

## SYMPOSIUM

---

November 21 - December 3, 2020

### Symposium Organizers

Jonathan Rivnay, Northwestern University  
Kaitlyn Sadtler, National Institute of Health  
Yun Shen, University of California Riverside  
Elizabeth Wayne, Carnegie Mellon University

### Symposium Support

**Bronze**  
Goodfellow Corporation  
MilliporeSigma

---

\* Invited Paper

SESSION F.GI01.06: Live Panel on Technology Development and Translation During a Pandemic  
Session Chairs: Kaitlyn Sadtler and Elizabeth Wayne  
Sunday Afternoon, November 29, 2020  
F.GI01

**1:30 PM PANELIST JOE DESIMONE; BETH VASY; WILLIAM HEETDERKS**

SESSION F.GI01.07: Live Keynote I: Diagnostics/Sensing  
Session Chair: Jonathan Rivnay  
Tuesday Morning, December 1, 2020  
F.GI01

**8:00 AM \*F.GI01.03.03**

**Homogeneous Bioluminescent Immunoassays: Cheap, Fast, and Sensitive Alternatives for ELISA in Point of Care Diagnostics** Maarten Merckx; Eindhoven University of Technology, Netherlands

The widely recognized need for more personalized, patient-centered healthcare requires the development of cheap, easy-to-use, yet reliable biomedical devices that are capable of detecting specific diseases. The current COVID-19 pandemic has made this need abundantly clear and has shown that we are ill-prepared for this and future viral pandemics. Immunoassays form the cornerstone of today's clinical biomolecular diagnosis. Their success is rooted in their modularity and the possibility to generate specific and high-affinity antibodies for almost any molecular target. However, translation of traditional heterogeneous immunoassays into point-of-care assays has proven challenging, because they require multiple incubation and washing steps, the addition of exogenous reagents, and external calibration. Laminar flow immune assays (LFIA) have been introduced as cheap and relatively easy-to-use POC immunoassays, but they suffer from limited sensitivity and are primarily used as qualitative tests.

In recent years our group pioneered the development of bioluminescent sensor proteins that allow affinity-based detection of antibodies, proteins, small molecules, and DNA/RNA directly in blood plasma using the camera of a smart phone as the sole piece of equipment. Unlike fluorescence, whose dependence on external illumination gives rise to autofluorescence and scattering, bioluminescence is ideally suited to measure analytes directly in complex media such as blood with minimal sample handling. In my presentation I'll focus on the development of a generic bioluminescent sandwich immunoassay platform that combines the analytical performance of a laboratory-based immunoassay such as ELISA with the speed and ease-of-use of laminar flow immunoassays. RAPPID (Ratiometric Plug-and-Play Immunodiagnostics) combines ratiometric bioluminescent detection with antibody-based target recognition into an easy-to-implement standardized workflow, and

therefore represents an attractive, fast, and low-cost alternative to traditional immunoassays, both in an academic setting and in clinical laboratories for point-of-care applications. The modularity of the RAPPID workflow also enables rapid development of point of diagnostics for newly emerging analytes, as demonstrated here by development of RAPPID assays for SARS-CoV-2 spike proteins and anti-SARS-CoV-2 antibodies. To allow further development for point-of-care diagnostic applications, RAPPID can be integrated in cheap and simple paper- or thread-based analytical devices or integrated into microfluidic cartridges, and dedicated readers could be developed to further increase sensitivity.

**8:20 AM \*F.GI01.03.01**

**Skin-Integrated Wireless Biosensors for Symptom Tracking** John A. Rogers; Northwestern University, United States

Rigorous and widespread testing remains a critical component of strategies for containing the COVID-19 pandemic. The limited availability of molecular diagnostics, however, creates a gap between requirements for population level testing and the availability of tests, likely to persist for the foreseeable future. These circumstances motivate the development of complementary technologies for diagnosing and monitoring COVID-19 infections. Consumer-grade wearables may have some utility in this context, but intrinsic shortcomings prevent measurements of the key symptoms of the disease: fever (98%), cough (65%) and shortness of breath (55%). This talk describes the custom development of a soft, hybrid electronic device, originally designed to track patients with aphasia and dysphagia, that mounts on the suprasternal notch to track all of these symptoms, continuously and with clinical-grade accuracy. Uses range from detecting early signs of symptoms in high risk populations, to monitoring the progression of patients with the disease in the hospital and in the home. Deployments on more than 250 healthcare workers and COVID-19 patients across the medical complex in Chicago over the last 20 weeks demonstrate the power of this technology, particularly when paired with HIPAA-compliant cloud data services and advanced analytics. Current and future activities will be discussed.

**8:40 AM \*F.GI01.03.02**

**High-Quality Factor (“High-Q”) Nanophotonics for COVID-19 Diagnostics** Jennifer A. Dionne, Jack Hu, Fareeha Safir, Jefferson Dixon, John M. Abendroth, Mark Lawrence, Scott Boyd, Benjamin Pinsky and Stefanie S. Jeffrey; Stanford University, United States

The emergence of COVID-19 has underscored the importance of rapid, frequent, sensitive and specific diagnostics for tracking and containing an infectious disease. Current detection methods including polymerase chain reaction (PCR) and enzyme-linked immunosorbent assays (ELISA) are robust and sensitive, but generally either rapid and qualitative or quantitative and slow; they are also constrained to measuring one analyte, such as a gene sequence or antibody isotype, at a time, and cannot correlate viral load to antibody type and level. Here, we present a new photonic chip-based technology that uses optical characterization to rapidly and quantitatively measure gene sequences and antibodies, and determine the corresponding viral load from the same patient. Our platform relies on high-quality-factor (“high-Q”) nanostructured dielectric substrates, known as metasurfaces. These high Q metasurfaces produce a large amplification of the electromagnetic field intensity, increasing the response to minute refractive index changes from targeted binding of a nucleic acid sequence or antibody; simultaneously, the optical signal is beam-steered for multiplexed detection. We will present the design and development of this quantitative optical assay, as well as application to clinical nasal-pharyngeal and serological samples from Stanford’s Clinical Virology Lab.

SESSION F.GI01.08: Live Panel Discussion I: Diagnostics/Sensing  
Session Chair: Jonathan Rivnay  
Tuesday Morning, December 1, 2020  
F.GI01

**9:00 AM PANELISTS: MAARTEN MERKS, JOHN ROGERS, JENNIFER DIONNE**

SESSION F.GI01.09: Live Keynote II: PPE/Surfaces  
Session Chairs: Jonathan Rivnay and Yun Shen  
Wednesday Morning, December 2, 2020  
F.GI01

**11:30 AM \*F.GI01.02.01**

**Leveraging Nanotechnology for Controlling SARS-CoV-2 Transmission** Danmeng Shuai; George Washington University, United States

COVID-19 has raised serious global public health concerns. The causative agent, SARS-CoV-2, has found to be environmentally persistent, and it can be transmitted through droplets or aerosols from an infected person and indirect contact via fomites. Nanotechnology has emerged as a promising tool for fighting against COVID-19, including but not limited to disease diagnosis, drug delivery, vaccine development, and pathogen detection and inactivation. In this talk, we will highlight recent progresses in controlling and inactivating pathogens in different environmental media, including SARS-CoV-2, by harnessing the power of nanotechnology. Specifically, electrospun nanofibrous membranes are developed to capture SARS-CoV-2-laden aerosols and they can be used for HVAC filters and masks/respirators. Photocatalysis that takes the advantage of environmental light can be implemented for effectively inactivating persistent pathogens on contact surfaces at an ambient condition.

**11:50 AM \*F.GI01.02.02**

**Harnessing Synthetic Biology to Address the COVID-19 Pandemic** James J. Collins; Massachusetts Institute of Technology, United States

Synthetic biology is bringing together engineers, physicists and biologists to model, design and construct biological circuits out of proteins, genes and other bits of DNA, and to use these circuits to rewire and reprogram organisms as well as create novel biomaterials. These biological circuits, living materials and re-engineered organisms are going to change our lives in the coming years, leading to cheaper drugs, rapid diagnostic tests, and synthetic probiotics to treat infections and a range of complex diseases. In this talk, we highlight recent efforts to create synthetic gene networks and programmable cells as new classes of diagnostics, therapeutics and vaccines for fighting pathogens, including SARS-CoV-2.

**12:10 PM \*F.GI01.02.03**

**Facial Masks during COVID-19: Imaging, Disinfection, Homemaking, and Future Materials Design** Yi Cui<sup>1,2</sup>; <sup>1</sup>Stanford University, United States; <sup>2</sup>SLAC National Accelerator Laboratory, United States

Facial masks are among the most important personal protection equipment to fight COVID-19. This talk covers our exciting progress related to facial masks including: 1) We utilized X-ray tomography and deep learning to perform 3D imaging and analysis of facial masks and the particle filtration to provide critical understanding how facial masks work. 2) We developed heating methods (dry and humid) as the most efficiency methods to disinfect N-95 level facial masks while maintaining their high filtration efficiency for over 20 times. 3) We studied a variety of household textiles and identify the most effective ones for homemade masks; 4) We propose that nanofiber filtration technology would afford the next generation high performance facial masks with high filtration efficiency and great breathability.

SESSION F.GI01.10: Live Panel Discussion II: PPE/Surfaces  
Session Chairs: Jonathan Rivnay and Yun Shen  
Wednesday Afternoon, December 2, 2020  
F.GI01

**12:30 PM PANELIST: DANMENG SHUAI, JAMES COLLINS, YI CUI**

SESSION F.GI01.11: Live Keynote III: Fundamentals/Therapeutics  
Session Chairs: Kaitlyn Sadtler and Elizabeth Wayne  
Thursday Afternoon, December 3, 2020  
F.GI01

**6:30 PM \*F.GI01.01.01**

**Microneedles Arrays for Effective and Efficient Mass Vaccinations** Burak Ozdoganlar; Carnegie Mellon University, United States

An effective mass vaccination strategy against SARS-CoV-2 and future pandemics requires both an efficacious vaccine and a reliable delivery method. To this end, intradermal (ID) delivery offers significant advantages over intramuscular (IM) or subcutaneous (SC) routes for developing rapid, potent, and long-lasting immunity. However, current ID delivery methods are unreliable and inconsistent, particularly for replication-competent and/or live attenuated vaccines. An effective way to address this problem is to use *microneedle arrays* (MNAs) for safe, reliable, efficient, and clinically relevant intradermal delivery of vaccines into the skin. MNAs include hundreds of micro-scale needles in a patch form. Vaccination using MNAs facilitates reproducible delivery of a high concentration of antigen to skin microenvironments for efficient and effective presentation of antigens to the skin's immune cells. In this talk, we will discuss the different type of MNA technologies, associated fabrication approaches for scalable manufacturing of MNAs, and their effectiveness in delivering surrogate vaccines to the human skin *ex vivo* and animal skin *in vivo*. One of those technologies include our new approach that uses Hybrid-MNAs, which combines advantages of other MNA technologies while addressing their drawbacks to realize significant advantages in regulation, manufacturing, application, and distribution aspects. Hybrid-MNAs will be inexpensive and patient friendly, will minimize cold-chain requirements and eliminate biohazardous sharps disposal. This would be transformational for global immunization programs.

**6:50 PM \*F.GI01.01.02**

**Insight from the Physical Sciences on Coronavirus Host Entry and Therapeutic Interventions** Susan Daniel; Cornell University, United States

The coronavirus disease 2019 (COVID-19) pandemic has focused attention on the need to develop effective therapies against the causative agent, SARS-CoV-2, and also against other pathogenic coronaviruses (CoV) that have yet to emerge. Focusing on steps in the CoV replication cycle, in particular the entry steps involving membrane fusion that are vulnerable to inhibition by broad-spectrum or specific antiviral agents, is an astute choice because of the conserved nature of the fusion machinery and mechanism across the CoV family. For coronavirus, entry into a host cell is mediated by a single glycoprotein protruding from its membrane envelope, called spike (S). Within S, the region that directly interacts with the membrane is called the fusion peptide, FP. It is the physico-chemical interactions of the FP with the host membrane that anchors it, thus enabling the necessary deformations of the membrane that lead to delivery of the viral genome into the cell when a fusion pore opens. Understanding of thermodynamics, kinetics, and intermolecular interactions are useful to describe FP interactions with the host membrane at the most fundamental molecular level. This knowledge in turn, can be used to facilitate the development of strategies to limit those interactions to stop the spread of infection. In this talk, I will describe our work on understanding the impact of calcium ions on CoV infection. Using cell infectivity, biophysical assays, and spectroscopic methods, we found that calcium ions serve to stabilize the fusion peptide structure during conformational change that then allows its insertion into the host membrane, resulting in increased lipid ordering in the membrane. This lipid ordering precedes membrane fusion and has been shown to correlate with increased fusion activity and higher levels of infection in the presence of calcium. As such, depletion of calcium ions leads to structure and activity changes in the fusion peptide that correlate well with *in vitro* experiments using calcium-chelating agents to block cell infection. In a final set of experiments, we used calcium channel blockers that are FDA approved for cardiac conditions to test their ability to block virus infection in lung cells. In some cases, these drugs eliminated infection, pointing to the possibility for re-purposing these drugs to treat COVID-19.

**7:10 PM \*F.GI01.01.03**

**Membrane Based Affinity Capture to Quantify Antibodies to COVID-19** Merlin Bruening; University of Notre Dame, United States

We are developing porous membranes containing affinity molecules to quantitatively capture antibodies and determine their concentration. Previously, we immobilized peptide mimotopes to bind therapeutic antibodies in serum. Flow through the membrane rapidly brings antibodies to binding sites to enable their capture with high efficiencies. In an effort to apply this to quantitation of COVID-19 antibodies, we are immobilizing COVID-19 proteins and capturing their antibodies. Subsequent binding of a fluorescently labelled secondary antibody provides a signal that we hope will be proportional to the quantity of polyclonal antibody. Moreover, because capture rates are high we will try to use a monoclonal antibody as a standard to estimate the absolute antibody concentration, whereas most analyses give a relative or qualitative value for antibody concentration. The presentation will present preliminary results and explain the method.



SESSION F.GI01.12: Live Panel Discussion III: Fundamentals/Therapeutics  
Session Chairs: Kaitlyn Sadtler and Elizabeth Wayne  
Thursday Afternoon, December 3, 2020  
F.GI01

**7:30 PM PANELIST: BURAK OZDOGANLAR, SUSAN DANIEL, MERLIN BRUENING**

SESSION F.GI01.01: Fundamental Studies/Modeling and Therapeutic Approaches  
On Demand Abstracts Available for Viewing Starting Saturday Morning, November 21, 2020  
F-GI01

**5:00 AM \*F.GI01.01.01**

**Microneedles Arrays for Effective and Efficient Mass Vaccinations** Burak Ozdoganlar; Carnegie Mellon University, United States

An effective mass vaccination strategy against SARS-CoV-2 and future pandemics requires both an efficacious vaccine and a reliable delivery method. To this end, intradermal (ID) delivery offers significant advantages over intramuscular (IM) or subcutaneous (SC) routes for developing rapid, potent, and long-lasting immunity. However, current ID delivery methods are unreliable and inconsistent, particularly for replication-competent and/or live attenuated vaccines. An effective way to address this problem is to use *microneedle arrays* (MNAs) for safe, reliable, efficient, and clinically relevant intradermal delivery of vaccines into the skin. MNAs include hundreds of micro-scale needles in a patch form. Vaccination using MNAs facilitates reproducible delivery of a high concentration of antigen to skin microenvironments for efficient and effective presentation of antigens to the skin's immune cells. In this talk, we will discuss the different type of MNA technologies, associated fabrication approaches for scalable manufacturing of MNAs, and their effectiveness in delivering surrogate vaccines to the human skin *ex vivo* and animal skin *in vivo*. One of those technologies include our new approach that uses Hybrid-MNAs, which combines advantages of other MNA technologies while addressing their drawbacks to realize significant advantages in regulation, manufacturing, application, and distribution aspects. Hybrid-MNAs will be inexpensive and patient friendly, will minimize cold-chain requirements and eliminate biohazardous sharps disposal. This would be transformational for global immunization programs.

**5:15 AM \*F.GI01.01.02**

**Insight from the Physical Sciences on Coronavirus Host Entry and Therapeutic Interventions** Susan Daniel; Cornell University, United States

The coronavirus disease 2019 (COVID-19) pandemic has focused attention on the need to develop effective therapies against the causative agent, SARS-CoV-2, and also against other pathogenic coronaviruses (CoV) that have yet to emerge. Focusing on steps in the CoV replication cycle, in particular the entry steps involving membrane fusion that are vulnerable to inhibition by broad-spectrum or specific antiviral agents, is an astute choice because of the conserved nature of the fusion machinery and mechanism across the CoV family. For coronavirus, entry into a host cell is mediated by a single glycoprotein protruding from its membrane envelope, called spike (S). Within S, the region that directly interacts with the membrane is called the fusion peptide, FP. It is the physico-chemical interactions of the FP with the host membrane that anchors it, thus enabling the necessary deformations of the membrane that lead to delivery of the viral genome into the cell when a fusion pore opens. Understanding of thermodynamics, kinetics, and intermolecular interactions are useful to describe FP interactions with the host membrane at the most fundamental molecular level. This knowledge in turn, can be used to facilitate the development of strategies to limit those interactions to stop the spread of infection. In this talk, I will describe our work on understanding the impact of calcium ions on CoV infection. Using cell infectivity, biophysical assays, and spectroscopic methods, we found that calcium ions serve to stabilize the fusion peptide structure during conformational change that then allows its insertion into the host membrane, resulting in increased lipid ordering in the membrane. This lipid ordering precedes membrane fusion and has been shown to correlate with increased fusion activity and higher levels of infection in the presence of calcium. As such, depletion of calcium ions leads to structure and activity changes in the fusion peptide that correlate well with *in vitro* experiments using calcium-chelating agents to block cell infection. In a final set of experiments, we used calcium channel blockers that are FDA approved for cardiac conditions to test their ability to block virus infection in lung cells. In some cases, these drugs eliminated infection, pointing to the possibility for re-purposing these drugs to treat COVID-19.

### 5:30 AM \*F.GI01.01.03

**Membrane Based Affinity Capture to Quantify Antibodies to COVID-19** Merlin Bruening; University of Notre Dame, United States

We are developing porous membranes containing affinity molecules to quantitatively capture antibodies and determine their concentration. Previously, we immobilized peptide mimotopes to bind therapeutic antibodies in serum. Flow through the membrane rapidly brings antibodies to binding sites to enable their capture with high efficiencies. In an effort to apply this to quantitation of COVID-19 antibodies, we are immobilizing COVID-19 proteins and capturing their antibodies. Subsequent binding of a fluorescently labelled secondary antibody provides a signal that we hope will be proportional to the quantity of polyclonal antibody. Moreover, because capture rates are high we will try to use a monoclonal antibody as a standard to estimate the absolute antibody concentration, whereas most analyses give a relative or qualitative value for antibody concentration. The presentation will present preliminary results and explain the method.

### 5:45 AM F.GI01.01.04

**Vent-Lock—A Bioinspired Ventilator Splitter to Enhance the Capacity of Treating Patients with COVID-19** Helen Xun<sup>1</sup>, Christopher Shallal<sup>1</sup>, Justin Unger<sup>1</sup>, Runhan Tao<sup>1</sup>, Alberto Torres<sup>1</sup>, Michael Vladimirov<sup>1</sup>, Jenna Frye<sup>2</sup>, Bo Soo Kim<sup>1</sup>, Broc Burke<sup>3</sup>, Michael Talcott<sup>3</sup>, Michael Montana<sup>3</sup>, Justin M. Sacks<sup>3</sup>, Julie Caffrey<sup>1</sup>, Jamie Guest<sup>1</sup> and Sung H. Kang<sup>1</sup>; <sup>1</sup>Johns Hopkins University, United States; <sup>2</sup>Maryland Institute College of Art, United States; <sup>3</sup>Washington University in St. Louis, United States

Due to the COVID-19 outbreak, many critical supplies for patient care and disease prevention are becoming increasingly scarce. One area that is increasingly in demand is ventilators. Ventilators are the mainstay treatment for COVID-19 patients that develop ARDS (Acute Respiratory Distress Syndrome), one of the primary causes of death of COVID-19. There exists an enormous gap between demand and supply. It is predicted that there is a global shortage of 880,000 ventilators. This is especially concerning in developing countries, where ventilators are already in short supply, and the hospitals may not have resources to meet those demands. Ventilator splitters are the most feasible option to increase capacity rapidly but face many challenges in inpatient care. The Society of Critical Care Medicine released a statement listing the challenges of splitting ventilators. Despite these challenges, ventilator splitting has already happened globally, including in New York City, as “the other option is death.” We have worked with anesthesiologists, clinicians, and ICU intensivists at Johns Hopkins Hospital to address pressing needs through materials research.

We will present our approaches to provide safe treatments for each patient by addressing the challenges associated with splitting ventilators. Due to the unstable supply chain, we have prototyped de novo ventilator splitters (“Vent-lock”) with flow restriction valve via 3D printing using biocompatible and easily sterilizable materials. Inspired by the shape and angles of the human bronchi, we designed the splitter to minimize turbulent airflow. We have used the ventilator splitter and flow restriction valve in a circuit containing filters, one-way valves, continuous monitoring, and positive end-expiratory pressure (PEEP) valves to safely allow clinicians to split ventilators for patients. Our 1+n(1) system is compatible with most ventilators and anesthesia machines.

We have tested our breathing circuits using a ventilator for two simulated patients with differing lung compliances, with continuous intrapulmonary data collection. We validated our airtight breathing circuit, and also produced one-way valves integrated into the ventilator splitter and filter drawers with replaceable filters to minimize aerosolization or cross-contamination of viruses. Our device was also validated for splitting anesthesia machines in in-vivo swine studies. Two swine were stably ventilated for five hours by one anesthesia gas machine, as confirmed by arterial blood gases, continuous airflow monitoring, and final lung histopathology. Our device is currently under review by the U.S. Food and Drug Administration for Emergency Use Authorization.

We envision that our study can contribute to increasing ventilator capacity safely to meet urgent ventilator shortages and provide another example that materials scientists and engineers contribute to addressing societal challenges such as COVID-19 by working with stakeholders from healthcare, government, and industry. Due to the multidisciplinary and collaborative nature of the materials research, the materials community is well-positioned to enable advances in medicine and public health.

### 5:55 AM F.GI01.01.05

**Late News: The pH-Varying Conformational States of SARS-CoV-2 Spike Glycoprotein** Ziyuan Niu, Miriam H. Rafailovich, Marcia Simon, Yuefan Deng and Peng Zhang; Stony Brook University, United States

**Introduction:** The coronavirus SARS-CoV-2 is postulated to infect cells by attaching its outer membrane S-protein (spike glycoprotein) [1] to the host cell targets such as ACE2, CD26, Ezrin, and cyclophilins [2]. Structurally altering the S-protein may mitigate or even block the infectivity of coronavirus. One way to alter the S-protein's physicochemical properties including structures and function is to surgically change the protonation and deprotonation state of each ionizable group to control the pH value[3]. The pH values of the aerosol droplets environment are known to change the chemical form, distribution, and reactivity [4-6] of the protein. Performing such study, e.g., immersing the virus and especially the S-protein in a solution of given pH values, is dangerous and nebulous. Our all-atomic molecular dynamics simulations, with their own challenges of long computation, allow us to examine the conformational states of the S-protein at extreme pH values. This is what we report in this work.

**Contributions:** We have performed our MD simulations of S-protein for five pH values in 3, 4, 5, 7, 11 for longer than the microsecond scales. With the current rate of simulation progress, we expect to reach a record simulated time and obtain the states of the S-protein for the first time. As the first attempt to control the pH values during MD simulation by protonation and deprotonation state of the amino acid sidechain residues in the S-protein, we may corroborate the simulated conformational states with the properties obtained in the lab bench experiments. We examine the detailed conformational states change at different pH values of the entire S-protein as well as the individual residues of interest.

**Methodologies:** We use the Gromacs program [7] to perform the MD simulation on the IBM Power9-based AiMOS supercomputer. The S-protein structure data is taken from the protein data bank (6VXX.pdb) and the force field for the S-protein and water molecule is from the CHARMM27. The S-protein is  $12 \times 13 \times 16 \text{ nm}^3$  in size which is placed in the water box of size  $21 \times 21 \times 21 \text{ nm}^3$ . Every simulation is controlled at the normal human body temperature of  $37^\circ\text{C}$  and a control group at this temperature and the neutral pH7 is run. Our MD simulations away from this neutral pH require the addition of the  $\text{Na}^+$  or  $\text{Cl}^-$  ions in the solvent to balance the charges and ensure the protonation state accuracy [8].

**Results:** The protein structure changes measured by RMSD for backbone and RMSF for individual residue were performed. Here is a list of brief observations: (1) The states of protein show significant RMSD increases for pH3 and pH11. We expect the protein to denature as we continue the simulation. (2) The conformational states for pH4 and pH5 appear to be quite similar to those of the pH7, at least for the simulated time we reached so far. (3) After 500ns, the protein at pH3 and pH11 showed obvious structural changes in specific residues. For pH3, ARG-466 and ASP-467 in Chain B are extremely active. Moreover, this is on the S1 domain, for binding the host cell [9]. For pH11, in both Chain A and Chain C, ASP-1146 and SER-1147 are more active than others. This part is on the S2 domain, which is for membrane fusion [9].

**Conclusion and Future Work:** The first studies of the effects of pH on S-protein at the microsecond scales provide us detailed pictures of the structural changes of whole S-protein and its individual residues. We continue the MD simulations to collect more data for various analyses of structures and functions of the S-protein and corroborate them with laboratory results.

SESSION F.GI01.02: Personal Protective Equipment and Surface Sanitization  
On Demand Abstracts Available for Viewing Starting Saturday Morning, November 21, 2020  
F-GI01

#### 5:00 AM \*F.GI01.02.01

**Leveraging Nanotechnology for Controlling SARS-CoV-2 Transmission** [Danmeng Shuai](#); George Washington University, United States

COVID-19 has raised serious global public health concerns. The causative agent, SARS-CoV-2, has found to be environmentally persistent, and it can be transmitted through droplets or aerosols from an infected person and indirect contact via fomites. Nanotechnology has emerged as a promising tool for fighting against COVID-19, including but not limited to disease diagnosis, drug delivery, vaccine development, and pathogen detection and inactivation. In this talk, we will highlight recent progresses in controlling and inactivating pathogens in different environmental media, including SARS-CoV-2, by harnessing the power of nanotechnology. Specifically, electrospun nanofibrous membranes are developed to capture SARS-CoV-2-laden aerosols and they can be used for HVAC filters and masks/respirators. Photocatalysis that takes the advantage of environmental light can be implemented for effectively inactivating persistent pathogens on contact surfaces at an ambient

condition.

**5:15 AM \*F.GI01.02.02**

**Harnessing Synthetic Biology to Address the COVID-19 Pandemic** [James J. Collins](#); Massachusetts Institute of Technology, United States

Synthetic biology is bringing together engineers, physicists and biologists to model, design and construct biological circuits out of proteins, genes and other bits of DNA, and to use these circuits to rewire and reprogram organisms as well as create novel biomaterials. These biological circuits, living materials and re-engineered organisms are going to change our lives in the coming years, leading to cheaper drugs, rapid diagnostic tests, and synthetic probiotics to treat infections and a range of complex diseases. In this talk, we highlight recent efforts to create synthetic gene networks and programmable cells as new classes of diagnostics, therapeutics and vaccines for fighting pathogens, including SARS-CoV-2.

**5:30 AM \*F.GI01.02.03**

**Facial Masks during COVID-19: Imaging, Disinfection, Homemaking, and Future Materials Design** [Yi Cui](#)<sup>1,2</sup>; <sup>1</sup>Stanford University, United States; <sup>2</sup>SLAC National Accelerator Laboratory, United States

Facial masks are among the most important personal protection equipment to fight COVID-19. This talk covers our exciting progress related to facial masks including: 1) We utilized X-ray tomography and deep learning to perform 3D imaging and analysis of facial masks and the particle filtration to provide critical understanding how facial masks work. 2) We developed heating methods (dry and humid) as the most efficiency methods to disinfect N-95 level facial masks while maintaining their high filtration efficiency for over 20 times. 3) We studied a variety of household textiles and identify the most effective ones for homemade masks; 4) We propose that nanofiber filtration technology would afford the next generation high performance facial masks with high filtration efficiency and great breathability.

**5:45 AM F.GI01.02.04**

**Facile Post-Process Coating for 3D Printed Nasopharyngeal Collection Swabs for Lubrication and Enhanced Specimen Collection** [Jason Hoffman-Bice](#) and Randall M. Erb; Northeastern University, United States

The disruption of the COVID-19 global pandemic has caused severe supply-chain disruption within several industries, to include food and medical devices. Due to supply shortages, focusing on medical devices, innovative solutions in additive manufacturing have been expedited through FDA approval, specifically in the arena of nasopharyngeal (NP) swabs, to increase testing rates of suspected COVID-19 patients. Further, there are other innovations, such as touchless door handles, allowing individuals to avoid hand contact with entry points if desired, leading to more hygienic interactions with public spaces. These provide strong examples that 3D printing can provide end-use products beyond prototyping. However, like many such manufacturing processes, additional processing techniques are required to produce the end-use products. The technology leading 3D printed NP swabs are SLA/DLP printers with acrylic based resins. This chemistry exhibits many drawbacks including both poor lubrication that leads to patient discomfort as well as less than desired wettability with specimens of patient sputum. This study investigated and screened biocompatible and hydrophilic coatings that may be applied to NP swabs in post-processing to increase lubrication and improve upon specimen collection quantity. Notably, the study was conducted during COVID lockdown which offers some additional supply chain learnings. To this end, a biocompatible modified poly(vinyl alcohol) (PVA) coating was applied to a 3D printed swab with a current marketed NP swab printing material already in use. The coating results showed an improvement in wettability as demonstrated by a 43.9% lowering of contact angle and a 39.3% improvement of specimen collection using synthetic saliva. This test case study was completed to help provide an additional solution to the manufacturing bottleneck for NP swabs. Additionally some further COVID case studies that are enabled by 3D printing will be briefly highlighted.

**5:55 AM F.GI01.02.05**

**Self-Limiting Electrospray Deposition to Create Bioactive Coatings** Lin Lei, Emran Lallow, Catherine Nachtigal, Hao Lin and [Jonathan P. Singer](#); Rutgers University, United States

Electrospray deposition (ESD) is a well-established technique for the creation of thin films from the spray of highly-charged droplets loaded with the materials to be deposited. While a majority of ESD research has focused on droplet evolution in air, the dissipation of charge on arrival at the substrate is critical in determining the macro- and micro-scale morphology of the final spray. Recently, we have categorized various modes of ESD, including self-limiting electrospray deposition (SLED). In SLED, specific manipulation of the electrostatic repulsion, hydrodynamic forces, and evaporation kinetics can be employed to conformally cover 3D architectures with microcoatings. The generated coatings are hierarchical, possessing either

nanoshell or nanoparticle microstructure. The initial demonstrations of SLED employed single glassy polymers as the solutes and simple cm-scale geometries as substrates. Here, I will discuss opportunities to create bioactive conformal coatings on medically-relevant architectures by employing blending, self-assembly, and complex geometries. Specifically, we explore coating transdermal microneedles with blends of DNA vaccines and rapid-dissolving matrices as a high-efficiency, scalable alternative to dip or inkjet coating. We demonstrate that we can deposit up to 70 wt% viable coatings of DNA in a sugar matrix that quickly dissolve upon insertion into the skin and show expression of GFP (pEGFP-N1). This method is compatible with rapid continuous manufacturing and is a route to shelf-stable, low-training vaccination administration for the current and future pandemic crises.

#### 6:05 AM F.GI01.02.07

**Late News: Binding Dynamics of SARS-CoV-2 Spike Glycoprotein to Polylactic Acid** Karin Hasegawa, Bernard Essuman, Fan Yang, Marcia Simon, Miriam H. Rafailovich, Yuefan Deng and Peng Zhang; Stony Brook University, United States

The personal protective equipment (PPE) may help reduce the risk of infection of the front-line healthcare workers of COVID-19 patients and others but the virus in aerosols, PPE and other materials' surfaces may also cause infections<sup>1,2</sup>. Studying the dynamics of the binding of SARS-CoV-2 spike glycoprotein (S-protein) to various substrates such as polylactic acid (PLA), the common material used in PPE, by *in silico* and *in vitro* experiments is essential. The S-protein, the key receptor for binding and promoting entry to host cells, is the main subject of our study that correlates *in silico* and *in vitro* data for validating the analysis of guidelines for improving PPE and other protection measures.

For *in silico* experiment, GROMACS is used for the MD simulations that are carried out at the reference room temperature (297K). The initial structure of the S-protein is obtained from the Protein Data Bank (PDB: 6VXX). CHARMM22/CMAP is used as the force field to perform MD for 200 ns for the structural relaxation of the S-protein in the NPT ensemble in the water system. PLA substrate is built with repeating optimized unit cells, where each unit cell is made of a set of lactic acid monomer which is generated using AVOGADRO and LigParGen. The structure of the PLA sheet is relaxed in a vacuum box in the NVT ensemble using OPLS-AA. To achieve the desired structure of the sheet, additional relaxation is performed in the NVT ensemble with CHARMM36. The well-relaxed S-protein and the PLA sheet are placed in a water box of size 21×27×21 nm<sup>3</sup> and the initial distance between two species is set to 0.8 nm. CHARMM36 is adapted to this system and Van der Waals radii of the carbon atom are increased to 0.51 nm to prevent the H<sub>2</sub>O molecules from erroneously slipping into the PLA substrate. The substrate is restrained during the equilibriums. The NPT production run is carried and the RMSD of the S-protein and the system trajectory are monitored to ensure the stability of the system. For *in vitro* experiment, the H1N1 is used as an alternative to the SARS-CoV-2 due to the laboratory restrictions. The viruses are placed on a plate and the plate is left at room temperature (297K) for an arbitrary period.

The relaxed S-protein-PLA system allows us to do an analysis of binding by i) counting the number of the atomic contacts among S-protein and PLA atoms and quantify the binding intensity. ii) calculating the binding force as a function of time to extract the binding dynamics. The analysis of *in vitro* experiment is done by washing the virus adhered to the plate with water every arbitrary period. The number of remaining viruses on the plate is counted accordingly and the results are plotted over time. Finally, both *in silico* and *in vitro* data are correlated with statistical tools and both results are cross-validated.

The data we obtain from our *in silico* and *in vitro* experiments provide a vital understanding of the binding dynamics of the protein and the guidelines for the protection of the contagion. We will expand our research to a matrix of various environmental conditions including temperature, pH values, and salinities on various substrates including inorganic, organic, and living cells, beyond our current studies with only one temperature (297K) and one material (PLA). In addition to understanding the elusive virus-substrate properties for the S-protein, our methodology and the resulting platform can be extended to the study of other viruses and substrates at other conditions.

The project is supported by OVPR&IEDM COVID-19 Grant and SUNY-IBM Consortium Award.

<sup>1</sup> van Doremalen, Neeltje et al. "Aerosol and Surface Stability of SARS-CoV-2 as Compared with SARS-CoV-1." *The New England journal of medicine* vol. 382,16 (2020): 1564-1567. doi:10.1056/NEJMc2004973

<sup>2</sup> Vasickova, P. et al. "Issues Concerning Survival of Viruses on Surfaces." *Food and Environmental Virology* vol. 2,1 (2010): 24-34. doi:10.1007/s12560-010-9025-6

#### 6:15 AM F.GI01.02.08

**Late News: Towards the Design of a Novel Antimicrobial/Antiviral Filtration System** Antwine W. McFarland, Chris Miller, Anusha Elumalai, Ahmed Humayun and David K. Mills; Louisiana Tech University, United States

With the COVID-19 pandemic, we face a global health crisis not seen since the influenza pandemic of 1918. It is believed

that the transmission of COVID-19 is thought to occur through respiratory droplets. As such, current CDC guidelines recommend using N95 masks for healthcare providers managing the care of patients infected with SARS-CoV-2 or persons under investigation (PUI) for COVID-19. The shortage of N95 style masks that could effectively protect health care professionals against harmful pathogens is of critical need in halting the current pandemic's trajectory and containing future outbreaks.

Using modified halloysite nanotubes (HNTs), we manufactured two products that work in conjunction with each other. We applied a simple, novel, and effective electrodeposition method for coating the surfaces of HNTs with metal nanoparticles (copper, silver, and zinc). Each metal is known to possess potent antiviral and antimicrobial properties. Metal-coated HNTs (mHNTs) were then added to polylactic acid and extruded to form a mHNT/PLA 3D printer filament. Furthermore, the halloysite's inner lumen was vacuum loaded with an additional antibacterial agent before the extrusion process.

Our antimicrobial/antiviral mHNT/polymer composite 3D printer filament was used to fabricate an N95-style mask with an interchangeable filter with surfaces that will deactivate a virus and reduce or eliminate adhesion, prevent bacterial growth, and reduce deadly infections. Antibacterial studies were conducted using methods that tested the efficacy of our design in a liquid medium and as a surface. Testing discs were 3D printed using the antimicrobial polymer composite. *E. coli* and *S. aureus* were the bacteria used in our experiments as they represent fast-growing gram-positive and gram-negative bacteria. The samples containing non-doped mHNTs showed a marked inhibition in the growth of both bacteria. However, the samples containing doped mHNTs showed an even greater ability to inhibit bacterial growth.

The filter respirator was made using the same ratio of PLA to mHNTs. Once dissolved in the solvent, the mixture was sprayed onto sterile gauze using a commercially available airbrush. Following the blow spraying of the gauze, the new filter was allowed to dry before another layer of treated gauze was added to the filter to make a three-layer sandwich consisting of gauze, blow spun antimicrobial fibers, and gauze. Simultaneously, the mask can be sanitized by alcohol or hydrogen peroxide solution, or UV light radiation and reused. The *National Institute for Occupational Safety and Health (NIOSH) guidelines require that a mask must be able to protect people with different facial features. Our mask can be form-fitted to an individual's unique facial features due to our mask's unique design.* Merely placing the mask in warm water will momentarily make the mask moldable. Once cooled, the shape is preserved for a custom fit. Additionally, masks were manufactured in smaller sizes that could accommodate children and young adults.

The technology developed for the respirator has additional uses. Utilizing the airbrushing method to cover a filter material, air-conditioning filters can be coated with the antimicrobial coating. Using preexisting air conditioning filters as a building platform, this technology can be used to keep areas such as hospitals, clean rooms, and quarantine areas free of contaminants. Moreover, the air can be filtered on its way out using a different filtration system to keep harmful pathogens from exiting those closed-off areas.

Future studies will include antiviral studies. We are confident in our mask and filter system's ability to perform as designed and eliminate the viruses promptly. Fit testing to become NIOSH certified will also be conducted. A qualitative study will rate the degree of discomfort the wearer experiences while wearing the mask for long periods, ranging between 4, 8, and 10 hours.

#### 6:25 AM F.GI01.02.09

**Late News: Artificial Intelligence Accelerated Design of Antimicrobial/Antiviral Surfaces—A Promising Route to Mitigate SARS-COV-2 Fomite Transmission** Heesoo Park<sup>1</sup>, El Tayeb Bentría<sup>1</sup>, Abdelilah Arredouani<sup>2</sup>, Halima Bensmail<sup>3</sup> and Fadwa El Mellouhi<sup>1</sup>; <sup>1</sup>Qatar Environment and Energy Research Institute, Hamad Bin Khalifa University, Qatar; <sup>2</sup>Qatar Biomedical Research Institute, Qatar; <sup>3</sup>Qatar Computing Research Institute, Qatar

Coronavirus disease 19 (Covid-19), caused by severe acute respiratory syndrome coronavirus 2 (SARS-CoV-2) infection, is the worst global pandemic of the 21st century to date, and continues to infect and kill many individuals worldwide. SARS-CoV-2 remains intact and contagious in small droplets (<5µm) and can be suspended in the air for up to three hours. Therefore, airborne isolation, room ventilation, and appropriate application of disinfectant might restrict aerosol spread of the virus. However, the virus-laden droplets that are too heavy to remain in the air would rather fall on nearby floors or surfaces, creating fomites (or contaminated surfaces). Recent studies have evaluated the stability of SARS-CoV-2 on different surfaces, and it was found that the virus could survive from 24h on cardboard to 2 days on stainless steel and wood and even to 7 days on outside of surgical masks. This indicates that the fomites can represent a considerable mode of transmission mainly in closed areas.

Nowadays, most experiments to synthesize and test antimicrobial/antiviral materials are based on trial and error, and often it is not known how the inhibitors act on the microorganism. In this work we will showcase how artificial intelligence and machine learning methods could be used to speed the design and optimization of antimicrobial/antiviral surfaces. Using computational methods, namely electronic structure calculations combined with data analytics and machine learning algorithms, we build a model able to estimate the activity of pathogen inhibitors. We focus our attention on photocatalytic systems that can be tailored to give a balanced production of Reactive Oxygen Species (ROS) upon illumination while taking into consideration the cost associated with a large-scale deployment of this solution. We built an artificial intelligence model that is able to predict the rates of ROS production while varying the composition and properties of the photocatalytic system. The proposed candidate materials, predicted from the computational modeling, may find application for high touch surfaces to avoid fomite viral and bacterial transmission, and also as coating for air conditioning and air cleaning filters to mitigate the viral transmission via aerosol.

### 6:35 AM F.GI01.02.10

**Late News: Thermal Analysis of the SARS-CoV-2 Spike Glycoprotein by *In Silico* and *In Vitro* Experiments** Meichen Song, Fan Yang, Miriam H. Rafailovich, Marcia Simon, Yuefan Deng and Peng Zhang; Stony Brook University, The State University of New York, United States

**Objectives:** The SARS-CoV-2 engulfs the world from tropical countries like India [1] at 51°C to cold supply chains [2, 3] at 3-4°C. Our molecular dynamics (MD) analysis of the temperature-dependent structural changes of the virus' spike glycoprotein (S-protein) [4-6] help bridge the data gaps from *in vitro* experiments to viral transmission assessment. Our thermolability studies of the protein immersing in H<sub>2</sub>O, differing from most protein binding simulations as the percentage of drug bound or unbound fraction [7, 8], complement the sparse and inconsistent *in vitro* experiments with high-infectious virus cultivation [9-12]. Correlating the *in vitro* and *in silico* experiments allows us to establish a deep neural network model for relating the virus's survival time or metamorphosis to the ambient temperatures.

**Methods and Materials:** Our *in silico* experiments of S-protein (PDB file 6VXX) involve immersing it in a H<sub>2</sub>O box of 21×21×21 nm<sup>3</sup> using the CHARMM27 force field under NVT ensemble. We calculate the S-protein's thermal instabilities based on RMSD of backbone, at eventful or purposeful temperatures: 3°C, 20°C, 37°C, 60°C, 80°C, 95°C, and 300°C. The *in vitro* experiments, where the infectivity is determined by a TCID<sub>50</sub> assay, is reported [12, 13]. The curve of RMSD vs. temperatures of the *in silico* data is corroborated with that of the inactivation time vs. temperature of the *in vitro*. The *in vitro* and *in silico* data are applied to cluster the distributions of RMSD of both experiments to generate a rough grouping of the protein's survival duration from weeks to milliseconds.

**Results:** The *in vitro* experiments and the *in silico* results can complement and verify each other:

Stable at low temperature: The average of RMSD at 3°C is 38% lower than it at 20°C with the small variance, agreeing with *in vitro* experiments that salmon-attached coronavirus at 4°C remain infectious for more than a week [3] and there was only around a 0.7 log-unit reduction of infectious titer on day 14 at 4°C [13].

Sensitive at 60°C~80°C: the distribution of RMSD at 20°C is similar to it at 37°C but different with it at 60°C. Two peaks in distribution at 60°C indicate the structure instability is shifting from a lower to higher level. The average of RMSD increases 30% with temperature from 60°C and 80°C, serving as a signal for the presence of a critical heat denaturation in that range. Those *in silico* results perfectly agree with *in vitro* results that the inactivation time at 37°C, 56°C and 70°C change from 24h, 30min to 5min [12, 13].

3) The *in vitro* survival time vs. temperature [12] agrees with the curve of RMSD vs. temperatures *in silico* experiments, showing a zone of substantial structural variation, suggesting existence of a critical temperature.

4) Correlate with *in vitro* data [12, 13], the clustering distributions of RMSD roughly group the virus' survival time at temperature ranges: 60°C-70°C, 80°C-95°C, and 300°C groups to week-, day-, hour-, minute- and microsecond-scales, respectively.

**Discussions:** Our millisecond-scale MD simulations help reveal the thermal properties of the S-protein. These *in silico* experiments corroborate well with the *in vitro* ones and, conversely, guide additional *in vitro* experiments, showing the benefits of "amalgamating" these two experiments. The 10-ms runs are expected to enhance the correlation and prediction accuracy. Our continued simulations at higher temperatures will likely capture the denaturation. This vital ground truth, coupled with *in vitro* experiments, will allow us to develop machine learning algorithms to predict the virus' survival duration at a given temperature and make quicker and wider discovery of properties of the coronavirus and, potentially, other materials.

**Acknowledgment:** The project is supported by OVPR&IEDM COVID-19 Grant and SUNY-IBM Consortium Award.

**5:00 AM \*F.GI01.03.01**

**Skin-Integrated Wireless Biosensors for Symptom Tracking** John A. Rogers; Northwestern University, United States

Rigorous and widespread testing remains a critical component of strategies for containing the COVID-19 pandemic. The limited availability of molecular diagnostics, however, creates a gap between requirements for population level testing and the availability of tests, likely to persist for the foreseeable future. These circumstances motivate the development of complementary technologies for diagnosing and monitoring COVID-19 infections. Consumer-grade wearables may have some utility in this context, but intrinsic shortcomings prevent measurements of the key symptoms of the disease: fever (98%), cough (65%) and shortness of breath (55%). This talk describes the custom development of a soft, hybrid electronic device, originally designed to track patients with aphasia and dysphagia, that mounts on the suprasternal notch to track all of these symptoms, continuously and with clinical-grade accuracy. Uses range from detecting early signs of symptoms in high risk populations, to monitoring the progression of patients with the disease in the hospital and in the home. Deployments on more than 250 healthcare workers and COVID-19 patients across the medical complex in Chicago over the last 20 weeks demonstrate the power of this technology, particularly when paired with HIPAA-compliant cloud data services and advanced analytics. Current and future activities will be discussed.

**5:15 AM \*F.GI01.03.02**

**High-Quality Factor (“High-Q”) Nanophotonics for COVID-19 Diagnostics** Jennifer A. Dionne, Jack Hu, Fareeha Safir, Jefferson Dixon, John M. Abendroth, Mark Lawrence, Scott Boyd, Benjamin Pinsky and Stefanie S. Jeffrey; Stanford University, United States

The emergence of COVID-19 has underscored the importance of rapid, frequent, sensitive and specific diagnostics for tracking and containing an infectious disease. Current detection methods including polymerase chain reaction (PCR) and enzyme-linked immunosorbent assays (ELISA) are robust and sensitive, but generally either rapid and qualitative or quantitative and slow; they are also constrained to measuring one analyte, such as a gene sequence or antibody isotype, at a time, and cannot correlate viral load to antibody type and level. Here, we present a new photonic chip-based technology that uses optical characterization to rapidly and quantitatively measure gene sequences and antibodies, and determine the corresponding viral load from the same patient. Our platform relies on high-quality-factor (“high-Q”) nanostructured dielectric substrates, known as metasurfaces. These high Q metasurfaces produce a large amplification of the electromagnetic field intensity, increasing the response to minute refractive index changes from targeted binding of a nucleic acid sequence or antibody; simultaneously, the optical signal is beam-steered for multiplexed detection. We will present the design and development of this quantitative optical assay, as well as application to clinical nasal-pharyngeal and serological samples from Stanford’s Clinical Virology Lab.

**5:30 AM \*F.GI01.03.03**

**Homogeneous Bioluminescent Immunoassays: Cheap, Fast, and Sensitive Alternatives for ELISA in Point of Care Diagnostics** Maarten Merkx; Eindhoven University of Technology, Netherlands

The widely recognized need for more personalized, patient-centered healthcare requires the development of cheap, easy-to-use, yet reliable biomedical devices that are capable of detecting specific diseases. The current COVID-19 pandemic has made this need abundantly clear and has shown that we are ill-prepared for this and future viral pandemics. Immunoassays form the cornerstone of today’s clinical biomolecular diagnosis. Their success is rooted in their modularity and the possibility to generate specific and high-affinity antibodies for almost any molecular target. However, translation of traditional heterogeneous immunoassays into point-of-care assays has proven challenging, because they require multiple incubation and washing steps, the addition of exogenous reagents, and external calibration. Laminar flow immune assays (LFIA) have been introduced as cheap and relatively easy-to-use POC immunoassays, but they suffer from limited sensitivity and are primarily used as qualitative tests.

In recent years our group pioneered the development of bioluminescent sensor proteins that allow affinity-based detection of antibodies, proteins, small molecules, and DNA/RNA directly in blood plasma using the camera of a smart phone as the sole piece of equipment. Unlike fluorescence, whose dependence on external illumination gives rise to autofluorescence and scattering, bioluminescence is ideally suited to measure analytes directly in complex media such as blood with minimal sample handling. In my presentation I’ll focus on the development of a generic bioluminescent sandwich immunoassay



platform that combines the analytical performance of a laboratory-based immunoassay such as ELISA with the speed and ease-of-use of laminar flow immunoassays. RAPPID (Ratiometric Plug-and-Play Immunodiagnosics) combines ratiometric bioluminescent detection with antibody-based target recognition into an easy-to-implement standardized workflow, and therefore represents an attractive, fast, and low-cost alternative to traditional immunoassays, both in an academic setting and in clinical laboratories for point-of-care applications. The modularity of the RAPPID workflow also enables rapid development of point of diagnostics for newly emerging analytes, as demonstrated here by development of RAPPID assays for SARS-CoV-2 spike proteins and anti-SARS-CoV-2 antibodies. To allow further development for point-of-care diagnostic applications, RAPPID can be integrated in cheap and simple paper- or thread-based analytical devices or integrated into microfluidic cartridges, and dedicated readers could be developed to further increase sensitivity.

#### **5:45 AM F.GI01.03.04**

**Low Cost Paper-Based Immunoassays for COVID-19 Diagnostics** [Kimberly Hamad-Schifferli](#); University of Massachusetts Boston, United States

The COVID-19 pandemic has suffered from a lack of rapid diagnostic tests, where the need far exceeds current supplies. Tests are required both for diagnosing infections as well those that can test for the presence of antibodies, which will aid in determining immunity. To meet what is expected to be an extreme demand for mass testing, there needs to be point of care tests that can be run by non-experts and go from sample to answer within minutes. Also, because the supply chain for reagents has been unable to meet the needs for testing, a diversified portfolio of biological reagents tests is also needed.

Paper based immunoassays are attractive for use as rapid diagnostics for COVID-19 and many other infectious diseases because they are low cost and can be administered at point of care and in field settings. Readout by eye is made possible by the gold nanoparticle-antibody conjugates, which have a strong absorption due to the nanoparticle surface plasmon resonance, thus providing sample-to-answer times of minutes. We describe the development of gold nanoparticle-antibody conjugates for use in COVID-19 tests, and how the physical properties of the nanoparticle can impact test performance and sensitivity.

In addition, preparation for the next emerging outbreak requires the ability to develop tests in a nimble manner. We describe a route for repurposing stockpiled antibodies to make immunoassays for new diseases for which antibodies have not yet been developed. We leverage cross reactive antibodies and the size- and material- dependent properties of gold nanoparticles, demonstrating it for multiplexed diagnostics for yellow fever, dengue, and zika viruses. By adapting immunoassays for selective sensing as opposed to specific sensing and using machine learning of the color test lines, we are able to construct an assay for yellow fever non structural protein 1(NS1) using cross-reactive antibodies raised for dengue and zika.

#### **5:55 AM F.GI01.03.05**

**Screening and Management of COVID-19 with Paper-Based Nanoparticle Tests** [Roberto de la Rica](#)<sup>1,2</sup>, Antonio Clemente<sup>1</sup>, Cristina Adrover-Jaume<sup>1,2</sup>, Alejandra Alba-Patiño<sup>1,2</sup>, Andreu Vaquer<sup>1</sup> and Giulia Santopolo<sup>1,2</sup>; <sup>1</sup>IdISBa (Health Research Institute of the Balearic Islands), Spain; <sup>2</sup>University of the Balearic Islands, Spain

The global COVID-19 pandemic strains healthcare systems with a sharp increase in critical care demand coupled with a decrease in available staff as healthcare workers are more likely to fall ill as well. To prevent these strains from leading to collapse, it is essential to find new ways to quickly detect new infections and closely monitor disease progression. Quick detection would greatly assist in the process of contact tracing. As for monitoring, one critical point in the healthcare chain is to identify patients who are developing severe COVID-19 and to provide treatment before critical care becomes necessary in order to avoid oversaturation of ICUs (1). There is a common consensus that a hyper-inflammatory syndrome or a “cytokine storm” is responsible for poor outcomes in COVID-19. Thus, it is crucial to develop rapid point-of-care tests for cytokine detection so that patients with a poor prognosis can be detected early and eschew the need for critical care. At the same time, healthcare workers must be tested regularly to limit contagions. While this is currently done with RT-PCR, it would be desirable to find alternative ways to screen for new infections for hospital staff.

In this presentation I introduce a diagnostic platform for monitoring disease severity and new SARS-CoV-2 infections. It is based on modifying conventional filter paper with polymers so that it can store antibody-decorated gold nanoparticles (2). The polymer treatment also ensures a highly efficient transfer to other substrates such as cellulose or polypropylene, which is the basis for the diverse family of diagnostic tests presented here. For example, we have developed tests for detecting IL-6 at the point of care using cellulose as the substrate. IL-6 is a key player in the COVID-19 cytokine storm as well as a therapeutic target for immunomodulating drugs. Our tests can detect alarming levels of this biomarker in the blood of

COVID-19 patients in less than 20 min. They can also detect IL-6 in respiratory samples (bronchial aspirate, sputum) of COVID-19 patients rapidly thanks to our method for sample liquefaction. This approach could greatly improve the evidence base for the coronavirus management by revealing fluctuations in local inflammatory biomarkers. We have also developed diagnostic tests based on the detection of viral proteins attached to a medical face mask. In this approach, biomarkers adsorbed to the propylene fibers inside the filter of the mask are detected by pressing our paper-based tests against them. This transfers antibody-decorated nanoparticles to the mask, which then generate a colored spot on it if the target proteins are present. This approach could be an inexpensive alternative to RT-PCR for COVID-19 screening. All our analytical platforms benefit from smartphone-based detection approaches developed in our lab, which makes them highly portable and easy to implement at the bedside. Because the assays are paper-based, they can be easily disposed of by incineration, therefore circumventing biosafety issues. These features, along with the versatile design for detecting antigens in different sample types, make our diagnostic tests excellent candidates for managing and screening COVID-19 at the point of care.

(1) ACS Sensors DOI: 10.1021/acssensors.0c00979

(2) ACS Sensors 2020, 5, 1, 147-153.

#### 6:05 AM F.GI01.03.07

**Late News: Molecular Imprinted Biosensor for SARS-CoV-2 Detection** Won-Il Lee<sup>1</sup>, Robert Wong<sup>1</sup>, Steffen Mueller<sup>2</sup>, Chang-Yong Nam<sup>3</sup>, Michelle Chang<sup>4</sup>, Nishanth Chinnadurai<sup>5</sup>, Jolene Huey<sup>6</sup>, James Kim<sup>7</sup>, Udithi Kothapalli<sup>8</sup>, Hugo Onghai<sup>9</sup>, Jeannie She<sup>10</sup> and Miriam H. Rafailovich<sup>1</sup>; <sup>1</sup>Stony Brook University, The State University of New York, United States; <sup>2</sup>Codagenix Inc, United States; <sup>3</sup>Center for Functional Nanomaterials, Brookhaven National Laboratory, United States; <sup>4</sup>Seoul International School, Korea (the Republic of); <sup>5</sup>East Meadow High School, United States; <sup>6</sup>Arcadia High School, United States; <sup>7</sup>Great Neck South High School, United States; <sup>8</sup>Saint Anthony's High School, United States; <sup>9</sup>Earl L. Vandermeulen High School, United States; <sup>10</sup>Walt Whitman High School, United States

The proliferation of cases during the COVID-19 pandemic has increased the urgency for point-of-care (POC) diagnostic tests. A rapid, accurate, affordable, and accessible diagnostic system in the field is necessary to extensively monitor an affected population to suppress the spread of the epidemics effectively. In this study, an electrochemical diagnostic sensor was developed to be capable of detecting entire virions or virion-associated proteins, which can be applied for rapid POC detection of SARS-CoV-2. The molecular imprinting (MI) technique was utilized on the surface of a gold substrate with virions and hydroxyl-terminated alkanethiol chains to form a self-assembled-monolayer (SAM) crystallized to the specific shape of targeted analytes. The crystalline SAM behaved as a footprint by forming cavities on the surface, and it allows specificity can be attributed to the cavities formed in the thiol layer based upon the size, orientation, and hydrophilicity of the analytes. Real-time detection of the target virus was possible by measuring the potential difference through the re-adsorbing of the analyte with the imprinted pattern to generate a surface charge on the chip. The technique was previously shown to be comparable to Elisa in accuracy of CEA cancer marker detection in humans but with 1/100 of the test volume [1]. In a recent publication, we also demonstrated that the technique could detect ZIKV in saliva at sub infectious concentrations of less than 10 PFU/mL and accurately discriminate against DENV [2]. Here we show that the sensor could selectively detect the influenza A viruses H1N1 and H3N2, which are morphologically similar to SARS-CoV-2, as well as the four capsid SARS-COV-2 proteins, in phosphate-buffered saline and human saliva without any sample manipulation. Heat inactivated H1N1 and H3N2 will also be tested and compared to results from heat inactivated SARS-COV-2 virus. These results demonstrate that the molecular imprinting technique has the potential to become a POC detection system for rapid and accurate screening of SARS-CoV-2.

This work was performed in part at the Center for Functional Nanomaterials (CFN) of Brookhaven National Laboratory (BNL).

[1] Yingjie Yu, et al. "Quantitative real-time detection of carcinoembryonic antigen (CEA) from pancreatic cyst fluid using 3-D surface molecular imprinting." *Analyst*, 2016, 141, 4424-4431

[2] Vincent Ricotta, et al. "A chip-based potentiometric sensor for a Zika virus diagnostic using 3D surface molecular imprinting." *Analyst*, 2019, 144, 4266-4280

#### 6:15 AM F.GI01.03.08

**Late News: Point-of-Care Biosensor for Rapid SARS-CoV-2 S1 Spike Protein Detection Using Aerosol Jet Printed Organic Electrochemical Transistor** Jiaxin Fan, Sheldon Parr, Seongdae Kang and Manisha Gupta; University of Alberta, Canada

Severe acute respiratory syndrome coronavirus 2 (SARS-CoV-2) has spread across the world and led to more than 924,000 deaths to date according to John Hopkins Coronavirus Resource Centre (September 14, 2020). Researchers and scientists around the world are actively working on developing therapeutics and vaccines for coronavirus disease 2019 (COVID-19).

The rapid transmission from asymptomatic infected people has made COVID-19 such a widespread and deadly pandemic compared to SARS or MERS. Relying on “social-distancing” measures comes at enormous economic and social cost; this type of compliance is not a sustainable long-term solution. Rapid large population screening to determine the confirmed cases and contact tracing are vital for controlling the spread. The current essential technology for confirmation of SARS-CoV-2 infection is nucleic acid amplification. Nucleic acid amplification-based diagnostics are reliable and highly sensitive, however, the time required for sample transportation, preparation, and completion of the assay does not provide the high throughput capacity for quick and mass population screening. Hence, developing a rapid and accurate sensing platform for SARS-CoV-2 detection is still an urgent need.

In this work, we have developed a prototype point-of-care device for rapid SARS-CoV-2 subunit 1 (S1) spike protein detection using organic electrochemical transistor (OECT) based biosensors. These sensors are being developed to work with saliva samples. The OECTs were fabricated using Optomec Aerosol Jet 5X 3D printer on flexible polyimide substrate, with Au nanoparticle ink for source, drain and gate electrodes, PEDOT:PSS channel, and UV-curable PDMS as the insulator. The printed in-plane Au gate electrode was chemically modified and immobilized with a specific antibody against the SARS-CoV-2 S1 spike protein. A distinctive shift in the transfer characteristics of OECT before and after the chemical modification and the antibody immobilization. Spike test was performed with biasing the OECT at constant voltages and adding SARS-CoV-2 S1 spike protein with different concentrations. The biosensors being developed are single use disposable chips. In addition, a small measurement kit has been developed which will provide the readout result from the chip indicating a positive or negative test result. As the proposed biosensors are printed using aerosol jet 3D printer and they can economically be scaled while maintaining their quality. The sensor can be deployed quickly at workplaces, schools, hospitals, airports, etc. for immediate test results.

SESSION F.GI01.04: Poster Session: Special Symposium on Materials Approaches for Tackling COVID-19  
On Demand Abstracts Available for Viewing Starting Saturday Morning, November 21, 2020  
5:00 AM - 8:00 AM  
F-GI01

#### **F.GI01.04.01**

**Substrate-Free PEDOT:PSS Fibre Arrays as Breath Sensor** Wenyu Wang and Yan Yan Shery Huang; University of Cambridge, United Kingdom

The development of a portable, rapid and efficient breath detector could potentially benefit the study of human respiration. This is of particular interest under the background of a global pandemic which could be spread through the respiratory system. Herein, we report an integrated, low-cost breath analyser that is composed of multi-layered, suspended PEDOT:PSS microfibre arrays, fabricated by original inflight fluidic fibre printing technique. Based on that the resistance of PEDOT:PSS is sensitive to the moisture change, this breath analyser offers a direct signal read-out. Thanks to the small diameter and large surface-to-volume ratio, the microfibres are much more responsive to the dynamics of moisture flow in air compared with planer or film based moisture sensor. Moreover, the ultrathin diameter and substrate-free feature enable the entire fibre array to be transparent and air permissive; thus, this sensor could be directly mounted in front of a camera, allowing visualisation at the same time. We demonstrate that this human breath analyser could be able to detect and distinguish the human breath level, when talking, breathing and coughing. In addition, we show that the breath sensor is also able to distinguish the human breath level change when wearing various face masks.

#### **F.GI01.04.02**

**Combat COVID-19—Sterilize and Recharge Masks Simultaneously for Safe Reuse** Sriram Sundar Shankara Narayanan, Xudong Wang, Zijian Weng, Vladislav Paley, Libin Ye and Ying Zhong; University of South Florida, United States

To rapidly respond to the COVID-19 pandemic and address the extreme shortage of proper sterilization methods for Personal Protective Equipment (PPE) and surfaces, we have urgently advanced safe, sustainable and high-efficiency corona discharge (CD) based sterilization technology. Filtering facepiece respirators (FFRs) like N95 masks and surgical masks are essential for reducing the spread of the virus. FFRs are primarily made of hydrophobic melt blown polypropylene layers. In addition to small pore sizes (<1µm), the filtration efficiency of N95 masks are also attributed to the electrostatic charges embedded in the fibers. These charges result in electrostatic attraction of small droplets carrying micro-organisms, effectively trapping them between the fibers. There are several attempts to decontaminate and reuse masks using existing sterilization techniques like heat, UV, etc. Although, these methods are effective in killing the virus, they negatively affect the filtration efficiency over

time.

In this study, we use CD to effectively sterilize masks and renew their filtration efficiency to make masks reusable. A high voltage is applied to a sharp electrode leading to dielectric breakdown of air. Electron and ion pairs are generated due to the avalanche effect. The combination of high electric field, ion bombardment and reactive species leads to effective sterilization of FFRs. The ions also renew the electrostatic charges on the surface of the fibers, thus recovering the filtration efficiency of the masks. Sterilization effect and mechanisms are being tested against *E. coli*, spores and SARS-CoV-2 virus. The sterility assurance level (SAL) has reached  $10^{-3}$  with single spot electrode discharge, which is the requirement for safe mask reuse. Masks are also successfully recharged after CD treatment within seconds, sterilizing them simultaneously, making them safe to reuse. We are also developing portable devices for sterilization of FFRs and other kinds of surfaces.

#### F.GI01.04.03

**Late News: Investigation of the COVID-19 Spike Glycoprotein at Varied Salt Concentrations—Correlating *In Silico* Modelling with *In Vitro* Droplet Drying Experiments** [Kaitlyn Swayze](#)<sup>1</sup>, Jacob Myers<sup>2</sup>, Fan Yang<sup>1</sup>, Miriam H. Rafailovich<sup>1</sup>, Marcia Simon<sup>1</sup>, Robert Elder<sup>3</sup>, Yuefan Deng<sup>1</sup> and Peng Zhang<sup>1,1</sup>; <sup>1</sup>Stony Brook University, The State University of New York, United States; <sup>2</sup>University of Scranton, United States; <sup>3</sup>U.S. Food and Drug Administration, United States

SARS-CoV-2 is transmitted by respiratory droplets containing protein surfactants and NaCl, which relates to virus transmission when surfactants are in negligible amounts. These droplets land on surfaces and evaporate depending on environmental factors such as relative humidity, temperature, and contact surface causing NaCl concentration to increase as the droplet dries. We aim to examine the effect of electrostatic interactions on the conformation of the spike glycoprotein (S-protein), as has been done *in vitro* with other respiratory viruses, showing a decrease in viability [2] throughout evaporation. This is a leading investigation correlating the results of *in silico* modelling and *in vitro* droplet drying dynamic experiments to analyze the transmission of SARS-CoV-2.

Saline droplets of 1-2 $\mu$ l are pipetted onto paper, PLA, glass, and aluminum and left to evaporate at 297K, 1 atm, and 48% relative humidity. Concentration is extrapolated from droplet mass using a microbalance. The S-protein structure was retrieved from the Protein Data Bank (PDB: 6VXX), cleaned, and placed into a system using the AMBERsb14 force field with Joung and Cheatham ion parameters [1], placed 2.0nm from the box edge in 0M, 0.5M, 1M and 4.0nm from the box edge in 1.5M. The system was solvated with TIP3P water and ions were added by replacing water molecules. Equilibration steps were carried out with a timestep of 2.0fs. Energy minimization was performed for 50,000 steps followed by NVT equilibration for 100ps to heat the system to the temperature of *in vitro* experiments. NPT equilibration was employed for 100ps and the system was brought to 1 atm. The equilibrated structure is input to the production run using an NPT ensemble and Parrinello-Rahman pressure coupling. Density is monitored to ensure no system collapse or changes in concentration. Raw trajectories from the run are processed by re-centering the protein in the box and realigning with the first frame as the reference structure.

Benchtop experiments indicate that a 2 $\mu$ l droplet of saline reaches 1M in 45 minutes and fully desiccates over several hours with concentrations between 0.15M and 6M. The evaporation rate of saline on different surfaces is constant regardless of NaCl concentration. On non-metal substrates, the evaporation rate is negatively correlated to the water contact angle of the substrate and on metal substrates the evaporation rate remains lowest of all the substrates, although it has a higher water contact angle than glass. The *in silico* model is analyzed by calculating the RMSD of atomic positions for the S-protein backbone yielding that the 1.5M increases more rapidly.

Simulation of the S-protein in varied NaCl concentrations is consistent with droplet drying experiments and depicts how Na<sup>+</sup> and Cl<sup>-</sup> ions interact with S-protein structure. We aim to correlate the volume and concentration from *in vitro* droplet drying experiments with the structural analysis from *in silico* experiments and to eventually utilize machine learning to predict the relationship between NaCl concentration and S-protein conformation over longer time, and to conduct further structural analysis on the S-protein. Simulation at higher salt concentrations (above 1.5M) has yet to be validated due to the need for a large number of monovalent ions, currently crashing our simulations. Future benchtop work will include plaque assays with the BSL-2 coronavirus OC-43 in drying saline droplets.

The project is supported by OVPR&IEDM COVID-19 Grant and SUNY-IBM Consortium Award.

[1] Joung, I. S., & Cheatham, T. E., 3rd. (2008). Determination of alkali and halide monovalent ion parameters for use in explicitly solvated biomolecular simulations. *J Phys Chem B*, 112(30), 9020-9041. doi:10.1021/jp8001614

[2] Yang, W., Elankumaran, S., & Marr, L. C. (2012). Relationship between humidity and influenza A viability in droplets and implications for influenza's seasonality. *PLoS One*, 7(10), e46789. doi:10.1371/journal.pone.0046789

#### F.GI01.04.05

**Late News: Characterizing Viral Lifetimes from Droplet-Surface Interactions** [Junsang Yoon](#)<sup>1</sup>, Jacob Myers<sup>2</sup>, Anand Srinivasan<sup>3</sup>, Fan Yang<sup>4</sup> and Miriam H. Rafailovich<sup>4</sup>; <sup>1</sup>Cupertino High School, United States; <sup>2</sup>The University of Scranton, United States; <sup>3</sup>The Westminster Schools, United States; <sup>4</sup>Stony Brook University, The State University of New York, United States

SARS-CoV-2 (CoV) has sickened millions and killed hundreds of thousands since emerging less than a year ago. Aerosol transmission of CoV in respiratory droplets is well-established, but its capacity for fomite transmission is not well defined [1,2]. Fomite transmission of viruses are generally impacted by two factors: surface materials and droplet composition. However, both mechanisms are not well defined. For example, viral lifetimes may be affected by different surface-droplet interactions which influence the amount of water retained in a dried droplet residue, or through distribution patterns that create the localization of dried droplet solutes. Thus, this study aims to better characterize the expected lifetime of CoV by simulating various surface-droplet interactions frequent in real life.

Droplets of distilled water, saline, DMEM+10%FBS, lung fluid, and human saliva, with volumes ranging from 0.25 - 2.0 uL, were deposited onto paper, glass, polylactic acid (PLA), and aluminum. All samples were analyzed using contact angle goniometry and microbalance data; the changes in droplet volume over time were recorded, from which the evaporation rate and concentration of solutes were determined. Images of the drying pattern of each surface-droplet interaction were generated using confocal laser scanning. Plaque assays are now being performed at 10-minute time intervals to determine virus lifetimes.

Results indicate that the surface material greatly affects the drying rate. Significantly different evaporation rates were obtained when placing distilled water on aluminum, glass, and PLA. More importantly, fluids relevant to virus transmission, such as saliva and lung fluid, evaporated significantly slower on paper and faster on glass than they did on PLA and aluminum, with rabbit lung fluid evaporating at 0.164ul/min on glass and 0.051 ul/min on paper. Droplet composition also impacted the drying rates. Based on the contents of the droplets, two different drying mechanisms have been observed. Distilled water and human saliva dried at a linear rate, but in saline, DMEM+10%FBS and lung fluid, an initial linear decrease in volume followed by a slower asymptotic approach to the volume of the solutes was observed. Droplets with the asymptotic mechanism could keep viruses hydrated for a much longer time than previously predicted. Saline droplets retained 3.75% of their starting mass and porcine lung fluid retained 12.08% after 50 minutes, compared to 0.08% for water droplets after only 39 minutes. This contrast suggests increased hydration, and potentially lengthened virus lifetimes, for droplets that dry by the asymptotic mechanism. Images taken using confocal laser scanning show that both the surface and the composition of the liquid droplet affect the distribution of droplet solutes. On aluminum, glass, and PLA, droplets of saline and rabbit lung fluid showed a pinned contact line, leading to the buildup of solutes near the edge of the droplet, while saliva droplets created a buildup of solutes in the center of the droplet. The localization of solutes in saline, rabbit lung, and saliva droplets may also indicate an ability to hold water for a longer period of time.

Continued experiments using plaque assays of droplets and droplet residues containing H1N1 and the coronavirus OC43 deposited on different surfaces will reveal more directly the lifetime of CoV on different surfaces over time.

[1] Aboubakr HA, Sharafeldin TA, Goyal SM. Stability of SARS CoV 2 and other coronaviruses in the environment and on common touch surfaces and the influence of climatic conditions: A review. *Transboundary and emerging diseases*.

[2] Firquet, S., Beaujard, S., Lobert, P. E., Sané, F., Caloone, D., Izard, D., & Hober, D. (2015). Survival of Enveloped and Non-Enveloped Viruses on Inanimate Surfaces. *Microbes and environments*, 30(2), 140–144.

We gratefully acknowledge support from the Louis Morin Charitable Trust

#### **F.GI01.04.06**

**Late News: SARS-CoV-2 Biosensor Development—Exhaled Particle Measurements Using OPC, QMS, QCM and Potential for Hydrophilic LiNbO<sub>3</sub> Biosensor Substrate** Finn O'Hara, Bart Checinski, [Guenevere O'Hara](#) and Jozef Ociepa; OCI Vacuum Microengineering Inc., Canada

In light of the global need for COVID-19 testing there is a need for much faster testing device and the exhaled breath present significant potential to be used for this purpose. SARS-CoV-2 19 attacks the upper respiratory tract (nose and throat) and progresses down to the lower respiratory tract (lungs). SARS-CoV-2 causes lung inflammation increasing the number of particles in an individual's exhale. Pathogens present in respiratory fluid can be carried in aerosol particles. It is uncertain if SARS-CoV-2 stays viable in droplet nuclei particles; some studies that claim that droplet nuclei particles remain viable, presenting the threat of airborne transmission [1, 2]. Air samples tested positive in a Wuhan hospital confirming aerosol transmission [3]. SARS-CoV-2 microdroplets exhaled from infectious patients can be detected by specially developed breath analyzer. This analyzer is based on the biosensor to detect viral SARS-CoV-2 microdroplets from exhaled breath. The aim of the present work is examining the characteristic of exhaled air samples from healthy individuals and finding

suitable substrate that can be used for further development of SARS-CoV-2 biosensor. We are using three techniques to measure the quantity and composition of exhaled air samples such as Optical Particle Counter (OPC), Quartz Crystal Microbalance (QCM) and Quadrupole Mass Spectrometer (QMS). The LiNbO<sub>3</sub> crystal was selected to the biosensor substrate and characterized with Low Energy Electron Diffraction (LEED) and Auger Electron Spectroscopy (AES) for the capturing of the microdroplets from exhaled breath. In order to work as SARS-CoV-2 biosensor the LiNbO<sub>3</sub> substrate has to be developed further to be functionalized with ACE2 receptor.

OPC tests confirm the possibility of significant exhale particle generation -356% of inhaled air. High concentration of background particles induce a greater difference in exhale to inhale than low particle concentration background. Low relative humidity (RH) influences the amount of particles added by the breath to be lower. This indicates that that the amount of exhaled particles produced increases when worse air quality is inhaled. QMS data confirm that less gaseous water is in exhale than in inhaled air suggesting exhaled microdroplets agglomeration. QCM data shows difficulties in adsorption and holding the microdroplets on the crystal sensor. A LiNbO<sub>3</sub> crystal was selected for the biosensor suitable substrate because it is strongly hydrophilic and has a very stable surface crystalline structure even after exposure to ambient air, water, and alcohol as was confirmed with LEED and AES study.

References:

- [1] N. M. Wilson, A. Norton, F. P. Young, and D. W. Collins, "Airborne transmission of severe acute respiratory syndrome coronavirus 2 to healthcare workers: a narrative review," *Anaesthesia*, 2020.
- [2] M. Yao, L. Zhang, J. Ma, and L. Zhou, "On airborne transmission and control of SARS-CoV-2," *Science of The Total Environment*, vol. 731, p. 139178, 2020.
- [3] Z.-D. Guo et al., "Aerosol and Surface Distribution of Severe Acute Respiratory Syndrome Coronavirus 2 in Hospital Wards, Wuhan, China, 2020," *Emerging Infectious Diseases*, vol. 26, no. 7, 2020.

#### **F.GI01.04.07**

**Late News: Molecular Dynamics Prediction of SARS-CoV-2 Spike Glycoproteins at Varying Temperature Using Machine Learning Models** [David Liang](#)<sup>1</sup>, Meichen Song<sup>2</sup>, Ziyuan Niu<sup>2</sup>, Peng Zhang<sup>2</sup>, Miriam H. Rafailovich<sup>2</sup> and Yuefan Deng<sup>2</sup>; <sup>1</sup>Ward Melville High School, United States; <sup>2</sup>Stony Brook University, The State University of New York, United States

**As the SARS-CoV-2 pandemic continues to spread, the effects of environmental factors on the molecular level remain unclear. While molecular dynamics (MD) simulations are a widely-used technique in modeling complex nanoscale interactions, its high computation requirements limit capabilities in long-term modeling.**

**This work explores a machine learning (ML) solution to predicting long-term properties of SARS-CoV-2 spike glycoproteins through the analysis of nanosecond S-protein backbone RMSD (root-mean-square deviation) MD simulation data at varying temperatures. The changes in the spike glycoprotein structure as time progresses are key to understanding the behavior and functionality of the virus under specific conditions.**

**Our data consists of 5000 RMSD values from 750ns to 1250ns. The data processing is characterized primarily with the denoising of the data with fast Fourier transforms (FFT) through filtering the Fourier terms or frequencies from the power spectrum. In addition to the data denoising, various statistical models, such as the autoregressive integrated moving average (ARIMA) and neural network models incorporating LSTM (Long short-term memory), GRU (Gated Recurrent Unit), and CNN (Convolutional neural network), were evaluated in performance on recursive forecasts. This work experiments with specific models including CNN-LSTM and CNN-GRU hybrid models and evaluates the incorporation of multi-step prediction features. Certain models were also trained on sliding window distributions of the data, where each window was characterized by a mean and standard deviation (SD) value, thus reducing the effect of variability in simulations. The performance of these distribution models was measured as overlap coefficients between actual and predicted windowed distributions. In predicting both the RMSD values and distributions, the hybrid CNN-LSTM and CNN-GRU, along with their multi-step counterparts, were more suitable for capturing and retaining the trends. The Multi-step CNN-LSTM model was able to achieve RMSE (root mean square error) scores of 0.0077 on actual value forecasts of 1230 points (123 ns), along with overlap coefficients of around 0.15 on 1105 distribution value forecasts, showing promise in predicting long-term RMSD values. This work essentially demonstrated the feasibility of using ML to predict long-term properties of SARS-CoV-2 spike glycoproteins from MD simulation data.**

**We gratefully acknowledge support from the Louis Morin Charitable Trust**

#### **F.GI01.04.08**

**Late News: Monte Carlo Simulation Studies of SARS-CoV-2 Spike Glycoproteins** [Clarise Han](#)<sup>1</sup>, Karin Hasegawa<sup>2</sup>, Peng Zhang<sup>2</sup> and Miriam H. Rafailovich<sup>2</sup>; <sup>1</sup>Mission San Jose High School, United States; <sup>2</sup>Stony Brook University, The State

University of New York, United States

Given the severity of the COVID-19 pandemic caused by the novel SARS-CoV-2 coronavirus, it is essential to develop effective approaches for treatment and prevention. The improvement of personal protective equipment (PPE) for front-line healthcare workers also relies on comprehensive binding analysis of surface stability and binding intensity of the virus on certain substrates<sup>1</sup>. As the SARS-CoV-2 spike glycoprotein (S protein) is the key receptor for promoting entry to host cells and binding, we investigate its conformational transitions during binding using computer simulations to inform development and improvement of drugs and PPE to treat and prevent infection.

Our plan is to use Monte Carlo methods for our simulations. Two main methods for such computer simulations are molecular dynamics (MD) and MC. MD simulations are based on trajectories determined by Newton's equations of motion and use small time steps typically on the order of femtoseconds. This makes the simulations computationally expensive. MC simulations generate random movements based on probability distributions at each step. This has often been found to be more computationally efficient. As such, we are motivated to employ MC methods to greatly increase the efficiency of the S protein simulations. Our first step is to simulate the S protein in an aerosol environment. Our next steps include simulating the binding of the S protein-aerosol system onto various substrates such as polylactic acid (PLA), the common material used in PPE. We plan to correlate the *in silico* results with *in vitro* experiments to better inform and improve PPE guidelines. Our current step is simulating the closed state 6vxx S protein in its aerosol environment. The Cassandra and GOMC (GPU-optimized MC) softwares were employed. Using Cassandra, data files such as the molecular connectivity file (MCF) needed to be generated. However, due to the complex nature of the S protein creating difficulties in generating the MCF file and the fact that Cassandra is not specifically designed for such large systems, we concluded that Cassandra was not suited for our simulation studies. As such, we decided to employ GOMC. We overcame difficulties with generating the appropriate PDB and PSF files. However, we discovered that there were limitations with GOMC for this type of simulation that prevented us from successfully running the entire simulation, including the fact that it does not support simulations for proteins with multiple residues. We are currently working on adjusting the source code with the help of the GOMC developers to support this type of simulation. We made some progress, and we expect to complete the simulations within the next few months. Ultimately, these simulations of the conformational changes of the S protein during binding will allow scientists to make more informed decisions on developments of drugs and PPE to treat and prevent infection. However, as time is of the essence, the need for efficient simulations using MC methods is vital to studying the S protein binding at a larger scale.

- [1] Stewart CL, Thornblade LW, Diamond DJ, Fong Y, Melstrom LG. Personal Protective Equipment and COVID-19: A Review for Surgeons. *Ann Surg*.
- [2] Walls AC, Park YJ, Tortorici MA, Wall A, McGuire AT, Velesler D. Structure, Function, and Antigenicity of the SARS-CoV-2 Spike Glycoprotein. *Cell*. 2020;181(2):281-292.e6.
- [3] Shah JK, Marin-Rimoldi E, Mullen RG, et al. Cassandra: An open source Monte Carlo package for molecular simulation. *J Comput Chem*. 2017;38(19):1727-1739.
- [4] Nejahi Y, Barhaghi MS, Mick J, Jackman B, Rushaidat K, Li Y, Schwiebert L, Potoff J. GOMC: GPU Optimized Monte Carlo for the Simulation of Phase Equilibria and Physical Properties of Complex Fluids. *SoftwareX* 2019;9:20-27.

We gratefully acknowledge support from the Louis Morin Charitable Trust

SESSION F.GI01.05: Live The Biology and Pathology of COVID-19—An Immunology Primer  
Session Chairs: Kaitlyn Sadtler and Elizabeth Wayne  
Sunday Afternoon, November 29, 2020  
F.GI01

### 12:30 PM \*F.GI01.05.01

**The Biology and Pathology of COVID-19: An Immunology Primer** [Bryan Bryson](#); Massachusetts Institute of Technology, United States

The SARS-CoV-2 pandemic has quickly spread throughout the globe in 2020. As such, engineers have applied their knowledge in materials design to approach prevention of infection, testing to diagnose infections, and treatment after an individual has COVID-19. These advancements rely on an understanding of the basic biology of SARS-CoV-2 from virology to immunology. Here, we will focus on a general overview of what is known about SARS-CoV-2 biology, focusing on components that are critical for materials design in prevention, diagnostics, and treatments.

SESSION F.LP06.05: Live Poster Session: General Information (F.GI01)

Session Chair: Jonathan Rivnay  
Wednesday Afternoon, December 2, 2020  
7:30 PM - 9:30 PM  
F.GI01

**F.GI01.04.01**

**Substrate-Free PEDOT:PSS Fibre Arrays as Breath Sensor** Wenyu Wang and Yan Yan Shery Huang; University of Cambridge, United Kingdom

The development of a portable, rapid and efficient breath detector could potentially benefit the study of human respiration. This is of particular interest under the background of a global pandemic which could be spread through the respiratory system. Herein, we report an integrated, low-cost breath analyser that is composed of multi-layered, suspended PEDOT:PSS microfibre arrays, fabricated by original inflight fluidic fibre printing technique. Based on that the resistance of PEDOT:PSS is sensitive to the moisture change, this breath analyser offers a direct signal read-out. Thanks to the small diameter and large surface-to-volume ratio, the microfibres are much more responsive to the dynamics of moisture flow in air compared with planer or film based moisture sensor. Moreover, the ultrathin diameter and substrate-free feature enable the entire fibre array to be transparent and air permissive; thus, this sensor could be directly mounted in front of a camera, allowing visualisation at the same time. We demonstrate that this human breath analyser could be able to detect and distinguish the human breath level, when talking, breathing and coughing. In addition, we show that the breath sensor is also able to distinguish the human breath level change when wearing various face masks.

**F.GI01.04.02**

**Combat COVID-19—Sterilize and Recharge Masks Simultaneously for Safe Reuse** Sriram Sundar Shankara Narayanan, Xudong Wang, Zijian Weng, Vladislav Paley, Libin Ye and Ying Zhong; University of South Florida, United States

To rapidly respond to the COVID-19 pandemic and address the extreme shortage of proper sterilization methods for Personal Protective Equipment (PPE) and surfaces, we have urgently advanced safe, sustainable and high-efficiency corona discharge (CD) based sterilization technology. Filtering facepiece respirators (FFRs) like N95 masks and surgical masks are essential for reducing the spread of the virus. FFRs are primarily made of hydrophobic melt blown polypropylene layers. In addition to small pore sizes ( $<1\mu\text{m}$ ), the filtration efficiency of N95 masks are also attributed to the electrostatic charges embedded in the fibers. These charges result in electrostatic attraction of small droplets carrying micro-organisms, effectively trapping them between the fibers. There are several attempts to decontaminate and reuse masks using existing sterilization techniques like heat, UV, etc. Although, these methods are effective in killing the virus, they negatively affect the filtration efficiency over time.

In this study, we use CD to effectively sterilize masks and renew their filtration efficiency to make masks reusable. A high voltage is applied to a sharp electrode leading to dielectric breakdown of air. Electron and ion pairs are generated due to the avalanche effect. The combination of high electric field, ion bombardment and reactive species leads to effective sterilization of FFRs. The ions also renew the electrostatic charges on the surface of the fibers, thus recovering the filtration efficiency of the masks. Sterilization effect and mechanisms are being tested against *E. coli*, spores and SARS-CoV-2 virus. The sterility assurance level (SAL) has reached  $10^{-3}$  with single spot electrode discharge, which is the requirement for safe mask reuse. Masks are also successfully recharged after CD treatment within seconds, sterilizing them simultaneously, making them safe to reuse. We are also developing portable devices for sterilization of FFRs and other kinds of surfaces.

**F.GI01.04.03**

**Late News: Investigation of the COVID-19 Spike Glycoprotein at Varied Salt Concentrations—Correlating *In Silico* Modelling with *In Vitro* Droplet Drying Experiments** Kaitlyn Swayze<sup>1</sup>, Jacob Myers<sup>2</sup>, Fan Yang<sup>1</sup>, Miriam H. Rafailovich<sup>1</sup>, Marcia Simon<sup>1</sup>, Robert Elder<sup>3</sup>, Yuefan Deng<sup>1</sup> and Peng Zhang<sup>1,1</sup>; <sup>1</sup>Stony Brook University, The State University of New York, United States; <sup>2</sup>University of Scranton, United States; <sup>3</sup>U.S. Food and Drug Administration, United States

SARS-CoV-2 is transmitted by respiratory droplets containing protein surfactants and NaCl, which relates to virus transmission when surfactants are in negligible amounts. These droplets land on surfaces and evaporate depending on environmental factors such as relative humidity, temperature, and contact surface causing NaCl concentration to increase as



the droplet dries. We aim to examine the effect of electrostatic interactions on the conformation of the spike glycoprotein (S-protein), as has been done in vitro with other respiratory viruses, showing a decrease in viability [2] throughout evaporation. This is a leading investigation correlating the results of in silico modelling and in vitro droplet drying dynamic experiments to analyze the transmission of SARS-CoV-2.

Saline droplets of 1-2 $\mu$ l are pipetted onto paper, PLA, glass, and aluminum and left to evaporate at 297K, 1 atm, and 48% relative humidity. Concentration is extrapolated from droplet mass using a microbalance. The S-protein structure was retrieved from the Protein Data Bank (PDB: 6VXX), cleaned, and placed into a system using the AMBERsb14 force field with Joung and Cheatham ion parameters [1], placed 2.0nm from the box edge in 0M, 0.5M, 1M and 4.0nm from the box edge in 1.5M. The system was solvated with TIP3P water and ions were added by replacing water molecules. Equilibration steps were carried out with a timestep of 2.0fs. Energy minimization was performed for 50,000 steps followed by NVT equilibration for 100ps to heat the system to the temperature of in vitro experiments. NPT equilibration was employed for 100ps and the system was brought to 1 atm. The equilibrated structure is input to the production run using an NPT ensemble and Parrinello-Rahman pressure coupling. Density is monitored to ensure no system collapse or changes in concentration. Raw trajectories from the run are processed by re-centering the protein in the box and realigning with the first frame as the reference structure.

Benchtop experiments indicate that a 2 $\mu$ l droplet of saline reaches 1M in 45 minutes and fully desiccates over several hours with concentrations between 0.15M and 6M. The evaporation rate of saline on different surfaces is constant regardless of NaCl concentration. On non-metal substrates, the evaporation rate is negatively correlated to the water contact angle of the substrate and on metal substrates the evaporation rate remains lowest of all the substrates, although it has a higher water contact angle than glass. The in silico model is analyzed by calculating the RMSD of atomic positions for the S-protein backbone yielding that the 1.5M increases more rapidly.

Simulation of the S-protein in varied NaCl concentrations is consistent with droplet drying experiments and depicts how Na<sup>+</sup> and Cl<sup>-</sup> ions interact with S-protein structure. We aim to correlate the volume and concentration from in vitro droplet drying experiments with the structural analysis from in silico experiments and to eventually utilize machine learning to predict the relationship between NaCl concentration and S-protein conformation over longer time, and to conduct further structural analysis on the S-protein. Simulation at higher salt concentrations (above 1.5M) has yet to be validated due to the need for a large number of monovalent ions, currently crashing our simulations. Future benchtop work will include plaque assays with the BSL-2 coronavirus OC-43 in drying saline droplets.

The project is supported by OVPR&IEDM COVID-19 Grant and SUNY-IBM Consortium Award.

[1] Joung, I. S., & Cheatham, T. E., 3rd. (2008). Determination of alkali and halide monovalent ion parameters for use in explicitly solvated biomolecular simulations. *J Phys Chem B*, 112(30), 9020-9041. doi:10.1021/jp8001614

[2] Yang, W., Elankumaran, S., & Marr, L. C. (2012). Relationship between humidity and influenza A viability in droplets and implications for influenza's seasonality. *PLoS One*, 7(10), e46789. doi:10.1371/journal.pone.0046789

#### **F.GI01.04.05**

**Late News: Characterizing Viral Lifetimes from Droplet-Surface Interactions** [Junsang Yoon](#)<sup>1</sup>, Jacob Myers<sup>2</sup>, Anand Srinivasan<sup>3</sup>, Fan Yang<sup>4</sup> and Miriam H. Rafailovich<sup>4</sup>; <sup>1</sup>Cupertino High School, United States; <sup>2</sup>The University of Scranton, United States; <sup>3</sup>The Westminster Schools, United States; <sup>4</sup>Stony Brook University, The State University of New York, United States

SARS-CoV-2 (CoV) has sickened millions and killed hundreds of thousands since emerging less than a year ago. Aerosol transmission of CoV in respiratory droplets is well-established, but its capacity for fomite transmission is not well defined [1,2]. Fomite transmission of viruses are generally impacted by two factors: surface materials and droplet composition. However, both mechanisms are not well defined. For example, viral lifetimes may be affected by different surface-droplet interactions which influence the amount of water retained in a dried droplet residue, or through distribution patterns that create the localization of dried droplet solutes. Thus, this study aims to better characterize the expected lifetime of CoV by simulating various surface-droplet interactions frequent in real life.

Droplets of distilled water, saline, DMEM+10%FBS, lung fluid, and human saliva, with volumes ranging from 0.25 - 2.0  $\mu$ L, were deposited onto paper, glass, polylactic acid (PLA), and aluminum. All samples were analyzed using contact angle goniometry and microbalance data; the changes in droplet volume over time were recorded, from which the evaporation rate and concentration of solutes were determined. Images of the drying pattern of each surface-droplet interaction were generated using confocal laser scanning. Plaque assays are now being performed at 10-minute time intervals to determine virus lifetimes.

Results indicate that the surface material greatly affects the drying rate. Significantly different evaporation rates were

obtained when placing distilled water on aluminum, glass, and PLA. More importantly, fluids relevant to virus transmission, such as saliva and lung fluid, evaporated significantly slower on paper and faster on glass than they did on PLA and aluminum, with rabbit lung fluid evaporating at 0.164ul/min on glass and 0.051 ul/min on paper. Droplet composition also impacted the drying rates. Based on the contents of the droplets, two different drying mechanisms have been observed. Distilled water and human saliva dried at a linear rate, but in saline, DMEM+10%FBS and lung fluid, an initial linear decrease in volume followed by a slower asymptotic approach to the volume of the solutes was observed. Droplets with the asymptotic mechanism could keep viruses hydrated for a much longer time than previously predicted. Saline droplets retained 3.75% of their starting mass and porcine lung fluid retained 12.08% after 50 minutes, compared to 0.08% for water droplets after only 39 minutes. This contrast suggests increased hydration, and potentially lengthened virus lifetimes, for droplets that dry by the asymptotic mechanism. Images taken using confocal laser scanning show that both the surface and the composition of the liquid droplet affect the distribution of droplet solutes. On aluminum, glass, and PLA, droplets of saline and rabbit lung fluid showed a pinned contact line, leading to the buildup of solutes near the edge of the droplet, while saliva droplets created a buildup of solutes in the center of the droplet. The localization of solutes in saline, rabbit lung, and saliva droplets may also indicate an ability to hold water for a longer period of time. Continued experiments using plaque assays of droplets and droplet residues containing H1N1 and the coronavirus OC43 deposited on different surfaces will reveal more directly the lifetime of CoV on different surfaces over time.

[1] Aboubakr HA, Sharafeldin TA, Goyal SM. Stability of SARS CoV 2 and other coronaviruses in the environment and on common touch surfaces and the influence of climatic conditions: A review. *Transboundary and emerging diseases*.

[2] Firquet, S., Beaujard, S., Lobert, P. E., Sané, F., Caloone, D., Izard, D., & Hober, D. (2015). Survival of Enveloped and Non-Enveloped Viruses on Inanimate Surfaces. *Microbes and environments*, 30(2), 140–144.

We gratefully acknowledge support from the Louis Morin Charitable Trust

#### **F.GI01.04.06**

**Late News: SARS-CoV-2 Biosensor Development—Exhaled Particle Measurements Using OPC, QMS, QCM and Potential for Hydrophilic LiNbO<sub>3</sub> Biosensor Substrate** Finn O'Hara, Bart Checinski, [Guenevere O'Hara](#) and Jozef Ociepa; OCI Vacuum Microengineering Inc., Canada

In light of the global need for COVID-19 testing there is a need for much faster testing device and the exhaled breath present significant potential to be used for this purpose. SARS-CoV-2 19 attacks the upper respiratory tract (nose and throat) and progresses down to the lower respiratory tract (lungs). SARS-CoV-2 causes lung inflammation increasing the number of particles in an individual's exhale. Pathogens present in respiratory fluid can be carried in aerosol particles. It is uncertain if SARS-CoV-2 stays viable in droplet nuclei particles; some studies that claim that droplet nuclei particles remain viable, presenting the threat of airborne transmission [1, 2]. Air samples tested positive in a Wuhan hospital confirming aerosol transmission [3]. SARS-CoV-2 microdroplets exhaled from infectious patients can be detected by specially developed breath analyzer. This analyzer is based on the biosensor to detect viral SARS-CoV-2 microdroplets from exhaled breath.

The aim of the present work is examining the characteristic of exhaled air samples from healthy individuals and finding suitable substrate that can be used for further development of SARS-CoV-2 biosensor. We are using three techniques to measure the quantity and composition of exhaled air samples such as Optical Particle Counter (OPC), Quartz Crystal Microbalance (QCM) and Quadrupole Mass Spectrometer (QMS). The LiNbO<sub>3</sub> crystal was selected to the biosensor substrate and characterized with Low Energy Electron Diffraction (LEED) and Auger Electron Spectroscopy (AES) for the capturing of the microdroplets from exhaled breath. In order to work as SARS-CoV-2 biosensor the LiNbO<sub>3</sub> substrate has to be developed further to be functionalized with ACE2 receptor.

OPC tests confirm the possibility of significant exhale particle generation -356% of inhaled air. High concentration of background particles induce a greater difference in exhale to inhale than low particle concentration background. Low relative humidity (RH) influences the amount of particles added by the breath to be lower. This indicates that that the amount of exhaled particles produced increases when worse air quality is inhaled. QMS data confirm that less gaseous water is in exhale than in inhaled air suggesting exhaled microdroplets agglomeration. QCM data shows difficulties in adsorption and holding the microdroplets on the crystal sensor. A LiNbO<sub>3</sub> crystal was selected for the biosensor suitable substrate because it is strongly hydrophilic and has a very stable surface crystalline structure even after exposure to ambient air, water, and alcohol as was confirmed with LEED and AES study.

References:

[1] N. M. Wilson, A. Norton, F. P. Young, and D. W. Collins, "Airborne transmission of severe acute respiratory syndrome coronavirus 2 to healthcare workers: a narrative review," *Anaesthesia*, 2020.

[2] M. Yao, L. Zhang, J. Ma, and L. Zhou, "On airborne transmission and control of SARS-CoV-2," *Science of The Total Environment*, vol. 731, p. 139178, 2020.

[3] Z.-D. Guo et al., "Aerosol and Surface Distribution of Severe Acute Respiratory Syndrome Coronavirus 2 in Hospital Wards, Wuhan, China, 2020," *Emerging Infectious Diseases*, vol. 26, no. 7, 2020.

#### F.GI01.04.07

**Late News: Molecular Dynamics Prediction of SARS-CoV-2 Spike Glycoproteins at Varying Temperature Using Machine Learning Models** [David Liang](#)<sup>1</sup>, Meichen Song<sup>2</sup>, Ziyuan Niu<sup>2</sup>, Peng Zhang<sup>2</sup>, Miriam H. Rafailovich<sup>2</sup> and Yuefan Deng<sup>2</sup>; <sup>1</sup>Ward Melville High School, United States; <sup>2</sup>Stony Brook University, The State University of New York, United States

As the SARS-CoV-2 pandemic continues to spread, the effects of environmental factors on the molecular level remain unclear. While molecular dynamics (MD) simulations are a widely-used technique in modeling complex nanoscale interactions, its high computation requirements limit capabilities in long-term modeling.

This work explores a machine learning (ML) solution to predicting long-term properties of SARS-CoV-2 spike glycoproteins through the analysis of nanosecond S-protein backbone RMSD (root-mean-square deviation) MD simulation data at varying temperatures. The changes in the spike glycoprotein structure as time progresses are key to understanding the behavior and functionality of the virus under specific conditions.

Our data consists of 5000 RMSD values from 750ns to 1250ns. The data processing is characterized primarily with the denoising of the data with fast Fourier transforms (FFT) through filtering the Fourier terms or frequencies from the power spectrum. In addition to the data denoising, various statistical models, such as the autoregressive integrated moving average (ARIMA) and neural network models incorporating LSTM (Long short-term memory), GRU (Gated Recurrent Unit), and CNN (Convolutional neural network), were evaluated in performance on recursive forecasts. This work experiments with specific models including CNN-LSTM and CNN-GRU hybrid models and evaluates the incorporation of multi-step prediction features. Certain models were also trained on sliding window distributions of the data, where each window was characterized by a mean and standard deviation (SD) value, thus reducing the effect of variability in simulations. The performance of these distribution models was measured as overlap coefficients between actual and predicted windowed distributions. In predicting both the RMSD values and distributions, the hybrid CNN-LSTM and CNN-GRU, along with their multi-step counterparts, were more suitable for capturing and retaining the trends. The Multi-step CNN-LSTM model was able to achieve RMSE (root mean square error) scores of 0.0077 on actual value forecasts of 1230 points (123 ns), along with overlap coefficients of around 0.15 on 1105 distribution value forecasts, showing promise in predicting long-term RMSD values. This work essentially demonstrated the feasibility of using ML to predict long-term properties of SARS-CoV-2 spike glycoproteins from MD simulation data.

We gratefully acknowledge support from the Louis Morin Charitable Trust

#### F.GI01.04.08

**Late News: Monte Carlo Simulation Studies of SARS-CoV-2 Spike Glycoproteins** [Clarise Han](#)<sup>1</sup>, Karin Hasegawa<sup>2</sup>, Peng Zhang<sup>2</sup> and Miriam H. Rafailovich<sup>2</sup>; <sup>1</sup>Mission San Jose High School, United States; <sup>2</sup>Stony Brook University, The State University of New York, United States

Given the severity of the COVID-19 pandemic caused by the novel SARS-CoV-2 coronavirus, it is essential to develop effective approaches for treatment and prevention. The improvement of personal protective equipment (PPE) for front-line healthcare workers also relies on comprehensive binding analysis of surface stability and binding intensity of the virus on certain substrates<sup>1</sup>. As the SARS-CoV-2 spike glycoprotein (S protein) is the key receptor for promoting entry to host cells and binding, we investigate its conformational transitions during binding using computer simulations to inform development and improvement of drugs and PPE to treat and prevent infection.

Our plan is to use Monte Carlo methods for our simulations. Two main methods for such computer simulations are molecular dynamics (MD) and MC. MD simulations are based on trajectories determined by Newton's equations of motion and use small time steps typically on the order of femtoseconds. This makes the simulations computationally expensive. MC simulations generate random movements based on probability distributions at each step. This has often been found to be more computationally efficient. As such, we are motivated to employ MC methods to greatly increase the efficiency of the S protein simulations. Our first step is to simulate the S protein in an aerosol environment. Our next steps include simulating the binding of the S protein-aerosol system onto various substrates such as polylactic acid (PLA), the common material used in PPE. We plan to correlate the in silico results with in vitro experiments to better inform and improve PPE guidelines. Our current step is simulating the closed state 6vxx S protein in its aerosol environment. The Cassandra and GOMC (GPU-optimized MC) softwares were employed. Using Cassandra, data files such as the molecular connectivity file (MCF) needed to be generated. However, due to the complex nature of the S protein creating difficulties in generating the MCF file and the

fact that Cassandra is not specifically designed for such large systems, we concluded that Cassandra was not suited for our simulation studies. As such, we decided to employ GOMC. We overcame difficulties with generating the appropriate PDB and PSF files. However, we discovered that there were limitations with GOMC for this type of simulation that prevented us from successfully running the entire simulation, including the fact that it does not support simulations for proteins with multiple residues. We are currently working on adjusting the source code with the help of the GOMC developers to support this type of simulation. We made some progress, and we expect to complete the simulations within the next few months. Ultimately, these simulations of the conformational changes of the S protein during binding will allow scientists to make more informed decisions on developments of drugs and PPE to treat and prevent infection. However, as time is of the essence, the need for efficient simulations using MC methods is vital to studying the S protein binding at a larger scale.

- [1] Stewart CL, Thornblade LW, Diamond DJ, Fong Y, Melstrom LG. Personal Protective Equipment and COVID-19: A Review for Surgeons. *Ann Surg*.
- [2] Walls AC, Park YJ, Tortorici MA, Wall A, McGuire AT, Veesler D. Structure, Function, and Antigenicity of the SARS-CoV-2 Spike Glycoprotein. *Cell*. 2020;181(2):281-292.e6.
- [3] Shah JK, Marin-Rimoldi E, Mullen RG, et al. Cassandra: An open source Monte Carlo package for molecular simulation. *J Comput Chem*. 2017;38(19):1727-1739.
- [4] Nejahi Y, Barhaghi MS, Mick J, Jackman B, Rushaidat K, Li Y, Schwiebert L, Potoff J. GOMC: GPU Optimized Monte Carlo for the Simulation of Phase Equilibria and Physical Properties of Complex Fluids. *SoftwareX* 2019;9:20-27.

We gratefully acknowledge support from the Louis Morin Charitable Trust

## SYMPOSIUM F.BI01

---

Early Career Development—Insights from Academia and Industry  
November 21 - December 4, 2020

### Symposium Organizers

Babak Anasori, Indiana University-Purdue University  
Mayra Castro, Springer Nature  
Jorge Nicolas Hernandez Charpak, STROBE NSF Science and Technology Center  
Hortense Le Ferrand, Nanyang Technological University

---

\* Invited Paper

SESSION F.BI01.04: Live Panel Discussion I: Early Career Development—Insights from Academia and Industry  
Session Chairs: Babak Anasori and Mayra Castro  
Thursday Morning, December 3, 2020  
F.BI01

**11:30 AM GET PUBLISHED AND FUNDED: STEWART BLAND; Y.SHIRLEY MENG; MARIA MARAGKOU; DAVID STEEP; LINDA SAPOCHAK**

**12:15 PM BREAK**

**12:30 PM GETTING READY FOR YOUR FUTURE CAREER: EVA HEMMER; MONICA JUNG DE ANDRADE; KAMALIKA CHATTERJEE; REMI DREYFUS**

SESSION F.BI01.05: Live Panel Discussion II: Early Career Development—Insights from Academia and Industry  
Session Chairs: Babak Anasori and Mayra Castro  
Friday Afternoon, December 4, 2020  
F.BI01

**1:45 PM CAREER OPTIONS FOR THE MATERIALS RESEARCHER: SUVEEN MATHAUDHU, MAX KORY, ROBIN HAYNES, PASCALINE HAYOUN, JOE SABOL**

**2:40 PM BREAK**

**2:50 PM FACULTY PATH: FROM APPLICATION TO THE TENURE-TRACK LIFE: SUSAN SINNOTT; DAVID BAHR; STEVEN YALISOVE**

SESSION F.BI01.01: Publishing Your Work and Funding Your Research and Future Plans  
On Demand Abstracts Available for Viewing Starting Saturday Morning, November 21, 2020  
F-BI01

**5:00 AM \*F.BI01.01.01**

**Publishing Insights from Materials Today** Stewart R. Bland; Elsevier | Materials Today, United Kingdom

In this session we will discuss the information flow in materials science and the broader publishing landscape, including the varied roles of Authors, Editors, Referees, and Publishers in connecting communities, providing perspectives on best practices for publication in journals such as those in the *Materials Today* family. We'll try to elucidate the most significant trends in the information landscape, including open access, article transfer, novel article formats, data sharing, and wider dissemination to society and decision makers.

Dr Stewart Bland is a former Editor-in-Chief and currently Executive Publisher in Elsevier's *Materials Today* family, responsible for journals including high impact titles such as *Materials Today*, *Applied Materials Today*, and *Progress in Materials Science*.

**5:15 AM F.BI01.01.02**

**Publishing with MRS Journals—Engaging with Our Community at Early Career Stage** Y. Shirley Meng; University of California, San Diego, United States

Publishing scholarly research articles is one of the most effective ways to engage with our materials research community and disseminate our work to our peers. MRS is a member-driven organization of approximately 14,000 materials researchers from academia, industry and government. I will present my perspectives as the editor-in-chief for MRS Energy & Sustainability how young researchers can fully leverage with the platforms MRS offer to maximize the impact of one's scholarly work.

**5:25 AM \*F.BI01.01.03**

**Inside Nature Materials** Maria Maragkou; Nature Materials, United Kingdom

Since its launch in 2002, Nature Materials remains a leading journal in the field of materials science across many disciplines, aiming at publishing cutting edge science for the relevant scientific communities as well as disseminating exciting results among the wider readership of materials scientists. This talk will describe how these principles shape the editorial process in *Nature Materials* and other journals within the *Nature* family, amidst a rapidly changing scientific publishing landscape, underlining the key points from submission of original research papers to publication.

**5:40 AM \*F.BI01.01.04**

**Publishing in Wiley Materials Science Journals** Bo Weng; Wiley, China

A highly competitive research environment with increasingly limited research funding has created a “Publish or Perish” attitude among scientists who are judged on the quantity rather than quality of their research articles. This presentation provides a brief overview of current trends and challenges in scientific publishing, some ethical considerations, how publishers and authors interact and influence each other, and how the publishing arena is being transformed. Tips will be presented on how to select an appropriate journal for your paper, what aspects of preparation and presentation to focus on from an editor’s and referee’s perspective, and hints for increasing the discoverability of your paper after publication.

**5:55 AM \*F.BI01.01.05**

**NSF Early Career Opportunities in Materials Research** Linda S. Sapochak; National Science Foundation, United States

The National Science Foundation (NSF) is an independent federal agency created by Congress in 1950 "to promote the progress of science; to advance the national health, prosperity, and welfare; to secure the national defense..." NSF is vital because it supports basic research and people from all science and engineering disciplines. The Division of Materials Research (DMR) in the Directorate for Mathematical and Physical Sciences (MPS) has eight topical materials research programs (TMRPs) that participate in the NSF-wide Faculty Early Career Development (CAREER) program. Materials research is also supported in other divisions in MPS and in the Directorate for Engineering. This presentation will provide an overview of NSF programs supporting materials research and the early career opportunities they offer.

**6:10 AM F.BI01.01.06**

**Late News: Finding Funding—A Glimpse into Science Funding in the Philippines** Bryan G. Alamani; University of the Philippines Diliman, Philippines

Science funding in the Philippines is guided by roadmaps and advices from the Department of Science and Technology. Early career scientists often apply for this funding call and find themselves working in a system that require broad range of knowledge and experience in project management and legalities that surround government funded calls. The complexity of the funding application process presents challenges to early career scientists who are not familiar navigating through the system. Funding agencies have also preference on proposals that will lead to technologies or innovations that can be implemented to society, and this entails some challenges to principal investigators who aim to answer fundamental scientific questions. Here, I will present some insights on the funding landscape in the Philippines for early career scientists by looking at scientists' roles in academe, support from the administration, and impact of government policy on R&D priorities. I shall also present certain coping mechanisms of early career scientists in obtaining support when their field is not considered top priority for funding.

SESSION F.BI01.02: Getting Ready for Your Future Career—Creating Your Next Research Environment  
On Demand Abstracts Available for Viewing Starting Saturday Morning, November 21, 2020  
F-BI01

**5:00 AM \*F.BI01.02.01**

**Finding Your Career Pathway in a Foreign Country—A Minority Perspective** Monica Jung de Andrade; The University of Texas at Dallas, United States

There is no ‘one path fits all’ as we are all different. With patented technologies and as one of the pioneers on carbon nanotube glass nanocomposites, I will share my ongoing career path. Being in a foreign country as a minority, the challenges are different: support system and cultural background, are just a few. Thus, one shall not just follow the flow, but forge one’s path aligned to their values, background, and passions. This is the ongoing story of a family’s first scientist enriched with different cultural exposures while finding her path. It is an unfinished story of challenges, failures, and learnings to be shared.

**5:15 AM \*F.BI01.02.02**

**Should I Stay or Should I Move? Thoughts about Early Career Mobility** Eva Hemmer; University of Ottawa, Canada

This presentation will provide a snapshot on the journey of a materials scientist from Germany moving via Japan to Canada. It will not only tell about the geographical, but also about the scientific and academic journey, and how studying materials science and engineering can lead to an academic position in a chemistry department, conducting research on multifunctional lanthanides in molecules and nanomaterials.

In this context, some experience from the time being a PhD student and the period discovering new countries and research areas as a postdoctoral fellow and how these may lead to a position in academia will be shared with the audience. This will include a personal answer to the question many young researchers may ask themselves: “*Should I stay or should I move?*”. It will also address some ongoing adventures (aka challenges) of starting an independent research group as assistant professor – because: having landed your first position does not mean to stand still, even when remaining in the same geographical location.

**5:30 AM \*F.BI01.02.03**

**Navigating an Academic Career in an Evolving Landscape** Susan B. Sinnott; The Pennsylvania State University, United States

This presentation will summarize the ways in which materials science and engineering in academia has evolved over the last decade, including abrupt changes over the last few months in response to the COVID-19 pandemic. It will review the implications of these changes for the field and provide some projections for the future. The objective is to prepare listeners for a career in higher education and to help them navigate the many choices available.

**5:45 AM \*F.BI01.02.04**

**Drawing Inspiration from Industrial Problematics in Academia—Examples of Water Retention and Microsensing** Remi Dreyfus; CNRS, United States

In the last 10 years, the University of Pennsylvania, the French CNRS and the chemical company Solvay teamed up in a joint laboratory in Philadelphia. The goal of the laboratory was to design sustainable solutions for “real-world” applications. Through two specific examples, I will show how members of the laboratory on the academic side gained inspirations from industrial problematics. The first example revolves around soil treatment, which can modify water retention for agricultural applications; the second example shows how smart formulations can lead to cheap dispersible sensors for monitoring bacterial growth.

**6:00 AM \*F.BI01.02.05**

**Useful Skill-Set Outside of the Employment Arena—Best Practices for the Solo Practitioner** Joe Sabol; Chemical Consultant, United States

The 2020 business cycle presented employment terms much different from previous times. Even if you are employed and have an enjoyable and challenging career, the global COVID recession of 2020, like what occurred in 2009, shows that the economy turn down quickly. Advice for anyone is to have skills that are marketable, i.e., you can get paid money for in the “1099-gig” economy. You don’t need a complicated business plan, extensive intellectual property, or even a physical footprint. Setting up a business does not have to be complicated, but there are some fundamental decisions around the way a business is structured and taxed and regulatory requirements that must be followed. Being aware of the issues will make it easier for you to define your core products and/or services and establish the necessary marketing, resources, and effort required to keep your operation afloat. This presentation holds the speaker’s perspective on the technical, business, and regulatory elements that were encountered when opening a start-up and maintaining a 20-year solo business, serving science and engineering-related customers.

**6:15 AM \*F.BI01.02.06**

**My Journey from Academia to Industry—Useful Tips and Tricks** Kamalika Chatterjee; Intel Corporation, United States

In this talk, I will go over my journey from being a PhD student at University of Illinois at Urbana-Champaign to a postdoctoral researcher at Cornell and finally becoming a process development engineer at Intel. I will discuss in detail the possible options I had or did not have, some struggles as an international student, how and why I decided to move from academia to industry and the process of mental preparation. Then, I will talk about my job application process, the successes and failures, why I decided to choose Intel and some experiences after starting at Intel. There will be useful tips for students preparing for a career in industry.

SESSION F.BI01.03: Multiple Career Options for the Materials Researcher—Academia, Industry, Governmental Agencies, Private Institutes

**5:00 AM \*F.BI01.03.01**

**Life as a Program Manager in the U.S. DOE's Office of Science** Robin L. Hayes; U.S. Department of Energy—Office of Basic Energy Sciences, United States

Ever wonder what it is like to work as a federal program manager in the U. S. Department of Energy (DOE)? Join Dr. Robin Hayes as she shares her journey from a graduate student to program manager in the DOE Office of Science via an American Association for the Advancement of Science (AAAS) Science and Technology Policy Fellowship. In addition, learn about fundamental materials research funding opportunities for early career professionals in the DOE Office of Basic Energy Sciences (<https://science.osti.gov/bes>).

**5:15 AM \*F.BI01.03.02**

**Behind the Curtain" at the Army Research Office, and How We Can Help You** David M. Stepp; U.S. Army Research Office, United States

Early career decisions can be daunting and often appear to be ill-posed. Concurrently, maneuvering the diverse and complex funding pipelines can often seem a challenge that threatens the very future of innovative materials science research. David Stepp brings more than twenty years of experience at the U.S. Army Research Office to share his career story (including some key failures) and provide insight and perspective on the "why" behind one of the preeminent materials science funding agencies. This talk will also include a discussion of some of the most common misunderstandings held by proposal authors.

**5:30 AM \*F.BI01.03.03**

**What to Consider When Switching to Industry** Pascaline Hayoun; Saint-Gobain, United States

Doctoral graduates are attractive for an ever-growing number of Research & Development (R&D) and Innovation roles across manifold companies and industries. PhD graduates possess the technical expertise and unique mindset that many companies find critical in order to cultivate innovative thinking and achieve their strategic objectives. Ask yourself: why are recruiters and hiring managers targeting academic candidates? The answer lies within the transferable skill sets that PhD candidates have developed throughout their studies and their early career positions within Academia. There are key aspects within a typical PhD CV that recruiters tease out and use to quickly identify the value add of hiring a PhD candidate and their impact on the job market. Whether PhD student or Post-doc, fully decided or still shaping their Academia or Industry career paths, I will draw on my personal experience at Saint-Gobain to help you decide if Industry is right for you. I have vast experience as an Innovation Manager and strategic & technical leader and will share tips and recommendations on what to expect while considering a job in Industry. Notably, I will discuss drivers that can motivate you to make the transition, as well as discuss the technical and non-technical transferable skills that are applicable to a corporate environment, the importance of building a network both in Academia and Industry and how to find a company that is suited right for you. Finally, I will paint an overview of the range of opportunities for career progression in Industry to pursue a fulfilling professional journey.

**5:45 AM \*F.BI01.03.04**

**Navigating the Academic Hiring Process at a Top Research University** Steven M. Yalisove; University of Michigan, United States

Getting hired as a faculty member at a top research university is not an easy thing to do. Yes you have to be an excellent researcher and teacher. Yes you need to understand how to fit into the department, university, and worldwide community through service. Yes you have to be a passionate and excellent teacher. But, those are only the first, necessary steps. Sadly, it is far from sufficient to land a top faculty position. This talk will go over the many things that must align for a candidate to get an in person interview and actually land the position. There is no guarantee, nor should there be any regrets when you start a search for a position. The real truth in getting hired as a faculty member is that once you reach the necessary conditions, the rest is really all about fit and the goals of each individual department that is looking for a faculty member to hire. Can a candidate influence this process? Yes. But it is not always possible to influence it enough. This talk will discuss how a candidate should at least consider a few things. In short, they are: why should a department believe that you will be successful in bringing in research funding?, How will your hire help bring in center grant funding? How will your hire have a positive impact on the culture of the department and make it more diverse, inclusive, and equitable? How will your hire help



the department increase its ranking? How will your hire improve the teaching of the entire department? How will your hire lead to “the next big thing?”, Why is it that you can convince a department of all of the last few topics and still not get hired?

**6:00 AM \*F.BI01.03.05**

**Navigating Towards a Faculty Position in Materials Engineering—Application To Appointment** David F. Bahr; Purdue University, United States

The initial stages of approaching a career in academia can be daunting to the candidate (just like any career path choice), and at times may seem opaque. This presentation will address some of the common stages that occur in becoming a faculty member in engineering in general, both when considering a materials engineering program, and the case where a materials researcher is joining a unit which does not offer an MSE (or related) degree. Common points in application materials for faculty positions for a range of departments, schools, and universities will be noted; addressing both a “direct” application route (right after PhD or post-doc) and applying after some time in other sectors (industry, government, or non-profit). In particular the presentation will highlight the need to demonstrate independent thought and ownership of research activities, maturity and dedication to education at the appropriate level of the institution, and articulating a vision of career success that covers both short- and long-term time scales. The presentation will strive to engage discussion points on topics that often arise during phone and in-person interviews, including addressing your vision for student advising, balancing teamwork versus independence within a unit, and identifying audiences in the hiring process. The need to speak directly to the variety of audiences, and to pivot your delivery while maintaining consistency amongst the range of groups you’d be speaking with. Finally, some details of perceived pitfalls in the process will be presented.

**6:15 AM \*F.BI01.03.06**

**Black Sheep—The Choice is Yours (Revisited)** Suveen N. Mathaudhu; University of California, Riverside, United States

Some may recognize that this title matches a classic 1991 track from the Black Sheep with the lyrics, “You can get with this, or you can get with that.” This rap group name represents the struggles of the members of a group who are often perceived as outliers, and the term often implies waywardness. This specific song presents listeners with concepts of key choices in life. The pathways to success for “black sheep” (may it be race, gender, ethnicity, sexual orientation, educational background, religion, physical ability, nationality and many others) are decidedly different from those who align with majority “preferable” groups across disciplines, and the Materials Science and Engineering community is not immune to these biases. Through the lens of this song and anecdotal stories, this talk will present career choices that can be made to overcome the “black sheep effect” in materials science and engineering industry and academia. Further, strategies on exploiting the factors that make one unique for positive outcomes in your research, teaching, mentoring and service activities will be discussed.

**6:30 AM \*F.BI01.03.07**

**From Academia to Startup—Insights to Starting a Technology-Driven Company** Max Kory; Batrion AG, Switzerland

Finishing my PhD I asked myself: "What next? Similar to the time years before, when I decided what I was going to study, I was facing once more a deeply personal question, what should I do with my life? Should I continue with a postdoc, go to industry, or do something completely different?"

It was the idea of founding a startup that somehow had sparked my interest already for quite some time.

During my PhD I had developed a novel 2D material with interesting properties, and so I decided to extend the time in my research group to determine whether the material could be applied somewhere in a useful way, hoping it may lead to the foundation of a company - It didn't. As time passed, I came to the conclusion that the material was interesting in the context of basic research, but far away from any useful application. Meanwhile a friend of mine who had finished his PhD on lithium-ion batteries was in a different situation, his research had what mine was lacking, a real application in sight. When he asked me in 2015, if I was interested in co-founding a startup, I said yes.

Founding a technology-driven company is very challenging on many different levels. In this talk, I would like to share my personal startup experience, hoping I can help answer some questions relevant to young researchers thinking about starting a company.

**SYMPOSIUM F.EL01**

---

Diamond and Diamond Heterojunctions—From Growth to Applications  
November 21 - December 3, 2020

Symposium Organizers

Robert Nemanich, Arizona State University  
Emmanuel Scorsone,  
Mariko Suzuki, Cornes Technologies Ltd  
Oliver Williams, Cardiff University

---

\* Invited Paper

SESSION F.EL01.10: Live Keynote I: Diamond and Diamond Heterojunctions—From Growth to Application  
Session Chairs: Emmanuel Scorsone and Oliver Williams  
Tuesday Morning, December 1, 2020  
F.EL01

**8:00 AM \*F.EL01.07.02**

**Molecular Transducers for Spin-Sensitive Optical Sensing Using Nitrogen-Vacancy Centers** Petr Cigler; Institute of Organic Chemistry and Biochemistry, Czech Academy of Sciences, Czechia

Non-perturbing sensing techniques applicable to biological systems currently are of central interest in the biosciences. Nanodiamond is a highly biocompatible nanomaterial for construction of nanosensors, which can accommodate various photoluminescent crystal defects. Nitrogen-vacancy (NV) centers show high photostability and unique electronic sensitivity to magnetic field. Their spin properties can be read by optical means, which enables construction of various probes based on quantum mechanical interactions. If embedded in nanodiamond particles, NV centers can be exposed to biological environment and report sensitively on the spin-related processes occurring in a close vicinity of the particle. Molecular transducers designed for NV centers transposing the presence of particular analytes to a selective and unambiguous readout will be presented. Different types of surface architectures will be shown [1, 2]. Optical nanosensors designed for selective measurements of pH, redox potential, and ascorbate under physiological conditions will be discussed.

**References**

Rendler T., Neburkova J., Zemek O., Kotek J., Zappe A., Chu Z., Cigler P., Wrachtrup J. (2017). Optical imaging of localized chemical events using programmable diamond quantum nanosensors. *Nat. Commun.*, 8, 14701.  
Vavra J., Rehor I., Rendler T., Jani M., Bednar J., Baksh M. M., Zappe A., Wrachtrup J., Cigler P. (2018). Supported Lipid Bilayers on Fluorescent Nanodiamonds: A Structurally Defined and Versatile Coating for Bioapplications. *Adv. Funct. Mater.* 28, 1803406.

**8:15 AM F.EL01.02.01**

**Optimization of NV Centers Density in Pink Irradiated-CVD Diamond** Lahcene Mehmél<sup>1</sup>, Ovidiu Brinza<sup>1</sup>, Alexandre Tallaire<sup>1,2</sup>, Fabien Bénédic<sup>1</sup>, Gabriel Hetet<sup>3</sup>, Clément Pellet-Mary<sup>3</sup>, Paul Huillery<sup>3</sup>, Bernd Abel<sup>4</sup>, Robert Staacke<sup>4</sup>, Jan Meijer<sup>4</sup> and Jocelyn Achard<sup>1</sup>; <sup>1</sup>LSPM-CNRS, France; <sup>2</sup>IRCP, France; <sup>3</sup>LPENS-CNRS, France; <sup>4</sup>Leipzig University, Germany

NV centers in diamond are point like defects that have attracted a lot of attention as one of the best candidates for quantum technologies particularly for sensing and imaging nanoscale magnetic fields. For this application, the use of an ensemble of NV centers with a high concentration in a high quality diamond layer is of prime interest. In previous works, it has been demonstrated that N<sub>2</sub>O doping rather than N<sub>2</sub>, allows improving diamond quality by limiting the formation of macroscopic defects and NV's photobleaching [1]. More recently, the growth of N<sub>2</sub>O doped samples thicker than 1.5 mm has been achieved with substitutional nitrogen (Ns) concentration as high as a few tens of ppm which is very difficult to obtain by a CVD process using a conventional N<sub>2</sub> precursor. After irradiation by a 10 MeV electron beam, a conversion ratio of 20% has been obtained leading to a CVD grown layer with 4 ppm of NV<sup>-</sup>. A decrease of the longitudinal spin relaxation time T<sub>1</sub> observed when the magnetic field is aligned along the [100] direction (i.e. when all NV centers classes are equally degenerate) indicates that NV-NV dipolar coupling becomes a dominant mechanism in such highly doped samples. In this work, we will more particularly focus on the optimization of N<sub>2</sub>O concentration in the gas phase in order to limit NV-

NV<sup>-</sup> interaction while maximizing density and spin properties. In the same time, samples grown in the presence of N<sub>2</sub> + O<sub>2</sub> and N<sub>2</sub> only will be compared in order to investigate the benefit of the use of N<sub>2</sub>O. We aim at evaluating the maximum sensitivity achievable in a magnetic quantum sensor using such defect ensembles.

[1] A. Tallaire, L. Mayer, O. Brinza, M.A. Pinault-Thaury, T. Debuisschert, J. Achard, Highly photostable NV centre ensembles in CVD diamond produced by using N<sub>2</sub>O as the doping gas, *Appl. Phys. Lett.*, 111 (2017) 143101.

### 8:25 AM F.EL01.02.02

**Stabilizing the Charge State of the Tin-Vacancy Center by Defect Engineering** Johannes Görlitz<sup>1</sup>, Dennis Herrmann<sup>1</sup>, Philipp Fuchs<sup>1</sup>, Michael Kieschnick<sup>2</sup>, Sebastien Pezzagna<sup>2</sup>, Jan Meijer<sup>2</sup> and Christoph Becher<sup>1</sup>; <sup>1</sup>Universität des Saarlandes, Germany; <sup>2</sup>University Leipzig, Germany

The recently discovered negatively charged tin-vacancy center (SnV<sup>-</sup>) in diamond combines high brightness single photon emission [1,2], large Debye-Waller factors and Fourier-limited linewidths [3,4]. Furthermore, the ground state fine structure splitting exceeds 800 GHz which potentially suppresses phonon mediated decoherence of the lowest ground state's spin doublet, which is the predominant decoherence mechanism for other negatively charged group-IV – vacancy centers (Silicon-vacancy center (SiV<sup>-</sup>) and germanium-vacancy center (GeV<sup>-</sup>)). Therefore, the SnV<sup>-</sup> center supposedly combines the advantages of the most established colour centers, namely the long spin coherence time of the nitrogen vacancy center and the large Debye-Waller factor and insensitivity to first order stark shifts of the silicon vacancy center. The exploitation of these very promising features for quantum information processing is up to now limited by the charge instability of the center under resonant optical excitation [4]. This instability results in termination of the fluorescence and therefore inhibits the use of coherent manipulation protocols.

We here present studies on stabilizing the SnV<sup>-</sup> charge state based on the recently discovered Coulomb-driven single defect engineering by co-implantation of charge donors into diamond [5]. We co-implant oxygen, sulfur and boron together with tin and find a suppression of bleaching (reduction of fluorescence intensity under continuous illumination) and fluorescence termination together with increased photo-luminescence intensity for sulfur co-doping. These results pave the way for application of the SnV center in coherent optical spin control experiments.

[1] Iwasaki T. et al., *Phys. Rev. Lett.* 119, 253601 (2017)

[2] Tchernij S. D. et al., *ACS Photonics* 4, 25802586 (2017)

[3] Trusheim M. E. et al., *Phys. Rev. Lett.* 124, 023602 (2020)

[4] Görlitz J. et al., *New J. Phys.* 22, 013048 (2019)

[5] T. Lühmann et al., *Nat. Commun.* 10, 4956 (2019)

### 8:35 AM F.EL01.02.03

**Generation of Nitrogen-Vacancy Ensembles in Diamond for Use in Magnetic-Field Sensing Applications** Matthew Markham, Andrew Edmonds, Pierre-Olivier Colard and William Hillman; Element Six Ltd, United Kingdom

Ensembles of negatively-charged nitrogen-vacancy (NV<sup>-</sup>) centres in diamond constitute a promising platform for magnetometry applications. However, the sensitivity of present NV-ensemble devices and the need for diamond material with reproducible properties have hindered progress toward many envisioned applications. The work presented here addresses these challenges by optimising a chemical vapor deposition (CVD) growth process to produce material at scale with improved NV-ensemble properties.

Through development of the CVD process it is shown that nitrogen incorporation can be increased without an increase in the density of unwanted vacancy-related defects which act as charge acceptors, reducing the  $[N_s^0]/[N_s]$  and  $[NV^-]/[NV]$  ratios, and limiting the dephasing time,  $T_2^*$ . The process of irradiation and annealing is optimised and subsequent measurements of the NV concentration, charge ratio and contrast suggest that these grown-in defects have a detrimental impact on the NV-ensemble properties. Strain is also demonstrated to be a critical parameter to control.

This work also investigated the potential to produce material with reproducible NV concentration, NV charge ratio, strain homogeneity, and  $T_2^*$  by characterising a batch of samples containing approx. 4 ppm NV. The measured NV<sup>-</sup> and NV<sup>0</sup> concentrations in the batch of samples varied by less than 7% (1 standard deviation) and exhibited well-controlled strain inhomogeneity. The resulting  $T_2^* = 1 \mu s$  in material enriched with >99.99% <sup>12</sup>C was as expected for the concentration of N, establishing that other sources of decoherence have been controlled.

The material reported in this work enables immediate sensitivity improvements for present quantum-sensing devices and the correlations observed between material properties at different stages of processing provide efficient metrics for future work

targeting other NV densities or sample geometries such as micron-scale, NV-rich layers for magnetic imaging.

#### 8:45 AM F.EL01.02.04

**Enhanced Emission from Silicon-Vacancy Centers in Ag-Diamond Core-Shell Nanostructures** Shuo Li<sup>1,2</sup>, Nicholas Melosh<sup>3</sup> and Robert Hamers<sup>2</sup>; <sup>1</sup>SLAC National Accelerator Laboratory, United States; <sup>2</sup>University of Wisconsin-Madison, United States; <sup>3</sup>Stanford University, United States

Color centers in diamond are promising candidates for emerging quantum sensing and quantum information processing applications due to their exceptional properties. Coupling diamond color centers with metal plasmonic nanostructures is reported to enhance the optical properties of color centers effectively, but the plasmonic metal structures of previous studies are vulnerable to the environment, making the diamond-metal system unstable. Here, we demonstrate a novel and highly-tunable structure of Ag nanospheres coated with a layer of diamond containing SiV centers. The Ag was grown by thermal vapor deposition and then plasma treated to form uniform nanospheres, which were protected by the stable diamond shell grown by plasma-enhanced chemical vapor deposition (PECVD) method. This enhances the emission rate and brightness of SiV in diamond drastically. The structure also shows great stability to extreme corrosive and high-temperature conditions. Our finding is promising for developing ultrabright quantum sensing, high-efficiency imaging, and surface plasmon-quantum emitter waveguide.

#### 8:55 AM BREAK

#### 9:00 AM \*F.EL01.07.05

**How the Surface Orientation of Diamond Crystals Influences its Interaction with Biological Matter** Romana Schirhagl<sup>1</sup>, Viraj Damle<sup>1</sup>, Kaiqi Wu<sup>1</sup>, Oreste De Luca<sup>1</sup>, Natalia Orti Casan<sup>1</sup>, Neda Norouzi<sup>1</sup>, Aryan Morita<sup>1</sup>, Joop de Vries<sup>1</sup>, Hans Kaper<sup>1</sup>, Inge Zuhorn<sup>1</sup>, Ulrich Eisel<sup>1</sup> and Danny Vanpouke<sup>2</sup>; <sup>1</sup>Groningen University, Netherlands; <sup>2</sup>Hasselt University, Belgium

Here we show how the diamond crystal orientation influences the interaction with biological systems[1]. More specifically we are investigating the interaction between the <100>, <110> and <111> surfaces of single crystal diamond with biomolecules, cell culture medium, mammalian cells and bacteria. We show that the crystal orientation significantly alters these biological interactions. Most surprising is the two orders of magnitude difference in the number of bacteria adhering on <111> surface compared to <100> surface when both the surfaces were maintained under the same conditions. We also observe differences in how small biomolecules attach to the surfaces. Neurons or HeLa cells on the other hand do not have clear preferences for either of the surfaces. To explain the observed differences, we theoretically estimated the surface charge for these three low index diamond surfaces and followed by the surface composition analysis using x-ray photoelectron spectroscopy (XPS). We conclude that the differences in negative surface charge, atomic composition and functional groups of the different surface orientations lead to significant variations in how the single crystal diamond surface interacts with the studied biological entities.

[1] Damle, V., Wu, K., De Luca, O., Ortí-Casañ, N., Norouzi, N., Morita, A., de Vries, J., Kaper, H., Zuhorn, I.S., Eisel, U. and Vanpoucke, D.E., 2020. Influence of diamond crystal orientation on the interaction with biological matter. *Carbon*, 162, pp.1-12.

#### 9:15 AM \*F.EL01.07.01

**Identifying the Multiple Classes of Diamond Nanoparticles Using Machine Learning** Amanda Barnard<sup>1</sup> and Amanda J. Parker<sup>2</sup>; <sup>1</sup>The Australian National University, Australia; <sup>2</sup>CSIRO, Australia

Diamond nanoparticles are complicated materials, presenting a diverse range of sizes, shapes, speciation and defects that cannot easily be controlled during synthesis. Each of these features contribute to structure/property relationships, but in different ways. Attempts to purify samples to tune the properties often fail due to lack of specificity, and polydispersivity usually persists. An alternative approach is to separate classes of nanodiamonds based on their properties, rather than seeking monodispersed samples based on their structure. To investigate if this approach has merit we have used machine learning to classify nanodiamonds and identify class-dependent properties and characteristics. Using a fully reconstructed data set that spans the experimentally observed size range from 1 nm to 4.5 nm we find that there are multiple classes of particles, based on their similarity in the high dimensional feature space. By using an interpretable classifier, with excellent accuracy, precision and recall, we also identify possible purification pathways based on the important features ranked by the AI.

#### 9:30 AM F.EL01.07.04

**Surface Functionalized Nanodiamond with Improved Protein Repulsion for Drug Delivery and Sensing** Julia Puck, Viktor Merz and Anke Krueger; Wuerzburg University, Germany

For many applications the surface chemistry of nanodiamond (ND) is a key factor for the control of properties such as the wetting behavior, biocompatibility and functionality[1]. By attaching appropriate moieties, the interaction with physiological environments can be controlled.

An important point for biomedical applications is the inhibition of a nonspecific protein corona. This shell of e.g. serum proteins masks the desired functions and renders the physiological properties of the nanoparticle uncontrollable[2].

Here we report on the grafting of zwitterionic moieties enabling the formation of NDs without protein corona [3] that enable the specific grafting of antibodies, targeting peptides and CO releasing drug molecules using visible light. The resulting constructs have been characterized using IR, Raman, x-ray spectroscopies as well as particle analysis, TGA and electron microscopy.

The ND conjugates have been tested in vitro as well as in cell assays and demonstrated their functionality in the cellular environment. Additionally, these NDs have been functionalized with pyrene moieties for fluorescence sensing in solution with strong ion background and demonstrated colloidal stability, sensitivity and specificity for the detection of heavy metal ions against a background of ions present in physiological environments.

This research has received funding from Volkswagenstiftung under Grant Agreement no. 88393.

### References

[1] A. Krueger, D. Lang, *Adv. Funct. Mater.* 22 (2012), 890.

[2] W. C. W. Chan, C. D. Walkey, *J. Am. Chem. Soc.* 134 (2012), 2139.

[3] V. Merz, J. Lenhart, Y. Vonhausen, M. E. Ortiz Soto, J. Seibel, A. Krueger, *Small* (2019) 1901551.

### 9:40 AM F.EL01.07.03

**Scalable Assembly of Fluorescent Nanodiamonds for Quantum Sensing** Henry J. Shulevitz, Tzu-Yung Huang, Steven Neuhaus, Lee Bassett and Cherie Kagan; University of Pennsylvania, United States

Milled fluorescent nanodiamonds containing nitrogen-vacancy (NV) centers provide an excellent platform for sensing applications due to their quantum sensitivity to a variety of external fields at nanometer length scales. Currently, the irregularity in crystal morphology and the difficulty of functionalizing the nanodiamond surface impede efforts to realize scalable assemblies of nanodiamonds, or to create heteroassemblies with other materials. Poor control over the nanodiamond composition and surface chemistry also creates significant heterogeneity in their optical and quantum characteristics. We will present scalable strategies to form ordered arrays of nanodiamonds using template-directed capillary assembly. This method enables the precise spatial arrangement of primary nanodiamonds with diameters below 50 nm, and it is compatible with the assembly of other compositions of colloidal nanoparticles. Large-scale arrays facilitate automated, repeatable measurements of the nanodiamonds' optical, structural, and quantum characteristics, enabling improved statistical understanding of these key properties and their heterogeneity. The flexible assembly method will allow for detailed studies of chemical treatments, integration of nanodiamonds within photonic and electronic devices, and the realization of quantum heterostructure devices composed from complementary nanomaterials.

### 9:50 AM F.EL01.05.05

**Surface Contamination Impact on Nanodiamond Seeding of Plasma-Treated Tantalum Films** Paulius Pobedinskas<sup>1,2</sup>, Wim Dexters<sup>1,2</sup>, Jan D'Haen<sup>1,2</sup> and Ken Haenen<sup>1,2</sup>; <sup>1</sup>Hasselt University, Belgium; <sup>2</sup>IMEC vzw, Belgium

The deposition of closed nanocrystalline diamond (NCD) thin films on non-diamond substrates requires diamond nucleation sites. An established technique for creating nucleation sites is a surface treatment with a water-based colloidal solution of ultra-dispersed nanodiamond (ND) particles.<sup>1</sup> In ND seeding the most important factors are the surface charge of the substrate and the zeta-potential of the used colloid. Together, they determine the nucleation density, which can lead to an extreme difference in the observed seeding density.<sup>2-6</sup> However, surface contamination by hydrocarbons, which is an unavoidable and quick process even in a cleanroom environment,<sup>7</sup> is often not taken into consideration. Such contamination can alter the surface wetting properties<sup>8</sup> and surface charge<sup>9</sup>, and thus the eventual seeding density. In this work we investigate and model the impact such surface contamination has on the ND seeding efficiency.

Tantalum is a metal well known for its resistivity to corrosion, bioinertness, biocompatibility and excellent osteoconductivity.<sup>10</sup> After sputtering a thin film of Ta on silicon substrates, these stacks were exposed to the ambient atmosphere for different times, allowing to achieve various degrees of surface contamination. Then, the Ta surface wettability was measured, samples were seeded with NDs, and the subsequent seeding density evaluated. As surface coverage by

hydrocarbons increased, the wetting properties gradually turned from hydrophilic to hydrophobic. The ND seeding density first decreased and then increased again. To understand this correlation, we propose an analytical model that describes the dynamics of surface contamination and hydrocarbon contaminant interaction with the surface, and the resulting ND seeding density.

We assume that when a hydrocarbon (HC) molecule lands on the Ta surface it attracts negative surface charge towards it, while creating a positive surface charge around it. Due to said dipole formation, the top part of the HC molecule is charging negatively. Solving differential equations for the dynamics of the normalized surface coverage number density of the HC molecules,  $n$ , and surface charge density,  $\sigma$ , we derive  $\sigma(n, \eta) = n + (1 - n)^{(1 + \eta)}$ , where  $\eta$  is a ratio between an area of the depleted charge around the HC molecule and the area of the HC molecule itself. The assumption that the contact angle,  $\theta$ , is linearly proportional to the surface coverage by HC,  $n = \theta / \theta_{\text{sat}}$ , makes wettability measurements a valid method for determining the degree of surface contamination. If the sum of electrostatic double-layer and Van der Waals interaction energies becomes positive, a potential energy barrier for a ND particle approaching a surface exists. ND particles must surmount a positive potential peak for a deposition onto the surface to occur. This occurs with a probability exponentially proportional to the potential barrier. By fitting the experimental data, we find that the ND seeding density is exponentially proportional to the calculated positive surface charge number density, which forms around HC molecules. This constitutes 57% of the HC molecule area, while the created barrier height is estimated to be  $\sim 0.18$  eV.

## References

- [1] O.A. Williams, *et al.*, Chem. Phys. Lett. **445**, 255 (2007).
- [2] O.A. Williams, *et al.*, ACS Nano **4**, 4824 (2010).
- [3] P. Pobedinskas, *et al.*, Appl. Phys. Lett. **102**, 201609 (2013).
- [4] J. Hees, *et al.*, Nanotechnology **24**, 025601 (2013).
- [5] G. Degutis, *et al.*, Chem. Phys. Lett. **640**, 50 (2015).
- [6] S. Mandal, *et al.*, ACS Appl. Mater. Interfaces **11**, 40826 (2019).
- [7] K. Takeda, *et al.*, Proc. 44<sup>th</sup> Annual Technical Meeting of the IEST and ISCC, 556 (1998).
- [8] Ch. Mücksch, *et al.*, J. Phys. Chem. C **119**, 12496 (2015).
- [9] A. Khachatourian, *et al.*, J. Chem. Phys. **140**, 074107 (2014).
- [10] H. Matsuno, *et al.*, Biomaterials **22**, 1253 (2001).

SESSION F.EL01.11: Live Keynote II: Diamond and Diamond Heterojunctions—From Growth to Applications  
Session Chairs: Robert Nemanich and Mariko Suzuki  
Wednesday Afternoon, December 2, 2020  
F.EL01

### 5:15 PM \*F.EL01.06.01

#### The Role of Interfaces and Heterogenous Integration in the Thermal Management of Wide Bandgap

**Semiconductors** Samuel Graham<sup>1</sup>, Zhe Cheng<sup>1</sup>, Mark Goorsky<sup>2</sup>, Fengwen Mu<sup>3</sup>, Jim Speck<sup>4</sup> and Tadatomo Suga<sup>3</sup>; <sup>1</sup>Georgia Institute of Technology, United States; <sup>2</sup>University of California, Los Angeles, United States; <sup>3</sup>Meisei University, Japan; <sup>4</sup>University of California, Santa Barbara, United States

Wide bandgap electronics made from GaN and Ga<sub>2</sub>O<sub>3</sub> are currently under development due to their potential to create advanced RF and power electronics. However, the performance and reliability of these devices are often controlled by their electrothermal response during device operation. A key feature which limits thermal control of the peak temperature is the thermal resistance that is encountered intrinsically from the material as well as across material interfaces with these devices. One method that has shown promise for mitigating the high thermal resistance of these devices is through their heterogenous integration with other materials which assist in heat dissipation and aid thermal management. For this, thermal transport across interfaces and novel integration methods are necessary.

In this work we will present modeling efforts which guide the impact of heterogenous integration on the thermal performance of UWBG devices. Thermal metrology methods used to measure interfacial thermal conductance will be discussed and new insights into the control of thermal boundary conductance given. Techniques such as surface activated bonding will be presented to demonstrate the integration of GaN and Ga<sub>2</sub>O<sub>3</sub> with high thermal conductivity substrates such as SiC and diamond. The use of other high thermal conductivity dielectrics for improved heat dissipation from the top side and bottom

side of the devices will be discussed. Finally, the prospects for the future development of thermal management via heterogenous integration will be presented.

### 5:30 PM F.EL01.06.02

**Formation Process of High Thermal-Stability Diamond/Si and Diamond/GaAs Heterointerfaces by Surface Activated Bonding** Yutaka Ohno<sup>1</sup>, Jianbo Liang<sup>2</sup>, Yasuo Shimizu<sup>1</sup>, Hideto Yoshida<sup>3</sup> and Naoteru Shigekawa<sup>2</sup>; <sup>1</sup>Tohoku University, Japan; <sup>2</sup>Osaka City University, Japan; <sup>3</sup>Osaka University, Japan

Diamond is a promising candidate for a base material of high power electronic devices, as well as for a superior heat spreading substrate, due to its excellent physical properties such as the highest electrical breakdown field strength, the highest thermal conductivity, and a high RF power capability that is 3 times higher in comparison with SiC. For the practical application toward power devices, we need diamond/semiconductor heterointerfaces with high thermal stability and can withstand the temperature rise of power devices during operating. Recently, Liang has demonstrated that diamond/Si [1] and diamond/GaAs [2] heterointerfaces with high thermal stability can be fabricated by surface activated bonding (SAB) at room temperature (RT). In this work, we have examined the bonding mechanism using cross-sectional scanning transmission electron microscopy (STEM) combined with electron energy loss spectroscopy (EELS) and energy dispersive x-ray spectroscopy (EDX).

In the SAB process, surfaces of diamond and Si (or GaAs) wafers are activated at RT before bonding by creating dangling bonds via the irradiation of high-energy Ar atoms in a high vacuum, and the surfaces are then bonded by the contact most of the time under pressure to form strong chemical bonds even for imperfect surfaces. For diamond/Si heterointerfaces, atomic diffusion at the interfaces, presumably due to the transient enhanced diffusion assisted by the point defects introduced in the surface activation process [3], is confirmed during the bonding process. The crystallinity at the diffusing region is rather low, and it is recovered by 1000 °C annealing via the formation of SiC layers, that would play a pivotal role in the relaxation process of residual stress due to the misfit of thermal expansion coefficient between diamond and Si [1]. Therefore, the defect-assisted atomic diffusion at the interfaces would be a key concept for the formation of high thermal-stability diamond/Si heterointerfaces. Similar atomic diffusion is also confirmed at diamond/GaAs heterointerfaces during the SAB process.

[1] J. Liang, S. Masuya, M. Kasu, and N. Shigekawa, Appl. Phys. Lett. 110 (2017)111603.

[2] Y. Nakamura, Y. Shimizu, Y. Ohno, K. Shirasaki, Y. Nagai, M. Kasu, N. Shigekawa, and J. Liang, 13th Topical Workshop on Heterostructure Microelectronics (Toyama, Japan, 2019) 11-7.

[3] Y. Ohno, H. Yoshida, N. Kamiuchi, R. Aso, S. Takeda, Y. Shimizu, Y. Nagai, J. Liang, and N. Shigekawa, Jpn. J. Appl. Phys. 59 (2020) SBBB05.

### 5:40 PM F.EL01.06.03

**The Impact of Polycrystalline Diamond Growth Nucleation on N-Polar GaN Channel Performance** Mohamadali Malakoutian<sup>1,2</sup>, Chenhao Ren<sup>1,2</sup>, Kelly Woo<sup>2</sup>, Shubhra Pasayat<sup>3</sup> and Srabanti Chowdhury<sup>2</sup>; <sup>1</sup>University of California, Davis, United States; <sup>2</sup>Stanford University, United States; <sup>3</sup>University of California, Santa Barbara, United States

N-polar gallium nitride (GaN) high electron mobility transistors (HEMTs) have shown superior performances when scaling for W-band frequencies over Ga-polar GaN HEMTs [1]. However, due to the shorter channel and closer gate fingers its ability to dissipate the heat from the channel to the heat-sink is limited. Polycrystalline (PC) diamond due to its very large thermal conductivity (TC) is one of the solutions for self-heating problem in high-power high-frequency devices. PC Diamond can be grown in a closed proximity to high temperature spot in the channel and spread the heat efficiently [2]. The standard Si<sub>3</sub>N<sub>4</sub> thickness as a gate dielectric for W-band N-polar HEMTs is 5 nm, which can be used as thermal interface material to reduce thermal boundary resistance (TBR < 2 m<sup>2</sup>K/GW) between diamond and GaN as well [3]. As diamond growth takes place in a high temperature hydrogen plasma environment using MPCVD, it can decompose both Si<sub>3</sub>N<sub>4</sub> and GaN layers by reacting with silicon, nitrogen, and gallium and making volatile gases (SiH<sub>4</sub>, NH<sub>3</sub>, and GaH, respectively) [4]. Any damage to GaN channel may result in a degradation of device performance after the growth. In this work, we investigated the impact of diamond growth nucleation and main stages on 2-dimensional electron gas (2DEG) properties such as electron mobility, sheet carrier concentration, and sheet resistivity (before growth:  $\mu_n=1200$  cm<sup>2</sup>/V.s,  $n_s=1.34E13$  cm<sup>-2</sup>, and  $\rho_s=388$  Ω/sq).

The main goal of the growth nucleation stage is to guarantee no damage to the 2DEG by covering the substrate (Si<sub>3</sub>N<sub>4</sub>/GaN) with thinnest possible nano-crystalline diamond (NCD) in shortest possible time as NCD has a poor TC (<100 W/m.K). The 2DEG has been characterized using Hall mobility measurement, and the thickness of nucleation layer has been measured by high resolution TEM. The nucleation layer can prevent diffusion of hydrogen radicals into the substrate which is highly dependent on the microwave power and gas pressure. To increase the diamond growth rate and decrease substrate etching rate the sample holder was redesigned to provide higher temperature (~700 C) with minimum power (600 W) and pressure

(20 Torr). The CH<sub>4</sub>% and time were changed from 3 to 10% and 10 to 15 min, respectively for nucleation stage followed by the same main growth for all samples (2% CH<sub>4</sub>, 1600 W, 60 Torr, 45 min). We observed no degradation in 2DEG by using >5% CH<sub>4</sub> and 15 min growth, while by lowering the time to 10 min we started to see about 20-30% reduction in  $\mu_n$  and 50-150  $\Omega/\text{sq}$  increase in  $\rho_s$ . This degradation varies with different cap layers on top of the channel; no cap layer, 1-2 nm AlN, or 1-2 nm 46% AlGaIn.

To study the impact of main growth on 2DEG, we have chosen 5% CH<sub>4</sub> and 15 min for nucleation stage and changed main growth parameters including CH<sub>4</sub>% (0.5-2%), power (600-1600 W), pressure (20-90 Torr), and sample holder design. CH<sub>4</sub>% showed the highest impact in determination of damage level to 2DEG and pressure had the lowest impact. With the sample holder same as nucleation stage, 1% CH<sub>4</sub> is the minimum required for no damage. For the case with original sample holder, 1.5% CH<sub>4</sub> is the lowest acceptable value for the first 45 min of the growth.

In this work, we were able to achieve a smooth interface between diamond and GaN (including 5 nm Si<sub>3</sub>N<sub>4</sub> interfacial layer) without using argon or nitrogen in the gas mixture by redesigning the sample holder and modifying growth parameters for lower etch rate of the substrate. This recipe is compatible with W-band N-polar GaN HEMTs as maintains device performance after the growth.

This work was supported by the Semiconductor Research Corporation (SRC) and DARPA under the JUMP program.

[1] B. Romanczyk *et al.*, *IEEE Electron Device Lett.*, vol. 41, no. 3, pp. 349–352, 2020.

[2] M. Malakoutian *et al.*, *Crystals*, vol. 9, no. 10, pp. 1–14, 2019.

[3] J. Cho *et al.*, *J. Appl. Phys.*, vol. 121, no. 5, 2017.

[4] Y. S. Zou *et al.*, *Cryst. Growth Des.*, vol. 8, no. 5, pp. 1770–1773, 2008.

#### 5:50 PM \*F.EL01.03.01

**Microfabrication of Sensors and Nanodiamond Structures on Diamond Substrates for Extreme Environments** Yogesh K. Vohra; University of Alabama-Birmingham, United States

Maskless lithography has been combined with the microwave plasma chemical vapor deposition (CVD) of diamond to fabricate a variety of micro-sensors that can be deposited on substrates and encapsulated in a protective CVD diamond layer to survive extreme conditions of high-pressure, high- and low-temperatures, corrosive, and high radiation environments. These hardened sensors provide electrical conductivity, magnetic susceptibility, and stress data on a variety of metallic and superconducting materials under extreme conditions of pressures and temperatures in diamond anvil cell devices. In addition, boron-doping of CVD diamond also enables the fabrication of micro-heaters in diamond anvil cell devices. Microfabrication techniques have also been utilized to selectively grow localized nanodiamond structures on single crystalline diamond substrates. Since nanodiamond structures lack the cleavage planes representative of single crystal diamond; ultrahigh pressures of over 500 GPa can be generated in this nanodiamond/single crystal diamond structures. The studies on materials under extreme conditions using these diamond-based sensors and nanodiamond structures are carried out at the Advanced Photon Source, Argonne National Laboratory. Future research directions in vertical integration of multiple sensors, wireless communications, and controlling the sp<sup>3</sup> bonded content in nanodiamond microstructures will be presented.

#### 6:05 PM BREAK

#### 6:15 PM F.EL01.04.06

**Diamond Electronics for the Surface of Venus** Robert J. Nemanich<sup>1</sup>, Mohamadali Malakoutian<sup>2,3</sup>, Harshad Surdi<sup>1</sup>, Manpuneet Benipal<sup>4</sup>, Franz A. Koeck<sup>1</sup>, Srabanti Chowdhury<sup>3</sup>, Stephen M. Goodnick<sup>1</sup> and James Lyons<sup>1</sup>; <sup>1</sup>Arizona State University, United States; <sup>2</sup>University of California - Davis, United States; <sup>3</sup>Stanford University, United States; <sup>4</sup>Advent Diamond, United States

The surface temperature of Venus is ~460 C, with a corrosive atmosphere including CO<sub>2</sub> and sulfuric acid at a pressure of 92 bar. A number of missions to Venus are being considered or planned that would include surface or atmosphere probes, and high temperature electronics would be required for power control, mechanical system control, and sensor electronics. While it is long been recognized that the wide bandgap of diamond would result in a negligible increase in the intrinsic carrier concentration, at high temperature the devices based on Schottky barriers would show a great reduction in the forward-reverse current rectification ratio. This research presents results of diamond diodes with a thin n-type layer in a Schottky-n-i-p structure, which achieves high current density, high breakdown field and a designed on-off rectification ration. The metal-n-i-p diamond diodes were prepared on single crystal p-type, boron doped (100) or (111) substrates, with undoped intrinsic epitaxial layers and phosphorus doped epitaxial layers prepared by microwave plasma CVD. The electrical results and simulations show regimes with low drift layer resistance where the contact resistance limits the current. The diodes have been confined in a high pressure CO<sub>2</sub> atmosphere for over 100 hrs. After removal, inspection of the surfaces shows dark regions thought to be carbon containing layers, which did not result in evident changes of the current-voltage characteristics. More



extensive Venus atmosphere testing planned at the NASA GEER facility will include active electrical measurements. The results establish that with control of p- and n-type doping optimal device designs can be achieved for diamond electronics at high temperature.

This research supported by NASA through grant NNX17AG45G as part of the HOTTech program.

#### 6:25 PM \*F.EL01.05.03

**Electrical and Quantum Application of Diamond—From the Viewpoint of Diamond CVD Growth and Device Fabrication** Satoshi Yamasaki<sup>1,2</sup>, Toshiharu Makino<sup>1</sup>, Hiromitsu Kato<sup>1</sup>, Masahiko Ogura<sup>1</sup>, Daisuke Takeuchi<sup>1</sup>, Yukako Kato<sup>1</sup>, Norio Tokuda<sup>2</sup> and Tsubasa Matsumoto<sup>2</sup>; <sup>1</sup>National Institute of Advanced Industrial Science and Technology, Japan; <sup>2</sup>Kanazawa University, Japan

Diamond has many unique physical properties. Due to these unique properties diamond has high potential for applications; electrical devices, quantum devices, etc. Depending on the target application we need to develop the growth and fabrication technique, In this talk, we introduce the electronic applications and the quantum application using nitrogen-vacancy centers from the viewpoint of diamond growth and fabrication technique.

#### 6:40 PM \*F.EL01.04.01

**Nuclear Battery Applications of Diamond Junction Devices** Takehiro Shimaoka<sup>1,2</sup>, Hitoshi Umezawa<sup>2,3</sup>, Kimiyoshi Ichikawa<sup>1</sup>, Julien Pernot<sup>3</sup> and Satoshi Koizumi<sup>1</sup>; <sup>1</sup>National Institute for Materials Science, Japan; <sup>2</sup>National Institute of Advanced Industrial Science and Technology, Japan; <sup>3</sup>Université Grenoble Alpes, France

Betavoltaic cells directly convert the energy of beta particles into electricity.[1] The operation principle of a betavoltaic cell is similar to that of a solar cell, except that the energy source is beta-emitting isotopes. In betavoltaic cells, semiconductor junctions play the role of energy conversion. These cells have the advantage of longevity, which is determined by the half-life ( $T_{1/2}$ ) of the beta-emitting radioisotopes. The cells can operate for several years to a decade. Betavoltaic cells are expected to be utilized for battery applications in remote locations such as outer space and underground.

Diamond is advantageous material for betavoltaic cells because the wide bandgap could offer high open circuit voltage due to large built-in potential of the junction, which improves the conversion efficiency of the cells. From theoretical perspective, ultrawidebandgap materials such as diamond and BN have potential to realize extreme conversion efficiency of the cells.[2] Moreover, diamond has durability against radiation and high temperature. Diamond betavoltaic cells could be utilized to application under extreme condition. In this study, we show the highest semiconductor conversion efficiency among the betavoltaic cells reported thus far by utilizing the large built-in potential of a diamond *pn* junction.

We formed pseudo-vertical diamond *pn* diodes. Homoepitaxial  $p^+$ ,  $p$ ,  $n^-$ , and  $n^+$  diamond layers were grown on a {111} high-pressure high-temperature (HPHT) type-Ib diamond substrate by using microwave plasma-assisted chemical vapor deposition (MPCVD). Each B- ( $p$ -type) and P- doped ( $n$ -type) diamond layer were grown with the use of individual MPCVD systems. The thickness of the  $p^+$ ,  $p$ ,  $n^-$ , and  $n^+$  layers were, respectively, 2, 0.1, 1.8, and <0.1  $\mu\text{m}$ . The impurity concentrations confirmed by secondary ion mass spectrometry (SIMS) were [B]:  $3 \times 10^{19} \text{ cm}^{-3}$  for the  $p^+$  layer, [B]:  $2 \times 10^{18} \text{ cm}^{-3}$  for the  $p$  layer, [P]:  $1 \times 10^{16} \text{ cm}^{-3}$  for the  $n^-$  layer, and [P]:  $1 \times 10^{20} \text{ cm}^{-3}$  for the  $n^+$  layer. Highly P- doped diamond was grown using homemade CVD reactor to enhance P incorporation into diamond to reduce series resistance. After the growth, mesa structures were formed by induction coupling plasma etching with oxygen gas. Subsequently, Ohmic contacts were formed by electron beam deposition of Ti/Mo/Au both on the mesa structure of the  $n^+$ -layer and on the  $p^+$ -layer. The diameters of the mesa and electrodes were, respectively, 240 and 150  $\mu\text{m}$ .

Then we evaluated power – voltage ( $P$ - $V$ ) and current-voltage ( $I$ - $V$ ) characteristics under electron-beam irradiation. For electron-beam irradiation, a scanning electron microscope was used as the electron source. Electron beams at accelerating voltages of 15 kV were irradiated on top of the  $n^+$  layer. The open-circuit voltage ( $V_{oc}$ ) under the electron-beam irradiation was 4.26 V, which is the highest among the betavoltaic cells reported thus far. The output power at the maximum point ( $P_{MP}$ ) was 10.7 nW. Fill factor ( $FF$ ) and semiconductor conversion efficiency ( $\eta_s$ ) calculated as following eqs (1) and (2)

$$FF = P_{MP}/I_{sc}V_{oc}, \dots(1)$$

$$\eta_s = VocFF/\varepsilon, \dots(2)$$

where  $\varepsilon$  is the electron–hole pair creation energy. Here, we substitute  $\varepsilon = 13 \text{ eV}$  in eq. (2). The  $FF$  and the semiconductor conversion efficiency  $\eta_s$  were respectively, 0.85 and 28%. Among the semiconductors, the diamond *pn* junction achieved the highest  $\eta_s$ , which enables to be utilized to energy efficient and long-life cells for remote sensing applications. In the talk, we will also present charge collection efficiency and total conversion efficiency of diamond *pn* diode against different energy of electrons.

## References

- [1] P. Rappaport, The electron-voltaic effect in p-n junctions induced by beta-particle bombardment, *Phys. Rev.* **93**, 246 (1954).  
[2] S. Maximenko, J. Moore, C. Affouda, P. Jenkins, Optimal semiconductors for  $^3\text{H}$  and  $^{63}\text{Ni}$  betavoltaics, *Sci. Rep.* **9**, 10892 (2019).

### 6:55 PM F.EL01.08.02

#### Stabilizing Diamond's Surface Conduction with Mixed-Oxide ALD Films and Deuterium Surface

**Termination** Michael Geis<sup>1</sup>, Joseph Varghese<sup>1</sup>, Yichen Yao<sup>2</sup>, Robert J. Nemanich<sup>2</sup>, Mark Hollis<sup>1</sup>, Charles H. Wuorio<sup>1</sup>, Xingyu Zhang<sup>1</sup>, George W. Turner<sup>1</sup>, Shireen M. Warnock<sup>1</sup>, Steven A. Vitale<sup>1</sup>, Richard J. Molnar<sup>1</sup>, Thomas Osadchy<sup>1</sup> and Beijia Zhang; <sup>1</sup>Massachusetts Institute of Technology, United States; <sup>2</sup>Arizona State University, United States

When the surface of diamond is H-terminated, a p-type surface conductive layer is formed. Atmospheric impurities,  $\text{NO}_2$ ,  $\text{O}_3$ , fluoropolymer, transition metal oxides and  $\text{Al}_2\text{O}_3$  adhere to the diamond surface and activate diamond's surface conductance by generating and trapping negative charges on the diamond surface. These charges increase the positive p-type carrier densities in the diamond surface and reduce its resistance. High drain current field effect transistors (FETs) of 1.2 to 1.3 A  $\text{mm}^{-1}$ , high frequency  $f_T$  of 75 GHz, and high voltage, >2000 V, devices have been demonstrated with these activation surface chemistries. However, these devices degraded in a few days or when stressed with high voltage.

Research to stabilize diamond's surface conductance has met with some success. H-terminated diamonds overcoated using atomic layer deposition (ALD)  $\text{Al}_2\text{O}_3$  have the best demonstrated stability, but the surface resistance is high (5 to 12  $\text{k}\Omega \text{sq}^{-1}$ ). Diamonds coated with transition metal oxides such as  $\text{WO}_2$ ,  $\text{MoO}_3$ , and  $\text{V}_2\text{O}_5$  have lower resistances of 2.5 to 3.5  $\text{k}\Omega \text{sq}^{-1}$  [1,2]. Their stability has been demonstrated although these oxides are conductive, have several oxidation states, and may electrochemically degrade under the high electric fields associated with FETs. This presentation will discuss the use of a mixed-oxide ( $\text{Al}_2\text{O}_3$ - $\text{SiO}_2$ ) ALD film to generate resistances between 1.5 and 3.5  $\text{k}\Omega \text{sq}^{-1}$  with demonstrated stability in excess of half a year.

The low surface resistance obtained with this mixed oxide is a result of a change in the structure of  $\text{Al}_2\text{O}_3$  when mixed with  $\text{SiO}_2$ . The electron trap surface density of  $\text{Al}_2\text{O}_3$  is  $\sim 7 \times 10^{12} \text{cm}^{-2}$  while the mixed oxide surface density is  $3 \times 10^{13}$  to  $8 \times 10^{13} \text{cm}^{-2}$  [3,4] with an estimated trap depth of 5.4 eV. This mixed oxide is just one of a group of oxides [5] with deep, > 5 eV, high-density electron traps.

Increased stability of the diamond surface is obtained by terminating the surface with deuterium atoms instead of hydrogen atoms. This additional stability is beneficial during device fabrication. This presentation will discuss diamond's surface conduction with  $\text{Al}_2\text{O}_3$ - $\text{SiO}_2$  combined with deuterium atom termination.

#### References

- [1] C. Verona, F. Arciprete, M. Foffi, E. Limiti, et. al. *Appl. Phys. Lett.* 112 (2018), 181602.  
[2] K. G. Crawford, D. Qi, J. McGlynn, T. G. Ivanov, et. al. *Sci. Rep.* 8 (2018), 3342.  
[3]. K. Raghavan, P. Sabu, K. Vijayachandra, C. Rao C. G. Ramachandran. *Bull Chem. Soc. Jpn.* 64 (1991), 1920.  
[4] A. Satsuma, Y. Westi, Y. Kamiya, T. Hattori, Y. Murakami. *Bull Chem. Soc. Jpn.* 70 (1997), 1311.  
[5] A. Corma. *Chem. Rev.* 95 (1995), 559.

DISTRIBUTION STATEMENT A. Approved for public release. Distribution is unlimited.

This material is based upon work supported by the Under Secretary of Defense for Research and Engineering under Air Force Contract No. FA8702-15-D-0001. Any opinions, findings, conclusions or recommendations expressed in this material are those of the author(s) and do not necessarily reflect the views of the Under Secretary of Defense for Research and Engineering.

© 2020 Massachusetts Institute of Technology.

Delivered to the U.S. Government with Unlimited Rights, as defined in DFARS Part 252.227-7013 or 7014 (Feb 2014). Notwithstanding any copyright notice, U.S. Government rights in this work are defined by DFARS 252.227-7013 or DFARS 252.227-7014 as detailed above. Use of this work other than as specifically authorized by the U.S. Government may violate any copyrights that exist in this work.

### 7:05 PM F.EL01.08.01

#### Investigation of Li Doping and SnO Termination on the Diamond (100) Surface for Thermionic Emission

**Application** Sami Ullah, Liam Cullingford, Tongfie Zhang, Jing Ren Wong, Gary Wan, Mattia Cattelan and Neil Fox; University of Bristol, United Kingdom

Diamond electrodes terminated with surface layers can impart significant changes to the electronic properties of a diamond

interface and we have previously reported on studies of the tunability of surface work function by substituting hydrogen with oxygen under controlled conditions [1]. Engineering a functionalised diamond surface that is stable and reproducible is of technological importance to future diamond electronic devices such as Schottky junctions and electron-emitting electrodes for field emission, thermionic energy converters, secondary electron multipliers.

O'Donnell and his group have demonstrated the formation of a stable Li-O termination of diamond by physical vapour deposition of a monolayer of Li on the diamond surface which develops and exhibits Negative electron affinity (NEA) and hence lowers the work function, even at an elevated temperature of 800 °C [2]. In this work we are seeking an alternative method, a novel and easy chemical means of introducing and coordinating lithium with oxygen on the diamond surface to realize a more controlled approach of creating a stable –O-Li dipole, with uniformity over the diamond surface which also serves as a means to study and visualize for the first time the effect of temperature on the concentration of Li atoms in the diamond surface and on the Li-O species on the surface of diamond sample.

Also, Tin monoxide has been considered as potential material for battery anodes, coating, gas sensing, catalysis, etc. The application area of SnO extends over photovoltaics, displays, information storage, etc. as it has a large optical bandgap of 4.12 eV, high transparency (~90%) non-toxic and abundant [3]. SnO has been found to form a layered structure in a crystallographic direction of [001] with a monolayer thickness of 0.48 nm. Sn 5s form a lone pair of electrons which point towards the interlayer spacing and result in dipole-dipole interaction leading to a Van der Waals gap of 2.52 Å between the layers. Various groups have demonstrated the growth of SnO mono and multiple layers by various methods but many of these result in an upper SnO<sub>2</sub> layer that forms as soon as the sample is taken into the oxygen environment as SnO is metastable and hence rapidly converts into SnO<sub>2</sub>.

We are doping oxygen terminated Boron doped Polycrystalline diamond and Nitrogen doped HPHT diamond (111) with Li atoms using microwave plasma technique. The oxygen termination was induced by acid washing. We analyze the sample with X-Ray Photoemission Spectroscopy (XPS) and Raman spectroscopy. The main aim of this study is to analyze the change in concentration of Li atoms in the bulk and on the surface of diamond with annealing temperature. We have produced sub ML SnO on conductive, p-type single crystal diamond under ultra-high vacuum (UHV) conditions by e-beam evaporation. The samples will be characterised in-situ by Spot Profile Analysis Low-Energy electron diffraction (SPA-LEED) and Energy Filtered Photo Emission Electron Microscopy (EF-PEEM) and X-ray Photoemission Spectroscopy (XPS). We quantify the change in work function between mono and few layer SnO and its effect upon the barrier height of a p-type diamond Schottky junction.

## References

[1] Wan, G., Cattelan, M. & Fox, N. A. Electronic structure tunability of diamonds by surface functionalization. *J. Phys. Chem. C* (2019). doi:10.1021/acs.jpcc.8b11232

[2] K. M. O'Donnell et al., "Diamond Surfaces with Air-Stable Negative Electron Affinity and Giant Electron Yield Enhancement," *Adv. Funct. Mater.*, vol. 23, no. 45, pp. 5608–5614, Dec. 2013.

[3] Pei, Y., Liu, W., Shi, J., Chen, Z. & Wang, G. Fabrication and Characterization of p-Type SnO Thin Film with High c-Axis Preferred Orientation. **45**,

SESSION F.EL01.01: Characterization of Diamond

On Demand Abstracts Available for Viewing Starting Saturday Morning, November 21, 2020

F-EL01

### 5:00 AM F.EL01.01.01

**A Study on Photoconductive Properties of Boron Doped Diamond** Kelly Woo<sup>1</sup>, Mohamadali Malakoutian<sup>1,2</sup>, Diego R. Yankelevich<sup>2</sup> and Srabanti Chowdhury<sup>1</sup>; <sup>1</sup>Stanford University, United States; <sup>2</sup>University of California, Davis, United States

In photoconductive semiconductor switches (PCSS), the conductance, measured between the two electrodes placed on the semiconductor, is modulated by the absorption of optical radiation in the gap between them. This switching device can be applied to pulsed power technology for high speed and jitter free switching. These may include radar, particle acceleration, and pulsed high-power lasers. However, typical materials studied for photoconductive switching, such as Si and GaAs suffer from thermal runaway effects at high power [1]. Since diamond is an ideal material for high power electronics due to its large bandgap (5.47 eV), high breakdown electric field (10 MV/cm), high carrier mobility, high thermal conductivity (10-20 W/cm.K), and low coefficient of thermal expansion (~1.1µm/mK) [2], we chose to study its photoconductive properties and

potential as a high power optoelectronic switch. Past studies have shown photoconductivity in intrinsic diamond by UV-band excimers in high electric fields up to 2 MV/cm [3].

In this work, however, we utilized boron-doped diamond substrates to excite carriers by sub-bandgap photon energies while maintaining the desirable properties of diamond that would facilitate higher breakdown field and better thermal management. Boron is the only known p-type dopant occupying substitutional sites and has an activation energy of 0.3-0.37eV above the valence band [4].

In designing extrinsic PCSS, on/off current ratios should be maximized for high performance switching. In the off state, the material conductance primarily depends on the number of ionized dopants, which decreases with lower doping levels or compensation. In the on state, the conduction is increased due to the photogeneration of free carriers through dopants and traps, which increases with doping concentration. However, on conductance is also limited by the number of excitable carriers based on the surface area of the substrate and absorption depth at the excitation wavelength. Thus, by analyzing the conduction as a function of doping concentration between the on and off state, a doping level of  $10^{18}$  cm<sup>-3</sup> was chosen in efforts to maximize the on/off current ratio in fabricated devices.

In this work, we have fabricated lateral electrodes on the surface of boron doped single crystalline diamond substrates and analyzed the photoresponse. The 1 $\mu$ m doped epilayer was grown by MPCVD on a diamond HPHT seed. Then, electron-beam evaporation was used to deposit ohmic Ti/Pt/Au contacts on its surface to form planar devices. Testing of the extrinsic diamond substrate was performed by exciting with a frequency doubled (532nm) Nd:YAG pulsed laser with an output energy of 20mJ and ~10ns duration. Our experiments with these devices have shown a pulsed photoresponse with a full width half maximum of 11.5 ns. Furthermore, sharper rise times and slower fall times were observed, which could be explained by the presence of traps. Aided by residual heating from the source, its captured carriers could still be thermally excited leading to a current tail. Through this work, photoconductivity was successfully shown in extrinsic homoepitaxial diamond using a lower energy, below bandgap Vis-NIR excitation source.

This work was supported by Precourt Institute, Stanford under the Bits and Watts initiative. Fabrication was done in the Stanford Nanofabrication Facility.

[1] S. Feng, et al., IEEE Transactions on Electron Devices, 37, 12, 2511-2516, (1990).

[2] Tsao, J. Y., et al., *Adv. Electron. Mater.*, 4, 1600501 (2018).

[3] Yoneda, H., et al., *Appl. Opt.* 40, 6733-6736 (2001)

[4] M. Dutta, et al., IEEE Electron Device Letters, 37, 9, 1170-1173 (2016).

#### 5:10 AM F.EL01.01.02

**Raman Spectroscopy of Boron-Doped Diamond** Vincent Mortet, Ivan Gregora, Andrew Taylor, Nicolas Lambert, Petr Ashcheulov, Marina Davydova, Zuzana Gedeonova and Pavel Hubik; Fyzikální ústav AV ČR, Czechia

Although a Raman spectroscopy presents a basis for an effective assessment of the atomic boron concentration in the boron-doped diamond, determination of further physical properties of diamond using non-destructive Raman approach requires advancement in the Raman analysis. In this work, we analyze Raman spectra of heavily boron-doped epitaxial (113) diamond layers measured at temperatures up to 600 °C based on the interaction between phonon and electronic Raman scattering effects. Raman spectra are modelled using a combination of multiple decoupled Fano-functions and the established “dirty-metal” electronic Raman scattering cross section model. The presented analysis demonstrates the imperative contribution of the electronic Raman scattering to the Raman spectrum and opens a new practical route towards determination of electronic transport properties in boron-doped diamond.

#### 5:20 AM F.EL01.01.03

**Investigating Diamond Defect Formation with Quantitative Birefringence** Benjamin M. Farris<sup>1,2</sup>, Matthias Muehle<sup>2</sup> and Elias Garratt<sup>1,2</sup>; <sup>1</sup>Michigan State University, United States; <sup>2</sup>Fraunhofer USA, United States

Lab-grown diamonds are candidate materials for several emerging technologies, including next-generation high-power electronics. These diamonds can be grown using high-pressure high-temperature (HPHT) synthesis or chemical vapor deposition (CVD). However, these methods produce defects in the diamond crystal structure, impairing the diamond's performance. To better understand defect formation in diamonds, the Fraunhofer USA Center for Coatings and Diamond Technologies (CCD) is developing a quantitative birefringence setup capable of imaging these defects. Because a defect-free diamond has an isotropic crystal structure, it transmits all polarizations of light identically. However, when defects are present, the resulting strain produces birefringence, in which the polarization of transmitted light is distorted. Diamond

samples are measured in an imaging polarimeter. By analyzing the raw data with Mueller calculus, the amount and orientation of birefringence are mapped across the diamond, revealing crystal defects. Not only can defects, such as threading edge dislocations, be visualized, the relative strain produced by defects can be quantified. Furthermore, statistical analysis on defect type and strength within the diamond can be performed, enabling distributions, concentrations, and types of defects to be identified and analyzed relative to reactor conditions. This analysis is part of a larger effort to develop data pipelines for diamond research. These pipelines will be integrated into an overall diamond database to enable cross-correlative analysis across different measurement techniques such as x-ray rocking curve or Raman mapping on diamond samples grown using specific processes. Cross-comparisons using statistical analysis (data science) on these data sets are predicted to yield deeper insights into process-structure relationships of diamond growth.

#### 5:30 AM F.EL01.01.04

**Relaxation of Compressive Stress in Diamond Nanomembranes** [Paulius Pobedinskas](#)<sup>1,2</sup> and Ken Haenen<sup>1,2</sup>; <sup>1</sup>Institute for Materials Research (IMO), Hasselt University, Belgium; <sup>2</sup>IMOMECE, IMEC vzw, Belgium

Nanomembranes (NMs) are very thin ( $\leq 500$  nm) and have very high aspect ratios of thickness to lateral dimension ( $\geq 10^4$ ). This makes them extremely flexible due to the linear decrease of bending strain with thickness. At the extreme thinness, materials fold much easier [1]. When nanocrystalline diamond (NCD) thin films are grown on substrates, which have a higher thermal expansion coefficient than diamond, unavoidably, compressive stress is generated. When a NCD NM is released from such substrate a pattern of wrinkles and wrinkles evolves. The out-of-plane deformation is associated with the onset of an elastic instability, where the total energy is best minimized by the film bending rather than straining in-plane. These deformations strongly affect the electrical properties of B-doped NCD NMs [2]. Therefore, one cannot disregard the influence of wrinkles when dealing with any type of device that is based on NMs.

In this work, we present finite element simulations of compressive stress relaxation under gravity in a diamond NM as it is released from a supporting substrate. As NCD consists of hard diamond grains and soft grain boundaries, the Young's modulus and Poisson's ratio are not expected to be the same as in bulk diamond [3]. To study the impact of elastic constants on wrinkling, the calculations were made with different Young's moduli ( $E = 300, 600, 900,$  and  $1200$  GPa) and Poisson's ratios ( $\nu = 0, 0.07, 0.14,$  and  $0.21$ ). The initial compressive stress of the NM was varied in the range from  $0$  Pa up to  $-6$  GPa. NCD thin film, which is  $150$  nm thick and has a compressive stress of up to  $-10^4$  Pa, relaxes without forming wrinkles when is released from the substrate as the NCD membrane. Symmetrical wrinkles form when the membrane relaxes from  $-10^5$  Pa and higher compression. At absolute stresses larger than  $-1$  GPa the asymmetric wrinkling is dominant. Young's modulus and Poisson's ratio does not have notable impact on the relaxed membrane shape as stress does. However, the Young's modulus has higher impact on the relaxed membrane area and out-of-plane deformation range than Poisson's ratio. The higher the Young's modulus (or Poisson's ratio) the smaller the area (and out-of-plane deformation range) of the NM is obtain after the compressive stress relaxation. Finally, the obtained results on wrinkling phenomena are explain through the system's energy minimization when stretching, bending and twisting events are competing.

#### References

- [1] J.A. Rogers, *et al.*, Nature **477**, 45 (2011).
- [2] S. Drijkoningen, *et al.*, Scientific Reports **6**, 35667 (2016).
- [3] C.A. Klein and G.F. Cardinale, Diamond and Related Materials **2**, 918 (1993).

SESSION F.EL01.02: Color Centers in Diamond

On Demand Abstracts Available for Viewing Starting Saturday Morning, November 21, 2020

F-EL01

#### 5:00 AM F.EL01.02.01

**Optimization of NV Centers Density in Pink Irradiated-CVD Diamond** Lahcene Mehmel<sup>1</sup>, Ovidiu Brinza<sup>1</sup>, Alexandre Tallaire<sup>1,2</sup>, Fabien Bénédic<sup>1</sup>, Gabriel Hetet<sup>3</sup>, Clément Pellet-Mary<sup>3</sup>, Paul Huillery<sup>3</sup>, Bernd Abel<sup>4</sup>, Robert Staacke<sup>4</sup>, Jan Meijer<sup>4</sup> and [Jocelyn Achard](#)<sup>1</sup>; <sup>1</sup>LSPM-CNRS, France; <sup>2</sup>IRCP, France; <sup>3</sup>LPENS-CNRS, France; <sup>4</sup>Leipzig University, Germany

NV centers in diamond are point like defects that have attracted a lot of attention as one of the best candidates for quantum technologies particularly for sensing and imaging nanoscale magnetic fields. For this application, the use of an ensemble of NV centers with a high concentration in a high quality diamond layer is of prime interest. In previous works, it has been

demonstrated that N<sub>2</sub>O doping rather than N<sub>2</sub>, allows improving diamond quality by limiting the formation of macroscopic defects and NV<sup>-</sup>'s photobleaching [1]. More recently, the growth of N<sub>2</sub>O doped samples thicker than 1.5 mm has been achieved with substitutional nitrogen (N<sub>s</sub>) concentration as high as a few tens of ppm which is very difficult to obtain by a CVD process using a conventional N<sub>2</sub> precursor. After irradiation by a 10 MeV electron beam, a conversion ratio of 20% has been obtained leading to a CVD grown layer with 4 ppm of NV<sup>-</sup>. A decrease of the longitudinal spin relaxation time T<sub>1</sub> observed when the magnetic field is aligned along the [100] direction (i.e. when all NV centers classes are equally degenerate) indicates that NV-NV dipolar coupling becomes a dominant mechanism in such highly doped samples. In this work, we will more particularly focus on the optimization of N<sub>2</sub>O concentration in the gas phase in order to limit NV<sup>-</sup>-NV<sup>-</sup> interaction while maximizing density and spin properties. In the same time, samples grown in the presence of N<sub>2</sub> + O<sub>2</sub> and N<sub>2</sub> only will be compared in order to investigate the benefit of the use of N<sub>2</sub>O. We aim at evaluating the maximum sensitivity achievable in a magnetic quantum sensor using such defect ensembles.

[1] A. Tallaire, L. Mayer, O. Brinza, M.A. Pinault-Thaury, T. Debuisschert, J. Achard, Highly photostable NV centre ensembles in CVD diamond produced by using N<sub>2</sub>O as the doping gas, *Appl. Phys. Lett.*, 111 (2017) 143101.

### 5:10 AM F.EL01.02.02

**Stabilizing the Charge State of the Tin-Vacancy Center by Defect Engineering** Johannes Görlitz<sup>1</sup>, Dennis Herrmann<sup>1</sup>, Philipp Fuchs<sup>1</sup>, Michael Kieschnick<sup>2</sup>, Sebastien Pezzagna<sup>2</sup>, Jan Meijer<sup>2</sup> and Christoph Becher<sup>1</sup>; <sup>1</sup>Universität des Saarlandes, Germany; <sup>2</sup>University Leipzig, Germany

The recently discovered negatively charged tin-vacancy center (SnV<sup>-</sup>) in diamond combines high brightness single photon emission [1,2], large Debye-Waller factors and Fourier-limited linewidths [3,4]. Furthermore, the ground state fine structure splitting exceeds 800 GHz which potentially suppresses phonon mediated decoherence of the lowest ground state's spin doublet, which is the predominant decoherence mechanism for other negatively charged group-IV – vacancy centers (Silicon-vacancy center (SiV<sup>-</sup>) and germanium-vacancy center (GeV<sup>-</sup>)). Therefore, the SnV<sup>-</sup> center supposedly combines the advantages of the most established colour centers, namely the long spin coherence time of the nitrogen vacancy center and the large Debye-Waller factor and insensitivity to first order stark shifts of the silicon vacancy center. The exploitation of these very promising features for quantum information processing is up to now limited by the charge instability of the center under resonant optical excitation [4]. This instability results in termination of the fluorescence and therefore inhibits the use of coherent manipulation protocols.

We here present studies on stabilizing the SnV<sup>-</sup> charge state based on the recently discovered Coulomb-driven single defect engineering by co-implantation of charge donors into diamond [5]. We co-implant oxygen, sulfur and boron together with tin and find a suppression of bleaching (reduction of fluorescence intensity under continuous illumination) and fluorescence termination together with increased photo-luminescence intensity for sulfur co-doping. These results pave the way for application of the SnV center in coherent optical spin control experiments.

[1] Iwasaki T. et al., *Phys. Rev. Lett.* 119, 253601 (2017)

[2] Tchernij S. D. et al., *ACS Photonics* 4, 25802586 (2017)

[3] Trusheim M. E. et al., *Phys. Rev. Lett.* 124, 023602 (2020)

[4] Görlitz J. et al., *New J. Phys.* 22, 013048 (2019)

[5] T. Lühmann et al., *Nat. Commun.* 10, 4956 (2019)

### 5:20 AM F.EL01.02.03

**Generation of Nitrogen-Vacancy Ensembles in Diamond for Use in Magnetic-Field Sensing Applications** Matthew Markham, Andrew Edmonds, Pierre-Olivier Colard and William Hillman; Element Six Ltd, United Kingdom

Ensembles of negatively-charged nitrogen-vacancy (NV<sup>-</sup>) centres in diamond constitute a promising platform for magnetometry applications. However, the sensitivity of present NV-ensemble devices and the need for diamond material with reproducible properties have hindered progress toward many envisioned applications. The work presented here addresses these challenges by optimising a chemical vapor deposition (CVD) growth process to produce material at scale with improved NV-ensemble properties.

Through development of the CVD process it is shown that nitrogen incorporation can be increased without an increase in the density of unwanted vacancy-related defects which act as charge acceptors, reducing the [N<sub>s</sub><sup>0</sup>]/[N<sub>s</sub>] and [NV<sup>-</sup>]/[NV] ratios, and limiting the dephasing time, T<sub>2</sub>\*. The process of irradiation and annealing is optimised and subsequent measurements of the NV concentration, charge ratio and contrast suggest that these grown-in defects have a detrimental impact on the NV-ensemble properties. Strain is also demonstrated to be a critical parameter to control.

This work also investigated the potential to produce material with reproducible NV concentration, NV charge ratio, strain homogeneity, and  $T_2^*$  by characterising a batch of samples containing approx. 4 ppm NV. The measured NV<sup>-</sup> and NV<sup>0</sup> concentrations in the batch of samples varied by less than 7% (1 standard deviation) and exhibited well-controlled strain inhomogeneity. The resulting  $T_2^* = 1 \mu\text{s}$  in material enriched with >99.99% <sup>12</sup>C was as expected for the concentration of N, establishing that other sources of decoherence have been controlled.

The material reported in this work enables immediate sensitivity improvements for present quantum-sensing devices and the correlations observed between material properties at different stages of processing provide efficient metrics for future work targeting other NV densities or sample geometries such as micron-scale, NV-rich layers for magnetic imaging.

#### 5:30 AM F.EL01.02.04

**Enhanced Emission from Silicon-Vacancy Centers in Ag-Diamond Core-Shell Nanostructures** [Shuo Li](#)<sup>1,2</sup>, Nicholas Melosh<sup>3</sup> and Robert Hamers<sup>2</sup>; <sup>1</sup>SLAC National Accelerator Laboratory, United States; <sup>2</sup>University of Wisconsin-Madison, United States; <sup>3</sup>Stanford University, United States

Color centers in diamond are promising candidates for emerging quantum sensing and quantum information processing applications due to their exceptional properties. Coupling diamond color centers with metal plasmonic nanostructures is reported to enhance the optical properties of color centers effectively, but the plasmonic metal structures of previous studies are vulnerable to the environment, making the diamond-metal system unstable. Here, we demonstrate a novel and highly-tunable structure of Ag nanospheres coated with a layer of diamond containing SiV centers. The Ag was grown by thermal vapor deposition and then plasma treated to form uniform nanospheres, which were protected by the stable diamond shell grown by plasma-enhanced chemical vapor deposition (PECVD) method. This enhances the emission rate and brightness of SiV in diamond drastically. The structure also shows great stability to extreme corrosive and high-temperature conditions. Our finding is promising for developing ultrabright quantum sensing, high-efficiency imaging, and surface plasmon-quantum emitter waveguide.

#### 5:40 AM F.EL01.02.05

**Late News: The Spin-Flip Bethe-Salpeter Equation Approach, and Applications to Defects in Diamond** [Bradford A. Barker](#) and David A. Strubbe; University of California, Merced, United States

The NV<sup>-</sup> center in diamond is a notable example of a system that has open-shell electronic structure. The challenge in describing open-shell systems for computational methods is that the wavefunctions for the ground-state and excited-states are composed of two or more electronic configurations. Wavefunction-based techniques to describe these multi-configurational systems, then, will necessarily be sums of multiple Slater determinants, called “multi-reference wavefunctions.” Their calculation is quite expensive for all but the smallest molecular systems. The Spin-Flip ansatz, however, allows for electronic structure methods based on an initial single-reference calculation that can capture contributions from the multiple configurations for open-shell systems. This method was originally applied to the Configuration Interaction and Equation-of-Motion Coupled-Cluster approaches, and then later applied to density-functional techniques, called Spin-Flip Time Dependent Density Functional Theory (or SF-TDDFT). In this work, we consider the Spin-Flip method being adapted for electronic structure calculations from the framework of the *GW*/BSE approach, which gives the Spin-Flip Bethe-Salpeter Equation, a method with lower scaling than Coupled Cluster Singles-Doubles and other similar wavefunction-based methods. SF-BSE is also *ab initio* and is accurate in solids. The SF-BSE Hamiltonian resembles that of SF-TDDFT but with an *ab initio* kernel. We present results for the open-shell test systems of ethylene under torsion and the NV<sup>-</sup> center defect in diamond. The excitation energies calculated for the NV<sup>-</sup> center in diamond compare reasonably well with both experiment and Configuration Interaction-based theoretical methods.

This work was supported by the U.S. Department of Energy, Office of Science, Basic Energy Sciences, CTC and CPIMS Programs, under Award DE-SC0019053.

SESSION F.EL01.03: Diamond Detectors and Sensors

On Demand Abstracts Available for Viewing Starting Saturday Morning, November 21, 2020  
F-EL01

#### 5:00 AM \*F.EL01.03.01

**Microfabrication of Sensors and Nanodiamond Structures on Diamond Substrates for Extreme Environments** Yogesh K. Vohra; University of Alabama-Birmingham, United States

Maskless lithography has been combined with the microwave plasma chemical vapor deposition (CVD) of diamond to fabricate a variety of micro-sensors that can be deposited on substrates and encapsulated in a protective CVD diamond layer to survive extreme conditions of high-pressure, high- and low-temperatures, corrosive, and high radiation environments. These hardened sensors provide electrical conductivity, magnetic susceptibility, and stress data on a variety of metallic and superconducting materials under extreme conditions of pressures and temperatures in diamond anvil cell devices. In addition, boron-doping of CVD diamond also enables the fabrication of micro-heaters in diamond anvil cell devices. Microfabrication techniques have also been utilized to selectively grow localized nanodiamond structures on single crystalline diamond substrates. Since nanodiamond structures lack the cleavage planes representative of single crystal diamond; ultrahigh pressures of over 500 GPa can be generated in this nanodiamond/single crystal diamond structures. The studies on materials under extreme conditions using these diamond-based sensors and nanodiamond structures are carried out at the Advanced Photon Source, Argonne National Laboratory. Future research directions in vertical integration of multiple sensors, wireless communications, and controlling the sp<sup>3</sup> bonded content in nanodiamond microstructures will be presented.

**5:15 AM F.EL01.03.02**

**The Use of Diamond in the Detection of High Energy Neutrons** Hank M. Thurston and Elias Garratt; Michigan State University, United States

Current state of the art scintillating neutron detectors are typically of large form factor, or detection node, on the order of cubic metres to achieve efficiencies of ~70%. This results in spatial resolutions of cm<sup>2</sup>, which relatively low for detecting certain particle species. However, detectors with a lower form factor (mm<sup>2</sup>) built into an array are expected to provide an order of magnitude increase in spatial resolution. Moreover, placing such detectors in series will enable higher resolution in for energy spectrum as well as tracking of scattered particles. Diamond is a highly favorable material for sensing radiation in very harsh environments, such as the beamlines of high energy particle colliders and space environments. This is primarily due to the strong covalent carbon-carbon bonding in the sp<sup>3</sup> hybridized orbital structure of diamond. Arranged in a periodic lattice this molecular structure also give rise to high electron mobilities and thermal transport properties which have the net effect of simplifying radiation sensor device design while maintaining a fast response rate and low dark current. A design consisting of a high cross-section neutron activation layer sandwiched by layers intrinsic CVD diamond and Boron doped semi-conducting diamond has been proposed.

The “sandwich” design takes advantage of the molecular density of diamond, allowing for detection in either the intrinsic or semiconducting layers. The activation layer material can be chosen to optimize detection at a desired energy. This device will be built and commissioned for use with the Facility for Rare Isotope Beams. To facilitate nuclear experiments at the FRIB’s capacity of 400MeV per nucleon, we plan to provide high efficiency detection of neutrons up to 250 MeV, in a form factor allowing for modular addition of neutron detection to experiments which otherwise would not have the capability. Due to the radiation hardness of diamond, the device could also effectively be employed as a permanent beamline monitoring or veto detector. The development of the device requires several stages of work, beginning with design optimization through computer modeling.

The current stage of work develops Monte Carlo simulations of atomic and nuclear processes inside of diamond crystal using several simulation frameworks. We simulate irradiation of diamond of neutrons and a variety of heavy ions. Using the GEANT 4 framework we are able to model the crystal lattice structure and monitor structure damage through the simulation. Through judicious selection of GEANT 4 physics lists we are able to model non-ionizing energy loss, both elastic and inelastic scattering, and nuclear interactions during irradiation. Secondary and tertiary effects and interactions can also be monitored. This allows us to identify points of lattice damage; creation of vacancies and interstitial ions. Throughout development, simulations were benchmarked against SRIM 2013. These benchmarks, discrepancies, and improvements are discussed.

**5:25 AM F.EL01.03.04**

**Electrochemiluminescence at Hybrid Boron Doped Diamond Electrodes** Samuel Stewart, Emmanuel Scorsone and Matthieu Hamel; CEA-LIST, France

Electrochemiluminescence (ECL) is a phenomenon in which photons are emitted during electrochemical reactions. It already proved to be a very promising analytical tool for sensing applications where both high sensitivity and selectivity are needed. Indeed, it merges the advantages of chemiluminescent analysis with the absence of background optical signal, with wide possibilities for reaction control using diverse electrochemical protocols. ECL can be observed in organic solvents where both oxidized and reduced forms of luminescent species are produced, e.g. by sweeping electrode potential between anodic



and cathodic. Excitation energy is then obtained from recombination of oxidized and/or reduced species. As an example, superoxide ions may be involved through electrochemical reduction of dissolved oxygen. In aqueous environments, simultaneous oxidation and reduction of luminescent species is difficult to achieve due to electrochemical splitting of water, implying the use of a co-reactant. In this case luminescent species are oxidized at the electrode together with the co-reactant, which gives a strong reducing agent after some chemical transformations. In this context, Boron Doped Diamond electrodes offer numerous advantages that have been little explored for ECL analytical applications. They display high electrochemical stability together with resilience to fouling, and good optical transparency. Furthermore, in aqueous media electro-generated hydroxyl radicals play important roles in ECL, implying that a co-reactant family can be expanded by taking advantage of the strong oxidation ability of electrogenerated hydroxyl radicals at boron doped diamond electrodes. The potential of diamond electrodes for ECL analytical applications will be discussed and illustrated through a comparative study using different electrode materials, including both highly textured electrodes and BDD electrodes functionalized with transition metal nanoparticles.

#### 5:35 AM F.EL01.03.05

**Boron-Doped Diamond/Pd-SnO<sub>2</sub> Heterojunction Gas Sensor for Enhanced Room-Temperature NO<sub>2</sub> Detection** [Marina Davydova](#)<sup>1</sup>, Alexandra Palla Papavlu<sup>2</sup>, Alexandr Laposa<sup>3</sup>, Andrew Taylor<sup>1</sup>, Ladislav Klimša<sup>1</sup>, Jiri Kroutil<sup>3</sup>, Petr Ashcheulov<sup>1</sup> and Thomas Lippert<sup>4,5</sup>; <sup>1</sup>FZU-Institute of Physics of the Czech Academy of Sciences, Czechia; <sup>2</sup>National Institute for Lasers, Plasma, and Radiation Physics, Romania; <sup>3</sup>Czech Technical University in Prague, Czechia; <sup>4</sup>Paul Scherrer Institut, Switzerland; <sup>5</sup>ETH Zürich, Switzerland

In recent years, wide band gap semiconductors have been recognized as very promising sensitive materials for detection of toxic pollutants and hazardous gases. A majority of research work has been carried out on metal oxide (MO) semiconductors by simple change of resistance measurements. However, the main issues for MO chemiresistor sensors are high operating temperature (above 300°C) and cross-sensitivity/selectivity. These drawbacks can be partially solved by utilizing the combination of two or more types of semiconductor materials (p-n heterostructures). The use of the combination of *n*-type and *p*-type semiconductor materials is a relatively recent field of research within chemiresistors. Such bilayer structures offer a variety of advantageous characteristics, including a large surface area, improved crystallinity, defect-free interface, and enhanced electrical properties.

In this work we report on the development of heterostructures based on *n*-type Pd-doped SnO<sub>2</sub> and *p*-type boron doped diamond (BDD) for room-temperature NO<sub>2</sub> detection. Here, three different gas sensor devices were developed based on (i) BDD, (ii) Pd-SnO<sub>2</sub>, and (iii) Pd-SnO<sub>2</sub>/BDD heterojunction structures using a combination of ink-jet printing, microwave linear antenna plasma enhanced chemical vapour deposition, and reactive laser induced forward transfer (rLIFT) techniques. The gas sensing properties of fabricated sensor devices were tested in oxidizing/reducing gases (NO<sub>2</sub>, CO, NH<sub>3</sub>) at various analyte concentrations (5-20 ppm) in the dark and under UV light illumination. It was found that all sensor structures measured under UV light illumination demonstrate significant enhancement of gas sensor response in comparison to the measurements performed in dark. Moreover, the sensors demonstrate high sensitivity to NO<sub>2</sub> gas and showed dependence on the intensity of UV light, fast response, and reversible character. The Pd-SnO<sub>2</sub>/BDD heterojunction structure exhibited a remarkable NO<sub>2</sub> gas sensor response in comparison to Pd-SnO<sub>2</sub> based structure (i.e., 280% for Pd-SnO<sub>2</sub>/BDD and 12% for Pd-SnO<sub>2</sub>). Finally, the Pd-SnO<sub>2</sub>/BDD structures possess the highest response to 10 ppm NO<sub>2</sub>, complete reversibility, and reproducible character under UV light illumination.

*This work was supported by the Czech Science Foundation (GAČR) contract no. 19-09784Y.*

#### 5:45 AM F.EL01.03.06

**Boron-Doped Diamond Electrodes—The Role of Doping Level, Surface Treatment and Porosity in the Electrooxidation of Cresol Environmental Contaminants** [Andrew Taylor](#)<sup>1</sup>, Vincent Mortet<sup>1</sup>, Ladislav Klimša<sup>1</sup>, Jaromír Kopeček<sup>1</sup>, Silvia Sedláková<sup>1</sup>, Simona Baluchová<sup>2</sup>, Michal Nedvěd<sup>2</sup>, Jana Vosáhlová<sup>2</sup> and Karolina Schwarzová-Pecková<sup>2</sup>; <sup>1</sup>FZU - Institute of Physics of the Czech Academy of Sciences, Czechia; <sup>2</sup>Charles University, Faculty of Science, Czechia

Due to its excellent properties in comparison with other carbon-based materials, boron doped diamond (BDD) has become a popular electrode material especially for electrooxidation. These include low background current, wide potential window in the region of positive potentials, mechanical robustness and low proclivity to electrode passivation. Cresols are classified by the US Environmental Protection Agency as a toxic and persistent chemical, exhibiting chronic effects at 12 mg.L<sup>-1</sup>, however they are commonly used for wood impregnation, production of polymers, disinfection and herbicides. Wastewater from these industries along with coal conversion contains a high concentration of cresols and is therefore a problematic environmental contaminant, which requires monitoring.

In this work, the influence of, 1- boron-doping levels (B/C ratio in the gas phase (ppm): 500, 1000, 2000, 4000, and 8000), 2- surface termination (H- vs. O-) and 3- *ex-situ* polishing with alumina, of planar BDD on its electrochemical properties and voltammetric behaviour of cresols was thoroughly investigated. In addition, we compare planar BDD with porous BDD samples for changes in their electrochemical properties. We show that all examined factors have a significant impact on cresol electrooxidation, and therefore should be carefully considered when designing BDD electrodes for electrochemical sensing of these environmental contaminants.

BDD deposition methods will be described together with BDD structural and composition characterisation, and the electrochemical methods used.

SESSION F.EL01.04: Diamond Electronics  
On Demand Abstracts Available for Viewing Starting Saturday Morning, November 21, 2020  
F-EL01

#### 5:00 AM \*F.EL01.04.01

**Nuclear Battery Applications of Diamond Junction Devices** Takehiro Shimaoka<sup>1,2</sup>, Hitoshi Umezawa<sup>2,3</sup>, Kimiyoshi Ichikawa<sup>1</sup>, Julien Pernot<sup>3</sup> and Satoshi Koizumi<sup>1</sup>; <sup>1</sup>National Institute for Materials Science, Japan; <sup>2</sup>National Institute of Advanced Industrial Science and Technology, Japan; <sup>3</sup>Université Grenoble Alpes, France

Betavoltaic cells directly convert the energy of beta particles into electricity.[1] The operation principle of a betavoltaic cell is similar to that of a solar cell, except that the energy source is beta-emitting isotopes. In betavoltaic cells, semiconductor junctions play the role of energy conversion. These cells have the advantage of longevity, which is determined by the half-life ( $T_{1/2}$ ) of the beta-emitting radioisotopes. The cells can operate for several years to a decade. Betavoltaic cells are expected to be utilized for battery applications in remote locations such as outer space and underground.

Diamond is advantageous material for betavoltaic cells because the wide bandgap could offer high open circuit voltage due to large built-in potential of the junction, which improves the conversion efficiency of the cells. From theoretical perspective, ultrawidebandgap materials such as diamond and BN have potential to realize extreme conversion efficiency of the cells.[2] Moreover, diamond has durability against radiation and high temperature. Diamond betavoltaic cells could be utilized to application under extreme condition. In this study, we show the highest semiconductor conversion efficiency among the betavoltaic cells reported thus far by utilizing the large built-in potential of a diamond *pn* junction.

We formed pseudo-vertical diamond *pn* diodes. Homoepitaxial  $p^+$ ,  $p$ ,  $n^-$ , and  $n^+$  diamond layers were grown on a {111} high-pressure high-temperature (HPHT) type-Ib diamond substrate by using microwave plasma-assisted chemical vapor deposition (MPCVD). Each B- ( $p$ -type) and P- doped ( $n$ -type) diamond layer were grown with the use of individual MPCVD systems. The thickness of the  $p^+$ ,  $p$ ,  $n^-$ , and  $n^+$  layers were, respectively, 2, 0.1, 1.8, and <0.1  $\mu\text{m}$ . The impurity concentrations confirmed by secondary ion mass spectrometry (SIMS) were [B]:  $3 \times 10^{19} \text{ cm}^{-3}$  for the  $p^+$  layer, [B]:  $2 \times 10^{18} \text{ cm}^{-3}$  for the  $p$  layer, [P]:  $1 \times 10^{16} \text{ cm}^{-3}$  for the  $n^-$  layer, and [P]:  $1 \times 10^{20} \text{ cm}^{-3}$  for the  $n^+$  layer. Highly P- doped diamond was grown using homemade CVD reactor to enhance P incorporation into diamond to reduce series resistance. After the growth, mesa structures were formed by induction coupling plasma etching with oxygen gas. Subsequently, Ohmic contacts were formed by electron beam deposition of Ti/Mo/Au both on the mesa structure of the  $n^+$ -layer and on the  $p^+$ -layer. The diameters of the mesa and electrodes were, respectively, 240 and 150  $\mu\text{m}$ .

Then we evaluated power – voltage ( $P$ - $V$ ) and current-voltage ( $I$ - $V$ ) characteristics under electron-beam irradiation. For electron-beam irradiation, a scanning electron microscope was used as the electron source. Electron beams at accelerating voltages of 15 kV were irradiated on top of the  $n^+$  layer. The open-circuit voltage ( $V_{oc}$ ) under the electron-beam irradiation was 4.26 V, which is the highest among the betavoltaic cells reported thus far. The output power at the maximum point ( $P_{MP}$ ) was 10.7 nW. Fill factor ( $FF$ ) and semiconductor conversion efficiency ( $\eta_s$ ) calculated as following eqs (1) and (2)

$$FF = P_{MP}/I_{sc}V_{oc}, \dots(1)$$

$$\eta_s = VocFF/\varepsilon, \dots(2)$$

where  $\varepsilon$  is the electron–hole pair creation energy. Here, we substitute  $\varepsilon = 13 \text{ eV}$  in eq. (2). The  $FF$  and the semiconductor conversion efficiency  $\eta_s$  were respectively, 0.85 and 28%. Among the semiconductors, the diamond *pn* junction achieved the highest  $\eta_s$ , which enables to be utilized to energy efficient and long-life cells for remote sensing applications. In the talk, we will also present charge collection efficiency and total conversion efficiency of diamond *pn* diode against different energy of

electrons.

#### References

- [1] P. Rappaport, The electron-voltaic effect in p-n junctions induced by beta-particle bombardment, *Phys. Rev.* **93**, 246 (1954).  
[2] S. Maximenko, J. Moore, C. Affouda, P. Jenkins, Optimal semiconductors for  $^3\text{H}$  and  $^{63}\text{Ni}$  betavoltaics, *Sci. Rep.* **9**, 10892 (2019).

#### 5:15 AM F.EL01.04.03

**A Simulation Study of Vertical Diamond FinFETs for Power Switching and RF Electronics** John P. Niroula<sup>1</sup>, Heyi Li<sup>1</sup>, Qingyun Xie<sup>1</sup>, Garrett Schlenvogt<sup>2</sup>, Thomas Jokinen<sup>2</sup> and Tomas Palacios<sup>1</sup>; <sup>1</sup>Massachusetts Institute of Technology, United States; <sup>2</sup>Silvaco, United States

The introduction of wide-bandgap semiconductors such as GaN and SiC have revolutionized the semiconductor electronics industry, especially in the areas of power switching and high frequency RF power amplifiers. While these materials have provided orders of magnitude improvements relative to silicon devices, today we are beginning to see the limitations of these wide-bandgap materials.

Consequently, electronic devices based on diamond, an ultra-wide-bandgap semiconductor, are increasingly explored due to diamonds' extraordinary material properties. A number of promising lateral [1],[2] and vertical diamond transistors [3] have been demonstrated; however, so far all diamond devices rely solely on surface conduction, either through a hydrogen terminated surface or a surface accumulation layer. The use of these transistors for power and RF applications may result in a number of issues, such as current collapse induced by surface trapping and poor reliability caused by non-uniform heat generation. A fin-based vertical transistor based in part on bulk conduction would allow us to take advantage of the superior material properties of diamond while mitigating these issues.

In this work, we use TCAD simulations in Silvaco to explore the potential of vertical diamond FinFETs [4] and compare it to an equivalent vertical GaN FinFET device. In our TCAD framework we incorporate several effects unique to diamond, including incomplete ionization, the metal-insulator transition of boron in diamond [5], and variable range hopping conduction [6].

For power applications, a vertical diamond FinFET of fin width 0.2  $\mu\text{m}$ , fin pitch 0.9  $\mu\text{m}$ , and fin height 0.8  $\mu\text{m}$  was simulated along with an optimized GaN structure. Assuming a critical electric field of 10 MV/cm for diamond and 3.3MV/cm for GaN, we find that to achieve a breakdown voltage of 1200 V, a drift region thicknesses of 1.4  $\mu\text{m}$  and 4.7  $\mu\text{m}$  are needed for diamond and GaN devices, respectively. For such relatively large drift regions, the incomplete ionization of boron in diamond in the on-state leads to a higher specific on-resistance for diamond (1.21  $\text{m}\Omega\text{cm}^{-2}$ ) than GaN (0.35  $\text{m}\Omega\text{cm}^{-2}$ ). We note, however, that if the dopants were completely ionized for diamond, the specific on-resistance would drop to 0.063  $\text{m}\Omega\text{cm}^{-2}$ , approximately 5x lower than GaN. This could potentially be done by raising the device nominal temperature, by optical activation of boron acceptors, or by high electric fields.

In addition, 200 V breakdown (60 V DC bias operation) devices for high frequency RF applications were simulated with dimensions of fin width 0.1  $\mu\text{m}$ , fin pitch 0.6  $\mu\text{m}$ , and fin height 0.2  $\mu\text{m}$ . In this case, the optimized drift region thicknesses were 0.25  $\mu\text{m}$  and 0.85  $\mu\text{m}$  for diamond and GaN, respectively. Compared with the GaN device, the diamond device exhibited a higher  $J_{\text{maz}}$  (640 vs. 240  $\text{kA}/\text{cm}^2$ ), lower  $V_{\text{knee}}$  (25 vs. 30 V), and higher  $f_T$  (53 vs. 42 GHz). As a result, the calculated linear power density of diamond was 7.36MW/cm<sup>2</sup> (44.2 W/mm per fin), which is about 2.7x higher than the GaN calculated linear power density at 2.7 MW/cm<sup>2</sup> (16.2W/mm per fin). In the case of the RF diamond device, as the drift region was relatively thin, the large number of holes injected from the channel lead to a significant carrier density in the drift region, which made up for the lack of carriers from unionized acceptors.

In summary, we have simulated a novel vertical fin transistor in diamond along with a reference GaN device, one set for power switching applications and one set for high power RF applications. We identify key priorities and initial results show great promise for vertical diamond FinFETs

Acknowledgement.- This work was partially funded by DARPA through a program monitored by Dr. Young-Kai Chen.

#### References

- Huang et al. Scientific Reports 2018  
Imanishi et al. EDL 2019  
Iwataki et al. EDL 2020  
Zhang et al. EDL 2019  
Thonke et al. Semicond. Sci. Technol. 2003  
Hathwar et al. JAP 2016.

#### 5:25 AM F.EL01.04.04

**Diamond Based High Temperature and High Power Electronics** Yuelin Wu<sup>1</sup>, Cristian J. Herrera-Rodriguez<sup>1</sup>, Aaron Hardy<sup>2</sup>, Matthias Muehle<sup>2</sup>, Tom Zimmermann<sup>1</sup> and Timothy Grotjohn<sup>1,2</sup>; <sup>1</sup>Michigan State University, United States; <sup>2</sup>Fraunhofer USA Center for Coatings and Diamond Technologies (CCD), United States

Diamond is a promising semiconductor material for high temperature and high power electronics due to its following properties: ultra-wide bandgap (5.45 eV), high electric breakdown field, and high thermal conductivity. Additionally, doped semiconducting diamond has a unique inverse temperature versus resistance correlation. Unlike many other semiconductors, the resistivity of diamond decreases with rising temperature until 150°C and remains low through 400°C. As a result, diamond device has lower theoretical "ON-resistance" and power loss than similar SiC and GaN device at temperatures higher than 150°C.

Diamond field effect transistors (FETs) can operate through surface or bulk conduction. Surface conduction is achieved via a two-dimensional hole gas (2DHG) formed on hydrogen-terminated diamond surface. Bulk conduction is typically achieved via holes generated in p-type boron-doped diamond. Surface conduction diamond FETs, also referred to as hydrogen-terminated diamond FETs, have attracted the most interest due to its current capability being close to commercial SiC and GaN MOSFETs of similar size. However, maintaining stability of the 2DHG at elevated temperatures can be challenging. Generally, hydrogen-terminated diamond FETs are not recommended to operate at temperatures higher than 400°C even with surface passivation.

In this study, our primary interest is to design and optimize bulk conduction diamond FETs with superior thermal stability and competitive power electronics capability. Three types of boron-doped conduction FETs were fabricated: lateral metal-semiconductor FET (MESFET), lateral metal-oxide-semiconductor FET (MOSFET), and vertical junction FET (JFET). The performance of the MESFET was demonstrated at elevated temperatures up to 430°C. It operated as a normally-on device at 0 V gate voltage,  $V_{GS}$  and became pinched-off at  $V_{GS} = 6V$ . The drain current density,  $I_{DS}$  increased rapidly with the increasing temperature until ~150°C. An  $I_{DS}$  value had approximately a 100-time increase from room temperature to 150°C and is attributed to the increase in the activated boron concentration because the boron acceptor level is deep at a value of 0.36 eV. The  $I_{DS}$  value peaked at 150°C and remained high until 430°C. Despite the high thermal stability, the metal-semiconductor junction limits the applicable gate forward bias to its Schottky turn-on voltage, which is around -1 V. This also limits the maximum drain current at a given drain voltage. To improve the current capability, a similar MOSFET structure was fabricated. With the introduction of an insulating  $Al_2O_3$  layer between the gate metal and diamond, a higher gate forward bias could be applied and a higher maximum drain current could be obtained. For instance, at 150°C, the maximum drain current of the MOSFET at -10  $V_D$ , achieved at -14  $V_{GS}$ , was more than two times of that obtained from the MESFET. However, the thermal stability of  $Al_2O_3$  deteriorated with rising temperature. Its electric breakdown field decreased from above 5 MV/cm at room temperature to 1 MV/cm at 250°C. The lateral transistors had breakdown voltages demonstrated to above 500 V.

Both lateral MESFET and MOSFET exhibited relatively low current capability due to high channel resistance. To significantly reduce the channel resistance while maintain the high thermal stability and high breakdown voltage, a vertical JFET structure without oxide was designed. A TCAD simulation estimated the "ON-resistance" to be less than 1  $m\Omega \cdot cm^2$  with a targeted 1200 V breakdown voltage. A key fabrication step, selective n-type phosphor doped layer of diamond, was successfully conducted through diamond etching and subsequent re-growth. Preliminary results for the vertical JFET will be presented.

### 5:35 AM F.EL01.04.05

**Increasing the Phase Purity of the Cubic Boron Nitride and Boron Doped Polycrystalline Diamond Heterojunction for Device Applications** Jesse Brown and Robert J. Nemanich; Arizona State University, United States

The properties of cubic boron nitride (c-BN) and diamond make them ideal materials for applications in a variety of extreme conditions, such as thermal or corrosive protection, ionizing radiation detection, and high-power high frequency electronics. One of the persistent challenges preventing many electronic applications of epitaxial c-BN on diamond is an interfacial hexagonal boron nitride (h-BN). While local epitaxy has been observed previously, a uniform interface for electronic grade applications has not been realized. Understanding the nucleation and subsequent growth of c-BN films on an atomic level at the growth interface and the properties across that interface is fundamentally critical to fully realize the materials' electronic properties.

Research at Arizona State University has studied the effects of hydrogen concentration during the growth of c-BN on diamond via electron cyclotron resonance plasma enhance chemical vapor deposition, and have found that, by forcing the hydrogen to be the limiting reactant in the growth environment, the reaction favors c-BN while suppressing the formation of h-BN impurities. In-Situ X-ray Photoelectron Spectroscopy (XPS) was used to characterize the interface, and Ultraviolet Photoelectron Spectroscopy (UPS) was used to determine the valence band offset of the pure interface. In this presentation we show that minimizing the hydrogen concentration during the deposition maximizes the cubic boron nitride phase purity at

the diamond interface.

This research is supported by The National Science Foundations (NSF) and Northrop Grumman.

#### 5:45 AM F.EL01.04.06

**Diamond Electronics for the Surface of Venus** Robert J. Nemanich<sup>1</sup>, Mohamadali Malakoutian<sup>2,3</sup>, Harshad Surdi<sup>1</sup>, Manpuneet Benipal<sup>4</sup>, Franz A. Koeck<sup>1</sup>, Srabanti Chowdhury<sup>3</sup>, Stephen M. Goodnick<sup>1</sup> and James Lyons<sup>1</sup>; <sup>1</sup>Arizona State University, United States; <sup>2</sup>University of California - Davis, United States; <sup>3</sup>Stanford University, United States; <sup>4</sup>Advent Diamond, United States

The surface temperature of Venus is ~460 C, with a corrosive atmosphere including CO<sub>2</sub> and sulfuric acid at a pressure of 92 bar. A number of missions to Venus are being considered or planned that would include surface or atmosphere probes, and high temperature electronics would be required for power control, mechanical system control, and sensor electronics. While it is long been recognized that the wide bandgap of diamond would result in a negligible increase in the intrinsic carrier concentration, at high temperature the devices based on Schottky barriers would show a great reduction in the forward-reverse current rectification ratio. This research presents results of diamond diodes with a thin n-type layer in a Schottky-n-i-p structure, which achieves high current density, high breakdown field and a designed on-off rectification ration. The metal-n-i-p diamond diodes were prepared on single crystal p-type, boron doped (100) or (111) substrates, with undoped intrinsic epitaxial layers and phosphorus doped epitaxial layers prepared by microwave plasma CVD. The electrical results and simulations show regimes with low drift layer resistance where the contact resistance limits the current. The diodes have been confined in a high pressure CO<sub>2</sub> atmosphere for over 100 hrs. After removal, inspection of the surfaces shows dark regions thought to be carbon containing layers, which did not result in evident changes of the current-voltage characteristics. More extensive Venus atmosphere testing planned at the NASA GEER facility will include active electrical measurements. The results establish that with control of p- and n-type doping optimal device designs can be achieved for diamond electronics at high temperature.

This research supported by NASA through grant NNX17AG45G as part of the HOTTech program.

#### SESSION F.EL01.05: Diamond Growth

On Demand Abstracts Available for Viewing Starting Saturday Morning, November 21, 2020

F-EL01

#### 5:00 AM F.EL01.05.01

**Boundary Condition Effects on Epitaxial Lateral Outgrowth of Single Crystal Diamond** Shengyuan Bai<sup>1</sup>, Yun Hsiung<sup>2</sup>, Karli Deutscher<sup>1</sup>, Ramón D. Díaz<sup>1</sup> and Elias Garratt<sup>1,2</sup>; <sup>1</sup>Michigan State University, United States; <sup>2</sup>Fraunhofer USA Center for Coatings and Diamond, United States

For decades, diamond has shown superior properties that make it desirable for novel electronic materials. However, fabricating large size high quality single crystal diamond wafers faces multiple challenges. Single crystal diamond (SCD) is a promising wide bandgap semiconductor material. Epitaxial lateral outgrowth (ELO) using microwave plasma assisted chemical vapor deposition (MPACVD) has shown its advantages in synthesizing large size high quality SCD. This research details experiments focused on the impact of physical boundary conditions on the epitaxial lateral growth of SCD using MPACVD. Growth dynamics, such as lateral growth rates, and as grown diamond crystal structural properties, such as X-ray rocking curves (XRC), relative to pocket holder boundaries is discussed. The boundary conditions of ELO are established relative to growth rate, and internal structure (planar alignment and mosaicity of the lattice) of outgrown areas are discussed. Results indicate the time varying effects of holder boundaries on growth rate can be parameterized into an exponential decay function based on the kinetics of phase change to predict the total lateral outgrowth possible for a given holder design. As expected, these results, in turn, will enable the design next generation reactors to accommodate continuous larger area single crystal diamond growth. Additionally, the structural characteristics of the internal lattice are discussed relative to reactor conditions of holder geometry, temperature, and gas pressure.

Among diamond growth methods, MPACVD has distinct advantages compared to high pressure high temperature (HPHT) growth, but primarily its ability to synthesize diamond at relatively low pressure and temperature makes it attractive as a scale-up method for diamond growth. While a plethora of literature on the chemical and macroscale mechanisms of diamond growth exists, synthesizing large size high quality SCD remains a significant challenge due to the emergence of

heterogeneous structure and morphology from uncontrolled nucleation based on reactor design. This research reveals how the pocket holder and the boundary conditions it creates influence the morphology that a CVD diamond (type IIa) growth on HPHT substrate (type Ib) assume. Crystal structure characteristics reflected from XRC mapping on both peak position and FWHM for both (400) diamond crystal planes shows the importance of the geometry of the sample holder. Further growth results of SCD using multiple types sample holders and their crystal structural measurement and analysis will be shown at the conference. This will give feedbacks on growth processing and lay the foundation for the real large size high quality SCD growth in the near future.

#### 5:10 AM F.EL01.05.02

##### **Diamondization of Multilayer Graphene/Graphitic Structures through a Shear Assisted Phase**

**Transformation** Shiddartha Paul<sup>1</sup>, Kasra Momeni<sup>1,2</sup> and Valery I. Levitas<sup>3</sup>; <sup>1</sup>Louisiana Tech University, United States; <sup>2</sup>The University of Alabama, United States; <sup>3</sup>Iowa State University, United States

Atomically thin diamond has various industrial applications because of their extreme hardness and excellent thermal conductivity. In this study, we have investigated the possibility of a novel synthesis technique for diamond and diamond thin films from multilayer graphene at pressures far below the graphite → diamond transformation pressure using the atomistic modeling approach. We have used the Molecular Dynamics technique with reactive force fields to study the formation mechanism of diamond. Our results demonstrate a drastic reduction (by a factor of two) in the graphite → diamond transformation stress upon using a combined shear and axial compression. The shear deformation in the multilayer graphene lowers the phase transformation energy barrier and plays the role of thermal fluctuations, which itself promotes the formation of diamond. We revealed weak temperature dependence of the transformation strain and stresses. The transformation stress vs. strain curve for the bulk graphite drops exponentially for finite temperatures. Therefore, our results support the proposition that shear strain plays a vital role in graphite → diamond phase transformation.

#### 5:20 AM \*F.EL01.05.03

##### **Electrical and Quantum Application of Diamond—From the Viewpoint of Diamond CVD Growth and Device**

**Fabrication** Satoshi Yamasaki<sup>1,2</sup>, Toshiharu Makino<sup>1</sup>, Hiromitsu Kato<sup>1</sup>, Masahiko Ogura<sup>1</sup>, Daisuke Takeuchi<sup>1</sup>, Yukako Kato<sup>1</sup>, Norio Tokuda<sup>2</sup> and Tsubasa Matsumoto<sup>2</sup>; <sup>1</sup>National Institute of Advanced Industrial Science and Technology, Japan; <sup>2</sup>Kanazawa University, Japan

Diamond has many unique physical properties. Due to these unique properties diamond has high potential for applications; electrical devices, quantum devices, etc. Depending on the target application we need to develop the growth and fabrication technique, In this talk, we introduce the electronic applications and the quantum application using nitrogen-vacancy centers from the viewpoint of diamond growth and fabrication technique.

#### 5:35 AM F.EL01.05.04

##### **Exploring the Role of Etching During CVD Diamond Growth Using Kinetic Monte Carlo Modelling** Max D.

Williams<sup>1,2</sup>, Neil L. Allan<sup>1,1</sup> and Paul May<sup>1,2</sup>; <sup>1</sup>University of Bristol, United Kingdom; <sup>2</sup>University of Warwick, United Kingdom

Using a simplified kinetic Monte Carlo (KMC) model of CVD diamond growth, the diamond and computational chemistry groups at the University of Bristol have previously reported simulating many atomic layers of diamond growth at relatively low computational cost. These simulations have been found to reproduce many of the growth features seen experimentally, including growth rates, while keeping the computational time required on the order of hours.<sup>1</sup> However, one limitation of such a simplified model is the use of a cubic representation of the diamond atomic lattice. Although this allows low calculation times and simplified methods, the geometries of specific adsorbates or surface defects thought to be important in the diamond growth mechanism cannot be correctly modelled.

Transitioning the model from a simple cubic lattice to a true tetrahedral diamond structure allows a more realistic representation for the diamond lattice, allowing implementation and testing of more complicated CVD growth reaction schemes, with application of modern software development strategies to maintain computational efficiency. Visualisation of the diamond surface as CVD growth progresses in true tetrahedral co-ordination is also now possible, allowing robust and powerful analysis of implemented reaction schemes and their effect on surface morphology development as a function of time.

Experimental observations of (100) CVD diamond growth have suggested the presence of species incorporation and etching mechanisms whose interplay results in step-flow growth<sup>2</sup> and aligned dimer row domains,<sup>3</sup> implying the presence of an

anisotropic etching mechanism.<sup>4</sup> Previous theoretical models have included etching mechanisms which facilitate the removal of isolated surface species,<sup>5-7</sup> but there has yet to be theoretical modelling studying each mechanism operates as growth conditions and mechanism energetics are varied.

Using our kMC model for (100) CVD diamond growth, we aim to investigate the various etching mechanisms and their associated energetics reported in the literature within a consistent growth model to assess how experimental growth rates can best be reproduced while observing commonly seen experimental surface features.

## References

1. W. J. Rodgers, P. W. May, N. L. Allan, and J. N. Harvey: Three-dimensional kinetic Monte Carlo simulations of diamond chemical vapor deposition. *J. Chem. Phys.* **142**(21), 214707 (2015).
2. K. Hayashi, S. Yamanaka, H. Okushi, and K. Kajimura: Stepped growth and etching of (001) diamond. *Diam. Relat. Mater.* **5**(9), 1002 (1996).
3. R. E. Stallcup and J. M. Perez: Scanning Tunneling Microscopy Studies of Temperature-Dependent Etching of Diamond (100) by Atomic Hydrogen. *Phys. Rev. Lett.* **86**(15), 3368 (2001).
4. C. L. Cheng, H. C. Chang, J. C. Lin, K. J. Song, and J. K. Wang: Direct observation of hydrogen etching anisotropy on diamond single crystal surfaces. *Phys. Rev. Lett.* **78**(19), 3713 (1997).
5. A. Netto and M. Frenklach: Kinetic Monte Carlo simulations of CVD diamond growth—Interplay among growth, etching, and migration. *Diam. Relat. Mater.* **14**(10), 1630 (2005).
6. M. Grujicic and S. G. Lai: Atomistic simulation of chemical vapor deposition of (111)-oriented diamond film using a kinetic Monte Carlo method. *J. Mater. Sci.* **34**(111), 7 (1999).
7. C. C. Battaile, D. J. Srolovitz, I. I. Oleinik, D. G. Pettifor, A. P. Sutton, S. J. Harris, and J. E. Butler: Etching effects during the chemical vapor deposition of (100) diamond. *J. Chem. Phys.* **111**(9), 4291 (1999).

## 5:45 AM F.EL01.05.05

**Surface Contamination Impact on Nanodiamond Seeding of Plasma-Treated Tantalum Films** Paulius Pobedinskas<sup>1,2</sup>, Wim Dexters<sup>1,2</sup>, Jan D'Haen<sup>1,2</sup> and Ken Haenen<sup>1,2</sup>; <sup>1</sup>Hasselt University, Belgium; <sup>2</sup>IMEC vzw, Belgium

The deposition of closed nanocrystalline diamond (NCD) thin films on non-diamond substrates requires diamond nucleation sites. An established technique for creating nucleation sites is a surface treatment with a water-based colloidal solution of ultra-dispersed nanodiamond (ND) particles.<sup>1</sup> In ND seeding the most important factors are the surface charge of the substrate and the zeta-potential of the used colloid. Together, they determine the nucleation density, which can lead to an extreme difference in the observed seeding density.<sup>2-6</sup> However, surface contamination by hydrocarbons, which is an unavoidable and quick process even in a cleanroom environment,<sup>7</sup> is often not taken into consideration. Such contamination can alter the surface wetting properties<sup>8</sup> and surface charge<sup>9</sup>, and thus the eventual seeding density. In this work we investigate and model the impact such surface contamination has on the ND seeding efficiency.

Tantalum is a metal well known for its resistivity to corrosion, bioinertness, biocompatibility and excellent osteoconductivity.<sup>10</sup> After sputtering a thin film of Ta on silicon substrates, these stacks were exposed to the ambient atmosphere for different times, allowing to achieve various degrees of surface contamination. Then, the Ta surface wettability was measured, samples were seeded with NDs, and the subsequent seeding density evaluated. As surface coverage by hydrocarbons increased, the wetting properties gradually turned from hydrophilic to hydrophobic. The ND seeding density first decreased and then increased again. To understand this correlation, we propose an analytical model that describes the dynamics of surface contamination and hydrocarbon contaminant interaction with the surface, and the resulting ND seeding density.

We assume that when a hydrocarbon (HC) molecule lands on the Ta surface it attracts negative surface charge towards it, while creating a positive surface charge around it. Due to said dipole formation, the top part of the HC molecule is charging negatively. Solving differential equations for the dynamics of the normalized surface coverage number density of the HC molecules,  $\mathbf{n}$ , and surface charge density,  $\sigma$ , we derive  $\sigma(\mathbf{n}, \eta) = \mathbf{n} + (\mathbf{1} - \mathbf{n})^{(1 + \eta)}$ , where  $\eta$  is a ratio between an area of the depleted charge around the HC molecule and the area of the HC molecule itself. The assumption that the contact angle,  $\theta$ , is linearly proportional to the surface coverage by HC,  $\mathbf{n} = \theta / \theta_{\text{sat}}$ , makes wettability measurements a valid method for determining the degree of surface contamination. If the sum of electrostatic double-layer and Van der Waals interaction energies becomes positive, a potential energy barrier for a ND particle approaching a surface exists. ND particles must surmount a positive potential peak for a deposition onto the surface to occur. This occurs with a probability exponentially proportional to the potential barrier. By fitting the experimental data, we find that the ND seeding density is exponentially proportional to the calculated positive surface charge number density, which forms around HC molecules. This constitutes

57% of the HC molecule area, while the created barrier height is estimated to be ~ 0.18 eV.

## References

- [1] O.A. Williams, *et al.*, Chem. Phys. Lett. **445**, 255 (2007).
- [2] O.A. Williams, *et al.*, ACS Nano **4**, 4824 (2010).
- [3] P. Pobedinskas, *et al.*, Appl. Phys. Lett. **102**, 201609 (2013).
- [4] J. Hees, *et al.*, Nanotechnology **24**, 025601 (2013).
- [5] G. Degutis, *et al.*, Chem. Phys. Lett. **640**, 50 (2015).
- [6] S. Mandal, *et al.*, ACS Appl. Mater. Interfaces **11**, 40826 (2019).
- [7] K. Takeda, *et al.*, Proc. 44<sup>th</sup> Annual Technical Meeting of the IEST and ISCC, 556 (1998).
- [8] Ch. Mücksch, *et al.*, J. Phys. Chem. C **119**, 12496 (2015).
- [9] A. Khachatourian, *et al.*, J. Chem. Phys. **140**, 074107 (2014).
- [10] H. Matsuno, *et al.*, Biomaterials **22**, 1253 (2001).

## SESSION F.EL01.06: Diamond Integration

On Demand Abstracts Available for Viewing Starting Saturday Morning, November 21, 2020

F-EL01

### 5:00 AM \*F.EL01.06.01

#### The Role of Interfaces and Heterogenous Integration in the Thermal Management of Wide Bandgap

**Semiconductors** Samuel Graham<sup>1</sup>, Zhe Cheng<sup>1</sup>, Mark Goorsky<sup>2</sup>, Fengwen Mu<sup>3</sup>, Jim Speck<sup>4</sup> and Tadatomo Suga<sup>3</sup>; <sup>1</sup>Georgia Institute of Technology, United States; <sup>2</sup>University of California, Los Angeles, United States; <sup>3</sup>Meisei University, Japan; <sup>4</sup>University of California, Santa Barbara, United States

Wide bandgap electronics made from GaN and Ga<sub>2</sub>O<sub>3</sub> are currently under development due to their potential to create advanced RF and power electronics. However, the performance and reliability of these devices are often controlled by their electrothermal response during device operation. A key feature which limits thermal control of the peak temperature is the thermal resistance that is encountered intrinsically from the material as well as across material interfaces with these devices. One method that has shown promise for mitigating the high thermal resistance of these devices is through their heterogenous integration with other materials which assist in heat dissipation and aid thermal management. For this, thermal transport across interfaces and novel integration methods are necessary.

In this work we will present modeling efforts which guide the impact of heterogenous integration on the thermal performance of UWBG devices. Thermal metrology methods used to measure interfacial thermal conductance will be discussed and new insights into the control of thermal boundary conductance given. Techniques such as surface activated bonding will be presented to demonstrate the integration of GaN and Ga<sub>2</sub>O<sub>3</sub> with high thermal conductivity substrates such as SiC and diamond. The use of other high thermal conductivity dielectrics for improved heat dissipation from the top side and bottom side of the devices will be discussed. Finally, the prospects for the future development of thermal management via heterogenous integration will be presented.

### 5:15 AM F.EL01.06.02

#### Formation Process of High Thermal-Stability Diamond/Si and Diamond/GaAs Heterointerfaces by Surface Activated

**Bonding** Yutaka Ohno<sup>1</sup>, Jianbo Liang<sup>2</sup>, Yasuo Shimizu<sup>1</sup>, Hideto Yoshida<sup>3</sup> and Naoteru Shigekawa<sup>2</sup>; <sup>1</sup>Tohoku University, Japan; <sup>2</sup>Osaka City University, Japan; <sup>3</sup>Osaka University, Japan

Diamond is a promising candidate for a base material of high power electronic devices, as well as for a superior heat spreading substrate, due to its excellent physical properties such as the highest electrical breakdown field strength, the highest thermal conductivity, and a high RF power capability that is 3 times higher in comparison with SiC. For the practical application toward power devices, we need diamond/semiconductor heterointerfaces with high thermal stability and can withstand the temperature rise of power devices during operating. Recently, Liang has demonstrated that diamond/Si [1] and diamond/GaAs [2] heterointerfaces with high thermal stability can be fabricated by surface activated bonding (SAB) at room temperature (RT). In this work, we have examined the bonding mechanism using cross-sectional scanning transmission electron microscopy (STEM) combined with electron energy loss spectroscopy (EELS) and energy dispersive x-ray spectroscopy (EDX).



In the SAB process, surfaces of diamond and Si (or GaAs) wafers are activated at RT before bonding by creating dangling bonds via the irradiation of high-energy Ar atoms in a high vacuum, and the surfaces are then bonded by the contact most of the time under pressure to form strong chemical bonds even for imperfect surfaces. For diamond/Si heterointerfaces, atomic diffusion at the interfaces, presumably due to the transient enhanced diffusion assisted by the point defects introduced in the surface activation process [3], is confirmed during the bonding process. The crystallinity at the diffusing region is rather low, and it is recovered by 1000 °C annealing via the formation of SiC layers, that would play a pivotal role in the relaxation process of residual stress due to the misfit of thermal expansion coefficient between diamond and Si [1]. Therefore, the defect-assisted atomic diffusion at the interfaces would be a key concept for the formation of high thermal-stability diamond/Si heterointerfaces. Similar atomic diffusion is also confirmed at diamond/GaAs heterointerfaces during the SAB process.

[1] J. Liang, S. Masuya, M. Kasu, and N. Shigekawa, *Appl. Phys. Lett.* 110 (2017)111603.

[2] Y. Nakamura, Y. Shimizu, Y. Ohno, K. Shirasaki, Y. Nagai, M. Kasu, N. Shigekawa, and J. Liang, 13th Topical Workshop on Heterostructure Microelectronics (Toyama, Japan, 2019) 11-7.

[3] Y. Ohno, H. Yoshida, N. Kamiuchi, R. Aso, S. Takeda, Y. Shimizu, Y. Nagai, J. Liang, and N. Shigekawa, *Jpn. J. Appl. Phys.* 59 (2020) SBBB05.

### 5:25 AM F.EL01.06.03

**The Impact of Polycrystalline Diamond Growth Nucleation on N-Polar GaN Channel Performance** Mohamadali Malakoutian<sup>1,2</sup>, Chenhao Ren<sup>1,2</sup>, Kelly Woo<sup>2</sup>, Shubhra Pasayat<sup>3</sup> and Srabanti Chowdhury<sup>2</sup>; <sup>1</sup>University of California, Davis, United States; <sup>2</sup>Stanford University, United States; <sup>3</sup>University of California, Santa Barbara, United States

N-polar gallium nitride (GaN) high electron mobility transistors (HEMTs) have shown superior performances when scaling for W-band frequencies over Ga-polar GaN HEMTs [1]. However, due to the shorter channel and closer gate fingers its ability to dissipate the heat from the channel to the heat-sink is limited. Polycrystalline (PC) diamond due to its very large thermal conductivity (TC) is one of the solutions for self-heating problem in high-power high-frequency devices. PC Diamond can be grown in a closed proximity to high temperature spot in the channel and spread the heat efficiently [2]. The standard Si<sub>3</sub>N<sub>4</sub> thickness as a gate dielectric for W-band N-polar HEMTs is 5 nm, which can be used as thermal interface material to reduce thermal boundary resistance (TBR < 2 m<sup>2</sup>K/GW) between diamond and GaN as well [3]. As diamond growth takes place in a high temperature hydrogen plasma environment using MPCVD, it can decompose both Si<sub>3</sub>N<sub>4</sub> and GaN layers by reacting with silicon, nitrogen, and gallium and making volatile gases (SiH<sub>4</sub>, NH<sub>3</sub>, and GaH, respectively) [4]. Any damage to GaN channel may result in a degradation of device performance after the growth. In this work, we investigated the impact of diamond growth nucleation and main stages on 2-dimensional electron gas (2DEG) properties such as electron mobility, sheet carrier concentration, and sheet resistivity (before growth:  $\mu_n=1200$  cm<sup>2</sup>/V.s,  $n_s=1.34E13$  cm<sup>-2</sup>, and  $\rho_s=388$  Ω/sq).

The main goal of the growth nucleation stage is to guarantee no damage to the 2DEG by covering the substrate (Si<sub>3</sub>N<sub>4</sub>/GaN) with thinnest possible nano-crystalline diamond (NCD) in shortest possible time as NCD has a poor TC (<100 W/m.K). The 2DEG has been characterized using Hall mobility measurement, and the thickness of nucleation layer has been measured by high resolution TEM. The nucleation layer can prevent diffusion of hydrogen radicals into the substrate which is highly dependent on the microwave power and gas pressure. To increase the diamond growth rate and decrease substrate etching rate the sample holder was redesigned to provide higher temperature (~700 C) with minimum power (600 W) and pressure (20 Torr). The CH<sub>4</sub>% and time were changed from 3 to 10% and 10 to 15 min, respectively for nucleation stage followed by the same main growth for all samples (2% CH<sub>4</sub>, 1600 W, 60 Torr, 45 min). We observed no degradation in 2DEG by using >5% CH<sub>4</sub> and 15 min growth, while by lowering the time to 10 min we started to see about 20-30% reduction in  $\mu_n$  and 50-150 Ω/sq increase in  $\rho_s$ . This degradation varies with different cap layers on top of the channel; no cap layer, 1-2 nm AlN, or 1-2 nm 46% AlGaIn.

To study the impact of main growth on 2DEG, we have chosen 5% CH<sub>4</sub> and 15 min for nucleation stage and changed main growth parameters including CH<sub>4</sub>% (0.5-2%), power (600-1600 W), pressure (20-90 Torr), and sample holder design. CH<sub>4</sub>% showed the highest impact in determination of damage level to 2DEG and pressure had the lowest impact. With the sample holder same as nucleation stage, 1% CH<sub>4</sub> is the minimum required for no damage. For the case with original sample holder, 1.5% CH<sub>4</sub> is the lowest acceptable value for the first 45 min of the growth.

In this work, we were able to achieve a smooth interface between diamond and GaN (including 5 nm Si<sub>3</sub>N<sub>4</sub> interfacial layer) without using argon or nitrogen in the gas mixture by redesigning the sample holder and modifying growth parameters for lower etch rate of the substrate. This recipe is compatible with W-band N-polar GaN HEMTs as maintains device performance after the growth.

This work was supported by the Semiconductor Research Corporation (SRC) and DARPA under the JUMP program.

[1] B. Romanczyk *et al.*, *IEEE Electron Device Lett.*, vol. 41, no. 3, pp. 349–352, 2020.

[2] M. Malakoutian *et al.*, *Crystals*, vol. 9, no. 10, pp. 1–14, 2019.

[3] J. Cho *et al.*, *J. Appl. Phys.*, vol. 121, no. 5, 2017.

[4] Y. S. Zou *et al.*, *Cryst. Growth Des.*, vol. 8, no. 5, pp. 1770–1773, 2008.

#### 5:35 AM F.EL01.06.04

##### **Correlation Between Linear Antenna Microwave Plasma CVD Reactor Parameters and the Diamond-on-GaN**

**Films** Awadesh K. Mallik<sup>1,2</sup>, Paulius Pobedinskas<sup>1,2</sup>, Jan D'Haen<sup>1,2</sup> and Ken Haenen<sup>1,2</sup>; <sup>1</sup>Hasselt University, Belgium; <sup>2</sup>imec vzw, Belgium

Compared to classical resonant cavity CVD, linear antenna microwave plasma enhanced CVD (LA MW CVD) is a relatively new route of depositing diamond films onto different vulnerable substrates [1]. It has been reported earlier that GaN surfaces are prone to etching under conventional CVD diamond deposition parameters. So, it was envisaged that due to the low pressure and low temperature regimes of LA MW CVD, it might be possible to deposit diamond onto otherwise reactive GaN surfaces. Although it is a regular practice to put an intermediate SiN buffer layer for successful deposition of diamond films on GaN [2], there are only few reports of such deposition onto bare GaN substrates [3], and not by a LA MW CVD reactor, which could potentially solve the problem associated with an additional SiN barrier layer, i.e. an extra thermal barrier. In the present work, the effect of different LA MW CVD processing parameters on the optimal deposition of the diamond films has been systematically studied. First of all, the distances between the quartz tube and the samples were varied, which has direct impact on the substrate temperature. Thereafter, the microwave input power was altered to attain varied substrate temperatures. There is an upper limit of the substrate temperature beyond which the microwave plasma alone is insufficient to increase the temperature further. Hence, an additional heater was used under the stage for attaining various substrate temperatures. Moreover, the microwave power input was also used in pulsed mode for further optimization of the film properties. The microstructure of the deposited films was observed in the scanning electron microscope (SEM) and the elemental analysis of the film surfaces was done by electron diffraction spectroscopy (EDX). Moreover the diamond film quality and crystallinity was evaluated by Raman spectroscopy. It will be shown that the said parameters have a significant impact on the grown films, both in terms of their quality and microstructure. It was found that the optimum film quality without GaN surface etching was obtained under the pulsed microwave power regime.

#### References

[1] S. Drijkoningen, P. Pobedinskas, S. Korneychuk, A. Momot, Y. Balasubramaniam, M.K. Van Bael, S. Turner, J. Verbeeck, M. Nesládek, K. Haenen, *Crystal Growth & Design*, 17, 4306 (2017).

[2] Y. Zhou, R. Ramaneti, J. Anaya, S. Korneychuk, J. Derluyn, H. Sun, J. Pomeroy, J. Verbeeck, K. Haenen, M. Kuball, *Applied Physics Letters*, 111, 041901 (2017).

[3] S. Mandal, Evan L. H. Thomas, C. Middleton, L. Gines, J. T. Griffiths, M. J. Kappers, R. A. Oliver, D. J. Wallis, L. E. Goff, S. A. Lynch, M. Kuball, O. A. Williams, *ACS Omega*, 2, 7275 (2017).

#### 5:45 AM F.EL01.06.05

**Nitrogen and Phosphorous Doping of Diamond Films on GaN Substrates** Awadesh K. Mallik<sup>1,2</sup>, Rozita Rouzbahani<sup>1,2</sup>, Giridharan Krishnamurthy<sup>1,2</sup>, Paulius Pobedinskas<sup>1,2</sup>, Wen-Ching Shih<sup>1,3</sup> and Ken Haenen<sup>1,2</sup>; <sup>1</sup>Hasselt University, Belgium; <sup>2</sup>imec vzw, Belgium; <sup>3</sup>Tatung University, Taiwan

In the present work, doped diamond films have been grown on GaN substrates. The CVD diamond processing is not straight forward, as GaN is susceptible to H<sub>2</sub> plasma etching, with formation of elemental Ga in the resulting diamond film, which can thereby enhance the electron emission properties of the stack. However, the electrical resistivity across the CVD grown film surface was found to become very high (~MΩ) after depositing diamond on GaN substrates. So, in order to induce electrical conduction on the top surface film, the diamond films were doped with nitrogen inside a 2.45 GHz resonant cavity reactor [1], and with phosphorous [2] inside a linear antenna CVD chamber [3]. 1%, 3% and 5% N<sub>2</sub> gas was added to the conventional H<sub>2</sub>/CH<sub>4</sub> gas mixture. On the other hand, 0.1% PH<sub>3</sub> gas diluted in H<sub>2</sub> was used as precursor gas for phosphorous doping. Different types of microstructures were produced while doping with two different dopants. Nitrogen gas changes the diamond film microstructure from faceted to spherical grains with signs of GaN substrate etching, whereas, the phosphorous doping produced much smaller nanocrystalline grains with strong Ga peaks in their EDX spectra. Nitrogen incorporation in the diamond lattice can happen easily at lower substrate temperatures of 500–600°C, as found from their photoluminescence data, but phosphorus doping was only possible at a high substrate temperature of 900°C, as evidenced from its XPS signal at 132 eV. The porous nanocrystalline grains in the doped diamond could possibly enhance the field emission characteristics in comparison to the bare GaN substrate. The electrical conductivities of the coated and uncoated GaN substrates will also be presented.

#### References

1. J. A. Cuenca; K. J. Sankaran ; P. Pobedinskas ; K. Panda, I. N. Lin, A. Porch, K. Haenen, O. A. Williams, *Carbon*, 145 (2019) 740-750
2. W. Janssen, S. Turner, G. Sakr, F. Jomard, J. Barjon, G. Degutis, Y-G. Lu, J. D'Haen, A. Hardy, M. Van Bael, J. Verbeeck, G. Van Tendeloo,; K. Haenen, *Physica Status Solidi-Rapid Research Letters*, 8 (2014) 705-709..
3. S. Drijkoningen, P. Pobedinskas, S. Korneychuk, A. Momot, Y. Balasubramaniam, M.K. Van Bael, S. Turner, J. Verbeeck, M. Nesládek, K. Haenen, *Crystal Growth & Design*, 17 (2017) 4306.

SESSION F.EL01.07: Diamond Nanoparticles  
On Demand Abstracts Available for Viewing Starting Saturday Morning, November 21, 2020  
F-EL01

**5:00 AM \*F.EL01.07.01**

**Identifying the Multiple Classes of Diamond Nanoparticles Using Machine Learning** Amanda Barnard<sup>1</sup> and Amanda J. Parker<sup>2</sup>; <sup>1</sup>The Australian National University, Australia; <sup>2</sup>CSIRO, Australia

Diamond nanoparticles are complicated materials, presenting a diverse range of sizes, shapes, speciation and defects that cannot easily be controlled during synthesis. Each of these features contribute to structure/property relationships, but in different ways. Attempts to purify samples to tune the properties often fail due to lack of specificity, and polydispersivity usually persists. An alternative approach is to separate classes of nanodiamonds based on their properties, rather than seeking monodispersed samples based on their structure. To investigate if this approach has merit we have used machine learning to classify nanodiamonds and identify class-dependent properties and characteristics. Using a fully reconstructed data set that spans the experimentally observed size range from 1 nm to 4.5 nm we find that there are multiple classes of particles, based on their similarity in the high dimensional feature space. By using an interpretable classifier, with excellent accuracy, precision and recall, we also identify possible purification pathways based on the important features ranked by the AI.

**5:15 AM \*F.EL01.07.02**

**Molecular Transducers for Spin-Sensitive Optical Sensing Using Nitrogen-Vacancy Centers** Petr Cigler; Institute of Organic Chemistry and Biochemistry, Czech Academy of Sciences, Czechia

Non-perturbing sensing techniques applicable to biological systems currently are of central interest in the biosciences. Nanodiamond is a highly biocompatible nanomaterial for construction of nanosensors, which can accommodate various photoluminescent crystal defects. Nitrogen-vacancy (NV) centers show high photostability and unique electronic sensitivity to magnetic field. Their spin properties can be read by optical means, which enables construction of various probes based on quantum mechanical interactions. If embedded in nanodiamond particles, NV centers can be exposed to biological environment and report sensitively on the spin-related processes occurring in a close vicinity of the particle. Molecular transducers designed for NV centers transposing the presence of particular analytes to a selective and unambiguous readout will be presented. Different types of surface architectures will be shown [1, 2]. Optical nanosensors designed for selective measurements of pH, redox potential, and ascorbate under physiological conditions will be discussed.

**References**

- Rendler T., Neburkova J., Zemek O., Kotek J., Zappe A., Chu Z., Cigler P., Wrachtrup J. (2017). Optical imaging of localized chemical events using programmable diamond quantum nanosensors. *Nat. Commun.*, 8, 14701.
- Vavra J., Rehor I., Rendler T., Jani M., Bednar J., Baksh M. M., Zappe A., Wrachtrup J., Cigler P. (2018). Supported Lipid Bilayers on Fluorescent Nanodiamonds: A Structurally Defined and Versatile Coating for Bioapplications. *Adv. Funct. Mater.* 28, 1803406.

**5:30 AM F.EL01.07.03**

**Scalable Assembly of Fluorescent Nanodiamonds for Quantum Sensing** Henry J. Shulevitz, Tzu-Yung Huang, Steven Neuhaus, Lee Bassett and Cherie Kagan; University of Pennsylvania, United States

Milled fluorescent nanodiamonds containing nitrogen-vacancy (NV) centers provide an excellent platform for sensing applications due to their quantum sensitivity to a variety of external fields at nanometer length scales. Currently, the irregularity in crystal morphology and the difficulty of functionalizing the nanodiamond surface impede efforts to realize scalable assemblies of nanodiamonds, or to create heteroassemblies with other materials. Poor control over the nanodiamond

composition and surface chemistry also creates significant heterogeneity in their optical and quantum characteristics. We will present scalable strategies to form ordered arrays of nanodiamonds using template-directed capillary assembly. This method enables the precise spatial arrangement of primary nanodiamonds with diameters below 50 nm, and it is compatible with the assembly of other compositions of colloidal nanoparticles. Large-scale arrays facilitate automated, repeatable measurements of the nanodiamonds' optical, structural, and quantum characteristics, enabling improved statistical understanding of these key properties and their heterogeneity. The flexible assembly method will allow for detailed studies of chemical treatments, integration of nanodiamonds within photonic and electronic devices, and the realization of quantum heterostructure devices composed from complementary nanomaterials.

#### 5:40 AM F.EL01.07.04

**Surface Functionalized Nanodiamond with Improved Protein Repulsion for Drug Delivery and Sensing** Julia Puck, Viktor Merz and Anke Krueger; Wuerzburg University, Germany

For many applications the surface chemistry of nanodiamond (ND) is a key factor for the control of properties such as the wetting behavior, biocompatibility and functionality[1]. By attaching appropriate moieties, the interaction with physiological environments can be controlled.

An important point for biomedical applications is the inhibition of a nonspecific protein corona. This shell of e.g. serum proteins masks the desired functions and renders the physiological properties of the nanoparticle uncontrollable[2]. Here we report on the grafting of zwitterionic moieties enabling the formation of NDs without protein corona [3] that enable the specific grafting of antibodies, targeting peptides and CO releasing drug molecules using visible light. The resulting constructs have been characterized using IR, Raman, x-ray spectroscopies as well as particle analysis, TGA and electron microscopy.

The ND conjugates have been tested in vitro as well as in cell assays and demonstrated their functionality in the cellular environment. Additionally, these NDs have been functionalized with pyrene moieties for fluorescence sensing in solution with strong ion background and demonstrated colloidal stability, sensitivity and specificity for the detection of heavy metal ions against a background of ions present in physiological environments.

This research has received funding from Volkswagenstiftung under Grant Agreement no. 88393.

#### References

- [1] A. Krueger, D. Lang, *Adv. Funct. Mater.* 22 (2012), 890.
- [2] W. C. W. Chan, C. D. Walkey, *J. Am. Chem. Soc.* 134 (2012), 2139.
- [3] V. Merz, J. Lenhart, Y. Vonhausen, M. E. Ortiz Soto, J. Seibel, A. Krueger, *Small* (2019) 1901551.

#### 5:50 AM \*F.EL01.07.05

**How the Surface Orientation of Diamond Crystals Influences its Interaction with Biological Matter** Romana Schirhagl<sup>1</sup>, Viraj Damle<sup>1</sup>, Kaiqi Wu<sup>1</sup>, Oreste De Luca<sup>1</sup>, Natalia Orti Casan<sup>1</sup>, Neda Norouzi<sup>1</sup>, Aryan Morita<sup>1</sup>, Joop de Vries<sup>1</sup>, Hans Kaper<sup>1</sup>, Inge Zuhorn<sup>1</sup>, Ulrich Eisel<sup>1</sup> and Danny Vanpouke<sup>2</sup>; <sup>1</sup>Groningen University, Netherlands; <sup>2</sup>Hasselt University, Belgium

Here we show how the diamond crystal orientation influences the interaction with biological systems[1]. More specifically we are investigating the interaction between the <100>, <110> and <111> surfaces of single crystal diamond with biomolecules, cell culture medium, mammalian cells and bacteria. We show that the crystal orientation significantly alters these biological interactions. Most surprising is the two orders of magnitude difference in the number of bacteria adhering on <111> surface compared to <100> surface when both the surfaces were maintained under the same conditions. We also observe differences in how small biomolecules attach to the surfaces. Neurons or HeLa cells on the other hand do not have clear preferences for either of the surfaces. To explain the observed differences, we theoretically estimated the surface charge for these three low index diamond surfaces and followed by the surface composition analysis using x-ray photoelectron spectroscopy (XPS). We conclude that the differences in negative surface charge, atomic composition and functional groups of the different surface orientations lead to significant variations in how the single crystal diamond surface interacts with the studied biological entities.

- [1] Damle, V., Wu, K., De Luca, O., Ortí-Casañ, N., Norouzi, N., Morita, A., de Vries, J., Kaper, H., Zuhorn, I.S., Eisel, U. and Vanpoucke, D.E., 2020. Influence of diamond crystal orientation on the interaction with biological matter. *Carbon*, 162, pp.1-12.

**5:00 AM F.EL01.08.01**

**Investigation of Li Doping and SnO Termination on the Diamond (100) Surface for Thermionic Emission**

**Application** Sami Ullah, Liam Cullingford, Tongfie Zhang, Jing Ren Wong, Gary Wan, Mattia Cattelan and Neil Fox; University of Bristol, United Kingdom

Diamond electrodes terminated with surface layers can impart significant changes to the electronic properties of a diamond interface and we have previously reported on studies of the tunability of surface work function by substituting hydrogen with oxygen under controlled conditions [1]. Engineering a functionalised diamond surface that is stable and reproducible is of technological importance to future diamond electronic devices such as Schottky junctions and electron-emitting electrodes for field emission, thermionic energy converters, secondary electron multipliers.

O'Donnell and his group have demonstrated the formation of a stable Li-O termination of diamond by physical vapour deposition of a monolayer of Li on the diamond surface which develops and exhibits Negative electron affinity (NEA) and hence lowers the work function, even at an elevated temperature of 800 °C [2]. In this work we are seeking an alternative method, a novel and easy chemical means of introducing and coordinating lithium with oxygen on the diamond surface to realize a more controlled approach of creating a stable –O-Li dipole. with uniformity over the diamond surface which also serves as a means to study and visualize for the first time the effect of temperature on the concentration of Li atoms in the diamond surface and on the Li-O species on the surface of diamond sample.

Also, Tin monoxide has been considered as potential material for battery anodes, coating, gas sensing, catalysis, etc. The application area of SnO extends over photovoltaics, displays, information storage, etc. as it has a large optical bandgap of 4.12 eV, high transparency (~90%) non-toxic and abundant [3]. SnO has been found to form a layered structure in a crystallographic direction of [001] with a monolayer thickness of 0.48 nm. Sn 5s form a lone pair of electrons which point towards the interlayer spacing and result in dipole-dipole interaction leading to a Van der Waals gap of 2.52 Å between the layers. Various groups have demonstrated the growth of SnO mono and multiple layers by various methods but many of these result in an upper SnO<sub>2</sub> layer that forms as soon as the sample is taken into the oxygen environment as SnO is metastable and hence rapidly converts into SnO<sub>2</sub>.

We are doping oxygen terminated Boron doped Polycrystalline diamond and Nitrogen doped HPHT diamond (111) with Li atoms using microwave plasma technique. The oxygen termination was induced by acid washing. We analyze the sample with X-Ray Photoemission Spectroscopy (XPS) and Raman spectroscopy. The main aim of this study is to analyze the change in concentration of Li atoms in the bulk and on the surface of diamond with annealing temperature. We have produced sub ML SnO on conductive, p-type single crystal diamond under ultra-high vacuum (UHV) conditions by e-beam evaporation. The samples will be characterised in-situ by Spot Profile Analysis Low-Energy electron diffraction (SPA-LEED) and Energy Filtered Photo Emission Electron Microscopy (EF-PEEM) and X-ray Photoemission Spectroscopy (XPS). We quantify the change in work function between mono and few layer SnO and its effect upon the barrier height of a p-type diamond Schottky junction.

References

[1] Wan, G., Cattelan, M. & Fox, N. A. Electronic structure tunability of diamonds by surface functionalization. *J. Phys. Chem. C* (2019). doi:10.1021/acs.jpcc.8b11232

[2] K. M. O'Donnell et al., "Diamond Surfaces with Air-Stable Negative Electron Affinity and Giant Electron Yield Enhancement," *Adv. Funct. Mater.*, vol. 23, no. 45, pp. 5608–5614, Dec. 2013.

[3] Pei, Y., Liu, W., Shi, J., Chen, Z. & Wang, G. Fabrication and Characterization of p-Type SnO Thin Film with High c-Axis Preferred Orientation. **45**,

**5:10 AM F.EL01.08.02**

**Stabilizing Diamond's Surface Conduction with Mixed-Oxide ALD Films and Deuterium Surface**

**Termination** Michael Geis<sup>1</sup>, Joseph Varghese<sup>1</sup>, Yichen Yao<sup>2</sup>, Robert J. Nemanich<sup>2</sup>, Mark Hollis<sup>1</sup>, Charles H. Wuorio<sup>1</sup>, Xingyu Zhang<sup>1</sup>, George W. Turner<sup>1</sup>, Shireen M. Warnock<sup>1</sup>, Steven A. Vitale<sup>1</sup>, Richard J. Molnar<sup>1</sup>, Thomas Osadchy<sup>1</sup> and Beijia Zhang; <sup>1</sup>Massachusetts Institute of Technology, United States; <sup>2</sup>Arizona State University, United States

When the surface of diamond is H-terminated, a p-type surface conductive layer is formed. Atmospheric impurities, NO<sub>2</sub>, O<sub>3</sub>,

fluoropolymer, transition metal oxides and Al<sub>2</sub>O<sub>3</sub> adhere to the diamond surface and activate diamond's surface conductance by generating and trapping negative charges on the diamond surface. These charges increase the positive p-type carrier densities in the diamond surface and reduce its resistance. High drain current field effect transistors (FETs) of 1.2 to 1.3 A mm<sup>-1</sup>, high frequency f<sub>T</sub> of 75 GHz, and high voltage, >2000 V, devices have been demonstrated with these activation surface chemistries. However, these devices degraded in a few days or when stressed with high voltage.

Research to stabilize diamond's surface conductance has met with some success. H-terminated diamonds overcoated using atomic layer deposition (ALD) Al<sub>2</sub>O<sub>3</sub> have the best demonstrated stability, but the surface resistance is high (5 to 12 kW sq<sup>-1</sup>). Diamonds coated with transition metal oxides such as WO<sub>2</sub>, MoO<sub>3</sub>, and V<sub>2</sub>O<sub>5</sub> have lower resistances of 2.5 to 3.5 kW sq<sup>-1</sup> [1,2]. Their stability has been demonstrated although these oxides are conductive, have several oxidation states, and may electrochemically degrade under the high electric fields associated with FETs. This presentation will discuss the use of a mixed-oxide (Al<sub>2</sub>O<sub>3</sub>-SiO<sub>2</sub>) ALD film to generate resistances between 1.5 and 3.5 kW sq<sup>-1</sup> with demonstrated stability in excess of half a year.

The low surface resistance obtained with this mixed oxide is a result of a change in the structure of Al<sub>2</sub>O<sub>3</sub> when mixed with SiO<sub>2</sub>. The electron trap surface density of Al<sub>2</sub>O<sub>3</sub> is ~7x10<sup>12</sup> cm<sup>-2</sup> while the mixed oxide surface density is 3x10<sup>13</sup> to 8x10<sup>13</sup> cm<sup>-2</sup> [3,4] with an estimated trap depth of 5.4 eV. This mixed oxide is just one of a group of oxides [5] with deep, > 5 eV, high-density electron traps.

Increased stability of the diamond surface is obtained by terminating the surface with deuterium atoms instead of hydrogen atoms. This additional stability is beneficial during device fabrication. This presentation will discuss diamond's surface conduction with Al<sub>2</sub>O<sub>3</sub>-SiO<sub>2</sub> combined with deuterium atom termination.

#### References

- [1] C. Verona, F. Arciprete, M. Foffi, E. Limiti, et. al. *Appl. Phys. Lett.* 112 (2018), 181602.
- [2] K. G. Crawford, D. Qi, J. McGlynn, T. G. Ivanov, et. al. *Sci. Rep.* 8 (2018), 3342.
- [3]. K. Raghavan, P. Sabu, K. Vijayachandra, C. Rao C. G. Ramachandran. *Bull Chem. Soc. Jpn.* 64 (1991), 1920.
- [4] A. Satsuma, Y. Westi, Y. Kamiya, T. Hattori, Y. Murakami. *Bull Chem. Soc. Jpn.* 70 (1997), 1311.
- [5] A. Corma. *Chem. Rev.* 95 (1995), 559.

DISTRIBUTION STATEMENT A. Approved for public release. Distribution is unlimited.

This material is based upon work supported by the Under Secretary of Defense for Research and Engineering under Air Force Contract No. FA8702-15-D-0001. Any opinions, findings, conclusions or recommendations expressed in this material are those of the author(s) and do not necessarily reflect the views of the Under Secretary of Defense for Research and Engineering.

© 2020 Massachusetts Institute of Technology.

Delivered to the U.S. Government with Unlimited Rights, as defined in DFARS Part 252.227-7013 or 7014 (Feb 2014). Notwithstanding any copyright notice, U.S. Government rights in this work are defined by DFARS 252.227-7013 or DFARS 252.227-7014 as detailed above. Use of this work other than as specifically authorized by the U.S. Government may violate any copyrights that exist in this work.

SESSION F.EL01.09: Poster Session: Diamond and Diamond Heterojunctions—From Growth to Applications  
On Demand Abstracts Available for Viewing Starting Saturday Morning, November 21, 2020  
5:00 AM - 8:00 AM  
F-EL01

#### F.EL01.09.01

**Diamond and Silicon Carbide as Passivation Layers for Packageless SAW Sensors** Lucie Drbohlavová<sup>1,2</sup>, Abdelkrim Talbi<sup>3</sup>, Yuxin Liu<sup>3</sup>, Cecile Ghouila-Houri<sup>3</sup>, Olivier Bou Matar<sup>3</sup>, Andrew Taylor<sup>1</sup> and Vincent Mortet<sup>1,2</sup>; <sup>1</sup>FZU - Institute of Physics of the Czech Academy of Sciences, Czechia; <sup>2</sup>Czech Technical University, Faculty of Biomedical Engineering, Czechia; <sup>3</sup>University Lille, CNRS, France

Surface acoustic waves (SAWs) and bulk acoustic waves are two of MEMS technologies of industrial relevance and can be found in a myriad of devices. Acoustic RF filters, for instance, are integral parts of wireless communication systems. SAW devices have been adapted as sensors which can be configured to operate both passively and wirelessly. For example, SAWs find applications in life sciences, in structural health monitoring, etc. In particular, SAW devices can also be operated in extremely confined environments such as implantable sensors to monitor or to provide real-time treatment. In this case, it

would make sense to protect the sensor surface and leave only the functionalized area visible for detection. This is true for implantable sensors where space is a major constraint and therefore requires the development of an intrinsically protected design. Also, this is true for biosensors where the surface is continuously exposed to the analysed biofluid.

In this work, we propose the use of a shear surface wave guided between the semi-infinite substrate and high acoustic velocity thin film materials. The upper high acoustic velocity layer works as an acoustically isolating layer, protecting the guided surface shear wave from undesired mechanical damping and eliminate the need for packaging. With very high acoustic velocities, diamond and silicon carbide (SiC) are excellent candidates for packageless SAW sensors applications. In previous studies, we have already demonstrated the possibility of diamond coating of SAW devices using Microwave Plasma Enhanced Chemical Vapor Deposition with Linear Antennas (MW-LA-PECVD) at low temperature [1, 2].

Here we investigate, theoretically and experimentally, the use of diamond and SiC as a passivation layer for SAW devices. Theoretical calculations were carried out using COMSOL Multiphysics FEM simulation software. Two different piezoelectric materials were investigated, ST-cut quartz and 36°YX LiTaO<sub>3</sub> as well as two common guiding layer materials – zinc oxide (ZnO) and silicone oxide (SiO<sub>2</sub>). Theoretical calculations show, that 2 μm thick diamond or SiC layers are sufficient to confine the acoustic wave in the guiding layer at a wavelength close to 10 μm. From the displacement curve we could see, that for 36°YX LiTaO<sub>3</sub> substrates the acoustic wave is very well confined for both guiding layer materials. On the contrary, shear wave disperses within the ST-cut quartz bulk with the addition of a passivation layer.

Based on theoretical results, SAW devices were fabricated on 36°YX LiTaO<sub>3</sub> substrates with 10 nm/190 nm Ti/Au electrodes patterned by RF sputtering, photolithography and chemical wet etching techniques. The SiO<sub>2</sub> layer was deposited using low temperature plasma enhanced chemical vapor deposition with a resulting normalized thickness equal to  $h_{SiO_2}/\lambda = 0.2$ . Depositions of nano-crystalline diamond (NCD) and SiC layers were carried out by MW-LA-PECVD with resulting normalized thicknesses of  $h/\lambda = 0.2$ . All depositions were carried out at a temperature below 500 °C to preserve the piezoelectric properties of substrates.

Our results are promising for waveguide protection applications as well as opening other directions, such as the introduction of the local sensitive zone in the diamond layer, which can be interesting for bio or electrochemical sensing applications.

This work has been supported by the Grant Agency of the Czech Republic (GACR) contract 19-09784Y, Czech Science Foundation (project 20-03187S) and by the Czech Technical University in Prague project SGS20/084/OHK4/1T/17.

#### References:

- [1] TALBI, A., A. SOLTANI, A. RUMEAU, et al., *Physica status solidi (a)*, 2015, **212**(11), 2606-2610 DOI: 10.1002/pssa.201532188. ISSN 18626300.
- [2] DRBOHLAVOVÁ, L., L. FEKETE, V. BOVTUN, et al., *Sensors and Actuators A: Physical*, 2019, **298**, DOI: 10.1016/j.sna.2019.111584. ISSN 09244247.

#### F.EL01.09.02

**Enhancing the Sensitivity of SAW Sensors Using the Diamond Surface Phononic Metamaterials** Lucie Drbohlavová<sup>1,2</sup>, Yuxin Liu<sup>3</sup>, Abdelkrim Talbi<sup>3</sup>, Cecile Ghouila-Houri<sup>3</sup>, Olivier Bou Matar<sup>3</sup>, Andrew Taylor<sup>1</sup> and Vincent Mortet<sup>1,2</sup>; <sup>1</sup>FZU - Institute of Physics of the Czech Academy of Sciences, Czechia; <sup>2</sup>Czech Technical University, Faculty of Biomedical Engineering, Czechia; <sup>3</sup>University Lille, CNRS, France

Phononic metamaterials (PnMs), analogue to photonic and plasmonic in optics, have attracted a great deal of attention in the last two decades. Based on phononic band-gap and local resonance mechanisms, these artificial materials enabled advanced control of elastic waves in solid condensed matter including wave-guiding, trapping, multiplexing, demultiplexing, etc. They offer the possibility to confine and focus an acoustic wave in an ultra-small region of sub-wavelength dimensions and to extend mechanical resonance lifetimes (high quality factor (Q)). For biosensing applications, Shear surface wave (Sh-SAW) and Antisymmetric Lamb waves are the most interesting, as they are compatible with liquid environments. Diamond is an attractive material for biosensing applications thanks to its chemical inertness, biocompatibility and prolonged stability of covalently attached biomolecules. Therefore, combining diamond PnMs and shear surface waveguides is of great interest to enhance the performance of biosensor.

In this work, we investigated the properties of Sh-SAW sensors with diamond pillar PnMs. Band structures and sensitivity were calculated with the finite element method (FEM, COMSOL Multiphysics). The sensitivity of studied structures was

investigated by adding 200 nm thick polymethyl methacrylate layer on top of the structure. The studied structure consists of 60  $\mu\text{m}$  high and 10  $\mu\text{m}$  wide block of 90ST-cut quartz substrate, which supports shear wave propagation. For comparison of sensitivity either a 2  $\mu\text{m}$  thick continuous  $\text{SiO}_2$  guiding layer or the diamond pillars with radius = 1  $\mu\text{m}$  and height = 1 or 2  $\mu\text{m}$  were introduced on top of the quartz substrate. For the diamond PnMs, the slowest shear wave mode is completely localized in the pillar for both heights. The sensitivity is significantly increased for diamond pillar phononic crystals (4.4 % for 2  $\mu\text{m}$  height pillar) in comparison with plain ST-cut quartz (0.9 %) and also ST-cut quartz + 2  $\mu\text{m}$   $\text{SiO}_2$  guiding layer (2.5 %). These results are very promising for the fabrication of highly sensitive LW-SAW sensor for biosensing applications.

This work has been supported by the Grant Agency of the Czech Republic (GACR) contract 19-09784Y, Czech Science Foundation (project 20-03187S) and by the Czech Technical University in Prague project SGS20/084/OHK4/1T/17.

#### **F.EL01.09.03**

**Spice Model Parameter Extraction for Diamond Schottky P-I-N Diodes** Mohammad Faizan Ahmad, Harshad Surdi, Vishal Jha, Franz A. Koeck, Robert J. Nemanich, Stephen M. Goodnick and Trevor Thornton; Arizona State University, United States

To develop practical applications for diamond-based electronics it will be important to have calibrated device models for use in circuit simulators such as LTSpice and Cadence. These Spice models consist of lumped-element components with values extracted by DC and RF measurements for bias conditions that represent typical operating conditions. Of particular importance for PN junction diodes are the on-resistance,  $R_{on}$ , and off-state capacitance,  $C_{off}$ . The product  $R_{on}C_{off}$  is a useful figure of merit that is minimized by careful optimization of the device design. While  $C_{off}$  is controlled largely by the thickness of the intrinsic region of the diode, there are several factors that contribute to the on-resistance, including the contact resistance present at the interfaces between the metal contacts and the doped semiconductor. To minimize the contact resistance, high doping concentration is required in the *n*- and *p*-type diamond regions. To further minimize on-resistance, smaller *i*-layer thickness is required. We have fabricated vertical diamond P-I-N diodes by plasma enhanced chemical vapor deposition of intrinsic and heavily phosphorus doped diamond films on boron doped diamond <111> substrates. Secondary ion mass spectroscopy (SIMS) confirms that the boron doping in the substrate exceeds  $10^{20} \text{ cm}^{-3}$ , the unintentional *p*-type doping in the *i*-layer is  $\sim 10^{16} \text{ cm}^{-3}$ , while the peak concentration at the surface of the *n*-layer is  $\sim 10^{19} \text{ cm}^{-3}$ . The thickness of the intrinsic layer was 300 nm and that of the heavily doped *n*-layer was 50 nm. Despite the heavy doping of the *n*-layer it is thin enough to be fully depleted by the metal contact resulting in a Schottky PIN diode.

The diodes were fabricated with ground-signal-ground (GSG) contacts on the top surface allowing for DC and RF probing. To electrically isolate the devices a partial mesa etch was performed using  $\text{O}_2/\text{SF}_6$  reactive ion-etching to define the diode area and top anode contact. A second RIE step etched through the *i*-layer to expose the p-type substrate on the top surface. Electron-beam evaporation of Ti/Ni/Au (50 nm/50 nm/300 nm) metals form the top cathode and anode contacts to the n and p-layer diamond respectively.

A combination of DC, and S-parameter measurements were used to extract the small-signal parameters for a diode Spice model. At a forward bias of 15 V the diode supports a current density in excess of 36  $\text{kA/cm}^2$ , with an on-resistance of  $9 \times 10^{-5} \text{ Ohm-cm}^2$ . The S-parameter measurements were converted to Z-parameters from which the diode off-capacitance was found to be 17.5 nF/cm<sup>2</sup>. The FOM is 1.6 ps corresponding to a frequency of 101 GHz. The full diode model provides excellent agreement with the measured current-voltage characteristics up to a forward bias of 15 V/3 A. It also reproduces the one-port s-parameter, S11, up to 25 GHz over all DC bias conditions.

This research is supported, in part, by NSF contract ECCS-1542160.

#### **F.EL01.09.04**

**Late News: Crystal Orientation Dependence of Local Electrical Characteristics on CVD-Grown Poly-Crystalline Diamond: Combined SPM and EBSD Study** Daichi Yoshii, Mami Fujii and Yukiharu Uraoka; Nara Institute of Science and Technology, Japan

Hydrogen-terminated surfaces of diamond are known to exhibit p-type conductivity, and power devices are being considered as an application that will take advantage of this property. Recently, poly-crystalline diamond devices have been attracting attention because it was reported that high breakdown voltage (>1 kV) MOSFETs can be fabricated<sup>[1]</sup> despite its lower cost compared to single-crystalline diamond. This property originates from non-doped hydrogen-terminated poly-crystalline diamond. However, the electrical characteristics variability depends on the crystal orientation. In this study, the correlation between the local electrical characteristics obtained by scanning probe microscopy (SPM) and the crystal orientation obtained



by electron backscattering diffraction (EBSD) was evaluated in order to clarify the electrical defect state of each crystal orientation.

Poly-crystalline diamond substrates (size: 3 mm × 3 mm, thickness: 0.33 mm) manufactured by Diamond Materials GmbH were used in this experiment. After cleaning the substrate in the order of aqua regia (80 °C, 5 min.), piranha solution (120 °C, 10 min.) and HNO<sub>3</sub> and H<sub>2</sub>SO<sub>4</sub> mixed acid (240 °C, 30 min.), the substrate was subjected to microwave plasma CVD with 199.5 sccm of CH<sub>4</sub> and 0.5 sccm of H<sub>2</sub> to grow diamond films. The hydrogen termination was processed by the same CVD equipment. Afterwards, the substrate surfaces were measured by current-AFM (c-AFM), and the same area was measured by EBSD. We used SPM-9600 (Shimadzu Corp.) for c-AFM measurement, using PtIr-coated conductive cantilever to measure surface morphology and c-AFM current images at bias of -0.05 V.

As a result of the measurements using c-AFM, it was confirmed that there were spots with different current flow patterns. These current spots were concentrated at the grain boundaries, and they were also confirmed in some parts of the grain. In addition, variation in the current spots density was confirmed. Next, we measured the same area as the c-AFM site with SEM/EBSD to investigate the correlation between the current spots in the grains and the crystal orientation. The surface morphology images and current images obtained from c-AFM measurements were compared with the inverse pole figure (IPF) map obtained from SEM/EBSD measurements. These results suggest that there is a correlation between the current spot density distribution and crystal orientation, ex, (111) oriented crystal shows lower current spots density, and (101) oriented crystal shows high current spots density. The results suggest that this is caused by the difference in the etching and/or growing condition of each crystal orientation. This study can reveal the suitable crystal orientation for electrical device fabrication that requires low electrical defect density.

[Reference]

[1] M. Syamsul et al., IEEE Electron Device Lett. 38, 5, 607-610 (2017)

[Acknowledgements]

This work is supported by JSPS KAKENHI JP18K13804 and the NAIST Special Fund

#### **F.EL01.09.05**

**Late News: Development of Nanodiamond-Based Multifunctional Biosensors** Yoobeen Lee; Hanyang University, Korea (the Republic of)

Nanodiamonds (NDs) have excited a lot of interest in the field of biomedical application as they can be used as spin probes for optical magnetic sensing and biological environments. Due to their optical and biological properties, NDs are expected to be employed as multitasking markers for the accurate visualization of biophysical parameters such as and magnetic fields and temperature. However, the engineered NDs to intracellular structures of interest within a complicated biological environment remains a challenge.

In this work, we investigated each property of the 4 types of nanodiamonds like SEM, PL spectra and then the NDs were transfected into human skin cells (WS1) using silicon nanopillar. For the development of nanodiamonds as multifunctional biosensor, researchers are still engaged in the in-depth study of NDs and their effect on life interfaces.

SESSION F.LP05.03: Live Poster Session: Electronics and Optics (F.EL01, F.EL02, F.EL03 and F.EL06)

Session Chairs: Stefaan De Wolf, Alex Martinson, Monica Morales-Masis, Philip Schulz and Feng Yan

Thursday Morning, December 3, 2020

11:30 AM - 1:30 PM

F.EL01

#### **F.EL01.09.01**

**Diamond and Silicon Carbide as Passivation Layers for Packageless SAW Sensors** Lucie Drbohlavová<sup>1,2</sup>, Abdelkrim Talbi<sup>3</sup>, Yuxin Liu<sup>3</sup>, Cecile Ghouila-Houri<sup>3</sup>, Olivier Bou Matar<sup>3</sup>, Andrew Taylor<sup>1</sup> and Vincent Mortet<sup>1,2</sup>; <sup>1</sup>FZU - Institute of Physics of the Czech Academy of Sciences, Czechia; <sup>2</sup>Czech Technical University, Faculty of Biomedical Engineering, Czechia; <sup>3</sup>University Lille, CNRS, France

Surface acoustic waves (SAWs) and bulk acoustic waves are two of MEMS technologies of industrial relevance and can be found in a myriad of devices. Acoustic RF filters, for instance, are integral parts of wireless communication systems. SAW devices have been adapted as sensors which can be configured to operate both passively and wirelessly. For example, SAWs

find applications in life sciences, in structural health monitoring, etc. In particular, SAW devices can also be operated in extremely confined environments such as implantable sensors to monitor or to provide real-time treatment. In this case, it would make sense to protect the sensor surface and leave only the functionalized area visible for detection. This is true for implantable sensors where space is a major constraint and therefore requires the development of an intrinsically protected design. Also, this is true for biosensors where the surface is continuously exposed to the analysed biofluid.

In this work, we propose the use of a shear surface wave guided between the semi-infinite substrate and high acoustic velocity thin film materials. The upper high acoustic velocity layer works as an acoustically isolating layer, protecting the guided surface shear wave from undesired mechanical damping and eliminate the need for packaging. With very high acoustic velocities, diamond and silicon carbide (SiC) are excellent candidates for packageless SAW sensors applications. In previous studies, we have already demonstrated the possibility of diamond coating of SAW devices using Microwave Plasma Enhanced Chemical Vapor Deposition with Linear Antennas (MW-LA-PECVD) at low temperature [1, 2].

Here we investigate, theoretically and experimentally, the use of diamond and SiC as a passivation layer for SAW devices. Theoretical calculations were carried out using COMSOL Multiphysics FEM simulation software. Two different piezoelectric materials were investigated, ST-cut quartz and 36°YX LiTaO<sub>3</sub> as well as two common guiding layer materials – zinc oxide (ZnO) and silicone oxide (SiO<sub>2</sub>). Theoretical calculations show, that 2 μm thick diamond or SiC layers are sufficient to confine the acoustic wave in the guiding layer at a wavelength close to 10 μm. From the displacement curve we could see, that for 36°YX LiTaO<sub>3</sub> substrates the acoustic wave is very well confined for both guiding layer materials. On the contrary, shear wave disperses within the ST-cut quartz bulk with the addition of a passivation layer.

Based on theoretical results, SAW devices were fabricated on 36°YX LiTaO<sub>3</sub> substrates with 10 nm/190 nm Ti/Au electrodes patterned by RF sputtering, photolithography and chemical wet etching techniques. The SiO<sub>2</sub> layer was deposited using low temperature plasma enhanced chemical vapor deposition with a resulting normalized thickness equal to  $h_{SiO_2}/\lambda = 0.2$ . Depositions of nano-crystalline diamond (NCD) and SiC layers were carried out by MW-LA-PECVD with resulting normalized thicknesses of  $h/\lambda = 0.2$ . All depositions were carried out at a temperature below 500 °C to preserve the piezoelectric properties of substrates.

Our results are promising for waveguide protection applications as well as opening other directions, such as the introduction of the local sensitive zone in the diamond layer, which can be interesting for bio or electrochemical sensing applications.

This work has been supported by the Grant Agency of the Czech Republic (GACR) contract 19-09784Y, Czech Science Foundation (project 20-03187S) and by the Czech Technical University in Prague project SGS20/084/OHK4/1T/17.

#### References:

- [1] TALBI, A., A. SOLTANI, A. RUMEAU, et al., *Physica status solidi (a)*, 2015, **212**(11), 2606-2610 DOI: 10.1002/pssa.201532188. ISSN 18626300.
- [2] DRBOHLAVOVÁ, L., L. FEKETE, V. BOVTUN, et al., *Sensors and Actuators A: Physical*, 2019, **298**, DOI: 10.1016/j.sna.2019.111584. ISSN 09244247.

#### F.EL01.09.02

**Enhancing the Sensitivity of SAW Sensors Using the Diamond Surface Phononic Metamaterials** Lucie Drbohlavová<sup>1,2</sup>, Yuxin Liu<sup>3</sup>, Abdelkrim Talbi<sup>3</sup>, Cecile Ghouila-Houri<sup>3</sup>, Olivier Bou Matar<sup>3</sup>, Andrew Taylor<sup>1</sup> and Vincent Mortet<sup>1,2</sup>; <sup>1</sup>FZU - Institute of Physics of the Czech Academy of Sciences, Czechia; <sup>2</sup>Czech Technical University, Faculty of Biomedical Engineering, Czechia; <sup>3</sup>University Lille, CNRS, France

Phononic metamaterials (PnMs), analogue to photonic and plasmonic in optics, have attracted a great deal of attention in the last two decades. Based on phononic band-gap and local resonance mechanisms, these artificial materials enabled advanced control of elastic waves in solid condensed matter including wave-guiding, trapping, multiplexing, demultiplexing, etc. They offer the possibility to confine and focus an acoustic wave in an ultra-small region of sub-wavelength dimensions and to extend mechanical resonance lifetimes (high quality factor (Q)). For biosensing applications, Shear surface wave (Sh-SAW) and Antisymmetric Lamb waves are the most interesting, as they are compatible with liquid environments. Diamond is an attractive material for biosensing applications thanks to its chemical inertness, biocompatibility and prolonged stability of covalently attached biomolecules. Therefore, combining diamond PnMs and shear surface waveguides is of great interest to enhance the performance of biosensor.

In this work, we investigated the properties of Sh-SAW sensors with diamond pillar PnMs. Band structures and sensitivity were calculated with the finite element method (FEM, COMSOL Multiphysics). The sensitivity of studied structures was investigated by adding 200 nm thick polymethyl methacrylate layer on top of the structure. The studied structure consists of 60  $\mu\text{m}$  high and 10  $\mu\text{m}$  wide block of 90ST-cut quartz substrate, which supports shear wave propagation. For comparison of sensitivity either a 2  $\mu\text{m}$  thick continuous  $\text{SiO}_2$  guiding layer or the diamond pillars with radius = 1  $\mu\text{m}$  and height = 1 or 2  $\mu\text{m}$  were introduced on top of the quartz substrate. For the diamond PnMs, the slowest shear wave mode is completely localized in the pillar for both heights. The sensitivity is significantly increased for diamond pillar phononic crystals (4.4 % for 2  $\mu\text{m}$  height pillar) in comparison with plain ST-cut quartz (0.9 %) and also ST-cut quartz + 2  $\mu\text{m}$   $\text{SiO}_2$  guiding layer (2.5 %). These results are very promising for the fabrication of highly sensitive LW-SAW sensor for biosensing applications.

This work has been supported by the Grant Agency of the Czech Republic (GACR) contract 19-09784Y, Czech Science Foundation (project 20-03187S) and by the Czech Technical University in Prague project SGS20/084/OHK4/1T/17.

#### F.EL01.09.03

**Spice Model Parameter Extraction for Diamond Schottky P-I-N Diodes** Mohammad Faizan Ahmad, Harshad Surdi, Vishal Jha, Franz A. Koeck, Robert J. Nemanich, Stephen M. Goodnick and Trevor Thornton; Arizona State University, United States

To develop practical applications for diamond-based electronics it will be important to have calibrated device models for use in circuit simulators such as LTSpice and Cadence. These Spice models consist of lumped-element components with values extracted by DC and RF measurements for bias conditions that represent typical operating conditions. Of particular importance for PN junction diodes are the on-resistance,  $R_{on}$ , and off-state capacitance,  $C_{off}$ . The product  $R_{on}C_{off}$  is a useful figure of merit that is minimized by careful optimization of the device design. While  $C_{off}$  is controlled largely by the thickness of the intrinsic region of the diode, there are several factors that contribute to the on-resistance, including the contact resistance present at the interfaces between the metal contacts and the doped semiconductor. To minimize the contact resistance, high doping concentration is required in the  $n$ - and  $p$ -type diamond regions. To further minimize on-resistance, smaller  $i$ -layer thickness is required. We have fabricated vertical diamond P-I-N diodes by plasma enhanced chemical vapor deposition of intrinsic and heavily phosphorus doped diamond films on boron doped diamond  $\langle 111 \rangle$  substrates. Secondary ion mass spectroscopy (SIMS) confirms that the boron doping in the substrate exceeds  $10^{20} \text{ cm}^{-3}$ , the unintentional  $p$ -type doping in the  $i$ -layer is  $\sim 10^{16} \text{ cm}^{-3}$ , while the peak concentration at the surface of the  $n$ -layer is  $\sim 10^{19} \text{ cm}^{-3}$ . The thickness of the intrinsic layer was 300 nm and that of the heavily doped  $n$ -layer was 50 nm. Despite the heavy doping of the  $n$ -layer it is thin enough to be fully depleted by the metal contact resulting in a Schottky PIN diode.

The diodes were fabricated with ground-signal-ground (GSG) contacts on the top surface allowing for DC and RF probing. To electrically isolate the devices a partial mesa etch was performed using  $\text{O}_2/\text{SF}_6$  reactive ion-etching to define the diode area and top anode contact. A second RIE step etched through the  $i$ -layer to expose the  $p$ -type substrate on the top surface. Electron-beam evaporation of Ti/Ni/Au (50 nm/50 nm/300 nm) metals form the top cathode and anode contacts to the  $n$  and  $p$ -layer diamond respectively.

A combination of DC, and S-parameter measurements were used to extract the small-signal parameters for a diode Spice model. At a forward bias of 15 V the diode supports a current density in excess of  $36 \text{ kA/cm}^2$ , with an on-resistance of  $9 \times 10^{-5} \text{ Ohm-cm}^2$ . The S-parameter measurements were converted to Z-parameters from which the diode off-capacitance was found to be  $17.5 \text{ nF/cm}^2$ . The FOM is 1.6 ps corresponding to a frequency of 101 GHz. The full diode model provides excellent agreement with the measured current-voltage characteristics up to a forward bias of 15 V/3 A. It also reproduces the one-port s-parameter, S11, up to 25 GHz over all DC bias conditions.

This research is supported, in part, by NSF contract ECCS-1542160.

#### F.EL01.09.04

**Late News: Crystal Orientation Dependence of Local Electrical Characteristics on CVD-Grown Poly-Crystalline Diamond: Combined SPM and EBSD Study** Daichi Yoshii, Mami Fujii and Yukiharu Uraoka; Nara Institute of Science and Technology, Japan

Hydrogen-terminated surfaces of diamond are known to exhibit  $p$ -type conductivity, and power devices are being considered as an application that will take advantage of this property. Recently, poly-crystalline diamond devices have been attracting attention because it was reported that high breakdown voltage ( $>1 \text{ kV}$ ) MOSFETs can be fabricated<sup>[1]</sup> despite its lower cost compared to single-crystalline diamond. This property originates from non-doped hydrogen-terminated poly-crystalline

diamond. However, the electrical characteristics variability depends on the crystal orientation. In this study, the correlation between the local electrical characteristics obtained by scanning probe microscopy (SPM) and the crystal orientation obtained by electron backscattering diffraction (EBSD) was evaluated in order to clarify the electrical defect state of each crystal orientation.

Poly-crystalline diamond substrates (size: 3 mm × 3 mm, thickness: 0.33 mm) manufactured by Diamond Materials GmbH were used in this experiment. After cleaning the substrate in the order of aqua regia (80 °C, 5 min.), piranha solution (120 °C, 10 min.) and HNO<sub>3</sub> and H<sub>2</sub>SO<sub>4</sub> mixed acid (240 °C, 30 min.), the substrate was subjected to microwave plasma CVD with 199.5 sccm of CH<sub>4</sub> and 0.5 sccm of H<sub>2</sub> to grow diamond films. The hydrogen termination was processed by the same CVD equipment. Afterwards, the substrate surfaces were measured by current-AFM (c-AFM), and the same area was measured by EBSD. We used SPM-9600 (Shimadzu Corp.) for c-AFM measurement, using PtIr-coated conductive cantilever to measure surface morphology and c-AFM current images at bias of -0.05 V.

As a result of the measurements using c-AFM, it was confirmed that there were spots with different current flow patterns. These current spots were concentrated at the grain boundaries, and they were also confirmed in some parts of the grain. In addition, variation in the current spots density was confirmed. Next, we measured the same area as the c-AFM site with SEM/EBSD to investigate the correlation between the current spots in the grains and the crystal orientation. The surface morphology images and current images obtained from c-AFM measurements were compared with the inverse pole figure (IPF) map obtained from SEM/EBSD measurements. These results suggest that there is a correlation between the current spot density distribution and crystal orientation, ex, (111) oriented crystal shows lower current spots density, and (101) oriented crystal shows high current spots density. The results suggest that this is caused by the difference in the etching and/or growing condition of each crystal orientation. This study can reveal the suitable crystal orientation for electrical device fabrication that requires low electrical defect density.

[Reference]

[1] M. Syamsul et al., IEEE Electron Device Lett. 38, 5, 607-610 (2017)

[Acknowledgements]

This work is supported by JSPS KAKENHI JP18K13804 and the NAIST Special Fund

#### **F.EL01.09.05**

**Late News: Development of Nanodiamond-Based Multifunctional Biosensors** Yoobeen Lee; Hanyang University, Korea (the Republic of)

Nanodiamonds (NDs) have excited a lot of interest in the field of biomedical application as they can be used as spin probes for optical magnetic sensing and biological environments. Due to their optical and biological properties, NDs are expected to be employed as multitasking markers for the accurate visualization of biophysical parameters such as and magnetic fields and temperature. However, the engineered NDs to intracellular structures of interest within a complicated biological environment remains a challenge.

In this work, we investigated each property of the 4 types of nanodiamonds like SEM, PL spectra and then the NDs were transfected into human skin cells (WS1) using silicon nanopillar. For the development of nanodiamonds as multifunctional biosensor, researchers are still engaged in the in-depth study of NDs and their effect on life interfaces.

#### **F.EL02.13.01**

**Triple-Wavelength Emission from Mn<sup>2+</sup>/Yb<sup>3+</sup> Codoped CsPbCl<sub>3</sub> Perovskite Nanocrystals and Luminescent Solar Concentrator Applications** Tong Cai, Junyu Wang and Ou Chen; Brown University, United States

Doping metal ions into lead halide perovskite nanocrystals (NCs) has attracted great attention over the past few years due to the emergence of novel properties relevant to optoelectronic applications. Current studies focus mostly on doping a single type of metal ions into the host perovskite NCs, while few research efforts have been made on simultaneous doping more than one type of metal ions into the same perovskite hosts and to study their synergic effects with intra-particle energy transfer processes. Here, a facile synthesis of Mn<sup>2+</sup>/Yb<sup>3+</sup> codoped CsPbCl<sub>3</sub> NCs through a hot-injection technique is firstly reported. Owing to the completely separated energy relaxation channels among the intrinsic bandgap (BG), Mn<sup>2+</sup> and Yb<sup>3+</sup> dopant emissions, the obtained Mn<sup>2+</sup>/Yb<sup>3+</sup> codoped CsPbCl<sub>3</sub> perovskite NCs exhibit a unique triple-wavelength emission profile simultaneously covering UV/blue (BG-PL), visible (Mn-PL) and NIR (Yb-PL) spectral regions. By optimizing the dopant concentrations, the total photoluminescence quantum yield (PL QY) of the codoped NCs can reach up to ~125.3% due to quantum cutting effects. Mechanism studies reveal different natures of emission mechanisms can be involved in a single batch of Mn<sup>2+</sup>/Yb<sup>3+</sup> codoped perovskite NCs: (i) electronic inter-band transition (BG-PL); (ii) electronic transition of ion centers within local molecular complexes (Mn-PL); and (iii) defect-induced energy transfer and subsequent

quantum cutting scheme (Yb-PL). Owing to the high PL QYs and minimal reabsorption loss, the codoped perovskite NCs are demonstrated to be used as efficient emitters in luminescent solar concentrators, with greatly enhanced external optical efficiency compared to that of using solely Mn<sup>2+</sup> doped CsPbCl<sub>3</sub> NCs. Therefore, co-doping both Mn<sup>2+</sup> and Yb<sup>3+</sup> ions into perovskite NCs can serve as a unique model system for studies of host-to-dopant and inter-dopant energy transfer mechanisms, as well as associated radiative and non-radiative decay pathways at each step. Most importantly, such codoped NCs with multiple emission channels hold a high potential to be applied in a wide range of applications, including multiplexed biological labelling and sensing, multi-channel photodetectors, stimuli-responsive inks for coding, encryption and decryption, and photon management devices in the future.

#### F.EL02.13.02

**Control of Excitonic Spin States via Magnetic Interactions with Transition-Metal Dopants in Ruddlesden-Popper Hybrid Perovskites** Jonathan Zerhoch, Timo Neumann, Martin S. Brandt, Jonathan Finley, Andreas Stier and Felix Deschler; Walter Schottky Institut and Physik-Department, Technische Universität München, Germany

Combining the advantageous electrical and optical properties of semiconductors with magnetic characteristics gives access to extraordinary phenomena and applications. Fully inorganic dilute magnetic semiconductors (DMS) have been known for decades, which show diverse functionalities like control of magnetism by electrical fields. The material class of DMS is obtained by introducing a substantial number of magnetic ions to an otherwise non-magnetic host semiconductor.

Due to their outstanding optoelectronic properties and high defect tolerance, organo-metal halide perovskites form an ideal system for efficient magnetic doping. We produced a selection of magnetic perovskites using simple solution processing techniques by doping of the host material, Ruddlesden-Popper hybrid perovskite ((PEA)<sub>2</sub>PbX<sub>4</sub> with X = Cl, Br, I), with different magnetic ions like Mn<sup>2+</sup>, Fe<sup>2+</sup>, Co<sup>2+</sup>, Ni<sup>2+</sup> and Eu<sup>2+</sup>. We investigated the influence of both halides and magnetic impurities on the long-range magnetic ordering of the materials with respect to the structural and optical properties. We investigate how localized excitons couple with the magnetic moments of the introduced impurities by detecting a dependence of the emitted lights polarization on the magnetization. We perform structural, magnetic, optical and magneto-optical temperature-dependent measurements to verify a successful magnetic doping of the perovskite and to show how photoluminescence and magnetization properties relate.

#### F.EL02.13.04

**Illuminating the Structural and Optical Changes Behind Photo-Induced Degradation in Mixed-Halide Perovskites** Gabriel C. Halford, Annie Gomez, Jill Mankoff and Rebecca Belisle; Wellesley College, United States

**While mixed-halide perovskites are ideal for use in tandem solar cells due to their tunable band gap, they are limited by reversible photo-induced degradation. While the impacts of photo-induced segregation on optical properties have been well documented, the underlying impacts on perovskite structure remain less clear. Structural changes that result in optical changes may come from halide migration and subsequent segregation in the perovskite. Utilizing grazing-incidence wide angle x-ray scattering (GIWAXS), we have observed in situ reversible structural changes that occur over time scales of 30 minutes to an hour in mixed-halide methylammonium perovskite thin films as a result of light soaking at approximately 1 sun intensity. Looking at a range of different compositions with varying ratios of bromine to iodine, we are able to observe the kinetics of photo-induced unmixing of mixed-halide perovskites and the formation of multiple distinct crystalline phases.. Data taken in the dark after illumination demonstrates the reversibility of this process, as the crystal structures relax back to approximately their original structure. Analyzing the x-ray diffraction data, we see multiple distinct phases we quantify as bromine-dominated and iodine-dominated crystal structures. Correlating our x-ray diffraction results with in situ photoluminescence, we are able to present a timeline of photo-induced halide segregation that captures changes in local structure with observed optoelectronic performance. Photoluminescence shifts occur during photo-induced halide segregation such that majority iodine films shift toward lower intensity, lower energy peaks and majority bromine films shift toward higher intensity, lower energy peaks. While optical changes appear to occur before structural changes are visible in the GIWAXS data, both optical and structural changes saturate at time scales approaching one hour. Looking forward we may be able to demonstrate whether this is a surface or a bulk phenomenon. Understanding the origins of the structural changes behind photo-induced degradation could help find strategies to mitigate the optical changes it causes to produce more stable mixed-halide perovskite solar cells. Overall, this work demonstrates more fully the correlation between structural and optical changes related to light-induced halide migration and gives the possibility of finding targeted solutions to minimizing degradation.**

### F.EL02.13.05

#### **High Affinity Polysalt Ligands Promote Long Term Stability While Enhancing the Quantum Yields of CsPbBr<sub>3</sub> Nanocrystals** Sisi Wang, Liang Du and Hedi M. Mattoussi; Florida State University, United States

Recently, cesium lead halide perovskite quantum dots (PQDs) have generated tremendous interests, due to the great promise they offer for use in optoelectronic applications. However, their poor colloidal stability, which can be traced to the ionic nature of the crystal cores and the high desorption rates of the native ligands, has impeded progress in fundamental research and slowed integration of such materials in devices. Developing novel surface ligands with strong coordination to both passivate surface traps and enhance fluorescence performance, while improving colloidal stability is urgently needed. Here, we detail the synthesis of a new family of multifunctional polymer ligands and their use for surface engineering of the CsPbBr<sub>3</sub> nanocrystals. The ligand synthesis relies on the ring opening reaction between distinct nucleophiles and poly(isobutylene-alt-maleic anhydride), PIMA. The modular ligand stoichiometrically displays multiple ammonium and/or imidazolium anchors for coordination onto PQD surfaces, along with several alkyl chains with different length to promote affinity to various organic solvents. The results show that the PQDs coated with those polysalts exhibit great colloidal stability and significantly enhanced photoluminescence. The coating also allows the resulting colloids to be dispersed a wide range of solvent conditions, including ethanol and methanol, while maintaining strong fluorescence and preserving the nanocrystal integrity after ligand substitution.

### F.EL02.13.06

#### **Polar Solvent Mediated Shape Control of CsPbBr<sub>3</sub> Perovskite Nanocrystals for Applications in LEDs** Arkajyoti Chakrabarty, Parvez Akhtar, Samridhi Satija, Upanshu Gangwar, Jitendra Kumar, Madhusudan Singh and Sameer Sapra; IIT Delhi, India

Nanocrystals (NCs) with different shapes, are of tremendous interest to material chemists, and precise control of their shapes and sizes through colloidal synthetic routes, with further solution-processability of the NCs, provides us with a great opportunity to tune their optoelectronic behaviour for advanced applications.<sup>1</sup> Interestingly, polar solvents are known to play crucial roles in determining the shapes of CsPbBr<sub>3</sub> perovskite NCs owing to the prevailing anisotropic growth conditions. However, to induce polar environment in the perovskite synthesis, a suitable precursor soluble in the desired polar solvent, is primarily required. In this work, we describe an efficient, MeOH-soluble steroidal Cs-precursor: cesium cholate and the different shapes of CsPbBr<sub>3</sub> NCs (nanorods, nanocubes and nanoplatelets) obtained from it, utilizing miniscule amount of polar solvents (methanol and methanol-water) in conjunction with commonly used 1-octadecene solvent and varying the reaction temperatures (90 °C and 180 °C). The resulting NCs exhibit very high photoluminescence (PL) quantum yields (94% for nanoplatelets and 96% for nanocubes), due to mitigation of Br vacancies by large cholate molecules, slowing down the complex nucleation and lattice construction processes in the synthetic pathway.<sup>2</sup> To study the application of these luminophores for application in perovskite light emitting diodes (PeLEDs), powdered CsPbBr<sub>3</sub> nanocubes were dispersed in toluene at different concentrations to prepare inks. Inks were spin-coated at different speeds (500, 1000 and 1500 rpm) and film quality was optimized to produce uniform and pinhole free films on an ITO substrate. Thin films produced at optimal deposition conditions and ink compositions were characterized using thin film photoluminescence measurements at 325 nm. A sharp and highly intense peak at 514 nm was observed. Initial device fabrication employing a spin-coated hole transport layer (poly (9-vinylcarbazole), and an electron transport layer (2,2',2''-(1,3,5-Benzinetriyl)-tris(1-phenyl-1-*H*-benzimidazole)) produced promising initial results. These initial results with perovskite nanocubes based thin films invite more studies of complete devices, possibly with other nanomaterial geometries (nanorods and nanoplatelets).

#### **References:**

- (1) Pan, A.; He, B.; Fan, X.; Liu, Z.; Urban, J. J.; Alivisatos, A. P.; He, L.; Liu, Y. Insight into the Ligand-Mediated Synthesis of Colloidal CsPbBr<sub>3</sub> Perovskite Nanocrystals: The Role of Organic Acid, Base, and Cesium Precursors. *ACS Nano* **2016**, *10*, 7943–7954.
- (2) Chakrabarty, A.; Satija, S.; Gangwar, U.; Sapra, S. Precursor-Mediated Synthesis of Shape-Controlled Colloidal CsPbBr<sub>3</sub> Perovskite Nanocrystals and Their Nanofiber-Directed Self-Assembly. *Chem. Mater.* **2020**, *32*, 721–733.

### F.EL02.13.07

#### **Chemically-Casted MoO<sub>3</sub> Hole Transport Active Layer for Perovskite Solar Cells** Taliya Gunawansa, Messaoud Bahoura and Sangram K. Pradhan; Norfolk State University, United States

Perovskite solar cells (PSCs) are promising contenders in the solar cell technology market having achieved photo-conversion efficiencies greater than 25%. The role of the hole transport layer in perovskite solar cells is essential for incredible

enhancement of their significant photo-conversion efficiency. Iron oxide is one of the interesting hole transport materials that can potentially improve the performance; however, the frequently used chemical synthesis technique of the micaceous iron oxide (MIO) precursors is very toxic, harmful and time-consuming. Molybdenum dioxide ( $\text{MoO}_3$ ) is a commonly studied hole transport layer utilized in perovskite solar cell; This study analyzes a chemically casted process preferably hot-casting technique to prepare a non-toxic molybdenum dioxide precursor that would fabricate a highly effective and densely packed  $\text{MoO}_3$  films. Various temperatures below  $100^\circ\text{C}$  results in intermittent deposition of the  $\text{MoO}_3$  films. When the hot-casting temperature is increased, the  $\text{MoO}_3$  thin film are uniformed and resulted in greater charge extraction and insignificant light soaking. Photoluminescence spectroscopy (PL), ultraviolet-visible spectroscopy (UV-VIS), and scanning electron microscopy (SEM) are the characterization techniques utilized to observe the opto-electronic properties of the  $\text{MoO}_3$  films. The capacitance, frequency dispersion, and leakage current measurements display stable performance of the  $\text{MoO}_3$  perovskite solar cells.

#### F.EL02.13.08

**Material Development And Emission Spectroscopy of Mn Doped  $\text{CsPbCl}_3$  Bulk Crystals and Nanoparticles for Light Source Applications** Uwe Hommerich<sup>1</sup>, Jihaad Barnett<sup>1</sup>, Kesete Ghebreyessus<sup>1</sup>, Al Amin Kabir<sup>1</sup>, Khalid Hampton<sup>1</sup>, Samuel Uba<sup>1</sup>, Ikemefuna Uba<sup>1</sup>, Demetris Geddis<sup>1</sup>, Clayton S. Yang<sup>2</sup>, Sudhir Trivedi<sup>2</sup>, Seth Fraden<sup>3</sup> and S. Ali Aghvami<sup>3</sup>; <sup>1</sup>Hampton University, United States; <sup>2</sup>Brimrose Technology Corporation, United States; <sup>3</sup>Brandeis University, United States

Manganese doped inorganic halide perovskites continue to be of current interest for applications in light emitting devices and down-converters in solar cells. In this work we prepared Mn doped  $\text{CsPbCl}_3$  (Mn: CPC) bulk crystals and nano-particles (NPs) and compared their emission properties. Bulk crystals were grown from the melt by vertical Bridgman technique and NPs were synthesized using a microwave assisted method. Under ultra-violet excitation at 350 nm, bulk crystal and NPs of Mn: CPC exhibited a broad orange emission centered at  $\sim 605$  nm at room temperature. The broadband emission was assigned to the intra-3d transition  ${}^4T_1 \rightarrow {}^6A_1$  of  $\text{Mn}^{2+}$  ions incorporated in the CPC host lattice. The  $\text{Mn}^{2+}$  emission lifetimes were nearly exponential with values of 1.07 ms for NPs and 0.73 ms for the bulk crystal. Mn: CPC NPs also showed exciton emission peaking at  $\sim 402$  nm, whereas the bulk crystal exhibited no significant emission near the band edge. Instead, the bulk material of Mn: CPC revealed a weak below-gap emission in the 450-550 nm region suggesting the existence of defect states. The excitation spectra for the orange  $\text{Mn}^{2+}$  emission from Mn: CPC NPs and bulk crystals were significantly different indicating distinct excitation pathways. The excitation spectrum of the orange  $\text{Mn}^{2+}$  emission for Mn: CPC NPs showed excitonic structure similar to the absorption spectrum suggesting energy transfer from excitons to  $\text{Mn}^{2+}$  ions. In contrast, UV excitation was less efficient for the bulk Mn: CPC crystal and the excitation was dominated by well defined below-gap excitation bands centered at  $\sim 425$  and  $\sim 530$  nm. More details of the material preparation emission spectroscopy, and initial hybrid LED experiments will be discussed at the conference.

#### F.EL02.13.09

**Red Light Emitting Ytterbium Activated  $\text{Sr}_3\text{Al}_2\text{O}_6$  Nanophosphor for LED Applications** Chitra Mallela; Tumkur University, India

Present study analyses the salient features of the newly synthesized phosphor powders of 1, 3, 5, 7, 9 and 11 molar concentrations of Ytterbium activated Strontium Aluminate by solution Combustion method using Urea. The prepared phosphors were calcined at  $950^\circ\text{C}$  for 4 hours. The Powder X-ray diffraction (PXRD) profiles of nanophosphors showed crystalline face centered cubic phase. The average crystallite sizes of the phosphors were in the range 34 to 48 nm. The samples showed pores and voids on their surface that formed by the escaping gases during the combustion method. The morphology showed the inherent nature of combustion process. The Scanning electron microscope (SEM) images showed non-uniform and irregular shapes of the particles. The Particle sizes were further confirmed by Transmission electron microscope (TEM). Energy dispersive analysis of X-ray techniques were used to study the structural characteristics of calcined phosphors. Fourier infrared spectral studies were carried out to evaluate the stretching and vibrational bonds in the product. They showed an absorption peak at  $1456\text{ cm}^{-1}$  that indicates the formation of crystallized Strontium Aluminate and a sharp peak at  $3670\text{ cm}^{-1}$  due to the presence of  $\text{AlO}_4$  group in the powders. Energy dispersive X-ray analysis (EDAX) with SEM image, revealed the uniform distribution of  $\text{Yb}^{3+}$  ions. The energy band gaps of the prepared phosphors from Kubelka-Munk plots of the Diffused reflectance Studies (DRS) were found to be in the range 5.31 eV to 5.78 eV. The Photoluminescence studies showed an emission peak at 708 nm when phosphors were excited with 355 nm. All the phosphors were found to emit red light as their Commission Internationale de L'Eclairage (CIE) co-ordinates have fallen in red region of chromaticity diagram. The average correlated color temperature of the phosphors was found to be  $3950^\circ\text{K}$ .

#### F.EL02.13.11

**Support for the Self-Trapped-Exciton Hypothesis in Multi-Layered ( $n > 1$ ) Two-Dimensional Lead Iodide Perovskites** Watcharaphol Paritmongkol, Eric Powers, Nabeel Dahod and William Tisdale; Massachusetts Institute of Technology, United States

Two-dimensional (2D) lead halide perovskites have been shown to exhibit broadband or white-light emission under certain conditions. Broadband emission in lead iodide 2D perovskites has been alternately attributed to self-trapped excitons (STEs) or permanent structural defects and/or impurities. Here, we investigate the photophysical characteristics of broadband emission in six different multi-layered ( $n > 1$ ) 2D lead iodide perovskites as a function of sample temperature from 5 K to 300 K. We distinguish shallow defect-associated emission from a broad near-infrared (NIR) spectral feature, which we assign to the STE. Sub-gap photoexcitation experiments and NIR transient absorption spectroscopy rule out permanent structural defects as the origin of this feature. When we varied the thickness ( $n = 2, 3, 4$ ), A-site cation (methylammonium vs. formamidinium), and organic cation spacer (butylammonium vs. hexylammonium vs. phenylethylammonium), we found that the temperature dependence of broad NIR emission was strongly correlated with both the strength of electron-phonon coupling and the extent of structural deformation of the ground state lattice, strongly supporting the assignment of this spectral feature to a STE.

#### F.EL02.13.12

**Thermal Impact on InAs Quantum Dots Covered by Different Capping Layers in GaAs/AlGaAs Structures** Georgiy Polupan<sup>1</sup>, Ricardo Cisneros Tamayo<sup>2</sup>, Tetyana V. Torchynska<sup>1</sup>, Ingrid. J. Guerrero Moreno<sup>1</sup> and Arturo Escobosa Echavarría<sup>3</sup>; <sup>1</sup>Instituto Politecnico Nacional, Mexico; <sup>2</sup>Universidad Politécnica del Valle de México,, Mexico; <sup>3</sup>CINVESTAV-IPN, Mexico

InAs quantum dots (QDs) embedded in MBE grown GaAs/Al<sub>0.30</sub>Ga<sub>0.70</sub>As/AlGaInAs heterostructures have been investigated in as grown state and after thermal annealing at 640°C or 710°C for two hours. Two types of QD structures with the different compositions of AlGaInAs capping layers (GaAs (#1) or Al<sub>0.10</sub>Ga<sub>0.75</sub>In<sub>0.15</sub>As (#2)) and the same composition of buffer layers (In<sub>0.15</sub>Ga<sub>0.85</sub>As) are compared and studied by means of photoluminescence (PL), X-ray diffraction (XRD) and high resolution HR-XRD methods. XRD and HR-XRD techniques are applied with the aim to control the crystal structures, the material compositions and elastic strains in quantum well (QW) layers.

The highest PL intensity, smaller PL band half width and lower energy of ground state (GS) emission are detected in the structure with the Al<sub>0.10</sub>Ga<sub>0.75</sub>In<sub>0.15</sub>As capping layer. Thermal annealing leads to the shift of PL spectra into higher energy range and the value of this shift is more essential in the structure with the Al<sub>0.10</sub>Ga<sub>0.75</sub>In<sub>0.15</sub>As capping layer as well.

The variation of GS emission peak versus temperature has been monitored within the range of 10-450K for as grown and annealed states and it compared with temperature shrinkage of band gap in the InAs and GaAs bulk crystals. It permits to reveal the QD composition that in #2 was closer to InAs than in #1. Finally, the reasons of PL spectrum transformation at annealing, the mechanism of PL thermal decay, and the advantages of the QD structure with strain reduced Al<sub>0.10</sub>Ga<sub>0.75</sub>In<sub>0.15</sub>As capping layer have been analyzed and discussed. The composition variation of QDs and QWs at annealing has been modeled using the simulation of HR-XRD results with Xpert Expitaxy software.

#### F.EL02.13.14

**Superparamagnetic Properties of Metal-Free Nitrogen Doped Graphene Quantum Dots Synthesized by Pulsed Laser Ablation** Muhammad Shehzad Sultan<sup>1</sup>, Vladimir I. Makarov<sup>1</sup>, Muhammad Sajjad<sup>2</sup>, Wojciech Jadwisieniczak<sup>3</sup>, Brad R. Weiner<sup>1</sup> and Gerardo Morell<sup>1</sup>; <sup>1</sup>University of Puerto Rico - Río Piedras, United States; <sup>2</sup>Indiana University Northwest, United States; <sup>3</sup>Ohio University, United States

In this study, we developed a novel approach to synthesize high-quality metal-free Nitrogen-doped graphene quantum dots (N-GQDs) with high quantum yield, via irradiation of s-triazene in a solution with benzene by using pulsed laser. The TEM, HRTEM, XPS, XRD, Raman spectroscopy and FTIR were carried out to observe the morphology, size distribution, crystalline structure and to prove successful doping of GQDs with nitrogen atoms. Furthermore, for the first time, to our knowledge, their magnetic properties were investigated. The results indicate that N-GQDs exhibit superparamagnetic behavior. The specific size, shape and zigzag edge structure of N-GQDs were considered to explain the origin of the observed magnetism. The magnetization dependence led to estimating the N-GQD material magnetic permeability for different ambient temperatures. From the zero-field-cooled (ZFC) and field-cooled (FC) magnetization measurements, carried out at 50 Oe magnetic field strength, we estimated the blocking temperature  $T_B$  to be around 300 K. Based on the experimental data analysis, the magnetic permeability, number of correlated spins per single N-GQD, and number density of superparamagnetic N-GQD per gram of material were estimated. The excellent superparamagnetic properties together with optical properties



manifested by N-QDs have the potential to lead to high performance biomedical applications.

#### F.EL02.13.15

**Highly Stable Luminescent Encapsulation Material Using Quantum Dot/Siloxane Hybrid for Reliable and Wide Color Gamut Light-Emitting Diode** Junho Jang, Da-Eun Yoon, Doh C. Lee and Byeong-Soo Bae; Korea Advanced Institute of Science and Technology, Korea (the Republic of)

Semiconducting nanocrystals, also known as quantum dots (QDs), are a promising color converting materials for next-generation display application due to their unique photophysical properties such as size-dependent color tunability, narrow spectral bandwidth, and high photoluminescence (PL) quantum yield (QY). However, the vulnerability of QDs to oxygen and moisture is a huge obstacle to practical applications. The commercialized QD for display has been a form of color converting QD films in liquid crystal display (LCD) backlight unit (BLU) using blue light-emitting diode (LED) (*i.e.*, On-Surface type), where QDs were physically blended in polymer matrixes sandwiched between two barrier layers. It is more desirable for LCD BLU using LEDs encapsulated the QDs directly into the packaging (*i.e.*, On-Chip type) in terms of performance, amount of QDs, and cost. Nevertheless, LEDs that are directly encapsulated by QDs have not been used in display applications due to their fatal instability. Therefore, reliable LEDs using highly stable luminescent encapsulation material that contains uniformly dispersed QDs in optical resin should be developed without additional protecting layers (such as SiO<sub>2</sub> or Al<sub>2</sub>O<sub>3</sub>) and ligand-exchange processes.

Herein, we developed luminescent LED encapsulation material (TSE-QD) using CdSe/CdZnS core/shell QDs (passivated by oleic acid) dispersed in a thermally resistant sol-gel derived siloxane matrix with high refractive index (> 1.57) [1,2]. The TSE-QD was fabricated via hydrosilylation of QD dispersed siloxane resin that was synthesized via *in situ* sol-gel reactions of silane precursors in the presence of QDs. The QDs were uniformly distributed in a linear-structured siloxane matrix in which functional groups of siloxane matrix is chemically cross-linked with ligands of the surface on QDs, and retained their initial optical properties during the fabrication processes [3]. Notably, we achieved dramatically enhanced thermal (at 120 °C in ambient air) and chemical stability (in acid or base solutions and alcohol) without additional barrier films and ligand-exchange process. We demonstrated a natural-white emitting LED using a blue LED chip directly encapsulated (*i.e.*, On-Chip type) by yellow-emitting TSE-QD that consist of red and green QDs in a siloxane matrix. Fabricated white LED exhibited wide color gamut (116% of NTSC 1931), excellent reliability (under 85 °C & 85% relative humidity), and high photostability (under continuous blue light irradiation).

[1] H. Y. Kim et al., *J. Am. Chem. Soc.*, **138**, 16478-16485 (2016).

[2] J.-Y. Bae et al., *RSC Adv.*, **3**, 8871-8877 (2013).

[3] J. Jang et al., *Nanoscale*, **11**, 2828-2834 (2019).

#### F.EL02.13.16

**Cs<sub>4</sub>Cd<sub>1-x</sub>Mn<sub>x</sub>Bi<sub>2</sub>Cl<sub>12</sub>—A Vacancy Ordered Halide Perovskite Phosphor with High Efficiency Orange-Red Emission** Noah P. Holzapfel<sup>1</sup>, Jackson Majher<sup>1</sup>, T. Amanda Strom<sup>2</sup>, Curtis Moore<sup>1</sup> and Patrick Woodward<sup>1</sup>; <sup>1</sup>The Ohio State University, United States; <sup>2</sup>University of California Santa Barbara, United States

The structural, optical, and magnetic properties of the vacancy-ordered quadruple perovskites Cs<sub>4</sub>CdBi<sub>2</sub>Cl<sub>12</sub> and Cs<sub>4</sub>MnBi<sub>2</sub>Cl<sub>12</sub> and their solid solution have been investigated. Both compounds are found to crystallize with *R-3m* space group symmetry that arises from ordering of Bi<sup>3+</sup>, Mn<sup>2+</sup>/Cd<sup>2+</sup>, and cation vacancies into layers that run perpendicular to the <111> direction of the cubic perovskite structure. Magnetic measurements reveal that Cs<sub>4</sub>MnBi<sub>2</sub>Cl<sub>12</sub> is paramagnetic down to 2 K with a Weiss constant of -2.88(3) K and an effective moment of 5.840(1) μ<sub>B</sub>. This compound exhibits weak orange-red luminescence, which involves Bi<sup>3+</sup> ions absorbing near UV photons followed by energy transfer to Mn<sup>2+</sup> ions and finally radiative decay that is attributed to a spin-forbidden <sup>4</sup>T<sub>1</sub>(G) to <sup>6</sup>A<sub>1</sub>(S) d-d transition. The emission peak is centered near 605 nm and has a full-width-half-maximum of ~90 nm and a photoluminescent quantum yield (PLQY) of ~4%. The isostructural Cs<sub>4</sub>CdBi<sub>2</sub>Cl<sub>12</sub> is neither magnetic nor does it show detectable photoluminescence at room temperature. Replacing Mn<sup>2+</sup> with Cd<sup>2+</sup> to form Cs<sub>4</sub>Cd<sub>1-x</sub>Mn<sub>x</sub>Bi<sub>2</sub>Cl<sub>12</sub> leads to a zero-dimensional electronic structure that inhibits energy migration to defect sites where non-radiative decay can occur, increasing the room temperature PLQY to 57% in the x = 0.27 sample. Cs<sub>4</sub>Cd<sub>1-x</sub>Mn<sub>x</sub>Bi<sub>2</sub>Cl<sub>12</sub> phosphors are easily synthesized from solution, free of rare-earth ions, and possess emission spectra that compare favorably to narrow-band red emitting phosphors based on Eu<sup>2+</sup> ions.

#### F.EL02.13.17

**Fluorene-Based Organic Phosphorescent Materials for LECs** C KY, Maxime Remond, Donghwan Kim and Eunyoung Kim; Yonsei University, Korea (the Republic of)

Fluorene-based organic phosphorescent materials (OPMs) were explored for organic light-emitting electrochemical cells

(LECs) taking advantages of their tunability in color and film processibility. TO tackle the problem of the apparent low emission efficiency of OPMS, compared to inorganic or organometallic materials, fluorene unit was designed as a  $\pi$ -bridge between halogen and n- $\pi$  transition groups. These OPMs provided a long-lived phosphorences at film state, possibly due to enhanced intersystem crossing (ISC) to the triplet state in the optimized structure. Thus OPMs were applied to light-emitting cells (LECs) along with a host and electrolyte, to show the highest luminescence among the organic phosphorescent LECs up to date. Synthesis of OPMs, mechanism of enhanced emission, and fabrication details on LECs will be presented.

#### F.EL02.13.18

**Synthesis of Efficient Blue Emitting CsPb(Br/Cl)<sub>3</sub> Nanoparticles via Post-Treatment with Short Organic Ligands and LED Fabrication** Jang Kyung Yeon, Jinwoo Park and Tae-Woo Lee; Seoul National University, Korea (the Republic of)

Perovskite nanoparticles (PeNPs) are promising emitters owing to their high color purity, low-cost synthesis, and facile wavelength control with halide composition control. However, chloride-based blue-emitting colloidal PeNPs have suffered from low photoluminescence quantum efficiency (PLQE) due to chloride-induced defect states. Their low PLQE hinders their use of blue-emitting devices.

In this work, we propose a method to improve the efficiency of blue PeNPs. At first, blue-emitting perovskite was synthesized by the hot injection method. Near Unity PLQE of as-synthesized PeNPs was obtained. For the efficient perovskite light-emitting diodes (PeLEDs), additional washing steps are required to remove excess ligands on the surface. But after washing steps, the PLQE rapidly decreased to ~50% because of surface defects.

A simple post-treatment process using short organic ligands solution was done after washing steps. PLQE increased again because the halide anions passivate defect sites. Moreover, those short organic ligands do not impede charge injection. By these methods, highly efficient blue-emitting PeNPs with PLQE > 92 % and high device efficiency of 2% was obtained.

#### F.EL02.13.19

**Water Passivation of Perovskite Nanocrystals Enables Air-Stable Intrinsically-Stretchable Color-Conversion Layers for Stretchable Displays** HuanYu Zhou<sup>1</sup>, Jinwoo Park<sup>1</sup>, Yeongjun Lee<sup>1</sup>, Jae-Man Park<sup>1</sup>, Jin-Hoon Kim<sup>2</sup>, Joo Sung Kim<sup>1</sup>, Hyeon-Dong Lee<sup>1</sup>, Seung Hyeon Jo<sup>1</sup>, Xue Cai<sup>1</sup>, Lizhu Li<sup>3</sup>, Xing Sheng<sup>3</sup>, Hyung Joong Yun<sup>4</sup>, Jin-Woo Park<sup>2</sup>, Jeong-Yun Sun<sup>1</sup> and Tae-Woo Lee<sup>1</sup>; <sup>1</sup>Seoul National University, Korea (the Republic of); <sup>2</sup>Yonsei University, Korea (the Republic of); <sup>3</sup>Tsinghua University, China; <sup>4</sup>Korea Basic Science Institute, Korea (the Republic of)

Despite organic light-emitting diode (OLED) technology has already left an indelible mark on the display industry, conventional OLEDs are still susceptible to degradation when exposed to air. A greater hurdle is to achieve the stretchable OLED as protecting devices from the penetration of moisture and oxygen is even more difficult under stretching. Here, we propose an air-stable intrinsically stretchable display without using any encapsulations by integrating a stretchable light-emitting device (SLED) with a stretchable color conversion layer that contains perovskites nanocrystals (PeNCs). PeNCs normally decay when exposed to air; counterintuitively, the moisture-assisted surface passivation of PeNCs is first observed. This work is believed to stimulate considerable research on fundamental aspects of PeNCs and furthermore into the practical applications both in academia and industries. The above-mentioned SLED can also open new ways toward intrinsically stretchable OLEDs.

#### F.EL02.13.20

**In Situ Fabrication of Highly Luminescent Halide Perovskite Thin Films Incorporating Organic Dispersing Agent** Eojin Yoon and Tae-Woo Lee; Seoul National University, Korea (the Republic of)

Recently, lead halide perovskite nanoparticles became promising candidates for light emitters due to narrow full-width at half maximum (FWHM), solution processability, easily tunable bandgap.<sup>1</sup> Excitons are well confined with the aids of long passivating ligands promoting radiative recombination, thus, lead halide perovskite nanoparticles exhibit high photoluminescence quantum yield (PLQY).<sup>2</sup> However, the synthesis of perovskite nanoparticles is complicated requiring several centrifugations and production yield is low because only the small amount of precipitate is utilized by reprecipitation method.

So, we took *in-situ* strategy for synthesizing perovskite nanoparticles by incorporating bulky ligand, phenyl ethyl ammonium bromide (PEABr).<sup>3</sup> To achieve stable in situ fabricated perovskite nanoparticles, dispersion of PEABr is essential because PEABr aggregates form local quasi-2D structure.<sup>4</sup> Here, we successfully synthesized perovskite nanoparticles by exploiting crown additive of 1,4,7,10,13,16-Hexaoxacyclooctadecane (18-crown-6) as a dispersing agent. From UV-vis spectroscopy, it was confirmed that low n phases (~440 nm) considerably decreased with 18-crown-6 and the average lifetime also enhanced due to reduced defect sites. Moreover, temperature-dependent PL represented increased exciton binding energy from 24.6 to

63.9 (meV) owing to the fine dispersion of PEABr and dielectric confinement effect. Finally, with optimized concentration, highly bright perovskite films with maximum PLQY of 93.036 % could be achieved, which is 47 times higher than pristine films.

## References

1. Kim Y-H, Cho H, Lee T-W. Metal halide perovskite light emitters. *Proc Natl Acad Sci*. 2016;113(42):11694-11702.
2. Kim YH, Cho H, Heo JH, et al. Multicolored organic/inorganic hybrid perovskite light-emitting diodes. *Adv Mater*. 2015;27(7):1248-1254. doi:10.1002/adma.201403751
3. Zhao L, Yeh YW, Tran NL, et al. In Situ Preparation of Metal Halide Perovskite Nanocrystal Thin Films for Improved Light-Emitting Devices. *ACS Nano*. 2017;11(4):3957-3964. doi:10.1021/acsnano.7b00404
4. Ban M, Zou Y, Rivett JPH, et al. Solution-processed perovskite light emitting diodes with efficiency exceeding 15% through additive-controlled nanostructure tailoring. *Nat Commun*. 2018;9(1):1-10. doi:10.1038/s41467-018-06425-5

### F.EL02.13.21

**Core-Shell Structure Perovskite Nanoparticles with Atomic Surface Passivation for Highly-Efficient Pure-Red Emitting Perovskite Light-Emitting Diodes** Jinwoo Park, Sinil Choi, Sungjin Kim, Joo Sung Kim and Tae-Woo Lee; Seoul National University, Korea (the Republic of)

Perovskite nanoparticles (PeNPs) is attractive next-generation sources for light-emitting diodes (LEDs) due to their efficient luminescent, solution processability, tunable bandgap and extremely high color purity which is superior to conventional light emitters (e.g. organic emitters, traditional quantum dots). However, due to halide segregation, emission wavelength shift while LED operation and precise control of emission wavelength is limited. Here, we develop facile atomic surface defect passivation method exploited post-synthesis treatment using high bandgap perovskite precursor. With this strategy, we synthesized color-stable and pure-red-emitting CsPbI<sub>3</sub> PeNPs with 630 nm of peak emission wavelength with core-shell structure. Highly efficient PeNP LEDs without electroluminescence wavelength shift was also demonstrated.

### F.EL02.13.22

**Late News: Maximizing the Photoluminescence Intensity in Quasi 2D Perovskites Through Surface Passivation of Defect States** - Yukta and Soumitra Satapathi; Indian Institute of Technology Roorkee, India

Quasi two-dimensional (2D) perovskites are currently considered as materials of choice for light emitting diodes (LEDs) due to their unique optoelectronic properties such as strong exciton binding energy, multiple quantum well structure, and reasonable ambient stability for practical applications. Tremendous progress has been achieved in 2D perovskites LEDs in terms of external quantum efficiency (EQE) (~17%), luminescence (6785 cd/m<sup>2</sup>) and stability through compositional and device engineering. However, the excessive surface defect states generated due to the reduced crystal size, the presence of un-coordinated Pb<sup>+2</sup> ions or shallow vacancy defects generated by MA or halide ions at the surface and grain boundaries, limits the radiative recombination and in turn the electro-luminescence (EL) efficiency of the LEDs. It has been realized that surface passivation with suitable organic/inorganic moieties can play a vital role in overcoming the adverse effect of defect states through their interaction with uncoordinated ions and can improve the stability.

In the present work, we have chosen n=4 composition quasi-2D perovskite (BA)<sub>2</sub>(MA)<sub>3</sub>Pb<sub>4</sub>Br<sub>13</sub> films as emissive layer by optimal phase engineering and have shown the order of magnitude enhancement of radiative emission after passivating them with two different molecules namely- triphenyl phosphine oxide (TPPO) and an insulating polymer polymethyl methacrylate (PMMA). Both the steady state and time resolved study confirm up to 400% enhancement in fluorescence intensity and improved average lifetime (=19.4 ns) after surface passivation. Additionally, the effect of passivating agents on film morphology and radiative emission efficiency is studied in details. Also, the interaction mechanism between layered perovskite and passivating agents has been probed with FTIR spectroscopy, XPS and KPFM study. Our systematic investigation with detailed mechanistic study will pave the way for further development of the highly efficient LEDs.

*References:-*

- Yang, Xiaolei *et.al Nat. Commun.* **2018**, 9 (1), 2–9.  
Bi, Wentao *et.al ACS Appl. Mater. Interfaces* **2020**, 12 (1), 1721–1727.  
Na Quan, L *et.al Nat. Commun.* **2020**, 11 (1), 1–9.

### F.EL02.13.23

**Late News: Quantum Confinement in Type I Heterostructure of Hybrid Lead Halide Perovskite Embedded in Organic Matrix** Amrita Dey<sup>1,2</sup>, Shivam Singh<sup>2</sup> and Dinesh Kabra<sup>2</sup>; <sup>1</sup>Ludwig-Maximilians-Universität, Germany; <sup>2</sup>Indian Institute of Technology Bombay, India

The type I heterostructure forms between Organic semiconductor molecule (4,4'-bis[9-dicarbazolyl]-2,2'-biphenyl [CBP] and bathocuproine [BCP]) and methylammonium lead halide (MAPbX<sub>3</sub>), assists easy growth of perovskite nanocrystals (PNCs) in an organic matrix. Herein, we present the modulation of electronic states of MAPbX<sub>3</sub> PNCs (MA = CH<sub>3</sub>NH<sub>3</sub><sup>+</sup> and X= Br<sup>-</sup> and I<sup>-</sup>) as a function of crystallite size. This results in the growth of MAPbX<sub>3</sub> PNCs of tunable sizes from ~110 nm to ~10 nm in the organic semiconductor matrix. A blue shift is observed in the photoluminescence peak (PL<sub>max</sub>) energy over a range of ~200 meV for MAPbI<sub>3</sub> PNCs embedded in the BCP matrix. However, PL<sub>max</sub> energy tunes over ~32 meV only with a similar volumetric concentration in the case of MAPbBr<sub>3</sub> PNCs in the same BCP matrix. Moreover, the PL blue shift is even lower in the case of the CBP matrix in comparison with the BCP matrix for both the perovskites. This discrepancy could be resolved by determining the resultant crystallite size using X-ray diffraction studies and the Debye–Scherrer formula. Results about the blue shift in the PL peak can be explained using the classic particle-in-a-box versus excitonic Bohr radius model under a weak confinement regime.

## References

1. S. Singh, A. Dey, S. Kolay and D. Kabra, Modulation of electronic states of Hybrid lead perovskites embedded in organic Matrix. *Energy Technol.* **2019**, 1900894.
2. D. Di, K. P. Musselman, G. Li, A. Sadhanala, Y. Ievskaya, Q. Song, Z.-K. Tan, M. L. Lai, J. L. MacManus-Driscoll, N. C. Greenham, R. H. Friend, Size-dependent photon emission from organometal halide perovskite nanocrystals embedded in organic matrix. *J. Phys. Chem. Lett.* **2015**, 6, 446.

### F.EL03.09.01

**Two-Dimensional Layered Germanium Monochalcogenides as Anode in Metal-Ion Batteries** Shakir Bin Mujib, Maren Ellis, Sophie Justus, Porter Herold and Gurpreet Singh; Kansas State University, United States

In this work, we investigate two-dimensional (2D) sheets of germanium sulfide (GeS) and germanium telluride (GeTe) as promising high-capacity and stable materials for energy storage. GeS and GeTe with layered structures are prepared via a simple liquid-phase exfoliation approach. As-synthesized 2D nanosheets can effectively increase the electrolyte-electrode interface area and facilitate metal ion transport. As a result, GeS and GeTe nanosheets deliver a high areal capacity of 1.76 mAh cm<sup>-2</sup> and 1.05 mAh cm<sup>-2</sup>, respectively as anodes in lithium-ion batteries (LIBs). Further analysis of GeS and GeTe in sodium-ion batteries (SIBs) and potassium-ion batteries (KIBs) suggest that layered germanium monochalcogenides can be potential anodes in other metal-ion batteries.

### F.EL03.09.02

**Two-Dimensional Nanosheet Inks Using Zwitterion Dispersants for Biocompatible and Scalable Inkjet Printing** Hyeokjung Lee, Seung Won Lee, Chanhoo Park, Kyuho Lee and Cheolmin Park; Yonsei University, Korea (the Republic of)

Inkjet printing of two-dimensional (2D) transition metal dichalcogenide (TMD) nanosheets fabricated by liquid-phase exfoliation (LPE) allows simple, low-cost, and mass-producible photo-electronic devices. Many LPE processes involving toxic and environmentally hazardous solvents; however, dispersants have restricted the extent of applications of 2D-TMD inks. Herein, various 2D-TMD nanosheets, including MoS<sub>2</sub>, MoSe<sub>2</sub>, WS<sub>2</sub>, and WSe<sub>2</sub>, in addition to few-layered graphene, are inkjet-printed using a LPE process based on zwitterionic dispersants in water. Zwitterions with cationic and anionic species are water-soluble, while alkyl chain moieties associated with two ionic species adhere universally on the surface of TMD nanosheets, resulting in high throughput liquid exfoliation of the nanosheets. The zwitterion-assisted TMD nanosheets in water are successfully employed as an ink without the need for additives to adjust the viscosity and surface tension of the ink for use in an office inkjet printer; this gives rise to A4 scale, large-area inkjet-printed images on diverse substrates, such as metals, oxides, and polymer substrates patchable onto human skin. The development of mechanically flexible, biocompatible-printed arrays of photodetectors with pixelated MoSe<sub>2</sub> channels and conductive graphene electrodes on a paper exhibits a photocurrent ON/OFF ratio of approximately 10<sup>3.8</sup> and photocurrent switching of 500 ms.

### F.EL03.09.03

**Effect of Bilayer Growth on the Thermoelectric Properties of Sb<sub>2</sub>Te<sub>3</sub> / Bi<sub>0.4</sub>Sb<sub>1.6</sub>Te<sub>3</sub> Thin Film** Andrew W. Howe, Mamadou T. Mbaye, Sangram K. Pradhan and Messaoud Bahoura; Norfolk State University, United States

Thermoelectric devices based on Sb<sub>2</sub>Te<sub>3</sub> and related alloys are of great interest to academia, industry, and government due to their efficiency in low-temperature applications such as micro-heating and small-scale refrigeration. The search for high performing thermoelectric devices is dominated by manipulating the electronic structure to boost the power factor through an increase in the density of states and/or reduction of the lattice thermal conductivity to maintain a large enough temperature

gradient. Superlattice structures are long heralded as potential candidates to increase the thermoelectric power factor as well as significantly reduce the lattice thermal conductivity. In this report, we compare the thermoelectric properties of bilayer p-type  $\text{Sb}_2\text{Te}_3/\text{Bi}_{0.4}\text{Sb}_{1.6}\text{Te}_3$  film and single layer p-type  $\text{Bi}_{0.4}\text{Sb}_{1.6}\text{Te}_3$  film of the same thickness. Preliminary Hall effect measurements showed that the carrier concentration of our bilayer and  $\text{Bi}_{0.4}\text{Sb}_{1.6}\text{Te}_3$  samples fall within the desired values common to heavily doped semiconductors. Carrier mobility and electrical conductivity are higher for our bilayer than the single-layer film. We noted a significant increase in the Seebeck coefficient values of our bilayer,  $202 \mu\text{V}/\text{K}$  compared to  $130 \mu\text{V}/\text{K}$  for our single-layer film. NanoTR thermoreflectance measurements revealed a significant reduction in the overall thermal conductivity of our bilayer system compared to our single-layer film. The low thermal conductivity reduction can be associated with, not only species intermixing -which allows phonon scattering events- interfacial boundary scatterings. When these observations are combined into a device, we would expect to see a great jump in the overall efficiency while maintaining the ease of fabrication allowing for quick scaling of production.

#### **F.EL03.09.04**

**Dimensionality Effects on Drift Resistivity of Nanoscale Phase-Change Memory (PCM) Cells in Reset State** Kazimierz J. Plucinski; Military University of Technology, Poland

Although the device physics related to the operation of PCM (Phase change Memory) have been widely studied since its discovery in the 1960s, questions relating to the nature of the physical principle responsible for the resistivity drift is still controversial [1, 4].

These problems are deepening at the transition to the nanoscale in the construction of PCM memory [2, 3].

Drift resistivity of the PCM in reset state in terms of subthreshold conductivity is analyzed.

This subthreshold conductivity is analyzed with respect to nanoscaling effects, especially:

the contribution of tunneling and trapping to electrical transport;

contribution of ballistic transport and diffusive transport;

analysis of the scattering in relation to dimension and mean free path in amorphous GST;

limitation of Poole-Frankel approach.

The results are verified on the base of present models of the subthreshold conduction and drift resistivity in reset state of the PCM memory [e.g. 4, 5].

#### References:

- 1.M. Le Gallo and A. Sebastian, An overview of phase-change memory device physics, Journal of Physics D: Applied Physics, 53 (2020), Issue 21, 213002
- 2.M. Le Gallo, Evidence for thermally assisted threshold switching behavior in nanoscale phase change memory cells, J. Appl. Phys. 119, 025704 (2016)
- 3.Xue-Peng Wang et al., Nanoscale amorphous interfaces in phase-change memory materials: structure, properties and design, J. Phys. D: Appl. Phys. 53 (2020) 114002 (8pp)
- 4.P. Noé et al., Phase-change materials for non-volatile memory devices: from technological challenges to materials science issues, Semicond. Sci. Technol. 33 (2018) 013002 (32pp)
- 5.A. Redaelli, Ed., Phase Change Memory Device Physics, Reliability and Applications, 2018, Springer, (Ch. 2, 4)

#### **F.EL06.08.01**

**Vacancy Defects Induced Changes in the Electronic and Optical Properties of NiO Studied by Spectroscopic Ellipsometry and First-Principles Calculations** Kingsley O. Egbo<sup>1</sup>, Chao Ping Liu<sup>2</sup>, Chinedu E. Ekuma<sup>3</sup> and Kin Man Yu<sup>1</sup>; <sup>1</sup>City University of Hong Kong, Hong Kong; <sup>2</sup>Shantou University, China; <sup>3</sup>Lehigh University, United States

Native defects in semiconductors are known to play an important role in determining their optoelectronic properties. Nickel oxide (NiO) is one of the few wide gap oxide semiconductors broadly applied as the hole transport layer in many optoelectronic devices. NiO exhibits *p*-type conductivity and its conductivity is believed to be controlled by Ni vacancy acceptors. Herein, we present a systematic study comparing the optical and electronic properties of *p*-type oxygen-rich NiO with Ni vacancies ( $\text{NiO}:V_{\text{Ni}}$ ) and insulating Ni-rich NiO with O vacancies ( $\text{NiO}:V_{\text{O}}$ ) and stoichiometric NiO. The optical properties were obtained by spectroscopic ellipsometry while valence band spectra were probed by high-resolution X-ray photoelectron spectroscopy. The experimental results are directly compared to first-principles DFT + *U* calculations. The absorption spectra for the  $\text{NiO}:V_{\text{Ni}}$  sample show significant defect-induced features below 3.0 eV compared to NiO, and  $\text{NiO}:V_{\text{O}}$  samples. The increase in sub-gap absorptions in the  $\text{NiO}:V_{\text{Ni}}$  can be attributed to gap states observed in the electronic

density of states. Computational results confirm that gap states in NiO:V<sub>o</sub> are predominantly Ni 3d states while those of NiO:V<sub>Ni</sub> is composed of both the Ni 3d and O 2p states. This work reveals the relations between native vacancy defects and optical properties of NiO and provides insights that would aid in designing optoelectronic devices utilizing NiO with native defects.

#### **F.EL06.08.02**

**Solvent Toolkit for Electrochemical Characterization of Hybrid Perovskite Films** Jason D. Slinker<sup>1</sup>, Alexander Zakhidov<sup>2</sup> and Sauraj Jha<sup>1</sup>; <sup>1</sup>The University of Texas at Dallas, United States; <sup>2</sup>Texas State University San Marcos, United States

Organohalide lead (hybrid) perovskites have emerged as competitive semiconducting materials for photovoltaic devices due to their high performance and low cost. To further the understanding and optimization of these materials, solution-based methods for interrogating and modifying perovskite thin films are needed. In this work, we report a hydrofluoroether (HFE) solvent-based electrolyte for electrochemical processing and characterization of organic-inorganic trihalide lead perovskite thin films. Organic perovskite films are soluble in most of the polar organic solvents, and thus until now, they were not considered suitable for electrochemical processing. We have enabled electrochemical characterization and demonstrated a processing toolset for these materials utilizing highly fluorinated electrolytes based on a HFE solvent. Our results show that chemically orthogonal electrolytes based on HFE solvents do not dissolve organic perovskite films and thus allow electrochemical characterization of the electronic structure, investigation of charge transport properties, and potential electrochemical doping of the films with in situ diagnostic capabilities

#### **F.EL06.08.04**

**Structural, Optical and Electrical Properties of NiO<sub>x</sub> Thin Films Obtained by Various Techniques** Jhonathan R. Castillo<sup>1,2</sup>, Nicola R. Nedev<sup>1</sup>, Benjamín Valdez<sup>1</sup> and Maria Bernechea<sup>2,3,4</sup>; <sup>1</sup>Institute of Engineering, Autonomous University of Baja California, Blvd. Benito Juárez s/n, Mexico; <sup>2</sup>Institute of Nanoscience of Aragon (INA), University of Zaragoza, Spain; <sup>3</sup>Instituto de Ciencia de Materiales de Aragón (ICMA-CISC), Spain; <sup>4</sup>ARAID, Spain

NiO<sub>x</sub> is a transparent conductive oxide (TCO) that has attracted a lot of attention because of its electrical and optical properties. Most of the available TCOs are n-type semiconductors, while the development of efficient p-type TCOs remains a challenge. NiO<sub>x</sub> is one of the promising p-type candidates, because of its superior chemical stability and optical transparency. Some potential optoelectronic applications of NiO<sub>x</sub> are as a p-type channel in transparent thin film transistors (TFTs) and as a hole transport layer in perovskite solar cells. In this work thin NiO<sub>x</sub> films were obtained by Pulsed Laser Deposition (PLD), d.c. sputtering, e-beam evaporation and sol-gel techniques.

All films were deposited on glass substrates with a size of 2×2 cm. The PLD films were deposited from a NiO target at room temperature. D.C sputtering and e-beam evaporation were used to deposit pure Ni films, which were then oxidized in air at various temperatures. The sol-gel NiO<sub>x</sub> was obtained by depositing chemical precursors and subsequent thermal treatment. Various parameters were varied in the experiments and it was found that the structural, optical and electrical properties of the PLD films depend strongly on the oxygen pressure. The most important parameter for the other three types of oxides was the annealing temperature.

All samples were characterized by UV-Vis spectroscopy, X-ray diffraction, X-ray photoelectron spectroscopy, scanning electron microscopy and atomic force microscopy. Results for the properties of NiO<sub>x</sub> films deposited by the above techniques will be presented and a discussion for their possible application in TFTs and solar cells will be given.

#### **F.EL06.08.05**

**The Role of Post Synthetic Treatment and Ligand Population on Optoelectronic Properties of PbS Quantum Dot Films and Devices** Fiaz Ahmed, Adam Roberge and Andrew B. Greytak; University of South Carolina, United States

Colloidal quantum dots (CQDs) are promising semiconducting materials to engineer photovoltaic and optoelectronic devices due to tunable size-dependent absorption and emission properties. Great efforts have been made to find suitable surface ligand to reduce spacing between the adjacent quantum dots to ease charge transport but there has been negligible attention given to purification strategies and systematic efforts to find the ideal ligand populations to optimize device performance. Charge transport could be hindered in the presence of excess free ligands forming interparticle barriers; on the contrary, an under-passivated QD can have high density of trap states and could also undermine the nanocrystal's stability toward coalescence. Precipitation and redissolution (PR) methods are widely used purification techniques that must typically be repeated to get clean CQDs with appropriate populations of surface-bound molecules (ligands). PR often results in loss of native ligands bound to the surface which induces more surface traps and/or compromise the chemical stability of these nanocrystals.

Gel permeation chromatography (GPC) has been proven to be an effective technique to remove the byproducts and impurities from CQDs without damaging the QDs surface. In this study, we demonstrate the effectiveness of GPC in removing byproducts and unbound ligands from pre and post ligand exchanged PbS CQDs.

NMR and UV-Vis-NIR spectroscopy of oleate-capped PbS quantum dots shows that despite removal of unbound surfactants, PbS QDs remain stable in solution following GPC. These purified nanocrystals were used to make CQDs photodetectors and photovoltaic devices.

We show that films fabricated using GPC purified PbS QD solutions exhibit higher charge transport, and low contact resistance, as investigated through in-plane conductivity and photoresponse. The charge carrier mobility was extracted from the mobility lifetime product and recombination lifetime determined by the spatial profiles of the photocurrent obtained through scanning photocurrent microscopy (SPCM), and transient photocurrent measurements, respectively. Furthermore, our findings show that post synthetic purification and optimum ligand population can significantly improve physical characteristics including reduced surface roughness, suggesting that impurities and optimum ligand coverage play an important role in film morphology and device performance.

#### **F.EL06.08.07**

**Revisiting *c*-type Screw Dislocations in GaN by First Principles—Implications on Nanopipes Formation** Liverios Lymperakis, Su-Hyun Yoo and Jorg Neugebauer; Max-Planck-Institut für Eisenforschung GmbH, Germany

Dislocations in III-Nitrides constitute a long standing controversial topic. The lattice and thermal mismatch associated with the heteroepitaxy of GaN results in high dislocation densities in the order of  $10^8$  to  $10^{10}$  cm<sup>-2</sup>. Although III-Nitride optoelectronic devices can operate even at these high dislocation densities, recent investigations indicate that *c*-type screw dislocations may have a detrimental effect on the properties and reliability of high-power electronic as well as of optoelectronic devices: For example, the observed high reverse (forward) leakage current in electronic (optoelectronic) devices is attributed to screw type dislocations [1]. Recently, it has been proposed that these defects are associated with open core structures, thus forming nanopipes with diameters of a few nms [2]. However, imaging screw dislocations at atomic resolution by electron microscopy to validate this model is not trivial. Moreover, first principles calculations that can accurately describe the energetics and atomic and electronic structure of these defects, have been restricted to MBE growth and/or did not explicitly consider the highly strained core region of these defects [3].

In the present study we combine density functional theory (DFT) with large scale empirical potential calculations within an Implicit Boundaries Multiscale Scheme calculations [4] to investigate the energetics, atomic structure and electronic properties of *c*-type screw dislocations in GaN. We explicitly consider both closed and open core screw dislocations as well as more than 100 different core reconstructions. Based on these calculations we construct a *c*-type screw dislocation phase diagram which describes the energetically most favorable core structures as function of the Ga, N and H chemical potentials. Our calculations indicate, in agreement with previous DFT studies, that growth under typical MBE growth conditions, i.e. metal rich growth, that these defects stabilize a Ga filled core. Moreover, under N rich conditions the core is stoichiometric, though a column of Ga-N dimers is removed from the core. However, the energy of the free *m*-plane surfaces under MBE conditions cannot be compensated by the core and strain energy and hence nanopipe formation is highly unfavorable. In contrast, under typical MOCVD or MOVPE growth conditions the Ga and N dangling bonds at the open core inner surfaces are passivated by NH<sub>x</sub> molecules and H atoms, respectively. This reduces considerably the surface energy under these conditions enabling the formation of nanopipes with hexagonal cross section and diameters ranging for ≈1 to ≈2 nm. Our calculations show that these nanopipes obey electron counting rule and hence are semiconducting. Nevertheless, they have important implications on the efficient diffusion and/or incorporation of impurities and/or dopants at the side facets and at the neighborhood of the open core, which will be discussed in detail. We will also discuss in detail the energetics and structure of superscrew dislocations and their implications on the diameter of the nanopipes as well as the potential implications of the nanopipes on the properties and the efficiency of the electronic devices.

[1] K. Nomoto *et al.*, IEEE Electron Device Lett. **37**, 161 (2016).

[2] S. Usami *et al.*, Appl. Phys. Lett. **112**, 182106 (2018).

[3] J. E. Northrup, Appl. Phys. Lett. **78**, 2288 (2001).

[4] L. Lymperakis *et al.*, Phys. Rev. Lett. **93**, 196401-1 (2004).

This project has received funding from the ECSEL Joint Undertaking (JU) project UltimateGaN under grant agreement No 826392. The JU receives support from the European Union's Horizon 2020 research and innovation programme and Austria, Belgium, Germany, Italy, Slovakia, Spain, Sweden, Norway, Switzerland.

#### **F.EL06.08.08**

**The Role of Third Cation Doping on Phase Stability, Carrier Transport and Carrier Suppression in Amorphous Oxide Semiconductors** Xingyu Wang<sup>1</sup>, Austin Reed<sup>2</sup>, Han Wook Song<sup>3</sup> and Sunghwan Lee<sup>1</sup>; <sup>1</sup>Purdue University, United States; <sup>2</sup>Baylor University, United States; <sup>3</sup>KRISS, Korea (the Republic of)

Transparent electronics and optoelectronics have been garnering increasing attention for use in high performance devices such as next generation displays, photovoltaics, electrochromic devices and sensors. Metal oxides are considered to be necessary components in these applications due to their excellent optical transparency ranging from visible to near infrared regime as well as pseudo-metallic electrical conductivity[1, 2]. These metal oxides have been implemented in devices, depending on their electrical conductivity, as transparent electrodes by degenerately-doped oxides such as InSnO and doped ZnO; semiconducting active layers based on indium oxides, ZnO or SnO<sub>2</sub>; and insulators (e.g., SiO<sub>2</sub>, Al<sub>2</sub>O<sub>3</sub>, HfO<sub>2</sub>) for dielectrics or encapsulations.

Thin film transistors (TFTs) are one of the key elements in displays as a pixel driving switch of which the required properties include high carrier mobility, low thermal budget processing, structural phase stability and reliable device performance in the presence of thermal and bias stress conditions. In recent years, amorphous oxide semiconductors based on indium oxides have been considerably investigated due to their promising carrier mobility, >5-25 cm<sup>2</sup>/Vs, compared to conventional amorphous Si (<1 cm<sup>2</sup>/Vs); low temperature processing; mechanical flexibility compared to the crystalline counterparts; and large area process-ability. Indium oxide-based binary and ternary cation material systems have shown tremendous promises for next generation displays since these materials meet the property and process needs that are described above. A binary cation material of indium zinc oxides (IZO) has been considered since the addition of Zn into In<sub>2</sub>O<sub>3</sub> stabilizes the amorphous phase of In<sub>2</sub>O<sub>3</sub> while the amorphous phase of undoped In<sub>2</sub>O<sub>3</sub> is rapidly crystallized at very low homologous temperatures (T/T<sub>m</sub><0.19) at 150 °C [3, 4]. The reported carrier mobility of IZO is as high as 20-50 cm<sup>2</sup>/Vs for both Hall and TFT field effect mobilities. A ternary cation system of InGaZnO (IGZO) [5, 6] has been more popular than binary systems since the addition of Ga in IGZO suppresses the channel carrier density in TFT application, which is preferred for TFT devices to obtain low device off-state current. Other third cation species such as Hf, Si and Zr were implemented. However, the carrier mobility of those ternary cation systems is significantly lower, 3-10 cm<sup>2</sup>/Vs, which is 3-10 fold lower than that of In<sub>2</sub>O<sub>3</sub> or IZO.

Therefore, securing strategies to develop a material system that maintains high carrier mobility (>20 cm<sup>2</sup>/Vs) and suppresses carrier generation for TFT channel application is of significant importance, which is expected to expedite the realization of next-generation transparent displays exhibiting reliable performance, fast switching speed and, consequently ultra high definition resolution.

Here, we report on a ternary cation material system of InAlZnO (IAZO) where the optimized carrier mobility is as high as 25-45 cm<sup>2</sup>/Vs. Further, the IAZO demonstrates an enhanced capability of stabilizing the amorphous phase during thermal stresses compared to InZnO. The effect of Al incorporation on the structural, electrical, optoelectronic and chemical properties of IAZO is systemically investigated and compared to those of IZO. The carrier transport behaviors (ionized impurity scattering; neutral scattering; charge screening) as well as the dominant mechanisms for carrier density and resistivity are discussed. The high mobility and greater phase stability may lead to high performance and sustainable device applications in next generation electronic and optoelectronic devices such as transparent displays.

## References

- [1] Lewis et al., MRS Bull., 25 (2000) 22-27.
- [2] Coutts et al., MRS Bull., 25 (2000) 58-65.
- [3] Paine et al., 85 (1999) 8445-8450.
- [4] Lee et al., Journal of Materials Research, 27 (2012) 2299-2308.
- [5] Nomura et al., Nature, 432 (2004) 488-492.
- [6] Hosono, Journal of Non-Crystalline Solids, 352 (2006) 851-858.

## F.EL06.08.09

**Investigation of Optical Bleaching Effect in InN-Based Films** Junjun Jia<sup>1</sup>, Takashi Yagi<sup>2</sup>, Taiki Ito<sup>1</sup> and Toshiki Makimoto<sup>1</sup>; <sup>1</sup>Waseda University, Japan; <sup>2</sup>National Institute of Advanced Industrial Science and Technology, Japan

Indium nitride (InN) was reported to have a large optical bleaching effect<sup>[1]</sup>, which provides potential application as high-speed and high-frequency optical switches in the optical communications. Due to its narrow direct bandgap (~0.7 eV), the bandgap engineering with GaN allows the ternary InGaIn system to cover a range of bandgap energies from the infrared of InN to the ultraviolet of GaN. Such wide bandgap tuning provides spectral flexibility for InGaIn as optical switches. In order



to materialize the potential of InGaN for optical device applications, we investigated the optical bleaching behavior and ultrafast carrier dynamics in epitaxial InN and InGaN films, and proposed a phenomenological model to explain the carrier relaxation behavior.

InN and InGaN films with the thickness of 300 nm were deposited on *c*-sapphire substrates by molecular beam epitaxy. The optical bleaching effect and ultrafast carrier dynamics in InN-based epitaxial films was investigated by using femtosecond time-resolved pump-probe transmittance/reflectance measurements with a photon energy of 1.50 eV, which is based on open-aperture Z-scan technique.

Both epitaxial InN and InGaN films show large optical bleaching effect from Z-scan measurements, where a nearly 3 times increase in transmittance was observed at 800 nm without the dependence of the film composition. The time-resolved pump-probe transmittance results indicate that hot carriers are relaxed within a time scale of subpicosecond. The carrier lifetime was found to be independent of the film composition and the fabrication condition. The maximum value in the transient transmittance shows a nonlinear increase with increasing the pump-beam power, which may be associated to a change in the nonlinear refractive index. The detailed mechanism on the carrier relaxation behavior will be given in the conference.

This work was supported by JSPS KAKENHI Grant-in-Aid for Scientific Research (C) (Grant No. 20K05368).

[1] V. Pacebutas, G. Alekseenko, and A. Krotkus, Appl. Phys. Lett. 88, 191109 (2006).

#### **F.EL06.08.10**

**Atomistic Insight in The Band Tailing of Kesterite Solar Absorbers** Wei Chen, Gian-Marco Rignanese and Geoffroy Hautier; Université catholique de Louvain, Belgium

The low open-circuit voltage  $V_{OC}$  of the earth-abundant kesterite  $Cu_2ZnSnS(Se)_4$  (CZTSSe) solar absorbers is often associated with the large band tails, the origin of which has been tentatively assigned to the Cu-Zn disorder. Such an assignment has recently been questioned by some experiments. Here, by using the cluster expansion method and first-principles calculations, we investigate the role of cation disorder in the band tailing of CZTS. Our results show that the formation of local Cu-Cu-Cu-Sn tetrahedral motif as a result of the disorder is responsible for the band-gap narrowing, leading to a redshift of optical absorption onset by up to 0.2 eV. The Urbach energy, however, is hardly modified by the cation disorder, thereby excluding Cu-Zn disorder as a main source of the large band tails observed in stoichiometric CZTS. On the other hand, we find that extensive Cu-Zn disorder could stabilize the formation of point defects to a large extent. In particular, the defect concentration of  $Sn_{Cu}$  can be as high as  $10^{12} \text{ cm}^{-3}$  under typical Cu-poor growth conditions. The defect level is found at 0.2 eV above the VBM, suggesting that  $Sn_{Cu}$  could be a hole trap.  $Sn_{Zn}$  remains the predominant deep donor with defect levels near the midgap and hence is responsible for nonradiative recombination. We show that Sn antisites could be the main culprit of the low  $V_{OC}$  and the persistence of the two donors in the presence of cation disorder presents a major challenge towards a high-efficiency CZTS absorber.

#### **F.EL06.08.11**

**Interface Engineering for Perovskite Solar Cells Based on Tin (IV) Oxide Nanostructures** Zhuldyz Yelzhanova<sup>1</sup>, Zhiwei Ren<sup>1</sup>, Damir Aidarkhanov<sup>1</sup>, Gaukhar Nigmatova<sup>1</sup>, Bakhytzhana Baptyayev<sup>1</sup>, Mannix Balanay<sup>1</sup>, Patrick W. K. Fong<sup>2</sup>, Aleksandra Djurisic<sup>3</sup> and Annie Ng<sup>1</sup>; <sup>1</sup>Nazarbayev University, Kazakhstan; <sup>2</sup>Hong Kong Polytechnic University, Kazakhstan; <sup>3</sup>The University of Hong Kong, China

Tin(IV) oxide ( $SnO_2$ ) is an n-type wide bandgap semiconductor, which is widely used as an electron transport layer (ETL) in organometal perovskite solar cells (PSCs) due to its promising properties such as high transmittance, high electron mobility, good photostability, good energy alignment and easy processing. In this work,  $SnO_2$  nanostructures were synthesized by a solvothermal technique. The impacts of each growth parameter for the  $SnO_2$  nanostructures were demonstrated. By investigating the relations among different growth conditions, optimized recipes were developed for  $SnO_2$  nanostructured ETLs employing in PSCs. Furthermore, the interfaces between the FTO/ETL and ETL/perovskite are optimized in order to enhance the charge extraction efficiency of the devices. Detailed characterizations such as scanning electron microscopy, electrochemical impedance spectroscopy, atomic force microscopy spectroscopy, X-ray diffraction,  $I-V$  characteristics etc. have been performed on the  $SnO_2$  ETL alone, material interfaces and the  $SnO_2$  nanostructures-based PSCs. The obtained results provide a valuable insight into the community for preparing desired PSCs with nanostructured ETL.

#### **F.EL06.08.12**

**Dual-Period Guided-Mode Resonance Filters for SWIR Multi-Spectral Image Sensors** Md Ataul Mamun, Rezwan

Mohammad Sayeed, Ümit Özgür and Vitaliy Avrutin; Virginia Commonwealth University, United States

Since their introduction in the early 1990s, subwavelength grating guided-mode resonance (GMR) filters have attracted considerable attention due to their simple and compact structures and versatile spectral characteristics. These outstanding features allow miniaturization of filters to pixel scale and high-density of integration for visible and short-wave infrared (SWIR) image sensors where a mosaic of transmission filters of different resonances can produce selective spectral signals to individual pixels of focal plane arrays. However, the conventional GMR-based transmission filter design, essentially unchanged for more than two decades, remains as a limiting factor for practical implementation of such an array of filters on the same substrate. The conventional design based on a single-period grating necessarily involves a homogeneous layer (of subwavelength thickness) underneath a subwavelength grating of a dielectric material to achieve a narrow transmission peak and a wide stop-band. Maintaining the other spectral characteristics, the transmission peak can then be tuned to the desired wavelength by scaling all the dimensions including the grating and homogeneous layer heights. However, to integrate different filters into a compact mosaic, this conventional design requires either different substrates of corresponding thicknesses or a very complicated non-planar fabrication process to use a single wafer leading to low throughput. In this work, we demonstrate a dual-period design to eliminate this issue by fetching additional design flexibilities. First, the dual-period filters possess two fill-fractions and thus unlike their single-period counterparts allow more degrees of freedom to vary the lateral profile parameters (e.g., fill-fractions and periods) for producing desired resonances at different wavelengths as well as to tune a resonance while keeping the grating height constant. Second, to produce a narrow passband with a wide stopband, these filters, unlike the single-period counterparts, do not require a homogeneous layer, allowing a planar fabrication process for integration of different filters on the same substrate. Moreover, dual-period filters show less sensitivity to the fabrication deviations such as sidewall roughness and to those related to grating and/or homogeneous layer heights where the latter, especially, remains as another limiting problem for the conventional narrow passband single-period based filters. For example, a small variation in grating and/or homogeneous layer thickness (while other parameters remain constant) causes the resonance peaks to disappear or be suppressed significantly and thus the fabrication requires very high precision. In this work, we report dual-period GMR filters of dimensions smaller than on silicon-on-quartz (SOQ) wafers using conventional electron beam lithography (EBL) and reactive ion etching (RIE). The filters demonstrate efficiencies as high as 80% at the peak transmission wavelength, e.g. 1550 nm. The passbands are as small as 15 nm with over 350-nm-wide stopband. The spectra of the fabricated filters are in a good agreement with the results of simulations using the finite element method (FEM) in COMSOL Multiphysics® software. Tunability of narrow passband resonances has also been achieved by only varying the fill-factors and/or period while keeping the substrate thickness constant. An array of four filters (all based on dual-period) have been demonstrated on same substrate to generate well-separated passbands in the SWIR region (1.2-1.6  $\mu\text{m}$ ) to work as a pixel. While smaller filter size would allow integration into compact chips, filters should be sufficiently spaced to eliminate the potential cross-talk. In order to produce an optimum pixel size to work in the concerned SWIR region, any potential cross-talk along with filter size effects are also analyzed theoretically and experimentally.

#### **F.EL06.08.13**

**High Power Generation of Double-Junction III-V Solar Cells by Strategically Designed Luminescent Waveguides** Shin Hyung Lee, Mun-Jong Kim and Sung-Min Lee; Kookmin University, Korea (the Republic of)

III-V compound solar cells have been considered as the leading photovoltaic devices due to their superior properties including the high carrier mobility, direct bandgap, and controllable bandgap against the solar spectrum. The extremely high solar-to-electric power conversion efficiency can be achieved with III-V solar cells by forming monolithic multi-junction structures through series processes of the epitaxial growth. Nevertheless, their prohibitively high materials and process (i.e. epitaxial growth) cost has limited the application to terrestrial photovoltaic systems. To reduce the cost per watts of III-V solar cells, several approaches have been suggested, such as transfer-printing-assisted assembly for re-using the expensive III-V substrate and solar light concentrator for boosting the power generation in a given cell area. A format of III-V solar cell arrays transfer-printed within the luminescent solar concentrator (LSC) has been particularly of interest due to the potential to mitigate the materials cost and simultaneously to augment the power generation. In spite of the successful demonstration with single-junction (e.g. GaAs) solar cells, the effect of power generation improvement by the LSC system cannot be simply achieved with multi-junction solar cells, because the balanced enhancement of photon absorption at each subcell is required for increasing overall photocurrent of series-connected multi-junction cells. In this regard, here we present a facile route to integrate the transfer-printed multi-junction III-V solar cells with the LSC medium for significantly raising their power generation. Monolithically grown indium gallium phosphide (InGaP)/gallium arsenide (GaAs) double-junction solar cells are completed implanted into a LSC printing medium by the transfer-printing-based fabrication assembly, where luminescent quantum dots (QDs) with the 610 nm emission wavelength are non-uniformly distributed in the LSC. Since the short-circuit current of InGaP/GaAs double-junction cells is limited by a level of photocurrent produced at the InGaP subcell, the LSC is designed for the emitted 610 nm photons of QDs to be preferentially guided into the InGaP subcell. At the optimal LSC

configuration, the power generation of 26%-efficient InGaP/GaAs solar cells can be considerably improved by ~50% compared to the identical cells but without add of the LSC.

#### **F.EL06.08.14**

**Selective Contacts Using Dipole Amino Acid Layers** Eloi Ros Costals, Gerard Masmitjà, Estefania Almache, Benjamin Pusay, Gema Lopez, Kunai Tiwari, Edgardo Saucedo, Pablo Ortega, Isidro Martin, Cristobal Voz and Joaquim Puigdollers; Universitat Politècnica de Catalunya, Spain

There has been a recent trend to use molecular dipole layers as a part of a novel strategy to fabricate selective contacts. Conceptually, a thin film of oriented molecular dipoles mimics a 2D capacitor, and the build-in voltage within the layer affects the final contact equilibrium state. When the dipoles are oriented in a certain direction one achieves larger accumulation of either holes or electrons by modifying the workfunction of the metal. Amongst many of the dipoles used amino acids have particularly interesting properties, for instance easy deposition by PVD methods such as spincoating and thermal evaporation and strong molecular dipole moment due to the presence within the molecule of a negatively charged carboxylic group and a positively charged amino group.

We tested the effect on the contact resistance of a Silicon/dipole/Aluminium stack using Transfer Length Method and testing different amino acids as the dipole layers (e.g. Cysteine, Glycine, Histidine...).

Preliminary results show an enhanced contact resistivity of orders of magnitude when dipoles are used on both p and n type silicon wafers, circumventing the problematic Fermi level pinning in Silicon aluminium as deposited contacts.

Finally, experiments on Histidine using different passivating layers show a clear difference in contact resistance with the change of the substrate dopant. Probably indicating that macroscopic orientation of the dipole layer can be promoted when using proper seed layers.

#### **F.EL06.08.15**

**Nucleation Site Tailoring at the 2D/3D Interface Using He-Ion Beam Patterning** Vera A. Zarubin, Kate Reidy, Joachim D. Thomsen, Julian Klein and Frances M. Ross; Massachusetts Institute of Technology, United States

For many of their applications, 2D materials must be connected to the macroscale world, implying interfaces between the 2D atomic layer and a 3D bulk material. The structure and defects at the interface between a 2D material and a 3D thin film influence (opto-)electronic properties of nanoscale devices such as contact resistance, photo-response and high frequency performance [1]. If the interface is between a 2D material and a 3D nanostructure, the ability to control the nanostructure geometry and lateral positioning is important in enabling nano-optoelectronic applications such as plasmonic arrays or arrays of wires or lines in individual circuits interfaced with 2D materials. When 3D nanoislands are grown on conventional, bulk substrates, “directed self-assembly” is a useful approach where growth takes place spontaneously but is favored at particular nucleation sites. The control of nucleation sites involves control of surface topography, geometry and local interactions [2]. Here we focus on extending this approach to the case of 3D nanoislands on 2D surfaces. We create specific defect locations on 2D materials (graphene, MoS<sub>2</sub>, WSe<sub>2</sub>) that act as heterogeneous nucleation sites for 3D metals (Au, Ti), and we tune the 3D metal deposition conditions to produce specific island shapes by self-assembly.

Since directed self-assembly requires avoidance of extraneous nucleation, as well as reliable nucleation at the patterned sites, we first discuss the control of metal island nucleation on unpatterned 2D materials. In particular, the nucleation density is expected to depend on the adatom diffusion distance on the 2D material surface. On 2D materials in the form of suspended layers, we use post-growth imaging by transmission electron microscopy (TEM) to measure the shape and distance between metal islands deposited in an ultra-high vacuum (UHV) evaporation system. We find that nucleation density and island shape depend on factors such as the substrate temperature, topography, background pressure, time, and partial pressure of the deposited material. We achieve the largest island diffusion distance (>2 μm) by removing polymeric residues in the 2D material transfer process, suspending the 2D material samples on TEM grids, using medium (100-200 °C) temperature deposition, and minimising defect sites such as wrinkles. We next induce locally reduced adatom diffusion distances using He-Ion beam patterning to create periodic defects in the 2D material. The He-Ion dose rates are calibrated and resulting defects characterised using high resolution scanning transmission electron microscopy. We show that these defects act as heterogeneous sites and we discuss the extent to which they can be exploited to produce patterned, periodic Au nanoisland

arrays. We develop automated image analysis techniques and perform statistical analysis of the nucleation site density and location. We believe that this templating and nucleation control opens routes towards self-assembled and tailored interface design. In particular, we discuss the possibilities of interface structures built from self-assembled 3D nanostructures for development of plasmonic nanoarrays with tunable and well-defined resonance frequencies.

[1] Wang, Y. et al. Van der Waals contacts between three-dimensional metals and two-dimensional semiconductors. *Nature* 568, 70–74 (2019).

[2] Gherasimova, M., Hull, R., Reuter, M. C. & Ross, F. M. Pattern-level assembly of Ge quantum dots on Si with focused ion beam templating. *Appl. Phys. Lett.* 93, 023106 (2008).

#### F.EL06.08.16

**Late News: Correlation of Nano-Morphology with Structural and Spectroscopic Studies in Organic Solar Cells** Urvashi Bothra<sup>1,2</sup>, Chris McNeill<sup>2</sup> and Dinesh Kabra<sup>1</sup>; <sup>1</sup>IIT Bombay, India; <sup>2</sup>Monash University, Australia

The nano-morphology of bulk heterojunction (BHJ) blends based on poly[[4,8-bis[(2-ethylhexyl)oxy]benzo[1,2-b:4,5-b']dithiophene-2,6-diyl][3-fluoro-2-[(2-ethylhexyl)carbonyl]thieno[3,4-b]thiophenediyl]] (PTB7) blended with [6,6]-phenyl-C<sub>71</sub>-butyric acid methyl ester (PC<sub>71</sub>BM) is systematically varied by changing the volume fraction of the solvent additive 1,8-diodooctane (DIO) from 0 vol% to 20 vol% in the casting solution to prepare organic solar cells (OSCs). With increasing addition of DIO, the photoluminescence (PL) from the blend is reduced; however, a relative increase in PL from 750 nm onwards is observed for blends with 20 vol% DIO. As quenching of the blend PL is related to the donor/acceptor (D/A) interface, structural characterizations in real-space (microscopy) and *k*-space (scattering) are performed to unravel the morphology of blend systems to correlate nano-morphology with photophysical and charge transport processes. Blends prepared with 0 vol% DIO form large phase separated domains of PC<sub>71</sub>BM, hundreds of nanometer in diameter. With the addition of 3 vol% DIO the size of PC<sub>71</sub>BM domains is suppressed resulting in a more mixed morphology due to the selective dissolution of DIO in PC<sub>71</sub>BM. On the addition of up to 20 vol% of DIO, the film becomes rougher with a finer interconnected morphology due to polymer aggregation, which contrasts with previous reports. Electron-transport length scales measured by scanning photocurrent microscopy (SPM) are found to increase with the addition of up to 3 vol% DIO associated with the break-up of the large PC<sub>71</sub>BM aggregates, while the hole-transport length is found to increase on adding DIO up to 20 vol% due to aggregation of polymer chains. Finite-difference time-domain (FDTD) simulations are performed to take into account for optical beam spread due to associated roughness of BHJ blend films which further strengthen the experimental findings to take into account for waveguiding/scattering components of excitation beam. The structural results are found to be in good agreement with the PL quenching and the effective transport lengths. Hence, this work represents a complete set of results systematically examining the effect of nanomorphology on structural and opto-electronic properties of BHJ blends, which can have a direct implication on better understanding of the emerging high efficiency OSC blend systems.

#### F.EL06.08.17

**Late News: Low Interfacial Thermal Resistance for BeO-on-Diamond** Kiumars Aryana<sup>1</sup>, Yoonseo Jang<sup>2</sup>, David Olson<sup>1</sup>, John Gaskins<sup>1</sup>, Dohwan Jung<sup>2</sup>, Jung H. Yum<sup>3</sup>, Eric S. Larsen<sup>4</sup>, Christopher W. Bielawski<sup>3,4,5</sup>, Sean King<sup>6</sup>, Jungwoo Oh<sup>2</sup> and Patrick Hopkins<sup>1,1,1</sup>; <sup>1</sup>University of Virginia, United States; <sup>2</sup>Yonsei University, Korea (the Republic of); <sup>3</sup>Institute for Basic Science (IBS), Korea (the Republic of); <sup>4</sup>Ulsan National Institute of Science and Technology, Korea (the Republic of); <sup>5</sup>Ulsan National Institute of Science and Technology (UNIST), Korea (the Republic of); <sup>6</sup>Intel Corporation, United States

Diamond, by far, is the most thermally conductive material at room temperature and a great candidate for thermal management applications in microelectronic devices. Yet, its application has been discouragingly hindered due to its large thermal barrier at the interface when paired with other CMOS materials. Beryllium oxide (BeO) is a potential material candidate to bridge this thermal barrier between diamond and other wide bandgap semiconductors such as gallium nitride (GaN) and Silicon carbide (SiC) owing to its large bandgap, high thermal conductivity, and large spectral phonon overlap with diamond. In this study, using time-domain thermoreflectance we report the thermal conductivity and interfacial thermal resistance at BeO/diamond and BeO/Si interface across various temperatures. We measure the thermal conductivity of amorphous BeO for thicknesses below 30 nm to be ~10 ± 0.7 W/mK, which is significantly lower than its bulk crystalline value. Our results suggest that the interfacial thermal resistance at BeO/diamond interface is significantly lower than that of GaN/diamond and BeO/Si. This observation paves the way towards more thermally efficient integrated circuits.

#### F.EL06.08.18

**Late News: The High Near-Infrared Transparency of Silver Nanowire Transparent Electrodes** Jon Atkinson and Irene Goldthorpe; University of Waterloo, Canada

Transparent electrodes are a necessary component of many optoelectronic devices. Networks of silver nanowires have emerged as a promising alternative to commonly-used metal oxides such as indium tin oxide (ITO). Their transparency and conductivity values are as high as ITO, while being mechanically flexible, less expensive and can be fabricated using high-throughput roll-to-roll methods. In this talk I will outline an additional advantage that has thus far received less attention: the high transparency of silver nanowire networks in the near-infrared region (NIR). This property is highly desirable for some applications such as window coatings and solar cells. I will show that for electrodes that are 96% transparent in the visible, ones made from ITO are only 35% transparent at a wavelength of 2500 nm, whereas those made from silver nanowires maintain a transparency as high as 94%. I will present results that show that the nanowires in the network should be sparse and larger in diameter to maximize NIR transparency. Modelling of the nanowire networks will also be shown and help demonstrate the physical reasons this is the case.

At the end of my talk I will present my results on passivating silver nanowire electrodes for capacitive-type devices such as smart windows and displays. To fully realize the advantages of silver nanowire electrodes, candidate passivation materials must be optically transparent (including in the NIR range), inexpensive, mechanically flexible and simple to deposit using high-throughput methods. I will present our findings of the passivation effectiveness of polyurethane, PMMA, a commercial optical adhesive and cyclotene passivation layers on silver nanowire networks.

#### **F.EL06.08.19**

**Late News: Reduced Non-Radiative Losses via Charge Selectivity Enhancement by Using a Fullerene Anodic Interlayer in Organic Photovoltaics** Donato Spoltore<sup>1</sup>, Manasi Pranav Ram<sup>1</sup>, Johannes Benduhn<sup>1</sup>, Mathias Nyman<sup>2</sup>, Jonas Kublitski<sup>1</sup> and Karl Leo<sup>1</sup>; <sup>1</sup>TU Dresden, Germany; <sup>2</sup>Abo Akademi, Finland

Charge transport layers play a fundamental role for efficient charge carrier injection and extraction in opto-electronic devices. Using interfacial layers, the open circuit voltage ( $V_{OC}$ ) and fill factor (FF) of organic solar cells can improve significantly. Here we show experimentally that the extent of contact between a Molybdenum Oxide ( $MoO_3$ ) hole extraction layer and the donor molecules in the photoactive layer of organic solar cells causes a proportional increase in non-radiative recombination losses. We quantify this effect by using several planar and bulk heterojunction solar cells device architectures, assigning it to surface recombination. We demonstrate that such losses can be suppressed by inserting a thin fullerene anodic interlayer. This interfacial layer enhances the built-in potential and reduces the presence of minority charge carriers at the electrodes: a new perspective on the principle of selective charge extraction layers. The improvement to device efficiency is limited by a critical interlayer thickness, which depends on the donor material in bilayer devices. These findings are relevant to different branches of organic electronics, given the popularity of  $MoO_3$  as an efficient hole extraction and injection layer, providing insights for future device design.

### **SYMPOSIUM F.EL02**

---

Emerging Light-Emitting Materials and Devices—Halide Perovskites, Quantum Dots and Other Nanoscale Emitters  
November 21 - December 1, 2020

#### Symposium Organizers

Hanwei Gao, Florida State University  
Maksym Kovalenko, ETH Zurich  
Tae-Woo Lee, Seoul National University  
Jiangeng Xue, University of Florida

#### Symposium Support

#### **Bronze**

The Journal of Physical Chemistry Letters | ACS Publications

---

\* Invited Paper

SESSION Tutorial F.EL02: Novel Perovskite Compounds as Classical and Quantum Light Sources  
Session Chair: Tae-Woo Lee  
Sunday Morning, November 29, 2020  
F.EL02

**8:00 AM \***

**Understanding Photophysics on Light-Emitting Properties at Different Length and Time Scales in Organic-Inorganic Hybrid Halide Perovskites** Bin Hu; University of Tennessee, United States

This tutorial lecture will focus on the photophysics to discuss controlling light-emitting and lasing properties in hybrid halide perovskites by considering orbit-orbit interaction between excited states in spontaneous and coherent regimes. Hybrid halide perovskites are defined as multifunctional semiconducting materials with strong orbital momentum, known as strong orbital materials. Orbit-orbit interaction can occur through long-range polarization and short-range magnetic dipole between excited states during developing light-emitting and lasing actions. Essentially, the long-range and short-range orbit-orbit interactions can determine the dynamics of light-emitting states through energy, polarization, and spin parameters. This tutorial lecture will present the fundamental analysis and experimental studies on photophysics involved in light-emitting and lasing actions in hybrid perovskites based on energy, polarization, and spin processes.

**9:30 AM BREAK**

**9:45 AM \***

**Perovskite Nanocrystals as Quantum Light Sources** Gabriele Raino; ETH Zurich, Switzerland

Besides conventional optoelectronic devices (LEDs and laser), colloidal quantum dots (QDs) are pursued as non-classical light sources (i.e. single photon emitters) that play a pivotal role in future quantum technologies, such as quantum cryptography and quantum sensing.

Due to strongly reduced charge trapping on surface states and their defect-tolerant character, perovskite QDs become attractive as alternative quantum light sources. Indeed, very stable, blinking-free emission has been observed at cryogenic temperatures with ultrafast radiative lifetime and very long coherence time. In addition, when organized in highly-ordered three-dimensional superlattices, perovskite NCs exhibit superfluorescence (SF), a cooperative emission of individual emitters that arises due to a coherent collective coupling to a common light field. Single NC spectroscopy has also revealed peculiar optical properties of perovskite compounds offering detailed information of the band-edge exciton fine structure and multi-excitons dynamics.

The tutorial lecture will review the main experimental methods used to perform single NC optical spectroscopy, with special focus on the recent achievements obtained at cryogenic and room temperature. Future prospects for the generation of complex quantum light sources will be also delineated.

SESSION F.EL02.14/F.EL08: Live Joint Session: Light Emission Mechanisms and Processes  
Session Chairs: Tae-Woo Lee and Samuel Stranks  
Tuesday Morning, December 1, 2020  
F.EL02

**11:30 AM \*F.EL02.12/F.EL08.12.01**

**Alloying and Slicing Halide Double Perovskites** Adam Slavney<sup>1</sup>, Bridget Connor<sup>1</sup>, Kurt P. Lindquist<sup>1</sup>, Linn Leppert<sup>2</sup>, Jeffrey Neaton<sup>3</sup> and Hemamala Karunadasa<sup>1,4</sup>; <sup>1</sup>Stanford University, United States; <sup>2</sup>University of Twente, Netherlands; <sup>3</sup>Lawrence Berkeley National Laboratory, United States; <sup>4</sup>SLAC National Accelerator Laboratory, United States

Halide double perovskites provide a flexible platform for manipulating electronic structure through synthetic design. I will present some recent studies from our group, where we have attempted to increase the compositional and structural complexity of halide perovskites through chemical substitution. In our quest to understand the electronic structure of double perovskites, we developed a simple model that allows us to predict the bandgap symmetry based on chemical composition.

Our work constructs an intuitive picture of how the molecular orbitals of metal-halide coordination complexes give rise to electronic bands in the extended perovskite lattice and describes how these molecular orbitals vary across the bands to give rise to the overall band structure. Although the effects of quantum confinement of Pb and Sn perovskites have been well studied, 2D analogs of 3D double perovskites are notably lacking. I will present a series of 2D double perovskites and discuss the optical and electronic consequences of dimensional reduction of the 3D double perovskite lattice to 2D derivatives.

**11:50 AM \*F.EL02.12/F.EL08.12.02**

**Hot Carriers in Halide Perovskites** Tze Chien Sum; Nanyang Technological University, Singapore

Halide Perovskites exhibit outstanding light-harvesting and emissive properties. Presently, record power conversion efficiencies (PCE) >25% in solar cells and external quantum efficiencies (EQE) >20% in light-emitting devices have been demonstrated. The perovskite field has since expanded well beyond photovoltaics and LEDs into other optoelectronic domains of lasers, x-ray detectors, memristors etc. Emerging frontier areas include multiphoton, multi-exciton generation and hot carrier applications. In this talk, I will focus on the hot carrier phenomena in halide perovskites and our recent work in this area.

**12:10 PM \*F.EL02.12/F.EL08.12.03**

**Defects Engineering and Photophysical Processes in 2D Perovskites** Annamaria Petrozza; Istituto Italiano di Tecnologia, Italy

Low-dimensional perovskites are rapidly emerging due to their distinctive emission properties. Here, first I will present the fundamental properties of pristine 2D perovskites, such as the nature of the primary photo-excitations, their relaxation through electronic states and their diffusion across thin films. Such properties will be correlated and modulated by the structural characteristics of the 2D perovskites. Then, I will discuss the possibility of perovskite doping by controlled addition of impurity ions which may enable new electronic, magnetic, and optical performances. I will explore new doping strategies based on transition and rare earth metals for tuning of the emission wavelength (from UV to NIR, further extending the typical range covered with perovskites) and luminescent enhancement. The suitability of doping for the realization of 4 level perovskite lasers will be assessed. Doping with heterovalent ions will be tested to selectively increase  $p$  and  $n$  type conductivity of the material. The addition of alkaline-earth metals as B-site dopants will be tested to improve the material stability

**12:30 PM F.EL02.12/F.EL08.12.04**

**High-Efficiency Blue Photoluminescence in the  $\text{Cs}_2\text{NaInCl}_6:\text{Sb}^{3+}$  Double Perovskite Phosphor** Matthew Gray<sup>1</sup>, Shruti Hariyani<sup>2</sup>, T. Amanda Strom<sup>3</sup>, Jackson Majher<sup>1</sup>, Jakoah Brgoch<sup>2</sup> and Patrick Woodward<sup>1</sup>; <sup>1</sup>The Ohio State University, United States; <sup>2</sup>University of Houston, United States; <sup>3</sup>University of California, Santa Barbara, United States

In this report, the photoluminescent properties of a lead-free double perovskite  $\text{Cs}_2\text{NaInCl}_6$  doped with  $\text{Sb}^{3+}$  are explored. The host crystal structure is a cubic double perovskite with Fm-3m symmetry,  $a = 10.53344(4)$  Å, and rock salt ordering of  $\text{Na}^+$  and  $\text{In}^{3+}$ . It is a wide bandgap compound ( $E_g \approx 5.1$  eV), and substitution with  $\text{Sb}^{3+}$  leads to strong absorption in the UV due to localized  $5s^2 \rightarrow 5s^15p^1$  transitions on  $\text{Sb}^{3+}$  centers. Radiative relaxation back to the  $5s^2$  ground state, via a  $^3P_1 \rightarrow ^1S_0$  transition, leads to intense blue luminescence, centered at 445 nm, with a photoluminescent quantum yield of 79%. The Stokes shift of 0.94 eV is roughly 33% smaller than it is in the related vacancy ordered double perovskite  $\text{Cs}_2\text{SnCl}_6$ . The reduction in Stokes shift is likely due to a change in coordination number of  $\text{Sb}^{3+}$  from 6-coordinate in  $\text{Cs}_2\text{NaInCl}_6$  to 5-coordinate in  $\text{Cs}_2\text{SnCl}_6$ . In addition to the high quantum yield,  $\text{Cs}_2\text{NaInCl}_6:\text{Sb}^{3+}$  exhibits excellent air/moisture stability and can be prepared from solution; characteristics make it a promising blue phosphor for applications involving near-UV excitation.

**12:45 PM F.EL02.12/F.EL08.12.07**

**Tuning the Photophysical Behavior of 2D Perovskites by Engineering the Nature of the Organic Component** Ferdinand C. Grozema; Delft University of Technology, Netherlands

Two-dimensional (2D) halide perovskites are a class of emitter materials that are enjoying growing attention recently. The materials are related to 3D halide perovskites but either part or all of the small A-site cations are replaced by large organic molecules with an ammonium binding moiety, for example butylammonium or phenyl-ethylammonium. This (generally) leads to the formation of a layered structure where a layer of metal-halide octahedra is formed and the large organic cations separate the layers from each other. Mixing of large and small A-site cations can lead to quasi-2D multi-layer materials where multiple layers of metal halide octahedra are separated by the organic molecules, for instance forming Ruddlesden-Popper or

Dion-Jacobson structures. The emissive properties of these materials are intricately linked to the structural dynamics and formation of possible defects in the inorganic layers.

In this work we explore how modifications of the large organic ammonium ion can affect the structural dynamics of the inorganic layer, combining molecular dynamics simulations with time-resolved spectroscopy. Using time-resolved fluorescence and ultrafast transient absorption spectroscopy we have studied the photophysical behavior of 2D perovskites with a range of different organic cations in order to gain insight in the relation between the structure and the excited state dynamics. These measurements indicate marked differences that can not solely be attributed to changes in the average structure of the materials.

To explain these differences we have performed classical molecular dynamics simulations for a variety of structures, for instance aliphatic alkyl chains, ammonium ions containing aromatic moieties such as phenyls or perylene, but also di-functional ions containing two binding sites that can connect to an inorganic perovskite layer on both sides. The results indicate that there are marked differences between the different structures in terms of their structural rigidity. Multi-layer Ruddlesden-Popper structures are generally more rigid than single layers, however, the rigidity of the single layer structures can be strongly enhanced by engineering of the interactions between organic cations, for instance by introduction of large conjugated ions. In addition, di-functional ligands resulting in Dion-Jacobson like structures also lead to more rigid structures. Comparison with the experimental results allows us to derive some design rules that indicate how engineering of the organic part of the structure can help in improving the emissive properties of the materials that is mostly due to the inorganic layer structure.

SESSION F.EL02.01: Emerging Low-Dimensional and Perovskite Emitters for Light-Emission Application  
On Demand Abstracts Available for Viewing Starting Saturday Morning, November 21, 2020  
F-EL02

#### 5:00 AM F.EL02.01.01

**Near-Infrared-Emitting CIZSe/CIZS/ZnS Colloidal Heteronanostructures** Xue Bai, Finn Purcell-Milton and Yurii Goun'ko; Trinity College Dublin, Ireland

Quantum dots (QDs) are very important light emitting materials that can be used in various applications (LED, bioimaging, luminescent solar concentrators and so forth)[1]. The photophysical properties of QDs are not only size and composition dependent, but also determined by the shape and morphology of the sample[2]. The investigation on the synthesis of Cd-based binary anisotropic nanorod QDs have been well explored to date, but using of heavy toxic metal (Cd) in the reaction impede the practical application of Cd-based QDs regarding serious environmental concerns and the unavoidable health damage for biomedical applications. Therefore, there is an urgent need for the development of toxic metal free fluorescent Cu-based quantum nanostructures with anisotropic morphology.

In this project, anisotropic fluorescent Cu-based multicomponent core/shell/shell heteronanostructures (HNNs) have been prepared by using the CIZSe/CIZS core/shell structure with wurtzite (WZ) crystal structure as the seed to coat the ZnS shell with a seeded growth method under fine control. Aliquots have been taken out from the reaction vessel at certain time intervals for further characterization and the growth mechanism of the particular anisotropic nanorod structure has been proposed based on the characterization results. Then the Au nanoparticles have been deposited on the surface of the preformed HNNs to give the Au-CIZSe/CIZS/ZnS nanocomposites. These nanomaterials are expected to find important applications in energy harvesting, sensing and nanobiotechnology.

References:

- [1] X. Bai, F. Purcell-Milton, Y. K. Gun'ko, *Nanomaterials* (Basel) 2019, 9.
- [2] D. Sahin, B. Ilan, D. F. Kelley, *Journal of Applied Physics* 2011, 110.

#### 5:10 AM F.EL02.01.02

**Chemically Reversible Isomerization in Inorganic Cluster-Molecules** Richard Robinson; Cornell University, United States

The ability to dynamically tune light emission through controlled structural transformations has promise in research and



application areas. Structural transformations are ubiquitous at all length scales in chemistry, spanning from isomerization reactions of small molecules to solid-solid transformations in bulk crystals, which have generally been studied in isolation. Despite attempts to merge understanding of these disparate regimes by reducing domain size in solids to nanocrystalline dimensions, bulk-like solid-solid transformation behavior still predominates at length scales approaching those of molecules. In-between small molecules and nanocrystals, magic-sized clusters (MSCs) provide an advantageous experimental platform to study isomerization in well-defined atomically precise systems. Additionally, MSCs are atomically identical species, with a narrow optical absorption and potential for precise color emission. Here we show here that a reversible transformation between CdS cluster isomers with distinct stable configurations possesses essential characteristics of both solid-solid transformations and molecular isomerization reactions. These isomers, termed  $\alpha$ - and  $\beta$ -(Cd<sub>2</sub>S)<sub>x</sub>, interconvert ( $\alpha$ -to- $\beta$ / $\beta$ -to- $\alpha$ ) reversibly, as identified by a 140 meV shift in the species' excitonic energy gap, that is, the absorption edge and peak emission wavelength is precisely tunable and reversible. A characteristic displacive reconfiguration of the inorganic core (solid-solid transformation), as evidenced by our reconstruction of the atomic pair distribution function from x-ray scattering, accompanies the change in electronic structures. The first order kinetics of the transformation—indicative of molecular isomerization—are driven by a distortion of the ligand binding motifs due to the presence of hydroxyl species in the ligand shell. Chemical control over the surface energy boundary conditions *via* adsorbates appears to be the exclusive determinant of “phase” stability in this system. The reversible transformation of MSCs reported here presents the missing bridge between molecular isomerization and solid-solid transformations. Manipulation of MSCs, which serve as seeds and as a monomer reservoir in nanocrystal growth, will provide an additional strategy for control over the structure of colloidal nanocrystals.

### 5:20 AM F.EL02.01.03

**Solvent Effect on Structural Elucidation of Photoluminescent Graphitic Carbon Nanodots** Almaz Jalilov; King Fahd University of Petroleum and Minerals, Saudi Arabia

Fluorescent carbon nanoparticles are stable materials that offer wide application potential ranging from the health to sustainable catalysis. Various carbon nanodots (CNDs) already reported, mainly synthesized from organic molecular precursors as a carbon source, and variety of amines as a nitrogen dopant. Photoluminescence (PL) emission of CNDs proposed to originate from the polycyclic aromatic carbon-core and in-situ synthesized molecular fluorophores. Higher temperatures and longer times of pyrolysis known to form higher order of polycyclic aromatic carbon-core. This work reports the CNDs and their fluorescence emission parameters in variety of solvents by means of steady state and time-resolved emission spectroscopies. Response of fluorescence emission lifetime and emission quenching rate constants to changes in solvent parameters such as polarity and tumbling lifetime were essentially independent, unlike molecular fluorophores that display solvent-dependent emission parameters. Fluorescence emission quenched in nitromethane additionally indicating to the polycyclic aromatic carbon-core as a predominant structural feature of the CNDs. The quenching of CNDs emission in the presence of benzophenone that has strong triplet component in excited state was observed. Quenching demonstrate the Stern-Volmer behavior and reveals the additional nonradiative decay pathways of CNDs. The main photophysical features of CNDs are discussed in terms of fluorescence emission originated from the excited state of the polycyclic aromatic carbon-core where contribution from the potential molecular fluorophores considered minimal. Contribution of the molecular fluorophores to emission mechanism of CNDs brings extra complexity and has strong impact on further development of CNDs, therefore, considering the importance of their minimal effect in emission parameters is discussed.

### 5:30 AM F.EL02.01.05

**Long-Term Effects of Impurities on the Particle Size and Optical Emission of Carbon Dots.** Nasir Javed and Deirdre O'Carroll; Rutgers, The State University of New Jersey, United States

Carbon dots (CDs) are nanoparticles that exhibit strong photoluminescence (PL) emission throughout the visible spectrum. In addition to strong PL emission, they possess several other promising properties, e.g., high water solubility, easy functionalization, excellent biocompatibility, electron donating and accepting capabilities, and low toxicity. Due to these attractive properties, with easy and low-cost synthesis, and abundance of the raw materials, they have been extensively studied as an alternative to conventional semiconductor quantum dots. Different top-down and bottom-up synthesis methods have been utilized to synthesize CDs. Recent studies highlight the presence of fluorescent byproducts in CD dispersions, especially in CDs synthesized by chemical methods.

Here, we synthesize CDs using citric acid and 1,5-diaminonaphthlene by the solvothermal method, and study their optical and structural properties utilizing UV-visible, PL, Raman and Fourier Transform-Infrared (FTIR) spectroscopy techniques. The long-term impact of reaction byproducts on the stability of the physical and optical properties of CDs is also studied. A significant increase in particle size is observed as a function of time after synthesis. Transmission electron microscopy analysis of unpurified CDs shows their average size increases from  $23.5 \pm 9.7$  nm to  $63.2 \pm 16.5$  nm during the 13-month

period after synthesis. UV-visible and FTIR spectra show strong absorption bands associated with C=O bonds. These absorption bands become less intense with time after synthesis, implying that C=O states decrease with time. PL emission from CD dispersions is measured using different excitation wavelengths. CDs that have not been purified show strong blue emission with a quantum yield of 30%, which is attributed to C=O states mostly associated with molecular fluorophores. In addition to blue emission, CDs also show weak green emission which becomes distinctive only at excitation wavelengths longer than 400 nm. With storage time, the blue emission is substantially reduced (quantum yield of 3% after 13 weeks) as C=O states decrease. This reduction in C=O states is accompanied by an increase in the average size of the CDs. From these observations it is concluded that the blue emission is mostly from the molecular fluorophores which slowly decompose and attach to the CDs, and cause an increase in particle size.

When CDs are properly purified, the intensities of absorption bands in UV-visible and FTIR spectra corresponding to C=O states and the blue PL emission decrease considerably. The quantum yield of purified CDs is just 2.6 %. Besides the blue emission, a solvent-dependent yellow emission arises, which is almost negligible when CDs are dispersed in water; however, the intensity of yellow emission increases significantly when CDs are dispersed in ethanol. This emission is attributed to solvent-activated surface states on CDs. Considerable reduction of blue PL emission along with C=O states after purification is accompanied by stable particle size. These observations strengthen our conclusions that the blue emission originates from free floating molecular fluorophores instead of CDs, and particle size increase is caused by deposition of impurities and subsequent deposition on the CD surface.

#### 5:40 AM F.EL02.01.07

**Low-Order Phases Suppressed Quasi-2D Perovskites for Efficient and Stable Blue Light Emitting Diodes** Zhenwei Ren and Wallace C. Choy; The University of Hong Kong, Hong Kong

Quasi-two-dimensional (quasi-2D) perovskite is rising as an efficient luminescent material for blue light emitting diodes (LEDs). However, typically reported quasi-2D perovskites with a wide distribution of small-n phases show low LED efficiency owing to the inefficient internal energy transfer. Meanwhile, the inevitable defects and traps generated during the perovskite crystallization increase non-radiative recombination, which further aggravate the emission efficiency. In this work, we demonstrate a new class of mixed ligand quasi-2D perovskite system of  $\text{PEA}_{2-x}\text{PA}_2(\text{CsPbBr}_3)_{n-1}\text{PbBr}_4$  (where PEA is phenethylammonium and PA is propylamine) by introducing a 2D perovskite ( $\text{PEA}_2\text{PbBr}_4$ ) into  $\text{PA}_2(\text{CsPbBr}_3)_{n-1}\text{PbBr}_4$  quasi-2D perovskite solution. The mixed ligand quasi-2D perovskite shows the unique feature of simultaneous suppression of low-order perovskite phase and defect passivation in quasi-2D perovskite for achieving efficient energy transfer and light emission. We theoretically and experimentally unveil the phase transformation mechanism. By fabricating blue perovskite light-emitting diodes (PeLEDs) from the mixed ligand quasi-2D perovskites, a high external quantum efficiency (EQE) of 7.51% with a brightness of  $1765 \text{ cd m}^{-2}$  and a very low turn-on voltage of 3.07 V is achieved for the blue perovskite light-emitting diodes (PeLEDs). Our most recent result show that by further modifying the mixed ligand quasi-2D perovskites, EQE can reach over 10%, which is among the highest efficiency of blue PeLEDs. Equally important, the PeLEDs show a very long operational stability of 3961 sec under continuous constant driving current together with very stable EL spectra without any peak shift during the entire stability test [1], which are superior to the reported blue PeLEDs with unstable EL spectra during operation, and thus contribute to the evolution of highly efficient and stable PeLEDs.

[1] Z. Ren, L. Li, J. Yu, R. Ma, X. Xiao, W. Yin, R. Chen, K Wang, X.W. Sun, and W. C. H. Choy\*. submitted.

#### 5:50 AM F.EL02.01.08

**Blue-Emitting CsPbBr<sub>3</sub> Nanoplates with Great Stability and High Quantum Yield Promoted by a Polysalt-Coating** Sisi Wang and Hedi M. Mattoussi; Florida State University, United States

Lead halide perovskite nanocrystals exhibit tunable photoemission properties across the entire visible spectrum, which make them highly promising materials for use in photovoltaic and light-emitting devices. Whereas green-emitting perovskite nanocrystals have achieved near-unity photoluminescence quantum yield (PLQY), their blue-emitting counterparts still lag-behind in terms of both PLQY and colloidal stability. Recently, two-dimensional colloidal perovskite nanoplates (NPLs), with strong 2-D confinement of charge carriers and large exciton binding energy, have attracted attention as an alternative to the mixed-halide core nanocrystals; these tend to experience phase segregation when used as light-emitting materials, for example. However, colloidal NPLs are strongly susceptible to surface defects, resulting in low PLQYs. They also spontaneously undergo morphological transformation manifesting in a shift of their emission to the green region of the spectrum.

Herein, we introduce a surface ligand-engineering strategy that enhances the PLQY, while preserving the shape of perovskite NPLs, using multi-coordinating poly-salts as ligand based on quaternary ammonium or imidazolium anchoring groups. These

ligands are prepared using ring opening reaction starting from polymaleic anhydride copolymers. When complexed with  $\text{PbBr}_2$  these salt groups strongly interact with the NPL surfaces, which significantly enhances structural stability while increasing the PLQY of these blue-emitting materials up to 70-80%. As such, these nanocrystals can be stored and processed using a wide range of solvents, while maintaining color purity. These findings are highly promising for use in developing blue light emitting devices.

SESSION F.EL02.02: Engineering of Perovskite Composition and Light-Emitting Devices  
On Demand Abstracts Available for Viewing Starting Saturday Morning, November 21, 2020  
F-EL02

**5:00 AM \*F.EL02.02.01**

**Large Cation Ethylammonium Incorporated Perovskite for Efficient and Spectra Stable Blue Light-Emitting Diodes** Jingbi You; Chinese Academy of Sciences, China

Perovskite light-emitting diodes (PeLEDs) have showed significant progresses in recent years, the external quantum efficiency (EQE) of electroluminescence in green and red regions have been beyond 20%, while the efficiency in blue is far lag behind. Here, we propose to add a large cation  $\text{CH}_3\text{CH}_2\text{NH}_2^+$  (EA) into the  $\text{Cs}^+$  site in  $\text{PEA}_2(\text{CsPbBr}_3)_2\text{PbBr}_4$  perovskite with green emission to decrease the Pb-Br orbit coupling and increase the bandgap for blue emission. X-ray diffraction and nuclear magnetic resonance results confirmed that the EA has been successfully incorporated into  $\text{CsPbBr}_3$  lattice for formation a  $\text{PEA}_2(\text{Cs}_{1-x}\text{EA}_x\text{PbBr}_3)_2\text{PbBr}_4$  perovskite. This method provide a versatile tool to modulate the photoluminescence from green region (508 nm) into blue (466 nm), and over than 70% photoluminescence quantum yield (PLQY) in blue is obtained. In addition, the emission spectra is stable under light and thermal stress. While configuration of PeLEDs with 60% EABr, as high as 12.1% EQE of sky-blue electroluminescence located at 488 nm has been demonstrated. As we know, this is the highest efficiency for PeLEDs in blue region up to now, which will pave the way for the full color display for the PeLEDs.

**5:15 AM \*F.EL02.02.02**

**Improving Perovskite Light Emitting Diodes via Doping Effects** Mahesh Gangishetty, Shaocong Hou, Samuel Sanders, Qimin Quan and Dan Congreve; Rowland Institute at Harvard, United States

Perovskite Light Emitting Diodes (LEDs) are a rapidly exploding field, driven by their low cost, facile synthesis, and color purity. Indeed, quantum efficiencies over 20% in both red and green emission have been demonstrated. Yet, key weaknesses in both spectral and operational stability hinder the long term application of these materials, and these issues are particularly exacerbated in blue devices, where both efficiencies and stabilities remain quite low. In this talk, we will demonstrate how atomic doping into the perovskite structure allows us to address these challenges, imparting improved efficiency and stability across different emission wavelengths and compositions. Doping is an effective strategy to drive perovskite LEDs towards commercial applications.

**5:30 AM \*F.EL02.02.03**

**Optoelectronic Applications and Fundamental Studies of Metal Halide Perovskite Nanostructures** Song Jin; University of Wisconsin-Madison, United States

The remarkable solar performance of lead halide perovskites can be attributed to their excellent physical properties that present many mysteries, challenges, as well as opportunities. Better control over the crystal growth of these fascinating materials and better understanding of their complex solid state chemistry would further enhance their applications. Here I will first report new insights on the crystal growth of perovskite materials and the solution growth of single crystal nanowires and nanoplates of various 3D lead halides perovskites ( $\text{APbX}_3$ , A = MA, FA, Cs) *via* a dissolution-recrystallization pathway. These perovskite nanowires have demonstrated high performance room temperature lasing with broad tunability of emission. Moreover, chemical strategies to stabilize the metastable perovskite phases, such as  $\text{FAPbI}_3$  and  $\text{CsPbI}_3$ , have been developed by using surface ligands to manipulate the delicate thermodynamic and kinetic balance between 3D and 2D layered perovskites. Such stabilization also allows the incorporation of unconventional large A site cations, such as guanidinium (GA) to be incorporated into n 2D Ruddlesden-Popper (RP) perovskites, and their effects on the physical properties of perovskites are studied. The excellent properties of these nanostructures of diverse families of perovskite materials with

different cations, anions, and dimensionality make them ideal for fundamental physical studies of carrier transport and decay mechanisms, and for enabling high performance lasers, LEDs, and other optoelectronic applications.

#### 5:45 AM F.EL02.02.04

**Impact of In Content on Optical Characteristics and Deep Defect Evolution in ZnO:In Nanocrystal Films** Brahim El Filali<sup>1</sup>, Tetyana V. Torchynska<sup>1</sup>, Juan A. Jaramillo Gomez<sup>2</sup>, Georgiy Polupan<sup>2</sup> and Lyudmyla Shcherbyna<sup>3</sup>; <sup>1</sup>Instituto Politecnico Nacional, Mexico; <sup>2</sup>Instituto Politécnico Nacional, Mexico; <sup>3</sup>V.Lashkaryov Institute of Semiconductor Physics at the National Academy of Sciences of Ukraine, Ukraine

ZnO nanocrystal films grown at ultrasonic spray pyrolysis and doped by In atoms have been investigated. The In impact on optical and structural parameters, and the evolution of O- and In- related defects versus In contents have been studied by means of the scanning electron microscopy, Raman scattering, photoluminescence and X ray photoelectron spectroscopy (XPS) methods.

Raman scattering spectra revealed the first and second order Raman peaks at In doping 0.5-2.5at% In. Raman peaks shift to higher energy, such as: 231, 245, 285, 324, 438, 481 and 481cm<sup>-1</sup> owing to decreasing the inter-planar distances in crystal lattice in comparison with un-doped ZnO stimulated by elastic strains. Simultaneously, the intensity of near band edge (NBE) bands enlarges. At In contents (1.0-3.0at%) the PL band (3.034eV) appears in PL spectra and its peak shifts to lower energy with increasing In concentrations. At higher In contents (3.0-5.5at%) the intensities of Raman peaks and NBE bands falling down owing to the formation of O- and In-related defects and decreasing the ZnO film crystallinity.

To analysis In – complex defects the high resolution XPS spectra were measured for lines: i) In 3d<sub>3/2</sub> and In3d<sub>5/2</sub>, and ii) In4d<sub>3/2</sub> and In4d<sub>5/2</sub>. In the XPS spectrum of ZnO:1.0%In NCs the doublets: In 3d<sub>3/2</sub> and In3d<sub>5/2</sub> with the energies of 451.7eV and 444.2eV, and overlapped In4d<sub>3/2</sub> and In4d<sub>5/2</sub> doublet peaks with the energies of 18.48eV and 17.28eV, respectively, have been detected. These peaks are typical for In<sup>3+</sup> ions in the In<sub>2</sub>O<sub>3</sub> crystal lattice. The In3d and In4d doublets shift to lower binding energies versus In contents, approaching the energies of 450.9 and 443.5 eV, as well as 17.58eV and 16.38eV, respectively, in the ZnO:5.5% In NC films. The last peaks are closer to the In<sup>0</sup> doublet lines in the metallic In crystal. Thus, this is a trend connected with the In atom coagulation and formation of In complex defects at higher In contents in ZnO:In NCs. Simultaneously, the oxygen vacancies have appeared in the studied films together with film lattice disordering. The optimal In concentration range to fabricate the ZnO films with the high optical parameters has been estimated.

#### 5:55 AM F.EL02.02.05

**Colloidal Manganese-Doped Hybrid Perovskite Nanoplatelets with Tunable Dual Color Emission** Seung Kyun Ha, Wenbi Shcherbakov-Wu and William Tisdale; Massachusetts Institute of Technology, United States

Two-dimensional (2D) perovskite nanoplatelets have attracted interest for light-emitting applications due to their strong quantum- and dielectric-confinement, directional emission, and tunable color throughout the visible spectrum. In this work, we demonstrate room-temperature synthesis of atomically-thin colloidal organic-inorganic hybrid perovskite nanoplatelets (Chemical formula: L<sub>2</sub>[ABX<sub>3</sub>]<sub>n-1</sub>BX<sub>4</sub>, L: alkylammonium, A: methylammonium or formamidinium, B: lead, X: halide, n(=1 or 2): number of PbBr<sub>6</sub><sup>4-</sup> octahedral layers in out-of-plane direction) incorporating manganese (Mn<sup>2+</sup>) dopants using the ligand-assisted reprecipitation method. Substitutional doping of manganese for lead enhances the photoluminescence quantum yield (PLQY) and introduces a broad, red-shifted emission feature in bromide nanoplatelets. We find that the choice of organic cation – in addition to the Pb:Mn ratio - strongly affects the final dopant concentration and the overall emission spectrum. We investigate the photophysics of Mn-doped lead bromide nanoplatelets (varying thickness and A-site cation) using time-resolved photoluminescence, excitation intensity-dependent PLQY, and spectral analysis, and we propose a kinetic model describing exciton dynamics between free-exciton and dopant-bound excitonic states. This work demonstrates a materials platform for tunable dual-wavelength emission from a 2D material and provides new understanding of photophysical interactions between localized Mn<sup>2+</sup> dopants and delocalized band-edge excitons in 2D perovskites.

#### 6:05 AM F.EL02.02.06

**Showerhead-Assisted Chemical Vapor Deposition of Organo-Metal-Halide Perovskite Films for Optoelectronic Application** Simon Sanders<sup>1</sup>, Dominik Stümmeler<sup>1</sup>, Gintautas Simkus<sup>1,2</sup>, Michael Heuken<sup>1,2</sup>, Andrei Vescan<sup>1</sup> and Holger Kalisch<sup>1</sup>; <sup>1</sup>RWTH Aachen University, Germany; <sup>2</sup>AIXTRON SE, Germany

Besides photovoltaics, which represents the main application focus of metal halide perovskites in the last decade, lighting has emerged as another appealing field. Perovskite films demonstrate readily tunable emission color, sharp luminescence spectra

and high external quantum efficiencies exceeding 21 % as emissive layers in perovskite LED (PeLED). Limited long-term stability of perovskite layers under electrical stress and the lack of deposition tools with process control on an industrial level remain as the critical obstacles for the commercialization of PeLED. Chemical vapor deposition (CVD) is an attractive highly scalable alternative to established solution-based techniques, enabling thin-film fabrication with high purity and reproducibility on large-area substrates.

Here, we introduce a custom-developed perovskite hot-wall showerhead CVD tool along with an optimized low-vacuum (5 hPa) CVD process to obtain dense perovskite films. We employ the organo-halide  $\text{CH}_3\text{NH}_3\text{Br}$  (MABr) and the metal-halide  $\text{PbBr}_2$  which are simultaneously introduced into the reactor to synthesize  $\text{MAPbBr}_3$  layers. To achieve this, the individual halide precursors are thermally sublimed (MABr: 175 °C,  $\text{PbBr}_2$ : 410 °C) and transported via separate  $\text{N}_2$  carrier gas flows (100 sccm each) to a static mixing unit. Due to a laminar flow regime, forced intermixing is essential to obtain uniformly distributed precursor molecules in the merged gas stream. A high-temperature run-vent system is employed to prevent undesired deposition during heat-up and cool-down phases. The heated showerhead spreads the carrier gas flow, enabling homogeneous deposition on temperature-controlled substrates up to 108  $\text{cm}^2$  in area. The substrates consist of a layer stack of poly(bis(4-phenyl)(2,4,6-trimethylphenyl)amine) (PTAA, 10 nm) / ITO (100 nm) / glass (substrate size 2.5 cm x 2.5 cm). We investigated the influence of the substrate temperature in the range of 60 °C – 110 °C on the morphology, optical and photophysical properties of the deposited films. The 110 °C-sample exhibits a highly porous morphology and a pronounced vertical growth mode, being unsuitable for device integration. Photoluminescence (PL) spectroscopy reveals green light emission at 530 nm, which is characteristic for  $\text{MAPbBr}_3$ . However, the emission is of low intensity, which likely can be attributed to increased non-radiative recombination losses induced by thermal perovskite degradation, e. g. during reactor cool-down. A reduction of substrate temperature provides a lower energy barrier of nucleation, leading to the formation of smaller crystallites and less porous layers at 100 °C. Besides light emission at 530 nm, a second peak at 500 nm is observed in PL measurements. Decreasing the substrate temperature further to 60 °C leads to dense films and light emission exclusively at 500 nm. The blueshift of 30 nm may be attributed to the formation of  $\text{MAPbBr}_3$ -nanoparticles with a size of 7 – 8 nm, emitting higher-energy photons due to the quantum confinement effect. Furthermore, the emission peak of the 60 °C-sample features a 200x enhanced intensity. The lower substrate temperature induces stronger MABr condensation, passivating perovskite grain boundaries. Thus, the high-intensity PL at 500 nm can be explained by suppressed non-radiative recombination due to  $\text{MAPbBr}_3$ -nanoparticles incorporated in an MABr matrix.

Ongoing work will examine the electrical properties of fabricated CVD layers in PeLED structures and will also focus on  $\text{CsPbBr}_3$  as a thermally more robust perovskite compound.

SESSION F.EL02.03: Mechanism and Physics of Perovskite Light-Emitting Devices  
On Demand Abstracts Available for Viewing Starting Saturday Morning, November 21, 2020  
F-EL02

#### 5:00 AM \*F.EL02.03.01

**High-Efficiency Perovskite Light-Emitting Diodes—Emission Mechanisms and Device Design** Dawei Di<sup>1,2</sup>; <sup>1</sup>Zhejiang University, China; <sup>2</sup>University of Cambridge, United Kingdom

Perovskite light-emitting diodes have recently exceeded the 20% external quantum efficiency (EQE) milestone. In particular, we have shown in our recent work that with careful device design, it is possible to achieve near-unity internal quantum efficiencies (IQEs) [1], demonstrating the potential of perovskite materials for extremely efficient electroluminescence. In this presentation, we discuss some design considerations behind the high IQEs, and for achieving EQEs that can approach the theoretical limits [1, 2]. We discuss the lessons learned from our recent studies in high-efficiency OLEDs [3, 4], and the important role of charge-transport interfaces in the realization of this goal [5]. Transient spectroscopy experiments are carried out to illustrate how radiative and non-radiative processes play their roles in the high-efficiency devices. Our work on perovskite LEDs may provide useful implications in the design of high-performance perovskite solar cells.

1. B. Zhao, R. H. Friend\*, D. Di\* *et al*, “High-efficiency perovskite-polymer bulk heterostructure light-emitting diodes”, *Nature Photonics* 12, 783–789 (2018).
2. C. Cho, R. H. Friend, D. Di\*, F. Deschler\*, N. C. Greenham\* *et al*, “The role of photon recycling in perovskite light-emitting diodes”, *Nature Communications* 11, 611 (2020).
3. D. Di, A. S. Romanov, L. Yang, R. H. Friend, M. Linnolahti, M. Bochmann, D. Credgington *et al*, “High-performance light-emitting diodes based on carbene-metal-amides”, *Science* 356, 159-163 (2017).
4. L. Yang, V. Kim, Y. Lian, B. Zhao, D. Di\* , “High-efficiency dual-dopant polymer light-emitting diodes with ultrafast

inter-fluorophore energy transfer", *Joule* 3, 2381-2389 (2019).  
5. B. Zhao, D. Di\*, R. H. Friend\* *et al*, under review (2020).

### 5:15 AM F.EL02.03.02

**Bright and Color-Tunable Single Layer Perovskite Host-Ionic Guest Light Emitting Electrochemical Cells** Jason D. Slinker<sup>1</sup>, Aditya Mishra<sup>1</sup>, Stephen DiLuzio<sup>2</sup>, Masoud Alahbakhshi<sup>1</sup>, Anvar Zakhidov<sup>1</sup> and Stefan Bernhard<sup>2</sup>; <sup>1</sup>The University of Texas at Dallas, United States; <sup>2</sup>Carnegie Mellon University, United States

Perovskite light emitting devices have drawn considerable attention for their favorable optoelectronic properties. High carrier mobilities make perovskites excellent candidates as host materials in electroluminescent devices, and iridium complexes serve as highly efficient triplet emitters. To achieve high performance in a simple single layer device, we employed a CsPbBr<sub>3</sub> perovskite host and a novel ionic iridium complex guest along with a polyelectrolyte to demonstrate efficient light emitting electrochemical cells (PeLECs). For an optimal guest/host blend, 10600 cd/m<sup>2</sup> luminance at 11.6 cd/A and 9.04 Lm/W were achieved. These devices showed voltage-dependent electroluminescence color proceeding from orange-red to green, facilitated by the reconfigurable ionic materials blend. Optimized devices exhibited enhanced stability under constant current driving. Our rationally-designed ionic guest at an optimal concentration of the host produced efficient (>90%) Förster energy transfer and improved thin film morphologies for high performance PeLEC operation enabled by ionic migration to interfaces.

### 5:25 AM F.EL02.03.03

**The Arrival of Optical Computers with Photonic CMOS—Techniques for Optoelectronic RF Signal Processors, Digital Switching Circuits and Optical Memories** James Pan<sup>1,2</sup>; <sup>1</sup>American Enterprise and License Company, United States; <sup>2</sup>Northrop Grumman Electronic Systems, United States

Traditionally, CMOS is not considered a light emitting device. Electronic instruments based on advanced CMOS technology function without lights in closed dark packages. Similar to laser or LED, photonic CMOS is a light emitting device. A laser is fabricated in the MOSFET drain region. A photon sensor or avalanche photo diode (APD) is fabricated in the MOSFET channel / well region. CMOS, laser and photon sensor are manufactured as one integral device. When the MOSFET is off, laser and photon sensor are also off. When the MOSFET is on, light from the laser is absorbed by the photon sensor or avalanche photo diode, triggering a large photonic current flowing back to the MOSFET drain to produce more lights. This process forms a positive feedback loop for conversion of light and electrons, and reduces heats.

Very low series resistance laser diodes, with forward voltage near 0V, are available, and suitable for the photonic CMOS.

In this paper we will discuss techniques to process small RF light signals with photonic CMOS under certain DC biases. In order to process the light signals, optical waveguide or air optical paths need to be created in an RF ASIC or analog ULSI circuit.

Additional features, such as polarization, optical filter, and grating thin films, can be added to the circuit for processing lights.

For digital switching devices in ULSI or ASIC, the design of a CMOS circuit may need to be optimized for optical processing. For traditional ICs, an electronic voltage is applied to the CMOS gate to turn the transistors on. In a optoelectronic IC, in addition to the electronic voltage, an optical voltage can be generated by directing a laser beam to the CMOS gate. Together electronic and photonic voltage may switch the CMOS inverter to "on". This new function not only increases the CMOS speed, but also reduces heat and power consumption.

A traditional SRAM is a 4 or 6 transistor bi-stable circuit, which consists of two back-to-back CMOS invertors. The speed of SRAM depends on how efficiently the pull-up and pull-down transistors operate for transferring electrons. A "pre-charging" step is always necessary prior to memory operations (WRITE / READ / ERASE).

In theory, the speed of an optoelectronic SRAM, which consists of two back-to-back photonic CMOS invertors, may surpass a traditional SRAM, because it takes less time to remove photon-generated electronics. For instance, when a positive voltage is applied to a pull down NMOSFET, holes need to be removed from the pull-up PMOSFET. If part of the holes are generated by laser from a photonic MOSFET, they can be more quickly removed when the laser is off.

To accomplish this much higher speed photonic SRAM, local interconnect must include optical waveguide or air optical paths, in addition to the traditional metal wires.

Finally, we would like to discuss how to expand the functions of photonic signal processors using nonlinear optics.

Nonlinear optical films can be fabricated in a photonic CMOS device in the isolation, buried oxide (in the case of FDSOI or UTSOI), or as optical waveguides connecting the CMOS. The nonlinear optical operation may increase the photon absorption rate of the embedded photon sensor or APD in a photonic CMOS, and quantum efficiencies. Promising near IR nonlinear optical materials will be illustrated, and the requirements for efficient second harmonic generation (SHG).

#### 5:35 AM F.EL02.03.04

**Operationally Stable Perovskite Light Emitting Diodes with High Radiance** Karim Elkhoully<sup>1,2</sup>, Iakov Goldberg<sup>1,2</sup>, Nirav Annavarapu<sup>1,2</sup>, Robert Gehlhaar<sup>1</sup>, Jan Genoe<sup>1,2</sup>, Paul Heremans<sup>1,2</sup> and Weiming Qiu<sup>1,2</sup>; <sup>1</sup>imec, Belgium; <sup>2</sup>KU Leuven, Belgium

Although perovskite light emitting diodes (PeLEDs) have shown fast advances in external quantum efficiency (EQE), their operational stability is still low compared to other light emitting diode (LED) technologies. Here, we show that by engineering the device stack for optimal band alignment and high mobility, the operating voltage of the PeLED is remarkably reduced, i.e. reaching high current density at low voltage. In depth analysis of the device characteristics shows that the low operating voltage of the stack leads to a significant mitigation of Joule heating. This mitigation leads to a better device performance at high current densities where the PeLED shows < 10% EQE roll-off at 800 mA/cm<sup>2</sup>. Furthermore, pulsed excitation and low temperature measurements allow us to show that ion-migration is the root cause for device degradation, while Joule heating accelerates this process. Based on this understanding, we resort to a perovskite layer with high ion-migration activation energy. Together with the optimized device stack, this allows us to demonstrate an unprecedented half-life time (T<sub>50</sub>) of 110 hours at room temperature, when biased at 100 mA/cm<sup>2</sup>. At 163 K, it even displays T<sub>98</sub> = 90 h at 300 mA/cm<sup>2</sup>. Our optimal device shows an EQE of 10.5% at 400 mA/cm<sup>2</sup> and a radiance of 351 W Sr<sup>-1</sup> m<sup>-2</sup> at 3.15 V, which rivals some of the highest performing stacks. Achieving an operationally stable high-performance PeLED at high current densities is crucial for a potential demonstration of an electrically pumped perovskite laser. To this end, we fabricate scaled PeLEDs down to 20 μm in diameter, and demonstrate reliable electrical pulsing at current densities > 1 kA/cm<sup>2</sup>. Pulsed excitation provides important insights about EQE roll-off at current densities relevant for injection lasing. Furthermore, unlike commonly used PeLED stacks, our PeLED shows optimal charge injection at low temperatures down to 163 K, which provides an opportunity to study PeLEDs at intense excitation at low temperatures.

#### 5:45 AM F.EL02.03.05

**Highly Efficient and Stable Perovskite Light-Emitting Diodes by Plasmon Effect Using Hydrophobic PVP Capped Gold Nanoparticles** Changmin Lee, Dong hyun Kim, Hyung Ju Chae, Jun Su Yang, Gyu Chan Lee, Ui Jun Lee and Seung Yoon Ryu; Korea University, Korea (the Republic of)

Noble metal nanoparticles are well-known for presenting plasmonic coupling with molecular excitons to enhance the performances of opto-electronic devices, especially light emitting diodes and solar cells. The higher momentum associated with metal surface plasmons can alter the lifetime of molecular excitons, thereby increasing the efficiency in the respective devices and enhancing the outcoupling. Solution processed metal nanoparticles are usually capped with selective surfactants which play significant role in their applications. In particular, for perovskite light-emitting diodes (PeLEDs), this kind of application positively contributes to the efficiency and stability and helps overcome the interface and charge transfer problems between hole injection layer (HTL) and emission layer (EML).

Herein, we have investigated the effect of incorporating size dependent gold nanoparticles (AuNPs) for altering the charge balance in PeLEDs. In addition, we studied the far-field interaction of AuNPs plasmons and charge trap by AuNPs through theoretical and experimental tools. To clearly understand the efficiency improvement tactics, we have fabricated PeLED samples with methylammonium lead bromide (MAPbBr<sub>3</sub>). AuNPs were incorporated in PeLED through the poly(3,4-ethylenedioxythio-phenylene):poly(styrene sulfonate) (PEDOT:PSS) solution as hole injection layer (HIL). To understand size dependent behaviors, AuNPs with sizes 10, 50, 90, 100 nm were inserted in PEDOT:PSS. Interestingly, even though we used the conventional perovskite (MAPbBr<sub>3</sub>) material, the obtained results speculated the possibility of enhancement in other perovskite materials such as CsPbBr<sub>3</sub> or FAPbBr<sub>3</sub>. By controlling the size of Au-NPs, we got the highest efficient inflection point at Au-NPs 90 nm.

By monitoring the lifetime of the excitons through time resolved photoluminescence (TRPL), the effect of plasmon over the perovskite photons can be delved. Each sample except the reference (w/o AuNPs) showed improved exciton lifetime, owing to far-field scattering effect by the AuNPs. We analyzed the modifications by AuNPs in the PEDOT:PSS thin film using ultraviolet photoelectron spectroscopy (UPS) and observed that the work function increment with increased AuNP size. It is

beneficial for reducing the hole injection barrier between HTL and the deep HOMO of perovskite. As expected, an increase in efficiency was observed with the increase in size of AuNPs, however the AuNPs with 90nm size was the inflection point. Using  $LT_{50}$  measurement, it was cross-evaluated that the efficiency of the device and the AuNPs size are directly proportional. To further investigate this issue, we fabricated hole-only-device (HOD) for the Richardson-schottky equation. It contains variables for carrier trapping or defect, so additional analysis was conducted to confirm the effects of trap and defect through the temperature-dependent I-V curve.

Device lifetime increase with the addition of AuNP might attributed to the capping layer PVP. We believed that the hydrophobic nature of PVP ligand on top of AuNPs helps to obstruct the indium diffusion from ITO as well as halide ion from MAPbBr<sub>3</sub>. Even though PVP serves as a capping layer, it exhibits hydrophobic passivation which prevented water penetration into perovskite. By applying PVP-capped AuNPs, we demonstrated the improved device efficiency and stability in perovskite LED in parallel.

#### 5:55 AM F.EL02.03.06

**Perovskite Light Emitting Diode Characteristics—The Effects of Electroluminescence Transient and Hysteresis** Karim Elkhoully<sup>1,2</sup>, Robert Gehlhaar<sup>1</sup>, Jan Genoe<sup>1,2</sup>, Paul Heremans<sup>1,2</sup> and Weiming Qiu<sup>1,2</sup>; <sup>1</sup>imec, Belgium; <sup>2</sup>KU Leuven, Belgium

The reproducibility of results is one of the corner stones of scientific research. However, often in emerging technologies, the reported results tend to be sensitive to the chosen measurement protocol. This can stem from measurement artifacts or from poorly understood complex underlying phenomena. Since their rise as an exciting material system for optoelectronic devices, metal halide perovskites have shown anomalous hysteresis effects in the current density-voltage ( $J$ - $V$ ) characteristics. In the case of perovskite solar cells, it has been shown that this anomalous hysteresis effect, which is highly dependent on the voltage scan rate, range, direction as well as the device structure, could significantly influence the extracted device metrics and the reported power conversion efficiency value. This has triggered wide discussions about the best practices to report perovskite solar cell performance to achieve consistency between different research groups. On the other hand, less attention is so far given to the anomalous effects that can affect the reporting of the characteristics of perovskite light emitting diodes (PeLEDs). Here, we show that even for PeLEDs with little  $J$ - $V$  hysteresis, the electroluminescence (EL) intensity changes by an order of magnitude on a timescale ranging from 10 msec to few seconds. This change is directly observed in the measured value of external quantum efficiency (EQE). Such reversible EL transient which is likely caused by ion-migration, can be followed by a roll-off regime dominated by Joule heating, and potentially device degradation when measured at high current densities. Naturally, this transient response leads to significantly different device characteristics depending on the measurement procedures for the same device. We directly explain those implications using the commonly used  $J$ - $V$ - $R$  scans with different sweep parameters, and show that these scans are not portraying unique device characteristics, but rather a snapshot in which the true device characteristics are entangled with inter-dependent underlying processes of ion-migration, Joule heating and device degradation in a non-linear way. Therefore, we propose a method based on pulsed excitation that allows better reproducibility and interpretation of the measured device characteristics. Furthermore, we also provide suggestions on reporting PeLED characteristics, as input for further discussions in the scientific community.

#### 6:05 AM F.EL02.03.07

**Late News: Perovskite LEDs with Nanostructures for Better Light Out-Coupling and Stability** Qianpeng Zhang, Daquan Zhang, Yu Fu, Lei Shu, Bryan Cao, Xiaofei Sun and Zhiyong Fan; Hong Kong University of Science and Technology, Hong Kong

In the past six years, perovskite light-emitting diodes (LEDs) have experienced rapid development. Thanks to the superior optoelectronic properties, perovskite material has made itself as a competitive candidate for next-generation displays and lighting. With the great efforts of researchers in this field, the external quantum efficiencies (EQEs) have already surpassed the 20% milestone for both red and green colored perovskite LEDs. Lately, the blue perovskite LEDs have been reported to achieve an EQE higher than 12%.

With the fantastic material quality, perovskite material can achieve a very high photoluminescent quantum efficiency (PLQY); therefore, the internal QE for perovskite LEDs can also reach the level as high as more than 90%. As a result, the key solution to the further enhancement of the perovskite LEDs performance lies in the light extractions/ outcoupling for perovskite LEDs.

During the past few years, our group has devoted ourselves to the development of nanophotonic strategies for the performance enhancement of the perovskite LEDs. The strategies include two main categories. The first kind is to use a nanophotonic substrate for perovskite LEDs devices. The structure we designed was a combination of a nanodome coupler and the photonic crystal optical antennas. When the geometry of the structure was properly optimized, the light originally trapped inside the active layer can be first coupled into the photonic crystals. After that, the photonic crystals, working as optical antennas, can convert the guided modes to the leaky modes and finally couple out the leaky modes to the air. With



this delicate strategy, we successfully improved the EQE of the perovskite LEDs from about 8% to 17.5%, which was the record for the MAPbBr<sub>3</sub> based perovskite LEDs at that time.

The second category of the nanophotonic strategies is making nanostructured active materials instead of using the nanostructured out-coupling substrates. With the exploration of varieties of nanostructures, we finally decided to use the nanowire arrays for the perovskite LEDs study. Very intriguingly, we found a solution method with the nanoporous template for perovskite nanowires growth. By studying the growth with different template geometries, we found out that the nanowire growth had a strong relationship with the capillary effect. Then we carefully designed the template thickness and the nanowire lengths, and we made the three-dimensional nanowire arrays based perovskite LEDs. Compared to the planar counterparts, the nanowire-based perovskite LEDs showed an enhanced EQE (from 11% to 16%), which is due to the improved light coupling inside the nanowires (from about 20% to about 45%). More importantly, the operational stability of the nanowire-based perovskite LEDs was also enhanced (T50 increased from 9 min to 35 min). And the long-term stability of the nanowire-based perovskite LEDs was also increased with an enhancement factor of 3 times. It's also worth noting that, the mechanical robustness of the nanowire-based perovskite LEDs was also enhanced a lot due to the protection of the porous template, and much fewer cracks were caused inside nanowires during bendings when compared to the planar counterparts. With the above mentioned two nanophotonic strategies for perovskite LEDs performance (both light-coupling efficiency and stability) enhancement, we demonstrated the advantages of applying nanostructures in perovskite LEDs. By further developing the perovskite material qualities and meanwhile improving the deposition techniques that are more compatible with nanostructures, we believe the EQEs of perovskite LEDs can be further improved to a much higher milestone soon. Last but not least, the nanophotonic strategies we developed here are not just limited to LEDs; they might be also applied for other device applications such as solar cells, photodetectors, and lasers.

#### 6:15 AM F.EL02.03.08

**Late News: Inkjet-Printed Metal Halide Perovskite LEDs** Felix Hermerschmidt<sup>1</sup>, Florian Mathies<sup>2</sup>, Vincent Schröder<sup>2</sup>, Carolin Rehermann<sup>2</sup>, Nicolas Zorn Morales<sup>1</sup>, Eva Unger<sup>2,3</sup> and Emil List-Kratochvil<sup>1,2</sup>; <sup>1</sup>Humboldt-Universität zu Berlin, Germany; <sup>2</sup>Helmholtz-Zentrum Berlin, Germany; <sup>3</sup>Lund University, Sweden

Solution-processable metal halide perovskites have sparked major interest for their use in (opto)electronic applications, but until now metal halide perovskite light emitting diodes (PeLEDs) have not been fabricated by inkjet printing. This is because of the difficulty in printing defect-free perovskite films as opposed to other printable optoelectronic materials.

Our work represents the first demonstration of inkjet-printed PeLEDs by specifically templating the crystallization behaviour within the perovskite. This effect is achieved by adding KCl to the commonly used hole injection material poly(3,4-ethylenedioxythiophene) polystyrene sulfonate (PEDOT:PSS) underneath the inkjet-printed perovskite layer, which significantly influences the device performance of the PeLEDs.

Firstly, the resulting "salty" PEDOT:PSS works as a seeding template to induce crystal nucleation of the metal halide perovskites inkjet-printed on top. It does so while having only a minor effect on the intrinsic electrical properties of the PEDOT:PSS. Secondly, the perovskite-polymer composite ink specifically developed for inkjet printing renders the commonly used antisolvent treatment unnecessary to induce favourable perovskite crystallization.

PeLEDs incorporating this PEDOT:PSS/KCl layer with the MAPbBr<sub>3</sub>:PEG perovskite composite show greatly improved performance, predominantly due to improved crystallization compared to PeLEDs containing only PEDOT:PSS. In particular, KCl-modified PEDOT:PSS contact layers enabled the realization of inkjet-printed PeLEDs with a 30-fold increased luminance at the same operating voltage. Using this approach, the first inkjet-printed metal halide PeLEDs with comparable performance parameters to spin-coated reference devices were produced [1].

[1] F. Hermerschmidt, F. Mathies, V. R. F. Schröder, C. Rehermann, N. Zorn Morales, E. L. Unger, E. J. W. List-Kratochvil, Mater. Horiz. 7 (2020) 1773.

SESSION F.EL02.04: Surface and Defect Passivation in Perovskite and Low-Dimensional Light Emitters  
On Demand Abstracts Available for Viewing Starting Saturday Morning, November 21, 2020  
F-EL02

#### 5:00 AM \*F.EL02.04.01

**Light-Emitting Metal Halide Perovskites and Perovskite-Related Hybrid Materials** Biwu Ma; Florida State University, United States

Metal halide perovskites and perovskite-related hybrid materials have emerged as new classes of light emitting materials with exceptional structural and property tunability. In these materials, various types of molecular metal halide building blocks can be assembled to form distinct crystalline structures with different dimensionalities at the molecular level, ranging from zero-dimensional (0D) clusters, to one-dimensional (1D) wires, two-dimensional (2D) layers, and three-dimensional (3D) networks. The rich combinations of compositions and structures afford these materials with a wide range of optical characteristics, for instance, direct band narrow emissions from 3D metal halide perovskites, and below-gap broadband emissions from 0D organic metal halide hybrids. In this talk, I will present our recent efforts on the development and study of highly efficient metal halide based light emitting materials, from synthetic control to device integration. The major subjects will include (i) color tuning and surface passivation of metal halide perovskite nanocrystals, (ii) single crystalline multicomponent organic metal halide hybrids with white emissions, and (iii) the applications of metal halide perovskites and perovskite-related hybrid materials in light-emitting diodes and radiation detectors.

**5:15 AM \*F.EL02.04.02**

**High-Efficiency Perovskite LEDs and Their Applications** Feng Gao; Linköping Univ, Sweden

A major efficiency limit for solution-processed perovskite optoelectronic devices (e.g. light-emitting diodes, LEDs) is trap-mediated non-radiative losses. Defect passivation using organic molecules has been identified as an attractive approach to tackle this issue. We significantly enhance the interaction with defects sites and minimize non-radiative recombination losses. Consequently, we achieve high-performance near infrared perovskite LEDs (PeLEDs) with a high external quantum efficiency (EQE) of 21.6%. We find that our devices can also work efficiently in an emitting/detector switchable mode, with tens-megahertz speed for both functions. Benefiting from the small Stokes shift of perovskites, the diode shows high specific detectivity ( $>2 \times 10^{12}$  Jones) at its peak emission ( $\sim 800$  nm), allowing optical signal exchange between two identical diodes. We further demonstrate the potential of the dual-functional diode for biomedicine diagnosis applications (as a monolithic heart pulse sensor) and for inter- and intra-chip bidirectional optical communications.

**5:30 AM F.EL02.04.03**

**New Quantum Dot Precursor Chemistry for Controllable Modulation of Reactivity by Lewis Base** Joonhyuck Park<sup>1</sup>, Arun Jayaraman<sup>1</sup>, Gyu Weon Hwang<sup>2</sup> and Hee-Sun Han<sup>1</sup>; <sup>1</sup>University of Illinois at Urbana-Champaign, United States; <sup>2</sup>Korea Institute of Science and Technology, Korea (the Republic of)

The optical and electronic properties of quantum dots (QDs) are mainly governed not only by their size distribution but also structural quality. Although the synthetic strategies for size control of QDs are well established for the last few decades, no systematic approach yet exists to achieve high structural quality nanocrystals. Here we show that reaction temperature and precursor reactivity must be independently tuned to achieve high crystallinity, uniform morphology, high quantum yield, and a well-defined core-shell structure. Reaction temperature governs the surface instability of QDs and lattice rearrangement. Precursor reactivity determines reaction kinetics at the surface, affecting the crystallinity and morphology of the resulting crystals. Prior to this work, the reactivity of conventional precursors has not been modulated in temperature-independent manner. As a result, the simultaneous optimization of reaction temperature and precursor reactivity has not been possible. Accordingly, growth conditions for QDs with various sizes and materials are optimized by trial-and-error. To allow temperature-independent modulation of precursor reactivity, we designed a new sulfur precursor employing a boron-sulfur bond, 9-mercapto-9-borabicyclo[3.3.1]nonane. The reactivity of the precursor is predictably modulated by the addition of a Lewis base, which modifies the boron-sulfur bond strength upon coordination to the boron atom. The new precursor chemistry enables the systematic optimization of growth conditions at a wide range of reaction temperatures. Adapting the growth method established here, high-quality QDs were grown from cores of various sizes and materials. The QD growth principles using the new design of precursors are universally applicable to different types of nanoparticles, including non-sulfur-based QDs. This work provides critical insights into the nanoparticle growth process, the design of new precursors, and the optimization of reaction conditions for high-quality QD synthesis.

**5:40 AM F.EL02.04.04**

**Proton-Transfer-Induced 3D/2D Hybrid Perovskites Suppress Ion Migration and Reduce Luminance Overshoot** Hobeom Kim<sup>1</sup>, Joo Sung Kim<sup>1</sup>, Jung-Min Heo<sup>1</sup>, Mingyuan Pei<sup>2</sup>, In-Hyeok Park<sup>3</sup>, Zhun Liu<sup>4</sup>, Hyung Joong Yun<sup>5</sup>, Min-Ho Park<sup>1</sup>, Su-Hun Jeong<sup>1</sup>, Young-Hoon Kim<sup>1</sup>, Jinwoo Park<sup>1</sup>, Emad Oveisi<sup>6</sup>, Satyawan Nagane<sup>7</sup>, Aditya Sadhanala<sup>7</sup>, Lijun Zhang<sup>4</sup>, Jin Jung Kweon<sup>1</sup>, Sung Keun Lee<sup>1</sup>, Hoichang Yang<sup>2</sup>, Hyun Myung Jang<sup>1</sup>, Richard Friend<sup>7</sup>, Kian Ping Loh<sup>3</sup>, Mohammad Nazeeruddin<sup>6</sup>, Nam-Gyu Park<sup>8</sup> and Tae-Woo Lee<sup>1</sup>; <sup>1</sup>Seoul National University, Korea (the Republic of); <sup>2</sup>Inha University, Korea (the Republic of); <sup>3</sup>National University of Singapore, Singapore; <sup>4</sup>Jilin University, China; <sup>5</sup>Korea Basic Science Institute, Korea (the Republic of); <sup>6</sup>École Polytechnique Fédérale de Lausanne, Switzerland; <sup>7</sup>University of Cambridge, United Kingdom; <sup>8</sup>Sungkyunkwan University, Korea (the Republic of)

Metal-halide perovskites (MHPs) has been considered as a promising candidate for solid-state light emission because of their superior optoelectronic properties such as extremely high color purity (full-width at half maximum (FWHM)  $\approx$  20 nm at room temperature), high photoluminescence quantum efficiency  $>$  90%, and easily tunable bandgap.<sup>1</sup> Further, the efficiency of perovskite light-emitting diodes (PeLEDs) based on three-dimensional (3D) polycrystalline perovskites has been greatly increased reaching external quantum efficiency (EQE) over 20% within only 5 years since the first high-efficiency PeLEDs reported in 2015.<sup>2-4</sup> However, a short operational lifetime of PeLEDs has been a critical drawback for their practical applications and commercialization.<sup>5</sup> One of the most critical causes of the problem is ion migration. PeLEDs' behavior can be more significantly influenced by ion migration as it requires higher bias to operate compared to perovskite solar cells. Here, we demonstrate a proton-transfer-induced 3D/2D hybrid perovskite by adding a small amount of neutral molecule, benzylamine (BnA). The proton transfer from organic ammonium in a precursor to the added BnA enabled the crystallization of 2D perovskite without destroying the 3D phase. As a result, the lifetime of PeLEDs was highly extended by more than 20 times, and an overshooting of electroluminescence at the initial stage of device operation was extremely suppressed; the 2D perovskite passivates trap sites of the 3D perovskite and blocks possible pathways of ion migration in the emitter. We also identified the mechanism of the suppressed luminance overshooting and the lifetime extension by relating with the retarded reorientation of BnA<sup>+</sup> in the perovskite lattice. Our work provides a helpful guideline to improve the stability of PeLEDs with important insights regarding defect engineering.

### Reference

1. Kim, Y.-H., Cho, H. & Lee, T.-W. Metal halide perovskite light emitters. *Proc. Natl. Acad. Sci. U. S. A.* **113**, 11694–11702 (2016).
2. Cho, H. *et al.* Overcoming the electroluminescence efficiency limitations of perovskite light-emitting diodes. *Science* (80-). **350**, 1222–1225 (2015).
3. Park, M.-H. *et al.* Boosting Efficiency in Polycrystalline Metal Halide Perovskite Light-Emitting Diodes. *ACS Energy Lett.* **4**, 1134–1149 (2019).
4. Xu, W. *et al.* Rational molecular passivation for high-performance perovskite light-emitting diodes. *Nat. Photonics* **13**, 418–424 (2019).
5. Quan, L. N., García de Arquer, F. P., Sabatini, R. P. & Sargent, E. H. Perovskites for Light Emission. *Adv. Mater.* **30**, 1801996 (2018).

### 5:50 AM F.EL02.04.05

#### Enhanced Stabilization and Easy Phase Transfer of CsPbBr<sub>3</sub> Perovskite Quantum Dots via Surface Ligand Engineering Sisi Wang, Liang Du, Zhicheng Jin and Hedi M. Mattoussi; Florida State University, United States

Colloidal nanocrystals made of all-inorganic lead halide cores, referred to as perovskite quantum dots (PQDs), exhibit quantum confinement of charge carriers. This endows these materials with size- and composition-dependent photophysical and electronic properties. They have been successfully grown using high temperature reaction routes. Along with organic metal halide compounds, PQDs are highly sought for applications that include light-emitting and photovoltaic devices. However, tangible progress in probing their fundamental properties and/or their integration in device design, has been hampered by issues of colloidal and photophysical instability. These problems can be traced to the ionic nature of the cores combined with the fast desorption rate of the surface capping ligands.

To address those problems, we introduce a promising surface coating strategy relying on a poly-zwitterionic polymer, where high affinity binding onto the QDs is driven by multi-coordinating electrostatic interactions with the ion-rich surfaces of CsPbBr<sub>3</sub> PQDs. The polymer ligands were synthesized by grafting a stoichiometric mixture of amine-modified sulfobetaine anchors and solubilizing motifs on a poly(isobutylene-alt-maleic anhydride), PIMA, via nucleophilic addition reaction. We find that this coating imparts enhanced colloidal stability to the nanocrystals over a broad range of solvent conditions and in powder form. It allows easy phase transfer of the PQDs to an array of solutions with varying polarities and properties. Additionally, this stabilization strategy preserves the photophysical and structural characteristics of the nanocrystals in a variety of polar solvents over a period extending to 1.5 years.

### 6:00 AM F.EL02.04.06

#### Equilibrium Crystal Shapes of InP Quantum Dots upon Ligand Adsorption and Synthesis Conditions Sangtae Kim<sup>1</sup>, Hyeri Yoo<sup>2,3</sup> and Gyu Weon Hwang<sup>2</sup>; <sup>1</sup>Hanyang University, Korea (the Republic of); <sup>2</sup>Korea Institute of Science and Technology, Korea (the Republic of); <sup>3</sup>Korea University, Korea (the Republic of)

InP quantum dots emerge as a non-toxic and industrially-applicable alternative to CdSe quantum dots in light-emitting materials. While the recent progress in synthesis and optimization of InP quantum dots led to quantum yields above 90%, the industrial goal of 95% quantum yield remains yet to be achieved, especially for the blue light-emitting quantum dots. As a viable strategy towards further optimizing quantum yields, reducing the trap states originating from the surfaces has been proposed. Dissimilar to CdSe quantum dots, controlling the surface facets and equilibrium crystal shapes of InP have been difficult, with largely spherical quantum dots synthesized and reported in the literature. In this work, we discuss and examine the thermodynamic stability of (100), (110) and (111) surfaces according to the ligand adsorption of  $\text{CH}_3\text{COO}^-$ ,  $\text{P}(\text{CH}_3)_3$  and  $\text{CH}_3\text{NH}_2$ , using density functional theory calculations. The change in equilibrium crystal shapes are examined with respect to the ligand species, concentration and the chemical potential of In, in order to account for the various synthesis conditions

SESSION F.EL02.05: Mechanism and Physics of Organic Light-Emitting Devices  
On Demand Abstracts Available for Viewing Starting Saturday Morning, November 21, 2020  
F-EL02

**5:00 AM \*F.EL02.05.01**

**High-Performance Light-Emitting Devices Based on Metal Halide Hybrid Perovskites** Toshinori Matsushima; Kyushu University, Japan

Metal halide perovskites have been widely used as the light absorber of solar cells, with the highest certified power conversion efficiency has reaching 25.2%, which is comparable to silicon-based solar cell technology. This high efficiency is inherent in perovskite's characteristics, such as high absorption coefficient, bandgap tunability, long carrier diffusion length, high carrier mobility, and compatibility with simple solution processing or vacuum evaporation. By taking these characteristics, perovskites can be used as the emitter of light-emitting diodes (LEDs) and laser devices. In this context, we show our recent results on such optoelectronic applications based on perovskites.

We found that singlet and triplet excitons are formed in quasi-two dimensional perovskite films with many domains of different phase orders (Nat. Photon., 14, 70, 2020). When we used organic cations with the low triplet energy for the fabrication of quasi-two dimensional perovskite films, the triplets generated by the recombination of electrons and holes injected from electrodes are strongly quenched. On the other hand, the use of organic cations with the sufficiently high triplet energy enabled the generated triplets to be harvested for emission as a result of efficient reverse intersystem crossing. With this method, we demonstrated a four-fold increase in external quantum efficiency of quasi-two-dimensional perovskite LEDs. To demonstrate the potential of using perovskites for other applications, we used the wide-energy-gap perovskite as the host layer of organic LEDs (Adv. Mater., 30, 1802662, 2018). We doped an organic fluorescent emitter into the perovskite host layer. The fluorescent molecules could exist at grain boundaries of perovskite films. Because of the better overlap between the emission band of the perovskite and the absorption band of the fluorescent molecules, the energy transfer from the perovskite to the organic emitter happened. We obtained low-voltage driving in the LEDs because of the high hole and electron mobilities of the perovskite. The radiative singlet exciton generation efficiency of the LEDs achieved ~40%, which is higher than the theoretical limit (25%) of emission from single excitons. We already demonstrated ~100% radiative singlet generation efficiency in a similar fluorescence/perovskite composite system.

To overcome poor carrier transport in organic films, we used the perovskite as the transport layers of organic LEDs (Nature, 572, 502, 2019). We were able to increase the total organic LED thickness by more than 10 times without reducing efficiency or operational durability or increasing driving voltage. This overturns 30 years of thinking that organic LEDs are limited to thin organic films. Additionally, some of thick organic LEDs with the perovskite transport layers had the same electroluminescence color from every viewing angle because of the absence of the optical interference. These results open new paths for low-cost, reliable, and uniform fabrication of organic LED displays and lighting.

We found that thresholds of amplified spontaneous emission under optical pumping strongly depend upon phase orders of perovskite films; thresholds decrease when a higher phase order is used and a typical three-dimensional perovskite with the highest phase order has the lowest threshold (Phys. Chem. Chem. Phys. 20, 15030, 2018). By embedding three-dimensional perovskite films into two-dimensional distributed feedback grating substrates, we saw lasing from the perovskite under optical pumping, with a peak width being lower than 1 nm (ACS Photon. 6, 460, 2019). We demonstrated a way of replicating grating patterns in lasing perovskite films on low-cost plastic substrates, which can reduce complexity and cost of the perovskite laser fabrication in the future (Appl. Phys. Lett. 115, 141106, 2019).

**5:15 AM F.EL02.05.02**

**Colorless and Transparent OLED with Solution Processable Electron Transport Layer** Je-Heon Oh and Jin-Woo Park;

Yonsei University, Korea (the Republic of)

Transparent displays have attracted considerable interest as the next-generation display technology in various fields, such as automotive industries, defense or military technology, and internet of things (IoT) applications. These applications require simultaneous projection or display of information and visibility of the surroundings through the device. However, the widely commercialized organic light-emitting diodes (OLEDs) are only used in semi-transparent displays due to their opaque and reflective metal thin film cathodes using Al and Ag despite the numerous excellent properties of OLEDs such as high color contrast, wide viewing angles and low-cost solution-based fabrication. For the transparent OLEDs (T-OLEDs), all the electrodes and organic functional materials in an OLED should be transparent. Especially, the opaque metal cathode should be replaced by a transparent material and blue EML materials owing to their wide electronic band gap should be used for the colorless characteristic. This study presents transparent organic light-emitting diodes (T-OLEDs) with excellent light-emission performance achieved by virtue of optically transparent functional layers. In this T-OLED, blue polymer poly(9,9-di-n-octylfluorenyl-2,7-diyl) (PFO) is used as a host material for the emission layer (EML) of the T-OLEDs, to achieve a high optical light transmittance in the visible range of the light spectrum. By controlled blending of the commercial emitting material Super Yellow with the PFO, the light-emission efficiency of the EML was significantly improved and the electroluminescence color could be changed from blue to green through a Förster resonance energy transfer (FRET). Furthermore, indium tin oxide (ITO) thin films was used not only as a transparent bottom anode but also as a transparent top cathode. Indium tin oxide (ITO) is one of the best candidates for transparent cathodes, owing to its excellent combination of optical transparency and electrical conductivity, along with its highly developed and mature deposition technology. However, the direct-current (DC) magnetron sputtering deposition approaches cause detrimental plasma damages to the organic layers ITO is deposited. Hence, solution-processable electron-transport composed of the zinc oxide (ZnO) nanoparticle layers and cesium carbonate-doped polyethyleneimine ethoxylated (d-PEIE), which aside from facilitating the efficient injection of electrons into the T-OLED, protected the organic emission layer (EML) of the T-OLED against the plasma damage during top ITO cathode sputtering deposition. Furthermore, semi-hydrophilic poly(methyl methacrylate) (PMMA) interlayer coated between the EML and ETL insured the good wettability and contact of the hydrophilic ETL with the hydrophobic EML. The even distribution of ZnO-NPs in the uniformly coated newly designed solution-processable composite ETL significantly enhanced the blue light emission performance of the conventionally structured T-OLED with top ITO cathode. The solution-processed T-OLED emitted the total maximum luminance ( $L_{\max}$ ) of about 2,417  $\text{cd m}^{-2}$  (bottom ITO anode emission at 1,455  $\text{cd m}^{-2}$  and top ITO cathode emission at 962  $\text{cd m}^{-2}$ ), total maximum current efficiency ( $\epsilon_{\max}$ ) at 3.12  $\text{cd A}^{-1}$  (bottom and top emissions at about 1.78 and 1.34  $\text{cd A}^{-1}$ , respectively), and total maximum power efficiency ( $\eta_{\max}$ ) at 1.64  $\text{lm W}^{-1}$  (bottom and top emissions at about 0.95 and 0.69  $\text{lm W}^{-1}$ , respectively) while having a very high optical transmittance of around 85% at 550 nm light wavelength.

#### 5:25 AM F.EL02.05.04

**Electroluminescent Metal-Organic-Framework Films with Thermally-Activated Delayed Fluorescence** Mariana Kozłowska<sup>1</sup>, Ritesh Haldar<sup>2</sup>, Marius Jakob<sup>3</sup>, Ian A. Howard<sup>4,3</sup>, Christof Wöll<sup>2</sup> and Wolfgang Wenzel<sup>1</sup>; <sup>1</sup>Institute of Nanotechnology, Karlsruhe Institute of Technology, Germany; <sup>2</sup>Institute of Functional Interfaces, Karlsruhe Institute of Technology, Germany; <sup>3</sup>Institute of Microstructure Technology, Karlsruhe Institute of Technology, Germany; <sup>4</sup>Light Technology Institute, Karlsruhe Institute of Technology, Germany

Light-emission efficiency of organic light emitting diodes (OLEDs) strongly depends on the photophysical processes: charge recombination, population of triplet excitons, nonradiative decay, steered by the electronic structure of molecules, their orientation and morphology. Various techniques to enhance luminescence and device quantum yield were reported. Among them, incorporation of thermally activated delayed fluorescent (TADF) chromophores allowing to convert unwanted triplets to singlets through reverse intersystem crossing (RISC) is a promising approach. Yet, controlled and stable assembly of TADF chromophores, modulating their functionality, is still not known, therefore, it is highly desirable to find a synthetic platform promoting the achievement of theoretically predicted device efficiencies.

Due to their vast chemical composition space, metal organic frameworks (MOFs) have emerged as a versatile class of functional materials with tunable properties for various applications. Here, we demonstrate new surface-anchored MOF (SURMOF) thin films with TADF activation, which results in efficient green electroluminescence of a LED device with luminance of 270  $\text{Cd/m}^2$  at 14.25 V. The TADF functionality of films originates from controlled aggregation of chromophores during their packing in a MOF scaffold. There, restriction of the rotational freedom of MOF linkers triggers new photophysical phenomena based on the “hot-exciton” RISC, enabling high population of singlet excited states and efficient SURMOF emitting layer [1].

In my talk, in depth explanation of the observed RISC processes and emission efficiency on the basis of the time-dependent

density functional theory calculations within quantum mechanics/molecular mechanics (QM/MM) approach will be given. The temperature dependence of RISC will be demonstrated as a function of the microscopic parameters between singlet and triplet excited states, i.e. energy splitting, reorganization energy and spin-orbit coupling, as predicted from the Marcus theory of charge transport. Perspectives of future computational screening of TADF chromophores [2] leading to a pronounced increase in luminescence of SURMOF-LEDs will be shown.

#### References

- [1] R. Haldar, M. Jakoby, M. Kozłowska, M. R. Khan, H. Chen, Y. Pramudya, B. S. Richards, L. Heinke, W. Wenzel, F. Odobel, S. Diring, I. A. Howard, U. Lemmer, C. Wöll, *JACS*, submitted.
- [2] R. Haldar, A. Mazel, M. Krstić, Q. Zhang, M. Jakoby, I. Howard, B. S. Richards, N. Jung, D. Jacquemin, W. Wenzel, S. Diring, F. Odobel, C. Wöll, A de novo strategy for predictive crystal engineering to tune excitonic coupling, *Nat. Commun.* (2019) 10:2048.

#### 5:35 AM F.EL02.05.07

**Modulation of Electronic, Structural and Photophysical Properties of Alkoxyphenyl Thiazolothiazole Based Materials for OLED Applications** Abhishek Shibu, Carly Kwiatkowski, Sean Jones, Daniel Jones and Michael Walter; University of North Carolina at Charlotte, United States

Organic light emitting diodes (OLEDs) are becoming ubiquitous with applications in television and computer screens, smart windows and wearable diagnostic tools due to their high resolution, energy efficiency and novel flexibility. However, the growth of this \$48Bn industry is facing stagnation due to dearth of suitable blue emitters. OLEDs need excellent red, green and blue emitters. Although the industry has high performing red and green emitters, the search is still ongoing for suitable blue emitters in solid state.

Presently, blue emission is obtained from rare-earth metal complexes which have complex synthesis routes and difficult processability. These materials have low thermal stability and poor operation lifetimes. As a result, the final devices are inefficient and expensive.

Among other potential candidates, thiazolothiazole (TTz) based materials have been widely reported as a molecular semiconductor that can emit blue. This blue emission has been used for a plethora of applications. TTzs are solution processible materials with facile synthesis routes using inexpensive and environment friendly precursors. They are thermally stable, and their planar structure enhances conduction of charge carriers in devices. Despite these properties, TTzs have been relatively unexplored for OLED applications. We hypothesize that TTz based materials can represent a new generation of affordable display materials with high device efficiency. In this study, we report the effect of different molecular spacers on electronic, structural and photophysical properties of seven novel TTz materials to help identify most suitable candidate for OLEDs.

We have explored the effect of molecular spacers on TTz packing, by resolving the crystal structures of the synthesized materials using single crystal X-ray diffractometry. Combined with fluorescence studies, we have thus correlated the tuning of inter-TTz core distances in a unit cell to their emission properties. We have determined their thermal stability using thermogravimetry and differential scanning calorimetry.

We have also determined their quantum yield and photoluminescence emission lifetime decay profiles. To establish exciton diffusion through these molecules, we have determined their singlet exciton diffusivity coefficient and the exciton diffusion length by employing a time resolved bulk quenching model with Monte Carlo eDiffusion computation simulation. We have also explored the molecular orientation of these materials in spin cast thin films using grazing incidence wide angle X-ray scattering. We establish the crystal orientation in thin films and how it affects charge mobilities in devices. This study will enable future researchers to engage in further possibilities with these materials, within and beyond the scope of OLEDs.

#### 5:45 AM F.EL02.05.08

**Late News: High Efficiency Pure Blue Fluorescent Organic Light Emitting Diode with CBP - BSB4 Emissive Layer** Dhruvajyoti Barah, Inaganti N. Manoj, Subhamoy Sahoo, HariPriya Kesavan, Jayeeta Bhattacharyya and Debduitta Ray; Indian Institute of Technology Madras, India

We present a pure blue fluorescent organic light emitting diode (OLED) where the device structure is optimized to yield a Commission Internationale de l'Eclairage (CIE) coordinate of (0.15, 0.13) which is very close to the National Television Standards Committee (NTSC) standard of blue color (0.14, 0.08). The emissive layer (EML) is composed of a host-guest matrix of 4,4'-di[N-carbazolyl] diphenyl (CBP, host) and 4,4'-Bis[(N-carbazole) styryl] biphenyl (BSB4, guest). We show, from photoluminescence (PL) studies, a blue-shift in the emission spectrum of the host-guest matrix from that of the pristine guest molecules resulting in a pure blue emission suitable for display application. We demonstrate methods to balance the electron and hole concentration in the EML of the OLED in order to improve the efficiency and its roll-off and optimize the

device to obtain a maximum external quantum efficiency (EQE) of 4.08%. This is very close to the theoretical limit for EQE (5%) of fluorescent OLEDs without the use of any light extraction layer. This is achieved by the choice of organic materials and their thicknesses in the OLED stack. The charge carrier mobility and molecular energy levels of the organic materials are taken into consideration for this optimization.

SESSION F.EL02.06: Low-Dimensional Nanoscale Materials for Photovoltaic Applications  
On Demand Abstracts Available for Viewing Starting Saturday Morning, November 21, 2020  
F-EL02

**5:00 AM \*F.EL02.06.01**

**Tailoring Phase Purity in 2D Halide Perovskites for High-Efficiency Optoelectronic Devices** Aditya D. Mohite; Rice University, United States

**Two-dimensional (2D) perovskites are a class of halide perovskites offering a pathway for realizing efficient and durable optoelectronic devices. One of key challenges has been the limited understanding of film formation, which have led to quasi-2D perovskite films with a high degree of polydispersity. Here we describe a novel technique, which leads to 2D perovskite thin-films with a high degree of phase purity as we go from precursors to thin-films. Photovoltaic devices fabricated with such films, yields an efficiency of 17.1% and 1.20V open-circuit voltage, while preserving 98% of their peak-performance after 800 hours under illumination without any external thermal management.**

**5:15 AM \*F.EL02.06.02**

**Metal Halide Perovskite Nanocrystals: Stability Improvement, Spectral Range Tuning via B-Site Substitution and Applications in Solar Energy Conversion** Yueli Liu<sup>1</sup>, Sudarsan Tamang<sup>2</sup>, Dmitry Aldakov<sup>3</sup> and Peter Reiss<sup>3</sup>; <sup>1</sup>Wuhan University of Technology, China; <sup>2</sup>Sikkim University, India; <sup>3</sup>CEA Grenoble, France

Metal halide perovskite nanocrystals (MHP NCs) exhibit many novel and unique phenomena both in terms of photophysics and materials chemistry. For NIR emission and solar energy conversion, the use of all-inorganic CsPbI<sub>3</sub> NCs is especially appealing, combining a narrow band gap with improved stability due to the absence of volatile organic constituents. However, the cubic black phase of CsPbI<sub>3</sub> is not thermodynamically stable at room temperature and transformation to the yellow orthorhombic phase occurs. This problem can be overcome by the use of molecular iodine as the halogen source during synthesis. It results in an improved surface passivation of the NCs and long-term air- and phase-stability of CsPbX<sub>3</sub> NCs.

Substitution of lead by the lighter group-14 homologue tin enables to shift the absorption onset and photoluminescence peak further to the near infrared, beyond 900 nm. However, Sn<sup>2+</sup> is much more prone to oxidation to the +IV state than Pb<sup>2+</sup> and can give rise to the formation of undesired intraband trap states. In this regard, mixed Cs(Pb,Sn)I<sub>3</sub> NCs exhibit enhanced stability and further possibilities of luminescence and morphology control, which will be discussed. Complete substitution of lead is also possible with europium, which gives access to nanoparticles strongly emitting in the deep blue spectral range (400-420 nm).

Finally, the application of the obtained MHP NCs in two approaches for solar energy conversion will be presented. First, they are incorporated into mesoporous TiO<sub>2</sub>, which constitutes to date the best performing electron transport material in perovskite solar cells. Efficient migration of the NCs into the mesoporous structure is achieved by means of interface engineering, enhancing at the same time significantly the electron injection rate. As a result, highly reproducible perovskite NC solar cells with an efficiency exceeding 14% could be obtained.

As an example for a further emerging application, the obtained air-stable MHP NCs can also be used as photocatalysts in organic syntheses. As an example, we demonstrate their use as efficient visible-light photocatalyst for the oxidative aromatization of a wide range of heterocyclic substrates.

**5:30 AM F.EL02.06.04**

**Denatured M13 Bacteriophage-Templated Perovskite Solar Cells Exhibiting High Efficiency** Il Jeon<sup>1,2</sup>, Haosheng Lin<sup>1</sup>, Yutaka Matsuo<sup>1</sup> and Jin-Woo Oh<sup>2</sup>; <sup>1</sup>The University of Tokyo, Japan; <sup>2</sup>Pusan National University, Korea (the Republic of)

The M13 bacteriophage, a nature-inspired environmentally friendly biomaterial, is used as the perovskite crystal growth template and the grain boundary passivator in perovskite solar cells. The amino groups and carboxyl groups of the four types

of amino acids on the M13 bacteriophage surface function as Lewis bases, interacting with the perovskite materials. The M13 bacteriophage-added perovskite films show a larger grain size and reduced trap-sites compared with the reference perovskite films. In addition, the existence of the M13 bacteriophage induces light scattering effect, which enhances the light absorption particularly in the long-wavelength region around 825 nm. Both the passivation effect of the M13 bacteriophage coordinating to the perovskite defect sites and the light scattering effect of the M13 bacteriophage intensify when the M13 virus-added perovskite precursor solution is heated at a temperature of 90 °C prior to the film formation. Heating the solution denatures the M13 bacteriophage by breaking their inter- and intra-molecular bondings. The denatured M13 bacteriophage-added perovskite solar cells exhibit a power conversion efficiency of 20.1% while the reference devices without the addition of the virus give a power conversion efficiency of 17.8%. The great improvement in efficiency comes from all of the three photovoltaic parameters, namely short-circuit current, open-circuit voltage, and fill factor, which corresponds to the perovskite grain size, trap-site passivation, and charge transport, respectively.

#### 5:40 AM F.EL02.06.05

**Study of The Synergetic Effects of Chloride and Surfactants Additions on Perovskite Crystallisation, in a Slot-Die Coating Process for Large-Scale Fabrication** Sophie Bernard<sup>1,2,3</sup>, Sébastien Juteau<sup>1,2</sup>, Armelle Yaiche<sup>1,2</sup>, Stefania Cacovich<sup>4</sup>, Frederic Sauvage<sup>3</sup> and Jean Rousset<sup>1,2</sup>; <sup>1</sup>EDF R&D, France; <sup>2</sup>IPVF (Institut Photovoltaïque d'Ile de France), France; <sup>3</sup>CNRS, UPJV Université Picardie Jules Verne, France; <sup>4</sup>CNRS UMR 9006, France

For the past ten years, perovskite solar cells have known a tremendous development among photovoltaic technologies, rapidly increasing from 3.8% [1] to 25.2% [2] power conversion efficiency (PCE). However, before transferring this technology to commercial applications, one of the main challenges to overcome is the fabrication of high quality perovskite absorber films on large surfaces. Various alternatives to spin-coating have been explored in the literature such as blade coating [3], inkjet coating [4], roll-to-roll [5] or spray coating [6]. But, slot-die coating is one of the most promising techniques. It is easily compatible with high rate fabrication technique like roll-to-roll and allows a sharp control over the uniformity on large surfaces.

In this work, we emphasis on the influence of the drying method upon the absorber properties. After the slot-die coating deposition, we chose to use a vacuum quench method, which allow a uniform extraction of the solvent, few minutes before annealing. The change of the quench system, from anti-solvent to vacuum aspiration, modify the speed with which the solvent is extracted. Then, it is possible to influence the crystallization mechanisms to fit the new drying environment by changing the perovskite ink composition. We herein propose a method to fabricate CsFA perovskite with a double-additives protocol, combining a surfactant and chloride addition through MACl.

A particular difficult challenge is to isolate the action of the surfactant and the chloride during crystallization. We combined PL and morphological characterisations, under different annealing and quench conditions, in order to successfully bring their respective effects out. For example, including MACl into precursor solutions seem to increase the film coverage and grain sizes during secondary grain growth, generating a smooth and pinhole-free perovskite layer with large grain size while surfactant enhance film uniformity and passivate surface defects. We reached over 16% PCE on small-scale cells (0.09 cm<sup>2</sup> aperture) with optimized ratio of chloride, thermal annealing and vacuum conditions.

This approach offers a better understanding of perovskite growth under large-scale fabrication conditions and is an important step towards industrial perovskite devices.

[1] A. Kojima, et al., J. Am. Chem. Soc., vol. 131, no. 17, pp. 6050–6051, May 2009, doi: 10.1021/ja809598r.

[2] NREL, 'Best research-cells efficiency', 2020.

[3] Y. Deng, et al., Energy & Environmental Science, vol. 8, no. 5, pp. 1544–1550, 2015, doi: 10.1039/C4EE03907F.

[4] F. Mathies, et al., ACS Applied Energy Materials, vol. 1, no. 5, pp. 1834–1839, May 2018, doi: 10.1021/acsaem.8b00222.

[5] C. Zuo, et al., Nano Energy, vol. 46, pp. 185–192, Apr. 2018, doi: 10.1016/j.nanoen.2018.01.037.

[6] Y. Jiang et al., Nano Energy, vol. 53, pp. 440–448, Nov. 2018, doi: 10.1016/j.nanoen.2018.08.062.

#### 5:50 AM F.EL02.06.06

**Ultrafast State-Resolved Pump-Probe Spectroscopy of CsPbBr<sub>3</sub> Nanocrystals Reveals Lineshape Dynamics and Quantum Confinement** Colin Sonnichsen, Dallas Strandell, Patrick Brosseau and Patanjali Kambhampati; McGill University, Canada

Disorder is intrinsic to ionic systems and gives rise to specific electronic processes. In recently developed perovskite ionic crystals, this dynamic lattice disorder is inferred to give rise to properties of interest, such as defect tolerance. Here, the



elementary excitation of interest is the polaron, a localized lattice distortion. We employ state resolved pump-probe spectroscopy to monitor electron and lattice dynamics in bulk CsPbBr<sub>3</sub> perovskite nanocrystals. The data report spectral lineshape dynamics that monitor the system from optical birth through polaron formation and exciton formation to fully thermalized, confined exciton. The formation of quantum confined excitons arises from the liquid-like polaronic potential. This polaronic confinement creates a quantum drop, as opposed to physical confinement creating a quantum dot. Disorder is intrinsic to ionic systems and gives rise to specific electronic processes. In recently developed perovskite ionic crystals, this dynamic lattice disorder is inferred to give rise to properties of interest, such as defect tolerance. Here, the elementary excitation of interest is the polaron, a localized lattice distortion. We employ state resolved pump-probe spectroscopy to monitor electron and lattice dynamics in bulk CsPbBr<sub>3</sub> perovskite nanocrystals. The data report spectral lineshape dynamics that monitor the system from optical birth through polaron formation and exciton formation to fully thermalized, confined exciton. The formation of quantum confined excitons arises from the liquid-like polaronic potential. This polaronic confinement creates a quantum drop, as opposed to physical confinement creating a quantum dot.

#### 6:00 AM F.EL02.06.07

**Ligand-Engineered Perovskite Nanoparticles for Photovoltaic Application** Seung Hyeon Jo<sup>1</sup>, Soyeong Ahn<sup>2</sup> and Tae-Woo Lee<sup>1</sup>; <sup>1</sup>Seoul National University, Korea (the Republic of); <sup>2</sup>Pohang University of Science and Technology, Korea (the Republic of)

Metal halide perovskites (MHPs) are promising materials for active layers in solar cells (SCs) because they have outstanding advantages such as low exciton binding energy (~14 meV for CH(NH<sub>2</sub>)<sub>2</sub>PbI<sub>3</sub>)<sup>[1]</sup> and high carrier mobility (100 cm<sup>2</sup>/(Vs))<sup>[2]</sup>. Despite the superior properties of MHPs, MHP polycrystalline (PC) bulk film based SCs had bad reproducibility due to bad surface morphology of MHP PC films. Furthermore, controlling the surface morphology of MHP PC films is very difficult because the environmental conditions such as temperature and moisture have a strong influence on the morphology. Here, we present MHP nanoparticles (NPs) synthesized by hot injection method and purified with ligand-engineering method. Moreover, perovskite NP layers with uniform morphology were fabricated by using a ligand washing method. The ligand engineering methods which reduce the amount of ligand improved the charge extraction/transport characteristics in MHP NP films. Also, more ligands can be removed by washing MHP NP films with organic solvent. The washing method is applied by dropping the organic solvent onto the film followed by subsequent spin-coating. Our research suggests a promising way to increase PCE of perovskite NP SCs.

#### 6:10 AM F.EL02.06.08

**A Near-Infrared Te-Doped GaAsSb Ensemble Nanowire Schottky Barrier Photodetector** Shisir Devkota<sup>1</sup>, Rabin Pokharel<sup>1</sup>, Mehul Parakh<sup>1</sup>, Sean Johnson<sup>1</sup>, Priyanka Ramaswamy<sup>1</sup>, Aubrey Penn<sup>2,2</sup>, Lewis Reynolds<sup>2</sup> and Shanthi Iyer<sup>1</sup>; <sup>1</sup>North Carolina A&T State University, United States; <sup>2</sup>North Carolina State University, United States

In this work, we report on a systematic investigation of the effect of tellurium (Te)-doping on the morphological, optical, and electrical properties of the GaAsSb nanowires (NWs) grown by Ga-assisted molecular beam epitaxy (MBE) and realization of the ensemble device. Te-incorporation in the NWs was assessed qualitatively from the structural, optical, and electrical properties, whereas the quantitative assessment was made based on the dark I-V simulations. Schottky barrier ensemble photodetector (PD) fabricated by capitalizing on optimized Te-doped NW exhibited a broad spectral range with the longer wavelength cutoff at ~1.2 μm, responsivity in the range of 580- 620 A/W and detectivity in the 1-3x 10<sup>12</sup> Jones. Padovani-Stratton parameter (E<sub>00</sub>) revealed field emission mechanism being dominant current conduction mechanism, backed by the higher ideality factor. Low-frequency noise (LFN) spectroscopy revealed the generation-recombination noise being the dominant noise source attributed to the Te induced localized states. The doped GaAsSb NWs have tremendous potential for further improvement, paving the path for high-performance NIR photodetection applications.

Author for correspondence: iyer@ncat.edu

#### **Acknowledgment:**

This work is supported by the Air Force Office of Scientific Research (AFOSR) under (grant# W911NF1910002) and National Science Foundation (grant# ECCS-1832117).

#### 6:20 AM F.EL02.06.09

**Late News: Synthesis of Lead-Free FASnI-based Perovskite Nanoparticles for Solar Cell and Lighting Applications** Zeying Chen<sup>1,2,2</sup> and Tara Dhakal<sup>1,2,2</sup>; <sup>1</sup>Binghamton University, United States; <sup>2</sup>Binghamton University, The State University of New York, United States

Metal halide perovskites with optimal opto-electronic properties contain lead (Pb). The replacement of lead with less toxic or nontoxic element, such as tin, has been studied in bulk thin film, but few in nanocrystal form. In this research, we synthesized

lead-free FASnI-based (FA: formamidinium) perovskite nanoparticles through the ligand-assisted reprecipitation method (LARP) at low temperature, and studied the impact of precursor solution molarity, the precursor solvent and the “poor” solvent on the phase of perovskite nanoparticle as well as optical properties. Different kinds of ligand were used and their function during the synthesis process were investigated. By controlling the molarity of precursor solution, we were able to tune the bandgap of FASnI-based perovskite from 700nm (1.77eV) to more than 830nm (1.49eV). For the same synthesis condition, the compositional variation of precursor solvent affected the phase of perovskite with either blue or red shift in PL spectra. For example, when 20% of DMSO was introduced into precursor solution, there is a ~70nm blue shift in photoluminescence spectra. A series of “poor solvents” were used in this research, such as chlorobenzene, chloroform, toluene, and hexane, among which the synthesis with toluene exhibited the better performance. With the interplay between precursor molarity, type of solvents, and ligands, we were able to achieve a low temperature synthesis of single phase FAPbI<sub>3</sub> nanoparticles. The PL, XRD and TEM data will be presented along with synthesis details.

SESSION F.EL02.07: Physics and Lasing Properties of Nanoscale Emitters  
On Demand Abstracts Available for Viewing Starting Saturday Morning, November 21, 2020  
F-EL02

#### 5:00 AM \*F.EL02.07.01

**Status and Prospects of Colloidal Quantum Dot Lasers** Victor I. Klimov; Los Alamos National Laboratory, United States

Colloidal semiconductor quantum dots (CQDs) are attractive materials for realizing highly flexible, solution-processable optical gain media with readily tunable operational wavelengths [1, 2]. However, CQDs are difficult to use in lasing due to extremely short optical gain lifetimes limited by nonradiative multicarrier Auger recombination [3]. This, in particular, is a serious obstacle for realizing cw optically and electrically pumped lasing devices. Recently, we have explored several approaches for mitigating the problem of Auger decay by taking advantage of a new generation of core/multi-shell CQDs with a radially graded composition that allow for considerable (nearly complete) suppression of Auger recombination [4, 5]. Using these specially engineered CQDs, we have been able to realize optical gain with direct-current electrical pumping [4], which has been a long-standing goal in the field of colloidal nanostructures. Further, we have applied these dots to practically demonstrate the viability of a ‘*zero-threshold optical gain*’ concept using not neutral but negatively charged particles wherein the pre-existing electrons block either partially or completely ground-state absorption [5, 6]. Such charged QDs are optical-gain-ready without excitation, which has allowed us to reduce the lasing threshold to record-low values that are well below the fundamental single-exciton-per-dot limit [6]. Most recently, we have developed CQD devices that operate as both an electroluminescent (EL) structure and a distributed feedback optically pumped laser [7]. By carefully engineering a refractive-index profile across the device stack, we have been able to demonstrate low-threshold lasing even with a very thin EL-active region, which comprises only three monolayers of the QDs. Yet another recent advance has been the realization of CQD-LEDs that achieve ultrahigh current densities exceeding 1,000 A cm<sup>-2</sup>. This has allowed us to inject ~10 excitons per dot and thereby realize population inversion of both the ground-state (1S) and the excited-state (1P) transitions. All of these recent developments suggest that CQD laser diodes (QLDs) are just around the corner. The availability of such devices will benefit numerous fields from integrated photonic circuits and optical interconnects to lab-on-a-chip platforms and wearable devices.

[1] V.I. Klimov, A.A. Mikhailovsky, S. Xu, A. Malko, J.A. Hollingsworth, C.A. Leatherdale, H.J. Eisler, M.G. Bawendi, *Science* **290**, 314 (2000).

[2] V.I. Klimov, S.A. Ivanov, J. Nanda, M. Achermann, I. Bezel, J.A. McGuire, A. Piryatinski, *Nature* **447**, 441 (2007).

[3] V.I. Klimov, A.A. Mikhailovsky, D.W. McBranch, C.A. Leatherdale, M.G. Bawendi, *Science* **287**, 1011 (2000).

[4] J. Lim, Y.-S. Park, V.I. Klimov, *Nature Materials* **17**, 42 (2018).

[5] K. Wu, Y.-S. Park, J. Lim, V.I. Klimov, *Nature Nanotechnology* **12**, 1140 (2017).

[6] O.V. Kozlov, Y.-S. Park, J. Roh, I. Fedin, V.I. Klimov, *Science* **365**, 672 (2019).

[7] J. Roh, Y.-S. Park, J. Lim, V.I. Klimov, *Nature Communications* **11**, 271 (2020).

#### 5:15 AM F.EL02.07.02

**On-Chip Light-Emitting Diodes and Lasers Integrated in the Final Back-End Processing Step** John P. Murphy, Alex J. Grede, Hoyeon Kim, Robert Cawthorn and Noel C. Giebink; The Pennsylvania State University, United States

Silicon photonic integrated circuits operating at visible and near-infrared wavelengths have enormous application potential; however, a scalable on-chip light source remains elusive. We address this challenge by introducing a new paradigm for halide perovskite light-emitting diodes (LEDs) and lasers that enables them to be integrated on silicon in a final solution processing step in the back-end-of-line (BEOL). In contrast to traditional sandwich-type device architectures, our approach makes use of co-planar interdigitated electrodes with ~100 nm spacing that facilitates both low voltage current injection and first order distributed feedback for lasing. This strategy overcomes the limited compatibility of perovskite materials with silicon processing by essentially pre-fabricating all components for LEDs and lasers except light-emitting materials so that they become functional once the perovskite is deposited from solution in the last step.

We demonstrate this approach by fabricating methylammonium lead iodide (MAPI) perovskite LEDs on SiO<sub>2</sub>/Si using alumina-coated Au interdigitated electrodes patterned by electron beam lithography. Despite the nominally-symmetric electrical structure of the devices, we achieve bipolar injection and bright MAPI electroluminescence with turn-on voltages below 2V. We propose that ionic conduction in MAPI, which is often viewed as detrimental for photovoltaics, is advantageous in this case because it can be exploited to break the electrical symmetry of the device by accumulating ions at the anode and cathode contacts so that the resultant interfacial band-bending facilitates hole and electron injection, respectively. We go on to investigate the operation of these devices under GHz bandwidth electrical pulsing enabled by an on-chip graded-impedance matching network and discuss the remaining hurdles that must be overcome to achieve electrically-pumped lasing.

#### 5:25 AM F.EL02.07.03

##### **Lasing in the Space Charge-Limited Current Regime—Implications for Organic and Halide-Perovskite Laser Diodes** Alex J. Grede and Noel C. Giebink; The Pennsylvania State University, United States

Organic and halide-perovskite semiconductors are capable of low threshold optically-pumped lasing over a wide range of wavelengths. Combined with their capacity for non-epitaxial deposition, these materials could facilitate a new range of coherent light sources for integrated photonics if electrically-pumped lasing can be established. In contrast to mature III-V laser diode technology where gain is achieved by diffusion current in a pn junction, the active layer in organic lasers cannot be doped because the dopants severely quench emission, and simply doping perovskites remains an ongoing challenge to begin with. In both cases, this means that gain will need to be achieved in an undoped active layer by a space charge-limited (SCL) *drift* current – a fundamentally different regime for diode lasing than III-V lasers operate in. While unipolar SCL current frequently occurs in organic materials and bipolar SCL current has been claimed in some organic light-emitting diodes, the implications of bipolar SCL current for lasing in organic and perovskite semiconductors has not been explored. Here, we establish analytical bounds on the threshold current, voltage, and power density for laser diodes operating in the bipolar SCL current regime. This formalism also provides useful insight into scaling relationships for SCL lasing in regard to electric field strength, carrier concentrations, recombination uniformity, and the impact of mobility imbalance on bimolecular quenching processes such as exciton-polaron annihilation (organics) and Auger recombination (perovskites). Importantly, we show how sub-Langevin recombination in perovskite semiconductors implies substantially higher threshold current density than in organics and motivates the need for quantum dot/well-like architectures to exploit carrier concentration/funneling effects. Our results establish basic bounds for the operation of organic and perovskite laser diodes and provide analytical guidelines for designing devices and identifying materials that are best suited for lasing in the SCL current regime.

#### 5:35 AM F.EL02.07.04

**Room-Temperature Lasing in Colloidal Nanoplatelets via Mie-Resonant Bound States in the Continuum** Mengfei Wu<sup>1</sup>, Son Tung Ha<sup>1</sup>, Sushant Shendre<sup>2</sup>, Emek Durmusoglu<sup>2</sup>, Weon-Kyu Koh<sup>2</sup>, Diego Abujetas<sup>3</sup>, José Sánchez-Gil<sup>3</sup>, Ramon Paniagua Dominguez<sup>1</sup>, Hilmi Volkan Demir<sup>2</sup> and Arseniy Kuznetsov<sup>1</sup>; <sup>1</sup>Institute of Materials Research and Engineering, A\*STAR, Singapore; <sup>2</sup>LUMINOUS! Centre of Excellence for Semiconductor Lighting and Displays, Nanyang Technological University, Singapore; <sup>3</sup>Instituto de Estructura de la Materia (IEM-CSIC), Consejo Superior de Investigaciones Científicas, Singapore

Solid-state room-temperature lasing with tunability in a wide range of wavelengths is desirable for many applications. To achieve so, besides an efficient gain material with a tunable emission wavelength, a high quality-factor optical cavity is essential. Here, we combine a film of colloidal CdSe/CdZnS core-shell nanoplatelets with square arrays of nanocylinders made of TiO<sub>2</sub> to achieve optically-pumped lasing at visible wavelengths and room temperature. The all-dielectric arrays support bound states in the continuum (BICs), which result from lattice-mediated Mie resonances and boast infinite quality factors in theory. In particular, we demonstrate lasing from a BIC that originates from out-of-plane magnetic dipoles oscillating in phase. By adjusting the diameter of the cylinders, we tune the lasing wavelength across the gain bandwidth of the nanoplatelets. The spectral tunability of both the cavity resonance and nanoplatelet gain, together with efficient light confinement in BICs, promises low-threshold lasing with wide selectivity in wavelengths.

5:45 AM F.EL02.07.05

**Identifying Spin Alignment between Coherent Light-Emitting Excitons Occurring in Amplified Spontaneous Emission in Perovskites** Miaosheng Wang; The University of Tennessee, Knoxville, United States

Amplified spontaneous emission (ASE) have become a common phenomenon in hybrid perovskites by establishing coherent light-emitting states. This paper reports a new phenomenon where spin alignment is occurred between coherent light-emitting excitons in the ASE regime in the perovskites. It is observed that the ASE exhibits higher and lower amplitudes when spin alignment is operated differently by using circularly and linearly polarized pumping. This shows as an increase on ASE amplitude upon switching pumping beam from linear to circular polarization, leading to a positive  $\Delta$ ASE. Essentially, this positive  $\Delta$ ASE identifies that the orbital magnetic dipoles between coherent light-emitting excitons are conserved during ASE development, realizing spin-aligned coherent light-emitting excitons. Furthermore, increasing pumping fluence gives rise to an enhancement on  $\Delta$ ASE phenomenon, proportionally following the ASE trend. This result indicates that the spin alignment can be gradually established between coherent light-emitting excitons by increasing pumping density. Clearly, our studies present a fundamental understanding on spin alignment between coherent light-emitting excitons towards developing spin-dependent lasing actions in metal halide perovskites.

5:55 AM F.EL02.07.06

**Late News: Whispering-Gallery Mode Lasing in Perovskite Nanocrystals Chemically Bound to Silicon Dioxide Microspheres** Nathaniel J. Davis; Victoria University of Wellington, New Zealand

Cesium lead halide perovskite nanocrystals exhibit high photoluminescence quantum efficiencies and tunability across the visible spectrum. This makes these crystals ideal candidates for solar panels, light-emitting diodes, lasers, and especially nanolasers. Due to the versatility of cation substitution in perovskite nanocrystals, they can be grown on amine-functionalized silicon dioxide nanoparticles, where the amine linker replaces the standard cation structure. Selectively growing luminescent nanocrystals on spherical silicon dioxide microspheres results in the opportunity to populate whispering-gallery modes in these spherical silica microspheres. In this case, the nanocrystal halide composition can be used to selectively tune the emission wavelength mode, and microsphere radius to tune the mode spacing. This silicon dioxide attachment also adds to the overall stability of the system. Through photoluminescence microscopy measurements, we show whispering gallery modes in individual perovskite-coated microspheres for CsPbBr<sub>3</sub> and CsPbI<sub>3</sub> nanocrystals on 9.2  $\mu$ m diameter silica spheres and compare these to theoretically predicted optical modes. In CsPbBr<sub>3</sub>, we provide evidence that these modes will lase under optical excitation, with a threshold of 750  $\mu$ J/cm<sup>2</sup>. This study presents a novel system that, through optimization, could be a promising pathway to achieve facile and stable perovskite nanolasers.

SESSION F.EL02.08: Optical Properties of Low-Dimensional Emitters and Light-Emitting Applications  
On Demand Abstracts Available for Viewing Starting Saturday Morning, November 21, 2020  
F-EL02

5:00 AM \*F.EL02.08.01

**Photon Upconversion—Effect of Material Dimensionality** Zachary VanOrman and Lea Nienhaus; Florida State University, United States

Photon upconversion describes the process of shortening the wavelength of the light emitted upon irradiation, resulting in a gain in photon energy. To comply with energy conservation laws, this occurs by combining two or more low energy photons through triplet states. Since triplet states are ‘spin-forbidden’, so-called sensitizers are required to indirectly populate the triplet state. Triplet sensitizers span a broad range of material classes including from metal-organic complexes, nanomaterials and bulk films. Understanding the energy transfer mechanism is crucial for the advancement of optoelectronic devices based on this process. In particular, tailoring the role of trap states in the sensitizer is key to further increase the device efficiency. The exact triplet sensitization mechanism varies depending on several factors including: (i) the absolute alignments of the sensitizer and acceptor energy levels. (ii) The exciton binding energy in the sensitizer, resulting in excited states in form of excitons or free carriers. (iii) Energetic polydispersity of a sample, which varies the energetic driving force for triplet transfer. I will present the current understanding of the triplet sensitization mechanism based on sensitizer materials with different dimensionalities including 0D quantum dots, 1D nanorods and 2D nanoplatelets and highlight the differences of each upconversion system. We obtain upconversion efficiencies exceeding 15% for quantum dot based green-to-blue

upconversion and 5% for nanoplatelet-based green-to-blue upconversion.

#### 5:15 AM F.EL02.08.03

**Green-to-Blue Triplet Fusion Upconversion Sensitized by Anisotropic CdSe Nanoplatelets** Zachary VanOrman, Alexander S. Bieber, Sarah Wieghold and Lea Nienhaus; Florida State University, United States

Photon upconversion (UC) resulting in blue and ultraviolet wavelengths has been studied for application in photocatalysis, as these high energy wavelengths could be transiently generated from lower energy excitation, thus avoiding photobleaching effects. Specifically, this can occur through the process of triplet-triplet annihilation based upconversion (TTA-UC), where the combination of two spin-triplet states results in a higher energy spin-singlet excited state. TTA-UC, however, requires triplet sensitization from another source, as triplets cannot be directly excited, as given by spin-selection rules.

We investigate 2D CdSe nanoplatelets (NPLs) as potential triplet sensitizers in a TTA-UC scheme. NPLs only have one dimension of quantum confinement, allowing for finer control of the band gap emission. Additionally, as NPLs have not been substituted for QDs previously, we looked to examine if their unique properties, like their giant oscillator strengths and ability to form stacks and other microstructures, would have an effect on TTA-UC.

We investigated the NPLs as a triplet sensitizer while taking advantage of 9-anthracenecarboxylic acid (ACA) as a transmitter ligand to increase the efficiency of energy transfer between the sensitizer and the triplet annihilator, 9,10-diphenylanthracene, while comparing a system sensitized by a CdSe QD for the sake of comparison. While NPL stacking and parasitic singlet back transfer still limit the achievable UC efficiency, we obtain a promising UC quantum yield of 5.4% and a low efficiency threshold,  $I_{th} = 237 \text{ mW/cm}^2$ . [1]

#### References:

[1] VanOrman, Z.; Bieber, A.; Wieghold, S.; Nienhaus, L.; Green-to-blue Triplet Fusion Upconversion Sensitized by Anisotropic CdSe Nanoplatelets. *Chem. Mater.* **2020**. <https://doi.org/10.1021/acs.chemmater.0c01354>

#### 5:25 AM F.EL02.08.05

**Optical Properties of Alloyed Quantum Dots: Experiment and Simulation** Erick I. Hernandez Alvarez, Andre Schleife and Andrew M. Smith; University of Illinois at Urbana-Champaign, United States

Quantum dots (QDs) are popular materials for applications that require stable photoluminescence with narrow-band emission. Biological imaging applications impose restrictions on QD size, while significant advantages are gained by tuning emission to the biological near-infrared (NIR) window (700 - 2000 nm) where tissue transparency is high and autofluorescence noise is low. Mercury cadmium chalcogenide alloy QDs are promising materials for these applications because their emission wavelength can be tuned continuously throughout the visible and NIR spectra through cation exchange-mediated alloying without changing the QD physical dimensions. However, precise selection of emission wavelengths through alloying remains challenging. In this context, atomic scale modeling of QD photophysical properties with varying size and composition can inform experimental QD designs. Here we combine first principles simulations of alloyed zinc blende  $\text{Hg}_x\text{Cd}_{1-x}(\text{S},\text{Se})$  QDs with experimental results to describe the optical properties of these materials. First we present experimental results for a series of size- and composition-controlled  $\text{Hg}_x\text{Cd}_{1-x}\text{S}$  and  $\text{Hg}_x\text{Cd}_{1-x}\text{Se}$  QDs, including optical spectra and materials analysis. We further apply density functional theory to compute the ground state properties and simulated optical spectra of QDs with varying size and composition. In this talk, we will interpret the combination of results from both approaches to inform alloyed QD design.

#### 5:35 AM F.EL02.08.06

**Combining Machine Learning and First-Principles Methods for the Accurate Calculation of Emission Spectra of Realistic-Size Quantum Dots** Sungwoo Kang<sup>1</sup>, Yongwook Kim<sup>2</sup>, Eunjoo Jang<sup>2</sup>, Youngho Kang<sup>3</sup> and Seungwu Han<sup>1</sup>; <sup>1</sup>Seoul National University, Korea (the Republic of); <sup>2</sup>Samsung Advanced Institute of Technology, Korea (the Republic of); <sup>3</sup>Incheon National University, Korea (the Republic of)

Semiconductor quantum dots (QDs) have attracted significant interest for wide color gamut display applications. Narrow emission linewidths are required to be achieved for the optical performance. As synthetic techniques have been improved, inhomogeneous linewidths can be reduced close to the single-dot level. However, the ultimate limit and the mechanism of homogeneous broadening of QDs are not clarified yet.

In this study, we develop an ab initio method to calculate the single-dot emission spectra of QDs originated from exciton-

phonon coupling (EPC) [1]. We calculate emission linewidths of core CdSe QDs, and demonstrate that the results are consistent with the CdSe/Cd<sub>x</sub>Se<sub>1-x</sub>Zn<sub>x</sub> QD [2]. In addition, the effect of charged surface traps on linewidth is studied. The partial Huang-Rhys factors of QDs show that the acoustic modes are dominant in EPC for perfectly passivated QDs, while the contribution of optical modes becomes significant with surface defects due to the internal field. Next, to simulate actual-size InP/ZnSe core/shell QD (3,506 atoms), we develop the theoretical framework combining machine learning and density functional theory (DFT) calculations: the structural relaxation and phonon calculations are performed by neural network potential (NNP), and the exciton is described by constrained DFT in single-particle level. We train NNP over reference structures made of various bulk, surface, and interface of InP and ZnSe using SIMPLE-NN code [3]. Trained NNP is tested for ZnSe QD and InP/ZnSe QD, not included in the training set, and verified to provide a precise description of phonon spectra in similar accuracy to DFT. Combining trained NNP with DFT, we calculate the emission spectrum of InP/ZnSe QD, and find that the result is in good agreement with the experimental measurement on the same size of InP/ZnSe/ZnS QD [4,5]. In addition, we find that the contribution of optical modes significantly increases when introducing ZnSe shell due to the mismatch between electron and hole wave functions.

[1] S. Kang, Y. Kim, E. Jang, Y. Kang and S. Han, *ACS Appl. Mater. Interfaces*, 12(19), 22012 (2020).

[2] Y.-S. Park, J. Lim and V. I. Klimov, *Nat. Mater.*, 18(3), 249 (2019).

[3] K. Lee, D. Yoo, W. Jeong and S. Han, *Comput. Phys. Commun.*, 242, 95 (2019).

[4] S. H. Lee, Y. Kim, H. Jang, J. H. Min, J. Oh, E. Jang and D. Kim, *Nanoscale*, 11(48), 23251 (2019).

[5] Y. Kim, S. Ham, H. Jang, J. H. Min, H. Chung, J. Lee, D. Kim and E. Jang, *ACS Appl. Nano Mater.*, 2(3), 1496 (2019).

#### 5:45 AM F.EL02.08.07

**Nanocrystal Precursor Incorporating Separated Reaction Mechanisms for Nucleation and Growth to Unleash the Full Potential of Heat-Up Synthesis** Joonhyuck Park<sup>1</sup>, Arun Jayaraman<sup>1</sup>, Xudong Wang<sup>2</sup>, Jing Zhao<sup>2</sup> and Hee-Sun Han<sup>1</sup>; <sup>1</sup>University of Illinois at Urbana-Champaign, United States; <sup>2</sup>University of Connecticut, United States

In the past few decades, many products incorporating quantum dots (QDs) have been introduced to the market. This has led to increasing demands for a simple, economical, and scalable synthesis method to produce high-quality core/shell QDs. The heat-up approach, involving bulk delivery of precursors at low temperature, is simple, scalable, and less sensitive to mixing limitations compared to the commonly used injection method. Its applications, however, have been limited because it inevitably yields a strong overlap between the nucleation and growth stages. We addressed this long-standing problem by introducing a new type of precursor having separated reaction paths for nucleation and growth. Unlike existing precursors, which employs a shared intermediate for both reactions, the new precursor have well-separated reaction mechanisms for growth and nucleation; growth proceeds via surface-assisted bond cleavage while nucleation requires the formation of metal-sulfur clusters in solution. Moreover, this precursor chemistry embeds an efficient mechanism to suppress nucleation during growth, enabling nucleation-free growth even at high precursor concentrations. Another unique benefit is temperature-independent tunability of precursor reactivity; the reactivity of the new precursor can be controllably tuned by chemical additives. By independently varying reaction temperature and precursor reactivity, researchers can systematically identify the optimal growth condition for various cores. We show that the new precursor grows high quality shells during heat up synthesis, comparable to those prepared by the continuous injection protocol. Lastly, we established a simple, economical, and scalable scheme for core/shell QDs by streamlining quantitative core synthesis and heat-up-based shell growth using the new precursor. The chemical insight obtained from this work inspires the design of other new precursors to unleash the full potential of heat-up synthesis as well as the development of a synthesis scheme that yields scale-independent reaction outcomes.

#### 5:55 AM F.EL02.08.08

**Electron Field Emission Behavior of Nitrogen Doped Graphene Quantum Dots Synthesized by Pulsed Laser Ablation** Muhammad Shehzad Sultan<sup>1</sup>, Vladimir I. Makarov<sup>1</sup>, Muhammad Sajjad<sup>2</sup>, Wojciech Jadwisnienczak<sup>3</sup>, Brad R. Weiner<sup>1</sup> and Gerardo Morell<sup>1</sup>; <sup>1</sup>University of Puerto Rico - Río Piedras, United States; <sup>2</sup>Indiana University Northwest, United States; <sup>3</sup>Ohio University, United States

Electron field emission is a process where the electrons are ejected from the material surface through quantum mechanical tunneling under the effect of high electric field. There is a great deal of research on the field emission properties of various nanomaterials, for example carbon nanomaterials, metal oxides, metal nitrides and metal tips. Among these cold cathode materials, carbon nanomaterials including carbon nanotubes (CNTs), graphene and diamond-like carbon are extensively investigated in order to seek high current density, stable and long-life cold cathodes. As expected, the carbon nanomaterials display unique advantages in field electron emission and carbon nanomaterials can potentially be used in cold-electron-source-based vacuum micro/nanoelectronics. Nitrogen doped graphene quantum dots (N-GQDs), chemically stable and with

potentially low toxic zero-dimensional nanostructure, are extensively studied in various fields, especially in energy storage, bio-imaging, photodetectors. So far the electron field emission behavior of individual N-GQDs has not been studied so in this research, a facile synthesis of nitrogen doped graphene quantum dots (N-GQDs) and its electron field emission performance will be carried out. Transmission Electron Microscopy (TEM), X-ray Photoelectron Spectroscopy (XPS), Raman and FTIR Spectroscopy, UV-vis and PL Spectra characterizations were carried out to study the structural and optical properties of as synthesized N-GQDs. The Current vs. Voltage (J-E) Curve of the N-GQDs Coated on Si Substrate was measured and Fowler-Nordheim (FN) plot was analyzed to check the Emission Stability of the N-GQDs Cathode with the objectives to achieve Outstanding Emission Stability of the N-GQDs Cathode and Low Turn-on Field ( $E_{10}$ ) and Threshold Field ( $E_{th}$ ).

SESSION F.EL02.09: Photophysical Properties of Low-Dimensional Material and Perovskite  
On Demand Abstracts Available for Viewing Starting Saturday Morning, November 21, 2020  
F-EL02

**5:00 AM \*F.EL02.09.02**

**Dielectric Confinement and Excitonic Effects in Two-Dimensional Nanoplatelets** Alexander Efros<sup>1</sup>, B. Ji<sup>2</sup>, E. Rabani<sup>3</sup>, R. Vaxenburg<sup>4</sup>, D. Azulay<sup>2</sup>, U. Banin<sup>2</sup> and O. Millo<sup>2</sup>; <sup>1</sup>U.S. Naval Research Laboratory, United States; <sup>2</sup>The Hebrew University of Jerusalem, Israel; <sup>3</sup>University of California, Berkeley, United States; <sup>4</sup>Howard Hughes Medical Institute, United States

Quasi-two-dimensional (2D) semiconductor nano-platelets manifest strong quantum confinement with exceptional optical characteristics of narrow photoluminescence peaks with energies tunable by thickness with monolayer precision.[1] We employed scanning tunneling spectroscopy (STS) in conjunction with optical measurements to probe the thickness-dependent band gap and density of excited states in a series of CdSe nanoplatelets.[2] The tunneling spectra, measured in the double-barrier tunnel junction configuration, reveal the effect of quantum confinement on the band gap taking place mainly through a blue-shift of the conduction band edge, along with a signature of 2D electronic structure intermixed with finite lateral-size and/or defects effects. The STS fundamental band gaps are larger than the optical gaps as expected from the contributions of exciton binding in the absorption, as confirmed by theoretical calculations. The calculations also point to strong valence band mixing between the light- and split-off hole levels. Strikingly, the energy difference between the heavy-hole and light-hole levels in the tunneling spectra are significantly larger than the corresponding values extracted from the absorption spectra. We have shown that this difference is mainly connected with enhancing of dielectric confinement of light holes relative to the heavy hole observed in STS measurement and an increase of light hole exciton binding energy relative to heavy hole exciton binding energy observed in absorption spectra.[2]

1. S. Ithurria, M. D. Tessier, B. Mahler, R. P. S. M. Lobo, B. Dubertret, and Al. L. Efros, A. L. Nat. Mater. 2011, 10, 936–941.
2. B. Ji, E. Rabani, Al. L. Efros, R. Vaxenburg, O. Ashkenazi, D. Azulay, U. Banin, and O. Milo ACS Nano, 2020 <https://dx.doi.org/10.1021/acsnano.0c01950>.

**5:15 AM \*F.EL02.09.03**

**Late News: Circular Dichroism in Non-Chiral Metal Halide Perovskite Nanostructures** Peter C. Sercel<sup>1</sup>, Valy Vardeny<sup>2</sup> and Alexander Efros<sup>3</sup>; <sup>1</sup>California Institute of Technology, United States; <sup>2</sup>The University of Utah, United States; <sup>3</sup>U.S. Naval Research Laboratory, United States

We have demonstrated theoretically that non-chiral perovskite layers can exhibit circular dichroism (CD) in the absence of a magnetic field and without chiral activation by chiral molecules [1]. The exciton dispersion in orthorhombic perovskites in the presence of Rashba spin-orbit terms creates helical exciton states, which are split from each other. The splitting can be described as a Zeeman effect in an effective magnetic field, whose direction and magnitude depend on the exciton momentum. The selective excitation of these states by helical light gives rise to CD. Using experimentally determined material parameters, we calculate significant circular dichroism of order 30% in orthorhombic perovskites under off-normal, top illumination. These calculations suggest the effect is observable and CD can be measured in non-chiral perovskite nanostructures such as layered-2D perovskites or nanoplatelets.

[1] P.C.Sercel, Z.V. Vardeny, Al.L. Efros, Nanoscale 2020, DOI/10.1039/D0NR05232A

**5:30 AM \*F.EL02.09.04**

**Excitonic and Vibrational Phenomena in Emerging 2D Light-Emitting Materials** William Tisdale; Massachusetts

Institute of Technology, United States

In this talk, I will present recent results from our lab exploring the excitonic and vibrational properties of emerging 2D light-emitting materials, including hybrid organic-inorganic perovskites, few-layer black phosphorous, and hybrid chalcogenides. Topics may include: 1) interlayer vibrational coupling and superlattice modes of layered 2D structures; 2) tunable exciton binding energy in layered perovskites; 3) origin of broadband emission in multilayer ( $n > 2$ ) lead halide perovskites; and 4) demonstration of novel materials with strong excitonic anisotropy.

#### 5:45 AM F.EL02.09.05

**Light-Induced Magnetism in Mn-Doped CsPbI<sub>3</sub> Perovskite Quantum Dots** Tian Qiao<sup>1</sup>, Daniel P. Rossi<sup>2</sup>, Xiaohan Liu<sup>1</sup>, Mohit Khurana<sup>1</sup>, Alexey Akimov<sup>1,3,4</sup> and Dong Hee Son<sup>1,2</sup>; <sup>1</sup>Texas A&M University, United States; <sup>2</sup>Center for Nanomedicine, Korea (the Republic of); <sup>3</sup>Russian Quantum Center, Russian Federation; <sup>4</sup>PN Lebedev Institute RAS, Russian Federation

Magnetic doping of semiconductor quantum dots has generated new materials that can couple magnetism with light, which are attractive for various applications such as spintronics. Here, we report the synthesis of strongly quantum-confined CsPbI<sub>3</sub> quantum dots doped with paramagnetic Mn<sup>2+</sup> ions and the characterization of their optical and magneto-optic properties evidencing the creation of light-induced magnetism. The magnetic order of the dopant ions forms via exchange interaction of the dopants and long-lived dark exciton at cryogenic temperatures. At the temperature of 5 K, CsPbI<sub>3</sub> quantum dots exhibited photoluminescence (PL) from dark exciton PL with lifetime of 1.5 microsecond in the absence of Mn dopant indicating that the lowest exciton state in this system is dipole forbidden dark state, which is beneficial in obtaining longer-lived light-induced magnetism. In Mn-doped CsPbI<sub>3</sub> quantum dots, the dark exciton PL lifetime decreased by 30 %, which is similar to the effect of applying external magnetic field, suggesting the creation of magnetic order from the doped paramagnetic Mn<sup>2+</sup> ions. Comparison of the temperature-dependent PL spectra of Mn-doped and undoped CsPbI<sub>3</sub> quantum dots showed that Mn-doped quantum dots have smaller PL energy due to magnified Zeeman splitting under light-induced magnetism. Our results suggest Mn-doped CsPbI<sub>3</sub> quantum dots, combined with long-lived dark ground exciton state, could become a promising material platform for obtaining optically generated magnetism.

#### 5:55 AM F.EL02.09.06

**Structure-Property Relationships for 2D Halide Perovskites with Large Cage Cations** Xiaotong Li<sup>1</sup>, Yongping Fu<sup>1</sup>, Pedesseau Laurent<sup>2</sup>, Peijun Guo<sup>3</sup>, Shelby Cuthriell<sup>1</sup>, Ido Hadar<sup>1</sup>, Jacky Even<sup>2</sup>, Claudine Katan<sup>2</sup>, Constantinos Stoumpos<sup>1</sup>, Richard D. Schaller<sup>3</sup>, Elad Harel<sup>1</sup> and Mercouri G. Kanatzidis<sup>1</sup>; <sup>1</sup>Northwestern University, United States; <sup>2</sup>University of Rennes, France; <sup>3</sup>Argonne National Laboratory, United States

In 2D perovskites, the choice of the A-site perovskitizer cations is not entirely limited by the so-called Goldschmidt tolerance factor. The stabilizing effect of the spacer cations makes it possible to tolerate larger A-site cations as perovskitizers. By solving the single-crystal structures of (BA)<sub>2</sub>(A)Pb<sub>2</sub>I<sub>7</sub> where BA = butylammonium, and A = methylammonium (MA), formamidinium (FA), dimethylammonium (DMA) or guanidinium (GA), we have proven that the relatively large DMA and GA can serve as the A-site cation of 2D perovskites despite the fact that they are too large to formally satisfy the Goldschmidt rule. As the size of the A-site cations across these compounds increases, the Pb-I bonds are elongated, which reduces the orbital overlap of Pb s- and I p-orbitals, thus decreasing the electronic bandwidths and increasing the bandgaps, as confirmed by DFT calculations. This increases the local distortions of the PbI<sub>6</sub> coordination environment and leads to a decrease of PL intensity and shortening of PL lifetime. The expanded cages also result in soft and anharmonic lattices, as supported by Raman spectra. Exciton-exciton annihilation processes occur in these systems with the rates being slower in the structures with larger A cations.

#### 6:05 AM F.EL02.09.08

**Late News: Transfer of Direct to Indirect Bound Excitons by Electron Intervalley Scattering in Cs<sub>2</sub>AgBiBr<sub>6</sub> Double Perovskite Nanocrystals** Amrita Dey, Alexander F. Richter, Tushar Debnath, He Huang, Lakshminarayana Polavarapu and Jochen Feldmann; Ludwig-Maximilians-Universität, Germany

Lead halide perovskites have gained a lot of popularity in the field of optoelectronics in recent times. Where the toxicity of lead remains a major issue, an emerging non-toxic alternative proposed is lead-free double perovskites with the generic stoichiometric formula A<sub>2</sub>M<sup>I</sup>M<sup>III</sup>X<sub>6</sub>. In double perovskite the divalent lead is replaced with one monovalent (M<sup>I</sup>) and one trivalent (M<sup>III</sup>) metal cation. Cs<sub>2</sub>AgBiBr<sub>6</sub> is one the stable double perovskite with an indirect bandgap where the optical properties and the charge carrier relaxation processes are not fully understood. We applied time-resolved photoluminescence and differential transmission spectroscopy to explore the photo-excited charge carrier dynamics within the indirect band



structure of Cs<sub>2</sub>AgBiBr<sub>6</sub> nanocrystals. We observed a high energetic emission at the direct bandgap, alongside the emission from the indirect bandgap transition. We assigned this emission to the radiative recombination of the direct bound excitons originating due to trapping of holes. Due to the electron intervalley scattering process, the emission maximum from this direct bound excitons redshifts over 1 eV within 10 ps, leading to its transfer from direct to indirect bound exciton. We conclude that this direct bound exciton has giant oscillator strength which causes the higher energetic emission to occur at the direct bandgap despite the prevailing intervalley scattering process. These results expand the current understanding of the optical properties and the charge carrier relaxation process in double perovskites family, thus, facilitating the further development of optoelectronic devices harnessing lead-free perovskites.

**6:15 AM F.EL02.09.09**

**Late News: Growth of Perovskite CsPbBr<sub>3</sub> Nanocrystals and Their Formed Superstructures Revealed by *In Situ* Spectroscopy** He Huang; Ludwig-Maximilians-Universität München, Germany

Metal halide perovskites have attracted substantial interest due to their promising properties for optoelectronic applications. Despite much progress made in the field, the exact growth mechanism of perovskite nanocrystals (e.g. CsPbBr<sub>3</sub>) remains elusive and further improvement of their controllable synthesis is challenging. Herein, we point out different phenomena during the processes of growth, cooling and purification of high-quality CsPbBr<sub>3</sub> nanocrystals using *in-situ* PL spectroscopy. The as-synthesized materials have been further characterized by time-resolved differential transmission and photoluminescence spectroscopies. Using X-ray scattering, we confirm that nanocrystals form superstructures during the process of cooling already in dispersion, which is frequently ignored. The purification process is explained by a proposed model based on the self-size-selection. On the one hand, such superstructures pave a potential pathway to the fabrication of high-quality devices such as LEDs. On the other hand, the approach to reveal their formation process benefits the comparison and understanding of the difference between nanocrystals and supercrystals. The fact that superstructures form already during synthesis may also apply to the different perovskite systems and thus help to improve the quality of as-prepared nanocrystals.

**6:25 AM F.EL02.09.10**

**Late News: Semiconductor Nanocrystal Scintillators for Fast Neutron Imaging** Kyle M. McCall<sup>1,2</sup>, Kostiantyn Sakhatskyi<sup>1,2</sup>, Eberhard Lehmann<sup>3</sup>, Bernhard Walfort<sup>4</sup>, Adrian Losko<sup>5</sup>, Federico Montanarella<sup>1,2</sup>, Maryna Bodnarchuk<sup>1,2</sup>, Franziska Krieg<sup>1,2</sup>, Yusuf Kelestemur<sup>1,2,6</sup>, David Mannes<sup>3</sup>, Yevhen Shynkarenko<sup>1,2</sup>, Sergii Yakunin<sup>1,2</sup> and Maksym V. Kovalenko<sup>1,2</sup>; <sup>1</sup>ETH Zürich, Switzerland; <sup>2</sup>Empa–Swiss Federal Laboratories for Materials Science and Technology, Switzerland; <sup>3</sup>Paul Scherrer Institut, Switzerland; <sup>4</sup>RC Tritec AG, Switzerland; <sup>5</sup>Forschungs-Neutronenquelle Heinz Maier-Leibnitz, Germany; <sup>6</sup>Atılım University, Turkey

Radiographical imaging with X-rays, gamma-rays, and thermal neutrons (~25 meV) has transformed fields including medical imaging, industrial inspection, and nuclear security over the past century. Fast neutron (> 1 MeV) imaging is a rising technique which benefits from the high penetration capabilities of fast neutrons which offer low interaction cross sections relative to other radiation sources. This penetrative power makes fast neutrons ideal for imaging large-scale objects such as large fossils, nuclear fuel, and as-built plane turbines, but widespread application of fast neutron imaging is hindered by inefficient fast neutron detection. The current detection scheme is based on detection of recoil protons generated by neutrons scattering off hydrogen, with the leading material in the field consisting of ZnS:Cu embedded in hydrogen-dense plastic. However, these scintillation plate detectors rely on microscale phosphors with drawbacks including significant light scattering at the plastic-phosphor interface, strong absorption of (and sensitivity to) gamma-rays, and long-lived afterglows on the order of minutes. Thus, alternative solutions are required to enhance the performance of detectors for fast neutron imaging.

Separately, the development of semiconductor nanocrystals (NCs) has ushered in a golden age for nanoscale emissive materials with quantum yields near unity and enhanced recombination rates for short decay times, promising maximal detector efficiency while eliminating problematic afterglow. Here, we demonstrate the efficacy of nanocrystals as scintillators for fast neutron imaging, utilizing colloidal nanocrystals in hydrogen-dense solvents to detect recoil protons generated by scattering of fast neutrons. The light yield, spatial resolution, and neutron-vs.-gamma sensitivity of several representative compositions are compared, including both chalcogenide (CdSe and CuInS<sub>2</sub>)-based and halide perovskite-based NCs, revealing the key parameters for optimized fast neutron detection.

FAPbBr<sub>3</sub> NCs exhibit the brightest total light output at 19.3% of the commercial ZnS:Cu(PP) standard (consisting of ZnS:Cu embedded in PP = polypropylene), the light output of the other compositions ranged from 1.5% for CuInS<sub>2</sub> NCs to 6.0% for CdSe/CdS quantum dots. Colloidal NCs also showed significantly lower gamma-ray sensitivity than ZnS:Cu, with the ratio of detected neutrons to gamma-rays ranging from 2.2 in CsPbBrCl<sub>2</sub>:Mn NCs to 4.1 for CsPbBr<sub>3</sub> NCs, well above the 1.0-1.1

reported for ZnS:Cu(PP). This permits the use of less gamma-ray shielding and therefore enables a higher flux of fast neutrons, for example, 79% of the FAPbBr<sub>3</sub> light yield results from neutron-induced radioluminescence and hence the neutron-specific light yield of FAPbBr<sub>3</sub> is 30.4% of that of ZnS:Cu(PP), despite the tenfold higher phosphor load of ZnS:Cu(PP). Metal blocks with sharp edges were used to estimate the spatial resolution, with the high Stokes shift CsPbBrCl<sub>2</sub>:Mn NCs offering the best spatial resolution at ~2.6 mm while that of FAPbBr<sub>3</sub> NCs is doubled at ~5.2 mm due to reabsorption and re-emission. Importantly, all NCs showed no evidence for afterglow on the order of seconds, in contrast to the minutes-long afterglow of the ZnS:Cu(PP) standard. Concentration and thickness-dependent measurements highlight the importance of increasing concentrations and reducing self-absorption, yielding design principles to optimize and foster an era of NC-based scintillators for fast neutron imaging.

#### 6:35 AM F.EL02.09.11

**Water Stable 1D Hybrid Tin(II) Iodide Emits Broad Light with 36% Photoluminescence Quantum Yield** Ioannis Spanopoulos<sup>1</sup>, Ido Hadar<sup>1</sup>, Weijun Ke<sup>1</sup>, Peijun Guo<sup>2</sup>, Siraj Sidhik<sup>3</sup>, Mikaël Kepenekian<sup>4</sup>, Jacky Even<sup>4</sup>, Aditya D. Mohite<sup>3</sup>, Richard D. Schaller<sup>1</sup> and Mercouri G. Kanatzidis<sup>1</sup>; <sup>1</sup>Northwestern University, United States; <sup>2</sup>Argonne National Laboratory, United States; <sup>3</sup>Rice University, United States; <sup>4</sup>Univ Rennes, France

Low dimensional (2D, 1D, 0D) lead halide materials have proven to be quite promising in terms of strong broad light emission with PLQY values above 90%, rendering them suitable for solid state lighting applications. These materials in order to be utilized in real applications must be environmentally stable and of non-toxic composition. Tin(II) based compounds pose as an excellent choice for addressing toxicity issues, however they are moisture and oxygen sensitive.

Addressing the above concerns, we report a new air-stable one-dimensional (1D) hybrid tin(II) halide material (DAO)Sn<sub>2</sub>I<sub>6</sub> (DAO: 1,8-octyldiammonium), that is resistant to water for more than 15h.[1] The material exhibits a sharp absorption edge at 2.70 eV and a strong broad orange light emission centered at 634 nm, with a full width at half maximum (FWHM) of 142 nm (0.44 eV). The corresponding emission has a high photoluminescence (PL) quantum yield (PLQY) of at least 20.3% at RT, being among the highest reported for lead-free low-dimensional 2D and 1D perovskites and metal halides, which is coupled by a very long PL lifetime of 582 ns. Additionally, the PL emission intensity and linewidth is constant over a very broad temperature range (145-415 K), underscoring the beneficial high temperature PL robustness. The corresponding CIE chromaticity coordinates are (0.55, 0.42), with a correlated color temperature (CCT) of 1822 K (warm orange light), and a color-rendering index (CRI) value of 75, meaning that this material is suitable for outdoor lighting.

We further evaluated the ability of (DAO)Sn<sub>2</sub>I<sub>6</sub> to fabricate thin films, the first step prior to device assembly. Apparently, the corresponding films exhibited the same optical properties of the bulk crystals, yet enhanced with an improved PLQY of 36%, and a much longer PL lifetime of 1100 ns, for a 60 nm thick film. These results demonstrate the versatile nature of hybrid halide materials, laying the path for the design of next generation of water stable lead-free semiconductors.

#### References

[1] Spanopoulos, I.; Hadar, I.; Ke, W.; Guo, P.; Sidhik, S.; Kepenekian, M.; Even, J.; Mohite, A. D.; Schaller, R. D.; Kanatzidis, M. G., *J. Am. Chem. Soc.* **2020**, 142, 9028-9038

#### 6:45 AM F.EL02.09.12

**Photocatalytic Inactivation of Escherichia Coli under UV Light Irradiation Using Large Surface Area Anatase TiO<sub>2</sub> Quantum Dots** Faheem Ahmed and Adil Alshoaibi; King Faisal University, Saudi Arabia

In this study, high specific surface areas (SSAs) of anatase titanium dioxide (TiO<sub>2</sub>) quantum dots (QDs) were successfully synthesized through a novel one-step microwave-hydrothermal method in rapid synthesis time (20 min) without further heat treatment. XRD analysis and HR-TEM images showed that the as-prepared TiO<sub>2</sub> QDs of approximately 2 nm size have high crystallinity with anatase phase. Optical properties showed that the energy band gap (E<sub>g</sub>) of as-prepared TiO<sub>2</sub> QDs was 3.60 eV, which is higher than the standard TiO<sub>2</sub> band gap, which might be due to the quantum size effect. Raman studies showed shifting and broadening of the peaks of TiO<sub>2</sub> QDs due to the reduction of the crystallite size. The obtained Brunauer-Emmett-Teller specific surface area (381 m<sup>2</sup> g<sup>-1</sup>) of TiO<sub>2</sub> QDs is greater than the surface area (181 m<sup>2</sup> g<sup>-1</sup>) of commercial TiO<sub>2</sub>

nanoparticles. The photocatalytic activities of TiO<sub>2</sub> QDs were conducted by the inactivation of Escherichia coli under ultraviolet light irradiation and compared with commercially available anatase TiO<sub>2</sub> nanoparticles. The photocatalytic inactivation ability of E. coli was estimated to be 91% at 60 µg ml<sup>-1</sup> for TiO<sub>2</sub> QDs, which is superior to the commercial TiO<sub>2</sub> nanoparticles. Hence, the present study provides new insight into the rapid synthesis of TiO<sub>2</sub> QDs without any annealing treatment to increase the absorbance of ultraviolet light for superior photocatalytic inactivation ability of E. coli.

#### 6:55 AM F.EL02.09.13

**Design Strategies for Achieving Efficient Wide Bandgap Halide Perovskite Phosphors via Analysis of the Halide Double Perovskite  $\text{Cs}_2\text{NaBiCl}_6\text{:Mn}^{2+}$  Orange-Emitting Phosphor System** [Jackson Majher](#)<sup>1</sup>, Matthew Gray<sup>1</sup>, Amanda Strom<sup>2</sup> and Patrick Woodward<sup>1</sup>; <sup>1</sup>The Ohio State University, United States; <sup>2</sup>University of California, Santa Barbara, United States

Recently wide bandgap halide double perovskites have emerged as promising phosphor materials for white light LED applications. These materials demonstrate enhanced photoluminescence properties compared to bulk  $\text{APbX}_3$  ( $\text{A} = \text{NH}_3\text{CH}_3^+$ ,  $\text{Cs}$ ;  $\text{X} = \text{Cl}, \text{Br}, \text{I}$ ) perovskites due in large part to their higher exciton binding energy, thereby reducing extensive nonradiative decay at defects and grain boundaries.  $\text{Cs}_2\text{NaBiCl}_6$  is an example of a halide double perovskite which in the pure form exhibits no photoluminescence. Upon doping  $\text{Mn}^{2+}$  into the lattice (0.06-7.2 mol%) bright orange luminescence emerges under UV excitation originating from the  ${}^4\text{T}_1$  to  ${}^6\text{A}_1$  transition of  $\text{Mn}^{2+}$  ions in an octahedral environment. Analysis of absorption and excitation measurements indicate absorption of the host material is dominated by localized  $6s^2$  to  $6s^16p^1$  transitions of  $\text{Bi}^{3+}$  ions, indicating a zero-dimensional electronic structure. The localized nature of  $\text{Bi}^{3+}$  absorption in the perovskite structure is identified as a crucial component for efficient energy transfer to  $\text{Mn}^{2+}$  sites. Partial replacement of  $\text{Cl}^-$  with  $\text{Br}^-$  in the structure forming  $\text{Cs}_2\text{NaBiCl}_{6-x}\text{Br}_x\text{:Mn}^{2+}$  is demonstrated to relax the crystal field around  $\text{Bi}^{3+}$  ions thereby shifting the excitation range towards the visible where it can be excited by conventional GaInN blue LEDs. Lessons learned in this study extend towards several other double perovskite and perovskite-derivative materials, including systems exhibiting intrinsic luminescence via self-trapped excitons as well as activator-doped materials. Routes to optimize photoluminescence in these systems are addressed.

#### 7:05 AM F.EL02.09.14

**Annealing Effects on the Optical and Luminescent Properties of Erbium Doped AZO Thin Films** [Paul Llontop](#), Miguel Piñeiro, Kevin Lizárraga, Jan Amaru Töfflinger, Rolf Grieseler and Jorge A. Guerra; Pontificia Universidad Católica del Perú, Peru

Rare-earth doped wide bandgap (WBG) semiconductors have attracted great attention as efficient luminescent materials for optoelectronic applications, such as photon downshift, down- and up-conversion systems, a new generation of low voltage light-emitting devices, non-contact luminescent temperature sensors and photonic structures.

However, these luminescent mechanisms have yet to be successfully implemented in transparent conductive oxide (TCO) films with a WBG, such as indium tin oxide (ITO) or aluminum zinc oxide (AZO) which often form part of these devices. Such optically active TCOs would therefore be advantageous for these applications since layers of the same TCO are already being used in said devices.

Our work focuses on the production and characterization of terbium (Tb) doped AZO thin films, keeping a high optical transmittance in the visible region and exhibiting Tb related luminescent properties. The effect of Tb doping on the optical and luminescent properties was investigated for different post-deposition annealing conditions. Films were produced on silicon and fused silica substrates by radiofrequency magnetron co-sputtering employing high purity AZO and Tb targets and a rotary sample holder. After deposition, samples were annealed between 200°C - 1000°C in steps of 100°C. The annealing processes were carried out in air or argon atmosphere. Optical transmittance, photoluminescence (PL) and energy dispersive X-ray spectroscopy experiments were made after each annealing step. Characteristic  $\text{Tb}^{3+}$  related light emission peaks were found in the as grown, as well as in the annealed samples. To the best of our knowledge, this is the first demonstration of  $\text{Tb}^{3+}$  emission in AZO as host matrix. Absorption coefficient, band gap and Urbach energies were estimated using computational methods and models developed in our group. Furthermore, temperature dependent PL experiments, ranging from 80K to 530K, were carried out on representative samples to discuss possible energy transfer mechanisms between  $\text{Tb}^{3+}$  ions and AZO matrix.

#### 7:15 AM F.EL02.09.15

**Structure-Property Correlation, Luminescence Enhancement and Excited-State Dynamics in Near-Infrared Emitting Gold Nanoclusters** [Qi Li](#); Stanford University, United States

The origin of the near-infrared photoluminescence (PL) from thiolate-protected gold nanoclusters (Au NCs, <2 nm) has long been controversial, and the exact mechanism for the enhancement of quantum yield (QY) in many works remains elusive. It is still a major challenge for researchers to map out a definitive relationship between the atomic structure and the PL property and understand how the Au kernel and Au-S surface contribute to the PL of Au NCs.

Herein, we first provide a paradigm study to address the above critical issues. By using a correlated series of “mono-cuboctahedral kernel” Au NCs and combined analyses of steady-state, temperature-dependence, femtosecond transient absorption, and Stark spectroscopy measurements, we have explicitly mapped out a kernel-origin mechanism and clearly elucidate the surface–structure effect, which establishes a definitive atomic-level structure–emission relationship. A ~100-fold enhancement of QY is realized via suppression of two effects: (i) the ultrafast kernel relaxation and (ii) the surface vibrations. The new insights into the PL origin, QY enhancement, wavelength tunability, and structure–property relationship constitute a major step toward the fundamental understanding and structural-tailoring-based modulation and enhancement of PL from Au NCs.

Furthermore, we report the emergence of a photo-induced structural distortion accompanied by an electron redistribution in a series of bi-tetrahedral gold nanoclusters. Such unexpected slow process of excited-state transformation results in near-infrared dual emission with extended photoluminescent lifetime. We demonstrate that this dual emission exhibits highly sensitive and ratiometric response to solvent polarity, viscosity, temperature and pressure. Thus, a versatile luminescent nano-sensor for multiple environmental parameters has been developed based on this strategy. Furthermore, we fully unravel the atomic-scale structural origin of this unexpected excited-state transformation, and demonstrate control over the transition dynamics by tailoring the bi-tetrahedral core structures of gold nanoclusters.

**7:25 AM F.EL02.09.16**

**Intense Microsecond-Lived Dark Exciton Emission from Strongly Quantum Confined Perovskite Nanocrystals** Dong Hee Son; Texas A&M University, United States

Dark exciton as the lowest-energy (ground) exciton state in metal halide perovskite nanocrystals is a subject of much interest. This is because the superior performance of perovskites as the photon source combined with long lifetime of dark exciton is very attractive for the applications such as quantum information processing. However, the direct observation of the long-lived dark exciton emission confirming the accessibility to dark ground exciton state has remained elusive. In this presentation, we discuss the observation of the intense photoluminescence (PL) from dark exciton with lifetime of 1-10 microsecond in strongly confined CsPbBr<sub>3</sub> nanocrystals of varying dimensionality of confinement. Strongly confined quantum dots, nanowires and nanoplatelets of cesium lead halide perovskite showed dark exciton emission that dominates the PL at cryogenic temperatures with bright-dark splitting energy ( $\Delta E$ ) of ~20 meV, which contrasts to the behavior of weakly confined nanocrystals that exhibit little dark exciton PL. The lifetime of dark exciton PL shortened under magnetic field as expected.  $\Delta E$  increased with increasing quantum confinement giving an easier access to the dark exciton PL at the higher temperatures, which is also consistent with the prediction from the earlier theoretical prediction. This work establishes the potential of strongly quantum confined perovskite nanostructures as the excellent platform to harvest the benefits of extremely long-lived and intense dark exciton PL.

**7:35 AM F.EL02.09.17**

**Late News: Green Solvent Assisted Synthesis of Cesium Bismuth Halide Perovskite Nanocrystals and Insights into the Effects of Slow and Fast Anion Exchange Rates** Rana Faryad Ali, Byron Gates and Irene Andreu; Simon Fraser University, Canada

The replacement of lead in halide perovskites with alternative halide perovskite materials has been driven by the concerns of lead toxicity. Lead-free all-inorganic cesium bismuth halide (Cs<sub>3</sub>Bi<sub>2</sub>X<sub>9</sub>) perovskites nanocrystals have attracted much attention in recent years due to their air-stability and the relatively non-toxic nature of bismuth. Common solvents used to prepare Cs<sub>3</sub>Bi<sub>2</sub>X<sub>9</sub> nanomaterials under ambient conditions have included dimethyl sulfoxide (DMSO) and dimethylformamide (DMF), which are also desired to be avoided for their own hazards. Herein, we demonstrate a facile, sonication-assisted approach for the preparation of all-inorganic cesium bismuth iodide (Cs<sub>3</sub>Bi<sub>2</sub>I<sub>9</sub>) perovskite nanocrystals (NCs) using propylene carbonate as a green solvent. The photoluminescence (PL) spectra of the Cs<sub>3</sub>Bi<sub>2</sub>X<sub>9</sub> NCs are further tuned from 410 to 550 nm by controlling the composition of the NCs through anion exchange reactions using tetraalkylammonium halides as a source of halide ions. The rate of reaction for the anion exchange process significantly influences the dimensions of the resulting NCs in contrast to their parent Cs<sub>3</sub>Bi<sub>2</sub>I<sub>9</sub> NCs. Absolute photoluminescence quantum efficiency (PLQE) of the Cs<sub>3</sub>Bi<sub>2</sub>I<sub>9</sub> NCs was also determined, and their PL emission was determined to be predominately due to exciton recombination processes. The NCs also exhibited an excellent air-stability for at least 150 days.

SESSION F.EL02.10: Mechanism and Physics of Perovskite and Low-Dimensional Light-Emitting Materials  
On Demand Abstracts Available for Viewing Starting Saturday Morning, November 21, 2020  
F-EL02

### 5:00 AM \*F.EL02.10.01

**Nanoscale Effects in Metal Halide Perovskites for Light-Emitting Applications.** Laura Herz; University of Oxford, United Kingdom

Organic-inorganic metal halide perovskites have emerged as attractive materials for light-emitting and light-harvesting devices. We discuss the fundamental processes that have underpin light-matter interactions enabling these applications.

Photon recycling is shown to slow charge losses from thin hybrid perovskite films, depending on light outcoupling. Interestingly, for thin films comprising a quasi-two-dimensional (2D) perovskite region interfaced with a 3D MAPbI perovskite layer the blue-shifted emission originating from quasi-2D regions overlaps significantly with the absorption spectrum of the 3D perovskite, allowing for highly effective “heterogeneous photon recycling”. We show that this combination fully compensates for the adverse effects of electronic confinement, yielding quasi-2D perovskites with highly efficient charge transporting properties.

We further discuss how vibrational, charge-carrier recombination and mobility is altered in thin films of perovskite nanocrystals films with respect to the bulk film. We show in thin films, carrier mobilities are still mostly dominated by intra-particle motion rather than inter-particle hops.

In tunable bandgaps across the entire visible light emission range, we discuss the mechanisms underlying detrimental halide segregation in mixed halide lead perovskites.

*S. G. Motti, T. Crothers, R. Yang, Y. Cao, R. Li, M. B. Johnston, J. Wang, and L. M. Herz, Nano Lett. 19, 3953 (2019).*

*S. G. Motti, F. Krieg, A. J. Ramadan, J. B. Patel, H. J. Snaith, M. V. Kovalenko, M. B. Johnston, and L. M. Herz, Adv. Func. Mater. 30, 1909904 (2020).*

*E. S. Parrott, J. B. Patel, A.-A. Haghghirad, H. J. Snaith, M. B. Johnston, and L. M. Herz, Nanoscale 11, 14276 (2019).*

*A. Knight, A. D. Wright, J. B. Patel, D. McMeekin, H. J. Snaith, M. B. Johnston, and L. M. Herz, ACS Energy Lett. 4, 75 (2019).*

*A. J. Knight, J. B. Patel, H. J. Snaith, M. B. Johnston, and L. M. Herz, Adv. Energy Mater. 10, 1903488 (2020).*

### 5:15 AM F.EL02.10.02

**Toward On-Demand Electrically-Driven Single-Photon Source That Can Be Triggered in Less Than 0.2 ns** Igor A. Khramtsov and Dmitry Y. Fedyanin; Moscow Institute of Physics and Technology, Russian Federation

On-demand single-photon sources (SPSs) operating at room temperature under electrical pumping play a crucial role in the emerging quantum applications ranging from linear quantum computing [1] to unconditionally secure communication lines [2]. Color centers in silicon carbide are now considered as a promising platform for the realization of such electrically-pumped SPSs operating at room temperature. In the steady-state, they are brighter than other quantum emitters, such as color centers in diamond or epitaxial quantum dots [3]. At the same time, steady-state emission of single photons almost does not have practical quantum applications, and an on-demand SPS is highly needed. However, very little is known about how to control, dynamically tune and quickly switch on and off the single-photon electroluminescence (SPEL) of color centers in SiC that will allow to meet the on-demand requirement when exactly one photon is emitted per excitation pulse.

Here, we propose and numerically demonstrate the SiC gate-tunable single-photon emitting diode (GT-SPED) with a silicon antisite near stacking fault (Si<sub>C</sub>-SF) defect placed underneath the gate [4]. Its emission can be controlled via source/drain and gate contacts. When no voltage is applied to the gate, the GT-SPED acts as a conventional p-i-n single-photon emitting diode, where the SPEL of Si<sub>C</sub>-SF cannot be switched between ON and OFF states fastly due to the high diode capacitance.

However, if one applies voltage to the gate contact and change it in the range of several volts at a fixed source voltage, he can not only control and dynamically tune the SPEL of Si<sub>C</sub>-SF center from 0.16 Mcps (OFF state) to 40 Mcps (ON state) but what is more important, switch between ON and OFF states of Si<sub>C</sub>-SF SPEL in less than 0.2 ns, which is less than the radiative lifetime of the Si<sub>C</sub>-SF center and other defects in solids. These possibilities allow to trigger single-photon emission from the Si<sub>C</sub>-SF center by applying small voltage pulses to the gate contact. If the width of such a voltage pulse is chosen

correctly, a single photon will be emitted with the probability of multiphoton events of less than 2%. Hence, the proposed device lays the solid foundation for the development of electrically-driven on-demand single-photon sources operating at room temperature.

## References

- [1] T. D. Ladd, F. Jelezko, R. Laflamme, Y. Nakamura, C. Monroe, and J. L. O'Brien, *Nature* 464, 45 (2010).
- [2] A. V. Sergienko, *Quantum Communications and Cryptography* (CRC Press, 2018).
- [3] A. Lohrmann, N. Iwamoto, Z. Bodrog, S. Castelletto, T. Ohshima, T. J. Karle, A. Gali, S. Prawer, J. C. McCallum, and B. C. Johnson, *Nat. Commun.* 6, 7783 (2015).
- [4] I. A. Khramtsov and D. Y. Fedyanin, *ACS Applied Electronic Materials* 1, 1859 (2019).

### 5:25 AM F.EL02.10.03

**Enhanced Room Temperature Photoluminescence Quantum Yield in Morphology-Controlled J-Aggregates** Surendra B. Anantharaman<sup>1,2</sup>, Joachim Kohlbrecher<sup>3</sup>, Gabriele Raino<sup>4,5</sup>, Sergii Yakunin<sup>4,5</sup>, Thilo Stöferle<sup>6</sup>, Jay Patel<sup>1</sup>, Maksym V. Kovalenko<sup>4,5</sup>, Rainer F. Mahrt<sup>6</sup>, Frank Nuesch<sup>1,2</sup> and Jakob Heier<sup>1</sup>; <sup>1</sup>Swiss Federal Laboratories for Materials Science and Technology, Empa, Switzerland; <sup>2</sup>École Polytechnique Fédérale de Lausanne EPFL, Switzerland; <sup>3</sup>Paul Scherrer Institute, Switzerland; <sup>4</sup>ETH Zürich, Switzerland; <sup>5</sup>Swiss Federal Laboratories of Materials Science and Technology, Empa, Switzerland; <sup>6</sup>IBM Research–Zurich, Switzerland

Narrow-band photoluminescence (PL) together with high quantum efficiency from organic molecules is essential for high-color-purity emitters. Supramolecular assemblies like J-aggregates are promising materials due to their narrow PL signal with full-width at half maximum <20 nm. However, their microcrystalline nature and coherent exciton migration results in strong nonradiative exciton recombination at the grain boundaries that diminish the photoluminescence quantum yield (PLQY), and possibilities for improving the crystallinity by tuning the growth mechanism are limited. Here, two distinct routes to grow different J-aggregate morphologies like platelets and lamellar crystals with improved crystallinity by surface-guided molecular assembly are demonstrated, thereby suppressing nonradiative decay and improving PLQY (upto 5% at room temperature). Both platelets and lamellar crystals show similar absorbance at room temperature. However, temperature-dependent PL studies show sevenfold (twofold) higher PLQY for lamellar films compared to platelets at 6 K (300 K). Using time-resolved PL spectroscopy, different nonradiative decay pathways are identified.<sup>1</sup>

Revisiting the J-aggregates formation in solution, we demonstrate that cyanine J-aggregates can reach an order of magnitude higher photoluminescence quantum yield (increase from 5% to 60%) in blend solutions of water and alkylamines at room temperature.<sup>2</sup> By means of time-resolved photoluminescence (TRPL) studies we show an increase in the exciton lifetime as a result of the suppression of non-radiative processes. Small-angle neutron scattering studies suggest a necessary condition for the formation of such highly emissive J-aggregates: the presence of a sharp water/amine interface for J-aggregate assembly and the coexistence of nanoscale-sized water and amine domains to restrict the J-aggregate size and solubilize monomers, respectively.

## References

- 1. Anantharaman, S. B., Stöferle, T., Nüesch, F. A., Mahrt, R. F. & Heier, J. Exciton Dynamics and Effects of Structural Order in Morphology-Controlled J-Aggregate Assemblies. *Adv. Funct. Mater.* 29, 1806997 (2019).
- 2. Anantharaman, S. B. et al. Enhanced Room Temperature Photoluminescence Quantum Yield in Morphology-controlled J-aggregates. Under Revision. (2020).

### 5:35 AM F.EL02.10.04

**Terahertz Emission with Plasmonic Photomixer in an InGaAs-Based Dual-Grating-Gate High-Electron-Mobility Transistor** Tomotaka Hosotani, Akira Satou and Taiichi Otsuji; Tohoku University, Japan

Plasmonic terahertz (THz) emitters are expected as on-chip and coherent THz sources. Up to the present, THz emissions stimulated by plasmonic instability with dc-current-driven Doppler-shift (DS) type and electron-transit-time (ETT) type have been experimentally observed in high-electron-mobility transistors (HEMTs). These instabilities could stimulate resonant-mode THz emission. Here we experimentally investigate the dc-current-driven plasmonic boom instability, the third plasmonic instability that occurs when the electron drift velocity exceeds the plasma velocity. The plasmonic boom instability generates shockwaves so that it stimulates rather broadband THz emission. To obtain a coherent narrow-band emission, a pertinent cavity structure needs to be installed. We use an original dual-grating-gate (DGG) HEMT structure based on an InGaAs high electron mobility channel under photoexcitation of photomixed dual-cw infrared (IR) lasers irradiation.

The InGaAs DGG-HEMT photomixer incorporates two types of grating-gate electrodes having a finger size of 100 nm and spacing between the adjacent fingers of 200 nm. The DGG structure modulates the electron drift velocity and plasma velocity in a complementary manner. One gate G1 (the other gate G2) are high (low) biased working as plasmonic cavities (as high-field, depleted regions) wherein the plasma velocity is higher (lower) than the electron drift velocity. The difference frequency ( $\delta f$ ) of the dual-cw-IR lasers was set around the plasmon resonant frequency determined by the G1 grating finger size and the electron density. As above mentioned, the plasmonic boom instability generates a shockwave of rather broadband plasmonic displacement current. Since the photomixed dual-cw-IR lasers irradiation generates coherent narrow spectral photocurrent component around the frequency  $\delta f$ , one can expect the broad plasmonic ac current could be injection-locked to the photogenerated  $\delta f$  component, resulting in an enhanced coherent THz emission around  $\delta f$ . We set  $\delta f$  at 2, 3, and 4 THz. The THz emission from the fabricated device was measured at 100K using a Fourier Transform IR (FTIR) spectrometer and a 4.2-K cooled Si bolometer.

The bias for G1 (VG1) was set at 0 V whereas that for G2 (VG2) was set at -0.5 V. The drain bias (VD) was set at 1V. We compared the THz emission beyond the background blackbody radiation at a fixed biases (VG1, VG2, VD) condition among the different photomixed  $\delta f$  conditions. With laser irradiation, rather broad THz emissions were observed. The observed spectral peaks are mostly independent of  $\delta f$  because of rather high-level of thermally-excited incoherent plasmons. However, the emission spectra for  $\delta f = 2$  and 4 THz exhibited a higher intensity at a narrow frequency range around 4-to-6 THz than that for  $\delta f = 3$  THz. To see these intensity differences in detail, the enhancement of mono-peak emission around 5 THz showed a weak blue shift from the emission for  $\delta f = 2$  THz to that for  $\delta f = 4$  THz. From these results, in the plasmonic cavities under G1 region, plasmonic resonant modes are situated close to 2 and 4 THz, and a plasmonic anti-resonant mode is situated close to 3 THz. It is worth noting that neither DS type nor ETT type current-driven instability emission could originate such an observed broadband emission. Since the drift velocity could exceed the plasma velocity at the cavity boundaries between G1 and G2, the results suggest that the photomixing-originated THz emission is amplified by stimulated emission of plasmons originated by the plasmonic boom instability.

In summary, the radiation spectra observed at 100K showed two distinctive emission components beyond the black-body radiation, one promoted by  $\delta f$ -independent thermally excited incoherent plasmons and the other promoted by  $\delta f$ -dependent coherent plasmons. The results suggest the occurrence of the plasmonic instability stimulated by the dc current flow in the channel.

#### 5:45 AM F.EL02.10.05

##### **Temperature-Independent Dielectric Constant In CsPbBr<sub>3</sub> Nanocrystals Revealed by Linear Absorption**

**Spectroscopy** Wenbi Shcherbakov-Wu<sup>1</sup>, Peter C. Serce<sup>2,3</sup>, Franziska Krieg<sup>4,5</sup>, Maksym V. Kovalenko<sup>4,5</sup> and William Tisdale<sup>1</sup>; <sup>1</sup>Massachusetts Institute of Technology, United States; <sup>2</sup>Center for Hybrid Organic Inorganic Semiconductors for Energy, United States; <sup>3</sup>California Institute of Technology, United States; <sup>4</sup>ETH Zürich, Switzerland; <sup>5</sup>Empa–Swiss Federal Laboratories for Materials Science and Technology, Switzerland

CsPbBr<sub>3</sub> nanocrystals (NCs) have attracted much attention over the past five years due to their exceptional optoelectronic properties and potential applications in devices such as light-emitting diodes (LEDs), lasers, and single-photon emitters. However, their fundamental photophysical properties, especially at low temperatures, are still under active debate. To date, almost all of the reports have used photoluminescence (PL) alone to infer the lattice dynamics in these materials. Here, we measure both the temperature-dependent (35 K - 300 K) absorption and PL spectra of zwitterionic ligand-capped CsPbBr<sub>3</sub> NCs with four different edge lengths ( $L = 4.9 - 13.2$  nm). The excitonic transitions observed in the absorption spectra can be explained with an effective mass model considering the quasicubic NC shape and non-parabolicity of the electronic bands. We observe a temperature-dependent Stokes shift; while the trend is similar to the Stokes shift observed in both MAPbBr<sub>3</sub> and CsPbBr<sub>3</sub> single crystals, it does not approach zero at cryogenic temperatures, pointing to an additional contribution intrinsically present in the NCs. Surprisingly, the effective dielectric constant determined from the best fit model parameters is independent of temperature, contrary to the previous report that the change in dielectric constant leads to the Stokes shift temperature dependence. Overall, our study sheds light on the fundamental lattice dynamics in these materials, and can potentially be used to guide future material optimization for device applications.

#### 5:55 AM F.EL02.10.07

##### **How Exciton Localization Enhances Radiative Recombination in Manganese-Doped Perovskite Nanocrystals**

Sascha Feldmann<sup>1</sup>, Bartomeu Monserrat<sup>1</sup>, Richard Friend<sup>1</sup> and Felix Deschler<sup>2</sup>; <sup>1</sup>University of Cambridge, United Kingdom; <sup>2</sup>Technische Universität München, Germany

Chemical doping of perovskites holds promise for enhancing luminescence efficiencies, which is crucial for applications such as efficient light-emitting diodes (LEDs). Using transient optical spectroscopy we study the recombination dynamics in manganese-doped Cs(Mn:Pb)(Cl,Br)<sub>3</sub> perovskite nanocrystals. We find an increased excitonic radiative recombination rate

upon doping, together with reduced non-radiative losses. Supported by ab initio calculations, we propose the enhanced luminescent recombination to arise from an increased electron hole overlap induced by the dopant ions. Thus, the stronger exciton localization leads to a higher probability of luminescent decay, important for optimising LED efficiencies.

**6:05 AM \*F.EL02.10.08**

**Band Gap Tuning in Halide Perovskites** Selina Olthof<sup>1,2</sup>; <sup>1</sup>University of Cologne, Germany; <sup>2</sup>Shaanxi Normal University, China

In recent years, the interest in halide perovskites rose at a rapid pace due to their tremendous success in the field of photovoltaic while other fields, like light emitting diodes, show great potential as well. One intriguing property of this material class is the wide tunability of the band-gap that can be induced by changing the perovskite composition. While changes in band gap are regularly reported, it is unclear how the respective conduction and valence band positions change and what the underlying origins of these changes are. Knowing the band positions is however crucial for device design, i.e. ensuring efficient charge transport across the various interfaces.

In this talk, I will present our results regarding variations in valence and conduction band position for a wide variety of lead and tin based perovskites [1]. Next to the primary ABX<sub>3</sub> type composition, also mixed metal structures will be shown. Using a combination of photoelectron spectroscopy and density functional theory we are able to explain the origin of these energy level and band gap changes based on changes in hybridization strength, atomic level positions, and lattice distortion.

References

[1] S. Tao, Ines Schmidt, G. Brocks, J. Jiang, I. Tranca, K. Meerholz, and S. Olthof, Absolute energy level positions in tin- and lead-based halide perovskites, Nature Communications 10, 2560 (2019)

**6:20 AM \*F.EL02.10.09**

**Controlling Light Emission in Halide Perovskite Device Structures** Samuel D. Stranks; University of Cambridge, United Kingdom

Halide perovskites exhibit a smorgasbord of emission properties, including tunable emission energies, linewidths and luminescence yields through judicious composition and dimensionality choice. This opens up a number of exciting applications in lighting and displays, as well as highly efficient solar cells. Achieving absolute control over the emission properties will further enable these novel semiconductors.

In this talk, I will cover recent developments in our group focusing on the light emission from halide perovskite semiconductors. I will demonstrate several approaches to dynamically control energy or charge transfer processes and ultimately tune emission colour, yields and carrier recombination by tuning either the 2D/3D components, halide components on the surface and/or bulk of thin films, or synthesizing well-passivated nanoplatelet structures. I will also show that local chemical variations in alloyed perovskites used in solar cells allow accumulation of photo-excited holes in small regions, leading to high emission yields even at low carrier densities in those regions. Finally, I will present new optical spectroscopy approaches to quantify luminescence yields and related device parameters in both solar cells and light-emitting diodes, providing unique insight into power loss processes in devices.

SESSION F.EL02.11: Light-Emitting Devices for Wearable Technologies  
On Demand Abstracts Available for Viewing Starting Saturday Morning, November 21, 2020  
F-EL02

**5:00 AM \*F.EL02.11.01**

**Efficient Near-Infrared Electroluminescent Devices for Wearable Technologies** Zhi Kuang Tan; National University of Singapore, Singapore

Near-infrared optoelectronic devices have found significant applications in facial recognition, eye tracking, motion sensing and health monitoring technologies. In this talk, I will discuss some of our new developments on efficient near-infrared light-emitting devices based on colloidal semiconductor quantum dots and metal halide perovskites. I will also highlight some of the design principles, synthesis and processing methods that we have employed to achieve high-performance devices with improved efficiency, radiance and reliability. Finally, I will showcase some novel implementations of large-area and flexible NIR devices in new wearable devices and technologies.



#### 5:15 AM F.EL02.11.02

**Aromatic Interaction-Induced Nonpolar Organogels for Soft, Efficient and Stable Perovskite Nanocomposites and Their Applications in Intrinsically Stretchable Light-Emitting Devices** Jae-Man Park and Jeong-Yun Sun; Seoul National University, Korea (the Republic of)

Existing gels are mostly polar, whose nature limits their role in soft devices. The intermolecular interactions of the nonpolar polymer-liquid system are typically weak, which makes the gel brittle or opaque. Here we report highly soft and transparent nonpolar organogels. Even though their elements are only carbon and hydrogen, their elastic modulus (~30 kPa), transparency (~98 %), and stretchability (~1000 %) are comparable to common soft hydrogels. A key strategy is introducing aromatic interaction into the polymer-solvent system, resulting in a high swelling ratio that enables efficient plasticization of the polymer networks. As a proof of applicability, soft perovskite nanocomposites are synthesized, where the organogels are in-situ polymerized with the two types of perovskite nanocrystals: physically dispersible or chemically addressable. The highly nonpolar environment of organogels enables stable formation and preservation of highly concentrated perovskite nanocrystals without mechanical sacrifice, and especially the chemically anchored perovskite-nonpolar organogel nanocomposites show high photoluminescence quantum efficiency (PLQE) that reaches 92.1 %, while their luminescence properties are environmentally stable against air, water, acid, base, heat, ultraviolet light, and mechanical deformation. Furthermore, when exposed to water, the chemically anchored nanocomposites show luminescence increasing behavior that their PLQE reaches near unity (~99.8 %) and is maintained for more than 110 days, which performance in the form of elastomeric perovskite emitters has not been reported. These superb properties enable the demonstration of fully soft electroluminescent devices that stably emit bright and pure green light under diverse deformations with no luminescence hysteresis. The aromatic interaction-induced nonpolar organogels may enable a step forward in soft optoelectronics.

#### 5:25 AM F.EL02.11.03

**Direct Growth of Light-Emitting III-V Nanowires on Flexible Plastic Substrates** Vladislav Khayrudinov<sup>1</sup>, Maxim Remennyi<sup>2</sup>, Vidur Raj<sup>3</sup>, Prokhor Alekseev<sup>2</sup>, Boris Matveev<sup>2</sup>, Harri Lipsanen<sup>1</sup> and Tuomas Haggren<sup>1,3</sup>; <sup>1</sup>Aalto University, Finland; <sup>2</sup>Ioffe Institute, Russian Federation; <sup>3</sup>The Australian National University, Australia

Semiconductor nanowires are routinely grown on high-priced crystalline substrates as it is extremely challenging to grow directly on plastics and flexible substrates due to high temperature requirements and substrate preparation. At the same time, plastic substrates can offer many advantages such as extremely low price, light weight, mechanical flexibility, shock and thermal resistance, and biocompatibility. We explore the direct growth of high-quality III-V nanowires on flexible plastic substrates by metal-organic vapor phase epitaxy (MOVPE). We synthesize InAs, InP, InSb and InAlAs nanowires on polyimide and show that the fabricated NWs are optically active with strong light emission in the mid-infrared range. We create a monolithic flexible nanowire-based p-n junction device on plastic in just two fabrication steps. Overall, we demonstrate that III-V nanowires can be synthesized directly on flexible plastic substrates inside a MOVPE reactor, and we believe that our results will further advance the development of the nanowire-based flexible electronic devices.

#### 5:35 AM F.EL02.11.04

**Ultrathin Perovskite Light-Emitting Diodes for Foldable and Conformable Light Sources** Junho Kim, Eungjun Kim, Hanul Moon and Seunghyup Yoo; KAIST, Korea (the Republic of)

Highly flexible ultrathin light sources and displays can play a key role in realizing future optoelectronic devices owing to their outstanding form factors. They may be utilized in wearable, body-attachable, and imperceptible electronic devices. Foldable displays are a good example of such devices that make most of such form-factor advantages. With the emerging interest in folding displays, it is expected that the market of foldable devices is growing bigger and bigger over the next few decades. Organic light-emitting diodes (OLEDs) or quantum-dot light-emitting diodes (QLEDs) are regarded as promising candidates for foldable displays because these light-sources are surface-emitting and their low-temperature processing is compatible with flexible substrates. Among these light-sources, perovskite light-emitting diodes (PeLEDs) exhibit excellent light-emitting properties such as high color purity thanks to their exceptional optoelectronic properties. For example, PeLEDs using organic-inorganic hybrid perovskite as light-emitting material have shown not only high external quantum efficiency over 20% but also narrow full width at half maximum (FWHM). For their superb material properties, several studies have been conducted to realize highly flexible light sources using perovskite as a light-emitting material. However, the bending radii in most of the initial attempts were larger than 1mm, which is the bench-mark number desired by foldable or imperceptible devices. Even if the bending radius was smaller than 1mm, the devices had shown a quick degradation upon repeated bending cycles.

In this study, we propose ultrathin perovskite light-emitting diodes using a substrate formed from UV-curable resins. In order to reduce the bending radius below 1mm, the thickness of the substrate should be decreased to a few tens of microns. Mechanical design has been done carefully to retain the device performance even after the repeated bending test by considering the crack onset strain (COS) for each layer. To this end, we measured COS for each layer including the perovskite emitting layer. The COS value of the perovskite layer is found to be ca. 3%, which is greater than that of typical transparent conductive oxides. Furthermore, to overcome any fabrication issues such as carrier leakage or solution penetration between a substrate and a carrier substrate, we ensured each layer to be formed as uniform as possible.

With these considerations, we were able to fabricate foldable perovskite light-emitting diodes that were shown to retain its EQE after 10,000 repeated bending cycles at the bending radius as small as 0.1 mm. The overall thickness was 20  $\mu\text{m}$  including the top encapsulation layer which was used for forming a neutral plane in the middle of the device, as well as protecting the device from ambient air. We believe the proposed foldable perovskite light-emitting diodes can be an important component for wearable or body-attachable devices, which can play a key role in realizing human-centric Internet-of-Things (IoT) applications.

SESSION F.EL02.12/F.EL08.12: Joint Session: Light Emission Mechanisms and Processes  
On Demand Abstracts Available for Viewing Starting Saturday Morning, November 21, 2020  
F-EL02

#### 5:00 AM \*F.EL02.12/F.EL08.12.01

**Alloying and Slicing Halide Double Perovskites** Adam Slavney<sup>1</sup>, Bridget Connor<sup>1</sup>, Kurt P. Lindquist<sup>1</sup>, Linn Leppert<sup>2</sup>, Jeffrey Neaton<sup>3</sup> and Hemamala Karunadasa<sup>1,4</sup>; <sup>1</sup>Stanford University, United States; <sup>2</sup>University of Twente, Netherlands; <sup>3</sup>Lawrence Berkeley National Laboratory, United States; <sup>4</sup>SLAC National Accelerator Laboratory, United States

Halide double perovskites provide a flexible platform for manipulating electronic structure through synthetic design. I will present some recent studies from our group, where we have attempted to increase the compositional and structural complexity of halide perovskites through chemical substitution. In our quest to understand the electronic structure of double perovskites, we developed a simple model that allows us to predict the bandgap symmetry based on chemical composition. Our work constructs an intuitive picture of how the molecular orbitals of metal-hexahalide coordination complexes give rise to electronic bands in the extended perovskite lattice and describes how these molecular orbitals vary across the bands to give rise to the overall band structure. Although the effects of quantum confinement of Pb and Sn perovskites have been well studied, 2D analogs of 3D double perovskites are notably lacking. I will present a series of 2D double perovskites and discuss the optical and electronic consequences of dimensional reduction of the 3D double perovskite lattice to 2D derivatives.

#### 5:15 AM \*F.EL02.12/F.EL08.12.02

**Hot Carriers in Halide Perovskites** Tze Chien Sum; Nanyang Technological University, Singapore

Halide Perovskites exhibit outstanding light-harvesting and emissive properties. Presently, record power conversion efficiencies (PCE) >25% in solar cells and external quantum efficiencies (EQE) >20% in light-emitting devices have been demonstrated. The perovskite field has since expanded well beyond photovoltaics and LEDs into other optoelectronic domains of lasers, x-ray detectors, memristors etc. Emerging frontier areas include multiphoton, multi-exciton generation and hot carrier applications. In this talk, I will focus on the hot carrier phenomena in halide perovskites and our recent work in this area.

#### 5:30 AM \*F.EL02.12/F.EL08.12.03

**Defects Engineering and Photophysical Processes in 2D Perovskites** Annamaria Petrozza; Istituto Italiano di Tecnologia, Italy

Low-dimensional perovskites are rapidly emerging due to their distinctive emission properties. Here, first I will present the fundamental properties of pristine 2D perovskites, such as the nature of the primary photo-excitations, their relaxation through electronic states and their diffusion across thin films. Such properties will be correlated and modulated by the structural characteristics of the 2D perovskites. Then, I will discuss the possibility of perovskite doping by controlled addition of impurity ions which may enable new electronic, magnetic, and optical performances. I will explore new doping

strategies based on transition and rare earth metals for tuning of the emission wavelength (from UV to NIR, further extending the typical range covered with perovskites) and luminescent enhancement. The suitability of doping for the realization of 4 level perovskite lasers will be assessed. Doping with heterovalent ions will be tested to selectively increase  $p$  and  $n$  type conductivity of the material. The addition of alkaline-earth metals as B-site dopants will be tested to improve the material stability

#### 5:45 AM F.EL02.12/F.EL08.12.04

**High-Efficiency Blue Photoluminescence in the  $\text{Cs}_2\text{NaInCl}_6\text{:Sb}^{3+}$  Double Perovskite Phosphor** Matthew Gray<sup>1</sup>, Shruti Hariyani<sup>2</sup>, T. Amanda Strom<sup>3</sup>, Jackson Majher<sup>1</sup>, Jakoah Brgoch<sup>2</sup> and Patrick Woodward<sup>1</sup>; <sup>1</sup>The Ohio State University, United States; <sup>2</sup>University of Houston, United States; <sup>3</sup>University of California, Santa Barbara, United States

In this report, the photoluminescent properties of a lead-free double perovskite  $\text{Cs}_2\text{NaInCl}_6$  doped with  $\text{Sb}^{3+}$  are explored. The host crystal structure is a cubic double perovskite with Fm-3m symmetry,  $a = 10.53344(4)$  Å, and rock salt ordering of  $\text{Na}^+$  and  $\text{In}^{3+}$ . It is a wide bandgap compound ( $E_g \approx 5.1$  eV), and substitution with  $\text{Sb}^{3+}$  leads to strong absorption in the UV due to localized  $5s^2 \rightarrow 5s^15p^1$  transitions on  $\text{Sb}^{3+}$  centers. Radiative relaxation back to the  $5s^2$  ground state, via a  $^3P_1 \rightarrow ^1S_0$  transition, leads to intense blue luminescence, centered at 445 nm, with a photoluminescent quantum yield of 79%. The Stokes shift of 0.94 eV is roughly 33% smaller than it is in the related vacancy ordered double perovskite  $\text{Cs}_2\text{SnCl}_6$ . The reduction in Stokes shift is likely due to a change in coordination number of  $\text{Sb}^{3+}$  from 6-coordinate in  $\text{Cs}_2\text{NaInCl}_6$  to 5-coordinate in  $\text{Cs}_2\text{SnCl}_6$ . In addition to the high quantum yield,  $\text{Cs}_2\text{NaInCl}_6\text{:Sb}^{3+}$  exhibits excellent air/moisture stability and can be prepared from solution; characteristics make it a promising blue phosphor for applications involving near-UV excitation.

#### 5:55 AM F.EL02.12/F.EL08.12.07

**Tuning the Photophysical Behavior of 2D Perovskites by Engineering the Nature of the Organic Component** Ferdinand C. Grozema; Delft University of Technology, Netherlands

Two-dimensional (2D) halide perovskites are a class of emitter materials that are enjoying growing attention recently. The materials are related to 3D halide perovskites but either part or all of the small A-site cations are replaced by large organic molecules with an ammonium binding moiety, for example butylammonium or phenyl-ethylammonium. This (generally) leads to the formation of a layered structure where a layer of metal-halide octahedra is formed and the large organic cations separate the layers from each other. Mixing of large and small A-site cations can lead to quasi-2D multi-layer materials where multiple layers of metal halide octahedra are separated by the organic molecules, for instance forming Ruddlesden-Popper or Dion-Jacobson structures. The emissive properties of these materials are intricately linked to the structural dynamics and formation of possible defects in the inorganic layers.

In this work we explore how modifications of the large organic ammonium ion can affect the structural dynamics of the inorganic layer, combining molecular dynamics simulations with time-resolved spectroscopy. Using time-resolved fluorescence and ultrafast transient absorption spectroscopy we have studied the photophysical behavior of 2D perovskites with a range of different organic cations in order to gain insight in the relation between the structure and the excited state dynamics. These measurements indicate marked differences that can not solely be attributed to changes in the average structure of the materials.

To explain these differences we have performed classical molecular dynamics simulations for a variety of structures, for instance aliphatic alkyl chains, ammonium ions containing aromatic moieties such as phenyls or perylene, but also di-functional ions containing two binding sites that can connect to an inorganic perovskite layer on both sides. The results indicate that there are marked differences between the different structures in terms of their structural rigidity. Multi-layer Ruddlesden-Popper structures are generally more rigid than single layers, however, the rigidity of the single layer structures can be strongly enhanced by engineering of the interactions between organic cations, for instance by introduction of large conjugated ions. In addition, di-functional ligands resulting in Dion-Jacobson like structures also lead to more rigid structures. Comparison with the experimental results allows us to derive some design rules that indicate how engineering of the organic part of the structure can help in improving the emissive properties of the materials that is mostly due to the inorganic layer structure.

SESSION F.EL02.13: Poster Session: Emerging Light-Emitting Materials and Devices—Halide Perovskites, Quantum Dots and Other Nanoscale Emitters

#### F.EL02.13.01

##### **Triple-Wavelength Emission from Mn<sup>2+</sup>/Yb<sup>3+</sup> Codoped CsPbCl<sub>3</sub> Perovskite Nanocrystals and Luminescent Solar Concentrator Applications** Tong Cai, Junyu Wang and Ou Chen; Brown University, United States

Doping metal ions into lead halide perovskite nanocrystals (NCs) has attracted great attention over the past few years due to the emergence of novel properties relevant to optoelectronic applications. Current studies focus mostly on doping a single type of metal ions into the host perovskite NCs, while few research efforts have been made on simultaneous doping more than one type of metal ions into the same perovskite hosts and to study their synergic effects with intra-particle energy transfer processes. Here, a facile synthesis of Mn<sup>2+</sup>/Yb<sup>3+</sup> codoped CsPbCl<sub>3</sub> NCs through a hot-injection technique is firstly reported. Owing to the completely separated energy relaxation channels among the intrinsic bandgap (BG), Mn<sup>2+</sup> and Yb<sup>3+</sup> dopant emissions, the obtained Mn<sup>2+</sup>/Yb<sup>3+</sup> codoped CsPbCl<sub>3</sub> perovskite NCs exhibit a unique triple-wavelength emission profile simultaneously covering UV/blue (BG-PL), visible (Mn-PL) and NIR (Yb-PL) spectral regions. By optimizing the dopant concentrations, the total photoluminescence quantum yield (PL QY) of the codoped NCs can reach up to ~125.3% due to quantum cutting effects. Mechanism studies reveal different natures of emission mechanisms can be involved in a single batch of Mn<sup>2+</sup>/Yb<sup>3+</sup> codoped perovskite NCs: (i) electronic inter-band transition (BG-PL); (ii) electronic transition of ion centers within local molecular complexes (Mn-PL); and (iii) defect-induced energy transfer and subsequent quantum cutting scheme (Yb-PL). Owing to the high PL QYs and minimal reabsorption loss, the codoped perovskite NCs are demonstrated to be used as efficient emitters in luminescent solar concentrators, with greatly enhanced external optical efficiency compared to that of using solely Mn<sup>2+</sup> doped CsPbCl<sub>3</sub> NCs. Therefore, co-doping both Mn<sup>2+</sup> and Yb<sup>3+</sup> ions into perovskite NCs can serve as a unique model system for studies of host-to-dopant and inter-dopant energy transfer mechanisms, as well as associated radiative and non-radiative decay pathways at each step. Most importantly, such codoped NCs with multiple emission channels hold a high potential to be applied in a wide range of applications, including multiplexed biological labelling and sensing, multi-channel photodetectors, stimuli-responsive inks for coding, encryption and decryption, and photon management devices in the future.

#### F.EL02.13.02

##### **Control of Excitonic Spin States via Magnetic Interactions with Transition-Metal Dopants in Ruddlesden-Popper Hybrid Perovskites** Jonathan Zerhoch, Timo Neumann, Martin S. Brandt, Jonathan Finley, Andreas Stier and Felix Deschler; Walter Schottky Institut and Physik-Department, Technische Universität München, Germany

Combining the advantageous electrical and optical properties of semiconductors with magnetic characteristics gives access to extraordinary phenomena and applications. Fully inorganic dilute magnetic semiconductors (DMS) have been known for decades, which show diverse functionalities like control of magnetism by electrical fields. The material class of DMS is obtained by introducing a substantial number of magnetic ions to an otherwise non-magnetic host semiconductor. Due to their outstanding optoelectronic properties and high defect tolerance, organo-metal halide perovskites form an ideal system for efficient magnetic doping. We produced a selection of magnetic perovskites using simple solution processing techniques by doping of the host material, Ruddlesden-Popper hybrid perovskite ((PEA)<sub>2</sub>PbX<sub>4</sub> with X = Cl, Br, I), with different magnetic ions like Mn<sup>2+</sup>, Fe<sup>2+</sup>, Co<sup>2+</sup>, Ni<sup>2+</sup> and Eu<sup>2+</sup>. We investigated the influence of both halides and magnetic impurities on the long-range magnetic ordering of the materials with respect to the structural and optical properties. We investigate how localized excitons couple with the magnetic moments of the introduced impurities by detecting a dependence of the emitted lights polarization on the magnetization. We perform structural, magnetic, optical and magneto-optical temperature-dependent measurements to verify a successful magnetic doping of the perovskite and to show how photoluminescence and magnetization properties relate.

#### F.EL02.13.04

##### **Illuminating the Structural and Optical Changes Behind Photo-Induced Degradation in Mixed-Halide Perovskites** Gabriel C. Halford, Annie Gomez, Jill Mankoff and Rebecca Belisle; Wellesley College, United States

**While mixed-halide perovskites are ideal for use in tandem solar cells due to their tunable band gap, they are limited**

by reversible photo-induced degradation. While the impacts of photo-induced segregation on optical properties have been well documented, the underlying impacts on perovskite structure remain less clear. Structural changes that result in optical changes may come from halide migration and subsequent segregation in the perovskite. Utilizing grazing-incidence wide angle x-ray scattering (GIWAXS), we have observed in situ reversible structural changes that occur over time scales of 30 minutes to an hour in mixed-halide methylammonium perovskite thin films as a result of light soaking at approximately 1 sun intensity. Looking at a range of different compositions with varying ratios of bromine to iodine, we are able to observe the kinetics of photo-induced unmixing of mixed-halide perovskites and the formation of multiple distinct crystalline phases.. Data taken in the dark after illumination demonstrates the reversibility of this process, as the crystal structures relax back to approximately their original structure. Analyzing the x-ray diffraction data, we see multiple distinct phases we quantify as bromine-dominated and iodine-dominated crystal structures. Correlating our x-ray diffraction results with in situ photoluminescence, we are able to present a timeline of photo-induced halide segregation that captures changes in local structure with observed optoelectronic performance. Photoluminescence shifts occur during photo-induced halide segregation such that majority iodine films shift toward lower intensity, lower energy peaks and majority bromine films shift toward higher intensity, lower energy peaks. While optical changes appear to occur before structural changes are visible in the GIWAXS data, both optical and structural changes saturate at time scales approaching one hour. Looking forward we may be able to demonstrate whether this is a surface or a bulk phenomenon. Understanding the origins of the structural changes behind photo-induced degradation could help find strategies to mitigate the optical changes it causes to produce more stable mixed-halide perovskite solar cells. Overall, this work demonstrates more fully the correlation between structural and optical changes related to light-induced halide migration and gives the possibility of finding targeted solutions to minimizing degradation.

#### F.EL02.13.05

**High Affinity Polysalt Ligands Promote Long Term Stability While Enhancing the Quantum Yields of CsPbBr<sub>3</sub> Nanocrystals** Sisi Wang, Liang Du and Hedi M. Mattoussi; Florida State University, United States

Recently, cesium lead halide perovskite quantum dots (PQDs) have generated tremendous interests, due to the great promise they offer for use in optoelectronic applications. However, their poor colloidal stability, which can be traced to the ionic nature of the crystal cores and the high desorption rates of the native ligands, has impeded progress in fundamental research and slowed integration of such materials in devices. Developing novel surface ligands with strong coordination to both passivate surface traps and enhance fluorescence performance, while improving colloidal stability is urgently needed. Here, we detail the synthesis of a new family of multifunctional polymer ligands and their use for surface engineering of the CsPbBr<sub>3</sub> nanocrystals. The ligand synthesis relies on the ring opening reaction between distinct nucleophiles and poly(isobutylene-alt-maleic anhydride), PIMA. The modular ligand stoichiometrically displays multiple ammonium and/or imidazolium anchors for coordination onto PQD surfaces, along with several alkyl chains with different length to promote affinity to various organic solvents. The results show that the PQDs coated with those polysalts exhibit great colloidal stability and significantly enhanced photoluminescence. The coating also allows the resulting colloids to be dispersed a wide range of solvent conditions, including ethanol and methanol, while maintaining strong fluorescence and preserving the nanocrystal integrity after ligand substitution.

#### F.EL02.13.06

**Polar Solvent Mediated Shape Control of CsPbBr<sub>3</sub> Perovskite Nanocrystals for Applications in LEDs** Arkajyoti Chakrabarty, Parvez Akhtar, Samridhi Satija, Upanshu Gangwar, Jitendra Kumar, Madhusudan Singh and Sameer Sapa; IIT Delhi, India

Nanocrystals (NCs) with different shapes, are of tremendous interest to material chemists, and precise control of their shapes and sizes through colloidal synthetic routes, with further solution-processability of the NCs, provides us with a great opportunity to tune their optoelectronic behaviour for advanced applications.<sup>1</sup> Interestingly, polar solvents are known to play crucial roles in determining the shapes of CsPbBr<sub>3</sub> perovskite NCs owing to the prevailing anisotropic growth conditions. However, to induce polar environment in the perovskite synthesis, a suitable precursor soluble in the desired polar solvent, is primarily required. In this work, we describe an efficient, MeOH-soluble steroidal Cs-precursor: cesium cholate and the different shapes of CsPbBr<sub>3</sub> NCs (nanorods, nanocubes and nanoplatelets) obtained from it, utilizing miniscule amount of polar solvents (methanol and methanol-water) in conjunction with commonly used 1-octadecene solvent and varying the reaction temperatures (90 °C and 180 °C). The resulting NCs exhibit very high photoluminescence (PL) quantum yields (94% for nanoplatelets and 96% for nanocubes), due to mitigation of Br vacancies by large cholate molecules, slowing down the complex nucleation and lattice construction processes in the synthetic pathway.<sup>2</sup> To study the application of these

luminophores for application in perovskite light emitting diodes (PeLEDs), powdered CsPbBr<sub>3</sub> nanocubes were dispersed in toluene at different concentrations to prepare inks. Inks were spin-coated at different speeds (500, 1000 and 1500 rpm) and film quality was optimized to produce uniform and pinhole free films on an ITO substrate. Thin films produced at optimal deposition conditions and ink compositions were characterized using thin film photoluminescence measurements at 325 nm. A sharp and highly intense peak at 514 nm was observed. Initial device fabrication employing a spin-coated hole transport layer (poly (9-vinylcarbazole), and an electron transport layer (2,2',2''-(1,3,5-Benzinetriyl)-tris(1-phenyl-1-*H*-benzimidazole)) produced promising initial results. These initial results with perovskite nanocubes based thin films invite more studies of complete devices, possibly with other nanomaterial geometries (nanorods and nanoplatelets).

#### References:

- (1) Pan, A.; He, B.; Fan, X.; Liu, Z.; Urban, J. J.; Alivisatos, A. P.; He, L.; Liu, Y. Insight into the Ligand-Mediated Synthesis of Colloidal CsPbBr<sub>3</sub> Perovskite Nanocrystals: The Role of Organic Acid, Base, and Cesium Precursors. *ACS Nano* **2016**, *10*, 7943–7954.
- (2) Chakrabarty, A.; Satija, S.; Gangwar, U.; Sapra, S. Precursor-Mediated Synthesis of Shape-Controlled Colloidal CsPbBr<sub>3</sub> Perovskite Nanocrystals and Their Nanofiber-Directed Self-Assembly. *Chem. Mater.* **2020**, *32*, 721–733.

#### F.EL02.13.07

**Chemically-Casted MoO<sub>3</sub> Hole Transport Active Layer for Perovskite Solar Cells** Taliya Gunawansa, Messaoud Bahoura and Sangram K. Pradhan; Norfolk State University, United States

Perovskite solar cells (PSCs) are promising contenders in the solar cell technology market having achieved photo-conversion efficiencies greater than 25%. The role of the hole transport layer in perovskite solar cells is essential for incredible enhancement of their significant photo-conversion efficiency. Iron oxide is one of the interesting hole transport materials that can potentially improve the performance; however, the frequently used chemical synthesis technique of the micaceous iron oxide (MIO) precursors is very toxic, harmful and time-consuming. Molybdenum dioxide (MoO<sub>3</sub>) is a commonly studied hole transport layer utilized in perovskite solar cell; This study analyzes a chemically casted process preferably hot-casting technique to prepare a non-toxic molybdenum dioxide precursor that would fabricate a highly effective and densely packed MoO<sub>3</sub> films. Various temperatures below 100 °C results in intermittent deposition of the MoO<sub>3</sub> films. When the hot-casting temperature is increased, the MoO<sub>3</sub> thin film are uniformed and resulted in greater charge extraction and insignificant light soaking. Photoluminescence spectroscopy (PL), ultraviolet-visible spectroscopy (UV-VIS), and scanning electron microscopy (SEM) are the characterization techniques utilized to observe the opto-electronic properties of the MoO<sub>3</sub> films. The capacitance, frequency dispersion, and leakage current measurements display stable performance of the MoO<sub>3</sub> perovskite solar cells.

#### F.EL02.13.08

**Material Development And Emission Spectroscopy of Mn Doped CsPbCl<sub>3</sub> Bulk Crystals and Nanoparticles for Light Source Applications** Uwe Hommerich<sup>1</sup>, Jihaad Barnett<sup>1</sup>, Kesete Ghebreyessus<sup>1</sup>, Al Amin Kabir<sup>1</sup>, Khalid Hampton<sup>1</sup>, Samuel Uba<sup>1</sup>, Ikemefuna Uba<sup>1</sup>, Demetris Geddis<sup>1</sup>, Clayton S. Yang<sup>2</sup>, Sudhir Trivedi<sup>2</sup>, Seth Fraden<sup>3</sup> and S. Ali Aghvami<sup>3</sup>; <sup>1</sup>Hampton University, United States; <sup>2</sup>Brimrose Technology Corporation, United States; <sup>3</sup>Brandeis University, United States

Manganese doped inorganic halide perovskites continue to be of current interest for applications in light emitting devices and down-converters in solar cells. In this work we prepared Mn doped CsPbCl<sub>3</sub> (Mn: CPC) bulk crystals and nano-particles (NPs) and compared their emission properties. Bulk crystals were grown from the melt by vertical Bridgman technique and NPs were synthesized using a microwave assisted method. Under ultra-violet excitation at 350 nm, bulk crystal and NPs of Mn: CPC exhibited a broad orange emission centered at ~605 nm at room temperature. The broadband emission was assigned to the intra-3d transition <sup>4</sup>T<sub>1</sub> → <sup>6</sup>A<sub>1</sub> of Mn<sup>2+</sup> ions incorporated in the CPC host lattice. The Mn<sup>2+</sup> emission lifetimes were nearly exponential with values of 1.07 ms for NPs and 0.73 ms for the bulk crystal. Mn: CPC NPs also showed exciton emission peaking at ~402 nm, whereas the bulk crystal exhibited no significant emission near the band edge. Instead, the bulk material of Mn: CPC revealed a weak below-gap emission in the 450-550 nm region suggesting the existence of defect states. The excitation spectra for the orange Mn<sup>2+</sup> emission from Mn: CPC NPs and bulk crystals were significantly different indicating distinct excitation pathways. The excitation spectrum of the orange Mn<sup>2+</sup> emission for Mn: CPC NPs showed excitonic structure similar to the absorption spectrum suggesting energy transfer from excitons to Mn<sup>2+</sup> ions. In contrast, UV excitation was less efficient for the bulk Mn: CPC crystal and the excitation was dominated by well defined below-gap excitation bands centered at ~425 and ~530 nm. More details of the material preparation emission spectroscopy, and initial hybrid LED experiments will be discussed at the conference.

#### F.EL02.13.09

**Red Light Emitting Ytterbium Activated Sr<sub>3</sub>Al<sub>2</sub>O<sub>6</sub> Nanophosphor for LED Applications** Chitra Mallela; Tumkur

University, India

Present study analyses the salient features of the newly synthesized phosphor powders of 1, 3, 5, 7, 9 and 11 molar concentrations of Ytterbium activated Strontium Aluminate by solution Combustion method using Urea. The prepared phosphors were calcined at 950 degree celcius for 4 hours. The Powder X-ray diffraction (PXR) profiles of nanophosphors showed crystalline face centered cubic phase. The average crystallite sizes of the phosphors were in the range 34 to 48 nm. The samples showed pores and voids on their surface that formed by the escaping gases during the combustion method. The morphology showed the inherent nature of combustion process. The Scanning electron microscope (SEM) images showed non-uniform and irregular shapes of the particles. The Particle sizes were further confirmed by Transmission electron microscope (TEM). Energy dispersive analysis of X-ray techniques were used to study the structural characteristics of calcined phosphors. Fourier infrared spectral studies were carried out to evaluate the stretching and vibrational bonds in the product. They showed an absorption peak at  $1456\text{ cm}^{-1}$  that indicates the formation of crystallized Strontium Aluminate and a sharp peak at  $3670\text{ cm}^{-1}$  due to the presence of  $\text{AlO}_4$  group in the powders. Energy dispersive X-ray analysis (EDAX) with SEM image, revealed the uniform distribution of  $\text{Yb}^{3+}$  ions. The energy band gaps of the prepared phosphors from Kubelka-Munk plots of the Diffused reflectance Studies (DRS) were found to be in the range 5.31 eV to 5.78 eV. The Photoluminescence studies showed an emission peak at 708 nm when phosphors were excited with 355 nm. All the phosphors were found to emit red light as their Commission Internationale de L'Eclairage (CIE) co-ordinates have fallen in red region of chromaticity diagram. The average correlated color temperature of the phosphors was found to be 3950 degree Kelvin.

#### F.EL02.13.11

**Support for the Self-Trapped-Exciton Hypothesis in Multi-Layered ( $n > 1$ ) Two-Dimensional Lead Iodide Perovskites** Watcharaphol Paritmongkol, Eric Powers, Nabeel Dahod and William Tisdale; Massachusetts Institute of Technology, United States

Two-dimensional (2D) lead halide perovskites have been shown to exhibit broadband or white-light emission under certain conditions. Broadband emission in lead iodide 2D perovskites has been alternately attributed to self-trapped excitons (STEs) or permanent structural defects and/or impurities. Here, we investigate the photophysical characteristics of broadband emission in six different multi-layered ( $n > 1$ ) 2D lead iodide perovskites as a function of sample temperature from 5 K to 300 K. We distinguish shallow defect-associated emission from a broad near-infrared (NIR) spectral feature, which we assign to the STE. Sub-gap photoexcitation experiments and NIR transient absorption spectroscopy rule out permanent structural defects as the origin of this feature. When we varied the thickness ( $n = 2, 3, 4$ ), A-site cation (methylammonium vs. formamidinium), and organic cation spacer (butylammonium vs. hexylammonium vs. phenylethylammonium), we found that the temperature dependence of broad NIR emission was strongly correlated with both the strength of electron-phonon coupling and the extent of structural deformation of the ground state lattice, strongly supporting the assignment of this spectral feature to a STE.

#### F.EL02.13.12

**Thermal Impact on InAs Quantum Dots Covered by Different Capping Layers in GaAs/AlGaAs Structures** Georgiy Polupan<sup>1</sup>, Ricardo Cisneros Tamayo<sup>2</sup>, Tetyana V. Torchynska<sup>1</sup>, Ingrid. J. Ingrid. J. Guerrero Moreno<sup>1</sup> and Arturo Escobosa Echavarría<sup>3</sup>; <sup>1</sup>Instituto Politecnico Nacional, Mexico; <sup>2</sup>Universidad Politécnica del Valle de México,, Mexico; <sup>3</sup>CINVESTAV-IPN, Mexico

InAs quantum dots (QDs) embedded in MBE grown GaAs/ $\text{Al}_{0.30}\text{Ga}_{0.70}\text{As}$ /AlGaInAs heterostructures have been investigated in as grown state and after thermal annealing at  $640^\circ\text{C}$  or  $710^\circ\text{C}$  for two hours. Two types of QD structures with the different compositions of AlGaInAs capping layers (GaAs (#1) or  $\text{Al}_{0.10}\text{Ga}_{0.75}\text{In}_{0.15}\text{As}$  (#2)) and the same composition of buffer layers ( $\text{In}_{0.15}\text{Ga}_{0.85}\text{As}$ ) are compared and studied by means of photoluminescence (PL), X-ray diffraction (XRD) and high resolution HR-XRD methods. XRD and HR-XRD techniques are applied with the aim to control the crystal structures, the material compositions and elastic strains in quantum well (QW) layers.

The highest PL intensity, smaller PL band half width and lower energy of ground state (GS) emission are detected in the structure with the  $\text{Al}_{0.10}\text{Ga}_{0.75}\text{In}_{0.15}\text{As}$  capping layer. Thermal annealing leads to the shift of PL spectra into higher energy range and the value of this shift is more essential in the structure with the  $\text{Al}_{0.10}\text{Ga}_{0.75}\text{In}_{0.15}\text{As}$  capping layer as well.

The variation of GS emission peak versus temperature has been monitored within the range of 10-450K for as grown and annealed states and it compared with temperature shrinkage of band gap in the InAs and GaAs bulk crystals. It permits to reveal the QD composition that in #2 was closer to InAs than in #1. Finally, the reasons of PL spectrum transformation at

annealing, the mechanism of PL thermal decay, and the advantages of the QD structure with strain reduced  $\text{Al}_{0.10}\text{Ga}_{0.75}\text{In}_{0.15}\text{As}$  capping layer have been analyzed and discussed. The composition variation of QDs and QWs at annealing has been modeled using the simulation of HR-XRD results with Xpert Expitaxy software.

#### F.EL02.13.14

**Superparamagnetic Properties of Metal-Free Nitrogen Doped Graphene Quantum Dots Synthesized by Pulsed Laser Ablation** Muhammad Shehzad Sultan<sup>1</sup>, Vladimir I. Makarov<sup>1</sup>, Muhammad Sajjad<sup>2</sup>, Wojciech Jadwisieniczak<sup>3</sup>, Brad R. Weiner<sup>1</sup> and Gerardo Morell<sup>1</sup>; <sup>1</sup>University of Puerto Rico - Río Piedras, United States; <sup>2</sup>Indiana University Northwest, United States; <sup>3</sup>Ohio University, United States

In this study, we developed a novel approach to synthesize high-quality metal-free Nitrogen-doped graphene quantum dots (N-GQDs) with high quantum yield, via irradiation of s-triazene in a solution with benzene by using pulsed laser. The TEM, HRTEM, XPS, XRD, Raman spectroscopy and FTIR were carried out to observe the morphology, size distribution, crystalline structure and to prove successful doping of GQDs with nitrogen atoms. Furthermore, for the first time, to our knowledge, their magnetic properties were investigated. The results indicate that N-GQDs exhibit superparamagnetic behavior. The specific size, shape and zigzag edge structure of N-GQDs were considered to explain the origin of the observed magnetism. The magnetization dependence led to estimating the N-GQD material magnetic permeability for different ambient temperatures. From the zero-field-cooled (ZFC) and field-cooled (FC) magnetization measurements, carried out at 50 Oe magnetic field strength, we estimated the blocking temperature  $T_B$  to be around 300 K. Based on the experimental data analysis, the magnetic permeability, number of correlated spins per single N-GQD, and number density of superparamagnetic N-GQD per gram of material were estimated. The excellent superparamagnetic properties together with optical properties manifested by N-GQDs have the potential to lead to high performance biomedical applications.

#### F.EL02.13.15

**Highly Stable Luminescent Encapsulation Material Using Quantum Dot/Siloxane Hybrid for Reliable and Wide Color Gamut Light-Emitting Diode** Junho Jang, Da-Eun Yoon, Doh C. Lee and Byeong-Soo Bae; Korea Advanced Institute of Science and Technology, Korea (the Republic of)

Semiconducting nanocrystals, also known as quantum dots (QDs), are a promising color converting materials for next-generation display application due to their unique photophysical properties such as size-dependent color tunability, narrow spectral bandwidth, and high photoluminescence (PL) quantum yield (QY). However, the vulnerability of QDs to oxygen and moisture is a huge obstacle to practical applications. The commercialized QD for display has been a form of color converting QD films in liquid crystal display (LCD) backlight unit (BLU) using blue light-emitting diode (LED) (*i.e.*, On-Surface type), where QDs were physically blended in polymer matrixes sandwiched between two barrier layers. It is more desirable for LCD BLU using LEDs encapsulated the QDs directly into the packaging (*i.e.*, On-Chip type) in terms of performance, amount of QDs, and cost. Nevertheless, LEDs that are directly encapsulated by QDs have not been used in display applications due to their fatal instability. Therefore, reliable LEDs using highly stable luminescent encapsulation material that contains uniformly dispersed QDs in optical resin should be developed without additional protecting layers (such as  $\text{SiO}_2$  or  $\text{Al}_2\text{O}_3$ ) and ligand-exchange processes.

Herein, we developed luminescent LED encapsulation material (TSE-QD) using CdSe/CdZnS core/shell QDs (passivated by oleic acid) dispersed in a thermally resistant sol-gel derived siloxane matrix with high refractive index ( $> 1.57$ ) [1,2]. The TSE-QD was fabricated via hydrosilylation of QD dispersed siloxane resin that was synthesized via *in situ* sol-gel reactions of silane precursors in the presence of QDs. The QDs were uniformly distributed in a linear-structured siloxane matrix in which functional groups of siloxane matrix is chemically cross-linked with ligands of the surface on QDs, and retained their initial optical properties during the fabrication processes [3]. Notably, we achieved dramatically enhanced thermal (at 120 °C in ambient air) and chemical stability (in acid or base solutions and alcohol) without additional barrier films and ligand-exchange process. We demonstrated a natural-white emitting LED using a blue LED chip directly encapsulated (*i.e.*, On-Chip type) by yellow-emitting TSE-QD that consist of red and green QDs in a siloxane matrix. Fabricated white LED exhibited wide color gamut (116% of NTSC 1931), excellent reliability (under 85 °C & 85% relative humidity), and high photostability (under continuous blue light irradiation).

[1] H. Y. Kim et al., *J. Am. Chem. Soc.*, **138**, 16478-16485 (2016).

[2] J.-Y. Bae et al., *RSC Adv.*, **3**, 8871-8877 (2013).

[3] J. Jang et al., *Nanoscale*, **11**, 2828-2834 (2019).

#### F.EL02.13.16

**$\text{Cs}_4\text{Cd}_{1-x}\text{Mn}_x\text{Bi}_2\text{Cl}_{12}$ —A Vacancy Ordered Halide Perovskite Phosphor with High Efficiency Orange-Red Emission** Noah P. Holzapfel<sup>1</sup>, Jackson Majher<sup>1</sup>, T. Amanda Strom<sup>2</sup>, Curtis Moore<sup>1</sup> and Patrick Woodward<sup>1</sup>; <sup>1</sup>The Ohio State



University, United States; <sup>2</sup>University of California Santa Barbara, United States

The structural, optical, and magnetic properties of the vacancy-ordered quadruple perovskites  $\text{Cs}_4\text{CdBi}_2\text{Cl}_{12}$  and  $\text{Cs}_4\text{MnBi}_2\text{Cl}_{12}$  and their solid solution have been investigated. Both compounds are found to crystallize with  $R-3m$  space group symmetry that arises from ordering of  $\text{Bi}^{3+}$ ,  $\text{Mn}^{2+}/\text{Cd}^{2+}$ , and cation vacancies into layers that run perpendicular to the  $\langle 111 \rangle$  direction of the cubic perovskite structure. Magnetic measurements reveal that  $\text{Cs}_4\text{MnBi}_2\text{Cl}_{12}$  is paramagnetic down to 2 K with a Weiss constant of  $-2.88(3)$  K and an effective moment of  $5.840(1) \mu_B$ . This compound exhibits weak orange-red luminescence, which involves  $\text{Bi}^{3+}$  ions absorbing near UV photons followed by energy transfer to  $\text{Mn}^{2+}$  ions and finally radiative decay that is attributed to a spin-forbidden  $^4T_1(G)$  to  $^6A_1(S)$  d-d transition. The emission peak is centered near 605 nm and has a full-width-half-maximum of  $\sim 90$  nm and a photoluminescent quantum yield (PLQY) of  $\sim 4\%$ . The isostructural  $\text{Cs}_4\text{CdBi}_2\text{Cl}_{12}$  is neither magnetic nor does it show detectable photoluminescence at room temperature. Replacing  $\text{Mn}^{2+}$  with  $\text{Cd}^{2+}$  to form  $\text{Cs}_4\text{Cd}_{1-x}\text{Mn}_x\text{Bi}_2\text{Cl}_{12}$  leads to a zero-dimensional electronic structure that inhibits energy migration to defect sites where non-radiative decay can occur, increasing the room temperature PLQY to 57% in the  $x = 0.27$  sample.  $\text{Cs}_4\text{Cd}_{1-x}\text{Mn}_x\text{Bi}_2\text{Cl}_{12}$  phosphors are easily synthesized from solution, free of rare-earth ions, and possess emission spectra that compare favorably to narrow-band red emitting phosphors based on  $\text{Eu}^{2+}$  ions.

#### F.EL02.13.17

**Fluorene-Based Organic Phosphorescent Materials for LECs** C KY, Maxime Remond, Donghwan Kim and Eunkyong Kim; Yonsei University, Korea (the Republic of)

Fluorene-based organic phosphorescent materials (OPMs) were explored for organic light-emitting electrochemical cells (LECs) taking advantages of their tunability in color and film processibility. TO tackle the problem of the apparent low emission efficiency of OPMS, compared to inorganic or organometallic materials, fluorene unit was designed as a  $\pi$ -bridge between halogen and  $n-\pi$  transition groups. These OPMs provided a long-lived phosphorescence at film state, possibly due to enhanced intersystem crossing (ISC) to the triplet state in the optimized structure. Thus OPMs were applied to light-emitting cells (LECs) along with a host and electrolyte, to show the highest luminescence among the organic phosphorescent LECs up to date. Synthesis of OPMs, mechanism of enhanced emission, and fabrication details on LECs will be presented.

#### F.EL02.13.18

**Synthesis of Efficient Blue Emitting  $\text{CsPb}(\text{Br}/\text{Cl})_3$  Nanoparticles via Post-Treatment with Short Organic Ligands and LED Fabrication** Jang Kyung Yeon, Jinwoo Park and Tae-Woo Lee; Seoul National University, Korea (the Republic of)

Perovskite nanoparticles (PeNPs) are promising emitters owing to their high color purity, low-cost synthesis, and facile wavelength control with halide composition control. However, chloride-based blue-emitting colloidal PeNPs have suffered from low photoluminescence quantum efficiency (PLQE) due to chloride-induced defect states. Their low PLQE hinders their use of blue-emitting devices.

In this work, we propose a method to improve the efficiency of blue PeNPs. At first, blue-emitting perovskite was synthesized by the hot injection method. Near Unity PLQE of as-synthesized PeNPs was obtained. For the efficient perovskite light-emitting diodes (PeLEDs), additional washing steps are required to remove excess ligands on the surface. But after washing steps, the PLQE rapidly decreased to  $\sim 50\%$  because of surface defects.

A simple post-treatment process using short organic ligands solution was done after washing steps. PLQE increased again because the halide anions passivate defect sites. Moreover, those short organic ligands do not impede charge injection. By these methods, highly efficient blue-emitting PeNPs with PLQE  $> 92\%$  and high device efficiency of 2% was obtained.

#### F.EL02.13.19

**Water Passivation of Perovskite Nanocrystals Enables Air-Stable Intrinsically-Stretchable Color-Conversion Layers for Stretchable Displays** HuanYu Zhou<sup>1</sup>, Jinwoo Park<sup>1</sup>, Yeongjun Lee<sup>1</sup>, Jae-Man Park<sup>1</sup>, Jin-Hoon Kim<sup>2</sup>, Joo Sung Kim<sup>1</sup>, Hyeon-Dong Lee<sup>1</sup>, Seung Hyeon Jo<sup>1</sup>, Xue Cai<sup>1</sup>, Lizhu Li<sup>3</sup>, Xing Sheng<sup>3</sup>, Hyung Joong Yun<sup>4</sup>, Jin-Woo Park<sup>2</sup>, Jeong-Yun Sun<sup>1</sup> and Tae-Woo Lee<sup>1</sup>; <sup>1</sup>Seoul National University, Korea (the Republic of); <sup>2</sup>Yonsei University, Korea (the Republic of); <sup>3</sup>Tsinghua University, China; <sup>4</sup>Korea Basic Science Institute, Korea (the Republic of)

Despite organic light-emitting diode (OLED) technology has already left an indelible mark on the display industry, conventional OLEDs are still susceptible to degradation when exposed to air. A greater hurdle is to achieve the stretchable OLED as protecting devices from the penetration of moisture and oxygen is even more difficult under stretching. Here, we propose an air-stable intrinsically stretchable display without using any encapsulations by integrating a stretchable light-emitting device (SLED) with a stretchable color conversion layer that contains perovskites nanocrystals (PeNCs). PeNCs

normally decay when exposed to air; counterintuitively, the moisture-assisted surface passivation of PeNCs is first observed. This work is believed to stimulate considerable research on fundamental aspects of PeNCs and furthermore into the practical applications both in academia and industries. The above-mentioned SLED can also open new ways toward intrinsically stretchable OLEDs.

#### F.EL02.13.20

##### ***In Situ* Fabrication of Highly Luminescent Halide Perovskite Thin Films Incorporating Organic Dispersing Agent** Eojin Yoon and Tae-Woo Lee; Seoul National University, Korea (the Republic of)

Recently, lead halide perovskite nanoparticles became promising candidates for light emitters due to narrow full-width at half maximum (FWHM), solution processability, easily tunable bandgap.<sup>1</sup> Excitons are well confined with the aids of long passivating ligands promoting radiative recombination, thus, lead halide perovskite nanoparticles exhibit high photoluminescence quantum yield (PLQY).<sup>2</sup> However, the synthesis of perovskite nanoparticles is complicated requiring several centrifugations and production yield is low because only the small amount of precipitate is utilized by reprecipitation method.

So, we took *in-situ* strategy for synthesizing perovskite nanoparticles by incorporating bulky ligand, phenyl ethyl ammonium bromide (PEABr).<sup>3</sup> To achieve stable *in situ* fabricated perovskite nanoparticles, dispersion of PEABr is essential because PEABr aggregates form local quasi-2D structure.<sup>4</sup> Here, we successfully synthesized perovskite nanoparticles by exploiting crown additive of 1,4,7,10,13,16-Hexaoxacyclooctadecane (18-crown-6) as a dispersing agent. From UV-vis spectroscopy, it was confirmed that low n phases (~440 nm) considerably decreased with 18-crown-6 and the average lifetime also enhanced due to reduced defect sites. Moreover, temperature-dependent PL represented increased exciton binding energy from 24.6 to 63.9 (meV) owing to the fine dispersion of PEABr and dielectric confinement effect. Finally, with optimized concentration, highly bright perovskite films with maximum PLQY of 93.036 % could be achieved, which is 47 times higher than pristine films.

#### References

1. Kim Y-H, Cho H, Lee T-W. Metal halide perovskite light emitters. *Proc Natl Acad Sci.* 2016;113(42):11694-11702.
2. Kim YH, Cho H, Heo JH, et al. Multicolored organic/inorganic hybrid perovskite light-emitting diodes. *Adv Mater.* 2015;27(7):1248-1254. doi:10.1002/adma.201403751
3. Zhao L, Yeh YW, Tran NL, et al. In Situ Preparation of Metal Halide Perovskite Nanocrystal Thin Films for Improved Light-Emitting Devices. *ACS Nano.* 2017;11(4):3957-3964. doi:10.1021/acsnano.7b00404
4. Ban M, Zou Y, Rivett JPH, et al. Solution-processed perovskite light emitting diodes with efficiency exceeding 15% through additive-controlled nanostructure tailoring. *Nat Commun.* 2018;9(1):1-10. doi:10.1038/s41467-018-06425-5

#### F.EL02.13.21

##### **Core-Shell Structure Perovskite Nanoparticles with Atomic Surface Passivation for Highly-Efficient Pure-Red Emitting Perovskite Light-Emitting Diodes** Jinwoo Park, Sinil Choi, Sungjin Kim, Joo Sung Kim and Tae-Woo Lee; Seoul National University, Korea (the Republic of)

Perovskite nanoparticles (PeNPs) is attractive next-generation sources for light-emitting diodes (LEDs) due to their efficient luminescent, solution processability, tunable bandgap and extremely high color purity which is superior to conventional light emitters (e.g. organic emitters, traditional quantum dots). However, due to halide segregation, emission wavelength shift while LED operation and precise control of emission wavelength is limited. Here, we develop facile atomic surface defect passivation method exploited post-synthesis treatment using high bandgap perovskite precursor. With this strategy, we synthesized color-stable and pure-red-emitting CsPbI<sub>3</sub> PeNPs with 630 nm of peak emission wavelength with core-shell structure. Highly efficient PeNP LEDs without electroluminescence wavelength shift was also demonstrated.

#### F.EL02.13.22

##### **Late News: Maximizing the Photoluminescence Intensity in Quasi 2D Perovskites Through Surface Passivation of Defect States** - Yukta and Soumitra Satapathi; Indian Institute of Technology Roorkee, India

Quasi two-dimensional (2D) perovskites are currently considered as materials of choice for light emitting diodes (LEDs) due to their unique optoelectronic properties such as strong exciton binding energy, multiple quantum well structure, and reasonable ambient stability for practical applications. Tremendous progress has been achieved in 2D perovskites LEDs in terms of external quantum efficiency (EQE) (~17%), luminescence (6785 cd/m<sup>2</sup>) and stability through compositional and device engineering. However, the excessive surface defect states generated due to the reduced crystal size, the presence of un-coordinated Pb<sup>+2</sup> ions or shallow vacancy defects generated by MA or halide ions at the surface and grain boundaries,

limits the radiative recombination and in turn the electro-luminescence (EL) efficiency of the LEDs. It has been realized that surface passivation with suitable organic/inorganic moieties can play a vital role in overcoming the adverse effect of defect states through their interaction with uncoordinated ions and can improve the stability.

In the present work, we have chosen  $n=4$  composition quasi-2D perovskite  $(BA)_2(MA)_3Pb_4Br_{13}$  films as emissive layer by optimal phase engineering and have shown the order of magnitude enhancement of radiative emission after passivating them with two different molecules namely- triphenyl phosphine oxide (TPPO) and an insulating polymer polymethyl methacrylate (PMMA). Both the steady state and time resolved study confirm up to 400% enhancement in fluorescence intensity and improved average lifetime ( $\approx 19.4$  ns) after surface passivation. Additionally, the effect of passivating agents on film morphology and radiative emission efficiency is studied in details. Also, the interaction mechanism between layered perovskite and passivating agents has been probed with FTIR spectroscopy, XPS and KPFM study. Our systematic investigation with detailed mechanistic study will pave the way for further development of the highly efficient LEDs.

*References:* -

Yang, Xiaolei *et.al Nat. Commun.* **2018**, 9 (1), 2–9.

Bi, Wentao *et.al ACS Appl. Mater. Interfaces* **2020**, 12 (1), 1721–1727.

Na Quan, L *et.al Nat. Commun.* **2020**, 11 (1), 1–9.

### F.EL02.13.23

**Late News: Quantum Confinement in Type I Heterostructure of Hybrid Lead Halide Perovskite Embedded in Organic Matrix** Amrita Dey<sup>1,2</sup>, Shivam Singh<sup>2</sup> and Dinesh Kabra<sup>2</sup>; <sup>1</sup>Ludwig-Maximilians-Universität, Germany; <sup>2</sup>Indian Institute of Technology Bombay, India

The type I heterostructure forms between Organic semiconductor molecule (4,4'-bis[9-dicarbazolyl]-2,2'-biphenyl [CBP] and bathocuproine [BCP]) and methylammonium lead halide (MAPbX<sub>3</sub>), assists easy growth of perovskite nanocrystals (PNCs) in an organic matrix. Herein, we present the modulation of electronic states of MAPbX<sub>3</sub> PNCs (MA = CH<sub>3</sub>NH<sub>3</sub><sup>+</sup> and X = Br<sup>-</sup> and I<sup>-</sup>) as a function of crystallite size. This results in the growth of MAPbX<sub>3</sub> PNCs of tunable sizes from  $\sim 110$  nm to  $\sim 10$  nm in the organic semiconductor matrix. A blue shift is observed in the photoluminescence peak (PL<sub>max</sub>) energy over a range of  $\sim 200$  meV for MAPbI<sub>3</sub> PNCs embedded in the BCP matrix. However, PL<sub>max</sub> energy tunes over  $\sim 32$  meV only with a similar volumetric concentration in the case of MAPbBr<sub>3</sub> PNCs in the same BCP matrix. Moreover, the PL blue shift is even lower in the case of the CBP matrix in comparison with the BCP matrix for both the perovskites. This discrepancy could be resolved by determining the resultant crystallite size using X-ray diffraction studies and the Debye–Scherrer formula. Results about the blue shift in the PL peak can be explained using the classic particle-in-a-box versus excitonic Bohr radius model under a weak confinement regime.

### References

1. S. Singh, A. Dey, S. Kolay and D. Kabra, Modulation of electronic states of Hybrid lead perovskites embedded in organic Matrix. *Energy Technol.* **2019**, 1900894.
2. D. Di, K. P. Musselman, G. Li, A. Sadhanala, Y. Ievskaya, Q. Song, Z.-K. Tan, M. L. Lai, J. L. MacManus-Driscoll, N. C. Greenham, R. H. Friend, Size-dependent photon emission from organometal halide perovskite nanocrystals embedded in organic matrix. *J. Phys. Chem. Lett.* **2015**, 6, 446.

## SYMPOSIUM F.EL03

---

Emerging Low-Dimensional Chalcogenides for Electronics and Photonics  
November 21 - December 3, 2020

### Symposium Organizers

Jon Major, University of Liverpool  
Xiaofeng Qian,  
Feng Yan, The University of Alabama  
Qian Zhang, Harbin Institute of Technology

\* Invited Paper

SESSION F.EL03.10: Live Keynote I: Emerging Low-Dimensional Chalcogenides for Electronics and Photonics  
Session Chairs: Jon Major, Xiaofeng Qian, Feng Yan and Qian Zhang  
Tuesday Afternoon, December 1, 2020  
F.EL03

**1:45 PM \*F.EL03.02.04**

**Hot Carrier Optoelectronics with 2D Transition Metal Dichalcogenides** Goki Eda; National University of Singapore, Singapore

One of the most distinct features of van der Waals (vdW) heterostructures based on two-dimensional (2D) materials is the ultrafast photo-induced interlayer charge transfer, which is known to occur in sub-picosecond time scales. Such ultrafast dynamics offers promise for the realization of novel hot carrier optoelectronic devices where non-thermalized photocarriers are harnessed to achieve unconventional functions. In this talk, we will discuss a few examples of hot carrier optoelectronic phenomena in heterostructures of 2D transition metal dichalcogenides. First, we will discuss realization of near-infrared (NIR) to visible light upconversion in a metal-insulator-semiconductor (MIS) vdW heterostack tunnel diode [1]. We show that the upconversion is enabled by interlayer transfer of non-thermalized photoexcited holes and its dynamics can be tuned by orders of magnitude by applied electric fields. Second, we will discuss unique photoresponse of these MIS devices arising from hot carriers generated by efficient exciton-exciton annihilation (EEA) in monolayer MoS<sub>2</sub> [2]. We describe how EEA can result in highly energetic electrons and holes due to uneven distribution of annihilation energies following energy- and momentum-conserving scattering.

[1] Linaryd et al. "Electro-Optic Upconversion in van der Waals Heterostructures via Nonequilibrium Photocarrier Tunneling" *Adv. Mater.* In Press (DOI: 10.1002/adma.202001543).

[2] Linaryd et al. "Harnessing Exciton-Exciton Annihilation in Two-Dimensional Semiconductors" *Nano Lett.* 2020, 20, 1647.

**2:10 PM \*F.EL03.05.05**

**Revealing Defect Passivation Mechanisms in Sb<sub>2</sub>Se<sub>3</sub>** David Tilley; University of Zurich, Switzerland

Antimony selenide (Sb<sub>2</sub>Se<sub>3</sub>) has emerged as a strong candidate for practical water splitting due to its suitable bandgap, excellent optoelectronic properties, and resistance to photocorrosion in strongly acidic electrolyte solutions. In this talk, I will discuss the synthesis of Sb<sub>2</sub>Se<sub>3</sub> thin films by selenization of antimony metal and the photoelectrochemical properties of these films after coating with a molybdenum sulfide hydrogen evolution catalyst. The performance of these photocathodes was greatly enhanced by a relatively low temperature sulfurization treatment with elemental sulfur, greatly improving the photovoltage and the fill factor. The origin of the improvement upon sulfurization was investigated with time-resolved microwave conductivity (TRMC) measurements and photoluminescence. TRMC of our Sb<sub>2</sub>Se<sub>3</sub> reveals high mobilities of the photogenerated charge carriers (>10 cm<sup>2</sup> V<sup>-1</sup> s<sup>-1</sup>) and a low trap density, in contrast to other emerging photoelectrochemical materials such as Fe<sub>2</sub>O<sub>3</sub>, CuFeO<sub>2</sub>, and BiVO<sub>4</sub>. We find that the sulfurization treatment of the Sb<sub>2</sub>Se<sub>3</sub> thin films yields improved charge carrier lifetimes. Not only is surface recombination curtailed, but deep traps in the bulk are eliminated (most likely Sb-Se antisite defects), which reduces non-radiative recombination of the photogenerated charge carriers. A low temperature sulfurization treatment is thereby identified as a simple method to remove bulk traps in Sb<sub>2</sub>Se<sub>3</sub> thin films.

**2:35 PM \*F.EL03.02.08**

**New Low-Dimensional Metal Chalcogenides and Their Optoelectronic Properties** Mercouri G. Kanatzidis; Northwestern University, United States

Two-dimensional (2D) materials have seen a surge of interest ever since the discovery of graphene, a single 2D layer of carbon atoms (graphene), more than a decade ago. 2D chalcogenides are a fundamental class in the study of low-dimensional science and their synthesis is an important goal of solid state chemistry. The presentation will focus on how novel chalcogenides can form using design concepts such as the "dimensional reduction". The new materials exhibit diverse

centrosymmetric and noncentrosymmetric structures that lead to a variety of attractive optoelectronic properties such as direct bandgaps, high X-ray absorption, neutron detection and strong nonlinear optical responses.

### 3:00 PM \*F.EL03.03.01

**Optical Properties and Refractive Uses of Phase-Change Phenomena in Layered Chalcogenides** Rafael Jaramillo; Massachusetts Institute of Technology, United States

Layered chalcogenides hold promise for manipulating light in confined geometry, such as in photonic integrated circuits, where key material properties include strong and controllable light-matter interaction, and limited optical loss. Layered materials feature strong anisotropy and a panoply of polymorphs that suggest a rich design space for highly-nonperturbative photonic integrated devices based on functional martensitic transformations: phase changes and ferroelastic domain switching. These phenomena are manifest in materials with band gap above the photonics-relevant near-infrared (NIR) spectral band ( $\sim 0.5 - 1$  eV), meaning that they can be harnessed in refractive (*i.e.* non-absorptive) applications.

Transition metal dichalcogenides (TMDs) offer a vast composition space within which to optimize refractive index contrast, optical loss, and switching energy. We are using a strategy of alloy design to optimize new, active materials for optical phase shifters. We will present our theoretical predictions of thermodynamics and optical properties of binary systems of sulfur-based TMDs:  $ZrS_2-MoS_2$ ,  $TiS_2-MoS_2$ ,  $TiS_2-ZrS_2$ , and  $MoS_2-CrS_2$ . We will present our experimental measurements of the NIR optical properties of single crystals. We will then present progress on making large-area thin films of sulfur-based TMDs, including the theoretically-predicted alloys, by a two-step method of metal sulfurization. Finally, we will present the optical properties and phase-change functionality of our designed TMD alloy thin films.

We will also present an alternative paradigm of strong, non-perturbative refractive index modulation: electric field-driven ferroelastic domain switching in low-symmetry layered materials. We predict that in materials such as SnSe, a sufficiently-strong electric field will induce rotation between equivalent crystallographic domains, with strong refractive index contrast for linearly-polarized light. We will present simulation-based design of photonic integrated devices utilizing the birefringence of materials such as SnSe and black phosphorous, and experimental results demonstrating non-thermal domain switching triggered by fast laser pulses.

SESSION F.EL03.12: Live Keynote III: Emerging Low-Dimensional Chalcogenides for Electronics and Photonics  
Session Chairs: Jon Major, Xiaofeng Qian, Feng Yan and Qian Zhang  
Thursday Afternoon, December 3, 2020  
F.EL03

### 6:30 PM \*F.EL03.05.07

**Chemical Trends and Electronic Engineering of V-VI-VII Metal Chalcohalides** Aron Walsh<sup>1,2</sup>; <sup>1</sup>Imperial College London, United Kingdom; <sup>2</sup>Yonsei University, Korea (the Republic of)

Metal chalcohalides are candidates for next-generation technologies including energy conversion, information storage, and quantum computing. I will present an exploration of V-VI-VII ternary chalcohalides, where V = Sb, Bi; VI = O, S, Se, Te; and VII = F, Cl, Br, I. These include the photoferroic compound SbSI [1,2] and the solar fuels photoelectrode BiOBr [3,4]. We consider 32 elemental combinations in 4 spacegroups using a combination of density functional theory (structural and thermochemistry) and many-body QSGW theory (relativistic electronic band structures). The materials are found to exhibit a wide range of electronic structures and bandgaps from metallic to over 5 eV. The large spin-orbit coupling in the heavy cations strongly influences the electronic structure. This research is part of a collaboration with the groups of David Scanlon (UCL) and Mark van Schilfgaarde (KCL), and used the UK National Supercomputer ARCHER.

[1] "Ferroelectric materials for solar energy conversion: photoferroics revisited" K. T. Butler et al, Energy Environ. Sci. 8, 838 (2015)

[2] "Quasi-particle electronic band structure and alignment of the V-VI-VII semiconductors SbSI, SbSBr, and SbSeI for solar cells" K. T. Butler et al, Appl. Phys. Lett. 108, 112103 (2016)

[3] "Bismuth oxyhalides: synthesis, structure and photoelectrochemical activity" D. S. Bhachu et al, Chem. Sci. 7, 4832

(2016)

[4] "Interplay of orbital and relativistic effects in bismuth oxyhalides: BiOF, BiOCl, BiOBr, and BiOI" A. M. Ganose et al, Chem. Mater. 28, 7, 1980 (2016)

**6:54 PM \*F.EL03.06.06**

**Synthesis of Two-Dimensional Materials via Chemical Vapor Deposition** Jing Kong; Massachusetts Institute of Technology, United States

In recent years tremendous efforts have been devoted to the research on two dimensional materials. Their unique structures and remarkable properties have offered great potential for a wide range of applications in electronics, optoelectronics, valleytronics, catalysis, etc. The synthesis of high quality large area mono- and few-layer 2D materials is highly desirable for their applications. In this talk I will present our recent development on novel 2D material and structures, together with further understanding regarding the chemical vapour deposition (CVD) synthesis process of monolayer MoS<sub>2</sub>.

**7:18 PM \*F.EL03.07.02**

**Systematic Exploration of Structure and Properties in Homologous Series of Nanoscale Chalcogenide Superlattices** Sage Bauers<sup>1</sup>, Danielle Hamann<sup>2</sup>, Dennice Roberts<sup>1</sup>, Andriy Zakutayev<sup>1</sup> and David Johnson<sup>2</sup>; <sup>1</sup>National Renewable Energy Laboratory, United States; <sup>2</sup>University of Oregon, United States

An exciting prospect for 2D materials is their ability to be integrated into heterostructures, where the selection and sequencing of stacked layers facilitate tailored properties. One form of such heterostructures are non-epitaxial chalcogenide superlattices with constituents interleaved at nanometer length scales. These materials can be prepared from amorphous—but intentionally layered—thin films which are gently heated to crystallize into a superlattice that mimicks the layer sequence of the precursor. Such facile synthesis enables superlattices with nearly limitless permutational flexibility, allowing for systematic explorations of how different layer arrangements affect the structure and properties of the composite material.

This talk will primarily focus on materials containing  $n$  monolayers of TiSe<sub>2</sub> interleaved with  $m$  monolayers of PbSe and/or SnSe in a repeating superlattice. These structures can be described by the chemical formula [(MSe)<sub>1+δ</sub>] <sub>$m$</sub> [TiSe<sub>2</sub>] <sub>$n$</sub> , where M=Sn or Pb and  $\delta$  is a compositional misfit parameter. We will discuss several homologous series wherein the relative fractions of constituents are successively modified by changing the integral number of layers ( $m$  and  $n$ ).

Changes to [(MSe)<sub>1+δ</sub>] <sub>$m$</sub> [TiSe<sub>2</sub>] <sub>$n$</sub>  layer sequencing induce changes to the composite materials' semi-metallic transport properties. In both [(PbSe)<sub>1+δ</sub>] <sub>$m$</sub> [TiSe<sub>2</sub>] <sub>$n$</sub>  and [(SnSe)<sub>1+δ</sub>] <sub>$m$</sub> [TiSe<sub>2</sub>] <sub>$n$</sub>  electrons exchanged between the layers are the primary source of mobile carriers while the amount of charge exchange required to equilibrate the chemical potential across the interface is dependent on the thicknesses and identities of layers. Thus,  $m$  and  $n$  can be used to tune the carrier density with minimal change to carrier mobility since no ionized dopants are introduced into conduction paths. In some cases, the sequencing can also affect the local structure within the layers. For example, in [(PbSe)<sub>1+δ</sub>] <sub>$m$</sub> [TiSe<sub>2</sub>] <sub>$n$</sub>  superlattices both constituents are structurally rigid and insensitive to the thickness of the layers. Conversely, in [(SnSe)<sub>1+δ</sub>] <sub>$m$</sub> [TiSe<sub>2</sub>] <sub>$n$</sub>  the nanolayers of SnSe exhibit a rich polymorphism dependent on thickness, which is attributed to a combination of low polymorph energies and strong interfacial interactions with TiSe<sub>2</sub>.

Motivated by successful synthesis of superlattice materials in several selenide systems, we have recently reported on [(SnS)<sub>1+δ</sub>] <sub>$m$</sub> [TaS<sub>2</sub>] <sub>$1$</sub>  superlattices, marking the first application of this synthesis approach to sulfur-based chemistries. As part of this work, we employ graded precursor films that enable parallel preparation of multiple stacking sequences with similar monolayer control. These results are a promising first step towards similar systematic investigation of structure and properties in another chalcogenide class.

**8:06 PM \*F.EL03.08.01**

**A Method to Reliably Measure Energy Conversion Efficiency without Making Contact for Confirmation of Thermoelectric Figure-of-Merit** Zhifeng Ren; University of Houston, United States

Thermoelectric figure-of-merit (ZT) is the overall most important physical quantity for a thermoelectric material. It ultimately determines the energy conversion efficiency. However, over the years, higher and higher ZTs were reported without confirmation since it requires zero-resistance contact that is as difficult as, if not more than, the material improvement. Therefore, how to confirm the ZT of any material without making the needed contact is urgently needed. In

this report I will present our detailed study on reliable efficiency measurement on materials without making the needed contact.

SESSION F.EL03.11: Live Keynote II: Emerging Low-Dimensional Chalcogenides for Electronics and Photonics  
Session Chairs: Jon Major, Xiaofeng Qian, Feng Yan and Qian Zhang  
Wednesday Morning, December 2, 2020  
F.EL03

**8:00 AM \*F.EL03.03.02**

**Optical Properties of Transition Metal Dichalcogenide Bilayers** Xiaoqin E. Li; The University of Texas at Austin, United States

Optical properties of atomically thin transition metal dichalcogenides are dominated by exciton resonances exhibiting large oscillator strength and binding energies. In vertically stacked bilayers, a host of new exciton resonances emerge, lending new opportunities to discover new science and enable new devices. In this talk, I will focus on how moire superlattices change exciton resonances and diffusion. We discovered recently that phonon spectra are renormalized in moire superlattices as well. A rich variety of properties can be controlled by tuning the twist angle between the bilayers. I make some comparisons between samples that are grown using chemical vapor deposition and those prepared by mechanical exfoliation and stacking. Our work is supported by DOE under grant DE-SC0019398, NSF DMR-1808042, DMR-1720595, and the Welch Foundation F-1662.

**8:30 AM OPEN SLOT**

**9:00 AM \*F.EL03.02.06**

**Chirality-Dependent Second Harmonic Generation of MoS<sub>2</sub> Nanoscroll with Enhanced Efficiency** Qingkai Qian<sup>1</sup>, Rui Zu<sup>1</sup>, Qingqing Ji<sup>2</sup>, Jing Kong<sup>2</sup>, Venkatraman Gopalan<sup>1</sup> and Shengxi Huang<sup>1</sup>; <sup>1</sup>The Pennsylvania State University, United States; <sup>2</sup>Massachusetts Institute of Technology, United States

Second harmonic generation (SHG), as a nonlinear optical effect, has important applications in photonics for frequency conversion and light modulations. Materials with high SHG efficiency and reduced dimensions are favorable for integrated photonics and novel nonlinear optical applications. Here, we fabricate MoS<sub>2</sub> nanoscrolls with different chiralities and study their SHG performances. As a 1D material, MoS<sub>2</sub> nanoscroll shows reduced symmetry and strong chirality dependency in the polarization-resolved SHG characterizations, which is in stark contrast with the 2D MoS<sub>2</sub> layers. This SHG performance can be well explained by the coherent superposition theory of second harmonic field of the nanoscroll walls. MoS<sub>2</sub> nanoscrolls with certain chiralities in our experiment can have SHG intensity up to 98 times stronger than that of monolayer MoS<sub>2</sub>. The same chirality-dependent SHG can be expected for nanoscrolls or nanotubes composed of other non-centrosymmetric 2D materials, such as WS<sub>2</sub>, WSe<sub>2</sub>, and hBN. The characterization and analysis results presented here can also serve as a non-destructive technique to determine the chiralities of these nanoscrolls and nanotubes.

SESSION F.EL03.01: Characterization of Low-Dimensional Chalcogenides  
On Demand Abstracts Available for Viewing Starting Saturday Morning, November 21, 2020  
F-EL03

**5:00 AM F.EL03.01.01**

**On the Nature of the Surface of Semiconductor Nanocrystals** Patanjali Kambhampati; McGill University, Canada

By virtue of their size, the surface must be one of the dominant aspects of semiconductor nanocrystals. Yet the surface remains the most poorly understood aspect of their basic science. Here, we exploit simple temperature dependence photoluminescence and electron transfer theory to rationalize the nature of surface emission from all nanocrystals. Moreover this work enables prediction of how to rationally generate white light from a single nanocrystal by virtue of mixing emission

from the excitonic core and the self trapped excitonic states at the surface.

#### 5:10 AM F.EL03.01.02

#### **Transrotational Bent-Lattice Nanostructures in Crystallizing Amorphous Nanoribbon Films Revealed by TEM** Vladimir Y. Kolosov; Ural Federal University, Russian Federation

The paper summarizes our recent TEM (transmission electron microscopy) studies and main former data on novel microcrystals, nanostructures with unexpected, dislocation independent, regular internal bending of the crystal lattice planes [1]. Usually it is revealed in thin films or layers after amorphous – crystalline transitions. Such **perfect crystals/grains with regularly bent lattice** (built up by simultaneous *translation* and small regular *rotation* of the unit cell) **demonstrate a new “transrotational” [2] type of solid state order realized in thin films**. It is primarily dislocation independent and takes place round an axis (or 2 axes) lying in the film plane of the growing crystal. The maximal values correspond to essential lattice orientation gradients (up to 300 degrees per  $\mu\text{m}$ ) resulting to several whole rotations for the crystal about 10  $\mu\text{m}$  in length (in film plane).

Thin (10 - 100 nm) crystallized areas with transrotation we study vary from small crystals (0.1 - 100 microns), ribbons, whiskers or spherulites to large-scaled polycrystalline areas with a complex texture. They are grown by heat treatment (or by self-organization upon aging) and local annealing by focused electron/laser beam in amorphous films most easily formed for chalcogenides. The films were prepared primarily by vacuum evaporation mostly with thickness or/and composition gradients across TEM grids (to study these factors directly). We used mainly TEM, primarily bend-contour method [3], *in situ* studies, and HREM. Correlative TEM-AFM studies were also performed.

The geometry and the magnitude of transrotation can be regulated by film preparation and crystallization conditions, orientation of the crystal nucleus, sublayers, composition and film thickness.

*In situ* studies in particular include HREM of amorphous-crystalline interface propagation and multiple reversible local transformations "amorphous – transrotational crystalline" inside the fingers in *Se*-based vacuum deposits. Dynamic changes of TEM diffraction contrast fit the mechanism of transrotation formation based on the surface nucleation that we proposed earlier.

Atomistic mathematical model (based on instrument of conformal transformations) for the atom positions in "transrotational" single crystal and the probable physical reasons are discussed. Transrotational microstructure can be considered as an intermediate one between amorphous and crystalline structures (likewise the structure of liquid crystals, intermediate between crystalline structure and liquid one). We suppose it as one of the reasons for easy phase changes in chalcogen-based films that tend to crystallize in such manner. Transrotational crystals have been eventually recognized/studied in a large variety of thin film systems and well-known chalcogenide compositions [4, 5] used for non-volatile memory and prospective for other kinds of storage and phase-change materials applications (including photonics).

Opposite to other unusual regular nano aggregations of atoms widely recognized by the community in recent 35 years (quasi-crystals, fullerenes and nanotubes and alike nano derivatives as well as graphene-like layers) our less known “transrotational” crystals/structures are less confined in dimensions. Bent atom layers in fine areas can be described as similar to that of hypothetical 2+D halves ( $180^\circ$ ) of endless (continuous in film plane) multiwall nano- tubes/onions/tori.

The transrotation phenomenon is the basis for novel lattice-rotation crystal nanoengineering of functional, smart thin-film materials including tunable and switchable low-D structures with some features suitable also for strain engineering.

[1] I E Bolotov, V Y Kolosov and A V Kozhyn, Phys. Stat. Sol. **72a** (1982) 645.

[2] V Y Kolosov and A R Thölen, Acta Mat. **48** (2000) 1829.

[3] I E Bolotov and V Y Kolosov, Phys. Stat. Sol. **69a** (1982) 85

[4] B J Kooi and J T M De Hosson, J. App. Phys. **95** (2004) 4714.

[5] E Rimini *et al.*, J. App. Phys. **105** (2009) 123502.

#### 5:20 AM F.EL03.01.03

#### **Understanding the Optical Properties of Monolayer Transition Metal Mono- and Dichalcogenides Materials** Nicholas Pike<sup>1,2</sup> and Ruth Pachter<sup>2</sup>; <sup>1</sup>UES, Inc., United States; <sup>2</sup>Air Force Research Laboratory, United States

With the advent of applications for two-dimensional materials in electronics and photonics, a number of theoretical investigations on the optical properties of have emerged. However, these investigations often focus on the linear optical properties with very few focused on the nonlinear optical properties of these two-dimensional materials. For example, measurements on the second harmonic generation (SHG) in monolayer transition metal dichalcogenides (TMDs), primarily MoS<sub>2</sub>, WS<sub>2</sub>, and WSe<sub>2</sub>, have shown promise due to the large second-order susceptibilities. SHG measurements of stacked twisted TMD bilayers, as well as from transition metal monochalcogenide (TMM) monolayers, e.g. GaSe and InSe, have also been reported. Yet, theoretical predictions of these second-order quantities are scarce. Here, we summarize a theoretical analysis of the linear and nonlinear susceptibilities of a series of monolayer TMDs and TMMs in comparison to experiment.



Aspects on the importance of including spin-orbit coupling and many-body effects to study excitonic effects in these materials will be discussed in detail. Finally, results for TMD and TMM heterostructures will be described, particularly with respect to the optical response upon changing the relative orientation of the stacked monolayers.

#### 5:30 AM F.EL03.01.04

**Strain-Induced Spontaneous Centroidal Voronoi Tessellation in Few-Layer MoS<sub>2</sub>** Yichao Zhang, Moon-Ki Choi, Ellad Tadmor and David J. Flannigan; University of Minnesota, United States

Due to the anisotropic bonding states inherent to transition metal dichalcogenides (TMDs), these materials can withstand as large as 10% elastic strains and display an associated wide range of variable optical and electronic properties [1]. In addition to interests in fundamental behaviors, such properties have driven efforts to develop strain-tunable devices and applications. While spontaneous wrinkle formation in few to monolayer specimens generates local strain variations, controllable and predictable strain-pattern requires rational engineering design and processing principles [2,3]. Nascent approaches have focused on either whole-flake deformation (*e.g.*, indirect handling of elastomer substrates) or single, site-specific mechanical indentation to modulate the global or local strain through repeatable stress application [4,5]. Spatially periodic strain patterning has been introduced to produce predictable, highly-symmetric local structural modulations in a passive, non-continuous manner, *e.g.*, through flake deposition on periodic nanostructures [6,7], or through moiré patterns in twisted layered heterostructures [8,9]. In this way, local strain patterning can be controlled by manipulating nanostructure geometry and patterning periodicity.

Here we report a method for highly-symmetric, spontaneous strain patterning of few-layer MoS<sub>2</sub> using patterned holey substrates based on the principle of tessellation. In this approach, uniformly-spaced substrate holes of the same size, arranged in a hexagonal array throughout the substrate, serve as the tessellation seeds. The resulting tessellation pattern with six-fold symmetry is well-described by centroidal Voronoi tessellation (CVT). In a TEM bright-field image, the tessellation manifests as strongly-scattering bend contours between the holes forming three-fold vertices at the center of sets of three holes. Further, twelve-fold bend contours, indexed to first- and second-order Bragg spots, radiate from the seeds and arise from curvature of the crystal over the hole, as confirmed with correlated bright- and dark-field imaging. Atomistic simulations of a bilayer MoS<sub>2</sub> crystal on a holey substrate show a change in the relative height and display similar bend contour patterns in the hole region [10]. Spatially-averaged strains of 2% to 4% are present, as determined with selected-area diffraction. Further, spatial mapping of relative strain was obtained with nanobeam electron diffraction with a 10-nm beam size. Strains were maximal near the hole centers with a steep decrease toward the substrate, as observed in both experiment and simulation, before increasing again when approaching the hexagonal tessellation patterns over the substrate. In addition to spontaneous formation, tessellated strain-patterning is also influenced by polymer residue from crystal transfer for thicker flakes within the holes. These results suggest a simple, highly-repeatable method based on the principles of CVT for producing highly-symmetric, strain-patterned films of high regular periodicity in TMDs, other layered materials, and generally in ultrathin films and crystals [11].

[1] H.-Y. Chang, *et al.*, ACS Nano **7** (2013), p. 5446.

[2] P. Miró, M. Ghorbani-Asl, and T Heine, Adv. Mater. **25** (2013), p. 5473.

[3] J. Brivio, D. T. L. Alexander, and A. Kis, Nano Lett. **11** (2011), p. 5148.

[4] S. Bertolazzi, J. Brivio, and A. Kis, ACS Nano **5** (2011), p. 9703.

[5] A. Castellanos-Gomez, *et al.*, Nano Lett. **13** (2013), p. 5361.

[6] H. Li, *et al.*, Nat. Commun. **6** (2015), 7381.

[7] Y. Zhang, *et al.*, Nano Lett. **18** (2018), p. 2098.

[8] K. Zhang and E. B. Tadmor, J. Mech. Phys. Solids **112** (2018), p. 225.

[9] H. Yoo, *et al.*, Nature Materials, **18** (2019), p. 448.

[10] Y. Zhang, *et al.*, submitted (2020).

[11] This work was supported primarily by the National Science Foundation through the University of Minnesota MRSEC under Award Number DMR-1420013 and partially by the National Science Foundation under Grant No. DMR-1654318.

#### 5:40 AM F.EL03.01.05

**Structural Origin of Size and Parity Effects Observed by NanoDSC in 2D Organic Metal Chalcogenides—Atomic Resolution Crystallography via Diffraction and *Ab Initio* Calculation** Jie Zhao, Zichao Ye, Kisung Kang, Scott J. McCormack, Yu-Tsun Shao, Mike Efremov, Andre Schleife, Jian-Min Zuo, Waltraud M. Kriven and Leslie Allen; University of Illinois at Urbana-Champaign, United States

The emerging characteristics of two categories of nanoscale materials with increasing interests, organic metal chalcogenides

(OMC) and two-dimensional (2D) van der Waals layers, can both be elucidated by studying the structure-property-relationship of 2D metal alkanethiolate layers. A detailed study of the crystal structure of this inorganic-organic hybrid system is critical to understand its size and odd/even effect observed in properties such as melting point/enthalpy (NanoDSC), luminescence, and band structures. Crystallography determination with atomic resolution is often challenging for beam-sensitive hybrid materials that do not grow into large scale single crystals (e.g. silver alkanethiolate, AgSC<sub>n</sub>, in this work). Here we describe a novel methodology combining synchrotron powder X-ray diffraction, nanobeam electron diffraction, and *ab initio* calculations. Unit cell level information and atomic coordinates of Ag-S segments are well uncovered by diffraction techniques, whereas density functional theory calculations suggest the complete atomic basis including the light/soft organic segments. Crystallography results of AgSC<sub>n</sub> (n=2-10) show odd/even effect in lamellar thickness consistent with prior experiments. Our preliminary findings of AgSC<sub>n</sub> structure suggest modifications to the initial simplified model, and consists of three segments: (i) Ag-S backbone: we first report an inorganic backbone deformation modulated by organic chain length, as a result of lattice mismatch between Ag-S framework and the epitaxial hydrocarbon chains that incline towards optimal packing. Such modulation probably leads to various optical luminescence properties inherent in the argentophilic interactions found in the backbone, an emerging topic in gold/silver chemistry. (ii) Interlayer interface: the structural origin of odd/even effect in this layered OMC system lies in the parity-dependent C-H orientations and H-H interactions exhibited among the terminal methyl groups. The resulting denser packing of odd-chain interface explains its higher melting enthalpy. (iii) Alkyl chains: the epitaxial accommodation between the backbone structure (sp<sup>3</sup> hybridized sulfur bonding) and the density of alkyl chains triggers the evolution of local chain tilting and twisting towards the optimal packing with longer chain length. This further provides clues that drive the similar variations of chain configurations in other hybrid systems such as self-assembled monolayers.

#### References:

- [1] Ye, Z, de la Rama, L.P., Efremov, M. Y., Schleife, A., and Allen, L.H. J. Phys. Chem. C. **121** (2017): 13916.
- [2] Ye, Z., de la Rama, L. P., Efremov, M. Y., Zuo, J.-M., and Allen, L. H. Dalton Trans. **45** (2016): 18954.
- [3] de la Rama, L. P., Hu, L., Ye, Z., Efremov, M. Y. and Allen, L. H. J. Am. Chem. Soc. **135** (2013): 14286
- [4] Lai, S. L., Guo, J. Y., Petrova, V., Ramanath, G., and Allen, L. H. Phys. Rev. Lett. **77** (1996): 99.
- [5] Zuo, J.-M., and Spence, J. CH. Advanced Transmission Electron Microscopy, ISBN 978-1-4939-6605-9. Springer Science+ Business Media New York, (2017).
- [6] Kisung, K., Kononov, A, Lee, C. W., Leveillee, J. A., Shapera, E. P., Zhang, X., and Schleife, A. Comput. Mater. Sci. **160** (2019): 207.

#### 5:50 AM F.EL03.01.06

**Late News: Room-Temperature Ferromagnetism in Single Layers of MoSe<sub>2</sub> Decorated with Manganese Oxide Nanoparticles** Nalaka A. Kapuruge, Vijaysankar Kalappattil, Florence A. Nugera, Valery O. Jimenez, Manh-Huong Phan and Humberto R. Gutierrez; University of South Florida, United States

Ferromagnetism in two-dimensional (2D) van der Waals materials has attracted increasing attention due to its potential for developing a new generation of spintronic devices. One route that has been explored to induce 2D ferromagnetism is substitutional doping in transition metal dichalcogenides (TMD) with V or with magnetic atoms. In this work, we propose an alternative approach that consists in decorating 2D TMD materials with nanoparticles of manganese oxide. The nanoparticles were deposited on the surface of monolayer MoSe<sub>2</sub> using a chemical vapor deposition technique. Micro-Raman and PL spectroscopy were used to study their optical properties; while the morphology, chemical composition and thickness of the samples were characterized via SEM, STEM and AFM, respectively. Magnetic measurements reveal a weak ferromagnetic behavior in individual MoSe<sub>2</sub> films, probably arising from the presence of selenium vacancies. Similarly, weak ferromagnetism is observed for MnO<sub>x</sub> nanoparticles deposited on a SiO<sub>2</sub> substrate. However, when the MnO<sub>x</sub> nanoparticles are deposited on 2D MoSe<sub>2</sub>, the hybrid MnO<sub>x</sub>/MoSe<sub>2</sub> system displays enhanced room-temperature ferromagnetism, suggesting a strong magnetic exchange coupling between the two material components. A detailed analysis on the temperature dependence of saturation magnetization and coercive field indicates stronger magnetic coupling at lower temperatures. Our results provide an alternative route to induce room-temperature ferromagnetism in 2D systems.

SESSION F.EL03.02: Optoelectronic Properties of Low-Dimensional Chalcogenides  
On Demand Abstracts Available for Viewing Starting Saturday Morning, November 21, 2020  
F-EL03

### 5:00 AM F.EL03.02.01

**Hybrid Exciton-Plasmon-Polaritons in van der Waals Semiconductor Gratings** Huiqin Zhang<sup>1</sup>, Bhaskar Abhiraman<sup>1,1</sup>, Qing Zhang<sup>2</sup>, Jinshui Miao<sup>1</sup>, Kiyoun Jo<sup>1</sup>, Stefano Roccasecca<sup>1</sup>, Mark W. Knight<sup>3</sup>, Artur Davoyan<sup>4</sup> and Deep M. Jariwala<sup>1</sup>; <sup>1</sup>University of Pennsylvania, United States; <sup>2</sup>National University of Singapore, Singapore; <sup>3</sup>Northrop Grumman Corporation, United States; <sup>4</sup>University of California, Los Angeles, United States

Van der Waals materials and heterostructures that manifest strongly bound exciton states at room temperature are of great promise for optoelectronic applications. 2D transitional metal dichalcogenides (TMDCs) of Mo and W are of particular interest since the strong exciton binding manifests in high refractive indices and extinction coefficients near the exciton resonance. Light-exciton interaction has been extensively studied in monolayer direct-band gap TMDC films (Schneider et al. 2018, *Nat. Comm.*; Brar et al. 2018, *Chem. Soc. Rev.*). Nevertheless, light-interaction with monolayer films is challenged by the very large disparity between optical wavelength and film thickness; without an external cavity, a TMDC monolayer only achieves 8-10% exciton resonance absorption.

In this work, we demonstrate that nanostructured, multilayer transition metal dichalcogenides by themselves provide an ideal platform for excitation and control of excitonic modes, paving the way to exciton-photonics. We first study reflection spectra of unpatterned micromechanically exfoliated WS<sub>2</sub> flakes on a template-stripped Au substrate. For a WS<sub>2</sub> thickness of 15 nm, we observe an avoided crossing of the A-exciton resonance and an optical cavity mode with a large splitting energy of 170 meV. We then introduced periodic one-dimensional gratings into the WS<sub>2</sub> with e-beam lithography and dry-etching. We measured spectra for grating periods ranging from 300 to 750 nm, WS<sub>2</sub> thicknesses from 5 to 30 nm, and grating widths from 200 to 300 nm. In these heterostructures, we observed hybrid modes in addition to strong dispersion of optical cavity modes and several orders of plasmon polariton modes. For a period of 600 nm, a grating width of 300 nm, and a WS<sub>2</sub> thickness of 10 nm, we observe exciton couplings to optical grating and optical cavity modes with strengths of 116 meV and 89 meV respectively. In addition, we observe complete suppression of the inherently strong exciton absorption resonance as a result of coupled optical modes and their interference. We supplement these experimental results with transfer matrix calculations and finite-difference time-domain simulation. We also model the resonances of this heterostructure with a coupled oscillator model; with this model, we recreate the exciton resonance suppression we observe in experiment, showing that the suppression is indeed due to two polaritonic couplings.

Our results highlight a previously unexplored aspect of TMDC excitonics and optics, opening a new regime in exploring strong light-matter interactions where the TMDC serves as a host for both excitonic and cavity modes (without the need for an external cavity). This work paves the way to a next generation of integrated exciton optoelectronic nano-devices and applications in light generation, computing, and sensing.

#### References:

Huiqin Zhang, Bhaskar Abhiraman, Qing Zhang, Jinshui Miao, Kiyoun Jo, Stefano Roccasecca, Mark W. Knight, Artur R. Davoyan, Deep Jariwala: "Hybrid Exciton-Plasmon-Polaritons in van der Waals Semiconductor Gratings", 2019; arXiv:1912.13442. (accepted) *Nature Communications*

### 5:10 AM F.EL03.02.03

**Binary Superlattices of Plasmonic and Excitonic Nanocrystals for Infrared Optical Metamaterials** Sarah Britzman, Nadeemullah A. Mahadik, Syed Qadri, Patrick Y. Yee, Joseph Tischler and Janice E. Boercker; U.S. Naval Research Laboratory, United States

Self-assembled nanocrystal superlattices offer exceptional control over the coupling between nanocrystals, just as solid-state crystals tailor the bonding between atoms. Because nanocrystals are much smaller than the wavelength of light, superlattices that integrate nanocrystals of different properties (e.g. metals, semiconductors, dielectrics) have the potential to generate new light-matter interactions that are not achievable in natural materials [1,2].

In this work [3], we add infrared plasmonic Cu<sub>2-x</sub>S nanocrystals to the relatively limited library of materials that have been successfully incorporated into binary superlattices. We create a variety of binary superlattices with small plasmonic (Cu<sub>2-x</sub>S) nanocrystals and large excitonic (PbS) nanocrystals, both resonant in the infrared. Then, by controlling the surface chemistry of large Cu<sub>2-x</sub>S nanocrystals, we are able to produce structurally analogous superlattices of large Cu<sub>2-x</sub>S and small PbS nanocrystals. Transmission electron microscopy (TEM) and grazing-incidence small-angle X-ray scattering (GISAXS) are used to characterize the superlattices. This synthetic achievement is the first step toward understanding how infrared

plasmonic and excitonic nanocrystals couple in well-defined lattices that display a variety of symmetries and stoichiometries.

## References

- [1] F. X. Redl, K.-S. Cho, C. B. Murray, & S. O'Brien, *Three-dimensional binary superlattices of magnetic nanocrystals and semiconductor quantum dots*. *Nature* **423**, 968-971 (2003).
- [2] M. A. Boles, M. Engel, & D. V. Talapin, *Self-Assembly of Colloidal Nanocrystals: From Intricate Structures to Functional Materials*. *Chemical Reviews* **116**, 11220-11289 (2016).
- [3] S. Brittan, N. A. Mahadik, S. B. Qadri, P. Y. Yee, J. G. Tischler, & J. E. Boercker, Binary Superlattices of Infrared Plasmonic and Excitonic Nanocrystals, *ACS Applied Materials & Interfaces* **12**, 24271-24280 (2020).

### 5:20 AM \*F.EL03.02.04

**Hot Carrier Optoelectronics with 2D Transition Metal Dichalcogenides** Goki Eda; National University of Singapore, Singapore

One of the most distinct features of van der Waals (vdW) heterostructures based on two-dimensional (2D) materials is the ultrafast photo-induced interlayer charge transfer, which is known to occur in sub-picosecond time scales. Such ultrafast dynamics offers promise for the realization of novel hot carrier optoelectronic devices where non-thermalized photocarriers are harnessed to achieve unconventional functions. In this talk, we will discuss a few examples of hot carrier optoelectronic phenomena in heterostructures of 2D transition metal dichalcogenides. First, we will discuss realization of near-infrared (NIR) to visible light upconversion in a metal-insulator-semiconductor (MIS) vdW heterostack tunnel diode [1]. We show that the upconversion is enabled by interlayer transfer of non-thermalized photoexcited holes and its dynamics can be tuned by orders of magnitude by applied electric fields. Second, we will discuss unique photoresponse of these MIS devices arising from hot carriers generated by efficient exciton-exciton annihilation (EEA) in monolayer MoS<sub>2</sub> [2]. We describe how EEA can result in highly energetic electrons and holes due to uneven distribution of annihilation energies following energy- and momentum-conserving scattering.

[1] Linardy et al. "Electro-Optic Upconversion in van der Waals Heterostructures via Nonequilibrium Photocurrent Tunneling" *Adv. Mater.* In Press (DOI: 10.1002/adma.202001543).

[2] Linardy et al. "Harnessing Exciton-Exciton Annihilation in Two-Dimensional Semiconductors" *Nano Lett.* 2020, 20, 1647.

### 5:35 AM F.EL03.02.05

**Direct Hot Carrier Collection in Monolayer WS<sub>2</sub>** Pan Adhikari<sup>1</sup>, Peijian Wang<sup>2</sup>, Kanishka Kobbekaduwa<sup>1</sup>, Hao Zeng<sup>2</sup> and Jianbo Gao<sup>1</sup>; <sup>1</sup>Clemson University, United States; <sup>2</sup>University at Buffalo, The State University of New York, United States

Hot carriers have significant impact to energy conversion/storage and photodetection. For instance, a hot carrier solar cell will lead to a ~ 67 % power conversion efficiency (PCE) to overcome the famous Shockley-Queisser (SQ) limit. For purposes of energy conversion and storage, the hot carriers trigger a more energetic and dynamic chemical reaction to split the water molecules and generate hydrogen molecules, leading to an efficient photoelectrochemical (PEC) cell. This is particularly important and urgent to 2D transition metal dichalcogenides (TMDCs) family, such as MoS<sub>2</sub>, WS<sub>2</sub>, MoSe<sub>2</sub> and MoTe<sub>2</sub>, which have great potential applications in quantum emitters, high performance photo or chemical detector and lithium-ion batteries. However, collecting and utilizing the hot carriers remains one of major challenges in ultrafast phenomena in quantum materials because the hot carriers have a super-short lifetime within couple picoseconds.

In this report, we directly collected hot carrier in monolayer WS<sub>2</sub> semiconductor as a photocurrent using ultrafast photocurrent spectroscopy. The hot carriers generation is resulted from the multiple exciton Auger recombination, demonstrated by the ultrafast photocurrent dependence on laser intensity, and temperature.

### 5:45 AM \*F.EL03.02.06

**Chirality-Dependent Second Harmonic Generation of MoS<sub>2</sub> Nanoscroll with Enhanced Efficiency** Qingkai Qian<sup>1</sup>, Rui Zu<sup>1</sup>, Qingqing Ji<sup>2</sup>, Jing Kong<sup>2</sup>, Venkatraman Gopalan<sup>1</sup> and Shengxi Huang<sup>1</sup>; <sup>1</sup>The Pennsylvania State University, United States; <sup>2</sup>Massachusetts Institute of Technology, United States

Second harmonic generation (SHG), as a nonlinear optical effect, has important applications in photonics for frequency conversion and light modulations. Materials with high SHG efficiency and reduced dimensions are favorable for integrated photonics and novel nonlinear optical applications. Here, we fabricate MoS<sub>2</sub> nanoscrolls with different chiralities and study their SHG performances. As a 1D material, MoS<sub>2</sub> nanoscroll shows reduced symmetry and strong chirality dependency in the polarization-resolved SHG characterizations, which is in stark contrast with the 2D MoS<sub>2</sub> layers. This SHG performance can be well explained by the coherent superposition theory of second harmonic field of the nanoscroll walls. MoS<sub>2</sub> nanoscrolls with certain chiralities in our experiment can have SHG intensity up to 98 times stronger than that of monolayer MoS<sub>2</sub>. The same chirality-dependent SHG can be expected for nanoscrolls or nanotubes composed of other non-centrosymmetric 2D materials, such as WS<sub>2</sub>, WSe<sub>2</sub>, and hBN. The characterization and analysis results presented here can also serve as a non-destructive technique to determine the chiralities of these nanoscrolls and nanotubes.

#### 6:00 AM F.EL03.02.07

**Direct Optical and Electronic Imaging of Atomically-Thin Semiconductor-Metal Buried Interfaces** Kiyoung Jo<sup>1</sup>, Joseph Orr<sup>2</sup>, Jinshui Miao<sup>1</sup>, Huiqin Zhang<sup>1</sup> and Deep M. Jariwala<sup>1</sup>; <sup>1</sup>University of Pennsylvania, United States; <sup>2</sup>Villanova University, United States

Metal contacts to two-dimensional (2D) semiconductors are critical for high performance and highly scaled devices. Yet, despite several years of effort they remain unoptimized and poorly understood from the perspective of metal semiconductor interface chemistry. Most existing studies rely on cross section electron microscopy images or device transport both of which are indirect ways to measure contact resistance. A key reason for this is because metal-semiconductor contacts are buried interfaces which are difficult to probe directly, at least in the case of bulk semiconductors. However, 2D semiconductors such as transition metal dichalcogenides (TMDCs) of Mo and W offer a unique opportunity to directly probe the metal semiconductor interface from the semiconductor side due to the atomically thin nature of the semiconductor.<sup>1</sup> In this talk, we will present spatially varying electrical and optical characteristics of TMDC-bulk metal buried interface using a simple metal-assisted flipping technique that inverts the interface for direct electronic and optical access of the buried interface.<sup>2</sup> Using a combination of scanning Kelvin Probe Force Microscopy (KPFM), conductive-AFM and tip enhanced Raman and Photoluminescence Spectroscopy (TERS/TEPL) we concurrently map surface potential, conductivity, charge density dependent-vibration and emission spectra of the interface with ~20 nm spatial resolution. We use three different Au deposition methods (Thermal, e-beam, Sputter) to compare and contrast the quality of different contacts in addition to direct van der Waals stamping. We observe that thermal metal evaporation results in formation of the most uniform, ohmic and lowest resistance contacts ( $1.49 \times 10^6 \Omega$ ) in comparison to e-beam evaporation ( $7.20 \times 10^8 \Omega$ ), whereas van der Waals stamping forms Schottky contacts ( $5.00 \times 10^{11} \Omega$ ). KPFM and TERS data of each buried interfaces reveals distinct change of carrier concentration as a function of evaporation technique.<sup>3</sup> We attribute different levels of metal semiconductor intimacy at the interface and different levels of defect creation during metal evaporation to these differences in contact quality. Our result highlights the importance of metal deposition schemes and paves a path forward towards engineering low resistance contacts and also presents a facile method for probing them in atomically thin channel materials.

[1] 2D Mater. 2018, 5, 035003

[2] ACS Appl. Mater. Interfaces, 2019, 11, 38218

[3] Phys. Rev. B, 2012, 85, 161403(R)

#### 6:10 AM \*F.EL03.02.08

**New Low-Dimensional Metal Chalcogenides and Their Optoelectronic Properties** Mercouri G. Kanatzidis; Northwestern University, United States

Two-dimensional (2D) materials have seen a surge of interest ever since the discovery of graphene, a single 2D layer of carbon atoms (graphene), more than a decade ago. 2D chalcogenides are a fundamental class in the study of low-dimensional science and their synthesis is an important goal of solid state chemistry. The presentation will focus on how novel chalcogenides can form using design concepts such as the “dimensional reduction”. The new materials exhibit diverse centrosymmetric and noncentrosymmetric structures that lead to a variety of attractive optoelectronic properties such as direct bandgaps, high X-ray absorption, neutron detection and strong nonlinear optical responses.

#### 6:25 AM F.EL03.02.09

**Valley-Mechanical Transduction in 2D Semiconductors** Haokun Li, King Yan Fong and Xiang Zhang; University of California, Berkeley, United States

The interaction of macroscopic mechanical object with electron charge and spin plays an important role in today's

information technology and fundamental studies of quantum mechanics. Recently emerged valleytronics encodes information to the electron valley degree-of-freedom and promises exciting applications in computation and communication. Exploring the interplay between the valley physics and macroscopic mechanics will bring new perspectives for valley information processing and exploration of the quantum-classical boundary. Here, for the first time, we realize valley-mechanical interaction in a monolayer MoS<sub>2</sub> resonator and demonstrate direct transduction of the valley information to mechanical states. The valley-mechanical coupling is achieved by exploiting the magnetic moment of valley carriers with a magnetic field gradient. We optically populate the valleys and observe the resulting mechanical actuation using laser interferometry. We are thus able to control the valley-mechanical interaction with the pump laser, the magnetic field gradient and temperature. Our experiment lays the foundation for a new class of valley-controlled mechanical devices. It also facilitates hybridization of valley pseudospin with other quantum information carriers such as two-level qubits and microwave photons.

#### 6:35 AM F.EL03.02.10

**Bandgap Tuning of Monolayer and Bilayer MoS<sub>2</sub> for Broadband UV-VIS-NIR Photodetection Using an Electric Double Layer Device Structure** [Roda Nur](#)<sup>1,2</sup>, Takashi Tsuchiya<sup>2</sup>, Mitsuru Takenaka<sup>1,2</sup> and Kazuya Terabe<sup>2</sup>; <sup>1</sup>The University of Tokyo, Japan; <sup>2</sup>National Institute for Materials Science, Japan

Transition Metal Dichalcogenides (TMDCs) have been under intensive research due to their unique electronic and optoelectronic properties. Due to their layered structure via weak van der Waals interactions, their bandgap can be modified by the number of layers[1] which directly impacts the range of wavelengths it can intrinsically detect. For the case of MoS<sub>2</sub>, monolayer has a direct bandgap of 1.8 eV with a cut-off wavelength of red light (~690 nm) and bulk has an indirect bandgap of 1.2 eV with a cut-off wavelength of ~1 μm. Photodetectors using MoS<sub>2</sub> as a photoactive material have been reported to offer very large responsivities (high light sensitivity) in photodetection applications[2]; however, the larger bandgaps of monolayer and bilayer MoS<sub>2</sub> limits its ability to detect wavelengths deeper in the near-infrared band. One technique to lower the bandgap of these materials is to introduce a very large perpendicular electric field. Unfortunately, conventional dielectric materials like SiO<sub>2</sub> and high-k metal oxides like HfO<sub>2</sub> and Al<sub>2</sub>O<sub>3</sub> cannot provide the required high electric fields to enable this effect. However, the use of an electric double layer (EDL) device structure can offer nano-gap capacitances resulting in generating very large electric fields. In this study, we investigated the bandgap tuning of monolayer and bilayer MoS<sub>2</sub> utilizing an electrical double layer device structure. In this structure, under the application of an applied gate bias, Li<sup>+</sup> ions migrate in the electrolyte layer to form an EDL with MoS<sub>2</sub>. As a result, we were able to detect NIR wavelengths and characterize its photoresponse behavior. We further confirmed our results with Density Functional Theory. This work shows the possibility of extending the intrinsic light detection of low dimensional chalcogenide materials for future optoelectronic devices.

[1] H. S. Lee et al., Nano Lett., 12, 3695, 2012.

[2] J.-Y., Wu et al., Adv. Mater., 30, 1705880, 2018.

#### 6:45 AM F.EL03.02.11

**Tellurium Doped III-V Dilute Nitride GaAsSbN NW Heterostructure for Room-Temperature Photodetector Applications in the Near-Infrared Region** [Rabin Pokharel](#)<sup>1</sup>, Priyanka Ramaswamy<sup>1</sup>, Shisir Devkota<sup>1</sup>, Kendall Dawkins<sup>1</sup>, Aubrey Penn<sup>2,2</sup>, Matthew Cabral<sup>2,2</sup>, Lewis Reynolds<sup>2</sup> and Shanthi Iyer<sup>1</sup>; <sup>1</sup>North Carolina A&T State University, United States; <sup>2</sup>North Carolina State University, United States

Nanowire (NW) based photodetectors in the near-infrared wavelength range is of great interest for next-generation single-photon-sources and photodetectors to be used in quantum networks, nanophotonic integrated circuits and solar cell applications. Bandgap engineering in the near-infrared region is facilitated by large bandgap bowing and increased electron confinement upon dilute (<2%) nitrogen incorporation. By leveraging these advantages, this work showcases optimized intrinsic and tellurium (Te)-doped dilute nitride GaAsSbN NW based photodetection. Compensation of point defects in the doped configuration is evidenced by a significant improvement in photoluminescence characteristics, Raman vibrational mode shifts, and spectral shape with improved photodetector device performance relative to intrinsic dilute nitride NWs. Transmission electron microscopy was used further to quantify the quality and composition of NW heterostructures, confirming a planar-defect-free zincblende crystal structure. The first successful demonstration of vertically aligned Te-doped GaAsSbN NW based PD device with a responsivity of ~5 A/W (@860 nm) on single NW configuration and ~3800 A/W (@1100 nm) on an ensemble NW device is reported. Further, a detectivity of  $3.2 \times 10^{10}$  Jones in ensemble configuration was confirmed from low-frequency noise characteristics. The responsivity of these NWs is comparable with the best reported values in this wavelength region, though the detectivity needs significant improvement. Encouraging prospects are seen for further bandgap engineering of this material system to develop improved quality and multicolor photodetection spanning the entire near-infrared-region range with potential for further red-shifting photodetection capability to 1.55 μm. A gallium

telluride (GaTe) captive source is used as the Te-dopant and molecular beam epitaxy (MBE) is the enabling technology that is used to realize Ga-catalyzed nanowires in axial configuration.

#### 6:55 AM F.EL03.02.12

**Low-Dimensional Sulvanites for Optoelectronic Applications** Cheng-Yu Lai<sup>1</sup>, Mimi Liu<sup>1</sup>, Chen-Yu Chang<sup>1</sup>, Gurpreet Singh Selopal<sup>2,3</sup> and Daniela R. Radu<sup>1</sup>; <sup>1</sup>Florida International University, United States; <sup>2</sup>Centre Énergie Matériaux Télécommunications (INRS-EMT), Canada; <sup>3</sup>Institute of fundamental and Frontier Sciences (IFFS) University of Electronic Science and Technology, China

The family of ternary chalcogenide compounds  $\text{Cu}_3\text{MX}_4$  (where M is V, Nb, or Ta and X is S, Se, or Te), also known as sulvanites, recently came to light due to their possible multiple uses in optoelectronic devices.<sup>1-3</sup> The compounds are isostructural and crystallize in the cubic structure with space group P-43m. They are characterized by significant values of refractive index, high ionic and electronic conductivity, as well as remarkable photoconductivity and photoluminescence.<sup>4</sup> Some reports show that  $\text{Cu}_3\text{TaS}_4$  is transparent in the visible region, having an absorption onset in the range of 2.8-3.0 eV, which could prove useful in light modulators, solar cells, optoelectronic and photocatalytic devices.<sup>1,3</sup> In general, the sulvanites are p-type semiconductors and show ionic conductivity that is attributed to a small number of interstitial Cu(I) ions.<sup>5,6</sup>

To take advantage of these excellent optoelectronic properties, processability of these materials would be highly desirable. We demonstrated facile solution-phase routes<sup>7</sup> to synthesize the entire sulfide and selenide suite of compounds, revealing fascinating nanocrystal morphologies, from 2D nanoplates to cubic and pyramidal quantum dots. Photoluminescence measurements reveal strong light emission in both vanadium and niobium compounds. Synthetic and characterization data will be presented in detail, and free-form sensor applications will be discussed.

#### References

- (1) Newhouse, P. F.; Hersh, P. A.; Zakutayev, A.; Richard, A.; Platt, H. A. S.; Keszler, D. A.; Tate, J. Thin film preparation and characterization of wide band gap  $\text{Cu}_3\text{TaQ}_4$  (Q = S or Se) p-type semiconductors. *Thin Solid Films* **2009**, *517*, 2473-2476.
- (2) Tate, J.; Newhouse, P. F.; Kykyneshi, R.; Hersh, P. A.; Kinney, J.; McIntyre, D. H.; Keszler, D. A. Chalcogen-based transparent conductors. *Thin Solid Films* **2008**, *516*, 5795-5799.
- (3) Lv, X. S.; Deng, Z. H.; Miao, F. X.; Gu, G. X.; Sun, Y. L.; Zhang, Q. L.; Wan, S. M. Fundamental optical and electrical properties of nano- $\text{Cu}_3\text{VS}_4$  thin film. *Optical Materials* **2012**, *34*, 1451-1454.
- (4) Bougherara, K.; Litimein, F.; Khenata, R.; Ucgun, E.; Ocak, H. Y.; Ugur, S.; Ugur, G.; Reshak, A.; Soyalp, F.; Omran, S. B. Structural, Elastic, Electronic and Optical Properties of  $\text{Cu}_3\text{TMSe}_4$  (TM = V, Nb and Ta) Sulvanite Compounds via First-Principles Calculations. *Science of Advanced Materials* **2013**, *5*, 97-106.
- (5) Arribart, H.; Sapoval, B.; Gorochoy, O.; LeNagard, N. Fast ion transport at room temperature in the mixed conductor  $\text{Cu}_3\text{VS}_4$ . *Solid State Communications* **1978**, *26*, 435-439.
- (6) Arribart, H.; Sapoval, B. Theory of mixed conduction due to cationic interstitials in the p-type semiconductor  $\text{Cu}_3\text{VS}_4$ . *Electrochimica Acta* **1979**, *24*, 751-754.
- (7) Liu, M.; Lai, C.-Y.; Selopal, G. S.; Radu, D. R. Synthesis and optoelectronic properties of  $\text{Cu}_3\text{VSe}_4$  nanocrystals. *PloS one* **2020**, *15*, e0232184.

#### 7:05 AM F.EL03.02.14

**Electrostatically Gated Multi-Functional  $\text{WSe}_2$  Transistor to Enable Multi-Bit Communication Schemes** Kartikay M. Thakar and Saurabh Lodha; Indian Institute of Technology, Bombay, India

There has been a surge in research interests in two-dimensional (2D) materials, and transition metal dichalcogenides (TMDs) in particular, owed to their unique physical, electrical and optical properties. [1,2] Although 2D materials are not at the par with present technologies in terms of device performance, they easily outperform them in terms of functionality in both electronic and optoelectronic applications. TMDs provide a plethora of novel physical properties such as flake-thickness dependent band structure, improved light-matter interaction and easy tuning of transport properties. With the possibility to go below 1-nm channel thickness, mechanically flexible devices and ease of making heterostructures, they have emerged as attractive candidates for next generation (opto)electronic technology.

Tungsten diselenide ( $\text{WSe}_2$ ) has been studied in detail due to its ambipolar transport, large carrier mobility values and good optical response. [3,4] In addition, we can easily dope the TMD channel with electrostatic gating providing us with freedom to easily tune the device performance with applied voltages. [5]

In this abstract, we present a simple yet effective method to leverage the ability to electrostatically tune the device transport to achieve a multi-functional device. The device consists of two set of gates – one to control the  $\text{WSe}_2$  channel and two

shorted gates under each contact to control the Schottky contact barriers. We are able to achieve not only conventional n-FET and p-FET characteristics, but also ambipolar as well as anti-ambipolar current trends with help of specific gate biasing schemes. Such device can be readily used for modulation of input signals (applied at the two gates) to get phase and frequency coded output current waveforms. Clubbed with an option to illuminate the channel, we can achieve an increased degree of freedom in device operation. We have been able to demonstrate in-phase, out-of-phase and double frequency signals on both ambipolar and anti-ambipolar current trends under dark and illumination condition. These waveforms have been experimentally demonstrated to be useful in two distinct 2-bit symbol encoding schemes. One of these schemes involves transition between ambipolar to anti-ambipolar transport in dark condition using electrostatic gating. This is not possible in conventional ambipolar or anti-ambipolar devices reported on 2D materials due to lack of tunable operation limited by device architecture. The other scheme uses illumination status along with frequency coding to identify frequency shift enabled by light-tunable anti-ambipolar current transport.

We further analysed the output current waveforms to better understand the information coding possibilities. By using a combination of phase, frequency and amplitude coding, we can potentially achieve up to 4-bit coded symbols with appropriate input gate-bias signals and illumination status (on/off). 2-bit and 3-bit transmission schemes are also examined with the same methodology. Phase-amplitude and phase-frequency polar plots are created to observe the constellation chart for any given transmission scheme.

To summarize, a novel device operation is proposed to leverage the tunable operation of 2D TMD channel material enabling both ambipolar and anti-ambipolar transport in the same device. With proper gate biasing schemes and incorporating illumination, we can generate distinct output current waveforms that can be used as modulated signals for multi-bit communication schemes.

#### References

- [1] Y. Cui et al., Adv. Funct. Mater., 1900040 (2019).
- [2] M. Long et al., Adv. Funct. Mater., 29, 1803807 (2018).
- [3] H. J. Chuang et al., Nano Lett., 14, 3594 (2014).
- [4] H. Kim et al., Sci. Adv., 5, 1, eaau4728 (2019).
- [5] D. J. Groenendijk et al., Nano Lett., 14, 5846 (2014).

#### 7:15 AM \*F.EL03.02.15

**Low-Dimensional Chalcogenides Materials: Physical Properties and Device Applications** Han Wang; University of Southern California, United States

Recent research progress has led to the successful synthesis of numerous low dimensional chalcogenides materials that demonstrate unique electronic and optical properties. In this talk, I will discuss our work in studying the ferroelectric, optical and phonon properties of such materials including  $\text{CuInP}_2\text{S}_4$  and  $\text{BaTiS}_3$ . The former demonstrates interesting ferroelectric properties in its layered van der Waals crystal lattice and the latter exhibits quasi-1-dimensional crystal structure giving rise to strong linear dichroism in the infrared and visible wavelength as well as unique phonon properties. I will also discuss the device applications of the respective materials, specifically the application of ferroelectric  $\text{CuInP}_2\text{S}_4$  in non-volatile memory and infrared detectors based on  $\text{BaTiS}_3$ . The promising future research directions, challenges and their potential applications in electronics and photonics technologies will also be discussed.

This work is supported in part by the Army Research Office (Grant no. W911NF1910111) and the National Science Foundation (Grant no. ECCS-1653870).

#### 7:30 AM F.EL03.02.16

**Late News: High Broadband Photoconductivity of Few-Layered  $\text{MoS}_2$  Field-Effect Transistor Measured in Multi-Terminal Method—Effect of Contact Resistance** Priyanka Das<sup>1</sup>, Jawnaye Nash<sup>1</sup>, Micah Webb<sup>1</sup>, Raelyn Burns<sup>1</sup>, Varun Mapara<sup>2</sup>, Govinda Ghimire<sup>1</sup>, Daniel Rosenmann<sup>3</sup>, Ralu Divan<sup>3</sup>, Denis Karaiskaj<sup>2</sup>, Stephen McGill<sup>4</sup>, Anirudha Sumant<sup>3</sup>, Qilin Dai<sup>1</sup>, Paresh Ray<sup>1</sup>, Bhausheb Tawade<sup>5</sup>, Dharmaraj Raghavan<sup>5</sup>, Alamgir Karim<sup>6</sup> and Nihar Pradhan<sup>1</sup>; <sup>1</sup>Jackson State University, United States; <sup>2</sup>University of South Florida, United States; <sup>3</sup>Argonne National Laboratory, United States; <sup>4</sup>National High Magnetic Field Laboratory, United States; <sup>5</sup>Howard University, United States; <sup>6</sup>University of Houston, United States

Among the layered two dimensional semiconductors, molybdenum disulfide ( $\text{MoS}_2$ ) is considered to be an excellent candidate for applications in optoelectronics and integrated circuits due to the layer-dependent tunable bandgap in the visible region, high ON/OFF current ratio in field-effect transistors (FET) and strong light-matter interaction properties. In this study, using multi-terminal measurements, we report high broadband photocurrent response ( $R$ ) and external quantum



efficiency (EQE) of few-atomic layered MoS<sub>2</sub> phototransistors using multi-terminal measurements, fabricated on a SiO<sub>2</sub> dielectric substrate and encapsulated with a thin transparent polymer film of Cytop. The photocurrent response was measured using a white light source as well as monochromatic light of wavelength  $\lambda = 400 \text{ nm} - 900 \text{ nm}$ . We measured responsivity in 2-terminal configuration as high as  $R = 1 \times 10^3 \text{ A/W}$  under white light illumination with optical power  $P_{\text{opt}} = 0.02 \text{ nW}$ . The  $R$  value increased to  $3.5 \times 10^3 \text{ A/W}$  when measured using a 4-terminal configuration. Using monochromatic light on the same device, the measured values of  $R$  were  $10^3$  and  $6 \times 10^3 \text{ A/W}$  under illumination of  $\lambda = 400 \text{ nm}$  when measured in 2- and 4-terminal methods, respectively. The highest EQE values obtained using  $\lambda = 400 \text{ nm}$  were  $10^5 \%$  and  $10^6 \%$  measured in 2- and 4-terminal configurations, respectively. The wavelength dependent responsivity decreased from 400 nm to the near-IR region at 900 nm. The observed photoresponse, photocurrent-dark current ratio (PDCR), detectivity as a function of applied gate voltage, optical power, contact resistances and wavelength were measured and are discussed in detail.

7:40 AM F.EL03.02.17

**Late News: Quasi-BIC Resonant Enhancement of Radiative Rate in Two-Dimensional Molybdenum Diselenide for Active Metasurfaces** Melissa Li, Souvik Biswas, Cora Went and Harry Atwater; California Institute of Technology, United States

Active metasurfaces composed of tunable subwavelength structures enable versatile light manipulation on ultrathin devices. Previously, electrically gated indium tin oxide-based metasurfaces have demonstrated dynamic amplitude and phase control of reflected light. However, these devices operate at around 1550nm, which limits their applications to infrared optoelectronics. Two-dimensional transition metal dichalcogenides (2D TMDs) are promising candidates for phase and amplitude modulation of visible light due to their strong excitonic resonances in the visible. Here, we investigate the gate-tunability of the complex index and the corresponding phase and amplitude modulation of the reflected light from 2D Molybdenum Diselenide (MoSe<sub>2</sub>). Our structure uses the large excitonic reflectivity that is dominated by radiative decay at low temperatures. By measuring the gate dependent change in the reflectivity of the MoSe<sub>2</sub>, we develop a model for the change in the complex dielectric function. We then enhance the emission of the TMD by integrating the monolayer with a metasurface comprised of subwavelength AlGaAs cylinders that support high quality factor quasi bound states in the continuum (BIC) modes. The subwavelength structure is based on a cylinder that utilizes the destructive interference between optical modes to obtain a significant enhancement in the quality factor of the cavity. The gate tunability of the MoSe<sub>2</sub> monolayer coupled to the high Q resonator allows us to electrically modulate the phase and amplitude of the reflected light. This monolayer TMD-based active metasurface could be a potential platform for ultrathin visible light modulators.

SESSION F.EL03.03: Phase Change Low Dimensional Chalcogenides  
On Demand Abstracts Available for Viewing Starting Saturday Morning, November 21, 2020  
F-EL03

5:00 AM \*F.EL03.03.01

**Optical Properties and Refractive Uses of Phase-Change Phenomena in Layered Chalcogenides** Rafael Jaramillo; Massachusetts Institute of Technology, United States

Layered chalcogenides hold promise for manipulating light in confined geometry, such as in photonic integrated circuits, where key material properties include strong and controllable light-matter interaction, and limited optical loss. Layered materials feature strong anisotropy and a panoply of polymorphs that suggest a rich design space for highly-nonperturbative photonic integrated devices based on functional martensitic transformations: phase changes and ferroelastic domain switching. These phenomena are manifest in materials with band gap above the photonics-relevant near-infrared (NIR) spectral band ( $\sim 0.5 - 1 \text{ eV}$ ), meaning that they can be harnessed in refractive (*i.e.* non-absorptive) applications.

Transition metal dichalcogenides (TMDs) offer a vast composition space within which to optimize refractive index contrast, optical loss, and switching energy. We are using a strategy of alloy design to optimize new, active materials for optical phase shifters. We will present our theoretical predictions of thermodynamics and optical properties of binary systems of sulfur-based TMDs: ZrS<sub>2</sub>-MoS<sub>2</sub>, TiS<sub>2</sub>-MoS<sub>2</sub>, TiS<sub>2</sub>-ZrS<sub>2</sub>, and MoS<sub>2</sub>-CrS<sub>2</sub>. We will present our experimental measurements of the NIR optical properties of single crystals. We will then present progress on making large-area thin films of sulfur-based TMDs, including the theoretically-predicted alloys, by a two-step method of metal sulfurization. Finally, we will present the

optical properties and phase-change functionality of our designed TMD alloy thin films.

We will also present an alternative paradigm of strong, non-perturbative refractive index modulation: electric field-driven ferroelastic domain switching in low-symmetry layered materials. We predict that in materials such as SnSe, a sufficiently-strong electric field will induce rotation between equivalent crystallographic domains, with strong refractive index contrast for linearly-polarized light. We will present simulation-based design of photonic integrated devices utilizing the birefringence of materials such as SnSe and black phosphorous, and experimental results demonstrating non-thermal domain switching triggered by fast laser pulses.

**5:15 AM \*F.EL03.03.02**

**Optical Properties of Transition Metal Dichalcogenide Bilayers** Xiaoqin E. Li; The University of Texas at Austin, United States

Optical properties of atomically thin transition metal dichalcogenides are dominated by exciton resonances exhibiting large oscillator strength and binding energies. In vertically stacked bilayers, a host of new exciton resonances emerge, lending new opportunities to discover new science and enable new devices. In this talk, I will focus on how moire superlattices change exciton resonances and diffusion. We discovered recently that phonon spectra are renormalized in moire superlattices as well. A rich variety of properties can be controlled by tuning the twist angle between the bilayers. I make some comparisons between samples that are grown using chemical vapor deposition and those prepared by mechanical exfoliation and stacking. Our work is supported by DOE under grant DE-SC0019398, NSF DMR-1808042, DMR-1720595, and the Welch Foundation F-1662.

**5:30 AM F.EL03.03.03**

**Reconfigurable Linear and Nonlinear Focusing Using All-Dielectric Metalenses Based on Phase-Change Materials** Muliang Zhu, Sajjad Abdollahramezani, Omid Hemmatyar and Ali Adibi; Georgia Institute of Technology, United States

Metalenses are flat surfaces that incorporate subwavelength structures to replace conventional bulky curved lenses. Metasurfaces with the capability of manipulating light-matter interaction at subwavelength are the core components of the metalenses that attract broad research attention. Metalenses are more convenient to be designed with tunable foci than conventional lenses with additional tunability brought by nanoscale features. Nonlinear metalenses are rarely investigated compared to linear counter-parts due to limited efficiency. However, to our interest, nonlinear metalenses provide a future platform for applications in nonlinear information processing, all-optical higher-order Fourier transformations, short laser pulse diagnostics, *etc.* [1]. Moreover, metalenses conveying information at both linear and nonlinear frequencies could potentially reveal more information of the imaging object. Generating nonlinear signal confocal with linear signal is difficult to realize for conventional high-index material due to material dispersion. Low-loss phase change chalcogenides such as Antimony Sulfide ( $\text{Sb}_2\text{S}_3$ ), which introduces substantial change in the refractive index with high-speed thermal-controllable phase changes [2] in addition to intrinsic large third-order nonlinearities, are potential candidates for efficient reconfigurable-foci metalenses that can realize third-harmonic generation (THG) signal co-focusing with the linear signal. We demonstrate a reconfigurable all-dielectric metalens by making use of a unique dispersion relationship between the amorphous state and the crystalline state of  $\text{Sb}_2\text{S}_3$ . The device works at the fundamental wavelength ( $\lambda_f$ ) of 950 nm, where the refractive index of amorphous  $\text{Sb}_2\text{S}_3$  ( $n_{a-\text{Sb}_2\text{S}_3}$ ) at  $\lambda_f$  is close to that of crystalline  $\text{Sb}_2\text{S}_3$  ( $n_{c-\text{Sb}_2\text{S}_3}$ ) at THG wavelength ( $\lambda_{\text{THG}}$ ) whereas  $n_{c-\text{Sb}_2\text{S}_3}$  at  $\lambda_f$  is close to  $n_{a-\text{Sb}_2\text{S}_3}$  at  $\lambda_{\text{THG}}$ . The principle of phase delay makes THG signal from the metalens of one crystallinity state confocal with the transmitted fundamental signal of the other crystallinity state. The reconfigurable metalens can inspire effective capture of double-frequency imaging of objects.

References

- [1] C. Schlickriede, *et al.* Nano Lett. 20, 4370 (2020).
- [2] W. Dong, *et al.* Adv. Funct. Mater. 29, 1806181 (2019).

SESSION F.EL03.04: Photocatalyst Application of Low-Dimensional Chalcogenides  
On Demand Abstracts Available for Viewing Starting Saturday Morning, November 21, 2020  
F-EL03

### 5:00 AM F.EL03.04.01

**Cu/Cd<sub>0.5</sub>Zn<sub>0.5</sub>S on a Fixed Bed Photocatalytic Reactor for CO<sub>2</sub> Reduction** Shengjie Bai and Liejin Guo; Xi'an Jiaotong University, China

The photo-induced conversion of CO<sub>2</sub> to chemical fuels in aqueous solution is limited by the electron transfer efficiency and the mass transfer of the reactants. Herein, Cu was decorated on a Cd<sub>0.5</sub>Zn<sub>0.5</sub>S twin nanocrystals by photo-deposition, and fixed it on a gas dispenser for photocatalytic CO<sub>2</sub> reduction (CO<sub>2</sub>RR). The quartz gas dispenser was used as a support for fixing catalysts, which accelerated the diffusion and mass transfer of CO<sub>2</sub> in the electrolyte, thus increasing the energy conversion efficiency of the reaction. Cd<sub>0.5</sub>Zn<sub>0.5</sub>S provides photovoltage for driving photocatalytic reactions. While Cu provides active sites for the conversion of CO<sub>2</sub>. Compared with undecorated Cd<sub>0.5</sub>Zn<sub>0.5</sub>S, Cu/Cd<sub>0.5</sub>Zn<sub>0.5</sub>S have a smaller band gap (~ -1.98 eV) and a higher selectivity for multi-carbon products (78%). Among the products, the selectivity of ethanol and acetic acid were 45% and 30%, respectively. Moreover, this work provides an efficiently strategy to integrate synthesis and assembly for photocatalytic conversion CO<sub>2</sub>.

### 5:10 AM F.EL03.04.02

**Selective Vapor Phase Syntheses of Low-Dimensional Metal Chalcogenides for Catalytic Water Splitting** Lasse Jurgensen, Michael Frank, David Graf, Veronika Brune, Isabel Gessner and Sanjay Mathur; University of Cologne, Germany

Investigation of the interplay of metal-organic chemistry will enrich the state-of-the-art of chemical vapor deposition (CVD) technology and open new possibilities for the generation of nanostructured metal sulfide and selenide nanostructures. Therefore, novel *single-source* precursors exhibiting high volatility and defined thermal decomposition under (plasma-enhanced) CVD conditions through targeted synthesis strategies are reported to elaborate the **precursor chemistry – materials synthesis – functional property** chain. Synergistic reactivity and sufficient stability through unique ligand design to provide a precise control over compositional purity of metal chalcogenides in CVD deposits without additional chalcogenide sources. CVD-grown ME<sub>x</sub> (M = Fe, Co, Ni, Cu, Sn, In; E = S, Se) 2 D nanostructures were tested towards their (electro)catalytic applications, particular in the oxygen evolution reactions (OER). The presented CVD data opens new possibilities in the vapor phase synthesis of chalcogenide nanostructures facilitating the application as mutable earth abundant electro- or photocatalysts in OER and hydrogen evolution reactions (HER).

### 5:20 AM F.EL03.04.03

**Late News: Understanding the Photocatalytic Activity of La<sub>5</sub>Ti<sub>2</sub>AgS<sub>5</sub>O<sub>7</sub> and La<sub>5</sub>Ti<sub>2</sub>CuS<sub>5</sub>O<sub>7</sub>—Computational Insights** Katarina Brlec<sup>1,2</sup>, Christopher Savory<sup>1,2</sup> and David O. Scanlon<sup>1,2,3</sup>; <sup>1</sup>Department of Chemistry, UCL, United Kingdom; <sup>2</sup>Thomas Young Centre, United Kingdom; <sup>3</sup>Diamond Light Source Ltd, United Kingdom

Hydrogen gas is one of the most important chemical precursors with a wide variety of uses. Currently, over 90% of hydrogen is produced using energy-intensive hydrocarbon reforming. Photocatalytic water splitting introduces an alternative, environmentally friendly pathway for hydrogen production. Water is split into hydrogen and oxygen using energy provided from the absorption of light photons by a photocatalytically active semiconductor. Thermodynamically, splitting of water requires 1.23 eV of energy per molecule of water. However, to overcome the associated overpotential, in semiconductors this energy requirement corresponds to an optimum band gap of 1.8 eV to 2.2 eV. [1] The electronic band structure of a promising material must allow for good mobility of charge carriers as well as align the band edges so that they straddle the redox window of water. [2]

La<sub>5</sub>Ti<sub>2</sub>AgS<sub>5</sub>O<sub>7</sub> (LTA) and La<sub>5</sub>Ti<sub>2</sub>CuS<sub>5</sub>O<sub>7</sub> (LTC) were experimentally shown to exhibit photocatalytic activity for both oxidation and reduction of water. [3,4] The complex crystal structures of systems exhibit one-dimensional chains of perovskite-like Ti-centred octahedra and rock-salt-like metal sulphide tetrahedra. Some experimental studies show the systems' electronic structure could support high mobility of charge carriers through the structure via these one-dimensional channels. [4]

To better understand the photocatalytic activity, we investigated the electronic structure of bulk LTA and LTC using plane wave density functional theory (DFT) with hybrid functionals as implemented in Vienna ab initio Simulation Package. Low effective charge carrier masses in b-directions were observed with spatial separation of the band edges centred on the Ti octahedra and metal tetrahedra, which confirmed good mobility of charge carriers along the one-dimensional channels with lowered probability of recombination taking place.

All non-polar symmetric surfaces up to a maximum Miller index of 2 were then evaluated to obtain their surface energies and

band alignments using generalised gradient approximation (GGA) and hybrid functionals. Wulff constructions based on the GGA surface energies visualised predicted nanoparticle shape, matching the experimental descriptions of crystallites. Combining the Wulff shapes with hybrid DFT band alignment showed the largest surfaces on the sides of columnar shapes had inadequate band edge alignment, so only the ends of crystallites were suitable for photocatalysis. This gave an important insight as photocatalytic activity of LTA and LTC would be greatly improved if the particles length in b-direction decreased in combination with an increase in the area of columnar crystallites' blunt ends which have more suitable band alignment.

[1] T. Hisatomi and K. Domen, *Nat. Catal.*, 2019, **2**, 387–399.

[2] T. Le Bahers, M. Rérat and P. Sautet, *J. Phys. Chem. C*, 2014, **118**, 5997–6008.

[3] V. Meignen, L. Cario, A. Lafond, Y. Moëlo, C. Guillot-Deudon and A. Meerschaut, *J. Solid State Chem.*, 2004, **177**, 2810–2817.

[4] T. Suzuki, T. Hisatomi, K. Teramura, Y. Shimodaira, H. Kobayashi and K. Domen, *Phys. Chem. Chem. Phys.*, 2012, **14**, 15475.

#### 5:30 AM F.EL03.04.04

**Late News: Computational Exploration of Low-Dimensional Chalcogenide and Oxychalcogenide Photocatalysts** [Syam Kumar](#)<sup>1</sup>, Heesoo Park<sup>2</sup>, Akinlolu Akande<sup>1</sup>, Stefano Sanvito<sup>3</sup> and Fadwa El Mellouhi<sup>2</sup>; <sup>1</sup>Institute of Technology Sligo, Ireland; <sup>2</sup>Hamad Bin Khalifa University, Qatar; <sup>3</sup>Trinity College Dublin, Ireland

Chalcogenides have recently attracted attention as alternate materials for photonic applications suffering less from stability and toxicity issues encountered in lead halide perovskites [1]. Also, in the past few years, the computer-aided design of metal chalcogenide semiconductors led to the discovery and synthesis of very promising compounds for numerous application such as light absorbers in the thin-film photovoltaic devices [2–4]. In this presentation, aiming at in-depth exploration for light absorbers and related devices, we discuss the potential of Nb- and Ta-based perovskites ( $\text{NaMO}_{(3-x)}\text{Q}_x$ ; M = Nb, Ta and Q = S, Se) [3], and Bi-based chalcogenides ( $\text{ABiX}_{2/3}$ ; A = Na, K and X = O, S) [5] for photocatalysis on the grounds of their structural and electronic dimensionality. Our interest focuses on the potential of these materials for hydrogen production from photocatalytic water splitting as well as  $\text{CO}_2$  conversion.

To select a photocatalyst, one must look into its photon absorption and charge separation, governed by their electronic properties such as the bandgap, band edge positioning, and the photogenerated charge carrier mobility. Although our density functional theory (DFT) calculation at the Heyd-Scuseria-Ernzerhof functional (HSE06) indicates the materials as good light absorbers, the analysis of effective masses of the charge carriers, along with the electronic dimensionality, imply that several of the considered compounds exhibit a reduced electronic dimensionality despite showing high structural dimensionality.

Analysis of the effective masses of the photogenerated charge carriers along the dominant directions or channels of charge transport show that most of the Bi-chalcogenides, except  $\text{NaBiS}_3$  and  $\text{KBiS}_3$ , could perform well as photocatalysts in terms of charge separation and transport. Even more promising, Nb- and Ta-perovskites have lower effective masses of the photogenerated charge carriers than their Bi-based compounds indicating their superior carrier transport properties. Turning into assessing the electrochemical performance of the Nb-/Ta- and Bi-based chalcogenides for hydrogen evolution reactions and  $\text{CO}_2$  conversions, we investigated the band edge alignments with respect to  $\text{O}_2/\text{H}_2\text{O}$ ,  $\text{H}^+/\text{H}_2$ ,  $\text{CO}_2/\text{CO}$ ,  $\text{CO}_2/\text{HCHO}$ ,  $\text{CO}_2/\text{CH}_3\text{OH}$ , and  $\text{CO}_2/\text{CH}_4$  redox levels considering aqueous media of different pH (acidic, neutral and alkaline), for photocatalysis reactions. This work provides a comprehensive insight into the Nb-/Ta- and Bi-based compounds on the grounds of relevant properties for hydrogen evolution and  $\text{CO}_2$  conversion reactions, calling for a careful analysis of both structural and electronic dimensionality metrics.

#### References

[1] Buffiere, M., Dhawale, D., El-Mellouhi, F. (2019). *Energy Technology* 7(11), 1900819.

[2] Park, H., Alharbi, F., Sanvito, S., Tabet, N., El-Mellouhi, F. (2018). *The Journal of Physical Chemistry C* 122(16), 8814 - 8821.

[3] Park, H., Alharbi, F., Sanvito, S., Tabet, N., El-Mellouhi, F. (2018). *ChemPhysChem* 19(6), 703 - 714.

[4] El-Mellouhi, F., Tabet, N., Alharbi, F. H., Sanvito, S., Park, H., US10553367B2,

[5] R, S., Akande, A., El-Mellouhi, F., Park, H., Sanvito, S. (2020) *Physical Review Materials* 4, 075401.

#### Acknowledgements

AA and SKR thanks Institute of Technology Sligo President's Bursary Award for the funding through the grant PPRES050. FE and HP thank the Qatar National Research Fund (QNRF) through the National Priorities Research Program (NPRP8-090-2-047). SS thanks the Irish Research Council (IRCLA/2019/127) for the financial support. Computational resources have

been provided by the research computing group at Texas A&M University at Qatar, Trinity Centre for High Performance Computing (TCHPC) (Project Code: HPC 16 00953), and Irish Centre for High-End Computing (ICHEC) (Project Codes: isphy002c and isphy003c).

SESSION F.EL03.05: Photovoltaic Application of Low-Dimensional Chalcogenides  
On Demand Abstracts Available for Viewing Starting Saturday Morning, November 21, 2020  
F-EL03

#### 5:00 AM F.EL03.05.01

**Heavy-Metal-Free Quantum Dot Inks for Thin-Film Solar Cells** Filip Dinic, Larissa Levina and Oleksandr Voznyy; University of Toronto, Canada

A newer generation of solar cells is emerging based on solution-processed materials, primarily PbS colloidal quantum dots (CQD) and lead halide perovskites. However, both contain toxic lead, posing significant safety concerns. Here, we propose to utilize chalcogenide based colloidal quantum dot (CQD) inks to achieve scalable and low-cost solution processing of the state-of-the-art photovoltaic materials. CQDs are used as a means in obtaining bulk direct bandgap semiconductors, which have been demonstrated to be highly efficient light absorbing layers by means of thermally annealing and sintering the QDs

The key challenges in this field revolve around improving CQD packing and further reducing the defect densities. We will demonstrate that inorganic atomic ligands can eliminate the need for organic long chain ligands required for colloidal stability. Furthermore, these inorganic ligands can be used as abundant passivating agents while promoting the sintering of CQDs in the resulting films. We will demonstrate proof-of-principle results with PV devices based on lead-free chalcogenide based CQDs, primarily CuInS<sub>2</sub>.

#### 5:10 AM F.EL03.05.02

**Chemical Variation Dependent Growth Behavior of Sb<sub>2</sub>Se<sub>3</sub> Thin Films by Close-Space Sublimation** Liping Guo and Feng Yan; The University of Alabama, United States

Sb<sub>2</sub>Se<sub>3</sub> has emerged as a promising absorber material for photovoltaic applications owing to its excellent optoelectronic properties such as suitable bandgap and high absorption coefficient as well as its low-toxic and earth-abundant constituents. Sb<sub>2</sub>Se<sub>3</sub> is comprised of quasi-one-dimensional (Q1D) ribbons stacked by weak van der Waals (vdW) interactions without dangling bonds, rendering the Sb<sub>2</sub>Se<sub>3</sub> grain boundaries (GBs) self-passivated and intrinsically benign. Various growth techniques have been used for the Sb<sub>2</sub>Se<sub>3</sub> absorber layer growth, such as close-space sublimation (CSS). However, due to the fast sublimation rate and confined CSS chamber space, the evaporated gas lacks a full and uniform mixture before condensing on the substrates. In the meantime, Se has a much higher saturated vapor pressure than that of Sb<sub>2</sub>Se<sub>3</sub>, making Se element release first during CSS deposition and dominates the chamber gas at the very initial stage. As a result, the chemical composition (ratio of Se and Sb) of the gas mixture varies with time, causing the deposited films at different growth stages to exhibit different chemical compositions. In this work, the chemical composition (Se and Sb), microstructure, and device performance of Sb<sub>2</sub>Se<sub>3</sub> films deposited at different growth stages were systematically investigated. It is demonstrated that the chemical variation dependent growth behavior can be used to control the carrier transport and lead to improved device performance. The work also paves a way to further improve the device performance of Sb<sub>2</sub>Se<sub>3</sub> based photovoltaic devices by tuning the scaleable vapor deposition.

#### 5:20 AM F.EL03.05.03

**Controlling the Preferred Orientation of Layered BiOI Solar Absorbers** Rob Jagt<sup>1</sup>, Tahmida Huq<sup>1</sup>, Katharina Börsig<sup>1</sup>, Daniella Sauven<sup>1</sup>, Lana C. Lee<sup>1</sup>, Judith MacManus-Driscoll<sup>1</sup> and Robert Hoyer<sup>2</sup>; <sup>1</sup>University of Cambridge, United Kingdom; <sup>2</sup>Imperial College London, United Kingdom

Bismuth oxyiodide (BiOI) has gained attention for photovoltaics, photocatalysis and photodetectors owing to its composition of non-toxic elements, tolerance to point defects, and highly-suitable optical properties.<sup>1,2</sup> But like many other bismuth-based compounds, BiOI is a layered material with anisotropic transport properties, making control over the preferred orientation critical for achieving optimal device performance. In this work, we develop new insights into the growth mechanism of BiOI synthesized by chemical vapor deposition (CVD) and show how the preferred orientation can be controlled. By adjusting the

precursor and substrate temperatures to tune whether or not we are in a nucleation- or growth-controlled regime, we reproducibly vary the ratio of the (001) and (110) orientations by over two orders of magnitude. As a result, we achieve highly c-axis oriented films, which leads to less shunting than a/b-axis oriented films, resulting in improved open-circuit voltages from a median value of 0.7 V (a/b-axis oriented) to 0.9 V (c-axis oriented) in BiOI solar cells. More broadly, the described mechanisms can be used to control the preferred orientation in other low-dimensional materials, which will be important for achieving improved performance across a wide variety of devices.

[1] *Adv. Mater.*, **2017**, *29*, 1702176

[2] *Adv. Funct. Mater.*, **2020**, *30*, 1909983

### 5:30 AM \*F.EL03.05.04

**Emerging Chalcogenides for Photovoltaics** David O. Scanlon; University College London, United Kingdom

The field of photovoltaics is undergoing a surge of interest following the recent discovery of the lead hybrid perovskites as a remarkably efficient class of solar absorber. Of these, methylammonium lead iodide (MAPI) has garnered significant attention due to its record breaking efficiencies, however, there are lingering concerns surrounding its long-term stability and toxicity. Compounding these problems is a more fundamental limitation: the hybrid perovskite structure shows a severe lack of compositional tunability. Beyond minor changes to the halide and A site composition it has not been possible to significantly supersede the original MAPI formulation, because the hybrid perovskite structure is not accommodating to significant changes to composition of the A or B sites.[1]

Many of the excellent properties seen in hybrid perovskites are thought to derive from the  $6s^2$  electronic configuration of lead, a configuration found in a range of post-transition metal compounds.[2] In this presentation I will outline our computational studies on  $Sb_2Se_3$ , a material which has displayed power conversion efficiencies approaching 10% from a limited number of studies,[3] and GeSe, a semiconductor whose fundamental band gap has been the source of much debate. Our results highlight the complex nature of the defect chemistry of the “simple” binary  $Sb_2Se_3$ , [4] explain why as deposited  $Sb_2Se_3$  is n-type, [5] and rationalise the nature of the band gap of GeSe. [6]

[1] W. Travis et al., *Chemical Science*, **7**, 4548 (2016)

[2] A. M. Ganose, C. N. Savory, and D. O. Scanlon, *Chemical Communications*, **53**, 20 (2017)

[3] L. J. Philips et al., *IEEE Journal of Photovoltaics*, **9**, 544 (2019)

[4] C. N. Savory and D. O. Scanlon, *Journal of Materials Chemistry A*, **7**, 10739 (2019)

[5] T. D. C. Hobson et al., *Chemistry of Materials*, **32**, 2621 (2020)

[6] P. A. E. Murgatroyd et al., *Chemistry of Materials*, **32**, 3245 (2020)

### 5:45 AM \*F.EL03.05.05

**Revealing Defect Passivation Mechanisms in  $Sb_2Se_3$**  David Tilley; University of Zurich, Switzerland

Antimony selenide ( $Sb_2Se_3$ ) has emerged as a strong candidate for practical water splitting due to its suitable bandgap, excellent optoelectronic properties, and resistance to photocorrosion in strongly acidic electrolyte solutions. In this talk, I will discuss the synthesis of  $Sb_2Se_3$  thin films by selenization of antimony metal and the photoelectrochemical properties of these films after coating with a molybdenum sulfide hydrogen evolution catalyst. The performance of these photocathodes was greatly enhanced by a relatively low temperature sulfurization treatment with elemental sulfur, greatly improving the photovoltage and the fill factor. The origin of the improvement upon sulfurization was investigated with time-resolved microwave conductivity (TRMC) measurements and photoluminescence. TRMC of our  $Sb_2Se_3$  reveals high mobilities of the photogenerated charge carriers ( $>10 \text{ cm}^2 \text{ V}^{-1} \text{ s}^{-1}$ ) and a low trap density, in contrast to other emerging photoelectrochemical materials such as  $Fe_2O_3$ ,  $CuFeO_2$ , and  $BiVO_4$ . We find that the sulfurization treatment of the  $Sb_2Se_3$  thin films yields improved charge carrier lifetimes. Not only is surface recombination curtailed, but deep traps in the bulk are eliminated (most likely Sb-Se antisite defects), which reduces non-radiative recombination of the photogenerated charge carriers. A low temperature sulfurization treatment is thereby identified as a simple method to remove bulk traps in  $Sb_2Se_3$  thin films.

### 6:00 AM F.EL03.05.06

**Impact of Pre Annealing Synthesis and Post Deposition Treatments With IA and IVA Group Elements in  $Sb_2Se_3$  Thin-Film Solar Cells** Pedro Vidal-Fuentes<sup>1</sup>, Yudania Sánchez González<sup>1</sup>, Joaquim Puigdollers<sup>2</sup>, Alejandro Pérez Rodríguez<sup>1,3</sup>, Victor Izquierdo-Roca<sup>1</sup> and Edgardo Saucedo<sup>2</sup>; <sup>1</sup>Catalonia Institute for Energy Research (IREC), Spain; <sup>2</sup>Polytechnic University of Catalonia (UPC), Spain; <sup>3</sup>Universitat de Barcelona, Spain

$Sb_2Se_3$  is becoming a relevant thin film chalcogenide semiconductor with different technological applications such as:

superconductivity, electronic component, electrode for sodium-ion batteries, photodetectors and as photovoltaic (PV) absorber. In particular,  $\text{Sb}_2\text{Se}_3$  have recently experienced incredible progresses as emerging photovoltaic material with a certified record efficiency of 9.2%. This technology has a promising interest due to good optoelectronic properties, earth-abundant and low toxicity constituents. Additionally, the quasi one-dimensional atomic structure provides interesting properties like improved charge carrier transport and minimization of grain boundaries recombination.

Up to date, most of the works in literature have been focused on device structure modifications, synthesis conditions optimization and understanding the fundamental properties of the material itself, to obtain the best self-standing photovoltaic performance. But little attention has been paid on explore new strategies to include extrinsic element that modify the physico-chemical properties of the devices (like doping, recrystallization, passivation, etc.) in order to improve the optoelectronic properties of the devices. In other more mature thin film PV technologies as  $\text{Cu}(\text{In,Ga})\text{Se}_2$ ,  $\text{Cu}_2\text{ZnSn}(\text{S,Se})_4$ , the inclusion of extrinsic elements by pre annealing synthesis (PAS) and post deposition treatment (PDT) during the device fabrication have a critical role in the improvement of the optoelectronics properties. These approaches are critical for high efficiency  $\text{Cu}(\text{In,Ga})\text{Se}_2$  technology, where the inclusion of alkali based treatments (Rb and Na) are critical to achieve record PCE up to 23%, or in the case of the  $\text{Cu}_2\text{ZnSnSe}_4$  based in sputtered metallic precursor, the introduction of nanometric Ge layer before the synthesis of the absorber and the soft thermal treatment after the synthesis of the complete devices allow to homogenize the material and achieve PCE over 11%, close to record devices.

In this work we propose to explore the effects of the PDT and PAS approaches to include IA and IVA group elements into the  $\text{Sb}_2\text{Se}_3$  and analyze the effects on its properties. In this case we explored the possibility of alkali inclusion with LiF, NaF and KF, as well as Ge and Sn, using PVD processes. Our synthesis process consists on the reactive annealing under Se atmosphere of antimony layers to obtain a Glass/Mo/ $\text{Sb}_2\text{Se}_3$ /CdS/i-ZnO/ITO system in substrate configuration. In the case of alkali-fluorides we compare post deposition treatments (PDT), consisting in the deposition of alkali fluorides by thermal evaporation on top of the as growth SLG/Mo/ $\text{Sb}_2\text{Se}_3$  stack and then performing a further soft annealing routine; with pre annealing treatments (PAS) in which the alkali-fluorides are thermally evaporated on top of the Sb layers prior to  $\text{Sb}_2\text{Se}_3$  synthesis. In the case of Ge and Sn the approach is more flexible and we could explore the PAS and PDT together with the inclusion of  $\text{GeSe}_2$  and  $\text{SnSe}$  during the reactive annealing, in order to obtain more homogeneous incorporation. Additionally, the study is complemented with a wide characterization of the  $\text{Sb}_2\text{Se}_3$  layers and devices using morphological and physico-chemical characterization (XRF, XRD and Raman spectroscopy), and with a complete analysis of the impact of the doping strategies correlated with the optoelectronic characterization (JV, IQE, CV) of the solar cells.

In the case of the IA inclusion, the optoelectronic characterization shows an improvement of the  $J_{sc}$  for NaF and LiF PDT treatments, and a  $V_{oc}$  increment for NaF PDT treatment, while KF is detrimental for the device performance. The NaF PDT allows slightly increase the power conversion efficiency from the 4.5% for reference devices to 4.9%. In the other hand the case of IVA inclusion, the effect of the  $\text{SnSe}$  approach do not show impact in the device performance in comparison with a huge degradation observed for the Sn PAS approach.

**6:10 AM \*F.EL03.05.07**

**Chemical Trends and Electronic Engineering of V-VI-VII Metal Chalcogenides** [Aron Walsh](#)<sup>1,2</sup>; <sup>1</sup>Imperial College London, United Kingdom; <sup>2</sup>Yonsei University, Korea (the Republic of)

Metal chalcogenides are candidates for next-generation technologies including energy conversion, information storage, and quantum computing. I will present an exploration of V-VI-VII ternary chalcogenides, where V = Sb, Bi; VI = O, S, Se, Te; and VII = F, Cl, Br, I. These include the photoferroic compound  $\text{SbSI}$  [1,2] and the solar fuels photoelectrode  $\text{BiOBr}$  [3,4]. We consider 32 elemental combinations in 4 spacegroups using a combination of density functional theory (structural and thermochemistry) and many-body QSGW theory (relativistic electronic band structures). The materials are found to exhibit a wide range of electronic structures and bandgaps from metallic to over 5 eV. The large spin-orbit coupling in the heavy cations strongly influences the electronic structure. This research is part of a collaboration with the groups of David Scanlon (UCL) and Mark van Schilfgaarde (KCL), and used the UK National Supercomputer ARCHER.

[1] "Ferroelectric materials for solar energy conversion: photoferroics revisited" K. T. Butler et al, Energy Environ. Sci. 8, 838 (2015)

[2] "Quasi-particle electronic band structure and alignment of the V-VI-VII semiconductors  $\text{SbSI}$ ,  $\text{SbSBr}$ , and  $\text{SbSeI}$  for solar cells" K. T. Butler et al, Appl. Phys. Lett. 108, 112103 (2016)

[3] "Bismuth oxyhalides: synthesis, structure and photoelectrochemical activity" D. S. Bhachu et al, Chem. Sci. 7, 4832

(2016)

[4] "Interplay of orbital and relativistic effects in bismuth oxyhalides: BiOF, BiOCl, BiOBr, and BiOI" A. M. Ganose et al, Chem. Mater. 28, 7, 1980 (2016)

SESSION F.EL03.06: Processing of Low-Dimensional Chalcogenides  
On Demand Abstracts Available for Viewing Starting Saturday Morning, November 21, 2020  
F-EL03

#### 5:00 AM F.EL03.06.01

**Design, Stability and Properties of Binary and High Entropy Transition Metal Dichalcogenide Alloys** John D. Cavin and Rohan Mishra; Washington University in St. Louis, United States

The diverse properties of transition metal dichalcogenides (TMDCs) make them a materials platform where alloying is an attractive option for tuning properties such as band gaps, charge density waves, superconductivity, and electrochemical activities. Of the many possible combinations of TMDCs, the small subset of Mo- and W-based quasi-binary semiconducting alloys has garnered widespread attention. Outside this limited subset, the synthesizability of alloys remains largely unknown. Furthermore, the usage of multiple principal elements to form so-called high entropy alloys (HEAs) of TMDCs has not been previously explored. Using first-principles calculations, we present a comprehensive analysis of the stability of 25 quasi-binary transition metal- and chalcogen-site TMDC alloys and a select number of 4- and 5-component transition metal-site TMDC HEAs. Critically, we expand knowledge of TMDC alloys beyond group VI transition metals Mo and W to include group V transition metals V, Nb, and Ta, opening the possibility of magnetic, superconducting, and charge density wave phases. We verify our stability predictions through evidence of the successful synthesis of many alloys, including new group VI quasi-binary alloys,<sup>1</sup> and the first synthesized TMDC HEA. First-principle calculations are also used to explain exciting experimental tuning of properties including thermal expansion, catalytic activity, and charge density wave transitions.

Acknowledgements: This work was supported by National Science Foundation (NSF) through grants: DMREF-1729787.

#### Reference:

1. Z. Hemmat, et al., Quasi-Binary Transition Metal Dichalcogenide Alloys: Thermodynamic Stability Prediction, Scalable Synthesis, and Application. *Advanced Materials* (2020).

#### 5:10 AM F.EL03.06.02

**Vapour Phase Formation of Freestanding One-Dimensional Molybdenum Disulphide** Matthias K. Grosch, Sanjay Mathur, Thomas Fischer and Rene Weißing; University of Cologne, Germany

Transition metal dichalcogenides (TMDCs) are of continuing research interest because of their interesting opto-electronical properties as well as catalytic application potential<sup>1</sup>. While two-dimensional TMDCs are well investigated one-dimensional micro and nanostructures are sparsely described in literature<sup>2</sup>. When structured in one-dimension these materials offer great potential for catalytic applications like the hydrogen evolution reaction (HER)<sup>1</sup> as they possess the materials intrinsic catalytic property while having additionally a high aspect-ratio. Herein, we report the synthesis of micro and nano-scaled one-dimensional molybdenum disulphide by vapour phase. A proposed mechanism for one dimensional growth is given and discussed.

1) S. R. Kadam, A. N. Enyashin, L. Houben, R. Bar-Ziv, M. Bar-Sadan, *J. Mater. Chem. A* **2020**, 8, 1403–1416.

2) W.-J. Li, E.-W. Shi, J.-M. Ko, Z. Chen, H. Ogino, T. Fukuda, *J. Cryst. Growth* **2003**, 250, 418–422.

#### 5:20 AM F.EL03.06.03

**Tertiary Hierarchical Complexity in Assemblies of Chiral Nanoclusters** Haixiang Han, Yuan Yao and Richard Robinson; Cornell University, United States

Low-dimensional metal chalcogenides with atomic homogeneity are emerging as promising materials due to their unique electronic and optical properties. One of the most interesting behaviors of such ultrasmall inorganic nanocrystals is their ability of self-assembly into higher level structure complexity, which is dictated by the intra/inter molecular interactions through the surfactant ligands. Here, we demonstrate the synthesis and assembly of atomically precise 1.2 nm sulfur-bridged



copper (SB-Cu) clusters with tertiary hierarchical complexity, characterized and confirmed with high accuracy through single-crystal X-ray diffraction. The primary structure is clockwise/counterclockwise chiral caps and cores. The caps and cores combine to form full clusters and, due to the cap-core interaction, only two enantiomeric isomers are formed (secondary structure). A tertiary hierarchical architecture is achieved through the self-assembly of alternating enantiomers. More importantly, the hierarchical assembly of SB-Cu clusters is inherently conductive due to the conjugated MBO ligand (MBO = 2-Mercaptobenzoxazole) and the effective intermolecular interactions. The SB-Cu cluster has a characteristic absorption peak at 333 nm and emission at 380 nm, both of which, due to the conductivity of the SB-Cu clusters network, could vary in response to photoirradiation at different wavelengths. These clusters and assemblies make for an interesting nanomaterial for photoconductive devices and optical applications.

#### 5:30 AM F.EL03.06.04

**Selenization of Ultrathin Pt Layers for PtSe<sub>2</sub> Growth in Molecular Beam Epitaxy** [Maria Hulse](#), Ke Wang and Roman Engel-Herbert; The Pennsylvania State University, United States

PtSe<sub>2</sub> was recently proposed as promising material for low-power, high-performance, and ultra-thin-body electronic application because of its sizeable band gap up to 1.2 eV, high carrier mobility in the order of 1,000 cm<sup>2</sup>/Vs, stability in air, and possibility of low-temperature fabrication compatible with CMOS back-end-of-line (BEOL) processing. First experimental values of its high carrier mobility of 210 cm<sup>2</sup>/Vs, that outperforms other 2-dimensional materials such as black phosphorus, MoS<sub>2</sub> and WSe<sub>2</sub>, demonstrate the great potential of optimizing the deposition process in order to grow high-quality PtSe<sub>2</sub> material. This work employed molecular beam epitaxy (MBE) to take advantage of its excellent in-situ control and monitoring capabilities to shine light on the kinetic processes involved and to optimize material properties, a strategy that is proven to produce high-quality and large size layers of various transition metal chalcogenides.

In the first step, we show growth of ultrathin Pt layers on c-plane Al<sub>2</sub>O<sub>3</sub>. We demonstrate how deposition parameters affect the morphology and crystallinity of the Pt films. In-situ reflection high energy electron diffraction (RHEED) and ex-situ atomic force microscopy (AFM) show single crystal film growth with smooth surfaces for growth in the temperature range from 300 to 600 °C, which is confirmed by X-ray diffraction (XRD) and transmission electron microscopy (TEM). We are addressing the epitaxial orientation relationship between Pt and the substrate and determine the growth to proceed in an island growth mode as observed by RHEED, XRD, and TEM.

In the second part we demonstrate the BEOL compatible selenization process done in MBE by exposing optimized Pt layers of 3 nm and 3 monolayer (ML) thickness to Se flux. We discuss the influence of Pt layer configuration and substrate temperature on the selenization process. For 3 nm thick Pt layers, selenization in the optimum temperature range of 200 to 300 °C leads to the formation of epitaxial, smooth, single crystal, PtSe<sub>2</sub> as determined by RHEED, AFM and Raman investigation. We elucidate the epitaxial orientation relationship between PtSe<sub>2</sub> and the underlying Pt as presented in RHEED. We find however from RHEED and Raman, that the thickness of the so formed PtSe<sub>2</sub> is limited to the mono/few-layer regime regardless of the selenization temperature and the Se flux exposure time. We conclude that the reason for the observed self-limited selenization process in the MBE environment is the compared to other physical vapor deposition techniques extremely small Se flux accessible within MBE. With the goal to form a layer of purely PtSe<sub>2</sub> on the Al<sub>2</sub>O<sub>3</sub> by the selenization method, we report on the transformation process of 3 ML thick Pt films by Se flux exposure. Using RHEED, AFM and Raman, we still find the transformation rate to be smaller than 100 %, in addition we see that the crystal quality of the PtSe<sub>2</sub> is inferior compared to the PtSe<sub>2</sub> layers formed by selenization of 3 nm thick Pt films. However, we present a post-selenization annealing process in Se atmosphere that enhances the crystallinity of the PtSe<sub>2</sub> significantly as confirmed by Raman investigation.

#### 5:40 AM F.EL03.06.05

**Precisely Controlled Surface Charge Transfer Doping for Enhancing Electrical Performance of MoS<sub>2</sub>-FETs Using Selective Inkjet-Printing** [Inho Jeong](#)<sup>1,2</sup>, [Minwoo Song](#)<sup>3</sup>, [Gyu-Tae Kim](#)<sup>2</sup>, [Takhee Lee](#)<sup>3</sup> and [Seungjun Chung](#)<sup>1</sup>; <sup>1</sup>Korea Institute of Science and Technology, Korea (the Republic of); <sup>2</sup>Korea University, Korea (the Republic of); <sup>3</sup>Seoul National University, Korea (the Republic of)

Chemical vapor deposition (CVD)-grown molybdenum disulfide (MoS<sub>2</sub>), one of the most widely used transition metal dichalcogenides (TMDs), have attracted much attention as an emerging semiconductor layer to realize field-effect transistors (FETs) and thin-film optoelectronic devices due to its unique characteristics, such as a high carrier mobility, chemical and thermal stability, absence of dangling bond, and tunable electronic energy band depending on a number of layers.[1] For the last decade, there have been a lot of effort for tuning its intrinsic properties and enhancing device performance via surface charge transfer doping, with exploring its fundamental electrical characteristics.[2,3] The surface charge transfer doping follows the charge transfer mechanism between deposited dopants and host materials which allows to modulate the electrical and optical characteristics of the TMDs by tuning the Fermi level.[4] Especially, the one of the key advantage of surface

charge transfer doping is that the electronic structure of the host materials is not changed. This doping strategy is typically conducted via a solution-immersion or vapor-phase doping methods to deposit organic dopants onto the surface of TMDs. However, because the modulation of their electrical characteristics are only determined by immersion time and the dopant concentration, therefore, the effective amount of dopants which critically affects the characteristics of host MoS<sub>2</sub> cannot be precisely controlled.[5]

In this presentation, we will report surface charge transfer doping by using drop-on-demand selective inkjet printing with the use of benzyl viologen (BV) as a surface charge transfer donor. To perform a reliable doping process onto CVD-grown MoS<sub>2</sub> with inkjet printing, we will report how to obtain a stable BV ink droplet considering a specific range of the inverse Ohnesorge number, which is a dominant parameter to determine inkjetability. In addition, systematically analyzed the solvent characteristics depending on the organic dopant candidates will be presented. With these efforts, we can enhance the electrical performance of MoS<sub>2</sub>-FETs via surface charge transfer doping using inkjet printing which allows precisely controlled effective doping concentrations.

[1] Z. Yu, Z.-Y. Ong, S. Li, J.-B. Xu, G. Zhang, Y.-W. Zhang, Y. Shi, X. Wang, *Adv. Funct. Mater.*, 27, 1604093 (2017).

[2] X. Zhang, Z. Shao, X. Zhang, Y. He, J. Jie, *Adv. Mater.*, 28, 10409 (2016).

[3] F.-Z. Li, L.-B. Luo, Q.-D. Yang, D. Wu, C. Xie, B. Nie, J.-S. Jie, C.-Y. Wu, L. Wang, S.-H. Yu, *Adv. Energy Mater.*, 3, 579 (2013).

[4] S. Andleeb, A.K. Singh, J. Eom, *Sci. Technol. Adv. Mater.* 16, 035009 (2015).

[5] D. Kiriya, M. Tosun, P. Zhao, J.S. Kang, A. Javey, *J. Am. Chem. Soc.* 136, 7853 (2014).

#### 5:50 AM \*F.EL03.06.06

**Synthesis of Two-Dimensional Materials via Chemical Vapor Deposition** Jing Kong; Massachusetts Institute of Technology, United States

In recent years tremendous efforts have been devoted to the research on two dimensional materials. Their unique structures and remarkable properties have offered great potential for a wide range of applications in electronics, optoelectronics, valleytronics, catalysis, etc. The synthesis of high quality large area mono- and few-layer 2D materials is highly desirable for their applications. In this talk I will present our recent development on novel 2D material and structures, together with further understanding regarding the chemical vapour deposition (CVD) synthesis process of monolayer MoS<sub>2</sub>.

#### 6:05 AM F.EL03.06.07

**III-V Heterostructure N-Type Contacts to CVD Monolayer MoS<sub>2</sub>** Aravindh Kumar, Alvin Tang, Pranav Ramesh and Krishna Saraswat; Stanford University, United States

As transistor channels scale below 100 nm, the drive current would be limited by the contact resistance. Transition metal dichalcogenides, including MoS<sub>2</sub>, are promising candidates for ultra-short (< 10 nm) channels as they are immune to mobility degradation in the < 5nm thickness regime, due to the absence of surface roughness scattering. When making metal contacts to MoS<sub>2</sub>, the metal Fermi level pins slightly below the conduction band edge, leading to n-type Schottky contacts. On the other hand, the problem of n-type contacts has been solved in InAs, a III-V semiconductor, since the metal Fermi level pins above the conduction band edge, leading to ohmic contacts. In this study, we discuss the fabrication of heterostructure contacts to MoS<sub>2</sub> by depositing InAs on to monolayer MoS<sub>2</sub>. The MoS<sub>2</sub> has been synthesized at 850 C using the Chemical Vapor Deposition technique and InAs is deposited using the Metalorganic-CVD technique. We fabricate Transmission Line Model (TLM) structures using electron-beam lithography to extract the contact resistance and to study the contacts using temperature-dependent current-voltage (I-V) measurements. We also model the interface using Density Functional Theory (DFT) to gain insight into the physics at the interface.

#### 6:15 AM F.EL03.06.08

**Novel Synthetic Path to Ternary and Quaternary 2D Chalcogenides and Optoelectronic Applications** Mahyar Mohammadnezad<sup>1</sup>, Mimi Liu<sup>2</sup>, Gurpreet Singh Selopal<sup>1</sup>, Fabiola Navarro-Pardo<sup>1</sup>, Zhiming M. Wang<sup>3</sup>, Barry Stansfield<sup>1</sup>, Haiguang Zhao<sup>4</sup>, Cheng-Yu Lai<sup>2</sup>, Daniela R. Radu<sup>2</sup> and Federico Rosei<sup>1</sup>; <sup>1</sup>Centre Énergie Matériaux Télécommunications (INRS-EMT), Canada; <sup>2</sup>Florida International University, United States; <sup>3</sup>Institute of Fundamental and Frontier Sciences, University of Electronic Science and Technology of China, China; <sup>4</sup>Qingdao University, China

Reduced dimensionality in known chalcogenides such as the quaternary Cu<sub>2</sub>ZnSnSe (CZTSe), enhances the usefulness of these materials, including this known photovoltaic material. Past reports of platinum (Pt)-free counter electrodes for dye-sensitized solar cells (DSSCs) showed that they lacked the high surface area and electrocatalytic activity that could truly drive Pt replacement. CZTSSe, a sulfo-selenide kesterite was synthesized in a cascade reaction path to CZTSe, starting with the binary SnSe<sub>2</sub> nanosheets that were sequentially treated with copper and zinc in solution. The templated synthesis enabled

retention of the morphology, thus resulting in stand-alone, large area, CZTSSe nanosheets. CZTSSe nanosheets deposited on fluorine-doped tin oxide (FTO) substrates were used as Pt replacement in a dye-sensitized solar cell, yielding a power conversion efficiency of (5.73%), comparable to the performance of a cell using a Pt-based CE (5.78%). [1] An excellent electrocatalytic performance (4.60%) [1] was also recorded for a CZTSSe/carbon paper (CP) utilized as a replacement of Pt/FTO-free CE. Fabrication of CZTSSe nanosheets as well characterization data will be presented.

(1) Mohammadnezhad, M.; Liu, M.; Selopal, G. S.; Navarro-Pardo, F.; Wang, Z. M.; Stansfield, B.; Zhao, H.; Lai, C.-Y.; Radu, D. R.; Rosei, F. Synthesis of highly efficient  $\text{Cu}_2\text{ZnSnS}_x\text{Se}_{4-x}$  (CZTSSe) nanosheet electrocatalyst for dye-sensitized solar cells. *Electrochimica Acta* **2020**, *340*, 135954.

#### 6:25 AM F.EL03.06.09

**Synthesis of Blue-Emitting Silver Phenylselenolate in Thin Film and Crystal Forms** Watcharaphol Paritmongkol, Wenbi Shcherbakov-Wu, Woo Seok Lee and William Tisdale; Massachusetts Institute of Technology, United States

Silver phenylselenolate (AgSePh) is an emerging two-dimensional semiconducting member of a hybrid metal-organic chalcogenolate family. In addition to its two-dimensional structure with high exciton binding energy, strong in-plane anisotropy, and a narrow emission spectrum at 467 nm, AgSePh can be synthesized by a scalable vapor-phase method as well as a solution-phase reaction. Here, we show by testing 24 solvents – with different polarities, boiling points and functional groups – that complexation between silver cations and solvent molecules is the key to an increasing size of AgSePh crystals. With the introduction of amine solvents, we are able to increase the size of AgSePh thin films prepared by the vapor-phase tarnish reaction from ~200 nm to >1  $\mu\text{m}$  and that of AgSePh crystals grown by the solution-phase biphasic reaction from ~3  $\mu\text{m}$  to >150  $\mu\text{m}$ . Moreover, the addition of solvent vapors to the vapor-phase tarnish reaction allows the control of crystal orientations between perpendicular and parallel to substrates' surfaces. The improved syntheses reported in this work will allow easy integrations of AgSePh in both thin-film electronic and nanoelectronic applications and the exploration of strong excitonic anisotropy.

#### 6:35 AM F.EL03.06.10

**Easy Fabricated Large Area Thin Film Based Thermo-Electric Generator for Waste Heat Harvesting to Electricity** Sangram K. Pradhan, G Kogo and Messaoud Bahoura; Norfolk State University, United States

Highly crystalline and conformal growth of metal dichalcogenide based large surface area thin films thermoelectric generator were successfully grown on different substrates using RF sputtering technique. Surface morphology, crystal structure, and electrical properties of both p and n type thin films have been studied thoroughly. X-ray diffraction data revealed that crystallites of  $\text{MoS}_2$  and  $\text{WS}_2$  films are highly oriented in 001 plane with grain size distribution ranging from 40nm-130nm. Surface roughness study from AFM confirms that it increases with rise in substrate temperature and it plays a big role in electronic and phonon scattering. Interestingly,  $\text{MoS}_2$  films also shows low thermal conductivity at room temperature and strongly favors achievement of higher thermoelectric figure of merit value of up to 1.98. Raman spectroscopy data shows two distinct  $\text{MoS}_2$  vibrational modes at  $380\text{ cm}^{-1}$  for  $E_{2g}^1$  and  $410\text{ cm}^{-1}$  for  $A_{1g}$ . Thermoelectric transport studies further demonstrated that  $\text{MoS}_2$  films show p-type thermoelectric characteristics, while  $\text{WS}_2$  is an n-type material. We demonstrated high efficient pn-junction thermoelectric generator device for waste heat recovery and cooling applications.

#### 6:45 AM F.EL03.06.11

**Designing Non-Enzymatic Electrochemical Sensors for Human Health Monitoring from Nanostructured Chalcogenide Composites** Harish Singh and Manashi Nath; Missouri University of Science and Technology, United States

Body-integrated electronic sensing devices is getting great attention in field of human healthcare. Especially, wearable health monitoring sensors allows access to effective and affordable diagnostic tools for sensitive, rapid and accurate detection for biologically relevant molecules such as dopamine (DA) and glucose. In this current work, efforts have been made to develop non-enzymatic direct electrochemical sensors based on transition metal chalcogenides electrocatalyst loaded on flexible polymeric film and graphitic substrate for DA and glucose. Among all the niche applications and properties of transition metal chalcogenides, recently these materials have gained attention due to their favorable electrochemical properties owing to tunable redox behavior of the transition metal center. Binary metal selenides and tellurides grown on different flexible substrates through electrodeposition, hydrothermal synthesis as well as by chemical vapor deposition exhibits exceptional activity for DA detection and electrocatalytic glucose oxidation at low applied potential. These chalcogenides also show enhanced sensing parameters including low limit of detection for glucose concentration and high sensitivity (~19 mA mM

<sup>1</sup> cm<sup>-2</sup> for copper selenide catalyst). The electrochemical studies shows long-term stability as well as sensitivity with a detection region from 5 nm to 2 μM, rapid response time to a set of DA concentrations with excellent reproducibility. Furthermore, for practical application, human blood serum was also tested for accurate detection of DA and glucose level. The results suggested that such nanostructured metal chalcogenides-based sensor may be a potential candidate for electrochemical detection of DA and glucose in practical analysis. Through these studies, we have explored transition metal chalcogenides as electrocatalysts for dopamine sensing and direct glucose oxidation along with an understanding of their structure-property relationship.

#### 6:55 AM F.EL03.06.12

**ALD of MoSe<sub>2</sub> Using New Precursors** Raul Zazpe<sup>1,2</sup>, Richard Krumpolec<sup>3</sup>, Jaroslav Charvot<sup>4</sup>, Ludek Hromadko<sup>1,2</sup>, Hanna Sopha<sup>1,2</sup>, Martin Motola<sup>1</sup>, David Pavlinak<sup>3</sup>, Milos Krbal<sup>1</sup>, Filip Bures<sup>4</sup> and Jan Macak<sup>1,2</sup>; <sup>1</sup>Center of Materials and Nanotechnologies, Faculty of Chemical Technology, University of Pardubice, Czechia; <sup>2</sup>Central European Institute of Technology, Brno University of Technology, Czechia; <sup>3</sup>R & D Center for Low-Cost Plasma and Nanotechnology Surface Modifications, Department of Physical Electronics, Faculty of Science, Masaryk University, Czechia; <sup>4</sup>Institute of Organic Chemistry and Technology, Faculty of Chemical Technology, University of Pardubice, Czechia

2D semiconductor transition metal dichalcogenides (TMDs) have attracted considerable attention due to their layered structure, suitable band gap for visible light absorption, high carrier mobility, electrochemically active unsaturated edges and relatively good stability against photocorrosion [1]. Recently, 2D MoSe<sub>2</sub> has been gaining considerable interest due to its higher electrical conductivity as compared to MoS<sub>2</sub>, its wider inter-layer distance (~0.65 nm), narrow bandgap (1.33–1.72 eV), high resistance to photo-corrosion, high surface area layer, electrochemically active unsaturated Se-edges and close to zero Gibbs free energy edges for hydrogen adsorption. These properties are promising for different applications of MoSe<sub>2</sub> including hydrogen evolution [2], photocatalysis [3] and Li-ion batteries [4]. However, their low light absorption efficiency, recombination issues of the photogenerated electron-hole pairs and slow charge transfer of the intrinsic semiconducting 2H-phase are a handicap. An efficient strategy to surpass those intrinsic limitations are hybrid nanostructures using conducting supporting materials. In this regard, anodic TiO<sub>2</sub> nanotubes (TNTs) are excellent photoactive supporting material providing a high surface area, unique directionality for the charge separation, and highly effective charge collection [5]. Accordingly, we present anodic TiO<sub>2</sub> nanotubes homogeneously decorated with MoSe<sub>2</sub> nanosheets by atomic layer deposition (ALD). In parallel, we address the current scarcity of convenient ALD Se precursors by the synthesis a set of new selenium precursors - alkylsilyl (R<sub>3</sub>Si)<sub>2</sub>Se and alkytin (R<sub>3</sub>Sn)<sub>2</sub>Se, and cyclic silylselenides compounds. Those Se precursors were extensively characterized and their reliability as ALD Se precursors explored [6,7]. Several compounds exhibited promising results to be convenient ALD Se precursor as will be presented in the presentation. The synthesis of the MoSe<sub>2</sub> nanosheets and their composites with TiO<sub>2</sub> NTs, their physical and electrochemical characterization, and encouraging results in electrochemical characterization, hydrogen evolution reaction (HER) and photocatalysis will be presented and discussed.

[1] W. Choi, N. Choudhary, G. H. Han, J. Park, D. Akinwande, Y. H. Lee, *Materials Today* 20 (2017) 116–130.

[2] S. Mao, Z. Wen, S. Ci, X. Guo, K. Ostrikov, J. Chen, *Small* 11 (2015) 414–419

[3] Y. Zhao, J. Tu, Y. Sun, X. Hu, J. Ning, W. Wang, F. Wang, Y. Xu, L. He, *J. Phys. Chem. C* 122 (2018) 26570–26575

[4] Y. Liu, M. Zhu, D. Chen, *J. Mater. Chem. A*, 3 (2015) 11857–11862

[5] J. M. Macak, H. Tsuchiya, A. Ghicov, K. Yasuda, R. Hahn, S. Bauer, P. Schmuki, *Curr. Opin. Solid State Mater. Sci.* 11 (2007) 3

[6] , R. Zazpe, J. Charvot, R. Krumpolec, L. Hromadko, D. Pavlinák, F. Dvorak, P. Knotek, J. Michalicka, J. Prikryl, S. Ng, V. Jelínková, F. Bures, J.M. Macak, *FlatChem* 21 (2020) 100166

[7] J. Charvot, D. Pokorný, R. Zazpe, R. Krumpolec, D. Pavlinák, L. Hromádsko, J. Prikryl, J. Rodriguez-Pereira, M. Klikar, V. Jelínková, J. M. Macak, F. Bures, *ChemPlusChem* 85 (2020) 576–579

#### 7:05 AM F.EL03.06.13

**Late News: Charge Transport in MBE-Grown MoTe<sub>2</sub> Bilayers with Enhanced Stability Provided by AlO<sub>x</sub> Capping** Zuzanna W. Ogorzalek<sup>1</sup>, Bartłomiej Seredyński<sup>1</sup>, Sławomir Kret<sup>2</sup>, Adam Kwiatkowski<sup>1</sup>, Krzysztof Korona<sup>1</sup>, Magdalena Grzeszczyk<sup>1</sup>, Janusz Mierzejewski<sup>1</sup>, Dariusz Wasik<sup>1</sup>, Wojciech Pacuski<sup>1</sup>, Janusz Sadowski<sup>1,2,3</sup> and Marta Gryglas-Borysiewicz<sup>1</sup>; <sup>1</sup>University of Warsaw, Poland; <sup>2</sup>Polish Academy of Sciences, Poland; <sup>3</sup>Linnaeus University, Sweden

MoTe<sub>2</sub> is a transition metal dichalcogenide (TMD), which has been intensively studied in the last few years. It exists in several crystalline phases among which the semimetallic T<sub>d</sub> and semiconducting 2H exhibit numerous intriguing physical properties. It is well known however, that MoTe<sub>2</sub> shows significant sensitivity to air, which makes ex-situ experiments, involving sample preparation and processing, very challenging. [1-3] The question of stability is especially important in the

case of ultra-thin, single and few-layer samples, which provide access to the most interesting physics. In this paper we address the problem of low stability of MoTe<sub>2</sub> and propose a very efficient protective capping, that stabilizes transport properties of the layers. A molecular beam epitaxy technique has been used to grow ultra-thin MoTe<sub>2</sub> films in 2H-semiconducting phase on large area GaAs (111)B substrates. A transmission electron microscopy study reveals the high quality of the MoTe<sub>2</sub> films. Directly after the growth, MoTe<sub>2</sub> films have been in-situ capped with a thin (3 nm) layer of Al, which oxidizes after exposure to ambient conditions. This oxide serves as a protective layer to the underlying MoTe<sub>2</sub> and it is thin enough to make good-quality electrical contacts. Wide range temperature resistivity studies showed that charge transport in MoTe<sub>2</sub> is realized by hopping with an anomalous hopping exponent of  $x \approx 0.66$ , reported also previously for ultra-thin, metallic layers. We demonstrate that this approach provides a significant improvement of the MoTe<sub>2</sub> stability. Upon exposure to pure nitrogen and air atmospheres, the resistivity of unprotected sample changes by more than 900%, whereas the protected sample shows electrical stability at the level of 1% over one week and 5% in the timescale of several months. [4]

[1] H. Diaz et al., **2015**, *2D Materials* 2

[2] M. Yamamoto et al., **2013**, *J. Phys. Chem.*, 117

[3] G. Mirabelli et al., **2016**, *J. Appl. Phys.*, 2016, 120, 125102

[4] Z. Ogorzalek et al., *Nanoscale*, **2020**, 12, 16535-16542

#### 7:15 AM F.EL03.06.14

**Late News: Atomically Precise Fabrication of 1D Transition Metal Chalcogenides Inside Nanotubes** Yusuke Nakanishi<sup>1</sup>, Naoyuki Kanda<sup>1</sup>, Zheng Liu<sup>2</sup>, Yasumitsu Miyata<sup>1</sup>, Kazutomo Suenaga<sup>2</sup> and Nori Shinohara<sup>3</sup>; <sup>1</sup>Tokyo Metropolitan University, Japan; <sup>2</sup>AIST, Japan; <sup>3</sup>Nagoya University, Japan

Since the discovery of buckminsterfullerene in 1985, nanocarbon materials have played a crucial role in modern materials science. Recently, significant efforts have been redirected towards exploring ‘post-nanocarbons’. Over the past decade, 2D layers of transition metal chalcogenides (TMCs) have been widely recognized as ‘beyond graphene’ owing to their versatile chemistry. On the other hand, their 1D counterparts such as nanoribbons, nanotubes, and nanowires could exhibit the unique electrical and optical properties, significantly distinct from 2D TMCs as well as 1D nanocarbons. However, exploring their potential has been hampered by their limited availability. Although these materials have been prepared using chemical and lithographic methods, the reliable production of well-defined 1D TMCs remains a significant challenge.

Here we report atomically precise fabrication of 1D TMCs within carbon/boron-nitride nanotubes (CNTs/BNNTs). Chemical reactions confined inside the NTs promote and stabilize the bottom-up growth of 1D TMCs, allowing their easy handling and characterization. We found that choosing suitable precursors and diameters of the host NTs provides a variety of morphologies including nanoribbons, nanotubes, and nanowires. Atomic-level transmission electron microscopy enabled us to observe dynamic torsions of the nanowires inside CNTs, not seen in the bulk (M. Nagata et al., *Nano Lett.* 2019; N. Kanda et al., *Nanoscale* 2020). Furthermore, we have recently investigated electronic structures of 1D TMCs within BNNTs. Our findings suggest that these 1D TMCs could provide new building blocks for future nanoelectronics.

#### 7:25 AM F.EL03.06.15

**Late News: Electron Transport of Transition Metal Chalcogenide Nanowire Networks** Hiroshi Shimizu<sup>1</sup>, Jiang Pu<sup>2</sup>, Hong En Lim<sup>1</sup>, Yusuke Nakanishi<sup>1</sup>, Zheng Liu<sup>3</sup>, Takahiko Endo<sup>1</sup>, Taishi Takenobu<sup>2</sup> and Yasumitsu Miyata<sup>1</sup>; <sup>1</sup>Tokyo Metropolitan University, Japan; <sup>2</sup>Nagoya University, Japan; <sup>3</sup>National Institute of Advanced Industrial Science and Technology, Japan

Transition metal chalcogenide (TMC) nanowires have attracted much attention in recent years because of their one-dimensional (1D) metallic properties and electronic device applications [1-5]. To date, many groups have reported the preparation and properties of individual and bundled TMC nanowires including as Mo<sub>6</sub>S<sub>6</sub>[2], Mo<sub>6</sub>Se<sub>6</sub>[3], and Mo<sub>6</sub>Te<sub>6</sub> [4,5]. Recently, our group has achieved large-area growth of TMC nanowires using chemical vapor deposition (CVD) [6]. Depending on the affinity with substrate surface, this technique also enables network formation of either aligned atomically thin two-dimensional (2D) sheets or random network of three dimensional (3D) bundles composing of individual nanowires. For these samples, it is expected that the morphology such as bundle size will strongly affect the electron transport properties of TMC nanowire networks.

In this study, we have investigated the temperature dependence electron transport of WTe nanowire networks with different bundle sizes. The samples were grown on SiO<sub>2</sub> or Al<sub>2</sub>O<sub>3</sub> surface using CVD, and the network formation was confirmed using scanning electron microscope (SEM). At room temperature, the sheet resistances of samples vary from 2 kΩ to 75 MΩ depending on the nanowire density and bundle size. The thick bundle network shows a metallic behavior from room temperature to 20 K, whereas a power-law dependence is observed for the thin bundle network. In the presentation, we will discuss a possible mechanism derived from 1D metallic behavior for the power-law dependence.

- [1] L. Venkataraman et al., Phys. Rev. Lett., 83, 5334 (1999).  
 [2] L. Venkataraman et al., Phys. Rev. Lett., 96, 076601 (2006).  
 [3] J. Kibsgaard et al., Nano Lett., 8, 11 (2008).  
 [4] J. Lin et al., Nat. Nanotechnol., 9, 436 (2014).  
 [5] M. Nagata et al., Nano Lett., 19, 4845–4851 (2019).  
 [6] H.-E. Lim et al. Submitted.

SESSION F.EL03.07: Theory and Modeling of Low-Dimensional Chalcogenide  
 On Demand Abstracts Available for Viewing Starting Saturday Morning, November 21, 2020  
 F-EL03

**5:00 AM F.EL03.07.01**

**Structural Modeling of 2D van der Waals Materials via X-Ray Dynamical Diffraction Simulation—Application to an Intrinsic Antiferromagnetic Topological Insulator** Yori G. Camillo da Silva<sup>1</sup>, Celso I. Fornari<sup>2</sup>, Sergio L. Morelhao<sup>1</sup>, Philipp Kagerer<sup>2</sup>, Sebastian Sebastian Buchberger<sup>2</sup>, Hendrik Bentmann<sup>2</sup> and Friedrich Reinert<sup>2</sup>; <sup>1</sup>University of Sao Paulo, Brazil; <sup>2</sup>Julius-Maximilians-Universität Würzburg, Denmark

Two-dimensional (2D) van der Waals (vdW) materials has experienced an explosive growth after graphene, and new families of 2D systems and block-layered bulk materials have been discovered [1]. The possibility of tuning their electronic properties via structural parameters make the layered vdW materials attractive from both fundamental and device engineering points of view. However, the weakness of vdW interlayer forces lead in general to systems undergoing drastic changes as a function of subtle variation in growth conditions. Finding controllable fabrication processes of such systems has proven challenging [2,3]. Within the scope of exploiting intriguing phenomena related to topological surface states and symmetry-breaking magnetic states, epitaxy of topological insulator materials having atomic layers of Mn has been pursued [4]. Simulations of X-ray scattering and diffraction are well-established procedures for structural analysis at nanometer and subnanometer length scales of layered materials, ranging from amorphous films to crystalline ones such as epitaxial layers on single-crystal substrates. Higher are the ordering in stacking sequences of the atomic layers, the more pronounced are the diffracted intensities at higher angles allowing more refined model structures. X-ray theories are well comfortable at the limiting cases, either amorphous films or perfect periodic layer sequences, that is crystalline films. However, in developing new materials and processing technologies, layered materials with random layer sequences of large d-spacing can often be found. Combined with the very high dynamical range of advanced X-ray sources and instruments, this kind of material represent a challenging in theoretical approach for X-ray diffraction simulation [5].

In this work, we describe how to adapt a general recursive equation for simulating X-ray dynamical diffraction in layered materials to the case of thin films of  $Mn_xBi_2Te_{3+x}$  grown by molecular beam epitaxy on BaF<sub>2</sub> (111) substrates as a function of MnTe source temperature. The films are staking of  $n$  vdW bounded  $MnBi_2Te_4$  septuple layers (SLs) where the occurrence of  $m$   $Bi_2Te_3$  quintuple layers (QLs) lead to composition  $x = n/(n+m)$ . Interface quality, random stacking sequences, surface finishing, and evolution of defects during growth are parameters investigated by curve fitting with the recursive equation. It demonstrates the effectiveness of this approach for describing X-ray diffraction in layered systems ranging from random to perfect periodic stacking sequences of atomic layers.

- [1] M. M. Otrokov, I. P. Rusinov, M. Blanco-Rey, M. Hoffmann, A. Yu. Vyazovskaya, S. V. Ereemeev, A. Ernst, P. M. Echenique, A. Arnau, E. V. Chulkov. Phys. Rev. Lett. 122, 107202 (2019).  
 [2] S. L. Morelhão, S. W. Kycia, S. Netzke, C. I. Fornari, P. H. O. Rappl, E. Abramof. J. Phys. Chem. C 123, 24818 (2019).  
 [3] C. I. Fornari, E. Abramof, P. H. O. Rappl, S. W. Kycia, S. L. Morelhão. MRS Advances (2020). doi: 10.1557/adv.2020.202.  
 [4] J. A. Hagmann, X. Li, S. Chowdhury, S.-N. Dong, S. Rouvimov, S. J. Pookpanratana, K. M. Yu, T. A. Orlova, T. B. Bolin, C. U. Segre, D. G. Seiler, C. A. Richter, X. Liu, M. Dobrowolska, J. K. Furdyna. New J. Phys. 19, 085002 (2017).  
 [5] S. L. Morelhão, C. I. Fornari, P. H. O. Rappl, E. Abramof. J. Appl. Cryst. 50, 399-410 (2017).

**5:10 AM \*F.EL03.07.02**

**Systematic Exploration of Structure and Properties in Homologous Series of Nanoscale Chalcogenide Superlattices** Sage Bauers<sup>1</sup>, Danielle Hamann<sup>2</sup>, Dennice Roberts<sup>1</sup>, Andriy Zakutayev<sup>1</sup> and David Johnson<sup>2</sup>; <sup>1</sup>National Renewable Energy Laboratory, United States; <sup>2</sup>University of Oregon, United States

An exciting prospect for 2D materials is their ability to be integrated into heterostructures, where the selection and sequencing of stacked layers facilitate tailored properties. One form of such heterostructures are non-epitaxial chalcogenide superlattices with constituents interleaved at nanometer length scales. These materials can be prepared from amorphous—but intentionally layered—thin films which are gently heated to crystallize into a superlattice that mimicks the layer sequence of the precursor. Such facile synthesis enables superlattices with nearly limitless permutational flexibility, allowing for systematic explorations of how different layer arrangements affect the structure and properties of the composite material.

This talk will primarily focus on materials containing  $n$  monolayers of  $\text{TiSe}_2$  interleaved with  $m$  monolayers of  $\text{PbSe}$  and/or  $\text{SnSe}$  in a repeating superlattice. These structures can be described by the chemical formula  $[(\text{MSe})_{1+\delta}]_m[\text{TiSe}_2]_n$ , where  $\text{M}=\text{Sn}$  or  $\text{Pb}$  and  $\delta$  is a compositional misfit parameter. We will discuss several homologous series wherein the relative fractions of constituents are successively modified by changing the integral number of layers ( $m$  and  $n$ ).

Changes to  $[(\text{MSe})_{1+\delta}]_m[\text{TiSe}_2]_n$  layer sequencing induce changes to the composite materials' semi-metallic transport properties. In both  $[(\text{PbSe})_{1+\delta}]_m[\text{TiSe}_2]_n$  and  $[(\text{SnSe})_{1+\delta}]_m[\text{TiSe}_2]_n$ , electrons exchanged between the layers are the primary source of mobile carriers while the amount of charge exchange required to equilibrate the chemical potential across the interface is dependent on the thicknesses and identities of layers. Thus,  $m$  and  $n$  can be used to tune the carrier density with minimal change to carrier mobility since no ionized dopants are introduced into conduction paths. In some cases, the sequencing can also affect the local structure within the layers. For example, in  $[(\text{PbSe})_{1+\delta}]_m[\text{TiSe}_2]_n$  superlattices both constituents are structurally rigid and insensitive to the thickness of the layers. Conversely, in  $[(\text{SnSe})_{1+\delta}]_m[\text{TiSe}_2]_n$  the nanolayers of  $\text{SnSe}$  exhibit a rich polymorphism dependent on thickness, which is attributed to a combination of low polymorph energies and strong interfacial interactions with  $\text{TiSe}_2$ .

Motivated by successful synthesis of superlattice materials in several selenide systems, we have recently reported on  $[(\text{SnS})_{1+\delta}]_m[\text{TaS}_2]_1$  superlattices, marking the first application of this synthesis approach to sulfur-based chemistries. As part of this work, we employ graded precursor films that enable parallel preparation of multiple stacking sequences with similar monolayer control. These results are a promising first step towards similar systematic investigation of structure and properties in another chalcogenide class.

### 5:25 AM F.EL03.07.03

**Data-Driven Creation of an Inorganic Nanotube Database** Felix Tim Bølle, August E. G. Mikkelsen, Tejs Vegge and [Ivano E. Castelli](#); Technical University of Denmark, Denmark

Reducing dimensionality has led to a new realm of materials exhibiting interesting structural, electronic, and catalytic properties. While two-dimensional materials are the focus of many theoretical and experimental research groups, one-dimensional materials are less well studied. Most of the theoretical work on 1D materials is focused on explaining phenomena at the atomic scale rather than performing a high-throughput search of new inorganic nanotube materials.

Here, we investigate by means of density functional theory (DFT) sub-nanometer tubes that exhibit different properties compared to their 2D counterparts while being selective in size and composition. These nanotubes are obtained by rolling up 2D Janus dichalcogenide sheets, where the strain between the two sides of the 2D layer is the driving force for the formation of the nanotube. We will elucidate designing rules to produce nanotubes with controlled dimensions and to guide the search towards nanotubes that can be used in a variety of applications. In detail, we focus on properties like bandgaps, stabilities, and adsorption energies that lead to predictive models assisting in designing new nanotubes before doing DFT calculations. The generalization from existing data helps to accelerate the search for novel materials for applications in batteries, (photo-)catalysis, chemical storage, and nanofluidics.

### 5:35 AM F.EL03.07.04

**Assessing the Defect Tolerance of Non-Tetrahedral I<sub>2</sub>-II-IV-VI<sub>4</sub> Chalcogenides** [Andrea Crovetto](#)<sup>1,2</sup>, [Sunghyun Kim](#)<sup>3</sup>, [Moritz Fischer](#)<sup>1</sup>, [Nicolas Stenger](#)<sup>1</sup>, [Aron Walsh](#)<sup>3</sup>, [Ib Chorkendorff](#)<sup>1</sup> and [Peter Vesborg](#)<sup>1</sup>; <sup>1</sup>Technical University of Denmark, Denmark; <sup>2</sup>Helmholtz-Zentrum Berlin, Germany; <sup>3</sup>Imperial College London, United Kingdom

The  $\text{Cu}_2\text{BaSnS}_4$  (CBTS) and  $\text{Cu}_2\text{SrSnS}_4$  (CSTS) compounds have been recently investigated as wide band gap photovoltaic absorbers for tandem solar cells. Unlike their parent compound  $\text{Cu}_2\text{ZnSnS}_4$ , which crystallizes in a fully tetrahedral zincblende-like structure, the large size of Sr and Ba leads to a less-than-3D trigonal structure in CBTS and CSTS. While Cu and Sn remain tetrahedrally coordinated, Ba and Sr are 8-fold coordinated, and their coordinating S atoms form square antiprisms with open spaces between them.

By combining photoluminescence experiments and first-principles defect calculations, we show that the defect properties of CBTS and CSTS are staggeringly different from the defect properties of the much-investigated CZTS compound. Such differences can be explained in terms of their unconventional crystal structure, as well as in terms of cation size mismatch. We demonstrate that the sub-band gap tail states plaguing CZTS photoabsorbers have almost completely disappeared in both CBTS and CSTS. Nevertheless, a high density of (probably interstitial) defects are observed deep into the band gap, due to the open spaces available in the complex crystal structure of CBTS and CSTS.

Based on these observations, we develop a theory to explain the defect properties of a large set of I<sub>2</sub>-II-IV-VI<sub>4</sub> chalcogenide semiconductors and predict the most promising chemical spaces to find defect-tolerant compounds. Our analysis includes defects responsible for sub-band gap tail states, as well as defects responsible for deep recombination centers.

**5:45 AM F.EL03.07.05**

**Machine Learning for Deep Elastic Strain Engineering of Electronic Band Structure of 3D and Low-Dimensional Materials** Zhe Shi<sup>1</sup>, Ming Dao<sup>1</sup>, Evgenii Tsymbalov<sup>2</sup>, Alexander Shapeev<sup>2</sup>, Ju Li<sup>1</sup> and Subra Suresh<sup>1,3</sup>; <sup>1</sup>Massachusetts Institute of Technology, United States; <sup>2</sup>Skolkovo Institute of Science and Technology, Russian Federation; <sup>3</sup>Nanyang Technological University, Singapore

Nanoscale specimens of electronic materials as diverse as 2D graphene and MoS<sub>2</sub> and 3D silicon and diamond are known to be deformable to large strains without inelastic relaxation. The introduction of strain within the elastic regime has become a widely employed strategy for providing unique and exciting electronic and photonic properties in both 3D and low-dimensional materials. These discoveries harbingers a new age of deep elastic strain engineering of the band structure and device performance of electronic materials. Many possibilities remain to be investigated as to what graphene can do as the most versatile 2D material or what semiconductor materials such as MoS<sub>2</sub> and hBN can offer after overcoming their present commercial immaturity.

Deep elastic strain engineering explores full six-dimensional (6D) space of admissible nonlinear elastic strain and its effects on physical properties. However, the complexity of controllably engineering materials properties by strains necessitates first-principles computations to first screen for a desirable figure-of-merit and then design an optimal straining pathway. The reduced dimension strain space accessible to low-dimensional materials would thus become easy to navigate if we have the model for the much larger 6D strain space. In our work, to map the 6D strain space fully, we first developed a general method that combines machine learning and ab initio calculations to guide strain engineering whereby properties and performance for 3D and 2D materials could be designed. This method invokes machine learning algorithms and utilizes a limited amount of ab initio data for the training of a surrogate model, predicting electronic bandgap within an accuracy of 8 meV [1]. On top of this, attempts have been made by us in developing a more versatile machine learning framework that adopts convolutional neural networks, solid-state physics informed data representation scheme, and a new active learning algorithm to discover the indirect-to-direct bandgap transition in a material by scanning the entire strain space [2]. Through this framework, we considerably improve the state-of-the-art set by ourselves and achieve enhanced performance in every front, including more accurate bandgap and band structure prediction, band extrema detection, and effective mass calculation. Combining this method with experimentally validated finite-element simulations, we identified the most energy-efficient strain pathways that would reversibly transform an ultrawide-bandgap material, such as hBN or diamond, to a metalized state without phonon stability [3]. Our approach could also be used in finding phase transitions within six-dimensional strain space for different crystallographic orientations of a target material. As an example, we explored the phonon-instability conditions that promote phase transition to graphite in diamond.

The fast and reliable inference of the proposed model opens a path towards analyzing and scrutinizing general band structures (electronic, phonon, magnon, photonic bands) in the vast 6D strain space. Our AI-driven model is even easier to be applied for studying 2D materials such as chalcogenides that are accessible to a lower strain space dimension, auguring unique opportunities for tailoring low-dimensional materials properties via strain engineering for electronic, photonic, quantum and energy applications.

[1] Z. Shi, E. Tsymbalov, M. Dao, S. Suresh, A. Shapeev, J. Li. *Proc. Natl. Acad. Sci.*, (2019) 116, 4117-4122

[2] E. Tsymbalov, Z. Shi, M. Dao, S. Suresh, J. Li, A. Shapeev (2020) *submitted*

[3] Z. Shi, M. Dao, E. Tsymbalov, A. Shapeev, J. Li, S. Suresh (2020) *under review*

**5:55 AM F.EL03.07.07**

**Computational Design of Thermodynamically-Enhanced Metathesis Reactions for Difficult-to-Synthesize**



**Chalcogenides and Pnictides** Wenhao Sun<sup>1</sup> and Akira Miura<sup>2</sup>; <sup>1</sup>University of Michigan, United States; <sup>2</sup>Hokkaido University, Japan

Complex inorganic materials are usually synthesized by an ‘addition’ approach, whereby simple precursors are reacted to form a target multicomponent phase. However, if the simple precursors are already very stable themselves, then there may be little free energy left to drive a chemical reaction to a higher-component phase, which often results in slow kinetics and long-lived reaction impurities. Here, we demonstrate that metathesis reactions operate in a fundamentally different synthesis paradigm. Instead of a conventional reaction of  $M + X \rightarrow MX$ , a metathesis reaction is driven by a salt byproduct like NaCl, in a reaction typified by  $MCl + NaX \rightarrow MX + NaCl$ . Because  $Na^+$  and  $Cl^-$  are separated in the precursor, but are then rejoined in the product, these metathesis reactions are often highly exothermic. The inclusion of additional species like  $Na^+$  and  $Cl^-$  can also relocate the ‘thermodynamic sink’ of the phase diagram to a new composition—enhancing structure-selectivity towards a target multicomponent phase. Here, we demonstrate how metathesis reactions facilitate the synthesis of metastable ternary molybdenum nitrides [1] and the difficult-to-synthesize  $MgCr_2S_4$  thiospinel chalcogenide for Mg-battery applications [2]. Not only can metathesis reactions facilitate the synthesis of the desired phase, they are also routes to low-dimensional nanoparticles and nano-porous compounds. The additional degrees of freedom afforded by including extra elements into the synthesis reaction opens up a vast and promising design space for creative new metathesis reactions to chalcogenides and pnictides.

[1] J. Odahara *et al.*, "Self-Combustion Synthesis of Novel Metastable Ternary Molybdenum Nitrides." *ACS Materials Letters* (2019).

[2] A. Miura, et al. "Selective metathesis synthesis of  $MgCr_2S_4$  by control of thermodynamic driving forces." *Materials Horizons* 7.5 (2020).

#### 6:05 AM F.EL03.07.08

**Late News: DFT, GW and BSE Calculations for Charged Defects in N-Doped Monolayer  $WS_2$**  Anne Marie Z. Tan<sup>1</sup>, Yuanxi Wang<sup>2</sup>, Qingkai Qian<sup>2</sup>, Shengxi Huang<sup>2</sup> and Richard Hennig<sup>1</sup>; <sup>1</sup>University of Florida, United States; <sup>2</sup>The Pennsylvania State University, United States

Two-dimensional (2D) semiconducting transition metal dichalcogenides (TMDCs) have attracted extensive research interests for applications in optoelectronics, spintronics, photovoltaics, and catalysis. Just as in bulk semiconductors, 2D semiconductors contain both intrinsic defects, e.g., vacancies and antisites, and extrinsic defects, e.g., substitutional and interstitial dopants and impurities. Due to the reduced electronic screening in 2D materials, point defects are expected to have an even stronger impact on the electronic properties of these systems compared to in bulk semiconductors. Understanding the effect of defects, dopants, and impurities and how they respond to synthesis and processing conditions is critical to fully realize the potential of 2D TMDCs for applications in electronic and optoelectronic devices.

In this talk, we present first-principles calculations at multiple theory levels to investigate the energetics, electronic structure, and optical response of nitrogen-doped monolayer  $WS_2$ . We perform density-functional theory (DFT) calculations with the PBE, SCAN, and HSE functionals to determine the defect formation energies and charge transition levels (CTLs), utilizing the Freysoldt-Neugebauer charge correction [1] to restore the appropriate electrostatic boundary conditions for charged defects in 2D materials. Many-body perturbation theory calculations within the  $GW$  approximation using a novel convergence acceleration technique provide accurate quasiparticle levels to correct the DFT band edge positions and CTLs. We show that it is energetically favorable for N atoms to substitute at S sites, forming a paramagnetic defect with a CTL close to the middle of the bandgap. When aligned to a common electrostatic potential reference, the absolute position of the CTL remains almost consistent across all levels of theory, while the positions of the band edges exhibit a strong dependence. Finally, we model the optical response of N-doped  $WS_2$ , including excitonic effects, by solving the Bethe-Salpeter equation on top of  $GW$ . Based on our results, we suggest possible optical transitions between the defect level and the valence or conduction bands, which may be observable with photoluminescence and other optical spectroscopy techniques. The approach used in this study can be extended to study other defects and dopants in  $WS_2$  and other 2D TMDCs [2].

[1] C. Freysoldt and J. Neugebauer, *Phys. Rev. B* 97, 205425 (2018)

[2] A. M. Z. Tan, C. Freysoldt, and R. G. Hennig, *Phys. Rev. Mater.* 4, 064004 (2020)

**5:00 AM \*F.EL03.08.01**

**A Method to Reliably Measure Energy Conversion Efficiency without Making Contact for Confirmation of Thermoelectric Figure-of-Merit** Zhifeng Ren; University of Houston, United States

Thermoelectric figure-of-merit (ZT) is the overall most important physical quantity for a thermoelectric material. It ultimately determines the energy conversion efficiency. However, over the years, higher and higher ZTs were reported without confirmation since it requires zero-resistance contact that is as difficult as, if not more than, the material improvement. Therefore, how to confirm the ZT of any material without making the needed contact is urgently needed. In this report I will present our detailed study on reliable efficiency measurement on materials without making the needed contact.

**5:15 AM F.EL03.08.02**

**Layer Dependent Thermal Properties of WSe<sub>2</sub>** Annie Xian Zhang; Stevens Institute of Technology, United States

Following the interest in graphene since its first isolation by mechanical exfoliation in 2004, the broader family of two dimensional (2D) materials has been the subject of extensive attention thanks to their unique properties and atomically thin structure. In particular, transition metal dichalcogenides (TMDC) materials have shown unique optical and electrical properties, such as band structure transitions, semiconducting transport behavior, and strong photoluminescence, which are distinct from those of graphene and other carbon allotropes. TMDC materials are also intriguing for optical, electrical, and thermoelectric applications, especially in few-layer forms. Although electron transport in TMDC materials has been widely studied, there have been only limited experimental data published on thermal transport in WSe<sub>2</sub> which is the crucial parameter in their thermoelectric applications. Therefore, more robust experiments and modeling are needed to explain this trend or to provide more accurate values. Meanwhile, the large disparity in thermal conductivities predicted by theory also motivates further experimental investigation. Here we demonstrate an improved experimental method for measuring thermal conductivities of thin TMDCs. This is used to provide new measurements of the thermal conductivity of single-, bi-, and tri-layer WSe<sub>2</sub> (1L, 2L, 3L WSe<sub>2</sub>). The systematic experimental results enable comparisons of experimental results between different layer number, different material conditions.

The optothermal Raman technique has been the most successful method for measurement of thermal conductivity of 2D materials. In this technique, a laser is focused at the center of a flake and used to measure the position of a Raman-active mode. As the laser power is increased, the sample is heated, which enables red-shift Raman mode due to thermal softening. Thermal modeling can then be used to extract the thermal conductivity from the measured shift rate.

The thermal modeling used for determination of thermal conductivity requires additional input of a number of parameters: the rate of mode softening with temperature; optical absorption; and the thermal conductance of the supported area of the flake. However, in previous work, typically only the mode softening rate is directly measured, whereas the values of other parameters are derived from published values or assumed. Here we present measurements of the thermal conductivity of WSe<sub>2</sub> in which all of these parameters are determined experimentally. Molecular Dynamics simulations are performed to confirm the thermal transport properties trend from 1L to 3L, and supports the theoretical model building.

In conclusion, we have used optothermal Raman technique to study thermal transport properties of 1L to 3L WSe<sub>2</sub>, an emergent efficient thermoelectric material. This work addresses several important issues in the measurement of thermal conductivity of the 2D materials WSe<sub>2</sub> using Raman spectroscopy. We derive the thermal conductivity values of 1L to 3L WSe<sub>2</sub> and their interfacial thermal conductance with substrate. These results are of significance to discover the thermal transport properties of 2D transition metal dichalcogenides with thermoelectric applications, and thus develop the efficient 2D thermoelectric materials.

#### **F.EL03.09.01**

**Two-Dimensional Layered Germanium Monochalcogenides as Anode in Metal-Ion Batteries** Shakir Bin Mujib, Maren Ellis, Sophie Justus, Porter Herold and Gurpreet Singh; Kansas State University, United States

In this work, we investigate two-dimensional (2D) sheets of germanium sulfide (GeS) and germanium telluride (GeTe) as promising high-capacity and stable materials for energy storage. GeS and GeTe with layered structures are prepared via a simple liquid-phase exfoliation approach. As-synthesized 2D nanosheets can effectively increase the electrolyte-electrode interface area and facilitate metal ion transport. As a result, GeS and GeTe nanosheets deliver a high areal capacity of 1.76 mAh cm<sup>-2</sup> and 1.05 mAh cm<sup>-2</sup>, respectively as anodes in lithium-ion batteries (LIBs). Further analysis of GeS and GeTe in sodium-ion batteries (SIBs) and potassium-ion batteries (KIBs) suggest that layered germanium monochalcogenides can be potential anodes in other metal-ion batteries.

#### **F.EL03.09.02**

**Two-Dimensional Nanosheet Inks Using Zwitterion Dispersants for Biocompatible and Scalable Inkjet Printing** Hyeokjung Lee, Seung Won Lee, Chanho Park, Kyuho Lee and Cheolmin Park; Yonsei University, Korea (the Republic of)

Inkjet printing of two-dimensional (2D) transition metal dichalcogenide (TMD) nanosheets fabricated by liquid-phase exfoliation (LPE) allows simple, low-cost, and mass-producible photo-electronic devices. Many LPE processes involving toxic and environmentally hazardous solvents; however, dispersants have restricted the extent of applications of 2D-TMD inks. Herein, various 2D-TMD nanosheets, including MoS<sub>2</sub>, MoSe<sub>2</sub>, WS<sub>2</sub>, and WSe<sub>2</sub>, in addition to few-layered graphene, are inkjet-printed using a LPE process based on zwitterionic dispersants in water. Zwitterions with cationic and anionic species are water-soluble, while alkyl chain moieties associated with two ionic species adhere universally on the surface of TMD nanosheets, resulting in high throughput liquid exfoliation of the nanosheets. The zwitterion-assisted TMD nanosheets in water are successfully employed as an ink without the need for additives to adjust the viscosity and surface tension of the ink for use in an office inkjet printer; this gives rise to A4 scale, large-area inkjet-printed images on diverse substrates, such as metals, oxides, and polymer substrates patchable onto human skin. The development of mechanically flexible, biocompatible-printed arrays of photodetectors with pixelated MoSe<sub>2</sub> channels and conductive graphene electrodes on a paper exhibits a photocurrent ON/OFF ratio of approximately 10<sup>3.8</sup> and photocurrent switching of 500 ms.

#### **F.EL03.09.03**

**Effect of Bilayer Growth on the Thermoelectric Properties of Sb<sub>2</sub>Te<sub>3</sub> / Bi<sub>0.4</sub>Sb<sub>1.6</sub>Te<sub>3</sub> Thin Film** Andrew W. Howe, Mamadou T. Mbaye, Sangram K. Pradhan and Messaoud Bahoura; Norfolk State University, United States

Thermoelectric devices based on Sb<sub>2</sub>Te<sub>3</sub> and related alloys are of great interest to academia, industry, and government due to their efficiency in low-temperature applications such as micro-heating and small-scale refrigeration. The search for high performing thermoelectric devices is dominated by manipulating the electronic structure to boost the power factor through an increase in the density of states and/or reduction of the lattice thermal conductivity to maintain a large enough temperature gradient. Superlattice structures are long heralded as potential candidates to increase the thermoelectric power factor as well as significantly reduce the lattice thermal conductivity. In this report, we compare the thermoelectric properties of bilayer p-type Sb<sub>2</sub>Te<sub>3</sub> / Bi<sub>0.4</sub>Sb<sub>1.6</sub>Te<sub>3</sub> film and single layer p-type Bi<sub>0.4</sub>Sb<sub>1.6</sub>Te<sub>3</sub> film of the same thickness. Preliminary Hall effect measurements showed that the carrier concentration of our bilayer and Bi<sub>0.4</sub>Sb<sub>1.6</sub>Te<sub>3</sub> samples fall within the desired values common to heavily doped semiconductors. Carrier mobility and electrical conductivity are higher for our bilayer than the single-layer film. We noted a significant increase in the Seebeck coefficient values of our bilayer, 202 μV/K compared to 130 μV/K for our single-layer film. NanoTR thermoreflectance measurements revealed a significant reduction in the overall thermal conductivity of our bilayer system compared to our single-layer film. The low thermal conductivity reduction can be associated with, not only species intermixing -which allows phonon scattering events- interfacial boundary scatterings. When these observations are combined into a device, we would expect to see a great jump in the overall efficiency while maintaining the ease of fabrication allowing for quick scaling of production.

#### **F.EL03.09.04**

**Dimensionality Effects on Drift Resistivity of Nanoscale Phase-Change Memory (PCM) Cells in Reset State** Kazimierz

J. Plucinski; Military University of Technology, Poland

Although the device physics related to the operation of PCM (Phase change Memory) have been widely studied since its discovery in the 1960s, questions relating to the nature of the physical principle responsible for the resistivity drift is still controversial [1, 4].

These problems are deepening at the transition to the nanoscale in the construction of PCM memory [2, 3].

Drift resistivity of the PCM in reset state in terms of subthreshold conductivity is analyzed.

This subthreshold conductivity is analyzed with respect to nanoscaling effects, especially:

the contribution of tunneling and trapping to electrical transport;

contribution of ballistic transport and diffusive transport;

analysis of the scattering in relation to dimension and mean free path in amorphous GST;

limitation of Poole-Frankel approach.

The results are verified on the base of present models of the subthreshold conduction and drift resistivity in reset state of the PCM memory [e.g. 4, 5].

References:

1.M. Le Gallo and A. Sebastian, An overview of phase-change memory device physics, Journal of Physics D: Applied Physics, 53 (2020), Issue 21, 213002

2.M. Le Gallo, Evidence for thermally assisted threshold switching behavior in nanoscale phase change memory cells, J. Appl. Phys. 119, 025704 (2016)

3.Xue-Peng Wang et al., Nanoscale amorphous interfaces in phase-change memory materials: structure, properties and design, J. Phys. D: Appl. Phys. 53 (2020) 114002 (8pp)

4.P. Noé et al., Phase-change materials for non-volatile memory devices: from technological challenges to materials science issues, Semicond. Sci. Technol. 33 (2018) 013002 (32pp)

5.A. Redaelli, Ed., Phase Change Memory Device Physics, Reliability and Applications, 2018, Springer, (Ch. 2, 4)

## **SYMPOSIUM F.EL04**

---

Beyond Graphene 2D Materials—Synthesis, Properties and Device Applications  
November 21 - December 4, 2020

### Symposium Organizers

Zakaria Al Balushi, University of California, Berkeley

Susan Fullerton, Univ of Pittsburgh

Jieun Lee, Ajou University

Tania Roy, University of Central Florida

### Symposium Support

#### **Bronze**

Pittsburgh Quantum Institute (University of Pittsburgh)

Two-Dimensional Crystal Consortium -

Materials Innovation Platform (2DCC-MIP)

---

\* Invited Paper

SESSION F.EL04.09: Magnetism in 2D—Properties and Devices  
On Demand Abstracts Available for Viewing Starting Saturday Morning, November 21, 2020  
F-EL04

### 5:00 AM \*F.EL04.09.01

**Distinct Magneto-Raman Signatures of Spin-Flip Phase Transitions in CrI<sub>3</sub>** Amber McCreary<sup>1</sup>, Thuc Mai<sup>1</sup>, Franz Utermohlen<sup>2</sup>, Jeffrey Simpson<sup>1,3</sup>, Kevin Garrity<sup>1</sup>, Xiaozhou Feng<sup>2</sup>, Dmitry Shcherbakov<sup>2</sup>, Yanglin Zhu<sup>4</sup>, Jin Hu<sup>5</sup>, Daniel Weber<sup>2</sup>, Kenji Watanabe<sup>6</sup>, Takashi Taniguchi<sup>6</sup>, Joshua Goldberger<sup>2</sup>, Zhiqiang Mao<sup>4</sup>, Jeanie Lau<sup>2</sup>, Yuanming Lu<sup>2</sup>, Nandini Trivedi<sup>2</sup>, Rolando Valdes Aguilar<sup>2</sup> and Angela Hight Walker<sup>1</sup>; <sup>1</sup>National Institute of Standards and Technology, United States; <sup>2</sup>The Ohio State University, United States; <sup>3</sup>Towson University, United States; <sup>4</sup>The Pennsylvania State University, United States; <sup>5</sup>University of Arkansas–Fayetteville, United States; <sup>6</sup>National Institute for Materials Science, Japan

The discovery of 2-dimensional (2D) materials, such as CrI<sub>3</sub>, that retain magnetic ordering at monolayer thickness has resulted in a surge of both pure and applied research in 2D magnetism. In this talk, I will detail our magneto-Raman spectroscopy study on multilayered CrI<sub>3</sub>, focusing on two additional features in the spectra that appear below the magnetic ordering temperature and were previously assigned to high frequency magnons. Instead, we conclude these modes are actually zone-folded phonons. We observe a striking evolution of the Raman spectra with increasing magnetic field applied perpendicular to the atomic layers in which clear, sudden changes in intensities of the modes and their polarization dependence are attributed to the interlayer ordering changing from antiferromagnetic to ferromagnetic at a critical magnetic field. Our work highlights the sensitivity of the Raman modes to weak interlayer spin ordering in CrI<sub>3</sub>.

### 5:15 AM \*F.EL04.09.02

**Optical Spectroscopy of Antiferromagnetic Two-Dimensional Materials** Hyeonsik Cheong; Sogang University, Korea (the Republic of)

Two-dimensional magnetic van der Waals materials have attracted much interest recently. Magnetism in low dimensional systems is an interesting topic for the fundamental physics, and atomically thin magnetic materials are promising candidates for novel spintronic devices. Antiferromagnetic 2-dimensional materials are particularly interesting both for fundamental physics and also for antiferromagnetism-based spintronic devices. However, traditional research tools such as neutron scattering to probe antiferromagnetic ordering cannot be employed for atomically thin materials due to the small sample volume. Although magneto-optical Kerr effect measurements can be used to monitor the magnetic ordering in ferromagnetic materials, the lack of net magnetization precludes the use of the Kerr effect in probing antiferromagnetic ordering. Optical spectroscopy is becoming increasingly important for the study of antiferromagnetic 2-dimensional materials. Raman spectroscopy, for example, has been established as an invaluable tool to probe the magnetic transition in antiferromagnetic van der Waals materials as it has been found that the magnetic ordering can be reliably monitored by Raman spectroscopy [1]. Furthermore, recent spectroscopic studies revealed a novel coherent state in some of these materials stabilized by the antiferromagnetic ordering. In this presentation, I will review recent achievements in the study of antiferromagnetism in 2 dimensions using optical spectroscopy. FePS<sub>3</sub> exhibits an Ising-type antiferromagnetic ordering down to the monolayer limit, in good agreement with the Onsager solution for a 2-dimensional order-disorder transition [2]. The transition temperature remains almost independent of the thickness from bulk to the monolayer limit, indicating that the weak interlayer interaction has little effect on the antiferromagnetic ordering. On the other hand, NiPS<sub>3</sub>, which shows an XXZ-type antiferromagnetic ordering in bulk, exhibits antiferromagnetic ordering down to 2 layers with a slight decrease in the transition temperature, but the magnetic ordering is suppressed in the monolayer limit [3]. Furthermore, an almost resolution-limited, sharp optical transition was observed in photoluminescence and optical absorption measurements on NiPS<sub>3</sub>, which is interpreted as being due to a novel excitonic state coupled with the antiferromagnetic ordering [4]. Furthermore, a Heisenberg-type antiferromagnet MnPS<sub>3</sub> also exhibits ordering down to 2 layers [5] with a weak dependence of the Néel temperature on the thickness [6].

#### References

- [1] Kim K, Lee J-U, Cheong H, *Nanotechnology* (2019); **30**, 452001.
- [2] Lee J-U, *et al.*, *Nano Letters* (2016); **16**, 7433.
- [3] Kim K, *et al.*, *Nature Communications* (2019); **10**, 345.
- [4] Kang S, *et al.*, *in press*.
- [5] Kim K, *et al.*, *2D Materials* (2019); **6**, 041001.
- [6] Lim S, *et al.*, *submitted*.

### 5:30 AM \*F.EL04.09.03

## Electrostatic Control of Magnetism in 2D Cr<sub>2</sub>Ge<sub>2</sub>Te<sub>6</sub> Goki Eda; National University of Singapore, Singapore

Electrical manipulation of spin in a magnetic material is a fundamental challenge for future spintronics. In this respect, recent discoveries of gate-tunable magnetism in ferromagnetic two-dimensional (2D) materials such as CrI<sub>3</sub> and Fe<sub>3</sub>GeTe<sub>2</sub> demonstrate that they are an excellent platform for the study of interplay between charge and magnetic order. In this talk, we will discuss electrostatic control of Cr<sub>2</sub>Ge<sub>2</sub>Te<sub>6</sub> (CGT), a van der Waals ferromagnetic semiconductor, in an electric double-layer transistor (EDLT) geometry [1]. We show that degenerately electron-doped CGT exhibits peculiar magnetoresistance (MR) curves with pronounced hysteresis and abrupt switching features, which is characteristic of spontaneous magnetic order. Remarkably, the hysteresis persists up to 200 K, well above the Curie temperature of 61 K for pristine CGT, indicating enhancement of exchange energy by free carriers. Further, we find that the easy axis of the doping-induced ferromagnetic state lies in the 2D plane, in contrast to the out-of-plane easy axis of the pristine material. We will discuss the role of doping on the magnetic anisotropy and prospects for observing similar effects in other magnetic 2D materials.

[1] I. Verzhbitskiy et al. "Controlling the magnetic anisotropy in Cr<sub>2</sub>Ge<sub>2</sub>Te<sub>6</sub> by electrostatic gating" Nat. Electron. In Press (<https://doi.org/10.1038/s41928-020-0427-7>).

### 5:45 AM F.EL04.09.04

**Synthesis of Iron-Doped Monolayer MoS<sub>2</sub> Enabling Room Temperature Ferromagnetism** Shichen Fu<sup>1</sup>, Kyungnam Kang<sup>1</sup>, Kamran Shayan<sup>2,1,1</sup>, Anthony Yoshimura<sup>3</sup>, Siamak Dadras<sup>2</sup>, Siwei Chen<sup>1</sup>, Lihua Zhang<sup>4</sup>, Na Liu<sup>1,1</sup>, A. Nick Vamivakas<sup>2</sup>, Vincent Meunier<sup>3</sup>, Stefan Strauf<sup>1,1</sup> and Eui-Hyeok Yang<sup>1,1</sup>; <sup>1</sup>Stevens Institute of Technology, United States; <sup>2</sup>University of Rochester, United States; <sup>3</sup>Rensselaer Polytechnic Institute, United States; <sup>4</sup>Brookhaven National Laboratory, United States

Inspired by the recent discovery of ferromagnetism in two-dimensional atomically thin layers, such as chromium triiodide (CrI<sub>3</sub>)<sup>1,2</sup>, chromium germanium telluride (Cr<sub>2</sub>Ge<sub>2</sub>Te<sub>6</sub>)<sup>3</sup>, and other van der Waals materials<sup>4-6</sup> has moved the emphasis of studies from bulk crystals to low-dimensional materials. Two-dimensional semiconductors, including transition metal dichalcogenides, are of interest in electronics and photonics but remain nonmagnetic in their intrinsic form. Previous efforts to form two-dimensional dilute magnetic semiconductors utilized extrinsic doping techniques<sup>7</sup>, bulk crystal growth<sup>8</sup> or liquid precursor based chemical vapor deposition<sup>9</sup>, detrimentally affecting uniformity, scalability, or Curie temperature ( $T_C$ ).

Here, we demonstrate successful in situ substitutional doping of Fe atoms into MoS<sub>2</sub> monolayers via low-pressure chemical vapor deposition (LPCVD)<sup>10</sup>. We uncover an unambiguous Fe-related spectral feature in the luminescence of Fe:MoS<sub>2</sub> monolayers, which is stable up to room temperature. The origin of the Fe-related luminescence peak is further supported by results obtained from a density functional theory (DFT) calculation of dipole-allowed transitions. In addition, we find that monolayer Fe:MoS<sub>2</sub> displays ferromagnetism by probing the hysteresis in the magnetic circular dichroism (MCD) of the Fe-related emission. Moreover, by using nitrogen-vacancy center magnetometry and magnetization measurement using superconducting quantum interference devices (SQUID), we provide clear evidence for room temperature ferromagnetism in our synthesized Fe:MoS<sub>2</sub> monolayers and also quantitatively determine a  $0.5 \pm 0.1$  mT local magnetic field.

#### Reference:

1. Huang, B. *et al. Nature* **546**, 270–273 (2017).
2. Jiang, S., Shan, J. & Mak, K. F. *Nat. Mater.* **17**, 406–410 (2018).
3. Gong, C. *et al. Nature* **546**, 265–269 (2017).
4. Deng, Y. *et al. Nature* **563**, 94–99 (2018).
5. Bonilla, M. *et al. Nat. Nanotechnol.* **13**, 289–293 (2018).
6. O'Hara, D. J. *et al. Nano Lett.* **18**, 3125–3131 (2018).
7. Coelho, P. M. *et al. Adv. Electron. Mater.* **5**, 1900044 (2019).
8. Li, B. *et al. Nat. Commun.* **8**, 1–7 (2017).
9. Yun, S. J. *et al. Adv. Sci.* **7**, 1903076 (2020).
10. Fu, S. *et al. Nat. Commun.* **11**, 2034 (2020).

### 5:55 AM F.EL04.09.05

**The Influence of Global and Local Magnetic Fields on the Optical Properties of Lamellar Semiconductors** Adam K. Budniak<sup>1</sup>, Ellenor Geraffy<sup>1</sup>, Esty Ritov<sup>1</sup>, Faris Horani<sup>1</sup>, Yaron Amouyal<sup>1</sup>, Szymon J. Zelewski<sup>2</sup>, Robert Kudrawiec<sup>2</sup> and Efrat Lifshitz<sup>1</sup>; <sup>1</sup>Technion-Israel Institute of Technology, Israel; <sup>2</sup>Wroclaw University of Science and Technology, Poland

Magnetism is a topic of a wide interest since the discoveries of motors/generators, through magneto-resistance and up to modern times, where low dimensional materials offer a support for new magnetic phenomena. The talk will focus on the influence of magnetic moments and magnetism on the optical magneto-properties of semiconductors in an ultimate two-dimensional limit found in van der Waals transition metal phosphorous tri-chalcogenides. A few types of magnetic properties will be discussed: the long-range magnetic order, ferromagnetism, anti-ferromagnetism or special spin textures; an interfacial developed Rashba spin-orbit effect; nuclear spin Overhauser effect; magnetic polaron, all gaining special stabilization by the size confinement and a shape anisotropy. The mentioned intrinsic fields lead to a lift of energy or momentum degeneracy at band-edge states with selective spin orientation in the ground or/and excited state, being of a special interest in emerging technologies of spin-electronics and quantum computation. The lecture will include the study of *long-range magnetic order and valley effects in single layer of metal phosphor tri-chalcogenide compounds*. Metal phosphor tri-chalcogenides with the general chemical formula  $MPX_3$  (M=metal, X=chalcogenide) closely resembling the metal di-chalcogenides, but the metal being paramagnetic elements, while one-third of them are replaced by phosphor pairs. The metal ions within a single layer produce a ferromagnetic or anti-ferromagnetic arrangement, endowing those materials with unique magnetic and magneto-optical properties. Most recent magneto-optical measurements will be reported, exposing the existence of valley degree of freedom in a few  $MPX_3$  (e.g.,  $FePS_3$ ,  $MnPS_3$ ), that reveals a protection of the spin helicity of each valley however, the coupling to an anti-ferromagnetism lifts the valleys' energy degeneracy. The phenomenon was also examined in magnetically doped diamagnetic  $MPX_3$  layers. The results indicated the occurrence of coupling between photo-generated carriers and magnetic impurities and the formation of magnetic polaron.

#### References:

[1] A.K. Budniak, N.A. Killilea, S.J. Zelewski, M. Sytnyk, Y. Kauffmann, Y. Amouyal, R. Kudrawiec, W. Heiss, E. Lifshitz; *Small*, **2020**, 16 (1), 1905924

#### 6:05 AM F.EL04.09.06

**Late News: Air-Stable 2D Magnets Harvested from Iron-Rich Talc Minerals** Aleksandar Matkovic<sup>1</sup>, Kevin P. Gradwohl<sup>1</sup>, Oleg E. Peil<sup>2</sup>, Apoorva Sharma<sup>3</sup>, Markus Kratzer<sup>1</sup>, Jakob Genser<sup>4</sup>, Evelin Fisslthaler<sup>5</sup>, Daniel Knez<sup>5</sup>, Christoph Gammer<sup>6</sup>, Ferdinand Hofer<sup>5</sup>, Alois Lugstein<sup>4</sup>, Ronald Bakker<sup>1</sup>, Johann Raith<sup>1</sup>, Lorenz Romaner<sup>2</sup>, Georgeta Salvan<sup>3</sup>, Dietrich R. Zahn<sup>3</sup> and Christian Teichert<sup>1</sup>; <sup>1</sup>University of Leoben, Austria; <sup>2</sup>Materials Center Leoben, Austria; <sup>3</sup>Chemnitz University of Technology, Germany; <sup>4</sup>TU Wien, Austria; <sup>5</sup>Graz University of Technology, Austria; <sup>6</sup>Austrian Academy of Sciences, Austria

Since the first reports on intrinsically magnetic two-dimensional (2D) materials in 2017 [1,2], the price-to-pay for accessing their monolayers is the lack of ambient stability and that magnetic ordering persists only at cryogenic temperatures. We discovered in a mineral aggregate – mainly composed of hematite, magnetite, and chalcopyrite – soft layers of which macroscopic flakes easily could be peeled off that stuck to a permanent magnet. Employing mechanical exfoliation, we succeeded in thinning and transferring micrometer sized – mainly hexagonally shaped – flakes to  $SiO_2$  substrates. Energy-dispersive x-ray spectroscopy (EDS) revealed magnesium and silica as major components of the flakes. Raman spectroscopy indicated the presence of hydroxide groups, pointing towards talc, a hydrated magnesium phyllosilicate mineral. Long-term EDS and Raman revealed that in the flakes about 10 % of the Mg atoms are substituted by Fe. With atomic force microscopy, a minimum flake thickness of 1 nm was determined indicating cleavage down to a talc monolayer. Combined magnetic force microscopy and superconducting quantum interference device magnetometry measurements imply that Fe-rich talc exhibits superparamagnetic behavior in the explored Fe concentration range. As convincingly demonstrated by electron diffraction, the Fe-rich flakes are also showing long-term stability under ambient conditions in contrast to the 2D magnets reported so far.

[1] C. Gong, et al., *Nature* 546, 265 (2017).

[2] B. Huang, et al., *Nature* 546, 270 (2017).

#### 6:15 AM F.EL04.09.07

**Late News: Computational Prediction of Strong Anisotropy and Magnetostriction in Two-Dimensional Stoner Ferromagnet MnTe** Biswas Rijal<sup>1</sup>, Joshua T. Paul<sup>2</sup>, Michael Ashton<sup>3</sup> and Richard G. Hennig<sup>1</sup>; <sup>1</sup>University of Florida, United States; <sup>2</sup>Argonne National Laboratory, United States; <sup>3</sup>Max-Planck-Gesellschaft, Germany

We identify through chemical substitutions and density-functional theory (DFT) calculations a family of 27 metastable single-layer transition metal monochalcogenides,  $MX$  (M = Mn, Co, Ni, Cu, Rh, Pd, Ag, Cd, Au; X = S, Se, Te), whose structures are based on the monolayer form of bulk layered CuTe. DFT calculations with the generalized-gradient PBE and hybrid HSE06 functionals of these 20 materials in four candidate 2D structures determine the thermodynamic stability and groundstate structure and characterize their electronic properties. We predict that the CuTe parent compound is indeed the

most stable structure of this family. Thirteen of these two-dimensional (2D) materials display sufficiently low formation energies to be stable as free-standing 2D materials and could be mechanically exfoliated from their bulk parent phases, while several more could be grown on substrates. All the stable 2D materials are metallic, and 2D MnTe, CoS, and CoSe are magnetic. We determine that MnTe exhibits a particularly large magnetocrystalline anisotropy, a preferred out-of-plane magnetization, and strong magnetostriction. These materials may be suitable for applications as metallic contacts and wires in nanoscale or magnetic layers in semiconductor and spintronics devices.

SESSION Tutorial F.EL04: 2D Layered Materials for Quantum—From Growth to Quantum Properties and Applications  
Session Chairs: Zakaria Al Balushi, Susan Fullerton and Tania Roy  
Sunday Morning, November 29, 2020  
F.EL04

**8:00 AM \***

**Topological and Quantum Phenomena in 2D Layered Materials** Jeanie Lau; The Ohio State University, United States

As a material's thickness is reduced to a single or few atomic layers, the interplay of quantum confinement, electronic interactions and Berry's curvature endow it with properties that are often dramatically different from the bulk. A particularly striking aspect of these materials is the tunability – the carrier density, Coulomb interaction strength, spin orbit coupling, band gaps, effective mass, and band structure can be tuned by stacking, proximity, gating and twisting. New quantum collective phases, such as ferromagnetism, superconductivity, quantum Hall and quantum spin Hall insulators, with topologically non-trivial attributes, also emerge in the monolayer or few-layer limit. In this tutorial, I will introduce and review the latest development in two-dimensional materials as quantum materials, the unexpected emergent phases in these systems, experimental techniques to explore these phases, and their applications towards quantum information science.

**9:00 AM BREAK**

**9:15 AM \***

**Challenges in the Growth and Fabrication to Topological Materials for Quantum Devices** Anthony Richardella and Nitin Samarth; The Pennsylvania State University, United States

The discovery of topological phases in strongly spin orbit coupled materials has been accompanied by a broad range of predictions of exotic physics. Some, such as the quantum anomalous Hall effect (QAHE) in magnetically doped topological insulators, have been unambiguously demonstrated, while others like Majorana fermion excitations, have been far harder to distinguish from more trivial phenomena. And new topological materials such as Dirac and Weyl semimetals have continued to broaden the range of materials in which novel quantum effects have been observed. In this tutorial, we will give a background to the range of topological phases and materials that have been identified and discuss the promise and challenges of using them for applications ranging from spin torque memory devices to topological quantum computing. Among these are the challenges of raising the observable temperatures of effects such as QAHE, common defects in the growth of van der Waals layered materials and heterostructures, and the prediction and identification of promising next generation materials.

**10:15 AM BREAK**

**10:30 AM \***

**“Straintronics” and “Twistronics”—New Paradigms for Tuning the Electronic Correlations in Two-Dimensional van der Waals Materials by Architected Nanostructures** Nai-Chang Yeh; California Institute of Technology, United States

There has been a surge of research activities in the studies of two-dimensional (2D) crystals of van der Waals (vdW) materials and heterostructures because of their novel properties and great promises for technological applications. The physical properties 2D vdW materials are highly susceptible to their structural distortions and interlayer coupling, which opens up new opportunities to manipulate the electronic, magnetic and optical properties of these materials. In this tutorial, we will first review a new paradigm of *straintronics* that involves nanoscale strain engineering of 2D materials by means of architected nanostructures, which can either create desirable pseudo-magnetic fields in monolayer graphene for tunable electronic correlations, or modify the spatial distributions of energy gaps in monolayer semiconducting transition-metal



dichalcogenides (TMDs) for tunable excitonic lifetimes. We will also review the paradigm of *twistronics* that involves controlling the relative twist angle of different monolayers of 2D crystals to achieve Moiré potentials that can result in correlated electronic phases such as Mott insulator, superconductivity and ferromagnetism. Finally, we will describe realistic devices, with tunable electronic correlations based on the aforementioned paradigms, that manifest a range of intriguing quantum phenomena such as quantized Landau levels, quantum valley Hall effect and quantum anomalous Hall effect, all in the absence of external magnetic fields.

SESSION F.EL04.20/F.MT06.07: Joint Session Live Keynote and Panel Discussion I: Quantum Phenomena in Atomically Thin Materials

Session Chairs: Susan Fullerton, SungWoo Nam, Yaguo Wang and Ke Xu  
Tuesday Afternoon, December 1, 2020  
F.EL04

### 5:15 PM WELCOME, ANNOUNCEMENTS, INTRODUCTION

#### 5:18 PM \*F.EL04.13/F.MT06.03.05

**THz-Driven Irreversible Topological Phase Transition in Monolayer MoTe<sub>2</sub>** Keith A. Nelson; Massachusetts Institute of Technology, United States

The availability of intense tabletop terahertz-frequency pulses and simple field-enhancement structures that enable peak electric fields of tens of MV/cm have led to demonstrations of highly nonlinear THz-induced responses from a wide variety of materials. THz-driven electronic, magnetic, and structural phase transitions and domain switching have illustrated novel possibilities for control over collective properties and dynamics. In experiments on single-layer and few-layer MoTe<sub>2</sub>, we have found that irradiation with just one sufficiently strong THz pulse induces an irreversible phase transition [1]. The initial, noncentrosymmetric 2H phase disappears, as shown by the disappearance of characteristic Raman lines and second harmonic generation. After further THz irradiation, the topological insulator phase appears, revealed by its distinct Raman spectrum. Single-shot measurements of the MoTe<sub>2</sub> evolution as a function of time after THz irradiation reveal complex dynamics over many-picosecond time scales. Theoretical calculations show that the transition is induced through THz-induced liberation of carriers which stabilize the new phase and reduce the energy barrier between the two phases. The result illustrates the prospects for THz control over complex multiphase landscapes in quantum materials.

[1] "Terahertz-driven irreversible topological phase transition in two-dimensional MoTe<sub>2</sub>," J. Shi, Y.-Q. Bie, W. Chen, S. Fang, J. Han, Z. Cao, T. Taniguchi, K. Watanabe, V. Bulović, E. Kaxiras, P. Jarillo-Herrero, and K. A. Nelson, *arXiv*:1901.13609 (2019).

#### 5:48 PM \*F.EL04.13/F.MT06.03.06

**Conformal, Area-Specific and Switchable Graphene Nanowrinkles** Teri W. Odom; Northwestern University, United States

Selective patterning and functionalization of graphene can produce spatially-defined properties. Buckling or wrinkling of graphene on polymeric substrates enables a direct approach to tune the physical properties without lithographic steps, and the resulting curvature of the wrinkles can control local chemical reactivity. However, most buckling methods have been limited by the range of wavelength tunability, only global control of the wrinkled patterns, and delamination and cracks in the graphene. This talk will describe a scalable approach to achieve area-specific reactivity and patterning of conformal graphene wrinkles. We will discuss how a fluoropolymer layer sandwiched between graphene and different polymer substrates can facilitate crack-free and switchable graphene nanostructures. Such patterned areas with different curvatures show different reactivities based on a plasma fluorination reaction. Our approach for large-area, fine control over graphene wrinkle topographies has prospects for other two-dimensional electronic materials and optoelectronics and plasmonics applications.

### 6:08 PM BREAK

#### 6:18 PM \*F.EL04.13/F.MT06.03.04

**Quantum Anomalous Hall Effect in Intrinsic Magnetic Topological Insulator MnBi<sub>2</sub>Te<sub>4</sub>** Yuanbo Zhang; Fudan University, China

In a magnetic topological insulator, nontrivial band topology conspires with magnetic order to produce exotic states of matter that are best exemplified by quantum anomalous Hall (QAH) insulators and axion insulators. Up till now, such magnetic topological insulators are obtained by doping topological insulators with magnetic atoms. The random magnetic dopants, however, inevitably introduce disorders that hinder further exploration of topological quantum effects in the material. We resolve this dilemma by probing quantum transport in  $\text{MnBi}_2\text{Te}_4$  thin flake—a topological insulator with intrinsic magnetic order. In this layered van der Waals crystal, the ferromagnetic layers couple anti-parallel to each other, so bulk  $\text{MnBi}_2\text{Te}_4$  is an antiferromagnet. Atomically thin  $\text{MnBi}_2\text{Te}_4$ , however, becomes ferromagnetic when the sample has odd number of septuple layers (a septuple layer represents a single structural unit in the out-of-plane direction). We observe zero-field QAH effect in a five-septuple-layer specimen; an external magnetic field further enhance the QAH quantization by forcing all layers to align ferromagnetically.  $\text{MnBi}_2\text{Te}_4$  therefore becomes the first intrinsic magnetic topological insulator exhibiting QAH effect.

## 6:38 PM PANEL DISCUSSION

SESSION F.EL04.21: Live Keynote II: Beyond Graphene 2D Materials—Synthesis, Properties and Device Applications  
Session Chairs: Zakaria Al Balushi, Dana Kern and Jierui Liang  
Wednesday Morning, December 2, 2020  
F.EL04

## 11:30 AM WELCOME AND ANNOUNCEMENTS

### 11:31 AM \*F.EL04..16.01

**Enabling 2D Heterostructure Development with Atomic Resolution Imaging—Studies of Twist Reconstruction and Degradation** [Sarah J. Haigh](#), David Hopkinson, Nick Clark, Astrid Weston and Yichao Zou; University of Manchester, United Kingdom

2D materials and their heterostructures provide an exciting playground for pioneering science. In this talk I will demonstrate how atomic resolution scanning transmission electron microscopy (STEM) imaging and analysis is being used to support the advancement of these systems.

For example, I will discuss new results revealing the structural relaxation that occurs when two transition metal dichalcogenide (TMDC) monolayers are misoriented by a small twist (rotation angle). Many high profile experimental measurements of the exciting physics present in twisted TMDCs have necessarily neglected the potential for local structural relaxation. We have used atomic resolution STEM to reveal that TMDCs bilayers twisted to a small angle, less than  $\sim 3$  degrees, reconstruct into energetically favourable stacking domains separated by a network of stacking faults, and that this behaviour is more complex than is observed in graphene [1]. For crystal alignments close to 3R stacking, we find that a tessellated pattern of mirror reflected triangular 3R domains while for alignments close to 2H stacking, stable 2H domains dominate, with nuclei of an earlier unnoticed metastable phase limited to  $\sim 5\text{nm}$  in size. This appears as a kagome-like pattern at twist angles less than 1 degree, transitioning to a hexagonal array of screw dislocations separating large-area 2H domains as the twist angle approaches 0 degrees. Tunneling spectroscopy measurements reveals that such reconstruction creates strong piezoelectric textures and pseudo-magnetic fields, opening new avenues for engineering of 2D material properties on the nanometre scale [1].

As the range of 2D materials increases rapidly, many of those with the most the promising magnetic or optoelectronic properties are found to be unstable in air or moisture, which makes fabrication challenging and hampers their use. Even relatively stable 2D crystals like  $\text{MoSe}_2$  and  $\text{WSe}_2$  are found to have perfect interfaces only when processed in an inert environment [2]. These materials can be stabilised to ambient conditions by encapsulating with stable 2D layers, such as graphene and hexagonal boron nitride. [3] For example, we have applied the encapsulation approach to study the presence and behaviour of point and extended defects in the 2D monochalcogenides,  $\text{GaSe}$  and  $\text{InSe}$  which are of interest due to their relatively high electron mobilities, strong second harmonic generation and quasi-direct bandgap when reduced to the monolayer limit.[4] Nonetheless the properties of  $\text{InSe}$  and  $\text{GaSe}$  crystals often degrade on exposure to air, light, and/or moisture, thought to be the result of oxidation induced defects. We have used atomic resolution STEM together with electron energy loss spectroscopy (EELS) and energy dispersive X-ray spectroscopy to characterise individual point and extended

defects in InSe and GaSe [5]. We observe that both materials contain multiple point and extended defects, even when exfoliated in argon and encapsulated in graphene. Point vacancies are observed to be healable under the electron beam, while extended defects and stacking faults have symmetries not found in bulk samples and which could be used to tune the properties of 2D post-transition-metal monochalcogenide materials for optoelectronic applications. We also demonstrate the nanopatterning of black phosphorus using electron beam lithography via etching protocols developed in the STEM [6], and recent work revealing oxidation induce improvement of superconductivity in few layer TaS<sub>2</sub> [7].

## References

- [1] A. Weston et al, Nature Nanotechnology (2020) doi: 10.1038/s41565-020-0682-9
- [2] A.P. Rooney et al, Nano Letters, 17, 5222, (2017)
- [3] Y. Cao et al, Nano Letters, 15, 8, 4914-4921 (2015)
- [4] M.J. Hamer et al., ACS nano 13 (2), 2136-2142 (2019)
- [5] D G Hopkinson et al, ACS nano, 13 (5), 5112-5123 (2019)
- [6] N. Clark et al, Nano Letters, 18 (9), 5373-5381, (2018)
- [7] J Bekaert, et al, Nano Letters, 20 (5), 3808-3818 (2020)

### 11:51 AM \*F.EL04.16.02

#### **Twistrionic Structures and Moire Superlattices in Homo- & Heterobilayers of Transition Metal Dichalcogenides** Vladimir Falko; University of Manchester, United Kingdom

We apply a multiscale modelling approach to study moiré superlattice in twisted homo- and heterobilayers of transition metal dichalcogenides (TMD), taking into account the interlayer hybridisation of the electronic orbital and lattice reconstruction due to stacking-dependent adhesion. First of all, we develop DFT-parametrized interpolation formulae for interlayer adhesion energies of MoSe<sub>2</sub>, WSe<sub>2</sub>, MoS<sub>2</sub>, and WS<sub>2</sub> with both parallel and antiparallel orientation of their unit cells and arbitrary offset of the honeycomb lattices in the adjacent layers. Then, we combine those interpolation formulae with elasticity theory and analyze the bilayer lattice relaxation into mesoscale domain structures. We find that 3R and 2H stacking domains develop for, respectively, bilayers with parallel (P) and antiparallel (AP) orientation of the monolayer unit cells, separated by a network of dislocations, for twist angles  $\theta < \theta_P \sim 2.5$  and  $\theta < \theta_{AP} \sim 1$ . Such lattice reconstruction has been verified by STEM imaging. We also show that the triangular domain structures of P-oriented homobilayers would manifest itself in local tunnelling characteristics of marginally twisted. For AP bilayer, we show that the deformation of the lattices around domain walls (which resemble twist dislocations oriented along the planes of in bulk 2H crystals) generate piezo-electric charges, reaching local density up to  $\pm 0.5 \times 10^{12} \text{e/cm}^2$  at the junctions of the honeycomb domain wall network. Finally, we use DFT modelling of bandstructure of bilayers with various stacking configurations and interlayer distances to develop and parametrise interpolation formulae for the interlayer hopping between the layers for the relevant parts of the Brillouin zone, and, then, establish the electronic structure of the bilayer across the moire supercell, taking into account the piezoelectric potentials.

### 12:11 PM \*F.EL04.16.04

#### **Surface and Strain Control of 2D Materials—From Fundamental Properties to Nanomanufacturing** Joel W. Ager<sup>1,2</sup>; <sup>1</sup>Lawrence Berkeley National Laboratory, United States; <sup>2</sup>University of California, Berkeley, United States

In the monolayer limit transition metal dichalcogenides (TMDs) such as MoS<sub>2</sub> and WS<sub>2</sub> have direct bandgaps, leading to significant interest in the use of these materials for opto-electronic applications. Their internal photoluminescence (PL) quantum efficiency (QE) is a sensitive measure of their quality. While some III-V thin films and II-VI quantum dot structures can achieve near-unity values of this metric, most semiconductor materials have QEs which are much smaller. We have discovered that treatment of sulfur-based TMDs with an organic superacid dissolved in a non-polar solvent suppresses non-radiative recombination at low pump powers, leading to near 100% QE. [1]. Similar, near-unity, QE values can be achieved via electrostatic gating by lowering the Fermi level to near mid-gap to suppress the formation of non-radiative trions [2]. Tuning of band parameters with strain is a common motif in semiconductor devices. Chemical vapor deposition of some monolayer TMDs on thermal expansion coefficient mismatched substrates can induce strains on the order of 1%, in spite of the weak van der Waals interaction [3]. Larger strains can be envisioned: Au grows epitaxially on MoS<sub>2</sub> with a predicted mismatch strain of 10% [4]. Further, the strain is predicted to be confined to the monolayer in contact with the Au, while other layers in the structure remain unstrained. This effect weakens the bonding between the top layer and the bulk [5], which enables exfoliation of large areas of monolayer material with defined patterns [6,7]. Further optimization of this nano-manufacturing process has improved the yield to nearly 50% and has led to the ability to form defined TMD heterostructures [8].

<sup>1</sup>M. Amani, D.-H. Lien, D. Kiriya, J. Xiao, A. Azcatl, J. Noh, S.R. Madhupathy, R. Addou, S. KC, M. Dubey, K. Cho, R.M. Wallace, S.-C. Lee, J.-H. He, J.W. Ager, X. Zhang, E. Yablonovitch, and A. Javey, *Science* **2015**, 350, 1065.

<sup>2</sup>Lien, D.-H.; Uddin, S. Z.; Yeh, M.; Amani, M.; Kim, H.; Ager, J. W.; Yablonovitch, E.; Javey, A. *Science* **2019**, 364, 468–471.

<sup>3</sup>Ahn, G. H.; Amani, M.; Rasool, H.; Lien, D.-H.; Mastandrea, J. P.; Ager III, J. W.; Dubey, M.; Chrzan, D. C.; Minor, A. M.; Javey, A. *Nat. Commun.* **2017**, 8, 608.

<sup>4</sup>Y. Zhou, D. Kiriya, E.E. Haller, J.W. Ager, A. Javey, and D.C. Chrzan, *Phys. Rev. B* **93**, 054106 (2016).

<sup>5</sup>Sun, H.; Sirott, E. W.; Mastandrea, J.; Gramling, H. M.; Zhou, Y.; Poschmann, M.; Taylor, H. K.; Ager, J. W.; Chrzan, D. C. *Phys. Rev. Mater.* **2018**, 2, 094004.

<sup>6</sup>S.B. Desai, S.R. Madhupathy, M. Amani, D. Kiriya, M. Hettick, M. Tosun, Y. Zhou, M. Dubey, J.W. Ager, D. Chrzan, and A. Javey, *Adv. Mater.* **28**, 4053 (2016).

<sup>7</sup>Gramling, H. M.; Towle, C. M.; Desai, S. B.; Sun, H.; Lewis, E. C.; Nguyen, V. D.; Ager, J. W.; Chrzan, D.; Yeatman, E. M.; Javey, A.; Taylor, H. *ACS Appl. Electron. Mater.* **2019**, 1, 407–416.

<sup>8</sup>Nguyen, V.; Gramling, H.; Towle, C.; Li, W.; Lien, D.-H.; Kim, H.; Chrzan, D. C.; Javey, A.; Xu, K.; Ager, J.; Taylor, H. *J. Micro Nano-Manufacturing* **2019** 7 041006.

### 12:31 PM \*F.EL04.16.03

**Interplay Between Intra- and Inter-Layer Interactions in Stacked Two-Dimensional Crystals** Young-Woo Son; Korea Institution for Advanced Study, Korea (the Republic of)

Interlayer interactions in stacked 2D crystals are one of key ingredients in exhibiting their qualitative distinct physical properties, differing from their single layer physics [1]. For example, a well-known 2D quantum spin Hall insulating transition metal dichalcogenide (TMDC) can show either topological Weyl metallic phase or trivial one depending on a minute stacking order difference [1,2]. Recent advances in fabricating stacked 2D crystals enable us to perform controlled studies on interesting electronic, magnetic and topological properties in low dimensional heterostructures. In this talk, I will first discuss interplay between intralayer correlation, interlayer interaction, and magnetism in layered materials [3-5]. To understand magnetic properties, I will introduce a new computationally efficient method to calculate various correlation effects in layered materials [3]. Another interesting examples revealing intriguing interlayer interactions will be discussed for graphene bilayer systems [6,7] and TMDCs [8]. For a graphene bilayer system with a rotation angle of 30 degrees, it is shown that a quasicrystalline order through a perfect incommensurate interlayer interaction shows localized 12 fold resonant states with fractal scaling [6]. For a bilayer MoS<sub>2</sub> system, I will demonstrate a intrinsic coupling between strain and shear in the system that can alter its low energy Raman modes, thereby providing a way to obtain its almost all fundamental mechanical constants through light-matter interactions.

#### References

- 1) Y.-W. Son, *Nature* **565**, 32 (2019).
- 2) H.-J. Kim, S.-H. Kang, I. Hamada, and Y.-W. Son, *Phys. Rev. B* **95**, 180101 (R) (2017).
- 3) S. Lee and Y.-W. Son, arXiv.org:1911.05967 (2019).
- 4) S. Lee and Y.-W. Son, *in preparation* (2020).
- 5) E. Ko and Y.-W. Son, *in preparation* (2020).
- 6) S. J. Ahn *et al*, *Science* **361**, 782 (2018).
- 7) P. Moon, M. Koshino, Y.-W. Son, *Phys. Rev. B* **99**, 165430 (2019).
- 8) J. Lee *et al.*, *Nat. Comm.* **8**, 1370 (2017).

### 12:51 PM \*F.EL04.17.01

**Imaging Carrier Inhomogeneities in Active 2D Material Devices** Samuel Berweger; National Institute of Standards and Technology, United States

Scanning microwave microscopy (SMM, often called scanning microwave impedance microscopy, sMIM) is a scanning probe implementation that can directly probe free carriers with nanometer spatial resolution using tip-localized GHz fields. With the subsurface sensitivity inherent to near-field techniques and the ability to measure electrically isolated systems, SMM is well-suited for studying electronic inhomogeneities in 2D semiconducting materials and their devices. We begin by highlighting SMM measurements of photogenerated free carriers in transition metal dichalcogenide lateral heterostructures.

We then focus on the application of SMM to studying ambipolar field effect transistors of 2D films of the 1D van der Waals material tellurium (tellurene). Tellurene can be solution processed, exhibits high bipolar mobilities, and is stable under ambient conditions, which makes it an attractive alternative to conventional 2D semiconductors. We combine SMM with a differential implementation to image spatial variations in conductivity as well as the associated carrier type as a function of

the applied backgate voltage in tellurene devices. We reveal spatial inhomogeneities in carrier type and conductivity and show that the measured backgate-dependent device conduction minimum in fact arises from the simultaneous coexistence of n-type and p-type regions in an overall minimum conductivity configuration. We further show that the spatial inhomogeneities in conductivity and carrier type in four-terminal devices results in differing transport characteristics between different terminals across the same device in well-defined backgate-controlled p-type and n-type conduction channels. While these results highlight the challenges facing the reproducible fabrication of 2D material devices, the possibilities of solution-based doping and deterministic weighting of multiple inputs into the same device hold future promise.

**1:11 PM \*F.EL04.12.01**

**What Governs the “Efficiency“ of Liquid Phase Exfoliation of Layered Crystals?** [Claudia Backes](#); Heidelberg University, Germany

Liquid phase exfoliation has become an important top down production technique giving access to large quantities of nanosheets in colloidal dispersion. Importantly, this is a highly versatile technique that can be applied to numerous layered materials from graphite to transition metal dichalcogenides, h-BN, III-VI semiconductors, hydroxides etc. All materials can be exfoliated in a similar way using aqueous surfactant or suitable solvents as stabilisers. Nanosheets in dispersion are extremely polydisperse with broad lateral size and thickness distributions. To narrow size and thickness distributions, liquid cascade centrifugation has proven to be a powerful tool for efficient size selection yielding nanosheet dispersions with well-defined dimensions.

Building on these established methodologies of exfoliation and size selection, it became possible in recent years to address some fundamental questions regarding the exfoliation process, such as: In which way is the yield, nanosheet size and layer number dependent on the liquid medium? What is a good descriptor for the exfoliation efficiency and what does it depend on? What is the role of defects? In this talk, these fundamental questions will be addressed and a picture of the current understanding will be drawn.

SESSION F.EL04.22: Live Keynote III: Beyond Graphene 2D Materials—Synthesis, Properties and Device Applications  
Session Chairs: Jieun Lee, Mehrnaz Mojtavavi and Alexander Vera  
Thursday Morning, December 3, 2020  
F.EL04

## **8:00 AM WELCOME AND ANNOUNCEMENTS**

**8:01 AM \*F.EL04.09.02**

**Optical Spectroscopy of Antiferromagnetic Two-Dimensional Materials** [Hyeonsik Cheong](#); Sogang University, Korea (the Republic of)

Two-dimensional magnetic van der Waals materials have attracted much interest recently. Magnetism in low dimensional systems is an interesting topic for the fundamental physics, and atomically thin magnetic materials are promising candidates for novel spintronic devices. Antiferromagnetic 2-dimensional materials are particularly interesting both for fundamental physics and also for antiferromagnetism-based spintronic devices. However, traditional research tools such as neutron scattering to probe antiferromagnetic ordering cannot be employed for atomically thin materials due to the small sample volume. Although magneto-optical Kerr effect measurements can be used to monitor the magnetic ordering in ferromagnetic materials, the lack of net magnetization precludes the use of the Kerr effect in probing antiferromagnetic ordering. Optical spectroscopy is becoming increasingly important for the study of antiferromagnetic 2-dimensional materials. Raman spectroscopy, for example, has been established as an invaluable tool to probe the magnetic transition in antiferromagnetic van der Waals materials as it has been found that the magnetic ordering can be reliably monitored by Raman spectroscopy [1]. Furthermore, recent spectroscopic studies revealed a novel coherent state in some of these materials stabilized by the antiferromagnetic ordering. In this presentation, I will review recent achievements in the study of antiferromagnetism in 2 dimensions using optical spectroscopy. FePS<sub>3</sub> exhibits an Ising-type antiferromagnetic ordering down to the monolayer limit, in good agreement with the Onsager solution for a 2-dimensional order-disorder transition [2]. The transition temperature remains almost independent of the thickness from bulk to the monolayer limit, indicating that the weak interlayer interaction has little effect on the antiferromagnetic ordering. On the other hand, NiPS<sub>3</sub>, which shows an XXZ-type antiferromagnetic ordering in bulk, exhibits antiferromagnetic ordering down to 2 layers with a slight decrease in the transition temperature, but the magnetic ordering is suppressed in the monolayer limit [3]. Furthermore, an almost resolution-limited, sharp optical

transition was observed in photoluminescence and optical absorption measurements on NiPS<sub>3</sub>, which is interpreted as being due to a novel excitonic state coupled with the antiferromagnetic ordering [4]. Furthermore, a Heisenberg-type antiferromagnet MnPS<sub>3</sub> also exhibits ordering down to 2 layers [5] with a weak dependence of the Néel temperature on the thickness [6].

#### References

- [1] Kim K, Lee J-U, Cheong H, *Nanotechnology* (2019); **30**, 452001.
- [2] Lee J-U, *et al.*, *Nano Letters* (2016); **16**, 7433.
- [3] Kim K, *et al.*, *Nature Communications* (2019); **10**, 345.
- [4] Kang S, *et al.*, *in press*.
- [5] Kim K, *et al.*, *2D Materials* (2019); **6**, 041001.
- [6] Lim S, *et al.*, *submitted*.

#### 8:21 AM \*F.EL04.09.01

**Distinct Magneto-Raman Signatures of Spin-Flip Phase Transitions in CrI<sub>3</sub>** Amber McCreary<sup>1</sup>, Thuc Mai<sup>1</sup>, Franz Utermohlen<sup>2</sup>, Jeffrey Simpson<sup>1,3</sup>, Kevin Garrity<sup>1</sup>, Xiaozhou Feng<sup>2</sup>, Dmitry Shcherbakov<sup>2</sup>, Yanglin Zhu<sup>4</sup>, Jin Hu<sup>5</sup>, Daniel Weber<sup>2</sup>, Kenji Watanabe<sup>6</sup>, Takashi Taniguchi<sup>6</sup>, Joshua Goldberger<sup>2</sup>, Zhiqiang Mao<sup>4</sup>, Jeanie Lau<sup>2</sup>, Yuanming Lu<sup>2</sup>, Nandini Trivedi<sup>2</sup>, Rolando Valdes Aguilar<sup>2</sup> and Angela Hight Walker<sup>1</sup>; <sup>1</sup>National Institute of Standards and Technology, United States; <sup>2</sup>The Ohio State University, United States; <sup>3</sup>Towson University, United States; <sup>4</sup>The Pennsylvania State University, United States; <sup>5</sup>University of Arkansas–Fayetteville, United States; <sup>6</sup>National Institute for Materials Science, Japan

The discovery of 2-dimensional (2D) materials, such as CrI<sub>3</sub>, that retain magnetic ordering at monolayer thickness has resulted in a surge of both pure and applied research in 2D magnetism. In this talk, I will detail our magneto-Raman spectroscopy study on multilayered CrI<sub>3</sub>, focusing on two additional features in the spectra that appear below the magnetic ordering temperature and were previously assigned to high frequency magnons. Instead, we conclude these modes are actually zone-folded phonons. We observe a striking evolution of the Raman spectra with increasing magnetic field applied perpendicular to the atomic layers in which clear, sudden changes in intensities of the modes and their polarization dependence are attributed to the interlayer ordering changing from antiferromagnetic to ferromagnetic at a critical magnetic field. Our work highlights the sensitivity of the Raman modes to weak interlayer spin ordering in CrI<sub>3</sub>.

#### 8:41 AM F.EL04.14.06

**Monolayer Half-van der Waals Heavy Metals Enabled by Confinement Heteroepitaxy** Alexander Vera<sup>1</sup>, Siavash Rajabpour<sup>1</sup>, Timothy Bowen<sup>1</sup>, Boyang Zheng<sup>1</sup>, Wilson Yanez Parreno<sup>1</sup>, Hesham El-Sherif<sup>2</sup>, Chaoxing Liu<sup>1</sup>, Nabil M. Bassim<sup>2</sup>, Nitin Samarth<sup>1</sup>, Vincent Crespi<sup>1</sup> and Joshua Robinson<sup>1</sup>; <sup>1</sup>The Pennsylvania State University, United States; <sup>2</sup>McMaster University, Canada

Due to relativistic effects, heavy metals (Pb, Bi, etc.) demonstrate strong spin orbit coupling (SOC) effects, making them promising elemental precursors to broken spin degeneracy and non-trivial topology. Atomically thin heavy metal layers exhibit large Rashba effects, translating to large spin Hall angles suitable for spin pumping, memory, and other spintronic applications. Atomically thin lead (Pb) in particular may support superconductivity along with non-trivial topology, potentially serving as a route to exotic superconducting states. However, typical synthesis techniques do not provide a platform for scalable, stackable, and air-stable 2D metals, necessary for *ex-situ* device work. To answer this challenge, we demonstrate the synthesis of an air-stable 1ML-Pb with strong (~500meV) spin splitting within a graphene/silicon-carbide interface through confinement heteroepitaxy. We expect this material to exhibit a large spin Hall angle suitable for spintronic applications.

#### 9:01 AM \*F.EL04.09.03

**Electrostatic Control of Magnetism in 2D Cr<sub>2</sub>Ge<sub>2</sub>Te<sub>6</sub>** Goki Eda; National University of Singapore, Singapore

Electrical manipulation of spin in a magnetic material is a fundamental challenge for future spintronics. In this respect, recent discoveries of gate-tunable magnetism in ferromagnetic two-dimensional (2D) materials such as CrI<sub>3</sub> and Fe<sub>3</sub>GeTe<sub>2</sub> demonstrate that they are an excellent platform for the study of interplay between charge and magnetic order. In this talk, we will discuss electrostatic control of Cr<sub>2</sub>Ge<sub>2</sub>Te<sub>6</sub> (CGT), a van der Waals ferromagnetic semiconductor, in an electric double-layer transistor (EDLT) geometry [1]. We show that degenerately electron-doped CGT exhibits peculiar magnetoresistance (MR) curves with pronounced hysteresis and abrupt switching features, which is characteristic of

spontaneous magnetic order. Remarkably, the hysteresis persists up to 200 K, well above the Curie temperature of 61 K for pristine CGT, indicating enhancement of exchange energy by free carriers. Further, we find that the easy axis of the doping-induced ferromagnetic state lies in the 2D plane, in contrast to the out-of-plane easy axis of the pristine material. We will discuss the role of doping on the magnetic anisotropy and prospects for observing similar effects in other magnetic 2D materials.

[1] I. Verzhbitskiy et al. "Controlling the magnetic anisotropy in  $\text{Cr}_2\text{Ge}_2\text{Te}_6$  by electrostatic gating" Nat. Electron. In Press (<https://doi.org/10.1038/s41928-020-0427-7>).

#### **9:21 AM \*F.EL04.14.10**

**Large-Area Growth of 2D Layered Materials—Chalcogenides, Oxides and Halides** Kibum Kang; Korea Advanced Institute of Science and Technology, Korea (the Republic of)

The 2D layered materials are the potential components in next-generation semiconductor devices and quantum devices. For the integration of 2D layered materials into such functional devices, it is necessary to develop a high-quality large-area growth process.

In this talk, I will introduce the MOCVD growth of 2D layered materials, including transition metal dichalcogenides, metal oxides, and metal halides. Furthermore, I will discuss the MOCVD grown 2D layered materials and their heterostructures that could potentially be utilized in a single-photon source for quantum devices.

#### **9:41 AM \*F.EL04.14.11**

**Electronics with Nobel Metal Dichalcogenides Applications** Georg Düsberg; Universität der Bundeswehr München, Germany

Two-dimensional materials such as transition metal dichalcogenides (TMDs) are intensively investigated because of their potential applications in future electronics. So far mainly group six (Mo/W) TMDs have been investigated, which show thickness depend electronic and optical properties. Metal-to-semiconductor transitions, high mobilities, and high potential for various sensing applications, now raised interest to the group 10 (Pt/Pd) TMDs or Nobel Metal Dichalcogenides (NMDs). In this presentation, the low temperature synthesis of various TMDs by thermally assisted conversion (TAC) is presented. [1] The composition and morphology of the resulting large-scale layers are investigated by a multitude of characterization techniques including Raman spectroscopy, [2] AFM and X-ray photoelectron spectroscopy (XPS). In particular, the low temperature TAC synthesis PtSe<sub>2</sub> potentially allows back end of line (BEOL) integration compatible with silicon technology. The effects of growth on the underlying substrates or investigated by TOF-SIMS and transmission electron microscopy. Further, as pre-patterned structures can be grown by the TAC, which allows to fabricate electronic devices using standard micro-fabrication technology. [3] PtSe<sub>2</sub> has shown potential for a range of novel electronics devices. Examples for high performance chemical sensors, [1] IR-photodetectors[4] and MEMS[5] devices based on PtSe<sub>2</sub> will be presented.

References

[1] Yim et al. ACS Nano, 10 (10), 9550 2016.

[2] O'Brien et al., 2D Materials, 3, 021004, 2016.

[3] Yim, et al. NPJ 2D Materials and Applications 5 (2) 2018.

[4] Yim, et al. Nano Letters, 3 (18), 1794 2018

[5] Wagner et al. Nano Letters, 8 (6), 3738 2018

SESSION F.EL04.23: Live Keynote IV: Beyond Graphene 2D Materials—Synthesis, Properties and Device Applications

Session Chairs: Nathan Frey and Tania Roy

Friday Afternoon, December 4, 2020

F.EL04

#### **4:00 PM WELCOME AND ANNOUNCEMENTS**

#### **4:01 PM \*F.EL04.15.01**

**Tailoring 2D Chalcogenide Interfaces for Heterostructure Growth and Device Optimization** Lincoln J. Lauhon; Northwestern University, United States

Understanding and control of surfaces and interfaces is necessary to exploit the potential of 2D metal chalcogenides in electronics and optical devices. The ubiquity and scalability of vapor-phase processing in particular provides a wealth of opportunities, from the growth of van der Waals heterostructures to the chemical tailoring of interfaces to optimize device performance, including devices made from "composite" 2D materials such as those printed from inks. This talk will describe research to leverage interfaces for devices via two routes: atomic layer deposition (ALD) of metal oxides to modify dichalcogenide properties and pulsed chemical vapor deposition of ferroelectric monochalcogenides. In prior work, tuning of ALD oxide stoichiometry was shown to tune the Fermi level of MoS<sub>2</sub>. [1] More recently, in situ monitoring of MoS<sub>2</sub> and MoSe<sub>2</sub> transistor performance during deposition of an oxide dielectric enabled the disentangling of changes in carrier concentration and mobility during the alternating dosing of the metal-organic precursor and oxidant.[2] Intriguingly, we find a substantial enhancement in field effect mobility with sub-monolayer coverage. Variable temperature transport measurements indicate that charged impurity scattering is reduced by screening even prior to formation of a complete dielectric, pointing to the importance of seeding conditions in maximizing mobility. Vapor deposition processes also provide scalable routes to van der Waals heterostructures whose properties can be engineered by band-offsets and dimensionality. Building on prior work demonstrating low-temperature epitaxy of SnS on MoS<sub>2</sub>[3], a range of processing conditions were explored to understand how SnS film morphology is influenced by substrates including amorphous SiO<sub>2</sub>, mica, MoS<sub>2</sub>, and hexagonal boron nitride (hBN). Control over film thickness and morphology is particularly important to harness the in-plane ferroelectricity of SnS for devices. Large area monolayer regions are readily achieved on MoS<sub>2</sub> substrates by targeting temperatures and purge times that enhance selective growth at edges. Due to the relative inertness of the vdW surface of hBN, modified surface preparation and pulsing schemes are necessary to favor lateral growth of SnS, and monolayers growth is more challenging. However, isolated islands of epitaxial SnS on hBN are relatively easy to achieve, providing a path towards highly scaled memristive devices based on ferroelectric switching.

[1] Chem. Mater. 2018, 30, 3628. [2] ACS Appl. Electron. Mater. 2020, 2, 1273. [3] ACS Appl. Mater. Interfaces 2019, 43, 40543.

#### 4:21 PM \*F.EL04.02.01

##### **Lithium-Ion Electrolytic Substrates—TMD Growth and 1V High-Performance Transistors and Amplifiers** Md.

Hasibul Alam and [Deji Akinwande](#); The University of Texas at Austin, United States

This talk will present our latest progress on materials, transistor and memory devices based on 2D atomically-thin films. In particular, we explore a new substrate, namely, solid lithium-ion electrolytic substrates, for the direct growth and realization of high-performance TMD devices and amplifiers. Electrostatic gating with ionic liquids (ILs), leading to the accumulation of high surface charge carrier densities, has been often exploited in thin-film transistors. However, the intrinsic liquid nature of ILs inhibit it from constituting an ideal platform. In this regard, a lithium-ion solid electrolyte, often used for battery applications, offers similar advantages as ionic-liquids, with the added benefit of solid-state compatibility. With the solid electrolyte, we demonstrate its application in high-performance n-type MoS<sub>2</sub> and p-type WSe<sub>2</sub> transistors with sub-threshold values approaching the ideal limit of 60 mV/dec and complementary inverter amplifier gain of 34, the highest among comparable amplifiers with a 1 V power supply. These results establish lithium-ion substrates as a promising alternative to ionic liquids for the study of thin-film devices.

#### 4:41 PM \*F.EL04.03.01

##### **Probing Two-Dimensional Materials Using Focused Angle-Resolved Photoemission Spectroscopy** [Jyoti Katoch](#);

Carnegie Mellon University, United States

Two-dimensional (2D) materials offer the freedom to create novel condensed matter systems, with unique properties, by mechanically assembling different (or same) 2D materials layer-by-layer to form atomically sharp vertical or lateral heterostructures. The van der Waals (vdW) heterostructures with small lattice mismatch and a relatively small twist angle between the constituent layers, have shown to exhibit coexisting complex phases of matter including Mott insulating state, superconductivity, bound quasiparticles, and topological states. In addition, the extreme surface sensitivity of two-dimensional (2D) materials provides an unprecedented opportunity to engineer the physical properties of these materials using external perturbations. In this talk, I will discuss the utilization of angle-resolved photoemission spectroscopy (ARPES) with high spatial resolution to investigate the electronic band structure of 2D heterostructures and their devices. This can shed light on the intricate relationship between controlled external perturbations, substrate, and electronic properties of 2D materials [1, 2]. In particular, I will discuss our *in-operando* nanoARPES results that exhibit highly tunable many-body effects in graphene devices [3] and tunable van Hove singularities in twisted bilayer graphene [4].

##### **References:**

[1] Katoch et. al., Nature Physics 14, 355-359 (2018).



- [2] Ulstrup, et. al., Science Advances, Vol. 6, no. 14, eaay6104, (2020).  
[3] Muzzio, et. al., Physical review B Rapid Communications 101, 201409(R) (2020).  
[4] Jones, et. al., arXiv:2006.00791 (2020). Accepted for publication in Advanced Materials.

#### 5:01 PM \*F.EL04.11.01

#### **“Valley Noise” and Rydberg Excitons in Monolayer Semiconductors—Insights from (Really) High Magnetic Fields** Scott Crooker; National High Magnetic Field Lab, United States

Much of the current interest in atomically-thin transition metal dichalcogenide (TMD) semiconductors such as MoS<sub>2</sub> and WSe<sub>2</sub> is driven by the physics of coupled spin & valley degrees of freedom and the potential for new spin- and valley-based devices. This talk will discuss recent optical studies that probe the valley-related physics of electrons, holes, and excitons in monolayer TMD semiconductors.

In a first study [1,2], we measure the polarized magneto-absorption spectra of high-quality exfoliated TMD monolayers in very large magnetic fields to 91 tesla, which allows to follow the diamagnetic shifts of not only the 1s ground state of the neutral exciton but also its excited 2s, 3s, ..., ns Rydberg states. The energies and diamagnetic shifts provide a direct determination of the effective (reduced) exciton masses and also the dielectric properties of these monolayer semiconductors – fundamental material parameters that until now were available only from theoretical calculations. Moreover, we also measure other important material properties, including exciton binding energies, exciton radii, and free-particle bandgaps. These results provide essential and quantitative parameters for the rational design of opto-electronic van der Waals heterostructures incorporating 2D semiconductor monolayers.

In a second study, we introduce an entirely passive, noise-based approach for exploring intrinsic valley dynamics in monolayer TMD semiconductors [3]. Under conditions of strict thermal equilibrium, we use optical Faraday rotation to “listen” to the thermodynamic fluctuations of the valley polarization in a Fermi sea of resident electrons or holes, due to their spontaneous scattering between the *K* and *K'*. Frequency spectra of this valley noise reveal narrow Lorentzian lineshapes and therefore very long intrinsic valley relaxation, especially for holes (~microseconds). These results provide quantitative measurements of intrinsic valley dynamics, free from any external perturbation, pumping, or excitation.

*\*In collaboration with Mateusz Goryca, Jing Li, & Andreas Stier (NHMFL), Nathan Wilson & Xiaodong Xu (University of Washington), and Cedric Robert, Bernhard Urbaszek, & Xavier Marie (INSA-Toulouse)*

- [1] M. Goryca *et al.*, *Nature Communications* **10**, 4172 (2019).  
[2] A. V. Stier *et al.*, *Phys. Rev. Lett.* **120**, 057405 (2018).  
[3] M. Goryca, N. P. Wilson, P. Dey, X. Xu, & S. A. Crooker, *Science Advances* **5**, eaau4899 (2019).

#### 5:21 PM \*F.EL04.11.02

#### **Isotropic and Anisotropic Polaritons in van der Waals Materials** Qiaoliang Bao and Qingdong Ou; Monash University, Australia

Polaritons, hybrid light-matter excitations, enable nanoscale control of light. Particularly large polariton field confinement and long lifetimes can be found in graphene and van der Waals materials, opening new avenues for low-loss photonic applications. Here, we present our recent progress in the discovery on engineering of these nanoscale polaritons in 2D materials [1,2]. First, plasmon polaritons arising from graphene and topological insulators were investigated in graphene/Bi<sub>2</sub>Te<sub>3</sub>, topological insulator Bi<sub>2</sub>Te<sub>3</sub>, graphene nanoribbon and 3D graphene using either spectroscopic or real space imaging techniques [3-6]. We show how the plasmonic coupling happens in two Dirac materials, how high-order plasmonic modes are observed in 3D graphene structure, how multiple plasmonic modes at sub-wavelength are achieved in graphene nanoribbon and how edge chirality controls the plasmonic shift.

We would also like to highlight our progress on the observation of anisotropic and ultra-low-loss polariton propagation along the surface of natural vdW material  $\alpha$ -MoO<sub>3</sub> [7]. We visualized and verified phonon polaritons with elliptic and hyperbolic in-plane dispersion, which have been theoretically predicted but never experimentally observed in natural materials before. To better utilize the low-loss directional polaritons, we developed a chemical intercalation method to reversibly control and switch the phonon polaritons while maintaining their long lifetimes [8]. Combined with photolithography, spatially controlled polariton switching was achieved with various in-plane heterostructure configurations and patterns. Most recently, we show

how the hyperbolic polaritons in  $\alpha$ -MoO<sub>3</sub> thin slabs were delicately manipulated by controlling the interlayer twist angle [9]. We experimentally observed tunable topological transitions from open (hyperbolic) to closed (elliptical) dispersion contours in twisted  $\alpha$ -MoO<sub>3</sub> bilayers at a photonic magic twist angle. The theoretical analysis showed these transitions of in-plane hyperbolic polaritons are controlled by a topological quantity. At the transitions, the photonic dispersion of the resulting topological polaritons flattens, exhibiting low-loss tunable polariton canalization and diffractionless propagation. In summary, biaxial van der Waals semiconductors like  $\alpha$ -MoO<sub>3</sub>[7, 9] and V<sub>2</sub>O<sub>5</sub>[10] represent an emerging family of material supporting exotic polaritonic behaviors and these natural-born hyperbolic materials offer an unprecedented platform for controlling the flow of energy at the nanoscale.

**5:41 PM \*F.EL04.11.03**

**Nanophotonics with Low-Dimensional Excitonic Materials** Deep M. Jariwala; University of Pennsylvania, United States

The isolation of a growing number of two-dimensional (2D) materials has inspired worldwide efforts to study their fundamental physical properties and integrate distinct 2D materials into van der Waals (vdW) heterostructures.<sup>1-2</sup> While the few atoms thick structure of 2D semiconductors naturally makes their electronic structure quantum confined, it also has profound implications on their optical properties.<sup>3-4</sup> Further being 2D in nature it also presents opportunities for engineering them into 0D and 1D quantum confined structures.<sup>5</sup> My talk will discuss our group's more recent work on optical phenomena and photonic devices made from 2D semiconductors. I will present how 1D nanostructuring of excitonic 2D semiconductors into nanophotonic dielectric gratings can enable exploration of new regimes of light-matter confinement including formation of hybrid exciton-plasmon-polariton states.<sup>6</sup> I will extend this discussion of light-matter interaction to excitonic/dielectric superlattices which are scalable over large areas. I will extend this concept to other excitonic materials and show dynamic tunability of their optical properties. If time permits, I will also discuss new approaches and methods for nanostructuring 2D semiconductors down to  $\sim 5$  nm lateral dimensions with superior control of crystallinity and structure.<sup>7</sup> I will conclude by giving a broad perspective on future prospects of 2D materials from fundamental science to applications.

**References:**

1. Jariwala, D.; Marks, T. J.; Hersam, M. C., *Nature Materials* **2017**, *16*, 170-181.
2. Jariwala, D.; et al. *ACS Nano* **2014**, *8*, 1102–1120.
3. Brar, V. W.; Sherrott, M. C.; Jariwala, D., *Chemical Society Reviews* **2018**, *47*, 6824-6844.
4. Jariwala, D.; et al. *ACS Photonics* **2017**, *4*, 2692-2970.
5. Stanford, M. G.; Rack, P. D.; Jariwala, D., *npj 2D Materials and Applications* **2018**, *2*, 20.
6. Zhang, H.; ...Jariwala, D., et al. Hybrid Exciton-Plasmon-Polaritons in van der Waals Semiconductor Gratings. *Nature Communications* **2020**, (*in press*).
7. Kumar, P....Stach, E. A.; Jariwala, D., et al. *Npj 2D Materials and Applications* **2020**, <https://doi.org/10.1038/s41699-020-0150-2>.

SESSION F.EL04.01: 2D Materials for Application in Biology

On Demand Abstracts Available for Viewing Starting Saturday Morning, November 21, 2020

F-EL04

**5:00 AM F.EL04.01.01**

**Two-Dimensional Gadolinium Oxide Nanoplates as T<sub>1</sub> MRI Contrast Agents** Jake Villanova<sup>1</sup>, Nasim Taheri<sup>2</sup>, Gary Stinnett<sup>3</sup>, Arash Bohloul<sup>2</sup>, Xiaoting Guo<sup>1</sup>, Edward Esposito<sup>1</sup>, Zhen Xiao<sup>1</sup>, Deanna Stueber<sup>1</sup>, Carolina Avendano<sup>2</sup>, Paolo Decuzzi<sup>4,5</sup>, Robia Pautler<sup>3</sup> and Vicki L. Colvin<sup>1</sup>; <sup>1</sup>Brown University, United States; <sup>2</sup>Rice University, United States; <sup>3</sup>Baylor College of Medicine, United States; <sup>4</sup>The Methodist Research Institute, United States; <sup>5</sup>Instituto Italiano di Tecnologia, Italy

Gadolinium-containing nanocrystals as T<sub>1</sub> MRI contrast agents (CA) offer the potential for intracellular accumulation, active targeting, and clearance pathways that avoid the kidneys. However, the most efficient T<sub>1</sub> relaxation mechanism requires that water protons come within a few angstroms of surface Gd<sup>3+</sup>, a difficult condition to meet as these surfaces are necessarily covered with polymers that prevent aggregation in biological environments. This problem is resolved with two-dimensional Gd<sub>2</sub>O<sub>3</sub> nanoplates (GONP) which, due to their shape, possess accessible edge Gd<sup>3+</sup> for inner-sphere water interactions. A novel sulfonated surface coating further contributes to water-surface exchange and second-sphere interactions while also providing colloidal stability over a wide range of conditions. At clinically relevant field strengths ( $\geq 1.4$  T), these nanoplates exhibit ionic T<sub>1</sub> relaxivities an order of magnitude greater ( $r_1 = 63.0$  mM-Gd<sup>-1</sup>s<sup>-1</sup> at 1.4 T) than commercial gadolinium-

chelates and significant performance even at 9.4 T ( $r_1 = 32.6 \text{ mM-Gd}^{-1}\text{s}^{-1}$ ). Systematic size and magnetic field dependence studies suggest while inner-sphere relaxation processes at nanoplate edges contribute to  $r_1$ , second-sphere interactions are also important and become more significant at higher fields. Nanoplates are readily taken into cells where they maintain contrast performance and exhibit minimal cytotoxicity. *In vivo*, nanoplates preferentially accumulate in the liver and their circulation half-life is 1.5 times faster than commercial gadolinium-chelates. These features allow for the novel demonstration that nanoscale  $T_1$  MRI contrast agents can be applied to detect non-alcoholic fatty liver disease (NAFLD) in mice.

#### 5:10 AM F.EL04.01.02

**Bio-Imaging with Photoluminescence of Single-Layer MoS<sub>2</sub> Transistor** Yuhei Hayamizu, Takakazu Seki and Sakaya Tezuka; Tokyo Institute of Technology, Japan

Visualizing biological activity in real time poses a novel way for biosensing. Single-layer Molybdenum disulfide (MoS<sub>2</sub>) shows strong photoluminescence (PL) under photo-excitation due to its direct bandgap property [1]. The PL intensity of MoS<sub>2</sub> transistors has been demonstrated to change with the internal electron density by applying a back-gate voltage [2]. It has also been reported that the PL intensity of mechanically exfoliated MoS<sub>2</sub> was modulated by pH changes in aqueous solution [3]. In this work, we demonstrate pH-sensitive photoluminescence of single-layer MoS<sub>2</sub> grown by chemical vapor deposition (CVD). While CVD MoS<sub>2</sub> grown from MoS<sub>2</sub> powder did not have a strong pH sensitivity, MoS<sub>2</sub> grown from MoO<sub>3</sub> powder exhibited a sensitivity to the solution pH in its PL intensity [4]. Next, we utilized the single-layer MoS<sub>2</sub> as the active layer of an imaging sensor to monitor the activity of individual bacteria by the MoS<sub>2</sub> PL. For the demonstration, we employed *Lactobacillus*. It is one of the most studied probiotic bacteria which consumes glucose and produces lactic acid by fermentation. The bacteria were placed on a single-layer MoS<sub>2</sub> and its PL intensity was monitored in real time. Experiments were performed in the following ways. For device fabrication, CVD MoS<sub>2</sub> grown on a Si substrate was transferred onto a cover glass with patterned gold micro-electrodes. An electrolyte solution was placed on the MoS<sub>2</sub> with electrode. A reference electrode was also inserted into the solution to apply a voltage between the MoS<sub>2</sub> and the reference electrode. Using these three electrodes, the MoS<sub>2</sub> acted as an electrochemical transistor. The PL image was observed through the cover glass by an inverse microscope with an oil immersion lens under a controlled voltage of the reference electrode. The PL intensity of the MoS<sub>2</sub> transistor was modulated by the applied voltage from the reference electrode in the buffer solution. As decreasing the voltage at the reference electrode, the PL intensity was appeared at a threshold voltage and increased monotonically. We observed that the threshold voltage changed depending on the concentration of lactic acid in the bulk solution. Next, we placed a solution of *Lactobacillus rhamnosus* GG (LGG) onto MoS<sub>2</sub>. We found that LGG specifically adhered onto MoS<sub>2</sub> rather than glass substrate. PL images of MoS<sub>2</sub> with LGG showed a pattern that correlates with LGG adhesion. The contrast of the PL images was tuned via the applied voltage. Furthermore, PL intensity at the vicinity of the adhered LGG changed over time, which is probably due to a change of lactic acid concentration. We assume that the local pH change caused by the lactic acid possibly modulated the carrier density in MoS<sub>2</sub>. In this work, we demonstrated that PL imaging of MoS<sub>2</sub> has the potential to visualize activity of living individual bacteria label-freely [5].

Mak KF, He K, Lee C, et al. *Nat Mater*. 12(3):207-211 (2012).

Mouri S, Miyauchi Y, Matsuda K. *Nano Lett*. 13(12):5944-5948 (2013).

Zhang W, Matsuda K, Miyauchi Y. *J Phys Chem C*. 122(24):13175-13181.(2018).

Seki T, Ihara T, Kanemitsu Y, Hayamizu Y. *2D Mater*. 7 034001 (2020).

Tezuka S, Seki T, et.al. *2D Mater*. 7 024002 (2020).

#### 5:20 AM F.EL04.01.04

**Atomically-Thin Sensing Surfaces from 2D Materials for Detecting Cellular Gaps** Volodymyr Koman, Xun Gong, Naveed Bakh and Michael Strano; Massachusetts Institute of Technology, United States

Cellular layers play critical role as barriers, filters, and membranes in our bodies. The performance of cellular layers is found to be determined by the properties of individual cellular gaps. Yet these gaps often fall below the diffraction limit, hampering their detection. Here, we develop a novel sensing modality, where the diffusion of a harmless chemical tracer is used to reveal cellular gaps in human umbilical vein endothelial cellular (HUVEC) layers. For the readout, we employ atomically-thin and optically-active MoS<sub>2</sub>, whose two-dimensional form-factor enables it to serve as an array of 20,164 wireless sensors over 420×420 μm<sup>2</sup> area. A rigorous screening of 30 analytes identifies several tracer candidates with MoS<sub>2</sub> dynamic range spanning over five orders of magnitude in tracer concentration. In a single layer of HUVEC cells, we find local spots with diffusivities ranging from  $1 \times 10^{-9}$ - $3 \times 10^{-8} \text{ cm}^2/\text{s}$  that are spatially correlated with immunofluorescence of vascular endothelial (VE)-cadherin proteins found on cell membrane. These spots correspond to breaks in nanoscale cellular junctions with <40 nm in length. This platform enables future studies on properties and dynamics of cellular gaps of various tissues.

### 5:30 AM F.EL04.01.05

**MXene Nanopores with In-Plane Cation Reservoir for High-Resolution Biomolecular Sensing** Mehrnaz Mojtabavi<sup>1</sup>, Armin VahidMohammadi<sup>2</sup>, Wentao Liang<sup>3</sup> and Meni Wanunu<sup>1</sup>; <sup>1</sup>Northeastern University, United States; <sup>2</sup>University of Connecticut, United States; <sup>3</sup>Kostas Advanced Nano-Characterization Facility, United States

Nanopore biosensing technology has been developed over the past two decades as a label-free, single-molecule sensing platform of biopolymers (DNA, RNA, and proteins). In this technology, a nanometer-sized pore, either a naturally-occurring biological channel self-assembled in an organic membrane (biological nanopore) or a synthetically-fabricated channel in a solid-state membrane (solid-state nanopore), is the only liquid junction between two buffer bath chambers. A charged biopolymer, such as DNA, is then threaded through the nanopore by applying a voltage across the nanopore, resulting in partial physical obstruction of the pore detected as a transient drop in the ionic current. This event is used to electrically and/or optically probe structural features of the DNA or determining its nucleic acid sequence. A key feature in this technology is the geometry of the nanopore (diameter and thickness in solid-state nanopores) that defines the total sensing resolution. For instance, two geometric requirements for DNA sequencing are a pore with comparable geometry to the width of a single strand of DNA (~1 nm in diameter), and a pore thickness of 0.5 nm (distance between bases on a DNA strand) to provide single base resolution. The one-atom-thick monolayer graphene with a thickness of 0.3 nm has been a candidate for this application since it was first introduced in 2010<sup>1</sup>. However, despite the atomically-thin pore, a phenomenon known as “access resistance” still dominates, producing a sensing region longer than the physical pore thickness and reducing the resolution<sup>2</sup>. Moreover, other challenges associated with graphene nanopores such as surface hydrophobicity and poor mechanical stability have phased out its application in nanopore technology.

Recently, we have demonstrated that “MXene nanopores” with high mechanical robustness, long-time stability, and low-noise ion current recordings could serve as an alternative to graphene<sup>3</sup>. MXenes are an emerging family of two-dimensional transition metal carbides and nitrides with a general formula of  $M_{n+1}X_nT_x$  (i.e.  $Ti_3C_2T_x$ ), where M is a transition metal, X represents carbon or nitrogen (n=1, 2, and 3), and  $T_x$  indicates different functional groups (O, OH, F) present on MXene surface. An intriguing property of MXenes is the ability to accommodate various kinds of organic molecules and cations into their interlayer spacing which has led to the high performance of MXenes electrodes and films in energy storage and sensing applications. In this work, we have harnessed this property of  $Ti_3C_2T_x$  MXene along with its in-plane electrical conductivity to engineer a novel nanopore sensing device with increased sensing resolution by eliminating the access resistance. In this design, bilayer  $Ti_3C_2T_x$  films serve as an embedded electrode and reservoir of cations, intercalated in the interlayer space, and support membrane of the nanopore, where the cations enter the pore from within the plane of the membrane rather than the bulk solution. By elimination of the access resistance contribution, this technology could reach the resolution of detecting three DNA bases at the pore sensing region, surpassing the commercially available nanopore technology with sensing resolution of four bases at the pore constriction.

1. Garaj, S., Hubbard, W., Reina, A. *et al. Nature* **467**, 190–193 (2010). DOI:10.1038/nature09379
2. Comer, J., Aksimentiev, A. *Nanoscale* **8**, 9600–9613 (2016). DOI:10.1039/c6nr01061j
3. Mojtabavi, M., VahidMohammadi, A. *et al. ACS Nano* **13**, 3042–3053 (2019). DOI:10.1021/acsnano.8b08017

SESSION F.EL04.02: 2D Materials for Capacitors, Cathodes, Transistors and Memory  
On Demand Abstracts Available for Viewing Starting Saturday Morning, November 21, 2020  
F-EL04

### 5:00 AM \*F.EL04.02.01

**Lithium-Ion Electrolytic Substrates—TMD Growth and 1V High-Performance Transistors and Amplifiers** Md. Hasibul Alam and Deji Akinwande; The University of Texas at Austin, United States

This talk will present our latest progress on materials, transistor and memory devices based on 2D atomically-thin films. In particular, we explore a new substrate, namely, solid lithium-ion electrolytic substrates, for the direct growth and realization of high-performance TMD devices and amplifiers. Electrostatic gating with ionic liquids (ILs), leading to the accumulation of high surface charge carrier densities, has been often exploited in thin-film transistors. However, the intrinsic liquid nature of ILs inhibit it from constituting an ideal platform. In this regard, a lithium-ion solid electrolyte, often used for battery applications, offers similar advantages as ionic-liquids, with the added benefit of solid-state compatibility. With the solid electrolyte, we demonstrate its application in high-performance n-type MoS<sub>2</sub> and p-type WSe<sub>2</sub> transistors with sub-threshold

values approaching the ideal limit of 60 mV/dec and complementary inverter amplifier gain of 34, the highest among comparable amplifiers with a 1 V power supply. These results establish lithium-ion substrates as a promising alternative to ionic liquids for the study of thin-film devices.

#### 5:15 AM F.EL04.02.03

**Large Area Monolayer MoS<sub>2</sub> and WS<sub>2</sub> Field-Effect Transistors—A Statistical Approach** Amritanand Sebastian, Rahul Pendurthi, Tanushree Choudhury, Joan Redwing and Saptarshi Das; The Pennsylvania State University, United States

Field-effect transistors (FETs) based on atomically thin transition metal dichalcogenides (TMDs) such as molybdenum disulfide (MoS<sub>2</sub>) and tungsten disulfide (WS<sub>2</sub>) have attracted immense attention in the scientific community due to their superior electronic properties.[1] The immense promise provided by the TMD FETs needs to be complemented by a thorough statistical and benchmarking study of relevant device parameters. In this regard, we report a comprehensive study of the carrier transport in monolayer MoS<sub>2</sub> and WS<sub>2</sub>, which were grown over a large area using metal-organic chemical vapour deposition (MOCVD) process. 160 WS<sub>2</sub> FETs and 230 MoS<sub>2</sub> FETs with channel length ranging from 100 nm to 5 μm were investigated for benchmarking field-effect carrier mobility, maximum current, threshold voltage, saturation velocity, device linearity, contact resistance, subthreshold slope (SS), current, ON/OFF ratio, and drain induced barrier lowering (DIBL). Our study shows low device-to-device variation owing to high growth quality. We are also able to demonstrate record high carrier mobility of 33 cm<sup>2</sup>V<sup>-1</sup>s<sup>-1</sup> in WS<sub>2</sub> FETs, with over 1.5X improvement compared to the best reported in the literature. [2-4] This work also demonstrates the first comprehensive statistical study on WS<sub>2</sub> films, showing comparable performance to MoS<sub>2</sub> films. Our experimental demonstrations confirm the technological viability of two dimensional (2D) semiconductors for use in commercial electronics.

#### References

- [1] D. S. Schulman, A. J. Arnold, and S. Das, "Contact engineering for 2D materials and devices," *Chem Soc Rev*, vol. 47, pp. 3037-3058, May 8 2018.
- [2] Y. Gong, V. Carozo, H. Li, M. Terrones, and T. N. Jackson, "High flex cycle testing of CVD monolayer WS<sub>2</sub> TFTs on thin flexible polyimide," *2D Materials*, vol. 3, p. 021008, 2016.
- [3] K. Kang, S. Xie, L. Huang, Y. Han, P. Y. Huang, K. F. Mak, *et al.*, "High-mobility three-atom-thick semiconducting films with wafer-scale homogeneity," *Nature*, vol. 520, pp. 656-60, Apr 30 2015.
- [4] S. J. Yun, S. H. Chae, H. Kim, J. C. Park, J. H. Park, G. H. Han, *et al.*, "Synthesis of centimeter-scale monolayer tungsten disulfide film on gold foils," *ACS Nano*, vol. 9, pp. 5510-9, May 26 2015.

SESSION F.EL04.03: Advanced Characterization of 2D Materials  
On Demand Abstracts Available for Viewing Starting Saturday Morning, November 21, 2020  
F-EL04

#### 5:00 AM \*F.EL04.03.01

**Probing Two-Dimensional Materials Using Focused Angle-Resolved Photoemission Spectroscopy** Jyoti Katoch; Carnegie Mellon University, United States

Two-dimensional (2D) materials offer the freedom to create novel condensed matter systems, with unique properties, by mechanically assembling different (or same) 2D materials layer-by-layer to form atomically sharp vertical or lateral heterostructures. The van der Waals (vdW) heterostructures with small lattice mismatch and a relatively small twist angle between the constituent layers, have shown to exhibit coexisting complex phases of matter including Mott insulating state, superconductivity, bound quasiparticles, and topological states. In addition, the extreme surface sensitivity of two-dimensional (2D) materials provides an unprecedented opportunity to engineer the physical properties of these materials using external perturbations. In this talk, I will discuss the utilization of angle-resolved photoemission spectroscopy (ARPES) with high spatial resolution to investigate the electronic band structure of 2D heterostructures and their devices. This can shed light on the intricate relationship between controlled external perturbations, substrate, and electronic properties of 2D materials [1, 2]. In particular, I will discuss our *in-operando* nanoARPES results that exhibit highly tunable many-body effects in graphene devices [3] and tunable van Hove singularities in twisted bilayer graphene [4].

#### References:

- [1] Katoch *et. al.*, *Nature Physics* 14, 355-359 (2018).
- [2] Ulstrup, *et. al.*, *Science Advances*, Vol. 6, no. 14, eaay6104, (2020).

[3] Muzzio, et. al., Physical review B Rapid Communications 101, 201409(R) (2020).

[4] Jones, et. al., arXiv:2006.00791 (2020). Accepted for publication in Advanced Materials.

### 5:15 AM F.EL04.03.02

#### **Visualizing Ultrafast Lattice Dynamics in Photoexcited 2D Heterostructures Using Femtosecond Electron**

**Diffraction** Aditya Sood<sup>1</sup>, Jonah Haber<sup>2</sup>, Johan Carlstroem<sup>3</sup>, Elizabeth Peterson<sup>2</sup>, Alexander Reid<sup>4</sup>, Xiaozhe Shen<sup>4</sup>, Marc Zajac<sup>1</sup>, Suji Park<sup>4</sup>, Michael Kozina<sup>4</sup>, Emma Regan<sup>2</sup>, Jie Yang<sup>4</sup>, Stephen Weathersby<sup>4</sup>, Feng Wang<sup>2</sup>, X.J. Wang<sup>4</sup>, Tony Heinz<sup>1</sup>, Jeffrey Neaton<sup>3</sup>, Felipe da Jornada<sup>1</sup>, Aaron Lindenberg<sup>1</sup> and Archana Raja<sup>3</sup>; <sup>1</sup>Stanford University, United States; <sup>2</sup>University of California, Berkeley, United States; <sup>3</sup>Lawrence Berkeley National Laboratory, United States; <sup>4</sup>SLAC National Accelerator Laboratory, United States

Two dimensional (2D) van der Waals semiconductors are exciting candidates for next generation optoelectronics. The layer-by-layer assembly of 2D monolayers enables the creation of heterostructures with unique and controllable properties. It has been shown previously that photoexcitation of 2D heterostructures induces ultrafast charge transfer across the van der Waals junction on timescales faster than 100 fs, resulting in the formation of interlayer excitons. However, the coupling between this charge transfer process and thermal excitations of the lattice is so far unexplored. Here, using mega electron volt (MeV) ultrafast electron diffraction (UED), we make the first direct measurements of atomic vibrations within the individual layers of a type II van der Waals heterostructure following femtosecond photoexcitation. The UED technique employs ~4 MeV electron pulses to probe a large range of reciprocal space up to  $\sim 12 \text{ \AA}^{-1}$ , with a time resolution of  $\sim 100$  fs. We track the propagation of energy from one layer to the next by measuring the changes in intensities of Bragg peaks. First principles calculations link the measured differential intensities with thermally-activated atomic displacements, providing a sub-nanometer temperature scale. Our results provide insights into the role of ultrafast charge transfer on lattice dynamics, and decouple the vibrational and electronic pathways for energy transfer across a van der Waals interface.

### 5:25 AM F.EL04.03.03

#### **Insights on the Bulk and Surface Chemistry of the Niobium MAX and MXene Phases from Multinuclear Solid-State**

**NMR Spectroscopy** Kent J. Griffith<sup>1,2</sup>, Michael Hope<sup>2</sup>, Philip Reeves<sup>2</sup>, Mark Anayee<sup>3</sup>, Yury Gogotsi<sup>3</sup> and Clare Grey<sup>2</sup>; <sup>1</sup>Northwestern University, United States; <sup>2</sup>University of Cambridge, United Kingdom; <sup>3</sup>Drexel University, United States

MXenes, derived from metallic MAX phases, are a class of two-dimensional materials with emerging applications in energy storage, electronics, and catalysis due to their high surface areas and attractive electronic properties. MXene properties are heavily influenced by their surface chemistry but a detailed understanding of the surface functionalization for the niobium MXenes  $\text{Nb}_2\text{CT}_x$  and  $\text{Nb}_4\text{C}_3\text{T}_x$  is still lacking. The parent MAX phases,  $\text{Nb}_2\text{AlC}$  and  $\text{Nb}_4\text{AlC}_3$ , exhibit interesting structural and electrical properties but can be sensitive to oxidation. Solid-state NMR allows us to probe the interfacial chemistry, as well as the connectivity using correlation experiments; the phase purity including the presence of amorphous/nanocrystalline phases; and the electronic properties of the MXene and MAX phases with quantitative chemical sensitivity. In this work, we systematically study of the chemistry of Nb MAX and MXenes using solid-state NMR spectroscopy and examine a variety of nuclei ( $^1\text{H}$ ,  $^{13}\text{C}$ ,  $^{19}\text{F}$ ,  $^{27}\text{Al}$  and  $^{93}\text{Nb}$ ) with a range of techniques ( $T_1$ -filtering, QCPMG, MATPASS, HETCOR, TRAPDOR, robot-automated VOCS). Hydroxide and fluoride terminations were identified, found to be intimately mixed, and their chemical shifts compared with other MXenes. In addition to the identification of surface species and their spatial distribution, this multinuclear NMR study demonstrates that diffraction alone is insufficient to characterize the phase composition of MAX and MXene samples as numerous amorphous or nanocrystalline phases were identified including NbC,  $\text{AlO}_6$  species, aluminum nitride or oxycarbide,  $\text{AlF}_3 \times n\text{H}_2\text{O}$ , Nb metal, and unreacted MAX phase. To the best of our knowledge, this is the first work to examine the metal resonances directly in MXene samples, and the first  $^{93}\text{Nb}$  NMR of any MAX phase. Insights from the  $^{93}\text{Nb}$  even enabled the previously-elusive assignment of the complex overlapping  $^{47/49}\text{Ti}$  spectrum of  $\text{Ti}_3\text{AlC}_2$ . The results and methodology presented here provide fundamental insights on MAX and MXene phases and can be used to obtain a more complete picture of MAX and MXene chemistry, to prepare realistic structure models for computational screening, and to guide the analysis of property measurements.

### 5:35 AM F.EL04.03.04

#### **Double Moiré Superlattices at the 2D/3D Interface—STEM Observations and Electronic Implications**

Kate Reidy<sup>1</sup>, Georgios Varnavides<sup>1,2</sup>, Joachim D. Thomsen<sup>1</sup>, Abinash Kumar<sup>1</sup>, Thang Pham<sup>1</sup>, Arthur M. Blackburn<sup>3</sup>, Polina Anikeeva<sup>1</sup>, Prineha Narang<sup>2</sup>, James M. LeBeau<sup>1</sup> and Frances M. Ross<sup>1</sup>; <sup>1</sup>Massachusetts Institute of Technology, United States; <sup>2</sup>Harvard

University, United States; <sup>3</sup>University of Victoria, Canada

Following the success of moiré engineering in modulating (opto-)electronic properties of twisted bilayer graphene and graphene/hBN heterostructures, studies have extended the moiré toolbox; from double bilayer, to trilayer graphene, transition metal dichalcogenide (TMDC/TMDC), and hexagonal boron nitride (hBN)-graphene-hBN vdW heterostructures [1]. Moiré engineering has yet to be explored in ‘quasi-vdW’ systems, such as the interface of a two-dimensional (2D) material and three-dimensional (3D) metal, despite its influence on contact resistance, photo-response, and high-frequency performance [2]. Herein, we report moiré modulation at a ‘quasi-vdW’ interface between a 3D metal and 2D material, in the model system of  $0 \pm 0.1^\circ$  epitaxially aligned Au{111}/MoS<sub>2</sub>.

By applying a predictive geometric convolution technique and four-dimensional (4D) scanning transmission electron microscopy (STEM) to epitaxially aligned Au{111}/MoS<sub>2</sub>, we demonstrate double moiré periodicity (18 Å and 32 Å) at the 2D/3D interface. 4D STEM allows us to decouple these multiple moirés and image weaker moiré superlattices, otherwise hidden in conventional (S)TEM. Using *ab initio* electronic structure calculations, we find that charge density is modulated with a period of 32 Å, illustrating electronic conductivity and (opto-)electronic modulation via moiré engineering at the 2D/3D interface. With growing potential for tunability in quasi-vdW layers, these results highlight the potential for moiré engineering at the 2D/3D interface, as well as showcasing the growing opportunities for advanced (S)TEM techniques in multiple moiré direct imaging.

[1] Balents, L., Dean, C.R., Efetov, D.K. et al. Superconductivity and strong correlations in moiré flat bands. *Nat. Phys.* (2020).

[2] Wang, Y. et al. Van der Waals contacts between three-dimensional metals and two-dimensional semiconductors. *Nature* 568, 70–74 (2019).

#### 5:45 AM F.EL04.03.08

**Cleaning and Smoothing the Interfaces of Hexagonal Boron Nitride Encapsulated Monolayer MoS<sub>2</sub> with Contact Mode Atomic Force Microscopy** [Sihan Chen](#)<sup>1</sup>, Jangyup Son<sup>1</sup>, Siyuan Huang<sup>1</sup>, Kenji Watanabe<sup>2</sup>, Takashi Taniguchi<sup>2</sup>, Rashid Bashir<sup>1</sup>, Arend M. van der Zande<sup>1</sup> and William King<sup>1</sup>; <sup>1</sup>University of Illinois at Urbana-Champaign, United States; <sup>2</sup>National Institute for Materials Science, Japan

The quality of the interfaces is critical for two-dimensional (2D) materials, as atomically thick 2D materials do not have any bulk to screen impurities.<sup>1</sup> For electronic devices based on 2D heterostructures, it is thus vital to have clean and smooth interfaces. Mechanical assembly is the most common and versatile way to assemble 2D heterostructures,<sup>2,3</sup> which often traps contaminants at the interfaces during assembly and does not yield high quality devices. Contact mode atomic force microscopy (AFM) cleaning is a reliable and controllable technique to remove interface contaminants of 2D heterostructures after assembly.<sup>4-6</sup> Reduction of nanometer scale corrugations was surmised to be responsible for improved electrical performance of 2D heterostructures after contact mode AFM cleaning.<sup>5</sup> Direct observation of the flattening of nanometer-scale interfacial roughness would help elucidate how contact mode AFM cleaning improves the electrical performance of 2D heterostructures.

This work reports the reduction of nanometer-scale roughness and improvement of interface qualities of 2D heterostructures, by scanning the heterostructure with an AFM tip in contact mode. The prototypical heterostructure system consists of monolayer MoS<sub>2</sub> encapsulated by top monolayer hBN and bottom multilayer hBN. We detected spatial height fluctuations ~ 1 nm with a lateral dimension of tens of nanometer in bubble-free areas of the heterostructures with AFM, which were minimized by contact mode AFM cleaning. The AFM cleaning process also reduced the photoluminescence (PL) linewidth of monolayer MoS<sub>2</sub>, indicating a reduction of interface impurities. The optimal cleaning force for the heterostructure was found to be 70 nN. One MoS<sub>2</sub> field-effect transistor (FET) fabricated on AFM-cleaned heterostructure achieved a high mobility of 73 cm<sup>2</sup>/Vs, which can be further improved by passivation with thick hBN or high-k dielectrics for better electrostatic environment. The mobility of four hBN encapsulated monolayer MoS<sub>2</sub> FETs fabricated on as-assembled heterostructure improved from 21±2 cm<sup>2</sup>/Vs to 37±6 cm<sup>2</sup>/Vs after AFM cleaning. Combining the results from AFM, PL and electrical measurements, we infer that contact mode AFM cleaning is effective in reducing interface disorders and enhancing the mobility of hBN encapsulated monolayer MoS<sub>2</sub>. Finally, we anticipate that contact mode AFM cleaning will significantly improve the quality of most mechanically assembled van der Waals heterostructures by cleaning and smoothing their interfaces.

#### References:

(1) Dean, C. R.; Young, A. F.; Meric, I.; Lee, C.; Wang, L.; Sorgenfrei, S.; Watanabe, K.; Taniguchi, T.; Kim, P.; Shepard, K. L.; et al. Boron Nitride Substrates for High-Quality Graphene Electronics. *Nat. Nanotechnol.* **2010**, 5 (10), 722–726.

- (2) Novoselov, K. S.; Mishchenko, A.; Carvalho, A.; Castro Neto, A. H. 2D Materials and van Der Waals Heterostructures. *Science* **2016**, *353* (6298), aac9439.
- (3) Weston, A.; Zou, Y.; Enaldiev, V.; Summerfield, A.; Clark, N.; Zólyomi, V.; Graham, A.; Yelgel, C.; Magorrian, S.; Zhou, M.; et al. Atomic Reconstruction in Twisted Bilayers of Transition Metal Dichalcogenides. *Nat. Nanotechnol.* **2020**, 1–6.
- (4) Schwartz, J. J.; Chuang, H. J.; Rosenberger, M. R.; Sivaram, S. V.; McCreary, K. M.; Jonker, B. T.; Centrone, A. Chemical Identification of Interlayer Contaminants within van Der Waals Heterostructures. *ACS Appl. Mater. Interfaces* **2019**, *11* (28), 25578–25585.
- (5) Kim, Y.; Herlinger, P.; Taniguchi, T.; Watanabe, K.; Smet, J. H. Reliable Postprocessing Improvement of van Der Waals Heterostructures. *ACS Nano* **2019**, *13* (12), 14182–14190.
- (6) Rosenberger, M. R.; Chuang, H. J.; McCreary, K. M.; Hanbicki, A. T.; Sivaram, S. V.; Jonker, B. T. Nano-"Squeegee" for the Creation of Clean 2D Material Interfaces. *ACS Appl. Mater. Interfaces* **2018**, *10* (12), 10379–10387.

SESSION F.EL04.04: Chemical Vapor Deposition of 2D Materials  
 On Demand Abstracts Available for Viewing Starting Saturday Morning, November 21, 2020  
 F-EL04

#### 5:00 AM F.EL04.04.01

**High Yield, Bottom-Up/Top-Down Synthesis of 2D Layered Metal Sulfides, Phosphides and Selenides Using Chemical Vapor Deposition with Applications in Electronics and Electrochemistry** Gilbert D. Nessim; Bar Ilan University, Israel

Since the excitement about graphene, a monolayer of graphite, with its 2010 Nobel Prize, there has been extensive research in the synthesis of other non-carbon few/mono-layers exhibiting a variety of bandgaps and semiconducting properties (e.g., n or p type). The main approaches to deposit few/monolayers on a substrate are: (a) bottom-up synthesis from precursors using chemical vapor deposition (CVD) or (b) top-down exfoliation (liquid or mechanical) of bulk layered material. Using a Lego approach of superposing monolayers, we can envisage the fabrication of heterojunctions with original electronic behavior. Here we show a combined bottom-up and top-down approach where (a) we synthesize in one step high yields of bulk layered materials by annealing a metal in the presence of a gas precursor (sulfur, phosphorous, or selenium) using chemical vapor deposition (CVD) and (b) we exfoliate and deposited (dropcast or Langmuir Blodgett) few/mono-layers on a substrate from a sonicated mixture of our material in a specific solvent. It is interesting to note that, besides the structure being 2D layered, the properties of the nanomaterials synthesized slightly differ from the materials with the same stoichiometry synthesized using conventional chemical methods (e.g., solvothermal).

In this talk, we will discuss the chemical synthesis, the very extensive characterizations, and the lessons we learned in making multiple metal sulfides (Cu-S, Ag-S, Ni-S), metal phosphides (Ni-P, Cu-P), and metal selenides (Ag-Se, Cu-Se, W-Se). We will see how we integrated these new materials into electrochemical devices. We will also explore how to deposit large mono/few layers of these materials using techniques such as dropcasting or Langmuir-Blodgett and to connect them to circuits using focused ion beam (FIB) to test their electrical properties with the goal build heterojunctions.

#### 5:10 AM F.EL04.04.02

**Precursor Vapor Pressure Control Strategies on the APCVD Growth of Molybdenum Disulfide** Guodong Meng, Feihong Wu, Jinan Xie, Changling Wang, Chengye Dong and Yonghong Cheng; Xi'an Jiaotong University, China

Molybdenum disulfide (MoS<sub>2</sub>) is known as promising 2D material with a tunable band-gap which is an ideal for optoelectronic devices. Uniform, crystalline and atomic layers of MoS<sub>2</sub> can be produced by the chemical vapor deposition method. The commonly used MoS<sub>2</sub> CVD system is a system with the substrate facing down toward the molybdenum source. A new kind of CVD system which loads and protects the molybdenum source with a separate quartz tube in order to avoid poisoning of molybdenum trioxide has been designed in recent years. Here we report and compare the strategies of precursor vapor pressure control under this two typical MoS<sub>2</sub> preparation systems. In order to obtain high crystalline MoS<sub>2</sub>, we studied the heating temperature of the precursor, the flow rate of the carrier gas, the horizontal distance and the vertical distance between the molybdenum source and the substrate during the growth of MoS<sub>2</sub> in this two different preparation systems. The results indicate the heating temperature of the precursor has the greatest influence on the growth of MoS<sub>2</sub>. The lower heating temperature of the precursor contributes to lower growth rate, which makes the thickness of MoS<sub>2</sub> is easily controlled. When the heating temperature is more than 650 °C, the thickness and morphology of MoS<sub>2</sub> differs under the two preparation systems. Nevertheless, the flow rate of carrier gas has little influence on growth of MoS<sub>2</sub>, but proper carrier gas flow rate can



prevent precursor poisoning. The horizontal distance and the vertical distance between the molybdenum source and the substrate affect the vapor concentration of the molybdenum source and the nucleation density of MoS<sub>2</sub> during the growth of MoS<sub>2</sub>.

#### 5:20 AM F.EL04.04.03

**Correlation Between Surface Processes and Reaction Kinetics for Predictive Growth of Monolayer MoS<sub>2</sub>** Ankit Rao, Kranthi Kumar V, Shashwat Rathkanthiwar and Srinivasan Raghavan; Indian Institute of Science, India

Modeling of physico-chemical processes such as adsorption-desorption equilibrium, adatom diffusion and attachment are required to correlate the change in supersaturation to the growth kinetics on the surface. We demonstrate an approach to predictively control the grain size and nucleation density of monolayer MoS<sub>2</sub> by employing such correlation via modeling the reaction kinetics in a true CVD system. The adatom concentration, on which this supersaturation depends, on the growth surface, is governed by the reaction kinetics of the precursor and the concentration gradients across the boundary layer at the growth surface. The varied dependencies of the rate of nucleation and edge growth rate on supersaturation and surface kinetics have been exploited to reduce nucleation density from 10<sup>7</sup> to 10<sup>3</sup> cm<sup>-2</sup> and simultaneously increasing the growth rates of the edges to a significant value of 3.3 μm/s. We show that to obtain large grain sizes in small time frames, we identify the physico-chemical windows in which the nucleation kinetics are suppressed but those which govern the growth of edges are enhanced. As in the case of graphene, we observe from the analysis of the rate of nucleations that with an increase in temperature, the availability of adatoms on the growth surface is reduced which in turn results in control of nucleation rate and hence a decrease in nucleation density. We thus simulate the dependence of pressure and temperature on the degree of such pre-reactions to determine the concentration gradients for three substrates placed at different lengths across the reactor tube so as to determine the effect of reaction kinetics on nucleation density. Mass transfer calculations were performed by using the combined convection-diffusion solver. Owing to the vapor phase reactions close to the inlet, the initial precursor concentration was found to reduce from 6x10<sup>-3</sup> to about 2.5x10<sup>-3</sup> for all the cases within about 2 cm from the inlet. The simulations indicate that despite the vapor phase reactions, in the considered pressure and temperature range, the Mo(CO)<sub>6</sub> precursor concentration at substrates placed across the length of the tube varies only by a factor of 2. This is not expected to alter the nucleation density significantly. This is in accordance with the experimental results. The simulation results thus rule out the impact of vapor phase reactions on the observed variations in nucleation density (and grain size) with temperature, pressure, and flow rates. Thus we show that the nucleation density of MoS<sub>2</sub> domains in a CVD process can be controlled in a predictive manner by tuning the supersaturation and surface kinetics.

#### 5:30 AM F.EL04.04.04

**CVD Growth of Monolayer N-Doped WSe<sub>2</sub> from Solid State Inorganic Precursors** Mauro Oeh<sup>1</sup>, Giulia Z. Zemignani<sup>1</sup>, Kostantinos Anastasiou<sup>2</sup>, Pawel Palczynski<sup>1</sup>, Evgeny Alexeev<sup>3</sup>, Alexander Tartakovskii<sup>3</sup>, Saverio Russo<sup>2</sup> and Cecilia Mattevi<sup>1</sup>; <sup>1</sup>Imperial College London, United Kingdom; <sup>2</sup>University of Exeter, United Kingdom; <sup>3</sup>The University of Sheffield, United Kingdom

Doping is fundamental to tune the properties of 2D transition metal dichalcogenides for their future integration in the CMOS architecture, hence achieving substitutional doping during growth is of paramount importance. N-type monolayer WSe<sub>2</sub> is often exfoliated from bulk crystals and a procedure to directly dope the material is yet to be established. Here, we demonstrate the synthesis of monolayer n-WSe<sub>2</sub> via CVD starting from tungstic acid (H<sub>2</sub>WO<sub>4</sub>) and zinc selenide (ZnSe). We achieved large WSe<sub>2</sub> triangular monolayer flakes, which exhibit n-type of transport which is attribute to donor states due to the incorporation of Zn ions in the lattice. The doping is very stable and the material exhibits good electron mobilities reaching the highest value at 50 cm<sup>2</sup>V<sup>-1</sup>s<sup>-1</sup>. The substitutional doping has been confirmed via atomic probe tomography (APT), showing Zn inclusions into the individual WSe<sub>2</sub> layers. Our material is of high crystal quality characterized by a sharp room temperature photoluminescence (PL) assessed by the PL spectra evolution from 10 K to room temperature that shows the contribution of neutral and defect-bound excitons, a signal so far reported only in mechanically exfoliated material.

#### 5:40 AM F.EL04.04.05

**Universal Approach Towards 2D Van der Waals Heterostructures of Metal Chalcogenides from Molecular Building Blocks** Veronika Brune, Lasse Jurgensen, Michael Wilhelm, Michael Frank and Sanjay Mathur; University of Cologne, Germany

Layered materials beyond omnipresent graphene such as chalcogenide-based materials that possess tunable and defined crystallographic structures and elemental compositions offer a broad portfolio of potential applications. The lacking control of large scale and homogeneous formation of 2D layered materials MX<sub>2</sub> (X = S, Se) in commercial formation processes motivated us to develop a unique synthetic approach to layered 2D materials. Complete characterization of synthesized

complexes enabled their controlled decomposition to desired materials.

Herein we report a uniform synthesis of molecular building blocks to form stable precursor classes  $[M(\text{SEtN}(\text{Me})\text{EtS})_x]$  ( $M = \text{Mo}^{\text{IV}}, \text{W}^{\text{IV}}, \text{Ti}^{\text{IV}}, \text{Zr}^{\text{IV}}, \text{Hf}^{\text{IV}}, \text{Sn}^{\text{IV}}, x = 2; M = \text{Ge}^{\text{II}}, \text{Sn}^{\text{II}}, \text{Pb}^{\text{II}}, x = 1$ ), which can be decomposed to layered 2D van der Waal heterostructures.

Following a simple synthetic protocol, the reaction of tridentate  $(\text{HSEt})_2\text{NMe}$  donor ligand with suitable metal compounds resulted in (air)stable molecular precursors, which were isolated and characterized by NMR, XRPD and single crystal analysis. Thermal decomposition experiments of synthesized metal precursors were analyzed by TG-DTA measurements and the formation of desired  $\text{MS}_2$  and  $\text{MS}$  ( $\text{W}, \text{Mo}, \text{Ti}, \text{Sn}, \text{Pb}$ ) materials was confirmed by XRPD analysis. SEM, XRD and TEM analysis of CVD deposited molecular precursors confirmed the formation of homogeneous crystalline layered sulfur based heterostructures. The number of deposited  $\text{MX}_2$  layers was calculated from a combination of TEM and AFM measurements. Moreover, prepared precursors were suitable for wet chemical syntheses as demonstrated via microwave assisted decomposition which resulted in homogeneous spherical  $\text{SnS}_2$  particles.

These molecular building blocks provide an extraordinary synthetic approach to a unique molecular precursor class, which reliably delivered chalcogenide-based *van der Waals* heterostructures of metal chalcogenide 2D materials.

#### 5:50 AM F.EL04.04.06

**Direct Synthesis of Bilayer  $\text{MoS}_2$  Nanoribbons with Sub-10nm Width** Xufan Li<sup>1</sup>, Raymond Unocic<sup>2</sup>, Emmanuel Okogbue<sup>1</sup> and Avetik Harutyunyan<sup>1</sup>; <sup>1</sup>Honda Research Institute USA Inc., United States; <sup>2</sup>Oak Ridge National Laboratory, United States

Nanoribbons of atomically thin transition metal dichalcogenides (TMDs) provide an additional space confinement in the two-dimensional plane and a more prominent edge effect compared to two-dimensional (2D) sheets, which have a potential to show even more unprecedented properties according to theoretical predictions. Etching from 2D sheets through lithography has realized TMD nanoribbons with a width down to ~30 nm. However, contamination introduced by lithography process can alter or even diminish their properties. Therefore, direct, lithography-free synthesis of atomically thin TMD nanoribbons are highly desired. In this work, we demonstrate for the first time a direct growth of  $\text{MoS}_2$  bilayer nanoribbons with a width down to less than 10 nm and a length up to 300  $\mu\text{m}$  through a chemical vapor deposition method using nickel clusters as nucleation seeds. These sub-10 nm bilayer nanoribbons allow us to study not only the quantum confinement and edge effect but also the effect of a second layer on the electronic structures as well as electrical and optical properties of the nanoribbons. Nickel nanoparticle that terminates the tip of each bilayer nanoribbon, serves as a nucleation seed, defines the width, and drives the tip growth mechanism. More insights of the growth mechanism are provided based on XPS, XRD, AES (Auger electron spectroscopy), SEM, and STEM studies. The synthesis method has been successfully applied on a variety of substrates including  $\text{SiO}_2/\text{Si}$ , sapphire, and mica. Our synthesis method introduces a new family of TMD nanoribbons i.e. bilayer nanoribbons, which opens an avenue for discovery of new phenomena and properties.

#### 6:00 AM F.EL04.04.08

**High Temperature CVD Growth of Crystalline Hexagonal Boron Nitride** Anushka Bansal, Maria Hilde, Benjamin Huet, Roman Engel-Herbert and Joan Redwing; The Pennsylvania State University, United States

Hexagonal Boron Nitride (hBN) is a 2D, III-nitride wide bandgap semiconductor that has a structure very similar to graphene. Due to its extraordinary physical properties, such as high resistivity, high thermal conductivity, stability in air up to 1000°C and large bandgap ( $E_g \sim 5.9$  eV), hBN appears to be a promising material for emerging applications, including deep UV (DUV) optoelectronics, single photon emitters and neutron detectors. There is also significant interest in monolayer and few-layer hBN as an encapsulating layer for 2D devices based on graphene and transition metal dichalcogenides.

While high quality hBN bulk crystals are available for exfoliation, the size of the crystals is limited, consequently there is continued interest in the epitaxial growth of large area hBN films on sapphire using chemical vapor deposition (CVD). However, high quality hBN film growth typically requires high growth temperatures (1100°C-1500°C). It has been reported that this temperature range alters the sapphire surface under ultra-high vacuum (UHV) conditions. In case of chemical vapor deposition (CVD), the presence of hydrogen in the growth ambient is expected to also modify the sapphire surface. However, its impact on hBN growth has not yet been explored.

In this work, we studied the growth of crystalline and epitaxial hBN in a vertical cold wall MOCVD reactor using diborane ( $\text{B}_2\text{H}_6$ ) and ammonia ( $\text{NH}_3$ ) as precursors for B and N, respectively using  $\text{H}_2$  as a carrier gas. The growths were performed on substrates with different plane directions (C-plane v/s A-plane) at a growth temperature of 1350°C under a pressure of 50 Torr. Sequential pulsing of the  $\text{B}_2\text{H}_6$  (2 sec) and  $\text{NH}_3$  (1 sec) precursors using N/B ratio of ~4000 resulted in a growth rate of ~300 nm/hr due to reduction in the extent of parasitic gas phase reactions. Continuous thin films of hBN were obtained on C-plane as well as A-plane sapphire along with wrinkles due to thermal expansion coefficient (CTE) difference between sapphire and hBN. The  $E_{2g}$  Raman active mode of hBN was observed at 1368.2  $\text{cm}^{-1}$  with a FWHM of 24.6  $\text{cm}^{-1}$  on C-plane

sapphire. Residual compressive stress due to CTE mismatch between film and the substrate (wrinkles) along with other inhomogeneities in the film (such as substrate's surface roughness) could be one of the possible reasons for the red shift in the Raman peak position (from bulk crystal Raman peak position at  $1365\text{cm}^{-1}$ ) and a broader FWHM. Therefore, the film was transferred on to Si/SiO<sub>2</sub> substrate using PMMA based transfer technique to release residual stress. After film transfer, Raman peak position was measured to be  $1365\text{cm}^{-1}$  with a FWHM of  $18.5\text{cm}^{-1}$  (FWHM of the best quality bulk crystal obtained is  $\sim 7\text{cm}^{-1}$ ). Also, pre-growth H<sub>2</sub> annealing of C-plane sapphire at the growth temperature alters the surface lattice parameter as confirmed by RHEED and is believed to induce a chemical change as well. RHEED pattern of the obtained hBN film suggests rotationally oriented, crystalline hBN film with [ ]<sub>h-BN</sub> || [ ]<sub>sapphire</sub> epitaxial relation. However, for hBN on A-plane sapphire, wrinkle density was higher compared to C-plane sapphire. Also, E<sub>2g</sub> mode was observed at  $1366.4\text{cm}^{-1}$  (corresponding well with AFM results showing higher wrinkle density indicating lesser residual stress in the film) with a FWHM of  $24.8\text{cm}^{-1}$ . The cause is still unknown; however, further studies are underway to provide additional insights into the role of crystallographic symmetry and surface preparation to form highly crystalline hBN films on sapphire.

#### 6:10 AM F.EL04.04.09

**Large-Area PtTe<sub>2</sub>/Silicon Heterojunction Devices with Ultrafast Photodetection and Enhanced Photovoltaics by Water Droplet Integration** Mashiyat Sumaiya Shawkat<sup>1,1</sup>, Tanvir Ahmed Chowdhury<sup>1</sup>, Hee-Suk Chung<sup>2</sup>, Shahid Sattar<sup>3</sup>, Tae-Jun Ko<sup>1</sup>, Shawn Putnam<sup>1</sup>, J. Andreas Larsson<sup>3</sup> and Yeonwoong Jung<sup>1,1,1</sup>; <sup>1</sup>University of Central Florida, United States; <sup>2</sup>Korea Basic Science Institute, Korea (the Republic of); <sup>3</sup>Luleå University of Technology, Sweden

Recently, interests in a family of noble metals-based 2D crystals are on the rise exploiting their superior electrical properties beyond conventional 2D transition metal dichalcogenides (TMDs). 2D platinum (Pt) ditelluride (PtTe<sub>2</sub>) layers are particularly promising due to their unique band structure and topological nature as well as remarkably high conductivity ( $>10^6\text{S/m}$ ), surpassing most of previously explored 2D TMD layers. Such intrinsic superiority can be leveraged to practical applications by integrating them with matured 3D semiconductors, which has remained largely unexplored. In this report, we explored PtTe<sub>2</sub>/silicon hetero-junction devices and unveiled their electrical and opto-electrical applications. We directly grew a large-area ( $> \text{cm}^2$ ) highly metallic 2D PtTe<sub>2</sub> layers on doped silicon wafers via a low-temperature chemical vapor deposition (CVD) process, achieving high-quality 2D/3D hetero-interfaces. The integrated devices incorporating the PtTe<sub>2</sub>/silicon vertical junctions exhibit excellent Schottky transport characteristics such as high rectification ratio ( $\sim 10^5$ ), small ideality factor ( $\sim 1.9$ ), and Schottky barrier height of  $0.67\text{eV}$ . These devices present strong photovoltaic properties and photo-responsiveness despite their large ( $0.5\text{cm}^2$ ) lateral junction area, i.e., a well-balanced attribute of high photo-detectivity ( $>10^{13}$  Jones) and short photo-response time ( $\sim 1\text{ }\mu\text{s}$ ), significantly outperforming most of the previously explored 2D/3D or 2D layers-based devices. Furthermore, we identified that the CVD 2D PtTe<sub>2</sub> layers exhibit unusually strong hydrophobicity which has been utilized to further improve the device photovoltaic performances; i.e.,  $\sim 300\%$  and  $\sim 200\%$  increase of short circuit current density and power conversion efficiency have been achieved respectively upon an integration of water droplet. Underlying principles for the Schottky junction characteristics, as well as the water-assisted performance enhancement will be discussed.

#### 6:20 AM F.EL04.04.10

**The (Mostly) Unwelcome Guest in 2D Chalcogenides—Native Oxidation Rates and the Effects of Oxygen During Processing MoS<sub>2</sub>, TiS<sub>2</sub>, and Zr(S,Se)<sub>2</sub>** Seong Soon Jo<sup>1</sup>, Yifei Li<sup>1</sup>, Akshay Singh<sup>2</sup>, Liqiu Yang<sup>3</sup>, Subodh C. Tiwari<sup>3</sup>, Sungwook Hong<sup>4</sup>, Aravind Krishnamoorthy<sup>3</sup>, Maria Sales<sup>5</sup>, Sean Oliver<sup>6</sup>, Patrick Vora<sup>6</sup>, Stephen McDonnell<sup>5</sup>, Priya Vashishta<sup>3</sup>, Rajiv Kalia<sup>3</sup>, Aiichiro Nakano<sup>3</sup> and Rafael Jaramillo<sup>1</sup>; <sup>1</sup>Massachusetts Institute of Technology, United States; <sup>2</sup>Indian Institute of Science, India; <sup>3</sup>University of Southern California, United States; <sup>4</sup>California State University, Los Angeles, United States; <sup>5</sup>University of Virginia, United States; <sup>6</sup>George Mason University, United States

A thorough understanding of the properties of native oxides and the role of oxygen during processing is essential for designing semiconductor devices. This is no less true for nanomaterials than it is for legacy semiconductors such as silicon, for which control of the native oxide was a seminal achievement of 20th century materials science. Being a very hard anion, oxygen bonds very differently to transition metals than do the chalcogens. Trace oxygen in a transition metal dichalcogenide (TMD) has a substantial impact on material processing and properties, much more so than for instance trace selenium in a sulfide. Since oxygen is all around us, even in our high-vacuum chambers, it is essential to understand and control the effects of oxygen on processing 2D materials. Here we report three studies of the effect of oxygen on processing TMDs. We find that lowering trace oxygen concentration in the reactor makes it possible to lower the processing temperature for large-area TiS<sub>2</sub> films, made by reacting Ti thin films with H<sub>2</sub>S gas. We quantify how lowering oxygen concentration enables faster metal sulfurization at lower temperatures (down to  $500\text{ }^\circ\text{C}$ ), leading to thin films that are smooth and homogeneous. In contrast, we find the opposite trend for MoS<sub>2</sub>: adding trace oxygen enables lower processing temperatures (down to  $375$

°C) for large-area MoS<sub>2</sub> films, made by sulfurizing Mo thin films. We understand these contrasting effects in the light of particulars of Ti-O and Mo-O bonds, including molecular dynamics (MD) simulations that suggest that oxygen is a catalyst for Mo-S bond formation.

We also report a quantitative study of the rate of native oxidation of pristine TMD surfaces. Layered transition metal dichalcogenides nominally have inert, fully-passivated surfaces, but it is well-known that this is an oversimplification and that many TMDs oxidize readily. MoS<sub>2</sub> surfaces remain pristine for over a year in laboratory ambient conditions, without a trace of oxide formation. In contrast, Zr(S,Se)<sub>2</sub> alloys oxidize rapidly, with the native oxide growing at a rate up to 0.5 Å/min. MD simulations reveal the kinetic mechanisms that limit native oxide growth for MoS<sub>2</sub> and promote it for Zr(S,Se)<sub>2</sub>, despite oxide formation in ambient conditions being thermodynamically-favorable in all cases.

Our results provide quantitative detail and atomistic understanding of the role of oxygen during TMD synthesis and processing, and may be broadly useful to ongoing efforts at film synthesis and device integration.

### 6:30 AM F.EL04.04.11

**Late News: Synthesis of 2D GaS Films on Versatile Substrates for High-Performance Electronic and Optoelectronic Devices** Yang Lu<sup>1</sup> and Jamie Warner<sup>2</sup>; <sup>1</sup>University of Oxford, United Kingdom; <sup>2</sup>The University of Texas at Austin, United States

A chemical vapor deposition method is developed for uniform and continuous gallium(II) sulfide (GaS) films on SiO<sub>2</sub> featuring both thickness-controlled (one to four layers), as well as defect-controlled (defective GaS<sub>0.87</sub> and stoichiometric GaS). We identify stoichiometry and concentration as two key elements in the growth mechanism. The 2D GaS films show sensitive layer-dependent Raman and optoelectronic properties. Furthermore, an enhanced stability of the stoichiometric GaS is demonstrated under laser and strong UV light, and by controlling defects in GaS, the photoresponse range can be changed from vis-to-UV to UV-discriminating. The stoichiometric GaS is suitable for large-scale, UV-sensitive, high-performance photodetector arrays for information encoding under large vis-light noise, with short response time (<66 ms), excellent UV photoresponsivity (4.7 A W<sup>-1</sup> for trilayer GaS), and 26-times increase of signal-to-noise ratio compared with small-bandgap 2D semiconductors. A defect-induced band further appears within the bandgap of GaS<sub>0.87</sub>, which can tune the band alignment of bilayer GaS-WS<sub>2</sub> from type-I heterojunction to type-II heterojunction.

We further synthesized GaS crystals on various substrates including sapphire, Si and other 2D materials such as graphene and MoS<sub>2</sub>. The morphology of various GaS crystals is influenced by different surface properties. By comprehensive characterizations from atomic-scale structures to large-scale device performances in 2D semiconductors, the study shows that both layer-controlled defective GaS<sub>0.87</sub> and stoichiometric GaS prove to be promising platforms for study of novel phenomena and new applications.

#### Reference:

[1] Lu, Y., Chen, J., Chen, T., Shu, Y., Chang, R.-J., Sheng, Y., Shautsova, V., Mkhize, N., Holdway, P., Bhaskaran, H., Warner, J. H., Controlling Defects in Continuous 2D GaS Films for High-Performance Wavelength-Tunable UV-Discriminating Photodetectors. *Adv. Mater.* 2020, 32, 1906958.

[2] Lu, Y., Warner, J. H., et al., Controlled Growth of Monolayer GaS Crystals on Versatile Substrates. In preparation.

### SESSION F.EL04.05: Defect Engineering and Detection

On Demand Abstracts Available for Viewing Starting Saturday Morning, November 21, 2020

F-EL04

### 5:00 AM F.EL04.05.01

**Machine Learning-Enabled Design of Point Defects in 2D Materials for Quantum and Neuromorphic Information Processing** Nathan Frey<sup>1</sup>, Deji Akinwande<sup>2</sup>, Deep M. Jariwala<sup>1</sup> and Vivek Shenoy<sup>1</sup>; <sup>1</sup>University of Pennsylvania, United States; <sup>2</sup>The University of Texas at Austin, United States

Engineered point defects in two-dimensional (2D) materials offer an attractive platform for solid-state devices that exploit tailored opto-electronic, quantum emission, and resistive properties. Naturally occurring defects are also unavoidably important contributors to material properties and performance. The immense variety and complexity of possible defects makes it challenging to experimentally control, probe, or understand atomic-scale defect-property relationships. Here, we develop an approach based on deep transfer learning, machine learning, and first-principles calculations to rapidly predict key properties of point defects in 2D materials. Properties including band gap and bulk formation energy are predicted for over

4,000 2D materials using deep transfer learning. 10,000 dopant, vacancy, divacancy, and antisite defect structures are generated in 150 wide band-gap materials and more than 1,000 defect band structures are computed *via* first-principles methods. We use physics-informed featurization to generate a minimal description of defect structures and present a general picture of defects across materials systems. We identify over 100 promising, unexplored dopant defect structures in layered metal chalcogenides, hexagonal nitrides, and metal halides including GeS, h-AlN, and MgI<sub>2</sub>. These defects have low formation energies and host material band-gaps calculated to be greater than 2 eV. We also find ten optimal substitutional defects for nonvolatile resistive switching in atomically thin memristor devices, where metal dopants substitute for chalcogen atoms in materials including WSe<sub>2</sub> and MoTe<sub>2</sub>. Au and Ag substitutions in WTe<sub>2</sub>- and MoTe<sub>2</sub>-based devices are predicted to have switching voltages as low as 110 meV. These defect structures are prime candidates for quantum emission, resistive switching, and neuromorphic computing.

#### 5:10 AM F.EL04.05.02

**Site-Selectively Generated Defects as Highly Scalable Quantum Emitters in Encapsulated Monolayer MoS<sub>2</sub>** Julian Klein<sup>1,2</sup>, Lukas Sigl<sup>1</sup>, Alexander Hötger<sup>1</sup>, Samuel Gyger<sup>3</sup>, Katija Barthelmi<sup>1</sup>, Matthias Florian<sup>4</sup>, Alexander Kerelsky<sup>5</sup>, Elmar Mitterreiter<sup>1</sup>, Christoph Kastl<sup>1</sup>, Sergio Rey<sup>1</sup>, Takashi Taniguchi<sup>6</sup>, Kenji Watanabe<sup>6</sup>, Frank Jahnke<sup>4</sup>, Valery Zwiller<sup>3</sup>, Klaus D. Jöns<sup>3</sup>, Abhay Pasupathy<sup>5</sup>, Frances M. Ross<sup>2</sup>, Kai Müller<sup>1</sup>, Ursula Wurstbauer<sup>7</sup>, Jonathan Finley<sup>1</sup> and A.W. Holleitner<sup>1</sup>; <sup>1</sup>Technical University of Munich, Germany; <sup>2</sup>Massachusetts Institute of Technology, United States; <sup>3</sup>KTH Royal Institute of Technology, Department of Applied Physics, Albanova University Centre, Sweden; <sup>4</sup>University of Bremen, Germany; <sup>5</sup>Columbia University, United States; <sup>6</sup>National Institute for Materials Science, Japan; <sup>7</sup>University of Münster, Germany

Two-dimensional materials offer a wide range of perspectives for hosting functional and highly localized zero-dimensional states, e.g. vacancy defects, that offer great potential for nano-photonics applications [1]. The site-selective generation of such defects and the fundamental understanding of their optical and electronic properties are of key importance for integrated quantum photonic devices.

In this talk, we will demonstrate the highly local formation of individual single-photon sources in a monolayer MoS<sub>2</sub> van der Waals heterostructure [2,3]. Individual defects that act as our single-photon emitters are created by He-ion irradiation. Irradiation after encapsulation of the MoS<sub>2</sub> with hBN reveals spectrally narrow and spatially localized spectral lines that exhibit anti-bunched emission at the defect characteristic energy of ~1.75 eV (194 meV redshifted from 2D exciton). The emission is highly homogeneous and background-free due to the encapsulation [4]. We investigate these individual single-photon emitters spectroscopically using photoluminescence excitation spectroscopy and temperature-dependent measurements. The line shape reveals a strong asymmetry resembling the interaction with LA/TA phonons. Applying the independent boson model to our emission lines, we find that the emitters are spatially localized to a length scale of 2 nm. We attribute the emission to atomistic defects induced by the He-ion irradiation and discuss their microscopic origin in the light of scanning tunneling microscopy measurements [5,6]. Moreover, we further demonstrate spatial integration and electrical control of single-photon sources in field-switchable van der Waals devices. Our work firmly establishes 2D materials as a highly scalable material platform for integrated quantum photonics.

#### References:

- [1] J. Klein *et al.*, 2D Mater. **5**, 1 (2017)
- [2] J. Klein *et al.*, Nature Comm. **10**, 2755 (2019)
- [3] J. Klein and L. Sigl *et al.*, submitted (2020)
- [4] J. Wierzbowski and J. Klein *et al.*, Sci. Rep. **7**, 12383 (2017)
- [5] J. Klein *et al.*, Appl. Phys. Lett. **115**, 261603 (2019)
- [6] E. Mitterreiter *et al.*, Nano Lett. **20**, 4437 (2020)

#### 5:20 AM F.EL04.05.03

**Elimination of Defect States in 2D Transition Metal Dichalcogenides via Doped Organic/Transition Metal Oxide Mixtures** Xiaheng Huang, Zidong Li, Xiao Liu, Jize Hou, Jongchan Kim, Stephen R. Forrest and Parag B. Deotare; University of Michigan, United States

Due to intrinsic defects, transition metal dichalcogenides (TMD) monolayers have low (< 0.1%) photoluminescence quantum yield (PLQY), hindering their potential for optoelectronic device applications. Here, we report a passivation method of monolayer TMD using organic/transition metal oxide (TMO) mixtures with laser soaking. A 10 nm mixed layer of 3,3',5,5'-Tetra[(m-pyridyl)-phen-3-yl]biphenyl (BP4mPy) and MoO<sub>3</sub> is vacuum deposited onto a MoS<sub>2</sub> monolayer, which is followed by laser soaking for tens of minutes in ambient. For 1:4 vol% BP4mPy:MoO<sub>3</sub>, the passivated MoS<sub>2</sub> monolayer shows up to 250 times enhancement in PL intensity as compared to exfoliated MoS<sub>2</sub>. The PLQY reaches ~ 5 % at excitation power

density  $< 10 \text{ W/cm}^2$  and rolls off as power density increases, reaching 1 % at  $10^3 \text{ W/cm}^2$ . These values are comparable to those achieved by recently reported superacid-treated<sup>1</sup> samples with PLQY reaching 3 % at  $10 \text{ W/cm}^2$  and 1 % at  $10^2 \text{ W/cm}^2$ . In addition, the passivated MoS<sub>2</sub> is stable in air, vacuum, and solvents (e.g. acetone, isopropanol). Using low temperature PL and transient spectroscopy, we find that the mid-gap defect states of MoS<sub>2</sub> are eliminated by passivation, concomitant with a decrease of exciton-exciton annihilation.

Mechanisms of passivation are studied by varying the photon energy of the soaking laser, and as a function of the structures: 5 nm BP4mPy/*d* nm MoO<sub>3</sub>/MoS<sub>2</sub>, where *d* is varied from 3 to 12nm. The effectiveness of the passivation is found to be determined by the polaron-pair generation at the BP4mPy/MoO<sub>3</sub> interface and polaron-diffusion efficiency from the interface to MoS<sub>2</sub>. This passivation method has been generalized to other organic/TMO capping layers, where organic molecules serve as the electron donor while TMO as the acceptor. It is also applicable to passivating other sulfur-based TMDs (e.g. WS<sub>2</sub>), offering a potential platform for next generation 2D device applications.

This work was supported in part by the Army Research Office (ARO) under Award Number W911NF-17-1-0312 and Air Force Office of Scientific Research (AFOSR) Award Number FA9550-17-1-0208

Xiaheng Huang and Zidong Li contributed equally to this work.

[1] Amani, Matin, et al. "Near-unity photoluminescence quantum yield in MoS<sub>2</sub>." *Science* 350.6264 (2015): 1065-1068.

### 5:30 AM F.EL04.05.04

**MoS<sub>2</sub> Defect Insights Using Raman Spectroscopy** Kirstin E. Schauble, Ryan Grady and Eric Pop; Stanford University, United States

Two-dimensional (2D) semiconductors, such as MoS<sub>2</sub>, are promising for electronics due to their good mobility in ultrathin channels. However, current synthesis methods result in defective films which hinder their electrical performance and can influence doping and reactivity. Therefore, it is important to have a quick and nondestructive method to analyze defect densities in MoS<sub>2</sub>.

Past studies used transmission electron microscopy [1] or scanning tunneling microscopy [2] to probe MoS<sub>2</sub> defects, but these methods are time consuming, destructive, and cannot be applied to large-area films. On the other hand, Raman spectroscopy has been used to probe graphene defects, particularly through the D-peak [3]. A similar Raman feature exists in MoS<sub>2</sub> as the LA(M) peak, however this only appears at very large defect densities ( $>10^{13} \text{ cm}^{-2}$ ) [4].

Here, we use Raman spectroscopy for rapid, large-area analysis of MoS<sub>2</sub> defect densities in the range of interest for electronic applications. We use a simple Raman peak fitting procedure as well as the phonon confinement (RWL) model [4-6] to compare disorder in monolayer MoS<sub>2</sub> prepared by exfoliation, chemical vapor deposition (CVD), and atomic layer deposition (ALD). Importantly, we uncover a correlation between Raman-based defect metrics and electrical mobility of MoS<sub>2</sub>, for the first time.

Non-resonant MoS<sub>2</sub> Raman spectra (532 nm laser) typically have two peaks, E' and A<sub>1</sub>'. However, the E' peak is comprised of two optical phonon modes (LO and TO) which almost overlap at the Gamma point. Thus, additional information on defects can be gained by fitting two E' peaks, including the E' shoulder. We use this approach and observe subtle changes in the Raman spectra of MoS<sub>2</sub> prepared by different methods, i.e. peak broadening, shifting, and increased E' peak shoulder intensity, which correlate with increased defect densities [4,6]. Based on these, we find that exfoliated monolayer MoS<sub>2</sub> is the least defective, followed by CVD-grown, and ALD-grown MoS<sub>2</sub> is the most defective material.

To quantitatively understand how defects change the MoS<sub>2</sub> Raman spectra, we use the RWL model [4-6], which posits that defects spatially confine Gamma point phonons, broadening their k-space participation and thus broadening the Raman peak. Non-Gamma point phonons which participate depend on the phonon dispersion, and a steeper dispersion near the Gamma point causes increased Raman peak broadening and asymmetry due to defects. Here we used a fit to the MoS<sub>2</sub> phonon dispersion based on [7].

By comparing Raman data across various MoS<sub>2</sub> samples with the RWL model, we find that as the defect density increases, the E' peak (with LO and TO modes) shifts and asymmetrically broadens. Fitting this model to Raman data from various MoS<sub>2</sub> sources, we can estimate the defect density in each sample and relate it to the relative E' peak positions and intensities. Importantly, we correlate these changes in Raman features with electrical mobility data for various samples from our lab and from the literature, providing a rapid evaluation of the quality of a 2D semiconductor film. This is an important advance, which allows us to distinguish between samples with, e.g. 10 and 30 cm<sup>2</sup>/V/s mobility using Raman analysis, without the need for extensive fabrication and electrical measurements. Our approach could also be extended to other 2D semiconductors, in particular WSe<sub>2</sub>, which also has a steep phonon dispersion near the Gamma point.

[1] J. Hong et al., *Nat. Comm.* 6, 6293 (2015)

- [2] P. Vancso et al., *Sci. Rep.* 6, 29726 (2016)  
 [3] A. Ferrari and D. Basko, *Nat. Nano* 8, 235 (2013)  
 [4] S. Mignuzzi et al., *Phys. Rev. B* 91, 195411 (2015)  
 [5] H. Richter et al., *Solid State Comm.* 39, 625 (1981)  
 [6] W. Shi et al., *Chin. Phys. Lett.* 33, 057801 (2016)  
 [7] H. Tornatzky et al., *Phys. Rev. B* 99, 144309 (2019)

SESSION F.EL04.06: Doping and Alloying of 2D Materials  
 On Demand Abstracts Available for Viewing Starting Saturday Morning, November 21, 2020  
 F-EL04

#### 5:00 AM F.EL04.06.01

**Single versus Dual Ion Conductors for Electric Double Layer Gating of Two-Dimensional Materials** Ke Xu<sup>1</sup>, Aaron Woeppel<sup>2</sup>, Jierui Liang<sup>1</sup>, Azimkhan Kozhakhmetov<sup>3</sup>, Shubham Sukumar Awate<sup>1</sup>, Joshua Robinson<sup>3</sup> and Susan Fullerton<sup>1</sup>; <sup>1</sup>University of Pittsburgh, United States; <sup>2</sup>Purdue University, United States; <sup>3</sup>The Pennsylvania State University, United States

Electric double layer (EDL) gating using a single-ion conductor is compared to a dual-ion conductor using both finite element modeling and experimentally on two-dimensional (2D) crystals based field effect transistors (FETs). A modified version of the Nernst-Planck Poisson (mNPP) equations are used to calculate the ion density per unit area in a parallel plate capacitor geometry with a bulk ion concentration  $215 \leq c_{\text{bulk}} \leq 1650 \text{ mol/m}^3$ . With electrodes of equal size at a 2 V potential difference, the EDL ion density of the single-ion conductor is  $\sim 7 \times 10^{13} \text{ ions/cm}^2$ , which is approximately 50% of the ion density induced in the dual-ion conductor. However, this difference is reduced to 8% when the electrode at which the cationic EDL forms is 10 times smaller than the anionic electrode. Thus, for a FET gated by a single-ion conductor, it is especially important to have a large gate-to-channel size ratio to achieve strong ion doping. I will also show that the numerical modeling results can be approximated by a simple analysis of capacitors in series, where the EDLs are modeled as capacitors with thickness estimated by the sum of the Debye screening length and the Stern Layer. The modeled ion densities are validated by Hall-effect measurements on graphene FETs gated by a polyethylene oxide (PEO)-based single-ion conductor. The sheet carrier density ( $n_s$ ), which is reported for the first time for a single-ion conductor, is  $\sim 2 \times 10^{13} \text{ cm}^{-2}$  at  $V_g = 2 \text{ V}$ , which is 3.5 times smaller than the predicted value, and on the same order of magnitude as the  $n_s$  measured for a PEO-based dual-ion conductor on the same graphene. Our results suggest single-ion conductor-gated 2D FETs can achieve  $n_s$  up to  $10^{14} \text{ cm}^{-2}$ , which is theoretically predicted to be able to induce sufficient strain required to achieve the semiconducting  $2H$  to metallic  $1T$  phase transition in  $\text{MoTe}_2$ . Therefore, in the last part I will discuss the ongoing work focused on the fabrication of single-ion conductor-gated  $\text{MoTe}_2$  FETs with suspended channels, and the in-situ characterization of the phase transition induced by the strain via the bending of single-ion conductor under an applied field.

This work is supported by the NSF DMR under grant #1607935.

#### 5:10 AM F.EL04.06.02

**Ion-Locking in Solid Polymer Electrolytes for Reconfigurable Gateless Electrostatic Doping** Jierui Liang, Ke Xu, Swati Arora, Jennifer Laaser and Susan Fullerton; University of Pittsburgh, United States

Electrostatic doping by ions relies on the formation of an electric double layer (EDL) at the electrolyte/channel interface where the image charges induced by the ions serve as dopants in the channel. Electrostatic doping can induce sheet carrier densities in two-dimensional (2D) crystals exceeding  $10^{14} \text{ cm}^{-2}$  without altering the intrinsic bandgap, and the doping is reconfigurable between  $p$ - and  $n$ -type or  $p$ - $n/n$ - $p$  junctions by redistributing ions under the field. However, in conventional electrolytes such as ionic liquids/gels, a gate voltage must be continuously applied to hold the ions in place and therefore set the doping state. What would be useful is a “gateless” electrostatic doping wherein the doping could be programmed by ions and then locked into position via a trigger until the ions could be unlocked and reconfigured again on demand. Herein, we report a newly developed doubly polymerizable ionic liquid (DPIL) that can perform ion-locking by a chemical trigger to achieve the gateless electrostatic doping. The structure of DPIL is similar to the ionic liquid, [EMIM][TFSI], but with polymerizable functional groups on both charged species to perform ion-locking. Before polymerization, the DPIL monomers behave as a typical electrolyte with mobile ions that can be drifted by an applied field to form EDLs. To lock the ions, and therefore the EDL into place, either UV or thermal initiated polymerization is used. Once locked, the electric field is removed

and EDL does not dissipate. Here, ion locking to create a gateless, lateral *p-n* junction is demonstrated on graphene.<sup>1</sup> The junction is set by an applied field and DPIL is polymerized to lock the doping; the junction is measured at room temperature. The results are compared to a common locking approach: thermally quenching a polyethylene oxide-based electrolyte to a temperature below the glass transition temperature ( $T_g$ ) and then measuring the junction at low temperature. Both approaches require only the source/drain terminals to create the junction, and a gate is not required to maintain the doping after ion-locking. Backgated transfer characteristics of both approaches show two current minima – the signature of a *p-n* junction in graphene. We have also made progress towards reconfigurable doping (i.e., locking and unlocking) by incorporating thermally-labile linkers into DPIL to allow ions to be released again after polymerization.<sup>2</sup>

[1] Liang, J., Xu, K., Arora, S., Laaser, J. and Fullerton-Shirey, S. "Ion-Locking in Solid Polymer Electrolytes for Reconfigurable Gateless Lateral Graphene *p-n* Junctions." *Materials* 13.5 (2020): 1089.

[2] Arora, S., Liang, J., Fullerton-Shirey, S. and Laaser, J. "Triggerable Ion Release in Polymerized Ionic Liquids Containing Thermally-Labile Diels-Alder Linkages." *ACS Materials Letters* (2020).

#### 5:20 AM F.EL04.06.03

**Near-Unity Molecular Doping Efficiency in Monolayer MoS<sub>2</sub>** Milad Yarali<sup>1,1</sup>, Yiren Zhong<sup>1,1</sup>, Serrae N. Reed<sup>1,1</sup>, Juefan Wang<sup>2</sup>, Kanchan A. Ulman<sup>2</sup>, David Charboneau<sup>1</sup>, Julia B. Curley<sup>1</sup>, David Hynek<sup>1,1</sup>, Joshua V. Pondick<sup>1,1</sup>, Sajad Yazdani<sup>1,1</sup>, Nilay Hazari<sup>1</sup>, Su Ying Quek<sup>2,2</sup>, Hailiang Wang<sup>1,1</sup> and Judy Cha<sup>1,1</sup>; <sup>1</sup>Yale University, United States; <sup>2</sup>National University of Singapore, Singapore

Surface functionalization with organic electron donors (OEDs) is an effective doping strategy for two-dimensional (2D) materials, which can achieve doping levels beyond those possible with conventional electric field gating. While the effectiveness of surface functionalization has been demonstrated in many 2D systems, the doping efficiencies of OEDs have largely been unmeasured, which is in stark contrast to their precision syntheses and tailored redox potentials. Here, using monolayer MoS<sub>2</sub> as a model system and an organic reductant based on 4,4'-bipyridine (DMAP-OED) as a strong organic dopant, we establish that the doping efficiency of DMAP-OED to MoS<sub>2</sub> is in the range of 0.63 to 1.26 electrons per molecule. We also achieve the highest doping level to date in monolayer MoS<sub>2</sub> with a carrier density of  $5.8 \pm 1.9 \times 10^{13} \text{ cm}^{-2}$  by surface functionalization with DMAP-OED at the maximum functionalization conditions. This is four times greater than the previous best system based on benzyl viologen, demonstrating that DMAP-OED is a stronger dopant than benzyl viologen. The measured range of the doping efficiency is in good agreement with the values predicted from first-principles calculations. We show that multiple factors, such as reduction potential, size, and binding mode of the dopant molecule, as well as interactions between the molecules and 2D materials and among the molecules themselves play an important role when considering the design of strong molecular dopants. The ability to dope MoS<sub>2</sub> beyond its degenerate limit *via* an organic super electron donor provides opportunities to access correlated electronic phases, such as superconductivity at the degenerate level, and offers an alternative to ionic gating and lithium intercalation for carrier density control, which may produce unwanted electrochemical reactions. Our work provides a basis for the rational design of OEDs for high-level doping of 2D materials.

#### 5:30 AM F.EL04.06.04

**Molecular Dopant Dependent Charged Impurity Scattering in Charge-Transfer-Doped WSe<sub>2</sub>** Jae-Keun Kim<sup>1</sup>, Jung-hoon Lee<sup>2</sup>, Kyungjune Cho<sup>1</sup>, Keehoon Kang<sup>1</sup> and Takhee Lee<sup>1</sup>; <sup>1</sup>Seoul National University, Korea (the Republic of); <sup>2</sup>Korea Institute of Science and Technology, Korea (the Republic of)

Transition metal dichalcogenides (TMDCs) has attracted great attention as a promising semiconductor of next generation nanoelectronics due to unique properties such as atomically flat nature and tunable band gap property. To utilize TMDCs for complementary logic circuit and various homo/heterojunction devices, controlling of the conductivity and the carrier type is necessary. In order to modulate carrier concentration and carrier type, surface charge transfer doping (SCTD) on TMDCs using functionalized organic molecules has been extensively studied. However, the molecular dopant could limit the electrical performance of TMDCs like in graphene [1] leading to charged impurity scattering. In this regard, a thorough understanding of the effect of SCTD on the charge transport of TMDCs is essential.

In this presentation, we report the effect of surface charge transfer doping on the transport properties of tungsten diselenide (WSe<sub>2</sub>) by using three types of p-type molecular dopants, 2,3,5,6-tetrafluoro-7,7,8,8-tetracyanoquinodimethane (denoted as F<sub>4</sub>-TCNQ), molybdenum tris(1,2-bis(trifluoromethyl)ethane-1,2-dithiolene) (denoted as Mo(tfd-COCF)<sub>3</sub>), and Tris(4-bromophenyl)ammoniumyl hexachloroantimonate (denoted as magic blue). These strong molecular acceptors have different



electron affinities, and thus the doping strength among the molecular dopants vary significantly, which we characterized with WSe<sub>2</sub> field-effect transistors (FETs). In particular, we measured four-point probe mobility at variable temperature from 10 K to 300 K to investigate the doping effect on the intrinsic charge transport of WSe<sub>2</sub>. Comparing to pristine WSe<sub>2</sub>, the mobility of molecular doped WSe<sub>2</sub> FETs is significantly reduced at low temperature regime. This result implies that the dopants can induce impurity scattering in the transport of WSe<sub>2</sub> FETs. It is found that magic blue molecule induces the least impurity scattering in WSe<sub>2</sub> FETs among the three molecular dopants. This study can help developing suitable molecular dopants for controlling the electrical properties of TMDC devices by understanding dopant-induced effects on the charge transport.

[1] Chen et al. *Nat. Phys.* **4**, 377 (2008)

#### 5:40 AM F.EL04.06.05

##### **Structure and Properties of Ni-Doped MoS<sub>2</sub> from DFT—Phase Diagrams, Raman Spectra, Defect States and Solid Lubrication** Enrique Guerrero, Rijan Karkee and David A. Strubbe; University of California, Merced, United States

Doping of MoS<sub>2</sub> can introduce novel functionality in terms of electronic, optical, magnetic, or mechanical properties. Experimental resolution of the doped structures have been challenging and often inconclusive, showing an important role for theory. In this work we study Ni-doped MoS<sub>2</sub>, motivated specifically by its exploration as a solid lubricant in the low-temperature and low-pressure environment in space, where liquid lubricants fail [MR Vazirisereshk, A Martini, DA Strubbe, and MZ Baykara, *Lubricants* **7**, 57 (2019)]. Some preliminary studies suggest that doping with transition metals (especially Ni) can improve tribology performance by reducing friction and wear, but the structure and mechanisms remain unclear. We use density functional theory (DFT) calculations to determine the structure and properties of Ni-doped MoS<sub>2</sub> in bulk and monolayer form, in various polytypes and doping levels. We consider formation energies for different sites for Mo or S substitution, intercalation, or adsorption, to create a phase diagram in chemical potential space to inform synthesis efforts. Our calculations identify structural changes on doping and which are the most stable structures. Stable Ni-doped MoS<sub>2</sub> phases and cases where phase segregation is favorable are identified. We compute infrared and Raman spectra to enable experimental identification of the doped structures coming from various growth methods. We additionally calculate elastic properties and potential energy for sliding to connect to atomic-force microscopy friction experiments, and use our DFT data to parametrize classical force fields for larger-scale reactive molecular dynamics simulations that can directly address friction and wear on larger length and time scales.

#### 5:50 AM F.EL04.06.07

##### **Preferred Distribution of Dopant Atoms in an Anisotropic Transition Metal Dichalcogenide** Amin Azizi<sup>1,1</sup>, Mehmet Dogan<sup>1,2</sup>, Jeffrey Cain<sup>1,1,2</sup>, Alessandro Varieschi<sup>1</sup>, Marvin L. Cohen<sup>1,2</sup> and Alex Zettl<sup>1,1,2</sup>; <sup>1</sup>University of California, Berkeley, United States; <sup>2</sup>Lawrence Berkeley National Laboratory, United States

Doping provides a key scheme for tuning materials' functional properties. The atomic-scale control of the position, distribution, and concentration of dopants is crucially important in engineering the material's behavior. Two-dimensional (2D) crystals provide an extremely rich materials platform to study the behaviors of dopant atoms in different lattices and their impacts on material's properties. While there has been remarkable progress in the synthesis and atomic-scale characterization of doped 2D transition metal dichalcogenides (TMDs), most studies have focused on isotropic TMDs with a hexagonal structure. However, anisotropic TMD material systems with a 1T' structure offer a more versatile platform to study the behaviors of dopant atoms. For example, while there is only one atomic site for metal atoms in hexagonal TMDs with the 1H structure, there are two different atomic sites for metal atoms in anisotropic TMDs with the 1T' structure. Here, we dope an anisotropic TMD crystal and probe individual and coupled dopant atoms in its lattice using aberration-corrected scanning transmission electron microscopy (STEM) with sub-Ångstrom resolution. Statistical analyses on the atomically-resolved images reveal the preference of dopant atoms for specific atomic sites. Using density functional theory calculations, we develop a model to describe the preferred distribution of atomic species.

#### 6:00 AM F.EL04.06.08

##### **Two-Dimensional As<sub>x</sub>P<sub>1-x</sub> Alloys—Structural and Thermoelectric Properties** Jacek B. Jasinski, Bhupendra Karki, Manthila Rajapakse and Gamini Sumanasekera; University of Louisville, United States

In recent years, van der Waals layered materials, especially their two-dimensional (2D) forms (monolayers, bilayers, and few-layers), have attracted significant attention as novel high-performance structures for a variety of applications, including thermoelectric devices, e.g. structures that are based on efficient conversion between heat and electricity. Thermoelectric properties and the performance of different 2D materials, such as SnSe, Bi<sub>2</sub>Te<sub>3</sub>, and MoS<sub>2</sub>, have been studied extensively. Owing to its unique properties, such as high carrier mobility (1000 cm<sup>2</sup>(Vs)<sup>-1</sup> at room temperature), a tunable thickness-

dependent bandgap (0.3–2.0 eV), a large Seebeck coefficient (335  $\mu\text{V K}^{-1}$  at room temperature), and a strong in-plane anisotropy, black phosphorus (BP) and its 2D form, phosphorene, are among the most prospective thermoelectric materials. Recent investigations have indicated that the thermoelectric properties of BP can be further enhanced by alloying or doping. For example, a very high  $ZT$  value of 6.0 has been predicted by first-principle calculations in black phosphorous with 1/4 of its P atoms substituted with Sb atoms. Here, motivated by these works, we have synthesized a series of  $\text{As}_x\text{P}_{1-x}$  alloys and conducted a comparative study of their structural and thermoelectric properties. Raman measurements of these samples show the presence of 3 types of atomic vibrational modes arising from As-As bonding ( $< 270 \text{ cm}^{-1}$ ), As-P bonding ( $270 \text{ cm}^{-1} - 350 \text{ cm}^{-1}$ ), and P-P bonding ( $> 350 \text{ cm}^{-1}$ ), respectively. For a wide range of As concentration, these materials are found to crystallize in the orthorhombic puckered structure and are alloy analogs of BP. Furthermore, it is found that the crystal structure of these  $\text{As}_x\text{P}_{1-x}$  alloys expands and their vibrational modes red-shift systematically with the increase of As. These changes are accompanied by the systematic changes of the electrical transport properties, especially the thermoelectric power. Temperature-dependent transport measurements show that, at room temperature, the samples with lower and intermediate As concentration exhibit very high thermopower (as high as 803  $\mu\text{V/K}$  for  $x = 0.2$  compared to 323  $\mu\text{V/K}$  for BP) and high power factor (as high as 317  $\mu\text{Wm}^{-1}\text{K}^{-2}$  for  $x = 0.5$  compared to 22  $\mu\text{Wm}^{-1}\text{K}^{-2}$  for BP). Overall, the study suggests that the thermoelectric properties of BP can be greatly improved by alloying, resulting in comparable or even better performance than some of the reported outstanding thermoelectric materials. Additional benefits of  $\text{As}_x\text{P}_{1-x}$  alloys include enhanced durability and higher resistance against degradation than those of BP. Finally, their unique in-plane anisotropy provides an opportunity for decoupling thermal and electronic transport pathways and therefore further enhancing thermoelectric properties.

SESSION F.EL04.07: Exploring 2D Crystal Phase Transitions  
On Demand Abstracts Available for Viewing Starting Saturday Morning, November 21, 2020  
F-EL04

#### 5:00 AM F.EL04.07.01

##### **Temperature-Dependent Raman Scattering and X-Ray Diffraction Study of Phase Transitions in Layered**

**Multiferroic  $\text{CuCrP}_2\text{S}_6$**  Michael A. Susner<sup>1,2</sup>, Rahul Rao<sup>1</sup>, Anthony Pelton<sup>1,2</sup>, Michael V. McLeod<sup>1,3</sup> and Benji Maruyama<sup>1</sup>; <sup>1</sup>Air Force Research Laboratory, United States; <sup>2</sup>UES, Inc., United States; <sup>3</sup>University of Dayton Research Institute, United States

Functional van der Waals layered materials, which exhibit interesting phenomena such as magnetism and ferroelectricity, have been proposed for use in next-generation nanoscale devices and sensors. Metal thiophosphates are an interesting class of 2D van der Waals gapped materials that contain a common structural framework where altering the cation composition can induce different types of ferroic ordering, including ferroelectricity and magnetism, making this family arguably the 2D equivalent of complex oxides. The compound  $\text{CuCrP}_2\text{S}_6$  is a promising 2D material that evinces *multiferroic* behavior where the  $\text{Cu}^+$  and  $\text{Cr}^{+3}$  cations are responsible for antiferroelectric and antiferromagnetic ordering, respectively, which are theoretically predicted to couple. In this study, we use X-ray diffraction and Raman spectroscopy to map out these phase transitions in the range 70-400 K. The antiferroelectric phase transition is complex and shows a gradual transition to complete antipolar order with an intermediate quasi-antipolar step. X-ray diffraction studies reveal evidence for negative thermal expansion across the antipolar phase transition around 140 K. This is accompanied by a drastic reduction in rotational and translational mode frequencies of the anion groups in  $\text{CuCrP}_2\text{S}_6$ . Our temperature-dependent structural data provides an important reference for subsequent research into this promising 2D multiferroic material.

#### 5:10 AM F.EL04.07.03

**Active Learning of Fast Bayesian Mapped Gaussian Processes—Application to 2D to 3D Structural Phase Transition of Stanene** Yu Xie, Jonathan Vandermause, Lixin Sun, Andrea Cepellotti and Boris Kozinsky; Harvard University, United States

Understanding metastability and phase transitions of 2D materials requires long and large-scale molecular dynamics simulations, but this is hindered by lack of accurate force fields capable of describing the vast variety of configurations and phases. Machine learning techniques are attractive for developing force field models because these powerful function-fitting schemes are capable of reaching first principles accuracy at a small fraction of computational cost. Gaussian process (GP) regression is one promising technique among them, whose remarkable competitive advantage is the built-in uncertainty quantification based on Bayesian posterior inference, which can be used to monitor the quality of model predictions. A

current limitation of existing GP force fields is that the prediction cost grows linearly with the size of the training data set, making accurate GP predictions slow. In this work, we exploit the special structure of the kernel function to construct a mapping of the trained Gaussian process model, including both forces and their uncertainty predictions, onto a spline functions of low-dimensional structural features. This method extends previous proposals of mapping only the forces by incorporating uncertainty at constant scaling cost, accelerating the active learning workflow for training of Bayesian force fields. To demonstrate the capabilities of this method, we construct a force field for 2D stanene and perform large scale dynamics simulation of its structural evolution as a function of temperature. We discover an unusual phase transformation mechanism of stanene, where the 2D metastable structure distorts, buckles and transforms into 3D tin or a liquid phase depending on the temperature. By monitoring the uncertainty of the prediction we are able to systematically improve the force field during the simulation, demonstrating a path to autonomous learning of fast models for studying phase transformations of complex systems

#### 5:20 AM F.EL04.07.05

**Late News: Metal to Semiconductor Transition in  $\text{MoTe}_2(1-x)\text{S}_2x$  Ternary Alloys** [Florence A. Nugera](#), Adrian Popescu, Lilia M. Woods and Humberto R. Gutierrez; University of South Florida, United States

$\text{MoTe}_2$  has received much attention due to its unique physical properties that make it good candidate for spintronics, thermoelectric and piezoelectric applications.  $\text{MoTe}_2$  is stable in both the 2H and 1T' phase. In general, the 1T' phase displays metallic behavior, making  $\text{MoTe}_2$  also interesting candidate for in-plane interconnects when combined with 2D semiconductors. In this study, we successfully synthesize large-area few-layers  $\text{MoTe}_2$  using a simple tellurization CVD process. Subsequently, the as-grown transition metal ditelluride was chemically modified using an in situ laser-assisted method recently developed in our group. The entire process takes place within a home-made mini chamber with an optical quartz window, where the samples are exposed to a laser beam in the presence of a controlled environment rich in different chalcogen atoms. For an optimized set of parameters (e.g. exposure time and laser power), the tellurium atoms are replaced by sulfur atoms. The chemical exchange process is monitored in real time via Raman spectroscopy. The site-selective replacement of the chalcogen atoms generate metal-semiconductor heterojunctions. 2D field effect transistors were fabricated to study the electrical response of these lateral heterojunctions. Additionally, we performed first-principle calculations for different chalcogen compositions in the ternary system  $\text{MoTe}_2(1-x)\text{S}_2x$  and found that the band structure evolves with increasing sulfur composition revealing a systematic transition from metal to semiconductor.

SESSION F.EL04.08: Fundamental Properties of 2D Materials—Computational Studies  
On Demand Abstracts Available for Viewing Starting Saturday Morning, November 21, 2020  
F-EL04

#### 5:00 AM F.EL04.08.02

**The Role of Li Intercalation Played in the Structural Transition from Layered Black Phosphorene to Layered Blue Phosphorene—A First Principle Study** [Md Rajib Khan K. Musa](#)<sup>1</sup>, Congyan Zhang<sup>1</sup>, Manthila C. Rajapakse<sup>1</sup>, Jacek B. Jasinski<sup>2</sup>, Gamini Sumanasekera<sup>1,2</sup> and Ming Yu<sup>1</sup>; <sup>1</sup>University of Louisville, United States; <sup>2</sup>Conn Center for Renewable Energy Research, University of Louisville, United States

Blue phosphorene, a new allotrope of 2D phosphorus material, has been theoretically predicted to be energetically as stable as black phosphorene with energy difference less than 2meV. It has a wide fundamental bandgap (> 2 eV) compared to black phosphorene, tunable gap depending on the number of layers, semiconducting-semimetal transition under strain, possible high carrier mobility, higher in-plane rigidity, and superconductivity with metal intercalation, which would become a worthy contender in the emerging field of post-graphene 2D electronics, such as photodetectors, transistors, and other novel devices. The next task is to synthesize the newly predicted blue phosphorene and to utilize its unique properties in the next generation of nanolithography devices. However, it is a big challenge to simply exfoliate blue phosphorene from its bulk counterpart since blue phosphorus can only exist at high pressure (>5GPa). Alternatively, recent efforts by epitaxial growth method have produced a single layer of blue phosphorus, but it strongly depends on the surface structures of Au, Al, and Te substrates. Therefore, it is extremely desirable if we can develop a new pathway to produce freestanding blue phosphorene. Here, we proposed a novel kinetic pathway to grow layered blue phosphorene from layered black phosphorene via Li intercalation, based on first principle study. This study points out that Li atoms could play as 'catalysts' to drive P atoms in the 'reactive region' undergoing a bond-breaking process and lead to a local structural transformation from orthorhombic lattice to an assembly of parallel narrow nanoribbons with rhombohedra-like symmetry. After delithiation, these nanoribbons are self-

mended and a layered blue phosphorene is formed. The interlayer distance of the obtained blue phosphorene layers was given by  $\sim 3.56 \text{ \AA}$ , indicating a monolayer blue phosphorene could be obtained by mechanical exfoliation. This theoretical study not only reveals the novel transition mechanism from layered black phosphorene to layered blue phosphorene induced by Li interaction, but also provides a fundamental guidance for synthesizing blue phosphorene.

#### 5:10 AM F.EL04.08.03

**Why Do 2D Semiconductors Generally Have Low Electron Mobility?** Yuanyue Liu; The University of Texas at Austin, United States

Atomically-thin (2D) semiconductors have shown great potential as the fundamental building blocks for next-generation electronics. However, all the 2D semiconductors that have been experimentally made so far have room-temperature electron mobility lower than that of bulk silicon. Although materials-specific explanations have been made [1,2], the "universality" of the low mobility is not well understood. Here, by using first-principles calculations and re-formulating the transport equations, we show that the universally low mobility of 2D semiconductors originates from the large "density of scatterings", which is intrinsic to 2D system. The "density of scatterings" characterizes the number of phonons that can interact with the electrons, and can be fully determined from the electron and phonon band structures without knowledge of electron-phonon coupling strength. Our work reveals the underlying physics limiting the electron mobility of 2D semiconductors, and offers a descriptor to quickly assess the mobility.[3]

[1] L. Cheng, C. Zhang, Y. Liu\*

"The Optimal Electronic Structure for High-Mobility 2D Semiconductors: Exceptionally High Hole Mobility in 2D Antimony"

J. Am. Chem. Soc., 2019, DOI: 10.1021/jacs.9b05923

[2] L. Cheng and Y. Liu\*

"What Limits the Intrinsic Mobility of Electrons and Holes in Two Dimensional Metal Dichalcogenides?"

J. Am. Chem. Soc., 2018, 140, 17895-17900

[3]. L. Cheng, C. Zhang, Y. Liu, in preparation.

#### 5:20 AM F.EL04.08.05

**Pre-Equilibrium Effects in 2D Materials Under Particle Radiation** Alina Kononov and Andre Schleife; University of Illinois at Urbana-Champ, United States

Ion beams in high-resolution imaging and patterning techniques can be used efficiently to manipulate and characterize 2D materials. Achieving higher precision control of the structure and properties necessitates a detailed understanding of the excited electron dynamics occurring in the material in response to the irradiation. Unfortunately, most existing knowledge concerning an energetic ion's interaction with a material is limited to bulk. While many real-life radiation effects, such as electron emission, inherently involve surface processes also for thick materials, the case is particularly compelling for ion-irradiated 2D materials: Their myriad potential applications oftentimes rely on precise control of defects that can be achieved with ion irradiation. In this context, first-principles simulations are an ideal tool to characterize the elusive fundamental physics of ion-irradiated surfaces and inform ion beam microscopy and patterning techniques for 2D materials.

Here we discuss our recent application of real-time time-dependent density functional theory simulations to two examples: (i) As an ion approaches and traverses a surface, it is expected to exchange charge with the material and transition into a steady-state. We model this pre-equilibrium behavior for protons with 0.5 - 1.5 atomic units of velocity impacting few-layer aluminum sheets. This allows us to interpret an enhancement of energy deposition in the sheet, observed from our simulation results, as being tied to surface plasmons and we derive electron escape depths with important implications for optimization of focused ion beam techniques. (ii) We study energy transfer, charge induced, and electrons emitted for monolayer and trilayer graphene as  $\text{H}^+$ ,  $\text{He}^{2+}$ ,  $\text{Si}^{4+}$ ,  $\text{Si}^{12+}$ , and  $\text{Xe}^{8+}$  ions with velocities of 0.5 - 4.6 au traverse the material. In particular, we study the emerging excited charge dynamics and its dependence on projectile velocity, trajectory, species, and charge as well as graphene thickness, with important implications for defect formation through particle radiation.

#### 5:30 AM F.EL04.08.06

**Unveiling Oxidation Mechanism of Bulk  $\text{ZrS}_2$  and  $\text{MoS}_2$**  Liqiu Yang<sup>1</sup>, Subodh C. Tiwari<sup>1</sup>, Seong Soon Jo<sup>2</sup>, Sungwook Hong<sup>3</sup>, Ankit Mishra<sup>1</sup>, Aravind Krishnamoorthy<sup>1</sup>, Rajiv Kalia<sup>1</sup>, Aiichiro Nakano<sup>1</sup>, Rafael Jaramillo<sup>2</sup> and Priya Vashishta<sup>1</sup>; <sup>1</sup>University of Southern California, United States; <sup>2</sup>Massachusetts Institute of Technology, United States; <sup>3</sup>California State University, Los Angeles, United States

Transition metal dichalcogenides (TMDC) are known to show great potential for next-generation electric and optoelectronic

devices. In TMDC family, ZrS<sub>2</sub> has shown a superior electrical properties and chemical catalytic properties. However, native oxidation remains a major issue to improve its long-term stability and thus an active area of research. Here, we develop first-principles informed reactive force field for Zr/O/S and perform reactive molecular dynamics simulations to study oxidation of ZrS<sub>2</sub> and MoS<sub>2</sub> to elucidate the reaction mechanisms of oxidation process. Our results show a significantly larger oxidation rate for ZrS<sub>2</sub> in comparison with MoS<sub>2</sub>. We find that the oxidation pathway of bulk ZrS<sub>2</sub> involves adsorption of oxygen on ZrS<sub>2</sub> surface, followed by amorphization and oxygen transport into bulk, leading to a continuous oxidation. In contrast, bulk MoS<sub>2</sub> remains inert due to the absence of oxygen transport into bulk. Our results show a valuable insight into the atomistic-scale mechanisms of native oxide formation and provide guidance for processing devices based on MoS<sub>2</sub> and ZrS<sub>2</sub>.

This work was supported as part of the Computational Materials Sciences Program funded by the U.S. Department of Energy, Office of Science, Basic Energy Sciences, under Award Number DE-SC0014607. Computations were performed at the Argonne Leadership Computing facility under the DOE INCITE and Aurora Early Science programs and at the Center for High Performance Computing of the University of Southern California.

#### 5:40 AM F.EL04.08.07

**Late News: Atlas of 2D Metals Epitaxial to SiC—Gapping Conditions and Alloying Rules** Yuanxi Wang and Vincent Crespi; The Pennsylvania State University, United States

Although common in the periodic table, monoelemental metals appear severely under-represented in known families of 2D materials. Their recent realization in air-stable 2D form (e.g. Ga, In, and Sn), epitaxial to SiC and capped by graphene [1], suggests an immense chemical space of possible 2D metals and alloys that could expand the physics of 2D metals beyond what is known for graphene and Nb/Ta chalcogenides, including unusual nonlinear optical response [2] and 2D superconductivity with doped-semiconductor characters. Here we present a first-principles computational survey predicting the favorabilities of *all* metals in the periodic table in intercalating graphene/SiC. All experimentally known metal intercalant structures agree with predicted 2D metal ground states. This stability survey not only reveals conspicuous trends related to metal cohesive energies and metal-silicon bonding, but also identifies special groups of metals stabilized by opening a bandgap. We discuss conditions required for gapping, including electron counts and in-plane mirror symmetry breaking. From this gapping stabilization, alloying rules unique to 2D metals are derived.

[1] N. Briggs, Nat. Mater. 19, 637 (2020)

[2] M. A. Steves, arXiv:2004.01809 (2020)

#### 5:50 AM F.EL04.08.08

**Late News: Datamining for Substrate Materials** Joshua T. Paul<sup>1,2</sup>, Alice Galdi<sup>3,3</sup> and Richard G. Hennig<sup>1</sup>; <sup>1</sup>University of Florida, United States; <sup>2</sup>Northwestern University, United States; <sup>3</sup>Cornell University, United States

The design of 2D materials and thin-film devices requires the ability to grow high-quality films consistently and systematically. The selection of substrates is critical to this goal, as a poor match will result in undesired defects and other difficulties during synthesis. To systematically identify potential substrate materials, we apply a topological algorithm and data mining approach to the Materials Project database in search of low-energy surfaces that can act as substrates. Inspired by the recent high-throughput searches for exfoliable 2D materials, we develop a topological algorithm to cleave bonds in fully periodic crystals. If the bond cleaving generates a surface, we isolate the cleaved monolayer and calculate the energy needed to break these bonds. This algorithm is applied to all metastable crystals in the MaterialsProject database with five or fewer atoms in the primitive cell, identifying 4,703 unique surfaces across 2,136 crystals. We compare the cleavage energy to commonly used substrates to identify over 3,000 surfaces with cleavage energy below (0001) AlN. We follow by characterizing trends between cleavage energy and the precursor phase bandgap. We summarize the breadth of materials using the precursor bandgaps and lattice parameters of cleaved surfaces, establishing a computational substrate database. We test the applicability of this database by searching for epitaxial matches to (100) BaSnO<sub>3</sub>, identifying several matches including (001) Rb<sub>2</sub>NiO<sub>2</sub>, (001) NiO, and (001) CaSe. We finalize by looking forward to ways to improve the computational prediction of thin-film and substrate interactions. We make this data freely available at MaterialsWeb.org and the software used to cleave the surfaces available in the open-source software package MPInterfaces.

**5:00 AM F.EL04.10.01**

**Synthesis of Two-Dimensional Janus Crystals and Their Superlattices** Mohammed Yasir Sayyad, Ying Qin and Sefaattin (Sef) Tongay; Arizona State University, United States

Two dimensional (2D) Janus Transition Metal Dichalcogenides (TMDs) are a new class of atomically thin polar materials. In these materials, the top and the bottom atomic layer are made of different chalcogen atoms. To date, several theoretical studies have shown that a broken mirror symmetry induces a colossal electrical field in these materials, which leads to unusual quantum properties. Despite these new properties, the current knowledge in their synthesis is limited only through two independent studies; both works rely on high-temperature processing techniques and are specific to only one type of 2D Janus material - MoSSe. Therefore, there is an urgent need for the development of a new synthesis method to (1) Extend the library of Janus class materials. (2) Improve the quality of 2D crystals. (3) Enable the synthesis of Janus heterostructures. The central hypothesis in this work is that the processing temperature of 2D Janus synthesis can be significantly lowered down to room temperatures by using reactive hydrogen and sulfur radicals while stripping off selenium atoms from the 2D surface. To test this hypothesis, a series of controlled growth studies were performed, and several complementary characterization techniques were used to establish a process–structure-property relationship. The results show that the newly proposed technique, namely Selective Epitaxy and Atomic Replacement (SEAR) is effective in reducing the growth temperature down to ambient conditions. The proposed technique benefits in achieving highly crystalline 2D Janus layers with an excellent optical response. Further studies herein show that this technique can form highly sophisticated lateral and vertical heterostructures of 2D Janus layers. Overall results establish an entirely new growth technique for 2D Janus layers, which pave ways for the realization of exciting quantum effects in these materials such as Skyrmion formation, 2D ferromagnetic ordering, topological superconductivity, and Majorana Zero Modes.

**5:10 AM F.EL04.10.02**

**Abnormal van der Waals Interlayer Coupling Tailored through Janus MoSSe** Kunyan Zhang<sup>1</sup>, Yunfan Guo<sup>2</sup>, Qingqing Ji<sup>2</sup>, Shiang Fang<sup>3</sup>, Efthimios Kaxiras<sup>4</sup>, Jing Kong<sup>2</sup> and Shengxi Huang<sup>1</sup>; <sup>1</sup>The Pennsylvania State University, United States; <sup>2</sup>Massachusetts Institute of Technology, United States; <sup>3</sup>Rutgers University, United States; <sup>4</sup>Harvard University, United States

Janus transition metal dichalcogenide (TMD) differs from conventional TMDs by its out-of-plane mirror asymmetry and intrinsic dipole moment. The dipole moment of Janus TMD monolayer, MoSSe as an example, affects the interlayer coupling of their van der Waals heterostructures (HSs). Here, we present the unexpected interfacial interactions of Janus MoS<sub>2</sub>/MoSSe HS by direct synthesis and twist stacking using low-frequency Raman spectroscopy. The interlayer coupling strength of Janus HS with 2H and 3R stackings is found to be strongly enhanced compared with their pristine MoS<sub>2</sub> counterparts through the linear chain model and density functional theory (DFT) calculations. Both experimental and DFT results indicate that the enhancement is attributed to the reduced interlayer distance due to the intrinsic dipole moment and the compressive strain of Janus MoSSe. On the other hand, low-frequency Raman modes of twisted MoS<sub>2</sub>/MoSSe heterobilayers exhibit characteristic dependence on the twisting angles that the shear and breathing modes are both observable only at high-symmetry angles. All these spectroscopic features along with DFT calculations serve as a fingerprint of the strong interlayer coupling in Janus HSs and indicate the potential in tuning the interlayer coupling strength through Janus heterostacking.

**5:20 AM F.EL04.10.04**

**2D Layered MOFs—The Response of a Flexible Platform to Dynamics of Confined Water** Farnaz A. Shakib, Mohammad Reza Momeni Taheri, Yuliang Shi, Zeyu Zhang and Yen-Jui Chen; New Jersey Institute of Technology, United States

Conductive layered metal-organic frameworks (MOFs) are a new family of 2D materials which offer electrical conductivity in addition to the other known fascinating properties of MOFs including permanent porosity and high surface area. Making progress towards application of these materials as field effect transistors, semiconductors and supercapacitors depends on a deep understanding of the structural, electronic and dynamical behavior of 2D MOFs at the atomistic level. Here, we answer to the open question of the structural stability of 2D MOFs subject to humidity with emphasis on Co<sub>3</sub>(HHTP)<sub>2</sub> and Cu<sub>3</sub>(HHTP)<sub>2</sub>, HHTP=2,3,6,7,10,11-hexahydroxytriphenylene, which show stark structural differences in aqueous solution. *Static* electronic structure methods are too perfect for reflecting the flexible nature of these layered materials

while *ab initio* molecular dynamics (AIMD) simulations are too expensive for providing a reliable picture of the complex dynamics in these systems. To tame the flexible and ever-changing layered structures of 2D MOFs, we develop *ab initio* parametrized force fields (AIFF) that allow large-scale/long-time simulations of the dynamics of both dry and hydrated MOFs. Our molecular dynamics simulations reproduces the structural properties of both MOFs as well as selective hydrolysis of metal nodes in hydrated  $\text{Co}_3(\text{HHTP})_2$  vs. intact metal nodes in hydrated  $\text{Cu}_3(\text{HHTP})_2$ , in agreement with experimental reports. Our developed AIFFs reveal that the reason behind this behavior is the presence of \textit{intrinsic defect sites} in dry  $\text{Co}_3(\text{HHTP})_2$ . Quantum mechanical calculations on cluster models cut from crystal structures confirm the higher tendency of  $\text{Co}^{2+}$  for coordination to water molecules compared to  $\text{Cu}^{2+}$  which prefers HHTP linkers. Our multi-faceted strategy paves the way toward simulation of realistic MOF-based materials and their interface with confined water molecules which is especially relevant to designing more robust water stable materials with desired properties and applications.

#### 5:30 AM F.EL04.10.05

**A Study on Electronic Properties of 2D MOFs Affected by Structural Deformations** Zeyu Zhang and Farnaz A. Shakib; New Jersey Institute of Technology, United States

Introduction of a highly stable metal organic framework (MOF) in the late 90s has inspired a wide range of interest in these porous structures. Their high surface area and permanent porosity has stimulated a spectrum of applications for gas adsorption/storage, water treatment, heterogeneous catalysis, and even defunctionalization of chemical warfare agents. Synthesis of conductive 2D layered MOFs, where extended  $\pi$ - $\pi$  conjugation creates possible intra- and inter-layer charge transfer path, opened another venue of potential applications for these intriguing materials. Tuning electronic properties of 2D MOFs for any specific application such as supercapacitors, field-effect transistors and electronically-induced chemical sensors can be a complicated challenge due to the flexibility of the layered structure that is composed of weak van der Waals interactions. The continuous strive for unravelling the electronic characteristics of 2D MOFs is most illustrated in the ongoing researches on  $\text{Ni}_3(\text{HITP})_2$ , HITP= 2,3,6,7,10,11-hexaiminotriphenylene, which since its synthesis in 2014 has been the subject of a continuous debate on being a metallic or semiconductor material. This debate arise from the fact that most theoretical studies and experimental deductions neglect the flexibility and structural dynamics of 2D MOFs, the two characteristics which should be fully addressed before trying to tune their electronic properties for any specific applications. Here, we employ a range of theoretical tools to elucidate different structural aspects of 2D MOFs and their individual effect on the electronic properties and overall conductivity of the material. By obtaining the  $1 \times 1 \times 1$   $\text{Ni}_3(\text{HITP})_2$  initial cell from experimental results, we construct a  $2 \times 2 \times 2$  unit cell and optimize it with periodic electronic structure calculation to get the most stable coordination geometry for metal site. According to this optimization, we develop an *ab initio* force field (AIFF) based on the most accurate quantum chemical calculations. Classical molecular dynamics based on the developed AIFF elucidate different structural deformations in specific environments. Then, we apply *ab initio* molecular dynamics (AIMD) to mimic same structural dynamics individually and determine their effects on electronic properties with subsequent periodic electronic structure calculations. Taking advantage of a combination of theoretical and computational tools, we create a general methodology to understand the electronic properties of 2D MOFs at an atomistic level.

#### 5:40 AM F.EL04.10.06

**Effect of BN Nanosheets on Mechanical and Thermal Properties of Polyethylene Nanocomposites** Md Golam Rasul<sup>1</sup>, Alper Kiziltas<sup>2</sup>, Reza Shahbazian-Yassar<sup>1</sup> and Babak Arfaei<sup>2</sup>; <sup>1</sup>University of Illinois at Chicago, United States; <sup>2</sup>Ford Motor Company, United States

Hexagonal boron nitride (BN) is an excellent 2D nanomaterial due to possessing with impressive mechanical property (e.g. Young's modulus  $\sim 1$  TPa), thermal stability up to 800 °C, high thermal conductivity (600 W/m-K), and electrically insulative properties (band gap  $\sim 5.97$  eV) (Boldrin *et al.*, 2011). These make BN a suitable reinforcement filler for the application of electrically insulating but thermally conductive polymer composite materials. While polymer nanocomposite offers a wide range of application including packaging to the automotive due to its exceptional low cost and lightweights with improved performances, one of the main challenges is the weak interfacial molecular interaction between reinforcement fillers and polymer matrix, affecting nanocomposite properties (Wang *et al.*, 2014).

In this work, we report a novel method to functionalize BNs by coupling agent silane (3-aminopropyltriethoxy) in order to assess the role of silane functional groups at the interface of polyethylene (PE) and BNs. We studied the effect of non-modified (pBN), and silane modified BNs (sBN) on the melt-extruded PE-BN composite performances by evaluating mechanical and thermal properties. While, both pBN and sBN nanomaterials enhance PE-BN nanocomposite performances, sBN have comparatively higher molecular interaction between PE matrix and BN fillers, resulting a significant improvement to the nanocomposite performances when compared with pBN composites. In comparison with PE materials, addition of 5 wt. % BN increases tensile modulus of elasticity by 37.4 and 42.2 %, tensile strength by 14.5 and 26.9 %, flexural modulus

of elasticity by 24 and 30.5 %, and storage modulus by 80 and 90.6 % for pBN and sBN nanocomposites, respectively. In addition to the mechanical reinforcement, thermal properties were also evaluated for PE-BN nanocomposites. While thermal stability of PE-pBN and PE-sBN nanocomposites was comparable, coefficient of thermal expansion was decreased by 11.7 and 20.3 % at 5 wt. % pBN and sBN loading, respectively. These results confirm enhanced molecular interaction of BN fillers with PE polymer matrix at the interface, affecting mechanical and thermal properties of the nanocomposites. The enhanced interfacial molecular interaction further reduced phonon scattering, resulting an increased thermal conductivity (14% increment for sBN composites when compared with pBN). However, low thermal stability of silane molecules makes it less attractive for limiting PE-BN nanocomposite thermal degradation. With 5 wt.% BN loading, PE-pBN nanocomposites show 4 °C increase in maximum degradation temperature while PE-sBN is increased by 2 °C. These polymer nanocomposites with enhanced mechanical and thermal properties can be an excellent choice for application in insulation materials, particularly for cables in automotive vehicles.

SESSION F.EL04.11: Photonics and Optoelectronic Properties and Devices  
On Demand Abstracts Available for Viewing Starting Saturday Morning, November 21, 2020  
F-EL04

**5:00 AM \*F.EL04.11.01**

**“Valley Noise” and Rydberg Excitons in Monolayer Semiconductors—Insights from (Really) High Magnetic Fields** Scott Crooker; National High Magnetic Field Lab, United States

Much of the current interest in atomically-thin transition metal dichalcogenide (TMD) semiconductors such as MoS<sub>2</sub> and WSe<sub>2</sub> is driven by the physics of coupled spin & valley degrees of freedom and the potential for new spin- and valley-based devices. This talk will discuss recent optical studies that probe the valley-related physics of electrons, holes, and excitons in monolayer TMD semiconductors.

In a first study [1,2], we measure the polarized magneto-absorption spectra of high-quality exfoliated TMD monolayers in very large magnetic fields to 91 tesla, which allows to follow the diamagnetic shifts of not only the 1s ground state of the neutral exciton but also its excited 2s, 3s, ..., ns Rydberg states. The energies and diamagnetic shifts provide a direct determination of the effective (reduced) exciton masses and also the dielectric properties of these monolayer semiconductors – fundamental material parameters that until now were available only from theoretical calculations. Moreover, we also measure other important material properties, including exciton binding energies, exciton radii, and free-particle bandgaps. These results provide essential and quantitative parameters for the rational design of opto-electronic van der Waals heterostructures incorporating 2D semiconductor monolayers.

In a second study, we introduce an entirely passive, noise-based approach for exploring intrinsic valley dynamics in monolayer TMD semiconductors [3]. Under conditions of strict thermal equilibrium, we use optical Faraday rotation to “listen” to the thermodynamic fluctuations of the valley polarization in a Fermi sea of resident electrons or holes, due to their spontaneous scattering between the *K* and *K'*. Frequency spectra of this valley noise reveal narrow Lorentzian lineshapes and therefore very long intrinsic valley relaxation, especially for holes (~microseconds). These results provide quantitative measurements of intrinsic valley dynamics, free from any external perturbation, pumping, or excitation.

*\*In collaboration with Mateusz Goryca, Jing Li, & Andreas Stier (NHMFL), Nathan Wilson & Xiaodong Xu (University of Washington), and Cedric Robert, Bernhard Urbaszek, & Xavier Marie (INSA-Toulouse)*

[1] M. Goryca *et al.*, *Nature Communications* **10**, 4172 (2019).

[2] A. V. Stier *et al.*, *Phys. Rev. Lett.* **120**, 057405 (2018).

[3] M. Goryca, N. P. Wilson, P. Dey, X. Xu, & S. A. Crooker, *Science Advances* **5**, eaau4899 (2019).

**5:15 AM \*F.EL04.11.02**

**Isotropic and Anisotropic Polaritons in van der Waals Materials** Qiaoliang Bao and Qingdong Ou; Monash University, Australia

Polaritons, hybrid light-matter excitations, enable nanoscale control of light. Particularly large polariton field confinement and long lifetimes can be found in graphene and van der Waals materials, opening new avenues for low-loss photonic



applications. Here, we present our recent progress in the discovery on engineering of these nanoscale polaritons in 2D materials [1,2]. First, plasmon polaritons arising from graphene and topological insulators were investigated in graphene/Bi<sub>2</sub>Te<sub>3</sub>, topological insulator Bi<sub>2</sub>Te<sub>3</sub>, graphene nanoribbon and 3D graphene using either spectroscopic or real space imaging techniques [3-6]. We show how the plasmonic coupling happens in two Dirac materials, how high-order plasmonic modes are observed in 3D graphene structure, how multiple plasmonic modes at sub-wavelength are achieved in graphene nanoribbon and how edge chirality controls the plasmonic shift.

We would also like to highlight our progress on the observation of anisotropic and ultra-low-loss polariton propagation along the surface of natural vdW material  $\alpha$ -MoO<sub>3</sub> [7]. We visualized and verified phonon polaritons with elliptic and hyperbolic in-plane dispersion, which have been theoretically predicted but never experimentally observed in natural materials before. To better utilize the low-loss directional polaritons, we developed a chemical intercalation method to reversibly control and switch the phonon polaritons while maintaining their long lifetimes [8]. Combined with photolithography, spatially controlled polariton switching was achieved with various in-plane heterostructure configurations and patterns. Most recently, we show how the hyperbolic polaritons in  $\alpha$ -MoO<sub>3</sub> thin slabs were delicately manipulated by controlling the interlayer twist angle [9]. We experimentally observed tunable topological transitions from open (hyperbolic) to closed (elliptical) dispersion contours in twisted  $\alpha$ -MoO<sub>3</sub> bilayers at a photonic magic twist angle. The theoretical analysis showed these transitions of in-plane hyperbolic polaritons are controlled by a topological quantity. At the transitions, the photonic dispersion of the resulting topological polaritons flattens, exhibiting low-loss tunable polariton canalization and diffractionless propagation. In summary, biaxial van der Waals semiconductors like  $\alpha$ -MoO<sub>3</sub>[7, 9] and V<sub>2</sub>O<sub>5</sub>[10] represent an emerging family of material supporting exotic polaritonic behaviors and these natural-born hyperbolic materials offer an unprecedented platform for controlling the flow of energy at the nanoscale.

#### 5:30 AM \*F.EL04.11.03

**Nanophotonics with Low-Dimensional Excitonic Materials** Deep M. Jariwala; University of Pennsylvania, United States

The isolation of a growing number of two-dimensional (2D) materials has inspired worldwide efforts to study their fundamental physical properties and integrate distinct 2D materials into van der Waals (vdW) heterostructures.<sup>1-2</sup> While the few atoms thick structure of 2D semiconductors naturally makes their electronic structure quantum confined, it also has profound implications on their optical properties.<sup>3-4</sup> Further being 2D in nature it also presents opportunities for engineering them into 0D and 1D quantum confined structures.<sup>5</sup> My talk will discuss our group's more recent work on optical phenomena and photonic devices made from 2D semiconductors. I will present how 1D nanostructuring of excitonic 2D semiconductors into nanophotonic dielectric gratings can enable exploration of new regimes of light-matter confinement including formation of hybrid exciton-plasmon-polariton states.<sup>6</sup> I will extend this discussion of light-matter interaction to excitonic/dielectric superlattices which are scalable over large areas. I will extend this concept to other excitonic materials and show dynamic tunability of their optical properties. If time permits, I will also discuss new approaches and methods for nanostructuring 2D semiconductors down to ~5 nm lateral dimensions with superior control of crystallinity and structure.<sup>7</sup> I will conclude by giving a broad perspective on future prospects of 2D materials from fundamental science to applications.

#### References:

1. Jariwala, D.; Marks, T. J.; Hersam, M. C., *Nature Materials* **2017**, *16*, 170-181.
2. Jariwala, D.; et al. *ACS Nano* **2014**, *8*, 1102-1120.
3. Brar, V. W.; Sherrott, M. C.; Jariwala, D., *Chemical Society Reviews* **2018**, *47*, 6824-6844.
4. Jariwala, D.; et al. *ACS Photonics* **2017**, *4*, 2692-2970.
5. Stanford, M. G.; Rack, P. D.; Jariwala, D., *npj 2D Materials and Applications* **2018**, *2*, 20.
6. Zhang, H.; ...Jariwala, D., et al. Hybrid Exciton-Plasmon-Polaritons in van der Waals Semiconductor Gratings. *Nature Communications* **2020**, (in press).
7. Kumar, P....Stach, E. A.; Jariwala, D., et al. *Npj 2D Materials and Applications* **2020**, <https://doi.org/10.1038/s41699-020-0150-2>.

#### 5:45 AM F.EL04.11.04

**Tailoring B-Exciton Emission in a Mixed Dimensional MoS<sub>2</sub>:AgPO<sub>3</sub> Nanoheterojunctions** Abdus S. Sarkar<sup>1</sup>, Emmanuel Stratakis<sup>1,2</sup>, Ioannis Konidakis<sup>1</sup>, Ioanna Demeridou<sup>1,2</sup>, Efthymis Serpetzoglou<sup>1,2</sup> and George Kioseoglou<sup>2</sup>; <sup>1</sup>Foundation for Research and Technology Hellas, Greece; <sup>2</sup>University of Crete, Greece

Tailoring the photoluminescence (PL) in two dimensional (2D) transition metal dichalcogenide (TMDs) using external factors is one of the remarkable interest for its use in emerging valleytronics, nanophotonic and optoelectronic applications.<sup>1,2</sup> Significant effort have been devoted to enhance or manipulate the excitonic emission in a monolayer MoS<sub>2</sub>. However, it has limited to the nanoscale fundamental studies for nanoelectronics and photonics applications. Here, we will

talk about a novel van der Waals nano- hybrid/heterojunctions system fabricated with a non-lithographic process to manipulate the PL emission, which is composed of a few layer MoS<sub>2</sub> integrated into a transparent semiconducting silver metaphosphate glass matrix. Successful isolation and formation of heterojunction revealed the preservation of phase integrity and the crystallinity. The heterojunctions demonstrated exotic intrinsic A- and B- excitonic peak emission. More interestingly we are able to tailor a dominant B- excitonic emission over A excitonic emission. A significant 6-fold enhancement in PL spectrum (van der Waals heterojunctions) over a control sample was recorded (Figure 1).<sup>3</sup> Furthermore, exciton plasmon coupling was undertaken to demonstrate the enhancement in B-excitonic emission of the van der Waals nanoheterojunctions. Finally, an ultrafast time-resolved spectroscopy interpreted the plasmon-enhanced electron transfer that takes place in Ag nanoparticles-MoS<sub>2</sub> nanoheterojunctions is behind the enhancement of the excitonic emission. No doubt, the efficient coupling of exciton-plasmon and tunability of B- excitonic emission pave great attention in emerging valleytronic and light emitting devices working with B excitons.

#### References

1. Sajede Manzeli, D. Ovchinnikov, D. Pasquier, O. V. Yazyev, & A. Kis, *Nat. Rev. Mater.*, 2, 17033 (2017).
2. G. M. Akselrod, T. Ming, C. Argyropoulos, T. B. Hoang, Y. Lin, X. Ling, D. R. Smith, J. Kong, and M. H. Mikkelsen, *Nano Lett.*, 15, 3578-3584 (2015).
3. A. S. Sarkar, I. Konidakis, I. Demeridou, G. Kioseoglou and E. Stratakis, Under review, 2020, <https://arxiv.org/abs/2005.02852>

#### 5:55 AM F.EL04.11.05

**Observation of Polaronic Trions in MoS<sub>2</sub>/SrTiO<sub>3</sub> Heterostructures** Soumya Sarkar, Maxim Trushin, Sinu Mathew, Sreetosh Goswami, Shaffiue Adam and T. Venky Venkatesan; National University of Singapore, Singapore

The reduced electrical screening in two-dimensional (2D) materials provides an ideal platform for realization of exotic quasiparticles, that are robust and whose functionalities can be exploited for future electronic, optoelectronic and valleytronic applications. Recent examples include an interlayer exciton, where an electron from one layer binds with a hole from another, and a Holstein polaron, formed by an electron dressed by a sea of phonons. Here, we report a new quasiparticle, ‘polaronic trion’ in a heterostructure of MoS<sub>2</sub>/SrTiO<sub>3</sub>. This emerges as the Fröhlich bound state of the trion in the atomically thin monolayer of MoS<sub>2</sub> and the very unique low energy soft phonon mode ( $\leq 7$  meV, which is temperature and field tunable) in the quantum paraelectric substrate SrTiO<sub>3</sub> (STO), arising below its structural antiferrodistortive (AFD) phase transition temperature. This dressing of the trion with soft phonons manifests in an anomalous temperature dependence of photoluminescence emission leading to a huge enhancement of the trion binding energy ( $\sim 70$  meV). The soft phonons in STO are sensitive to electric field, which enables field control of the interfacial trion-phonon coupling and resultant polaronic trion binding energy. Lastly, these results suggest evidence of Rotational Fröhlich Coupling a result of the counter intuitive interplay between the rotational axis of the MoS<sub>2</sub> trion and STO phonon mode. Polaronic trions could provide a platform to realize quasiparticle based tunable optoelectronic applications driven by many body effects.

#### References:

1. Sarkar, S., Goswami, S., Trushin, M., Saha, S., Panahandeh-Fard, M., Prakash, S., Tan, S.J.R., Scott, M., Loh, K.P., Adam, S. and Mathew, S., 2019. Polaronic Trions at the MoS<sub>2</sub>/SrTiO<sub>3</sub> Interface. *Advanced Materials*, 31(41), p.1903569.
2. Trushin, M., Sarkar, S., Mathew, S., Goswami, S., Adam, S. and Venkatesan, T., 2019. Evidence of Rotational Fröhlich Coupling in Polaronic Trions. *arXiv preprint arXiv:1911.09118*.
3. <https://www.advancedsciencenews.com/discovery-of-an-unusual-quasiparticle-in-a-2d-material/>
4. <https://www.sciencedaily.com/releases/2019/08/190827095049.htm>

#### 6:05 AM F.EL04.11.06

**Dispersion-Free Estimation of Color and Spectrum of Visible Light Using 2D Materials and Machine Learning** Davoud Hejazi, Sarah Ostadabbas and Swastik Kar; Northeastern University, United States

Recognizing color is a primary means of object identification – both in biological and non-biological systems. In the latter case, i.e. conventional photodetection or imaging, arbitrary color-identification is not an inherent function. On one hand, a color-camera can disperse incident light into its red, green and blue (RGB) components (using filters) and merely record the voltage-response the RGB-filter-covered detectors in a 0-255 scale. However, either a classification algorithm or a human observer of the regenerated image is needed to recognize the color. For pure machine-based color recognition, the set of recorded RGB responses can be used to estimate the nearest color of the incident light without the observer’s mediation. Spectral estimation on the other hand, usually carried out using dispersion-based spectrometers, is the process of breaking the incident light into its wavelength components via diffraction-grating and finding the intensity at each wavelength. These two types of tools, camera and spectrometers, however, cannot be used interchangeably and each have their limitations. We report

on a dispersion-free 2D materials-based and machine learning-enabled color and spectrum-estimator, that can mimic the color-estimation ability of the eye by learning to perceive new colors, as well as spectral estimation capability in the spectral range of 350 nm – 800 nm. This technique, where we use optical transmittance of a few transition-metal-dichalcogenide (TMD)-based thin-film filters -present an alternative for the estimation problem, and can reduce the manufacturing costs and the design complexities of the conventional color-estimation and spectrum-estimation tools, and also introduce the learning capacity to the estimator.

Through a comprehensive simulation scheme that led to the selection of an ideal set of filters, we have shown the importance of excitonic features of the transmittance curves in the estimation problem, and have designed and fabricated the thin-film filters based on outcome of these simulations. We have also studied the efficacy of various machine learning algorithms and identified the key advantages and limitations of each algorithm for color and spectrum estimation. Finally, by modeling the temporal drift of spectral transmittance of the filters over the period of one year, we have shown that it is possible to overcome the drift-induced inaccuracies over extended times.

#### **6:15 AM F.EL04.11.07**

**Isotropic, Stronger Light Absorption in Atomically Thin Materials by Geometry Design** Jong-Hoon Kang, Myungjae Lee, Fauzia Mujid and Jiwoong Park; The University of Chicago, United States

Two-dimensional (2D) materials are promising candidates for optoelectronics. Previous studies have shown that light absorption in 2D materials can be enhanced by generating multilayers using layer-by-layer stacking or integration with cavity resonators. However, these approaches have critical limitations as they may lead to optical properties that differ from the intrinsic properties of monolayers and they are still governed by the anisotropic thin film absorption with little control over light with different polarizations and incident angles. Here, we show that adding three-dimensional (3D) textures with controlled geometry to 2D materials, demonstrated with monolayers of transition metal dichalcogenides (TMDs), is a powerful solution to these challenges. For this, monolayer TMDs ( $\text{MoS}_2$ ,  $\text{WS}_2$ , and  $\text{WSe}_2$ ) were conformally grown on surfaces with nanoscale half-spherical textures, producing wafer-scale optical films with distinct geometry at different length scales: globally they behave as an optically flat substrate, whereas they possess isotropic bubble-like surfaces at the sub-wavelength limit. Spectrally-resolved, angle- and polarization-dependent absorption and reflection measurements confirm that all our TMD films with 3D textures have enhanced absorption for all visible wavelengths with a more pronounced enhancement for higher incident angles and p-polarization that flat optical films do not absorb strongly. This suggests that our TMD monolayers provide flat optoelectronic films with enhanced and isotropic light absorption, which can be precisely predicted by the geometric design of the surface texture parametrized by the aspect ratio of the domes in our experiment. This approach will advance the development of integrated optoelectronic circuitry with customizable light absorption.

#### **6:25 AM F.EL04.11.08**

**Bulk Transition Metal Dichalcogenides for Integrated Photonics** Haonan Ling, Renjie Li and Artur Davoyan; University of California, Los Angeles, United States

Transition metal dichalcogenide materials (TMDCs) are an emerging type of van der Waals semiconductors that possess unique electronic and optical properties<sup>1,2</sup> making them promising candidates for future photonic devices. Previous studies focused on monolayer/few layer structures, while, at the same time, properties of bulk materials and their applications have received little attention. Here we study theoretically light interaction with and propagation in bulk TMDCs materials. We show that owing to their high refractive index<sup>3</sup>, TMDCs may pave the way to a new generation of optical components with higher light confinement and smaller footprint, when compared to traditional Si and III/V photonic devices.

We begin our analysis with a study of light guiding in a simple planar waveguide made of bulk TMDCs ( $\text{MoS}_2$ ,  $\text{MoSe}_2$ ,  $\text{WS}_2$  and  $\text{WSe}_2$ ) and conventional semiconductors (Si, InP and GaAs). In our analysis we focus on the near-infrared and telecom frequencies, that is, below the band gap of the semiconductors, where materials are transparent. By analyzing the dispersion and mode properties of such waveguides, we find that the waveguide footprint may be reduced almost twice when compared to counterparts made of Si. Next we extended our analysis to other waveguide structures, including ridge, rib and slot waveguides. We show that deeply subwavelength and highly confined light guiding is possible in waveguides made out of TMDCs. These findings may pave the way to novel subwavelength optical devices based on TMDC materials.

We further discuss light interaction with photonic crystals made of TMDC materials. Specifically, we have designed and analyzed a 2D photonic crystal slab with a cavity in it. We find that the size of such a cavity can be made significantly smaller (~30%) than that for a comparable Si or GaAs structures, while demonstrating higher resonator quality factor. Small device size and significant concentration of electromagnetic field have profound implications for quantum and nonlinear optics. Specifically, as we show, such cavities demonstrate a threefold enhancement of Purcell factor when compared to analogous Si resonators. We then demonstrate that strong optical confinement in a small volume leads to a strong light-materials interaction and can be utilized to create more energy efficient active devices, such as modulators. In particular, we

demonstrate that two-fold reduction in both cross-sectional area and switching energy consumption are possible with TMDC structures.

Finally we discuss a potential roadmap for integrated photonics based on TMDC structures. We show that owing to an enhanced light-materials interaction in TMDC nanostructures novel opportunities for highly integrated and energy efficient photonic devices emerge.

#### References:

1. Mak, K. F.; Shan, J. J. N. P., Photonics and optoelectronics of 2D semiconductor transition metal dichalcogenides. 2016, 10 (4), 216.
2. Xia, F.; Wang, H.; Xiao, D.; Dubey, M.; Ramasubramaniam, A. J. N. P., Two-dimensional material nanophotonics. 2014, 8 (12), 899.
3. Wilson, J. A.; Yoffe, A. J. A. i. P., The transition metal dichalcogenides discussion and interpretation of the observed optical, electrical and structural properties. 1969, 18 (73), 193-335.

#### 6:35 AM F.EL04.11.09

**Anisotropic MoS<sub>2</sub> Nanoscale Patterns for Light Interaction by Design** Christian Martella<sup>1</sup>, Andrea Camellini<sup>2</sup>, Mukul Bhatnagar<sup>3</sup>, Marina Caterina Giordano<sup>3</sup>, Carlo Mennucci<sup>3</sup>, Pinaka Pani Tummala<sup>1</sup>, Debasree Chowdhury<sup>3</sup>, Andrea Mazzanti<sup>2</sup>, Margherita Zavelani Rossi<sup>2,1</sup>, Giuseppe Della Valle<sup>2,1</sup>, Francesco Buatier de Mongeot<sup>3</sup>, Alessio Lamperti<sup>1</sup> and Alessandro Molle<sup>1</sup>; <sup>1</sup>Consiglio Nazionale delle Ricerche, Italy; <sup>2</sup>Politecnico di Milano, Italy; <sup>3</sup>Università degli Studi di Genova, Italy

Two-dimensional flat MoS<sub>2</sub> retains an outstanding interest as active material to manipulate light via modulation or harvesting, owing to its thickness dependent optical response. Starting from this background, MoS<sub>2</sub> layers nanostructured in anisotropic layouts gain an extra-control of the optical characteristics enabling fabrication of novel metasurfaces or flat-optic configurations for light harvesting [1]. Here we illustrate two possible methodologies to reduce ultra-thin MoS<sub>2</sub> to different anisotropic structural fashions. One consists of rippling MoS<sub>2</sub> by means of pattern-assisted chemical vapour deposition [2]. This way, we prove MoS<sub>2</sub> can be continuously grown on a one-directional pre-patterned substrate by means of chemical vapor deposition or sulfurization schemes therein mimicking the anisotropic shape feature [3]. This results in a strongly dichroic optical response that is concomitant with an anisotropic strain redistribution in the MoS<sub>2</sub> layer (revealed by 2D Raman mapping and Kelvin-probe force microscopy) [2] and with a peculiar exciton dynamics (revealed by transient optical spectroscopy) [4]. As an alternative, a second layout is based on physically separated MoS<sub>2</sub> stripes with nanoscale thickness (few nm) produced by sulfurization of a Mo ribbon-like pattern prefabricated by laser interference lithography. Spatial confinement in the stripe pattern results in an enhanced ultrabroadband amplification of the optical absorption throughout the visible spectrum following a guided-mode anomaly. This layout is also presented as a suitable platform where to engineer hybrid plasmonic systems as, for instance, coming from the interplay of MoS<sub>2</sub> nanostripes and Au nanoparticles. Overall, we show that MoS<sub>2</sub> (and expectedly other 2D transition metal dichalcogenides with similar features) is strikingly suitable to anisotropy design expanding the edges of light-matter interactions with potential in applications for optical modulation, large-area flat optics, and light harvesting.

[1] C. Martella et al., Adv. Mater. (2018) 1, 1705615

[2] C. Martella et al., Adv. Mater. (2017) 29, 1605785

[3] C. Martella et al., Nano Res. (2019) 12, 1851

[4] A. Camellini et al., ACS Photon. (2018) 5, 3363

#### 6:45 AM F.EL04.11.10

**Study of Transmission Properties of Distorted 1T ReS<sub>2</sub> Based Type-II van der Waals Heterostructures** Dipankar Saha and Saurabh Lodha; Indian Institute of Technology Bombay, India

For the last few years we have been witnessing significant progress in micro and nano photonics due to successful fabrication of atomically thin optoelectronic devices based on two-dimensional (2D) layered materials and their vertical stacks [1-5]. Considering near infrared (NIR)/short-wave infrared (SWIR) photodetection, we find a theoretical study reported in [6] which describes various possible combinations of group-6 and group-7 monolayer TMDs. Among different combinations of type-II van der Waals (vdW) heterointerfaces, owing to efficient generation, separation, and collection of charge carriers, it has been found that both ReS<sub>2</sub>/WSe<sub>2</sub> and ReS<sub>2</sub>/MoSe<sub>2</sub> emerge as potentially promising candidates for the next generation ultrathin optoelectronic devices [6].

However, the analysis of electronic transmission through ReS<sub>2</sub>/WSe<sub>2</sub> and ReS<sub>2</sub>/MoSe<sub>2</sub> heterostructures is required for further insights on their conductance at near-equilibrium. In this work, employing density functional theory (DFT) and nonequilibrium Green's function (NEGF) combination, we have computed zero bias transmission spectra of the two-port devices with monolayer ReS<sub>2</sub>/monolayer WSe<sub>2</sub> and monolayer ReS<sub>2</sub>/monolayer MoSe<sub>2</sub> channels. In order to conduct first-

principles based DFT calculations, we have utilized the "QuantumATK" software package [7]. For a small energy range (-2 eV to 2 eV) near the Fermi level, we find that the electronic transmission through ReS<sub>2</sub>/MoSe<sub>2</sub> heterointerface is slightly better than that in ReS<sub>2</sub>/WSe<sub>2</sub>. Besides, the near-direct bandgap and superior optical absorption of the constituent MoSe<sub>2</sub> layer are the other key features which make ReS<sub>2</sub>/MoSe<sub>2</sub> heterostructure suitable for NIR/SWIR photodetection [6]. However, the electronic structure calculations reveal that the larger band offset values at the interface can ensure better separation of charge carriers for ReS<sub>2</sub>/WSe<sub>2</sub> vertical stack.

\* This work was funded by the Department of Science & Technology, Govt. of India through the grant DST/SJF/ETA-01/2016-17. D.S. acknowledges the Department of Electrical Engineering, Indian Institute of Technology (IIT) Bombay for the Institute Post Doctoral Fellowship.

#### References:

- [1] F. H. L. Koppens et al., *Nature Nanotechnology*, 9, 780-793, 2014.
- [2] T. C. Berkelbach and D. R. Reichman, *Annu. Rev. Condens. Matter Phys.*, 9, 379-396, 2018.
- [3] The International Technology Roadmap For Semiconductors 2.0, "Outside System Connectivity," 2015.
- [4] A. K. Geim and I. V. Grigorieva, *Nature*, 499, 419-425, 2013.
- [5] C-H. Lee et al., *Nature Nanotechnology*, 9, 676-681, 2014.
- [6] D. Saha, A. Varghese, and S. Lodha, *ACS Appl. Nano Mater.*, 3, 820-829, 2020.
- [7] QuantumATK version 2018.06, Synopsys Quantumwise A/S, Available at <http://quantumwise.com/>.

#### 6:55 AM F.EL04.11.11

**Optics in Crystalline Atomically-Thin Films—Nonlinear and Nonlocal Phenomena** Alvaro Rodriguez Echarr<sup>1</sup>, Joel Cox<sup>2,3</sup> and Javier Garcia de Abajo<sup>1,4</sup>; <sup>1</sup>ICFO - The institute of Photonic Sciences, Spain; <sup>2</sup>Center for Nano Optics, University of Southern Denmark, Denmark; <sup>3</sup>Danish Institute for Advanced Study, University of Southern Denmark, Denmark; <sup>4</sup>ICREA – Institutió Catalana de Recerca i Estudis Avançats, Spain

Crystalline metallic films are attracting significant attention within the nanophotonics community as a material platform for plasmonics that offers light concentration and manipulation on extreme subwavelength scales with lower intrinsic losses than for plasmons in amorphous metal films. Recent advances in nanotechnology now enable the fabrication of such crystalline films with nanometer-scale thickness, down to the level of only several atomic monolayers, further boosting plasmon confinement for the miniaturization of next-generation electronic and photonic devices. However, in very thin crystalline metallic films, quantum mechanical effects play a non-negligible role in the dynamics of electrons and their interaction with external electromagnetic fields, manifesting in the spectral features associated with its linear optical response that depend on film thickness and crystallographic orientation. These effects are anticipated to become even more significant when dealing with nonlinear optical phenomena, which necessitate intense optical fields that access additional transitions among quantized electronic states.

Here we reveal quantum and finite-size effects in the nonlinear optical response associated with plasmons supported by few-atom-thick crystalline noble metal films. In particular, we employ a quantum-mechanical description that captures the main features in the electronic band structure associated with the various crystal facets of noble metals to simulate their nonlinear optical response by extending the random-phase approximation to higher orders. Our results demonstrate strong signatures of film thickness and crystallographic orientation in the linear plasmonic response that are amplified in nonlinear optical processes such as harmonic generation and two-photon absorption, with additional effects attributed to surface states, electron spill out, and the directional band gap associated with bulk atomic-layer corrugation. These findings are of key importance in the characterization of atomically-thin crystalline films and their applications for nonlinear plasmonic nanophotonic devices.

#### 7:05 AM F.EL04.11.12

**Exfoliated CrPS<sub>4</sub> with Promising Photoconductivity** Adam K. Budniak<sup>1</sup>, Niall A. Killilea<sup>2</sup>, Szymon J. Zelewski<sup>3</sup>, Mykhailo Sytnyk<sup>2</sup>, Yaron Kauffmann<sup>1</sup>, Yaron Amouyal<sup>1</sup>, Robert Kudrawiec<sup>3</sup>, Wolfgang Heiss<sup>2</sup> and Efrat Lifshitz<sup>1</sup>; <sup>1</sup>Technion--Israel Institute of Technology, Israel; <sup>2</sup>Friedrich-Alexander Universitat Erlangen-Nurnberg, Germany; <sup>3</sup>Wroclaw University of Science and Technology, Poland

Layered semiconductors attract significant attention due to their diverse physical properties controlled by their composition and the number of stacked layers. Herein, large crystals of the ternary layered semiconductor chromium thiophosphate (CrPS<sub>4</sub>) are prepared by a vapor transport synthesis. Optical properties are determined using photoconduction, absorption, photorefectance, and photoacoustic spectroscopy exposing the semiconducting properties of the material. A simple, one-step protocol for mechanical exfoliation onto transmission electron microscope grid is developed [1,2] and multiple layers are

characterized by advanced electron microscopy methods, including atomic resolution elemental mapping confirming the structure by directly showing the positions of the columns of different elements' atoms. CrPS<sub>4</sub> is also liquid exfoliated and in combination with colloidal graphene, an ink-jet printed photodetector is created. This all-printed graphene/CrPS<sub>4</sub>/graphene heterostructure detector demonstrates specific detectivity of  $8.3 \times 10^8$  (D\*). This study shows a potential application of both bulk crystal as well as individual flakes of CrPS<sub>4</sub> as active components in light detection, when introduced as ink printable moieties with a large benefit for manufacturing [1].

#### References:

- [1] A.K. Budniak, N.A. Killilea, S.J. Zelewski, M. Sytnyk, Y. Kauffmann, Y. Amouyal, R. Kudrawiec, W. Heiss, E. Lifshitz; *Small*, **2020**, 16 (1), 1905924  
[2] M. Shentcis, A.K. Budniak, R. Dahan, Y. Kurman, X. Shi, M. Kalina, H.H. Sheinfux, M. Blei, M.K. Svendsen, Y. Amouyal, F. Koppens, S. Tongay, K.S. Thygesen, E. Lifshitz, F.J.G. de Abajo, L.J. Wong, I. Kaminer; *Under revision in Nature Photonics*

#### Acknowledgments:

This work was supported by the European Commission via the Marie-Sklodowska Curie action Phonsi (H2020-MSCA-ITN-642656)

This work was performed within the grant of the National Science Centre Poland (OPUS 11 no. 2016/21/B/ST3/00482). S.J.Z. also acknowledges the support within the ETIUDA 5 grant from National Science Center Poland (no. 2017/24/T/ST3/00257).

#### 7:15 AM F.EL04.11.13

**Charge Carrier Relaxation Dynamics and Phonon Coupling in Layered Bismuth Halide Semiconductors** Lissa Eyre<sup>1</sup>, Tahmida Huq<sup>2</sup>, Lana C. Lee<sup>2</sup>, Robert Hoye<sup>3</sup>, Hannah Joyce<sup>2</sup> and Felix Deschler<sup>1</sup>; <sup>1</sup>Technical University Munich, Germany; <sup>2</sup>University of Cambridge, United Kingdom; <sup>3</sup>Imperial College London, United Kingdom

A promising class of lead-free semiconductors for photovoltaic applications include the bismuth halides, such as bismuth iodide [1], bismuth oxyiodide [2] and the double perovskite Cs<sub>2</sub>AgBiBr<sub>6</sub> [3]. Although these materials have been predicted to exhibit defect tolerance, as seen in lead-halide perovskites, and already display improved stabilities and long charge carrier lifetimes, the power conversion efficiencies of the corresponding devices have not reached the level of lead-based perovskites. Potential reasons for this are explored, for example, the disconnected nature of the bismuth halide octahedra in the crystal structure, which limits carrier mobility, and the lower levels of absorption due to indirect bandgaps. Phonons have been shown to play a crucial role in carrier transport and hot carrier cooling in the lead halides [4], and there are many reports of strong carrier-phonon coupling, especially in low-dimensional morphologies [5]. The effect of phonons is expected to be even greater in the bismuth based perovskites due to their indirect bandgaps, as carriers will emit phonons to cool to the band extrema separated in momentum space from the excitation point, as well as to recombine. The combined effects of quantum confinement and coupling to phonons could allow carriers to overcome this distance in momentum space. The relative rates of these processes are vital for device efficiency, therefore we probe the early-time excited states in many bismuth halide semiconductors using transient absorption, Raman and photoluminescence spectroscopy. Overall, this work indicates that bismuth-based materials have the potential to be used in efficient optoelectronic devices, but there is a need to account for the effects of strong carrier-phonon coupling and localisation of electronic states on carrier scattering rates. We therefore present charge carrier-lattice interaction strength as an important design criterion for efficient next-generation solar cells.

[1] R. Brandt et al., *J. Phys. Chem. Lett.* **6**, 4297–4302 (2015).

[2] R. Hoye et al., *Adv. Mater.* **1702176** (2017).

[3] R. Hoye et al., *Adv. Mater. Interfaces* **1800464** (2018).

[4] M. Price et al., *Nat. Commun.* **6**, 8420 (2015).

[5] F. Thouin et al., *Nature Materials* **18**, 349–356 (2019).

#### 7:25 AM F.EL04.11.14

**Coupling between Light and 2D Polaritons—Fundamental Limits and How to Overcome Them** Eduardo Brioso Dias<sup>1</sup> and F. Javier Garcia de Abajo<sup>1,2</sup>; <sup>1</sup>ICFO—The Institute of Photonic Sciences, Spain; <sup>2</sup>ICREA - Institutió Catalana de Recerca i Estudis Avançats, Spain

Polaritons in 2D materials have been extensively studied over the past decade due to their fundamental interest and as a

platform for applications in telecommunications and sensing [1]. The wavelength of these polaritons is generally small compared to that of a photon of the same frequency [2], making them very attractive to manipulate light at deep-subwavelength distances. However, it simultaneously introduces a challenge in the coupling between propagation light and plasmonic modes, since the momentum mismatch between the two makes the in/out-coupling of this process intrinsically weak [2].

In this work, we address some fundamental limits in the coupling of radiation to 2D polaritons [3]. We study the scattering properties of 0D and 1D scatterers over a 2D or finite-thickness layer and quantify the coupling of light-to-polaritons cross-section for this process as a function of the scatterer effective polarizability. We find a generalization of the optical theorem to 2D polaritons, which allows us to determine the maximum possible value of their effective polarizability, which is remarkably independent of material. We present our results in the form of simple and rigorous analytical expressions, delivering an exact quantitative measure of photon-to/from-polariton coupling and polariton-to-polariton scattering. To that end, we first introduce a universal characterization of 2D SPs and their associated optical fields in terms of a single parameter – the ratio of their wavelength  $\lambda_p$  to the film thickness – regardless of the physical nature of the material's response. This allows us to determine the efficiency of different optical scattering channels involving incident light and polaritons, expressed in terms of universal light-polariton coupling strengths and fundamental limits to the scatterer polarizability. We write the result as a universal curve that is applicable to any layer thickness in the electrostatic approximation. Additionally, this result leads to a maximum light-to-polariton coupling cross-section which we explore, particularly by directly comparing the coupling efficiency of 0D and 1D scatterers and finding that the latter are up to 100 times more efficient than the former. We formulate our results for both 0D and 1D scatterers, including material edges, and present them in simple closed-form expressions. We finally propose coupling light to plasmons using a graphene edge as a configuration which maximizes the coupling efficiency, and address the case of scatterers with intrinsic losses to propose an optimum distance between the surface and the scatterer which maximizes the efficiency.

We find the maximum possible photon-to-polariton cross section to be of the order of  $\lambda_p^3/\lambda_0$  and  $\lambda_p^2/\lambda_0$  for point and line scatterers, respectively ( $\lambda_0$  is the light wavelength). For graphene, the limits to in-coupling are quantified by the maximum possible ratio between the numbers of generated plasmons and incident photons  $N_{\text{plasmon}}/N_{\text{photon}} \sim \alpha^3$  and  $\alpha^2$  for point and line scatterers, where  $\alpha \approx 1/137$  is the fine structure constant. Besides their fundamental interest, our results provide useful tools for the design of optical devices involving the in/out-coupling of propagating light and 2D SPs.

[1] J. García de Abajo, "Graphene Plasmonics: Challenges and Opportunities," ACS Photonics 1, 135 (2014).

[2] A.H. Castro Neto, F. Guinea, N.M.R. Peres, K.S. Novoselov, and A.K. Geim, "The electronic properties of graphene," Rev. Mod. Phys. 81, 109 (2009).

[3] E.J.C. Dias and F.J. García de Abajo, "Fundamental Limits to the Coupling between Light and 2D Polaritons by Small Scatterers." ACS Nano 13, 5184 (2019).

### 7:35 AM F.EL04.11.15

**Late News: Interlayer Excitons in Bilayer MoS<sub>2</sub>** [Shivangi Shree](#)<sup>1</sup>, Ioannis Paradisanos<sup>1</sup>, Nadine Leisgang<sup>2</sup>, Antony George<sup>3</sup>, Lukas Sponfeldner<sup>2</sup>, Cedric Robert<sup>1</sup>, Kenji Watanabe<sup>4</sup>, Takashi Taniguchi<sup>4</sup>, Richard J. Warburton<sup>2</sup>, Andrey Turchanin<sup>3</sup>, Xavier Marie<sup>1</sup>, Iann C. Gerber<sup>1</sup> and Bernhard Urbaszek<sup>1</sup>; <sup>1</sup>CNRS LPCNO INSA-CNRS-UPS, France; <sup>2</sup>University of Basel, Switzerland; <sup>3</sup>Institute of Physical Chemistry, Friedrich Schiller University, Germany; <sup>4</sup>National Institute for Materials Science, Japan

Transition metal dichalcogenides (TMDs) are ideal for exploring fundamental physics and applied optics as they are semiconductors with a direct bandgap in the monolayer limit. Chemical vapor deposition (CVD) allows growing wafer scale thin films of TMDs. The improved optical quality of MoS<sub>2</sub> monolayers with a reduced transition linewidth below 5 meV at low temperature (T = 4 K) by reducing dielectric disorder allows combining CVD grown MoS<sub>2</sub> monolayers to form multilayers to access new functionalities [1,2].

We examine the correlation between the stacking order and the interlayer coupling of valence states in high quality MoS<sub>2</sub> as grown CVD bilayers and artificially stacked bilayers from CVD monolayers. We show that hole delocalization over the bilayer in 2H stacking is allowed and results in strong interlayer exciton absorption and also in a larger A-B exciton separation as compared to 3R bilayers, where both holes and electrons are confined to the individual layers [2,3]. Comparing white light reflectivity spectra for 2H and 3R stacking allows extracting an interlayer coupling energy of about 50 meV. Obtaining very similar results for as-grown and artificially stacked bilayers is promising for assembling large area van der Waals structures with CVD material, using inter layer exciton formation and A-B exciton separation as indicators for interlayer coupling [2].

In bilayer MoS<sub>2</sub> the interlayer exciton has an out-of-plane static electric dipole. We show that as a result the interlayer exciton transition energies are widely tunable in applied electric fields, which is impossible for excitons in monolayers.

We show tuning over 120 meV of interlayer excitons with a high oscillator strength in bilayer MoS<sub>2</sub> due to the quantum-confined Stark effect [4]. We optically probed the interaction between intra- and interlayer excitons as they were energetically tuned into resonance. Interlayer excitons interact strongly with intralayer B excitons, as demonstrated by a clear avoided crossing, whereas the interaction with intralayer A excitons is substantially weaker. Our observations are supported by density functional theory (DFT) calculations, which include excitonic effects.

[1] S. Shree, A. George et al., 2D Materials, 7, 1 (2019).

[2] I. Paradisanos, S. Shree, Nature Communications, 11, 2391 (2020).

[3] I. C. Gerber, E. Courtade, S. Shree et al., Physical Review B, 99, 035443 (2019).

[4] N. Leisgang, S. Shree, I. Paradisanos, L. Sponfeldner, Nature Nanotechnology, 2612, 63 (2020).

#### 7:45 AM F.EL04.11.16

#### Late News: Two-Dimensional Material-Based Nanocomposites for Photocatalytic Environmental and Energy Applications Qingzhe Zhang, Mohamed Chaker and Dongling Ma; INRS, Canada

Following the graphene breakthrough, many other 2D materials have been discovered and extensively studied due to their exceptional physicochemical properties arising from the unique layered structure. Therein, 2D graphitic carbon nitride (g-C<sub>3</sub>N<sub>4</sub>) nanosheet has attracted dramatically increasing attention as a photocatalyst because of its nontoxicity, low cost, high stability and large surface, etc. However, g-C<sub>3</sub>N<sub>4</sub> is still suffering from fast recombination of photo-induced charge carriers and insufficiently broad photoresponse range.<sup>1-2</sup> Herein, we will present some of our recent development in efficient and broadband 2D g-C<sub>3</sub>N<sub>4</sub> nanosheet-based photocatalysts. One example is about our synthesized nanocomposites based on plasmonic Au nanoparticles (NPs) and in-situ synthesized lanthanide-doped NaYF<sub>4</sub> on g-C<sub>3</sub>N<sub>4</sub>. It showed enhanced ultraviolet (UV)-, visible- and near infrared (NIR)-light photocatalytic activity in the degradation of organic pollutants.<sup>3</sup> The used Au and rare-earth metals in this work are still expensive. To utilize solar energy more efficiently and cost-effectively, a 0D/2D heterojunction based on NIR-responsive quantum dots loaded g-C<sub>3</sub>N<sub>4</sub> nanosheets was constructed, which showed a record NIR photocatalytic activity in wastewater treatment.<sup>4</sup> The use of heavy-metal based QDs constitutes a big concern in the environmental application. To utilize solar energy more environmentally-friendly, a completely metal-free 2D/2D heterojunction of black phosphorus (BP)/g-C<sub>3</sub>N<sub>4</sub> was synthesized.<sup>5</sup> The 2D/2D heterojunction showed high activity and long-term stability in solar H<sub>2</sub> evolution. It is noteworthy that we developed an innovative, “organic ice”-assisted exfoliation method,<sup>6</sup> which led to the high-yield and high-quality few-layer BP with largely reduced energy inputs and processing time. In addition to yielding novel and interesting materials and properties, the current work also provides physical insights that can contribute to the future development of broadband photocatalysts and their applications in energy and environmental areas.

1. Q. Zhang, et al., J. Materiomics 2017, 3, 33-50.

2. Q. Zhang, et al., Nanoscale Horiz. 2019, 4, 579-591.

3. Q. Zhang, et al., ACS Catal., 2017, 7, 6225-6234.

4. Q. Zhang, et al., Appl. Catal., B 2020, 270, 118879.

5. Q. Zhang, et al., Adv. Funct. Mater. 2019, 1902486.

6. Q. Zhang, et al., United States Patent, Application No. 62/685,371; International Patent, Application No. PCT/CA2019/050813.

SESSION F.EL04.12: Progress in Liquid Exfoliation and 2D Reaction Chemistry  
On Demand Abstracts Available for Viewing Starting Saturday Morning, November 21, 2020  
F-EL04

#### 5:00 AM \*F.EL04.12.01

What Governs the “Efficiency“ of Liquid Phase Exfoliation of Layered Crystals? Claudia Backes; Heidelberg University, Germany



Liquid phase exfoliation has become an important top down production technique giving access to large quantities of nanosheets in colloidal dispersion. Importantly, this is a highly versatile technique that can be applied to numerous layered materials from graphite to transition metal dichalcogenides, h-BN, III-VI semiconductors, hydroxides etc. All materials can be exfoliated in a similar way using aqueous surfactant or suitable solvents as stabilisers. Nanosheets in dispersion are extremely polydisperse with broad lateral size and thickness distributions. To narrow size and thickness distributions, liquid cascade centrifugation has proven to be a powerful tool for efficient size selection yielding nanosheet dispersions with well-defined dimensions.

Building on these established methodologies of exfoliation and size selection, it became possible in recent years to address some fundamental questions regarding the exfoliation process, such as: In which way is the yield, nanosheet size and layer number dependent on the liquid medium? What is a good descriptor for the exfoliation efficiency and what does it depend on? What is the role of defects? In this talk, these fundamental questions will be addressed and a picture of the current understanding will be drawn.

#### 5:15 AM F.EL04.12.03

##### **Crystal Phase Engineering in Ternary $W_xMo_{1-x}Se_2$ Colloidal Nanoflowers for Efficient Catalytic Hydrogen**

**Reduction** [Maria S. Sokolikova](#), Gang Cheng, Mauro Och, Pawel Palczynski and Cecilia Mattevi; Imperial College London, United Kingdom

Layered transition metal dichalcogenides (TMDs) exhibit a rich diversity of structural polymorphs defined by the coordination symmetry of transition metal atoms.<sup>1</sup> Tailoring the lattice symmetry within individual TMD layers enables disparate electronic properties ranging from semiconducting (2H phase) to metallic and semimetallic (1T/1T' phases) for the same material composition. The metastable 1T/1T' polymorphs are generally obtained by destabilisation of the thermodynamically stable 2H phase, for instance, via electron transfer. The metastable 1T/1T' phases are particularly appealing for the heterogeneous catalysis as they demonstrate higher electrical conductivity and higher density of catalytically active sites compared to the semiconducting 2H counterparts.<sup>2</sup> Yet to date, obtaining the metastable 1T/1T' phases of high purity and in measurable quantities remains challenging. In our previous work, we demonstrated a successful colloidal synthesis of the 1T' phase of  $WSe_2$ .<sup>3</sup> Here, we report on how the designed colloidal approach can be expanded to synthesise  $W_xMo_{1-x}Se_2$  ( $x = 0-1$ ) nanostructures. Although colloidal  $MoSe_2$  nanoflowers are attained in the 2H phase, alloying with tungsten, which under the same synthesis conditions forms the 1T' phase of  $WSe_2$ , allowed us to stabilise the 1T' phase in the ternary  $W_xMo_{1-x}Se_2$  nanostructures. Moreover, the  $W_xMo_{1-x}Se_2$  nanostructures display tunable 1T'/2H crystal phase ratio that depends on their chemical composition. A set of the  $W_xMo_{1-x}Se_2$  ( $x = 0-1$ ) working electrodes was tested for the catalytic hydrogen evolution reaction (HER). The ternary 1T'/2H  $W_xMo_{1-x}Se_2$  ( $x \sim 0.5$ ) nanoflowers demonstrate an enhanced catalytic activity and faster reaction kinetics compared to either the pristine 2H  $MoSe_2$  or the 1T'  $WSe_2$  nanoflowers. We suggest that the presence of the metastable 1T' phase in the ternary  $W_xMo_{1-x}Se_2$  ( $x \sim 0.5$ ) nanoflowers may cause the observed improvement in the catalytic performance.

#### References:

1. Yang, H., Kim, S. W., Chhowalla, M. & Lee, Y. H. Structural and quantum-state phase transition in van der Waals layered materials. *Nat. Phys.* **13**, 931–937 (2017).
2. Tang, Q. & Jiang, D. Mechanism of hydrogen evolution reaction on 1T-MoS<sub>2</sub> from first principles. *ACS Catal.* **6**, 4953–4961 (2016).
3. Sokolikova, M. S., Sherrell, P. C., Palczynski, P., Bemmer, V. L. & Mattevi, C. Direct solution-phase synthesis of 1T'  $WSe_2$  nanosheets. *Nat. Commun.* **10**, 712 (2019).

#### 5:25 AM F.EL04.12.04

##### **Exfoliation and Deposition of 2D Phosphorene Nanosheets via Bipolar Electrochemistry for High-Performance Capacitive Energy Storage Applications**

[Amin Rabiei Baboukani](#)<sup>1</sup>, Iman Khakpour<sup>1</sup>, Vadym Drozd<sup>2</sup> and Chunlei Wang<sup>1</sup>; <sup>1</sup>Florida International University, United States; <sup>2</sup>Center for the Study of Matter at Extreme Conditions (CeSMEC), United States

Black phosphorus (BP), which was discovered by Bridgman back in 1914, has recaptured attention due to its promising physical and chemical properties. BP is the thermodynamically stable allotrope of phosphorous under ambient conditions. It is a layered material that can be exfoliated into a monolayer two-dimensional (2D) material similar to graphene. As a rising star in 2D materials, few-layer phosphorene is considered a strong competitor against other 2D materials and can be applied in an increasing number of fields such as energy storage and biomedical devices. To realize its real properties, the wide application of phosphorene nanosheets depends on the development and optimization of exfoliation methods. Fabricating BP with a high level of quality, uniformity, and producibility is of crucial importance for its large-scale application. Among

various top-down and bottom-up exfoliation methods, electrochemical exfoliation has emerged as an attractive approach for exfoliating 2D materials with high quality and high yields. However, they are multi-step and time-consuming procedures, and thus less attractive for practical applications. It is, therefore, necessary to develop alternative techniques that can fabricate and deposit phosphorene nanosheets on substrates in a facile, single-step, scalable, and eco-friendly manner for energy storage devices. In this study, we propose a novel and straightforward two-in-one process to exfoliate bulk BP into phosphorene nanosheets in DI water, which are then dragged electrophoretically to be deposited on a conductive substrate. The procedure is based on the mechanism of bipolar electrochemistry (BPE), which is based on applying a sufficiently high voltage to generate electrochemical reactions between two feeding electrodes and a conductive bipolar electrode placed wirelessly between them. The difference in the electric potential between the solution and the bipolar electrode drive redox reactions on the cathodic and anodic poles of the bipolar electrode. Due to the concept of BPE, in general, the induced voltage on the two poles of bulk BP depends on the applied voltage, length of the BP electrode, and distance between the two feeding electrodes. After 24 hours of BPE, bulk BP did not show any noticeable change; however, obvious deposition of a thin film on the feeding electrodes of the bipolar cell can be observed. The exfoliated-and-deposited BP nanosheets were characterized with different microscopic and spectroscopic techniques (SEM, Raman, XPS, and HR-TEM analysis), revealing thin layers of 2D phosphorene with the orthorhombic crystal structure and lateral dimensions up to a few hundreds of nanometers. SEM images showed the high-quality 2D morphology of phosphorene nanosheets on the feeding electrodes. TEM images confirmed that the crystal structure of BP appears to be not affected by the bipolar exfoliation, which confirms a low defect concentration in the produced phosphorene nanosheets. Owing to the 2D structure of the exfoliated-and deposited phosphorene, the electrochemical performance of the phosphorene nanosheets was evaluated for capacitive energy storage application in a two-electrode symmetric configuration (EIS, CV, and GCD). The deposited 2D phosphorene nanosheets delivered high specific capacitance of  $11 \text{ mF cm}^{-2}$  at the scan rate of  $2 \text{ mV s}^{-1}$  and specific capacitance of 8.57, 7.62, 6.66, 5.0, 4.65, 4.01, 3.32, and  $2.86 \text{ mF cm}^{-2}$  at the scan rate of 5, 10, 20, 50, 100, 200, 500, and  $1000 \text{ mV s}^{-1}$ , respectively, which is superior than most of the 2D materials-based devices such as MXene, 2D  $\text{MnO}_2$ , graphene or graphene oxide. This non-toxic, straightforward, and inexpensive novel method could be applied for other 2D materials for energy storage and biomedical application. In this conference, detailed novel bipolar exfoliation and deposition of phosphorene nanosheets and its electrochemical characterization will be presented.

SESSION F.EL04.13/F.MT06.03: Joint Session: Quantum Phenomena in Atomically Thin Materials  
On Demand Abstracts Available for Viewing Starting Saturday Morning, November 21, 2020  
F-EL04

**5:00 AM \*F.EL04.13/F.MT06.03.01**

**Interlayer Excitons in van der Waals Heterostructures** [Philip Kim](#); Harvard University, United States

A pair of electron and hole across the interface of semiconductor heterostructure can form a bound quantum state of the interlayer exciton. In a coupled interface between atomically thin van der Waals layers (vdW), the Coulomb interaction of the interlayer exciton increases further. In this presentation, we will discuss observing interlayer exciton formation in semiconducting transition metal dichalcogenide (TMDC) layers. Unlike conventional semiconductor heterostructures, charge transport in of the devices is found to critically depend on the interlayer charge transport, electron-hole recombination process mediated by tunneling across the interface. We demonstrate the enhanced electronic, optoelectronic performances in the vdW heterostructures, tuned by applying gate voltages, suggesting that these a few atom thick interfaces may provide a fundamental platform to realize novel physical phenomena. Furthermore, complete experimental control of density, displacement and magnetic fields in our graphene double layer system enables us to explore the rich phase diagram of several superfluid exciton phases with the different internal quantum degrees of freedom.

**5:15 AM \*F.EL04.13/F.MT06.03.02**

**Tunable Quantum Transport High Mobility 2D Materials** [Jeanie Lau](#); The Ohio State University, United States

One of the most alluring features of 2D materials is their tunability, as their carrier density, effective mass, band gap, and electronic phases can be tuned in situ by external parameters such as electric field, magnetic field and strain. Here we will present transport studies of high quality 2D materials. For instance, we demonstrate large tunable SOC and zero-field spin-splitting in atomically thin InSe with unprecedented mobility. From beating patterns in quantum oscillations, we establish

that the SOC parameter  $a$  is thickness-dependent; it can be continuously modulated over a large range by an out-of-plane electric field, achieving zero-field splitting tunable between 0 and 20 meV. Surprisingly,  $a$  could be enhanced by an order of magnitude in some devices, suggesting that SOC can be further manipulated by variations in interlayer spacing induced by stacking and/or electrostatic compression. Our work highlights the extraordinary tunability of SOC in 2D materials, which can be harnessed for *in operando* spintronic and topological devices and applications.

**5:30 AM \*F.EL04.13/F.MT06.03.03**

**Electron Interactions in 2D Materials—Correlated Multi-Particle Excitations and Optical Field Driven ARPES** Steven G. Louie<sup>1,2</sup>; <sup>1</sup>University of California, Berkeley, United States; <sup>2</sup>Lawrence Berkeley National Laboratory, United States

Many-electron interaction effects dominate many spectroscopic properties of reduced-dimensional systems, leading often to manifestation of novel phenomena not seen in the bulk. In this talk, I present some of our recent work on electron interaction effects in atomically thin quasi 2D materials: (1) strongly bounded correlated multi-particle excitations, such as trions and bi-excitons, in quasi 1D and 2D materials; (2) giant excitonic effects in shift currents, a nonlinear optical phenomenon, in non-centrosymmetric quasi 2D semiconductors; and (3) excitons and band renormalization in optical field driven angle-resolved photoemission spectroscopy (ARPES). Studies of these novel phenomena are made possible because of newly developed theoretical methods which incorporate higher-order many-electron correlation effects from first principles, using an interacting Green's function approach.

**5:45 AM \*F.EL04.13/F.MT06.03.04**

**Quantum Anomalous Hall Effect in Intrinsic Magnetic Topological Insulator  $\text{MnBi}_2\text{Te}_4$**  Yuanbo Zhang; Fudan University, China

In a magnetic topological insulator, nontrivial band topology conspires with magnetic order to produce exotic states of matter that are best exemplified by quantum anomalous Hall (QAH) insulators and axion insulators. Up till now, such magnetic topological insulators are obtained by doping topological insulators with magnetic atoms. The random magnetic dopants, however, inevitably introduce disorders that hinder further exploration of topological quantum effects in the material. We resolve this dilemma by probing quantum transport in  $\text{MnBi}_2\text{Te}_4$  thin flake—a topological insulator with intrinsic magnetic order. In this layered van der Waals crystal, the ferromagnetic layers couple anti-parallel to each other, so bulk  $\text{MnBi}_2\text{Te}_4$  is an antiferromagnet. Atomically thin  $\text{MnBi}_2\text{Te}_4$ , however, becomes ferromagnetic when the sample has odd number of septuple layers (a septuple layer represents a single structural unit in the out-of-plane direction). We observe zero-field QAH effect in a five-septuple-layer specimen; an external magnetic field further enhance the QAH quantization by forcing all layers to align ferromagnetically.  $\text{MnBi}_2\text{Te}_4$  therefore becomes the first intrinsic magnetic topological insulator exhibiting QAH effect.

**6:00 AM \*F.EL04.13/F.MT06.03.05**

**THz-Driven Irreversible Topological Phase Transition in Monolayer  $\text{MoTe}_2$**  Keith A. Nelson; Massachusetts Institute of Technology, United States

The availability of intense tabletop terahertz-frequency pulses and simple field-enhancement structures that enable peak electric fields of tens of MV/cm have led to demonstrations of highly nonlinear THz-induced responses from a wide variety of materials. THz-driven electronic, magnetic, and structural phase transitions and domain switching have illustrated novel possibilities for control over collective properties and dynamics. In experiments on single-layer and few-layer  $\text{MoTe}_2$ , we have found that irradiation with just one sufficiently strong THz pulse induces an irreversible phase transition [1]. The initial, noncentrosymmetric 2H phase disappears, as shown by the disappearance of characteristic Raman lines and second harmonic generation. After further THz irradiation, the topological insulator phase appears, revealed by its distinct Raman spectrum. Single-shot measurements of the  $\text{MoTe}_2$  evolution as a function of time after THz irradiation reveal complex dynamics over many-picosecond time scales. Theoretical calculations show that the transition is induced through THz-induced liberation of carriers which stabilize the new phase and reduce the energy barrier between the two phases. The result illustrates the prospects for THz control over complex multiphase landscapes in quantum materials.

[1] “Terahertz-driven irreversible topological phase transition in two-dimensional  $\text{MoTe}_2$ ,” J. Shi, Y.-Q. Bie, W. Chen, S. Fang, J. Han, Z. Cao, T. Taniguchi, K. Watanabe, V. Bulović, E. Kaxiras, P. Jarillo-Herrero, and K. A. Nelson, *arXiv*:1901.13609 (2019).

**6:15 AM \*F.EL04.13/F.MT06.03.06**

**Conformal, Area-Specific and Switchable Graphene Nanowrinkles** Teri W. Odom; Northwestern University, United States

Selective patterning and functionalization of graphene can produce spatially-defined properties. Buckling or wrinkling of graphene on polymeric substrates enables a direct approach to tune the physical properties without lithographic steps, and the resulting curvature of the wrinkles can control local chemical reactivity. However, most buckling methods have been limited by the range of wavelength tunability, only global control of the wrinkled patterns, and delamination and cracks in the graphene. This talk will describe a scalable approach to achieve area-specific reactivity and patterning of conformal graphene wrinkles. We will discuss how a fluoropolymer layer sandwiched between graphene and different polymer substrates can facilitate crack-free and switchable graphene nanostructures. Such patterned areas with different curvatures show different reactivities based on a plasma fluorination reaction. Our approach for large-area, fine control over graphene wrinkle topographies has prospects for other two-dimensional electronic materials and optoelectronics and plasmonics applications.

SESSION F.EL04.14: Scalable 2D Materials Synthesis  
On Demand Abstracts Available for Viewing Starting Saturday Morning, November 21, 2020  
F-EL04

#### 5:00 AM F.EL04.14.01

**Scalable Synthesis of Few-Layered 2D Tungsten Di-Selenide (2H-WSe<sub>2</sub>) Nanosheets Directly Grown on Tungsten (W) Foil Using Ambient Pressure Chemical Vapor Deposition for Reversible Li-Ion Storage** Rajashree Konar<sup>1</sup>, Rosy Sharma<sup>1</sup>, Ilana Perelshtein<sup>1</sup>, Eti Teblum<sup>1</sup>, Madina Telkhozhayeva<sup>1</sup>, Maria Tkachev<sup>1</sup>, Jonathan J. Richter<sup>1</sup>, Elti Cattaruzza<sup>2</sup>, Andrea P. Charmet<sup>2</sup>, Paolo Stoppa<sup>2</sup>, Malachi Noked<sup>1</sup> and Gilbert D. Nessim<sup>1</sup>; <sup>1</sup>Bar Ilan University, Israel; <sup>2</sup>Ca'Foscari University of Venice, Italy

Sustainable energy storage devices demand new materials for energy storage systems which alleviate their cost and increase longevity. A prominent energy storage technology for modern applications is Lithium-ion batteries. In this regard, two-dimensional (2D) materials attracted substantial and considerable attention due to their unique properties and abundant potential in various applications, including batteries<sup>1</sup>. Controllable synthesis of 2D materials with high quality and better efficiency is essential for their large scale applications, such as their functions as electrode material in batteries. The methods for synthesis of two-dimensional materials include exfoliation, solvothermal, and chemical vapor deposition (CVD) routes, among which, CVD offers better quality, efficiency, and consistency. In this perspective, the family of 2D transition metal dichalcogenides (TMDCs) gained significant attention for their ability to store metal ions such as Li, Na, and Mg. TMDCs of group 6 transition metals (MX<sub>2</sub> where M = Mo, W, and X = S, Se, Te) have a lamellar structure (space group P6<sub>3</sub>/mmc) similar to graphite but with larger interlayer spacing. Tungsten di-chalcogenides are significant here because of the larger size of W that provides a further alteration of the 2D structure and has been successfully utilized for various applications such as photodetectors, field-effect transistors (FETs), etc. The typical group 6 TMDC lattice structure show W atoms confined in a trigonal prismatic coordination sphere neighbored to Se atoms. Because of its very high density (~9.32 g cm<sup>-3</sup>), WSe<sub>2</sub> also has a high volumetric capacity thereby proving it as a prospective LiB electrode material<sup>2</sup>.

Our work focuses on a facile synthesis of 2H-WSe<sub>2</sub> on W foil in the ambient-pressure chemical vapor deposition system using only Argon as carrier gas during the reaction. Extensive characterization of the bulk and exfoliated material confirm that the as-synthesized 2H-WSe<sub>2</sub> is layered (i.e. 2D). XRD (X-Ray Diffraction) confirms the phase while HRSEM (High-Resolution Scanning Electron Microscopy), HRTEM (High-Resolution Scanning Electron Microscopy), and AFM (Atomic Force Microscopy) clarifies morphology of the material. FIB-SEM (Focused-Ion Beam Scanning Electron Microscopy) estimates the depth of the 2H-WSe<sub>2</sub> formation on W foil around 5-8 μm and Raman/UV-Vis measurements prove the quality of the exfoliated 2H-WSe<sub>2</sub>. The redox processes of Lithium-ion Battery (LiB) studies show an increase in capacity until 500 cycles. On prolonged cycling the discharge capacity till the 50th cycle at 250 mA/g the material shows a stable capacity of 550 mAh/g. These observations indicate exfoliated 2H-WSe<sub>2</sub> has promising applications as LiB electrode material.

#### References

- (1) Xia, H.; Xu, Q.; Zhang, J. Recent Progress on Two-Dimensional Nanoflake Ensembles for Energy Storage Applications. *Nano-Micro Lett.* **2018**, *10* (4), 1–30. <https://doi.org/10.1007/s40820-018-0219-z>.
- (2) Share, K.; Lewis, J.; Oakes, L.; Carter, R. E.; Cohn, A. P.; Pint, C. L. Tungsten Diselenide (WSe<sub>2</sub>) as a High Capacity, Low Overpotential Conversion Electrode for Sodium-Ion Batteries. *RSC Adv.* **2015**, *5* (123), 101262–101267. <https://doi.org/10.1039/C5RA19717A>.

### 5:10 AM F.EL04.14.03

**Facile and Scalable Ambient Pressure Chemical Vapor Deposition-Assisted Synthesis of Layered Silver Selenide ( $\beta$ -Ag<sub>2</sub>Se) on Ag Foil as an Oxygen Reduction Catalyst in Alkaline Medium** Rajashree Konar<sup>1</sup>, Suparna Das<sup>1</sup>, Eti Teblum<sup>1</sup>, Arindam Modak<sup>2</sup>, Ilana Perelshtein<sup>1</sup>, Jonathan J. Richter<sup>1</sup>, Alex Schechter<sup>2</sup> and Gilbert D. Nessim<sup>1</sup>; <sup>1</sup>Bar Ilan University, Israel; <sup>2</sup>Ariel University, Israel

To alleviate the adverse impacts of utilizing fossil fuel reserves on the environment (global warming, greenhouse emissions), extensive research is being devoted to the development of alternative/renewable energy systems, which include: photovoltaics, fuel cells, batteries, etc. Among them, fuel cells are an excellent solution for energy conversion, where, proton exchange membrane (PEM) fuel cells have a wide variety of applications. Some of these applications are being portable systems, automotive, etc., where an important reaction occurring at the cathode is the oxygen reduction reaction (ORR). At the current stage in fuel cell technology, platinum (Pt)-based materials are the most practical catalysts<sup>1</sup>, which, undoubtedly are the prime choice as the cathode catalyst for the electro-reduction of oxygen but Pt-based catalysts are expensive. To reduce such costs in commercially viable fuel cells, extensive research is focused on developing alternative catalysts. Silver-based catalysts show a comparatively high thermodynamic stability and excellent catalytic activity over a wide pH range. The TMCs (O, S, Se, and among them especially Se-based chalcogenides) have attracted significant attention since the work on selenium-based cluster compounds. Selenium-based metal-rich TMCs catalysts exhibit good electrocatalytic activity which is mainly attributed to Se because it helps to improve the electronic structure of the metal by preventing the electrochemical oxidation of metals in most transition metal chalcogenides, as seen for the cases of cobalt selenide and ruthenium selenide. Here, we present a high yield, industrially scalable, and the first-time report on the synthesis of silver selenide from silver foil and selenium powder using a two furnace atmospheric pressure-chemical vapor deposition (AP-CVD) system. We grew low temperature, LT- $\beta$ -Ag<sub>2</sub>Se on Ag foil in the AP-CVD system using thermal annealing and leading to a hollow fern-like morphology material, and its first-ever reported application as an ORR cathode catalyst. The exfoliated  $\beta$ -Ag<sub>2</sub>Se is characterized using XRD, EDS, HRTEM, AFM, and HRSEM, to determine its stoichiometry and its hollow layered fern-like morphology. Differential scanning calorimetry (DSC) further confirms that the final product is the low-temperature phase  $\beta$ -Ag<sub>2</sub>Se. Electrochemical oxygen reduction reaction (ORR) of exfoliated  $\beta$ -Ag<sub>2</sub>Se exhibits sharp oxygen reduction current with an onset potential of 0.88 V/RHE under alkaline condition, indicating oxygen reduction property of  $\beta$ -Ag<sub>2</sub>Se. The large value of limiting current (3 mA cm<sup>-2</sup>) as well as small Tafel slope (68.5 mV dec<sup>-1</sup>) corroborates  $\beta$ -Ag<sub>2</sub>Se as a superior layered transition metal chalcogenide cathode material suitable for such energy-related applications (typically fuel cells and/or metal-air batteries).

#### References

(1) Ostroverkh, A.; Johánek, V.; Dubau, M.; Kúš, P.; Khalakhan, I.; Šmíd, B.; Fiala, R.; Václavu, M.; Ostroverkh, Y.; Matolín, V. Optimization of Ionomer-Free Ultra-Low Loading Pt Catalyst for Anode/Cathode of PEMFC via Magnetron Sputtering. *Int. J. Hydrogen Energy* **2019**, *44* (35), 19344–19356. <https://doi.org/10.1016/j.ijhydene.2018.12.206>.

### 5:20 AM F.EL04.14.04

**cm<sup>2</sup>-Scale Synthesis of MoTe<sub>2</sub> Thin Films with Layer Control** David Hynek<sup>1,1</sup>, Raviat M. Singhanian<sup>2</sup>, Shiyu Xu<sup>1,1</sup>, Benjamin Davis<sup>2</sup>, Lei Wang<sup>1</sup>, Milad Yarali<sup>1,1</sup>, Joshua Pondick<sup>1,1</sup>, John Woods<sup>1,1</sup>, Nick C. Strandwitz<sup>2</sup> and Judy Cha<sup>1,1</sup>; <sup>1</sup>Yale University, United States; <sup>2</sup>Lehigh University, United States

2D transition metal dichalcogenide MoTe<sub>2</sub> has recently gained much attention due to its wide-ranging electronic states including the 2H semiconducting state and 1T' semimetallic state at room temperature, and the T<sub>d</sub> Weyl semimetallic state and superconductivity at low temperatures. Due to small energy differences between the polymorphs, phase transition between distinct electronic states can be achieved easily, making MoTe<sub>2</sub> a model system for fundamental studies of phase transformation and structure-property relationship as well as for potential applications such as low-power, non-volatile phase-change memory. Currently however, large-scale synthesis of high-crystalline MoTe<sub>2</sub> thin films with precise thickness control is largely lacking.

Here, we demonstrate cm<sup>2</sup>-scale synthesis of 2H-MoTe<sub>2</sub> thin films with layer control down to a monolayer and grain size that spans several microns. Layer precision is achieved by controlling the initial thickness of the precursor MoO<sub>x</sub> thin films, which are deposited on sapphire and SiO<sub>2</sub> substrates by atomic layer deposition (ALD) and subsequently converted to MoTe<sub>2</sub> through annealing in a tellurium-rich atmosphere. During the reactions, it is found that the precursor-substrate interface is critical in determining the uniformity in thickness and grain size of the resulting MoTe<sub>2</sub> films: Robust, uniform film growth is achieved on sapphire down to a monolayer of MoTe<sub>2</sub> while incomplete conversion and island growth of MoTe<sub>2</sub> is observed on SiO<sub>2</sub>. Surface characterization of the MoTe<sub>2</sub> films using atomic force microscopy indicates that the MoTe<sub>2</sub> films converted on sapphire are uniform in its thickness to within one layer thickness variation. Furthermore, using

dark-field transmission electron microscopy, we show that the films are highly crystalline with grains spanning over tens of microns. Thus, we show that by precisely controlling the number of ALD cycles for the precursor MoO<sub>x</sub> films on sapphire, we can achieve MoTe<sub>2</sub> thin films with thickness control.

The synthesis strategy we present decouples the layer control from the variabilities of growth conditions, creating a robust growth method that is applicable to other transition metal dichalcogenides. Our MoTe<sub>2</sub> films thus enable systematic studies of layer-dependent properties of MoTe<sub>2</sub> and other transition metal dichalcogenides.

### 5:30 AM F.EL04.14.05

**Orientation-Controlled Growth of Wafer Scale WSe<sub>2</sub> by Metalorganic Chemical Vapor Deposition** Haoyue Zhu, Tanushree Choudhury, Benjamin Huet, Nicholas Trainor, Saiphaneendra Bachu, Danielle R. Hickey, Nasim Alem and Joan Redwing; The Pennsylvania State University, United States

Two-dimensional (2D) transition metal dichalcogenides (TMDCs) with desired properties are ideal candidates for novel applications as 3D integrated devices on Si CMOS, sensors, and optoelectronics.<sup>1-4</sup> Due to the low yield of mechanical exfoliation, metalorganic chemical vapor deposition (CVD) has emerged one of the most promising approaches to synthesize WSe<sub>2</sub> monolayers because of its ability to tightly control source concentrations and scale to wafer size. In order to achieve single crystals monolayers, however, the orientation of domains must be controlled at the nucleation stage so that they grow laterally and coalesce without the formation of high angle or inversion domain boundaries.

In this study, we demonstrate the orientation-controlled growth of WSe<sub>2</sub> on 2" diameter c-plane sapphire by metalorganic chemical vapor deposition (MOCVD) in a cold-wall reactor. We used a multi-step growth protocol to independently control the WSe<sub>2</sub> nucleation density and domain lateral growth.<sup>5</sup> By controlling the growth temperature and ratio of H<sub>2</sub>Se and W(CO)<sub>6</sub>, the WSe<sub>2</sub> triangular domains grow epitaxially on the sapphire substrate with >85% of the domains exhibiting a preferred crystallographic direction after 5 minutes of growth. With continued lateral growth time up to 30 minutes, the WSe<sub>2</sub> monolayer becomes fully coalesced with a low surface coverage (2%) of bilayer domains. Dark-field TEM combined with high resolution imaging of WSe<sub>2</sub> removed from the sapphire substrate, demonstrates that the films are nearly single crystal with a low density of inversion domain boundaries. Low temperature (4K) photoluminescence of the WSe<sub>2</sub> monolayer transferred to oxidized silicon reveals emission peaks associated with biexcitons, negative trions, and neutral excitons for which the peak width ranges from 8 to 11 meV. The results demonstrate the potential of MOCVD to produce wafer-scale epitaxial TMD monolayers with structural and optical properties approaching that of single crystal exfoliated flakes.

(1) Acerce, M.; Voiry, D.; Chhowalla, M. Metallic 1T Phase MoS<sub>2</sub> Nanosheets as Supercapacitor Electrode Materials. *Nat. Nanotechnol.* **2015**, *10* (4), 313–318. <https://doi.org/10.1038/nnano.2015.40>.

(2) Late, D. J.; Doneux, T.; Bougouma, M. Single-Layer MoSe<sub>2</sub> Based NH<sub>3</sub> Gas Sensor. *Appl. Phys. Lett.* **2014**, *105* (23), 3–7. <https://doi.org/10.1063/1.4903358>.

(3) Tan, H.; Fan, Y.; Zhou, Y.; Chen, Q.; Xu, W.; Warner, J. H. Ultrathin 2D Photodetectors Utilizing Chemical Vapor Deposition Grown WS<sub>2</sub> with Graphene Electrodes. *ACS Nano* **2016**, *10* (8), 7866–7873. <https://doi.org/10.1021/acsnano.6b03722>.

(4) Akinwande, D.; Huyghebaert, C.; Wang, C. H.; Serna, M. I.; Goossens, S.; Li, L. J.; Wong, H. S. P.; Koppens, F. H. L. Graphene and Two-Dimensional Materials for Silicon Technology. *Nature* **2019**, *573* (7775), 507–518. <https://doi.org/10.1038/s41586-019-1573-9>.

(5) Zhang, X.; Choudhury, T. H.; Chubarov, M.; Xiang, Y.; Jariwala, B.; Zhang, F.; Alem, N.; Wang, G. C.; Robinson, J. A.; Redwing, J. M. Diffusion-Controlled Epitaxy of Large Area Coalesced WSe<sub>2</sub> Monolayers on Sapphire. *Nano Lett.* **2018**, *18* (2), 1049–1056. <https://doi.org/10.1021/acs.nanolett.7b04521>.

### 5:40 AM F.EL04.14.06

**Monolayer Half-van der Waals Heavy Metals Enabled by Confinement Heteroepitaxy** Alexander Vera<sup>1</sup>, Siavash Rajabpour<sup>1</sup>, Timothy Bowen<sup>1</sup>, Boyang Zheng<sup>1</sup>, Wilson Yanez Parreno<sup>1</sup>, Hesham El-Sherif<sup>2</sup>, Chaoxing Liu<sup>1</sup>, Nabil M. Bassim<sup>2</sup>, Nitin Samarth<sup>1</sup>, Vincent Crespi<sup>1</sup> and Joshua Robinson<sup>1</sup>; <sup>1</sup>The Pennsylvania State University, United States; <sup>2</sup>McMaster University, Canada

Due to relativistic effects, heavy metals (Pb, Bi, etc.) demonstrate strong spin orbit coupling (SOC) effects, making them promising elemental precursors to broken spin degeneracy and non-trivial topology. Atomically thin heavy metal layers exhibit large Rashba effects, translating to large spin Hall angles suitable for spin pumping, memory, and other spintronic applications. Atomically thin lead (Pb) in particular may support superconductivity along with non-trivial topology,

potentially serving as a route to exotic superconducting states. However, typical synthesis techniques do not provide a platform for scalable, stackable, and air-stable 2D metals, necessary for *ex-situ* device work. To answer this challenge, we demonstrate the synthesis of an air-stable 1ML-Pb with strong (~500meV) spin splitting within a graphene/silicon-carbide interface through confinement heteroepitaxy. We expect this material to exhibit a large spin Hall angle suitable for spintronic applications.

#### 5:50 AM F.EL04.14.07

**Growth of Large Edge Length WS<sub>2</sub> for Photodetector Applications** Mohd Samim Reza, Parvez Akhtar, Sandeep Kumar, Henam Sylvia Devi and Madhusudan Singh; IIT Delhi, India

Tungsten disulfide (WS<sub>2</sub>) has a tunable bandgap predicted to go from its measured value of 1.3 eV (indirect) in bulk to 2.1 eV (direct) in monolayer form, and is thus of potential interest for photodetectors. In this work, we report an atmospheric pressure chemical vapor deposition (APCVD) approach to synthesize large domain size WS<sub>2</sub> on SiO<sub>2</sub> (University Wafers) substrates, using a custom-designed and locally fabricated 12-zone horizontal split furnace (Quazar Technologies) and solid phase precursors: tungsten trioxide (WO<sub>3</sub>) and elemental sulfur (S). A series of experiments were carried out at temperatures between 900-1100 °C and in the presence of a carrier gas (Ar) flow (0-400 sccm). Thermal coupling between neighboring heating zones for precursors were controlled using tuned distances between precursor boats. At optimized conditions, growths of monolayer (edge size~ 63 μm), multilayer spiral and pyramidal structural WS<sub>2</sub> were observed on the substrate. Raman measurements were carried out with a laser source (Horiba Labram, 514 nm, 1mW) and spot size of 4 μm. In-plane (E<sub>12g</sub>) and out-of-plane mode (A<sub>1g</sub>) peaks at 352/cm and 420/cm confirmed monolayer growth. In other samples, bilayer and multilayer WS<sub>2</sub> growth was observed with Raman shifts 353/cm, 420/cm and 354/cm,421/cm. Field emission scanning electron microscopy (FEI Quanta 200 F SEM, 10 kV) and optical imaging (Olympus BX53M) confirms locally uniform growth of sharp edged WS<sub>2</sub>, with some visible upstream dependence of edge sizes (variation from 10 μm to 60 μm). Multilayer growth and non-coincidental triangles are observed at the center of the substrate with large edge sizes exceeding 60 μm. Use of vapor trapping techniques increases area coverage, though growth is then primarily multilayer, consistent with expectations from precursor supply limits during synthesis. Work is continuing towards our aim of achieving large edge size monolayer WS<sub>2</sub> suitable for photodetector applications.

#### 6:00 AM F.EL04.14.08

**Chemical Kinetics and Mechanisms for the Synthesis of 2D Polymers via Irreversible Solution-Phase Reactions** Ge Zhang, Yuwen Zeng and Michael Strano; Massachusetts Institute of Technology, United States

Novel organic two-dimensional materials synthesized from polymerization of molecular units have recently attracted much attention, due to their versatile and exotic chemical, mechanical, electronic and magnetic properties. However, large scale and facile synthesis of 2D polymers in homogeneous solution, albeit common for conventional linear polymers, remains challenging despite rapid progress in this field. Previously, two-dimensional, covalently bonded polymers have been made by: reversible crystallization under hydrothermal conditions, templated growth on flat surfaces or interfaces, and polymerization after non-covalent assembly. These methods are relatively slow and hard to scale up. In comparison, irreversible reactions in a homogeneous solution phase is attractive due to its potential to synthesize large quantities of chemically stable product. Unfortunately, such reactions are more likely to produce amorphous 3D structures rather than 2D polymers. The lack of restriction on bond rotation can turn a 2D polymer into 3D, and those defects are permanent due to the irreversibility of reaction. Moreover, a 3D polymer grows much faster than a 2D polymer with the same size.

In this work, we propose and compare two possible mechanisms for making two-dimensional polymers from irreversible reactions in solution phase: the autocatalysis effect, and the bond-planarity effect. Autocatalysis could be achieved by self-templated growth on the surface of as-formed 2D molecules, which increases the rates of 2D growth; while bond-planarity would limit the bond rotation and therefore reduce the probability of 3D growth. By modelling the reaction networks as systems of differential equations, we are able to calculate the reaction time, the size distribution function of the product, and the yield of 2D polymer. The autocatalysis and bond planarity effects are parametrized by two factors:  $\beta$  and  $\gamma$ , respectively.

The results show that both mechanisms can significantly increase the size and yield of 2D polymer, and suppress the formation of 3D product. Without the aid of either effect, the average size of 2D polymer will be minuscule (<10), and the yield is negligible. In contrast, when either of the two effect is strong enough ( $\beta > 10^4$  and  $\gamma > 10^3$ ), a yield close to unity and a much larger average size (>100) could be achieved for 2D polymer. We find that bond-planarity effect would limit the bond rotation and therefore restore the behaviour of 2D polymerization confined to a plane. On the other hand, autocatalysis could dramatically increase the rates of 2D growth, which leads to sizes even bigger than the ideal 2D polymerization without competition from 3D growth. We also study the combined effect of both mechanisms, and obtain further enhancement in the

average size (>1000) and near-unity yield, indicating a potential synergy between the two factors.

Our calculation show for the first time from theory, the feasibility of producing two-dimensional polymers from irreversible polymerization in solution. The framework is independent of the detailed pathways of reactions and structures/functionality of molecules, hence the results are expected to be general and applicable for all types of 2D polymerization process that happen irreversibly in solution. Latest experimental work from our group has successfully demonstrated the synthesis of mechanically strong 2D polymer from irreversible polymerization in solution, via the bond-planarity mechanism, which provides validation for our calculation.

#### **6:10 AM F.EL04.14.09**

**An Irreversible Route to an Ultra-Strong Two-Dimensional Polymer** Yuwen Zeng, Ge Zhang and Michael Strano; Massachusetts Institute of Technology, United States

Polymers that extend covalently in two dimensions have attracted recent attention as a means of combining the mechanical strength and in-plane energy conduction of layered nanomaterials with the low densities, synthetic processability, and organic composition of their one-dimensional counterparts. Efforts to date have proven successful in forms that do not allow that full realization of these properties, such as polymerization at flat interfaces or fixation of monomers in immobilized 2D lattices. A frequently employed synthetic route is to introduce microscopic reversibility, at the cost of bond stability, to achieve 2D crystals after extensive error corrections. Herein we demonstrate a synthetic route to 2D irreversible polycondensation directly in the solution phase, resulting in covalently bonded 2D polymer platelets that are chemically stable, acid-soluble, and allowed to be further fabricated into highly oriented thin films and membranes. The resulting films of 30-nm thickness exhibit exceptional film strength at 2.52 GPa as well as a highly oriented nature, demonstrated by polarized in-plane photoluminescence study. This synthetic route provides new opportunities to 2D polymers with applications to composite materials and molecular sieving membranes.

#### **6:20 AM \*F.EL04.14.10**

**Large-Area Growth of 2D Layered Materials—Chalcogenides, Oxides and Halides** Kibum Kang; Korea Advanced Institute of Science and Technology, Korea (the Republic of)

The 2D layered materials are the potential components in next-generation semiconductor devices and quantum devices. For the integration of 2D layered materials into such functional devices, it is necessary to develop a high-quality large-area growth process.

In this talk, I will introduce the MOCVD growth of 2D layered materials, including transition metal dichalcogenides, metal oxides, and metal halides. Furthermore, I will discuss the MOCVD grown 2D layered materials and their heterostructures that could potentially be utilized in a single-photon source for quantum devices.

#### **6:35 AM \*F.EL04.14.11**

**Electronics with Nobel Metal Dichalcogenides Applications** Georg Düsberg; Universität der Bundeswehr München, Germany

Two-dimensional materials such as transition metal dichalcogenides (TMDs) are intensively investigated because of their potential applications in future electronics. So far mainly group six (Mo/W) TMDs have been investigated, which show thickness depend electronic and optical properties. Metal-to-semiconductor transitions, high mobilities, and high potential for various sensing applications, now raised interest to the group 10 (Pt/Pd) TMDs or Nobel Metal Dichalcogenides (NMDs). In this presentation, the low temperature synthesis of various TMDs by thermally assisted conversion (TAC) is presented. [1] The composition and morphology of the resulting large-scale layers are investigated by a multitude of characterization techniques including Raman spectroscopy, [2] AFM and X-ray photoelectron spectroscopy (XPS). In particular, the low temperature TAC synthesis PtSe<sub>2</sub> potentially allows back end of line (BEOL) integration compatible with silicon technology. The effects of growth on the underlying substrates or investigated by TOF-SIMS and transmission electron microscopy. Further, as pre-pattered structures can be grown by the TAC, which allows to fabricate electronic devices using standard micro-fabrication technology. [3] PtSe<sub>2</sub> has shown potential for a range of novel electronics devices. Examples for high performance chemical sensors, [1] IR-photodetectors[4] and MEMS[5] devices based on PtSe<sub>2</sub> will be presented.

References

[1] Yim et al. ACS Nano, 10 (10), 9550 2016.

[2] O'Brien et al., 2D Materials, 3, 021004, 2016.

[3] Yim, et al. NPJ 2D Materials and Applications 5 (2) 2018.

[4] Yim, et al. Nano Letters, 3 (18), 1794 2018



**5:00 AM \*F.EL04.15.01**

**Tailoring 2D Chalcogenide Interfaces for Heterostructure Growth and Device Optimization** Lincoln J. Lauhon;  
Northwestern University, United States

Understanding and control of surfaces and interfaces is necessary to exploit the potential of 2D metal chalcogenides in electronics and optical devices. The ubiquity and scalability of vapor-phase processing in particular provides a wealth of opportunities, from the growth of van der Waals heterostructures to the chemical tailoring of interfaces to optimize device performance, including devices made from "composite" 2D materials such as those printed from inks. This talk will describe research to leverage interfaces for devices via two routes: atomic layer deposition (ALD) of metal oxides to modify dichalcogenide properties and pulsed chemical vapor deposition of ferroelectric monochalcogenides. In prior work, tuning of ALD oxide stoichiometry was shown to tune the Fermi level of MoS<sub>2</sub>. [1] More recently, in situ monitoring of MoS<sub>2</sub> and MoSe<sub>2</sub> transistor performance during deposition of an oxide dielectric enabled the disentangling of changes in carrier concentration and mobility during the alternating dosing of the metal-organic precursor and oxidant.[2] Intriguingly, we find a substantial enhancement in field effect mobility with sub-monolayer coverage. Variable temperature transport measurements indicate that charged impurity scattering is reduced by screening even prior to formation of a complete dielectric, pointing to the importance of seeding conditions in maximizing mobility. Vapor deposition processes also provide scalable routes to van der Waals heterostructures whose properties can be engineered by band-offsets and dimensionality. Building on prior work demonstrating low-temperature epitaxy of SnS on MoS<sub>2</sub>[3], a range of processing conditions were explored to understand how SnS film morphology is influenced by substrates including amorphous SiO<sub>2</sub>, mica, MoS<sub>2</sub>, and hexagonal boron nitride (hBN). Control over film thickness and morphology is particularly important to harness the in-plane ferroelectricity of SnS for devices. Large area monolayer regions are readily achieved on MoS<sub>2</sub> substrates by targeting temperatures and purge times that enhance selective growth at edges. Due to the relative inertness of the vdW surface of hBN, modified surface preparation and pulsing schemes are necessary to favor lateral growth of SnS, and monolayers growth is more challenging. However, isolated islands of epitaxial SnS on hBN are relatively easy to achieve, providing a path towards highly scaled memristive devices based on ferroelectric switching.

[1] Chem. Mater. 2018, 30, 3628. [2] ACS Appl. Electron. Mater. 2020, 2, 1273. [3] ACS Appl. Mater. Interfaces 2019, 43, 40543.

**5:15 AM F.EL04.15.02**

**Atomic Layer Deposition of Al Doped MoS<sub>2</sub>—A *p*-Type 2D Semiconductor with Tunable Carrier Density and Control Over the Doping Profile** Vincent Vandalon<sup>1</sup>, Marcel Verheijen<sup>1,2</sup>, Erwin Kessels<sup>1</sup> and Ageeth Bol<sup>1</sup>; <sup>1</sup>Eindhoven University of Technology, Netherlands; <sup>2</sup>Eurofins Material Science, Netherlands

Two-dimensional layered transition metal dichalcogenides (TMD) such as MoS<sub>2</sub> and WS<sub>2</sub> are of interest for nanoelectronics because of their promising electronic characteristics and their predictable properties even in the few- and monolayer regime. The merits of TMDs for transistor applications have already been demonstrated by fabrication of field-effect transistors (FET) mainly using intrinsic MoS<sub>2</sub>. However, doped variants of these TMDs are essential for the fabrication of high-performance devices and the realization of advanced transistors concepts. To allow adoption in actual device fabrication workflows, both the doped and the undoped material has to be fabricated with scalable synthesis methods. So far, it has proven difficult to synthesize doped TMDs with good control over the carrier density. Consequently, control over the doping profile is even farther out of reach.

Here we present a synthesis method for Al doped MoS<sub>2</sub> based on plasma-enhanced atomic-layer deposition (ALD) with good control over both the carrier density and doping profile. Using this method *p*-type doped MoS<sub>2</sub> was deposited with an precisely tunable carrier density between 10<sup>17</sup> and 10<sup>21</sup> cm<sup>-3</sup>. The Al dopant was introduced using an ALD supercycle concept which consisted of *N* MoS<sub>2</sub> ALD cycles followed by 1 AlS<sub>x</sub> ALD cycle. With this approach the Al concentration is controlled simply by varying the *N* parameter and the supercycle can be repeated as often as needed to deposit the desired film thickness. Both the doped and undoped films showed virtually no N, C, and O impurities and the Mo:S ratio was not

impacted by the Al incorporation. The films were crystalline and showed the typical 2D layered structure, even at high Al concentration, as observed with cross-section transmission electron microscopy (TEM) imaging. This, combined with the minimal impact of the Al doping on the mobility, suggests that the introduction of Al does not disrupt the layered nature of the TMD and it acts like a well behaved dopant.

The excellent control over the doping profile of this approach was demonstrated in a combined TEM and energy-dispersive X-ray spectroscopy (EDX) study. A stack of 5 alternatingly doped and undoped regions, each 10 nm thick, was synthesized for characterization. The crystal structure was not interrupted by the transition between doped and undoped regions. On the other hand, the Al concentration showed a sharp transition between the doped and undoped regions, demonstrating the control over the doping profile.

To conclude, *p*-type doped MoS<sub>2</sub> was synthesized with a widely tunable carrier density and good control over the doping profile. Compatibility with large-scale fabrication was ensured by the conformality, uniformity, and the sub-nm thickness control inherent of ALD. This approach is therefore of interest for the fabrication of nanoelectronics based on doped MoS<sub>2</sub>. Moreover, *p*-type doped TMDs are of interest in other fields including photovoltaics and catalysis.

#### 5:25 AM F.EL04.15.03

**From Mono- to Multilayers: Adjustable Layer Thickness of Hexagonal Boron Nitride Thin Films by Atomic Layer Deposition (ALD)** [Rene Weißing](#), Daniel Stadler, David Graf, Heechae Choi and Sanjay Mathur; University of Cologne, Germany

Hexagonal boron nitride (h-BN) with its atomically flat structure, excellent stability and large band gap energy (~ 6 eV) is an ideal insulator for 2D electronics and an outstanding material for the growth and encapsulation of transition metal dichalcogenides (TMdCs). Fabrication of h-BN thin films is dominated by exfoliation of multi-layer or bulk crystals and chemical vapor deposition (CVD) via thermal decomposition and surface nucleation of single-source precursors such as amino boranes and borazine. While mechanical exfoliation and chemical transfer procedures typically deliver h-BN flakes of several tens of micrometers that come along with significant interfacial impurities, a precise thickness control in the Ångström region by CVD grown thin films is hardly achievable. ALD, a vapor phase deposition technique based on self-limiting gas-surface reactions, is the ideal choice for a precise thickness control and high uniformity over areas in the centimeter regions. Therefore, we have developed ALD processes based on DFT calculations regarding the kinetics of film formation to grow h-BN layers in the centimeter region with a precise thickness control relevant for electronic applications. The synthetic access was achieved by two complementary half-reactions of B and N precursors with respect to adsorption energy calculation for each decomposition reaction step confirmed by mass spectroscopy. In addition to an insight into the growth mechanism, parameter-dependent layer thickness optimization was obtained.

#### 5:35 AM F.EL04.15.07

**3D Printed Networks of 2D Nanosheets for On-Chip Supercapacitors** [Apostolos Panagiotopoulos](#), Stefano Tagliaferri, Maria S. Sokolikova and Cecilia Mattevi; Imperial College London, United Kingdom

Miniaturization over three-dimensions is very attractive for future on-chip technologies where efficiencies need to be optimized over millimetre sized areas. This is a new challenge, as device fabrication is mainly developed to achieve planar-geometries. Direct Ink Writing is a cost-effective, industrially scalable route that brings the possibility of making electrodes and energy storage devices in a three-dimensional geometry.

Here, we demonstrate 3D printed supercapacitors from highly concentrated, water-based inks. The active materials are atomically thin sheets of transition metal dichalcogenides, either exfoliated from bulk or obtained via direct synthesis in solution. To ensure rapid prototyping as well as streamlined manufacturing, we formulated viscoelastic slurries with tailored rheological properties allowing printability and mechanical integrity of the printed structures in various resolutions. The printed architectures, from woodpile and serpentine structures to interdigitated electrodes, are extended over a few mm in three-dimensions and present structural integrity with as low as 100microns sized struts. Following electrode optimisation via thermal annealing, we formed high-surface area mechanically robust networks of 2D nanosheets. They combine electrochemical surface controlled kinetic processes to deliver high amounts of energy, in short bursts, to power electronics as standalone or in conjunction with other energy conversion/storage devices

#### 5:45 AM F.EL04.15.08

**Towards the Rational Design of Printed 2D Materials** [Zhehao Zhu](#), Joon-Seok Kim and Lincoln J. Lauhon; Northwestern University, United States

The formulation of inks based on 2D materials could provide new functional behaviors to printed electronics while retaining

scalable manufacturing processes. Recent advances in solution-based exfoliation have demonstrated that the electronic properties of single semiconducting 2D nanosheets can be preserved during ink processing, but there remain several challenges to the production of thin film transistors based on printed 2D materials. In addition to minimizing interface resistance and preserving bulk-like mobilities, the microstructure of the composite material must be optimized. To rationally guide the development of 2D inks and related processing, we integrated device modeling with electrical and scanning probe characterization of transistors with “composite” 2D channels. Experiments and finite element modeling were guided by a gate-dependent resistor network model that quantifies performance trade-offs determined by nanosheet thickness, degree of overlap, and interface resistivity. We measured the electrical characteristics of model  $\text{MoS}_2/\text{MoS}_2$  homojunctions created by mechanical exfoliation to validate model parameters. Kelvin probe force microscopy (KPFM) was used to measure the surface potential profiles in transistor channels as a function of applied bias conditions and morphological characteristics such as sheet thickness. Finite element device simulations, using parameters derived from experiments, were used to interpret both the experiments and trends observed in the resistor network model. We find that screening of the upper portions of overlapping nanosheets produces current crowding at junctions between the edge of one nanosheet and the basal plane of another. Reducing the nanosheet thickness (i.e. the number of layers) distributes the current over larger areas and facilitates efficient charge transfer, increasing the effective mobility and on/off ratio, providing further motivation to develop exfoliation schemes that preserve intrinsic monolayer properties. Detailed analysis of potential drops measured in KPFM provides indirect evidence that weakly screened trapped charges at edge states further limit charge transfer, suggesting that passivation and/or functionalization schemes targeting the edges of nanosheets could greatly improve transistor performance.

**5:55 AM F.EL04.15.09**

**Late News: Rapid Time-Resolved Laser Crystallization and Patterning of 2D Quantum Materials on Flexible Substrates** Zabihollah Ahmadi, Parvin Fathi-Hafshejani, Emre Kayali, Majid Beidaghi and Masoud Mahjouri-Samani; Auburn University, United States

Rapid direct writing of geometrically complex patterns of two dimensional (2D) quantum materials is critical for applications in a variety of areas, including flexible and wearable electronics and sensors. However, the available synthesis methods (e.g., CVD, MOCVD, MBE) are neither capable of direct writing nor possible to integrate onto flexible substrates due to high growth temperatures. Here, we demonstrate a rapid laser-based crystallization and complex patterning of 2D quantum materials ( $\text{MoS}_2$ ,  $\text{WS}_2$ ) on flexible substrates. A thin layer of solid-state stoichiometric amorphous 2D film is first pulsed laser deposited onto the flexible substrates – e.g., polydimethylsiloxane (PDMS) and polyethylene terephthalate (PET) - followed by a time-resolved infrared laser crystallization to controllably couple a precise amount of energy to locally heat and crystallize the amorphous 2D materials. The influence of pulse duration, frequency, and the number of pulses on the crystallization of 2D materials is investigated, and the spectroscopy and structural investigations verify the quality of crystallized 2D materials on the flexible substrates. Moreover, ultrathin 2D devices on stretchable PDMS substrate are fabricated, and their electrical characteristics under tensile strains and stretching cycles are measured. This novel method opens up a new opportunity for the future 2D materials-based wearable, transparent, and flexible optoelectronic and photonic devices.

Mr. Zabihollah Ahmadi is currently a Ph.D. student in the Department of Electrical and Computer Engineering (ECE) at Auburn University (AU). His research in the Laser-Assisted Science and Engineering (LASE), Lab under the supervision of Prof. Mahjouri-Samani, focuses on developing novel laser-based approaches for the synthesis and processing of 2D quantum materials and heterostructures on the flexible platform for optoelectronic and photonic applications.

SESSION F.EL04.16: Strain and Twist—Properties and Devices  
On Demand Abstracts Available for Viewing Starting Saturday Morning, November 21, 2020  
F-EL04

**5:00 AM \*F.EL04.16.01**

**Enabling 2D Heterostructure Development with Atomic Resolution Imaging—Studies of Twist Reconstruction and Degradation** Sarah J. Haigh, David Hopkinson, Nick Clark, Astrid Weston and Yichao Zou; University of Manchester, United Kingdom

2D materials and their heterostructures provide an exciting playground for pioneering science. In this talk I will demonstrate how atomic resolution scanning transmission electron microscopy (STEM) imaging and analysis is being used to support the

advancement of these systems.

For example, I will discuss new results revealing the structural relaxation that occurs when two transition metal dichalcogenide (TMDC) monolayers are misoriented by a small twist (rotation angle). Many high profile experimental measurements of the exciting physics present in twisted TMDCs have necessarily neglected the potential for local structural relaxation. We have used atomic resolution STEM to reveal that TMDCs bilayers twisted to a small angle, less than  $\sim 3$  degrees, reconstruct into energetically favourable stacking domains separated by a network of stacking faults, and that this behaviour is more complex than is observed in graphene [1]. For crystal alignments close to 3R stacking, we find that a tessellated pattern of mirror reflected triangular 3R domains while for alignments close to 2H stacking, stable 2H domains dominate, with nuclei of an earlier unnoticed metastable phase limited to  $\sim 5$ nm in size. This appears as a kagome-like pattern at twist angles less than 1 degree, transitioning to a hexagonal array of screw dislocations separating large-area 2H domains as the twist angle approaches 0 degrees. Tunneling spectroscopy measurements reveals that such reconstruction creates strong piezoelectric textures and pseudo-magnetic fields, opening new avenues for engineering of 2D material properties on the nanometre scale [1].

As the range of 2D materials increases rapidly, many of those with the most the promising magnetic or optoelectronic properties are found to be unstable in air or moisture, which makes fabrication challenging and hampers their use. Even relatively stable 2D crystals like MoSe<sub>2</sub> and WSe<sub>2</sub> are found to have perfect interfaces only when processed in an inert environment [2]. These materials can be stabilised to ambient conditions by encapsulating with stable 2D layers, such as graphene and hexagonal boron nitride. [3] For example, we have applied the encapsulation approach to study the presence and behaviour of point and extended defects in the 2D monochalcogenides, GaSe and InSe which are of interest due to their relatively high electron mobilities, strong second harmonic generation and quasi-direct bandgap when reduced to the monolayer limit.[4] Nonetheless the properties of InSe and GaSe crystals often degrade on exposure to air, light, and/or moisture, thought to be the result of oxidation induced defects. We have used atomic resolution STEM together with electron energy loss spectroscopy (EELS) and energy dispersive X-ray spectroscopy to characterise individual point and extended defects in InSe and GaSe [5]. We observe that both materials contain multiple point and extended defects, even when exfoliated in argon and encapsulated in graphene. Point vacancies are observed to be healable under the electron beam, while extended defects and stacking faults have symmetries not found in bulk samples and which could be used to tune the properties of 2D post-transition-metal monochalcogenide materials for optoelectronic applications. We also demonstrate the nanopatterning of black phosphorus using electron beam lithography via etching protocols developed in the STEM [6], and recent work revealing oxidation induce improvement of superconductivity in few layer TaS<sub>2</sub> [7].

## References

- [1] A. Weston et al, Nature Nanotechnology (2020) doi: 10.1038/s41565-020-0682-9
- [2] A.P. Rooney et al, Nano Letters, 17, 5222, (2017)
- [3] Y. Cao et al, Nano Letters, 15, 8, 4914-4921 (2015)
- [4] M.J. Hamer et al., ACS nano 13 (2), 2136-2142 (2019)
- [5] D G Hopkinson et al, ACS nano, 13 (5), 5112-5123 (2019)
- [6] N. Clark et al, Nano Letters, 18 (9), 5373-5381, (2018)
- [7] J Bekaert, et al, Nano Letters, 20 (5), 3808-3818 (2020)

**5:15 AM \*F.EL04.16.02**

### **Twistronic Structures and Moire Superlattices in Homo- & Heterobilayers of Transition Metal Dichalcogenides** Vladimir Falko; University of Manchester, United Kingdom

We apply a multiscale modelling approach to study moiré superlattice in twisted homo- and heterobilayers of transition metal dichalcogenides (TMD), taking into account the interlayer hybridisation of the electronic orbital and lattice reconstruction due to stacking-dependent adhesion. First of all, we develop DFT-parametrized interpolation formulae for interlayer adhesion energies of MoSe<sub>2</sub>, WSe<sub>2</sub>, MoS<sub>2</sub>, and WS<sub>2</sub> with both parallel and antiparallel orientation of their unit cells and arbitrary offset of the honeycomb lattices in the adjacent layers. Then, we combine those interpolation formulae with elasticity theory and analyze the bilayer lattice relaxation into mesoscale domain structures. We find that 3R and 2H stacking domains develop for, respectively, bilayers with parallel (P) and antiparallel (AP) orientation of the monolayer unit cells, separated by a network of dislocations, for twist angles  $\theta < \theta_P \sim 2.5$  and  $\theta < \theta_{AP} \sim 1$ . Such lattice reconstruction has been verified by STEM imaging. We also show that the triangular domain structures of P-oriented homobilayers would manifest itself in local tunnelling characteristics of marginally twisted. For AP bilayer, we show that the deformation of the lattices around domain walls (which resemble twist dislocations oriented along the planes of in bulk 2H crystals) generate piezo-electric charges, reaching local density up to  $\pm 0.5 \times 10^{12} \text{e/cm}^2$  at the junctions of the honeycomb domain wall network. Finally, we use DFT

modelling of bandstructure of bilayers with various stacking configurations and interlayer distances to develop and parametrise interpolation formulae for the interlayer hopping between the layers for the relevant parts of the Brillouin zone, and, then, establish the electronic structure of the bilayer across the moire supercell, taking into account the piezoelectric potentials.

**5:30 AM \*F.EL04.16.03**

**Interplay Between Intra- and Inter-Layer Interactions in Stacked Two-Dimensional Crystals** Young-Woo Son; Korea Institution for Advanced Study, Korea (the Republic of)

Interlayer interactions in stacked 2D crystals are one of key ingredients in exhibiting their qualitative distinct physical properties, differing from their single layer physics [1]. For example, a well-known 2D quantum spin Hall insulating transition metal dichalcogenide (TMDC) can show either topological Weyl metallic phase or trivial one depending on a minute stacking order difference [1,2]. Recent advances in fabricating stacked 2D crystals enable us to perform controlled studies on interesting electronic, magnetic and topological properties in low dimensional heterostructures. In this talk, I will first discuss interplay between intralayer correlation, interlayer interaction, and magnetism in layered materials [3-5]. To understand magnetic properties, I will introduce a new computationally efficient method to calculate various correlation effects in layered materials [3]. Another interesting examples revealing intriguing interlayer interactions will be discussed for graphene bilayer systems [6,7] and TMDCs [8]. For a graphene bilayer system with a rotation angle of 30 degrees, it is shown that a quasicrystalline order through a perfect incommensurate interlayer interaction shows localized 12 fold resonant states with fractal scaling [6]. For a bilayer MoS<sub>2</sub> system, I will demonstrate a intrinsic coupling between strain and shear in the system that can alter its low energy Raman modes, thereby providing a way to obtain its almost all fundamental mechanical constants through light-matter interactions.

#### References

- 1) Y.-W. Son, *Nature* **565**, 32 (2019).
- 2) H.-J. Kim, S.-H. Kang, I. Hamada, and Y.-W. Son, *Phys. Rev. B* **95**, 180101 (R) (2017).
- 3) S. Lee and Y.-W. Son, arXiv.org:1911.05967 (2019).
- 4) S. Lee and Y.-W. Son, *in preparation* (2020).
- 5) E. Ko and Y.-W. Son, *in preparation* (2020).
- 6) S. J. Ahn *et al*, *Science* **361**, 782 (2018).
- 7) P. Moon, M. Koshino, Y.-W. Son, *Phys. Rev. B* **99**, 165430 (2019).
- 8) J. Lee *et al.*, *Nat. Comm.* **8**, 1370 (2017).

**5:45 AM \*F.EL04.16.04**

**Surface and Strain Control of 2D Materials—From Fundamental Properties to Nanomanufacturing** Joel W. Ager<sup>1,2</sup>; <sup>1</sup>Lawrence Berkeley National Laboratory, United States; <sup>2</sup>University of California, Berkeley, United States

In the monolayer limit transition metal dichalcogenides (TMDs) such as MoS<sub>2</sub> and WS<sub>2</sub> have direct bandgaps, leading to significant interest in the use of these materials for opto-electronic applications. Their internal photoluminescence (PL) quantum efficiency (QE) is a sensitive measure of their quality. While some III-V thin films and II-VI quantum dot structures can achieve near-unity values of this metric, most semiconductor materials have QEs which are much smaller. We have discovered that treatment of sulfur-based TMDs with an organic superacid dissolved in a non-polar solvent suppresses non-radiative recombination at low pump powers, leading to near 100% QE. [1]. Similar, near-unity, QE values can be achieved via electrostatic gating by lowering the Fermi level to near mid-gap to suppress the formation of non-radiative trions [2]. Tuning of band parameters with strain is a common motif in semiconductor devices. Chemical vapor deposition of some monolayer TMDs on thermal expansion coefficient mismatched substrates can induce strains on the order of 1%, in spite of the weak van der Waals interaction [3]. Larger strains can be envisioned: Au grows epitaxially on MoS<sub>2</sub> with a predicted mismatch strain of 10% [4]. Further, the strain is predicted to be confined to the monolayer in contact with the Au, while other layers in the structure remain unstrained. This effect weakens the bonding between the top layer and the bulk [5], which enables exfoliation of large areas of monolayer material with defined patterns [6,7]. Further optimization of this nano-manufacturing process has improved the yield to nearly 50% and has led to the ability to form defined TMD heterostructures [8].

<sup>1</sup>M. Amani, D.-H. Lien, D. Kiriya, J. Xiao, A. Azcatl, J. Noh, S.R. Madhupathy, R. Addou, S. KC, M. Dubey, K. Cho, R.M. Wallace, S.-C. Lee, J.-H. He, J.W. Ager, X. Zhang, E. Yablonovitch, and A. Javey, *Science* **2015**, 350, 1065.

<sup>2</sup>Lien, D.-H.; Uddin, S. Z.; Yeh, M.; Amani, M.; Kim, H.; Ager, J. W.; Yablonovitch, E.; Javey, A. *Science* **2019**, 364, 468–471.

<sup>3</sup>Ahn, G. H.; Amani, M.; Rasool, H.; Lien, D.-H.; Mastandrea, J. P.; Ager III, J. W.; Dubey, M.; Chrzan, D. C.; Minor, A. M.;

Javey, A. *Nat. Commun.* **2017**, *8*, 608.

<sup>4</sup> Y. Zhou, D. Kiriya, E.E. Haller, J.W. Ager, A. Javey, and D.C. Chrzan, *Phys. Rev. B* **93**, 054106 (2016).

<sup>5</sup> Sun, H.; Sirott, E. W.; Mastandrea, J.; Gramling, H. M.; Zhou, Y.; Poschmann, M.; Taylor, H. K.; Ager, J. W.; Chrzan, D. C. *Phys. Rev. Mater.* **2018**, *2*, 094004.

<sup>6</sup> S.B. Desai, S.R. Madhvapathy, M. Amani, D. Kiriya, M. Hettick, M. Tosun, Y. Zhou, M. Dubey, J.W. Ager, D. Chrzan, and A. Javey, *Adv. Mater.* **28**, 4053 (2016).

<sup>7</sup> Gramling, H. M.; Towle, C. M.; Desai, S. B.; Sun, H.; Lewis, E. C.; Nguyen, V. D.; Ager, J. W.; Chrzan, D.; Yeatman, E. M.; Javey, A.; Taylor, H. *ACS Appl. Electron. Mater.* **2019**, *1*, 407–416.

<sup>8</sup> Nguyen, V.; Gramling, H.; Towle, C.; Li, W.; Lien, D-H; Kim, H.; Chrzan, D. C.; Javey, A.; Xu, K.; Ager, J.; Taylor, H. J. *Micro Nano-Manufacturing* **2019** 7 041006.

#### 6:00 AM F.EL04.16.05

**Charge Carrier Funneling and Radiative Trion Production in Nano-Pillar Strained MoS<sub>2</sub>** Mounika Vutukuru<sup>1</sup>, Zhuofa Chen<sup>1</sup>, Hossein Ardekani<sup>2</sup>, Zhangcheng Yao<sup>1</sup>, Kenan Gundogdu<sup>2</sup> and Anna Swan<sup>1</sup>; <sup>1</sup>Boston University, United States; <sup>2</sup>North Carolina State University, United States

We investigate the strain-driven localization of electrons and enhanced photoluminescence (PL) response of trions and excitons in monolayer MoS<sub>2</sub> strained by SiO<sub>2</sub> nanopillars. Using spatially resolved PL and Raman mapping, we observe the well-recognized red shift in the PL and Raman on the apex of the pillars due to the strain response, together with an overall 6-fold increase in the PL intensity and an increased fraction of radiative trions. The increased trion fraction in the strained areas is attributed to more efficient electron strain-funneling than exciton funneling, which increases the trion production relative to the A excitons. The large overall PL intensity increase on the pillars is due to a combination of interference enhancements and charge and exciton funneling. Using time-resolved PL, we also study radiative lifetimes of excitons and charge carriers to explore the effect of strain on the intrinsic radiative lifetime of each species which leads to increased production of trions on the strained site. The results demonstrate that strain-induced local energy minima affect diffusion of excitons and free charge carriers differently, as in the case of non-uniformly strained WS<sub>2</sub> [1]. Our results show that strain control could be used in addition to the electric field, as part of the toolbox for quasiparticle manipulation in 2D systems.

[1] M. G. Harats, J. N. Kirchoff, M. Qiao, K. Greben, and K. I. Bolotin, "Dynamics and efficient conversion of excitons to trions in non-uniformly strained monolayer WS<sub>2</sub>," *Nat. Photonics*, 2020, doi: 10.1038/s41566-019-0581-5.

#### 6:10 AM F.EL04.16.06

**The Role of Bubble Geometry and Thickness on Luminescence Properties of 2D Multilayers** Haeyeon Lee, Frances M. Ross and Silvija Gradečak; Massachusetts Institute of Technology, United States

In-plane and out-of-plane deformation of 2D materials, especially of van der Waals (vdW) heterostructures, occurs readily during the fabrication process and it modifies their optical and electronic properties. Bubbles that form between layers in vdW heterostructures have been viewed as an inconvenience, with research focusing on how to avoid them during fabrication. On the other hand, practical applications of bubbles have been recently reported including quantum dot-like emitters and single photon emitters. Therefore, understanding mechanical properties of bubbles is necessary to manipulate their geometry and optoelectronic properties. Bubbles formed by monolayers are found to exhibit universal shape and aspect ratio depending on the elastic stiffness of each monolayer. However, studies on bubbles formed by multilayers have not been established yet due to non-negligible bending modulus and unconventional lubricant interfaces.

Here, we present that the geometry of bubbles formed by hexagonal boron nitride (hBN) multilayers is strongly correlated to the thickness of multilayers, which enables us to manipulate the aspect ratio of bubbles by the thickness. Since the bending rigidity of 2D multilayers is no more negligible as in the case of monolayers, two phenomena in multilayer bubbles are observed, which are distinct to monolayer bubble with fixed aspect ratio: the aspect ratio of multilayer bubble (1) decreases with the thickness of multilayer and (2) increases with the radius of bubbles. In addition, significant enhancement of luminescence is observed by cathodoluminescence from the bubbles in ultraviolet region owing to a large band gap nature of hBN. Moreover, Fabry-Perot interference is created where the pattern largely depends on the geometry of bubbles. We believe that optical properties and/or strain could be efficiently manipulated by designing the geometry of multilayer bubbles with desirable thickness.

#### 6:20 AM F.EL04.16.07

**Coherent Lattice Wobbling and Dynamic Breaking of Friedel's Law Observed in Layered Gallium Telluride by Ultrafast Electron Diffraction** Qingkai Qian<sup>1</sup>, Xiaozhe Shen<sup>2</sup>, Duan Luo<sup>2</sup>, X.J. Wang<sup>2</sup> and Shengxi Huang<sup>1</sup>; <sup>1</sup>The Pennsylvania State University, United States; <sup>2</sup>SLAC National Accelerator Laboratory, United States

The inspection of Friedel's law in ultrafast electron diffraction (UED) is important to gain a comprehensive understanding of material atomic structure and its dynamic response. Here, monoclinic gallium telluride (GaTe), as a low-symmetry, layered crystal in contrast to many other 2D materials, is investigated by mega-electron-volt UED. Strong out-of-phase oscillations of Bragg peak intensities are observed for Friedel pairs, which has dynamically violated the Friedel's law. As evidenced by the preserved mirror symmetry and supported by both kinematic and dynamic scattering simulations, the intensity oscillations are provoked by the lowest-order longitudinal acoustic breathing phonon. Our results provide a generalized understanding of Friedel's law in UED, and demonstrate that by designed misalignment of surface normal and primitive lattice vectors, coherent lattice wobbling and effective shear strain can be generated in crystal films by laser pulse excitation, which is otherwise hard to achieve and can be further utilized to dynamically tune and switch material properties.

**6:30 AM F.EL04.16.09**

**Late News: Interplay Between Direct and Indirect Exciton in Strained Monolayers of Transition Metal**

**Dichalcogenides** [Navendu Mondal](#)<sup>1</sup>, Yuri Gartstein<sup>1</sup>, Masoud Mahjouri-Samani<sup>2</sup> and Anton Malko<sup>1</sup>; <sup>1</sup>The University of Texas at Dallas, United States; <sup>2</sup>Auburn University, United States

Owing to the spatial and dielectric confinement, monolayers of transition metal dichalcogenides (TMDs) undergo strong many-body Columbic interactions yielding into large binding energies for the exciton (>0.1 eV) and higher order exciton-complexes compared to the conventional semiconductors. However, local environments experienced by these tightly bound excitons often drive the optoelectronic properties of these TMDs. These TMDs often exhibit low photoluminescence quantum yield (PLQY) and short intrinsic radiative lifetime due to the presence of large impurities, defects and efficient phonon assisted non-radiative Auger recombination processes. Currently researchers in the community are exploring various routes to modulate the bandgaps and tailor optoelectronic properties of these TMDs to make them more suitable for the real device applications.

In this context, an interesting avenue continuously evolving in this field is that modulation of the bandgap (even upto 0.5 eV) of these semiconductors by inducing strain (tensile & compressive). This has understood by means of controlling the mechanical stress on those monolayers and studies in this line are largely limited within the PL properties and dynamics. While the effects of strain on the fate of those excitons (in ultrashort timescale) including excitonic many-body events remains less unexplored.

To unravel the effect of stress on those excitons and their dynamics, we first study the excitonic properties of high-quality monolayer MoS<sub>2</sub>, WS<sub>2</sub> & WSe<sub>2</sub> (grown by laser-assisted evaporation technique; analogous to CVD-method) samples both under substrate and suspended condition employing ultrafast optical (namely transient absorption, TA) spectroscopy as a major tool. Optical characterization data reveals that these as-synthesized monolayer flakes in fused silica substrates possess highly red-shifted absorption/PL w.r.t. the typical excitonic position. This characteristic low-band-gap signature is attributed to the effect of strain that presumably arises from the thermal expansion coefficient mismatch between the TMDs and substrate. It is quite common to observe this sort of unavoidable strain on TMDs during the CVD growth process. This is further corroborated when the strains were released from those monolayers by means of exfoliating them from the as-grown substrate. These suspended monolayer samples exhibit an enhanced PL intensity and the abs./PL position shifts back near to the typical excitonic position. TA spectroscopic measurement (for a representative case of WS<sub>2</sub> in fused silica) reveals that under low-excitation density, sharp excitonic bleach signal (~ 640 nm) decays quickly within 200 ps, consistent with earlier reports. Interestingly, under higher excitation density, even though spectral features remain similar, but the overall TA signal becomes long-lived and hardly decays within 2000 ps. This slowing down signature at higher exciton density is found to be similar for MoS<sub>2</sub> and WSe<sub>2</sub> as well. This observation contrasts with the typically observed faster bleach recovery dynamics (due to exciton-exciton annihilation events) at higher excitation fluence for large no of semiconductors including TMDs. This slow dynamic is anticipated as a typical signature of strain induced formation of indirect exciton. As the intervalley scattering dominates at higher exciton density, large number of direct excitons quickly scatter into the other-valley (indirect) and thus contribution of the long-lived TA signal increases. This is further evident from the TA measurements of suspended (strain-reduced) samples in which slowing down effect of the TA signal (at higher exciton density) is relatively suppressed. This interesting finding of controlling the population of direct and indirect excitons by means of optical excitation will open exciting areas in potential optoelectronic applications.

SESSION F.EL04.17: Transport in 2D Materials and Heterostructures  
On Demand Abstracts Available for Viewing Starting Saturday Morning, November 21, 2020  
F-EL04

**5:00 AM \*F.EL04.17.01**

**Imaging Carrier Inhomogeneities in Active 2D Material Devices** Samuel Berweger; National Institute of Standards and Technology, United States

Scanning microwave microscopy (SMM, often called scanning microwave impedance microscopy, sMIM) is a scanning probe implementation that can directly probe free carriers with nanometer spatial resolution using tip-localized GHz fields. With the subsurface sensitivity inherent to near-field techniques and the ability to measure electrically isolated systems, SMM is well-suited for studying electronic inhomogeneities in 2D semiconducting materials and their devices. We begin by highlighting SMM measurements of photogenerated free carriers in transition metal dichalcogenide lateral heterostructures.

We then focus on the application of SMM to studying ambipolar field effect transistors of 2D films of the 1D van der Waals material tellurene (tellurene). Tellurene can be solution processed, exhibits high bipolar mobilities, and is stable under ambient conditions, which makes it an attractive alternative to conventional 2D semiconductors. We combine SMM with a differential implementation to image spatial variations in conductivity as well as the associated carrier type as a function of the applied backgate voltage in tellurene devices. We reveal spatial inhomogeneities in carrier type and conductivity and show that the measured backgate-dependent device conduction minimum in fact arises from the simultaneous coexistence of n-type and p-type regions in an overall minimum conductivity configuration. We further show that the spatial inhomogeneities in conductivity and carrier type in four-terminal devices results in differing transport characteristics between different terminals across the same device in well-defined backgate-controlled p-type and n-type conduction channels. While these results highlight the challenges facing the reproducible fabrication of 2D material devices, the possibilities of solution-based doping and deterministic weighting of multiple inputs into the same device hold future promise.

**5:15 AM F.EL04.17.02**

**Long Continuous Electroluminescence in All 2D van der Waals Vertical Heterostructure Devices** Linlin Hou<sup>1</sup>, Qianyang Zhang<sup>1</sup>, Viktoryia Shautsova<sup>1</sup> and Jamie Warner<sup>2</sup>; <sup>1</sup>University of Oxford, United Kingdom; <sup>2</sup>The University of Texas at Austin, United States

2D materials can be assembled into various vertical heterostructure stacks to emit strong electroluminescence. However, until now, most work has been done using mechanical exfoliated materials, with little insights gained into the operation mechanisms when using synthetically grown crystals by chemical vapour deposition (CVD). In particular, the operation lifetime/duration of electroluminescence and subsequent failure mechanisms are poorly understood, mainly due to lack of abundance in device numbers that can shed statistical significance into the ensemble response. Here, we demonstrate that all 2D vertical layered heterostructures (Gr:hBN:WS<sub>2</sub>:hBN:Gr) using CVD grown materials can generate strong red electroluminescence (EL). Here, graphene acts as a transparent electrode, WS<sub>2</sub> works as an ultrathin photo-active material, and h-BN serves as a tunnelling barrier for carrier injection. Tens of the devices are produced across a single chip, with the success rate of working devices over 90%. EL starts to be detected at bias values of ~5 V, with a bright red EL dot located at the junction area. Continuous operation of the devices generate EL for more than 2 hours without significant degradation of WS<sub>2</sub> under high bias. Further investigation on breakdown tests reveal that the dominant reason for the device failure is local heating accumulation on top-graphene electrodes. This study provides a viable way for wafer-scale fabrication of high performance 2D LED arrays for ultra-thin and flexible optoelectronic devices and detailed insights about the mechanisms of failure and operation limits of EL devices made with CVD grown 2D materials within ambient conditions.

**5:25 AM F.EL04.17.04**

**Monolayer/Multilayer Homojunctions in Transition Metal Dichalcogenides Enhance Photoinduced Charge Generation in Heterostructures with Carbon Nanotubes** Dana Kern, Hanyu Zhang, Zhaodong Li and Jeffrey L. Blackburn; National Renewable Energy Laboratory, United States

Increasing the lifetimes and yields of photoexcited charge carriers in quantum-confined heterostructures is an important goal for realizing efficient next-generation energy conversion and storage devices. One-dimensional single-walled carbon nanotubes (SWCNTs) and two-dimensional transition metal dichalcogenides (TMDCs) are fascinating materials classes with possible applications in photovoltaic and photoelectrochemical technologies. However, the photophysics in heterostructures containing these materials are not well understood. Here, we explore a model Type-II heterojunction with (6,5)-SWCNTs as the electron donor and MoS<sub>2</sub> as the acceptor, where the energy level offsets at these interfaces provide a promising strategy to separate charge and overcome the ultrafast decay of tightly bound excitons that are inherent to these materials. We find that the TMDC microstructure affects the charge photogeneration pathways in MoS<sub>2</sub>/SWCNT heterojunctions, where a small fraction of multilayer islands in monolayer MoS<sub>2</sub> leads to longer-lived charge carriers and higher carrier yields, despite the emergence of a defect-associated spectral signature. We combine transient absorption spectroscopy with time-resolved



microwave photoconductivity to explore the interplay between defect states and the generation of mobile carriers. Global fitting of our transient absorption spectra enables us to separately analyze exciton, charge, and defect evolution on the MoS<sub>2</sub> and SWCNT layers, and microwave photoconductivity distinguishes between free and trapped charge. Our comparisons between multilayer-containing and monolayer-only MoS<sub>2</sub>/SWCNT heterostructures provide valuable insight for understanding the impact of local TMDC thickness variations on charge generation pathways.

#### 5:35 AM F.EL04.17.05

**Electron-Phonon Coupling Enhances Thermal Boundary Conductance of 2D-3D Interfaces** Arnab K. Majee, Cameron Foss and Zlatan Aksamija; University of Massachusetts Amherst, United States

Devices made of two-dimensional (2D) van der Waals (vdW) materials, including graphene, transition metal dichalcogenides (TMDs, e.g. MoS<sub>2</sub>, MoSe<sub>2</sub>, WS<sub>2</sub> etc.) and beyond-graphene materials (e.g. phosphorene, silicene, germanene, etc.), hold tremendous potential for next-generation nanoelectronics applications. The prospect of vertically stacking<sup>1</sup>--both homogeneous and heterogeneous--vdW materials has opened numerous avenues to engineer them for superior device performance. However, practical realization of electronic devices made of 2D vdW materials is limited by the inefficient thermal dissipation from the 2D material to the substrate. The high interface thermal resistance can cause unreliable performance and even lead to device failure. Significant research interests have been invested towards improving the electronic properties such as mobility, subthreshold slope, etc.,<sup>2-4</sup> but heat dissipation has received less attention. Heat removal in 2D field-effect transistors is mainly cross-plane through the substrate, owing to the small thermal healing length<sup>5</sup> and large lateral/vertical aspect ratio.<sup>6</sup> Heat dissipated by electrons is carried from the 2D material to the substrate via flexural out-of-plane lattice vibrations (ZA phonons) and the efficiency of heat transfer is quantified by thermal boundary conductance (TBC). Our previous studies suggest that the TBC of graphene and MoS<sub>2</sub> monolayers on various substrates can be improved by encapsulation.<sup>6</sup> However, encapsulation is not a viable alternative to improve TBC in optoelectronic devices. A recent study demonstrated lowering of in-plane thermal conductivity of 2D materials via phonon-electron interactions, opening a new avenue to modulate heat transfer by electrostatic gating;<sup>7</sup> however, the impact of electron-phonon coupling on cross-plane heat transfer through the 2D-substrate interface is not yet fully understood.

Here we demonstrate the role of phonon-electron scattering as a tool to tune TBC of 2DvdW materials on SiO<sub>2</sub> substrate. We calculate the electronic bandstructures and phonon dispersions of 2D materials from first principles Density Functional Theory using the QUANTUM ESPRESSO package.<sup>8</sup> Then we compute phonon-electron rates ( $\Gamma$ ) from Fermi's Golden rule.  $\Gamma$  is combined with the anharmonic phonon rates in our thermal model<sup>9</sup> to obtain TBC of the 2D-3D interface. We found that TBCs of MoS<sub>2</sub> and MoSe<sub>2</sub> are improved by 21.4% and 23.6%, respectively, when the carrier density is varied from 10<sup>10</sup> cm<sup>-2</sup> to 10<sup>14</sup> cm<sup>-2</sup> at 300K. On the other hand, WS<sub>2</sub> and WSe<sub>2</sub> show a weaker dependence on phonon-electron coupling with an improvement of 2.4% and 5.4%, respectively, which is due to dominant phonon-phonon scattering in these materials. The maximum enhancement in TBC due to phonon-electron coupling is obtained for TMDs composed of transition metals with smaller atomic mass and heavier chalcogen atoms. We also found that TMDs with smaller effective masses exhibit better TBC. From a fundamental perspective, we found that in all these 2D materials TBC is limited by the rate at which ZA phonons are replenished in the monolayer and not by the rate at which they scatter with the substrate. This study provides a novel tool to dynamically tune TBC by gating.

**References:** <sup>1</sup>A.K. Geim, I.V. Grigorieva, Nature 499, 419-425, 2013. <sup>2</sup>Bolotin et al., Solid State Commun. 146, 351, 2008. <sup>3</sup>Radisavljevic et al., Nat. Nanotechnol. 6, 147-150, 2011. <sup>4</sup>Perello et al., Nat. Commun. 6, 7809, 2015. <sup>5</sup>S.V. Suryavanshi and E. Pop, J.Appl. Phys. 120, 224503, 2016. <sup>6</sup>Yasaei et al., Adv. Mater. Interfaces 4, 1700334, 2017. <sup>7</sup>S.-Y. Yue, R. Yang, B. Liao, Phys. Rev. B 100, 115408, 2019. <sup>8</sup>Giannozzi et al., J. Phys. Condens. Matter 21, 395502, 2009. <sup>9</sup>C.J. Foss and Z. Aksamija, 2D Mater. 6, 025019, 2019.

#### 5:45 AM F.EL04.17.06

**Exciton Transport under Periodic Potential in TMD Heterostructures** Zidong Li<sup>1</sup>, Xiaobo Lu<sup>2</sup>, Darwin Cordovilla Leon<sup>1</sup>, Zhengyang Lyu<sup>1</sup>, Jize Hou<sup>1</sup>, Yanzhao Lu<sup>1</sup>, Austin Kaczmarek<sup>1</sup>, Takashi Taniguchi<sup>3</sup>, Kenji Watanabe<sup>3</sup>, Liuyan Zhao<sup>2</sup>, Li Yang<sup>2</sup> and Parag B. Deotare<sup>1,1</sup>; <sup>1</sup>University of Michigan, United States; <sup>2</sup>Washington University in St. Louis, United States; <sup>3</sup>National Institute for Materials Science, Japan

In this work, we unravel the mechanism that affects exciton transport in a periodic potential created by stacking two lattice mismatched transition metal dichalcogenide (TMD) monolayers. The confined periodic excitonic states (moiré excitons<sup>1-3</sup>) in the heterostructure creates a diffusion barrier that impacts the energy transport and dynamics of interlayer excitons (electron and hole spatially separated in different monolayers).

We experimentally quantify the diffusion barrier experienced by interlayer excitons in both R-type and H-type, h-BN encapsulated MoSe<sub>2</sub>/WSe<sub>2</sub> heterostructures. We further support the observations with density functional theory (DFT) simulations and a three-level model that represents the exciton dynamics at various temperatures. By measuring the diffusion

of interlayer excitons at various bath temperatures, we observe that the effective diffusivity of excitons can be significantly lower than their intrinsic diffusivity in the absence of the periodic potential. In fact, at low temperatures, most of the excitons remain immobile, ceasing exciton transport completely. We conclude that the strong localization of interlayer excitons at low temperature and the temperature activated Arrhenius type of diffusivity are inherent to the deep periodic potentials arising from the moiré superlattice. Based on the temperature dependent diffusivity and lifetime of interlayer excitons, we extracted the moiré potential of  $20 \pm 4$  meV for the H-type (54 degree twisted angle) heterostructure and  $34 \pm 3$  meV for the R-type heterostructure (5 degree twisted angle).

We believe the results will significantly advance the understanding of exciton transport in van der Waals heterostructures and will aid in the design of room-temperature efficient excitonic devices that leverage the various regimes of diffusivity based on twisted angle.

This work was supported through the National Science Foundation (NSF) grant No. DMR- 1904541 and Air Force Office of Scientific Research (AFOSR) Award Number FA9550-17-1-0208.

1. Seyler, K. L. *et al.* Signatures of moiré-trapped valley excitons in MoSe<sub>2</sub>/WSe<sub>2</sub> heterobilayers. *Nature* **567**, 66–70 (2019).
2. Tran, K. *et al.* Evidence for moiré excitons in van der Waals heterostructures. *Nature* **567**, 71–75 (2019).
3. Jin, C. *et al.* Observation of moiré excitons in WSe<sub>2</sub>/WS<sub>2</sub> heterostructure superlattices. *Nature* **567**, 76–80 (2019).

### 5:55 AM F.EL04.17.07

**Thermal Boundary Conductance of Buckled Group IV,V, and III-V Two-Dimensional Materials** Cameron Foss and Zlatan Aksamija; University of Massachusetts Amherst, United States

In the last decade, entire families of novel two-dimensional (2D) materials have been theoretically predicted and subsequently synthesized. The combination of their ultrathin geometry, environmental sensitivity, and mechanical robustness make 2D materials an exciting framework from which improved device performance and novel functionalities can be realized. While much of the attention on 2D materials focused on their electronic, magnetic, and optical properties, heat dissipation in these materials remains a major concern for their future implementation. The primary pathway for heat removal in 2D-based devices is the thermal pathway from the 2D layer to its underlying 3D substrate. Since 2D-3D interfaces are governed by weak van der Waals interactions, the interface thermal pathways can be one to two orders of magnitude more resistive than 3D-3D covalently bonded interface counterparts. Therefore, developing solutions to boost 2D-3D thermal boundary conductance (TBC) and identifying 2D material properties that favor interface thermal transport are critical to the future implementation of 2D-based devices.

The TBC between graphene, boron nitride (BN), and transitional metal dichalcogenides on several substrates have been studied rigorously. However, more recently synthesized 2D materials such as buckled group IV, V, and III-V 2D materials have not been investigated. Previously [2D Mater. 6 (2019) 025019] we have shown that 2D-3D TBC depends strongly on the overlap of available phonon modes in the long-wavelength regime and found selection criteria for choosing the best substrate for TBC. Here we turn our focus to 2D material features and report theoretical predictions of TBC for silicene, blue phosphorene, black phosphorene, and boron arsenide (BAs) on SiO<sub>2</sub> (with comparisons to graphene and BN). Our TBC model is driven by ab initio phonon dispersions and takes into account the two mechanisms that govern TBC: (i) an external resistance between ZA phonons in the 2D layer and the substrate which depopulates the ZA phonon population of the 2D layer and (ii) an internal resistance between ZA phonons and other thermal energy carriers which replenishes the ZA phonon population. Weak internal scattering can lead to a large internal resistance which effectively reduces the overall TBC. However, encapsulation has been shown to increase the internal scattering of ZA phonons effectively reducing the internal resistance and increasing the overall TBC [Adv. Mater. 30 (2018) 1801629].

We predict the external TBC, which is an upper bound on the effective TBC, of 2D/SiO<sub>2</sub> of (a) graphene, (b) BN, (c) blue phosphorene, (d) black phosphorene, (e) silicene, and (f) BAs interfaces without encapsulation to be (a) 20, (b) 32, (c) 70, (d) 80, (e) 100, and (f) 130 MW.m<sup>-2</sup>.K<sup>-1</sup>, respectively. On the other hand, the effective TBC values are approximately 50% ((a) 54%, (b) 52.5%, (c) 45%, (d) 51.6%, (e) 48%, and (f) 50.3%, respectively) of the external TBC because of additional internal resistance due to a slow repopulation of ZA phonons. However, upon encapsulation, which increases the damping and repopulation of ZA phonons, nearly half ((a) 26%, (b) 25.7%, (c) 21%, (d) 26%, (e) 20.1%, and (f) 16.6%) of those losses are regained at room temperature. Furthermore, the effective TBC of encapsulated samples shows a far weaker temperature dependence than the uncoated counterparts which is most significant at low temperatures where a near order of magnitude increase in the total TBC for temperatures below 50 K is seen for some cases. We also see that the TBC can vary over nearly an order of magnitude depending on the phonon bandwidth of the ZA branch. Our results help highlight the role of encapsulation on the temperature dependence of TBC and we find that 2D materials with narrower ZA branch bandwidths correlate strongly to high TBC.

**5:00 AM F.EL04.18.01**

**Vibrational Properties of Black Phosphorous under Intercalation and High-Pressure—An *In Situ* Study** Manthila C. Rajapakse, Rajib Musa, Usman Abu, Bhupendra Karki, Ming Yu, Gamini Sumanasekera and Jacek B. Jasinski; University of Louisville, United States

This work reports a systematic study of electrochemical Li intercalation and high-pressure studies of black phosphorous (BP). In-situ Raman spectroscopy is used to analyze the time evolution of vibrational modes of BP under lithiation during galvanostatic discharge in a dedicated electrochemical cell. At a constant current, discharge time accounts for the number of Li ions transferred to BP cathode, hence providing good control over the composition of  $\text{Li}_x\text{P}$  compound. Black phosphorous has three fundamental vibrational modes. The study shows that all three fundamental vibrational modes, A1g, B2g and A2g red-shift as a result of lithiation and in-plane modes (B2g and A2g) are red-shifting about 1.6 times more than out-of-plane mode A1g. The results also indicate the structural expansion measured using electron diffraction of ex-situ lithiated samples. Further analysis using optical and electron microscopy shows also that the intercalation of BP is highly anisotropic, where channels along the zigzag direction are found to be the easy direction for intercalation. The diffusion along these channels also leads to a formation of weakly connected nanoribbons, which could be used as an alternative route to fabricate phosphorene nanoribbons. X-ray diffraction on intercalated samples indicates a reduction of thickness as lithiation weakens interlayer bonding, thus resulting in a partial exfoliation of BP flakes. The experimental results show a random filling of Li atoms between BP layers rather than a periodic filling assumed in the first principle calculations based on density function theory which explains the discrepancy between the theoretical and experimental Raman peak positions. Furthermore, studying vibrational modes of BP under high-pressure is important and adds to the knowledge on mechanical properties and strain engineering in this material which could also lead to a structural phase transition towards blue phosphorous, as predicted by first principle calculations. A diamond anvil cell (DAC) is used to apply high pressure (up to  $\approx 15$  GPa) on BP. In this method, sample is stressed against two transparent diamond anvils via a liquid pressure transfer medium. Transparency of the diamond anvils allow in-situ Raman spectroscopy to monitor changes in phonon modes under pressure. High-pressure in-situ experiments are underway on both pristine and Li intercalated BP samples, also with a systematic study on the effect of different pressure media to study the possible structural phase changes of this intriguing material under high-pressure.

**5:10 AM F.EL04.18.02**

**Modifying Energetic Disorder and Hot Exciton Dynamics Through Cation Modification in Excitonic 2D Hybrid Perovskites** Daniel B. Straus<sup>1,2</sup>, Sebastian Hurtado Parra<sup>2</sup>, Natasha Iotov<sup>2</sup>, Michael R. Gau<sup>2</sup>, Qinghua Zhao<sup>2</sup>, Patrick J. Carroll<sup>2</sup>, James M. Kikkawa<sup>2</sup> and Cherie Kagan<sup>2</sup>; <sup>1</sup>Princeton University, United States; <sup>2</sup>University of Pennsylvania, United States

We report a family of two-dimensional hybrid perovskites (2DHPs) based on phenethylammonium lead iodide ( $(\text{PEA})_2\text{PbI}_4$ ) that exhibit complex cation-dependent optical properties. By replacing the 4-position (*para*) H on the phenyl moiety of the phenethylammonium cation with F, Cl,  $\text{CH}_3$ , or Br, we increase the length of the cation but leave the cross-sectional area unchanged, resulting in structurally similar  $\text{PbI}_4^{2-}$  frameworks with increasing interlayer spacing. Longer cations result in broader, blue-shifted excitonic absorption spectra with reduced or eliminated structure, indicating greater energetic disorder. Photoluminescence spectra are largely invariant and insensitive to cation length, suggesting polaron formation stabilizes a structural and electronic minimum. Temperature-dependent linewidth analysis reveals excitons couple to a vibration on the organic framework that is weakly sensitive to these cation substitutions, and Raman spectra and electronic structure calculations support the presence of such a cationic mode. Despite carriers being confined to the inorganic framework, the length of the organic cation alters the optical and electronic properties of 2DHPs.

If instead we replace the 2-position (*ortho*) H with F, Cl, or Br, we increase the cation's cross-sectional area. Unlike the 4-position substitutions, these single-atom substitutions substantially change the observable number of and spacing between discrete resonances in the excitonic absorption and PL spectra and drastically increase the amount of hot exciton PL that violates Kasha's rule by over an order of magnitude. To fit the progressively larger cations, the inorganic framework distorts and is strained, reducing the Pb-I-Pb bond angles and increasing the 2DHP band gap. Correlation between the 2DHP structure and steady-state and time-resolved spectra suggests the complex structure of resonances arises from one or two manifolds of states, depending on the 2DHP Pb-I-Pb bond angle (as)symmetry, and the resonances within a manifold are

regularly spaced with an energy separation that decreases as the mass of the cation increases. The uniform separation between resonances and the dynamics that show excitons can only relax to the next-lowest state are consistent with a vibronic progression caused by a vibrational mode on the cation. These results demonstrate that simple changes to the cation can be used to tailor the properties and dynamics of the confined excitons without directly modifying the inorganic framework.

#### 5:20 AM F.EL04.18.03

**Radiation Hardness of Atomically Thin Proton Irradiated Monolayer MoS<sub>2</sub>** Burcu Ozden; Penn State Abington, United States

We live in an era where space tourism finally becomes a reality. Space tourism is expected to become a large industry within the next decade along with the more and more private sector companies promoting it. These ambitious goals can only be achieved through the development of technologies, which are resilient to damage due to high, persistent fluxes of ionizing radiation in the extreme space environment. In this regard, two-dimensional materials (2DMs) have attracted great attention in the electrical device research for space applications due to potential use as a replacement of traditional semiconductor substrates for next-generation electronic devices and circuits. Studying the effects of proton irradiation on MoS<sub>2</sub> can help us to understand the response of optoelectronic devices fabricated from these materials operating in radiation hard environments such as space radiation environment, high-altitude flights, military aircraft, satellites, nuclear reactors, and particle accelerators. In this research, proton irradiation-induced effects on monolayer MoS<sub>2</sub> were studied by emulating a certain space radiation environment using a relatively low energies (150 and 590keV) proton beam with the same fluence of  $1 \times 10^{12}$  protons/cm<sup>2</sup>. The pristine and irradiated monolayer MoS<sub>2</sub> samples were characterized by comparing the phenomenological changes in the optical and morphological properties. The crystal quality was examined with x-ray diffraction (XRD) analysis and micro-Raman spectroscopy. The possible effects on defects/ traps were probed using photoluminescence (PL) spectroscopy. The surface compositional analysis was performed via x-ray photoelectron spectroscopy (XPS), and surface morphology was inspected using atomic force microscopy (AFM), scanning electron microscopy (SEM), and transmission electron microscopy (TEM). The MoS<sub>2</sub> material grown with the facilitation of sodium bromide by the chemical vapor deposition shows the negligible change in optical and morphological characteristics after the irradiation. Our results open the way for the use of robust and reliable MoS<sub>2</sub> based devices in space environments.

#### 5:30 AM F.EL04.18.04

**Fluoric Self-Assembled Monolayer (FSAM) for Enhancing the Electrical Properties of Graphene on Arbitrary Substrates** Shih-Ming He, Hsin-Yin Lin and Ching Yuan Su; National Central University, Taiwan

Charge scattering, impurities, wrinkles, and polymer residues among the substrate decline the electrical properties, such as carrier mobility and n/p-type doping, has been a challenge for graphene-based electronic devices. Self-assembled monolayers (SAMs) have been widely used to tailoring the electronic structure of substrate-supported graphene due to the effective modifications such as the extremely flatten surface or dipole at the interface. Also, the fluoric self-assembly monolayer (FSAM) used to promoting the electrical properties due to the hydrophobic so that it can eliminate the residue of water molecules between the substrate and graphene during the transferring process. In this study, the trichloro(1H,1H,2H,2H-perfluorooctyl)silane (FDTS) was selected as the precursor followed by the formation of the FSAM layers through the dip-coating and spin-coating methods on arbitrary substrates such as Si, SiO<sub>2</sub>/Si, PET, and glass. As the result, it was found out that the surface roughness of the FSAM/SiO<sub>2</sub> substrate significantly reduce from 2.96 to 0.29 nm with the optimized condition by dip-coating, on which the graphene mobility measured from Hall measurement increases about 1.77 times from 894.6 cm<sup>2</sup>/Vs to 1588cm<sup>2</sup>/Vs; the calculated mobility of graphene/FSAM with a top-gated field effect transistor (FET) is about 15 times higher than that of device without SAM-modified substrate. The increased mobility is mainly due to the lower surface roughness and dipole effect when graphene on FSAM layer, which is observed on other versatile substrates. The dipole at the interface of graphene or other 2D(MoS<sub>2</sub> and WSe<sub>2</sub>) and FSAM layer were comprehensively studied, where it allows for altering the carrier transport properties especially in FETs. This method provides a new strategy through the substrate modification to enhancing the electrical performance on graphene or 2D-based FETs, which could pave a way toward next-generation high-performance nanoelectronics.

SESSION F.EL04.19: Poster Session: Beyond Graphene 2D Materials—Synthesis, Properties and Device Applications  
On Demand Abstracts Available for Viewing Starting Saturday Morning, November 21, 2020

#### F.EL04.19.01

##### **Ice Templated and Directed Assembly to Construct 3D Boron Nitride and Graphene Oxide Nanosheet Topological Networks for Property Enhancement** Sanju Gupta<sup>1,2</sup>; <sup>1</sup>CCNY, United States; <sup>2</sup>Western Kentucky University, United States

Inspired by the nano/microscale hierarchical structure, topological network and precise inorganic/organic interfaces, we fabricated artificial 'nacre-like' papers and aerogels based on noncovalent functionalized boron nitride nanosheets (NF-BNNSs) and varying poly(vinyl alcohol) (PVA) concentration via vacuum-assisted self-assembly and freeze-drying (or ice-templating) techniques. The electron microscopy showed an ordered 'brick-and-mortar' arrangement of NF-BNNSs and PVA paper and aerogels, in which the long-chain PVA molecules act as the bridge to link NF-BNNSs via hydrogen bonds. Likewise, due to the need for heat removal in modern electronic devices, polymer composites with high thermal conductivity have drawn much attention. However, the traditional method to enhance polymers' thermal conductivity by random addition of nanofillers usually creates composites with not only limited thermal conductivity but also other detrimental effects due to a large amount of fillers required. Here, novel polymer composites are prepared by first constructing 3D boron nitride nanosheets (3D-BNNS) network using an ice-templated approach with varying BNNS sheets concentration and then infiltrating them with epoxy matrix. The thermal and mechanical properties of resulting free-standing nacre-like papers, aerogels and composites are investigated. They elucidated high glass transition temperature, low interfacial thermal resistance, or high thermal conductivity with relatively low BNNS loading thus revealing their superiority as flexible substrates. These results demonstrate that this approach opens a new avenue for the design and preparation of polymer composites with high thermal conductivity useful in advanced electronic packaging techniques, namely, thermal interface materials, underfill materials, and molding compounds.

#### F.EL04.19.02

##### **Development of New Nanofiltration Membranes Using 2D Nanomaterials** Natalia Garcia Domenech<sup>1,2</sup>, Yurii Goun'ko<sup>1,2</sup> and Finn Purcell-Milton<sup>1,2</sup>; <sup>1</sup>Trinity College Dublin, Ireland; <sup>2</sup>BiOrbic Bioeconomy Research Centre, Ireland

Nanofiltration has gained much attention in recent years due to its possible applications as a highly efficient and low-energy usage separation and purification technology[1,2]. Moreover, nanofiltration has shown to be potentially superior and more cost-effective than other filtration techniques. Nanofiltration was initially adapted for wastewater treatment, but has been implemented by other industries, such as the pharmaceutical and the food industries, where the standard for high quality products and stringent safety requirements necessitate further and more specialised separation approaches[1,3]. The main aim of this project was to use inorganic 2D nanomaterials in order to develop new membranes for nanofiltration applications, in particular, boron nitride (BN). In this project, BN was exfoliated by liquid assisted exfoliation and the membranes were prepared by vacuum filtration using hydrophilic polytetrafluoroethylene as template. Boron nitride was also partially oxidised before exfoliation proving new chemically functionalised BN materials. All membranes were tested using different dyes and calculating the rejection of each one. Almost 100% rejection rates have been achieved for optimised BN membranes demonstrating the superb nanofiltration performance for selected dyes. The new membranes are to be used for the separation of D- and L- lactic acid and various mono- and disaccharides from agricultural residues.

#### References:

- [1] B. Van der Bruggen, M. Manttari, M. Nystrom, Drawbacks of applying nanofiltration and how to avoid them: A review, Sep. Purif. Technol. 63 (2008) 251–263. doi:10.1016/j.seppur.2008.05.010.
- [2] P. Eriksson, Nanofiltration extends the range of membrane filtration, Environ. Prog. 7 (1988) 58–62. doi:10.1002/ep.3300070116.
- [3] N. Garcia Doménech, F. Purcell-Milton, Y.K. Gun'ko, Recent progress and future prospects in development of advanced materials for nanofiltration, Mater. Today Commun. 23 (2020) 100888. doi:https://doi.org/10.1016/j.mtcomm.2019.100888.

#### F.EL04.19.03

##### **Raman Studies of a Natural van der Waals Heterostructure** Viviane Z. Costa<sup>1</sup>, Addison Miller<sup>1</sup>, Sam Vaziri<sup>2</sup>, Shirin Jamil<sup>1</sup>, Andrew Ichimura<sup>1</sup>, Eric Pop<sup>2,2,2</sup> and Akm Newaz<sup>1</sup>; <sup>1</sup>San Francisco State University, United States; <sup>2</sup>Stanford University, United States

Van der Waals heterostructures comprised of two-dimensional (2D) materials offer a platform to obtain materials by design with unique electronic properties. Until recently, these van der Waals heterostructures (vdWH) materials were synthesized in

the laboratory by vertically stacking different atomically thin materials, which often leads to stacks with the presence of fabrication defects and air contaminants between layers. Franckeite is a naturally occurring vdWH comprised of two distinct alternately stacked semiconducting layers. Because it is naturally heterostructured, it enables the study of a complex layered system without the presence of fabrication defects, and where the crystal orientation between layers has been preserved. Unlike other layered sulfide-based 2D materials, Franckeite is a grained-textured layered solid composed of few-millimeters flakes in random orientation. For this reason, mechanical exfoliation of thin flakes with uniform and large surface area for optical characterization and transfer techniques is especially challenging, leading to a knowledge gap of the fundamental properties of Franckeite. Raman spectroscopy is a widely and powerful method to characterize and study the fundamental properties of molecules in 2D crystals. All of the power that Raman spectroscopy provides in characterizing 2D materials stems from a large and well-established literature on the Raman signature of these crystals, which is lacking for Franckeite. In this work, we performed an extensive micro-Raman spectroscopy study of Franckeite. At room temperature, Raman spectroscopy data were acquired for a large sample size of flakes with thickness ranging from 6 to 100 nm prepared by mechanical exfoliation on SiO<sub>2</sub> substrates. The Raman signature of Franckeite is detected for flakes thicker than 10 nm. We observed that the position of all Raman peaks is independent of sample thickness. As expected, signal intensity is enhanced for flakes prepared on ultra-flat gold (Au) substrates (root-mean-square (rms) surface roughness < 0.2 nm), but different Raman modes undergo different rates of enhancements when comparing flakes of the same thickness on SiO<sub>2</sub> and Au. Raman data was acquired for excitation sources of both 532 and 633 nm of wavelength. Comparison data plots indicate resonance-enhanced Raman scattering with 633 nm of excitation, confirmed by additional absorption measurements. Temperature-dependent data was acquired from room temperature to 225 °C. All Raman modes present redshift with increasing temperature, suggesting that the chemical bond length of Franckeite increases with increasing temperature, and therefore the bond's vibrational force constant decreases. Moreover, we observed new low-frequency shearing and breathing modes in the Raman spectra. These low-frequency vibrational modes of Franckeite can provide a broader understanding of interlayer vibrational modes in 2D crystals, and especially in van der Waals heterostructures.

#### References

1. Molina-Mendoza, A. J. *et al.* Franckeite as a naturally occurring van der Waals heterostructure. *Nat. Commun.* **8**, (2017).
2. Velický, M. *et al.* Exfoliation of natural van der Waals heterostructures to a single unit cell thickness. *Nat. Commun.* **8**, 1–11 (2017).
3. Ray, K. *et al.* Photoresponse of Natural van der Waals Heterostructures. *ACS Nano* **11**, 6024–6030 (2017).
4. Liang, L. *et al.* Low-Frequency Shear and Layer-Breathing Modes in Raman Scattering of Two-Dimensional Materials. *ACS Nano* **11**, 11777–11802 (2017).

#### F.EL04.19.05

##### Measuring Thermal Expansion Coefficient of Monolayer Molybdenum Disulfide Using Micro-Raman

**Spectroscopy** Lenan Zhang, Zhengmao Lu, Youngsup Song, Lin Zhao, Bikram Bhatia, Kevin Bagnall and Evelyn Wang; Massachusetts Institute of Technology, United States

Atomically thin two-dimensional (2D) molybdenum disulfide (MoS<sub>2</sub>) is highly attractive due to its unique properties and promising applications in nanoscale electronics. Characterization of thermal expansion coefficient (TEC) of 2D MoS<sub>2</sub> is ubiquitous for reducing the thermal mismatch and improving the thermal management of MoS<sub>2</sub>-based devices. However, measuring the TEC of 2D MoS<sub>2</sub> is particularly challenging owing to its nanoscale thickness, microscale area and optical transparency properties. As a result, the thermal expansion on 2D MoS<sub>2</sub> still extensively relies on simulation. In this work, we report a pure experimental approach to characterize the TEC of monolayer MoS<sub>2</sub> using micro-Raman spectroscopy. We analyzed the stress and temperature dependent phonon frequency of monolayer MoS<sub>2</sub> using the perturbation theory and symmetry analysis. To decouple the effect of thermal stress on phonon frequency shift, monolayer MoS<sub>2</sub> flakes were transferred on fused silica, pure copper and micro-hole patterned thermal oxide substrates. We characterized the temperature coefficients on three substrates through the temperature-dependent Raman measurement. The in-plane TEC of monolayer MoS<sub>2</sub> was then extracted by comparing these coefficients. The resulting in-plane TECs were  $(7.6 \pm 0.9) \times 10^{-6}$  1/K and  $(7.4 \pm 0.5) \times 10^{-6}$  1/K, which were independently obtained from two different phonon modes of MoS<sub>2</sub> and in reasonable agreement with previous first-principle reported values. This work provides accurate measurement on the TEC of monolayer MoS<sub>2</sub>. Additionally, the general experimental approach can be widely applied to study many other 2D materials or thin films in a simple way.

#### F.EL04.19.06

##### Luminescence Properties of Hexagonal Boron Nitride Powders Probed by Deep UV Photoluminescence

**Spectroscopy** Nikesh Maharjan and Mim Nakarmi; Brooklyn College and The Graduate Center of CUNY, United States

Hexagonal boron nitride (h-BN) is an ultrawide (~ 6.0 eV) semiconductor that has potential applications for developing

electronic, optoelectronic and nanophotonic devices including source of ultraviolet emitters. A key issue in these applications is understanding the effect of impurities, especially carbon and oxygen on its properties. Deep UV photoluminescence spectroscopy was employed for optical characterization of irregular-shaped h-BN crystal powders. Fourth harmonic laser (195 nm) generated from the Ti: sapphire laser was used for optical excitation in the experiments. The luminescence properties are investigated by annealing the sample at different temperatures under different conditions. The deep UV photoluminescence spectra from h-BN samples annealed at 700 °C in ambient air reveals a strong phonon-assisted band-edge emissions along with a sharp atomic-like emission line at 4.09 eV, and its phonon replicas at 3.89 and 3.69 eV. In addition to these peaks, sharp multi-phonon peaks are observed adjacent to them. The PL spectra of the sample shows the broadening of the main peaks as the annealing temperature exceeds 900 °C. We will present our findings of atomic-like features that could have potential applications as quantum sources in UV regions for quantum information technologies.

#### **F.EL04.19.08**

**Quantification of Surface Reactivity and Step-Selective Etching Chemistry on Single-Crystal BiOI** Julia Martin, Roy Stoflet, Alexander Carl, Katarina Himmelberger and Ronald L. Grimm; Worcester Polytechnic Institute, United States

We synthesized single-crystal BiOI via vapor transport, subjected the resulting crystals to a series of surface treatments, and quantified the resulting chemical states and electronic properties. Vapor transport methods included both physical vapor transport from single-source BiOI, as well as chemical vapor transport from  $\text{Bi}_2\text{O}_3 + \text{BiI}_3$  and from  $\text{Bi} + \text{I}_2 + \text{Bi}_2\text{O}_3$ . Surface treatments included tape cleaving, rinsing in water, sonication in acetone, an aqueous HF etch, and a sequential HF etch with subsequent sonication in acetone. X-ray diffraction, XRD, and X-ray photoelectron spectroscopy, XPS, probed the resulting bulk crystalline species and interfacial chemical states, respectively. In comparison with overlayer models of idealized oxide-terminated or iodide-terminated BiOI, angle-resolved XPS elucidated surface terminations as a function of each treatment. Ultraviolet photoelectron spectroscopy, UPS, established work-function and Fermi-level energies for each treatment. Data reveal that HF etching yields interfacial  $\text{BiI}_3$  at BiOI steps that is subsequently removed with acetone sonication. UPS establishes n-type behavior for the vapor-transport-synthesized BiOI, and surface work function and Fermi level shifts for each chemical treatment under study. We discuss the implications for processing BiOI nanofilms for PV and photocatalysis applications.

#### **F.EL04.19.09**

**Impact of Salt and Solvent Identity on the Deposition of a Cobalt Crown Ether Phthalocyanine Monolayer Electrolyte** Huiran Wang, Shubham Sukumar Awate and Susan Fullerton; University of Pittsburgh, United States

A monolayer electrolyte, developed by our group, has been used to demonstrate a solid-state nonvolatile two-dimensional (2D) crystal memory based on an electric-double-layer (EDL) gated field effect transistor. (Nano Lett., 19, 8911, 2019) The monolayer electrolyte consists of cobalt crown ether phthalocyanine (CoCrPc), with four crown ethers that can solvate one lithium ion each. By simply drop-casting and annealing, CoCrPc forms a flat and ordered array on 2D crystals including graphene and  $\text{WSe}_2$ . The key mechanism of the nonvolatile memory is the toggling of lithium ions up and down through the cavity of crown ether (i.e., away from or nearby the channel). This toggling is accomplished by an applied electric field to overcome the diffusion barrier for ion movement. Our previous experimental work focused on one combination of materials: CoCrPc with 15-crown 5-ether (15C5),  $\text{LiClO}_4$ , and ethanol as the solvent for the salt. However, additional material combinations should result in varying diffusion barriers, thereby offering a path to tune the voltage required to toggle the ions. In this study, we investigate CoCrPc with 15C5 combined with two kinds of salts, LiCl and LiI, and three solvents: anhydrous acetone, acetonitrile, and nitromethane. LiCl and LiI were chosen to isolate the impact of anion identity (Cl vs. I vs.  $\text{ClO}_4$ ) on the quality of the monolayer, and the three solvents were chosen for their reported tendency to promote ion-crown complexation. Monolayer quality is evaluated by measuring the thickness and surface roughness with atomic force microscopy (AFM) after deposition on 2D crystals in a water and oxygen-free glovebox. This study establishes the design rules for monolayer electrolyte deposition on 2D crystals, which can be used to engineer devices with multiple diffusion barriers in monolayer electrolyte random-access memory (MERAM). This work is supported by the NSF under Grant # NSF-DMR-EPM CAREER: 1847808.

#### **F.EL04.19.10**

**Monolayer Xene Films Synthesized by Molecular-Beam Epitaxy** Kaylyn Holmes, Ruizhe Kang, Qi Song, Charles Brooks, Jennifer E. Hoffman and Julia Mundy; Harvard University, United States

Single element atomic monolayer honeycomb lattice films (also called “Xene” films) are a quickly-growing topic in condensed matter physics and materials science. In contrast to graphene, Xene films from higher  $Z$  elements such as

bismuthene (from bismuth) and stanene (from tin) are predicted to exhibit quantum spin Hall effects at temperatures closer to room temperature due to their larger topological band gaps, making them more useful for potential applications in next generation electronics. Although these two Xene films have strong theoretical and computational evidence supporting their candidacy for higher temperature quantum spin Hall effects and topologically protected edge states, they are both very difficult to produce because hexagonal unit cells are unstable configurations for the crystallization of these elements. Here, we present our work on using molecular-beam epitaxy (MBE) to synthesize monolayers and thin layers of bismuthene.

#### F.EL04.19.11

##### **2D Nanostructured Tetrasilicates with Cr(II) and Cr(II)/Fe(II) in Square Planar Coordination—Preparation and Magnetic Properties** Harshani Rathnaweera and Tina Salguero; University of Georgia, United States

The chromium-containing alkaline earth metal tetrasilicates,  $ACrSi_4O_{10}$  ( $A = Ca, Sr, \text{ and } Ba$ ), are noteworthy as examples of rare, high spin Cr(II) in square-planar coordination complexes in chromium oxide-crystal chemistry. Though the synthesis of  $ACrSi_4O_{10}$  has been known in the literature for several decades, much of the chemistry surrounding  $ACrSi_4O_{10}$  formation remains unknown. In this contribution, we describe magnetic properties of all  $ACrSi_4O_{10}$  phases prepared through improved synthetic routes as well as the subsequent nanostructuring of them into nanosheets by exfoliation. For flux-based routes, we utilize a metal envelope made from folded Cr foil to maintain a low oxygen fugacity in the reaction environment to avoid the formation of highly oxidized Cr species. We further extend the chemistry of  $BaCrSi_4O_{10}$  to include mixed metal centers, specifically Cr(II) and Fe(II). The incorporation of mixed metal centers in  $ABSi_4O_{10}$  phase is new territory in metal tetrasilicate chemistry, and this is the first example of transition metal substitution in any of the known  $ABSi_4O_{10}$  systems ( $B = Cu, Fe, Cr$ ). We find that the targeted stoichiometry of  $Ba(Cr,Fe)Si_4O_{10}$  crystals yields an experimentally-determined composition with up to a ~40% incorporation of Fe(II), which appears to constitute the maximum incorporation of Fe(II) into  $BaCrSi_4O_{10}$ . Interestingly,  $Ba(Cr,Fe)Si_4O_{10}$  crystals show a different magnetic infrastructure due to the interaction of antiferromagnetic Cr(II) and ferromagnetic Fe(II) centers in a single lattice. In this paper, we characterize the magnetic properties of  $Ba(Cr,Fe)Si_4O_{10}$  crystals and nanosheets using Mössbauer and EPR spectroscopies.

#### F.EL04.19.16

##### **Fabrication of Large-Area $MoS_2$ Nanosheets by Salt-Assisted Mechanical Milling Process and Chemical Exfoliation in Cosolvent** Hsiang-Chun Yu and Tsung-Eong Hsieh; National Chiao Tung University, Taiwan

Salt-assisted mechanical milling and chemical exfoliation in cosolvent were adopted to prepare the large-area  $MoS_2$  nanosheets with a few layers in thickness. First, the  $MoS_2$  powder was blend with salt, *e.g.*, potassium chloride (KCl), calcium chloride ( $CaCl_2$ ) or sodium carbonate ( $Na_2CO_3$ ), and sent to a ball mill containing zirconia beads with 1 cm in diameter. The milling process was carried out at 300 rpm for 2 hrs so as to generate numerous dangling bonds at the edges of  $MoS_2$ . The dangling bonds would react with the salt to form the functionalized groups which may induce the electrical repulsion for the dispersion of  $MoS_2$  in subsequent chemical exfoliation process. The functionalized  $MoS_2$  powder was added in a centrifuge tube containing the cosolvent comprised of water and alcohol at the weight ratio of 1:1. After the ultrasonic vibration for 30 mins at room temperature, the  $MoS_2$  nanosheets with thickness of 1-2 nm could be obtained *via* the centrifugation of solution. Most studies of chemical exfoliation reported the  $MoS_2$  nanosheets with the lateral size smaller than 1  $\mu m$ . However, our study observed the  $MoS_2$  nanosheets which average area of  $12 \times 5.6 \mu m^2$  using  $Na_2CO_3$  and average area of  $14 \times 6 \mu m^2$  using KCl. Presently, the  $MoS_2$  FET devices containing the large-area  $MoS_2$  nanosheets are prepared and their electrical properties are measured.

#### F.EL04.19.18

##### **An Exfoliation of Mixed Dimensional van der Waals Organic/ $WS_2$ Heterojunctions Ink for Emerging Electronics** Abdus S. Sarkar<sup>1,2</sup> and Suman Kalyan Pal<sup>1</sup>; <sup>1</sup>Indian Institute of Technology Mandi, India; <sup>2</sup>Foundation For Research and Technology Hellas, Greece

Since, the isolation of single layer graphene, a great attention has been paid to integrate distinct emerging beyond graphene 2D materials into van der Waals (vdW) heterostructures. The emerging 2D transition metal dichalcogenides (TMDCs), such as semiconducting (2H-phase) tungsten sulfide ( $WS_2$ ) and their mixed dimensional heterojunctions have drawn most vibrant areas of nanoscience/photonic research because of fascinating optical and electrical properties in their low dimensional interface. [1-3] However, most of the preparation (chemical) methods do not preserve the semiconductive properties of  $WS_2$ . Here, we have prepared a novel mixed dimensional 2D semiconductor p-n heterojunction of few layer  $WS_2$ , which is exfoliated in the presence of an organic semiconductor (OS) and characterized by various experimental techniques. Our results revealed that the few hundred nanometer size, few layer (4-5 layers) thick  $WS_2$  sheets are grafted with OS. Hexagonal pattern in HR-TEM image intimate the preservation of 2H-phase  $WS_2$ . Significant changed in the electrical behavior in the p-



n nanoheterojunctions are presented. The insight spectroscopic analysis indicated the possible hybrid optoelectronic applications. Furthermore, the heterojunction dispersion WS<sub>2</sub> sheets are quite stable with prior little aggregation after 180 days.

#### Reference

- [1] D. Jariwala, T.J. Marks and M. C. Hersam, *Nat. Mater.*, 2017, 16, 170-181.
- [2] A. S. Sarkar, S. K Pal, *J. Phys. Chem. C*, 2017, 121, 21945-21954.
- [3] A. S. Sarkar, I. Konidakis, I. Demeridou, E. Serpetzoglou, G. Kioseoglou and E. Stratakis, 2020, <https://arxiv.org/abs/2005.02852>

#### F.EL04.19.19

**Mechanisms of Molybdenum Trioxide Sulfurization in the Growth of Two-Dimensional Molybdenum Disulfide** Joshua Maurer, Thierry Tsafack and Stephen F. Bartolucci; US Army CCDC AC, United States

Powder vaporization is a common method for the generation of large-area, single-crystal, two-dimensional molybdenum disulfide. While commonly employed as a growth method, the fundamental molecular mechanisms are not well understood. Recent ab initio analyses have shown that molybdenum oxysulfide rings play a key role in the sulfurization of molybdenum trioxide from elemental sulfur. Here, we present the utilization of molecular dynamics simulations with a reactive force field and ab initio calculations to elucidate the reaction pathway of sulfur with molybdenum trioxide. The molecular dynamics simulations demonstrated that for all sulfur allotropes the reaction pathway could be reduced to that of disulfur, trisulfur, or a combination of the two, and that molybdenum trioxide can catalyze the decomposition of larger sulfur allotropes. Ab initio calculations were used to illuminate the intermediates and transition states in the reaction pathways for disulfur and trisulfur. Analysis of the temperature dependence of the transition state energies show that the maximum reaction rates occur between 1000 and 1100 K, which corresponds with commonly reported experimental growth temperatures for molybdenum disulfide.

#### F.EL04.19.20

**Influence of Solvent Properties on the Morphology of Ultra-Thin Tin Monoxide Nanomaterials for Next-Generation Energy Storage Applications** Seán Kavanagh<sup>1,2,3</sup>, Sonia Jaskaniec<sup>3</sup>, João Coelho<sup>3</sup>, Sean Ryan<sup>3</sup> and Valeria Nicolosi<sup>3</sup>; <sup>1</sup>Imperial College London, United Kingdom; <sup>2</sup>University College London, United Kingdom; <sup>3</sup>Trinity College Dublin, Ireland

Two-dimensional (2D) nanomaterials, especially those with controlled size and shape, have attracted significant attention over the last decade, due to their enhanced performance in comparison to their bulk counterparts.<sup>1-3</sup> One such chemical compound is tin monoxide (SnO), whose layered crystal structure renders it amenable to the fabrication of 2D architectures. SnO has demonstrated promising performance in many relevant applications, including thin-film transistors,<sup>4-</sup> photocatalysis,<sup>7</sup> gas sensing<sup>8</sup> and, primarily, energy storage - as next-generation battery anode materials.<sup>9-11</sup> However, the synthesis of SnO nanomaterials with controlled morphology still poses a considerable challenge in the field.<sup>9,12-17</sup> In this work, we provide a comprehensive study of the complex relationship between wet chemistry synthesis conditions and resulting nanoparticle morphology. The solvent nature is observed to strongly influence the kinetics of nucleation and crystal growth in solution, and thus the final morphological and electrochemical properties.

Extensive characterization of the precipitate nanomaterial has been performed, including scanning electron microscopy (SEM), high-resolution transmission electron microscopy (HRTEM), selected area electron diffraction (SAED), x-ray diffraction (XRD) and thermogravimetric analysis (TGA), in order to comprehensively describe the solvent-morphology dependence. Furthermore, high-level electronic structure theory, including dispersion corrections to account for Van der Waal's effects, were employed to augment our understanding of the underlying chemical mechanisms. Using supercell calculations, electronic vacuum alignment and surface energies were determined, allowing the prediction of the thermodynamically-favored crystal shape (Wulff construction) and surface-weighted work function, important parameters for battery performance. Finally, the synthesized nanomaterials were tested as battery materials, illustrating the impact of particle morphology on electrochemical performance.

Our results reveal promising pathways to the controlled synthesis of nanomaterials with tailored morphologies for enhanced performance in specific applications.

<sup>1</sup> S. Suresh, *Nanoscience and Nanotechnology* **3**, 62 (2013).

<sup>2</sup> Y.W. Jun, J.S. Choi, and J. Cheon, *ANGEW CHEM (INT ED ENGL)* **45**, 3414 (2006).

<sup>3</sup> Z. Wu, S. Yang, and W. Wu, *Nanoscale* **8**, 1237 (2016).

<sup>4</sup> K.J. Saji, K. Tian, M. Snure, and A. Tiwari, *Advanced Electronic Materials* **2**, 1 (2016).

- <sup>5</sup> Y. Ogo, H. Hiramatsu, K. Nomura, H. Yanagi, T. Kamiya, M. Kimura, M. Hirano, and H. Hosono, *Physica Status Solidi (A) Applications and Materials Science* **206**, 2187 (2009).
- <sup>6</sup> S.S. Lin, Y.S. Tsai, and K.R. Bai, *Applied Surface Science* **380**, 203 (2016).
- <sup>7</sup> L. Liang, Y. Sun, F. Lei, S. Gao, and Y. Xie, *Journal of Materials Chemistry A* **2**, 10647 (2014).
- <sup>8</sup> I. Sm, N. St, N. Yh, B. Dk, S. Fj, M. Rs, R. Ns, G. Sk, A. Dk, and P. Vb, *J Colloid Interface Sci* **493**, 162 (2017).
- <sup>9</sup> F. Zhang, J. Zhu, D. Zhang, U. Schwingenschlögl, and H.N. Alshareef, *Nano Lett.* **17**, 1302 (2017).
- <sup>10</sup> C.S. Lim, Z. Sofer, O. Jankovský, H. Wang, and M. Pumera, *RSC Advances* **5**, 101949 (2015).
- <sup>11</sup> Y.C. Lu, C. Ma, J. Alvarado, T. Kidera, N. Dimov, Y.S. Meng, and S. Okada, *Journal of Power Sources* **284**, 287 (2015).
- <sup>12</sup> Y.-H. Sun, P.-P. Dong, X. Lang, and J.-M. Nan, *Chinese Chemical Letters* **25**, 915 (2014).
- <sup>13</sup> H. Uchiyama, H. Ohgi, and H. Imai, *Crystal Growth and Design* **6**, 2186 (2006).
- <sup>14</sup> S.C. Wang, R.K. Chiang, and P.J. Hu, *Journal of the European Ceramic Society* **31**, 2447 (2011).
- <sup>15</sup> W. Liu, L. Yin, R. Zhang, H. Yang, J. Ma, and W. Cao, *Nanotechnology* **29**, 284002 (2018).
- <sup>16</sup> J. Ning, T. Jiang, K. Men, Q. Dai, D. Li, Y. Wei, B. Liu, G. Chen, B. Zou, and G. Zou, *Journal of Physical Chemistry C* **113**, 14140 (2009).
- <sup>17</sup> S. Wang, S. Xie, H. Li, S. Yan, K. Fan, and M. Qiao, *Chemical Communications* 507 (2005).

#### F.EL04.19.21

**Effect of Aliovalent Doping on Epitaxial Growth, Structure and Properties of Triple-Layered Ruddlesden-Popper Phase Lanthanum Nickelate** Akifumi Matsuda<sup>1</sup>, Tomoaki Oga<sup>1</sup>, Shohei Hisatomi<sup>1</sup>, Nobuo Tsuchimine<sup>2</sup>, Satoru Kaneko<sup>3,1</sup> and Mamoru Yoshimoto<sup>1</sup>; <sup>1</sup>Tokyo Institute of Technology, Japan; <sup>2</sup>Toshima Manufacturing Co., Ltd., Japan; <sup>3</sup>Kanagawa Institute of Industrial Science and Technology, Japan

Ruddlesden-Popper phase lanthanum nickelates ( $\text{La}_{n+1}\text{Ni}_n\text{O}_{3n+1}$ ) with two-dimensional perovskite structure have attracted interests for their electronic properties related to the structure and mixed valence Ni-ions [1]. These two-dimensional perovskites are also expected as precursors to develop infinite-layer nickelate superconductors such as Sr-doped  $\text{NdNiO}_3$  [2]. Development of epitaxial thin films of lanthanum nickelate with multilayered structure and modifying their structure, electronic state, and properties according to interfacial strain and substitutional doping would contribute to develop further understanding and application of their solid-state physics. There are some reports of triple-layered  $\text{La}_4\text{Ni}_3\text{O}_{10}$  for its metal-insulator-transition due to oxygen deficiency and possible application to such as SOFCs and gas sensors [1,3]. However, aliovalent doping in  $\text{La}_4\text{Ni}_3\text{O}_{10}$  epitaxial thin films similar to  $\text{La}_2\text{NiO}_4$  and  $\text{La}_3\text{Ni}_2\text{O}_7$  still requires further researches to explain its effect on structure and properties [4,5]. In this study, effect of aliovalent dopants substituting  $\text{La}^{3+}$  in triple-layered  $\text{La}_4\text{Ni}_3\text{O}_{10}$  on its epitaxial growth as well as on the structure and electric properties of the thin films was investigated. The lanthanum nickelate thin films were prepared by pulsed laser deposition technique equipped with a KrF excimer laser ( $\lambda=248$  nm,  $d=20$  ns, and  $E\sim 1.0$  J/cm<sup>2</sup>). The films were deposited on atomically stepped  $\text{SrTiO}_3$  and  $\text{NdGaO}_3$  single crystal substrates at 700–750°C in  $\text{O}_2$  atmosphere (10 Pa) using sintered targets of  $\text{La}_4\text{Ni}_3\text{O}_{10}$  doped with Hf and Sn. The thin films were then thermally treated at  $\sim 950^\circ\text{C}$  for 2 hours in high-purity  $\text{O}_2$  atmosphere (1 atm, 200 sccm) to modify the crystal phases and the valence of Ni-ions. X-ray diffraction results indicated epitaxy of  $\text{La}_4\text{Ni}_3\text{O}_{10}$  (001) thin films after annealing in  $\text{O}_2$ , while epitaxial growth of  $\text{La}_2\text{NiO}_4$  (100) was observed for the as-grown films. The formation of  $\text{La}_2\text{O}_3$  buffer layer at the interface was suggested to have contribution on the epitaxy of  $\text{La}_4\text{Ni}_3\text{O}_{10}$  phase. The Hf and Sn-doped  $\text{La}_4\text{Ni}_3\text{O}_{10}$  (001) thin films with thickness of  $\sim 100$  nm demonstrated low resistivity of  $\sim 5$  m $\Omega\text{cm}$  at room-temperature measured by a 4-probe DC method. Further detailed structural analyses of the lanthanum nickelate thin films, and the effect of the aliovalent doping on the electronic property related to the structure would also be discussed.

[1] K.-T. Wu et al., *J. Mater. Chem. A*, **5** (2017) 9003–9013.

[2] D. Li et al., *Nature*, **572** (2019) 624–627.

[3] V. Pardo et al., *Phys. Rev. B*, **83** (2011) 245128.

[4] R. J. CaVa et al., *Phys. Rev. B*, **43** (1991) 1229–1232.

[5] S. A. Nedilko et al., *J. Alloys Compd.*, **367** (2004) 251–254.

#### F.EL04.19.22

**Thermoelectric Effect of Conductive Polymer Films from Functionalized Graphene** Byeonggwon Kim, Cheolhyun Cho and Eunkyong Kim; Yonsei University, Korea (the Republic of)

Thermoelectric effects in conductive polymers (CPs) have received significant attention owing to its high electrical conductivity, high Seebeck coefficient, and low thermal conductivity. Among the CPs, poly(3,4-ethylenedioxythiophene) (PEDOT) is a notable material by taking advantage of solution processability, high degree of crystallinity, and bipolaronic network. We prepared a PEDOT grafted graphene film by solution casting polymerization using surface functionalized graphenes, to provide thermoelectric PEDOT on graphene (PEOG) film. The PEOG showed a high degree of crystallinity,

which enhanced both electrical conductivity and Seebeck coefficient. Taking advantage of graphene functionality, TE properties were modulated via several external stimuli. This result reinforced the application potential of CP-based TE materials in a multifunctional energy conversion.

#### **F.EL04.19.23**

**A Novel Approach to Synthesize 2D Materials by Direct Heating of Bulk Sources and Detailed Photoluminescence Study in Comparison to Most Popular Synthesis Techniques** Davoud Hejazi, Renda Tan and Swastik Kar; Northeastern University, United States

Semiconducting 2D materials are becoming more and more attractive for various optoelectronics and sensing applications; however, synthesis of high-quality 2D materials for lab-scale research is not often practical for many research laboratories, since the synthesis process often requires reactors, carrier gases, or furnaces of various levels of complexities. A simple method of growing various types of 2D materials or their combined structures (i.e. heterostructure, alloys etc.) that is easy to set up and run can further accelerate 2D research. We report on a new synthesis technique, finding that single and multilayered 2D materials of various types can be easily fabricated by direct thermal evaporation of bulk sources under an inert atmosphere. This is in stark contrast with conventional vapor-phase techniques which require chemical reactions of precursors, and a flow of one or more inert carrier gases, thereby substantially reducing the cost and complexities involved. In this study, sources of target nanomaterials are taken in their commercial bulk form, reduced to a powder for convenience and placed on a clean container in close proximity of the target substrate inside an inert environment, then heated to a range of high temperature values and held at those temperatures for material-specific durations. The nanomaterials evaporate from the source and deposit directly on the substrate in the form of well-formed crystals that can be evaluated for quality or modified for basic research or proof-of-concept applications. This synthesis methodology is much simpler than the other synthesis techniques such as CVD, MBE, ME, etc. We present detailed analysis (AFM, optical images, Raman, photoluminescence) of the various types of 2D materials and structures possible through direct, mixed, and sequential evaporation of bulk powders.

By studying the photoluminescence (PL) spectra of the 2D materials fabricated with this method and comparing them with the PL spectra of the 2D materials synthesized by other methods, found in the literature, we show that the quality of these samples, observable in FWHM of the A-exciton, is comparable with the samples grown with the best synthesis techniques. Furthermore, by detailed analysis of the PL spectra of these samples, we observe metrology-dependent variations in quantum properties of these crystals, where the relative distance of the A-exciton and A<sup>-</sup>-trion becomes smaller for the specific crystals with high PL intensity, which appear to have wrinkles that may have originated from spacial confinement, induced by seed in the nucleation site.

#### **F.EL04.19.24**

**Enhanced Charge Separation with Insulator Mediation in Vertically Stacked InSe/GeS Heterostructures** Christy Roshini Paul Inbaraj<sup>1,2,3</sup>, Roshan Jesus Mathew<sup>1,2</sup>, Raman Sankar<sup>2</sup>, Chih-Hao Lee<sup>1</sup> and Yang-Fang Chen<sup>3</sup>; <sup>1</sup>National Tsing Hua University, Taiwan; <sup>2</sup>Academia Sinica, Taiwan; <sup>3</sup>National Taiwan University, Taiwan

Modulating the physical properties of two-dimensional materials by stacking different layers to form vertical heterostructures gives rise to the new exciting phenomenon. In this work, we developed a method to improve charge separation in the type-II band aligned heterostructures (InSe/GeS) by using thin dielectric spacers (h-BN). The optical transitions at the junctions exhibit quenched emission without h-BN layers indicating indirect recombination due to the strong interlayer coupling. However, the InSe/GeS heterojunction with h-BN layers in-between exhibits strongly enhanced emission granting an additional degree of freedom to modulate the optical property. The photoresponse of the heterostructures showing enhanced photocurrent density for InSe/h-BN/GeS device by refraining interlayer charge recombination backs up the argument. Thus, the improved charge separation with h-BN mediation demonstrates a higher photoresponsivity and detectivity in the order of  $10^2$  A W<sup>-1</sup> and  $10^{14}$  Jones, respectively. Furthermore, the high electron detection is evident from the photogain estimated in the order of  $10^3$ . In addition, the negative short-circuit current reveals the photovoltaic effect of the device. Therefore, our semiconductor-insulator-semiconductor (InSe/h-BN/GeS) device structure will be a promising candidate for future optoelectronics.

#### **F.EL04.19.25**

**Surface Characterization of Atomic Layer Deposited Molybdenum Oxide Films Using High Sensitivity Low Energy Ion Scattering** Raivat Singhania<sup>1</sup>, Benjamin Davis<sup>1</sup>, David Hynek<sup>2</sup>, Judy Cha<sup>2</sup> and Nick C. Strandwitz<sup>1</sup>; <sup>1</sup>Lehigh University, United States; <sup>2</sup>Yale University, United States

Transition metal dichalcogenides (TMDC), such as MoTe<sub>2</sub>, are a promising new class of materials with wide ranging

applications in the computing, optics, and photovoltaic industries. The deposition quality of these films has a drastic effect on overall film properties, and therefore device performance. In particular, achieving uniform and reproducible nucleation is important for creation of single monolayer films. However, islanding often occurs during film growth in which isolated regions of the film form initially, creating a discontinuous film and/or non-uniform film thickness, both of which are undesirable. We have investigated the uniformity and thickness control of molybdenum oxide films that are deposited via atomic layer deposition (ALD) and are precursors to MoTe<sub>2</sub> TMDCs. High-sensitivity low energy ion spectroscopy (HS-LEIS) was used to assess surface coverage and islanding of a variety of film MoO<sub>x</sub> films ranging in thickness from 0.2 nm to over 7 nm. HS-LEIS is used for this purpose due to its ability to selectively detect and differentiate between atoms in the outermost atomic layer and subsurface atoms. Absence of a signal from the substrate indicated that uniform nucleation and coverage of the surface with MoO<sub>x</sub> occurred at film thicknesses of approximately 0.5 nm. Ongoing research is focused on using Monte-Carlo simulations to predict LEIS spectra, which would allow for more quantitative analysis of nucleation and film growth. Quantitative analysis of nucleation and film growth is of great importance for next generation electronics that rely on layers that are only one or several atomic layers in thickness.

#### F.EL04.19.26

**Air Stable 2D Halide Perovskite/Transition Metal Dichalcogenide Heterostructures for Improved Optoelectronics** Abin Varghese<sup>1,2</sup>, Yuefeng Yin<sup>1</sup>, Saurabh Lodha<sup>2</sup> and Nikhil Medhekar<sup>1</sup>; <sup>1</sup>Monash University, Australia; <sup>2</sup>Indian Institute of Technology Bombay, India

Low-dimensional materials such as monolayer transition metal dichalcogenides (TMD) and two-dimensional (2D) perovskites have demonstrated enormous potential for optoelectronic applications.<sup>[1,2]</sup> TMDs have been explored for fast, high-responsivity photodetection owing to their sizeable bandgaps and high optical absorption coefficients, but their photovoltaic efficiency is quite low.<sup>[3]</sup> On the other hand, 2D Ruddlesden-Popper phase hybrid organic-inorganic perovskites have exhibited encouraging solar cell power conversion efficiencies and better ambient stability compared to the typical 3D perovskites.<sup>[4]</sup> However, the major challenges in realizing 2D perovskite based photovoltaic devices are its vulnerability to oxygen/humidity, large exciton binding energy, as well as poor optical absorption in the visible wavelengths.<sup>[2]</sup> In this work, using first-principles calculations, we propose a new strategy of employing TMD/2D perovskite heterostructures for optoelectronic applications to mitigate the intrinsic drawbacks of using TMD or 2D perovskite independently. These heterostructures formed via van der Waals (vdW) interaction between the constituents could be custom-designed for specific applications.

We show that the stacking of air stable TMDs like MoS<sub>2</sub> on top of the 2D perovskite (e.g., BA<sub>2</sub>PbBr<sub>4</sub>, BA is Butylammonium) could lead to improved ambient stability in addition to novel properties of the heterojunction. The calculated electronic band structure of the MoS<sub>2</sub>/BA<sub>2</sub>PbBr<sub>4</sub> heterostructure shows a type-II band alignment with good charge separation at the heterojunction. The effective bandgap at the heterointerface is ~ 0.8 eV, much lower than the intrinsic bandgaps of BA<sub>2</sub>PbBr<sub>4</sub> (~ 3 eV) and monolayer MoS<sub>2</sub> (1.9 eV).<sup>[1,4]</sup> Also, the calculated fermi level alignments of MoS<sub>2</sub> and BA<sub>2</sub>PbBr<sub>4</sub> show that the TMD can function as a selective electron transport layer resulting in improved solar cell performance with enhanced air stability. On the other hand, selenide based WSe<sub>2</sub>/BA<sub>2</sub>PbBr<sub>4</sub> heterointerface demonstrates a type-I alignment with a comparatively higher hetero-bandgap at ~ 1.5 eV, useful for light emitting applications at visible wavelengths.

In summary, this study explores the properties of TMD/2D perovskite heterostructures and provides new insights towards realizing high-performance next-generation optoelectronic devices. The high tensile strength of TMDs and molecular softness provided by the large organic chains could further enable the use of these heterostructures for flexible solar cells or light emitting devices.

#### References

- [1] K. F. Mak, J. Shan, *Nat. Photonics* **2016**, *10*, 216.
- [2] G. Grancini, M. K. Nazeeruddin, *Nat. Rev. Mater.* **2019**, *4*, 4.
- [3] D. Jariwala, A. R. Davoyan, J. Wong, H. A. Atwater, *ACS Photonics* **2017**, *4*, 2962.
- [4] L. Dou, A. B. Wong, Y. Yu, M. Lai, N. Kornienko, S. W. Eaton, A. Fu, C. G. Bischak, J. Ma, T. Ding, N. S. Ginsberg, L. W. Wang, A. P. Alivisatos, P. Yang, *Science (80-. )*. **2015**, *349*, 1518.

#### F.EL04.19.27

**Magnetic Properties in Correlated 2D van der Waals Metal Phosphosulfides Due to Suppression of Antiferromagnetic Ordering** Nitish Mathur<sup>1</sup>, Fengmei Wang<sup>1,2</sup>, Aurora Janes<sup>1</sup>, Peng He<sup>2</sup>, Xueli Zheng<sup>3</sup>, Tofik A. Shifa<sup>2</sup>, Peng Yu<sup>2</sup>, J.R. Schmidt<sup>1</sup>, Jun He<sup>2</sup> and Song Jin<sup>1</sup>; <sup>1</sup>University of Wisconsin--Madison, United States; <sup>2</sup>CAS Center for Excellence in Nanoscience, CAS Key Laboratory of Nanosystem and Hierarchical Fabrication, National Center for Nanoscience and Technology, China; <sup>3</sup>Stanford University, United States

Two-dimensional (2D) van der Waals (vdW) materials offer a versatile platform to explore their potential applications in electronic, photonic, and spintronic devices. Among them, the family of vdW layered metal phosphosulfides (MPS<sub>3</sub>, M = Ni, Fe, Co, Mn, etc.) show intriguing electronic physics, potential magnetic properties, and electrocatalysis applications. Recently, it has been reported that a strong long-range coupling between the electronic and magnetic structures results from super-exchange mechanism in 2D vdW NiPS<sub>3</sub> antiferromagnet (AFM). In this work, we demonstrate a new chemical route for suppression of AFM ordering in NiPS<sub>3</sub> system. Composition-tunable Ni<sub>1-x</sub>Co<sub>x</sub>PS<sub>3</sub> (0 ≤ x < 0.50) few-layered nanosheets (NSs) are successfully synthesized. Significantly, obvious suppression of AFM ordering below Néel temperature (T<sub>N</sub> ~ 143-155 K) in magnetic susceptibility measurements were observed in Ni<sub>1-x</sub>Co<sub>x</sub>PS<sub>3</sub> NSs, which contrast with the magnetic properties observed in bulk single crystals of Ni<sub>1-x</sub>Co<sub>x</sub>PS<sub>3</sub>. These findings provide a new direction for disruption of AFM long range ordering and opens a new window of opportunities for investigation of correlated physics and magnetism in 2D materials systems.

#### **F.EL04.19.29**

**High-Performance Ideal PN Photodiode Using Directly Grown CVD Heterostructure** Jieun Kim and Woo Jong Yu; Sungkyunkwan University, Korea (the Republic of)

As silicon-based field effect transistors (FET) face miniaturization limitations, various two-dimensional (2D) material-based FETs are promising for next-generation electronic and optoelectronic devices. These days, not only study to produce high performance 2D-FETs, but also to implement integrated circuits with 2D materials has been reported. In terms of integrated circuits, PN junction is essential for complementary circuit. To fabricate 2D PN junction, usually transferring and stacking with exfoliated flakes has been used. Even if the flakes electronic quality is good, it needs trained skills and is time consuming. In addition, it is hard to ensure interface quality and has residue problems which deteriorate device performances.

In this paper, we report the direct growth of PN heterostructures with transition metal dichalcogenide (Nb doped WSe<sub>2</sub>/MoSe<sub>2</sub>) on SiO<sub>2</sub>/Si substrates with chemical vapor deposition (CVD) method with one mixed solution source. To confirm the composition and structural properties of our as-grown heterojunction sample Raman, PL, XPS and AFM analysis is done. At inner and outer domain, obviously different center Raman and PL peaks are observed. The niobium (Nb) doping signal also confirmed by Raman peaks and XPS peaks. In AFM height profile data, inner and outer height show no difference which represents lateral heterostructure. To obtain electronic properties at inner, outer and junction region, multi electrodes are evaporated. At junction, current rectification behavior is shown as a PN diode with 1.3 ideality factor which is close to ideal ideality factor of 1. Also the current level between P (Nb doped WSe<sub>2</sub>) and N (MoSe<sub>2</sub>) domain is similar. Under lasers illumination, optoelectronic characteristic is shown. Several properties such as built-in potential across the junction, type-II band alignment of the materials (WSe<sub>2</sub> and MoSe<sub>2</sub>), low lattice mismatch and atomically sharp interface from directly growth mechanism, allow high advantages in optoelectronic devices. Additionally, the niobium acceptor dopants allow wide range of absorption wavelength from ultraviolet (UV) to near infrared (NIR) which overcomes the limitation of the TMD photodetectors. Additionally, back gated PN photodiode can effectively suppress dark current through gate voltage modulation, thus realizing very high detectivity.

Thus, our direct grown Nb doped WSe<sub>2</sub>/MoSe<sub>2</sub> PN heterostructure photodiode shows outstanding optoelectronic performances, such as high detectivities (10<sup>15</sup> Jones), I<sub>light</sub>/I<sub>dark</sub> (10<sup>5</sup>) under V<sub>DS</sub> = 0 V. Our approach of direct grown PN heterostructure photodiode allows fabricate high quality and easy integrated optoelectronic 2D atomic layer devices.

#### **F.EL04.19.31**

**Two-Dimensional ZnO Nanoplates Grown on r-plane Oriented Al<sub>2</sub>O<sub>3</sub> and Their Photocatalytic Properties** Shota Sakurai and Junghyun Cho; Binghamton University, The State University of New York, United States

Two-dimensional (2-D) nanomaterials have recently received considerable attention with their unique characteristics, which were not seen in their bulk and 1-D nanomaterials. Zinc oxide (ZnO) is chemically stable, non-toxic, and available at low cost, which makes it into one of the most intriguing materials. Since the surface is surrounded largely by basal c-planes, 2-D ZnO nanomaterials have the good potential for tailoring the functional properties through adjusting their surface morphologies. To achieve the growth of such 2-D ZnO nanoplatelets, the growth direction must be along the a-axis, while suppressing the growth along the c-axis. This growth is challenging because the growth along the c-axis is energetically favorable. To control the growth direction, a seed layer plays a significant role. r-plane (1-102) aluminum oxide (Al<sub>2</sub>O<sub>3</sub>) can serve as a good seed layer for 2-D ZnO growth as the lattice mismatch between r-plane Al<sub>2</sub>O<sub>3</sub> and a-plane ZnO is only 1.53% along ZnO [0001] and Al<sub>2</sub>O<sub>3</sub> [2-201] directions. In this study, we prepared r-plane oriented Al<sub>2</sub>O<sub>3</sub> on Si (111) substrate as a seed layer by spin coating followed by annealing at high temperatures. r-plane Al<sub>2</sub>O<sub>3</sub> also has an epitaxial relationship with Si (111). 2-D ZnO nanoplates were then grown on the seed layer by the hydrothermal method. The c-plane of ZnO nanoplates

contains a high concentration of the surface defects and is off-stoichiometric; therefore, the thinner the nanoplate is, the more it is influenced by the defects on the c-plane. It makes these 2-D nanoplates very attractive as an effective photocatalytic surface for the degradation of organic contaminants. As a result, the templated growth of the 2-D ZnO nanoplates shows the great potential to form functional surfaces that can be very sensitive to external stimuli such as light and environment by controlling the concentration and type of defects. Photoluminescence (PL) and Raman spectra are used to characterize defect characteristics of various nanoplate morphologies. This presentation highlights current research progresses made for the control of the defect population, size, aspect ratio, and packing density of the ZnO nanoplates at various conditions and the effect of the resulting morphologies of the nanoplates on their photocatalytic properties.

#### **F.EL04.19.33**

**Resonance Raman Signatures of Atomically-Thin Black Phosphorus** Nannan Mao<sup>1,1</sup>, Xi Ling<sup>2</sup>, Liangbo Liang<sup>3</sup>, William Tisdale<sup>1</sup> and Jing Kong<sup>1</sup>; <sup>1</sup>Massachusetts Institute of Technology, United States; <sup>2</sup>Boston University, United States; <sup>3</sup>Oak Ridge National Laboratory, Oak Ridge, United States

Black phosphorus (BP) is an elemental two-dimensional semiconductor with quantized electronic structure, high mobility and tightly bonded exciton. Especially, due to the quantum confinement in the out-of-plane direction and significant interlayer interaction, BP has direct band gap for all thicknesses that is highly tunable from visible region to mid-infrared region. Besides, the conduction band and valence band in phosphorene split into quantized subbands, which constitute a series of thickness-dependent interband electronic transitions. These pronounced subband transitions, evidenced by sharp thickness-dependent absorption peaks in the visible region and infrared region, give rise to strong coupling with photons and phonons in few-layer BP. Here we investigated the electron-photon and electron-phonon coupling in few-layer BP samples by resonance Raman spectroscopy. Firstly, we observed Raman splitting effect in atomically thin-BP, and the origin of this phenomenon will be revealed. Secondly, based on the collective interlayer vibration modes, the accurate interlayer interaction of BP was measured in experiment. Thirdly,  $A_g^1$  mode shows much smaller resonance effect than  $A_g^2$  mode when the incident polarization is along armchair direction of BP, which can be explained by the symmetry-dependent electron-phonon coupling. These investigations give direct evidence of the significant interlayer interaction and deep insights into fundamental electron-photon and electron-phonon coupling in atomically-thin BP.

#### **F.EL04.19.34**

**Raman Scattering of Electrocatalytic 2D MoS<sub>2</sub> Nanosheets in Water Splitting** Kit Sze, Mikel Tucker, Saroj Pramanik and Yucheng Lan; Morgan State University, United States

Molybdenum disulfide (MoS<sub>2</sub>) is one of the most promising hydrogen-evolution-reaction (HER) electrocatalysts to replace noble metals in water splitting. Raman scattering is one non-destructive, efficient, and mature technique to characterize renewable energy materials. Here, the 2D MoS<sub>2</sub> nanosheets with various crystallinity are prepared and their electrocatalytic behaviors are *in-situ* investigated by Raman scattering under varied electric fields and temperatures. The results would enlighten the electrocatalytic mechanism of MoS<sub>2</sub> nanosheets and help us to improve its HER activities over the Pt catalyst.

#### **F.EL04.19.35**

**The Thermal Oxidation of Hexagonal Boron Nitride Single Crystals—Dry and Ambient Air Compared** Neelam Khan<sup>1</sup>, Michael B. Katz<sup>2</sup>, Albert Davydov<sup>2</sup> and James H. Edgar<sup>3</sup>; <sup>1</sup>Georgia Gwinnett College, United States; <sup>2</sup>National Institute of Standards and Technology, United States; <sup>3</sup>Kansas State University, United States

Hexagonal boron nitride (hBN), a layered van-der-Waals material, is employed as a template and an insulator to improve the performance of devices made from graphene and other two-dimensional (2D) materials. Moreover, due to its oxidation resistance, it is used to protect 2D materials devices from the environment through encapsulation. This study aims to understand the ultimate protective qualities of hBN layers at high temperatures in dry vs. ambient air. Single crystals of hBN were thermally oxidized at different temperatures ranging from 800 °C to 1100 °C for different durations, from 20 min to 100 min. Atomic force microscopy analysis revealed surface pits of about 50-100 nm in width, and 1-2 nm in depth, for the layers exposed to 900 °C for 20 minutes in dry air. Increasing the temperature and duration did not significantly change the surface pit sizes, in contrast to the thermal oxidation in ambient air, where longer oxidation times and higher temperatures, produced larger etch pits. Having no effect of thermal oxidation as a function of temperature and duration in dry air could be due to formation of the surface oxide layer, which slows down the etching process. Complimentary transmission electron microscopy will be employed to compare the extent of surface oxidation in ambient versus dry air and to study the origin and morphology of the surface pit formation.

#### F.EL04.19.36

**Late News: Efficient Electron Doping of Monolayer MoS<sub>2</sub> by Salt-Crown Ether Treatment** Hiroto Ogura<sup>1</sup>, Yoshiyuki Nonoguchi<sup>2</sup>, Toshifumi Irisawa<sup>3</sup>, Takahiko Endo<sup>1</sup>, Hong En Lim<sup>1</sup>, Yusuke Nakanishi<sup>1</sup> and Yasumitsu Miyata<sup>1</sup>; <sup>1</sup>Tokyo Metropolitan University, Japan; <sup>2</sup>Nara Institute of Science and Technology, Japan; <sup>3</sup>AIST, Japan

Atomic layers of transition metal dichalcogenides (TMDCs) have attracted much attention because of their unique two-dimensional structure and high electrical performance. For electronics applications, it is essential to develop a sophisticated way to control their carrier density of materials. So far, carrier control of TMDCs is achieved via surface charge transfer by using chemical doping. To further improve doping concentration, it is highly desired to find any stable and efficient dopants for TMDCs. Recently, Nonoguchi et al. have reported the electron doping of carbon nanotubes using a series of ordinary salts with crown ethers. In this study, we have applied this technique to monolayer MoS<sub>2</sub> and investigated the transport and optical properties of such chemically-doped MoS<sub>2</sub>.

Monolayer MoS<sub>2</sub> films were grown on SiO<sub>2</sub>/Si substrates by using chemical vapor deposition method. Electron doping was conducted by spin coating of butanol solution of KOH and benzo-18-crown-6. The doping process changes the transfer curves of MoS<sub>2</sub> field-effect transistors (FETs) from a typical n-type semiconducting state to metallic one in air. We also found photoluminescence quenching and peak shift in the A<sub>1</sub>' Raman mode for doped MoS<sub>2</sub>. These results indicate that the salt-based doping provides an effective way for the electron doping of MoS<sub>2</sub>. In the presentation, the details of transport and optical properties will be discussed.

#### F.EL04.19.37

**Late News: Few-Layered Two-Dimensional Ruddlesden-Popper Organic-Inorganic Hybrid Perovskite Magnets** Ki-Yeon Kim<sup>1</sup>, Garam Park<sup>1</sup>, Jaehun Cho<sup>2</sup>, Joonwoo Kim<sup>2</sup>, June-Seo Kim<sup>2</sup>, Jinyong Jung<sup>2</sup>, Kwonjin Park<sup>2</sup> and In-Hwan Oh<sup>1</sup>; <sup>1</sup>KAERI, Korea (the Republic of); <sup>2</sup>Daegu Gyeongbuk Institute of Science and Technology, Korea (the Republic of)

Atomically thin two-dimensional (2D) Van der Waals (vdw) magnets have received extensive attention due to their interesting magnetic phenomena inherent to low-dimensional magnetism such as Berezinskii-Kosterlitz-Thouless transition in 2D XY models and Mermin-Wagner Theorem. However, it is not until 2017 that the first 2D ferromagnetic magnets such as Cr<sub>2</sub>Ge<sub>2</sub>Te<sub>6</sub> and CrI<sub>3</sub> were experimentally realized via mechanical exfoliation method using Scotch tape. Since then, although a number of potential 2D vdw magnets have been theoretically predicted a very limited number of atomically thin or few-layered 2D vdw magnets still have been experimentally available. Specifically, since 1960's, 2D Ruddlesden-Popper organic-inorganic halide perovskites (RH-OIHP) have been considered as the ideal model closest to 2D Heisenberg model. Recent theoretical calculation using first principle density functional theory shows that the cleavage energy of (R-NH<sub>3</sub>)<sub>2</sub>CuCl<sub>4</sub> (R = a monovalent organic moiety such as C<sub>n</sub>H<sub>2n+1</sub> or C<sub>6</sub>H<sub>5</sub>C<sub>2</sub>H<sub>4</sub>) is smaller by a factor of 2-2.5 than that of graphite (0.36 J/m<sup>2</sup>). It means that 2D RP-OIHP monolayer by mechanical exfoliation from bulk crystals would be experimentally feasible. However, until now, there has not been successful report on fabrication of atomically thin or few-layered 2D RP-OIHP thin films with intrinsic magnetism at all. We will demonstrate the few-layered 2D OIHP magnets via solvent engineering based on spin coating technique.

#### F.EL04.19.38

**Late News: First-Principles Study of Interaction of O<sub>3</sub> with Silicene** Lokanath Patra<sup>1</sup>, Geeta Sachdeva<sup>1</sup>, Ravindra Pandey<sup>1</sup> and Shashi Karna<sup>2</sup>; <sup>1</sup>Michigan Technological University, United States; <sup>2</sup>CCDC Army Research Laboratory, Weapons, and Materials Research Directorate, United States

Silicene, an analogous silicon counterpart of graphene with unique physical properties, has attracted a great deal of attention. Its interaction with environmental molecules, e.g ozone needs to be investigated thoroughly as it has a great role to play for silicon-based technology at the nanoscale. In this study, we study the interaction of O, O<sub>2</sub>, and O<sub>3</sub> with silicene using density functional theory. We find that O, being more electronegative than Si, draws electrons from the Si-Si bond. Consequently, it is chemisorbed at the bridge site forming an epoxide like Si-O-Si configuration with a binding energy of 5.76 eV. On the other hand, O<sub>2</sub> and O<sub>3</sub> interacting with silicene dissociate at the surface, in contrast to what has been reported for graphene. Moreover, the dissociation process is spontaneous and exothermic without any energy barrier leading to the formation of Si-O bonds at the surface.

#### F.EL04.19.39

**Late News: Mild Condition Synthesis of Nanosized Bismuth Vanadate and Polyoxometalates Composite** Boon Chong Ong, Teik Thye Lim and Zhili Dong; Nanyang Technological University, Singapore

Nanosized materials often possess unique characteristics compared to their bulk counterpart and are useful in various

applications. Bismuth vanadate ( $\text{BiVO}_4$ ), a type of mixed-metal oxide, gains popularity in the field of catalysis reaction, especially the light-induced related process. They are active towards visible light irradiation and able to stimulate a catalytic reaction, for example, the water oxidation process. However, the main drawback of  $\text{BiVO}_4$  is the photogenerated electron-hole pairs tend to recombine in a very short period, which negatively impacts their catalytic performance. Coupling metal oxide with other materials is often regarded as one of the promising methods to alter their properties and improve catalytic performance. In the field of catalysis, polyoxometalates (POMs) have a distinctive property to act as electron and hole scavengers, which can retard the recombination of photogenerated electron-hole pairs effectively. They belong to a large class of nanosized metal-oxygen anion complexes of early transition elements with tunable structure, their properties greatly influence by the type of metals present in their structure. In this experiment, all the materials were synthesized in mild condition, without the use of strong base and acid. By avoiding a harsh environment, the complexity in the synthesis process can be reduced and are safer. A nanocomposite of  $\text{BiVO}_4$  and cobalt-based POMs is produced to integrate the excellent properties of both materials for the application in photochemical water oxidation. Characterization tests are performed, such as field emission scanning electron microscopy (FESEM) to study the shape and size of composites materials, X-ray diffraction (XRD) for confirming the crystal lattice structure and Fourier-transform infrared spectroscopy to identify the types of chemical bonds. A sheet-like behavior of  $\text{BiVO}_4$  can be noticed from the FESEM analysis. The synthesized  $\text{BiVO}_4$  is in a monoclinic phase as confirmed by the XRD result, in which intense peaks are noticed for (130) and (040) planes, while the POMs produced are in the triclinic phase. It is believed that the  $\text{BiVO}_4$ /POMs composite is able to improve the photocatalytic water oxidation reaction.

Keywords: Bismuth Vanadate, Nanomaterials, Polyoxometalate, Mild condition

#### F.EL04.19.40

**Late News: Optical Absorbance in Multilayer Two-Dimensional Materials—Graphene and Antimonene** Geeta Sachdeva<sup>1</sup>, Ashok Kumar<sup>1</sup>, Ravindra Pandey<sup>1</sup> and Shashi Karna<sup>2</sup>; <sup>1</sup>Michigan Technological University, United States; <sup>2</sup>CCDC Army Research Laboratory, United States

Antimonene, one of the group V elemental monolayers, has attracted intensive interest due to their intriguing optical properties. Considering the case of atomically-flat antimonene for which directional bonding between Sb atoms appears to be analogous to C-C bonds in graphene, we present its optical absorption properties from near IR to visible spectral regime. The results based on density functional theory predict that absorbance in multilayer antimonene is equivalent to or higher than that calculated for multilayer graphene. Specifically, the IR absorption in antimonene is significantly higher with a prominent peak at about 4  $\mu\text{m}$  associated with the dipole-allowed interband transitions. Moreover, a strong dependence of absorbance on topology is predicted for both antimonene and graphene which can be attributed to the subtle variations in their stacking-dependent band structures. Our results suggest the possibility of multilayer antimonene coating be realized as effective optical limiting material in the IR region for optoelectronic materials.

#### F.EL04.19.41

**Late News: Impact of Partial Reduction on Electrical Properties in Graphene Oxide Films** Akiko Ohata<sup>1</sup>, Francisco Romero<sup>2</sup> and Noel Rodriguez<sup>2</sup>; <sup>1</sup>Institute of Astronautical Science, Japan; <sup>2</sup>Granada university, Spain

Graphene-based composite materials and nanostructures have been intensively studied in terms of unique electrical properties and a wide spectrum of applications. Among them, reduced graphene oxide (rGO) has attractive advantages of flexibility, electrical and thermal conductivity, and low-cost production. We have already reported memristive properties in rGO films partially reduced by the laser irradiation to graphene oxide (GO). However, the resistance switching mechanism has not been fully understood. In this study, by electrically characterizing the transition region from GO to the laser-irradiated rGO, a possible mechanism for the memristive properties is discussed.

**Reduced GO film preparation:** The GO films prepared by drop-casting commercially available GO colloid (4mg/mL) on PET film were placed on a 3D-shaker at room temperature until the water was fully evaporated. A PC-driven 405nm laser (scan speed 3 min/cm<sup>2</sup>) was used for the photothermal reduction of GO films with a rectangular shape (~1.5mm width).

**Electrical characterization:** GO films were initially non-conductive, while it became conductive with the laser-power increase. Interestingly, when GO films were reduced at the threshold laser-power for GO reduction, memristive properties were clearly observed. Around this region, on/off ratio was rather sharp (digital change) and large (maximum ratio was nearly 12). In addition, hysteric I-V characteristics (continuous change) were also detected. In this study, we mainly discuss the continuous hysteresis observed in the transition region between laser-irradiated and non-irradiated GO films.

The electrical measurements were performed by two-probe measurement. The probe-head was made of tungsten carbide with  $r = 25\mu\text{m}$ . The probe distance was 1 mm and the probe weight was fixed at 50g. The current was monitored by a source-measure unit. Two probes were set in parallel to the laser-irradiated side region.

Two-probe resistance systematically changes from 6M ohm to 3kohm, as the probes were approached from off region to



laser-irradiated one. Furthermore, the continuous hysteresis was observed, which means the resistance changed from the high( $R_{up}$ ) to low states( $R_{down}$ ) by increasing and decreasing the applied voltage. At the distance of 1mm from the laser-reduced parts,  $R_{up}/R_{down}$ , i.e., (resistance when applied voltage increases)/(resistance when applied voltage decreases after increasing) is quite large(very large hysteresis). Around or on the laser reduced GO area,  $R_{up}$  even becomes smaller than  $R_{down}$ .

As the mechanism of electrical conduction in rGO films, the hopping conduction between highly conductive  $sp^2$  domains has been proposed. The  $sp^2$  domain created by the laser irradiation are electrically connected by the hopping conduction in fully reduced area. When the current increases by applying voltage, the carrier trapping that can be the potential barrier for the transport could occur. It can cause the increase in the resistance, resulting in  $R_{up}/R_{down} < 1$ . On the other hand, at the area with the short distance (0.5~1mm) from the laser-irradiated GO, as the remained  $sp^2$  domains due to the imperfect reduced graphene oxide could be critically connected, small current still flows and large continuous hysteresis is observed. As conduction paths cannot respond to the applied voltage instantaneously,  $R_{up}$  could be larger than  $R_{down}$  by the voltage sweeping.

Summary: We systematically investigated the electrical transport in partially-reduced GO films by changing the distance from the laser-reduced area. We characterized electrical properties in the partially reduced area between GO to rGO and found the continuous hysteresis. Our results show that GO film can be a resistor with memory function by laser assisted reduction; an inexpensive and simple method. The memory effect is basically originated from graphene and oxygen-containing functional groups bonded to carbon. Therefore, this type of resistor can be scaled down to the atomic level.

SESSION F.LP05.01: Live Poster Session: Electronics and Optics (F.EL04 and F.EL05)

Session Chairs: Zakaria Al Balushi, Chris Bardeen, Susan Fullerton, Nathalie Katsonis, Jieun Lee, Javier Read de Alaniz, Tania Roy and Yanlei Yu

Thursday Afternoon, December 3, 2020

3:00 PM - 5:00 PM

F.EL04

#### F.EL04.19.01

**Ice Templated and Directed Assembly to Construct 3D Boron Nitride and Graphene Oxide Nanosheet Topological Networks for Property Enhancement** Sanju Gupta<sup>1,2</sup>; <sup>1</sup>CCNY, United States; <sup>2</sup>Western Kentucky University, United States

Inspired by the nano/microscale hierarchical structure, topological network and precise inorganic/organic interfaces, we fabricated artificial 'nacre-like' papers and aerogels based on noncovalent functionalized boron nitride nanosheets (NF-BNNSs) and varying poly(vinyl alcohol) (PVA) concentration via vacuum-assisted self-assembly and freeze-drying (or ice-templating) techniques. The electron microscopy showed an ordered 'brick-and-mortar' arrangement of NF-BNNSs and PVA paper and aerogels, in which the long-chain PVA molecules act as the bridge to link NF-BNNSs via hydrogen bonds. Likewise, due to the need for heat removal in modern electronic devices, polymer composites with high thermal conductivity have drawn much attention. However, the traditional method to enhance polymers' thermal conductivity by random addition of nanofillers usually creates composites with not only limited thermal conductivity but also other detrimental effects due to a large amount of fillers required. Here, novel polymer composites are prepared by first constructing 3D boron nitride nanosheets (3D-BNNS) network using an ice-templated approach with varying BNNS sheets concentration and then infiltrating them with epoxy matrix. The thermal and mechanical properties of resulting free-standing nacre-like papers, aerogels and composites are investigated. They elucidated high glass transition temperature, low interfacial thermal resistance, or high thermal conductivity with relatively low BNNS loading thus revealing their superiority as flexible substrates. These results demonstrate that this approach opens a new avenue for the design and preparation of polymer composites with high thermal conductivity useful in advanced electronic packaging techniques, namely, thermal interface materials, underfill materials, and molding compounds.

#### F.EL04.19.02

**Development of New Nanofiltration Membranes Using 2D Nanomaterials** Natalia Garcia Domenech<sup>1,2</sup>, Yurii Goun'ko<sup>1,2</sup> and Finn Purcell-Milton<sup>1,2</sup>; <sup>1</sup>Trinity College Dublin, Ireland; <sup>2</sup>BiOrbic Bioeconomy Research Centre, Ireland

Nanofiltration has gained much attention in recent years due to its possible applications as a highly efficient and low-energy usage separation and purification technology[1,2]. Moreover, nanofiltration has shown to be potentially superior and more cost-effective than other filtration techniques. Nanofiltration was initially adapted for wastewater treatment, but has been

implemented by other industries, such as the pharmaceutical and the food industries, where the standard for high quality products and stringent safety requirements necessitate further and more specialised separation approaches[1,3]. The main aim of this project was to use inorganic 2D nanomaterials in order to develop new membranes for nanofiltration applications, in particular, boron nitride (BN). In this project, BN was exfoliated by liquid assisted exfoliation and the membranes were prepared by vacuum filtration using hydrophilic polytetrafluoroethylene as template. Boron nitride was also partially oxidised before exfoliation proving new chemically functionalised BN materials. All membranes were tested using different dyes and calculating the rejection of each one. Almost 100% rejection rates have been achieved for optimised BN membranes demonstrating the superb nanofiltration performance for selected dyes. The new membranes are to be used for the separation of D- and L- lactic acid and various mono- and disaccharides from agricultural residues.

#### References:

- [1] B. Van der Bruggen, M. Manttari, M. Nystrom, Drawbacks of applying nanofiltration and how to avoid them: A review, *Sep. Purif. Technol.* 63 (2008) 251–263. doi:10.1016/j.seppur.2008.05.010.
- [2] P. Eriksson, Nanofiltration extends the range of membrane filtration, *Environ. Prog.* 7 (1988) 58–62. doi:10.1002/ep.3300070116.
- [3] N. García Doménech, F. Purcell-Milton, Y.K. Gun'ko, Recent progress and future prospects in development of advanced materials for nanofiltration, *Mater. Today Commun.* 23 (2020) 100888. doi:https://doi.org/10.1016/j.mtcomm.2019.100888.

#### F.EL04.19.03

**Raman Studies of a Natural van der Waals Heterostructure** Viviane Z. Costa<sup>1</sup>, Addison Miller<sup>1</sup>, Sam Vaziri<sup>2</sup>, Shirin Jamil<sup>1</sup>, Andrew Ichimura<sup>1</sup>, Eric Pop<sup>2,2,2</sup> and Akm Newaz<sup>1</sup>; <sup>1</sup>San Francisco State University, United States; <sup>2</sup>Stanford University, United States

Van der Waals heterostructures comprised of two-dimensional (2D) materials offer a platform to obtain materials by design with unique electronic properties. Until recently, these van der Waals heterostructures (vdWH) materials were synthesized in the laboratory by vertically stacking different atomically thin materials, which often leads to stacks with the presence of fabrication defects and air contaminants between layers. Franckeite is a naturally occurring vdWH comprised of two distinct alternately stacked semiconducting layers. Because it is naturally heterostructured, it enables the study of a complex layered system without the presence of fabrication defects, and where the crystal orientation between layers has been preserved. Unlike other layered sulfide-based 2D materials, Franckeite is a grained-textured layered solid composed of few-millimeters flakes in random orientation. For this reason, mechanical exfoliation of thin flakes with uniform and large surface area for optical characterization and transfer techniques is especially challenging, leading to a knowledge gap of the fundamental properties of Franckeite. Raman spectroscopy is a widely and powerful method to characterize and study the fundamental properties of molecules in 2D crystals. All of the power that Raman spectroscopy provides in characterizing 2D materials stems from a large and well-established literature on the Raman signature of these crystals, which is lacking for Franckeite. In this work, we performed an extensive micro-Raman spectroscopy study of Franckeite. At room temperature, Raman spectroscopy data were acquired for a large sample size of flakes with thickness ranging from 6 to 100 nm prepared by mechanical exfoliation on SiO<sub>2</sub> substrates. The Raman signature of Franckeite is detected for flakes thicker than 10 nm. We observed that the position of all Raman peaks is independent of sample thickness. As expected, signal intensity is enhanced for flakes prepared on ultra-flat gold (Au) substrates (root-mean-square (rms) surface roughness < 0.2 nm), but different Raman modes undergo different rates of enhancements when comparing flakes of the same thickness on SiO<sub>2</sub> and Au. Raman data was acquired for excitation sources of both 532 and 633 nm of wavelength. Comparison data plots indicate resonance-enhanced Raman scattering with 633 nm of excitation, confirmed by additional absorption measurements. Temperature-dependent data was acquired from room temperature to 225 °C. All Raman modes present redshift with increasing temperature, suggesting that the chemical bond length of Franckeite increases with increasing temperature, and therefore the bond's vibrational force constant decreases. Moreover, we observed new low-frequency shearing and breathing modes in the Raman spectra. These low-frequency vibrational modes of Franckeite can provide a broader understanding of interlayer vibrational modes in 2D crystals, and especially in van der Waals heterostructures.

#### References

1. Molina-Mendoza, A. J. *et al.* Franckeite as a naturally occurring van der Waals heterostructure. *Nat. Commun.* **8**, (2017).
2. Velický, M. *et al.* Exfoliation of natural van der Waals heterostructures to a single unit cell thickness. *Nat. Commun.* **8**, 1–11 (2017).
3. Ray, K. *et al.* Photoresponse of Natural van der Waals Heterostructures. *ACS Nano* **11**, 6024–6030 (2017).
4. Liang, L. *et al.* Low-Frequency Shear and Layer-Breathing Modes in Raman Scattering of Two-Dimensional Materials. *ACS Nano* **11**, 11777–11802 (2017).

#### F.EL04.19.05

**Measuring Thermal Expansion Coefficient of Monolayer Molybdenum Disulfide Using Micro-Raman Spectroscopy** Lenan Zhang, Zhengmao Lu, Youngsup Song, Lin Zhao, Bikram Bhatia, Kevin Bagnall and Evelyn Wang; Massachusetts Institute of Technology, United States

Atomically thin two-dimensional (2D) molybdenum disulfide ( $\text{MoS}_2$ ) is highly attractive due to its unique properties and promising applications in nanoscale electronics. Characterization of thermal expansion coefficient (TEC) of 2D  $\text{MoS}_2$  is ubiquitous for reducing the thermal mismatch and improving the thermal management of  $\text{MoS}_2$ -based devices. However, measuring the TEC of 2D  $\text{MoS}_2$  is particularly challenging owing to its nanoscale thickness, microscale area and optical transparency properties. As a result, the thermal expansion on 2D  $\text{MoS}_2$  still extensively relies on simulation. In this work, we report a pure experimental approach to characterize the TEC of monolayer  $\text{MoS}_2$  using micro-Raman spectroscopy. We analyzed the stress and temperature dependent phonon frequency of monolayer  $\text{MoS}_2$  using the perturbation theory and symmetry analysis. To decouple the effect of thermal stress on phonon frequency shift, monolayer  $\text{MoS}_2$  flakes were transferred on fused silica, pure copper and micro-hole patterned thermal oxide substrates. We characterized the temperature coefficients on three substrates through the temperature-dependent Raman measurement. The in-plane TEC of monolayer  $\text{MoS}_2$  was then extracted by comparing these coefficients. The resulting in-plane TECs were  $(7.6 \pm 0.9) \times 10^{-6}$  1/K and  $(7.4 \pm 0.5) \times 10^{-6}$  1/K, which were independently obtained from two different phonon modes of  $\text{MoS}_2$  and in reasonable agreement with previous first-principle reported values. This work provides accurate measurement on the TEC of monolayer  $\text{MoS}_2$ . Additionally, the general experimental approach can be widely applied to study many other 2D materials or thin films in a simple way.

**F.EL04.19.06**

**Luminescence Properties of Hexagonal Boron Nitride Powders Probed by Deep UV Photoluminescence Spectroscopy** Nikesh Maharjan and Mim Nakarmi; Brooklyn College and The Graduate Center of CUNY, United States

Hexagonal boron nitride (h-BN) is an ultrawide ( $\sim 6.0$  eV) semiconductor that has potential applications for developing electronic, optoelectronic and nanophotonic devices including source of ultraviolet emitters. A key issue in these applications is understanding the effect of impurities, especially carbon and oxygen on its properties. Deep UV photoluminescence spectroscopy was employed for optical characterization of irregular-shaped h-BN crystal powders. Fourth harmonic laser (195 nm) generated from the Ti: sapphire laser was used for optical excitation in the experiments. The luminescence properties are investigated by annealing the sample at different temperatures under different conditions. The deep UV photoluminescence spectra from h-BN samples annealed at 700 °C in ambient air reveals a strong phonon-assisted band-edge emissions along with a sharp atomic-like emission line at 4.09 eV, and its phonon replicas at 3.89 and 3.69 eV. In addition to these peaks, sharp multi-phonon peaks are observed adjacent to them. The PL spectra of the sample shows the broadening of the main peaks as the annealing temperature exceeds 900 °C. We will present our findings of atomic-like features that could have potential applications as quantum sources in UV regions for quantum information technologies.

**F.EL04.19.08**

**Quantification of Surface Reactivity and Step-Selective Etching Chemistry on Single-Crystal BiOI** Julia Martin, Roy Stoflet, Alexander Carl, Katarina Himmelberger and Ronald L. Grimm; Worcester Polytechnic Institute, United States

We synthesized single-crystal BiOI via vapor transport, subjected the resulting crystals to a series of surface treatments, and quantified the resulting chemical states and electronic properties. Vapor transport methods included both physical vapor transport from single-source BiOI, as well as chemical vapor transport from  $\text{Bi}_2\text{O}_3 + \text{BiI}_3$  and from  $\text{Bi} + \text{I}_2 + \text{Bi}_2\text{O}_3$ . Surface treatments included tape cleaving, rinsing in water, sonication in acetone, an aqueous HF etch, and a sequential HF etch with subsequent sonication in acetone. X-ray diffraction, XRD, and X-ray photoelectron spectroscopy, XPS, probed the resulting bulk crystalline species and interfacial chemical states, respectively. In comparison with overlayer models of idealized oxide-terminated or iodide-terminated BiOI, angle-resolved XPS elucidated surface terminations as a function of each treatment. Ultraviolet photoelectron spectroscopy, UPS, established work-function and Fermi-level energies for each treatment. Data reveal that HF etching yields interfacial  $\text{BiI}_3$  at BiOI steps that is subsequently removed with acetone sonication. UPS establishes n-type behavior for the vapor-transport-synthesized BiOI, and surface work function and Fermi level shifts for each chemical treatment under study. We discuss the implications for processing BiOI nanofilms for PV and photocatalysis applications.

**F.EL04.19.09**

**Impact of Salt and Solvent Identity on the Deposition of a Cobalt Crown Ether Phthalocyanine Monolayer Electrolyte** Huiran Wang, Shubham Sukumar Awate and Susan Fullerton; University of Pittsburgh, United States

A monolayer electrolyte, developed by our group, has been used to demonstrate a solid-state nonvolatile two-dimensional (2D) crystal memory based on an electric-double-layer (EDL) gated field effect transistor. (Nano Lett., 19, 8911, 2019) The monolayer electrolyte consists of cobalt crown ether phthalocyanine (CoCrPc), with four crown ethers that can solvate one lithium ion each. By simply drop-casting and annealing, CoCrPc forms a flat and ordered array on 2D crystals including graphene and WSe<sub>2</sub>. The key mechanism of the nonvolatile memory is the toggling of lithium ions up and down through the cavity of crown ether (i.e., away from or nearby the channel). This toggling is accomplished by an applied electric field to overcome the diffusion barrier for ion movement. Our previous experimental work focused on one combination of materials: CoCrPc with 15-crown 5-ether (15C5), LiClO<sub>4</sub>, and ethanol as the solvent for the salt. However, additional material combinations should result in varying diffusion barriers, thereby offering a path to tune the voltage required to toggle the ions. In this study, we investigate CoCrPc with 15C5 combined with two kinds of salts, LiCl and LiI, and three solvents: anhydrous acetone, acetonitrile, and nitromethane. LiCl and LiI were chosen to isolate the impact of anion identity (Cl vs. I vs. ClO<sub>4</sub>) on the quality of the monolayer, and the three solvents were chosen for their reported tendency to promote ion-crown complexation. Monolayer quality is evaluated by measuring the thickness and surface roughness with atomic force microscopy (AFM) after deposition on 2D crystals in a water and oxygen-free glovebox. This study establishes the design rules for monolayer electrolyte deposition on 2D crystals, which can be used to engineer devices with multiple diffusion barriers in monolayer electrolyte random-access memory (MERAM). This work is supported by the NSF under Grant # NSF-DMR-EPM CAREER: 1847808.

#### **F.EL04.19.10**

**Monolayer Xene Films Synthesized by Molecular-Beam Epitaxy** Kaylyn Holmes, Ruizhe Kang, Qi Song, Charles Brooks, Jennifer E. Hoffman and Julia Mundy; Harvard University, United States

Single element atomic monolayer honeycomb lattice films (also called “Xene” films) are a quickly-growing topic in condensed matter physics and materials science. In contrast to graphene, Xene films from higher *Z* elements such as bismuthene (from bismuth) and stanene (from tin) are predicted to exhibit quantum spin Hall effects at temperatures closer to room temperature due to their larger topological band gaps, making them more useful for potential applications in next generation electronics. Although these two Xene films have strong theoretical and computational evidence supporting their candidacy for higher temperature quantum spin Hall effects and topologically protected edge states, they are both very difficult to produce because hexagonal unit cells are unstable configurations for the crystallization of these elements. Here, we present our work on using molecular-beam epitaxy (MBE) to synthesize monolayers and thin layers of bismuthene.

#### **F.EL04.19.11**

**2D Nanostructured Tetrasilicates with Cr(II) and Cr(II)/Fe(II) in Square Planar Coordination—Preparation and Magnetic Properties** Harshani Rathnaweera and Tina Salguero; University of Georgia, United States

The chromium-containing alkaline earth metal tetrasilicates, ACrSi<sub>4</sub>O<sub>10</sub> (A= Ca, Sr, and Ba), are noteworthy as examples of rare, high spin Cr(II) in square-planar coordination complexes in chromium oxide-crystal chemistry. Though the synthesis of ACrSi<sub>4</sub>O<sub>10</sub> has been known in the literature for several decades, much of the chemistry surrounding ACrSi<sub>4</sub>O<sub>10</sub> formation remains unknown. In this contribution, we describe magnetic properties of all ACrSi<sub>4</sub>O<sub>10</sub> phases prepared through improved synthetic routes as well as the subsequent nanostructuring of them into nanosheets by exfoliation. For flux-based routes, we utilize a metal envelope made from folded Cr foil to maintain a low oxygen fugacity in the reaction environment to avoid the formation of highly oxidized Cr species. We further extend the chemistry of BaCrSi<sub>4</sub>O<sub>10</sub> to include mixed metal centers, specifically Cr(II) and Fe(II). The incorporation of mixed metal centers in ABSi<sub>4</sub>O<sub>10</sub> phase is new territory in metal tetrasilicate chemistry, and this is the first example of transition metal substitution in any of the known ABSi<sub>4</sub>O<sub>10</sub> systems (B = Cu, Fe, Cr). We find that the targeted stoichiometry of Ba(Cr,Fe)Si<sub>4</sub>O<sub>10</sub> crystals yields an experimentally-determined composition with up to a ~40% incorporation of Fe(II), which appears to constitute the maximum incorporation of Fe(II) into BaCrSi<sub>4</sub>O<sub>10</sub>. Interestingly, Ba(Cr,Fe)Si<sub>4</sub>O<sub>10</sub> crystals show a different magnetic infrastructure due to the interaction of antiferromagnetic Cr(II) and ferromagnetic Fe(II) centers in a single lattice. In this paper, we characterize the magnetic properties of Ba(Cr,Fe)Si<sub>4</sub>O<sub>10</sub> crystals and nanosheets using Mössbauer and EPR spectroscopies.

#### **F.EL04.19.16**

**Fabrication of Large-Area MoS<sub>2</sub> Nanosheets by Salt-Assisted Mechanical Milling Process and Chemical Exfoliation in Cosolvent** Hsiang-Chun Yu and Tsung-Eong Hsieh; National Chiao Tung University, Taiwan

Salt-assisted mechanical milling and chemical exfoliation in cosolvent were adopted to prepare the large-area MoS<sub>2</sub> nanosheets with a few layers in thickness. First, the MoS<sub>2</sub> powder was blend with salt, *e.g.*, potassium chloride (KCl),

calcium chloride (CaCl<sub>2</sub>) or sodium carbonate (Na<sub>2</sub>CO<sub>3</sub>), and sent to a ball mill containing zirconia beads with 1 cm in diameter. The milling process was carried out at 300 rpm for 2 hrs so as to generate numerous dangling bonds at the edges of MoS<sub>2</sub>. The dangling bonds would react with the salt to form the functionalized groups which may induce the electrical repulsion for the dispersion of MoS<sub>2</sub> in subsequent chemical exfoliation process. The functionalized MoS<sub>2</sub> powder was added in a centrifuge tube containing the cosolvent comprised of water and alcohol at the weight ratio of 1:1. After the ultrasonic vibration for 30 mins at room temperature, the MoS<sub>2</sub> nanosheets with thickness of 1-2 nm could be obtained *via* the centrifugation of solution. Most studies of chemical exfoliation reported the MoS<sub>2</sub> nanosheets with the lateral size smaller than 1 μm. However, our study observed the MoS<sub>2</sub> nanosheets which average area of 12×5.6 μm<sup>2</sup> using Na<sub>2</sub>CO<sub>3</sub> and average area of 14×6 μm<sup>2</sup> using KCl. Presently, the MoS<sub>2</sub> FET devices containing the large-area MoS<sub>2</sub> nanosheets are prepared and their electrical properties are measured.

#### **F.EL04.19.18**

##### **An Exfoliation of Mixed Dimensional van der Waals Organic/WS<sub>2</sub> Heterojunctions Ink for Emerging**

**Electronics** Abdus S. Sarkar<sup>1,2</sup> and Suman Kalyan Pal<sup>1</sup>; <sup>1</sup>Indian Institute of Technology Mandi, India; <sup>2</sup>Foundation For Research and Technology Hellas, Greece

Since, the isolation of single layer graphene, a great attention has been paid to integrate distinct emerging beyond graphene 2D materials into van der Waals (vdW) heterostructures. The emerging 2D transition metal dichalcogenides (TMDCs), such as semiconducting (2H-phase) tungsten sulfide (WS<sub>2</sub>) and their mixed dimensional heterojunctions have drawn most vibrant areas of nanoscience/photonic research because of fascinating optical and electrical properties in their low dimensional interface. [1-3] However, most of the preparation (chemical) methods do not preserve the semiconductive properties of WS<sub>2</sub>. Here, we have prepared a novel mixed dimensional 2D semiconductor p-n heterojunction of few layer WS<sub>2</sub>, which is exfoliated in the presence of an organic semiconductor (OS) and characterized by various experimental techniques. Our results revealed that the few hundred nanometer size, few layer (4-5 layers) thick WS<sub>2</sub> sheets are grafted with OS. Hexagonal pattern in HR-TEM image intimate the preservation of 2H-phase WS<sub>2</sub>. Significant changed in the electrical behavior in the p-n nanoheterojunctions are presented. The insight spectroscopic analysis indicated the possible hybrid optoelectronic applications. Furthermore, the heterojunction dispersion WS<sub>2</sub> sheets are quite stable with prior little aggregation after 180 days.

#### **Reference**

[1] D. Jariwala, T.J. Marks and M. C. Hersam, Nat. Mater., 2017, 16, 170-181.

[2] A. S. Sarkar, S. K Pal, J. Phys. Chem. C, 2017, 121, 21945-21954.

[3] A. S. Sarkar, I. Konidakis, I. Demeridou, E. Serpetzoglou, G. Kioseoglou and E. Stratakis, 2020, <https://arxiv.org/abs/2005.02852>

#### **F.EL04.19.19**

##### **Mechanisms of Molybdenum Trioxide Sulfurization in the Growth of Two-Dimensional Molybdenum Disulfide** Joshua Maurer, Thierry Tsafack and Stephen F. Bartolucci; US Army CCDC AC, United States

Powder vaporization is a common method for the generation of large-area, single-crystal, two-dimensional molybdenum disulfide. While commonly employed as a growth method, the fundamental molecular mechanisms are not well understood. Recent ab initio analyses have shown that molybdenum oxysulfide rings play a key role in the sulfurization of molybdenum trioxide from elemental sulfur. Here, we present the utilization of molecular dynamics simulations with a reactive force field and ab initio calculations to elucidate the reaction pathway of sulfur with molybdenum trioxide. The molecular dynamics simulations demonstrated that for all sulfur allotropes the reaction pathway could be reduced to that of disulfur, trisulfur, or a combination of the two, and that molybdenum trioxide can catalyze the decomposition of larger sulfur allotropes. Ab initio calculations were used to illuminate the intermediates and transition states in the reaction pathways for disulfur and trisulfur. Analysis of the temperature dependence of the transition state energies show that the maximum reaction rates occur between 1000 and 1100 K, which corresponds with commonly reported experimental growth temperatures for molybdenum disulfide.

#### **F.EL04.19.20**

##### **Influence of Solvent Properties on the Morphology of Ultra-Thin Tin Monoxide Nanomaterials for Next-Generation Energy Storage Applications** Seán Kavanagh<sup>1,2,3</sup>, Sonia Jaskaniec<sup>3</sup>, João Coelho<sup>3</sup>, Sean Ryan<sup>3</sup> and Valeria Nicolosi<sup>3</sup>; <sup>1</sup>Imperial College London, United Kingdom; <sup>2</sup>University College London, United Kingdom; <sup>3</sup>Trinity College Dublin, Ireland

Two-dimensional (2D) nanomaterials, especially those with controlled size and shape, have attracted significant attention over the last decade, due to their enhanced performance in comparison to their bulk counterparts.<sup>1-3</sup> One such chemical

compound is tin monoxide (SnO), whose layered crystal structure renders it amenable to the fabrication of 2D architectures. SnO has demonstrated promising performance in many relevant applications, including thin-film transistors,<sup>4</sup> photocatalysis,<sup>7</sup> gas sensing<sup>8</sup> and, primarily, energy storage - as next-generation battery anode materials.<sup>9-11</sup> However, the synthesis of SnO nanomaterials with controlled morphology still poses a considerable challenge in the field.<sup>9,12-17</sup> In this work, we provide a comprehensive study of the complex relationship between wet chemistry synthesis conditions and resulting nanoparticle morphology. The solvent nature is observed to strongly influence the kinetics of nucleation and crystal growth in solution, and thus the final morphological and electrochemical properties.

Extensive characterization of the precipitate nanomaterial has been performed, including scanning electron microscopy (SEM), high-resolution transmission electron microscopy (HRTEM), selected area electron diffraction (SAED), x-ray diffraction (XRD) and thermogravimetric analysis (TGA), in order to comprehensively describe the solvent-morphology dependence. Furthermore, high-level electronic structure theory, including dispersion corrections to account for Van der Waal's effects, were employed to augment our understanding of the underlying chemical mechanisms. Using supercell calculations, electronic vacuum alignment and surface energies were determined, allowing the prediction of the thermodynamically-favored crystal shape (Wulff construction) and surface-weighted work function, important parameters for battery performance. Finally, the synthesized nanomaterials were tested as battery materials, illustrating the impact of particle morphology on electrochemical performance.

Our results reveal promising pathways to the controlled synthesis of nanomaterials with tailored morphologies for enhanced performance in specific applications.

<sup>1</sup> S. Suresh, *Nanoscience and Nanotechnology* **3**, 62 (2013).

<sup>2</sup> Y.W. Jun, J.S. Choi, and J. Cheon, *ANGEW CHEM (INT ED ENGL)* **45**, 3414 (2006).

<sup>3</sup> Z. Wu, S. Yang, and W. Wu, *Nanoscale* **8**, 1237 (2016).

<sup>4</sup> K.J. Saji, K. Tian, M. Snure, and A. Tiwari, *Advanced Electronic Materials* **2**, 1 (2016).

<sup>5</sup> Y. Ogo, H. Hiramatsu, K. Nomura, H. Yanagi, T. Kamiya, M. Kimura, M. Hirano, and H. Hosono, *Physica Status Solidi (A) Applications and Materials Science* **206**, 2187 (2009).

<sup>6</sup> S.S. Lin, Y.S. Tsai, and K.R. Bai, *Applied Surface Science* **380**, 203 (2016).

<sup>7</sup> L. Liang, Y. Sun, F. Lei, S. Gao, and Y. Xie, *Journal of Materials Chemistry A* **2**, 10647 (2014).

<sup>8</sup> I. Sm, N. St, N. Yh, B. Dk, S. Fj, M. Rs, R. Ns, G. Sk, A. Dk, and P. Vb, *J Colloid Interface Sci* **493**, 162 (2017).

<sup>9</sup> F. Zhang, J. Zhu, D. Zhang, U. Schwingenschlögl, and H.N. Alshareef, *Nano Lett.* **17**, 1302 (2017).

<sup>10</sup> C.S. Lim, Z. Sofer, O. Jankovský, H. Wang, and M. Pumera, *RSC Advances* **5**, 101949 (2015).

<sup>11</sup> Y.C. Lu, C. Ma, J. Alvarado, T. Kidera, N. Dimov, Y.S. Meng, and S. Okada, *Journal of Power Sources* **284**, 287 (2015).

<sup>12</sup> Y.-H. Sun, P.-P. Dong, X. Lang, and J.-M. Nan, *Chinese Chemical Letters* **25**, 915 (2014).

<sup>13</sup> H. Uchiyama, H. Ohgi, and H. Imai, *Crystal Growth and Design* **6**, 2186 (2006).

<sup>14</sup> S.C. Wang, R.K. Chiang, and P.J. Hu, *Journal of the European Ceramic Society* **31**, 2447 (2011).

<sup>15</sup> W. Liu, L. Yin, R. Zhang, H. Yang, J. Ma, and W. Cao, *Nanotechnology* **29**, 284002 (2018).

<sup>16</sup> J. Ning, T. Jiang, K. Men, Q. Dai, D. Li, Y. Wei, B. Liu, G. Chen, B. Zou, and G. Zou, *Journal of Physical Chemistry C* **113**, 14140 (2009).

<sup>17</sup> S. Wang, S. Xie, H. Li, S. Yan, K. Fan, and M. Qiao, *Chemical Communications* 507 (2005).

#### F.EL04.19.21

**Effect of Aliovalent Doping on Epitaxial Growth, Structure and Properties of Triple-Layered Ruddlesden-Popper Phase Lanthanum Nickelate** Akifumi Matsuda<sup>1</sup>, Tomoaki Oga<sup>1</sup>, Shohei Hisatomi<sup>1</sup>, Nobuo Tsuchimine<sup>2</sup>, Satoru Kaneko<sup>3,1</sup> and Mamoru Yoshimoto<sup>1</sup>; <sup>1</sup>Tokyo Institute of Technology, Japan; <sup>2</sup>Toshima Manufacturing Co., Ltd., Japan; <sup>3</sup>Kanagawa Institute of Industrial Science and Technology, Japan

Ruddlesden-Popper phase lanthanum nickelates ( $\text{La}_{n+1}\text{Ni}_n\text{O}_{3n+1}$ ) with two-dimensional perovskite structure have attracted interests for their electronic properties related to the structure and mixed valence Ni-ions<sup>[1]</sup>. These two-dimensional perovskites are also expected as precursors to develop infinite-layer nickelate superconductors such as Sr-doped  $\text{NdNiO}_3$ <sup>[2]</sup>. Development of epitaxial thin films of lanthanum nickelate with multilayered structure and modifying their structure, electronic state, and properties according to interfacial strain and substitutional doping would contribute to develop further understanding and application of their solid-state physics. There are some reports of triple-layered  $\text{La}_4\text{Ni}_3\text{O}_{10}$  for its metal-insulator-transition due to oxygen deficiency and possible application to such as SOFCs and gas sensors<sup>[1,3]</sup>. However, aliovalent doping in  $\text{La}_4\text{Ni}_3\text{O}_{10}$  epitaxial thin films similar to  $\text{La}_2\text{NiO}_4$  and  $\text{La}_3\text{Ni}_2\text{O}_7$  still requires further researches to explain its effect on structure and properties<sup>[4,5]</sup>. In this study, effect of aliovalent dopants substituting  $\text{La}^{3+}$  in triple-layered  $\text{La}_4\text{Ni}_3\text{O}_{10}$  on its epitaxial growth as well as on the structure and electric properties of the thin films was investigated.

The lanthanum nickelate thin films were prepared by pulsed laser deposition technique equipped with a KrF excimer laser ( $\lambda=248$  nm,  $d=20$  ns, and  $E\sim 1.0$  J/cm<sup>2</sup>). The films were deposited on atomically stepped SrTiO<sub>3</sub> and NdGaO<sub>3</sub> single crystal substrates at 700–750°C in O<sub>2</sub> atmosphere (10 Pa) using sintered targets of La<sub>4</sub>Ni<sub>3</sub>O<sub>10</sub> doped with Hf and Sn. The thin films were then thermally treated at  $\sim 950^\circ\text{C}$  for 2 hours in high-purity O<sub>2</sub> atmosphere (1 atm, 200 sccm) to modify the crystal phases and the valence of Ni-ions. X-ray diffraction results indicated epitaxy of La<sub>4</sub>Ni<sub>3</sub>O<sub>10</sub> (001) thin films after annealing in O<sub>2</sub>, while epitaxial growth of La<sub>2</sub>NiO<sub>4</sub> (100) was observed for the as-grown films. The formation of La<sub>2</sub>O<sub>3</sub> buffer layer at the interface was suggested to have contribution on the epitaxy of La<sub>4</sub>Ni<sub>3</sub>O<sub>10</sub> phase. The Hf and Sn-doped La<sub>4</sub>Ni<sub>3</sub>O<sub>10</sub> (001) thin films with thickness of  $\sim 100$  nm demonstrated low resistivity of  $\sim 5$  m $\Omega\text{cm}$  at room-temperature measured by a 4-probe DC method. Further detailed structural analyses of the lanthanum nickelate thin films, and the effect of the aliovalent doping on the electronic property related to the structure would also be discussed.

[1] K.-T. Wu et al., *J. Mater. Chem. A*, 5 (2017) 9003–9013.

[2] D. Li et al., *Nature*, 572 (2019) 624–627.

[3] V. Pardo et al., *Phys. Rev. B*, 83 (2011) 245128.

[4] R. J. CaVa et al., *Phys. Rev. B*, 43 (1991) 1229–1232.

[5] S. A. Nedilko et al., *J. Alloys Compd.*, 367 (2004) 251–254.

#### **F.EL04.19.22**

**Thermoelectric Effect of Conductive Polymer Films from Functionalized Graphene** Byeongwan Kim, Cheolhyun Cho and Eunkyong Kim; Yonsei University, Korea (the Republic of)

Thermoelectric effects in conductive polymers (CPs) have received significant attention owing to its high electrical conductivity, high Seebeck coefficient, and low thermal conductivity. Among the CPs, poly(3,4-ethylenedioxythiophene) (PEDOT) is a notable material by taking advantage of solution processability, high degree of crystallinity, and bipolaronic network. We prepared a PEDOT grafted graphene film by solution casting polymerization using surface functionalized graphenes, to provide thermoelectric PEDOT on graphene (PEOG) film. The PEOG showed a high degree of crystallinity, which enhanced both electrical conductivity and Seebeck coefficient. Taking advantage of graphene functionality, TE properties were modulated via several external stimuli. This result reinforced the application potential of CP-based TE materials in a multifunctional energy conversion.

#### **F.EL04.19.23**

**A Novel Approach to Synthesize 2D Materials by Direct Heating of Bulk Sources and Detailed Photoluminescence Study in Comparison to Most Popular Synthesis Techniques** Davoud Hejazi, Renda Tan and Swastik Kar; Northeastern University, United States

Semiconducting 2D materials are becoming more and more attractive for various optoelectronics and sensing applications; however, synthesis of high-quality 2D materials for lab-scale research is not often practical for many research laboratories, since the synthesis process often requires reactors, carrier gases, or furnaces of various levels of complexities. A simple method of growing various types of 2D materials or their combined structures (i.e. heterostructure, alloys etc.) that is easy to set up and run can further accelerate 2D research. We report on a new synthesis technique, finding that single and multilayered 2D materials of various types can be easily fabricated by direct thermal evaporation of bulk sources under an inert atmosphere. This is in stark contrast with conventional vapor-phase techniques which require chemical reactions of precursors, and a flow of one or more inert carrier gases, thereby substantially reducing the cost and complexities involved. In this study, sources of target nanomaterials are taken in their commercial bulk form, reduced to a powder for convenience and placed on a clean container in close proximity of the target substrate inside an inert environment, then heated to a range of high temperature values and held at those temperatures for material-specific durations. The nanomaterials evaporate from the source and deposit directly on the substrate in the form of well-formed crystals that can be evaluated for quality or modified for basic research or proof-of-concept applications. This synthesis methodology is much simpler than the other synthesis techniques such as CVD, MBE, ME, etc. We present detailed analysis (AFM, optical images, Raman, photoluminescence) of the various types of 2D materials and structures possible through direct, mixed, and sequential evaporation of bulk powders.

By studying the photoluminescence (PL) spectra of the 2D materials fabricated with this method and comparing them with the PL spectra of the 2D materials synthesized by other methods, found in the literature, we show that the quality of these samples, observable in FWHM of the A-exciton, is comparable with the samples grown with the best synthesis techniques. Furthermore, by detailed analysis of the PL spectra of these samples, we observe metrology-dependent variations in quantum properties of these crystals, where the relative distance of the A-exciton and A<sup>-</sup>-trion becomes smaller for the specific crystals with high PL intensity, which appear to have wrinkles that may have originated from spacial confinement, induced by seed in the nucleation site.

#### F.EL04.19.24

**Enhanced Charge Separation with Insulator Mediation in Vertically Stacked InSe/GeS Heterostructures** Christy Roshini Paul Inbaraj<sup>1,2,3</sup>, Roshan Jesus Mathew<sup>1,2</sup>, Raman Sankar<sup>2</sup>, Chih-Hao Lee<sup>1</sup> and Yang-Fang Chen<sup>3</sup>; <sup>1</sup>National Tsing Hua University, Taiwan; <sup>2</sup>Academia Sinica, Taiwan; <sup>3</sup>National Taiwan University, Taiwan

Modulating the physical properties of two-dimensional materials by stacking different layers to form vertical heterostructures gives rise to the new exciting phenomenon. In this work, we developed a method to improve charge separation in the type-II band aligned heterostructures (InSe/GeS) by using thin dielectric spacers (h-BN). The optical transitions at the junctions exhibit quenched emission without h-BN layers indicating indirect recombination due to the strong interlayer coupling. However, the InSe/GeS heterojunction with h-BN layers in-between exhibits strongly enhanced emission granting an additional degree of freedom to modulate the optical property. The photoresponse of the heterostructures showing enhanced photocurrent density for InSe/h-BN/GeS device by refraining interlayer charge recombination backs up the argument. Thus, the improved charge separation with h-BN mediation demonstrates a higher photoresponsivity and detectivity in the order of  $10^2 \text{ A W}^{-1}$  and  $10^{14}$  Jones, respectively. Furthermore, the high electron detection is evident from the photogain estimated in the order of  $10^3$ . In addition, the negative short-circuit current reveals the photovoltaic effect of the device. Therefore, our semiconductor-insulator-semiconductor (InSe/h-BN/GeS) device structure will be a promising candidate for future optoelectronics.

#### F.EL04.19.25

**Surface Characterization of Atomic Layer Deposited Molybdenum Oxide Films Using High Sensitivity Low Energy Ion Scattering** Raivat Singhania<sup>1</sup>, Benjamin Davis<sup>1</sup>, David Hynek<sup>2</sup>, Judy Cha<sup>2</sup> and Nick C. Strandwitz<sup>1</sup>; <sup>1</sup>Lehigh University, United States; <sup>2</sup>Yale University, United States

Transition metal dichalcogenides (TMDC), such as  $\text{MoTe}_2$ , are a promising new class of materials with wide ranging applications in the computing, optics, and photovoltaic industries. The deposition quality of these films has a drastic effect on overall film properties, and therefore device performance. In particular, achieving uniform and reproducible nucleation is important for creation of single monolayer films. However, islanding often occurs during film growth in which isolated regions of the film form initially, creating a discontinuous film and/or non-uniform film thickness, both of which are undesirable. We have investigated the uniformity and thickness control of molybdenum oxide films that are deposited via atomic layer deposition (ALD) and are precursors to  $\text{MoTe}_2$  TMDCs. High-sensitivity low energy ion spectroscopy (HS-LEIS) was used to assess surface coverage and islanding of a variety of film  $\text{MoO}_x$  films ranging in thickness from 0.2 nm to over 7 nm. HS-LEIS is used for this purpose due to its ability to selectively detect and differentiate between atoms in the outermost atomic layer and subsurface atoms. Absence of a signal from the substrate indicated that uniform nucleation and coverage of the surface with  $\text{MoO}_x$  occurred at film thicknesses of approximately 0.5 nm. Ongoing research is focused on using Monte-Carlo simulations to predict LEIS spectra, which would allow for more quantitative analysis of nucleation and film growth. Quantitative analysis of nucleation and film growth is of great importance for next generation electronics that rely on layers that are only one or several atomic layers in thickness.

#### F.EL04.19.26

**Air Stable 2D Halide Perovskite/Transition Metal Dichalcogenide Heterostructures for Improved Optoelectronics** Abin Varghese<sup>1,2</sup>, Yuefeng Yin<sup>1</sup>, Saurabh Lodha<sup>2</sup> and Nikhil Medhekar<sup>1</sup>; <sup>1</sup>Monash University, Australia; <sup>2</sup>Indian Institute of Technology Bombay, India

Low-dimensional materials such as monolayer transition metal dichalcogenides (TMD) and two-dimensional (2D) perovskites have demonstrated enormous potential for optoelectronic applications.<sup>[1,2]</sup> TMDs have been explored for fast, high-responsivity photodetection owing to their sizeable bandgaps and high optical absorption coefficients, but their photovoltaic efficiency is quite low.<sup>[3]</sup> On the other hand, 2D Ruddlesden-Popper phase hybrid organic-inorganic perovskites have exhibited encouraging solar cell power conversion efficiencies and better ambient stability compared to the typical 3D perovskites.<sup>[4]</sup> However, the major challenges in realizing 2D perovskite based photovoltaic devices are its vulnerability to oxygen/humidity, large exciton binding energy, as well as poor optical absorption in the visible wavelengths.<sup>[2]</sup> In this work, using first-principles calculations, we propose a new strategy of employing TMD/2D perovskite heterostructures for optoelectronic applications to mitigate the intrinsic drawbacks of using TMD or 2D perovskite independently. These heterostructures formed via van der Waals (vdW) interaction between the constituents could be custom-designed for specific applications.

We show that the stacking of air stable TMDs like  $\text{MoS}_2$  on top of the 2D perovskite (e.g.,  $\text{BA}_2\text{PbBr}_4$ , BA is Butylammonium) could lead to improved ambient stability in addition to novel properties of the heterojunction. The



calculated electronic band structure of the MoS<sub>2</sub>/BA<sub>2</sub>PbBr<sub>4</sub> heterostructure shows a type-II band alignment with good charge separation at the heterojunction. The effective bandgap at the heterointerface is ~ 0.8 eV, much lower than the intrinsic bandgaps of BA<sub>2</sub>PbBr<sub>4</sub> (~ 3 eV) and monolayer MoS<sub>2</sub> (1.9 eV).<sup>[1,4]</sup> Also, the calculated fermi level alignments of MoS<sub>2</sub> and BA<sub>2</sub>PbBr<sub>4</sub> show that the TMD can function as a selective electron transport layer resulting in improved solar cell performance with enhanced air stability. On the other hand, selenide based WSe<sub>2</sub>/BA<sub>2</sub>PbBr<sub>4</sub> heterointerface demonstrates a type-I alignment with a comparatively higher hetero-bandgap at ~ 1.5 eV, useful for light emitting applications at visible wavelengths.

In summary, this study explores the properties of TMD/2D perovskite heterostructures and provides new insights towards realizing high-performance next-generation optoelectronic devices. The high tensile strength of TMDs and molecular softness provided by the large organic chains could further enable the use of these heterostructures for flexible solar cells or light emitting devices.

#### References

[1] K. F. Mak, J. Shan, *Nat. Photonics* **2016**, *10*, 216.

[2] G. Grancini, M. K. Nazeeruddin, *Nat. Rev. Mater.* **2019**, *4*, 4.

[3] D. Jariwala, A. R. Davoyan, J. Wong, H. A. Atwater, *ACS Photonics* **2017**, *4*, 2962.

[4] L. Dou, A. B. Wong, Y. Yu, M. Lai, N. Kornienko, S. W. Eaton, A. Fu, C. G. Bischak, J. Ma, T. Ding, N. S. Ginsberg, L. W. Wang, A. P. Alivisatos, P. Yang, *Science (80-. )*. **2015**, *349*, 1518.

#### F.EL04.19.27

**Magnetic Properties in Correlated 2D van der Waals Metal Phosphosulfides Due to Suppression of Antiferromagnetic Ordering** Nitish Mathur<sup>1</sup>, Fengmei Wang<sup>1,2</sup>, Aurora Janes<sup>1</sup>, Peng He<sup>2</sup>, Xueli Zheng<sup>3</sup>, Tofik A. Shifa<sup>2</sup>, Peng Yu<sup>2</sup>, J.R. Schmidt<sup>1</sup>, Jun He<sup>2</sup> and Song Jin<sup>1</sup>; <sup>1</sup>University of Wisconsin--Madison, United States; <sup>2</sup>CAS Center for Excellence in Nanoscience, CAS Key Laboratory of Nanosystem and Hierarchical Fabrication, National Center for Nanoscience and Technology, China; <sup>3</sup>Stanford University, United States

Two-dimensional (2D) van der Waals (vdW) materials offer a versatile platform to explore their potential applications in electronic, photonic, and spintronic devices. Among them, the family of vdW layered metal phosphosulfides (MPS<sub>3</sub>, M = Ni, Fe, Co, Mn, etc.) show intriguing electronic physics, potential magnetic properties, and electrocatalysis applications. Recently, it has been reported that a strong long-range coupling between the electronic and magnetic structures results from super-exchange mechanism in 2D vdW NiPS<sub>3</sub> antiferromagnet (AFM). In this work, we demonstrate a new chemical route for suppression of AFM ordering in NiPS<sub>3</sub> system. Composition-tunable Ni<sub>1-x</sub>Co<sub>x</sub>PS<sub>3</sub> (0 ≤ x < 0.50) few-layered nanosheets (NSs) are successfully synthesized. Significantly, obvious suppression of AFM ordering below Néel temperature (T<sub>N</sub> ~ 143-155 K) in magnetic susceptibility measurements were observed in Ni<sub>1-x</sub>Co<sub>x</sub>PS<sub>3</sub> NSs, which contrast with the magnetic properties observed in bulk single crystals of Ni<sub>1-x</sub>Co<sub>x</sub>PS<sub>3</sub>. These findings provide a new direction for disruption of AFM long range ordering and opens a new window of opportunities for investigation of correlated physics and magnetism in 2D materials systems.

#### F.EL04.19.29

**High-Performance Ideal PN Photodiode Using Directly Grown CVD Heterostructure** Jieun Kim and Woo Jong Yu; Sungkyunkwan University, Korea (the Republic of)

As silicon-based field effect transistors (FET) face miniaturization limitations, various two-dimensional (2D) material-based FETs are promising for next-generation electronic and optoelectronic devices. These days, not only study to produce high performance 2D-FETs, but also to implement integrated circuits with 2D materials has been reported. In terms of integrated circuits, PN junction is essential for complementary circuit. To fabricate 2D PN junction, usually transferring and stacking with exfoliated flakes has been used. Even if the flakes electronic quality is good, it needs trained skills and is time consuming. In addition, it is hard to ensure interface quality and has residue problems which deteriorate device performances.

In this paper, we report the direct growth of PN heterostructures with transition metal dichalcogenide (Nb doped WSe<sub>2</sub>/MoSe<sub>2</sub>) on SiO<sub>2</sub>/Si substrates with chemical vapor deposition (CVD) method with one mixed solution source. To confirm the composition and structural properties of our as-grown heterojunction sample Raman, PL, XPS and AFM analysis is done. At inner and outer domain, obviously different center Raman and PL peaks are observed. The niobium (Nb) doping signal also confirmed by Raman peaks and XPS peaks. In AFM height profile data, inner and outer height show no difference which represents lateral heterostructure. To obtain electronic properties at inner, outer and junction region, multi electrodes are evaporated. At junction, current rectification behavior is shown as a PN diode with 1.3 ideality factor which is close to ideal ideality factor of 1. Also the current level between P (Nb doped WSe<sub>2</sub>) and N (MoSe<sub>2</sub>) domain is similar. Under lasers illumination, optoelectronic characteristic is shown. Several properties such as built-in potential across the junction, type-II

band alignment of the materials (WSe<sub>2</sub> and MoSe<sub>2</sub>), low lattice mismatch and atomically sharp interface from directly growth mechanism, allow high advantages in optoelectronic devices. Additionally, the niobium acceptor dopants allow wide range of absorption wavelength from ultraviolet (UV) to near infrared (NIR) which overcomes the limitation of the TMD photodetectors. Additionally, back gated PN photodiode can effectively suppress dark current through gate voltage modulation, thus realizing very high detectivity.

Thus, our direct grown Nb doped WSe<sub>2</sub>/MoSe<sub>2</sub> PN heterostructure photodiode shows outstanding optoelectronic performances, such as high detectivities ( $10^{15}$  Jones),  $I_{\text{light}}/I_{\text{dark}}$  ( $10^5$ ) under  $V_{\text{DS}} = 0$  V. Our approach of direct grown PN heterostructure photodiode allows fabricate high quality and easy integrated optoelectronic 2D atomic layer devices.

#### F.EL04.19.31

**Two-Dimensional ZnO Nanoplates Grown on r-plane Oriented Al<sub>2</sub>O<sub>3</sub> and Their Photocatalytic Properties** Shota Sakurai and Junghyun Cho; Binghamton University, The State University of New York, United States

Two-dimensional (2-D) nanomaterials have recently received considerable attention with their unique characteristics, which were not seen in their bulk and 1-D nanomaterials. Zinc oxide (ZnO) is chemically stable, non-toxic, and available at low cost, which makes it into one of the most intriguing materials. Since the surface is surrounded largely by basal c-planes, 2-D ZnO nanomaterials have the good potential for tailoring the functional properties through adjusting their surface morphologies. To achieve the growth of such 2-D ZnO nanoplatelets, the growth direction must be along the a-axis, while suppressing the growth along the c-axis. This growth is challenging because the growth along the c-axis is energetically favorable. To control the growth direction, a seed layer plays a significant role. r-plane (1-102) aluminum oxide (Al<sub>2</sub>O<sub>3</sub>) can serve as a good seed layer for 2-D ZnO growth as the lattice mismatch between r-plane Al<sub>2</sub>O<sub>3</sub> and a-plane ZnO is only 1.53% along ZnO [0001] and Al<sub>2</sub>O<sub>3</sub> [2-201] directions. In this study, we prepared r-plane oriented Al<sub>2</sub>O<sub>3</sub> on Si (111) substrate as a seed layer by spin coating followed by annealing at high temperatures. r-plane Al<sub>2</sub>O<sub>3</sub> also has an epitaxial relationship with Si (111). 2-D ZnO nanoplates were then grown on the seed layer by the hydrothermal method. The c-plane of ZnO nanoplates contains a high concentration of the surface defects and is off-stoichiometric; therefore, the thinner the nanoplate is, the more it is influenced by the defects on the c-plane. It makes these 2-D nanoplates very attractive as an effective photocatalytic surface for the degradation of organic contaminants. As a result, the templated growth of the 2-D ZnO nanoplates shows the great potential to form functional surfaces that can be very sensitive to external stimuli such as light and environment by controlling the concentration and type of defects. Photoluminescence (PL) and Raman spectra are used to characterize defect characteristics of various nanoplate morphologies. This presentation highlights current research progresses made for the control of the defect population, size, aspect ratio, and packing density of the ZnO nanoplates at various conditions and the effect of the resulting morphologies of the nanoplates on their photocatalytic properties.

#### F.EL04.19.33

**Resonance Raman Signatures of Atomically-Thin Black Phosphorus** Nannan Mao<sup>1,1</sup>, Xi Ling<sup>2</sup>, Liangbo Liang<sup>3</sup>, William Tisdale<sup>1</sup> and Jing Kong<sup>1</sup>; <sup>1</sup>Massachusetts Institute of Technology, United States; <sup>2</sup>Boston University, United States; <sup>3</sup>Oak Ridge National Laboratory, Oak Ridge, United States

Black phosphorus (BP) is an elemental two-dimensional semiconductor with quantized electronic structure, high mobility and tightly bonded exciton. Especially, due to the quantum confinement in the out-of-plane direction and significant interlayer interaction, BP has direct band gap for all thicknesses that is highly tunable from visible region to mid-infrared region. Besides, the conduction band and valence band in phosphorene split into quantized subbands, which constitute a series of thickness-dependent interband electronic transitions. These pronounced subband transitions, evidenced by sharp thickness-dependent absorption peaks in the visible region and infrared region, give rise to strong coupling with photons and phonons in few-layer BP. Here we investigated the electron-photon and electron-phonon coupling in few-layer BP samples by resonance Raman spectroscopy. Firstly, we observed Raman splitting effect in atomically thin-BP, and the origin of this phenomenon will be revealed. Secondly, based on the collective interlayer vibration modes, the accurate interlayer interaction of BP was measured in experiment. Thirdly,  $A_g^1$  mode shows much smaller resonance effect than  $A_g^2$  mode when the incident polarization is along armchair direction of BP, which can be explained by the symmetry-dependent electron-phonon coupling. These investigations give direct evidence of the significant interlayer interaction and deep insights into fundamental electron-photon and electron-phonon coupling in atomically-thin BP.

#### F.EL04.19.34

**Raman Scattering of Electrochemical 2D MoS<sub>2</sub> Nanosheets in Water Splitting** Kit Sze, Mikel Tucker, Saroj Pramanik and Yucheng Lan; Morgan State University, United States

Molybdenum disulfide ( $\text{MoS}_2$ ) is one of the most promising hydrogen-evolution-reaction (HER) electrocatalysts to replace noble metals in water splitting. Raman scattering is one non-destructive, efficient, and mature technique to characterize renewable energy materials. Here, the 2D  $\text{MoS}_2$  nanosheets with various crystallinity are prepared and their electrocatalytic behaviors are *in-situ* investigated by Raman scattering under varied electric fields and temperatures. The results would enlighten the electrocatalytic mechanism of  $\text{MoS}_2$  nanosheets and help us to improve its HER activities over the Pt catalyst.

#### F.EL04.19.35

**The Thermal Oxidation of Hexagonal Boron Nitride Single Crystals—Dry and Ambient Air Compared** [Neelam Khan](#)<sup>1</sup>, Michael B. Katz<sup>2</sup>, Albert Davydov<sup>2</sup> and James H. Edgar<sup>3</sup>; <sup>1</sup>Georgia Gwinnett College, United States; <sup>2</sup>National Institute of Standards and Technology, United States; <sup>3</sup>Kansas State University, United States

Hexagonal boron nitride (hBN), a layered van-der-Waals material, is employed as a template and an insulator to improve the performance of devices made from graphene and other two-dimensional (2D) materials. Moreover, due to its oxidation resistance, it is used to protect 2D materials devices from the environment through encapsulation. This study aims to understand the ultimate protective qualities of hBN layers at high temperatures in dry vs. ambient air. Single crystals of hBN were thermally oxidized at different temperatures ranging from 800 °C to 1100 °C for different durations, from 20 min to 100 min. Atomic force microscopy analysis revealed surface pits of about 50-100 nm in width, and 1-2 nm in depth, for the layers exposed to 900 °C for 20 minutes in dry air. Increasing the temperature and duration did not significantly change the surface pit sizes, in contrast to the thermal oxidation in ambient air, where longer oxidation times and higher temperatures, produced larger etch pits. Having no effect of thermal oxidation as a function of temperature and duration in dry air could be due to formation of the surface oxide layer, which slows down the etching process. Complimentary transmission electron microscopy will be employed to compare the extent of surface oxidation in ambient versus dry air and to study the origin and morphology of the surface pit formation.

#### F.EL04.19.36

**Late News: Efficient Electron Doping of Monolayer  $\text{MoS}_2$  by Salt-Crown Ether Treatment** [Hiroto Ogura](#)<sup>1</sup>, Yoshiyuki Nonoguchi<sup>2</sup>, Toshifumi Irisawa<sup>3</sup>, Takahiko Endo<sup>1</sup>, Hong En Lim<sup>1</sup>, Yusuke Nakanishi<sup>1</sup> and Yasumitsu Miyata<sup>1</sup>; <sup>1</sup>Tokyo Metropolitan University, Japan; <sup>2</sup>Nara Institute of Science and Technology, Japan; <sup>3</sup>AIST, Japan

Atomic layers of transition metal dichalcogenides (TMDCs) have attracted much attention because of their unique two-dimensional structure and high electrical performance. For electronics applications, it is essential to develop a sophisticated way to control their carrier density of materials. So far, carrier control of TMDCs is achieved via surface charge transfer by using chemical doping. To further improve doping concentration, it is highly desired to find any stable and efficient dopants for TMDCs. Recently, Nonoguchi et al. have reported the electron doping of carbon nanotubes using a series of ordinary salts with crown ethers. In this study, we have applied this technique to monolayer  $\text{MoS}_2$  and investigated the transport and optical properties of such chemically-doped  $\text{MoS}_2$ .

Monolayer  $\text{MoS}_2$  films were grown on  $\text{SiO}_2/\text{Si}$  substrates by using chemical vapor deposition method. Electron doping was conducted by spin coating of butanol solution of KOH and benzo-18-crown-6. The doping process changes the transfer curves of  $\text{MoS}_2$  field-effect transistors (FETs) from a typical n-type semiconducting state to metallic one in air. We also found photoluminescence quenching and peak shift in the  $A_1'$  Raman mode for doped  $\text{MoS}_2$ . These results indicate that the salt-based doping provides an effective way for the electron doping of  $\text{MoS}_2$ . In the presentation, the details of transport and optical properties will be discussed.

#### F.EL04.19.37

**Late News: Few-Layered Two-Dimensional Ruddlesden-Popper Organic-Inorganic Hybrid Perovskite Magnets** [Ki-Yeon Kim](#)<sup>1</sup>, Garam Park<sup>1</sup>, Jaehun Cho<sup>2</sup>, Joonwoo Kim<sup>2</sup>, June-Seo Kim<sup>2</sup>, Jinyong Jung<sup>2</sup>, Kwonjin Park<sup>2</sup> and In-Hwan Oh<sup>1</sup>; <sup>1</sup>KAERI, Korea (the Republic of); <sup>2</sup>Daegu Gyeongbuk Institute of Science and Technology, Korea (the Republic of)

Atomically thin two-dimensional (2D) Van der Waals (vdw) magnets have received extensive attention due to their interesting magnetic phenomena inherent to low-dimensional magnetism such as Berezinskii-Kosterlitz-Thouless transition in 2D XY models and Mermin-Wagner Theorem. However, it is not until 2017 that the first 2D ferromagnetic magnets such as  $\text{Cr}_2\text{Ge}_2\text{Te}_6$  and  $\text{CrI}_3$  were experimentally realized via mechanical exfoliation method using Scotch tape. Since then, although a number of potential 2D vdw magnets have been theoretically predicted a very limited number of atomically thin or few-layered 2D vdw magnets still have been experimentally available. Specifically, since 1960's, 2D Ruddlesden-Popper organic-inorganic halide perovskites (RH-OIHP) have been considered as the ideal model closest to 2D Heisenberg model. Recent theoretical calculation using first principle density functional theory shows that the cleavage energy of (R-

$\text{NH}_3)_2\text{CuCl}_4$  (R = a monovalent organic moiety such as  $\text{C}_n\text{H}_{2n+1}$  or  $\text{C}_6\text{H}_5\text{C}_2\text{H}_4$ ) is smaller by a factor of 2-2.5 than that of graphite ( $0.36 \text{ J/m}^2$ ). It means that 2D RP-OIHP monolayer by mechanical exfoliation from bulk crystals would be experimentally feasible. However, until now, there has not been successful report on fabrication of atomically thin or few-layered 2D RP-OIHP thin films with intrinsic magnetism at all. We will demonstrate the few-layered 2D OIHP magnets via solvent engineering based on spin coating technique.

#### F.EL04.19.38

**Late News: First-Principles Study of Interaction of O<sub>3</sub> with Silicene** Lokanath Patra<sup>1</sup>, Geeta Sachdeva<sup>1</sup>, Ravindra Pandey<sup>1</sup> and Shashi Karna<sup>2</sup>; <sup>1</sup>Michigan Technological University, United States; <sup>2</sup>CCDC Army Research Laboratory, Weapons, and Materials Research Directorate, United States

Silicene, an analogous silicon counterpart of graphene with unique physical properties, has attracted a great deal of attention. Its interaction with environmental molecules, e.g ozone needs to be investigated thoroughly as it has a great role to play for silicon-based technology at the nanoscale. In this study, we study the interaction of O, O<sub>2</sub>, and O<sub>3</sub> with silicene using density functional theory. We find that O, being more electronegative than Si, draws electrons from the Si-Si bond. Consequently, it is chemisorbed at the bridge site forming an epoxide like Si-O-Si configuration with a binding energy of 5.76 eV. On the other hand, O<sub>2</sub> and O<sub>3</sub> interacting with silicene dissociate at the surface, in contrast to what has been reported for graphene. Moreover, the dissociation process is spontaneous and exothermic without any energy barrier leading to the formation of Si-O bonds at the surface.

#### F.EL04.19.39

**Late News: Mild Condition Synthesis of Nanosized Bismuth Vanadate and Polyoxometalates Composite** Boon Chong Ong, Teik Thye Lim and Zhili Dong; Nanyang Technological University, Singapore

Nanosized materials often possess unique characteristics compared to their bulk counterpart and are useful in various applications. Bismuth vanadate (BiVO<sub>4</sub>), a type of mixed-metal oxide, gains popularity in the field of catalysis reaction, especially the light-induced related process. They are active towards visible light irradiation and able to stimulate a catalytic reaction, for example, the water oxidation process. However, the main drawback of BiVO<sub>4</sub> is the photogenerated electron-hole pairs tend to recombine in a very short period, which negatively impacts their catalytic performance. Coupling metal oxide with other materials is often regarded as one of the promising methods to alter their properties and improve catalytic performance. In the field of catalysis, polyoxometalates (POMs) have a distinctive property to act as electron and hole scavengers, which can retard the recombination of photogenerated electron-hole pairs effectively. They belong to a large class of nanosized metal-oxygen anion complexes of early transition elements with tunable structure, their properties greatly influence by the type of metals present in their structure. In this experiment, all the materials were synthesized in mild condition, without the use of strong base and acid. By avoiding a harsh environment, the complexity in the synthesis process can be reduced and are safer. A nanocomposite of BiVO<sub>4</sub> and cobalt-based POMs is produced to integrate the excellent properties of both materials for the application in photochemical water oxidation. Characterization tests are performed, such as field emission scanning electron microscopy (FESEM) to study the shape and size of composites materials, X-ray diffraction (XRD) for confirming the crystal lattice structure and Fourier-transform infrared spectroscopy to identify the types of chemical bonds. A sheet-like behavior of BiVO<sub>4</sub> can be noticed from the FESEM analysis. The synthesized BiVO<sub>4</sub> is in a monoclinic phase as confirmed by the XRD result, in which intense peaks are noticed for (130) and (040) planes, while the POMs produced are in the triclinic phase. It is believed that the BiVO<sub>4</sub>/POMs composite is able to improve the photocatalytic water oxidation reaction.

Keywords: Bismuth Vanadate, Nanomaterials, Polyoxometalate, Mild condition

#### F.EL04.19.40

**Late News: Optical Absorbance in Multilayer Two-Dimensional Materials—Graphene and Antimonene** Geeta Sachdeva<sup>1</sup>, Ashok Kumar<sup>1</sup>, Ravindra Pandey<sup>1</sup> and Shashi Karna<sup>2</sup>; <sup>1</sup>Michigan Technological University, United States; <sup>2</sup>CCDC Army Research Laboratory, United States

Antimonene, one of the group V elemental monolayers, has attracted intensive interest due to their intriguing optical properties. Considering the case of atomically-flat antimonene for which directional bonding between Sb atoms appears to be analogous to C-C bonds in graphene, we present its optical absorption properties from near IR to visible spectral regime. The results based on density functional theory predict that absorbance in multilayer antimonene is equivalent to or higher than that calculated for multilayer graphene. Specifically, the IR absorption in antimonene is significantly higher with a prominent peak at about 4 μm associated with the dipole-allowed interband transitions. Moreover, a strong dependence of absorbance on topology is predicted for both antimonene and graphene which can be attributed to the subtle variations in their stacking-

dependent band structures. Our results suggest the possibility of multilayer antimonene coating be realized as effective optical limiting material in the IR region for optoelectronic materials.

#### F.EL04.19.41

**Late News: Impact of Partial Reduction on Electrical Properties in Graphene Oxide Films** Akiko Ohata<sup>1</sup>, Francisco Romero<sup>2</sup> and Noel Rodriguez<sup>2</sup>; <sup>1</sup>Institute of Astronautical Science, Japan; <sup>2</sup>Granada university, Spain

Graphene-based composite materials and nanostructures have been intensively studied in terms of unique electrical properties and a wide spectrum of applications. Among them, reduced graphene oxide(rGO) has attractive advantages of flexibility, electrical and thermal conductivity, and low-cost production. We have already reported memristive properties in rGO films partially reduced by the laser irradiation to graphene oxide(GO). However, the resistance switching mechanism has not been fully understood. In this study, by electrically characterizing the transition region from GO to the laser-irradiated rGO, a possible mechanism for the memristive properties is discussed.

**Reduced GO film preparation:** The GO films prepared by drop-casting commercially available GO colloid (4mg/mL) on PET film were placed on a 3D-shaker at room temperature until the water was fully evaporated. A PC-driven 405nm laser (scan speed 3 min/cm<sup>2</sup>) was used for the photothermal reduction of GO films with a rectangular shape(~1.5mm width).

**Electrical characterization:** GO films were initially non-conductive, while it became conductive with the laser-power increase. Interestingly, when GO films were reduced at the threshold laser-power for GO reduction, memristive properties were clearly observed. Around this region, on/off ratio was rather sharp (digital change) and large (maximum ratio was nearly 12). In addition, hysteric I-V characteristics (continuous change) were also detected. In this study, we mainly discuss the continuous hysteresis observed in the transition region between laser-irradiated and non-irradiated GO films.

The electrical measurements were performed by two-probe measurement. The probe-head was made of tungsten carbide with  $r = 25\mu\text{m}$ . The probe distance was 1 mm and the probe weight was fixed at 50g. The current was monitored by a source-measure unit. Two probes were set in parallel to the laser-irradiated side region.

Two-probe resistance systematically changes from 6M ohm to 3kohm, as the probes were approached from off region to laser-irradiated one. Furthermore, the continuous hysteresis was observed, which means the resistance changed from the high( $R_{up}$ ) to low states( $R_{down}$ ) by increasing and decreasing the applied voltage. At the distance of 1mm from the laser-reduced parts,  $R_{up}/R_{down}$ , i.e., (resistance when applied voltage increases)/(resistance when applied voltage decreases after increasing) is quite large(very large hysteresis). Around or on the laser reduced GO area,  $R_{up}$  even becomes smaller than  $R_{down}$ .

As the mechanism of electrical conduction in rGO films, the hopping conduction between highly conductive  $sp^2$  domains has been proposed. The  $sp^2$  domain created by the laser irradiation are electrically connected by the hopping conduction in fully reduced area. When the current increases by applying voltage, the carrier trapping that can be the potential barrier for the transport could occur. It can cause the increase in the resistance, resulting in  $R_{up}/R_{down} < 1$ . On the other hand, at the area with the short distance (0.5~1mm) from the laser-irradiated GO, as the remained  $sp^2$  domains due to the imperfect reduced graphene oxide could be critically connected, small current still flows and large continuous hysteresis is observed. As conduction paths cannot respond to the applied voltage instantaneously,  $R_{up}$  could be larger than  $R_{down}$  by the voltage sweeping.

**Summary:** We systematically investigated the electrical transport in partially-reduced GO films by changing the distance from the laser-reduced area. We characterized electrical properties in the partially reduced area between GO to rGO and found the continuous hysteresis. Our results show that GO film can be a resistor with memory function by laser assisted reduction; an inexpensive and simple method. The memory effect is basically originated from graphene and oxygen-containing functional groups bonded to carbon. Therefore, this type of resistor can be scaled down to the atomic level.

#### F.EL05.05.01

**Photothermal Effect of Porphyrin Compounds for Optical Thermal Insulation** Jou Lin<sup>1</sup>, Yuan Zhao<sup>2</sup>, David Kundrat<sup>1</sup>, Mathias Bonmarin<sup>3</sup>, John Krupczak<sup>4</sup>, Som V. Thomas<sup>1</sup>, Mengyao Lyu<sup>1</sup> and Donglu Shi<sup>1</sup>; <sup>1</sup>University of Cincinnati, United States; <sup>2</sup>The Pennsylvania State University, United States; <sup>3</sup>Zurich University of Applied Sciences, Switzerland; <sup>4</sup>Hope College, United States

The photothermal effect has been found in some porphyrin compounds including chlorophyll, chlorophyllin, hemoglobin, and phthalocyanine, all of which share similar structural characteristics. The porphyrin compounds are typically composed of four modified subunits bounded with carbon atoms forming a “ring-like” structure, therefore also known as “porphyrin rings.” Upon white light irradiation, these compounds can selectively observe light in a wide range of frequency from UV to NIR, and convert it to thermal energy. One of the major applications of these porphyrin compounds is in the energy-efficient windows via a newly developed concept of optical thermal insulation (OTI). Most of the thermally insulated windows in cold climate regions are double-paned, sandwiching transparent insulating materials (such as gases), creating additional and

unnecessary volume and weight. Thermal transmittance (U-factor) is proportional to the temperature difference,  $\Delta T$ , between the center of room and window interior surface. OTI does not rely on any conventional thermal insulating materials or gases, such as air or argon, as often used in conventional double-pane windows, but achieves its effectiveness via photothermally-heated building skins. If a spectral-selective thin film is applied on a window inner surface that exhibits strong UV/NIR absorptions and high visible transmittance, the pronounced photothermal (PT) effect will be photonically-activated to increase the surface temperature, resulting in much reduced heat transfer through the window. In this study, we report recent experimental results on deposition of transparent thin films of porphyrin compounds and show much lowered U-factors via OTI under simulated solar irradiation. Also identified is the operating mechanism of the photothermal effects for different porphyrin compounds.

#### **F.EL05.05.02**

**Effect of Incident Light Angle on the Photothermal Properties of Iron Oxide and Porphyrin-Based Thin Films for Energy-Efficient Single-Pane Window Applications** Mengyao Lyu<sup>1</sup>, Jou Lin<sup>1</sup>, John Krupczak<sup>2</sup> and Donglu Shi<sup>1</sup>; <sup>1</sup>University of Cincinnati, United States; <sup>2</sup>Hope College, United States

Photothermal experiments of incident light angle dependence were carried out by using solar-simulated light on iron oxides ( $\text{Fe}_3\text{O}_4$  and  $\text{Fe}_3\text{O}_4@\text{Cu}_{2-x}\text{S}$ ) and porphyrin compounds (chlorophyll and chlorophyllin) thin films. All thin films were deposited on glass substrates by spin-coating method with the photothermal materials evenly dispersed in polymethyl methacrylate (PMMA) solutions. The  $\text{Fe}_3\text{O}_4$  film was found to exhibit a strong absorption peak near the UV region but only with background absorptions in the visible and NIR regions. A broad NIR absorption was observed in the  $\text{Fe}_3\text{O}_4@\text{Cu}_{2-x}\text{S}$  thin film. Both chlorophyll and chlorophyllin showed pronounced peaks near UV and NIR characterized with the U-shaped spectra, ideal for energy-efficient single-pane window applications that require efficient solar harvest and high transparency. Thermal transmittance through the window can be significantly reduced by decreasing the temperature difference,  $\Delta T$ , between the window inner surface and the room interior based on a so-called “optical thermal insulation” (OTI) without any intervention medium, such as air/argon. Upon solar irradiation,  $\Delta T$  is reduced by increasing the inner surface temperature of the window through the photothermal heating of the iron oxide and porphyrin coatings. It is therefore possible to replace double- or triple- panes with single panes based on OTI. As the seasonal changes of sunlight inevitably affect OTI, an incident light angle dependence of the photothermal effect was carried on the oxide ( $\text{Fe}_3\text{O}_4$  and  $\text{Fe}_3\text{O}_4@\text{Cu}_{2-x}\text{S}$ ) and porphyrin (chlorophyll and chlorophyllin) thin films. It was found that their heating curves all reached maximum temperatures at small angles of incidence while that of which considerably reduced at large angles. The angle dependence data provides important references for OTI that the window exposure to the sun is higher at the winter solstice (small angle) and lower in summer (large angle). The enhanced solar harvesting at winter solstice can induce a stronger photothermal effect for effective optical thermal insulation of single-pane windows.

#### **F.EL05.05.03**

**Reconfigurable Azo-LCN/rGO Bilayers with Tailorable Mechanical and Electrical Properties** Woongbi Cho<sup>1</sup>, Jisoo Jeon<sup>1</sup>, Wonsik Eom<sup>2</sup>, Tae Hee Han<sup>2</sup>, Dong Gyun Kim<sup>3</sup>, Yong Seok Kim<sup>3</sup> and Jeong Jae Wie<sup>1</sup>; <sup>1</sup>Inha university, Korea (the Republic of); <sup>2</sup>Hanyang University, Korea (the Republic of); <sup>3</sup>Korea Research Institute of Chemical Technology, Korea (the Republic of)

Azo-benzene functionalized polymers have tremendously been studied owing to the advantages of battery-free light trigger shape reconfigurable properties. However, the trade-off relationship between mechanical strength and deformability and insulating properties are great limitations of azo-functionalized polymer for shape reconfigurable devices. In this presentation, we introduce bilayered structure of azobenzene functionalized liquid crystalline polymer networks (Azo-LCN) with reduced graphene oxide (rGO) toward drastic enhancement in mechanical and electrical properties without sacrifice of strain responsivity. The Young's modulus of the Azo-LCN/rGO bilayer increases by 5 times (6.4 GPa) in comparison with the neat Azo-LCN, and the electrical conductivity is recorded to be 340 S/cm. Remarkably, the Azo-LCN/rGO bilayer overcomes the tradeoff relationship between mechanical stiffness and elongational responsivity by mismatch of structural character of each layers. Upon exposure to broadband UV, the bending angle of azo-LCN/rGO bilayer is enhanced in forward and backward bending, respectively 2.4 times (97.5 to 229.5 degree) and 12 times (5.4 to 65.2 degree) compared to the neat Azo-LCN. In addition to in-plane bending, twisting actuation mode is achieved by simply adjusting the cutting angle of the linearly patterned azo-LCN/rGO bilayers. The Azo-LCN/rGO bilayer can also be shape-reconfigurable by thermal stimuli including near infrared (NIR), sunlight and lighter. The photothermal effect is selectively induced on the rGO layer by irradiation of NIR stimuli which drive bending actuation of azo-LCN/rGO bilayer. Then, spatially localized actuation of azo-LCN/rGO bilayer is demonstrated by focused irradiation of solar ray. Finally, a rapid and large actuation is also demonstrated by direct heat energy transfer by operation of a lighter.

#### **F.EL05.05.04**

**Light-Driven Manipulation of Microdroplet on a GeSbTe Substrate** Yuka Takamatsu<sup>1</sup>, Eiji Yamamoto<sup>1</sup>, Keiko Esashika<sup>1</sup>, Masashi Kuwahara<sup>2</sup> and Toshiharu Saiki<sup>1</sup>; <sup>1</sup>Keio University, Japan; <sup>2</sup>Nanoelectronics Research Institute, National Institute of Advanced Industrial Science & Technology, Japan

The phenomena related to droplet migration at the micro-scale is expected to be applied to micro medical robots, new printing technologies, and basic research for the locomotion mechanisms of active matter such as cells or microbial populations. One of the main driving forces of droplet motion is Marangoni flow, which takes place from lower to higher surface tension regions. There are many studies on droplet manipulation based on Marangoni flow by generating surface tension difference under temperature gradient. Since, generally, surface tension decreases with temperature, a droplet moves from higher to lower temperature regions. In this study, we demonstrated light-driven microdroplet formation and transportation in a two-dimensional slit on a Ge<sub>2</sub>Sb<sub>2</sub>Te<sub>5</sub> (GST) substrate. GST as a substrate material is suitable for local laser heating due to its large light absorption and low thermal conductivity. We found an inverse Marangoni effect, which refers to the droplet motion from lower to higher temperature regions. The inverse Marangoni mechanism is more advantageous for droplet manipulation by laser beam positioning.

As a droplet material, polyethylene glycol (PEG) was mixed with toluene at a volume ratio of 7:1 to control the temperature dependence of surface tension of the droplet. The toluene/PEG solution was sandwiched with two coverslips, one of which was coated with GST. Droplet formation and transportation was observed under an inverse optical microscope. A local temperature gradient was induced by focusing subnanosecond pulsed laser ( $\lambda=532$  nm) onto the GST layer through the microscope objective.

When the interface area between bulk-like toluene/PEG and its vapor was irradiated with the laser spot, many small droplets of toluene/PEG were generated in the vapor side and they merged together at the center of the laser spot to form a single larger droplet. When slightly shifting the laser spot, we found that the droplet immediately moved to follow the spot. The result implies that the droplet moved towards higher temperature region, which direction is opposite to that expected from the conventional Marangoni effect. When the laser was turned off, the droplet spread to its equilibrium diameter. We can control the diameter of droplet simply by changing the laser intensity.

We show possible explanation for the mechanism of inverse Marangoni effect. In the toluene/PEG mixed droplet under laser irradiation, the volume ratio of PEG becomes larger in the higher temperature region because the vapor pressure of PEG is much lower than that of toluene and evaporates more slowly. Also importantly, the surface tension of PEG is larger than that of toluene. Considering these facts, we can expect that the surface tension of droplet in the higher temperature side is larger and thereby Marangoni flow is directed towards the center of laser spot. In order to support this explanation, the same experiment was conducted using pure toluene.

The droplet moved towards the opposite direction with respect to the case of mixed solution. The result can be explained by conventional Marangoni effect. The efficient inverse Marangoni effect we obtained may be also attributed to the significantly low surface energy and its temperature dependence of GST.

#### **F.EL05.05.05**

**Enhanced Magnetic Actuation of Micropillar Arrays via Anisotropic Stress Distribution** Jeong Eun Park<sup>1</sup>, Jisoo Jeon<sup>1</sup>, Sei Jin Park<sup>2</sup>, Sukeyoung Won<sup>1</sup>, Zahyun Ku<sup>3</sup> and Jeong Jae Wie<sup>1</sup>; <sup>1</sup>Inha University, Korea (the Republic of); <sup>2</sup>Lawrence Livermore National Laboratory, United States; <sup>3</sup>Air Force Research Laboratory, United States

Recently, magnetically reconfigurable micropillar arrays have been documented by aligning magnetic particles within the microstructure. When the orientation axis of magnetic particles is deviated from the external magnetic field axis, micropillars undergo directional twisting and bending deformation according to the alignment of magnetic particles. Previous studies have mostly been focused on cylindrical micropillars, resulting in identical actuation regardless of magnetic field direction. In this presentation, we discuss a strategy of anisotropic stress distribution by employing anisotropic pillar geometry in order to introduce a preferential direction for strain responsivity. Under the linear external magnetic field, the effects of geometric anisotropy on magnetic actuation will be investigated by comparing experimental results with magneto-mechanical simulation for rectangular and triangular micropillars. Furthermore, we will discuss the anisotropic liquid spreading and wetting on magnetically actuated micropillar arrays where the pillars twist and bend.

#### **F.EL05.05.06**

**Multi-Functional and Transparent 3D Shape-Morphing by Patterned Adhesive Tapes via Photothermal Effects** Jae Gyeong Lee, Sukeyoung Won, Jeong Eun Park and Jeong Jae Wie; Inha University, Korea (the Republic of)

Construction of 3-dimensional (3D) architectures from 2-dimensional (2D) sheets has recently been drawn a great attention. In particular, printing of black ink hinges on pre-strained polymers provides facile and contactless shape-morphing by selective light absorption via photothermal effects. However, remaining ink hinges obstruct transparency and can cause undesirable over-actuation by thermal conduction to unpatterned regions. In this study, we suggest a facile strategy for formation of transparent non-Euclidean structures from pre-strained polystyrene (PS) sheets by employing adhesive tape. Upon exposure to near infrared (NIR) light, pre-stretched PS below the adhesive tape pattern undergoes relaxation of polymer segment into a random conformation above the glass transition temperature on account of local light absorption. Contraction of patterned areas induces 3D shape morphing and remaining tape patterns can simply be removed on-demand after the construction of the targeted 3D structures. Herein, we employed radial and chiral patterns to generate complex 3D architectures and conjugated the multi-material to endow heterogeneous strain-responsivity for each material in a single curvilinear structure. We will also discuss sequential folding by control of light absorption time with sequential removal of adhesive tapes.

#### **F.EL05.05.07**

**Optical Properties of Si Doped ta-C Anti-Reflective Coatings for Photovoltaic Applications** SangYul Lee<sup>1</sup>, Jung-Wan Kim<sup>2</sup> and HoeKun Kim<sup>1</sup>; <sup>1</sup>Korea Aerospace University, Korea (the Republic of); <sup>2</sup>Incheon National University, Korea (the Republic of)

Metal containing carbon nanocomposite coatings (Me doped DLC coatings) which include metal or metal carbide phase embedded in amorphous carbon matrix have attracted a significant attention for the past few decades. The association between the carbon matrix and the encapsulated metallic or metal carbide phase not only improve the overall mechanical properties of the nanocomposite coatings, but also attribute the optical properties by accompanying phase and microstructure changes in the coatings. Recently, it has been shown that DLC based coatings are very promising anti-reflection (AR) and protective coatings for photovoltaic applications due to their high chemical stability, radiation stability and high hardness with the possibility of changing their optical properties. Among the various DLC coating classification, tetrahedral amorphous carbon (ta-C) coatings, which showed high sp<sup>3</sup>/sp<sup>2</sup> fraction over 60%, with extremely high hardness, excellent wear resistance, and better radiation stability have been paid much attention to an alternative anti-reflection protective coating materials. So in this study, various contents of Si metal were doped in the ta-C coating to improve optical properties of the ta-C coatings. Filtered cathodic vacuum arc (FCVA) and sputter hybrid PVD system was conducted to synthesize the metal doped ta-C coating. As increasing of Si content in ta-C coating, microstructure of the coatings changed from a dense featureless amorphous to a columnar “moth-eye” like structure by a formation of rhomb silicon carbide (SiC) phase, and that is especially useful for reducing reflections and increasing transmission between materials by the roll of light absorption. Raman spectroscopy analysis showed that all the coatings had high sp<sup>3</sup>/sp<sup>2</sup> fraction about 63%, and the hardness showed high values of 47.5 GPa. The ta-C coating with 4at.% Si showed improved transmittance (over 93.4%) in the field of ultraviolet, and this value was higher than that of other carbon based coatings. These results indicate that the Si doped ta-C coating could be applied for protective & AR coating for photovoltaic applications.

#### **F.EL05.05.08**

**Late News: Supramolecular Modulation of  $\pi$ -Stacking in Anthracene Crystals—Toward Photoactive Organic Semiconductors** Gonzalo Campillo-Alvarado and Ying Diao; University of Illinois at Urbana-Champaign, United States

Organic semiconductors (OSCs) are a rapidly emerging field in molecular electronics. Specifically, single crystals of OSCs have received considerable attention due to unique properties associated with long-range order, absence of grain boundaries, and extremely low defect density [1] leading to a wide range of multi-functional materials (e.g., field-effect transistors, light-emitting diodes, photovoltaics). However, the lack of strategies to control and promote  $\pi$ -stacking in single crystals of OSCs has limited their tunability and application. While covalent modification of OSCs has arguably received the most attention [2], the noncovalent approach (e.g., supramolecular modulation) has been largely unexplored [3].

In this contribution, we introduce of efforts in the use of small molecules (e.g., templates) to promote  $\pi$ -stacking of a pyridyl-containing anthracene through weak non-covalent interactions. Modulation of the geometry of  $\pi$ -stacking in the crystalline solid state is accompanied by changes in the photophysical properties. We envisage the supramolecular control of  $\pi$ -stacking in single crystals of OSCs could lead to rapid developments and diversification of multifunctional crystalline electronics.

#### References:

[1] Zhang, X., Dong, H., Hu, W., *Adv. Mater.* **2018**, *30*, 1801048.

[2] Anthony, J., *Angew. Chem. Int. Ed.*, **2008**, *47*, 452.

[3] Ray, K. K., Campillo-Alvarado, G., Morales-Rojas, H., Höpfl, H., MacGillivray, L. R., Tivanski, A. V., *Cryst. Growth*



## SYMPOSIUM F.EL05

---

Putting Photons to Work—Progress in Photomechanical Materials and Applications  
November 21 - December 2, 2020

### Symposium Organizers

Chris Bardeen, University of California, Riverside  
Nathalie Katsonis, University of Twente  
Javier Read de Alaniz, University of California, Santa Barbara  
Yanlei Yu, Fudan University

### Symposium Support

**Platinum**  
Office of Naval Research

---

\* Invited Paper

SESSION F.EL05.06: Live Lightning/Flash I: Putting Photons to Work—Progress in Photomechanical Materials and Applications

Session Chairs: Chris Bardeen, Nathalie Katsonis, Javier Read de Alaniz and Yanlei Yu  
Tuesday Afternoon, December 1, 2020  
F.EL05

### 7:30 PM INTRODUCTION AND WELCOME

#### 7:33 PM \*F.EL05.03.05

**Light-Induced Curvature of a Landscape to Drive Mechanics Applications** Daniel Duffy, Fan Feng, John Biggins and Mark Warner; University of Cambridge, United Kingdom

Light-driven strains can be large, controlled by colour and polarisation of light, and quickly activated in liquid crystalline solids, both rubbery and glassy.

The challenge for applications is to make the response strong, typically involving stretch rather than bend energies if the distortions are loaded. To achieve stretch in both pull and in push without instabilities, the director needs to be programmed in the solid to change the Gaussian curvature of sheet and shell-like objects.

We make contact with current experiments and suggest new Gaussian-curved evolving landscapes, including those arising from curved fold non-isometric origami objects, for effective applications.

#### 7:43 PM \*F.EL05.03.01

**Coupling Molecular and Material Photomechanical Response** Ruobing Bai, Kevin Korner and Kaushik Bhattacharya; California Institute of Technology, United States

Actuation by light is attractive for a number of reasons: Objects can be actuated from a distance, distinct frequencies can be used to actuate and control distinct modes with minimal interference, and significant power can be transmitted over long distances through corrosion-free, lightweight fiber optic cables. Azobenzene and other molecules that are known to change conformation when exposed to light are the building blocks of photomechanical actuation. An important challenge is how the change of conformation of individual molecules can be harnessed into a robust change of deformation of the material. Approaches range from mean-field entropic coupling as in photoactive nematic elastomers to direct chemical bond coupling

as in molecular crystal to hybrid composite approaches where molecular crystals are embedded an elastic matrix. The mean-field entropic coupling can lead to weak coupling while the stiffness of molecular crystal can inhibit actuation or cause them to shatter on actuation. This talk will present a series of theoretical models to understand various aspects of this molecular to material coupling, illustrate them with experimental observations and discuss how ideas from these studies can be harnessed in real materials and devices.

### 7:53 PM \*F.EL05.02.03

**Self-Regulating Photoactive Materials for Actuation** Megan T. Valentine; University of California-Santa Barbara, United States

Light is an attractive source of remote control and power: it is non-invasive, wavelength-selective, and provides high spatial and temporal resolution. However, the development of new materials is required to fully exploit these advantages by optimizing light energy transduction pathways and/or the light-mediated modulation of materials properties. In this talk, I will present my group's collaborative efforts to advance the incorporation of donor-acceptor Stenhouse adducts (DASAs) into materials designed for light-driven generation and control of material motion. DASAs present unique advantages for actuation. These highly-absorbing, negatively photochromic molecules have highly tunable reaction kinetics and respond to visible light. We have shown them to be effective photothermal and photochemical agents that can drive the motion of amorphous polymeric materials as well as liquid flows. In particular, through control of DASA reaction kinetics and the applied light field, it is possible create self-regulating flow fields that hold promise for valveless optofluidic devices and soft robotics.

### 8:03 PM \*F.EL05.01.02

**Mechanically Flexible Crystals—Crystal Engineering** Malla Reddy Chilla; IISER Kolkata, India

In recent times various intriguing dynamic single crystals that respond to external stimuli such as mechanical stress, heat, light, solvent, humidity, have been reported, but their systematic design remained a challenge. In my talk, I will demonstrate a variety of mechanically reconfigurable and certain other stimuli responsive organic single crystals, where a range of supramolecular weak interactions such as van der Waals (vdW) and  $\pi$ -stacking, play a crucial role in absorbing the internal and external stresses generated.<sup>1-3</sup> I shall present a detailed case study of photomechanical work (i.e. mechanical bending) done by a crystal using visible light mediated photopolymerization chemical reaction, and recovery of the original shape in a reversible manner by a thermal depolymerization reaction.<sup>4</sup> A few other examples covering waveguides and mechanochromic luminescence will be discussed. Our study demonstrated the potential of soft interactions for designing mechanical behaviour of ordered molecular materials, including those from  $\pi$ -conjugated semiconducting systems, which are of paramount importance for achieving flexible smart materials.

- (1) Reddy, C. M.; Krishna, G. R.; Ghosh, S. *CrystEngComm* **2010**, *12*, 2296.
- (2) Panda, M. K.; Ghosh, S.; Yasuda, N.; Moriwaki, T.; Mukherjee, G. D.; Reddy, C. M.; Naumov, P. *Nature Chem.* **2015**, *7*, 65-72.
- (3) Krishna, G. R.; Devarapalli, R.; Lal, G. Reddy, C. M.; *J. Am. Chem. Soc.* **2016**, *138*, 13561–13567.
- (4) R. Samanta, S. Ghosh, R. Devarapalli, C. M. Reddy, *Chem. Mater.* **2018**, *30*, 577–581.

*CMR thanks DST for Swarnajayanti Fellowship and CSIR for research funding. IISER Kolkata is thanked for central facilities.*

### 8:13 PM \*F.EL05.04.06

**Photo-Steered Deformation and Locomotion of Nanocomposite Hydrogels** Qing Li Zhu, Zhi Jian Wang, Chen Fei Dai, Qiang Zheng and Zi Liang Wu; Zhejiang University, China

Inspired by the natural activated systems, realization of programmed deformations and locomotion in artificial materials has recently attracted great interest due to their promising applications in biomedical devices, soft robotics, and flexible electronics. Photo-responsive hydrogels are recognized as one ideal material to construct soft actuators and robots owing to their drastic volume change induced by contactless light irradiation with high spatial and temporal resolutions. The challenge is how to construct composite hydrogel with gradient structure and dynamically activate the specific regions of the gel toward

programmed deformation and locomotion. We present here a photolithographic method to fabricate patterned composite hydrogel sheets with heterogeneous structures by embedding the photo-responsive hydrogel in a preformed nonresponsive hydrogel. Under photo irradiation, the swelling/contraction mismatch results in the built-up of internal stress and thus programmed deformations of the composite hydrogel. Furthermore, a moving light beam is imposed on the composite hydrogel to spatiotemporally actuate the gel that shows sophisticated motions, including crawling, walking, and turning. Experimental and simulation results reveal that multigait locomotion is realized by the mutual coordination of shape-morphing and dynamic friction of the gel against a substrate under the spatiotemporal light stimulation. The programmed deformations of motions of photo-responsive hydrogels should be instructive for the development of soft robotics with advanced technologies and versatile applications.

**8:23 PM \*F.EL05.01.10**

**Photo-Induced Cooperative Supramolecular Nanosheets** [Shenqiang Ren](#); SUNY Buffalo, United States

Photostrictive compounds are promising device materials because of their fundamental photophysical properties and light-induced cooperative behaviors. Although molecular charge-transfer crystals exhibiting light-matter interactions have been successfully deployed in optoelectronics, an air-stable molecular material that couples photons and electrons, achieving photostriction through the coupling of light and mechanical degrees of freedom, has not yet been discovered. Herein, we report a substantial light-induced dilation in a molecular material at room temperature, which is accompanied by simultaneous photocurrent generation. This finding opens avenues for coupling optical, electronic, and mechanical functionalities for possible use in remote wireless photoswitchable devices.

**8:33 PM \*F.EL05.03.03**

**Magnifying Photomechanical Actuation Using Mechanical Instabilities** [Ravi Shankar](#); University of Pittsburgh, United States

The ability to harness light for photochromic switching that directs mechanical work generation within a macromolecular network is a platform for envisioning photomechanical machines, which are neither encumbered by onboard power sources, nor require microfabricated components and mechanisms. Light offers multiple control knobs for photomechanical regulation, including spatiotemporal modulation of intensity, direction, polarization and chirality. Unfortunately for actuators driven with light, the length over which the photons are attenuated (typically, few micrometers) limits the thickness of the photoactuators. The photomechanical strain generation is via bending, resulting from the gradation in the strains that are generated. Slender structures that respond by bending make for weak actuators. Work content that can be accessed is intrinsically bounded in the characteristically micrometer-scale thickness actuators.

Unusual opportunities emerge when we move beyond flat photoactive geometries, where the patterning of the molecular switches and the graded photomechanical strains conspire to result in non-linear mechanical responses. Snap-through in rod-like structures are one example. Creasing instabilities are another, where the bending of liquid crystalline polymers that are photoresponsive is used to drive non-linear transformations of curved shells, which are confined at their periphery. Torque densities  $>100$  Nm/kg and flexural actuation rates  $>100$  radians/s can be produced. Profiles of these photomechanical actuators places them in a property space that competes favorably with electromechanical systems. A third example is that of photoactuated tape-spring mimicking structures. Here, ms-scale actuation is triggered in shells that switch their principal curvatures, via a snap-through mechanism. Beyond these illustrations, opportunities also exist for utilizing a broader class of latch and torque-inversion mechanisms to magnify actuation by integrating active and passive (structural) materials.

Overall, accessing 3-dimensionally patterned freeform actuators is useful for magnifying photomechanical actuation. Realizing these geometries is simplified by the availability of an additive manufacturing platform, wherein the molecular order can be patterned voxel-by-voxel during the composition of multimaterial architectures. The interplay of magnetically assisted alignment and site-specific photopolymerization is a vehicle for achieving this in an inverted stereolithographic setup. In comparison to say, extrusion-based methods, decoupling the material accretion from the endowment of molecular order is key to expanding the design-space, which can be fabricated.

Magnifying photoactuation in monolithic polymeric structures, which can be scaled from the micrometer to mm-scale form factors holds implications for enabling photomechanical machines. It is possible to envision optically powered and reconfigurable devices in applications ranging from microrobotics, biomedicine and manipulation in environments hostile to electromechanical systems.

**8:42 PM BREAK**

8:46 PM \*F.EL05.03.04

**Characterizing the Photomechanical Response of Materials** Peter Palffy-Muhoray, Anastasia Svanidze, Seung-Won Oh, Tianyi Guo and Xiaoyu Zheng; Kent State University, United States

When illuminated, photomechanical materials move and demonstrate forces which cause motion. This response indicates that they have acquired momentum as consequence of photoexcitation. We characterize their response by identifying and quantifying the effectiveness of the physical mechanisms connecting photoexcitation and the mechanical response. We are particularly interested in the details of how photostress results from the exciting flux of photons, whose momentum is negligible compared to what is observed in the response, and how photostresses produced in the bulk are transported to the sample surfaces and do mechanical work. We introduce a simple relation linking a stress in light to the photostress, and propose that elements of the tensor relating these serve as measures of the effectiveness of the different aspects of the photoresponse, both in transforming photon energy to stress and in storing photon energy and making it available for mechanical work. Using this metric, we compare the performance of different classes of photomechanical materials using data from the published literature.

8:56 PM F.EL05.01.04

**Hybrid Organic-Inorganic Photoactuators Based on Molecular Crystals** Chris Bardeen and Xinning Dong; University of California, Riverside, United States

Crystals organize photoreactive molecules and coordinate their motions, leading to photoinduced deformations like expansion, bending, twisting, peeling and coiling. This class of materials provides a path to photomechanical actuators that can be scaled down to micro- or nanoscale dimensions, but along the way several challenges must be addressed: 1) optimization of the molecular structure to control the rate and mechanism of reversibility (photon versus thermal activation); 2) control of crystal morphology to generate actuating structures with a variety of shapes and sizes; and 3) the hierarchical organization of nano-scale and micro-scale crystals into a macroscopic actuator structure, usually by templated growth and organization. Recent progress in all three areas have led to the development of composite organic-inorganic structures with unprecedented power-to-weight ratios: under light illumination, less than 1 mg of a diarylethene photochrome can move a load weighing more than 100 g. These materials consist of organic photochromic crystals aligned in the pores of various types of inorganic host materials, including  $\text{Al}_2\text{O}_3$  and  $\text{SiO}_2$ . The effects of the inorganic matrix material, organic photochromic molecule, and crystal alignment and orientation are all analyzed. The potential of these hybrid materials as practical photoactuators will be assessed.

9:06 PM F.EL05.01.06

**Photoinduced Picosecond Nonthermal Amorphization in  $\text{Sb}_2\text{Te}_3$**  Subodh C. Tiwari<sup>1</sup>, Rajiv Kalia<sup>1</sup>, Aiichiro Nakano<sup>1</sup>, Fuyuki Shimojo<sup>2</sup>, Priya Vashishta<sup>1</sup> and Paulo Branicio<sup>1</sup>; <sup>1</sup>University of Southern California, United States; <sup>2</sup>Kumamoto University, Japan

Phase change materials are of great interest for low-power high-throughput storage devices and next-generation neuromorphic computing technologies due to their contrasting properties between amorphous and crystalline phases and fast switching rate. Notably,  $\text{Sb}_2\text{Te}_3$ , an archetypical Ge-Sb-Te alloy, displays a fast and energy-efficient crystallization-amorphization cycle, due to its growth-dominated crystallization and low melting point. Here, we demonstrate a new nonthermal amorphization pathway of  $\text{Sb}_2\text{Te}_3$  which can further reduce time required for amorphization from nanoseconds to picoseconds. We employ non-adiabatic quantum molecular dynamics simulations to investigate the time evolution of  $\text{Sb}_2\text{Te}_3$  at a constant temperature of 500 K with 2.6%, 5.2%, 7.5%, 10.3%, and 15% photoexcited valence electron-hole carriers. Results reveal picosecond nonthermal amorphization at and above a critical excitation of 7.5% valence electrons. The rapid amorphization originates from an instantaneous charge transfer from Te-*p* orbitals to Sb-*p* orbitals upon photoexcitation. Subsequent evolution of the excited state, within picosecond timescale, indicates a Sb-Te bonding to antibonding transition. Concurrently, Sb-Sb and Te-Te antibonding decreases, leading to the formation of wrong bonds. For 7.5% valence electron photoexcitation or larger, the electronic changes destabilize the crystal structure, leading to large atomic diffusion and loss of long-range order. These results highlight an ultrafast energy-efficient amorphization pathway that could be used to enhance the performance of phase change materials based opto-electronic devices.

This work was supported as part of the Computational Materials Sciences Program funded by the U.S. Department of Energy, Office of Science, Basic Energy Sciences, under Award Number DE-SC0014607. The simulations were performed at the Argonne Leadership Computing Facility under the DOE INCITE and Aurora Early Science programs and at the Center for High Performance Computing of the University of Southern California.

### 9:12 PM F.EL05.01.07

**Understanding and Control of Giant Opto-Mechanics in Wide-Band Gap Compound Semiconductors** Yifei Li<sup>1</sup>, Yuying Zhou<sup>2,3</sup>, Haowei Xu<sup>1</sup>, Alan F. Schwartzman<sup>1</sup>, Ju Li<sup>1</sup> and Rafael Jaramillo<sup>1</sup>; <sup>1</sup>Massachusetts Institute of Technology, United States; <sup>2</sup>Shanghai Institute of Applied Physics, Chinese Academy of Science, China; <sup>3</sup>University of Chinese Academy of Sciences, China

The coupling between mechanical and optical properties can be surprisingly large, and has a long history of study. Optical absorption resonances are related to breaking, reforming, and rearranging bonds, on an energy scale of 1 eV/molecule, and it stands to reason that the effects of optical absorption on mechanical properties may be substantial; still these effects continue to surprise, and are often overlooked. Opto-mechanical effects may be especially strong when mediated by optically-active defects that store charge, induce local lattice distortions, and interact with modes of plastic deformation. The connection between defects and opto-mechanics provides a handle for controlling opto-mechanical effects through materials processing, and suggests new applications.

Here we show that the wide-band gap compound semiconductors ZnO, ZnS, and CdS all feature large opto-mechanical coupling that is mediated by point defects. We measure the mechanical properties of sintered and single crystal samples using a nanoindenter equipped with a purpose-built variable wavelength and intensity illumination system. We find that both elasticity and plasticity vary strongly with moderate illumination. For instance, the hardness and stiffness of ZnO can increase by up to 40-80% due to blue illumination of intensity 3 mW/cm<sup>2</sup>. The wavelength-dependence shows that band-edge absorption (*e.g.* UV light) has the strongest effect, and the relative size of the effect of sub-band gap illumination varies between samples – a clear sign of defect-mediated processes. We further show that these giant opto-elastic and opto-plastic effects can be tuned by materials processing, and that the processing-dependence can be understood within a framework of point defect equilibrium. We tune point defect concentrations by annealing treatments, and measure composition by direct (inductively-coupled plasma optical emission spectroscopy, ICP-OES) and indirect (X-ray diffraction, XRD) methods. Our composition measurements for ZnO, ZnS and CdS all show that the magnitude of the optomechanical response varies with anion vacancy concentration. This is consistent with the hypothesis that photoconductivity and photoplasticity are positively correlated, and provides a rational guideline for engineering optomechanical response. We use density functional theory (DFT) calculations to interpret our experimental results. DFT suggests that photo-induced charge carriers migrate along strain gradients, and gather around anion vacancies. The high local net charge concentrations ( $10^{21} \sim 10^{22} \text{ cm}^{-3}$ ) create pseudo-tensile-strain (~5%), which opposes the compressive strain from the indenter, thereby enhancing the elastic modulus. We will conclude with an outlook on opto-mechanical effects in wide-band gap semiconductors, and with several proposed, new applications for these still-surprising effects.

### 9:18 PM F.EL05.01.08

**Casimir Heat Transfer and Strong Phonon Coupling** Haokun Li, King Yan Fong and Xiang Zhang; University of California, Berkeley, United States

In 1948, Casimir described a bizarre force that acts between neutral objects based on quantum fluctuations of electromagnetic fields. This effect is of both fundamental interest in quantum field theory and practical importance in nanotechnology. Recently, it has been predicted that Casimir force can induce phonon coupling between nearby objects and thus transfer heat across a vacuum gap. Revealing this unique quantum effect experimentally would bring fundamental insights to quantum thermodynamics and practical implications to nanoscale thermal management. Here, we present the first experimental demonstration of the Casimir heat transfer. We use nanomechanical systems to realize strong Casimir phonon coupling and observe the exchange of thermal energy between individual phonon modes. The experimental observation agrees well with our theoretical calculations and is unambiguously distinguished from other effects such as near-field radiation and electrostatic interaction. This experiment opens up new opportunities for studying nanoscale energy transport and quantum thermodynamics.

## 9:24 PM F.EL05.01.09

**Late News: Synthesis of Anthracene-Based Next-Generation Photomechanical Molecular Crystals.** Rabih O. Al-Kaysi<sup>1,2</sup>, Fei Tong<sup>3</sup> and Chris Bardeen<sup>3</sup>; <sup>1</sup>King Saud bin Abdulaziz University for Health Sciences, Saudi Arabia; <sup>2</sup>King Abdullah International Medical Research Center, Saudi Arabia; <sup>3</sup>University of California, Riverside, United States

Photomechanical organic crystals are fast becoming the next generation smart-materials that can convert light energy into mechanical work. While the majority of these photomechanical crystals are made from diarylethene or azobenzene derivatives our group has focused on the synthesis of anthracene-based compounds that can be grown into photomechanical crystals. These crystals can expand, bend, twist, curl, peel, or jump when exposed to UV or visible light. We will survey the synthetic routes used to make these anthracene derivatives. We will also describe how we made the corresponding photomechanical crystals using different techniques such as solvent annealing inside Anodic Aluminum Oxide (AAO) templates and aqueous surfactant-mediated precipitation technique.

Esterification of 9-Anthracenecarboxylic acid with aliphatic alcohols gives a family of photomechanically active anthracene derivatives. When these derivatives are grown into crystalline nanowires via solvent annealing inside AAO templates, the resulting nanowires expand anisotropically along their long axis when exposed to UV light. The intermolecular [4+4] photocycloaddition between parallel anthracene rings is the driving force behind the crystal expansion. A thoroughly studied molecule is the photomechanical expansion of tert-butyl anthracene-9-carboxylate (**9TBAE**) nanowires by 15% upon irradiation with 365 nm light. Crystalline microribbons grown from the commercially available 9-Anthracenecarboxylic acid (**9AC**) can twist reversibly (T-type) when exposed UV light. The microribbons require several minutes to reset by reversing the thermally unstable [4+4] photocycloaddition. The introduction of substituents on the **9AC** anthracene ring helps expand our toolbox of T-type photomechanical crystals. Multi-step synthesis was used to introduce substituents on different positions of the **9AC** anthracene ring. These substituents (F, Cl, or Br, NO<sub>2</sub>, CH<sub>3</sub>, etc.) either suppress or enhance the T-type character of the substituted 9-anthracene carboxylic acid crystals. While the 4-fluoro-9-anthracene carboxylic acid (**4F9AC**) shortened the reset time of the crystal by an order of magnitude, the 10-fluoro-9-anthracene carboxylic acid (**10F9AC**) derivative did the exact opposite. Extending the conjugation of the anthracene ring at the 9-position by attaching propenal using Mizoroki–Heck or Wittig reaction yields the very useful 3-(9-Anthryl)acrolein which was used as a building block for the synthesis of second-generation photomechanical anthracene derivatives. Adding different electron-withdrawing groups to the 3-(9-Anthryl)acrolein aldehyde via Knoevenagel condensation leads to a novel type of photomechanical crystals that are driven by trans/cis photochemistry. These crystals are dominantly P-type. For example, 2-(3-anthracene-9-yl-allylidene)-malononitrile (**9DVAM**) crystals and nanowires exhibit P-type photomechanical response under visible and UV light. When these crystals are grown into microwires from an aqueous surfactant they exhibit continuous photo-induced wiggling-like motion resembling flagella. Block-like microcrystals composed of *cis*-dimethyl-2(3-(anthracene-9-yl)allylidene)malonate (**DMAAM**) can peel off amorphous layers upon UV-light exposure while similar analog derivatives can super expand by transforming from crystalline-to-gel like material under intense green light exposure. The introduction of fluorine on the **9DVAM** anthracene ring yields derivatives with P-type photosensitive crystals and nanowires that may find future application in light-driven microactuators.

Synthesis of Anthracene-based photomechanical crystals coupled with non-classical crystal growth techniques has shown to be essential for both understanding the basic principles and advancing the field of photomechanical smart-crystals.

## 9:29 PM DISCUSSION, ADDITIONAL QUESTIONS AND WRAP-UP

SESSION F.EL05.07: Live Lightning/Flash II: Putting Photons to Work—Progress in Photomechanical Materials and Applications

Session Chairs: Chris Bardeen, Nathalie Katsonis, Javier Read de Alaniz and Yanlei Yu

Wednesday Morning, December 2, 2020

F.EL05

## 11:30 AM INTRODUCTION AND WELCOME

### 11:33 AM \*

**Robotic Soft Materials Activated by Photons and Magnetic Fields** Samuel I. Stupp; Northwestern University, United States

The development of soft synthetic materials that can emulate living organisms in their capacity to translate in space, change shape, and perform useful tasks with small energy inputs is a great challenge for materials science. Such “robotic soft matter” could be used to assist in productive functions that may range from robotics to smart management of chemical reactions and even communication with cells. This lecture will describe the development of molecularly designed hydrogels that can exhibit mechanical actuation in response to visible light or the combined action of photons and magnetic fields. The materials are created using components such as hybrid bonding polymers, which consist of supramolecular polymers integrated with light responsive covalent polymer networks. Relative to polymer networks, exposure of HBPs to photons results in faster bending and flattening actuation of objects, as well as longer steps during their light-driven crawling motion. In systems containing polymer networks and ferromagnetic nanostructures we have observed fast walking motion of macroscopic objects on surfaces with programmable trajectories and external activation of cargo delivery.

**11:42 AM \*F.EL05.04.01**

**Light-Induced Actuation of Hybrid Crystalline/Polymeric Photomechanical Materials** [Ryan C. Hayward](#); University of Colorado Boulder, United States

Materials capable of directly converting photon energy into mechanical deformation offer promise in a wide variety of contexts including adaptive optics, remotely operated swimmers, and actuators controlled via lightweight optical cables that resist corrosion and electromagnetic interference. Organic photoswitches offer significant potential in this regard, thanks to their ability to undergo large changes in molecular conformation upon excitation, and their highly tailorable absorption spectra. To date, efforts have focused largely on either crystalline lattices of small photomechanical molecules, which offer the possibility for greater work output due to their high density and well-organized nature, or on polymer matrices containing a modest concentration of photochromes, which generally have superior processability and mechanical properties. We have recently considered two classes of hybrid materials that combine many of the advantages of these disparate approaches. In one case, we have studied the growth of micrometer-scale photomechanical diarylethene crystals within the pores of polymer membranes. For appropriately controlled orientations of the crystals, such materials can exhibit photomechanical work outputs rivalling the best previously reported systems, while enabling facile processing into mechanically robust samples with cm-scale lateral dimensions. In a second case, we have developed a new class of structurally regular addition polymers bearing photoisomerizable azobenzene groups alternating with chain extenders. These materials form semicrystalline solids that exhibit fundamentally interesting temperature- and light-dependent melting and recrystallization behaviors, and that can be processed into aligned films and fibers exhibiting two-way optical shape memory properties.

**11:51 AM \*F.EL05.02.01**

**Hydrazone-Based Switches and Functional Materials** [Ivan Aprahamian](#); Dartmouth College, United States

For the past few years we have been developing structurally simple, easy to make, modular, and tunable hydrazone-based functional materials (*e.g.*, switches, sensors and fluorophores).<sup>1</sup> This presentation will deal with our recent advances with these systems, with an emphasis on newly developed photochromic compounds<sup>2</sup> that exhibit many interesting properties, including emission ON/OFF toggling in solution (see below) and the solid-state.<sup>3</sup> The integration of these photochromic compounds into liquid crystals<sup>4</sup> and liquid crystalline elastomers<sup>5</sup> will also be discussed.

**Representative references:**

1. I. Aprahamian *ChemCommun* **2017**, 53, 6674–6684
2. (a) H. Qian, S. Pramanik, I. Aprahamian *J. Am. Chem. Soc.* **2017**, 139, 9140–9143  
(b) Q. Li, H. Qian, B. Shao, R. P. Hughes, I. Aprahamian *J. Am. Chem. Soc.* **2018**, 140, 11829–11835
3. B. Shao, M. Baroncini, H. Qian, L. Bussotti, M. Di Donato, A. Credi, I. Aprahamian *J. Am. Chem. Soc.* **2018**, 140, 12323–12327
4. M. J. Moran, M. Magrini, D. Walba, I. Aprahamian *J. Am. Chem. Soc.* **2018**, 140, 13623–13627
5. A. Ryabchun, Q. Li, F. Lancia, I. Aprahamian, N. Katsonis *J. Am. Chem. Soc.* **2019**, 141, 1196–1200

**12:00 PM \*F.EL05.04.03**

**Eliciting Diverse Deformation Modes from a Compositionally Uniform Liquid Crystalline Elastomer Microstructure** Shucong Li, Michael M. Lerch and [Joanna Aizenberg](#); Harvard University, United States

The type of deformations and range of motion, which microstructures can undergo, determines their function, be it for soft

robotics, for sensing or for changing properties in optical or metamaterials. While composite, multimaterial architectures allow imprinting of pre-determined deformation behaviors, their fabrication at the microscale is difficult and the deformation modes are fixed once fabricated. Herein, we demonstrate the use of an alternative strategy – the generation of a transient bilayer architecture within microstructures by an external light stimulus, – and a variety of deformation behaviors that the same structure can display as a result. Changing the direction of UV-irradiation of high-aspect-ratio compositionally uniform microstructures fabricated from photoresponsive liquid crystalline elastomers gives access to a wide range of sophisticated deformations such as clockwise and counter-clockwise twisting, light seeking and avoiding, particularly if rotational symmetry is broken. Light intensity is demonstrated to be a further control parameter that allows one to tap into non-monotonic bending motions and combinations of twisting, bending and expansions/contractions. Finally, because the light-generated layered architectures are transient, they adapt and evolve as the deformation proceeds, leading to highly complex, yet controllable, self-regulated deformation behaviors. The described LCE microstructures are rapidly and easily fabricated and they offer exciting opportunities to further explore essential features of their finely controllable deformation abilities for applications in next generation smart materials.

**12:09 PM \*F.EL05.02.02**

**New Photochromes for Efficient Transduction of Photonic Energy to Potential Energy for Bond-Breaking and Bond-Making Processes** Jeffrey Rack; University of New Mexico, United States

We will describe our latest efforts to create new photochromic compounds based on sulfoxides and sulfoxide mimics. We will also detail our advances in the creation of first row transition metals, where we propose that isomerization is capable of stabilizing of high spin states available for first row transition metal complexes. In addition, we will detail our spectroscopic studies of these new materials, both in solution and in solid state.

**12:18 PM \*F.EL05.03.02**

**Modeling Photo-Mechanical Actuation in Liquid Crystal Polymers** Robin L. Selinger<sup>1</sup>, Michael Varga<sup>1</sup>, Youssef M. Golestani<sup>1</sup> and Sajedeh Afghah<sup>1,2</sup>; <sup>1</sup>Kent State University, United States; <sup>2</sup>Microsoft / OptoFidelity, United States

Liquid crystal polymer networks undergo reversible shape change in response to any stimulus that affects the strength of nematic order. These soft actuators can be fabricated as thin films, surface coatings, or 4D printed solids and have potential applications in soft robotics, biomedical devices, microfluidics, and sensors. Trajectories for shape change are “programmed” by patterning the nematic director when the polymer is cross-linked. Actuation is induced when the strength of nematic order is modulated by stimuli such as a change of temperature or chemical environment; for example, heating induces contraction along the nematic director and expansion in orthogonal directions. The addition of azobenzene derivatives that undergo photo-isomerization produces a soft actuator that flexes like an artificial muscle in response to illumination; if the cis-to-trans thermal relaxation is fast enough, the material can also flex rapidly back toward its original shape when illumination is removed. Such reversible photo-mechanical actuation is a highly attractive option to control a soft robot as it combines both control and power for induced motion without need for tethering or onboard batteries.

Modeling the dynamics of photo-mechanical actuation in these materials is important both to explain the mechanisms behind experimental observations and for device design. To model photo-mechanical actuation at the device scale, we use nonlinear finite element method (FEM) elastodynamics simulation based on a Hamiltonian approach. This method can simulate underdamped motion where momentum plays an important role. The code was developed in-house and implemented in CUDA for execution on a GPU-enabled computer.

We used this approach to model oscillatory mechanical wave motion in a soft robot whose motion was both controlled and powered by light [1]. We use a simplified ray tracing algorithm to determine which parts of the device were illuminated and which in shadow, and used a kinetic model of photo-isomerization/relaxation to describe the time evolution of nematic order. We found that the directionality of light-induced mechanical wave propagation is controlled by a self-shadowing mechanism and periodic pop-through transitions.

We also model a variety of other prototype devices including surface-adhered nematic polymer coatings that transform from flat to complex surface profiles with microchannels, spikes, or dimples recently observed in experiments by Babakhanova et al [2]. Next we model polymer coatings patterned with biomimetic “octopus-like” suckers, designed to grasp and release



nonporous objects on command. Such a device would have the potential to achieve strong, reversible adhesion. Our results demonstrate that actuation geometry produced by a disclination in a nematic polymer is controlled not only by the defect's topological charge and orientation but also by the details of its defect core structure. We compare our modeling results with relevant experiments by collaborators and discuss potential applications.

[1] Gelebart, A.H., Mulder, D.J., Varga, M., Konya, A., Vantomme, G., Meijer, E.W., Selinger, R.L.B., Broer, D.J., (2017) Making waves in a photoactive polymer film, *Nature* 546, 632 (2017) <https://doi.org/10.1038/nature22987>

[2] Babakhanova, G., Turiv, T., Guo, Y. *et al.* Liquid crystal elastomer coatings with programmed response of surface profile. *Nat Commun* 9, 456 (2018). <https://doi.org/10.1038/s41467-018-02895-9>

Work supported by NSF CMMI-1663041, NSF DMR-1409658, and NSF-CMMI 1436565; computer resources provided by the Ohio Supercomputer Center.

#### 12:27 PM \*F.EL05.04.05

**Photomechanical Effects in Liquid Crystalline Polymer Networks and Elastomers** Timothy White; University of Colorado Boulder, United States

Photons have been “put to work” in polymeric materials for more than 50 years. Photogeneration of work has been observed in a range of polymeric materials spanning the continuum from soft elastomers to rigid, high performance materials. Of particular importance is the organization of the polymer chains within the network which can affect magnitude, rate, and directionality of photoinduced deformation. Photomechanical effects in liquid crystalline polymer networks and elastomers are particularly appealing in enabling distinctive conversion of light into work. This presentation will summarize the salient benefits of using light as an actinic stimulus as well as highlight recent developments in this topical area of materials research from our laboratory.

#### 12:35 PM BREAK

#### 12:39 PM \*F.EL05.03.06

**Understanding the Photochemistry of Donor-Acceptor Stenhouse Adducts** David Sanchez, Umberto Raucci, Katherine Ferreras and Todd J. Martínez; Stanford University, United States

Donor-acceptor Stenhouse adducts (DASA) are a promising new chromophore for photomechanical applications. We detail studies of the photochemistry of this chromophore, including both the initial light-induced isomerization and the thermal ring-closing reaction. We further provide details on a framework for modeling excited state dynamics under force, combining the ab initio multiple spawning formalism for nonadiabatic dynamics with the force-modified potential energy surface framework developed for ground state mechanochemistry. We discuss the role of external force (either compressive or extensional) on the photodynamics of the DASA chromophore and its implications for the use of DASA chromophores in light-triggered mechanical actuators.

#### 12:48 PM \*F.EL05.04.02

**Twist Again—Dynamically and Reversibly Controllable Chirality in Liquid Crystalline Elastomer Microposts** Anna C. Balazs<sup>1</sup>, James T. Waters<sup>1</sup>, Shucong Li<sup>2</sup>, Yuxing Yao<sup>2</sup>, Michael M. Lerch<sup>2</sup>, Michael Aizenberg<sup>2</sup> and Joanna Aizenberg<sup>2</sup>; <sup>1</sup>University of Pittsburgh, United States; <sup>2</sup>Harvard University, United States

Photo-responsive liquid crystalline elastomers (LCEs) constitute ideal actuators for soft robots because their light-induced macroscopic shape changes can be harnessed to perform mechanical work. Conventional LCEs, however, do not typically exhibit complex modes of bending and twisting necessary to perform sophisticated maneuvers. Here, we model LCE microposts encompassing side-chain mesogens oriented along a specific axis characterized by the nematic director, and azobenzene crosslinkers, which determine the deformations of illuminated posts. On altering the nematic director from 90° to 0° relative to the underlying substrate, the post's bending respectively changes from light-seeking to light-avoiding. Moreover, with the director tilted at 45°, the initially achiral post reversibly twists into a right- or left-handed chiral structure, controlled by the angle of incident light. We exploit this photo-induced chirality to design “chimera” posts (encompassing two regions with distinct director orientations) that exhibit simultaneous bending and twisting, mimicking motions exhibited by the human musculoskeletal system.

12:57 PM F.EL05.02.05

**Designable, Responsive Non-Linear Optics of Light-Responsive, Spiropyran-Functionalized Hydrogels** Amos Meeks<sup>1</sup>, Rebecca Mac<sup>2</sup>, Simran Chathanat<sup>2</sup> and Joanna Aizenberg<sup>1</sup>; <sup>1</sup>Harvard University, United States; <sup>2</sup>University of Waterloo, Canada

We demonstrate the potential of spiropyran-functionalized, light-responsive hydrogels to be a promising new platform for nonlinear optical materials. Nonlinear optical behavior in these materials arises from the swelling/deswelling and resulting refractive index changes that occur due to photoisomerization between the hydrophilic ring-open merocyanine isomer and the hydrophobic ring-closed spiropyran isomer. These materials show an unprecedented combination of reversibility, soft easily processed material, low laser powers, and long-range interactions. These long-range interactions are especially promising for potential applications in all-optical computing or sensing. We show that the long-range interactions can be explained by thermal swelling or deswelling of the gel. The presence of a secondary temperature gradient that influences beam behavior leads to novel repulsive long-range interactions, which are not possible in conventional nonlinear optical materials in the absence of external symmetry breaking. Furthermore, the direction and magnitude of a hydrogel's thermal response can be controlled by changing the gel composition, which allows the behavior of single and multiple beams in these gel materials to be rationally designed over a potentially vast design space. We demonstrate this potential by exploring two beam interactions in poly(N-isopropylacrylamide-co-acrylic acid) gels which contract rather than swelling as function of increasing temperature. We observe a lack of long-range interactions in these gels along with behaviors indicative of short-range attractive interactions, such as spiraling and beam fusion. This tunable diversity of behaviors suggests the enormous potential for photoresponsive hydrogels as extremely versatile, rationally designable, soft, nonlinear optical materials.

1:03 PM F.EL05.04.07

**Light-Fueled Rolling and Jumping of Polymers** Jeong Jae Wie, Jisoo Jeon and Jae Gwang Kim; Inha University, Korea (the Republic of)

Light-fueled soft robots have recently demonstrated untethered manipulation of locomotion without the complex mechanical and electrical design principles of conventional robotic systems[1-2]. To achieve photomechanical motility, we photopolymerized light active molecular machines along with reactive liquid crystalline monomers. For energy effective and rapid photomotility, rolling is employed as an in-plane locomotive mode to reduce friction with the substrates in comparison with crawling. In this presentation, we will also discuss design strategy to implement and program jumping motion of liquid crystalline polymers by controlling the molecular alignment for miniaturized yet high-performance untethered soft robots.

**Acknowledgements:** This work was funded by NRF-2016R1D1A1B03931678 and NRF-2019R1A2C1004559.

**References:**

- [1] J.J. Wie, M.R. Shankar, T.J. White, Nat .Commun., 7:13260 (2016)
- [2] J.G. Kim, J.E. Park et al., Materials, **12**, 19, 3065-3086, (2019)

1:09 PM F.EL05.04.08

**Programmable Photothermal Actuation Driven by Visible Light Using Negative Photochromic Donor-Acceptor Stenhouse Adduct (DASA) Polymers** Jaejun Lee, Miranda M. Sroda, Younghoon Kwon, Sara El-Arid, Serena Seshadri, Luke F. Gockowski, Elliot W. Hawkes, Megan T. Valentine and Javier Read de Alaniz; University of California, Santa Barbara, United States

The demonstration of tunable actuation performance at a single light intensity by the simple remodeling of material properties advances the field of light responsive materials one step closer to the development of "life-like" actuators. We introduce a novel approach for programmable actuation using negatively photochromic molecular photoswitches, termed donor-acceptor Stenhouse adducts (DASAs), capable of tuning the photothermal actuation amplitude under constant light intensity based on photochemically programmed logic. We present a synthetic pathway for chemically attaching DASA conjugates to polymers through Diels-Alder click chemistry. We report a visible light-responsive bilayer actuator that can lift weight against gravity, as well as a simple light-powered crawler, that exploit photothermal energy conversion. Programmable control of the magnitude of actuation is achieved by slowly converting a highly-absorbing DASA photochrome into a non-absorbing form upon irradiation. Our results highlight the promising benefits of high molar

absorptivity, negative photochromism, and broadband visible light absorption of DASAs for programmable actuation.

**1:15 PM F.EL05.02.06**

**From Appendage to Crosslinker—Self-Regulation of Spiropyran Isomerizations in Volume-Changing Hydrogels** Michael M. Lerch, Amos Meeks, Ankita Shastri, Shucong Li and Joanna Aizenberg; Harvard University, United States

Molecular photoswitches – molecules that can switch between multiple states of differing properties – are useful to impart actuation and changes in optical properties of soft materials. The chemistry of these photoswitches can be conveniently tuned to control the resulting material properties and have found application in soft actuators, non-linear optics, and optical memories. Yet, there is often a mutual interaction between photoswitch and embedding matrix, in which the photoswitch not only determines material functionality, but in turn the embedding matrix influences photoswitching behavior, enabling self-regulated behaviors through feedback loops. Here, we show how such self-regulated behavior arises in spiropyran-functionalized hydrogels and what effects govern this behavior. We are able to disentangle influences of hydrogel chemistry, type of photoswitch attachment, ionic strength, changes in hydrogel volume, and aggregation on the isomer-distribution of the photoswitch. In particular, we find that by changing the spiropyran from appendage to crosslinker, we can not only control feedback in hydrogel swelling behavior, but also control the non-linear optical properties of the hydrogel. These studies directly inform how such feedback loops can be leveraged for the fabrication of evermore sophisticated self-regulated optical materials.

**1:21 PM F.EL05.04.09**

**Molecular Engineering of Liquid Crystalline Elastomers to Enhance Phototropic Disruption of Order** Taylor Hebner and Timothy White; University of Colorado Boulder, United States

Liquid crystal elastomers (LCEs) can be functionalized with photochromic moieties to sensitize these materials to light exposure. Prior work has demonstrated that phototropic disruption of order via photochemical adjustment of the isomeric state of azobenzene (for example) disrupts the anisotropic chain configurations of the polymer network. The phototropic disruption of order in azobenzene-functionalized LCEs (azo-LCEs) with UV light via *trans-cis* isomerization generates comparatively large strain, exceeding 20%.

Fundamentally, the strength of intermolecular interactions between polymer chains defines the thermotropic response of both low molar mass and polymeric liquid crystal compositions. Here we show that by adjusting the intermolecular interaction by introducing a nontraditional liquid crystalline monomer, light irradiation can induce photomechanical responses in azo-LCE at lower energy inputs to achieve equivalent mechanical output.

**1:26 PM DISCUSSION, ADDITIONAL QUESTIONS AND WRAP-UP**

SESSION F.EL05.01: Hard Material Actuation

On Demand Abstracts Available for Viewing Starting Saturday Morning, November 21, 2020  
F-EL05

**5:00 AM \*F.EL05.01.01**

**Photoresponsive Diarylethene Molecular Crystals for Photoactuators** Seiya Kobatake; Osaka City University, Japan

Photochromic compounds undergo a photochemically reversible transformation reaction between two isomers. Such molecules in organic crystals, which are regularly oriented and fixed in the crystal lattice, may be potentially useful for optoelectronic devices. To apply photochromic diarylethene crystals to functional materials in photonics, electronics, mechanics, and medical fields, the materials are required to change large physical property by photoirradiation. We have reported photoinduced crystal shape change of diarylethene crystals.<sup>1</sup> In the photoinduced crystal shape changes, there are contraction/expansion, bending, twisting, and so on,<sup>2</sup> which depend on the crystal structure and the size of the crystal. In this work, we have focused on the photoinduced crystal shape changes of diarylethene crystals depending on the crystal size, irradiation power, irradiation wavelength, irradiation direction with polarized UV light, and the direction of the incident light.

The rod-like crystals composed of the diarylethene derivatives showed the crystal bending away from the incident UV light or toward the incident UV light, depending on the molecular structure or the crystal packing. The bending velocity depended on the crystal thickness, and the curvature change against the crystal thickness was well fitted to Timoshenko's bimetal model.<sup>3</sup> When the irradiation power was changed, the bending velocity was proportional to the power of the UV irradiation, indicating that local strain acts cumulatively due to the structural changes in the individual diarylethene molecule at the initial stage of the photochromic reaction.<sup>4</sup> Moreover, the bending behavior depended on the wavelength of the incident light.<sup>5</sup> When the crystal was irradiated under polarized UV light, the bending speed depended on the polarization angles.<sup>6</sup> A unique mechanical behavior of a molecular crystal was induced by a combination of a photochromic reaction and a reversible single-crystal-to-single-crystal phase transition.<sup>7</sup> The photoinduced reversible crystal twisting of a diarylethene crystal was observed upon alternating irradiation with UV and visible light. The crystal twisting takes place in both a left-handed helix and a right-handed helix. The direction of the twisting depends on the face irradiated with UV light. The control of the photomechanical twisting of a diarylethene crystal was studied from the viewpoint of illumination direction.<sup>8</sup> Changing the UV illumination direction for the crystal resulted in different twisting modes, ranging from helicoid to cylindrical. The control of photomechanical crystal deformation by illumination direction provides a convenient and useful way to generate a variety of photomechanical motions from a single crystal.

#### References

1. Kobatake, S.; Takami, S.; Muto, H.; Ishikawa, T.; Irie, M. *Nature* **2007**, *446*, 778–781.
2. Irie, M.; Fukaminato, T.; Matsuda, K.; Kobatake, S. *Chem. Rev.* **2014**, *114*, 12174–12277.
3. Kitagawa, D.; Kobatake, S. *J. Phys. Chem. C* **2013**, *117*, 20887–20892.
4. Hirano, A.; Hashimoto, T.; Kitagawa, D.; Kono, K.; Kobatake, S. *Cryst. Growth Des.* **2017**, *17*, 4819–4825.
5. Kitagawa, D.; Tanaka, R.; Kobatake, S. *Phys. Chem. Chem. Phys.* **2015**, *17*, 27300–27305.
6. Hirano, A.; Kitagawa, D.; Kobatake, S. *CrystEngComm* **2019**, *21*, 2495–2501.
7. Kitagawa, D.; Kawasaki, K.; Tanaka, R.; Kobatake, S. *Chem. Mater.* **2017**, *29*, 7524–7532.
8. Kitagawa, D.; Tsujioka, H.; Tong, F.; Dong, X.; Bardeen, C. J.; Kobatake, S. *J. Am. Chem. Soc.* **2018**, *140*, 4208–4212.

#### 5:15 AM \*F.EL05.01.02

##### Mechanically Flexible Crystals—Crystal Engineering Malla Reddy Chilla; IISER Kolkata, India

In recent times various intriguing dynamic single crystals that respond to external stimuli such as mechanical stress, heat, light, solvent, humidity, have been reported, but their systematic design remained a challenge. In my talk, I will demonstrate a variety of mechanically reconfigurable and certain other stimuli responsive organic single crystals, where a range of supramolecular weak interactions such as van der Waals (vdW) and  $\pi$ -stacking, play a crucial role in absorbing the internal and external stresses generated.<sup>1-3</sup> I shall present a detailed case study of photomechanical work (i.e. mechanical bending) done by a crystal using visible light mediated photopolymerization chemical reaction, and recovery of the original shape in a reversible manner by a thermal depolymerization reaction.<sup>4</sup> A few other examples covering waveguides and mechanochromic luminescence will be discussed. Our study demonstrated the potential of soft interactions for designing mechanical behaviour of ordered molecular materials, including those from  $\pi$ -conjugated semiconducting systems, which are of paramount importance for achieving flexible smart materials.

- (1) Reddy, C. M.; Krishna, G. R.; Ghosh, S. *CrystEngComm* **2010**, *12*, 2296.
- (2) Panda, M. K.; Ghosh, S.; Yasuda, N.; Moriwaki, T.; Mukherjee, G. D.; Reddy, C. M.; Naumov, P. *Nature Chem.* **2015**, *7*, 65-72.
- (3) Krishna, G. R.; Devarapalli, R.; Lal, G. Reddy, C. M.; *J. Am. Chem. Soc.* **2016**, *138*, 13561–13567.
- (4) R. Samanta, S. Ghosh, R. Devarapalli, C. M. Reddy, *Chem. Mater.* **2018**, *30*, 577–581.

*CMR thanks DST for Swarnajayanti Fellowship and CSIR for research funding. IISER Kolkata is thanked for central facilities.*

#### 5:30 AM \*F.EL05.01.03

##### Converting Light Into Displacement Through Multifunctional Materials Nelson Sepulveda; Michigan State University, United States

Phase-change materials have demonstrated to be capable of the largest energy densities in micrometer-sized actuators. Vanadium dioxide-based devices, for example, have shown energy densities near 1 MJ per cubic meter only within a temperature change of only 10 degrees. Comparable work/volume characteristics can only be obtained using difference thermal expansion mechanisms through temperature changes of hundreds of degrees, or by shape memory alloys. Another intrinsic advantages of using vanadium dioxide in micro-actuators include reversibility and ability to use the material's

hysteretic behavior to program mechanical states. However, even though vanadium dioxide is the solid-solid phase change material with the transition temperature closest to room temperature, micrometer-sized actuators based on this material still suffer from low efficiencies, especially when photothermal actuation is used. Designing vanadium dioxide-based photothermal actuators has typically involved unavoidable trade-offs that hinder the demonstration of ubiquitous devices with high energy density, speed, flexibility, efficiency, sensitivity, and multifunctionality. This talk will show techniques that use carbon nanotube thin films of different chiralities to overcome this low-efficiency issue; which also produced faster devices with increased sensitivity, and the demonstration of wavelength-selective photothermal actuators.

#### 5:45 AM F.EL05.01.04

**Hybrid Organic-Inorganic Photoactuators Based on Molecular Crystals** Chris Bardeen and Xinning Dong; University of California, Riverside, United States

Crystals organize photoreactive molecules and coordinate their motions, leading to photoinduced deformations like expansion, bending, twisting, peeling and coiling. This class of materials provides a path to photomechanical actuators that can be scaled down to micro- or nanoscale dimensions, but along the way several challenges must be addressed: 1) optimization of the molecular structure to control the rate and mechanism of reversibility (photon versus thermal activation); 2) control of crystal morphology to generate actuating structures with a variety of shapes and sizes; and 3) the hierarchical organization of nano-scale and micro-scale crystals into a macroscopic actuator structure, usually by templated growth and organization. Recent progress in all three areas have led to the development of composite organic-inorganic structures with unprecedented power-to-weight ratios: under light illumination, less than 1 mg of a diarylethene photochrome can move a load weighing more than 100 g. These materials consist of organic photochromic crystals aligned in the pores of various types of inorganic host materials, including  $\text{Al}_2\text{O}_3$  and  $\text{SiO}_2$ . The effects of the inorganic matrix material, organic photochromic molecule, and crystal alignment and orientation are all analyzed. The potential of these hybrid materials as practical photoactuators will be assessed.

#### 5:55 AM F.EL05.01.05

**Cooperative Reaction Dynamics in Molecular Crystals and Optical Control of the Photomechanical Response** Chris Bardeen<sup>1</sup>, Rabih Al-Kaysi<sup>2</sup> and Connor J. Easley<sup>1</sup>; <sup>1</sup>University of California, Riverside, United States; <sup>2</sup>King Saud bin Abdulaziz University, Saudi Arabia

In molecular crystals, reaction at one site can influence the reaction probability at other sites. This cooperative photochemistry can lead to interesting and possibly useful phenomena. The fluoro-9-anthracenecarboxylic acids comprise a family of thermally reversible (T-type) photomechanical molecular crystals. Their photomechanical response is driven by a [4+4] photodimerization reaction, while the dimer dissociation determines the reset time. A microscopic fluorescence-recovery-after-photobleaching experiment is used to monitor the kinetics of dimer dissociation and mechanical bending in single crystals. The recovery kinetics depend strongly on the initial concentration of photodimer, slowing down and becoming nonexponential at high dimer concentrations. A new feature in the photomechanical behavior is identified: the ability of a very weak control beam to suppress dimer dissociation after large initial dimer conversions. This phenomenon provides a way to optically control the mechanical response of this photomechanical crystal. To gain physical insight into the origin of the nonexponential recovery curves, the experimental results were analyzed in terms of a standard first-order kinetic model and a nonlinear Finke-Watzky (FW) model, but neither model can reproduce the suppression of the recovery in the presence of a weak holding beam. More sophisticated theoretical treatments that explicitly take spatial heterogeneity into account are probably required to analyze the role of cooperative molecular phenomena in solid-state crystalline reactions and their photomechanical response.

#### 6:05 AM F.EL05.01.06

**Photoinduced Picosecond Nonthermal Amorphization in  $\text{Sb}_2\text{Te}_3$**  Subodh C. Tiwari<sup>1</sup>, Rajiv Kalia<sup>1</sup>, Aiichiro Nakano<sup>1</sup>, Fuyuki Shimojo<sup>2</sup>, Priya Vashishta<sup>1</sup> and Paulo Branicio<sup>1</sup>; <sup>1</sup>University of Southern California, United States; <sup>2</sup>Kumamoto University, Japan

Phase change materials are of great interest for low-power high-throughput storage devices and next-generation neuromorphic computing technologies due to their contrasting properties between amorphous and crystalline phases and fast switching rate. Notably,  $\text{Sb}_2\text{Te}_3$ , an archetypical Ge-Sb-Te alloy, displays a fast and energy-efficient crystallization-amorphization cycle, due to its growth-dominated crystallization and low melting point. Here, we demonstrate a new

nonthermal amorphization pathway of  $\text{Sb}_2\text{Te}_3$  which can further reduce time required for amorphization from nanoseconds to picoseconds. We employ non-adiabatic quantum molecular dynamics simulations to investigate the time evolution of  $\text{Sb}_2\text{Te}_3$  at a constant temperature of 500 K with 2.6%, 5.2%, 7.5%, 10.3%, and 15% photoexcited valence electron-hole carriers. Results reveal picosecond nonthermal amorphization at and above a critical excitation of 7.5% valence electrons. The rapid amorphization originates from an instantaneous charge transfer from Te-*p* orbitals to Sb-*p* orbitals upon photoexcitation. Subsequent evolution of the excited state, within picosecond timescale, indicates a Sb-Te bonding to antibonding transition. Concurrently, Sb-Sb and Te-Te antibonding decreases, leading to the formation of wrong bonds. For 7.5% valence electron photoexcitation or larger, the electronic changes destabilize the crystal structure, leading to large atomic diffusion and loss of long-range order. These results highlight an ultrafast energy-efficient amorphization pathway that could be used to enhance the performance of phase change materials based opto-electronic devices.

This work was supported as part of the Computational Materials Sciences Program funded by the U.S. Department of Energy, Office of Science, Basic Energy Sciences, under Award Number DE-SC0014607. The simulations were performed at the Argonne Leadership Computing Facility under the DOE INCITE and Aurora Early Science programs and at the Center for High Performance Computing of the University of Southern California.

#### 6:15 AM F.EL05.01.07

**Understanding and Control of Giant Opto-Mechanics in Wide-Band Gap Compound Semiconductors** Yifei Li<sup>1</sup>, Yuying Zhou<sup>2,3</sup>, Haowei Xu<sup>1</sup>, Alan F. Schwartzman<sup>1</sup>, Ju Li<sup>1</sup> and Rafael Jaramillo<sup>1</sup>; <sup>1</sup>Massachusetts Institute of Technology, United States; <sup>2</sup>Shanghai Institute of Applied Physics, Chinese Academy of Science, China; <sup>3</sup>University of Chinese Academy of Sciences, China

The coupling between mechanical and optical properties can be surprisingly large, and has a long history of study. Optical absorption resonances are related to breaking, reforming, and rearranging bonds, on an energy scale of 1 eV/molecule, and it stands to reason that the effects of optical absorption on mechanical properties may be substantial; still these effects continue to surprise, and are often overlooked. Opto-mechanical effects may be especially strong when mediated by optically-active defects that store charge, induce local lattice distortions, and interact with modes of plastic deformation. The connection between defects and opto-mechanics provides a handle for controlling opto-mechanical effects through materials processing, and suggests new applications.

Here we show that the wide-band gap compound semiconductors ZnO, ZnS, and CdS all feature large opto-mechanical coupling that is mediated by point defects. We measure the mechanical properties of sintered and single crystal samples using a nanoindenter equipped with a purpose-built variable wavelength and intensity illumination system. We find that both elasticity and plasticity vary strongly with moderate illumination. For instance, the hardness and stiffness of ZnO can increase by up to 40-80% due to blue illumination of intensity 3 mW/cm<sup>2</sup>. The wavelength-dependence shows that band-edge absorption (*e.g.* UV light) has the strongest effect, and the relative size of the effect of sub-band gap illumination varies between samples – a clear sign of defect-mediated processes. We further show that these giant opto-elastic and opto-plastic effects can be tuned by materials processing, and that the processing-dependence can be understood within a framework of point defect equilibrium. We tune point defect concentrations by annealing treatments, and measure composition by direct (inductively-coupled plasma optical emission spectroscopy, ICP-OES) and indirect (X-ray diffraction, XRD) methods. Our composition measurements for ZnO, ZnS and CdS all show that the magnitude of the optomechanical response varies with anion vacancy concentration. This is consistent with the hypothesis that photoconductivity and photoplasticity are positively correlated, and provides a rational guideline for engineering optomechanical response. We use density functional theory (DFT) calculations to interpret our experimental results. DFT suggests that photo-induced charge carriers migrate along strain gradients, and gather around anion vacancies. The high local net charge concentrations ( $10^{21} \sim 10^{22} \text{ cm}^{-3}$ ) create pseudo-tensile-strain (~5%), which opposes the compressive strain from the indenter, thereby enhancing the elastic modulus. We will conclude with an outlook on opto-mechanical effects in wide-band gap semiconductors, and with several proposed, new applications for these still-surprising effects.

#### 6:25 AM F.EL05.01.08

**Casimir Heat Transfer and Strong Phonon Coupling** Haokun Li, King Yan Fong and Xiang Zhang; University of California, Berkeley, United States

In 1948, Casimir described a bizarre force that acts between neutral objects based on quantum fluctuations of electromagnetic fields. This effect is of both fundamental interest in quantum field theory and practical importance in nanotechnology. Recently, it has been predicted that Casimir force can induce phonon coupling between nearby objects and thus transfer heat across a vacuum gap. Revealing this unique quantum effect experimentally would bring fundamental insights to quantum

thermodynamics and practical implications to nanoscale thermal management. Here, we present the first experimental demonstration of the Casimir heat transfer. We use nanomechanical systems to realize strong Casimir phonon coupling and observe the exchange of thermal energy between individual phonon modes. The experimental observation agrees well with our theoretical calculations and is unambiguously distinguished from other effects such as near-field radiation and electrostatic interaction. This experiment opens up new opportunities for studying nanoscale energy transport and quantum thermodynamics.

#### 6:35 AM F.EL05.01.09

**Late News: Synthesis of Anthracene-Based Next-Generation Photomechanical Molecular Crystals.** [Rabih O. Al-Kaysi](#)<sup>1,2</sup>, Fei Tong<sup>3</sup> and Chris Bardeen<sup>3</sup>; <sup>1</sup>King Saud bin Abdulaziz University for Health Sciences, Saudi Arabia; <sup>2</sup>King Abdullah International Medical Research Center, Saudi Arabia; <sup>3</sup>University of California, Riverside, United States

Photomechanical organic crystals are fast becoming the next generation smart-materials that can convert light energy into mechanical work. While the majority of these photomechanical crystals are made from diarylethene or azobenzene derivatives our group has focused on the synthesis of anthracene-based compounds that can be grown into photomechanical crystals. These crystals can expand, bend, twist, curl, peel, or jump when exposed to UV or visible light. We will survey the synthetic routes used to make these anthracene derivatives. We will also describe how we made the corresponding photomechanical crystals using different techniques such as solvent annealing inside Anodic Aluminum Oxide (AAO) templates and aqueous surfactant-mediated precipitation technique.

Esterification of 9-Anthracenecarboxylic acid with aliphatic alcohols gives a family of photomechanically active anthracene derivatives. When these derivatives are grown into crystalline nanowires via solvent annealing inside AAO templates, the resulting nanowires expand anisotropically along their long axis when exposed to UV light. The intermolecular [4+4] photocycloaddition between parallel anthracene rings is the driving force behind the crystal expansion. A thoroughly studied molecule is the photomechanical expansion of tert-butyl anthracene-9-carboxylate (**9TBAE**) nanowires by 15% upon irradiation with 365 nm light. Crystalline microribbons grown from the commercially available 9-Anthracenecarboxylic acid (**9AC**) can twist reversibly (T-type) when exposed UV light. The microribbons require several minutes to reset by reversing the thermally unstable [4+4] photocycloaddition. The introduction of substituents on the **9AC** anthracene ring helps expand our toolbox of T-type photomechanical crystals. Multi-step synthesis was used to introduce substituents on different positions of the **9AC** anthracene ring. These substituents (F, Cl, or Br, NO<sub>2</sub>, CH<sub>3</sub>, etc.) either suppress or enhance the T-type character of the substituted 9-anthracene carboxylic acid crystals. While the 4-fluoro-9-anthracene carboxylic acid (**4F9AC**) shortened the reset time of the crystal by an order of magnitude, the 10-fluoro-9-anthracene carboxylic acid (**10F9AC**) derivative did the exact opposite. Extending the conjugation of the anthracene ring at the 9-position by attaching propenal using Mizoroki–Heck or Wittig reaction yields the very useful 3-(9-Anthryl)acrolein which was used as a building block for the synthesis of second-generation photomechanical anthracene derivatives. Adding different electron-withdrawing groups to the 3-(9-Anthryl)acrolein aldehyde via Knoevenagel condensation leads to a novel type of photomechanical crystals that are driven by trans/cis photochemistry. These crystals are dominantly P-type. For example, 2-(3-anthracene-9-yl-allylidene)-malononitrile (**9DVAM**) crystals and nanowires exhibit P-type photomechanical response under visible and UV light. When these crystals are grown into microwires from an aqueous surfactant they exhibit continuous photo-induced wiggling-like motion resembling flagella. Block-like microcrystals composed of *cis*-dimethyl-2(3-(anthracene-9-yl)allylidene)malonate (**DMAAM**) can peel off amorphous layers upon UV-light exposure while similar analog derivatives can super expand by transforming from crystalline-to-gel like material under intense green light exposure. The introduction of fluorine on the 9DVAM anthracene ring yields derivatives with P-type photosalient crystals and nanowires that may find future application in light-driven microactuators.

Synthesis of Anthracene-based photomechanical crystals coupled with non-classical crystal growth techniques has shown to be essential for both understanding the basic principles and advancing the field of photomechanical smart-crystals.

#### 6:45 AM \*F.EL05.01.10

**Photo-Induced Cooperative Supramolecular Nanosheets** [Shenqiang Ren](#); SUNY Buffalo, United States

Photostrictive compounds are promising device materials because of their fundamental photophysical properties and light-induced cooperative behaviors. Although molecular charge-transfer crystals exhibiting light–matter interactions have been successfully deployed in optoelectronics, an air-stable molecular material that couples photons and electrons, achieving photostriction through the coupling of light and mechanical degrees of freedom, has not yet been discovered. Herein, we report a substantial light-induced dilation in a molecular material at room temperature, which is accompanied by simultaneous photocurrent generation. This finding opens avenues for coupling optical, electronic, and mechanical functionalities for possible use in remote wireless photoswitchable devices.

**5:00 AM \*F.EL05.02.01**

**Hydrazone-Based Switches and Functional Materials** Ivan Aprahamian; Dartmouth College, United States

For the past few years we have been developing structurally simple, easy to make, modular, and tunable hydrazone-based functional materials (*e.g.*, switches, sensors and fluorophores).<sup>1</sup> This presentation will deal with our recent advances with these systems, with an emphasis on newly developed photochromic compounds<sup>2</sup> that exhibit many interesting properties, including emission ON/OFF toggling in solution (see below) and the solid-state.<sup>3</sup> The integration of these photochromic compounds into liquid crystals<sup>4</sup> and liquid crystalline elastomers<sup>5</sup> will also be discussed.

**Representative references:**

1. I. Aprahamian *ChemCommun* **2017**, *53*, 6674–6684
2. (a) H. Qian, S. Pramanik, I. Aprahamian *J. Am. Chem. Soc.* **2017**, *139*, 9140–9143  
(b) Q. Li, H. Qian, B. Shao, R. P. Hughes, I. Aprahamian *J. Am. Chem. Soc.* **2018**, *140*, 11829–11835
3. B. Shao, M. Baroncini, H. Qian, L. Bussotti, M. Di Donato, A. Credi, I. Aprahamian *J. Am. Chem. Soc.* **2018**, *140*, 12323–12327
4. M. J. Moran, M. Magrini, D. Walba, I. Aprahamian *J. Am. Chem. Soc.* **2018**, *140*, 13623–13627
5. A. Ryabchun, Q. Li, F. Lancia, I. Aprahamian, N. Katsonis *J. Am. Chem. Soc.* **2019**, *141*, 1196–1200

**5:15 AM \*F.EL05.02.02**

**New Photochromes for Efficient Transduction of Photonic Energy to Potential Energy for Bond-Breaking and Bond-Making Processes** Jeffrey Rack; University of New Mexico, United States

We will describe our latest efforts to create new photochromic compounds based on sulfoxides and sulfoxide mimics. We will also detail our advances in the creation of first row transition metals, where we propose that isomerization is capable of stabilizing of high spin states available for first row transition metal complexes. In addition, we will detail our spectroscopic studies of these new materials, both in solution and in solid state.

**5:30 AM \*F.EL05.02.03**

**Self-Regulating Photoactive Materials for Actuation** Megan T. Valentine; University of California-Santa Barbara, United States

Light is an attractive source of remote control and power: it is non-invasive, wavelength-selective, and provides high spatial and temporal resolution. However, the development of new materials is required to fully exploit these advantages by optimizing light energy transduction pathways and/or the light-mediated modulation of materials properties. In this talk, I will present my group's collaborative efforts to advance the incorporation of donor-acceptor Stenhouse adducts (DASAs) into materials designed for light-driven generation and control of material motion. DASAs present unique advantages for actuation. These highly-absorbing, negatively photochromic molecules have highly tunable reaction kinetics and respond to visible light. We have shown them to be effective photothermal and photochemical agents that can drive the motion of amorphous polymeric materials as well as liquid flows. In particular, through control of DASA reaction kinetics and the applied light field, it is possible create self-regulating flow fields that hold promise for valveless optofluidic devices and soft robotics.

**5:45 AM \*F.EL05.02.04**

**Light-Activated Molecular Machines That Work at All Scales** Nicolas Giuseppone; University of Strasbourg, France

Making molecular machines that can be useful in the macroscopic world is a challenging long-term goal of nanoscience. Inspired by the protein machinery found in biological systems, and based on the theoretical understanding of the physics of motion at the nanoscale, organic chemists have developed a number of molecules that can produce work when triggered by



various external chemical or physical stimuli. In particular, basic molecular switches that commute between at least two thermodynamic minima and more advanced molecular motors that behave as dissipative units working out-of-equilibrium when fueled with external energy have been reported. However, the ultimate challenge of coordinating individual molecular motors in a continuous mechanical process that can have a measurable effect at the macroscale has remained elusive until very recently. We will discuss advances developed by our group on light-activated molecular machines and involving their mechanical coupling within dynamic polymer systems. We will show that it is now possible to amplify their individual motions to achieve macroscopic functions in materials. In particular, we will present a dual-light controlled system operating fully out-of-equilibrium, and in which the integrated motions of two types of mechanically active units can be tuned by modulation of frequencies. Finally, we will discuss the possibility to use similar ideas to get control over mechanotransduction in living cells.

(1) E. Moulin, L. Faour, C. Carmona-Vargas, N. Giuseppone, *Adv. Mat.* **2020**, 32, 201906036.

(2) D. Dattler, G. Fuks, J. Heiser, E. Moulin, A. Perrot, Y. Xuyang, N. Giuseppone, *Chem. Rev.* **2020**, 120, 310.

#### 6:00 AM F.EL05.02.05

**Designable, Responsive Non-Linear Optics of Light-Responsive, Spiropyran-Functionalized Hydrogels** Amos Meeks<sup>1</sup>, Rebecca Mac<sup>2</sup>, Simran Chathanat<sup>2</sup> and Joanna Aizenberg<sup>1</sup>; <sup>1</sup>Harvard University, United States; <sup>2</sup>University of Waterloo, Canada

We demonstrate the potential of spiropyran-functionalized, light-responsive hydrogels to be a promising new platform for nonlinear optical materials. Nonlinear optical behavior in these materials arises from the swelling/deswelling and resulting refractive index changes that occur due to photoisomerization between the hydrophilic ring-open merocyanine isomer and the hydrophobic ring-closed spiropyran isomer. These materials show an unprecedented combination of reversibility, soft easily processed material, low laser powers, and long-range interactions. These long-range interactions are especially promising for potential applications in all-optical computing or sensing. We show that the long-range interactions can be explained by thermal swelling or deswelling of the gel. The presence of a secondary temperature gradient that influences beam behavior leads to novel repulsive long-range interactions, which are not possible in conventional nonlinear optical materials in the absence of external symmetry breaking. Furthermore, the direction and magnitude of a hydrogel's thermal response can be controlled by changing the gel composition, which allows the behavior of single and multiple beams in these gel materials to be rationally designed over a potentially vast design space. We demonstrate this potential by exploring two beam interactions in poly(N-isopropylacrylamide-co-acrylic acid) gels which contract rather than swelling as function of increasing temperature. We observe a lack of long-range interactions in these gels along with behaviors indicative of short-range attractive interactions, such as spiraling and beam fusion. This tunable diversity of behaviors suggests the enormous potential for photoresponsive hydrogels as extremely versatile, rationally designable, soft, nonlinear optical materials.

#### 6:10 AM F.EL05.02.06

**From Appendage to Crosslinker—Self-Regulation of Spiropyran Isomerizations in Volume-Changing Hydrogels** Michael M. Lerch, Amos Meeks, Ankita Shastri, Shucong Li and Joanna Aizenberg; Harvard University, United States

Molecular photoswitches – molecules that can switch between multiple states of differing properties – are useful to impart actuation and changes in optical properties of soft materials. The chemistry of these photoswitches can be conveniently tuned to control the resulting material properties and have found application in soft actuators, non-linear optics, and optical memories. Yet, there is often a mutual interaction between photoswitch and embedding matrix, in which the photoswitch not only determines material functionality, but in turn the embedding matrix influences photoswitching behavior, enabling self-regulated behaviors through feedback loops. Here, we show how such self-regulated behavior arises in spiropyran-functionalized hydrogels and what effects govern this behavior. We are able to disentangle influences of hydrogel chemistry, type of photoswitch attachment, ionic strength, changes in hydrogel volume, and aggregation on the isomer-distribution of the photoswitch. In particular, we find that by changing the spiropyran from appendage to crosslinker, we can not only control feedback in hydrogel swelling behavior, but also control the non-linear optical properties of the hydrogel. These studies directly inform how such feedback loops can be leveraged for the fabrication of evermore sophisticated self-regulated optical materials.

**5:00 AM \*F.EL05.03.01**

**Coupling Molecular and Material Photomechanical Response** Ruobing Bai, Kevin Korner and Kaushik Bhattacharya; California Institute of Technology, United States

Actuation by light is attractive for a number of reasons: Objects can be actuated from a distance, distinct frequencies can be used to actuate and control distinct modes with minimal interference, and significant power can be transmitted over long distances through corrosion-free, lightweight fiber optic cables. Azobenzene and other molecules that are known to change conformation when exposed to light are the building blocks of photomechanical actuation. An important challenge is how the change of conformation of individual molecules can be harnessed into a robust change of deformation of the material. Approaches range from mean-field entropic coupling as in photoactive nematic elastomers to direct chemical bond coupling as in molecular crystal to hybrid composite approaches where molecular crystals are embedded in an elastic matrix. The mean-field entropic coupling can lead to weak coupling while the stiffness of molecular crystal can inhibit actuation or cause them to shatter on actuation. This talk will present a series of theoretical models to understand various aspects of this molecular to material coupling, illustrate them with experimental observations and discuss how ideas from these studies can be harnessed in real materials and devices.

**5:15 AM \*F.EL05.03.02**

**Modeling Photo-Mechanical Actuation in Liquid Crystal Polymers** Robin L. Selinger<sup>1</sup>, Michael Varga<sup>1</sup>, Youssef M. Golestani<sup>1</sup> and Sajedah Afghah<sup>1,2</sup>; <sup>1</sup>Kent State University, United States; <sup>2</sup>Microsoft / OptoFidelity, United States

Liquid crystal polymer networks undergo reversible shape change in response to any stimulus that affects the strength of nematic order. These soft actuators can be fabricated as thin films, surface coatings, or 4D printed solids and have potential applications in soft robotics, biomedical devices, microfluidics, and sensors. Trajectories for shape change are “programmed” by patterning the nematic director when the polymer is cross-linked. Actuation is induced when the strength of nematic order is modulated by stimuli such as a change of temperature or chemical environment; for example, heating induces contraction along the nematic director and expansion in orthogonal directions. The addition of azobenzene derivatives that undergo photo-isomerization produces a soft actuator that flexes like an artificial muscle in response to illumination; if the cis-to-trans thermal relaxation is fast enough, the material can also flex rapidly back toward its original shape when illumination is removed. Such reversible photo-mechanical actuation is a highly attractive option to control a soft robot as it combines both control and power for induced motion without need for tethering or onboard batteries.

Modeling the dynamics of photo-mechanical actuation in these materials is important both to explain the mechanisms behind experimental observations and for device design. To model photo-mechanical actuation at the device scale, we use nonlinear finite element method (FEM) elastodynamics simulation based on a Hamiltonian approach. This method can simulate underdamped motion where momentum plays an important role. The code was developed in-house and implemented in CUDA for execution on a GPU-enabled computer.

We used this approach to model oscillatory mechanical wave motion in a soft robot whose motion was both controlled and powered by light [1]. We use a simplified ray tracing algorithm to determine which parts of the device were illuminated and which in shadow, and used a kinetic model of photo-isomerization/relaxation to describe the time evolution of nematic order. We found that the directionality of light-induced mechanical wave propagation is controlled by a self-shadowing mechanism and periodic pop-through transitions.

We also model a variety of other prototype devices including surface-adhered nematic polymer coatings that transform from flat to complex surface profiles with microchannels, spikes, or dimples recently observed in experiments by Babakhanova et al [2]. Next we model polymer coatings patterned with biomimetic “octopus-like” suckers, designed to grasp and release nonporous objects on command. Such a device would have the potential to achieve strong, reversible adhesion. Our results demonstrate that actuation geometry produced by a disclination in a nematic polymer is controlled not only by the defect’s topological charge and orientation but also by the details of its defect core structure. We compare our modeling results with relevant experiments by collaborators and discuss potential applications.

[1] Gelebart, A.H., Mulder, D.J., Varga, M., Konya, A., Vantomme, G., Meijer, E.W., Selinger, R.L.B., Broer, D.J., (2017)

Making waves in a photoactive polymer film, *Nature* 546, 632 (2017) <https://doi.org/10.1038/nature22987>  
[2] Babakhanova, G., Turiv, T., Guo, Y. *et al.* Liquid crystal elastomer coatings with programmed response of surface profile. *Nat Commun* 9, 456 (2018). <https://doi.org/10.1038/s41467-018-02895-9>

Work supported by NSF CMMI-1663041, NSF DMR-1409658, and NSF-CMMI 1436565; computer resources provided by the Ohio Supercomputer Center.

### 5:30 AM \*F.EL05.03.03

**Magnifying Photomechanical Actuation Using Mechanical Instabilities** Ravi Shankar; University of Pittsburgh, United States

The ability to harness light for photochromic switching that directs mechanical work generation within a macromolecular network is a platform for envisioning photomechanical machines, which are neither encumbered by onboard power sources, nor require microfabricated components and mechanisms. Light offers multiple control knobs for photomechanical regulation, including spatiotemporal modulation of intensity, direction, polarization and chirality. Unfortunately for actuators driven with light, the length over which the photons are attenuated (typically, few micrometers) limits the thickness of the photoactuators. The photomechanical strain generation is via bending, resulting from the gradation in the strains that are generated. Slender structures that respond by bending make for weak actuators. Work content that can be accessed is intrinsically bounded in the characteristically micrometer-scale thickness actuators.

Unusual opportunities emerge when we move beyond flat photoactive geometries, where the patterning of the molecular switches and the graded photomechanical strains conspire to result in non-linear mechanical responses. Snap-through in rod-like structures are one example. Creasing instabilities are another, where the bending of liquid crystalline polymers that are photoresponsive is used to drive non-linear transformations of curved shells, which are confined at their periphery. Torque densities  $>100$  Nm/kg and flexural actuation rates  $>100$  radians/s can be produced. Profiles of these photomechanical actuators places them in a property space that competes favorably with electromechanical systems. A third example is that of photoactuated tape-spring mimicking structures. Here, ms-scale actuation is triggered in shells that switch their principal curvatures, via a snap-through mechanism. Beyond these illustrations, opportunities also exist for utilizing a broader class of latch and torque-inversion mechanisms to magnify actuation by integrating active and passive (structural) materials.

Overall, accessing 3-dimensionally patterned freeform actuators is useful for magnifying photomechanical actuation. Realizing these geometries is simplified by the availability of an additive manufacturing platform, wherein the molecular order can be patterned voxel-by-voxel during the composition of multimaterial architectures. The interplay of magnetically assisted alignment and site-specific photopolymerization is a vehicle for achieving this in an inverted stereolithographic setup. In comparison to say, extrusion-based methods, decoupling the material accretion from the endowment of molecular order is key to expanding the design-space, which can be fabricated.

Magnifying photoactuation in monolithic polymeric structures, which can be scaled from the micrometer to mm-scale form factors holds implications for enabling photomechanical machines. It is possible to envision optically powered and reconfigurable devices in applications ranging from microrobotics, biomedicine and manipulation in environments hostile to electromechanical systems.

### 5:45 AM \*F.EL05.03.04

**Characterizing the Photomechanical Response of Materials** Peter Palffy-Muhoray, Anastasia Svanidze, Seung-Won Oh, Tianyi Guo and Xiaoyu Zheng; Kent State University, United States

When illuminated, photomechanical materials move and demonstrate forces which cause motion. This response indicates that they have acquired momentum as consequence of photoexcitation. We characterize their response by identifying and quantifying the effectiveness of the physical mechanisms connecting photoexcitation and the mechanical response. We are particularly interested in the details of how photostress results from the exciting flux of photons, whose momentum is negligible compared to what is observed in the response, and how photostresses produced in the bulk are transported to the sample surfaces and do mechanical work. We introduce a simple relation linking a stress in light to the photostress, and propose that elements of the tensor relating these serve as measures of the effectiveness of the different aspects of the photoresponse, both in transforming photon energy to stress and in storing photon energy and making it available for mechanical work. Using this metric, we compare the performance of different classes of photomechanical materials using data from the published literature.

**6:00 AM \*F.EL05.03.05**

**Light-Induced Curvature of a Landscape to Drive Mechanics Applications** Daniel Duffy, Fan Feng, John Biggins and Mark Warner; University of Cambridge, United Kingdom

Light-driven strains can be large, controlled by colour and polarisation of light, and quickly activated in liquid crystalline solids, both rubbery and glassy.

The challenge for applications is to make the response strong, typically involving stretch rather than bend energies if the distortions are loaded. To achieve stretch in both pull and in push without instabilities, the director needs to be programmed in the solid to change the Gaussian curvature of sheet and shell-like objects.

We make contact with current experiments and suggest new Gaussian-curved evolving landscapes, including those arising from curved fold non-isometric origami objects, for effective applications.

**6:15 AM \*F.EL05.03.06**

**Understanding the Photochemistry of Donor-Acceptor Stenhouse Adducts** David Sanchez, Umberto Raucci, Katherine Ferreras and Todd J. Martínez; Stanford University, United States

Donor-acceptor Stenhouse adducts (DASA) are a promising new chromophore for photomechanical applications. We detail studies of the photochemistry of this chromophore, including both the initial light-induced isomerization and the thermal ring-closing reaction. We further provide details on a framework for modeling excited state dynamics under force, combining the ab initio multiple spawning formalism for nonadiabatic dynamics with the force-modified potential energy surface framework developed for ground state mechanochemistry. We discuss the role of external force (either compressive or extensional) on the photodynamics of the DASA chromophore and its implications for the use of DASA chromophores in light-triggered mechanical actuators.

SESSION F.EL05.04: Soft Material Actuation

On Demand Abstracts Available for Viewing Starting Saturday Morning, November 21, 2020

F-EL05

**5:00 AM \*F.EL05.04.01**

**Light-Induced Actuation of Hybrid Crystalline/Polymeric Photomechanical Materials** Ryan C. Hayward; University of Colorado Boulder, United States

Materials capable of directly converting photon energy into mechanical deformation offer promise in a wide variety of contexts including adaptive optics, remotely operated swimmers, and actuators controlled via lightweight optical cables that resist corrosion and electromagnetic interference. Organic photoswitches offer significant potential in this regard, thanks to their ability to undergo large changes in molecular conformation upon excitation, and their highly tailorable absorption spectra. To date, efforts have focused largely on either crystalline lattices of small photomechanical molecules, which offer the possibility for greater work output due to their high density and well-organized nature, or on polymer matrices containing a modest concentration of photochromes, which generally have superior processability and mechanical properties. We have recently considered two classes of hybrid materials that combine many of the advantages of these disparate approaches. In one case, we have studied the growth of micrometer-scale photomechanical diarylethene crystals within the pores of polymer membranes. For appropriately controlled orientations of the crystals, such materials can exhibit photomechanical work outputs rivalling the best previously reported systems, while enabling facile processing into mechanically robust samples with cm-scale lateral dimensions. In a second case, we have developed a new class of structurally regular addition polymers bearing photoisomerizable azobenzene groups alternating with chain extenders. These materials form semicrystalline solids that exhibit fundamentally interesting temperature- and light-dependent melting and recrystallization behaviors, and that can be processed into aligned films and fibers exhibiting two-way optical shape memory properties.

**5:15 AM \*F.EL05.04.02**

**Twist Again—Dynamically and Reversibly Controllable Chirality in Liquid Crystalline Elastomer Microposts** Anna C. Balazs<sup>1</sup>, James T. Waters<sup>1</sup>, Shucong Li<sup>2</sup>, Yuxing Yao<sup>2</sup>, Michael M. Lerch<sup>2</sup>, Michael Aizenberg<sup>2</sup> and Joanna Aizenberg<sup>2</sup>; <sup>1</sup>University of Pittsburgh, United States; <sup>2</sup>Harvard University, United States

Photo-responsive liquid crystalline elastomers (LCEs) constitute ideal actuators for soft robots because their light-induced

macroscopic shape changes can be harnessed to perform mechanical work. Conventional LCEs, however, do not typically exhibit complex modes of bending and twisting necessary to perform sophisticated maneuvers. Here, we model LCE microposts encompassing side-chain mesogens oriented along a specific axis characterized by the nematic director, and azobenzene crosslinkers, which determine the deformations of illuminated posts. On altering the nematic director from 90° to 0° relative to the underlying substrate, the post's bending respectively changes from light-seeking to light-avoiding. Moreover, with the director tilted at 45°, the initially achiral post reversibly twists into a right- or left-handed chiral structure, controlled by the angle of incident light. We exploit this photo-induced chirality to design “chimera” posts (encompassing two regions with distinct director orientations) that exhibit simultaneous bending and twisting, mimicking motions exhibited by the human musculoskeletal system.

**5:30 AM \*F.EL05.04.03**

**Eliciting Diverse Deformation Modes from a Compositionally Uniform Liquid Crystalline Elastomer**

**Microstructure** Shucong Li, Michael M. Lerch and Joanna Aizenberg; Harvard University, United States

The type of deformations and range of motion, which microstructures can undergo, determines their function, be it for soft robotics, for sensing or for changing properties in optical or metamaterials. While composite, multimaterial architectures allow imprinting of pre-determined deformation behaviors, their fabrication at the microscale is difficult and the deformation modes are fixed once fabricated. Herein, we demonstrate the use of an alternative strategy – the generation of a transient bilayer architecture within microstructures by an external light stimulus, – and a variety of deformation behaviors that the same structure can display as a result. Changing the direction of UV-irradiation of high-aspect-ratio compositionally uniform microstructures fabricated from photoresponsive liquid crystalline elastomers gives access to a wide range of sophisticated deformations such as clockwise and counter-clockwise twisting, light seeking and avoiding, particularly if rotational symmetry is broken. Light intensity is demonstrated to be a further control parameter that allows one to tap into non-monotonic bending motions and combinations of twisting, bending and expansions/contractions. Finally, because the light-generated layered architectures are transient, they adapt and evolve as the deformation proceeds, leading to highly complex, yet controllable, self-regulated deformation behaviors. The described LCE microstructures are rapidly and easily fabricated and they offer exciting opportunities to further explore essential features of their finely controllable deformation abilities for applications in next generation smart materials.

**5:45 AM \*F.EL05.04.05**

**Photomechanical Effects in Liquid Crystalline Polymer Networks and Elastomers** Timothy White; University of Colorado Boulder, United States

Photons have been “put to work” in polymeric materials for more than 50 years. Photogeneration of work has been observed in a range of polymeric materials spanning the continuum from soft elastomers to rigid, high performance materials. Of particular importance is the organization of the polymer chains within the network which can affect magnitude, rate, and directionality of photoinduced deformation. Photomechanical effects in liquid crystalline polymer networks and elastomers are particularly appealing in enabling distinctive conversion of light into work. This presentation will summarize the salient benefits of using light as an actinic stimulus as well as highlight recent developments in this topical area of materials research from our laboratory.

**6:00 AM \*F.EL05.04.06**

**Photo-Steered Deformation and Locomotion of Nanocomposite Hydrogels** Qing Li Zhu, Zhi Jian Wang, Chen Fei Dai, Qiang Zheng and Zi Liang Wu; Zhejiang University, China

Inspired by the natural activated systems, realization of programmed deformations and locomotion in artificial materials has recently attracted great interest due to their promising applications in biomedical devices, soft robotics, and flexible electronics. Photo-responsive hydrogels are recognized as one ideal material to construct soft actuators and robots owing to their drastic volume change induced by contactless light irradiation with high spatial and temporal resolutions. The challenge is how to construct composite hydrogel with gradient structure and dynamically activate the specific regions of the gel toward programmed deformation and locomotion. We present here a photolithographic method to fabricate patterned composite hydrogel sheets with heterogeneous structures by embedding the photo-responsive hydrogel in a preformed nonresponsive hydrogel. Under photo irradiation, the swelling/contraction mismatch results in the built-up of internal stress and thus programmed deformations of the composite hydrogel. Furthermore, a moving light beam is imposed on the composite hydrogel to spatiotemporally actuate the gel that shows sophisticated motions, including crawling, walking, and turning. Experimental and simulation results reveal that multigait locomotion is realized by the mutual coordination of shape-morphing and dynamic friction of the gel against a substrate under the spatiotemporal light stimulation. The programmed

deformations of motions of photo-responsive hydrogels should be instructive for the development of soft robotics with advanced technologies and versatile applications.

**6:15 AM F.EL05.04.07**

**Light-Fueled Rolling and Jumping of Polymers** Jeong Jae Wie, Jisoo Jeon and Jae Gwang Kim; Inha University, Korea (the Republic of)

Light-fueled soft robots have recently demonstrated untethered manipulation of locomotion without the complex mechanical and electrical design principles of conventional robotic systems[1-2]. To achieve photomechanical motility, we photopolymerized light active molecular machines along with reactive liquid crystalline monomers. For energy effective and rapid photomotility, rolling is employed as an in-plane locomotive mode to reduce friction with the substrates in comparison with crawling. In this presentation, we will also discuss design strategy to implement and program jumping motion of liquid crystalline polymers by controlling the molecular alignment for miniaturized yet high-performance untethered soft robots.

**Acknowledgements:** This work was funded by NRF-2016R1D1A1B03931678 and NRF-2019R1A2C1004559.

**References:**

- [1] J.J. Wie, M.R. Shankar, T.J. White, Nat .Commun., 7:13260 (2016)
- [2] J.G. Kim, J.E. Park et al., Materials, **12**, 19, 3065-3086, (2019)

**6:25 AM F.EL05.04.08**

**Programmable Photothermal Actuation Driven by Visible Light Using Negative Photochromic Donor-Acceptor Stenhouse Adduct (DASA) Polymers** Jaejun Lee, Miranda M. Sroda, Younghoon Kwon, Sara El-Arid, Serena Seshadri, Luke F. Gockowski, Elliot W. Hawkes, Megan T. Valentine and Javier Read de Alaniz; University of California, Santa Barbara, United States

The demonstration of tunable actuation performance at a single light intensity by the simple remodeling of material properties advances the field of light responsive materials one step closer to the development of “life-like” actuators. We introduce a novel approach for programmable actuation using negatively photochromic molecular photoswitches, termed donor-acceptor Stenhouse adducts (DASAs), capable of tuning the photothermal actuation amplitude under constant light intensity based on photochemically programmed logic. We present a synthetic pathway for chemically attaching DASA conjugates to polymers through Diels-Alder click chemistry. We report a visible light-responsive bilayer actuator that can lift weight against gravity, as well as a simple light-powered crawler, that exploit photothermal energy conversion. Programmable control of the magnitude of actuation is achieved by slowly converting a highly-absorbing DASA photochrome into a non-absorbing form upon irradiation. Our results highlight the promising benefits of high molar absorptivity, negative photochromism, and broadband visible light absorption of DASAs for programmable actuation.

**6:35 AM F.EL05.04.09**

**Molecular Engineering of Liquid Crystalline Elastomers to Enhance Phototropic Disruption of Order** Taylor Hebner and Timothy White; University of Colorado Boulder, United States

Liquid crystal elastomers (LCEs) can be functionalized with photochromic moieties to sensitize these materials to light exposure. Prior work has demonstrated that phototropic disruption of order via photochemical adjustment of the isomeric state of azobenzene (for example) disrupts the anisotropic chain configurations of the polymer network. The phototropic disruption of order in azobenzene-functionalized LCEs (azo-LCEs) with UV light via *trans-cis* isomerization generates comparatively large strain, exceeding 20%.

Fundamentally, the strength of intermolecular interactions between polymer chains defines the thermotropic response of both low molar mass and polymeric liquid crystal compositions. Here we show that by adjusting the intermolecular interaction by introducing a nontraditional liquid crystalline monomer, light irradiation can induce photomechanical responses in azo-LCE at lower energy inputs to achieve equivalent mechanical output.

SESSION F.EL05.05: Poster Session: Putting Photons to Work—Progress in Photomechanical Materials and Applications  
On Demand Abstracts Available for Viewing Starting Saturday Morning, November 21, 2020

5:00 AM - 8:00 AM

F-EL05

#### F.EL05.05.01

**Photothermal Effect of Porphyrin Compounds for Optical Thermal Insulation** Jou Lin<sup>1</sup>, Yuan Zhao<sup>2</sup>, David Kundrat<sup>1</sup>, Mathias Bonmarin<sup>3</sup>, John Krupczak<sup>4</sup>, Som V. Thomas<sup>1</sup>, Mengyao Lyu<sup>1</sup> and Donglu Shi<sup>1</sup>; <sup>1</sup>University of Cincinnati, United States; <sup>2</sup>The Pennsylvania State University, United States; <sup>3</sup>Zurich University of Applied Sciences, Switzerland; <sup>4</sup>Hope College, United States

The photothermal effect has been found in some porphyrin compounds including chlorophyll, chlorophyllin, hemoglobin, and phthalocyanine, all of which share similar structural characteristics. The porphyrin compounds are typically composed of four modified subunits bounded with carbon atoms forming a “ring-like” structure, therefore also known as “porphyrin rings.” Upon white light irradiation, these compounds can selectively observe light in a wide range of frequency from UV to NIR, and convert it to thermal energy. One of the major applications of these porphyrin compounds is in the energy-efficient windows via a newly developed concept of optical thermal insulation (OTI). Most of the thermally insulated windows in cold climate regions are double-paned, sandwiching transparent insulating materials (such as gases), creating additional and unnecessary volume and weight. Thermal transmittance (U-factor) is proportional to the temperature difference,  $\Delta T$ , between the center of room and window interior surface. OTI does not rely on any conventional thermal insulating materials or gases, such as air or argon, as often used in conventional double-pane windows, but achieves its effectiveness via photothermally-heated building skins. If a spectral-selective thin film is applied on a window inner surface that exhibits strong UV/NIR absorptions and high visible transmittance, the pronounced photothermal (PT) effect will be photonically-activated to increase the surface temperature, resulting in much reduced heat transfer through the window. In this study, we report recent experimental results on deposition of transparent thin films of porphyrin compounds and show much lowered U-factors via OTI under simulated solar irradiation. Also identified is the operating mechanism of the photothermal effects for different porphyrin compounds.

#### F.EL05.05.02

**Effect of Incident Light Angle on the Photothermal Properties of Iron Oxide and Porphyrin-Based Thin Films for Energy-Efficient Single-Pane Window Applications** Mengyao Lyu<sup>1</sup>, Jou Lin<sup>1</sup>, John Krupczak<sup>2</sup> and Donglu Shi<sup>1</sup>; <sup>1</sup>University of Cincinnati, United States; <sup>2</sup>Hope College, United States

Photothermal experiments of incident light angle dependence were carried out by using solar-simulated light on iron oxides ( $\text{Fe}_3\text{O}_4$  and  $\text{Fe}_3\text{O}_4@\text{Cu}_{2-x}\text{S}$ ) and porphyrin compounds (chlorophyll and chlorophyllin) thin films. All thin films were deposited on glass substrates by spin-coating method with the photothermal materials evenly dispersed in polymethyl methacrylate (PMMA) solutions. The  $\text{Fe}_3\text{O}_4$  film was found to exhibit a strong absorption peak near the UV region but only with background absorptions in the visible and NIR regions. A broad NIR absorption was observed in the  $\text{Fe}_3\text{O}_4@\text{Cu}_{2-x}\text{S}$  thin film. Both chlorophyll and chlorophyllin showed pronounced peaks near UV and NIR characterized with the U-shaped spectra, ideal for energy-efficient single-pane window applications that require efficient solar harvest and high transparency. Thermal transmittance through the window can be significantly reduced by decreasing the temperature difference,  $\Delta T$ , between the window inner surface and the room interior based on a so-called “optical thermal insulation” (OTI) without any intervention medium, such as air/argon. Upon solar irradiation,  $\Delta T$  is reduced by increasing the inner surface temperature of the window through the photothermal heating of the iron oxide and porphyrin coatings. It is therefore possible to replace double- or triple- panes with single panes based on OTI. As the seasonal changes of sunlight inevitably affect OTI, an incident light angle dependence of the photothermal effect was carried on the oxide ( $\text{Fe}_3\text{O}_4$  and  $\text{Fe}_3\text{O}_4@\text{Cu}_{2-x}\text{S}$ ) and porphyrin (chlorophyll and chlorophyllin) thin films. It was found that their heating curves all reached maximum temperatures at small angles of incidence while that of which considerably reduced at large angles. The angle dependence data provides important references for OTI that the window exposure to the sun is higher at the winter solstice (small angle) and lower in summer (large angle). The enhanced solar harvesting at winter solstice can induce a stronger photothermal effect for effective optical thermal insulation of single-pane windows.

#### F.EL05.05.03

**Reconfigurable Azo-LCN/rGO Bilayers with Tailorable Mechanical and Electrical Properties** Woongbi Cho<sup>1</sup>, Jisoo Jeon<sup>1</sup>, Wonsik Eom<sup>2</sup>, Tae Hee Han<sup>2</sup>, Dong Gyun Kim<sup>3</sup>, Yong Seok Kim<sup>3</sup> and Jeong Jae Wie<sup>1</sup>; <sup>1</sup>Inha university, Korea (the Republic of); <sup>2</sup>Hanyang University, Korea (the Republic of); <sup>3</sup>Korea Research Institute of Chemical Technology, Korea (the Republic of)

Azo-benzene functionalized polymers have tremendously been studied owing to the advantages of battery-free light trigger shape reconfigurable properties. However, the trade-off relationship between mechanical strength and deformability and

insulating properties are great limitations of azo-functionalized polymer for shape reconfigurable devices. In this presentation, we introduce bilayered structure of azobenzene functionalized liquid crystalline polymer networks (Azo-LCN) with reduced graphene oxide (rGO) toward drastic enhancement in mechanical and electrical properties without sacrifice of strain responsivity. The Young's modulus of the Azo-LCN/rGO bilayer increases by 5 times (6.4 GPa) in comparison with the neat Azo-LCN, and the electrical conductivity is recorded to be 340 S/cm. Remarkably, the Azo-LCN/rGO bilayer overcomes the tradeoff relationship between mechanical stiffness and elongational responsivity by mismatch of structural character of each layers. Upon exposure to broadband UV, the bending angle of azo-LCN/rGO bilayer is enhanced in forward and backward bending, respectively 2.4 times (97.5 to 229.5 degree) and 12 times (5.4 to 65.2 degree) compared to the neat Azo-LCN. In addition to in-plane bending, twisting actuation mode is achieved by simply adjusting the cutting angle of the linearly patterned azo-LCN/rGO bilayers. The Azo-LCN/rGO bilayer can also be shape-reconfigurable by thermal stimuli including near infrared (NIR), sunlight and lighter. The photothermal effect is selectively induced on the rGO layer by irradiation of NIR stimuli which drive bending actuation of azo-LCN/rGO bilayer. Then, spatially localized actuation of azo-LCN/rGO bilayer is demonstrated by focused irradiation of solar ray. Finally, a rapid and large actuation is also demonstrated by direct heat energy transfer by operation of a lighter.

#### **F.EL05.05.04**

**Light-Driven Manipulation of Microdroplet on a GeSbTe Substrate** Yuka Takamatsu<sup>1</sup>, Eiji Yamamoto<sup>1</sup>, Keiko Esashika<sup>1</sup>, Masashi Kuwahara<sup>2</sup> and Toshiharu Saiki<sup>1</sup>; <sup>1</sup>Keio University, Japan; <sup>2</sup>Nanoelectronics Research Institute, National Institute of Advanced Industrial Science & Technology, Japan

The phenomena related to droplet migration at the micro-scale is expected to be applied to micro medical robots, new printing technologies, and basic research for the locomotion mechanisms of active matter such as cells or microbial populations. One of the main driving forces of droplet motion is Marangoni flow, which takes place from lower to higher surface tension regions. There are many studies on droplet manipulation based on Marangoni flow by generating surface tension difference under temperature gradient. Since, generally, surface tension decreases with temperature, a droplet moves from higher to lower temperature regions. In this study, we demonstrated light-driven microdroplet formation and transportation in a two-dimensional slit on a Ge<sub>2</sub>Sb<sub>2</sub>Te<sub>5</sub> (GST) substrate. GST as a substrate material is suitable for local laser heating due to its large light absorption and low thermal conductivity. We found an inverse Marangoni effect, which refers to the droplet motion from lower to higher temperature regions. The inverse Marangoni mechanism is more advantageous for droplet manipulation by laser beam positioning.

As a droplet material, polyethylene glycol (PEG) was mixed with toluene at a volume ratio of 7:1 to control the temperature dependence of surface tension of the droplet. The toluene/PEG solution was sandwiched with two coverslips, one of which was coated with GST. Droplet formation and transportation was observed under an inverse optical microscope. A local temperature gradient was induced by focusing subnanosecond pulsed laser ( $\lambda=532$  nm) onto the GST layer through the microscope objective.

When the interface area between bulk-like toluene/PEG and its vapor was irradiated with the laser spot, many small droplets of toluene/PEG were generated in the vapor side and they merged together at the center of the laser spot to form a single larger droplet. When slightly shifting the laser spot, we found that the droplet immediately moved to follow the spot. The result implies that the droplet moved towards higher temperature region, which direction is opposite to that expected from the conventional Marangoni effect. When the laser was turned off, the droplet spread to its equilibrium diameter. We can control the diameter of droplet simply by changing the laser intensity.

We show possible explanation for the mechanism of inverse Marangoni effect. In the toluene/PEG mixed droplet under laser irradiation, the volume ratio of PEG becomes larger in the higher temperature region because the vapor pressure of PEG is much lower than that of toluene and evaporates more slowly. Also importantly, the surface tension of PEG is larger than that of toluene. Considering these facts, we can expect that the surface tension of droplet in the higher temperature side is larger and thereby Marangoni flow is directed towards the center of laser spot. In order to support this explanation, the same experiment was conducted using pure toluene.

The droplet moved towards the opposite direction with respect to the case of mixed solution. The result can be explained by conventional Marangoni effect. The efficient inverse Marangoni effect we obtained may be also attributed to the significantly low surface energy and its temperature dependence of GST.

#### **F.EL05.05.05**

**Enhanced Magnetic Actuation of Micropillar Arrays via Anisotropic Stress Distribution** Jeong Eun Park<sup>1</sup>, Jisoo Jeon<sup>1</sup>, Sei Jin Park<sup>2</sup>, Sukyoung Won<sup>1</sup>, Zahyun Ku<sup>3</sup> and Jeong Jae Wie<sup>1</sup>; <sup>1</sup>Inha University, Korea (the Republic of); <sup>2</sup>Lawrence Livermore National Laboratory, United States; <sup>3</sup>Air Force Research Laboratory, United States



Recently, magnetically reconfigurable micropillar arrays have been documented by aligning magnetic particles within the microstructure. When the orientation axis of magnetic particles is deviated from the external magnetic field axis, micropillars undergo directional twisting and bending deformation according to the alignment of magnetic particles. Previous studies have mostly been focused on cylindrical micropillars, resulting in identical actuation regardless of magnetic field direction. In this presentation, we discuss a strategy of anisotropic stress distribution by employing anisotropic pillar geometry in order to introduce a preferential direction for strain responsivity. Under the linear external magnetic field, the effects of geometric anisotropy on magnetic actuation will be investigated by comparing experimental results with magneto-mechanical simulation for rectangular and triangular micropillars. Furthermore, we will discuss the anisotropic liquid spreading and wetting on magnetically actuated micropillar arrays where the pillars twist and bend.

#### **F.EL05.05.06**

**Multi-Functional and Transparent 3D Shape-Morphing by Patterned Adhesive Tapes via Photothermal Effects** Jae Gyeong Lee, Sukyoung Won, Jeong Eun Park and Jeong Jae Wie; Inha University, Korea (the Republic of)

Construction of 3-dimensional (3D) architectures from 2-dimensional (2D) sheets has recently been drawn a great attention. In particular, printing of black ink hinges on pre-strained polymers provides facile and contactless shape-morphing by selective light absorption via photothermal effects. However, remaining ink hinges obstruct transparency and can cause undesirable over-actuation by thermal conduction to unpatterned regions. In this study, we suggest a facile strategy for formation of transparent non-Euclidean structures from pre-strained polystyrene (PS) sheets by employing adhesive tape. Upon exposure to near infrared (NIR) light, pre-stretched PS below the adhesive tape pattern undergoes relaxation of polymer segment into a random conformation above the glass transition temperature on account of local light absorption. Contraction of patterned areas induces 3D shape morphing and remaining tape patterns can simply be removed on-demand after the construction of the targeted 3D structures. Herein, we employed radial and chiral patterns to generate complex 3D architectures and conjugated the multi-material to endow heterogeneous strain-responsivity for each material in a single curvilinear structure. We will also discuss sequential folding by control of light absorption time with sequential removal of adhesive tapes.

#### **F.EL05.05.07**

**Optical Properties of Si Doped ta-C Anti-Reflective Coatings for Photovoltaic Applications** SangYul Lee<sup>1</sup>, Jung-Wan Kim<sup>2</sup> and HoeKun Kim<sup>1</sup>; <sup>1</sup>Korea Aerospace University, Korea (the Republic of); <sup>2</sup>Incheon National University, Korea (the Republic of)

Metal containing carbon nanocomposite coatings (Me doped DLC coatings) which include metal or metal carbide phase embedded in amorphous carbon matrix have attracted a significant attention for the past few decades. The association between the carbon matrix and the encapsulated metallic or metal carbide phase not only improve the overall mechanical properties of the nanocomposite coatings, but also attribute the optical properties by accompanying phase and microstructure changes in the coatings. Recently, it has been shown that DLC based coatings are very promising anti-reflection (AR) and protective coatings for photovoltaic applications due to their high chemical stability, radiation stability and high hardness with the possibility of changing their optical properties. Among the various DLC coating classification, tetrahedral amorphous carbon (ta-C) coatings, which showed high sp<sup>3</sup>/sp<sup>2</sup> fraction over 60%, with extremely high hardness, excellent wear resistance, and better radiation stability have been paid much attention to an alternative anti-reflection protective coating materials. So in this study, various contents of Si metal were doped in the ta-C coating to improve optical properties of the ta-C coatings. Filtered cathodic vacuum arc (FCVA) and sputter hybrid PVD system was conducted to synthesize the metal doped ta-C coating. As increasing of Si content in ta-C coating, microstructure of the coatings changed from a dense featureless amorphous to a columnar “moth-eye” like structure by a formation of rhomb silicon carbide (SiC) phase, and that is especially useful for reducing reflections and increasing transmission between materials by the roll of light absorption. Raman spectroscopy analysis showed that all the coatings had high sp<sup>3</sup>/sp<sup>2</sup> fraction about 63%, and the hardness showed high values of 47.5 GPa. The ta-C coating with 4at.% Si showed improved transmittance (over 93.4%) in the field of ultraviolet, and this value was higher than that of other carbon based coatings. These results indicate that the Si doped ta-C coating could be applied for protective & AR coating for photovoltaic applications.

#### **F.EL05.05.08**

**Late News: Supramolecular Modulation of  $\pi$ -Stacking in Anthracene Crystals—Toward Photoactive Organic Semiconductors** Gonzalo Campillo-Alvarado and Ying Diao; University of Illinois at Urbana-Champaign, United States

Organic semiconductors (OSCs) are a rapidly emerging field in molecular electronics. Specifically, single crystals of OSCs

have received considerable attention due to unique properties associated with long-range order, absence of grain boundaries, and extremely low defect density [1] leading to a wide range of multi-functional materials (e.g., field-effect transistors, light-emitting diodes, photovoltaics). However, the lack of strategies to control and promote  $\pi$ -stacking in single crystals of OSCs has limited their tunability and application. While covalent modification of OSCs has arguably received the most attention [2], the noncovalent approach (e.g., supramolecular modulation) has been largely unexplored [3].

In this contribution, we introduce efforts in the use of small molecules (e.g., templates) to promote  $\pi$ -stacking of a pyridyl-containing anthracene through weak non-covalent interactions. Modulation of the geometry of  $\pi$ -stacking in the crystalline solid state is accompanied by changes in the photophysical properties. We envisage the supramolecular control of  $\pi$ -stacking in single crystals of OSCs could lead to rapid developments and diversification of multifunctional crystalline electronics.

References:

[1] Zhang, X., Dong, H., Hu, W., *Adv. Mater.* **2018**, *30*, 1801048.

[2] Anthony, J., *Angew. Chem. Int. Ed.*, **2008**, *47*, 452.

[3] Ray, K. K., Campillo-Alvarado, G., Morales-Rojas, H., Höpfl, H., MacGillivray, L. R., Tivanski, A. V., *Cryst. Growth Des.* **2020**, *20*, 3.

## SYMPOSIUM F.EL06

---

Contacting Materials and Interfaces for Optoelectronic Devices  
November 21 - December 3, 2020

Symposium Organizers

Stefaan De Wolf, King Abdullah University of Science and Technology  
Alex Martinson, Argonne National Laboratory  
Monica Morales-Masis, University of Twente  
Philip Schulz, CNRS IPVF

---

\* Invited Paper

SESSION Tutorial F.EL06: Research Methods and Best Practices to Study and Optimize Contacts and Interfaces  
Session Chairs: Robert Hoye, Thomas Kirchartz and Sebastian Siol  
Sunday Morning, November 29, 2020  
F.EL06

**8:00 AM \***

**Fabrication, Processing and Characterization of Interfacial Layers for Optoelectronic Devices** Robert Hoye; Imperial College London, United Kingdom

The instructor will cover growth of oxide charge transport layers by chemical- and physical-based methods for photovoltaics and light-emitting diodes; characterization and mitigation of loss processes at interfaces; and ex-situ and in-situ methods to determine the band alignment of the active material with the charge transport layers.

**9:30 AM BREAK**

**9:45 AM \***

**Interface Design and Characterization using Photoelectron Spectroscopy** Sebastian Siol; Swiss Federal Institute of Materials Science and Technology, Switzerland

The instructor will cover characterization of semiconductor interfaces using photoelectron spectroscopy; high-throughput experiments and band alignment engineering; and advanced chemical state analysis and characterization of buried interfaces using Hard X-ray Photoelectron Spectroscopy.

### 11:15 AM BREAK

### 11:30 AM \*

**Optoelectronic Device Physics—Quantifying Electrical and Optical Losses in Solar Cells and LEDs** Thomas Kirchartz; Forschungszentrum Jülich GmbH, IEK-5 Photovoltaics, Germany

The instructor will cover fundamental efficiency limits of photovoltaic devices (Shockley-Queisser model) and deviations from the Shockley-Queisser model that lead to efficiency losses; characterizing losses due to interfaces and contact layers and methods of characterizing these losses in different material systems; terminology used to quantify the ability of contacts and interfaces that lead to lossless photovoltaic or optoelectronic operation (selectivity, passivity and resistivity of contacts and how these parameters are eventually related to performance).

SESSION F.EL06.09/F.EN02: Live Keynote Joint Session I: Contacts and Interfaces in Silicon Solar Cells  
Session Chairs: Stefaan De Wolf and David Young  
Tuesday Morning, December 1, 2020  
F.EL06

### 11:30 AM \*F.EL06.06.01

**Improved Infrared Light Management with Amorphous Silicon in High Efficiency Silicon Heterojunction Solar Cells** Weiyuan Duan, Karsten Bittkau, Andreas Lambertz, Paul Steuter, zhirong yao, Kaifu Qiu and Kaining Ding; IEK5-Photovoltaik, Forschungszentrum Jülich GmbH, Germany

Silicon heterojunction (SHJ) solar cells coupled with hydrogenated intrinsic amorphous silicon (a-Si:H) layers enable high open-circuit voltages ( $V_{oc}$ ) of up to 750 mV, but suffer from short-circuit current density ( $J_{sc}$ ) losses due to parasitic absorption in a-Si:H, transparent conductive oxide (TCO) layers and shadowing of the metal fingers. Significant improvement in  $V_{oc}$  is expected only for thinner wafer. Increasing  $J_{sc}$  is a more promising route to further improve cell efficiency. Besides the use of high bandgap materials such as nanocrystalline silicon oxide or low carrier density TCO layers to reduce parasitic absorption, an improved light trapping that enables more light to be absorbed within the silicon wafer represents another important opportunity for  $J_{sc}$  improvement, which becomes even more significant when thinner wafers are used. In this work, a thin intrinsic a-Si:H layer was introduced after metallization of SHJ solar cell, formed a TCO/a-Si:H back reflector. Unlike sophisticated structures such as diffraction gratings, black silicon or other kind of nanophotonics, TCO/a-Si:H back reflector is much easier to be fabricated. Compared with the very often used silver back reflector, a-Si:H is less expensive and can still keep some of the bifaciality of the cells.

The intrinsic a-Si:H layer was deposited by plasma enhanced chemical vapor deposition (PECVD). It has a refractive index of around 4 at infrared (IR) wavelengths extracted from ellipsometry measurement. Sentaurus TCAD simulation was used for the rear optics in terms of optimizing the thickness of TCO/a-Si:H stack. We systematically investigated how the TCO/a-Si:H back reflector increases rear internal reflectance by measuring reflectance and external quantum efficiency before and after deposition of the a-Si:H layer. As predicted from simulation, due to increased IR reflection,  $J_{sc}$  was 0.4 mA/cm<sup>2</sup> higher with TCO/a-Si:H back reflector when applied on SHJ solar cells using 110 mm thickness wafer, while fill factor ( $FF$ ) and  $V_{oc}$  remained constant. Combined with an optimized front MgF<sub>2</sub> double antireflection coating, we could demonstrate a 0.9 mA/cm<sup>2</sup> improvement in  $J_{sc}$ , which boosts the cell efficiency by 0.5%. Ultimately, a M2 size total area cell efficiency of 23.7% has been achieved with  $V_{oc}$  of 745 mV,  $J_{sc}$  of 39.4 mA/cm<sup>2</sup> and  $FF$  of 80.8% on 110 um thin wafer. It's worth noting that the cell still kept a bifaciality of more than 50%. The reflector concept introduced here has a possibility to be used in advanced double-glass module encapsulation.

### 11:50 AM \*F.EN03.04.06

**Efficient Hole-Selective Passivating Contacts for Si Photovoltaics** Takuya Matsui and Hitoshi Sai; AIST, Japan

Hydrogenated amorphous silicon (a-Si:H) is a key material in realizing efficient passivating contacts for Si solar cells known

as the silicon heterojunction (SHJ) technology. However, one drawback of the SHJ solar cells is that the a-Si:H, particularly when doped with boron, gives rise to a parasitic optical absorption loss due to its high absorption coefficients in the visible wavelengths. This adverse effect is pronounced in bifacial solar cells, as this type of device allows illumination from both the front and the rear surfaces. Here we pursued alternative materials focusing on hole-selective passivating contacts: one is the hydrogenated nanocrystalline Si (nc-Si:H) and the other is the novel metal-oxide material. For the nc-Si:H material, it is demonstrated that the replacement of (p)a-Si:H by (p)nc-Si:H provides not only an increase of  $J_{sc}$ , but also improvements in  $V_{oc}$  and FF. This results in an efficiency increase by 0.6% absolute compared to our reference cell with (p)a-Si:H, and a best cell efficiency of 23.5%. The factors that alter the optimum hole contact layer thickness depending on the material and deposition condition will be discussed. For the metal-oxide material, we have developed an atomic-layer-deposited  $TiO_x$  nanolayer that functions as an efficient and transparent hole-selective passivating contact, leading to proof-of-concept solar cells with efficiencies above 20%. This new function of  $TiO_x$  is opposite from the previous understanding that it acts solely as electron contact.

#### 12:10 PM \*F.EL06.06.05

**Organic-Silicon Heterojunction for Solar Cell and Integrated Flexible Energy Devices** Baoquan Sun; Soochow University, China

Numerous alternative materials and solar cell device structures have been widely explored in order to reduce the cost of photovoltaic (PV) manufacture. Organic-inorganic component solar cells based on nanostructured semiconductor have built up in past two decades, which may promise the potentially low cost and high performance. However, the device performances are generally lower than its pristine all-inorganic PV devices, resulting from the numerous surface defect and improper organic-inorganic phase segregation. Here, we demonstrate that hybrid PVs based on organic conjugated molecular and nanostructured silicon can achieve a high power conversion efficiency by controlling the interface contact as well as surface passivation.

An advantage of this type heterojunction devices presents the excellent light harvest capability of nanostructured as well as benefiting likely simple fabrication process. Especially, the composite of conjugated organic materials and nanostructured inorganic materials are potential candidates for cost-effective and efficient solar-energy-harvesting devices<sup>1</sup>. This device can be operated by a light-modulated field effect solar cell, which can improve the device performance under accumulation of light illumination<sup>2</sup>. In addition, this type device can be easily integrated with other type energy device, for example, an energy harvesting structure that integrates an organic-silicon heterojunction solar cell and a triboelectric nanogenerator (TENG) device is built to realize power generation from both sunlight and raindrop<sup>3</sup>. In addition, a self-charging power unit based on an organic-Si heterojunction solar cell and an organic supercapacitor, which simultaneously achieved both photoelectric conversion and energy storage<sup>4</sup>. Finally, we will demonstrate that low temperature processed conductive silver-based ink has wide application usage for low temperature processed solar cell and related plastic electronics.

1. Sun, B.; Shao, M.; Lee, S.-T. *Advanced Materials* **2016**, 28, (47), 10539-10547.
2. Wang, Y.; Xia, Z.; Liu, L.; Xu, W.; Yuan, Z.; Zhang, Y.; Siringhaus, H.; Lifshitz, Y.; Lee, S. T.; Bao, Q.; Sun, B. *Advanced Materials* **2017**, 29, (18), 1606370.
3. Liu, Y.; Sun, N.; Liu, J.; Wen, Z.; Sun, X.; Lee, S.-T.; Sun, B. *ACS Nano* **2018**, *ACS Nano* **2018**, 12 (3), 2893-2899.
4. Liu, R.; Wang, J.; Sun, T.; Wang, M.; Wu, C.; Zou, H.; Song, T.; Zhang, X.; Lee, S.-T.; Wang, Z. L.; Sun, B. *Nano Letters* **2017**, 17, (7), 4240-4247.

#### 12:50 PM PLACEHOLDER FOR 2 EN02 SPEAKERS

SESSION F.EL06.10/F.EL08: Live Keynote Joint Session II: Contacts and Interfaces in Halide Perovskite Devices  
Session Chairs: Philip Schulz and Yuanyuan Zhou  
Wednesday Afternoon, December 2, 2020  
F.EL06

#### 5:15 PM \*F.EL06.04/F.EL08.11.03

**Vacuum Deposited Perovskite Solar Cells with Multilayer Charge Selective Contacts** Michele Sessolo, Sang-Hyun Chin, Chris Dreessen, Lidón Gil-Escrig, Ana M. Igual-Muñoz, Beom-Soo Kim, Daniel Perez-del-Rey, Isidora Susic, Kassio P. Zaroni and Henk Bolink; Universitat de València, Spain

In solar cells, perovskite films are typically sandwiched in between charge selective layers, either organic or inorganic semiconductors, as well as their combinations. Electron/hole selectivity results from appropriate alignment of the electronic transport levels of these layers with the electronic bands of the perovskite. While transport layers should efficiently extract the photogenerated charge carriers, they should also not quench the perovskite luminescence to avoid a reduction of the quasi-Fermi level splitting and hence the maximum attainable photovoltage. Finally, ohmic charge injection/extraction and a high built-in potential are desirable to maximize fill factor both in single junction and tandem perovskite solar cells. We will review these design rules using fully vacuum deposited solar cells as a platform, as every layer can be fine-tuned or exchanged without substantially alter the device fabrication. The focus will be on wide bandgap, mixed halide perovskite solar cells, which suffer from a higher voltage deficit as compared to narrow bandgap analogous. We will highlight the importance of using non-quenching, energetically-matched hole and electron transport layers in order to reduce non-radiative charge recombination losses. Novel strategies and multilayers structures (including inorganic, organic and ionic compounds) to improve the device functioning will be presented. The implication for the perovskite compositional stability as well as for the device lifetime will also be discussed.

**5:35 PM \*F.EL06.04/F.EL08.11.02**

**Implications of Defects in Defect Tolerant Materials—Understanding Surfaces in Metal Halide Perovskite Solar Materials, Device and Related Systems** Joseph J. Berry<sup>1,2</sup>; <sup>1</sup>National Renewable Energy Laboratory, United States; <sup>2</sup>University of Colorado Boulder, United States

Photovoltaic (PV) devices based on metal halide perovskite (MHP) absorbers have reached outstanding performance over the past few years, surpassing power conversion efficiency of over 25% for lab cells and with large area devices in excess of 16%. For the solar application stability, the most demanding requirement to assess for PV, remains the outstanding issue. The problem of stability motivates basic science driven work on MHP based PV at NREL. Material and device insight can enable MHP PV stability along with the associated opportunities to further improve efficiency, scalability and realize unique device architectures. This talk will highlight work at NREL to develop understanding of defects and interfaces in MHPs and what these experiments indicate regarding the requirements to enhance stability of HPSCs. Discussion will focus on efforts to more carefully understand the implications of processing on a range of defects and interfaces to provide a foundation for enabling the technological requirements for PV and other devices. Ongoing efforts make, measure and ultimately control defects via material formation and processing in the context of high-volume manufacturing will also be touched upon. Hypothesized links between device architecture choices, questions regarding materials integration and coupling of formation along with resulting defects to stability will be discussed. More importantly approaches to move from hypothesis to insight using different experimental approaches will be presented. Work at NREL along these lines to provide critical insight regarding interface formation and passivation that appears to have direct implications for performance and its evolution over time in the resulting devices will be presented. New approaches to understanding the critical physical, chemical and electronic properties to provide predictive insight will also be discussed.

**5:55 PM \*F.EL06.04/F.EL08.11.04**

**Approaches to Defect Mitigation in Halide Perovskites** Nakita K. Noel; Princeton University, United States

Within a decade, there has been a surge of interest into halide perovskite semiconductors. With tuneable bandgaps, versatile and facile deposition processes and excellent optoelectronic properties, these materials have found applications in photovoltaics (PV), broad-spectrum photodetectors, light-emitting diodes and lasers. While research into using these materials for emission and X-ray detection applications is now beginning to surge; currently, halide perovskites are most well known for their remarkable PV performance, with perovskite solar cells achieving certified power conversion efficiencies exceeding 25% in a remarkably short developmental timescale. Despite the truly impressive device performance, these materials have not yet reached their full potential. The major obstacle to this is an incomplete understanding of crystallisation processes, as well as defects which exist on the surfaces and interfaces of perovskite thin-films. Deficiencies at these interfaces, likely formed during the crystallisation process, are responsible for the major losses in perovskite-based optoelectronic devices; limiting charge extraction, increasing non-radiative recombination, contributing to hysteresis and increasing the voltage-loss of perovskite photovoltaics. Herein, I will present various effective strategies to reduce the defect densities of perovskite films and thus improve the performance of perovskite optoelectronic devices. First, I will discuss how manipulating precursor solutions can have significant impact on the quality of the perovskite films, through enabling reduced defect density. Consequently, this is one approach which can be used to boost device performance. Next, I will focus on a strategy in which we extrinsically modify the bottom interface of perovskite solar cells such that the crystallization of the perovskite yields films with fewer defects. Specifically, we show that ionic liquids can have a dramatic effect on the interfacial trap density in a perovskite solar cell. And finally, I will illustrate an approach in which we manipulate the charge-

carrier density in the perovskite thin-film after its fully crystallized. We utilise molecular dopants to significantly alter the interfacial energetics in order to suppress non-radiative recombination losses. As a result, we observe a boost in both performance and stability. Importantly, these interface modification strategies can be used in tandem, resulting in further improvements in device efficiency. The utility of these defect mitigation strategies can readily be applied beyond perovskite PV and is likely to also improve the performance of a range of other perovskite-based optoelectronic devices.

**6:15 PM \*F.EL06.04/F.EL08.11.01**

**Passivated Interfaces and Surface Recombination Velocities in Mixed Cation Mixed Halide Perovskites** David S. Ginger; University of Washington, United States

Surfaces and charge-extracting contacts remain major sources of non-radiative recombination loss; limiting the performance of perovskite PV compared to theoretical limits. We investigate mixed-cation mixed-halide perovskites and demonstrate that, with chemical surface passivation, they can achieve  $>4 \mu\text{s}$  minority carrier lifetimes, and  $>20\%$  external PL quantum yields (PLQY), and nearly single-exponential decay kinetics. This high PLQY observed corresponds to  $\sim 97\%$  of the Shockley-Queisser theoretical quasi-fermi level splitting, a first for MA-free mixed-cation mixed-halide compositions. The high PLQY and long PL lifetimes allow us to measure average surface recombination velocities (SRV)  $<10\text{cm/s}$ , with a champion low of  $\sim 1\text{cm/s}$  (a conservative estimate). We show how such improvements in SRV should lead to an absolute improvement in PCE of  $>4\%$  even with the best of contact alignments. We investigate different MA-free high bandgap compositions, including bandgaps relevant for tandem applications (1.7-1.8eV), and demonstrate performance improvements across all these compositions with our surface passivation strategy. Lastly, using a combination of surface characterization techniques, we show Lewis base interactions of the passivating agent with the perovskite surfaces.

**6:35 PM \*F.EL08.01.06**

**Processing Dependent Signature of Electronic States in the Gap of Metal Halide Perovskites** Antoine Kahn; Princeton University, United States

An important area of research on metal halide perovskites (MHP) concerns the presence and role of surface and interface electronic gap states introduced by defects inherent to film processing, degradation under stress (T, irradiation, environment) or chemical reaction with neighboring layers, and the restrictions that these states impose on device performance, i.e., limit in Fermi level split, or aid carrier recombination, leading to reduction of solar cell open circuit voltage. This talk reports results on the determination of the presence and density of electronic states tailing above the valence band maximum of several MHPs, e.g., MAPbI<sub>3</sub>, CsPbI<sub>3</sub>, and FA<sub>0.85</sub>MA<sub>0.15</sub>Pb(I<sub>0.85</sub>Br<sub>0.15</sub>)<sub>3</sub>. Detailed measurements of the top of the valence band of these materials are performed using high-sensitivity UPS achieved in logarithmic detection. We focus specifically on MAPbI<sub>3</sub> films processed with different additives mixed in the precursor-DMF solution: (i) no additives; (ii) DMSO; (iii) NH<sub>4</sub><sup>++</sup>DMA<sup>+</sup>; and (iv) N-methyl-2-pyrrolidone thione (NMPT). The latter, an S-donor solvent, was investigated for its stronger coordination to Pb<sup>2+</sup> as compared to the O-donor solvent DMSO, the additive widely used for improving film morphology. Significant differences are revealed between films processed with DMSO and NMPT. Once carefully treated via (experimental) background and parasitic satellite line contribution subtraction, the DMSO processed film exhibits a clear density of gap states extending from the valence band maximum to the Fermi level, whereas the NMPT processed film does not. The study was then complemented by Kelvin probe-based contact potential difference measurements to address the issue of surface photovoltage (SPV) during UPS. KP-based SPV measurements on these films show a significantly larger SPV (150 mV) and EF-VBM on the DMSO-treated films than on the NMPT-treated ones (SPV= 40 mV), confirming both the presence of the gap states and their impact on the electronic structure of the MHP films. The origin and nature of these gap states are still under investigation.

**6:55 PM PLACEHOLDER FOR 1 MORE PERSON FROM EL06?**

SESSION F.EL06.11: Live Keynote: Contacting Materials and Interfaces for Optoelectronic Devices  
Session Chairs: Alex Martinson and Monica Morales-Masis  
Thursday Afternoon, December 3, 2020  
F.EL06

**3:00 PM \*F.EL06.01.01**

**Multifunctionality of Interfacial Agents in Organic and Inorganic Electronics** Norbert Koch<sup>1,2</sup>; <sup>1</sup>Humboldt-Universität

zu Berlin, Germany; <sup>2</sup>Helmholtz-Zentrum Berlin für Materialien und Energie, Germany

The electronic properties of interfaces in (opto-) electronic devices play a key role to reach the desired functionality and high efficiency. A wide range of organic and inorganic materials to tune interfacial properties is available today, and a comprehensive understanding of how they interact at interfaces is a prerequisite for realizing their full potential, particularly motivating their use in novel settings. This is exemplified here for the widely used interface modification agent polyethylenimine (PEI), which helps reducing electron injection barriers between electrodes and organic semiconductors. It is shown that PEI mixed with a polymer semiconductor in solution in fact serves two beneficial purposes simultaneously. PEI phase-separates from the semiconductor upon spin-coating and forms low work function bottom and top layers, which enhance electron injection. At the same time, minute amounts of PEI slightly n-dope poly{[N,N'-bis(2-octyldodecyl)naphthalene-1,4,5,8-bis(dicarboximide)-2,6-diyl]-alt-5,5'-(2,2'-bithiophene)} [P(NDI2OD-T2)] in the bulk film, thereby also increasing the electron mobility and boosting the conductivity overall by four orders of magnitude. The full capability of PEI interlayers for optimized electron injection at contacts, however, can only be reached by carefully excluding water during processing and applying mild annealing for improved surface coverage. With this, PEI interlayers reduce the work function of ZnO and graphite electrodes to a record low value of 2.3 eV.

Also the combination of organic conductive polymers and inorganic semiconductors provides a rich playground for interface manipulation. It has been demonstrated before that n-type Si coated with a layer of poly(3,4-ethylenedioxythiophene):poly(styrenesulfonate) (PEDOT:PSS) actually returns fully functional solar cells, despite the absence of a pn-junction in Si. We could now provide direct evidence that PEDOT:PSS induces indeed a large upward band bending in n-Si, even reaching inversion conditions. From a variation of processing conditions, suggestions on further improvements for this attractive approach to surface-dope inorganic semiconductors to the extreme can be derived.

It will further be noted how molecular photochromic switches, in the form of a monolayer at the interface between electrodes and an organic semiconductor, can be employed to facilitate multifunctionality of a device. As an example, an organic light emitting diode (OLED) will be discussed, whose brightness can be controlled reversibly during operation by both applied bias and external short-time light irradiation.

**3:20 PM \*F.EL06.05.07**

**Schottky Barriers and Selective Contacts Using Atomic Layer Deposited Interface Layers** [Nick C. Strandwitz](#); Lehigh University, United States

Electrical contacts are critical to nearly all semiconductor devices, and the behavior of these contacts can have massive implications to overall device performance. Decades of research into metal-semiconductor contacts continues today because of their complexity and our modern ability to control and probe these interfaces.

Our work, primarily in the context of photovoltaics, examines two classifications of modified metal-semiconductor contacts: Metal-insulator-semiconductor (MIS) Schottky barriers, and selective contacts based on metal oxides. MIS contacts were indeed the foundation of some of the first PV devices, but quickly gave way to p-n junction architectures because of greater stability and power conversion efficiency in the latter architecture. Using device physics simulations, we show that if proper junction properties can be created (Schottky barrier height, interface passivation), MIS-type PV devices can approach efficiencies of p-n homo- and hetero-junction cells. Our work exploring the interface properties of MIS structures for PV makes use of purposeful chemical surface preparation and the deposition of well-controlled oxide insulators using atomic layer deposition (ALD). I will discuss several observations including the role of fixed interface charge and interface layer thickness on Schottky barrier height.

Secondly, so-called "selective contacts" have been examined to boost efficiency of p-n and heterojunction silicon PV, and also to provide PV junctions without the need for traditional p-n junctions, similar to the MIS Schottky barrier case. In both cases, it can be argued that such contacts may reduce processing costs due to the low temperatures for the deposition of these materials. Notable developments include electron and hole-selective thin films that provide selective transport for one carrier while often reducing interfacial recombination rates. Our studies explore the introduction of aluminum oxide tunnel layers sandwiched between crystalline silicon and selective contact materials such as MoO<sub>x</sub>. The potential impact of this configuration is to 1) increase in stability of the junction and 2) and increase in performance through minimization of carrier recombination at the contact. We have examined the role of the alumina layer thickness on interface quality and specific contact resistance. We also examined the role of several deposition techniques and explore the different processing conditions that modify the interfacial electronic properties of these passivated contacts.

**3:40 PM \*F.EL06.03.12**

**Machine Learning and Design of Impurity Levels and Band Alignments in Optoelectronic Materials** Arun Kumar Mannodi Kanakkithodi and [Maria Chan](#); Argonne National Laboratory, United States

The prediction of electronic levels introduced by impurities and electronic level alignment at interfaces is critical to the design of optoelectronic materials, particularly for photovoltaic applications, for optimal function. Such prediction is possible using first principles density functional theory (DFT) calculations. Due to both a need to reduce computational cost and a desire to extract design principles, machine learning has increasingly been used to extract relationships between these computed quantities and physical or chemical descriptors of the semiconductor system. In this talk, we will discuss our work on machine learning (ML) of impurity levels in optoelectronic materials including classical II-VI [1], III-V, and group IV semiconductors, as well as hybrid perovskite halides. We will discuss the accuracy and uncertainty quantifications of different approaches for ML. We will also discuss the extension of this approach to prediction of electronic band alignments at interfaces.

[1] Arun Mannodi-Kanakkithodi, Michael Y Toriyama, Fatih G Sen, Michael J Davis, Robert F Klie, Maria KY Chan, "Machine-learned impurity level prediction for semiconductors: the example of Cd-based chalcogenides," *npj Comput Mater* 6, 39 (2020). <https://doi.org/10.1038/s41524-020-0296-7>

**4:00 PM \*F.EL06.03.07**

**Optoelectronic Properties of Halide Perovskites from First Principles—Challenges, Results and Surprises** Linn Leppert; University of Twente, Netherlands

Halide perovskites are a chemically and electronically diverse class of compounds. They encompass 3D materials like the hybrid organic-inorganic  $\text{CH}_3\text{NH}_3\text{PbI}_3$  and the all-inorganic double perovskite  $\text{Cs}_2\text{BiAgBr}_6$ , solar absorbers with excellent features for photovoltaic applications and beyond. This diversity of structures and optoelectronic properties is further expanded when reducing the dimensionality of these systems, as exemplified by the Ruddlesden-Popper perovskite  $(\text{BA})_4\text{AgBiBr}_8$  (BA=butylammonium), which can be thought of as a double perovskite monolayer with alternating  $\text{AgBr}_6$  and  $\text{BiBr}_6$  octahedra, separated by an organic spacer layer [1,2].

Accurately predicting the fundamental band gaps and excited state properties of this zoo of materials from *first principles* is challenging because of the intricate coupling of structural and electronic degrees of freedom [3], complex structural dynamics and strong spin-orbit interactions. In this contribution, I will discuss our recent progress in describing the optoelectronic properties of halide perovskites using density functional theory (DFT) and Green's function-based many-body perturbation theory [4]. DFT-based molecular dynamics simulations allow us to consider temperature dynamics of halide perovskites and design structural models for our electronic structure calculations. A particular focus of this talk will be our calculations of the electronic structure and optical excitations of the double perovskite series  $\text{Cs}_2\text{AgBX}_6$  (B=Bi, Sb; X=Br, Cl) and their 2D derivatives – a set of materials with unusual and highly tunable optoelectronic properties.

[1] B. A. Connor, L. Leppert, M. D. Smith, J. B. Neaton, H. I. Karunadasa, *J. Am. Chem. Soc.* **140**, 5235 (2018).

[2] B. A. Connor, R. I. Biega, L. Leppert, H. I. Karunadasa, *Chem. Science*, Accepted Manuscript (2020).

[3] L. Leppert, S. E. Reyes-Lillo, J. B. Neaton, *J. Phys. Chem. Lett.* **7**, 3683 (2016).

[4] L. Leppert, T. Rangel, J. B. Neaton, *Phys. Rev. Materials* **3**, 103803 (2019).

**4:20 PM \*F.EL06.03.01**

**Searching for Materials with Exceptional Opto-Electronic Properties Using *Ab Initio* High-Throughput Computing** Geoffroy Hautier; Université Catholique de Louvain, Belgium

New opto-electronic devices from solar cells to transparent transistors require high performance materials. *Ab initio* high-throughput computations offer an accelerated path towards the discovery of these exceptional materials. We can now screen thousands of materials by their computed properties even before the experiments. This computational paradigm allows experimentalists to focus on the most promising candidates, and enable researchers to efficiently and rapidly explore new chemical spaces.

In this talk, I will present the challenges and opportunities in materials discovery offered by high-throughput *ab initio* computing in searching for materials with exceptional opto-electronic properties. Recent examples from our work in the fields of transparent conducting materials and solar absorbers will be used to illustrate the approach. I will discuss the materials highlighted by these computational searches but also show how trends and design rules can be extracted from high-throughput data sets. Finally, I will report on our efforts in scaling up to high-throughput new properties from point defects to carrier mobilities.

**4:40 PM \*F.EL06.02.01**

**Interfacing Scandium Nitride with GaN and AlN for Enhanced Performance** Chris G. Van de Walle; University of California, Santa Barbara, United States



Scandium nitride (ScN) is a semiconducting nitride that has the rocksalt crystal structure, but with a lattice parameter that provides a close match to GaN; the lattice mismatch is less than 1%. One reason ScN has attracted recent interest is because adding ScN to AlN enhances the piezoelectric properties, and may even lead to ferroelectricity. Here I will focus on interfaces between ScN and GaN. ScN can be highly *n*-type doped and can thus serve as an almost metallic contact or current spreading layer to GaN. If rocksalt ScN is grown along the [111] direction on top of *c*-axis-oriented wurtzite GaN, interesting phenomena related to spontaneous polarization occur. GaN is polar with a large spontaneous polarization, while ScN is centrosymmetric. This suggests the possibility of a very large spontaneous polarization difference at the interface. We have examined the properties of such interfaces using first-principles calculations based on density functional theory [1]. We first apply the modern theory of polarization to obtain the bulk properties of the individual materials. The resulting difference in polarization constants yields a polarization discontinuity at the ScN/GaN interface of  $-1.358 \text{ C/m}^2$ . As a result, we expect a high-density electron gas on the N-polar GaN/ScN interface, and a high-density hole gas on the Ga-polar GaN/ScN interface, with carrier concentrations up to  $8.5 \times 10^{14} \text{ /cm}^2$ . This value is over an order of magnitude larger than what can be achieved at GaN/AlGaN interfaces. We have confirmed the presence of strong electric fields and bound interface charges in explicit interface calculations. The large polarization difference and small strain makes ScN a promising material for applications in polarization-enhanced *p*-GaN/ScN/*n*-GaN tunnel junctions. Current tunnel junctions make use of InGaN interlayers to reduce the effective barrier and increase the polarization field across the *p-n* junction to reduce the junction width. ScN is a promising alternative, with a higher polarization field, smaller bandgap, and much smaller strain.

Work performed in collaboration with N. L. Adamski and C. E. Dreyer, and supported by AFOSR.

[1] N. L. Adamski, C. E. Dreyer, C. G. Van de Walle, *Appl. Phys. Lett.* 115, 232103 (2019).

SESSION F.EL06.01: Interface Characterization of Optoelectronic Devices  
On Demand Abstracts Available for Viewing Starting Saturday Morning, November 21, 2020  
F-EL06

#### 5:00 AM \*F.EL06.01.01

**Multifunctionality of Interfacial Agents in Organic and Inorganic Electronics** Norbert Koch<sup>1,2</sup>; <sup>1</sup>Humboldt-Universität zu Berlin, Germany; <sup>2</sup>Helmholtz-Zentrum Berlin für Materialien und Energie, Germany

The electronic properties of interfaces in (opto-) electronic devices play a key role to reach the desired functionality and high efficiency. A wide range of organic and inorganic materials to tune interfacial properties is available today, and a comprehensive understanding of how they interact at interfaces is a prerequisite for realizing their full potential, particularly motivating their use in novel settings. This is exemplified here for the widely used interface modification agent polyethylenimine (PEI), which helps reducing electron injection barriers between electrodes and organic semiconductors. It is shown that PEI mixed with a polymer semiconductor in solution in fact serves two beneficial purposes simultaneously. PEI phase-separates from the semiconductor upon spin-coating and forms low work function bottom and top layers, which enhance electron injection. At the same time, minute amounts of PEI slightly *n*-dope poly{[N,N'-bis(2-octyldodecyl)naphthalene-1,4,5,8-bis(dicarboximide)-2,6-diyl]-alt-5,5'-(2,2'-bithiophene)} [P(NDI2OD-T2)] in the bulk film, thereby also increasing the electron mobility and boosting the conductivity overall by four orders of magnitude. The full capability of PEI interlayers for optimized electron injection at contacts, however, can only be reached by carefully excluding water during processing and applying mild annealing for improved surface coverage. With this, PEI interlayers reduce the work function of ZnO and graphite electrodes to a record low value of 2.3 eV.

Also the combination of organic conductive polymers and inorganic semiconductors provides a rich playground for interface manipulation. It has been demonstrated before that *n*-type Si coated with a layer of poly(3,4-ethylenedioxythiophene):poly(styrenesulfonate) (PEDOT:PSS) actually returns fully functional solar cells, despite the absence of a *pn*-junction in Si. We could now provide direct evidence that PEDOT:PSS induces indeed a large upward band bending in *n*-Si, even reaching inversion conditions. From a variation of processing conditions, suggestions on further improvements for this attractive approach to surface-dope inorganic semiconductors to the extreme can be derived.

It will further be noted how molecular photochromic switches, in the form of a monolayer at the interface between electrodes and an organic semiconductor, can be employed to facilitate multifunctionality of a device. As an example, an organic light emitting diode (OLED) will be discussed, whose brightness can be controlled reversibly during operation by both applied bias and external short-time light irradiation.

### 5:15 AM F.EL06.01.02

**Interfacial Doping in Organic Semiconductors with Self Assembled Monolayers at Electrodes** [Kalyani Patrikar](#)<sup>1</sup>, Valipe Ramgopal Rao<sup>1,2</sup> and Dinesh Kabra<sup>1</sup>; <sup>1</sup>IIT Bombay, India; <sup>2</sup>IIT Delhi, India

Organic semiconductors (OSC) have a low intrinsic carrier density. Devices based on OSC thinfilms require carriers to be doped by chemical, optical, or electrical means. Many types of devices such as light emitting diodes or transistors consist of metal electrodes which inject the carriers that are conducted across the thinfilm. For hole transporting OSC devices, electrodes of metals with high work function are needed for efficient injection. However, at any metal-OSC interface, mismatch in energy levels creates an energy barrier to hole injection. Energy barrier at interface introduces an additional resistance at interface, hampering device performance. Self Assembled Monolayers (SAM) of polar molecules are used as interlayers at metal-OSC interface to reduce the energy barrier.<sup>[1]</sup> We show that SAM can act as an agent for interfacial doping along with for work function tuning, thus having dual mechanism for reducing device resistance.

We show this with the case of bottom contact field effect transistor (FET) of the OSC pentacene. Copper electrodes are used for source-drain, and are coated with SAM of different fluorine containing molecules perfluorobenzenethiol (PFBT) or perfluorodecanethiol (PFDT). We find that work function of copper increases from ~4.82 eV to ~5.2 eV for PFBT/Cu and ~5.4 eV for PFDT/Cu. Drain current was found to be higher with SAM/Cu electrodes as compared with unmodified Cu electrodes, however the trends were in contradictory to those of work function. We show that the drain current increase can be explained on the basis of interfacial carrier doping of pentacene by SAM/Cu. During interface formation, holes are transported from high work function electrode to OSC, accompanied by bending of energy levels, which increases its the equilibrium hole density. We obtain doping profiles by applying a solution to Poisson's equation, and find that the excess hole concentration decreases exponentially away from interface. PFBT/Cu leads to larger average hole concentration ( $10^{16} \text{ cm}^{-3}$ ) as compared to PFDT/Cu ( $10^{14} \text{ cm}^{-3}$ ) which is in accordance with trends of drain current.

We thus show, by experimental device characteristics and applying analytical models, that interfacial SAM at electrodes can influence characteristics of OSC based devices by a two-fold mechanism of doping along with electrode work function tuning. Depending on the molecules SAM comprise of, doping amount and profile can be controlled. SAM thus has the twin advantage of enabling us to enhance device characteristics due to doping, as well as control device behaviour by doping amount.

### References

[1] Dario Natali, Mario Caironi, *Adv. Mater.* 2012, 24, 1357–1387

### 5:25 AM \*F.EL06.01.03

**Interface Engineering Materials and Methods for Efficient and Stable Perovskite Solar Cells** [Nam-Gyu Park](#); Sungkyunkwan University, Korea (the Republic of)

Since the seminal report on the 9.7% efficient and 500 h-stable solid-state perovskite solar cell (PSC) in 2012, following two seed reports on perovskite-sensitized liquid junction solar cells in 2009 and 2011, perovskite photovoltaics has been surged swiftly due to high power conversion efficiency (PCE) obtainable via facile fabrication procedure. As a result, a PCE of 25.2% was recorded in 2019. According to Web of Science, number of publications on PSCs increases exponentially since 2012, leading to the accumulated publications of more than 16,500, which indicates that PSC, needless to say, is promising next-generation photovoltaics. High photovoltaic performance was realized by compositional engineering, device architecture and fabrication methodologies for the past 10 years. Toward theoretical efficiency over 30% and commercialization of PSC, further studies on removal of recombination and scalable technologies are required for next 10 years. In this talk, importance of interface engineering is emphasized to reach the theoretical efficiency with voltage over 1.3 V and fill factor over 0.9. Material selection rule and interface engineering methodologies will be introduced. For commercialization, materials may be issued because the current precursor mixture is problematic due to the underlying aging effect. We developed cost-effective materials based on delta FAPbI<sub>3</sub> powder for reproducibly high efficiency PSC. Large-area uniform perovskite coating is also important in upscaling PSC. Acetonitrile-based and 2-methoxy ethanol-based coating solutions were developed for large-area perovskite films. In addition, additive engineering and bifacial stamping technique were found to be effective ways for the upscaling PSC. A paradoxical approach is discussed for improving stability of PSCs. PCEs over 23% could be achieved by the interface engineering, the additive engineering and the topographical approach.

### 5:40 AM \*F.EL06.01.04

## Perovskite Solar Cells—Lessons from a Device Model Lambert Jan Anton Koster; University of Groningen, Netherlands

To improve the performance of existing perovskite solar cells (PSCs), a detailed understanding of the underlying device physics during their operation is essential. We have developed and validated a numerical device model that describes the operation of PSCs and quantitatively explains the role of contacts and of (doped) transport layers (TLs), ionic movement, carrier generation, drift and diffusion of carriers and recombination. We fit the simulation to experimental data of various perovskite solar cells to identify the main losses and routes to optimization.

The performance of PSCs can be limited by losses due to the poor transport properties of the commonly used TLs. State-of-the-art TLs suffer from rather low mobilities when compared to the mobilities of perovskites. We introduce a conductivity criterion to guarantee the design of a good TL through a combination of experimental and modelling data.

We use large-scale drift-diffusion simulations to get a better understanding of the light intensity dependence of the open-circuit voltage and how it correlates to the dominant recombination process. We introduce an automated identification tool using machine learning methods to pinpoint the dominant loss using the light intensity-dependent performances as an input. The machine learning was trained using over 150,000 simulations and gives an accuracy of the prediction up to 80%.

Space-charge limited current (SCLC) measurements have been widely used to study the mobility and trap density in semiconductors. While such measurements have proven to be valuable to investigate the properties of organic semiconductors, their applicability to perovskite materials is not straightforward.

We present a description of the pitfalls of SCLC measurements when considering perovskite semiconductors with an emphasis on the effect of mobile ions, inherent properties of these materials, on the measurements. We show using drift-diffusion simulations that the presence of ions strongly affects the measurement and that the usual analysis and interpretation of the values extracted from SCLC needs to be refined. In particular, the trap density and mobility cannot be directly quantified using classical methods. We also discuss the advantages of pulsed SCLC measurements to get reliable data that are less influenced by ionic motion and degradation of the perovskite under voltage stress. Fitting the pulsed SCLC measurement using drift-diffusion modelling appears to be a reliable method to extract simultaneously mobility, trap and ion densities. We were able to obtain a trap density of  $10^{13} \text{ cm}^{-3}$ , ion density of  $10^{13} \text{ cm}^{-3}$  and mobility of  $13 \text{ cm}^2/\text{Vs}$  for  $\text{MAPbBr}_3$  single-crystal.

### 5:55 AM F.EL06.01.05

**Photoelectron Spectroscopy Investigation of the Electronic and Chemical Properties of Perovskite-Based Devices Under Operating Conditions** Maryline Ralajarisoa<sup>1</sup>, Johannes Frisch<sup>2,3</sup>, Mathieu Frégnaux<sup>4</sup>, Armelle Yaiche<sup>5</sup>, Jean Rousset<sup>5</sup>, Muriel Bouttemy<sup>4</sup>, Arnaud Etcheberry<sup>4</sup>, Regan Wilks<sup>2,3</sup>, Marcus Bär<sup>2,3,6</sup> and Philip Schulz<sup>1</sup>; <sup>1</sup>Helmholtz-Zentrum für Materialien und Energie GmbH, Germany; <sup>2</sup>Helmholtz-Zentrum Berlin für Materialien und Energie GmbH (HZB), Germany; <sup>3</sup>Helmholtz-Zentrum Berlin, Germany; <sup>4</sup>Université de Versailles Saint-Quentin en Yvelines, Université Paris-Saclay CNRS, France; <sup>5</sup>EDF R&D, France; <sup>6</sup>Friedrich-Alexander-Universität Erlangen-Nürnberg, Germany

The long-term viability of perovskite-based solar cells is contingent on the evolution of their performance and the improvement of their stability, which primarily require a deep understanding of their property-function relationships. A comprehensive description of the electronic and chemical properties of the device layers and interfaces is particularly relevant, since these properties ultimately dictate the charge transport across the interfaces and throughout the device. Still, an accurate understanding of the mechanisms governing device operation requires a controlled *operando* monitoring of the respective layers' electronic properties, i.e. when indispensable biases such as light and electrical bias are applied. In our study, in order to establish an X-ray photoelectron spectroscopy (XPS) *operando* procedure, we primarily designed and investigated perovskite half-devices consisting of a multi-cation mixed halide perovskite layer between a FTO/TiO<sub>2</sub> substrate and a partial Au top electrode. We consistently monitor the electronic and chemical properties across the surface of the device sample, which reveals a change of the iodine and lead species from the Au to perovskite side, consistent with a previously observed underpotential deposition process[1]. Then, we use synchrotron-based photoelectron spectroscopy (PES) that allows investigation under operating conditions. The X-ray beam provided by the synchrotron light source also provides the spatial resolution required to use the designed sample configuration and to monitor the changes of the electronic and chemical properties as a function of applied electrical bias and illumination.. A positive electrical bias applied to the Au anode produces a shift in binding energy of the core levels of the perovskite layer, as expected, although it is consistently smaller than the bias. This effect could be attributed to inhomogeneous electric potential across the surface, as it is notably observable close to the Au/perovskite boundary, highlighting the importance of sample design for *operando* studies. We further discuss the possible implications of transient and dynamic processes in these changes. Moreover, by varying

measurement parameters and monitoring the effects on chemical reactions - that may be at the core of degradation processes in perovskite solar cells -, we attempt to disentangle these effects from those induced by the external biases. Importantly, our results indicate a gradual shift of the core level binding energy towards lower values over the early course of the measurements on the perovskite side, potentially indicating an X-ray-induced photovoltage effect. The results provide first insight into perovskite device electronic properties under operating conditions and guidelines for XPS *operando* studies.

[1] Kerner et al., APL Materials 7, 041103 (2019)

#### 6:05 AM F.EL06.01.06

**Late News: Tuning the Work Function of Electrodes through Elucidation of Coordination Reaction at Organic/Inorganic Interfaces** Tsubasa Sasaki<sup>1</sup>, Kazuma Suzuki<sup>2</sup>, Hirokazu Ito<sup>2</sup>, Kaito Inagaki<sup>2</sup>, Taku Oono<sup>1</sup>, Munehiro Hasegawa<sup>3</sup>, Katsuyuki Morii<sup>3,4</sup>, Takahisa Shimizu<sup>1</sup> and Hirohiko Fukagawa<sup>1</sup>; <sup>1</sup>NHK Science & Technology Research Laboratories, Japan; <sup>2</sup>Tokyo University of Science, Japan; <sup>3</sup>Nippon Shokubai Co., Ltd., Japan; <sup>4</sup>Nippon Shokubai Research Alliance Laboratories, Osaka University, Japan

Understanding the carrier injection/extraction mechanism at organic/inorganic interfaces is of pivotal importance for the future progress of organic optoelectronic devices such as organic light-emitting diodes (OLEDs), organic thin-film transistors (OTFTs), organic solar cells (OSCs), perovskite solar cells (PSCs), and organic semiconductor laser diodes (OSLDs). Since barrier-free contacts for holes and electrons are essential for efficient organic optoelectronic devices, the method of tuning the work function (WF) of electrodes and related phenomena has been intensively studied. A higher WF is ideal for efficient hole injection/extraction, and the surface WF of anodes has been tuned to above 5 eV by using metal oxides such as p-type dopants and molybdenum trioxide, both of which have relatively high electron affinity. On the other hand, a cathode surface WF has been mainly tuned using reactive materials such as alkali elements with low WFs of less than 3 eV. Because such alkali elements are highly chemically reactive and easily oxidize in the presence of ambient oxygen and moisture, there is a strong desire to eliminate reactive materials from devices, especially flexible optoelectronic devices.

As a promising electron injection/extraction technique, the utilization of a coordination reaction between phenanthroline derivatives and metals has been studied. Yoshida [1] reported that the high electron injection and current collection efficiency at the Ag electrode/batocuproin (BCP) interface is due to the formation of Ag-BCP complexes. Very recently, Bin et al. [2] have reported that the electron injection efficiency of Ag-doped 4,7-dimethoxy-1,10-phenanthroline (p-MeO-Phen) films is higher than that of not only Ag-doped BPhen films, but also Cs-doped p-MeO-Phen films. It was also reported that the introduction of an electron-donating dimethoxy substituent in Phen results in greater electron exchange between p-MeO-Phen and Ag than between BCP and Ag, therefore improving the electron injection efficiency. However, the coordination reaction around the cathode is not yet systematically understood, and a feasible alternative material to reactive metals has not yet been found.

Here, we have found a novel phenanthroline derivative that can be a feasible alternative to reactive metals in electron injection through an in-depth elucidation of the coordination reaction [3]. The surface WF of the ITO/ZnO electrode with 4.10 eV can be tuned in the range of 3.29–2.43 eV by forming thin films of the Phen derivative on ITO/ZnO. From density functional theory (DFT) calculations, the change in WF ( $\Delta$ WF) was found to be strongly correlated with the amount of electron transfer associated with the coordination reaction compared with the other physical properties that likely affect WF, such as the molecular dipole moment of Phen derivatives. The electrode modified with 4,7-bis(1-pyrrolidinyl)-1,10-phenanthroline (p-Pyrrd-Phen) shows a lower WF than the electrode modified with p-MeO-Phen and a higher electron injection efficiency than LiF. Furthermore, the air stability of the p-Pyrrd-Phen-modified electrode is about 10 times higher than that of LiF, and the operational stability of the OLED using the p-Pyrrd-Phen-modified electrode is comparable to that of the OLED using LiF. Since both the air stability and operational stability of this phenanthroline-modified cathode was demonstrated to be high, our findings open the way to the fabrication of electronic systems that do not require air-sensitive materials.

[1] H. Yoshida, J. Phys. Chem. C vol.119, p.24459 (2015).

[2] Z. Bin et al., Nat. Commun. vol.10, p.866 (2019).

[3] H. Fukagawa et al., Nat. Commun. vol.11, p.3700 (2020).

#### 6:15 AM F.EL06.01.07

**Late News: Surface Ligand Penetration into Methylammonium Lead Iodide Perovskites and the Impact on Interfacial Energetics and Photovoltaic Performance** So Min Park, Ashkan Abtahi, Alex Boehm and Kenneth R. Graham; University of Kentucky, United States

Surface ligand treatment of organic metal halide perovskites is a promising route to passivate surface defect states, improve

material and device stability, alter interfacial energetics, and ultimately increase the perovskite solar cell (PSC) performance. In this work surface ligands with different binding groups are investigated to determine their extent of surface coverage, whether they form a surface monolayer or penetrate into MAPbI<sub>3</sub>, how they influence MAPbI<sub>3</sub> surface energetics and photoluminescence, and how this combination of factors affects PSC performance. Using angle-dependent X-ray photoelectron spectroscopy (XPS) we show that surface ligands with ammonium and phosphonic acid binding groups often penetrate into MAPbI<sub>3</sub>, which can significantly impact surface energetics, as determined through ultraviolet and inverse photoelectron spectroscopy measurements. These changes in surface energetics significantly impact the PSC performance, with solar cell performance decreasing for ligands that create less favorable energy landscapes for electron transfer from MAPbI<sub>3</sub> to the electron transport layer, C<sub>60</sub>. Through investigating a series of ammonium containing surface ligands, we propose guidelines to select ligands that will either penetrate into MAPbI<sub>3</sub> or remain only on the MAPbI<sub>3</sub> surface.

SESSION F.EL06.02: Contact Materials for LEDs and Beyond  
On Demand Abstracts Available for Viewing Starting Saturday Morning, November 21, 2020  
F-EL06

#### 5:00 AM \*F.EL06.02.01

**Interfacing Scandium Nitride with GaN and AlN for Enhanced Performance** Chris G. Van de Walle; University of California, Santa Barbara, United States

Scandium nitride (ScN) is a semiconducting nitride that has the rocksalt crystal structure, but with a lattice parameter that provides a close match to GaN; the lattice mismatch is less than 1%. One reason ScN has attracted recent interest is because adding ScN to AlN enhances the piezoelectric properties, and may even lead to ferroelectricity. Here I will focus on interfaces between ScN and GaN. ScN can be highly *n*-type doped and can thus serve as an almost metallic contact or current spreading layer to GaN. If rocksalt ScN is grown along the [111] direction on top of *c*-axis-oriented wurtzite GaN, interesting phenomena related to spontaneous polarization occur. GaN is polar with a large spontaneous polarization, while ScN is centrosymmetric. This suggests the possibility of a very large spontaneous polarization difference at the interface. We have examined the properties of such interfaces using first-principles calculations based on density functional theory [1]. We first apply the modern theory of polarization to obtain the bulk properties of the individual materials. The resulting difference in polarization constants yields a polarization discontinuity at the ScN/GaN interface of -1.358 C/m<sup>2</sup>. As a result, we expect a high-density electron gas on the N-polar GaN/ScN interface, and a high-density hole gas on the Ga-polar GaN/ScN interface, with carrier concentrations up to 8.5E14/cm<sup>2</sup>. This value is over an order of magnitude larger than what can be achieved at GaN/AlGaIn interfaces. We have confirmed the presence of strong electric fields and bound interface charges in explicit interface calculations. The large polarization difference and small strain makes ScN a promising material for applications in polarization-enhanced *p*-GaN/ScN/*n*-GaN tunnel junctions. Current tunnel junctions make use of InGaIn interlayers to reduce the effective barrier and increase the polarization field across the *p-n* junction to reduce the junction width. ScN is a promising alternative, with a higher polarization field, smaller bandgap, and much smaller strain.

Work performed in collaboration with N. L. Adamski and C. E. Dreyer, and supported by AFOSR.

[1] N. L. Adamski, C. E. Dreyer, C. G. Van de Walle, Appl. Phys. Lett. 115, 232103 (2019).

#### 5:15 AM F.EL06.02.02

**Solution-Processed Ceria Quantum Dots as Interface Layer for Enhancing Performance of Avalanche Amorphous-Selenium Photodetectors** Haripriya Kannan<sup>1</sup>, Jann Stavro<sup>2</sup>, Atreyo Mukherjee<sup>2</sup>, Sebastien Leveille<sup>3</sup>, Kim Kisslinger<sup>4</sup>, Lizhu Guan<sup>5,1</sup>, Wei Zhao<sup>6</sup>, Ayaskanta Sahu<sup>1</sup> and Amir H. Goldan<sup>6</sup>; <sup>1</sup>New York University, Tandon School of Engineering, United States; <sup>2</sup>Stony Brook University, College of Engineering and Applied Sciences, United States; <sup>3</sup>Analogic Canada, Canada; <sup>4</sup>Brookhaven National Laboratory, United States; <sup>5</sup>Harbin University of Science and Technology, China; <sup>6</sup>Stony Brook University, School of Medicine, United States

Photo-sensing devices using amorphous-selenium (a-Se) have gained significant attention in medical imaging due to their avalanche phenomena. a-Se photodetectors are wide bandgap ( $E_g$ ) semiconductor with high fill-factor, offers a high-gain ( $\sim 10^2 - 10^3$ ) with negligible low excess noise, and has  $\sim 90\%$  quantum efficiency to blue wavelength facilitating a scintillator-based conversion detector for gamma rays and X-rays. At electric fields above 70 V/ $\mu\text{m}$ , holes in a-Se undergo impact ionization which increases the effective sensitivity of the photodetector. However, at these high electric fields required for

avalanche gain, dark current due to charge injection from the metallic electrode can become a significant source of noise, limiting the dynamic range of the photodetector. Hole-blocking layer (HBL)/ electron transport layer (ETL) is an n-type semiconductor typically incorporated at the interface between positive electrode and a-Se to minimize the dark current from charge injection while conducting only electrons. However, the avalanche gain of the a-Se sensor has been limited so far by the use of inefficient hole-blocking layers. Two factors are necessary to achieve efficient a-Se devices with HBL. One is, the device should be fabricated with HBL on top of a-Se (*p-i-n* fabrication sequence where 'p' denotes p-type electron-blocking layer, 'i' is for intrinsic a-Se and 'n' for n-type HBL) to develop a scalable imager that is compatible with pixelated read-outs. Second, a-Se crystallizes at ~50°C which emphasizes a room-temperature deposition technique of HBL on a-Se. Among previously reported HBLs/ETLs, vacuum-deposited bulk cerium dioxide (CeO<sub>2</sub>) has been successfully utilized in avalanche a-Se sensors. Bulk CeO<sub>2</sub> cannot be directly deposited on a-Se, as the high-temperature required for the vacuum deposition crystallizes a-Se and is fabricated in the *n-i-p* sequence, with a-Se deposited on top of CeO<sub>2</sub>. a-Se with bulk CeO<sub>2</sub> suffers from the high dark current due to a lower effective hole barrier of CeO<sub>2</sub> (2.8 eV). In our work, we successfully synthesized colloidal CeO<sub>2</sub> quantum dots (QDs) with a large bandgap ( $E_g = 3.77$  eV), which are electronically passivated by surfactants/ligands and spin-coated directly on a-Se at room temperature without inducing any crystallization. As a large bandgap semiconductor, CeO<sub>2</sub> is extremely transparent at the 450 nm wavelength during photo-response measurement of a-Se. Our best performing device with 40 nm thick CeO<sub>2</sub> HBL achieved an avalanche gain of 42. Also, our prototype device of 150 nm thick CeO<sub>2</sub> achieved an ultra-low dark current of 30 pA/cm<sup>2</sup> at 70 V/μm which is three orders of magnitude lower than any avalanche a-Se device previously reported and might be the lowest dark current ever recorded for an avalanche device operated at room temperature.

### 5:25 AM F.EL06.02.03

**Generic Electroluminescent Device for Emission from Long-Wave Infrared to Ultraviolet Wavelength** Yingbo zhao<sup>1,2</sup>, Der-Hsien Lien<sup>1,2</sup>, Vivian Wang<sup>1,2</sup> and Ali Javey<sup>1,2</sup>; <sup>1</sup>University of California, Berkeley, United States; <sup>2</sup>Lawrence Berkeley National Laboratory, United States

The scope of luminescent materials that can be used for electroluminescent devices has been limited due to material processability and band alignment considerations. These limitations impede the development of electroluminescent devices at extreme wavelengths and hinder the use of electroluminescence (EL) spectroscopy as an analytical technique. Herein we report a device that can excite EL from various materials independent of their physical form and chemical composition. The device produces EL from the long-wave infrared (0.13 eV) to ultraviolet (3.3 eV) range depending on the emitting layer drop casted on top, with onset voltages closely approaching the optical energy gap of the emitting materials. The two-terminal device employs a carbon nanotube network as the source contact and utilizes an AC gate voltage to achieve charge injection through transient band bending. The concept of EL spectroscopy is demonstrated by probing a chemical reaction in a liquid droplet and an EL sensor is developed for detecting organic vapors.

### 5:35 AM F.EL06.02.04

**Pushing Correlated Metals Towards UV Transparency** Joseph Roth<sup>1</sup>, Arpita Paul<sup>2</sup>, Turan Biro<sup>2</sup> and Roman Engel-Herbert<sup>1</sup>; <sup>1</sup>The Pennsylvania State University, United States; <sup>2</sup>University of Minnesota, United States

The development of ultraviolet (UV) LEDs has long been a focus due to the wide application space including germicidal disinfection of water, medical sterilization of surfaces, UV polymer curing, DNA sensing, and solar blind detectors. The COVID-19 pandemic has further fueled the need for a time effective and economic solution to disinfect public areas from the coronavirus. Current UV-light disinfection devices use mercury-based gas discharge lamps because high-performance UV LEDs require an electrically conducting electrode material that is highly transparent in the UV range.<sup>1</sup> In this talk we will demonstrate that the correlated metal SrNbO<sub>3</sub> is an ideal transparent electrode for UV applications due to its high optical transmission coupled with a metallic like electrical conductivity superior to indium tin oxide. We will present electrical and optical properties of SrNbO<sub>3</sub> films grown by pulsed laser deposition<sup>2</sup> and by magnetron sputtering.<sup>3</sup> The optical transmission was found to be in excess of 80% throughout the visible range and near ultraviolet down to 270 nm for films with thicknesses smaller than 12 nm while maintaining an electrical resistivity lower than  $2 \times 10^{-5}$  Ωcm, giving rise to a sheet resistance of about 68Ω/sq due to its metal-like carrier concentration of  $\sim 1 \times 10^{22}$  cm<sup>-3</sup>, comparing favorably to conventional UV transparent conductor materials such as doped Ga<sub>2</sub>O<sub>3</sub> or ZnGa<sub>2</sub>O<sub>4</sub>. In addition, we will share insights obtained by density functional theory and experiments how sizeable Sr vacancy concentrations affect electrical and optical properties of SrNbO<sub>3</sub> films.

1. Hirayama, H. Recent Progress in AlGaIn Deep-UV LEDs. in *Light-Emitting Diode - An Outlook On the Empirical Features and Its Recent Technological Advancements* (InTech, 2018). doi:10.5772/intechopen.79936.

2. Park, Y. *et al.* SrNbO<sub>3</sub> as Transparent Conductor in the Visible and Ultraviolet Spectrum. *Commun. Phys.* **3**, 102 (2020).
3. Roth, J. *et al.* Sputtered Sr<sub>x</sub>NbO<sub>3</sub> as a UV transparent conducting film. *Accepted to ACS Appl. Mater. Interfaces.*

#### 5:45 AM F.EL06.02.05

##### **Comparison of the Performance and Stability of Top-Emitting and Bottom-Emitting Polymer Light Emitting Devices** Sumant R. Wasule and Deirdre O'Carroll; Rutgers University, United States

Organic light emitting devices (OLEDs) are one of the fascinating topics in both academic and industrial fields. Certain properties of OLEDs make them exciting prospects for next generation lighting and display applications, such as the large-area emission characteristics not found in other light sources. OLEDs are fabricated in either a conventional configuration or an inverted configuration. In the conventional configuration, the anode is the transparent electrode and the cathode is the metal electrode. For the inverted configuration the cathode and anode materials are reversed (metal as anode, transparent electrode as cathode). OLEDs are also divided based on the direction of light emitted from the device - bottom-emitting (BE) or top-emitting (TE). Most BE OLEDs are fabricated on indium-tin-oxide (ITO) coated glass substrates; however, this device type has some disadvantages. For example, the emitted light has to pass through a high refractive index ITO layer and a thick glass substrate to exit the device, which traps light in these layers. Additionally, ITO is brittle so this limits its application in flexible OLEDs. TE OLEDs are more compatible with n-type active matrix display-driven OLED technologies. In these devices, the top transparent electrode can be very thin (<100 nm) and the bottom metal layer is thicker so that it acts a reflecting surface. Therefore, TE OLEDs have reduced light trapping, and, therefore, increased light-extraction efficiency compared to BE OLEDs.

In this work, the main objective is to compare the performance and stability of both inverted BE and TE OLEDs fabricated using organic light-emitting polymer semiconductor active layers. The inverted BE OLED has the following layers in order from bottom to top: glass, ITO, zinc oxide (ZnO), cesium carbonate (Cs<sub>2</sub>CO<sub>3</sub>), poly(9, 9-dioctylfluorene-alt-BT) (F8BT), molybdenum trioxide (MoO<sub>3</sub>), aluminium (Al). ITO and Al are the cathode and anode respectively; ZnO and Cs<sub>2</sub>CO<sub>3</sub> are the electron injection layers; F8BT is the light-emitting polymer where electron and holes combine to emit light; and MoO<sub>3</sub> is the hole injection layer. Cs<sub>2</sub>CO<sub>3</sub> is deposited on ZnO because it lowers the barrier for electron injection into thick polymer films [1]. The inverted TE OLED has the following layers in order from bottom to top: glass, silver (Ag), titanium dioxide (TiO<sub>2</sub>), F8BT, MoO<sub>3</sub>, silver (Ag) [2]. The performance and stability of both devices is compared by studying current-voltage, current-light flux and voltage-light flux variations. In addition, optoelectronic simulations are employed to aid in optimization of the thickness of the device layers and to validate the experimental results.

#### References

- [1] D. Kabra, L. P. Lu, M. H. Song, H. J. Snaith, and R. H. Friend, "Efficient single-layer polymer light-emitting diodes.," *Adv. Mater.*, vol. 22, no. 29, pp. 3194–3198, 2010, doi: 10.1002/adma.201000317.
- [2] C. M. Carter, J. Cho, A. Glanzer, N. Kamcev, and D. M. O'Carroll, "Cost, energy and emissions assessment of organic polymer light-emitting device architectures," *J. Clean. Prod.*, vol. 137, pp. 1418–1431, 2016, doi: 10.1016/j.jclepro.2016.07.186.

#### 5:55 AM F.EL06.02.06

##### **Elucidating the PEDOT:PSS/Perovskite Interface for Perovskite Light-Emitting Diodes** Simon Sandrez<sup>1,2</sup>, Lionel Hirsch<sup>1</sup>, Tony Maindron<sup>2</sup> and Guillaume Wantz<sup>1</sup>; <sup>1</sup>Université de Bordeaux, France; <sup>2</sup>CEA-LETI, France

Lead halide perovskites have witnessed in the last few years a major progress as active materials for light-emitting applications. In only four years, efficiencies of perovskite light-emitting diodes (PeLEDs) soared up from less than 1% in 2014<sup>1</sup> to more than 20%<sup>2-4</sup> in 2018. These high efficiencies, together with remarkable properties such as cheap solution processes at low temperatures, efficient charge injection/transport, high color purity and easy wavelength tuning, make perovskite materials a very promising route for future display application. Especially, the use of quasi-2D perovskites forming multi-quantum well structures has enabled to improve radiative recombination probability by increasing the exciton binding energy and by inducing energy transfer within the perovskite material<sup>5</sup>. However, the efficiency and stability of PeLEDs are still lagging behind those of more established technologies like OLEDs. One of the main hurdles for the fabrication of efficient and stable PeLEDs is related to interfacial layer properties, adjacent to the perovskite material. Although the Poly(3,4-ethylenedioxythiophene)-poly(styrenesulfonate) (PEDOT:PSS) is famous as an easy-to-use excellent hole injection and transport layer, it is also known that luminescence quenching in perovskite emitter layers can appear when

deposited onto PEDOT:PSS films, which affect performances of the PeLED<sup>6</sup>. Up to now though, exact interactions occurring at the PEDOT:PSS/perovskite interface are not fully understood.

In this contribution, we use a  $\text{PEA}_2(\text{FAPbBr}_3)_n\text{-PbBr}_4$  quasi-2D perovskite and discover a very significant conductivity doping phenomenon located at this PEDOT:PSS/perovskite interface. It translates into unwanted light emission outside of the delimited active area of the PeLED, which may lead to calculation error of device efficiencies. It is demonstrated that this doping is specific to the association of perovskite and PEDOT:PSS materials through a singular behavior. In addition, a study of different interlayers is proposed in order to eliminate the interactions at the PEDOT:PSS/perovskite interface, with emphasis on deposition issues we encountered such as wettability of the perovskite material on those interlayers, which can drastically affect PeLED performances and the manufacture reproducibility from one batch to another.

#### References

1. Tan, Z. et al. Bright light-emitting diodes based on organometal halide perovskite. *Nat. Nanotechnol.* 1–6 (2014). doi:10.1038/nnano.2014.149
2. Zhao, B. et al. High-efficiency perovskite-polymer bulk heterostructure light-emitting diodes. *Nat. Photonics* 1–10 (2018).
3. Cao, Y. et al. Perovskite light-emitting diodes based on spontaneously formed submicrometre- scale structures. *Nature* 562, 249–253 (2018).
4. Lin, K. et al. Perovskite light-emitting diodes with external quantum efficiency exceeding 20 per cent. *Nature* 562, 245–248 (2018).
5. Yang, X. et al. Efficient green light-emitting diodes based on quasi-two-dimensional composition and phase engineered perovskite with surface passivation. *Nat. Commun.* 9, 2–9 (2018).
6. Meng, Y. et al. High performance and stable all-inorganic perovskite light emitting diodes by reducing luminescence quenching at PEDOT:PSS/Perovskites interface. *Org. Electron.* 64, 47– 53 (2019).

#### 6:05 AM \*F.EL06.02.07

**Transparent Oxide Semiconductors for Contact in OLEDs and Halide Perovskite LEDs** Hideo Hosono<sup>1,2</sup>; <sup>1</sup>Tokyo Institute of Technology, Japan; <sup>2</sup>National Institute for Materials Science, Japan

Contact materials for electron injection is critical for OLEDs and halide perovskite LEDs. This type of materials requires several properties; low work function, chemically stable, optically transparent and ohmic contact formation with cathode. In this talk, I would like to show 3 new transparent amorphous semiconductors which were developed for OLEDs/QLEDs along with materials design concepts. First is amorphous electride C12A7:e with very small work function and chemical stability [1]. Second is X-ray amorphous ZnO-SiO<sub>2</sub> thin films with small work function and easy Ohmic contact formation with various metals and semiconductors [2,3]. Such a feature makes it possible to fabricate tandem-type OLED devices without significant voltage drop [4]. The last is amorphous transparent p-type semiconductor, Cu-Sn-I with large mobility (~10cm<sup>2</sup>/Vs) which can be fabricated by spin-coating at low temperature [4]. Applying a-ZSO as the electron injection layer [5]. led very high green and red light emission from perovskite LEDs, revealing the critical role of exciton confinement and carrier injection.

- [1] H.Hosono, J.Kim, Y.Toda, T. Kamiya, and S.Watanabe, *Proc. Natl. Acad. Sci. USA*, 114(2), 233 (2017).
- [2] N.Nakamura, J. Kim, H.Hosono, *Adv. Electron. Mater.*, 4, 1700352, (2018).
- [3] N.Nakamura, J. Kim, K.Yamamoto, S. Watanabe, and H. Hosono. *Org.Electro.* 51, 103-110(2017).
- [3] H.Yang, J.Kim, K.Yamamoto, H.Hosono, *Org.Elect.*46, 133(2017).
- [4] T. Jun, J. Kim, M. Sasase, H. Hosono, *Adv. Mater.*, 30, 1706573 (2018).
- [5] K. Sim, T. Jun, J.Bang, H. Kamioka, J. Kim, H. Hiramatsu, H. Hosono, *Appl.Phys.Rev.* 6, 031402 (2019)

#### 6:20 AM F.EL06.02.08

**Micro LED Defect Analysis via Photoluminescent and Cathodoluminescent Imaging** Keith Behrman<sup>1</sup>, Julie Fouilloux<sup>2</sup>, Terry Ireland<sup>2</sup>, George R. Fern<sup>2</sup>, Jack Silver<sup>2</sup> and Ioannis Kymissis<sup>1</sup>; <sup>1</sup>Columbia University, United States; <sup>2</sup>Brunel University London, United Kingdom

**Micro light-emitting diodes (micro LEDs) are a promising technology for next-generation displays given their high brightness and efficiency, color gamut coverage and self-emissive design. Most applications require red, green and blue (RGB) pixel integration, which is currently not possible from a single epitaxially grown LED wafer in a fully self-emissive design [1]. To overcome this limitation, several transfer methods have been proposed to allow integration of singulated micro LEDs from red, green, and blue LED wafers [2]. These transfer methods result in lesser fabrication yields and a higher percentage of displays with inactive pixels requiring the display to either be discarded or repaired**



[3]. Device short-circuits can be caused by chlorine-based dry etching-related damage or redeposited GaN/GaAs during mesa formation [4]. Defects in the wiring or interconnects can also cause inactive pixels. A non-destructive method to examine for pixel damage would significantly improve yield and fabrication quality. Here we investigate the viability of photoluminescence (PL) and cathodoluminescence (CL) imaging as two non-destructive test methods for defects in micro LED displays.

Blue LEDs (448 nm) of epitaxially grown GaN and InGaN on sapphire were formed into 800 square pixels of side lengths varying from 5 to 500  $\mu\text{m}$  by dry etching in a chlorine plasma. CL images were taken using a Zeiss Supra 35VP field-emission scanning electron microscope [5]. PL images were recorded using a LEICA SP8 stimulated emission depletion microscope. After both non-destructive images were collected, we continued device fabrication to electrically connect individual pixels to wire bond pads for attachment to a driving PCB. We recorded electroluminescence (EL) images to compare to PL and CL as defect predictors.

All 800 pixels showed luminescent activity centered at 448 nm under PL imaging. While 582 pixels showed bright luminescence from CL imaging, the remainder showed dim or faded luminescence. An LED with little or no luminescence is indicative of a defect causing an electrical short between the anode and cathode. This provides a shunt resistance current return path around the emissive InGaN multiple quantum wells (MQWs). We explored this phenomenon further by examining the edges from a subset of the inactive pixels under SEM with a SE detector and found dry-etching related damage to the pixel sidewalls.

When comparing these results to the EL images, CL is a strong predictor of inactive pixels in EL. Additional pixels beyond those predicted from CL were inactive so we reexamined a subset of the devices with CL imaging with the die attached to the PCB creating a new measurement paradigm with multiple current return paths for incident electrons. The second set of CL images showed a variety of brightness levels from the individual LED pixels. The average brightness value of each LED was measured using a script in MATLAB and was found to correlate to the inactive pixels from EL imaging and could also predict the nature of the defect as a short or open circuit.

We found that PL imaging did not provide any information on predicting defects in micro LEDs. However, by comparing CL imaging results after mesa etching and after wire and bump fabrication, we show for the first time that it is possible to identify micro LED defects as either shorts from dry etching related damage, shorts from wiring defects, or open circuits from wiring defects. CL imaging is a promising solution for robust and non-destructive analysis for micro LED fabrication.

[1] F. Templier et al., SID, vol. 47, no. 1, pp. 1013–1016, 2016.

[2] A. Carlson et al., Adv. Mater., vol. 24, no. 39, pp. 5284–5318, Oct. 2012.

[3] M. Meitl et al., SID, vol. 47, no. 1, pp. 743–746, May 2016.

[4] S. J. Pearton et al., MRS, vol. 5, no. 1, p. e11, 2000.

[5] D. D. Engelsen et al., Ultramicroscopy, vol. 157, pp. 27–34, October 2015.

**6:30 AM F.EL06.02.09**

**Laser-Induced Graphene Electrodes for Biosensor Application** [Elvira Fortunato](#); Universidade NOVA de Lisboa, Portugal

Graphene has emerged as a novel material with enhanced electrical and structural properties that can be used for a multitude of applications from super-capacitors to biosensors. In this context, an ultra-sensitive biosensor was developed using a low-cost, simple and mask-free method based on laser-induced graphene technique for electrodes patterning. The graphene was produced on a polyimide substrate, showing a porous multi-layer structure with a resistivity of  $102.4 \pm 7.3 \Omega/\text{square}$ . The biosensor was designed as a 3-electrode system. Auxiliary and working electrodes were made of graphene by laser patterning and the reference electrode was handmade by casting a silver ink. A molecularly-imprinted polymer (MIP) was produced at the working electrode by direct electropolymerization of eriochrome black T (EBT). As proof-of-concept, the MIP film was tailored for chloramphenicol (CAP), a common contaminant in aquaculture.

**6:40 AM F.EL06.02.10**

**Industrial Waste Residue Converted into Value-Added ZnO for Optoelectronic Applications** [Elvira Fortunato](#); Universidade NOVA de Lisboa, Portugal

The present study shows a simple, fast and cost-effective way of converting industrial waste into a lightweight optoelectronic

device to detect UV radiation. An innovative recycling process of ZnO-rich (> 95% ZnO) residues from the brass industry has been investigated through the preparation of ceramic targets to be used in the deposition of ZnO thin films. A comparison between optical, structural and morphological properties of ZnO thin films deposited by sputtering technique on glass and polyimide substrates was carried out. The ZnO thin films deposited on polyimide substrates were used as seed layers for an ultrafast growth of ZnO nanorods arrays by hydrothermal method assisted by microwave radiation. Laser-induced graphene electrodes were fabricated on the polyimide substrates prior to the ZnO thin film deposition for UV sensor characterization. The produced UV sensor exhibits a responsivity around 12  $\mu\text{A/W}$  for an UV light of 365 nm under 10 V bias. The photoresponse measurements showed a stable UV sensor without significant variations in the sensor's responsivity when tested for long periods of time.

SESSION F.EL06.03: Theory and Experiments for Novel Contact and Absorber Materials  
On Demand Abstracts Available for Viewing Starting Saturday Morning, November 21, 2020  
F-EL06

**5:00 AM \*F.EL06.03.01**

**Searching for Materials with Exceptional Opto-Electronic Properties Using *Ab Initio* High-Throughput Computing** Geoffroy Hautier; Université Catholique de Louvain, Belgium

New opto-electronic devices from solar cells to transparent transistors require high performance materials. Ab initio high-throughput computations offer an accelerated path towards the discovery of these exceptional materials. We can now screen thousands of materials by their computed properties even before the experiments. This computational paradigm allows experimentalists to focus on the most promising candidates, and enable researchers to efficiently and rapidly explore new chemical spaces.

In this talk, I will present the challenges and opportunities in materials discovery offered by high-throughput ab initio computing in searching for materials with exceptional opto-electronic properties. Recent examples from our work in the fields of transparent conducting materials and solar absorbers will be used to illustrate the approach. I will discuss the materials highlighted by these computational searches but also show how trends and design rules can be extracted from high-throughput data sets. Finally, I will report on our efforts in scaling up to high-throughput new properties from point defects to carrier mobilities.

**5:15 AM F.EL06.03.03**

**Enabling and Boosting Size Convergence for Surface Calculations of Materials Exhibiting Spontaneous Polarization** Su-Hyun Yoo<sup>1</sup>, Mira Todorova<sup>1</sup>, Chris Van de Walle<sup>2</sup> and Jorg Neugebauer<sup>1</sup>; <sup>1</sup>Max-Planck-Institut für Eisenforschung GmbH, Germany; <sup>2</sup>University of California, Santa Barbara, United States

The most common approach to describe surfaces in density-functional theory is the repeated slab geometry based on periodic boundary conditions. A common strategy to avoid artificial charge transfer from one side of the slab to the other when modelling semiconductor surfaces is to passivate partially filled surface dangling bonds at the backside of the slab. Using the example of wurtzite (0001) surfaces we demonstrate that conventionally used passivation schemes (e.g. pseudo H or surface reconstructions) break down for materials exhibiting spontaneous polarization. We have therefore developed a generalized passivation method that accounts for the effect of spontaneous polarization and correctly describes the asymptotic bulk limit for pyroelectric materials. It is robust and ensures quick convergence of total energies and electronic structure with respect to system size. The performance of our approach will be demonstrated using the example of wurtzite ZnO polar surfaces.

This work is supported by the Cluster of Excellence RESOLV (EXC 2033) funded by the Deutsche Forschungsgemeinschaft. This project has received funding from the ECSEL Joint Undertaking (JU) project UltimateGaN under grant agreement No 826392. The JU receives support from the European Union's Horizon 2020 research and innovation programme and Austria, Belgium, Germany, Italy, Slovakia, Spain, Sweden, Norway, Switzerland.

**5:25 AM F.EL06.03.04**

**Graphene Oxide Encapsulated Silver Nanowire Transparent Electrodes—Stability and Device Applications** Woo Hyun Chae, Thomas Sanniccolo and Jeffrey C. Grossman; Massachusetts Institute of Technology, United States

Among many candidate materials that can overcome the high cost and brittleness of indium tin oxide (ITO), silver nanowire (AgNW) networks appear as a promising substitute. The percolating networks of AgNWs exhibit high flexibility and excellent optoelectronic properties, with sheet resistance of a few  $\Omega/\text{sq}$  and total transmittance of 90% at 550 nm, fulfilling the requirements for many applications such as solar cells or transparent heaters.<sup>1,2</sup> In addition, the fabrication of these electrodes can be achieved by scalable solution-based methods. However, AgNW's susceptibility to corrosion and thermal instability remain limiting factors to its widespread market adoption. Depending on the application target, bare AgNW networks usually require stabilization by encapsulation layers to increase resilience to chemical or electrical stress.

In this study, we present a scalable and economically viable process involving electrophoretic deposition (EPD) to fabricate a highly stable hybrid transparent electrode with a sandwich-like structure where the AgNW network is covered by GO on both sides.<sup>3</sup> The newly developed process allows the conductive transparent film to be transferred to an arbitrary surface after deposition and demonstrates excellent sheet resistance (15  $\Omega/\text{sq}$ ) and transmittance (87% at 550 nm) on glass substrates. Unlike the uncoated AgNW network, the hybrid electrode was found to retain its original conductivity under long-term storage at 80°C. This chemical resilience was explained by the absence of major silver corrosion products for the AgNW encapsulated by GO as indicated by X-ray photoelectron spectroscopy (XPS).

*In situ* electrical ramping and resistance measurement up to 20V combined with Infrared Thermography were also conducted in order to assess the electrical stability of our electrodes. The electrical behavior of bare AgNW networks typically undergoes distinct phases comprising “optimization” (Joule-effect-induced sintering of the junctions) at first,<sup>4</sup> then “degradation” (Joule-effect-induced morphological instabilities of some AgNWs), and finally “breakdown”. It was demonstrated experimentally that the latter breakdown stage involves the formation and propagation of a crack parallel to the contact electrodes.<sup>5</sup> On the other hand when encapsulating in GO, the results indicate a novel stabilization mechanism enabled by the presence of GO that prevents abrupt divergence of the resistance to the M $\Omega$  range.

Finally, we will explain the benefits of using these transferrable GO-stabilized AgNW networks in devices by giving some examples of successful integration into organic solar cells (OSC). Importantly, our film can be used as a transparent top electrode for OSC, paving the way for transparent photovoltaics with longer lifetimes. Our unique double-sided EPD-GO/AgNW/GO design where GO is already integrated with the AgNW network serves a dual purpose of encapsulating the entire device as well as enhancing the contact between AgNW and underlying device stack. This results in an enhanced device performance along with increased lifetime by a factor of 5 compared to an unencapsulated device with sprayed AgNWs as top contact.

- (1) T. Sannicolo, M. Lagrange, A. Cabos, C. Celle, J.-P. Simonato, D. Bellet, 2016. *Small*, 12 (44), 6052–6075
- (2) M. Lagrange, T. Sannicolo, D. Muñoz-Rojas, B.G. Lohan, A. Khan, M. Anikin, C. Jiménez, F. Bruckert, Y. Bréchet, D. Bellet, 2017. *Nanotechnology*, 28 (5), 55709
- (3) W.H. Chae, T. Sannicolo, J.C. Grossman, 2020, *ACS Applied Materials and Interfaces*, 12 (15), 17909-17920
- (4) T. Sannicolo, D. Muñoz-Rojas, N.D. Nguyen, S. Moreau, C. Celle, J.-P. Simonato, Y. Bréchet, D. Bellet, 2016. *Nano Letters*, 16 (11), 7046–7053
- (5) T. Sannicolo, N. Charvin, L. Flandin, S. Kraus, D.T. Papanastasiou, C. Celle, J.-P. Simonato, D. Muñoz-Rojas, C. Jiménez, D. Bellet, 2018. *ACS Nano*, 2018, 12, 4648–4659

### 5:35 AM F.EL06.03.05

**BaBi<sub>2</sub>O<sub>6</sub>—A Novel Sustainable, Solution-Processable Electron Transport Layer** Alex M. Ganose, Kieran B. Spooner, Winnie Leung, John Buckeridge, Benjamin A. Williamson, Robert Palgrave and David O. Scanlon; University College London, United Kingdom

A vast array of modern electronic devices require electron transport layers (ETLs), including photovoltaic cells and batteries. In order to be efficient, various constraints need to be fulfilled with respect to material it is contacting, including structural compatibility and band alignment, so a wide range of different possible electron transport layers is needed for current and future technologies. It is also vital that these materials are produced sustainably, to minimise resource depletion and global heating.

Here, BaBi<sub>2</sub>O<sub>6</sub> has been synthesised by a solution-based method at ambient temperatures from relatively non-toxic elements. BaBi<sub>2</sub>O<sub>6</sub> was shown to crystallise in the layered PbSb<sub>2</sub>O<sub>6</sub> structure, which is shared by a number of other materials,<sup>1</sup> some of which have magnetic and catalytic capabilities; and is stable up to around 600°C.

Hybrid density functional theory (DFT) calculations were then used to analyse its potential as an ETL. The electronic transport properties were calculated from two codes, BoltzTraP,<sup>2</sup> which solves the Boltzmann transport equations using the relaxation time approximation (RTA); and AMSET, a new code which does not use this approximation. Using AMSET, the

rates of polar optical phonon, acoustic deformation potential and ionised impurity scattering were each calculated, leading to a much more accurate approximation of the electrical conductivity compared to BoltzTraP. Via AMSET it is estimated that BaBi<sub>2</sub>O<sub>6</sub> possesses an electrical conductivity of around 6,800 S m<sup>-1</sup> with 10<sup>-19</sup> electrons cm<sup>-3</sup> at 300 K in the in-plane direction, or a mobility of approximately 42 cm<sup>2</sup> V<sup>-1</sup> s<sup>-1</sup>. By calculating the full set of intrinsic defects using hybrid DFT, it was then shown that BaBi<sub>2</sub>O<sub>6</sub> is intrinsically n-type, and by also calculating extrinsic La and F defects, it was shown La in particular is an effective donor dopant.

Overall, we show to a high level of theory that BaBi<sub>2</sub>O<sub>6</sub> is a sustainable material which possesses the high electron mobility and dopability required to be a promising ETL.

[1] Blasse, G. & De Pauw, A. D. M. *J. Inorg. Nucl. Chem.*, **1970**, 32, 2533.

[2] Madsen, G. K. H.; Singh, D. J. *Comput. Phys. Commun.* **2006**, 175, 67.

#### 5:45 AM F.EL06.03.06

**Growth of Transparent Conductor SrMoO<sub>3</sub> via Molecular Beam Epitaxy** [Tatiana Kuznetsova](#), Joseph Roth and Roman Engel-Herbert; The Pennsylvania State University, United States

The search for a cheaper and more efficient alternative to transparent conductor tin-doped indium oxide (ITO) in light-emitting devices, displays, and solar cells is still going. Strontium molybdate (SrMoO<sub>3</sub>) is known to be a transparent conductor with the lowest electrical resistivity among all known perovskite oxides and might be a better substitute for ITO. Optical transparency and electrical conductivity greatly depend on the concentration of defects; therefore, materials of exceptional quality are desirable. Currently used techniques for the growth of SrMoO<sub>3</sub>, such as pulsed laser deposition and electron beam evaporation, are based on the use of high energy species, and it may lead to the unintentional formation of defects and degraded quality of the material. Molecular beam epitaxy enables the growth of single-crystalline thin films of exceptional quality, provides unparalleled control over film stoichiometry and only utilizes low-energy particles; therefore, it is a suitable technique for the growth of SrMoO<sub>3</sub>.

However, it is challenging to grow high quality SrMoO<sub>3</sub> thin films via MBE because molybdenum has very low vapor pressure, making it difficult to supply Mo atoms through a conventional effusion cell. One solution might be to use MoO<sub>3</sub> as a source of molybdenum atoms instead of a pure metal. In this talk, I will provide the results of the growth of transparent conductor SrMoO<sub>3</sub> thin films via molecular beam epitaxy (MBE) using MoO<sub>3</sub> pellets as a source of molybdenum atoms. Thermodynamic calculations of vapor pressure and stability of MoO<sub>3</sub> will be presented. I will show the images of custom-built effusion cell we used to prevent the reduction of volatile MoO<sub>3</sub> to non-volatile MoO<sub>2</sub> in vacuum. Additionally, I will present reflection high energy electron diffraction, x-ray diffraction, and atomic force microscopy data, as well as the results of optical and electrical measurements to prove that high-quality transparent conducting SrMoO<sub>3</sub> thin films can be grown via MBE in a self-regulated manner.

#### 5:55 AM \*F.EL06.03.07

**Optoelectronic Properties of Halide Perovskites from First Principles—Challenges, Results and Surprises** [Linn Leppert](#); University of Twente, Netherlands

Halide perovskites are a chemically and electronically diverse class of compounds. They encompass 3D materials like the hybrid organic-inorganic CH<sub>3</sub>NH<sub>3</sub>PbI<sub>3</sub> and the all-inorganic double perovskite Cs<sub>2</sub>BiAgBr<sub>6</sub>, solar absorbers with excellent features for photovoltaic applications and beyond. This diversity of structures and optoelectronic properties is further expanded when reducing the dimensionality of these systems, as exemplified by the Ruddlesden-Popper perovskite (BA)<sub>4</sub>AgBiBr<sub>8</sub> (BA=butylammonium), which can be thought of as a double perovskite monolayer with alternating AgBr<sub>6</sub> and BiBr<sub>6</sub> octahedra, separated by an organic spacer layer [1,2].

Accurately predicting the fundamental band gaps and excited state properties of this zoo of materials from *first principles* is challenging because of the intricate coupling of structural and electronic degrees of freedom [3], complex structural dynamics and strong spin-orbit interactions. In this contribution, I will discuss our recent progress in describing the optoelectronic properties of halide perovskites using density functional theory (DFT) and Green's function-based many-body perturbation theory [4]. DFT-based molecular dynamics simulations allow us to consider temperature dynamics of halide perovskites and design structural models for our electronic structure calculations. A particular focus of this talk will be our calculations of the electronic structure and optical excitations of the double perovskite series Cs<sub>2</sub>AgBX<sub>6</sub> (B=Bi, Sb; X=Br, Cl) and their 2D derivatives – a set of materials with unusual and highly tunable optoelectronic properties.

[1] B. A. Connor, L. Leppert, M. D. Smith, J. B. Neaton, H. I. Karunadasa, *J. Am. Chem. Soc.* **140**, 5235 (2018).

[2] B. A. Connor, R. I. Biega, L. Leppert, H. I. Karunadasa, *Chem. Science*, Accepted Manuscript (2020).

[3] L. Leppert, S. E. Reyes-Lillo, J. B. Neaton, *J. Phys. Chem. Lett.* **7**, 3683 (2016).

[4] L. Leppert, T. Rangel, J. B. Neaton, *Phys. Rev. Materials* **3**, 103803 (2019).

### 6:10 AM F.EL06.03.08

**Bottom-up Filling of Nanosized Trenches with Silver to Fabricate Transparent Conducting Electrodes** Yorick Bleijl, Andrea Cordaro, Stefan W. Tabernig, Albert Polman and Esther Alarcon-Llado; AMOLF, Netherlands

Transparent conducting electrodes (TCEs) are essential in many optoelectronic devices including solar cells, LEDs, sensors and displays. The most common approach for TCEs is the use of transparent metal oxide layers, in particular Indium tin oxide (ITO). However, ITO comes with numerous drawbacks such as the relatively high cost, fragility, rarity of Indium, strong UV absorption and relatively high sheet resistance. An exciting TCE alternative is the use of interconnected metallic nanowires, where their sub-wavelength cross-sections makes them transparent to visible light [1,2,3].

In this work, we show a promising cost-effective method to fabricate metal nanowire structures using selective-area electrochemical deposition (SAEC). SAEC is based on electrochemical deposition through an insulating template onto a conductive substrate. Next to the low fabrication cost, electrochemical depositions is a bottom-up method with numerous advantages such as scalability, ambient operation conditions, control over nucleation and high purity. While submicron sized features have been already demonstrated by SAEC [4,5], obtaining homogeneous void free filling of features below 100 nm using direct plating is a major challenge because of the terminal effect and the poor control of nucleation of the seed layer.

Here, we have explored the SAEC fabrication of silver nanowire grids over a large area by using soft-conformal imprint lithography as means to fabricate the template on ITO or Si substrates. Numerical simulations of the full electrochemical 3D system have been performed to highlight the influence of ion diffusion, concentration, kinetic parameters and trench aspect ratio on the homogeneous bottom-up filling of the trenches in the template. Finally, we compare the optical and electrical properties of the SAEC-fabricated metal grids with those fabricated using conventional thermal or e-beam evaporation followed by lift-off. This work represents a low-cost and scalable strategy to fabricate sub 100 nm predefined metal structures, enabling the commercial viable fabrication of nanowire based transparent conductive electrodes for optoelectronic devices.

[1]: J. van de Groep, P. Spinelli, A. Polman, *Nano Letters*, **12**, 3138-3144, (2012)

[2]: B. Sciacca, J. van de Groep, A. Polman, E.C. Garnett, *Adv. Matt.*, **28**, 905-909, (2016)

[3]: M.W. Knight, J. van de Groep, P.C.P. Bronsveld W.C. Sinke, A. Polman, *Nano Energy*, **30**, 398-406, (2016)

[4]: D. Josell, S. Ambrozik, M.E. Williams, A.E. Hollowell, C. Arrington, S. Muramoto, T.P. Moffat, *J. Electrochem.*, **166**, D898-D907, (2019)

[5]: T.P. Moffat, J.E. Bonevich, W.H. Huber, A. Stanishevsky, D.R. Kelly, G.R. Stafford, D. Josell, *J. Electrochem.*, **147**, 4524-4535, (2000)

### 6:20 AM \*F.EL06.03.09

**Computationally Driven Design of Improved Transparent Conducting Oxides** David O. Scanlon; University College London, United Kingdom

The combination of electrical conductivity and optical transparency in a single material gives transparent conducting oxides (TCOs) an important role in modern optoelectronic applications such as in solar cells, flat panel displays, and smart coatings. The most commercially successful TCO so far is tin doped indium oxide (Indium Tin Oxide – ITO), which has become the industrial standard TCO for many optoelectronics applications; the ITO market share was 93% in 2013. Its widespread use stems from the fact that lower resistivities have been achieved in ITO than in any other TCO; resistivities in ITO have reached as low as  $7.2 \times 10^{-5} \Omega \text{ cm}$ , while retaining >90% visible transparency. In recent years, the demand for ITO has increased considerably, however, indium is quite a rare metal, having an abundance in the Earth's crust of only 160 ppb by weight, compared with abundances for Zn and Sn of 79000 ppb and 2200 ppb respectively, and is often found in unstable geopolitical areas. The overwhelming demand for ITO has led to large fluctuations in the cost of indium over the past decade. There has thus been a drive in recent years to develop reduced-indium and indium-free materials which can replace ITO as the dominant industrial TCO.[1,2] In this talk I will outline the strategies that we use in the Materials Theory Group to look beyond the current TCO materials, highlighting the interplay of theory and experiment.[3,4]

[1] J. E. N. Swallow et al., *Advanced Functional Materials*, **28**, 1701900 (2018)

[2] M. J. Powell et al., *Chemical Science*, **9**, 7968 (2018)

[3] J. E. N. Swallow et al., *Materials Horizons*, **7**, 236 (2020)

[4] B. A. D. Williamson et al., *Chemistry of Materials*, **32**, 1964 (2020)

### 6:35 AM F.EL06.03.10

**Combinatorial Development of P-Type Transparent Conductive Phosphides** Andrea Crovetto<sup>1,2</sup>, Thomas Unold<sup>1</sup> and Andriy Zakutayev<sup>2</sup>; <sup>1</sup>Helmholtz-Zentrum Berlin, Germany; <sup>2</sup>National Renewable Energy Laboratory, United States

Despite long-standing research efforts to develop p-type transparent conductive materials (TCMs), the current generation of optoelectronic devices still relies exclusively on n-type TCM contacts due to their much better trade-off between conductivity and transparency. An important issue in oxide-based p-type TCMs is the deep energy and localized nature of the 2p oxygen states in the valence band, which has negative consequences on both hole dopability and hole mobility in most oxides.

Recent computational work [1,2] has identified several phosphides (particularly BP and CaCuP) that could potentially outperform the existing p-type TCMs. These phosphides have shallow, disperse valence bands that are ideal for high hole dopability and mobility. Although their indirect band gaps are rather low (around 2 eV), their direct band gaps are much wider and could ensure transparency in thin film samples. However, thin films of CaCuP have not been made yet, and previously reported BP thin films have not been thoroughly evaluated as transparent contacts [3].

Using a unique combinatorial sputter chamber with reactive PH<sub>3</sub> gas, we have mapped the compositional and thermal phase space in BP and CaCuP. To evaluate their potential as p-type TCMs, we have characterized their application-relevant properties (optical transmission, carrier concentration, and mobility) with high-throughput methods.

In this contribution, we will discuss the pros and cons of sputter-deposited BP and CaCuP as prospective p-type TCMs. We will also contextualize their performance metrics by considering their thermal budget, air stability, and compatible substrates. Based on our experience, we will propose potential search strategies for new p-type transparent phosphides.

[1] B. Williamson et al., *Chem. Mater.*, **29**, 2402–2413 (2017).

[2] J. Varley et al., *Chem. Mater.*, **29**, 2568–2573 (2017).

[3] A. Fioretti, M. Morales-Masis, *J. Photonics Energy*, **10**, 042002 (2020)

### 6:45 AM F.EL06.03.11

**Optically Transparent Electrodes Based on Electrically Conductive Boron-Doped Diamond Films for Photoelectrochemical and Optoelectronic Applications** Petr Ashcheulov<sup>1</sup>, Andrew Taylor<sup>1</sup>, Vincent Mortet<sup>1,2</sup>, Ondrej Hak<sup>1</sup>, Marina Davydova<sup>1</sup>, Pavel Hubik<sup>1</sup> and Zdenek Remes<sup>1</sup>; <sup>1</sup>FZU - Institute of Physics of the Czech Academy of Sciences, Czechia; <sup>2</sup>Czech Technical University, Czechia

Transparent conductive electrodes based on metal oxide layers (such as indium tin oxide - ITO and fluorine-doped tin oxide - FTO) are commonly used materials in a variety of optoelectronic devices as they offer adjustable electrical and optical characteristics. However, these conventional transparent conductive oxide (TCO) electrodes possess several drawbacks, such as chemical and/or thermal instability. Such obstacles limit application of TCO's in advanced device structures, which require suitable optoelectronic characteristics following high temperature or chemical treatment [1].

A broad range of carbon-based materials is currently under development as a promising alternative to conventional TCO electrodes. Particularly, synthetic diamond in the form of thin polycrystalline films doped with boron can be optimized for suitable optical transparency and electrical conductivity, such that it enables favorable chemical and thermal characteristics over conventional TCO electrodes [1,2]. Tunable electrical, optical and chemical properties of boron-doped diamond (BDD) predestine the potential for BDD based electrodes for implementation in optoelectronic and energy conversion devices [2,3]. In this work, we report on the development of optically transparent BDD electrodes synthesized using microwave plasma enhanced chemical vapor deposition. The BDD layers with a nanocrystalline form (thickness below 500 nm) were grown on transparent glass substrates and optimized for high optical transmission and low electrical resistivity. To expand potential applicability of fabricated electrodes in various temperature-sensitive structures, synthesis temperature was varied between 250 and 750 °C. The effect of the BDD synthesis temperature on the structural, morphological and optoelectronic properties of fabricated BDD electrodes is discussed. The BDD electrodes were examined by scanning electron microscopy, Raman spectroscopy, optical transmission measurements, Hall effect measurements and secondary ion mass spectroscopy. Additionally, electrochemical characteristics of synthesized BDD electrodes is presented, to highlight applicability of such electrodes in integrated photoelectrochemical systems as a multi-functional coating [2].

This work has been supported by the Grant Agency of the Czech Republic (GACR) contract 19-09784Y.

[1] T.H. Stuchlikova et al., *Phys. Status Solidi B*, 2020, 1900247

[2] P. Ashcheulov et al., *ACS Appl. Mater. Interfaces* 2018, 10, 35, 29552–29564

[3] A. Kovalenko et al., *Sol. Energ. Mat. Sol. C.*, 2015, 134, 73–79.

**6:55 AM \*F.EL06.03.12**

**Machine Learning and Design of Impurity Levels and Band Alignments in Optoelectronic Materials** Arun Kumar Mannodi Kanakkithodi and Maria Chan; Argonne National Laboratory, United States

The prediction of electronic levels introduced by impurities and electronic level alignment at interfaces is critical to the design of optoelectronic materials, particularly for photovoltaic applications, for optimal function. Such prediction is possible using first principles density functional theory (DFT) calculations. Due to both a need to reduce computational cost and a desire to extract design principles, machine learning has increasingly been used to extract relationships between these computed quantities and physical or chemical descriptors of the semiconductor system. In this talk, we will discuss our work on machine learning (ML) of impurity levels in optoelectronic materials including classical II-VI [1], III-V, and group IV semiconductors, as well as hybrid perovskite halides. We will discuss the accuracy and uncertainty quantifications of different approaches for ML. We will also discuss the extension of this approach to prediction of electronic band alignments at interfaces.

[1] Arun Mannodi-Kanakkithodi, Michael Y Toriyama, Fatih G Sen, Michael J Davis, Robert F Klie, Maria KY Chan, "Machine-learned impurity level prediction for semiconductors: the example of Cd-based chalcogenides," *npj Comput Mater* 6, 39 (2020). <https://doi.org/10.1038/s41524-020-0296-7>

**7:10 AM F.EL06.03.13**

**Late News: Modifying the Surface of NiO for Perovskite Solar Cells** Sofia Apergi<sup>1</sup>, Geert Brocks<sup>2,1</sup> and Shuxia Tao<sup>1</sup>; <sup>1</sup>Eindhoven University of Technology, Netherlands; <sup>2</sup>University of Twente, Netherlands

During the last decade, metal halide perovskites have revolutionized the area of renewable energy research. However, the performance of a perovskite solar cell (PSC) depends, not only on the perovskite, but also on the combination and alignment of all its comprising layers, such as electrodes and charge transport layers. NiO is a very promising hole transport layer and its electronic levels need to be optimally aligned with a given perovskite for maximum PSC efficiency. Applying surface modifiers is one of the most widespread strategies to tune its energy levels. Here, we investigate the effect of single layer adsorption of twenty different alkali halides on the electronic levels of NiO, using Density Functional Theory (DFT). Our results show that alkali halides can shift the position of the valence band maximum (VBM) of NiO to a surprisingly large extend in both directions, from -3.10 eV to +1.59 eV. Our results indicate that with alkali halide surface modifiers, the electronic levels of NiO can be tuned robustly and potentially match those of many perovskite compositions in perovskite solar cells.

SESSION F.EL06.04/F.EL08.11: Joint Session: Contacts and Interfaces in Halide Perovskite Drives  
On Demand Abstracts Available for Viewing Starting Saturday Morning, November 21, 2020  
F-EL06

**5:00 AM \*F.EL06.04/F.EL08.11.01**

**Passivated Interfaces and Surface Recombination Velocities in Mixed Cation Mixed Halide Perovskites** David S. Ginger; University of Washington, United States

Surfaces and charge-extracting contacts remain major sources of non-radiative recombination loss; limiting the performance of perovskite PV compared to theoretical limits. We investigate mixed-cation mixed-halide perovskites and demonstrate that, with chemical surface passivation, they can achieve  $>4 \mu\text{s}$  minority carrier lifetimes, and  $>20\%$  external PL quantum yields (PLQY), and nearly single-exponential decay kinetics. This high PLQY observed corresponds to  $\sim 97\%$  of the Shockley-Queisser theoretical quasi-fermi level splitting, a first for MA-free mixed-cation mixed-halide compositions. The high PLQY and long PL lifetimes allow us to measure average surface recombination velocities (SRV)  $<10\text{cm/s}$ , with a champion low of  $\sim 1\text{cm/s}$  (a conservative estimate). We show how such improvements in SRV should lead to an absolute improvement in PCE of  $>4\%$  even with the best of contact alignments. We investigate different MA-free high bandgap compositions, including bandgaps relevant for tandem applications (1.7-1.8eV), and demonstrate performance improvements across all these compositions with our surface passivation strategy. Lastly, using a combination of surface characterization techniques, we show Lewis base interactions of the passivating agent with the perovskite surfaces.

**5:15 AM \*F.EL06.04/F.EL08.11.02**

**Implications of Defects in Defect Tolerant Materials—Understanding Surfaces in Metal Halide Perovskite Solar Materials, Device and Related Systems** Joseph J. Berry<sup>1,2</sup>; <sup>1</sup>National Renewable Energy Laboratory, United States; <sup>2</sup>University of Colorado Boulder, United States

Photovoltaic (PV) devices based on metal halide perovskite (MHP) absorbers have reached outstanding performance over the past few years, surpassing power conversion efficiency of over 25% for lab cells and with large area devices in excess of 16%. For the solar application stability, the most demanding requirement to assess for PV, remains the outstanding issue. The problem of stability motivates basic science driven work on MHP based PV at NREL. Material and device insight can enable MHP PV stability along with the associated opportunities to further improve efficiency, scalability and realize unique device architectures. This talk will highlight work at NREL to develop understanding of defects and interfaces in MHPs and what these experiments indicate regarding the requirements to enhance stability of HPSCs. Discussion will focus on efforts to more carefully understand the implications of processing on a range of defects and interfaces to provide a foundation for enabling the technological requirements for PV and other devices. Ongoing efforts make, measure and ultimately control defects via material formation and processing in the context of high-volume manufacturing will also be touched upon. Hypothesized links between device architecture choices, questions regarding materials integration and coupling of formation along with resulting defects to stability will be discussed. More importantly approaches to move from hypothesis to insight using different experimental approaches will be presented. Work at NREL along these lines to provide critical insight regarding interface formation and passivation that appears to have direct implications for performance and its evolution over time in the resulting devices will be presented. New approaches to understanding the critical physical, chemical and electronic properties to provide predictive insight will also be discussed.

**5:30 AM \*F.EL06.04/F.EL08.11.03**

**Vacuum Deposited Perovskite Solar Cells with Multilayer Charge Selective Contacts** Michele Sessolo, Sang-Hyun Chin, Chris Dreessen, Lidón Gil-Escrig, Ana M. Igual-Muñoz, Beom-Soo Kim, Daniel Perez-del-Rey, Isidora Susic, Kassio P. Zaroni and Henk Bolink; Universitat de València, Spain

In solar cells, perovskite films are typically sandwiched in between charge selective layers, either organic or inorganic semiconductors, as well as their combinations. Electron/hole selectivity results from appropriate alignment of the electronic transport levels of these layers with the electronic bands of the perovskite. While transport layers should efficiently extract the photogenerated charge carriers, they should also not quench the perovskite luminescence to avoid a reduction of the quasi-Fermi level splitting and hence the maximum attainable photovoltage. Finally, ohmic charge injection/extraction and a high built-in potential are desirable to maximize fill factor both in single junction and tandem perovskite solar cells. We will review these design rules using fully vacuum deposited solar cells as a platform, as every layer can be fine-tuned or exchanged without substantially alter the device fabrication. The focus will be on wide bandgap, mixed halide perovskite solar cells, which suffer from a higher voltage deficit as compared to narrow bandgap analogous. We will highlight the importance of using non-quenching, energetically-matched hole and electron transport layers in order to reduce non-radiative charge recombination losses. Novel strategies and multilayers structures (including inorganic, organic and ionic compounds) to improve the device functioning will be presented. The implication for the perovskite compositional stability as well as for the device lifetime will also be discussed.

**5:45 AM \*F.EL06.04/F.EL08.11.04**

**Approaches to Defect Mitigation in Halide Perovskites** Nakita K. Noel; Princeton University, United States

Within a decade, there has been a surge of interest into halide perovskite semiconductors. With tuneable bandgaps, versatile and facile deposition processes and excellent optoelectronic properties, these materials have found applications in photovoltaics (PV), broad-spectrum photodetectors, light-emitting diodes and lasers. While research into using these materials for emission and X-ray detection applications is now beginning to surge; currently, halide perovskites are most well known for their remarkable PV performance, with perovskite solar cells achieving certified power conversion efficiencies exceeding 25% in a remarkably short developmental timescale. Despite the truly impressive device performance, these materials have not yet reached their full potential. The major obstacle to this is an incomplete understanding of crystallisation processes, as well as defects which exist on the surfaces and interfaces of perovskite thin-films. Deficiencies at these interfaces, likely formed during the crystallisation process, are responsible for the major losses in perovskite-based optoelectronic devices; limiting charge extraction, increasing non-radiative recombination, contributing to hysteresis and increasing the voltage-loss of perovskite photovoltaics. Herein, I will present various effective strategies to reduce the defect densities of perovskite films and thus improve the performance of perovskite optoelectronic devices. First, I will discuss how



manipulating precursor solutions can have significant impact on the quality of the perovskite films, through enabling reduced defect density. Consequently, this is one approach which can be used to boost device performance. Next, I will focus on a strategy in which we extrinsically modify the bottom interface of perovskite solar cells such that the crystallization of the perovskite yields films with fewer defects. Specifically, we show that ionic liquids can have a dramatic effect on the interfacial trap density in a perovskite solar cell. And finally, I will illustrate an approach in which we manipulate the charge-carrier density in the perovskite thin-film after its fully crystallized. We utilise molecular dopants to significantly alter the interfacial energetics in order to suppress non-radiative recombination losses. As a result, we observe a boost in both performance and stability. Importantly, these interface modification strategies can be used in tandem, resulting in further improvements in device efficiency. The utility of these defect mitigation strategies can readily be applied beyond perovskite PV and is likely to also improve the performance of a range of other perovskite-based optoelectronic devices.

#### 6:00 AM F.EL06.04/F.EL08.11.05

**Transparent Conducting Oxides for Upscalable Solar Cells—Assessing Deposition Methods** Yury Smirnov<sup>1</sup>, Laura Schmengler<sup>1</sup>, Riemer Kuik<sup>1</sup>, Pierre-Alexis Repecaud<sup>1</sup>, Mehrdad Najafi<sup>2</sup>, Sjoerd Veenstra<sup>2</sup>, Erkan Aydin<sup>3</sup>, Stefaan De Wolf<sup>3</sup> and Monica Morales-Masis<sup>1</sup>; <sup>1</sup>University of Twente, Netherlands; <sup>2</sup>TNO-Solliance, Netherlands; <sup>3</sup>King Abdullah University of Science and Technology (KAUST), Saudi Arabia

Transparent electrodes are essential components of several kinds of high-efficiency solar cells. The photovoltaic devices working in the broadband spectra, from the ultraviolet (UV) to the near-infrared (NIR), require minimized parasitic absorption and high conductivity for these electrodes. Transparent conductive oxide (TCO) thin films are widely accepted choices for such applications. Among various successful TCOs, recently, Zr-doped indium oxide (IZrO) has been demonstrated as a broadband transparent and conductive material suitable for silicon heterojunction (SHJ) and silicon/perovskite tandem solar cells.<sup>1,2</sup> The main advantage of IZrO is combining specifications of wide bandgap, high carrier density, and high electron mobility in the same material.

Magnetron sputtering is by far the most established technique to fabricate TCO layers. During sputtering target material is removed in a ballistic process that sensitively depends on many interconnected processing parameters. This makes a stoichiometric transfer of target material challenging, while high kinetic energies of the arriving species may damage sensitive functional layers beneath. Conversely, in Pulsed Laser Deposition (PLD), the energy source for material ablation is physically decoupled from the vacuum equipment. This favors the stoichiometric transfer of the target material as well as provides a larger choice for deposition pressures and thermalizing the arriving species.

Despite these advantages, PLD is still considered an exotic fabrication method within the photovoltaic community due to the common concerns about the scalability of the technique reasoned by the small sample size for uniform coating and low deposition rates. In fact, significant progress in the upscaling of PLD<sup>3</sup> has already allowed fabrication of high-quality films by on 200 mm circular wafers and fabrication of superconducting tape with deposition rates  $> 750 \text{ nm/min}^4$ , which is considerably high deposition rate.

In our work, we introduce wafer-scale (4") room-temperature fabrication of high-mobility IZrO by PLD with deposition rates on par ( $>3 \text{ nm/min}$ ) with lab-scale RF sputtering equipment. We studied the optoelectronic properties and microstructure of the films and made a comparison with IZrO films grown by RF sputtering, both fabricated from an IZrO solid target with the same composition.

X-ray diffraction (XRD) reveals that as-deposited IZrO films are amorphous with small embedded nanocrystals. Their orientation is preserved as the preferred one after solid-phase crystallization at 200 °C. IZrO films exhibit excellent optoelectrical properties combining low absorptance ( $<10\%$ ) in the measured range (300-1500 nm) with high mobility ( $>60 \text{ cm}^2/\text{Vs}$ ) leading to impressive sheet resistivity ( $R_{\text{sh}}$ ) of  $<20 \text{ Ohm/sq}$  for a 100-nm PLD grown film.

When applied as a front electrode in solar cells, IZrO enables high short circuit currents and the possibility to reduce the amount of indium by reducing the thickness of the films compared to standard ITO, which is critical considering the large scale utilization of such materials. On the other hand, higher deposition pressures during PLD fabrication offer a promising way to mitigate the sputter-induced damage for the deposition of rear transparent electrodes on top of sensitive functional layers as in the perovskite solar cells, which opens new opportunities for the development of high-efficiency tandem solar cells.

#### References

1. M. Morales-Masis *et al.*, *IEEE J. Photovoltaics*, vol. 8, no. 5, p. 1202–1207, 2018.
2. E. Aydin *et al.*, *Advanced Functional Materials*, vol. 29, no. 25, p. 1901741, 2019.
3. J. A. Greer, *Journal of Physics D: Applied Physics*, vol. 47, no. 3, p. 034005, 2013.
4. S. Lee *et al.*, *Superconductor Science and Technology*, vol. 27, no. 4, p. 044022, 2014.

#### 6:10 AM F.EL06.04/F.EL08.11.06

**Overcoming Redox Reactions at Perovskite/Nickel Oxide Interfaces to Boost Voltages in Perovskite Solar Cells** Caleb C. Boyd<sup>1</sup>, R. C. Shallcross<sup>2</sup>, Neal R. Armstrong<sup>2</sup> and Michael McGehee<sup>3</sup>; <sup>1</sup>Stanford University, United States; <sup>2</sup>The University of Arizona, United States; <sup>3</sup>University of Colorado Boulder, United States

Metal halide perovskite solar cells have largely fulfilled their potential of combining III-V-like optoelectronic properties with low-cost, solution-processing deposition techniques, achieving single-junction power conversion efficiencies (PCEs) >25%. A semiconducting nickel oxide (NiO<sub>x</sub>) thin film is a highly desirable wide bandgap hole harvesting contact for perovskite solar cells and organic solar cells because it is low-cost, stable, and readily scalable. (1) Perovskite solar cells with NiO<sub>x</sub> HTLs have delivered some of the best reported stability results under a variety of stressors, including the 85°C/85% relative humidity damp heat test, temperature cycling from -40°C to 85°C, and extended operational stability at elevated illumination and temperature. (2, 3) However, perovskite solar cells made with NiO<sub>x</sub> HTLs typically result in lower open-circuit voltages ( $V_{OC}$ ) compared to ultra-thin, undoped organic hole transport layers, which are more expensive and present problems for both scalability and stability. Enhancing the  $V_{OC}$  and increasing efficiency of NiO<sub>x</sub>-based devices will directly result in a decreased photovoltaic module cost (\$/W).

Here, we identify a surface-assisted electron transfer-proton transfer (ET-PT) mechanism at the NiO<sub>x</sub>/perovskite interface leading to barriers for hole harvesting and device  $V_{OC}$  loss. Specifically, under-coordinated metal cation sites (Ni<sup>2+3+</sup>) act both as a Lewis acid/oxidant towards dissociated lead halide precursors (i.e. I) and as a Brønsted base (proton-acceptor) with protonated amine precursors, forming A-site deficient – and therefore PbI<sub>2-x</sub>Br<sub>x</sub>-rich – perovskite at the perovskite/NiO<sub>x</sub> interface. This defective perovskite region both increases recombination at the interface and acts as a hole extraction barrier, resulting in device  $V_{OC}$  loss.

We demonstrate the elimination of the extraction barrier via a simple, easily scaled approach: titration of surface oxide proton-acceptor sites by incorporating 1-5 mol% excess A-site cation to the perovskite precursor solution. This amount is sufficient to counteract the loss of organic cation, preventing formation of a PbI<sub>2-x</sub>Br<sub>x</sub> layer at the interface, ultimately leading to a  $V_{OC}$  increase >200 mV. We demonstrate that this mechanism applies to all forms of NiO<sub>x</sub>, including thin films created from sol-gel precursors, nanoparticles, atomic layer deposition (ALD), and radio frequency (RF) sputtering, and is generalizable across multiple perovskite active layers, including state-of-the-art single junction and tandem relevant compositions. A p-i-n perovskite solar cell with 19.7% PCE at maximum power point (MPP) and  $V_{OC}$  up to 1.15 V is achieved. Devices maintain >90% of their initial performance after 2000 hours of thermal stability testing at 85 °C or >80% of their initial performance after 400 hours of accelerated operational stability testing under illumination and 55 °C in nitrogen. Our results extend the generality of acid/base-coupled oxidation-reduction reactions as the driving force for interface equilibration at metal oxide/perovskite interfaces, suggesting that metal halide perovskites have similar reactions with many types of metal oxide layers.

1. M. D. Irwin, D. B. Buchholz, A. W. Hains, R. P. H. Chang, T. J. Marks, p-Type semiconducting nickel oxide as an efficiency-enhancing anode interfacial layer in polymer bulk-heterojunction solar cells. *Proc. Natl. Acad. Sci.* **105**, 2783–2787 (2008).
2. C. C. Boyd, R. Cheacharoen, T. Leijtens, M. D. McGehee, Understanding Degradation Mechanisms and Improving Stability of Perovskite Photovoltaics. *Chem. Rev.* **119**, 3418–3451 (2019).
3. J. Xu, C. C. Boyd, Z. J. Yu, A. F. Palmstrom, D. J. Witter, B. W. Larson, R. M. France, J. Werner, S. P. Harvey, E. J. Wolf, W. Weigand, S. Manzoor, M. F. A. M. van Hest, J. J. Berry, J. M. Luther, Z. C. Holman, M. D. McGehee, Triple-halide wide-band gap perovskites with suppressed phase segregation for efficient tandems. *Science*. **367**, 1097–1104 (2020).

**6:20 AM F.EL06.04/F.EL08.11.07**

**Balancing the Electronic Structure of Flexography-Printed NiO for Rapid Scaling of Perovskite Solar Cells** Julia Huddy, Andrew B. Hamlin, Francesco Guarnieri and William J. Scheideler; Dartmouth College, United States

Perovskite solar cells (PSCs) have potential to deliver TW-scale energy via low-cost manufacturing. However, scaling is limited by slow, high temperature annealing of the inorganic transport layers and insufficient understanding of how scalable processing impacts interfacial device physics. This study addresses the NiO, a leading hole transport layer (HTL) for both high-stability single junction architectures and tandem cells. We present a method for scaling ultrathin NiO HTLs by pairing high-speed (60 m/min) flexographic printing with a rapid annealing Cu:NiO sol-gel ink. By engineering precursor rheology for rapid film-leveling, large area (> 50 cm<sup>2</sup>) NiO HTLs were flexographically printed with high uniformity and photovoltaic performance matching that of spin coated films. Doping and the combustion precursor design enables 30X faster annealing while reducing intrinsic variability of work function and conductivity originating from NiOH surface species.

Integrating these printed transport layers in planar inverted PSCs allows rapid fabrication of high-efficiency (PCE > 16 %) Cs<sub>x</sub>FA<sub>1-x</sub>PbI<sub>1-y</sub>Br<sub>y</sub> solar cells with low hysteresis and open circuit voltages ( $V_{OC}$ ) of 1.11 V. XPS studies of the transition from

Ni-OH to Ni-O bonding for low-temperature annealed NiO clarify the balance required for both effective carrier collection and high photostability. Paired with variable illumination intensity measurements and detailed transient photovoltage characterization, these measurements provide an improved understanding of the intrinsic defects present at the NiO-perovskite interface and the impact of scalable synthesis of interfacial charge transport layers.

#### 6:30 AM F.EL06.04/F.EL08.11.08

**Late News: Interfacial Engineering in High Efficiency Vacuum Deposited Perovskite Solar Cells—From Metal Oxide Extraction Layers to Large Area Devices** Daniel Perez-del-Rey<sup>1</sup>, Henk Bolink<sup>1</sup> and Pablo P. Boix<sup>2</sup>; <sup>1</sup>University of Valencia, Spain; <sup>2</sup>Institut de ciència del materials, Spain

Vacuum deposition is a key technique in the field of perovskite photovoltaics due to the advantages it presents with respect to the classical deposition methods such as solution processed perovskites. The lack of solvents and the need of annealing makes it a good candidate for industrialization and upscaling as it has already been demonstrated in the OLED field. Despite its advantages, tuning the interfaces is essential to reach the high power conversion efficiencies found in solution processed perovskite solar cells. Metal oxides are an interesting choice for extraction layers due to their improved stability and reduced parasitic absorption. In this work we present our recent advances in using metal oxides as extraction layers optimising the interfaces in order to reach record open circuit voltages in CH<sub>3</sub>NH<sub>3</sub>PbI<sub>3</sub> perovskite and using MoO<sub>3</sub> as extraction layer by molecular passivation in both PIN and NiP structure improving the stability and opening new possibilities for tandem applications. We also show how we implemented this stable pinhole-free bottom layers in large area devices and mini modules, which is very promising for future industrial purposes.

SESSION F.EL06.05: Deposition Methods for PV and Optoelectronic Contact Materials  
On Demand Abstracts Available for Viewing Starting Saturday Morning, November 21, 2020  
F-EL06

#### 5:00 AM \*F.EL06.05.01

**Atomic Layer Deposition of Electron and Hole Transport Layers for Perovskite Solar Cells** Stacey F. Bent; Stanford University, United States

The power conversion efficiency (PCE) of metal halide perovskite solar cells has shown rapid improvement since their inception over a decade ago, recently surpassing 25%. Stabilizing these devices for long-term operation is needed for their future commercial success. In addition to good external encapsulation, engineering electron and hole contact layers and their interfaces with the perovskite absorber are a means to achieving this goal. Atomic layer deposition (ALD) has emerged as a powerful tool for the growth of these contact layers due to the nanoscale control it affords over film thickness and composition. In this work, we will describe the significant impact that ALD metal oxide contacts can have on improving the long-term operational stability of perovskite solar cells. We show that unencapsulated, single-junction p-i-n perovskite devices with metal electrodes that incorporate ALD SnO<sub>2</sub> electron contacts exhibit high initial PCEs (up to 18.5%), and maintain on average 82% of their initial PCE following 250 hours of continuous, illuminated operation at maximum power in air at 60 °C. This result is a marked improvement over devices with only organic contacts, which lose all PCE after only 20 hours in the same harsh testing conditions. We also describe the development of ALD VO<sub>x</sub> hole contact layers for n-i-p perovskite solar cells. We demonstrate that unencapsulated devices with ALD VO<sub>x</sub>, a more stable alternative to the commonly used material of evaporated MoO<sub>x</sub>, retain on average 71% of their initial PCE when aged for 1100 hours in ambient atmosphere with constant illumination and bias at 70 °C. The vapor deposition strategies described in this work can be applied to various perovskite solar cell designs, including tandem or non-planar devices, and provide a framework for improving the quality of barrier/encapsulation layers in other optoelectronic technologies.

#### 5:15 AM F.EL06.05.02

**Scalable Open-Air Deposition of Compact ETL TiO<sub>x</sub> on Perovskite for Fullerene-Free Solar Cells** Justin P. Chen<sup>1</sup>, Florian Hilt<sup>2</sup>, Nicholas Rolston<sup>1</sup> and Reinhold H. Dauskardt<sup>1</sup>; <sup>1</sup>Stanford University, United States; <sup>2</sup>Institut Photovoltaïque d'Île-de-France, France

Inorganic charge transport layers have not been readily adopted as the sole charge transport layer on top of perovskite in inverted P-I-N architectures because processing methods that involve high temperature annealing, particle bombardment, or

sol-gels damage the perovskite layer. We report on a scalable, low-temperature TiO<sub>x</sub> electron transport layer (ETL) produced directly on top of perovskite in an inverted architecture device by an open-air chemical vapor deposition (OA-CVD) process. It is an attractive low-energy and low-temperature alternative involving simple equipment that can be adopted for roll-to-roll and sheet-to-sheet processing, compatible with industrial manufacturing.

The OA-CVD pyrolysis of a titanium ethoxide precursor forms a fully inorganic, conformal, and compact TiO<sub>x</sub> film while preserving the underlying perovskite structure. The resultant film is mechanically robust and exhibits a fracture toughness 30-fold higher than commonly used fullerene-based ETL films. The TiO<sub>x</sub> is an effective barrier layer against environmental degradation—unencapsulated devices with the TiO<sub>x</sub> ETL retain 60% of their initial efficiency after 1000 hours in ambient aging conditions—compared to devices with a fullerene ETL which were inoperable after 144 hours. TiO<sub>x</sub> ETL films on top perovskite demonstrate comparable photoluminescence responses with a commonly used organic C<sub>60</sub> ETL counterpart. Inverted architecture devices with an optimized TiO<sub>x</sub> ETL thickness of 70nm exhibited high open-circuit voltages of 1.08V. We comment on the photocatalytic properties of TiO<sub>x</sub> and the influence of an amorphous film on maximum power point stability.

### 5:25 AM F.EL06.05.03

**Rapid Vapor-Phase Deposition of High-Mobility *p*-type Buffer Layers on Perovskite Photovoltaics for Efficient Semi-Transparent Devices** Rob Jagt<sup>1</sup>, Tahmida Huq<sup>1</sup>, Sam A. Hill<sup>1</sup>, Maung Thway<sup>2</sup>, Tianyuan Liu<sup>2</sup>, Mari Napari<sup>1</sup>, Bart Roose<sup>1</sup>, Krzysztof Galkowski<sup>1</sup>, Weiwei Li<sup>1</sup>, Serena Fen Lin<sup>2</sup>, Samuel D. Stranks<sup>1</sup>, Judith MacManus-Driscoll<sup>1</sup> and Robert Hoye<sup>3</sup>; <sup>1</sup>University of Cambridge, United Kingdom; <sup>2</sup>Solar Energy Research Institute of Singapore, Singapore; <sup>3</sup>Imperial College London, United Kingdom

Perovskite solar cells (PSCs) with transparent electrodes can be integrated with existing solar panels in tandem configurations to increase the power conversion efficiency. A critical layer in semi-transparent PSCs is the inorganic buffer layer, which protects the PSC against damage when the transparent electrode is sputtered on top. The development of *n-i-p* structured semi-transparent PSCs has been hampered by the lack of suitable *p*-type buffer layers. In this presentation we develop a *p*-type CuO<sub>x</sub> buffer layer, which can be grown uniformly over the perovskite device without damaging the perovskite or organic charge transport layers, can be grown using industrial scalable techniques and has high hole mobility ( $4.3 \pm 2 \text{ cm}^2 \text{ V}^{-1} \text{ s}^{-1}$ ), high transmittance (>95%), and a suitable valence band maximum for hole extraction ( $5.3 \pm 0.2 \text{ eV}$ ). Semi-transparent PSCs with efficiencies up to 16.7% are achieved using the CuO<sub>x</sub> buffer layer. Using these as top-cells, we demonstrate four-terminal tandems with two types of silicon bottom cells made using industrially-relevant methods, achieving efficiencies reaching 24.4%. Our work provides a new approach to integrate the most efficient architecture for PSCs in tandems, as well as other applications requiring semi-transparent devices, such as photoanodes for bias-free solar fuel production, transistors with transparent electrodes, or for spectroscopy on devices under operation.

### 5:35 AM F.EL06.05.06

**Uniform Deposition of 1D and 2D Materials Driven by Superhydrophilicity for Transparent Conductive Interfaces** David W. Fox, Anthony Schropp, Trisha Joseph, Nilab Azim, Yuen Yee Li Sip and Lei Zhai; University of Central Florida, United States

Transparent conductive film (TCF) materials have become a critical area of research in the field of optoelectronics. Although indium tin oxide (ITO) has traditionally excelled as such a material, device specifications have moved towards flexible designs with milder treatments, and with indium a scarce resource, other materials have begun to replace ITO. Electrodes composed of 1D and 2D materials have matched the high performance of ITO, with very mild deposition processes. We utilized a superhydrophilic antireflective surface to investigate the impact of nanocapillary forces on the deposition of 1D and 2D materials using silver nanowires (AgNWs) and graphene oxide (GO), as model 1D and 2D materials, respectively. A layer-by-layer deposition of silica nanoparticles (SiNPs) and poly(allylamine hydrochloride) (PAH) was used to produce the superhydrophilic antireflective surfaces. The influence of the nanocapillary forces on the deposition of AgNWs and GO from their suspensions solution processed films was investigated. It was discovered that the coffee-ring effect during deposition was suppressed by the nanocapillary forces. The performance of our TCFs prepared with AgNWs on the superhydrophilic antireflective coatings was evaluated. A TCF of  $25.0 \Omega \text{ sq}^{-1}$  with a transparency of 92.1 % transmittance was obtained without removing the substrate background. This TCF reached a figure of merit of  $1.76 \times 10^{-2}$  and retained the wetting properties of the nanoporous coating. The superhydrophilic antireflective surfaces with AgNWs showed an areal root mean square roughness ( $S_q$ ) 28.41 nm, and the roughness was brought down to 15.67 nm with gradual coating of GO.

### 5:45 AM \*F.EL06.05.07

**Schottky Barriers and Selective Contacts Using Atomic Layer Deposited Interface Layers** Nick C. Strandwitz; Lehigh

University, United States

Electrical contacts are critical to nearly all semiconductor devices, and the behavior of these contacts can have massive implications to overall device performance. Decades of research into metal-semiconductor contacts continues today because of their complexity and our modern ability to control and probe these interfaces.

Our work, primarily in the context of photovoltaics, examines two classifications of modified metal-semiconductor contacts: Metal-insulator-semiconductor (MIS) Schottky barriers, and selective contacts based on metal oxides. MIS contacts were indeed the foundation of some of the first PV devices, but quickly gave way to p-n junction architectures because of greater stability and power conversion efficiency in the latter architecture. Using device physics simulations, we show that if proper junction properties can be created (Schottky barrier height, interface passivation), MIS-type PV devices can approach efficiencies of p-n homo- and hetero-junction cells. Our work exploring the interface properties of MIS structures for PV makes use of purposeful chemical surface preparation and the deposition of well-controlled oxide insulators using atomic layer deposition (ALD). I will discuss several observations including the role of fixed interface charge and interface layer thickness on Schottky barrier height.

Secondly, so-called “selective contacts” have been examined to boost efficiency of p-n and heterojunction silicon PV, and also to provide PV junctions without the need for traditional p-n junctions, similar to the MIS Schottky barrier case. In both cases, it can be argued that such contacts may reduce processing costs due to the low temperatures for the deposition of these materials. Notable developments include electron and hole-selective thin films that provide selective transport for one carrier while often reducing interfacial recombination rates. Our studies explore the introduction of aluminum oxide tunnel layers sandwiched between crystalline silicon and selective contact materials such as  $\text{MoO}_x$ . The potential impact of this configuration is to 1) increase in stability of the junction and 2) and increase in performance through minimization of carrier recombination at the contact. We have examined the role of the alumina layer thickness on interface quality and specific contact resistance. We also examined the role of several deposition techniques and explore the different processing conditions that modify the interfacial electronic properties of these passivated contacts.

#### 6:00 AM F.EL06.05.09

##### **High-Performance Perovskite Optoelectronic Devices with Inorganic Nanopillar Arrays Functioning as Charge Transport Layers** Zhifeng Huang; Hong Kong Baptist University, Hong Kong

One-dimensional (1D) nano-arrays can reduce light reflection loss, suppress recombination dynamics, guide charge carrier transport, and relax stress and strain in flexible optoelectronic devices, and thus result in improving optoelectronic function and stability under mechanical bending. However, *in-situ* fabrication of 1D nano-arrays, especially on polymer-based flexible electrodes, is very challenging, mainly due to degradation of the flexible electrodes at high temperature of the *in-situ* growth. In this talk, I will present that nanopillar arrays (NaPAs), made of  $\text{NiO}_x$  (function as hole transport layers)[1] and  $\text{TiO}_2$ ,  $\text{SnO}_2$  and metal Ti (serving as electron transport layers), are *in-situ* deposited onto a rigid/flexible electrode by glancing angle deposition (GLAD), and then are hybridized with perovskite to generate solar cells and photodetectors. The as-grown NaPAs enhance light transmittance, facilitate light harvesting in perovskite, facilitate the formation of large perovskite grains, prohibit exciton recombination dynamics, promote charge carrier transport and collection, and prevent the perovskite decomposition. All these advanced features lead to excellent performance of the hybrid perovskite-based optoelectronic devices with good anti-aging and mechanic stability. We devise an advanced technique of low-substrate-temperature GLAD generally adapted to *in-situ* deposit charge carrier transport layers made of inorganic NaPAs on flexible electrodes, to significantly enhance optoelectronic performance of flexible devices.

#### References

[1] S. Cong, G. F. Zou,\* Y. H. Lou, H. Yang, Y. Su, J. Zhao,\* C. Zhang, P. P. Ma, Z. Lu, H. Y. Fan,\* and **Z. F. Huang,\*** Fabrication of Nickel Oxide Nanopillar Arrays on Flexible Electrodes for High-Efficient Perovskite Solar Cells, *Nano Lett.* 2019, 19, 3676-3683.

#### 6:10 AM \*F.EL06.05.10

##### **Progress in Perovskites, Quantum Dots and Interfaces** Edward H. Sargent; University of Toronto, Canada

I will discuss progress in interface management in, and among, perovskites and quantum dots, especially in relation to photovoltaics.

**5:00 AM \*F.EL06.06.01**

**Improved Infrared Light Management with Amorphous Silicon in High Efficiency Silicon Heterojunction Solar Cells** Weiyuan Duan, Karsten Bittkau, Andreas Lambertz, Paul Steuter, zhirong yao, Kaifu Qiu and Kaining Ding; IEK5-Photovoltaik, Forschungszentrum Jülich GmbH, Germany

Silicon heterojunction (SHJ) solar cells coupled with hydrogenated intrinsic amorphous silicon (a-Si:H) layers enable high open-circuit voltages ( $V_{oc}$ ) of up to 750 mV, but suffer from short-circuit current density ( $J_{sc}$ ) losses due to parasitic absorption in a-Si:H, transparent conductive oxide (TCO) layers and shadowing of the metal fingers. Significant improvement in  $V_{oc}$  is expected only for thinner wafer. Increasing  $J_{sc}$  is a more promising route to further improve cell efficiency. Besides the use of high bandgap materials such as nanocrystalline silicon oxide or low carrier density TCO layers to reduce parasitic absorption, an improved light trapping that enables more light to be absorbed within the silicon wafer represents another important opportunity for  $J_{sc}$  improvement, which becomes even more significant when thinner wafers are used. In this work, a thin intrinsic a-Si:H layer was introduced after metallization of SHJ solar cell, formed a TCO/a-Si:H back reflector. Unlike sophisticated structures such as diffraction gratings, black silicon or other kind of nanophotonics, TCO/a-Si:H back reflector is much easier to be fabricated. Compared with the very often used silver back reflector, a-Si:H is less expensive and can still keep some of the bifaciality of the cells.

The intrinsic a-Si:H layer was deposited by plasma enhanced chemical vapor deposition (PECVD). It has a refractive index of around 4 at infrared (IR) wavelengths extracted from ellipsometry measurement. Sentaurus TCAD simulation was used for the rear optics in terms of optimizing the thickness of TCO/a-Si:H stack. We systematically investigated how the TCO/a-Si:H back reflector increases rear internal reflectance by measuring reflectance and external quantum efficiency before and after deposition of the a-Si:H layer. As predicted from simulation, due to increased IR reflection,  $J_{sc}$  was 0.4 mA/cm<sup>2</sup> higher with TCO/a-Si:H back reflector when applied on SHJ solar cells using 110 mm thickness wafer, while fill factor ( $FF$ ) and  $V_{oc}$  remained constant. Combined with an optimized front MgF<sub>2</sub> double antireflection coating, we could demonstrate a 0.9 mA/cm<sup>2</sup> improvement in  $J_{sc}$ , which boosts the cell efficiency by 0.5%. Ultimately, a M2 size total area cell efficiency of 23.7% has been achieved with  $V_{oc}$  of 745 mV,  $J_{sc}$  of 39.4 mA/cm<sup>2</sup> and  $FF$  of 80.8% on 110 um thin wafer. It's worth noting that the cell still kept a bifaciality of more than 50%. The reflector concept introduced here has a possibility to be used in advanced double-glass module encapsulation.

**5:15 AM \*F.EL06.06.02**

**Efficient Hole-Selective Passivating Contacts for Si Photovoltaics** Takuya Matsui and Hitoshi Sai; AIST, Japan

Hydrogenated amorphous silicon (a-Si:H) is a key material in realizing efficient passivating contacts for Si solar cells known as the silicon heterojunction (SHJ) technology. However, one drawback of the SHJ solar cells is that the a-Si:H, particularly when doped with boron, gives rise to a parasitic optical absorption loss due to its high absorption coefficients in the visible wavelengths. This adverse effect is pronounced in bifacial solar cells, as this type of device allows illumination from both the front and the rear surfaces. Here we pursued alternative materials focusing on hole-selective passivating contacts: one is the hydrogenated nanocrystalline Si (nc-Si:H) and the other is the novel metal-oxide material. For the nc-Si:H material, it is demonstrated that the replacement of (p)a-Si:H by (p)nc-Si:H provides not only an increase of  $J_{sc}$ , but also improvements in  $V_{oc}$  and  $FF$ . This results in an efficiency increase by 0.6% absolute compared to our reference cell with (p)a-Si:H, and a best cell efficiency of 23.5%. The factors that alter the optimum hole contact layer thickness depending on the material and deposition condition will be discussed. For the metal-oxide material, we have developed an atomic-layer-deposited TiO<sub>x</sub> nanolayer that functions as an efficient and transparent hole-selective passivating contact, leading to proof-of-concept solar cells with efficiencies above 20%. This new function of TiO<sub>x</sub> is opposite from the previous understanding that it acts solely as electron contact.

**5:30 AM F.EL06.06.03**

**Atomic Layer Deposited Metal Oxide Bilayers for Metal-Insulator-Semiconductor Photovoltaics** Benjamin Davis and Nick C. Strandwitz; Lehigh University, United States

The use of metal-insulator-semiconductor (MIS) tunnel diodes as photovoltaics (PVs) relies on the Schottky barrier between the metal and semiconductor, which induces band bending in the semiconductor absorber allowing for efficient separation of

electrons and holes. In the years following early MIS PV research in the 1970s and 1980s, the advent of atomic layer deposition (ALD) has provided a tool for enhanced control of ultrathin film deposition. One method to potentially improve MIS PV performance is the use of ALD oxide bilayers as tunnel insulators. Oxides with different oxygen areal densities have been demonstrated to form interfacial dipoles, manipulating the Schottky barrier. Previous studies have only explored the impact of dipoles between a single ALD oxide and interfacial SiO<sub>x</sub>. The present work combines two ALD oxides, one (AlO<sub>x</sub>) with oxygen areal density higher than that of SiO<sub>x</sub> and another (LaO<sub>x</sub>) with oxygen areal density lower than that of SiO<sub>x</sub> according to literature. It has been hypothesized that the greater oxygen areal density difference would result in a greater impact on the Schottky barrier. It is demonstrated that, compared to AlO<sub>x</sub> alone, an ALD LaO<sub>x</sub>/AlO<sub>x</sub> stack increases the average n-Si/Ni Schottky barrier height from 0.63 to 0.70 eV, and the average p-Si/Al barrier height from 0.81 to 0.90 eV. LaO<sub>x</sub> was the oxide in direct contact with the Si substrate. The observation that the barrier height increases for both substrate types suggests that the effect is due to the ability of LaO<sub>x</sub> to depin the Fermi level rather than an interfacial dipole.

#### 5:40 AM F.EL06.06.04

**Exploiting Fixed Charge to Control Schottky Barrier Height in Si|Al<sub>2</sub>O<sub>3</sub>|MoO<sub>x</sub>—Based Tunnel Diodes** Ben Garland, Benjamin Davis and Nick C. Strandwitz; Lehigh University, United States

Carrier selective contacts have become one of the leading advancements in photovoltaics with the most efficient structures exceeding 26% conversion efficiency. Selective carrier conduction implies that one type of charge carrier is preferentially collected at an electrical contact. Carrier selectivity increases the efficiency of solar cells by reducing recombination at metal contacts and avoiding highly doped emitter layers. Popular selective contact materials are often transition metal oxides (TMOs) due to high optical transparencies and large work functions that are useful for hole selective contacts to silicon. In contrast to previous articles, recent studies have indicated that the interface of p-type silicon and the molybdenum oxide (MoO<sub>x</sub>) exhibits a significant Schottky barrier that decreases the efficiency of hole-selective contacts by impeding majority carrier hole collection. To alleviate this issue, atomic layer deposited (ALD) alumina (Al<sub>2</sub>O<sub>3</sub>) might be added between Si wafer and MoO<sub>x</sub> with the expectation to generate a negative interface fixed charge ( $N_f$ ) after annealing, decreasing band bending. ALD Al<sub>2</sub>O<sub>3</sub> also has the ability to passivate interface traps with diffusion of precursor hydrogen during annealing. In this work, we hypothesize that insertion of a tunneling ALD Al<sub>2</sub>O<sub>3</sub> layer between MoO<sub>x</sub> and p-type Si will enable Schottky barrier height ( $\Phi_{bh}$ ) minimization that is tunable with  $N_f$ , enabling a high efficiency hole-selective contact. Since there should not be quantifiable  $N_f$  in tunneling Al<sub>2</sub>O<sub>3</sub> using capacitance-voltage (C-V) analysis, non-tunneling n-Si|Al<sub>2</sub>O<sub>3</sub>|Al MOSCAP structures were used to determine ideal processing for maximum negative  $N_f$ . The ALD growth of Al<sub>2</sub>O<sub>3</sub> utilized trimethylaluminum and H<sub>2</sub>O at 4 deposition temperatures. Half of the samples were annealed at 425°C in a nitrogen atmosphere prior to the application of Al contacts. After  $N_f$  quantification, p-Si|Al<sub>2</sub>O<sub>3</sub>|MoO<sub>x</sub>|Al tunnel diodes with thin (~1 nm) as-deposited and annealed Al<sub>2</sub>O<sub>3</sub> layers were fabricated to determine  $\Phi_{bh}$ . Current density-voltage-temperature (J-V-T) and Mott-Schottky  $1/C^2$ -V measurements were used to establish a range for  $\Phi_{bh}$ . Both methods showed that the as-deposited tunneling Al<sub>2</sub>O<sub>3</sub> diodes had a higher  $\Phi_{bh}$  compared to the diodes with annealed tunneling Al<sub>2</sub>O<sub>3</sub>, and therefore also supported the existence of a  $\Phi_{bh}$  at the Si|MoO<sub>x</sub> interface. Future work will involve using larger barrier height diodes using n-Si to more accurately calculate  $\Phi_{bh}$  and confirm or reject the phenomenon observed.

#### 5:50 AM \*F.EL06.06.05

**Organic-Silicon Heterojunction for Solar Cell and Integrated Flexible Energy Devices** Baoquan Sun; Soochow University, China

Numerous alternative materials and solar cell device structures have been widely explored in order to reduce the cost of photovoltaic (PV) manufacture. Organic-inorganic component solar cells based on nanostructured semiconductor have built up in past two decades, which may promise the potentially low cost and high performance. However, the device performances are generally lower than its pristine all-inorganic PV devices, resulting from the numerous surface defect and improper organic-inorganic phase segregation. Here, we demonstrate that hybrid PVs based on organic conjugated molecular and nanostructured silicon can achieve a high power conversion efficiency by controlling the interface contact as well as surface passivation.

An advantage of this type heterojunction devices presents the excellent light harvest capability of nanostructured as well as benefiting likely simple fabrication process. Especially, the composite of conjugated organic materials and nanostructured inorganic materials are potential candidates for cost-effective and efficient solar-energy-harvesting devices<sup>1</sup>. This device can be operated by a light-modulated field effect solar cell, which can improve the device performance under accumulation of light illumination<sup>2</sup>. In addition, this type device can be easily integrated with other type energy device, for example, an energy harvesting structure that integrates an organic-silicon heterojunction solar cell and a triboelectric nanogenerator (TENG) device is built to realize power generation from both sunlight and raindrop<sup>3</sup>. In addition, a self-charging power unit based on an organic-Si heterojunction solar cell and an organic supercapacitor, which simultaneously achieved both

photoelectric conversion and energy storage<sup>4</sup>. Finally, we will demonstrate that low temperature processed conductive silver-based ink has wide application usage for low temperature processed solar cell and related plastic electronics.

1. Sun, B.; Shao, M.; Lee, S.-T. *Advanced Materials* **2016**, 28, (47), 10539-10547.
2. Wang, Y.; Xia, Z.; Liu, L.; Xu, W.; Yuan, Z.; Zhang, Y.; Siringhaus, H.; Lifshitz, Y.; Lee, S. T.; Bao, Q.; Sun, B. *Advanced Materials* **2017**, 29, (18), 1606370.
3. Liu, Y.; Sun, N.; Liu, J.; Wen, Z.; Sun, X.; Lee, S.-T.; Sun, B. *ACS Nano* **2018**, *ACS Nano* **2018**, 12 (3), 2893-2899.
4. Liu, R.; Wang, J.; Sun, T.; Wang, M.; Wu, C.; Zou, H.; Song, T.; Zhang, X.; Lee, S.-T.; Wang, Z. L.; Sun, B. *Nano Letters* **2017**, 17, (7), 4240-4247.

#### 6:05 AM F.EL06.06.06

**Evaluation of Carrier Transport Mechanism by Systematic Defect Level Modulation in TiO<sub>x</sub> Protective Layers of n-Si/TiO<sub>x</sub>/Ni Photoanodes for Water Splitting** [Songwoung Hong](#)<sup>1,2</sup>, Woo Lee<sup>1,2</sup>, Seungwoo Song<sup>1</sup> and Ansoon Kim<sup>1,2</sup>; <sup>1</sup>Korea Research Institute of Standards & Science, Korea (the Republic of); <sup>2</sup>University of Science and Technology, Korea (the Republic of)

Photo-corrosion of anode participating the oxygen evolution reaction (OER) in photoelectrochemical cell (PEC) for water splitting is one of the obstacles for the long term stability and efficient solar to hydrogen conversion. In order to prevent the phot-corrosion, “electrically leaky” thick TiO<sub>2</sub> film was deposited onto a n-Si photoanode surface. However, the carrier transport mechanism through the thick dielectric layer and the influence of oxygen vacancy-related midgap states on the mechanism are still unclear. In order to verify the carrier transport through the midgap states of thick TiO<sub>2</sub> film, we only modulated the defect density of the protective TiO<sub>2</sub> film with no significant change of optical, physical, and chemical properties. It has been demonstrated that the defect density of the TiO<sub>2</sub> film is proportional to water-splitting activity. This result enables to explain the hole transport mechanism of the previously reported electrically leaky TiO<sub>2</sub> protection layer in n-Si photoanode. For the defect-level optimization, titanium sub-oxide (*sub*-TiO<sub>x</sub>) protection layer with higher defect density compared to the TiO<sub>2</sub> layer was also investigated. The controlled incorporation of defects into TiO<sub>x</sub> dramatically enhances the hole transport from the photoanode surface to electrolyte solution. The relationship between band structure and PEC activity of the photoanode system was explored depending on the defect density of the protection layer. Mott-Schottky analysis of this system suggests that the defect level of TiO<sub>x</sub> films influences the band bending of n-Si, which governs the accessible density of defect states and the carrier recombination.

#### 6:15 AM F.EL06.06.07

**Improvement in the Passivation Quality of Titanium Oxide Electron-Selective Contacts by Tantalum Doping** [Seira Yamaguchi](#)<sup>1</sup>, Hyunju Lee<sup>1,2</sup> and Yoshio Ohshita<sup>1</sup>; <sup>1</sup>Toyota Technological Institute, Japan; <sup>2</sup>Meiji University, Japan

We report on improvement in the passivation quality of titanium oxide (TiO<sub>x</sub>) by doping with tantalum (Ta). TiO<sub>x</sub> has been considered one of the most promising materials for electron-selective contacts (ESCs) for crystalline silicon (c-Si) solar cells. There has been a high efficiency of 23.1% successfully achieved for a c-Si solar cell with a TiO<sub>x</sub> rear-side ESC [1]. To realize higher efficiencies, it is necessary to further improve the passivation quality. One possible candidate for realizing such improvements is Ta doping. Ta doping reportedly causes a negative shift of the flat band voltage of TiO<sub>x</sub> films [2], and the passivation quality of TiO<sub>2</sub> ESCs can therefore be improved by Ta doping. In addition, tantalum oxide (TaO<sub>x</sub>) has long-term stability against UV light irradiation [3,4], and it is possible that Ta doping may also improve the long-term stability. In this work, we focus on an improvement in the passivation quality of TiO<sub>x</sub> ESCs by doping with Ta.

We deposited TiO<sub>x</sub>:Ta films by atomic-layer deposition on the both-sides of n-type c-Si substrates which were in advance oxidized in 30% hydrogen peroxide solution at 80 °C. Ta doping was realized by inserting a unitcycle of TaO<sub>x</sub> monolayer into unitcycles of TiO<sub>x</sub>. In this study, Ta doping concentration is characterized by a ratio of the number of TaO<sub>x</sub> unitcycles to that of TiO<sub>x</sub> unitcycles. The thickness of TiO<sub>x</sub>:Ta passivation films was basically set to 3.5 nm. After the deposition, the TiO<sub>x</sub>:Ta-passivated c-Si substrates were annealed at 130 °C in air. The effective minority-carrier lifetimes ( $\tau_{\text{eff}}$ s) were acquired from quasi steady-state photoconductance measurements, which were used as an indicator for the passivation qualities of the TiO<sub>x</sub>:Ta ESCs.

The All the samples passivated with undoped TiO<sub>x</sub> films and with TiO<sub>x</sub>:Ta films with unitcycle ratios of 0.05, 0.09, 0.17, and 0.50 showed improvements in the  $\tau_{\text{eff}}$  by annealing at 130 °C. However, the  $\tau_{\text{eff}}$  of samples with TiO<sub>x</sub>:Ta after annealing was, in most cases, higher than that of samples with undoped TiO<sub>x</sub>. This indicates that doping with Ta improves the passivation quality of TiO<sub>x</sub> ESCs. In addition, TiO<sub>x</sub>:Ta with a relatively low amount of Ta doping tended to have high passivation



qualities. The  $\text{TiO}_x\text{:Ta}$  with a unitcycle ratio of 0.05 showed the highest  $\tau_{\text{eff}}$  of 784  $\mu\text{s}$  in this study, which corresponded to an effective surface recombination quality of 24.9 cm/s. The  $\text{TiO}_x\text{:Ta}$  with a unitcycle ratio of 0.50 exhibited a rather lower passivation quality than that of the undoped  $\text{TiO}_x$ , which indicates excess Ta doping rather degrades the passivation quality.

The above results imply that  $\text{TiO}_x\text{:Ta}$  is one of the promising materials for ESCs. The results of experiments to elucidate the mechanism of the improvements in the passivation quality will be presented.

[1] J. Bullock et al., *Adv. Energy Mater.* **9** (2019) 1803367.

[2] X. Feng et al., *Angew. Chem. Int. Ed.* **48** (2009) 8095.

[3] Y. Wan et al., *ACS Energy Lett.* **3** (2018) 125.

[4] T. Wang et al., *Ind. Eng. Chem. Res.* **58** (2019) 5510.

SESSION F.EL06.07/F.EL08.10/F.EN02.08: Joint Session: Emerging Tandem PV Technologies  
On Demand Abstracts Available for Viewing Starting Saturday Morning, November 21, 2020  
F-EL06

**5:00 AM \*F.EL06.07/F.EL08.10/F.EN02.08.01**

**Advances in Material Properties for Perovskite-Perovskite Tandems** Giles Eperon<sup>1,2</sup>; <sup>1</sup>Swift Solar, United States; <sup>2</sup>National Renewable Energy Laboratory, United States

Multijunction all-perovskite solar cells offer a route towards efficiencies of III-V materials at low cost by combining the advantages of low thermalization loss in multijunction architectures with the beneficial properties of perovskites - namely low processing cost, high throughput fabrication, and compatibility with flexible substrates. Here, I will discuss why flexible all-perovskite tandems are a very attractive iteration of the perovskite technology. I will focus on what is needed to make a good perovskite-perovskite tandem on a flexible substrate, and the advances that we have made towards this goal. I will cover advances including a) the development and understanding of wide bandgap materials that leverage a novel bandgap-tuning strategy (without increasing bromine, hence avoiding significant phase segregation) to reach the ideal bandgaps for all-perovskite tandems, resulting in efficient devices that are stable to the combined stresses of heat and light; b) advances that we have made in interlayer design, working towards more ideal material properties for reducing shunt resistance; and c) the integration of these approaches to develop >23% efficient monolithic all-perovskite tandems on rigid substrates and 21% efficient devices on flexible plastic substrates.

**5:15 AM \*F.EL06.07/F.EL08.10/F.EN02.08.02**

**The Many Faces of Characterization in Developing a Commercial Perovskite on Silicon Tandem Solar Cell** Laura Miranda; Oxford PV, United Kingdom

Perovskite solar absorbers have the potential to disrupt the photovoltaic industry predominantly with their simultaneous promise of high efficiency and low cost. Whilst these two properties ensure a steady stream of research and development opportunities, commercial scaling requires assuring that the devices are sufficiently characterized to be confident of their long-term performance. Oxford PV has been addressing the challenges associated with commercially scaling its perovskite on silicon tandem solar cell design. Key practices that have been adopted during the development of highly efficient, reliable, and cost-competitive solar cells are the use of rigorous characterization tools and techniques, and the development of necessary models. This talk will highlight some of the challenges and considerations associated with bringing perovskite on silicon tandem solar cells from a laboratory prototype to a commercial product ready for manufacturing and how characterization has shaped and continues to inform that process.

**5:30 AM \*F.EL06.07/F.EL08.10/F.EN02.08.03**

**Passivation Strategies and Interlayers for Perovskite-Based Tandem Photovoltaics** Ulrich W. Paetzold, Saba Gharibzadeh, Tobias Abzieher, Ihtezaz M. Hossain, Hang Hu, Thomas Feeney, Somayeh Moghadamzadeh, Mahdi Malekshahi Byranvand, Bahram Abdollahi Nejand, Paul Fassel and Bryce Sydney Richards; Karlsruhe Institute of Technology, Germany

Single-junction crystalline silicon solar cells dominate the photovoltaics market today, but their power conversion efficiencies (PCEs) are approaching the practical limit for this technology. The emergence of hybrid organic-inorganic metal

halide perovskite semiconductors over the past decade has opened a window of opportunity to advance the performance of the market-dominating photovoltaic technologies through the development of tandem solar cells. These tandem solar cells promise high PCEs (>33%). To reach this landmark, a number of scientific and technological challenges related to high-efficiency perovskite-based tandem solar cell architectures, stable and high-quality perovskite semiconductor materials, and light management concepts need to be addressed. In this presentation, our progress on passivation strategies and novel interlayers to reduce the voltage losses in wide-bandgap and low-bandgap perovskite solar cells (PSCs), and in turn to increase the PCE of perovskite-based tandem photovoltaics, will be presented.

The search for efficient passivation interlayers for wide-bandgap perovskite top solar cells in *n-i-p* architecture directed our research in the past towards solution-processed 2D/3D perovskite heterostructures. Making use of these heterostructures for interface passivation, wide-bandgap PSCs ( $E_g \sim 1.72$  eV) with record open-circuit voltage for this bandgap and very high PCEs of up to 19.4% were demonstrated [1]. The reduced voltage deficit is a result of the decreased non-radiative recombination losses at the perovskite/hole-transport layer (HTL) interface. The solution-processed 2D/3D perovskite heterostructure is compatible with 3D perovskite absorber layers of a wide range of bandgaps ( $1.65$  eV  $\leq E_g \leq 1.85$  eV) [2]. Using this strategy in 4-terminal perovskite/silicon and perovskite/CIGS tandem solar cells, high PCEs > 27% [3], and > 25% [2] were demonstrated, respectively, thereby significantly exceeding the record PCEs reported for the respective single-junction solar cell technologies.

Beyond these past results, at the MRS fall meeting we will further present our latest work on novel interlayers and passivation strategies to minimize the voltage loss in wide-bandgap ( $1.65$  eV  $\leq E_g \leq 1.75$  eV) as well as low-bandgap ( $E_g \sim 1.26$  eV) perovskite solar cells in *p-i-n* architecture. The *p-i-n* architecture is a key to realize high-performance 2-terminal perovskite/silicon as well as perovskite/perovskite tandem solar cells. Moreover, we will present a novel route to deposit uniform ultra-thin polymer passivation layers onto perovskite thin films by chemical vapor deposition (CVD) [4]. The CVD polymerization promises reliable, scalable, and homogeneous deposition for future large-area processing of perovskite-based tandem solar cells.

#### References:

- [1] Gharibzadeh, S. *et al.* Record Open-Circuit Voltage Wide-Bandgap Perovskite Solar Cells Utilizing 2D/3D Perovskite Heterostructure. *Adv. Energy Mater.* **9**, 1–10 (2019).
- [2] Gharibzadeh, S.; Hossain I. M. *et al.* 2D/3D Heterostructure for Semitransparent Perovskite Solar Cells with Engineered Bandgap Enables Efficiencies Exceeding 25% in Four-Terminal Tandems with Silicon and CIGS. *Adv. Funct. Mater.* **30**, (2020).
- [3] Duong, T. *et al.* High Efficiency Perovskite-Silicon Tandem Solar Cells: Effect of Surface Coating versus Bulk Incorporation of 2D Perovskite. *Adv. Energy Mater.* **10**, 1903553 (2020).
- [4] Malekshahi Byranvand M.; Behboodi-Sadabad F. *et al.* Chemical Vapor Deposited Polymer Layer for Efficient Passivation of Planar Perovskite Solar Cells. *submitted*

#### 5:45 AM \*F.EL06.07/F.EL08.10/F.EN02.08.05

**Towards Highly Efficient Monolithic 2- and 3-Terminal Perovskite Silicon Tandem Solar Cells** [Lars Korte](#), Eike Koehnen, Philipp Wagner, Philipp Tockhorn, Marko Jost, Amran Al-Ashouri, Lukas Kegelmann, Marcel Roß, Bernd Stannowski and Steve Albrecht; Helmholtz-Zentrum Berlin für Materialien und Energie, Germany

Integrating metal halide perovskite top cells with crystalline silicon (c Si) bottom cells into monolithic tandem devices has recently attracted increased attention due to the high efficiency potential of these cell architectures. To further increase the tandem device performance to a level well above the best single junctions, optical and electrical optimizations as well as a detailed device understanding for such architectures need to be developed [1]. Here we present our recent results on such monolithic tandem cells in the common 2-terminal (2T) as well as in a novel 3-terminal (3T) contacting scheme.

In the 2T design, we recently demonstrated a certified power conversion efficiency (PCE) of 29.15% [2,3]. I will discuss some key elements to this result: using a silicon heterojunction cell electron contact on the rear side, enabling the integration of a perovskite top cell in the *p-i-n* configuration; employing self-assembled monolayers (SAMs) as hole selective contacts for further reduction of non-radiative recombination losses, etc. With the latter, efficiencies of up to ~ 21 % were demonstrated for *p-i-n* perovskite single junctions [3].

In 3T tandems, one of the three contacts is shared by both subcells, allowing for the individual operation of both subcells in a monolithic device with a single substrate, thus combining the characteristic advantages of 2T and 4-terminal (4T) devices: high combined photogeneration currents as in state-of-the-art 2T tandems, and ideally independent electrical operation similar to 4T tandems, making the cell more robust against varying spectra. I will discuss our recent proof-of-concept study [4], demonstrating a 3T perovskite/silicon tandem cell by manufacturing an *n-i-p* perovskite top cell on an interdigitated back contact (IBC) silicon heterojunction solar cell. In our proof-of-concept device, the combined PCE of ~ 17% is still limited both optically and electrically, and it will be discussed how optimizations of the cell stack can bring this architecture to a

PCE level comparable to 2T tandems. Furthermore, I will demonstrate that the subcells can indeed be operated largely independently at their individual maximum power points, allowing to extract the maximum power output for varying spectral conditions similar to 4T cells. A minimized series resistance at the shared electron contact on the cell's rear side is identified as the crucial parameter for independent operation of the subcells, and I will discuss pathways to approach the simulated efficiency potential by an optimized device design.

#### References:

- [1] Jost, Kegelman, Korte, Albrecht, Adv. Energy Materials, 2020, doi: 10.1002/aenm.201904102
- [2] NREL Best Research-Cell Efficiency Chart, <https://www.nrel.gov/pv/cell-efficiency.html>
- [3] Köhnen, Jost, Stannowski, Albrecht et al., Sustainable Energy and Fuels, doi: 10.1039/C9SE00120D
- [3] Al-Ashouri, Magomedov, Korte, Albrecht et al., En. Env. Sci, 2019, doi: 10.1039/C9EE02268F
- [4] Tockhorn, Wagner, Korte et al., ACS Appl. En. Mat., 2020, doi: 10.1021/acsaem.9b01800

#### 6:00 AM \*F.EL06.07/F.EL08.10/F.EN02.08.06

##### **Solution Processed Perovskite Subcell in Monolithic Perovskite/Si Tandem Solar Cells and Their Cost and Stability Concerns** Qi Chen<sup>1</sup> and Huanping Zhou<sup>2</sup>; <sup>1</sup>Beijing institute of Technology, China; <sup>2</sup>Peking University, China

Among all commercialization routes for perovskite photovoltaics (PV), the perovskite/Si tandem is of particular interest as it capitalizes the mature silicon industry with decades of experience. Here we report low-temperature solution process for efficient two-terminal perovskite/Si tandem solar cells, wherein electrical and optical properties of the tunneling junction are carefully modulated. Moreover, we improve materials stability by introducing  $\text{Eu}^{2+}/\text{Eu}^{3+}$  “redox shuttle” to suppress the  $\text{Pb}^0/\text{I}^0$  impurities which inevitably occurred during device operation. In addition, we carefully analyze the cost of tandem devices in terms of levelized cost of energy (LCOE) by adopting the “bottom-up cost model”. It reveals perovskite PV exhibit low materials cost, which reduces the LCOE substantially in tandem devices. We conclude that further efforts are required to simultaneously improve the efficiency and lifetime of perovskite modules, which ultimately endows the competitiveness of perovskite tandem solar cells.

SESSION F.EL06.08: Poster Session: Contacting Materials and Interfaces for Optoelectronic Devices  
On Demand Abstracts Available for Viewing Starting Saturday Morning, November 21, 2020  
5:00 AM - 8:00 AM  
F-EL06

#### F.EL06.08.01

##### **Vacancy Defects Induced Changes in the Electronic and Optical Properties of NiO Studied by Spectroscopic Ellipsometry and First-Principles Calculations** Kingsley O. Egbo<sup>1</sup>, Chao Ping Liu<sup>2</sup>, Chinedu E. Ekuma<sup>3</sup> and Kin Man Yu<sup>1</sup>; <sup>1</sup>City University of Hong Kong, Hong Kong; <sup>2</sup>Shantou University, China; <sup>3</sup>Lehigh University, United States

Native defects in semiconductors are known to play an important role in determining their optoelectronic properties. Nickel oxide (NiO) is one of the few wide gap oxide semiconductors broadly applied as the hole transport layer in many optoelectronic devices. NiO exhibits *p*-type conductivity and its conductivity is believed to be controlled by Ni vacancy acceptors. Herein, we present a systematic study comparing the optical and electronic properties of *p*-type oxygen-rich NiO with Ni vacancies ( $\text{NiO}:V_{\text{Ni}}$ ) and insulating Ni-rich NiO with O vacancies ( $\text{NiO}:V_{\text{O}}$ ) and stoichiometric NiO. The optical properties were obtained by spectroscopic ellipsometry while valence band spectra were probed by high-resolution X-ray photoelectron spectroscopy. The experimental results are directly compared to first-principles DFT + *U* calculations. The absorption spectra for the  $\text{NiO}:V_{\text{Ni}}$  sample show significant defect-induced features below 3.0 eV compared to NiO, and  $\text{NiO}:V_{\text{O}}$  samples. The increase in sub-gap absorptions in the  $\text{NiO}:V_{\text{Ni}}$  can be attributed to gap states observed in the electronic density of states. Computational results confirm that gap states in  $\text{NiO}:V_{\text{O}}$  are predominantly Ni 3*d* states while those of  $\text{NiO}:V_{\text{Ni}}$  is composed of both the Ni 3*d* and O 2*p* states. This work reveals the relations between native vacancy defects and optical properties of NiO and provides insights that would aid in designing optoelectronic devices utilizing NiO with native defects.

#### F.EL06.08.02

##### **Solvent Toolkit for Electrochemical Characterization of Hybrid Perovskite Films** Jason D. Slinker<sup>1</sup>, Alexander Zakhidov<sup>2</sup> and Sauraj Jha<sup>1</sup>; <sup>1</sup>The University of Texas at Dallas, United States; <sup>2</sup>Texas State University San Marcos, United

States

Organohalide lead (hybrid) perovskites have emerged as competitive semiconducting materials for photovoltaic devices due to their high performance and low cost. To further the understanding and optimization of these materials, solution-based methods for interrogating and modifying perovskite thin films are needed. In this work, we report a hydrofluoroether (HFE) solvent-based electrolyte for electrochemical processing and characterization of organic-inorganic trihalide lead perovskite thin films. Organic perovskite films are soluble in most of the polar organic solvents, and thus until now, they were not considered suitable for electrochemical processing. We have enabled electrochemical characterization and demonstrated a processing toolset for these materials utilizing highly fluorinated electrolytes based on a HFE solvent. Our results show that chemically orthogonal electrolytes based on HFE solvents do not dissolve organic perovskite films and thus allow electrochemical characterization of the electronic structure, investigation of charge transport properties, and potential electrochemical doping of the films with in situ diagnostic capabilities

#### **F.EL06.08.04**

**Structural, Optical and Electrical Properties of NiO<sub>x</sub> Thin Films Obtained by Various Techniques** Jhonathan R. Castillo<sup>1,2</sup>, Nicola R. Nedev<sup>1</sup>, Benjamín Valdez<sup>1</sup> and Maria Bernechea<sup>2,3,4</sup>; <sup>1</sup>Institute of Engineering, Autonomous University of Baja California, Blvd. Benito Juárez s/n, Mexico; <sup>2</sup>Institute of Nanoscience of Aragon (INA), University of Zaragoza, Spain; <sup>3</sup>Instituto de Ciencia de Materiales de Aragón (ICMA-CISC), Spain; <sup>4</sup>ARAID, Spain

NiO<sub>x</sub> is a transparent conductive oxide (TCO) that has attracted a lot of attention because of its electrical and optical properties. Most of the available TCOs are n-type semiconductors, while the development of efficient p-type TCOs remains a challenge. NiO<sub>x</sub> is one of the promising p-type candidates, because of its superior chemical stability and optical transparency. Some potential optoelectronic applications of NiO<sub>x</sub> are as a p-type channel in transparent thin film transistors (TFTs) and as a hole transport layer in perovskite solar cells. In this work thin NiO<sub>x</sub> films were obtained by Pulsed Laser Deposition (PLD), d.c. sputtering, e-beam evaporation and sol-gel techniques.

All films were deposited on glass substrates with a size of 2×2 cm. The PLD films were deposited from a NiO target at room temperature. D.C sputtering and e-beam evaporation were used to deposit pure Ni films, which were then oxidized in air at various temperatures. The sol-gel NiO<sub>x</sub> was obtained by depositing chemical precursors and subsequent thermal treatment. Various parameters were varied in the experiments and it was found that the structural, optical and electrical properties of the PLD films depend strongly on the oxygen pressure. The most important parameter for the other three types of oxides was the annealing temperature.

All samples were characterized by UV-Vis spectroscopy, X-ray diffraction, X-ray photoelectron spectroscopy, scanning electron microscopy and atomic force microscopy. Results for the properties of NiO<sub>x</sub> films deposited by the above techniques will be presented and a discussion for their possible application in TFTs and solar cells will be given.

#### **F.EL06.08.05**

**The Role of Post Synthetic Treatment and Ligand Population on Optoelectronic Properties of PbS Quantum Dot Films and Devices** Fiaz Ahmed, Adam Roberge and Andrew B. Greytak; University of South Carolina, United States

Colloidal quantum dots (CQDs) are promising semiconducting materials to engineer photovoltaic and optoelectronic devices due to tunable size-dependent absorption and emission properties. Great efforts have been made to find suitable surface ligand to reduce spacing between the adjacent quantum dots to ease charge transport but there has been negligible attention given to purification strategies and systematic efforts to find the ideal ligand populations to optimize device performance. Charge transport could be hindered in the presence of excess free ligands forming interparticle barriers; on the contrary, an under-passivated QD can have high density of trap states and could also undermine the nanocrystal's stability toward coalescence. Precipitation and redissolution (PR) methods are widely used purification techniques that must typically be repeated to get clean CQDs with appropriate populations of surface-bound molecules (ligands). PR often results in loss of native ligands bound to the surface which induces more surface traps and/or compromise the chemical stability of these nanocrystals.

Gel permeation chromatography (GPC) has been proven to be an effective technique to remove the byproducts and impurities from CQDs without damaging the QDs surface. In this study, we demonstrate the effectiveness of GPC in removing byproducts and unbound ligands from pre and post ligand exchanged PbS CQDs.

NMR and UV-Vis-NIR spectroscopy of oleate-capped PbS quantum dots shows that despite removal of unbound surfactants, PbS QDs remain stable in solution following GPC. These purified nanocrystals were used to make CQDs photodetectors and photovoltaic devices.

We show that films fabricated using GPC purified PbS QD solutions exhibit higher charge transport, and low contact resistance, as investigated through in-plane conductivity and photoresponse. The charge carrier mobility was extracted from

the mobility lifetime product and recombination lifetime determined by the spatial profiles of the photocurrent obtained through scanning photocurrent microscopy (SPCM), and transient photocurrent measurements, respectively. Furthermore, our findings show that post synthetic purification and optimum ligand population can significantly improve physical characteristics including reduced surface roughness, suggesting that impurities and optimum ligand coverage play an important role in film morphology and device performance.

#### F.EL06.08.07

##### **Revisiting *c*-type Screw Dislocations in GaN by First Principles—Implications on Nanopipes Formation** Liverios Lymperakis, Su-Hyun Yoo and Jorg Neugebauer; Max-Planck-Institut für Eisenforschung GmbH, Germany

Dislocations in III-Nitrides constitute a long standing controversial topic. The lattice and thermal mismatch associated with the heteroepitaxy of GaN results in high dislocation densities in the order of  $10^8$  to  $10^{10}$   $\text{cm}^{-2}$ . Although III-Nitride optoelectronic devices can operate even at these high dislocation densities, recent investigations indicate that *c*-type screw dislocations may have a detrimental effect on the properties and reliability of high-power electronic as well as of optoelectronic devices: For example, the observed high reverse (forward) leakage current in electronic (optoelectronic) devices is attributed to screw type dislocations [1]. Recently, it has been proposed that these defects are associated with open core structures, thus forming nanopipes with diameters of a few nms [2]. However, imaging screw dislocations at atomic resolution by electron microscopy to validate this model is not trivial. Moreover, first principles calculations that can accurately describe the energetics and atomic and electronic structure of these defects, have been restricted to MBE growth and/or did not explicitly consider the highly strained core region of these defects [3].

In the present study we combine density functional theory (DFT) with large scale empirical potential calculations within an Implicit Boundaries Multiscale Scheme calculations [4] to investigate the energetics, atomic structure and electronic properties of *c*-type screw dislocations in GaN. We explicitly consider both closed and open core screw dislocations as well as more than 100 different core reconstructions. Based on these calculations we construct a *c*-type screw dislocation phase diagram which describes the energetically most favorable core structures as function of the Ga, N and H chemical potentials. Our calculations indicate, in agreement with previous DFT studies, that growth under typical MBE growth conditions, i.e. metal rich growth, that these defects stabilize a Ga filled core. Moreover, under N rich conditions the core is stoichiometric, though a column of Ga-N dimers is removed from the core. However, the energy of the free *m*-plane surfaces under MBE conditions cannot be compensated by the core and strain energy and hence nanopipe formation is highly unfavorable. In contrast, under typical MOCVD or MOVPE growth conditions the Ga and N dangling bonds at the open core inner surfaces are passivated by  $\text{NH}_x$  molecules and H atoms, respectively. This reduces considerably the surface energy under these conditions enabling the formation of nanopipes with hexagonal cross section and diameters ranging for  $\approx 1$  to  $\approx 2$  nm. Our calculations show that these nanopipes obey electron counting rule and hence are semiconducting. Nevertheless, they have important implications on the efficient diffusion and/or incorporation of impurities and/or dopants at the side facets and at the neighborhood of the open core, which will be discussed in detail. We will also discuss in detail the energetics and structure of superscrew dislocations and their implications on the diameter of the nanopipes as well as the potential implications of the nanopipes on the properties and the efficiency of the electronic devices.

[1] K. Nomoto *et al.*, IEEE Electron Device Lett. **37**, 161 (2016).

[2] S. Usami *et al.*, Appl. Phys. Lett. **112**, 182106 (2018).

[3] J. E. Northrup, Appl. Phys. Lett. **78**, 2288 (2001).

[4] L. Lymperakis *et al.*, Phys. Rev. Lett. **93**, 196401-1 (2004).

This project has received funding from the ECSEL Joint Undertaking (JU) project UltimateGaN under grant agreement No 826392. The JU receives support from the European Union's Horizon 2020 research and innovation programme and Austria, Belgium, Germany, Italy, Slovakia, Spain, Sweden, Norway, Switzerland.

#### F.EL06.08.08

##### **The Role of Third Cation Doping on Phase Stability, Carrier Transport and Carrier Suppression in Amorphous Oxide Semiconductors** Xingyu Wang<sup>1</sup>, Austin Reed<sup>2</sup>, Han Wook Song<sup>3</sup> and Sunghwan Lee<sup>1</sup>; <sup>1</sup>Purdue University, United States; <sup>2</sup>Baylor University, United States; <sup>3</sup>KRISS, Korea (the Republic of)

Transparent electronics and optoelectronics have been garnering increasing attention for use in high performance devices such as next generation displays, photovoltaics, electrochromic devices and sensors. Metal oxides are considered to be necessary components in these applications due to their excellent optical transparency ranging from visible to near infrared regime as well as pseudo-metallic electrical conductivity[1, 2]. These metal oxides have been implemented in devices,

depending on their electrical conductivity, as transparent electrodes by degenerately-doped oxides such as InSnO and doped ZnO; semiconducting active layers based on indium oxides, ZnO or SnO<sub>2</sub>; and insulators (e.g., SiO<sub>2</sub>, Al<sub>2</sub>O<sub>3</sub>, HfO<sub>2</sub>) for dielectrics or encapsulations.

Thin film transistors (TFTs) are one of the key elements in displays as a pixel driving switch of which the required properties include high carrier mobility, low thermal budget processing, structural phase stability and reliable device performance in the presence of thermal and bias stress conditions. In recent years, amorphous oxide semiconductors based on indium oxides have been considerably investigated due to their promising carrier mobility, >5-25 cm<sup>2</sup>/Vs, compared to conventional amorphous Si (<1 cm<sup>2</sup>/Vs); low temperature processing; mechanical flexibility compared to the crystalline counterparts; and large area process-ability. Indium oxide-based binary and ternary cation material systems have shown tremendous promises for next generation displays since these materials meet the property and process needs that are described above. A binary cation material of indium zinc oxides (IZO) has been considered since the addition of Zn into In<sub>2</sub>O<sub>3</sub> stabilizes the amorphous phase of In<sub>2</sub>O<sub>3</sub> while the amorphous phase of undoped In<sub>2</sub>O<sub>3</sub> is rapidly crystallized at very low homologous temperatures (T/T<sub>m</sub><0.19) at 150 °C [3, 4]. The reported carrier mobility of IZO is as high as 20-50 cm<sup>2</sup>/Vs for both Hall and TFT field effect mobilities. A ternary cation system of InGaZnO (IGZO) [5, 6] has been more popular than binary systems since the addition of Ga in IGZO suppresses the channel carrier density in TFT application, which is preferred for TFT devices to obtain low device off-state current. Other third cation species such as Hf, Si and Zr were implemented. However, the carrier mobility of those ternary cation systems is significantly lower, 3-10 cm<sup>2</sup>/Vs, which is 3-10 fold lower than that of In<sub>2</sub>O<sub>3</sub> or IZO.

Therefore, securing strategies to develop a material system that maintains high carrier mobility (>20 cm<sup>2</sup>/Vs) and suppresses carrier generation for TFT channel application is of significant importance, which is expected to expedite the realization of next-generation transparent displays exhibiting reliable performance, fast switching speed and, consequently ultra high definition resolution.

Here, we report on a ternary cation material system of InAlZnO (IAZO) where the optimized carrier mobility is as high as 25-45 cm<sup>2</sup>/Vs. Further, the IAZO demonstrates an enhanced capability of stabilizing the amorphous phase during thermal stresses compared to InZnO. The effect of Al incorporation on the structural, electrical, optoelectronic and chemical properties of IAZO is systemically investigated and compared to those of IZO. The carrier transport behaviors (ionized impurity scattering; neutral scattering; charge screening) as well as the dominant mechanisms for carrier density and resistivity are discussed. The high mobility and greater phase stability may lead to high performance and sustainable device applications in next generation electronic and optoelectronic devices such as transparent displays.

## References

- [1] Lewis et al., MRS Bull., 25 (2000) 22-27.
- [2] Coutts et al., MRS Bull., 25 (2000) 58-65.
- [3] Paine et al., 85 (1999) 8445-8450.
- [4] Lee et al., Journal of Materials Research, 27 (2012) 2299-2308.
- [5] Nomura et al., Nature, 432 (2004) 488-492.
- [6] Hosono, Journal of Non-Crystalline Solids, 352 (2006) 851-858.

## F.EL06.08.09

**Investigation of Optical Bleaching Effect in InN-Based Films** Junjun Jia<sup>1</sup>, Takashi Yagi<sup>2</sup>, Taiki Ito<sup>1</sup> and Toshiki Makimoto<sup>1</sup>; <sup>1</sup>Waseda University, Japan; <sup>2</sup>National Institute of Advanced Industrial Science and Technology, Japan

Indium nitride (InN) was reported to have a large optical bleaching effect<sup>[1]</sup>, which provides potential application as high-speed and high-frequency optical switches in the optical communications. Due to its narrow direct bandgap (~0.7 eV), the bandgap engineering with GaN allows the ternary InGaN system to cover a range of bandgap energies from the infrared of InN to the ultraviolet of GaN. Such wide bandgap tuning provides spectral flexibility for InGaN as optical switches. In order to materialize the potential of InGaN for optical device applications, we investigated the optical bleaching behavior and ultrafast carrier dynamics in epitaxial InN and InGaN films, and proposed a phenomenological model to explain the carrier relaxation behavior.

InN and InGaN films with the thickness of 300 nm were deposited on *c*-sapphire substrates by molecular beam epitaxy. The optical bleaching effect and ultrafast carrier dynamics in InN-based epitaxial films was investigated by using femtosecond time-resolved pump-probe transmittance/reflectance measurements with a photon energy of 1.50 eV, which is based on open-aperture Z-scan technique.

Both epitaxial InN and InGaN films show large optical bleaching effect from Z-scan measurements, where a nearly 3 times increase in transmittance was observed at 800 nm without the dependence of the film composition. The time-resolved pump-probe transmittance results indicate that hot carriers are relaxed within a time scale of subpicosecond. The carrier lifetime was found to be independent of the film composition and the fabrication condition. The maximum value in the transient transmittance shows a nonlinear increase with increasing the pump-beam power, which may be associated to a change in the nonlinear refractive index. The detailed mechanism on the carrier relaxation behavior will be given in the conference.

This work was supported by JSPS KAKENHI Grant-in-Aid for Scientific Research (C) (Grant No. 20K05368).

[1] V. Pacebutas, G. Alekseenko, and A. Krotkus, Appl. Phys. Lett. 88, 191109 (2006).

#### **F.EL06.08.10**

**Atomistic Insight in The Band Tailing of Kesterite Solar Absorbers** Wei Chen, Gian-Marco Rignanese and Geoffroy Hautier; Université catholique de Louvain, Belgium

The low open-circuit voltage  $V_{OC}$  of the earth-abundant kesterite  $Cu_2ZnSnS(Se)_4$  (CZTSSe) solar absorbers is often associated with the large band tails, the origin of which has been tentatively assigned to the Cu-Zn disorder. Such an assignment has recently been questioned by some experiments. Here, by using the cluster expansion method and first-principles calculations, we investigate the role of cation disorder in the band tailing of CZTS. Our results show that the formation of local Cu-Cu-Cu-Sn tetrahedral motif as a result of the disorder is responsible for the band-gap narrowing, leading to a redshift of optical absorption onset by up to 0.2 eV. The Urbach energy, however, is hardly modified by the cation disorder, thereby excluding Cu-Zn disorder as a main source of the large band tails observed in stoichiometric CZTS. On the other hand, we find that extensive Cu-Zn disorder could stabilize the formation of point defects to a large extent. In particular, the defect concentration of  $Sn_{Cu}$  can be as high as  $10^{12} \text{ cm}^{-3}$  under typical Cu-poor growth conditions. The defect level is found at 0.2 eV above the VBM, suggesting that  $Sn_{Cu}$  could be a hole trap.  $Sn_{Zn}$  remains the predominant deep donor with defect levels near the midgap and hence is responsible for nonradiative recombination. We show that Sn antisites could be the main culprit of the low  $V_{OC}$  and the persistence of the two donors in the presence of cation disorder presents a major challenge towards a high-efficiency CZTS absorber.

#### **F.EL06.08.11**

**Interface Engineering for Perovskite Solar Cells Based on Tin (IV) Oxide Nanostructures** Zhuldyz Yelzhanova<sup>1</sup>, Zhiwei Ren<sup>1</sup>, Damir Aidarkhanov<sup>1</sup>, Gaukhar Nigmatova<sup>1</sup>, Bakhytzhann Baptyayev<sup>1</sup>, Mannix Balanay<sup>1</sup>, Patrick W. K. Fong<sup>2</sup>, Aleksandra Djuricic<sup>3</sup> and Annie Ng<sup>1</sup>; <sup>1</sup>Nazarbayev University, Kazakhstan; <sup>2</sup>Hong Kong Polytechnic University, Kazakhstan; <sup>3</sup>The University of Hong Kong, China

Tin(IV) oxide ( $SnO_2$ ) is an n-type wide bandgap semiconductor, which is widely used as an electron transport layer (ETL) in organometal perovskite solar cells (PSCs) due to its promising properties such as high transmittance, high electron mobility, good photostability, good energy alignment and easy processing. In this work,  $SnO_2$  nanostructures were synthesized by a solvothermal technique. The impacts of each growth parameter for the  $SnO_2$  nanostructures were demonstrated. By investigating the relations among different growth conditions, optimized recipes were developed for  $SnO_2$  nanostructured ETLs employing in PSCs. Furthermore, the interfaces between the FTO/ETL and ETL/perovskite are optimized in order to enhance the charge extraction efficiency of the devices. Detailed characterizations such as scanning electron microscopy, electrochemical impedance spectroscopy, atomic force microscopy spectroscopy, X-ray diffraction,  $I-V$  characteristics etc. have been performed on the  $SnO_2$  ETL alone, material interfaces and the  $SnO_2$  nanostructures-based PSCs. The obtained results provide a valuable insight into the community for preparing desired PSCs with nanostructured ETL.

#### **F.EL06.08.12**

**Dual-Period Guided-Mode Resonance Filters for SWIR Multi-Spectral Image Sensors** Md Ataul Mamun, Rezwan Mohammad Sayeed, Ümit Özgür and Vitaliy Avrutin; Virginia Commonwealth University, United States

Since their introduction in the early 1990s, subwavelength grating guided-mode resonance (GMR) filters have attracted considerable attention due to their simple and compact structures and versatile spectral characteristics. These outstanding features allow miniaturization of filters to pixel scale and high-density of integration for visible and short-wave infrared (SWIR) image sensors where a mosaic of transmission filters of different resonances can produce selective spectral signals to individual pixels of focal plane arrays. However, the conventional GMR-based transmission filter design, essentially unchanged for more than two decades, remains as a limiting factor for practical implementation of such an array of filters on

the same substrate. The conventional design based on a single-period grating necessarily involves a homogeneous layer (of subwavelength thickness) underneath a subwavelength grating of a dielectric material to achieve a narrow transmission peak and a wide stop-band. Maintaining the other spectral characteristics, the transmission peak can then be tuned to the desired wavelength by scaling all the dimensions including the grating and homogeneous layer heights. However, to integrate different filters into a compact mosaic, this conventional design requires either different substrates of corresponding thicknesses or a very complicated non-planar fabrication process to use a single wafer leading to low throughput. In this work, we demonstrate a dual-period design to eliminate this issue by fetching additional design flexibilities. First, the dual-period filters possess two fill-fractions and thus unlike their single-period counterparts allow more degrees of freedom to vary the lateral profile parameters (e.g., fill-fractions and periods) for producing desired resonances at different wavelengths as well as to tune a resonance while keeping the grating height constant. Second, to produce a narrow passband with a wide stopband, these filters, unlike the single-period counterparts, do not require a homogeneous layer, allowing a planar fabrication process for integration of different filters on the same substrate. Moreover, dual-period filters show less sensitivity to the fabrication deviations such as sidewall roughness and to those related to grating and/or homogeneous layer heights where the latter, especially, remains as another limiting problem for the conventional narrow passband single-period based filters. For example, a small variation in grating and/or homogeneous layer thickness (while other parameters remain constant) causes the resonance peaks to disappear or be suppressed significantly and thus the fabrication requires very high precision. In this work, we report dual-period GMR filters of dimensions smaller than on silicon-on-quartz (SOQ) wafers using conventional electron beam lithography (EBL) and reactive ion etching (RIE). The filters demonstrate efficiencies as high as 80% at the peak transmission wavelength, e.g. 1550 nm. The passbands are as small as 15 nm with over 350-nm-wide stopband. The spectra of the fabricated filters are in a good agreement with the results of simulations using the finite element method (FEM) in COMSOL Multiphysics® software. Tunability of narrow passband resonances has also been achieved by only varying the fill-factors and/or period while keeping the substrate thickness constant. An array of four filters (all based on dual-period) have been demonstrated on same substrate to generate well-separated passbands in the SWIR region (1.2-1.6  $\mu\text{m}$ ) to work as a pixel. While smaller filter size would allow integration into compact chips, filters should be sufficiently spaced to eliminate the potential cross-talk. In order to produce an optimum pixel size to work in the concerned SWIR region, any potential cross-talk along with filter size effects are also analyzed theoretically and experimentally.

#### **F.EL06.08.13**

**High Power Generation of Double-Junction III-V Solar Cells by Strategically Designed Luminescent Waveguides** Shin Hyung Lee, Mun-Jong Kim and Sung-Min Lee; Kookmin University, Korea (the Republic of)

III-V compound solar cells have been considered as the leading photovoltaic devices due to their superior properties including the high carrier mobility, direct bandgap, and controllable bandgap against the solar spectrum. The extremely high solar-to-electric power conversion efficiency can be achieved with III-V solar cells by forming monolithic multi-junction structures through series processes of the epitaxial growth. Nevertheless, their prohibitively high materials and process (i.e. epitaxial growth) cost has limited the application to terrestrial photovoltaic systems. To reduce the cost per watts of III-V solar cells, several approaches have been suggested, such as transfer-printing-assisted assembly for re-using the expensive III-V substrate and solar light concentrator for boosting the power generation in a given cell area. A format of III-V solar cell arrays transfer-printed within the luminescent solar concentrator (LSC) has been particularly of interest due to the potential to mitigate the materials cost and simultaneously to augment the power generation. In spite of the successful demonstration with single-junction (e.g. GaAs) solar cells, the effect of power generation improvement by the LSC system cannot be simply achieved with multi-junction solar cells, because the balanced enhancement of photon absorption at each subcell is required for increasing overall photocurrent of series-connected multi-junction cells. In this regard, here we present a facile route to integrate the transfer-printed multi-junction III-V solar cells with the LSC medium for significantly raising their power generation. Monolithically grown indium gallium phosphide (InGaP)/gallium arsenide (GaAs) double-junction solar cells are completed implanted into a LSC printing medium by the transfer-printing-based fabrication assembly, where luminescent quantum dots (QDs) with the 610 nm emission wavelength are non-uniformly distributed in the LSC. Since the short-circuit current of InGaP/GaAs double-junction cells is limited by a level of photocurrent produced at the InGaP subcell, the LSC is designed for the emitted 610 nm photons of QDs to be preferentially guided into the InGaP subcell. At the optimal LSC configuration, the power generation of 26%-efficient InGaP/GaAs solar cells can be considerably improved by ~50% compared to the identical cells but without add of the LSC.

#### **F.EL06.08.14**

**Selective Contacts Using Dipole Amino Acid Layers** Eloi Ros Costals, Gerard Masmitjà, Estefania Almache, Benjamin Pusay, Gema Lopez, Kunai Tiwari, Edgardo Saucedo, Pablo Ortega, Isidro Martin, Cristobal Voz and Joaquim Puigdollers; Universitat Politècnica de Catalunya, Spain



There has been a recent trend to use molecular dipole layers as a part of a novel strategy to fabricate selective contacts. Conceptually, a thin film of oriented molecular dipoles mimics a 2D capacitor, and the build-in voltage within the layer affects the final contact equilibrium state. When the dipoles are oriented in a certain direction one achieves larger accumulation of either holes or electrons by modifying the workfunction of the metal. Amongst many of the dipoles used amino acids have particularly interesting properties, for instance easy deposition by PVD methods such as spincoating and thermal evaporation and strong molecular dipole moment due to the presence within the molecule of a negatively charged carboxylic group and a positively charged amino group.

We tested the effect on the contact resistance of a Silicon/dipole/Aluminium stack using Transfer Length Method and testing different amino acids as the dipole layers (e.g. Cysteine, Glycine, Histidine...).

Preliminary results show an enhanced contact resistivity of orders of magnitude when dipoles are used on both p and n type silicon wafers, circumventing the problematic Fermi level pinning in Silicon aluminium as deposited contacts.

Finally, experiments on Histidine using different passivating layers show a clear difference in contact resistance with the change of the substrate dopant. Probably indicating that macroscopic orientation of the dipole layer can be promoted when using proper seed layers.

#### **F.EL06.08.15**

**Nucleation Site Tailoring at the 2D/3D Interface Using He-Ion Beam Patterning** Vera A. Zarubin, Kate Reidy, Joachim D. Thomsen, Julian Klein and Frances M. Ross; Massachusetts Institute of Technology, United States

For many of their applications, 2D materials must be connected to the macroscale world, implying interfaces between the 2D atomic layer and a 3D bulk material. The structure and defects at the interface between a 2D material and a 3D thin film influence (opto-)electronic properties of nanoscale devices such as contact resistance, photo-response and high frequency performance [1]. If the interface is between a 2D material and a 3D nanostructure, the ability to control the nanostructure geometry and lateral positioning is important in enabling nano-optoelectronic applications such as plasmonic arrays or arrays of wires or lines in individual circuits interfaced with 2D materials. When 3D nanoislands are grown on conventional, bulk substrates, “directed self-assembly” is a useful approach where growth takes place spontaneously but is favored at particular nucleation sites. The control of nucleation sites involves control of surface topography, geometry and local interactions [2]. Here we focus on extending this approach to the case of 3D nanoislands on 2D surfaces. We create specific defect locations on 2D materials (graphene, MoS<sub>2</sub>, WSe<sub>2</sub>) that act as heterogeneous nucleation sites for 3D metals (Au, Ti), and we tune the 3D metal deposition conditions to produce specific island shapes by self-assembly.

Since directed self-assembly requires avoidance of extraneous nucleation, as well as reliable nucleation at the patterned sites, we first discuss the control of metal island nucleation on unpatterned 2D materials. In particular, the nucleation density is expected to depend on the adatom diffusion distance on the 2D material surface. On 2D materials in the form of suspended layers, we use post-growth imaging by transmission electron microscopy (TEM) to measure the shape and distance between metal islands deposited in an ultra-high vacuum (UHV) evaporation system. We find that nucleation density and island shape depend on factors such as the substrate temperature, topography, background pressure, time, and partial pressure of the deposited material. We achieve the largest island diffusion distance (>2 μm) by removing polymeric residues in the 2D material transfer process, suspending the 2D material samples on TEM grids, using medium (100-200 °C) temperature deposition, and minimising defect sites such as wrinkles. We next induce locally reduced adatom diffusion distances using He-Ion beam patterning to create periodic defects in the 2D material. The He-Ion dose rates are calibrated and resulting defects characterised using high resolution scanning transmission electron microscopy. We show that these defects act as heterogeneous sites and we discuss the extent to which they can be exploited to produce patterned, periodic Au nanoisland arrays. We develop automated image analysis techniques and perform statistical analysis of the nucleation site density and location. We believe that this templating and nucleation control opens routes towards self-assembled and tailored interface design. In particular, we discuss the possibilities of interface structures built from self-assembled 3D nanostructures for development of plasmonic nanoarrays with tunable and well-defined resonance frequencies.

[1] Wang, Y. et al. Van der Waals contacts between three-dimensional metals and two-dimensional semiconductors. *Nature* 568, 70–74 (2019).

[2] Gherasimova, M., Hull, R., Reuter, M. C. & Ross, F. M. Pattern-level assembly of Ge quantum dots on Si with focused

ion beam templating. Appl. Phys. Lett. 93, 023106 (2008).

#### F.EL06.08.16

**Late News: Correlation of Nano-Morphology with Structural and Spectroscopic Studies in Organic Solar Cells** Urvashi Bothra<sup>1,2</sup>, Chris McNeill<sup>2</sup> and Dinesh Kabra<sup>1</sup>; <sup>1</sup>IIT Bombay, India; <sup>2</sup>Monash University, Australia

The nano-morphology of bulk heterojunction (BHJ) blends based on poly[[4,8-bis[(2-ethylhexyl)oxy]benzo[1,2-b:4,5-b']dithiophene-2,6-diyl][3-fluoro-2-[(2-ethylhexyl)carbonyl]thieno[3,4-b]thiophenediyl]] (PTB7) blended with [6,6]-phenyl-C<sub>71</sub>-butyric acid methyl ester (PC<sub>71</sub>BM) is systematically varied by changing the volume fraction of the solvent additive 1,8-diiodooctane (DIO) from 0 vol% to 20 vol% in the casting solution to prepare organic solar cells (OSCs). With increasing addition of DIO, the photoluminescence (PL) from the blend is reduced; however, a relative increase in PL from 750 nm onwards is observed for blends with 20 vol% DIO. As quenching of the blend PL is related to the donor/acceptor (D/A) interface, structural characterizations in real-space (microscopy) and *k*-space (scattering) are performed to unravel the morphology of blend systems to correlate nano-morphology with photophysical and charge transport processes. Blends prepared with 0 vol% DIO form large phase separated domains of PC<sub>71</sub>BM, hundreds of nanometer in diameter. With the addition of 3 vol% DIO the size of PC<sub>71</sub>BM domains is suppressed resulting in a more mixed morphology due to the selective dissolution of DIO in PC<sub>71</sub>BM. On the addition of up to 20 vol% of DIO, the film becomes rougher with a finer interconnected morphology due to polymer aggregation, which contrasts with previous reports. Electron-transport length scales measured by scanning photocurrent microscopy (SPM) are found to increase with the addition of up to 3 vol% DIO associated with the break-up of the large PC<sub>71</sub>BM aggregates, while the hole-transport length is found to increase on adding DIO up to 20 vol% due to aggregation of polymer chains. Finite-difference time-domain (FDTD) simulations are performed to take into account for optical beam spread due to associated roughness of BHJ blend films which further strengthen the experimental findings to take into account for waveguiding/scattering components of excitation beam. The structural results are found to be in good agreement with the PL quenching and the effective transport lengths. Hence, this work represents a complete set of results systematically examining the effect of nanomorphology on structural and opto-electronic properties of BHJ blends, which can have a direct implication on better understanding of the emerging high efficiency OSC blend systems.

#### F.EL06.08.17

**Late News: Low Interfacial Thermal Resistance for BeO-on-Diamond** Kiumars Aryana<sup>1</sup>, Yoonseo Jang<sup>2</sup>, David Olson<sup>1</sup>, John Gaskins<sup>1</sup>, Dohwan Jung<sup>2</sup>, Jung H. Yum<sup>3</sup>, Eric S. Larsen<sup>4</sup>, Christopher W. Bielawski<sup>3,4,5</sup>, Sean King<sup>6</sup>, Jungwoo Oh<sup>2</sup> and Patrick Hopkins<sup>1,1,1</sup>; <sup>1</sup>University of Virginia, United States; <sup>2</sup>Yonsei University, Korea (the Republic of); <sup>3</sup>Institute for Basic Science (IBS), Korea (the Republic of); <sup>4</sup>Ulsan National Institute of Science and Technology, Korea (the Republic of); <sup>5</sup>Ulsan National Institute of Science and Technology (UNIST), Korea (the Republic of); <sup>6</sup>Intel Corporation, United States

Diamond, by far, is the most thermally conductive material at room temperature and a great candidate for thermal management applications in microelectronic devices. Yet, its application has been discouragingly hindered due to its large thermal barrier at the interface when paired with other CMOS materials. Beryllium oxide (BeO) is a potential material candidate to bridge this thermal barrier between diamond and other wide bandgap semiconductors such as gallium nitride (GaN) and Silicon carbide (SiC) owing to its large bandgap, high thermal conductivity, and large spectral phonon overlap with diamond. In this study, using time-domain thermoreflectance we report the thermal conductivity and interfacial thermal resistance at BeO/diamond and BeO/Si interface across various temperatures. We measure the thermal conductivity of amorphous BeO for thicknesses below 30 nm to be  $\sim 10 \pm 0.7$  W/mK, which is significantly lower than its bulk crystalline value. Our results suggest that the interfacial thermal resistance at BeO/diamond interface is significantly lower than that of GaN/diamond and BeO/Si. This observation paves the way towards more thermally efficient integrated circuits.

#### F.EL06.08.18

**Late News: The High Near-Infrared Transparency of Silver Nanowire Transparent Electrodes** Jon Atkinson and Irene Goldthorpe; University of Waterloo, Canada

Transparent electrodes are a necessary component of many optoelectronic devices. Networks of silver nanowires have emerged as a promising alternative to commonly-used metal oxides such as indium tin oxide (ITO). Their transparency and conductivity values are as high as ITO, while being mechanically flexible, less expensive and can be fabricated using high-throughput roll-to-roll methods. In this talk I will outline an additional advantage that has thus far received less attention: the high transparency of silver nanowire networks in the near-infrared region (NIR). This property is highly desirable for some applications such as window coatings and solar cells. I will show that for electrodes that are 96% transparent in the visible, ones made from ITO are only 35% transparent at a wavelength of 2500 nm, whereas those made from silver nanowires maintain a transparency as high as 94%. I will present results that show that the nanowires in the network should be sparse

and larger in diameter to maximize NIR transparency. Modelling of the nanowire networks will also be shown and help demonstrate the physical reasons this is the case.

At the end of my talk I will present my results on passivating silver nanowire electrodes for capacitive-type devices such as smart windows and displays. To fully realize the advantages of silver nanowire electrodes, candidate passivation materials must be optically transparent (including in the NIR range), inexpensive, mechanically flexible and simple to deposit using high-throughput methods. I will present our findings of the passivation effectiveness of polyurethane, PMMA, a commercial optical adhesive and cyclotene passivation layers on silver nanowire networks.

#### **F.EL06.08.19**

##### **Late News: Reduced Non-Radiative Losses via Charge Selectivity Enhancement by Using a Fullerenic Anodic**

**Interlayer in Organic Photovoltaics** Donato Spoltore<sup>1</sup>, Manasi Pranav Ram<sup>1</sup>, Johannes Benduhn<sup>1</sup>, Mathias Nyman<sup>2</sup>, Jonas Kublitski<sup>1</sup> and Karl Leo<sup>1</sup>; <sup>1</sup>TU Dresden, Germany; <sup>2</sup>Abo Akademi, Finland

Charge transport layers play a fundamental role for efficient charge carrier injection and extraction in opto-electronic devices. Using interfacial layers, the open circuit voltage ( $V_{OC}$ ) and fill factor (FF) of organic solar cells can improve significantly. Here we show experimentally that the extent of contact between a Molybdenum Oxide ( $MoO_3$ ) hole extraction layer and the donor molecules in the photoactive layer of organic solar cells causes a proportional increase in non-radiative recombination losses. We quantify this effect by using several planar and bulk heterojunction solar cells device architectures, assigning it to surface recombination. We demonstrate that such losses can be suppressed by inserting a thin fullerenic anodic interlayer. This interfacial layer enhances the built-in potential and reduces the presence of minority charge carriers at the electrodes: a new perspective on the principle of selective charge extraction layers. The improvement to device efficiency is limited by a critical interlayer thickness, which depends on the donor material in bilayer devices. These findings are relevant to different branches of organic electronics, given the popularity of  $MoO_3$  as an efficient hole extraction and injection layer, providing insights for future device design.

### **SYMPOSIUM F.EL07**

---

Coulomb Interactions in Functional Organic Materials and Devices—A Curse or a Blessing?

November 21 - December 3, 2020

#### Symposium Organizers

Lay-Lay Chua, National University of Singapore

Seth Marder, Georgia Institute of Technology

Thuc-Quyen Nguyen, University of California, Santa Barbara

Frank Ortman, Technische Universität Dresden

---

\* Invited Paper

SESSION F.EL07.05: Live Keynote I: Doping Transport and Electronic Materials

Session Chairs: Seth Marder and Frank Ortman

Tuesday Morning, December 1, 2020

F.EL07

### **8:00 AM WELCOME AND INTRODUCTION**

#### **8:10 AM \*F.EL07.01.07**

##### **Doping of Organic and Inorganic Semiconductors—A Novel Dopant and the Impact of the Dielectric**

**Environment** Norbert Koch<sup>1,2</sup>; <sup>1</sup>Humboldt-Universität zu Berlin, Germany; <sup>2</sup>Helmholtz-Zentrum Berlin für Materialien und Energie, Germany

Controlled doping of semiconductors is crucial for the functionality and efficiency of modern (opto-) electronic devices. For organic semiconductors, the use of strong molecular electron donors and acceptors is meanwhile established as viable approach for doping. However, diffusion and poor thermal stability of most presently used dopants poses a challenge in applications. It turns out that the salt of the mesitylene-borinium cation ( $\text{Mes}_2\text{B}^+$ ) and tetrakis(penta-fluorophenyl)borate anion  $[\text{B}(\text{C}_6\text{F}_5)_4]^-$  is a superior p-type dopant for polymer semiconductors, and doping occurs *via* a charge-exchange reaction. Remarkably, the  $[\text{B}(\text{C}_6\text{F}_5)_4]^-$  anion enables the stabilization of polarons *and* bipolarons in poly(3-hexylthiophene), and the effective electron affinity of  $\text{Mes}_2\text{B}^+[\text{B}(\text{C}_6\text{F}_5)_4]^-$  is estimated to be 5.9 eV. The comparably high molecular weight and bulkiness of  $[\text{B}(\text{C}_6\text{F}_5)_4]^-$  is expected to reduce diffusion, and no negative impact on doped polymer conductivity is observed up to 100 °C.

Notably, many of the molecular dopants used for organic semiconductors can also be employed for doping of transition metal dichalcogenides (TMDCs). When thinned to the monolayer, many are direct semiconductors, e.g.,  $\text{MoS}_2$  and  $\text{WS}_2$ , with superior optical properties. Due to the pronounced excitonic nature of TMDCs, their exciton energy and band gap depend strongly on the dielectric constant ( $\epsilon$ ) of the mechanical support used for the monolayer. Moreover, the electrical nature of the substrate plays a critical role for the mechanism by which doping with molecules occurs. Three fundamentally different charge transfer mechanisms between  $\text{MoS}_2$  and molecular dopants have been identified and will be discussed.

Finally, the impact of residual water in conductive polymer films on their work function will receive attention. The high  $\epsilon$  of water reduces the polymer's work function by screening of local charge transfer induced dipoles, and the work function varies with temperature as does  $\epsilon$  of water. This effect should thus be considered when device characterization includes temperature variation.

**8:35 AM \*F.EL07.01.05**

**Chemistry of Dimeric and Hydride-Donor n-Dopants for Organic Electronics** [Stephen Barlow](#); Georgia Institute of Technology, United States

Molecular n-dopants can play useful roles in controlling conductivity and charge injection/extraction in organic semiconductors, in lowering the work functions (WFs) of electrode materials, and in controlling the properties of low-dimensional materials such as graphene. However, even molecules that can n-dope  $\text{C}_{60}$ , which has a fairly high electron affinity of ca. 4.0 eV, through simple one-electron transfer are inevitably sensitive to air and water, while stronger one-electron reductants are even more sensitive. Coupling bond breaking and/or formation to electron transfer provides a way of circumventing this issue. One such approach is based on the dimers,  $\text{D}_2$ , formed by certain odd-electron species,  $\text{D}$ , formed on alkali-metal reduction of the corresponding cations,  $\text{D}^+$ . Another class of relatively stable n-dopant molecules,  $\text{DH}$ , can be formally regarded as hydride-reduced derivatives of  $\text{D}^+$  cations. We have synthesized a range of both organic and organometallic  $\text{D}_2$  and  $\text{DH}$  derivatives, in particular, derivatives of 2-substituted-1,3-dimethylbenzimidazolium cations ( $\text{Y-DMBI}^+$ ), and of 18-electron cationic sandwich compounds such as 1,2,3,4,5-pentamethylrhodocenium and ruthenium pentamethylcyclopentadienyl mesitylene cations. This talk will describe the diversity of structures and reactivity that we have obtained, and will compare the advantages and disadvantages of the organic and organometallic dopants, and of the  $\text{D}_2$  and  $\text{DH}$  approaches, from the point of view of synthesis, stability, dopant strength, kinetics, dopant ion size and shape, and the extent to which these properties can be tuned.

**9:00 AM \*F.EL07.02.12**

**Coulomb Interaction in Organic Semiconductor Blends** [Karl Leo](#); TU Dresden, Germany

Organic semiconductor systems offer many new exciting device applications with attractive features such as flexibility, low cost, low-temperature processing etc. One key difference to inorganic semiconductors is the usually quite small dielectric constant of organics, leading to much stronger Coulomb interactions. For instance, the exciton binding energy in organic semiconductors is significantly greater than the room temperature thermal energy, thus having profound influence on the optical properties. In this talk, I will discuss the influence of these strong Coulomb interactions on two phenomena, both related to blends of organic materials: First, I will discuss controlled electrical doping where the strong Coulomb interaction might be a curse and should, at least in simple hydrogen-like model, make efficient doping unlikely. I will discuss recent results which clarify that doping is indeed efficient, mainly because of disorder effects. Second, I will discuss how the Coulomb interaction can be a blessing by using it for “band structure engineering” of organic semiconductors: Long range Coulomb interactions allow to continuously tune the energy levels, allowing finely adjustable energy levels without synthesis of new molecules. The electrostatic nature of these phenomena is directly proven by experiments which show the strong influence of these quadrupole effects at interfaces. Finally, I will discuss recent results which show that the energy gap of organic semiconductors can be tuned in a similar way.

9:25 AM \*F.EL07.02.07

**Enlightening Polymer Electronic Devices** Paolo Samorì; University of Strasbourg, France

The development of multifunctional devices capable to respond to multiple and independent stimuli is one among the grand challenges in organic electronics. The combination of multiple components, with each one conferring a specific function to the ensemble, is a facile strategy to impart a multifunctional nature to electronic devices. The controlled combination of such components and their integration in real devices can be achieved by mastering the supramolecular approach.

In my lecture I will review our recent works on the combination of carbon-based nanomaterials, in particular comprising organic semiconductors, with photochromic molecules (diarylethenes or azobenzenes) in order to fabricate smart, high-performing and light-sensitive (opto)electronic devices such as field-effect transistors and light-emitting transistors and as well as flexible non-volatile optical memory thin-film transistor device with over 256 distinct levels.

### References

- [1] For reviews see: (a) X. Zhang, L. Hou, P. Samorì, *Nat. Commun.* **2016**, *7*, 11118. (b) E. Orgiu, P. Samorì, *Adv. Mater.* **2014**, *26*, 1827-1845.
- [2] For modulating charge injection at metal-organic interface with a chemisorbed photochromic SAM see: (a) N. Crivillers, E. Orgiu, F. Reinders, M. Mayor, P. Samorì, *Adv. Mater.* **2011**, *23*, 1447-1452. (b) T. Mosciatti, M.G. del Rosso, M. Herder, J. Frisch, N. Koch, S. Hecht, E. Orgiu, P. Samorì, *Adv. Mater.* **2016**, *28*, 6606.
- [3] For hybrid structure combining organic semiconductors blended with Au nanoparticles coated with a photochromic SAM see: C. Raimondo, N. Crivillers, F. Reinders, F. Sander, M. Mayor, P. Samorì, *Proc. Natl. Acad. Sci. U.S.A.* **2012**, *109*, 12375-12380.
- [4] For blends energy level phototuning in a photochromic - organic semiconductor blend see: (a) E. Orgiu, N. Crivillers, M. Herder, L. Grubert, M. Pätz, J. Frisch, E. Pavlica, G. Bratina, N. Koch, S. Hecht, and P. Samorì, *Nat. Chem.* **2012**, *4*, 675-679. (b) M. El Gemayel, K. Börjesson, M. Herder, D.T. Duong, J.A. Hutchison, C. Ruzié, G. Schweicher, A. Salleo, Y. Geerts, S. Hecht, E. Orgiu, P. Samorì, *Nat. Commun.* **2015**, *6*, 6330.
- [5] For the fabrication of memory devices: T. Leydecker, M. Herder, E. Pavlica, G. Bratina, S. Hecht, E. Orgiu, P. Samorì, *Nat. Nanotech.* **2016**, *11*, 769-775.
- [6] For the novel nanomesh scaffold based photodetector: (a) L. Zhang, X. Zhong, E. Pavlica, S. Li, A. Klekachev, G. Bratina, T.W. Ebbesen, E. Orgiu, P. Samorì, *Nat. Nanotech.* **2016**, *11*, 900-906. (b) L. Zhang, N. Pasthukova, Y. Yao, X. Zhong, E. Pavlica, G. Bratina, E. Orgiu, P. Samorì, *Adv. Mater.* **2018**, *30*, 1801181.
- [7] For optically switchable light-emitting transistors: L. Hou, X. Zhang, G. F. Cotella, G. Carnicella, M. Herder, B. M. Schmidt, M. Pätz, S. Hecht, F. Cacialli, P. Samorì, *Nat. Nanotechnol.*, **2019**, *14*, 347-353.

SESSION F.EL07.06: Live Keynote II: Excitons and TADF and Solar Cells

Session Chairs: Seth Marder and Frank Ortmann

Thursday Morning, December 3, 2020

F.EL07

11:30 AM WELCOME

11:35 AM \*F.EL07.03.09

**Coherent Photoexcited Dynamics and Intermolecular Conical Intersections** Sergei Tretiak; Los Alamos National Laboratory, United States

In this talk, I will overview some applications of Non-adiabatic EXcited-state Molecular Dynamics (NEXMD) framework recently developed at LANL. The NEXMD code is able to simulate tens of picoseconds photoinduced dynamics in large molecular systems with hundreds of atoms in size and dense manifold of interacting and crossing excited states. In particular, I will exemplify ultrafast excitonic dynamics guided by intermolecular conical intersections (CoIns). Both simulations and time-resolved two-dimensional electronic spectroscopy track the coherent motion of a vibronic wave packet passing through CoIns within 40 fs, a process that governs the ultrafast energy transfer dynamics in molecular aggregates. Our results suggest that intermolecular CoIns may effectively steer energy pathways in functional nanostructures. Observed relationships between spatial extent/properties of electronic wavefunctions and resulting electronic functionalities allow us to understand and potentially manipulate excited state dynamics and energy transfer pathways toward optoelectronic applications.

**12:00 PM \*F.EL07.03.02**

**Emissive and Charge-Generating Donor–Acceptor Interfaces for Organic Optoelectronics with Low Voltage Losses** Koen Vandewal; Hasselt University, Belgium

Charge transfer (CT) states at the interface between electron-donating (D) and electron-accepting (A) materials in organic thin films are characterized by absorption and emission bands within the optical gap of the interfacing materials. Depending on the used donor and acceptor materials, CT states can be very emissive, or generate free carriers at high yield. The former can result in rather efficient organic light emitting diodes, via thermally activated delayed fluorescence, while the latter property is exploited in organic photovoltaic (OPV) devices. In this talk, I will show that proper control of CT state properties allows simultaneous occurrence of a high photovoltaic and emission quantum yield within a single, visible-light-emitting D–A system. This leads to ultralow-emission turn-on voltages as well as significantly reduced voltage losses upon solar illumination.

**12:25 PM \*F.EL07.04.10**

**Understanding and Minimizing Voltage Losses in High-Efficiency Organic Solar Cells** Feng Gao; Linköping University, Sweden

Compared with inorganic or perovskite photovoltaics, the key limiting factor for organic solar cells (OSCs) is large voltage loss, which is usually over 0.7 V. A significant contribution of the large voltage loss in OSCs is due to strong non-radiative recombination, the origin of which has been puzzling the community for a long time, limiting rational design of materials to overcome this critical issue. We systematically investigate a range of low voltage loss systems, where the voltage loss is around or below 0.6 V. We find that the quantum efficiency of electroluminescence in these systems have been significantly increased, leading to decreased non-radiative voltage losses below 0.20 V. Combining spectroscopic and quantum chemistry approaches, we formulate the key rules for minimizing voltage losses: (i) low energy offset between donor and acceptor molecular states, and (ii) high photoluminescence yield of the low-gap material in the blend. We further demonstrate that there is no intrinsic limit for efficient charge separation in OSCs with small voltage losses.

SESSION F.EL07.01: Doping and Transport

On Demand Abstracts Available for Viewing Starting Saturday Morning, November 21, 2020

F-EL07

**5:00 AM \*F.EL07.01.01**

**Doping of Organic Systems Explored with the Embedded Many-Body GW and Bethe-Salpeter Formalisms** Xavier Blase<sup>1</sup>, Ivan Duchemin<sup>2</sup>, Jing Li<sup>1,3</sup>, David Beljonne<sup>4</sup> and Gabriele D'Avino<sup>1</sup>; <sup>1</sup>Institut Néel, CNRS, Grenoble, France; <sup>2</sup>CEA-IRIG-L\_SIM, France; <sup>3</sup>CEA-LETI, France; <sup>4</sup>Laboratory for Chemistry of Novel Materials, Belgium

We study the electronic properties of dopants in organic systems on the basis of state-of-the-art many-body GW and Bethe-Salpeter formalisms accounting for proper electrostatic and dielectric environments. [1,2] We show in particular that the absolute energy position of doping levels and band edges of organic semiconductors can be obtained with accuracy both in the bulk and at the surface. Our calculations reveal in particular that the energy levels of a molecular impurity strongly depend on the host environment as a result not only of the proper environment dielectric properties, but crucially as well on electrostatic intermolecular interactions. [3] Concerning doping mechanisms, we demonstrate that ionisation of the dopants can occur even in situations of very deep acceptor (donor) levels thanks to strong electron-hole Coulomb interactions stabilizing charge-transfer states. [4] The increase of conductivity requires from then on to understand the charge separation of these bound electron-hole pairs in order to generate free carriers. An initial blessing, Coulomb interactions turn into a curse that needs to be overcome.

[1] J. Li, G. D'Avino, I. Duchemin, D. Beljonne, X. Blase, *J. Phys. Chem. Lett.* 2016, **7**, 2814.

[2] J. Li, G. D'Avino, I. Duchemin, D. Beljonne, X. Blase, *Phys. Rev. B* 2018, **97**, 035108.

[3] J. Li, I. Duchemin, O. M. Roscioni, P. Friederich *et al.*, *Materials Horizons* 2019, **6**, 107-114.

[4] J. Li, G. D'Avino, A. Pershin, D. Jacquemin, I. Duchemin, D. Beljonne, X. Blase, *Phys. Rev. Materials* 2017, **1**, 025602.

**5:15 AM F.EL07.01.02**

### **An Organic Borate Salt with Superior *p*-Doping Capability for Polymer Semiconductors** Berthold

Wegner<sup>1,2</sup>, Dominique Lungwitz<sup>1</sup>, Ahmed E. Mansour<sup>1,2</sup>, Claudia Tait<sup>3</sup>, Naoki Tanaka<sup>4</sup>, Tianshu Zhai<sup>5</sup>, Steffen Duhm<sup>5</sup>, Michael Forster<sup>6</sup>, Jan Behrends<sup>3</sup>, Yoshiaki Shoji<sup>4</sup>, Andreas Opitz<sup>1</sup>, Ullrich Scherf<sup>6</sup>, Emil List-Kratochvil<sup>1</sup>, Takanori Fukushima<sup>4</sup> and Norbert Koch<sup>1,2,5</sup>; <sup>1</sup>Humboldt-Universität zu Berlin, Germany; <sup>2</sup>Helmholtz-Zentrum Berlin für Materialien und Energie, Germany; <sup>3</sup>Freie Universität Berlin, Germany; <sup>4</sup>Tokyo Institute of Technology, Japan; <sup>5</sup>Soochow University, China; <sup>6</sup>Bergische Universität Wuppertal, Germany

Molecular doping is of central technological relevance for organic (opto-) electronics since it allows enhancement and precise control of electrical properties of organic semiconductors. Nevertheless, it is currently challenging to efficiently *p*-dope host materials with ionization energies (IEs) higher than 5.5 eV.

Here, we demonstrate the unique potential of an organic salt consisting of a borinium cation ( $\text{Mes}_2\text{B}^+$ ; Mes - mesitylene) and the tetrakis(penta-fluorophenyl)borate anion  $[\text{B}(\text{C}_6\text{F}_5)_4]^-$  as *p*-type dopant for high ionization energy polymer semiconductors, i.e., methylated poly(para-phenylene) (MeLPPP,  $\text{IE} \approx 5.4$  eV) and the donor-acceptor polymer poly(9,9-dioctylfluorene-alt-benzothiadiazole) (F8BT,  $\text{IE} \approx 5.9$  eV). Optical absorption spectroscopy, ultraviolet photoelectron spectroscopy (UPS), X-ray photoelectron spectroscopy (XPS), and conductivity measurements were performed in order to verify successful *p*-type doping. This range of experimental methods allows to identify the doping mechanism, namely electron transfer from the polymer to  $\text{Mes}_2\text{B}^+$  combined with stabilization of the positive charge on the polymer chain by  $[\text{B}(\text{C}_6\text{F}_5)_4]^-$ . From doping studies with further polymer semiconductors, we estimate the EA of  $\text{Mes}_2\text{B}^+[\text{B}(\text{C}_6\text{F}_5)_4]^-$  to amount to an impressive 5.9 eV. Especially, our studies on  $\text{Mes}_2\text{B}^+[\text{B}(\text{C}_6\text{F}_5)_4]^-$ -doped poly(3-hexylthiophene) (P3HT) demonstrate the capability of the organic salt to form bipolarons with a high proportion beyond ca. 10% dopant concentration [1]. Thus, the parameter space for doping of polymer semiconductors is significantly extended.

[1] B. Wegner, D. Lungwitz, A. E. Mansour, C. E. Tait, N. Tanaka, T. Zhai, S. Duhm, M. Forster, J. Behrends, Y. Shoji, A. Opitz, U. Scherf, E. J. W. List-Kratochvil, T. Fukushima, N. Koch, *Adv. Sci.* **2020**, 7, 2001322.

### **5:25 AM F.EL07.01.03**

**Electrical Conductivity of Doped Organic Semiconductors Limited by Coulomb Carrier-Carrier Interactions** Marten Koopmans<sup>1</sup>, Miina A. Leiviskä<sup>1</sup>, Jian Liu<sup>1</sup>, Jingjin Dong<sup>1</sup>, Sylvia Rousseva<sup>1,1</sup>, Jan C. Hummelen<sup>1,1</sup>, Giuseppe Portale<sup>1</sup>, Michael C. Heiber<sup>2</sup> and Lambert Jan Anton Koster<sup>1</sup>; <sup>1</sup>University of Groningen, Netherlands; <sup>2</sup>Northwestern University, United States

High electrical conductivity is a prerequisite for advancing the performance of organic semiconductors for various applications and can be achieved through molecular doping. However, it is often observed that the conductivity is enhanced only up to a certain optimum doping concentration, beyond which it decreases significantly. This is typically attributed to morphological changes upon increasing dopant loading.

Here we address and elucidate the effect of morphology, dopant-carrier interactions, and carrier-carrier interactions on the conductivity of doped organic semiconductors. We first show that the conductivity increases, maximizes and then decreases with increasing doping density for a molecularly doped fullerene derivative. We use grazing-incidence wide-angle X-ray scattering (GIWAXS) measurements to investigate the microstructural changes upon doping and find that even though the conductivity decreases at high doping density, the microstructure does not deteriorate. In other words, the loss of electrical conductivity in this system cannot be explained by changes to the microstructure.

We combine analytical work and Monte-Carlo simulations to demonstrate that repulsive Coulomb interactions between charge carriers can cause this decrease in conductivity. We use Efros-Shklovskii theory on carrier-carrier interactions to predict the carrier density at which the maximum of conductivity occurs.[1] Next, we show kinetic Monte-Carlo simulations exhibiting a maximum in conductivity at a charge carrier density that corresponds to that observed experimentally. The maximum is observed both in the presence and absence of dopants. Overall, we show that carrier-carrier interactions lower the conductivity by orders of magnitude at high doping densities and therefore propose the suppression of carrier-carrier interactions as a key strategy in order to create higher conductivity organic semiconductors.

[1] A. L. Efros, and B.I. Shklovskii, *Coulomb gap and low temperature conductivity of disordered systems*, J. Phys. C Solid State Phys. **8**, 1 (1975).

### **5:35 AM \*F.EL07.01.04**

**Charge Transport Through Redox and Magnetically Active Molecules** Jaume Veciana; ICMAB (CSIC)/CIBER-BBN, Spain

Open-shell organic molecules, like free radicals and radical-cations, exhibit magnetic and optical properties due to the presence of an unpaired electron in a Single Occupied Molecular Orbital (SOMO) with an accessible Single Unoccupied Molecular Orbital (SUMO). This characteristics together with their low spin-orbit couplings and weak hyperfine interactions make them good candidates for molecular spintronics insofar the radical character is preserved in solid state and the molecules are properly arranged on a solid state device. To achieve these properties we used functionalized substituted polychlorinated triphenylmethyl (PTM) radicals attached, as self-assembled monolayers (SAMs), on metallic surfaces, like Au, Ag, Cu, or graphene, exploring the transport properties through such spin-containing organic hybrid systems. [1] In all studied metal-organic systems the conductance through the radical molecules is enhanced two orders of magnitude with respect the corresponding non-radical ones, a result that can be explained by a mediated electron transport through the SUMO orbitals in the open-shell systems. [2-3] These results paves the way towards the use of all-organic neutral radical molecules in spintronics.

In this contribution the use of such radical molecules to attain metallic surfaces with rectifying properties [4,5] as well as to manipulate the electronic properties of metallic surfaces, like the work function, will be presented. Remarkable is the possibility to switch reversibly the work function of the metallic surfaces using an external input like NIR light. [6] Also molecular junctions based on self-assembled monolayers with a strong donor molecule, like benzotetrafulvalene (BTTF), linked to Au, Ag, and Pt surfaces have been prepared and fully characterized exhibiting rectifying properties. Interestingly these solid-state molecular tunnel junctions show a switching of the direction of rectification by controlling the direction of charge transfer between the BTTF redox unit and the bottom-electrode that depend on the nature of the metallic surfaces. [7]

## References

- [1] L. Yuan, C. Franco, N. Crivillers, M. Mas-Torrent, L. Cao, C. S. Suchand Sangeeth, C. Rovira, J. Veciana, C. A. Nijhuis, *Nature Comm.*, **7**, 12066 (2016).
- [2] M. Souto, L. Yuan, D. C. Morales, L. Jiang, I. Ratera, C. A. Nijhuis, J. Veciana. *J. Am. Chem. Soc.*, **139**, 4262, (2017).
- [3] F. Bejarano I.J. Olavarria-Contreras, A. Droghetti, I. Rungger, A. Rudnev, D. Gutierrez, M. Mas Torrent, J. Veciana, H.S. J. van der Zant, C. Rovira, E. Burzuri, N. Crivillers, *J. Am. Chem. Soc.* **140**, 1691 (2018).
- [4] M. Souto, V. Diez-Cabanes, L. Yuan, A. R. Kyvik, I. Ratera, C. A. Nijhuis, J. Cornil, J. Veciana, *Phys.Chem.Chem.Phys.*, **20**, 25638 (2018).
- [5] V. Diez-Cabanes, D.C. Morales, M. Souto, M. Paradinas, F. Delchiaro, A. Painelli, C. Ocal, D. Cornil, J. Cornil, J. Veciana, I. Ratera, *Adv. Mater. Technol.* **2018**, 1800152 (2018).
- [6] V. Diez-Cabanes, A. Gómez, M. Souto, N. González-Pato, J. Cornil, J. Veciana, I. Ratera, *J. Mater. Chem. C*, **7**, 7418-7424 (2019).
- [7] Y. Han, M.S. Maglione, V. Diez Cabanes, J. Casado-Montenegro, X. Yu, S.K. Karuppannan, Z. Zhang, N. Crivillers, M. Mas-Torrent, C. Rovira, J. Cornil, J. Veciana, Ch.A. Nijhuis, submitted (2020).

## 5:50 AM \*F.EL07.01.05

**Chemistry of Dimeric and Hydride-Donor n-Dopants for Organic Electronics** [Stephen Barlow](#); Georgia Institute of Technology, United States

Molecular n-dopants can play useful roles in controlling conductivity and charge injection/extraction in organic semiconductors, in lowering the work functions (WFs) of electrode materials, and in controlling the properties of low-dimensional materials such as graphene. However, even molecules that can n-dope  $C_{60}$ , which has a fairly high electron affinity of ca. 4.0 eV, through simple one-electron transfer are inevitably sensitive to air and water, while stronger one-electron reductants are even more sensitive. Coupling bond breaking and/or formation to electron transfer provides a way of circumventing this issue. One such approach is based on the dimers,  $D_2$ , formed by certain odd-electron species,  $D$ , formed on alkali-metal reduction of the corresponding cations,  $D^+$ . Another class of relatively stable n-dopant molecules,  $DH$ , can be formally regarded as hydride-reduced derivatives of  $D^+$  cations. We have synthesized a range of both organic and organometallic  $D_2$  and  $DH$  derivatives, in particular, derivatives of 2-substituted-1,3-dimethylbenzimidazolium cations ( $Y\text{-DMBI}^+$ ), and of 18-electron cationic sandwich compounds such as 1,2,3,4,5-pentamethylrhodocenium and ruthenium pentamethylcyclopentadienyl mesitylene cations. This talk will describe the diversity of structures and reactivity that we have obtained, and will compare the advantages and disadvantages of the organic and organometallic dopants, and of the  $D_2$  and  $DH$  approaches, from the point of view of synthesis, stability, dopant strength, kinetics, dopant ion size and shape, and the extent to which these properties can be tuned.



## 6:05 AM F.EL07.01.06

**Fingerprints of Strong Coulomb Interactions and Disorder in Doped Organic Semiconductors** Artem Fediai<sup>1</sup>, Jonas Armleder<sup>1</sup>, Franz Symalla<sup>2</sup>, Anne Emering<sup>1</sup>, Timo Strunk<sup>2</sup>, Tobias Neumann<sup>2</sup> and Wolfgang Wenzel<sup>1</sup>; <sup>1</sup>Karlsruhe Institute of Technology, Germany; <sup>2</sup>Nanomatch GmbH, Germany

Doping is a key technology in both organic and inorganic electronics, allowing to control the type and the magnitude of the conductivity over many orders of magnitude. In organic electronics, it is primarily used to reduce injection barriers and voltage drop on the electron/hole transporting layers of organic light-emitting diodes (OLEDs). Doped organic semiconductors, comprising a lot of charged molecules, represent an ideal laboratory for both theoretical and experimental studies on strong Coulomb interactions.

In this talk, I will present several effects, which appear in the doped organic semiconductors due to the cooperative effect of strong Coulomb interactions and energetic disorder: appearance of doping-induced gap states, disorder-driven doping activation [Fediai et al, PCCP, 22, 10256-10264 (2020)] and the superlinear increase of electric conductivity due to the disorder-compensation effect [Fediai et al. Nature Comm. 10, 4547 (2019)]. We predict and consistently explain these experimentally observed features using a kinetic Monte Carlo (kMC) method. In this method, electrons and their interactions are treated individually, so that dynamic Coulomb correlations are taken into account. Moreover, the movement of charge carriers is simulated in the characteristic disordered energy landscape, allowing to study cooperative effects, such as the correlation of the doping-induced and intrinsic material disorder. Remarkably, taking into account only a model morphology and empirical hopping rates, this method qualitatively predicts the vast majority of the experimentally observed doping effects, including the temperature and doping rate dependence of the Fermi level shift, conductivity and ionized dopant rates. It also predicts passivation of the trap states in the ultralow doping regime and other previously reported experimental findings.

Second, I will present a multiscale method that allows to establish a direct link between the type of dopant and host molecules and the properties of the constituent doped material. In this method, the kMC method acts as the last component of the multi-scale approach, in which the morphology of doped materials is generated using the Deposit method (Monte-Carlo protocol that mimics the vacuum deposition [J. Comput. Chem. 2013, 34, 2716-2725]) and the Coulomb interaction in host-dopant charge-transfer complexes are computed using ab-initio methods, based on the previously reported Quantum Patch method [J. Chem. Theory Comput. 2014, 10, 9, 3720-3725]. The latter has been extended here to also treat charge-transfer complexes embedded into morphology. As a use case, we have computed the density of states and the ionized dopant fraction of the prototypical amorphous doped organic material  $\alpha$ -NPD:F<sub>4</sub>TCNQ. Due to well-balanced approximations, our multiscale approach allows to calculate the Coulomb interaction energies of several tens of host-dopant pairs and obtain the distribution of the charge-transfer states energies, which is of great practical importance for amorphous organic semiconductors, with every host and dopant molecule having a unique conformation and electrostatic environment. In the future these methods offer the opportunities to design materials and devices for optimal performance.

## 6:15 AM \*F.EL07.01.07

**Doping of Organic and Inorganic Semiconductors—A Novel Dopant and the Impact of the Dielectric Environment** Norbert Koch<sup>1,2</sup>; <sup>1</sup>Humboldt-Universität zu Berlin, Germany; <sup>2</sup>Helmholtz-Zentrum Berlin für Materialien und Energie, Germany

Controlled doping of semiconductors is crucial for the functionality and efficiency of modern (opto-) electronic devices. For organic semiconductors, the use of strong molecular electron donors and acceptors is meanwhile established as viable approach for doping. However, diffusion and poor thermal stability of most presently used dopants poses a challenge in applications. It turns out that the salt of the mesitylene-borinium cation (Mes<sub>2</sub>B<sup>+</sup>) and tetrakis(penta-fluorophenyl)borate anion [B(C<sub>6</sub>F<sub>5</sub>)<sub>4</sub>]<sup>-</sup> is a superior p-type dopant for polymer semiconductors, and doping occurs *via* a charge-exchange reaction. Remarkably, the [B(C<sub>6</sub>F<sub>5</sub>)<sub>4</sub>]<sup>-</sup> anion enables the stabilization of polarons *and* bipolarons in poly(3-hexylthiophene), and the effective electron affinity of Mes<sub>2</sub>B<sup>+</sup>[B(C<sub>6</sub>F<sub>5</sub>)<sub>4</sub>]<sup>-</sup> is estimated to be 5.9 eV. The comparably high molecular weight and bulkiness of [B(C<sub>6</sub>F<sub>5</sub>)<sub>4</sub>]<sup>-</sup> is expected to reduce diffusion, and no negative impact on doped polymer conductivity is observed up to 100 °C.

Notably, many of the molecular dopants used for organic semiconductors can also be employed for doping of transition metal dichalcogenides (TMDCs). When thinned to the monolayer, many are direct semiconductors, e.g., MoS<sub>2</sub> and WS<sub>2</sub>, with superior optical properties. Due to the pronounced excitonic nature of TMDCs, their exciton energy and band gap depend strongly on the dielectric constant ( $\epsilon$ ) of the mechanical support used for the monolayer. Moreover, the electrical nature of the substrate plays a critical role for the mechanism by which doping with molecules occurs. Three fundamentally different charge transfer mechanisms between MoS<sub>2</sub> and molecular dopants have been identified and will be discussed.

Finally, the impact of residual water in conductive polymer films on their work function will receive attention. The high  $\epsilon$  of water reduces the polymer's work function by screening of local charge transfer induced dipoles, and the work function varies

with temperature as does  $\epsilon$  of water. This effect should thus be considered when device characterization includes temperature variation.

### 6:30 AM \*F.EL07.01.08

**Interplay of Polaron Density and Conductivity of Strongly Doped Conjugated Polymers** Christian Muller; Chalmers University of Technology, Sweden

Molecular doping of conjugated polymers generates polarons and counterions that can act as charge carriers and Coulomb scattering sites. Knowledge about the charge-carrier density is needed to rationalize the electrical properties that are observed for different degrees of doping. This talk will explore how the charge-carrier density can be estimated through a comparison of the UV-vis-IR absorbance spectra of molecularly doped polymers and electrochemically oxidized material, using a combination of spectroelectrochemistry and chronoamperometry. The interplay of charge-carrier density and electrical conductivity will be discussed for a range of doped polymers. P-doping of polymers with ionization energies ranging from about 4.5 eV to 5.5 eV will be evaluated, using a series of dopants with electron affinities up to 5.8 eV in case of the strong oxidant Magic Blue.

### 6:45 AM F.EL07.01.09

**Towards Molecular Implantation Doping for Enhancing Charge Injection Properties in Organic Field-Effect Transistors** Keehoon Kang<sup>1</sup>, Youngrok Kim<sup>1</sup>, Katharina Broch<sup>2</sup>, Woocheol Lee<sup>1</sup>, Heebeom Ahn<sup>1</sup>, Jonghoon Lee<sup>1</sup>, Daekyoung Yoo<sup>1</sup>, Junwoo Kim<sup>1</sup>, Seungjun Chung<sup>3</sup>, Henning Sirringhaus<sup>4</sup> and Takhee Lee<sup>1</sup>; <sup>1</sup>Seoul National University, Korea (the Republic of); <sup>2</sup>University of Tuebingen, Germany; <sup>3</sup>Korea Institute of Science and Technology, Korea (the Republic of); <sup>4</sup>University of Cambridge, United Kingdom

In organic device applications, contact doping has been commonly used method for circumventing a high contact resistance between metal electrodes and organic semiconductors prevents an efficient charge injection and extraction, which fundamentally limits the device performance. We have recently employed an efficient doping method based on solid-state diffusion of 2,3,5,6-tetrafluoro-7,7,8,8-tetracyanoquinodimethane (F<sub>4</sub>-TCNQ) in poly(2,5-bis(3-hexadecylthiophen-2-yl)thieno[3,2-b]thiophene) (PBTTT) [1] to selectively bulk-dope contact regions of PBTTT organic field effect transistors (OFETs), which significantly enhanced the charge injection properties [2]. However, adopting such extensive contact doping method compromises the device stability of OFETs due to dopant diffusion problem, which significantly degrades the device stability by damaging the ON/OFF switching performance despite a . In this presentation, we show a significantly improved stability of the contact doping method by incorporating “dopant-blockade molecules” in PBTTT film in order to suppress the diffusion of the dopant molecules. By carefully selecting the dopant-blockade molecules for effectively blocking the dopant diffusion paths, the ON/OFF ratio of PBTTT OFETs can be maintained over 2 months. This result will maximize the potential of contact doping in OFETs by providing a promising route toward achieving stable and low-contact-resistance OFETs.

#### References:

- [1] K. Kang, S. Watanabe, K. Broch, A. Sepe, A. Brown, I. Nasrallah, M. Nikolka, Z. Fei, M. Heeney, D. Matsumoto, K. Marumoto, H. Tanaka, S. Kuroda and H. Sirringhaus, Nat. Mater. 15, 896 (2016).
- [2] Y. Kim, S. Chung, K. Cho, D. Harkin, W.-T. Hwang, D. Yoo, J.-K. Kim, W. Lee, Y. Song, H. Ahn, Y. Hong, H. Sirringhaus, K. Kang and T. Lee, Adv. Mater. 31, <a href="tel:10 1806697">10 1806697</a> (2019).
- [3] Y. Kim, K. Broch, W. Lee, H. Ahn, J. Lee, D. Yoo, J. Kim, S. Chung, H. Sirringhaus, K. Kang and T. Lee, Adv. Funct. Mater. 2000058 (2020)

### 6:55 AM F.EL07.01.11

**Coulombic Interactions and Charge Transport Dynamics in Organic Thermoelectrics** Meenakshi Upadhyaya, Michael Lu-Diaz, Dhandapani Venkataraman and Zlatan Aksamija; University of Massachusetts Amherst, United States

Organic semiconductors (OSC) hold tremendous potential to address the demand for cheap and sustainable thermoelectric (TE) materials. They are cost-efficient, environmentally friendly, and have a low lattice thermal conductivity well below their inorganic counterparts. Their lightweight and flexibility also make them a promising choice for self-powered wearable medical monitors and sensing electronics.

Polymers are intrinsically insulators and need to be electrochemically doped to induce high levels of carrier density to improve their electrical conductivity. This simple process, however, introduces complexities in the electronic structure because of the charge-charge Coulombic interactions between the dopant and the polymer. Poor screening of the dopant-

polymer interactions increases the energetic disorder, alters the width and the shape of the density of states (DOS) [1-2], and suppresses the density of free charge carriers. In this work, we investigate the effect of the dopant-polymer Coulombic interactions on the DOS and subsequently on the charge transport dynamics and the trend of the Seebeck vs. conductivity trade-off curve. Our charge transport model is based on electron hopping between localized sites with a modified Gaussian disorder model to account for the impact of dopant size and density, and the clustering of dopants on the energies. We iteratively solve the non-linear Pauli's master equation to compute the time-averaged occupational probabilities of the sites from which relevant transport quantities are calculated [3-4].

We find that the energetic disorder caused by doping which results in an increase in the width of the DOS distribution closely follows the Coulomb interaction energy with the nearest dopant. Also, the deep coulombic traps cause an additional tail in the otherwise Gaussian DOS which is further enhanced with dopant clustering [1]. The spread in site energies due to a broadened DOS causes a larger difference in energies between neighboring localized sites which reduces the carrier hopping rate and thus the electron mobility [2]. We find that at low doping the carrier mobility first decreases with doping, due to the trap states in the tail of the DOS being filled first, followed by rapidly increasing at high doping levels. Furthermore, our results show that the effect of dopant-polymer Coulombic interactions on the width and tail of the DOS dictate the slope of the Seebeck vs. conductivity plots. We conclude that reducing the dopant-carrier Coulomb interactions and minimizing dopant clustering can have a beneficial impact on the conductivity and the thermoelectric power factor of OSCs.

**REFERENCES:** [1] V. I. Arkhipov, P. Heremans, E. V. Emelianova, and H. Bässler, Phys. Rev. B 71, 045214 (2005). [2] G. Zuo, H. Abdalla, and M. Kemerink, Phys. Rev. B 93, 235203 (2016). [3] C. J. Boyle, M. Upadhyaya, P. Wang, L. Renna, M. Lu-Diaz, S. P. Jeong, N. Hight-Huf, Lj. Korugic-Karasz, M. Barnes, Z. Aksamija, and D. Venkataraman, Nat. Comm. 10, 2827 (2019). [4] M. Upadhyaya, C. J. Boyle, D. Venkataraman, and Z. Aksamija, Scientific Reports 9, 5820 (2019).

**7:05 AM F.EL07.01.12**

**Late News: Quantum Sensing of Current Flow Perpendicular to DNA Helix** [Hashem Mohammad](#) and M. P. Anantram; University of Washington, United States

Sensing of quantum mechanical current in DNA is important to the fields of molecular devices, disease detection and next generation of sequencing techniques. Molecular recognition and self-assembly properties exhibited by DNA offer a bottom-up fabrication process as opposed to silicon-based electronics which requires a top-down approach. These properties along with the possibility for long-range charge transport makes DNA an attractive material for nanoelectronics. Further, the self-assembly property is exploited to form complex 3D structures known as DNA Origami. This enables us to potentially create a new class of molecular electronic devices that occupy cross-wired 3D configurations. In addition, the ability to sense changes in current due to modifications in the quantum mechanical interaction between bases as a function of sequence raises the possibility for its use in next generation sequencing techniques.

Quantum tunnel current which flows both along and perpendicular to the helical axis are essential to describing DNA-based materials. For molecular electronics applications involving double strand DNA (ds-DNA), current flow along the helical axis is important. However, for sequencing applications and origami based nanostructures, tunneling both along and perpendicular to the helical axis are crucial.

The fundamental questions in this field relate to the sensitivity of the quantum tunneling rate through a base to (1) changing a single neighboring base as a function of distance and (2) the DNA-substrate or DNA-contact interface. DNA maintains its structure at room temperature in a solvent, so to begin answering these questions it is essential to understand the role of decoherence in altering the coherent quantum tunneling process at room temperature.

We model the effect of decoherence in studying the effect of contact-location and interstrand coupling in a system consisting of a ds-DNA lying on a substrate. Our model allows us to modulate the strength of DNA-substrate binding to simulate DNA lying on a gold surface, which also forms the first electrical contact. The second electrical contact is a gold tip that is perpendicular to the substrate. An example of a simulated sequence is a 15 base pair long, 3'-GGGAAAAAAAAAAGGGG-5' double strand. This sequence allows us to probe the effect of the tunnelling current when the tip makes contact to a single base while its nearest neighbors gradually change. For example, we calculate the tunnelling current through a tip making contact to an adenine either at distant or close proximity to a guanine.

Our results show that the effect of the contact location on charge transport is dependent on the energy and spatial distribution of the HOMO band between two contacts via multiple trajectories through the DNA. Resonant tunneling peaks when a contact is made to an adenine can increase by ten times depending on the nearest neighbor bases. Moreover, a sufficient coupling between adenine and the neighboring guanine is required to maintain the large resonant tunneling peak. Therefore,

by moving the tip to an adenine that is only weakly coupled to a guanine, the resonant tunneling peak almost disappears. We also find that the tunneling current decays more significantly as a function of the neighboring bases in the coherent regime. Our results clearly establish the sensitive nature of tunnelling current to the nearest neighbor bases even in a direction perpendicular to the helical axis. We find that the delocalization of the frontier molecular orbitals responsible for charge transport are significantly affected by the nearest neighbors. To summarize, our results demonstrate the dependence of tunneling current on the local environment which is of relevance to DNA sequencing. We also expect these results to help design DNA nanowires with tolerance to the location of the cross-linking between multiple structures while maintaining the desired conductance value.

#### 7:15 AM F.EL07.01.13

**Late News: High Performing N-Type Polymer Thermoelectrics Realized Though Heavy P-Doping** Zhiming Liang<sup>1</sup>, Hyun Ho Choi<sup>2</sup>, Xuyi Luo<sup>3</sup>, Tuo Liu<sup>1</sup>, Ashkan Abtahi<sup>1</sup>, Uma Shantini<sup>1</sup>, J. Andrew Hitron<sup>1</sup>, Kyle Baustert<sup>1</sup>, Jacob Hempel<sup>1</sup>, Alex Boehm<sup>1</sup>, Armin Ansary<sup>1</sup>, Doug Strachan<sup>1</sup>, Jianguo Mei<sup>3</sup>, Chad Risko<sup>1</sup>, Vitaly Podzorov<sup>2</sup> and Kenneth R. Graham<sup>1</sup>; <sup>1</sup>University of Kentucky, United States; <sup>2</sup>Rutgers, The State University of New Jersey, United States; <sup>3</sup>Purdue University, United States

Designing doped  $\pi$ -conjugated polymers (CPs) for organic thermoelectric remains a challenging pursuit, in part because of the difficulty in understanding the complete details of charge transport. For example, it is typically assumed that charge-carrier transport in CPs is dominated by one type of charge carrier, either holes or electrons, as determined by whether the dopant reduces or oxidizes the polymer. However, we find that this is not always a correct assumption, as several polymers that are heavily doped with dopants that oxidize the polymer (i.e., *p*-type dopants) show *n*-type charge transport, which is supported by negative Seebeck coefficients and negative (*n*-type) Hall voltages. Here, we show that moderate *p*-doping of a DPP-containing polymer with FeCl<sub>3</sub> leads to a *p*-type power factor of 24.5  $\mu\text{W m}^{-1} \text{K}^{-2}$ , while further increases in doping concentration lead to an *n*-type power factor of 9.2  $\mu\text{W m}^{-1} \text{K}^{-2}$ , where 9.2  $\mu\text{W m}^{-1} \text{K}^{-2}$  is a record power factor for an *n*-type donor-acceptor (D-A) conjugated polymer. Notably, *n*-type behavior upon heavy doping with oxidizing dopants can be realized with multiple dopants (FeCl<sub>3</sub> and NOBF<sub>4</sub>) and with all five of the D-A polymers examined. A mechanistic explanation for the origin of *n*-type charge-carrier transport is presented based on the Seebeck coefficient measurements, Hall effect measurements, density functional theory calculations, ultraviolet and inverse photoelectron spectroscopy (UPS and IPES, respectively), UV-Vis-NIR absorbance, and electron paramagnetic resonance (EPR) spectra. Ultimately, the combination of data points to the presence of hopping-type holes in the amorphous regions and delocalized electrons in the crystalline regions. With two carrier types present the Seebeck coefficient is determined by the energy-weighted contributions of each carrier type to the total electrical conductivity. This work provides fundamental insight to charge-carrier transport in highly doped polymers while presenting a new approach to developing high-performance *n*-type organic thermoelectrics.

#### SESSION F.EL07.02: Electronic Materials

On Demand Abstracts Available for Viewing Starting Saturday Morning, November 21, 2020

F-EL07

#### 5:00 AM F.EL07.02.01

**Conductive Polymer Work Function Changes Due to Residual Water—Impact of Water's Temperature Dependent Dielectric Constant** Ahmed E. Mansour<sup>1,2</sup>, Hongwon Kim<sup>3</sup>, Sohyung Park<sup>1,2,4</sup>, Thorsten Schultz<sup>1,2</sup>, David X. Cao<sup>5</sup>, Thuc-Quyen Nguyen<sup>5</sup>, Wolfgang Brütting<sup>3</sup>, Andreas Opitz<sup>2</sup> and Norbert Koch<sup>1,2</sup>; <sup>1</sup>Helmholtz-Zentrum Berlin für Materialien und Energie, Germany; <sup>2</sup>Humboldt-Universität zu Berlin, Germany; <sup>3</sup>Universität Augsburg, Germany; <sup>4</sup>Korea Institute of Science and Technology, Korea (the Republic of); <sup>5</sup>University of California, United States

The development of low-cost and flexible organic electronic and optoelectronic devices is enabled by solution-processed conducting polymer thin films. Residual water present in organic devices and their surrounding environment influences the properties of their polymer thin film components, which accelerates devices degradation and limits their lifetime and reproducibility. For example, poly(3,4-ethylenedioxythiophene)-poly(styrenesulfonate) (PEDOT:PSS) is a high work function conducting polymer, commonly used to achieve Ohmic contacts for holes with many semiconductors. However, it has been shown that residual water in PEDOT:PSS films lowers their work function [1, 2] and is detrimental for device lifetime.[3]

Here, we investigate the fundamental role of residual water in changing the work function of conducting polymers and

confirm an earlier proposed model,[1] which involves the dielectric screening of PEDOT:PSS surface dipoles due to the high dielectric constant ( $\epsilon$ ) of water.

Photoemission spectroscopy and electrical conductivity measurements in the temperature range from -100 °C to 100 °C were conducted on thin films of different formulations of PEDOT, as well as, molecularly doped polymers. Our results reveal that the work function of PEDOT:PSS films containing residual water follows the same trend as a function of temperature as does  $\epsilon$  of water, in the range between 25 °C and -100 °C. For instance, the work function at -100 °C decreases by ca. 270 meV from its value at room temperature and recovers its initial value once the thin film is warmed up to room temperature. After removal of residual water from PEDOT:PSS films by annealing in ultrahigh vacuum, the work function of thin films is much higher as before (reaching 6.1 eV) and, notably, independent of temperature. These findings are further supported by investigating a water-free variant of PEDOT, which shows no temperature dependence of the work function even without annealing. In contrast, we find no indication that the presence of residual water has any impact on the electrical conductivity. From a device perspective, the hole injection barrier at the interface with PEDOT:PSS can be lowered by increasing its work function once residual water is removed. However, from studies of PEDOT:PSS interfaces with the molecular semiconductor 2,2',7,7'-tetrakis(carbazol-9-yl)-9,9-spirobifluorene (s-CBP) we find that the water-removing annealing step should be done prior to molecular deposition, since water desorption is significantly reduced in the presence of s-CBP layer as thin as 5 nm. Furthermore, we find a similar correlation between thin film work function and temperature for the molecularly doped conjugated polymer poly[2,6-(4,4-bis-(2-ethylhexyl)-4H-cyclopenta[2,1-b;3,4-b']dithiophene)-alt-4,7(2,1,3-benzothiadiazole)] (PCPDTBT) films to that seen for PEDOT:PSS, which might thus be caused by a similar dielectric screening mechanism involving unanticipated residual water.

[1] N. Koch, A. Vollmer, A. Elschner, *Appl. Phys. Lett.* 2007, 90, 043512.

[2] E. S. Muckley, C. B. Jacobs, K. Vidal, J. P. Mahalik, R. Kumar, B. G. Sumpter, I. N. Ivanov, *ACS Appl. Mater. Interfaces* 2017, 9, 15880

[3] M. P. De Jong, L. J. Van Ijzendoorn, M. J. A. De Voigt, *Appl. Phys. Lett.* 2000, 77, 2255.

#### 5:10 AM F.EL07.02.03

**Ordered Donor-Acceptor Complex Formation and Electron Transfer in Co-Deposited Films of Structurally Dissimilar Molecules** Andreas Opitz<sup>1</sup>, Clea Peter<sup>1</sup>, Berthold Wegner<sup>1,2</sup>, H.S.S. Ramakrishna Matte<sup>1</sup>, Adriana Röttger<sup>1</sup>, Timo Florian<sup>1</sup>, Xiaomin Xu<sup>1</sup>, Paul Beyer<sup>1</sup>, Lutz Grubert<sup>1</sup>, Stefan Hecht<sup>1</sup>, Valentina Belova<sup>3</sup>, Alexander Hinderhofer<sup>3</sup>, Frank Schreiber<sup>3</sup>, Christian Kasper<sup>4</sup>, Jens Pflaum<sup>4</sup>, Yadong Zhang<sup>5</sup>, Stephen Barlow<sup>5</sup>, Seth R. Marder<sup>5</sup> and Norbert Koch<sup>1,2</sup>; <sup>1</sup>Humboldt-Universität zu Berlin, Germany; <sup>2</sup>Helmholtz-Zentrum Berlin für Materialien und Energie, Germany; <sup>3</sup>Universität Tübingen, Germany; <sup>4</sup>Julius-Maximilians-Universität Würzburg, Germany; <sup>5</sup>Georgia Institute of Technology Atlanta, United States

By mixing two molecular materials in thin films the electrical and optoelectronic properties of organic semiconductors can be tailored. Resulting morphologies include phase separation or mixed crystals, which can form either solid solutions or ordered complexes. At the moment it is difficult to predict *a priori* the resulting morphology for a selected material combination. Here, we study electron transfer between planar, rod-like electron donor molecules and a non-planar electron acceptor molecule in co-evaporated films by analyzing morphological, vibrational and optical properties. [1] For the donor under study here without ground-state electron transfer to the acceptor we find phase separation in the mixed film. If ground-state electron transfer is observed, the relation of the crystal binding energy of the single component materials and the Coulomb attraction between ions formed in the co-deposited film drives these films either into phase separation or mixed crystal formation. The resulting morphology of the co-deposited films can be rationalized within the laws of thermodynamics. Therefore, it is necessary to consider structural incompatibility of the molecules in terms of interaction energies between the molecules as well as the Coulomb attraction between molecular ions after the formation via ground-state electron transfer.

[1] A. Opitz et al. *J. Phys. Chem. C* **124** (2020) 11023–11031.

#### 5:20 AM F.EL07.02.04

**Real-Time Monitoring of Charge Carrier Traps Leads to High-Performance, Stable Organic Field-Effect Transistors** Hamna Haneef<sup>1</sup>, Qianxiang Ai<sup>2</sup>, Karl Thorley<sup>2</sup>, Chad Risko<sup>2</sup>, John Anthony<sup>2</sup> and Oana D. Jurchescu<sup>1</sup>; <sup>1</sup>Wake Forest University, United States; <sup>2</sup>University of Kentucky, United States

Organic semiconductors (OSCs) are gradually integrated into our lives as parts of various optoelectronic devices given their low-cost processing, light weight, and the opportunities that they offer for the versatile design of new materials with “on-demand” properties. These systems undergo considerable electronic and structural transformations during device fabrication and operation which can profoundly impact their performance and stability. Characterization techniques that can elucidate the mechanisms of the time-dependent transformations occurring in these materials and devices could guide the processing and

design to yield high performance and stable organic devices. Here we introduce a highly efficient methodology to elucidate the microscopic processes occurring within the OSC when deliberately exposed to different external stimuli by accessing in real-time the trap density of states spectrum of the OSC using organic field-effect transistor (OFET) measurements. In the first example, we monitored the generation/annihilation of charge carrier traps in a high-mobility small molecule OSC, 2,8-difluoro-5,11-bis (triethylsilylethynyl) anthradithiophene (diF TES ADT), as a result of microstructural changes occurring in the film during exposure to solvent vapors. The time-dependent changes in charge carrier mobility are correlated with the density and energetic distribution of the electronic states in the bandgap of the OSC providing unprecedented access to processes taking place in all intermediate states during the microstructural transformations. Given the strong dependence of the electrical properties on the film microstructure, such information is instrumental in identifying performance-limiting processes in devices and subsequently guiding material processing to achieve intrinsic limits. The discovery of defect-tolerant intermediate crystalline motifs can provide pathways for fabricating stable, high-performance devices for the next generation of low-cost electronics. We further employed this methodology to investigate the underlying physical process impacting the operational stability of OFETs based on a small molecule trimer, tri(*n*-hexyl) silylethynyl benzodithiophene (TnHS BDT) trimer. A large shift in threshold voltage and a drastic decrease in mobility observed during prolonged transistor operation in ambient air coincided remarkably with the establishment of a peak in the DOS spectrum at ca. 0.3 eV from the valence band edge after 20 min of repetitive transistor measurements. The peak is indicative of charge carrier trapping in discrete electronic states generated in the bandgap of the OSC during operation, which in turn is responsible for the device degradation. This information provided us with unparalleled insights into the microscopic mechanisms leading to device degradation which allowed us to devise a strategy that completely suppressed the formation of the discrete peak in the DOS spectrum, subsequently yielding highly stable OFETs with constant mobilities and threshold voltage shifts below 1 V during 500 min of continuous transistor operation in ambient air.

**5:30 AM \*F.EL07.02.05**

**Accessing the Dynamics of the Energetic Disorder in Organic Semiconductors—Implications to Radiation Detection for Medical Applications** Oana D. Jurchescu; Wake Forest University, United States

Organic semiconductors bring key advantages to integration into next generation flexible and bendable optoelectronics due to ease of processing and compatibility with arbitrary substrates. These properties are a direct consequence of their van der Waals intermolecular interactions, yet these interactions are also the main cause of the formation of localized electronic states in the band gap, which are responsible for the modest performance and reduced stability of organic semiconductor devices. In this talk, I will discuss the dynamics of trap formation and healing under several different pre, post deposition or in operando stimuli and relate it to the performance and long-term stability of the organic field-effect transistor devices. Charge carrier trapping can also provide a platform for developing sensors and radiation detectors by recording the changes in the trap DOS spectra upon interaction with external factors like impurities (chemical and biological), temperature, light, or radiation. In the second part of my talk, I will introduce radiation dosimeters for medical applications which exploit trap generation/annihilation in organic transistors. These X-ray medical imaging systems are robust and highly sensitive for doses relevant to a variety of medical investigations, including cancer diagnosis and therapy. Placement of the sensor directly onto the human body, coupled with the similarity in the atomic number *Z* between the electronically active layer and the human tissue, greatly enhances the precision and reduces the complexity of the medical equipment. These findings uncover new opportunities for organic circuits that will not only improve the quality of healthcare, but can have other applications, including wearable personal dosimeters.

**5:45 AM \*F.EL07.02.06**

**Exploring Structural Transitions During Ion-Injection into Conjugated Polymers** Christine Luscombe; University of Washington, United States

Mixed organic ionic and electronic conductors are being explored for a wide range of applications, from bioelectronics to neuromorphic computing, artificial muscles and energy storage applications. These materials exploit the simultaneous transport properties of ionic and electronic carriers to enable novel device functions. Recently, polymer semiconductors have received significant amounts of attention because of their flexibility, biological compatibility and ease of fabrication. These materials, particularly thiophene-based polymers such as poly(3,4-ethylenedioxythiophene)-poly(styrenesulfonate)(PEDOT:PSS) and related derivatives, have demonstrated significant enhancements in performance in a relatively short amount of time, with transconductance values of PEDOT:PSS transistors surpassing those achieved even with graphene.

We explore how small changes in ethylene-glycol functionalized polythiophenes alter ion injection. Specifically, their thin film morphology, and their ionic and electronic conductivities, and comparisons against theoretical predictions will be

discussed. In this talk, the effect on the density of the ethylene-glycol side chains and their pattern of placement on ionic conductivity will be discussed.

#### 6:00 AM \*F.EL07.02.07

**Enlightening Polymer Electronic Devices** Paolo Samorì; University of Strasbourg, France

The development of multifunctional devices capable to respond to multiple and independent stimuli is one among the grand challenges in organic electronics. The combination of multiple components, with each one conferring a specific function to the ensemble, is a facile strategy to impart a multifunctional nature to electronic devices. The controlled combination of such components and their integration in real devices can be achieved by mastering the supramolecular approach.

In my lecture I will review our recent works on the combination of carbon-based nanomaterials, in particular comprising organic semiconductors, with photochromic molecules (diarylethenes or azobenzenes) in order to fabricate smart, high-performing and light-sensitive (opto)electronic devices such as field-effect transistors and light-emitting transistors and as well as flexible non-volatile optical memory thin-film transistor device with over 256 distinct levels.

#### References

- [1] For reviews see: (a) X. Zhang, L. Hou, P. Samorì, *Nat. Commun.* **2016**, *7*, 11118. (b) E. Orgiu, P. Samorì, *Adv. Mater.* **2014**, *26*, 1827-1845.
- [2] For modulating charge injection at metal-organic interface with a chemisorbed photochromic SAM see: (a) N. Crivillers, E. Orgiu, F. Reinders, M. Mayor, P. Samorì, *Adv. Mater.* **2011**, *23*, 1447-1452. (b) T. Mosciatti, M.G. del Rosso, M. Herder, J. Frisch, N. Koch, S. Hecht, E. Orgiu, P. Samorì, *Adv. Mater.* **2016**, *28*, 6606.
- [3] For hybrid structure combining organic semiconductors blended with Au nanoparticles coated with a photochromic SAM see: C. Raimondo, N. Crivillers, F. Reinders, F. Sander, M. Mayor, P. Samorì, *Proc. Natl. Acad. Sci. U.S.A.* **2012**, *109*, 12375-12380.
- [4] For blends energy level phototuning in a photochromic - organic semiconductor blend see: (a) E. Orgiu, N. Crivillers, M. Herder, L. Grubert, M. Pätz, J. Frisch, E. Pavlica, G. Bratina, N. Koch, S. Hecht, and P. Samorì, *Nat. Chem.* **2012**, *4*, 675-679. (b) M. El Gemayel, K. Börjesson, M. Herder, D.T. Duong, J.A. Hutchison, C. Ruzié, G. Schweicher, A. Salleo, Y. Geerts, S. Hecht, E. Orgiu, P. Samorì, *Nat. Commun.* **2015**, *6*, 6330.
- [5] For the fabrication of memory devices: T. Leydecker, M. Herder, E. Pavlica, G. Bratina, S. Hecht, E. Orgiu, P. Samorì, *Nat. Nanotech.* **2016**, *11*, 769-775.
- [6] For the novel nanomesh scaffold based photodetector: (a) L. Zhang, X. Zhong, E. Pavlica, S. Li, A. Klekachev, G. Bratina, T.W. Ebbesen, E. Orgiu, P. Samorì, *Nat. Nanotech.* **2016**, *11*, 900-906. (b) L. Zhang, N. Pashukova, Y. Yao, X. Zhong, E. Pavlica, G. Bratina, E. Orgiu, P. Samorì, *Adv. Mater.* **2018**, *30*, 1801181.
- [7] For optically switchable light-emitting transistors: L. Hou, X. Zhang, G. F. Cotella, G. Carnicella, M. Herder, B. M. Schmidt, M. Pätz, S. Hecht, F. Cacialli, P. Samorì, *Nat. Nanotechnol.*, **2019**, *14*, 347-353.

#### 6:15 AM F.EL07.02.08

**One-Dimensional Nanowires of Non-Centrosymmetric Molecular Semiconductors Grown by Physical Vapor Deposition** Kwang-Won Park, David Bilger and Trisha L. Andrew; University of Massachusetts Amherst, United States

Understanding how dipolar, non-centrosymmetric organic semiconductors self-assemble, nucleate, and crystallize is indispensable for designing new molecular solids with unique physical properties and light-matter interactions. However, some intermolecular interactions, such as dipole-dipole and van der Waals interactions compete to direct the assembly of these compounds, making them difficult to predict how solids are formed from individual molecules. Here, we investigate four small molecules (**TpCPD**, **TpDCF**, **AcCPD**, and **AcDCF**) featuring anisotropic with large dipole moments, and establish robust algorithms to control their molecular self-assembly via simple physical vapor deposition technique. Each molecule contains a central polar moiety, consisting of either a cyclopentadienone (CPD, ca. 3.5 D dipole moment) or dicyanofulvene (DCF, ca. 7.0 D dipole moment) core, that is surrounded by either four twisted phenyl (tetraphenyl, Tp) groups or a fused aromatic (acenaphthene, Ac) ring system. We find that only molecules possessing extended  $\pi$  system form one-dimensional (1D) nanowires due to the stronger van der Waals associations, originating from the planar acenaphthene moieties. We examine the kinetics of self-assembly for **AcDCF** and create diverse 1D morphologies, including both curved and linear nanostructures. Finally, conductive AFM (c-AFM) measurements show that 1D **AcDCF** wires support their higher current densities relative to randomly-oriented clusters lacking long-range order.

#### 6:25 AM F.EL07.02.09

**Zooming in on the Microstructure of Glycolated Polythiophenes with Molecular Dynamics Simulations** Micaela Matta<sup>1,2</sup>, Bryan D. Paulsen<sup>2</sup>, Jonathan Rivnay<sup>2</sup>, George C. Schatz<sup>2</sup> and Alessandro Troisi<sup>1</sup>; <sup>1</sup>University of Liverpool, United

Kingdom; <sup>2</sup>Northwestern University, United States

Organic electrochemical transistors (OECTs) are ionic-to-electronic transducers that rely on the ability of the organic active layer to transport both ions and electrons. These devices consist of an aqueous electrolyte in direct contact with a  $\pi$ -conjugated polymer channel. In order to maximize both electronic and ionic transport, a balance between ordered  $\pi$ -stacking and the swelling promoted by the glycolated side chain must be achieved.<sup>1</sup>

Molecular dynamics (MD) simulations offer a unique perspective into the microstructure of conjugated polymers. In this work, we provide an atomistic picture of the polymer-electrolyte interface in the 'off' state of an OECT. Using a combination of MD simulations and X-ray fluorescence, we show how different anions effectively tune the coordination and chelation of cations by the glycolated polymer p(g2T-TT). At the same time, softer and hydrophobic anions such as TFSI and ClO<sub>4</sub> are found to preferentially interact with the p(g2T-TT) phase, further enhancing polymer-cation coordination. These trends are confirmed by X-ray Fluorescence experiments on p(g2T-TT) thin films undergoing passive swelling.<sup>2</sup>

We then use MD to simulate the swelling of another glycolated polymer, p(g3T2-T), mapping the phase diagram of a water-glycolated polymer mix as a function of the water content. This allows us to predict the microstructure changes associated to passive swelling and how different electrolytes penetrate the polymer morphology.

Finally, we discuss the challenges associated to the modelling of ionic doping of glycolated polymers, and analyse the interactions between polymer-electrolyte using a combination of electronic structure and classical simulations.

1. Rivnay, J.; Inal, S.; Salleo, A.; Owens, R. M.; Berggren, M.; Malliaras, G. G. Organic Electrochemical Transistors. *Nat. Rev. Mater.* 2018, 3 (2), 17086.

2. Matta, M.; Wu, R.; Paulsen, B. D.; Petty, A.; Sheelamantula, R.; McCulloch, I.; Schatz, G. C.; Rivnay, J. Ion Coordination and Chelation in a Glycolated Polymer Semiconductor: Molecular Dynamics and X-ray Fluorescence Study, 2020. <https://doi.org/10.26434/chemrxiv.12264308.v2>

### 6:35 AM F.EL07.02.11

**Role of Pendant Group in Organic Semiconductor Charge Transport Rate and Energetics** Kalyani Patrikar<sup>1</sup>, Nakul Jain<sup>1</sup>, Dwaipayan Chakraborty<sup>2</sup>, Priya Johari<sup>2</sup>, Valipe Ramgopal Rao<sup>1,3</sup> and Dinesh Kabra<sup>1</sup>; <sup>1</sup>IIT Bombay, India; <sup>2</sup>Shiv Nadar University, India; <sup>3</sup>IIT Delhi, India

Increasing the charge carrier mobility of organic semiconductors has been a dominating challenge in the field for over a decade, as typical values of mobility of organic materials are orders of magnitude lower than their inorganic counterparts. Various advances in molecular design as well as device fabrication have enabled mobility of organic materials to reach 10 cm<sup>2</sup>V<sup>-1</sup>s<sup>-1</sup> in recent times. However, the innovations in molecular design have focused on modifying main chain properties. Side chain groups have been considered to play a role in solubility and thin film morphology rather than charge transport energetics. Charge transport in organic semiconductor thinfilms occurs by thermally assisted hopping mechanism, wherein charge carriers are temporally localized on sites, such as a repeat unit of polymer chain, and subsequently hop to energetically favorable neighboring sites. A high mobility represents a higher speed of hopping as applied electric field is increased. Hopping rate is enhanced when orbital overlap between neighboring sites is high, which is achieved by repeat units of high area of conjugation, and when activation energy of hopping is low. Accommodating an incoming hopping charge carrier causes stretching and rotation of the chemical bonds in the newly charged polymer repeat unit. Energy consumed for this physical rearrangement, known as the reorganization energy, acts as an activation barrier to charge hopping process. We present the first report of how changing pendant group connecting the side chain to backbone chain may drastically change the field-effect-mobility of a polymer via reduction of its reorganization energy.<sup>[1]</sup>

We demonstrate this with the case of two structurally similar polymers with only pendant group different. Polymers PTB7 and PTB7-Th are common solar cell donor polymers.<sup>[2]</sup> Structure of both polymers are identical, except the pendant group is an oxygen atom in PTB7 while it is a thiophene unit in PTB7-Th.<sup>[3]</sup> In spite of only a minor difference in the polymer structure, we found charge carrier mobility of PTB7-Th (0.11 cm<sup>2</sup>V<sup>-1</sup>s<sup>-1</sup>) to be a magnitude higher than PTB7 (0.01 cm<sup>2</sup>V<sup>-1</sup>s<sup>-1</sup>) in respective thin film transistors. We show this to be due to the lower reorganization energy of PTB7-Th (0.157 eV) as compared to PTB7 (0.346 eV) as found by calculating from first principles. The values of reorganization energy predict the ratio of rate of charge carrier hopping between the two polymers to be ~10, consistent with our observation of experimental field effect mobility. We find this to be related to rigidity of the thiophene unit of PTB7-Th. During cation formation of polymer segment, side chains in PTB7-Th rotate less (~9°) as compared to PTB7 (~19°), thus requiring less energy to attain charged state molecular configuration. This lowers the activation barrier, and hence increases rate of hopping, and consequently the mobility.



We assert the role of reorganization energy as a dominant parameter controlling mobility of conjugated polymer semiconductors, and provide a key to tuning it via molecular design: an efficient pendant group.

## References

- [1] Patrikar, K., Jain, N., Chakraborty, D., Johari, P., Rao, V. R., Kabra, D., *Adv. Funct. Mater.* 2019, 29, 1805878.
- [2] Nakul Jain, Naresh Chandrasekaran, Aditya Sadhanala, Richard H. Friend, Christopher R. McNeill, Dinesh Kabra, *J. Mater. Chem. A*, 2017, 5, 24749-24757
- [3] Kedar D. Deshmukh, Shyamal K. K. Prasad, Naresh Chandrasekaran, Amelia C. Y. Liu, Eliot Gann, Lars Thomsen, Dinesh Kabra, Justin M. Hodgkiss, and Christopher R. McNeill *Chemistry of Materials* 2017, 29 (2), 804-816

## 6:45 AM \*F.EL07.02.12

**Coulomb Interaction in Organic Semiconductor Blends** [Karl Leo](#); TU Dresden, Germany

Organic semiconductors systems offer many new exciting device applications with attractive features such as flexibility, low cost, low-temperature processing etc. One key difference to inorganic semiconductors is the usually quite small dielectric constant of organics, leading to much stronger Coulomb interactions. For instance, the exciton binding energy in organic semiconductors is significantly greater than the room temperature thermal energy, thus having profound influence on the optical properties. In this talk, I will discuss the influence of these strong Coulomb interactions on two phenomena, both related to blends of organic materials: First, I will discuss controlled electrical doping where the strong Coulomb interaction might be a curse and should, at least in simple hydrogen-like model, make efficient doping unlikely. I will discuss recent results which clarify that doping is indeed efficient, mainly because of disorder effects. Second, I will discuss how the Coulomb interaction can be a blessing by using it for “band structure engineering” of organic semiconductors: Long range Coulomb interactions allow to continuously tune the energy levels, allowing finely adjustable energy levels without synthesis of new molecules. The electrostatic nature of these phenomena is directly proven by experiments which show the strong influence of these quadrupole effects at interfaces. Finally, I will discuss recent results which show that the energy gap of organic semiconductors can be tuned in a similar way.

## 7:00 AM F.EL07.02.13

**Late News: Reaching Double-Digit Dielectric Constants for Molecular Semiconductors** [Sylvia Rousseva](#), Felien S. van Kooij, Hugo den Besten, Ryan C. Chiechi and Jan C. Hummelen; University of Groningen, Netherlands

In most presently known organic semiconductors (OSCs), the relative dielectric constant ( $\epsilon_r$ ) is low ( $\epsilon_r \approx 3-4$ ) compared to crystalline inorganic semiconductors such as silicon ( $\epsilon_r \approx 11$ ). As a result, charges in the material experience strong Coulombic forces which can have a profound effect on the performance of OSC based devices. For instance, at high carrier densities such as found in organic field effect transistors (OFETs), simulations suggest that Coulomb interactions between charge carriers significantly reduce their mobility. Meanwhile, in doped organic semiconductors, the low  $\epsilon_r$  can lead to the formation of Coulomb traps and to lower doping efficiencies due to the formation of stable host-dopant charge-transfer complexes. For organic photovoltaics (OPVs), the low  $\epsilon_r$  has a significant effect on the exciton binding energy, which represents a crucial barrier to charge separation and extraction. Despite the relevance for many OSC based devices, the effect of  $\epsilon_r$  on the electronic and optoelectronic properties of organic materials is largely unexplored due to the scarcity of known organic semiconductors with  $\epsilon_r$  higher than 6. Furthermore,  $\epsilon_r$  is a frequency dependent property, and it remains unclear which frequency regime (timescale) is most relevant for the different device applications.

In this presentation, a homologous series of fullerene derivatives with varying length and geometrical arrangement of polar ethylene glycol (EG) side chains is investigated and the low-frequency  $\epsilon_r$  is measured using impedance spectroscopy. The low frequency  $\epsilon_r$  is found to correlate with length for the symmetrical adducts whereas for the unsymmetrical branched adducts, there is no significant difference. For BTrEG-2, the  $\epsilon_r$  reaches 10, which is unprecedented in an intrinsic molecular organic semiconductor film. The temperature dependence of the low frequency dielectric response and the optical constants (high frequency  $\epsilon_r$ ) are also investigated.

## 7:10 AM F.EL07.02.14

**Late News: Superelastic Organic Semiconductors—The Molecular Mechanisms** [Hong Sun](#); Purdue University, United States

Organic semiconductors are emerging in printable and flexible electronics. Nevertheless, the charge transport in crystal organic semiconductors is attained at the cost of the deformability. Superelastic organic semiconductors (SOSs) is a recently discovered phenomenon that provides a possibility to achieve the high mechanical deformability yet retaining the molecular

ordering. Compared to the well-studied martensitic phase transition in metallic alloys, superelasticity and ferroelasticity in solid-state organic molecules through polymorphic changes are much less understood. Here we leverage the phase transformation theory, genetic algorithm refined molecular modeling, and experimental validation to study the versatile cooperative transitions in bis(triisopropylsilylethynyl)-pentacene semiconductor crystal. The molecular rotation governed thermoelasticity, interconvertible super- and ferroelastic transitions, and molecular twinning are systematically studied by integrating both the lattice crystallography and molecular motions. The fundamental understanding promotes polymorphism to modulate the optoelectronic properties of organic semiconductors and can breed a new avenue of environmentally responsive organic devices.

**7:20 AM F.EL07.02.15**

**Late News: LO-TO Splitting, Coulomb Interactions and Ferroelectricity in Organic Ferroelectrics** [Sanghamitra Mukhopadhyay](#)<sup>1,2</sup>; <sup>1</sup>ISIS Neutron and Muon Facility, United Kingdom; <sup>2</sup>Rutherford Appleton Laboratory, United Kingdom

Organic ferroelectrics are in the focus of current research for their potential technological applications as materials to address global challenges. These lightweight, flexible and nontoxic ferroelectrics have potential applications as ferroelectric random access memories in computers, super capacitors for energy storage, transducers for medical ultrasound imaging and functional materials in flexible electronics [1-4]. As a result of their excellent dielectric, pyro- and piezo-electric properties comparable to traditional inorganic ferroelectrics, and with unique coexistence of flexibility and ferroelectricity, organic ferroelectrics are candidates of intense research promising of designing new bespoke functional materials. These materials are often hydrogen or halogen bonded molecular crystals [5,6] and dynamics or movements of protons from the centro symmetric to non-centrosymmetric positions are considered as the key mechanisms of their functionality. In case of inorganic ferroelectrics, large LO-TO splitting of normal modes helps to identify modes responsible for the ferroelectric functionality. A large LO-TO splitting is a manifestation of strong coupling with the electric field and contributes more to the dynamical effective charge. The effect of electric field on long range Coulomb interaction can also be identified by inspecting the splitting of LO-TO vibrational modes. Thus to understand the microscopic origin of ferroelectricity the knowledge of these normal modes are crucial.

We have done inelastic neutron scattering (INS) spectroscopy experiments on a number of hydrogen and halogen bonded ferroelectric materials, such as croconic acid ( $C_5O_5H_2$ ), 1-cyclobutene-1,2-dicarboxylic acid (CBDC,  $C_6H_8O_4$ ) and 2-phenylmalondialdehyde (PhMDA,  $C_9H_8O_2$ ) and dichloromethylimidazole ( $C_4H_4Cl_2N_2$ ). Calculations are done using plane wave pseudo potential density functional theory (DFT) using CASTEP code. Temperature dependent INS spectra are interpreted using first principles lattice dynamics within quasi harmonic approximations. Structures and dynamics of these functional materials are correlated to understand the role of hydrogen bonds for ferroelectric polarisation at room temperatures. A large LO-TO splitting of the O-H stretching mode around  $2500\text{ cm}^{-1}$  is identified as the mode that has significant contribution to the ferroelectric polarisation. Although this long range Coulomb interaction can be considered as blessings for ferroelectricity in this class of materials, any defect or grain boundary affecting this interaction can kill the ferroelectricity.

In this talk I will present structure and dynamics of few organic ferroelectrics using vibrational neutron spectroscopy and first principles DFT based simulations to find out the finger print of ferroelectricity in this class of materials [7-10]. From INS experiments and DFT simulations, modes sensitive to long range Coulomb interactions and responsible for ferroelectric properties of the material are identified. I would propose vibrational spectroscopy combined with DFT calculations as a characterisation tool to investigate ferroelectric properties in these molecular crystals.

#### References:

- [1] S. Horiuchi et. al, Nat. Mat. **2008**, 7, 267,
- [2] S. Horiuchi et. al, Nature **2010**, 463, 789.
- [3] W. Qin et. al., Nanoscale, **2015**, 7, 9122.
- [4] F. Kagawa et. al., Nat. Phys. **2010**, 6, 169.
- [5] A. Stroppa et. al., Phys. Rev. B, 2011, 84, 014101.
- [6] M. Owczarek et al. Nature Commn **2016**, 7, 1308.
- [7] S. Mukhopadhyay et. al., Phys. Chem. Chem. Phys. **2014**, 16, 26234.
- [8] F. Fernandez-Alonso et. al, J. Phys. Soc. Japan, **2013**, 82, SA001,.
- [9] S. Mukhopadhyay et. al., Chem Phys., **2013**, 427, 95.
- [10] S. Mukhopadhyay et. al., Phys. Chem. Chem. Phys. **2017**, 19, 32147.

**7:30 AM F.EL07.02.16**

**Late News: Optical Distance Measurement by Exploiting Irradiance-Dependent Photoresponse of Organic Near Infrared Photodetectors** Yazhong Wang, Johannes Benduhn, Karl Leo and Donato Spoltore; Dresden Integrated Center of Applied Physics and Photonic Materials (IAPP), Technische Universität Dresden, Germany, Germany

In organic semiconductor devices, extraction barriers are usually undesired since they lead to a reduced device performance. In this work, by intentionally introducing an extraction barrier for holes, near infrared (NIR) organic photodetectors (OPDs) dedicated for distance measurement are realized. The extraction barrier is introduced by replacing the hole transporting layer (HTL) material with a deeper highest occupied molecular orbital (HOMO) HTL material within a well-performing organic solar cell device. Holes pile up at the extraction barrier introducing additional charge recombination. With increasing irradiance, achieved by decreasing the illumination spot area on the OPD, the probability of charge recombination is rising. This allows to determine the distance between the OPD and light source from the irradiance-dependent, non-linear response of the OPD. We extend here this principle to the NIR: We demonstrate fully vacuum-deposited organic NIR optical distance photodetectors with a detection area up to 2.56 cm<sup>2</sup> and detection wavelengths at 850 nm and 1060 nm. Such NIR OPDs have high potential to be utilized as robust, low-cost and simple optical distance measurement setup.

SESSION F.EL07.03: Excitons and TADF

On Demand Abstracts Available for Viewing Starting Saturday Morning, November 21, 2020

F-EL07

**5:00 AM F.EL07.03.01**

**Hyperfine versus Spin-Vibronic Coupling—Or Do Both Drive TADF?** Bluebell H. Drummond<sup>1,2</sup>, William K. Myers<sup>2</sup>, Naoya Aizawa<sup>3</sup>, Leah R. Weiss<sup>4</sup>, Seth R. Marder<sup>5</sup>, Richard Friend<sup>1</sup> and Emrys W. Evans<sup>1</sup>; <sup>1</sup>University of Cambridge, United Kingdom; <sup>2</sup>University of Oxford, United Kingdom; <sup>3</sup>RIKEN, Japan; <sup>4</sup>The University of Chicago, United States; <sup>5</sup>Georgia Institute of Technology, United States

Thermally-activated delayed fluorescence (TADF) organic molecules undergo more efficient light emission than traditional organic fluorescent emitters, making them attractive materials for OLEDs. In TADF devices, indirect emission from dark triplet states via bright singlet excitons is activated and leads to boosted electroluminescence efficiencies.<sup>1</sup> There is general agreement that TADF emitters should be designed to have small singlet-triplet exchange energies that promote forward and reverse intersystem crossing (ISC) between singlet and triplet excited states. However, there is not agreement on the spin interactions and spin-flip mechanisms responsible for singlet-triplet interconversion, with suggestions of hyperfine- and spin-vibronic-based design rules.<sup>2,3</sup> Most studies of TADF use optical spectroscopies which can examine the photophysics and interconversion rates but do not shed light on the critical spin physics.<sup>4</sup> Here we use transient electron spin resonance spectroscopy to study TADF triplets and the role of hyperfine and spin-vibronic couplings on the critical ISC for efficient TADF.

We designed a series of TADF emitters with molecular modifications that led to systematic changes of TADF efficiencies. Solution-based studies of this series revealed the importance of low-lying triplet states and the spin-vibronic mechanism was dominant for ISC. However, in device-relevant thin-films, we find additional signatures of hyperfine coupling mediated triplet formation, proposed to arise from solid-state intermolecular interactions. Our work shows that the singlet-triplet-ground state picture for TADF should be expanded to understand the overall luminescent efficiencies of these materials. Understanding the interplay between molecular design and spin interactions for efficient spin interconversion is integral in establishing the structure-function relationships for the rational design of new TADF emitters.

1. Uoyama, H., Goushi, K., Shizu, K., Nomura, H. & Adachi, C. Highly efficient organic light-emitting diodes from delayed fluorescence. *Nature* **492**, 234–238 (2012).
2. Evans, E. W. *et al.* Vibrationally Assisted Intersystem Crossing in Benchmark Thermally Activated Delayed Fluorescence Molecules. *J. Phys. Chem. Lett.* **9**, 4053–4058 (2018).
3. Ogiwara, T., Wakikawa, Y. & Ikoma, T. Mechanism of Intersystem Crossing of Thermally Activated Delayed Fluorescence Molecules. *J. Phys. Chem. A* **119**, 3415–3418 (2015).
4. Etherington, M. K., Gibson, J., Higginbotham, H. F., Penfold, T. J. & Monkman, A. P. Revealing the spin–vibronic coupling mechanism of thermally activated delayed fluorescence. *Nat. Commun.* **7**, 13680 (2016).

**5:10 AM \*F.EL07.03.02**

## **Emissive and Charge-Generating Donor–Acceptor Interfaces for Organic Optoelectronics with Low Voltage Losses** Koen Vandewal; Hasselt University, Belgium

Charge transfer (CT) states at the interface between electron-donating (D) and electron-accepting (A) materials in organic thin films are characterized by absorption and emission bands within the optical gap of the interfacing materials. Depending on the used donor and acceptor materials, CT states can be very emissive, or generate free carriers at high yield. The former can result in rather efficient organic light emitting diodes, via thermally activated delayed fluorescence, while the latter property is exploited in organic photovoltaic (OPV) devices. In this talk, I will show that proper control of CT state properties allows simultaneous occurrence of a high photovoltaic and emission quantum yield within a single, visible-light-emitting D–A system. This leads to ultralow-emission turn-on voltages as well as significantly reduced voltage losses upon solar illumination.

### **5:25 AM F.EL07.03.03**

**Radical Design for Efficient Light-Emitting Diodes with Doublet Emission** Alim Abdurahman<sup>1</sup>, T. J. Cambridge<sup>2</sup>, Q. Gu<sup>2</sup>, Jiangbin Zhang<sup>2</sup>, Qiming Peng<sup>1,3</sup>, Ming Zhang<sup>1</sup>, Richard Friend<sup>2</sup>, Feng Li<sup>1</sup> and Emrys W. Evans<sup>2,4</sup>; <sup>1</sup>Jilin University, China; <sup>2</sup>University of Cambridge, United Kingdom; <sup>3</sup>Nanjing Tech University, China; <sup>4</sup>Swansea University, United Kingdom

Radical materials have unpaired electrons, leading to unusual physics that could be exploited in next-generation organic electronics. We have previously shown that luminescent radicals can be used for overcoming the spin statistical efficiency limit for electroluminescence (EL) in organic light-emitting diodes (OLEDs) due to their quantum-mechanical doublet-spin character<sup>1,2</sup>. However, suitable radical emitters for OLEDs are generally limited in terms of chemistry and color to tris[2,4,5-trichlorophenyl]methyl derivatives and the near-infrared (> 700 nm). Additionally, the presence of the singly-occupied molecular orbital (SOMO) leads to potential efficiency losses in charge trapping mechanisms for EL. Here we present general design rules to increase the absorption and luminescence yields of organic radicals<sup>3</sup>. These insights were used to design a series of radical molecules with pure-red emission, up to 90% photoluminescence quantum yields and over 12% external quantum efficiency in OLEDs. Doublet exciton quenching processes were probed for radical OLEDs in operation by optical spectroscopy. This work may be beneficial for the rational design and discovery of highly luminescent radical materials with new colors and motifs, as well as informing new device strategies for more efficient radical optoelectronics.

<sup>1</sup>Ai, X., Evans, E.W., Dong, S., Gillett, A.J., Guo, H., Chen, Y., Hele, T.J.H., Friend, R.H. & Li, F. Efficient radical-based light-emitting diodes with doublet emission. *Nature* (2018).

<sup>2</sup>Guo, H., Peng, Q., Chen, X.-K., Gu, Q., Dong, S., Evans, E.W., Gillett, A.J., Ai, X., Zhang, M., Credgington, D., Coropceanu, V., Friend, R.H., Bredas, J.-L. & Li, F. High stability and luminescence efficiency in donor-acceptor neutral radicals not following the Aufbau principle. *Nature Materials* (2019).

<sup>3</sup>Abdurahman, A., Hele, T.J.H., Gu, Q., Zhang, J., Peng, Q., Zhang, M., Friend, R.H., Li, F. & Evans, E.W. Understanding the luminescent nature of organic radicals for efficient doublet emitters and pure-red light-emitting diodes. *Nature Materials* (2020).

### **5:35 AM F.EL07.03.04**

**Controlling the Self-Assembly of Cyanine Dyes into Two-Dimensional Excitonic Molecular Aggregates Across Visible and Shortwave Infrared Wavelengths** Arundhati P. Deshmukh<sup>1</sup>, Austin D. Bailey<sup>1</sup>, Niklas Geue<sup>1</sup>, Leandra Forte<sup>1</sup>, Xingyu Shen<sup>1,2</sup>, Ellen M. Sletten<sup>1</sup> and Justin R. Caram<sup>1</sup>; <sup>1</sup>University of California, Los Angeles, United States; <sup>2</sup>Peking University, China

Molecular aggregates are non-covalent self-assemblies of chromophores where long range coulomb coupling of transition dipole moments leads to delocalized excitons with extreme blue or red shifts, called as H- or J-aggregates respectively. Cyanine dye aggregates have garnered tremendous interest due to their robust excitons, chemical tunability and biocompatibility (1). As a result, these materials have exciting applications in shortwave infrared (SWIR) imaging, plexitonics and excitation energy transfer (2–4). Our research aims to chemically control the excitons in cyanine dye aggregates by leveraging the long range coulomb coupling, which in turn, can be controlled via aggregate morphology as well as energetic disorder. In our previous work, we uncovered design principles for tuning the photophysics of 2-dimensional (2D) aggregates by chemically controlling the position of bright state within the excitonic band (5). However, control over the supramolecular self-assembly of cyanine dyes to push the aggregates to a desired H- or J-aggregated structure is still a challenge. Here, we give general principles to tune the self-assembly of cyanine dyes across a vast range of conditions enabling new experimental tools such as diffusion ordered spectroscopy. We predictably stabilize H- or J-aggregate state by independent control of solvent to non-solvent ratio, dye concentration and ionic strength. We observe universal trends in aggregation that can be understood using a simple three component equilibrium model where the

monomers go via an H-aggregated dimer state to form extended 2D J-aggregates. Comparing the model with our vast experimental aggregation space, we provide thermodynamic insights into the underlying principles that govern the self-assembly. We further show the universal applicability of these principles across the broad set of cyanine dyes, including benzothiazole (THIATS) and benzimidazole cyanines (TDBC), and stabilize H-aggregated dimers or extended J-aggregated sheets with absorptions across the visible and SWIR. Additionally, we perform temperature dependent absorption of sugar matrix stabilized 2D aggregates across this library and shed light on the effect of static and dynamic disorder in 2D aggregates. Overall, we will provide structure-property relationships that employ the ubiquitous coulomb coupling to chemically control the excitons in molecular aggregates.

References:

1. J. L. Bricks *et al.*, *Methods Appl. Fluoresc.* **6**, 012001 (2017).
2. X. Zhong *et al.*, *Angew. Chemie Int. Ed.* **55**, 6202–6206 (2016).
3. W. Chen *et al.*, *J. Am. Chem. Soc.* **141**, 12475–12480 (2019).
4. C. Wang, E. A. Weiss, *Nano Lett.* **17**, 5666–5671 (2017).
5. A. P. Deshmukh *et al.*, *J. Phys. Chem. C.* **123**, 18702–18710 (2019).

#### 5:45 AM \*F.EL07.03.05

**Emissive Isostructural Crystals of Organic Charge-Transfer Complex—Fine-Tuning of Isometric Donor-Acceptor Pairs** Soo Young Park<sup>1</sup>, Sangyoon Oh<sup>1</sup>, Johannes Gierschner<sup>2</sup> and Roland Resel<sup>3</sup>; <sup>1</sup>Seoul National University, Korea (the Republic of); <sup>2</sup>IMDEA nanoscience, Spain; <sup>3</sup>TU Graz, Austria

In this work, we report isostructural systems of mixed-stack CT complexes focusing on the D-A structure-property correlation under identical morphology condition with an aim to unveil the pure electronic mechanism of CT emission. For this, isometric motifs of two donors (D) and two acceptors (A) were rationally designed, of which cocrystals form bright luminescent D:A CT complexes with record high PL quantum yields of 83 %. Notably, four different CT pairs made of isometric D and A molecules all showed the quasi-isostructural intra-stack crystal structure, which allowed us to correlate the electronic CT interaction and their photophysical properties aside from the complicated morphological effect. Our isostructural concept of CT crystals is thus shown to be a crucial strategy for the targeted design of highly emissive CT cocrystals.

#### 6:00 AM F.EL07.03.06

**Photon Recycling in Organic Semiconductor Thin Films** Zhongkai Cheng, Nasir Javed and Deirdre O'Carroll; Rutgers, The State University of New Jersey, United States

Photon recycling (PR), whereby photons generated by radiative recombination in semiconductors result in the regeneration of electron-hole pairs, plays an important role in the study of optoelectronic semiconductor materials and significantly affects the properties of their applications. Excitons are expected to play important roles in PR because they promote high luminescence quantum yields, which are necessary for the observation of PR. However, PR in low-dielectric-constant excitonic materials, such as organic semiconductors, has not been studied to date. In this work, we investigate the mechanisms of PR in organic semiconductor thin films. We study PR in three different organic semiconducting polymer media (regiorandom poly(3-hexylthiophene-2,5-diyl) (RRa-P3HT), regioregular poly(3-hexylthiophene-2,5-diyl) (RR-P3HT), and poly(9,9-dioctylfluorene-alt-benzothiadiazole) (F8BT)) because of their different quantum efficiencies, morphologies and broadband absorptions. In order to study PR, we fabricate different nanostructured surfaces including silver nanoparticle (AgNP) metasurfaces and silver nanograting (AgNG) metasurfaces. In addition, we also use glass, planar Ag and PMMA/Ag surfaces as control groups to analyze the results of PR in the organic thin films compared to the results from nanostructured plasmonic metasurfaces. Surface photoluminescence (PL) emission spectra and edge PL emission spectra are employed to characterize PR because they show strongly red-shifted peaks from surface emission to edge emission when PR is strong. Surface and edge PL emission spectra also play important roles in calculating photon recycling efficiencies and in evaluating reabsorption coefficients. Finally, PL lifetime and PL quantum yield results are used to further explain the PR effect in the different organic semiconductor media. This work is expected to lead to greater understanding of the role of PR in affecting the performance of organic optoelectronic devices.

#### 6:10 AM \*F.EL07.03.07

**Quantum Dynamics of Exciton and Charge Migration in Functional Organic Materials—From Coherent to Diffusive Regimes** Irene Burghardt; Goethe University Frankfurt, Germany

We report on quantum dynamical studies of ultrafast photo-induced energy and charge transfer in functional organic materials, complementing time-resolved spectroscopic observations that underscore the coherent nature of the ultrafast

elementary transfer events in these molecular aggregate systems. Our approach combines first-principles parametrized Hamiltonians [1], with accurate quantum dynamics simulations using the Multi-Layer Multi-Configuration Time-Dependent Hartree (MCTDH) method [2], along with semiclassical approaches [3]. The talk will focus on (i) exciton dissociation and free carrier generation in regioregular donor-acceptor assemblies [1,4], and (ii) the elementary mechanism of exciton migration [3,5-7] and creation of charge-transfer excitons [8] in polythiophene and poly(para-phenylene vinylene) type materials. Special emphasis is placed on the interplay of trapping due to high-frequency phonon modes, and thermal activation due to low-frequency "soft" modes which drive a diffusive dynamics [6].

[1] M. Polkehn, P. Eisenbrandt, H. Tamura, I. Burghardt, *Int. J. Quantum Chem.* 118:e25502. (2018).

[2] H. Wang, *J. Phys. Chem. A* 119, 7951 (2015).

[3] R. Liang, S. J. Cotton, R. Binder, I. Burghardt, W. H. Miller, *J. Chem. Phys.* 149, 044101 (2018).

[4] M. Polkehn, H. Tamura, I. Burghardt, *J. Phys. B: At. Mol. Opt. Phys.* 51, 014003 (2018).

[5] R. Binder, D. Lauvergnat, I. Burghardt, *Phys. Rev. Lett.*, 120, 227401 (2018).

[6] R. Binder, I. Burghardt, *Faraday Discuss.*, 221, 406 (2020).

[7] R. Binder et al., *J. Chem. Phys.* 152, 204119 (2020), *ibid.* 152, 204120 (2020).

[8] W. Popp, M. Polkehn, R. Binder, I. Burghardt, *J. Phys. Chem. Lett.*, 10, 3326 (2019).

### 6:25 AM F.EL07.03.08

**Modification of Photoinduced Electron Transfer in the Strong Light-Matter Coupling Regime** [Nina Krainova](#) and Noel C. Giebink; Pennsylvania State University, United States

The notion that optical environment can change the nature of a chemical reaction emerges in the strong coupling regime when molecular electronic (or vibrational) transitions hybridize with light to form polariton states that have different energies, coherence, and dynamical characteristics than the bare (uncoupled) molecules themselves. Photoinduced charge transfer is arguably one of the most important areas to explore such modification since it underlies processes ranging from photolithography to photosynthesis. Here, we explore this possibility by measuring the photoconductivity of a p-doped organic semiconductor in which charged, rather than neutral molecules (i.e. polaronic rather than excitonic states) are strongly coupled to a Fabry-Perot microcavity.

We confirm the existence of polaron polariton modes in the photoconductivity action spectrum and find that their magnitude evolves differently with applied bias than photocurrent that originates from exciting uncoupled polarons in the same cavity. Importantly, the difference in functional dependence changes systematically with the polariton detuning. We explain these observations on the basis of Onsager theory, where strong coupling effectively changes the thermalization length of photoexcited holes that must escape their dopant counter-ions to contribute to the photoconductivity. We propose that this increase originates from an acceleration of the initial electron transfer event associated with the delocalized nature of the polaritonic excitation, which can effectively sample many more intermolecular electronic couplings in the disordered thin film than a localized excitation can. Access to a wider range of intermolecular electronic couplings in the film allows the polariton to benefit from the largest, thereby speeding up the overall rate of charge transfer.<sup>1</sup>

Reference:

<sup>1</sup>N. Krainova, A.J. Grede, D. Tsokkou, N. Banerji, and N.C. Giebink, *Phys. Rev. Lett.* 124, 177401 (2020)

### 6:35 AM \*F.EL07.03.09

**Coherent Photoexcited Dynamics and Intermolecular Conical Intersections** [Sergei Tretiak](#); Los Alamos National Laboratory, United States

In this talk, I will overview some applications of Non-adiabatic EXcited-state Molecular Dynamics (NEXMD) framework recently developed at LANL. The NEXMD code is able to simulate tens of picoseconds photoinduced dynamics in large molecular systems with hundreds of atoms in size and dense manifold of interacting and crossing excited states. In particular, I will exemplify ultrafast excitonic dynamics guided by intermolecular conical intersections (CoIns). Both simulations and time-resolved two-dimensional electronic spectroscopy track the coherent motion of a vibronic wave packet passing through CoIns within 40 fs, a process that governs the ultrafast energy transfer dynamics in molecular aggregates. Our results suggest that intermolecular CoIns may effectively steer energy pathways in functional nanostructures. Observed relationships between spatial extent/properties of electronic wavefunctions and resulting electronic functionalities allow us to understand and potentially manipulate excited state dynamics and energy transfer pathways toward optoelectronic applications.

### 6:50 AM F.EL07.03.11

**Sharp Thermally Activated Delayed Fluorescence Emission Despite a Rather Large Singlet-Triplet Energy**

**Gap Ramin Ansari**, Jinsang Kim and John Kieffer; University of Michigan, United States

Despite the ability of TADF materials to fully utilize triplet excitons, their inherent limitation is the broad emission spectrum. The torsional mobility about the twist angle between donor and acceptor is considered the principal cause of color impurity, since conventional TADF molecules involve large dihedral angles to facilitate intramolecular charge transfer. However, according to the Franck-Condon principle, electronic transitions are instantaneous compared to nuclear motions, and the emission characteristics should not be subject to molecular rotation. Conversely, there is ample experimental evidence that emission from charge transfer states is broad and diffuse. We submit that the dramatic change of electron configuration between ground and charge-transfer excited states causes the broad emission, as confirmed by our computational and experimental findings. Accordingly, to constrict emission broadening it is preferable to control the charge-transfer character by introducing chromophores with localized emission (LE) character, exhibiting minimal change in electron configuration upon emission. However, molecules with LE emitter states tend to have large singlet-triplet energy gaps ( $\Delta E_{ST}$ ), making TADF pathway inefficient. We have shown that ISC can be further enhanced with a process called “heavy atom oriented El-Sayed rule”, which allows us to design TADF emitters with rather large  $\Delta E_{ST}$  and still result in sharp emission. In this design approach, we incorporate a  $n-\pi^*$  triplet state below the emissive singlet state to boost the reverse ISC, and compensate for the larger  $\Delta E_{ST}$  of the LE emitter state. Our results can be used to design molecular organic alternatives with sharp emissions for LED applications.

#### 7:00 AM F.EL07.03.13

**Late News: Modelling of Ultra-Fast Processes in Organic Semiconductors Using Tensor Network Methods** [Antonios Alvertis](#)<sup>1</sup>, Christoph Schnedermann<sup>1</sup>, Andrew J. Musser<sup>2</sup>, Akshay Rao<sup>1</sup> and Alex W. Chin<sup>3</sup>; <sup>1</sup>University of Cambridge, United Kingdom; <sup>2</sup>Cornell University, United States; <sup>3</sup>Sorbonne Université, France

Ultrafast photo-induced processes in organic materials are crucial to several applications, including organic solar cells and LEDs. Such processes include exciton transport and singlet fission. Understanding the microscopic mechanism of these processes from a theoretical perspective is crucial in order to formulate molecular design rules and efficiently guide the experimental search for those structures that optimise them. However, the simulation of the real-time dynamics of ultrafast processes poses a significant challenge, due to the hundreds of molecular vibrations that interact very strongly with the excited charge carriers, often constituting traditional perturbative methods insufficient, and causing commonly employed approximations such as the Markov and Born-Oppenheimer approximations to break down.

In this talk, I will present a novel theoretical framework based on tensor network methods, for the simulation of the full quantum mechanical non-perturbative dynamics of ultrafast processes, which does not rely on any of the aforementioned approximations. This methodology is applied to very large molecules with up to 108 atoms. The large size of the studied molecules has allowed us to study them experimentally, subjecting our theoretical approach to a rigorous comparison with experimental results, and revealing its accuracy. We uncover the full microscopic mechanism of singlet fission in a covalent pentacene dimer and find that two different groups of vibrational modes coordinate in a precise manner in order to enable efficient fission through an avoided crossing [1].

For a dimer of tetracene, we reveal the impact of the specific pathway of vibrational relaxation on charge transfer, and show that selective excitation of vibrations can increase its efficiency by up to 26% [2].

Finally, we combine the insights from the above studies to build a simple model for singlet fission, which combines the effects of excess energy photoexcitation, molecular vibrations and the polarity of the molecular environment. We show that utilising the subtle interplay between these factors allows for switching into the coherent regime of singlet fission in a controlled manner, accelerating the process by an order of magnitude, as also confirmed experimentally [3].

[1] A molecular movie of ultrafast singlet fission, *Nature Communications* (2019)10:4207;

[2] Non-equilibrium relaxation of hot states in organic semiconductors: impact of mode-selective excitation on charge transfer, *J. Chem. Phys.* 151, 084104 (2019)

[3] Switching between coherent and incoherent singlet fission via solvent-induced symmetry-breaking, *Journal of the American Chemical Society* 2019, 141, 44, 17558-17570

#### 7:10 AM F.EL07.03.14

**Late News: Influence of Energy Gap Between Charge-Transfer and Locally Excited States on Organic Long Persistence Luminescence** [Zesen Lin](#)<sup>1</sup>, Ryota Kabe<sup>1</sup> and Chihaya Adachi<sup>2,2</sup>; <sup>1</sup>Okinawa Institute of Science and Technology

Graduate University, Japan; <sup>2</sup>Kyushu University, Japan

Long-persistent luminescence (LPL), also known as the glow-in-the-dark effect, noctilucous or long afterglow, is a self-sustained light emission phenomenon by which a material emits light for a very long time (longer than several minutes) after removal of the excitation sources which are typically visible light, ultraviolet (UV) light, electron beams or high energy radiation such as X-,  $\alpha$ -,  $\beta$ - or  $\gamma$ -rays. Although the LPL phenomenon is often confused with phosphorescence owing to the confusing terminology in history, the LPL is different with phosphorescence reflected in two apparent features: (i) the almost identical spectra between photoluminescence and LPL; (ii) their decay follows the different law: the LPL (refer in particular to the isothermal luminescence) obeys a power law ( $I(t) \sim t^{-m}$ , with  $m = 0.5 \sim 2$ , mostly 1, hyperbola) in the long time scale, while the phosphorescence follows an exponential law. Therefore, LPL materials can realize long emission duration from minutes to even days after cutoff excitation sources, which is quite longer than phosphorescence. Organic LPL (OLPL) materials have significant superiority over inorganic LPL materials in terms of functionality, flexibility, transparency, and solution-processability. OLPL excited by UV-visible light can be regarded as a recombination luminescence in a special organic solar cell. However, the material design strategies for the OLPL is still not clear. Here, we systematically investigate changes in the LPL duration and spectra for three donor materials having similar molecular structures but different energy levels and find that the LPL performance is significantly influenced by the energy gap between the lowest localized triplet excited-state and the lowest singlet charge-transfer excited-state in the exciplex system. When the energy level of the lowest localized triplet excited-state is much lower than that of the charge-transfer excited state, the system exhibits a short LPL duration under the same excitation condition and clear two distinct emission features originating from exciplex fluorescence and donor phosphorescence.

#### SESSION F.EL07.04: Solar Cells

On Demand Abstracts Available for Viewing Starting Saturday Morning, November 21, 2020

F-EL07

##### 5:00 AM F.EL07.04.01

**Tailoring Energy Levels of Thienothiophene Molecules to Study Photocurrent Generation Mechanism in Fullerene-Based Organic Solar Cells** Lakshmi Narayanan Mosur Saravana Murthy<sup>1</sup>, Aaron Kramer<sup>1</sup>, Jing-Mei Su<sup>2</sup>, Yi-Sheng Chen<sup>2</sup>, Boya Zhang<sup>1</sup>, Ken-Tsung Wong<sup>2,3</sup>, William Vandenberghe<sup>1</sup> and Julia W. Hsu<sup>1</sup>; <sup>1</sup>The University of Texas at Dallas, United States; <sup>2</sup>National Taiwan University, Taiwan; <sup>3</sup>Institute of Atomic and Molecular Science, Academia Sinica, Taiwan

Fullerene-based organic solar cells (OSCs), which consist of a dilute amount of donor molecules (< 5 wt.%) in a fullerene matrix, exhibit high open-circuit voltage ( $V_{oc}$ ) and short circuit current density ( $J_{sc}$ ) simultaneously, thus overcoming the intrinsic  $J_{sc}$ - $V_{oc}$  trade-off observed in traditional bulk heterojunction OSCs. The high  $V_{oc}$  in fullerene-based OSCs has been attributed to reduced bimolecular recombination or the Schottky barrier height between fullerene matrix and the anode. However, the origin of the high  $J_{sc}$  in these OSCs with a donor concentration much lower than the percolation threshold is still unclear. To investigate the photocurrent generation mechanism, we design and synthesize four variations of thienothiophene (TT) molecules with different center and end groups, tuning their HOMO levels from -6.1 to -5.2 eV. We perform experimental studies and density functional theory (DFT) calculations to understand TT:PC<sub>71</sub>BM devices with donor concentration varying from 0 to 10 wt.%. We show that photocurrent generation depends strongly on the center groups, which are either cyano (CN) or hexyloxy (OHex). With 1 wt.% donor, TTOHex:PC<sub>71</sub>BM devices show ten times higher photocurrent than neat PC<sub>71</sub>BM devices. In contrast, TTCN:PC<sub>71</sub>BM devices do not generate additional photocurrent even with 10 wt.% donor. The results are the same for both end group, dicyanovinylene (DC) or rhodamine (RH). DFT results also show TTOHex-PC<sub>71</sub>BM dimers have a shallower HOMO energy than PC<sub>71</sub>BM monomers, while TTCN-PC<sub>71</sub>BM dimers have a deeper HOMO energy than PC<sub>71</sub>BM monomers. Using photoelectron spectroscopy in air (PESA) to measure HOMO levels, we find that the difference between photocurrent in TTOHex:PC<sub>71</sub>BM and TTCN:PC<sub>71</sub>BM devices are strongly correlated with the HOMO offset between donor and acceptor. Since HOMO offset is required to dissociate excitons at the donor-acceptor interface, these results indicate that the first requirement of photocurrent generation is efficient exciton dissociation. We then analyze the possibility of three possible hole transport mechanisms—tunneling, percolation pathways, and hole back transfer—for the TT:PC<sub>71</sub>BM systems. Following exciton dissociation, we find that hole back transfer from donor molecules to PC<sub>71</sub>BM is primarily responsible for photocurrent generation for the TT:PC<sub>71</sub>BM devices.

##### 5:10 AM F.EL07.04.03



**Effects of Acceptor Unit Side Chain Bulk on Electronic Processes and Device Performance of Donor Polymers for Organic Solar Cells** Abigail A. Advincula, Ian Pelse and John Reynolds; Georgia Institute of Technology, United States

Semiconducting polymers are considered highly promising for next generation large area organic solar cell (OSC) devices because of their potential for solution processing and film forming ability. This work explores the effect of increasing side chain steric bulk (methyl, isopropyl, isobutyl, and cyclohexylmethyl) on the acceptor unit of a family of donor-acceptor polymers based on thienopyrroledione (TPD) and investigates the steric effects on electronic properties and device performance. Steric effects on solution-state aggregation properties, solid-state microstructures, optical properties, and thermal properties are also explored. Electronic properties (i.e. hole mobilities, ionization potentials, and electron affinities) were found to be relatively invariant, an effect due to the distance of the side chains from the main backbones of the polymers. When tested in photovoltaic devices with PC<sub>71</sub>BM, the devices fabricated from the polymers demonstrated subtle changes in short-circuit current, fill factor, and OSC device efficiency. In contrast to the electronic properties and photovoltaic statistics, the aggregation, thermal, and morphological properties demonstrated pronounced differences. By UV-vis absorption spectroscopy, we found that changes in steric bulk caused substantial differences in solution-state aggregation, with the bulkier side chain TPD polymers aggregating to a lesser extent. The thermal and morphological properties of neat thin films and blend thin films with PC<sub>71</sub>BM were investigated. By differential scanning calorimetry (DSC), melting/crystallization point depression could be observed with increasing acceptor unit side chain steric bulk, while the heats of fusion/crystallization remained the same. By grazing incidence wide angle x-ray scattering (GIWAXS), out-of-plane lamellar spacing distances (*d*) correlated directly with acceptor-unit side chain bulk – TPD-methyl (*d* = 24.4 Å) and TPD-cyclohexylmethyl (*d* = 26.6 Å). In this work, we demonstrate a unique example of side chain engineering that alters a polymer's solution and solid-state properties but ultimately has little effect on device performance.

**5:20 AM \*F.EL07.04.04**

**Precise Measurements of Hole-Electron Coulomb Binding Energy in Functional Organic Materials** Yoshida Hiroyuki; Chiba University, Japan

Owing to the low dielectric constants, the hole and electron pairs in functional organic materials are strongly bound by the Coulomb interaction. It is therefore crucial to measure precisely the Coulomb bounding energies. This energy is the difference between the bound state and the free hole/electron state. While the bound state energy can often be measured by optical spectroscopies, the energy of the free charge state was difficult to determine in organic materials. The free hole and electron energies correspond to the ionization energy and electron affinity, respectively. Thus, the energy of the free hole-electron pair without mutual interaction can be determined as the difference of the ionization energy and electron affinity measured separately. The ionization energies of organic solid materials are routinely examined by ultraviolet photoelectron spectroscopy (UPS). Therefore, the precise value of the electron affinity was the missing piece for the hole-electron interaction energy.

In 2012, we developed low-energy inverse photoelectron spectroscopy (LEIPS) which enable to determine the electron affinity of organic material as precise as the ionization energy determined by UPS. Using the combination of UPS/LEIPS for the free hole-electron energy together with the existing methods for the bound state energy, we are able to measure the hole-electron interaction energy with the uncertainty of 0.1 eV. We have applied this procedure to examine the Coulomb interaction energy of various functional organic materials. In this presentation, I focus on the following two topics:

1. Exciton binding energy

When the hole-electron pair stays in the same material, the interaction energy is the exciton binding energy. We have determined the exciton binding energies of organic materials used for organic light emitting diode (OLED) and organic solar cell (OSC) as well as prototypical organic semiconductors. The exciton binding energies of OLED materials exceeds 1 eV while those of the OSC materials are less than 0.5 eV. The large exciton binding energy may facilitate binding of the free holes and electrons to generate photons in OLED. In contrast, the small exciton binding energy is preferential to the free carrier generation in OSC. Interestingly, we found no distinct differences in the exciton binding energies among the state-of-the-art non-fullerene acceptors, conventional fullerene acceptors and low-bandgap polymers.

2. Charge dissociation energy in organic solar cell (OSC)

If the hole and electron stay in the donor and acceptor, respectively, at the donor/acceptor interface, the Coulomb interaction energy corresponds to the charge dissociation energy in OSC. A simple consideration based on the Coulomb interaction in continuum dielectric media gives a charge dissociation energy of around 0.5 eV. As this estimated value is much larger than

the thermal energy, there has been a long-standing debate how the strongly bound hole-electron pair at the donor/acceptor interface spontaneously dissociate into the free carriers. However, the reliable dissociation energy has never been determined experimentally. We applied the above-mentioned method to the bulk-heterojunction of the low-bandgap polymer/fullerene acceptor and low-bandgap polymer/non-fullerene acceptor. The determined charge dissociation energies (enthalpy difference) are always less than 0.3 eV which is small enough to dissociate the hole/electron pair by the thermal energy with the assistance of the entropy.

#### 5:35 AM \*F.EL07.04.05

##### **The Importance of Terahertz Short-Range Mobility for Free Charge Generation in NFA-Based Organic Solar Cells** Natalie Banerji; University of Bern, Switzerland

In the field of organic photovoltaics, efficiencies beyond 17% have recently been achieved by combining low bandgap conjugated polymers with small-molecule non-fullerene acceptors (NFAs). To understand what differentiates non-fullerenes from conventional fullerenes in terms of the charge separation and transport processes, we have used ultrafast transient absorption spectroscopy (TAS), electro-modulated differential absorption spectroscopy (EDA) and terahertz measurements (THz). We have thus investigated how the charge generation and separation processes depend on parameters such as the charge-transfer and recombination energetics, the short-range charge mobility and the morphology. Moreover, to simplify the complexity of the process caused by the phase morphology of bulk heterojunction blends, we have worked with bilayers of the donor polymer with the NFA, and with blends containing dilute concentrations of the acceptor. Our results are combined into a kinetic model that explains the efficiency of free charge generation in various polymer:NFA blends.

#### 5:50 AM F.EL07.04.06

##### **Influence Molecular Orientation on Charge Separation at Organic Donor/Acceptor Interface** Jeong Won Kim<sup>1</sup>, Heeseon Lim<sup>1</sup>, Sena Yang<sup>1</sup>, Sang-Hoon Lee<sup>2</sup>, Jung-Yong Lee<sup>2</sup>, Yeonhee Lee<sup>2</sup> and Yong-Hyun Kim<sup>2</sup>; <sup>1</sup>KRISS, Korea (the Republic of); <sup>2</sup>Korea Advanced Institute of Science and Technology, Korea (the Republic of)

For highly efficient organic photovoltaics (OPVs), control of molecular orientation is of prime importance. While molecular orientation within a film influences charge conduction, relative configuration at donor/acceptor interface determines energy level alignment as well as electron-hole separation. Here, we report the change in molecular orientation of planar-shape donor molecules, metal phthalocyanine (CuPc or ZnPc) on ITO by adding CuI templating layer. Near edge X-ray absorption fine structure measurement can estimate average tilt angle of the planar molecules with and without CuI underlayer. CuPc reveals a noticeable change from standing-up to lying-down orientation by CuI, but ZnPc keeps standing-up geometry. Ionization potential for both molecular films measured by ultraviolet photoelectron spectroscopy shows consistent results as well. To explain the different templating effect of CuI, we compare chemical interaction between CuI and the two different metal phthalocyanine molecules by DFT calculation. The stronger interaction between Cu-Cu atoms in CuPc and CuI, respectively, might be reason for the distinct influence on the molecular orientation change of CuPc film. Furthermore, the exciton dynamics at MPC/C<sub>60</sub> (donor/acceptor) interface is studied by time-resolved two-photon photoemission spectroscopy. On CuI layer, the lying-down CuPc molecules show a clear charge transfer (CT) exciton characteristics at the CuPc/C<sub>60</sub> interface, while ZnPc molecules only show long-lived singlet peak even at the ZnPc/C<sub>60</sub> interface. Thus, face-on interface of CuPc/C<sub>60</sub> induces CT exciton by strong  $\pi$ - $\pi$  overlap between donor and acceptor. Finally, we discuss the influence of molecular orientation on the enhanced carrier transport and overall OPV cell efficiency by measuring device performance.

#### 6:00 AM F.EL07.04.08

##### **Molecular Absorption and Exciton Hybridization Improve the Maximum Achievable Photovoltage in Organic Solar Cells** Michel Panhans<sup>1</sup> and Frank Ortman<sup>1,2</sup>; <sup>1</sup>Technische Universität Dresden, Germany; <sup>2</sup>Technische Universität München, Germany

Understanding optical absorption and excitonic properties is crucial for organic solar cells (OSCs). We study the microscopic origin of exciton bands in molecular blends and investigate their role in OSCs [1]. We simulate low-energy absorption features including molecular excitons, CT-excitons and hybrids including multi-exciton hybridization as well as low-frequency molecular vibrations. For model donor-acceptor blends featuring charge-transfer excitons, our numerical calculations agree very well with temperature-dependent experimental absorption spectra. We are able to predict the low-energy spectral lineshape, which we connect to radiative voltage losses that limit the solar cell's performance. In addition, we unveil that the quantum effect of zero-point vibrations, mediated by electron-phonon interaction plays a significant role. It causes a substantial exciton bandwidth and reduces the open-circuit voltage, which is predicted from

electronic and vibronic molecular parameters. This effect is surprisingly strong at room temperature and can substantially reduce the OSC's efficiency.

To circumvent such radiative voltage losses, we elaborate on a better understanding of their connection to OSC parameters such as the electronic coupling or the driving force for CT exciton formation. Radiative open circuit voltages are affected by exciton hybridization and delocalization on the order 100 mV or more, depending on the system.

We finally extend our theoretical predictions for a set of different donor-acceptor systems including non-fullerene donor-acceptor blends and different heterojunction and interface geometries. Our proposed strategies to reduce the radiative voltage losses are supported by excellent agreement of the present simulation approach to existing experimental data for the low-energy absorption.

[1] Panhans, M., Hutsch, S., Benduhn, J., Schellhammer, K. S., Nikolis, V. C., Vangerven, T., Vandewal, K., Ortmann, F. Molecular vibrations reduce the maximum achievable photovoltage in organic solar cells. *Nat Commun* **11**, 1488 (2020).

#### **6:10 AM \*F.EL07.04.10**

**Understanding and Minimizing Voltage Losses in High-Efficiency Organic Solar Cells** [Feng Gao](#); Linköping University, Sweden

Compared with inorganic or perovskite photovoltaics, the key limiting factor for organic solar cells (OSCs) is large voltage loss, which is usually over 0.7 V. A significant contribution of the large voltage loss in OSCs is due to strong non-radiative recombination, the origin of which has been puzzling the community for a long time, limiting rational design of materials to overcome this critical issue. We systematically investigate a range of low voltage loss systems, where the voltage loss is around or below 0.6 V. We find that the quantum efficiency of electroluminescence in these systems have been significantly increased, leading to decreased non-radiative voltage losses below 0.20 V. Combining spectroscopic and quantum chemistry approaches, we formulate the key rules for minimizing voltage losses: (i) low energy offset between donor and acceptor molecular states, and (ii) high photoluminescence yield of the low-gap material in the blend. We further demonstrate that there is no intrinsic limit for efficient charge separation in OSCs with small voltage losses.

#### **6:25 AM \*F.EL07.04.11**

**Self Organization in Vacuum Deposited Oligomer-Fullerene Blends for Efficient Organic Photovoltaics** [Martin P. Pfeiffer](#); Heliatek GmbH, Germany

Organic solar cells offer the unique opportunity to prepare flexible photovoltaic films based exclusively on abundantly available raw materials in an energy-efficient low-temperature process compatible with low-cost PET as a substrate foil. Due to their light weight and their attractive appearance, the films are especially suitable for building integration in facades and roofs of buildings that cannot bear the weight of traditional solar cells.

Heliatek has chosen the approach to prepare organic solar cells by a clean and solvent-free vacuum based on oligomer absorbers. It enables to manufacture p-i-n-type tandem or triple junction architectures in a fully integrated additive roll-to-roll process including laser-structuring and encapsulation. After the ramp of a 30cm wide pilot line using tailored organic conjugated oligomer absorbers developed within Heliatek, a production line for 120cm wide PET web is currently set up and starts to become productive within 2020.

To get optimum efficiency, we need strong absorption with steep absorption edges, efficient charge separation and good charge transport perpendicular to the substrate. This requires a nanocrystalline morphology with suitable preferential orientation, a close p-stacking mode within the donor domains and a phase separation on the order of at least 10-20nm between donor and acceptor domains. Moreover, the degree of slipping in x and y direction within pairs of p-stacked molecules plays a critical role both for the steepness of the absorption spectra and for the distribution of subgap states (Urbach tail) which strongly influences the achievable open circuit voltage. We will discuss the influence of non-classical hydrogen bridges and specific interactions such as sulfur-nitrogen attractions on self-organization processes. It turns out that these partly Coulombic interactions are essential for the desired growth mode.

We will summarize the state of the art of organic vacuum deposited photovoltaics reaching currently up to 13.2% efficiency and discuss the potential for further breakthroughs. Finally we report on a new small molecule absorber that combines fill factors above 70%, a very steep absorption edge, a low Urbach energy (22meV) and optimum energetic alignment to fullerene C<sub>60</sub> with excellent processability at high deposition rates.

#### **6:40 AM F.EL07.04.12**

**Late News: Lateral Alternating Multilayered Junction for Organic Solar Cells** [Masahiro Hiramoto](#); Institute for Molecular Science, Japan

Blended junctions are indispensable for organic solar cells. However, the fabrication of electron and hole transport routes in blended junction remains quite challenging. In this work, we proposed a novel concept of the junction structure of organic solar cell, namely, a lateral alternating multilayered junction [1]. An essential point is that the photogenerated holes and electrons are laterally transported and extracted to the respective electrodes.

Minimum units of proposed junction are hole highway and electron highway. At first, the lateral extraction of photogenerated holes and electrons of the order of 1 mm in the hole and electron highways using ultra-high mobility organic films was demonstrated. Observed macroscopic value of milli-meter order is surprising long compared to the conventional value below 1 mm. Next, the successful operation of organic solar cell having a lateral alternating multilayered junction by combining the hole highway and electron highway was demonstrated. A total of 93% of the photogenerated electrons and holes are laterally collected over a surprising long distance (0.14 mm). The exciton-collection efficiency reaches 75% in a lateral alternating multilayered junction with a layer thickness of 10 nm. Therefore, the lateral junction is proved to have an ability to collect both excitons and carriers almost completely.

A lateral alternating multilayered junction can be regarded to be an alternative blended junction for organic solar cells. Advantage of a lateral cell is its unlimited thickness in the vertical direction. Therefore, tandem solar cells that can utilize the full solar spectrum can be freely designed.

[1] M. Kikuchi, S. Izawa, M. Hiramoto et al., *ACS Appl. Energy Mater.*, **2**, 2087 (2019).

#### 6:50 AM F.EL07.04.13

**Late News: Nonradiative Voltage Losses in Fullerene-Free, Vacuum Deposited Organic Solar Cells** Lukasz K. Baisinger, Donato Spoltore and Karl Leo; Dresden Integrated Center for Applied Physics and Photonic Materials (IAPP), Germany

Organic Solar Cells (OSCs) have been gaining more and more momentum, starting to exhibit efficiencies close to the ones of their inorganic and perovskite counterparts, with recent achievements of certified Power Conversion Efficiency (PCE) above 17% for single-junction devices. The great flexibility in tailoring organic molecules, allowed to design systems that achieve strong absorption with External Quantum Efficiency (EQE) of 80% over whole visible spectrum, while still maintaining efficient charge generation with Fill Factor (FF) above 75%. On the other hand, the open-circuit voltage is still much lower as compared to the most efficient technologies, mainly due to large nonradiative losses, which were identified as intrinsic to devices based on organic molecules. The origin of those losses was proposed to be mainly due to electronic and molecular parameters of the donor and the acceptor molecules.

To study the effect of molecular parameters on nonradiative losses, we built Planar-Heterojunction (PHJ) devices carefully choosing material systems with identical Charge Transfer (CT) state energies while providing different Open-Circuit Voltages ( $V_{oc}$ ). Moreover, by keeping the optical gap constant thanks to red-absorbing SubNc donor, driving force for all material systems is kept the same. This allows to exclude several mechanisms influencing the overall nonradiative losses and focus only on molecular parameters such as reorganization energies and static dipole moment.

Calculated nonradiative voltage losses are indeed larger for the material systems with smaller  $V_{oc}$ , varying by about 100 mV. Subsequent Transient Photovoltage (TPV) measurement further confirm those results, indicating faster decay of free charges in systems with larger voltage losses. To make sure that the TPV is probing bulk recombination kinetics we make use of the novel Transient Photocharge (TPQ) technique, which allows to reliably measure the recombination lifetime of the charge carriers in the bulk.

#### SYMPOSIUM F.EL08

---

Frontiers of Halide Perovskites—Linking Fundamental Properties to Devices  
November 21 - December 4, 2020

Symposium Organizers  
Laura Herz,

Yabing Qi, Okinawa Institute of Science and Technology  
Samuel Stranks, University of Cambridge  
Yuanyuan Zhou, Hong Kong Baptist University

Symposium Support

**Silver**

PicoQuant

**Bronze**

ACS Energy Letters | ACS Publications  
Oxford PV

---

\* Invited Paper

SESSION Tutorial F.EL08: Fundamentals of Halide Perovskite Semiconductors  
Session Chairs: Matthew Beard, Nitin Padture, Laura Schelhas, Su-Huai Wei and Yuanyuan Zhou  
Sunday Afternoon, November 29, 2020  
F.EL08

**2:45 PM \***

**Atomistic Stimulation of Halide Perovskites** Su-Huai Wei; Beijing Computational Science Research Center, China

Basic DFT methods, origin of band structures, defect properties, multiscale stimulation, new materials screening, etc.

**4:00 PM \***

**Photophysics of Halide Perovskites** Matthew Beard; National Renewable Energy Laboratory, United States

Basic photospectroscopy, photophysical processes, coupling effects of photon, electronic, and spin perovskites, emergent photophysics, new tools and methods, etc.

**5:15 PM \***

**Microstructure of Halide Perovskites** Nitin Padture; Brown University, United States

Materials-science description of microstructures, grain boundaries, mechanisms of microstructure evolution, effects of microstructures, microstructure-property relations, etc.

**6:30 PM \***

**X-Ray Characterization of Halide Perovskites** Laura Schelhas; SLAC National Accelerator Laboratory, United States

Basic tutorial of X-ray characterization and synchrotron facilities, advanced x-ray characterization, rational application of x-ray characterization for understanding halide perovskites, etc.

SESSION F.EL08.22: Live Keynote I: Micro- and Nanoscale Characterization of Halide Perovskites  
Session Chairs: Juan Pablo Correa Baena and Libai Huang  
Tuesday Afternoon, December 1, 2020  
F.EL08

**5:15 PM \*F.EL08.01.07**

**Nanoscale Effects in Perovskite Solar Cells Observed by Scanning Force Microscopy** Stefan Weber; Max Planck

Institute for Polymer Research, Germany

Perovskite solar cells have electrified the solar cell research community with astonishing performance and surprising material properties. However, the widespread commercialization of perovskites in solar cells and other optoelectronic applications still requires a more detailed knowledge about fundamental material properties. My group is specialized in the investigation of these properties on nanometer length scales using scanning force microscopy. We recently discovered a distinct nanoscale stripe domain structure in the piezoresponse on perovskite crystals [1]. The pattern is characteristic for ferro-elastic twin domains. We are currently investigating the influence of the domain walls on the charge carrier dynamics. Next to fundamental physical properties of photovoltaic perovskites, we investigate complete solar cell devices under operation conditions. To map and follow the vertical charge distribution across the functional layers of an operating device, we developed a method to prepare smooth cuts across the device [2]. We subsequently map the potential distribution across the device using a time-resolved Kelvin probe force microscopy (tr-KPFM) [2,3]. We can simulate open- or short circuit conditions, apply an external voltage or illuminate the device. In particular, we found that thin layers of localized charge formed and stabilized at the electrode interfaces when we changed the external voltage or illuminated the device. We could show that ion migration itself is too fast to influence device hysteresis. Instead, the formation and release of ionic interface charges determine the time scales for current-voltage hysteresis in perovskite solar cells. Our results demonstrate that a precise control over the interfaces in perovskite solar cells is the key, not only for controlling and suppressing hysteresis but also for their long-term stability in perovskite solar cells. [1] *J. Phys. Chem C*, 120(10), 5724 (2016). [2] *ACS Appl. Mat. Interfaces*, 8(30), 19402 (2016). [3] *Energy Environmental Science*, 11, 2404 (2018).

#### 5:35 PM \*F.EL08.01.08

**Beyond Dilute Imperfections—Extended Defects in Halide Perovskites** Aron Walsh<sup>1,2</sup>; <sup>1</sup>Imperial College London, United Kingdom; <sup>2</sup>Yonsei University, Korea (the Republic of)

Defects come in a several flavours: conductivity-promoting defects create free carriers that enable electronics; killer defects (deep, charged centres) trigger recombination; and charge scattering defects reduce mobility [1]. Our understanding of the defect processes in halide perovskites is gradually improving through a combination of high-resolution measurements and materials modelling [2]. However, evidence is building for the importance of point defect aggregates and structural defects in higher dimensions. I will discuss recent progress, from theory and experiment, to identify, characterise and control extended defects in metal halide perovskites. In particular, I will cover the role of grain boundaries [3] stacking faults [4]. The use of defect tolerance as a metric to develop and screen post-perovskite materials will be critically addressed. This research is part of a collaboration with the group of Sam Stranks (Cambridge), and used the UK National Supercomputer ARCHER.

[1] "Instilling defect tolerance in new compounds" *Nature Mater.* 16, 964 (2017); <https://www.nature.com/articles/nmat4973>

[2] "Performance-limiting nanoscale trap clusters at grain junctions in halide perovskites" *Nature* 580, 260 (2020); <https://www.nature.com/articles/s41586-020-2184-1>

[3] "Accumulation of deep traps at grain boundaries in halide perovskites" *ACS Energy Lett.* 4, 1321 (2019); <https://doi.org/10.1021/acsenerylett.9b00840>

[4] "Hexagonal stacking faults act as hole blocking layers in lead halide perovskites" *ACS Energy Lett.* In Press (2020); <https://doi.org/10.1021/acsenerylett.0c01124>

#### 5:55 PM \*F.EL08.01.04

**Unraveling the Dynamic Behavior of Halide Perovskites from the Macro- to the Nanoscale** Marina S. Leite; University of California, Davis, United States

The dynamic optical and electrical responses of halide perovskites are currently not fully understood, and are closely related to the irreversible changes frequently observed in devices. We determine the individual and combined effects of extrinsic (humidity and oxygen) and intrinsic (light, bias, and temperature) stressors in the physical behavior of the archetypal MAPbBr<sub>3</sub> and MAPbI<sub>3</sub>, and Cs-mixed perovskites. First, a detailed comparison between MAPbBr<sub>3</sub> and MAPbI<sub>3</sub> through time-dependent voltage measurements reveals that, upon illumination, high-energy photons leads to a > 10x slower voltage decline toward equilibrium than low-energy photons in MAPbBr<sub>3</sub>. Yet, MAPbI<sub>3</sub> shows wavelength-independent decay rate, resulting from ion migration. Second, through in situ photoluminescence (PL) under environmentally controlled conditions, we resolve a humidity-induced PL hysteresis. Further, we apply a machine learning algorithm to predict the luminescence response for > 12 hs. Concerning the unique behavior of multi-cation perovskites, a correlative microscopy approach is

realized, combined with environmental-controlled PL measurements.

**6:15 PM \*F.EL08.01.10**

**3D Nanoscale Photoconduction in Hybrid Perovskite Thin-Film Grains and Grain Boundaries as Revealed by Tomographic Atomic Force Microscopy** Jingfeng Song<sup>1</sup>, Yuanyuan Zhou<sup>2</sup>, Nitin Padture<sup>2</sup> and Bryan D. Huey<sup>1</sup>; <sup>1</sup>University of Connecticut, United States; <sup>2</sup>Brown University, United States

Although grain boundaries and other interfaces in photovoltaics are generally detrimental for photogenerated carrier transport, their role remains contentious in hybrid perovskite semiconductors. The uncertainty is partially due to the practical challenge that most experimental approaches are performed at the top surface, which is not only insensitive to depth-dependent inhomogeneities but also may be influenced by topographic artifacts. Accordingly, we have developed tomographic atomic force microscopy (T-AFM) for fully 3-Dimensional mapping of photogenerated carrier transport in hybrid perovskite thin films. Via progressive nanoscale planarization and photoconduction mapping during *in-situ* illumination in an AFM, this unambiguously reveals grain boundaries serving as highly interconnected conducting channels for carrier transport in MAPbI<sub>3</sub>. Voltage dependent measurements reveal enhanced carrier mobilities at most grain boundaries, although careful analysis also reveals the coexistence of 5-10% insipid interfaces. Depth dependencies in photocurrent through the grains, and the grain boundaries, are also assessed. Such insights are critical for engineering hybrid perovskites to be optimized for future solar cells, photodetectors, and light sources.

**6:35 PM \*F.EL08.01.03**

**A Bird's Eye View of Composition-Performance Relationships in Halide Perovskites via Correlative Microscopy** David P. Fenning and Yanqi Luo; University of California, San Diego, United States

Halide perovskite thin films and devices exhibit a remarkable degree of heterogeneity in structure and composition at the nanoscale, varying frequently from nominal synthesis targets in ways that can be difficult to detect using ubiquitous laboratory analysis. Leveraging synchrotron-based *in situ* X-ray microscopies to sample composition, structure, and optoelectronic quality at the nanoscale, we reveal the dependence of nanoscale phase separation and variations in charge collection on the local chemistry of A-site perovskite alloys. At times, these stoichiometric variations arise in the as-fabricated film, revealing important chemical dependencies. However, we also find significant evolution in the microstructure of high-performance perovskites during operation and under environmental stress, leading to insights into mechanistic pathways of degradation and new avenues for stabilization in high-performance alloyed perovskites.

**6:55 PM \*F.EL08.01.02**

**Nanoscale Heterostructures of Halide Perovskites and the Study of Charge Transfer Mechanisms** Song Jin, Dongxu Pan and Matthew P. Hautzinger; University of Wisconsin-Madison, United States

The remarkable solar performance of lead halide perovskites can be attributed to their excellent physical properties that present many mysteries, challenges, as well as opportunities. Better control over the crystal growth of these fascinating materials and fabrication of heterostructures using various halide perovskites with different bandgaps would open up opportunities for exploring new properties and device applications. After a brief summary on the nanowires and nanoplates of various metal halide perovskites we have developed and their lasing properties, I will focus my discussion on the growth of heterostructures of 2D Ruddlesden-Popper (RP) layered lead iodide perovskites with defined n phases and atomically sharp interfaces both in 2D/3D perovskite heterostructures and also as multi-layered multi-colored vertical heterostructures, in which the long chain ammonium ligands serve as the barriers to prevent ion migration across the junctions. We have used these well-defined heterostructures to study the carrier transfer mechanisms between 2D and 3D perovskites and between different RP phases. The excellent properties of these single-crystal perovskite nanostructures of diverse families of perovskite materials with different cations, anions, and dimensionality make them ideal for fundamental physical studies of carrier transport and decay mechanisms, and for enabling high performance lasers, LEDs, and other optoelectronic applications.

SESSION F.EL08.23: Live Keynote II: Spectroscopy and Photophysics

Session Chairs: Laura Herz and Samuel Stranks

Wednesday Morning, December 2, 2020

F.EL08

**8:00 AM \*F.EL08.02.25**

**Many-Body Elastic Scattering of Excitons in Two-Dimensional Hybrid Metal-Halide Perovskites** Carlos Silva; Georgia Institute of Technology, United States

We quantify the role of many-body elastic scattering effects on exciton dephasing rates in two-dimensional hybrid metal-halide perovskites by means of nonlinear coherent excitation spectroscopy at a temperature of 5 K. We find that the exciton-density dependence of excitation-induced dephasing (EID) is two to three orders of magnitude lower than in other atomic monolayer semiconductors such as transition metal dichalcogenides. We find that, EID is different for the multiple excitons evident in the excitation line shape, as is their phonon-mediated temperature dependence. We ascribe these observations to screening effects due to polaronic dressing by the lattice. We further examine the evolution of the two-dimensional coherent exciton lineshape at 5 K with population waiting time. We find that the 2D coherent lineshape evolves with over time windows in which the population itself is static, in a manner that indicates time-dependent EID. Specifically, we find that the dephasing slows down with population waiting time. This spectral evolution invokes time-varying inter-exciton coherences, and we discuss the possible role of dark exciton states in these quantum dynamics.

**8:20 AM \*F.EL08.02.24**

**Carrier and Spin Dynamics in Perovskite 2D Layered and Nanocrystal Systems** Matthew Beard; National Renewable Energy Laboratory, United States

Lead-iodide based perovskite semiconductors are emerging as promising light absorbers for solution-processed thin-film photovoltaic applications. In addition, these materials are also intensively studied for light-emitting diodes, photodetectors, and lasers. Recently, hybrid organic-inorganic perovskite (HOIP) semiconductors are being considered as candidates for spintronic applications due to a large spin-orbit coupling (SOC) and controllable Rashba-splitting. Here we discuss the spin-coherence lifetimes in single crystals of 2D Ruddlesden-Popper perovskites  $\text{PEA}_2\text{PbI}_4(\text{MAPbI}_3)_n$  (PEA, phenethylammonium; MA, methylammonium;  $n = 1, 2, 3, 4$ ). Room temperature spin-coherence times show a nonmonotonic layer thickness dependence with an increasing spin-coherence lifetime with increasing layer thickness from  $n = 1$  to 4, followed by a decrease in lifetime from  $n = 4$  to  $n = 1$ . Our results are consistent with two contributions; Rashba-splitting increases the spin-coherence lifetime going from the  $n = 1$  to the layered systems, while phonon-scattering which increases for smaller layers decreases the spin-coherence lifetime. The unique tunability of HOIPs offers an unprecedented opportunity to directly incorporate chiral organic molecules in the production of a 2D-layered hybrid perovskite thin film and/or crystal that induces chirality into the inorganic sub-lattice bandedge states. Thus, there is an interesting opportunity to explore how chiral molecules embedded into the multilayers provide spin-control within these hybrid semiconductors. Here, we focus on controlling spin-transport within 2D-layered chiral Pb-I perovskite systems. We demonstrate spin-polarization of charge-transport through the chiral perovskites by showing that the injected current is preferential to one of the spin-states and depends upon the handedness of the incorporated chiral organic molecules; thus, the hybrid chiral system acts as a spin-filter.

**8:40 AM \*F.EL08.02.26**

**Harnessing Free Carriers for Photon Upconversion—Using Lead Halide Perovskites for Triplet Sensitization** Lea Nienhaus and Sarah Wieghold; Florida State University, United States

Solid-state nanocrystal-based upconversion (UC) systems have disadvantages with respect to poor exciton diffusion lengths, strong singlet reabsorption and the low resulting achievable UC efficiencies. To circumvent these issues, we employ bulk lead halide perovskite (LHPs) thin films as triplet sensitizers for near-infrared-to-visible UC. The sensitized UC process is based on triplet-triplet annihilation (TTA) in the organic semiconductor rubrene. Conservative estimates result in reported UC efficiencies upwards of 3%. However, to further boost the UC efficiency, it is required to understand and mitigate the effects of shallow trap states in the LHP sensitizer. Here, we investigate the underlying mechanism of energy transfer at the LHP/rubrene interface, and the effect of the LHP perovskite film thickness on the UC dynamics and efficiency threshold. In the LHP/rubrene bilayer device, we observe two opposing effects caused by interactions between the LHP and rubrene: i) passivation of surface defects by rubrene, which results in a longer native photoluminescence (PL) lifetime, and ii) quenching of the PL lifetime due to energy transfer to the triplet state of rubrene. Our observations indicate that non-radiative trap filling in the LHP film and charge transfer to rubrene are likely competitive quenching pathways. As a result, the threshold  $I_{th}$  at which the UC process becomes efficient, observed as a slope change in the power-dependent upconverted PL, shifts to lower values with increasing film thickness. In contrast to previous reported systems, the slope change is directly dependent on the underlying LHP dynamics: i) below  $I_{th}$ , we find a slope twice the value of the LHP PL, and ii) above  $I_{th}$ , the upconverted PL follows the same power-law as the underlying recombination of electrons and holes in the LHP thin films. However, two



unusual effects are also observed in the system: i) two distinct rise times in the upconverted emission, indicating two distinct triplet sensitization rates. ii) A reversible photobleach of the upconverted emission, which cannot be correlated to a physical degradation of the system. By manipulating the triplet population, we are able to show that a higher triplet population does not necessarily result in a higher UC yield for the LHP/rubrene system demonstrated here, rather can be detrimental to the efficiency due to strong singlet reabsorption.<sup>3</sup> (1) Nienhaus, L.; Correa-Baena, J.-P.; Wieghold, S.; Einzinger, M.; Lin, T.-A.; Shulenberger, K. E.; Klein, N. D.; Wu, M.; Bulovi?, V.; Buonassisi, T.; et al. Triplet-Sensitization by Lead Halide Perovskite Thin Films for Near-Infrared-to-Visible Upconversion. *ACS Energy Lett.* 2019, 4, 888-895. (2) Wieghold, S.; Bieber, A. S.; VanOrman, Z. A.; Daley, L.; Leger, M.; Correa-Baena, J.-P.; Nienhaus, L. Triplet Sensitization by Lead Halide Perovskite Thin Films for Efficient Solid-State Photon Upconversion at Subsolar Fluxes. *Matter* 2019, 1, 705-719. (3) Wieghold, S.; Bieber, A. S.; VanOrman, Z. A.; Nienhaus, L. Influence of Triplet Diffusion on Lead Halide Perovskite-Sensitized Solid-State Upconversion. *J. Phys. Chem. Lett.* 2019, 10, 3806-3811.

**9:00 AM \*F.EL08.02.17**

**Photophysics of Methylammonium Lead Bromide Perovskite** Natalie Banerji, Nikolaos Drosos and Dimitra Tsokkou; University of Bern, Switzerland

Methylammonium Lead Bromide (MAPbBr<sub>3</sub>) is the most investigated 3D Perovskite for visible LED applications. It is characterized by a much higher exciton binding energy compared to its Iodide equivalent (MAPbI<sub>3</sub>). This leads to complex excited-state phenomena, with free-carriers, excitons and defect states contributing to the photoluminescence (PL) properties. We have used a variety of spectroscopic techniques to study photoexcited MAPbBr<sub>3</sub> films, including time-resolve PL measurements, femtosecond transient absorption (TA) spectroscopy and optical-probe-terahertz-pump (THz) experiments. The co-existence of free carriers and excitons is demonstrated at low excitation densities in as-cast polycrystalline MAPbBr<sub>3</sub> (crystal size of the order of few ?m). The excitation wavelength and density are then varied in order to access different free-carrier to exciton ratios in order to evaluate their recombination dynamics and THz conductivities. Finally, we show how reducing the grain size of the Perovskite to the micro- and nanoscale (by using different additives during solution-processing) increases the PL quantum yield, which we explain by the presence of a bright exclusively excitonic population even at low excitation densities, together with reduced surface trapping thanks to passivation by the additives.

**9:20 AM \*F.EL08.02.01**

**Novel Hybrid Perovskites for Spin Control and Magneto-Optics** Felix Deschler; Technische Universität München, Germany

Functional materials combining the optoelectronic functionalities of semiconductors with control of the spin degree of freedom are highly sought after for the advancement of quantum technology devices and provide exciting avenues for polarized light-emission. Previous work towards this goal introduced small amounts of magnetic elements into crystalline semiconductor, e.g. through vacuum-based deposition, to obtain dilute magnetic semiconductors (DMS).

In my talk, I will present our efforts on gaining control over spin dynamics and spin interactions through compositional and structural tuning in solution-processable hybrid perovskite semiconductors. We aim to exploit the exceptional optoelectronic properties of these hybrid perovskites, together with their tolerance in the electronic states to dopants and defects, to make advances towards high-performance DMS. I will further discuss how we employ ultrafast optical spectroscopy to gain insights into fundamental excitation and spin dynamics in our novel materials, highlighting the potential of magneto-optic control.

I will present first results on chemical doping of layered Ruddlesden-Popper hybrid perovskites with transition metals. I will report how optical excitations interact with elemental spins in these materials, also on ultrafast timescales, to achieve control over exciton emission through magnetic proximity effects. Harnessing spin-orbit coupling effects, we achieved circular polarization up to 15% in the excitonic photoluminescence at low temperatures and high fields, which keeps a strong magnetic field dependence below 1 Tesla. Our finding constitutes the first example of optical polarization control in magnetically-doped hybrid perovskites and will stimulate research on this highly-tuneable material platform that promises tailored interactions between magnetic moments and electronic states.

**9:40 AM \*F.EL08.02.02**

**Ultrafast Studies of Two-Dimensional Hybrid Metal Halide Perovskites** Rebecca L. Milot; University of Warwick, United Kingdom

Two-dimensional Ruddlesden-Popper phase hybrid metal halide perovskites have been investigated for use in a range of optoelectronic devices including photovoltaic cells. Their main appeal for photovoltaics is improved aqueous stability, which is enabled by their incorporation of organic cations which are more hydrophobic than those usually used in 3D perovskites. However, quantum and dielectric confinement effects increase the exciton binding energies in these materials to as much as 100s of meV. These increased binding energies correspond to an increase in exciton population at ambient temperatures which can greatly alter the optoelectronic properties. Optical Pump/THz-probe (OPTP) spectroscopy measurements have revealed decreased effective charge-carrier mobilities and significantly shortened charge-carrier lifetimes for 2D perovskites (1). In hybrid 2D-3D materials, incorporating small amounts of the 2D material can improve optoelectronic properties (2), suggesting a balance between excitons and free charges is achievable by tuning the composition. OPTP and other ultrafast spectroscopic techniques are further used to elucidate the interplay between free charges and excitons in these materials and comment on the limits these properties impose on charge transport in devices.

1. R. L. Milot et al., "Charge-Carrier Dynamics in 2D Hybrid Metal–Halide Perovskites," *Nano Lett.* **16**(11), 7001-7007 (2016).
2. L. R. V. Buizza et al., "Charge-Carrier Dynamics, Mobilities, and Diffusion Lengths of 2D–3D Hybrid Butylammonium–Cesium–Formamidinium Lead Halide Perovskites," *Adv. Funct. Mater.*, 1902656 (2019).

SESSION F.EL08.24: Live Keynote III: Materials and Chemistry/Materials Discovery  
Session Chairs: Yabing Qi and Yuanyuan Zhou  
Thursday Afternoon, December 3, 2020  
F.EL08

### 6:30 PM \*F.EL08.04.03

**Insight into Layered and Deficient Metal Halide Perovskites from First Principles and Symmetry** Claudio Quarti<sup>1</sup>, Mikael Kepenekian<sup>1</sup>, Pedesseau Laurent<sup>2</sup>, Boubacar Traore<sup>2</sup>, Nicolas Mercier<sup>3</sup>, Mercouri G. Kanatzidis<sup>4</sup>, Constantinos Stoumpos<sup>5</sup>, Jacky Even<sup>2</sup> and Claudine Katan<sup>1</sup>; <sup>1</sup>Univ Rennes, ENSCR, INSA, CNRS, ISCR, France; <sup>2</sup>Univ Rennes, INSA Rennes, CNRS, Institut Foton, France; <sup>3</sup>Université d'Angers, France; <sup>4</sup>Northwestern University, United States; <sup>5</sup>University of Crete, Greece

Currently, many different perovskite -with corner-sharing octahedra- as well as non-perovskite metal-halide solids are synthesized worldwide entailing the need for in-depth understanding of their structure/property relationships. In this regard, combining the huge accumulated knowledge over the last decades, on halide but also oxide perovskites, with modern atomic scale modeling as well as symmetry analysis has proved useful. Among others, new compositions such as  $A'_2A_{n-1}M_nX_{3n+1}$  (where A and A' are cations, X is halide and M is metal) afford layered structures with a controlled number (n, currently  $\leq 7$ ) of octahedra in the perovskite layer. Those correspond to innate heterostructures that offer an ideal platform for fundamental understanding such as effect of quantum or dielectric confinement.<sup>[1]</sup>

Efforts have also been successful in building new perovskite structures with cations surpassing the Goldschmidt tolerance factor. For instance, this has been recently demonstrated for layered perovskites with the use of ethylammonium, isopropylammonium or dimethylammonium as perovskitizer, having a perovskite sheet retaining its continuous corner-sharing connectivity.<sup>[2]</sup> On another note, new three dimensional networks have been achieved by mixing larger cations (e.g., hydroxyethylammonium) with the standard ones (e.g. methylammonium, formamidinium) leading to the formation of voids in the perovskite lattice, either disordered (Hollow perovskites) or with structural signature of a periodic pattern (Deficient perovskites).<sup>[3]</sup>

In this talk, I will discuss some of our recent theoretical results paying attention on newly discovered halide perovskite phases and opportunities to further engineer their properties in connection with their use in devices.

**References** including references therein: [1] C. Katan, N. Mercier, J. Even, *Quantum and dielectric Confinement Effects in Lower-Dimensional Hybrid Perovskite Semiconductors*, Chem. Rev. 119, 3140 (2019); [2] Y. Fu, X. Jiang, X. Li, B. Traore, I. Spanopoulos, C. Katan, J. Even, M. G. Kanatzidis, E. Harel, *Cation Engineering in Two-Dimensional Ruddlesden-Popper Lead Iodide Perovskites with Mixed Large A-Site Cations in the Cages*, J. Am. Chem. Soc. 142, 4008 (2020); X. Li, Y. Fu, L. Pedesseau, P. Guo, S. Cuthriell, I. Hadar, J. Even, C. Katan, C. C. Stoumpos, R. D. Schaller, E. Harel, M. G. Kanatzidis, *Negative Pressure Engineering with Large Cage Cations in 2D Halide Perovskites Causes Lattice Softening*, J.

Am. Chem. Soc. (2020) DOI: 10.1021/jacs.0c03860; [3] A. Leblanc, N. Mercier, M. Allain, J. Dittmer, T. Pauporté, V. Fernandez, F. Boucher, M. Kepenekian, C. Katan, *Enhanced Stability and Band Gap Tuning of  $\alpha$ -[HC(NH<sub>2</sub>)<sub>2</sub>]PbI<sub>3</sub> Hybrid*, ACS Appl. Mater. Interfaces, 11, 20743 (2019); C. Zheng, O. Rubel, M. Kepenekian, X. Rocquefelte, C. Katan, *Electronic properties of Pb-I deficient lead halide perovskites*, J. Chem. Phys. 151, 234704 (2019); C. Quarti, C. Katan and J. Even, *Physical properties of bulk, defective, 2D and 0D metal halide perovskite semiconductors from a symmetry perspective*, under revision.

#### 6:50 PM \*F.EL08.04.01

**Polyelemental, Multicomponent Perovskite Semiconductor Libraries Through Combinatorial Screening** Michael Saliba; Technical University of Darmstadt, Germany

Perovskites have emerged as low-cost, high efficiency photovoltaics with certified efficiencies of 25.2% approaching already established technologies. The perovskites used for solar cells have an ABX<sub>3</sub> structure where the cation A is methylammonium (MA), formamidinium (FA), or cesium (Cs); the metal B is Pb or Sn; and the halide X is Cl, Br or I. Unfortunately, single-cation perovskites often suffer from phase, temperature or humidity instabilities. This is particularly noteworthy for CsPbX<sub>3</sub> and FAPbX<sub>3</sub> which are stable at room temperature as a photoinactive “yellow phase” instead of the more desired photoactive “black phase” that is only stable at higher temperatures. Moreover, apart from phase stability, operating perovskite solar cells (PSCs) at elevated temperatures (of 85 °C) is required for passing industrial norms. Recently, double-cation perovskites (using MA, FA or Cs, FA) were shown to have a stable “black phase” at room temperature.(1,2) These perovskites also exhibit unexpected, novel properties. For example, Cs/FA mixtures suppress halide segregation enabling band gaps for perovskite/silicon or perovskite/perovskite tandems.(3) In general, adding more components increases entropy that can stabilize unstable materials (such as the “yellow phase” of FAPbI<sub>3</sub> that can be avoided using the also unstable CsPbI<sub>3</sub>). Here, we take the mixing approach further to investigate triple cation (with Cs, MA, FA) perovskites resulting in significantly improved reproducibility and stability.(4) We then use multiple cation engineering as a strategy to integrate the seemingly too small rubidium (Rb) (that never shows a black phase as a single-cation perovskite) to study novel multication perovskites.(5) One composition containing Rb, Cs, MA and FA resulted in a stabilized efficiency of 21.6% and an electroluminescence of 3.8%. The Voc of 1.24 V at a band gap of 1.63 eV leads to a very small loss-in-potential of 0.39 V, one of the lowest measured on any PV material indicating the almost recombination-free nature of the novel compound. Polymer-coated cells maintained 95% of their initial performance at 85°C for 500 hours under full illumination and maximum power point tracking. This is a crucial step towards industrialisation of perovskite solar cells. Lastly, to explore the theme of multicomponent perovskites further, molecular cations were reevaluated using a globularity factor. With this, we calculated that ethylammonium (EA) has been misclassified as too large. Using the multication strategy, we studied an EA-containing compound that yielded an open-circuit voltage of 1.59 V, one of the highest to date. Moreover, using EA, we demonstrate a continuous fine-tuning for perovskites in the “green gap” which is highly relevant for lasers and display technology. The last part elaborates on a roadmap on how to extend the multication to multicomponent engineering providing a series of new compounds that are highly relevant candidates for the coming years.(6) (1) Jeon et al. Nature (2015) (2) Lee et al. Advanced Energy Materials (2015) (3) McMeekin et al. Science (2016) (4) Saliba et al., Cesium-containing triple cation perovskite solar cells: improved stability, reproducibility and high efficiency. Energy & Environmental Science (2016) (5) Saliba et al., Incorporation of rubidium cations into perovskite solar cells improves photovoltaic performance. Science (2016). (6) Turren-Cruz et al. Methylammonium-free, high-performance and stable perovskite solar cells on a planar architecture Science (2018)

#### 7:10 PM \*F.EL08.03.02

**Real-Time Investigation of Crystallization Pathways of Organo-Metal-Halide Perovskites Solar** Michael F. Toney; University of Colorado Boulder, United States

Organic-inorganic hybrid perovskite solar cells (PSCs) have gained tremendous attention as materials for photovoltaics due to their high efficiencies and their compatibility with low-cost low-temperature fabrication methods (such as solution processing). Perovskite film formation is complex, involving the formation of intermediates and/or metastable phases that strongly affect the final perovskite film microstructure. Therefore, understanding the mechanism of perovskite formation and the crystallization pathways is key for facile control of perovskite formation. We are using time-resolved x-ray scattering to investigate the perovskite formation of MAPbI<sub>3</sub>-based perovskites and mixed cation (Cs, FA)PbI<sub>3</sub> perovskites *in-situ* during spin coating and the subsequent post-deposition treatments, where FA is formamidinium and MA is methylammonium. For Cs<sub>0.15</sub>FA<sub>0.85</sub>PbI<sub>3</sub> we study: i) the crystallization pathways during spin coating; ii) the subsequent post-deposition thermal annealing, and iii) crystallization during blade-coating. Our findings reveal that the formation of a non-perovskite FAPbI<sub>3</sub> phase during spin coating is initially dominant regardless of the processing and that the processing treatments has a significant impact on the as-cast film structure and affects the phase evolution during subsequent thermal treatment. We show

that blade-coating can be used to overcome the non-perovskite phase formation via solvothermal direct crystallization of perovskite phase. This work show how real-time investigation of perovskite formation can help to establish processing-microstructure-functionality relationships. Our work highlights the importance of real-time investigation of perovskite film formation which can aid in establishing processing-microstructure-functionality relationships and help to provide a fundamental understanding of the mechanisms of perovskite formation.

**7:30 PM \*F.EL08.03.01**

**Progress in Homologous 2D Halide Perovskites and Their Impact in Photovoltaics** Mercouri G. Kanatzidis; Northwestern University, United States

2D perovskites is a fascinating class of compounds where the 3D perovskite lattice is cut and spatially confined in two dimensions and an “inert” layer of intercalated organic ions is inserted between the layers. The 2D perovskites layers can be formed by the introduction of bulky organic cations that tend to interdigitate between the perovskite sheets. They exhibit a large compositional and structural phase space, which has led to novel and exciting physical properties. The variable thickness of the inorganic slabs presents natural quantum wells (QW) type structures with increased Coulombic shielding, lowering the exciton binding energy and increasing the effective charge carrier mobility. Because these materials have had a strong impact in how record breaking and stable solar cells are constructed, it is critical to understand the thermodynamic and chemical limitations of the maximum thickness that can be sandwiched between the organic bilayers while retaining the structural integrity of the 2D perovskite. What are the limits within which the 2D architecture that define the thickness of the inorganic slabs before the system diverts into the familiar 3D structure? To answer this fundamental question, we employed a combination of synthetic chemistry, calorimetry and crystallography to obtain and identify the thickest known 2D halide perovskite compound characterized to date and we use thermodynamics analysis to assess the enthalpy of formation for these compounds. The application of these low dimensional semiconductors in stable photovoltaics will be discussed.

**7:50 PM \*F.EL08.03.03**

**Is the Unit Cell of Solids, Including Halide Perovskites, as Small as the XRD Literature Says? Consequences of the Polymorphous Network** Alex Zunger<sup>1</sup>, Xingang Zhao<sup>1</sup>, Zhi Wang<sup>1</sup> and Gustavo M. Dalpian<sup>2</sup>; <sup>1</sup>University of Colorado Boulder, United States; <sup>2</sup>Universidade Federal do ABC, Brazil

Many common crystal structures can be described by a single (or very few) repeated structural motifs (“monomorphous structures”) such as octahedron in cubic halide perovskites. Interestingly, recent accumulated evidence suggests that electronic structure calculations based on such macroscopically averaged monomorphous cubic (Pm-3m) halide perovskites obtained from x-ray diffraction, show intriguing deviations from experiment. These include systematically too small band gaps, dielectric constants dominated by the electronic, negative mixing enthalpy of alloys, and significant deviations from the measured pair distribution function. We show here that a minimization of the systems  $T = 0$  internal energy via density functional theory reveals a distribution of different low-symmetry local motifs, including tilting, rotations, and B-atom displacements (“polymorphous networks”). This is found only if one allows for larger-than-minimal cell size that does not geometrically exclude low symmetry motifs. As the (super) cell size increases, the energy is lowered relative to the monomorphous cell, and stabilizes after  $\sim 32$  formula units (160 atoms) are included. Being a result of nonthermal energy minimization in the internal energy without entropy, this correlated set of displacements must represent the intrinsic geometry preferred by the underlying chemical bonding (lone pair bonding), and as such has a different origin than the normal, dynamic thermal disorder modeled by molecular dynamics. Indeed, the polymorphous network, not the monomorphous ansatz, is the kernel structure from which high temperature thermal agitation develops. The emerging physical picture is that the polymorphous network has an average structure with high symmetry, yet the local structural motifs have low symmetries. We find that, compared with monomorphous counterparts, the polymorphous networks have significantly lower predicted total energies, larger band gaps, and ionic dominated dielectric constants, and agree much more closely with the observed pair distribution functions. An analogous polymorphous situation is found in the paraelectric phase of a few cubic oxide perovskites where local polarization takes the role of local displacements in halide perovskites, and in the paramagnetic phases of a few 3d oxides where the local spin configuration takes that role. See PHYSICAL REVIEW B 101, 155137 (2020).

**8:10 PM \*F.EL08.03.14**

**Facets of Multicomponent Halide Perovskites—How *In Situ* Experiments Can Help us to Understand Formation, Stability and Composition** Ana F. Nogueira; University of Campinas, Brazil

Multicomponent perovskite solar cells have reached the recent efficiency breakthrough of 25.2%, higher than silicon polycrystalline photovoltaics. Such fantastic result was only possible due to a precise control and engineering of the

morphology, interfaces and the use of multiple cations in perovskite A-site, as Rb, Cs, MA (methylammonium) and FA (formamidinium). For tandem perovskite solar cells, a mixture of different anions, as Br and I is also desired to adjust the band gap. Such cocktail of different cations and anions influences the formation of intermediates, new phases, favours halide homogenization, etc; so that at the end, the efficiency of the device is closely related to not only the optical quality of the film (e.g. crystallinity), but morphology and composition.

In this presentation, we will summarize important results using *in situ* experiments to probe perovskite formation (2D and 3D), stability and composition. We employed time-resolved grazing incidence wide angle x-ray scattering (GIWAXS), small angle x-ray scattering (SAXS) and high-resolution XRD taken at the Brazilian Synchrotron National Laboratory and SSRL-Stanford.

*In situ* GIWAXS experiments allowed us to understand the influence of the relative humidity and time to drop the antisolvent during the preparation of perovskite films and get important information about final composition and morphology [1]. It is well known that a 2D layer on the top of a 3D bulk perovskite improves stability and performance. *In situ* GIWAXS revealed us that during thermal annealing the 2D layer transforms itself into a disorder layer, improving hole transfer and stability [2]. This technique was also employed to identify the first intermediates formed during the degradation of different Cs and Br perovskite compositions under ambient conditions [3].

*In situ* SAXS is another powerful technique to follow the first stages of the 2D perovskite's formation. Our results suggest that the formation of the individual slabs in  $\text{BA}_2[\text{FAPbI}_3]\text{PbI}_4$  is quite fast (within the first 10 s) and, then, these slabs self-assemble into bulk crystallites during the next 40 minutes [4].

Another topic of interest is the photoinduced phase segregation in FACs-based perovskite films. We investigated this phenomenon by photoluminescence (PL) studies and *in situ* high-resolution XRD (dark and under illumination). We found out that cubic-tetragonal transition is able to stabilize the samples with higher Br and Cs content, however this is not true for the films with 17% Br. Thus, other mechanisms must be operating and ruling phase segregation [5].

SESSION F.EL08.25: Live Keynote IV: Devices—Perovskite Photovoltaics/Vapor Deposition and Upscaling of Perovskites  
Session Chairs: Robert Hoyer and Samuel Stranks  
Friday Morning, December 4, 2020  
F.EL08

### 11:30 AM \*F.EL08.07.02

**Fabrication of Perovskite Solar Cells—Wet Solution Deposition vs Vacuum Evaporation** Shengzhong (Frank) Liu<sup>1,2</sup>, Jiangshan Feng<sup>1</sup> and Min Huang<sup>3</sup>; <sup>1</sup>Shaanxi Normal University, China; <sup>2</sup>Dalian Institute of Chemical Physics, Chinese Academy of Sciences, China; <sup>3</sup>Academy of Opto-Electronics, Chinese Academy of Sciences, China

With its rapidly increased cell efficiency to as high as over 25% and incredible suitability to process, equipment and operation, the perovskite is truly a rising star for next generation solar cells. In fact, its cell efficiency has surpassed all other thin film solar cells. We have studied a few different deposition technologies, including dry processing such as vacuum-based alternating precursor deposition, partial co-evaporation of inorganic components; dry atmospheric deposition by using direct contact reactive process; and wet solution processing such as small area spin-coating, large-area blade coating and high-throughput slot-die coating. At present, the wet solution deposition processes are well-advanced with significantly higher efficiencies over 23%. In comparison, the vacuum processes are under development with best cell efficiency still lower than 22%. This article is intended to compare and opt for the best one with most promises for future largescale processing by screening these technologies developed in research laboratories. With mature industrial equipment and engineering processes, we improved the vacuum deposited perovskite cell efficiency to 21.32%, highest for this type to our knowledge. In addition, the films produced using dry deposition seem to show better stability against high humidity, temperature and light-soaking.

### 11:50 AM \*F.EL08.07.03

**Cationic Management for Efficient and Stable FAPbI<sub>3</sub>-Based Perovskite Solar Cells** Sang Il Seok; Ulsan National Institute of Science and Technology (UNIST), Korea (the Republic of)

Highly efficient perovskite solar cells (PSCs) with power conversion efficiencies (PCEs) > 25% are fabricated with formamidinium (FA)-based lead triiodide (FAPbI<sub>3</sub>) perovskites. In general, mixed cations and anions containing FA, methylammonium (MA), Cs, I and Br ions are used to stabilize the black  $\alpha$ -phase against  $\delta$ -phase of the pristine FAPbI<sub>3</sub>. Disadvantageously, the additives such as MA, Cs and Br to FAPbI<sub>3</sub> widen its bandgap and reduce the thermal stability due to the lower thermal decomposition of MA to FA. Therefore, in order to further increase PCE through the enhanced

photocurrent density due to the increased light harvesting, stabilizing the  $\alpha$ -FAPbI<sub>3</sub> without blue-shift of the bandgap is needed. In addition, structural dimensions, distortion, and dielectric properties can vary significantly depending on the ionic radius and type of the A-site cation. In this presentation, I would like to introduce the impact of cationic management on the efficiency and long-term stability of perovskite solar cells.

**12:10 PM \*F.EL08.07.04**

**Defect Related Charge Traps and Doping in Perovskites, Solar Cells and Tandem Devices** Jinsong Huang; University of North Carolina-Chapel Hill, United States

In this talk, I will present our recent progress in understanding the fundamental properties of metal halide perovskites and the related device developments. First, the nature of defects induced charge traps and doping in perovskite materials will be discussed, and their chemical origin will be analyzed. A recent development in characterizing the spatial and energetic distributions of defects will be presented, which revealed the significant difference in trap density between single crystals and polycrystalline films, but similarity in distribution of the traps. Second, the healing of defects and tuning the doping in perovskites by multiple processes will be presented that boost the efficiency and stability of perovskite solar cells and modules. Finally, a new charge recombination layer for all perovskite tandem solar cells will be presented which not only simplifies the fabrication process, but also significantly enhances tandem solar cell efficiency and stability.

**12:30 PM \*F.EL08.07.01**

**Metal Halide Perovskite Materials Development at Hunt Perovskite Technologies, LLC** Michael Irwin; Hunt Perovskite Technologies, LLC, United States

An overview of Hunt Perovskite Technologies, LLC (HPT) metal halide perovskite (MHP) PV research program will be presented. Founded in 2013, HPT has focused their research on stabilizing the MHP material through better chemistry, as highlighted by stabilizing the pure  $\alpha$ -phase FAPbI<sub>3</sub> MHP material in 2015. In this materials study, we have come to appreciate the unique defect structure of the MHP material by way of its ionic composition. Descriptions of MHP macro and molecular defect structure will be discussed, as well as their effect on the material's durability and PV device performance.

**12:50 PM \*F.EL08.08.01**

**Halide Perovskites—Unprecedented Opportunities for Semiconductor Design and Processing** David Mitzi; Duke University, United States

Although known for many years, organic-inorganic hybrid and related inorganic halide-based perovskites have received extraordinary attention recently, in part due to the unique physical properties and chemical diversity offered by these structures, which make them outstanding candidates for applications in photovoltaic and other semiconductor devices (especially for systems based on Pb, Sn and Ge). Perovskite structures consist of networks of corner-sharing metal halide octahedra that can extend in three or lower dimensions, providing opportunity to probe how dimensionality of the inorganic framework impacts semiconducting character. Further, incorporation of more complex organic cations within lower-dimensional perovskites enables combining outstanding inorganic-derived semiconducting character with organic-derived properties (e.g., luminescence, chirality), a feature extending well-beyond what is attainable with more established inorganic semiconductors (e.g., Si or GaAs) and underlying the creation of multifunctional organic-inorganic compounds and electronics [1]. This talk will emphasize chemical/structural versatility [2] and implications for semiconductor design (both with regards to properties and processing), as well as new characterization approaches for elucidating materials properties. Examples of topics that may be covered include custom-designed organic cations that template or stabilize the formation of difficult-to-realize lead-free perovskite structures [3], merging computational/experimental approaches to predict/verify optoelectronic character and guide design of complex organic-inorganic hybrids [4] and the use of a new carrier-resolved photo-Hall (CRPH) technique [5] to explore the impact of additive engineering on majority/minority carrier properties in perovskite films. Outstanding functionality and versatile processing provide two pillars for future application and study of this exciting and evolving materials family. References: [1] D. B. Mitzi, K. Chondroudis, C. R. Kagan, IBM J. Res. & Dev. 45, 29 (2001). [2] B. Saparov, D. B. Mitzi, Chem. Rev. 116, 4558 (2016). [3] M. K. Jana, S. M. Janke, D. J. Dirkes, S. Dovletgeldi, C. Liu, X. Qin, K. Gundogdu, W. You, V. Blum, D. B. Mitzi, J. Am. Chem. Soc. 141, 7955 (2019). [4] W. A. Dunlap-Shohl, E. T. Barraza, A. Barrette, S. Dovletgeldi, G. Findik, D. J. Dirkes, C. Liu, M. K. Jana, V. Blum, W. You, K. Gundogdu, A. D. Stiff-Roberts, D. B. Mitzi, Mater. Horiz. 6, 1707 (2019). [5] O. Gunawan, S. R. Pae, D. M. Bishop, Y. Virgus, J. H. Noh, N. J. Jeon, Y. S. Lee, X. Shao, T. Todorov, D. B. Mitzi, B. Shin, Nature, <https://doi.org/10.1038/s41586-019-1632-2> (2019).

**1:10 PM \*F.EL08.07.06**

**Phase Stable and Less-Defect Perovskite Quantum Dots—Optical Property, Photoexcited Carrier Dynamics and Application to Solar Cells** Qing Shen, Feng Liu, Chao Ding and Yaohong Zhang; The University of Electro-Communications, Japan

Perovskite quantum dots (QDs) as a new type of colloidal nanocrystals have gained significant attention for both fundamental research and commercial applications owing to their appealing optoelectronic properties and excellent chemical processability.<sup>1</sup> For their wide range of potential applications, synthesizing colloidal QDs with high crystal quality is of crucial importance. However, like most common QD systems, those reported perovskite QDs still suffer from a certain density of trapping defects, giving rise to detrimental non-radiative recombination centers and thus low photoluminescence quantum yield (PL QY). Halide vacancy in perovskites has been widely accepted to be the main factor preventing near-unity PL QY by creating uncoordinated Pb octahedra and the subsequent localized deep trap states.<sup>2</sup> Very recently, we have succeeded in synthesis of phase-stable and less-defect perovskite QDs, including FAPbI<sub>3</sub> QDs, CsPbI<sub>3</sub> QDs and Sn-Pb alloyed QDs.<sup>3-6</sup> We have demonstrated that a high room-temperature PL QY of up to 100% can be obtained in FAPbI<sub>3</sub> and CsPbI<sub>3</sub> perovskite QDs, signifying the achievement of almost complete elimination of the trapping defects. This is realized by the modulation of halide precursor involved in the synthesis, in which trioctylphosphine (TOP) is used to dissolve halide salts. For Sn-Pb alloyed QDs, although the alloyed QDs possess much improved structural stability than that of the pure Pb- and Sn-based one, they still suffer from an extremely low PL QY of ~0.3%, indicative of the severe charge trapping in these Sn-containing perovskites. Such low PL QY is believed to result from the widely known facile oxidation of Sn<sup>2+</sup> to Sn<sup>4+</sup>. To address this issue, we have demonstrated very recently that the deep-level trap states in Sn-based perovskites can be well suppressed by Na<sup>+</sup> doping, which gives rise to a dramatically improved PL QY of ~28% without alerting their favorable electronic structure. X-ray photoelectron spectroscopy (XPS) studies suggest the formation of a stronger chemical interaction between I<sup>-</sup> and Sn<sup>2+</sup> ions upon Na doping. On the other hand, though the reported TOP-based route has demonstrated efficacy in producing CsSn<sub>x</sub>Pb<sub>1-x</sub>I<sub>3</sub> QDs (x = 0~0.6) with superior structural stability, such synthetic protocol can only find success in making these I-related QDs, preparing those pure Cl- and Br-based analogues remains challenging because of the insufficient solubility of PbBr<sub>2</sub> and PbCl<sub>2</sub> in TOP. Therefore, by taking advantage of the strong coordinating ability of trioctylphosphine oxide (TOPO), we have recently reported the first synthesis of ASn<sub>x</sub>Pb<sub>1-x</sub>X<sub>3</sub> QDs (A = Cs, FA, MA) with excellent tunability in both Sn/Pb ratio and a full range of halide covering. The ability to generate all possible, unique combinations has offered great material versatility for the perovskite QD family. Further, by employing ultrafast spectroscopic techniques, we have resolved the fundamental photoexcited charge carrier dynamics in these alloyed QDs, which shall pave the way for future study for enhancing their usefulness in optoelectronic applications.<sup>7-9</sup> We expect the successful synthesis of the “ideal” perovskite QDs will exert profound influence on their applications to both QD-based light-harvesting and -emitting devices in the near future.

1. Swarnkar, A. *et al.*, *Science* 2016, Vol. 354, pp. 92-95.
2. Alivisatos *et al.*, *J. Am. Chem. Soc.* 2018, Vol. 140, pp. 17760.
3. F. Liu, Q. Shen *et al.*, *ACS Nano*, Vol. 11, No. 10, pp. 10373-10383, 2017.
4. F. Liu, Q. Shen *et al.*, *J. Am. Chem. Soc.*, Vol. 139, No. 46, pp. 16708-16719, 2017.
5. F. Liu, Q. Shen *et al.*, *J. Phys. Chem. Lett.*, Vol. 9, No. 2, pp. 294-297, 2018.
6. F. Liu, Q. Shen *et al.*, *Chem. Mater.*, Vol. 31, No. 3, pp. 798-807, 2019.
7. F. Liu, Q. Shen *et al.*, *Angew. Chem. Int. Ed.*, Vol. 59, pp. 1-5, 2020.
8. F. Liu, Q. Shen *et al.*, *Chem. Mater.*, Vol. 32, No. 3, pp. 1089-1100, 2020.
9. C. Ding, Q. Shen *et al.*, *Nano Energy* 2020, 67, 104267.

SESSION F.EL08.26: Live Keynote V: Toward Pb-Free Perovskite Absorbers/Devices—Applications Beyond PV

Session Chairs: Robert Hoyer and Hemamala Karunadasa

Friday Afternoon, December 4, 2020

F.EL08

**1:45 PM \*F.EL08.09.01**

**Molecular Engineering of Two-Dimensional Organic-Inorganic Hybrid Perovskites** Letian Dou; Purdue University, United States

Two-dimensional halide perovskites are exciting new semiconductors that show great promising in low cost and high-performance optoelectronics devices including solar cells, LEDs, photodetectors, transistors, etc. In the first part of this talk, I

will present a molecular approach to the synthesis of high-quality organic-inorganic hybrid perovskite quantum wells through incorporating widely tunable organic semiconducting building blocks as the surface capping ligands. By introducing sterically tailored groups into the molecular motif, the strong self-aggregation of the conjugated organic molecules can be suppressed, and single crystalline organic-perovskite hybrid quantum wells and superlattices can be easily obtained via one-step solution-processing. Energy transfer and charge transfer between adjacent organic and inorganic layers are extremely fast and efficient, owing to the atomically-flat interface and ultra-small interlayer distance. In the second part, I will present the synthesis and characterization of a stable lead-free Sn (II)-based two-dimensional perovskite featuring a p-conjugated oligothiophene ligand. The conjugated ligands facilitate formation of micrometer-size large grains, improve charge injections, and stabilize the inorganic perovskite layers. Thin film field-effect transistors based on  $(4Tm)_2SnI_4$  exhibit enhanced hole mobility up to  $2.3 \text{ cm}^2V^{-1}s^{-1}$ , and dramatically improved stability over the previous benchmark material  $(PEA)_2SnI_4$ . Stabilization mechanisms were investigated via single crystal structure analysis as well as density functional theory calculations. It was found that the large conjugated organic layers not only serve as thick and dense barriers for moisture and oxygen, but also increase the crystal formation energy via strong intermolecular interactions.

**2:05 PM \*F.EL08.05.05**

**Bismuth-Based Colloidal Nanocrystals—Lead-Free Materials for Solution-Processed Solar Cells** [Maria Bernechea](#); INA - Institute of Nanoscience of Aragon, Spain

In the last years, the field of solution-processed solar cells based on inorganic semiconductors has seen a great progress, showing the highest efficiencies among the emerging photovoltaic technologies. Indeed, quantum dot solar cells have reached an efficiency over 16%, and solar cells based on perovskites have surpassed 25% efficiency. However, the future development of these cells could be limited due to the presence of highly toxic elements in their composition, more specifically lead (Pb). Efforts are thus required in searching for earth-abundant, and non-toxic materials. Inorganic colloidal nanocrystals (NCs) are attractive materials for their use as active layers in quantum dot solar cells. They are generally composed of earth-abundant elements, and they can be processed from solutions, allowing an easy and cheap fabrication of devices. Moreover, they have additional attractive properties, like high absorption coefficients, tunable bandgaps, and band energy level engineering through ligand exchange. In this context, bismuth-based colloidal NCs, appear as an attractive alternative for environmentally friendly, low cost solar cells. We have developed ways to modify the size and shape of the bismuth-based nanocrystals, and we have observed how this affects their optoelectronic properties. We have studied the modulation of Fermi level and energy bands introducing different ligands on the surface of the NCs. We have employed these NCs to fabricate solution-processed solar cells, focusing on completely non-toxic devices, achieving a certified efficiency of more than 6%, employing very thin layers ( $\sim 35 \text{ nm}$ ) of  $AgBiS_2$  NCs. A summary of these results will be presented and future directions will be discussed.

**2:25 PM \*F.EL08.05.01**

**Is There Any Hope for Efficient Sn-Based Perovskite Solar Cells?** [Maria Antonietta Loi](#); University of Groningen, Netherlands

Organic lead halide perovskite based solar cells (HPSCs) have achieved certified power conversion efficiency (PCE) over 25.0%. Despite the high efficiency achieved, there are still many concerns about the large-scale applicability of this solar cells because of the water soluble toxic  $Pb^{2+}$ . The simpler approach to address this issue is to find a benign or less toxic metal to replace the lead atom in the perovskite structure, with the resulting perovskite still showing the excellent optical and electrical properties. Theoretically, tin based perovskite holds the promise to produce similar or even higher PCE compared to their Pb counterpart. However, for relatively long time the tin-based HPSCs held a PCE lower than 7% though intensive research efforts were devoted to their investigation. The facile formation of tin vacancies and easy oxidation of  $Sn^{2+}$  have been identified as the main reason determining the low PCE. In my presentation I will report as a small amount of 2D tin perovskite templates the growth of highly crystalline and oriented 3D  $FASnI_3$  grains (2D/3D mixtures), suppressing effectively the appearance of tin vacancies and  $Sn^{2+}$  oxidation. As a consequence of the reduced background charge carrier density and trap assisted charge recombination, the device showed a 50% improvement in the PCE (up to 9%) compared to that using pure 3D tin perovskite. We further succeeded reducing the defects in the 2D/3D tin perovskite films by adding ethylammonium iodide (EAI) into the corresponding perovskite precursor solution. These films display larger crystalline grains and a more compact and uniform film morphology when compared to their counterparts without EA cation. These features lead to a much lower trap density, background charge carrier density and charge recombination loss in the corresponding devices. Results, which allow hopping for future highly efficient Sn-based hybrid perovskite solar cells.

**2:45 PM \*F.EL08.05.02**

**Data-Science Methods Enable Perovskite Stability and Performance Improvements** [Tonio Buonassisi](#), Shijing Sun, Clio



Batali, Antonio Buscemi, Alex Encinas, Janak Thapa, Noor Titan Putri Hartono, Felipe Oviedo and Armi Tiihonen; Massachusetts Institute of Technology, United States

Data-science methods, including advanced statistics and machine learning, can help researchers diagnose, optimize, and design more efficiently. In this talk, I'll summarize the MIT PVLab's recent progress optimizing bare films and record-efficiency perovskite devices with capping layers using data-science methods. These include combining density-functional theory (DFT) and Bayesian inference to accelerate the search for stable compositions, and optimizing capping layers for combined performance and stability. Lastly, I'll highlight our progress searching for lead-free perovskite-inspired, defect-tolerant semiconductors.

### 3:05 PM \*F.EL08.006.05

**Unravelling the Impacts of Mobile Ions on Perovskite Solar Cell Performance** Rebecca Belisle; Wellesley College, United States

Defect tolerance has emerged as a central theme for the success of halide perovskites as photovoltaics. Some current estimates put the number of mobile ionic defects in common halide perovskites above  $10^{17}$  cm<sup>-3</sup>, yet the halide perovskite band structure and resulting shallow nature of the hypothesized dominant defects limits their ability to act as recombination centers in these materials. However, this defect tolerance does not imply that these ionic defects have no impact on device performance. Current-voltage hysteresis, reverse-bias breakdown, photo-brightening, photodegradation, thermal stability, and other behaviors related to perovskite performance have all been attributed to the appreciably ionic transport in perovskites made possible by this large defect population. In this work I will present recent advances in both the development of experimental methods for analyzing the formation and behavior of mobile ions in halide perovskites, and our understanding of the effects of these mobile ions on device performance. I will discuss methods to investigate defect formation and transport, including our results using in situ photoluminescence and X-ray diffraction techniques to track ion movement and correlate that with the optoelectronic properties of methylammonium perovskites. Additionally, I will share our work looking at the impacts of mobile ions on device performance, particularly with regards to limits on the open-circuit voltage of perovskite solar cells. Finally, I will highlight the unique roles that contacts and surfaces can play in optimizing the performance and stability of perovskite solar cells in light of these mobile ionic defects.

### 3:20 PM F.EL08.05.06

**Enhancement of Efficiency for Pb Free Perovskite Solar Cells Consisting of Sn<sup>2+</sup> Doped with Ge<sup>2+</sup>** Shuzi Hayase<sup>1</sup>, Kohei Nishimura<sup>1</sup>, Muhammad Akmal Kamarudin<sup>1</sup>, Daisuke Hirofani<sup>2</sup>, Kengo Hamada<sup>2</sup>, Qing Shen<sup>1</sup>, Satoshi Iikubo<sup>2</sup>, Takashi Minemoto<sup>3</sup> and Kenji Yoshino<sup>4</sup>; <sup>1</sup>The University of Elector-Communications, Japan; <sup>2</sup>Kyushu Institute of Technology, Japan; <sup>3</sup>Ritsumeikan University, Japan; <sup>4</sup>Miyazaki University, Japan

The certified efficiency of Pb-perovskite solar cells with more than 1 cm<sup>2</sup> area is reported to be 20.9%(1). In the smaller cell, the cell efficiency with 25.2% has been reported, which is close to 22.3 % of multi Si solar cells (2). However, the use of Pb in electronic devices is limited according to the EU RoHS Directive. Thus, it is needed to develop Pb-free perovskite solar cells. Among Pb-free perovskite candidates, Sn perovskite is one of the most promising candidates for the light harvesting layer for the Pb-free perovskite, because they have perovskite structure similar to Pb-perovskite. However, the efficiency was not as high as those for Pb-perovskite solar cells. We have already reported that the efficiency was enhanced by Ge<sup>2+</sup> doping to the Sn-perovskite layer, because the carrier density in the Sn-perovskite layer was reduced (3,4). Now, we discuss the further enhancement of the Sn-perovskite solar cells from the view point of the lattice strain (disordering) relaxation and the surface passivation on the perovskite layer to show the direction of the research. We report post-treatment of Sn-perovskite layer with Lewis base (NH<sub>2</sub>-CH<sub>2</sub>-CH<sub>2</sub>-NH<sub>2</sub>) to suppress the recombination reaction in Sn-perovskite solar cells resulting in efficiencies of 10.2 %. Upon analyzing the X-ray photoelectron spectroscopy and impedance spectroscopy data, we came to the conclusion that the amine-group bonded the under-coordinated tin, passivating the dangling bonds and defects resulting in suppressed charge carrier recombination (5). This also has the effect of prolonged lifetime and higher charge carrier mobility. These findings provide the groundwork for improving the efficiency of Sn-halide PSCs to compete with that of lead-based PSCs by simple post-treatment with organic molecules (6). We and other research groups have reported that the efficiency of Sn-perovskite solar cells increases spontaneously during the storage, which we explained by the perovskite lattice strain (disordering) relaxation. This prompted us to examine the relationship between relative lattice strain and photovoltaic performances. It is shown that the efficiency of the Sn-perovskite solar cells has good relationship with the lattice strain (disordering). By decreasing the lattice strain (disordering), Ge doped Sn-perovskite solar cells with 11.7% was prepared. The mechanism will be discussed. 1. M.A. Green et al., Progress in Photovoltaics, 2019;27:565-575, version 54, 2. NREL efficiency Table, <https://www.nrel.gov/pv/cell-efficiency.html> 3. N. Ito, S. Hayase, et al., Journal of Physical Chemistry Letters, 9, p.1682-1688, 2018. 4. C. H. Ng, S. Hayase, et al., Nano Energy,

<https://doi.org/10.1016/j.nanoen.2019.01.026>, 2019 5. M. A. Kumarudin, S. Hayase, et al., J. Phys. Chem., Lett., DOI:10.1021/acs.jpcclett.9b02024, 2019. 6. K. Nishimura, S. Hayase, et al., ACS Appl. Mater. Interfaces, <https://doi.org/10.1021/acsami.9b09564> 2019.

SESSION F.EL08.01: Micro- and Nanoscale Characterization of Halide Perovskites  
On Demand Abstracts Available for Viewing Starting Saturday Morning, November 21, 2020  
F-EL08

**5:00 AM \*F.EL08.01.01**

**Microscopic Insights About Metal Halide Perovskite Surfaces** Yabing Qi; Okinawa Institute of Science and Technology, Japan

Metal halide perovskite solar cell research keep progressing on various fronts. My group at OIST uses surface science and advanced characterization to obtain fundamental understanding about perovskite materials and solar cells. Surfaces and interfaces play an important role in dictating performance and stability of perovskite solar cells. In this talk, I focus on surface science understanding and microscopic insights about perovskite surfaces [1-3]. [1] R. Ohmann, Y. Li\*, N.-G. Park\*, Y. B. Qi\* et al., J. Am. Chem. Soc. 137, 16049 (2015); [2] J. Hieulle, X. Wang, Y. Yan\*, Y. B. Qi\* et al., J. Am. Chem. Soc. 141, 3515 (2019); [3] C. Stecker, K. Liu, G. Wang\*, Y. B. Qi\* et al., ACS Nano (2019)  
<https://pubs.acs.org/doi/10.1021/acsnano.9b06585#>

**5:15 AM \*F.EL08.01.02**

**Nanoscale Heterostructures of Halide Perovskites and the Study of Charge Transfer Mechanisms** Song Jin, Dongxu Pan and Matthew P. Hautzinger; University of Wisconsin-Madison, United States

The remarkable solar performance of lead halide perovskites can be attributed to their excellent physical properties that present many mysteries, challenges, as well as opportunities. Better control over the crystal growth of these fascinating materials and fabrication of heterostructures using various halide perovskites with different bandgaps would open up opportunities for exploring new properties and device applications. After a brief summary on the nanowires and nanoplates of various metal halide perovskites we have developed and their lasing properties, I will focus my discussion on the growth of heterostructures of 2D Ruddlesden-Popper (RP) layered lead iodide perovskites with defined n phases and atomically sharp interfaces both in 2D/3D perovskite heterostructures and also as multi-layered multi-colored vertical heterostructures, in which the long chain ammonium ligands serve as the barriers to prevent ion migration across the junctions. We have used these well-defined heterostructures to study the carrier transfer mechanisms between 2D and 3D perovskites and between different RP phases. The excellent properties of these single-crystal perovskite nanostructures of diverse families of perovskite materials with different cations, anions, and dimensionality make them ideal for fundamental physical studies of carrier transport and decay mechanisms, and for enabling high performance lasers, LEDs, and other optoelectronic applications.

**5:30 AM \*F.EL08.01.03**

**A Bird's Eye View of Composition-Performance Relationships in Halide Perovskites via Correlative Microscopy** David P. Fenning and Yanqi Luo; University of California, San Diego, United States

Halide perovskite thin films and devices exhibit a remarkable degree of heterogeneity in structure and composition at the nanoscale, varying frequently from nominal synthesis targets in ways that can be difficult to detect using ubiquitous laboratory analysis. Leveraging synchrotron-based in situ X-ray microscopies to sample composition, structure, and optoelectronic quality at the nanoscale, we reveal the dependence of nanoscale phase separation and variations in charge collection on the local chemistry of A-site perovskite alloys. At times, these stoichiometric variations arise in the as-fabricated film, revealing important chemical dependencies. However, we also find significant evolution in the microstructure of high-performance perovskites during operation and under environmental stress, leading to insights into mechanistic pathways of degradation and new avenues for stabilization in high-performance alloyed perovskites.

**5:45 AM \*F.EL08.01.04**

**Nanoscale Spectroscopy of Halide Perovskite** Marina S. Leite; University of California, Davis, United States

Halide perovskites for optoelectronics are often composed by micro- and nano-scale inhomogeneous constructs. Therefore, high spatial resolution characterization methods are required for mapping and quantifying their electrical behavior. In this talk I will present our latest developments on atomic force microscopy (AFM) methods to assess the dynamic physical and chemical processes that take once perovskite materials and photovoltaic devices are exposed to light. Briefly, we realize a 4D imaging method that enables mapping open-circuit voltage (Voc) changes with in real-time (16 seconds per scan), and at the nanoscale (< 50 nm in spatial resolution) based on illuminated Kelvin probe force microscopy (KPFM). Using this paradigm, we have demonstrated ion motion within a single nanoscale grain in MAPbI<sub>3</sub> solar cells upon 1-sun illumination, which results in a residual Voc that lasts for several minutes even under dark conditions. For multi-cation structures, we found that Cs-based perovskites deliver fully reversible and stable nanoscale voltage response, in excellent agreement with macroscopic measurements. We correlate the Voc nanoscale maps with chemical imaging through nano-IR and discover that the local variations in voltage are related to the power conversion efficiency enhancement in KI-treated perovskite. The heterogeneity revealed in both the local electrical and chemical responses reveals that the KI additive migrates out of the perovskite films, yet surprisingly; does not affect device performance. Our functional imaging platform can be extended to other perovskite materials, including Pb-free options.

**6:00 AM \*F.EL08.01.05**

**Multi-Modal Microscopy Approaches to Probe Halide Perovskite Device Operation** [Samuel D. Stranks](#); University of Cambridge, United Kingdom

Halide perovskites are generating enormous excitement for their use in high-performance yet inexpensive optoelectronic applications. Nevertheless, a number of fundamental questions about these materials still remain and need to be answered to push devices to their theoretical performance limits. For example, we still know very little about the specific nature of the defects leading to trap states, carrier recombination pathways or anisotropies of carrier diffusion. I will present results on new techniques we are developing to address these open questions in 2D and 3D halide perovskite semiconductors. These techniques focus on understanding charge carrier behavior, including recombination, trapping and diffusion, and how these properties link to chemical and material properties. I will present high-resolution luminescence microscopy techniques employing two-photon excitation to allow us to visualize and time-resolve carrier diffusion in three-dimensions, revealing anisotropic and depth-dependent carrier diffusion properties. Furthermore, we link the local luminescence properties to high-resolution crystallographic and chemical properties using synchrotron nano-probe X-Ray beamlines and low-dose scanning electron diffraction measurements. Through these measurements, we reveal the nature of the defects associated with local non-radiative power losses and heterogeneous diffusion. Furthermore, we provide guidelines about how we can ultimately eliminate these unwanted loss pathways and homogenize carrier diffusion.

**6:15 AM \*F.EL08.01.06**

**Processing Dependent Signature of Electronic States in the Gap of Metal Halide Perovskites** [Antoine Kahn](#); Princeton University, United States

An important area of research on metal halide perovskites (MHP) concerns the presence and role of surface and interface electronic gap states introduced by defects inherent to film processing, degradation under stress (T, irradiation, environment) or chemical reaction with neighboring layers, and the restrictions that these states impose on device performance, i.e., limit in Fermi level split, or aid carrier recombination, leading to reduction of solar cell open circuit voltage. This talk reports results on the determination of the presence and density of electronic states tailing above the valence band maximum of several MHPs, e.g., MAPbI<sub>3</sub>, CsPbI<sub>3</sub>, and FA<sub>0.85</sub>MA<sub>0.15</sub>Pb(I<sub>0.85</sub>Br<sub>0.15</sub>)<sub>3</sub>. Detailed measurements of the top of the valence band of these materials are performed using high-sensitivity UPS achieved in logarithmic detection. We focus specifically on MAPbI<sub>3</sub> films processed with different additives mixed in the precursor-DMF solution: (i) no additives; (ii) DMSO; (iii) NH<sub>4</sub><sup>++</sup>DMA<sup>+</sup>; and (iv) N-methyl-2-pyrrolidone thione (NMPT). The latter, an S-donor solvent, was investigated for its stronger coordination to Pb<sup>2+</sup> as compared to the O-donor solvent DMSO, the additive widely used for improving film morphology. Significant differences are revealed between films processed with DMSO and NMPT. Once carefully treated via (experimental) background and parasitic satellite line contribution subtraction, the DMSO processed film exhibits a clear density of gap states extending from the valence band maximum to the Fermi level, whereas the NMPT processed film does not. The study was then complemented by Kelvin probe-based contact potential difference measurements to address the issue of surface photovoltage (SPV) during UPS. KP-based SPV measurements on these films show a significantly larger SPV (150 mV) and EF-VBM on the DMSO-treated films than on the NMPT-treated ones (SPV= 40 mV), confirming both the presence of the gap states and their impact on the electronic structure of the MHP films. The origin and nature of these gap states are still under investigation.

**6:30 AM \*F.EL08.01.07**

**Nanoscale Effects in Perovskite Solar Cells Observed by Scanning Force Microscopy** Stefan Weber; Max Planck Institute for Polymer Research, Germany

Perovskite solar cells have electrified the solar cell research community with astonishing performance and surprising material properties. However, the widespread commercialization of perovskites in solar cells and other optoelectronic applications still requires a more detailed knowledge about fundamental material properties. My group is specialized in the investigation of these properties on nanometer length scales using scanning force microscopy. We recently discovered a distinct nanoscale stripe domain structure in the piezoresponse on perovskite crystals [1]. The pattern is characteristic for ferro-elastic twin domains. We are currently investigating the influence of the domain walls on the charge carrier dynamics. Next to fundamental physical properties of photovoltaic perovskites, we investigate complete solar cell devices under operation conditions. To map and follow the vertical charge distribution across the functional layers of an operating device, we developed a method to prepare smooth cuts across the device [2]. We subsequently map the potential distribution across the device using a time-resolved Kelvin probe force microscopy (tr-KPFM) [2,3]. We can simulate open- or short circuit conditions, apply an external voltage or illuminate the device. In particular, we found that thin layers of localized charge formed and stabilized at the electrode interfaces when we changed the external voltage or illuminated the device. We could show that ion migration itself is too fast to influence device hysteresis. Instead, the formation and release of ionic interface charges determine the time scales for current-voltage hysteresis in perovskite solar cells. Our results demonstrate that a precise control over the interfaces in perovskite solar cells is the key, not only for controlling and suppressing hysteresis but also for their long-term stability in perovskite solar cells. [1] J. Phys. Chem C, 120(10), 5724 (2016). [2] ACS Appl. Mat. Interfaces, 8(30), 19402 (2016). [3] Energy Environmental Science, 11, 2404 (2018).

**6:45 AM \*F.EL08.01.08**

**Beyond Dilute Imperfections—Extended Defects in Halide Perovskites** Aron Walsh<sup>1,2</sup>; <sup>1</sup>Imperial College London, United Kingdom; <sup>2</sup>Yonsei University, Korea (the Republic of)

Defects come in a several flavours: conductivity-promoting defects create free carriers that enable electronics; killer defects (deep, charged centres) trigger recombination; and charge scattering defects reduce mobility [1]. Our understanding of the defect processes in halide perovskites is gradually improving through a combination of high-resolution measurements and materials modelling [2]. However, evidence is building for the importance of point defect aggregates and structural defects in higher dimensions. I will discuss recent progress, from theory and experiment, to identify, characterise and control extended defects in metal halide perovskites. In particular, I will cover the role of grain boundaries [3] stacking faults [4]. The use of defect tolerance as a metric to develop and screen post-perovskite materials will be critically addressed. This research is part of a collaboration with the group of Sam Stranks (Cambridge), and used the UK National Supercomputer ARCHER.

[1] "Instilling defect tolerance in new compounds" Nature Mater. 16, 964 (2017); <https://www.nature.com/articles/nmat4973>

[2] "Performance-limiting nanoscale trap clusters at grain junctions in halide perovskites" Nature 580, 260 (2020); <https://www.nature.com/articles/s41586-020-2184-1>

[3] "Accumulation of deep traps at grain boundaries in halide perovskites" ACS Energy Lett. 4, 1321 (2019); <https://doi.org/10.1021/acsenerylett.9b00840>

[4] "Hexagonal stacking faults act as hole blocking layers in lead halide perovskites" ACS Energy Lett. In Press (2020); <https://doi.org/10.1021/acsenerylett.0c01124>

**7:00 AM \*F.EL08.01.09**

**Unraveling the Dynamic Behavior of Halide Perovskites from the Macro- to the Nanoscale** Marina S. Leite; University of California, Davis, United States

The dynamic optical and electrical responses of halide perovskites are currently not fully understood, and are closely related to the irreversible changes frequently observed in devices. We determine the individual and combined effects of extrinsic (humidity and oxygen) and intrinsic (light, bias, and temperature) stressors in the physical behavior of the archetypal MAPbBr<sub>3</sub> and MAPbI<sub>3</sub>, and Cs-mixed perovskites. First, a detailed comparison between MAPbBr<sub>3</sub> and MAPbI<sub>3</sub> through time-dependent voltage measurements reveals that, upon illumination, high-energy photons leads to a > 10x slower voltage decline toward equilibrium than low-energy photons in MAPbBr<sub>3</sub>. Yet, MAPbI<sub>3</sub> shows wavelength-independent decay rate, resulting from ion migration. Second, through in situ photoluminescence (PL) under environmentally controlled conditions, we resolve a humidity-induced PL hysteresis. Further, we apply a machine learning algorithm to predict the luminescence

response for > 12 hs. Concerning the unique behavior of multi-cation perovskites, a correlative microscopy approach is realized, combined with environmental-controlled PL measurements.

**7:15 AM \*F.EL08.01.10**

**3D Nanoscale Photoconduction in Hybrid Perovskite Thin-Film Grains and Grain Boundaries as Revealed by Tomographic Atomic Force Microscopy** Jingfeng Song<sup>1</sup>, Yuanyuan Zhou<sup>2</sup>, Nitin Padture<sup>2</sup> and Bryan D. Huey<sup>1</sup>; <sup>1</sup>University of Connecticut, United States; <sup>2</sup>Brown University, United States

Although grain boundaries and other interfaces in photovoltaics are generally detrimental for photogenerated carrier transport, their role remains contentious in hybrid perovskite semiconductors. The uncertainty is partially due to the practical challenge that most experimental approaches are performed at the top surface, which is not only insensitive to depth-dependent inhomogeneities but also may be influenced by topographic artifacts. Accordingly, we have developed tomographic atomic force microscopy (T-AFM) for fully 3-Dimensional mapping of photogenerated carrier transport in hybrid perovskite thin films. Via progressive nanoscale planarization and photoconduction mapping during *in-situ* illumination in an AFM, this unambiguously reveals grain boundaries serving as highly interconnected conducting channels for carrier transport in MAPbI<sub>3</sub>. Voltage dependent measurements reveal enhanced carrier mobilities at most grain boundaries, although careful analysis also reveals the coexistence of 5-10% insipid interfaces. Depth dependencies in photocurrent through the grains, and the grain boundaries, are also assessed. Such insights are critical for engineering hybrid perovskites to be optimized for future solar cells, photodetectors, and light sources.

**7:30 AM F.EL08.01.11**

**Size-Dependent Lattice Structure and Confinement Properties in CsPbI<sub>3</sub> Perovskite Nanocrystals—Negative Surface Energy for Stabilization** Joseph Luther<sup>1</sup>, Qian Zhao<sup>1</sup>, Laura Schelhas<sup>2</sup>, Abhijit Hazarika<sup>1</sup>, Michael F. Toney<sup>2</sup> and Peter C. Sercel<sup>3</sup>; <sup>1</sup>National Renewable Energy Laboratory, United States; <sup>2</sup>SLAC National Accelerator Laboratory, United States; <sup>3</sup>California Institute of Technology, United States

CsPbI<sub>3</sub> nanocrystals are widely reported to be more stable in the perovskite phase than thin film CsPbI<sub>3</sub> which rapidly converts into the non-perovskite orthorhombic phase. In this work, we answer why the phase stability is enhanced at the nanoscale. In addition, contrary to many reports, we confirm that the actual perovskite phase for CsPbI<sub>3</sub> NCs is the gamma phase, rather than the alpha cubic phase. In this work, CsPbI<sub>3</sub> with narrow size distributions between 5 and 15 nm were prepared to study the size-dependent properties. The size dependent structural lattice constants were characterized and found to systematically vary by 3% across the size range, with unit cell volume increasing linearly with the inverse of size to 2.1% for the smallest size. This size dependent volume change correlates to negative surface energy between -3.0 to -5.1 eV nm<sup>-2</sup> for ligated CsPbI<sub>3</sub> nanocrystals. This negative surface energy leads to strain on the nanocrystals which, when present, causes stability in the perovskite phase, whereas thin film, strain-free CsPbI<sub>3</sub> is only metastable in the perovskite phase. Moreover, the size-dependent bandgap is also studied and found to be best described using a nonparabolic intermediate confinement model. Using this new model, we can experimentally determine constants such as the bulk bandgap, effective mass, and exciton binding energy, and conclude that many of these main material constants vary from the bulk  $\alpha$ -phase values. This work provides a robust route to understanding  $\gamma$ -phase properties of CsPbI<sub>3</sub>.

**7:40 AM F.EL08.01.12**

**CsPbBr<sub>3</sub> Nanocrystal Films—Charge Localization and Deviations from Bulk Properties** Silvia G. Motti<sup>1</sup>, Franziska Krieg<sup>2</sup>, Jay Patel<sup>1</sup>, Maksym V. Kovalenko<sup>2</sup>, Michael Johnston<sup>1</sup> and Laura Herz<sup>1</sup>; <sup>1</sup>University of Oxford, United Kingdom; <sup>2</sup>ETH Zürich, Switzerland

Metal halide perovskites are highly promising semiconductors for light-emitting and photovoltaic applications. The colloidal synthesis of nanocrystals (NC) is an effective approach for obtaining nearly defect-free semiconducting materials that can be processed into inks for low cost, high performance device fabrication. However, disentangling the effects of surface ligands, morphology and boundaries on charge-carrier transport in thin films fabricated with these high-quality NCs is inherently difficult. To overcome this fundamental challenge, here we employ terahertz (THz) spectroscopy to optically probe the photoconductivity of CsPbBr<sub>3</sub> nanocrystal films. We compare the vibrational and optoelectronic properties of the NCs with those of a corresponding bulk polycrystalline perovskite and find significant deviations. We demonstrate a dependence of the charge-carrier mobilities and recombination rates on the nanocrystal size that derives from the localized nature of charge-carriers within nanocrystals, with local mobilities dominating those associated with inter-particle transport. We further show that the colloidal synthesized NCs have distinct vibrational properties with respect to the bulk perovskite, exhibiting blue-shifted optical phonon modes with enhanced THz absorption strength that also manifest as strong modulations in the THz photoconductivity spectra. Such fundamental insights into NC versus bulk properties will guide the optimization of

nanocrystalline perovskite thin films for optoelectronic applications.

#### 7:50 AM F.EL08.01.13

##### ***In Situ and Operando* Strain and Defect Characterization Using Coherent X-Ray Diffractive Imaging in Bragg Geometry** Wonsuk Cha; Argonne National Laboratory, United States

Coherent x-ray diffractive imaging in Bragg geometry (BCDI) is a powerful technique to image three-dimensional morphology as well as internal deformation field distribution of nano-scaled materials [1]. Because of unique sensitivity to lattice, BCDI has been employed to map strain and defect distribution inside metal, metal oxide, and minerals with non-destructive measurements. In this talk, I will introduce current state-of-art of BCDI and the 34-ID-C beamline in the Advanced Photon Source where one can perform this experiment. This talk will also cover recent experimental results on in-situ and operando BCDI, e.g. unique lattice distortion in ZSM-5 zeolites [2], annealing effect on gold grains on gold thin films [3], oxidation induced strain and defects in magnetite [4], and defect dynamics on platinum during catalytic reaction [5]. In addition, some estimates of BCDI in the future will be discussed. [1] M. A. Pfeifer, et al., Nature 442, 63 (2006). [2] W. Cha, et al., Nat. Mater. 12, 729 (2013). [3] A. Yau, et al., Science 356, 739 (2017). [4] K. Yuan, et al., Nat. Commun. 10, 703 (2019). [5] D. Kim, et al., Nano Lett. 19, 5044 (2019).

#### 8:00 AM F.EL08.01.14

##### **Imaging Light-Induced Phase Separation Dynamics of Inorganic Halide Perovskites** Siyang Peng, Andrew Meng, Wanliang Tan, Michael Braun, Balreen Saini, Kayla Severson, Ann Marshall and Paul McIntyre; Stanford University, United States

Halide perovskites have emerged as promising materials for optoelectronics with superior photoconversion efficiency and low cost. Moreover, optical properties of halide perovskite with mixed bromide and iodide composition can be substantially tuned via light-induced ion migration. Bromide-rich and iodide-rich domains starts to form during the process, which can be initiated at low intensity of light. Phase separation is subsequently reversible under the dark. Photoluminescence emission energy redshifts as a result of phase separation, while optical constants also change. The tunability of photoluminescence emission and optical constants in a wide spectral range makes halide perovskite alloys a promising, dynamically tunable photonic materials system. Unlike conventional tunable photonic materials such as ITO, TCO, and VO<sub>2</sub>, which rely on tuning of carrier density or an abrupt structural transformation, the speed and degree of phase separation/optical property evolution of mixed halide perovskite alloys can be tuned monotonically by varying the photon intensity. Inorganic mixed halide perovskites have been widely investigated for high-efficiency solar cells, with a focus on improving stability of their light absorption by reducing ion migration. To integrate halide perovskites for tunable nanophotonics, it is essential to understand light-induced phase separation in halide perovskites such as the spacing of phase separated domains, the influence of perovskite crystallite size and orientation, etc. We have synthesized crystallographically-textured polycrystalline films of the inorganic halide perovskite alloy CsPb(BrxI1-x)<sub>3</sub> on SrTiO<sub>3</sub> (STO) substrates by chemical vapor transport (CVT) at 620°C (at the precursor position) with N<sub>2</sub> as the carrier gas. These perovskite films have large single crystal domains in the [001] orientation on the order of millimeters in lateral size and are stable under ambient laboratory conditions. X-ray diffraction confirms the perovskite phase of the film and the predominantly (001) orientation. EDX mapping shows a homogeneous initial distribution of Br, I as well as Cs and Pb. Photoluminescence characterization reveals initial light emission at 2.15 eV. By shining an HgXe lamp on the film, light emission at 2.0 eV starts to occur and dominate the emission spectrum. Time dependent photoluminescence characterization at 2.0 eV shows that the forward phase separation process has a time constant of 2000s and the reverse phase separation process also has a time constant on the order of 2000s. The film remains stable under many cycles of the forward and reverse phase separation process. In-situ X-ray diffraction confirms that halide perovskite film under phase separation has diffraction shoulders corresponding to iodide-rich and bromide-rich domains, while the initial film and reverse phase separated film show the same diffraction peak. In-situ ellipsometry reveals 0.2 difference in the refractive index before and after phase separation, with 50 nm blue shift of the excitonic features of the optical constants. To understand the length scale of phase separation, we CVT synthesized CsPb(BrxI1-x)<sub>3</sub> films with < 200nm thickness on TEM compatible Si<sub>3</sub>N<sub>4</sub> membranes, where the film exhibit similar optical properties to those deposited on STO. We probed the perovskite film before and after light-driven phase separation with the electron beam at cryogenic temperatures. The film showed no degradation while strong cathodoluminescence and STEM EELS signals were collected with nanometer scale spatial resolution. We compare the results with optical confocal microscopy which has subwavelength resolution. Efforts on mapping the phase separation length scale with X-ray diffraction will also be discussed.

#### 8:10 AM F.EL08.01.16

##### **Inhomogeneous Doping of Perovskite Materials by Dopants from Hole-Transport Layer** Chuanxiao Xiao; National Renewable Energy Laboratory, United States

Dopants, which are often indispensable in the organic hole-transport layer (HTL) in perovskite solar cells (PSCs), significantly impact the device performance, hysteresis, and stability. The primary roles of the HTL dopants are to enhance HTL conductivity and tune the energy level of HTLs. Here, we show that the lithium dopant from HTLs can significantly dope the perovskite absorber layer through diffusion. Kelvin probe force microscopy mapping shows that lithium diffusion increases the surface potential of the perovskite film. The potential at grain boundaries showed more increase than in grain interiors, indicating inhomogeneous distribution of Li dopant in the perovskite layer. Accumulation of Li at the grain boundaries was further confirmed by lateral elemental mapping using time-of-flight secondary-ion mass spectrometry. For both p-i-n and n-i-p device structures, the diffusion and nonuniform distribution of Li<sup>+</sup> ions are shown to influence the carrier-transport properties of perovskites and device characteristics. This work reveals the hidden doping effects of the HTL dopants on perovskite films and their impact on PSC performance. Property changes of the perovskite thin films in actual devices from their pristine states should be considered for future understanding of device physics, characterization studies, and device engineering.

**8:20 AM F.EL08.01.17**

**Development and Application of Novel Multi-Modal *In Situ* Probes to Reveal Precursor Chemistry-Property Dynamics of Halide Perovskites** Tze-Bin Song<sup>1</sup>, Shambhavi Pratap<sup>2</sup>, Nobumichi Tamura<sup>1</sup>, Jonathan Slack<sup>1</sup> and Carolyn M. Sutter-Fella<sup>1</sup>; <sup>1</sup>Lawrence Berkeley National Laboratory, United States; <sup>2</sup>Technische Universität München, Germany

Progress made to date in terms of higher efficiency and stability in the field of halide perovskites is based on increasing material complexity that is, formation of multicomponent halide perovskites comprising multiple cations and anions. Each precursor component and synthetic variable can influence the reaction pathway during the formation of halide perovskites as well as influence key properties such as morphology and radiative efficiency. Here, we present the development of a multi-modal platform that is attached to a synchrotron end station and capable of in situ monitoring the dynamic transformation processes from the chemical precursor to the final halide perovskite film. By remotely controlling the spin-coating process and precursor heating we are able to characterize perovskite formation already during spin coating and the very early stages of annealing. In two independent studies we investigate the influence of the Pb-salt on CH<sub>3</sub>NH<sub>3</sub>PbI<sub>3</sub> formation and the Br/(I+Br) concentration on the formation pathway of mixed CH<sub>3</sub>NH<sub>3</sub>Pb(I<sub>1-x</sub>Br<sub>x</sub>)<sub>3</sub> perovskites. We show the correlation between Pb-salt and morphology as well as Br-content and crystallization mechanisms. This multi-modal platform enables efficient screening of complex multicomponent precursors and establishing chemistry-property relationships.

**8:30 AM F.EL08.01.18**

**Photoexcited Carrier Dynamics on the Nanoscale in Perovskite Photovoltaics** Samuel Berweger<sup>1</sup>, Obadiah Reid<sup>2</sup>, Fei Zhang<sup>2</sup>, Axel Palmstrom<sup>2</sup>, Thomas M. Wallis<sup>1</sup>, Andrew Ferguson<sup>2</sup>, Kai Zhu<sup>2</sup>, Joseph J. Berry<sup>2</sup>, Sanjini Nanayakkara<sup>2</sup> and Pavel Kabos<sup>1</sup>; <sup>1</sup>National Institute of Standards and Technology, United States; <sup>2</sup>National Renewable Energy Laboratory, United States

We present time-domain conductivity measurements of optically excited free carriers in perovskite photovoltaics using microwave near-field microscopy. Using a pulsed excitation source that is continuously tunable through the visible spectrum we demonstrate the capability to measure local photoconductivity transients with 10 ns temporal resolution and spatial resolution as high as 50 nm. We study the effect of surface treatment on the local response of [(CsPbI<sub>3</sub>)<sub>0.05</sub>(FAPbI<sub>3</sub>)<sub>0.85</sub>(MAPbBr<sub>3</sub>)<sub>0.15</sub>] perovskite films as well as their deterioration. We find a strong dependence of the free carrier lifetimes on surface treatment, where the presence of an electron transport layer is seen to result in carrier lifetimes of less than 100 ns. Similarly, surface passivation using conformal alumina encapsulation leads to reduced carrier lifetimes compared to untreated films and imparts significant resistance to deterioration. We find that film deterioration leads to strong spatial inhomogeneities in the photoconductive response across films and results in overall longer carrier lifetimes and a redshift in the absorption onset as measured using local action spectra.

**8:40 AM F.EL08.01.19**

**Spatially Resolved Bulk and Interfacial Recombination Dynamics in Perovskite Optoelectronic Devices** Haralds Abolins<sup>1</sup>, Arjun Ashoka<sup>1</sup>, Yu-Hsien Chiang<sup>1</sup>, Gregory Tainter<sup>1,1</sup>, Bart Roose<sup>1</sup>, Hannah Joyce<sup>1</sup>, Stephan Hofmann<sup>1</sup>, Jack Alexander-Webber<sup>1</sup>, Richard Friend<sup>1</sup> and Felix Deschler<sup>2</sup>; <sup>1</sup>University of Cambridge, United Kingdom; <sup>2</sup>Technical University of Munich, Germany

We report the in-situ charge carrier recombination dynamics in perovskite bulk and at interfaces with electrodes by employing a novel photocurrent modulation technique, which enables us to achieve micrometre spatial and sub-microsecond temporal resolution of photocurrent transients. Our capacity to identify and isolate significant loss channels for device

operation, by characterizing the performance of individual electrodes and charge selective layers, has previously only been achieved via indirect techniques. We find a charge trapping length for holes in the perovskite bulk of 21  $\mu\text{m}$  with an associated trapping timescale of 2  $\mu\text{s}$ , demonstrating that bulk trapping is not a major limiting factor for long-distance charge transport in perovskite-based devices. We observe significant photocurrent losses on and near gold electrodes due to the formation of a reduced charge carrier mobility region near the perovskite-gold interface with an associated trapping timescale of 0.7  $\mu\text{s}$ . We further determine the length and timescales of carrier transport via diffusion and photon recycling. Our ability to expand the steady-state operation of the device in space and time allows us to characterise a broad range of processes in-situ with crucial insights into device operation, and paves the way for high throughput optimisation of interfaces for high-efficiency optoelectronics.

**8:50 AM F.EL08.01.21**

### **The Nanoscale Structural and Chemical Mass Spectrometry Imaging of Photovoltaic Perovskite**

**Semiconductors** Onovbaramwen J. Usiobo<sup>1</sup>, Hiroyuki Kanda<sup>2</sup>, Jean-Nicolas Audinot<sup>1</sup>, Tom Wirtz<sup>1</sup> and Mohammad Nazeeruddin<sup>2</sup>; <sup>1</sup>Luxembourg Institute of Science and Technology, Luxembourg; <sup>2</sup>École Polytechnique Fédérale de Lausanne, Switzerland

Solar power has a key role in the crucial transition to low carbon energy generation. Perovskite solar cells, in particular, are a great photovoltaic alternative as they exhibit excellent energy harvesting abilities and do not require energy-intensive manufacturing techniques [1]. The photo-conversion efficiency of perovskite photovoltaics rapidly increased like no other contemporary photovoltaic technology and as such, there is an industry-wide gap in the fundamental understanding of the relationship between microstructure and properties [2]. In addition, poor stability against UV light, moisture and elevated temperature during scale-up of perovskite photovoltaics limits and serves as an impediment for their widespread commercial use [3]. Nanoscale structural and chemical characterization is one alternative to better relate microstructural features to their resultant properties and to further fine-tune the perovskite properties beyond the current state of the art. For this to be achieved, a reliable and effective analytical strategy is not only necessary, but also key for resolving the microstructure of perovskite semiconductors at the nanoscale.

We have developed a magnetic sector Secondary Ion Mass Spectrometer (SIMS) and coupled it to a Helium Ion Microscope (HIM) [4]. Owing to this, we combine the best of both worlds; the high lateral resolution in secondary electron (SE) imaging of the HIM (<0.5 nm with He<sup>+</sup>) with the high detection limit of the SIMS technique (at least in ppm for a wide variety of elements and clusters). In SIMS mode, we are able to detect elements in the full mass range (from H to U) with a lateral resolution below 20 nm. With correlative microscopy, the chemical SIMS micrographs can be co-registered with sub-nm resolution secondary electron (SE) micrographs [5].

We will show several analytical studies completed with HIM-SIMS, among them, a cross-sectional chemical map of a mixed cation perovskite device where different thin films at the nanoscale can be distinguished morphologically and chemically. HIM-SIMS analysis in positive polarity reveals a heterogeneous distribution of Cs and Pb, where specific grains are depleted of these elements. Surface analysis of a multi-cation and multi-halide perovskite in both negative and positive polarity, show a different heterogeneous elemental distribution. Here, the chemical maps of the ions of Cs, Br, I and an organic cluster display a similar distribution while Pb enrichment occurs at selected grains. HIM-SIMS is a versatile and powerful technique for the improved understanding of the impact of microstructure, such as interfaces, grain boundaries and grains, on the photovoltaic stability and performance.

The authors gratefully acknowledge support by the Swiss National Science Foundation (SNF) under grant no 200020L\_172929/1, and the National Research Fund Luxembourg (FNR) through grant INTER/SNF/16/11534230

[1] A. R. Bin Mohd Yusoff, P. Gao, and M. K. Nazeeruddin, "Recent progress in organohalide lead perovskites for photovoltaic and optoelectronic applications," *Coord. Chem. Rev.*, vol. 373, pp. 258–294, 2018.

[2] "National Renewable Energy Laboratory (NREL) – National Center for Photovoltaics: 'Research Cell Record Efficiency Chart.'" [Online]. Available: <https://www.nrel.gov/pv/%0Aassets/images/efficiency-chart.png>.

[3] Y. Rong *et al.*, "Challenges for commercializing perovskite solar cells," *Science (80-. )*, vol. 361, no. 6408, 2018.

[4] T. Wirtz, O. De Castro, J.-N. Audinot, and P. Philipp, "Imaging and Analytics on the Helium Ion Microscope," *Annu. Rev. Anal. Chem.*, vol. 12, no. 1, pp. 523–543, 2019.

[5] F. Vollnhals *et al.*, "Correlative Microscopy Combining Secondary Ion Mass Spectrometry and Electron Microscopy: Comparison of Intensity-Hue-Saturation and Laplacian Pyramid Methods for Image Fusion," *Anal. Chem.*, vol. 89, no. 20, pp. 10702–10710, 2017.



**5:00 AM \*F.EL08.02.01**

**Novel Hybrid Perovskites for Spin Control and Magneto-Optics** Felix Deschler; Technische Universität München, Germany

Functional materials combining the optoelectronic functionalities of semiconductors with control of the spin degree of freedom are highly sought after for the advancement of quantum technology devices and provide exciting avenues for polarized light-emission. Previous work towards this goal introduced small amounts of magnetic elements into crystalline semiconductor, e.g. through vacuum-based deposition, to obtain dilute magnetic semiconductors (DMS).

In my talk, I will present our efforts on gaining control over spin dynamics and spin interactions through compositional and structural tuning in solution-processable hybrid perovskite semiconductors. We aim to exploit the exceptional optoelectronic properties of these hybrid perovskites, together with their tolerance in the electronic states to dopants and defects, to make advances towards high-performance DMS. I will further discuss how we employ ultrafast optical spectroscopy to gain insights into fundamental excitation and spin dynamics in our novel materials, highlighting the potential of magneto-optic control.

I will present first results on chemical doping of layered Ruddlesden-Popper hybrid perovskites with transition metals. I will report how optical excitations interact with elemental spins in these materials, also on ultrafast timescales, to achieve control over exciton emission through magnetic proximity effects. Harnessing spin-orbit coupling effects, we achieved circular polarization up to 15% in the excitonic photoluminescence at low temperatures and high fields, which keeps a strong magnetic field dependence below 1 Tesla. Our finding constitutes the first example of optical polarization control in magnetically-doped hybrid perovskites and will stimulate research on this highly-tuneable material platform that promises tailored interactions between magnetic moments and electronic states.

**5:15 AM \*F.EL08.02.02**

**Ultrafast Studies of Two-Dimensional Hybrid Metal Halide Perovskites** Rebecca L. Milot; University of Warwick, United Kingdom

Two-dimensional Ruddlesden-Popper phase hybrid metal halide perovskites have been investigated for use in a range of optoelectronic devices including photovoltaic cells. Their main appeal for photovoltaics is improved aqueous stability, which is enabled by their incorporation of organic cations which are more hydrophobic than those usually used in 3D perovskites. However, quantum and dielectric confinement effects increase the exciton binding energies in these materials to as much as 100s of meV. These increased binding energies correspond to an increase in exciton population at ambient temperatures which can greatly alter the optoelectronic properties. Optical Pump/THz-probe (OPTP) spectroscopy measurements have revealed decreased effective charge-carrier mobilities and significantly shortened charge-carrier lifetimes for 2D perovskites (1). In hybrid 2D-3D materials, incorporating small amounts of the 2D material can improve optoelectronic properties (2), suggesting a balance between excitons and free charges is achievable by tuning the composition. OPTP and other ultrafast spectroscopic techniques are further used to elucidate the interplay between free charges and excitons in these materials and comment on the limits these properties impose on charge transport in devices.

1. R. L. Milot et al., "Charge-Carrier Dynamics in 2D Hybrid Metal-Halide Perovskites," *Nano Lett.* **16**(11), 7001-7007 (2016).

2. L. R. V. Buizza et al., "Charge-Carrier Dynamics, Mobilities, and Diffusion Lengths of 2D-3D Hybrid Butylammonium-Cesium-Formamidinium Lead Halide Perovskites," *Adv. Funct. Mater.*, 1902656 (2019).

**5:30 AM F.EL08.02.03**

**Unveiling Hidden Carrier Dynamics in Hybrid-Halide Perovskites** Sean A. Bourelle<sup>1</sup>, Xie Zhang<sup>2</sup>, Sascha Feldmann<sup>1</sup>, Angus Mathieson<sup>1</sup>, Lissa Eyre<sup>1,3</sup>, Chris Van de Walle<sup>2</sup>, Felix Deschler<sup>3</sup> and Thomas Winkler<sup>4,1</sup>; <sup>1</sup>University of Cambridge,

United Kingdom; <sup>2</sup>University of California, United States; <sup>3</sup>Technische Universität München, Germany; <sup>4</sup>Aarhus University, Denmark

There remains debate on the nature of electronic states in hybrid metal-halide perovskite thin films, and their impact on charge-carrier dynamics, due to the unique dependence of its band structure on lattice deformations. Here, we present our unique combination of single- and two-photon transient absorption and photoluminescence spectroscopy experiments to map bright and dark transitions in the bulk and at the surface of methylammonium lead bromide thin films. Supported by first-principles calculations, we report a peculiar alignment of energy levels throughout the film, which efficiently funnels carriers away from trap-rich surface states and into the bulk, where an efficient and strong radiative recombination takes place. We show that, for operational carrier densities, these effects lead to high emission rates from heavily occupied bright states within Rashba split bands. Our findings unify the debate on the indirect-direct nature of the hybrid perovskites and have crucial relevance for charge extraction and injection processes at perovskite interfaces, which need to be optimized for maximum device efficiencies.

#### 5:40 AM F.EL08.02.04

**Light Induced Passivation in Triple Cation Mixed Halide Perovskites—Interplay Between Transport Properties and Surface Chemistry** [Stefania Cacovich](#)<sup>1</sup>, Davina Messou<sup>2,3</sup>, Adrien Bercegol<sup>4</sup>, Solène Béchu<sup>3</sup>, Armelle Yaiche<sup>4</sup>, Jean Rousset<sup>4</sup>, Philip Schulz<sup>1</sup>, Muriel Bouttemy<sup>3</sup> and Laurent Lombez<sup>1</sup>; <sup>1</sup>CNRS IPVF UMR 9006, France; <sup>2</sup>IPVF, France; <sup>3</sup>ILV, France; <sup>4</sup>EDF, France

Over the last years we have witnessed a tremendous interest into hybrid organic-inorganic perovskite solar cells (PSCs) research. However, the physical and chemical phenomena occurring in different regions in the film (electrode interface, air interface, grain boundaries) and time scales under different stresses (light, oxygen, moisture, temperature, potential) have been identified to limit the attainable device performance. Especially, the chemistry at the interfaces critically affects the fundamental optoelectronic properties of the perovskite-based absorber as well as the working principles of the corresponding solar cells.

Here, we employed advanced and complementary characterisation techniques, namely multidimensional absolute photoluminescence (PL) and X-Ray Photoelectron Spectroscopy (XPS), to correlate optoelectronic and chemical properties. On the one side, through hyperspectral imaging (HI) and time-resolved fluorescence imaging (TR-FLIM) we investigated intrinsic material and carrier transport properties with quantitative indicators such as Quasi Fermi Level Splitting (QFLS), carrier mobility and recombination rates. On the other side, complementary XPS analyses were implemented on the same batch of samples to precisely determine chemical changes to the surface but also in the bulk, as investigated by XPS depth profiling, to correlate the modification of optoelectronic properties with changes in the composition of the perovskite layer. We have investigated the behaviour of a triple cation mixed halide perovskite thin film deposited on a glass/FTO/c-TiO<sub>2</sub>/m-TiO<sub>2</sub> stack. A series of mixed halide multi-cations perovskite thin films were light soaked for 10 minutes, 1 hour, 5 hours and 15 hours in air. We found that light exposure for a short time (10 minutes or 1 hour) results in a net enhancement of the optoelectronic properties of the material. Indeed, the QFLS of the perovskite thin films increases from 1.31 to 1.36 eV, remaining the same for longer exposure times. Time-resolved PL measurements confirm that the passivated recombination centers are located at the front interface (perovskite/air). As such, both steady-state and transient measurements evidence a surface passivation effect. For longer light soaking times (5 and 15 hours), persistent changes to the perovskite layer composition are observed. The modifications of the chemical environments suggest the formation of a stable PbO<sub>x</sub> passivation layer starting from 5 hours of continuous light soaking in air atmosphere. The formation of this oxidized passivation layer goes along with sample degradation. Starting from 5 hours light soaking a phase segregation appears leading to a degradation of the transport properties of the material. XPS depth profiles indicate that the main responsible of this sample degradation is the oxygen diffusion through the perovskite active layer.

#### 5:50 AM F.EL08.02.05

**Dimensional Mixing and Formation Mechanisms of 2D/3D Perovskite Interfaces** [Andrew H. Proppe](#), Andrew Johnston, Sam Teale and Edward H. Sargent; University of Toronto, Canada

2D/3D heterojunction perovskite solar cells have demonstrated superior efficiency and stability compared to their fully 3D counterparts. These interfaces are formed by exposing the 3D perovskite surface to ligands that induce the formation of 2D layers, though this transformation is not yet understood. We used *in situ* Grazing-Incidence Wide-Angle X-Ray Scattering (GIWAXS) to identify intermediate states in the transformation from 3D to 2D. For (MAPbBr<sub>3</sub>)<sub>0.05</sub>(FAPbI<sub>3</sub>)<sub>0.95</sub> perovskites treated with a dilute ligand solution, we observe the initial formation of  $n = 3$  and  $n = 2$  quantum wells before the final formation of  $n = 1$  wells, suggesting a gradual reduction in dimensionality rather than immediate conversion to 2D perovskite monolayers. For MAPbI<sub>3</sub>, we instead observe intermediate PbI<sub>2</sub> sheets that eventually turn into ligated perovskite quantum

wells. A molecular picture of these transformations will help guide the design of superior 2D/3D interfaces for perovskite solar cell devices.

#### 6:00 AM F.EL08.02.06

***In Situ* Ultrafast Carrier Transport Dynamics in Perovskite Nanocrystal Film** Kanishka Kobbekaduwa<sup>1</sup>, Exian Liu<sup>1</sup>, Zhao Qian<sup>2</sup>, Pan Adhikari<sup>1</sup>, CHENDI XIE<sup>1</sup>, Joseph Luther<sup>3</sup>, Matthew Beard<sup>3</sup> and Jianbo Gao<sup>1</sup>; <sup>1</sup>Clemson University, United States; <sup>2</sup>Tianjin University, China; <sup>3</sup>National Renewable Energy Laboratory, United States

CsPbI<sub>3</sub> perovskite nanocrystals boost their promising applications in high efficiency solar cells, LEDs, and photodetectors because of low-cost, and solution-processing. However, for these optoelectronic applications, the fundamental question of carrier transport mechanism remain unclear, in particular, *in-situ* devices.

In this report, we use the ultrafast photocurrent spectroscopy with sub-20 ps time resolution to elucidate the nature of carrier transport. In early time before 200 ps, the ultrafast photocurrent dependence with temperature clearly demonstrates a phonon-scattering mechanism, wherein the photocurrent increase with decreasing temperature. This unusual transport mechanism, which is absent in the disordered system of nanocrystal arrays, is consistent with the high carrier mobility  $\sim 10$  cm<sup>2</sup>/Vs, and long carrier travelling length  $\sim 100$  nm. After 200 ps, the carriers carry out hopping transport mechanism, which is manifested by the defect scattering effect.

#### 6:10 AM F.EL08.02.07

**Quantifying Photon Recycling in Halide Perovskite Solar Cells and Light Emitting Diodes** Alan Bowman, Miguel Anaya, Neil Greenham and Samuel D. Stranks; University of Cambridge, United Kingdom

The re-absorption of emitted photons within a material, photon recycling, has received increased attention in recent years following its observation in halide perovskite thin films and light-emitting diodes<sup>1,2</sup>. It has been shown to lower the effective bimolecular recombination rate and thus increase excitation densities within a material<sup>3</sup>. However, the relationship of photon recycling to controllable device parameters is poorly understood, as is photon recycling's relative importance in different optoelectronic devices.

Here we present a general framework to quantify photon recycling in any material or device. Using experimental parameters, we apply our model to idealized methylammonium lead iodide (MAPbI<sub>3</sub>) solar cells and cesium lead iodide (CsPbI<sub>3</sub>) light-emitting diodes (LEDs) at operating voltages. Specifically, we explore the relationship of photon recycling to controllable parameters: thickness; charge-trapping rate; non-ideal interface transmission; and absorptance. We show that in MAPbI<sub>3</sub> solar cells the number of photon recycling events per absorbed photon at maximum power point is 0.4 in the (optimal) case of no charge trapping, due to most charges being extracted to the external circuit before they can radiatively recombine. Conversely, in a CsPbI<sub>3</sub> LED there can be up to 8 photon recycling events per injected charge in this optimal case (for emission into a full  $2\pi$  hemisphere and applied voltage giving emission of  $\sim 1000$  lm m<sup>-2</sup>). In both device types we demonstrate that photon recycling and device performance (efficiency or amount of emitted light for solar cells and LEDs respectively) improve with thicker cells, those with less charge-trapping and improved back reflection. However, while device performance improves with better front transmission and light scattering, the degree of photon recycling rapidly reduces. For example, for a solar cell with a high degree of light scattering (to improve absorptance), there is less than 0.1 photon recycling event per initially absorbed photon. Similarly, in LEDs, the number of photon recycling events reduces to less than 1 when the emitter has a rough surface, but there is a significant increase in the quantity of light emitted from the system due to fewer trapped photon modes.

Our experimentally parameterized simulations reveal that photon recycling is significantly more important in LEDs than solar cells at operating voltages. Furthermore, we show that maximizing absorption and emission processes remains paramount for optimizing devices, even if this is at the expense of photon recycling. We therefore demonstrate that photon recycling cannot always be seen as a beneficial process in perovskite solar cells and LEDs.

#### References

- 1 C. Cho, B. Zhao, G. D. Tainter, J. Y. Lee, R. H. Friend, D. Di, F. Deschler and N. C. Greenham, *Nat. Commun.*, 2020, **11**, 1–8.
- 2 L. M. Pazos-Outon, M. Szumilo, R. Lamboll, J. M. Richter, M. Crespo-Quesada, M. Abdi-Jalebi, H. J. Beeson, M. Vrućinić, M. Alsari, H. J. Snaith, B. Ehrler, R. H. Friend and F. Deschler, *Science (80-. )*, 2016, **351**, 1430–1433.
- 3 T. W. Crothers, R. L. Milot, J. B. Patel, E. S. Parrott, J. Schlipf, P. Müller-Buschbaum, M. B. Johnston and L. M. Herz, *Nano Lett.*, 2017, **17**, 5782–5789.

## 6:20 AM F.EL08.02.08

**Nonradiative Energy Transfer in Halide Perovskite Nanocrystal Heterosystems** Alexander S. Urban, Andreas Singldinger, Carola Lampe, Moritz Gramlich and Christoph Gruber; LMU Munich, Germany

Halide perovskite nanocrystals (NCs) hold great promise for optoelectronic applications because of their large absorption cross-sections and high photoluminescence quantum yields. Moreover, by varying either their halide composition or their size/dimensionality, the absorption onsets and emission maxima can be tuned throughout the entire visible spectrum. Commercialization is currently impeded however due to several issues. Susceptibility to environmentally-induced degradation necessitates the use of stabilizing and encapsulation, which hinders charge injection and halide ion diffusion impedes the realization of heterostructures.

In this presentation, we look at nonradiative energy transfer (FRET) in mixed halide perovskite nanosystems, for enhancing the stability and integration into optoelectronic devices and novel architectures. Halide perovskite nanoplatelets (NPLs) enable a precise tuning of absorption and emission by controlling the number of layers in the NPLs. We look at energy transfer between CsPbBr<sub>3</sub> NPLs of different thicknesses and analyze efficiency and transfer times.<sup>[1]</sup> Using this, we then look into realizing multi-layer heterojunctions comprising different NC thicknesses for concentrating charge carriers or promoting charge carrier collection. We also show how highly stable polymer micelle-encapsulated NCs can be integrated into light-emitting devices through energy transfer.<sup>[2]</sup> We specifically investigate how the polymer shell and NC size affect the transfer efficiencies and device performance. These results open up pathways for realizing new device architectures and enhance the stability of the perovskite NCs, both important for pushing perovskite NCs from a mainly scientific state toward commercialization.

[1] Singldinger, A.; Gramlich, M.; Gruber, C.; Lampe, C.; Urban, A. S. Nonradiative Energy Transfer between Thickness-Controlled Halide Perovskite Nanoplatelets. *ACS Energy Lett.* 2020, 5, 1380-1385.

[2] Hintermayr, V. A.; Lampe, C.; Low, M.; Roemer, J.; Vanderlinden, W.; Gramlich, M.; Bohm, A. X.; Sattler, C.; Nickel, B.; Lohmuller, T.; et al. Polymer Nanoreactors Shield Perovskite Nanocrystals from Degradation. *Nano Lett.* 2019, 19, 4928-4933.

## 6:30 AM F.EL08.02.09

**Femtosecond Charge Transfer Between the Organic and Inorganic Sub-Lattices in the Halide Perovskite Methylammonium Lead Tri-Iodide** Gabriel J. Man<sup>1</sup>, Pabitra Nayak<sup>2</sup>, Konstantin A. Simonov<sup>1</sup>, Sebastian Svanström<sup>1</sup>, Anders Sandell<sup>1</sup> and Håkan Rensmo<sup>1</sup>; <sup>1</sup>Uppsala University, Sweden; <sup>2</sup>Tata Institute of Fundamental Research, India

Halide perovskite (HaP) materials have attracted substantial renewed research interest for over a decade, largely due to initially dramatic gains in photovoltaic power conversion efficiencies demonstrated by lead HaP-based solar cells<sup>[1]</sup>. Efforts to commercialize HaP-based solar cells, light-emitting diodes (LED's) and other opto-electronic devices are currently underway around the globe. The prototypical hybrid organic-inorganic HaP is methylammonium lead tri-iodide (MAPbI<sub>3</sub> or MAPI) which features an organic cation (methylammonium or MA) located at the A-site embedded within a lead-iodide (B-X) inorganic sub-lattice. Since the early demonstrations of MAPI solar cells, device applications of HaPs have transitioned towards the use of mixed-cation (with/without MA plus other A-site cations) formulations due to concerns about the thermal and chemical stability of MA in device-relevant, ambient conditions<sup>[2]</sup>. The role of MA in the HaP matrix was considered by some to be structural only, which indirectly influences the optical and electrical properties of MAPI<sup>[3,4]</sup>. Density-functional theory (DFT) calculations of the electronic structure supported that view<sup>[5,6]</sup>. Selective thermal excitation of the MA did not alter the optical properties of MAPI<sup>[7]</sup>. Mechanical nano-indentation studies of APbBr<sub>3</sub> crystals showed that the type of A-site cation, be it organic or inorganic, has little effect on the chemical bonding in HaPs<sup>[8]</sup>.

In spite of the considerable evidence for the passive opto-electronic role and thermal instability of MA, the highest-performing HaP solar cells typically incorporated some fraction of MA in the absorber layer<sup>[9]</sup>. Hot fluorescence was observed from APbBr<sub>3</sub> crystals with an MA or FA, but not cesium, cation<sup>[10]</sup>. In this work, we demonstrate that MA is an active participant in the nitrogen 1s (N1s) core-excited electronic structure of MAPI. In doing so, we reveal the existence of additional mechanisms: (i) ultrafast <7 fs charge transfer between molecular unoccupied states in the MA and MAPI conduction band states and (ii) MA carrier lifetime > 7 fs. Using Resonant Photoelectron Spectroscopy (RPES), which involves resonantly exciting the nitrogen in MA with soft X-rays and measuring the N1s decay spectra (KVV Auger and autoionization), we convert MA into a core-excited microscopic probe of the electronic coupling to its environment. The N1s decay spectra corresponding to N1s-to-2p\* resonant excitations to bound states below the ionization threshold show evidence of spectator and participator autoionization and normal Auger decay. We find MA to be quasi-localized electronically,

meaning its electronic coupling to the Pb-I sub-lattice is intermediate between weak and strong coupling, since a fraction of the resonantly-excited N1s core electrons de-localize into the environment surrounding the MA with a timescale that is comparable to the N1s core hole lifetime (~7 fs). To access the intrinsic materials physics of MAPI, the experiments were performed with in-vacuum cleaved single crystals at a low photon flux synchrotron beamline. Beam-induced sample damage was judiciously checked with XPS and was found to be negligible.

The presence of MA-to-(Pb-I) charge transfer in the N1s core-excited state reveals that the MA cation is not chemically and electronically inert, and suggests that bi-directional MA-(Pb,I) charge transfer may be possible in valence-excited states, which is relevant for the operation of MA-based HaP solar cells, LED's, and other opto-electronic devices.

[1] NREL, 2020.

[2] M. Saliba *et al.*, *Science* **2016**, 354, 206.

[3] J. M. Frost *et al.*, *Nano Lett.* **2014**, 14, 2584.

[4] D. A. Egger *et al.*, *Adv. Mater.* **2018**, 30, 1800691.

[5] B. Philippe *et al.*, *JPCC* **2017**, 121, 26655.

[6] J. Endres *et al.*, *JPCL*. **2016**, 7, 2722.

[7] P. Guo *et al.*, *Nat. Commun.* **2019**, 10, 482.

[8] Y. Rakita, D. Cahen, G. Hodes, **2018**.

[9] Q. Jiang *et al.*, *Nat. Photonics* **2019**, 13, 460.

[10] H. Zhu *et al.*, *Science* **2016**, 353, 1409.

#### 6:40 AM F.EL08.02.10

**Deep-Level Transient Spectroscopies for the Detailed Experimental Assessment of Defect Tolerance in Lead-Free Perovskite-Inspired Semiconductors** Vincenzo Pecunia<sup>1</sup>, Chaewon Kim<sup>1</sup>, Jing Zhao<sup>1</sup>, Robert Hoye<sup>2</sup>, Tahmida Huq<sup>3</sup> and Judith MacManus-Driscoll<sup>3</sup>; <sup>1</sup>Soochow University, China; <sup>2</sup>Imperial College London, United Kingdom; <sup>3</sup>University of Cambridge, United Kingdom

The exploration of lead-free perovskite-inspired semiconductors for optoelectronic applications has captured ever-growing attention, driven by their promise to replicate the success of the lead-based counterparts, but without the toxicity concerns associated with the latter.<sup>1</sup> In the search for lead-free perovskite-inspired semiconductors, emphasis has been placed on the identification of materials with a defect-tolerant character, as this has been associated with a high optoelectronic potential.<sup>2</sup> While computational studies have been of fundamental importance in screening lead-free perovskite-inspired semiconductors for defect tolerance, the detailed experimental assessment of the defect tolerance in such materials is lacking in the field. This has been particularly limiting in regard to the experimental identification of the most promising lead-free perovskite-inspired semiconductors. In fact, at an experimental level, investigators have most often relied on phenomenological findings to probe the defect tolerance of such materials. For instance, device performance boosts achieved through specialized processing strategies have often been linked to defect passivation, while photoluminescence lifetimes have been regarded as the default indicator of defect tolerance.<sup>3,4</sup>

Recognizing that an experimental quantitative assessment of the defect parameters (volumetric densities, characteristic energies, and capture cross sections) is key to developing a detailed understanding of defect tolerance in perovskite-inspired semiconductors, in this study we have explored the applicability of deep-level transient spectroscopy methods to reliably characterize the defect properties of a range of lead-free perovskite-inspired compounds. In particular, we have focused on a number of antimony- and bismuth-based perovskite-inspired materials, as they have been generally associated with a defect-tolerant character.<sup>2</sup> Herein, we firstly examine the applicability of conventional deep-level transient spectroscopy (DLTS) for their experimental defect characterization. We then discuss current-based deep-level spectroscopy variants, of which we show the particular configurations that we have found to be widely applicable to the defect characterization of lead-free perovskite-inspired compounds. Finally, by comparing with the reported approaches for the quantitative defect characterization of lead-halide perovskites, we discuss the defect tolerance of the antimony- and bismuth-based perovskite-inspired materials we have characterized (e.g., A<sub>3</sub>Sb<sub>2</sub>I<sub>9</sub> absorbers with A being a monovalent cation, bismuth oxyiodide,<sup>5</sup> silver iodobismuthates). This study thus contributes to identifying a viable strategy for the experimental screening of defect tolerance in lead-free perovskite-inspired materials, potentially enabling the experimentally-grounded identification of the most promising compositions towards high-performance low-toxicity optoelectronics.

1 A. Abate, *Joule*, 2017, 1, 659–664.

2 R. E. Brandt, J. R. Poindexter, P. Gorai, R. C. Kurchin, R. L. Z. Hoye, L. Nienhaus, M. W. B. Wilson, J. A. Polizzotti, R. Sereika, R. Zaltauskas, L. C. Lee, J. L. MacManus-Driscoll, M. Bawendi, V. Stevanović and T. Buonassisi, *Chem. Mater.*, 2017, 29, 4667–4674.

3 B. Yang, J. Chen, F. Hong, X. Mao, K. Zheng, S. Yang, Y. Li, T. Pullerits, W. Deng and K. Han, *Angew. Chemie Int. Ed.*,

2017, **56**, 12471–12475.

4 J. Pal, S. Manna, A. Mondal, S. Das, K. V. Adarsh and A. Nag, *Angew. Chemie Int. Ed.*, 2017, **56**, 14187–14191.

5 T. N. Huq, L. C. Lee, L. Eyre, W. Li, R. A. Jagt, C. Kim, S. Fearn, V. Pecunia, F. Deschler, J. L. MacManus-Driscoll and R. L. Z. Hoye, *Adv. Funct. Mater.*, 2020, 1909983.

#### 6:50 AM F.EL08.02.11

**Investigation of Ion Migration in Methylammonium Lead Bromide (MAPbBr<sub>3</sub>) Perovskite Crystals Using Current Deep Level Transient Spectroscopy (I-DLTS)** Mmantsae M. Diale, Nosiselo Mrwetyana and Matshisa Legodi; University of Pretoria, South Africa

Despite the rapid development of halide perovskite with power conversion efficiency over 25% to date, there are many unresolved issues such as the identification and characterization of defects affecting device performance. This dearth of knowledge is inhibiting the commercialization of HAP solar cells. The migration of ionic species in HAPs influences the degradation of perovskite solar cells and their long-term reliability and robustness. In this work, we investigated ion migration in crystalline methylammonium lead bromide C/MAPbBr<sub>3</sub>/Au solar cells in the dark using the hp DC Voltage source 4140B picoAmmeter in the temperature range 255 K < T < 320 K and various bias pulse sequences. Arrhenius plots constructed from the data were used to determine ion migration activation energies for various ion species. Atypical temperature dependency of the current transients was observed: fast transients at low temperature and slower ones at elevated temperatures. In addition, characteristic features typical of ion migration such as scan rate and bias sensitivity with hysteresis accompanying temperature cycling were also observed. The ion transport mechanisms in the C/MAPbBr<sub>3</sub>/Au perovskite crystals agree with observations in the MAPbI<sub>3</sub> analogue. We conclude that the fast exponential corresponds to the migration of the negatively charged halide species, Br, with activation energy of 0.41 eV; and, the slower exponential is due to the positively charged lead (Pb<sup>2+</sup>) species with activation energy of 2.82 – 2.87 eV.

#### 7:00 AM F.EL08.02.12

**PbI<sub>2</sub> Phase Impurities Trap Electrons in Lead Halide Perovskites** Young-Kwang Jung<sup>1</sup> and Aron Walsh<sup>1,2</sup>; <sup>1</sup>Yonsei University, Korea (the Republic of); <sup>2</sup>Imperial College London, United Kingdom

The use of excess lead iodide (PbI<sub>2</sub>) during the synthesis and processing of lead halide perovskites has been exploited as a way to improve performance of perovskite solar cells [1,2]. On the other hand, it has also been proposed that excess PbI<sub>2</sub> can increase the trap-state density [3] and enhance the thermal decomposition to PbI<sub>2</sub> [4]. Although the presence of PbI<sub>2</sub> in perovskite films plays an important role, the current understanding of how PbI<sub>2</sub> phase impurities form interfaces with halide perovskites and affect their electronic properties is poor. Here, we model CsPbI<sub>3</sub>-PbI<sub>2</sub> superlattices and identify their interfacial geometry, thermodynamic stability, and electronic structure. Our first-principles density functional theory (DFT) calculations reveal that PbI<sub>2</sub> present in CsPbI<sub>3</sub> can induce electron trap state at the interface between these two phases. However, the electron trapping tendency is sensitive to the atomic nature of the phase boundary, which can explain the variation reported in different investigations.

[1] C. Roldán-Carmona, P. Gratia, I. Zimmermann, G. Grancini, P. Gao, M. Graetzel, and M. K. Nazeeruddin, *Energy Environ. Sci.* **8**, 3550 (2015); <https://doi.org/10.1039/C5EE02555A>

[2] Y. C. Kim, N. J. Jeon, J. H. Noh, W. S. Yang, J. Seo, J. S. Yun, A. Ho-Baillie, S. Huang, M. A. Green, J. Seidel, T. K. Ahn, and S. I. Seok, *Adv. Energy Mater.* **6**, 1502104 (2016); <https://doi.org/10.1002/aenm.201502104>

[3] H.-Y. Wang, M.-Y. Hao, J. Han, M. Yu, Y. Qin, P. Zhang, Z.-X. Guo, X.-C. Ai, and J.-P. Zhang, *Chem. Eur. J.* **23**, 3986 (2017); <https://doi.org/10.1002/chem.201605668>

[4] T. Matsui, T. Yamamoto, T. Nishihara, R. Morisawa, T. Yokoyama, T. Sekiguchi, and T. Negami, *Adv. Mater.* **31**, 1806823 (2019); <https://doi.org/10.1002/adma.201806823>

#### 7:10 AM F.EL08.02.13

**Microscopic Mechanisms of Halide Diffusion in Perovskite Solar Cells** Young Won Woo<sup>1</sup>, Young-Kwang Jung<sup>1</sup>, Sunghyun Kim<sup>2</sup> and Aron Walsh<sup>1,2</sup>; <sup>1</sup>Yonsei University, Korea (the Republic of); <sup>2</sup>Imperial College London, United Kingdom

It is now well established that metal halide perovskites are mixed ionic-electronic conductors. The halide ions are highly mobile at room temperature [1]. Ion migration is speculated to be the origin, or an important contributing factor, for many unusual phenomena in photovoltaic devices, such as current-voltage hysteresis, and photoinduced phase separation and transformations [2,3]. Illumination of a photovoltaic device will result in electrical and thermal changes. Absorption of light can access metastable charge states of defects due to the trapping of electrons or holes and result in hot carriers with excess

energy, which cool to the lattice temperature by phonon emission that could enhance the rate of ion migration [4]. Thus, these ionic migration processes must be suppressed in such device structures. The rate of halide ion jumps in halide perovskites depends not only on the activation energy but also on the pre-exponential factor of diffusion. Here, we report the microscopic mechanisms for iodine ion diffusion mediated by vacancies from first-principles density functional theory (DFT) calculations. We quantify the potential energy landscape for chemical transport including the activation energies of ions migration and the migration frequency at the room temperature.

[1] Ionic transport in hybrid lead iodide perovskite solar cells. *Nature commun.* **6**, 7495 (2016) ;

<https://doi.org/10.1038/ncomms8497>

[2] Anomalous hysteresis in perovskite solar cells. *J. Phys. Chem. Lett.* **5**, 1511 (2014) ; <https://doi.org/10.1021/jz500113x>

[3] Reversible photo-induced trap formation in mixed-halide hybrid perovskites for photovoltaics. *Chem. Sci.* **6**, 613 (2015) ; <https://doi.org/10.1039/c4sc03141e>

[4] Taking control of ion transport in halide perovskite solar cells. *ACS Energy Lett.* **3**, 1983 (2018);

<https://doi.org/10.1021/acsenergylett.8b00764>

### 7:20 AM F.EL08.02.14

#### Using Time-Resolved Photoconductivity Measurements to Reveal the Urbach Tail and Two Photon Absorption in MHPs

Valentina Caselli<sup>1</sup>, Dengyang Guo<sup>1</sup>, Zimu Wei<sup>1</sup>, Jos Thieme<sup>1</sup>, Claudine Katan<sup>2</sup>, Jacky Even<sup>2</sup> and Tom J. Savenije<sup>1</sup>; <sup>1</sup>Delft University of Technology, Netherlands; <sup>2</sup>Université Européenne de Bretagne, INSA, FOTON, France

The unprecedented rise in power conversion efficiency of solar cells based on metal halide perovskites (MHPs) has led to an enormously growing research effort over the last 6 years. In this paper, we report how the electrodeless transient microwave photoconductivity technique (TRMC) can reveal detailed information, regarding the interesting photo-physical properties of MHPs. First, we recorded two photon absorption (2PA) spectra of MHP thin films over a wavelength regime between  $0.5E_g$  and  $E_g$ , from which the 2PA coefficients have been calculated. A two-step upward trend is observed in the 2PA coefficient spectrum for  $\text{CH}_3\text{NH}_3\text{PbI}_3$ . Using a parameterized tight binding model, spectra were calculated by integration over all Brillouin zones showing compelling similarity with experimental results. We conclude that the second upward trend in the 2PA spectrum originates from additional optical transitions to the heavy and light electron bands formed by the strong spin-orbit coupling.

Next, we performed TRMC measurements using optical excitation above and below the band-gap on pristine  $\text{MAPbI}_3$ ,  $\text{MAPbI}_3/\text{C60}$ , and  $\text{MAPbI}_3/\text{Spiro-OMeTAD}$  thin films. In pristine  $\text{MAPbI}_3$  we have observed a band-like charge transport for photon energies down to 1.40 eV, from which we calculated an Urbach energy of approximately 16 meV, indicative of a relatively low structural disorder. Our TRMC measurements on the bilayers revealed that electrons in defect states close to the VB can be excited by photons with an energy as low as 1.30 eV. Their excitation leads to free electrons in the CB that undergo charge injection into the C60 yielding long-lived charge separation. In contrast, excitation of  $\text{MAPbI}_3/\text{Spiro-OMeTAD}$  at 1.3 eV shows a rapidly decaying signal implying that holes are localized and cannot be transferred over the interface to the Spiro-OMeTAD.

### 7:30 AM F.EL08.02.15

#### Below-Bandgap, Low-Frequency Raman Spectroscopy to Probe Lattice Vibrations in $\text{CsPbI}_3$ Polymorphs

Yi Yang, Jason Robbins, Lotanna Ezeonu, Yichen Ma, Nicholas Sparta, Xiaoqing Kong, Stefan Strauf, Simon G. Podkolzin and Stephanie Lee; Stevens Institute of Technology, United States

The coupling of electrons with lattice vibrations is thought to play a crucial role in determining the efficiency of optoelectronic processes in metal-halide perovskites. Herein, we report the first comparison of the low-frequency Raman (LFR) spectra of thermodynamically-stable, inactive  $\delta$ - $\text{CsPbI}_3$  and metastable, active  $\gamma$ - $\text{CsPbI}_3$  in the range of 5 – 150  $\text{cm}^{-1}$  [1]. While previous reports have suffered from material degradation during measurements, our successful recording of these spectra was enabled by a combination of nanoconfinement to stabilize the respective  $\text{CsPbI}_3$  phases against temperature- and humidity-induced polymorph transitions,[2] as well as the use of a below-bandgap 976-nm wavelength laser to avoid laser-induced degradation. Temperature-dependent LFR spectra confirmed that  $\gamma$ - $\text{CsPbI}_3$  could be stabilized to temperatures as low as 77 K upon nanoconfinement. The main vibrational modes at these low frequencies were determined via density functional theory calculations to primarily involve bending and stretching of Pb-I bonds. We further explored the compositional dependence of the  $\gamma$  phase phonon modes via systematic substitution of Cs cations with methylammonium cations ( $\text{Cs}_y\text{MA}_{1-y}\text{PbI}_3$ ) or I anions with Br anions ( $\text{CsPbI}_x\text{Br}_{3-x}$ ). The three main peaks exhibited in  $\gamma$ - $\text{CsPbI}_3$  were found to be present in all variations of the composition, with peak locations shifting to lower frequencies with expanding lattice dimensions. These results indicate that the phonon modes in these MHPs depend primarily on the structure of the metal-halide framework, not

the specific nature of the A-site cations and halide anions.

[1] Yang, Y., Robbins, J., Ezeonu, L., Ma, Y., Sparta, N., Kong, X., Strauf, S., Podkolzin, S., and Lee, S. “**Probing Lattice Vibrations of Stabilized CsPbI<sub>3</sub> Polymorphs via Low-Frequency Raman Spectroscopy**” *Journal of Materials Chemistry C* (2020): Available at <http://pubs.rsc.org/en/Content/ArticleLanding/2020/TC/D0TC02123G>.

[2] Kong, X., Shayan, K., Hua, S., Strauf, S., and Lee, S. S. “**Complete Suppression of Detrimental Polymorph Transitions in All-Inorganic Perovskites via Nanoconfinement**” *ACS Applied Energy Materials* 2, (2019): 2948–2955.

#### 7:40 AM F.EL08.02.16

##### **Late News: Phonon Vibrational Dynamics Reveals Intrinsic Lattice Anharmonicity in Hybrid Perovskite**

**Nanocrystals** Tushar Debnath<sup>1</sup>, Debalaya Sarker<sup>2</sup>, He Huang<sup>1</sup>, Zhong-Kang Han<sup>2</sup>, Amrita Dey<sup>1</sup>, Lakshminarayana Polavarapu<sup>1</sup>, Sergey V. Levchenko<sup>2</sup> and Jochen Feldmann<sup>1</sup>; <sup>1</sup>Ludwig-Maximilians-University (LMU), Germany; <sup>2</sup>Skolkovo Institute of Science and Technology, Russian Federation

Organic–inorganic halide perovskite nanocrystals (PNCs) are gaining increasing attention in contemporary research due to their promising optoelectronic performance. Photoexcitation of these PNCs with an ultrashort laser pulse can produce coherent phonons along the lattice displacement coordinate, leading to lattice vibrations. The halide ions of organic-inorganic hybrid perovskites can strongly influence the interaction between the central organic moiety and the inorganic metal halide octahedral units and thus their lattice vibrations. Here, we employ femtosecond pump–probe spectroscopy to initiate the photophysics by the formation of coherent phonons and to observe the subsequent coherent vibrational dynamics of formamidinium lead halide (FAPbX<sub>3</sub>, X=Br, I) PNCs. We find that the FAPbX<sub>3</sub> PNCs generate halide-dependent coherent vibronic wave packets upon non-resonant excitation, and the dominant contributions are attributed to the Pb–X bending and stretching modes of PbX<sub>6</sub><sup>4-</sup> octahedral units of the lattice. More importantly, for the first time, we observe higher harmonic vibrational modes in FAPbI<sub>3</sub> PNCs, which points to a more anharmonic potential energy surface in the case of FAPbI<sub>3</sub> as compared to FAPbBr<sub>3</sub> PNCs. This is likely due to the weaker interaction between the central FA moiety (which sits in a larger octahedral interstitial site) and the inorganic cage for FAPbI<sub>3</sub> PNCs, and thus the PbI<sub>6</sub><sup>4-</sup> unit can vibrate more freely. This weakening reveals the intrinsic anharmonicity in the Pb-I framework, and thus facilitating the energy transfer into overtone and combination bands. Furthermore, our control experiment with MAPbBr<sub>3</sub> reveals the energy transfer between framework phonons due to the intrinsic anharmonicity of the lead-halide framework is indeed influenced by the interaction between the framework and the organic molecules, and not only by the halide nature. The insights interestingly not only unravel the underlying reason for the halide-dependent stability of these materials but also shed light on their charge-carrier mobility and polaronic properties.

#### 7:50 AM \*F.EL08.02.17

**Photophysics of Methylammonium Lead Bromide Perovskite** Natalie Banerji, Nikolaos Droseros and Dimitra Tsokkou; University of Bern, Switzerland

Methylammonium Lead Bromide (MAPbBr<sub>3</sub>) is the most investigated 3D Perovskite for visible LED applications. It is characterized by a much higher exciton binding energy compared to its Iodide equivalent (MAPbI<sub>3</sub>). This leads to complex excited-state phenomena, with free-carriers, excitons and defect states contributing to the photoluminescence (PL) properties. We have used a variety of spectroscopic techniques to study photoexcited MAPbBr<sub>3</sub> films, including time-resolve PL measurements, femtosecond transient absorption (TA) spectroscopy and optical-probe-terahertz-pump (THz) experiments. The co-existence of free carriers and excitons is demonstrated at low excitation densities in as-cast polycrystalline MAPbBr<sub>3</sub> (crystal size of the order of few ?m). The excitation wavelength and density are then varied in order to access different free-carrier to exciton ratios in order to evaluate their recombination dynamics and THz conductivities. Finally, we show how reducing the grain size of the Perovskite to the micro- and nanoscale (by using different additives during solution-processing) increases the PL quantum yield, which we explain by the presence of a bright exclusively excitonic population even at low excitation densities, together with reduced surface trapping thanks to passivation by the additives.

#### 8:05 AM F.EL08.02.19

**Novel Absorption and Emission Processes in FAPbI<sub>3</sub>** Adam D. Wright; University of Oxford, United Kingdom

Due to a larger organic cation, formamidinium lead triiodide (FAPbI<sub>3</sub>) has a narrower, more optimal band gap than MAPbI<sub>3</sub>, which extends the photocurrent generation onset into the near-infrared. FAPbI<sub>3</sub> is also more resistant to heat stress than MAPbI<sub>3</sub> while retaining a comparable charge-carrier mobility[1] long charge-carrier diffusion length[2] and impressive solar cell efficiencies as high as 16%[3]. The current most efficient single-junction perovskite photovoltaics are based on FAPbI<sub>3</sub>,



albeit with chemical substitution to enhance the stability of the perovskite phase. Improving our understanding of the fundamental optoelectronic properties of FAPbI<sub>3</sub> is therefore essential to improving the performance of the semiconductor devices based on it. However, despite its remarkable promise, the photophysics of FAPbI<sub>3</sub> remains under-studied compared to MAPbI<sub>3</sub> [4]. In this study, I report on novel and intriguing emission and absorption processes in FAPbI<sub>3</sub>. First, we investigated [5] the influence of sub-bandgap trap states on charge-carrier recombination through an analysis of the low-temperature photoluminescence (PL) of FAPbI<sub>3</sub>. We observed a power-law time dependence in the emission intensity and an additional low-energy emission peak that exhibits an anomalous relative Stokes shift. Using a rate-equation model and a Monte Carlo simulation, we revealed that both phenomena arise from an exponential trap-density tail with characteristic energy scale of ~3 meV. Since charge-carrier recombination from sites deep within the tail causes emission with energy downshifted by up to several tens of meV, such phenomena may in part be responsible for Voc losses commonly observed in these materials. Secondly, we investigated the temperature-dependent absorption of FAPbI<sub>3</sub>, supported by first-principles modelling. Altogether, we elucidate how the polar FA cation affects the optoelectronic properties of FAPbI<sub>3</sub>. [1] W. Rehman, R. L. Milot, G. E. Eperon, C. Wehrenfennig, J. L. Boland, H. J. Snaith, M. B. Johnston, L. M. Herz, *Adv. Mater.* 2015, 27, 7938. [2] A. A. Zhumekenov, M. I. Saidaminov, M. A. Haque, E. Alarousu, S. P. Sarmah, B. Murali, I. Dursun, X.-H. Miao, A. L. Abdelhady, T. Wu, O. F. Mohammed, O. M. Bakr, *ACS Energy Lett.* 2016, 32. [3] J. W. Lee, D. J. Seol, A. N. Cho, N. G. Park, *Adv. Mater.* 2014, 26, 4991. [4] C. L. Davies, J. Borchert, R. L. Milot, H. Kraus, M. B. Johnston, L. M. Herz, *J. Phys. Chem. Lett.* 2018, 9, 4502. [5] A. D. Wright, R. L. Milot, G. E. Eperon, H. J. Snaith, M. B. Johnston, L. M. Herz, *Adv. Funct. Mater.* 2017, 27, 1700860.

### 8:15 AM F.EL08.02.20

**Charge-Carrier Cooling and Polarization Memory Loss in Formamidinium Tin Triiodide** Kimberley J. Savill, Matthew Klug, Rebecca L. Milot, Henry Snaith and Laura Herz; University of Oxford, United Kingdom

Reports of slow charge-carrier cooling in hybrid metal halide perovskites have prompted hopes of achieving higher photovoltaic cell voltages through hot-carrier extraction. However, observations of long-lived hot charge carriers even at low photoexcitation densities and an orders-of-magnitude spread in reported cooling times have been challenging to explain. In this work we present ultrafast time-resolved photoluminescence measurements on formamidinium tin triiodide, showing fast initial cooling over tens of picoseconds and demonstrating that a perceived secondary regime of slower cooling instead derives from electronic relaxation, state-filling, and recombination in the presence of energetic disorder. We identify limitations of some widely used approaches to determine charge-carrier temperature and make use of an improved model which accounts for the full photoluminescence line shape. The adoption of this model offers a path to more accurate determination of charge-carrier temperatures, and ready comparison between perovskite compositions to assess the true potential for hot-carrier solar cells. Further, we do not find any persistent polarization anisotropy in FASnI<sub>3</sub> within 270 fs after excitation, indicating that excited carriers rapidly lose both polarization memory and excess energy through interactions with the perovskite lattice. References Kimberley J. Savill, Matthew T. Klug, Rebecca L. Milot, Henry J. Snaith, and Laura M. Herz, *Charge-Carrier Cooling and Polarization Memory Loss in Formamidinium Tin Triiodide*. *J. Phys. Chem. Lett.* 2019, 10 (20), 6038-6047

### 8:25 AM F.EL08.02.21

**Excitonic Finestructure and Evidence of Dark States in Two-Dimensional Tin Iodide and Lead Iodide Perovskites** Ajay Ram Srimath Kandada<sup>1</sup>, Giulia Folpini<sup>2</sup>, Daniele Cortecchia<sup>2</sup> and Annamaria Petrozza<sup>2</sup>; <sup>1</sup>Wake Forest University, United States; <sup>2</sup>Istituto Italiano di Tecnologia, Italy

We report on the origin of the multiple excitonic states reported previously by us [1,2] in two-dimensional hybrid perovskites, by systematic analysis of the optical observables with the variation of the metal cation from lead to tin. We particularly discuss the temperature dependence of the exciton recombination dynamics obtained via time-resolved photoluminescence (PL) and transient absorption spectroscopies. We quantitatively analyze the monotonous increase in the exciton lifetime as well as PL quantum yield with increasing temperature in the range of 5 K — 290 K. We consider such a behaviour as an evidence for the presence of dark excitonic states within the finestructure that are de-populated at higher temperatures with an activation energy of ~8-10 meV. We discuss the role of the phonons in the exciton inter-conversion dynamics through non-adiabatic exciton-phonon couplings [3]. [1] A. R. Srimath Kandada and C. Silva, *Perspective: Exciton polarons in two-dimensional hybrid metal-halide perovskites*, arXiv:1908.03909[cond-mat.mtrl-sci] (2019). [2] F. Thouin, D. Valverde-Chavez, C. Quarti, D. Cortecchia, I. Bargigia, D. Beljonne, A. Petrozza, C. Silva and A. R. Srimath Kandada, *Phonon coherences reveal the polaronic character of the excitons in two-dimensional lead-halide perovskites*, *Nature Materials*, 18, 349-356 (2019). [3] F. Thouin, A. R. Srimath Kandada, D. Valverde-Chavez, D. Cortecchia, I. Bargigia, A. Petrozza, X. Yang, E. R. Bittner and C. Silva, *Electron-phonon couplings inherent in polarons drive exciton dynamics in two-dimensional metal-halide perovskites*, *Chem. Mater.*, 31, 7085-7091(2019).

### 8:35 AM F.EL08.02.22

**Spectroscopic Investigations of Hybrid 2D-3D and Lead-Free Perovskite Materials for Photovoltaics** Leonardo R. Buizza; University of Oxford, United Kingdom

Lead-halide perovskite solar cells have improved dramatically over the past decade, increasing in efficiency and overcoming hurdles of temperature- and humidity-induced instability [1]. Materials that combine the high charge-carrier lifetimes and mobilities, strong absorption and good crystallinity of 3D perovskites with the hydrophobic properties of 2D perovskites have become leading candidates for use in solar cells [2]. In order to fully understand the optoelectronic properties of these 2D-3D hybrid systems, we investigate the hybrid perovskite  $\text{BA}_x(\text{FA}_{0.83}\text{Cs}_{0.17})_{1-x}\text{Pb}(\text{I}_{0.6}\text{Br}_{0.4})_3$  across the compositional range  $0 < x < 0.8$ . Small amounts of butylammonium (BA) are found to help improve crystallinity and passivate grain boundaries, reducing trap-mediated recombination and enhancing charge-carrier mobilities. However, over-hybridisation leads to poor crystallinity and inhomogeneous film formation, greatly reducing charge-carrier mobilities. We find long charge-carrier diffusion lengths up to 7.7  $\mu\text{m}$  at low BA content of  $x = 0.167$ , paving the way for highly efficient and stable perovskite solar cells based on 2D-3D hybrid materials [3]. Separately, lead-free all-inorganic materials have become of interest in order to address issues surrounding the stability of lead-halide perovskites, and concerns around the toxicity of  $\text{PbI}_2$  [4]. Here we investigate a novel silver-bismuth material that shows ultrafast charge-carrier dynamics, observed via optical-pump terahertz-probe spectroscopy. A wide-ranging spectroscopic and temperature-based investigation of this material points towards localisation effects and strong charge-lattice interactions, whilst still showing good charge-carrier transport properties, lending promise for potential applications of this material to photovoltaics. References: [1] McMeekin, D.P., Sadoughi, G., Rehman, W., Eperon, G.E., Saliba, M., Hörlantner, M.T., Haghighirad, A., Sakai, N., Korte, L., Rech, B. and Johnston, M.B., 2016. A mixed-cation lead mixed-halide perovskite absorber for tandem solar cells. *Science*, 351(6269), 151-155. [2] Wang, Z., Lin, Q., Chmiel, F.P., Sakai, N., Herz, L.M. and Snaith, H.J., 2017. Efficient ambient-air-stable solar cells with 2D-3D heterostructured butylammonium-caesium-formamidinium lead halide perovskites. *Nature Energy*, 2(9), 17135. [3] Buizza, L.R., Crothers, T., Wang, Z., Patel, J.B., Milot, R., Snaith, H., Johnston, M. and Herz, L., 2019. Charge-carrier dynamics, mobilities and diffusion lengths of 2D-3D hybrid butylammonium-caesium-formamidinium lead halide perovskites. *Advanced Functional Materials*, 29, 1902656. [4] Volonakis, G., Filip, M.R., Haghighirad, A.A., Sakai, N., Wenger, B., Snaith, H.J. and Giustino, F., 2016. Lead-free halide double perovskites via heterovalent substitution of noble metals. *The journal of physical chemistry letters*, 7(7), 1254-1259.

### 8:45 AM F.EL08.02.23

**Reversible Photochromic and Photoluminescence in Iodide Perovskites** Md Wayesh Qarony<sup>1</sup>, Mohammad Kamal Hossain<sup>2</sup>, Mohammad Hossain<sup>1</sup> and Yuen Hong Tsang<sup>1</sup>; <sup>1</sup>The Hong Kong Polytechnic University, Hong Kong; <sup>2</sup>City University of Hong Kong, Hong Kong

Functional materials with photochromism behaviors are highly attractive for various potential applications, such as sensors, displays or lighting devices, clothing, decoration, memory, and commercial consumer products (e.g. photochromic cars, sunglasses, T-shirts, shoes, and umbrella), where a reversible color change occurs with changes in light intensity. Photochromic properties are commonly observed in large molecular organic compounds or polymer materials with several states of different colors. However, most of the materials exhibit photochromic behavior with various states in the solution state of that material, limiting the potential and extensive applications. Light-induced phase segregation with photoluminescence (PL) peak shift in mix-halide perovskites owing to reversible energy bandgap tunability of halide-rich domains under illuminations allows to obtain photochromic behaviors in solid-state materials beyond organic polymers. Inspired by this phenomenon, our color imaging experiment demonstrates a nice photochromic behavior of such mixed-halide perovskites upon dark and light excitation, while the color emitted by the crystals changes from red to yellow and vice versa with the intensity of excitation light source. Interestingly, this photochromic light-emitting characteristic can be well-matched with the laser light-induced reversible PL. Unlike the photochromic property commonly observed in solution-state polymer materials, solid-state perovskite materials with photochromic behavior might open wide applications in consumer products and electronic devices. In the next part, we report on a reversible PL peak in iodide-based organic-inorganic lead halide perovskite materials under a two-photon absorption (TPA) process, while tuning the excitation wavelength. This phenomenon occurs when the incoming femtosecond (fs) laser photon energy is higher than threshold energy. Intriguingly, two shorter wavelength peaks are visible and become prominent when the excitation photon energy is being tuned in the high energy spectrum, while laser power is remained constant. The same phenomenon of reversible PL peak is also observed in various iodine-based organic-inorganic halides as well as all-inorganic perovskite single crystals and polycrystals. We attribute to the reversible PL peak phenomenon to the photoinduced structural deformation and the associated change in the optical bandgap of iodide perovskites under the (fs) laser excitation. Our findings will introduce a new degree of freedom in future research as well as adding new functionalities to optoelectronic applications in these emerging perovskite materials.

**8:55 AM \*F.EL08.02.24**

**Carrier and Spin Dynamics in Perovskite 2D Layered and Nanocrystal Systems** Matthew Beard; National Renewable Energy Laboratory, United States

Lead-iodide based perovskite semiconductors are emerging as promising light absorbers for solution-processed thin-film photovoltaic applications. In addition, these materials are also intensively studied for light-emitting diodes, photodetectors, and lasers. Recently, hybrid organic-inorganic perovskite (HOIP) semiconductors are being considered as candidates for spintronic applications due to a large spin-orbit coupling (SOC) and controllable Rashba-splitting. Here we discuss the spin-coherence lifetimes in single crystals of 2D Ruddlesden-Popper perovskites  $\text{PEA}_2\text{PbI}_4(\text{MAPbI}_3)_n$  (PEA, phenethylammonium; MA, methylammonium;  $n = 1, 2, 3, 4$ ). Room temperature spin-coherence times show a nonmonotonic layer thickness dependence with an increasing spin-coherence lifetime with increasing layer thickness from  $n = 1$  to 4, followed by a decrease in lifetime from  $n = 4$  to  $n = 3$ . Our results are consistent with two contributions; Rashba-splitting increases the spin-coherence lifetime going from the  $n = 3$  to the layered systems, while phonon-scattering which increases for smaller layers decreases the spin-coherence lifetime. The unique tunability of HOIPs offers an unprecedented opportunity to directly incorporate chiral organic molecules in the production of a 2D-layered hybrid perovskite thin film and/or crystal that induces chirality into the inorganic sub-lattice bandedge states. Thus, there is an interesting opportunity to explore how chiral molecules embedded into the multilayers provide spin-control within these hybrid semiconductors. Here, we focus on controlling spin-transport within 2D-layered chiral Pb-I perovskite systems. We demonstrate spin-polarization of charge-transport through the chiral perovskites by showing that the injected current is preferential to one of the spin-states and depends upon the handedness of the incorporated chiral organic molecules; thus, the hybrid chiral system acts as a spin-filter.

**9:10 AM \*F.EL08.02.25**

**Many-Body Elastic Scattering of Excitons in Two-Dimensional Hybrid Metal-Halide Perovskites** Carlos Silva; Georgia Institute of Technology, United States

We quantify the role of many-body elastic scattering effects on exciton dephasing rates in two-dimensional hybrid metal-halide perovskites by means of nonlinear coherent excitation spectroscopy at a temperature of 5 K. We find that the exciton-density dependence of excitation-induced dephasing (EID) is two to three orders of magnitude lower than in other atomic monolayer semiconductors such as transition metal dichalcogenides. We find that, EID is different for the multiple excitons evident in the excitation line shape, as is their phonon-mediated temperature dependence. We ascribe these observations to screening effects due to polaronic dressing by the lattice. We further examine the evolution of the two-dimensional coherent exciton lineshape at 5 K with population waiting time. We find that the 2D coherent lineshape evolves with over time windows in which the population itself is static, in a manner that indicates time-dependent EID. Specifically, we find that the dephasing slows down with population waiting time. This spectral evolution invokes time-varying inter-exciton coherences, and we discuss the possible role of dark exciton states in these quantum dynamics.

**9:25 AM \*F.EL08.02.26**

**Harnessing Free Carriers for Photon Upconversion—Using Lead Halide Perovskites for Triplet Sensitization** Lea Nienhaus and Sarah Wieghold; Florida State University, United States

Solid-state nanocrystal-based upconversion (UC) systems have disadvantages with respect to poor exciton diffusion lengths, strong singlet reabsorption and the low resulting achievable UC efficiencies. To circumvent these issues, we employ bulk lead halide perovskite (LHPs) thin films as triplet sensitizers for near-infrared-to-visible UC. The sensitized UC process is based on triplet-triplet annihilation (TTA) in the organic semiconductor rubrene. Conservative estimates result in reported UC efficiencies upwards of 3%. However, to further boost the UC efficiency, it is required to understand and mitigate the effects of shallow trap states in the LHP sensitizer. Here, we investigate the underlying mechanism of energy transfer at the LHP/rubrene interface, and the effect of the LHP perovskite film thickness on the UC dynamics and efficiency threshold. In the LHP/rubrene bilayer device, we observe two opposing effects caused by interactions between the LHP and rubrene: i) passivation of surface defects by rubrene, which results in a longer native photoluminescence (PL) lifetime, and ii) quenching of the PL lifetime due to energy transfer to the triplet state of rubrene. Our observations indicate that non-radiative trap filling in the LHP film and charge transfer to rubrene are likely competitive quenching pathways. As a result, the threshold  $I_{th}$  at which the UC process becomes efficient, observed as a slope change in the power-dependent upconverted PL, shifts to lower values with increasing film thickness. In contrast to previous reported systems, the slope change is directly dependent on the underlying LHP dynamics: i) below  $I_{th}$ , we find a slope twice the value of the LHP PL, and ii) above  $I_{th}$ , the upconverted PL follows the same power-law as the underlying recombination of electrons and holes in the LHP thin films.<sup>2,3</sup> However, two unusual effects are also observed in the system: i) two distinct rise times in the upconverted emission, indicating two distinct

triplet sensitization rates. ii) A reversible photobleach of the upconverted emission, which cannot be correlated to a physical degradation of the system. By manipulating the triplet population, we are able to show that a higher triplet population does not necessarily result in a higher UC yield for the LHP/rubrene system demonstrated here, rather can be detrimental to the efficiency due to strong singlet reabsorption.<sup>3</sup> (1) Nienhaus, L.; Correa-Baena, J.-P.; Wieghold, S.; Einzinger, M.; Lin, T.-A.; Shulenberger, K. E.; Klein, N. D.; Wu, M.; Bulovi?, V.; Buonassisi, T.; et al. Triplet-Sensitization by Lead Halide Perovskite Thin Films for Near-Infrared-to-Visible Upconversion. *ACS Energy Lett.* 2019, 4, 888-895. (2) Wieghold, S.; Bieber, A. S.; VanOrman, Z. A.; Daley, L.; Leger, M.; Correa-Baena, J.-P.; Nienhaus, L. Triplet Sensitization by Lead Halide Perovskite Thin Films for Efficient Solid-State Photon Upconversion at Subsolar Fluxes. *Matter* 2019, 1, 705-719. (3) Wieghold, S.; Bieber, A. S.; VanOrman, Z. A.; Nienhaus, L. Influence of Triplet Diffusion on Lead Halide Perovskite-Sensitized Solid-State Upconversion. *J. Phys. Chem. Lett.* 2019, 10, 3806-3811.

SESSION F.EL08.03: Materials and Chemistry  
On Demand Abstracts Available for Viewing Starting Saturday Morning, November 21, 2020  
F-EL08

**5:00 AM \*F.EL08.03.01**

**Progress in Homologous 2D Halide Perovskites and Their Impact in Photovoltaics** Mercuri G. Kanatzidis;  
Northwestern University, United States

2D perovskites is a fascinating class of compounds where the 3D perovskite lattice is cut and spatially confined in two dimensions and an “inert” layer of intercalated organic ions is inserted between the layers. The 2D perovskites layers can be formed by the introduction of bulky organic cations that tend to interdigitate between the perovskite sheets. They exhibit a large compositional and structural phase space, which has led to novel and exciting physical properties. The variable thickness of the inorganic slabs presents natural quantum wells (QW) type structures with increased Coulombic shielding, lowering the exciton binding energy and increasing the effective charge carrier mobility. Because these materials have had a strong impact in how record breaking and stable solar cells are constructed, it is critical to understand the thermodynamic and chemical limitations of the maximum thickness that can be sandwiched between the organic bilayers while retaining the structural integrity of the 2D perovskite. What are the limits within which the 2D architecture that define the thickness of the inorganic slabs before the system diverts into the familiar 3D structure? To answer this fundamental question, we employed a combination of synthetic chemistry, calorimetry and crystallography to obtain and identify the thickest known 2D halide perovskite compound characterized to date and we use thermodynamics analysis to assess the enthalpy of formation for these compounds. The application of these low dimensional semiconductors in stable photovoltaics will be discussed.

**5:15 AM \*F.EL08.03.02**

**Real-Time Investigation of Crystallization Pathways of Organo-Metal-Halide Perovskites Solar** Michael F. Toney;  
University of Colorado Boulder, United States

Organic-inorganic hybrid perovskite solar cells (PSCs) have gained tremendous attention as materials for photovoltaics due to their high efficiencies and their compatibility with low-cost low-temperature fabrication methods (such as solution processing). Perovskite film formation is complex, involving the formation of intermediates and/or metastable phases that strongly affect the final perovskite film microstructure. Therefore, understanding the mechanism of perovskite formation and the crystallization pathways is key for facile control of perovskite formation. We are using time-resolved x-ray scattering to investigate the perovskite formation of MAPbI<sub>3</sub>-based perovskites and mixed cation (Cs, FA)PbI<sub>3</sub> perovskites *in-situ* during spin coating and the subsequent post-deposition treatments, where FA is formamidinium and MA is methylammonium. For Cs<sub>0.15</sub>FA<sub>0.85</sub>PbI<sub>3</sub> we study: i) the crystallization pathways during spin coating; ii) the subsequent post-deposition thermal annealing, and iii) crystallization during blade-coating. Our findings reveal that the formation of a non-perovskite FAPbI<sub>3</sub> phase during spin coating is initially dominant regardless of the processing and that the processing treatments has a significant impact on the as-cast film structure and affects the phase evolution during subsequent thermal treatment. We show that blade-coating can be used to overcome the non-perovskite phase formation via solvothermal direct crystallization of perovskite phase. This work show how real-time investigation of perovskite formation can help to establish processing-microstructure-functionality relationships. Our work highlights the importance of real-time investigation of perovskite film formation which can aid in establishing processing-microstructure-functionality relationships and help to provide a fundamental understanding of the mechanisms of perovskite formation.

### 5:30 AM \*F.EL08.03.03

**Is the Unit Cell of Solids, Including Halide Perovskites, as Small as the XRD Literature Says? Consequences of the Polymorphous Network** [Alex Zunger](#)<sup>1</sup>, Xingang Zhao<sup>1</sup>, Zhi Wang<sup>1</sup> and Gustavo M. Dalpian<sup>2</sup>; <sup>1</sup>University of Colorado Boulder, United States; <sup>2</sup>Universidade Federal do ABC, Brazil

Many common crystal structures can be described by a single (or very few) repeated structural motifs (“monomorphous structures”) such as octahedron in cubic halide perovskites. Interestingly, recent accumulated evidence suggests that electronic structure calculations based on such macroscopically averaged monomorphous cubic (Pm-3m) halide perovskites obtained from x-ray diffraction, show intriguing deviations from experiment. These include systematically too small band gaps, dielectric constants dominated by the electronic, negative mixing enthalpy of alloys, and significant deviations from the measured pair distribution function. We show here that a minimization of the systems  $T = 0$  internal energy via density functional theory reveals a distribution of different low-symmetry local motifs, including tilting, rotations, and B-atom displacements (“polymorphous networks”). This is found only if one allows for larger-than-minimal cell size that does not geometrically exclude low symmetry motifs. As the (super) cell size increases, the energy is lowered relative to the monomorphous cell, and stabilizes after  $\sim 32$  formula units (160 atoms) are included. Being a result of nonthermal energy minimization in the internal energy without entropy, this correlated set of displacements must represent the intrinsic geometry preferred by the underlying chemical bonding (lone pair bonding), and as such has a different origin than the normal, dynamic thermal disorder modeled by molecular dynamics. Indeed, the polymorphous network, not the monomorphous ansatz, is the kernel structure from which high temperature thermal agitation develops. The emerging physical picture is that the polymorphous network has an average structure with high symmetry, yet the local structural motifs have low symmetries. We find that, compared with monomorphous counterparts, the polymorphous networks have significantly lower predicted total energies, larger band gaps, and ionic dominated dielectric constants, and agree much more closely with the observed pair distribution functions. An analogous polymorphous situation is found in the paraelectric phase of a few cubic oxide perovskites where local polarization takes the role of local displacements in halide perovskites, and in the paramagnetic phases of a few 3d oxides where the local spin configuration takes that role. See PHYSICAL REVIEW B 101, 155137 (2020).

### 5:45 AM F.EL08.03.04

**TiO<sub>2</sub>-Assisted Halide Ion Segregation in Mixed Halide Perovskite Films** [Jeffrey DuBose](#)<sup>1,2</sup> and Prashant Kamat<sup>1,2</sup>; <sup>1</sup>University of Notre Dame, United States; <sup>2</sup>Radiation Laboratory, University of Notre Dame, United States

In metal halide perovskite solar cells, electron transport layers (ETLs) such as TiO<sub>2</sub> dictate the overall photovoltaic performance. However, the same electron capture property of ETL indirectly impacts halide ion mobility and overall phase stability, as is evident from the TiO<sub>2</sub>-assisted halide ion segregation in mixed halide perovskite (MHP) films under pulsed laser excitation (387 nm, 500 Hz). This segregation is only observed when deposited on an ETL such as TiO<sub>2</sub> but not on insulating ZrO<sub>2</sub> substrate. Injection of electrons from excited MHP into the ETL ( $k_{et} = 10^{11} \text{ s}^{-1}$ ) followed by scavenging of electrons by O<sub>2</sub> causes hole accumulation in the MHP film. Localization of holes on the iodide site in the MHP induces instability causing iodide from the lattice to move away toward grain boundaries. Suppression of segregation occurs when holes are extracted by a hole transport layer (spiro-OMeTAD) deposited on the MHP, thus avoiding hole build-up. These results provide further insight into the role of holes in the phase segregation of MHPs and hole mobility in perovskite solar cells.

### 5:55 AM F.EL08.03.05

**Enhanced Functionality in 2D Hybrid Halide Perovskites Through Engineering of the Organic Component** [Ferdinand C. Grozema](#); Delft University of Technology, Netherlands

Two-dimensional halide perovskites have properties that are markedly different than those of the corresponding 3D perovskites, for instance a considerably larger band gap and much stronger interactions between electrons and hole in the inorganic part of the material, i.e. a much large exciton binding energy. The exciton binding energy and other opto-electronic properties can be tuned by modifications in the composition of the inorganic layer, or by changing the layer thickness, for instance in Ruddlesden-Popper structures, as we have shown recently.

Until now, most of the large organic cations used in 2D or quasi-2D perovskite materials only act as a spacer, defining the dimensionality of the system. Their HOMO-LUMO gap is generally very large and the electronic properties of the resulting materials are fully determined by the properties of the inorganic layers. Currently, there is an increased interest in the introduction of specific functionality in the organic component of the material.

In this work, we aim to introduce such additional functionality in the organic part. An example of such functionality is the introduction of electron donors or acceptors resulting in enhanced charge separation. We have explored the introduction of functional organic chromophores theoretically by density functional theory calculations and show that it is possible to introduce conjugated molecules that have a significant effect on the electronic structure. Strong electron acceptors or donors lead to conduction band or valence band edges that are localized on the organic part of the materials. This could lead to enhanced charge separation.

In a subsequent step, several 2D perovskites with functional organic components have been synthesized. These systems include colloidal perovskite platelets with strongly electron accepting perylenebisimids on the surface, solid 2D materials with electron donating conjugated molecules such as benzothieno[3,2-b][1]benzothiophene (BTBT) and pyrene, and materials that include two-component charge transfer complexes (pyrene:TCNQ) between the inorganic layers. Using a combination of time resolved fluorescence spectroscopy and ultrafast transient absorption we show that introduction of such functional components can directly affect the excited state behavior, in several cases leading to charge separation between the inorganic perovskite layer and the organic layer. In a next step, we show that this can indeed lead to the formation of mobile charges in the perovskite layer with a much higher yield and a much longer lifetime than in the analogous materials without functionality in the organic component. This shows that careful engineering of the organic part in 2D perovskite materials shows a lot of promise for the programmed design of functionality in these materials.

#### **6:05 AM F.EL08.03.06**

**Dopants, Isotope, Pressure and Lead Sequestration for Hybrid Perovskite Materials** Tao Xu; Northern Illinois University, United States

The soaring power conversion efficiency (PCE) of solution process-based organic-inorganic hybrid perovskites solar cells (PSCs) assures their membership in the competitive photovoltaic technologies. However, stability, toxicity and scalability are the three grand challenges that still impedes the market adoption of PSCs. Careful fundamental studies on how their fascinating optoelectronic properties is related to their structures may provide leads to these challenges and also spin off new applications. In this talk, I will present our recent study on the dopants, isotope and pressure effects on hybrid perovskite materials (HPMs). We discovered an interesting bipolar electron injection in LiCl-doped MAPbI<sub>3</sub>-based UV detectors that respond to the energy of UV photons in distinguished photocurrents polarity. We also investigated how the underline interaction between the mass of the cationic rotors and the inorganic lattice in HPMs by isotope effect. In-situ synchrotron X-ray and time-resolved photoluminescence revealed abnormal optoelectronic properties of HPMs by modulating their bond angles and bond lengths using high pressure techniques. Moreover, I will also discuss our new technology to sequestrate lead leakage on perovskite solar cells that can absorb >96% leaked Pb ions under severe device damage while without sacrificing the PCE under normal operational conditions.

#### **6:15 AM F.EL08.03.07**

**Direct Backbone Attachment of Polyesters on Grain Boundaries Enhances Chemical Stability and Suppressing Ion Migration in CH<sub>3</sub>NH<sub>3</sub>PbI<sub>3</sub> Hybrid Perovskite Solar Cells** Chang-Yong Nam; Brookhaven National Laboratory, United States

Organic-inorganic halide perovskites feature excellent optoelectronic properties but poor chemical stability. While passivating perovskite grain boundary (GB) by polymers shows prospects on long-term performance of perovskite solar cells (PSCs), its detailed impact on the ion migration phenomenon, which largely deteriorates the PSC stability, remains less probed. Here, we introduce a new polar polymer, polycaprolactone (PCL), to passivate GBs of methylammonium lead triiodide (MAPbI<sub>3</sub>) perovskites with only 1 – 2 polymer monolayers via direct backbone attachment. The PSCs with passivated MAPbI<sub>3</sub>, using classic but less stable Spiro-OMeTAD (2,2',7,7'-tetrakis[N,N-di(4-methoxyphenyl)amino]-9,9'-spirobifluorene) hole transport layer (HTL), exhibit improved power conversion efficiencies up to 20.1 %, with 90 % of the initial PCE being preserved after 400-h ambient storage, and 80 % even after 100-h, 85 C aging. The improved PSC stability indicates critical roles of PCL GB passivation in retarding moisture-induced decomposition and suppressing ion migration within the perovskite. Time-of-flight secondary ion mass spectrometry reveals that I<sup>-</sup> ions can actively migrate into electrode, HTL, and their interface in non-passivated PSCs, even without externally applied electric field, while such migrations are significantly mitigated in PCL-passivated PSCs. This effective GB passivation by PCL suggests an important potential of polymer additives towards the development of stable high-performance PSCs.

#### **6:25 AM F.EL08.03.08**

**A Matter of Mixing—Chemical Heterogeneity in Mixed Perovskites** [Laura E. Mundt](#)<sup>1</sup>, Junwei Xu<sup>1</sup>, Leah L. Kelly<sup>1</sup>, Axel Palmstrom<sup>2</sup>, Joseph J. Berry<sup>2</sup> and Laura Schelhas<sup>1,2</sup>; <sup>1</sup>SLAC National Accelerator Laboratory, United States; <sup>2</sup>National Renewable Energy Laboratory, United States

One of the key features of halide perovskite photovoltaics (PV) is the absorber's ability to accommodate various ions of different sizes in the crystal lattice. Consequently, halide perovskite solar cells yield the highest efficiency and stability when absorbers comprised of a mixture of ions are utilized. However, some compositions such as FAPbI<sub>3</sub> (FA = formamidinium) or the fully inorganic composition CsPbI<sub>3</sub> exhibit non-ideal geometric conditions and are prone to form non-perovskite  $\delta$ -phases that are detrimental for their application in PV. Alloying compositions allows for a fine tuning of the geometric conditions and therefore the inherent structural stability.<sup>[1]</sup> Nevertheless, any chemical heterogeneity in the film can instigate phase segregation of the material into pure phases which as noted prefer their non-perovskite  $\delta$ -phases and consequently lead to degradation of the device performance. In this study, we present X-ray scattering-based characterization technique as a novel approach of probing the nanoscale heterogeneity.

Spatially resolved analyses have repeatedly revealed microscopic heterogeneity in halide perovskite thin films, including compositional heterogeneity. Evidence has been found that decomposition upon exposure to the aforementioned stress factors is triggered/facilitated by local compositional variation from the averaged mixed phase.<sup>[2]</sup> Consequently, a lack of homogeneity even on the nanoscale may eventually lead to decomposition and device degradation. Characterizing the chemical heterogeneity in these delicate materials on small length scales, however, has proven challenging and we herein present a novel approach of probing the nanoscale heterogeneity.

Analyzing the structural change across phase transitions allows us to probe the nanoscale heterogeneity in perovskite thin films. More precisely, we hypothesize that the cubic to tetragonal phase transition width is a measure of the chemical heterogeneity in the mixed perovskite composition. To analyze the perovskite phase transition from the tetragonal to the cubic phase at higher temperatures, temperature-dependent in situ wide angle X-ray scattering is utilized. Whereas the transition is abrupt for pure MAPbI<sub>3</sub> (MA = methyl ammonium), the transition is stretched over a temperature range for mixed compositions.<sup>[3]</sup> We hypothesize that this is due to heterogeneity in the probed area. Local variations in the chemical composition can exhibit slightly varying transition temperatures from the completely mixed phase and thereby lead to the observed "smearing" of the phase transition. To test our hypothesis, we prepare a set of FA<sub>0.83</sub>Cs<sub>0.17</sub>PbI<sub>3</sub> perovskite thin films, choosing a variation of annealing conditions. The annealing temperature has previously been shown to impact the compositional heterogeneity.

Here, we report a systematic study of the influence of annealing conditions on the phase transition in state-of-the-art perovskites, indicating a correlation between the thermodynamic limit of mixing and the processing conditions. If the slope in the tilt angle over temperature is an indicator for the nanoscale heterogeneity, we can expect this to be related to the device stability and therefore be of high relevance for future processing protocols.

[1] Z. Li et al., *Chem. Mater.* **2016**, 28, 284.

[2] L. T. Schelhas et al., *Energy Environ. Sci.* **2019**, 12, 1341.

[3] J. Barrier et al., *submitted n.d.*

### 6:35 AM F.EL08.03.09

**Understanding and Mitigating Damage in Hybrid Organic-Inorganic Perovskites Using Pulsed Electron Beams** [Elisah VandenBussche](#), Catherine P. Clark, Russell J. Holmes and David J. Flannigan; University of Minnesota, United States

Transmission electron microscopy (TEM) has significant potential to advance fundamental understanding of hybrid organic-inorganic perovskite (HOIP) behavior via high resolution characterization of structure and morphology, chemical analysis, beam-induced current mapping, or even ultrafast structural dynamics at high spatial resolution. However, the organic components and van der Waals bonding critical to the hybrid nature of the material renders HOIPs susceptible to degradation under various environmental conditions, including electron beam irradiation. One promising technique to mitigate this damage is through temporally modulated electron beams, which deliver electron doses with prescribed regularity in place of a thermionic beam in which electron emission is randomly distributed in time. In the present work, the temporally-modulated electron beam is created by training a femtosecond pulsed laser on the source material in the TEM gun region. Importantly, the range of pulsed-electron beam parameters that can be covered in this way is directly dependent upon the pulsed-laser properties, amounting to fine control over both the specimen relaxation time between packets and the instantaneous dose rate. This enables exploration of a host of factors, from spatially-localized specimen heating to complex cumulative, molecular to nanoscale energy-deposition effects. Here, we use a systematic approach to demonstrate the ways in which pulsed beams consisting of discrete packets of photoelectrons delivered to the specimen at precise times can be used to reduce damage to polycrystalline methyl-ammonium lead iodide (MAPbI<sub>3</sub>) specimens, demonstrated quantitatively by using Bragg-peak-intensity attenuation to track damage as a function of total dose and dose rate. We also discuss insights garnered from these

experiments into damage mechanisms in HOIPs, and report real-space imaging studies on the material using temporal modulation techniques. Because of the two-fold aspect of this work, in which damage is both mitigated and studied, it is of both fundamental and practical relevance.

#### 6:45 AM F.EL08.03.10

**Structure-Mechanical-Property Relationship of 2D Hybrid Organic-Inorganic Perovskites** [Qing Tu](#)<sup>1</sup>, Ioannis Spanopoulos<sup>2</sup>, Eugenia S. Vasileiadou<sup>2</sup>, Xiaotong Li<sup>2</sup>, Mercuri G. Kanatzidis<sup>2</sup>, Gajendra Shekhawat<sup>2</sup> and Vinayak Dravid<sup>2</sup>; <sup>1</sup>Texas A&M University, United States; <sup>2</sup>Northwestern University, United States

Mechanical stability of hybrid organic-inorganic perovskites (HOIPs) is essential to achieve long-term durable HOIP-based devices. While HOIPs in two-dimensional (2D) form offer numerous options in the structure and composition to tune their mechanical properties, little is known about the structure/mechanical-properties relationship in this family of materials. Here we investigated a series of 2D lead-halide HOIPs by nano-indentation to explore the impact of critical factors controlling the properties of both the organic and inorganic layers on the materials' out-of-plane mechanical performance. We find that the presence of soft organic layer and weak Van der Waals (VdW) interfaces renders 2D Ruddlesden-Popper (RP) HOIPs more compliant than their 3D counterparts. For 2D RP lead iodide HOIP crystals with n-alkylammonium as spacer molecules, shorter alkyl chain and higher n number (*i.e.*, thicker  $\text{PbI}_6^{4-}$  inorganic slab between organic layers) result in higher Young's Moduli and hardness values, which gradually converge to those of 3D HOIPs. We further discover that the lead-halide bond in the inorganic framework can significantly influence the mechanical properties of 2D RP HOIPs with  $n = 1$ . Like 3D HOIPs, stronger lead-halide bond strength leads to higher Young's modulus in these 2D HOIPs, *i.e.*  $E_{\text{Cl}} > E_{\text{Br}} > E_{\text{I}}$ , while the hardness of 2D RP HOIPs follows a trend different from that in 3D HOIPs (*i.e.*,  $H_{\text{Br}} > H_{\text{Cl}} > H_{\text{I}}$  for 2D HOIPs), probably due to the combined effects from the Pb-X bond strength and inorganic framework structural change (*e.g.*, symmetry and distortion). Moreover, we uncover that the interface between the organic layers in 2D HOIPs can be an effective route to engineer the materials' mechanical properties. Replacing the weak  $\text{CH}_3\text{-CH}_3$  VdW forces by covalent bonds or phenyl-phenyl interactions in the interface can lead to a much stiffer and harder 2D HOIPs. Finally, we show that the mechanical performance of 2D HOIPs with linear aliphatic diammonium spacer molecules is affected by the two basic structural parameters, *i.e.*, the thicknesses of the organic and inorganic layers. Thinner organic layer and thicker inorganic layer can result in 2D HOIPs with larger elastic modulus and hardness values, similar to what is found in 2D RP HOIPs. 2D HOIPs exhibit hybrid mechanical features of those from metals, ceramics and polymers, which are tunable over a wide range through the vast compositional choices. Our results offer intriguing insights into the structure-property relationship of 2D HOIPs from a mechanical perspective, providing guidelines and inspirations to achieve materials design with required mechanical properties for applications.

#### 6:55 AM F.EL08.03.11

**Probing Solution Dynamics in Organic-Inorganic and All-Inorganic Perovskite Solutions by  $^{207}\text{Pb}$  NMR Investigations** [Ferah Ünlü](#), Ufuk Atamtürk, Eunhwan Jung, Khan Lê and Sanjay Mathur; University of Cologne, Germany

Organic-inorganic lead halide perovskites with  $\text{ABX}_3$  structure, established as rapidly emergent energy materials for optoelectronic applications, such as photovoltaics (PV) and light emitting devices (LED). The power conversion efficiencies (PCE) of perovskite solar cells (PSC) reached threshold values beyond 25% competing with silicon counterparts. The versatility of compositions and structures lead to various application forms such as thin films for PSCs or nanocrystals for LEDs or quantum dot solar cells. To obtain the perovskite semi-conductor in preferred form, solution-based synthesis is done using a variety of lead precursors, solvents and additives. These perovskite inks dictate the crystallization and grain morphology of thin films or nanocrystals, however, the nucleation dynamics in solution are not well understood yet. For this purpose, perovskite precursor solutions were investigated via solution nuclear magnetic resonance (NMR) spectroscopy. The  $\text{Pb}^{2+}$  coordination behavior in perovskite solution was tracked very extensively for the first time by  $^{207}\text{Pb}$  NMR spectroscopy and chemical shifts in the range of -500 to 2500 ppm were obtained in deuterated DMF and DMSO solutions. Since the signals obtained by NMR spectroscopy are the direct response from the local electronic structure of the  $^{207}\text{Pb}$ -nuclei, any changes in the structural environment are reflected as chemical shift  $\delta^{207}\text{Pb}$ . The lead iodide species in solution are part of an equilibrium, which was investigated via detecting the chemical shift  $\delta^{207}\text{Pb}$  upon variation of accessible solution parameters, such as molarity, temperature, iodide amount and coordinating solvent. In DMSO, 2D and 3D structures of connected lead iodide octahedra are dominant, whereas structures of lower dimensionality are mainly found in DMF solutions. Therefore,  $^{207}\text{Pb}$  NMR spectroscopy acts as a valuable probe for studies on the solution species and dynamic processes, that are involved in the formation of the perovskite crystals.

#### 7:05 AM F.EL08.03.12

**Late News: Eppure si muove—Proton Diffusion in Halide Perovskite Single Crystals** [Davide R. Ceratti](#)<sup>1</sup>, Arava Zohar<sup>1</sup>,



Roman Kozlov<sup>2</sup>, Hao Dong<sup>3</sup>, Gennady Uraltsev<sup>4</sup>, Olga Girshevitz<sup>5</sup>, Iddo Pinkas<sup>1</sup>, Liat Avram<sup>1</sup>, Gary Hodes<sup>1</sup> and David Cahen<sup>1,5</sup>; <sup>1</sup>Weizmann Institute of Science, Israel; <sup>2</sup>Academician Semenov, Russian Federation; <sup>3</sup>Nanjing University, China; <sup>4</sup>Cornell University, United States; <sup>5</sup>Bar-Ilan University, Israel

Ion diffusion has been demonstrated to seriously affect the optoelectronic properties of Halide Perovskites (HaPs). Till now the fastest diffusion has been attributed to the movement of the halide anions, largely neglecting the contribution of mobile protons, on the basis of computed estimates of their density. In this talk, I will show the proofs of the process of proton diffusion inside HaPs following deuterium-hydrogen exchange and migration in MAPbI<sub>3</sub>, MAPbBr<sub>3</sub> and FAPbBr<sub>3</sub> single crystals through D/H NMR quantification, Raman spectroscopy and Elastic Recoil Detection Analysis, challenging the original assumption of halide-dominated diffusion. These results are confirmed by impedance spectroscopy, where MAPbBr<sub>3</sub>-based solar cells respond at very different voltage frequencies compared to CsPbBr<sub>3</sub>-based ones. I will show that water plays a key role in allowing the migration of protons as we do not detect deuteration in its absence. The water contribution is modeled to explain and forecast its effect as a function of its concentration in the perovskite structure. These findings are of great importance as they evidence how unexpected, water-dependent proton diffusion can be at the basis of the ~7 orders of magnitude spread of diffusion (attributed to I<sup>-</sup> and Br<sup>-</sup>) coefficient values, reported in the literature. The reported enhancement of the optoelectronic properties of HaP when exposed to small amounts of water, may be related to our finding.

**7:15 AM F.EL08.03.13**

**Late News: The Role of Additives in Efficient and Stable Perovskite Solar Cells—Atomistic Insights from Both Experiments and DFT Simulations** Shuxia Tao; TU Eindhoven, Netherlands

Perovskite solar cells have gained prominence for their high efficiency and ease of fabrication, yet are hampered by instability. While ion mixing improves device efficiency and stability in general, recent work is demonstrating that incorporation of ions of particularly small or large size (via applying additives in the fabrication process) enhances both further. However there is a lack of understanding of the mysterious mechanisms through which these ions modify material properties (either in the bulk or grain boundaries) or alter the crystallization pathways. In this talk, I will outline recent advances in material characterization (from both experiments and atomistic simulations using DFT) of the impact of several additives (organic salts (PEAI, BAI, GAI) or inorganic salts (alkali halide)) and investigate how they modify the microstructure of the perovskites. I will also discuss the proposed mechanisms and their prospects in the evolution of efficiency and long term stability perovskite solar cells.

**7:25 AM \*F.EL08.03.14**

**Facets of Multicomponent Halide Perovskites—How *In Situ* Experiments Can Help us to Understand Formation, Stability and Composition** Ana F. Nogueira; University of Campinas, Brazil

Multicomponent perovskite solar cells have reached the recent efficiency breakthrough of 25.2%, higher than silicon polycrystalline photovoltaics. Such fantastic result was only possible due to a precise control and engineering of the morphology, interfaces and the use of multiple cations in perovskite A-site, as Rb, Cs, MA (methylammonium) and FA (formamidinium). For tandem perovskite solar cells, a mixture of different anions, as Br and I is also desired to adjust the band gap. Such cocktail of different cations and anions influences the formation of intermediates, new phases, favours halide homogenization, etc; so that at the end, the efficiency of the device is closely related to not only the optical quality of the film (e.g. crystallinity), but morphology and composition.

In this presentation, we will summarize important results using *in situ* experiments to probe perovskite formation (2D and 3D), stability and composition. We employed time-resolved grazing incidence wide angle x-ray scattering (GIWAXS), small angle x-ray scattering (SAXS) and high-resolution XRD taken at the Brazilian Synchrotron National Laboratory and SSRL-Stanford.

*In situ* GIWAXS experiments allowed us to understand the influence of the relative humidity and time to drop the antisolvent during the preparation of perovskite films and get important information about final composition and morphology [1]. It is well known that a 2D layer on the top of a 3D bulk perovskite improves stability and performance. *In situ* GIWAXS revealed us that during thermal annealing the 2D layer transforms itself into a disorder layer, improving hole transfer and stability [2]. This technique was also employed to identify the first intermediates formed during the degradation of different Cs and Br perovskite compositions under ambient conditions [3].

*In situ* SAXS is another powerful technique to follow the first stages of the 2D perovskite's formation. Our results suggest that the formation of the individual slabs in BA<sub>2</sub>[FAPbI<sub>3</sub>]PbI<sub>4</sub> is quite fast (within the first 10 s) and, then, these slabs self-assemble into bulk crystallites during the next 40 minutes [4].

Another topic of interest is the photoinduced phase segregation in FACs-based perovskite films. We investigated this

phenomenon by photoluminescence (PL) studies and *in situ* high-resolution XRD (dark and under illumination). We found out that cubic-tetragonal transition is able to stabilize the samples with higher Br and Cs content, however this is not true for the films with 17% Br. Thus, other mechanisms must be operating and ruling phase segregation [5].

SESSION F.EL08.04: Materials Discovery—Theory, Experiment and Data  
On Demand Abstracts Available for Viewing Starting Saturday Morning, November 21, 2020  
F-EL08

#### 5:00 AM \*F.EL08.04.01

**Polyelemental, Multicomponent Perovskite Semiconductor Libraries Through Combinatorial Screening** Michael Saliba; Technical University of Darmstadt, Germany

Perovskites have emerged as low-cost, high efficiency photovoltaics with certified efficiencies of 25.2% approaching already established technologies. The perovskites used for solar cells have an ABX<sub>3</sub> structure where the cation A is methylammonium (MA), formamidinium (FA), or cesium (Cs); the metal B is Pb or Sn; and the halide X is Cl, Br or I. Unfortunately, single-cation perovskites often suffer from phase, temperature or humidity instabilities. This is particularly noteworthy for CsPbX<sub>3</sub> and FAPbX<sub>3</sub> which are stable at room temperature as a photoinactive “yellow phase” instead of the more desired photoactive “black phase” that is only stable at higher temperatures. Moreover, apart from phase stability, operating perovskite solar cells (PSCs) at elevated temperatures (of 85 °C) is required for passing industrial norms. Recently, double-cation perovskites (using MA, FA or Cs, FA) were shown to have a stable “black phase” at room temperature.(1,2) These perovskites also exhibit unexpected, novel properties. For example, Cs/FA mixtures suppress halide segregation enabling band gaps for perovskite/silicon or perovskite/perovskite tandems.(3) In general, adding more components increases entropy that can stabilize unstable materials (such as the “yellow phase” of FAPbI<sub>3</sub> that can be avoided using the also unstable CsPbI<sub>3</sub>). Here, we take the mixing approach further to investigate triple cation (with Cs, MA, FA) perovskites resulting in significantly improved reproducibility and stability.(4) We then use multiple cation engineering as a strategy to integrate the seemingly too small rubidium (Rb) (that never shows a black phase as a single-cation perovskite) to study novel multication perovskites.(5) One composition containing Rb, Cs, MA and FA resulted in a stabilized efficiency of 21.6% and an electroluminescence of 3.8%. The Voc of 1.24 V at a band gap of 1.63 eV leads to a very small loss-in-potential of 0.39 V, one of the lowest measured on any PV material indicating the almost recombination-free nature of the novel compound. Polymer-coated cells maintained 95% of their initial performance at 85°C for 500 hours under full illumination and maximum power point tracking. This is a crucial step towards industrialisation of perovskite solar cells. Lastly, to explore the theme of multicomponent perovskites further, molecular cations were reevaluated using a globularity factor. With this, we calculated that ethylammonium (EA) has been misclassified as too large. Using the multication strategy, we studied an EA-containing compound that yielded an open-circuit voltage of 1.59 V, one of the highest to date. Moreover, using EA, we demonstrate a continuous fine-tuning for perovskites in the “green gap” which is highly relevant for lasers and display technology. The last part elaborates on a roadmap on how to extend the multication to multicomponent engineering providing a series of new compounds that are highly relevant candidates for the coming years.(6) (1) Jeon et al. Nature (2015) (2) Lee et al. Advanced Energy Materials (2015) (3) McMeekin et al. Science (2016) (4) Saliba et al., Cesium-containing triple cation perovskite solar cells: improved stability, reproducibility and high efficiency. Energy & Environmental Science (2016) (5) Saliba et al., Incorporation of rubidium cations into perovskite solar cells improves photovoltaic performance. Science (2016). (6) Turren-Cruz et al. Methylammonium-free, high-performance and stable perovskite solar cells on a planar architecture Science (2018)

#### 5:15 AM \*F.EL08.04.03

**Insight into Layered and Deficient Metal Halide Perovskites from First Principles and Symmetry** Claudio Quarti<sup>1</sup>, Mikaël Kepenekian<sup>1</sup>, Pedesseau Laurent<sup>2</sup>, Boubacar Traore<sup>2</sup>, Nicolas Mercier<sup>3</sup>, Mercouri G. Kanatzidis<sup>4</sup>, Constantinos Stoumpos<sup>5</sup>, Jacky Even<sup>2</sup> and Claudine Katan<sup>1</sup>; <sup>1</sup>Univ Rennes, ENSCR, INSA, CNRS, ISCR, France; <sup>2</sup>Univ Rennes, INSA Rennes, CNRS, Institut Foton, France; <sup>3</sup>Université d'Angers, France; <sup>4</sup>Northwestern University, United States; <sup>5</sup>University of Crete, Greece

Currently, many different perovskite -with corner-sharing octahedra- as well as non-perovskite metal-halide solids are synthesized worldwide entailing the need for in-depth understanding of their structure/property relationships. In this regard, combining the huge accumulated knowledge over the last decades, on halide but also oxide perovskites, with modern atomic scale modeling as well as symmetry analysis has proved useful. Among others, new compositions such as A<sub>2</sub>A<sub>n</sub>.

$A_nM_nX_{3n+1}$  (where A and A' are cations, X is halide and M is metal) afford layered structures with a controlled number (n, currently  $\leq 7$ ) of octahedra in the perovskite layer. Those correspond to innate heterostructures that offer an ideal platform for fundamental understanding such as effect of quantum or dielectric confinement.<sup>[1]</sup>

Efforts have also been successful in building new perovskite structures with cations surpassing the Goldschmidt tolerance factor. For instance, this has been recently demonstrated for layered perovskites with the use of ethylammonium, isopropylammonium or dimethylammonium as perovskitizer, having a perovskite sheet retaining its continuous corner-sharing connectivity.<sup>[2]</sup> On another note, new three dimensional networks have been achieved by mixing larger cations (e.g., hydroxyethylammonium) with the standard ones (e.g. methylammonium, formamidinium) leading to the formation of voids in the perovskite lattice, either disordered (Hollow perovskites) or with structural signature of a periodic pattern (Deficient perovskites).<sup>[3]</sup>

In this talk, I will discuss some of our recent theoretical results paying attention on newly discovered halide perovskite phases and opportunities to further engineer their properties in connection with their use in devices.

**References** including references therein: [1] C. Katan, N. Mercier, J. Even, *Quantum and dielectric Confinement Effects in Lower-Dimensional Hybrid Perovskite Semiconductors*, Chem. Rev. 119, 3140 (2019); [2] Y. Fu, X. Jiang, X. Li, B. Traore, I. Spanopoulos, C. Katan, J. Even, M. G. Kanatzidis, E. Harel, *Cation Engineering in Two-Dimensional Ruddlesden-Popper Lead Iodide Perovskites with Mixed Large A-Site Cations in the Cages*, J. Am. Chem. Soc. 142, 4008 (2020); X. Li, Y. Fu, L. Pedesseau, P. Guo, S. Cuthriell, I. Hadar, J. Even, C. Katan, C. C. Stoumpos, R. D. Schaller, E. Harel, M. G. Kanatzidis, *Negative Pressure Engineering with Large Cage Cations in 2D Halide Perovskites Causes Lattice Softening*, J. Am. Chem. Soc. (2020) DOI: 10.1021/jacs.0c03860; [3] A. Leblanc, N. Mercier, M. Allain, J. Dittmer, T. Pauporté, V. Fernandez, F. Boucher, M. Kepenekian, C. Katan, *Enhanced Stability and Band Gap Tuning of  $\alpha$ -[HC(NH<sub>2</sub>)<sub>2</sub>]PbI<sub>3</sub> Hybrid*, ACS Appl. Mater. Interfaces, 11, 20743 (2019); C. Zheng, O. Rubel, M. Kepenekian, X. Rocquefelte, C. Katan, *Electronic properties of Pb-I deficient lead halide perovskites*, J. Chem. Phys. 151, 234704 (2019); C. Quarti, C. Katan and J. Even, *Physical properties of bulk, defective, 2D and 0D metal halide perovskite semiconductors from a symmetry perspective*, under revision.

#### 5:30 AM F.EL08.04.04

**AI-Driven Design of Novel Halide Perovskites** Arun Kumar Mannodi Kanakkithodi and Maria Chan; Argonne National Laboratory, United States

Halide perovskites have become increasingly popular semiconductors for application in photovoltaics, LEDs, transistors and electronics. While materials like methylammonium- or Cesium- lead halide perovskites are well studied, there remain vast regions of the ABX<sub>3</sub> chemical space that are unexplored in terms of stability, electronic structure and defect behavior. There have been several attempts to tune the properties of halide perovskites by partial substitution at the A-site by Rb, K or other large organic cations, at the B-site by Sn, Ge or other divalent cations with similar ionic radii as Pb such as Ba, and at the X site by mixing of I, Br and Cl. To discover new perovskite compositions with improved properties, materials scientists would traditionally use an Edisonian approach to synthesize and test one composition after another until a candidate is found that is stable, robust, processable, and possesses the required properties. Data-driven approaches have rendered brute-force experimentation nearly a thing of the past; today, we can leverage better-than-ever-before computing power and increasingly optimal machine learning methodologies to develop a knowledgebase of semiconductor materials that allows instant access to properties of existing compounds and efficient design of novel compositions for applications in solar cells, infrared sensors, wearable electronics and quantum information sciences. In this work, we combine first principles computations and machine learning to develop a general prediction and design framework for mixed composition halide perovskites with tailored structural, energetic, optoelectronic and defect properties. We consider a chemical space of cubic ABX<sub>3</sub> perovskites where A is selected from the set {FA, MA, Cs, Rb, K}, B from the set {Pb, Sn, Ge, Ba, Sr, Ca}, and X from {I, Br, Cl}. Density functional theory (DFT) computations are performed to generate a dataset of the pseudo-cubic crystal structure, formation and mixing energy, band gap, dielectric constant and cation/anion vacancy formation energy of several hundred known and hypothetical perovskite compositions. This compositionally diverse perovskite dataset along with a set of unique descriptors-based on tabulated elemental properties of constituent elements at the A, B and X site in the compound-serve as input to a neural network (NN) model with multiple output neurons to simultaneously predict each of the aforementioned properties. This model forms the material à properties 'forward prediction' half of the design framework and is applicable to any amount of mixing at the A, B and X sites, which opens up immediate access to extreme levels of alloying that are expensive to model computationally. Following this, the NN model is combined with a mathematical optimization scheme employing genetic algorithms (GA), Bayesian optimization (BO) and generative adversarial networks (GAN) to efficiently design novel compositions with a set of targeted structural, energetic, electronic and defect properties, completing the

properties to material 'inverse design' component. This AI-based design framework is used to quickly screen promising new perovskites which we study in greater detail using more expensive calculations at advanced levels of theory (eg. hybrid functionals that predict band gaps more accurately), and recommend such materials to experimental collaborators for synthesis, testing and characterization. With further expansions in terms of data, descriptors and learning strategies, this framework can lead to the definitive prediction and design methodology that covers the entire halide perovskite chemical universe and informs the creation of new materials that would have taken years of computation or experimentation to be discovered in the past. References 1. A. Mannodi-Kanakkithodi et al., *Chemistry of Materials* 31 (10), 3599-3612 (2019). 2. A. Mannodi-Kanakkithodi, et al., under review, preprint: <https://arxiv.org/abs/1906.02244>.

#### 5:40 AM F.EL08.04.05

**Resolving Rotational Stacking Disorder and Electronic Level Alignment in a 2D Oligothiophene-Based Lead Iodide Perovskite** Manoj K. Jana<sup>1</sup>, Chi Liu<sup>1</sup>, Sven Lidin<sup>2</sup>, David J. Dirkes<sup>3</sup>, Wei You<sup>3</sup>, Volker Blum<sup>1</sup> and David Mitzzi<sup>1</sup>; <sup>1</sup>Duke University, United States; <sup>2</sup>Lund University, Sweden; <sup>3</sup>University of North Carolina at Chapel Hill, United States

Two-dimensional (2D) hybrid organic-inorganic perovskites (HOIPs) represent diverse quantum well heterostructures composed of alternating inorganic and organic layers. While 2D HOIPs are nominally periodic in three dimensions for X-ray scattering, the inorganic layers can orient quasi-randomly, leading to rotational stacking disorder (RSD). RSD manifests as poorly resolved, diffuse X-ray scattering along the stacking direction, limiting the structural description to an apparently disordered subcell. However, local ordering preferences can still exist between adjacent unit cells and can considerably impact the properties, particularly the electronic structure. Here, we elucidate RSD and determine the preferred local ordering in the 2D [AE2T]PbI<sub>4</sub> HOIP (AE2T: 5,5'-bis(ethylammonium)-[2,2'-bithiophene]). We use first-principles calculations to determine energy differences between a set of systematically generated supercells with different order patterns. We show that interlayer ordering tendencies are weak, explaining the observed RSD in terms of differing in-plane rotation of PbI<sub>6</sub> octahedra in neighboring inorganic planes. In contrast, the ordering preference within a given organic layer is strong, favoring a herringbone-type arrangement of adjacent AE2T cations. The calculated electronic level alignments of proximal organic and inorganic frontier orbitals in the valence band vary significantly with the local arrangement of AE2T cations; only the most stable AE2T configuration leads to an interfacial type-Ib band alignment consistent with observed optical properties. The present study underscores the importance of resolving local structure arrangements in 2D HOIPs for reliable structure-property prediction.

#### 5:50 AM F.EL08.04.06

**Computational Design Rules for Novel Double Perovskites for Opto-Electronic Devices—The Analogy Between Cs<sub>2</sub>AgInCl<sub>6</sub> and Ba<sub>2</sub>AgIO<sub>6</sub>**, George Volonakis<sup>1,2</sup> and Feliciano Giustino<sup>3,2</sup>; <sup>1</sup>Université de Rennes 1, France; <sup>2</sup>University of Oxford, United Kingdom; <sup>3</sup>The University of Texas at Austin, United States

Recent computational design strategies towards designing new materials that do not contain Pb have been remarkably successful, and lead to the discovery of a series of novel compounds within the so-called halide double perovskites family. [1] Today there are five inorganic crystals that have been synthesized and characterized; Cs<sub>2</sub>BiAgCl<sub>6</sub>, Cs<sub>2</sub>BiAgBr<sub>6</sub>, Cs<sub>2</sub>SbAgCl<sub>6</sub>, Cs<sub>2</sub>SbAgBr<sub>6</sub>, and Cs<sub>2</sub>InAgCl<sub>6</sub>. Among these, Cs<sub>2</sub>BiAgBr<sub>6</sub> has the narrower indirect band gap of 1.9 eV, and Cs<sub>2</sub>InAgCl<sub>6</sub> is the only direct band gap semiconductor, yet with a large gap of 3.3 eV. All of them exhibit low carrier effective masses and consequently, are prominent candidates for opto-electronic applications including photovoltaics. Here, we probe oxide perovskites to look for potential promising oxide perovskites following our substitution-based computational design approach. We identify a new oxide double perovskite semiconductor: Ba<sub>2</sub>AgIO<sub>6</sub> (BAIO), and report on its synthesis by low-temp solution process. BAIO has a band gap in the visible range (i.e. 1.9 eV), and a broad PL spectrum. Surprisingly, BAIO has an electronic band structure remarkably similar to that of our recently discovered perovskite Cs<sub>2</sub>AgInCl<sub>6</sub>. This allows us to further develop a universal analogy concept that can be used to identify links between oxide and halide perovskites. As such example, we show how BAIO and Cs<sub>2</sub>AgInCl<sub>6</sub> are both analogs of the well-known transparent conductor BaSnO<sub>3</sub>, but the significantly lower band-gap of BAIO makes this new compound more promising for oxide-based optoelectronics and for novel monolithic halide/oxide devices.

[1] Patent WO 2017/037448 A1 (2015); JPCL 7 1254 (2016); JPCL 8 772 (2017); APL 112 243901 (2018)

[2] JPCL 8 3917 (2017)

[3] Patent Application 19386013.7 (2019) ; JPCL 10 1722 (2019)

#### 6:00 AM F.EL08.04.07

**Pronounced Nonlinear Bandgap Behavior in Mixed Cs<sub>2</sub>Ag(Sb<sub>x</sub>Bi<sub>1-x</sub>)Br<sub>6</sub> Double Perovskite Alloys** Zewei Li<sup>1</sup>, Seán Kavanagh<sup>2,3,2</sup>, Mari Napari<sup>4</sup>, Robert Palgrave<sup>2</sup>, Mojtaba A. Jalebi<sup>2</sup>, Zahra A. Garmaroudi<sup>1</sup>, Mikko Laitinen<sup>5</sup>, Jaakko Julin<sup>5</sup>,

Richard Friend<sup>1</sup>, David O. Scanlon<sup>2,6</sup>, Aron Walsh<sup>3,7</sup> and Robert Hoyer<sup>3</sup>; <sup>1</sup>University of Cambridge, United Kingdom; <sup>2</sup>University College London, United Kingdom; <sup>3</sup>Imperial College London, United Kingdom; <sup>4</sup>University of Southampton, United Kingdom; <sup>5</sup>University of Jyväskylä, Finland; <sup>6</sup>Harwell Science and Innovation Campus, United Kingdom; <sup>7</sup>Yonsei University, Korea (the Republic of)

Halide-based double perovskites have gained significant attention in recent years, owing to the ability to replace the toxic  $\text{Pb}^{2+}$  cation with a pair of more benign cations (e.g.  $\text{Ag}^+$  and  $\text{Bi}^{3+}$ ) while preserving the perovskite crystal structure. However, most double perovskites, including the prototypical  $\text{Cs}_2\text{AgBiBr}_6$ , have wide bandgaps, limiting photoconversion efficiencies. Recently, it has been demonstrated that the bandgap of  $\text{Cs}_2\text{AgBiBr}_6$  can be reduced through alloying with  $\text{Sb}^{3+}$ . But the bandgap of the pure Sb-based compound ( $\text{Cs}_2\text{AgSbBr}_6$ ) is also wide. A particular challenge with the Sb-Bi double perovskite alloy system is that materials with high Sb content are difficult to synthesize phase-pure due to the high formation energy of  $\text{Cs}_2\text{AgSbBr}_6$ . In this talk, we show a solution-based route we developed to achieve phase-pure  $\text{Cs}_2\text{Ag}(\text{Sb}_x\text{Bi}_{1-x})\text{Br}_6$  thin films with the mixing parameter  $x$  tunable over the entire composition range. In doing so, we reveal this system to disobey Vegard's law, exhibiting significant bandgap bowing, such that the mixed alloys ( $x$  between 0.5 and 0.9) demonstrate smaller bandgaps (down to 2.08 eV) than the pure Sb- (2.18 eV) and Bi-based (2.25 eV) double perovskites. Based on the calculated electronic band alignment, the origin of bandgap bowing in this double perovskite alloy is found to be electronic, rather than structural, in nature. The staggered bandgap alignment between  $\text{Cs}_2\text{AgBiBr}_6$  and  $\text{Cs}_2\text{AgSbBr}_6$ , in combination with non-linear mixing of electronic states, via either short-range ordering or spin-orbit effects, produces a bandgap lower than that of either pure material. This work demonstrates a method to reduce the bandgap of  $\text{Cs}_2\text{AgBiBr}_6$  double perovskites, such that it is better suited to photovoltaic or photocatalytic applications. More broadly, our results suggest that bandgap bowing could be found in other lead-free double perovskite alloys by pairing together materials with band positions forming a Type II heterojunction, thus offering a new route to engineer the bandgaps of these materials.

#### 6:10 AM F.EL08.04.09

**Efficient Lead-Free Perovskite Solar Cells Enabled by Polymer Induced Trap Passivation for  $\text{FA}_x\text{PEA}_{1-x}\text{SnI}_3$  Layer** Wenzhan Xu, Yu Gao, Feiyu Kang and Guodan Wei; Tsinghua University, China

Tin-based perovskites with excellent optoelectronic properties are promising candidates for fabricating efficient lead-free perovskite solar cells (PSCs). Unfortunately, Tin-based PSCs exhibited a low efficiency, which mainly arises from serious traps-induced non-radiative recombination, leading into large energy loss with a low voltage, more seriously,  $\text{Sn}^{2+}$  is easily oxidized to  $\text{Sn}^{4+}$ , which leads into p-type self-doping with devices having high dark current density. Herein, the polymer poly(ethylene glycol) diacrylate (PEGDA) is employed as a template-agent in  $\text{FASnI}_3$  to control nucleation and growth is reported. This  $\text{FASnI}_3$  layer showed a compact crystal with large grain size and reduced defects. As a result, the fabricated planar heterojunction device of ITO/PEDOT:PSS/ $\text{FA}_x\text{PEA}_{1-x}\text{SnI}_3$ /ICBA/BCP/Ag showed the power conversion efficiency (PCE) of 9.35% with voltage of 0.75 V. Moreover, corresponding perovskite solar cells exhibit an enhanced stability.

#### 6:20 AM F.EL08.04.10

**Compositional Optimization Strategies for Multi-Cation Perovskites Against Thin-Film Degradation** Shijing Sun<sup>1</sup>, Armi Tiihonen<sup>1</sup>, Felipe Oviedo<sup>1</sup>, Zhe Liu<sup>1</sup>, Janak Thapa<sup>1</sup>, Noor Titan Putri Hartono<sup>1</sup>, Anuj Goyal<sup>2</sup>, Jason J. Yoo<sup>1</sup>, Ruipeng Li<sup>3</sup>, Mounqi Bawendi<sup>1</sup>, Vladan Stevanovic<sup>2</sup>, John W. Fisher<sup>1</sup> and Tonio Buonassisi<sup>1</sup>; <sup>1</sup>Massachusetts Institute of Technology, United States; <sup>2</sup>National Renewable Energy Laboratory, United States; <sup>3</sup>Brookhaven National Laboratory, United States

Improving the heat–moisture–light stability of organic–inorganic perovskites, an outstanding semiconductor material class, is a critical challenge.[1] To identify the most stable multi-cation lead iodide perovskites containing Cs, formamidinium (FA) and methylammonium (MA), we fuse results from density functional theory (DFT) calculations and high-throughput *in situ* thin-film degradation test within a singular machine learning (ML) algorithm to inform the compositional optimization of  $\text{Cs}_x\text{MA}_y\text{FA}_{1-x-y}\text{PbI}_3$ . [2] We identify thin-film compositions centered at  $\text{Cs}_{0.17}\text{MA}_{0.03}\text{FA}_{0.80}\text{PbI}_3$  that achieve a 3x delay in macroscopic degradation onset under elevated temperature, humidity and light compared with the more complex  $\text{Cs}_{0.05}(\text{MA}_{0.17}\text{FA}_{0.83})_{0.95}\text{Pb}(\text{I}_{0.83}\text{Br}_{0.17})_3$ . [3] We find up to 8% of MA can be incorporated into the perovskite structure before stability is significantly compromised. Cs is beneficial at low concentrations, however beyond 17% is found to contribute to reduced stability. Synchrotron-based grazing-incidence wide-angle X-ray scattering (GIWAXS) further reveals that the  $\text{CsPbI}_3$  minority phase is both a degradation product and an accelerator for chemical decomposition in hot and humid environments, and our findings highlight this detrimental effect can be kinetically suppressed by co-optimising Cs and MA content. Our findings highlight the detrimental effect of  $\text{CsPbI}_3$  in hot and humid environments both as a degradation product and an accelerator for further chemical decomposition even in top-performing multi-cation compositions.[4] This indicates a limitation of Cs as a perovskite-stabilizing agent, despite it has been to date one of the most widely used cations for environmental stability and performance enhancement in perovskite optoelectronics.

## References

- [1] M. Saliba, “Polyelemental, Multicomponent Perovskite Semiconductor Libraries through Combinatorial Screening,” *Advanced Energy Materials*, vol. 9, no. 25, p. 1803754, May 2019.
- [2] L. T. Schelhas *et al.*, “Insights into operational stability and processing of halide perovskite active layers,” *Energy and Environmental Science*, vol. 12, no. 4, pp. 1341–1348, 2019.
- [3] J.-P. Correa-Baena *et al.*, “Homogenized Halides and Alkali Cation Segregation in Alloyed Organic-inorganic Perovskites,” *Science (New York, N.Y.)*, vol. 363, no. 6427, pp. 627–631, Feb. 2019.
- [4] M. V. Khenkin *et al.*, “Consensus statement for stability assessment and reporting for perovskite photovoltaics based on ISOS procedures,” *Nature Energy*, vol. 5, no. 1, pp. 35–49, Jan. 2020.

### 6:30 AM F.EL08.04.11

**Predicting Optoelectronic Failure in Hybrid Perovskites Using Machine Learning and Simple Optical Techniques** Wiley A. Dunlap-Shohl, Ryan Stoddard, Hongbo Qiao, Yuhuan Meng, Wylie Kau and Hugh W. Hillhouse; University of Washington, United States

Stability is one of the most pressing issues facing commercialization of hybrid perovskite solar cells. While there have been encouraging recent improvements in the longevity of efficient perovskite devices,<sup>1,2</sup> researchers have yet to demonstrate their ability to reach useful lifetimes on the order of decades, or even years. Key steps in reaching this goal include identifying behaviors that appear early in the life cycle of a perovskite film or device that are indicative of future failure, and developing quantitative links between these early-time features and metrics of sample lifetime. Accurate and general lifetime models that can bridge the gap between accelerated testing and normal operating conditions will enable more efficient troubleshooting of problems in state-of-the-art perovskite solar cells and hence be of great value to the photovoltaics community.

To address this challenge, we have developed techniques that monitor *in situ* the evolution of key optoelectronic figures of merit of perovskite thin films in response to varied environmental stresses. By combining measurements of photoluminescence, photoconductivity, and optical transmittance, we gather time-resolved information into carrier generation (quantified by quasi-Fermi level splitting/QFLS), carrier transport (quantified by mean carrier diffusion length  $L_D$ ), and material integrity, respectively.<sup>3</sup> We show that carrier transport failure is the primary mechanism curtailing photovoltaic performance of hybrid perovskites, evidenced by a rapid drop in  $L_D$  that, in most cases, occurs before the QFLS has reached a maximum. The time  $t_{LD75}$  at which  $L_D$  has decreased to 75% of its starting value is therefore a useful measure of the perovskite film’s effective lifetime. Machine learning models employing a greedy feature selection algorithm predict  $\ln(t_{LD75})$  for MAPbI<sub>3</sub> to within about 12%, with a dataset spanning a wide range of environmental stress conditions. The initial time derivative of transmittance has high predictive weight in these models, illustrating the importance of the connection between the material’s initial physical degradation rate and its eventual loss of connectivity between undegraded domains within the film. As an alternative means of characterizing material integrity, we have employed dark-field optical microscopy, which is sensitive to scattered light due to roughness or secondary phases, and unlike transmittance is compatible with *in situ* observations of devices with a metal back contact. Heterogeneity of the dark field images of degrading perovskite films evolves in a way that is highly correlated with their transmittance, showing that this technique can be used to connect changes in solar cell operating characteristics (such as shunt resistance) with local failure of the absorber material. These early successes demonstrate that simple *in situ* optical techniques provide extremely useful physical information that aids the task of forecasting perovskite failure.

#### References:

1. Bai, S.; Da, P.; Li, C.; Wang, Z.; Yuan, Z.; Fu, F.; Kawecki, M.; Liu, X.; Sakai, N.; Wang, J. T.; Huettner, S.; Buecheler, S.; Fahlman, M.; Gao, F.; Snaith, H. J., Planar Perovskite Solar Cells with Long-Term Stability Using Ionic Liquid Additives. *Nature* **2019**, *571* (7764), 245-250.
2. Christians, J. A.; Schulz, P.; Tinkham, J. S.; Schloemer, T. H.; Harvey, S. P.; Tremolet de Villers, B. J.; Sellinger, A.; Berry, J. J.; Luther, J. M., Tailored Interfaces of Unencapsulated Perovskite Solar Cells for >1,000 Hour Operational Stability. *Nat. Energy* **2018**, *3* (1), 68-74.
3. Stoddard, R. J.; Dunlap-Shohl, W. A.; Qiao, H.; Meng, Y.; Kau, W. F.; Hillhouse, H. W., Forecasting the Decay of Hybrid Perovskite Performance Using Optical Transmittance or Reflected Dark-Field Imaging. *ACS Energy Lett.* **2020**, *5* (3), 946-954.

### 6:40 AM F.EL08.04.12

**Late News: Efficient Lone Pair-Driven Luminescence: Structure-Property Relationships in Emissive 5s2 Metal Halides** Kyle M. McCall<sup>1,2</sup>, Viktoriia Morad<sup>1,2</sup>, Bogdan M. Benin<sup>1,2</sup> and Maksym V. Kovalenko<sup>1,2</sup>; <sup>1</sup>ETH Zürich, Switzerland; <sup>2</sup>Empa–Swiss Federal Laboratories for Materials Science and Technology, Switzerland

Low-dimensional metal halides have been the focus of intense investigations in recent years following the success of the three-dimensional (3D) hybrid lead halide perovskites as optoelectronic materials for solar cells, semiconductor radiation detectors, and narrow emitters. In particular, the light emission of zero-dimensional (0D) metal halides based on the  $5s^2$  cations  $\text{Sn}^{\text{II}}$  and  $\text{Sb}^{\text{III}}$  have found utility in a variety of applications (including X-ray scintillation and remote thermometry) that are complementary to those of the 3D halide perovskites, thanks to their unusual properties including intrinsic broadband emission and highly temperature-dependent lifetimes. These properties derive from the exceptional chemistry of the  $5s^2$  lone pair, which generates the appropriate atomic environments for efficient emission as it lies on the cusp of the static  $4s^2$  lone pair and the dynamic but less pronounced  $6s^2$  lone pair. However, the descriptions and terminology of this unusual emission vary significantly, complicating efforts of various researchers to build a cohesive understanding and enable the design such emissive materials.

Here, we provide a structural overview of these materials with a focus on the dynamics driven by the stereoactivity of the  $5s^2$  lone pair to identify the structural features that enable strong emission. The chemistry of the  $5s^2$  lone pairs in various halide environments is described and compared to those of the neighboring  $4s^2$  and  $6s^2$  cations to highlight the unique combination of stereoactivity and structural flexibility of these main group metals. We relate the different theoretical models which have been able to explain the success of these bright  $5s^2$  emission centers into a cohesive framework, which is then applied to the array of compounds recently developed by our group and other researchers, demonstrating its utility and generating a holistic picture of the field from the point of view of a materials chemist. We summarize the most promising materials to identify the common trends among them, finding that  $\text{Sn}(\text{II})$  bromides and  $\text{Sb}(\text{III})$  chlorides lead the field with the highest efficiencies, highlighting the importance of metal-halogen overlap in the lone pair dynamics. We highlight the state-of-the-art applications which demonstrate the unique capabilities of these versatile emissive centers, describing the current progress and challenges for each application to identify promising future directions in the field. This work introduces the field of low-dimensional  $5s^2$  metal halides, pointing the way towards an understanding that will enable the design of such materials for optoelectronic devices that deliver on the promise of these applications.

#### 6:50 AM F.EL08.04.13

**Late News: How Defect Tolerant are Halide Perovskites?** [Xie Zhang](#), Mark E. Turiansky, Jimmy-Xuan Shen and Chris G. Van de Walle; University of California, Santa Barbara, United States

“Defect tolerance” has been commonly considered as the origin of the high photovoltaic performance of halide perovskites. However, a rigorous assessment of this concept is still lacking. Based on accurate first-principles calculations, we quantitatively show that halide perovskites are not “defect tolerant”; defect-assisted nonradiative recombination is actually a key limitation of perovskite solar cells. The conventional wisdom suggests that only defects with charge-state transition levels deep in the band gap can be efficient nonradiative recombination center. We demonstrate that the presence of charge-state transition levels in the band gap is a prerequisite for being a nonradiative recombination center, but unlike in many conventional semiconductors the position of the level does not directly imply high or low capture rates because of exceptionally strong lattice coupling and anharmonicity in halide perovskites. Explicit calculations of the nonradiative capture rates are essential. We emphasize that accurate calculations, based on hybrid density functional theory and including spin-orbit coupling, are essential for obtaining reliable results. Our results show that iodine interstitials, although their transition levels are close to the band edges, can actually act as efficient nonradiative recombination centers in methylammonium-lead iodide, and are likely responsible for the experimentally observed nonradiative recombination rates. We also address the impact of impurities. The Bi impurity has been commonly believed to be an efficient recombination center. Our rigorous calculations show that while the Bi impurity does have a transition level in the band gap, it is, in fact, not a recombination center on its own. The observed impact on device performance occurs indirectly, via promoting the formation of iodine interstitials. These insights clarify misconceptions in the field, and point to fruitful directions for defect engineering toward enhanced performance.

SESSION F.EL08.05: Toward Pb-Free Perovskite Absorbers  
On Demand Abstracts Available for Viewing Starting Saturday Morning, November 21, 2020  
F-EL08

#### 5:00 AM \*F.EL08.05.01

**Is There Any Hope for Efficient Sn-Based Perovskite Solar Cells?** [Maria Antonietta Loi](#); University of Groningen,

Netherlands

Organic lead halide perovskite based solar cells (HPSCs) have achieved certified power conversion efficiency (PCE) over 25.0%. Despite the high efficiency achieved, there are still many concerns about the large-scale applicability of this solar cells because of the water soluble toxic  $Pb^{2+}$ . The simpler approach to address this issue is to find a benign or less toxic metal to replace the lead atom in the perovskite structure, with the resulting perovskite still showing the excellent optical and electrical properties. Theoretically, tin based perovskite holds the promise to produce similar or even higher PCE compared to their Pb counterpart. However, for relatively long time the tin-based HPSCs held a PCE lower than 7% though intensive research efforts were devoted to their investigation. The facile formation of tin vacancies and easy oxidation of  $Sn^{2+}$  have been identified as the main reason determining the low PCE. In my presentation I will report as a small amount of 2D tin perovskite templates the growth of highly crystalline and oriented 3D  $FASnI_3$  grains (2D/3D mixtures), suppressing effectively the appearance of tin vacancies and  $Sn^{2+}$  oxidation. As a consequence of the reduced background charge carrier density and trap assisted charge recombination, the device showed a 50% improvement in the PCE (up to 9%) compared to that using pure 3D tin perovskite. We further succeeded reducing the defects in the 2D/3D tin perovskite films by adding ethylammonium iodide (EAI) into the corresponding perovskite precursor solution. These films display larger crystalline grains and a more compact and uniform film morphology when compared to their counterparts without EA cation. These features lead to a much lower trap density, background charge carrier density and charge recombination loss in the corresponding devices. Results, which allow hopping for future highly efficient Sn-based hybrid perovskite solar cells.

**5:15 AM \*F.EL08.05.02**

**Data-Science Methods Enable Perovskite Stability and Performance Improvements** Tonio Buonassisi, Shijing Sun, Clio Batali, Antonio Buscemi, Alex Encinas, Janak Thapa, Noor Titan Putri Hartono, Felipe Oviedo and Armi Tiihonen; Massachusetts Institute of Technology, United States

Data-science methods, including advanced statistics and machine learning, can help researchers diagnose, optimize, and design more efficiently. In this talk, I'll summarize the MIT PVLab's recent progress optimizing bare films and record-efficiency perovskite devices with capping layers using data-science methods. These include combining density-functional theory (DFT) and Bayesian inference to accelerate the search for stable compositions, and optimizing capping layers for combined performance and stability. Lastly, I'll highlight our progress searching for lead-free perovskite-inspired, defect-tolerant semiconductors.

**5:30 AM \*F.EL08.05.05**

**Bismuth-Based Colloidal Nanocrystals—Lead-Free Materials for Solution-Processed Solar Cells** Maria Bernechea; INA - Institute of Nanoscience of Aragon, Spain

In the last years, the field of solution-processed solar cells based on inorganic semiconductors has seen a great progress, showing the highest efficiencies among the emerging photovoltaic technologies. Indeed, quantum dot solar cells have reached an efficiency over 16%, and solar cells based on perovskites have surpassed 25% efficiency. However, the future development of these cells could be limited due to the presence of highly toxic elements in their composition, more specifically lead (Pb). Efforts are thus required in searching for earth-abundant, and non-toxic materials. Inorganic colloidal nanocrystals (NCs) are attractive materials for their use as active layers in quantum dot solar cells. They are generally composed of earth-abundant elements, and they can be processed from solutions, allowing an easy and cheap fabrication of devices. Moreover, they have additional attractive properties, like high absorption coefficients, tunable bandgaps, and band energy level engineering through ligand exchange. In this context, bismuth-based colloidal NCs, appear as an attractive alternative for environmentally friendly, low cost solar cells. We have developed ways to modify the size and shape of the bismuth-based nanocrystals, and we have observed how this affects their optoelectronic properties. We have studied the modulation of Fermi level and energy bands introducing different ligands on the surface of the NCs. We have employed these NCs to fabricate solution-processed solar cells, focusing on completely non-toxic devices, achieving a certified efficiency of more than 6%, employing very thin layers (~35 nm) of  $AgBiS_2$  NCs. A summary of these results will be presented and future directions will be discussed.

**5:45 AM F.EL08.05.06**

**Enhancement of Efficiency for Pb Free Perovskite Solar Cells Consisting of  $Sn^{2+}$  Doped with  $Ge^{2+}$**  Shuzi Hayase<sup>1</sup>, Kohei Nishimura<sup>1</sup>, Muhammad Akmal Kamarudin<sup>1</sup>, Daisuke Hirotsu<sup>2</sup>, Kengo Hamada<sup>2</sup>, Qing Shen<sup>1</sup>, Satoshi Iikubo<sup>2</sup>, Takashi Minemoto<sup>3</sup> and Kenji Yoshino<sup>4</sup>; <sup>1</sup>The University of Elector-Communications, Japan; <sup>2</sup>Kyushu Institute of Technology, Japan; <sup>3</sup>Ritsumeikan University, Japan; <sup>4</sup>Miyazaki University, Japan



The certified efficiency of Pb-perovskite solar cells with more than 1 cm<sup>2</sup> area is reported to be 20.9%(1). In the smaller cell, the cell efficiency with 25.2% has been reported, which is close to 22.3 % of multi Si solar cells (2). However, the use of Pb in electronic devices is limited according to the EU RoHS Directive. Thus, it is needed to develop Pb-free perovskite solar cells. Among Pb-free perovskite candidates, Sn perovskite is one of the most promising candidates for the light harvesting layer for the Pb-free perovskite, because they have perovskite structure similar to Pb-perovskite. However, the efficiency was not as high as those for Pb-perovskite solar cells. We have already reported that the efficiency was enhanced by Ge<sup>2+</sup> doping to the Sn-perovskite layer, because the carrier density in the Sn-perovskite layer was reduced (3,4). Now, we discuss the further enhancement of the Sn-perovskite solar cells from the view point of the lattice strain (disordering) relaxation and the surface passivation on the perovskite layer to show the direction of the research. We report post-treatment of Sn-perovskite layer with Lewis base (NH<sub>2</sub>-CH<sub>2</sub>-CH<sub>2</sub>-NH<sub>2</sub>) to suppress the recombination reaction in Sn-perovskite solar cells resulting in efficiencies of 10.2 %. Upon analyzing the X-ray photoelectron spectroscopy and impedance spectroscopy data, we came to the conclusion that the amine-group bonded the under-coordinated tin, passivating the dangling bonds and defects resulting in suppressed charge carrier recombination (5). This also has the effect of prolonged lifetime and higher charge carrier mobility. These findings provide the groundwork for improving the efficiency of Sn-halide PSCs to compete with that of lead-based PSCs by simple post-treatment with organic molecules (6). We and other research groups have reported that the efficiency of Sn-perovskite solar cells increases spontaneously during the storage, which we explained by the perovskite lattice strain (disordering) relaxation. This prompted us to examine the relationship between relative lattice strain and photovoltaic performances. It is shown that the efficiency of the Sn-perovskite solar cells has good relationship with the lattice strain (disordering). By decreasing the lattice strain (disordering), Ge doped Sn-perovskite solar cells with 11.7% was prepared. The mechanism will be discussed. 1. M.A. Green et al., *Progress in Photovoltaics*, 2019;27:565-575, version 54, 2. NREL efficiency Table, <https://www.nrel.gov/pv/cell-efficiency.html> 3. N. Ito, S. Hayase, et al., *Journal of Physical Chemistry Letters*, 9, p.1682-1688, 2018. 4. C. H. Ng, S. Hayase, et al., *Nano Energy*, <https://doi.org/10.1016/j.nanoen.2019.01.026>, 2019 5. M. A. Kumarudin, S. Hayase, et al., *J. Phys. Chem., Lett.*, DOI:10.1021/acs.jpcclett.9b02024, 2019. 6. K. Nishimura, S. Hayase, et al., *ACS Appl. Mater. Interfaces*, <https://doi.org/10.1021/acsami.9b09564> 2019.

#### 5:55 AM F.EL08.05.07

##### **Carrier Dynamics and Recombination in Low-Dimensional Halide Perovskites—Role of Structural Fluctuations** Dibyajyoti Ghosh; University of Bath, United Kingdom

Low-dimensional halide perovskites have demonstrated promising luminescence properties for light-emitting diodes due to their high radiative recombination rate.[1] However, the lack of a complete understanding of the structure-property relationship hinders the systematic design of these materials to enhance their luminescence efficiency. Combining state-of-the-art nonadiabatic molecular dynamics and time-domain density functional theory, we explore the substantial effects of structural fluctuations on the excited state dynamics and carrier recombination in these perovskites. Here, I will demonstrate how structurally rigid perovskites experience weaker electron-phonon interactions, resulting in suppressed non-radiative carrier recombination and enhanced photoluminescence quantum yield (PLQY).[2,3] Our work revealed that stacking of the spacer cations, and halogen composition of the inorganic layers substantially tune the PLQY of these materials. Based on these understanding, we further propose a combination of suitable spacer cations and inorganic layer compositions to improve the PLQY of low-dimensional halide perovskites. References: 1. Smith et al. *Chem. Rev.* 2019, 119, 3104 2. Ghosh et al. Submitted, 2019 3. Leveillee et al. Under final review, *Nano Lett.* 2019

#### 6:05 AM F.EL08.05.08

**Late News: Enhanced Optical Absorption via Mixed-Valent Doping of Vacancy-Ordered A<sub>3</sub>B<sub>2</sub>X<sub>9</sub> Triple Perovskites** Seán Kavanagh<sup>1,2,3</sup>, David O. Scanlon<sup>1,4</sup>, Aron Walsh<sup>2,5</sup> and Robert Palgrave<sup>1</sup>; <sup>1</sup>University College London, United Kingdom; <sup>2</sup>Imperial College London, United Kingdom; <sup>3</sup>Centre for Doctoral Training in the Advanced Characterisation of Materials (CDT-ACM), United Kingdom; <sup>4</sup>Diamond Light Source, United Kingdom; <sup>5</sup>Yonsei University, Korea (the Republic of)

Vacancy-ordered triple perovskites have recently come under the scientific spotlight as promising materials for high-performance next-generation optoelectronic technologies.<sup>1,2</sup> Their A<sub>3</sub>B<sub>2</sub>X<sub>9</sub> stoichiometry facilitates the replacement of the toxic Pb<sup>2+</sup> cation with a benign isoelectronic B<sup>3+</sup> cation (e.g. Bi<sup>3+</sup> or Sb<sup>3+</sup>) while preserving the perovskite crystal structure. Unfortunately, however, these materials tend to exhibit large bandgaps (> 2 eV), impeding their application in many photocatalytic/voltaic devices.<sup>3,4</sup>

In this work, we demonstrate a drastic shift of over 1 eV in the optical absorption onset of Cs<sub>3</sub>Bi<sub>2</sub>Br<sub>9</sub> (from 2.58 eV to 1.39 eV), upon doping with tin. Through a combination of detailed theoretical and experimental characterization of this novel material, we elucidate the origin of broadband absorption. Sn is found to disproportionate in the doped material, inducing a

strong intervalence charge transfer (IVCT) transition, whilst preserving the structural integrity of the perovskite framework. Our work provides valuable insight regarding the effects of mixed-valency and structure-property relationships in perovskite-inspired materials, guiding design strategies and expanding the compositional space of candidate materials. Moreover, we anticipate that this massive reduction in absorption onset could aid charge transport and/or photo-catalytic performance, opening the door to unexplored applications of this material class.

<sup>1</sup> Y.-T. Huang, **S.R. Kavanagh**, D.O. Scanlon, A. Walsh, and R.L.Z. Hoyer, ArXiv:2008.08959 (2020).

<sup>2</sup> Z. Li, **S.R. Kavanagh**, M. Napari, R.G. Palgrave, M. Abdi-Jalebi, Z. Andaji-Garmaroudi, D.W. Davies, M. Laitinen, J. Julin, R.H. Friend, D.O. Scanlon, A. Walsh, and R.L.Z. Hoyer, ArXiv:2007.00388 (2020).

<sup>3</sup> K.K. Bass, L. Estergreen, C.N. Savory, J. Buckeridge, D.O. Scanlon, P.I. Djurovich, S.E. Bradforth, M.E. Thompson, and B.C. Melot, *Inorg. Chem.* **56**, 42 (2017).

<sup>4</sup> R. Nie, R.R. Sumukam, S.H. Reddy, M. Banavoth, and S.I. Seok, *Energy Environ. Sci.* **13**, 2363 (2020).

#### 6:15 AM F.EL08.05.09

##### **High Efficiency Pb-Free Cs<sub>2</sub>PtI<sub>6</sub> Halide Perovskite Photovoltaic Devices with > 2 Microseconds Carrier**

**Lifetime** Shubhra Bansal, Dakota Schwartz and Curtis Walkons; University of Nevada, Las Vegas, United States

Organic-inorganic hybrid halide perovskite solar cells (HPSCs) have attracted immense attention because of excellent optoelectronic properties and record power conversion efficiency (PCE) has reached 24.2% from 3.8% within a few years. Despite the very high efficiency already attained by HPSCs (ABX<sub>3</sub>; A = MA, FA, Cs; B = Pb, Sn; X=I, Br, Cl) resulting from high absorption coefficient and electron-hole diffusion lengths; toxicity of Pb and stability of these materials are veritable issues. Replacing MA<sup>+</sup> and FA<sup>+</sup> with PEA<sup>+</sup>, BA<sup>+</sup>, Cs<sup>+</sup> has shown to enhance the stability of hybrid perovskite solar cells against thermal and moisture related degradation. The superior optoelectronic properties of Pb-based halide perovskites are attributed to the inactive Pb 6s orbitals, and can be replaced by Ge<sup>2+</sup>, Sn<sup>2+</sup>, Sb<sup>3+</sup>, Bi<sup>3+</sup>, Cu<sup>2+</sup> with inactive s orbitals. Replacement of Pb<sup>2+</sup> with Sn<sup>2+</sup> and Ge<sup>2+</sup> seems to be a logical solution for addressing the toxicity issues and results in excellent optoelectronic properties such as high absorption coefficient, high hole mobility resulting in PCE of 9.6% for (GA,FA)SnI<sub>3</sub> and 7.9% for mixed (FA,MA)GeSnI<sub>3</sub> and 7.11% for CsSn<sub>0.5</sub>Ge<sub>0.5</sub>I<sub>3</sub>. However, a major challenge for Sn and Ge based Pb-free perovskites is poor power conversion efficiencies as divalent Sn<sup>2+</sup> and Ge<sup>2+</sup> tend to oxidize into 4+ oxidation state, generating excessive defects (Sn and Ge vacancies), and resultant short carrier diffusion lengths. The 2D structure Cs<sub>2</sub>SnI<sub>6</sub> has received attention as a more stable alternative to CsSnI<sub>3</sub> based halide-perovskites for photovoltaic applications due to stable Sn<sup>4+</sup> oxidation state and the strong covalency of Sn-I bonds in the [SnI<sub>6</sub>]<sup>2-</sup> octahedral. Cs<sub>2</sub>PdBr<sub>6</sub>, Cs<sub>2</sub>TiBr<sub>6</sub>, Cs<sub>2</sub>AgBiX<sub>6</sub>, CsGe<sub>0.5</sub>Sn<sub>0.5</sub>I<sub>3</sub>, AgBiI<sub>4</sub>, (MA,Cs,Rb)<sub>3</sub>Sb<sub>2</sub>I<sub>9</sub> have been shown to be unsuitable for PV applications due to many reasons such as bandgap > 2 eV, low minority carrier diffusion lengths, deep level defects, etc. We have reproducibly created high quality thin-films of Pb-free perovskite Cs<sub>2</sub>PtI<sub>6</sub> via atmospheric solution process with experimentally determined bandgap of ~ 1.4 eV. Cs<sub>2</sub>PtI<sub>6</sub> crystallizes in a cubic crystal structure with the space group with high {111} peak intensities. SEM analysis shows well-formed micron-sized crystallites with improved film density with the use of ethylene diamine treatment. These atmospherically processed films contains low oxygen levels (mostly surface CsOx) and Cl impurity from PtI<sub>4</sub> precursors as determined by EDS, ToFSIMS and XPS. Cs<sub>2</sub>PtI<sub>6</sub> shows enhanced stability and excellent optical absorption, hole mobility and minority carrier lifetimes. For the first time we have demonstrated a Pb-free halide perovskite material, Cs<sub>2</sub>PtI<sub>6</sub>, with high absorption coefficient compared to MAPbI<sub>3</sub> and minority carrier lifetime > 2 μs. The high absorption coefficient in Cs<sub>2</sub>PtI<sub>6</sub> results from the stronger d-p transitions as compared to the p-p transitions in MAPbI<sub>3</sub>. The combination of high absorption coefficient and high minority carrier diffusion lifetime in Cs<sub>2</sub>PtI<sub>6</sub> suggests presence of direct-indirect transition behavior similar to MAPbI<sub>3</sub>, perhaps due to high Z of Pt. Superstrate n-i-p devices with FTO/CdS/Cs<sub>2</sub>PtI<sub>6</sub>/carbon/Cu have been reported for the first time, with maximum PCE of 13.88% and low Voc deficit. Further improvement in device efficiency is envisioned with the improvement of Cs<sub>2</sub>PtI<sub>6</sub> film quality and better selection of ETL and HTL materials. It is noted that cost of Pt-based precursors is higher compared to Pb-based precursors, however, Pt offers a model system for Pb-free perovskite materials and may offer a pathway to ultra-thin wide bandgap top cells for tandem solar cells. The key advantages of Cs<sub>2</sub>PtI<sub>6</sub> over MAPbI<sub>3</sub> include high stability, absorption coefficient, minority carrier lifetimes and tunable bandgap for applications beyond photovoltaics such as water splitting, photocatalytic CO<sub>2</sub> reduction, and other optoelectronic devices.

SESSION F.EL08.06: Electronic Defects, Interfaces and Stability

On Demand Abstracts Available for Viewing Starting Saturday Morning, November 21, 2020

F-EL08

**5:00 AM \*F.EL08.06.01**

**Understanding Defect Physics to Stabilize Metal-Halide Perovskite Semiconductors for Optoelectronic Applications** [Annamaria Petrozza](#); Istituto Italiano di Tecnologia, Italy

Semiconducting metal-halide perovskites present various types of chemical interactions which give them a characteristic fluctuating structure sensitive to the operating conditions of the device, to which they adjust. This makes the control of structure-properties relationship, especially at interfaces where the device realizes its function, the crucial step in order to control devices operation. In particular, given their simple processability at relatively low temperature, one can expect an intrinsic level of structural/chemical disorder of the semiconductor which results in the formation of defects. Here, first I will summarize our understanding of the nature of defects and their photo-chemistry, which leverages on the cooperative action of density functional theory investigations and accurate experimental design. Then, I will show the correlation between the nature of defects and the observed semiconductor instabilities. Instabilities are manifested as light-induced ion migration and segregation, eventually leading to material degradation under prolonged exposure to light. Understanding, controlling and eventually blocking such material instabilities are fundamental steps towards large scale exploitation of perovskite in optoelectronic devices. Finally, based on such knowledge, I will discuss different synthetic and passivation strategies which are able to stabilize the perovskite layer towards photo, thermal and electrical instabilities, leading to improved optoelectronic material quality and enhanced device reliability

**5:15 AM \*F.EL08.06.02**

**Tools to Reveal the Energetic Losses in Perovskite Solar Cells** [Pablo P. Boix](#); University De Valencia, Spain

The rapid development of perovskite solar cells has been based on improvements in materials and device architectures, yet further progress towards their theoretical limit will require a detailed study of the main physical processes determining the photovoltaic performance. In this talk, we combine optical and electrical spectroscopy measurements to gain insight into the main losses in perovskite solar cells. The analysis of solution-processed devices with controlled precursor concentrations is the perfect platform to develop an impedance spectroscopy equivalent circuit.[1] The model provides a tool to evaluate the processes directly affecting the device performance, including charge recombination and charge transport. In-situ absolute photoluminescence measured during cell operation enables an alternative way to probe the device recombination mechanisms. Applied to vacuum deposited perovskite solar cells, it can directly assess radiative recombination, as well as the variation of the relative radiative /non-radiative along the measured potentials. Altogether, we provide a complete view of the main loss mechanisms in perovskite solar cells, yet in a pragmatic way which allows its application as a device evaluation tool. [1] Yoo et al., *Joule* 3, 2535-2549

**5:30 AM \*F.EL08.06.03**

**Bulk and Interface Engineering for Defect Passivation in Perovskites** [Kai Zhu](#); National Renewable Energy Laboratory, United States

Perovskite solar cells (PSCs) have become a competitive photovoltaic (PV) technology with rapid progress of efficiencies reaching a certified 25.2% for single-junction devices. The bandgap tunability through perovskite composition engineering is attractive for developing ultrahigh-efficiency tandem solar cells, including perovskite/perovskite, perovskite/silicon, or perovskite/thin-film absorber (e.g., CIGS). Toward this end, highly efficient wide-bandgap and low-bandgap perovskites solar cells need to be development. In this talk, I will discuss our recent progress on suppressing defects in perovskites covering both the wide-bandgap (~1.7–1.8 eV) and low-bandgap (~1.2–1.3 eV) perovskite compositions. Strategies on reducing the bulk defects by utilizing 2D perovskite passivation agents (2D-PPA) will be discussed. The precursor chemistry and growth conditions affect significantly the physical and optoelectronic properties of perovskites. Surface recombination at an interface in a device is also critical to device operation. Characterization and strategies to reduce surface recombination will be presented. Applications of perovskite absorbers in highly efficient tandem devices will be discussed. Finally, the potential toxicity issue of Pb and the corresponding mitigation approaches will be discussed.

**5:45 AM \*F.EL08.06.04**

**Intricacy of Photoinduced Halide Ion Segregation and Dark Remixing in Mixed Halide Perovskites** [Prashant Kamat](#); University of Notre Dame, United States

The intrinsic ionic defects, specifically halide ion vacancies, often dictate the mobility of halide species within the perovskite film during the operation of solar cells. Of particular interest is the halide ion mobility in metal halide perovskites, which

plays an important role in determining the performance of perovskite solar cells. Photoinduced phase segregation seen in mixed halide perovskite films under steady state irradiation offers a convenient way to visualize halide ion segregation. Interestingly, upon storage in dark, the process is reversed and the original mixed halide composition gets restored. Whereas entropy of mixing explain the thermally activated mixing of halide ions to yield mixed halide perovskite, the opposite trend observed during photoirradiation remains an intriguing phenomenon. The threshold energy of incident light to observe halide segregation increases with increasing temperature. The diffusion of these halide species, which is tracked through changes in the absorption spectra at different temperatures, offers a direct measurement of thermally activated halide diffusion in perovskite films. The increase in the rate constant of halide diffusion with increasing temperature (from  $5 \times 10^{-5} \text{ s}^{-1}$  at 23 °C to  $2.2 \times 10^{-3} \text{ s}^{-1}$  at 140 °C) follows an Arrhenius relationship with activation energy of 51 kJ/mole. The thermally activated halide exchange shows the challenges of employing layers of different metal halide perovskites in stable tandem solar cells

#### 6:00 AM \*F.EL08.06.05

**Unravelling the Impacts of Mobile Ions on Perovskite Solar Cell Performance** Rebecca Belisle; Wellesley College, United States

Defect tolerance has emerged as a central theme for the success of halide perovskites as photovoltaics. Some current estimates put the number of mobile ionic defects in common halide perovskites above  $10^{17} \text{ cm}^{-3}$ , yet the halide perovskite band structure and resulting shallow nature of the hypothesized dominant defects limits their ability to act as recombination centers in these materials. However, this defect tolerance does not imply that these ionic defects have no impact on device performance. Current-voltage hysteresis, reverse-bias breakdown, photo-brightening, photodegradation, thermal stability, and other behaviors related to perovskite performance have all been attributed to the appreciably ionic transport in perovskites made possible by this large defect population. In this work I will present recent advances in both the development of experimental methods for analyzing the formation and behavior of mobile ions in halide perovskites, and our understanding of the effects of these mobile ions on device performance. I will discuss methods to investigate defect formation and transport, including our results using in situ photoluminescence and X-ray diffraction techniques to track ion movement and correlate that with the optoelectronic properties of methylammonium perovskites. Additionally, I will share our work looking at the impacts of mobile ions on device performance, particularly with regards to limits on the open-circuit voltage of perovskite solar cells. Finally, I will highlight the unique roles that contacts and surfaces can play in optimizing the performance and stability of perovskite solar cells in light of these mobile ionic defects.

#### 6:15 AM F.EL08.06.06

**Mechanism of Surface Passivation of Methylammonium Lead Tribromide Single Crystals by Benzylamine** Herman Duim<sup>1</sup>, Hong-Hua Fang<sup>1</sup>, Sampson Adjokatse<sup>1</sup>, Gert H. Ten Brink<sup>1</sup>, Miguel A. Marques<sup>2</sup>, Bart J. Kooi<sup>1</sup>, Graeme R. Blake<sup>1</sup>, Silvana Botti<sup>3</sup> and Maria Antonietta Loi<sup>1</sup>; <sup>1</sup>University of Groningen, Netherlands; <sup>2</sup>Martin-Luther-Universität-Halle-Wittenberg, Germany; <sup>3</sup>Friedrich-Alexander-Universität Jena, Germany

Solar cells, light-emitting diodes and photodetectors are amongst the promising examples of the use of hybrid organic-inorganic perovskite semiconductors in optoelectronic applications. The surface of these materials plays a crucial role in the performance and stability of such devices as the presence of surface trap states strongly affects the recombination rate of excited charge carriers. It has previously been reported that molecular ligands, such as benzylamine, are capable of significantly reducing the amount of surface trap states in thin films. In this work, we aim to clarify the mechanisms that govern the surface passivation of hybrid perovskites by benzylamine. We use freshly cleaved single crystal to investigate the influence of benzylamine on a well-defined perovskite surface. We demonstrate that benzylamine permanently passivates surface trap states in these single crystals which results in enhanced photoluminescence and charge carrier lifetimes. Additionally, we show that, when exposed to benzylamine, the methylammonium cations are replaced by benzylammonium, thereby creating a thermodynamically more stable two-dimensional (2D) perovskite (BA)<sub>2</sub>PbBr<sub>4</sub> on the surface of the three-dimensional crystal. The formation of this 2D perovskite phase drives a highly anisotropic etching of the underlying crystal surface, with the {100} planes being most prone to etching. Initially, isolated square etching pits appear spread over the surface. As time elapses, these etching pits broaden and eventually merge to give rise to large flat terraces that are oriented normally to the cleaving plane. These results highlight that even a simple passivation procedure can have a marked effect on the morphology and composition of the perovskite material. A thorough understanding of the mechanisms governing the surface passivation is thus crucially important to optimize and design novel passivation schemes, with the ultimate goal of further advancing the efficiency of optoelectronic devices based on hybrid perovskites.

#### 6:25 AM F.EL08.06.08

**Multi-Messenger Stability Testing Using Environmental X-Ray Photoelectron Spectroscopy** Anthony Donakowski<sup>1</sup>, Wes Miller<sup>2</sup>, Nicholas Anderson<sup>2</sup>, Erin Sanehira<sup>2</sup>, Joseph J. Berry<sup>3</sup>, Michael Irwin<sup>2</sup>, Angus Rockett<sup>1</sup> and Xerxes

Steirer<sup>1</sup>; <sup>1</sup>Colorado School of Mines, United States; <sup>2</sup>HEE Solar LLC, United States; <sup>3</sup>National Renewable Energy Laboratory, United States

Using Environmental X-ray Photoelectron Spectroscopy (EXPS), we evaluate the solid and gas phase products from degradation of metal halide perovskites (MHPs) during interaction with water and light. The stability of novel MHPs is traditionally assessed under accelerated stress conditions in complete photovoltaic devices but the associated trial and error approach provides little insight into the chemical origin of device or material failure. Alternatively, EXPS addresses MHP instability head on, testing resilience against water and other stimuli monitored by surface chemistry and electronic structure. With the environmental chamber of the EXPS we control sample temperature, atmosphere, and illumination. A quadrupole mass spectrometer allows identification and quantification of gaseous products. We report time-resolved chemical information about interface reactions, changes to surface bonding, activation energies, and chemical pathways to determine degradation pathways in situ. Using the multi-messenger EXPS approach, we observe significant chemical changes under accelerated stress factor degradation tests within one working day and compare these results to MHPs degraded under standard water and light stress conditions. These results provide insight into previous studies describing the high defect tolerance of MHPs in juxtaposition to their instability under operating conditions after certain chemical thresholds are met. (Snaith, 2018; Steirer et al., 2016). Snaith, H.J., 2018. Present status and future prospects of perovskite photovoltaics. *Nat. Mater.* 17, 372-376. <https://doi.org/10.1038/s41563-018-0071-z>.

### 6:35 AM F.EL08.06.09

**Late News: Approaching the Limits of Optoelectronic Performance in Mixed Cation Mixed Halide Perovskites by Controlling Surface Recombination** Sarthak Jariwala<sup>1</sup>, Sven Burke<sup>1</sup>, Sean P. Dunfield<sup>2</sup>, R. C. Shallcross<sup>3</sup>, Margherita Taddei<sup>1</sup>, Jian Wang<sup>1</sup>, Giles Eperon<sup>2</sup>, Neal R. Armstrong<sup>3</sup>, Joseph J. Berry<sup>2</sup> and David S. Ginger<sup>1</sup>; <sup>1</sup>University of Washington, Seattle, United States; <sup>2</sup>National Renewable Energy Laboratory, United States; <sup>3</sup>The University of Arizona, United States

We demonstrate the critical role of surface recombination in mixed-cation, mixed-halide perovskite,  $\text{FA}_{0.83}\text{Cs}_{0.17}\text{Pb}(\text{I}_{0.85}\text{Br}_{0.15})_3$ . By passivating non-radiative defects with the polymerizable Lewis base (3-aminopropyl)trimethoxysilane (APTMS) we transform these thin films. We demonstrate average minority carrier lifetimes  $> 4 \mu\text{s}$ , nearly single exponential monomolecular PL decays, and concomitantly high external photoluminescence quantum efficiencies ( $>20\%$ , corresponding to  $\sim 97\%$  of the maximum theoretical quasi-Fermi-level splitting) at low excitation fluence. We confirm both the composition and valence band edge position of the  $\text{FA}_{0.83}\text{Cs}_{0.17}\text{Pb}(\text{I}_{0.85}\text{Br}_{0.15})_3$  perovskite using multi-institution, cross-validated, XPS and UPS measurements. We extend the APTMS surface passivation to higher bandgap double cation (FA,Cs) compositions (1.7 eV, 1.75 eV and 1.8 eV) as well as the widely used triple cation (FA,MA,Cs) composition and observe significant PL and PL lifetime improvements after surface passivation. Finally, we demonstrate that the average surface recombination velocity (SRV) decreases from  $\sim 1000 \text{ cm/s}$  to  $\sim 10 \text{ cm/s}$  post APTMS passivation for  $\text{FA}_{0.83}\text{Cs}_{0.17}\text{Pb}(\text{I}_{0.85}\text{Br}_{0.15})_3$ . Our results demonstrate that surface-mediated recombination is the primary non-radiative loss pathway in MA-free mixed-cation mixed-halide films with a range of different bandgaps, which is a problem observed for a wide range of perovskite active layers and reactive electrical contacts. This study indicates that surface passivation and contact engineering will enable near-theoretical device efficiencies with these materials.

SESSION F.EL08.07: Devices—Perovskite Photovoltaics  
On Demand Abstracts Available for Viewing Starting Saturday Morning, November 21, 2020  
F-EL08

### 5:00 AM \*F.EL08.07.01

**Metal Halide Perovskite Materials Development at Hunt Perovskite Technologies, LLC** Michael Irwin; Hunt Perovskite Technologies, LLC, United States

An overview of Hunt Perovskite Technologies, LLC (HPT) metal halide perovskite (MHP) PV research program will be presented. Founded in 2013, HPT has focused their research on stabilizing the MHP material through better chemistry, as highlighted by stabilizing the pure alpha-phase  $\text{FAPbI}_3$  MHP material in 2015. In this materials study, we have come to appreciate the unique defect structure of the MHP material by way of its ionic composition. Descriptions of MHP macro and molecular defect structure will be discussed, as well as their effect on the material's durability and PV device performance.

### 5:15 AM \*F.EL08.07.02

**Fabrication of Perovskite Solar Cells—Wet Solution Deposition vs Vacuum Evaporation** Shengzhong (Frank) Liu<sup>1,2</sup>, Jiangshan Feng<sup>1</sup> and Min Huang<sup>3</sup>; <sup>1</sup>Shaanxi Normal University, China; <sup>2</sup>Dalian Institute of Chemical Physics, Chinese Academy of Sciences, China; <sup>3</sup>Academy of Opto-Electronics, Chinese Academy of Sciences, China

With its rapidly increased cell efficiency to as high as over 25% and incredible suitability to process, equipment and operation, the perovskite is truly a rising star for next generation solar cells. In fact, its cell efficiency has surpassed all other thin film solar cells. We have studied a few different deposition technologies, including dry processing such as vacuum-based alternating precursor deposition, partial co-evaporation of inorganic components; dry atmospheric deposition by using direct contact reactive process; and wet solution processing such as small area spin-coating, large-area blade coating and high-throughput slot-die coating. At present, the wet solution deposition processes are well-advanced with significantly higher efficiencies over 23%. In comparison, the vacuum processes are under development with best cell efficiency still lower than 22%. This article is intended to compare and opt for the best one with most promises for future largescale processing by screening these technologies developed in research laboratories. With mature industrial equipment and engineering processes, we improved the vacuum deposited perovskite cell efficiency to 21.32%, highest for this type to our knowledge. In addition, the films produced using dry deposition seem to show better stability against high humidity, temperature and light-soaking.

**5:30 AM \*F.EL08.07.03**

**Cationic Management for Efficient and Stable FAPbI<sub>3</sub>-Based Perovskite Solar Cells** Sang Il Seok; Ulsan National Institute of Science and Technology (UNIST), Korea (the Republic of)

Highly efficient perovskite solar cells (PSCs) with power conversion efficiencies (PCEs) > 25% are fabricated with formamidinium (FA)-based lead triiodide (FAPbI<sub>3</sub>) perovskites. In general, mixed cations and anions containing FA, methylammonium (MA), Cs, I and Br ions are used to stabilize the black  $\alpha$ -phase against  $\delta$ -phase of the pristine FAPbI<sub>3</sub>. Disadvantageously, the additives such as MA, Cs and Br to FAPbI<sub>3</sub> widen its bandgap and reduce the thermal stability due to the lower thermal decomposition of MA to FA. Therefore, in order to further increase PCE through the enhanced photocurrent density due to the increased light harvesting, stabilizing the  $\alpha$ -FAPbI<sub>3</sub> without blue-shift of the bandgap is needed. In addition, structural dimensions, distortion, and dielectric properties can vary significantly depending on the ionic radius and type of the A-site cation. In this presentation, I would like to introduce the impact of cationic management on the efficiency and long-term stability of perovskite solar cells.

**5:45 AM \*F.EL08.07.04**

**Defect Related Charge Traps and Doping in Perovskites, Solar Cells and Tandem Devices** Jinsong Huang; University of North Carolina-Chapel Hill, United States

In this talk, I will present our recent progress in understanding the fundamental properties of metal halide perovskites and the related device developments. First, the nature of defects induced charge traps and doping in perovskite materials will be discussed, and their chemical origin will be analyzed. A recent development in characterizing the spatial and energetic distributions of defects will be presented, which revealed the significant difference in trap density between single crystals and polycrystalline films, but similarity in distribution of the traps. Second, the healing of defects and tuning the doping in perovskites by multiple processes will be presented that boost the efficiency and stability of perovskite solar cells and modules. Finally, a new charge recombination layer for all perovskite tandem solar cells will be presented which not only simply the fabrication process, but also significantly enhance tandem solar cell efficiency and stability.

**6:00 AM \*F.EL08.07.05**

**Efficient Perovskite Solar Cells with Various Bandgaps** Jingbi You; Chinese Academy of Sciences, China

Lead halide perovskite is a new type of semiconductor optoelectronic material, which owns large absorption coefficient, long diffusion length, which make it as an excellent photovoltaic material. Perovskite solar cells with different bandgaps of absorber need to be studied for making efficient single or tandem solar cells. In this talk, we will show: 1) By contact engineering, for the bandgap around 1.5 eV, we have achieved close to 25% efficiency, 2) By the composition engineering, we have pushed the PCE of inorganic perovskite CsPbI<sub>3</sub> based solar cells to 20% efficiency, 3) According to the defect engineering, over 20% efficiency of the perovskite solar cells have been demonstrated for the perovskite bandgap around 1.35 eV.

**6:15 AM \*F.EL08.07.06**

**Phase Stable and Less-Defect Perovskite Quantum Dots—Optical Property, Photoexcited Carrier Dynamics and Application to Solar Cells** Qing Shen, Feng Liu, Chao Ding and Yaohong Zhang; The University of Electro-

Perovskite quantum dots (QDs) as a new type of colloidal nanocrystals have gained significant attention for both fundamental research and commercial applications owing to their appealing optoelectronic properties and excellent chemical processability.<sup>1</sup> For their wide range of potential applications, synthesizing colloidal QDs with high crystal quality is of crucial importance. However, like most common QD systems, those reported perovskite QDs still suffer from a certain density of trapping defects, giving rise to detrimental non-radiative recombination centers and thus low photoluminescence quantum yield (PL QY). Halide vacancy in perovskites has been widely accepted to be the main factor preventing near-unity PL QY by creating uncoordinated Pb octahedra and the subsequent localized deep trap states.<sup>2</sup> Very recently, we have succeeded in synthesis of phase-stable and less-defect perovskite QDs, including FAPbI<sub>3</sub> QDs, CsPbI<sub>3</sub> QDs and Sn-Pb alloyed QDs.<sup>3-6</sup> We have demonstrated that a high room-temperature PL QY of up to 100% can be obtained in FAPbI<sub>3</sub> and CsPbI<sub>3</sub> perovskite QDs, signifying the achievement of almost complete elimination of the trapping defects. This is realized by the modulation of halide precursor involved in the synthesis, in which trioctylphosphine (TOP) is used to dissolve halide salts. For Sn-Pb alloyed QDs, although the alloyed QDs possess much improved structural stability than that of the pure Pb- and Sn-based one, they still suffer from an extremely low PL QY of ~0.3%, indicative of the severe charge trapping in these Sn-containing perovskites. Such low PL QY is believed to result from the widely known facile oxidation of Sn<sup>2+</sup> to Sn<sup>4+</sup>. To address this issue, we have demonstrated very recently that the deep-level trap states in Sn-based perovskites can be well suppressed by Na<sup>+</sup> doping, which gives rise to a dramatically improved PL QY of ~28% without alerting their favorable electronic structure. X-ray photoelectron spectroscopy (XPS) studies suggest the formation of a stronger chemical interaction between I<sup>-</sup> and Sn<sup>2+</sup> ions upon Na doping. On the other hand, though the reported TOP-based route has demonstrated efficacy in producing CsSn<sub>x</sub>Pb<sub>1-x</sub>I<sub>3</sub> QDs (x = 0~0.6) with superior structural stability, such synthetic protocol can only find success in making these I-related QDs, preparing those pure Cl- and Br-based analogues remains challenging because of the insufficient solubility of PbBr<sub>2</sub> and PbCl<sub>2</sub> in TOP. Therefore, by taking advantage of the strong coordinating ability of trioctylphosphine oxide (TOPO), we have recently reported the first synthesis of ASn<sub>x</sub>Pb<sub>1-x</sub>X<sub>3</sub> QDs (A = Cs, FA, MA) with excellent tunability in both Sn/Pb ratio and a full range of halide covering. The ability to generate all possible, unique combinations has offered great material versatility for the perovskite QD family. Further, by employing ultrafast spectroscopic techniques, we have resolved the fundamental photoexcited charge carrier dynamics in these alloyed QDs, which shall pave the way for future study for enhancing their usefulness in optoelectronic applications.<sup>7-9</sup> We expect the successful synthesis of the “ideal” perovskite QDs will exert profound influence on their applications to both QD-based light-harvesting and -emitting devices in the near future.

1. Swarnkar, A. *et al.*, *Science* 2016, Vol. 354, pp. 92-95.
2. Alivisatos *et al.*, *J. Am. Chem. Soc.* 2018, Vol. 140, pp. 17760.
3. F. Liu, Q. Shen *et al.*, *ACS Nano*, Vol. 11, No. 10, pp. 10373-10383, 2017.
4. F. Liu, Q. Shen *et al.*, *J. Am. Chem. Soc.*, Vol. 139, No. 46, pp. 16708-16719, 2017.
5. F. Liu, Q. Shen *et al.*, *J. Phys. Chem. Lett.*, Vol. 9, No. 2, pp. 294-297, 2018.
6. F. Liu, Q. Shen *et al.*, *Chem. Mater.*, Vol. 31, No. 3, pp. 798-807, 2019.
7. F. Liu, Q. Shen *et al.*, *Angew. Chem. Int. Ed.*, Vol. 59, pp. 1-5, 2020.
8. F. Liu, Q. Shen *et al.*, *Chem. Mater.*, Vol. 32, No. 3, pp. 1089-1100, 2020.
9. C. Ding, Q. Shen *et al.*, *Nano Energy* 2020, 67, 104267.

#### 6:30 AM \*F.EL08.07.07

**Linking Fundamental Properties to Devices by Multiscale Modelling** Alison B. Walker, Matthew J. Wolf, Lewis A. Irvine and Thijs J. Smolders; University of Bath, United Kingdom

Solar cells utilising a metal-halide perovskite (MHP) as the active layer boast maximum power conversion efficiencies rivalling those of commercial silicon based cells, despite the low temperature, solution-based processing methods used in their fabrication. However, those fabrication methods lead to structural and stoichiometric heterogeneity on multiple length scales, with high concentrations of mobile ionic defects, which are believed to underlie undesirable device characteristics such as current-voltage hysteresis and performance degradation.

To further development of perovskite based solar cells, an increased understanding of the complex and often intertwined phenomena underlying both their high performance and the degradation of this performance is essential. The insights and predictions provided by the application of multiscale modelling techniques to the study of phenomena occurring at multiple length- and time-scales continue to play a critical role in this effort.

In this talk I will focus on our use of atomic, mesoscale and continuum modelling techniques to explore aspects of electron and ion dynamics in MHPs and devices based on them. Applications include the effects of pressure and grain boundaries on ion motion; polaronic and hot carrier dynamics; and the influence of the electron and hole transporting layers on current-

voltage hysteresis in perovskite based solar cells.

**6:45 AM F.EL08.07.08**

**The Perovskite Database Project—Insights Gain from Pooling all the World’s Perovskite Device Data** Tor J. Jacobsson<sup>1,2</sup> and Eva Unger<sup>1</sup>; <sup>1</sup>Helmholtz-Zentrum Berlin für Materialien und Energie, Germany; <sup>2</sup>Uppsala University, Sweden

Over the last ten years, the halide perovskites have grown from an academic curiosity into one of the hottest topics in renewable energy research, and more than 15000 papers on perovskite solar cell have now been published. The sheer amount of papers makes it increasingly difficult to get a good overview of what has been going on in the field, and we firmly believe that much could be gained if the data in all those papers could be stored in one place where it would be easily accessible by the research community. Such a collection of data would lead to a better overview, better experimental design, as well as new insights that would be hard to get from data scattered over thousands of articles. It thus represents a way to accelerate the pace of development by applying scientific openness. In this project, we have with the help of a large group of volunteers manually extracted all extractable device data found in the over 15000 perovskite papers so far published. Around the time of presentation this data will be made available in the form of a web application together with interactive graphics enabling anyone to explore and learn from the completeness of the published perovskite device data. We will in this presentation describe what we have created, what can be conclude from the accumulated data, as well as the potential future benefits for the perovskite community if this approach to data sharing gets universally implemented.

Over the last ten years, the halide perovskites have grown from an academic curiosity into one of the hottest topics in renewable energy research, and more than 15000 papers on perovskite solar cell have now been published. The sheer amount of papers makes it increasingly difficult to get a good overview of what has been going on in the field, and we firmly believe that much could be gained if the data in all those papers could be stored in one place where it would be easily accessible by the research community. Such a collection of data would lead to a better overview, better experimental design, as well as new insights that would be hard to get from data scattered over thousands of articles. It thus represents a way to accelerate the pace of development by applying scientific openness. In this project, we have with the help of a large group of volunteers manually extracted all extractable device data found in the over 15000 perovskite papers so far published. Around the time of presentation this data will be made available in the form of a web application together with interactive graphics enabling anyone to explore and learn from the completeness of the published perovskite device data. We will in this presentation describe what we have created, what can be conclude from the accumulated data, as well as the potential future benefits for the perovskite community if this approach to data sharing gets universally implemented.

**6:55 AM F.EL08.07.09**

**Perovskite/Si Tandem Cells Enabled by Efficient and Stable Wide Bandgap Perovskite via Anion-Engineered Two-Dimensional Additives** Daehan Kim<sup>1</sup>, Hee Joon Jung<sup>2</sup>, Ik Jae Park<sup>3</sup>, Bryon W. Larson<sup>4</sup>, Sean P. Dunfield<sup>4</sup>, Chuanxiao Xiao<sup>4</sup>, Jekyung Kim<sup>1</sup>, Jinhui Tong<sup>4</sup>, Passarut Boonmongkolras<sup>1</sup>, Su Geun Ji<sup>3</sup>, Fei Zhang<sup>4</sup>, Seong Ryul Pae<sup>1</sup>, Min Kyu Kim<sup>1</sup>, Vinayak Dravid<sup>2</sup>, Joseph J. Berry<sup>4</sup>, Jin Young Kim<sup>3</sup>, Kai Zhu<sup>4</sup>, Dong Hoe Kim<sup>5</sup> and Byungha Shin<sup>1</sup>; <sup>1</sup>Korea Advanced Institute of Science and Technology, Korea (the Republic of); <sup>2</sup>Northwestern University, United States; <sup>3</sup>Seoul National University, Korea (the Republic of); <sup>4</sup>National Renewable Energy Laboratory, United States; <sup>5</sup>Sejong University, Korea (the Republic of)

Perovskite/Si tandem technology has been highlighted as the next technology to achieve ultrahigh efficiency, however progress has been deterred due to difficulties in optimizing the unstable and low-efficiency wide bandgap perovskite (~1.7 electron volts). Here, we have developed a wide bandgap perovskite that simultaneously improves the electrical properties and enhances the passivation effect using a novel strategy that involves tuning the anion of 2D additives (PEAI<sub>x</sub>SCN<sub>1-x</sub>).

We have observed the formation of defects in 2D phase via high-resolution TEM analysis and revealed that anion-engineering of 2D-forming additives leads to improved crystallinity and enhanced charge transport properties (higher mobility, longer carrier mobility, and uniform current flow through grains).

Additionally, we demonstrated a 20.7% efficient wide bandgap perovskite solar cell along with excellent long-term stability under continuous light illumination (80% of the initial efficiency was maintained after 1000 hours of illumination). This is the record efficiency among the reported wide bandgap perovskite solar cells. Using this anion-engineered wide bandgap perovskite cell as a top cell, we fabricated a monolithic 2-terminal perovskite/Si tandem cell with 26.7% efficiency (26.2% certified). Notably, the perovskite top cell in our champion tandem device contributes to ~64% of the total open-circuit voltage, which is the largest contribution from any perovskite top cell among the reported perovskite/Si tandem cells that identified relative contributions of each cell.



This work will be essential for future research on perovskite passivation using 2D additives and present a huge impact for the development of perovskite/Si tandem cells with efficiencies over 30%.

**7:05 AM F.EL08.07.10**

**Efficient Flexible Lead-Free Perovskite Solar Cells Enabled by Grain Boundaries Functionalization** Min Chen, Zhenghong Dai and Nitin Padture; Brown University, United States

Hybrid perovskites materials have been skyrocketing the field of new generation photovoltaics and immediately expanding into advanced optoelectronics. Among the tremendous efforts in commercialization for perovskite solar cell (PSC) technology, the flexible Lead-free PSCs has drawn a great attention from the public to meet with the increasing demands for portable and wearable electronic devices. However, the fracture behavior in the prepared perovskite thin film will typically occur within the grain boundaries, which will retard the PCE performance and negatively affect the mechanical stability during the bending test. Here, we functionalized the volatile and brittle grain boundaries by incorporating low-dimensional (LD) phase. The LD phase was in-situ grown within the grain boundaries. Such in-situ grown LD phase not only enhanced the stability by passivating the grain boundaries defects, but also avoided the crack within the grain boundaries by linking with the neighbored grains. As a result, the prepared flexible lead-free PSCs showed remarkable endurance to mechanical cyclic-bending fatigue, with a PCE retention of 80% after 2,000 cycles.

**7:15 AM F.EL08.07.11**

**Effects of Pressure on Photoconversion Efficiencies of FAI-Based Perovskite Solar Cells** Oluwaseun K. Oyewole<sup>1</sup>, Deborah Oyewole<sup>1</sup>, Benjamin Agyei-Tuffour<sup>2</sup>, Juan Martin Hinostroza Tamayo<sup>1</sup>, Richard Koech<sup>1</sup>, Reisia Ichwani<sup>1</sup>, Jaya Cromwell<sup>1</sup>, Nancy Burnham<sup>1</sup> and Winston Soboyejo<sup>1</sup>; <sup>1</sup>Worcester Polytechnic Institute, United States; <sup>2</sup>University of Ghana, Ghana

Power conversion efficiencies (PCEs) of perovskite photovoltaics now exceed 25%. Perovskite solar cells hold great promise because of their potential low cost, tunable optoelectronic properties, and the possibility of improving their stability. For their commercial success, it is important to keep improving both their performance characteristics and stability. In this paper, a combined experimental and theoretical technique is used to study the effects of pressure on efficiencies of formamidinium-based perovskite solar cells. The interfacial surface contacts in the multilayered structures are predicted before fabricating the perovskite solar cells. A range of pressures is then applied to heal both pre-existing cracks within layered films and along the multilayered interfaces. The results show that the PCEs of the perovskite solar cells increased from ~18% to ~23% for applied pressures between ~0 – 6 MPa. A decrease in the PCEs is observed for pressure applied beyond 6 MPa. The implications of the results are discussed for lamination and roll-to-roll fabrication of perovskite solar cells.

**7:25 AM F.EL08.07.13**

**Inverted Single-Crystal MAPbI<sub>3</sub> Solar Cells Efficient with 21.9% Efficiency by Lowering the Crystallization Temperature** Bekir Turedi; King Abdullah University of Science and Technology, Saudi Arabia

Single-crystal materials are playing a dominant role in shaping established solar cell technologies such as Silicon and GaAs. With their low concentrations of non-radiative carrier recombination centers, single-crystals have led the way in terms of efficiency and are on of the most promising paths forward to approaching the theoretical Shockley-Queisser (SQ) limit for solar cells. In theory, lead halide perovskite single-crystals, with their orders of magnitude lower defect density, longer carrier diffusion lengths, and superior light absorption compared to their polycrystalline counterparts, should offer a chance for perovskite solar cell (PSC) technology to overcome the limitations of polycrystalline thin films and get as close as practical to the SQ theoretical limit. Unfortunately, due to challenges in crystal growth and device integration conditions, the pace of progress (In comparison to polycrystalline PSCs) has been very slow in single-crystal devices. In a recent study, we demonstrated the potential of SC-PSCs by realizing ~21.1% efficient devices based on ~20 μm-thick methylammonium lead iodide monocrystalline absorber films. The preferred method, thus far, to grow MAPbI<sub>3</sub> single-crystal films for PSCs involves solution-processing at temperatures exceeding 120 °C, which adversely affects the film's crystalline quality, especially at the surface, primarily due to the loss of methylammonium iodide. Here, we devised an approach that enables the thin film MAPbI<sub>3</sub> crystal growth on a charge carrier transport layer at lower temperatures (<90 °C), and, thereby, limiting the escape of methylammonium iodide (MAI) from the crystal structure. We showed that this strategy extends the radiative charge carrier lifetime due to a significant reduction in non-radiative recombination channels. SC-PSCs fabricated with this method exhibit an enhanced V<sub>OC</sub> of up to 1.15 V (Control 1.08 V) and a champion PCE of 21.93%. With no grain-boundaries at play, our work indicates the importance of the surface in advancing perovskite photovoltaic technology and provides an approach to grow perovskite single-crystal films under more favorable conditions for better optoelectronic qualities. We believe that our findings will be of wide interest to the perovskite materials and solar cell communities.

SESSION F.EL08.08: Vapor Deposition and Upscaling of Perovskites  
On Demand Abstracts Available for Viewing Starting Saturday Morning, November 21, 2020  
F-EL08

**5:00 AM \*F.EL08.08.01**

**Halide Perovskites—Unprecedented Opportunities for Semiconductor Design and Processing** David Mitzi; Duke University, United States

Although known for many years, organic-inorganic hybrid and related inorganic halide-based perovskites have received extraordinary attention recently, in part due to the unique physical properties and chemical diversity offered by these structures, which make them outstanding candidates for applications in photovoltaic and other semiconductor devices (especially for systems based on Pb, Sn and Ge). Perovskite structures consist of networks of corner-sharing metal halide octahedra that can extend in three or lower dimensions, providing opportunity to probe how dimensionality of the inorganic framework impacts semiconducting character. Further, incorporation of more complex organic cations within lower-dimensional perovskites enables combining outstanding inorganic-derived semiconducting character with organic-derived properties (e.g., luminescence, chirality), a feature extending well-beyond what is attainable with more established inorganic semiconductors (e.g., Si or GaAs) and underlying the creation of multifunctional organic-inorganic compounds and electronics [1]. This talk will emphasize chemical/structural versatility [2] and implications for semiconductor design (both with regards to properties and processing), as well as new characterization approaches for elucidating materials properties. Examples of topics that may be covered include custom-designed organic cations that template or stabilize the formation of difficult-to-realize lead-free perovskite structures [3], merging computational/experimental approaches to predict/verify optoelectronic character and guide design of complex organic-inorganic hybrids [4] and the use of a new carrier-resolved photo-Hall (CRPH) technique [5] to explore the impact of additive engineering on majority/minority carrier properties in perovskite films. Outstanding functionality and versatile processing provide two pillars for future application and study of this exciting and evolving materials family. References: [1] D. B. Mitzi, K. Chondroudis, C. R. Kagan, *IBM J. Res. & Dev.* 45, 29 (2001). [2] B. Saparov, D. B. Mitzi, *Chem. Rev.* 116, 4558 (2016). [3] M. K. Jana, S. M. Janke, D. J. Dirkes, S. Dovletgeldi, C. Liu, X. Qin, K. Gundogdu, W. You, V. Blum, D. B. Mitzi, *J. Am. Chem. Soc.* 141, 7955 (2019). [4] W. A. Dunlap-Shohl, E. T. Barraza, A. Barrette, S. Dovletgeldi, G. Findik, D. J. Dirkes, C. Liu, M. K. Jana, V. Blum, W. You, K. Gundogdu, A. D. Stiff-Roberts, D. B. Mitzi, *Mater. Horiz.* 6, 1707 (2019). [5] O. Gunawan, S. R. Pae, D. M. Bishop, Y. Virgus, J. H. Noh, N. J. Jeon, Y. S. Lee, X. Shao, T. Todorov, D. B. Mitzi, B. Shin, *Nature*, <https://doi.org/10.1038/s41586-019-1632-2> (2019).

**5:15 AM F.EL08.08.02**

**ALD/MLD of 2-D Perovskite Passivation Layers** Jacob Vagott and Juan Pablo Correa Baena; Georgia Institute of Technology, United States

Atomic layer deposition (ALD) is a sequential thin film deposition technique with great potential for increasing the performance of high-efficiency perovskite solar cells (PSCs) through advantages such as high uniformity and thickness control. Although ALD is limited to inorganic precursors, molecular layer deposition (MLD) allows for the use of organic precursors and can be used in conjunction with ALD to result in high-quality hybrid organic—inorganic films. Organic—inorganic perovskite materials for PSCs are typically solution processed; this is undesirable when compared to vapor processes due to the use of toxic solvents which require careful control of the atmosphere, making it difficult to manufacture. This research focuses on the design of a process for depositing hybrid organic—inorganic perovskite films through a combined ALD/MLD process. There are currently no processes for depositing perovskite materials by ALD/MLD without some degree of solution processing. Since sequential deposition methods allow for precise thickness control, it would be possible to then deposit both methylammonium lead iodide and 2-D perovskites. 2-D perovskites have shown the potential to be effective surface passivators for perovskite solar cells. As passivation layers, 2-D perovskites improve long-term stability, decrease interfacial defects and charge recombination, and increase efficiency by enhanced charge extraction from the bulk perovskite.

**5:25 AM F.EL08.08.03**

**Triple-Halide Multi-Cation Perovskite Solar Cells via Hybrid Vapor-Solution Technique** Amir Zarean Afshord, Wiria Soltanpoor, Ummugulsum Gunes, Zenep Gozukara, Gorkem Gunbas and Selcuk Yerci; Middle East Technical University,

Turkey

Employing scalable deposition techniques adaptable to complex multi-cation halide perovskites is a significant step towards the commercialization of perovskite optoelectronics. The hybrid vapor-solution method has been shown to render uniform and conformal perovskite layers on textured surfaces such as random pyramids of Si substrates <sup>1,2</sup>. During that method, a seed layer containing Cs/Pb iodide is deposited by co-evaporating CsI and PbI<sub>2</sub> in a vacuum chamber followed by transformation into a perovskite layer by spin-coating an isopropanol solution of formamidinium/methylammonium-halide (FA/MA-halide). In this study, the deposition rate of CsI with respect to PbI<sub>2</sub> in terms of crystallinity and device performance was investigated. A CsI:PbI<sub>2</sub> rate ratio of 1:10 was found optimal. Later, the concentrations of FAI, MABr, and MACl were systematically optimized to deposit triple halide multi-cation perovskite solar cells. This is the first time a triple-halide multi-cation perovskite layer is fabricated using the hybrid vapor-solution method. A comparison between perovskites with double and triple halides showed a superior solar cell performance of Br-free triple cation perovskite compared to the other species. This is attributed to the wider absorption range of that perovskite with narrower bandgap. The champion devices showed efficiencies of 18.1% in the n-i-p and 17.6% in the p-i-n structure. The presented analysis exhibits good control on the halide composition during the hybrid vapor-solution method.

#### References

- (1) Sahli, F.; Werner, J.; Kamino, B. A.; Bräuninger, M.; Monnard, R.; Paviet-Salomon, B.; Barraud, L.; Ding, L.; Diaz Leon, J. J.; Sacchetto, D.; Cattaneo, G.; Despeisse, M.; Boccard, M.; Nicolay, S.; Jeangros, Q.; Niesen, B.; Ballif, C. Fully Textured Monolithic Perovskite/Silicon Tandem Solar Cells with 25.2% Power Conversion Efficiency. *Nat. Mater.* **2018**, *17* (9), 820–826. <https://doi.org/10.1038/s41563-018-0115-4>.
- (2) Schulze, P. S. C.; Wienands, K.; Bett, A. J.; Rafizadeh, S.; Mundt, L. E.; Cojocar, L.; Hermle, M.; Glunz, S. W.; Hillebrecht, H.; Goldschmidt, J. C. Perovskite Hybrid Evaporation/ Spin Coating Method: From Band Gap Tuning to Thin Film Deposition on Textures. *Thin Solid Films* **2020**, *704*, 137970. <https://doi.org/10.1016/j.tsf.2020.137970>.

#### 5:35 AM F.EL08.08.04

**Controllable Single-Source Flash Evaporation of Organic-Metal-Halide Perovskite Films with Wafer-Scale Uniformity** Jonghoon Lee, Woocheol Lee, Heebeom Ahn, Junwoo Kim, Youngrok Kim, Daekyoung Yoo, Keehoon Kang and Takhee Lee; Seoul National University, Korea (the Republic of)

Organic-inorganic halide perovskites (OHPs) are widely studied due to their excellent optoelectronic properties for solar cell and light-emitting diode applications. Conventional solution-processing techniques such as spin-coating method are commonly used in lab-scale device production but it is essential to explore other deposition techniques compatible for large-scale production. To overcome this, single-source flash evaporation technique, in which a single source of materials of interest is rapidly heated to be deposited in a few seconds, is one of the candidate techniques for large-scale thin film deposition of OHPs. [1.2] In this work, we investigated the reliability and controllability of the single-source flash evaporation technique for methylammonium lead iodide (MAPbI<sub>3</sub>) perovskite. In-depth statistical analysis was employed to demonstrate that the MAPbI<sub>3</sub> films prepared via the flash evaporation have an ultrasurface and uniform thickness throughout the 4-inch wafer scale. We also show that the thickness and grain size of the MAPbI<sub>3</sub> film can be controlled by adjusting the amount of the source and number of deposition steps. In addition, we demonstrate that the reliability of the technique has a direct impact on the device characteristics of the fabricated photodetector devices via statistical analysis.

#### References

- [1] Longo, G., Gil-Escrig, L., Degen, M., Sessolo, M., Bolink, H. *Chemical Communications*, 51, 7376 (2015).
- [2] Wei, H., Ma, H., Tai, M., Wei, Y., Li, D., Zhao, X., Lin, H., Fan, S., Jiang, K. *RSC Advances*, 7, 34795 (2017).

#### 5:45 AM F.EL08.08.06

**Improving the Performance of Solution-Sheared Perovskite Solar Cell with a Surface-Functionalized Coating Blade** Min Kyu Kim, Hyeon Seok Lee, Steve Park and Byungha Shin; Korea Advanced Institute of Science and Technology, Korea (the Republic of)

The currently prevailing technique to produce high quality perovskite films is one-step spin-coating with antisolvent dripping. However, this method has disadvantages when considering mass production due to large waste of precursor solution and poor coverage over a large substrate. Solution-shearing, a type of blade coating methods, is better suited for large scale production and has been applied to printing of halide perovskite. However, devices fabricated by spin-coating generally outperforms those by solution-shearing, which suggests that the quality of spin-coated films is better than solution-sheared films. Herein, we report on a simple modification of a shearing blade that enabled us to access a wider property-map

of the coated perovskite films, thereby improving device performance compared to a conventional glass blade. More specifically, the key was functionalization of the blade's surface into non-wetting. The non-wetting blade formed a thicker meniscus because a lower surface energy of the blade applied a weaker shearing force to the precursor solution compared to a wetting blade. The thicker meniscus yielded not only a thicker film but also a larger average domain size because of the reduced nucleation rate. Carrier lifetime, measured by time resolved photoluminescence, of the perovskite film with the non-wetting blade was twice as long as that with the conventional blade, suggesting much improved film quality with the surface modification of the blade. These structural and optoelectronic changes led to an improved power conversion efficiency of 19.0% while that of the reference device was 17.7%. Additionally, we have successfully coated a uniform perovskite film over 70 cm<sup>2</sup> using the non-wetting blade demonstrating large-scalability of solution shearing.

#### 5:55 AM F.EL08.08.07

**Laser Printed Metal Halide Perovskite** [Colin Tyznik](#)<sup>1</sup>, Zachary A. Lampion<sup>2</sup> and Oana D. Jurchescu<sup>1</sup>; <sup>1</sup>Wake Forest University, United States; <sup>2</sup>Columbia University, United States

The emergence of hybrid organic-inorganic perovskites (HOIPs) has been an exciting development in semiconductor research. Due to their cost-effective processing, high charge carrier mobilities, and band gap tunability, these materials have been incorporated in a wide array of applications such as solar cells, light emitting diodes, and photodetectors. HOIPs have been processed using a wide variety of methods: solution deposition, vacuum deposition, and even from a melt. Here, we report the first example of metal halide perovskite that has been deposited by laser printing on a flexible substrate. Laser printing is a solvent-free manufacturing method that is scalable and high-throughput, and that can be easily adopted and modified for flexible substrates of any shape and size. To formulate the toner, the CH<sub>3</sub>NH<sub>3</sub>PbI<sub>3</sub> powder was first obtained using standard procedures. This powder was combined with carnauba wax, hexamethyldisilazane (HMDS) treated fumed silica, and a charge control agent, to create a toner that was then printed onto polyethylene terephthalate (PET) using an office laser printer. Scanning electron microscope (SEM) electron dispersive X-ray spectroscopy (EDS) revealed that a vertical phase-separation of the toner components occurred in the printed film, with the perovskite layer segregated in the middle. Atomic force microscope (AFM) measurements were used to evaluate the morphology of the films as a function of processing conditions. Electrical measurements were performed in air and dark and an average resistivity of  $1.6 \times 10^7 \text{ } \Omega \cdot \text{m}$  was obtained, a value comparable with that of spin-coated films. Space-charge limited current (SCLC) mobilities were estimated to be 20 cm<sup>2</sup>/Vs. The current-voltage characteristics exhibit no hysteresis and the properties are constant over a large period of time, due to the fact that the non-perovskite toner components encapsulate the perovskite layer. Our work introduces an exciting new avenue for the fabrication of stable perovskite devices that is scalable and devoid of hazardous solvents.

#### 6:05 AM F.EL08.08.09

**Impurity Control as a Pathway Towards Controllable, Up-Scalable Co-Evaporation of Methylammonium Perovskite Thin-Film Solar Cells** [Juliane Borchert](#)<sup>1</sup>, Ievgen Levchuk<sup>2</sup>, Lavina C. Snoek<sup>1</sup>, Mathias U. Rothmann<sup>1</sup>, Henry Snaith<sup>1</sup>, Christoph J. Brabec<sup>2</sup>, Laura Herz<sup>1</sup> and Michael Johnston<sup>1</sup>; <sup>1</sup>University of Oxford, United Kingdom; <sup>2</sup>Friedrich-Alexander Universität Erlangen-Nürnberg, Germany

Since their emergence in 2009 perovskites solar cells have reached a remarkable efficiency of 25.2 % [1]. Metal-halide perovskites exhibit low Shockley-Read-Hall recombination rates, high absorption coefficients across much of the solar spectrum as well as high charge-carrier diffusion lengths and mobilities [2]. These properties are ideal for a wide range of applications, including solar cells, transistors, light-emitting devices and lasers. A particularly simple and popular design for perovskite solar cells is the planar architecture, which was first fabricated using co-evaporation of methylammonium lead iodide (MAI) and lead iodide (PbI<sub>2</sub>) [3]. Co-evaporation makes it possible to deposit perovskite thin-films that are smooth, very planar and pin-hole-free over large areas [4]. This makes evaporated thin-films advantageous for the fabrication of perovskite solar cells and for detailed studies of the optoelectronic properties of the material. Furthermore, no solvents are required which makes this method fully additive and prevents damage to underlying layers. This is important both for the manufacturing of tandem solar cells and the upscaling of perovskite solar cells. While this method was initially mainly used for the deposition of MAPbI<sub>3</sub>, it has recently been extended to other perovskite materials including formamidinium lead iodide (FAPbI<sub>3</sub>) [4], triple-cation perovskites [5] and perovskites incorporating tin [6]. Despite this progress, several hurdles remain on the way to large-area co-evaporated perovskite solar cells. One issue are challenges with the evaporation of MAI [7]. Especially the rate control with conventional quartz micro balances (QMBs) does not work reliably for this material. Furthermore, it has been reported that impurities in MAI influence the film morphology and efficiency of solution-processed perovskite solar cells [8]. Therefore it is important to study the evaporation mechanics of MAI and the influence of impurities in-depth, which we set out to do in this contribution [9]. We compared two different MAIs, an impure one, and a highly purified MAI. A wide range of techniques was employed to characterise the precursors and deposited films, including nuclear magnetic resonance (NMR), infra red spectroscopy and mass spectroscopy. We were able to identify impurities in MAI and

track their presence over the course of an evaporation. Furthermore, we characterised the purity of commercially available MAI and found drastic differences between manufacturers. Finally we fabricated solar cells with MAI of different purity and characterised their performance. We found that impurities critically influence the process control during the co-evaporation of perovskite thin-films. Based on this finding we give recommendations to improve the control over the evaporation and therefore the reproducibility of the process. These insights pave the way towards the upscaling of co-evaporated perovskite solar cells. [1] <https://www.nrel.gov/pv/cell-efficiency.html> [2] MB Johnston, LM Herz (2016) *Acc. Chem. Res.*, 49: [3] Liu, M., Johnston, M. B., & Snaith, H. J. (2013). *Nature*, 501(7467), [4] Borchert, J., Milot, R. L., Patel, J. B., Davies, C. L., Wright, A. D., Martínez Maestro, L., Johnston, M. B. (2017). *ACS En. Lett.*, 2(12), [5] Gil-Escrig, L., Momblona, C., La-Placa, M.-G., Boix, P. P., Sessolo, M., & Bolink, H. J. (2018). *Adv. En. Mat.*, 8(14), [6] Ball, J., Buizza, L., Sansom, H., Farrar, M., Klug, M., Borchert, J., Patel, J.B., Herz, L.M., Johnston, M.B. and Snaith, H.J., 2019. *ACS En. Lett.* (2019) 4, [7] Borchert, J., Boht, H., Fränzel, W., Csuk, R., Scheer, R. and Pistor, P., (2015). *J. of Mat. Chem. A*, 3(39), [8] Levchuk, I., Hou, Y., Gruber, M., Brandl, M., Herre, P., Tang, X., Hoegl, F., Batentschuk, M., Osvet, A., Hock, R. and Peukert, W., 2016 *Adv. Mat. Int.*, 3(22), [9] Borchert, J., Levchuk, I., Snoek, L.C., Rothmann, M.U., Haver, R., Snaith, H.J., Brabec, C.J., Herz, L.M. and Johnston, M.B., 2019. *ACS AMI*, 11(32)

#### 6:15 AM F.EL08.08.10

**Thermal Evaporation for Large-Area Perovskite Solar Cells** Andres Felipe Castro Mendez, Vivek Prakash, Carlo Andrea Riccardo Perini and Juan Pablo Correa Baena; Georgia Institute of Technology, United States

Perovskite Solar Cells (PSC) have achieved up to 25.2% efficiency in the lab-scale by solution processing. However, one of the barriers towards their commercialization is scalability. Achieving this is difficult because of the various layers that are commonly deposited through spin coating, a solution process that is undesirable in industry. The use of toxic solvents presents another challenge to fabricate perovskite modules. To overcome the limitations of solution processing, thermal evaporation has been explored as a robust deposition method that can be upscaled. Thermal evaporation provides three main advantages. First, it can provide scalability. Second, it allows better control and homogeneity of the thickness of the films. And third, it allows for the fabrication of graded compositions throughout the thin film. However, thermal evaporation of perovskites has been difficult to achieve due to the challenges associated with measuring accurately the deposition rate of organic cations such as methylammonium iodide. Here, we systematically study different approaches to coevaporate perovskites with various stoichiometries. We correlate film stoichiometry to the deposition temperature/rate of the organic precursors through XRD and XPS measurements, demonstrating good control and reproducibility of the films over a 10 cm<sup>2</sup> area. The films with varying stoichiometries were incorporated into solar devices where it was observed an improvement of efficiency in large areas with respect to the conventional deposition techniques.

#### 6:25 AM F.EL08.08.11

**2D-on-3D Hybrid Organic-Inorganic Perovskite Heterostructure Thin Films Deposited by RIR-MAPLE** Niara E. Wright<sup>1</sup>, Steven Harvey<sup>2</sup> and Adrienne Stiff-Roberts<sup>1</sup>; <sup>1</sup>Duke University, United States; <sup>2</sup>National Renewable Energy Laboratory, United States

Despite the exceptional increase in the power conversion efficiency of perovskite solar cells (PSCs) over the past decade, the feasibility of commercial systems depends upon achieving stable device performance over thousands of hours. While the crystalline structure of three-dimensional (3D) metal halide perovskites is responsible for unique semiconductor properties advantageous to photovoltaics, such as strong absorption and a tunable bandgap, this structure also leads to aggressive degradation by humidity, light, and oxygen that prevent the required stability. Fortunately, two-dimensional (2D) perovskites have been shown to have improved stability due to the hydrophobic nature of these materials.<sup>2,3</sup> Thus, work is being done to incorporate 2D perovskites as passivating layers for the photovoltaic active regions in 3D metal halide PSCs. While quasi-2D perovskite structures are widely studied, experimental investigations of 2D-on-3D interfaces have been limited due to processing challenges.<sup>4</sup> The purpose of this work is to investigate how resonant infrared, matrix-assisted pulsed laser evaporation (RIR-MAPLE) can overcome these processing challenges to create high-quality 2D-on-3D hybrid organic-inorganic perovskite heterostructures. Eventually, such structures could be used as passivation layers in PSCs. RIR-MAPLE is a vapor deposition technique that uses a low-power, Er:YAG (2.94 μm) laser to evaporate a matrix solvent in a frozen target, which gently ejects the precursor material onto the substrate without evaporating the precursor itself.<sup>5,6</sup> In this work, 2D-on-3D heterostructure thin films of (PEA)<sub>2</sub>PbBr<sub>4</sub> (PEA = phenethylammonium, C<sub>8</sub>H<sub>12</sub>N) on MAPbI<sub>4</sub> (MA = methylammonium, CH<sub>3</sub>NH<sub>2</sub>) are deposited by RIR-MAPLE. Growth conditions and in-situ annealing protocols at the interface of the two materials are investigated to achieve a heterostructure with little to no compositional mixing between the layers. X-ray diffraction spectroscopy and time-of-flight secondary ion mass spectrometry (TOF-SIMS) are performed to confirm that the films are compositionally distinct across the interface. UV-Vis absorbance spectroscopy of the 2D-on-3D heterostructures is conducted to determine the optical properties of the films. Furthermore, efficient charge transport in the

vertical direction is influenced by the quantum well orientation of the 2D perovskite layer. Wells oriented perpendicular to the 3D surface will assist in vertical transport, and wells that are parallel to the 3D surface will impede vertical transport. Spin-coated PEA-based 2D perovskites have been shown to have parallel orientation with respect to the substrate, while preliminary work has demonstrated that these materials have a random orientation of crystalline grains when deposited by RIR-MAPLE. To explore charge transport in the 2D-on-3D heterostructure, current measurements through an anode-heterostructure-cathode configuration are conducted to focus on the transport through the interface itself. In this way, additional variables related to full device architectures are minimized. Separate 2D and 3D hybrid perovskite films, as well as spin-coated heterostructures, are characterized as references for comparison to the RIR-MAPLE-deposited heterostructures. A. D. S.-R. and N. E. W. acknowledge research supported as part of the Center for Hybrid Organic Inorganic Semiconductors for Energy (CHOISE), an Energy Frontier Research Center funded by the U. S. Department of Energy, Office of Science, Basic Energy Sciences (BES) (MAPLE film deposition of 2D hybrid perovskites). References 1. Mitzi, D. B., J. Chem. Soc. Dalt. Trans. 1-12 (2001). 2. Milot, R. L. et al., Nano Lett. 16, 7001-7007 (2016). 3. Grancini, G. & Nazeeruddin, M. K., Nat. Rev. Mater. 4, 4-22 (2019). 4. Grancini, G. et al., Nat. Commun. 8, 15684 (2017). 5. Barraza, E. T. et al., J. Electron. Mat. 47, 917-926 (2018). 6. Stiff-Roberts, A. D. & Wright, N. in Low-Dimensional Materials and Devices. 11085, 26 (SPIE, 2019).

#### 6:35 AM F.EL08.08.13

**The Importance of Knowing Your Surface in Perovskites—When Methylammonium Iodide Content Alters the Structural, Surface, Electronic and Ionic Properties of CH<sub>3</sub>NH<sub>3</sub>PbI<sub>3</sub>** Thibaut Gallet and Alex Redinger; University of Luxembourg, Luxembourg

Optimizing hybrid perovskite devices has been a central research topic in the last few years. This usually is performed through a thorough band alignment engineering of the hole and electron extraction layers with respect to the absorber. This led to the emergence of an uncountable number of organic, inorganic and hybrid layers, usually suitable for specific absorbers, which makes it hard to repeat their improving effects on slightly different absorbers. This comes from the fact that surfaces and therefore interfaces are complex media that are still not well understood but are the major starting points for the fabrication of efficient working solar cells. Density of surface states, surface workfunction homogeneity, grains and grain boundaries properties, optoelectronic properties at the surface are the most important characteristics to determine in order to boost the power conversion efficiency. Kelvin Probe Force Microscopy (KPFM) is a suitable tool to access most of these properties but the measurements outcomes are delicate to interpret, especially for perovskites, essentially because they are often performed under ambient conditions. In this contribution we present our results obtained on methylammonium lead iodide perovskites (MAPI), grown by co-evaporation, where the methylammonium iodide (MAI) concentration is changed by varying the pressure inside the physical vapor deposition (PVD) chamber. We focus our work on the analysis of the surface of our samples without exposing them to air to minimize their contamination to moisture and oxygen. For that, we used Frequency Modulation KPFM (FM-KPFM) under ultra-high vacuum (UHV), photoluminescence (PL), time resolved-PL (TRPL), structural and compositional techniques to understand the impact of MAI concentration in MAPI on the surface. In a first part, we show the impact of varying the MAI pressure inside the PVD by looking at two different pressures. We compare the surface of these two samples by first using KPFM under UHV, which gives the impression that different compounds are deposited on the surface of the samples. For a better interpretation of our results, we additionally use X-ray diffraction (XRD) and Energy Dispersive Spectroscopy (EDS) which enables us to create a link between I/Pb ratio and the transition from a cubic to tetragonal structure. In a second part, we discuss the effect that annealing the samples under inert gas has on the surface workfunction. We see that depending on the initial MAI concentration, the outcome of annealing at several temperatures is different. We again use EDS and XRD for a better understanding but we also perform PL and TRPL. We start to illuminate our sample to access surface photovoltage values and we see how the difference in MAI concentration initially and through the annealing steps influence the ionic mobility at the surface, where different ionic species migrate depending on the absorber's state. Finally, we introduce PL and TRPL to potentially link minority carrier lifetime, PL bandgap and surface photovoltage and we perform a thickness study with KPFM to define an energy band diagram and summarize the key effects of varying the MAI concentration on the surface and why it is important to clearly identify the state of the surface before optimizing the device via band alignment engineering.

#### 6:45 AM F.EL08.08.14

**Vapor Deposition Enables Interface Design and Defect Passivation for Highly Efficient Perovskite Solar Cells** Carlo Andrea Riccardo Perini, Andres Felipe Castro Mendez, Jake Vargott, Juanita Hidalgo and Juan Pablo Correa Baena; Georgia Institute of Technology, United States

To go beyond the present 25.2 % solar cell efficiency record, halide perovskite point defects should be either reduced or passivated. Device interfaces need to be designed to minimize recombination and boost charge carrier extraction. 2D

perovskites are effective interface passivation layers which, included in solar cell device structures, enabled the highest published efficiencies. However, 2D perovskites are mostly processed via solution, which limits the control over the deposited film resulting in losses that manifest as increased series resistance or recombination. The requirement of solvent orthogonality for the 3D and 2D perovskite deposition limits the choice of possible material compositions, whereas the solution deposition of the 3D perovskite limits the use of the 2D passivation to the top 3D surface. Vapor deposition methods are established in manufacturing and enable us to overcome these limitations. Here, we demonstrate a vapor deposition route for 2D passivation of a 3D perovskite, which enables a down to monolayer control and conformal film uniformity. The quality of the 2D passivation layer is probed combining time resolved photoluminescence with spatially resolved hyperspectral luminescence imaging and X-ray beam induced current. Films are then incorporated in complete solar cell device structures demonstrating enhanced performances with respect to the solution processed counterparts. In addition, benefiting from a full vapor deposition of the 2D-3D perovskite stack, a bottom interface 2D passivation is demonstrated.

#### 6:55 AM F.EL08.08.15

**Solvent-Free Synthesis of Alternative Inorganic Halide Materials with Application in Optoelectronics** Paz Sebastia-Luna, Michele Sessolo, Franciso Palazon and Henk Bolink; University of Valencia, Spain

Lead halide perovskites have shown outstanding properties when applied in optoelectronic devices, such as solar cells and light-emitting diodes.[1,2] Nevertheless, the presence of highly toxic lead together with their low environmental stability might become a bottleneck for their commercialization. Herein we present different inorganic halides based on non-toxic metals with potential application in optoelectronics. Among these, Cu(I)-based fully inorganic ternary metal halides are particularly promising, especially for applications in light-emitting diodes (LEDs). Blue, highly luminescent materials (required for the fabrication of white light-emitting diodes) are commonly more challenging to obtain than red or green emitters, due to the increased probability of non-radiative recombination. We report the synthesis of two different series of inorganic cesium copper halides, with the general formulas  $Cs_3Cu_2X_5$  and  $CsCu_2X_3$  ( $X = Cl, Br, I$ , and mixtures thereof).  $Cs_3Cu_2I_5$  has been identified as the most promising material, as it maintains blue luminescence with photoluminescence quantum yield exceeding 40% even after being exposed to air for several days. Importantly, we employed a dry mechanochemical synthesis which avoids the use of solvents and high temperatures and allows the preparation of phase-pure compounds.[3] Homogeneous  $Cs_3Cu_2I_5$  thin-films were also fabricated by single-source vacuum deposition (SSVD) employing the pre-synthesized luminescent compounds. The emission spectrum and crystallinity is maintained in thin films, even without any further post-deposition treatment.[4] Using similar synthesis and thin-film processing techniques, we investigate several cesium bismuth halides and their potential use in thin-film solar cells. Finally, we present the synthesis and characterization of an unexplored family of materials, called anti-perovskites, which are based on silver chalcogenides compounds. These materials have potential applications in IR photodiodes and tandem solar cells, thanks to their narrow bandgap  $< 1$  eV. References: [1]. Leijtens, T., Bush, K. A., Prasanna, R., y McGehee, M. D. "Opportunities and challenges for tandem solar cells using metal halide perovskite semiconductors". *Nat. Energy*, 3, 828-838 (2018). [2]. Xing, J. et al. "Color-stable highly luminescent sky-blue perovskite light-emitting diodes". *Nat. Commun.* 9, 1-8 (2018). [3]. Palazon, F., El Ajjouri, Y., y Bolink, H. J. "Making by Grinding: Mechanochemistry Boosts the Development of Halide Perovskites and Other Multinary Metal Halides". *Adv. Energy Mater.* 1902499 (2019). [4]. Sebastia-Luna, P., Navarro-Alapont, J., Sessolo, M., Palazon, F., y Bolink, H. J. "Solvent-Free Synthesis and Thin-Film Deposition of Cesium Copper Halides with Bright Blue Photoluminescence". Submitted

SESSION F.EL08.09: Devices—Applications Beyond PV

On Demand Abstracts Available for Viewing Starting Saturday Morning, November 21, 2020

F-EL08

#### 5:00 AM \*F.EL08.09.01

**Molecular Engineering of Two-Dimensional Organic-Inorganic Hybrid Perovskites** Letian Dou; Purdue University, United States

Two-dimensional halide perovskites are exciting new semiconductors that show great promising in low cost and high-performance optoelectronics devices including solar cells, LEDs, photodetectors, transistors, etc. In the first part of this talk, I will present a molecular approach to the synthesis of high-quality organic-inorganic hybrid perovskite quantum wells through incorporating widely tunable organic semiconducting building blocks as the surface capping ligands. By introducing sterically tailored groups into the molecular motif, the strong self-aggregation of the conjugated organic molecules can be

suppressed, and single crystalline organic-perovskite hybrid quantum wells and superlattices can be easily obtained via one-step solution-processing. Energy transfer and charge transfer between adjacent organic and inorganic layers are extremely fast and efficient, owing to the atomically-flat interface and ultra-small interlayer distance. In the second part, I will present the synthesis and characterization of a stable lead-free Sn (II)-based two-dimensional perovskite featuring a p-conjugated oligothiophene ligand. The conjugated ligands facilitate formation of micrometer-size large grains, improve charge injections, and stabilize the inorganic perovskite layers. Thin film field-effect transistors based on  $(4Tm)_2SnI_4$  exhibit enhanced hole mobility up to  $2.3 \text{ cm}^2V^{-1}s^{-1}$ , and dramatically improved stability over the previous benchmark material  $(PEA)_2SnI_4$ . Stabilization mechanisms were investigated via single crystal structure analysis as well as density functional theory calculations. It was found that the large conjugated organic layers not only serve as thick and dense barriers for moisture and oxygen, but also increase the crystal formation energy via strong intermolecular interactions.

**5:15 AM \*F.EL08.09.02**

**Multiscale Structural Engineering of Luminescent Metal Halides for Thermography and Security Tags** [Maksym V. Kovalenko](#); ETH Zurich, Switzerland

Metal halides offer unique structural engineerability of practically useful optical functionalities. In particular, low-dimensional compounds often exhibit broadband emission from highly localized, self-trapped excitons. These compounds exhibit strong temperature dependence of the photoluminescence lifetime. Using a range of tin based halides,  $[C(NH_2)_3]_2SnBr_4$  to  $Cs_4SnBr_6$  and  $(C_4N_2H_{14})_4SnI_6$ , we show the radiative-lifetime-based thermal imaging [1]. The fluorescence lifetimes are governed by the phonon-assisted de-trapping of self-trapped excitons, and their values can be varied over several orders of magnitude by adjusting the temperature (up to  $20 \text{ ns } ^\circ C^{-1}$ ). The sensitive range conveniently spans up to  $100 \text{ }^\circ C$ . The resulting thermometric precision is as high as  $0.013 \text{ }^\circ C$ , using conventional TSCPC fluorescence lifetime imaging (FLI). We also showcase a great utility of the time-of-flight technology (ToF-FLI) for cost-effective fluorescence lifetime imaging. In our ongoing work, we find that analogous Sb(III) compounds as thermoluminophores are much more environmentally stable than easily oxidizable Sn(II) compounds and can be used to increase spatial resolution [2]. We also present unicolor security tags composed of lifetime-tunable lead-halide perovskite nanocrystals that can be deciphered with both existing time-correlated TCSPC-FLI microscopy and a novel ToF-FLI prototype. In particular, we partially substituted formamidinium for ethylenediammonium {en} to generate “hollow” {en}FAPbBr<sub>3</sub> NCs, which exhibit same PL spectrum but 3-fold longer fluorescence lifetimes [3].

#### References

- [1] S. Yakunin et al. Nature Materials, 2019, 18, 846-852
- [2] V. Morad et al. submitted
- [2] S. Yakunin et al. submitted

**5:30 AM \*F.EL08.09.03**

**Halide Perovskite Nano—Increasing Long Term Stability of Perovskite Nanoparticles and Exploring Synergies with Conventional Quantum Dots** [Ivan Mora-Sero](#); Universitat Jaume I, Spain

Halide perovskite have revolutionized not just photovoltaic field but the complete optoelectronic devices spectra for their outstanding properties as low-non radiative recombination, high absorption coefficient, good transport properties, facile material synthesis and huge versatility and tunability. When halide perovskites become nano the properties of their nanoparticles are also exceptional with impressive photoluminescence quantum yields (PLQY) close or even as high as 100%. However, the long term stability of perovskite nanoparticles is the Achilles' heel of these materials. In this presentation we analyze as with an appropriated synthesis routes, affecting the nanoparticle capping or the perovskite composition, is possible to produce ultra-stable halide perovskite nanoparticles for more than 15 months. On the other hand the interaction of halide perovskite and colloidal semiconductor quantum dots can produce interesting synergistic interactions. We show that the interaction of PbS quantum dots and nanoplatelets can produce the stabilization of FAPbI<sub>3</sub> perovskite black phase and also the increase of the efficiency, stability and reproducibility of the photovoltaic devices prepared with of FAPbI<sub>3</sub> with embedded QDs. The use of PbS nanoplatelets also improve the long term stability of CsFAPbI<sub>3</sub> perovskite. Incorporation of PbS QDs allows the dramatic decrease of the annealing temperature for the formation of black FAPbI<sub>3</sub> phase perovskite thin film, from the 170C required without QDs to 85C when QDs are present. This result points the interest of Perovskite-Quantum Dot Nanocomposites, for further development of advanced optoelectronic devices.

**5:45 AM \*F.EL08.09.04**

**Stability Improvement of Perovskite Light-Emitting Diodes Through Composition Engineering and Surface**



**Passivation** Ni Zhao, Yuwei Guo, Nan Li and Yongheng Jia; Chinese University of Hong Kong, Hong Kong

The past few years have seen a significant improvement in the efficiency of organometal halide perovskite-based light emitting diodes (PeLEDs). However, the poor operation stability of the devices still hinders the commercialization of this technology for practical applications. In this talk I will introduce our recent efforts in understanding the degradation mechanisms of PeLEDs and developing material strategies to improve the device stability. Firstly, using time-of-flight secondary ion mass spectrometry we find the degradation of FAPbI<sub>3</sub>- based PeLEDs during operation is directly associated with ion migration and incorporation of binary alkali cations, i.e., Cs<sup>+</sup> and Rb<sup>+</sup>, in FAPbI<sub>3</sub> could suppress ion migration and significantly enhance the lifetime of PeLEDs. Combining experimental and theoretical approaches, we further reveal that Cs<sup>+</sup> and Rb<sup>+</sup> ions stabilize the perovskite films by locating at different lattice positions, with Cs<sup>+</sup> ions present relatively uniformly throughout the bulk perovskite while Rb<sup>+</sup> ions preferentially on the surface and grain boundaries, both leading to strong Coulomb interactions between the cations and the inorganic framework and consequently greatly enhanced device stability. Secondly, we introduced electroabsorption spectroscopy (EA) to study the degradation process of PeLEDs during operation and directly evaluate the stability of each functional layer (i.e., charge transporting layers and light-emitting layer) by monitoring their unique optical signatures. The EA measurements unambiguously reveal that the degradation of the PeLEDs occurs predominantly in the perovskite layer. With finite element method-based device modeling, we further point out that the degradation is likely to initiate from the interface between the perovskite and hole transporting layers and that the interface defects could further accelerate the degradation. Inspired by these observations, a surface treatment step is introduced to passivate the perovskite surface with phenylalkylammonium iodide. After molecular optimization, the PeLEDs exhibit an external quantum efficiency of 17.5% and a long T50 lifetime of over 125 hours under a high biasing current density of 100 mA cm<sup>-2</sup>.

**6:00 AM F.EL08.09.05**

**Bright and Effectual Perovskite Light Emitting Electrochemical Cells Leveraging Ionic Additives** Masoud Alahbakhshi<sup>1</sup>, Aditya Mishra<sup>1</sup>, Ross Haroldson<sup>1</sup>, Arthur Ishteev<sup>2</sup>, Jiyoung Moon<sup>1</sup>, Qing Gu<sup>1</sup>, Jason D. Slinker<sup>1</sup> and Anvar Zakhidov<sup>1</sup>; <sup>1</sup>The University of Texas at Dallas, United States; <sup>2</sup>ITMO University, Russian Federation

Perovskite light emitting diodes (PeLEDs) have drawn considerable attention for their favorable optoelectronic properties. Perovskite light emitting electrochemical cells (PeLECs) - devices that utilize mobile ions - have recently been reported but have yet to reach the performance of the best PeLEDs. We leveraged a poly(ethylene oxide) electrolyte and a lithium salt in CsPbBr<sub>3</sub> thin films to produce PeLECs of improved brightness and efficiency. In particular, we found that a single layer PeLEC from CsPbBr<sub>3</sub>:PEO:LiPF<sub>6</sub> with 0.5% wt. LiPF<sub>6</sub> produced bright (~15000 cd/m<sup>2</sup>) electroluminescence of improved efficiency (3.0 Lm/W). To understand this improved performance among PeLECs, we characterized these perovskite thin films with photoluminescence (PL) spectroscopy, scanning electron microscopy (SEM), atomic force microscopy (AFM), X-ray photoelectron spectroscopy (XPS), and X-ray diffraction (XRD). These studies revealed that this optimal LiPF<sub>6</sub> concentration improves electrical double layer formation, reduces the occurrence of voids, charge traps, and pinholes, and increases grain size and packing density.

**6:10 AM F.EL08.09.06**

**Perovskite Light Emitting Electrochemical Cells** Jason D. Slinker, Aditya Mishra, Masoud Alahbakhshi, Ross Haroldson and Anvar Zakhidov; The University of Texas at Dallas, United States

Solution processed organic-inorganic metal halide perovskites with the chemical formula ABX<sub>3</sub> have emerged as next generation light emitting materials. Recently, ion migration has been demonstrated to significantly influence the performance of metal halide perovskite devices. The interplay between electronic and ionic currents provides a new pathway to utilize metal halide perovskites as emissive materials in light emitting electrochemical cells (PeLEC). Light emitting electrochemical cells (LECs) utilize ionic motion to generate electrical double layers for high carrier injection and potential doping effects to achieve efficient operation in single layer devices. Recently, our group demonstrated bright and effectual PeLECs with simple single layer architectures, leveraging a polyelectrolyte and a lithium ionic additive (LiPF<sub>6</sub>) to achieve devices with a high maximum luminance of >10000 cd m<sup>-2</sup> and operation exceeding 100 hours over 800 cd m<sup>-2</sup>. To understand this improved performance among PeLECs, we characterized these perovskite thin films with photoluminescence (PL) spectroscopy, scanning electron microscopy (SEM), atomic force microscopy (AFM), X-ray photoelectron spectroscopy (XPS), and X-ray diffraction (XRD). These studies revealed that this optimal LiPF<sub>6</sub> concentration improves electrical double layer formation, reduces the occurrence of voids, charge traps, and pinholes, and increases grain size and packing density. Electrochemical impedance spectroscopy with equivalent circuit modeling revealed that electrical double layer widths are minimized with an optimal LiPF<sub>6</sub> concentration and inversely correlate with efficient performance. These results demonstrate that an optimal LiPF<sub>6</sub> concentration improves stability and efficiency through improved double layer formation and retention

of perovskite structure.

#### 6:20 AM F.EL08.09.07

**Modulation of Growth Kinetics and Dimensional Control of Vacuum-Deposited Cs-Pb-Br Perovskite for Efficient Light-Emitting Diodes** Mingue Shin<sup>1</sup>, Ho Seung Lee<sup>1</sup>, Young Chul Sim<sup>1</sup>, Yong-Hoon Cho<sup>1</sup>, Kyung Cheol Choi<sup>1</sup>, Sung-Wook Nam<sup>2</sup>, Aditya Sadhanala<sup>3</sup>, Ravichandran Shivanna<sup>3</sup>, Miguel Anaya<sup>3</sup>, Alberto Jimenez-Solano<sup>4</sup>, Hyewon Yoon<sup>1</sup>, Seokwoo Yeon<sup>1</sup>, Samuel D. Stranks<sup>3</sup>, Robert Hoyer<sup>3</sup> and Byungha Shin<sup>1</sup>; <sup>1</sup>Korea Advanced Institute of Science and Technology, Korea (the Republic of); <sup>2</sup>Kyungpook National University, Korea (the Republic of); <sup>3</sup>University of Cambridge, United States; <sup>4</sup>Max Plank Institute for Solid State Research, Germany

Due to exceptional color purity and good thermal stability, all-inorganic halide perovskite (CsPbBr<sub>3</sub>) has been attracting interest as the next-generation materials for light-emitting diodes (LEDs). However, its low exciton binding energy is one of the factors limiting luminescence efficiency and spatial confinement of excitons is a promising way to resolve this issue. Here, we present two strategies of spatially confining excitons in vacuum-deposited Cs-Pb-Br light emitters. In the first part, we have modulated growth kinetics unique to thermal evaporation to form fine-grain-structured CsPbBr<sub>3</sub> polycrystalline films. By adjust the deposition rate, nucleation rate was controlled, which then influenced the final grain structure. With this strategy, we demonstrate a green light-emitting (at 524 nm) LED with a maximum current efficiency of 1.07 cd/A and an extremely narrow electroluminescence spectrum of 18 nm—the results that highlight the potential of vacuum-processed CsPbBr<sub>3</sub> films for high efficiency LEDs. In the second part, we have controlled dimensionality of by adjusting the flux ratio of the two source materials, CsPb and PbBr<sub>2</sub>, to deposit Cs-Pb-Br films. Under the excess flux of CsPb the so-called zero-dimensional Cs<sub>4</sub>PbBr<sub>6</sub> formed, producing strong green emission with high photoluminescence quantum yield close to 90%. The green emission from Cs<sub>4</sub>PbBr<sub>6</sub> is unusual considering its large bandgap of 3.9 eV. Through in-depth transmission electron microscopy study and optical measurement such as photothermal deflection spectroscopy and photoluminescence contour map, we identified the inclusion of trace amount of CsPbBr<sub>3</sub> "impurities" as the source of the green emission. We have achieved a 60-fold improvement in external quantum efficiency from an LED with a CsPbBr<sub>3</sub>-embedded Cs<sub>4</sub>PbBr<sub>6</sub> light emitter compared to the control device with CsPbBr<sub>3</sub>. Details of the materials characterization and device analysis will be discussed.

#### 6:30 AM F.EL08.09.08

**Origin of High Piezoelectricity and Energy Harvesting Performance in Inorganic Halide Thin Films** Da Bin Kim and Yong Soo Cho; Yonsei University, Korea (the Republic of)

Halide perovskite materials have been actively studied to chase other suitable applications with unveiled characteristics. Piezoelectricity-related applications using the halide perovskites are another area that may be suitable with unique potentials. However, the studies on piezoelectricity of the halide perovskites are very limited probably due to the difficulty in fabricating quality thin films or bulk specimens although the possession of ferroelectricity of the materials has been theoretically estimated with calculated polarization values in literature. Here, we report the high piezoelectricity of representative inorganic halides, CsPbBr<sub>3</sub>, which was optimized with poling process, and their energy harvesting characteristics in the form of thin film. This is the very first report of revealing effective piezoelectric coefficient for any inorganic halide perovskite and demonstrating piezoelectric energy harvesting performance using inorganic halides. So far, the piezoelectric coefficients of 6-25 pm/V were reported only for the methylammonium lead halides (MAPbX<sub>3</sub>) or formamidinium lead halides (FAPbX<sub>3</sub>)-based hybrid perovskite thin films. Our highest value of ~40.3 pm/V for the optimized CsPbBr<sub>3</sub> with film thickness and poling field was chased to understand origin of the high piezoelectricity via structural estimation associated with the changes in bonding angles. As expected from the high piezoelectricity, the electromechanical energy-harvesting performance was very competitive, such as 16.4 V output voltage and 604 nA output current for a larger size sample of 5 cm<sup>2</sup>. The values obtained for the inorganic CsPbBr<sub>3</sub> thin films are the highest ones compared to any reported values for inorganic-organic hybrid halide perovskite thin films.

#### 6:40 AM F.EL08.09.10

**Charge Transport in Lead Halide Perovskite Field-Effect Transistors** Amita Ummadisingu, Youcheng Zhang and Henning Sirringhaus; University of Cambridge, United Kingdom

In recent years, lead halide perovskites have been found to be interesting candidates for various applications such as solar cells and light-emitting diodes, due to their excellent optical and electronic properties(1, 2). However, a deeper understanding of the intrinsic charge transport in thin films of these materials is currently lacking and it is essential for the bottom-up design of opto-electronic devices(2). Here, we fabricated three-dimensional (3D) perovskite thin film field-effect transistors (FETs), and employed them to investigate the temperature-dependent charge transport. We explored several state-of-the-art 3D

perovskite compositions starting with methylammonium lead iodide, followed by numerous triple cation and Rb-incorporated perovskite compositions(3). A significant issue with these materials is the migration of ions and this results in partial screening of the applied gate field which gives a lower field-effect mobility than expected in these FETs(4). Initial trials resulted in FETs that did not display any modulation of the drain current with the gate voltage due to ion migration. This problem was suppressed through extensive optimization of both the deposition methods and the compositions using Design of Experiments (DOE) principles. The transfer characteristics of optimized FET devices show that these devices exhibit n-type behavior and low hysteresis even at room temperature. One of the triple cation compositions shows the best performance and it exhibits a good saturation electron field-effect mobility and an on/off ratio of  $\sim 10^4$  at room temperature. Our results bring us closer to achieving the high field-effect mobility values predicted for lead halide perovskites and in understanding the charge transport mechanism in thin films of these materials.

## References

1. Green, M. A.; Ho-Baillie, A.; Snaith, H. J. The emergence of perovskite solar cells. *Nature Photonics* 2014, **8**, 506-514.
2. J. Wang *et al.*, Investigation of electrode electrochemical reactions in  $\text{CH}_3\text{NH}_3\text{PbBr}_3$  perovskite single-crystal field-effect transistors. *Advanced Materials* 2019, **31**, 1902618.
3. M. Saliba *et al.*, Incorporation of rubidium cations into perovskite solar cells improves photovoltaic performance. *Science* 2016, **354**, 206-209.
4. S. P. Senanayak *et al.*, Understanding charge transport in lead iodide perovskite thin-film field-effect transistors. *Science Advances* 2017, **3**, e1601935.

## 6:50 AM F.EL08.09.11

**High-Quality  $\text{CuBi}_2\text{O}_4$  Photoelectrodes with Increased Stability by Rapid Thermal Processing of  $\text{Bi}_2\text{O}_3/\text{CuO}$  Grown by Pulsed Laser Deposition** Ronen Gottesman, Angang Song, Igal Levine, Maximilian Krause, Nazmul Islam, Daniel Abou-Ras, Thomas Dittrich, Roel Van de Krol and Abdelkrim Chemseddine; Helmholtz-Zentrum Berlin für Materialien und Energie, Germany

A new approach for fabricating high-quality ternary photoelectrodes such as  $\text{CuBi}_2\text{O}_4$  will be presented. Pulsed laser deposition (PLD)<sup>1</sup> is used to deposit the binary oxides  $\text{Bi}_2\text{O}_3$  and  $\text{CuO}$  on FTO substrates, and rapid thermal processing (RTP)<sup>2</sup> is used to achieve an efficient solid-state reaction between the two oxide films. It is shown that when  $\text{Bi}_2\text{O}_3$  is deposited first, the thin film photoelectrodes are comprised of single-phase, compact, crystalline, and well-defined  $\text{CuBi}_2\text{O}_4$  particles. A comparative study with conventional furnace heating reveals the significance of radiative heating in the processing of complex metal oxides photoelectrodes. Additionally, the much shorter heating times enable the use of FTO substrates at temperatures up to 650 °C, also resulting in a low thermal budget (the product of process temperature and processing duration at elevated temperatures). In a comparative study with  $\text{CuBi}_2\text{O}_4$  photoelectrodes produced by spray-pyrolysis, a benchmark synthesis technique of photoactive materials<sup>3</sup> and complex metal-oxide photoelectrodes,<sup>4</sup> the  $\text{CuBi}_2\text{O}_4$  layer fabricated by PLD + RTP photoelectrodes featured superior electronic properties, which were sustained even in cases of a secondary oxide co-existence in the film by deliberately altering the Bi:Cu stoichiometry ratio during the PLD stage. The photoelectrodes have shown an efficient charge separation, low tail energies, and band-gap energy virtually identical to that of a  $\text{CuBi}_2\text{O}_4$  single crystal, shown by modulated surface photovoltage analysis<sup>5</sup> and confocal Raman microscopy. Furthermore, bare photoelectrodes, without the addition of electron scavengers, protection layers, or catalysts, exhibited exceptional photoelectrochemical stability, substantially improving the prospects of implementing  $\text{CuBi}_2\text{O}_4$  photoelectrodes in photoelectrochemical devices towards high solar-to-hydrogen efficiency. References: (1) Christen, H. M.; Eres, G. Recent Advances in Pulsed-Laser Deposition of Complex Oxides. *J. Phys. Condens. Matter* 2008, **20** (26), 264005. (2) Fiory, A. T. Rapid Thermal Processing for Silicon Nanoelectronics Applications. *J. Miner. Met. Mater. Soc.* 2005, **57** (6), 21-26. (3) Hu, J.; Gouda, L.; Kama, A.; Tirosh, S.; Gottesman, R. Radiative Recombination Changes under Light-Soaking in  $\text{CsPbBr}_3$  Films on  $\text{TiO}_2$  and Insulating Glass Contacts: Interface vs. Bulk Effects. *ACS Appl. Energy Mater.* 2019, **2**, 3013-3016. (4) Song, A.; Plate, P.; Chemseddine, A.; Wang, F.; Abdi, F.; Wollgarten, M.; van de Krol, R.; Berglund, S.  $\text{Cu:NiO}$  as a Hole-Selective Back Contact to Improve the Photoelectrochemical Performance of  $\text{CuBi}_2\text{O}_4$  Thin Film Photocathodes. *J. Mater. Chem. A* 2019, **7**, 9183-9194. (5) Chen, R.; Fan, F.; Dittrich, T.; Li, C. Imaging Photogenerated Charge Carriers on Surfaces and Interfaces of Photocatalysts with Surface Photovoltage Microscopy. *Chem. Soc. Rev.* 2018, **47** (22), 8238-8262.

SESSION F.EL08.10/F.EL06.07/F.EN02.08: Joint Session: Emerging Tandem PV Technologies  
On Demand Abstracts Available for Viewing Starting Saturday Morning, November 21, 2020  
F-EL08

**5:00 AM \*F.EL08.10/F.EL06.07/F.EN02.08.01**

**Advances in Material Properties for Perovskite-Perovskite Tandems** Giles Eperon<sup>1,2</sup>; <sup>1</sup>Swift Solar, United States; <sup>2</sup>National Renewable Energy Laboratory, United States

Multijunction all-perovskite solar cells offer a route towards efficiencies of III-V materials at low cost by combining the advantages of low thermalization loss in multijunction architectures with the beneficial properties of perovskites - namely low processing cost, high throughput fabrication, and compatibility with flexible substrates. Here, I will discuss why flexible all-perovskite tandems are a very attractive iteration of the perovskite technology. I will focus on what is needed to make a good perovskite-perovskite tandem on a flexible substrate, and the advances that we have made towards this goal. I will cover advances including a) the development and understanding of wide bandgap materials that leverage a novel bandgap-tuning strategy (without increasing bromine, hence avoiding significant phase segregation) to reach the ideal bandgaps for all-perovskite tandems, resulting in efficient devices that are stable to the combined stresses of heat and light; b) advances that we have made in interlayer design, working towards more ideal material properties for reducing shunt resistance; and c) the integration of these approaches to develop >23% efficient monolithic all-perovskite tandems on rigid substrates and 21% efficient devices on flexible plastic substrates.

**5:15 AM \*F.EL08.10/F.EL06.07/F.EN02.08.02**

**The Many Faces of Characterization in Developing a Commercial Perovskite on Silicon Tandem Solar Cell** Laura Miranda; Oxford PV, United Kingdom

Perovskite solar absorbers have the potential to disrupt the photovoltaic industry predominantly with their simultaneous promise of high efficiency and low cost. Whilst these two properties ensure a steady stream of research and development opportunities, commercial scaling requires assuring that the devices are sufficiently characterized to be confident of their long-term performance. Oxford PV has been addressing the challenges associated with commercially scaling its perovskite on silicon tandem solar cell design. Key practices that have been adopted during the development of highly efficient, reliable, and cost-competitive solar cells are the use of rigorous characterization tools and techniques, and the development of necessary models. This talk will highlight some of the challenges and considerations associated with bringing perovskite on silicon tandem solar cells from a laboratory prototype to a commercial product ready for manufacturing and how characterization has shaped and continues to inform that process.

**5:30 AM \*F.EL08.10/F.EL06.07/F.EN02.08.03**

**Passivation Strategies and Interlayers for Perovskite-Based Tandem Photovoltaics** Ulrich W. Paetzold, Saba Gharibzadeh, Tobias Abzieher, Ihtezaz M. Hossain, Hang Hu, Thomas Feeney, Somayeh Moghadamzadeh, Mahdi Malekshahi Byranvand,, Bahram Abdollahi Nejad, Paul Fassel and Bryce Sydney Richards; Karlsruhe Institute of Technology, Germany

Single-junction crystalline silicon solar cells dominate the photovoltaics market today, but their power conversion efficiencies (PCEs) are approaching the practical limit for this technology. The emergence of hybrid organic-inorganic metal halide perovskite semiconductors over the past decade has opened a window of opportunity to advance the performance of the market-dominating photovoltaic technologies through the development of tandem solar cells. These tandem solar cells promise high PCEs (>33%). To reach this landmark, a number of scientific and technological challenges related to high-efficiency perovskite-based tandem solar cell architectures, stable and high-quality perovskite semiconductor materials, and light management concepts need to be addressed. In this presentation, our progress on passivation strategies and novel interlayers to reduce the voltage losses in wide-bandgap and low-bandgap perovskite solar cells (PSCs), and in turn to increase the PCE of perovskite-based tandem photovoltaics, will be presented.

The search for efficient passivation interlayers for wide-bandgap perovskite top solar cells in *n-i-p* architecture directed our research in the past towards solution-processed 2D/3D perovskite heterostructures. Making use of these heterostructures for interface passivation, wide-bandgap PSCs ( $E_g \sim 1.72$  eV) with record open-circuit voltage for this bandgap and very high PCEs of up to 19.4% were demonstrated [1]. The reduced voltage deficit is a result of the decreased non-radiative recombination losses at the perovskite/hole-transport layer (HTL) interface. The solution-processed 2D/3D perovskite heterostructure is compatible with 3D perovskite absorber layers of a wide range of bandgaps ( $1.65$  eV  $\leq E_g \leq 1.85$  eV) [2]. Using this strategy in 4-terminal perovskite/silicon and perovskite/CIGS tandem solar cells, high PCEs > 27% [3], and > 25% [2] were demonstrated, respectively, thereby significantly exceeding the record PCEs reported for the respective single-junction solar cell technologies.

Beyond these past results, at the MRS fall meeting we will further present our latest work on novel interlayers and

passivation strategies to minimize the voltage loss in wide-bandgap ( $1.65 \text{ eV} \leq E_g \leq 1.75 \text{ eV}$ ) as well as low-bandgap ( $E_g \sim 1.26 \text{ eV}$ ) perovskite solar cells in *p-i-n* architecture. The *p-i-n* architecture is a key to realize high-performance 2-terminal perovskite/silicon as well as perovskite/perovskite tandem solar cells. Moreover, we will present a novel route to deposit uniform ultra-thin polymer passivation layers onto perovskite thin films by chemical vapor deposition (CVD) [4]. The CVD polymerization promises reliable, scalable, and homogeneous deposition for future large-area processing of perovskite-based tandem solar cells.

#### References:

- [1] Gharibzadeh, S. *et al.* Record Open-Circuit Voltage Wide-Bandgap Perovskite Solar Cells Utilizing 2D/3D Perovskite Heterostructure. *Adv. Energy Mater.* **9**, 1–10 (2019).
- [2] Gharibzadeh, S.; Hossain I. M. *et al.* 2D/3D Heterostructure for Semitransparent Perovskite Solar Cells with Engineered Bandgap Enables Efficiencies Exceeding 25% in Four-Terminal Tandems with Silicon and CIGS. *Adv. Funct. Mater.* **30**, (2020).
- [3] Duong, T. *et al.* High Efficiency Perovskite-Silicon Tandem Solar Cells: Effect of Surface Coating versus Bulk Incorporation of 2D Perovskite. *Adv. Energy Mater.* **10**, 1903553 (2020).
- [4] Malekshahi Byranvand M.; Behboodi-Sadabad F. *et al.* Chemical Vapor Deposited Polymer Layer for Efficient Passivation of Planar Perovskite Solar Cells. *submitted*

#### 5:45 AM \*F.EL08.10/F.EL06.07/F.EN02.08.05

**Towards Highly Efficient Monolithic 2- and 3-Terminal Perovskite Silicon Tandem Solar Cells** Lars Korte, Eike Koehnen, Philipp Wagner, Philipp Tockhorn, Marko Jost, Amran Al-Ashouri, Lukas Kegelmann, Marcel Roß, Bernd Stannowski and Steve Albrecht; Helmholtz-Zentrum Berlin für Materialien und Energie, Germany

Integrating metal halide perovskite top cells with crystalline silicon (c Si) bottom cells into monolithic tandem devices has recently attracted increased attention due to the high efficiency potential of these cell architectures. To further increase the tandem device performance to a level well above the best single junctions, optical and electrical optimizations as well as a detailed device understanding for such architectures need to be developed [1]. Here we present our recent results on such monolithic tandem cells in the common 2-terminal (2T) as well as in a novel 3-terminal (3T) contacting scheme.

In the 2T design, we recently demonstrated a certified power conversion efficiency (PCE) of 29.15% [2,3]. I will discuss some key elements to this result: using a silicon heterojunction cell electron contact on the rear side, enabling the integration of a perovskite top cell in the *p-i-n* configuration; employing self-assembled monolayers (SAMs) as hole selective contacts for further reduction of non-radiative recombination losses, etc. With the latter, efficiencies of up to  $\sim 21\%$  were demonstrated for *p-i-n* perovskite single junctions [3].

In 3T tandems, one of the three contacts is shared by both subcells, allowing for the individual operation of both subcells in a monolithic device with a single substrate, thus combining the characteristic advantages of 2T and 4-terminal (4T) devices: high combined photogeneration currents as in state-of-the-art 2T tandems, and ideally independent electrical operation similar to 4T tandems, making the cell more robust against varying spectra. I will discuss our recent proof-of-concept study [4], demonstrating a 3T perovskite/silicon tandem cell by manufacturing an *n-i-p* perovskite top cell on an interdigitated back contact (IBC) silicon heterojunction solar cell. In our proof-of-concept device, the combined PCE of  $\sim 17\%$  is still limited both optically and electrically, and it will be discussed how optimizations of the cell stack can bring this architecture to a PCE level comparable to 2T tandems. Furthermore, I will demonstrate that the subcells can indeed be operated largely independently at their individual maximum power points, allowing to extract the maximum power output for varying spectral conditions similar to 4T cells. A minimized series resistance at the shared electron contact on the cell's rear side is identified as the crucial parameter for independent operation of the subcells, and I will discuss pathways to approach the simulated efficiency potential by an optimized device design.

#### References:

- [1] Jost, Kegelmann, Korte, Albrecht, *Adv. Energy Materials*, 2020, doi: 10.1002/aenm.201904102
- [2] NREL Best Research-Cell Efficiency Chart, <https://www.nrel.gov/pv/cell-efficiency.html>
- [3] Köhnen, Jost, Stannowski, Albrecht *et al.*, *Sustainable Energy and Fuels*, doi: 10.1039/C9SE00120D
- [3] Al-Ashouri, Magomedov, Korte, Albrecht *et al.*, *En. Env. Sci*, 2019, doi: 10.1039/C9EE02268F
- [4] Tockhorn, Wagner, Korte *et al.*, *ACS Appl. En. Mat.*, 2020, doi: 10.1021/acsaem.9b01800

#### 6:00 AM \*F.EL08.10/F.EL06.07/F.EN02.08.06

**Solution Processed Perovskite Subcell in Monolithic Perovskite/Si Tandem Solar Cells and Their Cost and Stability Concerns** Qi Chen<sup>1</sup> and Huanping Zhou<sup>2</sup>; <sup>1</sup>Beijing institute of Technology, China; <sup>2</sup>Peking University, China

Among all commercialization routes for perovskite photovoltaics (PV), the perovskite/Si tandem is of particular interest as it capitalizes the mature silicon industry with decades of experience. Here we report low-temperature solution process for efficient two-terminal perovskite/Si tandem solar cells, wherein electrical and optical properties of the tunneling junction are carefully modulated. Moreover, we improve materials stability by introducing  $\text{Eu}^{2+}/\text{Eu}^{3+}$  “redox shuttle” to suppress the  $\text{Pb}^0/\text{I}^0$  impurities which inevitably occurred during device operation. In addition, we carefully analyze the cost of tandem devices in terms of leveled cost of energy (LCOE) by adopting the “bottom-up cost model”. It reveals perovskite PV exhibit low materials cost, which reduces the LCOE substantially in tandem devices. We conclude that further efforts are required to simultaneously improve the efficiency and lifetime of perovskite modules, which ultimately endows the competitiveness of perovskite tandem solar cells.

SESSION F.EL08.11/F.EL06.04: Joint Session: Contacts and Interfaces in Halide Perovskite Devices  
On Demand Abstracts Available for Viewing Starting Saturday Morning, November 21, 2020  
F-EL08

**5:00 AM \*F.EL08.11/F.EL06.04.01**

**Implications of Defects in Defect Tolerant Materials—Understanding Surfaces in Metal Halide Perovskite Solar Materials, Device and Related Systems** Joseph J. Berry<sup>1,2</sup>; <sup>1</sup>National Renewable Energy Laboratory, United States; <sup>2</sup>University of Colorado Boulder, United States

Photovoltaic (PV) devices based on metal halide perovskite (MHP) absorbers have reached outstanding performance over the past few years, surpassing power conversion efficiency of over 25% for lab cells and with large area devices in excess of 16%. For the solar application stability, the most demanding requirement to assess for PV, remains the outstanding issue. The problem of stability motivates basic science driven work on MHP based PV at NREL. Material and device insight can enable MHP PV stability along with the associated opportunities to further improve efficiency, scalability and realize unique device architectures. This talk will highlight work at NREL to develop understanding of defects and interfaces in MHPs and what these experiments indicate regarding the requirements to enhance stability of HPSCs. Discussion will focus on efforts to more carefully understand the implications of processing on a range of defects and interfaces to provide a foundation for enabling the technological requirements for PV and other devices. Ongoing efforts make, measure and ultimately control defects via material formation and processing in the context of high-volume manufacturing will also be touched upon. Hypothesized links between device architecture choices, questions regarding materials integration and coupling of formation along with resulting defects to stability will be discussed. More importantly approaches to move from hypothesis to insight using different experimental approaches will be presented. Work at NREL along these lines to provide critical insight regarding interface formation and passivation that appears to have direct implications for performance and its evolution over time in the resulting devices will be presented. New approaches to understanding the critical physical, chemical and electronic properties to provide predictive insight will also be discussed.

**5:15 AM \*F.EL08.11/F.EL06.04.02**

**Passivated Interfaces and Surface Recombination Velocities in Mixed Cation Mixed Halide Perovskites** David S. Ginger; University of Washington, United States

Surfaces and charge-extracting contacts remain major sources of non-radiative recombination loss; limiting the performance of perovskite PV compared to theoretical limits. We investigate mixed-cation mixed-halide perovskites and demonstrate that, with chemical surface passivation, they can achieve  $>4 \mu\text{s}$  minority carrier lifetimes, and  $>20\%$  external PL quantum yields (PLQY), and nearly single-exponential decay kinetics. This high PLQY observed corresponds to  $\sim 97\%$  of the Shockley-Queisser theoretical quasi-fermi level splitting, a first for MA-free mixed-cation mixed-halide compositions. The high PLQY and long PL lifetimes allow us to measure average surface recombination velocities (SRV)  $<10\text{cm/s}$ , with a champion low of  $\sim 1\text{cm/s}$  (a conservative estimate). We show how such improvements in SRV should lead to an absolute improvement in PCE of  $>4\%$  even with the best of contact alignments. We investigate different MA-free high bandgap compositions, including bandgaps relevant for tandem applications (1.7-1.8eV), and demonstrate performance improvements across all these compositions with our surface passivation strategy. Lastly, using a combination of surface characterization techniques, we show Lewis base interactions of the passivating agent with the perovskite surfaces.

**5:30 AM \*F.EL08.11/F.EL06.04.03**

**Vacuum Deposited Perovskite Solar Cells with Multilayer Charge Selective Contacts** Michele Sessolo, Sang-Hyun

Chin, Chris Dreessen, Lidón Gil-Escrig, Ana M. Igual-Muñoz, Beom-Soo Kim, Daniel Perez-del-Rey, Isidora Susic, Kassio P. Zaroni and Henk Bolink; Universitat de València, Spain

In solar cells, perovskite films are typically sandwiched in between charge selective layers, either organic or inorganic semiconductors, as well as their combinations. Electron/hole selectivity results from appropriate alignment of the electronic transport levels of these layers with the electronic bands of the perovskite. While transport layers should efficiently extract the photogenerated charge carriers, they should also not quench the perovskite luminescence to avoid a reduction of the quasi-Fermi level splitting and hence the maximum attainable photovoltage. Finally, ohmic charge injection/extraction and a high built-in potential are desirable to maximize fill factor both in single junction and tandem perovskite solar cells. We will review these design rules using fully vacuum deposited solar cells as a platform, as every layer can be fine-tuned or exchanged without substantially alter the device fabrication. The focus will be on wide bandgap, mixed halide perovskite solar cells, which suffer from a higher voltage deficit as compared to narrow bandgap analogous. We will highlight the importance of using non-quenching, energetically-matched hole and electron transport layers in order to reduce non-radiative charge recombination losses. Novel strategies and multilayers structures (including inorganic, organic and ionic compounds) to improve the device functioning will be presented. The implication for the perovskite compositional stability as well as for the device lifetime will also be discussed.

**5:45 AM \*F.EL08.11/F.EL06.04.04**

**Approaches to Defect Mitigation in Halide Perovskites** Nakita K. Noel; Princeton University, United States

Within a decade, there has been a surge of interest into halide perovskite semiconductors. With tuneable bandgaps, versatile and facile deposition processes and excellent optoelectronic properties, these materials have found applications in photovoltaics (PV), broad-spectrum photodetectors, light-emitting diodes and lasers. While research into using these materials for emission and X-ray detection applications is now beginning to surge; currently, halide perovskites are most well known for their remarkable PV performance, with perovskite solar cells achieving certified power conversion efficiencies exceeding 25% in a remarkably short developmental timescale. Despite the truly impressive device performance, these materials have not yet reached their full potential. The major obstacle to this is an incomplete understanding of crystallisation processes, as well as defects which exist on the surfaces and interfaces of perovskite thin-films. Deficiencies at these interfaces, likely formed during the crystallisation process, are responsible for the major losses in perovskite-based optoelectronic devices; limiting charge extraction, increasing non-radiative recombination, contributing to hysteresis and increasing the voltage-loss of perovskite photovoltaics. Herein, I will present various effective strategies to reduce the defect densities of perovskite films and thus improve the performance of perovskite optoelectronic devices. First, I will discuss how manipulating precursor solutions can have significant impact on the quality of the perovskite films, through enabling reduced defect density. Consequently, this is one approach which can be used to boost device performance. Next, I will focus on a strategy in which we extrinsically modify the bottom interface of perovskite solar cells such that the crystallization of the perovskite yields films with fewer defects. Specifically, we show that ionic liquids can have a dramatic effect on the interfacial trap density in a perovskite solar cell. And finally, I will illustrate an approach in which we manipulate the charge-carrier density in the perovskite thin-film after its fully crystallized. We utilise molecular dopants to significantly alter the interfacial energetics in order to suppress non-radiative recombination losses. As a result, we observe a boost in both performance and stability. Importantly, these interface modification strategies can be used in tandem, resulting in further improvements in device efficiency. The utility of these defect mitigation strategies can readily be applied beyond perovskite PV and is likely to also improve the performance of a range of other perovskite-based optoelectronic devices.

**6:00 AM F.EL08.11/F.EL06.04.05**

**Transparent Conducting Oxides for Upscalable Solar Cells—Assessing Deposition Methods** Yury Smirnov<sup>1</sup>, Laura Schmengler<sup>1</sup>, Riemer Kuik<sup>1</sup>, Pierre-Alexis Repecaud<sup>1</sup>, Mehrdad Najafi<sup>2</sup>, Sjoerd Veenstra<sup>2</sup>, Erkan Aydin<sup>3</sup>, Stefaan De Wolf<sup>3</sup> and Monica Morales-Masis<sup>1</sup>; <sup>1</sup>University of Twente, Netherlands; <sup>2</sup>TNO-Solliance, Netherlands; <sup>3</sup>King Abdullah University of Science and Technology (KAUST), Saudi Arabia

Transparent electrodes are essential components of several kinds of high-efficiency solar cells. The photovoltaic devices working in the broadband spectra, from the ultraviolet (UV) to the near-infrared (NIR), require minimized parasitic absorption and high conductivity for these electrodes. Transparent conductive oxide (TCO) thin films are widely accepted choices for such applications. Among various successful TCOs, recently, Zr-doped indium oxide (IZrO) has been demonstrated as a broadband transparent and conductive material suitable for silicon heterojunction (SHJ) and silicon/perovskite tandem solar cells.<sup>1,2</sup> The main advantage of IZrO is combining specifications of wide bandgap, high carrier density, and high electron mobility in the same material.

Magnetron sputtering is by far the most established technique to fabricate TCO layers. During sputtering target material is

removed in a ballistic process that sensitively depends on many interconnected processing parameters. This makes a stoichiometric transfer of target material challenging, while high kinetic energies of the arriving species may damage sensitive functional layers beneath. Conversely, in Pulsed Laser Deposition (PLD), the energy source for material ablation is physically decoupled from the vacuum equipment. This favors the stoichiometric transfer of the target material as well as provides a larger choice for deposition pressures and thermalizing the arriving species.

Despite these advantages, PLD is still considered an exotic fabrication method within the photovoltaic community due to the common concerns about the scalability of the technique reasoned by the small sample size for uniform coating and low deposition rates. In fact, significant progress in the upscaling of PLD<sup>3</sup> has already allowed fabrication of high-quality films by on 200 mm circular wafers and fabrication of superconducting tape with deposition rates  $> 750 \text{ nm/min}^4$ , which is considerably high deposition rate.

In our work, we introduce wafer-scale (4") room-temperature fabrication of high-mobility IZrO by PLD with deposition rates on par ( $>3 \text{ nm/min}$ ) with lab-scale RF sputtering equipment. We studied the optoelectronic properties and microstructure of the films and made a comparison with IZrO films grown by RF sputtering, both fabricated from an IZrO solid target with the same composition.

X-ray diffraction (XRD) reveals that as-deposited IZrO films are amorphous with small embedded nanocrystals. Their orientation is preserved as the preferred one after solid-phase crystallization at  $200 \text{ }^\circ\text{C}$ . IZrO films exhibit excellent optoelectrical properties combining low absorptance ( $<10\%$ ) in the measured range (300-1500 nm) with high mobility ( $>60 \text{ cm}^2/\text{Vs}$ ) leading to impressive sheet resistivity ( $R_{\text{sh}}$ ) of  $<20 \text{ Ohm/sq}$  for a 100-nm PLD grown film.

When applied as a front electrode in solar cells, IZrO enables high short circuit currents and the possibility to reduce the amount of indium by reducing the thickness of the films compared to standard ITO, which is critical considering the large scale utilization of such materials. On the other hand, higher deposition pressures during PLD fabrication offer a promising way to mitigate the sputter-induced damage for the deposition of rear transparent electrodes on top of sensitive functional layers as in the perovskite solar cells, which opens new opportunities for the development of high-efficiency tandem solar cells.

## References

1. M. Morales-Masis *et al.*, *IEEE J. Photovoltaics*, vol. 8, no. 5, p. 1202–1207, 2018.
2. E. Aydin *et al.*, *Advanced Functional Materials*, vol. 29, no. 25, p. 1901741, 2019.
3. J. A. Greer, *Journal of Physics D: Applied Physics*, vol. 47, no. 3, p. 034005, 2013.
4. S. Lee *et al.*, *Superconductor Science and Technology*, vol. 27, no. 4, p. 044022, 2014.

## 6:10 AM F.EL08.11/F.EL06.04.06

**Overcoming Redox Reactions at Perovskite/Nickel Oxide Interfaces to Boost Voltages in Perovskite Solar Cells** Caleb C. Boyd<sup>1</sup>, R. C. Shallock<sup>2</sup>, Neal R. Armstrong<sup>2</sup> and Michael McGehee<sup>3</sup>; <sup>1</sup>Stanford University, United States; <sup>2</sup>The University of Arizona, United States; <sup>3</sup>University of Colorado Boulder, United States

Metal halide perovskite solar cells have largely fulfilled their potential of combining III-V-like optoelectronic properties with low-cost, solution-processing deposition techniques, achieving single-junction power conversion efficiencies (PCEs)  $>25\%$ . A semiconducting nickel oxide ( $\text{NiO}_x$ ) thin film is a highly desirable wide bandgap hole harvesting contact for perovskite solar cells and organic solar cells because it is low-cost, stable, and readily scalable. (1) Perovskite solar cells with  $\text{NiO}_x$  HTLs have delivered some of the best reported stability results under a variety of stressors, including the  $85^\circ\text{C}/85\%$  relative humidity damp heat test, temperature cycling from  $-40^\circ\text{C}$  to  $85^\circ\text{C}$ , and extended operational stability at elevated illumination and temperature. (2, 3) However, perovskite solar cells made with  $\text{NiO}_x$  HTLs typically result in lower open-circuit voltages ( $V_{\text{OC}}$ ) compared to ultra-thin, undoped organic hole transport layers, which are more expensive and present problems for both scalability and stability. Enhancing the  $V_{\text{OC}}$  and increasing efficiency of  $\text{NiO}_x$ -based devices will directly result in a decreased photovoltaic module cost ( $\$/\text{W}$ ).

Here, we identify a surface-assisted electron transfer-proton transfer (ET-PT) mechanism at the  $\text{NiO}_x$ /perovskite interface leading to barriers for hole harvesting and device  $V_{\text{OC}}$  loss. Specifically, under-coordinated metal cation sites ( $\text{Ni}^{2+3+}$ ) act both as a Lewis acid/oxidant towards dissociated lead halide precursors (i.e. I) and as a Brønsted base (proton-acceptor) with protonated amine precursors, forming A-site deficient – and therefore  $\text{PbI}_{2-x}\text{Br}_x$ -rich – perovskite at the perovskite/ $\text{NiO}_x$  interface. This defective perovskite region both increases recombination at the interface and acts as a hole extraction barrier, resulting in device  $V_{\text{OC}}$  loss.

We demonstrate the elimination of the extraction barrier via a simple, easily scaled approach: titration of surface oxide proton-acceptor sites by incorporating 1-5 mol% excess A-site cation to the perovskite precursor solution. This amount is sufficient to counteract the loss of organic cation, preventing formation of a  $\text{PbI}_{2-x}\text{Br}_x$  layer at the interface, ultimately leading to a  $V_{\text{OC}}$  increase  $>200 \text{ mV}$ . We demonstrate that this mechanism applies to all forms of  $\text{NiO}_x$ , including thin films created from sol-gel precursors, nanoparticles, atomic layer deposition (ALD), and radio frequency (RF) sputtering, and is



generalizable across multiple perovskite active layers, including state-of-the-art single junction and tandem relevant compositions. A p-i-n perovskite solar cell with 19.7% PCE at maximum power point (MPP) and  $V_{OC}$  up to 1.15 V is achieved. Devices maintain >90% of their initial performance after 2000 hours of thermal stability testing at 85 °C or >80% of their initial performance after 400 hours of accelerated operational stability testing under illumination and 55 °C in nitrogen. Our results extend the generality of acid/base-coupled oxidation-reduction reactions as the driving force for interface equilibration at metal oxide/perovskite interfaces, suggesting that metal halide perovskites have similar reactions with many types of metal oxide layers.

1. M. D. Irwin, D. B. Buchholz, A. W. Hains, R. P. H. Chang, T. J. Marks, p-Type semiconducting nickel oxide as an efficiency-enhancing anode interfacial layer in polymer bulk-heterojunction solar cells. *Proc. Natl. Acad. Sci.* **105**, 2783–2787 (2008).
2. C. C. Boyd, R. Cheacharoen, T. Leijtens, M. D. McGehee, Understanding Degradation Mechanisms and Improving Stability of Perovskite Photovoltaics. *Chem. Rev.* **119**, 3418–3451 (2019).
3. J. Xu, C. C. Boyd, Z. J. Yu, A. F. Palmstrom, D. J. Witter, B. W. Larson, R. M. France, J. Werner, S. P. Harvey, E. J. Wolf, W. Weigand, S. Manzoor, M. F. A. M. van Hest, J. J. Berry, J. M. Luther, Z. C. Holman, M. D. McGehee, Triple-halide wide-band gap perovskites with suppressed phase segregation for efficient tandems. *Science*. **367**, 1097–1104 (2020).

**6:20 AM F.EL08.11/F.EL06.04.07**

**Balancing the Electronic Structure of Flexography-Printed NiO for Rapid Scaling of Perovskite Solar Cells** Julia Huddy, Andrew B. Hamlin, Francesco Guarnieri and William J. Scheideler; Dartmouth College, United States

Perovskite solar cells (PSCs) have potential to deliver TW-scale energy via low-cost manufacturing. However, scaling is limited by slow, high temperature annealing of the inorganic transport layers and insufficient understanding of how scalable processing impacts interfacial device physics. This study addresses the NiO, a leading hole transport layer (HTL) for both high-stability single junction architectures and tandem cells. We present a method for scaling ultrathin NiO HTLs by pairing high-speed (60 m/min) flexographic printing with a rapid annealing Cu:NiO sol-gel ink. By engineering precursor rheology for rapid film-leveling, large area (> 50 cm<sup>2</sup>) NiO HTLs were flexographically printed with high uniformity and photovoltaic performance matching that of spin coated films. Doping and the combustion precursor design enables 30X faster annealing while reducing intrinsic variability of work function and conductivity originating from NiOH surface species.

Integrating these printed transport layers in planar inverted PSCs allows rapid fabrication of high-efficiency (PCE > 16 %) Cs<sub>x</sub>FA<sub>1-x</sub>PbI<sub>1-y</sub>Br<sub>y</sub> solar cells with low hysteresis and open circuit voltages ( $V_{OC}$ ) of 1.11 V. XPS studies of the transition from Ni-OH to Ni-O bonding for low-temperature annealed NiO clarify the balance required for both effective carrier collection and high photostability. Paired with variable illumination intensity measurements and detailed transient photovoltage characterization, these measurements provide an improved understanding of the intrinsic defects present at the NiO-perovskite interface and the impact of scalable synthesis of interfacial charge transport layers.

**6:30 AM F.EL08.11/F.EL06.04.08**

**Late News: Interfacial Engineering in High Efficiency Vacuum Deposited Perovskite Solar Cells—From Metal Oxide Extraction Layers to Large Area Devices** Daniel Perez-del-Rey<sup>1</sup>, Henk Bolink<sup>1</sup> and Pablo P. Boix<sup>2</sup>; <sup>1</sup>University of Valencia, Spain; <sup>2</sup>Institut de ciència del materials, Spain

Vacuum deposition is a key technique in the field of perovskite photovoltaics due to the advantages it presents with respect to the classical deposition methods such as solution processed perovskites. The lack of solvents and the need of annealing makes it a good candidate for industrialization and upscaling as it has already been demonstrated in the OLED field.

Despite its advantages, tuning the interfaces is essential to reach the high power conversion efficiencies found in solution processed perovskite solar cells. Metal oxides are an interesting choice for extraction layers due to their improved stability and reduced parasitic absorption. In this work we present our recent advances in using metal oxides as extraction layers optimising the interfaces in order to reach record open circuit voltages in CH<sub>3</sub>NH<sub>3</sub>PbI<sub>3</sub> perovskite and using MoO<sub>3</sub> as extraction layer by molecular passivation in both PiN and NiP structure improving the stability and opening new possibilities for tandem applications. We also show how we implemented this stable pinhole-free bottom layers in large area devices and mini modules, which is very promising for future industrial purposes.

**5:00 AM \*F.EL08.13/F.EL02..01**

**Alloying and Slicing Halide Double Perovskites** Adam Slavney<sup>1</sup>, Bridget Connor<sup>1</sup>, Kurt P. Lindquist<sup>1</sup>, Linn Leppert<sup>2</sup>, Jeffrey Neaton<sup>3</sup> and Hemamala Karunadasa<sup>1,4</sup>; <sup>1</sup>Stanford University, United States; <sup>2</sup>University of Twente, Netherlands; <sup>3</sup>Lawrence Berkeley National Laboratory, United States; <sup>4</sup>SLAC National Accelerator Laboratory, United States

Halide double perovskites provide a flexible platform for manipulating electronic structure through synthetic design. I will present some recent studies from our group, where we have attempted to increase the compositional and structural complexity of halide perovskites through chemical substitution. In our quest to understand the electronic structure of double perovskites, we developed a simple model that allows us to predict the bandgap symmetry based on chemical composition. Our work constructs an intuitive picture of how the molecular orbitals of metal-hexahalide coordination complexes give rise to electronic bands in the extended perovskite lattice and describes how these molecular orbitals vary across the bands to give rise to the overall band structure. Although the effects of quantum confinement of Pb and Sn perovskites have been well studied, 2D analogs of 3D double perovskites are notably lacking. I will present a series of 2D double perovskites and discuss the optical and electronic consequences of dimensional reduction of the 3D double perovskite lattice to 2D derivatives.

**5:15 AM \*F.EL08.13/F.EL02..02**

**Hot Carriers in Halide Perovskites** Tze Chien Sum; Nanyang Technological University, Singapore

Halide Perovskites exhibit outstanding light-harvesting and emissive properties. Presently, record power conversion efficiencies (PCE) >25% in solar cells and external quantum efficiencies (EQE) >20% in light-emitting devices have been demonstrated. The perovskite field has since expanded well beyond photovoltaics and LEDs into other optoelectronic domains of lasers, x-ray detectors, memristors etc. Emerging frontier areas include multiphoton, multi-exciton generation and hot carrier applications. In this talk, I will focus on the hot carrier phenomena in halide perovskites and our recent work in this area.

**5:30 AM \*F.EL08.13/F.EL02..03**

**Defects Engineering and Photophysical Processes in 2D Perovskites** Annamaria Petrozza; Istituto Italiano di Tecnologia, Italy

Low-dimensional perovskites are rapidly emerging due to their distinctive emission properties. Here, first I will present the fundamental properties of pristine 2D perovskites, such as the nature of the primary photo-excitations, their relaxation through electronic states and their diffusion across thin films. Such properties will be correlated and modulated by the structural characteristics of the 2D perovskites. Then, I will discuss the possibility of perovskite doping by controlled addition of impurity ions which may enable new electronic, magnetic, and optical performances. I will explore new doping strategies based on transition and rare earth metals for tuning of the emission wavelength (from UV to NIR, further extending the typical range covered with perovskites) and luminescent enhancement. The suitability of doping for the realization of 4 level perovskite lasers will be assessed. Doping with heterovalent ions will be tested to selectively increase  $p$  and  $n$  type conductivity of the material. The addition of alkaline-earth metals as B-site dopants will be tested to improve the material stability

**5:45 AM F.EL08.12/F.EL02.12.01**

**High-Efficiency Blue Photoluminescence in the  $\text{Cs}_2\text{NaInCl}_6\text{:Sb}^{3+}$  Double Perovskite Phosphor** Matthew Gray<sup>1</sup>, Shruti Hariyani<sup>2</sup>, T. Amanda Strom<sup>3</sup>, Jackson Majher<sup>1</sup>, Jakoah Brgoch<sup>2</sup> and Patrick Woodward<sup>1</sup>; <sup>1</sup>The Ohio State University, United States; <sup>2</sup>University of Houston, United States; <sup>3</sup>University of California, Santa Barbara, United States

In this report, the photoluminescent properties of a lead-free double perovskite  $\text{Cs}_2\text{NaInCl}_6$  doped with  $\text{Sb}^{3+}$  are explored. The host crystal structure is a cubic double perovskite with  $Fm\text{-}3m$  symmetry,  $a = 10.53344(4)$  Å, and rock salt ordering of  $\text{Na}^+$  and  $\text{In}^{3+}$ . It is a wide bandgap compound ( $E_g \approx 5.1$  eV), and substitution with  $\text{Sb}^{3+}$  leads to strong absorption in the UV due to localized  $5s^2 \rightarrow 5s^15p^1$  transitions on  $\text{Sb}^{3+}$  centers. Radiative relaxation back to the  $5s^2$  ground state, via a  $^3P_1 \rightarrow ^1S_0$  transition, leads to intense blue luminescence, centered at 445 nm, with a photoluminescent quantum yield of 79%. The Stokes shift of 0.94 eV is roughly 33% smaller than it is in the related vacancy ordered double perovskite  $\text{Cs}_2\text{SnCl}_6$ . The reduction in Stokes shift is likely due to a change in coordination number of  $\text{Sb}^{3+}$  from 6-coordinate in

Cs<sub>2</sub>NaInCl<sub>6</sub> to 5-coordinate in Cs<sub>2</sub>SnCl<sub>6</sub>. In addition to the high quantum yield, Cs<sub>2</sub>NaInCl<sub>6</sub>:Sb<sup>3+</sup> exhibits excellent air/moisture stability and can be prepared from solution; characteristics make it a promising blue phosphor for applications involving near-UV excitation.

#### 5:55 AM F.EL08.12/F.EL02.12.04

**Tuning the Photophysical Behavior of 2D Perovskites by Engineering the Nature of the Organic Component** Ferdinand C. Grozema; Delft University of Technology, Netherlands

Two-dimensional (2D) halide perovskites are a class of emitter materials that are enjoying growing attention recently. The materials are related to 3D halide perovskites but either part or all of the small A-site cations are replaced by large organic molecules with an ammonium binding moiety, for example butylammonium or phenyl-ethylammonium. This (generally) leads to the formation of a layered structure where a layer of metal-halide octahedra is formed and the large organic cations separate the layers from each other. Mixing of large and small A-site cations can lead to quasi-2D multi-layer materials where multiple layers of metal halide octahedra are separated by the organic molecules, for instance forming Ruddlesden-Popper or Dion-Jacobson structures. The emissive properties of these materials are intricately linked to the structural dynamics and formation of possible defects in the inorganic layers.

In this work we explore how modifications of the large organic ammonium ion can affect the structural dynamics of the inorganic layer, combining molecular dynamics simulations with time-resolved spectroscopy. Using time-resolved fluorescence and ultrafast transient absorption spectroscopy we have studied the photophysical behavior of 2D perovskites with a range of different organic cations in order to gain insight in the relation between the structure and the excited state dynamics. These measurements indicate marked differences that can not solely be attributed to changes in the average structure of the materials.

To explain these differences we have performed classical molecular dynamics simulations for a variety of structures, for instance aliphatic alkyl chains, ammonium ions containing aromatic moieties such as phenyls or perylene, but also di-functional ions containing two binding sites that can connect to an inorganic perovskite layer on both sides. The results indicate that there are marked differences between the different structures in terms of their structural rigidity. Multi-layer Ruddlesden-Popper structures are generally more rigid than single layers, however, the rigidity of the single layer structures can be strongly enhanced by engineering of the interactions between organic cations, for instance by introduction of large conjugated ions. In addition, di-functional ligands resulting in Dion-Jacobson like structures also lead to more rigid structures. Comparison with the experimental results allows us to derive some design rules that indicate how engineering of the organic part of the structure can help in improving the emissive properties of the materials that is mostly due to the inorganic layer structure.

SESSION F.EL08.13: Poster Session I: Micro- and Nanoscale Characterization of Halide Perovskites  
On Demand Abstracts Available for Viewing Starting Saturday Morning, November 21, 2020  
5:00 AM - 8:00 AM  
F-EL08

#### F.EL08.13.02

**Atomic Layer Deposition of 2D Perovskite Passivation Layers** Jacob Vagott, Carlo Andrea Riccardo Perini and Juan Pablo Correa Baena; Georgia Institute of Technology, United States

In order to further advance perovskite solar cell efficiency from the current record of 25.2%, it is important to minimize perovskite crystal defects and increase interface performance through passivation layers. 2-D perovskites have shown great potential as passivation layers but are primarily deposited by solution processing. Drawbacks of using solution processing for 2-D perovskite films include toxicity of the solvent, potential insolubility of the precursors, and lack of precise thickness control. Atomic layer deposition (ALD) could be a solution to these problems. ALD allows for the deposition of highly uniform layers of perovskite with great control over the final thickness of the film. Self-limiting in nature, ALD processes may allow for deposition of monolayers of perovskite with more control than solution processing techniques. Although an established deposition technique, ALD processes for perovskites have yet to be developed. Through this work, we consider ALD as a method of depositing 2-D perovskites as passivation layers for perovskite solar cells. These passivation layers are further incorporated into devices and their effect on solar cell efficiency is analyzed.

#### F.EL08.13.04

**Understanding the Effects of Sr Chemical Doping on Pb/Sn Based Perovskite Films** Hurriyet Yuce Cakir<sup>1,2</sup> and Juan Pablo Correa Baena<sup>2</sup>; <sup>1</sup>Izmir Institute of Technology, Turkey; <sup>2</sup>Georgia Institute of Technology, United States

Organometal halide perovskites have been in the spotlight of semiconductor science over the past decade. Their exceptional electronic-optical properties and easy production from solution give them an edge over the semiconductor applications. The organic-inorganic halide perovskite solar cells (PSCs) have attracted the incredible attention of the researchers working on solar cells owing to a rapid increase in the efficiency of 25.5% since 2009<sup>1,2</sup>.

Furthermore, tin/lead (Sn/Pb)-based perovskite offers lower toxicity compared to the lead-based perovskites<sup>3</sup>. Their bandgaps are close to 1.3-1.4 eV which is the ideal bandgap of an absorber layer in a solar cell regarding the Shockley-Queisser model<sup>4</sup>.

In this study, we have performed SrI<sub>2</sub> addition (ranging from 0.1% to 5.0% concentrations) to the (FASnI<sub>3</sub>)<sub>0.8</sub>(MAPbBr<sub>3</sub>)<sub>0.2</sub> perovskite to improve their physical properties. Moreover, we have investigated the incorporation of SrI<sub>2</sub> into perovskites impacts on the morphological and optical properties of perovskite films.

[1] NREL. Best Research-Cell Efficiencies. <https://www.nrel.gov/pv/assets/pdfs/bestresearch-cell-efficiencies.20200925.pdf>

[2] Correa-Baena, J.-P., et al., Science, 2017. 358(6364): p. 739-744.

[3] Tavakoli, M.M., et al., Advanced Materials, 2018. 30(11): p. 1705998.

[4] Zhou, X., et al., Advanced Materials, 2020. 32(14): p. 1908107.

#### F.EL08.13.06

**Revealing the Internal Luminescence Quantum Efficiency of Perovskite Films via Accurate Quantification of Photon Recycling** Paul Fassl<sup>1</sup>, Vincent Lami<sup>2</sup>, Ian Howard<sup>1</sup>, David Becker-Koch<sup>2</sup>, Felix Berger<sup>2</sup>, Lukas Falk<sup>2</sup>, Raphael Schmager<sup>1</sup>, Jana Zaumseil<sup>2</sup>, Bryce Sydney Richards<sup>1</sup>, Yana Vaynzof<sup>2</sup> and Ulrich W. Paetzold<sup>1</sup>; <sup>1</sup>Karlsruhe Institute of Technology, Germany; <sup>2</sup>Heidelberg University, Germany

The high refractive index of perovskite semiconductors at their emission wavelength ( $n \sim 2.3-2.6$ ) results in a narrow emission escape cone and a large amount of photoluminescence (PL) to be trapped within perovskite thin films. Due to strong band edge absorption and a very small luminescent Stokes shift, this effect leads to considerable photon reabsorption and reemission - an effect known as photon recycling (PR) [1] - as well as a concurrent red-shift of propagating PL due to emission filtering [2]. As recently highlighted, the self-absorption induced redistribution of charge carriers and outcoupling of propagated PL can lead to a significant misinterpretation of measurements of the intrinsic bimolecular recombination and charge carrier diffusion coefficients as well as of asymmetric PL spectral shapes [3, 4]. For perovskite films with low non-radiative recombination and parasitic absorption losses, PR can be of great advantage as it allows higher charge carrier densities at steady-state and thus increased device open-circuit voltage [5]. However, most current models still start from the simplified assumption that all initially trapped PL will be reabsorbed at some point without the possibility of being outcoupled, likely overestimating the effect of PR [6]. In this study, we show that in external photoluminescence quantum efficiency (PLQE) measurements employing an integrating sphere setup, the PL spectra of polycrystalline perovskite films with layer thicknesses typically employed for thin film solar cells (~150-500 nm) exhibit a notable red-shift and broadening. Such asymmetric PL spectra are often ignored or misinterpreted in the literature. We developed an all-optical model that considers both PR and outcoupling of initially trapped filtered PL due to scattering, which can reproduce spectral shapes with varying extents of red-shifts. We determined the true PL spectral shape as well as the absorption spectrum via high resolution confocal PL measurements and photothermal deflection spectroscopy respectively. Our model allows to estimate the total escape probability in addition to the initially generated internal PL intensity and thus to determine the internal PLQE of perovskite thin films. We confirm our assumptions by various control experiments and Monte Carlo simulations, benchmarking the model for perovskite thin films with different grain size, thickness and composition. Our approach serves as a new guideline for estimating these important parameters directly from measurements of the external PLQE and PL spectrum using an integrating sphere setup. [1] L. M. Pazos-Outon et al., Photon Recycling in Lead Iodide Perovskite Solar Cells. Science 2016, 351, 1430-1433. [2] B. Wenger et al., Consolidation of the Optoelectronic Properties of CH<sub>3</sub>NH<sub>3</sub>PbBr<sub>3</sub> Perovskite Single Crystals. Nat. Commun. 2017, 8, 590. [3] T. W. Crothers et al., Photon Reabsorption Masks Intrinsic Bimolecular Charge-Carrier Recombination in CH<sub>3</sub>NH<sub>3</sub>PbI<sub>3</sub> Perovskite. Nano Lett. 2017, 17, 5782-5789. [4] A. Bercegol et al., Quantitative Optical Assessment of Photonic and Electronic Properties in Halide Perovskite. Nat. Commun. 2019, 10 (1), 1586. [5] M. G. Abebe et al., Rigorous Wave-Optical Treatment of Photon Recycling in Thermodynamics of Photovoltaics: Perovskite Thin-Film Solar Cells. Phys. Rev. B 2018, 98, 075141. [6] J. M. Richter et al., Enhancing Photoluminescence Yields in Lead Halide Perovskites by Photon Recycling and Light Out-Coupling. Nat. Commun. 2016, 7, 13941.

### F.EL08.13.07

**Energy Level Alignment of Formamidinium Tin Iodide with Organic Contact Materials** Jonas Horn, Pascal Schweitzer and Derck Schlettwein; Justus Liebig University Giessen, Germany

The alignment of energy levels at the interface of perovskite absorber and adjacent hole- and electron-transporting material affects the formation of space-charge regions and interfacial recombination. These have consequences for charge transport in the layers and, therefore, for the efficiency of devices. We measured this alignment by the use of Kelvin-probe-force microscopy (KPFM) to gain a detailed understanding of this alignment of energy levels. This study is focused on Formamidinium tin iodide (FASnI<sub>3</sub>) as perovskite absorber. This material avoids the toxicity problems of lead and is known to yield the highest power conversion efficiencies amongst all lead free perovskite absorbers. The most common solar cell geometry for FASnI<sub>3</sub> implements C60 as electron-transporting material, which is prepared on FASnI<sub>3</sub> by physical vapor deposition (PVD). Intermittently to PVD, we use KPFM to simultaneously monitor morphology and work function of C60 during its growth on FASnI<sub>3</sub>. We show that a sufficiently high deposition rate is needed to avoid island formation of C60 and obtain a homogeneously covering film with constant work function. We further show that the width of the space charge layer in C60 is larger than the film thickness often implemented in perovskite solar cells (20 nm - 30 nm). A band bending in the range of 300 meV is observed and consequences for prospective device operation are discussed.

### F.EL08.13.08

**The Underlying Mechanism of Surface Defect Passivation Process for Organohalide-Lead Perovskite Nanocrystals** Artavazd Kirakosyan<sup>1</sup>, Duc Chinh Nguyen<sup>1</sup>, Min-Gi Jeon<sup>1</sup>, Jae Hyuck Jang<sup>2</sup>, Jihoon Choi<sup>1</sup> and MoonRyul Sihn<sup>1</sup>; <sup>1</sup>Chungnam National University, Korea (the Republic of); <sup>2</sup>Korea Basic Science Institute, Korea (the Republic of)

Organolead halide perovskite nanocrystals (NCs) have emerged as a versatile and promising active material for many optoelectronic applications such as solar energy harvesting, light-emitting device, and photodetectors owing to their size- and composition-dependent optoelectronic properties. Although the extensive studies on their optical and electronic properties have been studied in the last several years, their low stability, structural integrity, and poor luminescence stability associated with the fast attachment-detachment dynamics of surface capping molecules during post-processing limit their practical applications in optoelectronics. Therefore, an in-depth understanding of the surface chemical processes is required. We found that the amine group (-NH<sub>3</sub><sup>+</sup>) immobilizes Br<sup>-</sup> anion at the corner of undercoordinated PbBr<sub>6</sub><sup>4-</sup> octahedron on the MAPbBr<sub>3</sub> surface resulting in a charge-balanced Pb-Br framework where Br/Pb ratio is slightly higher than stoichiometry, and thus provides exciton radiative recombination and high photoluminescence quantum yield. In contrast, the oleic acid is not able to coordinate with the surface moieties of the perovskite, but rather carboxyl acid groups (-COO<sup>-</sup>) etch Pb<sup>2+</sup> into solution when only acid was used. Interestingly, a mixture of oleic acid and amine-functionalized surfactants was found to promote amine conversion to ammonium ion (-NH<sub>2</sub> + H<sup>+</sup> → -NH<sub>3</sub><sup>+</sup>), which is favorable for their localization on the surface. Our results show that the Br vacancies at the non-passivated surface result in a reduction of Pb<sup>2+</sup> to Pb<sup>0</sup> by trapping the electrons generated from the exciton dissociation, which provides the main pathway for exciton trapping. Acknowledgment This work is supported by the National Research Foundation of Korea (NRF) grant funded by the Korean government (No. NRF-2019R1I1A2A01060608) and by Nano-Material Technology Development Program through the National Research Foundation of Korea (NRF) funded by the Ministry of Science, ICT and Future Planning. (2009-0082580).

### F.EL08.13.11

**Impact of Temperature and Humidity on the Stability of the Optical Properties and Structure of Formamidinium Lead Iodide Thin Films and Solar Cells** Marie Solange Tumasange, Biwas Subedi, Cong Chen, Maxwell M. Junda, Juan Zuo, Zhaoning Song, Yanfa Yan and Nikolas Podraza; University of Toledo, United States

Organic-inorganic lead halide perovskite polycrystalline thin films used as absorber layers in high efficiency solar cells have direct band gaps, high absorption coefficients, and potentially low-cost solution-based fabrication processing. However, these materials are inclined to degradation with exposure to humidity, oxygen, heat, and ultraviolet light. Formamidinium lead iodide (FAPbI<sub>3</sub>) is an attractive composition perovskite as it has a more symmetric crystal structure due to a larger cation radius for FA compared to that for methylammonium (MA) as well as an elevated decomposition temperature for improved stability. Even though FAPbI<sub>3</sub> is among the more stable perovskite compositions, solar cells incorporating these absorbers still degrade with atmospheric exposure over time. Here we study the behavior of FAPbI<sub>3</sub> film structure and complex optical properties under controlled temperature variations and relative humidity (RH) exposure. In situ real time spectroscopic ellipsometry (RTSE) measurements are collected over the near infrared to ultraviolet spectral range (0.75-5.9 eV) for polycrystalline FAPbI<sub>3</sub> thin films deposited on glass substrates which are then held at different temperatures, ranging from 7 to 70°C, in a sealed nitrogen chamber with controlled 0, 26, and 85% RH introduced. From RTSE, the optical response in the form of complex dielectric function ( $\epsilon = \epsilon_1 + i\epsilon_2$ ) spectra is deduced using a parametric model accounting for above band

gap critical points, the direct band gap, an Urbach tail, and degradation induced sub-gap absorption due to defects. Variations in parameters describing spectra in  $\epsilon$  are tracked as functions of temperature, controlled RH, and the amount of time films are held under those conditions. Changes in bulk thickness, surface roughness thickness, and surface roughness relative density are also tracked with time under these conditions. For example, RTSE indicates no change in structure and minimal changes in  $\epsilon$  at 0% RH regardless of temperature. However, when FAPbI<sub>3</sub> is exposed to 26% RH at 70°C, RTSE indicates changes in parameters describing  $\epsilon$  and structure, such as increases in film thickness with time indicative of water intercalation. To the contrary, slight film densification is observed over time when held at 26% RH and 70°C. These RTSE studies show that deviations from near room temperature with controlled relative humidity induces more changes in optical and structural properties with time than when the sample is exposed to only humidity. In all cases of RH exposure sub-gap absorption increases with time, most notably in widening of the Urbach tail obtained from the parametric model for  $\epsilon$ . To further study how other ambient conditions affect perovskite stability, RTSE is performed for FAPbI<sub>3</sub> with exposure to controlled amounts of both oxygen and relative humidity as a function of temperature. RTSE is applied directly to measure a FAPbI<sub>3</sub> based solar cell to track changes in the perovskite absorber over time and identify potential correlations with device performance.

#### F.EL08.13.12

**Diagnosis of Optical and Electrical Losses in Organic-Inorganic Lead Halide Perovskite Photovoltaics via External Quantum Efficiency Modelling** Biwas Subedi, Chongwen Li, Zhaoning Song, Maxwell M. Junda, Kiran Ghimire, Yanfa Yan and Nikolas Podraza; University of Toledo, United States

Organic-inorganic lead halide perovskite-based photovoltaics (PV) exhibit high initial efficiency, can be processed at potentially low cost, and material bandgaps can be tuned by composition. Solution-processing enables fabrication of a range of different ABX<sub>3</sub> (A: methylammonium—MA, formamidinium—FA, Cs; B: Pb, Sn; X: I, Br, Cl) perovskite compositions to meet these needs in single or tandem junction PV. Unfortunately, these perovskites may degrade upon exposure to relative humidity and oxygen in ambient air, during device processing, and overtime during device operation. Like all PV devices, performance depends on the characteristics of each material and interfaces between layers to minimize sources of optical and electronic losses. External quantum efficiency (EQE) simulations of perovskite PV assess sources of parasitic optical losses with input complex optical response of all component materials and known multiple layer device structure. From these simulations, the optical performance of devices with different structures or component materials is predicted. Comparison of simulated EQE with experimental measurement validates the optical model when simulated and experimental EQE match but also more importantly identifies electronic losses such as incomplete carrier collection when experimental EQE is less than the simulation. Obtaining the most accurate input complex optical response of perovskite films and layer thicknesses in devices is necessary to maximize the amount of information gained from EQE and its modeling. Toward this end, spectroscopic ellipsometry (SE) over the near-infrared to the ultraviolet wavelength range (0.73-5.9 eV) is used to characterize the complex optical response of solution-processed perovskite films of different compositions. Photothermal deflection spectroscopy (PDS) and unpolarized transmittance complement SE by enhanced sensitivity to low values of absorption coefficient ( $\alpha$ ) in the vicinity of the bandgap. Extension to low values of  $\alpha$  enables detection of exponential band tailing and Urbach Energy (EU), with narrower EU indicative of more ordered and higher electronic quality material. A parametric optical property model has been developed which includes contributions from electronic transitions above the bandgap, the direct bandgap, an exponentially decaying Urbach tail, and sub-gap absorption due to defects. Complex optical properties of perovskite films, including wide-bandgap FA<sub>1-x</sub>Cs<sub>x</sub>Pb(I<sub>1-y</sub>Br<sub>y</sub>)<sub>3</sub> and narrow-bandgap (FASnI<sub>3</sub>)<sub>x</sub>(MAPbI<sub>3</sub>)<sub>1-x</sub> compositions, in both as-prepared and degraded states are determined. SE data is collected for complete perovskite PV to deduce layer thicknesses and perovskite complex optical properties within the device. This information serves as direct input for EQE simulation. Comparison with perovskite PV experimental EQE enables the deduction of optical and electronic device performance losses arising from perovskite composition and device architecture, variations in near bandgap perovskite optical response resulting from complete device processing, and perovskite degradation during solar cell operation. As an example, similar simulated and experimental EQE in (FASnI<sub>3</sub>)<sub>x</sub>(MAPbI<sub>3</sub>)<sub>1-x</sub> (0.3  $\leq$  x  $\leq$  0.7) perovskite PV validates the optical model and indicates minimal losses. In another case, for FAPbI<sub>3</sub> PV comparisons between simulation and experimental EQE indicate sources of both optical and electronic losses arising from device processing.

#### F.EL08.13.13

**Enhanced Charge Extraction Through Double-Layered Electron Transfer Films for Hybrid Perovskite Planar Solar Cells** Jihyun Kim, Hye Ri Jung, Yeon Soo Kim and William Jo; Ewha Womans University, Korea (the Republic of)

The electron transfer film (ETF) plays an important role in obstructing recombination of electrons and holes between the perovskite layer and fluorine-doped tin oxide in planar perovskite solar cells (PSCs). In addition, at the compact spin-coated SnO<sub>2</sub> ETF, morphological defects, such as pinholes and cracks, due to roughness of the substrate seriously impact on the performance of PSCs. Here, we investigate the variables that can control the charge extraction using spin-coated SnO<sub>2</sub>,

sputtered TiO<sub>2</sub> and double-layered (DL) ETF composed of TiO<sub>2</sub> on SnO<sub>2</sub> and SnO<sub>2</sub> on TiO<sub>2</sub>. We determined the resistance, mobility, conductivity and carrier concentration of double-layered ETF based on PSCs by a 4-probe method. The electrical properties show that the DL-ETF can effectively reduce the trap density at perovskite/ETF interface, promote the electron transfer, and suppress the interface recombination rather than SnO<sub>2</sub> alone. The band structure and the carrier transport mechanism at perovskite/DL-ETF interface were explained by conductive atomic force microscopy, Kelvin probe force microscopy and ultraviolet photoelectron spectroscopy. Complementary composite DL-ETF has been found to eliminate severe current leakage inside the device, reducing interface defects and hysteresis. More importantly, DL-ETF accelerates at electron extraction and transport owing to the excellent mobility. Finally, DL-ETF based PSCs yield higher power conversion efficiency with improved JSC than the device with SnO<sub>2</sub> alone. Therefore, these are beneficial for reducing the recombination of carriers in the electron traps, leading to the enhancement of device performance.

#### **F.EL08.13.17**

##### **Leveraging Electrochemical Techniques to Augment and Accelerate Halide Perovskite Technology**

**Development** Moses Kodur<sup>1</sup>, Ross Kerner<sup>2</sup>, Zachary Dorfman<sup>1</sup>, Justin H. Skaggs<sup>1</sup>, Taewoo Kim<sup>1</sup>, Joseph J. Berry<sup>2</sup> and David P. Fenning<sup>1</sup>; <sup>1</sup>University of California, San Diego, United States; <sup>2</sup>National Renewable Energy Laboratory, United States

Improving the repeatability and operational stability of interfaces in perovskite devices is crucial to extend device lifetime. With each sequential step in perovskite device fabrication comes a risk of a failed device integration or an interaction that leads to longer-term device instability. Here, we present simple electrochemical techniques to evaluate fundamental properties of charge transport layers and limits of stability before completion of a full device stack, with the objective of improving batch yield, deconvoluting the troubleshooting process, and accelerating the development of new perovskite absorbers, their contact layers, and high-efficiency devices.

We focus on two exemplary measurements using easily accessible aqueous electrolytes. First, we show that an outer sphere redox couple such as the ferro/ferricyanide system allows facile evaluation of the semiconducting properties (conduction band minimum position, doping level, etc.) of SnO<sub>x</sub> electron transport layers. The anodic and cathodic features in cyclic voltammograms of the SnO<sub>x</sub> are correlated to final solar cell efficiency and offer an early screen of quality. Second, we show that ionic permeability/reactivity of SnO<sub>x</sub> layers, which can lead to irreversible absorber degradation under bias, can be rapidly evaluated by potentiostatic measurements in the presence of organohalide salts. This technique reveals the influences of processing condition and deposition method on susceptibility to bias-induced degradation reactions.

These process control measurements can be readily adapted to devices of any area and are compatible with industry-scale fabrication techniques to improve process reliability and reproducibility. While our work focuses on the development and characterization of SnO<sub>x</sub> layers, the fundamental principles can be adapted for a wide variety of charge transport layers so long as the proper electrochemical set-up is implemented, making this method a powerful tool for halide perovskite development.

#### **F.EL08.13.18**

##### **Wide-Bandgap Perovskites in the Spotlight—Multimodal Study of Photo-Induced Halide Segregation in Solar**

**Cells** Kunal Datta, Bas T. van Gorkom, Matthew J. Dyson, Martijn M. Wienk and Rene A. Janssen; Eindhoven University of Technology, Netherlands

Segregation of illuminated mixed-halide perovskites into iodide- and bromide-rich domains presents a critical bottleneck in the application of wide-bandgap absorbers in single- and multi-junction architectures. And while its occurrence has been well-studied in thin films, the influence on operational solar cells lacks sufficient understanding.

This work employs a multimodal characterization procedure to observe the slow progression of halide segregation in efficient solar cells prepared in the p-i-n architecture using sequentially processed perovskite absorbers. Photoluminescence spectroscopy is used to identify the stages that demixing of halide ions entails while simultaneous tracking of photovoltaic parameters allows correlating performance degradation to the migration of ionic species in each stage. A new stage of the process is thus observed upon prolonged illumination. Characterization of sub-bandgap features reveals the occurrence of photo-induced defect formation whose suppression through cationic substitution provides a strategy for stabilization of wide-bandgap compositions against halide segregation.

#### **F.EL08.13.19**

##### **Elucidating the Role of Electrochemical Halide Reactions in Perovskite Optoelectronic Devices Under Prolonged**

**Reverse Bias** Jay B. Patel<sup>1,2</sup>, Luca Bertoluzzi<sup>3</sup>, Kevin A. Bush<sup>3</sup>, Caleb C. Boyd<sup>3,1</sup>, Ross Kerner<sup>1</sup> and Michael McGehee<sup>2,1</sup>; <sup>1</sup>National Renewable Energy Laboratory, United States; <sup>2</sup>University of Colorado Boulder, United

States; <sup>3</sup>Stanford University, United States

Partial shading of a solar module can bring a set of cells within the module to operate under reverse bias. When a solar cell is shaded in a module, the photogenerated current falls and a negative voltage (reverse bias) builds up as the other illuminated cells in series try to push current through it. Moreover, metal-halide perovskite photodetectors are regularly operated in reverse bias, and therefore it is critical to understand how these devices behave under reverse bias. Previous studies have shown that perovskite solar cells with a wide variety of compositions and contacts exhibit unusual behavior, compared to typical silicon solar cells, in reverse bias that includes both reversible performance loss and non-reversible degradation. [1, 2] Furthermore, we have shown that when a perovskite solar cell is held under reverse bias, the mobile ions move in a way such that there is favorable band energetics to allow for hole injection into the perovskite, yet the consequence of this process was unclear. [1]

Recent investigations have shown that photogenerated holes can induce electrochemical oxidation of halides into halogens. [3, 4] These halogens can leave the perovskite absorber and diffuse into contacts and cause further detrimental reactions with the electrodes. [5] To elucidate and understand the degradation mechanisms that occurs when perovskite solar cells are held under reverse bias, we have developed an advanced drift-diffusion model that incorporates an electrochemical term that can explain the short-circuit, open circuit and fill factor losses we experimentally measure. Our model conclusively shows that the injected holes can trigger the oxidation of halides to form neutral halogen interstitials. The density of halogen interstitials is much higher in reverse bias because there are hardly any electrons available to reduce the halogens back into halides. The resulting halogens act as bulk recombination centers and lead to a sharp decline in all the JV device characteristics. While the interstitial halogen density will decay when the cell is finally operated in forward bias, permanent degradation will occur if the halogen diffuses out of the perovskite layer into the transport layers or electrodes. Finally, we discuss how changing parameters such as the mobile ion density or the permeability of contacts can positively influence device performance and stability.

- [1] A. R. Bowring, L. Bertoluzzi, B. C. O'Regan and M. D. McGehee, *Adv. Energy Mater.*, 2018, 8, 1702365  
[2] R. A. Z. Razera, D. A. Jacobs, F. Fu, P. Fiala, M. Dussouillez, F. Sahli, T. C. J. Yang, L. Ding, A. Walter, A. F. Feil, H. I. Boudinov, S. Nicolay, C. Ballif and Q. Jeangros, *J. Mater. Chem. A*, 2020, 8, 242–250.  
[3] G. Y. Kim, A. Senocrate, T.-Y. Yang, G. Gregori, M. Grätzel and J. Maier, *Nat. Mater.*, 2018, 17, 445–449.  
[4] S. G. Motti, D. Meggiolaro, A. J. Barker, E. Mosconi, C. A. R. Perini, J. M. Ball, M. Gandini, M. Kim, F. De Angelis and A. Petrozza, *Nat. Photonics*, 2019, 13, 532–539.  
[5] R. A. Kerner and B. P. Rand, *ACS Appl. Energy Mater.*, 2019, 2, 6097–6101.

### F.EL08.13.20

**Anionic Diffusion in Two-Dimensional Halide Perovskite Heterostructures** Akriti Akriti<sup>1</sup>, Enzheng Shi<sup>1</sup>, Stephen B. Shiring<sup>1</sup>, Jiaqi Yang<sup>1</sup>, Yao Gao<sup>1</sup>, Cindy L. Atencio-Martinez<sup>2</sup>, Alan J. Pistone<sup>1</sup>, Peilin Liao<sup>1</sup>, Brett Savoie<sup>1</sup> and Letian Dou<sup>1</sup>; <sup>1</sup>Purdue University, United States; <sup>2</sup>University of Los Andes, Colombia

The soft crystal lattice of hybrid halide perovskites facilitates anionic diffusion which impacts material stability, optoelectronic properties and solid-state device performance. Two-dimensional (2D) halide perovskites with bulky organic barriers have been used for improving the extrinsic stability as well as suppressing intrinsic anionic diffusion. With this strategy, devices with enhanced stability and reduced hysteresis have been achieved. Nevertheless, a fundamental understanding of the role of organic cations in inhibiting anionic diffusion across the perovskite-ligand interface is missing. Through this study, we demonstrate a quantitative investigation of the anionic inter-diffusion in atomically sharp and flat 2D heterojunctions between two arbitrarily determined phase-pure halide perovskite single crystals. Stark differences are observed in anion diffusion across 2D halide perovskite lateral and vertical heterostructures. Halide inter-diffusion in lateral heterostructures is found to be similar to the classical Fickian diffusion featuring continuous concentration profile evolution. However, vertical heterostructures show a “quantized” layer-by-layer diffusion behavior governed by a local free energy minimum and ion-blocking effects of the organic cations. Surprisingly, halide inter-diffusion coefficients for 2D perovskites capped with short aliphatic organic cations (e.g. butylammonium) are only 1~2 order of magnitudes smaller than that of 3D perovskites, suggesting the ineffectiveness of these cations in blocking the anionic migration. Furthermore, we found that bulkier and more rigid  $\pi$ -conjugated organic cations inhibit halide inter-diffusion much more effectively ( $D < 10^{-20}$  m<sup>2</sup>/s) compared to aliphatic cations. These results offer significant insights into the mechanism of anionic diffusion in 2D perovskites and provide a new materials platform for heterostructure assembly and device integration.



SESSION F.EL08.14: Poster Session II: Tin-Based and Other Lead-Free Optoelectronic Materials  
On Demand Abstracts Available for Viewing Starting Saturday Morning, November 21, 2020  
5:00 AM - 8:00 AM  
F-EL08

#### F.EL08.14.01

##### **Chemical Diversity in Lead-Free, Layered Double Perovskites—A Combined Experimental and Computational**

**Approach** Brenda Vargas<sup>1</sup>, Raúl Torres<sup>1</sup>, Diana Reyes-Castillo<sup>1</sup>, Joelis Rodríguez-Hernández<sup>2</sup>, Milan Gembicky<sup>3</sup>, Eduardo Ménendez-Proupin<sup>4</sup> and Diego Solis-Ibarra<sup>1</sup>; <sup>1</sup>UNAM, Mexico; <sup>2</sup>Centro de Investigaciones en Química Aplicada, Mexico; <sup>3</sup>University of California, United States; <sup>4</sup>Universidad de Chile, Chile

Akin to the expansion in compositional diversity that halide double perovskites provided to three-dimensional perovskites [1-2], layered double perovskites could further expand the diversity of two-dimensional (2D) perovskites, and therefore, they could also enhance the properties or expand the possible applications of such materials [3]. Despite the great promise of halide 2D double perovskites, up to date, there are only four confirmed members of this family of materials [3-6]. Herein, we explore 90 hypothetical new members of this family of materials by a combined theoretical, computational, and experimental method. The combination of these tactics allowed us to predict several new materials, out of which we experimentally synthesized and characterized five new layered double perovskites, some of which show promising properties for their use in photovoltaics and optoelectronics. Further, our work highlights the vast diversity of compositions and therefore of applications that double-layered perovskites have yet to offer. References [1] X. Zhao, D. Yang, J. Ren, Y. Sun, Z. Xiao and L. Zhang, *Joule*, 2018, 2, 1-12. [2] L. Chiu et al, *Nano-Micro Lett*, 2019, 11:16. [3] B. Vargas, E. Ramos, E. Pérez-Gutiérrez, J.C. Alonso, D. Solis-Ibarra, *J. Am. Chem. Soc*, 2017, 139, 27, 9116-9119. [4] B. Vargas, R. Torres-Cadena, J. Rodríguez-Hernández, M. Gembicky, H. Xie, J. Jiménez-Mier, Y-S. Liu, E. Menéndez-Proupin, K. R. Dunbar, N. Lopez, P. Olalde-Velasco, D. Solis-Ibarra, *Chem. Mater*, 2018, 30, 5315-5321. [5] B. A. Connor, L. Leppert, M. D. Smith, J. B. Neaton, H. I. Karunadasa, *J. Am. Chem. Soc*, 2018, 140, 5235-5240. [6] C. Ortiz-Cervantes, P. Carmona-Monroy, D. Solis-Ibarra, *ChemSusChem*, 2019, 12, 1560-1575.

#### F.EL08.14.06

##### **Ion Exchange-Diffusion Mechanisms in Transforming Calcite into Lead (Pb)-Free Perovskite Light**

**Absorbers** Jonathan B. Junio, Marlon T. Conato and Candy C. Mercado; University of the Philippines Diliman, Philippines

The synthesis of perovskite materials has gone beyond the traditional wet chemistry routes into other methods such as a sequential ion exchange process that can produce perovskite materials from calcite in either thin film or bulk form. The use of lead (Pb), the most successful element in terms of PSC efficiency performance, was already successfully demonstrated in an ion exchange process. In this work, tin (Sn) is chosen since it has the most potential to replace Pb since they are on the same group and for the similarity in ionic radii of their ions (Pb<sup>2+</sup>, Sn<sup>2+</sup>) at 1.19 and 1.02 Å, respectively. Methyl ammonium tin triiodide (MASnI<sub>3</sub>) has a lower bandgap (1.2 to 1.4 eV) that induces broader absorption spectrum as compared with the benchmark MAPbI<sub>3</sub> counterpart (1.55 eV). The second alternative - strontium (Sr) has an ionic radius of 1.18 Å indicating possible ion exchange in the strontianite structure. The band gap for the Sr perovskite was estimated at 3.6 eV, considerably higher than that for the lead perovskite and therefore not suitable for direct solar cell applications but can be used as a top cell in tandem architectures. These ion exchange processes are observed using x-ray absorbance and photoelectron spectroscopies to elucidate the underlying mechanisms of the sequential ion exchange process. These will shed light into the material transformation with shape preservation from the raw shells or single crystal calcite towards the intermediate carbonate material and eventually, the Pb-free perovskite material.

SESSION F.EL08.15: Poster Session III: Vapor Deposition and Upscaling of Perovskites  
On Demand Abstracts Available for Viewing Starting Saturday Morning, November 21, 2020  
5:00 AM - 8:00 AM  
F-EL08

#### F.EL08.15.01

**A Comparison of Three Emerging Bi-Based (Oxy)Halide Absorbers Grown from Metallic Precursors** Andrea Crovetto, Alireza Hijjajafarassar, Ole Hansen, Brian Seger, Ib Chorkendorff and Peter Vesborg; Technical University of Denmark,

Denmark

The bismuth-based (oxy)iodides BiI<sub>3</sub>, BiOI and Ag<sub>x</sub>BiI<sub>x+3</sub> share similar layered crystal structures, optimal band gaps for top absorbers in tandem solar cells, and moderate growth temperatures. Similarly to halide perovskite absorbers, they contain a heavy cation with a lone pair of electrons (Bi<sup>3+</sup>) which has been proposed as one of the features enabling defect tolerance in perovskites. We have grown and characterized BiI<sub>3</sub>, BiOI, and Ag<sub>3</sub>BiI<sub>6</sub> absorbers and solar cells in a systematic manner by employing a consistent synthesis method ((oxy)iodization of metallic precursor) and a consistent analysis routine. In this way, the individual strengths and weaknesses of the three absorbers, as well as their common challenges, can be outlined. The radiative efficiency of the three materials is within the same order of magnitude, thus indicating a similar degree of defect tolerance. Control of growth orientation should be a priority for this class of materials in view of their anisotropic properties. P-type bulk doping and selection of hole transport layers with deep valence bands could also improve performance. At the device level, we report an improved open circuit voltage of BiI<sub>3</sub> solar cells with respect to the state of the art, and we report a proof-of-concept Ag<sub>3</sub>BiI<sub>6</sub>/silicon tandem cell. Beyond photovoltaics, the very low dark diode ideality factor in BiI<sub>3</sub> devices and the existence of both electronic and ionic conduction in Ag<sub>3</sub>BiI<sub>6</sub> may open up alternative unexpected applications in other fields.

### F.EL08.15.03

**Boosting the Self-Trapping Emissions in Zero-Dimensional Perovskite Heterojunctions** Jun Yin<sup>1</sup>, Jean-Luc Bredas<sup>2</sup>, Osman M. Bakr<sup>1</sup> and Omar F. Abdelsaboor<sup>1</sup>; <sup>1</sup>King Abdullah University of Science and Technology, Saudi Arabia; <sup>2</sup>Georgia Institute of Technology, United States

Zero-dimensional (0D) inorganic and hybrid perovskites have attracted great interest for white-light emitting applications due to their broadband emissions originating from the self-trapping excitonic states. In this work, we study a series of 0D inorganic perovskites, A<sub>4</sub>PbX<sub>6</sub> and A<sub>4</sub>SnX<sub>6</sub> (A = K, Rb, and Cs; X = Cl, Br, and I), under the theoretical framework of one-dimensional configuration coordinate diagram using density functional theory (DFT) calculations. We demonstrate that the formation of self-trapping excitonic states of A<sub>4</sub>PbX<sub>6</sub> and A<sub>4</sub>SnX<sub>6</sub> is attributed to the local structural distortion of individual [PbX<sub>6</sub>]<sup>4-</sup> and [SnX<sub>6</sub>]<sup>4-</sup> octahedron (i.e., the octahedral shrinking under photoexcitation). We further predict the broadband emissions of a new family of 0D A<sub>4</sub>PbX<sub>6</sub>/A<sub>4</sub>SnX<sub>6</sub> heterostructures, and find that among these crystal structures Rb<sub>4</sub>PbI<sub>6</sub>/Rb<sub>4</sub>SnI<sub>6</sub> exhibits an increased photoluminescence efficiency with good stability as compared to pristine Rb<sub>4</sub>SnI<sub>6</sub>. Our findings provide a new material design strategy for boosting the self-trapping emissions with improved stability using 0D inorganic perovskite heterostructures.

### F.EL08.15.05

**Single-Source Deposition of Double Perovskites for Optoelectronic Devices** Nathan Rodkey<sup>1,2</sup>, Stan Kaal<sup>2</sup>, Paz Sebastia-Luna<sup>1</sup>, Yorick A. Birkhölzer<sup>2</sup>, Franciso Palazon<sup>1</sup>, Henk Bolink<sup>1</sup> and Monica Morales-Masis<sup>2</sup>; <sup>1</sup>Universidad de Valencia, Spain; <sup>2</sup>University of Twente, Netherlands

As halide perovskites (PVKs) continue to garner scientific interest for their potential to enhance efficiencies of solar cells and LEDs, a push has been made towards lead-free and completely inorganic PVKs with increasingly complex stoichiometries. One example of this is the double PVK Cs<sub>2</sub>AgBiBr<sub>6</sub> and Sn:Cs<sub>2</sub>AgBiBr<sub>6</sub>. Synthesis of thin films with these complex stoichiometries is challenging due to the distinct volatility of the constituent elements, usually requiring multi-step or multi-source processes. Here we explore Pulsed Laser Deposition (PLD) as a route to grow these types of complex materials with a single source. PLD offers the advantage of being a volatility-insensitive thin film synthesis technique which we use to demonstrate single-source deposition of Cs<sub>2</sub>AgBiBr<sub>6</sub> and Sn:Cs<sub>2</sub>AgBiBr<sub>6</sub>. For this, solid targets are made first by mechanochemical synthesis of powders, followed by a uniaxial and isostatic pressing to form the powders into dense, compact targets. X-ray diffraction (XRD) is used to verify the desired PVK phase is maintained along each step of target fabrication. Laser-ablation of the double PVK targets in vacuum leads to formation of Cs<sub>2</sub>AgBiBr<sub>6</sub> and Sn:Cs<sub>2</sub>AgBiBr<sub>6</sub> double PVK films after optimization of the deposition parameters. We discuss the effects of deposition pressure and laser fluence on the formation of stoichiometric and phase-pure films, as well as the critical role of the thermalization of the source elements to achieve stoichiometric transfer. In addition to the structural properties, the optoelectronic properties of the films were studied by UV-Vis-NIR spectrophotometry and time-resolved photoluminescence. Notably, >1 μm thick films are deposited and all films present high structural stability over the course of 3 months, without the need for an annealing step. This work represents an important step forward in the development of controlled growth and future scalability of complex halide perovskites for efficient optoelectronic devices.

#### **F.EL08.16.06**

**Improving Blue Light Emission of CsPbBr<sub>3</sub> Nanoplatelets via Post-Synthesis Surface Passivation** Jinu Park, Joonyun Kim and Byungha Shin; Korea Advanced Institute of Science and Technology, Korea (the Republic of)

Lead halide perovskite is considered as a potential candidate for the next generation light emitting diodes (LEDs) due to its extremely narrow light emission spectrum with a typical full width half maximum (FWHM) < 20 nm. In particular, all-inorganic CsPbBr<sub>3</sub> has demonstrated the near unity photoluminescence quantum yield (PLQY) for green light emission. A more challenging, yet technologically important, task is developing a high performance blue light emitter. By partially replacing Br of CsPbBr<sub>3</sub> with Cl, the emission wavelength can be adjusted to the blue emission; however, CsPbBr<sub>3-x</sub>Cl<sub>x</sub>, suffers from ion migration and phase segregation which result in low PLQY and poor stability. Here, we present a synthesis method to produce nanostructure CsPbBr<sub>3</sub> in the form of nanoplatelets (NPLs) that is capable of emitting blue light without the need for anion-substitution. Nanoplatelets with 2 monolayer (ML) and 3 ML of thickness yielded photoluminescence (PL) peak at 435nm with an extremely narrow FWHM of 14.2 nm and PL peak at 456nm with FWHM of 19.6nm, respectively. The luminescence of these nanoplatelets was further improved by post-synthesis treatment with tetrafluoroborate salts-almost 1150% increase in PL intensity was observed without a noticeable broadening of the PL spectrum. Details of the results and discussion of a possible mechanism behind the improvement with the post-synthesis treatment will be presented.

#### **F.EL08.16.07**

**Highly Luminescent Vacuum-Evaporated All Inorganic CsPbBr<sub>3</sub> Perovskite Light Emitters with a Polymer Auxiliary Layer** Nakyung Kim, Mingue Shin and Byungha Shin; Korea Advanced Institute of Science and Technology, Korea (the Republic of)

All inorganic halide perovskite CsPbBr<sub>3</sub> has emerged as the next-generation material for light-emitting diodes (LEDs) due to its high color purity with a narrow spectral width (< 20 nm) and tunable band gap by adjusting the composition of halide anions, i.e. substitution of Br with I or Cl. Considering the needs for large-area scalability and fine control of the emitter thickness, vacuum-deposition will be a more commercialization-friendly technique to produce perovskite films for LEDs. Here, we prepare CsPbBr<sub>3</sub> light emitters by thermal co-evaporation of CsBr and PbBr<sub>2</sub> sources. The luminescence of the vacuum-deposited CsPbBr<sub>3</sub> films was greatly improved by introducing a poly-ethylene oxide (PEO) layer underneath the CsPbBr<sub>3</sub>-almost 300-fold increase in photoluminescence quantum yield (PLQY) with the PEO layer compared to the reference sample (CsPbBr<sub>3</sub>/glass). It is believed that the interaction between PEO and Pb<sup>2+</sup> ions leads to the passivation of non-radiative recombination defects. After the careful optimization of the PEO layer thickness and post-deposition thermal treatments of CsPbBr<sub>3</sub>, we have demonstrated PLQY of 30% from a peak at 521 nm with full-width-half-maximum of ~17nm. Furthermore, the samples exhibit excellent ambient stability. Details of the results and analysis will be discussed.

#### **F.EL08.16.08**

**Ultra Sensitive Perovskite Halide Based Room Temperature Ammonia Gas Sensor Using Flexible Paper Electronics** Avishek Maity and Barnali Ghosh; S.N. Bose National Centre for Basic Sciences, India

In current days, development and search of new materials for solid state thin film gas sensor to detect toxic gases, particularly using nanomaterial for their enhanced functionality, is growing rapidly as view point of both environmental and clinical application. Particularly, gas sensor with low power consumption, room temperature operation, portability and cost effectiveness is highly demandable. Perovskite halides, namely methyl ammonium lead iodide (CH<sub>3</sub>NH<sub>3</sub>PbI<sub>3</sub>) / MAPI is widely popular as photovoltaic and optoelectronic material. Recently we have found that MAPI can act also as an active material for gas sensing to trace hazards pollutants. Ammonia (NH<sub>3</sub>) not only is one of harmful pollutants in nature but also treated as a biomarker for kidney disease via exhaled breathe analysis in recent days. Thus a room temperature, cost effective, very high sensitivity NH<sub>3</sub> gas sensor could be extremely beneficial in view point of both environmental and clinical issues. The sensor using MAPI can trace ammonia gas (NH<sub>3</sub>) by a visual color change method as well as by electrical read out [1-2]. Here we have shown a MAPI based electrical sensor grown on a cheap paper as a substrate for tracing NH<sub>3</sub> gas. The paper sensor has a very high sensitivity (98% for 10 ppm NH<sub>3</sub>) towards NH<sub>3</sub> gas at room temperature and sub ppm (<1 ppm) detection capability (down to 10 ppb) by its noise limited detectability [2]. This ultra high response down to ppb level

can be extremely suitable for exhaled breathe analysis. Current through the sensor increases nearly by one order on exposure to only 10 ppm NH<sub>3</sub> gas with a bias voltage of 1 V DC and hence the sensor consumes extremely low power (~ few nano watts). The paper sensor is also highly selective to NH<sub>3</sub> gas and maintains stability over 150 days within decrease of 10% sensitivity. This could open up the possibility of perovskite halide (MAPI) as next generation solid state room temperature gas sensor for rapid and cost effective detection using paper electronics. References: [1] Maity, A; Ghosh,B; Fast Response paper based visual color change gas sensor for efficient ammonia detection at room temperature; Scientific Reports (2018), 8,16851 [2] Maity, A; Raychaudhuri, A.K.; Ghosh,B ; High sensitivity NH<sub>3</sub> gas sensor with electrical readout made on paper with perovskite halide as sensor material; Scientific Reports (2019) ,9,7777 I

SESSION F.EL08.17: Poster Session V: Materials and Chemistry  
On Demand Abstracts Available for Viewing Starting Saturday Morning, November 21, 2020  
5:00 AM - 8:00 AM  
F-EL08

### F.EL08.17.01

**Suppressing Cation Migration in Triple-Cation Lead Halide Perovskites** Iliia M. Pavlovec<sup>1</sup>, Michael Brennan<sup>1</sup>, Sergiu Draguta<sup>1</sup>, Anthony Ruth<sup>1</sup>, Jeffrey A. Christians<sup>2</sup>, Taylor Moot<sup>3</sup>, Steven Harvey<sup>3</sup>, Joseph Luther<sup>3</sup> and Masaru Kuno<sup>1,1</sup>; <sup>1</sup>University of Notre Dame, United States; <sup>2</sup>Hope College, United States; <sup>3</sup>National Renewable Energy Laboratory, United States

Mixed cation and anion APbX<sub>3</sub>-type lead halide perovskites [A<sup>+</sup>=Cs<sup>+</sup>, CH<sub>3</sub>NH<sub>3</sub><sup>+</sup> [MA<sup>+</sup>], or (NH<sub>2</sub>)<sub>2</sub>CH<sup>+</sup> [FA<sup>+</sup>]; X<sup>-</sup>=Br<sup>-</sup> or I<sup>-</sup>] have received extensive attention for use as low cost, efficient light harvesters in solar cells. Issues regarding long-term active layer stability, however, remain unresolved. Electric field-induced ion migration in perovskite solar cells is of particular concern because it results in current-voltage (J-V) hysteresis, metastable power conversion efficiencies and accelerated active layer degradation. Facile ion migration within the perovskite lattice stems from relatively fragile ionic bonding between heavy, low-valence ions. This results in small activation barriers and correspondingly moderate diffusion coefficients for halide anions and A-site cations. The mobile nature of A<sup>+</sup> cations and X<sup>-</sup> anions is thus an instability of all metal halide perovskites. While numerous recent studies have focused on halide migration and segregation, significantly less work has gone into investigating cation migration in metal halide perovskites. This is especially true of double- and triple-cation FA<sub>x</sub>MA<sub>y</sub>Cs<sub>1-x-y</sub>PbX<sub>3</sub> alloys.

Here, we demonstrate that bias-induced cation migration is mitigated in mixed  $\alpha$ -phase/ $\delta_{\text{ortho}}$ -CsPbI<sub>3</sub> triple-cation FA<sub>x</sub>MA<sub>y</sub>Cs<sub>1-x-y</sub>PbI<sub>3</sub> films (referred as  $\alpha/\delta$ -FA<sub>0.33</sub>MA<sub>0.33</sub>Cs<sub>0.33</sub>PbI<sub>3</sub>). We verify this by comparing cation movement in lateral devices and working solar cells made of pure  $\alpha$ -phase double-/triple-cation perovskite phase systems (FA<sub>0.85</sub>Cs<sub>0.09</sub>PbI<sub>3</sub> and FA<sub>0.76</sub>MA<sub>0.15</sub>Cs<sub>0.09</sub>PbI<sub>3</sub>) as well as  $\alpha/\delta$ -FA<sub>0.33</sub>MA<sub>0.33</sub>Cs<sub>0.33</sub>PbI<sub>3</sub>. The effects of bias-induced A<sup>+</sup> migration on perovskite stability and device performance are assessed via infrared photothermal heterodyne imaging (IR-PHI), time-of-flight secondary ion mass spectrometry (ToF-SIMS), and solar cell operational stability testing. Enhanced  $\alpha/\delta$ -FA<sub>0.33</sub>MA<sub>0.33</sub>Cs<sub>0.33</sub>PbI<sub>3</sub> cation stability likely stems from “post-perovskite”  $\delta_{\text{ortho}}$ -CsPbI<sub>3</sub> inclusions within parent thin films that act as barriers through which cations cannot easily migrate. This resistance to cation migration translates into improved device operational stability of  $\alpha/\delta$ -FA<sub>0.33</sub>MA<sub>0.33</sub>Cs<sub>0.33</sub>PbI<sub>3</sub> lateral devices and solar cells relative to complementary, triple-cation,  $\alpha$ -phase FA<sub>0.76</sub>MA<sub>0.15</sub>Cs<sub>0.09</sub>PbI<sub>3</sub> devices. This study therefore provides new insights into cation migration in working devices and outlines a materials design strategy for stabilizing metal halide perovskites against bias-induced cation migration.

### F.EL08.17.02

**Efficient of Ion Migration in Perovskite Solar Cells with Hexagonal Boron Nitride** Yifan Yin, Yuchen Zhou and Miriam H. Rafailovich; Stony Brook University, The State University of New York, United States

Organic-inorganic halide perovskite solar cells (PSCs) have been considered a viable member of next generation photovoltaics, which can address the scalability changes with a low-cost solution process. The energy lose in the hybrid system has been approved to be principally caused by defects/traps at grain boundaries and surfaces as well as point defects such as interstitial defects or vacancies in the perovskite compounds crystal lattice. Because of the presence of these defects, both anions (I) and cations (MA<sup>+</sup>) can migrate through the organic layer which provides a degradation pathway for perovskite materials even in those well-encapsulated devices: the halide ions can react with metal electrodes such as Ag, forming insulating components (AgI). In addition to the corrosion of electrode, halide ions migrating into organic hole transport layer (HTL) which is deleterious to transport properties, thus retarding device efficiency, especially under solar cell working

conditions. Inspired by the quasi-2D-perovskite which shows a great stability in photovoltaic performance, here, the hexagonal boron nitride (h-BN) was incorporated into the perovskite absorber as an ionic diffusion barrier. The lamellar structure of h-BN consists of a lattice similar to graphite which can be subjected to exfoliation leading to few-layers nanosheets. The exfoliated 2D-layered materials present high surface area and quantum confinement, and also high chemical stability. The integration of this low-cost, lower dimensional material enables a better device stability as the result from the efficient suppression on the ion-migration induced degradation. With the aid of time-of-flight secondary ion mass spectroscopy (TOF-SIMS) and energy dispersive x-ray spectroscopy (EDX). The h-BN/ perovskites has an initial PCE over 20% that shows no degradation exhibit in over 72 h and retained 80% of the original PCE after 800hr, whereas the PCE of pristine MAPI devices diminishes by more than 30% within the first 24 hr.

#### F.EL08.17.03

**Light-Induced Degradation of Hybrid Organic-Inorganic Perovskites Reveals Autocatalytic Kinetics and Increased Stability with Substitution of Larger Organic Cations** Emily C. Smith, Christie Ellis, Hamza Javaid and Dhandapani Venkataraman; University of Massachusetts Amherst, United States

Instability under illumination in hybrid organic-inorganic perovskite solar cells represents a major roadblock to the development and commercialization of this thin-film technology. Recently, it has been shown that varying the nature of the organic cation in the perovskite structure represents a potential pathway to tuning stability of materials under illumination. However, many potential mixed-cation perovskite compositions remain unexplored, and, much is still unknown about the degradation kinetics in mixed-cation thin-films. In this work, we successfully fabricated thin-films of substituted methylammonium lead triiodide (MAPI), where we substituted the methylammonium ion with varying percentages of three larger organic cations: imidazolium, dimethylammonium, and guanidinium. We achieved substitution of these large cations for compositions of up to 20-30% while maintaining the structure and optoelectronic properties of the films. We studied the degradation kinetics of the mixed-cation films under illumination using powder x-ray diffraction. We observed that the degradation is autocatalytic. Furthermore, we calculated rate coefficients for the degradation process and observed that the degradation was slowed in films which contained  $\leq 20\%$  of any of the larger cations compared to pristine MAPI films. A maximum decrease of 62% in the degradation rate coefficient was observed in the case of 5% guanidinium substitution. Ultimately, this work provides key insight into the degradation kinetics of mixed-cation perovskite films under illumination and provides a strategy for further stabilization of perovskite thin-films for improved photovoltaic performance.

#### F.EL08.17.04

**Effect of Pyrazine and Guanidinium Thiocyanate (GuaSCN) on the Structure and Bandgap of Pb and Pb-Free Halide Perovskites** Rubaiya Murshed and Shubhra Bansal; University of Nevada Las Vegas, United States

Perovskite solar cells (PSCs) research has been projected over the past decade due to its promising photovoltaic properties, increasing efficiency and low cost. With a need to eliminate toxic lead from prevailing halide perovskite solar cells, several low-toxicity cations have been proposed, among them Sn(II) is considered as one of the most suitable replacements due to its similar electronic configuration and ionic radius to Pb(II). But the Sn-based perovskites are still plagued with low efficiency, oxidation and phase instability. Here we demonstrate the use of atmospheric solution-processed lead-free all inorganic molecular iodide compound cesium tin iodide ( $\text{Cs}_2\text{SnI}_6$ ) as the light absorber in PSCs. The presence of excess  $\text{SnF}_2$  in precursor solution assists phase separation. Due to the good binding affinity to  $\text{SnF}_2$ , pyrazine is expected to reduce Sn vacancy thus restricts phase separation. The effect of GuaSCN results in increasing grain size and improving film morphology thus improves the structural and optoelectronic properties of low bandgap perovskites. The present work aims at analyzing the effect of pyrazine and guanidinium thiocyanate (GuaSCN) in oxidation reduction and fabrication of low bandgap (1.3 eV)  $\text{Cs}_2\text{SnI}_6$  films when used separately as a mediator during film fabrication in GBL. Initial results suggest both pyrazine and guanidinium thiocyanate give absorption onset at higher optical wavelength ( $>1000$  nm) and low bandgap ( $\sim 1.2$ -1.3 eV). Films in addition of Pyrazine both with and without  $\text{SnF}_2$  (0 mol% and 40 mol%) shows mostly cubic  $\text{Cs}_2\text{SnI}_6$  diffraction patterns in XRD analysis which implies that the effect of  $\text{SnF}_2$  is not considerable in this case. The SCN ions increases grain size and produces cubic  $\text{Cs}_2\text{SnI}_6$  crystals. Heating at higher temperature leads to samples with lower bandgap. Both the absorption vs. wavelength and tauc plot analyses show bandgap at around 1.25 eV. Most of the samples after dark testing for over 100 hours at 65 °C retain their properties and show similar absorption edge and bandgap patterns. Samples having exposure to light at 65 °C show higher bandgap over 2 eV. In this study, the effect of these additives in  $\text{Cs}(\text{Pb},\text{Sn})\text{I}_3$  perovskite with a Sn-Pb ratio of 60:40 is also included. Primary results show separately use of both pyrazine and GuaSCN in precursor solution in a mixture of GBL and DMF result in low bandgap perovskites. Both  $\text{Cs}(\text{Pb},\text{Sn})\text{I}_3$  and  $\text{Cs}_2\text{SnI}_6$  without these additives tend to have higher bandgap at around 2.3 eV when deposited on glass substrates. Further analysis of the effect of Pyrazine and GuaSCN additives in the stability, morphology and lifetime of  $\text{Cs}(\text{Pb},\text{Sn})\text{I}_3$  and

Cs<sub>2</sub>SnI<sub>6</sub> perovskite films will be continued in this study.

#### F.EL08.17.05

**Enabling High Photoconversion Efficiency in Lead-Free Antimony-Based Perovskite Derivatives by Tuning Crystallographic Dimensionality and Microstructure** Vincenzo Pecunia, Yueheng Peng and Fengzhu Li; Soochow University, China

The exploration of lead-free perovskite-inspired semiconductors for optoelectronic applications (e.g., single- and multi-junction solar cells, photocathodes for water splitting, photodetectors) has captured ever-growing attention, driven by their promise to replicate the success of the Pb-based counterparts without the toxicity concerns associated with the latter. In particular, an emerging approach to Pb replacement involves Sb, whose attractiveness resides in its highly-polarizable Sb<sup>3+</sup> cations with filled 5s orbitals, a stable oxidation state, and an ionic radius comparable to Pb<sup>2+</sup>. A number of antimony-halide perovskite derivatives with a formula A<sub>3</sub>Sb<sub>2</sub>X<sub>9</sub> (A<sup>+</sup>: monovalent cation; X<sup>-</sup>: halide anion) have thus been explored. Notwithstanding the rise in their reported performance, A-Sb-X absorbers are yet to deliver photoconversion efficiencies comparable to the Pb-based counterparts. Importantly, this has been linked to the zero-dimensional (0D) structure of most A-Sb-X embodiments, as the more attractive two-dimensional (2D) embodiments have been demonstrated only in very few instances, due to constraints on composition or processing conditions.

With the aim of contributing to the realization of the full potential of antimony-halide perovskite derivatives, we have investigated two such systems featuring a desirable 2D structure, exploring the impact of dimensionality, microstructure, and crystallographic orientation on their photoconversion behavior. Herein, we firstly focus on Rb<sub>3</sub>Sb<sub>2</sub>I<sub>9</sub>, the only ternary A-Sb-I with a direct bandgap, and also having the smallest exciton binding energy of all reported A-Sb-I embodiments.<sup>1</sup> In order to assess the role of microstructure on the photoconversion efficiency of Rb<sub>3</sub>Sb<sub>2</sub>I<sub>9</sub>, we have developed two strategies for its microstructural enhancement, which involve the control of the supersaturation level during the annealing step, or a high-temperature treatment in SbI<sub>3</sub> vapor. Both strategies deliver a dramatic improvement in the film morphology and microstructure.<sup>2</sup> Within sandwich-type planar devices, the resultant high-quality films enable a substantial improvement in external quantum efficiency (EQE), reaching up to 65.4% at short circuit, i.e., the highest to date for perovskite-inspired antimony-/bismuth-halide A<sub>3</sub>M<sub>2</sub>X<sub>9</sub> (M: Sb<sup>3+</sup>/Bi<sup>3+</sup>). Importantly, this is achieved without the aid of a mesoporous architecture for charge extraction, thereby revealing the inherent capability and potential of Rb<sub>3</sub>Sb<sub>2</sub>I<sub>9</sub> for efficient photoconversion.

We additionally discuss the impact of dimensionality on the photoconversion capabilities of the Cs<sub>3</sub>Sb<sub>2</sub>X<sub>9</sub> system. Departing from the dedicated high-temperature (≥ 230 °C) processing protocols pursued in the prior literature, we demonstrate that halide mixing enables the 0D-to-2D structural conversion of the Cs<sub>3</sub>Sb<sub>2</sub>X<sub>9</sub> system at temperatures < 150 °C.<sup>3</sup> The resultant 2D absorbers manifest a considerable photoconversion efficiency boost with respect to the 0D counterpart, attaining a peak EQE of 62.5%, which is at the state-of-the-art for all antimony-/bismuth-halide perovskite derivatives.

Through photocurrent-power characterization and Hall effect measurements, we finally reveal that the EQE boost achieved with both 2D Rb<sub>3</sub>Sb<sub>2</sub>I<sub>9</sub> and Cs<sub>3</sub>Sb<sub>2</sub>X<sub>9</sub> arises from their improved charge carrier transport, which we relate to the microstructural enhancement, dimensionality tuning, and crystallographic orientation. Such performance boost and mechanistic insight constitute an important step in realizing the full potential of lead-free antimony-halide perovskite derivatives and related bismuth-based homologs for their application in optoelectronics and photovoltaics.

1 J. P. Correa-Baena et al., *Chem. Mater.*, 2018, **30**, 3734–3742.

2 F. Li, Y. Wang, K. Xia, R. L. Z. Hoye and V. Pecunia, *J. Mater. Chem. A*, 2020, **8**, 4396–4406.

3 Y. Peng et al., *Appl. Mater. Today*, 2020, **19**, 100637.

#### F.EL08.17.06

**A Critical Assessment of the Use of Excess Lead Iodide in Lead Halide Perovskite Solar Cells** Bart Roose, Krishanu Dey, Yu-Hsien Chiang, Richard Friend and Samuel D. Stranks; University of Cambridge, United Kingdom

It is common practice in the lead halide perovskite solar cell field to add a small molar excess of lead iodide (PbI<sub>2</sub>) to the precursor solution in order to increase device performance. However, recent reports have shown that an excess of PbI<sub>2</sub> can accelerate performance loss. In addition, PbI<sub>2</sub> is photoactive (bandgap ~2.3 eV), which may lead to parasitic absorption losses in a solar cell.

We use XRD and SEM to show that incorporation of  $\text{PbI}_2$  into the perovskite film is not straightforward and can have very different effects, depending on how and where  $\text{PbI}_2$  is present. At low concentrations,  $\text{PbI}_2$  facilitates charge extraction and improves device performance. For higher concentrations,  $\text{PbI}_2$  influences how perovskite crystallises and a thick  $\text{PbI}_2$  layer can be formed that impedes charge extraction. We show that devices using an optimized quantity of excess  $\text{PbI}_2$  exhibit better device performance as compared to stoichiometric devices, both initially and for the duration of a stability test under operating conditions, primarily by enhancing charge extraction. However,  $\text{PbI}_2$  is gradually degraded during device operation, largely negating the beneficial effect on charge extraction and introducing trap states that are detrimental for device performance. We find that although excess  $\text{PbI}_2$  provides a good template for enhanced performance as compared to stoichiometric devices, it can not meet stability requirements needed for commercialization of perovskite solar cells. The community must continue to seek other additives or synthesis routes that fulfill the same beneficial role as excess  $\text{PbI}_2$ , but which do not suffer from light induced degradation.

#### F.EL08.17.07

**Understanding the Instability of the Halide Perovskite  $\text{CsPbI}_3$  Through Temperature-Dependent Structural Analysis** Daniel B. Straus<sup>1</sup>, Shu Guo<sup>1</sup>, AM Milinda Abeykoon<sup>2</sup> and Robert J. Cava<sup>1</sup>; <sup>1</sup>Princeton University, United States; <sup>2</sup>Brookhaven National Laboratory, United States

Despite the tremendous interest in halide perovskite solar cells, the structural reasons that cause the all-inorganic perovskite  $\text{CsPbI}_3$  to be unstable at room temperature remain mysterious especially since many tolerance factor-based approaches predict  $\text{CsPbI}_3$  should be stable as a perovskite. Here single-crystal X-ray diffraction and X-ray pair distribution function (PDF) measurements characterize bulk perovskite  $\text{CsPbI}_3$  from 100 to 295 K to elucidate its thermodynamic instability. While Cs occupies a single site from 100 to 150 K, it splits between two sites from 175 to 295 K with the second site having a lower effective coordination number, which along with other structural parameters suggests that Cs rattles in its coordination polyhedron. PDF measurements reveal that on the length scale of the unit cell, the Pb-I octahedra concurrently become greatly distorted, with one of the I-Pb-I angles approaching  $82^\circ$  compared to the ideal  $90^\circ$ . The rattling of Cs, low number of Cs-I contacts, and high degree of octahedral distortion cause the instability of perovskite-phase  $\text{CsPbI}_3$ . These results reveal the limitations of tolerance factors in predicting perovskite stability and provide detailed structural information that suggests methods to engineer stable  $\text{CsPbI}_3$ -based solar cells.

#### F.EL08.17.08

**Enhanced Bending Fracture Behavior of Flexible Halide Thin Films Processed with *In Situ* Stress** Da Bin Kim and Yong Soo Cho; Yonsei University, Korea (the Republic of)

Halide perovskites have emerged as attractive materials for electronic and optoelectronic applications because of their unique properties and low-temperature processing. However, the mechanical aspects of the halide thin films have been very limitedly reported although strong bending fracture behavior is required for the flexible system. Here, we suggest a very promising processing way to enhance the bending fracture behavior of the flexible halide thin films with fundamental definitions of the mechanical parameters of the halide materials that have been also unavailable thus far. The processing is based on the assignments of in-situ compressive or tensile stress during the film deposition with a controllable manner. As a result, a substantial improvement of the fracture resistance against the bending operation was observed for the compressively stressed halide thin films. For example as a result of bending fracture evaluation, cesium lead bromide ( $\text{CsPbBr}_3$ ) and methylammonium lead iodide ( $\text{MAPbI}_3$ ) thin films prepared on PEDOT:PSS-coated polyethersulfone (PES) substrates demonstrated high fracture mode I toughness of 1.18 and 1.66  $\text{MPa m}^{0.5}$  for the in-situ compressive strain of -1.09%, which correspond to the enhancements by ~97 and ~100 %, respectively, compared to those for the reference samples. The structural origins of the mechanical enhancements are elucidated with experimental evidences on the variations in lattice distortion and bonding length.

#### F.EL08.17.09

**Structural Evolution of Layered Hybrid Lead Iodide Perovskites—Colloidal Nanocrystals or Ruddlesden-Popper Phases?** Clayton J. Dahlman<sup>1</sup>, Naveen Venkatesan<sup>1</sup>, Patrick Corona<sup>2</sup>, Rhys M. Kennard<sup>1</sup>, Lingling Mao<sup>1</sup>, Noah Smith<sup>2</sup>, Jiamin Zhang<sup>2</sup>, Ram Seshadri<sup>1,2</sup>, Matthew Helgeson<sup>2</sup> and Michael Chabinye<sup>1</sup>; <sup>1</sup>The University of California, Santa Barbara, United States; <sup>2</sup>University of California, Santa Barbara, United States

Hybrid organic-inorganic perovskites (HOIPs) are promising semiconductors with long carrier lifetimes, synthetic tunability, remarkable defect tolerance and simple processing. Recently, 2D analogues have been made by adding insulating cations (e.g. butylammonium) to separate the perovskite structure into sheets. These 2D materials can be formed either in thin films,

large single crystals or as dispersed nanoplatelets of only a few PbX<sub>6</sub> octahedra thick. The number of PbX<sub>6</sub> octahedra confined between insulating layers (i.e. the ‘*n*-value’) can be tuned by varying precursor stoichiometry, enabling discrete tunability of the bandgap through dielectric and quantum confinement. Controlling the structure of layered hybrid metal halide perovskites, such as the Ruddlesden-Popper (R-P) phases, is challenging because of their tendency to form mixtures of varying composition. Colloidal growth techniques can form dispersions of particles with properties that match the bulk properties of layered R-P phases, but controlling the composition of these particles remains challenging.

In this talk, we explore the microstructure of particles of R-P phases of methylammonium lead iodide prepared by antisolvent precipitation from ternary mixtures of different alkylammonium cations, where one cation is able to form perovskite phases (CH<sub>3</sub>NH<sub>3</sub><sup>+</sup>) and the other two promote layered structures as spacers (e.g. C<sub>4</sub>H<sub>9</sub>NH<sub>3</sub><sup>+</sup> and C<sub>12</sub>H<sub>25</sub>NH<sub>3</sub><sup>+</sup>). We illustrate how competition between cations that act as spacers between layers, or as grain-terminating ligands, determines the colloidal particle size of R-P crystallites that form in solution. Optical measurements reveal that quantum well dimensions can be tuned by engineering the ternary cation composition. Transmission synchrotron wide-angle X-ray scattering and small angle neutron scattering reveal changes in the structure of colloids in solvent and after deposition into thin films. In particular, we find that spacers can alloy between R-P layers if they share common steric arrangements, but tend to segregate into polydisperse R-P phases if they do not mix. This study provides a framework to compare the microstructure of colloidal layered perovskites and suggests clear avenues to control phase and colloidal morphology.

#### F.EL08.17.10

**Adhesion and Interfacial Fracture of Perovskite Solar Cells** Reisya Ichwani, Vanessa Uzonwanne, Juan Martin Hinostroza Tamayo, Deborah Oyewole, Oluwaseun K. Oyewole, Nancy Burnham and Winston Soboyejo; Worcester Polytechnic Institute, United States

Emerging perovskite solar cells (PSCs) are not only required to be highly efficient, but also durable. The mechanical stability of PSCs also requires good adhesion and contacts across their interfaces. These are studied using atomic force microscopy (AFM) and fracture mechanics approaches. AFM pull-off forces are measured for bi-material interfaces that are present in model perovskite solar cells. These are then incorporated into adhesion models for the estimation of adhesion energies and mode I interfacial fracture energies. The mode mixity dependence of interfacial fracture toughness is also studied for interfaces between the perovskite and electron transport layers in PSCs. This is done using Brazil Disk specimens that are used to study the robustness of the interfaces across a range of mode mixities between pure mode I and pure mode II. The underlying crack/microstructure interactions and fracture modes are used to provide insights into the underlying crack-tip shielding due to crack bridging and microcracking. These are modeled using zone and row models that are used to predict the mode-mixity dependence of fracture toughness. The implications of the results are also discussed for the determination of crack path selection criteria in perovskite solar cells.

#### F.EL08.17.11

**Double Perovskite Nanofibers for Photovoltaic and Optoelectronic Applications** Nageh K. Allam; American University in Cairo, Egypt

Organic-inorganic hybrid perovskite compounds are currently the archetypal materials for high performance photovoltaic (PV) and optoelectronic devices. However, the remaining bottlenecks preventing their large scale production are their environmental/thermal instability and lead toxicity. Herein, we demonstrate a novel approach to synthesize single-phase electrospun Cs<sub>2</sub>SnI<sub>x</sub>Cl<sub>6-x</sub> double perovskites with varying halide content (I, Cl or mixed I/Cl) as active materials for potential application in perovskite solar cells (PSCs). The x-ray photoelectron spectroscopy and Raman spectroscopy analyses indicated the *in-situ* formation of graphene oxide (GO) during the annealing process. The GO layer was found to enhance the optical properties and thermal stability of the fabricated perovskites even at high Cl content. Moreover, the presence of GO as an insulating layer significantly decreases the bandgap energy of the resulting perovskites. The perovskites with a mix of iodide and chloride ions showed significantly improved optical properties with higher photoluminescence (PL) intensity than that of pure chloride or iodide counterparts. Moreover, the compound with low chloride content showed superior thermal stability to those reported in the literature. Therefore, the application of the electrospinning technique is a useful strategy to *in-situ* incorporate GO in a lead-free perovskite matrix for potential photovoltaic and optoelectronic applications.

#### F.EL08.17.12

**Organic-Inorganic Hybrid Perovskite Single-Crystal Thin Films—Synthesis and Photoluminescence** Xiaobing Tang<sup>1</sup>, Zhaojin Wang<sup>2</sup>, Kai Wang<sup>2</sup> and Fuqian Yang<sup>1</sup>; <sup>1</sup>University of Kentucky, United States; <sup>2</sup>Southern University of Science and



Technology, China

Metallic halide organic–inorganic hybrid perovskites with excellent optoelectrical properties have potential applications in optoelectronic devices and systems. In this work, we demonstrate the feasibility of preparing  $\text{CH}_3\text{NH}_3\text{PbBr}_3$  single crystal thin films on poly-TPD hole transport layer by controlling the heating rates. The crystallinity and trap state density of the  $\text{CH}_3\text{NH}_3\text{PbBr}_3$  thin films are characterized by X-ray diffraction and photoluminescence and time-resolved photoluminescence, respectively. The crystallinity with the peak intensity of (100) plane of the  $\text{CH}_3\text{NH}_3\text{PbBr}_3$  thin films prepared at 2 °C/h is nine times of that prepared at 10 °C/h. The  $\text{CH}_3\text{NH}_3\text{PbBr}_3$  thin films prepared at 2 °C/h exhibit a carrier lifetime of 21 ns, which is much larger than 0.6 ns for the  $\text{CH}_3\text{NH}_3\text{PbBr}_3$  thin films prepared at 10 °C/h, and an excellent structural stability. Acknowledgements: KW is grateful for the support from National Key Research and Development Program (No.2017YFE0120400) and National Natural Science Foundation of China (No.61875082). FY is grateful for the support from National Science Foundation (CMMI-1854554)

#### F.EL08.17.13

**Hybrid Lead Iodide Perovskites with Aromatic Diammonium Cations** Xiaotong Li<sup>1</sup>, Weijun Ke<sup>1</sup>, Yihui He<sup>1</sup>, Peijun Guo<sup>2</sup>, Mikael Kepenekian<sup>3</sup>, Boubacar Traore<sup>3</sup>, Jacky Even<sup>3</sup>, Claudine Katan<sup>3</sup>, Constantinos Stoumpos<sup>1</sup>, Richard D. Schaller<sup>2</sup> and Mercouri G. Kanatzidis<sup>1</sup>; <sup>1</sup>Northwestern University, United States; <sup>2</sup>Argonne National Laboratory, United States; <sup>3</sup>University of Rennes, France

Aromatic diammonium cation, x-(aminomethyl)pyridinium (AMPY, x = 3 or 4) can form 2D Dion-Jacobson lead iodide perovskite, which adopt the general formula of  $(x\text{AMPY})(\text{MA})_{n-1}\text{Pb}_n\text{I}_{3n+1}$  (MA = methylammonium, n = 1–4). By modifying the position of the  $-\text{CH}_2\text{NH}_3^+$  group from 4AMPY to 3AMPY, the stacking of the inorganic layers changes from exactly eclipsed to slightly offset. The perovskite octahedra tilts are also different between the two series, with the 3AMPY series exhibiting smaller bandgaps than the 4AMPY series. Compared to the aliphatic cation of the same size (AMP = (aminomethyl)piperidinium), the aromatic spacers increase the rigidity of the cation, reduce the interlayer spacing and decrease the dielectric mismatch between inorganic layer and the organic spacer, showing the indirect but powerful influence of the organic cations on the structure and consequently on the optical properties of the perovskite materials. Preliminary solar cell devices based on the n = 4 perovskites as absorbers of both series exhibit promising performances. More interestingly, when using 1:4 ratio of AMPY:PbO as starting materials, totally different structures with 3D connection motif form instead. However, because of the steric requirement of the Goldschmidt tolerance factor rule, it is impossible for  $(x\text{AMPY})\text{M}_2\text{I}_6$  to form proper perovskite structures. Instead, a combination of corner-sharing and edge-sharing connectivity is adopted in these compounds leading to the new 3D structures. Devices of  $(3\text{AMPY})\text{Pb}_2\text{I}_6$  crystals exhibit clear photoresponse under ambient light without applied bias, reflecting a high carrier mobility ( $\mu$ ) and long carrier lifetime ( $\tau$ ) and great potential for photo and X-ray detection applications.

#### F.EL08.17.14

**Exploring the Limit of Layer Thickness in 2D Hybrid Lead Halide Perovskites** Eugenia S. Vasileiadou<sup>1</sup>, Bin Wang<sup>2</sup>, Ioannis Spanopoulos<sup>1</sup>, Ido Hadar<sup>1</sup>, Alexandra Navrotsky<sup>3,2</sup> and Mercouri G. Kanatzidis<sup>1</sup>; <sup>1</sup>Northwestern University, United States; <sup>2</sup>University of California, Davis, United States; <sup>3</sup>Arizona State University, United States

Two-dimensional (2D) hybrid organic-inorganic halide perovskites are a rapidly emerging class of semiconductors whose structural tunability and optoelectronic properties have led to the successful fabrication of solar cell devices with high power conversion efficiency. The features of the 2D perovskite structure that are tuned are the organic “spacer” cation and the number of the inorganic layers (n). There is a significant interest to target higher n-member compounds for light harvesting applications, due to their attractive photophysical properties such as low bandgap value and high carrier mobility. Herein, we present a comprehensive study on exploring the limit of layer thickness of bulk 2D lead halide perovskites through structural and thermodynamic study. Phase-pure synthesis of a new n=6 perovskite compound is reported with the characterization of the single crystal structure and optical properties of the material. Thorough calorimetry studies examine the thermodynamic stability of 2D lead iodide perovskites with layer thickness n=2-6. The favorable enthalpy of formation n=6 crystals shows that higher n-layer thickness is dependent on specific structural aspects. Additionally, the systematic investigation of the variances on the structural parameters and optical properties between different structure types of 2D perovskites, offers guiding principles for the targeted design and synthesis of 2D perovskites for efficient solar cell fabrication. Lastly, the stability studies of thin films demonstrate consistent observations with the thermochemical findings, further shedding light on the behavior of high n-layer perovskite materials.

#### F.EL08.17.15

**Amorphous Halide Perovskite Thin Films** Susan Rigter<sup>1,2</sup> and Erik C. Garnett<sup>1,2</sup>; <sup>1</sup>AMOLF, Netherlands; <sup>2</sup>University of

Amsterdam, Netherlands

Lead halide perovskites are one of the most exciting and heavily researched classes of optoelectronic materials due to their unique ability to form high quality crystals with tunable band gaps in the visible and near infrared using simple solution precipitation reactions. This facile crystallization is driven by their ionic nature; just as with other salts, it is challenging to form amorphous halide perovskites, particularly in thin-film form where they can most easily be studied. Herein, we show that rapid desolvation promoted by addition of acetate precursors is a general method for making amorphous lead halide perovskite films with a wide variety of compositions, including those using all the common cations (cesium, methylammonium, formamidinium) and anions (bromide, iodide). We show that by controlling the amount of acetate, it is possible to tune from fully crystalline to fully amorphous films, with an interesting intermediate state consisting of crystalline islands embedded in an amorphous matrix. The amorphous lead halide perovskite has a large and tunable optical band gap and improves the optical properties of incorporated crystalline perovskite, opening up the intriguing possibility of using amorphous perovskite as a passivating window layer, as is currently done in record efficiency silicon solar cells.

#### F.EL08.17.16

**Facile Healing of Cracks in Organic-Inorganic Halide Perovskite Thin Films** Srinivas K. Yadavalli, Zhenghong Dai, Min Chen, Mingyu Hu, Yuanyuan Zhou and Nitin Padture; Brown University, United States

Organic-inorganic halide perovskite (OIHP) thin films have attracted a great deal of interest as photoactive materials in various optoelectronic devices due to their unprecedented photophysical properties, but their long-term reliability is likely to be limited by their poor mechanical properties. In this context, we explain different possible modes of fracture in OIHP based devices, and for the first time demonstrate facile healing of through-thickness cracks in OIHP thin films which can otherwise be detrimental to the device properties. This is achieved through application of either a moderate compressive stress at room-temperature or a simple heat treatment at moderate temperatures. Based on the findings from a series of *ex situ* residual stress measurements, crack-healing process is found to be time-dependent, which indicates that facile mass-transport in OIHPs plays a key role in this phenomenon. The mechanisms governing crack-healing process are explained based on the fundamentals of brittle fracture. This discovery has broad implications for the prevention and/or restoration of the overall performance, environmental stability, and mechanical reliability of OIHP based devices like solar cells which are poised for commercialization.

#### F.EL08.17.17

**Understanding the Effects of Moisture and Stoichiometry Variations on Composition and Structure in Halide Perovskite Solar Cells** Juanita Hidalgo<sup>1</sup>, Carlo Andrea Riccardo Perini<sup>1</sup>, Andres Felipe Castro Mendez<sup>1</sup>, Barry Lai<sup>2</sup>, Ruipeng Li<sup>3</sup>, Shijing Sun<sup>4</sup>, Antonio Abate<sup>5</sup> and Juan Pablo Correa Baena<sup>1</sup>; <sup>1</sup>Georgia Institute of Technology, United States; <sup>2</sup>Argonne National Laboratory, United States; <sup>3</sup>Brookhaven National Laboratory, United States; <sup>4</sup>Massachusetts Institute of Technology, United States; <sup>5</sup>Helmholtz-Zentrum Berlin für Materialien und Energie, Germany

Hybrid halide lead perovskites are promising materials for photovoltaic applications. Nonetheless, these materials are highly sensitive and degrade in various environmental conditions. Among these, moisture is a prime cause of material degradation, representing a threat to the commercialization of perovskite-based materials. Hence, it is essential to study how water interacts with a perovskite thin film, what factors trigger instability in the material, and loss in solar cell performances. In order to understand these degradation mechanisms, we expose  $\text{Cs}_{0.05}(\text{MA}_{0.17}\text{FA}_{0.83})_{0.95}\text{Pb}(\text{I}_{0.83}\text{Br}_{0.17})_3$  perovskite thin films with different precursor stoichiometries (organic to inorganic ratios) to a moisture treatment with high relative humidity. We monitor the evolution of perovskite crystalline structure, and we correlate it to changes in performances. Characterization with SEM images show morphological changes in the grain size, and XRD patterns evidence structural features that are further explained and understood by grazing incidence wide angle X-ray scattering (GIWAXS). Remarkably, we observe improved photovoltaic efficiency for treated films with an excess organic component, correlated with vertical orientation along the (001) plane. In addition, synchrotron-based X-ray fluorescence and X-ray beam induced current (XRF-XBIC) is used to correlate the elemental distribution with the current output of the devices.

SESSION F.EL08.18: Poster Session VI: Materials Discovery—Theory, Experiment, Data  
On Demand Abstracts Available for Viewing Starting Saturday Morning, November 21, 2020

### F.EL08.18.01

**HybriD<sup>3</sup> and MatD<sup>3</sup>: Curated Materials Data for Hybrid Organic-Inorganic Perovskites and a General Software Stack for Materials Data** Xiaochen Du<sup>1,1</sup>, Raul Laasner<sup>1</sup>, Xixi Qin<sup>1</sup>, Connor Clayton<sup>2</sup>, Svenja Janke<sup>1</sup>, Becca Lau<sup>1</sup>, Chi Liu<sup>1</sup>, Sampreeti Bhattacharya<sup>3</sup>, Juliana Mendes<sup>4</sup>, Jun Hu<sup>3</sup>, Dovletgeldi Seyitliyev<sup>4</sup>, Ruyi Song<sup>1</sup>, Manoj Jana<sup>1</sup>, Matti Ropo<sup>5</sup>, Franky So<sup>4</sup>, Kenan Gundogdu<sup>4</sup>, Wei You<sup>3</sup>, Yosuke Kanai<sup>3</sup>, David Mitzi<sup>1,1</sup> and Volker Blum<sup>1,1</sup>; <sup>1</sup>Duke University, United States; <sup>2</sup>Carnegie Mellon University, United States; <sup>3</sup>University of North Carolina at Chapel Hill, United States; <sup>4</sup>North Carolina State University, United States; <sup>5</sup>University of Turku, Finland

Materials research is generating a wealth of data across a vast community. Specifically, the volume of available data on hybrid organic-inorganic perovskites (HOIPs) and related growth in this area is now immense. Keeping track of data of different origins, sample types or levels of theory, with a diverse set of different relevant observables and discoveries, is a challenging task at best. We here present an open database, "HybriD<sup>3</sup>" (Design, discovery and dissemination (D<sup>3</sup>) of data related to hybrid materials, <https://materials.hybrid3.duke.edu>), aiming to collect, curate, and make available materials data related to HOIP. The database is designed to provide a broad set of data, i.e., experimental and computational, related to in principle any materials property of relevance to the community: structure, optical or electronic properties, and more. A key goal is to provide the ability to curate data, that is, identify property information closest to the actual properties of a real material prepared in a specific way (bulk crystalline, powder, thin film, nanocrystalline, ...). Importantly, the database is open to the community and designed to accept community input. While the "HybriD<sup>3</sup>" database is focused on a particular materials class, the problem of making materials data of all kinds available in a structured, reproducible way is general. The software underlying the HybriD<sup>3</sup> database is thus available as a separate open-source project "MatD<sup>3</sup>" (<https://github.com/HybriD3-database/MatD3>). We also describe this software stack, which can enable materials data at any scale, from small workgroups via focused projects all the way to large and general, open and reproducible materials data collections.

### F.EL08.18.02

**Ab Initio Characterization of the Cs<sub>2</sub>ZrX<sub>6</sub> (X=Cl, Br) Family, 0D Ordered Defect Perovskite Emitters** Christopher Savory<sup>1</sup>, Anna Abfalterer<sup>2</sup>, Javad Shamsi<sup>2</sup>, Samuel D. Stranks<sup>2</sup> and David O. Scanlon<sup>1</sup>; <sup>1</sup>University College London, United Kingdom; <sup>2</sup>University of Cambridge, United Kingdom

As halide perovskites have made their significant impact in the fields of photovoltaics, light emitters and other optical devices, research interest has been reignited in families of lead-free 2D, 1D and 0D perovskite-derived materials that, while poorer photovoltaics, can access some of the strong emissive properties of the halide perovskites, while also demonstrating emergent optoelectronic properties of their own.[1] The layered Cs<sub>3</sub>Pn<sub>2</sub>X<sub>9</sub> (Pn = Sb, Bi; X = Cl, Br, I) family demonstrates structured excitonic emission at room temperature[2,3] while the K<sub>2</sub>PtCl<sub>6</sub>-structured 'vacancy-ordered double perovskites' such as M<sub>2</sub>SnI<sub>6</sub> (M=Rb, Sn) have shown both evidence of defect tolerance similar to that seen in the lead halide perovskites as well as strong exciton-phonon coupling.[4,5] As such, the exploration of perovskite-inspired lower dimensionality compounds represents an exciting direction in the research of optical materials.

In this study, inspired by our experimental collaborators' colloidal synthesis of nanocrystals of Cs<sub>2</sub>ZrCl<sub>6</sub> and Cs<sub>2</sub>ZrBr<sub>6</sub>, which also belong to the K<sub>2</sub>PtCl<sub>6</sub> structure type and demonstrate broad white photoluminescence when formed into thin films, we perform hybrid Density Functional Theory (DFT) calculations in order to predict and rationalize the observed optical and electronic behavior of the Cs<sub>2</sub>ZrX<sub>6</sub> materials family, producing good agreement to experiment. By calculating the thermodynamic and luminescent properties of the intrinsic defects within the system, as well as excitonic properties within the QSGW method and the Bethe-Salpeter equation, we attempt to accurately predict the origin of such promising emissive properties. Finally, we present direct comparisons to the analogous M<sub>2</sub>SnX<sub>6</sub> family and draw conclusions on the feasibility of extending the field of lead-free perovskite-inspired emitters, and whether such optimal optical properties are available beyond the post-transition metals.

[1] Xiao, Z.; Song, Z.; Yan, Y. From Lead Halide Perovskites to Lead-Free Metal Halide Perovskites and Perovskite Derivatives. *Adv. Mater.* **2019**, *31*, 1803792

[2] Bass, K.K.; Estergreen, L.; Savory, C.N.; Buckeridge, J. et al. Vibronic Structure in Room Temperature Photoluminescence of the Halide Perovskite Cs<sub>3</sub>Bi<sub>2</sub>Br<sub>9</sub>. *Inorg. Chem.* **2017**, *56*, 42

[3] McCall, K.M.; Stoumpos, C.C.; Kostina, S.S.; Kanatzidis, M.G. and Wessels, B.W. Strong Electron-Phonon Coupling and Self-Trapped Excitons in the Defect Halide Perovskites A<sub>3</sub>M<sub>2</sub>I<sub>9</sub> (A=Cs,Rb; M=Bi,Sb). *Chem. Mater.* **2017**, *29*, 4129

[4] Maughan, A.E.; Ganose, A.M.; Almaker, M.A.; Scanlon, D.O. and Neilson, J.R. Tolerance Factor and Cooperative Tilting Effects in Vacancy-Ordered Double Perovskite Halides. *Chem. Mater.* **2018**, *30*, 3909

[5] Maughan, A.E.; Ganose, A.M.; Bordelon, M.M.; Miller, E.M. et al. Defect Tolerance to Intolerance in the Vacancy-Ordered Double Perovskite Semiconductors Cs<sub>2</sub>SnI<sub>6</sub> and Cs<sub>2</sub>TeI<sub>6</sub>. *J. Am. Chem. Soc.* **2016**, *138*, 8453

#### F.EL08.18.03

**Exploration of Compositional Space in Methylammonium-Free Lead Halogen Perovskites for High-Performance Solar Cells** Yu An<sup>1,2</sup>, Xianggao Li<sup>1</sup> and Juan Pablo Correa Baena<sup>2</sup>; <sup>1</sup>Tianjin University, China; <sup>2</sup>Georgia Institute of Technology, United States

The certified power conversion efficiency (PCE) of state-of-the-art organic-inorganic metal halide perovskite solar cells (PSCs) has surpassed 25%, coming after single crystalline silicon solar cells. The most widely studied methylammonium (MA) lead iodide undergoes a structural phase transition and degradation due to the volatile MA cation, detrimental to the long-term stability of the devices. Formamidinium (FA), used as the majority cation in most of PCE >20% PSCs, is thermally more stable and has an optimal red-shifted bandgap. However, FA with the relatively large radius induces tilted PbI<sub>6</sub> octahedra in FAPbI<sub>3</sub>, leading to the photoinactive yellow  $\delta$ -phase at room temperature. Herein, iodide and FA in FAPbI<sub>3</sub> were gradually replaced by bromide and cesium (Cs) with smaller radius to suppress the yellow  $\delta$ -phase and systematically explore the compositional space via regulating the tolerance factor, revealing the crucial link between the crystal structure and optoelectronic properties of the mixed-cation (FA/Cs) lead mixed-halide (I/Br) perovskite. An empirical expression for FA/Cs-Pb-I/Br bandgap as a function of composition was determined, which contributes to tailored bandgap suitable for tandem solar cells. In addition, the FA/Cs-Pb-I/Br films were probed by advanced synchrotron X-ray characterization to understand halide phase segregation, which has been found to be detrimental for solar cell performance.

#### F.EL08.18.04

**Interfacial States, Energetics and Atmospheric Stability of Large-Grain Antifluorite Cesium Titanium Bromide** Jocelyn Mendes, Julia Martin, Alexander Carl, Emma J. Pellerin and Ronald L. Grimm; Worcester Polytechnic Institute, United States

Cesium titanium bromide, Cs<sub>2</sub>TiBr<sub>6</sub>, has attracted research interest due to its ~1.8 eV band gap, which makes it desirable for forming tandem junctions with silicon. However, the instability of large-grain Cs<sub>2</sub>TiBr<sub>6</sub> in ambient atmosphere prompts further fundamental understanding of its surface chemistry and oxidation. To ascertain stability of the material in ambient atmosphere and establish band edge positions of the material we conducted controlled air exposure experiments and UHV cleaving of nascent material. X-ray photoelectron spectroscopy (XPS) established correct synthesis, effects of atmospheric exposure, and characterization of UHV cleaved samples. Ultraviolet photoelectron spectroscopy (UPS) established band edge positions of Cs<sub>2</sub>TiBr<sub>6</sub> with and without surface metal oxide species present. Powder X-ray diffraction (pXRD) quantified the effects of atmospheric exposure over time. The presence of metal oxides on Cs<sub>2</sub>TiBr<sub>6</sub> surfaces shifted band alignments towards TiO<sub>2</sub> while UHV cleaved, oxide-free surfaces demonstrated an intrinsically n-type semiconductor. These results elucidate the effects of surface oxides on Cs<sub>2</sub>TiBr<sub>6</sub> surfaces, and future routes through which interfacial reactivity may be used to improve atmospheric stability.

#### F.EL08.18.05

**Bandgap-Tailored Perovskite Capping Layer Design for Improving Stability and Passivation** Noor Titan Putri Hartono<sup>1</sup>, Marie-Hélène Tremblay<sup>2</sup>, Armi Tiihonen<sup>1</sup>, Janak Thapa<sup>1</sup>, Shijing Sun<sup>1</sup>, Seth R. Marder<sup>2</sup> and Tonio Buonassisi<sup>1</sup>; <sup>1</sup>Massachusetts Institute of Technology, United States; <sup>2</sup>Georgia Institute of Technology, United States

In recent years, the 3D/low-dimensional (LD) perovskite heterostructure consisting of LD perovskite called ‘capping layer’, deposited atop of 3D perovskite in a device [1], has emerged as a solution for improving perovskite solar cells’ (PSCs’) stability and interfacial passivation. However, the capping layer materials and processing conditions have been optimized for single-junction PSCs, and not for multi-junction PSCs. To apply the capping layer in multi-junction PSCs, research efforts are required to understand and optimize the bandgap-tailored capping layer material. We propose a detailed study exploring at least 10 different types of LD perovskite with various halides (I, Br, and Cl) and thicknesses, and CH<sub>3</sub>NH<sub>3</sub>Pb(I-Br)<sub>3</sub> absorber mixtures with increasing bandgap from 1.59 to 2.27 eV [2]. The samples are degraded in a well-controlled environmental chamber, under high humidity (85% RH), high heat (85°C), and low illumination (0.17 sun). The same set of samples are screened using photoconductivity, as a proxy for its interfacial passivation property. We also utilize decision tree-based machine learning models and Shapley values [3] to help determine which molecular properties in the capping layers significantly affect the absorber mixtures’ stability and conductivity. Our results indicate that capping layers needs to be tailored based on the perovskite absorbers’ composition, bandgap, and organic cation types to achieve high stability.

Furthermore, by comparing the optimum bandgap-tailored capping layers through X-ray photoelectron spectroscopy (XPS), Fourier-transform infrared spectroscopy (FTIR), and ultraviolet photoelectron spectroscopy (UPS), we can understand how the film stability is affected by inorganic and organic bonds on the surface of the capping layers, as well as how interfacial passivation is affected by band alignment. Our study suggests that capping layer tuning is a promising approach to increase the stability of perovskite-based tandem solar cells.

#### References

- [1] W. Huang, T. Bu, F. Huang, and Y. B. Cheng, “Stabilizing High Efficiency Perovskite Solar Cells with 3D-2D Heterostructures,” *Joule*, vol. 4, no. 5, pp. 975–979, May 2020, doi: 10.1016/j.joule.2020.04.009.
- [2] L. Atourki *et al.*, “Role of the chemical substitution on the structural and luminescence properties of the mixed halide perovskite thin MAPbI<sub>3-x</sub>Br<sub>x</sub> (0 ≤ x ≤ 1) films,” *Appl. Surf. Sci.*, vol. 371, pp. 112–117, May 2016, doi: 10.1016/j.apsusc.2016.02.207.
- [3] N. T. P. Hartono *et al.*, “How machine learning can help select capping layers to suppress perovskite degradation,” *ChemRxiv*, pp. 1–47, Jan. 2020, doi: 10.26434/CHEMRXIV.11766528.V1.

#### F.EL08.18.06

**Nonlinear Bandgap Behavior in Lead-Free Cs<sub>2</sub>Ag(Sb<sub>x</sub>Bi<sub>1-x</sub>)Br<sub>6</sub> Double Perovskite Alloys** Seán Kavanagh<sup>1,2,3</sup>, Zewei Li<sup>4</sup>, Robert Palgrave<sup>3</sup>, Richard Friend<sup>4</sup>, David O. Scanlon<sup>3</sup>, Aron Walsh<sup>2</sup> and Robert Hoye<sup>2</sup>; <sup>1</sup>Thomas Young Centre, UCL, ICL, KCL, QMUL, United Kingdom; <sup>2</sup>Imperial College London, United Kingdom; <sup>3</sup>University College London, United Kingdom; <sup>4</sup>University of Cambridge, United Kingdom

Double perovskites have emerged as promising candidate materials for high-performance next-generation optoelectronic technologies, owing to the ability to replace the toxic Pb<sup>2+</sup> cation with a pair of more benign cations (*e.g.* Ag<sup>+</sup> and Bi<sup>3+</sup>), while preserving the perovskite crystal structure.<sup>1</sup> However, most double perovskites, including the prototypical Cs<sub>2</sub>AgBiBr<sub>6</sub>, have prohibitively wide bandgaps, limiting photoconversion and photocatalytic efficiencies.<sup>2</sup> Recently, it has been demonstrated that the bandgap of Cs<sub>2</sub>AgBiBr<sub>6</sub> can be reduced through alloying with Sb<sup>3+</sup>,<sup>3</sup> yet the bandgap of the pure Sb-based double perovskite (Cs<sub>2</sub>AgSbBr<sub>6</sub>) remains excessively wide for photo-voltaic/catalytic applications. In this work, we develop a solution-based route to synthesize phase-pure Cs<sub>2</sub>Ag(Sb<sub>x</sub>Bi<sub>1-x</sub>)Br<sub>6</sub> thin films, with the mixing parameter *x* tunable over the entire composition range. In doing so, we observe this system to disobey Vegard’s law, exhibiting significant bandgap bowing, such that the mixed alloy (*x* = 0.9) demonstrates the smallest bandgap (2.08 eV, compared to 2.18 eV and 2.25 eV for the pure Sb- and Bi-based double perovskites, respectively). We investigate the possible mechanisms for this nonlinear bandgap variation through relativistic hybrid Density Functional Theory (DFT) calculations, combined with in-depth measurements of the composition, phase and grain structure to yield detailed understanding of the underlying physical origins. The energetic alignment of electron states within these materials is accurately calculated, including consideration of deformation potentials to adequately account for the spurious supercell effects associated with such calculations.<sup>4,5</sup> Our work reveals pathways to bandgap engineering in double perovskite alloys, such that it is better suited to photovoltaic or photocatalytic applications, which may be generally applicable to other mixed-metal double perovskite systems.

<sup>1</sup> C.N. Savory, A. Walsh, and D.O. Scanlon, *ACS Energy Lett.* **1**, 949 (2016).

<sup>2</sup> A.H. Slavney, T. Hu, A.M. Lindenberg, and H.I. Karunadasa, *Journal of the American Chemical Society* **138**, 2138 (2016).

<sup>3</sup> G. García-Espejo, D. Rodríguez-Padrón, R. Luque, L. Camacho, and G. de Miguel, *Nanoscale* **11**, 16650 (2019).

<sup>4</sup> K.T. Butler, C.H. Hendon, and A. Walsh, *Journal of the American Chemical Society* **136**, 2703 (2014).

<sup>5</sup> S.-H. Wei, S.B. Zhang, and A. Zunger, *Journal of Applied Physics* **87**, 1304 (2000).

#### F.EL08.18.08

**Tin Oxynitride-Based Ferroelectric Semiconductors for Solar Energy Conversion Applications** Steven T. Hartman, Arashdeep S. Thind and Rohan Mishra; Washington University in St. Louis, United States

Lead-halide perovskites have emerged as a promising class of semiconductors; however they suffer from issues related to lead-toxicity and instability. We report results of a first-principles-based design of heavy-metal-based oxynitrides as alternatives to lead-halide perovskites. We have used density-functional-theory calculations to search a vast composition space of ABO<sub>2</sub>N and ABON<sub>2</sub> compounds, where *B* is a *p*-block cation, and *A* is an alkaline, alkali-earth, rare-earth or transition metal cation, and identify 10 new ABO<sub>2</sub>N oxynitride semiconductors that we expect to be formable. Specifically, we discover a new family of ferroelectric semiconductors with ASnO<sub>2</sub>N stoichiometry (*A* = Y, Eu, La, In, Sc) in the LuMnO<sub>3</sub>-type structure, which combine the strong bonding of metal oxides with the low carrier effective mass and small,

tunable band gaps of the lead-halide perovskites. These tin oxynitrides have predicted direct band gaps ranging from 1.6 – 3.3 eV, and a sizeable electric polarization up to 17  $\mu\text{C}/\text{cm}^2$ , which is predicted to be switchable by an external electric field through a non-polar phase. With their unique combination of polarization, low carrier effective mass and band gaps spanning the entire visible spectrum, we expect  $\text{ASnO}_2\text{N}$  ferroelectric semiconductors will find useful applications as photovoltaics, photocatalysts, and for optoelectronics.

Acknowledgments: This work was supported by the National Science Foundation through grant number DMR-1806147.

#### **F.EL08.18.09**

**How to Design Defect Tolerant Devices** Basita Das<sup>1</sup>, Irene Aguilera<sup>1</sup>, Uwe Rau<sup>1</sup> and Thomas Kirchartz<sup>1,2</sup>; <sup>1</sup>Forschungszentrum Jülich GmbH, Germany; <sup>2</sup>University of Duisburg-Essen, Germany

Perovskite solar cells have emerged as a key photovoltaic technology given the remarkable rise in their efficiency in the past decade. Long non-radiative lifetimes as a result of slow defect-mediated recombination in perovskite materials are key in achieving high open-circuit voltages necessary for high efficiency solar cells.

The quantitative impact of bulk or interface defects on recombination is often estimated by defect statistics based on the model of Shockley, Read and Hall. However, defect statistics depend on defect capture coefficients to calculate defect occupancy and the recombination rate through the defect. Due to the lack of enough experimental data on capture coefficients of novel materials or, alternatively, models to calculate trap energy dependent capture coefficients it is frequently assumed that capture coefficients are symmetric, i.e,  $k_n = k_p$  for all defect levels within the bandgap in a device. However, equal or at least similar values of the capture coefficients are not necessarily a typical or even a likely scenario.

To go beyond the state-of-the-art device simulation in photovoltaics involving constant capture coefficients, we present a generalized microscopic model based on the Harmonic oscillator approximation to calculate defect capture coefficients as a function of the host material and the energetic position of the defects. Then we use this capture coefficients to classify the “deep” defects inside a device not merely based on the energetic position of the device but also as a function of the quantitative impact it has on the device. Furthermore, we discuss certain photovoltaic device design principles that can substantially reduce recombination through the dominant recombination centers.

#### **F.EL08.18.10**

**Enhancing Fundamental Understanding of Structure-Property Relationships in Chalcogenide Perovskite Semiconductors with Theoretical and Experimental Studies of Dielectric Response, X-Ray Absorption and Electronic Transport** Stephen Filippone<sup>1</sup>, Kevin Ye<sup>1</sup>, Boyang Zhao<sup>2</sup>, Shanyuan Niu<sup>2</sup>, Nathan Koocher<sup>3</sup>, Daniel Silevitch<sup>4</sup>, Ignasi Fina<sup>5</sup>, James Rondinelli<sup>3</sup>, Jayakanth Ravichandran<sup>2</sup> and Rafael Jaramillo<sup>1</sup>; <sup>1</sup>Massachusetts Institute of Technology, United States; <sup>2</sup>University of Southern California, United States; <sup>3</sup>Northwestern University, United States; <sup>4</sup>California Institute of Technology, United States; <sup>5</sup>Universitat Autònoma de Barcelona, Spain

Electronic materials in perovskite and related structure types are a rich field of study because they combine characteristics of ionic and covalent bonding in crystal structures that are tolerant of distortions and chemical substitution. Tremendous efforts are now underway to understand the structure-property relationships that underpin the photovoltaic performance of lead halide perovskites (LHPs), expanding on and linking decades of research on photovoltaic absorbers, on the one hand, and complex oxide physics on the other. Now we extend this spirit of interdisciplinary, fundamental inquiry to a much less-studied class of materials, the chalcogenide perovskites. Recent works have shown that chalcogenide perovskites have outstanding properties for optoelectronic applications, including: slow minority carrier recombination, strong light absorption, excellent environmental stability, and dopability. Efforts are just now beginning to develop a fundamental understanding of these phenomena and to exploit these exciting materials for applications.

We present a diverse set of studies of the atomistic origin of structure-property relationships in chalcogenide perovskites. We combine impedance spectroscopy, X-ray absorption spectroscopy (XAS), electronic transport, and first-principles theory to understand how atomic structure and particular chemical bonds support outstanding semiconducting properties. Our impedance spectroscopy measurements on single crystals reveal that chalcogenide perovskites are highly-polarizable semiconductors, with stronger dielectric response than any other family of semiconductors with band gap in the VIS-NIR, exceeding even LHPs. Our theoretical calculations agree quantitatively with our measurements, and illustrate the particular polar phonon modes responsible for the large dielectric response. Our XAS studies combining experiment and theory illustrate the importance of directional bonds in determining the near-band edge electronic structure (including the band gap), especially for layered variants in the Ruddlesden-Popper structure type. This electronic anisotropy is further illustrated by electronic transport measurements made on oriented single crystals.

Our results illustrate, in a fundamental and detailed level, the ways in which chalcogenide perovskites differ from their oxide

and halide cousins. We show that the structure-property relationships follow from covalent metal-chalcogen bonds and strong electron-phonon coupling. We conclude that chalcogenide perovskites are highly promising for optoelectronic and energy-conversion technologies.

[1] Jaramillo, R. & Ravichandran, J. In praise and in search of highly-polarizable semiconductors: Technological promise and discovery strategies. *APL Materials* 7, 100902 (2019).

SESSION F.EL08.19: Poster Session VII: Devices—Photoelectronics and Beyond  
On Demand Abstracts Available for Viewing Starting Saturday Morning, November 21, 2020  
5:00 AM - 8:00 AM  
F-EL08

#### **F.EL08.19.01**

**Novel C<sub>6</sub>H<sub>5</sub>NHNH<sub>3</sub>I Additive for Efficiency Acceleration in Organic-Inorganic Halide Perovskite Solar Cells** Md Ashiqur Rahman Laskar<sup>1,2</sup> and Qiquan (Quinn) Qiao<sup>1</sup>; <sup>1</sup>South Dakota State University, United States; <sup>2</sup>Arizona State University, United States

Different additive materials are widely used to improve the power conversion efficiency (PCE) of organic-inorganic halide perovskite solar cells. In this work, we report a novel organic additive material C<sub>6</sub>H<sub>5</sub>NHNH<sub>3</sub>I (Phenylhydrazinium Iodide) which is very effective to enhance the PCE of single cation-single halide based Methylammonium Lead Iodide perovskite solar cells (MLIPSC). In addition to that, we have found the additive is also effective for other types of perovskite composition such as double cation-double halide perovskite solar cells. C<sub>6</sub>H<sub>5</sub>NHNH<sub>3</sub>I promotes perovskite crystal growth and improves the light absorption capability of the active layer. Furthermore, because of reduced defects and charge traps in the additive treated perovskite film, charge carrier lifetime becomes almost double from 1.4 μs to 2.5 μs which ensures minimum recombination of the photogenerated electrons and holes. Besides, approximately 10% increased external quantum efficiency (EQE) and 14% improved built in potential (V<sub>bi</sub>) of the perovskite solar cells indicate superior device performance. Eventually, accelerated short circuit current density and open circuit voltage of the C<sub>6</sub>H<sub>5</sub>NHNH<sub>3</sub>I treated perovskite solar cells contribute to nearly 20% increment of PCE in MLIPSC.

#### **F.EL08.19.02**

**Understanding the Effect of Electrode Spacing on CsPbI<sub>2</sub>Br Interdigital Photodetector with Chromium Electrodes** Haider B. Salman; University of Arkansas, United States

Significant achievements were made in the past few years with perovskite material in optoelectronic applications. One of the advantages of the halide perovskite in photo detection applications is that the band gap of the material can be tuned to cover a wide range of wavelengths by halide mixing. In this paper, the research is focused on the fabrication and characterization of interdigital photodetectors made with CsPbI<sub>2</sub>Br. The photodetector consists of two interdigitate chromium electrodes deposited on glass substrates with the perovskite filling the spacing between the electrodes. The interdigital pattern of the device was fabricated using photolithography method to deposit 80 nm of chromium. To study the effect of the electrode spacing on the device performance, four types of photodetectors with four different spacing; 50, 20, 10, and 5 μm were fabricated. The perovskite was synthesized using one step deposition method with 0.6 molar concentration of CsPbI<sub>2</sub>Br precursor. The material was characterized by obtaining the absorbance, the photoluminescence, and the X-ray diffraction spectra. One single peak in the PL spectrum was observed at 648 nm indicating a band gap 1.91 eV. The current voltage curves of the photodetectors were obtained under dark and light conditions using Keithley 4200 semiconductor characterization system and Newport solar simulator. The spectral response of the device was obtained using Bruker IFS 125HR spectrometer. The device with 10 μm spacing showed ~370 on/off ratio at 5 V bias under 100 mW/cm<sup>2</sup> light intensity. Under the same conditions, the device with 5 μm showed an increase in the on/off ratio to 6800. The detectivities of the 10 and 5 μm devices were calculated to be 4.9 × 10<sup>9</sup>, and 2.46 × 10<sup>10</sup> Jones respectively.

#### **F.EL08.19.04**

**Enhancing Chemical Stability and Suppressing Ion Migration in CH<sub>3</sub>NH<sub>3</sub>PbI<sub>3</sub> Perovskite Solar Cells via Direct Backbone Attachment of Polyester on Grain Boundaries** Yuchen Zhou<sup>1</sup>, Yifan Yin<sup>1</sup>, Xianghao Zuo<sup>1</sup>, Likun Wang<sup>1</sup>, Chang-Yong Nam<sup>2</sup> and Miriam H. Rafailovich<sup>1</sup>; <sup>1</sup>Stony Brook University, United States; <sup>2</sup>Brookhaven National Laboratory,

United States

Grain boundary (GB) passivation by polymer additives has been shown effective in improving the performance of solution processed hybrid perovskite solar cells (PSCs). However, the critical stability issue associated with detrimental ion migration in PSCs remains less explored by polymer additives. Here, we show that a new linear polar polymer, polycaprolactone (PCL), can passivate GBs of methylammonium lead triiodide (MAPbI<sub>3</sub>) perovskites via direct backbone attachment, enabling significantly enhanced environmental stability of n-i-p type PSC. The champion PSC with optimal PCL concentration shows an improved power conversion efficiency (PCE) of 20.1 %. 90% of initial PCE was preserved after 400 h ambient storage. After 100 h thermal aging (85 °C), 80% of the original PCE has also been preserved. The tested PSCs use less stable Spiro-OMeTAD (2,2',7,7'-tetrakis[N,N-di(4-methoxyphenyl)amino]-9,9'-spirobifluorene) as hole transport layer (HTL), and, thus, the improved stability indicates critical roles of PCL in retarding moisture ingress as well as suppressing ion migration. Detailed structures of PCL GB passivation is visualized directly via lateral scanning force and transmission electron microscopies. Secondary ion mass spectrometry and ion conduction measurements confirm the PCL GB passivation significantly retards I<sup>-</sup> ion migration in MAPbI<sub>3</sub> PSCs, while without PCL, I<sup>-</sup> ions are actively accumulating in the organic HTL and at the interface between electrodes and the HTL even without externally applied electric field. We envision this passivation strategy by PCL GB functionalization can help the development of environmentally stable, high-performance PSCs. (This work was supported by the Morin Foundation Trust and the NSF, Inspire program #1344267)

#### F.EL08.19.06

**Effects of Annealing Temperature on Interdiffusion of Materials in Layered Perovskite Solar Cells** Deborah Oyewole<sup>1,2,1</sup>, Juan Martin Hinojosa Tamayo<sup>1,1</sup>, Oluwaseun K. Oyewole<sup>1,1</sup>, Benjamin Agyei-Tuffour<sup>3</sup>, Richard Koech<sup>4,1</sup>, Reisyah Ichwani<sup>1,1</sup>, Jaya Cromwell<sup>1</sup>, Nancy Burnham<sup>1,1</sup> and Winston Soboyejo<sup>1,1</sup>; <sup>1</sup>Worcester Polytechnic Institute, United States; <sup>2</sup>Sheda Science and Technology, Km 10 Abuja-Lokoja Road, Nigeria; <sup>3</sup>School of Engineering Sciences, University of Ghana, Ghana; <sup>4</sup>African University of Science and Technology, Nigeria

In order to design more efficient and durable perovskite solar cells (PSCs), the effects of annealing temperature on interdiffusion of the constituent elements in layered formamidinium-based PSCs were studied. First, the PSCs were fabricated by spin-coating lead (II) iodide solution onto the mesoporous electron transporting layer (ETL) followed by a mixture of formamidinium ammonium iodide, with small proportion methylammonium bromide and methylammonium chloride. The effect of varying annealing temperature of the perovskite films is then studied to gain insight into the changes that occur on the perovskite film and the overall effects of interdiffusion of constituent elements on photoconversion efficiencies of the PSCs. The results show there is diffusion of tin from fluorine-doped tin oxide to the mesoporous ETL due to sintering. The level of tin in the mesoporous layer decreases with increased annealing temperatures of the perovskite films. The quality of perovskite films is also improved with better uniformly distributed grain sizes for annealing temperatures between room temperature and 130 °C compared to higher annealing temperatures of 140 °C and 150 °C. The overall effects of the interdiffusion of layer constituents on photoconversion efficiencies are then discussed for the design of PSCs.

#### F.EL08.19.07

**A Hole Transport Bilayer for Highly Efficient and Stable Inverted Perovskite Solar Cells** Hamza Javaid, Volodymyr V. Duzhko and Dhandapani Venkataraman; University of Massachusetts Amherst, United States

Highly efficient and stable inverted, *i.e.* p-i-n, perovskite solar cells (PSCs) are fabricated by employing a novel hole transport bilayer. Compared to devices with single PTAA interlayer, which have an average power conversion efficiency (PCE) of 18.9%, an enhanced average PCE of 20.2% and a maximum PCE of 21.16% in the bilayer-based devices are observed. The XRD and AFM studies show an improved crystallinity and larger grain size of perovskite films on the bilayer surface. The ultraviolet photoelectron spectroscopy and Mott-Schottky analysis suggest an increased built-in potential with an enhanced upward band bending at the bilayer/perovskite interface. Compared to devices with single PTAA, CuI and PEDOT:PSS interlayer, the bilayer-based devices show significant suppression of *J-V* hysteresis and stable current output at maximum power point. The bilayer-based devices also demonstrate a remarkable long-term stability, as tested in inert atmosphere.

#### F.EL08.19.08

**Toward Rational Design of Stable and Robust Hybrid Perovskite Devices—The Role of Functionalized Organic Cations and Dimensionality Engineering** Arvin Kakekhani<sup>1</sup>, Marcos A. Reyes-Martinez<sup>2</sup>, Xiaoming Zhao<sup>2</sup>, Melissa Ball<sup>2,2</sup>, Peng Tan<sup>3,1</sup>, Sayan Banerjee<sup>1</sup>, Lynn Loo<sup>2,2</sup> and Andrew Rappe<sup>1</sup>; <sup>1</sup>University of Pennsylvania, United States; <sup>2</sup>Princeton University, United States; <sup>3</sup>Harbin Institute of Technology, China



Here, we discuss how density functional theory (DFT)-based methods can help us in designing strategies to mitigate the stability and efficiency challenges for hybrid organic-inorganic perovskite (HOIP) systems. On one front, we use first-principles theory to rationalize the elastic properties of layered hybrid perovskites, correlating such properties with interlayer organic-organic interactions and also the HOIP's structural properties e.g., its dimensionality or intrinsic interlayer defects and voids. [1] On a different but complementary front, we have studied fundamental chemistry behind the water degradation of 3D hybrid perovskites and have related this to the chemical properties of the organic cations. [2] We are now expanding this work to study water interactions in layered quasi-2D systems, unraveling the fundamental role of dimensionality in water stability of perovskites. Beyond the realm of bulk-like perovskites, we also study the determining role of organic cations' chemistry on surface stability and defect formation for HOIP nanoparticles. The role of organic cations goes further than directly influencing the inorganic backbone structure, and for some specific functionalized organic cations and through intricate hydrogen-bonding networks, the organic-organic interactions can become important at dictating the electronic and structural properties of layered perovskites. Having a multipronged approach in which we identify descriptors for elastic and electronic properties of perovskite, as well as their stability, allows us to rationalize and help improve experimentally-relevant pathways to create more robust HOIP-based devices capable of performing in real-world PV or LED applications. Few such possibilities which are discussed here include: surface passivation with mixed short organic cations, supramolecular interactions between long cations, secondary organic functionalities, and dimensionality engineering.

[1] Reyes-Martinez, Marcos A., Peng Tan, Arvin Kakekhani, Sayan Banerjee, Ayan A. Zhumekenov, Wei Peng, Osman M. Bakr, Andrew M. Rappe, and Yueh-Lin Loo. "Unraveling the Elastic Properties of (Quasi) Two-Dimensional Hybrid Perovskites: A Joint Experimental and Theoretical Study." *ACS Applied Materials & Interfaces* 12, no. 15 (2020): 17881-17892.

[2] Kakekhani, Arvin, Radhika N. Katti, and Andrew M. Rappe. "Water in hybrid perovskites: Bulk MAPbI<sub>3</sub> degradation via super-hydrous state." *APL Materials* 7, no. 4 (2019): 041112.

#### **F.EL08.19.09**

**Bilayer Perovskite Solar Cells by Grafted PDMS Transfer Process** [Anisha Mohapatra](#)<sup>1,2</sup> and Chih-Wei Chu<sup>1</sup>; <sup>1</sup>Academia Sinica, Taiwan; <sup>2</sup>National Tsing Hua University, Taiwan

Organic-Inorganic Perovskite solar cells has a great advantage to reach the radiative limit for PCE enhancement. The single junction devices are restricted to attain the radiative limit because of the energy losses. Multi-structure architectures like tandem, heterostructure are adapted to recover the thermodynamic energy loss. The variable bandgap of perovskite is an advantage, which varies from 1.5eV~1.8eV providing a complete solar spectrum coverage. Stacking of high-bandgap perovskite with low bandgap perovskites is a good approach for encountering the energy losses. The perovskite heterostructure is fabricated by sequential deposition of quantum dots and thermally evaporated p-n junctions. Till now, there is no demonstration of any solution process able method in perovskites for stacking perovskite absorbers because of the dissolution of perovskite precursors by the subsequent layers. Therefore, we demonstrated a PDMS printing technique for stacking perovskite layers inspired by multi-stacked organic solar cells. The printing technique is assisted with modification of surface energy of PDMS by grafting process, which facilitates printing of high crystalline pinhole free perovskite layers. On proving ground, we also stacked perovskite layers to form a perovskite heterostructures. We demonstrated the printing of multi-layer perovskite layers to encounter the thermodynamic losses. To understand the advantage of heterostructure for encountering the energy losses, a constant thickness of single layer and heterostructure was maintained for compared the photovoltaic performance. We achieved a photovoltaic performance of ~5%, ~9% for MaPbI<sub>3</sub> and MaPbBrI<sub>2</sub> layer and ~10% for MAPbBrI<sub>2</sub>/MAPbI<sub>3</sub> heterostructure. This gave us an indication that the heterostructure was able to suppress some non-radiative recombination to overcome the energy losses, which can be a great application for stacking perovskite layers to use in different optoelectronic applications.

#### **F.EL08.19.11**

**Fracture Behavior of Halide Perovskite Thin Films for Solar Cells** [Zhenghong Dai](#), Srinivas K. Yadavalli, Mingyu Hu, Min Chen, Yuanyuan Zhou and Nitin Padture; Brown University, United States

Organic-inorganic halide perovskites (OIHPs) have emerged as the most promising light-absorber materials in thin-film photovoltaic (PVs). However, the low formation energies of OIHPs render them unstable. While significant progress has been made in improving the stability of OIHPs, perovskite solar cells (PSCs) will also need to be mechanically reliable if they are to service satisfactorily for years. In this context, we have studied the fracture behavior of PSCs by measuring their cohesion energies using double cantilever beam method and report a novel approach to strategically enhance the interfacial adhesion and performance of PSCs by interface modification. This work points to a new route for designing mechanically

robust PSCs with long-term durability.

SESSION F.EL08.20: Poster Session VIII: Spectroscopy and Photophysics  
On Demand Abstracts Available for Viewing Starting Saturday Morning, November 21, 2020  
5:00 AM - 8:00 AM  
F-EL08

#### **F.EL08.20.01**

**Amplified Spontaneous Emission from All-Inorganic Quasi-2D Perovskites** Lei Lei, Dovletgeldi Seyitliyev, Kasra Darabi, Siliang He, Samuel Stuard, Qi Dong, Juliana Mendes, Harald Ade, Aram Amassian, Kenan Gundogdu and Franky So; North Carolina State University, United States

Recently, metal-halide perovskite materials are considered as a promising candidate for lasing applications since perovskites may overcome typical limitations showed in organic gain media and the “green-gap” in inorganic semiconductors. While lasing has been demonstrated based on perovskite materials with both 3D and low-dimensionalities, quasi-2D perovskites are a better gain media due to its unique properties such as large binding energy and self-assembled quantum wells. It has been shown that efficient energy funneling from low-dimensional domains to high-dimensional domains will not only enhance the radiative recombination but also facilitate population inversion. However, the trend of how the dimensionality of quasi-2D perovskites affects amplified spontaneous emission (ASE) threshold is still controversial. Here, we investigate ASE of all-inorganic quasi-2D perovskite thin films with different dimensionalities, and try to understand the role of dimensionality in both materials properties and charge carrier dynamics.

In this work, we formed quasi-2D perovskite thin films based on the all-inorganic 3D cesium lead halide perovskite framework due to the improved thermal and optical stability. The dimensionality of quasi-2D perovskites is tuned by varying the concentration of the organic spacer phenethylamine (PEA). In our work, the large organic cation PEA acts as a nucleation center facilitating the crystallization process of perovskites. Via grazing-incidence wide-angle X-ray scattering (GIWAXS) measurements and scanning electronic microscopy, we found that the addition of PEA also enhances the quality of the thin films by controlling the domain size and morphology. As a result, the PLQY increases with the PEA concentration. However, the ASE threshold is not correlated with the PLQY and it reaches to the lowest value ( $7 \mu\text{J}/\text{cm}^2$ ) at a moderate PEA concentration of 40%. To study the correlation between PEA concentration and ASE threshold, we used transient photoluminescence and transient absorption spectroscopy to study the photophysics of these films. Our results showed that with increasing PEA concentration to 40%, the non-radiative recombination is significantly reduced due to defect passivation, leading to the increasing PLQY and decreasing of ASE threshold. However, the existing of the low-dimensional domains became significant with a higher PEA concentration (60%), which acted as long-lived trap states for excitons and limited the population inversion process. Finally, by using the optimized PEA ratio, the ASE emission was observed over the broad visible range from red to blue, demonstrating its wide wavelength-tunability.

#### **F.EL08.20.02**

**Direct Observation of the Ultrafast Dynamics of Trapped Carriers in Organic Metal Halide Perovskite Films** Kanishka Kobbekaduwa<sup>1</sup>, Shreetu Shrestha<sup>2</sup>, Pan Adhikari<sup>1</sup>, Hsinhan Tsai<sup>2</sup>, Wanyi Nie<sup>2</sup> and Jianbo Gao<sup>1</sup>; <sup>1</sup>Clemson University, United States; <sup>2</sup>Los Alamos National Laboratory, United States

Despite the power conversion efficiency (PCE) of the perovskite solar cells soars more than 25 % in less than ten years, their limited stability remains one of the crucial hurdles on the path to commercialization. To improve the device stability, various trap state passivation strategies targeting the bulk perovskite, perovskite surface, and device interfaces have been employed. However, knowledge of the temporal, spatial, and energetic correlation of the defect/trap states is the foundation for fundamental and technical understanding of the impact of the trap/defect states, manifested by the device stability and PCE optimization.

In this report, we directly observe the ultrafast dynamics of trapped carriers in organic lead halide perovskite  $\text{MAPbI}_3$  thin film by ultrafast photocurrent spectroscopy (UPCS). Under low carrier density, the trapped carriers undergo a multiple trapping and release (MTR) transport mechanism among the shallow trap states and deep trap state, demonstrated by a time-dependent activation energy. Above the trap filling region, in addition to the MTR transport mechanism, the trap-assist Auger recombination occurs, which is demonstrated by the laser intensity dependent decay time. Our results elucidated the trapped carrier dynamics from sub-25 ps to couple ns in the solution-processed film with mobility of  $\sim 1 \text{ cm}^2/\text{Vs}$ .

### F.EL08.20.03

**Exciton Spin Relaxation in 2D Metal Halide Perovskites** Sean A. Bourelle; University of Cambridge, United Kingdom

Optoelectronic properties of 2D metal halide perovskites are dominated by the transitions and interactions between excitons. Here, we present a study on the spin relaxation mechanisms for these excitonic states and demonstrate how these mechanisms can be altered. Our analysis utilizes ultrafast spectroscopy methods including Faraday rotation and circularly polarised transient absorption spectroscopy.

### F.EL08.20.04

**Optical Studies of Mixed-Dimension Perovskites—Excitonic Effects and Morphological Changes with Alkyl-Ammonium Iodide Doping** Mohsin Raza Khan, Shahzad Akhtar Ali, Qurat ul Ain, Ataul Haq and Ammar A. Khan; Lahore University of Management Sciences, Pakistan

Organometal halide perovskites are promising materials for optoelectronic applications due to excellent light absorption, charge transport and emissive properties, coupled with potentially low-cost scalable fabrication [1][2]. Perovskite solar cells (PSCs), as well as other devices, currently suffer from moisture and thermal instability of the perovskite semiconductors [3]. There are several complimentary methodologies of increasing the stability of PSCs, and amongst these the formation of hybrid two/three dimensional Ruddleson Popper perovskites is one of the most promising [4]. Mixed dimension perovskites (MDPs) can be formed by the incorporation of long alkyl-chain cations into the crystal structure leading to the formation of a layered crystal structure [5]. The individual layers are separated by covalently linked cations, with a 3D intra layer geometry. The optical, crystalline, electrical and magnetic properties of 3D perovskites can be readily tuned by varying the stoichiometric concentration and chain length of the dopant, leading to a considerable scope for application dependent material engineering. However, exploring this large yet versatile parameter space of dopants requires an understanding of the underlying excitonic processes and morphological dependencies.

In this work, the formation of 2D/3D mixed alkylammonium lead iodide perovskites using Butylammonium (BAI) and Octylammonium (OAI) iodides as additives in methyl-ammonium lead iodide perovskites is demonstrated. A solvent annealing method is employed to improve film morphology. The effect of incorporating these cations on the optical properties of the films is investigated using micro-photoluminescence and absorption studies, and a left shift in band-gap with increasing 2D character is illustrated, in accordance with literature[6]. BAI and OAI demonstrate very different spectral properties, with much larger spectral shifts in the longer chain derivative, hinting towards a strong effect of the alkyl chain. We further utilise multi-gaussian fitting to reveal insights into edge-states as well as disorder in MDPs, which can have important consequences for photovoltaic and light-emitting device applications.

[1] N. Elumalai, M. Mahmud, D. Wang, and A. Uddin, “Perovskite Solar Cells: Progress and Advancements,” *Energies*, vol. 9, no. 11, p. 861, 2016, doi: 10.3390/en9110861.

[2] Z. Li *et al.*, “Scalable fabrication of perovskite solar cells,” *Nat. Rev. Mater.*, vol. 3, pp. 1–20, 2018, doi: 10.1038/natrevmats.2018.17.

[3] N. Grossiord, J. M. Kroon, R. Andriessen, and P. W. M. Blom, “Degradation mechanisms in organic photovoltaic devices,” *Org. Electron.*, vol. 13, no. 3, pp. 432–456, 2012, doi: 10.1016/j.orgel.2011.11.027.

[4] P. Gao, A. R. Bin Mohd Yusoff, and M. K. Nazeeruddin, “Dimensionality engineering of hybrid halide perovskite light absorbers,” *Nat. Commun.*, vol. 9, no. 1, pp. 1–14, 2018, doi: 10.1038/s41467-018-07382-9.

[5] R. L. Milot *et al.*, “Charge-Carrier Dynamics in 2D Hybrid Metal-Halide Perovskites,” *Nano Lett.*, vol. 16, no. 11, pp. 7001–7007, 2016, doi: 10.1021/acs.nanolett.6b03114.

[6] D. H. Cao, C. C. Stoumpos, O. K. Farha, J. T. Hupp, and M. G. Kanatzidis, “2D Homologous Perovskites as Light-Absorbing Materials for Solar Cell Applications,” *J. Am. Chem. Soc.*, vol. 137, no. 24, pp. 7843–7850, 2015, doi: 10.1021/jacs.5b03796.

### F.EL08.20.05

**Benefits of Disorder—Carrier Localisation in Alloyed Hybrid Perovskites for Efficient Luminescence** Sascha Feldmann<sup>1</sup>, Stuart Macpherson<sup>1</sup>, Richard Friend<sup>1</sup>, Henning Siringhaus<sup>1</sup>, David Beljonne<sup>2</sup>, Samuel D. Stranks<sup>1</sup> and Felix Deschler<sup>3</sup>; <sup>1</sup>University of Cambridge, United Kingdom; <sup>2</sup>Université de Mons, Belgium; <sup>3</sup>Technische Universität München, Germany

Metal halide perovskites have emerged as promising materials for optoelectronic applications like solar cells or light-emitting diodes (LEDs). Here, we investigate mixed-halide perovskites and control the cation alloying to enhance optoelectronic

performance through alteration of the charge carrier dynamics. In contrast to single-halide perovskites, we find high luminescence yields for photoexcited carrier densities far below solar illumination conditions. We employ time-resolved spectroscopy and show that the charge carrier recombination regime changes from second to effectively first order within the first tens of nanoseconds after excitation. Supported by microscale mapping of the optical bandgap, electrically gated transport measurements and first-principles calculations, we demonstrate that spatially varying energetic disorder in the electronic states causes local charge accumulation, creating p- and n-type photodoped regions, which unearths a strategy for efficient light emission at low charge-injection in solar cells. [1]

[1] Feldmann, Macpherson et al. *Nature Photonics* 14, 123–128 (2020).

#### F.EL08.20.06

**Performance Limiting Structural Heterogeneities in Metal Halide Perovskites** Tiarnan A. Doherty<sup>1</sup>, Stuart Macpherson<sup>1</sup>, Andrew Winchester<sup>2</sup>, Duncan Johnstone<sup>1</sup>, Miguel Anaya<sup>1</sup>, Aron Walsh<sup>3</sup>, Paul Midgley<sup>1</sup>, Keshav Dani<sup>2</sup> and Samuel D. Stranks<sup>1</sup>; <sup>1</sup>University of Cambridge, United Kingdom; <sup>2</sup>Okinawa Institute of Science and Technology, Japan; <sup>3</sup>Imperial College London, United Kingdom

Halide perovskite materials have promising performance characteristics for low-cost optoelectronic applications. Photovoltaic devices fabricated from perovskite absorbers have reached power conversion efficiencies above 25 per cent in single-junction devices and 28 per cent in tandem devices. Though widely considered defect tolerant materials, perovskites still exhibit a sizeable density of deep sub-gap non-radiative trap states, which create local variations in photoluminescence (1, 2) that fundamentally limit device performance. These trap states have also been associated with light-induced halide segregation in mixed halide perovskite compositions (3) and local strain (4), both of which can detrimentally impact device stability (5). Understanding the nature of these traps will be critical to ultimately eliminate losses and yield devices operating at their theoretical performance limits with optimal stability. We recently revealed that the majority of these trap states in state-of-the-art (CS<sub>0.05</sub>FA<sub>0.78</sub>MA<sub>0.17</sub>)Pb(I<sub>0.83</sub>Br<sub>0.17</sub>)<sub>3</sub> perovskites form in nanoscale clusters at grain boundaries of compositionally and structurally distinct entities [*Nature*, 2020].

In this talk we detail our low-dose, high-resolution and multimodal approach to link photophysical properties to nanoscale structural and compositional heterogeneities. By combining scanning electron microscopy techniques with spatially resolved photoemission measurements, we compare and contrast observed structural defects in (CS<sub>0.05</sub>FA<sub>0.78</sub>MA<sub>0.17</sub>)Pb(I<sub>0.83</sub>Br<sub>0.17</sub>)<sub>3</sub> and (CS<sub>0.05</sub>FA<sub>0.78</sub>MA<sub>0.17</sub>)PbI<sub>3</sub> halide perovskite thin films and discuss how they ultimately limit device performance. In so doing, we reveal the nature and origin of the “inhomogenous” perovskite grains that have been directly linked to non-radiative recombination and were previously unidentified (1). Finally, by combining scanning electron diffraction measurements with environmental chambers, we perform *in-situ* experiments to explore the local nanoscale structural modifications that occur in perovskite materials under real world operating conditions and how these structural modifications are linked to device degradation.

#### References

1. T. A. S. Doherty, A. J. Winchester, S. Macpherson, D. N. Johnstone, V. Pareek, E. M. Tennyson, S. Kosar, F. U. Kosasih, M. Anaya, M. Abdi-Jalebi, Z. Andaji-Garmaroudi, E. L. Wong, J. Madéo, Y.-H. Chiang, J.-S. Park, Y.-K. Jung, C. E. Petoukhoff, G. Divitini, M. K. L. Man, C. Ducati, A. Walsh, P. A. Midgley, K. M. Dani, S. D. Stranks, Performance-limiting nanoscale trap clusters at grain junctions in halide perovskites. *Nature*. **580**, 360–366 (2020).
2. D. W. de Quilettes, S. M. Vorpahl, S. D. Stranks, H. Nagaoka, G. E. Eperon, M. E. Ziffer, H. J. Snaith, D. S. Ginger, Impact of microstructure on local carrier lifetime in perovskite solar cells. *Science*. **348**, 683–686 (2015).
3. A. J. Knight, A. D. Wright, J. B. Patel, D. P. McMeekin, H. J. Snaith, M. B. Johnston, L. M. Herz, Electronic Traps and Phase Segregation in Lead Mixed-Halide Perovskite. *ACS Energy Lett.* **4**, 75–84 (2019).
4. T. W. Jones, A. Osherov, M. Alsari, M. Sponseller, B. C. Duck, Y.-K. Jung, C. Settens, F. Niroui, R. Brenes, C. V. Stan, Y. Li, M. Abdi-Jalebi, N. Tamura, J. E. Macdonald, M. Burghammer, R. H. Friend, V. Bulović, A. Walsh, G. J. Wilson, S. Lilliu, S. D. Stranks, Lattice strain causes non-radiative losses in halide perovskites. *Energy Environ. Sci.* **12**, 596–606 (2019).
5. J. Zhao, Y. Deng, H. Wei, X. Zheng, Z. Yu, Y. Shao, J. E. Shield, J. Huang, Strained hybrid perovskite thin films and their impact on the intrinsic stability of perovskite solar cells. *Science Advances*. **3**, eaao5616 (2017).

#### F.EL08.20.07

**Elucidating the Influence of Compositional Heterogeneity on Charge Carrier Accumulation and Photodoping in Metal Halide Perovskites** Stuart Macpherson, Jooyoung Sung, Tiarnan A. Doherty, Kyle Frohna, Elizabeth Tennyson, Miguel Anaya, Yu-Hsien Chiang, Akshay Rao and Samuel D. Stranks; University of Cambridge, United Kingdom

Metal halide perovskites are remarkable thin film semiconductors with numerous favorable properties that are optimal for photovoltaic and light emission applications<sup>1</sup>. These characteristics include high absorption coefficients, long charge carrier lifetimes and a tunable bandgap.

We have previously shown that the luminescence efficiency and charge carrier recombination behavior in mixed halide perovskites is significantly altered by the cation alloy employed during fabrication via facile solution processing<sup>2</sup>. The addition of alkali metal cations provides passivation of sub-bandgap defect states and also stabilizes an energetic landscape that facilitates photodoped carrier accumulation, leading to enhanced optoelectronic performance.

Our current work aims to further unveil the influence of microscopic compositional variations on local photoinduced carrier accumulation in (CsMAFA)Pb<sub>x</sub>Br<sub>3-x</sub> perovskite films. We combine Femtosecond Transient Absorption Microscopy with nanoscale X-ray Fluorescence and Atomic Force Microscopy to track carrier diffusion and recombination across a heterogeneous chemical and morphological landscape. We find that the complex interplay of local carrier recombination and diffusion will have important ramifications for solar cell and LED device performance.

[1] Stranks, S. D. & Snaith, H. *Nature Nanotech* **10**, 391-402 (2015)

[2] Feldmann, S., Macpherson S. et al. *Nature Photonics* **14**, 123-128 (2020)

#### **F.EL08.20.08**

**Ferroelastic Strain and Defect Behavior upon Repeated Bending of Flexible Methylammonium Lead Iodide Perovskite Films** Rhys M. Kennard, Clayton J. Dahlman, Ryan DeCrescent, Jon Schuller, Kunal Mukherjee, Ram Seshadri and Michael Chabinyo; University of California, Santa Barbara, United States

The highest solar cell efficiencies in halide perovskite devices are achieved using compositional derivatives of tetragonal methylammonium lead iodide (MAPbI<sub>3</sub>). Commercialization of flexible perovskite devices will require a thorough understanding of how applied strain modifies the perovskite structure and defect-related properties. A complication of studying strain behavior in tetragonal MAPbI<sub>3</sub> is that it is ferroelastic, meaning that it spontaneously forms multiple domains, also called “twins”. These twins exhibit identical crystal structure but different orientation, are inherently strained, and are separated by domain walls. The relative proportions of different twins can be semi-reversibly changed (“domain switching”) upon application of stress, via a process called ferroelastic hysteresis. Separate studies have shown that applying strain to MAPbI<sub>3</sub> films modifies defect-related properties such as the degradation rate, the activation energy of ion migration and the photoluminescence lifetime. However, potential correlations between changes to these properties in films and ferroelasticity have proven difficult to establish, as a detailed structural description of the ferroelastic behavior of MAPbI<sub>3</sub> under strain is missing.

In this work, we characterized in detail the ferroelastic hysteresis loop of MAPbI<sub>3</sub>. Films of MAPbI<sub>3</sub> were cast on polymer substrates. We used Grazing Incidence Wide-Angle X-ray Scattering (GIWAXS) to first identify twin type and to assess the impact of the polymer substrate on the twins formed. Changes in the populations of different ferroelastic twins, in the strain magnitudes of different lattice planes, and in minimum domain sizes were then characterized for increasingly large applied strains. We thus identified approximate locations for the coercive stress (onset of domain switching) and saturation (all possible domain switching has occurred) on the stress-strain curve of MAPbI<sub>3</sub>, as well as transformation strain magnitudes imparted by the hysteresis. Changes in the minimum domain sizes enabled deduction of evolution of the number of domain walls. The concentration of domain walls in films was found to closely correlate with previously-reported changes in the activation energy of ion migration, photoluminescence lifetime and degradation rate of MAPbI<sub>3</sub> films upon application of strain. The understanding gained by these results will aid design of more stable MAPbI<sub>3</sub> flexible devices with better-controlled ionic and electronic properties.

#### **F.EL08.20.10**

**Ultrafast Photophysics of Metal Halide Perovskite Multiple Quantum Wells—Device Implications and Reconciling Band Alignment** Andrew H. Proppe and Edward H. Sargent; University of Toronto, Canada

Metal halide perovskite quantum wells (QWs) have been used to fabricate efficient optoelectronic devices, and exhibit stability superior to that of their bulk 3D counterparts. The perovskite QWs are tuned in synthesis so that they possess different bandgaps and exciton binding energies owing to variable quantum confinement as a function of QW thickness. Accordingly, the device performance of these materials depends on the efficiency of various interwell carrier dynamical

processes, principally exciton and charge transfer. I will discuss the use of transient absorption and ultrafast two-dimensional electronic spectroscopy to probe interwell exciton transfer on timescales of 100s of femtoseconds, and show that interwell charge transfer occurs on timescales of 10s to 100s of picoseconds. These results, in addition to ultraviolet photoelectron spectroscopy experiments, are used to reconcile conflicting observations of type-I and type-II band alignment amongst perovskite QWs.

#### F.EL08.20.12

##### **Rashba Band Splitting in Methylammonium Lead Iodide—An Insight from Spin-Polarized Scanning Tunneling Spectroscopy** Abhishek Maiti, Salma Khatun and Amlan J. Pal; Indian Association for the Cultivation of Science, India

A low recombination rate of photogenerated carriers in methylammonium lead iodide (MAPbI<sub>3</sub>) enhancing the carrier lifetime and thereby diffusion length is believed to be occurred due to Rashba band splitting<sup>[1]</sup> which arises due to a large spin-orbit coupling (SOC) arising out of high-Z elements (lead and iodine) in the compound along with a lack of centrosymmetry which appears due to a tilted PbI<sub>6</sub> octahedra and rotating electric dipoles of the organic ions leading to an effective magnetic field and thereby lifting the Kramer's spin-degeneracy of the electrons.<sup>[2]</sup> Regarding the spin-rotation or spin-texture ( $\chi$ ) of the two split-levels, two schools of thought persist amongst theoreticians: (1) spin-forbidden transition model and (2) spin-allowed transition model. In the spin-forbidden transition model, after spin-split, the CB and VB closer to the Fermi energy possess opposite spin-textures. A recombination between electrons in CB-minimum and holes in VB-maximum is hence a spin-forbidden process leading to a low recombination rate and thereby an enhanced carrier lifetime and a longer diffusion length.<sup>[1]</sup> On the other hand, such possibility has been overruled in the spin-allowed transition model as CB and VB possess a similar type of spin-texture closer to the Fermi energy where the recombination of photo-excited carriers is apparently possible due to spin-allowed nature of the transition.<sup>[3]</sup> In this regard, we have reported an experimental observation of Rashba splitting in MAPbI<sub>3</sub> through spin-polarized scanning tunneling spectroscopy to probe the split bands.<sup>[4]</sup>  $dI/dV$  spectra recorded at many different points of the film allowed us to spot both the Rashba split-levels and also to deliberate on their spin-textures. We observe that the bands split in such a manner that the conduction and valence bands closer to the Fermi energy have the same type of spin-textures (a spin-allowed transition model). Still a low recombination rate of photogenerated carriers in MAPbI<sub>3</sub> has been analyzed by considering Wannier-type excitons, a molecular nature of spin-domains as observed from the  $dI/dV$  images, and therefore a spin-forbidden nature of inter-domain transition.

#### Reference

1. Zheng, F.; Tan, L. Z.; Liu, S.; Rappe, A. M., Rashba Spin–Orbit Coupling Enhanced Carrier Lifetime in CH<sub>3</sub>NH<sub>3</sub>PbI<sub>3</sub>. *Nano Lett.* 2015, 15 (12), 7794-7800.
2. Kepenekian, M.; Even, J., Rashba and Dresselhaus Couplings in Halide Perovskites: Accomplishments and Opportunities for Spintronics and Spin–Orbitronics. *The Journal of Physical Chemistry Letters* 2017, 8 (14), 3362-3370.
3. Zhang, X.; Shen, J.-X.; Van de Walle, C. G., Three-Dimensional Spin Texture in Hybrid Perovskites and Its Impact on Optical Transitions. *The Journal of Physical Chemistry Letters* 2018, 9 (11), 2903-2908.
4. **Maiti, A.**; Khatun, S.; Pal, A. J., Rashba Band Splitting in CH<sub>3</sub>NH<sub>3</sub>PbI<sub>3</sub>: An Insight from Spin-Polarized Scanning Tunneling Spectroscopy. *Nano Lett.* 2020, 20 (1), 292-299.

SESSION F.EL08.21: Poster Session IX: Frontiers of Halide Perovskites—Linking Fundamental Properties to Devices  
On Demand Abstracts Available for Viewing Starting Saturday Morning, November 21, 2020

5:00 AM - 8:00 AM

F-EL08

#### F.EL08.21.01

##### **Late News: Comparison of Different Functionals for First-Principles Calculations of Defects in Metal Halide**

**Perovskites** Haibo Xue<sup>1</sup>, Geert Brocks<sup>2,1</sup> and Shuxia Tao<sup>1</sup>; <sup>1</sup>Eindhoven University of Technology, Netherlands; <sup>2</sup>University of Twente, Netherlands

Being one of the most promising photovoltaic materials, the metal halide perovskites have attracted plenty of scientific effort in improving their optoelectronic properties and long-term stability. Both properties are highly sensitive to the nature and the concentration of the intrinsic defects in the perovskites. The first-principles calculation is very useful to predict the thermodynamics relevant to the formation of the defects and their consequences in the optoelectronic properties and plays an essential role in complementing experiments in understanding the defect chemistry and physics. However, due to the intrinsic complexity of the halide perovskites, i. e. hybrid composition and covalent-ionic bonds, diverse results were reported using

different functionals within the density functional theory framework. Here, using the typical perovskite, MAPbI<sub>3</sub>, as an example, we show a comprehensive comparison of a wide range of functionals including GGAs, meta-GGA (SCAN), and combination of them with atom-pairwise (DFT-D3) and non-local (rev-vdW-DF2 and rVV10) van der Waals (vdW) correction. Our results indicate meta-GGA (SCAN) predicts consistently more accurate geometries and energies than GGAs and the vdW correction is essential for describing the vdW bonds associated with the organic cations in the hybrid perovskites. Based on the above, we suggest the SCAN+rVV10 is the most promising functional and is expected to improve on the accuracy for other halide perovskites in this large family of materials.

#### F.EL08.21.02

**Late News: Machine Learning Framework for Accelerated Development of Halide Perovskites** [Meghna Srivastava](#)<sup>1</sup>, John Howard<sup>2,2</sup>, Tao Gong<sup>1</sup> and Marina S. Leite<sup>1</sup>; <sup>1</sup>University of California, Davis, United States; <sup>2</sup>University of Maryland, United States

Metal halide perovskite solar cells (PSC) are a high-efficiency, low-cost alternative to Si photovoltaics. However, various environmental stressors (light, humidity, temperature, bias, and oxygen) initiate degradation in perovskite devices, which limits device lifetimes and impedes commercialization. Discovering materials and fabrication parameters that provide a stable performance is therefore vital. Machine learning (ML) accelerates design at every level of the PSC development process while offering novel physical insight. We present a framework for applying ML to (A) perovskite compositional screening, (B) material synthesis and stability analysis, and (C) full device development and testing. Key parameters such as crystal lattice parameters, quasi-fermi-level splitting, and power conversion efficiency (PCE) are extracted from experimental data, including X-ray diffraction (XRD), photoluminescence (PL), and current-voltage (I-V) characteristics. Traditionally, these data lead to a time-consuming trial-and-error process that informs optimal perovskite compositions, fabrication processes, and device operating conditions. ML models expedite this process and, once trained, use easily acquired experimental data to immediately predict figures of merit or future material/device performance (including forecasting time-resolved behavior). These predictions then guide further experimental investigation. Our generalized roadmap involves (1) identifying the material question of interest, (2) obtaining data for model training, (3) data pre-processing, (4) feature engineering, and (5) model optimization and testing. We demonstrate this process from start-to-finish using several baseline models trained on currently available data from the perovskite community, noting potentials for fine-tuning and extension. As one example, we use past time-series PL and relative humidity (rH) data to forecast humidity-dependent light emission for methylammonium lead triiodide (MAPI), methylammonium lead tribromide, and triple-cation (formamidinium-methylammonium-cesium) perovskite thin films. For this task, we implement an echo state network (ESN), a type of recurrent neural network (RNN). The optimized model predicts PL output with <15% normalized root mean square error (NRMSE) for all compositions over 12+ hours. We train an additional ESN to forecast power output from a PSC with a triple-cation absorber, using light intensity and temperature data as inputs, and obtain an NRMSE of only 3.1%. In addition to time-series prediction, ML models can extrapolate from ground truth experimental data to novel conditions. This reduces laboratory time drastically and eliminates the need for exhaustive trial-and-error work. For example, we train a long short-term memory (LSTM) model on temperature-dependent aging data from a MAPI PSC. We generate degradation traces at unseen temperatures with <3% NRMSE. Finally, we show image-based machine learning, using a convolutional neural network (CNN) to extract hidden trends from dark-field images of spiro-OMeTAD (a common hole-transport layer in PSC devices) and predict film conductance. Although the images have no visual trends discernable by the human eye, the model achieves an NRMSE of 19%. These examples illustrate the versatility of ML as a tool in PSC research, and our workflow is easily generalizable to other facets of development. We propose integrating projects from all three levels of PSC design (composition, material, and device) into a streamlined ML pipeline that includes materials discovery, fabrication, characterization, and stability testing. This pipeline takes advantage of our current technological capabilities in ML, data science, and autonomous experimentation and presents a rational, accelerated pathway to PSC commercialization.

#### F.EL08.21.03

**Late News: Atomistic and Electronic Origin of Phase Instability of Metal Halide Perovskites** [Junke Jiang](#)<sup>1</sup>, Feng Liu<sup>2</sup>, Ionut Tranca<sup>1</sup>, Qing Shen<sup>2</sup> and Shuxia Tao<sup>1</sup>; <sup>1</sup>Eindhoven University of Technology, Netherlands; <sup>2</sup>The University of Electro-Communications, Japan

The excellent optoelectronic properties of metal halide perovskites (MHPs) have attracted extensive scientific interests and boosted their application in optoelectronic devices. Despite their attractive optoelectronic properties, their poor stability under ambient conditions remains the major challenge, hindering their large-scale practical applications. In particular, some MHPs undergo spontaneous phase transitions from perovskites to non-perovskites. Compositional engineering via mixing cations or anions has been widely reported to be effective in suppressing such unwanted phase transition. However, the atomistic and electronic origins of the stabilization effect remain unexplored. Here, by combining Density Functional Theory (DFT)

calculations and Crystal Orbital Hamilton Population (COHP) analysis, we provide insights for the undesired phase transition of pristine perovskites (FAPbI<sub>3</sub>, CsPbI<sub>3</sub>, and CsSnI<sub>3</sub>) and reveal the mechanisms of the improved phase stability of the mixed compounds (Cs<sub>x</sub>FA<sub>1-x</sub>PbI<sub>3</sub>, CsSn<sub>y</sub>Pb<sub>1-y</sub>I<sub>3</sub>, and CsSn(Br<sub>z</sub>I<sub>1-z</sub>)<sub>3</sub>). We identify that the phase transition is correlated with the relative strength of the M-X bonds as well as that of the hydrogen bonds (for hybrid compositions) in perovskite and non-perovskite phases. The phase transition can be suppressed by mixing ions, giving rise to either increased bond strength for the perovskite or decreased bond strength in their non-perovskite counterparts. Our results present a comprehensive understanding of the mechanisms for the phase instability of metal halide perovskites and provide design rules for engineering phase-stable perovskite compositions.

#### F.EL08.21.04

**Late News: Atmosphere Affecting Lattice and Degradation Mechanisms of High-Efficiency Perovskite Solar Cells** Renjun Guo<sup>1</sup>, Dan Han<sup>2</sup>, Wei Chen<sup>1</sup>, Manuel A. Scheel<sup>1</sup>, Lennart K. Reb<sup>1</sup>, Nian Li<sup>1</sup>, Shambhavi Pratap<sup>1</sup>, Tianxiao Xiao<sup>1</sup>, Suzhe Liang<sup>1</sup>, Christian L. Weindl<sup>1</sup>, Shanshan Yin<sup>1</sup>, Hubert Ebert<sup>2</sup>, Matthias Schwartzkopf<sup>3</sup>, Stephan V. Roth<sup>3,4</sup> and Peter Muller-Buschbaum<sup>1,5</sup>; <sup>1</sup>Technische Universität München, Germany; <sup>2</sup>Ludwig-Maximilians-Universität München, Germany; <sup>3</sup>Deutsches Elektronen-Synchrotron, Germany; <sup>4</sup>KTH Royal Institute of Technology, Sweden; <sup>5</sup>Heinz Maier-Leibnitz-Zentrum, Germany

Metal halide perovskites have shown a promising future for application in field-effect transistors, light-emitting diodes, sensors, solar cells, and photodetectors due to their excellent optic-electrical properties. Among the excellent properties of perovskites, for example, strong absorption, the long diffusion length of photo-generated charge carriers and low binding energies make it possible to realize next-generation solar cells with 25.2% power conversion efficiency (PCE) in a decade. At the same time, perovskite solar cells (PSCs) have shown a powerful photovoltaic application for replacing silicon solar cells not only due to high PCE but also because of its low processing costs. Despite such advantages, the application of PSCs is currently limited by combining high performance and operational stability, because the PCE of PSCs can degrade due to the presence of temperature, light, humidity, and oxygen. So far, the degradation research on PSCs is carried out without having an established standard protocol. The microscopic degradation mechanisms are not clear under operating conditions upon suggested inert atmospheres based on the International Summit on Organic Photovoltaic Stability protocols. Therefore, it is necessary to establish an improved standard protocol for the long-term degradation of PSCs.

In this respect, we investigate the degradation processes of PSCs under both, AM 1.5G and different atmosphere conditions (vacuum and nitrogen) with in-operando grazing incidence wide-angle X-ray scattering (GIWAXS) and grazing incidence small-angle X-ray scattering (GISAXS). With these approaches, we find that mixed cations lead mixed halides lattice exhibit the effect of photostriction when being operated in different atmospheres. In addition, the nature of photostriction can help the phase segregation of halide perovskites. Pressure conditions can suppress this photostriction behavior. Theoretical calculations based on density functional theory confirm that lattice photostriction behavior can suppress phase segregation induced by thermodynamic driving forces. A standard protocol is suggested based on our findings.

#### F.EL08.21.05

**Late News: Study of the Formation of Different Electron Transport Layer (ETL) Materials and Their Impacts on Perovskite Solar Cell (PSC) Performance** Luisa Pan<sup>1</sup>, Pranati Patnam<sup>2</sup>, Benjamin Roitman<sup>3</sup>, Yifan Yin<sup>4</sup>, Yuchen Zhou<sup>4</sup>, Miriam H. Rafailovich<sup>4</sup> and Chang-Yong Nam<sup>5</sup>; <sup>1</sup>The Harker School, United States; <sup>2</sup>Herricks High School, United States; <sup>3</sup>SAR High School, United States; <sup>4</sup>Stony Brook University, The State University of New York, United States; <sup>5</sup>Brookhaven National Laboratory, United States

Perovskite solar cells (PSC) are believed to be the core of next-generation solar cells due to their rapidly increasing efficiency and popularity as an alternative energy source to fossil fuels. However, the interfacial contact between the electron transport layer (ETL) and the perovskite layer in the cell often results in problems of hysteresis. This research investigates different ETL materials to remedy hysteresis in organic-inorganic CH<sub>3</sub>NH<sub>3</sub>PbI<sub>3</sub> (MAPbI<sub>3</sub>) PSCs. Compact TiO<sub>2</sub> (c-TiO<sub>2</sub>), SnO<sub>2</sub> (0.1M and 0.2M), and mesoporous TiO<sub>2</sub> (m-TiO<sub>2</sub>) (1:4 and 1:6 w:w) were deposited as the chosen ETL materials via spin-casting and followed by high-temperature annealing. The PSC devices were built using FTO glass, MAPbI<sub>3</sub>, and gold electrodes (80nm).

Scanning electron microscopy (SEM) was utilized to take cross-sectional images of the solar cell after depositing the perovskite layer. Higher values in the precursor ETL solution concentration correlated with increased ETL thickness. Qualitative analysis of the c-TiO<sub>2</sub>/m-TiO<sub>2</sub> bilayer SEM image demonstrated that the perovskite layer also effectively diffused into the porous m-TiO<sub>2</sub>, which increased the interfacial contact between the perovskite and the ETL. Although the control c-TiO<sub>2</sub> had a power conversion efficiency (PCE) of 14.5%, the sample had a hysteresis index of 0.400. In comparison, the 34mM TiO<sub>2</sub> sample had a PCE of 11.9% with a more desired hysteresis index of 0.034. The m-TiO<sub>2</sub> bilayer



sample, albeit having a PCE of 6.8%, had a hysteresis index of 0.121, suggesting that the mesoporous layer aided in reducing the hysteresis index of the original c-TiO<sub>2</sub> ETL.

We gratefully acknowledge support from the Louis Morin Charitable Trust.

#### F.EL08.21.06

**Late News: Ultralong Micro-Belts of Luminescent Lead Halide-Based Perovskites** [Fnu Parul](#); Indian Institute of Technology Roorkee, India

Ultralong micro-belts of MAPbI<sub>3</sub> show bright and stable fluorescence in solution. Luminescent perovskites have been synthesized through centrifugation of a solution-processed with a ligand-assisted reprecipitation technique (LARP). All electron spectroscopic analysis provided evidence for the stacking of nanocrystals as bundles of self-assembled micro-belts. Under an applied bias, migration of free charge carriers through the long axis is feasible. Thus, long micro-belts are promising channel materials for two-electrode nanodevices for good electrical conductivity.

#### F.EL08.21.07

**Late News: Compositional Effect on Water Adsorption on Metal Halide Perovskites** [Qihua Li](#), Zehua Chen, Ionut Tranca, Silvia Gaastra-Nedeaa, David Smeulders and Shuxia Tao; Eindhoven University of Technology, Netherlands

The moisture-induced instability of metal halide perovskites is one of the major challenges for perovskite devices. Although compositional engineering has been widely employed to improve the overall stability of perovskites, its effect on the moisture-induced instability received little attention. Here, we systematically study the interaction of water with the surfaces of primary perovskites, AMX<sub>3</sub> (A<sup>+</sup> = MA<sup>+</sup>, FA<sup>+</sup>, Cs<sup>+</sup>; M<sup>2+</sup> = Pb<sup>2+</sup>, Sn<sup>2+</sup>; X<sup>-</sup> = I<sup>-</sup>, Br<sup>-</sup>), by using Density Functional Theory (DFT) calculations and comprehensive chemical bonding analysis. We reveal that the hydrophilic group NH<sub>3</sub><sup>+</sup> of MA<sup>+</sup> cation may be the cause for instability issues. We find that the adsorption of water on FAPbI<sub>3</sub> and CsPbI<sub>3</sub> are much weaker than on MAPbI<sub>3</sub> due to the less polarity of FA<sup>+</sup> and Cs<sup>+</sup>. When exchanging M<sup>2+</sup> cations, water adsorption on MASnI<sub>3</sub> is also less energetically favorable than on MAPbI<sub>3</sub> because of the weaker ionic interaction of H<sub>2</sub>O-MASnI<sub>3</sub>. When exchanging X<sup>-</sup> anion, water adsorption on MAPbBr<sub>3</sub> is slightly weaker than on MAPbI<sub>3</sub> due to the slightly weaker covalent interaction of H<sub>2</sub>O-MAPbBr<sub>3</sub>. Our results present a comprehensive understanding of the compositional effect on the interactions of water with perovskites and provide rational design strategies to improve their stability against moisture via compositional engineering.

#### F.EL08.21.08

**Late News: Unified Thermodynamic Theory for Light-Induced Phase Separation in Mixed Halide Perovskites** [Zehua Chen](#)<sup>1</sup>, Geert Brocks<sup>2</sup>, Peter Bobbert<sup>1</sup> and Shuxia Tao<sup>1</sup>; <sup>1</sup>Eindhoven University of Technology, Netherlands; <sup>2</sup>University of Twente, Netherlands

In the dark and at room temperature most mixed halide perovskites are thermodynamically stable. Under illumination, however, funneling of photo-excited carriers to a phase with a lower band gap than the parent phase leads to halide demixing. This is problematic for the application of mixed halide perovskites in solar cells. Here, we present a unified thermodynamic theory for this light-induced phase separation and apply it to five mixed iodine-bromine perovskites. Under illumination, the spinodals separating the metastable and unstable regions in the composition-temperature phase diagrams show an upward shift in temperature, while the binodals separating the stable and metastable regions acquire an additional branch signaling the nucleation of a low-band gap iodine-rich phase. We find that the threshold illumination intensity is mainly governed by the band gap difference of the parent and iodine-rich phase. Partial replacement of organic cations by cesium reduces this difference and therefore has a stabilizing effect.

#### F.EL08.21.09

**Late News: Charge Carrier Dynamics in Two-Dimensional Hybrid Perovskites—Impact of Spacer Cations** [Dibyajyoti Ghosh](#); Los Alamos National Laboratory, United States

Two-dimensional (2D) halide perovskites are promising materials for environmentally stable next-generation optoelectronic device applications. However, there is very little atomistic understanding of the charge carrier dynamics at ambient conditions for these materials, limiting the possibilities to tune their optoelectronic performances through compositional engineering routes. *Here, by combining nonadiabatic molecular dynamics with time-domain density functional theory methods at room temperature, we study the dominant non-radiative carrier recombination and dephasing processes in monolayered lead halide perovskites.* Our systematic study demonstrates that performance-limiting nonradiative carrier recombination processes greatly depend on the electron-phonon interactions induced by structural fluctuations and instantaneous charge localization in these materials. *The stiffer interlayer packing in presence of selectively chosen spacer*

cations (benzene ring or cyclic dication based), which separates the lead iodide slabs, reduces the thermal fluctuations in these 2D-perovskites to a greater extent.<sup>[1-2]</sup> These reduce the inelastic electron-phonon scattering and enhance the photogenerated charge carrier lifetime in layered perovskites making them suitable for various optoelectronic devices. The computational insights gained from these studies allow us to outline a set of robust design principles for 2D halide perovskites to strategically tune their optoelectronic properties.

#### Reference:

1. Ghosh *et al.* J. Phys. Chem. Lett, **2020**, 11, 2955
2. Ghosh *et al.* J. Mater. Chem. A, **2020**, Just Accepted (DOI: 10.1039/D0TA07205B)

#### F.EL08.21.12

**Late News: Synthesis, Photocatalytic Properties and Phase Stability Studies of Full Inorganic CsPbBr<sub>3</sub> and CsPb<sub>2</sub>Br<sub>5</sub> Perovskites** [Anna L. Pellegrino](#)<sup>1,2</sup> and Graziella Malandrino<sup>1,2</sup>; <sup>1</sup>Università degli Studi di Catania, Italy; <sup>2</sup>INSTM, Italy

The compounds belonging to the family of perovskites show a great variety of mechanical, magnetic and optical properties, and for these reasons are nowadays key materials for many technologies, including piezoelectrics, photovoltaic solar cells and photocatalytic systems.

Among perovskites, the most studied crystal structure ABX<sub>3</sub> for photocatalysis and photovoltaic applications is composed of an organic/inorganic compounds made of: monovalent cation A = methylammonium (MA: CH<sub>3</sub>NH<sub>3</sub><sup>+</sup>); formamidinium (FA: CH(NH<sub>2</sub>)<sub>2</sub><sup>+</sup>); a divalent metal cation B = Pb<sup>2+</sup>, Sn<sup>2+</sup>; and an halide anion X = I<sup>-</sup>; Br<sup>-</sup>; Cl<sup>-</sup>. These hybrid lead-based materials have excellent properties and contain elements that are both cheap and abundant. However, they tend to partially decompose when exposed to air, water, ultra-violet light, or heat. For these reasons, several substitutions have been attempted to improve the properties and performances of these materials. One route to improve the stability of these structures is to explore the all-inorganic perovskite systems and thus finding alternatives to replace organic components. Particularly, our attention is devoted to the all-inorganic perovskites, i.e. CsPbBr<sub>3</sub> and CsPb<sub>2</sub>Br<sub>5</sub>, which do not have any labile or expensive components and show remarkable stability. Furthermore, unlike the hybrid structures, the entire fabrication process of all-inorganic analogous materials can be operated in ambient atmosphere without humidity control systems. Additionally, CsPbX<sub>3</sub> (X = Cl, Br, and I) perovskite family shows high performances for photocatalytic and photo-electrochemical degradation processes of different organic dye compounds, and are also exceptional candidates as photocatalysts for organic reactions. Among the different strategy developed for their synthesis, the surfactants-based solution route is widely applied, which also allows to control the stability and the growth kinetics according to the surface chemical phenomenon and the solubility equilibrium. Herein we report a novel synthetic strategy, which represents a facile, one-step, low-temperature and surfactant free approach to the synthesis of Cs-Pb-Br microcrystals, using Cs and Pb β-diketonate metallorganic complexes. The present precipitation approach represents an innovative and interesting strategy of synthesis, which avoids the use of surfactant species and toxic solvents, and, taking the advantages of the β-diketonate metalorganic Cs and Pb precursors reactivity, it allows, reproducibly and selectively, the synthesis of CsPbBr<sub>3</sub> and CsPb<sub>2</sub>Br<sub>5</sub> microcrystals. Structural, morphological and compositional analyses of the final products, addressed through X-ray diffraction (XRD), field-emission scanning electron microscopy (FE-SEM) and Energy Dispersive X-ray (EDX) analysis, show the formation of pure and stable CsPbBr<sub>3</sub> or CsPb<sub>2</sub>Br<sub>5</sub> systems characterized by squared microcrystals, with a grain size up to 3 μm. The stability of the two different phases has been tested as a function of heating treatment and UV exposure as well. Moreover, as a proof-of-concept, the photocatalytic properties of degradation processes have been tested using organic dye solutions, showing high degradation yield up to 70% under UV lamp (λ=360 nm).

#### F.EL08.21.13

**Late News: Synthesis of Lead-Free All-Inorganic Cs<sub>3</sub>Sb<sub>2</sub>Br<sub>9</sub> Perovskite Microplates by Two-Step Chemical Vapor Deposition for Fast Response Visible Light Photodetector Application** [Sujit Kumer Shil](#)<sup>1,2</sup>, Fei Wang<sup>1</sup>, Mohammad Kamal Hossain<sup>1</sup>, Cheuk Kai Gary Kwok<sup>1</sup>, Kingsley O. Egbo<sup>1</sup>, Ying Wang<sup>1</sup> and Kin Man Yu<sup>1,1</sup>; <sup>1</sup>City University of Hong Kong, Hong Kong; <sup>2</sup>Khulna University of Engineering & Technology, Bangladesh

Lead-based halide perovskites (CsPbX<sub>3</sub>, X=Cl, Br, I) are well-known for their attractive properties which make them suitable materials for many optoelectronic devices. But the toxicity of lead (Pb) undoubtedly hinders the development and commercialization of these devices. Therefore, Pb-free, environmental friendly all-inorganic halide perovskites are now the subject of enormous interest to the scientific community. It has been suggested that antimony (Sb) can be a possible replacement of Pb (Cs<sub>3</sub>Sb<sub>2</sub>X<sub>9</sub>) in these inorganic halide perovskites. Until now Sb-based all-inorganic perovskites have been synthesized by solution processes but properties are still inferior to Pb-based materials. However, due to the low melting point of Sb halides, synthesis of high quality Cs<sub>3</sub>Sb<sub>2</sub>X<sub>9</sub> using chemical vapor process is still a challenge. In this work, we present a report on the synthesis and properties of Pb-free all-inorganic Cs<sub>3</sub>Sb<sub>2</sub>Br<sub>9</sub> perovskite microplates by a two-step chemical vapor deposition (CVD) approach. In step-I, CsBr powder was vaporized at 530°C at a pressure of 4.8 Torr under

50 sccm of Ar flow for 10 minutes in a single-zone CVD furnace. In step-II, due to low melting point,  $\text{SbBr}_3$  powder was vaporized at  $90^\circ\text{C}$  under 15 sccm of Ar flow while the pressure and holding time were remained same as step-I. Substrates were placed at 22 cm downstream from the center. Finally  $\text{Cs}_3\text{Sb}_2\text{Br}_9$  microplates with average size  $20\ \mu\text{m}$  were obtained after annealing the as-grown materials at  $140^\circ\text{C}$  for 25 minutes. XRD analysis of the microplates shows the pure phase crystalline nature of the  $\text{Cs}_3\text{Sb}_2\text{Br}_9$  perovskite structure. The optical band gap was measured by spectroscopic ellipsometry to be 2.6 eV. The UV-vis absorption spectrum revealed the exciton absorption peak at around 2.82 eV. Simple photoconductive devices fabricated using these microplates exhibit current on/off ratio of  $10^2$  upon 450 nm photon irradiation with a fast response of rise and decay time down to 79 ms and 28 ms, respectively. All these results clearly suggest the technological potential of inorganic lead-free  $\text{Cs}_3\text{Sb}_2\text{Br}_9$  perovskite microplates for future optoelectronic devices.

#### F.EL08.21.15

**Late News: Interfacial Engineering by Double Decked Electron and Hole Extraction Layers for Reproducible and Thermally Stable Perovskite Solar Cells.** Shivam Singh and Dinesh Kabra; Indian Institute of Technology Bombay, India

**Abstract:** We present an interfacial engineering method to fabricate an efficient and thermally stable  $\text{MAPbI}_3$  based perovskite solar cell with a double decked hole ( $H$ ) and electron ( $E$ ) extraction layers (EL) in an inverted ( $p-i-n$ ) architecture. The double HEL film is fabricated by thermal evaporation of  $\text{MoO}_3$  and spin-coating of poly(3,4-ethylene dioxy-thiophene)-poly(styrene sulfonate) (PEDOT:PSS). The double EEL is formed by spin-coating of phenyl-C61-butyric acid methyl ester ( $\text{PC}_{61}\text{BM}$ ) and bathocuproine (BCP). The role of BCP as a buffer layer is quite established in the community to prevent the formation of metal induced charge state at the perovskite- EEL interface. Despite of presence of BCP interlayer, the thermal stability of  $p-i-n$  architecture still suffers. We observed that the underneath  $\text{MoO}_3$  layer provides an improved morphology for perovskite film and reduces the shunt path. However, the BCP buffer interlayer not only passivates the defects at the perovskite- EEL interface and but also helps to planarize the thin-films for better contact with Ag. Thus, double EEL and HEL facilitate better charge collection at the interfaces and shows improved power conversion efficiency (PCE) of  $\sim 15\%$ . Besides the improved PCE, double EEL and HEL based structures also provide an approach to have better reproducibility and high thermal stability of perovskite solar cells. We also address the issue of area dependent efficiency and explore the reasons behind the increased efficiency of smaller area devices. We believe reproducibility, stability and area dependence are the most important aspects for current perovskite PV research and thus this study will provide an important insight for further development.

**Keywords:**  $\text{MAPbI}_3$ , double extraction layer, thermal stability, solar cells, BCP,  $\text{MoO}_3$

#### References:

1. S. Singh, R. Shourie, and D. Kabra, Efficient and thermally stable  $\text{CH}_3\text{NH}_3\text{PbI}_3$  based perovskite solar cells with double electron and hole extraction layers. *J. Phys. D: Appl. Phys.* **2019**, 52, 255106.
2. Y. Zhao, A. M. Nardes and K. Zhu, Effective hole extraction using  $\text{MoO}_x$ -Al contact in perovskite  $\text{CH}_3\text{NH}_3\text{PbI}_3$  solar Cells. *Appl. Phys. Lett.* **2014**, 104 213906.

#### F.EL08.21.16

**Late News: GFN1-xTB Method for a Fast Calculation of Metal Halide Perovskites Properties for Solar Cells Applications** Jose Manuel Vicent-Luna, Sofia Apergi and Shuxia Tao; Eindhoven University of Technology, Netherlands

Metal halide perovskites (MHPs) for perovskite solar cells (PSCs) have gained great attention in just few years due to their rapid increase of photoconversion records of efficiency. In addition, MHPs exhibit a competitive fabrication cost together with a simple route to synthesize. Due to these facts, PSCs are recognized by scientists as a promising technology with enormous potential in the energy market. However, it is well known that many factors cause the degradation of PSCs, thus, industrial applications are critically hampered by instability issues.

Nowadays, experimental and theoretical researchers are investigating many possible alternatives to increase the stability of PSCs. In this context, computational techniques are being extremely useful to understand the properties of MHPs at microscopic level that cause instability of the material. Density functional theory (DFT) calculations are the key method for studying material properties, but the high computational cost limits the study to small systems and short time-scales. Classical simulations seem to be an option to overcome these limitations, but they suffer from other drawbacks such as classical simulations cannot describe electrons and chemical reactions. The study of many applications of MHPs requires the simultaneously modeling of electrons and ions in relatively large systems, sometimes not computationally affordable by the standard techniques. Therefore an intermediate approach between DFT and classical simulations is often desired. In this regard, semi-empirical Quantum Mechanics methods, such as density functional tight binding (DFTB), combine the

functionalities of describing both electrons and ions. Traditional DFTB methods are based on a simplification of the Kohn-Sham DFT total energy, using pre-computed interactions of element pairs, considerably reducing the computational cost. However, this parameterization lacks of transferability and is limited to a number of elements. A new extended tight binding method called GFN1-xTB has been recently developed to cover all the elements of the periodic table. This method was designed for the fast calculation of diverse physicochemical properties of systems of a few thousand atoms and has the advantageous of maintaining high accuracy and a limited number of parameters which can be refined for the study of a given application.

The performance of GFN1-xTB is benchmarked for a set of MHPs and compared with density functional theory calculations. We study organic and inorganic MHPs with formula  $ABX_3$ , with  $A = MA, FA,$  and  $Cs$ ;  $B = Pb$  and  $Sn$ ;  $X = I, Br,$  and  $Cl$ , being a total of 18 MHPs with cubic, tetragonal, and orthorhombic forms. We included the computation of structural, vibrational, and optoelectronic properties of these semiconductors. This work aims to provide a general overview of the performance of GFN1-xTB for the fast computation of the main features of MHPs. Our results indicate that this method can describe the targeted features of the MHPs, but performs worse for geometry relaxation calculations. We also identified the drawbacks of the method for particular compositions of MHPs, which hamper its use for solar cell applications.

#### F.EL08.21.17

**Late News: Lone-Pair Driven Ferroelectric and Piezoelectric Response of Germanium Halide Perovskites  $CsGeX_3$  ( $X = Cl, Br,$  and  $I$ )** Jiwoo Lee<sup>1</sup>, Young-Kwang Jung<sup>1</sup> and Aron Walsh<sup>1,2</sup>; <sup>1</sup>Yonsei University, Korea (the Republic of); <sup>2</sup>Imperial College London, United Kingdom

While much attention has been paid to halide perovskites based on  $Pb$  and  $Sn$  cations on the B-site,  $Ge$  compounds offer a distinct combination of structure and properties. All three cations feature the same  $s^2$  lone pair configuration; however, the stereochemical activity varies in each case. We performed a computational analysis via density-functional-theory and Berry phase calculations of the  $CsGeX_3$  ( $X = Cl, Br, I$ ) series. Our motivation is to clarify the existence and magnitude of ferroelectricity and piezoelectricity, which has important technological consequences such as polar nanodomains that can reduce the recombination of light-excited electron-hole pairs and extend the carrier lifetime [2]. The explanation for the origin of spontaneous polarization in  $Ge$  halide perovskites in terms of an on-site second-order Jahn-Teller effect has not been hitherto investigated [3]. In this work, we investigate the role of halide anions in spontaneous polarization within the modern first-principles theory of polarization. Our calculation results show that interaction between  $Ge$  lone-pair electrons and halogen  $p$ -orbital mainly determines the depth of the ferroelectric double well and the spontaneous polarization strength with  $Cl > Br > I$ . Further exploration of lone pair systems offers an exciting pathway to design novel photoelectric devices [4,5].

[1] Lead-free germanium iodide perovskite materials for photovoltaic applications. *J. Mater. Chem. A*, **3**, 23829-23832 (2015); <https://doi.org/10.1039/C5TA05741H>

[2] Atomistic origins of high-performance in hybrid halide perovskite solar cells. *Nano Lett.* **14**, 2584–2590 (2014); <https://doi.org/10.1021/nl500390f>

[3] Resolving the Physical Origin of Octahedral Tilting in Halide Perovskites. *Chem. Mater.* **28**, 4259–4266 (2016); <https://doi.org/10.1021/acs.chemmater.6b00968>

[4] Stereochemistry of post-transition metal oxides: revision of the classical lone pair model. *Chem. Soc. Rev.* **40**, 4455–4463 (2011); <https://doi.org/10.1039/C1CS15098G>

[5] The underappreciated lone pair in halide perovskites underpins their unusual properties. *MRS Bulletin.* **45**, 467-477 (2020); <https://doi.org/10.1557/mrs.2020.142>

#### F.EL08.21.19

**Late News: A Reactive Force Field for Large Scale Simulations of Metal Halide Perovskites** Mike Pols<sup>1,2</sup>, Jose Manuel Vicent-Luna<sup>1,2</sup>, Ivo Filot<sup>3,2</sup>, Adri v. Duin<sup>4</sup> and Shuxia Tao<sup>1,2</sup>; <sup>1</sup>Materials Simulation and Modelling, Department of Applied Physics, Eindhoven University of Technology, Netherlands; <sup>2</sup>Center for Computational Energy Research, Eindhoven University of Technology, Netherlands; <sup>3</sup>Laboratory of Inorganic Materials Chemistry, Schuit Institute of Catalysis, Eindhoven University of Technology, Netherlands; <sup>4</sup>Department of Mechanical Engineering, The Pennsylvania State University, United States

Metal halide perovskites have been the focus of many computational studies over the past few years. The bulk of these investigations were done using methods based on quantum mechanics (QM). However, the computational cost of QM methods is high, severely limiting the length and time scales of the systems that can be investigated. Molecular dynamics (MD) simulations have been successfully applied to simulate larger material systems and at longer time scales by making use of classical force fields (CFF). Nonetheless, the predefined connectivity in CFF makes them unsuited for the simulation of chemical reactions. A reactive force field (ReaxFF) is an extension to CFF by including a dynamic bond order that is calculated from the interatomic distances and allows for the simulation of bond breaking and formation. In this presentation, I will outline our progress in the creation of the first ReaxFF for halide perovskites, CsPbI<sub>3</sub>.

SESSION F.LP04.01: Live Poster Session I: Electronics and Optics I (F.EL08)

Session Chairs: Juan Pablo Correa Baena and Samuel Stranks

Wednesday Morning, December 2, 2020

11:30 AM - 1:30 PM

F.EL08

### F.EL08.13.02

**Atomic Layer Deposition of 2D Perovskite Passivation Layers** Jacob Vagott, Carlo Andrea Riccardo Perini and Juan Pablo Correa Baena; Georgia Institute of Technology, United States

In order to further advance perovskite solar cell efficiency from the current record of 25.2%, it is important to minimize perovskite crystal defects and increase interface performance through passivation layers. 2-D perovskites have shown great potential as passivation layers but are primarily deposited by solution processing. Drawbacks of using solution processing for 2-D perovskite films include toxicity of the solvent, potential insolubility of the precursors, and lack of precise thickness control. Atomic layer deposition (ALD) could be a solution to these problems. ALD allows for the deposition of highly uniform layers of perovskite with great control over the final thickness of the film. Self-limiting in nature, ALD processes may allow for deposition of monolayers of perovskite with more control than solution processing techniques. Although an established deposition technique, ALD processes for perovskites have yet to be developed. Through this work, we consider ALD as a method of depositing 2-D perovskites as passivation layers for perovskite solar cells. These passivation layers are further incorporated into devices and their effect on solar cell efficiency is analyzed.

### F.EL08.13.04

**Understanding the Effects of Sr Chemical Doping on Pb/Sn Based Perovskite Films** Hurriyet Yuce Cakir<sup>1,2</sup> and Juan Pablo Correa Baena<sup>2</sup>; <sup>1</sup>Izmir Institute of Technology, Turkey; <sup>2</sup>Georgia Institute of Technology, United States

Organometal halide perovskites have been in the spotlight of semiconductor science over the past decade. Their exceptional electronic-optical properties and easy production from solution give them an edge over the semiconductor applications. The organic-inorganic halide perovskite solar cells (PSCs) have attracted the incredible attention of the researchers working on solar cells owing to a rapid increase in the efficiency of 25.5% since 2009<sup>1,2</sup>.

Furthermore, tin/lead (Sn/Pb)-based perovskite offers lower toxicity compared to the lead-based perovskites<sup>3</sup>. Their bandgaps are close to 1.3-1.4 eV which is the ideal bandgap of an absorber layer in a solar cell regarding the Shockley-Queisser model<sup>4</sup>.

In this study, we have performed SrI<sub>2</sub> addition (ranging from 0.1% to 5.0% concentrations) to the (FASnI<sub>3</sub>)<sub>0.8</sub>(MAPbBr<sub>3</sub>)<sub>0.2</sub> perovskite to improve their physical properties. Moreover, we have investigated the incorporation of SrI<sub>2</sub> into perovskites impacts on the morphological and optical properties of perovskite films.

[1] NREL. Best Research-Cell Efficiencies. <https://www.nrel.gov/pv/assets/pdfs/bestresearch-cell-efficiencies.20200925.pdf>

[2] Correa-Baena, J.-P., et al., Science, 2017. 358(6364): p. 739-744.

[3] Tavakoli, M.M., et al., Advanced Materials, 2018. 30(11): p. 1705998.

[4] Zhou, X., et al., Advanced Materials, 2020. 32(14): p. 1908107.

### F.EL08.13.06

**Revealing the Internal Luminescence Quantum Efficiency of Perovskite Films via Accurate Quantification of Photon Recycling** Paul Fassl<sup>1</sup>, Vincent Lami<sup>2</sup>, Ian Howard<sup>1</sup>, David Becker-Koch<sup>2</sup>, Felix Berger<sup>2</sup>, Lukas Falk<sup>2</sup>, Raphael Schmagel<sup>1</sup>,

Jana Zaumseil<sup>2</sup>, Bryce Sydney Richards<sup>1</sup>, Yana Vaynzof<sup>2</sup> and Ulrich W. Paetzold<sup>1</sup>; <sup>1</sup>Karlsruhe Institute of Technology, Germany; <sup>2</sup>Heidelberg University, Germany

The high refractive index of perovskite semiconductors at their emission wavelength ( $n \sim 2.3-2.6$ ) results in a narrow emission escape cone and a large amount of photoluminescence (PL) to be trapped within perovskite thin films. Due to strong band edge absorption and a very small luminescent Stokes shift, this effect leads to considerable photon reabsorption and reemission - an effect known as photon recycling (PR) [1] - as well as a concurrent red-shift of propagating PL due to emission filtering [2]. As recently highlighted, the self-absorption induced redistribution of charge carriers and outcoupling of propagated PL can lead to a significant misinterpretation of measurements of the intrinsic bimolecular recombination and charge carrier diffusion coefficients as well as of asymmetric PL spectral shapes [3, 4]. For perovskite films with low non-radiative recombination and parasitic absorption losses, PR can be of great advantage as it allows higher charge carrier densities at steady-state and thus increased device open-circuit voltage [5]. However, most current models still start from the simplified assumption that all initially trapped PL will be reabsorbed at some point without the possibility of being outcoupled, likely overestimating the effect of PR [6]. In this study, we show that in external photoluminescence quantum efficiency (PLQE) measurements employing an integrating sphere setup, the PL spectra of polycrystalline perovskite films with layer thicknesses typically employed for thin film solar cells ( $\sim 150-500$  nm) exhibit a notable red-shift and broadening. Such asymmetric PL spectra are often ignored or misinterpreted in the literature. We developed an all-optical model that considers both PR and outcoupling of initially trapped filtered PL due to scattering, which can reproduce spectral shapes with varying extents of red-shifts. We determined the true PL spectral shape as well as the absorption spectrum via high resolution confocal PL measurements and photothermal deflection spectroscopy respectively. Our model allows to estimate the total escape probability in addition to the initially generated internal PL intensity and thus to determine the internal PLQE of perovskite thin films. We confirm our assumptions by various control experiments and Monte Carlo simulations, benchmarking the model for perovskite thin films with different grain size, thickness and composition. Our approach serves as a new guideline for estimating these important parameters directly from measurements of the external PLQE and PL spectrum using an integrating sphere setup. [1] L. M. Pazos-Outon et al., Photon Recycling in Lead Iodide Perovskite Solar Cells. *Science* 2016, 351, 1430-1433. [2] B. Wenger et al., Consolidation of the Optoelectronic Properties of  $\text{CH}_3\text{NH}_3\text{PbBr}_3$  Perovskite Single Crystals. *Nat. Commun.* 2017, 8, 590. [3] T. W. Crothers et al., Photon Reabsorption Masks Intrinsic Bimolecular Charge-Carrier Recombination in  $\text{CH}_3\text{NH}_3\text{PbI}_3$  Perovskite. *Nano Lett.* 2017, 17, 5782-5789. [4] A. Bercegol et al., Quantitative Optical Assessment of Photonic and Electronic Properties in Halide Perovskite. *Nat. Commun.* 2019, 10 (1), 1586. [5] M. G. Abeb et al., Rigorous Wave-Optical Treatment of Photon Recycling in Thermodynamics of Photovoltaics: Perovskite Thin-Film Solar Cells. *Phys. Rev. B* 2018, 98, 075141. [6] J. M. Richter et al., Enhancing Photoluminescence Yields in Lead Halide Perovskites by Photon Recycling and Light Out-Coupling. *Nat. Commun.* 2016, 7, 13941.

#### **F.EL08.13.07**

**Energy Level Alignment of Formamidinium Tin Iodide with Organic Contact Materials** Jonas Horn, Pascal Schweitzer and Derck Schlettwein; Justus Liebig University Giessen, Germany

The alignment of energy levels at the interface of perovskite absorber and adjacent hole- and electron-transporting material affects the formation of space-charge regions and interfacial recombination. These have consequences for charge transport in the layers and, therefore, for the efficiency of devices. We measured this alignment by the use of Kelvin-probe-force microscopy (KPFM) to gain a detailed understanding of this alignment of energy levels. This study is focused on Formamidinium tin iodide ( $\text{FASnI}_3$ ) as perovskite absorber. This material avoids the toxicity problems of lead and is known to yield the highest power conversion efficiencies amongst all lead free perovskite absorbers. The most common solar cell geometry for  $\text{FASnI}_3$  implements C60 as electron-transporting material, which is prepared on  $\text{FASnI}_3$  by physical vapor deposition (PVD). Intermittently to PVD, we use KPFM to simultaneously monitor morphology and work function of C60 during its growth on  $\text{FASnI}_3$ . We show that a sufficiently high deposition rate is needed to avoid island formation of C60 and obtain a homogeneously covering film with constant work function. We further show that the width of the space charge layer in C60 is larger than the film thickness often implemented in perovskite solar cells (20 nm - 30 nm). A band bending in the range of 300 meV is observed and consequences for prospective device operation are discussed.

#### **F.EL08.13.08**

**The Underlying Mechanism of Surface Defect Passivation Process for Organohalide-Lead Perovskite Nanocrystals** Artavazd Kirakosyan<sup>1</sup>, Duc Chinh Nguyen<sup>1</sup>, Min-Gi Jeon<sup>1</sup>, Jae Hyuck Jang<sup>2</sup>, Jihoon Choi<sup>1</sup> and MoonRyul Sihn<sup>1</sup>; <sup>1</sup>Chungnam National University, Korea (the Republic of); <sup>2</sup>Korea Basic Science Institute, Korea (the Republic of)

Organolead halide perovskite nanocrystals (NCs) have emerged as a versatile and promising active material for many optoelectronic applications such as solar energy harvesting, light-emitting device, and photodetectors owing to their size- and

composition-dependent optoelectronic properties. Although the extensive studies on their optical and electronic properties have been studied in the last several years, their low stability, structural integrity, and poor luminescence stability associated with the fast attachment-detachment dynamics of surface capping molecules during post-processing limit their practical applications in optoelectronics. Therefore, an in-depth understanding of the surface chemical processes is required. We found that the amine group ( $-\text{NH}_3^+$ ) immobilizes  $\text{Br}^-$  anion at the corner of undercoordinated  $\text{PbBr}_6^{4-}$  octahedron on the  $\text{MAPbBr}_3$  surface resulting in a charge-balanced Pb-Br framework where Br/Pb ratio is slightly higher than stoichiometry, and thus provides exciton radiative recombination and high photoluminescence quantum yield. In contrast, the oleic acid is not able to coordinate with the surface moieties of the perovskite, but rather carboxyl acid groups ( $-\text{COO}^-$ ) etch  $\text{Pb}^{2+}$  into solution when only acid was used. Interestingly, a mixture of oleic acid and amine-functionalized surfactants was found to promote amine conversion to ammonium ion ( $-\text{NH}_2 + \text{H}^+ \rightarrow -\text{NH}_3^+$ ), which is favorable for their localization on the surface. Our results show that the Br vacancies at the non-passivated surface result in a reduction of  $\text{Pb}^{2+}$  to  $\text{Pb}^0$  by trapping the electrons generated from the exciton dissociation, which provides the main pathway for exciton trapping. Acknowledgment This work is supported by the National Research Foundation of Korea (NRF) grant funded by the Korean government (No. NRF-2019R1I1A2A01060608) and by Nano-Material Technology Development Program through the National Research Foundation of Korea (NRF) funded by the Ministry of Science, ICT and Future Planning. (2009-0082580).

#### F.EL08.13.11

**Impact of Temperature and Humidity on the Stability of the Optical Properties and Structure of Formamidinium Lead Iodide Thin Films and Solar Cells** Marie Solange Tumasange, Biwas Subedi, Cong Chen, Maxwell M. Junda, Juan Zuo, Zhaoning Song, Yanfa Yan and Nikolas Podraza; University of Toledo, United States

Organic-inorganic lead halide perovskite polycrystalline thin films used as absorber layers in high efficiency solar cells have direct band gaps, high absorption coefficients, and potentially low-cost solution-based fabrication processing. However, these materials are inclined to degradation with exposure to humidity, oxygen, heat, and ultraviolet light. Formamidinium lead iodide (FAPbI<sub>3</sub>) is an attractive composition perovskite as it has a more symmetric crystal structure due to a larger cation radius for FA compared to that for methylammonium (MA) as well as an elevated decomposition temperature for improved stability. Even though FAPbI<sub>3</sub> is among the more stable perovskite compositions, solar cells incorporating these absorbers still degrade with atmospheric exposure over time. Here we study the behavior of FAPbI<sub>3</sub> film structure and complex optical properties under controlled temperature variations and relative humidity (RH) exposure. In situ real time spectroscopic ellipsometry (RTSE) measurements are collected over the near infrared to ultraviolet spectral range (0.75-5.9 eV) for polycrystalline FAPbI<sub>3</sub> thin films deposited on glass substrates which are then held at different temperatures, ranging from 7 to 70°C, in a sealed nitrogen chamber with controlled 0, 26, and 85% RH introduced. From RTSE, the optical response in the form of complex dielectric function ( $\epsilon = \epsilon_1 + i\epsilon_2$ ) spectra is deduced using a parametric model accounting for above band gap critical points, the direct band gap, an Urbach tail, and degradation induced sub-gap absorption due to defects. Variations in parameters describing spectra in  $\epsilon$  are tracked as functions of temperature, controlled RH, and the amount of time films are held under those conditions. Changes in bulk thickness, surface roughness thickness, and surface roughness relative density are also tracked with time under these conditions. For example, RTSE indicates no change in structure and minimal changes in  $\epsilon$  at 0% RH regardless of temperature. However, when FAPbI<sub>3</sub> is exposed to 26% RH at 70°C, RTSE indicates changes in parameters describing  $\epsilon$  and structure, such as increases in film thickness with time indicative of water intercalation. To the contrary, slight film densification is observed over time when held at 26% RH and 70°C. These RTSE studies show that deviations from near room temperature with controlled relative humidity induces more changes in optical and structural properties with time than when the sample is exposed to only humidity. In all cases of RH exposure sub-gap absorption increases with time, most notably in widening of the Urbach tail obtained from the parametric model for  $\epsilon$ . To further study how other ambient conditions affect perovskite stability, RTSE is performed for FAPbI<sub>3</sub> with exposure to controlled amounts of both oxygen and relative humidity as a function of temperature. RTSE is applied directly to measure a FAPbI<sub>3</sub> based solar cell to track changes in the perovskite absorber over time and identify potential correlations with device performance.

#### F.EL08.13.12

**Diagnosis of Optical and Electrical Losses in Organic-Inorganic Lead Halide Perovskite Photovoltaics via External Quantum Efficiency Modelling** Biwas Subedi, Chongwen Li, Zhaoning Song, Maxwell M. Junda, Kiran Ghimire, Yanfa Yan and Nikolas Podraza; University of Toledo, United States

Organic-inorganic lead halide perovskite-based photovoltaics (PV) exhibit high initial efficiency, can be processed at potentially low cost, and material bandgaps can be tuned by composition. Solution-processing enables fabrication of a range of different  $\text{ABX}_3$  (A: methylammonium—MA, formamidinium—FA, Cs; B: Pb, Sn; X: I, Br, Cl) perovskite compositions to meet these needs in single or tandem junction PV. Unfortunately, these perovskites may degrade upon exposure to relative humidity and oxygen in ambient air, during device processing, and overtime during device operation. Like all PV devices,

performance depends on the characteristics of each material and interfaces between layers to minimize sources of optical and electronic losses. External quantum efficiency (EQE) simulations of perovskite PV assess sources of parasitic optical losses with input complex optical response of all component materials and known multiple layer device structure. From these simulations, the optical performance of devices with different structures or component materials is predicted. Comparison of simulated EQE with experimental measurement validates the optical model when simulated and experimental EQE match but also more importantly identifies electronic losses such as incomplete carrier collection when experimental EQE is less than the simulation. Obtaining the most accurate input complex optical response of perovskite films and layer thicknesses in devices is necessary to maximize the amount of information gained from EQE and its modeling. Toward this end, spectroscopic ellipsometry (SE) over the near-infrared to the ultraviolet wavelength range (0.73-5.9 eV) is used to characterize the complex optical response of solution-processed perovskite films of different compositions. Photothermal deflection spectroscopy (PDS) and unpolarized transmittance complement SE by enhanced sensitivity to low values of absorption coefficient ( $\alpha$ ) in the vicinity of the bandgap. Extension to low values of  $\alpha$  enables detection of exponential band tailing and Urbach Energy (EU), with narrower EU indicative of more ordered and higher electronic quality material. A parametric optical property model has been developed which includes contributions from electronic transitions above the bandgap, the direct bandgap, an exponentially decaying Urbach tail, and sub-gap absorption due to defects. Complex optical properties of perovskite films, including wide-bandgap  $\text{FA}_{1-x}\text{Cs}_x\text{Pb}(\text{I}_{1-y}\text{Br}_y)_3$  and narrow-bandgap  $(\text{FASnI}_3)_x(\text{MAPbI}_3)_{1-x}$  compositions, in both as-prepared and degraded states are determined. SE data is collected for complete perovskite PV to deduce layer thicknesses and perovskite complex optical properties within the device. This information serves as direct input for EQE simulation. Comparison with perovskite PV experimental EQE enables the deduction of optical and electronic device performance losses arising from perovskite composition and device architecture, variations in near bandgap perovskite optical response resulting from complete device processing, and perovskite degradation during solar cell operation. As an example, similar simulated and experimental EQE in  $(\text{FASnI}_3)_x(\text{MAPbI}_3)_{1-x}$  ( $0.3 \leq x \leq 0.7$ ) perovskite PV validates the optical model and indicates minimal losses. In another case, for  $\text{FAPbI}_3$  PV comparisons between simulation and experimental EQE indicate sources of both optical and electronic losses arising from device processing.

#### **F.EL08.13.13**

**Enhanced Charge Extraction Through Double-Layered Electron Transfer Films for Hybrid Perovskite Planar Solar Cells** Jihyun Kim, Hye Ri Jung, Yeon Soo Kim and William Jo; Ewha Womans University, Korea (the Republic of)

The electron transfer film (ETF) plays an important role in obstructing recombination of electrons and holes between the perovskite layer and fluorine-doped tin oxide in planar perovskite solar cells (PSCs). In addition, at the compact spin-coated  $\text{SnO}_2$  ETF, morphological defects, such as pinholes and cracks, due to roughness of the substrate seriously impact on the performance of PSCs. Here, we investigate the variables that can control the charge extraction using spin-coated  $\text{SnO}_2$ , sputtered  $\text{TiO}_2$  and double-layered (DL) ETF composed of  $\text{TiO}_2$  on  $\text{SnO}_2$  and  $\text{SnO}_2$  on  $\text{TiO}_2$ . We determined the resistance, mobility, conductivity and carrier concentration of double-layered ETF based on PSCs by a 4-probe method. The electrical properties show that the DL-ETF can effectively reduce the trap density at perovskite/ETF interface, promote the electron transfer, and suppress the interface recombination rather than  $\text{SnO}_2$  alone. The band structure and the carrier transport mechanism at perovskite/DL-ETF interface were explained by conductive atomic force microscopy, Kelvin probe force microscopy and ultraviolet photoelectron spectroscopy. Complementary composite DL-ETF has been found to eliminate severe current leakage inside the device, reducing interface defects and hysteresis. More importantly, DL-ETF accelerates at electron extraction and transport owing to the excellent mobility. Finally, DL-ETF based PSCs yield higher power conversion efficiency with improved JSC than the device with  $\text{SnO}_2$  alone. Therefore, these are beneficial for reducing the recombination of carriers in the electron traps, leading to the enhancement of device performance.

#### **F.EL08.13.17**

**Leveraging Electrochemical Techniques to Augment and Accelerate Halide Perovskite Technology**

**Development** Moses Kodur<sup>1</sup>, Ross Kerner<sup>2</sup>, Zachary Dorfman<sup>1</sup>, Justin H. Skaggs<sup>1</sup>, Taewoo Kim<sup>1</sup>, Joseph J. Berry<sup>2</sup> and David P. Fenning<sup>1</sup>; <sup>1</sup>University of California, San Diego, United States; <sup>2</sup>National Renewable Energy Laboratory, United States

Improving the repeatability and operational stability of interfaces in perovskite devices is crucial to extend device lifetime. With each sequential step in perovskite device fabrication comes a risk of a failed device integration or an interaction that leads to longer-term device instability. Here, we present simple electrochemical techniques to evaluate fundamental properties of charge transport layers and limits of stability before completion of a full device stack, with the objective of improving batch yield, deconvoluting the troubleshooting process, and accelerating the development of new perovskite absorbers, their contact layers, and high-efficiency devices.

We focus on two exemplary measurements using easily accessible aqueous electrolytes. First, we show that an outer sphere



redox couple such as the ferro/ferricyanide system allows facile evaluation of the semiconducting properties (conduction band minimum position, doping level, etc.) of SnO<sub>x</sub> electron transport layers. The anodic and cathodic features in cyclic voltammograms of the SnO<sub>x</sub> are correlated to final solar cell efficiency and offer an early screen of quality. Second, we show that ionic permeability/reactivity of SnO<sub>x</sub> layers, which can lead to irreversible absorber degradation under bias, can be rapidly evaluated by potentiostatic measurements in the presence of organohalide salts. This technique reveals the influences of processing condition and deposition method on susceptibility to bias-induced degradation reactions.

These process control measurements can be readily adapted to devices of any area and are compatible with industry-scale fabrication techniques to improve process reliability and reproducibility. While our work focuses on the development and characterization of SnO<sub>x</sub> layers, the fundamental principles can be adapted for a wide variety of charge transport layers so long as the proper electrochemical set-up is implemented, making this method a powerful tool for halide perovskite development.

#### **F.EL08.13.18**

##### **Wide-Bandgap Perovskites in the Spotlight—Multimodal Study of Photo-Induced Halide Segregation in Solar Cells**

**Kunal Datta**, Bas T. van Gorkom, Matthew J. Dyson, Martijn M. Wienk and Rene A. Janssen; Eindhoven University of Technology, Netherlands

Segregation of illuminated mixed-halide perovskites into iodide- and bromide-rich domains presents a critical bottleneck in the application of wide-bandgap absorbers in single- and multi-junction architectures. And while its occurrence has been well-studied in thin films, the influence on operational solar cells lacks sufficient understanding.

This work employs a multimodal characterization procedure to observe the slow progression of halide segregation in efficient solar cells prepared in the p-i-n architecture using sequentially processed perovskite absorbers. Photoluminescence spectroscopy is used to identify the stages that demixing of halide ions entails while simultaneous tracking of photovoltaic parameters allows correlating performance degradation to the migration of ionic species in each stage. A new stage of the process is thus observed upon prolonged illumination. Characterization of sub-bandgap features reveals the occurrence of photo-induced defect formation whose suppression through cationic substitution provides a strategy for stabilization of wide-bandgap compositions against halide segregation.

#### **F.EL08.13.19**

##### **Elucidating the Role of Electrochemical Halide Reactions in Perovskite Optoelectronic Devices Under Prolonged Reverse Bias**

**Jay B. Patel**<sup>1,2</sup>, Luca Bertoluzzi<sup>3</sup>, Kevin A. Bush<sup>3</sup>, Caleb C. Boyd<sup>3,1</sup>, Ross Kerner<sup>1</sup> and Michael McGehee<sup>2,1</sup>; <sup>1</sup>National Renewable Energy Laboratory, United States; <sup>2</sup>University of Colorado Boulder, United States; <sup>3</sup>Stanford University, United States

Partial shading of a solar module can bring a set of cells within the module to operate under reverse bias. When a solar cell is shaded in a module, the photogenerated current falls and a negative voltage (reverse bias) builds up as the other illuminated cells in series try to push current through it. Moreover, metal-halide perovskite photodetectors are regularly operated in reverse bias, and therefore it is critical to understand how these devices behave under reverse bias. Previous studies have shown that perovskite solar cells with a wide variety of compositions and contacts exhibit unusual behavior, compared to typical silicon solar cells, in reverse bias that includes both reversible performance loss and non-reversible degradation. [1, 2] Furthermore, we have shown that when a perovskite solar cell is held under reverse bias, the mobile ions move in a way such that there is favorable band energetics to allow for hole injection into the perovskite, yet the consequence of this process was unclear. [1]

Recent investigations have shown that photogenerated holes can induce electrochemical oxidation of halides into halogens. [3, 4] These halogens can leave the perovskite absorber and diffuse into contacts and cause further detrimental reactions with the electrodes. [5] To elucidate and understand the degradation mechanisms that occurs when perovskite solar cells are held under reverse bias, we have developed an advanced drift-diffusion model that incorporates an electrochemical term that can explain the short-circuit, open circuit and fill factor losses we experimentally measure. Our model conclusively shows that the injected holes can trigger the oxidation of halides to form neutral halogen interstitials. The density of halogen interstitials is much higher in reverse bias because there are hardly any electrons available to reduce the halogens back into halides. The resulting halogens act as bulk recombination centers and lead to a sharp decline in all the JV device characteristics. While the interstitial halogen density will decay when the cell is finally operated in forward bias, permanent degradation will occur if the halogen diffuses out of the perovskite layer into the transport layers or electrodes. Finally, we discuss how changing parameters such as the mobile ion density or the permeability of contacts can positively influence device performance and stability.

- [1] A. R. Bowring, L. Bertoluzzi, B. C. O'Regan and M. D. McGehee, *Adv. Energy Mater.*, 2018, 8, 1702365
- [2] R. A. Z. Razera, D. A. Jacobs, F. Fu, P. Fiala, M. Dussouillez, F. Sahli, T. C. J. Yang, L. Ding, A. Walter, A. F. Feil, H. I. Boudinov, S. Nicolay, C. Ballif and Q. Jeangros, *J. Mater. Chem. A*, 2020, 8, 242–250.
- [3] G. Y. Kim, A. Senocrate, T.-Y. Yang, G. Gregori, M. Grätzel and J. Maier, *Nat. Mater.*, 2018, 17, 445–449.
- [4] S. G. Motti, D. Meggiolaro, A. J. Barker, E. Mosconi, C. A. R. Perini, J. M. Ball, M. Gandini, M. Kim, F. De Angelis and A. Petrozza, *Nat. Photonics*, 2019, 13, 532–539.
- [5] R. A. Kerner and B. P. Rand, *ACS Appl. Energy Mater.*, 2019, 2, 6097–6101.

#### F.EL08.13.20

**Anionic Diffusion in Two-Dimensional Halide Perovskite Heterostructures** Akriti Akriti<sup>1</sup>, Enzheng Shi<sup>1</sup>, Stephen B. Shiring<sup>1</sup>, Jiaqi Yang<sup>1</sup>, Yao Gao<sup>1</sup>, Cindy L. Atencio-Martinez<sup>2</sup>, Alan J. Pistone<sup>1</sup>, Peilin Liao<sup>1</sup>, Brett Savoie<sup>1</sup> and Letian Dou<sup>1</sup>; <sup>1</sup>Purdue University, United States; <sup>2</sup>University of Los Andes, Colombia

The soft crystal lattice of hybrid halide perovskites facilitates anionic diffusion which impacts material stability, optoelectronic properties and solid-state device performance. Two-dimensional (2D) halide perovskites with bulky organic barriers have been used for improving the extrinsic stability as well as suppressing intrinsic anionic diffusion. With this strategy, devices with enhanced stability and reduced hysteresis have been achieved. Nevertheless, a fundamental understanding of the role of organic cations in inhibiting anionic diffusion across the perovskite-ligand interface is missing. Through this study, we demonstrate a quantitative investigation of the anionic inter-diffusion in atomically sharp and flat 2D heterojunctions between two arbitrarily determined phase-pure halide perovskite single crystals. Stark differences are observed in anion diffusion across 2D halide perovskite lateral and vertical heterostructures. Halide inter-diffusion in lateral heterostructures is found to be similar to the classical Fickian diffusion featuring continuous concentration profile evolution. However, vertical heterostructures show a “quantized” layer-by-layer diffusion behavior governed by a local free energy minimum and ion-blocking effects of the organic cations. Surprisingly, halide inter-diffusion coefficients for 2D perovskites capped with short aliphatic organic cations (e.g. butylammonium) are only 1~2 order of magnitudes smaller than that of 3D perovskites, suggesting the ineffectiveness of these cations in blocking the anionic migration. Furthermore, we found that bulkier and more rigid  $\pi$ -conjugated organic cations inhibit halide inter-diffusion much more effectively ( $D < 10^{-20}$  m<sup>2</sup>/s) compared to aliphatic cations. These results offer significant insights into the mechanism of anionic diffusion in 2D perovskites and provide a new materials platform for heterostructure assembly and device integration.

#### F.EL08.14.01

**Chemical Diversity in Lead-Free, Layered Double Perovskites—A Combined Experimental and Computational Approach** Brenda Vargas<sup>1</sup>, Raúl Torres<sup>1</sup>, Diana Reyes-Castillo<sup>1</sup>, Joelis Rodríguez-Hernández<sup>2</sup>, Milan Gembicky<sup>3</sup>, Eduardo Ménéndez-Proupin<sup>4</sup> and Diego Solis-Ibarra<sup>1</sup>; <sup>1</sup>UNAM, Mexico; <sup>2</sup>Centro de Investigaciones en Química Aplicada, Mexico; <sup>3</sup>University of California, United States; <sup>4</sup>Universidad de Chile, Chile

Akin to the expansion in compositional diversity that halide double perovskites provided to three-dimensional perovskites [1-2], layered double perovskites could further expand the diversity of two-dimensional (2D) perovskites, and therefore, they could also enhance the properties or expand the possible applications of such materials [3]. Despite the great promise of halide 2D double perovskites, up to date, there are only four confirmed members of this family of materials [3-6]. Herein, we explore 90 hypothetical new members of this family of materials by a combined theoretical, computational, and experimental method. The combination of these tactics allowed us to predict several new materials, out of which we experimentally synthesized and characterized five new layered double perovskites, some of which show promising properties for their use in photovoltaics and optoelectronics. Further, our work highlights the vast diversity of compositions and therefore of applications that double-layered perovskites have yet to offer. References [1] X. Zhao, D. Yang, J. Ren, Y. Sun, Z. Xiao and L. Zhang, *Joule*, 2018, 2, 1-12. [2] L. Chiu et al, *Nano-Micro Lett*, 2019, 11:16. [3] B. Vargas, E. Ramos, E. Pérez-Gutiérrez, J.C. Alonso, D. Solis-Ibarra, *J. Am. Chem. Soc*, 2017, 139, 27, 9116-9119. [4] B. Vargas, R. Torres-Cadena, J. Rodríguez-Hernández, M. Gembicky, H. Xie, J. Jiménez-Mier, Y-S. Liu, E. Menéndez-Proupin, K. R. Dunbar, N. Lopez, P. Olalde-Velasco, D. Solis-Ibarra, *Chem. Mater*, 2018, 30, 5315-5321. [5] B. A. Connor, L. Leppert, M. D. Smith, J. B. Neaton, H. I. Karunadasa, *J. Am. Chem. Soc*, 2018, 140, 5235-5240. [6] C. Ortiz-Cervantes, P. Carmona-Monroy, D. Solis-Ibarra, *ChemSusChem*, 2019, 12, 1560-1575.

#### F.EL08.14.06

**Ion Exchange-Diffusion Mechanisms in Transforming Calcite into Lead (Pb)-Free Perovskite Light Absorbers** Jonathan B. Junio, Marlon T. Conato and Candy C. Mercado; University of the Philippines Diliman, Philippines

The synthesis of perovskite materials has gone beyond the traditional wet chemistry routes into other methods such as a sequential ion exchange process that can produce perovskite materials from calcite in either thin film or bulk form. The use of lead (Pb), the most successful element in terms of PSC efficiency performance, was already successfully demonstrated in an ion exchange process. In this work, tin (Sn) is chosen since it has the most potential to replace Pb since they are on the same group and for the similarity in ionic radii of their ions ( $\text{Pb}^{2+}$ ,  $\text{Sn}^{2+}$ ) at 1.19 and 1.02 Å, respectively. Methyl ammonium tin triiodide ( $\text{MASnI}_3$ ) has a lower bandgap (1.2 to 1.4 eV) that induces broader absorption spectrum as compared with the benchmark  $\text{MAPbI}_3$  counterpart (1.55 eV). The second alternative - strontium (Sr) has an ionic radius of 1.18 Å indicating possible ion exchange in the strontianite structure. The band gap for the Sr perovskite was estimated at 3.6 eV, considerably higher than that for the lead perovskite and therefore not suitable for direct solar cell applications but can be used as a top cell in tandem architectures. These ion exchange processes are observed using x-ray absorbance and photoelectron spectroscopies to elucidate the underlying mechanisms of the sequential ion exchange process. These will shed light into the material transformation with shape preservation from the raw shells or single crystal calcite towards the intermediate carbonate material and eventually, the Pb-free perovskite material.

#### **F.EL08.15.01**

**A Comparison of Three Emerging Bi-Based (Oxy)Halide Absorbers Grown from Metallic Precursors** [Andrea Crovetto](#), Alireza Hijjafarassar, Ole Hansen, Brian Seger, Ib Chorkendorff and Peter Vesborg; Technical University of Denmark, Denmark

The bismuth-based (oxy)iodides  $\text{BiI}_3$ ,  $\text{BiOI}$  and  $\text{Ag}_x\text{Bi}_{x+3}$  share similar layered crystal structures, optimal band gaps for top absorbers in tandem solar cells, and moderate growth temperatures. Similarly to halide perovskite absorbers, they contain a heavy cation with a lone pair of electrons ( $\text{Bi}^{3+}$ ) which has been proposed as one of the features enabling defect tolerance in perovskites. We have grown and characterized  $\text{BiI}_3$ ,  $\text{BiOI}$ , and  $\text{Ag}_3\text{BiI}_6$  absorbers and solar cells in a systematic manner by employing a consistent synthesis method ((oxy)iodization of metallic precursor) and a consistent analysis routine. In this way, the individual strengths and weaknesses of the three absorbers, as well as their common challenges, can be outlined. The radiative efficiency of the three materials is within the same order of magnitude, thus indicating a similar degree of defect tolerance. Control of growth orientation should be a priority for this class of materials in view of their anisotropic properties. P-type bulk doping and selection of hole transport layers with deep valence bands could also improve performance. At the device level, we report an improved open circuit voltage of  $\text{BiI}_3$  solar cells with respect to the state of the art, and we report a proof-of-concept  $\text{Ag}_3\text{BiI}_6$ /silicon tandem cell. Beyond photovoltaics, the very low dark diode ideality factor in  $\text{BiI}_3$  devices and the existence of both electronic and ionic conduction in  $\text{Ag}_3\text{BiI}_6$  may open up alternative unexpected applications in other fields.

#### **F.EL08.15.03**

**Boosting the Self-Trapping Emissions in Zero-Dimensional Perovskite Heterojunctions** [Jun Yin](#)<sup>1</sup>, Jean-Luc Bredas<sup>2</sup>, Osman M. Bakr<sup>1</sup> and Omar F. Abdelsaboor<sup>1</sup>; <sup>1</sup>King Abdullah University of Science and Technology, Saudi Arabia; <sup>2</sup>Georgia Institute of Technology, United States

Zero-dimensional (0D) inorganic and hybrid perovskites have attracted great interest for white-light emitting applications due to their broadband emissions originating from the self-trapping excitonic states. In this work, we study a series of 0D inorganic perovskites,  $\text{A}_4\text{PbX}_6$  and  $\text{A}_4\text{SnX}_6$  (A = K, Rb, and Cs; X = Cl, Br, and I), under the theoretical framework of one-dimensional configuration coordinate diagram using density functional theory (DFT) calculations. We demonstrate that the formation of self-trapping excitonic states of  $\text{A}_4\text{PbX}_6$  and  $\text{A}_4\text{SnX}_6$  is attributed to the local structural distortion of individual  $[\text{PbX}_6]^{4-}$  and  $[\text{SnX}_6]^{4-}$  octahedron (i.e., the octahedral shrinking under photoexcitation). We further predict the broadband emissions of a new family of 0D  $\text{A}_4\text{PbX}_6/\text{A}_4\text{SnX}_6$  heterostructures, and find that among these crystal structures  $\text{Rb}_4\text{PbI}_6/\text{Rb}_4\text{SnI}_6$  exhibits an increased photoluminescence efficiency with good stability as compared to pristine  $\text{Rb}_4\text{SnI}_6$ . Our findings provide a new material design strategy for boosting the self-trapping emissions with improved stability using 0D inorganic perovskite heterostructures.

#### **F.EL08.15.05**

**Single-Source Deposition of Double Perovskites for Optoelectronic Devices** [Nathan Rodkey](#)<sup>1,2</sup>, Stan Kaal<sup>2</sup>, Paz Sebastia-Luna<sup>1</sup>, Yorick A. Birkhölzer<sup>2</sup>, Franciso Palazon<sup>1</sup>, Henk Bolink<sup>1</sup> and Monica Morales-Masis<sup>2</sup>; <sup>1</sup>Universidad de Valencia, Spain; <sup>2</sup>University of Twente, Netherlands

As halide perovskites (PVKs) continue to garner scientific interest for their potential to enhance efficiencies of solar cells and LEDs, a push has been made towards lead-free and completely inorganic PVKs with increasingly complex stoichiometries. One example of this is the double PVK  $\text{Cs}_2\text{AgBiBr}_6$  and  $\text{Sn}:\text{Cs}_2\text{AgBiBr}_6$ . Synthesis of thin films with these complex

stoichiometries is challenging due to the distinct volatility of the constituent elements, usually requiring multi-step or multi-source processes. Here we explore Pulsed Laser Deposition (PLD) as a route to grow these types of complex materials with a single source. PLD offers the advantage of being a volatility-insensitive thin film synthesis technique which we use to demonstrate single-source deposition of  $\text{Cs}_2\text{AgBiBr}_6$  and  $\text{Sn}:\text{Cs}_2\text{AgBiBr}_6$ . For this, solid targets are made first by mechanochemical synthesis of powders, followed by a uniaxial and isostatic pressing to form the powders into dense, compact targets. X-ray diffraction (XRD) is used to verify the desired PVK phase is maintained along each step of target fabrication. Laser-ablation of the double PVK targets in vacuum leads to formation of  $\text{Cs}_2\text{AgBiBr}_6$  and  $\text{Sn}:\text{Cs}_2\text{AgBiBr}_6$  double PVK films after optimization of the deposition parameters. We discuss the effects of deposition pressure and laser fluence on the formation of stoichiometric and phase-pure films, as well as the critical role of the thermalization of the source elements to achieve stoichiometric transfer. In addition to the structural properties, the optoelectronic properties of the films were studied by UV-Vis-NIR spectrophotometry and time-resolved photoluminescence. Notably,  $>1$   $\mu\text{m}$  thick films are deposited and all films present high structural stability over the course of 3 months, without the need for an annealing step. This work represents an important step forward in the development of controlled growth and future scalability of complex halide perovskites for efficient optoelectronic devices.

#### **F.EL08.16.06**

**Improving Blue Light Emission of  $\text{CsPbBr}_3$  Nanoplatelets via Post-Synthesis Surface Passivation** Jinu Park, Joonyun Kim and Byungha Shin; Korea Advanced Institute of Science and Technology, Korea (the Republic of)

Lead halide perovskite is considered as a potential candidate for the next generation light emitting diodes (LEDs) due to its extremely narrow light emission spectrum with a typical full width half maximum (FWHM)  $< 20$  nm. In particular, all-inorganic  $\text{CsPbBr}_3$  has demonstrated the near unity photoluminescence quantum yield (PLQY) for green light emission. A more challenging, yet technologically important, task is developing a high performance blue light emitter. By partially replacing Br of  $\text{CsPbBr}_3$  with Cl, the emission wavelength can be adjusted to the blue emission; however,  $\text{CsPbBr}_{3-x}\text{Cl}_x$ , suffers from ion migration and phase segregation which result in low PLQY and poor stability. Here, we present a synthesis method to produce nanostructure  $\text{CsPbBr}_3$  in the form of nanoplatelets (NPLs) that is capable of emitting blue light without the need for anion-substitution. Nanoplatelets with 2 monolayer (ML) and 3 ML of thickness yielded photoluminescence (PL) peak at 435nm with an extremely narrow FWHM of 14.2 nm and PL peak at 456nm with FWHM of 19.6nm, respectively. The luminescence of these nanoplatelets was further improved by post-synthesis treatment with tetrafluoroborate salts-almost 1150% increase in PL intensity was observed without a noticeable broadening of the PL spectrum. Details of the results and discussion of a possible mechanism behind the improvement with the post-synthesis treatment will be presented.

#### **F.EL08.16.07**

**Highly Luminescent Vacuum-Evaporated All Inorganic  $\text{CsPbBr}_3$  Perovskite Light Emitters with a Polymer Auxiliary Layer** Nakyung Kim, Mingue Shin and Byungha Shin; Korea Advanced Institute of Science and Technology, Korea (the Republic of)

All inorganic halide perovskite  $\text{CsPbBr}_3$  has emerged as the next-generation material for light-emitting diodes (LEDs) due to its high color purity with a narrow spectral width ( $< 20$  nm) and tunable band gap by adjusting the composition of halide anions, i.e. substitution of Br with I or Cl. Considering the needs for large-area scalability and fine control of the emitter thickness, vacuum-deposition will be a more commercialization-friendly technique to produce perovskite films for LEDs. Here, we prepare  $\text{CsPbBr}_3$  light emitters by thermal co-evaporation of CsBr and PbBr<sub>2</sub> sources. The luminescence of the vacuum-deposited  $\text{CsPbBr}_3$  films was greatly improved by introducing a poly-ethylene oxide (PEO) layer underneath the  $\text{CsPbBr}_3$ -almost 300-fold increase in photoluminescence quantum yield (PLQY) with the PEO layer compared to the reference sample ( $\text{CsPbBr}_3/\text{glass}$ ). It is believed that the interaction between PEO and  $\text{Pb}^{2+}$  ions leads to the passivation of non-radiative recombination defects. After the careful optimization of the PEO layer thickness and post-deposition thermal treatments of  $\text{CsPbBr}_3$ , we have demonstrated PLQY of 30% from a peak at 521 nm with full-width-half-maximum of  $\sim 17$ nm. Furthermore, the samples exhibit excellent ambient stability. Details of the results and analysis will be discussed.

#### **F.EL08.16.08**

**Ultra Sensitive Perovskite Halide Based Room Temperature Ammonia Gas Sensor Using Flexible Paper Electronics** Avishek Maity and Barnali Ghosh; S.N. Bose National Centre for Basic Sciences, India

In current days, development and search of new materials for solid state thin film gas sensor to detect toxic gases, particularly using nanomaterial for their enhanced functionality, is growing rapidly as view point of both environmental and clinical application. Particularly, gas sensor with low power consumption, room temperature operation, portability and cost

effectiveness is highly demandable. Perovskite halides, namely methyl ammonium lead iodide ( $\text{CH}_3\text{NH}_3\text{PbI}_3$ ) / MAPI is widely popular as photovoltaic and optoelectronic material. Recently we have found that MAPI can act also as an active material for gas sensing to trace hazards pollutants. Ammonia ( $\text{NH}_3$ ) not only is one of harmful pollutants in nature but also treated as a biomarker for kidney disease via exhaled breathe analysis in recent days. Thus a room temperature, cost effective, very high sensitivity  $\text{NH}_3$  gas sensor could be extremely beneficial in view point of both environmental and clinical issues. The sensor using MAPI can trace ammonia gas ( $\text{NH}_3$ ) by a visual color change method as well as by electrical read out [1-2]. Here we have shown a MAPI based electrical sensor grown on a cheap paper as a substrate for tracing  $\text{NH}_3$  gas. The paper sensor has a very high sensitivity (98% for 10 ppm  $\text{NH}_3$ ) towards  $\text{NH}_3$  gas at room temperature and sub ppm (<1 ppm) detection capability (down to 10 ppb) by its noise limited detectability [2]. This ultra high response down to ppb level can be extremely suitable for exhaled breathe analysis. Current through the sensor increases nearly by one order on exposure to only 10 ppm  $\text{NH}_3$  gas with a bias voltage of 1 V DC and hence the sensor consumes extremely low power (~ few nano watts). The paper sensor is also highly selective to  $\text{NH}_3$  gas and maintains stability over 150 days within decrease of 10% sensitivity. This could open up the possibility of perovskite halide (MAPI) as next generation solid state room temperature gas sensor for rapid and cost effective detection using paper electronics. References: [1] Maity, A; Ghosh, B; Fast Response paper based visual color change gas sensor for efficient ammonia detection at room temperature; Scientific Reports (2018), 8,16851 [2] Maity, A; Raychaudhuri, A.K.; Ghosh, B; High sensitivity  $\text{NH}_3$  gas sensor with electrical readout made on paper with perovskite halide as sensor material; Scientific Reports (2019), 9,7777 I

### F.EL08.17.01

**Suppressing Cation Migration in Triple-Cation Lead Halide Perovskites** Iliia M. Pavlovets<sup>1</sup>, Michael Brennan<sup>1</sup>, Sergiu Draguta<sup>1</sup>, Anthony Ruth<sup>1</sup>, Jeffrey A. Christians<sup>2</sup>, Taylor Moot<sup>3</sup>, Steven Harvey<sup>3</sup>, Joseph Luther<sup>3</sup> and Masaru Kuno<sup>1,1</sup>; <sup>1</sup>University of Notre Dame, United States; <sup>2</sup>Hope College, United States; <sup>3</sup>National Renewable Energy Laboratory, United States

Mixed cation and anion  $\text{APbX}_3$ -type lead halide perovskites [ $\text{A}^+=\text{Cs}^+$ ,  $\text{CH}_3\text{NH}_3^+$  [ $\text{MA}^+$ ], or  $(\text{NH}_2)_2\text{CH}^+$  [ $\text{FA}^+$ ];  $\text{X}^-=\text{Br}^-$  or  $\text{I}^-$ ] have received extensive attention for use as low cost, efficient light harvesters in solar cells. Issues regarding long-term active layer stability, however, remain unresolved. Electric field-induced ion migration in perovskite solar cells is of particular concern because it results in current-voltage (J-V) hysteresis, metastable power conversion efficiencies and accelerated active layer degradation. Facile ion migration within the perovskite lattice stems from relatively fragile ionic bonding between heavy, low-valence ions. This results in small activation barriers and correspondingly moderate diffusion coefficients for halide anions and A-site cations. The mobile nature of  $\text{A}^+$  cations and  $\text{X}^-$  anions is thus an instability of all metal halide perovskites. While numerous recent studies have focused on halide migration and segregation, significantly less work has gone into investigating cation migration in metal halide perovskites. This is especially true of double- and triple-cation  $\text{FA}_x\text{MA}_y\text{Cs}_{1-x-y}\text{PbX}_3$  alloys.

Here, we demonstrate that bias-induced cation migration is mitigated in mixed  $\alpha$ -phase/ $\delta$ - $\text{ortho}$ - $\text{CsPbI}_3$  triple-cation  $\text{FA}_x\text{MA}_y\text{Cs}_{1-x-y}\text{PbI}_3$  films (referred as  $\alpha/\delta$ - $\text{FA}_{0.33}\text{MA}_{0.33}\text{Cs}_{0.33}\text{PbI}_3$ ). We verify this by comparing cation movement in lateral devices and working solar cells made of pure  $\alpha$ -phase double-/triple-cation perovskite phase systems ( $\text{FA}_{0.85}\text{Cs}_{0.09}\text{PbI}_3$  and  $\text{FA}_{0.76}\text{MA}_{0.15}\text{Cs}_{0.09}\text{PbI}_3$ ) as well as  $\alpha/\delta$ - $\text{FA}_{0.33}\text{MA}_{0.33}\text{Cs}_{0.33}\text{PbI}_3$ . The effects of bias-induced  $\text{A}^+$  migration on perovskite stability and device performance are assessed via infrared photothermal heterodyne imaging (IR-PHI), time-of-flight secondary ion mass spectrometry (ToF-SIMS), and solar cell operational stability testing. Enhanced  $\alpha/\delta$ - $\text{FA}_{0.33}\text{MA}_{0.33}\text{Cs}_{0.33}\text{PbI}_3$  cation stability likely stems from "post-perovskite"  $\delta$ - $\text{ortho}$ - $\text{CsPbI}_3$  inclusions within parent thin films that act as barriers through which cations cannot easily migrate. This resistance to cation migration translates into improved device operational stability of  $\alpha/\delta$ - $\text{FA}_{0.33}\text{MA}_{0.33}\text{Cs}_{0.33}\text{PbI}_3$  lateral devices and solar cells relative to complementary, triple-cation,  $\alpha$ -phase  $\text{FA}_{0.76}\text{MA}_{0.15}\text{Cs}_{0.09}\text{PbI}_3$  devices. This study therefore provides new insights into cation migration in working devices and outlines a materials design strategy for stabilizing metal halide perovskites against bias-induced cation migration.

### F.EL08.17.02

**Efficient of Ion Migration in Perovskite Solar Cells with Hexagonal Boron Nitride** Yifan Yin, Yuchen Zhou and Miriam H. Rafailovich; Stony Brook University, The State University of New York, United States

Organic-inorganic halide perovskite solar cells (PSCs) have been considered a viable member of next generation photovoltaics, which can address the scalability changes with a low-cost solution process. The energy loss in the hybrid system has been approved to be principally caused by defects/traps at grain boundaries and surfaces as well as point defects such as interstitial defects or vacancies in the perovskite compounds crystal lattice. Because of the presence of these defects, both anions ( $\text{I}^-$ ) and cations ( $\text{MA}^+$ ) can migrate through the organic layer which provides a degradation pathway for perovskite materials even in those well-encapsulated devices: the halide ions can react with metal electrodes such as Ag, forming insulating components ( $\text{AgI}$ ). In addition to the corrosion of electrode, halide ions migrating into organic hole transport layer

(HTL) which is deleterious to transport properties, thus retarding device efficiency, especially under solar cell working conditions. Inspired by the quasi-2D-perovskite which shows a great stability in photovoltaic performance, here, the hexagonal boron nitride (h-BN) was incorporated into the perovskite absorber as an ionic diffusion barrier. The lamellar structure of h-BN consists of a lattice similar to graphite which can be subjected to exfoliation leading to few-layers nanosheets. The exfoliated 2D-layered materials present high surface area and quantum confinement, and also high chemical stability. The integration of this low-cost, lower dimensional material enables a better device stability as the result from the efficient suppression on the ion-migration induced degradation. With the aid of time-of-flight secondary ion mass spectroscopy (TOF-SIMS) and energy dispersive x-ray spectroscopy (EDX). The h-BN/ perovskites has an initial PCE over 20% that shows no degradation exhibit in over 72 h and retained 80% of the original PCE after 800hr, whereas the PCE of pristine MAPI devices diminishes by more than 30% within the first 24 hr.

#### **F.EL08.17.03**

**Light-Induced Degradation of Hybrid Organic-Inorganic Perovskites Reveals Autocatalytic Kinetics and Increased Stability with Substitution of Larger Organic Cations** Emily C. Smith, Christie Ellis, Hamza Javaid and Dhandapani Venkataraman; University of Massachusetts Amherst, United States

Instability under illumination in hybrid organic-inorganic perovskite solar cells represents a major roadblock to the development and commercialization of this thin-film technology. Recently, it has been shown that varying the nature of the organic cation in the perovskite structure represents a potential pathway to tuning stability of materials under illumination. However, many potential mixed-cation perovskite compositions remain unexplored, and, much is still unknown about the degradation kinetics in mixed-cation thin-films. In this work, we successfully fabricated thin-films of substituted methylammonium lead triiodide (MAPI), where we substituted the methylammonium ion with varying percentages of three larger organic cations: imidazolium, dimethylammonium, and guanidinium. We achieved substitution of these large cations for compositions of up to 20-30% while maintaining the structure and optoelectronic properties of the films. We studied the degradation kinetics of the mixed-cation films under illumination using powder x-ray diffraction. We observed that the degradation is autocatalytic. Furthermore, we calculated rate coefficients for the degradation process and observed that the degradation was slowed in films which contained  $\leq 20\%$  of any of the larger cations compared to pristine MAPI films. A maximum decrease of 62% in the degradation rate coefficient was observed in the case of 5% guanidinium substitution. Ultimately, this work provides key insight into the degradation kinetics of mixed-cation perovskite films under illumination and provides a strategy for further stabilization of perovskite thin-films for improved photovoltaic performance.

#### **F.EL08.17.04**

**Effect of Pyrazine and Guanidinium Thiocyanate (GuaSCN) on the Structure and Bandgap of Pb and Pb-Free Halide Perovskites** Rubaiya Murshed and Shubhra Bansal; University of Nevada Las Vegas, United States

Perovskite solar cells (PSCs) research has been projected over the past decade due to its promising photovoltaic properties, increasing efficiency and low cost. With a need to eliminate toxic lead from prevailing halide perovskite solar cells, several low-toxicity cations have been proposed, among them Sn(II) is considered as one of the most suitable replacements due to its similar electronic configuration and ionic radius to Pb(II). But the Sn-based perovskites are still plagued with low efficiency, oxidation and phase instability. Here we demonstrate the use of atmospheric solution-processed lead-free all inorganic molecular iodide compound cesium tin iodide ( $\text{Cs}_2\text{SnI}_6$ ) as the light absorber in PSCs. The presence of excess  $\text{SnF}_2$  in precursor solution assists phase separation. Due to the good binding affinity to  $\text{SnF}_2$ , pyrazine is expected to reduce Sn vacancy thus restricts phase separation. The effect of GuaSCN results in increasing grain size and improving film morphology thus improves the structural and optoelectronic properties of low bandgap perovskites. The present work aims at analyzing the effect of pyrazine and guanidinium thiocyanate (GuaSCN) in oxidation reduction and fabrication of low bandgap (1.3 eV)  $\text{Cs}_2\text{SnI}_6$  films when used separately as a mediator during film fabrication in GBL. Initial results suggest both pyrazine and guanidinium thiocyanate give absorption onset at higher optical wavelength ( $>1000$  nm) and low bandgap ( $\sim 1.2$ -1.3 eV). Films in addition of Pyrazine both with and without  $\text{SnF}_2$  (0 mol% and 40 mol%) shows mostly cubic  $\text{Cs}_2\text{SnI}_6$  diffraction patterns in XRD analysis which implies that the effect of  $\text{SnF}_2$  is not considerable in this case. The SCN ions increases grain size and produces cubic  $\text{Cs}_2\text{SnI}_6$  crystals. Heating at higher temperature leads to samples with lower bandgap. Both the absorption vs. wavelength and tauc plot analyses show bandgap at around 1.25 eV. Most of the samples after dark testing for over 100 hours at 65 °C retain their properties and show similar absorption edge and bandgap patterns. Samples having exposure to light at 65 °C show higher bandgap over 2 eV. In this study, the effect of these additives in  $\text{Cs}(\text{Pb},\text{Sn})\text{I}_3$  perovskite with a Sn-Pb ratio of 60:40 is also included. Primary results show separately use of both pyrazine and GuaSCN in precursor solution in a mixture of GBL and DMF result in low bandgap perovskites. Both  $\text{Cs}(\text{Pb},\text{Sn})\text{I}_3$  and  $\text{Cs}_2\text{SnI}_6$  without these additives tend to have higher bandgap at around 2.3 eV when deposited on glass substrates. Further

analysis of the effect of Pyrazine and GuaSCN additives in the stability, morphology and lifetime of Cs(Pb,Sn)I<sub>3</sub> and Cs<sub>2</sub>SnI<sub>6</sub> perovskite films will be continued in this study.

#### F.EL08.17.05

**Enabling High Photoconversion Efficiency in Lead-Free Antimony-Based Perovskite Derivatives by Tuning Crystallographic Dimensionality and Microstructure** Vincenzo Pecunia, Yueheng Peng and Fengzhu Li; Soochow University, China

The exploration of lead-free perovskite-inspired semiconductors for optoelectronic applications (e.g., single- and multi-junction solar cells, photocathodes for water splitting, photodetectors) has captured ever-growing attention, driven by their promise to replicate the success of the Pb-based counterparts without the toxicity concerns associated with the latter. In particular, an emerging approach to Pb replacement involves Sb, whose attractiveness resides in its highly-polarizable Sb<sup>3+</sup> cations with filled 5s orbitals, a stable oxidation state, and an ionic radius comparable to Pb<sup>2+</sup>. A number of antimony-halide perovskite derivatives with a formula A<sub>3</sub>Sb<sub>2</sub>X<sub>9</sub> (A<sup>+</sup>: monovalent cation; X<sup>-</sup>: halide anion) have thus been explored. Notwithstanding the rise in their reported performance, A-Sb-X absorbers are yet to deliver photoconversion efficiencies comparable to the Pb-based counterparts. Importantly, this has been linked to the zero-dimensional (0D) structure of most A-Sb-X embodiments, as the more attractive two-dimensional (2D) embodiments have been demonstrated only in very few instances, due to constraints on composition or processing conditions.

With the aim of contributing to the realization of the full potential of antimony-halide perovskite derivatives, we have investigated two such systems featuring a desirable 2D structure, exploring the impact of dimensionality, microstructure, and crystallographic orientation on their photoconversion behavior. Herein, we firstly focus on Rb<sub>3</sub>Sb<sub>2</sub>I<sub>9</sub>, the only ternary A-Sb-I with a direct bandgap, and also having the smallest exciton binding energy of all reported A-Sb-I embodiments.<sup>1</sup> In order to assess the role of microstructure on the photoconversion efficiency of Rb<sub>3</sub>Sb<sub>2</sub>I<sub>9</sub>, we have developed two strategies for its microstructural enhancement, which involve the control of the supersaturation level during the annealing step, or a high-temperature treatment in SbI<sub>3</sub> vapor. Both strategies deliver a dramatic improvement in the film morphology and microstructure.<sup>2</sup> Within sandwich-type planar devices, the resultant high-quality films enable a substantial improvement in external quantum efficiency (EQE), reaching up to 65.4% at short circuit, i.e., the highest to date for perovskite-inspired antimony-/bismuth-halide A<sub>3</sub>M<sub>2</sub>X<sub>9</sub> (M: Sb<sup>3+</sup>/Bi<sup>3+</sup>). Importantly, this is achieved without the aid of a mesoporous architecture for charge extraction, thereby revealing the inherent capability and potential of Rb<sub>3</sub>Sb<sub>2</sub>I<sub>9</sub> for efficient photoconversion.

We additionally discuss the impact of dimensionality on the photoconversion capabilities of the Cs<sub>3</sub>Sb<sub>2</sub>X<sub>9</sub> system. Departing from the dedicated high-temperature (≥ 230 °C) processing protocols pursued in the prior literature, we demonstrate that halide mixing enables the 0D-to-2D structural conversion of the Cs<sub>3</sub>Sb<sub>2</sub>X<sub>9</sub> system at temperatures < 150 °C.<sup>3</sup> The resultant 2D absorbers manifest a considerable photoconversion efficiency boost with respect to the 0D counterpart, attaining a peak EQE of 62.5%, which is at the state-of-the-art for all antimony-/bismuth-halide perovskite derivatives.

Through photocurrent-power characterization and Hall effect measurements, we finally reveal that the EQE boost achieved with both 2D Rb<sub>3</sub>Sb<sub>2</sub>I<sub>9</sub> and Cs<sub>3</sub>Sb<sub>2</sub>X<sub>9</sub> arises from their improved charge carrier transport, which we relate to the microstructural enhancement, dimensionality tuning, and crystallographic orientation. Such performance boost and mechanistic insight constitute an important step in realizing the full potential of lead-free antimony-halide perovskite derivatives and related bismuth-based homologs for their application in optoelectronics and photovoltaics.

1 J. P. Correa-Baena et al., *Chem. Mater.*, 2018, **30**, 3734–3742.

2 F. Li, Y. Wang, K. Xia, R. L. Z. Hoye and V. Pecunia, *J. Mater. Chem. A*, 2020, **8**, 4396–4406.

3 Y. Peng et al., *Appl. Mater. Today*, 2020, **19**, 100637.

#### F.EL08.17.06

**A Critical Assessment of the Use of Excess Lead Iodide in Lead Halide Perovskite Solar Cells** Bart Roose, Krishanu Dey, Yu-Hsien Chiang, Richard Friend and Samuel D. Stranks; University of Cambridge, United Kingdom

It is common practice in the lead halide perovskite solar cell field to add a small molar excess of lead iodide (PbI<sub>2</sub>) to the precursor solution in order to increase device performance. However, recent reports have shown that an excess of PbI<sub>2</sub> can accelerate performance loss. In addition, PbI<sub>2</sub> is photoactive (bandgap ~2.3 eV), which may lead to parasitic absorption losses

in a solar cell.

We use XRD and SEM to show that incorporation of  $\text{PbI}_2$  into the perovskite film is not straightforward and can have very different effects, depending on how and where  $\text{PbI}_2$  is present. At low concentrations,  $\text{PbI}_2$  facilitates charge extraction and improves device performance. For higher concentrations,  $\text{PbI}_2$  influences how perovskite crystallises and a thick  $\text{PbI}_2$  layer can be formed that impedes charge extraction. We show that devices using an optimized quantity of excess  $\text{PbI}_2$  exhibit better device performance as compared to stoichiometric devices, both initially and for the duration of a stability test under operating conditions, primarily by enhancing charge extraction. However,  $\text{PbI}_2$  is gradually degraded during device operation, largely negating the beneficial effect on charge extraction and introducing trap states that are detrimental for device performance. We find that although excess  $\text{PbI}_2$  provides a good template for enhanced performance as compared to stoichiometric devices, it can not meet stability requirements needed for commercialization of perovskite solar cells. The community must continue to seek other additives or synthesis routes that fulfill the same beneficial role as excess  $\text{PbI}_2$ , but which do not suffer from light induced degradation.

#### F.EL08.17.07

**Understanding the Instability of the Halide Perovskite  $\text{CsPbI}_3$  Through Temperature-Dependent Structural Analysis** Daniel B. Straus<sup>1</sup>, Shu Guo<sup>1</sup>, AM Milinda Abeykoon<sup>2</sup> and Robert J. Cava<sup>1</sup>; <sup>1</sup>Princeton University, United States; <sup>2</sup>Brookhaven National Laboratory, United States

Despite the tremendous interest in halide perovskite solar cells, the structural reasons that cause the all-inorganic perovskite  $\text{CsPbI}_3$  to be unstable at room temperature remain mysterious especially since many tolerance factor-based approaches predict  $\text{CsPbI}_3$  should be stable as a perovskite. Here single-crystal X-ray diffraction and X-ray pair distribution function (PDF) measurements characterize bulk perovskite  $\text{CsPbI}_3$  from 100 to 295 K to elucidate its thermodynamic instability. While Cs occupies a single site from 100 to 150 K, it splits between two sites from 175 to 295 K with the second site having a lower effective coordination number, which along with other structural parameters suggests that Cs rattles in its coordination polyhedron. PDF measurements reveal that on the length scale of the unit cell, the Pb-I octahedra concurrently become greatly distorted, with one of the I-Pb-I angles approaching  $82^\circ$  compared to the ideal  $90^\circ$ . The rattling of Cs, low number of Cs-I contacts, and high degree of octahedral distortion cause the instability of perovskite-phase  $\text{CsPbI}_3$ . These results reveal the limitations of tolerance factors in predicting perovskite stability and provide detailed structural information that suggests methods to engineer stable  $\text{CsPbI}_3$ -based solar cells.

#### F.EL08.17.08

**Enhanced Bending Fracture Behavior of Flexible Halide Thin Films Processed with *In Situ* Stress** Da Bin Kim and Yong Soo Cho; Yonsei University, Korea (the Republic of)

Halide perovskites have emerged as attractive materials for electronic and optoelectronic applications because of their unique properties and low-temperature processing. However, the mechanical aspects of the halide thin films have been very limitedly reported although strong bending fracture behavior is required for the flexible system. Here, we suggest a very promising processing way to enhance the bending fracture behavior of the flexible halide thin films with fundamental definitions of the mechanical parameters of the halide materials that have been also unavailable thus far. The processing is based on the assignments of in-situ compressive or tensile stress during the film deposition with a controllable manner. As a result, a substantial improvement of the fracture resistance against the bending operation was observed for the compressively stressed halide thin films. For example as a result of bending fracture evaluation, cesium lead bromide ( $\text{CsPbBr}_3$ ) and methylammonium lead iodide ( $\text{MAPbI}_3$ ) thin films prepared on PEDOT:PSS-coated polyethersulfone (PES) substrates demonstrated high fracture mode I toughness of 1.18 and 1.66  $\text{MPa m}^{0.5}$  for the in-situ compressive strain of -1.09%, which correspond to the enhancements by ~97 and ~100 %, respectively, compared to those for the reference samples. The structural origins of the mechanical enhancements are elucidated with experimental evidences on the variations in lattice distortion and bonding length.

#### F.EL08.17.09

**Structural Evolution of Layered Hybrid Lead Iodide Perovskites—Colloidal Nanocrystals or Ruddlesden-Popper Phases?** Clayton J. Dahlman<sup>1</sup>, Naveen Venkatesan<sup>1</sup>, Patrick Corona<sup>2</sup>, Rhys M. Kennard<sup>1</sup>, Lingling Mao<sup>1</sup>, Noah Smith<sup>2</sup>, Jiamin Zhang<sup>2</sup>, Ram Seshadri<sup>1,2</sup>, Matthew Helgeson<sup>2</sup> and Michael Chabinye<sup>1</sup>; <sup>1</sup>The University of California, Santa Barbara, United States; <sup>2</sup>University of California, Santa Barbara, United States

Hybrid organic-inorganic perovskites (HOIPs) are promising semiconductors with long carrier lifetimes, synthetic tunability, remarkable defect tolerance and simple processing. Recently, 2D analogues have been made by adding insulating cations



(e.g. butylammonium) to separate the perovskite structure into sheets. These 2D materials can be formed either in thin films, large single crystals or as dispersed nanoplatelets of only a few PbX<sub>6</sub> octahedra thick. The number of PbX<sub>6</sub> octahedra confined between insulating layers (i.e. the 'n-value') can be tuned by varying precursor stoichiometry, enabling discrete tunability of the bandgap through dielectric and quantum confinement. Controlling the structure of layered hybrid metal halide perovskites, such as the Ruddlesden-Popper (R-P) phases, is challenging because of their tendency to form mixtures of varying composition. Colloidal growth techniques can form dispersions of particles with properties that match the bulk properties of layered R-P phases, but controlling the composition of these particles remains challenging.

In this talk, we explore the microstructure of particles of R-P phases of methylammonium lead iodide prepared by antisolvent precipitation from ternary mixtures of different alkylammonium cations, where one cation is able to form perovskite phases (CH<sub>3</sub>NH<sub>3</sub><sup>+</sup>) and the other two promote layered structures as spacers (e.g. C<sub>4</sub>H<sub>9</sub>NH<sub>3</sub><sup>+</sup> and C<sub>12</sub>H<sub>25</sub>NH<sub>3</sub><sup>+</sup>). We illustrate how competition between cations that act as spacers between layers, or as grain-terminating ligands, determines the colloidal particle size of R-P crystallites that form in solution. Optical measurements reveal that quantum well dimensions can be tuned by engineering the ternary cation composition. Transmission synchrotron wide-angle X-ray scattering and small angle neutron scattering reveal changes in the structure of colloids in solvent and after deposition into thin films. In particular, we find that spacers can alloy between R-P layers if they share common steric arrangements, but tend to segregate into polydisperse R-P phases if they do not mix. This study provides a framework to compare the microstructure of colloidal layered perovskites and suggests clear avenues to control phase and colloidal morphology.

#### **F.EL08.17.10**

**Adhesion and Interfacial Fracture of Perovskite Solar Cells** Reisya Ichwani, Vanessa Uzonwanne, Juan Martin Hinostroza Tamayo, Deborah Oyewole, Oluwaseun K. Oyewole, Nancy Burnham and Winston Soboyejo; Worcester Polytechnic Institute, United States

Emerging perovskite solar cells (PSCs) are not only required to be highly efficient, but also durable. The mechanical stability of PSCs also requires good adhesion and contacts across their interfaces. These are studied using atomic force microscopy (AFM) and fracture mechanics approaches. AFM pull-off forces are measured for bi-material interfaces that are present in model perovskite solar cells. These are then incorporated into adhesion models for the estimation of adhesion energies and mode I interfacial fracture energies. The mode mixity dependence of interfacial fracture toughness is also studied for interfaces between the perovskite and electron transport layers in PSCs. This is done using Brazil Disk specimens that are used to study the robustness of the interfaces across a range of mode mixities between pure mode I and pure mode II. The underlying crack/microstructure interactions and fracture modes are used to provide insights into the underlying crack-tip shielding due to crack bridging and microcracking. These are modeled using zone and row models that are used to predict the mode-mixity dependence of fracture toughness. The implications of the results are also discussed for the determination of crack path selection criteria in perovskite solar cells.

#### **F.EL08.17.11**

**Double Perovskite Nanofibers for Photovoltaic and Optoelectronic Applications** Nageh K. Allam; American University in Cairo, Egypt

Organic-inorganic hybrid perovskite compounds are currently the archetypal materials for high performance photovoltaic (PV) and optoelectronic devices. However, the remaining bottlenecks preventing their large scale production are their environmental/thermal instability and lead toxicity. Herein, we demonstrate a novel approach to synthesize single-phase electrospun Cs<sub>2</sub>SnI<sub>x</sub>Cl<sub>6-x</sub> double perovskites with varying halide content (I, Cl or mixed I/Cl) as active materials for potential application in perovskite solar cells (PSCs). The x-ray photoelectron spectroscopy and Raman spectroscopy analyses indicated the *in-situ* formation of graphene oxide (GO) during the annealing process. The GO layer was found to enhance the optical properties and thermal stability of the fabricated perovskites even at high Cl content. Moreover, the presence of GO as an insulating layer significantly decreases the bandgap energy of the resulting perovskites. The perovskites with a mix of iodide and chloride ions showed significantly improved optical properties with higher photoluminescence (PL) intensity than that of pure chloride or iodide counterparts. Moreover, the compound with low chloride content showed superior thermal stability to those reported in the literature. Therefore, the application of the electrospinning technique is a useful strategy to *in-situ* incorporate GO in a lead-free perovskite matrix for potential photovoltaic and optoelectronic applications.

#### **F.EL08.17.12**

**Organic-Inorganic Hybrid Perovskite Single-Crystal Thin Films—Synthesis and Photoluminescence** Xiaobing Tang<sup>1</sup>,

Zhaojin Wang<sup>2</sup>, Kai Wang<sup>2</sup> and Fuqian Yang<sup>1</sup>; <sup>1</sup>University of Kentucky, United States; <sup>2</sup>Southern University of Science and Technology, China

Metallic halide organic–inorganic hybrid perovskites with excellent optoelectrical properties have potential applications in optoelectronic devices and systems. In this work, we demonstrate the feasibility of preparing CH<sub>3</sub>NH<sub>3</sub>PbBr<sub>3</sub> single crystal thin films on poly-TPD hole transport layer by controlling the heating rates. The crystallinity and trap state density of the CH<sub>3</sub>NH<sub>3</sub>PbBr<sub>3</sub> thin films are characterized by X-ray diffraction and photoluminescence and time-resolved photoluminescence, respectively. The crystallinity with the peak intensity of (100) plane of the CH<sub>3</sub>NH<sub>3</sub>PbBr<sub>3</sub> thin films prepared at 2 °C/h is nine times of that prepared at 10 °C/h. The CH<sub>3</sub>NH<sub>3</sub>PbBr<sub>3</sub> thin films prepared at 2 °C/h exhibit a carrier lifetime of 21 ns, which is much larger than 0.6 ns for the CH<sub>3</sub>NH<sub>3</sub>PbBr<sub>3</sub> thin films prepared at 10 °C/h, and an excellent structural stability. Acknowledgements: KW is grateful for the support from National Key Research and Development Program (No.2017YFE0120400) and National Natural Science Foundation of China (No.61875082). FY is grateful for the support from National Science Foundation (CMMI-1854554)

#### F.EL08.17.13

**Hybrid Lead Iodide Perovskites with Aromatic Diammonium Cations** Xiaotong Li<sup>1</sup>, Weijun Ke<sup>1</sup>, Yihui He<sup>1</sup>, Peijun Guo<sup>2</sup>, Mikael Kepenekian<sup>3</sup>, Boubacar Traore<sup>3</sup>, Jacky Even<sup>3</sup>, Claudine Katan<sup>3</sup>, Constantinos Stoumpos<sup>1</sup>, Richard D. Schaller<sup>2</sup> and Mercouri G. Kanatzidis<sup>1</sup>; <sup>1</sup>Northwestern University, United States; <sup>2</sup>Argonne National Laboratory, United States; <sup>3</sup>University of Rennes, France

Aromatic diammonium cation, x-(aminomethyl)pyridinium (AMPY, x = 3 or 4) can form 2D Dion-Jacobson lead iodide perovskite, which adopt the general formula of (xAMPY)(MA)<sub>n-1</sub>Pb<sub>n</sub>I<sub>3n+1</sub> (MA = methylammonium, n = 1–4). By modifying the position of the -CH<sub>2</sub>NH<sub>3</sub><sup>+</sup> group from 4AMPY to 3AMPY, the stacking of the inorganic layers changes from exactly eclipsed to slightly offset. The perovskite octahedra tilts are also different between the two series, with the 3AMPY series exhibiting smaller bandgaps than the 4AMPY series. Compared to the aliphatic cation of the same size (AMP = (aminomethyl)piperidinium), the aromatic spacers increase the rigidity of the cation, reduce the interlayer spacing and decrease the dielectric mismatch between inorganic layer and the organic spacer, showing the indirect but powerful influence of the organic cations on the structure and consequently on the optical properties of the perovskite materials. Preliminary solar cell devices based on the n = 4 perovskites as absorbers of both series exhibit promising performances. More interestingly, when using 1:4 ratio of AMPY:PbO as starting materials, totally different structures with 3D connection motif form instead. However, because of the steric requirement of the Goldschmidt tolerance factor rule, it is impossible for (xAMPY)M<sub>2</sub>I<sub>6</sub> to form proper perovskite structures. Instead, a combination of corner-sharing and edge-sharing connectivity is adopted in these compounds leading to the new 3D structures. Devices of (3AMPY)Pb<sub>2</sub>I<sub>6</sub> crystals exhibit clear photoresponse under ambient light without applied bias, reflecting a high carrier mobility ( $\mu$ ) and long carrier lifetime ( $\tau$ ) and great potential for photo and X-ray detection applications.

#### F.EL08.17.14

**Exploring the Limit of Layer Thickness in 2D Hybrid Lead Halide Perovskites** Eugenia S. Vasileiadou<sup>1</sup>, Bin Wang<sup>2</sup>, Ioannis Spanopoulos<sup>1</sup>, Ido Hadar<sup>1</sup>, Alexandra Navrotsky<sup>3,2</sup> and Mercouri G. Kanatzidis<sup>1</sup>; <sup>1</sup>Northwestern University, United States; <sup>2</sup>University of California, Davis, United States; <sup>3</sup>Arizona State University, United States

Two-dimensional (2D) hybrid organic-inorganic halide perovskites are a rapidly emerging class of semiconductors whose structural tunability and optoelectronic properties have led to the successful fabrication of solar cell devices with high power conversion efficiency. The features of the 2D perovskite structure that are tuned are the organic “spacer” cation and the number of the inorganic layers (*n*). There is a significant interest to target higher *n*-member compounds for light harvesting applications, due to their attractive photophysical properties such as low bandgap value and high carrier mobility. Herein, we present a comprehensive study on exploring the limit of layer thickness of bulk 2D lead halide perovskites through structural and thermodynamic study. Phase-pure synthesis of a new *n*=6 perovskite compound is reported with the characterization of the single crystal structure and optical properties of the material. Thorough calorimetry studies examine the thermodynamic stability of 2D lead iodide perovskites with layer thickness *n*=2-6. The favorable enthalpy of formation *n*=6 crystals shows that higher *n*-layer thickness is dependent on specific structural aspects. Additionally, the systematic investigation of the variances on the structural parameters and optical properties between different structure types of 2D perovskites, offers guiding principles for the targeted design and synthesis of 2D perovskites for efficient solar cell fabrication. Lastly, the stability studies of thin films demonstrate consistent observations with the thermochemical findings, further shedding light on the behavior of high *n*-layer perovskite materials.

#### F.EL08.17.15

**Amorphous Halide Perovskite Thin Films** Susan Rigter<sup>1,2</sup> and Erik C. Garnett<sup>1,2</sup>; <sup>1</sup>AMOLF, Netherlands; <sup>2</sup>University of Amsterdam, Netherlands

Lead halide perovskites are one of the most exciting and heavily researched classes of optoelectronic materials due to their unique ability to form high quality crystals with tunable band gaps in the visible and near infrared using simple solution precipitation reactions. This facile crystallization is driven by their ionic nature; just as with other salts, it is challenging to form amorphous halide perovskites, particularly in thin-film form where they can most easily be studied. Herein, we show that rapid desolvation promoted by addition of acetate precursors is a general method for making amorphous lead halide perovskite films with a wide variety of compositions, including those using all the common cations (cesium, methylammonium, formamidinium) and anions (bromide, iodide). We show that by controlling the amount of acetate, it is possible to tune from fully crystalline to fully amorphous films, with an interesting intermediate state consisting of crystalline islands embedded in an amorphous matrix. The amorphous lead halide perovskite has a large and tunable optical band gap and improves the optical properties of incorporated crystalline perovskite, opening up the intriguing possibility of using amorphous perovskite as a passivating window layer, as is currently done in record efficiency silicon solar cells.

#### F.EL08.17.16

**Facile Healing of Cracks in Organic-Inorganic Halide Perovskite Thin Films** Srinivas K. Yadavalli, Zhenghong Dai, Min Chen, Mingyu Hu, Yuanyuan Zhou and Nitin Padture; Brown University, United States

Organic-inorganic halide perovskite (OIHP) thin films have attracted a great deal of interest as photoactive materials in various optoelectronic devices due to their unprecedented photophysical properties, but their long-term reliability is likely to be limited by their poor mechanical properties. In this context, we explain different possible modes of fracture in OIHP based devices, and for the first time demonstrate facile healing of through-thickness cracks in OIHP thin films which can otherwise be detrimental to the device properties. This is achieved through application of either a moderate compressive stress at room-temperature or a simple heat treatment at moderate temperatures. Based on the findings from a series of *ex situ* residual stress measurements, crack-healing process is found to be time-dependent, which indicates that facile mass-transport in OIHPs plays a key role in this phenomenon. The mechanisms governing crack-healing process are explained based on the fundamentals of brittle fracture. This discovery has broad implications for the prevention and/or restoration of the overall performance, environmental stability, and mechanical reliability of OIHP based devices like solar cells which are poised for commercialization.

#### F.EL08.17.17

**Understanding the Effects of Moisture and Stoichiometry Variations on Composition and Structure in Halide Perovskite Solar Cells** Juanita Hidalgo<sup>1</sup>, Carlo Andrea Riccardo Perini<sup>1</sup>, Andres Felipe Castro Mendez<sup>1</sup>, Barry Lai<sup>2</sup>, Ruipeng Li<sup>3</sup>, Shijing Sun<sup>4</sup>, Antonio Abate<sup>5</sup> and Juan Pablo Correa Baena<sup>1</sup>; <sup>1</sup>Georgia Institute of Technology, United States; <sup>2</sup>Argonne National Laboratory, United States; <sup>3</sup>Brookhaven National Laboratory, United States; <sup>4</sup>Massachusetts Institute of Technology, United States; <sup>5</sup>Helmholtz-Zentrum Berlin für Materialien und Energie, Germany

Hybrid halide lead perovskites are promising materials for photovoltaic applications. Nonetheless, these materials are highly sensitive and degrade in various environmental conditions. Among these, moisture is a prime cause of material degradation, representing a threat to the commercialization of perovskite-based materials. Hence, it is essential to study how water interacts with a perovskite thin film, what factors trigger instability in the material, and loss in solar cell performances. In order to understand these degradation mechanisms, we expose  $\text{Cs}_{0.05}(\text{MA}_{0.17}\text{FA}_{0.83})_{0.95}\text{Pb}(\text{I}_{0.83}\text{Br}_{0.17})_3$  perovskite thin films with different precursor stoichiometries (organic to inorganic ratios) to a moisture treatment with high relative humidity. We monitor the evolution of perovskite crystalline structure, and we correlate it to changes in performances. Characterization with SEM images show morphological changes in the grain size, and XRD patterns evidence structural features that are further explained and understood by grazing incidence wide angle X-ray scattering (GIWAXS). Remarkably, we observe improved photovoltaic efficiency for treated films with an excess organic component, correlated with vertical orientation along the (001) plane. In addition, synchrotron-based X-ray fluorescence and X-ray beam induced current (XRF-XBIC) is used to correlate the elemental distribution with the current output of the devices.

SESSION F.LP05.05: Live Poster Session II: Electronics and Optics II (F.EL08)  
Session Chairs: Robert Hoyer and Libai Huang

Thursday Afternoon, December 3, 2020  
3:00 PM - 5:00 PM  
F.EL08

### F.EL08.18.01

**HybriD<sup>3</sup> and MatD<sup>3</sup>: Curated Materials Data for Hybrid Organic-Inorganic Perovskites and a General Software Stack for Materials Data** Xiaochen Du<sup>1,1</sup>, Raul Laasner<sup>1</sup>, Xixi Qin<sup>1</sup>, Connor Clayton<sup>2</sup>, Svenja Janke<sup>1</sup>, Becca Lau<sup>1</sup>, Chi Liu<sup>1</sup>, Sampreeti Bhattacharya<sup>3</sup>, Juliana Mendes<sup>4</sup>, Jun Hu<sup>3</sup>, Dovletgeldi Seyitliyev<sup>4</sup>, Ruyi Song<sup>1</sup>, Manoj Jana<sup>1</sup>, Matti Ropo<sup>5</sup>, Franky So<sup>4</sup>, Kenan Gundogdu<sup>4</sup>, Wei You<sup>3</sup>, Yosuke Kanai<sup>3</sup>, David Mitzi<sup>1,1</sup> and Volker Blum<sup>1,1</sup>; <sup>1</sup>Duke University, United States; <sup>2</sup>Carnegie Mellon University, United States; <sup>3</sup>University of North Carolina at Chapel Hill, United States; <sup>4</sup>North Carolina State University, United States; <sup>5</sup>University of Turku, Finland

Materials research is generating a wealth of data across a vast community. Specifically, the volume of available data on hybrid organic-inorganic perovskites (HOIPs) and related growth in this area is now immense. Keeping track of data of different origins, sample types or levels of theory, with a diverse set of different relevant observables and discoveries, is a challenging task at best. We here present an open database, "HybriD<sup>3</sup>" (Design, discovery and dissemination (D<sup>3</sup>) of data related to hybrid materials, <https://materials.hybrid3.duke.edu>), aiming to collect, curate, and make available materials data related to HOIP. The database is designed to provide a broad set of data, i.e., experimental and computational, related to in principle any materials property of relevance to the community: structure, optical or electronic properties, and more. A key goal is to provide the ability to curate data, that is, identify property information closest to the actual properties of a real material prepared in a specific way (bulk crystalline, powder, thin film, nanocrystalline, ...). Importantly, the database is open to the community and designed to accept community input. While the "HybriD<sup>3</sup>" database is focused on a particular materials class, the problem of making materials data of all kinds available in a structured, reproducible way is general. The software underlying the HybriD<sup>3</sup> database is thus available as a separate open-source project "MatD<sup>3</sup>" (<https://github.com/HybriD3-database/MatD3>). We also describe this software stack, which can enable materials data at any scale, from small workgroups via focused projects all the way to large and general, open and reproducible materials data collections.

### F.EL08.18.02

**Ab Initio Characterization of the Cs<sub>2</sub>ZrX<sub>6</sub> (X=Cl, Br) Family, 0D Ordered Defect Perovskite Emitters** Christopher Savory<sup>1</sup>, Anna Abfalterer<sup>2</sup>, Javad Shamsi<sup>2</sup>, Samuel D. Stranks<sup>2</sup> and David O. Scanlon<sup>1</sup>; <sup>1</sup>University College London, United Kingdom; <sup>2</sup>University of Cambridge, United Kingdom

As halide perovskites have made their significant impact in the fields of photovoltaics, light emitters and other optical devices, research interest has been reignited in families of lead-free 2D, 1D and 0D perovskite-derived materials that, while poorer photovoltaics, can access some of the strong emissive properties of the halide perovskites, while also demonstrating emergent optoelectronic properties of their own.[1] The layered Cs<sub>3</sub>Pn<sub>2</sub>X<sub>9</sub> (Pn = Sb, Bi; X = Cl, Br, I) family demonstrates structured excitonic emission at room temperature[2,3] while the K<sub>2</sub>PtCl<sub>6</sub>-structured 'vacancy-ordered double perovskites' such as M<sub>2</sub>SnI<sub>6</sub> (M=Rb, Sn) have shown both evidence of defect tolerance similar to that seen in the lead halide perovskites as well as strong exciton-phonon coupling.[4,5] As such, the exploration of perovskite-inspired lower dimensionality compounds represents an exciting direction in the research of optical materials.

In this study, inspired by our experimental collaborators' colloidal synthesis of nanocrystals of Cs<sub>2</sub>ZrCl<sub>6</sub> and Cs<sub>2</sub>ZrBr<sub>6</sub>, which also belong to the K<sub>2</sub>PtCl<sub>6</sub> structure type and demonstrate broad white photoluminescence when formed into thin films, we perform hybrid Density Functional Theory (DFT) calculations in order to predict and rationalize the observed optical and electronic behavior of the Cs<sub>2</sub>ZrX<sub>6</sub> materials family, producing good agreement to experiment. By calculating the thermodynamic and luminescent properties of the intrinsic defects within the system, as well as excitonic properties within the QSGW method and the Bethe-Salpeter equation, we attempt to accurately predict the origin of such promising emissive properties. Finally, we present direct comparisons to the analogous M<sub>2</sub>SnX<sub>6</sub> family and draw conclusions on the feasibility of extending the field of lead-free perovskite-inspired emitters, and whether such optimal optical properties are available beyond the post-transition metals.

[1] Xiao, Z.; Song, Z.; Yan, Y. From Lead Halide Perovskites to Lead-Free Metal Halide Perovskites and Perovskite Derivatives. *Adv. Mater.* **2019**, *31*, 1803792

[2] Bass, K.K.; Estergreen, L.; Savory, C.N.; Buckeridge, J. et al. Vibronic Structure in Room Temperature Photoluminescence of the Halide Perovskite Cs<sub>3</sub>Bi<sub>2</sub>Br<sub>9</sub>. *Inorg. Chem.* **2017**, *56*, 42

[3] McCall, K.M.; Stoumpos, C.C.; Kostina, S.S.; Kanatzidis, M.G. and Wessels, B.W. Strong Electron-Phonon Coupling

and Self-Trapped Excitons in the Defect Halide Perovskites A<sub>3</sub>M<sub>2</sub>I<sub>9</sub> (A=Cs,Rb; M=Bi,Sb). *Chem. Mater.* **2017**, *29*, 4129  
[4] Maughan, A.E.; Ganose, A.M.; Almaker, M.A.; Scanlon, D.O. and Neilson, J.R. Tolerance Factor and Cooperative Tilting Effects in Vacancy-Ordered Double Perovskite Halides. *Chem. Mater.* **2018**, *30*, 3909  
[5] Maughan, A.E.; Ganose, A.M.; Bordelon, M.M.; Miller, E.M. et al. Defect Tolerance to Intolerance in the Vacancy-Ordered Double Perovskite Semiconductors Cs<sub>2</sub>SnI<sub>6</sub> and Cs<sub>2</sub>TeI<sub>6</sub>. *J. Am. Chem. Soc.* **2016**, *138*, 8453

#### F.EL08.18.03

**Exploration of Compositional Space in Methylammonium-Free Lead Halogen Perovskites for High-Performance Solar Cells** Yu An<sup>1,2</sup>, Xianggao Li<sup>1</sup> and Juan Pablo Correa Baena<sup>2</sup>; <sup>1</sup>Tianjin University, China; <sup>2</sup>Georgia Institute of Technology, United States

The certified power conversion efficiency (PCE) of state-of-the-art organic-inorganic metal halide perovskite solar cells (PSCs) has surpassed 25%, coming after single crystalline silicon solar cells. The most widely studied methylammonium (MA) lead iodide undergoes a structural phase transition and degradation due to the volatile MA cation, detrimental to the long-term stability of the devices. Formamidinium (FA), used as the majority cation in most of PCE >20% PSCs, is thermally more stable and has an optimal red-shifted bandgap. However, FA with the relatively large radius induces titled PbI<sub>6</sub> octahedra in FAPbI<sub>3</sub>, leading to the photoinactive yellow  $\delta$ -phase at room temperature. Herein, iodide and FA in FAPbI<sub>3</sub> were gradually replaced by bromide and cesium (Cs) with smaller radius to suppress the yellow  $\delta$ -phase and systematically explore the compositional space via regulating the tolerance factor, revealing the crucial link between the crystal structure and optoelectronic properties of the mixed-cation (FA/Cs) lead mixed-halide (I/Br) perovskite. An empirical expression for FA/Cs-Pb-I/Br bandgap as a function of composition was determined, which contributes to tailored bandgap suitable for tandem solar cells. In addition, the FA/Cs-Pb-I/Br films were probed by advanced synchrotron X-ray characterization to understand halide phase segregation, which has been found to be detrimental for solar cell performance.

#### F.EL08.18.04

**Interfacial States, Energetics and Atmospheric Stability of Large-Grain Antifluorite Cesium Titanium Bromide** Jocelyn Mendes, Julia Martin, Alexander Carl, Emma J. Pellerin and Ronald L. Grimm; Worcester Polytechnic Institute, United States

Cesium titanium bromide, Cs<sub>2</sub>TiBr<sub>6</sub>, has attracted research interest due to its ~1.8 eV band gap, which makes it desirable for forming tandem junctions with silicon. However, the instability of large-grain Cs<sub>2</sub>TiBr<sub>6</sub> in ambient atmosphere prompts further fundamental understanding of its surface chemistry and oxidation. To ascertain stability of the material in ambient atmosphere and establish band edge positions of the material we conducted controlled air exposure experiments and UHV cleaving of nascent material. X-ray photoelectron spectroscopy (XPS) established correct synthesis, effects of atmospheric exposure, and characterization of UHV cleaved samples. Ultraviolet photoelectron spectroscopy (UPS) established band edge positions of Cs<sub>2</sub>TiBr<sub>6</sub> with and without surface metal oxide species present. Powder X-ray diffraction (pXRD) quantified the effects of atmospheric exposure over time. The presence of metal oxides on Cs<sub>2</sub>TiBr<sub>6</sub> surfaces shifted band alignments towards TiO<sub>2</sub> while UHV cleaved, oxide-free surfaces demonstrated an intrinsically n-type semiconductor. These results elucidate the effects of surface oxides on Cs<sub>2</sub>TiBr<sub>6</sub> surfaces, and future routes through which interfacial reactivity may be used to improve atmospheric stability.

#### F.EL08.18.05

**Bandgap-Tailored Perovskite Capping Layer Design for Improving Stability and Passivation** Noor Titan Putri Hartono<sup>1</sup>, Marie-Hélène Tremblay<sup>2</sup>, Armi Tiihonen<sup>1</sup>, Janak Thapa<sup>1</sup>, Shijing Sun<sup>1</sup>, Seth R. Marder<sup>2</sup> and Tonio Buonassisi<sup>1</sup>; <sup>1</sup>Massachusetts Institute of Technology, United States; <sup>2</sup>Georgia Institute of Technology, United States

In recent years, the 3D/low-dimensional (LD) perovskite heterostructure consisting of LD perovskite called ‘capping layer’, deposited atop of 3D perovskite in a device [1], has emerged as a solution for improving perovskite solar cells’ (PSCs’) stability and interfacial passivation. However, the capping layer materials and processing conditions have been optimized for single-junction PSCs, and not for multi-junction PSCs. To apply the capping layer in multi-junction PSCs, research efforts are required to understand and optimize the bandgap-tailored capping layer material. We propose a detailed study exploring at least 10 different types of LD perovskite with various halides (I, Br, and Cl) and thicknesses, and CH<sub>3</sub>NH<sub>3</sub>Pb(I-Br)<sub>3</sub> absorber mixtures with increasing bandgap from 1.59 to 2.27 eV [2]. The samples are degraded in a well-controlled environmental chamber, under high humidity (85% RH), high heat (85°C), and low illumination (0.17 sun). The same set of samples are screened using photoconductivity, as a proxy for its interfacial passivation property. We also utilize decision tree-based machine learning models and Shapley values [3] to help determine which molecular properties in the capping layers significantly affect the absorber mixtures’ stability and conductivity. Our results indicate that capping layers needs to

be tailored based on the perovskite absorbers' composition, bandgap, and organic cation types to achieve high stability. Furthermore, by comparing the optimum bandgap-tailored capping layers through X-ray photoelectron spectroscopy (XPS), Fourier-transform infrared spectroscopy (FTIR), and ultraviolet photoelectron spectroscopy (UPS), we can understand how the film stability is affected by inorganic and organic bonds on the surface of the capping layers, as well as how interfacial passivation is affected by band alignment. Our study suggests that capping layer tuning is a promising approach to increase the stability of perovskite-based tandem solar cells.

#### References

- [1] W. Huang, T. Bu, F. Huang, and Y. B. Cheng, "Stabilizing High Efficiency Perovskite Solar Cells with 3D-2D Heterostructures," *Joule*, vol. 4, no. 5, pp. 975–979, May 2020, doi: 10.1016/j.joule.2020.04.009.
- [2] L. Atourki *et al.*, "Role of the chemical substitution on the structural and luminescence properties of the mixed halide perovskite thin MAPbI<sub>3-x</sub>Br<sub>x</sub> (0 ≤ x ≤ 1) films," *Appl. Surf. Sci.*, vol. 371, pp. 112–117, May 2016, doi: 10.1016/j.apsusc.2016.02.207.
- [3] N. T. P. Hartono *et al.*, "How machine learning can help select capping layers to suppress perovskite degradation," *ChemRxiv*, pp. 1–47, Jan. 2020, doi: 10.26434/CHEMRXIV.11766528.V1.

#### F.EL08.18.06

**Nonlinear Bandgap Behavior in Lead-Free Cs<sub>2</sub>Ag(Sb,Bi<sub>1-x</sub>)Br<sub>6</sub> Double Perovskite Alloys** Seán Kavanagh<sup>1,2,3</sup>, Zewei Li<sup>4</sup>, Robert Palgrave<sup>3</sup>, Richard Friend<sup>4</sup>, David O. Scanlon<sup>3</sup>, Aron Walsh<sup>2</sup> and Robert Hoye<sup>2</sup>; <sup>1</sup>Thomas Young Centre, UCL, ICL, KCL, QMUL, United Kingdom; <sup>2</sup>Imperial College London, United Kingdom; <sup>3</sup>University College London, United Kingdom; <sup>4</sup>University of Cambridge, United Kingdom

Double perovskites have emerged as promising candidate materials for high-performance next-generation optoelectronic technologies, owing to the ability to replace the toxic Pb<sup>2+</sup> cation with a pair of more benign cations (*e.g.* Ag<sup>+</sup> and Bi<sup>3+</sup>), while preserving the perovskite crystal structure.<sup>1</sup> However, most double perovskites, including the prototypical Cs<sub>2</sub>AgBiBr<sub>6</sub>, have prohibitively wide bandgaps, limiting photoconversion and photocatalytic efficiencies.<sup>2</sup> Recently, it has been demonstrated that the bandgap of Cs<sub>2</sub>AgBiBr<sub>6</sub> can be reduced through alloying with Sb<sup>3+</sup>,<sup>3</sup> yet the bandgap of the pure Sb-based double perovskite (Cs<sub>2</sub>AgSbBr<sub>6</sub>) remains excessively wide for photo-voltaic/catalytic applications. In this work, we develop a solution-based route to synthesize phase-pure Cs<sub>2</sub>Ag(Sb<sub>x</sub>Bi<sub>1-x</sub>)Br<sub>6</sub> thin films, with the mixing parameter *x* tunable over the entire composition range. In doing so, we observe this system to disobey Vegard's law, exhibiting significant bandgap bowing, such that the mixed alloy (*x* = 0.9) demonstrates the smallest bandgap (2.08 eV, compared to 2.18 eV and 2.25 eV for the pure Sb- and Bi-based double perovskites, respectively). We investigate the possible mechanisms for this nonlinear bandgap variation through relativistic hybrid Density Functional Theory (DFT) calculations, combined with in-depth measurements of the composition, phase and grain structure to yield detailed understanding of the underlying physical origins. The energetic alignment of electron states within these materials is accurately calculated, including consideration of deformation potentials to adequately account for the spurious supercell effects associated with such calculations.<sup>4,5</sup> Our work reveals pathways to bandgap engineering in double perovskite alloys, such that it is better suited to photovoltaic or photocatalytic applications, which may be generally applicable to other mixed-metal double perovskite systems.

<sup>1</sup> C.N. Savory, A. Walsh, and D.O. Scanlon, *ACS Energy Lett.* **1**, 949 (2016).

<sup>2</sup> A.H. Slavney, T. Hu, A.M. Lindenberg, and H.I. Karunadasa, *Journal of the American Chemical Society* **138**, 2138 (2016).

<sup>3</sup> G. García-Espejo, D. Rodríguez-Padrón, R. Luque, L. Camacho, and G. de Miguel, *Nanoscale* **11**, 16650 (2019).

<sup>4</sup> K.T. Butler, C.H. Hendon, and A. Walsh, *Journal of the American Chemical Society* **136**, 2703 (2014).

<sup>5</sup> S.-H. Wei, S.B. Zhang, and A. Zunger, *Journal of Applied Physics* **87**, 1304 (2000).

#### F.EL08.18.08

**Tin Oxynitride-Based Ferroelectric Semiconductors for Solar Energy Conversion Applications** Steven T. Hartman, Arashdeep S. Thind and Rohan Mishra; Washington University in St. Louis, United States

Lead-halide perovskites have emerged as a promising class of semiconductors; however they suffer from issues related to lead-toxicity and instability. We report results of a first-principles-based design of heavy-metal-based oxynitrides as alternatives to lead-halide perovskites. We have used density-functional-theory calculations to search a vast composition space of ABO<sub>2</sub>N and ABON<sub>2</sub> compounds, where *B* is a *p*-block cation, and *A* is an alkaline, alkali-earth, rare-earth or transition metal cation, and identify 10 new ABO<sub>2</sub>N oxynitride semiconductors that we expect to be formable. Specifically, we discover a new family of ferroelectric semiconductors with ASnO<sub>2</sub>N stoichiometry (*A* = Y, Eu, La, In, Sc) in the

LuMnO<sub>3</sub>-type structure, which combine the strong bonding of metal oxides with the low carrier effective mass and small, tunable band gaps of the lead-halide perovskites. These tin oxynitrides have predicted direct band gaps ranging from 1.6 – 3.3 eV, and a sizeable electric polarization up to 17  $\mu\text{C}/\text{cm}^2$ , which is predicted to be switchable by an external electric field through a non-polar phase. With their unique combination of polarization, low carrier effective mass and band gaps spanning the entire visible spectrum, we expect  $\text{ASnO}_2\text{N}$  ferroelectric semiconductors will find useful applications as photovoltaics, photocatalysts, and for optoelectronics.

Acknowledgments: This work was supported by the National Science Foundation through grant number DMR-1806147.

#### F.EL08.18.09

**How to Design Defect Tolerant Devices** Basita Das<sup>1</sup>, Irene Aguilera<sup>1</sup>, Uwe Rau<sup>1</sup> and Thomas Kirchartz<sup>1,2</sup>; <sup>1</sup>Forschungszentrum Jülich GmbH, Germany; <sup>2</sup>University of Duisburg-Essen, Germany

Perovskite solar cells have emerged as a key photovoltaic technology given the remarkable rise in their efficiency in the past decade. Long non-radiative lifetimes as a result of slow defect-mediated recombination in perovskite materials are key in achieving high open-circuit voltages necessary for high efficiency solar cells.

The quantitative impact of bulk or interface defects on recombination is often estimated by defect statistics based on the model of Shockley, Read and Hall. However, defect statistics depend on defect capture coefficients to calculate defect occupancy and the recombination rate through the defect. Due to the lack of enough experimental data on capture coefficients of novel materials or, alternatively, models to calculate trap energy dependent capture coefficients it is frequently assumed that capture coefficients are symmetric, i.e,  $k_n = k_p$  for all defect levels within the bandgap in a device. However, equal or at least similar values of the capture coefficients are not necessarily a typical or even a likely scenario.

To go beyond the state-of-the-art device simulation in photovoltaics involving constant capture coefficients, we present a generalized microscopic model based on the Harmonic oscillator approximation to calculate defect capture coefficients as a function of the host material and the energetic position of the defects. Then we use this capture coefficients to classify the “deep” defects inside a device not merely based on the energetic position of the device but also as a function of the quantitative impact it has on the device. Furthermore, we discuss certain photovoltaic device design principles that can substantially reduce recombination through the dominant recombination centers.

#### F.EL08.18.10

**Enhancing Fundamental Understanding of Structure-Property Relationships in Chalcogenide Perovskite Semiconductors with Theoretical and Experimental Studies of Dielectric Response, X-Ray Absorption and Electronic Transport** Stephen Filippone<sup>1</sup>, Kevin Ye<sup>1</sup>, Boyang Zhao<sup>2</sup>, Shanyuan Niu<sup>2</sup>, Nathan Koocher<sup>3</sup>, Daniel Silevitch<sup>4</sup>, Ignasi Fina<sup>5</sup>, James Rondinelli<sup>3</sup>, Jayakanth Ravichandran<sup>2</sup> and Rafael Jaramillo<sup>1</sup>; <sup>1</sup>Massachusetts Institute of Technology, United States; <sup>2</sup>University of Southern California, United States; <sup>3</sup>Northwestern University, United States; <sup>4</sup>California Institute of Technology, United States; <sup>5</sup>Universitat Autònoma de Barcelona, Spain

Electronic materials in perovskite and related structure types are a rich field of study because they combine characteristics of ionic and covalent bonding in crystal structures that are tolerant of distortions and chemical substitution. Tremendous efforts are now underway to understand the structure-property relationships that underpin the photovoltaic performance of lead halide perovskites (LHPs), expanding on and linking decades of research on photovoltaic absorbers, on the one hand, and complex oxide physics on the other. Now we extend this spirit of interdisciplinary, fundamental inquiry to a much less-studied class of materials, the chalcogenide perovskites. Recent works have shown that chalcogenide perovskites have outstanding properties for optoelectronic applications, including: slow minority carrier recombination, strong light absorption, excellent environmental stability, and dopability. Efforts are just now beginning to develop a fundamental understanding of these phenomena and to exploit these exciting materials for applications.

We present a diverse set of studies of the atomistic origin of structure-property relationships in chalcogenide perovskites. We combine impedance spectroscopy, X-ray absorption spectroscopy (XAS), electronic transport, and first-principles theory to understand how atomic structure and particular chemical bonds support outstanding semiconducting properties. Our impedance spectroscopy measurements on single crystals reveal that chalcogenide perovskites are highly-polarizable semiconductors, with stronger dielectric response than any other family of semiconductors with band gap in the VIS-NIR, exceeding even LHPs. Our theoretical calculations agree quantitatively with our measurements, and illustrate the particular polar phonon modes responsible for the large dielectric response. Our XAS studies combining experiment and theory illustrate the importance of directional bonds in determining the near-band edge electronic structure (including the band gap), especially for layered variants in the Ruddlesden-Popper structure type. This electronic anisotropy is further illustrated by electronic transport measurements made on oriented single crystals.

Our results illustrate, in a fundamental and detailed level, the ways in which chalcogenide perovskites differ from their oxide and halide cousins. We show that the structure-property relationships follow from covalent metal-chalcogen bonds and strong electron-phonon coupling. We conclude that chalcogenide perovskites are highly promising for optoelectronic and energy-conversion technologies.

[1] Jaramillo, R. & Ravichandran, J. In praise and in search of highly-polarizable semiconductors: Technological promise and discovery strategies. *APL Materials* 7, 100902 (2019).

#### **F.EL08.19.01**

**Novel C<sub>6</sub>H<sub>5</sub>NHNH<sub>3</sub>I Additive for Efficiency Acceleration in Organic-Inorganic Halide Perovskite Solar Cells** Md Ashiqur Rahman Laskar<sup>1,2</sup> and Qiquan (Quinn) Qiao<sup>1</sup>; <sup>1</sup>South Dakota State University, United States; <sup>2</sup>Arizona State University, United States

Different additive materials are widely used to improve the power conversion efficiency (PCE) of organic-inorganic halide perovskite solar cells. In this work, we report a novel organic additive material C<sub>6</sub>H<sub>5</sub>NHNH<sub>3</sub>I (Phenylhydrazinium Iodide) which is very effective to enhance the PCE of single cation-single halide based Methylammonium Lead Iodide perovskite solar cells (MLIPSC). In addition to that, we have found the additive is also effective for other types of perovskite composition such as double cation-double halide perovskite solar cells. C<sub>6</sub>H<sub>5</sub>NHNH<sub>3</sub>I promotes perovskite crystal growth and improves the light absorption capability of the active layer. Furthermore, because of reduced defects and charge traps in the additive treated perovskite film, charge carrier lifetime becomes almost double from 1.4 μs to 2.5 μs which ensures minimum recombination of the photogenerated electrons and holes. Besides, approximately 10% increased external quantum efficiency (EQE) and 14% improved built in potential (V<sub>bi</sub>) of the perovskite solar cells indicate superior device performance. Eventually, accelerated short circuit current density and open circuit voltage of the C<sub>6</sub>H<sub>5</sub>NHNH<sub>3</sub>I treated perovskite solar cells contribute to nearly 20% increment of PCE in MLIPSC.

#### **F.EL08.19.02**

**Understanding the Effect of Electrode Spacing on CsPbI<sub>2</sub>Br Interdigital Photodetector with Chromium Electrodes** Haider B. Salman; University of Arkansas, United States

Significant achievements were made in the past few years with perovskite material in optoelectronic applications. One of the advantages of the halide perovskite in photo detection applications is that the band gap of the material can be tuned to cover a wide range of wavelengths by halide mixing. In this paper, the research is focused on the fabrication and characterization of interdigital photodetectors made with CsPbI<sub>2</sub>Br. The photodetector consists of two interdigitate chromium electrodes deposited on glass substrates with the perovskite filling the spacing between the electrodes. The interdigital pattern of the device was fabricated using photolithography method to deposit 80 nm of chromium. To study the effect of the electrode spacing on the device performance, four types of photodetectors with four different spacing; 50, 20, 10, and 5 μm were fabricated. The perovskite was synthesized using one step deposition method with 0.6 molar concentration of CsPbI<sub>2</sub>Br precursor. The material was characterized by obtaining the absorbance, the photoluminescence, and the X-ray diffraction spectra. One single peak in the PL spectrum was observed at 648 nm indicating a band gap 1.91 eV. The current voltage curves of the photodetectors were obtained under dark and light conditions using Keithley 4200 semiconductor characterization system and Newport solar simulator. The spectral response of the device was obtained using Bruker IFS 125hr spectrometer. The device with 10 μm spacing showed ~370 on/off ratio at 5 V bias under 100 mW/cm<sup>2</sup> light intensity. Under the same conditions, the device with 5 μm showed an increase in the on/off ratio to 6800. The detectivities of the 10 and 5 μm devices were calculated to be 4.9 × 10<sup>9</sup>, and 2.46 × 10<sup>10</sup> Jones respectively.

#### **F.EL08.19.04**

**Enhancing Chemical Stability and Suppressing Ion Migration in CH<sub>3</sub>NH<sub>3</sub>PbI<sub>3</sub> Perovskite Solar Cells via Direct Backbone Attachment of Polyester on Grain Boundaries** Yuchen Zhou<sup>1</sup>, Yifan Yin<sup>1</sup>, Xianghao Zuo<sup>1</sup>, Likun Wang<sup>1</sup>, Chang-Yong Nam<sup>2</sup> and Miriam H. Rafailovich<sup>1</sup>; <sup>1</sup>Stony Brook University, United States; <sup>2</sup>Brookhaven National Laboratory, United States

Grain boundary (GB) passivation by polymer additives has been shown effective in improving the performance of solution processed hybrid perovskite solar cells (PSCs). However, the critical stability issue associated with detrimental ion migration in PSCs remains less explored by polymer additives. Here, we show that a new linear polar polymer, polycaprolactone (PCL), can passivate GBs of methylammonium lead triiodide (MAPbI<sub>3</sub>) perovskites via direct backbone attachment, enabling significantly enhanced environmental stability of n-i-p type PSC. The champion PSC with optimal PCL concentration shows



an improved power conversion efficiency (PCE) of 20.1 %. 90% of initial PCE was preserved after 400 h ambient storage. After 100 h thermal aging (85 °C), 80% of the original PCE has also been preserved. The tested PSCs use less stable Spiro-OMeTAD (2,2',7,7'-tetrakis[N,N-di(4-ethoxyphenyl)amino]-9,9'-spirobifluorene) as hole transport layer (HTL), and, thus, the improved stability indicates critical roles of PCL in retarding moisture ingress as well as suppressing ion migration. Detailed structures of PCL GB passivation is visualized directly via lateral scanning force and transmission electron microscopies. Secondary ion mass spectrometry and ion conduction measurements confirm the PCL GB passivation significantly retards I<sup>-</sup> ion migration in MAPbI<sub>3</sub> PSCs, while without PCL, I<sup>-</sup> ions are actively accumulating in the organic HTL and at the interface between electrodes and the HTL even without externally applied electric field. We envision this passivation strategy by PCL GB functionalization can help the development of environmentally stable, high-performance PSCs. (This work was supported by the Morin Foundation Trust and the NSF, Inspire program #1344267)

#### **F.EL08.19.06**

**Effects of Annealing Temperature on Interdiffusion of Materials in Layered Perovskite Solar Cells** Deborah Oyewole<sup>1,2,1</sup>, Juan Martin Hinojosa Tamayo<sup>1,1</sup>, Oluwaseun K. Oyewole<sup>1,1</sup>, Benjamin Agyei-Tuffour<sup>3</sup>, Richard Koech<sup>4,1</sup>, Rejsya Ichwani<sup>1,1</sup>, Jaya Cromwell<sup>1</sup>, Nancy Burnham<sup>1,1</sup> and Winston Soboyejo<sup>1,1</sup>; <sup>1</sup>Worcester Polytechnic Institute, United States; <sup>2</sup>Sheda Science and Technology, Km 10 Abuja-Lokoja Road, Nigeria; <sup>3</sup>School of Engineering Sciences, University of Ghana, Ghana; <sup>4</sup>African University of Science and Technology, Nigeria

In order to design more efficient and durable perovskite solar cells (PSCs), the effects of annealing temperature on interdiffusion of the constituent elements in layered formamidinium-based PSCs were studied. First, the PSCs were fabricated by spin-coating lead (II) iodide solution onto the mesoporous electron transporting layer (ETL) followed by a mixture of formamidinium ammonium iodide, with small proportion methylammonium bromide and methylammonium chloride. The effect of varying annealing temperature of the perovskite films is then studied to gain insight into the changes that occur on the perovskite film and the overall effects of interdiffusion of constituent elements on photoconversion efficiencies of the PSCs. The results show there is diffusion of tin from fluorine-doped tin oxide to the mesoporous ETL due to sintering. The level of tin in the mesoporous layer decreases with increased annealing temperatures of the perovskite films. The quality of perovskite films is also improved with better uniformly distributed grain sizes for annealing temperatures between room temperature and 130 °C compared to higher annealing temperatures of 140 °C and 150 °C. The overall effects of the interdiffusion of layer constituents on photoconversion efficiencies are then discussed for the design of PSCs.

#### **F.EL08.19.07**

**A Hole Transport Bilayer for Highly Efficient and Stable Inverted Perovskite Solar Cells** Hamza Javaid, Volodymyr V. Duzhko and Dhandapani Venkataraman; University of Massachusetts Amherst, United States

Highly efficient and stable inverted, *i.e.* p-i-n, perovskite solar cells (PSCs) are fabricated by employing a novel hole transport bilayer. Compared to devices with single PTAA interlayer, which have an average power conversion efficiency (PCE) of 18.9%, an enhanced average PCE of 20.2% and a maximum PCE of 21.16% in the bilayer-based devices are observed. The XRD and AFM studies show an improved crystallinity and larger grain size of perovskite films on the bilayer surface. The ultraviolet photoelectron spectroscopy and Mott-Schottky analysis suggest an increased built-in potential with an enhanced upward band bending at the bilayer/perovskite interface. Compared to devices with single PTAA, CuI and PEDOT:PSS interlayer, the bilayer-based devices show significant suppression of *J-V* hysteresis and stable current output at maximum power point. The bilayer-based devices also demonstrate a remarkable long-term stability, as tested in inert atmosphere.

#### **F.EL08.19.08**

**Toward Rational Design of Stable and Robust Hybrid Perovskite Devices—The Role of Functionalized Organic Cations and Dimensionality Engineering** Arvin Kakekhami<sup>1</sup>, Marcos A. Reyes-Martinez<sup>2</sup>, Xiaoming Zhao<sup>2</sup>, Melissa Ball<sup>2,2</sup>, Peng Tan<sup>3,1</sup>, Sayan Banerjee<sup>1</sup>, Lynn Loo<sup>2,2</sup> and Andrew Rappe<sup>1</sup>; <sup>1</sup>University of Pennsylvania, United States; <sup>2</sup>Princeton University, United States; <sup>3</sup>Harbin Institute of Technology, China

Here, we discuss how density functional theory (DFT)-based methods can help us in designing strategies to mitigate the stability and efficiency challenges for hybrid organic-inorganic perovskite (HOIP) systems. On one front, we use first-principles theory to rationalize the elastic properties of layered hybrid perovskites, correlating such properties with interlayer organic-organic interactions and also the HOIP's structural properties *e.g.*, its dimensionality or intrinsic interlayer defects and voids. [1] On a different but complementary front, we have studied fundamental chemistry behind the water degradation of 3D hybrid perovskites and have related this to the chemical properties of the organic cations. [2] We are now expanding this work to study water interactions in layered quasi-2D systems, unraveling the fundamental role of dimensionality in water

stability of perovskites. Beyond the realm of bulk-like perovskites, we also study the determining role of organic cations' chemistry on surface stability and defect formation for HOIP nanoparticles. The role of organic cations goes further than directly influencing the inorganic backbone structure, and for some specific functionalized organic cations and through intricate hydrogen-bonding networks, the organic-organic interactions can become important at dictating the electronic and structural properties of layered perovskites. Having a multipronged approach in which we identify descriptors for elastic and electronic properties of perovskite, as well as their stability, allows us to rationalize and help improve experimentally-relevant pathways to create more robust HOIP-based devices capable of performing in real-world PV or LED applications. Few such possibilities which are discussed here include: surface passivation with mixed short organic cations, supramolecular interactions between long cations, secondary organic functionalities, and dimensionality engineering.

[1] Reyes-Martinez, Marcos A., Peng Tan, Arvin Kakekhani, Sayan Banerjee, Ayan A. Zhumeckenov, Wei Peng, Osman M. Bakr, Andrew M. Rappe, and Yueh-Lin Loo. "Unraveling the Elastic Properties of (Quasi) Two-Dimensional Hybrid Perovskites: A Joint Experimental and Theoretical Study." *ACS Applied Materials & Interfaces* 12, no. 15 (2020): 17881-17892.

[2] Kakekhani, Arvin, Radhika N. Katti, and Andrew M. Rappe. "Water in hybrid perovskites: Bulk MAPbI<sub>3</sub> degradation via super-hydrous state." *APL Materials* 7, no. 4 (2019): 041112.

#### **F.EL08.19.09**

**Bilayer Perovskite Solar Cells by Grafted PDMS Transfer Process** Anisha Mohapatra<sup>1,2</sup> and Chih-Wei Chu<sup>1</sup>; <sup>1</sup>Academia Sinica, Taiwan; <sup>2</sup>National Tsing Hua University, Taiwan

Organic-Inorganic Perovskite solar cells has a great advantage to reach the radiative limit for PCE enhancement. The single junction devices are restricted to attain the radiative limit because of the energy losses. Multi-structure architectures like tandem, heterostructure are adapted to recover the thermodynamic energy loss. The variable bandgap of perovskite is an advantage, which varies from 1.5eV~1.8eV providing a complete solar spectrum coverage. Stacking of high-bandgap perovskite with low bandgap perovskites is a good approach for encountering the energy losses. The perovskite heterostructure is fabricated by sequential deposition of quantum dots and thermally evaporated p-n junctions. Till now, there is no demonstration of any solution process able method in perovskites for stacking perovskite absorbers because of the dissolution of perovskite precursors by the subsequent layers. Therefore, we demonstrated a PDMS printing technique for stacking perovskite layers inspired by multi-stacked organic solar cells. The printing technique is assisted with modification of surface energy of PDMS by grafting process, which facilitates printing of high crystalline pinhole free perovskite layers. On proving ground, we also stacked perovskite layers to form a perovskite heterostructures. We demonstrated the printing of multi-layer perovskite layers to encounter the thermodynamic losses. To understand the advantage of heterostructure for encountering the energy losses, a constant thickness of single layer and heterostructure was maintained for compared the photovoltaic performance. We achieved a photovoltaic performance of ~5%, ~9% for MaPbI<sub>3</sub> and MaPbBrI<sub>2</sub> layer and ~10% for MAPbBrI<sub>2</sub>/MAPbI<sub>3</sub> heterostructure. This gave us an indication that the heterostructure was able to suppress some non-radiative recombination to overcome the energy losses, which can be a great application for stacking perovskite layers to use in different optoelectronic applications.

#### **F.EL08.19.11**

**Fracture Behavior of Halide Perovskite Thin Films for Solar Cells** Zhenghong Dai, Srinivas K. Yadavalli, Mingyu Hu, Min Chen, Yuanyuan Zhou and Nitin Padture; Brown University, United States

Organic-inorganic halide perovskites (OIHPs) have emerged as the most promising light-absorber materials in thin-film photovoltaic (PVs). However, the low formation energies of OIHPs render them unstable. While significant progress has been made in improving the stability of OIHPs, perovskite solar cells (PSCs) will also need to be mechanically reliable if they are to service satisfactorily for years. In this context, we have studied the fracture behavior of PSCs by measuring their cohesion energies using double cantilever beam method and report a novel approach to strategically enhance the interfacial adhesion and performance of PSCs by interface modification. This work points to a new route for designing mechanically robust PSCs with long-term durability.

#### **F.EL08.20.01**

**Amplified Spontaneous Emission from All-Inorganic Quasi-2D Perovskites** Lei Lei, Dovletgeldi Seyitliyev, Kasra Darabi, Siliang He, Samuel Stuard, Qi Dong, Juliana Mendes, Harald Ade, Aram Amassian, Kenan Gundogdu and Franky So; North Carolina State University, United States

Recently, metal-halide perovskite materials are considered as a promising candidate for lasing applications since perovskites may overcome typical limitations showed in organic gain media and the “green-gap” in inorganic semiconductors. While lasing has been demonstrated based on perovskite materials with both 3D and low-dimensionalities, quasi-2D perovskites are a better gain media due to its unique properties such as large binding energy and self-assembled quantum wells. It has been shown that efficient energy funneling from low-dimensional domains to high-dimensional domains will not only enhance the radiative recombination but also facilitate population inversion. However, the trend of how the dimensionality of quasi-2D perovskites affects amplified spontaneous emission (ASE) threshold is still controversial. Here, we investigate ASE of all-inorganic quasi-2D perovskite thin films with different dimensionalities, and try to understand the role of dimensionality in both materials properties and charge carrier dynamics.

In this work, we formed quasi-2D perovskite thin films based on the all-inorganic 3D cesium lead halide perovskite framework due to the improved thermal and optical stability. The dimensionality of quasi-2D perovskites is tuned by varying the concentration of the organic spacer phenethylamine (PEA). In our work, the large organic cation PEA acts as a nucleation center facilitating the crystallization process of perovskites. Via grazing-incidence wide-angle X-ray scattering (GIWAXS) measurements and scanning electronic microscopy, we found that the addition of PEA also enhances the quality of the thin films by controlling the domain size and morphology. As a result, the PLQY increases with the PEA concentration. However, the ASE threshold is not correlated with the PLQY and it reaches to the lowest value ( $7 \mu\text{J}/\text{cm}^2$ ) at a moderate PEA concentration of 40%. To study the correlation between PEA concentration and ASE threshold, we used transient photoluminescence and transient absorption spectroscopy to study the photophysics of these films. Our results showed that with increasing PEA concentration to 40%, the non-radiative recombination is significantly reduced due to defect passivation, leading to the increasing PLQY and decreasing of ASE threshold. However, the existing of the low-dimensional domains became significant with a higher PEA concentration (60%), which acted as long-lived trap states for excitons and limited the population inversion process. Finally, by using the optimized PEA ratio, the ASE emission was observed over the broad visible range from red to blue, demonstrating its wide wavelength-tunability.

#### **F.EL08.20.02**

##### **Direct Observation of the Ultrafast Dynamics of Trapped Carriers in Organic Metal Halide Perovskite**

**Films** Kanishka Kobbekaduwa<sup>1</sup>, Shreetu Shrestha<sup>2</sup>, Pan Adhikari<sup>1</sup>, Hsinhan Tsai<sup>2</sup>, Wanyi Nie<sup>2</sup> and Jianbo Gao<sup>1</sup>; <sup>1</sup>Clemson University, United States; <sup>2</sup>Los Alamos National Laboratory, United States

Despite the power conversion efficiency (PCE) of the perovskite solar cells soars more than 25 % in less than ten years, their limited stability remains one of the crucial hurdles on the path to commercialization. To improve the device stability, various trap state passivation strategies targeting the bulk perovskite, perovskite surface, and device interfaces have been employed. However, knowledge of the temporal, spatial, and energetic correlation of the defect/trap states is the foundation for fundamental and technical understanding of the impact of the trap/defect states, manifested by the device stability and PCE optimization.

In this report, we directly observe the ultrafast dynamics of trapped carriers in organic lead halide perovskite MAPbI<sub>3</sub> thin film by ultrafast photocurrent spectroscopy (UPCS). Under low carrier density, the trapped carriers undergo a multiple trapping and release (MTR) transport mechanism among the shallow trap states and deep trap state, demonstrated by a time-dependent activation energy. Above the trap filling region, in addition to the MTR transport mechanism, the trap-assist Auger recombination occurs, which is demonstrated by the laser intensity dependent decay time. Our results elucidated the trapped carrier dynamics from sub-25 ps to couple ns in the solution-processed film with mobility of  $\sim 1 \text{ cm}^2/\text{Vs}$ .

#### **F.EL08.20.03**

##### **Exciton Spin Relaxation in 2D Metal Halide Perovskites** Sean A. Bourelle; University of Cambridge, United Kingdom

Optoelectronic properties of 2D metal halide perovskites are dominated by the transitions and interactions between excitons. Here, we present a study on the spin relaxation mechanisms for these excitonic states and demonstrate how these mechanisms can be altered. Our analysis utilizes ultrafast spectroscopy methods including Faraday rotation and circularly polarised transient absorption spectroscopy.

#### **F.EL08.20.04**

##### **Optical Studies of Mixed-Dimension Perovskites—Excitonic Effects and Morphological Changes with Alkyl-**

**Ammonium Iodide Doping** Mohsin Raza Khan, Shahzad Akhtar Ali, Qurat ul Ain, Ataul Haq and Ammar A. Khan; Lahore University of Management Sciences, Pakistan

Organometal halide perovskites are promising materials for optoelectronic applications due to excellent light absorption,

charge transport and emissive properties, coupled with potentially low-cost scalable fabrication [1][2]. Perovskite solar cells (PSCs), as well as other devices, currently suffer from moisture and thermal instability of the perovskite semiconductors [3]. There are several complimentary methodologies of increasing the stability of PSCs, and amongst these the formation of hybrid two/three dimensional Ruddleson Popper perovskites is one of the most promising [4]. Mixed dimension perovskites (MDPs) can be formed by the incorporation of long alkyl-chain cations into the crystal structure leading to the formation of a layered crystal structure [5]. The individual layers are separated by covalently linked cations, with a 3D intra layer geometry. The optical, crystalline, electrical and magnetic properties of 3D perovskites can be readily tuned by varying the stoichiometric concentration and chain length of the dopant, leading to a considerable scope for application dependent material engineering. However, exploring this large yet versatile parameter space of dopants requires an understanding of the underlying excitonic processes and morphological dependencies.

In this work, the formation of 2D/3D mixed alkylammonium lead iodide perovskites using Butylammonium (BAI) and Octylammonium (OAI) iodides as additives in methyl-ammonium lead iodide perovskites is demonstrated. A solvent annealing method is employed to improve film morphology. The effect of incorporating these cations on the optical properties of the films is investigated using micro-photoluminescence and absorption studies, and a left shift in band-gap with increasing 2D character is illustrated, in accordance with literature[6]. BAI and OAI demonstrate very different spectral properties, with much larger spectral shifts in the longer chain derivative, hinting towards a strong effect of the alkyl chain. We further utilise multi-gaussian fitting to reveal insights into edge-states as well as disorder in MDPs, which can have important consequences for photovoltaic and light-emitting device applications.

[1] N. Elumalai, M. Mahmud, D. Wang, and A. Uddin, "Perovskite Solar Cells: Progress and Advancements," *Energies*, vol. 9, no. 11, p. 861, 2016, doi: 10.3390/en9110861.

[2] Z. Li *et al.*, "Scalable fabrication of perovskite solar cells," *Nat. Rev. Mater.*, vol. 3, pp. 1–20, 2018, doi: 10.1038/natrevmats.2018.17.

[3] N. Grossiord, J. M. Kroon, R. Andriessen, and P. W. M. Blom, "Degradation mechanisms in organic photovoltaic devices," *Org. Electron.*, vol. 13, no. 3, pp. 432–456, 2012, doi: 10.1016/j.orgel.2011.11.027.

[4] P. Gao, A. R. Bin Mohd Yusoff, and M. K. Nazeeruddin, "Dimensionality engineering of hybrid halide perovskite light absorbers," *Nat. Commun.*, vol. 9, no. 1, pp. 1–14, 2018, doi: 10.1038/s41467-018-07382-9.

[5] R. L. Milot *et al.*, "Charge-Carrier Dynamics in 2D Hybrid Metal-Halide Perovskites," *Nano Lett.*, vol. 16, no. 11, pp. 7001–7007, 2016, doi: 10.1021/acs.nanolett.6b03114.

[6] D. H. Cao, C. C. Stoumpos, O. K. Farha, J. T. Hupp, and M. G. Kanatzidis, "2D Homologous Perovskites as Light-Absorbing Materials for Solar Cell Applications," *J. Am. Chem. Soc.*, vol. 137, no. 24, pp. 7843–7850, 2015, doi: 10.1021/jacs.5b03796.

#### F.EL08.20.05

**Benefits of Disorder—Carrier Localisation in Alloyed Hybrid Perovskites for Efficient Luminescence** [Sascha Feldmann](#)<sup>1</sup>, Stuart Macpherson<sup>1</sup>, Richard Friend<sup>1</sup>, Henning Sirringhaus<sup>1</sup>, David Beljonne<sup>2</sup>, Samuel D. Stranks<sup>1</sup> and Felix Deschler<sup>3</sup>; <sup>1</sup>University of Cambridge, United Kingdom; <sup>2</sup>Université de Mons, Belgium; <sup>3</sup>Technische Universität München, Germany

Metal halide perovskites have emerged as promising materials for optoelectronic applications like solar cells or light-emitting diodes (LEDs). Here, we investigate mixed-halide perovskites and control the cation alloying to enhance optoelectronic performance through alteration of the charge carrier dynamics. In contrast to single-halide perovskites, we find high luminescence yields for photoexcited carrier densities far below solar illumination conditions. We employ time-resolved spectroscopy and show that the charge carrier recombination regime changes from second to effectively first order within the first tens of nanoseconds after excitation. Supported by microscale mapping of the optical bandgap, electrically gated transport measurements and first-principles calculations, we demonstrate that spatially varying energetic disorder in the electronic states causes local charge accumulation, creating p- and n-type photodoped regions, which unearths a strategy for efficient light emission at low charge-injection in solar cells. [1]

[1] Feldmann, Macpherson et al. *Nature Photonics* 14, 123–128 (2020).

#### F.EL08.20.06

**Performance Limiting Structural Heterogeneities in Metal Halide Perovskites** [Tiarnan A. Doherty](#)<sup>1</sup>, Stuart Macpherson<sup>1</sup>, Andrew Winchester<sup>2</sup>, Duncan Johnstone<sup>1</sup>, Miguel Anaya<sup>1</sup>, Aron Walsh<sup>3</sup>, Paul Midgley<sup>1</sup>, Keshav Dani<sup>2</sup> and Samuel D. Stranks<sup>1</sup>; <sup>1</sup>University of Cambridge, United Kingdom; <sup>2</sup>Okinawa Institute of Science and Technology, Japan; <sup>3</sup>Imperial College London, United Kingdom

Halide perovskite materials have promising performance characteristics for low-cost optoelectronic applications. Photovoltaic devices fabricated from perovskite absorbers have reached power conversion efficiencies above 25 per cent in single-junction devices and 28 per cent in tandem devices. Though widely considered defect tolerant materials, perovskites still exhibit a sizeable density of deep sub-gap non-radiative trap states, which create local variations in photoluminescence (1, 2) that fundamentally limit device performance. These trap states have also been associated with light-induced halide segregation in mixed halide perovskite compositions (3) and local strain (4), both of which can detrimentally impact device stability (5). Understanding the nature of these traps will be critical to ultimately eliminate losses and yield devices operating at their theoretical performance limits with optimal stability. We recently revealed that the majority of these trap states in state-of-the-art  $(\text{Cs}_{0.05}\text{FA}_{0.78}\text{MA}_{0.17})\text{Pb}(\text{I}_{0.83}\text{Br}_{0.17})_3$  perovskites form in nanoscale clusters at grain boundaries of compositionally and structurally distinct entities [*Nature*, 2020].

In this talk we detail our low-dose, high-resolution and multimodal approach to link photophysical properties to nanoscale structural and compositional heterogeneities. By combining scanning electron microscopy techniques with spatially resolved photoemission measurements, we compare and contrast observed structural defects in  $(\text{Cs}_{0.05}\text{FA}_{0.78}\text{MA}_{0.17})\text{Pb}(\text{I}_{0.83}\text{Br}_{0.17})_3$  and  $(\text{Cs}_{0.05}\text{FA}_{0.78}\text{MA}_{0.17})\text{PbI}_3$  halide perovskite thin films and discuss how they ultimately limit device performance. In so doing, we reveal the nature and origin of the “inhomogenous” perovskite grains that have been directly linked to non-radiative recombination and were previously unidentified (1). Finally, by combining scanning electron diffraction measurements with environmental chambers, we perform *in-situ* experiments to explore the local nanoscale structural modifications that occur in perovskite materials under real world operating conditions and how these structural modifications are linked to device degradation.

#### References

1. T. A. S. Doherty, A. J. Winchester, S. Macpherson, D. N. Johnstone, V. Pareek, E. M. Tennyson, S. Kosar, F. U. Kosasih, M. Anaya, M. Abdi-Jalebi, Z. Andaji-Garmaroudi, E. L. Wong, J. Madéo, Y.-H. Chiang, J.-S. Park, Y.-K. Jung, C. E. Petoukhoff, G. Divitini, M. K. L. Man, C. Ducati, A. Walsh, P. A. Midgley, K. M. Dani, S. D. Stranks, Performance-limiting nanoscale trap clusters at grain junctions in halide perovskites. *Nature*. **580**, 360–366 (2020).
2. D. W. de Quilettes, S. M. Vorpahl, S. D. Stranks, H. Nagaoka, G. E. Eperon, M. E. Ziffer, H. J. Snaith, D. S. Ginger, Impact of microstructure on local carrier lifetime in perovskite solar cells. *Science*. **348**, 683–686 (2015).
3. A. J. Knight, A. D. Wright, J. B. Patel, D. P. McMeekin, H. J. Snaith, M. B. Johnston, L. M. Herz, Electronic Traps and Phase Segregation in Lead Mixed-Halide Perovskite. *ACS Energy Lett.* **4**, 75–84 (2019).
4. T. W. Jones, A. Osherov, M. Alsari, M. Sponseller, B. C. Duck, Y.-K. Jung, C. Settens, F. Niroui, R. Brenes, C. V. Stan, Y. Li, M. Abdi-Jalebi, N. Tamura, J. E. Macdonald, M. Burghammer, R. H. Friend, V. Bulović, A. Walsh, G. J. Wilson, S. Lilliu, S. D. Stranks, Lattice strain causes non-radiative losses in halide perovskites. *Energy Environ. Sci.* **12**, 596–606 (2019).
5. J. Zhao, Y. Deng, H. Wei, X. Zheng, Z. Yu, Y. Shao, J. E. Shield, J. Huang, Strained hybrid perovskite thin films and their impact on the intrinsic stability of perovskite solar cells. *Science Advances*. **3**, eaa05616 (2017).

#### F.EL08.20.07

**Elucidating the Influence of Compositional Heterogeneity on Charge Carrier Accumulation and Photodoping in Metal Halide Perovskites** Stuart Macpherson, Jooyoung Sung, Tiarnan A. Doherty, Kyle Frohna, Elizabeth Tennyson, Miguel Anaya, Yu-Hsien Chiang, Akshay Rao and Samuel D. Stranks; University of Cambridge, United Kingdom

Metal halide perovskites are remarkable thin film semiconductors with numerous favorable properties that are optimal for photovoltaic and light emission applications<sup>1</sup>. These characteristics include high absorption coefficients, long charge carrier lifetimes and a tunable bandgap.

We have previously shown that the luminescence efficiency and charge carrier recombination behavior in mixed halide perovskites is significantly altered by the cation alloy employed during fabrication via facile solution processing<sup>2</sup>. The addition of alkali metal cations provides passivation of sub-bandgap defect states and also stabilizes an energetic landscape that facilitates photodoped carrier accumulation, leading to enhanced optoelectronic performance.

Our current work aims to further unveil the influence of microscopic compositional variations on local photoinduced carrier accumulation in  $(\text{CsMAFA})\text{PbI}_x\text{Br}_{3-x}$  perovskite films. We combine Femtosecond Transient Absorption Microscopy with nanoscale X-ray Fluorescence and Atomic Force Microscopy to track carrier diffusion and recombination across a heterogeneous chemical and morphological landscape. We find that the complex interplay of local carrier recombination and diffusion will have important ramifications for solar cell and LED device performance.

[1] Stranks, S. D. & Snaith, H. *Nature Nanotech* **10**, 391-402 (2015)

[2] Feldmann, S., Macpherson S. et al. *Nature Photonics* **14**, 123-128 (2020)

#### **F.EL08.20.08**

**Ferroelastic Strain and Defect Behavior upon Repeated Bending of Flexible Methylammonium Lead Iodide Perovskite Films** Rhys M. Kennard, Clayton J. Dahlman, Ryan DeCrescent, Jon Schuller, Kunal Mukherjee, Ram Seshadri and Michael Chabiny; University of California, Santa Barbara, United States

The highest solar cell efficiencies in halide perovskite devices are achieved using compositional derivatives of tetragonal methylammonium lead iodide (MAPbI<sub>3</sub>). Commercialization of flexible perovskite devices will require a thorough understanding of how applied strain modifies the perovskite structure and defect-related properties. A complication of studying strain behavior in tetragonal MAPbI<sub>3</sub> is that it is ferroelastic, meaning that it spontaneously forms multiple domains, also called “twins”. These twins exhibit identical crystal structure but different orientation, are inherently strained, and are separated by domain walls. The relative proportions of different twins can be semi-reversibly changed (“domain switching”) upon application of stress, via a process called ferroelastic hysteresis. Separate studies have shown that applying strain to MAPbI<sub>3</sub> films modifies defect-related properties such as the degradation rate, the activation energy of ion migration and the photoluminescence lifetime. However, potential correlations between changes to these properties in films and ferroelasticity have proven difficult to establish, as a detailed structural description of the ferroelastic behavior of MAPbI<sub>3</sub> under strain is missing.

In this work, we characterized in detail the ferroelastic hysteresis loop of MAPbI<sub>3</sub>. Films of MAPbI<sub>3</sub> were cast on polymer substrates. We used Grazing Incidence Wide-Angle X-ray Scattering (GIWAXS) to first identify twin type and to assess the impact of the polymer substrate on the twins formed. Changes in the populations of different ferroelastic twins, in the strain magnitudes of different lattice planes, and in minimum domain sizes were then characterized for increasingly large applied strains. We thus identified approximate locations for the coercive stress (onset of domain switching) and saturation (all possible domain switching has occurred) on the stress-strain curve of MAPbI<sub>3</sub>, as well as transformation strain magnitudes imparted by the hysteresis. Changes in the minimum domain sizes enabled deduction of evolution of the number of domain walls. The concentration of domain walls in films was found to closely correlate with previously-reported changes in the activation energy of ion migration, photoluminescence lifetime and degradation rate of MAPbI<sub>3</sub> films upon application of strain. The understanding gained by these results will aid design of more stable MAPbI<sub>3</sub> flexible devices with better-controlled ionic and electronic properties.

#### **F.EL08.20.10**

**Ultrafast Photophysics of Metal Halide Perovskite Multiple Quantum Wells—Device Implications and Reconciling Band Alignment** Andrew H. Proppe and Edward H. Sargent; University of Toronto, Canada

Metal halide perovskite quantum wells (QWs) have been used to fabricate efficient optoelectronic devices, and exhibit stability superior to that of their bulk 3D counterparts. The perovskite QWs are tuned in synthesis so that they possess different bandgaps and exciton binding energies owing to variable quantum confinement as a function of QW thickness. Accordingly, the device performance of these materials depends on the efficiency of various interwell carrier dynamical processes, principally exciton and charge transfer. I will discuss the use of transient absorption and ultrafast two-dimensional electronic spectroscopy to probe interwell exciton transfer on timescales of 100s of femtoseconds, and show that interwell charge transfer occurs on timescales of 10s to 100s of picoseconds. These results, in addition to ultraviolet photoelectron spectroscopy experiments, are used to reconcile conflicting observations of type-I and type-II band alignment amongst perovskite QWs.

#### **F.EL08.20.12**

**Rashba Band Splitting in Methylammonium Lead Iodide—An Insight from Spin-Polarized Scanning Tunneling Spectroscopy** Abhishek Maiti, Salma Khatun and Amlan J. Pal; Indian Association for the Cultivation of Science, India

A low recombination rate of photogenerated carriers in methylammonium lead iodide (MAPbI<sub>3</sub>) enhancing the carrier lifetime and thereby diffusion length is believed to be occurred due to Rashba band splitting<sup>[1]</sup> which arises due to a large spin-orbit coupling (SOC) arising out of high-Z elements (lead and iodine) in the compound along with a lack of centrosymmetry which appears due to a tilted PbI<sub>6</sub> octahedra and rotating electric dipoles of the organic ions leading to an effective magnetic field and thereby lifting the Kramer’s spin-degeneracy of the electrons.<sup>[2]</sup> Regarding the spin-rotation or

spin-texture ( $\chi$ ) of the two split-levels, two schools of thought persist amongst theoreticians: (1) spin-forbidden transition model and (2) spin-allowed transition model. In the spin-forbidden transition model, after spin-split, the CB and VB closer to the Fermi energy possess opposite spin-textures. A recombination between electrons in CB-minimum and holes in VB-maximum is hence a spin-forbidden process leading to a low recombination rate and thereby an enhanced carrier lifetime and a longer diffusion length.<sup>[1]</sup> On the other hand, such possibility has been overruled in the spin-allowed transition model as CB and VB possess a similar type of spin-texture closer to the Fermi energy where the recombination of photo-excited carriers is apparently possible due to spin-allowed nature of the transition.<sup>[3]</sup> In this regard, we have reported an experimental observation of Rashba splitting in MAPbI<sub>3</sub> through spin-polarized scanning tunneling spectroscopy to probe the split bands.<sup>[4]</sup>  $dI/dV$  spectra recorded at many different points of the film allowed us to spot both the Rashba split-levels and also to deliberate on their spin-textures. We observe that the bands split in such a manner that the conduction and valence bands closer to the Fermi energy have the same type of spin-textures (a spin-allowed transition model). Still a low recombination rate of photogenerated carriers in MAPbI<sub>3</sub> has been analyzed by considering Wannier-type excitons, a molecular nature of spin-domains as observed from the  $dI/dV$  images, and therefore a spin-forbidden nature of inter-domain transition.

#### Reference

1. Zheng, F.; Tan, L. Z.; Liu, S.; Rappe, A. M., Rashba Spin–Orbit Coupling Enhanced Carrier Lifetime in CH<sub>3</sub>NH<sub>3</sub>PbI<sub>3</sub>. *Nano Lett.* 2015, 15 (12), 7794-7800.
2. Kepenekian, M.; Even, J., Rashba and Dresselhaus Couplings in Halide Perovskites: Accomplishments and Opportunities for Spintronics and Spin–Orbitronics. *The Journal of Physical Chemistry Letters* 2017, 8 (14), 3362-3370.
3. Zhang, X.; Shen, J.-X.; Van de Walle, C. G., Three-Dimensional Spin Texture in Hybrid Perovskites and Its Impact on Optical Transitions. *The Journal of Physical Chemistry Letters* 2018, 9 (11), 2903-2908.
4. **Maiti, A.**; Khatun, S.; Pal, A. J., Rashba Band Splitting in CH<sub>3</sub>NH<sub>3</sub>PbI<sub>3</sub>: An Insight from Spin-Polarized Scanning Tunneling Spectroscopy. *Nano Lett.* 2020, 20 (1), 292-299.

#### F.EL08.21.01

##### **Late News: Comparison of Different Functionals for First-Principles Calculations of Defects in Metal Halide**

**Perovskites** [Haibo Xue](#)<sup>1</sup>, Geert Brocks<sup>2,1</sup> and Shuxia Tao<sup>1</sup>; <sup>1</sup>Eindhoven University of Technology, Netherlands; <sup>2</sup>University of Twente, Netherlands

Being one of the most promising photovoltaic materials, the metal halide perovskites have attracted plenty of scientific effort in improving their optoelectronic properties and long-term stability. Both properties are highly sensitive to the nature and the concentration of the intrinsic defects in the perovskites. The first-principles calculation is very useful to predict the thermodynamics relevant to the formation of the defects and their consequences in the optoelectronic properties and plays an essential role in complementing experiments in understanding the defect chemistry and physics. However, due to the intrinsic complexity of the halide perovskites, i. e. hybrid composition and covalent-ionic bonds, diverse results were reported using different functionals within the density functional theory framework. Here, using the typical perovskite, MAPbI<sub>3</sub>, as an example, we show a comprehensive comparison of a wide range of functionals including GGAs, meta-GGA (SCAN), and combination of them with atom-pairwise (DFT-D3) and non-local (rev-vdW-DF2 and rVV10) van der Waals (vdW) correction. Our results indicate meta-GGA (SCAN) predicts consistently more accurate geometries and energies than GGAs and the vdW correction is essential for describing the vdW bonds associated with the organic cations in the hybrid perovskites. Based on the above, we suggest the SCAN+rVV10 is the most promising functional and is expected to improve on the accuracy for other halide perovskites in this large family of materials.

#### F.EL08.21.02

**Late News: Machine Learning Framework for Accelerated Development of Halide Perovskites** [Meghna Srivastava](#)<sup>1</sup>, John Howard<sup>2,2</sup>, Tao Gong<sup>1</sup> and Marina S. Leite<sup>1</sup>; <sup>1</sup>University of California, Davis, United States; <sup>2</sup>University of Maryland, United States

Metal halide perovskite solar cells (PSC) are a high-efficiency, low-cost alternative to Si photovoltaics. However, various environmental stressors (light, humidity, temperature, bias, and oxygen) initiate degradation in perovskite devices, which limits device lifetimes and impedes commercialization. Discovering materials and fabrication parameters that provide a stable performance is therefore vital. Machine learning (ML) accelerates design at every level of the PSC development process while offering novel physical insight. We present a framework for applying ML to (A) perovskite compositional screening, (B) material synthesis and stability analysis, and (C) full device development and testing. Key parameters such as crystal lattice parameters, quasi-fermi-level splitting, and power conversion efficiency (PCE) are extracted from experimental data, including X-ray diffraction (XRD), photoluminescence (PL), and current-voltage (I-V) characteristics. Traditionally, these data lead to a time-consuming trial-and-error process that informs optimal perovskite compositions, fabrication processes, and device operating conditions. ML models expedite this process and, once trained, use easily acquired experimental data to

immediately predict figures of merit or future material/device performance (including forecasting time-resolved behavior). These predictions then guide further experimental investigation. Our generalized roadmap involves (1) identifying the material question of interest, (2) obtaining data for model training, (3) data pre-processing, (4) feature engineering, and (5) model optimization and testing. We demonstrate this process from start-to-finish using several baseline models trained on currently available data from the perovskite community, noting potentials for fine-tuning and extension. As one example, we use past time-series PL and relative humidity (rH) data to forecast humidity-dependent light emission for methylammonium lead triiodide (MAPI), methylammonium lead tribromide, and triple-cation (formamidinium-methylammonium-cesium) perovskite thin films. For this task, we implement an echo state network (ESN), a type of recurrent neural network (RNN). The optimized model predicts PL output with <15% normalized root mean square error (NRMSE) for all compositions over 12+ hours. We train an additional ESN to forecast power output from a PSC with a triple-cation absorber, using light intensity and temperature data as inputs, and obtain an NRMSE of only 3.1%. In addition to time-series prediction, ML models can extrapolate from ground truth experimental data to novel conditions. This reduces laboratory time drastically and eliminates the need for exhaustive trial-and-error work. For example, we train a long short-term memory (LSTM) model on temperature-dependent aging data from a MAPI PSC. We generate degradation traces at unseen temperatures with <3% NRMSE. Finally, we show image-based machine learning, using a convolutional neural network (CNN) to extract hidden trends from dark-field images of spiro-OMeTAD (a common hole-transport layer in PSC devices) and predict film conductance. Although the images have no visual trends discernable by the human eye, the model achieves an NRMSE of 19%. These examples illustrate the versatility of ML as a tool in PSC research, and our workflow is easily generalizable to other facets of development. We propose integrating projects from all three levels of PSC design (composition, material, and device) into a streamlined ML pipeline that includes materials discovery, fabrication, characterization, and stability testing. This pipeline takes advantage of our current technological capabilities in ML, data science, and autonomous experimentation and presents a rational, accelerated pathway to PSC commercialization.

#### F.EL08.21.03

**Late News: Atomistic and Electronic Origin of Phase Instability of Metal Halide Perovskites** Junke Jiang<sup>1</sup>, Feng Liu<sup>2</sup>, Ionut Tranca<sup>1</sup>, Qing Shen<sup>2</sup> and Shuxia Tao<sup>1</sup>; <sup>1</sup>Eindhoven University of Technology, Netherlands; <sup>2</sup>The University of Electro-Communications, Japan

The excellent optoelectronic properties of metal halide perovskites (MHPs) have attracted extensive scientific interests and boosted their application in optoelectronic devices. Despite their attractive optoelectronic properties, their poor stability under ambient conditions remains the major challenge, hindering their large-scale practical applications. In particular, some MHPs undergo spontaneous phase transitions from perovskites to non-perovskites. Compositional engineering via mixing cations or anions has been widely reported to be effective in suppressing such unwanted phase transition. However, the atomistic and electronic origins of the stabilization effect remain unexplored. Here, by combining Density Functional Theory (DFT) calculations and Crystal Orbital Hamilton Population (COHP) analysis, we provide insights for the undesired phase transition of pristine perovskites (FAPbI<sub>3</sub>, CsPbI<sub>3</sub>, and CsSnI<sub>3</sub>) and reveal the mechanisms of the improved phase stability of the mixed compounds (Cs<sub>x</sub>FA<sub>1-x</sub>PbI<sub>3</sub>, CsSn<sub>y</sub>Pb<sub>1-y</sub>I<sub>3</sub>, and CsSn(Br<sub>z</sub>I<sub>1-z</sub>)<sub>3</sub>). We identify that the phase transition is correlated with the relative strength of the M-X bonds as well as that of the hydrogen bonds (for hybrid compositions) in perovskite and non-perovskite phases. The phase transition can be suppressed by mixing ions, giving rise to either increased bond strength for the perovskite or decreased bond strength in their non-perovskite counterparts. Our results present a comprehensive understanding of the mechanisms for the phase instability of metal halide perovskites and provide design rules for engineering phase-stable perovskite compositions.

#### F.EL08.21.04

**Late News: Atmosphere Affecting Lattice and Degradation Mechanisms of High-Efficiency Perovskite Solar Cells** Renjun Guo<sup>1</sup>, Dan Han<sup>2</sup>, Wei Chen<sup>1</sup>, Manuel A. Scheel<sup>1</sup>, Lennart K. Reb<sup>1</sup>, Nian Li<sup>1</sup>, Shambhavi Pratap<sup>1</sup>, Tianxiao Xiao<sup>1</sup>, Suzhe Liang<sup>1</sup>, Christian L. Weindl<sup>1</sup>, Shanshan Yin<sup>1</sup>, Hubert Ebert<sup>2</sup>, Matthias Schwartzkopf<sup>3</sup>, Stephan V. Roth<sup>3,4</sup> and Peter Muller-Buschbaum<sup>1,5</sup>; <sup>1</sup>Technische Universität München, Germany; <sup>2</sup>Ludwig-Maximilians-Universität München, Germany; <sup>3</sup>Deutsches Elektronen-Synchrotron, Germany; <sup>4</sup>KTH Royal Institute of Technology, Sweden; <sup>5</sup>Heinz Maier-Leibnitz-Zentrum, Germany

Metal halide perovskites have shown a promising future for application in field-effect transistors, light-emitting diodes, sensors, solar cells, and photodetectors due to their excellent optic-electrical properties. Among the excellent properties of perovskites, for example, strong absorption, the long diffusion length of photo-generated charge carriers and low binding energies make it possible to realize next-generation solar cells with 25.2% power conversion efficiency (PCE) in a decade. At the same time, perovskite solar cells (PSCs) have shown a powerful photovoltaic application for replacing silicon solar cells not only due to high PCE but also because of its low processing costs. Despite such advantages, the application of PSCs is



currently limited by combining high performance and operational stability, because the PCE of PSCs can degrade due to the presence of temperature, light, humidity, and oxygen. So far, the degradation research on PSCs is carried out without having an established standard protocol. The microscopic degradation mechanisms are not clear under operating conditions upon suggested inert atmospheres based on the International Summit on Organic Photovoltaic Stability protocols. Therefore, it is necessary to establish an improved standard protocol for the long-term degradation of PSCs.

In this respect, we investigate the degradation processes of PSCs under both, AM 1.5G and different atmosphere conditions (vacuum and nitrogen) with in-operando grazing incidence wide-angle X-ray scattering (GIWAXS) and grazing incidence small-angle X-ray scattering (GISAXS). With these approaches, we find that mixed cations lead mixed halides lattice exhibit the effect of photostriction when being operated in different atmospheres. In addition, the nature of photostriction can help the phase segregation of halide perovskites. Pressure conditions can suppress this photostriction behavior. Theoretical calculations based on density functional theory confirm that lattice photostriction behavior can suppress phase segregation induced by thermodynamic driving forces. A standard protocol is suggested based on our findings.

#### **F.EL08.21.05**

**Late News: Study of the Formation of Different Electron Transport Layer (ETL) Materials and Their Impacts on Perovskite Solar Cell (PSC) Performance** [Luisa Pan](#)<sup>1</sup>, Pranati Patnam<sup>2</sup>, Benjamin Roitman<sup>3</sup>, Yifan Yin<sup>4</sup>, Yuchen Zhou<sup>4</sup>, Miriam H. Rafailovich<sup>4</sup> and Chang-Yong Nam<sup>5</sup>; <sup>1</sup>The Harker School, United States; <sup>2</sup>Herricks High School, United States; <sup>3</sup>SAR High School, United States; <sup>4</sup>Stony Brook University, The State University of New York, United States; <sup>5</sup>Brookhaven National Laboratory, United States

Perovskite solar cells (PSC) are believed to be the core of next-generation solar cells due to their rapidly increasing efficiency and popularity as an alternative energy source to fossil fuels. However, the interfacial contact between the electron transport layer (ETL) and the perovskite layer in the cell often results in problems of hysteresis. This research investigates different ETL materials to remedy hysteresis in organic-inorganic CH<sub>3</sub>NH<sub>3</sub>PbI<sub>3</sub> (MAPbI<sub>3</sub>) PSCs. Compact TiO<sub>2</sub> (c-TiO<sub>2</sub>), SnO<sub>2</sub> (0.1M and 0.2M), and mesoporous TiO<sub>2</sub> (m-TiO<sub>2</sub>) (1:4 and 1:6 w:w) were deposited as the chosen ETL materials via spin-casting and followed by high-temperature annealing. The PSC devices were built using FTO glass, MAPbI<sub>3</sub>, and gold electrodes (80nm).

Scanning electron microscopy (SEM) was utilized to take cross-sectional images of the solar cell after depositing the perovskite layer. Higher values in the precursor ETL solution concentration correlated with increased ETL thickness. Qualitative analysis of the c-TiO<sub>2</sub>/m-TiO<sub>2</sub> bilayer SEM image demonstrated that the perovskite layer also effectively diffused into the porous m-TiO<sub>2</sub>, which increased the interfacial contact between the perovskite and the ETL. Although the control c-TiO<sub>2</sub> had a power conversion efficiency (PCE) of 14.5%, the sample had a hysteresis index of 0.400. In comparison, the 34mM TiO<sub>2</sub> sample had a PCE of 11.9% with a more desired hysteresis index of 0.034. The m-TiO<sub>2</sub> bilayer sample, albeit having a PCE of 6.8%, had a hysteresis index of 0.121, suggesting that the mesoporous layer aided in reducing the hysteresis index of the original c-TiO<sub>2</sub> ETL.

We gratefully acknowledge support from the Louis Morin Charitable Trust.

#### **F.EL08.21.06**

**Late News: Ultralong Micro-Belts of Luminescent Lead Halide-Based Perovskites** [Fnu Parul](#); Indian Institute of Technology Roorkee, India

Ultralong micro-belts of MAPbI<sub>3</sub> show bright and stable fluorescence in solution. Luminescent perovskites have been synthesized through centrifugation of a solution-processed with a ligand-assisted reprecipitation technique (LARP). All electron spectroscopic analysis provided evidence for the stacking of nanocrystals as bundles of self-assembled micro-belts. Under an applied bias, migration of free charge carriers through the long axis is feasible. Thus, long micro-belts are promising channel materials for two-electrode nanodevices for good electrical conductivity.

#### **F.EL08.21.07**

**Late News: Compositional Effect on Water Adsorption on Metal Halide Perovskites** [Qihua Li](#), Zehua Chen, Ionut Tranca, Silvia Gaastra-Nedea, David Smeulders and Shuxia Tao; Eindhoven University of Technology, Netherlands

The moisture-induced instability of metal halide perovskites is one of the major challenges for perovskite devices. Although compositional engineering has been widely employed to improve the overall stability of perovskites, its effect on the moisture-induced instability received little attention. Here, we systematically study the interaction of water with the surfaces of primary perovskites, AMX<sub>3</sub> (A<sup>+</sup> = MA<sup>+</sup>, FA<sup>+</sup>, Cs<sup>+</sup>; M<sup>2+</sup> = Pb<sup>2+</sup>, Sn<sup>2+</sup>; X<sup>-</sup> = I<sup>-</sup>, Br<sup>-</sup>), by using Density Functional Theory (DFT) calculations and comprehensive chemical bonding analysis. We reveal that the hydrophilic group NH<sub>3</sub><sup>+</sup> of MA<sup>+</sup> cation

may be the cause for instability issues. We find that the adsorption of water on FAPbI<sub>3</sub> and CsPbI<sub>3</sub> are much weaker than on MAPbI<sub>3</sub> due to the less polarity of FA<sup>+</sup> and Cs<sup>+</sup>. When exchanging M<sup>2+</sup> cations, water adsorption on MASnI<sub>3</sub> is also less energetically favorable than on MAPbI<sub>3</sub> because of the weaker ionic interaction of H<sub>2</sub>O-MASnI<sub>3</sub>. When exchanging X<sup>-</sup> anion, water adsorption on MAPbBr<sub>3</sub> is slightly weaker than on MAPbI<sub>3</sub> due to the slightly weaker covalent interaction of H<sub>2</sub>O-MAPbBr<sub>3</sub>. Our results present a comprehensive understanding of the compositional effect on the interactions of water with perovskites and provide rational design strategies to improve their stability against moisture via compositional engineering.

#### F.EL08.21.08

**Late News: Unified Thermodynamic Theory for Light-Induced Phase Separation in Mixed Halide Perovskites** [Zehua Chen](#)<sup>1</sup>, Geert Brocks<sup>2</sup>, Peter Bobbert<sup>1</sup> and Shuxia Tao<sup>1</sup>; <sup>1</sup>Eindhoven University of Technology, Netherlands; <sup>2</sup>University of Twente, Netherlands

In the dark and at room temperature most mixed halide perovskites are thermodynamically stable. Under illumination, however, funneling of photo-excited carriers to a phase with a lower band gap than the parent phase leads to halide demixing. This is problematic for the application of mixed halide perovskites in solar cells. Here, we present a unified thermodynamic theory for this light-induced phase separation and apply it to five mixed iodine-bromine perovskites. Under illumination, the spinodals separating the metastable and unstable regions in the composition-temperature phase diagrams show an upward shift in temperature, while the binodals separating the stable and metastable regions acquire an additional branch signaling the nucleation of a low-band gap iodine-rich phase. We find that the threshold illumination intensity is mainly governed by the band gap difference of the parent and iodine-rich phase. Partial replacement of organic cations by cesium reduces this difference and therefore has a stabilizing effect.

#### F.EL08.21.09

**Late News: Charge Carrier Dynamics in Two-Dimensional Hybrid Perovskites—Impact of Spacer Cations** [Dibyajyoti Ghosh](#); Los Alamos National Laboratory, United States

Two-dimensional (2D) halide perovskites are promising materials for environmentally stable next-generation optoelectronic device applications. However, there is very little atomistic understanding of the charge carrier dynamics at ambient conditions for these materials, limiting the possibilities to tune their optoelectronic performances through compositional engineering routes. *Here, by combining nonadiabatic molecular dynamics with time-domain density functional theory methods at room temperature, we study the dominant non-radiative carrier recombination and dephasing processes in monolayered lead halide perovskites.* Our systematic study demonstrates that performance-limiting nonradiative carrier recombination processes greatly depend on the electron-phonon interactions induced by structural fluctuations and instantaneous charge localization in these materials. *The stiffer interlayer packing in presence of selectively chosen spacer cations (benzene ring or cyclic dication based), which separates the lead iodide slabs, reduces the thermal fluctuations in these 2D-perovskites to a greater extent.*<sup>[1-2]</sup> These reduce the inelastic electron-phonon scattering and enhance the photogenerated charge carrier lifetime in layered perovskites making them suitable for various optoelectronic devices. The computational insights gained from these studies allow us to outline a set of robust design principles for 2D halide perovskites to strategically tune their optoelectronic properties.

#### Reference:

1. Ghosh *et al.* J. Phys. Chem. Lett, **2020**, 11, 2955
2. Ghosh *et al.* J. Mater. Chem. A, **2020**, Just Accepted (DOI: 10.1039/D0TA07205B)

#### F.EL08.21.12

**Late News: Synthesis, Photocatalytic Properties and Phase Stability Studies of Full Inorganic CsPbBr<sub>3</sub> and CsPb<sub>2</sub>Br<sub>5</sub> Perovskites** [Anna L. Pellegrino](#)<sup>1,2</sup> and Graziella Malandrino<sup>1,2</sup>; <sup>1</sup>Università degli Studi di Catania, Italy; <sup>2</sup>INSTM, Italy

The compounds belonging to the family of perovskites show a great variety of mechanical, magnetic and optical properties, and for these reasons are nowadays key materials for many technologies, including piezoelectrics, photovoltaic solar cells and photocatalytic systems.

Among perovskites, the most studied crystal structure ABX<sub>3</sub> for photocatalysis and photovoltaic applications is composed of an organic/inorganic compounds made of: monovalent cation A = methylammonium (MA: CH<sub>3</sub>NH<sub>3</sub><sup>+</sup>); formamidinium (FA: CH(NH<sub>2</sub>)<sub>2</sub><sup>+</sup>); a divalent metal cation B = Pb<sup>2+</sup>, Sn<sup>2+</sup>; and an halide anion X = I<sup>-</sup>; Br<sup>-</sup>; Cl<sup>-</sup>. These hybrid lead-based materials have excellent properties and contain elements that are both cheap and abundant. However, they tend to partially decompose when exposed to air, water, ultra-violet light, or heat. For these reasons, several substitutions have been attempted to improve the properties and performances of these materials. One route to improve the stability of these structures is to explore the all-inorganic perovskite systems and thus finding alternatives to replace organic components. Particularly, our attention is

devoted to the all-inorganic perovskites, i.e. CsPbBr<sub>3</sub> and CsPb<sub>2</sub>Br<sub>5</sub>, which do not have any labile or expensive components and show remarkable stability. Furthermore, unlike the hybrid structures, the entire fabrication process of all-inorganic analogous materials can be operated in ambient atmosphere without humidity control systems. Additionally, CsPbX<sub>3</sub> (X = Cl, Br, and I) perovskite family shows high performances for photocatalytic and photo-electrochemical degradation processes of different organic dye compounds, and are also exceptional candidates as photocatalysts for organic reactions. Among the different strategy developed for their synthesis, the surfactants-based solution route is widely applied, which also allows to control the stability and the growth kinetics according to the surface chemical phenomenon and the solubility equilibrium. Herein we report a novel synthetic strategy, which represents a facile, one-step, low-temperature and surfactant free approach to the synthesis of Cs-Pb-Br microcrystals, using Cs and Pb β-diketonate metallorganic complexes. The present precipitation approach represents an innovative and interesting strategy of synthesis, which avoids the use of surfactant species and toxic solvents, and, taking the advantages of the β-diketonate metalorganic Cs and Pb precursors reactivity, it allows, reproducibly and selectively, the synthesis of CsPbBr<sub>3</sub> and CsPb<sub>2</sub>Br<sub>5</sub> microcrystals. Structural, morphological and compositional analyses of the final products, addressed through X-ray diffraction (XRD), field-emission scanning electron microscopy (FE-SEM) and Energy Dispersive X-ray (EDX) analysis, show the formation of pure and stable CsPbBr<sub>3</sub> or CsPb<sub>2</sub>Br<sub>5</sub> systems characterized by squared microcrystals, with a grain size up to 3 μm. The stability of the two different phases has been tested as a function of heating treatment and UV exposure as well. Moreover, as a proof-of-concept, the photocatalytic properties of degradation processes have been tested using organic dye solutions, showing high degradation yield up to 70% under UV lamp (λ=360 nm).

#### F.EL08.21.13

**Late News: Synthesis of Lead-Free All-Inorganic Cs<sub>3</sub>Sb<sub>2</sub>Br<sub>9</sub> Perovskite Microplates by Two-Step Chemical Vapor Deposition for Fast Response Visible Light Photodetector Application** [Sujit Kumer Shil](#)<sup>1,2</sup>, Fei Wang<sup>1</sup>, Mohammad Kamal Hossain<sup>1</sup>, Cheuk Kai Gary Kwok<sup>1</sup>, Kingsley O. Egbo<sup>1</sup>, Ying Wang<sup>1</sup> and Kin Man Yu<sup>1,1</sup>; <sup>1</sup>City University of Hong Kong, Hong Kong; <sup>2</sup>Khulna University of Engineering & Technology, Bangladesh

Lead-based halide perovskites (CsPbX<sub>3</sub>, X=Cl, Br, I) are well-known for their attractive properties which make them suitable materials for many optoelectronic devices. But the toxicity of lead (Pb) undoubtedly hinders the development and commercialization of these devices. Therefore, Pb-free, environmental friendly all-inorganic halide perovskites are now the subject of enormous interest to the scientific community. It has been suggested that antimony (Sb) can be a possible replacement of Pb (Cs<sub>3</sub>Sb<sub>2</sub>X<sub>9</sub>) in these inorganic halide perovskites. Until now Sb-based all-inorganic perovskites have been synthesized by solution processes but properties are still inferior to Pb-based materials. However, due to the low melting point of Sb halides, synthesis of high quality Cs<sub>3</sub>Sb<sub>2</sub>X<sub>9</sub> using chemical vapor process is still a challenge. In this work, we present a report on the synthesis and properties of Pb-free all-inorganic Cs<sub>3</sub>Sb<sub>2</sub>Br<sub>9</sub> perovskite microplates by a two-step chemical vapor deposition (CVD) approach. In step-I, CsBr powder was vaporized at 530°C at a pressure of 4.8 Torr under 50 sccm of Ar flow for 10 minutes in a single-zone CVD furnace. In step-II, due to low melting point, SbBr<sub>3</sub> powder was vaporized at 90°C under 15 sccm of Ar flow while the pressure and holding time were remained same as step-I. Substrates were placed at 22 cm downstream from the center. Finally Cs<sub>3</sub>Sb<sub>2</sub>Br<sub>9</sub> microplates with average size 20 μm were obtained after annealing the as-grown materials at 140 °C for 25 minutes. XRD analysis of the microplates shows the pure phase crystalline nature of the Cs<sub>3</sub>Sb<sub>2</sub>Br<sub>9</sub> perovskite structure. The optical band gap was measured by spectroscopic ellipsometry to be 2.6 eV. The UV-vis absorption spectrum revealed the exciton absorption peak at around 2.82 eV. Simple photoconductive devices fabricated using these microplates exhibit current on/off ratio of 10<sup>2</sup> upon 450 nm photon irradiation with a fast response of rise and decay time down to 79 ms and 28 ms, respectively. All these results clearly suggest the technological potential of inorganic lead-free Cs<sub>3</sub>Sb<sub>2</sub>Br<sub>9</sub> perovskite microplates for future optoelectronic devices.

#### F.EL08.21.15

**Late News: Interfacial Engineering by Double Decked Electron and Hole Extraction Layers for Reproducible and Thermally Stable Perovskite Solar Cells.** [Shivam Singh](#) and Dinesh Kabra; Indian Institute of Technology Bombay, India

**Abstract:** We present an interfacial engineering method to fabricate an efficient and thermally stable MAPbI<sub>3</sub> based perovskite solar cell with a double decked hole (*H*) and electron (*E*) extraction layers (EL) in an inverted (*p-i-n*) architecture. The double HEL film is fabricated by thermal evaporation of MoO<sub>3</sub> and spin-coating of poly(3,4-ethylene dioxy-thiophene)-poly(styrene sulfonate) (PEDOT:PSS). The double EEL is formed by spin-coating of phenyl-C61-butyric acid methyl ester (PC<sub>61</sub>BM) and bathocuproine (BCP). The role of BCP as a buffer layer is quite established in the community to prevent the formation of metal induced charge state at the perovskite- EEL interface. Despite of presence of BCP interlayer, the thermal stability of *p-i-n* architecture still suffers. We observed that the underneath MoO<sub>3</sub> layer provides an improved morphology for perovskite film and reduces the shunt path. However, the BCP buffer interlayer not only passivates the defects at the perovskite- EEL interface and but also helps to plenaries the thin-films for better contact with Ag. Thus, double EEL and

HEL facilitate better charge collection at the interfaces and shows improved power conversion efficiency (PCE) of ~15%. Besides the improved PCE, double EEL and HEL based structures also provide an approach to have better reproducibility and high thermal stability of perovskite solar cells. We also address the issue of area dependent efficiency and explore the reasons behind the increased efficiency of smaller area devices. We believe reproducibility, stability and area dependence are the most important aspects for current perovskite PV research and thus this study will provide an important insight for further development.

**Keywords:** MAPbI<sub>3</sub>, double extraction layer, thermal stability, solar cells, BCP, MoO<sub>3</sub>

#### References:

1. S. Singh, R. Shourie, and D. Kabra, Efficient and thermally stable CH<sub>3</sub>NH<sub>3</sub>PbI<sub>3</sub> based perovskite solar cells with double electron and hole extraction layers. *J. Phys. D: Appl. Phys.* **2019**, 52, 255106.
2. Y. Zhao, A. M. Nardes and K. Zhu, Effective hole extraction using MoO<sub>x</sub>-Al contact in perovskite CH<sub>3</sub>NH<sub>3</sub>PbI<sub>3</sub> solar Cells. *Appl. Phys. Lett.* **2014**, 104 213906.

#### F.EL08.21.16

##### Late News: GFN1-xTB Method for a Fast Calculation of Metal Halide Perovskites Properties for Solar Cells

**Applications** Jose Manuel Vicent-Luna, Sofia Apergi and Shuxia Tao; Eindhoven University of Technology, Netherlands

Metal halide perovskites (MHPs) for perovskite solar cells (PSCs) have gained great attention in just few years due to their rapid increase of photoconversion records of efficiency. In addition, MHPs exhibit a competitive fabrication cost together with a simple route to synthesize. Due to these facts, PSCs are recognized by scientists as a promising technology with enormous potential in the energy market. However, it is well known that many factors cause the degradation of PSCs, thus, industrial applications are critically hampered by instability issues.

Nowadays, experimental and theoretical researchers are investigating many possible alternatives to increase the stability of PSCs. In this context, computational techniques are being extremely useful to understand the properties of MHPs at microscopic level that cause instability of the material. Density functional theory (DFT) calculations are the key method for studying material properties, but the high computational cost limits the study to small systems and short time-scales. Classical simulations seem to be an option to overcome these limitations, but they suffer from other drawbacks such as classical simulations cannot describe electrons and chemical reactions. The study of many applications of MHPs requires the simultaneously modeling of electrons and ions in relatively large systems, sometimes not computationally affordable by the standard techniques. Therefore an intermediate approach between DFT and classical simulations is often desired. In this regard, semi-empirical Quantum Mechanics methods, such as density functional tight binding (DFTB), combine the functionalities of describing both electrons and ions. Traditional DFTB methods are based on a simplification of the Kohn-Sham DFT total energy, using pre-computed interactions of element pairs, considerably reducing the computational cost. However, this parameterization lacks of transferability and is limited to a number of elements. A new extended tight binding method called GFN1-xTB has been recently developed to cover all the elements of the periodic table. This method was designed for the fast calculation of diverse physicochemical properties of systems of a few thousand atoms and has the advantageous of maintaining high accuracy and a limited number of parameters which can be refined for the study of a given application.

The performance of GFN1-xTB is benchmarked for a set of MHPs and compared with density functional theory calculations. We study organic and inorganic MHPs with formula ABX<sub>3</sub>, with A = MA, FA, and Cs; B = Pb and Sn; X = I, Br, and Cl, being a total of 18 MHPs with cubic, tetragonal, and orthorhombic forms. We included the computation of structural, vibrational, and optoelectronic properties of these semiconductors. This work aims to provide a general overview of the performance of GFN1-xTB for the fast computation of the main features of MHPs. Our results indicate that this method can describe the targeted features of the MHPs, but performs worse for geometry relaxation calculations. We also identified the drawbacks of the method for particular compositions of MHPs, which hamper its use for solar cell applications.

#### F.EL08.21.17

**Late News: Lone-Pair Driven Ferroelectric and Piezoelectric Response of Germanium Halide Perovskites CsGeX<sub>3</sub> (X = Cl, Br, and I)** Jiwoo Lee<sup>1</sup>, Young-Kwang Jung<sup>1</sup> and Aron Walsh<sup>1,2</sup>; <sup>1</sup>Yonsei University, Korea (the Republic of); <sup>2</sup>Imperial College London, United Kingdom

While much attention has been paid to halide perovskites based on Pb and Sn cations on the B-site, Ge compounds offer a distinct combination of structure and properties. All three cations feature the same s<sup>2</sup> lone pair configuration; however, the stereochemical activity varies in each case. We performed a computational analysis via density-functional-theory and Berry

phase calculations of the CsGeX<sub>3</sub> (X = Cl, Br, I) series. Our motivation is to clarify the existence and magnitude of ferroelectricity and piezoelectricity, which has important technological consequences such as polar nanodomains that can reduce the recombination of light-excited electron-hole pairs and extend the carrier lifetime [2]. The explanation for the origin of spontaneous polarization in Ge halide perovskites in terms of an on-site second-order Jahn-Teller effect has not been hitherto investigated [3]. In this work, we investigate the role of halide anions in spontaneous polarization within the modern first-principles theory of polarization. Our calculation results show that interaction between Ge lone-pair electrons and halogen *p*-orbital mainly determines the depth of the ferroelectric double well and the spontaneous polarization strength with Cl > Br > I. Further exploration of lone pair systems offers an exciting pathway to design novel photoelectric devices [4,5].

[1] Lead-free germanium iodide perovskite materials for photovoltaic applications. *J. Mater. Chem. A*, **3**, 23829–23832 (2015); <https://doi.org/10.1039/C5TA05741H>

[2] Atomistic origins of high-performance in hybrid halide perovskite solar cells. *Nano Lett.* **14**, 2584–2590 (2014); <https://doi.org/10.1021/nl500390f>

[3] Resolving the Physical Origin of Octahedral Tilting in Halide Perovskites. *Chem. Mater.* **28**, 4259–4266 (2016); <https://doi.org/10.1021/acs.chemmater.6b00968>

[4] Stereochemistry of post-transition metal oxides: revision of the classical lone pair model. *Chem. Soc. Rev.* **40**, 4455–4463 (2011); <https://doi.org/10.1039/C1CS15098G>

[5] The underappreciated lone pair in halide perovskites underpins their unusual properties. *MRS Bulletin.* **45**, 467–477 (2020); <https://doi.org/10.1557/mrs.2020.142>

#### F.EL08.21.19

**Late News: A Reactive Force Field for Large Scale Simulations of Metal Halide Perovskites** [Mike Pols](#)<sup>1,2</sup>, Jose Manuel Vicent-Luna<sup>1,2</sup>, Ivo Filot<sup>3,2</sup>, Adri v. Duin<sup>4</sup> and Shuxia Tao<sup>1,2</sup>; <sup>1</sup>Materials Simulation and Modelling, Department of Applied Physics, Eindhoven University of Technology, Netherlands; <sup>2</sup>Center for Computational Energy Research, Eindhoven University of Technology, Netherlands; <sup>3</sup>Laboratory of Inorganic Materials Chemistry, Schuit Institute of Catalysis, Eindhoven University of Technology, Netherlands; <sup>4</sup>Department of Mechanical Engineering, The Pennsylvania State University, United States

Metal halide perovskites have been the focus of many computational studies over the past few years. The bulk of these investigations were done using methods based on quantum mechanics (QM). However, the computational cost of QM methods is high, severely limiting the length and time scales of the systems that can be investigated. Molecular dynamics (MD) simulations have been successfully applied to simulate larger material systems and at longer time scales by making use of classical force fields (CFF). Nonetheless, the predefined connectivity in CFF makes them unsuited for the simulation of chemical reactions. A reactive force field (ReaxFF) is an extension to CFF by including a dynamic bond order that is calculated from the interatomic distances and allows for the simulation of bond breaking and formation. In this presentation, I will outline our progress in the creation of the first ReaxFF for halide perovskites, CsPbI<sub>3</sub>.

### SYMPOSIUM F.EN01

---

Emerging Dielectric Materials—Applications in Energy Transmission, Storage and Conversion  
November 21 - December 3, 2020

Symposium Organizers  
Jinbo Bai, CNRS ECPaaris  
Xingyi Huang, Shanghai Jiao Tong University

\* Invited Paper

SESSION F.EN01.07: Live Keynote I: Emerging Dielectric Materials—Applications in Energy Transmission, Storage and Conversion

Session Chairs: Jinbo Bai, Xingyi Huang, Qi Li and Linda Schadler  
Wednesday Morning, December 2, 2020  
F.EN01

**8:00 AM \*F.EN01.01.03**

**High Energy Density and High Temperature Multilayer Polymer Films for Electric Vehicle Applications** Lei Zhu and Eric Baer; Case Western Reserve University, United States

Current state-of-the-art biaxially oriented polypropylene (BOPP) film capacitors suffer from low temperature rating ( $<85\text{ }^{\circ}\text{C}$ ) and low energy density. At Case Western Reserve University, we have developed a novel multilayer film technology to meet the stringent requirements for next-generation dielectric film capacitors for electric vehicles. By multilayering a high breakdown strength polymer such as polycarbonate (PC) with a high dielectric constant polymer such as poly(vinylidene fluoride) (PVDF), we have achieved high breakdown strength ( $>600\text{ MV/m}$ ), high energy density at breakdown ( $16\text{ J/cm}^3$ ), and relatively low dielectric dissipation factor ( $\tan\delta < 0.005$ ) and hysteresis loss (15% loop area). In this presentation, we will identify and discuss fundamental issues for these multilayer dielectric films, which include polarization of amorphous and crystalline dipoles, polarization of impurity ions, and interfacial polarization to achieve enhanced breakdown strength and lifetime at high temperatures.

**8:20 AM \*F.EN01.01.05**

**Stabilization of High Energy Density Over a Wide Temperature Range by Blend Structure in Ferroelectric Polymers** Yongbin Liu and Jinghui Gao; Xi'an Jiaotong University, China

Achieving stable energy density at elevated temperature remains a great challenge for ferroelectric polymer-based capacitors. It seems that the emerging ferroelectric polymers (e.g. poly(vinylidene fluoride) (PVDF) and its copolymers), which possess spontaneous polarization and large permittivity, provide a promising solution to meet the ever-increasing requirement for high energy density. Nevertheless, the state-of-the-art PVDF-based ferroelectric polymer usually exhibits mediocre temperature stability in energy storage performance, which cannot fully satisfy the applications at elevated temperature caused by the energy consumption or nearby heat sources.

In this work, we report a strategy for stabilizing high energy density of ferroelectric polymer (PVDF) over a wide temperature range by blending with a miscible high- $T_g$  polymer (polymethyl methacrylate (PMMA)). The blending material forms an alternating lamellar structure consisting of high-polarization crystalline regions and strengthened amorphous regions. It is found that this special morphology is able to confine the constructional change of stacked lamellar structure at elevated temperatures. Accordingly, the associated energy storage performances, including energy density, energy storage efficiency and breakdown strength, are remarkably enhanced in a wide temperature range (30 to  $70^{\circ}\text{C}$ ). At  $70^{\circ}\text{C}$ , the energy density and efficiency of PVDF/PMMA(80/20) is  $9.8\text{ J cm}^{-3}$  and 67.8%, which surpasses most neat ferroelectric polymers at such an elevated temperature. This work reveals the relationship between lamellar confinement of polymer blend and electric properties under temperature variation, and might provide a valid approach to attain high energy density and temperature stability in ferroelectric polymers.

**8:40 AM \*F.EN01.01.06**

**Strategies of Enhancing Electric Breakdown Strength of Nanocomposites by Designing Fillers with Special Microstructure Structure** Shuhui Yu, Junyi Yu and Rong Sun; Shenzhen Institutes of Advanced Technology, Chinese Academy of Sciences, China

As one of the most important renewable energy storage technologies, film capacitors have been used in modern electronics and power industries such as wearable electronics, hybrid vehicles, and other fields due to their high power density, long working hours, and environmental friendliness. With the development of electronic devices toward miniaturization and high

performance, there is an urgent need for dielectric materials with high energy storage density. A high breakdown strength ( $E_b$ ) is crucial for dielectric materials to ensure reliability of electric circuits and to improve electrostatic energy storage density.  $E_b$  is the result of space charge movement in the dielectrics under the applied electric field. Effectively reducing the density of charge carriers in the dielectrics is one of the keys to enhancing  $E_b$ . In this study, hybrid nanoparticles with special physical microstructure were designed and fabricated. When they were used as fillers, these particles possessing isoelectronic traps or heterojunction have proved efficient in confining space charge carriers generated under applied electric field and meanwhile suppressing their movement through the whole polymer system. As a result, electrical conductivity was reduced and  $E_b$  was enhanced significantly, leading to improved energy storage density.

**9:00 AM \*F.EN01.07.01**

**Triboelectric Charging Mechanisms of Polymers** Andris Sutka; Riga Technical University, Latvia

Knowing the polymer triboelectrification mechanisms is the key to provide high-performance triboelectric nanogenerators for mechanical energy harvesting from movement or, vice versa, to eliminate charge accumulation on the surface for safety. Moreover, the triboelectric surface charge has attracted significant interest among scientists recently for particle separation and liquid droplet transport, as well as nanoparticle deposition and surface patterning.

The three main mechanisms considered for polymer electrification are (i) electron transfer [1], (ii) heterolytic covalent bond break and material transfer [2], and (iii) ion transfer [3]. The ion transfer, where ions are separated between water adsorbate layers on contacted polymers, seems not the dominating mechanism as the polymer triboelectrification has been observed in the complete absence of water and between identical materials which should exhibit the same affinity between cationic and ionic species in water. In the past few years, the debate has concentrated on electron transfer and covalent bond breaking as possible dominating polymer triboelectrification mechanisms.

Recently a vast number of triboelectrification experiments has been performed and reported for various polymers with the different structural state, surface adhesion, and morphology. The experimental results indicate that the triboelectrification mechanism for polymer insulators is heterolytic covalent bond cleavage (heterolysis or heterolytic fission) alongside material transfer [4-6]. The surface charge increases with decreasing cohesion energy [4] or increasing surface adhesion [5]. A dramatic three orders of magnitude increase in surface charge when passing the transition temperature from a glassy to a rubbery state also has been observed due to the adhesion, softness, and deformation increases, thus enhance the covalent bond cleavage, material transfer, and surface charge formation [6].

Herein we are highlighting these aspects and illuminating the pathways to enhance the triboelectrification avoiding expensive and complicated nanostructuring approaches.

References:

- [1] J. Chen and Z. L. Wang, Reviving vibration energy harvesting and self-powered sensing by a triboelectric nanogenerator, *Joule*, 1, 480-521, (2017).
- [2] H. T. Baytekin, A. Z. Patashinski, M. Branicki, B. Baytekin, S. Soh and B. A. Grzybowski, The mosaic of surface charge in contact electrification, *Science*, 333, 308, (2011).
- [3] L. S. McCarty and G. M. Whitesides, Electrostatic charging due to separation of ions at interfaces: contact electrification of ionic electrets, *Angew. Chem., Int. Ed.*, 47, 2188-2207, (2008).
- [4] A. Šutka, K. Mālnieks, L. Lapčinskis, P. Kaufelde, A. Linarts, A. Berzina, R. Zābels, V. Jurkāns, I. Gornevs, J. Blums and M. Knite, The role of intermolecular forces in contact electrification on polymer surfaces and triboelectric nanogenerators. *Energy Environ. Sci.*, 12, 2417-2421, (2019).
- [5] L. Lapčinskis, K. Mālnieks, J. Blums, M. Knite, S. Oras, T. Käämbre, S. Vlassov, M. Antsov, M. Timusk and A. Šutka, The Adhesion-Enhanced Contact Electrification and Efficiency of Triboelectric Nanogenerators, *Macromol. Mater. Eng.*, 305, 1900638, (2020).
- [6] A. Šutka, A. Linarts, K. Mālnieks, K. Stiprais and L. Lapčinskis, Dramatic increase in polymer triboelectrification by transition from a glassy to rubbery state, *Mater. Horiz.*, 7, 520-523, (2020).

**9:20 AM \*F.EN01.05.05**

**The Preparation and Dielectric Properties of 2D Nano-Sheets Materials and Composites Based on Electrospinning** Hua Deng; Sichuan University, China

Two dimensional dielectric fillers have been considered to serve as high performance fillers to enhance both the dielectric constant and breakdown strength of various dielectric polymer composites. Nevertheless, the fabrication of these 2D fillers is quite often complicated, and usually rely on the nature availability of these materials. Herein, we demonstrate systematic study on the fabrication of 2D TiO<sub>2</sub> nanofillers through tuning various processing condition of electrospinning. This research work was carried out to investigate the effects of different solution formulas and electrospinning conditions on the

morphology of the spinning fibers. The influence of calcination temperature on the preparation of dielectric fillers was studied, and it was applied to the preparation of dielectric composite materials based on PVDF and PI. The energy density of two-dimensional nano-sheets dielectric fillers was investigated, and shows high dielectric constant, high Effects, high breakdown strength and low dielectric loss. The extended application of 2D lamellar fillers in polyimide system under high temperature conditions is further discussed achieving an energy density of 3 J/cm<sup>3</sup> at 150 degree C; 3.5 J/cm<sup>3</sup> at 100 degree C; a charge-discharge efficiency of around 90%. This could provides a theoretical and technical guidelines for the practical application.

**9:40 AM \*F.EN01.02.08**

**Rational Design of Dielectric Materials for Flexible Capacitive Pressure Sensing Coatings** Jianing Wu, Tianyu Shao and Zhuo Li; Fudan University, China

Flexible pressure sensors are the basic components for many different applications, such as electronic skins, robotics, health-monitoring devices, and human-machine interfaces. Among different working mechanisms, capacitive pressure sensors are widely-used owing to their low energy consumption, simple structure, and high reliability. Pressure sensors in the form of coatings have the advantages of facile applications on various complex surfaces because of the flowability before solidification, capability for large scale production, and low cost. But how to prepare pressure sensing coatings to meet the requirements for different applications remains to be addressed. This talk covers our recent work to enhance the performances of pressure sensing coatings through the rational design of dielectric materials.

Firstly, I will discuss a highly sensitive capacitive pressure sensing coating using thermally expandable microspheres/polydimethylsiloxane (PDMS) composite as the dielectric layer. The microspheres can expand during the thermal curing process of PDMS, which greatly enhance the compressibility and thus increase the sensitivity of the pressure sensors. At the same time, it achieves a broad pressure sensing range from 10 Pa to 4.5 MPa and also features low hysteresis and good stability against repeated compression.

Secondly, I will discuss a strategy to achieve linear response of capacitive pressure sensor over a broad sensing range. Conventional capacitive pressure sensors usually exhibit a highly non-linear response as the sensitivity drops dramatically towards high pressure. Our strategy employs a percolative composite as the dielectric layer. The fast increase in dielectric constant during compression can compensate the sensitivity drop from the decreased compressibility, leading to a linear response. Owing to the nature of polymer composite, its dispersion not only can be conformally coated on surfaces with various complex shapes, but also can be molded into films with surface microstructures to achieve a unique combination of high sensitivity and linear response over a wide pressure sensing range.

SESSION F.EN01.08: Live Keynote II: Emerging Dielectric Materials—Applications in Energy Transmission, Storage and Conversion

Session Chairs: Jinbo Bai, Qi Li and Linda Schadler

Thursday Afternoon, December 3, 2020

F.EN01

**3:00 PM \*F.EN01.04.02**

**Electrical and Electromechanical Reliability of Lead Zirconate Titanate Piezoelectric Films** Betül Akkopru-Akgün<sup>1</sup>, Kathleen Coleman<sup>1</sup>, Wanlin Zhu<sup>1</sup>, Raul Bermejo<sup>2</sup> and Susan E. Trolier-McKinstry<sup>1</sup>; <sup>1</sup>The Pennsylvania State University, United States; <sup>2</sup>Montanuniversitaet Leoben, Austria

Use of dielectric materials such as lead zirconate titanate films for dielectric energy storage or for piezoelectric applications necessitates that they be able to sustain high DC electric fields. This paper will describe the coupled failure mechanisms that control these lifetimes for donor-doped, acceptor-doped, and films with graded doping. Curiously, the median failure time of PZT films can be increased on doping with either donors or Mn as an acceptor. It is found that lifetimes under DC fields are dominated by a combination of oxygen vacancy migration, coupled with changes in the interface barrier heights for conduction in thin films. This was assessed through a combination of highly accelerated lifetime testing, thermally stimulated depolarization currents, impedance spectroscopy, deep level transient spectroscopy, and electron energy loss spectroscopy. The relic defect chemistry of the film, including variations in this defect chemistry at interfaces strongly influences both the failure and the asymmetry of the failure as a function of the electrical polarity. As film thickness and/or the piezoelectric coefficients rise, the critical stress required for crack initiation decreases, and the failure modes can shift to electro-



mechanically induced failure. Ball-on-three ball mechanical testing demonstrates that the critical flaw size in the failure of the stack becomes the thickness of the piezoelectric layer itself.

### 3:20 PM \*F.EN01.03.06

**Low Temperature and High-Speed Processing of Oxide Dielectric Thin Films** Julia W. Hsu; The University of Texas at Dallas, United States

Thin film oxide dielectrics boast high breakdown voltages, low leakage current densities, and high dielectric constants making them ideal for use as gate dielectrics in thin film electronics. However, to fully realize the benefit of thin film electronics, low-cost high-throughput production is necessary. This means reducing not only processing time, but also processing temperature to allow for production on plastic substrates. In this work, we discuss the effects of low temperature UV-assisted processing and high-speed photonic curing on the properties of solution-deposited oxide dielectric films. First, we show the results from exposing sol gel precursor films to UV-ozone (UVO) through a shadow mask. This process accomplishes both lowering the conversion temperature to 250 °C and direct patterning the precursor film with exposed areas converted to oxide after final annealing. We find drastically different capacitance-frequency behavior between Al<sub>2</sub>O<sub>3</sub> and ZrO<sub>2</sub> dielectrics, which in turn affects the In<sub>2</sub>O<sub>3</sub> transistors' behavior. The origins of this finding are studied through Fourier transform infrared analysis and time dependent drain current measurements. Next, we adapt photonic curing, the use short but high intensity pulses of broadband light, to selectively heat and convert ZrO<sub>2</sub> precursor films on flexible polyethylene naphthalate (PEN) substrates. Photonic curing is typically used to sinter metal nanoparticle inks into conductive metal traces on plastic substrates, but it has not previously been used to fabricate oxide thin film dielectrics on plastic substrates. We demonstrate that the conversion time is reduced from 10s minutes to < 1s and patterning using a shadow mask during photonic curing does not need subsequent thermal annealing, unlike in the UVO processing. Furthermore, by adjusting the photonic curing conditions, the oxide film can be selectively converted on top of Al electrodes, which act as selective area heat absorbers, but not on the bare PEN substrate, resulting in a self-aligned oxide pattern. We achieve a ZrO<sub>2</sub> dielectric with breakdown field of 8 MV/cm and areal capacitance of 200 nF/cm<sup>2</sup> with little frequency dispersion. Finally, we show a pathway to converting ZrO<sub>2</sub> dielectric at a roll-to-roll web speed of up to 50 m/min.

### 3:40 PM \*F.EN01.04.07

**Solid-State Cooling Devices Based on Electrocaloric Polymers** Qibing Pei; University of California, Los Angeles, United States

Electrocaloric cooling is a solid-state cooling technology, offering several advantages over traditional cooling systems, but few EC devices have been reported with high specific cooling power and high coefficient of performance (COP). We have developed solution processes to fabricate poly(vinylidene fluoride-trifluoroethylene-chlororfluoroethylene) terpolymer thin films. Various material treatment and characterizations were conducted to study and optimize the performance of the terpolymer thin films. We present several EC cooling device designs with compact and desired form factors to transfer heat between a heat source and heat sink, with the ultimate objective to pave the way for new applications that cannot be obtained using existing technologies.

### 4:00 PM \*F.EN01.04.04

**Flexible Dielectric Nanocomposites—From Power Energy Storage to Mechanical Energy Harvesting** Jinkai Yuan; Ctrde Recherch Paul Pascal, France

Our research activities on the energy-related dielectric polymer nanocomposites will be reviewed. Micro-energy storage devices are highly demanded for diverse miniaturized electronic devices. [1,2] However, making high-energy microcapacitors with currently available printing technologies remains challenging. Based on a composite material of latex polyvinylidene fluoride and polyvinyl alcohol, we created high-energy microcapacitors with inkjet printing technique. A discharged energy density of 12 Jcm<sup>-3</sup> is achieved at 550 MVm<sup>-1</sup>. [3] The printed microcapacitors demonstrate mechanical robustness and dielectric stability over time. on the other hand, it is well known that all dielectric materials have electrostriction. They have capability of changing their dielectric properties upon an external mechanical deformation. Based on this effect, we have developed giant electrostriction soft nanocomposites which can serve as an active dielectric layers in a variable capacitor to convert the vibrational mechanical energy into electricity. To make such energy harvester, we prepare an electrostrictive nanocomposite composed of reduced graphene oxide in soft polydimethylsiloxane matrix. [4] The near percolated composite exhibits a large permittivity variation in response to small strain deformation, giving rise to a giant electrostrictive coefficient  $-4.3 \times 10^{-14} \text{ m}^2/\text{V}^2$ , [5] indicating that our materials are particularly promising for harvesting mechanical energy applications. Their implementation in actual MEMS generator devices has been also investigated. [6]

## References

- [1] Z. S. Wu, X. Feng, H. M. Cheng, *Natl. Sci. Rev.* 2014, 1, 277.
- [2] M. Beidaghi, Y. Gogotsi, *Energy Environ. Sci.* 2014, 7, 867.
- [3] F. Torres-Canas, et al, *Adv. Funct. Mater.* 2019, 1901884.
- [4] J. Yuan, et al, *Nat. Commun.* 2015, 6, 8700.
- [5] J. Yuan, et al. *ACS Nano* 2018, 12, 1688-1695
- [6]. Nessler, H. et al, *Nano Energy*, 2018, 44, 1–6.

### 4:20 PM \*F.EN01.03.02

**Dielectric Materials in Semiconductor Packages** Enis Tuncer; Texas Instruments, United States

It is important to determine the dielectric characteristics of semiconductor encapsulation materials based on epoxy resins. There are several such material systems employed to protect the active silicon circuitry. Some of the important properties of the materials are their glass transition temperature, filler content and the level of water absorption which leads to reliability challenges with respect to performance and lifetime. We study changes in the properties by investigating dielectric relaxation using broadband impedance spectroscopy techniques. It is known that the dielectric relaxation in polymeric systems influenced by the presence of water, which demands special attention in sensitive applications. We will present measurement and analysis methods based on time and frequency domain techniques. It would be appreciated within the materials science community to improve material selection and performance evaluation efforts. We will also share information on the glass transition temperature estimates for a number of composites employed in semiconductor packaging.

### 4:40 PM \*F.EN01.02.01

**Atomic Scale Simulation of Charge Transport Properties of Dielectric Polymers** Mikael Unge; NKT HV Cables AB, Technology Consulting, Sweden

Sustainable energy sources – such as wind, wave and solar – are attractive for reducing CO<sub>2</sub> emissions and tackling climate change. Often these energy sources are placed at large distances from where the energy is actually needed; off-shore wind farms and desert solar parks. To transfer the electrical power from such remote locations high voltage direct current (HVDC) is the preferred technology due to lower transmission losses. In the design of high voltage component the dielectric properties of the materials used are of significant importance. The conductivity of the leakage current in and the electrical breakdown field of the dielectric material impact and limits the design. To understand how these properties are affected by the materials chemical composition and morphology, material simulation is one approach to understand these phenomena in more detail.

Material simulation methods such as density functional theory (DFT) and molecular dynamics (MD) has an increased usage in literature to study dielectric properties of materials relevant for HV components. Basic properties such as band gaps and trap states, to more challenging properties to calculate such as mobility and electrical breakdown fields are reported. An additional important area is to include material simulation methods in multiscale simulation models to incorporate phenomena on longer time and length scales possible.

In this talk we will present result from several different studies of dielectric polymers using DFT, MD and kinetic Monte Carlo (KMC). Primarily the material of interest in these studies is polyethylene (PE) which is used as insulation in HVDC cables. PE is a semi crystalline material and have a complex structure at micrometer scale. Using linear scaling DFT (LSDFT) we have investigated the electronic structure of different parts of PE morphology. Band gaps and electron localization are calculated and used to determine electronic charge transport properties. A combination of DFT, MD and KMC are used to calculate mobility in PE. A coarse grained model for hopping transport in PE is also being developed. Recently we also applied LSDFT to investigate electronic structure of another dielectric polymer, poly(ethylene oxide), which may be used as polymer electrolyte in solid state batteries. Coupling to models at longer time and length scales are discussed.

SESSION F.EN01.01: Advanced Dielectrics for Electrical Energy Storage  
On Demand Abstracts Available for Viewing Starting Saturday Morning, November 21, 2020  
F-EN01

#### 5:00 AM F.EN01.01.01

##### **Enhancing the Dielectric Breakdown Strength of Solid-State Polymer Capacitors by Chain End**

**Manipulations** Maninderjeet Singh<sup>1</sup>, Wenjie wu<sup>1</sup>, Mei Dong<sup>2</sup>, David Tran<sup>2</sup>, Karen Wooley<sup>2</sup>, Nihar Pradhan<sup>3</sup>, Dharmaraj Raghavan<sup>4</sup> and Alamgir Karim<sup>1</sup>; <sup>1</sup>University of Houston, United States; <sup>2</sup>Texas A&M University, United States; <sup>3</sup>Jackson State University, United States; <sup>4</sup>Howard University, United States

The need for high power density, flexible, pulsed power and lightweight energy storage devices requires the use of polymer film-based dielectric capacitors. The maximum energy storage density of a dielectric capacitor is directly proportional to the square of the maximum voltage that can be applied to the dielectric without causing the electrical breakdown. Theoretically, it has been shown that chain ends contribute adversely to the electrical breakdown of polymer dielectrics at high electric fields, resulting in low energy density in polymer capacitors. In this work, we enhanced the dielectric breakdown voltage and hence the energy density of the polymer capacitor by using well-ordered high molecular weight block copolymers (BCP), in which the chain ends are segregated to narrow zones. The well-ordered and easily processable amorphous BCP based capacitors exhibit an energy density more than 5 J/cm<sup>3</sup>, which is higher than that of industrially used crystalline biaxially oriented polypropylene. Cyclic homopolymers (no chain ends) and linear homopolymers having chemistry-controlled chain ends also show enhanced dielectric breakdown strength, resulting in higher energy density as compared to their linear counterparts. These novel insights into manipulating chain end distribution such as in BCPs and with molecular topology to increase the energy density of polymers will help fulfill next-generation energy demands.

#### 5:10 AM F.EN01.01.02

**Gamma-Radiated Biochar Carbon for Improved Supercapacitor Performance** Ezaldeen Adhamash; South Dakota State University, United States

Biochar carbon YP-50 exposed to gamma radiation at 50 kGy, 100 KGy, and 150 kGy was used as an electrode for an electric double-layer capacitor. The gamma radiation affected the pore structure and pore volume of the biochar electrodes. The optimized surface morphology, pore structure, and pore volume of the biochar with an irradiation dose of 100 kGy showed outstanding specific capacitance of 246.2 F g<sup>-1</sup> compared to the untreated biochar (115.3 F g<sup>-1</sup>). The irradiation dose of 100 kGy exhibited higher specific power and specific energy of 0.1 kW kg<sup>-1</sup> and 34.2 W h kg<sup>-1</sup> respectively, with a capacity retention of above 96% after 10,000 cycles at a current density of 2 A g<sup>-1</sup>. This improvement can be attributed to the decrease in average particle size, an increase in the porosity of biochar carbon. Besides, the charge transfer resistance of supercapacitor is significantly reduced from 21.7 Ω to 7.4 Ω after treating the biochar carbon with 100 kGy gamma radiation, which implies an increase in conductivity. This gamma radiation strategy to pretreat the carbon material for improving the properties of carbon materials can be promising for the development of high-performance supercapacitors for large-scale applications.

#### 5:20 AM \*F.EN01.01.03

**High Energy Density and High Temperature Multilayer Polymer Films for Electric Vehicle Applications** Lei Zhu and Eric Baer; Case Western Reserve University, United States

Current state-of-the-art biaxially oriented polypropylene (BOPP) film capacitors suffer from low temperature rating (<85 °C) and low energy density. At Case Western Reserve University, we have developed a novel multilayer film technology to meet the stringent requirements for next-generation dielectric film capacitors for electric vehicles. By multilayering a high breakdown strength polymer such as polycarbonate (PC) with a high dielectric constant polymer such as poly(vinylidene fluoride) (PVDF), we have achieved high breakdown strength (>600 MV/m), high energy density at breakdown (16 J/cm<sup>3</sup>), and relatively low dielectric dissipation factor (tanδ <0.005) and hysteresis loss (15% loop area). In this presentation, we will identify and discuss fundamental issues for these multilayer dielectric films, which include polarization of amorphous and crystalline dipoles, polarization of impurity ions, and interfacial polarization to achieve enhanced breakdown strength and lifetime at high temperatures.

#### 5:35 AM F.EN01.01.04

**N-Doped Carbon Quantum Dots Boost the Electrochemical Supercapacitive Performance and Cyclic Stability of MoS<sub>2</sub>** Nageh K. Allam; American University in Cairo, Egypt

We report on the successful synthesis of flower-like MoS<sub>2</sub>/N-doped carbon dots (CDs) composite nanospheres *via* a facile solvothermal method making use of the layered structure of MoS<sub>2</sub> and the excellent conductivity of CDs. The structural, compositional, and morphological properties of the fabricated electrodes were investigated using XRD, XPS, EDS, Raman spectroscopy, FTIR, TEM, and FE-SEM techniques. The addition of carbon dots to MoS<sub>2</sub> improved the cyclic stability,

wettability, and conductivity of the fabricated composites upon their use as supercapacitor electrodes. The supercapacitor electrodes showed a specific capacitance as high as 250.55  $\text{Fg}^{-1}$  at a scan rate of 10 mV/s and 149.21  $\text{Fg}^{-1}$  at 0.5 A/g. A symmetric supercapacitor device composed of  $\text{MoS}_2/\text{NCDs}$  composite and activated carbon as the positive and negative electrodes, respectively delivered an energy density and a power density of 20.01 Wh/kg and 350 W/kg, respectively with 98% Coulombic efficiency after 5000 cycles, indicating the high performance of the fabricated electrodes.

**5:45 AM \*F.EN01.01.05**

**Stabilization of High Energy Density Over a Wide Temperature Range by Blend Structure in Ferroelectric Polymers** Yongbin Liu and Jinghui Gao; Xi'an Jiaotong University, China

Achieving stable energy density at elevated temperature remains a great challenge for ferroelectric polymer-based capacitors. It seems that the emerging ferroelectric polymers (e.g. poly(vinylidene fluoride) (PVDF) and its copolymers), which possess spontaneous polarization and large permittivity, provide a promising solution to meet the ever-increasing requirement for high energy density. Nevertheless, the state-of-the-art PVDF-based ferroelectric polymer usually exhibits mediocre temperature stability in energy storage performance, which cannot fully satisfy the applications at elevated temperature caused by the energy consumption or nearby heat sources.

In this work, we report a strategy for stabilizing high energy density of ferroelectric polymer (PVDF) over a wide temperature range by blending with a miscible high- $T_g$  polymer (polymethyl methacrylate (PMMA)). The blending material forms an alternating lamellar structure consisting of high-polarization crystalline regions and strengthened amorphous regions. It is found that this special morphology is able to confine the constructional change of stacked lamellar structure at elevated temperatures. Accordingly, the associated energy storage performances, including energy density, energy storage efficiency and breakdown strength, are remarkably enhanced in a wide temperature range (30 to 70°C). At 70°C, the energy density and efficiency of PVDF/PMMA(80/20) is 9.8J  $\text{cm}^{-3}$  and 67.8%, which surpasses most neat ferroelectric polymers at such an elevated temperature. This work reveals the relationship between lamellar confinement of polymer blend and electric properties under temperature variation, and might provide a valid approach to attain high energy density and temperature stability in ferroelectric polymers.

**6:00 AM \*F.EN01.01.06**

**Strategies of Enhancing Electric Breakdown Strength of Nanocomposites by Designing Fillers with Special Microstructure Structure** Shuhui Yu, Junyi Yu and Rong Sun; Shenzhen Institutes of Advanced Technology, Chinese Academy of Sciences, China

As one of the most important renewable energy storage technologies, film capacitors have been used in modern electronics and power industries such as wearable electronics, hybrid vehicles, and other fields due to their high power density, long working hours, and environmental friendliness. With the development of electronic devices toward miniaturization and high performance, there is an urgent need for dielectric materials with high energy storage density. A high breakdown strength ( $E_b$ ) is crucial for dielectric materials to ensure reliability of electric circuits and to improve electrostatic energy storage density.  $E_b$  is the result of space charge movement in the dielectrics under the applied electric field. Effectively reducing the density of charge carriers in the dielectrics is one of the keys to enhancing  $E_b$ . In this study, hybrid nanoparticles with special physical microstructure were designed and fabricated. When they were used as fillers, these particles possessing isoelectronic traps or heterojunction have proved efficient in confining space charge carriers generated under applied electric field and meanwhile suppressing their movement through the whole polymer system. As a result, electrical conductivity was reduced and  $E_b$  was enhanced significantly, leading to improved energy storage density.

**6:15 AM F.EN01.01.07**

**Late News: Layered Polymer Nanocomposites Reinforced by 2D Interfaces for Electrostatic Energy Storage and Conversion** Yifei Wang and Yang Cao; University of Connecticut, United States

Carbon dioxide emissions and ever-growing environmental issues have stimulated the exploration of new energy sources that are required to be renewable and environmentally friendly. Most of the energy in nature is intermittent, such as solar, wind, and tidal energy, which puts forward critical requirements for energy conversion systems with ultrahigh power densities. Among all energy conversion technologies, the electrostatic capacitor has the fastest charge-discharge speed, which has been utilized as the invertors/convertor in hybrid electric vehicles. However, polymers, as the main functional part in electrostatic capacitors, are severely limited by unsatisfied energy densities due to their low dielectric constants, compared with ceramic counterparts.

Although much research work has been done to improve the dielectric polarization, e.g., introducing ceramic nanoparticles with high dielectric constant to construct nanocomposites, the increase in energy storage density is still restricted due to the

compromise in electrical insulation capabilities. These ceramic nanoparticles generally have high electrical conductivity. When a large amount of the nanoparticles is introduced into polymers, conductive paths will be formed in the nanocomposites. As a result, charge migration will become easier, which will lead to not only a high energy loss but also a suppressed breakdown strength.

Here, to address this issue, layered nanocomposites reinforced by 2D interfaces are designed, which possess high dielectric polarization and insulation capabilities simultaneously. MMT nanosheets with anisotropic conductivities (surface conductivity > bulk conductivity) are adopted as the interface materials. It is demonstrated that this 2D interface plays different roles when it is interposed at different positions. In detail, it can block the charge injection when it locates between the electrodes and the surface of the polymers, while it tends to dissipate charges along the in-plane direction when they are inside of the polymers. The above two functions can simultaneously serve the purpose of preventing carriers from penetrating the polymer films. It causes a suppressed leakage current and energy loss, thus leading to an enhanced charge-discharge efficiency and energy density. This proposed method is applicable to a wide range of polymers. Favorable energy storage performance can be achieved in a harsh environment, e.g., high temperature (as high as 250°C), when high-temperature resistant polymers are selected as the matrix. For example, a high energy density of 4.3 J/cm<sup>3</sup> is found in an interface-enhanced barium titanate/polyamideimide nanocomposite at 150°C, which can still be 2.2 J/cm<sup>3</sup> even when the temperature is elevated to 250°C. This work systematically illustrates the impact of the interface reinforcement on the electrostatic energy storage performance and provides guidance for the exploration of high-performance dielectric nanocomposites for renewable energy storage and conversion.

SESSION F.EN01.02: Computational Modeling in Dielectric Materials  
On Demand Abstracts Available for Viewing Starting Saturday Morning, November 21, 2020  
F-EN01

#### 5:00 AM \*F.EN01.02.01

**Atomic Scale Simulation of Charge Transport Properties of Dielectric Polymers** Mikael Unge; NKT HV Cables AB, Technology Consulting, Sweden

Sustainable energy sources – such as wind, wave and solar – are attractive for reducing CO<sub>2</sub> emissions and tackling climate change. Often these energy sources are placed at large distances from where the energy is actually needed; off-shore wind farms and desert solar parks. To transfer the electrical power from such remote locations high voltage direct current (HVDC) is the preferred technology due to lower transmission losses. In the design of high voltage component the dielectric properties of the materials used are of significant importance. The conductivity of the leakage current in and the electrical breakdown field of the dielectric material impact and limits the design. To understand how these properties are affected by the materials chemical composition and morphology, material simulation is one approach to understand these phenomena in more detail.

Material simulation methods such as density functional theory (DFT) and molecular dynamics (MD) has an increased usage in literature to study dielectric properties of materials relevant for HV components. Basic properties such as band gaps and trap states, to more challenging properties to calculate such as mobility and electrical breakdown fields are reported. An additional important area is to include material simulation methods in multiscale simulation models to incorporate phenomena on longer time and length scales possible.

In this talk we will present result from several different studies of dielectric polymers using DFT, MD and kinetic Monte Carlo (KMC). Primarily the material of interest in these studies is polyethylene (PE) which is used as insulation in HVDC cables. PE is a semi crystalline material and have a complex structure at micrometer scale. Using linear scaling DFT (LSDFT) we have investigated the electronic structure of different parts of PE morphology. Band gaps and electron localization are calculated and used to determine electronic charge transport properties. A combination of DFT, MD and KMC are used to calculate mobility in PE. A coarse grained model for hopping transport in PE is also being developed. Recently we also applied LSDFT to investigate electronic structure of another dielectric polymer, poly(ethylene oxide), which may be used as polymer electrolyte in solid state batteries. Coupling to models at longer time and length scales are discussed.

#### 5:15 AM F.EN01.02.02

**Designing Polymers Resistant to Electric Field Extremes with Materials Modeling and Machine Learning** Deepak Kamal<sup>1</sup>, Yifei Wang<sup>2</sup>, Huan Tran<sup>1</sup>, Lihua Chen<sup>1</sup>, Rishi Gurnani<sup>1</sup>, Zongze Li<sup>2</sup>, Chao Wu<sup>2</sup>, Yang Cao<sup>2</sup> and Rampi

Ramprasad<sup>1</sup>; <sup>1</sup>Georgia Institute of Technology, United States; <sup>2</sup>University of Connecticut, United States

Breakdown strength (Ebd), the maximum electric field that can be applied on a dielectric polymer without destroying its insulating characteristics, sets an upper limit on the maximum energy that can be stored in this material. Despite its significance, the breakdown phenomena in polymers remain poorly understood owing to the complex nature of the phenomena. This is a major challenge in the development of new high-energy polymer dielectrics. In this work, we present a multi-step strategy to develop novel high breakdown polymers, sidestepping this challenge - by finding and improving properties that are correlated to Ebd (and easy to estimate) rather than directly attempting to improve Ebd. Specifically the steps involved include - (i) Identification of potential proxy properties correlated to Ebd utilizing available experimental data. (ii) Development and utilization of Density Functional Theory (DFT) based computational models to better understand the proxy properties and to create a dataset which can be used to build machine learning based prediction models of the proxy properties. (iii) Development of machine learning (ML) based prediction models capable of predicting the proxy properties of any given polymer. These models are used as screening tools to downselect potential high breakdown polymers from a candidate set which is much larger than what DFT can handle. (iv) Generation of novel potential high Ebd polymers utilizing optimization strategies (Genetic Algorithm, Graph to Graph translations etc.) and ML models. Finally, the obtained novel polymers are further down selected and suggested for synthesis.

#### 5:25 AM F.EN01.02.03

**Fast Simulations of Thermal Transport in Imperfect Dielectrics using Machine Learning and Bayesian Force Fields** Anders Johansson, Andrea Cepellotti and Boris Kozinsky; Harvard University, United States

Controlling thermal conductivities of materials is important for a wide range of applications, from thermoelectrics for clean energy generation to electronic devices and thermal barrier coatings. The thermal conductivity is commonly estimated using molecular dynamics simulations within the Green-Kubo formulation. This requires a force field that is both 1) an accurate estimate of the interatomic interactions and 2) fast enough to allow simulations with sufficiently large length and time scales. Traditionally, only empirical force fields have fulfilled both of these requirements, which severely limits the applicability of the method.

In this work, we employ the Gaussian Process-based FLARE force field, which automatically learns the interactions of more complex materials than empirical force fields. The resulting model can then be mapped to a low-dimensional, computationally efficient model. Through GPU-acceleration with LAMMPS and the Kokkos library, we achieve excellent performance and obtain well-converged estimates for the thermal conductivity. Furthermore, we investigate state-of-the-art sampling and spectral denoising methods for further acceleration of the simulations. We apply this machinery to dielectrics with high thermal conductivity and study the effect of impurities.

#### 5:35 AM F.EN01.02.04

**First-Principles Method for Temperature-Dependent Dielectric Permittivity and Curie Temperatures of Ferroelectric Materials** Woon ih Choi<sup>1</sup>, Dae Jin Yang<sup>2</sup> and Doh Won Jung<sup>2</sup>; <sup>1</sup>Samsung Electronics, Korea (the Republic of); <sup>2</sup>Samsung Advanced Institute of Technology, Korea (the Republic of)

High fidelity prediction of dielectric permittivity is of critical importance for the design of better performing devices. However, conventional calculations that are based on quasi-harmonic approximation, are known to incur huge error in particular for ultrahigh-k material such as SrTiO<sub>3</sub>. This is attributed to the missing of key physics i.e. lattice anharmonicity in the theory. To overcome this, we developed computational workflow that account for anharmonic contribution by performing self-consistent phonon (SCP) theory calculations using AlamoDe. Preceding preparation of higher order interatomic force constants are determined based on Hellmann-Feynman forces of standard DFT calculations. It turns out that efficient structure sampling is critical to reduce computational cost and maintaining errors in harmonic force constants as small as possible are very important for the accuracy of following SCP calculations. Resultant temperature dependency of transverse optical phonon frequency agrees well with experimentally measured ones. In addition, dielectric permittivity of SrTiO<sub>3</sub> calculated from phonon band structure is in good accord with values reported in literatures. We also confirmed that this workflow is able to predict para- to ferro-electric phase transition temperature of ferroelectric materials such as BaTiO<sub>3</sub> and PbTiO<sub>3</sub>.

#### 5:45 AM F.EN01.02.05

**High-Throughput Phase-Field Simulations and Machine Learning of Resistive Switching in Resistive Random-Access Memory** Kena Zhang<sup>1</sup>, Jianjun Wang<sup>2</sup>, Yuhui Huang<sup>3</sup>, Long-Qing Chen<sup>2</sup>, Panchapakesan Ganesh<sup>4</sup> and Ye Cao<sup>1</sup>; <sup>1</sup>The

University of Texas at Arlington, United States; <sup>2</sup>The Pennsylvania State University, United States; <sup>3</sup>Zhejiang University, China; <sup>4</sup>Oak Ridge National Laboratory, United States

Metal oxide-based Resistive Random-Access Memory (RRAM) exhibits multiple resistance states, arising from the activation/deactivation of a conductive filament (CF) inside a switching layer. Understanding CF formation kinetics is critical to achieving optimal functionality of RRAM. Here a phase-field model is developed, based on materials properties determined by *ab initio* calculations, to investigate the role of electrical bias, heat transport and defect-induced Vegard strain in the resistive switching behavior, using  $\text{MO}_{2-x}$  systems such as  $\text{HfO}_{2-x}$  as a prototypical model system. It successfully captures the CF formation and resultant bipolar resistive switching characteristics. High-throughput simulations are performed for RRAMs with different material parameters to establish a dataset, based on which a compressed-sensing machine learning is conducted to derive interpretable analytical models for device performance (current on/off ratio and switching time) metrics in terms of key material parameters (electrical and thermal conductivities, Vegard strain coefficients). These analytical models reveal that optimal performance (i.e. high current on/off ratio and low switching time) can be achieved in materials with a low Lorenz number. This work provides a fundamental understanding to the resistive switching in RRAM and demonstrates a computational data-driven methodology of materials selection for improved RRAM performance, which can also be applied to other electro-thermo-mechanical systems.

#### 5:55 AM F.EN01.02.06

##### **Mechanisms of Dielectric Breakdown at Metal Polymer Interfaces Using Reactive Molecular Dynamics Simulations**

**Simulations** Ankit Mishra<sup>1</sup>, Deepak Kamal<sup>2</sup>, Aravind Krishnamoorthy<sup>1</sup>, Subodh C. Tiwari<sup>1</sup>, Ruru Ma<sup>1</sup>, Liqiu Yang<sup>1</sup>, Ken-ichi Nomura<sup>1</sup>, Rampi Ramprasad<sup>2</sup>, Rajiv Kalia<sup>1</sup>, Aiichiro Nakano<sup>1</sup> and Priya Vashishta<sup>1</sup>; <sup>1</sup>University of Southern California, United States; <sup>2</sup>Georgia Institute of Technology, United States

The performance and reliability of organic dielectric devices depends critically on the chemistry and morphology of metal-organic semiconductor interfaces. Conjugated polymers represents a promising class of organic dielectrics due to their excellent electronic properties which can be tuned over 10 orders of magnitude through reversible doping processes. Aluminium (Al) is popular candidate for device electrodes on account of its low work function and capability to get thermally deposited on top these dielectric polymers to enable desired device architectures. The reliability and efficiency of these devices is dependent upon the stability of these Al-dielectric polymer interfaces since the charge injected from Al layer is a key contributor to polymer degradation and dielectric breakdown. Here, we perform a hybrid reactive molecular dynamics and density functional theory based study to understand how various interfacial features affect charge injection barriers. We utilize first-principles data on Al-polymer interfaces to design efficient ReaxFF force fields capable of simulating realistic interfaces. We demonstrate this approach on various dielectric polymers such as Polypropylene (PP), Polystyrene (PS), Polyethylene (PE) and Polyethylene terephthalate (PET) by carefully examining the effect of deposition rate and size of Al clusters, surface and bulk diffusion of Al clusters on polymer substrate and defects in polymer substrate.

#### **Acknowledgments**

This work was supported by the Office of Naval Research through a Multi-University Research Initiative (MURI) under grant number (N00014-17-1-2656). The simulations were performed at the Argonne Leadership Computing Facility under the DOE INCITE and Aurora Early Science programs and at the Centre for High Performance Computing of the University of Southern California.

#### 6:05 AM F.EN01.02.07

**Modelling Dielectric Energy Materials with Lone-Pair Cations Using a Novel Hybrid Approach—From One-Centre Quantum Mechanics to Interatomic Potentials** Woongkyu Jee, Scott Woodley and Alexey Sokol; University College London, United Kingdom

A wide range of dielectric energy materials exhibit unusual properties that are due to soft, or highly polarisable constituent cations, e.g., Sn(II), Pb(II) or Bi(III). An accurate account of their behaviour may cause in modern first-principles calculations both methodological and technical difficulties, and, in general, requires high computational costs. Results of such calculations in turn are often difficult to analyse and interpret using chemical or physical intuition that is, however, essential in applied research. The oxides of these heavy main-group elements typically have a medium to wide band gap, and their materials show potential applications in many energy applications including solar/fuel cells and batteries. Examples include: SnO in both bulk and nanoparticle form have been studied as a photoelectric material and rechargeable batteries; whereas PbO and Bi<sub>2</sub>O<sub>3</sub> have potential applications in thermoelectric materials and fuel cells, respectively; and SnTiO<sub>3</sub> and PbTiO<sub>3</sub> perovskites have ferro- and piezo-electric properties. Related compounds including transition metals show exciting multiferroic properties.

Modelling the effect of the local environment on the Sn(II), Pb(II) and Bi(III) cations at the quantum-mechanical level of theory requires an accurate representation of, at the very least, their valence *s* and *p* orbitals; that can hybridise and occupied by the valence electrons form an *sp*-lone pair in the environment of closed-packed oxides, which avoids forming any direct chemical bonding and makes the cations relatively more polarisable than other cations with closed valence electron configuration. As a result, the formation of an *sp*-lone pair typically induces a local structural distortion about such a cation, i.e., a reduction of the symmetry of the crystal structure, that may have a significant effect on the desired material property and is, therefore, crucial to model correctly. Alkaline earth metal oxides, for example, adopt the NaCl rock salt structure with the space group symmetry of *Fm3m* where each cation is at the centre of a regular octahedron composed of six oxygen anions at the vertices, whereas SnO and PbO have the space group symmetry of *P4/nmm* with the six nearest neighbour oxygen anions showing a breakdown of the octahedral symmetry.

Atomistic simulations, based on semi-empirical interatomic potentials – a useful conventional tool for the study of simple ionic materials – are many orders of magnitude cheaper to conduct than a full electronic structure approach, but, alas, cannot successfully reproduce the atomic structure and dielectric properties of materials containing Sn(II), Pb(II) or Bi(III). To resolve this difficulty and model the effect of the *sp*-lone pair electron density we introduce a simple quantum mechanical treatment to the lone pair cations based on a one-centre Hamiltonian approach with an *s* and *p* atomic basis set. Polarisation effects of the other species are captured using a well-known Shell Model. The new approach has been implemented in our in-house software *Sp-Lone pair involved Atomistic Model* (SLAM) code and could easily be implemented in popular molecular-mechanical codes such as GULP and LAMMPS. During this presentation we will demonstrate the accuracy and efficiency of our model by comparison of our results with those from first principles calculations using Density Functional Theory (DFT) and previous interatomic-potential models for bulk materials doped with Sn(II) and nanosized molecular SnO clusters.

6:15 AM \*F.EN01.02.08

**Rational Design of Dielectric Materials for Flexible Capacitive Pressure Sensing Coatings** Jianing Wu, Tianyu Shao and Zhuo Li; Fudan University, China

Flexible pressure sensors are the basic components for many different applications, such as electronic skins, robotics, health-monitoring devices, and human-machine interfaces. Among different working mechanisms, capacitive pressure sensors are widely-used owing to their low energy consumption, simple structure, and high reliability. Pressure sensors in the form of coatings have the advantages of facile applications on various complex surfaces because of the flowability before solidification, capability for large scale production, and low cost. But how to prepare pressure sensing coatings to meet the requirements for different applications remains to be addressed. This talk covers our recent work to enhance the performances of pressure sensing coatings through the rational design of dielectric materials.

Firstly, I will discuss a highly sensitive capacitive pressure sensing coating using thermally expandable microspheres/polydimethylsiloxane (PDMS) composite as the dielectric layer. The microspheres can expand during the thermal curing process of PDMS, which greatly enhance the compressibility and thus increase the sensitivity of the pressure sensors. At the same time, it achieves a broad pressure sensing range from 10 Pa to 4.5 MPa and also features low hysteresis and good stability against repeated compression.

Secondly, I will discuss a strategy to achieve linear response of capacitive pressure sensor over a broad sensing range. Conventional capacitive pressure sensors usually exhibit a highly non-linear response as the sensitivity drops dramatically towards high pressure. Our strategy employs a percolative composite as the dielectric layer. The fast increase in dielectric constant during compression can compensate the sensitivity drop from the decreased compressibility, leading to a linear response. Owing to the nature of polymer composite, its dispersion not only can be conformally coated on surfaces with various complex shapes, but also can be molded into films with surface microstructures to achieve a unique combination of high sensitivity and linear response over a wide pressure sensing range.

6:30 AM F.EN01.02.09

**Stochastic Computational Search of Capacitance Variance Mechanisms in Particle-Based Heterogeneous Dielectrics** Venkatesh Meenakshisundaram<sup>1,2</sup>, David Yoo<sup>1,2</sup>, Andrew Gillman<sup>1</sup>, Nicholas Glavin<sup>1</sup> and Phil Buskohl<sup>1</sup>; <sup>1</sup>Air Force Research Laboratory, United States; <sup>2</sup>UES, Inc., United States

Dielectric particles are often added to 3D printing inks to tailor the macro level permittivity of printed dielectric substrates and coatings. In these inks, the combined role of particle morphology, discrete spatial arrangement and material properties on variance is difficult to distinguish experimentally and hence poorly understood. This is primarily due to the large parameter space of processing variables as well as electrical sensitivity to local heterogeneities. We address this challenge by combining a finite element capacitor model with a neural network biased genetic algorithm (NBGA) to optimize the volume fraction, particle size and permittivity distributions of dielectric particles to identify systems with high capacitance variance. Analysis



of the database generated from the optimization process provided insights on effect of polydisperse particles on the variance of the system. Design rules/strategies were also identified for achieving target variance. Unsupervised machine learning techniques were applied to the NBGA-created database to extract correlations between the spatial/material distributions of the dielectric particles and the capacitance variance. Collectively, this study provides a useful framework to correlate electrical performance with both macro- and microstructural variation sources, which is key to accelerating the development of 3D printing materials.

SESSION F.EN01.03: Dielectric and Electrical Insulation Materials for Electronics  
On Demand Abstracts Available for Viewing Starting Saturday Morning, November 21, 2020  
F-EN01

**5:00 AM \*F.EN01.03.01**

**Highly Thermally Conductive and Electrically Insulating Polymer Composites Based on Functionalized Boron Nitride Nanosheets** Takuya Morishita; Toyota Central R&D Labs., Inc., Japan

Highly thermally conductive and electrically insulating polymer composites are strongly demanded for thermal management applications including next-generation electronics and electric power systems. Anisotropic nanocarbons such as carbon nanotubes (CNTs) and graphenes are excellent nanofillers for improving thermal conductivity (TC) of polymers. However, nanocarbons exhibit high electrical conductivity and the addition of even small amounts of them into polymer matrices leads to decreased electrical insulation. Therefore, morphologically controlled CNT/polymer composites having highly electrical insulation were designed and fabricated [1,2]. However, these composites have not actually been applied towards highly electrically insulating materials requiring much higher TC ( $>10 \text{ W m}^{-1} \text{ K}^{-1}$ ). Meanwhile, boron nitride nanosheet (BNNS) is analogous to graphene and has an increasing interest for the abovementioned applications because of its extremely high TC and highly electrical insulation. BNNSs were easily prepared by direct exfoliation of h-BNs using carefully selected solvents such as ionic liquids (ILs) [3,4] and superacids [5]. ILs and superacids showed strong physical adsorption on h-BN surfaces, giving exfoliated, noncovalently functionalized BNNSs (NF-BNNSs) in high yields. The obtained NF-BNNSs showed high solubility in various solvents and maintained perfect crystallinity of h-BN structure. Therefore, NF-BNNSs acted as excellent nanofillers for dramatically improving TC of polymers. Highly thermally conductive and electrically insulating NF-BNNS/thermoplastic (TP) polymer composite films were produced through a simple wet-process using NF-BNNS solutions. NF-BNNSs were uniformly dispersed in the TP polymers, enhancing both the in- and through-plane TCs. Noncovalent functionalization of BNNSs with ILs or superacids gave high affinity between BNNSs and TP polymer matrices in the composites, leading to extremely high TC ( $\geq 15 \text{ W m}^{-1} \text{ K}^{-1}$ ) and improved volume resistivity compared with those of previously reported BNNS/TP polymer composites. Moreover, the composites exhibited high flexibility. The proposed approach is very promising for preparation of electrically insulating materials for various thermal management applications.

[1] T. Morishita, et al., *J. Mater. Chem.* 21, 5610 (2011).

[2] T. Morishita, et al., *Compos. Sci. Technol.* 142, 41 (2017).

[3] T. Morishita, et al., *Chem. Commun.* 51, 12068 (2015).

[4] T. Morishita, et al., *RSC Adv.* 7, 36450 (2017).

[5] T. Morishita, et al., *ACS Appl. Mater. Interfaces* 8, 27064 (2016).

**5:15 AM \*F.EN01.03.02**

**Dielectric Materials in Semiconductor Packages** Enis Tuncer; Texas Instruments, United States

It is important to determine the dielectric characteristics of semiconductor encapsulation materials based on epoxy resins. There are several such material systems employed to protect the active silicon circuitry. Some of the important properties of the materials are their glass transition temperature, filler content and the level of water absorption which leads to reliability challenges with respect to performance and lifetime. We study changes in the properties by investigating dielectric relaxation using broadband impedance spectroscopy techniques. It is known that the dielectric relaxation in polymeric systems influenced by the presence of water, which demands special attention in sensitive applications. We will present measurement and analysis methods based on time and frequency domain techniques. It would be appreciated within the materials science community to improve material selection and performance evaluation efforts. We will also share information on the glass transition temperature estimates for a number of composites employed in semiconductor packaging.

### 5:30 AM F.EN01.03.03

**Ultra-Thin Doped HfO<sub>2</sub> Gate Dielectric for Ultra-Low Power Ubiquitous Electronics** Ahmad Zubair<sup>1</sup>, Winston Chern<sup>1</sup>, Nitul Rajput<sup>2</sup>, Kevin Limanta<sup>1</sup> and Tomas Palacios<sup>1</sup>; <sup>1</sup>Massachusetts Institute of Technology, United States; <sup>2</sup>Khalifa University of Science and Technology, United Arab Emirates

Ferroelectric materials are promising candidate for both conventional (e.g. low power, scalable and non-volatile memory) and emerging (e.g. in-memory computing, analog synapses, coupled oscillator networks, spiking neurons and quantum computing) nanoelectronics applications. Conventional ferroelectric materials suffer from lack of thickness scaling and compatibility with CMOS processing. Ultra-thin doped HfO<sub>2</sub> based ferroelectric thin-films have emerged as an attractive option for non-volatile memory and ultra-low power computing due to CMOS compatibility and precise thickness control through atomic layer deposition. In this work, we systematically investigate the scaling properties of ferroelectric Hf<sub>0.5</sub>Zr<sub>0.5</sub>O<sub>2</sub> in a metal/ferroelectric/insulator/semiconductor (MFIS) capacitors to identify the design space for logic and memory applications.

MFIS capacitors are fabricated on p-Si wafers using standard CMOS processing with different ferroelectric thickness. The ferroelectricity in the doped HfO<sub>2</sub> thin film is introduced by rapid thermal annealing. This high temperature annealing steps leads to structural phase change (monoclinic to orthorhombic) and non-centrosymmetric crystal structure in the doped HfO<sub>2</sub>. The dielectric constant,  $k$ , of the orthorhombic Hf<sub>0.5</sub>Zr<sub>0.5</sub>O<sub>2</sub> film is higher than those of HfO<sub>2</sub> and ZrO<sub>2</sub> ( $k = 25$ ) for all thicknesses as observed from the small signal capacitance-voltage (C-V) characteristics. At low gate biases, the Hf<sub>0.5</sub>Zr<sub>0.5</sub>O<sub>2</sub> film is hysteresis-free and shows negligible frequency dispersion indicating a high-quality interface. This observation indicates that orthorhombic Hf<sub>0.5</sub>Zr<sub>0.5</sub>O<sub>2</sub> can be a promising way to achieve high- $k$  gate dielectric. At high gate bias, the thinner Hf<sub>0.5</sub>Zr<sub>0.5</sub>O<sub>2</sub> films shows polarization switching when the effective electric field across the ferroelectric film exceeds the coercive field. However, in the thicker Hf<sub>0.5</sub>Zr<sub>0.5</sub>O<sub>2</sub> film required gate bias for polarization switching is higher the critical field for dielectric breakdown.

Our results indicate that orthorhombic Hf<sub>0.5</sub>Zr<sub>0.5</sub>O<sub>2</sub> can be an attractive option for gate dielectric for ubiquitous electronics. The high dielectric constant and relatively lower effective charge of the ferroelectric thin film can enable the polarization switching of the thinner dielectrics. However, to enable non-volatile memory with lower switching voltage additional materials and device engineering would be required as the switching voltage weakly scales with ferroelectric thickness.

### 5:40 AM F.EN01.03.04

**Superionic Charge Accumulation in the In-Plane Direction of Pt Nanoparticle Films Fabricated by Atomic Layer Deposition** Munekazu Motoyama<sup>1</sup> and An Jihwan<sup>2</sup>; <sup>1</sup>Nagoya University, Japan; <sup>2</sup>Seoul National University of Science and Technology, Korea (the Republic of)

Here we report the charge accumulation phenomena in Pt nanoparticle (NP) films deposited by the atomic layer deposition (ALD) on borosilicate glass (Pyrex®) substrates. The in-plane capacitance of Pt NP films was measured by AC impedance spectroscopy using Au electrodes patterned with an interval of 6.0 μm on Pyrex substrates. The experimental results show that annealed Pt NP films exhibit very high capacitance on Pyrex substrates. This phenomenon was observed in neither electron-beam-evaporation-deposited-Pt-NP films on Pyrex nor ALD-Pt-NP films on quartz. Although the mechanism of this charge accumulation phenomenon was not fully elucidated, it is considered that protons conduct in the in-plane direction of a Pt NP film via adsorbed water and behave like a supercapacitor to enhance the in-plane capacity. It is found that if the effective volume contributing to the charge accumulation is only the Pt NP film, quite large volume power and volume energy densities ( $6.3 \times 10^6 \text{ W L}^{-1}$ ,  $7.0 \times 10^2 \text{ Wh L}^{-1}$ ) are achieved.

### 5:50 AM \*F.EN01.03.06

**Low Temperature and High-Speed Processing of Oxide Dielectric Thin Films** Julia W. Hsu; The University of Texas at Dallas, United States

Thin film oxide dielectrics boast high breakdown voltages, low leakage current densities, and high dielectric constants making them ideal for use as gate dielectrics in thin film electronics. However, to fully realize the benefit of thin film electronics, low-cost high-throughput production is necessary. This means reducing not only processing time, but also processing temperature to allow for production on plastic substrates. In this work, we discuss the effects of low temperature UV-assisted processing and high-speed photonic curing on the properties of solution-deposited oxide dielectric films. First, we show the results from exposing sol gel precursor films to UV-ozone (UVO) through a shadow mask. This process accomplishes both lowering the conversion temperature to 250 °C and direct patterning the precursor film with exposed areas converted to oxide after final annealing. We find drastically different capacitance-frequency behavior between Al<sub>2</sub>O<sub>3</sub> and ZrO<sub>2</sub> dielectrics, which in turn affects the In<sub>2</sub>O<sub>3</sub> transistors' behavior. The origins of this finding are studied through Fourier transform infrared analysis and time dependent drain current measurements. Next, we adapt photonic curing, the use short but

high intensity pulses of broadband light, to selectively heat and convert ZrO<sub>2</sub> precursor films on flexible polyethylene naphthalate (PEN) substrates. Photonic curing is typically used to sinter metal nanoparticle inks into conductive metal traces on plastic substrates, but it has not previously been used to fabricate oxide thin film dielectrics on plastic substrates. We demonstrate that the conversion time is reduced from 10s minutes to < 1s and patterning using a shadow mask during photonic curing does not need subsequent thermal annealing, unlike in the UVO processing. Furthermore, by adjusting the photonic curing conditions, the oxide film can be selectively converted on top of Al electrodes, which act as selective area heat absorbers, but not on the bare PEN substrate, resulting in a self-aligned oxide pattern. We achieve a ZrO<sub>2</sub> dielectric with breakdown field of 8 MV/cm and areal capacitance of 200 nF/cm<sup>2</sup> with little frequency dispersion. Finally, we show a pathway to converting ZrO<sub>2</sub> dielectric at a roll-to-roll web speed of up to 50 m/min.

#### 6:05 AM F.EN01.03.07

***Ab Initio* Electronic Transport in Disordered Semiconductors** [Andrea Cepellotti](#) and Boris Kozinsky; Harvard University, United States

The field of disordered materials is experiencing a meteoritic rise within materials engineering. In particular, several computational and experimental efforts are aimed at synthesizing novel alloy and highly doped materials, and predictive modeling is a powerful tool to guide the materials space exploration. However, the modeling of charge transport in disordered materials presents a number of challenges. In fact, charge transport in disordered materials is often not well described by common semiclassical methods, such as the Boltzmann transport equation, which have instead been developed for simple dielectric crystals such as silicon. In this work, we present some of our recent efforts aimed at bridging this gap in the modeling of charge transport in disordered materials. In an alloy, in the regime of weak electron localization, the electronic band structure consists of several overlapping flat bands. Here, the prevalent conduction mechanism is due to vertical electronic transitions, rather than diffusion due to electron group velocity. We introduce an ab-initio formalism based on the Wigner distribution that corrects predictions of electronic conductivity by including the effect of these vertical transitions. We exemplify the method with an application to a narrow gap topological semiconductor, Bi<sub>2</sub>Se<sub>3</sub>, showing that bulk transport is dominated by vertical electronic transitions between the valence and the conduction bands, a phenomenon also known as Zener tunneling effect. Our approach is general, applies to any system and provides a step forward for the modeling of charge transport in disordered materials.

#### 6:15 AM F.EN01.03.08

**The Search for Enhanced Dielectric Strength of Polymer-Based Dielectrics** [Daniel Tan](#); Guangdong Technion Israel Institute of Technology, China

Remarkable progress has occurred over the past 15 years through nanodielectric engineering involving inorganic nanofillers, coatings, and polymer matrices. The challenges of dielectric polymers remain primarily toward breakdown strength in thin polymer films for capacitor applications. There reported several major technical approaches to enhance the dielectric strength of polymers and nanocomposites, including nanoparticle incorporation in polymers, filler polymer interface engineering, and film surface coating. This work will direct the attention to interface contributions, including the rational design of core-shell structures, the use of low-dimensional fillers and thermally conducting fillers, and the inorganic surface coating of polymer films. These efforts demonstrated the enhancement in dielectric strength by 40–160% when controlling the fillers below 5 wt% in polyvinylidenedifluoride composites. This work will also discuss the possible dielectric mechanisms and the positive role of interfaces against charge transport traps for attaining higher breakdown strength. The investigation of low-dimensional filler/coating materials of high thermal conductivity is considered to be a key scientific subject for future research.

#### 6:25 AM F.EN01.03.09

**The Impact of Chemical Modification on Charge Injection at Metal/Polyolefin Interfaces** [Yiyuan Wang](#)<sup>1</sup>, Mikael Unge<sup>2</sup>, Sari Laihonen<sup>3</sup> and Arash Mostofi<sup>1</sup>; <sup>1</sup>Imperial College London, United Kingdom; <sup>2</sup>NKT HV Cables AB, Sweden; <sup>3</sup>ABB Power Grids Sweden AB, Sweden

The process of charge injection at metal/polymer interfaces is crucial to many areas of research and technology, such as organic light emitting and harvesting devices, high-voltage capacitors and cables. In this work, we study charge injection at metal/polymer interfaces for two polymers commonly used in high-voltage applications, namely polyethylene (PE) and polypropylene (PP). Using first-principles electronic structure methods, we compute charge injection barriers at model aluminium/PE and aluminium/PP interfaces. We show that the introduction of polar chemical groups (e.g., -COOH, -CH<sub>2</sub>Cl, and -CHO) in the polymer chains at the interface can tune the intrinsic charge injection barrier significantly. We take into account of thermal disorder by averaging over a large ensemble of interface structures obtained from first-principles

molecular dynamics trajectories. Our results suggest the possibility of rational design of metal/polymer interfaces via localised chemical modification.

#### **6:35 AM F.EN01.03.11**

**Use of Ultrathin Atomic Layer Deposited Capping Layers to Increase Stability in Thermally Processed Metalcone Thin Films** Vamseedhara Vemuri and Nick C. Strandwitz; Lehigh University, United States

Molecular layer deposition (MLD) and atomic layer deposition (ALD) are sequential, self limiting thin film deposition techniques, used to fabricate organic, inorganic, and inorganic-organic hybrid thin films. The hybrid organic-inorganic films deposited using MLD are usually metal alkoxides that are also termed as metalcones. Metalcone films can be subjected to thermal processing to selectively remove the organic parts of the film and induce porosity to form porous dielectric materials. However the as deposited and thermally processed metalcone films are unstable in ambient atmosphere due to the moisture absorption and permeation, which alters the chemical properties of these films. Since the dielectric constant of the water is very high (70-80), the net dielectric constant of these films increases after moisture absorption thus affecting the electrical properties. To preserve the chemical stability and electrical properties of metalcones, this work examines the use of an ultra thin ALD film grown over the as deposited and thermally processed films.

We report the growth of alucone thin films using trimethylaluminum and ethylene glycol as precursors for MLD and water (H<sub>2</sub>O) as an oxygen source for ALD reactions. The as deposited MLD films are subjected to thermal processing from 150-350 C in inert atmosphere and under UV light to remove the organic components and induce porosity to form in-organic dielectric films. We examined the thermally induced changes in film's chemistry, thickness, density, etch rate and dielectric constant.

Incorporation of the organic components, formation of M-O-C bonding and water absorption is confirmed using FTIR in the as deposited MLD films. By subjecting MLD films to thermal processing the decrease in intensity of hydrocarbon bonds and changes in thickness, density compared to pure MLD films can be observed by FTIR and x-ray reflectivity respectively. The dielectric constant of these films is measured using capacitance-voltage measurements. The dielectric constant of the thermally processed films with a thin ALD layer decreases compared to only thermally processed films indicating that the thin ALD layer thus preserves electrical properties of the film. The as deposited and thermally processed films with and without the ultrathin ALD layer are subjected to CF<sub>4</sub>/O<sub>2</sub> plasma etch and the MLD films without an ALD layer shows more than double the etch rate compared to the MLD films with an ALD layer. Both the decreased dielectric constant and etch rates show that the ALD layer acts as a barrier to prevent moisture absorption and preserve the chemical stability and electrical properties of the film.

SESSION F.EN01.04: Materials for Thermal, Mechanical and Electrical Energy Interconversion  
On Demand Abstracts Available for Viewing Starting Saturday Morning, November 21, 2020  
F-EN01

#### **5:00 AM F.EN01.04.01**

**Dynamic Tuning of Near-Field Radiative Thermal Rectification** Fangqi Chen, Xiaojie Liu, Yanpei Tian and Yi Zheng; Northeastern University, United States

Taking advantage of phase transition and reconfigurable metamaterials, dynamic control of nanoscale thermal modulation can be achieved through the near-field radiative thermal rectification devices. An active-tuning near-field thermal rectifier using reconfigurable phase-transition metamaterials is explored. The rectifier has two terminals separated by vacuum, working under a controllable operational temperature around the critical temperature of the phase-transition material VO<sub>2</sub>. One of the terminals is a stretchable structure made of PDMS thin film and grating consisting of various types of phase-transition material. The effects of various inclusion forms and all the related geometric parameters are well analyzed. The controllable nanoscale thermal modulation can be achieved and the ultrahigh rectification ratios of 23.7 and 19.8, the highest values ever predicted, can be obtained for two deformation scenarios, respectively. It will shed light on the dynamic tuning of small-scale thermal transport and light manipulation.

#### **5:10 AM \*F.EN01.04.02**

**Electrical and Electromechanical Reliability of Lead Zirconate Titanate Piezoelectric Films** Betul Akkopru-Akgun<sup>1</sup>, Kathleen Coleman<sup>1</sup>, Wanlin Zhu<sup>1</sup>, Raul Bermejo<sup>2</sup> and Susan E. Trolier-McKinstry<sup>1</sup>; <sup>1</sup>The Pennsylvania State University, United States; <sup>2</sup>Montanuniversitaet Leoben, Austria

Use of dielectric materials such as lead zirconate titanate films for dielectric energy storage or for piezoelectric applications necessitates that they be able to sustain high DC electric fields. This paper will describe the coupled failure mechanisms that control these lifetimes for donor-doped, acceptor-doped, and films with graded doping. Curiously, the median failure time of PZT films can be increased on doping with either donors or Mn as an acceptor. It is found that lifetimes under DC fields are dominated by a combination of oxygen vacancy migration, coupled with changes in the interface barrier heights for conduction in thin films. This was assessed through a combination of highly accelerated lifetime testing, thermally stimulated depolarization currents, impedance spectroscopy, deep level transient spectroscopy, and electron energy loss spectroscopy. The relic defect chemistry of the film, including variations in this defect chemistry at interfaces strongly influences both the failure and the asymmetry of the failure as a function of the electrical polarity. As film thickness and/or the piezoelectric coefficients rise, the critical stress required for crack initiation decreases, and the failure modes can shift to electro-mechanically induced failure. Ball-on-three ball mechanical testing demonstrates that the critical flaw size in the failure of the stack becomes the thickness of the piezoelectric layer itself.

### 5:25 AM F.EN01.04.03

#### **Enhancement of Thermoelectric Power Factor Due to Electron-Phonon Interaction at High Carrier Concentrations** Natalya Fedorova, Andrea Cepellotti and Boris Kozinsky; Harvard University, United States

Thermoelectric materials directly convert waste heat to electricity and thus hold great potential for power generation with low environmental impact. To be able to compete with established technology and find broad applications, thermoelectric power generators must have high energy conversion efficiency, which is determined by their figure of merit  $ZT$ . This, in turn, is proportional to the material's power factor  $\sigma S^2$ , where  $\sigma$  is the electrical conductivity and  $S$  is Seebeck coefficient. Optimization of PF is a challenging task, since  $\sigma$  and  $S$  have conflicting dependencies on different tuning parameters such as carrier concentration and their effective masses.

In this work we employ *ab initio* calculations to investigate the effects of the electron-phonon interaction on the transport properties of thermoelectric materials, focusing on the example of half-Heusler semiconductors. We calculate electron-phonon scattering rates using Wannier-Fourier interpolation of electron-phonon matrix elements and the recently developed electron-phonon averaged approximation. We find that the electron-phonon scattering can lead to anomalous behavior of the transport coefficients, namely the conductivity decreases with increasing number of charge carriers, and Seebeck coefficient changes sign, leading to an unusual peak in the PF at high carrier concentrations. We discuss the origin and magnitude of this enhancement effect starting from the electronic band structure and identify design rules to maximize the material's performance.

### 5:35 AM \*F.EN01.04.04

#### **Flexible Dielectric Nanocomposites—From Power Energy Storage to Mechanical Energy Harvesting** Jinkai Yuan; Ctrde Recherch Paul Pascal, France

Our research activities on the energy-related dielectric polymer nanocomposites will be reviewed. Micro-energy storage devices are highly demanded for diverse miniaturized electronic devices. [1,2] However, making high-energy microcapacitors with currently available printing technologies remains challenging. Based on a composite material of latex polyvinylidene fluoride and polyvinyl alcohol, we created high-energy microcapacitors with inkjet printing technique. A discharged energy density of  $12 \text{ Jcm}^{-3}$  is achieved at  $550 \text{ MVm}^{-1}$ . [3] The printed microcapacitors demonstrate mechanical robustness and dielectric stability over time. on the other hand, it is well known that all dielectric materials have electrostriction. They have capability of changing their dielectric properties upon an external mechanical deformation. Based on this effect, we have developed giant electrostriction soft nanocomposites which can serve as an active dielectric layers in a variable capacitor to convert the vibrational mechanical energy into electricity. To make such energy harvester, we prepare an electrostrictive nanocomposite composed of reduced graphene oxide in soft polydimethylsiloxane matrix. [4] The near percolated composite exhibits a large permittivity variation in response to small strain deformation, giving rise to a giant electrostrictive coefficient  $-4.3 \times 10^{-14} \text{ m}^2/\text{V}^2$ , [5] indicating that our materials are particularly promising for harvesting mechanical energy applications. Their implementation in actual MEMS generator devices has been also investigated. [6]

### References

- [1] Z. S. Wu, X. Feng, H. M. Cheng, Natl. Sci. Rev. 2014, 1, 277.
- [2] M. Beidaghi, Y. Gogotsi, Energy Environ. Sci. 2014, 7, 867.
- [3] F. Torres-Canas, et al, Adv. Funct. Mater. 2019, 1901884.

- [4] J. Yuan, et al, Nat. Commun. 2015, 6, 8700.  
[5] J. Yuan, et al. ACS Nano 2018, 12, 1688-1695  
[6]. Nessler, H. et al, Nano Energy, 2018, 44, 1–6.

#### 5:50 AM F.EN01.04.05

**Lead-Free Relaxor-Ferroelectric Superlattice for Pyroelectric Energy Harvesting** Amrit Sharma, Sangram K. Pradhan, Carl E. Bonner, Jr. and Messaoud Bahoura; Norfolk State University, United States

To overcome the energy crisis and its efficient utilization, there is a great need to harvest clean and green energy from waste-heat, which is abundant, ubiquitous, and free. Energy harvesting, using waste-heat, is one of the most encouraging methods to capture freely accessible heat and converting it to electrical energy. Ferroelectric materials are the most suitable candidates to harvest energy for low power electronic devices, as they exhibit switchable polarization, excellent piezoelectric and pyroelectric coefficients. The most important characteristic of ferroelectric materials is their ability to generate electric power via the pyroelectric effect. In this work, we have grown superlattice of BaZr<sub>0.2</sub>Ti<sub>0.8</sub>O<sub>3</sub> (barium zirconium titanate, BZT)/Ba<sub>0.7</sub>Ca<sub>0.3</sub>TiO<sub>3</sub> (barium calcium titanate, BCT) on SrRuO<sub>3</sub> (strontium ruthenate, SRO) deposited on SrTiO<sub>3</sub> (strontium titanate, STO) single crystalline substrate via optimized pulsed laser deposition. We observed only the substrate peaks without any secondary peaks in the x-ray diffraction patterns, which confirms the epitaxial nature and phase purity of the grown material. Interface and domain engineering are integrated on these BZT / BCT structures for slim and well-saturated polarization-electric field (P-E) loops with improved saturation polarization.

Solid-state thin-film devices are demonstrated by the conversion of waste-heat into electrical energy by measuring P-E loops at various temperatures using pyroelectric Ericsson cycles and measured an energy conversion density ~ 10.97 MJ/m<sup>3</sup> per cycle. These devices exhibit a large pyroelectric current of ~ 600 nA with a temperature fluctuation of ~ 11°C. Our findings suggest that these lead-free relaxor-ferroelectric superlattices might be superior to the well-known thermoelectric materials for thermal energy harvesting.

#### 6:00 AM \*F.EN01.04.07

**Solid-State Cooling Devices Based on Electrocaloric Polymers** Qibing Pei; University of California, Los Angeles, United States

Electrocaloric cooling is a solid-state cooling technology, offering several advantages over traditional cooling systems, but few EC devices have been reported with high specific cooling power and high coefficient of performance (COP). We have developed solution processes to fabricate poly(vinylidene fluoride-trifluoroethylene-chlorofluoroethylene) terpolymer thin films. Various material treatment and characterizations were conducted to study and optimize the performance of the terpolymer thin films. We present several EC cooling device designs with compact and desired form factors to transfer heat between a heat source and heat sink, with the ultimate objective to pave the way for new applications that cannot be obtained using existing technologies.

#### 6:15 AM F.EN01.04.08

**Ultra-High Current Mechanical Energy Harvester Based on Lithium Cobalt Oxide** Xiujun Yue<sup>1</sup>, Alissa C. Johnson<sup>1</sup>, Zhimin Jiang<sup>1</sup>, Ryan R. Kohlmeyer<sup>2</sup>, Chadd T. Kiggins<sup>2</sup>, John Cook<sup>2</sup> and James H. Pikul<sup>1</sup>; <sup>1</sup>University of Pennsylvania, United States; <sup>2</sup>Xerion Advanced Battery Corporation, United States

Mechanical energy harvesters are important for powering wearable devices and microelectronics. Most mechanical energy harvesters supply high voltages (10<sup>0</sup>-10<sup>2</sup> V), low currents (10<sup>-4</sup>-10<sup>-2</sup> mA/cm<sup>2</sup>), and operate at high frequencies (~20-100 Hz). The high voltage and low current outputs, however, do not interface well with many microelectronics (which use low voltage and high current supplied from a battery). Additionally, the high operation frequency of mechanical energy harvesters does not match the low frequency of most mechanical energy sources in daily life.

Here, we report lithium cobalt oxide (LCO) based mechanical energy harvesters that deliver ultra-high current from low-frequency mechanical energy input. LCO is widely used as a cathode material for lithium ion batteries, where its crystal volume changes as lithium ions intercalate/deintercalate during battery cycling. We utilize the reverse process, where a change in volume in the crystal due to external stress causes a change in potential that drives a large current. LCO is conductive (9.25×10<sup>-4</sup> S/cm) and exhibits a piezoelectrochemical effect, like many dielectrics, that converts mechanical to chemical or electrical energy. Our energy harvester consists of a pair of LCO electrodes with identical composition and different thicknesses. When an external load is applied to the device, the corresponding stress is concentrated on the thick electrode. As the thick electrode volume changes, the free energy of LCO bonds is modified and results in a shift in the electrochemical voltage. When the unloaded LCO is electrically connected to the loaded LCO, the potential difference drives

a current through an external circuit while lithium ions migrate between electrodes through an electrolyte. The current continues until there is 0 V between the electrodes. When the pressure is removed, an opposite potential difference is generated between electrodes. The device can be cycled between low displacements (<100  $\mu\text{m}$ ) loads at a wide range of frequencies ( $10^{-4}$ - $10^{-1}$  Hz) to convert mechanical energy into ultra-high currents (0.87 mA/cm<sup>2</sup>) and low voltage (~10 mV) power.

Molten salt electrodeposition allowed the synthesis of up to 98% dense and hundreds of micrometer thick monolithic LCO electrodes with no additives, which improved the performance over slurry cast electrodes with binders found in battery electrodes. By reducing mechanical losses that occur in the polymer binders, the high density and single component electrodes enabled a high voltage output close to the theoretical value. Furthermore, the laser-based fabrication process enabled small electrode gaps which contribute to low internal resistance and high output current. The design can be scaled to form array of harvesters connected in series or parallel to generate higher current or voltage to meet the demands of different applications. The usage of aqueous electrolyte in our energy harvester decreases the potential toxic and combustion hazards of organic solvent based electrolytes and avoids the hermetic requirements for battery device packaging. Our work demonstrated an energy harvester with high current capabilities that will create new opportunities for powering wearables and microelectronics with increased functionality.

#### 6:25 AM F.EN01.04.09

**Unveiling the Origin of Relaxor Behavior in Ferroelectric Polymers** [Yang Liu](#)<sup>1</sup>, Bing Zhang<sup>2</sup>, Wenhan Xu<sup>1</sup>, Aziguli Haibibu<sup>1</sup>, Zhubing Han<sup>1</sup>, Wenchang Lu<sup>2</sup>, J Bernholc<sup>2</sup> and Qing Wang<sup>1</sup>; <sup>1</sup>The Pennsylvania State University, United States; <sup>2</sup>North Carolina State University, United States

Relaxor ferroelectric exhibits striking physical properties including ultrahigh piezoelectric coefficients, large dielectric permittivity over a broad temperature range, and strong frequency dependence in dielectric response, which enables a wide range of applications in acoustic sensors, transducers and actuators. Understanding of the origin of unusual properties in relaxor ferroelectrics, however, remains one of the central challenges in ferroelectric materials despite more than 50 years of investigations. Here we reveal that the relaxor behavior of ferroelectric polymers originates from conformational disorder (Y. Liu et al, Nature Materials, in press), which is completely different from classic perovskite relaxors typically characterized by the existence of chemical disorder. We show that chain chirality is essential to the formation of disordered helix conformation arising from local distortions of gauche torsional angles, which consequently give rise to relaxor ferroelectric properties in polymers. Our insights into the origin of relaxor ferroelectric properties in polymers shed new light on fundamental theory of relaxor ferroelectric materials and enable the investigation of the mechanisms of ferroelectric relaxor from a new perspective. The structural model established in this work provides unprecedented guidance for the design of new organic relaxor materials for flexible electronics and energy applications.

#### 6:35 AM F.EN01.04.10

**Late News: Nanomaterial-Induced Polarization Templating in Polymer Piezoelectric Generators** [Nick A. Shepelin](#)<sup>1,2</sup>, Peter C. Sherrell<sup>1,2</sup>, Eirini Goudeli<sup>1</sup>, Emmanuel N. Skountzos<sup>3,4</sup>, Joseph G. Shapter<sup>5</sup>, Joselito M. Raza<sup>6</sup> and Amanda V. Ellis<sup>1,2</sup>; <sup>1</sup>The University of Melbourne, Australia; <sup>2</sup>St Vincent's Hospital Melbourne, Australia; <sup>3</sup>University of Patras, Greece; <sup>4</sup>FORTH/ICE-HT, Greece; <sup>5</sup>The University of Queensland, Australia; <sup>6</sup>Deakin University, Australia

For the purposes of powering always-on, self-powered sensors and portable/wearable electronics, new reliable and sustainable energy harvesting technologies are required. Piezoelectric generators show exceptional promise to fill this gap, owing to their ability to convert mechanical energy from external sources to electricity, with energy conversion efficiencies >35%.<sup>1</sup> Recent advances in piezoelectric fluoropolymers (e.g., poly(vinylidene fluoride), PVDF) further enable the use of flexible polymer-based piezoelectric generators with tailored optical transmittance for wearable or implantable energy harvesting from the movements of the human body.

Despite the promising nature of piezoelectric polymers, the extraordinary energy input required during the manufacture steps limits the commercial applicability for energy harvesting. Namely, the electrical energy (>200 MV m<sup>-1</sup>) and thermal energy (>100 °C), applied to the fluoropolymer in order to align the dipole moments and induce polarization, negates the energy harvested over the device lifetime.<sup>2</sup> Hence, the elimination of this so-called electrical poling step will enable the commercial and environmental viability of flexible piezoelectric generators.

Here, we demonstrate for the first time the dipole templating and polarization locking of a copolymer of PVDF, poly(vinylidene fluoride-co-trifluoroethylene) (PVDF-TrFE), in the presence of 1D (carbon nanotube) and 2D (MXene) nanomaterials. The alignment of polarization at the interface, predicted by molecular dynamics models, improves energy

harvesting performance and decreases the energy input for the manufacture of flexible piezoelectric energy harvesters. The presence of single-walled carbon nanotubes (0.02 wt%) exhibits a generated power density of  $70.6 \mu\text{W cm}^{-3}$ , whereas the incorporation of  $\text{Ti}_3\text{C}_2\text{T}_x$  MXenes (0.50 wt%) results in a piezoelectric charge coefficient of  $52.0 \text{ pC N}^{-1}$ , without the use of electrical poling. The composites produced through this method are fully recyclable in acetone and can be reprinted into various form factors without loss of performance, enabling future use for designer energy harvesting systems.

1. Shepelin, N. A., *et al.*, *Energy Environ. Sci.* 2019, **12**, 1143-1176.
2. Lovinger, A. J., *Science* 1983, **220**, 1115-1121.

SESSION F.EN01.05: Novel Synthesis and Characterization Techniques of Dielectric Materials  
On Demand Abstracts Available for Viewing Starting Saturday Morning, November 21, 2020  
F-EN01

### 5:00 AM F.EN01.05.01

#### **Oleylamine Modified Boron Nitride Nanosheets as Efficient Nanofillers for Electrospun PVDF**

**Nanofibers** Madeshwaran Sekkarapatti Ramasamy and Byungki Kim; Korea University of Technology and Education, Korea (the Republic of)

Poly(vinylidene fluoride) (PVDF) have received applications in piezoelectric sensors, actuators and nanogenerators due to their flexibility and electroactive properties. In general, PVDF exhibit five crystalline polymorphs namely,  $\alpha$ ,  $\delta$ ,  $\beta$ ,  $\gamma$  and  $\epsilon$ , among them,  $\beta$  (TTTT conformation) and  $\gamma$  (TTTGTTG' conformation) phases are the electrically active phases. Moreover,  $\gamma$ -phase offers higher breakdown strength and discharge energy density as compared to  $\beta$ -phase, therefore, receiving greater attention as a ferroelectric material. Until now, various approaches such as, high electric field poling, mechanical stretching, electrospinning and incorporation of nanofillers have been established for fabricating PVDF with high content of electroactive phases. In comparison, incorporation of nanofillers can simultaneously enhance the mechanical properties of polymer matrix and can also promote the formation of preferred electroactive phases owing to the interaction between the surface of the fillers and dipoles of the PVDF chains. Recently, mono or few-layered two-dimensional (2D) boron nitride nanosheets (BNNS) have been actively applied as nanofillers for polymer composites because of their extraordinary properties such as, high thermal conductivity, bandgap, thermal stability, Young's modulus and piezoelectric properties. However, their main drawback is related with their poor dispersion in polymer matrix due to their Van der Waals forces. Herein, we report the fabrication of high performance PVDF nanofibers (PVDFNFs) based composites using oleylamine functionalized boron nitride nanosheets (OLABN) as nanofillers. First, PVDFNFs-OLABN composite nanofiber membranes were prepared by liquid-phase exfoliation (LPE) and electrospinning process, and then, the effect of OLABN on the crystalline phases, mechanical and piezoelectric properties of PVDFNFs were systematically investigated. FTIR results revealed that the OLABN promote the formation of polar  $\gamma$ -phase in PVDFNFs. Impressive 343% and 823% enhancements in tensile strength and Young's modulus can be achieved even with addition of only 0.1 wt% OLABN, respectively. The composites exhibited enhanced piezoelectric outputs as compared to reference PVDFNFs. Furthermore, rapid and sharp piezoelectric outputs can be achieved upon force applied by finger tapping/releasing on the PVDFNFs-OLABN (4 wt%) composite based piezo sensors. The output power density of the composites with 4 wt% OLABN was 133% higher than that of reference PVDFNFs. The findings of this study hold a great potential in high performance polymer based piezoelectric sensors/actuators and nanogenerators applications.

Keywords: Boron Nitride, Piezoelectric Sensing, Polymer Nanofibers, Nano Composites, Mechanical Properties

#### Acknowledgements

This work was supported by Grant NRF-2018R1A6A1A03025526 under the Priority Research Program through National Research Foundation of Korea(NRF) under Ministry of Education.

### 5:10 AM F.EN01.05.02

**Orientation Effects on Antiferroelectric Switching of PbZrO<sub>3</sub> Polycrystalline Films** Cosme Milesi-Brault<sup>1,2</sup>, Stéphanie Girod<sup>1</sup>, Sebastjan Glinsek<sup>1</sup>, Emmanuel Defay<sup>1</sup> and Mael Guennou<sup>2</sup>; <sup>1</sup>Luxembourg Institute of Science and Technology, Luxembourg; <sup>2</sup>University of Luxembourg, Luxembourg



The interest for antiferroelectric materials has been increasing over the last years, largely because of their potential for energy storage and electrocaloric applications, but also because they still are insufficiently known compared to ferroelectrics. Their key distinctive signature is the antiferroelectric switching revealed by a double hysteresis loop. However, this switching is not often demonstrated, largely due to the large electric fields involved. In particular, the details of the switching behavior of the model antiferroelectric perovskite  $\text{PbZrO}_3$  are still unclear.

Here, we synthesize and characterize polycrystalline films of  $\text{PbZrO}_3$ , with thicknesses ranging from 85 nm to 850 nm. The samples have been processed via chemical solution deposition on Pt/TiO<sub>x</sub>/SiO<sub>2</sub>/Si and fused silica substrates. For the films processed on platinized silicon, platinum top electrodes have been sputtered to apply the field out-of-plane in a metal/insulator/metal (MIM) geometry. For the samples deposited on fused silica substrates, interdigitated platinum electrodes (IDE) have been deposited to apply the field in-plane.

In both geometries, we could observe the double hysteresis loop, signature of antiferroelectric switching. We compare the switching characteristics in the two types of sample, with adequate corrections in order to take into account the differences in geometry in the calculation of the applied field. A saturation polarization of up to 36  $\mu\text{C}/\text{cm}^2$  was reached in the IDE geometry. The switching peaks in the current vs. voltage characteristic are generally broader in the IDE geometry as compared to the MIM geometry. Orientation effects alone decrease the switching fields in MIM geometry from 495 kV/cm to 286 kV/cm in the IDE geometry. We discuss these differences with a simple switching model. Additionally, in both geometries, the films display a “ferroelectric-like” contribution at lower fields. This work paves the way for possible applications based on antiferroelectric switching of polycrystalline  $\text{PbZrO}_3$  thin films.

#### 5:20 AM F.EN01.05.04

**Synthesis of Doped Hafnia by Metal-Organic Decomposition (MOD) of Low-Toxicity Chemical Solutions for Energy Harvesting Applications** Miguel A. Badillo-Avila, Beatriz Noheda and Mónica Acuautila; University of Groningen, Netherlands

Since the discovery of ferroelectricity in doped- $\text{HfO}_2$  by Böscke et. al in 2011, doped- $\text{HfO}_2$  has been regarded as an eventual replacement of lead zirconate titanate (PZT), and as a highly promising functional oxide for information storage devices, electromechanical systems, energy storage, and piezoelectric-power generation. Highly ordered, highly piezoelectric orthorhombic and rhombohedral doped- $\text{HfO}_2$  film structures have been obtained by physical deposition techniques such as ALD, PLD and sputtering deposition. Such methods have produced groundbreaking results and astonishing conceptual devices. Unfortunately, they require high-vacuum and expensive high-precision equipment. Chemical solution deposition methods have also yielded decent results, albeit less surprising. Yet, they are more suitable for large scale production, particularly for applications where large areas are needed. Nevertheless, current chemical approaches make use of highly unstable or toxic compounds, which require restrictive inert-atmosphere processing conditions. In our work, we have focused on the sustainable synthesis of piezoelectric doped- $\text{HfO}_2$  good-quality films by employing much less or non-toxic chemical precursors, and short/lower thermal treatments. Besides, no special synthesis conditions are required, which makes the processing cheaper.

We have employed Zr and Ca as dopants of  $\text{HfO}_2$  because such elements are relatively abundant and, like Hf, they do not present risks for human health or for the environment. Chemical precursor solutions of each corresponding metal oxide are prepared in normal air atmosphere from simple and low toxicity compounds dissolved in alcoholic solvents. Solvation-enhancing agents are used to suspend the precursor metal salts. Combustion-boosting compounds are also added to produce an increased annealing temperature, which promotes crystallization. The solutions are mixed in calculated ratios. Thin films of doped- $\text{HfO}_2$  are deposited in normal conditions via spin-coating on platinized silicon substrates. Each layer is dried at 200 to 400 °C for 5 minutes. The process is repeated several times for increased thickness. The films are later annealed in Ar or air ambience at temperatures between 500 and 800 °C. Top Pt electrodes are deposited by e-beam evaporation.

Uniform and dense doped- $\text{HfO}_2$  layers are deposited from the evaporation and Metal-Organic Decomposition (MOD) of the precursor solution components. The solution can be prepared and safely managed in normal ambient because it does not contain sol-gel-type precursors. The most stable crystalline phase of  $\text{HfO}_2$ , monoclinic, is obtained for drying temperatures of 200-300 °C after sintering at 500-800 °C under conventional annealing in Ar and air. However, cubic and/or tetragonal phases mixed with monoclinic phase can be obtained for drying temperature of 400 °C and annealing at 500 °C in Ar and air.

Interestingly, pure cubic or tetragonal phase is obtained at a drying temperature of 400 °C and Rapid Thermal Annealing (RTA) at 500 – 700 °C for 5 minutes. Cubic and/or tetragonal phase is required because it has been demonstrated each can undergo phase-transition to ferroelectric orthorhombic phase during wake-up polarization cycling. The cubic, tetragonal and

orthorhombic phases are stabilized by a small crystallite size. On the contrary, bigger crystals lead to the irreversible formation of the monoclinic phase. The use of a relatively high drying temperature of 400 °C promotes the nucleation of small HfO<sub>2</sub> crystals rather than growth. Besides, annealing in RTA does not allow enough time for such crystals to increase in size, thus stabilizing the higher symmetry phases of HfO<sub>2</sub>.

The fabrication method developed can be used to make films with piezoelectric response, of easy scalability, and with low-toxicity precursor materials.

**5:30 AM \*F.EN01.05.05**

**The Preparation and Dielectric Properties of 2D Nano-Sheets Materials and Composites Based on Electrospinning** Hua Deng; Sichuan University, China

Two dimensional dielectric fillers have been considered to serve as high performance fillers to enhance both the dielectric constant and breakdown strength of various dielectric polymer composites. Nevertheless, the fabrication of these 2D fillers is quite often complicated, and usually rely on the nature availability of these materials. Herein, we demonstrate systematic study on the fabrication of 2D TiO<sub>2</sub> nanofillers through tuning various processing condition of electrospinning. This research work was carried out to investigate the effects of different solution formulas and electrospinning conditions on the morphology of the spinning fibers. The influence of calcination temperature on the preparation of dielectric fillers was studied, and it was applied to the preparation of dielectric composite materials based on PVDF and PI. The energy density of two-dimensional nano-sheets dielectric fillers was investigated, and shows high dielectric constant, high Effects, high breakdown strength and low dielectric loss. The extended application of 2D lamellar fillers in polyimide system under high temperature conditions is further discussed achieving an energy density of 3 J/cm<sup>3</sup> at 150 degree C; 3.5 J/cm<sup>3</sup> at 100 degree C; a charge-discharge efficiency of around 90%. This could provides a theoretical and technical guidelines for the practical application.

**5:45 AM F.EN01.05.06**

**Ultrathin-Enhanced Ferroelectricity in Doped-HfO<sub>2</sub> Films Directly on Silicon** Suraj Cheema<sup>1</sup>, Daewoong Kwon<sup>1</sup>, Nirmaan Shanker<sup>1,1</sup>, Roberto dos Reis<sup>2</sup>, Shang-Lin Hsu<sup>2,2</sup>, Jun Xiao<sup>1</sup>, Cheng-Hsiang Hsu<sup>1</sup>, Haigang Zhang<sup>3</sup>, Ryan Wagner<sup>3</sup>, Ajay Yadav<sup>1</sup>, Claudy Serrao<sup>1</sup>, Golnaz Karbasian<sup>1</sup>, Margaret McCarter<sup>1</sup>, Apurva Mehta<sup>4</sup>, Evgenia Karapetrova<sup>5</sup>, Rajesh Chopdekar<sup>2</sup>, Padraic Shafer<sup>2</sup>, Elke Arenholz<sup>2,6</sup>, Xiang Zhang<sup>2,1</sup>, Chenming Hu<sup>1</sup>, Roger Proksch<sup>3</sup>, Ramamoorthy Ramesh<sup>1,1</sup>, Jim Ciston<sup>2</sup> and Sayeef Salahuddin<sup>1,2</sup>; <sup>1</sup>University of California, Berkeley, United States; <sup>2</sup>Lawrence Berkeley National Laboratory, United States; <sup>3</sup>Oxford Instruments, United States; <sup>4</sup>SLAC National Accelerator Laboratory, United States; <sup>5</sup>Argonne National Laboratory, United States; <sup>6</sup>Cornell University, United States

The critical size limit of ferroelectric order has extensive implications for the future scaling of energy-efficient electronics, particularly due to the intrinsic ability to control electric polarization with an applied voltage. As ferroelectric materials are made thinner however, polarization is typically suppressed, as size effects in ferroelectrics have been thoroughly investigated in the prototypical perovskite oxides. Furthermore, perovskites suffer from various chemical, thermal, electrical, and interfacial incompatibilities with silicon and modern semiconductor processes. Recently, fluorite-structure binary oxides have attracted considerable interest as they overcome many of the silicon compatibility issues afflicting its perovskite ferroelectric counterparts. Here we report ferroelectricity in ultrathin Zr-doped HfO<sub>2</sub> (HZO) [1], a fluorite-structure oxide grown by atomic layer deposition (ALD) on silicon. We demonstrate the persistence of inversion symmetry breaking and spontaneous, switchable polarization down to a thickness of one nanometer, equivalent to just two fluorite-structure unit cells. Second harmonic generation (SHG) and advanced scanning probe techniques – microwave-frequency scanning capacitance microscopy (SCM) and piezoresponse force microscopy (PFM) coupled with an interferometric displacement sensor (IDS) – establish the presence of inversion symmetry breaking and switchable electric polarization in one nanometer HZO films, respectively. Synchrotron X-ray characterization indicate that polar distortions increase in the ultrathin limit; diffraction markers (structural aspect ratio, interplanar lattice spacing) and spectroscopic signatures (orbital polarization, crystal field splitting) of polarization all demonstrate ultrathin enhancement.

These results indicate not only the absence of a ferroelectric critical thickness, but also ultrathin-enhanced ferroelectricity in HZO thin films on silicon. Notably, such ‘reverse’ size effects oppose conventional perovskite ferroelectric trends, which can be understood from the crystal symmetries involved in the competing fluorite-structure polymorphs. Therefore, this work shifts the search for the fundamental limits of ferroelectricity to simpler transition-metal oxide systems – that is, from perovskite-derived complex oxides to fluorite-structure binary oxides – in which ‘reverse’ size effects can counterintuitively stabilize polar symmetry in the ultrathin regime. From a synthesis perspective, these results suggest that harnessing confinement strain – required to crystallize ultrathin HZO into the metastable ferroelectric orthorhombic phase – offers a new

mechanism to control electric polarization at the atomic-scale beyond epitaxial strain. Furthermore, this approach to integrate nanoscale ferroelectricity in doped-HfO<sub>2</sub> thin films directly on silicon via ALD provides a route towards realizing emerging hyper-scaled energy-efficient nanoelectronics [2]. In particular, we have recently demonstrated ferroelectric tunnel junctions [1] and negative capacitance ferroelectric field-effect transistors [3,4] exploiting ultrathin ferroelectric HZO films on silicon, critical steps towards realistic polarization-driven resistive switching memories and ultralow-power advanced transistors, respectively.

[1] S Cheema\*, D Kwon\* [...] S Salahuddin. “Enhanced ferroelectricity in ultrathin films grown directly on silicon.” *Nature* **580**, 478–482 (2020).

[2] S Salahuddin, K Ni & S Datta. “The era of hyper-scaling in electronics.” *Nat. Electron.* **1**, 442–450 (2018).

[3] D Kwon\*, S Cheema\* [...] S Salahuddin. “Negative Capacitance FET with 1.8-nm-Thick Zr-Doped HfO<sub>2</sub> Oxide.” *IEEE Electron Device Lett.* **40**, 993–996 (2019).

[4] D Kwon\*, S Cheema\* [...] S Salahuddin. “Near Threshold Capacitance Matching in a Negative Capacitance FET with 1 nm Effective Oxide Thickness Gate Stack.” *IEEE Electron Device Lett.* **41**, 179–182 (2020).

### 5:55 AM F.EN01.05.07

**van der Waals Epitaxy of Highly (111)-Oriented BaTiO<sub>3</sub> on MXene** Andrew Bennett-Jackson<sup>1</sup>, Matthias Falmbigl<sup>1</sup>, Kanit Hantanasirisakul<sup>1,2</sup>, Gu Zongquan<sup>1,1</sup>, Dominic Imbrenda<sup>1,1</sup>, Aleksandr Plokhikh<sup>1</sup>, Alexandria Will-Cole<sup>1</sup>, Christine Hatter<sup>1,2</sup>, Liyan Wu<sup>3</sup>, Babak Anasori<sup>1,2</sup>, Yury Gogotsi<sup>1,2</sup> and Jonathan Spanier<sup>1,1,1</sup>; <sup>1</sup>Drexel University, United States; <sup>2</sup>A.J. Drexel Nanomaterials Institute, United States; <sup>3</sup>University of Pennsylvania, United States

We report on the high temperature thin film growth of BaTiO<sub>3</sub> on Ti<sub>3</sub>C<sub>2</sub>T<sub>x</sub> (where T<sub>x</sub> represents surface terminations, such as O and F) MXene flakes using van der Waals epitaxy on a degradable template layer. MXene was deposited on amorphous and crystalline substrates by spray- and dip-coating techniques, while the growth of BaTiO<sub>3</sub> at 700 °C was accomplished using pulsed laser deposition in an oxygen rich environment. We demonstrate that the MXene flakes act as a temporary seed layer, which promotes highly oriented BaTiO<sub>3</sub> growth along <111> independent of the underlying substrate. The lattice parameters of the BaTiO<sub>3</sub> films are close to the bulk value suggesting that the BaTiO<sub>3</sub> films remains unstrained, as expected for van der Waals epitaxy. The initial size of the MXene flakes has an impact on the orientation of the BaTiO<sub>3</sub> films with larger flake sizes promoting a higher fraction of the polycrystalline film to grow along the <111>. The deposited BaTiO<sub>3</sub> film adopts the same morphology as the original flakes and piezoresponse force microscopy shows a robust ferroelectric behavior for individual grains. Transmission electron microscopy results indicate that the Ti<sub>3</sub>C<sub>2</sub>T<sub>x</sub> MXene fully decomposes during the BaTiO<sub>3</sub> deposition and the surplus Ti atoms are readily incorporated into the BaTiO<sub>3</sub> film. Electrical measurements show a similar dielectric constant as a BaTiO<sub>3</sub> film grown without the MXene seed layer. The demonstrated process has the potential to overcome the longstanding issue of integrating highly oriented complex oxide thin films directly on any desired substrate. Work supported by the Hearst Foundation, the U.S. Dept. of Energy under DE-SC0018618, the ONR under N00014-15-11-2170, the ARO under W911NF-14-1-0500, the AFOSR under FA9550-13-1-0124, NSF under DMR 1608887, and the NSF under NNCI-1542153.

SESSION F.EN01.06: Poster Session: Emerging Dielectric Materials—Applications In Energy Transmission, Storage and Conversion

On Demand Abstracts Available for Viewing Starting Saturday Morning, November 21, 2020

5:00 AM - 8:00 AM

F-EN01

### F.EN01.06.03

**Novel Bi-Based Photocatalysts with Unprecedented Visible-Light-Driven Hydrogen Production Rate: Experimental and DFT Insights** Nageh K. Allam; American University in Cairo, Egypt

Green and efficient energy technologies are a key point where nanoscience could make a difference in the paradigm shift from fossil fuels to renewable sources. One attractive possibility is the utilization of solar energy to obtain electricity or chemical fuel based on the ability of semiconductor nanomaterials to function as photocatalysts promoting various oxidation and reduction reactions under sunlight. We report on a novel class of Bi-based photocatalysts for hydrogen production via water splitting. A screening DFT investigation was performed on the Bi<sub>2</sub>(MO<sub>4</sub>)<sub>3</sub> (M= Cr, Mo, and W) systems. The Bi<sub>2</sub>(CrO<sub>4</sub>)<sub>3</sub> system exhibits the smallest bandgap energy, the highest dielectric constant, and the highest absorption in the

visible region among the other counterpart materials. Consequently,  $\text{Bi}_2(\text{CrO}_4)_3$  nanoparticles were synthesized via a simple one-pot method at room temperature and characterized by XRD, XPS, DRS, FE-SEM, HR-TEM, and Raman spectroscopy. The as-prepared yellow  $\text{Bi}_2(\text{CrO}_4)_3$  nanoparticles exhibited direct bandgap energy of 2.45 eV. The photoactivity of the as-prepared  $\text{Bi}_2(\text{CrO}_4)_3$  nanoparticles was tested toward the photocatalytic hydrogen production, where reasonable rates of 522.44, 174.15, and 88.24  $\mu\text{mol/g/h}$  were achieved under UV, AM 1.5, and visible irradiations, respectively in the absence of any hole scavengers. Those rates are higher than those reported for Bi-based photocatalysts.

#### **F.EN01.06.04**

**Thermal–Stimulated Evolution of Structural and Optical Properties of Hafnia Films Co-Doped with Si, N and Nd Grown by Magnetron Sputtering** Larysa Khomenkova<sup>1,2</sup>, Tetyana V. Torchynska<sup>3</sup>, Nadiia Korsunskaya<sup>1</sup>, Leonardo G. Vega Macotela<sup>4</sup>, Oleksandr Melnichuk<sup>5</sup> and Fabrice Gourbilleau<sup>6</sup>; <sup>1</sup>V. Lashkaryov Institute of Semiconductor Physics at NASU, Ukraine; <sup>2</sup>National University “Kyiv-Mohyla Academy, Ukraine; <sup>3</sup>Instituto Politécnico Nacional, Mexico; <sup>4</sup>Instituto Politécnico Nacional, Mexico; <sup>5</sup>Mykola Gogol State University, Ukraine; <sup>6</sup>CIMAP, UMR CNRS/CEA/ENSICAEN/UNICAEN, France

Hafnium oxide and its silicates are considered mainly as gate dielectrics owing to their high dielectric constant. Recently, their ferroelectric properties were discovered, whereas optical application of these materials was rarely addressed in spite of promised optical parameters and mechanical and thermal stability. Usually, CVD or ALD approaches are used for the fabrication of hafnia-based films. At the same time magnetron sputtering was considered only by some research groups. In this work, we report on the utility of reactive magnetron sputtering for the fabrication of composite thin films based on  $\text{HfO}_2$  co-doped with Si, N, and Nd ions simultaneously.

The evolution of structural and optical properties of such films with annealing temperature was investigated by means of the scanning electron microscopy, energy-dispersive X-ray spectroscopy, X-ray diffraction, Raman scattering, and photoluminescence techniques. It is observed that sputtering of  $\text{HfO}_2$ -Si-Nd composed target in argon-nitrogen plasma allowed producing homogeneous, dense and smooth films. The analysis of film properties with annealing temperature revealed the stability of film structure up to 950°C.

The light emission in the visible and IR spectral range was detected. It was found that bright  $\text{Nd}^{3+}$ -related emission can be achieved at lower temperatures (about 950°C) contrary to that reported for Nd-doped Si-SiO<sub>2</sub> or Si-Si<sub>3</sub>N<sub>4</sub> materials. The  $\text{Nd}^{3+}$  PL intensity correlates with the evolution of  $\text{HfO}_2$  monoclinic phase. It is shown that the excitation channel of  $\text{Nd}^{3+}$  ions under non-resonant excitation involves host defects contained nitrogen ions. The desorption of nitrogen at high annealing temperature (1100°C) via the formation of volatile NO, as well as the formation of the Nd silicate phase results in the quenching of  $\text{Nd}^{3+}$  photoluminescence. This complex approach used for investigation of our films allowed demonstrating the utility of reactive magnetron sputtering for the fabrication of thin films with stable chemical composition and structure (up to 950°C). These results can be attractive for future applications of the hafnium silicate films (un-doped and doped with rare-earth ions) as emitting elements or waveguides.

#### **F.EN01.06.05**

**Strategy to Choose Best Building Blocks for Efficient Triboelectric Generator Devices** Linards Lapčinskis, Kaspars Malnieks, Artis Linarts, Māris Knite and Andris Sutka; Riga Technical University, Latvia

TEG devices have potential to satisfy growing energy needs in portable electronics and sensors providing a clean alternative to conventional batteries.<sup>1</sup> TEG devices are produced from cheap, lightweight, flexible, widely used polymer materials and offer promise to capture neglected and unutilized forms of mechanical energy. TEG device consists from two conductive electrodes from which at least one is covered with polymer insulator film.<sup>1</sup> The two electrodes in TEG are connected by outer circuit and upon electrode oscillation surface charge on polymer layers and electric potential is created that drive electrons to flow between two electrodes in order to balance this electric potential difference. TEG devices can be operated in different modes – vertical separation, sliding, rotating, single electrode etc.<sup>2</sup> but the key feature for high TEG efficiency is surface charge from contact electrification.<sup>3</sup>

Different mechanisms are responsible for contact electrification and depend on material used. It is well demonstrated, that on metal-metal, metal-semiconductor or semiconductor-semiconductor contact the electron transfer occurs,<sup>4,5</sup> but this is not so obvious for polymer insulators.<sup>6</sup> The three mechanisms for polymer insulator contact electrification are considered – electron transfer,<sup>7</sup> ionic transfer,<sup>6</sup> and covalent bond cleavage.<sup>8</sup> Electron transfer between polymers is doubtful, because there are no available free electrons in insulators. Usage of the term “effective work function” in connection to the driving force for charge exchange between polymer insulators is also questionable even if the polymer is contacted with metal.<sup>6</sup> Ion exchange between contacted polymer insulators has been considered, because water under ambient conditions is adsorbed even on hydrophobic polymers.<sup>9</sup> The water layers on contacted surfaces fuse together upon contacting and as different polymer materials may have different affinity towards cations and anions in water, the imbalance between ions form during

separation, thus creating surface charge.<sup>6</sup> However, it has been proven, that contact electrification of polymer insulators also occurs in complete absence of water.<sup>10</sup>

In our work we show that polymer contact-electrification can be predicted using their cohesive energy density. This allows us to select the most suitable materials as the building blocks for efficient TEG devices.

## References

- [1] Z.L. Wang, *ACS Nano*, 2013, 7, 9533-9557.
- [2] R. Hinchet, W. Seung, S.-W. Kim, *ChemSusChem*, 2015, 8, 2327-2344.
- [3] J. Wang, C. Wu, Y. Dai, Z. Zhao, A. Wang, T. Zhang, Z.L. Wang, *Nature Commun.*, 2017, 8, 88.
- [4] J. Lowell, *J. Phys. D: Appl. Phys.*, 1975, 8, 53-63.
- [5] J. Liu, A. Goswami, K. Jiang, F. Khan, S. Kim, R. McGee, Z. Li, Z. Hu, J. Lee, T. Thundat, *Nature Nanotechnol.*, 2018, 13, 112-116.
- [6] L.S. McCarty, G.M. Whitesides, *Angew. Chem. Int. Ed.*, 2008, 47, 2188-2207.
- [7] M. Willatzen, Z.L. Wang, *Nano Energy*, 2018, 52, 517-523.
- [8] H.T. Baytekin, A.Z. Patashinski, M. Branicki, B. Baytekin, S. Soh, B.A. Grzybowski, *Science*, 2011, 333, 308-312.
- [9] H.T. Baytekin, B. Baytekin, S.S., B.A. Grzybowski, *Angew. Chem. Int. Ed.*, 2011, 50, 6766-6770.
- [10] A.L. Sumner, E.J. Menke, Y. Dubowski, J.T. Newberg, R.M. Penner, J.C. Hemminger, L.M. Wingen, T. Brauers, B.J. Finlayson-Pitts, *Phys. Chem. Chem. Phys.*, 2004, 6, 604-613.

## F.EN01.06.06

**Characterization of Various High k Gate Dielectric Thin Films for TFT Applications** Kelsea Yarbrough, Sangram K. Pradhan and Messaoud Bahoura; Norfolk State University, United States

Traditional dielectric materials such as silicon dioxide ( $\text{SiO}_2$ ) is the first choice and mostly used in many electronic devices including Metal Oxide Semiconductor Field Effect Transistors, Thin Film Transistors, and VLSI technology. However,  $\text{SiO}_2$  has several disadvantages that researchers are currently looking for alternatives. Scaling down electronics are the most popular device approach where  $\text{SiO}_2$  will not be able to fit in these ultralow dimensional adjustments. One approach to scaling down electronics, while sustaining adequate dielectric properties is incorporating high k dielectrics. High k dielectrics refer to materials with a high dielectric constant, which denotes the material ability to store an electrical charge.

$\text{SiO}_2$  generally has a dielectric constant value of 4, while high k dielectrics have a dielectric constant greater than approximately 10. Noteworthy high k dielectrics include Hafnium Oxide ( $\text{HfO}_2$ ), Zirconium Oxide ( $\text{ZrO}_2$ ), and Aluminum Oxide ( $\text{Al}_2\text{O}_3$ ). In this study, we perform important characterization techniques to analyze  $\text{HfO}_2$ ,  $\text{ZrO}_2$ , and  $\text{Al}_2\text{O}_3$  for the possible replacement of  $\text{SiO}_2$ . These high k dielectric thin films exhibited leakage currents lower than  $9.45 \times 10^{-11}$  and with a thin film roughness of less than .5 nm. These high-quality high k dielectrics thin films were grown by Atomic Layer Deposition on n-type silicon at a different temperature and constant thickness for premise characterization. The effect of temperature on surface morphology, crystalline orientation, and dielectric properties were analyzed through Atomic Force Microscopy (AFM), X-ray Diffraction (XRD), Keithley 4200 SCS, and Four Point Probe measurement system. AFM provided thin film roughness, grain size, and surface morphology for thin films. XRD provided the crystalline orientation of these high k dielectrics with the effect of temperature. Keithley 4200 was used to show and calculate the dielectric properties including; dielectric constant, I-V plots (leakage current), and C-V plots. Lastly, Four Point probe measurement system provided electrical properties for these high k dielectrics. The present work will provide valuable scientific input dielectric performance for the improvement of TFT devices.

## F.EN01.06.07

**Mechanically Robust PVDF/Isocyanate-Treated Graphene Oxide Composite Nanofiber and Its Piezoelectric Sensor Applications** Madeshwaran Sekkarapatti Ramasamy and Byungki Kim; Korea University of Technology and Education, Korea (the Republic of)

Graphene, the two dimensional material with  $\text{sp}^2$ -hybridized carbon atoms arranged in honeycomb-like structure has attracted greatest research interests because of their excellent mechanical and electrical properties. In particular, graphene have been considered as one of the most promising reinforcing nanofillers for developing cost-effective, high performance polymer composites. However, their main drawback is associated with their poor solution processability in organic solvents and agglomeration in polymer matrix due to their Van der Waals forces. Graphene oxide (GO), derived from acidic oxidation of natural graphite possesses abundant oxygen containing functionalities exhibit good solution processability, and therefore, receiving attention as precursor to the graphene-based nanofillers. On the other hand, poly(vinylidene fluoride) (PVDF) have been actively applied in piezoelectric sensors and nanogenerators because of their electroactive properties and flexibility. Generally, PVDF present five crystalline phases such as,  $\alpha$ ,  $\delta$ ,  $\beta$ ,  $\gamma$  and  $\epsilon$ , among them,  $\beta$ -phase PVDF with TTTT

conformation shows the best piezoelectric properties, because all the dipoles are arranged parallel which resulted in highest dipole moment per unit cells. Incorporating GO into PVDF matrix can promote the formation of preferred  $\beta$ -phases owing to the interaction between the oxygen functionalities of GO and dipoles of the PVDF chains. In addition, the intrinsic high mechanical properties of GO can also enhance the mechanical properties of PVDF matrix. However, in most of the polymer composite systems, the strength and stiffness increased with the addition of nanofillers, meanwhile, the toughness decreased due to reduction in strain at break, which often restricts their applications in stretchable and flexible electronics. Herein, we report a method for fabricating PVDF/GO composite nanofibers with significantly enhanced mechanical strength and modulus without losing its toughness/stretchability. Isocyanate treated GO (i-GO) nanosheets were incorporated as nanofillers into PVDF nanofibers (PVDFNFs) using solution blending and electrospinning techniques. i-GO exhibit strong interfacial interaction with PVDF due to its reduced hydrophilicity and excellent dispersibility in organic solvents. FTIR results revealed that the addition of i-GO induce the formation of PVDFNFs with high content of electroactive phases. Interestingly, the tensile strength, modulus and as well as strain-at-break increased with the addition i-GO. Furthermore, the composites displayed enhanced piezoelectric outputs than that of reference PVDFNFs during the static load analysis. The enhanced performance of the composites can be attributed to the strong interaction between i-GO and PVDF achieved through incorporation of chemically modified GO. The reported composites in this study hold a great potential in the field of flexible and stretchable piezoelectric sensors and nanogenerators.

#### Acknowledgements

This work was supported by Grant NRF-2018R1A6A1A03025526 under the Priority Research Program through National Research Foundation of Korea(NRF) under Ministry of Education.

#### F.EN01.06.08

**Dramatic Increase in Polymer Triboelectrification by Transition from a Glassy to Rubbery State** Artis Linarts, Andris Sutka, Kaspars Malnieks and Linards Lapčinskis; Riga Technical University, Latvia

Triboelectric nanogenerators (TENG) are intriguing energy harvesting devices that convert mechanical energy into electricity and could power small portable devices or charge batteries [1]. Here we report contact electrification of glassy polymers at different temperatures and observing a dramatic three orders of magnitude increase in surface charge when passing the transition temperature to a rubbery state. Transition is accompanied by a larger force required for separation due to material softening and increased stickiness. This enhances material transfer during contact/separation cycles and indicates covalent bond breaking as the mechanism for increased polymer triboelectrification. Undeniably, surface roughness plays a great role in contact electrification, however in our study its impact is overrated when compared to the influence of physical properties.

[1] Z.L. Wang “Triboelectric Nanogenerators as New Energy Technology for Self-Powered Systems and as Active Mechanical and Chemical Sensors”, ACS Nano 7 (2013) 9533-9557.

#### F.EN01.06.09

**Matching the Directions of Electric Fields from Triboelectric and Ferroelectric Charges in Nanogenerator Devices for Boosted Performance** Kaspars Malnieks, Andris Sutka, Linards Lapčinskis and Artis Linarts; Riga Technical University, Latvia

The field related to triboelectricnanogenerator (TENG) devices is emerging rapidly. Many original and creative TENG concepts have been presented in the literature for harvesting mechanical energy and converting it into electricity (Lee et al., 2019). The working principle of TENG devices is straightforward. Due to electrode oscillation or movement, a potential difference is created, which causes a current flow in the external electric circuit. TENG devices can be integrated into fabrics, wearables, interior objects, membranes (to harvest energy from sound), and even implantable devices.

To enhance the performance of TENG, different approaches have been used. The most obvious way is to increase the specific contact area via nanostructuring (Zhang et al.). Another possibility is the modification of surface or physicochemical properties of the triboelectric material (Sutka et al., 2019). The performance can be also enhanced by using ferroelectric polymer or composite films as the contacting surfaces (Bai et al.). State-of-the-art performance of ferroelectric material-based TENG devices can be expected when the ferroelectric material layers on contacting sides of the device are inversely polarized (Sutka et al). However, previous works related to TENG devices based on ferroelectric materials overlook the dipole that forms between the triboelectric surface charges on contacting surfaces. As soon as we consider this additional factor, it follows that the electric field direction from ferroelectric dipoles should match the direction of the electric field from triboelectric surface charge to achieve maximum electric field strength and electrostatic induction.

Polydimethylsiloxane (PDMS), ethylene-vinyl acetate copolymer (EVA), poly(vinyl acetate) (PVAc), and poly(methyl methacrylate) (PMMA) were used in our studies to prepare TENG devices. The polymer films were spin coated on indium tin oxide (ITO) conductive electrode and contacted against another ITO. The polymer films were given ferroelectric properties by adding 7.5 vol% BaTiO<sub>3</sub> nanoparticles. The sign of triboelectric surface charges formed on pure polymers after contacting against ITO was determined by measuring the current between the underlying electrode and the ground in Faraday cup mode. Polymers PDMS, PVAc, and EVA obtain a negative charge on their surface whereas for PMMA a positive charge is observed when contacted ITO. The sign of the net triboelectric charge did not change when BaTiO<sub>3</sub> nanoparticles were incorporated into the polymers. All poled BaTiO<sub>3</sub>/polymer composites exhibit piezoelectric properties. The piezoelectric charges of 2.9 pC/cm<sup>2</sup>, 10.9 pC/cm<sup>2</sup>, 3.7 pC/cm<sup>2</sup>, and 2.4 pC/cm<sup>2</sup> were measured for BaTiO<sub>3</sub>/EVA, BaTiO<sub>3</sub>/PDMS, BaTiO<sub>3</sub>/PVAc, and BaTiO<sub>3</sub>/PMMA composites, respectively. The higher piezoelectric response of BaTiO<sub>3</sub>/PDMS could be attributed to its larger deformability under the constant loading force. Composite layer in each of these TENG devices was tested as non-poled and also positively and negatively poled, so that ferroelectric dipole is matched and mismatched with the previously determined surface charge.

As example BaTiO<sub>3</sub>/PDMS TENG device performed excellently, and the output was superior to any other presented in this study. The peak open-circuit voltage ( $V_{OC}$ ) of device with matched dipoles reached 460 V, instant energy and power densities of this TENG device reached 9.7 mJ/m<sup>2</sup> and 143.2 mW/m<sup>2</sup>, respectively. For comparison, a TENG device from the same polymers without BaTiO<sub>3</sub> NPs shows  $V_{OC}$  as small as 16 V and three orders of magnitude smaller energy and power densities of 0.012 mJ/m<sup>2</sup> and 0.104 mW/m<sup>2</sup>. Also, the TENG device from the same inversely polarized composite films but with mismatched dipoles exhibited significantly lower output— $V_{OC}$  of 300 V and instant energy and power densities of 4.0 mJ/m<sup>2</sup> and 91.6 mW/m<sup>2</sup> from the same contacting area.

#### **F.EN01.06.10**

##### **Towards Engineering Mixed Oxide Thin Films Using a Genomic Approach—A Case Study of Ta<sub>2</sub>O<sub>5</sub>-Based Coatings** Mariana A. Fazio, Le Yang and Carmen Menoni; Colorado State University, United States

Mixed oxide thin films have found their way into numerous applications ranging from high-k dielectrics to gas sensors to optical coatings with tunable properties. The field is vast and most research conducted on mixed oxide coatings has been approached from the experimental side, leading to an arduous and time-consuming trial-and-error process. In the last decade, emerging computational methods have been conducive to accelerated materials discovery. In particular, the genomics approach behind open access initiatives such as the Materials Project aims to provide materials scientists with a new set of tools: large databases of computational calculations of known and predicted materials. This web-based database leads the way for *in silico* material design that can guide experimentation.

In this work, we carried out an extensive study of tantalum (Ta<sub>2</sub>O<sub>5</sub>) amorphous thin films doped with Al, Si, Sc, Ti, Zn, Y, Zr, Nb and Hf grown by reactive sputtering. The influence of the dopant and post-deposition annealing on the film properties and structure was characterized by grazing-incidence x-ray diffraction, x-ray photoelectron spectroscopy and spectroscopic ellipsometry. Using the Materials Project database, compositional phase diagrams based on density functional theory calculations were constructed for all mixed oxide systems and the annealing process was evaluated via grand potential phase diagrams with varying oxygen chemical potential. The computational calculations agree well with experimental results, predicting formation of ternary compounds after annealing in some systems. When no ternary phase can be stabilized, the dopant acts as an amorphizer agent increasing the crystallization temperature of tantalum. In the case where the dopant forms an oxide with similar formation enthalpy to tantalum we experimentally observed effects of oxygen competition that lead to formation of phases that are predicted to be unstable. Overall, the predictions based on the Materials Project database provide valuable information for tailoring dopant type and concentration in mixed oxide thin films towards specific applications that might require increased thermal stability or to adjust processing conditions for ternary oxide production.

#### **F.EN01.06.11**

##### **Characterization of MnO<sub>2</sub>-MWCNT Nanocomposite Morphology for Supercapacitor Applications** Rian

Tucci<sup>1,2</sup>, Thomas Sadowski<sup>1,2</sup>, Rahul Singhal<sup>3,2</sup> and Christine Broadbridge<sup>1,2</sup>; <sup>1</sup>Southern Connecticut State University, United States; <sup>2</sup>Connecticut State Colleges and Universities (CSCU) Center for Nanotechnology, United States; <sup>3</sup>Central Connecticut State University, United States

Supercapacitors, with long cycle lives and long-term efficiency, have potential to become an appealing alternative to lithium-ion batteries; however, the specific energy of these devices lags well behind current state-of-the-art lithium-ion batteries. Nevertheless, numerous opportunities exist to optimize supercapacitors through the manipulation of the structure and morphology of novel materials. The implementation of hybrid supercapacitors, a device which combines a pseudo-capacitor

with an electrical double layer capacitor, are of interest because material composites have greater charge storage capabilities than their components alone. The most effective hybrid capacitors for charge storage are ones possessing high specific capacitance (capacitance per unit mass). The optimization of a composite for high specific capacitance requires changes to intrinsic material properties, either by changing chemical or physical structures. The current study was aimed at the manipulation of the nanostructure of a manganese dioxide ( $\text{MnO}_2$ ) – multi walled carbon nanotube (MWCNT) composite material via modulation of MWCNT composite concentration. The composite nanostructure was characterized using transmission electron microscopy (TEM), x-ray diffraction (XRD), charge-discharge tests, and cyclic voltammetry. Ten composites, each with different initial MWCNT concentrations, were synthesized via hydrothermal method. All ten concentrations were imaged via TEM. Of those ten, three were chosen to be characterized with electrochemical methods and XRD: 4.8%, 16.9%, and 33.7% mass MWCNT. TEM imaging reveals a nanostructure of polycrystalline  $\text{MnO}_2$  adsorbed onto MWCNT. Results indicated that, on average, the thickness of  $\text{MnO}_2$  coating decreased as percent mass MWCNT increased. At 33.7% MWCNT mass, MWCNT agglomeration became hard to mitigate and dominated  $\text{MnO}_2$  adsorption structure. This is supported by XRD of 33.7% sample showing emergence of (002) plane of CNT, indicating widespread non-coating of  $\text{MnO}_2$  in composite. Charge-discharge tests were conducted in with a 1 V window at 0.5, 1, and 2 A/g. Charge-discharge tests with 1 A/g indicate highest specific capacitance for 16.9% mass MWCNT at 150 F/g, compared to 70 and 45 F/g with 4.8% and 33.7% mass MWCNT, respectively. Preliminary results indicate that as MWCNT concentration increases, there is a decline in the average  $\text{MnO}_2$  aggregation thickness, with this thickness potentially impacting the specific capacitance of the resulting device.

#### F.EN01.06.12

**Emergent Polar Vortex and Light Switching Behavior in Nanolayered  $\text{SrTiO}_3/\text{PbTiO}_3$  Crystal** Ken-ichi Nomura<sup>1</sup>, Thomas Linker<sup>1</sup>, Rajiv Kalia<sup>1</sup>, Aravind Krishnamoorthy<sup>1</sup>, Aiichiro Nakano<sup>1</sup>, Kohei Shimamura<sup>2</sup>, Fuyuki Shimojo<sup>2</sup>, Subodh C. Tiwari<sup>1</sup> and Priya Vashishta<sup>1</sup>; <sup>1</sup>University of Southern California, United States; <sup>2</sup>Kumamoto University, Japan

Oxide perovskite is an excellent platform for energy, sensing, and electronics applications, and their dielectric property has been extensively studied to date. Recently, superlattices of dielectric (*e.g.*  $\text{SrTiO}_3$ ) and ferroelectric (*e.g.*  $\text{PbTiO}_3$ ) materials have been shown to exhibit various emergent properties. An example is a newly discovered materials state of which could overcome fundamental limitations on the power consumption of field-effect transistors. Another emergent property is novel topological states of polarization such as vortex-antivortex arrays and with quantized skyrmion number. The formation of the polarization structures involves nanometric domains with opposite polarization orientation separated by domain walls (DWs). Highly complex DW characteristics as well as DW interactions dictates the design and control of functional ferroelectric devices. Furthermore, these topological phases can be switched on and off by ultrafast light pulses, opening up a fascinating opportunity for light-activated pathways to thermally-inaccessible and emergent metastable states. The scientific challenge here is to understand the intricate interplay between lattice polarization, strains in complex superlattice and polarization-vortex geometries, and excited electrons which triggers the light-induced structural transitions from first principles. In this talk, I will discuss non-adiabatic quantum molecular dynamics (NAQMD) simulations of light switching behavior of topological states in a  $\text{SrTiO}_3/\text{PbTiO}_3$  superlattice, as well as artificial neural network (ANN) MD simulations to study the structure and dynamics of polar vortex arrays encompassing sufficient length scales to represent realistic supercrystalline dimensions.

This work was supported as part of the Computational Materials Sciences Program funded by the U.S. Department of Energy, Office of Science, Basic Energy Sciences, under Award Number The simulations were performed at the Argonne Leadership Computing Facility under the DOE INCITE and Aurora Early Science programs and at the Center for High Performance Computing of the University of Southern California.

#### F.EN01.06.13

**Lattice Dynamics and Raman Spectrum of  $\text{BaZrO}_3$**  Constance Toulouse and Mael Guennou; Université du Luxembourg, Luxembourg

$\text{BaZrO}_3$  is one of the end-members of remarkable perovskite systems: the binary  $\text{Ba}(\text{Zr},\text{Ti})\text{O}_3$ , studied for its relaxor-to-ferroelectric crossover, and the pseudo-ternary  $(\text{Ba},\text{Ca})(\text{Ti},\text{Zr})\text{O}_3$ , identified as promising for lead-free piezoelectrics. Pure  $\text{BaZrO}_3$  exhibits the simple cubic structure down to 2 K, but theoretical DFT studies show that the cubic phase is slightly unstable, with an unstable phonon mode that should give rise to an antiferrodistortive transition driven by octahedral tilts. It has been also suggested that such distortions exist as distorted nano-domains. Experimentally, because of its very high melting point, investigations of  $\text{BaZrO}_3$  have been mostly limited to polycrystalline samples. Here, we revisit its structure and properties using recently grown single crystals. In particular, we studied the unstable phonon mode by neutron scattering, and performed Raman measurements in a wide range of temperatures and pressures (up to 20 GPa). With the support of detailed



calculations of the lattice dynamics, we show that the Raman spectrum does not confirm the hypothesis of distorted nano-domains, but instead can be explained by second-order scattering.

#### **F.EN01.06.16**

**Cellulose Nanoparticles in Energy Storage Applications** Prathima P. Tumkur and Govindarajan Ramesh; Norfolk State University, United States

In recent years, environmentally friendly supercapacitors are gaining importance amongst researchers due to environmental concerns. Cellulose is one of the environmentally friendly biomaterials having properties such as renewability, degradability, biocompatibility, and cost-effectiveness that has drawn a considerable amount of attention in the energy applications. In the present work, chemically synthesized cellulose nanoparticles were used in the energy storage applications to develop a supercapacitor. A mixture of carbon and cellulose nanoparticles was used as the electrode materials which were coated on a stainless-steel disk and assembled in a coin cell to develop a supercapacitor. Various electrolytes were used in the assembly to determine the best suitable one to obtain improved specific capacitance with large cyclic stability.

#### **F.EN01.06.17**

**Late News: Controlled Synthesis, Piezoelectric, Magnetic and Dielectric Characterization of Novel Europium Titanate Nanoscale Structures—Implications for Energy Storage and Transfer** Benard Kavey and Gabriel Caruntu; Central Michigan University, United States

Europium titanate is known to crystallize in the pyrochlore crystal structure with the general formula  $A_2B_2O_7$ . Within the crystal structure, the A-site cations are occupied by  $Eu^{n+}$  ions whereas the B-sites are occupied by  $Ti^{n+}$  ions in which the spins of the atoms are arranged on the vertices of tetrahedrons linked together at their corners. The high degree of freedom of rotation and vibration in the three-dimensional framework of tetrahedrons allows for a stronger spin interaction in the crystal lattice. The result of this interaction brings about a variety of magnetic properties that largely depends on the A-site cations, in this case,  $Eu^{n+}$  ions. In this work, novel piezoelectric europium titanate nanorods have been synthesized by using a simple solvothermal route in the temperature range 160-180 °C. TEM micrographs of the as-prepared samples show nanorods with lengths ranging from 0.3 to 1.2  $\mu m$  and an average diameter of  $40 \pm 5$  nm. The nanorods become more elongated but rather thinner (length range = 0.5 – 1.6  $\mu m$ , and diameter =  $10 \pm 5$  nm) when the as-synthesized powder was annealed at 800 °C. Powder X-ray diffraction pattern of the nanorods showed pure and highly crystalline pattern consistent with the diffraction patterns seen in  $Eu_2Ti_2O_7$  nanocrystals. Dielectric spectroscopy of the pelletized  $Eu_2Ti_2O_7$  revealed high-k dielectric constant up to  $\epsilon = 4000$  at room temperature. In this study, scanning probe microscope was used to measure the magnetic interactions in the solution-processed  $Eu_2Ti_2O_7$  nanorods thin-film. AFM topography images showed that the fabricated nanocrystals thin-film have an average thickness of 180 nm on a silicon substrate. The corresponding magnetic force microscope (MFM) images, were obtained by raising the magnetized MFM probe by 25 nm (delta height) above the sample surface in the tapping/lift mode. Since the probe tip uniformly scans at a height of 25 nm above the sample surface, the topography signal of the sample surface was drastically minimized allowing for the magnetic interactions to be mapped. This method allowed for the detection of the nanoscopic magnetic domains by measuring the interaction between the cantilever tip and sample surface. The widespread magnetic interactions can be visibly seen as a change in contrast (phase shift) in the amplitude and phase images.

#### **F.EN01.06.18**

**Late News: MOCVD of Functional Dy-Doped BiFeO<sub>3</sub> Film Grown on Single Crystal** Quentin Micard<sup>1</sup>, Giacomo Clementi<sup>2</sup>, Ausrine Bartasyte<sup>2</sup>, Paul Muralt<sup>3</sup>, Guglielmo G. Condorelli<sup>1</sup> and Graziella Malandrino<sup>1</sup>; <sup>1</sup>University of Catania - INSTM, Italy; <sup>2</sup>FEMTO-ST Institute, University of Bourgogne Franche-Comté, France; <sup>3</sup>EPFL, Switzerland

The deposition of  $BiFeO_3$  has been widely investigated in the recent years. Among multiferroic materials  $BiFeO_3$  is of a special interest since its ferroelectric and magnetic transition temperatures are well above the room temperature ( $T_C \approx 1100$  K and  $T_N \approx 650$  K) [1]. Depositions of  $BiFeO_3$  films by chemical routes: sol-gel, chemical solution deposition (CSD) and physical methods: sputtering, pulsed laser deposition (PLD) on single crystals such as  $SrTiO_3$  or  $LaAlO_3$  are well established. Despite its major role in industry MOCVD process is not as much investigated as other deposition techniques, but it has the major advantage to be easily scaled up. Recent works have been focused on A-site doping with rare-earth ions [2].

This work reports a simple MOCVD process for Dy-doped  $BiFeO_3$  thin films on conductive Nb-doped  $SrTiO_3$  (100) substrates. A multicomponent mixture composed of  $Bi(phenyl)_3$ ,  $Dy(hfa)_3$  diglyme and  $Fe(tmhd)_3$  (phenyl =  $-C_6H_5$ , H-hfa = 1,1,1,5,5,5-hexafluoro-2,4-pentanedione, diglyme = 1-methoxy-2-(2-methoxyethoxy)ethane, H-tmhd = 2,2,6,6-tetramethyl-3,5-heptanedione), has been used as precursor source. Nb: $SrTiO_3$  is acting simultaneously as a substrate and a bottom

electrode, top gold electrodes have been sputtered after film deposition.

The piezoelectric, pyroelectric, and ferroelectric properties strongly depend on the structural and compositional properties of the deposited film with attention to the Dy doping. This correlation has been done using X-ray diffraction (XRD), for the structural characterization, field-emission scanning electron microscopy (FE-SEM), atomic force microscopy (AFM), and energy dispersive X-ray (EDX), X-ray photoelectron spectroscopy (XPX) analyses for the morphologic and chemical characterizations, respectively. For the functional study, the permittivity, piezo-, pyro- and ferro-electric response of deposited films have been investigated by impedance spectroscopy, Piezoelectric Force Microscopy (PFM), pyroelectric measurement and P-V loop, respectively. Significant correlation between Dy doping and film properties have been observed and promising pyro-electric coefficients were measured.

### Acknowledgment

This work is supported by the European Community under the Horizon 2020 Programme in the form of the MSCA-ITN-2016 ENHANCE project, Grant Agreement N.722496.

### References

- [1] T. Choi, S. Lee, Y. J. Choi, V. Kiryukhin, S.-W. Cheong, *Science* (2009), 324, 63  
[2] M. R. Catalano, G. Spedalotto, G. G. Condorelli, G. Malandrino, *Adv. Mater Interfaces* (2017), 1601025

**Corresponding author:** Graziella Malandrino, +39-095-7385055, gmalandrino@unicit.it

### F.EN01.06.19

**Late News: Synthesis of Novel Lithium Adducts as Precursors for Lithium Niobate Films by DLI-MOCVD** Nishant Peddagopu<sup>1</sup>, Patrizia Rossi<sup>2</sup>, Paola Paoli<sup>2</sup>, Ausrine Bartasyte<sup>3</sup> and Graziella Malandrino<sup>1</sup>; <sup>1</sup>INSTM, University of Catania, Italy; <sup>2</sup>University of Florence, Italy; <sup>3</sup>University of Franche-Comté, France

Lithium niobate (LiNbO<sub>3</sub>) nanomaterials have recently attracted considerable attention due to their wide range of applications in the fields of ferroelectrics, piezoelectrics, and nonlinear optics. This material has been referred to as the “silicon of photonics” due to its exceptional optical properties. Applications for quantum photonics, surface acoustic wave devices, ferroelectric based devices, etc. require the availability of LiNbO<sub>3</sub> in thin-film form. To this aim, various techniques have been applied such as capillary liquid epitaxial technique [1], RF- magnetron sputtering [2], spin-coating [3], and metalorganic chemical vapor deposition (MOCVD) [4]. MOCVD represents one of the most appealing processes in view of its easy scalability, but its application requires the use of precursors with appropriate mass transport properties. Despite these promising advantages, industrial applications of an MOCVD process are still limited, likely because the commercial availability of starting molecular compounds is insufficient. Very few lithium precursors are known for vapor phase processes, either MOCVD or atomic layer deposition.

In this work, we report on the syntheses, through a single-step reaction, of novel adducts of lithium hexafluoroacetylacetonato {Li(hfa)} with polyethers (monoglyme = {CH<sub>3</sub>OCH<sub>2</sub>CH<sub>2</sub>OCH<sub>3</sub>}, diglyme = {CH<sub>3</sub>O(CH<sub>2</sub>CH<sub>2</sub>O)<sub>2</sub>CH<sub>3</sub>}, triglyme = {CH<sub>3</sub>O(CH<sub>2</sub>CH<sub>2</sub>O)<sub>3</sub>CH<sub>3</sub>} and tetraglyme {CH<sub>3</sub>O(CH<sub>2</sub>CH<sub>2</sub>O)<sub>4</sub>CH<sub>3</sub>} [5]. They have been characterized by elemental analyses, FT-IR spectroscopy, <sup>1</sup>H, and <sup>13</sup>C NMR. Single crystal X-ray diffraction studies provide evidence of interesting coordination moieties [7]. Lithium niobate films have been deposited on sapphire and Si using direct liquid injection (DLI-) MOCVD reactor. X-ray diffraction and scanning electron microscopy characterizations have allowed assessing the film quality.

The mass transport properties of these adducts have been investigated through thermogravimetric (TG) analysis. The TG curve of the “Li(hfa)monoglyme” shows a step mass loss with a residue of 6% at 338 °C. Thermal analysis data revealed a discrete behavior, when precursors are used in a suited temperature range, regarding conventional MOCVD applications, while its solubility and clean decomposition make these complexes interesting precursors for liquid assisted processes such as liquid-delivery and aerosol-assisted MOCVD or sol-gel applications.

The depositions have been carried in a pulsed liquid injection MOCVD reactor using the different lithium precursors and a correlation between the precursor nature and film properties have been derived.

### Acknowledgments

This work is supported by the European Community under the Horizon 2020 Programme in the form of the MSCA-ITN-2016 ENHANCE project, Grant Agreement N.722496.

- [1] T. Fukuda, H. Hirano, *J. Cryst. Growth*, 50, (1980), 291.  
[2] J. Ye, X. Sun, Z. Wu, J. Liu, Y. An, *J. Alloys Comp.*, 768, (2018), 750.

- [3] M. A. Fakhri, E. T. Salim, A. W. Abdulwahhab, U. Hashim, Z. T. Salim, *Optics & Laser Technol.*, 103, (2018), 226.  
[4] A. Bartaszyte, S. Margueron, T. Baron, S. Oliveri, P. Boulet, *Adv. Mater. Interfaces*, 4, (2017), 1600998.  
[5] N. Peddagopu, P. Rossi, C. Bonaccorso, A. Bartaszyte, P. Paoli & G. Malandrino, *Dalton Trans.*, 49, (2020), 1002.

SESSION F.LP04.03: Live Poster Session: Energy (F.EN01, F.EN06 and F.EN09)  
Session Chairs: Katharine Page, Yuliya Preger, Linda Schadler, Donghai Wang and Markus Winterer  
Wednesday Afternoon, December 2, 2020  
5:15 PM - 7:15 PM  
F.EN01

#### F.EN01.06.03

##### **Novel Bi-Based Photocatalysts with Unprecedented Visible-Light-Driven Hydrogen Production Rate: Experimental and DFT Insights** Nageh K. Allam; American University in Cairo, Egypt

Green and efficient energy technologies are a key point where nanoscience could make a difference in the paradigm shift from fossil fuels to renewable sources. One attractive possibility is the utilization of solar energy to obtain electricity or chemical fuel based on the ability of semiconductor nanomaterials to function as photocatalysts promoting various oxidation and reduction reactions under sunlight. We report on a novel class of Bi-based photocatalysts for hydrogen production via water splitting. A screening DFT investigation was performed on the  $\text{Bi}_2(\text{MO}_4)_3$  (M= Cr, Mo, and W) systems. The  $\text{Bi}_2(\text{CrO}_4)_3$  system exhibits the smallest bandgap energy, the highest dielectric constant, and the highest absorption in the visible region among the other counterpart materials. Consequently,  $\text{Bi}_2(\text{CrO}_4)_3$  nanoparticles were synthesized via a simple one-pot method at room temperature and characterized by XRD, XPS, DRS, FE-SEM, HR-TEM, and Raman spectroscopy. The as-prepared yellow  $\text{Bi}_2(\text{CrO}_4)_3$  nanoparticles exhibited direct bandgap energy of 2.45 eV. The photoactivity of the as-prepared  $\text{Bi}_2(\text{CrO}_4)_3$  nanoparticles was tested toward the photocatalytic hydrogen production, where reasonable rates of 522.44, 174.15, and 88.24  $\mu\text{mol/g/h}$  were achieved under UV, AM 1.5, and visible irradiations, respectively in the absence of any hole scavengers. Those rates are higher than those reported for Bi-based photocatalysts.

#### F.EN01.06.04

##### **Thermal-Stimulated Evolution of Structural and Optical Properties of Hafnia Films Co-Doped with Si, N and Nd Grown by Magnetron Sputtering** Larysa Khomenkova<sup>1,2</sup>, Tetyana V. Torchynska<sup>3</sup>, Nadiia Korsunsk<sup>1</sup>, Leonardo G. Vega Macotela<sup>4</sup>, Oleksandr Melnichuk<sup>5</sup> and Fabrice Gourbilleau<sup>6</sup>; <sup>1</sup>V. Lashkaryov Institute of Semiconductor Physics at NASU, Ukraine; <sup>2</sup>National University "Kyiv-Mohyla Academy, Ukraine; <sup>3</sup>Instituto Politécnico Nacional, Mexico; <sup>4</sup>Instituto Politécnico Nacional, Mexico; <sup>5</sup>Mykola Gogol State University, Ukraine; <sup>6</sup>CIMAP, UMR CNRS/CEA/ENSICAEN/UNICAEN, France

Hafnium oxide and its silicates are considered mainly as gate dielectrics owing to their high dielectric constant. Recently, their ferroelectric properties were discovered, whereas optical application of these materials was rarely addressed in spite of promised optical parameters and mechanical and thermal stability. Usually, CVD or ALD approaches are used for the fabrication of hafnia-based films. At the same time magnetron sputtering was considered only by some research groups. In this work, we report on the utility of reactive magnetron sputtering for the fabrication of composite thin films based on  $\text{HfO}_2$  co-doped with Si, N, and Nd ions simultaneously.

The evolution of structural and optical properties of such films with annealing temperature was investigated by means of the scanning electron microscopy, energy-dispersive X-ray spectroscopy, X-ray diffraction, Raman scattering, and photoluminescence techniques. It is observed that sputtering of  $\text{HfO}_2$ -Si-Nd composed target in argon-nitrogen plasma allowed producing homogeneous, dense and smooth films. The analysis of film properties with annealing temperature revealed the stability of film structure up to 950°C.

The light emission in the visible and IR spectral range was detected. It was found that bright  $\text{Nd}^{3+}$ -related emission can be achieved at lower temperatures (about 950°C) contrary to that reported for Nd-doped Si-SiO<sub>2</sub> or Si-Si<sub>3</sub>N<sub>4</sub> materials. The  $\text{Nd}^{3+}$  PL intensity correlates with the evolution of  $\text{HfO}_2$  monoclinic phase. It is shown that the excitation channel of  $\text{Nd}^{3+}$  ions under non-resonant excitation involves host defects contained nitrogen ions. The desorption of nitrogen at high annealing temperature (1100°C) via the formation of volatile NO, as well as the formation of the Nd silicate phase results in the quenching of  $\text{Nd}^{3+}$  photoluminescence. This complex approach used for investigation of our films allowed demonstrating the utility of reactive magnetron sputtering for the fabrication of thin films with stable chemical composition and structure (up to 950°C). These results can be attractive for future applications of the hafnium silicate films (un-doped and doped with rare-

earth ions) as emitting elements or waveguides.

#### F.EN01.06.05

**Strategy to Choose Best Building Blocks for Efficient Triboelectric Generator Devices** Linards Lapčinskis, Kaspars Malnieks, Artis Linarts, Māris Knite and Andris Sutka; Riga Technical University, Latvia

TEG devices have potential to satisfy growing energy needs in portable electronics and sensors providing a clean alternative to conventional batteries.<sup>1</sup> TEG devices are produced from cheap, lightweight, flexible, widely used polymer materials and offer promise to capture neglected and unutilized forms of mechanical energy. TEG device consists from two conductive electrodes from which at least one is covered with polymer insulator film.<sup>1</sup> The two electrodes in TEG are connected by outer circuit and upon electrode oscillation surface charge on polymer layers and electric potential is created that drive electrons to flow between two electrodes in order to balance this electric potential difference. TEG devices can be operated in different modes – vertical separation, sliding, rotating, single electrode etc.<sup>2</sup> but the key feature for high TEG efficiency is surface charge from contact electrification.<sup>3</sup>

Different mechanisms are responsible for contact electrification and depend on material used. It is well demonstrated, that on metal-metal, metal-semiconductor or semiconductor-semiconductor contact the electron transfer occurs,<sup>4,5</sup> but this is not so obvious for polymer insulators.<sup>6</sup> The three mechanisms for polymer insulator contact electrification are considered – electron transfer,<sup>7</sup> ionic transfer,<sup>6</sup> and covalent bond cleavage.<sup>8</sup> Electron transfer between polymers is doubtful, because there are no available free electrons in insulators. Usage of the term “effective work function” in connection to the driving force for charge exchange between polymer insulators is also questionable even if the polymer is contacted with metal.<sup>6</sup> Ion exchange between contacted polymer insulators has been considered, because water under ambient conditions is adsorbed even on hydrophobic polymers.<sup>9</sup> The water layers on contacted surfaces fuse together upon contacting and as different polymer materials may have different affinity towards cations and anions in water, the imbalance between ions form during separation, thus creating surface charge.<sup>6</sup> However, it has been proven, that contact electrification of polymer insulators also occurs in complete absence of water.<sup>10</sup>

In our work we show that polymer contact-electrification can be predicted using their cohesive energy density. This allows us to select the most suitable materials as the building blocks for efficient TEG devices.

#### References

- [1] Z.L. Wang, *ACS Nano*, 2013, 7, 9533-9557.
- [2] R. Hinchet, W. Seung, S.-W. Kim, *ChemSusChem*, 2015, 8, 2327-2344.
- [3] J. Wang, C. Wu, Y. Dai, Z. Zhao, A. Wang, T. Zhang, Z.L. Wang, *Nature Commun.*, 2017, 8, 88.
- [4] J. Lowell, *J. Phys. D: Appl. Phys.*, 1975, 8, 53-63.
- [5] J. Liu, A. Goswami, K. Jiang, F. Khan, S. Kim, R. McGee, Z. Li, Z. Hu, J. Lee, T. Thundat, *Nature Nanotechnol.*, 2018, 13, 112-116.
- [6] L.S. McCarty, G.M. Whitesides, *Angew. Chem. Int. Ed.*, 2008, 47, 2188-2207.
- [7] M. Willatzen, Z.L. Wang, *Nano Energy*, 2018, 52, 517-523.
- [8] H.T. Baytekin, A.Z. Patashinski, M. Branicki, B. Baytekin, S. Soh, B.A. Grzybowski, *Science*, 2011, 333, 308-312.
- [9] H.T. Baytekin, B. Baytekin, S.S., B.A. Grzybowski, *Angew. Chem. Int. Ed.*, 2011, 50, 6766-6770.
- [10] A.L. Sumner, E.J. Menke, Y. Dubowski, J.T. Newberg, R.M. Penner, J.C. Hemminger, L.M. Wingen, T. Brauers, B.J. Finlayson-Pitts, *Phys. Chem. Chem. Phys.*, 2004, 6, 604-613.

#### F.EN01.06.06

**Characterization of Various High k Gate Dielectric Thin Films for TFT Applications** Kelsea Yarbrough, Sangram K. Pradhan and Messaoud Bahoura; Norfolk State University, United States

Traditional dielectric materials such as silicon dioxide (SiO<sub>2</sub>) is the first choice and mostly used in many electronic devices including Metal Oxide Semiconductor Field Effect Transistors, Thin Film Transistors, and VLSI technology. However, SiO<sub>2</sub> has several disadvantages that researchers are currently looking for alternatives. Scaling down electronics are the most popular device approach where SiO<sub>2</sub> will not be able to fit in these ultralow dimensional adjustments. One approach to scaling down electronics, while sustaining adequate dielectric properties is incorporating high k dielectrics. High k dielectrics refer to materials with a high dielectric constant, which denotes the material ability to store an electrical charge.

SiO<sub>2</sub> generally has a dielectric constant value of 4, while high k dielectrics have a dielectric constant greater than approximately 10. Noteworthy high k dielectrics include Hafnium Oxide (HfO<sub>2</sub>), Zirconium Oxide (ZrO<sub>2</sub>), and Aluminum Oxide (Al<sub>2</sub>O<sub>3</sub>). In this study, we perform important characterization techniques to analyze HfO<sub>2</sub>, ZrO<sub>2</sub>, and Al<sub>2</sub>O<sub>3</sub> for the possible replacement of SiO<sub>2</sub>. These high k dielectric thin films exhibited leakage currents lower than 9.45 x 10<sup>-11</sup> and with a thin film roughness of less than .5 nm. These high-quality high k dielectrics thin films were grown by Atomic Layer

Deposition on n-type silicon at a different temperature and constant thickness for premise characterization. The effect of temperature on surface morphology, crystalline orientation, and dielectric properties were analyzed through Atomic Force Microscopy (AFM), X-ray Diffraction (XRD), Keithley 4200 SCS, and Four Point Probe measurement system. AFM provided thin film roughness, grain size, and surface morphology for thin films. XRD provided the crystalline orientation of these high k dielectrics with the effect of temperature. Keithley 4200 was used to show and calculate the dielectric properties including; dielectric constant, I-V plots (leakage current), and C-V plots. Lastly, Four Point probe measurement system provided electrical properties for these high k dielectrics. The present work will provide valuable scientific input dielectric performance for the improvement of TFT devices.

#### **F.EN01.06.07**

**Mechanically Robust PVDF/Isocyanate-Treated Graphene Oxide Composite Nanofiber and Its Piezoelectric Sensor Applications** Madeshwaran Sekkarapatti Ramasamy and Byungki Kim; Korea University of Technology and Education, Korea (the Republic of)

Graphene, the two dimensional material with  $sp^2$ -hybridized carbon atoms arranged in honeycomb-like structure has attracted greatest research interests because of their excellent mechanical and electrical properties. In particular, graphene have been considered as one of the most promising reinforcing nanofillers for developing cost-effective, high performance polymer composites. However, their main drawback is associated with their poor solution processability in organic solvents and agglomeration in polymer matrix due to their Van der Waals forces. Graphene oxide (GO), derived from acidic oxidation of natural graphite possesses abundant oxygen containing functionalities exhibit good solution processability, and therefore, receiving attention as precursor to the graphene-based nanofillers. On the other hand, poly(vinylidene fluoride) (PVDF) have been actively applied in piezoelectric sensors and nanogenerators because of their electroactive properties and flexibility. Generally, PVDF present five crystalline phases such as,  $\alpha$ ,  $\delta$ ,  $\beta$ ,  $\gamma$  and  $\epsilon$ , among them,  $\beta$ -phase PVDF with TTTT conformation shows the best piezoelectric properties, because all the dipoles are arranged parallel which resulted in highest dipole moment per unit cells. Incorporating GO into PVDF matrix can promote the formation of preferred  $\beta$ -phases owing to the interaction between the oxygen functionalities of GO and dipoles of the PVDF chains. In addition, the intrinsic high mechanical properties of GO can also enhance the mechanical properties of PVDF matrix. However, in most of the polymer composite systems, the strength and stiffness increased with the addition of nanofillers, meanwhile, the toughness decreased due to reduction in strain at break, which often restricts their applications in stretchable and flexible electronics. Herein, we report a method for fabricating PVDF/GO composite nanofibers with significantly enhanced mechanical strength and modulus without losing its toughness/stretchability. Isocyanate treated GO (i-GO) nanosheets were incorporated as nanofillers into PVDF nanofibers (PVDFNFs) using solution blending and electrospinning techniques. i-GO exhibit strong interfacial interaction with PVDF due to its reduced hydrophilicity and excellent dispersibility in organic solvents. FTIR results revealed that the addition of i-GO induce the formation of PVDFNFs with high content of electroactive phases. Interestingly, the tensile strength, modulus and as well as strain-at-break increased with the addition i-GO. Furthermore, the composites displayed enhanced piezoelectric outputs than that of reference PVDFNFs during the static load analysis. The enhanced performance of the composites can be attributed to the strong interaction between i-GO and PVDF achieved through incorporation of chemically modified GO. The reported composites in this study hold a great potential in the field of flexible and stretchable piezoelectric sensors and nanogenerators.

Keywords: Graphene, PVDF Nanofibers, Piezoelectric Sensing, Nano Composites, Mechanical Properties

#### Acknowledgements

This work was supported by Grant NRF-2018R1A6A1A03025526 under the Priority Research Program through National Research Foundation of Korea(NRF) under Ministry of Education.

#### **F.EN01.06.08**

**Dramatic Increase in Polymer Triboelectrification by Transition from a Glassy to Rubbery State** Artis Linarts, Andris Sutka, Kaspars Malnieks and Linards Lapčinskis; Riga Technical University, Latvia

Triboelectric nanogenerators (TENG) are intriguing energy harvesting devices that convert mechanical energy into electricity and could power small portable devices or charge batteries [1]. Here we report contact electrification of glassy polymers at different temperatures and observing a dramatic three orders of magnitude increase in surface charge when passing the transition temperature to a rubbery state. Transition is accompanied by a larger force required for separation due to material softening and increased stickiness. This enhances material transfer during contact/separation cycles and indicates covalent bond breaking as the mechanism for increased polymer triboelectrification. Undeniably, surface roughness plays a great role

in contact electrification, however in our study its impact is overrated when compared to the influence of physical properties.

[1] Z.L. Wang “Triboelectric Nanogenerators as New Energy Technology for Self-Powered Systems and as Active Mechanical and Chemical Sensors”, ACS Nano 7 (2013) 9533-9557.

#### **F.EN01.06.09**

**Matching the Directions of Electric Fields from Triboelectric and Ferroelectric Charges in Nanogenerator Devices for Boosted Performance** Kaspars Malnieks, Andris Sutka, Linards Lapčinskis and Artis Linarts; Riga Technical University, Latvia

The field related to triboelectricnanogenerator (TENG) devices is emerging rapidly. Many original and creative TENG concepts have been presented in the literature for harvesting mechanical energy and converting it into electricity (Lee et al., 2019). The working principle of TENG devices is straightforward. Due to electrode oscillation or movement, a potential difference is created, which causes a current flow in the external electric circuit. TENG devices can be integrated into fabrics, wearables, interior objects, membranes (to harvest energy from sound), and even implantable devices.

To enhance the performance of TENG, different approaches have been used. The most obvious way is to increase the specific contact area via nanostructuring (Zhang et al.). Another possibility is the modification of surface or physicochemical properties of the triboelectric material (Sutka et al., 2019). The performance can be also enhanced by using ferroelectric polymer or composite films as the contacting surfaces (Bai et al.). State-of-the-art performance of ferroelectric material-based TENG devices can be expected when the ferroelectric material layers on contacting sides of the device are inversely polarized (Sutka et al). However, previous works related to TENG devices based on ferroelectric materials overlook the dipole that forms between the triboelectric surface charges on contacting surfaces. As soon as we consider this additional factor, it follows that the electric field direction from ferroelectric dipoles should match the direction of the electric field from triboelectric surface charge to achieve maximum electric field strength and electrostatic induction.

Polydimethylsiloxane (PDMS), ethylene-vinyl acetate copolymer (EVA), poly(vinyl acetate) (PVAc), and poly(methyl methacrylate) (PMMA) were used in our studies to prepare TENG devices. The polymer films were spin coated on indium tin oxide (ITO) conductive electrode and contacted against another ITO. The polymer films were given ferroelectric properties by adding 7.5 vol% BaTiO<sub>3</sub> nanoparticles. The sign of triboelectric surface charges formed on pure polymers after contacting against ITO was determined by measuring the current between the underlying electrode and the ground in Faraday cup mode. Polymers PDMS, PVAc, and EVA obtain a negative charge on their surface whereas for PMMA a positive charge is observed when contacted ITO. The sign of the net triboelectric charge did not change when BaTiO<sub>3</sub> nanoparticles were incorporated into the polymers. All poled BaTiO<sub>3</sub>/polymer composites exhibit piezoelectric properties. The piezoelectric charges of 2.9 pC/cm<sup>2</sup>, 10.9 pC/cm<sup>2</sup>, 3.7 pC/cm<sup>2</sup>, and 2.4 pC/cm<sup>2</sup> were measured for BaTiO<sub>3</sub>/EVA, BaTiO<sub>3</sub>/PDMS, BaTiO<sub>3</sub>/PVAc, and BaTiO<sub>3</sub>/PMMA composites, respectively. The higher piezoelectric response of BaTiO<sub>3</sub>/PDMS could be attributed to its larger deformability under the constant loading force. Composite layer in each of these TENG devices was tested as non-poled and also positively and negatively poled, so that ferroelectric dipole is matched and mismatched with the previously determined surface charge.

As example BaTiO<sub>3</sub>/PDMS TENG device performed excellently, and the output was superior to any other presented in this study. The peak open-circuit voltage ( $V_{OC}$ ) of device with matched dipoles reached 460 V, instant energy and power densities of this TENG device reached 9.7 mJ/m<sup>2</sup> and 143.2 mW/m<sup>2</sup>, respectively. For comparison, a TENG device from the same polymers without BaTiO<sub>3</sub> NPs shows  $V_{OC}$  as small as 16 V and three orders of magnitude smaller energy and power densities of 0.012 mJ/m<sup>2</sup> and 0.104 mW/m<sup>2</sup>. Also, the TENG device from the same inversely polarized composite films but with mismatched dipoles exhibited significantly lower output— $V_{OC}$  of 300 V and instant energy and power densities of 4.0 mJ/m<sup>2</sup> and 91.6 mW/m<sup>2</sup> from the same contacting area.

#### **F.EN01.06.10**

**Towards Engineering Mixed Oxide Thin Films Using a Genomic Approach—A Case Study of Ta<sub>2</sub>O<sub>5</sub>-Based Coatings** Mariana A. Fazio, Le Yang and Carmen Menoni; Colorado State University, United States

Mixed oxide thin films have found their way into numerous applications ranging from high-k dielectrics to gas sensors to optical coatings with tunable properties. The field is vast and most research conducted on mixed oxide coatings has been approached from the experimental side, leading to an arduous and time-consuming trial-and-error process. In the last decade, emerging computational methods have been conducive to accelerated materials discovery. In particular, the genomics approach behind open access initiatives such as the Materials Project aims to provide materials scientists with a new set of tools: large databases of computational calculations of known and predicted materials. This web-based database leads the way for *in silico* material design that can guide experimentation.

In this work, we carried out an extensive study of tantala ( $\text{Ta}_2\text{O}_5$ ) amorphous thin films doped with Al, Si, Sc, Ti, Zn, Y, Zr, Nb and Hf grown by reactive sputtering. The influence of the dopant and post-deposition annealing on the film properties and structure was characterized by grazing-incidence x-ray diffraction, x-ray photoelectron spectroscopy and spectroscopic ellipsometry. Using the Materials Project database, compositional phase diagrams based on density functional theory calculations were constructed for all mixed oxide systems and the annealing process was evaluated via grand potential phase diagrams with varying oxygen chemical potential. The computational calculations agree well with experimental results, predicting formation of ternary compounds after annealing in some systems. When no ternary phase can be stabilized, the dopant acts as an amorphizer agent increasing the crystallization temperature of tantala. In the case where the dopant forms an oxide with similar formation enthalpy to tantala we experimentally observed effects of oxygen competition that lead to formation of phases that are predicted to be unstable. Overall, the predictions based on the Materials Project database provide valuable information for tailoring dopant type and concentration in mixed oxide thin films towards specific applications that might require increased thermal stability or to adjust processing conditions for ternary oxide production.

#### **F.EN01.06.11**

##### **Characterization of $\text{MnO}_2$ -MWCNT Nanocomposite Morphology for Supercapacitor Applications** Rian

Tucci<sup>1,2</sup>, Thomas Sadowski<sup>1,2</sup>, Rahul Singhal<sup>3,2</sup> and Christine Broadbridge<sup>1,2</sup>; <sup>1</sup>Southern Connecticut State University, United States; <sup>2</sup>Connecticut State Colleges and Universities (CSCU) Center for Nanotechnology, United States; <sup>3</sup>Central Connecticut State University, United States

Supercapacitors, with long cycle lives and long-term efficiency, have potential to become an appealing alternative to lithium-ion batteries; however, the specific energy of these devices lags well behind current state-of-the-art lithium-ion batteries. Nevertheless, numerous opportunities exist to optimize supercapacitors through the manipulation of the structure and morphology of novel materials. The implementation of hybrid supercapacitors, a device which combines a pseudo-capacitor with an electrical double layer capacitor, are of interest because material composites have greater charge storage capabilities than their components alone. The most effective hybrid capacitors for charge storage are ones possessing high specific capacitance (capacitance per unit mass). The optimization of a composite for high specific capacitance requires changes to intrinsic material properties, either by changing chemical or physical structures. The current study was aimed at the manipulation of the nanostructure of a manganese dioxide ( $\text{MnO}_2$ ) – multi walled carbon nanotube (MWCNT) composite material via modulation of MWCNT composite concentration. The composite nanostructure was characterized using transmission electron microscopy (TEM), x-ray diffraction (XRD), charge-discharge tests, and cyclic voltammetry. Ten composites, each with different initial MWCNT concentrations, were synthesized via hydrothermal method. All ten concentrations were imaged via TEM. Of those ten, three were chosen to be characterized with electrochemical methods and XRD: 4.8%, 16.9%, and 33.7% mass MWCNT. TEM imaging reveals a nanostructure of polycrystalline  $\text{MnO}_2$  adsorbed onto MWCNT. Results indicated that, on average, the thickness of  $\text{MnO}_2$  coating decreased as percent mass MWCNT increased. At 33.7% MWCNT mass, MWCNT agglomeration became hard to mitigate and dominated  $\text{MnO}_2$  adsorption structure. This is supported by XRD of 33.7% sample showing emergence of (002) plane of CNT, indicating widespread non-coating of  $\text{MnO}_2$  in composite. Charge-discharge tests were conducted in with a 1 V window at 0.5, 1, and 2 A/g. Charge-discharge tests with 1 A/g indicate highest specific capacitance for 16.9% mass MWCNT at 150 F/g, compared to 70 and 45 F/g with 4.8% and 33.7% mass MWCNT, respectively. Preliminary results indicate that as MWCNT concentration increases, there is a decline in the average  $\text{MnO}_2$  aggregation thickness, with this thickness potentially impacting the specific capacitance of the resulting device.

#### **F.EN01.06.12**

##### **Emergent Polar Vortex and Light Switching Behavior in Nanolayered $\text{SrTiO}_3/\text{PbTiO}_3$ Crystal** Ken-ichi Nomura<sup>1</sup>,

Thomas Linker<sup>1</sup>, Rajiv Kalia<sup>1</sup>, Aravind Krishnamoorthy<sup>1</sup>, Aiichiro Nakano<sup>1</sup>, Kohei Shimamura<sup>2</sup>, Fuyuki Shimojo<sup>2</sup>, Subodh C. Tiwari<sup>1</sup> and Priya Vashishta<sup>1</sup>; <sup>1</sup>University of Southern California, United States; <sup>2</sup>Kumamoto University, Japan

Oxide perovskite is an excellent platform for energy, sensing, and electronics applications, and their dielectric property has been extensively studied to date. Recently, superlattices of dielectric (*e.g.*  $\text{SrTiO}_3$ ) and ferroelectric (*e.g.*  $\text{PbTiO}_3$ ) materials have been shown to exhibit various emergent properties. An example is a newly discovered materials state of which could overcome fundamental limitations on the power consumption of field-effect transistors. Another emergent property is novel topological states of polarization such as vortex-antivortex arrays and with quantized skyrmion number. The formation of the polarization structures involves nanometric domains with opposite polarization orientation separated by domain walls (DWs). Highly complex DW characteristics as well as DW interactions dictates the design and control of functional ferroelectric devices. Furthermore, these topological phases can be switched on and off by ultrafast light pulses, opening up a fascinating

opportunity for light-activated pathways to thermally-inaccessible and emergent metastable states. The scientific challenge here is to understand the intricate interplay between lattice polarization, strains in complex superlattice and polarization-vortex geometries, and excited electrons which triggers the light-induced structural transitions from first principles. In this talk, I will discuss non-adiabatic quantum molecular dynamics (NAQMD) simulations of light switching behavior of topological states in a SrTiO<sub>3</sub>/PbTiO<sub>3</sub> superlattice, as well as artificial neural network (ANN) MD simulations to study the structure and dynamics of polar vortex arrays encompassing sufficient length scales to represent realistic supercrystalline dimensions.

This work was supported as part of the Computational Materials Sciences Program funded by the U.S. Department of Energy, Office of Science, Basic Energy Sciences, under Award Number The simulations were performed at the Argonne Leadership Computing Facility under the DOE INCITE and Aurora Early Science programs and at the Center for High Performance Computing of the University of Southern California.

#### **F.EN01.06.13**

**Lattice Dynamics and Raman Spectrum of BaZrO<sub>3</sub>** Constance Toulouse and Mael Guennou; Université du Luxembourg, Luxembourg

BaZrO<sub>3</sub> is one of the end-members of remarkable perovskite systems: the binary Ba(Zr,Ti)O<sub>3</sub>, studied for its relaxor-to-ferroelectric crossover, and the pseudo-ternary (Ba,Ca)(Ti,Zr)O<sub>3</sub>, identified as promising for lead-free piezoelectrics. Pure BaZrO<sub>3</sub> exhibits the simple cubic structure down to 2 K, but theoretical DFT studies show that the cubic phase is slightly unstable, with an unstable phonon mode that should give rise to an antiferrodistortive transition driven by octahedral tilts. It has been also suggested that such distortions exist as distorted nano-domains. Experimentally, because of its very high melting point, investigations of BaZrO<sub>3</sub> have been mostly limited to polycrystalline samples. Here, we revisit its structure and properties using recently grown single crystals. In particular, we studied the unstable phonon mode by neutron scattering, and performed Raman measurements in a wide range of temperatures and pressures (up to 20 GPa). With the support of detailed calculations of the lattice dynamics, we show that the Raman spectrum does not confirm the hypothesis of distorted nano-domains, but instead can be explained by second-order scattering.

#### **F.EN01.06.15**

**Cellulose Nanoparticles in Energy Storage Applications** Prathima P. Tumkur and Govindarajan Ramesh; Norfolk State University, United States

In recent years, environmentally friendly supercapacitors are gaining importance amongst researchers due to environmental concerns. Cellulose is one of the environmentally friendly biomaterials having properties such as renewability, degradability, biocompatibility, and costeffectiveness that has drawn a considerable amount of attention in the energy applications. In the present work, chemically synthesized cellulose nanoparticles were used in the energy storage applications to develop a supercapacitor. A mixture of carbon and cellulose nanoparticles was used as the electrode materials which were coated on a stainless-steel disk and assembled in a coin cell to develop a supercapacitor. Various electrolytes were used in the assembly to determine the best suitable one to obtain improved specific capacitance with large cyclic stability.

#### **F.EN01.06.17**

**Late News: MOCVD of Functional Dy-Doped BiFeO<sub>3</sub> Film Grown on Single Crystal** Quentin Micard<sup>1</sup>, Giacomo Clementi<sup>2</sup>, Ausrine Bartasyte<sup>2</sup>, Paul Mural<sup>3</sup>, Guglielmo G. Condorelli<sup>1</sup> and Graziella Malandrino<sup>1</sup>; <sup>1</sup>University of Catania - INSTM, Italy; <sup>2</sup>FEMTO-ST Institute, University of Bourgogne Franche-Comté, France; <sup>3</sup>EPFL, Switzerland

The deposition of BiFeO<sub>3</sub> has been widely investigated in the recent years. Among multiferroic materials BiFeO<sub>3</sub> is of a special interest since its ferroelectric and magnetic transition temperatures are well above the room temperature ( $T_C \approx 1100$  K and  $T_N \approx 650$  K) [1]. Depositions of BiFeO<sub>3</sub> films by chemical routes: sol-gel, chemical solution deposition (CSD) and physical methods: sputtering, pulsed laser deposition (PLD) on single crystals such as SrTiO<sub>3</sub> or LaAlO<sub>3</sub> are well established. Despite its major role in industry MOCVD process is not as much investigated as other deposition techniques, but it has the major advantage to be easily scaled up. Recent works have been focused on A-site doping with rare-earth ions [2].

This work reports a simple MOCVD process for Dy-doped BiFeO<sub>3</sub> thin films on conductive Nb-doped SrTiO<sub>3</sub> (100) substrates. A multicomponent mixture composed of Bi(phenyl)<sub>3</sub>, Dy(hfa)<sub>2</sub>diglyme and Fe(tmhd)<sub>3</sub> (phenyl = -C<sub>6</sub>H<sub>5</sub>, H-hfa = 1,1,1,5,5,5-hexafluoro-2,4-pentanedione, diglyme = 1-methoxy-2-(2-methoxyethoxy)ethane, H-tmhd = 2,2,6,6-tetramethyl-3,5-heptandione), has been used as precursor source. Nb:SrTiO<sub>3</sub> is acting simultaneously as a substrate and a bottom electrode, top gold electrodes have been sputtered after film deposition.



The piezoelectric, pyroelectric, and ferroelectric properties strongly depend on the structural and compositional properties of the deposited film with attention to the Dy doping. This correlation has been done using X-ray diffraction (XRD), for the structural characterization, field-emission scanning electron microscopy (FE-SEM), atomic force microscopy (AFM), and energy dispersive X-ray (EDX), X-ray photoelectron spectroscopy (XPX) analyses for the morphologic and chemical characterizations, respectively. For the functional study, the permittivity, piezo-, pyro- and ferro-electric response of deposited films have been investigated by impedance spectroscopy, Piezoelectric Force Microscopy (PFM), pyroelectric measurement and P-V loop, respectively. Significant correlation between Dy doping and film properties have been observed and promising pyro-electric coefficients were measured.

### Acknowledgment

This work is supported by the European Community under the Horizon 2020 Programme in the form of the MSCA-ITN-2016 ENHANCE project, Grant Agreement N.722496.

### References

- [1] T. Choi, S. Lee, Y. J. Choi, V. Kiryukhin, S.-W. Cheong, *Science* (2009), 324, 63
- [2] M. R. Catalano, G. Spedalotto, G. G. Condorelli, G. Malandrino, *Adv. Mater Interfaces* (2017), 1601025

**Corresponding author:** Graziella Malandrino, +39-095-7385055, gmalandrino@unict.it

### F.EN01.06.18

**Late News: Controlled Synthesis, Piezoelectric, Magnetic and Dielectric Characterization of Novel Europium Titanate Nanoscale Structures—Implications for Energy Storage and Transfer** Benard Kavey and Gabriel Caruntu; Central Michigan University, United States

Europium titanate is known to crystallize in the pyrochlore crystal structure with the general formula  $A_2B_2O_7$ . Within the crystal structure, the A-site cations are occupied by  $Eu^{n+}$  ions whereas the B-sites are occupied by  $Ti^{n+}$  ions in which the spins of the atoms are arranged on the vertices of tetrahedrons linked together at their corners. The high degree of freedom of rotation and vibration in the three-dimensional framework of tetrahedrons allows for a stronger spin interaction in the crystal lattice. The result of this interaction brings about a variety of magnetic properties that largely depends on the A-site cations, in this case,  $Eu^{n+}$  ions. In this work, novel piezoelectric europium titanate nanorods have been synthesized by using a simple solvothermal route in the temperature range 160-180 °C. TEM micrographs of the as-prepared samples show nanorods with lengths ranging from 0.3 to 1.2  $\mu\text{m}$  and an average diameter of  $40\pm 5$  nm. The nanorods become more elongated but rather thinner (length range = 0.5 – 1.6  $\mu\text{m}$ , and diameter =  $10\pm 5$  nm) when the as-synthesized powder was annealed at 800 °C. Powder X-ray diffraction pattern of the nanorods showed pure and highly crystalline pattern consistent with the diffraction patterns seen in  $Eu_2Ti_2O_7$  nanocrystals. Dielectric spectroscopy of the pelletized  $Eu_2Ti_2O_7$  revealed high-k dielectric constant up to  $\epsilon = 4000$  at room temperature. In this study, scanning probe microscope was used to measure the magnetic interactions in the solution-processed  $Eu_2Ti_2O_7$  nanorods thin-film. AFM topography images showed that the fabricated nanocrystals thin-film have an average thickness of 180 nm on a silicon substrate. The corresponding magnetic force microscope (MFM) images, were obtained by raising the magnetized MFM probe by 25 nm (delta height) above the sample surface in the tapping/lift mode. Since the probe tip uniformly scans at a height of 25 nm above the sample surface, the topography signal of the sample surface was drastically minimized allowing for the magnetic interactions to be mapped. This method allowed for the detection of the nanoscopic magnetic domains by measuring the interaction between the cantilever tip and sample surface. The widespread magnetic interactions can be visibly seen as a change in contrast (phase shift) in the amplitude and phase images.

### F.EN01.06.19

**Late News: Synthesis of Novel Lithium Adducts as Precursors for Lithium Niobate Films by DLI-MOCVD** Nishant Peddagopu<sup>1</sup>, Patrizia Rossi<sup>2</sup>, Paola Paoli<sup>2</sup>, Ausrine Bartasyte<sup>3</sup> and Graziella Malandrino<sup>1</sup>; <sup>1</sup>INSTM, University of Catania, Italy; <sup>2</sup>University of Florence, Italy; <sup>3</sup>University of Franche-Comté, France

Lithium niobate ( $LiNbO_3$ ) nanomaterials have recently attracted considerable attention due to their wide range of applications in the fields of ferroelectrics, piezoelectrics, and nonlinear optics. This material has been referred to as the “silicon of photonics” due to its exceptional optical properties. Applications for quantum photonics, surface acoustic wave devices, ferroelectric based devices, etc. require the availability of  $LiNbO_3$  in thin-film form. To this aim, various techniques have been applied such as capillary liquid epitaxial technique [1], RF- magnetron sputtering [2], spin-coating [3], and metalorganic chemical vapor deposition (MOCVD) [4]. MOCVD represents one of the most appealing processes in view of its easy

scalability, but its application requires the use of precursors with appropriate mass transport properties. Despite these promising advantages, industrial applications of an MOCVD process are still limited, likely because the commercial availability of starting molecular compounds is insufficient. Very few lithium precursors are known for vapor phase processes, either MOCVD or atomic layer deposition.

In this work, we report on the syntheses, through a single-step reaction, of novel adducts of lithium hexafluoroacetylacetonato {Li(hfa)} with polyethers (monoglyme = {CH<sub>3</sub>OCH<sub>2</sub>CH<sub>2</sub>OCH<sub>3</sub>}, diglyme = {CH<sub>3</sub>O(CH<sub>2</sub>CH<sub>2</sub>O)<sub>2</sub>CH<sub>3</sub>}, triglyme = {CH<sub>3</sub>O(CH<sub>2</sub>CH<sub>2</sub>O)<sub>3</sub>CH<sub>3</sub>} and tetraglyme {CH<sub>3</sub>O(CH<sub>2</sub>CH<sub>2</sub>O)<sub>4</sub>CH<sub>3</sub>} [5]. They have been characterized by elemental analyses, FT-IR spectroscopy, <sup>1</sup>H, and <sup>13</sup>C NMR. Single crystal X-ray diffraction studies provide evidence of interesting coordination moieties [7]. Lithium niobate films have been deposited on sapphire and Si using direct liquid injection (DLI-) MOCVD reactor. X-ray diffraction and scanning electron microscopy characterizations have allowed assessing the film quality.

The mass transport properties of these adducts have been investigated through thermogravimetric (TG) analysis. The TG curve of the “Li(hfa)monoglyme” shows a step mass loss with a residue of 6% at 338 °C. Thermal analysis data revealed a discrete behavior, when precursors are used in a suited temperature range, regarding conventional MOCVD applications, while its solubility and clean decomposition make these complexes interesting precursors for liquid assisted processes such as liquid-delivery and aerosol-assisted MOCVD or sol-gel applications.

The depositions have been carried in a pulsed liquid injection MOCVD reactor using the different lithium precursors and a correlation between the precursor nature and film properties have been derived.

#### Acknowledgments

This work is supported by the European Community under the Horizon 2020 Programme in the form of the MSCA-ITN-2016 ENHANCE project, Grant Agreement N.722496.

[1] T. Fukuda, H. Hirano, *J. Cryst. Growth*, 50, (1980), 291.

[2] J. Ye, X. Sun, Z. Wu, J. Liu, Y. An, *J. Alloys Comp.*, 768, (2018), 750.

[3] M. A. Fakhri, E. T. Salim, A. W. Abdulwahhab, U. Hashim, Z. T. Salim, *Optics & Laser Technol.*, 103, (2018), 226.

[4] A. Bartaszyte, S. Margueron, T. Baron, S. Oliveri, P. Boulet, *Adv. Mater. Interfaces*, 4, (2017), 1600998.

[5] N. Peddagopu, P. Rossi, C. Bonaccorso, A. Bartaszyte, P. Paoli & G. Malandrino, *Dalton Trans.*, 49, (2020), 1002.

#### F.EN06.07.01

**Phosphorus-Based Anode Materials via Electrostatic Spray Deposition for High-Performance Lithium-Ion Batteries** Amin Rabiei Baboukani<sup>1</sup>, Iman Khakpour<sup>1</sup>, Vadym Drozd<sup>2</sup> and Chunlei Wang<sup>1</sup>; <sup>1</sup>Florida International University, United States; <sup>2</sup>Center for the Study of Matter at Extreme Conditions (CeSMEC), United States

In the past few years, due to rapidly increased global demand for energy storage devices such as advanced electronics, electric vehicles (EVs), and implantable medical devices, it is essential to develop novel materials for energy storage technologies. Lithium-ion batteries (LIBs) have been the most popular and commercially available energy storage devices. However, anodes of LIBs still suffer poor theoretical capacity of graphite (372 mAh g<sup>-1</sup>). Recently, phosphorus as an anode material has attracted much attention owing to its high theoretical capacity (2596 mAh/g) via Li<sub>3</sub>P alloying formation. White P (WP), black P (BP), and red P (RP) are the main three allotropes of solid phosphorus. WP is not stable in the air, flammable, and very toxic, which impose safety concerns for LIBs. BP is the most thermodynamically stable form of phosphorus with an orthorhombic crystal structure. However, the synthesis of BP via high-pressure and high-temperature process is expensive, which restricts its practical application. Compare to WP and BP, RP is non-toxic, low cost, eco-friendly, and easy to handle, making RP a promising anode for LIBs. Nevertheless, the application of RP in LIBs is obstructed by two serious issues: low electrical conductivity of RP (~ 10<sup>-14</sup> S cm<sup>-1</sup>), and huge volume change (more than 300 %) during lithiation and delithiation causing the pulverization of the active materials which leads to significant capacity fading, and poor cycling performance. Compositing phosphorous with carbonaceous materials and constructing stable architecture are the two main methods that have been evaluated to resolve the issues and improve the electrochemical performance of P-based electrode materials. Moreover, the chemical bond of P to the conductive matrix could contribute to the integrity of the electrode during cycling. In this research, for the first time we developed a binder-free P-based anode materials with sulfurized polyacrylonitrile (SPAN) as functional polymer composite fabricated through ball-milling and electrostatic spray deposition (ESD) method. SPAN-based electrodes have shown attractive electrochemical performance such as good cycling life and Coulombic efficiency due to its chemical compatibility for energy storage devices. In addition, due to the low bonding energy of S-S (265 kJ mol<sup>-1</sup>) and its high reactivity to form additional chemical bonds with RP, the conductive SPAN could be an ideal composite to increase the conductivity and control the volume expansion of RP in LIBs. The electrochemical performance of the fabricated anode materials evaluated via electrochemical impedance spectroscopy, cyclic voltammetry, and galvanostatic charge/discharge tests. The RP-SPAN hybrid electrode exhibited excellent specific capacity up to 1605 mAh g<sup>-1</sup> at 0.1 A g<sup>-1</sup> at 100 cycles, which is one of the best reported performances among the RP-based

composite electrode in LIBs. Moreover, a specific capacity of 320 mAh g<sup>-1</sup> was maintained at 3 A g<sup>-1</sup>. Due to the SEM images, the hybrid electrode still maintains its microstructural integrity without obvious degradation after cycling, indicating that the volume change didn't affect the structural stability. Our results show that the ESD method is an effective approach to prepare RP-based composite with favorable morphology and composition in order to buffer mechanical stress and alleviate crack formation during cycling. The RP-SPAN hybrid delivered high specific capacity, most likely due to the synergetic effect of chemical bonding and improved kinetics. The developed anode material and its material and electrochemical characterizations will be discussed in detail at the conference.

#### **F.EN06.07.03**

##### **Surface Modified Graphite Electrodes for Limiting Lithium Plating and Enabling Fast Charging of Li-Ion**

**Batteries** Killian Tallman<sup>1</sup>, Bingjie Zhang<sup>1</sup>, Shan S. Yan<sup>2</sup>, Amy Marschilok<sup>1,2</sup>, Kenneth Takeuchi<sup>1</sup>, David Bock<sup>2</sup> and Esther Takeuchi<sup>1,2</sup>; <sup>1</sup>Stony Brook University, United States; <sup>2</sup>Brookhaven National Laboratory, United States

Lithium metal plating on graphite anodes has been identified as a mechanism contributing to diminished capacity retention of Li-ion batteries under conditions of repeated fast charge. Due to mass transfer limitations, instead of lithium ion insertion in the graphite anode Li metal can deposit on the graphite anode surface when the electrode is highly polarized. The result is inactive Li metal which limits cell cycle life and raises risk of internal short-circuits due to dendrite growth. The objective of this research was to mitigate Li-plating during fast charging by increasing the overpotential of Li-deposition via interfacial surface modification. The hypothesis tested was that deposition of Cu or Ni metal on the surface of graphite electrodes can increase the Li nucleation overpotential due to crystalline mismatch and suppress Li-plating.

Thin metal films of Cu or Ni were deposited on graphite anodes. The films were characterized by a variety of methods including atomic force microscopy, scanning electron microscopy, X-ray photoelectron spectroscopy and X-ray absorption near edge structure spectroscopy. Lithium ion cells with the treated graphite anodes as well as control cells were assembled and evaluated using galvanostatic cycling. Benefit in capacity retention for the treated electrodes was demonstrated. Further, Li-plating was quantified over a series of experiments and supported the electrochemical results. The findings of this study establish that with rational design of an electrode interface, the overpotential for Li-deposition can be modulated, providing a new conceptual approach for reducing Li-plating on graphite anodes.

#### **F.EN06.07.04**

##### **Nanocomposite of SnO<sub>2</sub>/CeO<sub>2</sub> Nanostructured Electrode for Efficient Li-Ion Storage Application**

**Samuel Danquah**, Messaoud Bahoura and Sangram K. Pradhan; Norfolk State University, United States

Cerium oxide (CeO<sub>2</sub>) nanocomposite material for Li-ion battery is synthesized using hydrothermal method. To fabricate a hybrid nanostructure electrode, CeO<sub>2</sub> is coated on tin oxide (SnO<sub>2</sub>) nanorods (NR), which is grown using a vapor-liquid-solid (VLS) technique on a steel substrate. The structure of SnO<sub>2</sub>/CeO<sub>2</sub> nanocomposite was confirmed by X-ray diffraction (XRD), field emission scanning electron microscopy (FESEM). The surface morphology of the hybrid nanostructure electrode confirms that, single-crystalline SnO<sub>2</sub> nanorods are grown vertically with spine-like structures, a few microns in length, as evident from FESEM. The electrochemical performance of SnO<sub>2</sub>/CeO<sub>2</sub> shows an enhanced charge storage capability. The coin cell shows improved capacity with a higher number of charging and discharging cycles. This SnO<sub>2</sub>/CeO<sub>2</sub> hybrid composite electrode shows better specific capacitance value as compared to the pristine SnO<sub>2</sub> electrode and pristine CeO<sub>2</sub> electrode.

#### **F.EN06.07.06**

##### **Nanoscale Three-Dimensional Imaging of Degradation in Composite Si-Containing Anodes**

**Zoey Huey**<sup>1,2</sup>, Caleb Stetson<sup>1,2</sup>, Sang-Don Han<sup>1</sup>, Donal P. Finegan<sup>1</sup>, Yeyoung Ha<sup>1</sup>, Chun-Sheng Jiang<sup>1</sup>, Andrew Norman<sup>1</sup>, Steven DeCaluwe<sup>2</sup> and Mowafak Al-Jassim<sup>1</sup>; <sup>1</sup>National Renewable Energy Laboratory, United States; <sup>2</sup>Colorado School of Mines, United States

The use of silicon (Si) in the anodes of next-generation lithium ion batteries (LIBs) has the potential to dramatically improve electrochemical performance over current LIBs with graphite anodes, due to the higher specific capacity of silicon.<sup>1</sup> However, widespread implementation of Si-containing anodes is inhibited by issues such as significant volume expansion of Si during lithiation and an unstable solid-electrolyte interphase (SEI), resulting in unreliable performance and poor cycle life. Currently, composite anodes with both Si and graphite active materials are used to increase capacity and mitigate some of the limitations associated with Si. In composite electrodes with a heterogeneous distribution of components with varying electrical properties (including Si, graphite, conductive carbon additive, and binder), it is important to understand the local distribution of each component to correlate with electrochemical processes, particularly localized degradation and heterogeneous aging, and to optimize performance. The heterogeneous distribution of these components leads to localized lithiation, nonuniform SEI formation and material degradation, and complex electron transfer pathways,

which all impact anode cycling and performance.

To investigate Si-containing composite anodes in the nanoscale, we employ scanning spreading resistance microscopy (SSRM), a form of scanning probe microscopy (SPM) that probes local electronic resistivities. By examining the contrast in intrinsic electronic resistivity between the anode components, separate phases can be distinguished and understood within the composite structure. Previous work has been conducted on composite Si-graphite electrodes using SSRM, as well as with X-ray tomography, to study degradation after cycling.<sup>2,3</sup> SSRM is able to measure composite electrode components over a wide range of relative intrinsic resistivities with nanometer-scale resolution and a smaller sampling volume than X-ray based methods, making it ideal for distinguishing anode components and determining their spatial positions. This work studies the effects of electrochemical cycling on component distribution and aging by comparing the electrical and structural evolution of composite Si-graphite electrodes before and after charge-discharge cycling. Additionally, we compare the resistivity maps to STEM-EDS and EELS results for both pristine and cycled electrodes to understand chemical changes that occur within the observed structure. By analyzing structural and chemical changes that occur during cycling, we identify degradation mechanisms and potential design improvements to increase capacity and cycle life next-generation composite anodes.

1. W. J. Zhang. A review of the electrochemical performance of alloy anodes for lithium-ion batteries *J. Power Sources* **196** 13–24 (2011)
2. S.H. Kim, Y.S. Kim, W.J. Baek, S. Heo, D.J. Yun, S. Han and H. Jung. Nanoscale Electrical Degradation of Silicon-Carbon Composite Anode Materials for Lithium-Ion Batteries *ACS Appl. Mater. Interfaces* **10** 24549–53 (2018)
3. O.O. Taiwo, M. Loveridge, S.D. Beattie, D.P. Finegan, R. Bhagat, D.J.L. Brett and P.R. Shearing. Investigation of cycling-induced microstructural degradation in silicon-based electrodes in lithium-ion batteries using X-ray nanotomography *Electrochim. Acta* **253** 85–92 (2017)

#### **F.EN06.07.07**

**Multiscale Modeling of Ni-Rich Cathode Materials—From Electrons, Ions, Atoms to Particles** Yugin Wu and Yue Qi; Michigan State University, United States

Ni-rich Li[Ni-Mn-Co]O<sub>2</sub> is a promising cathode material due to its high discharge capacity, high voltage and low cost, but its application is hindered by the poor thermal stability and low capacity retention. To guide the design of Ni-rich cathode materials, multiscale modeling analysis was used to determine its atomic structure, band structure, open-circuit voltage, and mechanical properties and to predict the critical size of Ni-rich cathode single particles that are mechanically stable. First, density functional theory (DFT) calculations were performed to identify the base structure of pure LiNiO<sub>2</sub> layered compounds based on three different space groups, namely Rm, C<sub>2</sub>/m, and P<sub>2</sub>/c. It was found the calculated band structures of the widely applied Rm structure of LiNiO<sub>2</sub> is metallic, contrary to the experimentally reported insulating behavior. P<sub>2</sub>/c structure, which allows a disproportionation of the oxidation state of Ni (Ni<sup>2+</sup> and Ni<sup>4+</sup>), is the most energetically stable and insulating layered structure of LiNiO<sub>2</sub>. Therefore, model structures representing Ni-rich NMC cathode materials were built by partially replacing Ni with Co or Mn in the base P<sub>2</sub>/c LiNiO<sub>2</sub> structure. The electronic structure of model Ni-rich NMC cathode shows that Ni tends to be Ni<sup>3+</sup> when neighboring with Co<sup>3+</sup>, while becoming Ni<sup>2+</sup> next to an Mn<sup>4+</sup>. Based on the model Ni-rich cathode structures, the elastic constants and fracture energy were also computed from DFT. The information served as input to a continuum diffusion induced stress model to predict when a crack starts to propagate and leads to the fracture of a single Ni-rich NMC particle. The predicted results show good agreement with single-particle observations.

#### **F.EN06.07.08**

**Enabling Lithium Metal Anode in Non-Flammable Phosphate Electrolyte with Electrochemically-Induced Chemical Reactions** Haochuan Zhang, Jingru Luo, Miao Qi, Haoyi Li and Qi Dong; Boston College, United States

Lithium metal anode holds great promise in the next-generation battery but it suffers from great challenges in efficiency and safety. Previous research has developed various methods to mitigate these issues but most of them are still based on traditional flammable electrolyte systems. Here we demonstrate that reversible Li plating/stripping process, which cannot be implemented in non-flammable phosphate electrolyte previously, can be realized by introducing oxygen as an additive in triethyl phosphate (TEP) electrolyte. The symmetric Li||Li cell can achieve more than 300 cycles at current density of 0.5 mA/cm<sup>2</sup> with O<sub>2</sub> existence. Mechanistic study reveals that the electrochemically induced chemical reactions between reactive O<sub>2</sub> species and TEP molecules alter the decomposition pathway of TEP. The possible products, Li<sub>3</sub>PO<sub>4</sub>/poly-phosphate thereby serve as beneficial SEI components to enable stable Li metal operation in non-flammable electrolyte. Demonstration of Li-O<sub>2</sub> and Li-ion battery also shows that it is promising to deploy phosphate-based electrolyte in future high-energy density batteries efficiently and safely.

#### F.EN06.07.11

**Late News: A New Method for Evaluating Li-Ion Battery Anode Materials Based on Surface Compositional and Structural Characterization of Li Thermal Diffusion** Jozef Ociepa, Paige Harford, Ryan Charlinski, Guenevere O'Hara and Bart Checinski; OCI Vacuum Microengineering Inc., Canada

There is a global effort to develop safer lithium-ion batteries with a high energy density and long lifetime. Material properties, their mutual interactions, and active interfaces are key factors in battery performance. Popular methods involve the mixing of different ingredients and development of a suitable fabrication process. Significant effort has been spent to understand the reaction mechanism of battery materials, but this is very challenging due to high system complexity. Different techniques have been developed to follow these reactions, and most significantly, the reactions between Li and electrode materials. Our team has developed a new method to characterize Li thermal diffusion and structural interaction on the surfaces of potential anode and cathode materials. This method is based on surface crystallographic and compositional characterization of deposited ultra-thin film of Li on potential single crystal anode material. For surface crystallography we are using Low Energy Electron Diffraction (LEED) and for composition Auger Electron Spectroscopy (AES). This characterization monitors Li diffusion into the electrode surface and changes in surface crystalline structure and composition providing data on Li interaction with the crystalline anode material structure. This dynamic interaction of Li is monitored at the nanoscale level and gives the direct response how Li atoms interact with the substrate. The diffusion of evaporated Li on single crystals of HOPG, Si(111)-(211)-(100), SiC-6H, Diamond and LiNbO<sub>3</sub> have been performed. The results show that HOPG is the excellent reference substrate for this method as Li diffuses at room temperature and surface crystallography of HOPG remains unchanged. The structural reaction of Li with Si is very strong causing LEED pattern to disappear and there is no Li diffusion at room temperature. The data for SiC-6H and LiNbO<sub>3</sub> shows better Li diffusional behavior than on Si but not as good as on HOPG. This method of using a single crystal substrate and basic surface characterization techniques is providing simple nanoscale access into the chemical reactions between Li and the substrate material that will result in better understanding of diffusional Li response to high capacity anodes with new chemistry content.

#### F.EN06.07.12

**Late News: Structure and Electrochemistry of Transition Metal Substituted Lithium Vanadyl Phosphate for Lithium-Ion Batteries** Krystal J. Lee, Marc Francis V. Hidalgo, Yanxu Zhong, Mateusz Zuba, Natasha Chernova, Guangwen Zhou, Hao Liu and M.S. Whittingham; Binghamton University, United States

Li-ion intercalation compound enlisting multi-electron redox is a promising strategy to maximize the storage capacity of LIBs. Lithium vanadyl phosphate, LiVOPO<sub>4</sub>, is one such material that can intercalate up to two Li<sup>+</sup> ions per vanadium ion through the change in vanadium valence from V<sup>5+</sup> to V<sup>3+</sup>, which translates to a theoretical capacity of 305 mAh/g and an energy density above 900 Wh/kg. However, Li-ion intercalation in the high voltage region (V<sup>5+</sup>/V<sup>4+</sup>) is kinetically limited by the sluggish Li-ion diffusion, and thus impedes the use of LiVOPO<sub>4</sub> in practical applications. Transition metal substitution has been a technique used to enhance the performance of battery cathodes by changing its intrinsic properties and stabilizing the crystal structure. The goal of this work is to explore experimentally if substitution with chromium and niobium can enhance the electrochemical performance of LiVOPO<sub>4</sub>. X-ray diffraction and inductively coupled plasma atomic emission spectroscopy indicate the substituent is successfully incorporated into the structure. The effects of transition metal substitution on the crystal structure and the electrochemical performance of LiVOPO<sub>4</sub> will be discussed.

#### F.EN06.07.13

**Molybdenum Disulfide Anode of Lithium-Ion Battery for High Stability and Rate Capability** Chanho Park, Han S. Kang, Seung Won Lee, Hyeokjung Lee, Kyuho Lee and Cheolmin Park; Yonsei University, Korea (the Republic of)

Development of a lithium-ion battery (LIB) is of great interest with an anode based on transition metal dichalcogenide nanosheets due to their intrinsically high capacity. The stability of a LIB is, however, detrimental with the nanostructured MoS<sub>2</sub> anode resulting from the gradual decrease of electrical conductivity with time due to the re-stacking of the nanosheets. In this work, we present a novel MoS<sub>2</sub> anode with molecularly architecture graft polymer binder having functionalized groups, enabling the high stability of a LIB. The fluorinated graft polymer synthesized by one-step atomic transfer radical polymerization allows not only for exfoliating MoS<sub>2</sub> nanosheets in the liquid phase to guarantee the stable sheet-to-sheet separation by preventing re-aggregation but also for providing self-assembled ionic channels through which lithium ions in electrolyte readily reach close to the surface of the nanosheets. The electrochemical reduction of lithium ions efficiently occurs at the layered nanostructure of MoS<sub>2</sub> facilitated by the functionalized polymer binder, giving rise to a high-performance LIB with the high rate capability and stability. Our binary anode of MoS<sub>2</sub> nanosheets self-assembled with the graft polymer enables high cell capacity even without the requirement of conductive additives which are frequently employed

for ensuring high conductivity and thus comparable cell capacity, making our approach one-step closer to commercial energy applications.

#### F.EN09.11.02

**High Efficiency Water Oxidation Through Oxide Bilayers with Electronically Coupled Phase Boundaries** Aida Raaf, Dennis Grödler, Lasse Jurgensen and Sanjay Mathur; University of Cologne, Germany

New semiconductor metal oxides capable of driving water-splitting reactions by solar irradiation alone are required for sustainable hydrogen production. Whereas most metal oxides only marginally deliver the photochemical energy to split water molecules, uranium oxides are efficient photoelectrocatalysts due to their absorption properties ( $E_g \sim 2.0 - 2.6$  eV) and easy valence switching among uranium centers that additionally augment the photocatalytic efficiency. Although considered a scarce resource, the abundance of uranium compounds in the environment is manifested in the huge quantities of stored UF<sub>6</sub> gas, produced as waste streams in the nuclear fuel enrichment process. Here we demonstrate that thin films of depleted uranium oxide (U<sub>3</sub>O<sub>8</sub>) and their bilayers with hematite ( $\alpha$ -Fe<sub>2</sub>O<sub>3</sub>) are high activity water oxidation catalysts due to electronically coupled phase boundaries. The electronic structure of uranium oxides showed an optimal band edge alignment in U<sub>3</sub>O<sub>8</sub>/Fe<sub>2</sub>O<sub>3</sub> bilayers (DFT calculations) resulting in improved charge-transfer at the heterojunction as supported by TAS and XAS measurements. The enhanced photocurrent density of the heterostructures with respect to well-known hematite offers unexplored potential of uranium oxide in artificial photosynthesis.

#### F.EN09.11.03

**Enhanced Photocatalytic Oxygen Evolution Reaction—Surface Modification of the Multiferroics BiFeO<sub>3</sub> Nanostructure Using IrO<sub>2</sub> Nanoparticles** Wegdan Ramadan<sup>1</sup> and Detlef Bahnemann<sup>2,3,4</sup>; <sup>1</sup>Alexandria University, Egypt; <sup>2</sup>Institut für Technische Chemie, Leibniz Universität Hannover, Germany; <sup>3</sup>Saint-Petersburg State University, Laboratory “Photoactive Nanocomposite Materials”, Russian Federation; <sup>4</sup>Laboratorium für Nano- und Quantenengineering, Gottfried Wilhelm Leibniz Universität Hannover, Germany

BiFeO<sub>3</sub> (BFO) is a multiferroic that combines antiferromagnetic and ferroelectric order well above room temperature. It is narrow band gap semiconductor ( $\sim 2.2$ - $2.7$  eV) hence, it can harvest significant amount of visible light. Combining such desired properties on simple ternary compound makes it easier to utilize in many different folds. However, the performance of BFO in the field of photocatalysis is still poor due to the fast recombination of the photogenerated charges which will negatively affect their performance. Here we report on the photocatalytic oxygen evolution reaction, OER, of BiFeO<sub>3</sub> nanoparticles synthesized by sol gel. Oxygen evolution reaction is challenging because production of one molecule of gaseous oxygen, O<sub>2</sub>, requires four holes (oxidize two molecules of water), and occurs on a time scale approximately 5 orders of magnitude slower than that required for H<sub>2</sub> evolution. There are two important issues to address when photocatalysis intended for water redox reaction to takes place; sacrificial agents to be used and the co-catalyst to be loaded on surface. For the former and in case of OER a sacrificial agent acts as an electron acceptor. Although many choices of sacrificial electron donor are available for water reduction to produce H<sub>2</sub>, the choices are narrowing down to only few for sacrificial electron acceptors used for water oxidation to produce O<sub>2</sub>. Ag<sup>+</sup> and Fe<sup>+3</sup> ions are commonly used for this purpose and to a lower extend sodium persulfate, Na<sub>2</sub>S<sub>2</sub>O<sub>8</sub>. The redox potential of Ag<sup>+</sup>, Fe<sup>+3</sup> and S<sub>2</sub>O<sub>8</sub> at pH zero are 0.8 V, 0.77 V and 2.05 V, respectively. It is reported that both the quantum efficiency and the stability of the colloidal nanocrystals in solution improve with increasing redox potential of the scavenger. The higher redox potential leads to faster scavenging, which in turn increases quantum efficiency and stability of the catalyst since electron hole recombination and oxidation or reduction of the catalyst become less important. This finding is important for choosing hole/electron scavengers and for comparing efficiencies and stabilities for different photocatalytic nano systems. Hence the resolve to Na<sub>2</sub>S<sub>2</sub>O<sub>8</sub> as electron scavenger. Mott Schottky measurements and the UV-Vis spectroscopy showed that the band positions of BFO, the conduction band and valence band lie at 0.46V and 2.69 V with respect to NHE, respectively. To enhance BFO photocatalytic OER, IrO<sub>2</sub> nanoparticles as a co-catalyst were loaded on the surface using impregnation method. OER showed two folds enhancement upon loading with 2wt% IrO<sub>2</sub>. IrO<sub>2</sub> is one of the best catalysts for OER, unfortunately it is also one of the most expensive rare elements, so their applicability is limited by the high cost. Reducing IrO<sub>2</sub> content onto the system should be an option to make its application feasible and cost effective and loading on IrO<sub>2</sub> nanoparticles on the surface could be feasible solution. Scanning the loaded IrO<sub>2</sub> content on BFO from 0.5 wt% up to 4 wt% showed a maximum of the evolved oxygen at 2wt % followed by a decrease in activity. XPS showed the 4f peaks of Ir, it shows symmetric two peaks at binding energies 64.9 and 61.87 eV corresponding to the 4f 5/2 and 4f 7/2 of Ir (IV) respectively. TEM indicated non uniform distribution of it on the surface. Charge carrier lifetime and dynamics for pure BFO and IrO<sub>2</sub> loaded BFO have been studied by means of laser transient absorption spectroscopy, TAS, laser pulses of 20 ns and of  $\lambda = 540$  nm were used. 2wt.% IrO<sub>2</sub> loading showed the fastest decay of holes compared to other loading percentage indicating a significant role of the IrO<sub>2</sub> nanoparticles mediating the hole transfer process of the solar irradiated BFO system. This loading percentage corresponds to the observed highest OER. Band

positions between BFO and IrO<sub>2</sub> favors the formation of heterojunction at the interface between IrO<sub>2</sub> and BiFeO<sub>3</sub> that enhances the separation of the photogenerated charges and the photocatalytic OER performance.

#### **F.EN09.11.05**

##### **Probing the Effects of Electrolyte Anions on the Adsorption of CO on Polycrystalline Cu Electrodes with Surface-Enhanced Infrared Absorption Spectroscopy** Vincent J. Ovalle and Matthias Waegle; Boston College, United States

On Cu electrodes, the electrochemical conversion of CO<sub>2</sub> to hydrocarbons occurs via surface-adsorbed CO. Understanding the molecular factors that determine the adsorption of CO on Cu under electrochemical conditions is therefore essential to improving the product selectivity of this electrocatalytic process. Previous studies probing the adsorption of CO on Cu electrodes have suggested that, at low overpotentials, CO likely competes with anions from the electrolyte for surface sites. However, prior work has not systematically explored the effects of anion concentration and identity on the coverage of CO on the electrode. In this work, we examine the impact of adsorbing and non-adsorbing anions (Cl<sup>-</sup>, SO<sub>4</sub><sup>2-</sup>, ClO<sub>4</sub><sup>-</sup>) at varying concentrations (10 mM and 1 M) on the adsorption and desorption of CO from polycrystalline Cu electrodes. Using surface-enhanced infrared absorption spectroscopy (SEIRAS), we observed the interplay between adsorbed CO and interfacial anions through the lens of the anion hydration shells, CO coverage, and CO stretch frequency under electrochemical conditions. In the presence of 10 mM anion, the potential dependent CO coverage and stretch frequency during a cyclic voltammogram (CV) is virtually independent of the anion identity. By contrast, at 1 M anion, the CO coverage and stretch frequency are distinctly dependent on the anion identity of the electrolyte. With weakly adsorbing and non-adsorbing anions (SO<sub>4</sub><sup>2-</sup> and ClO<sub>4</sub><sup>-</sup>), the CO saturation coverage is lowered by ≈35% compared to the corresponding 10 mM experiments. We attribute the lower coverage to quasi-specifically adsorbed anions that block adsorption sites. With 1 M Cl<sup>-</sup>, the CO saturation coverage is only lowered by ≈12% relative to the coverage in the presence of 10 mM Cl<sup>-</sup>. This moderate decrease is attributed to a decrease in the binding strength of CO to Cu in the presence of co-adsorbed Cl<sup>-</sup>, which is evidenced by the ~19 cm<sup>-1</sup> blue shift in the CO stretch frequency. In contrast to all other electrolytes, there is no hysteresis in the adsorption/desorption profiles of CO in the presence of 1 M Cl<sup>-</sup>. This hysteresis between the forward and reverse scans in the CV is due to a CO-induced reversible reconstruction of the Cu electrode surface. In the presence of Cl<sup>-</sup>, this reconstruction is suppressed. We discuss our findings in the context of the effects of halides on the product selectivity of the CO<sub>2</sub> reduction reaction on Cu electrodes. Our study provides critical insight into the structure of the electric double layer and its evolution during the CO adsorption process.

#### **F.EN09.11.06**

##### **Identifying the Prevalent Surface Facets of Rough Cu Electrodes During CO Reduction Electrocatalysis** Charuni Gunathunge, Jingyi Li, Xiang Li, Julie Hong and Matthias M. Waegle; Boston College, United States

The surface morphology of rough Cu electrodes can profoundly affect the product selectivity and activity for the reduction of CO and CO<sub>2</sub> to hydrocarbons. Because of the scarcity of in situ methods for probing the atomic-level surface structure under electrochemical conditions, it is still debated how the atomic-level surface morphology gives rise to desirable catalytic activity and selectivity. In this work, we introduce a novel method for the determination of the prevalent surface facets on rough metal electrodes under electrochemical conditions. As model systems, we employed two types of rough Cu thin-film electrodes that are widely applied in surface-enhanced infrared absorption spectroscopy (SEIRAS). With differential electrochemical mass spectrometry (DEMS), we show that Cu films that are electrochemically deposited on Si-supported Au films (CuAu-Si) exhibit an onset potential for ethylene that is ~200 ± 65 mV more cathodic than the one of copper films (Cu-Si) that are electrolessly deposited onto Si crystals. With SEIRAS, we find that lineshapes of the CO stretch mode of surface-adsorbed CO exhibit greatly different potential-dependences for the two types of electrodes. Lineshape analysis reveals the presence of different prevalent terraces on these two types of electrodes. On the basis of this finding, we rationalize the higher overpotential for the formation of ethylene on the CuAu-Si film. We expect this novel methodology to be broadly applicable for the in situ surface characterization of rough metal electrodes. This structural information is critical for the development of rough metal electrodes with desirable catalytic characteristics.

#### **F.EN09.11.07**

##### **In Operando Study of the Role of Ni Nanoparticles and Their Coarsening on the Catalytic Activity of Solid Oxide Fuel Cell Anodes Using Distribution of Relaxation Times Analysis** Boshan Mo, Jillian Rix, Uday Pal, Srikanth Gopalan and Soumendra Basu; Boston University, United States

Mitigating activation polarization and maintaining long-term stability in solid oxide fuel cell (SOFC) electrodes represent major challenges in improving their intermediate-temperature operation and applications. It has been shown that the infiltration of nanoparticle electrocatalysts increases the number of electrochemically active sites to decrease charge transfer

polarization losses and improve performance. In this study, nickel and mixed ionic and electronic conducting (MIEC) phases were infiltrated into Ni-YSZ and Ni-doped YSZ anodes of symmetric cells, and their performances characterized in-operando using electrochemical impedance spectroscopy (EIS). The kinetics of various charge transfer processes are modeled by distribution of relaxation times (DRT) analysis of the EIS spectra, allowing for an understanding of the role of the nickel nanoparticles and the consequences of nickel coarsening on the catalytic activity of the anode.

#### F.EN09.11.09

**Electrochemomechanical Effects of Aqueous Cation Intercalation into Prussian Blue** Saeed M. Saeed<sup>1</sup>, Shelby Boyd<sup>1</sup>, Wan-Yu Tsai<sup>2</sup>, Ruocun Wang<sup>1</sup>, Nina Balke<sup>2</sup> and Veronica Augustyn<sup>1</sup>; <sup>1</sup>North Carolina State University, United States; <sup>2</sup>Oak Ridge National Laboratory, United States

Prussian blue ( $\text{Fe}_4[\text{Fe}(\text{CN})_6]_3$ ) and its analogues are of interest as electrode materials for electrochemical energy storage. The open cubic framework of Prussian blue allows for long cycle life and reversible intercalation kinetics during cation insertion/extraction with capacities of up to 125 mAh/g in aqueous electrolytes. However, this performance is highly dependent on the electrolyte cation, and prior results indicate that a smaller hydrated cation radius leads to the best cyclability. The hypothesis guiding this study is that the cycling stability with smaller hydrated cations is tied to lower structural deformation of Prussian blue during electrochemical intercalation. In this study, we investigate the electrochemomechanics of Prussian blue due to the intercalation of three different aqueous cations,  $\text{K}^+$ ,  $\text{Na}^+$ , and  $\text{Li}^+$ . *Operando* atomic force microscopy (AFM) is used to measure the mechanical deformation of the electrode during electrochemical cycling as a function of electrolyte and cyclic voltammetry sweep rate. This technique confirms that the electrochemical stability as well as the local deformation of the Prussian blue is dependent on the hydrated cation radius, with smaller cations giving rise to larger deformation. The superior cycling stability seen during  $\text{K}^+$  insertion is commensurate with the high mechanical stability measured via *operando* AFM. This presentation will provide an understanding of the coupling between electrolyte cation size and electrochemomechanical response of a framework-type energy storage material.

#### F.EN09.11.10

**Metal-Organic Frameworks as Sacrificial Template—Novel Bimetallic Co-W-S Chalcogenide Confined in N, S Codoped Porous Carbon Matrix for Highly Stable Electrochemical Supercapacitors** Aya M. Mohamed<sup>1,2</sup>, Ahmed O. Abo El Naga<sup>3</sup>, Hanna B. Hassan<sup>1</sup>, Tamer Zaki<sup>3</sup> and Nageh K. Allam<sup>2</sup>; <sup>1</sup>Cairo University, Egypt; <sup>2</sup>American University in Cairo, Egypt; <sup>3</sup>Egyptian Petroleum Research Inst, Egypt

Transition metal dichalcogenides are gaining much interest in the energy storage sector due to the 2D nature and conductivity of the materials. However, single transition metal dichalcogenides are not stable, preventing their practical use in real devices. Herein, we demonstrate the synthesis of binary metal dichalcogenides (Co-W-S) via carbonization of (ZIF-67) metal organic framework encapsulated with phosphotungstic acid (PTA@ZIF-67). The morphology and surface functional groups of the as-synthesized Co-W-S composite are characterized via (FESEM), (HRTEM), and (FTIR). Furthermore, the crystal structure and the elemental composition of the fabricated Co-W-S composite are elucidated using (XRD) and (XPS) analyses. Upon testing its electrochemical performance as a supercapacitor electrode, the fabricated Co-W-S@N,S co-doped porous carbon (N,S-PC) shows exceptional specific capacitance ( $1929 \text{ Fg}^{-1}$  at  $5 \text{ mVs}^{-1}$ ). Furthermore, the constructed asymmetric supercapacitor device using Co-W-S@N,S-PC and activated carbon as positive and negative poles, respectively displays superior energy density and power density of  $32.9 \text{ Wh Kg}^{-1}$  and  $700.2 \text{ W kg}^{-1}$ , respectively with a high Columbic efficiency over 10000 charge/discharge cycles at  $10 \text{ A g}^{-1}$ .

#### F.EN09.11.11

**In Situ Raman Scattering of Photovoltaic Iron-Hydroxide Nanostructures in Dye-Sensitized Solar Cells** Mikel Tucker, Kit Sze, Saroj Pramanik and Yucheng Lan; Morgan State University, United States

Iron hydroxide is a promising photovoltaic material because of its abundance on earth, chemical stability in aqueous media, and outstanding optical absorbance. Here, iron hydroxide nanostructures are synthesized by the atmospheric micro-plasma and characterized. The nanostructures are fabricated into dye-sensitized solar cells and their photovoltaic behaviors are measured. The *in-situ* Raman scattering of the integrated nanostructures is investigated under various experimental conditions. The *in-situ* investigation would enhance our understanding of the dynamic behaviors of the photovoltaic nanomaterial in solar cells.

#### F.EN09.11.12

**Operando Metrology with Photoelectron Spectroscopy and Organic Field-Effect Transistors for Interfacial Charge Transfers of Organic Semiconductor** Kyung-Geun Lim<sup>1</sup>, Jeong Won Kim<sup>1</sup> and Jaeyoon Baik<sup>2</sup>; <sup>1</sup>Korea Research Institution



of Standards and Science (KRISS), Korea (the Republic of); <sup>2</sup>Pohang Accelerator Laboratory (PAL), Korea (the Republic of)

Many chemical transitions of organic semiconductors occur at the interface during device operations. Charges are transferred or accumulated at the interface between organic semiconductors and intimate functional materials as function of operating conditions. However, the kinetic materials properties at the interface of organic semiconductor are hardly observed with real-time operational transition. Operando metrology is used to analyze charge transfers at the interface of organic semiconductors by photoelectron spectroscopy during operating bottom gate top electrode p-type organic field-effect transistors (OFETs). The interfacial chemical potential shift of organic semiconductor is simultaneously compared according to electrical behaviors. The electronic activation in the nearest effective monolayers of organic semiconductors at the interface is explained to correlate with gating, doping, or transporting behaviors of OFETs. This operando metrology will shed a light on many veiled intermediate transitions during the operation of organic semiconductors.

#### F.EN09.11.13

**Fabrication of Nanoscale Multilayered Thin-Film Thermoelectric Materials and Devices** Lauren Williams, Rodricka Miller, Alandria Henderson and Zhigang Xiao; Alabama A&M University, United States

We report the growth of nanoscale multilayered thermoelectric thin films and the fabrication of integrated thermoelectric devices for high-efficiency energy conversion and solid-state cooling. Nano multilayered Bi<sub>2</sub>Te<sub>3</sub>/Sb<sub>2</sub>Te<sub>3</sub>, Sb/Sb<sub>2</sub>Te<sub>3</sub>, and Te/Bi<sub>2</sub>Te<sub>3</sub> thermoelectric thin-film materials were grown using the e-beam evaporation. The multilayered thin films were prepared with 100 to 300 layers, where each layer is about 3 to 5 nm thick. The effects of DC substrate bias on the growth of films such as the crystalline structures in the films were studied. Integrated thermoelectric devices with a high density of thermoelectric elements were fabricated with the nanoscale multilayered thin films using the clean room-based microfabrication techniques such as UV lithography. Plasma-enhanced atomic layer deposition (PE-ALD) was used to grow zirconium dioxide (ZrO<sub>2</sub>) as the insulation layer in the device fabrication. X-ray diffraction and high-resolution tunneling electron micrograph (HR-TEM) were used to analyze the nanoscale multilayered thin films. The fabricated device was cooled in liquid nitrogen or annealed at 150 °C for 30 min, respectively. HR-TEM was used to analyze the cross-section of the nanoscale multilayered thin films for the three cases: as-grown, after being cooled in the liquid nitrogen, and after being annealed, showing that the cooling made the multilayer structures to be sharper while the annealing made the multilayer structures to become weaker. The thermoelectric characteristics of the devices were measured and analyzed for the three cases of as fabricated, after being cooled, and after being annealed, respectively, showing that the integrated thermoelectric device had the highest efficiency of thermal-to-electrical energy conversion after being cooled in the liquid nitrogen.

#### F.EN09.11.14

**Late News: Correlating Cu-Based Catalyst Properties to Activity and Selectivity from Operando Studies of CO Electroreduction in a Gas-Fed Device** SooHong Lee<sup>1</sup>, Ian Sullivan<sup>2</sup>, Chengxiang Xiang<sup>2</sup> and Walter Drisdell<sup>1</sup>; <sup>1</sup>Lawrence Berkeley National Laboratory, United States; <sup>2</sup>California Institute of Technology, United States

Identifying the catalyst properties that determine catalyst activity and selectivity is of significant importance, as an understating of the catalytic mechanism can provide a rational catalyst design principle for efficient energy devices. However, understanding the relationships between catalyst properties and performance remain challenges in general because of the co-existence of multiple factors that are irrelevant to the catalytic cycle, and the dynamic nature of the catalytic chemistry which is responsive to reaction rates. To investigate the complex dynamic catalyst structure, an *operando* characterization under realistic operation, particularly at electrochemical conditions approaching those used to evaluate and benchmark electrocatalysts, is needed. Here, we report a comprehensive study of catalyst properties that can determine the electrochemical CO reduction reaction (CORR) in a gas-fed cell. We first employed *operando* X-ray absorption spectroscopy (XAS) synchronized with simultaneous measurements of catalyst performance by gas chromatography (GC) to investigate the relationship between valence states of Cu-based catalysts and activity for ethylene (C<sub>2</sub>H<sub>4</sub>) production. By introducing an anodic oxidation process, which enhanced CORR performance, we demonstrated that the oxidation states do not correlate with the activity or selectivity of Cu-based catalysts. We also found that an increase in the number of active sites estimated by electrochemical surface area (ECSA) was not proportional to the C<sub>2</sub>H<sub>4</sub> yield, whereas hydrogen evolution reaction (HER) activity is positively correlated to the ECSA changes. Based on the post-mortem microscopic investigations of Cu-based catalysts, we suggest that the increased C<sub>2</sub>H<sub>4</sub> activity and selectivity may arise from a morphological reconstruction that originates from the electrochemical oxidation-reduction process. The rapid reduction of the initial oxide structure into metallic Cu at the early stage of the CORR could generate a more active structure. This electrochemical oxidation-reduction process was used as a regeneration method that recovered the original catalyst activity and selectivity in the gas-fed cell without requiring cell disassembly.

#### F.EN09.11.15

**Late News: Determining the Effect of Local Heterogeneity on the Activity and Selectivity of Au<sub>1</sub>-xPd<sub>x</sub> Particles for the Hydrogenation of Alkynes with *In Situ* and *Ex Situ* Transmission Electron Microscopy** Alexandre Foucher and Eric Stach; University of Pennsylvania, United States

Heterogeneous catalysis plays a crucial role in the production of chemicals and requires the design of active and selective nanostructures. In situ transmission electron microscopy (TEM) can determine morphology or chemistry changes in novel catalysts during a chemical reaction. In this work, bimetallic Au<sub>1</sub>-xPd<sub>x</sub> particles supported on a raspberry colloid templated (RCT) silica support were studied under oxidative and reactive conditions with a temperature of up to 500 °C and a pressure of 1 bar. Pd is the minority component, representing no more than 25 weight percent of the total metallic loading, and the particles have an average size of 5.5 nm. The remarkable stability of this system, with limited particle migration and coalescence phenomena, was demonstrated. Sharp facets perpendicular to [100] and [111] directions are present when Pd's concentration is below four atomic percent. When the concentration of Pd exceeds four atomic percent, the particles have a spherical shape, and high-resolution spectroscopy revealed the presence of small Pd clusters on the surface of the as-prepared particles with an average size of 1-2 nm. In situ results combined with ex situ TEM and infrared spectroscopy show the growth of small Pd clusters on the nanoparticles' surface that explain changes in activity and selectivity observed after treating the sample with oxygen or hydrogen. These observations demonstrate how a combination of operando methods, aberration-corrected microscopy, and direct electron detection can be used to guide the design of future catalytic structures.

#### F.EN09.11.16

**Late News: Assessing the Durability and Composition of Pt-Based Ternary Nanoalloys in Proton Exchange Membrane Fuel Cells Using *In-Situ/Operando* High-Energy XRD Technique** Dominic Caracciolo, Shiyao Shan and Chuan-Jian Zhong; SUNY Binghamton, United States

Due to the rising demand for sustainable energy, there has been a global drive for developing clean energy from renewable sources (solar, wind, etc.) which will reduce our dependence on fossil fuels. Fuel cells represent an important vector in the development of clean and renewable energy, but major challenges for the mass commercialization of fuel cells are the high cost and poor durability of the catalysts at the cathode, which requires the prohibitive Pt as a catalyst to overcome the sluggish oxygen reduction reaction kinetics. This presentation will discuss recent results of our investigations of low-Pt binary and ternary nanoalloy electrocatalysts using different characterization techniques, including in operando synchrotron X-ray diffraction technique in standard electrochemical cells and proton exchange membrane fuel cells (PEMFC). The focus is to develop the fundamental understanding of the nanophase structures of the catalysts, which provide insights into the correlation between the durability and the composition of the nanoalloy catalysts in the PEMFCs.

#### F.EN09.11.17

**Late News: Self-Constructed MnCo<sub>2</sub>O<sub>4</sub> via Atomic Layer Deposition as an Efficient Bifunctional Catalyst for Zn-Air Battery** Arim Seong and Guntae Kim; Ulsan National Institute of Science and Technology, United States

The discovery of electrocatalysts for efficient oxygen reduction reaction (ORR) and oxygen evolution reaction (OER) is pivotal to the growth of a new generation of energy technologies. In this study, for the first time, we present an effective strategy for a nano-dispersed low amount of Co<sub>3</sub>O<sub>4</sub> materials (*i.e.*, 2.67 wt %) on La<sub>0.5</sub>Sr<sub>0.5</sub>MnO<sub>3-δ</sub> catalyst substrate for synthesizing an efficient bifunctional ORR/OER catalyst by utilizing an advanced ALD technique. Interestingly, the cation diffusion between LSM and Co<sub>3</sub>O<sub>4</sub> introduces a self-intercalated MnCo<sub>2</sub>O<sub>4</sub> spinel structure at the interface. The existence of MnCo<sub>2</sub>O<sub>4</sub> was assisted by TEM-EDS, XANES. Benefiting from the MnCo<sub>2</sub>O<sub>4</sub> interlayer, the LSM-20-Co catalyst exhibits excellent maximum power density (146.5 mW cm<sup>-2</sup>), specific capacity (755.0 mA gZn<sup>-1</sup>) and outstanding stability over 450mn without any increase of charge-discharge voltage gap. Consequently, the LSM-20-Co catalyst is an attractive bifunctional catalyst as an efficient air cathode catalyst for the alkaline metal-air system and provides insight into the rational design of a thin metal oxide with the ALD process.

### SYMPOSIUM F.EN02

Silicon for Photovoltaics  
November 21 - December 4, 2020

Symposium Organizers

James Bullock, The University of Melbourne  
Kaining Ding, Research Center Juelich  
Eszter Voroshazi, imec  
David Young, National Renewable Energy Laboratory

---

\* Invited Paper

SESSION F.EN02.09: Live Panel Discussion I: Silicon for Photovoltaics  
Session Chairs: Kaining Ding and Eszter Voroshazi  
Wednesday Afternoon, December 2, 2020  
F.EN02

**5:15 PM INTRODUCTION; KAINING DIN**

**5:20 PM PLENARY - ARNO SMETS**

**6:05 PM BREAK**

**6:10 PM INTRODUCTION OF WAFER PANEL; KAINING DING**

**6:15 PM PANELIST: JASMIN HOFSTETTER; KWANGYONG SEO; VALERIE DEPAUW; FREDERIC DROSS**

**6:40 PM BREAK**

**6:45 PM INTRODUCTION OF MODULE PANEL DISCUSSION; ESZTER VOROSHAZI**

**6:50 PM PANELISTS: ALISON LENNON; KARSTEN WAMBACH; MARTIN HEINRICH; TERESA BARNES**

SESSION F.EN02.10: Live Panel Discussion II: Silicon for Photovoltaics  
Session Chairs: James Bullock and David Young  
Thursday Morning, December 3, 2020  
F.EN02

**8:00 AM INTRODUCTION OF MANUFACTURING PANEL DISCUSSION, DAVID YOUNG**

**8:05 AM PANELISTS: QI WANG; JIA CHEN; AKIRA TERAOKAWA**

**8:30 AM BREAK**

**8:35 AM INTRODUCTION OF CONTACT PANEL DISCUSSION, JAMES BULLOCK**

**8:40 AM PANELISTS: REBECCA SAIVE; MARTIN LEDINSKI; STEFAAN DE WOLF; BARBARA TERHEIDEN**

**9:05 AM BREAK**

**9:10 AM \*F.EN02.04.01**

**Lifetime Prediction of PV Modules—When is it Useful and When is it a Distraction? [Sarah R. Kurtz](#); University of**

California Merced, United States

Lifetime prediction is a critical first step as the basis of a warranty or risk assessment. Research that identifies a PV module's primary degradation or failure mechanism, quantifies the associated acceleration factors, and applies those to operating conditions is a straightforward approach to lifetime prediction. The value of this process is obvious and researchers around the world are investigating degradation and failure mechanisms of PV modules with this goal in mind. Making a lifetime prediction is actually quite easy: we can predict 25 years  $\pm$ 25 years for pretty much all PV products on the market, but such a prediction is useless. Making a lifetime prediction with a small uncertainty that leads to a useful prediction is much harder. This talk will describe why lifetime prediction is difficult, when it is essential, when it is a distraction, and how we expect lifetime prediction may evolve in the future.

**9:30 AM \*F.EN02.04.03**

**From Modules to Atoms—Characterization of Silicon Photovoltaic Module Reliability Guided by Luminescence and Thermal Imaging** [Dana Kern](#)<sup>1</sup>, Steve Johnston<sup>1</sup>, Helio Moutinho<sup>1</sup>, Dirk C. Jordan<sup>1</sup>, Jenya Meydbray<sup>2</sup>, Laura Spinella<sup>1</sup>, Michael Owen-Bellini<sup>1</sup>, Kent Terwilliger<sup>1</sup>, Archana Sinha<sup>3</sup>, Laura Schelhas<sup>3</sup>, Chun-Sheng Jiang<sup>1</sup>, Chuanxiao Xiao<sup>1</sup>, Matthew Young<sup>1</sup> and Mowafak Al-Jassim<sup>1</sup>; <sup>1</sup>National Renewable Energy Laboratory, United States; <sup>2</sup>PV Evolution Labs, United States; <sup>3</sup>SLAC National Accelerator Laboratory, United States

With the lifespans of photovoltaic (PV) modules expected to last >20 years, rapid and spatially-resolved characterization methods are essential for understanding module reliability and degradation processes. Luminescence and thermal imaging have been gaining popularity both for fast, outdoor-compatible module inspection and for more detailed post-mortem analysis of failure mechanisms. Importantly, many failure mechanisms are not evident by visual inspection, and characterization of electrical properties alone is insufficient to identify the weakest features of cell or module design. This is especially true as PV technologies and module packaging schemes become more advanced and degradation becomes more subtle. Here, we present various examples of PV module degradation mechanisms in field-weathered modules, where we (1) locate problem areas with luminescence and thermal imaging, (2) core these areas out of the module, and (3) use various microscopy methods to identify chemical and structural causes of power loss. We particularly highlight causes of voltage loss or series resistance increases that vary depending on the technology, and we show studies including conventional Al back surface field (Al-BSF), silicon heterojunction with intrinsic thin layer (HIT), and passivated emitter and rear contact (PERC) modules. These results highlight the utility of imaging methods for improving module reliability.

**9:50 AM CLOSING REMARKS; JAMES BULLOCK**

SESSION F.EN02.11/F.EL06/F.EL08: Live Keynote: Joint Session: Emerging Tandem PV Technologies  
Session Chairs: Kaining Ding and Robert Hoye  
Friday Afternoon, December 4, 2020  
F.EN02

**4:00 PM \*F.EN02.11/F.EL06/FEL08.01**

**The Many Faces of Characterization in Developing a Commercial Perovskite on Silicon Tandem Solar Cell** [Laura Miranda](#); Oxford PV, United Kingdom

Perovskite solar absorbers have the potential to disrupt the photovoltaic industry predominantly with their simultaneous promise of high efficiency and low cost. Whilst these two properties ensure a steady stream of research and development opportunities, commercial scaling requires assuring that the devices are sufficiently characterized to be confident of their long-term performance. Oxford PV has been addressing the challenges associated with commercially scaling its perovskite on silicon tandem solar cell design. Key practices that have been adopted during the development of highly efficient, reliable, and cost-competitive solar cells are the use of rigorous characterization tools and techniques, and the development of necessary models. This talk will highlight some of the challenges and considerations associated with bringing perovskite on silicon tandem solar cells from a laboratory prototype to a commercial product ready for manufacturing and how characterization has shaped and continues to inform that process.

**4:20 PM \*F.EN02.11/F.EL06/FEL08.02**

**Passivation Strategies and Interlayers for Perovskite-Based Tandem Photovoltaics** [Ulrich W. Paetzold](#), Saba

Gharibzadeh, Tobias Abzieher, Ihtez M. Hossain, Hang Hu, Thomas Feeney, Somayeh Moghadamzadeh, Mahdi Malekshahi Byranvand, Bahram Abdollahi Nejad, Paul Fassel and Bryce Sydney Richards; Karlsruhe Institute of Technology, Germany

Single-junction crystalline silicon solar cells dominate the photovoltaics market today, but their power conversion efficiencies (PCEs) are approaching the practical limit for this technology. The emergence of hybrid organic-inorganic metal halide perovskite semiconductors over the past decade has opened a window of opportunity to advance the performance of the market-dominating photovoltaic technologies through the development of tandem solar cells. These tandem solar cells promise high PCEs (>33%). To reach this landmark, a number of scientific and technological challenges related to high-efficiency perovskite-based tandem solar cell architectures, stable and high-quality perovskite semiconductor materials, and light management concepts need to be addressed. In this presentation, our progress on passivation strategies and novel interlayers to reduce the voltage losses in wide-bandgap and low-bandgap perovskite solar cells (PSCs), and in turn to increase the PCE of perovskite-based tandem photovoltaics, will be presented.

The search for efficient passivation interlayers for wide-bandgap perovskite top solar cells in *n-i-p* architecture directed our research in the past towards solution-processed 2D/3D perovskite heterostructures. Making use of these heterostructures for interface passivation, wide-bandgap PSCs ( $E_g \sim 1.72$  eV) with record open-circuit voltage for this bandgap and very high PCEs of up to 19.4% were demonstrated [1]. The reduced voltage deficit is a result of the decreased non-radiative recombination losses at the perovskite/hole-transport layer (HTL) interface. The solution-processed 2D/3D perovskite heterostructure is compatible with 3D perovskite absorber layers of a wide range of bandgaps ( $1.65$  eV  $\leq E_g \leq 1.85$  eV) [2]. Using this strategy in 4-terminal perovskite/silicon and perovskite/CIGS tandem solar cells, high PCEs > 27% [3], and > 25% [2] were demonstrated, respectively, thereby significantly exceeding the record PCEs reported for the respective single-junction solar cell technologies.

Beyond these past results, at the MRS fall meeting we will further present our latest work on novel interlayers and passivation strategies to minimize the voltage loss in wide-bandgap ( $1.65$  eV  $\leq E_g \leq 1.75$  eV) as well as low-bandgap ( $E_g \sim 1.26$  eV) perovskite solar cells in *p-i-n* architecture. The *p-i-n* architecture is a key to realize high-performance 2-terminal perovskite/silicon as well as perovskite/perovskite tandem solar cells. Moreover, we will present a novel route to deposit uniform ultra-thin polymer passivation layers onto perovskite thin films by chemical vapor deposition (CVD) [4]. The CVD polymerization promises reliable, scalable, and homogeneous deposition for future large-area processing of perovskite-based tandem solar cells.

#### References:

- [1] Gharibzadeh, S. *et al.* Record Open-Circuit Voltage Wide-Bandgap Perovskite Solar Cells Utilizing 2D/3D Perovskite Heterostructure. *Adv. Energy Mater.* **9**, 1–10 (2019).
- [2] Gharibzadeh, S.; Hossain I. M. *et al.* 2D/3D Heterostructure for Semitransparent Perovskite Solar Cells with Engineered Bandgap Enables Efficiencies Exceeding 25% in Four-Terminal Tandems with Silicon and CIGS. *Adv. Funct. Mater.* **30**, (2020).
- [3] Duong, T. *et al.* High Efficiency Perovskite-Silicon Tandem Solar Cells: Effect of Surface Coating versus Bulk Incorporation of 2D Perovskite. *Adv. Energy Mater.* **10**, 1903553 (2020).
- [4] Malekshahi Byranvand M.; Behboodi-Sadabad F. *et al.* Chemical Vapor Deposited Polymer Layer for Efficient Passivation of Planar Perovskite Solar Cells. *submitted*

#### 4:40 PM \*F.EN02.11/F.EL06/FEL08.03

**Towards Highly Efficient Monolithic 2- and 3-Terminal Perovskite Silicon Tandem Solar Cells** Lars Korte, Eike Koehnen, Philipp Wagner, Philipp Tockhorn, Marko Jost, Amran Al-Ashouri, Lukas Kegelmann, Marcel Roß, Bernd Stannowski and Steve Albrecht; Helmholtz-Zentrum Berlin für Materialien und Energie, Germany

Integrating metal halide perovskite top cells with crystalline silicon (c Si) bottom cells into monolithic tandem devices has recently attracted increased attention due to the high efficiency potential of these cell architectures. To further increase the tandem device performance to a level well above the best single junctions, optical and electrical optimizations as well as a detailed device understanding for such architectures need to be developed [1]. Here we present our recent results on such monolithic tandem cells in the common 2-terminal (2T) as well as in a novel 3-terminal (3T) contacting scheme.

In the 2T design, we recently demonstrated a certified power conversion efficiency (PCE) of 29.15% [2,3]. I will discuss some key elements to this result: using a silicon heterojunction cell electron contact on the rear side, enabling the integration of a perovskite top cell in the p-i-n configuration; employing self-assembled monolayers (SAMs) as hole selective contacts for further reduction of non-radiative recombination losses, etc. With the latter, efficiencies of up to ~ 21 % were demonstrated for p-i-n perovskite single junctions [3].

In 3T tandems, one of the three contacts is shared by both subcells, allowing for the individual operation of both subcells in a

monolithic device with a single substrate, thus combining the characteristic advantages of 2T and 4-terminal (4T) devices: high combined photogeneration currents as in state-of-the-art 2T tandems, and ideally independent electrical operation similar to 4T tandems, making the cell more robust against varying spectra. I will discuss our recent proof-of-concept study [4], demonstrating a 3T perovskite/silicon tandem cell by manufacturing an n-i-p perovskite top cell on an interdigitated back contact (IBC) silicon heterojunction solar cell. In our proof-of-concept device, the combined PCE of ~ 17% is still limited both optically and electrically, and it will be discussed how optimizations of the cell stack can bring this architecture to a PCE level comparable to 2T tandems. Furthermore, I will demonstrate that the subcells can indeed be operated largely independently at their individual maximum power points, allowing to extract the maximum power output for varying spectral conditions similar to 4T cells. A minimized series resistance at the shared electron contact on the cell's rear side is identified as the crucial parameter for independent operation of the subcells, and I will discuss pathways to approach the simulated efficiency potential by an optimized device design.

#### References:

- [1] Jost, Kegelmann, Korte, Albrecht, Adv. Energy Materials, 2020, doi: 10.1002/aenm.201904102
- [2] NREL Best Research-Cell Efficiency Chart, <https://www.nrel.gov/pv/cell-efficiency.html>
- [3] Köhnen, Jost, Stannowski, Albrecht et al., Sustainable Energy and Fuels, doi: 10.1039/C9SE00120D
- [3] Al-Ashouri, Magomedov, Korte, Albrecht et al., En. Env. Sci, 2019, doi: 10.1039/C9EE02268F
- [4] Tockhorn, Wagner, Korte et al., ACS Appl. En. Mat., 2020, doi: 10.1021/acsaem.9b01800

#### 5:00 PM \*F.EN02.11/F.EL06/FEL08.04

**Advances in Material Properties for Perovskite-Perovskite Tandems** Giles Eperon<sup>1,2</sup>; <sup>1</sup>Swift Solar, United States; <sup>2</sup>National Renewable Energy Laboratory, United States

Multijunction all-perovskite solar cells offer a route towards efficiencies of III-V materials at low cost by combining the advantages of low thermalization loss in multijunction architectures with the beneficial properties of perovskites - namely low processing cost, high throughput fabrication, and compatibility with flexible substrates. Here, I will discuss why flexible all-perovskite tandems are a very attractive iteration of the perovskite technology. I will focus on what is needed to make a good perovskite-perovskite tandem on a flexible substrate, and the advances that we have made towards this goal. I will cover advances including a) the development and understanding of wide bandgap materials that leverage a novel bandgap-tuning strategy (without increasing bromine, hence avoiding significant phase segregation) to reach the ideal bandgaps for all-perovskite tandems, resulting in efficient devices that are stable to the combined stresses of heat and light; b) advances that we have made in interlayer design, working towards more ideal material properties for reducing shunt resistance; and c) the integration of these approaches to develop >23% efficient monolithic all-perovskite tandems on rigid substrates and 21% efficient devices on flexible plastic substrates.

#### 5:20 PM \*F.EN02.11/F.EL06/FEL08.06

**Solution Processed Perovskite Subcell in Monolithic Perovskite/Si Tandem Solar Cells and Their Cost and Stability Concerns** Qi Chen<sup>1</sup> and Huanping Zhou<sup>2</sup>; <sup>1</sup>Beijing institute of Technology, China; <sup>2</sup>Peking University, China

Among all commercialization routes for perovskite photovoltaics (PV), the perovskite/Si tandem is of particular interest as it capitalizes the mature silicon industry with decades of experience. Here we report low-temperature solution process for efficient two-terminal perovskite/Si tandem solar cells, wherein electrical and optical properties of the tunneling junction are carefully modulated. Moreover, we improve materials stability by introducing Eu<sup>2+</sup>/Eu<sup>3+</sup> “redox shuttle” to suppress the Pb<sup>0</sup>/I<sup>0</sup> impurities which inevitably occurred during device operation. In addition, we carefully analyze the cost of tandem devices in terms of levelized cost of energy (LCOE) by adopting the “bottom-up cost model”. It reveals perovskite PV exhibit low materials cost, which reduces the LCOE substantially in tandem devices. We conclude that further efforts are required to simultaneously improve the efficiency and lifetime of perovskite modules, which ultimately endows the competitiveness of perovskite tandem solar cells.

SESSION F.EN02.01: Advanced Characterization and New Insights  
On Demand Abstracts Available for Viewing Starting Saturday Morning, November 21, 2020  
F-EN02

#### 5:00 AM \*F.EN02.01.01

## Thin Films for Silicon Based Photovoltaic Under Zoom Martin Ledinsky; Institute of Physics AS CR, Czechia

Thin films, based on amorphous and microcrystalline silicon or silicon oxides, are the key players in the future silicon photovoltaics. They very well passivate the surface of crystalline silicon, enabling high open circuit voltages and fill factors of finalized cells. Two most promising strategies are Silicon Heterojunction solar cell (SHJ) and Tunnel Oxide Passivated Contacts (TOPCon) based cells.

Interdigitated back contacted SHJ solar cell (IBC SHJ), is the current silicon efficiency world record holder with 26.7%. The record IBC SHJ cell is fabricated by many photolithography steps, not fully compatible with mass production. Thus straightforward shadow masks technology has been developed. In order to check the profiles of ~10 nm thin passivating/selective contacts prepared by shadow mask process on rough substrates, Raman spectroscopy based thickness measurement with resolution below 0.2 nm was introduced [1]. Alternative, industrially relevant way, to image the silicon film thickness by photoluminescence imaging will be introduced.

In the same time it is important to probe the structural and local electrical properties of these films. For this end conductive atomic force microscope (C-AFM) in the tomography regime is suitable for characterisation of mixed phase amorphous/nanocrystalline ultrathin films as well as the tunnelling oxide contacts. 3D visualisations of high temperature passivated back contacts (TOPCon) will be used as an example.

But since the silicon wafer based technology approaches the practical efficiency limit (the theoretical is at ~29%), the only way how to go beyond 30% is combination of two cells in a so called tandem. By doing that the theoretical limit is shifted to over 40%. Suitable candidates for the top cell accompanying well mastered silicon bottom cell are halide perovskites. We will discuss the extraordinary properties of this material family [2]. Finally, we introduce a simple semiconductor property dictating the maximal open circuit voltage obtainable with the given material [3]. In this way we can rapidly preselect suitable candidates for top tandem cell.

### References

- [1] M. Ledinsky, B. Paviet-Salomon, A. Vetushka, J. Geissbühler, A. Tomasi, M. Despeisse, S. De Wolf, C. Ballif and A. Fejfar: *Sci. Rep.* **6**, 37859 (2016).
- [2] De Wolf, S.; Holovsky, J.; Moon, S.-J.; Loeper, P.; Niesen, B.; Ledinsky, M.; Haug, F.-J.; Yum, J.-H.; Ballif, C. *J. Phys. Chem. Lett.*, **5**, 1035–1039 (2014).
- [3] Ledinsky, M.; Schönfeldová, T.; Holovský, J.; Aydin, E.; Hájková, Z.; Landová, L.; Neyková, N.; Fejfar, A.; De Wolf, S. Temperature Dependence of the Urbach Energy in Lead Iodide Perovskites. *J. Phys. Chem. Lett.*, **10**, 1368–1373 (2019).

### Acknowledgments

This work was supported by the Czech Science Foundation Project No. 17-26041Y, Operational Programme Research, Development, and Education financed by the European Structural and Investment Funds and the Czech Ministry of Education, Youth and Sports (Project No. CZ.02.1.01/0.0/0.0/16\_019/0000760 - SOLID21). This work is also supported by Operational Programme Research, Development and Education financed by EU Structural and Investment Funds and the MEYS CR Project No. CZ.02.1.01/0.0/0.0/16\_026/0008382 (CARAT).

### 5:15 AM F.EN02.01.02

**Spatial Mapping of Electrical Parameters with Micrometer Resolution in Interdigitated Back Contact Solar Cells** Siddhartha Garud<sup>1</sup>, Matevz Bokalič<sup>2</sup>, Cham thi Trinh<sup>1</sup>, Bernd Rech<sup>1</sup>, Daniel Amkreutz<sup>1</sup> and Marko Topič<sup>2</sup>; <sup>1</sup>Helmholtz-Zentrum Berlin, Germany; <sup>2</sup>University of Ljubljana, Slovenia

Light-beam induced current (*LBIC*) measurements with a bias voltage or current are used to obtain photogenerated charge collection profiles at different points in the I-V curve of a solar cell. Such measurements can be analysed to obtain local electrical parameters such as dark saturation current and series/shunt resistance and identify aspects for improving solar cell performance.

In the present work, such an analysis technique was developed for solar cells made from 14 μm liquid-phase-crystallized silicon. In particular, it compares a reference cell with the current best cell exhibiting 657 mV open-circuit voltage ( $V_{OC}$ ) and 32.7 mA/cm<sup>2</sup> short-circuit current density ( $J_{SC}$ ) (with an anti-reflection foil on the illumination side). Since the cell architecture used is ‘silicon heterojunction interdigitated back contact’ (SHJ-IBC), the implemented circuit model is designed for an IBC architecture. The circuit is fit to the measured data on a MATLAB script, which will be available for downloading and adapting to other solar cell architectures and materials. The *LBIC* setup was built in-house at the University of Ljubljana. It uses an alternating current (AC) measurement with a direct current (DC) bias and produces full cell images at different bias points. A 40 μm step size was used. The setup offers a minimum step size of 1 μm and an illumination spot diameter <= 10 μm.

Each pixel is treated as an independent one-diode model, surrounded by 2 one-diode model representing the remaining (dark) cell. With this approximation, full cell maps of the following parameters of a one diode model were obtained: dark saturation current ( $I_0$ ), ideality factor ( $n$ ), effective series resistance, shunt resistance and photo-generated current. While treating each pixel as an independent, illuminated solar cell, local I-V curves were simulated, giving full cell maps of  $V_{OC}$ ,  $J_{SC}$ , maximum power points ( $V_{MPP}$  and  $I_{MPP}$ ) and efficiency ( $\eta$ ). The following key observations were made:

1. Top 50 percentile of  $40 \mu\text{m} \times 40 \mu\text{m}$  pixels show a  $J_{SC}$  between 32-33.5 mA/cm<sup>2</sup>,  $V_{OC}$  between 600-640 mV, fill-factor ( $FF$ ) between 73-76 % and  $\eta$  14-15.1% in the reference cell and  $J_{SC}$  between 33.6-34 mA/cm<sup>2</sup>,  $V_{OC}$  between 658-700 mV,  $FF$  between 71-76% and  $\eta$  between 15.7 %-16.5% in the best cell. Due to the presence of crystal defects, local shunts and lower charge collection under the electron contact fingers, the resultant full cell parameters for the reference cell are  $J_{SC}$ : 28.5 mA/cm<sup>2</sup>,  $V_{OC}$ : 617 mV,  $FF$  65.4 % and  $\eta$  11.5 % and for the best cell are  $J_{SC}$ : 30.3 mA/cm<sup>2</sup>,  $V_{OC}$ : 652 mV,  $FF$  64.6 % and  $\eta$  12.8 % (as measured under a AAA-rated sun simulator).
2. Grain boundaries exhibit  $J_{SC}$  of approximately 7-9 mA/cm<sup>2</sup>,  $V_{OC}$  of approximately 340-400 mV, 50%-70%  $FF$  and 1.5-5 %  $\eta$ , subject to the size and recombination activity. Similarly, stacking faults in the reference cell exhibit average values of 26 mA/cm<sup>2</sup>  $J_{SC}$ , 515 mV  $V_{OC}$ , 70 %  $FF$  and 9.5 %  $\eta$ .
3. Laser firing used to lower contact resistance on the electron contact fingers does not lower the over-all  $V_{OC}$  of a cell because it is primarily limited by grain boundaries present in the cell.
4. Electroluminescence imaging shows a gradient towards the direction of the electron contact busbar primarily due to high series resistance in the electron contact fingers. This gradient is also visible in the  $LBIC$  images taken at voltage bias  $> 0.6 \text{ V}$  and is reflected in the local series resistance fitted by the model.

A comparison with the best efficiency cell (15.1 % with anti-reflection foil) is ongoing in which similar trends are expected, but with higher power conversion efficiency. In conclusion, this method successful models current paths of photogenerated charge carriers within the cell and to external electrodes in an IBC architecture. The high resolution maps of electrical parameters quantify the excellent performance of intra-grain regions and limitations primarily due to crystal defects and minority carrier (hole) diffusion length under the electron contact.

### 5:25 AM F.EN02.01.03

**Defect Analysis of Crystalline Si Solar Cells by Learning Radiation-induced Defects in Si** Masafumi Yamaguchi, Takefumi Kamioka, Nobuaki Kojima and Yoshio Ohshita; Toyota Technology Institute, Japan

Although 26.7% efficiency has been attained with hetero-junction and back contact (HBC) structure and by using bulk minority-carrier lifetime of around 10 msec, high efficiency of more than 29% is expected to be realized as a result of decreasing non-radiative recombination loss. This paper presents analytical results for high efficiency potential of crystalline Si solar cells, analyzed by using knowledge ( $C_i$ - $O_i$  center,  $B_i$ - $O_i$  center,  $E'$  center and Pb center), in radiation-induced defects in Si.

One of problems to attain the higher efficiency crystalline Si solar cells is to reduce non-radiative recombination loss. The open-circuit voltage drop compared to bandgap energy ( $E_g/q$ - $V_{oc}$ ) is dependent upon non-radiative voltage loss ( $V_{oc}$ , nrad) that is expressed by external radiative efficiency (ERE). Open-circuit voltage is expressed by

$$V_{oc} = V_{oc,rad} + (kT/q)\ln(ERE), (1)$$

where the second term shows non-radiative voltage loss, and  $V_{oc,rad}$  is radiative open-circuit voltage and 0.87V was used in this study. Correlation between  $V_{oc}$  values for HIT, HBC, PERL and multi-crystalline Si cells and ERE values in the references estimated by eq. (1) suggests that crystalline Si solar cells have still non-radiative loss and further improvements in efficiency are thought to be possible by improving minority-carrier lifetime [1]. Calculated values of minority-carrier lifetime is expressed by the following equation

$$1/\tau = BN + CN^2, (2)$$

where B is radiative recombination probability and  $2 \times 10^{-15} \text{ cm}^3/\text{s}$  for Si, N is carrier concentration and C is the Auger coefficient and is  $1.6 \times 10^{-30} \text{ cm}^6/\text{s}$  for Si. Correlation between calculated values and obtained values of minority-carrier lifetime suggests that further improvement in minority-carrier lifetime is expected to be realized. Really, high bulk lifetime of around 100 msec has been obtained by the MCZ (Magnetic-field-applied Czochralski) method and decreasing carbon concentration to less than  $10^{14} \text{ cm}^{-3}$  in Si.  $C_i$ - $O_i$  center induced by 1-MeV electron irradiations have been used for calibration of carbon concentration in Si. Higher minority-carrier lifetime of around 100msec by decreasing carbon and oxygen precipitate concentrations will provide lower voltage drop of around 0.3V and higher  $V_{oc}$  of around 800mV and thus higher efficiency Si solar cells of more than 28%.

Regarding light-induced degradation of Si solar cells, although  $B_i$ - $O_i$  center in Si was previously thought to act as defect center for light illumination degradation,  $B_i$ - $O_i$  center doesn't act as a non-radiative recombination center according to our



previous studies [2] for radiation-induced defects in Si. Defect introduction rates of  $B_i-O_{2i}$  center induced by light illumination are compared with those of  $B_i-O_i$  center induced by 1-MeV electron irradiations in this study.

Surface recombination degradation of Si solar cells under light illumination is also another important issue for realizing highly reliable Si solar cells. In this study, surface recombination degradation of Si solar cells due to 1-MeV electron irradiations is compared with surface degradation of Si solar cells under light illumination by considering Pb center generation due to 1-MeV electron and ultraviolet light exposures.

In summary, understanding defects in Si solar cells by learning radiation-induced defects in Si is thought to be useful for further development of high-efficiency and highly reliable Si solar cells.

#### References

[1] M. Yamaguchi et al., *J. Mater. Res.* **33**, 2621 (2018).

[2] M. Yamaguchi et al., *J. Appl. Phys.* **86**, 217 (1999).

#### 5:35 AM F.EN02.01.04

**Defect Phase Diagram of Facet and Line Junctions of  $\Sigma 3$  Grain Boundaries in Si** Liverios Lymperakis<sup>1</sup>, Masud Alam<sup>2,1</sup> and Jorg Neugebauer<sup>1</sup>; <sup>1</sup>Max-Planck-Institut für Eisenforschung GmbH, Germany; <sup>2</sup>Interdisciplinary Centre for Advanced Materials Simulation, Germany

Interfaces such as grain boundaries (GB) that break the translational symmetry of a crystal play a dominant role in the properties of materials. The role of GBs is substantial in multi- and polycrystalline optoelectronic and photovoltaic materials: Multi-crystalline Si (mc-Si), which nowadays dominates the Si based photovoltaics industry has a density of  $10^4/\text{cm}$  GBs. These defects, as well as their interaction with impurities constitute a major limiting factor in the efficiency of the aforementioned devices. More specifically it has been shown that recombination at GBs constitute a major channel for electrical losses in high performance mc-Si solar cells.  $\Sigma 3$  tilt GBs in Si is a family of interfaces with special fundamental and technological interest. The  $\Sigma 3\{111\}$  twin boundaries (TB) have negligible boundary energy and are electrically inactive. They are therefore preferred over other electrically active boundaries. However,  $\Sigma 3\{112\}$  GBs exist in two stable/metastable states, the symmetric (S- $\Sigma 3$ ) and the asymmetric (A- $\Sigma 3$ ), with the former having deep states into the fundamental bandgap. Furthermore, facet junctions of the TB with the A- $\Sigma 3$  show a unique anisotropic segregation mechanism, that goes beyond the classical picture of planar McLean type segregation [1]. Nevertheless, a prerequisite to get full control on the properties of these interfaces is to gather a deep understanding of the corresponding faceting mechanisms.

In the present work we employ density functional theory (DFT) and large scale modified embedded atom method (MEAM) potential calculations to investigate the structure, energetics and strain associated with these boundaries. Based on our DFT calculations we parametrize a MEAM potential suitable to describe GB energetics and long range elastic interactions in Si. Our calculations revealed that  $\Sigma 3$  tilt GBs with the  $[110]$  rotation axis are intrinsically unstable against faceting towards  $\{111\}$  and  $\{112\}$  facets. Furthermore, based on these calculations we derive a facet and line junction phase diagram that describes and predicts the reconstructions of these extended defects as function of facet length and boundary inclination angle. This diagram reveals that large (small) inclination angles with respect to  $\{111\}$  plane and/or large (small) facet lengths favor junctions with A- $\Sigma 3$  (S- $\Sigma 3$ ) facets, respectively. This is explained in terms of (i) the large anisotropy in the energies of S- and A- $\Sigma 3$  and (ii) the presence (lack) of extended defects at the  $\{111\}$  and A- (S-)  $\{112\}$  line junctions, respectively: While the low energy of the A- $\Sigma 3$  facets favors these boundaries over their symmetric counterparts, line junctions of TBs with A- $\{112\}$  facets are accommodated by edge type dislocations. The long range repulsive interactions make these facets highly unfavorable at small facet lengths. On the other hand, S- $\Sigma 3$  GBs are commensurate to the  $\Sigma 3$  coincidence site lattice and the energy of the corresponding faceted junction is independent of the facet length. These findings shed light upon GB faceting phenomena and have important implications on the GB mobility mechanisms, the electronic properties as well as on selective impurity segregation at line junctions and facets in mc-Si: At large inclination angles the A- $\Sigma 3$  GBs will adopt the maximum length allowed by the microstructure and grain size. Furthermore, the highly strained core region and its topology at the line junctions will strongly influence impurity segregation at these regions. On the other hand, at small inclination angles, the deep states introduced by the S- $\Sigma 3$  facets will act as recombination centers and will be detrimental for the device efficiency. Based on the aforementioned results we will further discuss the implications on impurity segregation at the flat and facet junctions  $\Sigma 3$ GBs as well as on their mobility.

[1] C. H. Liebscher, A. Stoffers, M. Alam, L. Lymperakis *et al.*, *Phys. Rev. Lett.* **121**, 015702 (2018).

#### 5:45 AM F.EN02.01.05

**Spectroscopic Investigation of Spin-Active Defect in Czochralski Silicon Responsible for Light-Induced Degradation** Abigail R. Meyer<sup>1</sup>, P. Craig Taylor<sup>1</sup>, Matthew Page<sup>2</sup>, David L. Young<sup>2</sup>, Paul Stradins<sup>2</sup> and Sumit

Agarwal<sup>1</sup>; <sup>1</sup>Colorado School of Mines, United States; <sup>2</sup>National Renewable Energy Laboratory, United States

Light-induced degradation (LID) is a decrease in the minority carrier lifetime in boron-doped Czochralski (Cz) silicon solar cells due to injection of excess carriers. It is well accepted that LID occurs due to a defect involving a substitutional boron atom and an oxygen dimer. There are three characteristic stages of LID: an annealed state where defects are metastable and non-recombination-active, a degraded state where defects are recombination active, and a stabilized state where defects are permanently non-recombination-active. While a technological solution to mitigate LID is slowly being implemented into industrial manufacturing lines, the fundamental mechanism for lifetime stabilization and the structure of the LID defect remain speculative. Empirical studies relate B and O to the defect structure, but atomistic evidence is lacking. If the defect structure and mechanism of LID is discovered, mitigation strategies could be quickly studied and implemented improving the long-term reliability of high-efficiency, B-doped Si solar cells.

In this work we utilize electron paramagnetic resonance (EPR) spectroscopy, magnetic susceptibility, and lifetime spectroscopy to study the structure of the LID defect and the degradation mechanism. We report on the EPR spectra of Cz and float-zone (FZ) Si in different stages of LID. Firstly, we show that the paramagnetic signal at low temperature (6 K) is dependent on the state of LID and on the sample doping. The light-degraded state in *p*-type Cz Si shows a strong, sharp paramagnetic defect signature ( $g$ -value = 2.003) compared to samples in the annealed state, where the EPR spectra is relatively featureless. In contrast, the broad EPR active signature related to boron interaction with lattice, is present in the annealed state but diminishes after light exposure. Both EPR signals change under indoor light exposure at room temperature and therefore are sensitive to initial stages of LID. We see a smaller decline in the wide-spectrum boron/lattice interaction EPR signal in *p*-type FZ Si and none in *n*-type Cz Si. We hypothesize the decrease in the oxygen concentration in the *p*-type FZ sample results in incomplete quenching of the boron acceptor spins. We suggest that these changes in the EPR spectra are related to the BO defect that causes LID. Additionally, we utilized *p*-type FZ with an order of magnitude higher B doping to investigate the effect of the B/O concentration ratio on extent of quenching of  $B_a$  spins after indoor light exposure. We observe that in the *p*-type FZ Si sample that is more heavily doped with B (B/O ~ 10:1) the  $B_a$  spin signal is almost unaffected by LID compared to the more lightly doped B-doped *p*-type FZ Si sample (B/O ~ 1:1). Therefore, if the B atoms are in excess, there are simply not enough O atoms to quench all the  $B_a$  spins and the EPR signal remains. Therefore, O is involved in this paramagnetic to diamagnetic transition of the  $B_a$  in the Si bulk and for this transition to occur, BO complexes are required. Finally, we show that magnetic susceptibility measurements confirm that in the annealed state of LID, the *p*-type Cz Si sample is paramagnetic, and in the degraded state, diamagnetic, which is consistent with our EPR findings. Thus, for the first time, EPR and magnetic susceptibility have been used to show manipulation of the LID defect after dark-annealing and light exposure.

#### 5:55 AM F.EN02.01.06

**A Scanning Nonlinear Dielectric Microscopic Investigation of Potential-Induced Degradation in Monocrystalline Silicon Solar Cells** Yasuo Cho<sup>1</sup>, Sachiko Jonai<sup>2</sup> and Atsushi Masuda<sup>2</sup>; <sup>1</sup>Tohoku University, Japan; <sup>2</sup>National Institute of Advanced Industrial Science and Technology, Japan

Crystalline silicon (Si) solar cells currently occupy an important place in the solar cell market. However, potential-induced degradation (PID) of crystalline Si photovoltaic (PV) modules has recently been observed in large systems comprising significant numbers of PV modules. In these PV systems, numerous such modules are interconnected in series, such that potential stress is imparted to some of the modules with consequent high power losses. PID in Si PV modules based on *p*-type crystalline Si solar cells has been previously investigated in detail [1]-[5].

About estimated changes in solar cell during PID, for example, it has been reported that, due to the penetration of Na into the solar cell, a deep level is formed in the depletion layer or the base layer (*p* layer) and, as a result, carrier recombination through the level occurs [4]. Na is known to create a level in Si at a position 0.35 eV from the valence band. It also has been suggested that current shunt path is formed by intrusion of Na into stacking faults penetrating the pn junction (or that Na invading Si forms stacking faults) [5].

Even so, there is still a lack of understanding of the PID mechanism in solar cells, and obtaining more information regarding this phenomenon will require measurements of carrier distributions on a microscopic scale. One of the authors previously succeeded in quantitatively analyzing such distributions in monocrystalline Si solar cells using scanning nonlinear dielectric microscopy (SNDM) [6][7].

In the present study, the microscopic carrier distributions in monocrystalline Si solar cells exhibiting PID were investigated using this same technique. In addition, an enhanced version of this technique referred to as super-higher-order (SHO)-SNDM was employed to visualize depletion layer distributions in such cells both with and without PID.

As a result, reductions in carrier density in accordance with the extent of PID were clearly observed, and quantitative measurements demonstrated that the electron concentration was reduced by several order of magnitude due to PID. Depth profile measurements showed that the solar cells were affected by PID to a significant depth of approximately 90  $\mu\text{m}$ , equal

to almost half the cell thickness, suggesting that Na<sup>+</sup> migration proceeded easily upon the application of a high voltage. The SHO-SNDM data showed that the depletion layer of the non-PID sample was thinner than that of a PID sample, indicating that the carrier concentration in the former was greater.

This work demonstrates that SNDM is a very useful means of investigating the PID effect through the measurement of carrier distributions in monocrystalline silicon solar cells.

#### References:

- [1] S. Jonai and A. Masuda, AIP Adv. 8, 115311 (2018).
- [2] Berghold, O. Frank, H. Hoehne, S. Pingel, B. Richardson and M. Winkler, Proceedings of the 25th European Photovoltaic Solar Energy Conference and Exhibition, Valencia, Spain, 3753 (2010).
- [3] P. Hacke, M. Kempe, K. Terwilliger, S. Glick, N. Call, S. Johnston, S. Kurtz, I. Bennett and M. Kloos, Proceedings of the 25th European Photovoltaic Solar Energy Conference and Exhibition, Valencia, Spain, 3760 (2010).
- [4] W. Luo, Y. Sheng Khoo, P. Hacke, V. Naumann, D. Lausch, S. P. Harvey, J. Prakash Singh, J. Chai, Y. Wang, A. G. Aberle and S. Ramakrishna, Energy Environ. Sci. 10, 43 (2017).
- [5] V. Naumann, D. Lausch, A. Hähnel, J. Bauer, O. Breitenstein, A. Graff, M. Werner, S. Swatek, S. Großer and J. Bagdahn, and C. Hagendorf, Sol. Energy Mater. Sol. Cells 120, 383 (2014).
- [6] K. Hirose, K. Tanahashi, H. Takato, and Y. Cho, Appl. Phys. Lett. 111, 032101 (2017).
- [7] Y. Cho, A. Kirihara, and T. Saeki, Rev. Sci. Instrum. 67, 2297 (1996).

#### 6:05 AM F.EN02.01.07

**Analysis of the Physical and Photoelectrochemical Properties of c-Si(p)/a-SiC:H(p) Photocathodes for Solar Water Splitting** María del Carmen Mejía, Luis Francisco Sanchez, Francisco Rumiche and Jorge A. Guerra; Pontificia Universidad Católica del Perú, Peru

In the present work, the effect of surface states and bulk opto-electronic properties of Al doped c-Si(p)/a-SiC:H(p) heterojunction photocathodes were evaluated on the photocatalytic performance for photoelectrochemical water splitting, before and after thermal treatments. The absorber a-SiC:H(p) thin film of around 320 nm was deposited onto p-type Si and fused silica substrates by reactive Radio frequency magnetron co-sputtering using high purity SiC and Al targets under Ar-H<sub>2</sub> atmosphere. a-SiC:H(p) thin films on Si substrates were chosen to perform morphological, structural and photoelectrochemical characterization. Whereas the samples prepared onto fused silica substrates, were used to perform optical characterization. The absorption coefficient and optical bandgap energy were determined since they play an important role in the device performance. Optical properties of the a-SiC:H(p) films were assessed systematically by means of UV-Vis transmittance measurements. Fourier transform infrared spectroscopy measurements were performed to track the hydrogen content, molecular bond-densities and changes in the structural properties of the a-SiC:H(p) layer for the distinct annealing temperatures. Van der Pauw electrical measurements revealed an improvement in the electrical behavior of the photocathode device after performing the annealing step at 600°C. Ohmic contact, which is a key requirement for an optimal photoelectrochemical cell performance, was achieved after the annealing step at this temperature.

Annealing treatments induced changes in electrical, structural and optical properties of the material. These changes were reflected in the achieved good photocathode performance. Thus, an abrupt enhancement of the photocurrent was observed during the device photoelectrochemical test in 1 M H<sub>2</sub>SO<sub>4</sub> solution under chopped light illumination. Reaching a saturation value of 17 mA/cm<sup>2</sup> at -1.75 V vs. Ag/AgCl (3.5 M KCl). In this research we propose that this enhancement is associated to a charge transfer kinetic mechanism influenced by surface states and the p-type Si substrate. The latter most likely due to the space charge region extension beyond the absorber layer until reaching the substrate, as it was demonstrated by means of electrochemical impedance spectroscopy measurements and some of our estimations. Current density-potential and electrochemical impedance spectroscopy measurements in dark, revealed a reduction of the SiO<sub>2</sub> native layer at cathodic potentials higher than -1 V vs. Ag/AgCl (3.5 M KCl). This last effect might contribute to the high charge transfer kinetic of the system. In that sense, our findings so far conduct to believe that SiO<sub>2</sub> layer reduction triggers a favorable semiconductor-electrolyte interface, possessing less overpotential barriers that facilitates photocurrent generation. We believe that these results will help to the developing of Si/SiC junction devices in tandem for solar-to-hydrogen energy conversion.

SESSION F.EN02.02: Emerging Materials and Concepts  
On Demand Abstracts Available for Viewing Starting Saturday Morning, November 21, 2020  
F-EN02

#### 5:00 AM \*F.EN02.02.01

**Neutral-Colored Transparent Crystalline Silicon Solar Cells** Kangmin Lee, Namwoo Kim, Han-don Um and Kwanyong Seo; Ulsan National Institute of Science and Technology, Korea (the Republic of)

Transparent solar cells, which combine visible transparency and solar energy conversion, are being developed for applications in which conventional opaque solar cells are unlikely to be feasible, such as windows of buildings or vehicles. However, transparent solar cells developed to date have limitations in efficiency and stability. Crystalline silicon (*c*-Si) is one of the best candidates to develop transparent solar cells with high efficiency and stability, because conventional *c*-Si solar cells are known to exhibit high efficiency and long-term stability compared with other solar cells. However, the opaque characteristic of the *c*-Si wafer hinders the development of transparent solar cells using *c*-Si. In this presentation, we introduce a novel approach to develop neutral-colored transparent *c*-Si solar cells that exhibit the highest efficiency among neutral-colored transparent solar cells developed to date. Also, we review recent progress in transparent solar cells along with strategies that enable the transparency of conventional solar cells, including thin film technology, selective light transmission technology, and luminescent solar concentrator technology. From fundamental research to commercialization of the transparent solar cells, three main perspectives should be considered: (1) high power conversion efficiency at the same average visible transmittance; (2) aesthetic factors, which should not detract from applications such as buildings and vehicles; and (3) feasibility for real-world applications, including modularization and stability evaluation. We present the distinct analysis criteria for these main perspectives and discuss their importance.

#### 5:15 AM F.EN02.02.02

**PV Cells Based on Arrays of Subwavelength Light Concentrators** Ashish Prajapati; Ben Gurion University of the Negev, Israel

Texturing the front surface of thin film photovoltaic cells with ordered or disordered arrangements of subwavelength structures is beneficial in terms of efficient light harvesting as well as efficient carrier extraction. Previous studies demonstrated efficient broadband absorption of solar radiation with surface arrays of subwavelength inverted cones (light funnels – LFs). In the current work, we use three-dimensional finite-difference time-domain electromagnetic calculations as well as three-dimensional device calculations to examine carrier extraction from photovoltaic cells that are composed of LF arrays on top of underlying substrates. For the selected geometry under examination, we show a broadband absorption enhancement of 14% for the LF photovoltaic cell compared with a cell based on the respective optically optimized nanopillar arrays. However, we show that the nominal power conversion efficiency is 60% higher in the LF cell which is due to the enhancement of both open-circuit voltage and short-circuit current. The higher open-circuit voltage in the LF cell is due to the higher injection of photocarriers, and the higher short-circuit current is a result of the unique LF geometry that supports efficient carrier extraction due to the naturally occurring gradients of the quasi-Fermi levels and minority carrier conductivity that allow for enhanced contact selectivity. We believe that this work paves the way towards a new approach for carrier collection in photonic devices for energy applications.

#### 5:25 AM F.EN02.02.03

**Multifunctional Effect of *p*-Doping, Anti-Reflection, and Encapsulation by Polymeric Acid for High Efficiency and Stable Carbon Nanotube-based Silicon Solar Cells** Il Jeon<sup>1,2</sup>, Yang Qian<sup>1</sup>, Esko Kauppinen<sup>3</sup>, Yoonmook Kang<sup>4</sup>, Haeseok Lee<sup>4</sup>, Donghwan Kim<sup>4</sup> and Shigeo Maruyama<sup>1</sup>; <sup>1</sup>The University of Tokyo, Japan; <sup>2</sup>Pusan National University, Korea (the Republic of); <sup>3</sup>Aalto University, Finland; <sup>4</sup>Korea University, Korea (the Republic of)

Silicon solar cells among different types of solar energy harvesters have entered the commercial market owing to their high power conversion efficiency and stability. By replacing the electrode and the p-type layer by a single layer of carbon nanotubes, the device can be further simplified. This greatly augments the attractiveness of silicon solar cells in the light of raw material shortages and the solar payback period, as well as lowering the fabrication costs. However, carbon nanotube-based silicon solar cells still lack device efficiency and stability. These can be improved by chemical doping, antireflection coating, and encapsulation. In this work, the multifunctional effects of p-doping, antireflection, and encapsulation are observed simultaneously, by applying a polymeric acid. This method increases the power conversion efficiency of single-walled carbon nanotube-based silicon solar cells from 9.5% to 14.4% and leads to unprecedented device stability of more than 120 days under severe conditions. In addition, the polymeric acid-applied carbon nanotube-based silicon solar cells show excellent chemical and mechanical robustness. The obtained stable efficiency stands the highest among the reported carbon nanotube-based silicon solar cells.

#### 5:35 AM F.EN02.02.04

**Indium Gallium Nitride-Silicon Heterojunction Schottky Barrier Solar Cells** Choudhury J. Praharaj; BandOptics Materials, United States

We present calculations of performance characteristics of Indium Gallium Nitride-Silicon Heterojunction Schottky barrier solar cells. The effect of growth axis and spontaneous and piezoelectric effects in the Indium Gallium Nitride are taken into account. We consider both wurtzite Indium Gallium Nitride layers on 111 silicon and cubic indium gallium nitride layers on 100 silicon. The short-circuit current generation as a function of depletion-layer thickness is studied along with the effect of Indium Gallium Nitride composition on the Schottky barrier dark current. The absorption of high energy solar photons in a wider band-gap indium gallium nitride layer with the absorption of lower energy photons in the silicon layer provides the best efficiencies for this device as the conduction and valence band discontinuities are of the right sign to provide unimpeded electron and hole flow for collection in a high-efficiency cell. We consider the effect of composition grading on solar cell characteristics.

#### 5:45 AM F.EN02.02.05

**Optimization of Silicon Clathrates Films for Photovoltaic Applications** Romain Vollandat<sup>1</sup>, Arechkik Ameur<sup>1</sup>, Stéphane Roques<sup>2</sup>, Jean-Luc Rehspringer<sup>2</sup>, Dominique Muller<sup>1</sup>, Céline Chevalier<sup>3</sup>, Abdelilah Slaoui<sup>1</sup> and Thomas Fix<sup>1</sup>; <sup>1</sup>CNRS and University of Strasbourg, ICube Laboratory, France; <sup>2</sup>CNRS and University of Strasbourg, Institut de Physique et Chimie des Matériaux de Strasbourg, France; <sup>3</sup>Institut des Nanotechnologies de Lyon, France

Common forms of elemental silicon (mono-, multi-crystalline and amorphous) materials have been playing a key role in photovoltaic technologies for almost seventy years and are studied thoroughly. Exotic, low-density forms of silicon have recently regained interest due to alluring semiconducting and optical properties as films in regard to the conventional ones. In this work, the focus is put on an allotrope of silicon: silicon clathrate films. Inorganic clathrates are intermetallic structures defined by a 3D porous framework (Si or group IV elements) of polyhedrons, which can enclose guest-atoms (Na or alkali metals). Due to this specific organization, some silicon clathrates can exhibit an interesting direct band-gap in the range of 1.8-2 eV<sup>[1]</sup>, at low guest-atom concentration, which is specifically beneficial for photovoltaic applications.

In this work, we will introduce the preparation and characterization of silicon clathrate films using different silicon reagents (p-doped and intrinsic c-Si (100) and (111) wafer, a-Si on sapphire...). The structural, electrical, optical, surface properties are analyzed and the fabrication conditions optimized to give the best properties and mechanical integrity. Furthermore, various post-synthesis processes are investigated in order to maximize the photovoltaic efficiency of silicon clathrates in regard to the first silicon clathrates basic solar-cell obtained<sup>[2]</sup>. From Ion implantation experiments and other doping techniques to annealing under press, we will discuss how these treatments could, not only help to strengthen the properties of silicon clathrates, but also to bring some enlightenment about the underlying mechanisms that are still unclear.

<sup>[1]</sup> Valeri I. Smelyansky, John S. Tse. (1997). *The electronic structure of metallo-silicon clathrates NaxSi136 (x = 0, 4, 8, 16 and 24)*. Chemical Physics Letters. **264** (5).

<sup>[2]</sup> Tetsuji. Kume et al. (2016). *Thin film of guest-free type-II silicon clathrate on Si (111) wafer*. Thin Solid Films. **609**.

#### 5:55 AM F.EN02.02.06

**Evaluation of Tellurium-Hyperdoped Silicon for Photovoltaic Applications** Sashini S. Dissanayake<sup>1</sup>, Shao Qi Lim<sup>2</sup>, Philippe Chow<sup>3</sup>, Jeffrey Warrender<sup>3</sup>, Jim S. Williams<sup>2</sup> and Meng-Ju Sher<sup>1</sup>; <sup>1</sup>Wesleyan University, United States; <sup>2</sup>The Australian National University, Australia; <sup>3</sup>Benet Laboratories - ARDEC, United States

Hyperdoped semiconductors are promising material candidates for intermediate band photovoltaic applications with theoretical efficiency exceeding 50% [1]. Despite of considerable amount of literature reports on the optical and structural characterizations, few studies focus on crucial parameters for device designs such as charge carrier lifetime and mobility. In recent years, ion implantation followed by non-equilibrium pulse laser melting has shown to produce high quality hyperdoped material. The resulting hyperdoped layer is highly substitutional, containing up to 1 atomic % of dopant exceeding the typical solid solubility limit [2]. Previous studies have reported Si hyperdoped with S, Se, Te and Au as promising materials to enhance light absorption to the order of  $\sim 10^4$  cm<sup>-1</sup> in sub-band gap wavelength range [3-5]. Furthermore, Te dopant exhibits higher thermal stability than S and Se, and less dopant segregation than Au [6]. This study aims at understanding charge carrier dynamics such as carrier lifetime and mobility of Te-hyperdoped silicon (Si:Te). We study Si:Te on both p-type and n-type substrates with varying laser processing conditions. The optical absorption spectroscopy and secondary ion-mass spectrometry were employed to investigate the sub band-gap absorption and concentration profile. The results show that the absorption values are comparable with the other well studied materials like Au-hyperdoped Si (Si:Au), where sub bandgap absorption increases with increasing dopant dose. Time resolved terahertz spectroscopy (TRTS) is used to study the charge carrier lifetime. Optical pump THz probe is a non-contact photoconductivity

measurement for probing carrier lifetime with picosecond time resolution. We found that Si:Te lifetimes are much longer, consisting of a rapid decay in the order of ps followed by a longer, ns-lifetime component. To explain the observed results, we study two different optical pump wavelengths at 400nm and 266nm to investigate surface recombination, carrier mobility and diffusion properties. The carrier lifetime and mobility results together with optical absorption and structural properties will be discussed to better understand and optimize Si:Te as a material candidate for intermediate band photovoltaics.

- [1] A. Luque, *et al.*, *Nature Photonics* **6**, 146 (2012).
- [2] J. P. Mailoa, *et al.*, *Nature Communications* **5**, 3011 (2014).
- [3] T. G. Kim, *et al.*, *Appl. Phys. Lett.* **88**, 241902 (2006).
- [4] M. Tabbal *et al.*, *Appl. Phys. A* **98**, 589 (2010).
- [5] W. Yang, *et al.*, *Phys. Rev. Mater.* **1**, 074602 (2017).
- [6] M. Wang, *et al.*, *Phys. Rev. Applied* **10**, 024054 (2018).

#### 6:05 AM F.EN02.02.07

**Thin-Film Synthesis and Characterization of Silicon Clathrate** Yinan Liu, William Schenken, Lakshmi Krishna, Ahmad A. A. Majid, Carolyn A. Koh, P. Craig Taylor and Reuben Collins; Colorado School of Mines, United States

Development of new materials with novel optical, electronic, and spin properties is critical to next generation electronic and photonic technologies. Although Si has been the most widely used element in this area, the most stable Si phase, diamond Si, offers an indirect band gap and weak absorption. A cage-like, crystalline Si allotrope, Si clathrate, has been reported to have a direct or nearly direct bandgap with potentially exciting optoelectronic properties. Room temperature and atmospheric pressure metastable clathrates are synthesized in the presence of alkali guest atoms, such as Na, which occupy the interstitial sites in the cages. Low Na concentration Type II Si clathrate  $\text{Na}_x\text{Si}_{136}$  in the powder form has been identified to be a heavily doped semiconductor with Na guest(s) as a shallow donor. Compared with clathrate powder, the thin-film clathrates are more interesting due to their potential for practical application. However, the synthesis of high-quality clathrate films with well-defined properties for studies of band structure, defects, dopant diffusion, and electronic transport has been difficult. A detailed understanding of tunable and controlled thin-film synthesis and its optical properties is critical to eventually realizing the potential of these semiconductors for electronic and optoelectronic devices.

Here, we present a protocol for silicon clathrate thin film synthesis that produces thin, uniform, well adhered type II clathrate films with low Na concentration and a low concentration of competing phases. The films have been formed using a two-step process: formation of the precursor NaSi film and thermal decomposition of the precursor into the clathrate phase. By adding an additional annealing process between the two steps above, Na content was reduced before the thermal decomposition in an effort to reduce the voids and holes in the final film due to Na removal. XRD in combination with Rietveld refinement was used to characterize film crystallinity, phase purity, and Na content. The effect of varying the time and temperature of each of the processing steps was explored. Also, films were formed directly on Si wafers and Si films on alternative substrates, such as sapphire, to simplify electrical and optical characterization. Post growth treatment procedures to remove residual Na contamination were also developed. The films are expected to grow randomly and SEM images confirm morphological variation, but also show regions with sufficient uniformity to allow further measurement with optical and electronic techniques that sample small areas (e.g. photoluminescence (PL) and Time of Flight SIMS). We also obtained the correlation between the thin film thickness and the annealing time of the first step which makes controllable synthesis possible. Characterization of the synthesized thin film samples was performed and compared to low Na content powder samples. The PL spectrum shows a wide emission peak centered around 2 eV, with a full width at half maximum of about 0.54 meV. This peak is near the reported direct bandgap of Si clathrates but extends to higher energy, suggesting a degenerately doped semiconductor with an impurity band moving into the conduction band. Moreover, similar to the Electron Paramagnetic Resonance spectra of the clathrate powder at low temperature, we observe a feature at  $g \sim 2.002$  associated with free carriers and four hyperfine lines with the splitting of 133mT in the thin film due to the interaction of the Na valence electron with the nuclear spin ( $I = 3/2$ ) of  $\text{Na}^{23}$ . The observation of the hyperfine lines suggests that the Na content in the films is below the metal-insulator transition. The findings in this work reinforce the notion that this Si allotrope could be a next-generation material for semiconductor technology.

This work was supported by the National Science Foundation Award #1810463.

#### 6:15 AM F.EN02.02.08

**Atomic Layer Deposition of Vanadium Oxide Films for Crystalline Silicon Solar Cells** Eloi Ros Costals, Gerard Masmitjà, Estefania Almache, Benjamin Pusay, Gema Lopez, Kunai Tiwari, Edgardo Saucedo, Joaquim Puigdollers, Isidro Martin, Cristobal Voz and Pablo Ortega; Universitat Politècnica de Catalunya, Spain

Deposition of TMOs for PV purposes on industrial techniques (e.g. Sputtering, ALD, etc) is a work that has been repeatedly

reported by relevant photovoltaic research groups[1][2], however so far literature results indicate that the hole selective properties of evaporated TMOs can not be successfully reproduced by other deposition methods. Oposing to this thesis we report the deposition of vanadium oxide (V<sub>2</sub>O<sub>5</sub>) films by ALD effectively performing as hole-selective contact for n-type crystalline silicon solar cells. Reasonable specific contact resistance of 100 mΩcm<sup>2</sup> was measured by transfer length method. In addition, capacitance-voltage measurements confirms the presence of a strong inversion layer at the c-Si/V<sub>2</sub>O<sub>5</sub> interface with a built in voltage of 683 mV. Furthermore, soft deposition of ALD achieved high effective lifetime values up to 800 μs as a result of passivation properties of the film. Finally, a proof-of-concept solar cells fabricated exhibiting efficiencies beyond 18% and with similar if not better photovoltaic parameters to evaporated TMOs without the use of any additional passivation layer in the front contact. The technological implementation of ALD as the deposition technique to state of the art TMO solar cells could be the key for the fabrication of full wafer high efficiency dopant free c-Si solar cells.

[1] Sputter-deposited WO<sub>x</sub> and MoO<sub>x</sub> for hole selective contacts, Martin Bivour et al, 10.1016/j.egypro.2017.09.259, Fraunhofer Institute for Solar Energy Systems ISE.

[2] Atomic layer deposited molybdenum oxide for the hole-selective contact of silicon solar cells, Martin Bivour et al, 10.1016/j.egypro.2016.07.125, Fraunhofer Institute for Solar Energy Systems ISE

#### 6:25 AM F.EN02.02.09

**Late News: *In Situ* Catalyst Doped Silicon Nanowires Solar Cells** Krishna Nama Manjunatha; De Montfort University, United Kingdom

Silicon nanowires (SiNWs) have gained great attention in various emerging applications that include solar cells, Li- & Na-ion batteries, electronic memory devices, supercapacitors, and thermoelectric generators [1-3]. Although the semiconductor industry is dictated by silicon, there are many limitations posed by the bulk material limiting its use in emerging electronic devices. Interestingly, these limitations are solved by its micro to nano-sized silicon. Smaller dimensions of SiNWs have provided opportunities in solar cells due to increased absorption by trapping of light, anti-reflection effect, effective charge separation, decoupling the path of light absorption and carrier separation [1, 2]. The use of SiNWs requires a fraction amount of silicon as compared with the traditional Si wafer-based devices, which minimises the cost of production. With the Use of Plasma Enhanced Chemical Vapor Deposition process (PECVD) it is possible to lower the energy consumption for the growth of crystalline SiNWs by efficiently dissociating precursors gases, controlling the process with plasma and growth rate is an order of magnitude faster as compared with the Chemical Vapour Deposition and Molecular Beam Epitaxy. Also, enables the use of relatively cheaper substrates such as glass and plastic. However, currently SiNWs are doped with diffusion processes and/or gaseous precursors (diborane and phosphine). However, our work proposes doping from a metal catalyst [2-3] that is already used as a seed for the growth of nanowires. This method has added advantages including the elimination of toxic gases, avoiding the complexity of counter-doping caused by the catalyst, and reducing costs. Thereby moving towards green manufacturing processes.

This research focuses on understanding and optimisation of controlled growth of self-doped SiNWs (both n-doped and p-doped) by a PECVD process at relatively low temperatures (<300°C). Metals used as a catalyst in the VLS growth process provides some additional advantages along with the nucleation and precipitation if carefully selected. Hence, the selection of catalyst (metal) with ionisation energy level closer to the valence and/or conduction band of Si will contribute to self-doping. In this study, various metals (such as gallium, indium as p-type dopant, and Bismuth as n-type dopant) are used to facilitate the growth and to dope the nanowires. This work also introduces and discusses the novel process to grow simultaneously and selectively *in situ* n- and p-type silicon nanowires in a single pump-down PECVD process without the use of dopant gases. To the best of our knowledge, such a process is not reported. Such nanowires are possible to be grown on plastic and glass substrates thus reducing cost and open up a number of opportunities. Optical and electrical analyses including Seebeck and resistivity measurements will be discussed to understand the properties of catalyst doped SiNWs. Morphology and crystallinity by various characterisation techniques such as transmission and scanning electron microscopy, X-Ray diffraction, and Raman spectroscopy are performed. This work is not just limited to the growth process, but also adapting SiNWs to fabricate solar cells. For example, fabricated SiNWs photovoltaic solar cells have shown an efficiency of 6% and there is still room for improvement as the study is at the exploratory stage.

[1] Manjunatha, Krishna Nama, et al. "Comparative Study of Silicon Nanowires Grown From Ga, In, Sn, and Bi for Energy Harvesting." IEEE Journal of Photovoltaics (2020).

[2] Manjunatha, Krishna Nama, and Shashi Paul. "In-situ catalyst mediated growth and self-doped silicon nanowires for use in nanowire solar cells." Vacuum 139 (2017): 178-184.

[3] Manjunatha, Krishna Nama, and Shashi Paul. "Carrier selective metal-oxides for self-doped silicon nanowire solar cells." *Applied Surface Science* 492 (2019): 856-861.

#### 6:35 AM F.EN02.02.10

**Late News: Energy Conversion of Yb<sup>3+</sup>, Pr<sup>3+</sup>-Doped BaF<sub>2</sub> Thin Films for Photovoltaics—Synthesis and Luminescent Studies** [Francesca Lo Presti](#)<sup>1</sup>, Anna L. Pellegrino<sup>1</sup>, Adolfo Speghini<sup>2</sup> and Graziella Malandrino<sup>1</sup>; <sup>1</sup>University of Catania, Italy; <sup>2</sup>University of Verona, Italy

Photovoltaic technology is considered one of the leading fields for sustainable solar energy production. In recent years, considerable efforts have been done in the development of functional materials for the fabrication of increasingly sophisticated and advanced photovoltaic devices (PV) that can ensure an efficient exploitation of solar spectrum. In this context, lanthanide (Ln)-doped fluoride materials are considered particularly promising for energy conversion applications due to their unique luminescent properties under light irradiation. A proper combination of doping elements allows an efficient luminescent pathway in a large spectral range through up-conversion (UC) or down-conversion (DC) mechanisms. UC and DC processes are the main mechanisms which enhance the efficiency of photovoltaic devices since they make possible to collect the radiation energy outside the absorption range of the photoactive material (usually silicon) by shifting the energy to a more suitable optical region. Among the fluoride-based systems, BaF<sub>2</sub> is considered a suitable host for the UC and DC luminescence of Ln<sup>3+</sup> ions because of its low phonon energy (similar or even lower than the extensively used hosts such as NaYF<sub>4</sub>), high chemical stability, wide transparency (i.e. BaF<sub>2</sub> is transparent from 150 nm to 15 μm) and versatile synthetic strategies. It should be mentioned that host materials require lattice matches with Ln<sup>3+</sup> dopant ions. Trivalent lanthanide ions in particular can be well incorporated into crystal structure of alkaline-earth fluorides due to the similar coordination sphere. However, a charge compensation mechanism is required to balance the additional charge introduced after the replacement of divalent alkaline-earth ions with trivalent Ln dopants.

In the present study, we report the synthesis of Ln<sup>3+</sup> co-doped BaF<sub>2</sub> thin films (Ln<sup>3+</sup> = Yb<sup>3+</sup>, Pr<sup>3+</sup>) on silicon and quartz substrates, using metalorganic chemical vapor deposition technique (MOCVD). The advantages of this approach include: simplified instrumental apparatus, high deposition rate, high purity and easy industrial scale-up. For the fabrication of BaF<sub>2</sub> thin films co-doped with Yb<sup>3+</sup>, Pr<sup>3+</sup>, a multicomponent mixture of metalorganic adducts in an appropriate molar ratio is used as a single molten source. It is possible to easily tune the chemical compositions of the films, to tailor the energy transfer processes, by changing the composition of the precursor mixture, that is the Ba:Yb:Pr ratio in the multicomponent source. X-ray diffraction analysis (XRD), field-emission scanning electron microscopy (FE-SEM) and energy dispersive X-ray analysis (EDX) allowed a structural, morphological and compositional characterization of the films. Finally, the film functional properties have been assessed through luminescence spectroscopy.

#### SESSION F.EN02.03: Heterojunction and Passivating Contact

On Demand Abstracts Available for Viewing Starting Saturday Morning, November 21, 2020  
F-EN02

#### 5:00 AM F.EN02.03.01

**Atomic Layer Deposited Niobium Oxide as a Passivating Layer and Selective Contact for Silicon-Based Photovoltaics** [Connor Leach](#), Benjamin Davis, Ben Garland and Nick C. Strandwitz; Lehigh University, United States

Atomic layer deposited (ALD) niobium oxide (NbO<sub>x</sub>) has shown potential for use as a passivating layer or as a selective contact for silicon-based photovoltaics (PVs). However, there is large gap in understanding of the synthesis-structure-electronic property relationships. It has been shown by Macco et. al. that ALD niobium oxide can provide effective passivation of silicon substrates with an interfacial oxide down to 1 nanometer layer thickness.<sup>1</sup> In a separate work it was also show that ALD niobium oxide can serve as an electron selective contact.<sup>2</sup> In this work, the ALD growth of niobium oxide is optimized for temperature and co-reactants of either ozone (O<sub>3</sub>) or water (H<sub>2</sub>O). The oxidation states are then determined via X-ray photoelectron spectroscopy (XPS) to determine the exact stoichiometry of the films. The surface recombination velocity of niobium oxide contacts to silicon is measured and related to deposition conditions, film thickness, and post-deposition processing. Some samples are annealed in both inert and oxygen atmospheres and the stoichiometry is determined as well as the crystal structures measured via X-ray diffraction (XRD). This work provides new insight into the applicability of niobium oxides for passivation and selective contact layers for Si photovoltaics.

1. Macco, B. *et al.* Effective passivation of silicon surfaces by ultrathin atomic-layer deposited niobium oxide. *Appl. Phys.*



*Lett.* **112**, (2018).

2. Macco, B. *et al.* Atomic-layer deposited Nb<sub>2</sub>O<sub>5</sub> as transparent passivating electron contact for c-Si solar cells. *Sol. Energy Mater. Sol. Cells* **184**, 98–104 (2018).

#### **5:10 AM F.EN02.03.04**

**Effect of Deposition Temperature and Post Deposition Treatment on Carrier Selectivity of Tunnel Oxide Passivated Phosphorus Doped APCVD Polysilicon Contact** Jannatul Ferdous Mousumi and Kristopher Davis; University of Central Florida, United States

Carrier selective contact enhances the efficiency of silicon (Si) solar cell by providing surface passivation and an effective majority carrier extraction. Recently, ultrathin silicon oxide (SiO<sub>x</sub>) passivated *n*<sup>+</sup> polysilicon (poly-Si) contact has drawn attention as a promising electron selective contact because of its excellent surface passivation quality, low contact resistivity and high thermal stability compared to amorphous Si (a-Si:H) layer. Record efficiency of 25.7 % has been reported for *n*-type silicon solar cell fabricated using this as a full area rear contact [1].

In this work, we present a tunnel oxide passivated phosphorus doped poly-Si electron selective contact for *n*-type silicon solar cell where the *in-situ* doped poly-Si layer (around 100 nm) is deposited using an in-line high-throughput atmospheric pressure chemical vapor deposition process (APCVD). This in-line APCVD system can perform single-sided deposition in atmospheric environment and is well-suited for industrial mass production. In this process, thermal dissociation of silane (SiH<sub>4</sub>) and phosphene (PH<sub>3</sub>) gases deposits the phosphorus doped Si layer on top of the ultrathin SiO<sub>x</sub> (<2nm) layer which is grown in a wet chemical process and acts as the tunnel oxide. Later, the as-deposited Si layer goes through different post deposition treatments such as annealing, firing, hydrogenation, etc. for solid phase crystallization and passivation quality improvement. We have studied the effect of the deposition temperature and different post deposition treatments on Si surface passivation quality and contact resistivity ( $\rho_c$ ) of this poly-Si contact. The change in microstructure, dopant profile and crystallinity of the APCVD Si layer due to change in process parameters are observed to understand the process-structure-property relationship of this electron selective contact.

1. Richter, Armin, Jan Benick, Frank Feldmann, Andreas Fell, Martin Hermle, and Stefan W. Glunz. "n-Type Si solar cells with passivating electron contact: Identifying sources for efficiency limitations by wafer thickness and resistivity variation." *Solar Energy Materials and Solar Cells* 173 (2017): 96-105.

#### **5:20 AM \*F.EN02.03.06**

**Evolution of Silicon Heterojunction Solar Cells** Akira Terakawa; Panasonic Corp, Japan

Amorphous/Crystalline Silicon heterojunction (SHJ), which has been invented in 1990 and has been industrialized in 1997 by Sanyo, is regarded as one of the ideal junction technologies for silicon-based solar cells. The conversion efficiencies are exceeding >24% for "standard" bifacial SHJ solar cells, and >25% for back contact SHJ solar cells, respectively, using industrially feasible processes. We are aiming to improve power generation efficiency and reduce power generation cost by combining thinner and larger wafering, reducing optical losses reduction, innovating texturing, hetero-junction and metallization technologies. We are also developing perovskite/SHJ tandem solar cells in order to break the "Silicon Limit." I will review our recent R&D activities.

#### **5:35 AM F.EN02.03.07**

**Impact of the Bulk Resistivity on Silicon Solar Cells at Different Temperatures and Light Conditions** Andre Augusto, Apoorva Srinivasa, Pradeep Balaji, Richard King and Stuart Bowden; Arizona State University, United States

We are reporting the findings of the 18 months project on impact of undoped substrates on high performance silicon solar cells supported by the U.S. Department of Energy. The aim of the project was to develop fundamental understanding and experimentally demonstrate the mechanisms in play when silicon solar cells are manufactured using different bulk resistivities (1 ohm.cm to over 15000 ohm.cm). The project focus was understanding how the performance of the solar cells, with different bulk resistivities, is impacted by in-field temperatures (up to 80 °C) and light conditions (0.1-1 suns). Today's highest-efficiency solar cells typically operate near the threshold between low and high injection. It is not well understood whether pushing the cell operation point further into a high injection regime throughout the day is beneficial for the solar cell performance. In this study, we present a comprehensive assessment, both experimental and by simulation, of how bulk resistivity, defects, light conditions, and operation temperature impact the performance of the silicon solar cell. Analytical simulations indicate that high bulk resistivity wafers (10 ohm.cm to over 15000 ohm.cm) require bulk Shockley-Read-Hall lifetimes in the millisecond range to outperform wafers with standard bulk resistivities (below 10 ohm.cm). Additionally, for bulk resistivities beyond 10 ohm.cm, the cell efficiency is shown to be weakly dependent of bulk resistivity. This study is

particularly relevant today, as solar cell architectures with better surface passivation and milliseconds lifetimes wafers are commercially available, leveraging potential benefits of using higher bulk resistivities. Previous studies on high bulk resistivities are limited, inconclusive and lacked experimental data above 100 ohm.cm. In this work, we fabricate silicon heterojunction solar cells and samples to study lifetimes on n-type wafers with bulk resistivities from 1 ohm.cm to over 15000 ohm.cm. We measured their performance at different operation temperatures between 30 °C and 80 °C and for light intensities between 0.1-1 suns. The temperature coefficients are calculated from voltages at open circuit and maximum power, and from fill factors as a function of temperature. They are shown to be independent of the bulk resistivity and exhibit similar values as previously reported on standard bulk resistivities wafers. The surface saturation current density increases by several orders of magnitude for all bulk resistivities and show a cubic dependence of temperature. This temperature dependence was previously reported on standard bulk resistivities wafers. The significant increase of the surface saturation current density with temperature can be partially explained with a similar increase of the effective intrinsic carrier concentration. We are currently in the last quarter of the project and finalizing the measurements at different light conditions, the conclusions of which will be reported at the conference.

SESSION F.EN02.04: Module Manufacturing and Characterization  
On Demand Abstracts Available for Viewing Starting Saturday Morning, November 21, 2020  
F-EN02

**5:00 AM \*F.EN02.04.01**

**Lifetime Prediction of PV Modules—When is it Useful and When is it a Distraction?** Sarah R. Kurtz; University of California Merced, United States

Lifetime prediction is a critical first step as the basis of a warranty or risk assessment. Research that identifies a PV module's primary degradation or failure mechanism, quantifies the associated acceleration factors, and applies those to operating conditions is a straightforward approach to lifetime prediction. The value of this process is obvious and researchers around the world are investigating degradation and failure mechanisms of PV modules with this goal in mind. Making a lifetime prediction is actually quite easy: we can predict 25 years  $\pm$ 25 years for pretty much all PV products on the market, but such a prediction is useless. Making a lifetime prediction with a small uncertainty that leads to a useful prediction is much harder. This talk will describe why lifetime prediction is difficult, when it is essential, when it is a distraction, and how we expect lifetime prediction may evolve in the future.

**5:15 AM \*F.EN02.04.02**

**Vehicle Integrated Photovoltaics—Past, Present and Future** Martin Heinrich, Christoph Kutter, Felix Basler, Christian Schill, Holger Neuhaus and Harry Wirth; Fraunhofer Institute for Solar Energy Systems ISE, Germany

Vehicle integrated photovoltaics has recently seen a rise in interest due to the increased employment of full or hybrid electric vehicles. The topic itself is not new, already in the 80ies first cars have been equipped with solar cells, such as for the "Tour de Sol" in 1985. However, only within the last few years there has been a peak in announcements and news about this topic. New car manufactures such as SonoMotors or Lightyear as well as established car manufacturers such as Toyota or Hyundai have announced sizeable plans to introduce cars with solar energy support. The current spike in interest is not odd, solar technologies have become historically low priced in recent years and electric cars are more and more available for which an addition of a solar support is most reasonable.

After a brief introduction of the topic with support of a historical review, we provide an overview on the current approach of vehicle-integrated photovoltaics (VIPV) at Fraunhofer ISE. While VIPV for cars focusses currently on the embedding of silicon solar cells within curved laminated glass, the approach for utility vehicles such as trucks and their trailers is vastly different. Here, lightweight and glass-free setups are preferred due to the crash behavior and less intense requirements regarding surface finish. As promising solar cell and interconnection technology for VIPV, we introduce the concept of shingled solar cells, offering benefits regarding efficiency, voltage level, curvature and the overall aesthetics.

To precisely calculate the potential benefits of VIPV we provide insights into the project "PV2Go", where we compile a solar register of roads in Germany, which provides a detailed overview of the shading on roads in Germany. The modelling approach using spatial, geographic as well as digital terrain models is supported by a measurement campaign, where 100 cars are equipped with irradiation sensors.

We round off the topic with an overview of the future potential prospects of VIPV, such as equipping further vehicle parts like motor hood, side doors or even the windows with solar cells. It is concluded that by utilizing next generation solar cells such as tandem cells and further advances in increasing the efficiency of electric vehicles could lead to affordable vehicles with solar as the main source for propulsion.

#### **5:30 AM \*F.EN02.04.03**

**From Modules to Atoms—Characterization of Silicon Photovoltaic Module Reliability Guided by Luminescence and Thermal Imaging** Dana Kern<sup>1</sup>, Steve Johnston<sup>1</sup>, Helio Moutinho<sup>1</sup>, Dirk C. Jordan<sup>1</sup>, Jenya Meydbray<sup>2</sup>, Laura Spinella<sup>1</sup>, Michael Owen-Bellini<sup>1</sup>, Kent Terwilliger<sup>1</sup>, Archana Sinha<sup>3</sup>, Laura Schelhas<sup>3</sup>, Chun-Sheng Jiang<sup>1</sup>, Chuanxiao Xiao<sup>1</sup>, Matthew Young<sup>1</sup> and Mowafak Al-Jassim<sup>1</sup>; <sup>1</sup>National Renewable Energy Laboratory, United States; <sup>2</sup>PV Evolution Labs, United States; <sup>3</sup>SLAC National Accelerator Laboratory, United States

With the lifespans of photovoltaic (PV) modules expected to last >20 years, rapid and spatially-resolved characterization methods are essential for understanding module reliability and degradation processes. Luminescence and thermal imaging have been gaining popularity both for fast, outdoor-compatible module inspection and for more detailed post-mortem analysis of failure mechanisms. Importantly, many failure mechanisms are not evident by visual inspection, and characterization of electrical properties alone is insufficient to identify the weakest features of cell or module design. This is especially true as PV technologies and module packaging schemes become more advanced and degradation becomes more subtle. Here, we present various examples of PV module degradation mechanisms in field-weathered modules, where we (1) locate problem areas with luminescence and thermal imaging, (2) core these areas out of the module, and (3) use various microscopy methods to identify chemical and structural causes of power loss. We particularly highlight causes of voltage loss or series resistance increases that vary depending on the technology, and we show studies including conventional Al back surface field (Al-BSF), silicon heterojunction with intrinsic thin layer (HIT), and passivated emitter and rear contact (PERC) modules. These results highlight the utility of imaging methods for improving module reliability.

#### **5:45 AM \*F.EN02.04.04**

**Advances in Silicon Photovoltaic Module Manufacturing—From Manual Tabbing to Cut Cells and High-Power Modules** Alison Lennon; University of New South Wales Sydney, Australia

Silicon solar cells have been interconnected by soldering and laminated into modules using essentially the same process that was used in the 1970's. When Suntech commenced the mass manufacture of silicon photovoltaic modules in China in 2006, soldering was performed manually due to the low-cost of labour. However, automated stringing and tabbing machines quickly became the norm in Chinese manufacturing for the commonly produced two-busbar cells. Since then we have seen numerous advances in module engineering as silicon photovoltaics has become a low-cost form of electricity generation across the world. Starting from 3 busbar patents to large-sized modules fabricated from cut-cells designed to increase the module area efficiency especially for utility scale photovoltaics. It is now not just the module power that matters, it is module specific yield or how much electricity (kWh) will be generated per unit of purchased power (kW). This presentation will trace the advances in silicon photovoltaic module manufacturing over the years and discuss the current challenges of rapidly changing module architectures to service both rooftop and utility-scale applications.

#### **6:00 AM \*F.EN02.04.05**

**Photovoltaics Crystalline Silicon Wafer Trends and Their Impact on Module Performance** Frederic Dross, Adrien Pellarin, Thibaut Lemoine, Jenny Yang and Alexandre Minuzzo; STS, United States

Despite being labelled as “first generation” by some of the most eminent experts, crystalline-silicon technology has been dominating the photovoltaics industry for several decades and shows no sign of giving up its leading position. There are many reasons for that and the fast ramp up of production volumes combined with an aggressive learning curve makes it hard for challengers to compete. But another element should not be underestimated when considering the dominance of crystalline silicon: the constant improvement of the base material, the crystalline silicon wafer.

In this presentation, we will identify the main trends the silicon wafers have experienced along the years: the secular battle between mono and multi, the reduction of thickness incentivized in periods of raw material shortage, the increase of grain size to reduce effect of grain boundaries followed by a reduction of the grain size to avoid intra-grain defects, etc. We will also discuss the market rationale as well as the technical implications of the most recent trends in this domain: rapid increase of the wafer size, cutting of wafers into smaller pieces and emerging interest for n-type technologies.

The discussion will rely 10-years of in-factory experience, and data collection (module bill-of-materials and performance metrics) that STS is enjoying to address the impact of each crystalline silicon wafer trend on all aspects of the module performance.

6:15 AM \*F.EN02.04.06

**DuraMAT—Leveraging Field Data, Advanced Characterization, Multi-Scale Modeling, Accelerated Testing and Material Development to Improve Module Reliability** Teresa M. Barnes; National Renewable Energy Laboratory, United States

The Durable Module Materials Consortium (DuraMAT) launched in November of 2016 with five years of funding as part of the Energy Materials Network. DuraMAT is a multi-lab consortium, led by NREL and Sandia with SLAC and LBL as core research labs. The overarching goal of DuraMAT is to discover, develop, de-risk, and enable the rapid commercialization of improved materials, designs, predictive tests and models for photovoltaic modules that increase performance, extend lifetime, and enable new applications. Our core objectives are focused on establishing and applying critical capabilities to address big challenges for PV module durability. These challenges include the community's inability to make meaningful service life and durability predictions for PV modules with our current testing protocols and knowledge. It is incredibly difficult to make meaningful predictions for 30+ year outdoor durability for cutting edge products with a six month product development cycle! Improving outdoor durability and our ability to predict it requires more durable materials and designs, better tests to screen for weaknesses, modeling, materials and module characterization data, and a way to combine all of this data with historical performance data to extract meaningful results.

6:30 AM F.EN02.04.07

**Multiscale Characterization to Gain Insight into Failure Modes and Degradation Mechanisms in Silicon Photovoltaics** Nafis Iqbal, Dylan Colvin and Kristopher Davis; University of Central Florida, United States

With the increasing global demand for silicon photovoltaics (PV), new cell and module technologies are quickly emerging in the market. The implementation of these technologies requires investigation of the long-term performance in order to maintain PV module reliability standards. In this work, we perform multiscale characterization to gain insight into the different failure modes and degradation mechanisms commonly observed in PV modules. Multiscale characterization methods can be used to link observed degradation to specific loss mechanisms (i.e., optical, recombination, resistive) and to the root causes (i.e., changes in chemistry and/or microstructure). We investigate a range of module types with different cell technologies like traditional Al-BSF (Aluminum Back Surface Field) and newly emerging mono/multi-crystalline PERC (Passivated Emitter and Rear Cell). Both field exposed and damp-heat aged modules are investigated to track the long-term degradation. Module and cell level current-voltage ( $I$ - $V$ ), Suns- $V_{OC}$ , photoluminescence (PL) and electroluminescence (EL) imaging have been performed on aged and control modules. For the aged modules, cell darkening has been observed in the EL images which can be related to high resistance and fill factor (FF) losses. For the older modules, this darkening happens across the entire cell area, whereas for newer modules with new generation silver (Ag) paste, the darkening is mainly observed to start from the busbars. Our analysis suggests this degradation is related to metallization corrosion. To gain more insight into this failure mode, samples have been cored out from the modules followed by the removal of encapsulation to perform materials characterization. Top-down and cross-sectional SEM and EDS analysis have been performed on the degraded Ag fingers. Furthermore, XPS analysis on the top of the bulk Ag finger and on the glass-layer (after etching away the Ag) has been performed. We observe that the degradation results in delamination of the Ag finger from the cell with voids and gaps forming within the metal-Si interface. EDS and XPS analysis show tin (Sn) in the busbar region and oxidation of the Ag finger. Further investigations are being performed to understand the effect of Sn migration and oxidation on the corrosion and delamination process.

SESSION F.EN02.05: Silicon Solar Cell Based Tandem

On Demand Abstracts Available for Viewing Starting Saturday Morning, November 21, 2020

F-EN02

5:00 AM \*F.EN02.05.01

**Building Efficient Single-Junction and Tandem Solar Cells from Silicon and Perovskites Using Passivating Contacts** Stefaan De Wolf; King Abdullah University of Science and Technology, Saudi Arabia

In silicon and perovskite solar cells, the presence of surface states at their electrical contacts is increasingly recognized as a key factor limiting device performance [1,2]. In this presentation, I will first discuss how such surface states result in Fermi-level pinning and surface recombination. Passivating-contact technology aims at minimizing the interface-gap state density,

resulting in improved operating voltages and low contact resistances. I will focus on recent advancements in this topic, both for crystalline silicon and perovskite solar cells. In a second part of my presentation, I will discuss the fabrication of efficient monolithic tandem solar cells, combining silicon and perovskite solar cells, aimed at very high-efficient photovoltaics at affordable cost. Specific emphasis will be laid on different possible strategies to build efficient tandems from fully-textured silicon bottom cells; the use of such macro-scale textured bottom cells brings optical advantages, but also brings perovskite/silicon tandems close to industrial implementation [3]. In a final part, I discuss the field performance of such devices and draw conclusions from this for future device development.

[1] E. Aydin, M. De Bastiani, and S. De Wolf, *Defect and Contact Passivation for Perovskite Solar Cells*, *Adv. Mater.* **31**, 1900428 (2019).

[2] T.G. Allen, J. Bullock, X. Yang, A. Javey, and S. De Wolf, *Passivating contacts for silicon solar cells*, *Nature Energy* **4** (2019).

[3] Y. Hou, E. Aydin, M. De Bastiani, C. Xiao, F.H. Isikgor, D.-J. Xue, B. Chen, H. Chen, B. Bahrami, A.H. Chowdury, A. Johnston, S.-W. Baek, Z. Huang, M. Wei, Y. Dong, J. Troughton, R. Jalmood, A.J. Mirabelli, T. Allen, E. Van Kerschaver, M.I. Saidaminov, D. Baran, Q. Qiao, K. Zhu, S. De Wolf, and E.H. Sargent, *Efficient Tandem Solar Cells with Solution-Processed Perovskite on Textured Crystalline Silicon*, *Science* **367**, 1135 (2020).

**5:15 AM \*F.EN02.05.02**

**Sustainability Aspects and Circular Economy Approaches of Modern Crystalline Silicon and Perovskite Silicon Tandem Modules** Karsten Wambach; bifa Umweltinstitut GmbH, Germany

Silicon PV modules have become a worldwide commodity nowadays. New module types and production technologies are rapidly introduced and the consumption of costly or valuable materials is minimized with increasing conversion efficiencies of sunlight to electricity. The latest approaches utilize, for example, advanced silicon and perovskite silicon tandem cells to increase the conversion efficiencies to more than 30% of the incident sunlight. These 2 examples are selected to assess the current and forthcoming challenges in the reuse and waste treatment sector of end-of-life modules in this presentation. The five topics covered are:

- Regulations and standards
- Economic and environmental aspects
- Decommissioning of PV plants
- Preparation for re-use
- Recycling and end-of-waste criteria

The PV modules have a long lifetime of beyond 25 years, but with increasing installations sound end-of-life treatment solutions have to be introduced and any potential environmental burdens have to be reduced as far as possible. Even though the waste amounts are rather small compared to other waste streams like electronics, a sound circular economy should be developed with a good eye for the market demands, resources, costs and environment. This approach requires a detailed analysis of the components and materials used in a PV module and an environmental risk and value analysis.

Usually end-of-life PV modules are considered as electronic waste. The approaches to establish a sound waste treatment economy are manifold. E.g., mandatory end-of-life collection and waste treatment systems are already in force in all EU countries and in some areas of USA. At the end of the life of a PV module the collection and treatment is frequently covered by general waste, waste electronic and electrical equipment (WEEE) laws. International and local regulations exist in trans-boundary shipments of used modules and wastes. The waste regulations are applied in combination with the globally harmonized system (GHS). Examples of current practices of waste treatment with recycling and/or landfill disposal are presented. A brief overview about a possible classification of the wastes according to the European list of wastes is presented for both example module types and their possible output materials. End-of-waste criteria for intact modules having entered the waste regime are discussed and, additionally, the major recycling outputs like glass, metals and semiconductor materials are included.

New standards like ANSI/NSF 457-2019 “Sustainability Leadership Standard for Photovoltaic Modules and Photovoltaic Inverters, or CENELEC EN50625-1-4 (2018) on collection, logistics & treatment requirements for WEEE, and other have been introduced. Like in the automotive and the electronics industry stewardship systems and product databases including the individual components are proposed and producer responsibility principles are realized. This is closely linked to the introduction of new assessment methodologies like the European Environmental Footprint (PEF). Recommendations for the cases of a second life of the modules including reuse and repair are under development. The presentation includes an

overview about these topics.

### 5:30 AM F.EN02.05.03

**Interplay Between Temperature and Bandgap Energies Determines Outdoor Performance of Perovskite/Silicon Tandem Solar Cells** [Erkan Aydin](#)<sup>1</sup>, Thomas G. Allen<sup>1</sup>, Michele De Bastiani<sup>1</sup>, Lujia Xu<sup>1</sup>, Jorge Avila<sup>2</sup>, Michael Salvador<sup>1</sup>, Emmanuel Van Kerschaver<sup>1</sup> and Stefaan De Wolf<sup>1</sup>; <sup>1</sup>King Abdullah University of Science and Technology, Saudi Arabia; <sup>2</sup>Universidad de Valencia, Spain

Perovskite/silicon tandem solar cells promise power conversion efficiencies (PCE) beyond the Shockley–Queisser limit of single-junction devices, however, their actual outdoor performance is yet to be studied and understood. Here we fabricate two-terminal (2T) monolithic perovskite/silicon tandem solar cells with certified PCE values of 25% and current densities of 19.8 mA/cm<sup>2</sup> and test them outdoors at elevated temperatures in a hot and sunny climate. With these data, we then calibrated a device-temperature model. By combining this model with relevant meteorological data, we simulated the tandem temperature over a complete year (2016), giving a realistic framework for tandem-performance analysis. Later, we experimentally characterized our tandems in a controlled laboratory environment under various temperatures and illumination spectra, with specific attention paid to their impact on current matching. Finally, to gain further insight, we developed a temperature-dependent radiative-efficiency model to support our findings. We find that the temperature dependence of the bandgaps ( $E_g$ ) of both crystalline silicon and perovskite – which follow opposing trends – shifts the devices away from current matching for 2T tandems optimized at standard test conditions (STC, *i.e.*, AM1.5G spectrum, 1000 W/m<sup>2</sup>, 25 °C). Consequently, we argue that the optimal perovskite bandgap at STC is lower compared to earlier findings. Through temperature-dependent radiative-efficiency modeling, we show that the ideal bandgap of the perovskite in perovskite/silicon tandems is  $E_g < 1.68$  eV (at STC) for optimal field performance at operational temperatures  $> 55$  °C. This implies that Br-lean perovskites with narrower bandgaps at STC – and, therefore, better phase stability – hold great promise for the commercialization of perovskite/silicon tandem solar cells.

### SESSION F.EN02.06: Thin Wafer and Light Management

On Demand Abstracts Available for Viewing Starting Saturday Morning, November 21, 2020  
F-EN02

### 5:00 AM \*F.EN02.06.01

**Internal and External Solar Cell Light Management—The Forgotten Photons** [Rebecca Saive](#); University of Twente, Netherlands

I will present different strategies to improve the efficiency and power yield of solar cells, both by reducing optical losses of the cell itself as well as by optical design of the surroundings.

As solar researchers during the past decade, we have been privileged to witness solar energy transitioning from a niche technology into the most promising and affordable way to meet our demand for electricity. In many regions of the world, solar cells have reached grid parity with conventional fossil fuel based electricity sources and the cost of solar energy is further declining. Finally, the transition to renewable energy sources is no longer driven by environmental concerns only, but also offers competitive return of investment.

Simultaneously to this rapid cost decline, the efficiency of solar cells has been increasing steadily. Thanks to very careful interface design and reduction of surface recombination, silicon solar cells are on a strong track to approach the practical Auger limit.

Nevertheless, creative approaches from many directions still enable new record efficiencies and power per cost enhancements. Here, I will present some of our strategies to improve the power output of conventional photovoltaic panels by controlling and managing the photon influx. First, I will talk about effectively transparent contacts (ETCs), the only front contact technology eliminating close to all shading losses while providing high conductivity. ETCs are triangular microscale silver contacts featuring high aspect ratio ( $>1:2.5$ ) and specular side walls which redirect incoming sunlight towards the active area of the solar cell instead of reflecting it away. We have integrated ETCs with different types of solar cells, and observed up to 7% power output enhancement. Upscaling and commercialization of the ETC technology by the start-up ETC Solar is underway.

As the second topic, I will present our experimental study of spectro-angular solar irradiance and the influence on the yield of solar power plants in different locations and configurations. In particular, I will present comparisons between monofacial and

bifacial solar cells with respect to the measured spectrum and angle dependent irradiance. Bifacial cells show to be superior both under cloudy as well as under sunny conditions. Under sunny conditions, the benefit mainly arises from ground reflection. The ability of surface to reflect light, also known as albedo, heavily influences the output of bifacial solar cells. The output is strongly dependent on the spectral reflection properties of the albedo material and it can be shown that an ideal spectral albedo material exists. We are designing and fabricating ideal albedo materials with the goal to achieve affordable low x concentration in bifacial solar cells.

#### 5:15 AM F.EN02.06.02

**Towards High Solar Cell Efficiency with Low Material Usage—15 % Efficiency with 14  $\mu\text{m}$  Liquid Phase Crystallized Silicon** Siddhartha Garud, Cham thi Trinh, Bernd Rech and Daniel Amkreutz; Helmholtz-Zentrum Berlin für Materialien und Energie, Germany

A bottom-up approach to creating silicon solar cells has the potential to not only avoid kerflosses incurring in wafer slicing, but also the energy involved in kerfless slicing techniques. Liquid-phase-crystallized silicon (LPC-Si) is one such approach in which amorphous/nanocrystalline silicon is deposited on glass up to a desired thickness (5-40  $\mu\text{m}$ ) and crystallized with a line-shaped energy source, which is a laser in this work. LPC-Si of  $\sim 14 \mu\text{m}$  has previously demonstrated power conversion efficiency up to 14.2 % despite illumination through glass, using a heterojunction interdigitated back contact cell architecture (HJ-IBC) [1]. The first part of this work reports efforts to create thicker heterojunction interfaces for better surface passivation. A 'multilayer' a-Si surface passivation is also shown which consists of three cycles of a-Si(i) deposition, each one followed by a short hydrogen plasma treatment but with different hydrogen dilution levels. The second part covers laser firing on the electron contact. It enables a controllable trade-off between charge collection and fill-factor by creating a low resistance Ag-Si electron contact, while preserving a-Si:H (i) passivation in other areas [2,3]. Short-circuit current density ( $J_{SC}$ ) was observed to be up to 33.1  $\text{mA}/\text{cm}^2$ , surpassing all previously recorded values for this technology. Open-circuit voltage ( $V_{OC}$ ) of up to 658 mV also exceeded every previous value published at a low bulk doping concentration of  $1 \times 10^{16} \text{cm}^{-3}$ . Laser firing reduced  $J_{SC}$  by 0.6  $\text{mA}/\text{cm}^2$  on average but improved fill-factor ( $FF$ ) by 22.5 % absolute on average, without any significant effect on  $V_{OC}$ . Collectively, these efforts have helped achieve a new in-house record efficiency for LPC-Si of 15.1 % with 31.4  $\text{mA}/\text{cm}^2$   $J_{SC}$ , 645 mV  $V_{OC}$  and 74.7 %  $FF$ . The best cell in terms of  $J_{SC}$  (32.7  $\text{mA}/\text{cm}^2$ ) and  $V_{OC}$  (657 mV) lacked only in series resistance and shows potential to surpass the current best cell performance in the near future. While excluding the effects of series resistance by measuring a Suns- $V_{OC}$  curve, this cell shows a pseudo-efficiency of 17 %. Therefore, current efforts are focused on creating larger electron contact widths and heterojunction layers optimised for lower contact resistance.

- [1] Trinh, Cham Thi, Natalie Preissler, Paul Sonntag, Martin Muske, Klaus Jäger, Martina Trahms, Rutger Schlatmann, Bernd Rech, and Daniel Amkreutz. "Potential of interdigitated back-contact silicon heterojunction solar cells for liquid phase crystallized silicon on glass with efficiency above 14%." *Solar Energy Materials and Solar Cells* 174 (2018): 187-195.
- [2] Garud, Siddhartha, Cham Thi Trinh, Holger Rhein, Sven Kuehnappel, Stefan Gall, Rutger Schlatmann, Bernd Rech, and Daniel Amkreutz. "Laser firing in silicon heterojunction interdigitated back contact architecture for low contact resistance." *Solar Energy Materials and Solar Cells* 203 (2019): 110201.
- [3] Garud, Siddhartha, Matevz Bokalič, Cham thi Trinh, Bernd Rech, Daniel Amkreutz, and Marko Topič. "Analysis of Surface Passivation and Laser Firing on thin-film silicon solar cells via Light-Beam Induced Current." *IEEE Journal of Photovoltaics* (2020) (Accepted for publication)

#### 5:25 AM \*F.EN02.06.03

**Lift-off Techniques for Kerfless and Thin Monocrystalline-Silicon Solar Cells—A Snapshot of History** Valerie Depauw and Hariharsudan Sivaramakrishnan Radhakrishnan; imec, Belgium

To be able to continue its steady reduction of solar module cost, the photovoltaic industry must keep increasing the usage efficiency of all the materials, particularly that of silicon (Si). For the latter, the three main levers are increasing cell efficiency, reducing cell thickness and reducing all the losses along the wafer manufacturing chain. To reach below today's average consumption of 4 g/Wp, incremental improvements can be still be envisaged. However, going far below that value, down to 1 g/Wp, requires disruptive technologies. The 2019 ITRPV roadmap is thus predicting the increase in appearance of kerfless multi- and monocrystalline wafers on the market.

A wide range of kerfless wafering methods have been developed as alternatives to the traditional Czochralski wafer manufacturing process. These disruptive concepts can supply wafers thinner than 100  $\mu\text{m}$  and increase the Si utilization rate by shortcutting the Cz process chain. These various methods can be classified according to the process step at which they introduce the shortcut, and at which silicon is available in different states: solid/ingot, liquid/melt or gas. At the end of the

chain, are kerfless wafering methods, such as spalling, that propose alternatives to wafer sawing. One step upstream are methods that enable growing multi- or monocrystalline wafers directly from the melt, without ingot growth, such as ribbon growth techniques or Epilift. And further upstream, skipping the energy-intensive poly-Si production step, are methods that grow wafers from the gas (silane) phase, such as epi-Si lift-off. Except for the ribbon-growth methods, all rely on the lift-off of a thin silicon wafer or seed layer with manifold re-uses of the parent substrate (wafer or ingot). The first reported lift-off silicon foil, by Milnes and Feucht, dates back to 1975. Forty-five years later, the concept has been explored in countless labs and has resulted in dozens of creative ways of producing thin and high-quality silicon layers. Only very few have the potential however to make it from lab to fab.

We have recently reviewed this rich field of silicon lift-off techniques for photovoltaics and propose to give an overview of all the different innovative ways that have been imagined and realized to fabricate thin silicon slabs with minimal silicon wastage, and to try and understand what has determined their fade-out or survival. And what may determine their survival or revival in the future. Today, even though the drive for the entry of kerfless lift-off methods in the PV market is still rather low and hindered by different technological hurdles, they may, with their lower carbon dioxide footprint, be better suited to the world of tomorrow.

#### 5:40 AM F.EN02.06.04

**Hyperuniform Designs for Enhanced Light Trapping in Ultra-Thin Si Solar Cells** Nasim Tavakoli<sup>1</sup>, R. J. Spalding<sup>2</sup>, Pepijn Koppejan<sup>1</sup>, G. Gkantzounis<sup>2</sup>, C. Wan<sup>2</sup>, Ruslan Rohrich<sup>1,3</sup>, Evgenia Kontoleta<sup>1</sup>, A. Femius Koenderink<sup>1</sup>, Riccardo Sapienza<sup>4</sup>, Marian Florescu<sup>2</sup> and Esther Alarcon-Llado<sup>1</sup>; <sup>1</sup>AMOLF, Netherlands; <sup>2</sup>Department of Physics, Advanced Technology Institute, University of Surrey, United Kingdom; <sup>3</sup>Advanced Research Center for Nanolithography (ARCNL), Netherlands; <sup>4</sup>Imperial College London, United Kingdom

Introducing thin, light-weight and high efficiency photovoltaics (PV) will make solar cells more suitable to be integrated in urban landscapes or even small gadgets and would largely contribute to solving the global warming threat that we are facing today. Stacking of solar cells with different characteristic bandgaps is the most common strategy to increase efficiency to surpass the Shockley-Queisser limit, but such tandem devices are typically heavy weight, rigid and costly. An effective approach to tackle this problem is nanopatterning the absorbing layer.

In this work we introduce various hyperuniform designs incorporated on a 1- $\mu\text{m}$  thin silicon film as an effective way to control scattered light into particular range of angles to be efficiently absorbed in silicon. These structures are first designed by a 6-fold optimization to achieve 2D designs, and later Meep simulations to optimize absorption spectra in 3D structures. We experimentally show the redirection of light into the engineered range of angles as a ring in the k-space, which matches greatly with the expected structure factors. Further, using an integrating sphere we measure 65% sunlight absorption in the free-standing 1  $\mu\text{m}$  c-Si with fabricated hyperuniform designs. The equivalent photocurrent derived from our measurement is far above the highest found in literature, and the estimated photovoltaic efficiency for a state-of-the-art ultra-thin solar cell incorporating our designed nanotexturing is above 20%. This is a highly remarkable efficiency for such a thin indirect-bandgap material and establishes a new breakthrough in thin light-weight and flexible solar cells.

SESSION F.EN02.07/F.EL06.06: Joint Session: Contacts and Interfaces in Silicon Solar Cells  
On Demand Abstracts Available for Viewing Starting Saturday Morning, November 21, 2020  
F-EN02

#### 5:00 AM \*F.EN02.07.01

**Improved Infrared Light Management with Amorphous Silicon in High Efficiency Silicon Heterojunction Solar Cells** Weiyuan Duan, Karsten Bittkau, Andreas Lambertz, Paul Steuter, zhirong yao, Kaifu Qiu and Kaining Ding; IEK5-Photovoltaik, Forschungszentrum Jülich GmbH, Germany

Silicon heterojunction (SHJ) solar cells coupled with hydrogenated intrinsic amorphous silicon (a-Si:H) layers enable high open-circuit voltages ( $V_{oc}$ ) of up to 750 mV, but suffer from short-circuit current density ( $J_{sc}$ ) losses due to parasitic absorption in a-Si:H, transparent conductive oxide (TCO) layers and shadowing of the metal fingers. Significant improvement in  $V_{oc}$  is expected only for thinner wafer. Increasing  $J_{sc}$  is a more promising route to further improve cell efficiency. Besides the use of high bandgap materials such as nanocrystalline silicon oxide or low carrier density TCO layers to reduce parasitic absorption, an improved light trapping that enables more light to be absorbed within the silicon wafer



represents another important opportunity for  $J_{sc}$  improvement, which becomes even more significant when thinner wafers are used. In this work, a thin intrinsic a-Si:H layer was introduced after metallization of SHJ solar cell, formed a TCO/a-Si:H back reflector. Unlike sophisticated structures such as diffraction gratings, black silicon or other kind of nanophotonics, TCO/a-Si:H back reflector is much easier to be fabricated. Compared with the very often used silver back reflector, a-Si:H is less expensive and can still keep some of the bifaciality of the cells.

The intrinsic a-Si:H layer was deposited by plasma enhanced chemical vapor deposition (PECVD). It has a refractive index of around 4 at infrared (IR) wavelengths extracted from ellipsometry measurement. Sentaurus TCAD simulation was used for the rear optics in terms of optimizing the thickness of TCO/a-Si:H stack. We systematically investigated how the TCO/a-Si:H back reflector increases rear internal reflectance by measuring reflectance and external quantum efficiency before and after deposition of the a-Si:H layer. As predicted from simulation, due to increased IR reflection,  $J_{sc}$  was 0.4 mA/cm<sup>2</sup> higher with TCO/a-Si:H back reflector when applied on SHJ solar cells using 110 mm thickness wafer, while fill factor ( $FF$ ) and  $V_{oc}$  remained constant. Combined with an optimized front MgF<sub>2</sub> double antireflection coating, we could demonstrate a 0.9 mA/cm<sup>2</sup> improvement in  $J_{sc}$ , which boosts the cell efficiency by 0.5%. Ultimately, a M2 size total area cell efficiency of 23.7% has been achieved with  $V_{oc}$  of 745 mV,  $J_{sc}$  of 39.4 mA/cm<sup>2</sup> and  $FF$  of 80.8% on 110 um thin wafer. It's worth noting that the cell still kept a bifaciality of more than 50%. The reflector concept introduced here has a possibility to be used in advanced double-glass module encapsulation.

#### 5:15 AM \*F.EN02.07.02

**Efficient Hole-Selective Passivating Contacts for Si Photovoltaics** Takuya Matsui and Hitoshi Sai; AIST, Japan

Hydrogenated amorphous silicon (a-Si:H) is a key material in realizing efficient passivating contacts for Si solar cells known as the silicon heterojunction (SHJ) technology. However, one drawback of the SHJ solar cells is that the a-Si:H, particularly when doped with boron, gives rise to a parasitic optical absorption loss due to its high absorption coefficients in the visible wavelengths. This adverse effect is pronounced in bifacial solar cells, as this type of device allows illumination from both the front and the rear surfaces. Here we pursued alternative materials focusing on hole-selective passivating contacts: one is the hydrogenated nanocrystalline Si (nc-Si:H) and the other is the novel metal-oxide material. For the nc-Si:H material, it is demonstrated that the replacement of (*p*)a-Si:H by (*p*)nc-Si:H provides not only an increase of  $J_{sc}$ , but also improvements in  $V_{oc}$  and  $FF$ . This results in an efficiency increase by 0.6% absolute compared to our reference cell with (*p*)a-Si:H, and a best cell efficiency of 23.5%. The factors that alter the optimum hole contact layer thickness depending on the material and deposition condition will be discussed. For the metal-oxide material, we have developed an atomic-layer-deposited TiO<sub>x</sub> nanolayer that functions as an efficient and transparent hole-selective passivating contact, leading to proof-of-concept solar cells with efficiencies above 20%. This new function of TiO<sub>x</sub> is opposite from the previous understanding that it acts solely as electron contact.

#### 5:30 AM F.EN02.07.03

**Atomic Layer Deposited Metal Oxide Bilayers for Metal-Insulator-Semiconductor Photovoltaics** Benjamin Davis and Nick C. Strandwitz; Lehigh University, United States

The use of metal-insulator-semiconductor (MIS) tunnel diodes as photovoltaics (PVs) relies on the Schottky barrier between the metal and semiconductor, which induces band bending in the semiconductor absorber allowing for efficient separation of electrons and holes. In the years following early MIS PV research in the 1970s and 1980s, the advent of atomic layer deposition (ALD) has provided a tool for enhanced control of ultrathin film deposition. One method to potentially improve MIS PV performance is the use of ALD oxide bilayers as tunnel insulators. Oxides with different oxygen areal densities have been demonstrated to form interfacial dipoles, manipulating the Schottky barrier. Previous studies have only explored the impact of dipoles between a single ALD oxide and interfacial SiO<sub>x</sub>. The present work combines two ALD oxides, one (AlO<sub>x</sub>) with oxygen areal density higher than that of SiO<sub>x</sub> and another (LaO<sub>x</sub>) with oxygen areal density lower than that of SiO<sub>x</sub> according to literature. It has been hypothesized that the greater oxygen areal density difference would result in a greater impact on the Schottky barrier. It is demonstrated that, compared to AlO<sub>x</sub> alone, an ALD LaO<sub>x</sub>/AlO<sub>x</sub> stack increases the average n-Si/Ni Schottky barrier height from 0.63 to 0.70 eV, and the average p-Si/Al barrier height from 0.81 to 0.90 eV. LaO<sub>x</sub> was the oxide in direct contact with the Si substrate. The observation that the barrier height increases for both substrate types suggests that the effect is due to the ability of LaO<sub>x</sub> to depin the Fermi level rather than an interfacial dipole.

#### 5:40 AM F.EN02.07.04

**Exploiting Fixed Charge to Control Schottky Barrier Height in Si|Al<sub>2</sub>O<sub>3</sub>|MoO<sub>x</sub>—Based Tunnel Diodes** Ben Garland, Benjamin Davis and Nick C. Strandwitz; Lehigh University, United States

Carrier selective contacts have become one of the leading advancements in photovoltaics with the most efficient structures exceeding 26% conversion efficiency. Selective carrier conduction implies that one type of charge carrier is preferentially collected at an electrical contact. Carrier selectivity increases the efficiency of solar cells by reducing recombination at metal contacts and avoiding highly doped emitter layers. Popular selective contact materials are often transition metal oxides (TMOs) due to high optical transparencies and large work functions that are useful for hole selective contacts to silicon. In contrast to previous articles, recent studies have indicated that the interface of p-type silicon and the molybdenum oxide ( $\text{MoO}_x$ ) exhibits a significant Schottky barrier that decreases the efficiency of hole-selective contacts by impeding majority carrier hole collection. To alleviate this issue, atomic layer deposited (ALD) alumina ( $\text{Al}_2\text{O}_3$ ) might be added between Si wafer and  $\text{MoO}_x$  with the expectation to generate a negative interface fixed charge ( $N_f$ ) after annealing, decreasing band bending. ALD  $\text{Al}_2\text{O}_3$  also has the ability to passivate interface traps with diffusion of precursor hydrogen during annealing. In this work, we hypothesize that insertion of a tunneling ALD  $\text{Al}_2\text{O}_3$  layer between  $\text{MoO}_x$  and p-type Si will enable Schottky barrier height ( $\Phi_{bh}$ ) minimization that is tunable with  $N_f$ , enabling a high efficiency hole-selective contact. Since there should not be quantifiable  $N_f$  in tunneling  $\text{Al}_2\text{O}_3$  using capacitance-voltage (C-V) analysis, non-tunneling n-Si/ $\text{Al}_2\text{O}_3$ /Al MOSCAP structures were used to determine ideal processing for maximum negative  $N_f$ . The ALD growth of  $\text{Al}_2\text{O}_3$  utilized trimethylaluminum and  $\text{H}_2\text{O}$  at 4 deposition temperatures. Half of the samples were annealed at  $425^\circ\text{C}$  in a nitrogen atmosphere prior to the application of Al contacts. After  $N_f$  quantification, p-Si/ $\text{Al}_2\text{O}_3$ / $\text{MoO}_x$ /Al tunnel diodes with thin ( $\sim 1$  nm) as-deposited and annealed  $\text{Al}_2\text{O}_3$  layers were fabricated to determine  $\Phi_{bh}$ . Current density-voltage-temperature (J-V-T) and Mott-Schottky  $1/C^2$ -V measurements were used to establish a range for  $\Phi_{bh}$ . Both methods showed that the as-deposited tunneling  $\text{Al}_2\text{O}_3$  diodes had a higher  $\Phi_{bh}$  compared to the diodes with annealed tunneling  $\text{Al}_2\text{O}_3$ , and therefore also supported the existence of a  $\Phi_{bh}$  at the Si/ $\text{MoO}_x$  interface. Future work will involve using larger barrier height diodes using n-Si to more accurately calculate  $\Phi_{bh}$  and confirm or reject the phenomenon observed.

5:50 AM \*F.EN02.07.05

**Organic-Silicon Heterojunction for Solar Cell and Integrated Flexible Energy Devices** [Baoquan Sun](#); Soochow University, China

Numerous alternative materials and solar cell device structures have been widely explored in order to reduce the cost of photovoltaic (PV) manufacture. Organic-inorganic component solar cells based on nanostructured semiconductor have built up in past two decades, which may promise the potentially low cost and high performance. However, the device performances are generally lower than its pristine all-inorganic PV devices, resulting from the numerous surface defect and improper organic-inorganic phase segregation. Here, we demonstrate that hybrid PVs based on organic conjugated molecular and nanostructured silicon can achieve a high power conversion efficiency by controlling the interface contact as well as surface passivation.

An advantage of this type heterojunction devices presents the excellent light harvest capability of nanostructured as well as benefiting likely simple fabrication process. Especially, the composite of conjugated organic materials and nanostructured inorganic materials are potential candidates for cost-effective and efficient solar-energy-harvesting devices<sup>1</sup>. This device can be operated by a light-modulated field effect solar cell, which can improve the device performance under accumulation of light illumination<sup>2</sup>. In addition, this type device can be easily integrated with other type energy device, for example, an energy harvesting structure that integrates an organic-silicon heterojunction solar cell and a triboelectric nanogenerator (TENG) device is built to realize power generation from both sunlight and raindrop<sup>3</sup>. In addition, a self-charging power unit based on an organic-Si heterojunction solar cell and an organic supercapacitor, which simultaneously achieved both photoelectric conversion and energy storage<sup>4</sup>. Finally, we will demonstrate that low temperature processed conductive silver-based ink has wide application usage for low temperature processed solar cell and related plastic electronics.

1. Sun, B.; Shao, M.; Lee, S.-T. *Advanced Materials* **2016**, 28, (47), 10539-10547.
2. Wang, Y.; Xia, Z.; Liu, L.; Xu, W.; Yuan, Z.; Zhang, Y.; Siringhaus, H.; Lifshitz, Y.; Lee, S. T.; Bao, Q.; Sun, B. *Advanced Materials* **2017**, 29, (18), 1606370.
3. Liu, Y.; Sun, N.; Liu, J.; Wen, Z.; Sun, X.; Lee, S.-T.; Sun, B. *ACS Nano* **2018**, *ACS Nano* **2018**, 12 (3), 2893-2899.
4. Liu, R.; Wang, J.; Sun, T.; Wang, M.; Wu, C.; Zou, H.; Song, T.; Zhang, X.; Lee, S.-T.; Wang, Z. L.; Sun, B. *Nano Letters* **2017**, 17, (7), 4240-4247.

6:05 AM F.EN02.07.06

**Evaluation of Carrier Transport Mechanism by Systematic Defect Level Modulation in TiOx Protective Layers of n-Si/TiOx/Ni Photoanodes for Water Splitting** [Songwoung Hong](#)<sup>1,2</sup>, Woo Lee<sup>1,2</sup>, Seungwoo Song<sup>1</sup> and Ansoon Kim<sup>1,2</sup>; <sup>1</sup>Korea Research Institute of Standards & Science, Korea (the Republic of); <sup>2</sup>University of Science and Technology, Korea (the Republic of)

Photo-corrosion of anode participating the oxygen evolution reaction (OER) in photoelectrochemical cell (PEC) for water splitting is one of the obstacles for the long term stability and efficient solar to hydrogen conversion. In order to prevent the phot-corrosion, “electrically leaky” thick TiO<sub>2</sub> film was deposited onto a n-Si photoanode surface. However, the carrier transport mechanism through the thick dielectric layer and the influence of oxygen vacancy-related midgap states on the mechanism are still unclear. In order to verify the carrier transport through the midgap states of thick TiO<sub>2</sub> film, we only modulated the defect density of the protective TiO<sub>2</sub> film with no significant change of optical, physical, and chemical properties. It has been demonstrated that the defect density of the TiO<sub>2</sub> film is proportional to water-splitting activity. This result enables to explain the hole transport mechanism of the previously reported electrically leaky TiO<sub>2</sub> protection layer in n-Si photoanode. For the defect-level optimization, titanium sub-oxide (*sub*-TiO<sub>x</sub>) protection layer with higher defect density compared to the TiO<sub>2</sub> layer was also investigated. The controlled incorporation of defects into TiO<sub>x</sub> dramatically enhances the hole transport from the photoanode surface to electrolyte solution. The relationship between band structure and PEC activity of the photoanode system was explored depending on the defect density of the protection layer. Mott-Schottky analysis of this system suggests that the defect level of TiO<sub>x</sub> films influences the band bending of n-Si, which governs the accessible density of defect states and the carrier recombination.

#### 6:15 AM F.EN02.07.07

#### **Improvement in the Passivation Quality of Titanium Oxide Electron-Selective Contacts by Tantalum Doping** Seira Yamaguchi<sup>1</sup>, Hyunju Lee<sup>1,2</sup> and Yoshio Ohshita<sup>1</sup>; <sup>1</sup>Toyota Technological Institute, Japan; <sup>2</sup>Meiji University, Japan

We report on improvement in the passivation quality of titanium oxide (TiO<sub>x</sub>) by doping with tantalum (Ta). TiO<sub>x</sub> has been considered one of the most promising materials for electron-selective contacts (ESCs) for crystalline silicon (c-Si) solar cells. There has been a high efficiency of 23.1% successfully achieved for a c-Si solar cell with a TiO<sub>x</sub> rear-side ESC [1]. To realize higher efficiencies, it is necessary to further improve the passivation quality. One possible candidate for realizing such improvements is Ta doping. Ta doping reportedly causes a negative shift of the flat band voltage of TiO<sub>x</sub> films [2], and the passivation quality of TiO<sub>2</sub> ESCs can therefore be improved by Ta doping. In addition, tantalum oxide (TaO<sub>x</sub>) has long-term stability against UV light irradiation [3,4], and it is possible that Ta doping may also improve the long-term stability. In this work, we focus on an improvement in the passivation quality of TiO<sub>x</sub> ESCs by doping with Ta.

We deposited TiO<sub>x</sub>:Ta films by atomic-layer deposition on the both-sides of n-type c-Si substrates which were in advance oxidized in 30% hydrogen peroxide solution at 80 °C. Ta doping was realized by inserting a unitcycle of TaO<sub>x</sub> monolayer into unitcycles of TiO<sub>x</sub>. In this study, Ta doping concentration is characterized by a ratio of the number of TaO<sub>x</sub> unitcycles to that of TiO<sub>x</sub> unitcycles. The thickness of TiO<sub>x</sub>:Ta passivation films was basically set to 3.5 nm. After the deposition, the TiO<sub>x</sub>:Ta-passivated c-Si substrates were annealed at 130 °C in air. The effective minority-carrier lifetimes ( $\tau_{\text{eff}}$ s) were acquired from quasi steady-state photoconductance measurements, which were used as an indicator for the passivation qualities of the TiO<sub>x</sub>:Ta ESCs.

The All the samples passivated with undoped TiO<sub>x</sub> films and with TiO<sub>x</sub>:Ta films with unitcycle ratios of 0.05, 0.09, 0.17, and 0.50 showed improvements in the  $\tau_{\text{eff}}$  by annealing at 130 °C. However, the  $\tau_{\text{eff}}$  of samples with TiO<sub>x</sub>:Ta after annealing was, in most cases, higher than that of samples with undoped TiO<sub>x</sub>. This indicates that doping with Ta improves the passivation quality of TiO<sub>x</sub> ESCs. In addition, TiO<sub>x</sub>:Ta with a relatively low amount of Ta doping tended to have high passivation qualities. The TiO<sub>x</sub>:Ta with a unitcycle ratio of 0.05 showed the highest  $\tau_{\text{eff}}$  of 784  $\mu$ s in this study, which corresponded to an effective surface recombination quality of 24.9 cm/s. The TiO<sub>x</sub>:Ta with a unitcycle ratio of 0.50 exhibited a rather lower passivation quality than that of the undoped TiO<sub>x</sub>, which indicates excess Ta doping rather degrades the passivation quality.

The above results imply that TiO<sub>x</sub>:Ta is one of the promising materials for ESCs. The results of experiments to elucidate the mechanism of the improvements in the passivation quality will be presented.

[1] J. Bullock et al., *Adv. Energy Mater.* **9** (2019) 1803367.

[2] X. Feng et al., *Angew. Chem. Int. Ed.* **48** (2009) 8095.

[3] Y. Wan et al., *ACS Energy Lett.* **3** (2018) 125.

[4] T. Wang et al., *Ind. Eng. Chem. Res.* **58** (2019) 5510.

**5:00 AM \*F.EN02.08/F.EL06.07/F.EL08.10.01**

**Advances in Material Properties for Perovskite-Perovskite Tandems** Giles Eperon<sup>1,2</sup>; <sup>1</sup>Swift Solar, United States; <sup>2</sup>National Renewable Energy Laboratory, United States

Multijunction all-perovskite solar cells offer a route towards efficiencies of III-V materials at low cost by combining the advantages of low thermalization loss in multijunction architectures with the beneficial properties of perovskites - namely low processing cost, high throughput fabrication, and compatibility with flexible substrates. Here, I will discuss why flexible all-perovskite tandems are a very attractive iteration of the perovskite technology. I will focus on what is needed to make a good perovskite-perovskite tandem on a flexible substrate, and the advances that we have made towards this goal. I will cover advances including a) the development and understanding of wide bandgap materials that leverage a novel bandgap-tuning strategy (without increasing bromine, hence avoiding significant phase segregation) to reach the ideal bandgaps for all-perovskite tandems, resulting in efficient devices that are stable to the combined stresses of heat and light; b) advances that we have made in interlayer design, working towards more ideal material properties for reducing shunt resistance; and c) the integration of these approaches to develop >23% efficient monolithic all-perovskite tandems on rigid substrates and 21% efficient devices on flexible plastic substrates.

**5:15 AM \*F.EN02.08/F.EL06.07/F.EL08.10.02**

**The Many Faces of Characterization in Developing a Commercial Perovskite on Silicon Tandem Solar Cell** Laura Miranda; Oxford PV, United Kingdom

Perovskite solar absorbers have the potential to disrupt the photovoltaic industry predominantly with their simultaneous promise of high efficiency and low cost. Whilst these two properties ensure a steady stream of research and development opportunities, commercial scaling requires assuring that the devices are sufficiently characterized to be confident of their long-term performance. Oxford PV has been addressing the challenges associated with commercially scaling its perovskite on silicon tandem solar cell design. Key practices that have been adopted during the development of highly efficient, reliable, and cost-competitive solar cells are the use of rigorous characterization tools and techniques, and the development of necessary models. This talk will highlight some of the challenges and considerations associated with bringing perovskite on silicon tandem solar cells from a laboratory prototype to a commercial product ready for manufacturing and how characterization has shaped and continues to inform that process.

**5:30 AM \*F.EN02.08/F.EL06.07/F.EL08.10.03**

**Passivation Strategies and Interlayers for Perovskite-Based Tandem Photovoltaics** Ulrich W. Paetzold, Saba Gharibzadeh, Tobias Abzieher, Ihtezaz M. Hossain, Hang Hu, Thomas Feeney, Somayeh Moghadamzadeh, Mahdi Malekshahi Byranvand,, Bahram Abdollahi Nejad, Paul Fassel and Bryce Sydney Richards; Karlsruhe Institute of Technology, Germany

Single-junction crystalline silicon solar cells dominate the photovoltaics market today, but their power conversion efficiencies (PCEs) are approaching the practical limit for this technology. The emergence of hybrid organic-inorganic metal halide perovskite semiconductors over the past decade has opened a window of opportunity to advance the performance of the market-dominating photovoltaic technologies through the development of tandem solar cells. These tandem solar cells promise high PCEs (>33%). To reach this landmark, a number of scientific and technological challenges related to high-efficiency perovskite-based tandem solar cell architectures, stable and high-quality perovskite semiconductor materials, and light management concepts need to be addressed. In this presentation, our progress on passivation strategies and novel interlayers to reduce the voltage losses in wide-bandgap and low-bandgap perovskite solar cells (PSCs), and in turn to increase the PCE of perovskite-based tandem photovoltaics, will be presented.

The search for efficient passivation interlayers for wide-bandgap perovskite top solar cells in *n-i-p* architecture directed our research in the past towards solution-processed 2D/3D perovskite heterostructures. Making use of these heterostructures for interface passivation, wide-bandgap PSCs ( $E_g \sim 1.72$  eV) with record open-circuit voltage for this bandgap and very high PCEs of up to 19.4% were demonstrated [1]. The reduced voltage deficit is a result of the decreased non-radiative recombination losses at the perovskite/hole-transport layer (HTL) interface. The solution-processed 2D/3D perovskite heterostructure is compatible with 3D perovskite absorber layers of a wide range of bandgaps ( $1.65$  eV  $\leq E_g \leq 1.85$  eV) [2]. Using this strategy in 4-terminal perovskite/silicon and perovskite/CIGS tandem solar cells, high PCEs > 27% [3], and > 25%

[2] were demonstrated, respectively, thereby significantly exceeding the record PCEs reported for the respective single-junction solar cell technologies.

Beyond these past results, at the MRS fall meeting we will further present our latest work on novel interlayers and passivation strategies to minimize the voltage loss in wide-bandgap ( $1.65 \text{ eV} \leq E_g \leq 1.75 \text{ eV}$ ) as well as low-bandgap ( $E_g \sim 1.26 \text{ eV}$ ) perovskite solar cells in *p-i-n* architecture. The *p-i-n* architecture is a key to realize high-performance 2-terminal perovskite/silicon as well as perovskite/perovskite tandem solar cells. Moreover, we will present a novel route to deposit uniform ultra-thin polymer passivation layers onto perovskite thin films by chemical vapor deposition (CVD) [4]. The CVD polymerization promises reliable, scalable, and homogeneous deposition for future large-area processing of perovskite-based tandem solar cells.

#### References:

- [1] Gharibzadeh, S. *et al.* Record Open-Circuit Voltage Wide-Bandgap Perovskite Solar Cells Utilizing 2D/3D Perovskite Heterostructure. *Adv. Energy Mater.* **9**, 1–10 (2019).
- [2] Gharibzadeh, S.; Hossain I. M. *et al.* 2D/3D Heterostructure for Semitransparent Perovskite Solar Cells with Engineered Bandgap Enables Efficiencies Exceeding 25% in Four-Terminal Tandems with Silicon and CIGS. *Adv. Funct. Mater.* **30**, (2020).
- [3] Duong, T. *et al.* High Efficiency Perovskite-Silicon Tandem Solar Cells: Effect of Surface Coating versus Bulk Incorporation of 2D Perovskite. *Adv. Energy Mater.* **10**, 1903553 (2020).
- [4] Malekshahi Byranvand M.; Behboodi-Sadabad F. *et al.* Chemical Vapor Deposited Polymer Layer for Efficient Passivation of Planar Perovskite Solar Cells. *submitted*

#### 5:45 AM \*F.EN02.08/F.EL06.07/F.EL08.10.05

**Towards Highly Efficient Monolithic 2- and 3-Terminal Perovskite Silicon Tandem Solar Cells** Lars Korte, Eike Koehnen, Philipp Wagner, Philipp Tockhorn, Marko Jost, Amran Al-Ashouri, Lukas Kegelmann, Marcel Roß, Bernd Stannowski and Steve Albrecht; Helmholtz-Zentrum Berlin für Materialien und Energie, Germany

Integrating metal halide perovskite top cells with crystalline silicon (c Si) bottom cells into monolithic tandem devices has recently attracted increased attention due to the high efficiency potential of these cell architectures. To further increase the tandem device performance to a level well above the best single junctions, optical and electrical optimizations as well as a detailed device understanding for such architectures need to be developed [1]. Here we present our recent results on such monolithic tandem cells in the common 2-terminal (2T) as well as in a novel 3-terminal (3T) contacting scheme.

In the 2T design, we recently demonstrated a certified power conversion efficiency (PCE) of 29.15% [2,3]. I will discuss some key elements to this result: using a silicon heterojunction cell electron contact on the rear side, enabling the integration of a perovskite top cell in the *p-i-n* configuration; employing self-assembled monolayers (SAMs) as hole selective contacts for further reduction of non-radiative recombination losses, etc. With the latter, efficiencies of up to ~ 21 % were demonstrated for *p-i-n* perovskite single junctions [3].

In 3T tandems, one of the three contacts is shared by both subcells, allowing for the individual operation of both subcells in a monolithic device with a single substrate, thus combining the characteristic advantages of 2T and 4-terminal (4T) devices: high combined photogeneration currents as in state-of-the-art 2T tandems, and ideally independent electrical operation similar to 4T tandems, making the cell more robust against varying spectra. I will discuss our recent proof-of-concept study [4], demonstrating a 3T perovskite/silicon tandem cell by manufacturing an *n-i-p* perovskite top cell on an interdigitated back contact (IBC) silicon heterojunction solar cell. In our proof-of-concept device, the combined PCE of ~ 17% is still limited both optically and electrically, and it will be discussed how optimizations of the cell stack can bring this architecture to a PCE level comparable to 2T tandems. Furthermore, I will demonstrate that the subcells can indeed be operated largely independently at their individual maximum power points, allowing to extract the maximum power output for varying spectral conditions similar to 4T cells. A minimized series resistance at the shared electron contact on the cell's rear side is identified as the crucial parameter for independent operation of the subcells, and I will discuss pathways to approach the simulated efficiency potential by an optimized device design.

#### References:

- [1] Jost, Kegelmann, Korte, Albrecht, *Adv. Energy Materials*, 2020, doi: 10.1002/aenm.201904102
- [2] NREL Best Research-Cell Efficiency Chart, <https://www.nrel.gov/pv/cell-efficiency.html>
- [3] Köhnen, Jost, Stannowski, Albrecht *et al.*, *Sustainable Energy and Fuels*, doi: 10.1039/C9SE00120D
- [3] Al-Ashouri, Magomedov, Korte, Albrecht *et al.*, *En. Env. Sci*, 2019, doi: 10.1039/C9EE02268F
- [4] Tockhorn, Wagner, Korte *et al.*, *ACS Appl. En. Mat.*, 2020, doi: 10.1021/acsaem.9b01800

#### 6:00 AM \*F.EN02.08/F.EL06.07/F.EL08.10.06

**Solution Processed Perovskite Subcell in Monolithic Perovskite/Si Tandem Solar Cells and Their Cost and Stability Concerns** Qi Chen<sup>1</sup> and Huanping Zhou<sup>2</sup>; <sup>1</sup>Beijing institute of Technology, China; <sup>2</sup>Peking University, China

Among all commercialization routes for perovskite photovoltaics (PV), the perovskite/Si tandem is of particular interest as it capitalizes the mature silicon industry with decades of experience. Here we report low-temperature solution process for efficient two-terminal perovskite/Si tandem solar cells, wherein electrical and optical properties of the tunneling junction are carefully modulated. Moreover, we improve materials stability by introducing  $\text{Eu}^{2+}/\text{Eu}^{3+}$  “redox shuttle” to suppress the  $\text{Pb}^0/\text{I}^0$  impurities which inevitably occurred during device operation. In addition, we carefully analyze the cost of tandem devices in terms of levelized cost of energy (LCOE) by adopting the “bottom-up cost model”. It reveals perovskite PV exhibit low materials cost, which reduces the LCOE substantially in tandem devices. We conclude that further efforts are required to simultaneously improve the efficiency and lifetime of perovskite modules, which ultimately endows the competitiveness of perovskite tandem solar cells.

**SYMPOSIUM F.EN03**

---

Overcoming the Challenges with Metal Anodes for High-Energy Batteries  
November 21 - December 3, 2020

Symposium Organizers

Rachel Carter, U.S. Naval Research Laboratory  
Nian Liu, Georgia Institute of Technology  
Munekazu Motoyama, Nagoya University  
Andrew Westover, Oak Ridge National Laboratory

---

\* Invited Paper

SESSION F.EN03.07: Live Keynote: Alkali Metal Plating and Stripping  
Session Chairs: Rachel Carter and Munekazu Motoyama  
Wednesday Afternoon, December 2, 2020  
F.EN03

**5:15 PM \*F.EN03.04.05**

**Mesoscale Interactions in Electrodeposition Stability of Metal Electrodes** Partha P. Mukherjee and Bairav S. Vishnugopi; Purdue University, United States

Lithium metal electrodes in the presence of liquid electrolytes suffer from unmitigated growth of dendrites that pose safety concerns and lead to electrochemical performance limitation. It necessitates fundamental understanding of the mechanistic origins of interface instability at the mesoscale. This work relies on a detailed mesoscale analysis of the role of disparate mechanisms including electrolyte transport, self-diffusion and electrochemical reaction on the nucleation and growth of electrodeposition. The contrasting influence of temperature on the electrodeposition stability is examined. Finally, the role of mesoscale interactions in devising potential pathways toward electrodeposition stability is elucidated.

**5:35 PM \*F.EN03.06.02**

**Magnesium Metal Electrodeposition and Electrodeposition with Polymer Electrolytes** Bumjun Park and Jennifer L. Schaefer; University of Notre Dame, United States

Lithium metal and magnesium metal batteries have potential for high system energy density due to the high gravimetric and volumetric charge capacity of these metal anodes. Magnesium metal offers several advantages and disadvantages with respect to lithium metal as an anode. Magnesium is more abundant and resources are geographically widespread. Magnesium

metal is less chemically reactive than lithium metal and electrodisolution/deposition happens at elevated potentials, yet issues with inefficiency and side reactions still remain. While lithium metal polymer batteries have been investigated intently for decades, magnesium metal polymer batteries have received little attention. There exist great difficulties in producing magnesium polymer electrolytes that both effectively transport magnesium and support reversible electrodeposition and dissolution of magnesium metal. In this talk, I will review our recent research on ion transport and electrochemistry in traditional salt-doped magnesium polymer electrolytes and magnesium poly(ionic liquid) electrolytes.

**5:55 PM \*F.EN03.04.06**

**Electrochemical Activation and Passivation of Magnesium Metal Anodes** Masaki Matsui; Kobe University, Japan

Magnesium metal anode has a high volumetric capacity of  $3833 \text{ mAh cm}^{-3}$ , rechargeable magnesium battery is expected as an advanced battery system alternate to Li-ion batteries. The SEI-free surface of the magnesium metal leads to the uniform nucleation process resulting in the dendrite free growth during the electrodeposition process. On the other hand, the passivation of the magnesium metal surface initiates the locally-focused current. As a consequence, a risk of dendritic growth of the magnesium metal remains in the electrodeposition process. Here we investigated the nucleation process of magnesium metal on magnesium metal substrates. The initial anodic polarization forms several corrosion pits at the surface of the magnesium substrate. We found that these pits become the preferable sites for the following magnesium deposition. The results suggest that the initial electrochemical activation process is crucial to obtain the uniform plating of magnesium metal.

**6:15 PM \*F.EN03.04.08**

**Interelectrode Temperature Differences used to Promote Reversible Lithium Electroplating and Stripping** Corey T. Love<sup>1</sup>, Robert Atkinson III<sup>2</sup>, Rachel Carter<sup>1</sup> and Todd Kingston<sup>3</sup>; <sup>1</sup>U.S. Naval Research Laboratory, United States; <sup>2</sup>EXCET, Inc., United States; <sup>3</sup>NRL/NRC Post-doctoral Research Associate, United States

The challenges with metal anodes for high-energy batteries will likely be overcome as a result of advancements in three research areas: materials structure-property relationships, electrode architectural design and informed operational controls. We have been focusing our efforts on the operational considerations, specifically temperature control, to promote reversible Li plating and stripping. Modulating temperature, both through thermal gradients and transients, has a direct effect on the performance and stability of the electrochemical plating and stripping processes of Li metal. Applying a modest thermal gradient impacts the lithium plating morphology and dictates whether unstable, one-dimensional Li electroplating or stable, more homogeneous electroplating occurs (1). This talk will expand upon our understanding of gradient-influenced plating/stripping behavior and present operational temperature controls necessary for prolonged battery performance and safety. Additionally, thermal regimes applied to improve electrode kinetics and diffusion will show the opportunity to enable fast charging of Li metal and metal-free electrodes coupled with a  $\text{LiFePO}_4$  positive electrode. We use a suite of materials and electrochemical characterization tools (XPS, XRD, optical microscopy, computed tomography and EIS) to guide our understanding of Li metal behaviors in the battery environment.

(1) R. W. Atkinson III, R. Carter and C. T. Love, *Energy Storage Materials*, **22**, 18 (2019).

**6:35 PM \*F.EN03.04.01**

**Chances and Challenges in Zinc Electrode Rechargeability** Hajime Arai and Atsunori Ikezawa; Tokyo Institute of Technology, Japan

Zinc is abundant, widely used as structural materials, non-toxic, safe and inexpensive. It has the most negative potential among metals that can be recharged in aqueous electrolyte solutions and high capacity density, and hence is an attractive candidate as a negative electrode material. In alkaline media, the thermodynamically stable discharge product is  $\text{ZnO}$ , a semiconductor (not insulator), and there is acceptable volume expansion upon its formation (ca. +60%). When anion conductors such as alkaline solutions are used as the electrolyte, as is often the case, the formation of  $\text{ZnO}$  is at the negative electrode side, which causes tolerable volume changes of the negative electrode when compared to the total metal dissolution and/or deposition at the positive electrode side. The corresponding positive electrode materials can be proton-acceptor types such as  $\text{NiOOH}$  and oxygen in aqueous alkaline electrolytes. Recent trials include zinc ion acceptors such as organic metal frameworks with zinc ion conductive ionic liquid electrolyte. This presentation mainly focuses on alkaline-based aqueous systems.

The main drawback of the zinc electrode is its insufficient durability, suffered from the morphology changes such as dendrite growth, shape change and densification. This is mostly caused by the formation of highly soluble species  $\text{Zn(OH)}_4^{2-}$ , a kinetically favorable discharge product, that diffuses away from the original positions and precipitates wherever it favors.

Even if zinc oxide is saturated in the alkaline electrolyte, zinc supersaturation occurs; it stays longer than the time scale of the charge-discharge reactions, even for months. There are several ways to restrict the zinc dissolution, such as complex formation (e.g. calcium zincate [1]), protective film formation (e.g. anion exchange membrane [2]) and the use of electrolyte additives (e.g. pH controller, indifferent salts and organic solvents [3-4]). Though the durability depends on the utilization rates and loaded mass (mAh/cm<sup>2</sup>), cycle life of more than several hundred cycles be achieved in ideal cases. Mechanical pressure on the electrode (e.g. separator wrapping) is a simple but effective way in restraining the morphology changes. In contrast to electrical charging, mechanical charging is a unique method for air battery systems, mostly for electric vehicles, where soluble zinc species are removed from the cell and regenerated by off-site processes [5].

Passivation during high rate discharging is also problematic, but can be mitigated by constructing composite electrodes with high surface areas. Hydrogen evolution as the self-discharge can be restricted by adding inhibitors such as indium and bismuth.

Analytical methods to clarify the zinc electrode reaction processes are of particular interest, since degradation proceeds with nearly no sign in the electrochemical responses. Since zinc is oxidized in air, in situ (in-cells) or operando (in-current-flow) analyses are favorable. *Operando* X-ray diffraction (XRD) is helpful in detecting the formation of crystalline ZnO during discharging [6]. XRD mapping analysis indicates how the shape change proceeds [7]. *Operando* X-ray fluorescence imaging, utilizing the zinc visibility in hard X-ray absorption, is effective in observing zinc behavior with space resolutions [8]. Optical analysis is promising to observe macroscopic changes of the zinc species that significantly affects the electrode durability [9].

[1] R. Jain, et al. *J. Appl. Electrochem.*, **22**, 1039 (1992).

[2] K. Miyazaki et al., *Electrochemistry*, **80**, 725 (2012).

[3] A. Nakata et al., *J. Electrochem. Soc.*, **163**, A50-A56 (2016).

[4] T. Takeya et al., *J. Power Sources*, **407**, 180 (2018).

[5] J. Goldstein et al., *J. Power Sources*, **80**, 171 (1999).

[6] A. Nakata et al., *Electrochim. Acta*, **166**, 82 (2015).

[7] A. Nakata et al., *APL Materials*, **6**, 047703 (2018).

[8] A. Nakata et al., *Electrochemistry*, **83**, 849 (2015).

[9] M. Horiuchi et al., *Abs. Batt. Symp. Japan*, 1E27 (2019).

#### 6:55 PM F.EN03.04.04

**Characteristic Electrochemical Features of Interfaces on Calcium Foils** [Aaron M. Melemed](#) and Betar Gallant; Massachusetts Institute of Technology, United States

Batteries based on calcium (Ca) metal anodes offer a possibility of improved sustainability and safety with attractive electrochemical metrics. However, Ca battery development is still in its infancy due to basic chemical limitations. When Ca metal comes in contact with an organic electrolyte, a native solid electrolyte interphase (SEI) forms which passivates, and in some instances fully deactivates, the electrode surface. Considering that Ca deposition and dissolution is widely believed to be a surface-film-controlled process, understanding Ca<sup>2+</sup> transport through this native SEI is paramount. In this talk, characteristic features occurring in cyclic voltammetry (CV) with Ca foils will be discussed as a function of interface composition in a benchmark electrolyte system, Ca(BH<sub>4</sub>)<sub>2</sub> in tetrahydrofuran (THF). This electrolyte was found recently by others to support reversible plating/stripping under continuous CV conditions (at 25 mV/s) on planar metal (Au or Pt) working electrodes. As opposed to plating/stripping onto a gold substrate, the first CV cycle on Ca foil reveals a persistent native passivation layer — reflective of the foil preparation process — which manifests as significant reduction and oxidation overpotentials. This native interface can be degraded through the initial electrochemical steps, by processes that depend on whether plating or stripping is first conducted, along with the associated electrochemical protocol. The effect of this first activation step on the resulting electrochemistry will be discussed. Subsequently, the interface evolves to reflect one predominantly governed by CaH<sub>2</sub>, which enables further study of the dynamics of this interface under different cycling conditions (scan rate and the imposition of various resting times) on Ca foil. Upon continued cycling, access into the underlying bulk Ca is possible. While this process remains limited by the interface and yields lower current densities than with fresh Ca plating/stripping on Au electrodes, the underlying Ca is not entirely deactivated as concluded by earlier studies, but rather depends on the surface conditioning process and the electrolyte. To further investigate the role of the interface, I will also describe experiments in which nanoscale CaF<sub>2</sub> (~100 nm), an inorganic component found to be present in other Ca SEI, was intentionally formed on Ca foils prior to immersion in an attempt to decouple the foil from the surrounding electrolyte and modulate interface behaviors. Critical differences in interface chemical and electrochemical stability, along with electrochemical performance under CV conditions, will be discussed, and prospects for improving the cyclability of practical Ca foil electrodes will be explored.



SESSION F.EN03.08: Live Keynote: Alkali Metal Mechanics  
Session Chairs: Nian Liu and Andrew Westover  
Thursday Morning, December 3, 2020  
F.EN03

**11:30 AM \*F.EN03.03.01**

**From Ion-to-Atom-to-Dendrite—Formation and Nanomechanical Behavior of Electrodeposited Lithium** Julia R. Greer<sup>1</sup>, Michael A. Citrin<sup>1</sup>, Heng Yang<sup>1</sup>, Simon Nieh<sup>2</sup>, Joel M. Berry<sup>3</sup> and David J. Srolovitz<sup>4</sup>; <sup>1</sup>California Institute of Technology, United States; <sup>2</sup>Front Edge Technology, United States; <sup>3</sup>Lawrence Livermore National Laboratory, United States; <sup>4</sup>City University of Hong Kong, Hong Kong

Lithium is an ideal battery anode, with theoretical specific capacity of 3860 mAh/g; replacing conventional graphitic anodes with Li in Li-ion batteries can increase energy density by ~50%. A significant drawback of Li anodes is dendrite formation during cycling, which can lead to short circuiting (a safety hazard and cell death) and to “dead Li,” which drastically reduces cycle life.

A complete dearth of experiments that probe mechanical behavior of electrodeposited Li exists. Most experiments on mechanical properties have focused on thin films and on Focused Ion Beam-carved Li. We developed *in-situ* experimental methodology that allows to electrochemically charge small-scale battery cells and to observe, in real-time, the formation of Li dendrites and to probe their mechanical response. Experiments reveal: (1) Li nano-deposits are single crystalline and (2) strengths of Li nano-pillars are  $16.0 \pm 6.82$  MPa, which is 24x greater than bulk. This strength enhancement can be explained in terms of the ubiquitous “smaller is stronger size effect” nano-sized single crystalline metals. This work expands the existing strength vs. size property space for Li and helps explain why dendrites can penetrate through much stiffer and harder ceramic solid electrolytes, theorized for several years but never unambiguously demonstrated

Development of high energy density solid-state batteries with Li metal anodes has been limited by uncontrollable growth of Li dendrites in liquid and solid electrolytes. This, in part, may be caused by a dearth of information about mechanical properties of Li, especially at the nano- and micro-length scales and microstructures relevant to Li batteries. We investigate formation, microstructure, and mechanical properties of nano-sized Li electrodeposited in a commercial LiCoO<sub>2</sub>/LiPON/Cu solid-state thin film cell, grown *in-situ* in a scanning electron microscope (SEM) equipped with nanomechanical capabilities. Experiments reveal that Li was preferentially deposited at the LiPON/Cu interface, along the valleys that mimic the domain boundaries of underlying LiCoO<sub>2</sub>. This pattern of Li formation is consistent with the higher driving force for Li nucleation at the valleys uncovered by electrochemical simulations of Li ion transport in this system. Further charging of the cell resulted in Li nuclei piercing through the 30 nm-thick Cu layer and growing into vacuum through the crack openings. Cryogenic electron microscopy analysis of electrodeposited Li revealed its single crystalline microstructure, and *in-situ* nano-compression experiments on individual Li nano-pillars with diameters of 360-759 nm revealed their average Young's modulus to be  $6.76 \pm 2.88$  GPa and an average yield stress of  $16.0 \pm 6.82$  MPa, ~24x higher than what has been reported for bulk polycrystalline Li. We discuss mechanical deformation mechanisms and strength of nano-sized electrodeposited Li in the framework of its microstructure and dislocation-governed nano-scale plasticity of crystals and place it in the parameter space of existing knowledge on small-scale Li mechanics. The enhanced strength of Li at small scales may help explain why Li can penetrate through and fracture much stiffer and harder ceramic solid electrolytes.

**11:50 AM \*F.EN03.03.02**

**On the Mechanisms of Stress Relaxation and Intensification at the Lithium/Solid-State Electrolyte Interface** Erik G. Herbert<sup>1</sup>, Nancy Dudney<sup>2</sup>, Maria Rochow<sup>1</sup>, Violet Thole<sup>1</sup> and Stephen Hackney<sup>1</sup>; <sup>1</sup>Michigan Technological University, United States; <sup>2</sup>Oak Ridge National Laboratory, United States

Under electrochemical cycling, stress intensification and relaxation within small, confined volumes at the Li/solid-state electrolyte (SSE) interface are thought to be critical factors contributing to mechanical failure of the SSE and subsequent short-circuiting of the device. Nanoindentation has been used to examine the diffusion limited pressure Li can support in the absence of active dislocation sources at high homologous temperatures. Based on the underlying physics of this deformation mechanism, a simple perturbation model coupling local current density, elastic stress and diffusional creep relaxation is introduced. Combining this analysis with the indentation results, it is possible to describe a ‘defect danger zone,’ a length scale which is too large for effective diffusional creep relaxation, but too small for efficient dislocation multiplication. In this instance, the properties of the SSE become critical in controlling localized pressure at the interface.

In contrast to the ‘first generation,’ pioneering analysis of the Li/electrolyte interface by Monroe and Newman, more recent analyses of the Li/SSE interface mechanics examine a similar but uniquely different problem in that they consider non-uniform electrochemical properties and/or filling of morphological defects at the interface during Li charging such that the initial amplitude of the Li protrusion is fixed by a pre-existing interface defect or undulation. Meaningful comparisons between multiple ‘second-generation’ approaches can be challenging. Although they generally address the same problem, assumptions about the interface defect geometry and the self-limiting mechanical and electrochemical behavior of Li place significant limitations on the conclusions and the general applicability of the proposed solution. Despite their differences, the second-generation approaches arrive at generally the same conclusion: Within confined or localized volumes of Li at the interface, Li can support pressures significantly higher than its bulk yield strength (stresses as high as 200 MPa). Such stress concentrations at the interface are of critical concern because they facilitate mechanical failure of the SSE by fracture. The key question then becomes, why is the stress concentration so large relative to the bulk yield strength of Li? Two potential explanations are offered by the second-generation approaches: geometry effects and length scale effects. These effects are not unique to Li. Any metallic anode will experience these effects in a manner that depends on its absolute melting temperature, elastic modulus, yield strength, and self-diffusion coefficient.

Although the length scale effects of high purity Li have only been recently documented, the basic concept of “smaller is stronger” is well documented. As described by Brenner in 1956 and later quantified by Phani et al. in 2013, the yield strength of a metal in small volumes can be described from a purely statistical point of view, as the stress required to plastically flow depends on the probability of finding the necessary dislocations within the stressed volume. Load-displacement data from nanoindentation experiments performed in high purity Li at a homologous temperature of 0.67 graphically illustrate this concept. Similar results obtained in high purity indium, a mechanical surrogate to Li, further illustrate the competition for stress relief. Collectively, an important outcome from these ‘second generation’ approaches is that SSEs with nominally uniform electrochemical properties and flat, smooth surfaces will promote planar, nominally stress-free plating and stripping of Li. Unfortunately, brittle SSE materials will likely experience the same statistical failure issues as structural ceramics. The most robust devices will also implement SSEs that are engineered to provide localized stress relief, potentially through mechanisms such as densification, shear banding and time dependent recovery.

#### 12:10 PM F.EN03.03.03

**A New Paradigm for Preventing Lithium Dendrite Penetration Through Solid Electrolytes** Yue Qi<sup>1</sup>, Chunmei Ban<sup>2</sup> and Stephen J. Harris<sup>3</sup>; <sup>1</sup>Michigan State University, United States; <sup>2</sup>University of Colorado Boulder, United States; <sup>3</sup>Lawrence Berkeley National Laboratory, United States

We introduce a new concept to suppress penetration of lithium dendrites through solid electrolytes (SE) by putting the surface of the SE into a state of compressive stress. For a sufficiently high residual compressive stress, cracks have difficulty forming at the surface, and cracks that do form tend to close, inhibiting dendrite penetration. Introduction of compressive surface residual stress solves stress corrosion cracking problems in metals and static fatigue problems in ceramics and glasses. An example of the latter is Gorilla Glass, which is strongly resistant to cracking because of surface compressive stresses. However, the technique will not work if Li ion transport through a SE in compression is substantially reduced. Our DFT and MD calculations for LLZO indicate that the introduction of even high residual compressive stresses (up to 10 GPa) will have only a very modest effect on Li ion transport kinetics, suggesting that the approach is viable. In addition to inhibiting penetration and fracture in solid electrolytes, compressive stresses on the order of GPa will tend to suppress lithium plating inside of solid electrolytes because of an increased overpotential for the Li ion reduction reaction. We discuss and compare several experimental methods for introducing compressive residual stresses at the surfaces of solid electrolytes. We believe that the information here can provide a new avenue for developing high-performance and stable solid electrolytes

#### 12:30 PM F.EN03.03.04

**In Situ Investigations of Stress Evolution During Plating and Stripping of Lithium Metal** Jung Hwi Cho<sup>1</sup>, Xingcheng Xiao<sup>2</sup>, Kai Guo<sup>3</sup>, Yuanpeng Liu<sup>4</sup>, Huajian Gao<sup>5</sup> and Brian Sheldon<sup>1</sup>; <sup>1</sup>Brown University, United States; <sup>2</sup>General Motors, United States; <sup>3</sup>Massachusetts Institute of Technology, United States; <sup>4</sup>Harbin Institute of Technology, China; <sup>5</sup>Nanyang Technological University, Singapore

Poor stability of Li metal / liquid electrolyte or Li metal / solid electrolyte interfaces leads to chronic problems, such as dendrite formation and capacity loss. The impact of electro-chemo mechanical phenomena on interface stability and dendrite formation are believed to be critical, but are challenging to investigate directly. In-situ curvature measurements are an important tool that can be used to monitor these stresses during battery cycling. Using this technique during Li plating and examining film thickness effects, it is possible to separate contributions from the bulk lithium metal and the solid electrolyte

interphase (SEI). These investigations show that the stresses created in the SEI films are much larger than those in the Li metal. Furthermore, these stresses in the SEI can destabilize the electrode / electrolyte interface. Recently, a variety of methods have been employed to improve the performance and safety of Li metal based batteries by using various artificial SEI layers and/or implementing solid electrolytes. Several of these approaches were also investigated with stress evolution measurements during lithium plating and stripping. This work includes the use of both soft (PEO) and hard (LiF) artificial surface layers. These results indicate that stresses in both the surface film and the bulk lithium evolve differently when artificial SEI layers are employed. Initial attempts to monitor stress evolution with oxide solid electrolytes will also be presented.

#### **12:50 PM F.EN03.03.05**

**Plastic Deformation and Microstructural Evolution of Pure Lithium Under Various Stress States** Juner Zhu<sup>1,1</sup>, Tobias Sedlatschek<sup>1</sup>, Junhe Lian<sup>1,2</sup>, Wei Li<sup>1</sup>, Tomasz Wierzbicki<sup>1</sup> and Martin Bazant<sup>1</sup>; <sup>1</sup>Massachusetts Institute of Technology, United States; <sup>2</sup>Aalto University, Finland

Pure lithium in lithium metal batteries is often examined in research projects aiming at improving today's battery technology significantly. But the knowledge about the mechanical properties and the microstructural evolution of pure lithium is incomplete with two particular limitations. First, the available data extensively focuses on the elastic-plastic behavior in some uniaxial loading conditions, the multi-axial plasticity and fracture of pure lithium are rarely taken into consideration. Second, existing studies are mostly performed at the two ends of the length scale axes, either at the nano-scale where dendritic initiation and growth happen or at the bulk-scale where lithium foil is used as an electrode. There is a clear gap at the scale of one single grain or microstructural imperfection. This work aims at providing a systematic study of the multi-axial plasticity and microstructural evolution of pure lithium at the scale of 100  $\mu\text{m}$  to 1 mm under various stress states. To manufacture the required complex-shaped experimental specimens for five different stress states including uniaxial tension, notch tension with two different radii, central hole tension, and pure shear, a method that allows safe laser cutting of thick lithium foils in argon atmosphere is developed. The tests are conducted in pure argon as well as in air to quantify the oxidation behavior of lithium. Two active slip systems are observed during deformation and cross-slip is regularly present. Lithium fractures in an extremely ductile manner when the thickness is reduced to zero due to necking. Numerical simulations of the five loading conditions were performed using a multi-axial plasticity model recently developed by Narayan and Anand, which shed light on the full-field deformation and stress information of the samples for fracture examinations. Finally, the developed plasticity model is applied to a lithium-solid electrolyte interface model that couples contact condition, mechanical deformation, and electrochemistry to study the effect of external pressure on the cycling performance of lithium-metal all-solid-state batteries.

#### **1:10 PM F.EN03.03.06**

**Mechanical Properties of Alkali Metal Anodes** Coleman D. Fincher<sup>1,2</sup>, George Pharr<sup>1</sup> and Matt Pharr<sup>1</sup>; <sup>1</sup>Texas A&M University, United States; <sup>2</sup>Massachusetts Institute of Technology, United States

While room temperature metallic anodes possess the potential to enable batteries with enormous capacities, their mechanical behavior ultimately plays a key role in the failure modes for both liquid and solid electrolyte battery systems. That is, not only do alkali metal deposits threaten to deform and penetrate the battery separator in liquid electrolyte systems, but the degree of interfacial contact at the solid-state electrolyte/ anode interface possesses significant pressure dependence for solid-state systems. In this talk, we present a comprehensive multi-length scale assessment of the mechanical behavior of lithium, sodium, and potassium metal. Beyond the mechanical properties, we also discuss some practical implications of the anode's mechanical properties in battery systems.

### SESSION F.EN03.01: Electrode Engineering

On Demand Abstracts Available for Viewing Starting Saturday Morning, November 21, 2020

F-EN03

#### **5:00 AM \*F.EN03.01.01**

**The Importance of Nothing in Porous, 3D-Wired Metal Anodes** Debra R. Rolison, Brandon J. Hopkins, Christopher Chervin, Jeffrey Long and Joseph Parker; US Naval Research Laboratory, United States

Our team uses an architectural design metaphor to redesign materials and electrodes relevant to electrochemical energy science. Because batteries must balance multiple functions (molecular mass transport, ionic/electronic/thermal conductivity,

and electron-transfer kinetics), wiring these functions in three dimensions can move established battery chemistries in new directions. By designing metallic zinc into a sponge form-factor, with co-continuous void and solid, zinc-based alkaline batteries are now rechargeable at high rate and to deep utilization of zinc — without forming separator-piercing dendrites. We solved the historic lack of rechargeability of the zinc anode in alkaline electrolytes because the local current density throughout the sponge never broaches that necessary to launch dendritic growth. All thanks to an inner core of metallic zinc that electronically wires the  $4 \text{ m}^2 \text{ g}^{-1}$  of zinc surface area while the pore structure retains the zincate/ZnO discharge product nearby for recovery on the charge step. The nonperiodic, metallically interconnected “sponge” form factor distributes current more uniformly than ad hoc powder composites and ensures extensive charge-discharge cycling without deleterious dendrite formation.

#### 5:15 AM F.EN03.01.02

**Vertically Aligned Nanotube Arrays Featured with Confined Space and Uniform Curvature Enabling Dendrite Free Li Metal Batteries** Daxian Cao<sup>1</sup>, Karnpiwat Tantratian<sup>2</sup>, Lei Chen<sup>2</sup> and Hongli Zhu<sup>1</sup>; <sup>1</sup>Northeastern University, United States; <sup>2</sup>University of Michigan-Dearborn, United States

In past decade, because of ultrahigh capacity and lowest reduction potential, Lithium (Li) metal anode has regained great interest aiming to meet the urgent demand for high energy density rechargeable batteries. However, the dendritic growth of Li during cycling causes serious safety concerns and fast performance decay, which primarily restricts its application. Among various strategies about dendrite suppression, the design that introducing Li in a scaffold to fabricate a 3D Li structure is widely accepted. Therefore, the structural features of the scaffold dominate the behavior of Li metal anode. Herein, low-tortuosity, vertically aligned, and well-spaced TiO<sub>2</sub> nanotube arrays with ultrauniform curvature are selected as the host for Li metal anode, and the effect of the surface curvature and nanotube spacing on Li deposition are studied from experiment to theory. The Li metal behaves a unique electrodeposition manner that Li metal homogeneously deposits on the nanotubular wall, causing each Li nanotube to grow in circumference without obvious sign of dendritic formation. The uniform curvature of the anode structure, as well as the space confinement, are the keys to achieve highly stable, dendrite-free Li metal anodes. When this novel Li metal anode was coupled with LiFePO<sub>4</sub> cathode in a full cell, an excellent specific capacity of 132 mAh g<sup>-1</sup> and coulombic efficiency of ~99.85% over 400 cycles are achieved under a high charging rate at 1C. This work sheds light on the effect of structure feature on the stabilization of Li metal anode and takes an inspiring step toward reliable Li metal anode.

#### 5:25 AM F.EN03.01.03

**3D Nanoporous Graphene Based Metal Anodes for High-Energy-Density Rechargeable Metal Batteries** Gang Huang<sup>1</sup>, Jiuhi Han<sup>1</sup>, Isaac Johnson<sup>2</sup> and Mingwei Chen<sup>2,1</sup>; <sup>1</sup>Tohoku University, Japan; <sup>2</sup>Johns Hopkins University, United States

The key bottlenecks hindering the practical implementations of metal anodes in high-energy-density rechargeable batteries are the uncontrolled dendrite growth and infinite volume changes during charging and discharging, which lead to short lifespan and catastrophic safety hazard. In principle, these problems can be mitigated or even solved by loading active metals, such as Li, Na and Zn, into a high-surface-area, conductive and porous scaffold. However, a suitable material that can synchronously host a large loading amount of these active metals and endure large current density has not been achieved. Here we report a three-dimensional bicontinuous nanoporous graphene, prepared by nanoporous metal based CVD, as the sought-after scaffold material for metal anodes. The high surface area, large porosity and high conductivity of the nanoporous graphene concede not only dendrite-free stripping/plating but also abundant open space accommodating volume fluctuation of active metals. This ingenious scaffold endows the composite anodes with a long-term cycling stability and ultrahigh rate capability, significantly improving the charge storage performance of high-energy-density rechargeable metal batteries.

#### 5:35 AM F.EN03.01.04

**In Operando Study for Lithium Metal Deposition in Porous Carbon Scaffolds with Different Lithiophilicity** Juran Noh, Jian Tan, Digvijay R. Yadav, Peng Wu, Kelvin Xie and Choongho Yu; Texas A&M University, United States

Conventional graphite anodes for Li-ion batteries are the most demanding targets for further improvement in order to increase their energy densities. Lithium metal anodes have a much higher energy density but suffer from dendrite formation and volume expansion. To alleviate these problems, three-dimensional (3D) porous carbon scaffolds could be attractive alternatives if lithium metal is deposited in the inside of the porous structures. Nevertheless lithium insertion into porous structures have not been well understood because of difficulties in direct observation during the process. Here we present in-operando study coupled with simultaneously recorded voltage/current profiles for clarifying lithium insertion into porous carbon nanotube (CNT) structures depending on surface characteristics, lithiophobic, lithiophilic, and hybridized

lithiophobic/philic surface properties. It was found that lithiophobic graphitic surfaces interfered lithium insertion into the porous media despite the high conductivity along the CNT scaffold. Lithiophilic 3D scaffolds rendered lithium deposited on the outer mouth of the porous electrode, clogging pores and engendering dendrites. This can be attributed to preferential deposition of lithium on lithium metal due to sluggish charge transfer through insulating carboxyl functional groups on graphitic layers. On the other hand, when lithiophilic trenches were created on the lithiophobic graphitic wall of CNT, lithium was uniformly deposited on the surface and then filled up the pores, reaching a high areal capacity of 16 mAh cm<sup>-2</sup> even with a high current density of 8 mA cm<sup>-2</sup> without noticeable dendrite appearance and volume expansion. The functional group near the trench attracts lithium ions into trenches/pores while the preserved graphitic surface allows for charge transfer, giving rise to promising high energy density anode with lithium-impregnated scaffolds by both lithium intercalation and deposition.

#### 5:45 AM F.EN03.01.05

**Late News: Electronegativity-Guided Atomic Doping for Air-Stable and Dendrite-Free Li Metal Anode** Tao Xu and Yingwen Cheng; Northern Illinois University, United States

The diverse electronegativity among metals provides a rich toolkit to modulate the reactivity of metals via doping different metals while still keeping their metallic behavior for electrochemical purposes. Here we describe a general approach for modulating Li metal properties and enabling stable Li metal batteries by doping with ~0.1 at% Ag or Al. Unlike alloys, our dopant metal (Ag or Al) are atomically dispersed in Li via a non-equilibrium ultrasonication and quenching method during the synthesis and the atomic level dispersion of Ag is evidenced by synchrotron X-ray absorption method. The dopants were atomically dispersed in the vacant face-centered sites of the body-centered cubic Li crystals and pull electrons strongly due to higher electronegativity (Ag: 1.98; Al: 1.61 vs. Li: 0.98). As a result, the doped Li anodes have increased work function with reduced chemical reactivity and remained shiny in dry air for months. They also exhibited enhanced Li<sup>+</sup>/Li redox kinetics and generated thinner but stronger solid-electrolyte interphases in carbonate electrolytes. The dopant atoms are lithophilic and have stronger binding with Li adatoms, which guide uniform Li deposition and ensures dendrite-free Li interface during battery cycling. Overall, the doped anodes enabled stable operations of not only high current symmetric cells but also practical full cells in which Ni-rich layered cathodes were paired with 30 mm anodes and 7 mL electrolytes. The doping approach is facile and scalable, and opens up new and promising opportunities for designing practical high energy density metal batteries.

#### SESSION F.EN03.02: Interface Engineering

On Demand Abstracts Available for Viewing Starting Saturday Morning, November 21, 2020  
F-EN03

#### 5:00 AM F.EN03.02.01

**Lithium Deposition Underneath Interfacial Coating Layers** Grace Whang<sup>1</sup>, Qizhang Yan<sup>2</sup>, Jian Luo<sup>2</sup> and Bruce S. Dunn<sup>1</sup>; <sup>1</sup>University of California, Los Angeles, United States; <sup>2</sup>University of California, San Diego, United States

The formation of lithium dendrites has long stood in the way of accessing lithium's unmatched combination of low reduction potential and high specific capacity for next generation lithium ion batteries. While there has been a body of research directed towards the use of interfacial coatings to improve upon lithium deposition morphologies, one interesting and often overlooked approach to circumvent dendritic growth is the possibility of plating lithium underneath the coating layers. The mechanism of lithium plating underneath offers a refreshing perspective on reframing the question of how to best suppress dendrites and furthermore presents a direction that could greatly benefit from more fundamental understanding.

In this study, we report on a novel mechanism that leads to plating of lithium underneath a coating layer. A lithium-tin system was chosen as a model coating system due to its ability to form lithium-rich intermetallic which exhibit high Li diffusivity and plays a critical role when considering lithium transport across microns length scale. To assess the role of the Lithium-Tin coating on the kinetics of the lithium electrode, Galvanostatic Linear Polarization (GLP) was used to extrapolate the exchange current density using a linear approximation of the Butler-Volmer equation. For the lithium electrode with a Li-Sn coating, the exchange current density of  $0.522 \pm 0.011$  mA cm<sup>-2</sup> was twice as large as that of a bare lithium control indicating that charge transfer kinetics for plating on the lithium tin coated electrodes are more favorable relative to bare lithium. This relationship can also be seen in the large differences in charge transfer resistance observed in impedance

measurements.

To study how the enhanced kinetics of the coating layer influences lithium plating, Li-Sn coated and bare lithium electrodes were plated at various current densities for a substantial plating capacity of  $4\text{mAh cm}^{-2}$  corresponding to  $\sim 20\ \mu\text{m}$  of lithium assuming uniform deposition. Unlike bare lithium which always plates on the lithium surface, lithium-tin composite coatings can lead to lithium plating underneath the Li-Sn layer given that there is favorable Li transport kinetics across it. From our studies, there exists a current density ‘transition point’ from which plating occurs below the surface of the coating layer. By combining planar SEM of the surface and cross section of the electrode using Cryo-FIB SEM, we show that current densities below the exchange current density lead to lithium deposition underneath the Li-Sn surface with no evidence of lithium deposits on the surface of the coating. The extension of this model to other systems is presented.

#### 5:10 AM F.EN03.02.02

##### **"Mirror-Like" Electrodeposition of Lithium Metal Under a Low-Resistance Artificial Solid Electrolyte Interphase Layer** Fei Hu, Zhuo Li, Shaofei Wang and Wyatt Tenhaeff; University of Rochester, United States

Lithium metal is one of the most promising anode materials for energy dense electrochemical energy storage. However, non-uniform electrodeposition and dendritic growth of Li metal result in low Coulombic efficiency and potential short circuits, which are critical challenges that impede development of practical Li metal batteries. To suppress dendrite growth of Li metal, one strategy is to encapsulate the Li metal with an artificial solid-electrolyte interface (ASEI) layer. The ideal ASEI layer should possess high mechanical strength to prevent the intrusion of Li dendrite, high Li transference number, low bulk/interfacial resistance, and high ionic yet negligible electronic conductivity. Moreover, recent studies show that the morphology of the ASEI layer is critical and that a smooth homogeneous surface is beneficial. A thin film solid electrolyte, lithium phosphorous oxynitride (LiPON), satisfies these requirements. It has a relatively high shear modulus of 7.7 GPa, unity  $\text{Li}^+$  transference number, wide electrochemical stability window (0 - 5.5V vs.  $\text{Li}/\text{Li}^+$ ), ionic conductivity of  $\sim 2 \times 10^{-6}\ \text{S cm}^{-1}$ , electronic conductivity of  $\sim 8 \times 10^{-13}\ \text{S cm}^{-1}$ , and can be fabricated as a smooth isotropic, homogeneous thin film via physical vapor deposition. However, it remains a challenge to observe uniform, mirror-like electrodeposition of Li metal under the sole protection of LiPON layers.

Herein we report a multifunctional ASEI design that combines the benefits of a LiPON coating with the enhanced Li morphology conferred by  $\text{Li}_x\text{Au}$  alloys. The 100 nm-thick Au interlayer alloy with Li into a solid buffer layer, which reduces the nucleation energy for Li electrodeposition, resulting in improved Li deposition uniformity. The LiPON layer prevents reactions between the deposited Li and liquid electrolyte. The integrity of the LiPON protective layer was assessed using *in operando* impedance spectroscopy and *ex situ* SEM and EDS measurements. At a current density of  $0.1\ \text{mA cm}^{-2}$ , it was shown that the LiPON layer remained intact for Li capacities of at least  $3\ \text{mAh cm}^{-2}$ . The deposited Li was confined under the LiPON layer creating a smooth, uniform interface, resulting in a shiny Li surface that was “mirror-like.” It was shown that the Au layer is essential to achieving this morphology; discrete, heterogeneous Li deposits were observed using Cu current collectors. At higher current densities (up to  $1\ \text{mA cm}^{-2}$ ) and capacities ( $6\ \text{mAh cm}^{-2}$ ), the LiPON protective coating fractured and nonuniform Li morphologies were observed. Efforts to further optimize this multifunctional ASEI design and engineering application towards long-cycling Li metal batteries will be discussed in the future.

#### 5:20 AM F.EN03.02.03

##### **Inter-Layer-Calated Thin Li Metal Electrode with Improved Battery Capacity Retention and Dendrite Suppression** Junjie Niu; University of Wisconsin-Milwaukee, United States

A light-weighting, stable Li metal is critical to high energy-density lithium ion batteries (LIBs). In this presentation, we introduce an inter-layer-calated thin Li metal (ILC-Li) electrode using non-delaminated 2D  $\text{Ti}_3\text{C}_2\text{T}_x$  MXene stacks coated on an ultra-thin Li host (*Nano Lett.* **2020**, *20*, 2639–2646). The excellent electrical conductivity (higher than graphite) and expanded inter-layer space of about 1.34 nm of the MXene provide a fast  $\text{e}^-/\text{Li}^+$  transport to allow Li homogeneous deposition while the layer limits the Li growth along perpendicular direction, thus largely mitigating the dendrite growth. Also, the large surface area of the multi-layer MXene stacks with high mechanical flexibility ensures a high Li capacity and reliable Li nucleation/growth upon plating/stripping. The highly reversible Li deposition/extraction through the confined 2D configuration greatly reduces the dead lithium and electrolyte consumption by forming a thin solid-electrolyte-interphase (SEI) layer. As the result, a small overpotential of less than 135 mV in symmetric cells was achieved after >1050 cycles (>2100 hours) with a very high current density of  $10\ \text{mA cm}^{-2}$  and an areal capacity of  $10\ \text{mAh cm}^{-2}$  while the cell with Li foil showed a larger potential over 400 mV in only 50 cycles with a low current density of  $3\ \text{mA cm}^{-2}$ . In a full cell paired with nickel-manganese-cobalt oxide (NMC) or nickel-cobalt-aluminum oxide (NCA) as cathode, the battery with ILC-Li electrode exhibited a clearly improved capacity retention when compared with Li foil, particularly with lean electrolyte

conditions of as low as 2.5  $\mu\text{l mAh}^{-1}$ . The less inorganic-rich SEI layer shown by X-ray photoelectron spectroscopy depth profiling indicates a reduced electrolyte consumption, thus leading to a high energy density up to 366.6 Wh/Kg. In contrast to other coating technologies, the current approach is manufacture scalable by using large sizes of MXene stacks via a facile process, which displays a promising potential in higher energy-density LIBs.

### 5:30 AM F.EN03.02.05

**A Dynamic, Electrolyte-Blocking and Single-Ion-Conductive Network as an Artificial Solid Electrolyte Interphase for Lithium Metal Anode** Zhiao Yu<sup>1</sup>, David Mackanic<sup>1</sup>, Yi Cui<sup>1,2</sup> and Zhenan Bao<sup>1</sup>; <sup>1</sup>Stanford University, United States; <sup>2</sup>SLAC National Accelerator Laboratory, United States

Lithium (Li) metal is an ideal candidate as the anode of Li batteries due to its potential to provide high specific energy. However, Li metal anode is challenging to implement due to several drawbacks. First, Li easily reacts with electrolytes to form a solid electrolyte interface (SEI). The heterogeneous nature of SEI results in local fluctuation of  $\text{Li}^+$  flux and current density, which lead to the formation of dendrites. Second, large volume change during Li stripping/plating creates cracks in the brittle SEI, forms dead Li, and causes further electrolyte consumption. These effects lower the Coulombic efficiency (CE) and devastate the cycle life of Li metal anodes. In order to mitigate the abovementioned degradation pathways, strategies pursued include modifying electrolyte components, utilizing solid electrolytes, employing a shielding cation layer, or chemically pretreating Li metal. Nevertheless, it remains challenging to achieve a stable SEI on Li metal; and therefore, the artificial SEI attracts more attention as an alternative strategy to replace the native SEI on Li.

An ideal artificial SEI must have several key properties. First, previous work proposed benefits of having high modulus coatings on Li; however, our recent work suggested flowability and dynamic property allow SEI to adapt to large volume change during Li stripping/deposition, and result in uniform Li deposition macroscopically. Second, uniform and fast  $\text{Li}^+$  single-ion conduction in the artificial SEI is found to be beneficial to reduce “hot spots”, increase critical Li deposit size, and stabilize the Li metal anode. Finally, the SEI needs to be both chemically and electrochemically inert itself and mitigate electrolyte penetration to minimize deleterious Li-coating and Li-electrolyte side reactions. Nevertheless, few artificial SEIs possess all the desirable properties such as dynamic adaptivity, high ion conductivity, and chemical passivation. Additionally, the majority of the reported Li-metal artificial SEIs are only compatible with ether-based electrolytes, making them incompatible with high-voltage, high-energy-density lithium nickel manganese cobalt oxide (NMC) cathodes that are used in today’s commercial Li-ion batteries.

Herein, we propose an artificial SEI design based on a dynamic polymeric network with high  $\text{Li}^+$  single-ion conductivity. In this network, tetrahedral  $\text{Al}(\text{OR})_4^-$  (R = soft organic linker) anions are used for the first time as a dynamic motif while providing counter anions for  $\text{Li}^+$ . With this dynamic single-ion-conductive network (DSN) as an artificial SEI, we demonstrate over 400 stable plating/stripping cycles in  $\text{Li}|\text{Cu}$  cell using commercial carbonate-based electrolyte. Greater than 85% capacity retention for over 160 cycles in a  $\text{Li}|\text{NMC}$  full battery was achieved using directly coated Li foils and commercial, high active material proportion NMC cathode sheets. This work demonstrates for the first time the promise of dynamic single-ion conductor as a stable and scalable artificial SEI for practical Li metal batteries.

### SESSION F.EN03.03: Mechanics

On Demand Abstracts Available for Viewing Starting Saturday Morning, November 21, 2020

F-EN03

### 5:00 AM \*F.EN03.03.01

**From Ion-to-Atom-to-Dendrite—Formation and Nanomechanical Behavior of Electrodeposited Lithium** Julia R. Greer<sup>1</sup>, Michael A. Citrin<sup>1</sup>, Heng Yang<sup>1</sup>, Simon Nieh<sup>2</sup>, Joel M. Berry<sup>3</sup> and David J. Srolovitz<sup>4</sup>; <sup>1</sup>California Institute of Technology, United States; <sup>2</sup>Front Edge Technology, United States; <sup>3</sup>Lawrence Livermore National Laboratory, United States; <sup>4</sup>City University of Hong Kong, Hong Kong

Lithium is an ideal battery anode, with theoretical specific capacity of 3860 mAh/g; replacing conventional graphitic anodes with Li in Li-ion batteries can increase energy density by ~50%. A significant drawback of Li anodes is dendrite formation during cycling, which can lead to short circuiting (a safety hazard and cell death) and to “dead Li,” which drastically reduces cycle life.

A complete dearth of experiments that probe mechanical behavior of electrodeposited Li exists. Most experiments on

mechanical properties have focused on thin films and on Focused Ion Beam-carved Li. We developed *in-situ* experimental methodology that allows to electrochemically charge small-scale battery cells and to observe, in real-time, the formation of Li dendrites and to probe their mechanical response. Experiments reveal: (1) Li nano-deposits are single crystalline and (2) strengths of Li nano-pillars are  $16.0 \pm 6.82$  MPa, which is 24x greater than bulk. This strength enhancement can be explained in terms of the ubiquitous “smaller is stronger size effect” nano-sized single crystalline metals. This work expands the existing strength vs. size property space for Li and helps explain why dendrites can penetrate through much stiffer and harder ceramic solid electrolytes, theorized for several years but never unambiguously demonstrated. Development of high energy density solid-state batteries with Li metal anodes has been limited by uncontrollable growth of Li dendrites in liquid and solid electrolytes. This, in part, may be caused by a dearth of information about mechanical properties of Li, especially at the nano- and micro-length scales and microstructures relevant to Li batteries. We investigate formation, microstructure, and mechanical properties of nano-sized Li electrodeposited in a commercial LiCoO<sub>2</sub>/LiPON/Cu solid-state thin film cell, grown *in-situ* in a scanning electron microscope (SEM) equipped with nanomechanical capabilities. Experiments reveal that Li was preferentially deposited at the LiPON/Cu interface, along the valleys that mimic the domain boundaries of underlying LiCoO<sub>2</sub>. This pattern of Li formation is consistent with the higher driving force for Li nucleation at the valleys uncovered by electrochemical simulations of Li ion transport in this system. Further charging of the cell resulted in Li nuclei piercing through the 30 nm-thick Cu layer and growing into vacuum through the crack openings. Cryogenic electron microscopy analysis of electrodeposited Li revealed its single crystalline microstructure, and *in-situ* nano-compression experiments on individual Li nano-pillars with diameters of 360-759 nm revealed their average Young’s modulus to be  $6.76 \pm 2.88$  GPa and an average yield stress of  $16.0 \pm 6.82$  MPa, ~24x higher than what has been reported for bulk polycrystalline Li. We discuss mechanical deformation mechanisms and strength of nano-sized electrodeposited Li in the framework of its microstructure and dislocation-governed nano-scale plasticity of crystals and place it in the parameter space of existing knowledge on small-scale Li mechanics. The enhanced strength of Li at small scales may help explain why Li can penetrate through and fracture much stiffer and harder ceramic solid electrolytes.

5:15 AM \*F.EN03.03.02

**On the Mechanisms of Stress Relaxation and Intensification at the Lithium/Solid-State Electrolyte Interface** [Erik G. Herbert](#)<sup>1</sup>, Nancy Dudney<sup>2</sup>, Maria Rochow<sup>1</sup>, Violet Thole<sup>1</sup> and Stephen Hackney<sup>1</sup>; <sup>1</sup>Michigan Technological University, United States; <sup>2</sup>Oak Ridge National Laboratory, United States

Under electrochemical cycling, stress intensification and relaxation within small, confined volumes at the Li/solid-state electrolyte (SSE) interface are thought to be critical factors contributing to mechanical failure of the SSE and subsequent short-circuiting of the device. Nanoindentation has been used to examine the diffusion limited pressure Li can support in the absence of active dislocation sources at high homologous temperatures. Based on the underlying physics of this deformation mechanism, a simple perturbation model coupling local current density, elastic stress and diffusional creep relaxation is introduced. Combining this analysis with the indentation results, it is possible to describe a ‘defect danger zone,’ a length scale which is too large for effective diffusional creep relaxation, but too small for efficient dislocation multiplication. In this instance, the properties of the SSE become critical in controlling localized pressure at the interface.

In contrast to the ‘first generation,’ pioneering analysis of the Li/electrolyte interface by Monroe and Newman, more recent analyses of the Li/SSE interface mechanics examine a similar but uniquely different problem in that they consider non-uniform electrochemical properties and/or filling of morphological defects at the interface during Li charging such that the initial amplitude of the Li protrusion is fixed by a pre-existing interface defect or undulation. Meaningful comparisons between multiple ‘second-generation’ approaches can be challenging. Although they generally address the same problem, assumptions about the interface defect geometry and the self-limiting mechanical and electrochemical behavior of Li place significant limitations on the conclusions and the general applicability of the proposed solution. Despite their differences, the second-generation approaches arrive at generally the same conclusion: Within confined or localized volumes of Li at the interface, Li can support pressures significantly higher than its bulk yield strength (stresses as high as 200 MPa). Such stress concentrations at the interface are of critical concern because they facilitate mechanical failure of the SSE by fracture. The key question then becomes, why is the stress concentration so large relative to the bulk yield strength of Li? Two potential explanations are offered by the second-generation approaches: geometry effects and length scale effects. These effects are not unique to Li. Any metallic anode will experience these effects in a manner that depends on its absolute melting temperature, elastic modulus, yield strength, and self-diffusion coefficient.

Although the length scale effects of high purity Li have only been recently documented, the basic concept of “smaller is stronger” is well documented. As described by Brenner in 1956 and later quantified by Phani et al. in 2013, the yield strength of a metal in small volumes can be described from a purely statistical point of view, as the stress required to plastically flow depends on the probability of finding the necessary dislocations within the stressed volume. Load-displacement data from



nanoindentation experiments performed in high purity Li at a homologous temperature of 0.67 graphically illustrate this concept. Similar results obtained in high purity indium, a mechanical surrogate to Li, further illustrate the competition for stress relief. Collectively, an important outcome from these 'second generation' approaches is that SSEs with nominally uniform electrochemical properties and flat, smooth surfaces will promote planar, nominally stress-free plating and stripping of Li. Unfortunately, brittle SSE materials will likely experience the same statistical failure issues as structural ceramics. The most robust devices will also implement SSEs that are engineered to provide localized stress relief, potentially through mechanisms such as densification, shear banding and time dependent recovery.

### 5:30 AM F.EN03.03.03

**A New Paradigm for Preventing Lithium Dendrite Penetration Through Solid Electrolytes** Yue Qi<sup>1</sup>, Chunmei Ban<sup>2</sup> and Stephen J. Harris<sup>3</sup>; <sup>1</sup>Michigan State University, United States; <sup>2</sup>University of Colorado Boulder, United States; <sup>3</sup>Lawrence Berkeley National Laboratory, United States

We introduce a new concept to suppress penetration of lithium dendrites through solid electrolytes (SE) by putting the surface of the SE into a state of compressive stress. For a sufficiently high residual compressive stress, cracks have difficulty forming at the surface, and cracks that do form tend to close, inhibiting dendrite penetration. Introduction of compressive surface residual stress solves stress corrosion cracking problems in metals and static fatigue problems in ceramics and glasses. An example of the latter is Gorilla Glass, which is strongly resistant to cracking because of surface compressive stresses. However, the technique will not work if Li ion transport through a SE in compression is substantially reduced. Our DFT and MD calculations for LLZO indicate that the introduction of even high residual compressive stresses (up to 10 GPa) will have only a very modest effect on Li ion transport kinetics, suggesting that the approach is viable. In addition to inhibiting penetration and fracture in solid electrolytes, compressive stresses on the order of GPa will tend to suppress lithium plating inside of solid electrolytes because of an increased overpotential for the Li ion reduction reaction. We discuss and compare several experimental methods for introducing compressive residual stresses at the surfaces of solid electrolytes. We believe that the information here can provide a new avenue for developing high-performance and stable solid electrolytes

### 5:40 AM F.EN03.03.04

**In Situ Investigations of Stress Evolution During Plating and Stripping of Lithium Metal** Jung Hwi Cho<sup>1</sup>, Xingcheng Xiao<sup>2</sup>, Kai Guo<sup>3</sup>, Yuanpeng Liu<sup>4</sup>, Huajian Gao<sup>5</sup> and Brian Sheldon<sup>1</sup>; <sup>1</sup>Brown University, United States; <sup>2</sup>General Motors, United States; <sup>3</sup>Massachusetts Institute of Technology, United States; <sup>4</sup>Harbin Institute of Technology, China; <sup>5</sup>Nanyang Technological University, Singapore

Poor stability of Li metal / liquid electrolyte or Li metal / solid electrolyte interfaces leads to chronic problems, such as dendrite formation and capacity loss. The impact of electro-chemo mechanical phenomena on interface stability and dendrite formation are believed to be critical, but are challenging to investigate directly. In-situ curvature measurements are an important tool that can be used to monitor these stresses during battery cycling. Using this technique during Li plating and examining film thickness effects, it is possible to separate contributions from the bulk lithium metal and the solid electrolyte interphase (SEI). These investigations show that the stresses created in the SEI films are much larger than those in the Li metal. Furthermore, these stresses in the SEI can destabilize the electrode / electrolyte interface.

Recently, a variety of methods have been employed to improve the performance and safety of Li metal based batteries by using various artificial SEI layers and/or implementing solid electrolytes. Several of these approaches were also investigated with stress evolution measurements during lithium plating and stripping. This work includes the use of both soft (PEO) and hard (LiF) artificial surface layers. These results indicate that stresses in both the surface film and the bulk lithium evolve differently when artificial SEI layers are employed. Initial attempts to monitor stress evolution with oxide solid electrolytes will also be presented.

### 5:50 AM F.EN03.03.05

**Plastic Deformation and Microstructural Evolution of Pure Lithium Under Various Stress States** Juner Zhu<sup>1,1</sup>, Tobias Sedlatschek<sup>1</sup>, Junhe Lian<sup>1,2</sup>, Wei Li<sup>1</sup>, Tomasz Wierzbicki<sup>1</sup> and Martin Bazant<sup>1</sup>; <sup>1</sup>Massachusetts Institute of Technology, United States; <sup>2</sup>Aalto University, Finland

Pure lithium in lithium metal batteries is often examined in research projects aiming at improving today's battery technology significantly. But the knowledge about the mechanical properties and the microstructural evolution of pure lithium is incomplete with two particular limitations. First, the available data extensively focuses on the elastic-plastic behavior in some uniaxial loading conditions, the multi-axial plasticity and fracture of pure lithium are rarely taken into consideration. Second, existing studies are mostly performed at the two ends of the length scale axes, either at the nano-scale where dendritic initiation and growth happen or at the bulk-scale where lithium foil is used as an electrode. There is a clear gap at the scale of

one single grain or microstructural imperfection. This work aims at providing a systematic study of the multi-axial plasticity and microstructural evolution of pure lithium at the scale of 100  $\mu\text{m}$  to 1 mm under various stress states. To manufacture the required complex-shaped experimental specimens for five different stress states including uniaxial tension, notch tension with two different radii, central hole tension, and pure shear, a method that allows safe laser cutting of thick lithium foils in argon atmosphere is developed. The tests are conducted in pure argon as well as in air to quantify the oxidation behavior of lithium. Two active slip systems are observed during deformation and cross-slip is regularly present. Lithium fractures in an extremely ductile manner when the thickness is reduced to zero due to necking. Numerical simulations of the five loading conditions were performed using a multi-axial plasticity model recently developed by Narayan and Anand, which shed light on the full-field deformation and stress information of the samples for fracture examinations. Finally, the developed plasticity model is applied to a lithium-solid electrolyte interface model that couples contact condition, mechanical deformation, and electrochemistry to study the effect of external pressure on the cycling performance of lithium-metal all-solid-state batteries.

#### 6:00 AM F.EN03.03.06

**Mechanical Properties of Alkali Metal Anodes** Coleman D. Fincher<sup>1,2</sup>, George Pharr<sup>1</sup> and Matt Pharr<sup>1</sup>; <sup>1</sup>Texas A&M University, United States; <sup>2</sup>Massachusetts Institute of Technology, United States

While room temperature metallic anodes possess the potential to enable batteries with enormous capacities, their mechanical behavior ultimately plays a key role in the failure modes for both liquid and solid electrolyte battery systems. That is, not only do alkali metal deposits threaten to deform and penetrate the battery separator in liquid electrolyte systems, but the degree of interfacial contact at the solid-state electrolyte/ anode interface possesses significant pressure dependence for solid-state systems. In this talk, we present a comprehensive multi-length scale assessment of the mechanical behavior of lithium, sodium, and potassium metal. Beyond the mechanical properties, we also discuss some practical implications of the anode's mechanical properties in battery systems.

#### SESSION F.EN03.04: Metal Plating and Stripping

On Demand Abstracts Available for Viewing Starting Saturday Morning, November 21, 2020  
F-EN03

#### 5:00 AM \*F.EN03.04.01

**Chances and Challenges in Zinc Electrode Rechargeability** Hajime Arai and Atsunori Ikezawa; Tokyo Institute of Technology, Japan

Zinc is abundant, widely used as structural materials, non-toxic, safe and inexpensive. It has the most negative potential among metals that can be recharged in aqueous electrolyte solutions and high capacity density, and hence is an attractive candidate as a negative electrode material. In alkaline media, the thermodynamically stable discharge product is ZnO, a semiconductor (not insulator), and there is acceptable volume expansion upon its formation (ca. +60%). When anion conductors such as alkaline solutions are used as the electrolyte, as is often the case, the formation of ZnO is at the negative electrode side, which causes tolerable volume changes of the negative electrode when compared to the total metal dissolution and/or deposition at the positive electrode side. The corresponding positive electrode materials can be proton-acceptor types such as NiOOH and oxygen in aqueous alkaline electrolytes. Recent trials include zinc ion acceptors such as organic metal frameworks with zinc ion conductive ionic liquid electrolyte. This presentation mainly focuses on alkaline-based aqueous systems.

The main drawback of the zinc electrode is its insufficient durability, suffered from the morphology changes such as dendrite growth, shape change and densification. This is mostly caused by the formation of highly soluble species  $\text{Zn}(\text{OH})_4^{2-}$ , a kinetically favorable discharge product, that diffuses away from the original positions and precipitates wherever it favors. Even if zinc oxide is saturated in the alkaline electrolyte, zinc supersaturation occurs; it stays longer than the time scale of the charge-discharge reactions, even for months. There are several ways to restrict the zinc dissolution, such as complex formation (e.g. calcium zincate [1]), protective film formation (e.g. anion exchange membrane [2]) and the use of electrolyte additives (e.g. pH controller, indifferent salts and organic solvents [3-4]). Though the durability depends on the utilization rates and loaded mass ( $\text{mAh}/\text{cm}^2$ ), cycle life of more than several hundred cycles be achieved in ideal cases. Mechanical pressure on the electrode (e.g. separator wrapping) is a simple but effective way in restraining the morphology changes. In contrast to electrical charging, mechanical charging is a unique method for air battery systems, mostly for electric vehicles, where soluble zinc species are removed from the cell and regenerated by off-site processes [5].

Passivation during high rate discharging is also problematic, but can be mitigated by constructing composite electrodes with

high surface areas. Hydrogen evolution as the self-discharge can be restricted by adding inhibitors such as indium and bismuth.

Analytical methods to clarify the zinc electrode reaction processes are of particular interest, since degradation proceeds with nearly no sign in the electrochemical responses. Since zinc is oxidized in air, in situ (in-cells) or operando (in-current-flow) analyses are favorable. *Operando* X-ray diffraction (XRD) is helpful in detecting the formation of crystalline ZnO during discharging [6]. XRD mapping analysis indicates how the shape change proceeds [7]. *Operando* X-ray fluorescence imaging, utilizing the zinc visibility in hard X-ray absorption, is effective in observing zinc behavior with space resolutions [8]. Optical analysis is promising to observe macroscopic changes of the zinc species that significantly affects the electrode durability [9].

- [1] R. Jain, et al. *J. Appl. Electrochem.*, **22**, 1039 (1992).
- [2] K. Miyazaki et al., *Electrochemistry*, **80**, 725 (2012).
- [3] A. Nakata et al., *J. Electrochem. Soc.*, **163**, A50-A56 (2016).
- [4] T. Takeya et al., *J. Power Sources*, **407**, 180 (2018).
- [5] J. Goldstein et al., *J. Power Sources*, **80**, 171 (1999).
- [6] A. Nakata et al., *Electrochim. Acta*, **166**, 82 (2015).
- [7] A. Nakata et al., *APL Materials*, **6**, 047703 (2018).
- [8] A. Nakata et al., *Electrochemistry*, **83**, 849 (2015).
- [9] M. Horiuchi et al., *Abs. Batt. Symp. Japan*, 1E27 (2019).

#### 5:15 AM \*F.EN03.04.02

##### **Morphological Evolution of Li Metal Anode in Lithium Metal Batteries—Studied by Synchrotron X-Ray Tomography** Fu Sun; Qingdao Institute of Bioenergy and Bioprocess Technology Chinese Academy of Sciences, China

The electrochemical performance and serviceable life-span of lithium metal batteries (LMBs) are largely governed by the Li metal anode. Particularly, low Columbic efficiency, inferior cycling stability, short life time and potential safety concerns of LMBs are acknowledged to be closely linked to the employed Li anode. As a result, tremendous efforts have been devoted to enhance the electrochemical cycling ability of Li anode and the performance of LMBs have been significantly improved during the last decade. Nevertheless, breakthroughs in propelling the LMB technology from laboratory research to practical commercialization are still missing, which can be mostly attributed to the incomplete understanding of the underlying working/decaying mechanisms of Li anode. To fill in this knowledge gap, a variety of probing techniques, e.g., (Cryo-) TEM, SEM, XPS, NMR, FTIR have been employed to study the underlying working/decaying mechanisms of Li anode during electrochemical cycling, yielding significant amount of valuable insights. Unfortunately, linking these novel insights of the Li anode to the LMB's performance is still challenging, hence, a comprehensive and in-depth understanding of the correlation between the Li anode and the overall LMB performance remains elusive.

In the current talk, the studies of the morphological evolution of Li anode and its correlation to the LMB's performance studied by Synchrotron X-ray tomography will be shown. *In operando* monitoring of the Li-Li symmetrical cells reveals the morphological evolution mechanism of the electrochemically generated/dissolved Li, as well as the underlying internal short circuits. In addition, the effect of the electrochemically generated Li on different types of separators has been also disclosed and it was found that both the mechanical and physical properties of the separator play an important role during Li electrodeposition. Moreover, the close correlation between the morphological evolution of Li anode and the LMB's electrochemical performance has been established: it was found that the irreversible transformation from original Li bulk to the electrochemically inactive Li electrodeposits results in the observed performance decay. It is hoped that these discoveries could open up new design principles and opportunities to accelerate the practical applications of LMBs.

#### 5:30 AM \*F.EN03.04.03

##### **Lithium Metal Anodes—The Dynamic Evolution of Electrochemical, Morphological and Mechanical Phenomena** Neil P. Dasgupta; University of Michigan, United States

Lithium (Li) metal anodes have experienced a resurgence of research in recent years, which has been fueled by advances in electrolyte chemistry (both solid and liquid), interfacial engineering, and rational design of electrode architectures<sup>1,2</sup>. This has enabled Coulombic efficiency values to push above 99.5%, and cycle life to extend into relevant ranges for transportation applications<sup>3</sup>. However, while performance metrics are beginning to approach relevant values for consideration of their use in electric vehicles, several fundamental questions remain on how Li metal anodes dynamically evolve during cycling, especially at high current densities. Towards this goal, there is a continued need for new methods to quantitatively measure the evolving morphology, mechanical response, and electrochemical overpotentials of Li metal anodes under realistic

conditions.

In this talk, I will discuss recent insights that have been gained on how morphological evolution of non-planar geometries couple with mechanical stresses, both during both electrodeposition and dissolution<sup>4</sup>. To contextualize the critical role of coupled electro-chemo-mechanical phenomena, examples of dynamic Li metal deformation will be discussed during cycling in solid and liquid electrolytes. Specifically, a multi-modal suite of *operando* analytical techniques will be employed to describe the role of mechanical stresses during the formation of “dead” Li, crack propagation in ceramic solid electrolytes during high-rate cycling, and reversible cycling of Li metal to achieve high Coulombic efficiencies<sup>5-8</sup>.

To compliment the cross-sectional perspective provided in our previous *operando* optical microscopy investigations, recent cell designs that enable plan-view *operando* of Li metal dynamics will be demonstrated for both liquid and solid electrolyte systems. In liquid electrolytes this allows for new insight into the influence of surface microstructure on nucleation of both dendrites and pits, and the critical role of surface heterogeneity on Coulombic efficiency<sup>9</sup>. In solid electrolytes, plan-view imaging enables direct visualization of Li metal filament propagation in garnet LLZO ceramics, and four distinct filament morphologies are identified<sup>10</sup>. Equipped with this fundamental understanding, the talk will aim to address the following critical question in the field: *how, when, where, and why* does “dead” Li form, and can we control this irreversible Li loss during battery operation?

## References

- (1) Wood, K. N.; Noked, M.; Dasgupta, N. P. *ACS Energy Lett.* **2017**, *2* (3), 664–672.
- (2) Hatzell, K. B. et al. *ACS Energy Letters.* **2020**, *5*, 922–934.
- (3) Chen, K.-H.; Sanchez, A. J.; Kazyak, E.; Davis, A. L.; Dasgupta, N. P. *Adv. Energy Mater.* **2019**, *9* (4), 1802534.
- (4) LePage, W. S.; Chen, Y.; Kazyak, E.; Chen, K.-H.; Sanchez, A. J.; Poli, A.; Arruda, E. M.; Thouless, M. D.; Dasgupta, N. P. *J. Electrochem. Soc.* **2019**, *166* (2), A89–A97.
- (5) Wood, K. N.; Kazyak, E.; Chadwick, A. F.; Chen, K.-H.; Zhang, J.-G.; Thornton, K.; Dasgupta, N. P. *ACS Cent. Sci.* **2016**, *2* (11).
- (6) Chen, K.-H.; Wood, K. N.; Kazyak, E.; LePage, W. S.; Davis, A. L.; Sanchez, A. J.; Dasgupta, N. P. *J. Mater. Chem. A* **2017**, *5* (23), 11671–11681.
- (7) Gupta, A.; Kazyak, E.; Craig, N.; Christensen, J.; Dasgupta, N. P.; Sakamoto, J. *J. Electrochem. Soc.* **2018**, *165* (11), A2801–A2806.
- (8) Davis, A. L.; Kazyak, E.; Sakamoto, J.; Dasgupta, N. P.; Garcia-Mendez, R.; Chen, K. H.; Sakamoto, J.; Wood, K. N.; Teeter, G.; Wood, K. N. *J. Mater. Chem. A* **2020**, *8* (13), 6291–6302.
- (9) Sanchez, A. J.; Kazyak, E.; Chen, Y.; Chen, K. H.; Pattison, E. R.; Dasgupta, N. P. *ACS Energy Lett.* **2020**, *5* (3), 994–1004.
- (10) Kazyak, E.; Garcia-Mendez, R.; LePage, W. S.; Sharafi, A.; Davis, A. L.; Sanchez, A. J.; Chen, K. H.; Haslam, C.; Sakamoto, J.; Dasgupta, N. P. *Matter* **2020**, *2* (4), 1025–1048.

## 5:45 AM F.EN03.04.04

**Characteristic Electrochemical Features of Interfaces on Calcium Foils** [Aaron M. Melemed](#) and Betar Gallant; Massachusetts Institute of Technology, United States

Batteries based on calcium (Ca) metal anodes offer a possibility of improved sustainability and safety with attractive electrochemical metrics. However, Ca battery development is still in its infancy due to basic chemical limitations. When Ca metal comes in contact with an organic electrolyte, a native solid electrolyte interphase (SEI) forms which passivates, and in some instances fully deactivates, the electrode surface. Considering that Ca deposition and dissolution is widely believed to be a surface-film-controlled process, understanding Ca<sup>2+</sup> transport through this native SEI is paramount. In this talk, characteristic features occurring in cyclic voltammetry (CV) with Ca foils will be discussed as a function of interface composition in a benchmark electrolyte system, Ca(BH<sub>4</sub>)<sub>2</sub> in tetrahydrofuran (THF). This electrolyte was found recently by others to support reversible plating/stripping under continuous CV conditions (at 25 mV/s) on planar metal (Au or Pt) working electrodes. As opposed to plating/stripping onto a gold substrate, the first CV cycle on Ca foil reveals a persistent native passivation layer — reflective of the foil preparation process — which manifests as significant reduction and oxidation overpotentials. This native interface can be degraded through the initial electrochemical steps, by processes that depend on whether plating or stripping is first conducted, along with the associated electrochemical protocol. The effect of this first activation step on the resulting electrochemistry will be discussed. Subsequently, the interface evolves to reflect one predominantly governed by CaH<sub>2</sub>, which enables further study of the dynamics of this interface under different cycling conditions (scan rate and the imposition of various resting times) on Ca foil. Upon continued cycling, access into the underlying bulk Ca is possible. While this process remains limited by the interface and yields lower current densities than

with fresh Ca plating/stripping on Au electrodes, the underlying Ca is not entirely deactivated as concluded by earlier studies, but rather depends on the surface conditioning process and the electrolyte. To further investigate the role of the interface, I will also describe experiments in which nanoscale  $\text{CaF}_2$  (~100 nm), an inorganic component found to be present in other Ca SEI, was intentionally formed on Ca foils prior to immersion in an attempt to decouple the foil from the surrounding electrolyte and modulate interface behaviors. Critical differences in interface chemical and electrochemical stability, along with electrochemical performance under CV conditions, will be discussed, and prospects for improving the cyclability of practical Ca foil electrodes will be explored.

**5:55 AM \*F.EN03.04.05**

**Mesoscale Interactions in Electrodeposition Stability of Metal Electrodes** Partha P. Mukherjee and Bairav S. Vishnugopi; Purdue University, United States

Lithium metal electrodes in the presence of liquid electrolytes suffer from unmitigated growth of dendrites that pose safety concerns and lead to electrochemical performance limitation. It necessitates fundamental understanding of the mechanistic origins of interface instability at the mesoscale. This work relies on a detailed mesoscale analysis of the role of disparate mechanisms including electrolyte transport, self-diffusion and electrochemical reaction on the nucleation and growth of electrodeposition. The contrasting influence of temperature on the electrodeposition stability is examined. Finally, the role of mesoscale interactions in devising potential pathways toward electrodeposition stability is elucidated.

**6:10 AM \*F.EN03.04.06**

**Electrochemical Activation and Passivation of Magnesium Metal Anodes** Masaki Matsui; Kobe University, Japan

Magnesium metal anode has a high volumetric capacity of  $3833 \text{ mAh cm}^{-3}$ , rechargeable magnesium battery is expected as an advanced battery system alternate to Li-ion batteries. The SEI-free surface of the magnesium metal leads to the uniform nucleation process resulting in the dendrite free growth during the electrodeposition process. On the other hand, the passivation of the magnesium metal surface initiates the locally-focused current. As a consequence, a risk of dendritic growth of the magnesium metal remains in the electrodeposition process. Here we investigated the nucleation process of magnesium metal on magnesium metal substrates. The initial anodic polarization forms several corrosion pits at the surface of the magnesium substrate. We found that these pits become the preferable sites for the following magnesium deposition. The results suggest that the initial electrochemical activation process is crucial to obtain the uniform plating of magnesium metal.

**6:25 AM \*F.EN03.04.08**

**Interelectrode Temperature Differences used to Promote Reversible Lithium Electroplating and Stripping** Corey T. Love<sup>1</sup>, Robert Atkinson III<sup>2</sup>, Rachel Carter<sup>1</sup> and Todd Kingston<sup>3</sup>; <sup>1</sup>U.S. Naval Research Laboratory, United States; <sup>2</sup>EXCET, Inc., United States; <sup>3</sup>NRL/NRC Post-doctoral Research Associate, United States

The challenges with metal anodes for high-energy batteries will likely be overcome as a result of advancements in three research areas: materials structure-property relationships, electrode architectural design and informed operational controls. We have been focusing our efforts on the operational considerations, specifically temperature control, to promote reversible Li plating and stripping. Modulating temperature, both through thermal gradients and transients, has a direct effect on the performance and stability of the electrochemical plating and stripping processes of Li metal. Applying a modest thermal gradient impacts the lithium plating morphology and dictates whether unstable, one-dimensional Li electroplating or stable, more homogeneous electroplating occurs (1). This talk will expand upon our understanding of gradient-influenced plating/stripping behavior and present operational temperature controls necessary for prolonged battery performance and safety. Additionally, thermal regimes applied to improve electrode kinetics and diffusion will show the opportunity to enable fast charging of Li metal and metal-free electrodes coupled with a  $\text{LiFePO}_4$  positive electrode. We use a suite of materials and electrochemical characterization tools (XPS, XRD, optical microscopy, computed tomography and EIS) to guide our understanding of Li metal behaviors in the battery environment.

(1) R. W. Atkinson III, R. Carter and C. T. Love, *Energy Storage Materials*, **22**, 18 (2019).

**6:40 AM \*F.EN03.04.10**

**Metallic Lithium as a Potential Electrode for High Energy Batteries with Metal Polysulfides** Hikari Sakaebe; National Institute of Advanced Industrial Science and Technology (AIST), Japan

Increase in the energy density of batteries has been a pressing issue, and metallic lithium is a key electrode material for

establishment of such high-energy battery systems. Long history of research has focused on the “dendritic morphology”, but we would still need to continue the basic research for full-scale practical use. Suppressing the dendritic morphology of electrodeposited lithium is so important and surface modification study has been intensively conducted.

In the basic theory of electrodeposition, balance of  $\text{Li}^+$  diffusion and charge transfer kinetics control the morphology and authors confirmed this by lithium plating experiments in ionic liquids [1-3]. Surface modification may adjust this balance or mechanically avoid the growth of dendritic lithium.

We have to consider another point, so called “cross-talk” in the cell. Lithium has the most negative potential among all elements, and electrolytes should be decomposed partly. This is strongly connected to the film formation and then to the cycling efficiency of lithium electrode. Furthermore, the side reaction products may affect the total performance of the cell. In the metal polysulfide/Li cell, a sign of the cross-talk was found and it would lead to the life of the cell [4, 5]. This is quite different from the shuttle mechanism of Li polysulfides in the conventional Li-S cell.

#### Acknowledgement

A part of this work was conducted by the financial support of JST-CREST and NEDO RISING2 project (JPNP16001).

#### References

- [1] H. Sano, H. Sakaebe, et al., *J. Power Sources*, 196, 6663-6669 (2011).
- [2] H. Sano, H. Sakaebe, et al., *ELECTROCHEMISTRY*, 80, 777-779 (2012).
- [3] H. Sano, H. Sakaebe, et al., *J. Electrochem. Soc.*, 161, A1236-A1240 (2014).
- [4] H. Mokudai, H. Sakaebe, et al., to be submitted for publication.
- [5] A. Yano, H. Sakaebe, et.al., abstract 3G02, The 87<sup>th</sup> ECSJ Spring Meeting, March 2020.

#### 6:55 AM F.EN03.04.11

**Lithium Dendrite Initiation in Penetration Microchannels** Youngju Lee and Peng Bai; Washington University in St. Louis, United States

Dendritic growth inside lithium metal batteries is the major issue that prevents the utilization of Li metal anode despite its high energy density. Due to the heterogeneous nature of dendritic growth, the penetrations inside practical batteries occur through few isolated channels, as analysis on multiple postmortem images of the penetrated separators or solid electrolytes advocates. Utilizing the pulled glass capillary cells and COMSOL simulations, we assessed the penetration dynamics focusing on the concentration polarization within the isolated channels with different geometries. We discovered that the varying cross-sectional area has a major impact on the characteristic time for ion depletion on the advancing electrode front, which was previously discovered as the initiation time of dendritic growth. While the ion depletion times still showed a power-law relationship with current densities as the classical Sand equation predicts, the scaling exponent varied, showing a monotonic relationship with the wall curvature near the electrode front. Our findings explain the presence of dendritic growth observed during the system-defined non-transport limited states, as well as deviations of the dendrite initiation time from the classical electro-diffusion equation behaviors. We also propose a new strategic direction for suppressing the dendritic growth and realizing stable lithium metal batteries based on our discovery.

#### 7:05 AM F.EN03.04.12

**Textured Metal Electrodeposition at Rechargeable Battery Anodes—Towards Affordable Energy Storage Systems** Kent Zheng and Lynden Archer; Cornell University, United States

The development of affordable energy harvesting and storage technology has in recent times emerged as a Grand challenge in addressing the irreversible depletion of fossil fuel supplies. It has also emerged as a crucial barrier that must be overcome to lower humanity’s carbon footprint by electrifying transportation and by utilizing renewables-sourced power on the electric grid. One promising solution is to build integrated Photovoltaics(PV)-Battery systems that are high-performing and cost-effective. Currently, the levelized cost of PV energy generation has dropped to \$0.05/kWh, which is comparable with gasoline, while the cost of energy storage (i.e. the battery) is over one order of magnitude higher, making the integrated system economically uncompetitive. Zn-ion battery has a low levelized cost of \$0.3/kWh relative to vanadium flow battery, Li-ion battery, lead-acid battery and sodium-ion battery(\$0.7, \$0.5, \$0.8, \$0.7/kWh, respectively).<sup>1</sup> It is obvious that one can further reduce the levelized cost of a battery by prolonging the cycle life in order to maximize its accumulated energy throughput.<sup>2</sup> Analyses show that, to attain this goal, an at least >99% reversibility must be achieved at the Zn metal anode; however this value is usually <80% in conventional Zn batteries.

In this talk, I will report a type of textured metal anodes that exhibit unprecedented levels of reversibility, > 99.9%. As a first demonstration, I will discuss my recent progress in creating Zn metal batteries that overcome the inherent propensity of the

metal to form highly porous microstructures composed of randomly oriented plates. The porous, loosely-connected metal electrodeposits can be only partially reused in the next discharge, leading to a considerable permanent materials lost and the <80% reversibility. Therefore, a compact, planar Zn metal electrodeposition morphology is necessary in order to meet the reversibility requirement. We then show that this characteristic morphology is attributable to the hexagonal close-pack crystal structure of Zn; it tends to expose its close-packed (002) crystal facet, which is parallel to the micro-plates observed. On this basis, we hypothesize that the desirable compact Zn morphology can be obtained by aligning the (002) Zn plates horizontally with respect to the electrode surface. As I will present in the talk, this goal can be fulfilled either by (a) designing an epitaxial substrate that has low lattice misfit with (002) Zn facet,<sup>3</sup> or by (b) introducing a hydrodynamic flow normal to the electrode surface.<sup>4</sup> The resultant (002)-textured Zn electrodes claim >99.9% reversibilities over 10,000 cycles. As a final note, we demonstrate that this concept of textured electrodeposition can be readily generalized to other metals of interest in batteries, e.g. Al.

## References

1 Lazard, L. Levelized Cost of Storage Analysis v.1.0 (2015).

2 Zheng, J. *et al.* Regulating electrodeposition morphology of lithium: towards commercially relevant secondary Li metal batteries. *Chemical Society Reviews* (2020).

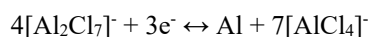
3 Zheng, J. *et al.* Reversible epitaxial electrodeposition of metals in battery anodes. *Science* **366**, 645, doi:10.1126/science.aax6873 (2019).

4 Zheng, J. *et al.* Spontaneous and field-induced crystallographic reorientation of metal electrodeposits at battery anodes. *Science Advances* (*in press*) (2020).

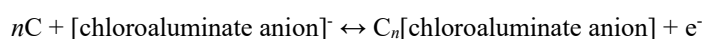
## 7:15 AM \*F.EN03.04.13

**Aluminum Metal Anode Rechargeable Batteries with Chloroaluminate Ionic Liquids** Tetsuya Tsuda<sup>1</sup>, Junya Sasaki<sup>1</sup>, Yuya Uemura<sup>1</sup>, Toshikatsu Kojima<sup>2</sup>, Hiroshi Senoh<sup>2</sup> and Susumu Kuwabata<sup>1</sup>; <sup>1</sup>Osaka University, Japan; <sup>2</sup>National Institute of Advanced Industrial Science and Technology, Japan

It is well-known that mass production of aluminum metal is conducted by Hall-Héroult process using high temperature Na<sub>3</sub>AlF<sub>6</sub>-AlF<sub>3</sub>-NaF (or LiF) molten salt system with Al<sub>2</sub>O<sub>3</sub>. Aluminum metal is one of the most widely used metallic materials for supporting our modern life. However, it is not easy to obtain Al metal without Hall-Héroult process, because Al<sub>2</sub>O<sub>3</sub> is thermodynamically very stable as shown in Ellingham diagram and handling temperature for the molten salt is ca. 1273 K. Interestingly, the use of organoaluminum compounds and aluminum halides make it an open possibility to electrochemically deposit Al metal at lower temperature, even below 298 K. Now, chloroaluminate melts consisting of aluminum halides and chemical compounds have attracted attention as Al electroplating baths. Among them, Lewis acidic AlCl<sub>3</sub>-1-ethyl-3-methylimidazolium chloride ionic liquid (IL) is mostly employed because of its favorable physicochemical properties including negligible vapor pressure, flame resistance, and high ionic conductivity.<sup>1</sup> Note that Lewis acidic means the AlCl<sub>3</sub> molar fraction is over 50 mol%. In this organic chloroaluminate IL electrolyte, Al metal deposition/stripping reversibly proceeds by the following reaction:



Similar electrochemical reaction is recognized in a Lewis acidic inorganic 61.0-26.0-13.0 mol% AlCl<sub>3</sub>-NaCl-KCl IL (eutectic point: 366 K).<sup>2</sup> The electrochemical behavior on the Al metal deposition/stripping in these ILs strongly suggests that we can use it for creating Al metal anode rechargeable batteries. Besides, Al metal has several advantages as an anode material, such as very high theoretical capacity (2980 mAh g<sup>-1</sup>, 8046 mAh cm<sup>-3</sup>), less expensive and mass consumable material, and moderate reactivity in air. Therefore, the number of publications on Al metal anode rechargeable battery (AARB) is increasing for this half a decade.<sup>3,4</sup> AARBs commonly use chloroaluminate anions to control both cathodic and anodic reactions. Cathode is a key for designing good AARBs. Currently layered sp<sup>2</sup> carbon materials, which can reversibly cause the insertion/deinsertion of chloroaluminate anions, [AlCl<sub>4</sub>]<sup>-</sup> and/or [Al<sub>2</sub>Cl<sub>7</sub>]<sup>-</sup>, are often employed as cathode active materials.<sup>1</sup>



Such carbon materials show desirable cathodic behaviors, for example, high coulomb efficiency and rapid charge-discharge. But, their charge-discharge capacities seem to be insufficient (~ 90 mAh g<sup>-1</sup> in Lewis acidic organic chloroaluminate ILs at 298 K;<sup>1,4</sup> ~ 130 mAh g<sup>-1</sup> in Lewis acidic inorganic ones at 393 K<sup>2</sup>). In this context, novel high capacity cathode active materials for AARB are being developed. Recently we found out that the sulfur-carbon composite material (SPEG) synthesized from the mixture of sulfur and polyethylene glycol<sup>5</sup> show appealing electrochemical behaviors, especially high

rate capability and excellent cycling durability, in an inorganic 61.0-26.0-13.0 mol% AlCl<sub>3</sub>-NaCl-KCl IL. In this presentation, features of the promising cathodes for the AARBs and impact of the ionic liquid electrolytes on the cathodes will be discussed.

Our research on AARBs is being supported by the MIRAI program (grant number JPMJMI17E9), Japan Science and Technology Agency (JST).

## References

1. T. Tsuda, G. R. Stafford, and C. L. Hussey, *J. Electrochem. Soc.*, **164**, H5007 (2017) and references therein.
2. C.-Y. Chen, T. Tsuda, S. Kuwabata, and C. L. Hussey, *Chem. Commun.*, **54**, 4164 (2018).
3. T. Tsuda, I. Kokubo, M. Kawabata, M. Yamagata, M. Ishikawa, S. Kusumoto, A. Imanishi, and S. Kuwabata, *J. Electrochem. Soc.*, **161**, A908 (2014).
4. M.-C. Lin, M. Gong, B. Lu, Y. Wu, D.-Y. Wang, M. Guan, M. Angell, C. Chen, J. Yang, B.-J. Hwang, and H. Dai, *Nature*, **520**, 324 (2015).
5. T. Kojima, H. Ando, N. Takeichi, and H. Senoh, *ECS Trans.*, **75**, 201 (2017).

SESSION F.EN03.05: Solid Electrolyte Interphase  
On Demand Abstracts Available for Viewing Starting Saturday Morning, November 21, 2020  
F-EN03

### 5:00 AM \*F.EN03.05.01

**Overcoming the Challenges of Sodium Metal Anodes for Low-Temperature Operation** Weiyang Li; Dartmouth College, United States

Low-temperature (LT) batteries using sodium (Na) metal anodes are highly promising for diverse applications under extreme climate conditions owing to the high specific capacity and low cost of the electrode materials. Unfortunately, the insufficient ionic conductivity of the electrolyte together with the Na dendrite growth at LT significantly influences the performance of Na metal anodes. Herein, we present a novel electrolyte, which not only possesses a superior ionic conductivity at  $-20\text{ }^{\circ}\text{C}$  but also can derive a robust SEI to effectively suppress the dendrite growth and electrolyte decomposition over cycling, contributing to the realization of battery operation under a lean electrolyte condition. Accordingly, the Na metal anode exhibits an ultrahigh reversible capacity of  $50\text{ mAh cm}^{-2}$  at  $2\text{ mA cm}^{-2}$  rate at  $-20\text{ }^{\circ}\text{C}$ . Furthermore, in the Na metal- $\text{Na}_3\text{V}_2(\text{PO}_4)_3$  full-cells, a relatively high capacity of  $98\text{ mAh g}^{-1}$  after 1000 cycles and stable Coulombic efficiency over 99.6% at 2C rate are achieved at  $-20\text{ }^{\circ}\text{C}$ .

### 5:15 AM F.EN03.05.02

**Degradation of Lithium Anode in Lithium-Sulfur Batteries—Evolution of SEI Layer and Loss of Lithium Inventory** Sanjay Nanda and Arumugam Manthiram; University of Texas-Austin, United States

The commercial viability of lithium-sulfur batteries is mainly caused by the poor plating and stripping efficiency of the lithium-metal anode. Lithium metal tends to deposit in mossy/dendritic morphology with high surface area. The liquid electrolyte irreversibly decomposes on the reducing lithium surface, consuming both the lithium and electrolyte supply in the cell. Nevertheless, the mechanisms underlying loss of lithium inventory and the role of the lithium-electrolyte interfacial layer (SEI) remain unclear. A clear mechanistic understanding of lithium degradation with cycling in Li-S batteries is necessary to develop strategies towards stabilizing lithium deposition in this unique system.

Here, the anode-free full cell configuration, which combines a fully lithiated Li<sub>2</sub>S cathode with a bare nickel foil as the current collector, is used to study the dynamics of lithium deposition. The cycle life of anode-free full cells is dependent on the active lithium inventory in the system, as there is no excess lithium in the system (N/P ratio = 1). By deconvoluting the cycling regimes limited by lithium and sulfur, the lithium inventory loss rate per cycle can be quantitatively estimated. This parameter provides a useful and reliable descriptor of lithium degradation with cycling in cells with a limited lithium inventory.

Analysis using time-of-flight secondary ion mass spectrometry (ToF-SIMS) of the deposited lithium in the anode-free full cells showed that the integrated intensity for Li<sub>2</sub><sup>-</sup>, which is indicative of metallic lithium, displayed almost no change with



cycling. Thus, a poor correlation between available lithium inventory and amount of metallic lithium detected is discovered. This indicates that the loss of lithium inventory is primarily due to the formation of electrochemically inactive “dead” metallic lithium ( $\text{Li}^0$ ), and not due to undesirable side reactions with the electrolyte forming SEI components ( $\text{Li}^+$ ). ToF-SIMS also revealed the growth of a thick layer of electrolyte decomposition products on the surface of the deposited lithium. Since the decomposition products are not ionically conducting, the metallic lithium underneath is rendered electrochemically inactive or “dead”.

It is also found that various hydrogen-containing decomposition products in the bulk of the deposited lithium, such as  $\text{LiH}$  and  $\text{LiOH}$ , show a sharp decrease in concentration with cycling. This may be ascribed to the considerable gas evolution that occurs during cycling. These gases include  $\text{H}_2$ ,  $\text{CH}_4$ , and  $\text{C}_2\text{H}_4$ . This could play an important role in lithium degradation by blocking off ionic and electronic conduction to the trapped metallic lithium, especially if the gases themselves are trapped in void spaces of the porous lithium deposit.

Thus, the mechanisms that underlie the loss of lithium inventory in Li-S batteries are illuminated by a novel application of the anode-free full cell configuration and analytical tools such as ToF-SIMS. The evolution of the lithium-electrolyte interfacial layer (SEI) and its role in causing lithium degradation is demonstrated. It is hoped that the insights generated in this work can motivate efforts towards enabling stable operation of lithium-metal anodes and long cycle life for energy-dense Li-S batteries.

#### 5:25 AM F.EN03.05.03

##### **Building Artificial Solid Electrolyte Interphase with High-Uniformity and Fast Ion Diffusion for Ultralong-Life**

**Sodium Metal Anodes** Qianwen Chen, Heng He, Weiman Zhuang and Limin Huang; Southern University of Science and Technology, China

Na metal is regarded as a promising anode for Na batteries owing to its high specific capacity and natural abundance. However, rapid dendrite growth and low reversibility hinder its practical applications. Building an artificial solid electrolyte interphase (SEI) is an effective strategy to stabilize a Na metal anode, yet it is still deficient at high current density and cycling capacity. Here, two artificial SEI layers were constructed through the analogous reactions between Na metal and pure  $\text{SnCl}_4$  liquid ( $\text{SnCl}_4$ -Na electrode) or diglyme solvent with  $\text{SnCl}_2$  additive ( $\text{SnCl}_2$ -Na electrode) to investigate the key parameters for an excellent artificial SEI. Both simulations and experiments demonstrate that high-uniformity and high  $\text{Na}^+$  diffusion properties of  $\text{SnCl}_4$ -derived protective layer are significant for stabilizing Na metal anodes under rigorous test conditions. Therefore, the  $\text{SnCl}_4$ -Na electrode protected by homogenous and high  $\text{Na}^+$  diffusion Na-Sn alloy and NaCl achieves an ultralong cycle life for 4000 h and small voltage hysteresis ( $\sim 100$  mV) with a cycling capacity of  $3 \text{ mAh cm}^{-2}$  at  $3 \text{ mA cm}^{-2}$ , which is much better than that of the  $\text{SnCl}_2$ -Na electrode. Moreover, even with a cycling capacity of  $5 \text{ mAh cm}^{-2}$  at  $5 \text{ mA cm}^{-2}$ , the  $\text{SnCl}_4$ -Na electrode still can stably run for  $\sim 1500$  h. Benefiting from the durable SEI layer, a stable capacity of  $\sim 350 \text{ mAh g}^{-1}$  is observed on a  $\text{SnCl}_4$ -Na| $\text{FeS}_2$  full cell for 380 cycles.

#### 5:35 AM \*F.EN03.05.05

**Structure and Dynamics of the Solid Electrolyte Interphase on Li Metal Anodes** Lauren Marbella; Columbia University in the City of New York, United States

Li metal batteries have the opportunity to enable high energy density technologies, including Li-air, Li-S, and all-solid-state batteries. However, Li metal anodes suffer from microstructural growth that leads to a loss of Coulombic efficiency and, in some cases, short circuiting and cell death. The composition and structure of the solid electrolyte interphase (SEI) that forms on the surface of Li metal is not well understood, but is believed to play a key role in controlling, and possibly initiating, Li microstructural growth. Here, we use solid-state NMR spectroscopy to provide a detailed characterization of discrete organic and inorganic species that comprise the SEI on Li metal anodes. We examine the SEI and Li ion dynamics through the interphase on Li metal after galvanostatic cycling/polarization in various electrolyte formulations and correlate these changes with differences in Li microstructural growth patterns. Insight into molecular-level changes in SEI composition and dynamics for distinct electrolyte mixtures allows us to rationalize how specific electrolyte components may mediate Li microstructural growth.

#### 5:50 AM F.EN03.05.06

**The Role of the Interface in Stabilizing Reaction Intermediates for Hydrogen Evolution and SEI Formation in Aprotic Electrolyte** Ivano E. Castelli; Technical University of Denmark, Denmark

Understanding the battery interface is a key-point for improving the lifetime of Li-ion batteries (LIB) as well as design novel

electrode materials, beyond LIB. Here, we investigate the SEI formation on the single-crystal metal facets in an organic aprotic electrolyte, by combining idealized experiments with realistic quantum mechanical simulations of the interface (ab-initio molecular dynamics, AIMD). We discover that the LiF formation, accompanied by H<sub>2</sub> evolution, is caused by a reduction of HF impurities and requires the presence of Li at the interface, which catalyzes the HF dissociation. The measured potential of the electrochemical response for these reduction reactions correlates with the work function of the electrode surfaces and that the work function determines the potential for Li<sup>+</sup> adsorption. The reaction path is investigated further by electrochemical simulations suggesting that the overpotential of the reaction is related to stabilizing the active structure of the interface having adsorbed Li<sup>+</sup>. Li<sup>+</sup> is needed to facilitate the dissociation of HF which is the source of protons. Further experiments on other proton sources, water, and methanesulfonic acid show that if the hydrogen evolution involves negatively charged intermediates, F<sup>-</sup> or HO<sup>-</sup>, a cation at the interface can stabilize them and facilitate the reaction kinetics. When the proton source is already significantly dissociated (in the case of a strong acid), there is no negatively charged intermediate and thus the hydrogen evolution can proceed at much lower overpotentials. This reveals a situation where the overpotential for electrocatalysis is related to stabilizing the active structure of the interface, facilitating the reaction rather than providing the reaction energy. Using these data, we generate neural network potentials to extend the length and time scale of AIMD and to fully understand the implications that these findings have for the SEI formation.

**6:00 AM \*F.EN03.05.07**

**Characterization of Solid Electrolyte Interphase Formed in the Electrolytes Developed for Rechargeable Lithium-Sulfur Battery** Yasushi Katayama, Takaaki Matsumoto, Tomohiro Uchiya, Mika Nishikawa and Nobuyuki Serizawa; Keio University, Japan

Rechargeable lithium sulfur battery has attracted much attention as a next generation battery due to a high theoretical energy density and low cost. In the discharge process, sulfur is reduced to Li<sub>2</sub>S with formation of polysulfides as intermediate species. In the case of conventional organic electrolytes used for commercial lithium-ion batteries, polysulfides dissolve in the electrolytes, leading to the self-discharge by the diffusion of polysulfides from the cathode to anode, namely a shuttle effect. The self-discharge has been reported to be prevented by forming a solid electrolyte interphase (SEI) based on functional additives like lithium nitrate. However, the consumption of the additives spoils the prevention of the shuttle effect for long-term cycling. It has been reported that the solubility of polysulfides is very low in the electrolytes composed of lithium bis(trifluoromethylsulfonyl)amide (LiTFSA) and such organic compounds as tetraglyme (G4) and sulfolane (SL). Although the superior performance of sulfur cathodes has been reported in these electrolytes, the applicability of a lithium anode in the electrolytes has not been investigated from a fundamental point of view. In the present study, SEIs formed in LiTFSA-G4 and LiTFSA-SL were characterized by electrochemical impedance spectroscopy (EIS), Fourier transform infrared spectroscopy (FT-IR), X-ray photoelectron spectroscopy (XPS), and transmission electron microscopy (TEM). The formation of a SEI on a Cu substrate was suggested by holding the potential at 0 V vs. Li|Li(I) in LiTFSA-G4 by EIS. The SEI is considered to grow with the elapse of time for holding the potential at 0 V, indicating the decomposition of the electrolyte was sluggish. The SEI with the thickness of about 100 nm was observed on the Cu substrate after the SEI formation. The SEI was suggested to be composed of the organic components derived from the reductive decomposition of the electrolyte. FT-IR and XPS indicated that TFSA<sup>-</sup> was included in the SEI. On the other hand, the formation of LiF was not confirmed by XPS, indicating the electrochemical decomposition of TFSA<sup>-</sup> was not predominant while the decomposition of TFSA<sup>-</sup> after Ar<sup>+</sup> etching was found to give a peak assignable to LiF. A similar SEI was also found to be formed on a Cu substrate in LiTFSA-SL with addition of a diluent, 1,1,2,2-tetrafluoroethyl 2,2,3,3-tetrafluoropropyl ether (HFE). The thickness of the SEI in LiTFSA-SL-HFE was thinner than that in LiTFSA-G4, suggesting the poor adhesion and/or partial dissolution of the SEI. The formation of LiF was not confirmed by XPS. These results suggested that the SEIs formed in these electrolytes are composed of the ionic species, which are immobilized in the matrix based on the decomposed products of the organic components of the electrolytes.

**Acknowledgment**

This study was supported by the Advanced Low Carbon Technology Research and Development of Program (ALCA) of the Japan Science and Technology Agency (JST).

**6:15 AM F.EN03.05.08**

**The Electronic Properties of Grain Boundaries in Solid Electrolyte Interphase and Their Impact on Li-Metal Electrode Passivation** Min Feng, Jie Pan and Yue Qi; Michigan State University, United States

Due to the highly reactive and reductive nature of Li-metal, the surface of Li-metal electrodes is typically covered by a layer of solid electrolyte interphase (SEI), which can be formed by electrolyte decomposition or artificial coating. If the SEI cannot passivate the Li-surface, continuous electron leakage through the SEI will lead to more electrolyte decomposition, SEI

growth, metallic Li formation and growth inside of the SEI, all of which contribute to the major durability and safety concerns for Li-metal electrodes. Given the multi-components and mosaic structures of SEI, the extended defects such as grain boundaries and interfaces in SEI are likely to be the electron conduction pathways, as the individual SEI components are wide-bandgap insulators in their single crystalline form. Therefore, in this work, the electronic properties of representative grain boundaries (GBs) of the main SEI components (LiF, Li<sub>2</sub>O, and Li<sub>2</sub>S) on Li in various electrolytes were investigated via density functional theory (DFT) calculations. The GB energy, GB bandgap, excess electron distribution were computed. The total density of states (DOS) of GBs was then aligned with Li Fermi level and Li<sup>+</sup>/Li<sup>0</sup> potential level to determine their ability to trap electrons from the Li metal electrode. For a systematic comparison, highly coherent tilt and twist GBs with the same  $\Sigma$  values ( $\Sigma 3$  and  $\Sigma 5$ ) in coincidence site lattices (CSL) model were studied to represent low energy special GBs; and GBs with melted GB region and the same orientation of the special GBs were used to demonstrate the influence of the amorphous GBs.

It was found that all the GB bandgaps were smaller than the corresponding bulk bandgaps, with an order of amorphous GBs < Tilt GBs < Twist GBs < single crystal. Among all the calculated GBs, the coherent Li<sub>2</sub>S Tilt  $\Sigma 3$  (-12-1)/[111] GB and the amorphous LiF GB showed empty electronic states lower than the Li<sup>+</sup>/Li<sup>0</sup> depositing level, suggesting that those GB states can trap electrons from Li metal, leading to nucleation of metallic Li inside of the SEI and contributing to the Li dendrite growth. Structural analysis revealed that more under-coordinated atoms in the GBs caused larger bandgap drops and more excess electron localization in the less dense GB regions. These insights suggested that dense SEI structures such as sharp interfaces and well-ordered GBs are preferred to design a fully electronically passivating SEI. Furthermore, to overcome the size limitation of DFT calculations for complex GB structures and facilitate the multiscale simulations, we proposed an analytical model to extrapolate the bandgaps of special GB structures based on the DFT-computable bulk and surface bandgaps. Our predictions of GB bandgaps can be used as inputs for phase field models to simulate Li dendrite growth morphology in both solid and liquid electrolytes.

#### 6:25 AM \*F.EN03.05.09

**Formation of a Spontaneous Passivation Layer at the Li Metal/Electrolyte Interface** Perla B. Balbuena, Francisco Ospina-Acevedo and Ningxuan Guo; Texas A&M University, United States

The promise of Li metal as one of the best imaginable anodes for the next generation of advanced batteries remains intact. However, this promise becoming a reality is not yet possible because of the various issues associated with its high reactivity. Obviously, the immediate expectation is that a great passivation layer will mitigate the problem. Indeed, the immediate contact of Li metal with a liquid electrolyte leads to the spontaneous formation of a “solid-electrolyte interphase” (SEI). The SEI results from the redox reactions where Li becomes oxidized and the electrolyte components become reduced. In this talk, we will discuss how the various anode and electrolyte properties affect such SEI. We have carried out classical reactive molecular dynamics simulations and density functional theory calculations for many different anode surfaces and various electrolyte compositions. As a result, we have observed nucleation and growth of the SEI under various important conditions. The conclusions are very important to understand the evolution of Li metal anodes during battery cycling.

#### 6:40 AM F.EN03.05.10

**The Identity and Role of Interphases in Regulating Mg Anode Morphology Evolution** Kevin R. Zavadil, Nathan Hahn, Scott A. McClary, Daniel Long and Katherine L. Jungjohann; Sandia National Laboratories, United States

The spontaneously formed and evolved interphase present on a metal anode dictates the Coulombic efficiency, capacity, rate, and lifetime (cycle and calendar) properties of this electrode. Ideally, we would design electrolytes with a detailed knowledge of interphase function to achieve optimum anode performance. Such knowledge is currently lacking for the more energy dense multivalent metal anodes, such as Mg and Ca, cycled in electrolytes that exhibit promise for viable, full cell chemistries. In this presentation, we describe interphase characterization of Mg metal anodes, where Mg serves as a test case for correlating interfacial phenomena with energy storage performance and morphological evolution. We show that Mg exhibits a range of electrolyte dependent behaviors from classic electrocrystallization, marked by near unity Coulombic efficiency and electrochemical epitaxy, to varying degrees of deposit density and crystallography determined by the interphases present at the anode surface. We employ transmission electron microscopy based on a cell to microscope approach to define the role the interphase plays in controlling metal grain size/shape, crystallography and microstructure with cycling and we relate these attributes to the interphase composition and structure. We demonstrate dramatic changes in deposition and dissolution morphology are possible with subtle changes in electrolyte composition, including controlled levels of trace water, added co-ions, and added co-solvents. Our results suggest a path exists toward directing interphase formation based on enhanced electrolyte design.

This work was supported by the Joint Center for Energy Storage Research, an Energy Innovation Hub funded by the U.S.

Department of Energy. Sandia National Laboratories is a multimission laboratory managed and operated by National Technology & Engineering Solutions of Sandia, LLC, a wholly owned subsidiary of Honeywell International Inc., for the U.S. Department of Energy's National Nuclear Security Administration under contract DE-NA0003525.

#### 6:50 AM F.EN03.05.11

**Self-Discharge in Lithium Metal Batteries as a Function of Electrolyte** Laura C. Merrill, Samantha G. Rosenberg and Katharine Harrison; Sandia National Laboratories, United States

Lithium metal anodes are of interest due to the high theoretical capacity of lithium (3800 mAh/g) making the lithium anode ideal for use in high energy density applications. Self-discharge is apparent when an electrochemical cell loses capacity at rest, subsequently lowering the energy density. In Li-ion batteries, this can represent up to a 100 % loss in capacity.<sup>1</sup> New Li-ion chemistries using silicon anodes also show evidence of self-discharge.<sup>2-3</sup> Recent work suggests that lithium metal batteries will experience significant capacity losses when at rest in the charged state.<sup>4-6</sup> One of the primary means of self-discharge identified is lithium metal corrosion. This work evaluates self-discharge phenomena in carbonate and ether-based electrolytes commonly used with lithium metal batteries. It is found that the interplay between the solid electrolyte interphase (SEI) and the chemical passivation layer, both of which are electrolyte dependent, determine the extent of self-discharge observed. Specifically, self-discharge is worsened in some electrolytes by the continual breakdown and repair of the SEI upon lithium electrodeposition and dissolution. The use of inorganic artificial SEIs are also studied to mitigate the capacitive losses.

Supported by the Laboratory Directed Research and Development program at Sandia National Laboratories, a multimission laboratory managed and operated by National Technology and Engineering Solutions of Sandia, LLC., a wholly owned subsidiary of Honeywell International, Inc., for the U.S. Department of Energy's National Nuclear Security Administration under contract DE-NA-0003525.

1. Reddy, T. B., *Linden's Handbook of Batteries*. Fourth ed.; McGraw-Hill Education: 2011.
2. Kalaga, K.; Rodrigues, M.-T. F.; Trask, S. E.; Shkorb, I. A.; Abraham, D. P., Calendar-life versus cycle-life aging of lithium-ion cells with silicon-graphite composite electrodes. *Electrochimica Acta* **2018**, *280*, 221-228.
3. Zilberman, I.; Sturm, J.; Jossen, A., Reversible self-discharge and calendar aging of 18650 nickel-rich, silicon-graphite lithium-ion cells. *Journal of Power Sources* **2019**, *425*, 217-226.
4. Lin, D.; Liu, Y.; Li, Y.; Li, Y.; Pei, A.; Xie, J.; Huang, W.; Cui, Y., Fast galvanic lithium corrosion involving a Kirkendall-type mechanism. *Nature Chemistry* **2019**, *11*, 382-389.
5. Harrison, K. L.; Zavadil, K. R.; Hahn, N. T.; Meng, X.; Elam, J. W.; Leenheer, A.; Zhang, J.-G.; Jungjohann, K. L., Lithium Self-Discharge and Its Prevention: Direct Visualization through In Situ Electrochemical Scanning Transmission Electron Microscopy. *ACS Nano* **2017**, *11*, 11194-11205.
6. Wood, S. M.; Fang, C.; Dufek, E. J.; Nagpure, S. C.; Sazhin, S. V.; Liaw, B.; Meng, Y. S., Predicting Calendar Aging in Lithium Metal Secondary Batteries: The Impacts of Solid Electrolyte Interphase Composition and Stability. *Advanced Energy Materials* **2018**, *8* (26).

SESSION F.EN03.06: Solid Electrolytes

On Demand Abstracts Available for Viewing Starting Saturday Morning, November 21, 2020

F-EN03

#### 5:00 AM \*F.EN03.06.01

**Challenges in Enabling Li Metal Anode—A Composite Electrolyte Approach** Xi C. Chen; Oak Ridge National Laboratory, United States

Li metal is the ultimate anode of choice to improve the energy and power densities of current lithium ion batteries due to its high theoretical capacity and low electrochemical potential. However, challenges associated with the high reactivity and dendrite growth of metallic Li must be addressed before its practical applications. The development of a solid-state electrolyte is the key to enabling Li anode. In order to achieve this goal, the solid-state electrolyte must have high ionic conductivity, adequate mechanical modulus, good chemical stability and adhesion with metallic lithium, and thin sheet processability.

Our strategy to enable Li metal anode is a composite electrolyte approach. The goal is to develop a composite solid electrolyte consisting of a processible soft polymer phase and a highly conductive hard ceramic phase to meet the challenging combination of physical, chemical and manufacturing requirements.

Here we introduce the fabrication of two types of composite electrolytes. One type is to disperse model  $\text{Li}^+$ -conducting ceramic particles (LICGC<sup>TM</sup>) within a polymer electrolyte matrix (poly(ethylene oxide)-based). Aqueous spray coating is used to produce thin, large area and dense composite films with high loadings of ceramic. The interfacial resistance for ion transport between the polymer and the ceramic is quantified using a trilayer model and methods to minimize the interfacial resistance is discussed. In this type of composite electrolyte, the main ion conduction pathway is through the polymer matrix. A second type of composite electrolyte involves creating a three-dimensionally interconnected structure of the ceramic with greatly reduced interparticle resistance. The main ion conduction pathway is through the ceramic in this case. Symmetrical cells and full cells using these electrolytes with Li metal will be compared.

Acknowledgements: The development of composite electrolytes was sponsored by the U.S. Department of Energy (DOE), Office of Energy Efficiency and Renewable Energy for the Vehicle Technologies Office's Advanced Battery Materials Research Program (Tien Duong, Program Manager). Neutron and solid state nuclear magnetic resonance experiments were sponsored by DOE's Office of Science, Basic Energy Sciences, Materials Science and Engineering Division.

#### 5:15 AM \*F.EN03.06.02

**Magnesium Metal Electrodeposition and Electrodeposition with Polymer Electrolytes** Bumjun Park and Jennifer L. Schaefer; University of Notre Dame, United States

Lithium metal and magnesium metal batteries have potential for high system energy density due to the high gravimetric and volumetric charge capacity of these metal anodes. Magnesium metal offers several advantages and disadvantages with respect to lithium metal as an anode. Magnesium is more abundant and resources are geographically widespread. Magnesium metal is less chemically reactive than lithium metal and electrodeposition/deposition happens at elevated potentials, yet issues with inefficiency and side reactions still remain. While lithium metal polymer batteries have been investigated intently for decades, magnesium metal polymer batteries have received little attention. There exist great difficulties in producing magnesium polymer electrolytes that both effectively transport magnesium and support reversible electrodeposition and dissolution of magnesium metal. In this talk, I will review our recent research on ion transport and electrochemistry in traditional salt-doped magnesium polymer electrolytes and magnesium poly(ionic liquid) electrolytes.

#### 5:30 AM \*F.EN03.06.03

**Chemo-Mechanics at Lithium Metal Interfaces in Solid-State Batteries** Matthew T. McDowell; Georgia Institute of Technology, United States

Incorporating lithium metal anodes into solid-state batteries (SSBs) is critical for enabling high energy density and specific energy. However, a variety of chemo-mechanical issues at the solid-state electrochemical interface, including interphase growth, contact loss, and lithium morphology evolution, have hindered development of efficient solid-state lithium anodes. Understanding and controlling the dynamic evolution of lithium interfaces is therefore necessary for further development of SSBs. Here, I discuss my group's efforts using *in situ* and *operando* methods to investigate the dynamic evolution of lithium metal and its interphase within SSBs. Multi-modal *in situ* investigation of interfacial reactions combined with electrochemical experiments reveal how the formation of the interphase is linked to chemo-mechanical cell failure in NASICON-based lithium metal cells. *In situ* transmission electron microscopy (TEM) shows that the reaction of  $\text{Li}_{1+x}\text{Al}_x\text{Ge}_{2-x}(\text{PO}_4)_3$  (LAGP) with lithium to form an interphase is similar to a conversion reaction, in which lithium insertion causes amorphization and volume expansion of ~130%. *In situ* X-ray tomography experiments of operating LAGP-based cells reveal that the growth of the interphase causes fracture, which is the underlying cause of impedance increase within the cell. Interestingly, we have found that deposited interfacial layers can alter the growth trajectory of the interphase and extend cycling stability of symmetric cells from ~30 hours with unprotected LAGP SSEs to >1000 hours with protected materials. Additional efforts have been focused on the use of *operando* synchrotron X-ray imaging to understand interfacial dynamics and overall cell evolution during cycling in SSBs with different chemistries. Finally, I will discuss our results on understanding lithium anode evolution at different temperatures in liquid and solid systems. Overall, these results provide fundamental insight into the evolution of the lithium/electrolyte interface, and they show that control over interfacial transformation processes could enable the development of solid-state lithium metal batteries.

#### 5:45 AM F.EN03.06.04

**Sodium Stripping and Plating from Na-β"-Alumina Ceramics Beyond 1000 mA/cm<sup>2</sup>** Daniel Landmann, Gustav Graeber, Meike Heinz and Corsin Battaglia; Empa–Swiss Federal Laboratories for Materials Science and Technology, Switzerland

Dendrite formation limits the cycle life of lithium and sodium metal anodes and remains a major challenge for their integration into next-generation batteries, even when replacing the liquid electrolyte by a solid electrolyte. Recent studies have pointed out that lithium and sodium metal creep rather than lithium and sodium diffusion is the primary mechanism for replenishing the voids forming in solid metal anodes at the interface to a solid electrolyte upon stripping. Void formation upon stripping causes current constrictions upon plating, promoting dendrite formation. Here we investigate plating and stripping of liquid sodium metal from a ceramic Na-β"-alumina electrolyte at 250 °C, thereby eliminating mass transport limitations due to creep. Employing a porous carbon electrode coating to (1) prevent dewetting of plated liquid sodium from and (2) to supply liquid sodium upon stripping to the sodiophobic Na-β"-alumina surface, we demonstrate extremely high current densities above 1000 mA/cm<sup>2</sup> and cumulative plated capacities of 10 Ah/cm<sup>2</sup> without dendrite formation [1]. These values are two orders of magnitude larger than the corresponding values measured at room temperature [2]. We further show that liquid sodium occupies 60% of the porosity of the carbon coating, while excess sodium accumulates on top of the coating. Increasing the thickness of the carbon coating from 50 μm to 200 μm does not affect the Coulombic efficiency, but reduces the constant current rate capability due to the increased flow resistance for liquid sodium in the porous coating. Our results confirm that eliminating void formation is effective in suppressing dendrite formation.

[1] D. Landmann, G. Graeber, M. V. F. Heinz, C. Battaglia, submitted

[2] M.-C. Bay, M. Wang, R. Grissa, M. V. F. Heinz, J. Sakamoto, C. Battaglia, *Adv. Energy Mater.* 2019, 201902889

5:55 AM \*F.EN03.06.06

**Factors Influencing Lithium Protrusion Nucleation and Cycle Life in Solid Polymer Electrolytes for Battery Applications** Alec S. Ho<sup>1,2</sup>, Jacqueline Maslyn<sup>1,2</sup> and Nitash P. Balsara<sup>1,2</sup>; <sup>1</sup>University of California, Berkeley, United States; <sup>2</sup>Lawrence Berkeley National Laboratory, United States

Successful prevention of lithium dendrite growth would enable the use of lithium metal as an anode material in next-generation secondary batteries. Mechanically stiff solid polymer electrolytes have been shown to prolong the life of lithium metal cells by partially suppressing lithium dendrite growth. However, we lack fundamental knowledge about the nature of lithium electrodeposition under different electrochemical and electrolyte conditions, as direct observation of this phenomenon is non-trivial.

Synchrotron X-ray microtomography was used to observe lithium metal plating through these solid polystyrene-*block*-poly(ethylene oxide)-LiTFSI electrolyte membranes under a range of electrochemical conditions: regimes of lithium plating behavior as functions of current density and electrolyte thickness through the block copolymer electrolyte were identified. Impurity particles in the lithium metal were observed at the nucleation sites of protrusions, as reported in other work. Next, stable lithium plating at low current density was used to treat the lithium layer at the electrode-electrolyte interface to investigate the effect of impurity particles on protrusion nucleation and lithium deposition. We show that this “lithium filtering” strategy increases the cycle life of lithium symmetric cells in an unexpected way.

## SYMPOSIUM F.EN04

---

Beyond Lithium-Ion Batteries—Materials, Architectures and Techniques  
November 21 - December 4, 2020

### Symposium Organizers

David Mitlin, The University of Texas at Austin

Dong Su, Chinese Academy of Sciences

Chunlei Wang, Florida International University

Yan Yu, University of Science and Technology of China

Symposium Support

**Platinum**

Samsung SDI

**Silver**

Materials Today | Elsevier

**Bronze**

MilliporeSigma

---

\* Invited Paper

SESSION F.EN04.30: Live Keynote I: Solid State Electrolytes

Session Chairs: Miaofang Chi and Daniel Steingart

Wednesday Afternoon, December 2, 2020

F.EN04

**7:30 PM \*F.EN04.01.01**

**Solid-State Ceramic Battery Electrolyte Processing** Jennifer Rupp; Massachusetts Institute of Technology, United States

Next generation of energy storage devices may largely benefit from fast and solid Li<sup>+</sup> ceramic electrolyte conductors to allow for safe and efficient batteries and fast data calculation. For those applications, the ability of Li-oxides to be processed as thin film structures and with high control over Lithiation and phases at low temperature is of essence to control conductivity. In particular, Li-garnet structures are attractive due to their fast transfer properties and safe operation over a wide electrochemical stability range for batteries. In the first part we focus on low temperature processing of Li-garnet thin films and nanostructures. Examining the structure-Li transport in solid state and asking the provocative question: How do Li-amorphous to crystalline structures conduct? How to alter processing of Li-oxide films to compensate for the challenge that most of Lithium phases lead to sluggish transport and hard phase stabilization? Bringing down battery solid electrolyte processing temperature and decreasing form factor opens new opportunities in battery design and new doors to give more functions for similar material classes for neuromorphic computing. Through the talk, we focus on new processing opportunities to Lithiate thin film structures in crystalline state and to assure cubic and fast conduction on the example of Li-garnet for thin film form using some active Lithiation strategies at film deposition<sup>1-3</sup>. For this we will review the field of thin film processing and introduce to new processing routes based on vacuum and wet-chemical techniques to control various strategies of Lithiation and phase evolution. Excitingly, one has the opportunity for Li-garnet solid state conductors to not only synthesize crystalline structures, but also amorphous films in various frozen-in states<sup>4</sup>. Insights on degree of amorphous to crystalline Li-garnet thin films are presented based on model experiments, incl. JMAK and TTT-diagram analysis of Li-garnet structure types. Dependent on either a vacuum or wet-chemical based method chosen the phase evolution differs when synthesizing the glass states, with significant impact on condensation and Li-transport<sup>5-6</sup>. We find that the different amorphous structures that Li-garnets are no Zachariasen glasses as they violate several of Zachariasen rules by text book: These amorphous Li-garnets differ therefore significantly from LIPON but have a wider room to arrange the higher coordinated polyhedral, network former and builders. In amorphous garnets there is room for manipulation in densification and Li-transport and one may potentially profit from high stability window to design batteries with no grain boundaries at the Li electrolyte interface. Collectively, the insights on solid state energy storage provide evidence for the functionalities that those Li-materials can have in the future. The challenges are deeply connected to low temperature processing and design of structure-transport properties, however, solving those allows us to dream a little more and give materials more functions. 1. A Low Ride on Processing Temperature for a Fast Li Conduction in Garnet Solid State Battery Films R Pfenninger, M. Struzik, I Garbayo, E Stilp, JLM Rupp, Nature Energy, 4, 475-4832019, 2019 2. Lithium-Containing Thin Films JLM Rupp, R Pfenninger, M. Struzik, A Nanning, I Garbayo, US 62/718,838 (2018) 3. Methods of Fabricating Thin Films Comprising Lithium-Containing Materials JLM Rupp, R Pfenninger, M. Struzik, A Nanning, I Garbayo, US 62/718,842 (2018) 4. Glass-Type Polyamorphism in Li-Garnet Thin Film Solid State Battery Conductors I Garbayo, M Struzik, WJ Bowman, R Pfenninger, JLM Rupp, Advanced Energy Materials, 1702265 (2018) 5. Solid-state Electrolyte and Method of Manufacture Thereof. ZD Hood, Y Zhu, L Miara, JLM Rupp. US 62/713,366 (2018) 6. Solution-Processed Solid-state Electrolyte and Method of Manufacture Thereof. Y Zhu, ZD Hood, L Miara, JLM Rupp US 62/713,428 (2018)

**8:00 PM \*F.EN04.20.04**

**Synthesis and Electrochemical Properties of Na-ion Conducting Pseudo-Solid State Ionogel Electrolytes** Ryan H. DeBlock<sup>1</sup>, David Ashby<sup>2</sup>, Grace Whang<sup>1</sup>, Danielle Butts<sup>1</sup>, Christopher Choi<sup>1</sup> and Bruce S. Dunn<sup>1</sup>; <sup>1</sup>University of California, Los Angeles, United States; <sup>2</sup>Sandia National Laboratories, United States

Ionogels are pseudo-solid state electrolytes in which an ionic liquid electrolyte confined in a mesoporous inorganic matrix leads to a material that possesses the electrochemical, thermal and chemical properties of the ionic liquid despite being a macroscopic solid. Because of their unique architecture, ionogels maintain a nanoscale fluidic state and thus mitigate the interfacial resistances which commonly arise at solid-solid interfaces. The use of sol-gel synthesis enables the materials to be prepared as liquids and to penetrate porous electrodes before becoming solid, an especially beneficial property for solid-state batteries. The incorporation of Li-ion conducting ionogel electrolytes into Li-ion batteries has been reported previously and generally show behavior comparable to that of the ionic liquid electrolyte.

In this work, we report on the development of Na-ion conducting ionogels, a topic which has received only limited investigation to date. We use sol-gel synthesis to form a siloxane-modified silica scaffold that traps an ionic liquid electrolyte comprised of 0.5M NaFSI in 1-Butyl-1-methylpyrrolidinium bis(trifluoromethanesulfonyl)imide [PYR14][TFSI]. The low vapor pressure of the ionic liquid ensures that a dense gel is formed. The interconnected porosity allows for good ionic conductivity ( $0.7 \text{ mS cm}^{-1}$ ), although it is somewhat less than the corresponding ionic liquid electrolyte. The activation energy for conduction of 0.3eV is, as expected, higher than that of Li-ion conducting ionogels. The material possesses a 5V electrochemical window and is thermally stable up to 150°C. Using the positive Na-ion electrode material,  $\text{Na}_3\text{V}_2(\text{PO}_4)_3$ , the charge transfer properties of the ionogel/NVP interface were characterized and found to exhibit low interfacial impedance. This led us to demonstrate the operation of a Na-ion solid state battery which contained a  $\text{NaTi}_2(\text{PO}_4)_3$  negative electrode in conjunction with the NVP. The results shown here underscore the versatility of ionogels as a thermally stable electrolyte with designed ion transport properties for use in future solid-state electrochemical devices

**8:30 PM \*F.EN04.03.01**

**Stabilizing Solid Li and Na Metal Anodes Using Ceramic Membrane Technology** Jeff Sakamoto<sup>1</sup>, Michael Wang<sup>1</sup>, Marie-Claude Bay<sup>2</sup> and Corsin Battaglia<sup>2</sup>; <sup>1</sup>University of Michigan, United States; <sup>2</sup>Empa–Swiss Federal Laboratories for Materials Science and Technology, Switzerland

There is tremendous interest in making the next super battery, but state-of-the-art Li-ion technology works well and has inertia in several commercial markets. Supplanting Li-ion will be difficult. Recent material breakthroughs in Li and Na metal solid-state electrolytes could enable a new class of non-combustible solid-state batteries (SSB) delivering twice the energy density (1,200 Wh/L) compared to Li-ion. However, technological and manufacturing challenges remain. The discussion will consist of recent milestones and attempts to bridge knowledge gaps to include: The physical and mechano-electrochemical phenomena that affect the stability and kinetics of the Li and Na metal-solid electrolyte interface Thin film processing and Li integration with LLZO Plating and stripping dynamics of Li and Na metal Despite the challenges, SSB technology is rapidly progressing. Multi-disciplinary research in the fields of materials science, solid-state electrochemistry, and solid-state mechanics will play an important role in determining if SSB will make the lab-to-market transition.

**9:00 PM \*F.EN04.20.09**

**Halide-Based Solid-State Batteries—Electrolyte, Stability, Interface and Electrode** Xueliang A. Sun; University of Western Ontario, Canada

All-state-state lithium batteries (ASSLBs) have gained worldwide attention because of intrinsic safety and increased energy density. Compared with other types of solid-state electrolytes including oxide-based, polymer-based and sulfide-based electrolytes, recently-developed halide-based solid-state electrolytes (SSEs) have garnered considerable attention for all-solid-state lithium batteries (ASSLBs) due to the high ionic conductivity, high oxidation voltage and good stability toward oxide cathode materials [1]. However, there are still many challenges in halide-based solid-state electrolytes for ASSLBs including controllable and mass-production synthesis, achieving high humidity tolerance and demonstrate high-performance of ASSLBs; in particular, increased understanding of mechanisms during synthesis and tuning their properties of the electrolytes as well as interface with electrode materials[1].

In this talk, **(i)** I will demonstrate synthesis strategy [2-3], in particular, new and salable water-mediated synthesis method [2]. **(ii)** I will report a systematic study on the correlations among structural evolution,  $\text{Li}^+$  migration properties, and humidity stability resulting of the halide-based electrolytes, along with in-situ characterization for understanding of the mechanisms [4], **(iii)** Full cell battery performance will be optimized [5], **(iv)** humidity ability [6] and **(v)** other applications such as Li-O<sub>2</sub> batteries [7]. In the end, energy densities of ASSLBs using different solid-state electrolytes in ASSLBs will be discussed.



## References:

1. X. Li, J. Liang, X. Yang, K. Adair, C. Wang, F. Zhao, X. Sun. Progress and Perspectives of Halide-based Lithium Conductors for All-Solid-State Batteries. **Energy Environ. Sci.**, 13, 1429-1461 (2020).
2. X. Li, J. Liang, X. Sun, et al., H<sub>2</sub>O-Mediated Synthesis of Superionic Halide Solid Electrolyte. **Angewandte Chemie International Edition**, 58, 16427-16432 (2019).
3. X. Li, J. Liang, X. Sun, et al., Air-Stable Li<sub>3</sub>InCl<sub>6</sub> Electrolyte with High Voltage Compatibility for All-Solid-State Batteries. **Energy Environ. Sci.**, 12, 2665 - 267 (2019).
4. X. Li, J. Liang, X. Sun, et al., Origin of Superionic Halide Solid Electrolytes with High Humidity Tolerance, **J. Am. Chem. Soc.** 142, 7012-7022 (2020).
5. C. Wang, X. Li, J. Liang, X. Sun, et al., Eliminating Interfacial Resistance in All-Inorganic Batteries by In-situ Interfacial Growth of Halide-based Electrolyte. **Nano Energy**, 2020, in press.
6. X. Li, J. Liang, X. Sun, et al., Origin of Superionic Li<sub>3</sub>Y<sub>1-x</sub>In<sub>x</sub>Cl<sub>6</sub> Halide Solid Electrolytes with High Humidity Tolerance, **Nano Letters**, in press, 2020.
7. Zhao, J. X. Sun, et al., Halide-based solid-state electrolyte as an interfacial modifier for high performance solid-state Li-O<sub>2</sub> batteries. **Nano Energy**, 2020, in press

SESSION F.EN04.31: Live Programming Session  
Thursday Afternoon, December 3, 2020  
F.EN04

## 3:00 PM LIVE SESSION

SESSION F.EN04.32: Live Programming Session  
Thursday Morning, December 3, 2020  
F.EN04

## 11:30 AM LIVE SESSION

SESSION F.EN04.33: Live Lithium Metal and Metal Alloy Batteries, Advanced Characterization and Modeling  
Session Chairs: Y. Shirley Meng and Gleb Yushin  
Friday Afternoon, December 4, 2020  
F.EN04

## 1:45 PM F.EN04.20.04

**Voids and Dendrites at the Alkali Metal/Solid Electrolyte Interface** Peter Bruce, Jitti Kasemchainan, Stefanie Zekoll, Dominic Spencer Jolly, Gareth Hartley, Ziyang Ning, Boyang Liu and Paul Adamson; University of Oxford, United Kingdom

Implementing alkali metal anodes and replacing flammable liquid electrolytes with solids promises to deliver higher energy densities and greater safety than conventional Li-ion batteries. However, challenges at both the metal-electrolyte and cathode-electrolyte interfaces must be addressed to realise this potential. It is imperative to maintain good interfacial contact between the solid-state components to achieve low interfacial resistances. Alkali metal dendrite growth, even at modest rates, when paired with dense, well-sintered solid electrolytes, leads to short circuits, and ultimately cell failure. We have used a number of techniques to investigate the effect of cycling conditions on the formation of voids and dendrites and how the latter is intimately connected to the former. These results and their implications for the operation of a failure free all-solid-state

battery will be discussed.

#### **2:25 PM \*F.EN04.03.05**

**Novel Additives and Polymer Coatings for Stabilizing Li-Metal Anodes** Zheng Chen; University of California, San Diego, United States

Li metal is considered as one of the most promising anode materials for high energy batteries, owing to its high theoretical specific capacity and low electrochemical potential. However, notorious issues with the formation of Li dendrites and insufficient coulombic efficiency (CE) during the plating/stripping process prevent its practical applications in rechargeable batteries. These limitations are primarily attributed to fragile and inhomogeneous solid electrolyte interphases (SEIs), which cause continuous consumption of fresh Li and electrolyte during cycling, leading to short battery life. Of late, many efforts have been taken to enhance CE and suppress Li dendrite growth, including design of three-dimensional current collectors, artificial SEI construction on the surface of Li, employment of solid-state electrolytes, separator modification and optimization of electrolyte compositions. In this talk, we will show some recent works in developing novel electrolyte additives and polymer coatings to improve the CE and cycling stability of Li-metal anodes. We demonstrate reasonably stable cell cycling performance under practical conditions such as lean electrolytes and low N/P ratios. The roles of these additives and polymer coatings were also explored to elucidate their function in tuning Li-metal morphology and SEI composition.

#### **3:05 PM OPEN DISCUSSION**

SESSION F.EN04.34: Live Keynote: 2D Atomic and Molecular Sheets—Electronic and Photonic Properties and Device Applications

Session Chairs: Albert Davydov, Jing Kong, Han Wang and Xinran Wang  
Friday Afternoon, December 4, 2020  
F.EN04

#### **6:30 PM F.EN04.10.06**

**Strong Adhesive Pick-up Technique with Polycaprolactone for Rare 2D Materials** Young Shin<sup>1</sup>, Suhan Son<sup>2</sup>, Sungmin Lee<sup>2</sup>, Dohun Kim<sup>2</sup>, Je-Geun Park<sup>2</sup> and Philip Kim<sup>3</sup>; <sup>1</sup>Brookhaven National Laboratory, United States; <sup>2</sup>Seoul National University, Korea (the Republic of); <sup>3</sup>Harvard University, United States

We introduce polycaprolactone (PCL) dry transfer which is a powerful material for picking up non-adhesive van der Waals materials such as NiPS<sub>3</sub>, NbSe<sub>2</sub>, Fe<sub>3</sub>GeTe<sub>2</sub>, ZnPS<sub>3</sub> and bismuth strontium calcium copper oxide (BSCCO) and etc. The heterostructures of Van der Waals were composed of layered atomically thin 2D materials that provide access to new properties important to the quantum information sciences. However, one of the main constraints is the stacking techniques. (PPC) has been known as the highest quality in dry transfer because PPC left less residue on vdW heterostructure through high temperature vacuum annealing but yield of the transfer was low. Here, we present the new polymer, polycaprolactone (PCL) for stacking vdW heterostructure with Rare layered 2D materials by dry transfer at low temperature. These 2D materials were easily detached from hexagonal boron nitride (hBN) assisted with PPC during dry transfer process. We succeeded to pick up many rare superconducting or magnetic 2D materials which were hard to be picked up by conventional dry transfer method from the oxide or silicon nitride substrates.

#### **6:50 PM \*F.EN04.34.01**

**Two-Dimensional Material Heterostructures and Applications** Mark Hersam; Northwestern University, United States

Abstract

#### **7:10 PM \*F.EN04.10.07**

**Strong Magnon-Phonon Hybridization in a 2D van der Waals Antiferromagnet** Thuc Mai<sup>1</sup>, Kevin Garrity<sup>1</sup>, Amber McCreary<sup>1</sup>, J. Argo<sup>2</sup>, Jeffrey Simpson<sup>1,3</sup>, V. Doan-Nguyen<sup>2</sup>, Rolando Valdes Aguilar<sup>2</sup> and Angela Hight Walker<sup>1</sup>; <sup>1</sup>National Institute of Standards and Technology, United States; <sup>2</sup>The Ohio State University, United States; <sup>3</sup>Towson University, United States

Low dimensional, van der Waals (vdW) materials, from graphene to 2D magnets such as  $\text{Fe}_3\text{GeTe}_2$  and  $\text{CrI}_3$ , show exotic behaviors at the atomic layer limit, including superconductivity, long range magnetism and topological edge states. Their “stackability” further creates new opportunities to explore quantum phenomena previously studied only in 3D crystals. Here we demonstrate that magneto-Raman spectroscopy is a unique measurement capability that is exceptionally well suited to study these exotic 2D materials.

Specifically, in the  $\text{MPX}_3$  ( $M=\text{Fe, Mn}$ ;  $X=\text{S, Se}$ ) compounds, inter-layer antiferromagnetic ordering has been suggested to survive in the monolayer limit through the measurement of spin-phonon coupling. Using temperature-, polarization-, and wavelength-dependent Raman scattering, we studied the Neel-type antiferromagnet  $\text{MnPSe}_3$  through its ordering temperature, and as a function of applied magnetic field. Surprisingly, the previously assigned one-magnon scattering peak showed no change in frequency with an increasing in-plane magnetic field. Instead, the Raman data revealed a more surprising story, including changes in resonant Raman scattering due to magnetic ordering as well as the hybridization of phonons with a 2-magnon scattering continuum. These results, which are supported using first-principles calculations, reveal the complex phase space of the interactions of phonons and magnons with regards to temperature, laser excitation wavelength, and magnetic field.

**7:30 PM \*F.EN04.13.02**

**Fundamental Properties of 2D Tellurium Films** Peide P. Ye; Purdue University, United States

Tellurium is one of the special elemental materials which have 1D helical atomic structures and formed by van der Waals force between helical atomic chains. 2D tellurium films can be synthesized in a liquid solution. [1,2] In this talk, we will review the fundamental studies of this new 2D material at atomic scale in terms of its electrical, optical, thermal and mechanical properties. The helical atomic structure offers strong anisotropic properties of this 1D van der Waals material. The band-structure of this 2D material also offers some excellent material properties such as a high value of thermoelectric figure-of-merit  $ZT$  [3] and high carrier mobilities for both electrons and holes. Magneto-transport properties, such as SdH oscillations and QHE in 2D tellurium, were reported before. [4] More interestingly, topological non-trivial properties as Weyl node at conduction band edge are also unveiled in magneto-transport under 45 Tesla at tens of mK temperatures, showing Berry phase and radial spin texture being significantly different from Rashba or Dresselhaus spin-orbit coupling materials [5,6] The work is in close collaborations with Prof. Wenzhuo Wu at Purdue University. References: [1] Wang, Y. et al., Nature Electronics 2018, 1, 228. [2] Du, Y. et al., Nano Letters 2017, 17, 3965. [3] Qiu, G. et al., Nano Letters 2019, 19, 1955. [4] Qiu, G. et al., Nano Letters 2018, 18, 5760. [5] Qiu, G. et al., arXiv. 1908.11495. [6] Niu, C. et al., arXiv. 1909.06659.

**7:50 PM \*F.EN04.10.12**

**Electronic Properties and Device Applications of Quasi-Two-Dimensional Charge-Density-Wave Materials** Alexander Balandin; University of California, Riverside, United States

The charge density wave (CDW) phase is a quantum state consisting of a periodic modulation of the electronic charge density accompanied by a periodic distortion of the atomic lattice in quasi-1D or quasi-2D metallic crystals. Several layered transition metal dichalcogenides (TMDs) exhibit unusually high transition temperatures to different CDW symmetry-reducing phases opening possibility for practical device applications. One of the most promising materials, 1T-TaS<sub>2</sub>, has the CDW transition between the nearly-commensurate (NC-CDW) and the incommensurate (IC-CDW) phases at 350 K. The transition from the IC-CDW phase to the normal metal phase is observed at even higher temperature. In this invited talk, I will review our recent experimental results on controlling the CDW phase transitions with an applied electric field and discuss device applications of quasi-2D CDW materials. We have demonstrated the room-temperature voltage controlled oscillators and logic circuits, which operate on the basis of the NC-to-IC CDW transition in 1T-TaS<sub>2</sub> channels, triggered by the applied voltage [1-2]. We found that the 1T-TaS<sub>2</sub> CDW devices reveal exceptional hardness against X-ray and proton radiations [3-4]. We explained this property of the CDW devices by the high carrier concentration in all their phase states, two-terminal design, and the thin-film channel geometry. The low-frequency electronic noise spectroscopy has been used as an effective tool for monitoring the CDW phase transitions, particularly the switching from the IC-CDW phase to the normal metal phase in 1T-TaS<sub>2</sub> [5]. The noise spectral density exhibits sharp increases at the phase transition points, which correspond to the step-like changes in resistivity. The noise spectroscopy was instrumental in revealing the “hidden phase transitions” in vertical 1T-TaS<sub>2</sub> devices [6]. Preliminary data on the “narrow-band noise” in quasi-2D CDW devices will also be presented.

This work was supported, in part, by the National Science Foundation (NSF) through the DMREF: Collaborative Research (UC Riverside – Stanford): Data Driven Discovery of Synthesis Pathways and Distinguishing Electronic Phenomena of van der Waals Bonded Solids, and by the University of California – National Laboratory Collaborative Research and Training

Program LFR-17-477237, and by the Semiconductor Research Corporation (SRC) contract 2018-NM-2796: One-Dimensional van-der-Waals Metals: Ultimately Downscaled Interconnects with Exceptional Current-Carrying Capacity and Reliability.

- [1] G. Liu, et al., A charge-density-wave oscillator based on an integrated tantalum disulfide–boron nitride–graphene device operating at room temperature, *Nature Nanotechnology*, 11, 845 (2016).
- [2] A. G. Khitun, et al., Transistor-less logic circuits implemented with 2-D charge density wave devices, *IEEE Electron Device Letters*, 39, 1449 (2018).
- [3] G. Liu, et al., Total-ionizing-dose effects on threshold switching in 1T-TaS<sub>2</sub> charge density wave devices, *IEEE Electron Device Letters*, 38, 1724 (2017).
- [4] A. K. Geremew, et al., Proton-irradiation-immune electronics implemented with two-dimensional charge-density-wave devices, *Nanoscale*, 11, 8380 (2019).
- [5] A. K. Geremew, et al., Bias-voltage driven switching of the charge-density-wave and normal metallic phases in 1T-TaS<sub>2</sub> thin-film devices, *ACS Nano*, 13, 7231 (2019).
- [6] R. Salgado, et al., Low-frequency noise spectroscopy of charge- density-wave phase transitions in vertical quasi-2D 1T-TaS<sub>2</sub> devices, *Appl. Phys. Express*, 12, 037001 (2019).

**8:10 PM \*F.MT06.01.02**

**Moire Superpotentials and Quantum Calligraphy of Single Photon Emitters in van der Waals Heterostructures** Berend T. Jonker; Naval Research Laboratory, United States

Single photon emitters (SPEs), or quantum emitters, are key components in a wide range of nascent quantum-based technologies. A solid state host offers many advantages for realization of a functional system, but creation and placement of SPEs are difficult to control. We describe here a novel paradigm for encoding strain into 2D materials to create and deterministically place SPEs in arbitrary locations with nanometer-scale precision [1]. We demonstrate the direct writing of SPEs in 2D semiconductors based on a materials platform consisting of a WSe<sub>2</sub> monolayer on a deformable substrate using an atomic force microscope nano-indentation process. This quantum calligraphy allows deterministic placement and real time design of arbitrary patterns of SPEs for facile coupling with photonic waveguides, cavities and plasmonic structures.

The weak interlayer bonding in van der Waals heterostructures (vdWh) enables one to rotate the layers at arbitrary azimuthal angles. For transition metal dichalcogenide vdWh, twist angle has been treated solely through the use of rigid-lattice moiré patterns. No atomic reconstruction has been observed to date, although reconstruction can be expected to have a significant impact on all measured properties, and its existence will fundamentally change our understanding of such systems. Here we demonstrate via conductive AFM and TEM that vdWh of MoSe<sub>2</sub>/WSe<sub>2</sub> and MoS<sub>2</sub>/WS<sub>2</sub> undergo significant atomic level reconstruction at twist angles  $\leq 1^\circ$  leading to discrete commensurate domains divided by narrow domain walls [2], rather than a smoothly varying rigid-lattice moiré pattern as has been assumed in prior work. We show that this occurs because the energy gained from adopting low energy vertical stacking configurations is larger than the accompanying strain energy [3]. Such reconstruction impacts both the local conductivity and the optical properties.

[1] M.R. Rosenberger et al, *ACS Nano* **13**, 904 (2019). DOI: 10.1021/acsnano.8b08730

[2] M.R. Rosenberger et al, *ACS Nano* **14**, 4550 (2020). <https://dx.doi.org/10.1021/acsnano.0c00088>

[3] M. Phillips and C.S. Hellberg, ArXiv 190902495 Cond-Mat (2019)

\*Work done in collaboration with Matthew R. Rosenberger, Hsun-Jen Chuang, Madeleine Phillips, Kathleen M. McCreary, and C. Stephen Hellberg of the *Naval Research Laboratory*, Washington DC, and Chandriker Kavir Dass and Joshua R. Hendrickson of the *Air Force Research Laboratory*, Wright-Patterson AFB, OH.

† This work was supported by AFOSR and core programs at NRL.

SESSION F.EN04.01: Technologies Enabling Alloying and Conversion Anodes  
On Demand Abstracts Available for Viewing Starting Saturday Morning, November 21, 2020  
F-EN04

**5:00 AM \*F.EN04.01.01**

## **Solid-State Ceramic Battery Electrolyte Processing** Jennifer Rupp; Massachusetts Institute of Technology, United States

Next generation of energy storage devices may largely benefit from fast and solid Li<sup>+</sup> ceramic electrolyte conductors to allow for safe and efficient batteries and fast data calculation. For those applications, the ability of Li-oxides to be processed as thin film structures and with high control over Lithiation and phases at low temperature is of essence to control conductivity. In particular, Li-garnet structures are attractive due to their fast transfer properties and safe operation over a wide electrochemical stability range for batteries. In the first part we focus on low temperature processing of Li-garnet thin films and nanostructures. Examining the structure-Li transport in solid state and asking the provocative question: How do Li-amorphous to crystalline structures conduct? How to alter processing of Li-oxide films to compensate for the challenge that most of Lithium phases lead to sluggish transport and hard phase stabilization? Bringing down battery solid electrolyte processing temperature and decreasing form factor opens new opportunities in battery design and new doors to give more functions for similar material classes for neuromorphic computing. Through the talk, we focus on new processing opportunities to Lithiate thin film structures in crystalline state and to assure cubic and fast conduction on the example of Li-garnet for thin film form using some active Lithiation strategies at film deposition<sup>1-3</sup>. For this we will review the field of thin film processing and introduce to new processing routes based on vacuum and wet-chemical techniques to control various strategies of Lithiation and phase evolution. Excitingly, one has the opportunity for Li-garnet solid state conductors to not only synthesize crystalline structures, but also amorphous films in various frozen-in states<sup>4</sup>. Insights on degree of amorphous to crystalline Li-garnet thin films are presented based on model experiments, incl. JMAK and TTT-diagram analysis of Li-garnet structure types. Dependent on either a vacuum or wet-chemical based method chosen the phase evolution differs when synthesizing the glass states, with significant impact on condensation and Li-transport<sup>5-6</sup>. We find that the different amorphous structures that Li-garnets are no Zachariasen glasses as they violate several of Zachariasen rules by text book: These amorphous Li-garnets differ therefore significantly from LIPON but have a wider room to arrange the higher coordinated polyhedral, network former and builders. In amorphous garnets there is room for manipulation in densification and Li-transport and one may potentially profit from high stability window to design batteries with no grain boundaries at the Li electrolyte interface. Collectively, the insights on solid state energy storage provide evidence for the functionalities that those Li-materials can have in the future. The challenges are deeply connected to low temperature processing and design of structure-transport properties, however, solving those allows us to dream a little more and give materials more functions. 1. A Low Ride on Processing Temperature for a Fast Li Conduction in Garnet Solid State Battery Films R Pfenninger, M. Struzik, I Garbayo, E Stilp, JLM Rupp, Nature Energy, 4, 475-483(2019), 2019 2. Lithium-Containing Thin Films JLM Rupp, R Pfenninger, M. Struzik, A Nanning, I Garbayo, US 62/718,838 (2018) 3. Methods of Fabricating Thin Films Comprising Lithium-Containing Materials JLM Rupp, R Pfenninger, M. Struzik, A Nanning, I Garbayo, US 62/718,842 (2018) 4. Glass-Type Polyamorphism in Li-Garnet Thin Film Solid State Battery Conductors I Garbayo, M Struzik, WJ Bowman, R Pfenninger, JLM Rupp, Advanced Energy Materials, 1702265 (2018) 5. Solid-state Electrolyte and Method of Manufacture Thereof. ZD Hood, Y Zhu, L Miara, JLM Rupp. US 62/713,366 (2018) 6. Solution-Processed Solid-state Electrolyte and Method of Manufacture Thereof. Y Zhu, ZD Hood, L Miara, JLM Rupp US 62/713,428 (2018)

### **5:15 AM F.EN04.01.02**

**Interface Engineering to Enhance the Performance of All-Solid-State Lithium Metal Batteries** Yang Li, Thad Druffel, Mahendra Mahendra Sunkara and Hui Wang; University of Louisville, United States

All-solid-state lithium (Li) metal batteries (ASSLMBs) attract increasing attention due to the use of high-capacity Li metal anode and solid electrolytes (SEs) with high safety. Recently, significant research achievements have been made in developing Li-ion conductors. In particular, sulphide SEs generally offer higher ionic conductivity ( $10^{-4}$ – $10^{-3}$  S cm<sup>-1</sup> at room temperature) and lower grain boundary resistance. However, the practical applications of sulfide-based ASSLMBs are significantly hampered due to the interfacial challenges originating from (1) poor solid-solid contact between SE and electrode; (2) significant reaction at SE/Li interface. To solve these issues and enhance the electrochemical performance of sulfide-based ASSLMBs, here, we employed a polymer interlayer between Li<sub>6</sub>PS<sub>5</sub>Cl SE and electrodes. It was found that the contact resistance was remarkably eliminated and the instability of SE against Li metal was resolved owing to the engineered polymer interlayer. In addition, long-term cycling stability was achieved due to the chemical compatibility between SE and this polymer interlayer. This method provides an effective strategy to address the interfacial challenge between sulfide SEs and Li metal, enabling the successful utilization of Li metal and sulfide SEs in ASSLMBs towards next-generation safe and high-energy density energy storage systems.

### **5:25 AM F.EN04.01.05**

**Mn<sub>1-x</sub>V<sub>x</sub>P Solid Solution Phosphides for Alloying/Insertion Dual Reaction Lithium-Ion Battery Anode** Kyeong-Ho Kim, Juhyun Oh, Chul-Ho Jung, Miyoung Kim and Seong-Hyeon Hong; Seoul National University, Korea (the Republic of)

Recently, the beneficial combination of two different lithium storage mechanisms in a single compound, referred to as conversion and alloying materials (CAMs), has been noticed to complement the shortcomings of the conversion and alloying mechanisms [1,2]. This could lead to the excellent synergistic effects due to their atomically homogeneous and finer distribution than the physically mixed nanocomposite between two materials. However, the combination between alloying and insertion reaction or conversion and insertion reaction materials has been rarely investigated even it is expected to show superior cycle retention with an intermediate specific capacity than that of CAMs or other anode materials. Unlike the known CAMs, the realization of dual reaction with insertion reaction in a single compound requires a consideration of the crystal structure relation between two different materials, not simple comprising elements in the compound. Since the insertion reaction anodes have sufficient spaces to accommodate the reversible lithium ion insertion/extraction in their crystal structure, the dual reaction material should be designed with the similar crystal structure, which could be the solid solution compounds exhibiting a high solubility limit with an insertion-reaction type structure. The lack of consideration for the structural relation prevents the realization of dual reaction anode with an insertion reaction mechanism in a single compound. In this study, we suggest a new concept of highly stable alloying/insertion dual reaction anode of  $Mn_{1-x}V_xP$  solid solution by combining alloying reaction type MnP and insertion reaction type VP based on their structural similarity. The crystal structures of MnP and VP are basically similar, but their electrochemical performance as anodes for lithium-ion batteries (LIBs) is entirely different [3,4]. In this regard, the combination of MnP and VP into a single compound could form a fascinating solid solution anode with synergistic effects on electrochemical performance through alloying/insertion dual reaction mechanism derived its structural similarity. The series of  $Mn_{1-x}V_xP$  compounds ( $x = 0, 0.25, 0.5, 0.75, \text{ and } 1.0$ ) are firstly synthesized with a facile high energy mechanical milling and their electrochemical properties as an anode for LIBs were systematically studied and compared with those of MnP/VP mixture composite, particularly focusing on the verification of simultaneous alloying/insertion dual anode reaction in the solid solution compounds. The  $Mn_{1-x}V_xP$  ( $x = 0.25$ ) solid solution electrode showed the excellent high-rate cyclability delivering the reversible capacity of 310 mAh g<sup>-1</sup> after 400 cycles with a negligible capacity fading at 2 A g<sup>-1</sup> by the synergistic effects of two reaction mechanisms. [1] D. Bresser et al., *Energy Environ. Sci.*, 9, 3348-3367 (2016). [2] F. Wu et al., *Nanoscale*, 7, 17211-17230 (2015). [3] L. Li et al., *Electrochim. Acta*, 95, 230 (2013). [4] C.-M. Park et al., *Chem. Mater.*, 21, 5566-5568 (2009).

#### 5:35 AM F.EN04.01.08

**Revisiting the Use of Square Root Scaling in Battery Analyses** [Stephen J. Harris](#)<sup>1</sup>, Peter Attia<sup>2</sup> and William C. Chueh<sup>2</sup>; <sup>1</sup>Lawrence Berkeley National Laboratory, United States; <sup>2</sup>Stanford University, United States

A number of Li battery processes, including growth of Li dendrites, growth of SEI, and the effect of pressure on the internal resistance in solid state batteries, have been understood using a square root scaling, in line with simple models such as diffusion-limited metal/semiconductor oxidation. This model performs sufficiently well for some empirical predictions of capacity fade via SEI growth in lithium-ion batteries, for example. However, the  $t^{0.5}$  model is not theoretically well-justified to describe SEI growth in many cases. Furthermore, this model is not necessarily the best-fitting empirical model for published literature data. In this work, we illustrate these limitations and suggest an alternative approach for accurate estimates and predictions of SEI growth: evaluating and comparing the performance of multiple models. We also provide other examples where a square root scaling has been improperly assumed.

#### SESSION F.EN04.02: Solid-State Batteries

On Demand Abstracts Available for Viewing Starting Saturday Morning, November 21, 2020

F-EN04

#### 5:00 AM F.EN04.02.01

**Void and Dendrites at the Alkali Metal/Solid Electrolyte Interface** [Peter Bruce](#), Jitti Kasemchainan, Stefanie Zekoll, Dominic Spencer Jolly, Gareth Hartley, Ziyang Ning, Boyang Liu and Paul Adamson; University of Oxford, United Kingdom

Implementing alkali metal anodes and replacing flammable liquid electrolytes with solids promises to deliver higher energy densities and greater safety than conventional Li-ion batteries. However, challenges at both the metal-electrolyte and cathode-electrolyte interfaces must be addressed to realise this potential. It is imperative to maintain good interfacial contact between the solid-state components to achieve low interfacial resistances. Alkali metal dendrite growth, even at modest rates, when paired with dense, well-sintered solid electrolytes, leads to short circuits, and ultimately cell failure. We have used a number of techniques to investigate the effect of cycling conditions on the formation of voids and dendrites and how the latter is

intimately connected to the former. These results and their implications for the operation of a failure free all-solid-state battery will be discussed.

#### **5:10 AM F.EN04.02.05**

**Pressure-Driven Evolution of the Interface Between Li-Metal and a Ceramic Solid Electrolyte Such as LLZO** Stephen J. Harris<sup>1</sup>, Xin Zhang<sup>2</sup>, Q. Jane Wang<sup>2</sup>, Katharine Harrison<sup>3</sup> and Scott A. Roberts<sup>3</sup>; <sup>1</sup>Lawrence Berkeley National Laboratory, United States; <sup>2</sup>Northwestern University, United States; <sup>3</sup>Sandia National Laboratories, United States

Recent experiments have shown that applying a stack pressure can strongly alter both the electrical and mechanical behavior of Li metal-solid electrolyte (SE) systems. To understand quantitatively the relationship between pressure, Li microstructure, and the Li-SE interface resistance, we have developed a 3D time-dependent contact model for describing the Li-SE interface evolution under a stack pressure. Our simulation simultaneously considers the surface roughness of the Li and the SE, Li elastoplasticity, Li creep, and the Li metal plating/stripping process. Our spatial scale runs from tens of nm to sub-mm, and our time scale runs from 50 ms to 50 hours. We describe quantitatively the competition between charge/discharge and creep, and how that competition controls the interfacial resistance. We demonstrate how to predict whether plating/stripping is stable or unstable under given conditions. And we describe a simple technique that can allow determination of the absolute area-specific resistance of the Li-SE interface. Simultaneous fitting to very recent experiments from two different research groups requires an effective yield strength of the Li used in those experiments of  $16 \pm 2$  MPa, substantially higher than traditional values.

#### SESSION F.EN04.03: Li-Metal Anode

On Demand Abstracts Available for Viewing Starting Saturday Morning, November 21, 2020

F-EN04

#### **5:00 AM \*F.EN04.03.01**

**Stabilizing Solid Li and Na Metal Anodes Using Ceramic Membrane Technology** Jeff Sakamoto<sup>1</sup>, Michael Wang<sup>1</sup>, Marie-Claude Bay<sup>2</sup> and Corsin Battaglia<sup>2</sup>; <sup>1</sup>University of Michigan, United States; <sup>2</sup>Empa–Swiss Federal Laboratories for Materials Science and Technology, Switzerland

There is tremendous interest in making the next super battery, but state-of-the-art Li-ion technology works well and has inertia in several commercial markets. Supplanting Li-ion will be difficult. Recent material breakthroughs in Li and Na metal solid-state electrolytes could enable a new class of non-combustible solid-state batteries (SSB) delivering twice the energy density (1,200 Wh/L) compared to Li-ion. However, technological and manufacturing challenges remain. The discussion will consist of recent milestones and attempts to bridge knowledge gaps to include: The physical and mechano-electrochemical phenomena that affect the stability and kinetics of the Li and Na metal-solid electrolyte interface Thin film processing and Li integration with LLZO Plating and stripping dynamics of Li and Na metal Despite the challenges, SSB technology is rapidly progressing. Multi-disciplinary research in the fields of materials science, solid-state electrochemistry, and solid-state mechanics will play an important role in determining if SSB will make the lab-to-market transition.

#### **5:15 AM F.EN04.03.04**

**Enabling Lithium Metal Anode for Solid-State Batteries by Mechanical Constriction Design Principle** Xin Li; Harvard University, United States

Mechanical constriction theory and simulation technique were recently developed by our group to quantitatively describe the expansion of voltage stability window and modification of instability decomposition for solid state batteries based on sulfide solid electrolyte.[1,2,3] In solid state batteries, lithium dendrites form when the applied current density is higher than a critical value. In this talk, an advanced mechanical constriction technique is applied on a solid-state battery constructed with Li<sub>10</sub>GeP<sub>2</sub>S<sub>12</sub> (LGPS) as the electrolyte and lithium metal as the anode. The decomposition pathway of LGPS at the anode interface is modified by this mechanical constriction and the growth of lithium dendrite is inhibited, leading to excellent rate and cycling performances. A combination of electrochemical battery tests, SEM, XPS and XRD characterizations, and DFT simulations were used. 1. Advanced sulfide solid electrolyte by core-shell structural design, Nature Communications, (9), 4037 (2018) 2. Strain-stabilized ceramic-sulfide electrolytes, Small, 15, 1901470 (2019) 3. The effects of mechanical constriction on the operation of sulfide based solid-state batteries, Journal of Materials Chemistry A: 7, 23604 - 23627 (2019)

**5:25 AM \*F.EN04.03.05**

**Novel Additives and Polymer Coatings for Stabilizing Li-Metal Anodes** Zheng Chen; University of California, San Diego, United States

Li metal is considered as one of the most promising anode materials for high energy batteries, owing to its high theoretical specific capacity and low electrochemical potential. However, notorious issues with the formation of Li dendrites and insufficient coulombic efficiency (CE) during the plating/stripping process prevent its practical applications in rechargeable batteries. These limitations are primarily attributed to fragile and inhomogeneous solid electrolyte interphases (SEIs), which cause continuous consumption of fresh Li and electrolyte during cycling, leading to short battery life. Of late, many efforts have been taken to enhance CE and suppress Li dendrite growth, including design of three-dimensional current collectors, artificial SEI construction on the surface of Li, employment of solid-state electrolytes, separator modification and optimization of electrolyte compositions. In this talk, we will show some recent works in developing novel electrolyte additives and polymer coatings to improve the CE and cycling stability of Li-metal anodes. We demonstrate reasonably stable cell cycling performance under practical conditions such as lean electrolytes and low N/P ratios. The roles of these additives and polymer coatings were also explored to elucidate their function in tuning Li-metal morphology and SEI composition.

**5:40 AM F.EN04.03.08**

**Cu<sub>2</sub>P a Novel Conversion Anode for Li Ion Batteries** Angela F. Harper<sup>1</sup>, Matthew Evans<sup>1</sup> and Andrew J. Morris<sup>2</sup>; <sup>1</sup>University of Cambridge, United Kingdom; <sup>2</sup>University of Birmingham, United Kingdom

By utilizing a combination of ab initio random structure searching, genetic algorithms, and prototyping, we have identified a new phase of copper phosphides, Fm-3m Cu<sub>2</sub>P, which is a potential candidate for a high capacity conversion anode [1]. Within the copper phosphide phase diagram, Cu<sub>3</sub>P is currently the highest capacity material with a capacity of 363 mAh/g, however Cu<sub>2</sub>P has a theoretical capacity of 508 mAh/g, which is higher than both Cu<sub>3</sub>P and the commonly used graphite anodes. Although many conversion anodes exhibit volume expansions above 150%, Cu<sub>2</sub>P has a limited volume expansion of 99%, similar to Cu<sub>3</sub>P which has been previously used as an anode for Li-ion and Na-ion batteries. We calculate the dynamical stability of Cu<sub>2</sub>P using the vibrational effects from 0 K phonon modes, which suggest that Cu<sub>2</sub>P is stable up to temperatures of 600 K. We predict that Cu<sub>2</sub>P, if synthesized experimentally, would therefore be a successful conversion anode for future battery applications, and outperform other conversion anodes within the copper phosphide phase diagram.

[1] Harper et al., Chem. Mater. 2020, 32, 15, 6629–6639

## SESSION F.EN04.04: Mg and Na Electrochemistry

On Demand Abstracts Available for Viewing Starting Saturday Morning, November 21, 2020

F-EN04

**5:00 AM F.EN04.04.02**

**Understanding the Role of Electrochemically Inactive Dopant in Layered Oxide Cathode Materials for Advanced Sodium-Ion Batteries** Junghoon Yang and Sang-Don Han; National Renewable Energy Laboratory, United States

The importance of electrochemical energy storage systems for large-scale application has been growing increasingly over the last decade. Due to high cost, limited source and several technical barriers of the lithium ion system, sodium ion batteries are considered as one of promising candidates for large-scale energy storage systems considering their cost-effective, earth abundant and recyclable characteristics.[1] As cathode materials for sodium ion batteries, sodium transition metal (TM) oxide with layered structures (Na<sub>x</sub>TMO<sub>2</sub>, 0.5 < x < 1.0) demonstrated high energy density similar to cathode for lithium ion batteries.[2] However, the capacity retention of the cell with layered structure cathode is not optimized especially when it is charged and discharged fully to obtain higher capacity. The major reason for this is a phase transition induced by gliding of transition metal slabs, which causes irreversible structural changes gradually during cycling.[3] To address this phase transition problem, we doped electrochemically inactive components in the transition metal sites with precise ratio control. The introduction of the inactive components (by substituting with existing transition metal(s)) consumed some of reversible capacity, but it is able to provide improved capacity retention due to their enhanced structural stability. In addition, we systematically studied the reversible capacity and corresponding phase transition behavior of layered type oxide materials with/without dopant(s) under various voltage window ranges to figure out the role of electrochemically inactive dopants. By



tracing the structural changes using in-situ XRD, we determined the optimized ratio of electrochemically inactive components to minimize and/or detain the phase transition. The results can provide the insights of the phase transition mechanism of layered type cathode materials and the strategies to suppress them by stabilizing the structure, thus enabling rational design of new cathode materials for the development of next generation advanced Na-ion batteries. [1] M. D. Slater, D. Kim, E. Lee, C. S. Johnson, *Adv. Funct. Mater.* 23 (2013) 947-958. [2] C. Delmas, C. Fouassier, P. Hagenuller, *Physica B+C* 99 (1980) 81-85. [3] E. Talaie, V. Duffort, H. L. Smith, B. Fultz, L. F. Nazar, *Energy Environ. Sci.*, 5 (2015) 2512.

#### 5:10 AM F.EN04.04.04

**Atomistic Mechanism of Na Intercalation into Amorphous Carbon—A First-Principles Study** Yu-Jen Tsai and Chin-Lung Kuo; National Taiwan University, Taiwan

Amorphous carbon is a promising anode materials for Na-ion batteries since it has been reported to exhibit high Na storage capacity (180~420 mAh g<sup>-1</sup>) as compared to graphite (~35 mAh g<sup>-1</sup>) and other potential candidates. Previous studies suggested that Na ions can be easily intercalated into amorphous carbon primarily because of its large interlayer distance as well as the presence of vacancy defects. However, the fundamental mechanisms remain unclear yet to date. In this work, we employed first-principles density functional theory calculations to investigate the atomistic mechanism of Na intercalation into amorphous carbon. Furthermore, we recalibrated the dispersion coefficients for C and Na in the DFT-D2 method to reproduce the d-spacing and the Na/Li storage capacity of bulk graphite measured in the experiments. This refined potential was then used to describe the van der Waals interactions between Na and amorphous carbon in this study. Our calculations first revealed that the interlayer spacing is not the main factor that hinders the intercalation of Na into the carbon-based electrodes. When the equilibrium d-spacing of graphite increased from 3.35 to 4.40 Å by weakening the C-C van der Waals interaction, the Na capacity was only slightly raised up from 35 to 70 mAh g<sup>-1</sup>, which is still much lower than the Na capacity of amorphous carbon. We next investigated the C vacancy effect on the Na capacity of graphene monolayer. Our results showed that the achievable Na capacity limit is only half of the achievable Li capacity limit on both monovacancy and divacancy defects in graphene, indicating a much weaker binding strength of Na to graphene as compared to Li. Moreover, our calculations showed that the Na storage capacity can be effectively enhanced by increasing the degree of structural disorders and non-hexagonal rings in the graphene sheets, which can even turn the neighboring hexagonal rings into the active sites for Na intercalation. Our results suggest that the presence of large amounts of non-hexagonal rings in the bond network is the main driving force that triggers the intercalation of Na into amorphous carbon, which can be more effective than creating vacancies on the surface of the carbon electrodes. It was also found that the amorphous bond network can become much softer as the number of non-hexagonal rings increases. The increased softness of the amorphous bond network can be beneficial in reducing the strain energy induced by Na intercalation, thereby contributing to the Na storage capacity of the amorphous carbon electrode. Accordingly, our study can provide a new insight toward a mechanistic understanding of Na intercalation into the amorphous carbon electrode.

#### 5:20 AM \*F.EN04.04.05

**Understanding the Influence of Adsorbed Water on Metal Oxides Operating in Non-Aqueous Mg-Ion Electrolytes** Veronica Augustyn; North Carolina State University, United States

There is a significant interest in understanding the factors that influence multivalent ion intercalation kinetics into oxide host materials. Recently, the addition of water into non-aqueous Mg<sup>2+</sup> electrolytes was proposed as a strategy to decrease interfacial charge transfer resistance and increase solid state Mg<sup>2+</sup> diffusion into different transition metal-based intercalation hosts. To investigate the role of this adsorbed water, we added known amounts of H<sub>2</sub>O to a non-aqueous magnesium ion electrolyte (Mg(ClO<sub>4</sub>)<sub>2</sub> in acetonitrile) and performed cyclic voltammetry with a tungsten oxide (WO<sub>3</sub>) electrode. Similar to other reports, we find increased kinetic reversibility as the electrolyte water content increases. The WO<sub>3</sub> electrode undergoes reversible electrochromism indicative of an intercalation process. We investigated the nature of the water in the non-aqueous electrolyte using solution <sup>1</sup>H NMR and molecular dynamics simulations. To investigate the nature of the intercalated species (and in particular, the potential for proton intercalation) and the energy storage mechanism, we performed ex situ X-ray diffraction, solid state <sup>1</sup>H NMR, and inductively coupled plasma-optical emission spectroscopy. Our combined results suggest that adsorbed water in non-aqueous electrolytes may increase the surface, and not solid-state, diffusivity and thus lead to enhanced energy storage kinetics.

#### 5:35 AM F.EN04.04.06

**Engineering an Aqueous Energy Dense Manganese Dioxide|Zinc Battery to Challenge Lithium-Ion's Dominance** Gautam G. Yadav; Urban Electric Power, United States

The current landscape of energy storage systems is dominated by lithium-ion batteries because of their high energy densities,

and continuous improvement in performance through the last few decades for use in a number of applications. They certainly have been a boon for rapid societal development; however, they also have had major disadvantages like high cost, severe toxicity, high chances of flammability and ethical concerns about the use of cobalt. Aqueous batteries containing manganese dioxide (MnO<sub>2</sub>) and zinc (Zn) have the theoretical capacities to deliver high energy densities comparable to some variations of lithium-ion batteries, have low cost and toxicity, and high material abundance to be used as an alternative battery compared to the current status quo. However, MnO<sub>2</sub> and Zn have been highly irreversible and accessing close to their theoretical capacities has been very challenging. The current status quo in aqueous batteries has been to intercalate Zn and H<sup>+</sup> ions into layered structures to deliver modest capacities, which also has unfortunately resulted in limited energy densities. These layered structures, although novel, face limitations like their layered counterparts in lithium (Li)-ion batteries, where the capacity is limited to the host's intercalation capacity. Low voltage of ~1.1-1.4V is another Achilles heel of aqueous Zn-anode batteries, where it is simply not comparable to the high voltage properties of Li-ion. MnO<sub>2</sub>/Zn batteries can compete with Li-ion because of its safe and abundant raw materials, nonflammable electrolyte and theoretical energy density, however, sufficient advances are required for it to be considered a true challenger. In this talk, we will present a new strategy to enable a new generation of energy dense aqueous-based batteries, where we exploit the conversion reactions of MnO<sub>2</sub> and Zn electrodes to extract significantly higher capacity compared to intercalation systems. Accessing the conversion reactions allows us to achieve theoretical capacities of 617 mAh/g (~30 mAh/cm<sup>2</sup>) from MnO<sub>2</sub> and 810 mAh/g (~30 mAh/cm<sup>2</sup>) from Zn anodes, respectively. The high areal capacities help to attain unprecedented energy densities of 210 Wh/L, which is the highest of all aqueous-based batteries. We will also present our work on identifying new Mn-based conversion compounds that give higher capacities and demonstrate its application in the case of small-scale automobile. We will also present our breakthrough work on breaking the 2V barrier in aqueous Zn batteries, where we have demonstrated for the first time in the field of energy storage 2.45V and 2.8V MnO<sub>2</sub>/Zn aqueous batteries capable of accessing the theoretical capacity, which can truly challenge Li-ion's dominance. Finally, we will briefly present our commercialization experience, and how market forces and application have guided the design and research of these batteries.

#### 5:45 AM F.EN04.04.07

**Characterizing Mechanical and Microstructural Properties of Novel Montmorillonite-Based Sodium-Ion Conductors** [Ryan C. Hill](#)<sup>1</sup>, Yang-Tse Cheng<sup>1</sup>, Erik Spoecke<sup>2</sup> and Amanda Peretti<sup>2</sup>; <sup>1</sup>University of Kentucky, United States; <sup>2</sup>Sandia National Laboratories, United States

Rapidly growing demands for electrical energy storage have motivated active research into new safe, low-cost technologies, such as sodium-based batteries. Solid-state sodium-ion conductors are central elements of emerging molten sodium, solid-state, and even sodium-ion batteries designed for effective long-term applications. Traditional sodium-ion conductors, such as  $\gamma$ -alumina or the sodium super ion conductor, NaSICON, however, can be expensive or difficult to process, they often suffer from limited ionic conductivity at desirable low to intermediate temperatures, and they can be mechanically fragile, limiting their long-term durability. A simple, low-cost alternative ion conducting candidate proposed by researchers at Sandia National Laboratories aims to utilize layered sodium-montmorillonite (MMT) clay and MMT/polymer composites. In this presentation, the microstructural, mechanical and electrochemical properties of the MMT-based solid electrolytes are investigated and correlated. Characterization methods such as x-ray diffraction, atomic force microscopy, and scanning electron microscopy together with measurement techniques such as nanoindentation and bulk and local electrochemical impedance spectroscopy (EIS) inform important structure-property relationships in materials with room temperature ionic conductivities rivaling conventional ceramic electrolytes. Utilizing these techniques, we have discovered that MMT processing can impact the layered microstructure, chemical integrity, and subsequently not only the ionic conductivity, but critically the elastic modulus and hardness of prepared bulk MMT ion conductors. Recognizing the importance of mechanical integrity for high performance, reliable solid-state ion conductors, these studies reveal that many of the processing parameters that degrade ionic conductivity also diminish the mechanical properties in these materials. Understanding these relationships will help guide new studies to engineer the development of robust, highly conductive MMT-based separators.

SESSION F.EN04.05: Advanced Electrodes

On Demand Abstracts Available for Viewing Starting Saturday Morning, November 21, 2020  
F-EN04

#### 5:00 AM F.EN04.05.01

***In Situ* and *Operando* Electrochemical Investigation of Cobalt-Free, Nickel-Rich Layered Oxide Cathode for Next Generation Lithium-Ion Batteries** [Shankar Aryal](#), Jessica Durham, Albert L. Lipson, Krzysztof Z. Puzek and Ozenur

Kahvecioglu; Argonne National Laboratory, United States

Nickel-rich layered oxide cathodes are promising candidates to achieve high energy density lithium ion batteries (LIB) because of lower content of expensive and toxic cobalt. However, transition metal dissolution, increased structural disorder, material amorphization upon cycling and parasitic reactions between organic electrolyte and nickel-rich composition lead to both capacity and voltage fading upon cycling. Extensive work has been reported on NMC532, NMC622 and NMC811 compositions, which are already commercialized. Recently, the battery research community is increasing nickel content in NMC based layered oxide cathodes to increase gravimetric capacity. Nickel-rich cathodes with nickel content above 80% aren't fully understood and their synthesis at larger scales requires optimization. This presentation reports cobalt-free, nickel-rich  $\text{LiNi}_{0.9}\text{Mn}_{0.1}\text{O}_2$  cathode material synthesized at a moderate level (500 g), using co-precipitation method in a 1 liter Taylor Vortex Reactor. The physical and chemical properties of the cathode material were measured with scanning electron microscopy (SEM), x-ray diffraction (XRD), and x-ray absorption spectroscopy (XAS). In-operando XAS was measured at Ni and Mn K-edges to examine oxidation state and local geometry of transition metal atoms as a function of state of charge. Additionally, ex-situ XAS and synchrotron XRD before and after long term cycling were utilized to understand the degradation mechanism and provide insight for designing cathode material with better performance.

#### 5:10 AM F.EN04.05.03

**Li-Ion Cathodes Based on Disordered Rock Salt Structures, Oxides and Oxyfluorides** Damien P. Guegan<sup>1</sup>, Jean-François Colin<sup>1</sup>, Adrien Boulineau<sup>1</sup>, Sebastien Martinet<sup>1</sup> and Pierre-Etienne Cabelguen<sup>2</sup>; <sup>1</sup>Université Grenoble Alpes, France; <sup>2</sup>Umicore, Belgium

This work explores a new class of material for Li-ion cathodes, based on disordered rock salt structures, in particular the composition  $\text{Li}_{1.2}\text{Mn}_{0.6}\text{Nb}_{0.2}\text{O}_2$  and the oxyfluoride versions  $\text{Li}_{1.2}\text{Mn}_{0.6}\text{Nb}_{0.2}\text{O}_{2-x}\text{Fx}$ . The classical approach of layered oxides, as their name indicates, consist in a superposition of separated layers of transition metals (TM) and Li in an oxygen network. On the contrary disordered rocksalt materials still compose of an oxygen network but in which all cations share their positions. This structure of material was ignored for a long time, the reason being that it generally did not seem to allow for Li ions conduction. However this structure very easily accommodate with Li-rich compositions. Based on previous studies carried out by the Ceder's group[1], it was demonstrated that in the case of Li-rich materials Li ions conduction was possible. Therefore, this class of materials was the perfect choice to attain higher energy densities via the increase of Li content. Considering that in Li-rich materials the redox capabilities of the TM are smaller than the Li content, we usually observe oxygen redox activity for these materials. Depending on the composition of the material, this contribution can go from very to hardly reversible[2]. Knowing that the oxygen contribution is inevitable, two approaches are valid to improve cycling performances: stabilise the oxygen or increase the redox part of the TM. To achieve both we introduce fluoride in the oxygen network. This work aims to deepen the understanding of the material structure and electrochemical behaviour via an experimental approach. We synthesised various samples of disordered rock salt materials using the solid-state approach. The oxide material is metastable and the synthesis requires special apparatus. The oxyfluoride is even more constrained with the use of high temperatures and corrosive precursors such as LiF and (TM)Fx. Materials synthesised were then characterised using advanced microscopy and spectroscopy technics, especially, a particular structure with short range order (SRO) was observed by TEM (transmission electron microscope) despite the long range order observed using XRD (X-ray diffraction). These structural observations are explained and are put in perspective with the electrochemical performances. In regards to oxygen stability, which is one of the main structural issues in Li-rich materials, we investigate the benefits of a fluoride doping. The cycling performances indicate an influence of surface reactivity and conductivity. To respond to such limitations new coating strategies were set in place. A carbon coating has led to improved electrochemical performances, which can come from either surface protection or enhanced electronic conductivity (or combination). [1] Urban, Lee, et Ceder, « The Configurational Space of Rocksalt-Type Oxides for High-Capacity Lithium Battery Electrodes ». [2] Yabuuchi, « Material Design Concept of Lithium-Excess Electrode Materials with Rocksalt-Related Structures for Rechargeable Non-Aqueous Batteries ».

#### 5:20 AM F.EN04.05.04

**Synergy of Epoxy Chemical Tethers and Defect-Free Graphene in Enabling Stable Lithium Cycling of Silicon Nanoparticles** David Mitlin; The University of Texas at Austin, United States

We report a new approach for nanosilicon-graphene hybrids with uniquely stable solid electrolyte interphase. Expanded graphite is gently exfoliated creating "defect-free" graphene that is non-catalytic towards electrolyte decomposition, simultaneously introducing high mass loading (48wt.%) Si nanoparticles. Silane surface treatment creates epoxy chemical tethers, mechanically binding nano-Si to CMC binder through epoxy ring-opening reaction while stabilizing the Si surface chemistry. Epoxy-tethered Silicon pristine-Graphene hybrid "E-Si-pG" exhibits state-of-the-art performance in full battery

opposing commercial mass loading (12 mg cm<sup>-2</sup>) LiCoO<sub>2</sub> (LCO) cathode. At 0.4 C, with areal capacity of 1.62 mAh cm<sup>-2</sup> and energy of 437 Wh kg<sup>-1</sup>, achieving 1.32 mAh cm<sup>-2</sup>, 340.4 Wh kg<sup>-1</sup> at 1C. After 150 cycles, it retains 1.25 mAh cm<sup>-2</sup>, 306.5 Wh kg<sup>-1</sup>. Sputter-down XPS demonstrates survival of surface C-Si-O-Si groups in E-Si-pG after repeated cycling. The discovered synergy between support defects, chemical-mechanical stabilization of Si surfaces, and SEI-related failure may become key LIB anode design rule.

### 5:30 AM F.EN04.05.06

**A Controllable, Affordable and Scalable Method for Synthesizing Silicon-Carbon Composites for Lithium-Ion Batteries** Joseph Schwan<sup>1</sup>, Giorgio Nava<sup>1</sup>, Matthew Boebinger<sup>2</sup>, Matthew T. McDowell<sup>2</sup> and Lorenzo Mangolini<sup>1</sup>; <sup>1</sup>University of California, Riverside, United States; <sup>2</sup>Georgia Institute of Technology, United States

From as far back as 1971 researchers have been intensively working on developing strategies for integrating silicon into commercial lithium-ion batteries with the goal of developing more energy-dense energy storage devices. Relatively quickly, the research community determined that silicon-carbon nanocomposites were a promising avenue to address this technical challenge, allowing for long cycle-life electrodes as well as overcoming the swelling experienced by silicon.<sup>1</sup> However, the majority of proposed synthesis methods of these complex and intricate nanostructures have proven to be too expensive, slow, or unable to scale to meet potential demand. Within this contribution we present a cost-effective solution suitable for large-volume production through a chemical vapor deposition -CVD- process based on a cheap acetylene precursor and largely available off-the-shelf silicon nanoparticles -SNPs. Key advantages of this method are the precise and decoupled control of both the carbon layer thickness and its graphitization degree. This is achieved by separating the CVD process into two steps: first the SNPs are placed into a furnace and exposed to pure acetylene at 650oC permitting thermal cracking of the precursor and causing a uniform deposition of amorphous carbon on the particles, with shell thickness depending on the amount of time spent in CVD; next the reactor is drained of acetylene, refilled with argon at low pressure, and brought up to 1000oC to instigate graphitization. Notably, this approach achieves the described result of a silicon-core coated with a uniform graphitic shell without any protective oxide shell or the formation of silicon carbide phases, both of which would negatively affect the battery performance. By taking advantage of the flexibility of the described approach, we were also able to delve into the effects on electrochemical performance and charging mechanism resulting from the interplay between a silicon-core and carbon-shell of varying graphitization degree. Through the use of core-shell particles with identical silicon cores and carbon layer thicknesses, but by varying the degree of shell graphitization (i.e. amorphous carbon and highly graphitic carbon), this work highlights how this simple property of the carbon-coating bears a profound influence on the material's electrochemical characteristics. In-situ TEM lithiation experiments revealed insights into the surprisingly poorly understood interaction between silicon and carbon in lithium-ion batteries, showing that a highly graphitized carbon layer significantly promotes the lithium ion diffusion dynamics into the silicon core with respect to an amorphous coating. As a result, lithium-ion battery anodes produced with graphitic-carbon coated SNPs exhibit markedly enhanced coulombic efficiencies and capacity retention upon cycling with respect to amorphous-carbon coated SNPs.<sup>2</sup> Finally, the optimized composite produced with our CVD method can operate both as a pure high-charge-density anode material as well as a "drop-in" additive for graphite-dominant anodes. The pure composite boasts 1800mAh g<sup>-1</sup> in half-cell testing and a first cycle coulombic efficiency -FCCE- of 87%, while replacing 10% in weight of a standard graphite anode increases capacity from 330mAh g<sup>-1</sup> to 600mAh g<sup>-1</sup> with FCCE of 90% and capacity retention of 81% over 100 cycles. [1] Zuo, X.; Zhu, J.; Muller-Buschbaum, P.; Cheng, Y.-J. Silicon based lithium-ion battery anodes: A chronicle perspective review. *Nano Energy*. 2017, 31, 113-143. [2] Nava, G.; Schwan, J.; Boebinger, M.; McDowell M.; Mangolini, L. Silicon-Core-Carbon-Shell Nanoparticles for Lithium Ion Batteries: Rational Comparison between Amorphous and Graphitic Carbon Coatings. *Nano Letters*. 2019, 19 (10), 7236-7245.

### SESSION F.EN04.06: Conversion-Type Electrotype Materials

On Demand Abstracts Available for Viewing Starting Saturday Morning, November 21, 2020

F-EN04

### 5:00 AM \*F.EN04.06.01

**The Vital Role of Electrolyte Design in Enabling Conversion Chemistries for Beyond Li-Ion Batteries** Graham Leverick<sup>1</sup>, Emily J. Crabb<sup>1</sup>, Arthur France-Lanord<sup>1</sup>, Ryan Stephens<sup>2</sup>, Jeffrey Grossman<sup>1</sup> and Yang Shao-Horn<sup>1</sup>; <sup>1</sup>Massachusetts Institute of Technology, United States; <sup>2</sup>Shell International Exploration and Production Inc., United States

While the modern Li-ion battery is a scientific and engineering marvel, having enabled substantial technological innovation

spanning from mobile electronics to commercially viable electric vehicles, the intercalation chemistry of the Li-ion battery has a fundamental upper limit on its achievable energy density owing to the fact that the same structure must remain stable in the fully lithiated and delithiated states. While further advances within the Li-ion chemistry are possible, significantly higher theoretical energy densities are achievable with conversion chemistries, such as Li-O<sub>2</sub> and Li-S batteries<sup>1</sup>, where the structure and/or phase of the electrode materials change with its state of charge. While the importance of electrolyte electrochemical/chemical stability and ionic conductivity has been known since the very first batteries, owing to the partial solubility of reaction intermediates in conversion chemistries (such as Li<sup>+</sup>-O<sub>2</sub><sup>-</sup> and Li<sub>2</sub>S<sub>x</sub>), electrolyte can play an even more critical role in determining their reaction pathway and kinetics. In this talk, the various mechanisms through which electrolyte has been found to interact with the Li-O<sub>2</sub> battery chemistry are explored. This includes recent results on the influence of solvent, counter anion and lithium ion concentration on the thermodynamics and kinetics of oxygen reduction<sup>2</sup> as well as solvent-water-halide interactions and their impact on the performance of lithium halide redox mediators<sup>3-5</sup>. This work highlights that a complex combination of solvent, salt and additives can alter the thermodynamics and kinetics of redox reactions, the understanding of which can be extended beyond the Li-O<sub>2</sub> battery reactions studied here to any small molecule redox reaction. References 1. P. G. Bruce, S. A. Freunberger, L. J. Hardwick, and J.-M. Tarascon: Li-O<sub>2</sub> and Li-S batteries with high energy storage. *Nature Materials* 11(1), 19 (2011). 2. G. Leverick, R. Tataru, S. Feng, E. Crabb, A. France-Lanord, M. Tulodziecki, J. Lopez, R. Stephens, J. Grossman, and Y. Shao-Horn: Solvent- and anion-dependent Li<sup>+</sup>-O<sub>2</sub><sup>-</sup> coupling strength and implications on the thermodynamics and kinetics of Li-O<sub>2</sub> batteries. Submitted (2019). 3. M. Tulodziecki, G. M. Leverick, C. V. Amanchukwu, Y. Katayama, D. G. Kwabi, F. Barde, P. T. Hammond, and Y. Shao-Horn: The role of iodide in the formation of lithium hydroxide in lithium-oxygen batteries. *Energy Environ. Sci.* 10(8), 1828 (2017). 4. G. Leverick, M. Tulodziecki, R. Tataru, F. Barde, and Y. Shao-Horn: Solvent-Dependent Oxidizing Power of LiI Redox Couples for Li-O<sub>2</sub> Batteries. *Joule* 3, 1 (2019). 5. G. Leverick and Y. Shao-Horn: In preparation (2019).

#### 5:15 AM F.EN04.06.03

**Transforming an Electrolyte into an Electrode—Fe Substituted Na  $\beta$ "-Al<sub>2</sub>O<sub>3</sub>** [Danielle Butts](#)<sup>1</sup>, Juergen Schoiber<sup>2</sup>, Günther Redhammer<sup>2</sup> and Bruce S. Dunn<sup>1</sup>; <sup>1</sup>University of California, Los Angeles, United States; <sup>2</sup>University of Salzburg, Austria

Na-ion batteries present a promising alternative to Li-ion batteries due to the low cost and abundance of sodium and the existence of well-studied Na-superionic conductors. The design of new Na-ion battery electrode materials, however, is severely limited by the larger size of Na<sup>+</sup> compared to Li<sup>+</sup>. One approach to designing new electrode materials for Na-ion solid-state batteries is to modify solid-state electrolytes. That is, because solid-state electrolyte materials are known for their high levels of ionic conductivity and minimal levels of electronic conductivity, they are not even considered as candidates for electrode materials which require both ionic and electronic conduction. However, if the chemistry of fast ion conductors can be suitably modified to produce electronic conduction and their defect structures are maintained so that their high ion conductivities are preserved, then these materials represent a unique opportunity to creating a new class of battery electrode materials. An electrolyte-centered material design method takes advantage of not only the inherently fast ionic conduction within the material but also of a more continuous chemical potential across the electrode-electrolyte interface for solid-state batteries, leading to increased interfacial stability. The research presented in this paper demonstrates that partial substitution of aluminum by iron in the superionic conductor Na  $\beta$ "-Al<sub>2</sub>O<sub>3</sub> (stabilized as Na<sub>1.67</sub>Li<sub>0.33</sub>Al<sub>11</sub>O<sub>17</sub>) results in a mixed ionic-electronic conductor. A series of Fe-substituted compositions exhibit reasonable capacities as a negative electrode for Na-ion batteries. Fe-substitution for up to 80% of the aluminum sites is possible through a combination of sol-gel chemistry and high-temperature heat treatment, resulting in Fe<sup>2+</sup>/Fe<sup>3+</sup> in both the octahedral (O) and tetrahedral (T) sites of the spinel block. Structural refinement and Mössbauer spectroscopy have helped to elucidate the nature of Fe-substitution within the structure and its limitations. Successful octahedral site doping with Fe-ions appears to be the key to appreciable electronic conduction due to the shorter bond distances between O-O sites compared to T-T and O-T of the spinel block. The electrochemical properties of ~50% Fe-substituted Na  $\beta$ "-Al<sub>2</sub>O<sub>3</sub> (Na<sub>1+x</sub>(Al,Fe)<sub>11</sub>O<sub>17</sub>) have been investigated in non-aqueous electrolytes, demonstrating 115 mAh g<sup>-1</sup> at C/5 and 72 mAh g<sup>-1</sup> at 20C (0.2-2.5 V vs Na/Na<sup>+</sup>) through Fe<sup>2+</sup>/Fe<sup>3+</sup> redox, while maintaining the  $\beta$ " structure. Electrochemical analysis indicates a capacitive-like charge storage mechanism and excellent capacity retention at high rates, despite the micron-sized particles.

#### 5:25 AM F.EN04.06.04

**Laminating Ti<sub>3</sub>C<sub>2</sub>T<sub>x</sub> MXene on Ultrathin Li-Metal as Li Storage Host in Lithium-Ion Batteries** [Xi Chen](#), Mingwei Shang and Junjie Niu; University of Wisconsin-Milwaukee, United States

Due to the high specific capacity of 3860 mAh g<sup>-1</sup> and low electrochemical potential of -3.04 V vs standard hydrogen electrode, Li metal as anode is one of most attractive approaches in high energy-density lithium ion batteries (LiBs). Nevertheless, mossy/dendritic Li growth induces numerous safety issues and the sustained SEI formation causes Li depletion,

which greatly limits further applications. We present the lamination of Ti<sub>3</sub>C<sub>2</sub>T<sub>x</sub> MXene film on 30 microns Li metal foil using a rolling process, which significantly improves the battery cycling performance in both symmetric and full cells. The excellent Li<sup>+</sup>/e<sup>-</sup> transport behavior of the 2D MXene provides the Li<sub>Cx</sub>-Ti intercalated surface, interlayer spacing and inter-block spacing for Li metal storage. The improved electrical conductivity also reduces un-uniform distribution of current density, leading to a homogeneous Li plating/stripping along with a suppressed mossy/dendritic Li growth and reduced Li and electrolyte depletion from continuous SEI formation. Moreover, the coexisted organic-rich and inorganic-rich SEI of both cycled MXene-Li and Li foil electrodes were investigated via XPS depth profiling spectroscopy. A full cell battery paired with commercial LiNi<sub>0.8</sub>Co<sub>0.15</sub>Al<sub>0.05</sub>O<sub>2</sub> (NCA) cathode with lean electrolyte condition and an N/P ratio as low as 1.5 was also studied. The 2D MXene coated Li metal anode presents a great potential in high energy-density batteries for portable devices and electric vehicles.

**5:35 AM \*F.EN04.06.06**

**High Capacity Conversion Materials—Operando Characterization of Key Factors Governing the Electrochemistry** Esther Takeuchi, Kenneth Takeuchi and Amy Marschilok; Stony Brook University, United States

There are multiple types of electrochemical storage mechanisms in energy storage materials. The most widely adopted is the insertion mechanism where on reduction, a positive ion inserts into the structure of the host material and is removed from the structural lattice upon oxidation. A second type of mechanism is conversion where a chemical reaction leads to a new material or phase on reduction with reformation of the original material on oxidation. Insertion materials contain space in the lattice to accommodate Li<sup>+</sup> or other positive ions and can be depicted as nLi<sup>+</sup> + ne<sup>-</sup> + M<sub>x</sub>O<sub>y</sub> → Li<sub>n</sub>M<sub>x</sub>O<sub>y</sub>. Functionally, these materials exhibit reversible or quasi-reversible electrochemistry with the transfer of limited numbers of electrons/lithium ions per metal center resulting in moderate lattice expansion but also providing moderate capacity. Conversion materials differ in that they often involve multielectron transfers per active center represented here for a metal oxide type material as M<sub>x</sub>O<sub>y</sub> + 2yLi<sup>+</sup> + 2ye<sup>-</sup> → yLi<sub>2</sub>O + xM resulting in significantly higher theoretical capacity. However, the challenge with many conversion reactions is the degradation of delivered capacity with continued electrochemical oxidation and reduction. The mechanisms of conversion reactions will be examined including those of densely packed ferrites with spinel or inverse spinel structures where the theoretical capacity exceeds 900 mAh/g. In-situ and operando methods that demonstrate the governing roles of crystallite size, aggregation, and interfacial reactivity on rate capability and capacity retention will be featured.

**5:50 AM F.EN04.06.07**

**Understanding the Conversion Mechanism of FeF<sub>2</sub> Cathodes Using Monodisperse, Single-Crystalline Nanorods** Albert W. Xiao, Hyeon Jeong Lee, Isaac Capone, Alex Robertson, Jack Fawdon and Mauro Pasta; University of Oxford, United Kingdom

Transition metal fluorides display the combination of high capacity and high electrode potential that are essential to boosting the energy density of lithium ion batteries. However, their application as cathode materials has been hindered by an incomplete understanding of their electrochemical capabilities and limitations. Herein, we present a system of single crystalline, monodisperse iron (II) fluoride nanorods and detail how their morphology and uniformity make them ideal for mechanistic study. High-resolution analytical transmission electron microscopy reveals intricate morphological features, lattice orientation relationships, and oxidation state changes that redefine the conversion reaction with unprecedented spatial resolution. We first introduce the presence of surface specific reactions and examine how they critically influence phase evolution, diffusion kinetics and cell failure. Next, we examine how the reversibility of the conversion reaction is governed by topotactic cation diffusion through an invariant lattice of fluoride anions and the nucleation of metallic particles on semi-coherent interfaces. Finally, we demonstrate how this new understanding informs a more effective application of metal fluorides and establishes a framework for improving reaction hysteresis, kinetics and reversibility. To ensure a pertinent result, ex-situ data was extracted from coin cells that deliver near theoretical capacity (570 mAh g<sup>-1</sup>) and extraordinary cycling stability (>90 % capacity retention after 100 cycles). The role of the electrolyte in enabling this performance as well as the collection of meaningful HRTEM data is briefly discussed.

**6:00 AM F.EN04.06.09**

**Fe<sub>2</sub>O<sub>3</sub> Coated with Thermally Etched Carbon Nanotubes as High Rate Capable Anode for Lithium-Ion Battery** Dipsikha Ganguly and Ramaprabhu Sundara; Indian Institute of Technology Madras, India

Over the past few decades lithium ion batteries have become utmost technological importance for energy storage devices for stationary applications and electric vehicles. Currently, Graphite is the widely used anode materials for lithium ion batteries due to its low intercalation voltage and high stability. But due to its low specific capacity research is focussed to find alternative anode materials for lithium ion batteries. Among the transition metal oxides, α-Fe<sub>2</sub>O<sub>3</sub> as anode material is

extensively studied owing to its high theoretical capacity (1006 mAh. g<sup>-1</sup>), environment-friendly, good catalytic properties and stability. But capacity fading is found to be inhibitory to be used as the anode materials for lithium ion battery. In order to reduce the capacity fading, different porous carbon supports have been reported in the literature. In this work, we have synthesised  $\gamma$ -Fe<sub>2</sub>O<sub>3</sub> coated with thermally etched carbon nanotubes ( $\gamma$ -Fe<sub>2</sub>O<sub>3</sub>/TECNTs) using solid state pyrolysis method. In the presence of nanotube structure, high rate capability is observed for  $\gamma$ -Fe<sub>2</sub>O<sub>3</sub>/TECNT anode material due to the fact that lithium insertion/de-insertion in carbon matrix at lower voltage is governed by the intercalation mechanism while for  $\gamma$ -Fe<sub>2</sub>O<sub>3</sub>, lithium interaction is mainly observed due to the conversion reaction. The rate capability studies in the range 0.05-20 A/g shows 100% retention of capacity even after extensive cycling. Also, good cyclic stability and 100 % coulombic efficiency are achieved in the presence of carbon matrix. Further to analyse the role of carbon nanotubes, amount of carbon matrix is varied which also corroborates the crucial role of carbon in enhancing the electrochemical performance of lithium ion battery.

#### **6:10 AM F.EN04.06.10**

**Deterministic Design of Energy Storage Electrodes Through Oxide Electrodeposition in CNT Foam Scaffolds** [Ishita Kamboj](#), Michael A. Spencer, Ozkan Yildiz, Philip D. Bradford and Veronica Augustyn; North Carolina State University, United States

The use of deterministic design is a growing area of interest to achieve both high energy and power density for energy storage electrodes. Traditionally manufactured energy storage electrodes consist of a multi-component slurry containing an electrochemically active material as well as conductive carbon and polymer binder additives cast onto a flat conductive substrate. Inhomogeneity in the dispersion of the slurry components limits areal power and energy densities due to tortuous and poorly controlled electron and ion transport pathways. In this work, a nanostructured, high capacity transition metal oxide (MoO<sub>3</sub>) is electrodeposited onto a conductive carbon nanotube (CNT) foam scaffold to attain high mass loading energy storage electrodes with fast Li<sup>+</sup> intercalation kinetics. CNT foams provide surface area for the electrodeposition of MoO<sub>3</sub> while maintaining sufficient electrical conduction throughout electrodes. Ample porosity between the CNTs provides good ion transport pathways. The MoO<sub>3</sub> is a model Li<sup>+</sup> intercalation oxide with a high gravimetric capacity that can be easily electrodeposited from aqueous solutions. This presentation will describe how control over the properties of the CNT foam and MoO<sub>3</sub> electrodeposition are used to tailor the energy storage performance of the electrode architecture, along with characterization to understand the how the structure of the electrode affects its energy storage behavior. Overall, this research seeks to understand the relationships between electrode architecture and energy storage behavior to achieve simultaneous high power and high energy density.

#### SESSION F.EN04.07: Beyond Li Electrochemistry

On Demand Abstracts Available for Viewing Starting Saturday Morning, November 21, 2020

F-EN04

#### **5:00 AM F.EN04.07.02**

**Gallium Nitride Based Nuclear Batteries—Long-Term Radiation Effects on the Contact Interface** [Lance Hubbard](#)<sup>1</sup>, Christian Cowles<sup>1</sup>, David Blanchard<sup>1</sup>, Jesse Johns<sup>1</sup>, Andrew Prichard<sup>1</sup>, Gary Sevigny<sup>1</sup>, Jarrod Allred<sup>1</sup>, Bethany Mathews<sup>1</sup>, Erin Fuller<sup>1</sup> and David Schwellenbach<sup>2</sup>; <sup>1</sup>Pacific Northwest National Laboratory, United States; <sup>2</sup>Mission Support and Test Services (MSTS), Los Alamos Office, United States

Nuclear batteries, or betavoltaic cells (BV), convert the energy of beta radiation directly into electricity via a semiconductor stack. The decades-long lifetime and high-energy density open a broad range of applications that are not able to use chemical batteries. Such low-power electronic applications (nW-mW) are the internet-of-things, internal medical devices, and unattended equipment in space and other hostile environments. We are developing simulation methods to model radiation sources and degradation of the contact interface under beta irradiation. Methods were developed to adequately simulate radiation sources for BVs with Monte Carlo N-Particle (MCNP) and CASINO. Methods were also developed to adequately simulate electron generation and device performance with ATLAS. The simulations have been used to design the accelerated aging experiments of tritium beta-induced degradation at a GaN contact.

#### **5:10 AM F.EN04.07.04**

**Engineering Ceramic Electrolyte Interfaces for Low-Temperature Molten Sodium Batteries** [Martha M. Gross](#), Amanda Peretti, Stephen Percival, Leo J. Small and Erik Spoorcke; Sandia National Laboratories, United States

Ceramic electrolytes exhibiting high sodium-ion conductivity are a key component in the development of low temperature molten sodium batteries. Traditionally, molten sodium batteries utilize Na<sup>+</sup>-ion conducting solid electrolytes such as  $\beta$ -Al<sub>2</sub>O<sub>3</sub> or NaSICON. These ceramics require high operating temperatures of ~300°C, not only for improved Na<sup>+</sup>-ion conductivity, but also to facilitate wetting of molten sodium on the solid electrolyte. Lowering the operating temperature to near 100°C drastically reduces interfacial wetting of the molten sodium to the ceramic electrolyte, increasing interfacial resistance in the cell and ultimately producing poor battery performance. Here, we describe the use of engineered coatings to enhance wetting of molten sodium on NaSICON ceramic electrolyte and improve charge transfer across this key interface. We observe that these coatings dramatically lower cell-limiting interfacial resistance, and thereby increase battery cycling current densities and overall battery performance at low operating temperatures. Continued optimization of such engineered, interfacial coatings promises continued advances of low temperature sodium batteries. Sandia National Laboratories is a multimission laboratory managed and operated by National Technology & Engineering Solutions of Sandia, LLC, a wholly owned subsidiary of Honeywell International Inc., for the U.S. Department of Energy's National Nuclear Security Administration under contract DE-NA0003525.

#### 5:20 AM F.EN04.07.05

**Spinel Structured High Entropy Oxide Nanoparticles as Bi-Functional Catalyst for Lithium-Air Batteries** Guruprasad S. Hegde and Ramaprabhu Sundara; Indian Institute of Technology Madras, India

High entropy materials are the "multi-metallic cocktails" in metallurgy, which are having five or more than five metals, all in equal proportions. Due to the high configurational entropy arising from such conditions, these types of materials form a simple single-phase structure. The high entropy alloys are high strength, corrosion resistant materials which find application in several industries. However, the exploration on the other class of high entropy oxides have caught the attention of the researchers only recently. High entropy oxide nanoparticles with multifunctional properties can have potential applications in several technologies. In this work, a high entropy oxide nanoparticle (HEO) in a simple bottom up process is synthesized and the possibility of application of such materials as cathode electrocatalysts in Li-O<sub>2</sub> batteries is explored. Reversible formation and decomposition of Li<sub>2</sub>O<sub>2</sub> during the respective discharge and charge operations is the main challenge in the development of a secondary Li-O<sub>2</sub> battery. Several approaches to address this issue include development of an efficient bifunctional catalyst material in aprotic media and liquid phase redox mediators. In the present work, we have prepared HEO containing Co, Cr, Ni, Al, Fe by a simple sol-gel process. The oxide crystallizes in spinel (Fd3m) phase. The synthesized material is characterized extensively to understand the structure and morphology. Li-O<sub>2</sub> cells are fabricated with synthesized HEO coated on a gas diffusion layer as cathode, a redox mediated electrolyte (1M LiTFSI and 0.1M LiI in tetraethylene glycol dimethyl ether) and lithium metal as anode. The detailed investigations result in a capacity of 1000 mAh g<sup>-1</sup> for a constant current of 250 mA g<sup>-1</sup> in the capacity limited cyclic stability test for 50 cycles.

SESSION F.EN04.08: Thermodynamics and Advanced Characterization  
On Demand Abstracts Available for Viewing Starting Saturday Morning, November 21, 2020  
F-EN04

#### 5:00 AM \*F.EN04.08.02

**Thermodynamic and Kinetic Aspects of Batteries** Joachim Maier; Max Planck Institute, Germany

Joachim Maier Max Planck Institute for Solid State Research, Physical Chemistry of Solids, Stuttgart, 70569, Germany, e-mail: office-maier@fkf.mpg.de One part of the contribution considers the various storage mechanisms (insertion, phase change and interfacial storage) together with thermodynamic and kinetic constraints [1-3]. Special emphasis is laid on the difference between Lithium and Sodium based battery systems [2]. The helpful role of nano-structuring and confinement is stressed. A second part of the contribution refers to the equally important role of the circuitry [4]. A detailed modelling of the storage kinetics provides useful guidelines of how to optimize the electrode morphology [5]. In all cases practical examples and experimental results are discussed. References [1] J. Maier, *Angewandte Chemie* 52 (2013) 4998 [2] Chen et al., *Nature* 536 (2016) 159 [3] Chen et al., *Nature Energy* 3 (2018) 102 [4] Zhu et al., *Science* 358 (2017) eaao2808(1--8) [5] Usiskin et al., *Physical Chemistry Chemical Physics* 20 (2018) 16449

#### 5:15 AM F.EN04.08.03

**ReaxFF—A Predictive Tool for Study of a Solid-Electrolyte Interphase on the Silicon-Based Anodes of a Lithium-Ion**



**Battery** Mahdi Khajeh Talkhoncheh and Adri v. Duin; The Pennsylvania State University, United States

Lithium-ion secondary batteries (LIBs) are one of the most popular electrochemical systems, especially in home-electronics and electric vehicles due to their relatively high energy density, high operating voltage, and low self-discharge. Further advancements of Lithium-ion batteries are imperative in order to improve their capacities and life cycles. Silicon anode materials are regarded as one of the most promising candidates for Lithium-ion batteries based on their substantial specific capacity in comparison with conventional graphite anodes. However, a severe drawback is the large volume changes of anodes during the charge (up to ~300% volume expansion during lithiation) and discharge (delithiation) cycles. These changes cause high mechanical stress, breakdown of the conductive layers of composite electrodes, and undesirable side reactions within batteries. In addition, the solid electrolyte interphase (SEI) formed on the silicon anodes surfaces are unstable and cannot efficiently protect the electrodes from reacting with electrolytes. The importance of SEI on battery performance motivates us to study the interphase interaction in batteries. In this work, the formation of SEI components such as C<sub>2</sub>H<sub>4</sub>, CO<sub>2</sub>, and CO gases, and organic and inorganic products are predicted by using Reactive molecular dynamics (ReaxFF) simulations. For this investigation, we analyzed the effect of different types of Si anodes (pristine Si and SiO<sub>x</sub>), compositions of various carbonate electrolytes and additives on SEI formation. Additionally, the degree of lithiation and temperature effects on gas evolution are investigated. Overall, these simulation results indicate that ReaxFF will be a very useful tool for the development of novel electrolytes or additives in Lithium-ion batteries.

**5:25 AM F.EN04.08.04**

***In Situ* TEM Observation of Structural and Chemical Evolution of Interphase in Rechargeable Batteries** Chongmin Wang; Pacific Northwest National Laboratory, United States

Electron microscopy and spectroscopy diagnosis, both in-situ and ex-situ, appears to be one of the essential methods for gaining insights as how an electrode material evolves and eventually fails, therefore feeding back for designing and creating new materials with enhanced battery performances. In this presentation, I will focus on recent progress on ex-situ, in-situ and operando S/TEM studies for probing into the structural and chemical evolution of electrode for lithium ion batteries, especially layer structured transition metal oxide cathode and Li metal anode. I will highlight several recent key observations, which appear to be well documented, while essentially are poorly understood, and therefore act as the bottleneck for the advances of cathode and anode for better batteries. It would be expected that this presentation can stimulate new ideas as how to attack these bottlenecks to advance the cathode based on layer structured materials and Li anode.

**5:35 AM F.EN04.08.05**

**Atomistic Modeling and Simulations of the Lithiation Behavior of the Si Anode in Li-Ion Batteries Using Reactive Force Field** Li-Yi Pan and Chin-Lung Kuo; National Taiwan University, Taiwan

Si-based materials have recently received great interest for their much higher theoretical Li capacity than graphite. However, their practical use is still largely hampered by many of their inherent problems, particularly for the massive volume expansion and the anisotropic lithiation behavior that result in the pulverization of the Si electrode upon lithiation. To solve this problem, it would require a detailed understanding of the fundamental mechanism of the Si-based anode during the lithiation processes. Regarding this aspect, molecular dynamic (MD) simulation is a powerful tool to explore the structural evolution and dynamic properties of the Si-based anode upon lithiation. However, molecular dynamic simulation requires a reliable force-field model to accurately describe the atomic interactions between the constituent elements. In this study, we have developed a new ReaxFF parameter set for the Li-Si alloy system based on first-principles calculations. This new potential parameter set has been examined through a series of validations, which has proved to accurately predict the fundamental properties of Li, Si, and Li<sub>x</sub>Si alloys, including the structure parameters, elastic moduli, and formation energies, etc. We then employed this newly developed model in conjunction with MD simulations to investigate the lithiation kinetics and the associated underlying mechanisms for the Si-based anode. Our MD simulations first show that this newly developed ReaxFF model can accurately describe the anisotropic lithiation behavior of the Si-based anode as observed in the experiments. The distinct properties in each facets were further analyzed to find out the mechanism of the anisotropic lithiation. More specifically, the Li insertion energy barrier is found to be the controlling factor in the initial stage lithiation. The high surface Si density of Si(111) facet leads to its high Li insertion energy barrier, which makes it "almost immobile" as observed in our MD simulations, consistent with the experimental results. Meanwhile, the local Li/Si ratio and the stress concentration generated at the Si/Li<sub>x</sub>Si interface (phase boundary layer), which affects the bond-breaking and Li insertion rate, was found to play a critical role in the steady-state lithiation process. These structural characteristics lead to the distinct lithiation rates and anisotropic morphologies on different crystallographic orientations of Si. Finally, our results show that the anisotropic lithiation behavior of the Si anode is primarily determined by the lithiation kinetics on different facets of Si rather than the thermodynamic factors as suggested by early first-principles calculations.

### 5:45 AM F.EN04.08.07

**Understanding the Lithiation Pathways in Si and Ge Clathrates Using Synchrotron X-Ray Characterization** Andrew M. Dopilka<sup>1</sup>, Candace K. Chan<sup>1</sup>, Amanda Childs<sup>2</sup> and Svilen Bobev<sup>2</sup>; <sup>1</sup>Arizona State University, United States; <sup>2</sup>University of Delaware, United States

Clathrates are comprised of a cage framework of covalently bonded Group IV elements in which guest atoms reside in the center of each cage. Clathrates are typically known for their superconducting or thermoelectric applications, while their electrochemical properties are relatively unexplored. Our group has been investigating the electrochemistry of Si and Ge clathrates for Li-ion battery anodes and have found that in some cases the Li-alloying pathways and reactions are distinctly different than those seen in the diamond Si/Ge case. For example, the Ba<sub>8</sub>Al<sub>16</sub>Si<sub>30</sub> Type I clathrate does not undergo a Li-alloying reaction<sup>1</sup> while the Ba<sub>8</sub>Ge<sub>43</sub> clathrate does<sup>2</sup>. In the case of Ba<sub>8</sub>Ge<sub>43</sub>, the reaction pathway appears to follow an amorphous phase transformation. This is different than diamond cubic Ge which undergoes several phase transformations to crystalline phases<sup>3</sup>. In the case of the Type II Si clathrate (Na<sub>x</sub>Si<sub>136</sub>), the alloying reaction depends on the Na content. When the cages are full of Na (Na<sub>24</sub>Si<sub>136</sub>), the alloying reaction looks similar to diamond cubic Si<sub>4</sub>, where if the cages are empty (Si<sub>136</sub>) the voltage profile is significantly more sloped<sup>5</sup>, more similar to the alloying of amorphous Si. In this work, we employ synchrotron x-ray pair-distribution function analysis (PDF), X-ray diffraction, and in-situ heating experiments to elucidate the structural differences between Ba<sub>8</sub>Ge<sub>43</sub> and Si<sub>136</sub> and their diamond cubic analogues at similar states of charge. The PDF method allows us to probe the local structure of the amorphous phases that are present in the lithiated samples. In situ heating experiments enable us to observe structural changes to amorphous phases upon moderate heating. The insight learned from the structural characterizations are then used to explain the differences in the electrochemistry between the Si and Ge clathrates and their diamond cubic analogues. The results show that at various states of lithiation of Ba<sub>8</sub>Ge<sub>43</sub>, Ba<sub>8</sub>Ge<sub>43</sub> is converted to an X-ray amorphous phase while diamond cubic Ge undergoes crystalline phase transformations similar to previous work<sup>3</sup>. Interesting, when heating the fully lithiated Ba<sub>8</sub>Ge<sub>43</sub> phase and monitoring with X-ray diffraction, crystalline peaks corresponding Li<sub>15</sub>Ge<sub>4</sub> appear at 420 K. Upon further heating to 480 K, the reflections corresponding to Ba<sub>4</sub>Li<sub>2</sub>Ge<sub>6</sub> and other binary Ge-Li phases appear. These results suggest that the amorphous phases that are part of the final lithiation state have local structures similar to that of crystalline phases which can then be accessed upon moderate heating (480 K). These results would aid in giving insight to the fundamentals of how the initial structure of group IV materials affect their Li-alloying properties and structures. (1) Zhao, R.; Bobev, S.; Krishna, L.; Yang, T.; Weller, J. M.; Jing, H.; Chan, C. K. Anodes for Lithium-Ion Batteries Based on Type I Silicon Clathrate Ba<sub>8</sub>Al<sub>16</sub>Si<sub>30</sub> - Role of Processing on Surface Properties and Electrochemical Behavior. *ACS Appl. Mater. Interfaces* 2017, 9, 41246-41257. (2) Dopilka, A.; Zhao, R.; Weller, J. M.; Bobev, S.; Peng, X.; Chan, C. K. Experimental and Computational Study of the Lithiation of Ba<sub>8</sub>Al<sub>y</sub>Ge<sub>46-y</sub> Based Type I Germanium Clathrates. *ACS Appl. Mater. Interfaces* 2018, 10, 37981-37993. (3) Jung, H.; Allan, P. K.; Hu, Y. Y.; Borkiewicz, O. J.; Wang, X. L.; Han, W. Q.; Du, L. S.; Pickard, C. J.; Chupas, P. J.; Chapman, K. W.; et al. Elucidation of the Local and Long-Range Structural Changes That Occur in Germanium Anodes in Lithium-Ion Batteries. *Chem. Mater.* 2015, 27, 1031-1041. (4) Wagner, N. A.; Raghavan, R.; Zhao, R.; Wei, Q.; Peng, X.; Chan, C. K. Electrochemical Cycling of Sodium-Filled Silicon Clathrate. *ChemElectroChem* 2014, 1, 347-353. (5) Langer, T.; Dupke, S.; Trill, H.; Passerini, S.; Eckert, H.; Pöttgen, R.; Winter, M. Electrochemical Lithiation of Silicon Clathrate-II. *J. Electrochem. Soc.* 2012, 159159, 1318-1322.

SESSION F.EN04.09: Li-S and Advanced Electrolytes

On Demand Abstracts Available for Viewing Starting Saturday Morning, November 21, 2020  
F-EN04

### 5:00 AM F.EN04.09.02

**Ab Initio Investigation of Li and Na Migration in Guest-Free, Type I Clathrates** Andrew M. Dopilka<sup>1</sup>, Candace K. Chan<sup>1</sup> and Xihong Peng<sup>2</sup>; <sup>1</sup>Arizona State University, United States; <sup>2</sup>Arizona State University Polytechnic Campus, United States

Group IV clathrates have cage structures that host guest atoms and exhibit a wide range of interesting properties including superconductivity, hydrogen storage, and thermoelectricity. Recently, there have been interest in the possibility of clathrates and other group IV frameworks as anodes for Li-ion and Na-ion batteries. The type and presence of guest atoms have a direct influence on the properties that are observed. For Li-ion battery applications, we found with DFT (density functional theory) calculations that the presence of Ba inside the clathrate cages in Ba<sub>8</sub>Ge<sub>43</sub> impedes Li mobility by raising the migration

barrier for diffusion. If Ba was absent, the barrier was much lower suggesting the need for guest atoms to be absent for diffusion to be feasible. In this work, the favorable Li and Na positions are determined in the type I clathrate frameworks (Si<sub>46</sub>, Ge<sub>46</sub>, and Sn<sub>46</sub>) and then the nudged elastic band (NEB) method is used to evaluate the Li and Na mobility. The results show that it is energetically favorable for a Li atom to occupy the center position inside the small Tt<sub>20</sub> cages while preferring the off-center positions in the larger Tt<sub>24</sub> cages. The lowest Li migration barriers are found to be 0.35, 0.13 and 0.37 eV for Si<sub>46</sub>, Ge<sub>46</sub>, and Sn<sub>46</sub>, respectively, with the dominant diffusion pathway along channels of Tt<sub>24</sub> cages connected by hexagonal faces. Li accessibility to the Si<sub>20</sub> cage in Si<sub>46</sub> appears to be restricted in the dilute regime due to a high energy barrier (2.0 eV) except for the case in which Li atoms are present in adjacent cages; this lowers the migration barrier to 0.77 eV via a mechanism where a Si-Si bond is temporarily broken. In contrast, Na atoms show preference for the cage centers and display higher migration barriers than Li. Overall, the Tt<sub>24</sub> channel sizes in the guest-free, type I clathrates are ideal for fast Li diffusion, while Na is too large to migrate effectively between cages, except in the case of hexagonal migration of Na in Sn<sub>46</sub> (0.43 eV). The energy landscape for Li inside the type I clathrates is uniquely different than that in diamond cubic structures, leading to significantly lower energy barriers for Li migration. These results suggest that open frameworks of group IV elements may enable facile Li migration and, in some cases, facile Na migration. By the gained understanding the structural requirements for fast ion diffusion in group IV open frameworks, new materials can be identified that have potential use as Li-ion or Na-ion anodes. (1) Dopilka, A.; Zhao, R.; Weller, J. M.; Bobev, S.; Peng, X.; Chan, C. K. Experimental and Computational Study of the Lithiation of Ba<sub>8</sub>AlyGe<sub>46</sub>-y Based Type I Germanium Clathrates. ACS Appl. Mater. Interfaces 2018, 10, 37981-37993.

#### 5:10 AM F.EN04.09.03

**High Energy Density and Ultrastable Lithium-Sulphur Batteries** Ying Chen<sup>1</sup>, Baozhi Yu<sup>1</sup>, Ye Fan<sup>1</sup>, Tao Tao<sup>1</sup> and Chunging Hou<sup>2</sup>; <sup>1</sup>Deakin University, Australia; <sup>2</sup>North Minzu University, China

Lithium-Sulfur (Li-S) batteries exhibit a very high theoretical specific capacity of 1675 mA h g<sup>-1</sup> and high energy density of 2650 W h Kg<sup>-1</sup>, which are 2~3 times higher than the current Li ion batteries and thus are considered next-generation batteries. The major challenges of current Li-S batteries are cathode degradation related to the "shuttle" effect and Li dendrite formation on anode surface, leading to the low Coulombic efficiency, poor cyclic stability, and serious safety problems. We have used new nanomaterials to solve these issues and improved substantially the performance of Li-S batteries. The shuttle effect has been reduced by adding a BN nanosheet-graphene interlayer on cathode surface to trap lithium polysulfide ions (Fan 2017). Coating the separator with a thin layer of negatively-charged BN nanosheets can prevent polysulfide migration through the separator effectively, further suppressing the shuttle effect (Fan 2019); Dendrite formation is successfully avoided by constructing a 3D Li anode using a 3D host of MnO<sub>2</sub>-decorated graphene foam (Yu 2018). These research effort have substantially improved the battery performance with a long cycle life of over 1000 cycles, a high Coulombic efficiency of 98.9%, and high rate capacities (7C) both in symmetric-cell and full-cell cells (Tao 2018). REFERENCES Fan, Y. Chen, Y. et al "Functionalized Boron Nitride Nanosheets/Graphene Interlayer for Fast and Long Life Lithium-Sulfur Batteries", Advanced Energy Materials, 2017, 7,1602380 Fan, Y, Chen, Y. et al "Repelling Polysulfide Ions by Boron Nitride Nanosheets Coated Separators in Lithium-Sulfur Batteries", ACS Applied Energy Materials, 2019, DOI: 10.1021/acsaem.8b02205 Yu, B. Chen, Y. et al "Nanoflake Arrays of Lithiophilic Metal Oxides for the Ultra Stable Anodes of Lithium-Sulfur Batteries", Advanced Functional Materials, 2018, 1803023. Tao, T. Chen, Y et al "Anode Improvement in Rechargeable Lithium-Sulfur Batteries", Advanced Materials, 2017, 29, 1700542.

#### 5:20 AM F.EN04.09.04

**High-Throughput Neural Potential Exploration of Ether-Ion Chemical Space** Wujie Wang, William H. Harris and Rafael Gomez-Bombarelli; Massachusetts Institute of Technology, United States

The use of ether species has shown great promises for equimolar (super-concentrated) ionic liquid for novel organic electrolyte applications and as model systems for solid-state polymer electrolyte [1-5]. However, the moderately-sized combinatorial space for designing supramolecular chemistry for ether-ion interactions is on the order of 10<sup>3</sup> ~ 10<sup>4</sup> and has remained largely unexplored. We applied graph neural network-based potentials to accelerate the exploration of novel species for equimolar ionic liquid using a self-consistent strategy that accelerates the sampling and training of transferable neural networks[6-10]. The proposed method combines deep neural network training and active sampling of both chemical and configurational space in an end-to-end fashion to 1) bypass expensive ab initio MD sampling and 2) leverage the transferable configurational information across species. This workflow has discovered novel molecules for potential novel organic electrolyte applications for several different ions including Lithium and Sodium and shows great promises in theory-guided engineering for supramolecular chemistry. [1]Seki, S., Serizawa, N., Takei, K., Dokko, K. & Watanabe, M. Charge/discharge performances of glyme-lithium salt equimolar complex electrolyte for lithium secondary batteries. J. Power Sources 243, 323-327 (2013). [2]Ueno, K. et al. Glyme-lithium salt equimolar molten mixtures: Concentrated solutions or solvate ionic

liquids? J. Phys. Chem. B 116, 11323-11331 (2012). [3]Ueno, K. et al. Li<sup>+</sup> solvation in glyme-Li salt solvate ionic liquids. Phys. Chem. Chem. Phys. 17, 8248-8257 (2015). [4]Westman, K. et al. Diglyme Based Electrolytes for Sodium-Ion Batteries. ACS Appl. Energy Mater. 1, 2671-2680 (2018). [5]Zhang, L., Han, J., Wang, H., Car, R. & E, W. Deep Potential Molecular Dynamics: a scalable model with the accuracy of quantum mechanics. (2017). [6]Schütt, K. T., Saucedo, H. E., Kindermans, P.-J., Tkatchenko, A. & Müller, K.-R. SchNet-A deep learning architecture for molecules and materials. J. Chem. Phys. 148, 241722 (2018). [7]Behler, J. & Parrinello, M. Generalized neural-network representation of high-dimensional potential-energy surfaces. Phys. Rev. Lett. 98, 1-4 (2007). [8]Yao, K., Herr, J. E., Toth, D. W., Mckintyre, R. & Parkhill, J. The TensorMol-0.1 model chemistry: a neural network augmented with long-range physics. Chem. Sci. 9, 2261-2269 (2018). [9]Smith, J. S., Isayev, O. & Roitberg, A. E. ANI-1: an extensible neural network potential with DFT accuracy at force field computational cost. Chem. Sci. 8, 3192-3203 (2017). [10]Smith, J. S., Nebgen, B., Lubbers, N., Isayev, O. & Roitberg, A. E. Less is more: Sampling chemical space with active learning. J. Chem. Phys. 148, 241733 (2018).48, 241733 (2018).

SESSION F.EN04.10: Material Synthesis, Properties and Scalable Devices  
On Demand Abstracts Available for Viewing Starting Saturday Morning, November 21, 2020  
F-EN04

**5:00 AM \*F.EN04.10.01**

**P-Type Contacts on 2D Semiconductors** Manish Chhowalla; University of Cambridge, United Kingdom

Ultra-clean van der Waals interfaces can be achieved between soft indium metal and monolayer 2D transition metal dichalcogenide semiconductors. Such interfaces lead to low contact resistance and n-type field effect transistors with high mobilities- in excess of 100 cm<sup>2</sup>-V<sup>-1</sup>-s<sup>-1</sup>. It has been, however, challenging to make similarly clean interfaces between refractory metals with high work functions to achieve efficient hole injection. Here, I will present our efforts on realizing p-type contacts using high work function metals and alloys. We show that it is possible to deposit a thin layer of indium and then a high work function metal on top of it to form an alloy by annealing at 200oC. This method preserves the ultra-clean interface between the monolayer semiconductor and alloy while increasing the work function so that p-type devices can be realized. We also demonstrate clean interfaces using metals such as Au and Pt via direct deposition. These interfaces reveal low contact resistance and also high mobility p-type devices.

**5:15 AM F.EN04.10.02**

**The Synthesis of Submillimeter and Two-Dimensional vdW Manganese Metal-Organic Framework via Bi-Phase Strategy** Yuxia Shen, Bin Mu and Sefaattin (Sef) Tongay; Arizona State University, United States

Synthesis of van der Waals (vdW) metal-organic framework (MOF) nanosheets with controlled crystallinity and interlayer coupling strength are one of the bottlenecks in 2D materials that have limited its successful transition to large-scale applications. Especially for MOFs involving transition metals possessed versatile oxidation states have been highly rated in electrocatalytic applications. Here, the synthesis of vdW MnBDC with huge crystal size through a novel bi-phase strategy is demonstrated. The results show Mn<sup>2+</sup> and BDC- species diffusing along vertical directions in described bi-phase system slows down the reaction speed and enhances the crystallinity of MnBDC significantly. Moreover, the existence of capping agent - pyridine promotes the nanosheets that are stacking in 2D landscape and controls over the crystallinity further by competing with ligands carboxylic acid. The attained MnBDC crystals exhibit classic vdW nature, submillimeter of lateral size and great crystallinity. The high quality of vdW MnBDC nanosheets enables us to perform thickness-dependent kelvin probe force microscopy and optical absorption to discover the electron transition and interlayer hybridization in 2D MOF nanosheets for the first time. Further, we conducted a series of electrocatalytic characterizations to investigate the catalytic water splitting efficiency of MnBDC. Theoretical calculation and experimental results highlighted the contributions of 2D crystal structure and multiple oxidation states of MnBDC crystals.

**5:25 AM F.EN04.10.05**

**Investigating Influence of Oriented Metal Films on Optical Properties and Excitonic Resonances of Suspended 2D Membranes** Todd H. Brintlinger, Jose Fonseca, Andrew Yeats, Joel Grim, Sam Carter, Jim C. Culbertson, Blake S. Simpkins, Daniel Ratchford, Maxim Zalalutdinov, Rhonda M. Stroud and Jeremy Robinson; U.S. Naval Research Laboratory, United States

The choice of growth substrate often has a profound influence on the electronic [1] and optical [2] behavior of atomically thin 2D crystals (2DCs). In order to exploit this influence, we have developed a synthetic technique for creating ordered, porous metal films with various suspended 2DCs, which we dub Oriented Porous mEtallic Networks (OPEN) [3]. These OPEN films exhibit characteristic optical phenomena, including enhanced photoluminescent (PL) intensity in suspended regions and remote quantum emission. Aberration-corrected scanning transmission electron microscopy (STEM) and electron energy loss spectroscopy (EELS) enables us to probe the various resonances of the suspended 2D crystals, the metal/2DC hybrid, and the interfacial region between these two distinct areas. Similar to recent work that uses gold films for generation of large-area 2DCs [4], OPEN films are synthesized by annealing metal films capped by 2DCs. The annealing causes lattice registry between the metal layer and the 2DCs. We show a single MoS<sub>2</sub> monolayer can affect the structural order of a comparatively thick (13-25nm) gold thin film. Electron back scatter diffraction and aberration-corrected STEM high-angle annular dark-field (HAADF) imaging of annealed MoS<sub>2</sub>/Au layers reveals that the gold films become highly textured and in close crystallographic registry with each other. With further annealing, the gold films can locally dewet beneath the MoS<sub>2</sub> layer to form the OPEN film structure with suspended regions of monolayer 2DC above the pore sites. The unique optical behavior of these hybrid systems include a 1000x increase in PL intensity in suspended 2DCs vs 2DCs on the metal film, and single-photon emitters manifests in remote quantum emission, with evidence for surface plasmon-polariton (SPP) propagation of > 10 μm. Further, low-loss EELS measurements at 60 kV, reveal that the OPEN films have resonances at ~ 2 eV, which are associated with the so-called A and B excitons in 2DCs, while resonances at several other energies occur in both the interfacial region and the "bulk" MoS<sub>2</sub>/Au regions. We will discuss the origin of these resonances, and how both the metal overlayer and disordered carbon contamination affect them. References: [1] W Bao et al., Appl Phys Lett 102 (2013), p. 042104. [2] M Buscema et al., Nano Research 7 (2014), p. 561. [3] J. Fonseca, submitted (2019) [4] MA Islam et al., Nano Lett 17 (2017), p. 6157.

#### 5:35 AM F.EN04.10.06

**Strong Adhesive Pick-up Technique with Polycaprolactone for Rare 2D Materials** Young Shin<sup>1</sup>, Suhan Son<sup>2</sup>, Sungmin Lee<sup>2</sup>, Dohun Kim<sup>2</sup>, Je-Geun Park<sup>2</sup> and Philip Kim<sup>3</sup>; <sup>1</sup>Brookhaven National Laboratory, United States; <sup>2</sup>Seoul National University, Korea (the Republic of); <sup>3</sup>Harvard University, United States

We introduce polycaprolactone (PCL) dry transfer which is a powerful material for picking up non-adhesive van der Waals materials such as NiPS<sub>3</sub>, NbSe<sub>2</sub>, Fe<sub>3</sub>GeTe<sub>2</sub>, ZnPS<sub>3</sub> and bismuth strontium calcium copper oxide (BSCCO) and etc. The heterostructures of Van der Waals were composed of layered atomically thin 2D materials that provide access to new properties important to the quantum information sciences. However, one of the main constraints is the stacking techniques. (PPC) has been known as the highest quality in dry transfer because PPC left less residue on vdW heterostructure through high temperature vacuum annealing but yield of the transfer was low. Here, we present the new polymer, polycaprolactone (PCL) for stacking vdW heterostructure with Rare layered 2D materials by dry transfer at low temperature. These 2D materials were easily detached from hexagonal boron nitride (hBN) assisted with PPC during dry transfer process. We succeeded to pick up many rare superconducting or magnetic 2D materials which were hard to be picked up by conventional dry transfer method from the oxide or silicon nitride substrates.

#### 5:45 AM \*F.EN04.10.07

**Strong Magnon-Phonon Hybridization in a 2D van der Waals Antiferromagnet** Thuc Mai<sup>1</sup>, Kevin Garrity<sup>1</sup>, Amber McCreary<sup>1</sup>, J. Argo<sup>2</sup>, Jeffrey Simpson<sup>1,3</sup>, V. Doan-Nguyen<sup>2</sup>, Rolando Valdes Aguilar<sup>2</sup> and Angela Hight Walker<sup>1</sup>; <sup>1</sup>National Institute of Standards and Technology, United States; <sup>2</sup>The Ohio State University, United States; <sup>3</sup>Towson University, United States

Low dimensional, van der Waals (vdW) materials, from graphene to 2D magnets such as Fe<sub>3</sub>GeTe<sub>2</sub> and CrI<sub>3</sub>, show exotic behaviors at the atomic layer limit, including superconductivity, long range magnetism and topological edge states. Their "stackability" further creates new opportunities to explore quantum phenomena previously studied only in 3D crystals. Here we demonstrate that magneto-Raman spectroscopy is a unique measurement capability that is exceptionally well suited to study these exotic 2D materials.

Specifically, in the MPX<sub>3</sub> (M=Fe, Mn; X=S, Se) compounds, inter-layer antiferromagnetic ordering has been suggested to survive in the monolayer limit through the measurement of spin-phonon coupling. Using temperature-, polarization-, and wavelength-dependent Raman scattering, we studied the Neel-type antiferromagnet MnPSe<sub>3</sub> through its ordering temperature, and as a function of applied magnetic field. Surprisingly, the previously assigned one-magnon scattering peak showed no change in frequency with an increasing in-plane magnetic field. Instead, the Raman data revealed a more surprising story, including changes in resonant Raman scattering due to magnetic ordering as well as the hybridization of phonons with a 2-magnon scattering continuum. These results, which are supported using first-principles calculations, reveal the complex phase space of the interactions of phonons and magnons with regards to temperature, laser excitation wavelength, and

magnetic field.

**6:00 AM F.EN04.10.08**

**Thermoreflectance Imaging of Thermionic Heating and Cooling at Source and Drain Contacts in  $\beta$ -Ga<sub>2</sub>O<sub>3</sub> and Graphene Nanoribbon Transistors** Kerry Maize; Purdue University, United States

Electronic devices based on 2D and quasi-2D materials promise several performance advantages. However, the physical properties and small length scales that enhance low dimensional electronic devices can also make them more susceptible to parasitic effects. Contact resistance and power dissipation [1] are notable challenges to making practical 2D devices. This study measures thermionic heating and cooling at heterojunctions of 2D nanoribbon semiconductor channel and metal contacts in both  $\beta$ -Ga<sub>2</sub>O<sub>3</sub> FET on insulator [2] and graphene FET on insulator. High resolution thermoreflectance microscope images show temperature difference of 60 K between gold drain and source contacts separated by a 15 micron long, two micron wide, 70 nm thick  $\beta$ -Ga<sub>2</sub>O<sub>3</sub> nanoribbon channel deposited on insulator substrate. [2] Current density was  $9 \times 10^4$  A/cm<sup>2</sup>, power was 3 mW. Thermionic effects at the metal-2D semiconductor contact interface were consistent with current flux, reversing heating and cooling at respective drain-source contacts when applied current polarity was reversed. Heating in the  $\beta$ -Ga<sub>2</sub>O<sub>3</sub> channel increased quadratically with current, consistent with Joule's law. However, temperature dependence on current at the gold- $\beta$ -Ga<sub>2</sub>O<sub>3</sub> contacts diverged significantly from a simple model combining Joule and Peltier contributions, suggesting thermionic effects at the metal-2D semiconductor interface dominate over any thermoelectric contribution from the  $\beta$ -Ga<sub>2</sub>O<sub>3</sub> channel. [3] Thermionic parasitics at the contacts may be exacerbated by use of low dimensional  $\beta$ -Ga<sub>2</sub>O<sub>3</sub> as channel. The high temperature gradient along the quasi-2D channel could impact transport properties, and device performance and reliability. Thermoreflectance images of a monolayer graphene nanoribbon FET modulated by backgate substrate revealed similar location, magnitude, and polarity dependent thermionic heating and cooling at the metal-graphene source and drain contacts. Thermionic heating and cooling, especially the large spatial temperature gradient between source and drain, would be difficult to measure using purely electrical methods. Future study will look at both geometric dependence and reliability considerations related to parasitic thermionic heating and cooling in 2D material electronic devices. [1] Zhou, H., Maize, K., Noh, J., Shakouri, A. & Ye, P. D. Thermodynamic Studies of  $\beta$ -Ga<sub>2</sub>O<sub>3</sub> Nanomembrane Field-Effect Transistors on a Sapphire Substrate. ACS Omega 2, 7723-7729 (2017). [2] Zhou, H., Maize, K., Qiu, G., Shakouri, A. & Ye, P. D.  $\beta$ -Ga<sub>2</sub>O<sub>3</sub> on insulator field-effect transistors with drain currents exceeding 1.5 A/mm and their self-heating effect. Applied Physics Letters 111, 092102 (2017). [3] Zeng, T. & Chen, G. Interplay between thermoelectric and thermionic effects in heterostructures. Journal of Applied Physics 92, 3152-3161 (2002).

**6:10 AM \*F.EN04.10.10**

**Two-Dimensional Alloys and Heterostructures** Pulickel Ajayan; Rice University, United States

There has been tremendous interest in recent years to study two-dimensional (2D) atomic layers which form building blocks of many bulk layered materials. This talk will focus on the use of 2D atomic layer building blocks to create various types of heterostructures and composite architectures that takes advantage of the varied properties of individual layers. The concept of nanoscale engineering and the goal of creating new artificially stacked van der Waals solids and 3D constructs will be discussed through a number of examples including graphene and other 2D layer compositions. The talk will explore the emerging landscape of multi-component 2D layers such as doped, intercalated and alloy systems. The anticipated multifunctional properties of these structures will be discussed.

**6:25 AM \*F.EN04.10.12**

**Electronic Properties and Device Applications of Quasi-Two-Dimensional Charge-Density-Wave Materials** Alexander Balandin; University of California, Riverside, United States

The charge density wave (CDW) phase is a quantum state consisting of a periodic modulation of the electronic charge density accompanied by a periodic distortion of the atomic lattice in quasi-1D or quasi-2D metallic crystals. Several layered transition metal dichalcogenides (TMDs) exhibit unusually high transition temperatures to different CDW symmetry-reducing phases opening possibility for practical device applications. One of the most promising materials, 1T-TaS<sub>2</sub>, has the CDW transition between the nearly-commensurate (NC-CDW) and the incommensurate (IC-CDW) phases at 350 K. The transition from the IC-CDW phase to the normal metal phase is observed at even higher temperature. In this invited talk, I will review our recent experimental results on controlling the CDW phase transitions with an applied electric field and discuss device applications of quasi-2D CDW materials. We have demonstrated the room-temperature voltage controlled oscillators and logic circuits, which operate on the basis of the NC-to-IC CDW transition in 1T-TaS<sub>2</sub> channels, triggered by the applied voltage [1-2]. We found that the 1T-TaS<sub>2</sub> CDW devices reveal exceptional hardness against X-ray and proton radiations [3-4]. We explained this property of the CDW devices by the high carrier concentration in all their phase states,

two-terminal design, and the thin-film channel geometry. The low-frequency electronic noise spectroscopy has been used as an effective tool for monitoring the CDW phase transitions, particularly the switching from the IC-CDW phase to the normal metal phase in 1T-TaS<sub>2</sub> [5]. The noise spectral density exhibits sharp increases at the phase transition points, which correspond to the step-like changes in resistivity. The noise spectroscopy was instrumental in revealing the “hidden phase transitions” in vertical 1T-TaS<sub>2</sub> devices [6]. Preliminary data on the “narrow-band noise” in quasi-2D CDW devices will also be presented.

This work was supported, in part, by the National Science Foundation (NSF) through the DMREF: Collaborative Research (UC Riverside – Stanford): Data Driven Discovery of Synthesis Pathways and Distinguishing Electronic Phenomena of van der Waals Bonded Solids, and by the University of California – National Laboratory Collaborative Research and Training Program LFR-17-477237, and by the Semiconductor Research Corporation (SRC) contract 2018-NM-2796: One-Dimensional van-der-Waals Metals: Ultimately Downscaled Interconnects with Exceptional Current-Carrying Capacity and Reliability.

- [1] G. Liu, et al., A charge-density-wave oscillator based on an integrated tantalum disulfide–boron nitride–graphene device operating at room temperature, *Nature Nanotechnology*, 11, 845 (2016).
- [2] A. G. Khitun, et al., Transistor-less logic circuits implemented with 2-D charge density wave devices, *IEEE Electron Device Letters*, 39, 1449 (2018).
- [3] G. Liu, et al., Total-ionizing-dose effects on threshold switching in 1T-TaS<sub>2</sub> charge density wave devices, *IEEE Electron Device Letters*, 38, 1724 (2017).
- [4] A. K. Geremew, et al., Proton-irradiation-immune electronics implemented with two-dimensional charge-density-wave devices, *Nanoscale*, 11, 8380 (2019).
- [5] A. K. Geremew, et al., Bias-voltage driven switching of the charge-density-wave and normal metallic phases in 1T-TaS<sub>2</sub> thin-film devices, *ACS Nano*, 13, 7231 (2019).
- [6] R. Salgado, et al., Low-frequency noise spectroscopy of charge- density-wave phase transitions in vertical quasi-2D 1T-TaS<sub>2</sub> devices, *Appl. Phys. Express*, 12, 037001 (2019).

#### SESSION F.EN04.11: Electronic Properties and Devices

On Demand Abstracts Available for Viewing Starting Saturday Morning, November 21, 2020  
F-EN04

#### SESSION F.EN04.12: Photonic Properties and Devices

On Demand Abstracts Available for Viewing Starting Saturday Morning, November 21, 2020  
F-EN04

#### 5:00 AM F.EN04.12.01

**Local Strain Associated Localized Exciton Energy in WSe<sub>2</sub>** Hyowon Moon<sup>1</sup>, Eric Bersin<sup>1</sup>, Chitrleema Chakraborty<sup>1</sup>, Ang-Yu Lu<sup>1</sup>, Gabriele Grosso<sup>2</sup>, Jing Kong<sup>1</sup> and Dirk R. Englund<sup>1</sup>; <sup>1</sup>Massachusetts Institute of Technology, United States; <sup>2</sup>The City University of New York, United States

The deterministic creation of single-photon emitters in a solid-state system is an important step towards scalable photonic quantum processors [1]. Two-dimensional materials transferred onto nanostructures are promising candidate thanks to their ability to host quantum emitters with high probability at specifically fabricated sites [2,3]. However, the emission energies of quantum emitters, a crucial factor for generating indistinguishable photons and entangled states, are broadly distributed, and the precise relationship between this strain and the resultant emission energy remains elusive. Here, we study the localized emitters hosted in monolayer WSe<sub>2</sub> transferred onto micron-sized structures, and the corresponding free-exciton energy shift induced by local strain. The localized emission energy show positive correlation with the strain-modulated free-exciton energy together with minimum offset value ~ 40 meV. Our results show local strain plays a crucial role not only in the formation but also in the emission energy of the localized emitters, elucidates the origin of single-photon emission in two-dimensional semiconductors. [1] I. Aharonovich, D. Englund, M. Toth, *Nature Photonics* 2016, 10, 631. [2] A. Branny, S. Kumar, R. Proux, B. D. Gerardot, *Nature Communications* 2017, 8, 15053. [3] C. Palacios-Berraquero, D. M. Kara, A. R.-P.

Montblanch, M. Barbone, P. Latawiec, D. Yoon, A. K. Ott, M. Loncar, A. C. Ferrari, M. Atatüre, Nat. Commun. 2017, 8, 15093.

#### 5:10 AM F.EN04.12.02

**Advanced 2D Material Optoelectronic Devices in Integrated Photonics** Volker J. Sorger<sup>1</sup>, Rishi Maiti<sup>1</sup>, Mario Miscuglio<sup>1</sup>, Tony Low<sup>2</sup> and Ritesh Agarwal<sup>3</sup>; <sup>1</sup>George Washington University, United States; <sup>2</sup>University of Minnesota, United States; <sup>3</sup>University of Pennsylvania, United States

2D materials have a number of intriguing value proposition that could be harnessed for compact, tunable, high-performance optoelectronic devices when heterogeneously integrated in photonic circuits. Here I review our latest work including: (1) tunable TMD-based microring resonator with engineered critical-coupling condition, (2) a broadband graphene plasmon-slot photodetector ( $R=0.7A/W$ ), (3) a 200mV bandgap-shifted strain-engineered absorption-enhanced MoTe2 photodetector ( $R=0.5A/W$ , low-dark-current  $<10nA@-1V$ ), (4) a record-high responsivity ( $R=1.36A/W$ ) slot-plasmon exciton-modulated MoTe2 photodetector, (5) a MoS2 electro-absorption modulator all enabled by our recently developed method of cross-contamination-free yet deterministic dry transfer 2D material 'printer' mimicking a 3D printer for enabling rapid prototyping. These devices are based on heterogeneous integration of 2D materials into Silicon and SiN photonics, with the latter used for on-exciton modulation or exciton absorption.

#### 5:20 AM F.EN04.12.04

**A Full Picture of Intrinsic Defects in Monolayer 2D Ferroelectric Materials** Bolong Huang; The Hong Kong Polytechnic University, Hong Kong

Following the developments of two-dimensional (2D) graphene with distinct properties, tremendous progress has been achieved for the broad applications of 2D materials in nanoscale electronics and optoelectronics. The layered metal chalcogenides (LMC) contribute to a dominant group of the layered 2D structure with various properties and applications. Pursuing the precise structural identification of functional two-dimensional (2D) layered metal chalcogenides (LMCs) are key factors dominating the origins of the unique electronic and ferroelectric properties. Presently, indium selenide ( $In_2Se_3$ ) has become one of the most studied LMC materials due to the flexible phases with broad applications in phase-change memory, lithium batteries, optoelectronic and even photovoltaic devices.  $In_2Se_3$  is particularly attractive in the atomically thin film research due to the flexible phase modulations and unique electronic behaviors. However, the complicated phase change of  $In_2Se_3$  and their high sensitivity towards the intrinsic defects still requires the advanced technology to identify the origins of the inhomogeneous charge distribution induced in-plane and out-of-plane ferroelectricity. In this work, we have presented comprehensive theoretical research to reveal the simulated scanning tunneling microscope (STM) images as a toolbox for the experimental results to distinguish the structural features. By detailed analysis of the simulated STM images and phonon behaviors under different defects, this work supplies the insightful structure clues of the nanoscale charge distribution fluctuations, explaining the unique electronic behaviors in mono-layered  $In_2Se_3$ . We also confirm the high possibility of surface defects in the few-layered  $In_2Se_3$  rather than sub-layered defects. Moreover, the corresponding electron-phonon behaviors of  $In_2Se_3$  with major intrinsic defects provide pivotal references to explain the unique in-plane and out-of-plane electronic and ferroelectric properties in different applications. The modulations of the electronic properties by different intrinsic defects regarding the charge couplings and bandgap have been revealed, which is of significance in the precise identification and modulation of the ultra-thin LMC based ferroelectric materials, shedding new light for the synthesis of other relevant functional materials for broad applications.

#### 5:30 AM F.EN04.12.05

**Laser Induced Transformation of PdSe2 for On-Demand Device Fabrication** Viktoryia Shautsova, Sapna Sinha, Linlin Hou, Qianyang Zhang, Martin Tweedie, Yang Lu, Yüewen Sheng, Benjamin Porter, Harish Bhaskaran and Jamie Warner; University of Oxford, United Kingdom

Two-dimensional materials with tunable band gap in the range of 0.3-1.5 eV are highly desirable for electronic and optoelectronic applications. Palladium diselenide ( $PdSe_2$ ), a less explored group-10 transition metal dichalcogenide, is one such material of particular interest that demonstrates a gradual transition from a semiconductor (monolayer) to semimetal (bulk) [1, 2]. In this work, we report our recent results on laser-induced phase transformation of a few layer  $PdSe_2$  films [3]. We demonstrate that controlled laser irradiation can be used to directly ablate  $PdSe_2$  thin films using high power or trigger the local transformation of  $PdSe_2$  into a metallic phase  $PdSe_{2-x}$  using lower laser power. Scanning transmission electron microscopy is used to reveal the laser-induced Se-deficient phases of  $PdSe_2$  material. The process sensitivity to the laser power allows patterning flexibility for resist-free device fabrication. The laser-patterned devices demonstrate that a laser-induced metallic phase  $PdSe_{2-x}$  is stable with increased conductivity by a factor of about 20 compared to  $PdSe_2$ . [1] L. H.



Zeng et al. Adv. Funct. Mater. 2019, 1806878, 1-9. [2] A. D.Oyedele et al. J. Am. Chem. Soc. 2017, 139, 14090-14097. [3] V. Shautsova et al. ACS Nano 2019, 13, 12, 14162-14171

SESSION F.EN04.13: Multiferroic Properties and Quantum Devices  
On Demand Abstracts Available for Viewing Starting Saturday Morning, November 21, 2020  
F-EN04

**5:00 AM \*F.EN04.13.01**

**Probing and Pressure Control of the Magnetic States in Atomically Thin van der Waals Magnets Zaiyao Fei and Xiaodong Xu; University of Washington, United States**

The discovery of two-dimensional (2D) magnets in van der Waals (vdW) crystals provide a new platform for studying fundamental 2D magnetism and spintronic devices. In this talk, I will first present 2D itinerant ferromagnetism in atomically thin Fe<sub>3</sub>GeTe<sub>2</sub> (FGT). FGT is a ferromagnetic metal in the bulk form, with a strong out-of-plane anisotropy and high Curie temperature of 220-230 K. Our layer-number-dependent studies reveal a crossover from 3D to 2D Ising ferromagnetism for thicknesses less than 4 nm (five layers), accompanied by a fast drop of the Curie temperature from 207 K to 130 K in the monolayer. For FGT flakes thicker than ~15 nm, a distinct magnetic behavior emerges in an intermediate temperature range, which we show is due to the formation of labyrinthine domain patterns. In the second part of my talk, I will present the pressure control of the magnetic states in bi- and tri-layer chromium triiodide (CrI<sub>3</sub>), which exhibits layered antiferromagnetic ground states at ambient pressure. In bilayer CrI<sub>3</sub>, pressure can change the stacking arrangement which induces a transition from layered antiferromagnetic to ferromagnetic phases. In trilayer CrI<sub>3</sub>, we found that pressure can create coexisting domains of three phases, one ferromagnetic and two distinct antiferromagnetic. Our work provides ample opportunities to engineer spintronic devices based on vdW magnets and heterostructures.

**5:15 AM \*F.EN04.13.02**

**Fundamental Properties of 2D Tellurium Films Peide P. Ye; Purdue University, United States**

Tellurium is one of the special elemental materials which have 1D helical atomic structures and formed by van der Waals force between helical atomic chains. 2D tellurium films can be synthesized in a liquid solution. [1,2] In this talk, we will review the fundamental studies of this new 2D material at atomic scale in terms of its electrical, optical, thermal and mechanical properties. The helical atomic structure offers strong anisotropic properties of this 1D van der Waals material. The band-structure of this 2D material also offers some excellent material properties such as a high value of thermoelectric figure-of-merit ZT [3] and high carrier mobilities for both electrons and holes. Magneto-transport properties, such as SdH oscillations and QHE in 2D tellurium, were reported before. [4] More interestingly, topological non-trivial properties as Weyl node at conduction band edge are also unveiled in magneto-transport under 45 Tesla at tens of mK temperatures, showing Berry phase and radial spin texture being significantly different from Rashba or Dresselhaus spin-orbit coupling materials [5,6] The work is in close collaborations with Prof. Wenzhuo Wu at Purdue University. References: [1] Wang, Y. et al., Nature Electronics 2018, 1, 228. [2] Du, Y. et al., Nano Letters 2017, 17, 3965. [3] Qiu, G. et al., Nano Letters 2019, 19, 1955. [4] Qiu, G. et al., Nano Letters 2018, 18, 5760. [5] Qiu, G. et al., arXiv. 1908.11495. [6] Niu, C. et al., arXiv. 1909.06659.

**5:30 AM F.EN04.13.03**

**Two-Dimensional Material Tunnel Barrier for Josephson Junctions and Superconducting Qubits Kan-Heng Lee<sup>1</sup>, Ariana Ray<sup>1</sup>, Hui Gao<sup>1</sup>, David A. Muller<sup>1</sup>, Srivatsan Chakram<sup>2</sup>, Shi En Kim<sup>2</sup>, Fauzia Mujid<sup>2</sup>, Chibeom Park<sup>2</sup>, Yu Zhong<sup>2</sup>, David I. Schuster<sup>2</sup> and Jiwoong Park<sup>2</sup>; <sup>1</sup>Cornell University, United States; <sup>2</sup>The University of Chicago, United States**

Recent developments in the device architecture and operation of state-of-the-art superconducting qubits has allowed the technology to advance to practical applications in quantum computing. However, the central circuit element in superconducting qubits, the Josephson junction, has mainly focused on using the amorphous AlO<sub>x</sub> tunnel barrier. New materials for fabricating Josephson junctions are expected to introduce novel functionalities and new circuit elements to superconducting qubits. Two-dimensional (2D) materials are one such promising candidate. The van der Waals layered structures of 2D materials can enable the precise design of the tunnel barrier at the sub-nanometer scale via layer-by-layer stacking of atomically thin monolayers, wherein each layer can be a different 2D material. This ability to generate heterostructure barriers would allow, for example, the design of the tunnel barrier's band structure using 2D materials with

different band gaps and band offsets, or the fabrication of novel quantum circuit components such as  $\pi$ -junctions using 2D magnets. In order to realize the implementation of 2D materials in these systems, it is essential to have a fabrication method that not only maintains oxide-free interfaces between the easily-oxidized superconductors and the 2D material tunnel barriers, but is also scalable for technological applications. Here, we demonstrate Josephson junctions and superconducting qubits that employ 2D materials as the tunnel barrier [1]. We batch-fabricate and tune the critical Josephson current of the device arrays over orders of magnitudes via layer-by-layer stacking of N layers of MoS<sub>2</sub>. In addition, we observe a transition of the junction J-V characteristics when N is increased. Based on these junctions, we demonstrate, for the first time, the engineering and operation of MoS<sub>2</sub> superconducting qubits using a bulk superconducting microwave resonator. Our work here allows Josephson junctions to access the diverse physical properties of 2D materials, offering a platform to study the effects of these properties in superconducting qubit circuits under different geometries, and engineer novel quantum circuit elements for quantum computing. [1] K. -H. Lee, S. Chakram, S. E. Kim, F. Mujid, A. Ray, H. Gao, C. Park, Y. Zhong, D. A. Muller, D. I. Schuster, J. Park, "Two-Dimensional Material Tunnel Barrier for Josephson Junctions and Superconducting Qubits," *Nano Letters*, <https://doi.org/10.1021/acs.nanolett.9b03886> (2019).

#### 5:40 AM F.EN04.13.04

**Purely In-Plane Ferroelectricity in SnS Down to the Monolayer Limit** Naoki Higashitarumizu<sup>1</sup>, Hayami Kawamoto<sup>1</sup>, Chien-Ju Lee<sup>2</sup>, Bo-Han Lin<sup>2</sup>, Fu-Hsien Chu<sup>2</sup>, Itsuki Yonemori<sup>3</sup>, Tomonori Nishimura<sup>1</sup>, Katsunori Wakabayashi<sup>3</sup>, Wen-Hao Chang<sup>2</sup> and Kosuke Nagashio<sup>1</sup>; <sup>1</sup>The University of Tokyo, Japan; <sup>2</sup>National Chiao Tung University, Taiwan; <sup>3</sup>Kwansei Gakuin University, Japan

Ferroelectric 2D materials have emerged as a promising platform for nonvolatile memories and nonlinear optoelectrical devices working at the ultimate atomic thickness. However, most of the experimental investigations have been limited in the 2D ferroelectric with out-of-plane polarization, which causes the depolarization field at the metal/ferroelectric interface with decreasing the thickness. Although monolayer SnS has been theoretically expected to be a purely in-plane multiferroic semiconductor with ferroelectricity and ferroelasticity,[1] experimental demonstration is challenging because it is difficult to obtain a high-quality monolayer SnS.[2,3] Bao et al. have recently reported a ferroelectric device of bulk SnS (~15 nm), utilizing an external electric field to break the centrosymmetry.[4] As the few layer SnS has been investigated only by probe measurements owing to its small size of several tens of nanometers, the ferroelectric characteristic of few-to-monolayer SnS is still unidentified. Here, we report an in-plane ferroelectric device of a micrometer-size monolayer SnS grown via physical vapor deposition, where the growth conditions are precisely controlled to balance the adsorption and desorption of SnS. The Raman spectrum for monolayer SnS indicates high crystalline quality and strong anisotropy. As a prerequisite for ferroelectricity, second harmonic generation (SHG) spectroscopy reveals a non-centrosymmetry in monolayer SnS. Room temperature ferroelectric switching in monolayer is successfully demonstrated by the ferroelectric evaluation system. SnS has been commonly regarded to exhibit the odd/even effect, where the centrosymmetry breaks only in the odd-number layers to exhibit ferroelectricity. Remarkably, however, both the SHG signal and ferroelectric switching are observed in both odd and even-number layers below a critical thickness (~15 layers), thus overcoming the odd/even effect. This suggests an unusual stacking sequence lacking centrosymmetry due to a strong interaction between SnS and mica substrate. Given that SnS is the semiconductor with multiferroicity, pyroelectricity, and piezoelectricity, this work will open up possibilities of providing novel multifunctionalities in van der Waals heterostructure devices. [1] M. Wu and X.C. Zeng, *Nano Lett.* 16, 3236 (2016). [2] N. Higashitarumizu et al., *MRS Adv.* 3, 2809 (2018). [3] N. Higashitarumizu et al., *Nanoscale* 10, 22474 (2018). [4] Y. Bao et al., *Nano Lett.* 19, 5109 (2019).

SESSION F.EN04.14: Electronic Properties and Quantum Devices  
On Demand Abstracts Available for Viewing Starting Saturday Morning, November 21, 2020  
F-EN04

#### 5:00 AM F.EN04.14.01

**Direct Graphene Growth for Si-Based Technology** Keun Wook Shin, Yeonchoo Cho, Minsu Seol and Hyeon Jin Shin; Samsung Advanced Institute of Technology, Korea (the Republic of)

Graphene is a 2-dimensional carbon layer. Because of its potential properties such as chemical inertness and atomically thin nature, graphene has been considered as a thin diffusion layer in metal interconnect structures. Furthermore, as the feature size of device is decreased to sub-nm size, the contact resistance between metal and Si in source/drain has become one of the critical issues. We demonstrated that reduced contact resistivity of 1.47 n $\Omega$ -cm<sup>2</sup> via insertion of graphene between metal

and Si which approaches the theoretical limit of 1.3 nohm-cm<sup>2</sup>. [1] In order to adapt graphene to source and drain, direct and selective graphene growth on semiconductor substrates is required. In our previous report, we have already suggested that the directly grown nanocrystalline graphene (nc-G) at 560 oC can act as a liner reducing the resistivity of W as well as a diffusion barrier in a W interconnect structure by realizing W/nc-G/TiN. [2] However, the selective graphene growth on the non-catalytic semiconductor-insulator substrates is barely reported. In this study, we addressed the origin of selective growth of graphene on a semiconductor over the dielectric materials. Based on Ab initio simulations, we found that the adsorption energy of CH<sub>4</sub> on SiO<sub>2</sub> is much higher than that on Si and Ge. The growth differences of graphene on Ge and SiO<sub>2</sub> were also experimentally confirmed. While a continuous graphene layer was formed on the Ge surface at the initial growth stage that became thicker at increasing growth times, an incubation time was required for the nucleation of graphene on SiO<sub>2</sub>. The interface analysis between nc-G and SiO<sub>2</sub> indicates that initially incorporated carbon onto SiO<sub>2</sub> cannot contribute to the nc-G growth because of its reaction with SiO<sub>2</sub> producing CO. Finally, we selectively grew 3 nm-thick nc-G layer on a SiO<sub>2</sub>-patterned Ge substrate. [3] In addition, as the feature size of semiconductor devices decreases, hard mask films with high etch selectivity are required to achieve fine pattern transfer during lithography. We are going to address the potential and properties of nc-G layer as a future hardmask film. [4] [1] M.-H. Lee et al.(SAIT) "Two-Dimensional Materials Inserted at the Metal/Semiconductor Interface: Attractive Candidates for Semiconductor Device Contacts", Nano Letters 18, 4878 (2018) [2] C.S. Lee et al.(SAIT) "Fabrication of Metal/Graphene Hybrid Interconnects by Direct Graphene Growth and Their Integration Properties", Advanced Electronic Materials 4, 170064 (2018). [3] K.W. Shin et al.(SAIT) "Study of Selective Graphene Growth on Non-Catalytic Hetero-Substrates", 2D Materials 7, 011002 (2020). [4] S. W Kim et al.(SAIT) (In preparation).

#### 5:10 AM F.EN04.14.02

**2D Material Enabled Colloidal Electronics** Albert Liu, Pingwei Liu, Daichi Kozawa, Volodymyr Koman, Jingfan Yang and Michael Strano; Massachusetts Institute of Technology, United States

Graphene and other 2D materials possess desirable mechanical and functional properties for incorporation into or onto novel colloidal particles, potentially granting them unique electronic and optical functions. However, this application has not yet been realized because conventional top-down lithography scales poorly for the production of colloidal solutions. Herein, we describe an "autoperforation" technique providing a means of spontaneous assembly for colloidal microparticles comprised of 2D molecular surfaces at scale. Such particles demonstrate remarkable chemical, mechanical and thermal stability. They can function as aerosolizable memristor arrays capable of storing digital information, as well as dispersible and recoverable probes for large-scale collection of chemical information in water and soil. Liu, A. T.;\* Liu, P.;\* Kozawa, D.; Dong, J.; Yang, J. F.; Koman, V. B.; Saccone, M.; Wang, S.; Son, Y.; Wong, M. H.; Strano, M. S.-Nature Materials (2018) 17, 1005-1012.

#### 5:20 AM \*F.EN04.14.03

**Scalable Synthesis Approaches Towards 2D Transition Metal Dichalcogenide-Based Molecular Sensors** Nicholas Glavin; Air Force Research Laboratory, United States

Two-dimensional (2D) transition metal dichalcogenides (TMDs) are some of the more promising material candidates for future sensors requiring detection of molecular species at extremely low concentrations. This is primarily due to the multifunctional properties including a high surface to volume ratio and strict control of surface reaction sites. In this talk, two different scalable synthesis approaches towards large area TMD films using magnetron sputtering are presented. Firstly, direct sputtering of MoS<sub>2</sub> and WSe<sub>2</sub> thin onto various substrate and subsequent laser crystallization was shown to enable local control of defect density and crystal structure. Additionally, wafer-scale crystallization of stretchable 2D photodetectors with the use of a broadband pulsed lamp source demonstrate the feasibility of large scale transformation as a means to create unique device constructs. The second large area technique to be discussed is the sputtering of metal precursor films and sulfurization/selenization using various gas phase reaction sources. Heterostructures and superlattice constructs using stacked metal layers with alternating materials were also demonstrated using this technique. Finally, the large area TMD films and heterostructures were evaluated in both electrical and optical molecular sensors constructs for future low analyte detection devices.

#### 5:35 AM \*F.EN04.14.04

**RF Energy Harvesters Based on Atomically Thin MoS<sub>2</sub> Phase Heterostructures** Xu Zhang<sup>1</sup>, Jesus Grajal<sup>2</sup>, Jose Luis Vazquez-Roy<sup>3</sup>, Ujwal Radhakrishna<sup>4</sup>, Han Wang<sup>5</sup>, Jing Kong<sup>4</sup>, Mildred Dresselhaus<sup>4</sup> and Tomas Palacios<sup>4</sup>; <sup>1</sup>Carnegie Mellon University, United States; <sup>2</sup>Universidad Politécnic de Madrid, Spain; <sup>3</sup>University Carlos III of Madrid, Spain; <sup>4</sup>Massachusetts Institute of Technology, United States; <sup>5</sup>University of Southern California, United States

The atomically thin two-dimensional materials have emerged as a new type of thin film semiconductors that are promising for flexible electronics, thanks to their unique electronic and mechanical properties. As many important components of flexible electronics (for example, transistors, sensors and memory devices based on two-dimensional materials) have been developed, an efficient, flexible and always-on energy-harvesting solution is highly desirable yet still missing. In this work, we present a fully flexible Wi-Fi band rectenna based on atomically thin MoS<sub>2</sub> semiconducting-metallic phase heterojunctions. Through a self-aligned phase engineering technology, we successfully improved the cutoff frequency of MoS<sub>2</sub>-based rectifiers to 10 gigahertz, which is high enough to cover the increasingly ubiquitous electromagnetic radiation from Wi-Fi and cellular systems. By integrating the MoS<sub>2</sub> rectifier with a flexible Wi-Fi band antenna, we realized wireless energy harvesting of electromagnetic radiation at zero external bias. In addition, the phase-engineered MoS<sub>2</sub> rectifier can also function as a flexible mixer, realizing frequency conversion beyond 10 gigahertz. This work provides a flexible energy-harvesting building block that can be integrated with various flexible electronic systems.

#### 5:50 AM \*F.EN04.14.05

**Hybrid van der Waals Interfaces for Photonics and Electronics** Deep M. Jariwala; University of Pennsylvania, United States

Van der Waals semiconductor materials and heterostructures possessing room temperature strongly bound exciton states exhibit emergent physical phenomena and are of a great promise for optoelectronic applications. Likewise, their self-passivated surfaces enable facile integration for novel heterostructures for device applications. In the first part of the talk, we will present novel light-matter interactions that are observed at the hybrid interface of two-dimensional (2D) semiconductors and bulk gold (Au) surface. We will demonstrate that nanostructured multilayer transition metal dichalcogenides (TMDCs) by themselves provide an ideal cavity-less platform for exciton-photonics. Hence, we show that by patterning the TMDCs into nanoresonators, strong dispersion and avoided crossing of excitons and photon-polaritons with interaction potentials exceeding 410 meV may be controlled with great precision. We further observe that inherently strong TMDC exciton absorption resonances may be completely suppressed due to excitation of hybrid photon states and their interference. In the second part of this talk we will demonstrate, hybrid 2D/3D semiconductor heterojunctions using MoS<sub>2</sub> as the prototypical 2D semiconductor laid upon Si and GaN as the heavily doped 3D semiconductor layers. At the interface of these junctions we demonstrate that Fermi-level is tunable in the transition metal dichalcogenides (TMDCs) to achieve highly tunable rectification ratios in the diodes across seven orders of magnitude i.e from 0.1 to 106. Concurrently, we have also demonstrated that these triodes can effectively serve the purpose of a switching device with on/off ratios exceeding 107. Our results suggest that the 2D/3D semiconductor heterojunction system is highly tunable, near-ideal and effective for electronic applications despite the lack the perfect passivation at the interface. Given the hybrid nature of the device it can serve the function in both switching and rectifying applications. With a wealth of 2D semiconductors now isolated and combined with the availability of controlled complementary doping in 3D semiconductors, our work opens up new opportunities in high performance and multi-functional, hybrid heterostructure devices.

SESSION F.EN04.15: Optoelectronics, Flexible Electronics and Other Devices  
On Demand Abstracts Available for Viewing Starting Saturday Morning, November 21, 2020  
F-EN04

#### 5:00 AM F.EN04.15.02

**Flexible Large-Scale LEDs Based on MOCVD-Grown WS<sub>2</sub> Monolayers as Luminescing Material** Dominik Andrzejewski<sup>1</sup>, Ruth Oliver<sup>1</sup>, Yannick Beckmann<sup>1</sup>, Michael Heuken<sup>2</sup>, Annika Grundmann<sup>3</sup>, Holger Kalisch<sup>3</sup>, Andrei Vescan<sup>3</sup>, Tilmar Kümmell<sup>1</sup> and Gerd Bacher<sup>1</sup>; <sup>1</sup>Universität Duisburg-Essen, Germany; <sup>2</sup>AIXTRON SE, Germany; <sup>3</sup>RWTH Aachen University, Germany

Semiconducting transition metal dichalcogenides (TMDs) represent a novel and sustainable material class for ultrathin optoelectronic devices. Although various approaches towards light emitting devices have been reported, e.g. based on exfoliated or chemical vapor deposited TMD monolayers, they all suffer from limited scalability required for practical applications. Recently, a first scalable approach has been suggested combining WS<sub>2</sub> monolayers grown in a commercial horizontal multi-wafer AIXTRON metal organic chemical vapor deposition (MOCVD) reactor on sapphire (0001) substrates [1] with a vertical p-n device concept [2]. With this, large-scale light emitting devices based on TMDs as active material, organic injection layers on the anode side and an inorganic supporting layer on the cathode side have been demonstrated.[3] One unique property of this ultra-thin semiconductor family is their flexibility. Taking advantage of this, we realized for the

first time a large-scale WS<sub>2</sub> monolayer based light emitting device on a flexible substrate. Our devices are fabricated in a vertical p-n architecture on ITO covered PEN foil, with PEDOT:PSS / poly-TPD hole injection layers on the anode side and a ZnO nanoparticle layer as an electron supporting layer on the cathode side. By applying an external voltage, those devices show diode-like behavior in their I-V characteristic and pronounced red electroluminescence purely originating from the WS<sub>2</sub> monolayer. Light emission starts at a turn-on voltage below 3 V from an emissive area of 6 mm<sup>2</sup>, which is just limited by the size of the cathode contact. By bending the device, an energy shift of the electroluminescence with a gauge factor of 30 meV/% is observed, caused by the strain-induced shift of the bandgap. These novel large-scale and flexible LEDs with a TMD emissive monolayer and an emission energy depending on the bending radius opens a new field of potential applications for flexible optoelectronics. References: [1] A. Grundmann et al., MRS Adv. 4, 593 (2019) [2] D. Andrzejewski et al., Nanoscale 11, 8372 (2019) [3] D. Andrzejewski et al., ACS Photonics 6, 1832 (2019)

#### 5:10 AM \*F.EN04.15.03

##### **High Performance OFETs Based on Meniscus Guide Coating—From Growth Mechanisms to Achievements** Paddy K. L. Chan; University of Hong Kong, Hong Kong

Organic field effect transistors (OFETs) are the major building blocks of the next generation flexible electronics. From logic gates to health monitoring sensors, different flexible electronics have been developed based on the OFETs. In this talk, I will focus on one of the most promising OFET fabrication methods which has excellent compatibility with large area deposition, the meniscus guided coating (MGC). Four elementary processing parameters (i) shearing speed ( $v$ ), (ii) solute concentration, (iii) deposition temperature ( $T$ ) and, (iv) solvent boiling point ( $T_b$ ) are utilized to analyze crystal growth behavior in the meniscus-guided coating. By carefully varying and studying these four key factors, we can confirm that  $v$  is the thickness regulation factor while  $c$  is proportional to crystal growth rate. The MGC crystal growth rate is also correlated to latent heat ( $L$ ) of solvents and deposition temperature in an Arrhenius form. The latent heat of solvents is proportional to  $T_b$ . I will also provide a generalized formula to estimate the effects of these fabrication parameters which can serve as the crystal growth guidelines for the MGC approach. It is also an important cornerstone towards scaling up the OFETs for the sophisticated organic circuits or mass production. Furthermore, I will also discuss how to use the ultra-low speed version of MGC to develop 2D monolayer organic crystal and long range in-plane ordering. By using this method, we can obtain 2,9-dicyclopentadithiophene (C10-DNTT) monolayer with single-crystalline domain size ranging from millimeters to centimeters. Intrinsic field-effect mobility around 12 cm<sup>2</sup>V<sup>-1</sup>s<sup>-1</sup> is achieved. More importantly, the ultrathin thickness minimizes the charge injection barrier for the top-contact electrodes, allowing an ohmic hole injection and a low contact resistance ( $R_cW$ ) of 40±15 ohm-cm, one of the lowest values reported for the n-shape organic semiconductors. The detailed analysis of this ohmic metal/organic contact will be also be discussed.

#### 5:25 AM F.EN04.15.04

##### **Waveguide-Integrated, Plasmonic Enhanced Photodetectors Based on the Photo-Thermoelectric Effect in CVD**

**Graphene** Jakob Muench<sup>1</sup>, Alfonso Ruocco<sup>1</sup>, Marco Giambra<sup>2</sup>, Vaidotas Miseikis<sup>2</sup>, Dengke Zhang<sup>1</sup>, Junjia Wang<sup>1</sup>, Hannah Watson<sup>1</sup>, Gyeong Cheol Park<sup>1</sup>, Shahab Akhavan<sup>1</sup>, Michele Midrio<sup>2</sup>, Andrea Tomadin<sup>3</sup>, Camilla Coletti<sup>4</sup>, Marco Romagnoli<sup>2</sup>, Ilya Goykhman<sup>1</sup> and Andrea C. Ferrari<sup>1</sup>; <sup>1</sup>University of Cambridge, United Kingdom; <sup>2</sup>Consorzio Nazionale per le Telecomunicazioni, Italy; <sup>3</sup>University of Pisa, Italy; <sup>4</sup>Center for Nanotechnology Innovation @ NEST, Italy

The integration of single layer graphene (SLG) with on-chip photonic circuitry may offer improved performance and new functionalities for active components in telecom modules [1]. Graphene based photodetectors (GPDs) promise high-speed [1,2], broad-band operation [3,4] and the direct generation of a photovoltage [1,2,4,5], potentially removing the need of using noise-prone trans-impedance amplifiers (TIAs) [1]. Here we present a micrometer scale, on-chip integrated, plasmonic enhanced photo-thermoelectric [6] GPD for telecom wavelengths operating at zero dark current [1,5]. The GPD is designed and optimized to directly generate a photovoltage and has an external responsivity  $\approx 12.2$  V/W with a 3dB bandwidth  $\approx 42$  GHz. We utilize Au split-gates with a  $\approx 100$  nm gap to electrostatically create a p-n-junction and simultaneously guide a surface plasmon polariton gap-mode. This increases light-graphene interaction and optical absorption and results in an increased electronic temperature and steeper temperature gradient across the channel. Implemented with scalable CVD SLG, our work paves the way to compact, on-chip integrated, power-efficient GPDs for receivers in tele/datacom. [1] M. Romagnoli et al., Nat. Rev. Mater., 3, 392, (2018). [2] S. Schuler et al., Nano Lett., 16, 7107, (2016) [3] F. Bonaccorso et al., Nat. Photonics, 4, 611, (2010). [4] F. H. L. Koppens et al., Nat. Nanotechnol., 9, 780, (2014). [5] J. E. Muench et al., arxiv: 1905.04639, (2019) [6] N. Gabor et al., Science, 334, 648, (2011).

#### 5:35 AM \*F.EN04.15.05

##### **Dimensional Control of Physical Properties in Perovskite Chalcogenides—From Optical Anisotropy to Ultra-Low Thermal Conductivity** Jayakanth Ravichandran; University of Southern California, United States

Perovskite Chalcogenides are a new class of semiconductors, which have tunable band gap in the visible to infrared part of the electromagnetic spectrum. Besides this band gap tunability, they offer a unique opportunity to realize large density of states semiconductors with high carrier mobility. In this talk, I will discuss some of the advances made both in my research group and in the research community on the theory, synthesis of these materials and understanding their optoelectronic properties. The basic building block of the perovskite structure is the octahedral cage and the nature of its connectivity gives rise to both the perovskite and related structures with varying dimensionality. I will discuss how low dimensional connectivity can influence areas spanning optoelectronics to thermal transport. First, I will show unusual band gap evolution in two dimensional Ruddlesden Popper perovskites; Second, I will discuss giant optical anisotropy in one dimensional perovskite-like phases, which also show ultralow thermal conductivity. These examples show unique opportunities to explore novel dimensional controlled physical properties in bulk materials. Finally, I will provide a general outlook for future studies on these exciting new class of materials. References: Nature Photonics, 12, 392-396 (2018). Advanced Materials 29, 1604733 (2017). Chemistry of Materials, 30 (15), 4897-4901 (2018). Chemistry of Materials, 30 (15), 4882-4886 (2018).

**5:50 AM \*F.EN04.15.07**

**Interface Engineering for 2D Layered Semiconductors** Kosuke Nagashio; Tokyo University, Japan

The insulator/2D channel interface property is highly detrimental for the performance of 2D field effect transistors. Although severe interface degradation has been reported so far, a common understanding of the origin of the interface states has not been obtained yet. Here, for the first time, we present the full energy spectra of interface states density for both n- and p-MoS<sub>2</sub> FETs, as shown below, based on the comprehensive and systematic studies, i.e., wide thickness range from monolayer to bulk and various gate stack structures including 2D heterostructure with h-BN as well as typical high-k top gate structure (more than 100 devices). For n-MoS<sub>2</sub>, the lowest interface states density ( $D_{it} = 5 \times 10^{11} \text{ cm}^{-2}\text{eV}^{-1}$ ) was achieved for the heterostructure FET with h-BN, while the interface states density remained high,  $\sim 10^{13} \text{ cm}^{-2}\text{eV}^{-1}$ , even for the heterostructure FET for p-MoS<sub>2</sub>. The systematic study elucidates that the strain induced externally through the substrate surface roughness and high-k deposition process is the origin for the interface degradation at the conduction band side, while sulfur-vacancy-induced defect-states dominate the interface degradation at the valence band side. The present understanding on the interface properties provides the key to further improving the performance of 2D FETs. Finally, based on the recent understanding, the perspective on 2D electronics will be discussed.

SESSION F.EN04.16: Electronic Devices for Memory and Computing

On Demand Abstracts Available for Viewing Starting Saturday Morning, November 21, 2020

F-EN04

**5:00 AM \*F.EN04.16.01**

**High Speed and Multifunctional Electronics Based on 2D Materials** Han Wang<sup>1</sup>, Yanqing Wu<sup>2</sup> and Xuefei Li<sup>3</sup>; <sup>1</sup>University of Southern California, United States; <sup>2</sup>Peking University, China; <sup>3</sup>Huazhong University of Science & Technology, China

Electronic devices based on atomic layered two-dimensional materials and related heterostructures have recently attracted great research attention due to their unique electronic properties and the feasibility of hybrid integration, which provide the unprecedented opportunities for various van der Waals heterojunctions. We have studied the performance improvement based on black phosphorus and molybdenum disulfide from the carrier velocity and operating frequency. High frequency transistor and circuits operating at gigahertz range based on molybdenum disulfide are demonstrated with record high maximum oscillation frequency. High hole velocity of up to  $1.5 \times 10^7 \text{ cm/s}$  has been demonstrated for short channel BP transistors and transport approaching ballistic limit are predicted for ultimately scaled channel length. Moreover, bandgap engineering using lateral heterojunctions has been carried out with multifunctionality for reconfigurable logic operations, showing great promise for future electronics. Ultrathin indium tin oxide has been also systematically investigated for high performance electronics with high on off rate and frequency response.

**5:15 AM \*F.EN04.16.02**

**From the Top or through the Edge—What is the Most Scalable Contact to 2D Semiconductors?** Aaron D. Franklin; Duke University, United States

The most common approach for establishing electrical contacts to 2D semiconductors, such as MoS<sub>2</sub>, is by fabricating metal contacts on top of the inert crystal surface. From an electron transport perspective, these top-contact interfaces can be awkward, with a van der Waals gap or some difficult-to-control form of interfacial bonding. Pure edge contacts (where the interface between the metal and 2D semiconductor occurs completely along the open bonds of the 2D crystal edge) provide a more natural bonding structure and potentially better carrier transport behavior; however, edge contacts have proven more difficult to realize. In this talk, recent success with establishing clean, pure edge contacts between metals and 2D semiconductors will be discussed, including an approach involving an in situ ion beam within a thin-film deposition system. Evaluation of these edge contacts compared to other approaches will be provided, along with demonstration of how edge-contact scaling affects the performance of 2D transistors compared to top-contact scaling. While there remains much to be learned about these interesting metal-2D edge interfaces, results thus far show significant promise for yielding a more scalable and potentially reproducible contact for 2D-based devices.

### 5:30 AM F.EN04.16.03

#### **The Applications of 2D Monolayer-Based Atomrystals in Non-Volatile Memory, RF Switches and Neuromorphic**

**Computing** Xiaohan Wu, Ruijing Ge, Myungsoo Kim, Deji Akinwande and Jack Lee; The University of Texas at Austin, United States

With the ever-increasing demand for new memory technologies, tremendous efforts have been made to develop non-volatile, high-density, fast-operation and flexible memory devices. To continue scaling and reducing cell size, our future towards high-density and flexible memory would be made up of cells with 2D materials. On the other hand, as the devices continue to scale down, the time and energy spent transporting data across a Von-Neumann bottleneck between memory and processor has become an unavoidable issue, which is believed to be resolved by non-Von Neumann computing system as in human brain. In the last few years, the scaling of dense non-volatile memory crossbar arrays, which has few-nm critical dimensions, has been recognized as one promising way to build the neuromorphic computing system that can mimic the massive parallelism and low-power operation in the human brain. In our work, we reported the observation of non-volatile resistive switching (NVRs) effect in various single-layer atomic sheets, including transition metal dichalcogenides (TMDs) and hexagonal boron nitride (h-BN) atomic sheets which can be labeled as atomrystal - memristor effect in atomically thin nanomaterials. The atomrystals in vertical metal-insulator-metal (MIM) device structure are fabricated using CVD-grown or high-quality exfoliated TMDs and h-BN with various process realization techniques. The memory devices show low switching voltage (down to < 1V), high on/off current ratio (up to ~ 6 orders of magnitude), fast switching speed (< 15ns) and good endurance and retention. What's more, the intrinsic low resistance values, approaching ~5 $\Omega$ , opens up a new application for low-power non-volatile electronic RF switches. With the utilization of MoS<sub>2</sub> and h-BN atomrystals, the RF switches can be realized with low insertion loss (< 0.2dB) and high isolation (> 15dB) up to 110 GHz. Importantly, the operating frequencies cover the RF, 5G and mm-wave bands, which is suitable for diverse communication and connectivity front-end systems. In this work, the application of the atomrystals in neuromorphic computing system will be presented and discussed. The energy consumption is expected to be minimized due to the fast switching speed. Moreover, as a result of the large on/off current ratio, more resistance states are committed to mimic the gradual analog-like change in neuromorphic computing. The discovery of atomrystals indicates a potential universal phenomenon of non-volatile resistance switching in 2D monolayers, inspiring the in-depth study of the intriguing mechanisms. In addition, with the desired characteristics presented, the atomrystals will stand out as a promising candidate in the applications of flexible electronics, non-volatile memory arrays, low-power RF switches and neuromorphic synapse.

### 5:40 AM F.EN04.16.05

**Ultra-Low Off-State Leakage Current in Monolayer WS<sub>2</sub> Transistors** Connor Bailey, Ryan Grady, Victoria Chen and Eric Pop; Stanford University, United States

Two-dimensional (2D) semiconducting transition metal dichalcogenides (TMDs) are promising for next-generation electronics due to their layered structure and electrical properties. In particular, they can maintain good carrier mobilities compared to silicon at sub-nanometer thickness [1], making them attractive for digital or flexible electronics applications. Often overlooked is the fact that monolayer (1L) TMDs also have relatively large electronic band gaps and large effective masses [2], potentially enabling transistors with ultra-low off-state currents ( $I_{off}$ ). These could enable significant improvements in standby power consumption, or in dynamic random access memory (DRAM) where retention and performance are dependent on minimizing leakage currents.  $I_{off}$  in exfoliated multilayer MoS<sub>2</sub> [3], and more recently in chemical vapor deposition (CVD) grown monolayer MoSe<sub>2</sub> and WSe<sub>2</sub> [4] have been reported. However, WS<sub>2</sub>, which possesses the largest band gap and thus the lowest expected  $I_{off}$ , has not been investigated. Here we measure, for the first time, record-low  $I_{off}$  in CVD-grown monolayer WS<sub>2</sub> transistors. We first grow such layers directly on amorphous SiO<sub>2</sub>/Si substrates by CVD utilizing a perylene-3,4,9,10 tetracarboxylic acid tetrapotassium salt (PTAS) seeding molecule alongside

solid sulfur and  $\text{WO}_3$  precursors [5]. Material quality was characterized using Raman spectroscopy and photoluminescence (PL), confirming monolayer uniformity. We note that the PL (optical) band gap of monolayer  $\text{WS}_2$  is  $\sim 1.9$  eV but its electronic band gap (on  $\text{SiO}_2$ ) is  $\sim 2.4$  eV [6], due to the large exciton binding energy in 2D semiconductors. Back-gated field-effect transistors (FETs) were fabricated using electron-beam lithography with channel lengths down to  $L \approx 100$  nm. Au contacts were used and devices were capped with  $\sim 15$  nm  $\text{Al}_2\text{O}_3$  by atomic layer deposition (ALD) to improve stability and hysteresis [7]. In order to avoid the noise floor of our instrumentation when measuring the true off-state leakage, ultra-wide FETs were fabricated with an interdigitated structure resulting in widths up to  $W = 2275$   $\mu\text{m}$ . These ultra-wide FETs enabled our measurement of  $I_{\text{off}}$  down to  $\sim 10$  aA/ $\mu\text{m}$  at drain bias of  $V_{\text{DS}} = 0.1$  V in a device with channel length  $L = 250$  nm. At higher drain bias, we measured  $I_{\text{off}}$  as low as 15 aA/ $\mu\text{m}$  in a FET with  $L = 750$  nm at  $V_{\text{DS}} = 1$  V, i.e. an average lateral field  $> 1$  V/ $\mu\text{m}$ . In both devices, on/off current ratios were  $> 1010$ , demonstrating viability for memory and power gating applications which require ultra-low leakage transistors. In comparison, silicon transistors have off-state leakage more than three orders of magnitude higher [8]. In summary, we demonstrated the first measurements of "true" off-state leakage current in monolayer  $\text{WS}_2$  transistors, reaching  $\sim 10$  aA/ $\mu\text{m}$  with on/off current ratio  $\sim 1010$ . These represent the lowest currents measured to date in any monolayer semiconductor, particularly at lateral fields  $> 1$  V/ $\mu\text{m}$ , and suggest significant advantages over silicon in ultra-low leakage applications such as DRAM and power gating. [1] C. English et al., Nano Lett. 16, 3824 (2016) [2] J. Kang et al., IEDM Tech. Dig., 32.2.1 (2017) [3] C. Kshirsagar et al., ACS Nano, 10, 8457 (2016) [4] C. Bailey et al., MRS-EMC, 125 (2019) [5] K. McCreary et al., Sci. Rep., 6, 19159 (2016) [6] H. Hill et al., Nano Lett. 16, 4831 (2016) [7] Y. Illarionov et al., IEEE-EDL, 38, 1763 (2017) [8] J. Song et al., ISDRS (2009)

#### 5:50 AM F.EN04.16.06

**Design Rules for Memories Based on Graphene Ferroelectric Field-Effect Transistors** Kamal Asadi; Max Planck Institute for Polymer Research, Germany

Despite the great progress of ferroelectric gated field-effect transistors (Fe-FETs) based on graphene and other 2D materials, a device model that accurately describes the hysteretic transfer characteristics and provides guidelines on performance enhancement of the Fe-FET is still lacking. Here, we present an experimentally validated analytical model that couples charge displacement of the ferroelectric layer with the charge transport in the graphene layer. The model describes hysteretic transfer characteristics of the FeFETs with good accuracy and predicts that the on/off ratio of the graphene Fe-FET is determined by Dirac bias and the charge carrier mobility. We show unsuitability of an ideal graphene layer for memory application and outline the conditions to achieve the best memory performance in graphene Fe-FETs. Using the insight gained from the model, we theoretically and experimentally demonstrate ternary and quaternary graphene memory elements. The model is generic and can be equally well used for Fe-FETs based on other 2D materials.

SESSION F.EN04.17: New Developments in Mg Batteries  
On Demand Abstracts Available for Viewing Starting Saturday Morning, November 21, 2020  
F-EN04

#### 5:00 AM F.EN04.17.01

**How Promising are Rechargeable Mg Batteries? A DFT Study on Li and Mg Intercalation in MXene Electrodes** Jacob Hadler-Jacobsen<sup>1</sup>, Frode H. Fagerli<sup>1</sup>, Henning Kaland<sup>1</sup>, Zhaohui Wang<sup>1,2</sup>, Sverre M. Selbach<sup>1</sup>, Kjell Wiik<sup>1</sup>, Nils Wagner<sup>1,3</sup> and Sondre Kvalvåg Schnell<sup>1</sup>; <sup>1</sup>NTNU Norwegian University of Science and Technology, Norway; <sup>2</sup>SINTEF Industry, Metal Production and Processing, Norway; <sup>3</sup>SINTEF Industry, Sustainable Energy Technology, Norway

Rechargeable Mg batteries present a "beyond lithium-ion" technology with high theoretical energy density and a comparatively small susceptibility for dendrite formation<sup>1,2</sup>. However, rechargeable Mg batteries suffer from slow migration and irreversible trapping of Mg ions in most cathode materials.

The MXene family is a group of electronically conductive 2D materials which have been investigated as electrode material for both Mg and Li batteries. Here, DFT is used to assess the voltage, specific capacity and migration barriers for Li and Mg ions in MXenes with compositions  $\text{V}_2\text{CO}_2$ ,  $\text{V}_2\text{CF}_2$ ,  $\text{V}_2\text{C}(\text{OH})_2$ ,  $\text{Ti}_3\text{C}_2\text{O}_2$ ,  $\text{Ti}_3\text{C}_2\text{F}_2$  and  $\text{Ti}_3\text{C}_2(\text{OH})_2$  as reported in our recent work<sup>3</sup>. Bader charge analysis and ionization energies are used to understand the differences in performance. Guidelines for MXene electrode design and views on how to best overcome the fundamental challenges with divalent battery chemistries are presented.



## References

1. M. Matsui, Journal of Power Sources 196 (2011), 7048-7055
2. P. Canepa, G. S. Gautam, D. C. Hannah, R. Malik, M. Liu, K. G. Gallagher, K. A. Persson, G. Ceder, Chemical Reviews 117 (2017) 4287-4341
3. H. Kaland, J. Hadler-Jacobsen, F. H. Fagerli, N. P. Wagner, Z. Wang, S. M. Selbach, F. Vullum-Bruer, K. Wiik, S. K. Schnell, Sustainable Energy Fuels, 2020, 4, 2956-2966

### 5:10 AM F.EN04.17.02

**Local Atomic and Electronic Structure's Influence on Migration Along Li and Mg Surfaces** Ingeborg Treu Roe, Sverre Magnus Selbach and Sondre Kvalvåg Schnell; Norwegian University of Science and Technology, Norway

Dendrite formation on Li metal anodes leads to reduced Coulombic efficiency, poor cycling stability and short-circuiting, and prevents commercialization of high energy density rechargeable Li metal batteries. The migration energy barrier for transport along the metal surface can describe the tendency of the surface to form dendrites. Density functional theory calculations of the migration energy barrier show inherent differences in transport properties between Li and Mg<sup>1</sup>, which may explain the higher propensity of Li to form dendrites compared to Mg<sup>2</sup>. We use density functional theory to show that differences in the atomic and electronic structure of the Li and Mg surface lead to different migration energy barriers<sup>3</sup>. The atomic and electronic surface structure of Li and Mg are in turn affected by the bulk crystal structure, the atomic and electronic structure of the substrate, and surface impurities. We investigate how and why these factors impact the migration energy barrier to shed light on the mechanisms of dendrite formation on the metal anodes. Thus, we may guide the development of dendrite-free metal anodes for battery applications.

## References:

1. M. Jäckle, A. Groß, J. Chem. Phys. 141 (2014) 174710
2. M. Matsui, K. Takahashi, K. Sakamoto, A. Hirano, Y. Takeda, O. Yamamoto, N. Imanishi, Dalton trans. 43 (2014) 1019
3. I. T. Roe, S. M. Selbach, S. K. Schnell, J. Phys. Chem. Lett. 11 (2020) 2891-2895

### 5:20 AM F.EN04.17.05

**Surface Termination Control of Two-Dimensional MXenes for Rechargeable Magnesium Battery Cathodes** Frode H. Fagerli<sup>1</sup>, Henning Kaland<sup>1</sup>, Jacob Hadler-Jacobsen<sup>1</sup>, Zhaohui Wang<sup>1,2</sup>, Sverre M. Selbach<sup>1</sup>, Tor Grande<sup>1</sup>, Nils Wagner<sup>1,2</sup> and Kjell Wiik<sup>1</sup>; <sup>1</sup>Norwegian University of Science and Technology, Norway; <sup>2</sup>SINTEF Industry, Norway

Rechargeable Mg batteries have the potential to take advantage of Mg metal anodes, as they are less prone to dendritic growth compared to Li metal [1]. This leads to the possibility of having high capacity batteries based on Mg-ions, with competitive energy density and materials cost compared to the state-of-the-art Li-ion batteries [2]. However, this requires a cathode material that allows for reversible reactions with significant amounts of Mg-ions at a sufficiently high operating potential. Since the first prototype of a rechargeable Mg battery was reported in 2000 [3], only a limited number of cathode materials have been demonstrated to work reversibly, and the energy density has not been sufficient to compete with Li-ion battery technology [2]. In this project, we have investigated the possibility of using two-dimensional MXenes as possible cathode materials for rechargeable Mg batteries, based on their previously reported ion intercalating properties [4,5]. Here, we present the synthesis and surface modification of two MXenes, Ti<sub>3</sub>C<sub>2</sub>T<sub>x</sub> and V<sub>2</sub>CT<sub>x</sub> (T = F, O or OH), in order to optimize the possibility for Mg-intercalation by increasing the O terminations [6]. Various methods, such as hydrolysis and vacuum annealing, were used to shift the surface terminations towards more oxygen content, where EDX and XPS were used to quantify the different termination groups. The surface modified MXenes demonstrate more promising electrochemical performance compared to the pristine MXene, which is assigned to the improved properties of the O-terminated surfaces.

## References:

- [1] M. Masaki, Journal of Power Sources 196 (2011), 7048-7055
- [2] P. Canepa et al., Chemical Reviews 117 (2017) 4287-4341
- [3] D. Aurbach et al., Nature 407 (2000) 724-727
- [4] Naguib et al., J. Am. Chem. Soc. 135 (2013) 15966-15969
- [5] C. Eames, M. S. Islam, J. Am. Chem. Soc. 136 (2015) 16270-16276
- [6] H. Kaland, J. Hadler-Jacobsen, F. H. Fagerli, et al., Sustainable Energy Fuels, 4 (2020) 2956-2966

### 5:30 AM F.EN04.17.07

**Late News: A Computational Comparison of Ca-Ion Battery Electrolytes—Tetrahydrofuran vs Ethylene Carbonate** [Diana Liepinya](#)<sup>1,2</sup> and Manuel Smeu<sup>2</sup>; <sup>1</sup>University of Maryland, United States; <sup>2</sup>Binghamton University, The State University of New York, United States

Secondary batteries are crucial to contemporary life, powering everything from personal electronics to electric vehicles. The growth of these technologies has led to an unprecedented demand for rechargeable batteries, a market currently dominated by Li-ion batteries. Despite its high performance, Li-ion is an unideal candidate for meeting this growing demand due to the scarcity of its component elements, resulting in higher costs and an inflexible supply chain. Ca-ion batteries would avoid these issues while providing higher volumetric energy density and the potential for improved safety through suppressed dendrite growth. However, their development is limited by a lack of suitable electrolytes. Many electrolytes decompose to form an impermeable layer at the anode, preventing plating and stripping and compromising the cyclability of the battery. Our work aims to elucidate the reactions occurring at the electrolyte-anode interface, which will allow for more informed Ca-ion battery electrolyte selection.

As a starting point for this analysis, we use *ab initio* molecular dynamics (AIMD) to simulate several anode-electrolyte systems. Motivated by recent successes in reversible Ca-ion plating and stripping, tetrahydrofuran (THF) is selected as one of the solvents. We contrast THF with ethylene carbonate (EC), a successful Li-ion solvent and popular choice for Ca-ion battery experiments. In addition to pure solvent, we also investigate 1.2 M solutions of four different salts (Ca(BH<sub>4</sub>)<sub>2</sub>; Ca(BF<sub>4</sub>)<sub>2</sub>; Ca(BCl<sub>4</sub>)<sub>2</sub>; and Ca(ClO<sub>4</sub>)<sub>2</sub>) in each solvent for a total of ten AIMD trajectories. Over a 15 ps trajectory at 450 K in the presence of a Ca anode, pure THF was found to be non-reactive, while pure EC decomposed soon upon contact with the anode. Preliminary results have shown that similar behavior persists upon addition of salt molecules. We supplement these trajectories with density functional theory (DFT) calculations of electronic structure and reaction barriers as well as charge analysis over time. Lastly, we include a final simulation to test the reactivity of THF while gradually adding electrons to the Ca-THF system, reflecting the changes in anode charge during battery cycling. Our multifaceted characterization will both illuminate past experiments' results as well as guide new research, shedding light on a major obstacle in the development of Ca-ion batteries.

SESSION F.EN04.18: Li-Sulfur Batteries

On Demand Abstracts Available for Viewing Starting Saturday Morning, November 21, 2020  
F-EN04

**5:00 AM F.EN04.18.01**

**Lithium Deposition in Lithium-Sulfur Batteries Stabilized by Tellurium as a Cathode Additive** [Sanjay Nanda](#), Amruth Bhargav and Arumugam Manthiram; University of Texas-Austin, United States

The lithium-metal anode is the main factor constraining the cyclability of energy-dense lithium-sulfur batteries. The irreversible plating and stripping of lithium in the liquid ether-based electrolyte engenders poor cycling efficiencies and severe parasitic side reactions with the electrolyte. Under conditions of limited lithium inventory and limited electrolyte supply, which are necessary for practically relevant cell designs, this leads to rapid capacity fade and premature cell failure. Commercially viable Li-S batteries with high energy density and long cycle life can only be realized by designing strategies towards stabilizing lithium deposition and reducing electrolyte decomposition.

The generation of soluble polysulfide intermediates that shuttle between the sulfur cathode and the lithium-metal anode renders the chemistry of Li-S batteries fundamentally unique compared to other systems. They transform the chemistry of the lithium-electrolyte interface by reducing on the lithium surface and forming lithium sulfide (Li<sub>2</sub>S) and lithium disulfide (Li<sub>2</sub>S<sub>2</sub>) as components of the SEI layer. These species have been observed to have a unique stabilizing effect on lithium deposition, which is intrinsic to Li-S batteries. This suggests that tuning polysulfide species with other elements or functional groups could be a potential pathway towards further stabilization of lithium deposition in this system.

We discovered that elemental tellurium (Te<sup>0</sup>) reacts with ethereal solutions of polysulfides to form mixed *polytellurosulfide* species that are also soluble in the ether-based solvent. On the reducing surface of lithium metal, these polytellurosulfide species decomposed to form red-colored lithium thiotellurate (Li<sub>2</sub>TeS<sub>3</sub>). As a lithium SEI component, Li<sub>2</sub>TeS<sub>3</sub> is anticipated to enable a homogenous lithium-ion flux on the lithium surface, thereby leading to uniform plating of lithium. This is due to the lower diffusion barrier for lithium ions through Li<sub>2</sub>TeS<sub>3</sub> when compared with Li<sub>2</sub>S, as the electron

density around sulfur is significantly softened when bonded with tellurium.

When  $\text{Te}^0$  was added to sulfur/ $\text{Li}_2\text{S}$  cathodes in a 1:10 molar ratio, polytellurosulfide species were generated *in-situ* during cell operation by the reaction of polysulfides with  $\text{Te}^0$  additive. These species crossed over to the lithium anode and formed  $\text{Li}_2\text{TeS}_3$  as a thin interfacial layer on the lithium surface. The favorable properties of this tellurized, sulfide-rich SEI allows lithium to be deposited without undesirable high-surface area mossy/dendritic growths. With a limited lithium inventory (N/P ratio = 1) in an anode-free full cell, which combines a fully-lithiated  $\text{Li}_2\text{S}$  cathode with a bare Ni foil current collector on the anode side, the enhancement in lithium cycling efficiency with the addition of  $\text{Te}^0$  drastically reduced capacity fade per cycle by a factor of 7.

It was also found using time-of-flight secondary ion mass spectroscopy (ToF-SIMS) that electrolyte decomposition on the lithium surface was significantly mitigated with the addition of tellurium to the cathode. This enabled the limited electrolyte supply to be maintained for a longer number of cycles. Under lean-electrolyte conditions (E/S ratio =  $4.5 \mu\text{l mg}^{-1}$ ) in large-area pouch cells employing a high-loading sulfur cathode ( $5.2 \text{ mg cm}^{-2}$ ), tellurium-stabilized lithium deposition allowed the cell to be stably operated for nearly 100 cycles. This was a nearly four-fold improvement over the control cell with no additive.

A unique and reliable strategy for stabilizing lithium deposition and reducing electrolyte decomposition in Li-S batteries is demonstrated. This is achieved by a simple and scalable addition of elemental tellurium to the cathode. The stabilizing layer is formed *in-situ* during cell operation and no expensive or complicated pre-treatments of the lithium surface are required. Importantly, a pathway for commercially viable Li-S batteries with high energy density and long cycle life is realized.

#### 5:10 AM F.EN04.18.03

**Sulfur-Inserted Polymer-Anchored Edge Exfoliated Graphite for High Performance Lithium-Sulfur Batteries** Nanami Uesugi<sup>1</sup>, Natsuho Kazahaya<sup>1</sup>, Hiroshi Yoshitani<sup>2</sup>, Takuya Wada<sup>2</sup>, Hiroji Fukui<sup>2</sup>, Yu Katayama<sup>1</sup> and Hiromori Tsutsumi<sup>1</sup>; <sup>1</sup>Yamaguchi University, Japan; <sup>2</sup>Sekisui Chemical Co., Ltd., Japan

Lithium-sulfur batteries hold promising potential for next-generation high-energy-density energy storage. One of their major technical problems is the loss of sulfur active material and its significant volume change during the charge-discharge process, resulting in rapid capacity fading. Here, we introduce sulfur-inserted polymer-anchored edge exfoliated graphite as a new class of positive electrode, which can accommodate the conflicting requirement of physically restrain sulfur dissolution while maintaining structural flexibility to cope with the volume expansion.

The introduction of sulfur between the flexible polymer-anchored graphene layer is achieved by a simple chemical reaction at ambient temperature. The obtained sulfur-carbon composite demonstrates superior sulfur efficiency and cyclability compare to mesoporous carbon-based counterparts. The strong interfacial attraction between sulfur and highly-conductive graphene sheet at the confined interlayer space enables (1) rapid charge transfer and (2) effective inhibition of the polysulfide dissolution, resulting in improved redox reaction reversibility and sulfur efficiency. Furthermore, the structural flexibility of layered structure, derived from polymer-anchor, guarantees the stable cycling by accommodating the significant volume expansion of sulfur active materials.

Therefore, our work provides a simple, proof-of-concept strategy for improving the overall performance of carbon-based positive electrode for lithium-sulfur batteries.

#### 5:20 AM F.EN04.18.04

**Preparation and Evaluation of Polymer Electrolytes with Low-solubility of Lithium-polysulfide for Li-S Batteries** Hibiki Miyauchi, Kohei Inaba, Keitaro Takahashi and Shiro Seki; Kogakuin University, Japan

##### Introduction

Lithium-Sulfur (Li-S) batteries are attracting attention as high energy density rechargeable battery. Elemental sulfur ( $\text{S}_8$ ) have high theoretical capacity ( $1,672 \text{ mAhg}^{-1}$ ) as positive electrode active material. However,  $\text{S}_8$  electrode is degraded by redox shuttle effect of lithium-polysulfide ( $\text{Li}_2\text{S}_n$ ), which are generated during charge-discharge reactions. To solve this problem, many electrolyte designs were proposed. As one of many designs, sulfolane (SL) based high Li salt concentration electrolyte solution was reported as low solubility electrolyte of  $\text{Li}_2\text{S}_n$  [1]. The aim of this concept is chemically protection of  $\text{Li}_2\text{S}_n$  dissolution into electrolyte solution. Therefore, we proposed new polymer electrolyte, which protects chemically and physically dissolution and diffusion of  $\text{Li}_2\text{S}_n$ . In this study, we prepared SL based solid gel polymer electrolytes (GPEs), and thermal and ionic conductive properties of the samples were evaluated. Furthermore, Li-S batteries containing GPEs were prepared and evaluated by charge-discharge measurements.

## Experimental

Sulfolane (SL),  $\text{LiN}(\text{SO}_2\text{CF}_3)_2$  (LiTFSA), and polyether-based P(EO/PO) macromonomer were used as electrolyte materials for GPEs. First, electrolyte solution samples were prepared by mixing LiTFSA and SL at each molar ratio of SL : LiTFSA =  $x : 1$  ( $x=1, 1.5$  and  $2$ , respectively). Next, prepared electrolyte solution and P(EO/PO) macromonomer were mixed at each weight ratio of electrolyte solution : polymer =  $y : (10-y)$  ( $y=7, 8$  and  $9$ , respectively), and added DMPA as photo initiator. After that, these materials were radical polymerized by UV irradiation. In this research, GPEs are expressed as  $(x)_y\text{El}+(10-y)\text{Po}$ . Thermal property and ionic conductivity of prepared GPEs were investigated by TG-DTA, DSC and AC impedance measurements.

## Results & Discussion

First, in TG-DTA, TG curves of all GPEs were exhibited 3 step weight trends of decreasing. First weight decreasing observed the range of 380 K to 490 K, which might due to evaporation or decomposition of SL. From first weight decreasing, thermal stability was improved with Li salt concentration and electrolyte solution amount. Therefore, a part of  $\text{Li}^+$  should be changed coordination site from SL to P(EO/PO).

Next, from impedance measurements, obtained ionic conductivity ( $\sigma$ ) showed non-Arrhenius type temperature dependence with all GPEs. All GPEs exhibited high  $\sigma$  compared with genuine solid polymer electrolyte (mixture of P(EO/PO) and LiTFSA) within a range of 244 K to 353 K. (2)<sub>9</sub>El+1Po sample observed relatively high  $\sigma$  ( $4.0 \times 10^{-4} \text{ Scm}^{-1}$ ) at 303 K.  $\sigma$  increased with decrease of Li salt concentration (inverse of  $x$ ). Also,  $\sigma$  increased with electrolyte solution composition ( $y$ ) at low temperature region. Therefore, ionic transport mechanism and thermal property should be affected by Li salt concentration and electrolyte solution amount into GPE.

In presentation, charge-discharge properties of Li-S batteries containing GPE will be also discussed.

## Reference

[1] A. Nakanishi *et al.*, *J. Phys. Chem. C*, **123**, 14229-14238 (2019).

### SESSION F.EN04.19: Metal-Air Batteries

On Demand Abstracts Available for Viewing Starting Saturday Morning, November 21, 2020

F-EN04

#### 5:00 AM F.EN04.19.02

**Pushing Zinc–Air to Outperform Lithium–Based Batteries** [Brandon J. Hopkins](#), Christopher Chervin, Jeffrey Long, Debra Rolison and Joseph Parker; U.S. Naval Research Laboratory, United States

Electrically rechargeable zinc–air may achieve higher rechargeable specific energy than Li-ion batteries, but today's air cathodes limit zinc–air performance. To overcome this challenge, researchers have investigated hundreds of air-cathode variations. Unfortunately, the efficacy of these variations remains ambiguous due to non-standardized cycling protocols. We show using a meta-analysis of 100 zinc–air cells that reported areal-energy values span five orders of magnitude. Based on an analytical model we present here, researchers should cycle zinc–air cells at  $35 \text{ mWh cm}_{\text{geo}}^{-2}$  to compete with lithium-ion and  $240 \text{ mWh cm}_{\text{geo}}^{-2}$  to compete with lithium–air. Once the community cycles zinc–air cells at relevant areal-energy values and understands failure mechanisms, lab-scale results will translate to practical advancements.

#### 5:10 AM F.EN04.19.03

**High-Performance Zinc–Air Batteries Realized by Apically Dominant Mechanism Controlled N-Doped Carbon Nanotube Arrays** [Zhao Li](#), Wenhan Niu and Yang Yang; University of Central Florida, United States

Presently, nitrogen-doped carbon nanotube (NCNT) has been widely considered as one of the promising carbon materials replacing the platinum group metal catalysts in energy conversion and storage technologies. It has been essentially concentrated on rational design of NTCNT to overcome the generalized limitations of hydrophobic surface and base-growth model for the enhancement of catalytic performance in renewable energy devices such as zinc–air battery (ZAB). Here, we demonstrated a concept of an apically dominant mechanism controlled NCNT, encapsulating CoNi nanoparticles (CoNi@NCNT) as highly efficient catalysts for ZAB. Density functional theory calculations reveals that the outstanding catalytic performance of CoNi@NCNT can be ascribed to the synergetic contributions from the apical active sites nearby CoNi and NCNT. Remarkably, the ZAB using CoNi@NCNT as air electrode exhibits an excellent battery performance with

a power density of 127 mW cm<sup>-2</sup> and energy density of 845 Wh kg<sub>zn</sub><sup>-1</sup>.

#### 5:20 AM F.EN04.19.04

**Importance of Equilibration Method and Sampling for *Ab Initio* Molecular Dynamics Simulations of Solvent - Lithium Salt Systems in Lithium Air Batteries** [Emily J. Crabb](#)<sup>1</sup>, Arthur France-Lanord<sup>1</sup>, Graham Leverick<sup>1</sup>, Ryan Stephens<sup>2</sup>, Yang Shao-Horn<sup>1</sup> and Jeffrey C. Grossman<sup>1</sup>; <sup>1</sup>Massachusetts Institute of Technology, United States; <sup>2</sup>Shell International Exploration & Production Inc., United States

Lithium-air batteries are an active area of research because of their potential to have a much higher energy density than traditional lithium-ion batteries. However, they are not yet commercially viable due to poor efficiency, high charging voltages, and low cycle lifetimes. Many of these issues could be addressed with a deeper fundamental understanding of the atomistic behavior of these batteries. One tool to model such atomic scale behavior is *ab initio* molecular dynamics (AIMD) simulations. However, AIMD simulations are limited to timescales of tens of picoseconds due to their high computational cost. As a result, equilibration and sampling methodologies can have a significant effect on the behavior of AIMD simulations. We thus compared two equilibration methods for AIMD simulations of systems of common solvents and salts found in lithium air batteries: (1) using an AIMD temperature ramp and (2) using a classical MD simulation followed by a short AIMD simulation all at the target simulation temperature of 300 K. We also compared two different classical all-atom force fields (PCFF+ and OPLS) and performed multiple simulations for each system. In this presentation, I will discuss how the differences between our simulation results and experimental results for properties such as coordination number illustrate the importance of both equilibration method and independent sampling for extracting experimentally relevant quantities from AIMD simulations.

#### 5:30 AM F.EN04.19.05

**Ion-Selective Separators in Alkaline Zinc Batteries for Grid Storage Applications** [Igor V. Kolesnichenko](#)<sup>1</sup>, Matthew Lim<sup>1</sup>, David J. Arnot<sup>1</sup>, Elijah I. Ruiz<sup>1</sup>, Gautam G. Yadav<sup>2</sup>, Michael Nyce<sup>2</sup>, Sanjoy Banerjee<sup>2</sup> and Timothy N. Lambert<sup>1</sup>; <sup>1</sup>Sandia National Laboratories, United States; <sup>2</sup>The City College of New York, United States

Rechargeable alkaline Zn–MnO<sub>2</sub> batteries are a promising candidate for grid-level energy storage owing to their high theoretical energy density rivaling Li-ion systems (~400 Wh/L), safe aqueous electrolyte, established supply chain, and projected costs as low as \$50/kWh at scale.[1] Unfortunately, due to inherent issues at both electrodes, the goal of a Zn–MnO<sub>2</sub> battery with long lifetime (5000+ cycles, equating to 10-15 years of service life) at appreciable energy densities (200+ Wh/L) has not yet been achieved. Over repeated cycling at high capacity utilization, Zn anodes suffer from irreversible redistribution of active material and passivation, while MnO<sub>2</sub> cathodes suffer from irreversible breakdown of the crystal structure and formation of inactive phases.

To mitigate anode degradation, we recently showed that pre-saturating the electrolyte with zincate [Zn(OH)<sub>4</sub>]<sup>2-</sup>, which is the soluble discharge product of the anode, improved cycle life of Zn–Ni cells by 100-200% at 14-35% Zn utilization.[2] However, this strategy alone cannot be used with MnO<sub>2</sub> cathodes because zincate reacts with Mn(III) species to irreversibly form ZnMn<sub>2</sub>O<sub>4</sub>, which is insulating and electrochemically inactive. Conventional cellophane and polyolefin separators used in alkaline batteries have no ability to block zincate from migrating to the cathode, whereas ceramic conductors such as NaSICON, which we previously studied in limited-depth-of-discharge Zn–MnO<sub>2</sub> batteries,[3] are impervious to zincate but are thick, brittle, and less conductive overall, limiting their utility.

To address this issue, this presentation will discuss various aspects of our efforts to develop flexible polymeric separators that selectively impede zincate transport without sacrificing overall conductivity. We have synthesized freestanding membranes of polymers incorporating charged functional groups, as well as thin films of ion-selective polymers on commercial separator materials. Using a rapid anodic stripping voltammetry assay,[4] our separator materials show a strong selectivity for hydroxide over zincate transport, while maintaining comparable ionic conductivity to commercial battery separators. Most importantly, our selective separators impart significant performance improvements to both Zn–Ni cells and Zn–MnO<sub>2</sub> cells with Bi/Cu-stabilized cathodes[5] that can be cycled at or near the full two-electron capacity of MnO<sub>2</sub> (617 mAh g<sup>-1</sup>). Notably, Zn–Ni cells show a 460+% and 115+% increase in cycle life at substantial Zn utilizations of 20% and 50% respectively. In Zn–MnO<sub>2</sub> cells, our separators not only slow down zincate poisoning of MnO<sub>2</sub> but also hinder growth of zinc through the separator pores, which can lead to shorting.

This work was supported by the U.S. Department of Energy, Office of Electricity, and the Laboratory Directed Research and Development program at Sandia National Laboratories. Sandia National Laboratories is a multimission laboratory managed and operated by National Technology and Engineering Solutions of Sandia, LLC, a wholly owned subsidiary of Honeywell

International, Inc., for the U.S. Department of Energy's National Nuclear Security Administration under contract DE-NA-0003525. The views expressed herein do not necessarily represent the views of the U.S. Department of Energy or the United States Government.

- [1] S. Banerjee, "Alkaline Zn-MnO<sub>2</sub> Battery Development: A University-Private-Public Partnership". U.S. Department of Energy Office of Electricity Peer Review, 2018. [https://eesat.sandia.gov/wp-content/uploads/2018/10/1\\_SanjoyBanerjee\\_Presentation.pdf](https://eesat.sandia.gov/wp-content/uploads/2018/10/1_SanjoyBanerjee_Presentation.pdf)
- [2] M. B. Lim, T. N. Lambert, E. I. Ruiz, *J. Electrochem. Soc.* **2020**, *167*, 060508.
- [3] J. Duay, M. Kelly, T. N. Lambert, *J. Power Sources* **2018**, *395*, 430.
- [4] J. Duay, T. N. Lambert, R. Aidun, *Electroanalysis* **2017**, *29*, 2261.
- [5] G. G. Yadav, J. W. Gallaway, D. E. Turney, M. Nyce, J. Huang, X. Wei, S. Banerjee, *Nat. Commun.* **2017**, *8*, 14424.

#### SESSION F.EN04.20: Solid States and Interface

On Demand Abstracts Available for Viewing Starting Saturday Morning, November 21, 2020  
F-EN04

#### 5:00 AM F.EN04.20.01

**Proposal of High Li Salt Concentration Solvate Ionic Liquid / PEO Matrix Solid-Gel Electrolytes for Keitaro Takahashi, Hibiki Miyachi, Yuji Yokomaku, Yusuke Ushioda and Shiro Seki; Kogakuin University, Japan**

#### Introduction

Lithium-sulfur (Li-S) batteries are attracted attention as new secondly battery system. The sulfur positive electrode of this system have theoretical capacity of 1672 mAhg<sup>-1</sup>, which shows approximately 10 times higher than conventional Li-ion battery positive electrode material (LiCoO<sub>2</sub>). A problem of the Li-S batteries is dissolution of sulfur component of positive electrode, which reached as state of reaction intermediate (Li<sub>2</sub>S<sub>m</sub>: m=2~8) into electrolyte during charge / discharge processes. The dissolution and diffusion of Li<sub>2</sub>S<sub>m</sub> into electrolyte solution lead significant degradation of cycle characteristics and irreversible side reaction of Li-S batteries. Currently, as functional electrolyte solution that suppresses dissolution of Li<sub>2</sub>S<sub>m</sub>, "Solvate Ionic Liquid (SIL)" has been proposed [1]. We propose further functional SIL electrolyte for high performance Li-S battery. In order to exhaustive suppress to dissolve/diffuse of Li<sub>2</sub>S<sub>m</sub> into electrolyte, and we investigated the increase of salt composition in the SIL electrolyte and the solidification by introducing polymer matrix.

#### Experimental

In this study, all procedures of sample preparation were conducted in an argon-filled glovebox. At first, as highly concentrated SILs, [Li<sub>a</sub>(G4)<sub>1</sub>]TFSA<sub>a</sub> (a = 1 and 1.25) (G4 : CH<sub>3</sub>-O-(C<sub>2</sub>H<sub>4</sub>O)<sub>4</sub>-CH<sub>3</sub>, LiTFSA: LiN(SO<sub>2</sub>CF<sub>3</sub>)<sub>2</sub> = 1 : a) were prepared [2]. Gel electrolyte were prepared by mixing of SILs (a = 1, 1.25), polyether-based P(EO/PO) macromonomer and photo initiator. Composition ratio of gel electrolyte were SILs : polymer = 7 : 3, 8 : 2, 9 : 1 (wt%), respectively. After stirring, samples casted to glass substrate and polymerized by UV irradiation to obtain thin-films, which was transparent and self-standing gel electrolyte films. Prepared electrolyte films were evaluated by differential scanning calorimetry (DSC) and AC impedance measurements.

#### Result and discussion

Thermal properties of prepared SILs and gel electrolytes were measured by DSC. For the results, all electrolytes exhibited glass transition temperatures (T<sub>g</sub>s). T<sub>g</sub> of SIL electrolytes was shifted high temperature with Li salt concentration in electrolyte. Gel electrolyte showed lower T<sub>g</sub> than that neat polymer electrolyte (without SIL). From the results, it was considered that mobility of PEO chain was increased by SIL electrolyte solutions. With increasing SIL amount into the gel electrolyte, T<sub>g</sub> appeared low temperature side, and therefore, the gel electrolyte with high SIL composition should indicate high ionic conductivity.

Prepared SILs and gel electrolyte was measured dependence temperature of ionic conductivity (s) by AC impedance method. Owing to increase of viscosity with Li salt concentration, s value of high Li salt composition SIL electrolyte (a=1.25) was lower than equimolar SIL (a=1). At 303 K, s of [Li<sub>1</sub>(G4)<sub>1</sub>]TFSA<sub>1</sub> : polymer = 8 : 2 electrolyte was 1.5×10<sup>-3</sup> Scm<sup>-1</sup>, which was almost same s value with SIL electrolyte solution. Generally, the introduction of polymer matrix in electrolyte solution should suppress the diffusion of Li<sup>+</sup>. However, our result exhibited another result.

Gel electrolyte of [Li<sub>1</sub>(G4)<sub>1</sub>]TFSA : polymer = 8 : 2 was applied for charge/discharge test in Li-S cell. The Li-S battery using the equimolar SIL of gel electrolyte was confirmed first discharge capacity of 1,100 mAhg<sup>-1</sup>. However, this system showed

unstable voltage profiles during charge process, and this charge capacity exhibited larger than that discharging capacity. From the unstable and large voltage in this charging process,  $\text{Li}_2\text{S}_m$  dissolution into gel electrolyte and side reactions were estimated. This result correlates with the report of the co-migration of glyme molecule and breaking of Li complex cation with introduction of PEO matrix by NMR spectroscopy [3].

#### Reference

- [1] K. Dokko *et. al.*, *J. Electrochem. Soc.*, **160**, A1304 (2013).
- [2] K. Takahashi *et.al.*, *RSC Adv.*, **9**, 24922 (2019).
- [3] R. Kido, *et.al.*, *Electrochem. Acta*, **170**, 5 (2015).

#### 5:10 AM F.EN04.20.03

##### **Solid-Electrolyte Interphases on Graphite Electrodes in Li- and K-Systems—A Comparison by Photoelectron Spectroscopy** Fabian Jeschull, Franziska Allgayer and Julia Maibach; Karlsruhe Institute of Technology (KIT), Germany

The solid-electrolyte interphase (SEI) formed at the negative electrode in Li-ion batteries (LIB) is a passivation layer that prevents recurrent electrolyte decomposition reactions at the electrode-electrolyte interface.<sup>1</sup> The consumption of the charge carrier inventory due to these irreversible reactions are the origin of capacity fading and increasing internal resistances and ultimately reduce the cycle life of a cell.

For more than three decades the SEI layer of LIB has been characterized and optimized in order to arrive at the outstanding cycle life of high energy density, state-of-the-art LIB. A major contribution to its success is the graphite negative electrode that offers high reversibility, electrode potentials close to that of Li metal at a small volume expansion of the active material particles.<sup>2</sup> Post-Li systems might also benefit from the stability of graphite intercalation compounds and are therefore an interesting material choice for Na- (in ether-electrolytes)<sup>3</sup> and K-batteries<sup>4</sup> as well. However, their performance has not yet reached that of a corresponding Li-cell.<sup>5</sup>

Li- and K-systems are highly comparable because, despite the alkali metal ion, the same electrode and electrolyte formulations can be employed. A comparison between the graphite-electrolyte interface formed in a Li- and K-system, respectively, can thus allow valuable insights on how to work towards a more benign SEI layer formation in K-batteries. For this study, the surface compositions of graphite electrodes cycled in Li- or K-half cells was investigated post-mortem by in-house X-ray photoelectron spectroscopy (XPS). Our results show a comparatively high degree of crosstalk originating from the K-metal counter electrode and a different distributions of the characteristic decomposition products in presence of K- instead of Li-ions. The presentation will further discuss strategies to mitigate charge losses related to SEI layer formation on graphite electrodes as negative electrodes in K-ion batteries.

#### References

- (1) Verma, P.; Maire, P.; Novák, P. A Review of the Features and Analyses of the Solid Electrolyte Interphase in Li-Ion Batteries. *Electrochim. Acta* **2010**, *55* (22), 6332–6341.
- (2) Berg, E. J.; Villevieille, C.; Streich, D.; Trabesinger, S.; Novák, P. Rechargeable Batteries: Grasping for the Limits of Chemistry. *J. Electrochem. Soc.* **2015**, *162* (14), A2468–A2475.
- (3) Jache, B.; Adelhelm, P. Use of Graphite as a Highly Reversible Electrode with Superior Cycle Life for Sodium-Ion Batteries by Making Use of Co-Intercalation Phenomena. *Angew. Chem. Int. Ed.* **2014**, *53* (38), 10169–10173.
- (4) Komaba, S.; Hasegawa, T.; Dahbi, M.; Kubota, K. Potassium Intercalation into Graphite to Realize High-Voltage/High-Power Potassium-Ion Batteries and Potassium-Ion Capacitors. *Electrochem. Commun.* **2015**, *60*, 172–175.
- (5) Carboni, M.; Naylor, A. J.; Valvo, M.; Younesi, R. Unlocking High Capacities of Graphite Anodes for Potassium-Ion Batteries. *RSC Adv.* **2019**, *9* (36), 21070–21074.

#### 5:20 AM \*F.EN04.20.04

##### **Synthesis and Electrochemical Properties of Na-ion Conducting Pseudo-Solid State Ionogel Electrolytes** Ryan H. DeBlock<sup>1</sup>, David Ashby<sup>2</sup>, Grace Whang<sup>1</sup>, Danielle Butts<sup>1</sup>, Christopher Choi<sup>1</sup> and Bruce S. Dunn<sup>1</sup>; <sup>1</sup>University of California, Los Angeles, United States; <sup>2</sup>Sandia National Laboratories, United States

Ionogels are pseudo-solid state electrolytes in which an ionic liquid electrolyte confined in a mesoporous inorganic matrix leads to a material that possesses the electrochemical, thermal and chemical properties of the ionic liquid despite being a macroscopic solid. Because of their unique architecture, ionogels maintain a nanoscale fluidic state and thus mitigate the interfacial resistances which commonly arise at solid-solid interfaces. The use of sol-gel synthesis enables the materials to be prepared as liquids and to penetrate porous electrodes before becoming solid, an especially beneficial property for solid-state batteries. The incorporation of Li-ion conducting ionogel electrolytes into Li-ion batteries has been reported previously and

generally show behavior comparable to that of the ionic liquid electrolyte.

In this work, we report on the development of Na-ion conducting ionogels, a topic which has received only limited investigation to date. We use sol-gel synthesis to form a siloxane-modified silica scaffold that traps an ionic liquid electrolyte comprised of 0.5M NaFSI in 1-Butyl-1-methylpyrrolidinium bis(trifluoromethanesulfonyl)imide [PYR14][TFSI]. The low vapor pressure of the ionic liquid ensures that a dense gel is formed. The interconnected porosity allows for good ionic conductivity ( $0.7 \text{ mS cm}^{-1}$ ), although it is somewhat less than the corresponding ionic liquid electrolyte. The activation energy for conduction of 0.3eV is, as expected, higher than that of Li-ion conducting ionogels. The material possesses a 5V electrochemical window and is thermally stable up to 150°C. Using the positive Na-ion electrode material,  $\text{Na}_3\text{V}_2(\text{PO}_4)_3$ , the charge transfer properties of the ionogel/NVP interface were characterized and found to exhibit low interfacial impedance. This led us to demonstrate the operation of a Na-ion solid state battery which contained a  $\text{NaTi}_2(\text{PO}_4)_3$  negative electrode in conjunction with the NVP. The results shown here underscore the versatility of ionogels as a thermally stable electrolyte with designed ion transport properties for use in future solid-state electrochemical devices

#### 5:35 AM F.EN04.20.05

**Molecular-Level Insights of Coupled Aluminum-Ion Intercalation and Charge Transfer Mechanism into Chevrel Phase Electrodes Using Solid-State NMR Spectroscopy** Ankur Jadhav, Jeffrey Xu and Robert J. Messinger; The City College of New York, United States

Rechargeable aluminum metal batteries have seen a resurgence of interest as an emerging energy storage technology. Aluminum (Al) is low cost, inherently safe, and the most abundant metal in the earth's crust. Despite these opportunities, technological development of rechargeable aluminum batteries has been hindered due to lack of cathode materials that permit reversible transport of aluminum ions, mainly due to high Coulombic charge on aluminum cations rendering solid-state diffusion of aluminum ions difficult into crystalline materials.

The chevrel phases  $\text{Mo}_6\text{X}_8$  (X= S, Se) are among the few materials known to electrochemically intercalate multitude of multivalent ions, including trivalent aluminum cations. Thus, understanding the ion intercalation and charge transfer mechanism within this unique structure may provide insights into the design of new intercalation electrodes for rechargeable aluminum-ion batteries. Here, electrochemical and multi-nuclear solid-state nuclear magnetic resonance (NMR) measurements of aluminum-ion intercalation into the chevrel  $\text{Mo}_6\text{S}_8$  are correlated and quantitatively analyzed, revealing new insights into the ion intercalation mechanism. Solid-state  $^{27}\text{Al}$  NMR measurements reveal aluminum ions in two different environments associated with distinct cavities in the chevrel framework. Quantitative analyses of their relative populations establish that they reversibly (de)intercalate into the cavities simultaneously, as opposed to sequentially, upon discharge (charge).

In addition, for  $\text{Mo}_6\text{Se}_8$  electrodes, we perform ex-situ  $^{77}\text{Se}$  and  $^{95}\text{Mo}$  Hahn-echo NMR measurements along with single-pulse  $^{27}\text{Al}$  NMR at charged and discharged states to probe the crystalline frameworks to experimentally determine the charge transfer mechanism during the intercalation process. Replacing S with Se in the chevrel phase  $\text{Mo}_6\text{X}_8$  (X=S, Se) enables use of  $^{77}\text{Se}$  and  $^{95}\text{Mo}$  NMR which reveal changes in the chemical shift of only the  $^{77}\text{Se}$  NMR signal suggesting that the electrons prefer going to the Se atoms rather than the Mo atoms, unlike traditional transition metal oxide cathodes where the electrons are stored within the d-orbitals of the transition metal. Thus, for the first time, we demonstrate reversible electrochemical anionic redox as a charge storage mechanism for rechargeable batteries, which preserves the crystalline framework structure and does not involve the breaking and forming of chemical bonds.

Overall, the results yield quantitative molecular-level understanding of aluminum ion intercalation and charge transfer mechanism in a model crystalline transition metal electrode and establish solid-state  $^{27}\text{Al}$  NMR as a powerful characterization tool for rechargeable aluminum-ion batteries.

#### 5:45 AM F.EN04.20.06

**Self-Assembled Nanostructures in Ionic Liquids Facilitate Charge Storage at Electrified Interfaces** Xianwen Mao<sup>1</sup> and T. Alan Hatton<sup>2</sup>; <sup>1</sup>Cornell University, United States; <sup>2</sup>Massachusetts Institute of Technology, United States

Driven by the potential applications of ionic liquids (ILs) in many emerging electrochemical technologies, recent research efforts have been directed at understanding the complex ion ordering in these systems, to uncover novel energy storage mechanisms at IL/electrode interfaces. Here, we discover that surface-active ionic liquids (SAILs), which contain amphiphilic structures inducing self-assembly, exhibit enhanced charge storage performance at electrified surfaces. Unlike conventional non-amphiphilic ILs (NAILs), for which ion distribution is dominated by Coulombic interactions, SAILs exhibit significant and competing van der Waals interactions owing to the nonpolar surfactant tails, leading to unusual interfacial ion distributions. We reveal that at an intermediate degree of electrode polarization SAILs display optimal performance, because the low-charge-density alkyl tails are effectively excluded from the electrode surfaces, whereas the



formation of nonpolar domains along the surface suppresses undesired overscreening effects. This work represents a crucial step towards understanding the unique interfacial behavior and electrochemical properties of amphiphilic liquid systems showing long-range ordering, and offers insights into the design principles for high-energy-density electrolytes based on spontaneous self-assembly behavior. (Reference: Mao *et al.*, *Nature Materials* **2019**, 18, 1350–1357.)

**5:55 AM \*F.EN04.20.07**

**Solid State Electrolyte and Interface Design from Multiscale Mechano-Electrochemical Interactions** Xin Li; Harvard University, United States

Different from commercial liquid electrolyte batteries, where multiple interfaces can react under no mechanical constriction, the close contact between electrolyte particles and between electrolyte and electrode particles enforces a local mechanical constriction inside these particles as well as on their interfaces. Our work shows how such mechanical constriction effect can modulate battery performances at the material particle, interface coating and device levels. Design principles for advanced solid state batteries based on various types of solid electrolytes and advanced electrodes will be discussed, including sulfide, halide, oxide electrolytes, high voltage cathodes and the lithium metal anode.

**6:10 AM \*F.EN04.20.09**

**Halide-Based Solid-State Batteries—Electrolyte, Stability, Interface and Electrode** Xueliang A. Sun; University of Western Ontario, Canada

All-state-state lithium batteries (ASSLBs) have gained worldwide attention because of intrinsic safety and increased energy density. Compared with other types of solid-state electrolytes including oxide-based, polymer-based and sulfide-based electrolytes, recently-developed halide-based solid-state electrolytes (SSEs) have garnered considerable attention for all-solid-state lithium batteries (ASSLBs) due to the high ionic conductivity, high oxidation voltage and good stability toward oxide cathode materials [1]. However, there are still many challenges in halide-based solid-state electrolytes for ASSLBs including controllable and mass-production synthesis, achieving high humidity tolerance and demonstrate high-performance of ASSLBs; in particular, increased understanding of mechanisms during synthesis and tuning their properties of the electrolytes as well as interface with electrode materials[1].

In this talk, **(i)** I will demonstrate synthesis strategy [2-3], in particular, new and salable water-mediated synthesis method [2]. **(ii)** I will report a systematic study on the correlations among structural evolution,  $\text{Li}^+$  migration properties, and humidity stability resulting of the halide-based electrolytes, along with in-situ characterization for understanding of the mechanisms [4], **(iii)** Full cell battery performance will be optimized [5], **(iv)** humidity ability [6] and **(v)** other applications such as Li-O<sub>2</sub> batteries [7]. In the end, energy densities of ASSLBs using different solid-state electrolytes in ASSLBs will be discussed.

#### References:

1. X. Li, J. Liang, X. Yang, K. Adair, C. Wang, F. Zhao, X. Sun. Progress and Perspectives of Halide-based Lithium Conductors for All-Solid-State Batteries. **Energy Environ. Sci.**, 13, 1429-1461 (2020).
2. X. Li, J. Liang, X. Sun, et al., H<sub>2</sub>O-Mediated Synthesis of Superionic Halide Solid Electrolyte. **Angewandte Chemie International Edition**, 58, 16427-16432 (2019).
3. X. Li, J. Liang, X. Sun, et al., Air-Stable Li<sub>3</sub>InCl<sub>6</sub> Electrolyte with High Voltage Compatibility for All-Solid-State Batteries. **Energy Environ. Sci.**, 12, 2665 - 267 (2019).
4. X. Li, J. Liang, X. Sun, et al., Origin of Superionic Halide Solid Electrolytes with High Humidity Tolerance, **J. Am. Chem. Soc.** 142, 7012-7022 (2020).
5. C. Wang, X. Li, J. Liang, X. Sun, et al., Eliminating Interfacial Resistance in All-Inorganic Batteries by In-situ Interfacial Growth of Halide-based Electrolyte. **Nano Energy**, 2020, in press.
6. X. Li, J. Liang, X. Sun, et al., Origin of Superionic Li<sub>3</sub>Y<sub>1-x</sub>In<sub>x</sub>Cl<sub>6</sub> Halide Solid Electrolytes with High Humidity Tolerance, **Nano Letters**, in press, 2020.
7. Zhao, J. X. Sun, et al., Halide-based solid-state electrolyte as an interfacial modifier for high performance solid-state Li-O<sub>2</sub> batteries. **Nano Energy**, 2020, in press

**6:25 AM F.EN04.20.10**

**Chemo-Mechanics of Alkali-Ion Intercalation into Iron Phosphate Composite Cathodes** Bertan Ozdogru, Hannah Dykes, Darrell Gregory and Omer O. Capraz; Oklahoma State University, United States

Sodium-ion and potassium-ion batteries have attracted attention in the search for cost-effective batteries with a minimum sacrifice on the performance. Similar to Li-ion batteries, performance of these batteries depends on mechanical integrity of the cathodes and interfacial stability associated with solid-electrolyte interface formation. However, larger alkali metal-ions are expected to cause greater volumetric changes and lattice distortions in the cathode structure. Even small changes in volume upon alkali metal-ion intercalation can cause particle fracturing in brittle cathode materials. Also, diffusion of these larger alkali metal ions is slower in the electrode matrix due to their larger ionic size, compared to the Li ions. Therefore, it is expected that Na-ion and K-ion cathodes experience more mechanical instabilities at faster scan rates due to diffusion-limited ion transport. Understanding the interplay between alkali-ion chemistry, structural stability and electrochemical performance of cathode materials is crucial to develop novel cathode structures, which are suitable for Na-ion and K-ion batteries.

In this study, we investigated electrochemical strain generation in composite iron phosphate ( $\text{FePO}_4$ ) cathode during  $\text{Li}^+$ ,  $\text{Na}^+$  and  $\text{K}^+$  ion intercalation. Strains were monitored using *in situ*, optical, full-field digital image correlation technique. A host  $\text{FePO}_4$  framework was initially formed by the electrochemical delithiation of the  $\text{LiFePO}_4$  composite electrode in order to establish the identical electrodes in terms of active material loading in composite electrode, particle size, binder, and porosity of the composite electrode.  $\text{FePO}_4$  composite electrodes were cycled at 1C, C/10 and C/25 in against Na and Li counter electrode, and K ions were only intercalated into  $\text{FePO}_4$  at C/25 rate.

Striking differences in the physical response of  $\text{FePO}_4$  were observed during the intercalation of three different alkali-metal ions. First of all, Li intercalation caused strain hysteresis at higher scan rates. Linear relationship between strains and capacity was observed during Na intercalation at any scan rate. However, the electrodes experience additional 0.05 and 0.15% more composite strains at C/10 and 1C rates compared to the electrode cycled at C/25 rate when the state of discharge was same during Na intercalation. An analytical model was developed to predict Na concentration gradients and misfit strain generation in the NFP particles. Second, only about 30 mAh/g discharge capacity was achieved at fourth cycle during the intercalation of potassium into  $\text{FePO}_4$ , whereas at the same scan rate, Li and Na intercalation delivered about 130 and 140 mAh/g, respectively. Despite of the size difference between Na and K ions, at the same discharge capacity, similar volumetric expansion was observed upon Na and K intercalation. Third, strain derivatives with respect to voltage were calculated using the finite difference method. Local minima in strain derivatives closely matched the current peaks during Li, Na and K insertion into the  $\text{FePO}_4$  structure. Phase transformation during Li and Na intercalation, measured by *ex-situ* XRD, corresponds well with the current peaks observed during the cycling. Intercalation of K into  $\text{FePO}_4$  was reported to cause amorphization in the crystalline  $\text{FePO}_4$ . Surprisingly, strain derivatives during K ion intercalation demonstrated distinct features, which aligned well with the electrochemical responses. Therefore, digital image correlation can be used to monitor electrochemical strains in other amorphous electrodes too. In conclusion, our results provide new insights about how Li, Na and K alkali ions influence the phase transitions and mechanical response of the iron phosphate cathodes.

#### 6:35 AM F.EN04.20.11

**Sulfide-Based Composite Electrolyte to Enhance the Performance of Solid-State Lithium Metal Batteries** [Yang Li](#), Thad Druffel, Mahendra Mahendra Sunkara and Hui Wang; University of Louisville, United States

Sulfide-based lithium (Li)-ion conductors represent one of the most popular solid electrolytes (SEs) for solid-state Li metal batteries (SSLMBs) with high safety. However, the practical application of sulfide-based SEs is significantly limited by their chemical instability in air and electrochemical instability with electrode materials (metallic Li anode and oxide cathodes). To address these difficulties, here, we design and demonstrate a novel sulfide-based composite electrolyte (SCE) through the combination of inorganic sulfide Li argyrodite ( $\text{Li}_7\text{PS}_6$ ) with a polymer matrix. The developed SCE achieves excellent air-stability, impressive flexibility, and great chemical/electrochemical stability. Meanwhile, the presence of sulfide fillers facilitates the Li-ion transport in SCE, leading to a superior ionic conductivity at room temperature. Using the SCE enables with enhanced stability in Li symmetric cells and excellent suppression of Li dendrites. In addition,  $\text{LiFePO}_4$  (LFP)/Li cells can deliver impressive specific capacity and excellent stability over long-term cycles. These features indicate this sulfide-based SCE as a promising candidate, and whose design will contribute to the practical development of SSLMBs.

#### 6:45 AM F.EN04.20.12

**Designing MOF-Based Nickel Cobaltite Composites for Energy Storage** [Ali Rashti](#) and Tae-Sik Oh; Auburn University, United States

Metal-organic frameworks (MOFs) are considered a novel type of crystalline porous structures. These structures are composed of inorganic vertices and organic linkers coupled through the coordination bonds. MOFs have distinct purposes such as high specific surface area, controllable pore size and good thermal stability that makes them good candidates to be

used as porous templates.

In this work, the designed synthesis of  $\text{NiCo}_2\text{O}_4(\text{Co}_3\text{O}_4)$  double shell nanocages (DSNCs) from zeolitic imidazolate framework-67 is studied. The DSNCs are later embedded with graphene to enhance their conductivity and electrochemical performance. The strategy includes the synthesis of zeolite imidazolate framework-67 (ZIF-67)/Ni-Co layer doubled hydroxide (LDH) precursor and subsequent transformation to  $\text{NiCo}_2\text{O}_4(\text{Co}_3\text{O}_4)$  DSNC by thermal annealing. The as-prepared DSNC structure is wrapped with graphene structure through a simple electrostatic self-assembly. Here, we focused on tuning the microstructure of  $\text{NiCo}_2\text{O}_4(\text{Co}_3\text{O}_4)$  DSNCs by controlling the crystal size of ZIF-67 and Ni-Co LDH formation while etching the initial MOF template.

Herein, we report  $\text{NiCo}_2\text{O}_4(\text{Co}_3\text{O}_4)\text{@rGO}$  composite structure with a capacity of  $969 \text{ F.g}^{-1}$  at current density of  $1 \text{ A.g}^{-1}$  showing a remarkable stability of showing 88% of initial capacitance after 10000 cycles of charge-discharge with a high mass loading of electrodes ( $\text{mg.cm}^{-2}$ ).

This work shows a universal process for controlled synthesis of different complex spinel structures that can be used for various applications.

#### 6:55 AM F.EN04.20.13

##### **Tailoring Electrode-Electrolyte Interfaces in Lithium-Ion Batteries using Molecularly Engineered Functional Polymers** Laisuo Su and B. Reeja Jayan; Carnegie Mellon University, United States

Understanding and tailoring electrode-electrolyte interfaces (EIs) is critical for enhancing the rate capability, cycling stability, and thermal safety of lithium ion batteries (LIBs). Although artificial coatings have been explored to tailor EIs, no clear mechanisms have been identified that explain how these coatings engineer the EIs of LIB electrodes. For the first time, we study  $\text{Li}^+$  kinetics in different polymer-based artificial coatings and at EIs using a combination of experimental techniques (electrochemical impedance, neutron reflectometry and depth profiling) and density functional theory (DFT) calculations. Small binding energy with  $\text{Li}^+$  and the presence of sufficient binding sites for  $\text{Li}^+$  allow poly(3,4-ethylenedioxythiophene) (PEDOT) based artificial coatings to enable fast charging of  $\text{LiCoO}_2$ . Operando synchrotron X-ray diffraction experiments suggest that the superior  $\text{Li}^+$  transport property of the PEDOT coating further improves current homogeneity in the  $\text{LiCoO}_2$  electrode during cycling, and, therefore, determines the electrochemical performance of the electrode. The  $\text{LiCoO}_2$  4.5 V cycle life tested at  $C/2$  is increased by over 1700 % after applying the PEDOT coating. In comparison, other polymer coatings have negligible or negative effects on  $\text{LiCoO}_2$  performance. Additionally, X-ray photoelectron spectroscopy and DFT calculations demonstrate that S, O present in PEDOT form chemical bonds with Co in  $\text{LiCoO}_2$ . These chemical bonds reduce Co dissolution and inhibit electrolyte decomposition, improving the cycling stability of  $\text{LiCoO}_2$ . These insights provide us practical design rules for polymer selection that will help shorten the research time and reduce the trial-and-error effort involved in tailoring EIs for developing advanced batteries.

#### 7:05 AM F.EN04.20.14

##### **Advancing Lithium-ion Capacitor Energy Storage with Composite Activated Carbon Cathodes** Jacob Strimaitis, Samuel Danquah, Sangram K. Pradhan and Messaoud Bahoura; Norfolk State University, United States

Hybrid supercapacitors, which exhibit the beneficial characteristics of both their battery (high energy density) and supercapacitor (high power density and durability) constituents, are in demand to meet current and future technological and infrastructural needs. While substantial efforts have already been made to modify the anode, commonly  $\text{Li}_4\text{Ti}_5\text{O}_{12}$  (LTO), to increase rate performance, lesser attention has been placed on the activated carbon (AC) cathode, which has been reported as the energy density limiting electrode and is so prime for optimization. Using galvanostatic charge-discharge cycling and high-resolution imaging techniques, it was determined that systematically adding  $\text{LiMn}_2\text{O}_4$  (LMO), a common battery cathode material, and Super P, a common conductive element, to the AC supercapacitor cathode changes the structure of the electrode and increases the energy density of a LTO//AC Li-ion capacitor without significantly impacting rate performance. Future work will help determine the energy storage kinetics of the composite cathode and how modifications to the LTO anode in tandem with the cathode may increase electrochemical capacity without affecting the capacitor's typical high-power density and long-term cyclability.

#### 7:15 AM F.EN04.20.15

##### **Inhibit of Lithium Dendrite Growth in Solid Composite Electrolyte by Phase-Field Modeling** Ye Cao<sup>1</sup>, Ren Yao<sup>1</sup> and Yue Zhou<sup>2</sup>; <sup>1</sup>The University of Texas at Arlington, United States; <sup>2</sup>South Dakota State University, United States

Lithium (Li) dendrite growth poses serious challenges for the development of Li metal batteries. Replacing liquid electrolyte with solid composite electrolyte embedded with nanofiller additives can potentially suppress the Li dendrite growth. However the underlying mechanism is still not fully understood, and most theoretical works focus on pure liquid electrolyte

and ignore the mechanical strain effects. Here we developed a phase-field model to simulate the Li dendrite growth by incorporating the microstructure of the solid composite electrolyte, and considering the mechanical effects of the electrolyte. Using aluminum oxide nanofiber embedded poly(vinylidene fluoride-co-hexafluoropropylene) (P(VDF-HFP)) as an example, we discovered two key factors, the elastic modulus and the electrolyte nanochannel width that govern the Li dendrite growth. The difference of the Young's modulus between the Li metal and solid electrolyte acts as the additional mechanical driving force, which partially offsets the electrochemical driving force to either promote or inhibit the dendrite growth. We also discovered that the introduction of the 1D nanofiber arrays could confine the Li ion transport along vertical direction, reduce the concentration gradient across the metal/electrolyte interface, and inhibit the Li dendrite growth. Finally the dependence of overall Li ion conductivity on the nanofiller is discussed. Our work provides deep understanding and designing strategy for the solid composite electrolyte for improved Li anode stability and Li ion conductivity.

7:25 AM \*F.EN04.20.16

**Design, Discovery and Structure-Property Relationship Investigation of Oxide, Sulfide and Halide Solid Electrolytes for All-Solid-State-Batteries** [Hailong Chen](#); Georgia Institute of Technology, United States

Solid electrolyte is the key component for all solid state batteries. Extensive research attentions are being attracted to the design and development of high performance solid electrolytes. An ideal solid electrolyte should simultaneously satisfy properties in multiple categories, including ionic and electronic conductivities, chemical stabilities against air and moisture, good mechanical properties, and good electrochemical stability and compatibility with both cathode and anode, etc. Cost and feasibility for scale production and battery fabrication are also important considerations.

Here we report our recent work on design and development of high performance novel solid electrolytes, including oxide, sulfide and halide compounds, and the comparison of their performances in batteries. These new materials are designed based on either computational prediction or empirical hypothesis. LiTaSiO<sub>5</sub> series oxide materials show good ionic conductivity and outstanding stability. The synthesis and processing of this material will be discussed. Novel sulfide and halide solid electrolytes will also be reported. They all show very high room temperature ionic conductivities and good performance in the cycling test of all solid state batteries. High resolution synchrotron X-ray and neutron scattering techniques, solid state NMR and electron microscopy were complementarily used to reveal the structure-property relationships in these compounds. The impacts of synthesis condition, chemical composition and processing to the ionic conductivity and battery performances will be discussed.

7:40 AM F.EN04.20.17

**Late News: Development of Water-Stable O<sub>3</sub>-type Transition Metal Oxide Enabling Long-Term Cyclic Stability with "Aqueous Processed" Cathodes for Na-Ion Batteries** [Bachu Sravan Kumar](#), Anagha Pradeep, Animesh Dutta and Amartya Mukhopadhyay; IIT Bombay, India

The upcoming Na-ion battery system has advantages over the Li-ion battery system in terms of the more widespread availability and lower cost of Na-precursors. Among the potential cathode material classes, O<sub>3</sub>-type layered Na<sub>x</sub>T<sub>M</sub>O<sub>2</sub> (T<sub>M</sub> => transition metal ion; x~1) is important due to the inherently high Na-storage capacity. However, the O<sub>3</sub>-type Na<sub>x</sub>T<sub>M</sub>O<sub>2</sub> suffers from instabilities caused due to multiple structural changes during Na-extraction/insertion, T<sub>M</sub>-dissolution into electrolyte and, more importantly, inherent sensitivity to moisture. The moisture sensitivity necessitates the usage of binders that dissolve only in toxic non-aqueous solvents like N-Methyl-2-pyrrolidone (NMP) during electrode preparation. Against this backdrop, a carefully designed composition has been developed here to address the aforementioned problems, in particular, the air/water-instability. Among other things, Ti-ion substitution for Mn-ion (partially/completely) has led to excellent air/water-stability; resulting in no phase/structural change (from the original O<sub>3</sub> structure) even after 40 days of exposure to air and 12 h of stirring in water. By contrast, under similar conditions, O<sub>3</sub> and P<sub>3</sub> phases progressively evolve for the predominantly Mn-ion containing counterparts. The excellent stability of the optimized O<sub>3</sub>-type NaT<sub>M</sub>O<sub>2</sub> enables the usage of environment/health friendly and economical 'aqueous-binder' (*viz.*, Na-alginate) and water (as solvent) for electrode preparation. Furthermore, Ti-substitution also prevented the presence of Mn-ion in its +3 oxidation state; thus, addressing the Mn-dissolution problem and concomitantly suppressing the increase in impedance, as well as voltage hysteresis, during electrochemical cycling. Overall, the 'aqueous-processed' cathode exhibits excellent long-term cyclic stability, with a capacity retention of ~56% after 750 cycles at C/5, including just ~4% capacity fade over the last 250 cycles investigated. Hence, this is a significant step towards the development of alkali metal-ion batteries having electrochemically stable electrodes being prepared in a health/environment friendly and cost-effective manner (by enabling the usage of water-based, as opposed to NMP-based, binder). A part of this work has been published as; Kumar *et al.*, *J. Mater. Chem. A* (2020; DOI: 10.1039/D0TA05169A).

Keywords: *Na-ion battery; layered transition metal oxide cathode; air/water-stability; aqueous processing; electrochemical behaviour*

7:50 AM F.EN04.20.18

**Late News: Bi-Phase Na-Titanate Based Composite with Excellent Long-Term Electrochemical Stability and Rate Capability as Anode for Na-Ion Batteries** Anagha Pradeep<sup>1</sup>, Bachu Sravan Kumar<sup>1</sup>, Ajay Kumar<sup>1</sup>, Velaga Srihari<sup>2</sup>, Himanshu Poswal<sup>2</sup> and Amartya Mukhopadhyay<sup>1</sup>; <sup>1</sup>IIT Bombay, India; <sup>2</sup>Bhabha Atomic Research Center, India

In contrast to the Li-ion battery system, graphite does not work as anode material for the upcoming Na-ion battery system. Even though hard carbon has been widely explored as anode material, it possesses safety issues since the Na-insertion potential is very low and close to that of Na-plating. In this context, the present work reports a bi-phase Na-titanate based composite anode material, which is safe, electrochemically stable, possesses very high 'rate-capability' and long-term cyclic stability, even at very high current densities. 'Bi-phase NTO', having ~66% Na<sub>2</sub>Ti<sub>3</sub>O<sub>7</sub> and ~34% Na<sub>2</sub>Ti<sub>6</sub>O<sub>13</sub> shows contributions from both the constituent phases, which is confirmed via *operando* synchrotron X-ray diffraction studies. 'Bi-phase NTO' is electrochemically more stable than Na<sub>2</sub>Ti<sub>3</sub>O<sub>7</sub> and its operating potential is well above the Na-plating potential. Furthermore, the performance of 'Bi-phase NTO' has been further improved by the addition of functionalized multi-walled carbon nanotubes (MWCNTs), which bestows the same with reversible Na-storage capacity of ~162 mAh g<sup>-1</sup> at C/5 and outstanding cyclic stability. The very stable 'charge-averaged' discharge/charge potentials and only minor increment in impedance over multiple electrochemical cycles support the excellent stability of 'bi-phase NTO'/MWCNTs composites. Of special note is that the composite electrode exhibits 1<sup>st</sup> cycle reversible capacity of >140 mAh g<sup>-1</sup> even at 50C, with capacity retentions of ~83% and ~58%, after 100 and 2000 cycles, respectively, including negligible capacity fade from the 300<sup>th</sup> cycle onwards. This indicates the feasibility for long-term cycling at very high current densities. Overall, this will allow the development of Na-ion cells possessing outstanding rate-capability and cyclic stability; thus addressing some of the major concerns associated with the same. A part of this work has been published as Pradeep *et al.*, *Electrochim. Acta* (2020).

SESSION F.EN04.21: Sodium Batteries

On Demand Abstracts Available for Viewing Starting Saturday Morning, November 21, 2020  
F-EN04

5:00 AM F.EN04.21.02

**Elucidating the Intergrowth of Octahedral and Prismatic Na Layers in Sodium Transition Metal Oxides** Jae Chul Kim<sup>1</sup>, Deok-Hwang Kwon<sup>2,3</sup>, Julia Yang<sup>2,3</sup> and Gerbrand Ceder<sup>2,3</sup>; <sup>1</sup>Stevens Institute of Technology, United States; <sup>2</sup>University of California, Berkeley, United States; <sup>3</sup>Lawrence Berkeley National Laboratory, United States

As an alternative to Li-based technologies to develop stationary energy storage systems, Na-ion batteries have attracted substantial interest. Unlike the Li-ion, layered sodium transition metal oxide (NaTMO<sub>2</sub>) cathodes can diversify their redox centers from expensive Co to cheap Mn and Fe to achieve high energy density, offering a wide variety of chemistry selection to design low-cost, high-performance batteries. These cathode materials often undergo discontinuous, yet reversible, phase transitions upon Na intercalation due to complex interatomic interactions, which result in multiple plateau-like features in their voltage profiles. However, large desodiation of Fe-containing Na-ion cathodes often leads to an unclarified, irreversible phase transition at high voltage, hindering the full use of Fe redox.

In this talk, we will discuss how transition metal selection affects the thermodynamic stability of desodiated structures of NaTMO<sub>2</sub>. Specifically, our recent findings on a quaternary transition metal system, NaTi<sub>0.25</sub>Fe<sub>0.25</sub>Co<sub>0.25</sub>Ni<sub>0.25</sub>O<sub>2</sub>, will be underlined. We will present structural evidence and characterization of the highly-desodiated, high-voltage phase that exhibits peculiar oxygen stacking. This phase consists of alternating octahedral and prismatic Na layers, namely OP2 stacking, in which formation is afforded by distortion-tolerant Ti and Jahn-Teller-active Fe. Moreover, we will demonstrate that this new phase participates in redox reaction reversibly, fundamentally distinct from inactive high-voltage phases in many Na-ion cathodes. Finally, a strategy to stabilize Fe-containing NaTMO<sub>2</sub> materials to create layered cathodes with high reversible Na capacity will be briefly discussed. Our results demonstrate that we can manipulate the redox reaction and associated structure change by transition metal mixing.

5:10 AM F.EN04.21.03

**Understanding the Reaction Mechanism of Sodium Vanadate for an Aqueous Zn Ion Battery by Transmission Electron Microscopy** Sung Joo Kim<sup>1</sup>, Christopher Tang<sup>2</sup>, Gurpreet Singh<sup>2</sup>, Lisa House<sup>2</sup>, Shize Yang<sup>1</sup>, Kenneth Takeuchi<sup>2</sup>, Amy Marschilok<sup>2</sup>, Esther Takeuchi<sup>2</sup> and Yimei Zhu<sup>1</sup>; <sup>1</sup>Brookhaven National Laboratory, United States; <sup>2</sup>Stony Brook

University, The State University of New York, United States

Layered metal vanadate, such as sodium vanadate ( $\text{Na}_{1+x}\text{V}_3\text{O}_8$  or NVO), has recently attracted immense interest as the promising aqueous Zn ion battery cathode material owing to its metal ion pillars that facilitate Zn ion diffusion within the structure. Here, reaction mechanisms of hydrated  $\text{Na}_2\text{V}_6\text{O}_{16} \cdot 2\text{H}_2\text{O}$  slabs and non-hydrated  $\text{Na}_{1.25}\text{V}_3\text{O}_8$  nanorods were investigated in detail by employing transmission electron microscopy. We observed the full discharge of the thin (30-50 nm)  $\text{Na}_2\text{V}_6\text{O}_{16} \cdot 2\text{H}_2\text{O}$  system with successful Zn ion insertion into the bulk while detecting Zn ion insertion only at the surface for thick (120-170 nm)  $\text{Na}_{1.25}\text{V}_3\text{O}_8$ , demonstrating that both the hydration and the nanostructure thickness determine the reaction mechanism of NVO. Interestingly, electrochemical cycling of Zn/NVO cells induced the irreversible formation of the novel by-product phase, Na-inserted Zinc pyrovanadate ( $\text{Zn}_3\text{Na}_x(\text{OH})_2\text{V}_2\text{O}_7$  or ZNVO), which is electrochemically active. Its presence could eventually lead to a bifurcated discharge/charge process, where Zn redox reactions happen in both NVO and ZNVO contributing to the overall cell capacity. This microscopy work offers important insights into the effects of morphology and hydration on reaction mechanisms of NVO, which hold some implications on its electrochemistry for aqueous Zn ion batteries.

**5:20 AM \*F.EN04.21.04**

**Optimization of Titanate Anodes for Sodium-Ion Batteries** Marca M. Doeff, Lawrence Berkeley National Laboratory, United States

Sodium-ion batteries (NIBs) are the nearest of the "Beyond Li-ion Batteries" systems to commercialization. Attractive features include the large abundance of sodium precursor materials, which reduce supply security worries and lower cost, and the ability to use Co-free cathodes and aluminum current collectors on the anode side. Further improvements require the identification of suitable replacements for the hard carbon anodes currently used, which limit energy density and present safety issues. We have recently been working with several types of sodium titanium oxides with stepped layered structures, which undergo reductive intercalation of sodium at extremely low potentials. These include "sodium nonatitanate", which can deliver up to 200 mAh/g at an average potential of about 0.3V vs.  $\text{Na}^+/\text{Na}$ , and lepidocrocite-structured titanates, whose redox properties vary depending on exact chemistry and structure. Both types of materials show excellent reversibility in sodium half-cells, making them appealing candidates for use as anode materials for NIBs. In this talk, we will discuss their structure, chemistry, and electrode optimization.

**5:35 AM F.EN04.21.07**

**Accurately Predicting Sodium Ion Cathode Voltages from Statistical and Ab-Initio Approaches** Arthur B. Youd, Daniel Davies, Christopher Savory and David O. Scanlon; University College London, United Kingdom

$\text{Na}_x\text{CoO}_2$  is a layered cathode material which shares many attributes with widely used  $\text{LiCoO}_2$ . Several geopolitical and economic factors make lithium a potentially unreliable raw material for rechargeable batteries therefore an earth abundant alternative is eagerly sought after. Sodium shares many chemical similarities with lithium however does underperform in the areas of specific energy and charge density<sup>1</sup>; as such understanding the electronic structure and electrochemical behaviour is an essential steppingstone to optimising said material and rationally designing new layered sodium ion cathode materials. A combination of structural dynamism, magnetic complexity and inter layer dispersion make  $\text{Na}_x\text{CoO}_2$  a challenging material to model; thus far its electrochemical voltage profile has not been convincingly reproduced by theoretical methods.<sup>2</sup> The motivation of this study is to ascertain the correct level of theory necessary to robustly reproduce experimental structures and voltage profiles of  $\text{Na}_x\text{CoO}_2$ , and thus guide the accurate simulation of other layered Na-ion cathodes.

This study simulates octahedral and prismatic structures of  $\text{Na}_x\text{CoO}_2$  within the stoichiometric range of  $0 \leq x \leq 1$  using the cluster expansion approach as implemented in the CASM code<sup>3-5</sup> as well as high throughput ab-initio calculation management within the *atomate* program.<sup>6</sup> The hierarchical survey of methodology uses both generalised-gradient and hybrid functionals to examine the role of electron exchange. Our hierarchical survey examines the voltage profile of  $\text{Na}_x\text{CoO}_2$  calculated with 6 different methodologies; these variously comprise hybrid DFT and GGA+U methods to correct for correlated d electrons, and include or exclude the effects of Van der Waals interactions to explicitly account for how each of these affects the voltage profile and thus establish the optimal ab-initio methodology to accurately reproduce such profiles in the future. This survey will inform predictions of future Na-ion cathodes, while detailed electronic structure analysis will develop our understanding of the redox processes present in  $\text{LiCoO}_2$ . DFT is also used to inform electronic structure analysis, specifically the composition of the valance band, with a view to ascertain the species participating in the redox process during cycling. Collectively, this approach will inform computational analyses into similar layered sodium open shell transition metal oxides for cathode applications to take the guess work out of voltage predictions.

## References

1. Sawicki, M. & Shaw, L. L., Advances and challenges of sodium ion batteries as post lithium ion batteries, RSC Adv., The Royal Society of Chemistry, 2015, 5, 53129-53154
2. Kaufman, J. L. & Van der Ven, A.,  $\text{Na}_x\text{CoO}_2$  phase stability and hierarchical orderings in the O3/P3 structure family, Phys. Rev. Materials, American Physical Society, 2019, 3, 015402
3. J. C. Thomas, A. Van der Ven, Finite-temperature properties of strongly anharmonic and mechanically unstable crystal phases from first principles, Physical Review B, 88, 214111 (2013).
4. B. Puchala, A. Van der Ven, Thermodynamics of the Zr-O system from first-principles calculations, Physical Review B, 88, 094108 (2013).
5. A. Van der Ven, J. C. Thomas, Q. Xu, J. Bhattacharya “Linking the electronic structure of solids to their thermodynamic and kinetic properties”, Mathematics and Computers in Simulation, 80(7) 1393-1410 (2010).
6. Mathew, K., Montoya, J. H., Faghaninia, A., Dwarakanath, S., Aykol, M., Tang, H., Chu, I., Smidt, T., Bocklund, B., Horton, M., Dagdelen, J., Wood, B., Liu, Z.-K., Neaton, J., Ong, S. P., Persson, K., Jain, A., Atomate: A high-level interface to generate, execute, and analyse computational materials science workflows. Comput. Mater. Sci. 139, 140–152 (2017)

### 5:45 AM F.EN04.21.08

#### First Principles Investigation on the Phase Stability of $\text{Na}_2\text{Ti}_3\text{O}_7$ Electrode During Hydrogenation Treatment for High Performance Na-ion Batteries Yong-Seok Choi<sup>1,2</sup>, Sara I. Costa<sup>3,2</sup>, Nuria Tapia-Ruiz<sup>3,2</sup> and David O.

Scanlon<sup>1,2,4</sup>; <sup>1</sup>University College London, United Kingdom; <sup>2</sup>The Faraday Institution, United Kingdom; <sup>3</sup>Lancaster University, United Kingdom; <sup>4</sup>Diamond Light Source Ltd., United Kingdom

The low cost and abundance of sodium have driven the growing interest in Na-ion batteries (NIBs) as a possible alternative for Li-ion batteries. However, NIBs are still in a developmental research phase and the exploration of proper electrode materials is necessary<sup>[1]</sup>. Among the candidate electrode materials,  $\text{Na}_2\text{Ti}_3\text{O}_7$  has emerged as a promising electrode material because of its low cost, nontoxicity<sup>[2,3]</sup>, and high theoretical capacity of 177 mAhg<sup>-1</sup><sup>[4]</sup>. Nevertheless,  $\text{Na}_2\text{Ti}_3\text{O}_7$  has not been used as main electrodes owing to its low electric/ionic conductivity and poor structural stability, which causes significant capacity fading upon cycling<sup>[5]</sup>. Efforts to improve the cycling stability of sodium titanates have discovered  $\text{Na}_2\text{Ti}_6\text{O}_{13}$  which has properties contradictory to  $\text{Na}_2\text{Ti}_3\text{O}_7$ ;  $\text{Na}_2\text{Ti}_6\text{O}_{13}$  exhibits high ionic conductivity and structural stability but suffers from low Na storage capacity<sup>[6]</sup>. In this regard, proper hybridization of  $\text{Na}_2\text{Ti}_3\text{O}_7$  and  $\text{Na}_2\text{Ti}_6\text{O}_{13}$  could break the limitations of each structure and offer a composite electrode for high performance NIBs<sup>[7]</sup>.

Hydrogenation treatment, which can transform  $\text{Na}_2\text{Ti}_3\text{O}_7$  into  $\text{Na}_2\text{Ti}_6\text{O}_{13}$ <sup>[8,9]</sup>, has recently emerged as a facile way to synthesize hybrid  $\text{Na}_2\text{Ti}_3\text{O}_7/\text{Na}_2\text{Ti}_6\text{O}_{13}$  electrode<sup>[7]</sup>. From this perspective, a comprehensive understanding of the phase stability of  $\text{Na}_2\text{Ti}_3\text{O}_7$  during hydrogenation treatment can enable further performance enhancements of sodium titanate electrodes. In this study, using hybrid HSE06 DFT functional implemented in VASP code, we have analyzed the phase stability of  $\text{Na}_2\text{Ti}_3\text{O}_7$  during hydrogenation treatment and its effect on battery performance. The ternary phase diagram of Na-Ti-O system and subsequent Gibbs free energy calculations reveal that, as a result of the thermal energy applied during hydrogenation treatment,  $\text{Na}_2\text{Ti}_3\text{O}_7$  can thermodynamically decompose into six different phases of  $\text{Na}_2\text{O}$ ,  $\text{Na}_4\text{TiO}_4$ ,  $\text{Na}_8\text{Ti}_5\text{O}_{14}$ ,  $\text{Na}_4\text{Ti}_5\text{O}_{12}$ ,  $\text{Na}_2\text{Ti}_6\text{O}_{13}$ , and  $\text{TiO}_2$ . The calculated band structures and their alignments show that the formation of  $\text{Na}_2\text{Ti}_6\text{O}_{13}$  can reduce the band gap of initial  $\text{Na}_2\text{Ti}_3\text{O}_7$  by up to 0.19 eV, which enhances electrochemical performances of the electrode. In addition to these results, the formation of defects (O vacancy and -OH group) associated with hydrogenation treatment and their effect on electrochemical performance will be also discussed. The results provided here can help designing high performance sodium titanate electrodes for future NIBs.

- (1) Chemical reviews 117.21 (2017): 13123-13186.
- (2) Advanced Functional Materials 26.21 (2016): 3703-3710.
- (3) Nano Energy 18 (2015): 20-27.
- (4) Journal of Materials Chemistry A 3.44 (2015): 22280-22286.
- (5) Advanced Energy Materials 6.11 (2016): 1502568.
- (6) Small 12.22 (2016): 2991-2997.
- (7) Advanced Science 5.9 (2018): 1800519.
- (8) The Journal of Physical Chemistry B 110.9 (2006): 4030-4038.
- (9) Journal of Raman Spectroscopy 41.10 (2010): 1331-1337.

### 5:55 AM F.EN04.21.09

#### An Experimental and Computational Investigation of Nickel Tellurate Cathode Materials for Na-ion and Li-ion Batteries Ieuan D. Seymour<sup>1,2</sup>, Nicholas Grundish<sup>1</sup>, Yutao Li<sup>1</sup>, John B. Goodenough<sup>1</sup> and Graeme Henkelman<sup>1</sup>; <sup>1</sup>The University of Texas at Austin, United States; <sup>2</sup>Imperial College London, United Kingdom

Layered transition-metal (TM) oxides have played a central role as cathodes for Na-ion and Li-ion rechargeable batteries. Alleviating the deleterious structural transitions that occur in these materials during electrochemical cycling is still a critical challenge which requires a fundamental understanding of the mechanisms taking place at the atomistic level. In this work we investigated how  $\text{Te}^{6+}$  doping into the  $A_x\text{NiO}_2$  ( $A=\text{Na}$  and  $\text{Li}$ ) family of materials leads to changes in the local structure and electrochemical performance. The Na-Ni-Te-O system provides an ideal case study into the link between local structure and electrochemical performance of Na-cathode materials. The inclusion of  $\text{Te}^{6+}$  results in the suppression of TM layer shearing during desodiation after an initial transformation from an O'3 to a P'3 structure. Using a combination of X-ray diffraction and solid-state paramagnetic NMR it can be shown that the inclusion of Na-ions into the TM layer suppresses long range Na-ordering in the P'3 structure which facilitates favorable electrochemical properties. Paramagnetic NMR measurements show that while the long-range Na ordering is suppressed in the Na-Ni-Te-O system, there is significant local ordering of the Na sites in the TM layer, with a strong preference for the formation of nearest neighbor Na-Na motifs that are distinct from analogous Li compounds.

Complimentary DFT calculations are used to understand energetics of local structural orderings and to assign the complex paramagnetic NMR spectra. The DFT calculations are coupled with an advanced basin-hopping methodology to probe the intricate relationship between structural transitions and Na-vacancy ordering as a function of sodium content in the O'3 and P'3 structures. The combined experimental and computational approach developed in this work is further extended to understand the changes in the local structure during desodiation of the isostructural Na-Ni-Fe-Sb-O family of materials.

In the analogous Li-Ni-Te-O family, two layered polymorphs and one disordered rock salt phase can be synthesized. In contrast to the Na-Ni-Te-O system,  $\text{Ni}^{2+}$  migration occurs in layered Li polymorphs which leads to rapid capacity fading. The disordered rock salt compound displayed the highest reversible capacity out of the three structures, which could be rationalized based on the presence of fast Li-transport on the partially ordered Li/Ni sublattice. The conclusions from this work have wider implications for the design of new Na-ion and Li-ion cathode materials.

[1] Grundish et al. *Chem. Mater.* 31 (2019)

#### 6:05 AM F.EN04.21.10

**Late News: "Na Ion Redistribution" in Layered Oxide Compound during Na/K Ion Exchange** Haegyeom Kim;  
Lawrence Berkeley National Laboratory, United States

Recently, new energy storage materials for K-ion batteries (KIBs), which emerged as a low cost alternative battery system, have been developed by using  $\text{Na}^+/\text{K}^+$  ion exchange. For example, P2-type  $\text{K}_{0.5}\text{CoO}_2$  was prepared from P2- $\text{Na}_{0.84}\text{CoO}_2$  via electrochemical  $\text{Na}^+/\text{K}^+$  ion exchange by Baskar *et al.*<sup>1</sup> P3-type  $\text{K}_x\text{CrO}_2$  and  $\text{K}_x\text{Cr}_{0.9}\text{Ru}_{0.1}\text{O}_2$ , both cathodes which display good cycle life, have been derived from their Na analogues through ion exchange.<sup>2-4</sup> There are many other examples.<sup>5-7</sup> In fact, ion exchange reaction has been widely used to produce metastable inorganic materials, unlike those prepared by direct chemical reactions at high temperature. New materials design for Li-ion batteries has frequently used  $\text{Li}^+/\text{Na}^+$  ion-exchange reactions to attain structural features of Na layered oxides not directly achievable via conventional synthesis methods for Li compounds. For example, Delmas *et al.* developed O2-type  $\text{LiCoO}_2$  from P2-type  $\text{Na}_{0.7}\text{CoO}_2$ , even though O3-type  $\text{LiCoO}_2$  is the commonly observed structure.<sup>8</sup> Similarly, layered  $\text{LiMnO}_2$  was first synthesized from  $\alpha$ - $\text{NaMnO}_2$  via  $\text{Li}^+/\text{Na}^+$  ion exchange by Armstrong *et al.* and Delmas *et al.*,<sup>9,10</sup> whereas an orthorhombic structure (space group Pmmn) is the stable form of  $\text{LiMnO}_2$  under typical synthesis conditions.<sup>11</sup> Nevertheless, the microscopic theory of solid-state ion-exchange is not well developed. The microscopic mechanism for  $\text{Na}^+/\text{K}^+$  ion-exchange has been even less investigated than that of  $\text{Li}^+/\text{Na}^+$ .

In this work, we investigate how ion-exchange occurs in compounds, using electrochemical  $\text{Na}^+/\text{K}^+$  ion exchange in  $\text{Na}_3\text{Ni}_2\text{SbO}_6$  as a model system. Using *in-situ* XRD we find a surprising and remarkable sequences of phase to occur as K is inserted into a compound with Na ions remaining. We establish that the origin of this remarkable behavior upon Na/K ion exchange is the strong repulsion between the two ions. We discover that K ion insertion into the desodiated  $\text{Na}_x\text{Ni}_2\text{SbO}_6$  pushes the remaining Na ions away and redistributes them, thereby separating Na-rich and K-rich phases in a particle. Interestingly, this phenomenon creates a complex three-phase equilibrium during most of the de-sodiation and potassiation of  $\text{Na}_x\text{K}_y\text{Ni}_2\text{SbO}_6$ : either one K-rich and two Na-rich phases or two K-rich and one Na-rich phase coexist, thereby perfectly satisfying the Gibbs phase rule. Our computational study further demonstrates that the phase separation originates from the large lattice mismatch along the *c*-axis between the two phases (K-rich and Na-rich phases). Our observations and interpretations demonstrate that "ion-exchange" systems may be more complex to interpret than previously understood. Our analysis should be applicable to other ion-exchange systems where the exchanged ions are not well miscible



in the host structure.

## References

- [1] S. Baskar et al. *ECS Transactions* 2017, 80, 357.
- [2] N. Naveen et al. *Chem. Mater.* 2018, 30, 2049.
- [3] J. Y. Hwang et al. *Energy Environ. Sci.* 2018, 11, 2821.
- [4] H. Zhang et al. *Chem. Commun.* 2019, 55, 7910.
- [5] B. Senthilkumar et al. *J. Power Sources.* 2020, 480, 228794.
- [6] H. Park et al. *Energy Storage Materials.* 2020, 28, 27.
- [7] H. Kim et al. *Chem. Mater.* 2020, 32, 4312.
- [8] C. Delmas et al. *Mater. Res. Bull.* 1982, 17, 117.
- [9] A. R. Armstrong et al. *Nature* 1996, 381, 499.
- [10] F. Capitaine et al. *Solid State Ionc.* 1996, 89, 197.
- [11] G. Dittrich et al. *Zeitschrift für anorganische und allgemeine Chemie* 1969, 368, 262.

### SESSION F.EN04.22: Sulfur Batteries

On Demand Abstracts Available for Viewing Starting Saturday Morning, November 21, 2020

F-EN04

#### 5:00 AM F.EN04.22.01

**Development of Non-deteriorating Lithium-Sulfur Battery** Kazuki Machida<sup>1</sup>, Yusuke Ushioda<sup>1</sup>, Hibiki Miyauchi<sup>1</sup>, Kohei Inaba<sup>1</sup>, Keitaro Takahashi<sup>1</sup> and Shiro Seki<sup>2</sup>; <sup>1</sup>Kogakuin University, Japan; <sup>2</sup>Kogakuin University, Japan

To resolve energy issues, the demand of large-scaled capacity storage batteries are increasing. Therefore, the realization of lithium-sulfur (Li-S) battery, which is one candidate of the next-generation high-performance innovative battery systems, is strongly desired. In general, lithium metal is used as the negative electrode for Li-S batteries. On the other hand, elemental sulfur (S<sub>8</sub>) is also used as the positive electrode, and it has high theoretical reversible capacity of 1,672 mAhg<sup>-1</sup>. However, effect of Li metal negative electrode is unclear due to their chemical properties with charge and discharge process. In this study, we applied Li-doped negative electrode for suppressing the Li-dendrite formation. Therefore, we obtained Li<sub>4</sub>Ti<sub>5</sub>O<sub>12</sub> (LTO) electrode as stable negative electrode, which is strain-free intercalation material, and high reversible characteristics of battery system are expected.

To applying LTO for Li-S batteries, electrochemical doping of Li into LTO is required owing to their deficiency of carrier ion into LTO. Therefore, at first [Li] electrolyte [LTO] cells were assembled by using disassemble cell, which can be easily taken out cell materials without short circuit into inert atmosphere (e.g., glove box). After takeoff of Li-doped LTO (Li-LTO), lithium (Li-doped) -sulfur battery was fabricated by using SPAN as sulfur positive electrode ([Li-LTO]IM-LiFSI EC/DEC=3/7[SPAN] cell). (SPAN: developed non-degraded S positive electrode). Charge and discharge performance of prepared cells were evaluated. Experimental conditions of prepared cells are weight of active material: 0.602 mgcm<sup>-2</sup>, current density: 328 mAcm<sup>-2</sup>, range of voltage: -0.5~1.5 V, temperature: 303K, respectively.

Although operating voltage and capacity are relatively low, charge and discharge over 2000 cycles were observed in the charge and discharge profiles. Therefore, this cell has suitable constitution in battery materials. Within 200 cycles, high coulombic efficiencies (about 99.9%) were always observed in the cycle number dependences of coulombic efficiency. Therefore, it suggests the possibility of realizing a non-degraded battery, which has high reversible characteristics by using both Li-LTO negative electrode and SPAN positive electrode.

#### 5:10 AM F.EN04.22.02

**High-loading Sulfur Cathodes in Low-electrolyte Lithium-sulfur** Sheng-Heng Chung; National Cheng Kung University, Taiwan

ies is a mature and successful energy-storage technology. The continuous development of lithium-ion battery cathodes has pushed the cathode performance approaching their theoretical values, which shows a challenge for the future development. A high-capacity sulfur cathode in the lithium-sulfur battery enables a complete two-electron conversion reaction per sulfur atom and therefore provides an order of magnitude higher theoretical capacity (1,672 mA h g<sup>-1</sup>) than the currently used oxide cathodes. Such a significant progress in the electrochemical characteristics let sulfur cathode getting a high attention. In

addition, sulfur is inexpensive and environmentally benign. However, as a new energy-storage technology, lithium-sulfur battery cathodes suffer from unique electrochemical challenges. The insulating nature of sulfur limits the high and reversible electrochemical utilization of the active material. The irreversible migration of polysulfides within the cells impact the cycle life and electrochemical stability of lithium-sulfur cells. These challenges further restrict the lithium-sulfur battery cathode to attain a sufficient sulfur loading and content of above 4.0 mg cm<sup>-2</sup> and 65 wt.%, respectively, in a cell with a reasonable low electrolyte-to-sulfur ratio of less than 10.0 uL mg<sup>-1</sup>.

In our presentation, we present innovations on electrode design enabling lithium-sulfur batteries to operate excellently with a high amount of sulfur (*i.e.*, 14.4 mg cm<sup>-2</sup> and 70 wt.%) and a low electrolyte-to-sulfur ratio of 4.0 uL mg<sup>-1</sup>. The cathode substrate is prepared by carbonized electrospinning nanofibers having 20 wt.%, 40 wt.%, and 100wt.% polyacrylonitrile mixing with Nafion as the sacrificial polymer. With a high content of the sacrificial Nafion, the carbonized nanofibers generate a high specific surface area of up to 640 m<sup>2</sup> g<sup>-1</sup> with 150 m<sup>2</sup> g<sup>-1</sup> contributed from micropores. Although a high surface area and micropores of the electrode substrate benefit the polysulfide retention, most of the electrolyte added in the cell is initially absorbed by this highly porous cathode substrate. This explains why a high amount of electrolyte that would cause a low energy density is needed in the lithium-sulfur research. This also expounds why our high-loading cathodes with a low amount of electrolyte either dry out in a short cycle life nor cannot get sufficient charges transferred *via* the electrolyte, resulting in a poor cell performance. On the other hand, the carbonized electrospinning nanofiber with no sacrificial polymer possesses a relatively low specific surface area of 130 m<sup>2</sup> g<sup>-1</sup> and no micropores. Benefiting from a unique electrode-design criterion, the limited surface area ameliorates the fast consumption of electrolyte, while still blocking the fast polysulfide diffusion. Therefore, the cells with the 100CNF substrate output a stable discharge capacity and Coulombic efficiency of above 650 mA h g<sup>-1</sup> and 98%, respectively, for 100 cycles. Such excellent electrochemical efficiency and stability demonstrate a high capacity retention of 98% with a high areal capacity and energy density of 10 mA h cm<sup>-2</sup> and 20 mW h cm<sup>-2</sup>, respectively, in a cell with a low electrolyte-to-sulfur ratio of only 4 uL mg<sup>-1</sup>. In conclusion, the electrochemical enhancements and engineering designs of the cathode substrates with limited nanopores make them advanced cathode designs for the development of high-loading/content sulfur cathodes in high-energy-density lithium-sulfur batteries.

#### 5:20 AM F.EN04.22.03

**Performance Evaluation of Li-Ion-Sulfur Battery Using Highly Composed S<sub>8</sub> Positive Electrode and Li-Doped C<sub>6</sub> Negative Electrode** Yusuke Ushioda<sup>1</sup>, Kohei Inaba<sup>1</sup>, Kazuki Machida<sup>1</sup>, Keitaro Takahashi<sup>1</sup>, Masayoshi Watanabe<sup>2</sup> and Shiro Seki<sup>1</sup>; <sup>1</sup>Kogakuin University, Japan; <sup>2</sup>Yokohama National University, Japan

Recently, large-scaled rechargeable batteries are expected as load-leveling systems for in/output natural energy, such as solar / wind power. Thus, lithium-sulfur(Li-S) batteries are attracted attention because of sulfur-based positive electrodes have high theoretical reversible capacity (1,672 mAh/g(S<sub>8</sub>)), low-cost of active material and so on. On the other hand, Li-S batteries still have some issues for practical use. For instance, dissolution of intermediate products (Li<sub>2</sub>S<sub>n</sub>) into electrolyte and deposition of Li-dendrite during charge process are serious problems for Li-S batteries. Then, we applied sulfolane (SL) based electrolyte because of their prevent properties for dissolution of Li<sub>2</sub>S<sub>n</sub>, and prepared Li-doped graphite (Li<sub>x</sub>C<sub>6</sub>) negative electrodes by electrochemical process to prevent deposition of Li-dendrite. However, Li<sub>x</sub>C<sub>6</sub> electrodes should be handled under inert atmosphere. Therefore, we used to disassemble-type cell, which can easily pick up Li<sub>x</sub>C<sub>6</sub> electrodes. In addition, increasing for loading amount of elemental S<sub>8</sub> positive electrodes are required for actual high-energy-density systems. Therefore, we fabricated 3D-S<sub>8</sub> electrode prepared by using 3D-Al current collector, which can easily obtain electron conductive pathway. In this study, we fabricated Li-S battery using 3D-S<sub>8</sub> positive electrode and Li<sub>x</sub>C<sub>6</sub> negative electrode (lithium-ion-sulfur battery), and evaluated by constant current charge-discharge cycle test.

S<sub>8</sub> and ketjen black (KB) were mixed in mortar, and mixed compound was heated at 438K into sealed bottle for compositing S<sub>8</sub> and KB. Slurry was prepared by the mixed compounds and binders (CMC+SBR) into H<sub>2</sub>O. 3D-S<sub>8</sub> electrodes were fabricated with putting on the slurry to 3D-Al cermet current collector. Prepared 3D-S<sub>8</sub> electrodes were dried, punched out /13 mm and pressed at 0.3t. First, [Li | electrolyte | C<sub>6</sub>] cells were prepared using disassemble-type cell, and examined with constant current charge-discharge tests. Li<sub>x</sub>C<sub>6</sub> (x<1) negative electrodes were picked out by disassemble-type cell in the inert Ar-filled glove box, and washed with DMC. [Li<sub>x</sub>C<sub>6</sub> | SL-based electrolyte | 3D-S<sub>8</sub>] cells were fabricated with 2032-type coin cell, and evaluated by constant current charge-discharge cycle test.

[Li<sub>x</sub>C<sub>6</sub> | SL based electrolyte | 3D-S<sub>8</sub>] cell showed good charge-discharge behavior and high discharge capacity (*ca.* 1,000 mAhg<sup>-1</sup>) at 1st cycle. Similar capacity and low over potential were observed comparison with normal Li-S batteries, because of low resistance derived from Li<sub>x</sub>C<sub>6</sub> electrode than Li-metal electrode. In addition, reaction resistances of second plateau of discharge process and beginning charge process declined gradually as cycle passes. Those phenomena are showed frequently normal Li-S battery using Li-metal negative electrode, and regard as constitution of ionic conductive pathway on positive electrode. Furthermore, capacity fluctuations of 1<sup>st</sup> plateaus were quite lower than 2<sup>nd</sup> plateaus during discharge process at

any cycles. Also, capacity degradation of 1<sup>st</sup> plateau during discharge process for Li-S battery using SL based electrolytes was reported. From the above, we considered that low capacity fluctuation was due to the balance between capacity increasing due to constitution of conductive pathway and capacity degradation. Moreover, this cell showed high cycle performance. Quite high coulombic efficiencies (*ca.* 98.5 %) were confirmed except for 1<sup>st</sup> cycle. Also, capacity retention at 50 cycles was high (*ca.* 87.8 %). Therefore, high performance lithium-ion-sulfur battery was achieved. In addition, we will report actual energy density of lithium-ion-sulfur battery for practical application.

#### 5:30 AM F.EN04.22.04

**Transition Metal Sulfide (MS, M = Mn, Zn) Nanoparticles as Conversion Cathode Materials for Rechargeable Magnesium-Sulfur Batteries** Michael Wilhelm, Tim Ludwig, Veronika Brune and Sanjay Mathur; University of Cologne, Germany

For the application in consumer electronics, magnesium metal can be used as anode material in a rechargeable magnesium batteries (RMB) which are proposed as one of the next generation batteries beyond lithium-ion batteries given their high capacity (3833 mAh\*L<sup>-1</sup> and 2205 mAh\*g<sup>-1</sup>). More advantages beside the dendrite-free stripping/plating of Mg with high reversibility (CE close to 100 % depending on the electrolyte) are high abundance, high standard reduction potential vs. SHE (-2.37 V) and safety. While significant advantages have been achieved in RMB electrolytes, especially for Mg-S battery architectures, Mg-based cathode materials are still challenging based on their low energy density and sluggish kinetics. MnS and ZnS as cathode materials follow a conversion-type storage mechanism to form MgS. The weaker coulombic attraction between the guest Mg<sup>2+</sup> and the host sulfur lattice enhances ion mobility, which is expected to enhance Mg<sup>2+</sup> diffusion. In this work, nanoparticles of MnS and ZnS were synthesized via hydrothermal synthesis and characterized by XRD, XPS, and SEM. These materials exhibited good theoretical specific densities (MnS: 569 Wh\*g<sup>-1</sup> and ZnS: 705 Wh\*g<sup>-1</sup>) and high energy densities (MnS: 1770 Wh\*L<sup>-1</sup> and ZnS: 2270 Wh\*L<sup>-1</sup>) in a RMB setup with a metallic Mg anode. Cyclic voltammetry and galvanostatic measurements were performed in conjunction with a non-nucleophilic Mg(HMDS)<sub>2</sub>\*2 AlCl<sub>3</sub> electrolyte and a salt electrolyte containing MgCl<sub>2</sub>\*AlCl<sub>3</sub>/THF (MACC) to investigate the electrochemical performance. To the best of our knowledge we present for the first time a MnS and a ZnS cathode material in a rechargeable magnesium battery with metallic Mg anode.

#### 5:40 AM F.EN04.22.05

**Proposal of Na Conductive New Solid Electrolyte and Their Physicochemical Properties and Na-S Battery Performance** Yuji Yokomaku, Koji Hiraoka, Masaki Kato, Kohei Inaba, Hibiki Miyauchi and Shiro Seki; Kogakuin University, Japan

##### <Introduction>

In general, sodium-sulfur (Na-S) battery operates at high temperature (*ca.* 573 K) using  $\beta$ -Al<sub>2</sub>O<sub>3</sub> ceramic as the membrane of Na-conductive electrolyte separated sodium negative electrode and sulfur positive electrode. During discharge in the Na-S battery, Na<sup>+</sup> migrates to the S electrode through the ceramic electrolyte and products sodium polysulfide. This system by operating high temperature increases the ionic conductivity of beta-alumina and ensures to form the interface between electrode and electrolyte. However, there is a concern about the fire risk attributable to an active reaction between molten sodium and molten sulfur in case of a rupture of the  $\beta$ -alumina ceramic membrane. To avoid these risks, we propose low-temperature operated Na-S battery using thermally stable organic gel electrolyte with polyether-based host polymer and sulfolane (SL)-based electrolyte solution. Herein, thermal stability and ionic conductivity of proposed Na conductive gel polymer electrolyte and charge-discharge property of Na-S cells were evaluated.

##### <Experimental>

Liquid electrolytes were prepared by mixing SL and NaTFSA using shading bottle in Ar-filled glove box. The molar ratio was changed to *x*SL:1NaTFSA (*x*=2,3,4,5 and 6, respectively). These liquid electrolytes and polyether-based macromonomer (P(EO)/(PO), polymer) were mixed with changing weight ratio as followed formula; *y* liquid electrolyte: (10-*y*)polymer (*y*=7 and 8). After added DMPA as photo-initiator, solid gel polymer electrolytes were fabricated by photo-polymerization by UV irradiation. Prepared samples were expressed as (*x*SL)<sub>*y*</sub>El+(10-*y*)Po. Thermophysical properties of fabricated gel polymer electrolytes were evaluated by thermogravimetric analysis (TG) and differential scanning calorimeter analysis (DSC). In addition, ionic conductivities were measured by electrochemical impedance method. The reversibility of Na-S batteries was evaluated by charge and discharge measurements at 333 K.

##### <Results and discussion>

The prepared gel electrolytes were transparent film and showed high flexibility. Therefore, the P(EO/PO) polymer matrix

might maintain electrolyte solvent as the framework of SL-based liquid electrolyte. Gel electrolyte of each composition of SL and polymer showed three-steps decreasing thermogravimetry by TG measurement and it was assumed thermally decomposed in the order SL, polymer, and NaTFSA. Moreover, the gel electrolytes showed the possibility of applying to room temperature operated Na-S battery because thermogravimetry decreasing wasn't observed by less than 373K. Ionic conductivity of the gel electrolytes showed a tendency of increasing with SL composition owing to decreasing viscosity of liquid electrolytes. Na-S cells using the gel electrolyte exhibited sufficient charge and discharge operations at relatively low temperature (333 K) and exhibited a high capacity of approximately 350 mAh g<sup>-1</sup>.

#### 5:50 AM F.EN04.22.06

**Sulfur and Selenium Electrodes for Rechargeable Aluminum Batteries—Investigation of Electrochemical Reaction Mechanisms by NMR Spectroscopy** Rahul Jay, Ankur Jadhav and Robert J. Messinger; City College of New York, United States

Rechargeable Al metal batteries have recently garnered significant interest due to its low cost, earth abundance, inherent safety, and high volumetric and gravimetric capacities due to the trivalent nature of Al<sup>3+</sup> ions. Commercialization of rechargeable aluminum battery systems has been limited, however, due to the small number of (i) electrolytes that enable reversible electrodeposition of Al metal and (ii) positive electrode materials that are compatible with the electrolytes while providing high capacity and cycle life. Sulfur (S) and selenium (Se) are promising positive electrode materials for rechargeable battery systems as they provide very high specific capacities. Although, sulfur is a very low-cost material and can provide a very high specific capacity. Battery systems with sulfur electrodes has been hindered due to its low electrical conductivity, high volume expansion during galvanostatic cycling, and deleterious polysulfide shuttle reactions during cycling. Selenium, a chalcogen like sulfur is a heavier element and consequently exhibits lower specific capacity, it possesses significantly higher electronic conductivity compared to sulfur that would be beneficial in mitigating key challenges that faces sulfur electrodes, such as low active material utilization and high charge transfer overpotentials during galvanostatic cycling. To date, there are few reports of Al-S, and Al-Se systems. There is no clear consensus on the electrochemical reaction mechanism during the charge/discharge process, while capacity fade plagues both systems during galvanostatic cycling.

Here, aluminum-sulfur (Al-S) and aluminum-selenium (Al-Se) cells were investigated with a chloroaluminate ionic liquid electrolyte, AlCl<sub>3</sub>:[EMIm][Cl] (molar ratio of 1.5:1), whose electrochemical reaction mechanisms and ensuing reaction products were analyzed via a combination of bulk (XRD, NMR) and surface (XPS) analyzation techniques. Electrochemical experiments for Al-S batteries showed high initial capacities close to 1200 mAh g<sup>-1</sup>. For Al-S batteries a higher capacity was observed upon charge, compared to discharge, pointing towards either an unwanted side reaction or polysulfide-shuttle-like behavior. This behavior occurred predominately at low current densities and affected the reversibility of the system. For the Al-Se batteries, the two different reaction mechanisms that have been previously reported were found to be dependent on (i) the applied current density and (ii) the crystallinity of the active material, as shown by XRD. We demonstrate that, with appropriate cycling conditions, both reaction mechanisms can occur during a single charge/discharge step, thus significantly increasing the capacity and the electrochemical window of the Al-Se cell. A significant capacity fade was also observed over a course of multiple cycles showing similar behavior compared to Al-S cells.

To understand the reaction mechanisms of Al-S and Al-Se batteries at a molecular level, solid-state magic-angle-spinning and liquid-state <sup>27</sup>Al NMR and <sup>77</sup>Se NMR measurements (on Al-Se systems) were acquired on the electrodes and electrolyte at different states-of-charge, respectively. In particular, <sup>27</sup>Al NMR measurements reveal aluminum moieties in different coordination environments and establish quantitatively their relative populations. Solid-state 2D <sup>27</sup>Al{<sup>27</sup>Al} multiple-quantum MAS NMR measurements also reveal information about the local electronic environments and extents of disorder of the solid discharge products. XPS was also performed on cycled chalcogen electrodes to understand surface compositions. This work establishes the potential of conversion-type aluminum-chalcogen batteries as high-energy-density energy storage systems and highlights the importance that molecular-level analytical tools like NMR spectroscopy can have in clarifying electrochemical mechanisms in emerging electrochemical systems.

#### 6:00 AM F.EN04.22.07

**Tailoring Atomistic Interactions in Li-S Battery via a Computational Multi-Scale-Data-Driven Approach** Rasha Atwi and Nav Nidhi Rajput; Tufts University, United States

A major breakthrough in battery materials is required to meet the ever-increasing proliferation of portable electronic devices, electric vehicles and their variants, as well as the need for incorporating renewable energy resources into the main energy supply [1]. In this context, lithium-sulfur (Li-S) batteries attract attention owing to their very high energy density (2,600 Wh kg<sup>-1</sup>) and specific capacity (1,675 mAh g<sup>-1</sup>) and significantly lower weight and cost, compared to lithium-ion batteries (LIBs) [2]. Fully packaged, it is expected that future Li-S batteries can operate at close to 500 Wh kg<sup>-1</sup>, which is more than twice the

energy density of LIBs ( $200 \text{ Wh kg}^{-1}$ ) [3]. The problem of realizing the expected high energy density is defined by several issues including the dissolution of Li-Polysulfide (PS) species into the electrolyte, insulating properties of sulfur and Li-PS species, and volume change at the cathode [4]. Overcoming these challenges requires a fundamental understanding of the interplay between events scaling over wide spatial and temporal scales, and accurate prediction of electrode and electrolyte properties to obtain design metrics for new improved materials. In this talk, I will present how we are utilizing a multi-scale-data-driven approach to gain mechanistic insight into Li-S battery by combining density functional theory (DFT) with molecular dynamics (MD) simulations. I will describe our group's newly developed computational workflow and analysis codes for generating data with high-throughput DFT and MD simulations within the framework of the Materials Project infrastructure [5]. I will discuss usage of these tools to mitigate dissolution of LiPS species by altering the atomistic interactions between electrode and electrolyte components through functionalizing the cathode material. This approach guides and accelerates our rational selection of functional groups that exhibit strong affinity with both the cathode material and LiPS moieties from a bigger set of available candidates through fully automated DFT calculations. We use the selected candidates in detailed MD studies to understand the effect of various electrolyte variables (components, PS chain length, salt concentration) on structural and dynamical properties at the functionalized interface [6, 7]. The approach allows for creating a database of well-characterized materials to be used in machine learning-based methods as well as for testing computationally identified structures in experiments. This work provides crucial information to alleviate the dissolution of PS species during cycling, which is the main reason for rapid capacity decay in Li-S batteries.

1. Larcher, D. and J.-M. Tarascon, *Towards greener and more sustainable batteries for electrical energy storage*. Nature chemistry, 2015. **7**(1): p. 19.
2. Manthiram, A., X. Yu, and S. Wang, *Lithium battery chemistries enabled by solid-state electrolytes*. Nature Reviews Materials, 2017. **2**(4): p. 1-16.
3. Fang, R., et al., *More reliable lithium-sulfur batteries: status, solutions and prospects*. Advanced materials, 2017. **29**(48): p. 1606823.
4. Manthiram, A., Y. Fu, and Y.-S. Su, *Challenges and prospects of lithium-sulfur batteries*. Accounts of chemical research, 2013. **46**(5): p. 1125-1134.
5. Jain, A., et al., *Commentary: The Materials Project: A materials genome approach to accelerating materials innovation*. Apl Materials, 2013. **1**(1): p. 011002.
6. Rajput, N.N., et al., *Elucidating the solvation structure and dynamics of lithium polysulfides resulting from competitive salt and solvent interactions*. Chemistry of Materials, 2017. **29**(8): p. 3375-3379.
7. Andersen, A., et al., *Structure and dynamics of polysulfide clusters in a nonaqueous solvent mixture of 1, 3-dioxolane and 1, 2-dimethoxyethane*. Chemistry of Materials, 2019. **31**(7): p. 2308-2319.

#### SESSION F.EN04.23: Developments in Electrodes

On Demand Abstracts Available for Viewing Starting Saturday Morning, November 21, 2020

F-EN04

#### 5:00 AM F.EN04.23.01

**Insights into the Design of High Energy Density  $\text{MnO}_2$  Cathodes for Rechargeable Alkaline Batteries** [Andrea M. Bruck](#), Matthew A. Kim and Joshua Gallaway; Northeastern University, United States

Recent advances in rechargeable Zn/ $\text{MnO}_2$  alkaline batteries have shown promise for scalable energy storage systems which provide a safe, low-cost alternative to current Li-ion technologies and have a demonstrated lifetime of thousands of cycles.<sup>1</sup> This cathode technology is based on a 2-electron Mn redox process where a layered birnessite-type phase has been shown to form after the first cycle with excellent reversibility between the discharge product,  $\text{Mn}(\text{OH})_2$  when  $\text{Bi}_2\text{O}_3$  and Cu constituents were added to the electrode architecture. For this system to reach costs  $< \$100/\text{kWh}$ , the complete reduction to  $\text{Mn}^{2+}$  must be reversible with high mass loading ( $>20 \text{ mAh/cm}^2$ ).<sup>2</sup> We investigate the reversible reaction between birnessite and  $\text{Mn}(\text{OH})_2$  with and without  $\text{Bi}_2\text{O}_3$  and Cu additives using multimodal structural characterization techniques during active battery cycling to provide a fundamental understanding of the structural properties critical to reversibility. Diffraction results provide evidence of  $\text{Bi}^{3+}$  residing in the interlayer of birnessite, which prevents irreversible  $\text{Mn}_3\text{O}_4$  formation by limiting  $\text{Mn}^{3+}$  diffusion within the crystal lattice. Also, upon charge no  $\text{MnOOH}$  intermediate phases are observed. Instead, X-ray absorption and Raman spectroscopy indicate a disordered, non-crystalline birnessite-type phase consisting of mostly neutral  $\text{H}_2\text{O}$  within the interlayer. Birnessite phases will reform without the constituents present, but  $\text{Mn}_3\text{O}_4$  formation severely polarizes the potential they are formed at, leading to capacity fade. Also, we discuss the reversible  $\text{Bi}_2\text{O}_3$  and Cu conversion

and their contribution to the observed capacity. We expect the results will provide crucial insight into the development of aqueous, rechargeable battery systems utilizing  $\text{MnO}_2$ .

## References

1. Yadav, G. G.; Gallaway, J. W.; Turney, D. E.; Nyce, M.; Huang, J.; Wei, X.; Banerjee, S., *Nature Communications* **2017**, *8*, 14424.
2. Gallaway, J. W.; Hertzberg, B. J.; Zhong, Z.; Croft, M.; Turney, D. E.; Yadav, G. G.; Steingart, D. A.; Erdonmez, C. K.; Banerjee, S., *J. Power Sources* **2016**, *321*, 135-142.

### 5:10 AM F.EN04.23.02

**A Nanoconfined Iron(III) Fluoride Cathode in a NaDFOB Electrolyte—Towards High-Performance Sodium-Ion Batteries** [Zifei Sun](#), Wenbin Fu, Michael Z. Liu and Peilin Lu; Georgia Institute of Technology, United States

Iron(III) fluoride ( $\text{FeF}_3$ ) is considered a potential cathode for sodium-ion batteries (SIBs) due to its high capacity and low cost. However, particle pulverization upon cycling generally results in poor cycling performance. Here, we introduce a free-standing nanoconfined  $\text{FeF}_3$  cathode and explore the effect of different salts and solvents on the improvement of its cycling performance. 1M sodium-difluoro(oxalato)borate (NaDFOB) in ternary electrolytes solvents shows the best performance compared with others in this case. The achieved high performance can be attributed to the synergic protection provided by the nanoconfined  $\text{FeF}_3$  electrode and the NaDFOB electrolyte. Post-mortem analysis and quantum mechanics show that DFOB anions facilitated the formation of a thin cathode electrolyte interphase (CEI) on the surface of  $\text{FeF}_3$ -carbon nanofibers (CNFs) *via* oligomerization.

### 5:20 AM F.EN04.23.04

**Designing New Cathode Materials with Unbiased Sampling of the Configuration Space** [Bonan Zhu](#) and David O. Scanlon; University College London, United Kingdom

Choice of the cathode materials underpins the overall performance ceiling of battery systems. Historically, the identification of new cathode materials had led to significant advances in the battery field. To achieve truly revolutionary advances, we can employ theoretical methods that explore cathode stoichiometries beyond those seen in traditional Li-ion batteries. Database-based structure prediction methods have been developed to automate the generation of unknown materials for a given chemical composition alone. However, they can suffer from significant bias originating from the databases themselves. In the current work, we apply *ab initio* random structure searching (AIRSS), an unbiased structure prediction method, to search for cathode materials in the under-explored regions of the chemical space. Our tests performed over a few known systems, such as  $\text{LiFePO}_4$  and  $\text{LiMnPO}_4$ , show that the method can rapidly rediscover the known phases and predict many previously unknown polymorphs. We will present a few newly identified promising cathode systems. The use of crystal structure prediction helps us construct fundamental structure-property relationships in cathodes, and thus will also help the field to explore and find new cathode paradigms in the future.

### 5:30 AM F.EN04.23.05

**Let's Do It an Easier Way—Molecular Precursors for  $\text{M}_2\text{S}$  (M = Li, Na, K) as Cathode Material** [Veronika Brune](#), Christoph Bohr, Tim Ludwig and Sanjay Mathur; University of Cologne, Germany

Air stable precursors for alkali metal sulfides provide an unpredicted molecular approach to sulfur-based materials for battery applications. These molecular precursors facilitate a more flexible preparation of the desired material via electrospinning, based on the appropriate solubility of molecular precursors in different protic solvents like alcohol or water and DMSO compared to conventional spinning systems. We describe the design and synthesis of molecular precursors of general formula  $(\text{MSEt})_2\text{NMe}$  (M = Li, Na, K) which were characterized by NMR analysis. Provision of suitable spinning solution enable the incorporation in 3D fiber mats forming networks of 1D electrospun polymer/ $(\text{MSEt})_2\text{NMe}$  fiber hybrids. The starting material, an ethanolic PVP/ $(\text{MSEt})_2\text{NMe}$  (M = Li, Na) spinning solution was stable under air and thus enabled simple handling and an innovative preparational approach of the desired materials, compared to literature known systems. These molecular precursors allow integration of  $\text{M}_2\text{S}$  (M = Li, Na) at the cathode side of the battery, which obviate the need of additionally  $\text{M}_2\text{S}$  materials at the anode side. Air stable 3D fiber mats of homogeneous 1D electrospun PVP/ $(\text{LiSEt})_2\text{NMe}$  fibers were isolated at ambient conditions and characterized by electron microscopy. Calcination of the prepared fibers at  $700^\circ\text{C}$  led to homogeneous crystalline carbon based  $\text{Li}_2\text{S}$  fibers which were confirmed by XRPD, SEM and TEM analysis. These fiber mats were tested in a battery half-cell, which performed good cycle stability and efficiency comparable to literature known systems.

#### 5:40 AM F.EN04.23.06

**Stability Enhanced Li<sub>2</sub>S Cathode Materials through Tailored 1D Electrode Design** Tim Ludwig, Christoph Bohr, Arun Ichangi and Sanjay Mathur; University of Cologne, Germany

Inspired from their high theoretical capacity (1675 mAh g<sup>-1</sup>) and high energy density (2600 Wh kg<sup>-1</sup>) lithium-sulfur (Li-S) batteries are one of the most attractive next generation energy storage solutions to meet the emerging market requirements. Nevertheless, some challenges like the poor electrical conductivity, volume expansion during the charge-discharge process, as well as the shuttling effect of soluble polysulfides retard the commercial success of Li-S batteries. Considering these challenges for the sulfur cathode, Li<sub>2</sub>S is an alternative cathode material for Li-S batteries, offering several advantages like avoiding structural damages and increase the safety of the battery cell.

In this work, Li<sub>2</sub>S/C nanofiber composites were synthesized via an electrospinning process to embed the active material in a defined, conductive 1D structure and additionally minimize the diffusion of polysulfides using metal oxides as trapping agents.

The high flexibility and mechanical stability of the fiber structure is expected to buffer the volume changes during electrochemical cycling and generates a freestanding electrode design making the use of a current collector and the preparation of a battery slurry obsolete.

Furthermore, changes in the setup of the electrospinning process allowed for the design of core/shell nanofibers, in which the active material Li<sub>2</sub>S was completely surrounded by a carbon shell rather than just being randomly distributed in the carbon matrix. This coaxial fiber architecture facilitated handling of the materials under atmospheric conditions, slowed down the degradation of the active material by traces of water, and lowered the shuttle effect of polysulfides.

#### SESSION F.EN04.24: Redox and Flow Batteries

On Demand Abstracts Available for Viewing Starting Saturday Morning, November 21, 2020

F-EN04

#### 5:00 AM F.EN04.24.01

**Disproving the Electrocatalytic Role of Initial Oxygen Functional Groups in Comparison to Stable Defects on Graphite Electrodes in Vanadium Redox Flow Batteries** Hannes Radinger, Ahmad Ghamlouche, Frieder Scheiba and Helmut Ehrenberg; Karlsruhe Institute of Technology, Germany

For many electrochemical applications in the energy sector such as batteries, water splitting, or supercapacitors, active oxygen functional groups (OFGs) at the electrode surface are considered essential. This has sparked a lot of scientific as well as industrial activities for instance in the domain of vanadium redox flow batteries, which focus on the optimization of the carbon electrodes by various oxidation treatments. The introduced OFGs are considered to catalyze the vanadium redox reactions effectively. However, these studies often disregard that the harsh attack of the surface also leads to an increase of graphitic edge sites which may also contribute to the observed catalytic activity. In a previous study, we could demonstrate that the relative amount of OFGs is less important for the catalysis than the electrochemical stability of structural defects. Further, the initial surface composition and defect structure was altered significantly in the electrochemical cell, which complicates a prediction of the electrode performance based on OFG composition. Therefore, a more systematic approach is taken to analyze the influence of OFGs and defects on the electrocatalytic activity. To separate the effect of OFGs and defects we took the reverse approach by thermally stripping oxygen groups under inert atmosphere of two different kinds of graphitic electrodes; a pristine one with a low amount of defects and oxygen species, and a thermally activated one with a high amount, respectively. By varying the stripping temperature and saturating resulting dangling bonds with hydrogen, specific OFGs were removed prior to electrochemical cycling experiments without changing surface area or defect density of the electrode. Subsequently, the electronic and defect structure of the samples was analyzed by X-Ray photoelectron and Raman spectroscopy. Cyclic voltammetry and impedance spectroscopy were used to study the electrochemical activity. Our results suggest that the initial amount or kind of OFG has no beneficial effect on the catalysis of the vanadium redox reactions. The pristine graphite felt exhibited even higher half-cell activity after the thermal treatment, which can be attributed to an increase of graphitic edge sites by the removal of OFGs. For the activated felt no remarkable change in activity was observed after stripping, most likely due to its already initially quite high amount of defects. However, both stripped samples showed an increase of the charge-transfer resistance during cycling by the formation of oxygen species. In a second step, the evolution of OFGs on the electrode was investigated by XPS after polarization experiments at the negative and positive half-cell as

well as storage in the electrolyte without polarization. The results of our study disprove the universal opinion about the role of carbonaceous OFGs for the catalysis of the vanadium redox reactions. It is much rather the defect density that is responsible for the activity of the electrode.

#### 5:10 AM F.EN04.24.03

**Accelerating the Design of Novel Materials for Aqueous Organic Redox Flow Batteries** Matthew M. Bliss and Nav Nidhi Rajput; Tufts University, United States

As more and more electricity is generated from renewable sources such as wind or solar, there is a growing demand for improved energy storage devices to mitigate the intermittent nature of these sources [1]. Of particular interest are organic redox flow batteries (RFBs) due to the organic active material's facility to undergo multiple electron transfers, its ability to be diversely sourced, and its tunability via functionalization [2]. The selection of optimal materials of such devices presents a challenge due to the sheer number of possible combinations of class of organic molecules, types and locations of functional group additions, solvents, and additives [2]. In the current work, our focus is on the selection of organic redox active materials in aqueous solvent, specifically the effect of type and position of functional groups attached to a base organic molecule on properties critical to battery performance. In particular, the effect of change in solvation structure around redox active molecules as a function of functional group and operating conditions (concentration, temperature) on the electrochemical and chemical stability, solubility, and transport properties is explored [3,4]. Such fundamental understanding allows establishing design rules to develop novel redox active molecules for flow batteries. Our approach involves using coupled high throughput ab initio and molecular dynamics simulations to estimate crucial properties of the electrolyte over a wide spatial and temporal scale and explore a large chemical and parameter space. We then develop computational databases of properties on which surrogate machine learning models can be trained to gain key insights into the effect of functional groups of the redox active species and the properties of the electrolyte, which is pivotal in the design of novel electrolytes for aqueous organic RFBs.

#### References:

[1] Després, J.; Mima, S.; Kitous, A.; Criqui, P.; Hadjsaid, N.; Noirot, I. Storage as a Flexibility Option in Power Systems with High Shares of Variable Renewable Energy Sources: A POLES-Based Analysis. *Energy Econ.* **2017**, *64*, 638–650.

[2] Leung, P.; Shah, A. A.; Sanz, L.; Flox, C.; Morante, J. R.; Xu, Q.; Mohamed, M. R.; Ponce de León, C.; Walsh, F. C. Recent Developments in Organic Redox Flow Batteries: A Critical Review. *J. Power Sources* **2017**, *360*, 243–283.

[3] Rajput, N. N.; Qu, X.; Sa, N.; Burrell, A. K.; Persson, K. A. The Coupling between Stability and Ion Pair Formation in Magnesium Electrolytes from First-Principles Quantum Mechanics and Classical Molecular Dynamics. *J. Am. Chem. Soc.* **2015**, *137* (9), 3411–3420.

[4] Han, S. D.; Rajput, N. N.; Qu, X.; Pan, B.; He, M.; Ferrandon, M. S.; Liao, C.; Persson, K. A.; Burrell, A. K. Origin of Electrochemical, Structural, and Transport Properties in Nonaqueous Zinc Electrolytes. *ACS Appl. Mater. Interfaces* **2016**, *8* (5), 3021–3031.

#### 5:20 AM F.EN04.24.04

**Bioinspired Nanoporous Ion Conducting Membranes for Next Generation Batteries** Ahmet Emre, Jinchen Fan, Emine Turali-Emre, Alycia Gerber, Volkan Cecen and Nicholas Kotov; University of Michigan, United States

Bioinspired ion transport membranes have been widely investigated for energy storage applications. High theoretical specific energy density (2600Wh/kg) and high specific capacity (1675mA/g) along with natural abundance and low toxicity of sulfur have been attracting significant attention for development of an alternative battery system to replace traditional lithium ion batteries which suffer from safety and capacity/energy density limitations in various applications. However, challenges such as polysulfide dissolution and shuttling prevent mass commercialization of metal sulfur batteries. Inspired from biological ion transport mechanisms, we show a practical yet comprehensive approach for development of highperformance metal sulfur batteries. Aramid nanofiber (ANF) based composite ion transport membranes not only prevent dendrite formation but also confine polysulfides on the cathode side. ANF composite battery separators provide diverse and opposing properties including high mechanical properties, high ionic conductivity and high thermal/chemical stability. Highly selective ion sieving properties of these biomimetic separators provide safe and high-performance batteries. Fabrication of such biocompatible, affordable, flexible and high energy density battery is quite crucial in powering next-generation electronics including but not limited to portable, wearable and implantable biomedical devices.



### 5:30 AM F.EN04.24.05

**1500 Wh/L and 580 W/L Lithium Cobalt Oxide Electrodes** Xiujun Yue<sup>1</sup>, Sungbong Kim<sup>2</sup>, Ryan R. Kohlmeier<sup>3</sup>, Chadd T. Kiggins<sup>3</sup>, Alissa C. Johnson<sup>1</sup>, Arghya Patra<sup>2</sup>, Aaron J. Blake<sup>3</sup>, Jessica A. Grzyb<sup>1</sup>, Akaash Padmanabha<sup>1</sup>, Min Wang<sup>1</sup>, John Cook<sup>3</sup>, Paul Braun<sup>2,2</sup> and James H. Pikul<sup>1</sup>; <sup>1</sup>University of Pennsylvania, United States; <sup>2</sup>University of Illinois at Urbana Champaign, United States; <sup>3</sup>Xerion Advanced Battery Corporation, United States

New battery architectures have enabled large improvements in battery energy and power density by improving ion and electron transport through multiple solid and liquid materials as well as maximizing the volume fraction of energy storage materials. The standard battery architecture for lithium ion battery electrodes is made of small particles (to reduce solid transport distances) tightly packed together (to increase energy density and reduce interfacial resistances) with a small fraction of fillers that increase conductivity, adhesion between particles, and processability. Although effective, this slurry cast particle architecture has important limitations on energy and power. Thick electrodes increase energy density and reduce fabrication costs, however, the associated long transport distances of Li ions and electrons in thick slurry cast electrodes greatly hinder the power output. Delamination issues also limit the thickness of slurry cast electrode below ~100  $\mu\text{m}$ . As a result, most electrode loadings are lower than 20  $\text{mg}/\text{cm}^2$ , which correspond to 2–3  $\text{mAh}/\text{cm}^2$ . Meanwhile, electrode porosity, carbon additives, and binder account for about one-third of the inactive volume in the electrode. These limitations in slurry cast particle electrodes cause significant trade-offs between energy, power, and cost for lithium and lithium-ion batteries.

Here, we demonstrate lithium cobalt oxide (LCO) based electrode architectures delivering 1516 Wh/L (over 3X higher capacity than typical slurry electrodes) electrode energy density at a loading of 52  $\text{mg}/\text{cm}^2$  (3X higher than typical slurry electrodes) while keeping a practical current density of 1.46  $\text{mA}/\text{cm}^2$ , which correspond to 580 W/L power density. To achieve this performance, we electrochemically deposited hundreds of micrometer thick and up to 98% dense LCO directly onto current collectors from molten salts. Since no carbon and polymer binder was required, and the electrodes were almost completely dense, our monolithic LCO cathodes delivered close to theoretical electrode energy densities. Traditional approaches suggest that cathodes need to be ~1-10  $\mu\text{m}$  thick to achieve good power density, but despite our electrode being over 100  $\mu\text{m}$  thick, we extracted 63% of the electrode capacity at 1C rates (7.3  $\text{mA}/\text{cm}^2$ ) because the electrode grains were aligned so that the fastest transport directions were normal to the current collector. With a working potential of 2.5-4.7 V, our 113  $\mu\text{m}$  thick (52  $\text{mg}/\text{cm}^2$ ) monolithic LCO electrode delivered 1516 Wh/L and 580 W/L at a current density of 1.46  $\text{mA}/\text{cm}^2$ . The electrode delivered 639 Wh/L at an ultra-high 14.6  $\text{mA}/\text{cm}^2$  current density (5025 W/L), which is about 15% more energy than conventional electrodes discharged at low current. We realized 60% of the above energy density over the working potential range of 3-4.3 V. In addition to improved performance, these electrodes allowed for new manufacturing methods. We demonstrated this by fabricating lithium metal primary microbatteries with 400 Wh/kg and 900 Wh/L energy densities. These microbatteries had 4x larger energy density than previous size-comparable batteries.

### 5:40 AM F.EN04.24.06

**Effect of Iron Substitution on Cobalt Oxide and Study of Its Electrochemical Performance** Deepa Guragain; The University of Memphis, United States

The application of metal oxides has been increasing for energy storage device due to excellent electrochemical properties, multifunctional energy application, environmentally friendly property and lower price. Due to rapid growth of energy use, there is very high demand for new ways to store energy. It is challenged to develop efficient way to store energy without polluting environment, which is possible by using transition metal oxide. We have prepared  $\text{Fe}_x\text{Co}_{3-x}\text{O}_4$  ( $x=0.0, 0.2, 0.4, 0.6, 0.8, 1$ ) successfully via hydrothermal method from which we can prepared electrode to make supercapacitor device. The structural properties were investigated by X-ray diffraction (XRD) and found phase pure  $\text{Fe}_x\text{Co}_{3-x}\text{O}_4$ . The morphology of the series obtained from scanning electron microscopy (SEM) varies from thinner nano-plates to thicker nano-plates as the concentration of Fe increase from  $x=0.0$  to  $x=1.0$ . Furthermore,  $\text{Fe}_x\text{Co}_{3-x}\text{O}_4$  were characterized by X-ray Photoelectron spectroscopy (XPS), Fourier Transform Infrared Spectroscopy (FTIR) and Quantachrome Surface area analyzer. The maximum BET surface area obtained from Quantachrome Instrument for  $x=1$  is 87.5  $\text{m}^2/\text{g}$ . The XPS gives elemental composition of  $\text{Fe}_x\text{Co}_{3-x}\text{O}_4$  as in desired amount. The higher specific capacitance of 268 F/g at a current density of 1 A/g, 856 F/g at 2 mV/s scan rate, the energy density of 16 Wh/kg and power density of 170 W/kg in 3M KOH electrolyte was observed for  $x=1$  sample. An increased retention capacity ~122 % measured at 5 A/g current density and Coulombic efficiency of 100%. All these results indicate Fe dope  $\text{Co}_3\text{O}_4$  composites electrode shows promising electrocatalytic activity results in the high intrinsic electronic conductivity, can largely improve the interfacial electroactive sites, increase charge transfer rates and help to stabilize the structure of compound.

### 5:50 AM F.EN04.24.07

**Porous Inorganic Electrode for High Performance Li-O<sub>2</sub> battery** Hyunpyo Lee, Tae Young Kim, Mokwon Kim and Wonsung Choi; Samsung Advanced Institute of Technology, Korea (the Republic of)

Li-O<sub>2</sub> batteries with high capacity have been studied for several decades because of their superior energy density compared to Li-ion batteries. The cathode composed of carbon materials and an liquid electrolyte could play a critical role for reducing the cathode weight. However, due to the limitation of carbon based cathode, the Li-O<sub>2</sub> cells can't achieve both a high energy density and long cycles. It is well known that discharge product, Li<sub>2</sub>O<sub>2</sub>, formed during a discharge reaction with lithium ions and oxygen molecules decomposes the carbon based materials to produce Li<sub>2</sub>CO<sub>3</sub>.

In this study, we propose a porous inorganic electrode without an organic liquid electrolyte. The LiNi<sub>2</sub>O<sub>4</sub> inorganic electrode is stable in saturated aqueous LiOH solution for 1 week. Porous LiNi<sub>2</sub>O<sub>4</sub> electrode was prepared by slurry-coating by doctor-blade with sacrificial Poly(styrene-divinyl benzene) (PS-DVB) microspheres having 3 μm diameter. After thermal treatment, PS-DVB microspheres are clearly removed and introduce the pore architecture which facilitates fast oxygen transport and increases the discharge-charge reaction surface area to achieve high current density during cycles. It also acts as a storage of the discharge products, LiOH monohydrate. The reversible reaction in cathode is observed by SEM and FT-IR. With this strategy, we achieved 55 cycles at high current density (0.6 mA/cm<sup>2</sup>) and high capacity (3 mAh/cm<sup>2</sup>)

**6:00 AM F.EN04.24.08**

**Incorporating a Br<sub>3</sub><sup>-</sup>/Br<sub>2</sub>-based Redox Mediator in Li-O<sub>2</sub>/CO<sub>2</sub> Batteries: Performance and Mechanism**

**Assessment** Filipe Marques Mota<sup>1</sup>, Hye Ryung Byon<sup>2</sup> and Dong Ha Kim<sup>1</sup>; <sup>1</sup>Ewha Womans University, Korea (the Republic of); <sup>2</sup>Korea Advanced Institute of Science and Technology, Korea (the Republic of)

A key step to assure the practical application of Li-air batteries involves replacing O<sub>2</sub> with air. The presence of CO<sub>2</sub> in the air (>400 ppm), however, critically alters the underlying O<sub>2</sub> chemistry of the Li-air battery.[1] CO<sub>2</sub> added to Li-O<sub>2</sub> cells in a tetraglyme-electrolyte was shown to swiftly shift the discharge reaction mechanism toward the formation of soluble CO<sub>4</sub><sup>2-</sup> and C<sub>2</sub>O<sub>6</sub><sup>2-</sup> products and solid-state Li<sub>2</sub>CO<sub>3</sub>. Surprisingly, CO<sub>2</sub> was shown to favorably act as an O<sub>2</sub><sup>-</sup> scavenger during discharge, with the resulting soluble products being also correlated with enhanced full capacity and cell cyclability.

Compared with the conventional Li-O<sub>2</sub> however, the introduced CO<sub>2</sub> resulted in higher recharge potentials (~4.5 V) required for the decomposition of Li<sub>2</sub>CO<sub>3</sub>, rendering impracticable the commercialization of these technologies.[2] In this study, we assessed the promise of incorporating a Br<sub>3</sub><sup>-</sup>/Br<sub>2</sub>-based redox mediator to suppress the overcharge potential.[3] Hindered overcharges (~0.5 V) driven by electrochemically-generated Br<sub>2</sub> were found to be a function of the LiBr concentration and the insulating Li<sub>2</sub>CO<sub>3</sub> structure. Coupled electrochemical and spectroscopic analyses additionally discerned involved redox shuttling steps at progressive states-of-charge and, for the first time, the prominent presence of Br<sub>2</sub>-Br<sub>3</sub><sup>-</sup> loosely-bound anionic complexes in the electrolyte during the recharge step. As opposed to discrete polar Br<sub>2</sub> irreversibly precipitated on the CNT surface, these soluble Br<sub>2</sub>-Br<sub>3</sub><sup>-</sup> species were proposed to operate as redox mediators with advantageous facile diffusion. These findings foment the evaluation of the appropriateness of redox mediators beyond an overcharge decrease, and shed light for the development of Li-air devices.

#### References

- [1] K. Takechi, T. Shiga, T. Asaoka, *Chem. Commun.* **2011**, 47(12), 3463.
- [2] Y. Qiao, J. Yi, S. Guo, Y. Sun, S. Wu, X. Liu, S. Yang, P. Hec, H. Zhou, *Energy Environ. Sci.* **2018**, 11(5), 1211.
- [3] F. Marques Mota, J.-H. Kang, Y. Jung, J. W. Park, M. Na, D. H. Kim, H. R. Byon, *Adv. Energy Mater.* **2020**, 10(9), 1903486.

SESSION F.EN04.25: 2D Materials for Battery Applications

On Demand Abstracts Available for Viewing Starting Saturday Morning, November 21, 2020

F-EN04

**5:00 AM F.EN04.25.01**

**A Fast Charge/Discharge And Wide-Temperature Battery With Ultra-Thin Germanium Oxide Layer On 2D TiCA<sub>3</sub> MXene Matrix As Anode** Junjie Niu; University of Wisconsin-Milwaukee, United States

In contrast to silicon, germanium shows an electrical conductivity of ~1.0 S m<sup>-1</sup> that is 100 times higher than silicon, and a fast lithium ion diffusivity of 10<sup>-12</sup>-10<sup>-8</sup> cm<sup>2</sup> s<sup>-1</sup> that is 400 times faster than silicon, leading to a promising potential in rapid charge/discharge batteries. Similar as silicon, the large volume expansion upon lithiation/delithiation leads to capacity decay

and thus poor cycling performance. The scalable production of complex nano-structures also pose a challenge. Recently MXene, a family of 2D transition-metal carbides, are attracting great interest in lithium-ion batteries due to their unique electrical, mechanical and electrochemical properties particularly with the high electrical conductivity. Here we present a novel 2D hybrid composite that is composed of 2D layered MXene as host covered with a thin layer of amorphous GeO<sub>x</sub>, which showed an improved rate capability as anode electrode in lithium ion batteries (*ACS Nano* 2020, 14, 3678–3686). The battery with hybrid composite as anode maintains 90% of the initial capacity with a coulombic efficiency of 99.4 % after charging/discharging 500 cycles at 0.5 C. A high capacity retention under 10.0 C and 20.0 C and a wide temperature between -40 and 80 C was achieved. A full-cell battery paired with NMC as cathode also exhibited a high capacity.

#### 5:10 AM F.EN04.25.02

**Microstructural Evolution and Electrochemical Properties of Arachis Hypogaea Shell Derived *Ex Situ* Nitrogen-Doped Activated Carbon for Energy Storage Applications as Supercapacitor** Balla D. Ngom<sup>1</sup>, Ndeye Fatou D. Sylla<sup>1</sup>, Ndeye Maty Ndiaye<sup>1</sup>, Mohamed Chaker<sup>2</sup> and Ncholu Manyala<sup>3</sup>; <sup>1</sup>Universté Cheikh Anta Diop de Dakar, Senegal; <sup>2</sup>INRS, Canada; <sup>3</sup>University of Pretoria, South Africa

We report on the correlation of the microstructural evolution and electrochemical properties of an ex-situ N-doping KOH activated carbon derived from Arachis Hypogaea Shell (NAC-AHS) and compared to the non-doped (AC-AHS). Interconnected cavities with irregular-shaped structure are reported by SEM analysis for AC-AHS. After nitrogen doping, the morphology of the NAC-AHS materials exhibited a less porous structure as compared to AC-AHS. The surface specific area (SSA) of NAC-AHS was found to be 1442 m<sup>2</sup> g<sup>-1</sup> lower than the value of AC-AHS (1557 m<sup>2</sup> g<sup>-1</sup>), the pore volumes were also found to follow the same trend since the reported values are as follow 0.76 cm<sup>3</sup> g<sup>-1</sup> and 0.69 cm<sup>3</sup> g<sup>-1</sup>, respectively for AC-AHS and NAC-AHS. The AC-AHS and NAC-AHS exhibited in a half cell a specific capacitance (C<sub>s</sub>) values of 167 F g<sup>-1</sup> and 216 F g<sup>-1</sup>, respectively at 1 A g<sup>-1</sup>, corresponding to an improvement of 30% after ex-situ N-doping, which agrees with the higher current response recorded in the CV profiles of the samples. A symmetric device fabricated from the NAC-AHS materials displayed a C<sub>s</sub> of 251.2 F g<sup>-1</sup> at 1 A g<sup>-1</sup> in a wide operating voltage of 2.0 V in 2.5 M KNO<sub>3</sub> aqueous electrolyte. In terms of stability, it achieved 83.2% as capacity retention up to 20,000 cycles, which was, improved through the floating/aging measurement at 5 A g<sup>-1</sup> over a long period of time (~7+ days). A specific energy of 35 Wh kg<sup>-1</sup> with a corresponding specific power of 1 kW kg<sup>-1</sup> at 1 A g<sup>-1</sup> was delivered with the device still retaining up to 22 Wh kg<sup>-1</sup> and a 20 kW kg<sup>-1</sup> specific power even at 20 A g<sup>-1</sup>.

#### 5:20 AM F.EN04.25.04

**MXene Nanosheets as Active Materials for Nonaqueous Monovalent-Ion Battery Electrodes** Davi Marcelo Soares<sup>1</sup>, Christopher Shuck<sup>2</sup>, Narendra Kurra<sup>2</sup>, Yury Gogotsi<sup>2</sup> and Gurpreet Singh<sup>1</sup>; <sup>1</sup>Kansas State University, United States; <sup>2</sup>Drexel University, United States

Two-dimensional (2D) materials are deemed as more efficient players regarding ionic intercalation compared to their bulk counterparts. This property makes 2D materials attractive for applications such as energy storage. Within this ever-ascending group, 2D transition metal carbides, carbonitrides and nitrides (MXenes) are studied since 2011 due to their versatile chemistry and consequent surface terminations, which provide hydrophilic surfaces, unlike graphene, for instance. Here we study three MXene species, namely Mo<sub>2</sub>TiC<sub>2</sub>, Mo<sub>2</sub>Ti<sub>2</sub>C<sub>3</sub>, and Ti<sub>3</sub>C<sub>2</sub> as anode materials for lithium (LIB), sodium (SIB), and potassium-ion batteries (KIB). In terms of electrochemical results, our findings indicate reasonable cycling stability under galvanostatic charge-discharge for all alkali metal ion batteries studied. Interestingly, Ti<sub>3</sub>C<sub>2</sub> potassium-ion presented the highest first cycle capacity drop; however, it also yielded the highest specific first cycle charge capacity of 305.6 mAh g<sup>-1</sup>. Detailed electrochemical impedance spectroscopy (EIS) studies are also presented for better understanding of the charge storage mechanisms taking place in the MXenes studied.

#### 5:30 AM F.EN04.25.05

**WTe<sub>2</sub>, a Semimetal Transition Metal Dichalcogenide Electrode for Potassium-Ion Batteries** Davi Marcelo Soares and Gurpreet Singh; Kansas State University, United States

Potassium-ion batteries have currently been in the spotlight as an alternative to lithium- and sodium-ion batteries due to abundant availability, low reduction potential, and high theoretical energy density. Although some chemistry correlation with other monovalent-ion batteries may exist, research on potassium-ion battery chemistry is still in its infancy. Hence, a relevant research aspect of potassium-ion rechargeable batteries is the development of electrode materials that may efficiently intercalate the larger size K<sup>+</sup> ions in its layered structure; thus, providing reasonable capacity and reversibility. With a peculiar electronic structure, here we report the semimetal tungsten ditelluride (WTe<sub>2</sub>) as anode material for potassium-ion batteries. This layered material presents reasonable cycling stability and specific capacity within 0 to 3 V potential range.

Results show that  $\text{WTe}_2$  may store up to  $3.3 \text{ K}^+$  per formula unit, at least 4 times of  $\text{WS}_2$  KIB electrode. In sum, this work unravels the potential of  $\text{WTe}_2$  as anode for potassium-ion batteries with respect to its physical and electrochemical properties.

#### 5:40 AM F.EN04.25.07

**On-Chip Interdigital 3D Carbon Microelectrode for High-Energy Lithium-Ion Capacitor** Ebenezer Adelowo, [Amin Rabiei Baboukani](#) and Chunlei Wang; Florida International University, United States

The need for high-performance microscale energy storage units for rapidly growing microelectronic devices have continued to attract much attention. Miniaturized batteries and electrochemical capacitors (ECs) are attractive candidates for on-chip energy storage applications. Typically, ECs can give advantageous characteristics such as higher power density, faster charge/discharge properties, and ultralong cyclability than batteries. However, the limited energy density of ECs represents a significant drawback. One strategy to overcome this issue is based on the combination of the bulk and surface storage mechanisms by a battery-type and a capacitor-type electrode. Lithium-ion capacitor (LIC) is one such systems, consisting of a high energy battery-type electrode and high power capacitor-type electrode. On-chip LICs could potentially be favorable for integration along with other components in microelectronic devices to provide a good combination of high energy and power densities within a limited footprint area. Carbon microelectromechanical systems (C-MEMS) technique is one of the most interesting 3D microelectrode fabrication approaches which generally involves photolithographic patterning and pyrolyzing photoresists in an inert atmosphere to obtain glassy carbon structures. C-MEMS process is a facile route of obtaining a wide variety of ordered 3D carbon microelectrode structures with high resolution. Given the prospects of providing enhanced areal capacity, this study demonstrates a novel first-generation 3D on-chip LIC based on C-MEMS-derived interdigital carbon microelectrodes. In this work, the total developed electrode geometric surface area of each side of the interdigital microelectrode was  $\sim 0.07 \text{ cm}^2$ . An aqueous on-chip LIC was fabricated using carbon microelectromechanical systems (C-MEMS) technique. Oxygen plasma-treated 3D carbon microelectrode arrays served as the capacitor-type electrode in the LIC, while  $\text{LiFePO}_4$  integrated on the 3D carbon microelectrode arrays was used as the battery-type cathode. Among the devices, the 5 min plasma-treated sample gives the highest discharge capacity. The discharge capacities calculated from the GCD curves for 0, 1, 5, and 10 min plasma treatment durations were about 0.001, 0.041, 0.297 and  $0.138 \mu\text{Ah cm}^{-2}$ , respectively, based on device footprint area. The rate performance results also shows that the 5 min plasma-treated device gave the highest discharge capacities at different current densities. The discharge capacities after the tenth cycle for the 5 min plasma-treated sample at current densities of 0.24, 0.48, and  $0.60 \text{ mA cm}^{-2}$  were about 0.63, 0.18, and  $0.13 \mu\text{Ah cm}^{-2}$ , respectively, based on device footprint area. The decreased discharge capacities of the device upon further increasing the oxygen plasma treatment duration from 5 to 10 min may be attributed to the reduced effective surface area of the interdigital microelectrodes. Electrochemical performance evaluation shows that the aqueous on-chip LIC can deliver an areal density up to  $\sim 5.03 \mu\text{Wh cm}^{-2}$ , which is  $\sim 5$  times higher than the oxygen plasma-treated symmetric carbon microelectrode-based electrochemical capacitor. Our work is an initial full cell study on the application of the C-MEMS technique for the development of on-chip LIC in aqueous electrolytes. The C-MEMS approach demonstrated in this study exhibits promising potential for the facile development of on-chip LICs with 3D microelectrodes. The on-chip LIC could potentially be favorable as a high-performance compact and integrable energy storage system for practical application in microelectronic devices. The developed electrode preparation and its material and electrochemical characterizations will be discussed in detail at the conference.

SESSION F.EN04.26: New Materials Developments and Characterizations  
On Demand Abstracts Available for Viewing Starting Saturday Morning, November 21, 2020  
F-EN04

#### 5:00 AM F.EN04.26.02

**Thick High Energy Density Electrode Fabrication and Active Material Synthesis Using Spark Plasma Sintering** [Arina Nadeina](#)<sup>1,2</sup>, Patrick Rozier<sup>3,2</sup> and Vincent Seznec<sup>1,2</sup>; <sup>1</sup>University of Picardie Jules Verne, France; <sup>2</sup>Réseau sur le Stockage Electrochimique de l'Énergie (RS2E), CNRS FR3459, France; <sup>3</sup>Université de Toulouse, France

Spark Plasma Sintering (SPS) has proven to be an effective, rapid, and energy-efficient tool in the sintering of a variety of materials, such as ultrahigh temperature ceramics, composites, thermoelectric and magnetic compounds. Its main difference from the traditional sintering techniques (hot pressing, pressureless sintering, microwave sintering, etc) consists in the use of

the direct pulsed current along with a uniaxial pressure to obtain well-compacted materials. Due to the fast heating/cooling rates and internally generated heat (resistive heating), the obtained compounds experience little to no particle growth while shortened sintering times ensure the absence of the unwanted side-reactions. Recently, SPS has been demonstrated to be used not only for the sintering of materials but also for their synthesis making it an attractive technique in the fabrication of thick high energy density electrodes for Li- or Na-ion battery application as well as in the synthesis of battery's active material compounds or the fabrication of all-solid-state batteries [1-5].

High energy density electrodes could be obtained by altering the electrodes' architectures. In pursuit of increasing the energy density, some methods suggest fabrication of (ultra)thick electrodes while others concentrate on the production of electrodes with a minimum amount of inactive materials (binder-free, conductive additive-free, integrated current collectors, etc).

Owing to a rapid and highly efficient sintering process, SPS offers a luxury of obtaining simultaneously binder-free and (ultra)thick electrodes which suffer no structural degradation. In 2018 Elango et. al reported a successful Spark Plasma Sintering of the  $\text{LiFePO}_4$  and  $\text{Li}_4\text{Ti}_5\text{O}_{12}$  electrodes with controlled porosity by hard templating method (NaCl leaching) [1]. Obtained by SPS and templating approach ultrathick electrodes (1 mm thick) showed remarkable electrochemical performance at C/20 against lithium metal delivering areal capacities 4 times higher than those of the conventional tape-casted electrodes. This study coming from our group demonstrated the proof-of-concept in the fabrication of Li-ion battery electrodes with an ultrathick design by means of SPS.

Such a fabrication technique is expected to be easily transferrable to other battery types like Na-ion batteries. However, commonly used Na-ion battery materials are not as widely produced as their Li counterparts and still require long and tedious synthesis procedures. In our work, we have recently demonstrated that SPS could be used to synthesize a common Na-ion battery cathode material –  $\text{Na}_3\text{V}_2(\text{PO}_4)_2\text{F}_3$  – in under only 40 min [2] which resembles a phase-pure compound with small particle size showing slightly enhanced electrochemical performance when compared to the solid-state synthesized NVPF. SPS-synthesized NVPF requires no further treatment and could be used directly as an active material component in the production of our thick binder-free electrodes.

In this presentation, apart from the Spark Plasma Sintering-assisted synthesis of active materials for Na-ion battery application, a new generation of thick binder-free electrodes will be presented. Correlation between the electrode architecture (porosity, pore size/shape distribution, tortuosity, etc), synthesis/sintering parameters, nature of precursors, and the electrochemical performance will be discussed.

[1] R. Elango *et al.*, *Advanced Energy Materials*, Vol 8 Issue 15 (2018)

[2] A. Nadeina *et al.*, *Energy Technol.*, 8: 1901304 (2020)

[3] F. Lalère, *et al*, *Journal of Power Sources*, 247, 975-980 (2014)

[4] G. Delaizir, *et al.*, *Adv. Funct. Mater.*, 22: 2140-2147 (2012)

[5] A. Aboulaich, *et al.*, *Adv. Energy Mater.*, 1: 179-183 (2011)

#### 5:10 AM F.EN04.26.04

**Mechanical Properties of Electrochemically Lithiated Tin** Chung Su Hong and Seung Min J. Han; Korea Advanced Institute of Science and Technology, Korea (the Republic of)

Sn possesses three times higher capacity in comparison to graphite anode ( $372 \text{ mAhg}^{-1}$ ) which makes it a promising candidate for enhanced performance Li ion batteries. Contrary to Si, Sn is compliant and ductile in nature and thus is expected to readily relax the Li diffusion-induced stresses. The low melting point of Sn additionally allows for stress relaxations from time-dependent or creep deformations even at room temperature. In this study, intrinsic mechanical properties of lithiated Sn at various stages in the lithiation were evaluated using nanoindentation experiments using a special setup. In order to avoid oxidation of the highly reactive lithiated Sn, nanoindentation was performed on specimens submerged in a mineral oil bath. After careful calibration, hardness and modulus of different phases of lithiated Sn were evaluated. With increasing in the lithium content, both the hardness and modulus of the lithiated tin decreased, as expected, where the hardness and modulus are 28.6 GPa and 0.37 GPa, respectively, for fully lithiated Sn ( $\text{Li}_{22}\text{Sn}_5$ ) and 58.0 GPa and 0.76 GPa, respectively, for unlithiated Sn. This is the first report on the mechanical properties of lithiated Sn, which is expected to be of importance in theoretical analysis of the diffusion induced stresses in Sn anodes.

#### 5:20 AM F.EN04.26.07

**Activation of Electrochemical Water-Splitting by Tuning the Polarity of Cu-Deposited Poly(vinylidene fluoride-co-hexafluoropropylene) Fibrous Catalyst** Shunsaku Uchiyama, Asuka Morinaga, Hiromori Tsutsumi and Yu Katayama; Yamaguchi University, Japan

Water electrolysis is an ideal method for producing hydrogen, which is expected as a next-generation energy carrier. However, the sluggish reaction kinetics of the oxygen evolution reaction (OER) limits the overall energy efficiency.<sup>1,2</sup>

We here present a highly-efficient water electrolyzer, consist of the metal-deposited fibrous electrode supported on a nonwoven polarized sheet, synthesized via simple and scalable electrospinning and electroless deposition methods. We selected PVdF-HFP with tunable polarity as catalyst support, to promote the diffusion of the ions in the electrolyte and optimize the reaction energetics. Cu was used as an electrocatalyst, owing to its low cost and excellent electrical conductivity. Various spectro(electro)chemical methods were performed, including infrared spectroscopy, X-ray photoelectron spectroscopy, and linear sweep voltammetry, to clarify the effect of the geometric structure of Cu and polarity of the catalyst support on the OER activity. It was found that the fibrous structure of Cu catalyst increases the active surface area as well as optimizes the mass transport and diffusion, which contributes to the improved OER activity. Furthermore, the high dipolar moment and large dielectric constant for a polarized PVdF-HFP can assist OER by its unique catalyst-support and reactant-support interaction, which can optimize the OH adsorption energetics and diffusion of the reactant (e.g., OH<sup>-</sup>), respectively. We successfully build a prototype water electrolyzer with a nonwoven fabric-fibrous electrode assembly, which achieved the stable water electrolysis for more than 24 h at 2.5 V.

This work opens up a new avenue to fabricate a flexible and durable water electrolyzer in a scalable way, which expands the applicability of the water electrolyzer and provides a new strategy to simplify the fabrication procedure of electrocatalysts for various energy conversion/storage reactions.

#### REFERENCES

- 1 Seh, W. Z. *et al.*, *Science*. **2017**, 355, eaad4998.
- 2 Fabbri, E. *et al.*, *Catal. Sci. Technol.* **2014**, 4, 3800–3821.

#### 5:30 AM F.EN04.26.08

**Universal Utilization of Charge-Transfer Complexes for High Power- and Energy-Density Organic Rechargeable Batteries** Sechan Lee<sup>1</sup>, Jihyun Hong<sup>2</sup> and Kisuk Kang<sup>1</sup>; <sup>1</sup>Seoul National University, Korea (the Republic of); <sup>2</sup>Korea Institute of Science and Technology, Korea (the Republic of)

Organic electrode materials hold great potential due to their low cost, minimal environmental footprint, and chemical diversity. However, their electrochemical performances could not reach the level of currently used electrode materials due to the relatively low redox potential, low electrical conductivity, and high solubility in organic solvents. Those drawbacks have not been simultaneously overcome with the single moiety-based tuning such as molecular tailoring and hybridization with conductive scaffolds. Herein, we report the novel design paradigm of organic charge-transfer complexes (OCTCs), an association of two or more types of organic molecules in which a fraction of electronic charge is transferred between the molecular entities, as a new category of organic electrode material candidates.[1, 2] The OCTCs exhibit superior electrochemical performances in terms of rate capability, energy density, and cyclability, compared to the single-moiety-based organic electrode materials discovered so far. The improved performances are attributed to the high electronic conductivity and structural stability. Well-ordered stacking of the molecular layers in OCTCs creates a charge-transport path through which electrons can move freely, and the strong intermolecular interaction such as hydrogen bonding and  $\pi$ - $\pi$  interaction secure structural stability.

We first introduce the OCTC through a combination of phenazine (PNZ) and 7,7,8,8-tetracyanoquinodimethane (TCNQ) via a room-temperature synthesis.[1] OCTC exhibited the enhancement in the electrical conductivity for 5 order magnitudes and reduction in the dissolution for 2-5 times, resulting in the high power and cycle performances that far outperform those of each single-moiety counterpart in Li-ion battery. In order to optimize the electrochemical performances in terms of energy- and power-density, two further steps were progressed in the molecular- and battery-level. First, dibenzo-1,4-dioxin (DD) is adopted due to the high redox potential of 4.1 V vs. Li/Li<sup>+</sup>, and DD-TCNQ OCTC showed the increased practical energy density of 560 Wh kg<sup>-1</sup>. [1] On the other hand, an aqueous electrolyte is applied to further enhance the rate performance of OCTC. Zinc aqueous batteries could achieve the ultrahigh level of active contents (80%) and loading density (10 mg cm<sup>-2</sup>) with fully utilizing the specific capacity (~250 mAh g<sup>-1</sup>) from both PNZ and TCNQ.[2] Surprisingly, it is observed that the redox mechanisms are different according to the electrolyte types, and we revealed that the formation of the TCNQ-electrolyte complex affects the redox reaction path. These findings demonstrate the general applicability of the OCTCs and open up an uncharted pathway toward the development of high-performance organic electrode materials via the exploration of various combinations of donor-acceptor monomers with different stoichiometry.

[1] S. Lee *et al.*, *Energy Storage Mater.* **20**, 462 (2019) [2] S. Lee *et al.*, In preparation to submit.

#### 5:40 AM F.EN04.26.09

**Understanding Length-Scale Dependence of Morphological Instability in Electrodeposition Processes** Snehashis Choudhury and Lynden Archer; Cornell University, United States

Advances in the basic science and engineering principles of electrochemical energy storage is imperative for significant

progress in portable electronic devices. In this regard, metal batteries based on a reactive metal (like Li, Na) as anode have attracted remarkable attention due to their promise of improving the gravimetric energy density by at least 3-folds, compared to the current Li-ion battery that uses graphitic anode. However, a persistent challenge with metal batteries is their propensity to fail by short-circuiting due to dendrite growth, and by runaway of cell resistance because of internal side reactions. In this talk, I will discuss my research that utilizes multiscale transport modeling and experiments to fundamentally understand and thereby develop rational designs for polymer electrolytes and electrochemical interfaces to overcome these challenges. Specifically, we utilized linear stability analysis of metal electrodeposition and showed that the length-scale on which transport occurs near the electrodes can be as important as electrolyte modulus in stabilizing metal deposition. To evaluate this concept, we designed cross-linked polymer electrolytes with tunable nanostructure and quantified corresponding dendritic growth. Direct visualization of electrodeposition using optical microscopy showed remarkable agreement with the theoretical predictions.

#### References:

- Choudhury, S., Mangal, R., Agrawal, A. & Archer, L. A. A highly reversible room-temperature lithium metal battery based on crosslinked hairy nanoparticles. *Nat. Commun.* **6**, 10101 (2015).
- Tikekar, M. D., Choudhury, S., Tu, Z. & Archer, L. A. Design principles for electrolytes and interfaces for stable lithium-metal batteries. *Nat. Energy* **1**, 16114 (2016).
- Tikekar, M. D., Archer, L. A. & Koch, D. L. Stabilizing electrodeposition in elastic solid electrolytes containing immobilized anions. *Sci. Adv.* **2**, (2016).
- Choudhury, S. *et al.* Confining electrodeposition of metals in structured electrolytes. *Proc. Natl. Acad. Sci.* **201803385**, (2018).

#### 5:50 AM F.EN04.26.10

**Modeling the Amorphous Na<sub>2</sub>Ge-GeSe<sub>2</sub> Chalcogenide System** Max S. Win<sup>1</sup>, Charles A. Sievers<sup>1</sup>, Riccardo Dettori<sup>1</sup>, Nir Goldman<sup>2</sup> and Davide Donadio<sup>1</sup>; <sup>1</sup>University of California, Davis, United States; <sup>2</sup>Lawrence Livermore National Laboratory, United States

Li-ion batteries with polymer-electrolytes still have several disadvantages related to costs, safety, and materials' availability. It would be desirable to develop alternative storage devices comprising solid-state electrolytes and sodium ions, which may replace current Li-ion batteries for certain applications. The Na<sub>2</sub>Ge-GeSe<sub>2</sub> chalcogenide glass-ceramic was proposed as a promising material to be used as a solid electrolyte for Na-ion batteries. The complex chemistry and structural heterogeneity of this material are hardly described by empirical potentials, calling for first-principles modeling. However, first-principles simulations involve high computational costs and cannot scale to the size and time scales necessary to characterize the functional behavior of this material, thus requiring a multiscale approach.

Initially, we show that parameter-free ab initio molecular dynamics (AIMD) simulations reproduce the experimental properties of Ge-Se melts at different stoichiometry, and predict the structural variations induced by the inclusion of Na. In this study, we overcome the size and time scale limitations of AIMD by constructing suitable machine-learning potentials - based on the Chebyshev Polynomials paradigm (ChIMES) - with which we can simulate quenching from the melt and Na diffusion. This study will allow us to finally characterize amorphous Na-intercalated GeSe<sub>2</sub> and predict its ionic conductivity at various conditions.

#### 6:00 AM \*F.EN04.26.11

**Recent Insights into Material Properties and Chemical Dynamics of the Lithium SEI** Betar Gallant; Massachusetts Institute of Technology, United States

Achieving a truly stable and reversible Li metal anode would enable a step-change in today's battery energy densities if key hurdles of reactivity, insufficiently high Coulombic Efficiency, parasitic electrolyte consumption and loss of active Li can be addressed. These challenges arise invariably from reactivity at the solid electrolyte interphase (SEI) on Li. After decades of study, the native SEI, which is highly chemically nonuniform, fragile, and nanoscopically thin (< 100 nm), remains notoriously difficult to experimentally probe. To identify strategies that may rationally address these challenges by interface or electrolyte design, improved understanding of the chemistry, structure, and function of the SEI are still needed.

In this talk, I present our recent studies on dynamic processes occurring in SEI-forming reactions and also within a nominally-established SEI. First, I describe our studies on single SEI components, which we have conducted to isolate and simplify the multi-phase SEI for experimental study. We have developed synthetic approaches based on Li reactions with oxide- and fluoride-donating reactants that permit formation of a compositionally uniform SEI consisting entirely of lithium fluoride (LiF) or lithium oxide (Li<sub>2</sub>O). The stability of LiF within the Li SEI is first examined. We find that, counter to some

assertions in literature, LiF does not fully protect Li from electrolyte reactions under even mild cycling conditions; its breakdown invites infiltration and repair from the electrolyte, causing the SEI to evolve over time to reflect the electrolyte chemistry more than the initial interphase. We compare these results to those obtained with fluorinated electrolyte, high-concentration LiFSI in FEC, and discuss our conclusions regarding the origin of improved cycling and high Coulombic Efficiency in fluorinated electrolyte systems. Next, I will discuss recent findings on transport properties of Li<sub>2</sub>O and LiF at the interface of Li. Using impedance measurements coupled to a transport model of the interface, we have extracted conductivity, diffusion coefficients, and carrier concentrations of these phases at the chemical potential of Li for the first time. Our results indicate significant differences between Li<sub>2</sub>O and LiF that help to identify less-resistive phases that may support more facile ion transport. Finally, I will present our emerging understanding of the chemical stability of these individual phases, Li<sub>2</sub>O and LiF, in contact with carbonate electrolytes. Using X-ray absorption near-edge spectroscopy, we have probed the reactivity of ionic SEI phases upon exposure to electrolyte, and find evidence of varying interfacial stability as a function of SEI and electrolyte composition due to reactions at the SEI-electrolyte interface. These results help illuminate the origins of commonly-observed changes in SEI impedance over hours or days in certain electrolytes, which have lacked chemical specificity to date, and identify motifs for improved stability. The integration of this knowledge to guide design of improved SEI chemistries will be discussed.

#### 6:15 AM F.EN04.26.12

**Flexible, Biocompatible Batteries for Bioelectronics** Patricia Jastrzebska-Perfect<sup>1,2</sup>, Georgios Spyropoulos<sup>1</sup>, Onni Rauhala<sup>1</sup>, Jennifer Gelinis<sup>1</sup>, Dion Khodagholy<sup>1</sup> and Richard Yao<sup>1</sup>; <sup>1</sup>Columbia University, United States; <sup>2</sup>Massachusetts Institute of Technology, United States

The wide range of operations performed by implantable bioelectronic devices mandates reliable, stable and biocompatible sources of power. Commercially available batteries, even those used in implantable devices, are predominantly based on toxic and volatile compounds that require bulky, rigid encapsulations to protect the body from exposure. Here, we introduce a battery that functions on the basis of the work-function difference between conducting polymers and inner metals, materials that are currently utilized clinically within implantable devices. To provide mechanical flexibility and high charge capacity, we developed physical processes that create dense particulate films from bulk material. Particles can slide freely within these films, ensuring flexibility that persists even when volume of material is substantially increased. We investigated how metal particle size affected anode conductivity, Young modulus, and battery discharge time. We further investigated how electrolyte membrane thickness affected metal dissolution, device capacitance, and battery cycling ability in digestive fluids. We evaluated the battery's performance and its potential application to medical devices by developing an ingestible "electronic pill" that allows wireless pH sensing and drug delivery within the gastrointestinal tract. Overall, the mechanical flexibility and biocompatibility of material used in such batteries should allow them to become a critical component of implantable bioelectronic devices.

#### 6:25 AM F.EN04.26.15

**Binder Preparation Method Influence on Silicon Anode Architecture as Probed by X-Ray Nanotomography** Mary K. Burdette-Trofimov<sup>1</sup>, Beth Armstrong<sup>1</sup>, Johanna Weker<sup>2</sup>, Alexander M. Rogers<sup>1</sup>, Guang Yang<sup>1</sup>, Ryan R. Armstrong<sup>1</sup>, Ethan C. Self<sup>1</sup> and Gabriel Veith<sup>1</sup>; <sup>1</sup>Oak Ridge National Laboratory, United States; <sup>2</sup>SLAC National Accelerator Laboratory, United States

In this work, x-ray tomography data of silicon anodes is used to reveal the distribution of poly(acrylic acid)-based binder and silicon. This data reveals that processing conditions directly mediate the electrode (in)homogeneity. X-ray nanotomography shows poor binder and silicon intermixing resulting in segregation of silicon and binder where the binder is in the middle of the electrode. Electrode homogeneity could be improved by adding a dispersant to the slurry, which, in turn produced better cycling performance. This data may shed light on some of the reasons behind the large variability observed in the literature with respect to silicon electrode performance and proposes a way to increase electrode homogeneity.

Acknowledgement: This work was supported by the US Department of Energy's Office of Energy Efficiency and Renewable Energy through the Vehicle Technology Office (Brian Cunningham Program Manager).

#### 6:35 AM F.EN04.26.16

**New Chemistries for Safe and High Energy Density Lithium Primary Batteries Using Condensed Fluorinated Reactants** Haining Gao and Betar Gallant; Massachusetts Institute of Technology, United States

For long-duration standalone power needs such as unmanned vehicles, space applications, and implantable/portable medical



devices, batteries need to have longer operation times and thus higher energy densities. Although today's state-of-the-art Li primary battery, Li-SOCl<sub>2</sub>, has high specific energy (~500 Wh/kg), it is highly toxic if vented or leaked. Therefore, research into safer primary batteries that can achieve high energy density remains essential. Our previous work into Li-perfluorinated gas batteries, such as Li-SF<sub>6</sub> and Li-NF<sub>3</sub> batteries, demonstrated that perfluorinated compounds that are nominally chemically inert (thus have high safety) can be electrochemically activated through multi-electron transfer reduction reactions, resulting in a high theoretical energy density (e.g. 3922 Wh/kg for SF<sub>6</sub>). However, the intrinsically low solubility of perfluorinated gases in typical battery electrolytes (< 5 mM) makes it necessary to have a gas reservoir present in the cell, resulting in difficulties to further optimize volumetric capacity. To overcome these issues induced by the gas phase, but still retain a multiple electron transfer reaction, we have subsequently studied new battery chemistries using liquid fluorinated reactants: an iodo-fluorocarbon series (C<sub>6</sub>F<sub>13</sub>I, C<sub>4</sub>F<sub>9</sub>I, and C<sub>3</sub>F<sub>7</sub>I), or 'Li-CFI'. This battery system utilizes lithium metal as the anode, and liquid CFI as both the electrolyte and active cathodic component. The Li-CFI batteries exhibit attractive electrochemical performance, with voltages up to 2.9 V and an areal capacity of > 5 mAh/cm<sup>2</sup> (at 0.3 mA/cm<sup>2</sup> on un-optimized low surface area gas diffusion layer (GDL) cathodes). The liquid nature of CFI also contributes to its outstanding rate capability: an areal capacity of ~3 mAh/cm<sup>2</sup> is achievable at a current density as high as 1 mA/cm<sup>2</sup> (on GDL). In addition to the cell configuration and performance, the discharge reaction mechanism, effect of molecular structure on the electrochemistry, and electrode/electrolyte balance strategy will be discussed. We will point to current challenges for the Li-CFI system, including relatively sluggish reduction kinetics after the first electron transfer and overpotential induced by electrode passivation. Strategies to address these issues in ongoing work will also be provided. In addition to the cathode reaction, the operation of the Li anode in these novel fluorinated electrolytes will be discussed, including the potential of using CFI to construct a stable solid electrolyte interface (SEI) on Li metal surface and improve the Li stability and cycle performance for secondary batteries.

**6:45 AM \*F.EN04.26.18**

**Designing Intercalation for High-Valent Redox** William C. Chueh; Stanford University, United States

Increasing the energy density of intercalation positive electrodes in Li- an Na-ion batteries necessitate high talent redox couples. Oxygen redox has emerged as a versatile and promising high-talent redox couple. However, the reversibility of this redox couple is low compared to conventional lower-valent transition metal redox couples. In this talk, I will present understandings of and design rules for high-talent redox in intercalation compounds.

**7:00 AM F.EN04.26.19**

**Overcoming Transport Limitations in Ionic Liquid Electrolytes through an Atomistic Understanding of Ionic Correlation and Transport** Nicola Molinari<sup>1</sup>, Jonathan P. Mailoa<sup>2</sup> and Boris Kozinsky<sup>1,2</sup>; <sup>1</sup>Harvard University, United States; <sup>2</sup>Robert Bosch LLC, United States

Electrolytes comprising a Li-salt (or other alkali metal salts) dissolved in ionic liquids (ILs) are often seen as attractive candidates to replace flammable organic solvents, mainly due to their superior safety. However, relatively poor transport properties hinder their applicability. Due to high salt concentrations and long-range Coulombic interactions, these systems possess high degrees of inter-species ionic correlation, thus posing a crucial and interesting challenge to understanding their transport properties. We investigate the transport properties of IL-based electrolytes through molecular dynamics computer simulations, and report two major findings. First, by adopting rigorous concentrated multicomponent solution theory, we uncover anomalously low and even negative Li transference numbers. This is due to the strong ionic interactions resulting in significant correlations and deviations from ideal solution behavior. We show that a negative transference number is to be expected in a wide range of chemistries, suggesting a universal behavior for this class of materials. Additionally, we study the anion-cation clusters and show that lithium-containing clusters carry an overall negative charge in a remarkably wide range of compositions and concentrations. Second, we leverage the microscopic understanding developed in the previous point to suggest and test modifications to increase the cation transference number. The results have significant implications for the adoption of IL-based electrolytes as they provide a recipe for optimizing transport properties in next-generation highly concentrated and correlated electrolytes.

**7:10 AM F.EN04.26.20**

**Computational Investigation of Earth Abundant Electrolytes of the M<sub>3</sub>AlP<sub>2</sub> (M = Li, Na) System** Arthur B. Youd, Daniel Davies, Christopher Savory and David O. Scanlon; University College London, United Kingdom

Earth abundant electrolytes are a vital paradigm in the realisation of truly sustainable solid-state rechargeable batteries. These materials must maintain a tight balancing act between chemical stability, ion mobility and earth abundance. Recent work has

shown promising Li ion mobility in phosphidoaluminates owing to the favourable alignment of  $\text{AlP}_4$  tetrahedra.<sup>1</sup> The final characterisation of this as well as the exact Li migration mechanism is not fully understood. The sodium analogue ( $\text{Na}_3\text{AlP}_2$ ) shares significant structural features which may make it a possible candidate for sodium ion electrolytes.<sup>2</sup>

In this study, we have performed ab initio Density Functional Theory calculations on  $\text{M}_3\text{AlP}_2$  ( $\text{M} = \text{Li}, \text{Na}$ ) to predict and critically assess their ion transport properties. The methodology makes use of an array of python-based tools to generate structures (pymatgen)<sup>3</sup>, defective supercells (bsym)<sup>4</sup> and create workflows (atomate)<sup>5</sup> to perform high throughput calculations. Ab initio molecular dynamics (AIMD) and nudged elastic band (NEB) approaches are employed to examine the ion mobility and diffusion coefficients of  $\text{M}_3\text{AlP}_2$  with a view to assessing its suitability as an electrolyte. The thermodynamic stability is window is calculated with electronic alignment relative to cathodes. Dynamic stability of these electrolytes is investigated with phonon analysis within the harmonic approximation.

While quantitative analysis of AIMD informs the extent of diffusion, qualitative directional analysis gives insights into the preferred route of diffusion as well as help propose specific mechanisms for ion diffusion. Through multiple AIMD runs we can extract temperature dependent behaviour and compare with microscopic activation barriers from NEB. These results allow us to elucidate the favourable mechanism in the phosphidoaluminates and thus draw conclusions on promising future developments for solid state electrolytes in both Li-ion and Na-ion batteries.

1. T. M. F. Restle, C. Sedlmeier, H. Kirzhain, W. Klein, G. Raudaschl-Sieber, V. L. Deringer, L. van Wüllen, H. A. Gasteiger, T. F. Fässler, *Angew. Chem. Int. Ed.* 2020, 59, 5665.

2. Somer, M., Carrillo-Cabrera, W., Peters, E.-M., Peters, K., & von Schnering, H. G. (1995). Crystal structure of trisodium catena-di- $\mu$ -phosphidoaluminate,  $\text{Na}_3\text{AlP}_2$ , *Zeitschrift für Kristallographie - Crystalline Materials*, 210(10), 777-777.

3. Shyue Ping Ong, William Davidson Richards, Anubhav Jain, Geoffroy Hautier, Michael Kocher, Shreyas Cholia, Dan Gunter, Vincent L. Chevrier, Kristin A. Persson, Gerbrand Ceder, Python Materials Genomics (pymatgen): A robust, open-source python library for materials analysis, *Computational Materials Science*, Volume 68, 2013, Pages 314-319.

4. Bsym: Morgan, (2017), bsym: A basic symmetry module, *Journal of Open Source Software*, 2(16), 370.

5. Mathew, K., Montoya, J. H., Faghaninia, A., Dwarakanath, S., Aykol, M., Tang, H., Chu, I., Smidt, T., Bocklund, B., Horton, M., Dagdelen, J., Wood, B., Liu, Z.-K., Neaton, J., Ong, S. P., Persson, K., Jain, A., Atomate: A high-level interface to generate, execute, and analyse computational materials science workflows. *Comput. Mater. Sci.* 139, 140–152 (2017).

#### 7:20 AM F.EN04.26.23

##### **Metal–Organic Frameworks Encapsulated with Vanadium-Substituted Heteropoly Acid for Highly Stable Asymmetric Supercapacitors** Nageh K. Allam; The American University in Cairo, Egypt

Herein, we report on a facile one-pot synthesis of polyoxometalates encapsulated zeolite imidazolate framework cages ( $\text{PMo}_{10}\text{V}_2@ZIF-67$ ). The morphological and structural properties of the as-synthesized materials were investigated *via* FESEM, EDS, XRD and FTIR techniques. Moreover,  $\text{N}_2$  adsorption/desorption isotherms, and XPS measurements were carried out to elucidate the textural properties and composition of the fabricated materials. Upon their use as supercapacitor electrodes, the  $\text{PMo}_{10}\text{V}_2@ZIF-67$  electrode exhibited a maximum specific capacitance of 765 F/g at a scan rate of 5 mV/s. Furthermore, a supercapacitor device was assembled using activated carbon as the negative electrode and  $\text{PMo}_{10}\text{V}_2@ZIF-67$  as the positive electrode, delivering a specific power of 702 W/kg and corresponding specific energy of 20.9 Wh/kg at a charging current density of 1 A/g. In addition, the device shows excellent long term stability and high Columbic efficiency over 5000 charging and discharging cycles at charging and discharging current density of 5 A/g.

#### 7:30 AM F.EN04.26.24

##### **Recycling of Li-Ni-Mn-Co Hydroxide from Spent Batteries to High-Performance Supercapacitors with Exceptional Stability** Nageh K. Allam; American University in Cairo, Egypt

The intensive implementation of Li-ion batteries in many markets makes it increasingly urgent to address the recycling of strategic materials from spent batteries. Batteries typically contain toxic chemicals and cannot be disposed of at will. In this study, Li-Ni-Mn-Co hydroxides are successfully recycled from spent Li-ion batteries electrodeposited on nickel foam and fully characterized using different techniques such as field emission scanning electron microscopy (FESEM), x-ray diffraction (XRD), energy-dispersive X-ray spectroscopy (EDXS), inductively coupled plasma (ICP), and X-ray photoelectron spectroscopy (XPS) techniques. The recycled nanostructured films are tested in a three-electrode electrochemical system to investigate their capacitance behavior. The recycled electrodes show a high capacitance of 951 F.g<sup>-1</sup> (Specific capacity of 523.5 C.g<sup>-1</sup>) at 1 A.g<sup>-1</sup>. Moreover, recycled materials are used as positive electrodes to construct asymmetric supercapacitor devices. The device shows a Columbic efficiency of 100%, capacitance retention reaching

~90% with excellent cycling stability after 10,000 cycles as well as reasonable power and energy densities.

#### 7:40 AM F.EN04.26.26

**Structural Control of Hard Carbons Synthesized from Resorcinol-Formaldehyde Xerogels with Application as New Anode Materials** Joelle Medinger, Marco Lattuada, Xavier Amantini and Pacifique Umubyeyi; University of Fribourg, Switzerland

The increase in demands of devices requiring batteries, which not only encompasses electronic devices, but also electric cars, is pushing towards the development of new materials and solutions for electrodes. Hard carbons obtained by pyrolysis of resorcinol-formaldehyde xerogels have gained in interest because of their promising properties as alternative anode materials in sodium ion batteries [1]. They are easily prepared, are non-toxic and have low production costs because a simple sol-gel process can be used to prepare them. The meso- and macroporosity and overall architecture of the xerogels can be controlled by tuning the composition of the sol mixture, and the concentration of the catalyst (pH) [2-3]. Aging and drying conditions also have a substantial effect on the final surface area and pore volume of these gels. Conversely, the microporosity is created during the pyrolysis step 800 °C for 1h under inert atmosphere, which leads to a fully carbonized porous xerogels [4]. The impact of the porosity and the pyrolysis step on the performance of the carbonized RF xerogels as electrodes have been extensively investigated.

Current synthetic methods do not permit to impart anisotropy to the macrostructure of the final material, and neither allow for a control of pores direction. By adapting a procedure developed by our group, in this work we show that the macroporous structure of carbon gels can be rendered naturally anisotropic by adding superparamagnetic colloids to the sol-gel precursor solution, and by applying a uniform magnetic field during the sol-gel transition. By ensuring that the superparamagnetic colloids are incorporated into the gel phase, the magnetic colloids will self-assemble into chain-like structures in the direction of the magnetic field and become templates for the growing gel phase [5]. The lower tortuosity brought by the structural anisotropy has known advantages [6]. As anode material, the structural control gives an optimized directional flow of the ions without interfering with the advantages brought by the well-engineered internal meso and microporous gel structure.

[1] Velez, V. *et al.*, *Carbon N. Y.*, 2019, **147**, 214–226.

[2] Pekala, R. W. *CA* 94550, 1990, **171**, 285–291.

[3] Al-Muhtaseb, S. A. & Ritter, J. A., *Advanced Materials*, 2003, **15**, 101–114.

[4] Hasegawa, G. *et al.*, *J. Power Sources*, 2016, **318**, 41–48.

[5] Furlan, M. & Lattuada, M., *Langmuir: the ACS Journal of surfaces and colloids*, 2012, **28**, 12655–12662.

[6] Billaud, J., Bouville, F., Magrini, T., Villeveuille, C. & Studart, A. R., *Nature Energy*, 2016, **1**, 8-14.

#### 7:50 AM F.EN04.26.27

**Controlling Charge Transport in Spinel Oxides through Manipulation of Cation Site Occupation** Anuj Bhargava and Richard Robinson; Cornell University, United States

Understanding how complex oxides conduct electronic charge has relevance to a wide range of energy materials. For instance, ternary spinel oxides are actively researched for applications in electronics, sensors, catalysis, data storage, and energy storage due to their useful magnetic, catalytic, and electronic properties. It is known that the most prominent mechanism of charge transport in oxides is through hopping that follows the polaron models. But the polaron hopping models are too crude to account for the configurational differences that can occur in complex oxides, like ternary transition metal spinels, where the two different cation types can exhibit large degrees of disorder between the two cation lattice sites, possess a variety of oxidation states, and have different energy barriers. The current model, the small polaron nearest neighbor hopping model, was proposed in 1961 and has multiple limitations. Understanding the mechanisms of charge transport in ternary and higher order spinels would enable design principles for enhancing their electronic and electrochemical properties for energy applications. Here, we develop a new method to characterize the donor/acceptor pairs that form the conduction pathway for polarons: advanced synchrotron x-ray emission spectroscopy (XES) is able to accurately determine both site location and oxidation state of the cations to a higher accuracy than other common methods such as XAS and XPS. We use XES to investigate colloidal nanoparticles of the ternary  $\text{Co}_x\text{Mn}_{3-x}\text{O}_4$  spinel system and determine the relationship between electronic properties and cation site occupation, based on the octahedral site, donor-acceptor formalization introduced in the polaron hopping model. We find that the stoichiometric volcano trend in electronic conductivity correlates well with the concentration of  $\text{Mn}^{4+}/\text{Mn}^{3+}$  hopping pairs, while the concentration of  $\text{Mn}^{3+}/\text{Mn}^{2+}$  pairs is unchanged with stoichiometry. We also find that Co does not directly contribute to conductivity, however, the Co does create configurational disorder that leads to the generation of hopping pairs for Mn at octahedral sites. From these results we conclude that  $\text{Mn}^{4+}/\text{Mn}^{3+}$  pairs are the dominant active species and the origin of the stoichiometry-dependent behavior for polaron charge transport. This work

provides a starting point for understanding and optimizing charge transport for higher order spinels to improve energy electrodes.

#### 8:00 AM F.EN04.26.29

**Molecular Dynamics Study of Ionic Conduction Mechanism in Network Glasses** Mirza C. Beg and John Kieffer; University of Michigan, United States

Combining a recently developed variant of transition state theory (TST) for ionic transport in amorphous structures with molecular dynamics (MD) simulations facilitates unprecedented insights into the local and medium-range structure of glasses. Realistic structural models of network glasses are generated using MD simulations based on a reactive force field, which allows for the accommodation of dynamically variable coordination numbers for a given network former and dynamic charge transfer upon formation or breakage of covalent bonds. The TST model, which relies on mean-field statistical measures, allows us to identify the size of the spatial region affected by the activated ion hopping process. In combination with MD simulations, we can identify the specific molecular configurations that participate in the jump process and onto which the thermal energy for activation must be focused. Thus, MD simulations allow us to observe the behavior of all atoms involved in the ionic transport process, and identify the underlying mechanisms in the context of glass structure, its chemical character, and its bonding topology. Cation jumps at room temperature are a rare event, but in the supercooled liquid near  $T_g$  each cation jumps once every 1-10 ns. Since, structural relaxation comes to a halt upon cooling at  $T_g$ , we can expect meaningful results for solid state ionic conduction when studying cation mobility in this temperature range. This allows us to observe a number of jump events that is statistically significant but typically too few to rely on standard measures such as the mean squared displacements to evaluate cation mobility. We explore a potentially novel approach for estimating cation mobility that is based on the analysis of deviatory modes of motion using the construct of the velocity autocorrelation function, which can be described as an oscillatory function whose amplitude decays with time. The integral of the velocity correlation function yields the diffusion coefficient. The existence of this non-zero diffusion coefficient is a consequence of damping or decay in the velocity correlation function. Here we establish a working connection between cation mobility and the damping coefficients as a means to rapidly screen materials structures for their potential to be good ion conductors. This knowledge is used towards the development of a materials design criteria for solid-state electrolytes. (Acknowledgment: NSF DMR-1610742.)

#### 8:10 AM F.EN04.26.30

**Late News: Novel Developments in MRI Diagnostics of Commercial Batteries** Stefan Benders<sup>1</sup>, Mona Mohammadi<sup>1</sup>, Roberta Pigliapochi<sup>1</sup>, Christopher A. Klug<sup>2,1</sup> and Alexej Jerschow<sup>1</sup>; <sup>1</sup>New York University, United States; <sup>2</sup>U.S. Naval Research Laboratory, United States

While batteries are an essential part of modern technology, diagnostic techniques for commercial batteries are still in high demand. Magnetic Resonance Imaging (MRI) is a powerful technique with a variety of contrast options and measurable parameters, but its application to batteries in conductive enclosures poses a major challenge. Recently, the inside-out (ioMRI) technique enabled the recovery of essential information by mapping the field caused by the (changing) susceptibility of the battery associated with state-of-charge (SOC) or defects [1]. Current distributions have been measured with this technique as well [2] and the technique has been demonstrated with the simple acquisition of free induction decays (FID) paired with statistical analysis as well. A common technique in battery diagnostics is electrical impedance spectroscopy (EIS), which lacks spatial resolution in the case of commercial batteries. A novel technique has been developed, which provides the ability to measure the oscillating fields caused by alternating currents in a battery at different frequencies [3].

Although the inside-out technique provides important parameters, direct measurements of e.g. the lithium within the battery are often desirable. Due to the inability of RF radiation to penetrate through the metal casing, other ways to access the interior noninvasively are sought for. A method to incorporate the aluminum casing of a pouch cell into a resonant circuit, essentially making it a low quality rf coil was developed recently [4]. Employing this method, signals from three different characteristic environments can be observed: Metallic lithium, intercalated lithium and lithium in the electrolyte. This approach can enable deeper insights into processes within commercial batteries.

[1] Illot *et al.*, Nat. Comm. **9** (1) (2018) 1-7; [2] Mohammadi *et al.*, J. Magn. Res. **209** (2019) 206601; [3] Benders *et al.*, J. Magn. Res. **319** (2020) 106811; [4] Benders *et al.*, Sci. Rep. **10**(2020) 13781.

#### 8:20 AM F.EN04.26.31

**Late News: New Sulfonamide-Based Electrolytes Enable High-Energy and Long-Cycling Practical High-Voltage Lithium-Metal Batteries** Weijiang Xue; Massachusetts Institute of Technology, United States

Current lithium-ion batteries (LIBs) based on a lithium transition metal oxide cathode (LiCoO<sub>2</sub>, LiMn<sub>2</sub>O<sub>4</sub>, etc) and a graphite anode (372 mAh g<sup>-1</sup>) are approaching their theoretical energy density (~ 300 Wh kg<sup>-1</sup>) and thus are unable to satisfy the increasing demand for high-energy-density power sources for electric vehicles, electronic devices, and other promising markets. A promising and feasible approach to boost energy density > 400 Wh kg<sup>-1</sup> is to turn to high-voltage rechargeable LMBs based on a Li metal anode (LMA) and a commercially-available high-Ni NMC (LiNi<sub>x</sub>M<sub>1-x</sub>O<sub>2</sub>, M=Mn, Co and x ≥ 0.6) cathode materials. However, it still remains a great challenge to for developing electrolytes that are compatible with both the Li metal anode (LMA) and the high-Ni NMC cathodes.

In order to overcome the challenge, a group of new sulfonamide-based electrolytes beyond traditional carbonate and ether-based ones are rationally designed and developed. They successfully enable a highly reversible LMA, exhibiting an excellent Coulombic efficiency with rapid ramp-up to >99% within several cycles. Furthermore, due to the excellent compatibility with high-Ni NMC cathodes, the sulfonamide-based electrolyte successfully reach a stable cycle and high energy efficiency of commercial NMC811 at an ultra-high cutoff voltage of 4.7 V vs. Li<sup>+</sup>/Li, which is first ever reported in the literature. Benefitting from these unique performances, a full-cell energy density exceeding 400 Wh kg<sup>-1</sup> has been achieved under practical conditions with industrial-level high-loading cathode, extremely low negative to positive (N/P) ratio, and lean electrolyte which demonstrates huge technological advances for practical LMBs.

**8:30 AM F.EN04.26.32**

**Late News: Anion Chaotropicity as Indicator for Water-in-Salt Electrolyte Stability** David Reber<sup>1</sup>, Maximilian Becker<sup>1,2</sup>, Ruben-Simon Kühnel<sup>1</sup> and Corsin Battaglia<sup>1</sup>; <sup>1</sup>Empa, Switzerland; <sup>2</sup>ETH Zürich, Switzerland

Water-in-salt electrolytes have enabled the development of novel high-voltage aqueous lithium-ion batteries due to their wide electrochemical stability window. In this study, we explore why analogous sodium electrolytes have struggled to reach the same level of electrochemical stability.<sup>[1-3]</sup> We compare solution structure and electrochemical stability for eleven sodium salts, selected among the major classes of salts proposed for highly concentrated electrolytes. We relate the water environment established for each anion to its position in the Hofmeister series and find a surprisingly strong correlation between the chaotropicity of the anion and the resulting electrochemical stability of the electrolyte. We also discuss the importance of the solid-electrolyte interphase for stable battery performance and how it relates to the anion. We further show that the search for suitable sodium salts is complicated by the fact that higher salt concentrations are needed than for their lithium equivalents.<sup>[4]</sup> Reaching such a high concentration of 25 to 30 mol/kg with one or a combination of multiple sodium salts that have the desired properties remains a major challenge. We conclude that alternative approaches such as mixed water/organic solvent or dual-cation electrolytes should be pursued to enable the development of high-voltage aqueous sodium-ion batteries. We demonstrate the potential of the mixed-solvent approach by showing that the water solubility of NaTFSI can be increased from 8 to 30 mol/kg in the presence of ionic liquids. Such a ternary electrolyte, based on highly chaotropic anions, enables stable cycling of a 2 V-class sodium-ion battery based on the NaTi<sub>2</sub>(PO<sub>4</sub>)<sub>3</sub>/Na<sub>2</sub>Mn[Fe(CN)<sub>6</sub>] electrode couple for 300 cycles at 1C with a Coulombic efficiency of >99.5%.<sup>[5]</sup>

References:

<sup>[1]</sup> Kühnel, R.-S.; Reber, D.; Battaglia, C., A High-Voltage Aqueous Electrolyte for Sodium-Ion Batteries. *ACS Energy Lett.* **2017**, *2*, 2005-2006.

<sup>[2]</sup> Reber, D.; Kühnel, R.-S.; Battaglia, C., Suppressing Crystallization of Water-in-Salt Electrolytes by Asymmetric Anions Enables Low-Temperature Operation of High-Voltage Aqueous Batteries. *ACS Materials Letters* **2019**, *1*, 44-51.

<sup>[3]</sup> Reber, D.; Takenaka, N.; Kühnel, R.-S.; Yamada, A.; Battaglia, C., Impact of Anion Asymmetry on Local Structure and Supercooling Behavior of Water-in-Salt Electrolytes. *J. Phys. Chem. Lett.* **2020**, *11*, 4720

<sup>[4]</sup> Reber, D.; Kühnel, R.-S.; Battaglia, C., Stability of aqueous electrolytes based on LiFSI and NaFSI. *Electrochim. Acta* **2019**, *321*, 134644

<sup>[5]</sup> Reber, D.; Becker, M.; Kühnel, R.-S.; Battaglia, C., Anion Chaotropicity as Indicator for Water-in-Salt Electrolyte Stability. *submitted*

**8:40 AM F.EN04.26.33**

**Development of Carbon-Based Nanostructures for High Performance Li Metal Anodes** Hansen Wang, Yuzhang Li and Yi Cui; Stanford University, United States

Development of Li metal anodes is critical to the realization of next generation high specific energy batteries.

Commercialization of Li metal anodes, however, is plagued by its poor cyclability. This is because Li metal inevitably reacts with electrolytes, forming mechanically vulnerable solid-electrolyte interphase (SEI). With the significant volume fluctuation during Li metal cycling, the SEI easily cracks, leading to dendritic growth and continuous capacity loss. Electrode structural design is one of the most promising approaches to address these issues. Various "host" frameworks have been developed to accommodate Li metal and ameliorate the volume fluctuation during cycling, enabling much improved SEI stability and Coulombic efficiency (CE). However, further optimizations of these "host" frameworks are still in demand. First, achieving completely zero volume change is still challenging. Second, most of current carbon-based structures possess decent electronic conductivity, promoting undesirable surface Li plating under high currents. Here, we report recently developed "host" frameworks that successfully address these issues, enabling further advancements in the Li metal anode cycling performance.

#### 1. Wrinkled graphene cages (WGCs)

We report WGCs as a "host" framework for Li metal anodes. Different from previously reported amorphous carbon spheres, WGCs show highly improved mechanical stability, Li-ion conductivity and robust SEI for continuous Li metal protection. With embedded gold nucleation seeds, Li metal preferentially deposits inside the cages with minimal exposure to the electrolyte. As a result, CEs of 98.0% in a carbonate electrolyte, 99.1% in a high concentration electrolyte are realized. A Li-WGC||LFP full cell can run for ~350 cycles with minimal capacity decay.

#### 2. Silicon (Si) nanoparticles embedded reduced graphene oxide (rGO)

A rGO "host" framework for Li metal anodes is further optimized by embedding Si nanoparticles between the graphene layers. These Si nanoparticles possess two critical functionalities. First, they serve as Li nucleation seeds to promote Li deposition within the framework even without pre-stored Li. Second, the  $\text{Li}_x\text{Si}$  alloy particles serve as supporting "pillars" between the graphene layers, enabling a negligible thickness shrinkage after full stripping of metallic Li. As a result, we achieve 99.4% Coulombic efficiency over ~600 cycles in Cu||Li half cells. Meanwhile, a Li-SirGO||NMC532 full cell runs for ~380 cycles with negligible capacity decay.

SESSION F.EN04.27: Poster Session I: Next-Generation Electrical Energy Storage—Beyond Intercalation-Type Lithium Ion  
On Demand Abstracts Available for Viewing Starting Saturday Morning, November 21, 2020  
5:00 AM - 8:00 AM  
F-EN04

#### F.EN04.27.01

##### **Structural Characterization of Solid-State Electrochemical Interfaces via Integrated Computation and**

**Spectroscopy** Deyu Lu<sup>1</sup>, Nongnuch Artrith<sup>2</sup>, Alexander Urban<sup>2</sup>, Shinjae Yoo<sup>1</sup> and Feng Wang<sup>1</sup>; <sup>1</sup>Brookhaven National Laboratory, United States; <sup>2</sup>Columbia University, United States

Solid-state batteries are attracting world-wide interest for their potential to enhance safety by eliminating the need for flammable liquid electrolytes and to increase the energy density by facilitating the use of Li metal anodes and high-capacity cathodes. When incorporated into real devices, the solid electrolyte interacts with Li anodes and cathodes to form a nanometer-thick amorphous/disordered interfacial layer known as the solid electrolyte interphase (SEI), which determines the resistivity and stability of the interfaces between the electrode and electrolyte. The inherent complexity and the dynamic evolution of the SEI cannot be handled directly with first-principles methods, such as density functional theory, because of the computational hurdle associated with the large system size (e.g., more than one thousand atoms) and time scale. In order to gain insights into the structural properties and the interfacial reactions at the SEI, an integrated approach that combines high-performance computing and machine learning tools with state-of-the-art synchrotron X-ray absorption/electron energy-loss spectroscopy, is developed to tackle the complex electrochemical interfaces. The approach and some recent results from the structural modeling and spectroscopy studies of the SEI at the LiTMO<sub>2</sub> (TM=Ni, Co, Mn) cathode/ Li<sub>7</sub>La<sub>3</sub>Zr<sub>2</sub>O<sub>12</sub> solid electrolyte interfaces will be presented.

#### F.EN04.27.02

**Realistic Modeling of AlCl<sub>4</sub> Intercalation in Strained Two-Dimensional Materials** Rizcky Tamarany<sup>1</sup>, Chan-Woo Lee<sup>1</sup>, Hana Yoon<sup>1</sup>, Chung-Yul Yoo<sup>2</sup> and Kanghoon Yim<sup>1</sup>; <sup>1</sup>Korea Institute of Energy Research, Korea (the Republic of); <sup>2</sup>Mokpo National University, Korea (the Republic of)

Graphite-based Al-ion battery has been attracted large attention due to its extremely fast charge/discharge rate and excellent cycle stability. However, the intercalation mechanism of AlCl<sub>4</sub> into graphite is still vague. The concern comes with the large

size of the  $\text{AlCl}_4$  molecule while the experimentally observed gallery height for graphite cathode is not large enough ( $\sim 5.7$  Å). In the past theoretical studies, the computational models mostly represent that the stable structure of intercalated  $\text{AlCl}_4$  is the tetragonal form which resulted in a large expansion of the intercalation gallery to 8–9 Å. In those studies, researchers commonly considered thermodynamically stable structures that allow free expansions of electrode structures. In this study, we suggest that a strain effect in a realistic electrode structure governs the stable form of intercalating  $\text{AlCl}_4$ . We have performed first-principles calculations to show a strain-structure relation of intercalated  $\text{AlCl}_4$  in graphite and found that a planar-shape of  $\text{AlCl}_4$  molecule is more probable in realistic conditions. Using the computational results, we made model energy for  $\text{AlCl}_4$  intercalation at given structural conditions such as volume expansion rate and stage number of graphite electrode. The model energy shows good agreements with the experimental observations on the structure-engineered graphite electrodes. In addition, to examine new candidate materials for Al-ion cathode, we also conduct calculations on  $\text{MoS}_2$  and  $\text{MoS}_2/\text{graphene}$  hetero-structure for  $\text{AlCl}_4$  intercalation. As a result, we believe our study provides a deeper understanding of the charging/discharging mechanism and a modeling rule to find more enhanced electrode materials in Al-ion batteries.

#### **F.EN04.27.04**

**Improved Cycle Lifetime of Lithium-Sulfur Battery by Polysulfide Entrapment Using a Surface Decorated Carbon Cloth** Saisaban Fahad and Akihiro Kushima; University of Central Florida, United States

Lithium sulfur batteries (LSBs) are attracting attention as a next generation energy storage device because of their high energy density, low cost, and environmental friendliness surpassing that of lithium ion batteries (LIBs). LIBs are considered insufficient for many applications such as grid energy storage and electric vehicles due to their high cost and low energy density. However, LSBs still have some problems that need to be overcome before they can be used commercially. The major problem that limits their capacity is the dissolution of long chain lithium polysulfide into the electrolyte which leads to a loss of active material and capacity decay during cycling. Here, we have developed a cost-effective method for the lithium polysulfide battery to achieve high performance by employing a nanostructured carbon black/ carbon cloth electrode that exhibits high electrical conductivity, good mechanical properties and high surface area. These benefits enable a high sulfur loading mass, capture the lithium polysulfide intermediate reaction products and avoid structural changes. As a result, this simple and novel design delivered a high specific discharge capacity exceeding 1350 mAhg<sup>-1</sup> at 0.2 C and good capacity retention, providing a promising path towards practical lithium sulfur batteries.

#### **F.EN04.27.07**

**Enhanced Polysulfide Conversion Using 2D Alloy Catalyst in Li-S Batteries** Sanket D. Bhoyate<sup>1</sup>, Junyoung Kim<sup>1</sup>, Eunji Lee<sup>2</sup>, Eunho Lee<sup>1</sup>, Juhong Park<sup>1</sup>, Jeongyong Kim<sup>2</sup> and Wonbong Choi<sup>1</sup>; <sup>1</sup>University of North Texas, United States; <sup>2</sup>SKKU, Korea (the Republic of)

The lithium sulfur battery presents unique polysulfide chemistry to exhibit high theoretical capacity of 2,600 Wh/kg. However, the life cycle of Li-S battery is greatly affected due to unwanted shuttling of soluble lithium polysulfides (LiPSs) such as  $\text{Li}_2\text{S}_8$  and  $\text{Li}_2\text{S}_6$ , that corrodes the Li anode by forming an inactive sulfide layer. Previously, pristine 2D materials with polar surface were used as a catalyst in sulfur cathodes to overcome this issue by acting as polysulfide anchor and prevent shuttling effect. However, the concentration and weight loading of catalyst was high and lack the practical applicability in Li-S battery. To overcome this issue, we adopted novel strategy of synthesizing 2D alloys with very low concentration loading on carbon nanotube paper as a sulfur host cathode to efficiently catalyze the polysulfide reactions. The 2D alloy with mixed 2H-1T phase exhibited synergetic properties and showed high specific capacity of 1,228 mAh/g at 0.1 C and improved the cyclic stability to 400 cycles, as compared to 100 cycles for pristine cathode. The reduced shuttle effect and increased life cycle was due to accelerated transformation of the dissolved polysulfides to the insoluble LiPSs and back to sulfur. Our study shows novel approach with binder-free ultra-light weight catalytic cathodes for practical application of Li-S battery.

#### **F.EN04.27.10**

**Improvement of Specific Capacitance in Lithium Batteries by Three-Dimensional Carbon Networks** Valerio Dorvilien<sup>1</sup>, Carolina Rojas<sup>2</sup>, Neida Santacruz<sup>3</sup>, Cid Marie Calderon Rodriguez<sup>3</sup>, Omayra Ortiz Alicea<sup>3</sup>, Genesis M. Ferrer<sup>1</sup>, Frank Martinez-Henriquez<sup>1</sup>, Daniel Fontanez<sup>1</sup>, Frank Mendoza<sup>1</sup>, Carolina Rojas Michea<sup>4</sup>, Brad R. Weiner<sup>2</sup> and Gerardo Morell<sup>1</sup>; <sup>1</sup>University of Puerto Rico-Rio Piedras Campus, United States; <sup>2</sup>University of Puerto Rico, San Juan, Puerto Rico; <sup>3</sup>University of Puerto Rico, Rio Piedras Campus, Puerto Rico; <sup>4</sup>Universidad Autónoma de Chile, Chile

We propose a low cost and simple method to prepare three-dimensional (3D) carbon structures by Chemical Vapor Deposition (CVD) and characterized their structural and electrochemical properties. The 3D pore system were obtained using different zeolites (NaY, SBA-15, and ZMS-5) as solid template structures to assist in the synthesis of 3D carbon network

structures. The carbon source consisted of radicals formed from the thermal decomposition of acetone, in a relatively facile and fast chemical deposition process. The 3D carbon network structures were characterized with X-ray diffraction, Raman spectroscopy, spectroscopy, surface area measurement, scanning electron microscopy, and transmission electron microscopy. The carbon networks deposited in the pores consist of reduced graphene oxide and multiwalled carbon nanotubes; their size distribution correlates with the size of the pores of zeolites. The electrical conductivity and dispersed morphology of the 3Ds carbon network structures -based conductive electrode were examined by atomic force microscope (AFM), scanning electron microscope (SEM) and transmission electron microscope (TEM). Using the standard method we assembled the Lithium Ion Battery in the Ar-filled glove box, we used LiPF<sub>6</sub> with EC:DMC::1:2 ratio as the electrolyte, lithium foil as the counter electrode and the 3D carbon network material. The specific capacity and cycle-life stability of the 3Ds carbon network-based lithium ion battery was investigated by cyclic voltammetry analysis.

#### **F.EN04.27.11**

**3D Carbon-Coated MXene Architectures with High Capacity and Ultrafast Lithium/Sodium Storage** Peng Zhang, Qizhen Zhu and Bin Xu; Beijing University of Chemical Technology, China

MXene is a promising candidate for energy storage devices owing to its versatile characteristics. However, as 2D structured material, layer restacking besides its surface oxidation is a serious issue. This re-stacking compromises significantly surface active sites, compelling the material to exhibit sluggish electro-kinetics behavior, and thus deterring the overall capacitive performance. Here, a tremella-like 3D architecture of carbon-coated Ti<sub>3</sub>C<sub>2</sub>T<sub>x</sub> MXene (T-MXene@C) is fabricated as an efficient anode material for lithium- (LIBs) and sodium-ion batteries (SIBs), respectively. The nanohybrid is synthesized via self-polymerization of dopamine over the surface of pristine Ti<sub>3</sub>C<sub>2</sub>T<sub>x</sub> MXene nanosheets succeeded by carbonization. The self-polymerization of dopamine in this case, facilitates the transformation of MXene sheets into 3D architectures where its post-carbonization subsequently forms a thin carbon layer over the structure, preserving the surface facets from oxidation and structural aggregation. The incursion of carbon layers within MXene not only contributes in provision of additional active area, but also enhances the structural durability of the material during charge/discharge process. Therefore, the T-MXene@C nanohybrid exhibits ultrahigh capacities, superior rate performance, and stable cyclability as anodes in both LIBs and SIBs. Moreover, the discussed strategy could be applied as general route to fabricate diverse MXene-based 3D structures with potential applications in many other areas.

#### **F.EN04.27.12**

**Tin Dioxide/Graphene/Graphene Oxide as Anode Material for Lithium-Ion Batteries** Valerio Dorvilien, Frank Martinez-Henriquez, Cid Marie Calderon Rodriguez, Daniel Fontanez, Genesis M. Ferrer, Omayra Ortiz Alicea, Frank Mendoza, Brad R. Weiner and Gerardo Morell; University of Puerto Rico-Rio Piedras Campus, United States

Graphene Oxide was synthesized using a Modified Hummer's Method. It is fairly known that SnO<sub>2</sub> is used as anode material for lithium-ion batteries applications due to their high specific capacity. Hence, we use a non-conventional synthesis route to obtain a final composite, G/GO/SnO<sub>2</sub>. G/GO, with its good surface-to-volume ratio, serves as a support and matrix for SnO<sub>2</sub> nanoparticles that buffers the huge volume changes the nanoparticles are used alone as anode for lithium ion batteries and then enhances its electrochemical properties. For the structural characterization of the synthesized material, scanning electron microscopy (SEM), energy dispersive spectroscopy (EDS) and Raman Spectroscopy were performed; showing a uniform distribution of the nanomaterial in the carbon matrix. Electrochemical analysis, such as charge/discharge profiles show that the composite can be used as anode in lithium ion batteries. In fact, at different current densities- 25, 75, 100, and 200 mA/g- the material deliver in the first cycle very high specific capacity-1808, 1253, 903, 886 mAhg<sup>-1</sup> respectively. After repeated cycling the composite is still offering reversible capacities over 400 mAhg<sup>-1</sup> for each current density, showing that G/GO is providing contact areas which results in more energy density at the interface electrode/electrolyte and that the SnO<sub>2</sub> provides additional ions to the EDL and the electrochemical process.

#### **F.EN04.27.13**

**Theoretical Intercalation Profiles of Layered NaMO<sub>2</sub> (M=Co, Ni, Fe) Cathodes—Learning from the Electronic Structure of LiMO<sub>2</sub>** Christopher Savory, Arthur B. Youd and David O. Scanlon; University College London, United Kingdom

Ab initio modelling can provide valuable insights into the electronic and structure behaviour of battery materials, including the prediction of sodium, potassium and magnesium cathodes.<sup>12</sup> Nevertheless, it is crucial that the accuracy of such ab initio calculations be established. The most common method to theoretically the strong correlation in the 3d valence electrons of transition metals is to use the addition of 'U' parameters to standard Density Functional Theory (DFT), enabling high throughput studies of Na-based materials;<sup>3</sup> however these parameters must be tuned to experimental measurements, and are



highly sensitive to changes in oxidation state and composition - crucial properties during the intercalation of  $AMO_2$  ( $A=Li, Na, K$ ) layered cathodes.<sup>4,5</sup> Recent high-level quasiparticle self-consistent GW (QSGW) calculations performed on the layered  $LiMO_2$  ( $M=Co, Ni, Mn$ ) cathodes suggest that the charge transfer transition in  $LiMO_2$  phases is underestimated, even when the inaccuracy of standard DFT at describing band gaps is accounted for, but it is well predicted by hybrid Density Functional Theory (DFT), which mixes exact exchange from Hartree-Fock theory.<sup>6</sup> In this study, we examine how electronic correlation is described in layered sodium cathode materials with various levels of theory. We calculate the electronic structures of  $NaCoO_2$ ,  $NaNiO_2$  (in direct comparison to their Li counterparts) and  $\delta$ - $NaFeO_2$  - ternaries typically alloyed to form stable and efficient sodium-based cathodes<sup>7</sup> -- using DFT+U, hybrid DFT (HSE06) and QSGW to establish a thorough comparison of the electronic properties at each level, and to establish that tuning is necessary to reproduce the valence electronic structure of such materials. We further demonstrate the practical impact of this theoretical description by calculating and comparing voltage intercalation profiles of these systems as a function of Na content, at both the DFT+U and hybrid DFT levels via a cluster expansion approach, in order to establish the most reliable comparison to experiment. We establish the necessity to use accurate, transferable methods to describe such systems, with an aim to inform ab initio studies on the future generation of first row transition metal-based cathodes. (1) Zhang, W.; Liu, Y.; Guo, Z. *Sci. Adv.* 2019, 5 (5), eaav7412. (2) Gao, Y.; Wang, Z.; Lu, G. J. *Mater. Chem. A* 2019, 7 (6), 2619. (3) Zhang, X.; Zhang, Z.; Yao, S.; Chen, A.; Zhao, X.; Zhou, Z. *npj Comput. Mater.* 2018, 4 (1), 13. (4) Urban, A.; Seo, D.-H.; Ceder, G. *npj Comput. Mater.* 2016, 2 (October 2015), 16002. (5) Zhou, F.; Cococcioni, M.; Marianetti, C. A.; Morgan, D.; Ceder, G. *Phys. Rev. B - Condens. Matter Mater. Phys.* 2004, 70 (23), 235121. (6) Savory, C. N.; Morgan, B.J., Walsh, A.; Scanlon, D. O. (in preparation) 2019 (7) Thorne, J. S.; Zheng, L.; Lee, C. L. D.; Dunlap, R. A.; Obrovac, M. N. *ACS Appl. Mater. Interfaces* 2018, 10 (26), 22013.

#### **F.EN04.27.16**

**Enhancement of Ionic Conductivity of Composite Electrolytes for All-Solid-State Lithium Rechargeable Batteries by Incorporating Gold Nanorods into a Polyethylene Oxide Matrix** Yifan Zhang, Nian Liu and John Zhang; Georgia Institute of Technology, United States

Solid state batteries have advantages such as safeness and high energy density. However, their conductivity at room temperature is low which limits their further commercialization. Gold nanorods can promote the Li ion transport by decreasing the crystallization of solid state electrolytes, and locally heat the electrolytes based on their photothermal conversion capability, providing a more efficient way to improve the performance of solid state batteries.

#### **F.EN04.27.17**

**Large-Scale Synthesis of Uniform and Extremely Small-Sized Cobalt Ferrite Nanoparticles as High-Performance Anode Materials for Lithium-Ion Batteries** Yifan Zhang, Nian Liu and John Zhang; Georgia Institute of Technology, United States

Spinel ferrites have emerged as an attracted class of materials that can find application in various fields, ranging from information storage, biomedical application to energy-related areas. As the anode in LIBs, spinel  $CoFe_2O_4$  attracts much attention because of its high theoretical specific capacity (916 mAh g<sup>-1</sup>). However, some issues impede its practical application such as drastic capacity fading and poor rate capability arising from an inherent low electronic conductivity, severe aggregation, and lithiation-induced volume expansion in the cycling process. Increasing surface-to-volume ratio could provide relatively short transport distance for lithium-ion diffusion and alleviate the volume expansion, which is one of the possible strategies to solve the above-mentioned problem. In this frame, an aminolytic method is described to synthesize ultra-small (<10 nm)  $CoFe_2O_4$  nanoparticles with good dispersion at a relatively low temperature without further annealing being required. Here, the 9.1 nm  $CoFe_2O_4$  nanoparticles synthesized by aminolytic method delivered a reversible specific capacity of 1238 mAh g<sup>-1</sup> after 100 cycles at a current density of 0.1C, a much better performance compared with  $CoFe_2O_4$  synthesized by traditional methods in previous reports. By adjusting the reaction temperature, 3.4 nm  $CoFe_2O_4$  nanoparticles could also be synthesized, delivering a slightly enhanced specific capacity (1343 mAh g<sup>-1</sup> after 100 cycles at 0.1C). For comparison, the  $CoFe_2O_4$  nanoparticles were also prepared by coprecipitation method and its electrochemical performance was studied in detail. It can be concluded that spinel  $CoFe_2O_4$  synthesized by aminolytic method is a promising anode for LIBs based on its superior lithium storage performance. Further, the aminolytic method can also be used to prepare other spinel materials in different fields. The systematically studied electrochemical performance of  $CoFe_2O_4$  nanoparticles is beneficial in the design of future anode materials for LIBs.

#### **F.EN04.27.23**

**Li<sub>2</sub>S<sub>x</sub>-CNT Electrode with Lean Electrolyte for High-Energy-Density Li-S Battery** Yuichi Yoshie, Keisuke Hori and Suguru Noda; Waseda University, Japan

Sulfur is a promising active material because of a high theoretical capacity (1675 mA h g<sup>-1</sup>) and low cost. Nevertheless, practical applications of S electrode have been hindered by low S fraction in a cell. Excess Li in negative electrode, auxiliary materials such as heavy current collectors of metals, and large amount of electrolyte (Electrolyte/Sulfur ratio (E/S) > 7) have been used in previous works [1], which lowers energy density of the Li-S cells based on total mass/volume (including electrodes, separator and electrolyte). We previously demonstrated the high gravimetric and volumetric energy densities based on an electrode using self-supporting sponge-like paper of few wall carbon nanotubes (FWCNTs) as current collector. The unique properties of FWCNTs with high conductivity of ~100 S cm<sup>-1</sup> and high surface area of ~500 m<sup>2</sup> g<sup>-1</sup> enhanced the sulfur utilization; however, E/S ratio was still high [2]. In this work, we report the Li<sub>2</sub>S<sub>x</sub>-CNT (4?x?8) positive electrode that works effectively even with lean electrolyte. Self-supporting paper of FWCNTs was fabricated by dispersion and filtration. Then, three types of Li<sub>2</sub>S<sub>x</sub> (x = 4, 6, 8) in 1,2-dimethoxyethane (DME) solution were drop-casted on the papers and dried for 1 h to obtain the Li<sub>2</sub>S<sub>x</sub>-CNT electrodes. As a reference, the S-CNT electrode was also prepared by the S vapor deposition method [2]. The Li<sub>2</sub>S<sub>x</sub>-CNT and S-CNT (areal density of 2 mgS cm<sup>-2</sup> and 1 mgCNT cm<sup>-2</sup>) electrodes were evaluated by assembling 2032-type coin cell with Li foil (50 μm thick) as a negative electrode, a polyethylene separator, and an electrolyte of 1 M LiTFSI + 0.2 M LiNO<sub>3</sub> in 1:1 (v/v) DOL/DME. Although the S-CNT exhibited very small capacity, the Li<sub>2</sub>S<sub>6</sub>-CNT exhibited 1471 mA h g<sup>-1</sup> with lean electrolyte of E/S ratio of 3.2 μL mgS<sup>-1</sup>. Furthermore, the Li<sub>2</sub>S<sub>6</sub>-CNT achieved 526 W h kgcell<sup>-1</sup> based on the cell including positive and negative electrodes, separator, and electrolyte at second discharge. The value is encouragingly high compared to the high-performance Li-ion battery of ~300 W h kgcell<sup>-1</sup> [1]. [1] M. Hagen et al., *Adv. Energy Mater.*, 5, 1401986 (2015). [2] K. Hori, et al., *J. Phys. Chem. C*, 123, 3951 (2019).

#### F.EN04.27.24

**Thin Li-Metal Negative Electrode Held in Self-Supporting Paper of Carbon Nanotubes for Stable, High Energy Density Rechargeable Batteries** Tomotaro Mae<sup>1</sup>, Keisuke Hori<sup>1</sup>, Yuki Yamada<sup>2</sup> and Suguru Noda<sup>1</sup>; <sup>1</sup>Waseda University, Japan; <sup>2</sup>The University of Tokyo, Japan

Li metal is a promising negative electrode because of its high theoretical capacity (3860 mAh gLi<sup>-1</sup>) and low potential (3.04 V vs SHE). However, it has a serious safety problem of Li dendrite which penetrates a separator and causes short circuit [1]. Surface modification of Li foils by texture or additional layer have shown effective in suppressing the dendrite growth [2] [3], but many of such methods make the electrode too thick (several hundred μm), and excessive Li were used (5 times or more). In this work, we propose thin and light-weight electrode to achieve high gravimetric, volumetric and areal capacities. Self-supporting paper of few-wall carbon nanotubes (FWCNTs; areal mass of 0.3 mg cm<sup>-2</sup> and thickness of ~15 μm), having high conductivity of 40 S cm<sup>-1</sup> and large specific surface area of ~500 m<sup>2</sup> g<sup>-1</sup>, was used as non-metal 3D current collector. Cu nanoparticles (25 nm; 0.1-0.2 mg cm<sup>-2</sup>) were held in this 3D matrix as seeds for stable Li plating/stripping. The Cu-CNT film was prepared by dispersion and filtration [4]. 2032 coin cells of symmetrical configurations (Li-CNT//Li-CNT and Li-Cu-CNT//Li-Cu-CNT) were prepared by performing electrochemical pre-cycling of the Li foil (50 μm)/CNT//CNT and Li foil (50 μm)/Cu-CNT//Cu-CNT stacks with polypropylene separator (25 μm). Charge-discharge test was performed with an areal capacity of 4 mA h cm<sup>-2</sup> and current density of 0.4 mA cm<sup>-2</sup>. The former cell showed unstable plating/stripping behavior in several cycles due to micro-short circuits while the latter worked stably over 20 cycles with small excess (1.5-2 times of the areal capacity) in Li. The Cu nanoparticles working as the nucleation sites and mesopores in the FWCNT paper working as growth sites realized the stable operation of the cells. [1] L. Wang, et al., *Energy Storage Mater.* 14, 22 (2018). [2] Rodrigo V. Salvatierra, et al., *Adv. Mater.* 30, 50, (2018). [3] Y. Zhao, et al., *Nano energy.* 43, 368, (2018). [4] K. Hori, et al., *J. Phys. Chem. C* 123, 3951 (2019).

#### F.EN04.27.25

**A Versatile Crosslinked Solid Polymer Electrolyte for Lithium, Calcium, Aluminum and Sodium-Ion Conduction** Francielli Genier, Jiayue Wang, Tianyi Yao, Saeid Biria and Ian D. Hosein; Syracuse University, United States

The development of high-performance batteries is fundamental to meeting global energy demands, while also storing energy affordably and safely. An area of intense research in the battery field has been the replacement of the liquid or gel electrolyte with a solid polymer material, namely a solid polymer electrolyte (SPE). SPEs can allow the use of metal anodes due to its suppression of dendrite formation, which could thereby double the energy density, besides further addressing concerns over the volatility and flammability of liquid electrolytes. Crosslinked polymer electrolytes are quite attractive owing to their ability to enhance conductivity, while also retaining mechanical stability.1 Studies on SPEs not only focus on different polymer systems, but also on improving the interaction of existing and new polymer networks to ions other than lithium-ion to achieve even less expensive and more efficient rechargeable batteries. Other univalent ions, in particular sodium cations, can be highlighted due to its wide availability and low cost comparing to lithium. Multivalent cations, such as Ca<sup>2+</sup> and Al<sup>3+</sup>, are also featured in SPE studies for their high energy density and mineral abundance.2 In those studies, poly(ethylene oxide) (PEO) has been extensively employed as the electrolyte's backbone. However, polytetrahydrofuran (PTHF) has been

reported as having a looser coordination with Li<sup>+</sup> than PEO, due to PTHF's fewer oxygen heteroatoms in its chain.<sup>3</sup> As a result, lower activation energy for ion motion is observed, leading to higher conductivity and transference numbers. In this work, we describe the synthesis of crosslinked SPEs for lithium, sodium, aluminum, and calcium conduction using a PTHF backbone. The SPEs were crosslinked through the photo-copolymerization of PTHF and 3,4-epoxycyclohexylmethyl 3,4-epoxycyclohexanecarboxylate. The crosslinked samples were evaluated for their ionic conductivity, thermal stability, amorphousness, and mechanical properties. Ionic conductivity of the order of 10<sup>-5</sup> - 10<sup>-4</sup> S/cm at room temperature was achieved, which is superior to some previously reported Ca, Na, and Al dry SPEs.<sup>4,5</sup> Thermogravimetric analysis of the electrolytes indicated that, within the operating temperature of a battery, all electrolytes were stable and showed minimal weight loss. Differential scanning calorimetry confirmed the amorphous feature of the polymer. The electrolytes also showed excellent mechanical stiffness and flexibility. Further electrochemical studies will be presented and discussed. This work represents a new route for cleaner and safer energy storage devices with the potential for a broad variety of applications. References 1. Placke, T., Kloepsch, R., Dühnen, S. & Winter, M. Lithium ion, lithium metal, and alternative rechargeable battery technologies: the odyssey for high energy density. *J. Solid State Electrochem.* 21, 1939-1964 (2017). 2. Xu, C. et al. Secondary batteries with multivalent ions for energy storage. *Nat. Publ. Gr.* 1-8 (2015). doi:10.1038/srep14120 3. Mackanic, D. G. et al. Crosslinked Poly ( tetrahydrofuran ) as a Loosely Coordinating Polymer Electrolyte. 1800703, 1-11 (2018). 4. Wang, J., Genier, F. S., Li, H., Biria, S. & Hosein, I. D. A Solid Polymer Electrolyte from Cross-Linked Polytetrahydrofuran for Calcium Ion Conduction. *ACS Appl. Polym. Mater.* 1, 1837-1844 (2019). 5. Yao, T., Genier, F. S., Biria, S. & Hosein, I. D. A solid polymer electrolyte for aluminum ion conduction. *Results Phys.* 10, 529-531 (2018).

SESSION F.EN04.28: Poster Session II: 2D Materials—Synthesis, Properties and Device Applications  
On Demand Abstracts Available for Viewing Starting Saturday Morning, November 21, 2020  
5:00 AM - 8:00 AM  
F-EN04

#### **F.EN04.28.02**

**MoS<sub>2</sub> Based High-Performance FET Devices for Memory Circuits on Flexible Platform** [Sayani Majumdar](#)<sup>1</sup>, Miika Soikkeli<sup>1</sup>, Ioannis Zeimpekis<sup>2</sup>, Nikolaos Aspiotis<sup>2</sup>, Chung-Che Huang<sup>2</sup>, Sanna Arpiainen<sup>1</sup> and Mika Prunnila<sup>1</sup>; <sup>1</sup>VTT Technical Research Centre, Finland; <sup>2</sup>University of Southampton, United Kingdom

Two-dimensional transition metal dichalcogenides (TMDs) are fertile ground for fundamental material science and emergent applications in high-performance electronics. The mechanical flexibility of 2D materials allows their incorporation in variable form factor designs such as smart wearables and foldable electronics, where their electronic and optical properties outperform conventional flexible materials such as organic polymers. In the current work, we present high-performance ALD grown MoS<sub>2</sub> based FET devices transferred on polyimide substrates. The growth method employs ALD to grow an MoO<sub>3</sub> layer on a 6 inch wafer which is subsequently annealed in an H<sub>2</sub>S atmosphere to convert to MoS<sub>2</sub>. The ALD allows for excellent uniformity and because the layer acts as a template the process is scalable to larger sizes. The resulting MoS<sub>2</sub> film is 2-3 layers thick. The film was transferred on the patterned target substrate using polystyrene assisted transfer of MoS<sub>2</sub> layer. More than 90% device yield, excellent current ON to OFF ratio of 106 and mobility values up to 32 cm<sup>2</sup> V<sup>-1</sup> s<sup>-1</sup> have been measured from micron scale devices with L/W in the range of two. We will present results on the yield and homogeneity on large area memory networks aiming for low power neuromorphic circuits.

#### **F.EN04.28.04**

**Infrared Permittivity of the Biaxial van der Waals Semiconductor  $\alpha$ -MoO<sub>3</sub> from Near- and Far-Field Correlative Studies** [Thomas Folland](#)<sup>1</sup>, Gonzalo Alvarez-Perez<sup>2</sup>, Ion Errea<sup>3</sup>, Javier Taboada-Gutierrez<sup>2</sup>, Ana I. Tresguerres-Mata<sup>2</sup>, Joseph R. Matson<sup>1</sup>, Andrei Bylinkin<sup>4</sup>, Mingze He<sup>1</sup>, Weiliang Ma<sup>5</sup>, Qiaoliang Bao<sup>6</sup>, Joshua D. Caldwell<sup>1</sup>, Alexey Nikitin<sup>4</sup> and Pablo Alonso-Gonzalez<sup>2</sup>; <sup>1</sup>Vanderbilt University, United States; <sup>2</sup>University of Oviedo, Spain; <sup>3</sup>University of Basque Country, Spain; <sup>4</sup>Donostia International Physics Center, Spain; <sup>5</sup>Huazhong University of Science & Technology, China; <sup>6</sup>Soochow University, China

The natural crystal anisotropy of van der Waals materials allows them to support a range of nanophotonic phenomena not observable in other natural materials. One such example is anisotropic phonon polaritons (PhPs), which form due to polar optic phonons in materials such as hexagonal boron nitride. Such hyperbolic polaritons have been shown to enable sub-diffraction guiding of light waves, sensing of ultra-thin analytes, and hyperlensing for super resolution imaging in the mid infrared (IR). Recently, the biaxial van der Waals semiconductor  $\alpha$ -phase molybdenum trioxide ( $\alpha$ -MoO<sub>3</sub>) has received

significant attention due to its ability to support PhPs which are anisotropic along all three crystal axes. These offer an unprecedented platform for controlling the flow of energy at the nanoscale, in particular for manipulating the polarization state of light. However, to fully exploit the extraordinary IR response of this material, an accurate dielectric function is required.

In this work, we report an accurate IR dielectric function of  $\alpha$ -MoO<sub>3</sub> by modelling far-field, polarized IR reflectance spectra acquired on a single thick flake of this material. Unique to our work, the far-field model is refined using the experimental dispersion and damping of PhPs revealed by using scattering-type scanning near-field optical microscopy (s-SNOM) on thin flakes of  $\alpha$ -MoO<sub>3</sub>. Through these correlative efforts, exceptional quantitative agreement is attained to both far- and near-field properties for multiple flakes, thus providing strong verification of the accuracy of our model. This also provides a novel approach to extracting dielectric functions of different 2D materials, usually too small or inhomogeneous for establishing accurate models only from standard far-field methods. Finally, by employing density functional theory (DFT), we provide insights into the various vibrational states dictating our dielectric function model and the intriguing optical properties of  $\alpha$ -MoO<sub>3</sub>.

#### **F.EN04.28.05**

**Feedback-Controlled Electroburning of MoS<sub>2</sub> Monolayers** Yan Qi Huan<sup>1</sup>, Yincheng Liu<sup>1</sup>, Choon Hwa Ken Goh<sup>1</sup>, Kuan Eng Johnson Goh<sup>1,2</sup>, Swee Liang Wong<sup>1,2</sup> and Chit Siong Lau<sup>1</sup>; <sup>1</sup>Institute of Materials Research and Engineering, Singapore; <sup>2</sup>National University of Singapore, Singapore

Two-dimensional materials have been identified as interesting candidates for various applications in nano-electronics, and the characterization of electrical breakdown limits is a crucial step in device development. However, methods for repeatable measurements have been scarce in two-dimensional materials, where breakdown studies have been limited to destructive methods. This lack of repeatability restricts our ability to fully account for variability in local electronic properties induced by the fabrication process and surface contaminants.

To tackle this, we implement a two-step deep-learning model to predict the breakdown mechanism and breakdown voltage of monolayer MoS<sub>2</sub> devices with varying channel lengths and resistances using current measured in the low-voltage regime as inputs. A deep neural network (DNN) first classifies between Joule and avalanche breakdown mechanisms with partial current traces from 0–20V. Following this, a convolutional long short-term memory network (CLSTM) predicts breakdown voltages of these classified devices based on user-defined partial current traces.

We test our model with feedback-controlled electrical measurements to achieve non-destructive electrical measurements that limit device damage and increase the amount of data collected. We show that the DNN classifier achieves an accuracy of 74% while the CLSTM model has a 14% error when requiring only 80% of the current trace as inputs. Our results indicate that information encoded in the current behavior far from the breakdown point can be used for predictions, thus enabling non-destructive and fast material characterization for 2D material device development.

#### **F.EN04.28.06**

**Synthesis and Characterization of MXene-WS<sub>2</sub> Heterostructure Devices** Venkata Surya N Chava, Aruna Narayanan Nair and Sreerasad T. Sreenivasan; The University of Texas at El Paso, United States

Atomically thin two-dimensional (2D) materials such as graphene, MoS<sub>2</sub>, WS<sub>2</sub> show excellent material properties and therefore studied extensively for a variety of applications including electronics, optoelectronics, electrocatalysis, energy storage, etc. More recently, there has been a growing interest in 2D heterostructure devices as they offer unique opportunities to design and study possibilities for controlling and manipulating the carrier confinement and transport of charge within these device structures. Tungsten disulfide (WS<sub>2</sub>) is an excellent material for optoelectronic applications such as photodetectors as monolayer WS<sub>2</sub> has a direct bandgap of  $\sim 2.05$  eV. Also, recently emerged as MXenes has shown great promise in energy storage and electromagnetic shielding applications due to excellent metallic conductivity. The MXenes can show either metallic or semiconducting behavior depending on the functional groups attached to the surface during the etching process. In particular, their tunable work function property can be exploited to control the properties of the heterostructure of MXenes with other layered 2D materials. Here, we report the characterization results of one such heterostructure formed by combining MXenes with WS<sub>2</sub>. MXene is synthesized by etching the Al layer from the parent MAX phase, and WS<sub>2</sub> is synthesized on SiO<sub>2</sub>/Si substrates using the CVD process. The electrical properties of these as-synthesized materials can be modified using different approaches such as chemical doping etc. We present results from different morphological, spectroscopic and electrical characterization techniques that are used to study the transport characteristics of these MXene-WS<sub>2</sub> heterostructure devices.

#### F.EN04.28.08

**Photo-Thermoelectric Effect along Waveguide-Integrated Graphene Photodetectors** Jakob Muench, Hannah Watson, Osman Balci, Alfonso Ruocco and Andrea C. Ferrari; Cambridge Graphene Centre, United Kingdom

The dominating mechanism of photodetection in a single-layer graphene (SLG) based device depends on the design of the detector [1,2,3], its chosen operation [1,3], and the band diagram in the photo-active region [2,4]. Here we demonstrate, over a  $\sim 0.5\text{eV}$  doping range, that the photo-thermoelectric effect [5] has a long-range (exceeding the cooling length in SLG) contribution, even in uniformly doped SLG, in the absence of a Seebeck coefficient gradient, whenever non-uniform absorption creates an electronic temperature gradient. This is achieved by integrating SLG with on-chip Si waveguides to generate an heterogeneous absorption profile over tens  $\mu\text{m}$  and placing electrical probes along the propagation direction of light. We show the presence of a photovoltage  $V_{\text{ph}}$  along the waveguide. The doping-dependence of  $V_{\text{ph}}$  suggests signal generation by hot electrons via the Seebeck effect. This has general implications for the design and optimization of optoelectronic devices based on SLG, in particular for integrated photonics, where planar integration of layered materials leads to non-uniform absorption. [1] F. H. L. Koppens et al., Nat. Nanotechnol., 9, 780, (2014). [2] T. Echtermeyer et al., Nano Lett., 7, 3733, (2014) [3] M. Romagnoli et al., Nat. Rev. Mater., 3, 392, (2018). [4] V. Shautsova et al., Nat. Comm., 9, 5190, (2018). [5] N. Gabor et al., Science, 334, 648, (2011).

#### F.EN04.28.12

**Unraveling Nonlinear Formation and Relaxation of Excitons in Atomically Thin 2D Semiconductors** Matthew C. Strasbourg<sup>1</sup>, Cory Johns<sup>1</sup>, Thomas Darlington<sup>2</sup>, James Hone<sup>2</sup>, P James Schuck<sup>2</sup> and Nicholas Borys<sup>1</sup>; <sup>1</sup>Montana State University, United States; <sup>2</sup>Columbia University, United States

Transition metal dichalcogenide (TMD) semiconductors are layered van der Waals materials that exhibit exceptional optoelectronic properties in monolayer form. Their atomically thin nature and reduced long-range dielectric screening make them ideal systems in which to study many-body electronic states. Notably, excitonic many-body phenomena govern the light-matter interactions in TMD semiconductors and open up new possibilities for novel optoelectronic devices, including new classes of quantum light sources. Thus, understanding the rich suite of many-body phenomena in these systems is motivated by potential applications in on-chip optoelectronics and by the insights that can be gained into the fundamental interactions that govern TMD material properties. Here, the dynamics of several higher-order excitons including trions, biexcitons, and charged biexcitons in monolayer-WSe<sub>2</sub> are probed using temperature-, energy-, and power-dependent time-resolved optical spectroscopy. The properties of these multiexciton states build on the unique many-body physics of the single-excitons in TMDs. These studies reveal a complex interplay between the multiexcitons and single-excitons that depends on both the density and excitation energy of the initial exciton population. In addition, the presence of defect-bound excitons is found to drastically alter the formation of multiexcitons. This competition between exciton trapping and multiexciton formation highlights the need for high-quality materials to enhance multiexciton physics. By exploring this parameter space of excitation energy, excitation density, and defect density, complex many-body interactions are revealed that suggest means to optimize multiexciton yields and thus capitalize on the emergent characteristics of multiexciton emission and exciton-multiexciton interactions that are unique to monolayer-WSe<sub>2</sub>. These observations open new doors to a number of applications such as entangle photon pair production and lasing, highlighting the importance of understanding the formation and relaxation dynamics of the rich manifold of excitons in order to leverage 2D semiconductors for advanced technologies.

#### F.EN04.28.13

**Computational Synthesis of 2D Materials—A High-Throughput Approach to Materials Design** Tara M. Boland and Arunima Singh; Arizona State University, United States

The emergence of two dimensional (2D) materials opened up many potential avenues for novel device applications such as nanoelectronics, topological insulators, field effect transistors, microwave and terahertz photonics and many more. To date there are over 1,000 theoretically predicted 2D materials. Of those theoretical materials, only 55 have been experimentally synthesized due to the difficulty in finding a suitable substrate which simultaneously stabilizes the 2D phase over of bulk phase while preserving the novel materials properties resulting from quantum confinement. One avenue to aid in the development of these novel 2D materials is to explore and predict suitable substrates which will stabilize the 2D growth using computational methods. In this work a high-throughput approach to density functional theory is used to explore the viability of various common substrates to stabilize and grow these novel theoretically predicted 2D materials. This work analyzes three key factors which determine the stability of synthesizing 2D materials via substrate assisted methods such as chemical vapor deposition. The results will provide guidance to future experimental efforts to synthesize these 2D materials.

Using various 2D materials databases and van der Waals corrected density functional theory we investigate the suitability of 12 substrates to stabilize 2D growth. First, the formation energy of the 2D material is computed relative to the most stable bulk phase. A 2D material with a high formation energy implies the material will likely only be synthesized via substrate assisted methods thus making it a good candidate material for this study. Computational synthesis can be broken down into a two-step process: the formation of the 2D flake from the bulk phase, the formation energy, and adsorption of the 2D material on a symmetry-matched and low lattice-matched substrate surface, the binding energy. When the adsorption energy, the difference between the formation from the binding energy, is less than zero the adsorption is spontaneous, exothermic, and stable. For materials which meet this criteria, the density of states is computed to characterize the electronic properties of these materials for device applications. 1. We gratefully acknowledge ASU's HPC staff for support and assistance with computing resources along with the Extreme Science and Engineering Discovery Environment (XSEDE), for support by National Science Foundation grant number ACI-1548562, through award number TG-DMR-150006. We gratefully acknowledge the National Science Foundation grant DMR-1308085 and Arizona State University for funding.

#### **F.EN04.28.14**

**Surface Protection of 2D Black Phosphorus with Greatly Enhanced Photoluminescence and Stability** Dongying Li and Cun-Zheng Ning; Arizona State University, United States

Black phosphorus (BP) has gained intense interests because of its tunable direct bandgap, leading to emission with photon energies from  $\sim 1.7\text{eV}$  for monolayer to  $\sim 0.35\text{eV}$  for bulk [1]. This makes few-layer BPs one of the very few 2D infrared materials, especially in communication wavelengths. Besides, BP has a strong anisotropy compared with other 2D materials due to its puckered honeycomb lattice. It leads to many interesting phenomena such as strong coupling between phonon and carriers [2]. Thus BP is an appealing 2D platform for investigating novel physics and device applications. However, few-layer BP degrades quickly in the ambient environment due to the interaction with oxygen under light excitation. Such instability causes great difficulty in investigating properties of few-layer BP and in exploring the practical applications. Although BP protection methods are reported with verified good electronic properties, there is no report on stabilized BP with enhanced photoluminescence (PL) under ambient environment. Here we report an approach to realize BP with greatly enhanced PL (by as much as 160 times) that can be stable under ambient environment for months. We adopt a three-step method to prepare BP covered by boron nitride (BN) from both sides. First, thin flakes of BP and BN are exfoliated onto PDMS layers, followed by successive transfers of the bottom BN and then BP onto SiO<sub>2</sub> (270nm)/ Si substrate. Second, oxygen plasma is used to thin down BP to desired thickness or numbers of layers. The oxygen plasma also leaves an oxide layer on top of the thinned-down BP at the end of the process. Third, we transfer the top BN onto the oxide covered BP which is then followed by thermal annealing. This process leads to oxygen doped few-layer BP with BN binding tightly from both sides to protect BP from the environment, highly improving the stability of BP. Raman spectroscopy indicates the sandwiched BP is defective. The breathing mode shows broadening and redshift. Ag1 and Ag2 modes both split into two subpeaks. These are the signs of introduction of oxygen defects in BP. PL of oxygen doped BP shows two-order of magnitude enhancement compared with freshly etched BP, which can be explained by bound exciton luminescence. Few-layer BP produced this way shows remarkable stability. The PL line-shape and intensity of sandwiched BP are barely changed when kept in the ambient environment under room temperature. A 3-layer BP sample prepared by such method, 5 months after preparation, PL intensity is still  $\sim 80\%$  of that measured as prepared. At an elevated temperature of  $90^\circ\text{C}$ , oxygen can escape from BP, which will result in redshift of PL peak and decreased PL intensity. 7 months after preparation, the 3-layer BP sample still shows strong PL, at  $\sim 70\%$  of the original PL intensity right before TEM measurement. TEM results show close contact between BP and BN and three BP layers can be clearly identified from side view. Quite low oxygen concentration in BP layers is consistent with the assumption that oxygen escapes from BP with time. A 4-layer BP with comparable intensity to that of the 3-layer sample made by this method shows the possible general validity of this approach. In summary, our method can produce highly stable BP with excellent PL intensity induced by oxygen defects, allowing the study of rich physics in defective BP. Furthermore, it can pave the way for research on BP-based photonic devices such as lasers, modulators, etc. [1] Li, Likai, et al. "Direct observation of the layer-dependent electronic structure in phosphorene." *Nature nanotechnology* 12.1 (2017): 21. [2] Pelant, Ivan, and Jan Valenta. *Luminescence spectroscopy of semiconductors*. Oxford University Press, 2012.

#### **F.EN04.28.15**

**Large Voltage Generation Through Liquid Motion on Single-Layer MoS<sub>2</sub>** Adha Sukma Aji<sup>1</sup>, Ryohei Nishi<sup>1</sup>, Hiroki Ago<sup>2</sup> and Yutaka Ohno<sup>1</sup>; <sup>1</sup>Nagoya University, Japan; <sup>2</sup>Kyushu University, Japan

Dynamics of water is one kind of clean energy source which readily available in our surrounding environment. Recently, the direct conversion of liquid motion energy into electricity by two-dimensional (2D) materials such as graphene has gained much interest [1-3]. However, the reported output voltage values generated by liquid motion on the graphene surface are

limited to millivolts order. With these output voltage values, the graphene nanogenerators might be difficult to drive conventional silicon-based electronics. Thus, an alternative to semimetallic graphene as an active material is needed to boost the output voltage. Here we report a single-layer MoS<sub>2</sub> nanogenerator to generate electricity from liquid movement on its surface. The centimeter-scale single-layer MoS<sub>2</sub> sheets were prepared by using chemical vapor deposition on sapphire substrate (3 × 1 cm) with MoO<sub>3</sub> and sulfur powder as precursors. Then, the MoS<sub>2</sub> was transferred onto polyethylene naphthalate (PEN) substrate. The device was finalized by applying silver epoxy as electrical contact on both ends of MoS<sub>2</sub> and a silicone film as electrode protection from liquid. To generate electricity, aqueous 1 M NaCl were dropped on the MoS<sub>2</sub> surface on a stage inclined at 45°. Due to the high hydrophobicity of MoS<sub>2</sub>, the droplets easily slid on the MoS<sub>2</sub> surface, generating an open-circuit voltage of ~6 V. This output voltage value is significantly higher than graphene nanogenerators previously reported [1-3]. The short-circuit current of ~5 nA was generated from liquid movement on the MoS<sub>2</sub> surface. The power produced by droplet movement is about 1.7 nW at load resistance of 200 MΩ. We also show the high scalability of our MoS<sub>2</sub> nanogenerator by arranging them in series and parallel connections. The open-circuit voltage and short-circuit current were multiplied about three times by connecting three identical MoS<sub>2</sub> nanogenerators in series and parallel connection, respectively. In conclusion, we showed the large-area single-layer MoS<sub>2</sub> nanogenerator, which is capable of generating output voltage more than 5 V from liquid motion. Seeing the exceptional mechanical and electrical property of single-layer MoS<sub>2</sub>, the realization of self-powering untethered wearable device based on 2D materials will soon become fulfilled. Reference: [1] J. Yin et al., Nat. Nanotechnol. 9, 378 (2014) [2] D. Park et al., Nano Energy 54, 66 (2018) [3] S. S. Kwak et al., ACS Nano 10, 7297 (2016)

#### **F.EN04.28.16**

##### **Greenhouse Gas Sensor Constructed with Two-Dimensional Quantum Dots Platform with Anchored Electroactive Conducting Polymer** Reeba Thomas and Kalathur Santhanam; Rochester Institute of Technology, United States

Recently, there has been active interest in developing greenhouse gas sensors for understanding the influence of these gases in controlling the atmosphere and the weather (1,2). We wish to report here, a greenhouse gas sensor that has been developed using 2D graphene quantum dots (3) platform on alumina substrate containing platinum interdigitated electrodes on one side and heating resistors on the other side of the platform with an electroactive conducting polymer, as the 2D structure provides a large surface area for the active material making it more sensitive for detection and measurements. The sensor operates in two stages; in the first stage the response of the interfering gases is measured and in the second stage a thermal pulse is applied corresponding to the desorption energies of the interfering gases. The temperature on the active material was measured using an infrared thermometer. The electroactive conducting polymer was electrochemically synthesized at a graphene quantum dots electrode by a potential step electrolysis at 1.00 V vs SCE. The experiments conducted with graphene quantum dots dispersed in the electrolytic medium, shows the monomer well coupled with graphene prior to the polymerization. The polymer coupled graphene shows D and G bands arising from graphene in Raman imaging spectroscopy. The mechanistic pathways has been unraveled by Raman imaging, Fourier transform infra-red spectroscopy, UV-VIS absorption spectroscopy, and scanning electron microscope. The results suggest that 2D platform for the active material for sensing enhances the performance of the sensor with a temperature-controlled selectivity. 1. D. Shukman, Greenland's ice faces melting 'death sentence', <https://www.bbc.com/news/science-environment-49483580> 2. K.S.V. Santhanam and N. Ahamed, Chemical Engineering (MDPI), 2,38 (2018) 3. K.S.V. Santhanam, S. Kandlikar, M. Valentina and Y. Yang, US patent No. 9840782, December 12, 2017

#### **F.EN04.28.20**

##### **Edge-Contacted 2D Transition Metal Dichalcogenide (TMD) Transistors** Hattan Abuzaid, Zhihui Cheng and Aaron D. Franklin; Duke University, United States

Two-dimensional (2D) transition metal dichalcogenides (TMDs) have emerged as a promising transistor channel material because of their inherent atomic thinness, which can allow further scaling of channel length. In order to miniaturize transistors in future technology nodes, not only the channel length, but also the contact length (L<sub>c</sub>) needs to be scaled as L<sub>c</sub> constitutes a significant portion of the device's integrated pitch/density. Researchers have suggested the use of edge contacts to enable maximum scalability; in this configuration, the channel is contacted via its side edges along the same lateral plane as the contacts. Since the injection area is practically independent of the actual L<sub>c</sub>, the performance of edge contacts can be L<sub>c</sub>-independent [1], thus allowing much better scalability compared to traditional top contacts. In addition, edge contacts are hypothesized to form covalent bonds with the TMD channel, which should translate to better carrier injection. Published work on edge-contacted TMD transistors has predominantly focused on MoS<sub>2</sub> as the channel material. Since chemically dissimilar TMDs interact distinctly with different metal contacts, further research on other promising TMDs, such as MoTe<sub>2</sub> and WSe<sub>2</sub> is warranted. In this work, we created clean edge contacts to TMD channels utilizing our previously established method [1] using an in-situ Ar<sup>+</sup> ion beam in an integrated electron beam evaporation chamber. We discovered that the

etching behavior of the TMDs varied, and thus the realization of clean edge contacts required custom fabrication processes. The role of contact metal is elucidated for each TMD, along with analysis of top- versus edge-contacted devices on the same TMD flake or domain. These results provide key insights on how metal selection and channel thickness influence the device performance for various edge-contacted TMD transistors. References [1] Cheng, Zhihui, et al. "Immunity to Contact Scaling in MoS<sub>2</sub> Transistors Using In Situ Edge Contacts." *Nano letters* 19.8 (2019): 5077-5085.

#### **F.EN04.28.21**

**Scalable and Stable Intercalation of Li<sup>+</sup> into Multi-Layer CVD Graphene for Controlled Optical and Electronic Properties** Joseph Andrade<sup>1</sup>, Jan Folkson<sup>1</sup>, Amanda Carr<sup>1</sup>, Mohamed Boukhicha<sup>2</sup> and Matthew Eisaman<sup>1</sup>; <sup>1</sup>Stony Brook University, The State University of New York, United States; <sup>2</sup>Brookhaven National Laboratory, United States

While graphitic intercalant compounds (GICs) have been thoroughly studied for application in battery technologies, use of these materials for transparent conductive electrodes (TCEs) has remained fairly unexplored. Although individual layers of 2D graphene promise high intrinsic mobility and transparency, its inherent properties do not rival those of current industry-standard materials. However, with lithium-ion intercalated multi-layer graphene grown via chemical vapor deposition (CVD), we produce large-scale LiC<sub>6</sub> films whose electrical and optical properties are expected to surpass TCE requirements. With the developed sample design, we present preliminary data suggesting a path toward scalable and stable films for TCE application.

#### **F.EN04.28.22**

**Steric and Electronic Effects at Polymer-2D Materials Interfaces** James Nicolas M. Pagaduan, Nicholas Hight-Huf, Avdhoot Datar, Reika Katsumata, Michael Barnes, Ashwin Ramasubramaniam and Todd Emrick; University of Massachusetts Amherst, United States

This presentation will describe the impacts of steric and electronic interactions of zwitterionic polymers in contact with two-dimensional (2D) materials. Modulation of the work function of 2D materials facilitates charge injection and improves device performance for several applications such as solar cells, electronic displays, and organic light emitting diodes. The work function of 2D materials has been tailored by gas absorption, mechanical strain, and chemical doping methods. Polymer coatings have also been applied to tune the work function of 2D materials via non-covalent adsorption, offering possibilities for designing novel hybrid organic-inorganic functional materials. However, little is known about the precise role of functional group orientation on work function modulation. Here, we select graphene as a model 2D system and systematically examine work function modulation arising from coatings of functional poly(sulfobetaine methacrylate) (PSBMA). This approach maintains the desirable structural and electronic properties of graphene while exclusively altering its surface potential via the polymer coating. Work function modulation was observed by ultraviolet photoelectron spectroscopy and Kelvin probe force microscopy. First-principles density functional theory calculations provided insights into the preferred configurations of zwitterionic SBMA pendent groups physically adsorbed on graphene sheet, resultant dipole moment, and possible range of work function shifts that are achievable. Overall, this method of work function engineering permits scalable patterning of polymer films and precise spatial control over carrier doping for fabrication of monolayer graphene-based devices.

#### **F.EN04.28.23**

**Ni-Decorated Graphene Microchannel for Self-Activated Gas Sensors with Enhanced Response to Ethanol** Taehoon Kim<sup>1</sup>, Yeonhoo Kim<sup>2</sup>, Seo Yun Park<sup>1</sup> and Ho Won Jang<sup>1</sup>; <sup>1</sup>Seoul National University, Korea (the Republic of); <sup>2</sup>Los Alamos National Laboratory, United States

Graphene, one of the most popular two-dimensional (2-D) materials, has been studied with high interests owing to its outstanding properties such as high thermal and electrical conductivity, easy surface decoration, and transparency with flexibility. These remarkable advantages led to the studies of graphene in varied applications including gas sensors. However, for various applications, graphene-based gas sensors have to solve various problems such as power consumption by external heaters, insufficient selectivity, and method of mass production. In this work, we report ethanol gas detection of nickel nanoparticles decorated on graphene layers which are self-activated by applied bias voltage from 1 to 5 V. The graphene is prepared by chemical vapor deposition (CVD) method and we designed a narrow graphene channel to generate heat by using a joule heating effect while working as a sensing area. Since graphene is a 2-D material, both active sensing area and electrodes composed of graphene could be easily defined by facile lithography processes. Nickel nanoparticles are deposited by the e-beam evaporator. The gas sensing properties to various gases such as NO<sub>2</sub>, H<sub>2</sub>, C<sub>2</sub>H<sub>5</sub>OH, and NH<sub>3</sub> have been tested at room temperature while regulating the input bias voltages. Our results show superior ethanol gas detection of nickel nanoparticles decorated graphene sensors at room temperature. These results broaden the potential of graphene-based gas



sensors for real applications.

#### **F.EN04.28.24**

**New Low Bandgap Graphenic Semiconductors for Solar Cells and Photocatalysts** Pawan Kumar<sup>1</sup>, Ryan Kisslinger<sup>1</sup>, Sheng Zeng<sup>1</sup>, Guy Bernard<sup>1</sup>, Sergey Gusarov<sup>2</sup>, Alexander Kobryn<sup>2</sup>, Kazi Alam<sup>1</sup>, Vladimir Michaelis<sup>1</sup> and Karthik Shankar<sup>1</sup>; <sup>1</sup>University of Alberta, Canada; <sup>2</sup>National Research Council Canada, Canada

Graphenic semiconductors (GSCs) are an emerging class of energy materials based on the sp<sup>2</sup>-hybridized graphene motif that either by themselves or in composites, have demonstrated excellent performance for the electrochemical reduction of CO<sub>2</sub>, the photoelectrochemical splitting of water to generate H<sub>2</sub>, and the photocatalytic reduction of CO<sub>2</sub>. GSCs have a range of astonishing properties such as high catalytic activity, strong visible light absorption, exceptional chemical stability, thermal stability until at least 350 deg. C, and facile compositional and electrical doping. GSCs are typically synthesized by low cost solvothermal and annealing processes that lend themselves to scale-up and mass production. The most prominent member of this family of compounds is g-C<sub>3</sub>N<sub>4</sub>, which has a relatively wide bandgap of 2.6 eV. Herein, we report on the synthesis, characterization and solar energy applications of a number of new GSCs [1-5]. C<sub>3</sub>N<sub>5</sub> is a novel modified carbon nitride framework with a remarkable 3:5 C:N stoichiometry and an electronic bandgap of 1.76 eV which was formed by thermal deamination of a precursor consisting of melem hydrazine [1]. The two s-heptazine units in the polymeric C<sub>3</sub>N<sub>5</sub> are bridged together with an azo linkage, which constitutes an unconventional bonding arrangement, different from g-C<sub>3</sub>N<sub>4</sub> where three heptazine units are linked together with tertiary nitrogen. C<sub>3</sub>N<sub>5</sub> exhibits extended conjugation due to overlap of azo nitrogens and increased electron density [1]. C<sub>3</sub>N<sub>5</sub> was found to be an excellent electron transport layer for perovskite solar cells, and a good photocatalyst for the photoreduction of 4-nitrobenzenethiol into 4,4'-dimercaptoazobenzene. Even lower bandgap analogs of C<sub>3</sub>N<sub>5</sub> were synthesized and characterized. We also formed highly luminescent quantum dots of g-C<sub>3</sub>N<sub>4</sub> doped with P, F or Cl. Intimate heterojunctions of doped g-C<sub>3</sub>N<sub>4</sub> quantum dots with BiOI and TiO<sub>2</sub> were demonstrated to be excellent photoanodes for visible light-driven water splitting, achieving photocurrent densities as high 2.5 mA cm<sup>-2</sup> under AM1.5G simulated sunlight [2-3]. REFERENCES 1. P Kumar, E Vahidzadeh, UK Thakur, P Kar, KM Alam, A Goswami, N Mahdi, K Cui, GM Bernard, VK Michaelis and K Shankar, "C<sub>3</sub>N<sub>5</sub>: A Low Bandgap Semiconductor Containing an Azo-Linked Carbon Nitride Framework for Photocatalytic, Photovoltaic and Adsorbent Applications", Journal of the American Chemical Society, 2019, 141, 13, 5415-5436. 2. P Kumar et al. "Noble Metal Free, Visible Light Driven Photocatalysis Using TiO<sub>2</sub> Nanotube Arrays Sensitized by P-doped C<sub>3</sub>N<sub>4</sub> Quantum Dots", Advanced Optical Materials (in press), 2019. 3. KM Alam, P. Kumar, P Kar, A Goswami, UK Thakur, S Zeng, E Vahidzadeh, K Cui and K Shankar, "Heterojunctions of halogen-doped carbon nitride nanosheets and BiOI for sunlight-driven water-splitting", Nanotechnology, 2019, doi: 10.1088/1361-6528/ab4e2c. 4. C Ott et al. "Flexible and Ultrasoft Inorganic 1D Semiconductor and Heterostructure Systems Based on SnIP", Advanced Functional Materials, 2019, 29, 1900233. 5. KM Alam, P Kumar, AP Manuel, E Vahidzadeh, A Goswami, S Zeng, W Wu, N Mahdi, K Cui, AE Kobryn, S Gusarov, Y Song and K Shankar, "CVD grown nitrogen doped graphene is an exceptional visible-light driven photocatalyst for surface catalytic reactions", 2D Materials, 2019, 7, 015002.

#### **F.EN04.28.25**

**Enhanced Environmental Stability Coupled with a 12.5% Power Conversion Efficiency in an Aluminum Oxide-Encapsulated n-Graphene/p-Silicon Solar Cell** Serdar Yavuz, Eric Martinez Loran, David P. Fenning and Prab Bandaru; University of California, San Diego, United States

A significant improvement in the power conversion efficiency (PCE) and the environmental stability of n-Graphene/p-Si solar cells is indicated through effective n-doping of graphene, using low work function oxide capping layers. AlOx, deposited through atomic layer deposition, is particularly effective for such doping and in addition serves as an antireflection coating and a cell encapsulating layer. It is shown that the related charge transfer doping and interfacial engineering was crucial to achieve a record PCE of 12.5%. The work indicates a path forward, through work function engineering, for further efficiency gains in Gr-based solar cells

#### **F.EN04.28.26**

**Electron Emission from Epitaxial Graphene Microribbons Towards Emission of Soft X-Rays** Daniel Lewis and Kevin Daniels; University of Maryland, United States

X-rays have been used for decades in medical diagnostic imaging, but the presence of metal scattering interference centers can limit their effectiveness. Longer wavelength sources may mitigate this effect, but risk poor imaging from low x-ray fluence. To produce a sufficient density of low-power x-rays to allow imaging of targets with metal inclusions, the x-ray current source would require a proportionate increase in output. Graphene nanoribbons crafted by CVD[1] or arc discharge[2]

have been shown to exhibit electron emission under bias, with theoretical outputs exceeding thermionic or field emission sources of similar dimensionality and applied bias conditions. Epitaxial graphene, able to be synthesized on the wafer-scale and compatible with current fabrication techniques, can be readily processed into ribbons with superior mechanical and electrical capabilities to its CVD or arc discharge counterparts. With even low applied bias (3 - 5 V) graphene nanoribbons (0.5 - 1  $\mu\text{m}$  long, 10-30 nm wide) suspended in high vacuum exhibited phonon-assisted electron emission (PAEE)[1][2], resulting in emission currents being produced at internal electric fields and external pulling voltages both nearly  $10^2$  less than comparable thermionic or field emission sources. Emissions exhibited repeatable directionality out of the plane of the ribbons, offering a means to mechanically control the orientation of the output current; ribbons crafted from epitaxial graphene, with deposited electrodes to provide the bias, would emit out of the plane of the substrate, enabling even macro-scale directional control. Fabrication of epitaxial graphene microribbons is readily accomplished via a combination of electron beam lithography and plasma etching, while relevant metal depositions are completed with electron beam evaporation. Patterned-photoresist masks allow for precise plasma etching to isolate the ribbons and electrodes in order to craft emission arrays of arbitrary numbers, dimensions, and positions, facilitating arrangements for rapid testing of device parameters and capabilities. Metals deposited on plasma-etched surfaces allow for external ball- and wedge-bonding of gold wire, resulting in test setup and device controls being significantly cheaper, faster, easier, and more robust than those presented in referenced works. Emission currents can be measured via a straightforward setup with the devices (cathodes) and a phosphor screen (anode) positioned in a vacuum chamber with feed-through contacts for control and measurement. Results of captured currents from various dimensions, arrangements, and applied biases of the graphene microribbon emitters and arrays are provided in both absolute terms, as well as normalized to more conventional dimensions and energizing voltages of comparable thermionic and field emission electron sources. By crafting microribbon emitters in various combinations of dimensions and arrangements, and isolating control circuits from each other, it should even be possible to craft a single physical device that could alternately function as multiple different sources, either independently or in concert as need dictates. Electron sources crafted in this fashion are expected to exhibit greater output, durability, flexibility, and cost savings compared to other electron sources of comparable dimensionality and power requirements. Presented here is a treatment of the preparation, fabrication, and testing of these epitaxial graphene microribbon electron emission arrays intended as sources for low-power x-ray imaging applications. 1. Wei, X. L.; Golberg, D.; Chen, Q.; Bando, Y.; Peng, L. M.; Phonon-Assisted Electron Emission from Individual Carbon Nanotubes. *Nano Lett.* 2011, 11, 734-739. 2. Wei, X.; Bando, Y.; Golberg, D.; Electron Emission from Individual Graphene Nanoribbons Driven by Internal Electric Field. *ACS Nano*, 2012, 6, 705.

#### F.EN04.28.27

**Full Consideration of Acoustic Phonon Scatterings in Two-Dimensional Dirac Materials** Yia-Chung Chang and Khoe Van Nguyen; Academia Sinica, Taiwan

The in-plane acoustic phonon scattering in graphene is solved by considering fully inelastic acoustic phonon scatterings in two-dimensional (2D) Dirac materials for large range of temperature ( $T$ ) and chemical potential ( $\mu$ ). Rigorous analytical solutions and symmetry properties of Fermionic and Bosonic functions are obtained. We illustrate how doping alters the temperature dependence of acoustic phonon scattering rates. It is shown that the quasi-elastic and ansatz equations previously derived for acoustic phonon scatterings in graphene are limiting cases of the inelastic-scattering equations derived here. For heavily-doped graphene, we found that the high- $T$  behavior of resistivity is better described by  $\rho(T, \mu) \sim T^{-1} [1 - \mu^2/3(k_B T)^2]$  rather than a linear  $T$  behavior, and in the low  $T$  regime we found  $\rho^{-1} \sim (k_B T)^4$  but with a different prefactor (i.e.  $\sim 3$  times smaller) in comparison with the existing quasi-elastic expressions. Furthermore, we found a simple analytic "semi-inelastic" expression of the form  $\rho^{-1} \sim (k_B T)^4 / (1 + cT^3)$  which matches nearly perfectly with the full inelastic results for any temperature up to 500 K and  $\mu$  up to 1 eV. Our simple analytic results agree well with previous first-principles studies and available experimental data. Our analyses pave a way for investigating scatterings between electrons and other fundamental excitations with linear dispersion relation in 2D Dirac material-based heterostructures such as bogolon-mediated electron scattering in graphene-based hybrid Bose-Fermi systems.

SESSION F.EN04.29: Poster Session III: Beyond Lithium-Ion Batteries—Materials, Architectures and Techniques  
On Demand Abstracts Available for Viewing Starting Saturday Morning, November 21, 2020  
5:00 AM - 8:00 AM  
F-EN04

#### F.EN04.29.01

### **Metal–Organic Frameworks Encapsulated with Vanadium-Substituted Heteropoly Acid for Highly Stable Asymmetric Supercapacitors** Nageh K. Allam; The American University in Cairo, Egypt

Herein, we report on a facile one-pot synthesis of polyoxometalates encapsulated zeolite imidazolate framework cages ( $\text{PMo}_{10}\text{V}_2@\text{ZIF-67}$ ). The morphological and structural properties of the as-synthesized materials were investigated *via* FESEM, EDS, XRD and FTIR techniques. Moreover,  $\text{N}_2$  adsorption/desorption isotherms, and XPS measurements were carried out to elucidate the textural properties and composition of the fabricated materials. Upon their use as supercapacitor electrodes, the  $\text{PMo}_{10}\text{V}_2@\text{ZIF-67}$  electrode exhibited a maximum specific capacitance of 765 F/g at a scan rate of 5 mV/s. Furthermore, a supercapacitor device was assembled using activated carbon as the negative electrode and  $\text{PMo}_{10}\text{V}_2@\text{ZIF-67}$  as the positive electrode, delivering a specific power of 702 W/kg and corresponding specific energy of 20.9 Wh/kg at a charging current density of 1 A/g. In addition, the device shows excellent long term stability and high Columbic efficiency over 5000 charging and discharging cycles at charging and discharging current density of 5 A/g.

#### **F.EN04.29.02**

### **Recycling of Li-Ni-Mn-Co Hydroxide from Spent Batteries to High-Performance Supercapacitors with Exceptional Stability** Nageh K. Allam; American University in Cairo, Egypt

The intensive implementation of Li-ion batteries in many markets makes it increasingly urgent to address the recycling of strategic materials from spent batteries. Batteries typically contain toxic chemicals and cannot be disposed of at will. In this study, Li-Ni-Mn-Co hydroxides are successfully recycled from spent Li-ion batteries electrodeposited on nickel foam and fully characterized using different techniques such as field emission scanning electron microscopy (FESEM), x-ray diffraction (XRD), energy-dispersive X-ray spectroscopy (EDXS), inductively coupled plasma (ICP), and X-ray photoelectron spectroscopy (XPS) techniques. The recycled nanostructured films are tested in a three-electrode electrochemical system to investigate their capacitance behavior. The recycled electrodes show a high capacitance of 951 F.g<sup>-1</sup> (Specific capacity of 523.5 C. g<sup>-1</sup>) at 1 A.g<sup>-1</sup>. Moreover, recycled materials are used as positive electrodes to construct asymmetric supercapacitor devices. The device shows a Coulombic efficiency of 100%, capacitance retention reaching ~90% with excellent cycling stability after 10,000 cycles as well as reasonable power and energy densities.

#### **F.EN04.29.03**

### **Effect of Iron Substitution on Cobalt Oxide and Study of Its Electrochemical Performance** Deepa Guragain; The University of Memphis, United States

The application of metal oxides has been increasing for energy storage device due to excellent electrochemical properties, multifunctional energy application, environmentally friendly property and lower price. Due to rapid growth of energy use, there is very high demand for new ways to store energy. It is challenged to develop efficient way to store energy without polluting environment, which is possible by using transition metal oxide. We have prepared  $\text{Fe}_x\text{Co}_{3-x}\text{O}_4$  ( $x=0.0, 0.2, 0.4, 0.6, 0.8, 1$ ) successfully via hydrothermal method from which we can prepared electrode to make supercapacitor device. The structural properties were investigated by X-ray diffraction (XRD) and found phase pure  $\text{Fe}_x\text{Co}_{3-x}\text{O}_4$ . The morphology of the series obtained from scanning electron microscopy (SEM) varies from thinner nano-plates to thicker nano-plates as the concentration of Fe increase from  $x=0.0$  to  $x=1.0$ . Furthermore,  $\text{Fe}_x\text{Co}_{3-x}\text{O}_4$  were characterized by X-ray Photoelectron spectroscopy (XPS), Fourier Transform Infrared Spectroscopy (FTIR) and Quantachrome Surface area analyzer. The maximum BET surface area obtained from Quantachrome Instrument for  $x=1$  is 87.5 m<sup>2</sup>/g. The XPS gives elemental composition of  $\text{Fe}_x\text{Co}_{3-x}\text{O}_4$  as in desired amount. The higher specific capacitance of 268 F/g at a current density of 1 A/g, 856 F/g at 2 mV/s scan rate, the energy density of 16 Wh/kg and power density of 170 W/kg in 3M KOH electrolyte was observed for  $x=1$  sample. An increased retention capacity ~122 % measured at 5 A/g current density and Coulombic efficiency of 100%. All these results indicate Fe dope  $\text{Co}_3\text{O}_4$  composites electrode shows promising electrocatalytic activity results in the high intrinsic electronic conductivity, can largely improve the interfacial electroactive sites, increase charge transfer rates and help to stabilize the structure of compound.

#### **F.EN04.29.04**

### **Microstructural Evolution and Electrochemical Properties of Arachis Hypogaea Shell Derived *Ex Situ* Nitrogen-Doped Activated Carbon for Energy Storage Applications as Supercapacitor** Balla D. Ngom<sup>1</sup>, Ndeye Fatou D. Sylla<sup>1</sup>, Ndeye Maty Ndiaye<sup>1</sup>, Mohamed Chaker<sup>2</sup> and Ncholu Manyala<sup>3</sup>; <sup>1</sup>Universté Cheikh Anta Diop de Dakar, Senegal; <sup>2</sup>INRS, Canada; <sup>3</sup>University of Pretoria, South Africa

We report on the correlation of the microstructural evolution and electrochemical properties of an ex-situ N-doping KOH

activated carbon derived from Arachis Hypogaea Shell (NAC-AHS) and compared to the non-doped (AC-AHS). Interconnected cavities with irregular-shaped structure are reported by SEM analysis for AC-AHS. After nitrogen doping, the morphology of the NAC-AHS materials exhibited a less porous structure as compared to AC-AHS. The surface specific area (SSA) of NAC-AHS was found to be  $1442 \text{ m}^2 \text{ g}^{-1}$  lower than the value of AC-AHS ( $1557 \text{ m}^2 \text{ g}^{-1}$ ), the pore volumes were also found to follow the same trend since the reported values are as follow  $0.76 \text{ cm}^3 \text{ g}^{-1}$  and  $0.69 \text{ cm}^3 \text{ g}^{-1}$ , respectively for AC-AHS and NAC-AHS. The AC-AHS and NAC-AHS exhibited in a half cell a specific capacitance ( $C_s$ ) values of  $167 \text{ F g}^{-1}$  and  $216 \text{ F g}^{-1}$ , respectively at  $1 \text{ A g}^{-1}$ , corresponding to an improvement of 30% after ex-situ N-doping, which agrees with the higher current response recorded in the CV profiles of the samples. A symmetric device fabricated from the NAC-AHS materials displayed a  $C_s$  of  $251.2 \text{ F g}^{-1}$  at  $1 \text{ A g}^{-1}$  in a wide operating voltage of 2.0 V in 2.5 M  $\text{KNO}_3$  aqueous electrolyte. In terms of stability, it achieved 83.2% as capacity retention up to 20,000 cycles, which was, improved through the floating/aging measurement at  $5 \text{ A g}^{-1}$  over a long period of time ( $\sim 7+$  days). A specific energy of  $35 \text{ Wh kg}^{-1}$  with a corresponding specific power of  $1 \text{ kW kg}^{-1}$  at  $1 \text{ A g}^{-1}$  was delivered with the device still retaining up to  $22 \text{ Wh kg}^{-1}$  and a  $20 \text{ kW kg}^{-1}$  specific power even at  $20 \text{ A g}^{-1}$ .

#### F.EN04.29.05

**Electrical Transport in Coconut Shell Charcoal** G. R. A. Kumara<sup>1</sup>, Kasun J. Wimalasena<sup>2</sup>, S. M. B. Dissanayake<sup>2</sup>, T. M. W. J. Bandara<sup>2</sup>, Ajith DeSilva<sup>3,4</sup>, A. G. U. Perera<sup>4</sup> and K. Tennakone<sup>1,4</sup>; <sup>1</sup>National Institute of Fundamental Studies, Sri Lanka; Sri Lanka; <sup>2</sup>University of Peradeniya, Sri Lanka; <sup>3</sup>University of West Georgia, United States; <sup>4</sup>Georgia State University, United States

Activated coconut charcoal is unique in meso and micro pore distribution, BET surface area exceeding  $2000 \text{ m}^2 \text{ g}^{-1}$  and pore volume  $\sim 1.3 \text{ cm}^3 \text{ g}^{-1}$ . It is the bio-derived carbon material of choice for supercapacitor electrodes, cryogenic gas absorption in vacuum technology and water purification. Coconut shell carbon is also the hardest biochar - hardness 3-4 in the Mohs scale. For supercapacitors, batteries and several other applications, high electrical conductivity is an advantageous parameter. Owing to large surface to volume ratio of the material, the carrier trapping sites on the surface play a crucial role in electrical transport. The DC electrical conductivity is found to be greatly influenced by mode of activation, surface treatments and impurities. The most studies on electrical conductivity of activated carbons were based on measurements conducted using compacted pellets. The higher hardness of coconut shell charcoal enable use of sizable samples made from uncrushed flakes to carry out chemical treatments and conduct measurements under varying conditions. The results of measurements and interpretations will be presented, emphasizing supercapacitor applications of coconut shell charcoal.

#### F.EN04.29.06

**Dielectric h-BN Separators for  $\text{Ti}_3\text{C}_2\text{-MnO}_2$  Supercapacitors** Alptekin Aydinli<sup>1,2</sup>, Xuehang Wang<sup>1</sup>, Husnu E. Unalan<sup>2</sup> and Yury Gogotsi<sup>1</sup>; <sup>1</sup>Drexel University, United States; <sup>2</sup>Middle East Technical University, Turkey

Electrochemical energy storage (EES) units are vital for mobile electronic devices that can provide high energy and power densities. Current studies mostly aim at improving the performance of the electrode active materials. Nevertheless, inert components such as electrolyte, separator and current collector occupy 70-80 wt.% of the EES devices and reducing their weight/volume can significantly improve the performance of these devices. Dielectric materials are used extensively in EES devices as separators such as ceramics in conventional capacitors. In supercapacitors, polypropylene membranes and glassy fiber films with typical thicknesses larger than  $25 \mu\text{m}$  are the common separator materials. Two dimensional (2D) dielectric materials with flat and smooth surfaces at a much smaller thickness can in fact be used as efficient separators. In this work, 2D hexagonal boron nitride (h-BN) thin films were utilized as efficient separator layers in asymmetric MXene supercapacitors. In these devices, titanium carbide ( $\text{Ti}_3\text{C}_2$ ) and manganese dioxide ( $\text{MnO}_2$ ) were used as the negative and positive electrodes, respectively. Electrochemical tests such as cyclic voltammetry, chronopotentiometry and electrochemical impedance spectroscopy were conducted to determine specific capacity, rate capability and cycling stability of the asymmetric supercapacitor devices. Fabricated supercapacitor devices showed promising electrochemical performance in a PVA/ $\text{H}_2\text{SO}_4$  gel electrolyte compared to the control device with conventional Celgard separator. The reduced thickness of the h-BN separator decreased the volume of an entire supercapacitor device and significantly improved the overall capacitance.

#### F.EN04.29.07

**Bioinspired Nanoporous Ion Conducting Membranes for Next Generation Batteries** Ahmet Emre, Jinchen Fan, Emine Turali-Emre, Alycia Gerber, Volkan Cecen and Nicholas Kotov; University of Michigan, United States

Bioinspired ion transport membranes have been widely investigated for energy storage applications. High theoretical specific energy density ( $2600 \text{ Wh/kg}$ ) and high specific capacity ( $1675 \text{ mA/g}$ ) along with natural abundance and low toxicity of sulfur have been attracting significant attention for development of an alternative battery system to replace traditional lithium ion

batteries which suffer from safety and capacity/energy density limitations in various applications. However, challenges such as polysulfide dissolution and shuttling prevent mass commercialization of metal sulfur batteries. Inspired from biological ion transport mechanisms, we show a practical yet comprehensive approach for development of highperformance metal sulfur batteries. Aramid nanofiber (ANF) based composite ion transport membranes not only prevent dendrite formation but also confine polysulfides on the cathode side. ANF composite battery separators provide diverse and opposing properties including high mechanical properties, high ionic conductivity and high thermal/chemical stability. Highly selective ion sieving properties of these biomimetic separators provide safe and high-performance batteries. Fabrication of such biocompatible, affordable, flexible and high energy density battery is quite crucial in powering next-generation electronics including but not limited to portable, wearable and implantable biomedical devices.

SESSION F.LP06.01: Live Poster Session: Energy (F.EN04)

Session Chair: Han Wang

Friday Morning, December 4, 2020

8:00 AM - 10:00 AM

F.EN04

#### F.EN04.28.02

**MoS<sub>2</sub> Based High-Performance FET Devices for Memory Circuits on Flexible Platform** Sayani Majumdar<sup>1</sup>, Miika Soikkeli<sup>1</sup>, Ioannis Zeimpekis<sup>2</sup>, Nikolaos Aspiotis<sup>2</sup>, Chung-Che Huang<sup>2</sup>, Sanna Arpiainen<sup>1</sup> and Mika Prunnila<sup>1</sup>; <sup>1</sup>VTT Technical Research Centre, Finland; <sup>2</sup>University of Southampton, United Kingdom

Two-dimensional transition metal dichalcogenides (TMDs) are fertile ground for fundamental material science and emergent applications in high-performance electronics. The mechanical flexibility of 2D materials allows their incorporation in variable form factor designs such as smart wearables and foldable electronics, where their electronic and optical properties outperform conventional flexible materials such as organic polymers. In the current work, we present high-performance ALD grown MoS<sub>2</sub> based FET devices transferred on polyimide substrates. The growth method employs ALD to grow an MoO<sub>3</sub> layer on a 6 inch wafer which is subsequently annealed in an H<sub>2</sub>S atmosphere to convert to MoS<sub>2</sub>. The ALD allows for excellent uniformity and because the layer acts as a template the process is scalable to larger sizes. The resulting MoS<sub>2</sub> film is 2-3 layers thick. The film was transferred on the patterned target substrate using polystyrene assisted transfer of MoS<sub>2</sub> layer. More than 90% device yield, excellent current ON to OFF ratio of 106 and mobility values up to 32 cm<sup>2</sup> V<sup>-1</sup> s<sup>-1</sup> have been measured from micron scale devices with L/W in the range of two. We will present results on the yield and homogeneity on large area memory networks aiming for low power neuromorphic circuits.

#### F.EN04.28.04

**Infrared Permittivity of the Biaxial van der Waals Semiconductor  $\alpha$ -MoO<sub>3</sub> from Near- and Far-Field Correlative Studies** Thomas Folland<sup>1</sup>, Gonzalo Alvarez-Perez<sup>2</sup>, Ion Errea<sup>3</sup>, Javier Taboada-Gutriérrez<sup>2</sup>, Ana I. Tresguerres-Mata<sup>2</sup>, Joseph R. Matson<sup>1</sup>, Andrei Bylinkin<sup>4</sup>, Mingze He<sup>1</sup>, Weiliang Ma<sup>5</sup>, Qiaoliang Bao<sup>6</sup>, Joshua D. Caldwell<sup>1</sup>, Alexey Nikitin<sup>4</sup> and Pablo Alonso-Gonzalez<sup>2</sup>; <sup>1</sup>Vanderbilt University, United States; <sup>2</sup>University of Oviedo, Spain; <sup>3</sup>University of Basque Country, Spain; <sup>4</sup>Donostia International Physics Center, Spain; <sup>5</sup>Huazhong University of Science & Technology, China; <sup>6</sup>Soochow University, China

The natural crystal anisotropy of van der Waals materials allows them to support a range of nanophotonic phenomena not observable in other natural materials. One such example is anisotropic phonon polaritons (PhPs), which form due to polar optic phonons in materials such as hexagonal boron nitride. Such hyperbolic polaritons have been shown to enable sub-diffraction guiding of light waves, sensing of ultra-thin analytes, and hyperlensing for super resolution imaging in the mid infrared (IR). Recently, the biaxial van der Waals semiconductor  $\alpha$ -phase molybdenum trioxide ( $\alpha$ -MoO<sub>3</sub>) has received significant attention due to its ability to support PhPs which are anisotropic along all three crystal axes. These offer an unprecedented platform for controlling the flow of energy at the nanoscale, in particular for manipulating the polarization state of light. However, to fully exploit the extraordinary IR response of this material, an accurate dielectric function is required.

In this work, we report an accurate IR dielectric function of  $\alpha$ -MoO<sub>3</sub> by modelling far-field, polarized IR reflectance spectra acquired on a single thick flake of this material. Unique to our work, the far-field model is refined using the experimental

dispersion and damping of PhPs revealed by using scattering-type scanning near-field optical microscopy (s-SNOM) on thin flakes of  $\alpha$ -MoO<sub>3</sub>. Through these correlative efforts, exceptional quantitative agreement is attained to both far- and near-field properties for multiple flakes, thus providing strong verification of the accuracy of our model. This also provides a novel approach to extracting dielectric functions of different 2D materials, usually too small or inhomogeneous for establishing accurate models only from standard far-field methods. Finally, by employing density functional theory (DFT), we provide insights into the various vibrational states dictating our dielectric function model and the intriguing optical properties of  $\alpha$ -MoO<sub>3</sub>.

#### **F.EN04.28.05**

**Feedback-Controlled Electroburning of MoS<sub>2</sub> Monolayers** Yan Qi Huan<sup>1</sup>, Yincheng Liu<sup>1</sup>, Choon Hwa Ken Goh<sup>1</sup>, Kuan Eng Johnson Goh<sup>1,2</sup>, Swee Liang Wong<sup>1,2</sup> and Chit Siong Lau<sup>1</sup>; <sup>1</sup>Institute of Materials Research and Engineering, Singapore; <sup>2</sup>National University of Singapore, Singapore

Two-dimensional materials have been identified as interesting candidates for various applications in nano-electronics, and the characterization of electrical breakdown limits is a crucial step in device development. However, methods for repeatable measurements have been scarce in two-dimensional materials, where breakdown studies have been limited to destructive methods. This lack of repeatability restricts our ability to fully account for variability in local electronic properties induced by the fabrication process and surface contaminants.

To tackle this, we implement a two-step deep-learning model to predict the breakdown mechanism and breakdown voltage of monolayer MoS<sub>2</sub> devices with varying channel lengths and resistances using current measured in the low-voltage regime as inputs. A deep neural network (DNN) first classifies between Joule and avalanche breakdown mechanisms with partial current traces from 0–20V. Following this, a convolutional long short-term memory network (CLSTM) predicts breakdown voltages of these classified devices based on user-defined partial current traces.

We test our model with feedback-controlled electrical measurements to achieve non-destructive electrical measurements that limit device damage and increase the amount of data collected. We show that the DNN classifier achieves an accuracy of 74% while the CLSTM model has a 14% error when requiring only 80% of the current trace as inputs. Our results indicate that information encoded in the current behavior far from the breakdown point can be used for predictions, thus enabling non-destructive and fast material characterization for 2D material device development.

#### **F.EN04.28.06**

**Synthesis and Characterization of MXene-WS<sub>2</sub> Heterostructure Devices** Venkata Surya N Chava, Aruna Narayanan Nair and Sreerasad T. Sreenivasan; The University of Texas at El Paso, United States

Atomically thin two-dimensional (2D) materials such as graphene, MoS<sub>2</sub>, WS<sub>2</sub> show excellent material properties and therefore studied extensively for a variety of applications including electronics, optoelectronics, electrocatalysis, energy storage, etc. More recently, there has been a growing interest in 2D heterostructure devices as they offer unique opportunities to design and study possibilities for controlling and manipulating the carrier confinement and transport of charge within these device structures. Tungsten disulfide (WS<sub>2</sub>) is an excellent material for optoelectronic applications such as photodetectors as monolayer WS<sub>2</sub> has a direct bandgap of ~ 2.05 eV. Also, recently emerged as MXenes has shown great promise in energy storage and electromagnetic shielding applications due to excellent metallic conductivity. The MXenes can show either metallic or semiconducting behavior depending on the functional groups attached to the surface during the etching process. In particular, their tunable work function property can be exploited to control the properties of the heterostructure of MXenes with other layered 2D materials. Here, we report the characterization results of one such heterostructure formed by combining MXenes with WS<sub>2</sub>. MXene is synthesized by etching the Al layer from the parent MAX phase, and WS<sub>2</sub> is synthesized on SiO<sub>2</sub>/Si substrates using the CVD process. The electrical properties of these as-synthesized materials can be modified using different approaches such as chemical doping etc. We present results from different morphological, spectroscopic and electrical characterization techniques that are used to study the transport characteristics of these MXene-WS<sub>2</sub> heterostructure devices.

#### **F.EN04.28.08**

**Photo-Thermoelectric Effect along Waveguide-Integrated Graphene Photodetectors** Jakob Muench, Hannah Watson, Osman Balci, Alfonso Ruocco and Andrea C. Ferrari; Cambridge Graphene Centre, United Kingdom

The dominating mechanism of photodetection in a single-layer graphene (SLG) based device depends on the design of the detector [1,2,3], its chosen operation [1,3], and the band diagram in the photo-active region [2,4]. Here we demonstrate, over

a  $\sim 0.5\text{eV}$  doping range, that the photo-thermoelectric effect [5] has a long-range (exceeding the cooling length in SLG) contribution, even in uniformly doped SLG, in the absence of a Seebeck coefficient gradient, whenever non-uniform absorption creates an electronic temperature gradient. This is achieved by integrating SLG with on-chip Si waveguides to generate an heterogeneous absorption profile over tens  $\mu\text{m}$  and placing electrical probes along the propagation direction of light. We show the presence of a photovoltage  $V_{\text{ph}}$  along the waveguide. The doping-dependence of  $V_{\text{ph}}$  suggests signal generation by hot electrons via the Seebeck effect. This has general implications for the design and optimization of optoelectronic devices based on SLG, in particular for integrated photonics, where planar integration of layered materials leads to non-uniform absorption. [1] F. H. L. Koppens et al., Nat. Nanotechnol., 9, 780, (2014). [2] T. Echtermeyer et al., Nano Lett., 7, 3733, (2014) [3] M. Romagnoli et al., Nat. Rev. Mater., 3, 392, (2018). [4] V. Shautsova et al., Nat. Comm., 9, 5190, (2018). [5] N. Gabor et al., Science, 334, 648, (2011).

#### **F.EN04.28.12**

**Unraveling Nonlinear Formation and Relaxation of Excitons in Atomically Thin 2D Semiconductors** Matthew C. Strasbourg<sup>1</sup>, Cory Johns<sup>1</sup>, Thomas Darlington<sup>2</sup>, James Hone<sup>2</sup>, P James Schuck<sup>2</sup> and Nicholas Borys<sup>1</sup>; <sup>1</sup>Montana State University, United States; <sup>2</sup>Columbia University, United States

Transition metal dichalcogenide (TMD) semiconductors are layered van der Waals materials that exhibit exceptional optoelectronic properties in monolayer form. Their atomically thin nature and reduced long-range dielectric screening make them ideal systems in which to study many-body electronic states. Notably, excitonic many-body phenomena govern the light-matter interactions in TMD semiconductors and open up new possibilities for novel optoelectronic devices, including new classes of quantum light sources. Thus, understanding the rich suite of many-body phenomena in these systems is motivated by potential applications in on-chip optoelectronics and by the insights that can be gained into the fundamental interactions that govern TMD material properties. Here, the dynamics of several higher-order excitons including trions, biexcitons, and charged biexcitons in monolayer-WSe<sub>2</sub> are probed using temperature-, energy-, and power-dependent time-resolved optical spectroscopy. The properties of these multiexciton states build on the unique many-body physics of the single-excitons in TMDs. These studies reveal a complex interplay between the multiexcitons and single-excitons that depends on both the density and excitation energy of the initial exciton population. In addition, the presence of defect-bound excitons is found to drastically alter the formation of multiexcitons. This competition between exciton trapping and multiexciton formation highlights the need for high-quality materials to enhance multiexciton physics. By exploring this parameter space of excitation energy, excitation density, and defect density, complex many-body interactions are revealed that suggest means to optimize multiexciton yields and thus capitalize on the emergent characteristics of multiexciton emission and exciton-multiexciton interactions that are unique to monolayer-WSe<sub>2</sub>. These observations open new doors to a number of applications such as entangle photon pair production and lasing, highlighting the importance of understanding the formation and relaxation dynamics of the rich manifold of excitons in order to leverage 2D semiconductors for advanced technologies.

#### **F.EN04.28.13**

**Computational Synthesis of 2D Materials—A High-Throughput Approach to Materials Design** Tara M. Boland and Arunima Singh; Arizona State University, United States

The emergence of two dimensional (2D) materials opened up many potential avenues for novel device applications such as nanoelectronics, topological insulators, field effect transistors, microwave and terahertz photonics and many more. To date there are over 1,000 theoretically predicted 2D materials. Of those theoretical materials, only 55 have been experimentally synthesized due to the difficulty in finding a suitable substrate which simultaneously stabilizes the 2D phase over of bulk phase while preserving the novel materials properties resulting from quantum confinement. One avenue to aid in the development of these novel 2D materials is to explore and predict suitable substrates which will stabilize the 2D growth using computational methods. In this work a high-throughput approach to density functional theory is used to explore the viability of various common substrates to stabilize and grow these novel theoretically predicted 2D materials. This work analyzes three key factors which determine the stability of synthesizing 2D materials via substrate assisted methods such as chemical vapor deposition. The results will provide guidance to future experimental efforts to synthesize these 2D materials. Using various 2D materials databases and van der Waals corrected density functional theory we investigate the suitability of 12 substrates to stabilize 2D growth. First, the formation energy of the 2D material is computed relative to the most stable bulk phase. A 2D material with a high formation energy implies the material will likely only be synthesized via substrate assisted methods thus making it a good candidate material for this study. Computational synthesis can be broken down into a two-step process: the formation of the 2D flake from the bulk phase, the formation energy, and adsorption of the 2D material on a symmetry-matched and low lattice-matched substrate surface, the binding energy. When the adsorption energy, the difference between the formation from the binding energy, is less than zero the adsorption is spontaneous, exothermic, and

stable. For materials which meet this criteria, the density of states is computed to characterize the electronic properties of these materials for device applications. 1. We gratefully acknowledge ASU's HPC staff for support and assistance with computing resources along with the Extreme Science and Engineering Discovery Environment (XSEDE), for support by National Science Foundation grant number ACI-1548562, through award number TG-DMR-150006. We gratefully acknowledge the National Science Foundation grant DMR-1308085 and Arizona State University for funding.

#### **F.EN04.28.14**

**Surface Protection of 2D Black Phosphorus with Greatly Enhanced Photoluminescence and Stability** Dongying Li and Cun-Zheng Ning; Arizona State University, United States

Black phosphorus (BP) has gained intense interests because of its tunable direct bandgap, leading to emission with photon energies from  $\sim 1.7\text{eV}$  for monolayer to  $\sim 0.35\text{eV}$  for bulk [1]. This makes few-layer BPs one of the very few 2D infrared materials, especially in communication wavelengths. Besides, BP has a strong anisotropy compared with other 2D materials due to its puckered honeycomb lattice. It leads to many interesting phenomena such as strong coupling between phonon and carriers [2]. Thus BP is an appealing 2D platform for investigating novel physics and device applications. However, few-layer BP degrades quickly in the ambient environment due to the interaction with oxygen under light excitation. Such instability causes great difficulty in investigating properties of few-layer BP and in exploring the practical applications. Although BP protection methods are reported with verified good electronic properties, there is no report on stabilized BP with enhanced photoluminescence (PL) under ambient environment. Here we report an approach to realize BP with greatly enhanced PL (by as much as 160 times) that can be stable under ambient environment for months. We adopt a three-step method to prepare BP covered by boron nitride (BN) from both sides. First, thin flakes of BP and BN are exfoliated onto PDMS layers, followed by successive transfers of the bottom BN and then BP onto SiO<sub>2</sub> (270nm)/ Si substrate. Second, oxygen plasma is used to thin down BP to desired thickness or numbers of layers. The oxygen plasma also leaves an oxide layer on top of the thinned-down BP at the end of the process. Third, we transfer the top BN onto the oxide covered BP which is then followed by thermal annealing. This process leads to oxygen doped few-layer BP with BN binding tightly from both sides to protect BP from the environment, highly improving the stability of BP. Raman spectroscopy indicates the sandwiched BP is defective. The breathing mode shows broadening and redshift. Ag1 and Ag2 modes both split into two subpeaks. These are the signs of introduction of oxygen defects in BP. PL of oxygen doped BP shows two-order of magnitude enhancement compared with freshly etched BP, which can be explained by bound exciton luminescence. Few-layer BP produced this way shows remarkable stability. The PL line-shape and intensity of sandwiched BP are barely changed when kept in the ambient environment under room temperature. A 3-layer BP sample prepared by such method, 5 months after preparation, PL intensity is still  $\sim 80\%$  of that measured as prepared. At an elevated temperature of  $90^\circ\text{C}$ , oxygen can escape from BP, which will result in redshift of PL peak and decreased PL intensity. 7 months after preparation, the 3-layer BP sample still shows strong PL, at  $\sim 70\%$  of the original PL intensity right before TEM measurement. TEM results show close contact between BP and BN and three BP layers can be clearly identified from side view. Quite low oxygen concentration in BP layers is consistent with the assumption that oxygen escapes from BP with time. A 4-layer BP with comparable intensity to that of the 3-layer sample made by this method shows the possible general validity of this approach. In summary, our method can produce highly stable BP with excellent PL intensity induced by oxygen defects, allowing the study of rich physics in defective BP. Furthermore, it can pave the way for research on BP-based photonic devices such as lasers, modulators, etc. [1] Li, Likai, et al. "Direct observation of the layer-dependent electronic structure in phosphorene." *Nature nanotechnology* 12.1 (2017): 21. [2] Pelant, Ivan, and Jan Valenta. *Luminescence spectroscopy of semiconductors*. Oxford University Press, 2012.

#### **F.EN04.28.15**

**Large Voltage Generation Through Liquid Motion on Single-Layer MoS<sub>2</sub>** Adha Sukma Aji<sup>1</sup>, Ryohei Nishi<sup>1</sup>, Hiroki Ago<sup>2</sup> and Yutaka Ohno<sup>1</sup>; <sup>1</sup>Nagoya University, Japan; <sup>2</sup>Kyushu University, Japan

Dynamics of water is one kind of clean energy source which readily available in our surrounding environment. Recently, the direct conversion of liquid motion energy into electricity by two-dimensional (2D) materials such as graphene has gained much interest [1-3]. However, the reported output voltage values generated by liquid motion on the graphene surface are limited to millivolts order. With these output voltage values, the graphene nanogenerators might be difficult to drive conventional silicon-based electronics. Thus, an alternative to semimetallic graphene as an active material is needed to boost the output voltage. Here we report a single-layer MoS<sub>2</sub> nanogenerator to generate electricity from liquid movement on its surface. The centimeter-scale single-layer MoS<sub>2</sub> sheets were prepared by using chemical vapor deposition on sapphire substrate ( $3 \times 1$  cm) with MoO<sub>3</sub> and sulfur powder as precursors. Then, the MoS<sub>2</sub> was transferred onto polyethylene naphthalate (PEN) substrate. The device was finalized by applying silver epoxy as electrical contact on both ends of MoS<sub>2</sub> and a silicone film as electrode protection from liquid. To generate electricity, aqueous 1 M NaCl were dropped on the MoS<sub>2</sub>



surface on a stage inclined at 45°. Due to the high hydrophobicity of MoS<sub>2</sub>, the droplets easily slid on the MoS<sub>2</sub> surface, generating an open-circuit voltage of ~6 V. This output voltage value is significantly higher than graphene nanogenerators previously reported [1-3]. The short-circuit current of ~5 nA was generated from liquid movement on the MoS<sub>2</sub> surface. The power produced by droplet movement is about 1.7 nW at load resistance of 200 MΩ. We also show the high scalability of our MoS<sub>2</sub> nanogenerator by arranging them in series and parallel connections. The open-circuit voltage and short-circuit current were multiplied about three times by connecting three identical MoS<sub>2</sub> nanogenerators in series and parallel connection, respectively. In conclusion, we showed the large-area single-layer MoS<sub>2</sub> nanogenerator, which is capable of generating output voltage more than 5 V from liquid motion. Seeing the exceptional mechanical and electrical property of single-layer MoS<sub>2</sub>, the realization of self-powering untethered wearable device based on 2D materials will soon become fulfilled. Reference: [1] J. Yin et al., Nat. Nanotechnol. 9, 378 (2014) [2] D. Park et al., Nano Energy 54, 66 (2018) [3] S. S. Kwak et al., ACS Nano 10, 7297 (2016)

#### **F.EN04.28.16**

##### **Greenhouse Gas Sensor Constructed with Two-Dimensional Quantum Dots Platform with Anchored Electroactive Conducting Polymer** Reeba Thomas and Kalathur Santhanam; Rochester Institute of Technology, United States

Recently, there has been active interest in developing greenhouse gas sensors for understanding the influence of these gases in controlling the atmosphere and the weather (1,2). We wish to report here, a greenhouse gas sensor that has been developed using 2D graphene quantum dots (3) platform on alumina substrate containing platinum interdigitated electrodes on one side and heating resistors on the other side of the platform with an electroactive conducting polymer, as the 2D structure provides a large surface area for the active material making it more sensitive for detection and measurements. The sensor operates in two stages; in the first stage the response of the interfering gases is measured and in the second stage a thermal pulse is applied corresponding to the desorption energies of the interfering gases. The temperature on the active material was measured using an infrared thermometer. The electroactive conducting polymer was electrochemically synthesized at a graphene quantum dots electrode by a potential step electrolysis at 1.00 V vs SCE. The experiments conducted with graphene quantum dots dispersed in the electrolytic medium, shows the monomer well coupled with graphene prior to the polymerization. The polymer coupled graphene shows D and G bands arising from graphene in Raman imaging spectroscopy. The mechanistic pathways has been unraveled by Raman imaging, Fourier transform infra-red spectroscopy, UV-VIS absorption spectroscopy, and scanning electron microscope. The results suggest that 2D platform for the active material for sensing enhances the performance of the sensor with a temperature-controlled selectivity. 1. D. Shukman, Greenland's ice faces melting 'death sentence', <https://www.bbc.com/news/science-environment-49483580> 2. K.S.V. Santhanam and N. Ahamed, Chemical Engineering (MDPI), 2,38 (2018) 3. K.S.V. Santhanam, S. Kandlikar, M. Valentina and Y. Yang, US patent No. 9840782, December 12, 2017

#### **F.EN04.28.20**

##### **Edge-Contacted 2D Transition Metal Dichalcogenide (TMD) Transistors** Hattan Abuzaid, Zhihui Cheng and Aaron D. Franklin; Duke University, United States

Two-dimensional (2D) transition metal dichalcogenides (TMDs) have emerged as a promising transistor channel material because of their inherent atomic thinness, which can allow further scaling of channel length. In order to miniaturize transistors in future technology nodes, not only the channel length, but also the contact length (L<sub>c</sub>) needs to be scaled as L<sub>c</sub> constitutes a significant portion of the device's integrated pitch/density. Researchers have suggested the use of edge contacts to enable maximum scalability; in this configuration, the channel is contacted via its side edges along the same lateral plane as the contacts. Since the injection area is practically independent of the actual L<sub>c</sub>, the performance of edge contacts can be L<sub>c</sub>-independent [1], thus allowing much better scalability compared to traditional top contacts. In addition, edge contacts are hypothesized to form covalent bonds with the TMD channel, which should translate to better carrier injection. Published work on edge-contacted TMD transistors has predominantly focused on MoS<sub>2</sub> as the channel material. Since chemically dissimilar TMDs interact distinctly with different metal contacts, further research on other promising TMDs, such as MoTe<sub>2</sub> and WSe<sub>2</sub> is warranted. In this work, we created clean edge contacts to TMD channels utilizing our previously established method [1] using an in-situ Ar<sup>+</sup> ion beam in an integrated electron beam evaporation chamber. We discovered that the etching behavior of the TMDs varied, and thus the realization of clean edge contacts required custom fabrication processes. The role of contact metal is elucidated for each TMD, along with analysis of top- versus edge-contacted devices on the same TMD flake or domain. These results provide key insights on how metal selection and channel thickness influence the device performance for various edge-contacted TMD transistors. References [1] Cheng, Zhihui, et al. "Immunity to Contact Scaling in MoS<sub>2</sub> Transistors Using in Situ Edge Contacts." Nano letters 19.8 (2019): 5077-5085.

#### **F.EN04.28.21**

**Scalable and Stable Intercalation of Li<sup>+</sup> into Multi-Layer CVD Graphene for Controlled Optical and Electronic Properties** Joseph Andrade<sup>1</sup>, Jan Folkson<sup>1</sup>, Amanda Carr<sup>1</sup>, Mohamed Boukhicha<sup>2</sup> and Matthew Eisaman<sup>1</sup>; <sup>1</sup>Stony Brook University, The State University of New York, United States; <sup>2</sup>Brookhaven National Laboratory, United States

While graphitic intercalant compounds (GICs) have been thoroughly studied for application in battery technologies, use of these materials for transparent conductive electrodes (TCEs) has remained fairly unexplored. Although individual layers of 2D graphene promise high intrinsic mobility and transparency, its inherent properties do not rival those of current industry-standard materials. However, with lithium-ion intercalated multi-layer graphene grown via chemical vapor deposition (CVD), we produce large-scale LiC<sub>6</sub> films whose electrical and optical properties are expected to surpass TCE requirements. With the developed sample design, we present preliminary data suggesting a path toward scalable and stable films for TCE application.

#### **F.EN04.28.22**

**Steric and Electronic Effects at Polymer-2D Materials Interfaces** James Nicolas M. Pagaduan, Nicholas Hight-Huf, Avdhoot Datar, Reika Katsumata, Michael Barnes, Ashwin Ramasubramaniam and Todd Emrick; University of Massachusetts Amherst, United States

This presentation will describe the impacts of steric and electronic interactions of zwitterionic polymers in contact with two-dimensional (2D) materials. Modulation of the work function of 2D materials facilitates charge injection and improves device performance for several applications such as solar cells, electronic displays, and organic light emitting diodes. The work function of 2D materials has been tailored by gas absorption, mechanical strain, and chemical doping methods. Polymer coatings have also been applied to tune the work function of 2D materials via non-covalent adsorption, offering possibilities for designing novel hybrid organic-inorganic functional materials. However, little is known about the precise role of functional group orientation on work function modulation. Here, we select graphene as a model 2D system and systematically examine work function modulation arising from coatings of functional poly(sulfobetaine methacrylate) (PSBMA). This approach maintains the desirable structural and electronic properties of graphene while exclusively altering its surface potential via the polymer coating. Work function modulation was observed by ultraviolet photoelectron spectroscopy and Kelvin probe force microscopy. First-principles density functional theory calculations provided insights into the preferred configurations of zwitterionic SBMA pendent groups physically adsorbed on graphene sheet, resultant dipole moment, and possible range of work function shifts that are achievable. Overall, this method of work function engineering permits scalable patterning of polymer films and precise spatial control over carrier doping for fabrication of monolayer graphene-based devices.

#### **F.EN04.28.23**

**Ni-Decorated Graphene Microchannel for Self-Activated Gas Sensors with Enhanced Response to Ethanol** Taehoon Kim<sup>1</sup>, Yeonhoo Kim<sup>2</sup>, Seo Yun Park<sup>1</sup> and Ho Won Jang<sup>1</sup>; <sup>1</sup>Seoul National University, Korea (the Republic of); <sup>2</sup>Los Alamos National Laboratory, United States

Graphene, one of the most popular two-dimensional (2-D) materials, has been studied with high interests owing to its outstanding properties such as high thermal and electrical conductivity, easy surface decoration, and transparency with flexibility. These remarkable advantages led to the studies of graphene in varied applications including gas sensors. However, for various applications, graphene-based gas sensors have to solve various problems such as power consumption by external heaters, insufficient selectivity, and method of mass production. In this work, we report ethanol gas detection of nickel nanoparticles decorated on graphene layers which are self-activated by applied bias voltage from 1 to 5 V. The graphene is prepared by chemical vapor deposition (CVD) method and we designed a narrow graphene channel to generate heat by using a joule heating effect while working as a sensing area. Since graphene is a 2-D material, both active sensing area and electrodes composed of graphene could be easily defined by facile lithography processes. Nickel nanoparticles are deposited by the e-beam evaporator. The gas sensing properties to various gases such as NO<sub>2</sub>, H<sub>2</sub>, C<sub>2</sub>H<sub>5</sub>OH, and NH<sub>3</sub> have been tested at room temperature while regulating the input bias voltages. Our results show superior ethanol gas detection of nickel nanoparticles decorated graphene sensors at room temperature. These results broaden the potential of graphene-based gas sensors for real applications.

#### **F.EN04.28.24**

**New Low Bandgap Graphenic Semiconductors for Solar Cells and Photocatalysts** Pawan Kumar<sup>1</sup>, Ryan Kisslinger<sup>1</sup>, Sheng Zeng<sup>1</sup>, Guy Bernard<sup>1</sup>, Sergey Gusarov<sup>2</sup>, Alexander Kobryn<sup>2</sup>, Kazi Alam<sup>1</sup>, Vladimir Michaelis<sup>1</sup> and Karthik Shankar<sup>1</sup>; <sup>1</sup>University of Alberta, Canada; <sup>2</sup>National Research Council Canada, Canada

Graphenic semiconductors (GSCs) are an emerging class of energy materials based on the sp<sup>2</sup>-hybridized graphene motif that either by themselves or in composites, have demonstrated excellent performance for the electrochemical reduction of CO<sub>2</sub>, the photoelectrochemical splitting of water to generate H<sub>2</sub>, and the photocatalytic reduction of CO<sub>2</sub>. GSCs have a range of astonishing properties such as high catalytic activity, strong visible light absorption, exceptional chemical stability, thermal stability until at least 350 deg. C, and facile compositional and electrical doping. GSCs are typically synthesized by low cost solvothermal and annealing processes that lend themselves to scale-up and mass production. The most prominent member of this family of compounds is g-C<sub>3</sub>N<sub>4</sub>, which has a relatively wide bandgap of 2.6 eV. Herein, we report on the synthesis, characterization and solar energy applications of a number of new GSCs [1-5]. C<sub>3</sub>N<sub>5</sub> is a novel modified carbon nitride framework with a remarkable 3:5 C:N stoichiometry and an electronic bandgap of 1.76 eV which was formed by thermal deammoniation of a precursor consisting of melem hydrazine [1]. The two s-heptazine units in the polymeric C<sub>3</sub>N<sub>5</sub> are bridged together with an azo linkage, which constitutes an unconventional bonding arrangement, different from g-C<sub>3</sub>N<sub>4</sub> where three heptazine units are linked together with tertiary nitrogen. C<sub>3</sub>N<sub>5</sub> exhibits extended conjugation due to overlap of azo nitrogens and increased electron density [1]. C<sub>3</sub>N<sub>5</sub> was found to be an excellent electron transport layer for perovskite solar cells, and a good photocatalyst for the photoreduction of 4-nitrobenzenethiol into 4,4'-dimercaptoazobenzene. Even lower bandgap analogs of C<sub>3</sub>N<sub>5</sub> were synthesized and characterized. We also formed highly luminescent quantum dots of g-C<sub>3</sub>N<sub>4</sub> doped with P, F or Cl. Intimate heterojunctions of doped g-C<sub>3</sub>N<sub>4</sub> quantum dots with BiOI and TiO<sub>2</sub> were demonstrated to be excellent photoanodes for visible light-driven water splitting, achieving photocurrent densities as high 2.5 mA cm<sup>-2</sup> under AM1.5G simulated sunlight [2-3].

REFERENCES 1. P Kumar, E Vahidzadeh, UK Thakur, P Kar, KM Alam, A Goswami, N Mahdi, K Cui, GM Bernard, VK Michaelis and K Shankar, "C<sub>3</sub>N<sub>5</sub>: A Low Bandgap Semiconductor Containing an Azo-Linked Carbon Nitride Framework for Photocatalytic, Photovoltaic and Adsorbent Applications", *Journal of the American Chemical Society*, 2019, 141, 13, 5415-5436. 2. P Kumar et al. "Noble Metal Free, Visible Light Driven Photocatalysis Using TiO<sub>2</sub> Nanotube Arrays Sensitized by P-doped C<sub>3</sub>N<sub>4</sub> Quantum Dots", *Advanced Optical Materials* (in press), 2019. 3. KM Alam, P. Kumar, P Kar, A Goswami, UK Thakur, S Zeng, E Vahidzadeh, K Cui and K Shankar, "Heterojunctions of halogen-doped carbon nitride nanosheets and BiOI for sunlight-driven water-splitting", *Nanotechnology*, 2019, doi: 10.1088/1361-6528/ab4e2c. 4. C Ott et al. "Flexible and Ultrasoft Inorganic 1D Semiconductor and Heterostructure Systems Based on SnIP", *Advanced Functional Materials*, 2019, 29, 1900233. 5. KM Alam, P Kumar, AP Manuel, E Vahidzadeh, A Goswami, S Zeng, W Wu, N Mahdi, K Cui, AE Kobryn, S Gusarov, Y Song and K Shankar, "CVD grown nitrogen doped graphene is an exceptional visible-light driven photocatalyst for surface catalytic reactions", *2D Materials*, 2019, 7, 015002.

#### **F.EN04.28.25**

**Enhanced Environmental Stability Coupled with a 12.5% Power Conversion Efficiency in an Aluminum Oxide-Encapsulated n-Graphene/p-Silicon Solar Cell** Serdar Yavuz, Eric Martinez Loran, David P. Fenning and Prab Bandaru; University of California, San Diego, United States

A significant improvement in the power conversion efficiency (PCE) and the environmental stability of n-Graphene/p-Si solar cells is indicated through effective n-doping of graphene, using low work function oxide capping layers. AlO<sub>x</sub>, deposited through atomic layer deposition, is particularly effective for such doping and in addition serves as an antireflection coating and a cell encapsulating layer. It is shown that the related charge transfer doping and interfacial engineering was crucial to achieve a record PCE of 12.5%. The work indicates a path forward, through work function engineering, for further efficiency gains in Gr-based solar cells

#### **F.EN04.28.26**

**Electron Emission from Epitaxial Graphene Microribbons Towards Emission of Soft X-Rays** Daniel Lewis and Kevin Daniels; University of Maryland, United States

X-rays have been used for decades in medical diagnostic imaging, but the presence of metal scattering interference centers can limit their effectiveness. Longer wavelength sources may mitigate this effect, but risk poor imaging from low x-ray fluence. To produce a sufficient density of low-power x-rays to allow imaging of targets with metal inclusions, the x-ray current source would require a proportionate increase in output. Graphene nanoribbons crafted by CVD[1] or arc discharge[2] have been shown to exhibit electron emission under bias, with theoretical outputs exceeding thermionic or field emission sources of similar dimensionality and applied bias conditions. Epitaxial graphene, able to be synthesized on the wafer-scale and compatible with current fabrication techniques, can be readily processed into ribbons with superior mechanical and electrical capabilities to its CVD or arc discharge counterparts. With even low applied bias (3 - 5 V) graphene nanoribbons (0.5 - 1 μm long, 10-30 nm wide) suspended in high vacuum exhibited phonon-assisted electron emission (PAEE)[1][2], resulting in emission currents being produced at internal electric fields and external pulling voltages both nearly 10<sup>2</sup> less than comparable thermionic or field emission sources. Emissions exhibited repeatable directionality out of the plane of the

ribbons, offering a means to mechanically control the orientation of the output current; ribbons crafted from epitaxial graphene, with deposited electrodes to provide the bias, would emit out of the plane of the substrate, enabling even macro-scale directional control. Fabrication of epitaxial graphene microribbons is readily accomplished via a combination of electron beam lithography and plasma etching, while relevant metal depositions are completed with electron beam evaporation. Patterned-photoresist masks allow for precise plasma etching to isolate the ribbons and electrodes in order to craft emission arrays of arbitrary numbers, dimensions, and positions, facilitating arrangements for rapid testing of device parameters and capabilities. Metals deposited on plasma-etched surfaces allow for external ball- and wedge-bonding of gold wire, resulting in test setup and device controls being significantly cheaper, faster, easier, and more robust than those presented in referenced works. Emission currents can be measured via a straightforward setup with the devices (cathodes) and a phosphor screen (anode) positioned in a vacuum chamber with feed-through contacts for control and measurement. Results of captured currents from various dimensions, arrangements, and applied biases of the graphene microribbon emitters and arrays are provided in both absolute terms, as well as normalized to more conventional dimensions and energizing voltages of comparable thermionic and field emission electron sources. By crafting microribbon emitters in various combinations of dimensions and arrangements, and isolating control circuits from each other, it should even be possible to craft a single physical device that could alternately function as multiple different sources, either independently or in concert as need dictates. Electron sources crafted in this fashion are expected to exhibit greater output, durability, flexibility, and cost savings compared to other electron sources of comparable dimensionality and power requirements. Presented here is a treatment of the preparation, fabrication, and testing of these epitaxial graphene microribbon electron emission arrays intended as sources for low-power x-ray imaging applications. 1. Wei, X. L.; Golberg, D.; Chen, Q.; Bando, Y.; Peng, L. M.; Phonon-Assisted Electron Emission from Individual Carbon Nanotubes. *Nano Lett.* 2011, 11, 734-739. 2. Wei, X.; Bando, Y.; Golberg, D.; Electron Emission from Individual Graphene Nanoribbons Driven by Internal Electric Field. *ACS Nano*, 2012, 6, 705.

#### F.EN04.28.27

**Full Consideration of Acoustic Phonon Scatterings in Two-Dimensional Dirac Materials** Yia-Chung Chang and Khoe Van Nguyen; Academia Sinica, Taiwan

The in-plane acoustic phonon scattering in graphene is solved by considering fully inelastic acoustic phonon scatterings in two-dimensional (2D) Dirac materials for large range of temperature ( $T$ ) and chemical potential ( $\mu$ ). Rigorous analytical solutions and symmetry properties of Fermionic and Bosonic functions are obtained. We illustrate how doping alters the temperature dependence of acoustic phonon scattering rates. It is shown that the quasi-elastic and ansatz equations previously derived for acoustic phonon scatterings in graphene are limiting cases of the inelastic-scattering equations derived here. For heavily-doped graphene, we found that the high- $T$  behavior of resistivity is better described by  $\rho(T, \mu) \sim T [1 - \alpha \frac{2}{3} (k_B T)^2]$  rather than a linear  $T$  behavior, and in the low  $T$  regime we found  $\rho^{-1} \sim (k_B T)^4$  but with a different prefactor (i.e.  $\sim 3$  times smaller) in comparison with the existing quasi-elastic expressions. Furthermore, we found a simple analytic "semi-inelastic" expression of the form  $\rho^{-1} \sim (k_B T)^4 / (1 + cT^3)$  which matches nearly perfectly with the full inelastic results for any temperature up to 500 K and  $\mu$  up to 1 eV. Our simple analytic results agree well with previous first-principles studies and available experimental data. Our analyses pave a way for investigating scatterings between electrons and other fundamental excitations with linear dispersion relation in 2D Dirac material-based heterostructures such as bogolon-mediated electron scattering in graphene-based hybrid Bose-Fermi systems.

#### F.EN04.29.01

**Metal–Organic Frameworks Encapsulated with Vanadium-Substituted Heteropoly Acid for Highly Stable Asymmetric Supercapacitors** Nageh K. Allam; The American University in Cairo, Egypt

Herein, we report on a facile one-pot synthesis of polyoxometalates encapsulated zeolite imidazolate framework cages ( $\text{PMo}_{10}\text{V}_2@ZIF-67$ ). The morphological and structural properties of the as-synthesized materials were investigated *via* FESEM, EDS, XRD and FTIR techniques. Moreover,  $\text{N}_2$  adsorption/desorption isotherms, and XPS measurements were carried out to elucidate the textural properties and composition of the fabricated materials. Upon their use as supercapacitor electrodes, the  $\text{PMo}_{10}\text{V}_2@ZIF-67$  electrode exhibited a maximum specific capacitance of 765 F/g at a scan rate of 5 mV/s. Furthermore, a supercapacitor device was assembled using activated carbon as the negative electrode and  $\text{PMo}_{10}\text{V}_2@ZIF-67$  as the positive electrode, delivering a specific power of 702 W/kg and corresponding specific energy of 20.9 Wh/kg at a charging current density of 1 A/g. In addition, the device shows excellent long term stability and high Columbic efficiency over 5000 charging and discharging cycles at charging and discharging current density of 5 A/g.

#### F.EN04.29.02

**Recycling of Li-Ni-Mn-Co Hydroxide from Spent Batteries to High-Performance Supercapacitors with Exceptional**

**Stability** Nageh K. Allam; American University in Cairo, Egypt

The intensive implementation of Li-ion batteries in many markets makes it increasingly urgent to address the recycling of strategic materials from spent batteries. Batteries typically contain toxic chemicals and cannot be disposed of at will. In this study, Li-Ni-Mn-Co hydroxides are successfully recycled from spent Li-ion batteries electrodeposited on nickel foam and fully characterized using different techniques such as field emission scanning electron microscopy (FESEM), x-ray diffraction (XRD), energy-dispersive X-ray spectroscopy (EDXS), inductively coupled plasma (ICP), and X-ray photoelectron spectroscopy (XPS) techniques. The recycled nanostructured films are tested in a three-electrode electrochemical system to investigate their capacitance behavior. The recycled electrodes show a high capacitance of  $951 \text{ F.g}^{-1}$  (Specific capacity of  $523.5 \text{ C.g}^{-1}$ ) at  $1 \text{ A.g}^{-1}$ . Moreover, recycled materials are used as positive electrodes to construct asymmetric supercapacitor devices. The device shows a Coulombic efficiency of 100%, capacitance retention reaching  $\sim 90\%$  with excellent cycling stability after 10,000 cycles as well as reasonable power and energy densities.

#### **F.EN04.29.03**

**Effect of Iron Substitution on Cobalt Oxide and Study of Its Electrochemical Performance** Deepa Guragain; The University of Memphis, United States

The application of metal oxides has been increasing for energy storage device due to excellent electrochemical properties, multifunctional energy application, environmentally friendly property and lower price. Due to rapid growth of energy use, there is very high demand for new ways to store energy. It is challenged to develop efficient way to store energy without polluting environment, which is possible by using transition metal oxide. We have prepared  $\text{Fe}_x\text{Co}_{3-x}\text{O}_4$  ( $x=0.0, 0.2, 0.4, 0.6, 0.8, 1$ ) successfully via hydrothermal method from which we can prepared electrode to make supercapacitor device. The structural properties were investigated by X-ray diffraction (XRD) and found phase pure  $\text{Fe}_x\text{Co}_{3-x}\text{O}_4$ . The morphology of the series obtained from scanning electron microscopy (SEM) varies from thinner nano-plates to thicker nano-plates as the concentration of Fe increase from  $x=0.0$  to  $x=1.0$ . Furthermore,  $\text{Fe}_x\text{Co}_{3-x}\text{O}_4$  were characterized by X-ray Photoelectron spectroscopy (XPS), Fourier Transform Infrared Spectroscopy (FTIR) and Quantachrome Surface area analyzer. The maximum BET surface area obtained from Quantachrome Instrument for  $x=1$  is  $87.5 \text{ m}^2/\text{g}$ . The XPS gives elemental composition of  $\text{Fe}_x\text{Co}_{3-x}\text{O}_4$  as in desired amount. The higher specific capacitance of  $268 \text{ F/g}$  at a current density of  $1 \text{ A/g}$ ,  $856 \text{ F/g}$  at  $2 \text{ mV/s}$  scan rate, the energy density of  $16 \text{ Wh/kg}$  and power density of  $170 \text{ W/kg}$  in  $3\text{M KOH}$  electrolyte was observed for  $x=1$  sample. An increased retention capacity  $\sim 122\%$  measured at  $5 \text{ A/g}$  current density and Coulombic efficiency of 100%. All these results indicate Fe dope  $\text{Co}_3\text{O}_4$  composites electrode shows promising electrocatalytic activity results in the high intrinsic electronic conductivity, can largely improve the interfacial electroactive sites, increase charge transfer rates and help to stabilize the structure of compound.

#### **F.EN04.29.04**

**Microstructural Evolution and Electrochemical Properties of Arachis Hypogaea Shell Derived *Ex Situ* Nitrogen-Doped Activated Carbon for Energy Storage Applications as Supercapacitor** Balla D. Ngom<sup>1</sup>, Ndeye Fatou D. Sylla<sup>1</sup>, Ndeye Maty Ndiaye<sup>1</sup>, Mohamed Chaker<sup>2</sup> and Ncholu Manyala<sup>3</sup>; <sup>1</sup>Universté Cheikh Anta Diop de Dakar, Senegal; <sup>2</sup>INRS, Canada; <sup>3</sup>University of Pretoria, South Africa

We report on the correlation of the microstructural evolution and electrochemical properties of an ex-situ N-doping KOH activated carbon derived from Arachis Hypogaea Shell (NAC-AHS) and compared to the non-doped (AC-AHS). Interconnected cavities with irregular-shaped structure are reported by SEM analysis for AC-AHS. After nitrogen doping, the morphology of the NAC-AHS materials exhibited a less porous structure as compared to AC-AHS. The surface specific area (SSA) of NAC-AHS was found to be  $1442 \text{ m}^2 \text{ g}^{-1}$  lower than the value of AC-AHS ( $1557 \text{ m}^2 \text{ g}^{-1}$ ), the pore volumes were also found to follow the same trend since the reported values are as follow  $0.76 \text{ cm}^3 \text{ g}^{-1}$  and  $0.69 \text{ cm}^3 \text{ g}^{-1}$ , respectively for AC-AHS and NAC-AHS. The AC-AHS and NAC-AHS exhibited in a half cell a specific capacitance ( $C_s$ ) values of  $167 \text{ F.g}^{-1}$  and  $216 \text{ F.g}^{-1}$ , respectively at  $1 \text{ A.g}^{-1}$ , corresponding to an improvement of 30% after ex-situ N-doping, which agrees with the higher current response recorded in the CV profiles of the samples. A symmetric device fabricated from the NAC-AHS materials displayed a  $C_s$  of  $251.2 \text{ F.g}^{-1}$  at  $1 \text{ A.g}^{-1}$  in a wide operating voltage of  $2.0 \text{ V}$  in  $2.5 \text{ M KNO}_3$  aqueous electrolyte. In terms of stability, it achieved 83.2% as capacity retention up to 20,000 cycles, which was, improved through the floating/aging measurement at  $5 \text{ A.g}^{-1}$  over a long period of time ( $\sim 7+$  days). A specific energy of  $35 \text{ Wh.kg}^{-1}$  with a corresponding specific power of  $1 \text{ kW.kg}^{-1}$  at  $1 \text{ A.g}^{-1}$  was delivered with the device still retaining up to  $22 \text{ Wh.kg}^{-1}$  and a  $20 \text{ kW.kg}^{-1}$  specific power even at  $20 \text{ A.g}^{-1}$ .

#### **F.EN04.29.05**

**Electrical Transport in Coconut Shell Charcoal** G. R. A. Kumara<sup>1</sup>, Kasun J. Wimalasena<sup>2</sup>, S. M. B. Dissanayake<sup>2</sup>, T. M. W. J. Bandara<sup>2</sup>, [Ajith DeSilva](#)<sup>3,4</sup>, A. G. U. Perera<sup>4</sup> and K. Tennakone<sup>1,4</sup>; <sup>1</sup>National Institute of Fundamental Studies, Sri Lanka, Sri Lanka; <sup>2</sup>University of Peradeniya, Sri Lanka; <sup>3</sup>University of West Georgia, United States; <sup>4</sup>Georgia State University, United States

Activated coconut charcoal is unique in meso and micro pore distribution, BET surface area exceeding 2000 m<sup>2</sup>g<sup>-1</sup> and pore volume ~ 1.3 cm<sup>3</sup>g<sup>-1</sup>. It is the bio-derived carbon material of choice for supercapacitor electrodes, cryogenic gas absorption in vacuum technology and water purification. Coconut shell carbon is also the hardest biochar - hardness 3-4 in the Mohs scale. For supercapacitors, batteries and several other applications, high electrical conductivity is an advantageous parameter. Owing to large surface to volume ratio of the material, the carrier trapping sites on the surface play a crucial role in electrical transport. The DC electrical conductivity is found to be greatly influenced by mode of activation, surface treatments and impurities. The most studies on electrical conductivity of activated carbons were based on measurements conducted using compacted pellets. The higher hardness of coconut shell charcoal enable use of sizable samples made from uncrushed flakes to carry out chemical treatments and conduct measurements under varying conditions. The results of measurements and interpretations will be presented, emphasizing supercapacitor applications of coconut shell charcoal.

#### **F.EN04.29.06**

**Dielectric h-BN Separators for Ti<sub>3</sub>C<sub>2</sub>-MnO<sub>2</sub> Supercapacitors** [Alptekin Aydinli](#)<sup>1,2</sup>, Xuehang Wang<sup>1</sup>, Husnu E. Unalan<sup>2</sup> and Yury Gogotsi<sup>1</sup>; <sup>1</sup>Drexel University, United States; <sup>2</sup>Middle East Technical University, Turkey

Electrochemical energy storage (EES) units are vital for mobile electronic devices that can provide high energy and power densities. Current studies mostly aim at improving the performance of the electrode active materials. Nevertheless, inert components such as electrolyte, separator and current collector occupy 70-80 wt.% of the EES devices and reducing their weight/volume can significantly improve the performance of these devices. Dielectric materials are used extensively in EES devices as separators such as ceramics in conventional capacitors. In supercapacitors, polypropylene membranes and glassy fiber films with typical thicknesses larger than 25 μm are the common separator materials. Two dimensional (2D) dielectric materials with flat and smooth surfaces at a much smaller thickness can in fact be used as efficient separators. In this work, 2D hexagonal boron nitride (h-BN) thin films were utilized as efficient separator layers in asymmetric MXene supercapacitors. In these devices, titanium carbide (Ti<sub>3</sub>C<sub>2</sub>) and manganese dioxide (MnO<sub>2</sub>) were used as the negative and positive electrodes, respectively. Electrochemical tests such as cyclic voltammetry, chronopotentiometry and electrochemical impedance spectroscopy were conducted to determine specific capacity, rate capability and cycling stability of the asymmetric supercapacitor devices. Fabricated supercapacitor devices showed promising electrochemical performance in a PVA/H<sub>2</sub>SO<sub>4</sub> gel electrolyte compared to the control device with conventional Celgard separator. The reduced thickness of the h-BN separator decreased the volume of an entire supercapacitor device and significantly improved the overall capacitance.

#### **F.EN04.29.07**

**Bioinspired Nanoporous Ion Conducting Membranes for Next Generation Batteries** [Ahmet Emre](#), Jinchun Fan, Emine Turali-Emre, Alycia Gerber, Volkan Cecen and Nicholas Kotov; University of Michigan, United States

Bioinspired ion transport membranes have been widely investigated for energy storage applications. High theoretical specific energy density (2600Wh/kg) and high specific capacity (1675mA/g) along with natural abundance and low toxicity of sulfur have been attracting significant attention for development of an alternative battery system to replace traditional lithium ion batteries which suffer from safety and capacity/energy density limitations in various applications. However, challenges such as polysulfide dissolution and shuttling prevent mass commercialization of metal sulfur batteries. Inspired from biological ion transport mechanisms, we show a practical yet comprehensive approach for development of high-performance metal sulfur batteries. Aramid nanofiber (ANF) based composite ion transport membranes not only prevent dendrite formation but also confine polysulfides on the cathode side. ANF composite battery separators provide diverse and opposing properties including high mechanical properties, high ionic conductivity and high thermal/chemical stability. Highly selective ion sieving properties of these biomimetic separators provide safe and high-performance batteries. Fabrication of such biocompatible, affordable, flexible and high energy density battery is quite crucial in powering next-generation electronics including but not limited to portable, wearable and implantable biomedical devices.

## SYMPOSIUM F.EN06

---

Advancement of Lithium-Based High-Energy Density Batteries at Multiple Scales, Factoring in Safety  
November 21 - December 3, 2020

### Symposium Organizers

Dongping Lu, Pacific Northwest National Laboratory  
Sagar Mitra, IITB  
Yuliya Preger, Sandia National Laboratories  
Donghai Wang, The Pennsylvania State University

### Symposium Support

#### **Bronze**

Sandia National Laboratories  
Thermo Fisher Scientific

---

\* Invited Paper

SESSION F.EN06.08: Live Keynote I: Advancement of Lithium-Based High-Energy Density Batteries at Multiple Scales, Factoring in Safety  
Session Chairs: Dongping Lu and Sagar Mitra  
Tuesday Afternoon, December 1, 2020  
F.EN06

### 7:30 PM INTRODUCTION

#### 7:35 PM \*F.EN06.01.10

**Late News: Rational Designed Materials for Energy Storage—From the View of Semiconductor Physics** Jiantao Zai;  
Shanghai Jiao Tong University, China

Semiconductor physics mainly discuss the energy band structures and the carrier behaviors in semiconductors. The carrier dynamics and the resulting conduction properties of semiconductors. As a semiconductor, the carrier transporting characteristics of Si has been well studied and adjusted via doping (n type, N, P; p type, B), which has been widely applied in electronics, solar cell and photocatalysis. In recent years, Si has been regarded as the most promising anode material for its highest theoretical specific capacity, and natural abundance. However, the poor conductivity of intrinsic Si still limits the rate performance of Si materials.

Previously, Yi and me found boron doping can obviously enhance the rate capability of Si-C composite. Recently, phosphorus-doped yolk-shell Si@C materials (P-doped Si@C) with balanced electron and Li<sup>+</sup> transportation dynamics are rational designed and prepared, which deliver high specific capacities (2709 mAh g<sup>-1</sup> @ 0.4 A g<sup>-1</sup>), great rate capability (510 mAh g<sup>-1</sup> @ 35 A g<sup>-1</sup>) and good retention of ~95% over 800 cycles at 4 A g<sup>-1</sup>. As a result, P-doped Si@C anode pairs with commercial activated carbon to assemble lithium-ion capacitor (high power density of ~61080 W kg<sup>-1</sup> at 20 A g<sup>-1</sup>). Junction is also an important concept in semiconductor physics, which refers to the interface region with rectification characteristics formed by the contact of two different semiconductor phases. The formation of semiconductor junction will change the charge state of atoms near the junction interface, and then regulate the adsorption and catalytic activity of active sites in the region. Our previous research reveals the space charge of p-n junction of p-type CoP and n-type FeNi LDH can be utilized to improve the adsorption of OH<sup>-</sup> and promote the OER process. With this in mind, The *in-situ* formed VS<sub>x</sub>@VO<sub>2</sub> junctions can designed to promote the absorption of polysulfide and result high volume specific Li-S batteries. Furthermore, a n-n-type CoS<sub>2</sub>-CoS heterojunction were designed to facilitate the electrocatalytic conversion of I<sup>-</sup>/I<sub>3</sub><sup>-</sup> and polysulfides, which can significantly improve the power density and lifetime of flow batteries. Therefore, it is possible to modulate the electronic configuration of active site by designing proper semiconductor junctions following the theories of solid physics.

In all, the semiconductor physics can offer useful theoretical guidance for rational design of high performance materials for energy storage.

Ref

- [1] R. Yi, J. Zai; F. Dai, et al., *Electrochem Commun*, 2013, 36,  
[2] M. Chen, B. Li, X. Liu, et al., *J Mater Chem A*, 2018, 6, 3022-3027.  
[3] K He, T. Tadesse Tsega, X. Liu, et al., *Angew. Chem. Int. Ed.*, 2019, 58, 34, 11903-11909.  
[4] L. Zhou, L. Yao, S. Li, et al., *J Mater Chem A* 2019, 7 (8), 3618-3623.  
[5] D. Ma, B. Hu Bo, W. Wu, et al., *Nat Commun*, 2019, 10, 1, 3367-3367.

#### 8:15 PM F.EN06.02.03

**Pressure-Tailored Lithium Deposition and Dissolution in Lithium Metal Batteries** Chengcheng Fang and Y. Shirley Meng; University of California, San Diego, United States

Lithium (Li) metal offers high theoretical capacity, lowest negative potential and light weight, making it the ideal anode material for high-energy-density batteries. Porous electrodes resulting from unregulated Li growth is believed to be the major cause of the low Coulombic efficiency (CE) and potential safety hazards of rechargeable Li metal batteries. Strategies aiming to achieve large granular Li deposits have been extensively explored; yet, the ideal Li deposits, which consist of large Li particles seamlessly packed on the electrode and can be reversibly deposited and stripped, have never been reported. Here, by using cryo-FIB-SEM, 3D reconstruction and MD simulation, we quantitatively revealed the role of stack pressure on Li nucleation, growth and stripping, and discovered that optimal pressure for approaching 100% dense Li deposition by establishing a pressure-morphology-performance correlation. Unprecedented, a dense Li deposition (99.49% electrode density) with an ideal columnar structure has been achieved and can be reversibly plated and stripped during extended cycles at room temperature. The tailored Li deposition and stripping by optimizing stack pressure opens new opportunities to rationally mitigate inactive Li formation, improve cycle life and enable fast charging for rechargeable Li metal batteries.

#### 8:35 PM BREAK

#### 8:50 PM \*F.EN06.05.01

**Ni-Rich Layered Cathodes for All-Solid-State Li Batteries—Effects of Microstructure and Solid Electrolyte** Yoon Jae Han, Sung Hoo Jung and Yoon Seok Jung; Hanyang University, Korea (the Republic of)

All-solid-state Li batteries (ASLBs) have been emerged as the enabler to achieve significantly enhanced safety and energy densities, as compared to conventional lithium-ion batteries (LIBs). Several classes of inorganic solid electrolyte (SE) materials have garnered much attention as they could be integrated with electrode active materials into ASLBs by a scalable process such as cold-pressing. Sulfides (or thiophosphates, e.g.,  $\text{Li}_6\text{PS}_5\text{Cl}$ ) and halides (e.g.,  $\text{Li}_3\text{YCl}_6$ ) satisfy critical features for scalable high-performance ASLBs; those are mechanically sinterability and high  $\text{Li}^+$  conductivity. However, they show different comparative advantages in multiple aspects. For example, while halides are heavier than sulfides, they show superior electrochemical oxidation stability to sulfides.

As is the case for advanced LIBs based on liquid electrolytes, Ni-rich cathode materials are the key to the practical ASLB technologies. Unfortunately, they suffer from par below electrochemical performances in ASLBs, which are attributed to the interfacial instabilities in terms of both electrochemical and electrochemo-mechanical effects.

In this presentation, we report on our recent findings on the electrochemo-mechanical effects for Ni-rich layered cathode materials for ASLBs. Microstructural effects of NCM particles on the performance of ASLBs are revealed. Moreover, the performances of NCM using halide SEs are extensively compared. These results shed light on a design strategy for high-performance practical ASLBs.

#### References

- [1] K. H. Park, Q. Bai, D. H. Kim, D. Y. Oh, Y. Zhu, Y. Mo, Y. S. Jung, *Adv. Energy Mater.* **2018**, 8, 1800035.  
[2] S. H. Jung, U.-H. Kim, J.-H. Kim, S. Jun, C. S. Yoon, Y. S. Jung, Y.-K. Sun, *Adv. Energy Mater.* **2020**, 10, 1903360.

#### 9:10 PM \*F.EN06.06.01

**Understanding for Charge/Discharge Curves of Commercial Lithium-Ion Batteries** Yuhao Lu and Xiao Jie; NingDe Amperex Technology Limited, China

Lithium ion batteries (LIBs) are wildly used for portable electronics and electric vehicles due to the favorable performance compared with other rechargeable batteries. However, their degradation deteriorate their service life remarkably. Fortunately, charge/discharge curves can provide quantitative information for understanding how such degradation correlates with usage conditions and environment of LIBs.

In general, the charge/discharge curves can be divided into two parts, i.e. the open circuit voltage (OCV) and the polarization in the cell. The OCV provides a thermodynamic fingerprint of the electrode which could be roughly estimated by



charge/discharge the cell at very low C-rate. With regards to a commonly used 2430 coin cell, the difference between charge/discharge curve and theoretical OCV is less than 30mV at the full range of SOC when a 1/25C current rate is used. In this presentation, the changes in OCV during long cycles will be exhibited, which offers a quantified information on active material decay as well as the side reactions in the cell. The polarization of the cell is strongly affected by the electron and lithium ion transport inside the electrode microstructure. In this work, both the time-domain and the frequency-domain electrochemical methods were applied to the analysis to distinguish each process onto the polarization in the cell, i.e. the contact problem between the solid phases, the mass transport through the interface and in the solid phase of the electrodes, along with the slow electrochemical reactions. Furthermore, the thermodynamic fingerprints of the positive and negative materials have strongly relation with the polarization in the cell. These relations generally becomes very complex, and thus a mathematical modeling is also used to understand and explain the charge/discharge curve for LIB in detail. Overall, it is proposed that more collaborations could be needed between the academia and industry so that the lithium ion battery degradation could be fully investigated.

SESSION F.EN06.09: Live Keynote II: Advancement of Lithium-Based High-Energy Density Batteries at Multiple Scales, Factoring in Safety

Session Chairs: Dongping Lu and Yuliya Preger

Wednesday Morning, December 2, 2020

F.EN06

## 11:30 AM INTRODUCTION

11:35 AM \*

**Organosilicon Compounds Improve the Thermal and Electrochemical Stability of Lithium-Ion Batteries** Robert Hamers<sup>1</sup>, Sarah Guillot<sup>2</sup>, Monica Usrey<sup>2</sup>, Louis Morris<sup>1</sup> and Cesar Ortiz Ledon<sup>1</sup>; <sup>1</sup>University of Wisconsin-Madison, United States; <sup>2</sup>Silatronix, Inc., United States

Incorporation of organosilicon (OS) compounds in modest concentrations as low as several percent in conventional carbonate electrolytes lead to substantial improvements in the thermal and electrochemical stability of the resulting lithium ion batteries. We have been investigating the fundamental chemical degradation pathways of organosilicon compounds in an effort to understand the chemical and electrochemical origins of these remarkable properties. The combination of NMR spectroscopy, in situ FTIR, AFM, and XPS provides unique insights into how organosilicon electrolytes reduce or eliminate autocatalytic chemical pathways associated with PF6 and its degradation products. OS compounds further alter the chemical nature of SEI layers on silicon, leading to improvements in overall performance. In this talk I will summarize some of our recent work characterizing organosilicon thermal stability and electrochemical stability against different materials, including silicon-based anodes and NMC-based cathodes.

11:55 AM \*

**Pairing Lithium-Metal Anode with High-Nickel NMC and Sulfur Cathodes—Fundamental Understanding and Engineering Solutions** Arumugam Manthiram; The University of Texas at Austin, United States

Lithium-metal anode holds tremendous potential for enabling next generation of rechargeable batteries due to their high storage capacity (3,861 mAh g<sup>-1</sup>) and low reduction potential (-3.04 V vs SHE). When paired with a high-capacity cathode, such as high-nickel NMC or sulfur, lithium-metal anode can help deliver energy-dense storage systems with ~ 500 Wh kg<sup>-1</sup>. However, the poor efficiency associated with lithium plating and stripping severely limits the cycle life. For realizing practical viability, reversible lithium deposition needs to be achieved by stabilizing the lithium-electrolyte interphase (SEI) layer and mitigating the extreme volume changes accompanying the cycling.

The chemistry of the lithium-electrolyte interface is rendered distinct by the choice of the cathode in a full cell, *viz.*, high-nickel NMC or sulfur. This is not only due to the different electrolyte formulations used, but also due to the crossover of species between the cathode and anode. The characteristics of deposited lithium can fundamentally vary across different cathode systems, and unique strategies must be employed to stabilize lithium deposition in each case. Hence, an in-depth fundamental study is necessary to develop a thorough understanding of the lithium-electrolyte interfacial chemistry, while creative engineering solutions are necessary to achieve highly efficient lithium plating and stripping. This presentation will focus both on a fundamental understanding and offering engineering solutions.

When paired with a high-nickel NMC cathode, the lithium-metal anode is affected by transition-metal dissolution at the cathode and crossover to the anode. However, we find that during initial cycling, crossover of electrolyte decomposition products from the anode to the cathode is more severe and plays a more critical role. Not only does it alter/thicken the cathode SEI layer, it also affects the anode itself as the lithium SEI components could continually dissolve. The magnitude of this crossover is expected to depend on the nickel content in the cathode.

When paired with a sulfur cathode, the lithium-metal anode is affected by polysulfide dissolution at the cathode and crossover to the anode. We use anode-free full cells, which contain no excess lithium at the anode, to investigate the dynamics of lithium deposition. With advanced surface characterization methodologies, *e.g.*, time-of-flight secondary ion spectrometry, we find that the depletion of cyclable lithium inventory is due to the formation of “dead” metallic lithium, which itself is caused by severe electrolyte decomposition on lithium-metal surface with cycling.

The presence of polysulfide intermediates is found to have an intrinsically stabilizing effect on lithium deposition in Li-S batteries. This motivates our strategies towards engineering further improvements in cycle life. With tellurium as a cathode additive, tellurium-substituted polysulfides are formed, which reduce on lithium surface to form  $\text{Li}_2\text{TeS}_3$  as a thin,  $\text{Li}^+$ -ion conducting SEI layer. This enables uniform deposition of lithium and mitigates electrolyte decomposition. A remarkable improvement in cyclability is achieved in energy-dense anode-free full cells and lean-electrolyte pouch cells. Similarly, using organosulfide molecules as electrolyte additives opens the possibility of favorably tuning the properties of lithium SEI layer by simply modifying the organic functional group.

The development of three-dimensional current collector matrices is also critical to achieving reversible lithium deposition. The highly conductive frameworks provide efficient electron/ion transport and guides a homogenous deposition of lithium, while the porous 3D architecture helps mitigate severe volume changes during cycling. The presentation will demonstrate various lithiophilic host materials that show considerable promise in improving the cyclability of lithium-metal anode when paired with both high-nickel NMC and sulfur cathodes.

**12:15 PM \***

**Building Ultra-Conformal Protective Layers on Both Secondary and Primary Particles of Layered Lithium Transition Metal Oxide Cathodes** Guiliang Xu and Khalil Amine; Argonne National Laboratory, United States

Nickel-rich layered lithium transition metal oxides are the most attractive cathode materials for the next generation lithium-ion batteries for automotive application. However, they suffer from crystal and interfacial structure instability under aggressive electrochemical and thermal driving force, leading to rapid performance degradation and severe safety concerns. In this talk, we reported a transformative approach by using an oxidative chemical vapour deposition technique to build a protective conductive polymer (PEDOT) skin on layered oxide cathode materials. The ultra-conformal PEDOT skin facilitates the transport of lithium ions and electrons, significantly suppresses the undesired layered to spinel/rock-salt phase transformation and the associated oxygen loss, mitigates intergranular and intragranular mechanical cracking, and effectively stabilizes cathode-electrolyte interface. This approach remarkably enhances the capacity and thermal stability under high-voltage operation. Building a protective skin at both secondary and primary particle levels of layered oxides offers a design strategy for the promising Ni-rich cathodes towards high-energy, long-life and safe lithium-ion batteries.

**12:35 PM BREAK**

**12:50 PM \***

**Thermal Conduction in Li-Ion Battery Materials** Ankur Jain; The University of Texas at Arlington, United States

Li-ion batteries offer excellent energy conversion rate and high energy storage density in electric vehicles, aircraft, consumer electronics and renewable energy storage. However, these batteries suffer from several safety related problems, as evidenced by recent product recalls and incidents of fires in electric cars and aircraft. Overheating due to poor thermal transport is at the heart of several of these challenges, and therefore, a fundamental understanding of heat transfer in Li-ion battery materials is critically needed. While Li-ion battery materials have been well optimized from the perspective of electrochemistry, the nature of thermal transport in these materials remains relatively less known.

This talk will summarize ongoing research on understanding and optimizing heat transfer in Li-ion battery materials through experiments and theoretical analysis. Measurement of orthotropic thermal conductivity of a Li-ion cell will be described. Measurements of thermal conductivity of the separator of a Li-ion cell will be discussed. Measurements that identify poor

thermal transport across the cathode-separator interface as the fundamental root cause of the low thermal conductivity of Li ion cells will be discussed. A molecular bridging approach that reduces this rate-limiting thermal contact resistance by 4X through improved interfacial thermal transport will be discussed. This approach is expected to significantly enhance thermal conductivity of a Li-ion cell. More recent work on enhancement of thermal transport in Gel Polymer Electrolytes (GPEs) through inclusion of BN/Al<sub>2</sub>O<sub>3</sub> nano/microparticles will also be discussed. While this approach is shown to improve thermal conduction in general, a careful optimization of thermal and ionic transport in GPEs will help fully utilize this promising class of materials for next-generation solid-state batteries. Related research on developing predictive models for onset of thermal runaway based on thermal properties of battery materials and kinetics of underlying electrochemical processes will also be discussed briefly.

**1:10 PM \***

**Performance of High Energy and High Power Commercial Li-Ion Cells for Space Missions** Ratnakumar Bugga;  
California Institute of Technology, United States

Li-ion batteries are being widely used in planetary space missions, owing to their impressive performance characteristics, including high specific energy, long life, and the ability to operate over a wide temperature range. Historically, batteries with custom large-format Li-ion cells of 10-55 Ah have been used in various Mars missions, e.g., Mars Exploration Rovers (Spirit and Opportunity), Mars Curiosity Rover, Mars landers (Phoenix and InSight), Mars and Jupiter orbiters and the upcoming Mars 2020 Rover. However, in several other robotic and human space missions, e.g., Europa Clipper, Artemis missions to moon, and Portable Life Support System (PLSS) for Extra-Vehicular Activities, commercial 18650 Li-ion cells are being used due to their improved specific energies of ~250 Wh/kg (20-50% over custom cells), improved safety from built-in safety devices, modularity, and excellent uniformity, which obviate the need for cell-level control during charging. Several cell types with different chemistries and from different manufacturers are being evaluated at JPL. The cell chemistries differ mostly in cathodes, i.e., either lithium nickel cobalt aluminum oxide (NCA), Li-rich nickel manganese cobalt oxide (Ni-rich NMC) or blends with lithium manganese spinel oxide (LMO). Various performance tests, including cycle life at different depths of discharge, radiation tolerance and high-power characterization at different temperatures are being carried out in conjunction with Electrochemical Impedance Spectroscopy (EIS). In addition, destructive physical analysis of the cells have been performed to analyze the electrode materials, and correlate them with the performance characteristics. Finally, low temperature charge characterization studies have been carried out to ascertain the propensity of lithium plating as a function of charge current and temperature.

SESSION F.EN06.10: Live Keynote III: Advancement of Lithium-Based High-Energy Density Batteries at Multiple Scales,  
Factoring in Safety  
Session Chairs: Sagar Mitra and Yuliya Preger  
Thursday Morning, December 3, 2020  
F.EN06

**8:00 AM INTRODUCTION**

**8:05 AM \*F.EN06.01.01**

**Progress Toward Safe Electrochemical Energy Storage Systems—The Benefits of Deliberate Materials-Focused Electrode Design and *Operando* Characterization** Amy Marschilok<sup>1,2</sup>; <sup>1</sup>Stony Brook University, United States; <sup>2</sup>Brookhaven National Laboratory, United States

Future applications for energy storage will demand high level function with long lifetime. As batteries increase in size and use requirements increase in complexity, safety takes on expanded importance for multiple applications including transportation and grid-level storage. Examples of electrode design approaches leading to improved safety based on materials chemistry will be highlighted in this presentation. Complementary *ex-situ*, *in-situ* and *operando* characterization approaches to understand energy storage material/composite degradation modes and relationship to cell level safety will also be described.

**8:25 AM F.EN06.01.02**

**A Scaling Law to Determine Phase Morphologies During Ion Intercalation** Dimitrios Fraggedakis, Martin Bazant and

Yang Shao-Horn; Massachusetts Institute of Technology, United States

Driven phase separation in ion intercalation materials is known to result in different non-equilibrium phase morphologies, such as intercalation waves and shrinking-core structures, but the mechanisms of pattern selection are poorly understood. Here, based on the idea that the coarsening of the slowest phase is the rate limiting step, we introduce a scaling law that quantifies the transition from quasi-equilibrium intercalation-wave to diffusion-limited shrinking-core behavior. The scaling law is validated by phase-field simulations of single  $\text{Li}_x\text{CoO}_2$  particles, *in situ* optical imaging of single  $\text{Li}_x\text{C}_6$  particles undergoing transitions between stage 1 ( $x = 1$ ) and 2 ( $x = 0.5$ ) at different rates, and all the available literature data for single-particle imaging of  $\text{Li}_x\text{CoO}_2$ ,  $\text{Li}_x\text{C}_6$  and  $\text{Li}_x\text{FePO}_4$ . The results are summarized in operational phase diagrams to guide simulations, experiments, and engineering applications of phase-separating active materials. Implications for Li-ion battery performance and degradation are discussed.

**8:45 AM \*F.EN06.02.01**

**Modeling of the Transfer Reactions at Li/SEI/Electrolyte Interface and Dendrite Free Morphology** Yue Qi<sup>1,2</sup>; <sup>1</sup>Brown University, United States; <sup>2</sup>Michigan State University, United States

The charge transfer reaction is the fundamental reaction for rechargeable batteries. The energy landscape of this reaction depicts the equilibrium and kinetics of the electrochemical process. Typically, a Li-metal electrode is always covered by a thin layer of solid electrolyte interphase (SEI), forming a complex Li/SEI/electrolyte interface. We first introduced a new half-cell model to predict the energy landscape of the electrochemical reaction of at the complex Li/SEI/electrolyte interface, with combined density functional theory (DFT) and tight-binding (DFTB) calculations. The simulated atomic details revealed that the Li-metal surface is negatively charged at the electrochemical equilibrium condition (the experimentally defined zero voltage for  $\text{Li}^+/\text{Li}^0$ ) due to the large solvation energy of  $\text{Li}^+$  in the EC-based electrolyte. The electric field created by the negatively charged surface can reorient the electrolyte into an ordered structure, lower the  $\text{Li}^+$  ion desolvation energy barrier, and help the  $\text{Li}^+$  ion transport through the SEI.

Further, the calculated energy landscape can be used to describe the electrochemical reaction kinetics with a Butler-Volmer equation, enabling a multiscale modeling approach. In this study, the DFT and DFTB predicted interfacial structures, desolvation processes, and the ion transfer energy barrier, were inputted into a non-linear phase-field model to capture the morphological evolution during the electroplating process. Specifically, this model captured the morphology difference between the dendritic Li plating in carbonate (EC)-electrolyte and faceted Mg plating in tetrahydrofuran(THF)-electrolyte under the similar current density. Furthermore, through systematical parametric analyses, we conclude that the cation desolvation-induced exchange current difference between Li and Mg is mainly responsible for their deposition morphological differences. This study provides a strategy of connecting the phase-field method and atomistic calculations and predicts that increasing the desolvation energy and lowering the equilibrium exchange current can help to achieve dendrite-free Li-metal anode.

**9:05 AM BREAK**

**9:20 AM \*F.EN06.02.04**

**Advances in Imaging Lithium Batteries at Different Length Scales** Herman Lemmens and Zhao Liu; Thermo Fisher Scientific, Netherlands

Imaging the microstructure of a battery cell at different length scales is important to understand the degradation processes through the battery cycle life. For example, investigating the formation of defects such as dendrites at the Li anode interface requires both high resolution imaging and large field of view. Ideally, imaging techniques cover the entire electrode thickness at submicron resolution with a method that preserves the sample interface. Here, we present an approach to probe the defects at the Li-metal battery interface. A coin cell has been sliced under cryo conditions with a laser inside the vacuum of the scanning electron microscope (SEM) chamber so a pristine surface is obtained and defect formation can be observed across the entire thickness of the cell.

In another example, transport properties for a thick NMC 811 cathode were obtained from focused ion beam (FIB) milling in combination with SEM. Because of the cathode thickness, an alternative to traditional Ga FIB milling was used. With a Xenon plasma beam, it was possible to obtain a 3D data set with more than 100  $\mu\text{m}$  field of view on a 70  $\mu\text{m}$  thick cathode. The microstructural characteristics extracted from such representative 3D volume help the understanding of the correlation between electrode microstructural evolution and performance deterioration.

**9:40 AM \*F.EN06.02.08**

**Thermal Runaway Propagation Study on Lithium-ion Cells as Packaged for Transportation** Judith Jeevarajan;

Underwriters Laboratories, United States

Thermal runaway in lithium-based cells and batteries have been a significant concern during transportation. The ICAO had set temporary restrictions on transportation to limit the SOC to 30% or less. In parallel, the ICAO commissioned the Society of Aerospace Engineers (SAE) to write a standard that would have test procedures that confirmed that li-based cells in the package as shipped will not become a fire hazard. The test procedure and the verification of test protocols have been looked into in this study. The results obtained as part of this test program will be presented.

SESSION F.EN06.01: Anodes—Graphite and Beyond  
On Demand Abstracts Available for Viewing Starting Saturday Morning, November 21, 2020  
F-EN06

**5:00 AM \*F.EN06.01.01**

**Progress Toward Safe Electrochemical Energy Storage Systems—The Benefits of Deliberate Materials-Focused Electrode Design and *Operando* Characterization** Amy Marschilok<sup>1,2</sup>; <sup>1</sup>Stony Brook University, United States; <sup>2</sup>Brookhaven National Laboratory, United States

Future applications for energy storage will demand high level function with long lifetime. As batteries increase in size and use requirements increase in complexity, safety takes on expanded importance for multiple applications including transportation and grid-level storage. Examples of electrode design approaches leading to improved safety based on materials chemistry will be highlighted in this presentation. Complementary *ex-situ*, *in-situ* and *operando* characterization approaches to understand energy storage material/composite degradation modes and relationship to cell level safety will also be described.

**5:15 AM F.EN06.01.02**

**A Scaling Law to Determine Phase Morphologies During Ion Intercalation** Dimitrios Fraggedakis, Martin Bazant and Yang Shao-Horn; Massachusetts Institute of Technology, United States

Driven phase separation in ion intercalation materials is known to result in different non-equilibrium phase morphologies, such as intercalation waves and shrinking-core structures, but the mechanisms of pattern selection are poorly understood. Here, based on the idea that the coarsening of the slowest phase is the rate limiting step, we introduce a scaling law that quantifies the transition from quasi-equilibrium intercalation-wave to diffusion-limited shrinking-core behavior. The scaling law is validated by phase-field simulations of single  $\text{Li}_x\text{CoO}_2$  particles, *in situ* optical imaging of single  $\text{Li}_x\text{C}_6$  particles undergoing transitions between stage 1 ( $x = 1$ ) and 2 ( $x = 0.5$ ) at different rates, and all the available literature data for single-particle imaging of  $\text{Li}_x\text{CoO}_2$ ,  $\text{Li}_x\text{C}_6$  and  $\text{Li}_x\text{FePO}_4$ . The results are summarized in operational phase diagrams to guide simulations, experiments, and engineering applications of phase-separating active materials. Implications for Li-ion battery performance and degradation are discussed.

**5:25 AM F.EN06.01.03**

**Low Tortuous, Highly Conductive and High-Areal-Capacity Battery Electrodes Enabled by Through-Thickness Aligned Carbon Structures** Kun Fu; University of Delaware, United States

Thick electrode with high-areal-capacity is a practical and promising strategy to increase the energy density of batteries, but development towards thick electrode is limited by the electrochemical performance, mechanical properties, and manufacturing approaches. In this talk, we overcome these limitations and report an ultra-thick electrode structure, called fiber-aligned thick or FAT electrode, which offers a novel electrode design and a scalable manufacturing strategy for high-areal-capacity batter electrodes. The FAT electrode uses aligned carbon fibers to construct a through-thickness fiber-aligned electrode structure, with feature of high electrode material loading, low tortuosity, high electrical and thermal conductivity, and good compression property. The low tortuosity of FAT electrode enables fast electrolyte infusion and rapid electron/ion transport, exhibiting a higher capacity retention and lower charge transfer resistance than conventional slurry-casted thick electrode design.

**5:35 AM F.EN06.01.06**

**Late News: Kinetic Pathways of Ionic Transport in Fast Charging Lithium Titanate** Tina Chen<sup>1,2</sup>, Wei Zhang<sup>3,4</sup>, Dong-

Hwa Seo<sup>1</sup>, Feng Wang<sup>4</sup> and Gerbrand Ceder<sup>1,2</sup>; <sup>1</sup>University of California, Berkeley, United States; <sup>2</sup>Lawrence Berkeley National Laboratory, United States; <sup>3</sup>Nankai University, China; <sup>4</sup>Brookhaven National Laboratory, United States

Fast-charging batteries typically employ electrodes capable of accommodating lithium continuously via solid-solution transformation because they have few kinetic barriers apart from Li<sup>+</sup> diffusion.[1, 2] One exception is lithium titanate, an anode that can cycle without the Li plating observed in graphite [3] and exhibits extraordinary rate capability seemingly inconsistent with its two-phase reaction and the sluggish diffusion within its endmembers [4]. Through first-principles calculations combined with nudged-elastic band calculations, we reveal that the kinetic pathway that enables facile ionic transport in lithium titanate consists of distorted face-sharing Li polyhedra in metastable intermediate states. The importance of the face-sharing Li polyhedral is further confirmed by real-time tracking of Li<sup>+</sup> local environments during migration using operando electron energy-loss spectroscopy. This study highlights that the rate capability of fast-charging electrodes may be controlled not solely by the intrinsic ionic diffusivity of macroscopic phases, but also by the transport pathways available via kinetically accessible low-energy states. Findings from this study, particularly on the improved kinetics originating from the face-sharing Li motifs in intermediate lithium titanate configurations, may open new directions for designing electrode materials for fast-charging batteries.

#### References:

- [1] H. Liu, F. C. Strobridge, O. J. Borkiewicz, K. M. Wiaderek, K. W. Chapman, P. J. Chupas, C. P. Grey, Capturing metastable structures during high-rate cycling of LiFePO<sub>4</sub> nanoparticle electrodes. *Science* **344**, 1252817 (2014).
- [2] R. Malik, F. Zhou, G. Ceder, Kinetics of non-equilibrium lithium incorporation in LiFePO<sub>4</sub>. *Nat. Mater.* **10**, 587-590 (2011).
- [3] T.-F. Yi, S.-Y. Yang, Y. Xie, Recent advances of Li<sub>4</sub>Ti<sub>5</sub>O<sub>12</sub> as a promising next generation anode material for high power lithium-ion batteries. *J. Mater. Chem. A* **3**, 5750-5777 (2015).
- [4] W. Schmidt, P. Bottke, M. Sternad, P. Gollob, V. Hennige, M. Wilkening, Small change-great Effect: steep increase of Li ion dynamics in Li<sub>4</sub>Ti<sub>5</sub>O<sub>12</sub> at the early stages of chemical Li insertion. *Chem. Mater.* **27**, 1740-1750 (2015).

#### 5:45 AM F.EN06.01.07

**Controlling Microstructure of Silicon-Based Anodes and Their Stress Evolution During Electrochemical Cycling** Mok Yun Jin<sup>1</sup>, Elizabeth Healy<sup>1</sup>, Xingcheng Xiao<sup>2</sup> and Brian Sheldon<sup>1</sup>; <sup>1</sup>Brown University, United States; <sup>2</sup>General Motors, United States

Composite electrodes that incorporate oxidized silicon are a cost-effective way to accommodate stresses and extend cycle life. To obtain fundamental information about chemo-mechanical phenomena in these composite structures, several different types of materials are being investigated through tuning the microstructures of Si nanoparticles and composite SiO<sub>x</sub> particles. The evolution of internal stresses in all of these structures was monitored with precise in-situ curvature in conjunction with parallel electrochemical measurements. Ex-situ characterization with electron microscopy, x-ray diffraction, and XPS provide important complementary information about changes in the materials. The different types of materials used for this work make it possible to systematically investigate key length scales, by independently varying the microstructures such as oxide layer thicknesses and particle/nano-cluster sizes. Analysis of these results requires assessments and models of both the chemical and mechanical effects of oxide surface layers and silicon encapsulation. The implications for optimizing these composite electrode structures will also be presented.

#### 5:55 AM F.EN06.01.08

**Evaluating Temperature Dependent Capacity Fade Mechanisms of Silicon-Graphite Electrodes** Yeyoung Ha<sup>1</sup>, Donal P. Finegan<sup>1</sup>, Andrew M. Colclasure<sup>1</sup>, Stephen E. Trask<sup>2</sup> and Matthew Keyser<sup>1</sup>; <sup>1</sup>National Renewable Energy Laboratory, United States; <sup>2</sup>Argonne National Laboratory, United States

One of the critical factors for determining the success of lithium-ion batteries (LiBs) in electric vehicles is their resilience to a wide range of environmental conditions. As batteries with higher energy densities are being developed, ensuring that they can withstand elevated temperatures without severe capacity fade is critical. Silicon (Si), which delivers higher specific capacity compared to graphite (Gr), is a promising anode material toward increasing the energy density of LiBs. Thus, evaluating the response of Si anodes to harsh temperatures that an electric vehicle might experience is crucial to ensure the development of safe, high energy density, and long life LiBs.

In this work, the performance of Si-Gr electrode is examined in half-cell (Si-Gr/Li), full cell (Si-Gr/LiNi<sub>0.5</sub>Mn<sub>0.3</sub>Co<sub>0.2</sub>O<sub>2</sub> and Si-Gr/LiFePO<sub>4</sub>), and symmetric cell (Si-Gr/Si-Gr) configurations at varying temperatures (25, 45, and 70°C). By examining the three different cell configurations, contributions from different cell components are deconvoluted and physical mechanism for each electrode (i.e., loss of lithium inventory or active material) are evaluated. In addition, the effect of

fluoroethylene carbonate (FEC) electrolyte additive on the thermal stability of Si is examined by testing two different electrolyte compositions (Gen2 (1.2 M LiPF<sub>6</sub> in ethylene carbonate (EC)/ethyl methyl carbonate (EMC) (3:7, w/w)) and GenF (Gen2 + 10 wt% FEC)). The degradation mechanisms in each system is further analyzed via incremental capacity analysis. As dQ/dV analysis of Si-Gr composites represent challenges not accounted for in Gr electrodes (i.e., hysteresis and path dependency), dQ/dV methods for Si-Gr electrodes are developed in this work. Detailed analyses of the electrochemical performance of Si-Gr electrodes, along with incremental capacity analysis and post-mortem analysis, provide insights into the critical factors affecting the performance of Si-Gr electrodes at elevated temperatures. Based on the results, we propose the appropriate cell configuration and protocol for testing the thermal stability of Si-based cells.

#### 6:05 AM F.EN06.01.09

**Silicon Oxycarbide as a Host Matrix of Choice to Stabilize Li-Ion Storage in Nanosized Alloying Elements** Romain J. Dubey<sup>1,2</sup>, Pradeep Vallachira Warriam Sasikumar<sup>2</sup>, Frank Krumeich<sup>1</sup>, Gurdial Blugan<sup>2</sup>, Kostiantyn Kravchyk<sup>1,2</sup>, Thomas Graule<sup>2</sup> and Maksym V. Kovalenko<sup>1,2</sup>; <sup>1</sup>ETH Zürich, Switzerland; <sup>2</sup>Empa–Swiss Federal Laboratories for Materials Science and Technology, Switzerland

The ever-increased demand in energy and consumable goods have led to a high necessity for sustainable catalysts<sup>[1,2]</sup> and innovative energy storage systems<sup>[3,4,5]</sup> with high energy densities, such as Li-ion batteries (LiBs). To maximize the anodic charge storage capacity of LiBs, alloying-type anode materials such as Sn and Sb have attracted considerable interest because of their high theoretical capacity of 992 and 660 mAh g<sup>-1</sup> and a suitable lithiation/delithiation voltage window of 0.01-1.5 V vs. Li<sup>+</sup>/Li. Recent advances in nanostructuring of the alloying-type anodes provide an effective way of mitigating the challenges of their volume expansion upon lithiation that severely hinder the cycling stability.<sup>[6]</sup> Besides, one of the prevailing approaches toward stabilization of such electrodes is the embedding of Sn or Sb in the form of nanoparticles (NPs) in a matrix. The matrix helps to buffer the volume changes, impart better electronic connectivity, and prevent particle aggregation upon lithiation/delithiation. In this context, polymer-derived ceramics, namely, silicon oxycarbide (SiOC), is an appealing candidate for stabilizing Sn and Sb inclusions. This matrix features a high Li-ion storage capacity ranging from 600 to 700 mAh g<sup>-1</sup>, low volume expansion upon lithiation of about 7%, and high electronic conductivity. In this study, we report a facile synthesis of Sn<sup>[7]</sup> and Sb<sup>[8]</sup> NPs embedded in a SiOC matrix via the pyrolysis of a cross-linked preceramic polymer. The NPs are formed *in-situ* via a carbothermal reduction during the pyrolysis. We determined that a key element to obtain a homogeneous distribution of NPs in SiOC is the employment of precursors with compatible polarities, allowing for an intimate blending of the functionalized polysiloxanes with the Sn or Sb precursors. This approach proved to be effective for buffering volume changes while retaining practical energy densities and high rate capabilities. For instance, SiOC/Sn nanocomposite exhibited a high rate capability, delivering a high capacity of 553 mAh g<sup>-1</sup> at a current density of 2232 mA g<sup>-1</sup> ( $\approx$  6C for a graphite anode). Additionally, the electrochemical performance of SiOC was assessed in full cell configuration using areal capacities of 1.3 mAh cm<sup>-2</sup> being relevant for high-power industrial applications. The mechanism of Sn lithiation in SiOC was evaluated by *in-situ* powder X-ray diffraction.

References:

- [1] R. Dubey, R. Comito, Z. Wu, G. Zhang, A. Rieth, C. Hendon, J. Miller, M. Dinca, *J. Amer. Chem. Soc.* **2017**, *139*, 12664.
- [2] E. Metzger, R. Comito, Z. Wu, G. Zhang, R. Dubey, W. Xu, J. Miller, M. Dinca, *ACS Sust. Chem. Eng.* **2019**, *7*, 6654.
- [3] R. Dubey, J. Nüssli, L. Piveteau, K. Kravchyk, M. Rossell, M. Campanini, R. Erni, M. Kovalenko, N. Stadie, *ACS Applied Mater. Interfaces* **2019**, *11*, 17686.
- [4] K. Kravchyk, R. Widmer, R. Erni, R. Dubey, F. Krumeich, M. Kovalenko *Sci. Rep.* **2019**, *9*, 1-8.
- [5] R. Dubey, T. Colijn, M. Aebli, E. Hanson, R. Widmer, K. Kravchyk, M. Kovalenko, *ACS Applied Mater. Interfaces* **2019**, *11*, 39902.
- [6] M. Nasir, T. Tianyu, H. Yanglong, *Adv. Energy Mater.* **2016**, *6*, 1600374.
- [7] R. Dubey, P. Vallachira, F. Krumeich, G. Blugan, J. Kuebler, K. Kravchyk, T. Graule, M. V Kovalenko, *Adv. Sci.* **2019**, *6*, 1901220. (featured as Frontispiece Cover)
- [8] R. Dubey et al. **2020**, *in revision*.

#### 6:15 AM \*F.EN06.01.10

**Late News: Rational Designed Materials for Energy Storage—From the View of Semiconductor Physics** Jiantao Zai; Shanghai Jiao Tong University, China

Semiconductor physics mainly discuss the energy band structures and the carrier behaviors in semiconductors. The carrier dynamics and the resulting conduction properties of semiconductors. As a semiconductor, the carrier transporting characteristics of Si has been well studied and adjusted via doping (n type, N, P; p type, B), which has been widely applied in electronics, solar cell and photocatalysis. In recent years, Si has been regarded as the most promising anode material for its highest theoretical specific capacity, and natural abundance. However, the poor conductivity of intrinsic Si still limits the rate

performance of Si materials.

Previously, Yi and me found boron doping can obviously enhance the rate capability of Si-C composite. Recently, phosphorus-doped yolk-shell Si@C materials (P-doped Si@C) with balanced electron and Li<sup>+</sup> transportation dynamics are rational designed and prepared, which deliver high specific capacities (2709 mAh g<sup>-1</sup> @ 0.4 A g<sup>-1</sup>), great rate capability (510 mAh g<sup>-1</sup> @ 35 A g<sup>-1</sup>) and good retention of ~95% over 800 cycles at 4 A g<sup>-1</sup>. As a result, P-doped Si@C anode pairs with commercial activated carbon to assemble lithium-ion capacitor (high power density of ~61080 W kg<sup>-1</sup> at 20 A g<sup>-1</sup>). Junction is also an important concept in semiconductor physics, which refers to the interface region with rectification characteristics formed by the contact of two different semiconductor phases. The formation of semiconductor junction will change the charge state of atoms near the junction interface, and then regulate the adsorption and catalytic activity of active sites in the region. Our previous research reveals the space charge of p-n junction of p-type CoP and n-type FeNi LDH can be utilized to improve the adsorption of OH<sup>-</sup> and promote the OER process. With this in mind, The *in-situ* formed VS<sub>x</sub>@VO<sub>2</sub> junctions can be designed to promote the absorption of polysulfide and result in high volume specific Li-S batteries. Furthermore, a n-n-type CoS<sub>2</sub>-CoS heterojunction was designed to facilitate the electrocatalytic conversion of I<sup>-</sup>/I<sub>3</sub><sup>-</sup> and polysulfides, which can significantly improve the power density and lifetime of flow batteries. Therefore, it is possible to modulate the electronic configuration of active site by designing proper semiconductor junctions following the theories of solid physics.

In all, the semiconductor physics can offer useful theoretical guidance for rational design of high performance materials for energy storage.

Ref

- [1] R. Yi, J. Zai; F. Dai, et al., *Electrochem Commun*, 2013, 36,
- [2] M. Chen, B. Li, X. Liu, et al., *J Mater Chem A*, 2018, 6, 3022-3027.
- [3] K He, T. Tadesse Tsega, X. Liu, et al., *Angew. Chem. Int. Ed.*, 2019, 58, 34, 11903-11909.
- [4] L. Zhou, L. Yao, S. Li, et al., *J Mater Chem A* 2019, 7 (8), 3618-3623.
- [5] D. Ma, B. Hu Bo, W. Wu, et al., *Nat Commun*, 2019, 10, 1, 3367-3367.

#### 6:30 AM F.EN06.01.11

**A Novel Cryogenic Milling Route to Fabricate Nanostructured Alloy Anodes with Improved Cycling Stability** Qizhang Yan<sup>1</sup>, Shu-Ting Ko<sup>1</sup>, Grace Whang<sup>2</sup>, Yumin Zhao<sup>1</sup>, Andrew Dawson<sup>2</sup>, Sarah H. Tolbert<sup>2</sup>, Bruce S. Dunn<sup>2</sup> and Jian Luo<sup>1</sup>; <sup>1</sup>University of California, San Diego, United States; <sup>2</sup>University of California, Los Angeles, United States

Alloys and intermetallics are of great interest as anode materials due to their high energy density, but they generally suffer from poor cycling life due to large volume expansion that leads to cracking. In this work, we demonstrate a new and facile route using cryogenic milling (cryomilling) to fabricate stable and high energy density anode materials. Because a ductile-to-brittle transition occurs for most metals at a low temperature, cryomilling can efficiently reduce the grain/particle size while adding a small amount of well-dispersed nanocarbon to stabilize the resulting nanostructures. Adding a minimum amount (1.2 wt%) of graphite during cryomilling produces SnSb anodes that demonstrate an initial coulombic efficiency of 83%, averaged efficiency >99.5%, and capacity retention of 90% over 100 cycles. Scanning electron microscopy (SEM), scanning transmission electron microscopy (STEM), and various electrochemical characterizations were employed to understand this high stability. The refined grain size (~10nm) and well-dispersed carbon matrix can alleviate the volume expansion and prevent particle cracking after cycling. Cryomilling is a cost-effective manufacturing method that is widely used in the food industry, plastic powder synthesis, and fabrication of nanostructured alloys. This work demonstrates the successful application of cryomilling to battery electrode materials for the first time and shows much-improved cycle life compared with conventional ball milling.

#### 6:40 AM F.EN06.01.12

**Translating a Material Discovery into a New High-Energy-Density Lithium-Ion Battery** Kent J. Griffith<sup>1</sup>, Rogério Ribas<sup>2</sup>, Robson Monteiro<sup>2</sup>, Robert J. Cava<sup>3</sup>, Robert Von Dreele<sup>4</sup>, Anthony K. Cheetham<sup>5</sup>, Clare Grey<sup>6</sup> and John B. Goodenough<sup>7</sup>; <sup>1</sup>Northwestern University, United States; <sup>2</sup>CBMM, Brazil; <sup>3</sup>Princeton University, United States; <sup>4</sup>Argonne National Laboratory, United States; <sup>5</sup>University of California Santa Barbara, United States; <sup>6</sup>University of Cambridge, United Kingdom; <sup>7</sup>The University of Texas at Austin, United States

Of the thousands of materials that have been investigated as prospective rechargeable lithium-ion battery electrodes, only a handful have successfully traversed the journey toward commercialization. Following the award of the 2019 Nobel Prize in Chemistry to Whittingham, Goodenough, and Yoshino “for the development of lithium-ion batteries”,<sup>1</sup> and owing to the global effort to develop advanced battery materials, we seek to chronicle a modern commercialization pathway via the tale of high-power and high-energy density titanium niobium oxide (TNO, TiNb<sub>2</sub>O<sub>7</sub>) a crystallographic shear structure.



The state-of-the-art material in the high-power and fast-charging performance space is LTO, commercialized by Toshiba as the SCiB™ battery and now used globally in applications including mild-hybrid electric passenger cars, electric buses and trolleys, electric trains, and grid energy storage systems. Relative to graphite,  $\text{Li}_4\text{Ti}_5\text{O}_{12}$  provides only 50% of the gravimetric capacity and sacrifices approximately 40% of the voltage when paired with a 4.0 V cathode. Despite their limited energy density,  $\text{Li}_4\text{Ti}_5\text{O}_{12}$ -based cells reached commercial success because they can be cycled over 20,000 times and operated safely at current densities and temperatures that are not suitable for graphite-based batteries.

Owing to the favorable properties of niobium,  $\text{TiNb}_2\text{O}_7$  is being developed as a high-energy-density alternative anode material to  $\text{Li}_4\text{Ti}_5\text{O}_{12}$ . It was first discovered by crystallographers in the 1950s and 1960s,<sup>2,3</sup> reported as a lithium-ion battery material by Bell Labs in 1983,<sup>4</sup> and “rediscovered” in the last decade by a team led by John Goodenough<sup>5,6</sup>. Since then, it has been the most studied crystallographic shear or Wadsley–Roth phase, the subject of numerous applied and fundamental studies on characteristics such as the mechanism of structure evolution,<sup>7–9</sup> ionic and electronic conduction,<sup>9</sup> and battery performance<sup>10,11</sup>. The lithiation reaction may proceed all the way to  $\text{Li}_5\text{Ti}^{\text{III}}\text{Nb}^{\text{III}}_2\text{O}_7$  with a theoretical capacity of  $387.7 \text{ mAh}\times\text{g}^{-1}$ . The multielectron redox chemistry of  $\text{TiNb}_2\text{O}_7$  puts it on par with the gravimetric capacity of graphite ( $371.9 \text{ mAh}\times\text{g}^{-1}$ ). It is worth mentioning that the crystal density of  $\text{TiNb}_2\text{O}_7$  ( $4.33 \text{ g}\times\text{cm}^{-3}$ ) is twice that of graphite ( $2.22 \text{ g}\times\text{cm}^{-3}$ ). Thus, the volumetric energy density of this oxide anode compares even more favorably than its gravimetric energy density. The high voltage of  $\text{TiNb}_2\text{O}_7$  (above 0.6 V vs.  $\text{Li}^+/\text{Li}$ ) enables safe charging under high current densities even in a heterogeneous electrode with large overpotentials and may be considered a necessary feature despite the cell voltage penalty. The high operating voltage may also mitigate surface–electrolyte interphase (SEI) formation as the voltage window is largely within the stability limits of standard electrolytes.

We will present the development, the state-of-the-art, and the future of  $\text{TiNb}_2\text{O}_7$  and Wadsley–Roth crystallographic shear structures as fast-charging and high-energy-density lithium-ion battery materials.

(1) Press release: The Nobel Prize in Chemistry 2019 <https://www.nobelprize.org/prizes/chemistry/2019/press-release>.

(2) Roth, R. S.; Coughanour, L. W. *J. Res. Natl. Bur. Stand.* **1955**, *55*, 209–213.

(3) Wadsley, A. D. *Acta Crystallogr.* **1961**, *14*, 660–664. <https://doi.org/10.1107/S0365110X61001996>.

(4) Cava, R. J.; Murphy, D. W.; Zahurak, S. M. *J. Electrochem. Soc.* **1983**, *130*, 2345–2351.

(5) Han, J.-T.; Huang, Y.-H.; Goodenough, J. B. *Chem. Mater.* **2011**, *23*, 2027–2029.

(6) Han, J.-T.; Goodenough, J. B. *Chem. Mater.* **2011**, *23*, 3404–3407.

(7) Lu, X.; Jian, Z.; Fang, Z.; Gu, L.; Hu, Y.-S.; Chen, W.; Wang, Z.; Chen, L. *Energy Environ. Sci.* **2011**, *4*, 2638–2644.

(8) Guo, B.; et al. *Energy Environ. Sci.* **2014**, *7*, 2220–2226.

(9) Griffith, K. J.; et al. *J. Am. Chem. Soc.* **2019**, *141*, 16706–16725.

(10) Ise, K.; Morimoto, S.; Harada, Y.; Takami, N. *Solid State Ion.* **2018**, *320*, 7–15.

(11) Takami, N.; et al. *Power Sources* **2018**, *396*, 429–436.

## 6:50 AM F.EN06.01.13

**Understanding the De-/Lithiation Mechanism of Iron-Doped Zinc Oxide—From Fundamentals to Practical Considerations** Jakob Asenbauer<sup>1,2</sup>, Tobias Eisenmann<sup>1,2</sup>, Adele Birrozzi<sup>1,2</sup>, Alexander Hoefling<sup>1,2</sup>, Joachim Binder<sup>3</sup>, Sylvio Indris<sup>1,3</sup>, Matthias Kuenzel<sup>1,2</sup>, Jens Tuebke<sup>1,2,4</sup>, Stefano Passerini<sup>1,2</sup> and Dominic Bresser<sup>1,2</sup>; <sup>1</sup>Helmholtz Institute Ulm (HIU), Germany; <sup>2</sup>Karlsruhe Institute of Technology (KIT), Germany; <sup>3</sup>Karlsruhe Institute of Technology–Institute for Applied Materials, Germany; <sup>4</sup>Fraunhofer Institute for Chemical Technology, Germany

The unique combination of high energy and power density made lithium-ion batteries the state-of-the-art energy storage technology to power small consumer electronics, as well as large-scale applications like electric vehicles.<sup>[1]</sup> However, especially the latter application, requires batteries that cannot only provide high energy density, but also the possibility for rapid recharging.<sup>[2]</sup> This is maybe the greatest challenge for the presently used graphite-based anodes, since the low lithiation potential ( $\sim 0.1 \text{ V}$  vs.  $\text{Li}/\text{Li}^+$ ) in combination with the sluggish lithium transport within the graphite structure and across the solid electrolyte interphase (SEI) provides the risk of lithium plating and dendrite formation during fast charging, especially at low temperatures.<sup>[3]</sup>

To solve this issue, alternative anodes, following, e.g., a conversion or an alloying mechanism, are being investigated.<sup>[4]</sup> These alternatives frequently possess higher capacities and rate capabilities; however, conversion materials still suffer from low energy efficiencies, due to a significant voltage hysteresis, and the extensive volume variation of alloying materials leads to rapid capacity fading and low coulombic efficiencies. Conversion/alloying-materials (CAMs), such as  $\text{Zn}_{0.9}\text{Fe}_{0.1}\text{O}$ , are a relatively new material class, that combines both, the conversion and alloying mechanism in a single material.<sup>[5]</sup> During the initial lithiation of CAMs, nanograins of an alloying element and a percolating conductive network of transition metal nanoparticles are formed *in situ* by the (reversible) conversion reaction. The metallic nano-network leads to fast de-/lithiation kinetics, making them a promising candidate for high-power applications. Yet, the

achievement of sufficiently high energy efficiencies and the volume variations occurring upon cycling are still remaining obstacles and there is still a lack of knowledge about how to potentially tackle these issues. Herein, we present our findings towards a detailed mechanistic understanding of the de-/lithiation of (carbon-coated)  $Zn_{0.9}Fe_{0.1}O$ . By combining *in situ* microcalorimetry, with *in situ* XRD, *ex situ*  $^7Li$  NMR and *ex situ*  $^{57}Fe$  Mössbauer spectroscopy we were able to propose a refined model for the initial de-/lithiation reaction. Furthermore, the volume variations of  $Zn_{0.9}Fe_{0.1}O$  electrodes upon cycling were studied by complementary *in situ* dilatometry and *ex situ* cross-sectional SEM analysis. These measurements reveal a continuous volume variation at the electrode level in the range of 10%. This is much lower than the theoretically predicted expansion when considering bulk densities only – even though the electrodes were cycled within a 3-V potential window. On the basis of these results we highlight the favorable effect of limiting the operational voltage window. We finally confirm this for  $Zn_{0.9}Fe_{0.1}O/LiNi_{0.5}Mn_{1.5}O_4$  full-cells, providing an energy and power density of  $284 Wh kg^{-1}$  and  $1105 W kg^{-1}$ , respectively, accompanied by an excellent energy efficiency of >93%.

[1] N. Nitta, F. Wu, J. T. Lee, G. Yushin, *Mater. Today* **2015**, *18*, 252–264.

[2] M. Li, J. Lu, Z. Chen, K. Amine, *Adv. Mater.* **2018**, *30*, 1800561.

[3] J. Asenbauer, T. Eisenmann, M. Kuenzel, A. Kazzazi, Z. Chen, D. Bresser, *Sustain. Energy Fuels* **2020**.

[4] N. Loeffler, D. Bresser, S. Passerini, M. Copley, *Johnson Matthey Technol. Rev.* **2015**, *59*, 34–44.

[5] D. Bresser, S. Passerini, B. Scrosati, *Energy Environ. Sci.* **2016**, *9*, 3348–3367.

#### SESSION F.EN06.02: Li-Metal Anodes

On Demand Abstracts Available for Viewing Starting Saturday Morning, November 21, 2020

F-EN06

##### 5:00 AM \*F.EN06.02.01

**Modeling of the Transfer Reactions at Li/SEI/Electrolyte Interface and Dendrite Free Morphology** Yue Qi<sup>1,2</sup>; <sup>1</sup>Brown University, United States; <sup>2</sup>Michigan State University, United States

The charge transfer reaction is the fundamental reaction for rechargeable batteries. The energy landscape of this reaction depicts the equilibrium and kinetics of the electrochemical process. Typically, a Li-metal electrode is always covered by a thin layer of solid electrolyte interphase (SEI), forming a complex Li/SEI/electrolyte interface. We first introduced a new half-cell model to predict the energy landscape of the electrochemical reaction of at the complex Li/SEI/electrolyte interface, with combined density functional theory (DFT) and tight-binding (DFTB) calculations. The simulated atomic details revealed that the Li-metal surface is negatively charged at the electrochemical equilibrium condition (the experimentally defined zero voltage for  $Li^+/Li^0$ ) due to the large solvation energy of  $Li^+$  in the EC-based electrolyte. The electric field created by the negatively charged surface can reorient the electrolyte into an ordered structure, lower the  $Li^+$  ion desolvation energy barrier, and help the  $Li^+$  ion transport through the SEI.

Further, the calculated energy landscape can be used to describe the electrochemical reaction kinetics with a Butler-Volmer equation, enabling a multiscale modeling approach. In this study, the DFT and DFTB predicted interfacial structures, desolvation processes, and the ion transfer energy barrier, were inputted into a non-linear phase-field model to capture the morphological evolution during the electroplating process. Specifically, this model captured the morphology difference between the dendritic Li plating in carbonate (EC)-electrolyte and faceted Mg plating in tetrahydrofuran(THF)-electrolyte under the similar current density. Furthermore, through systematical parametric analyses, we conclude that the cation desolvation-induced exchange current difference between Li and Mg is mainly responsible for their deposition morphological differences. This study provides a strategy of connecting the phase-field method and atomistic calculations and predicts that increasing the desolvation energy and lowering the equilibrium exchange current can help to achieve dendrite-free Li-metal anode.

##### 5:15 AM F.EN06.02.03

**Pressure-Tailored Lithium Deposition and Dissolution in Lithium Metal Batteries** Chengcheng Fang and Y. Shirley Meng; University of California, San Diego, United States

Lithium (Li) metal offers high theoretical capacity, lowest negative potential and light weight, making it the ideal anode material for high-energy-density batteries. Porous electrodes resulting from unregulated Li growth is believed to be the major cause of the low Coulombic efficiency (CE) and potential safety hazards of rechargeable Li metal batteries. Strategies aiming

to achieve large granular Li deposits have been extensively explored; yet, the ideal Li deposits, which consist of large Li particles seamlessly packed on the electrode and can be reversibly deposited and stripped, have never been reported. Here, by using cryo-FIB-SEM, 3D reconstruction and MD simulation, we quantitatively revealed the role of stack pressure on Li nucleation, growth and stripping, and discovered that optimal pressure for approaching 100% dense Li deposition by establishing a pressure-morphology-performance correlation. Unprecedented, a dense Li deposition (99.49% electrode density) with an ideal columnar structure has been achieved and can be reversibly plated and stripped during extended cycles at room temperature. The tailored Li deposition and stripping by optimizing stack pressure opens new opportunities to rationally mitigate inactive Li formation, improve cycle life and enable fast charging for rechargeable Li metal batteries.

#### 5:25 AM \*F.EN06.02.04

**Advances in Imaging Lithium Batteries at Different Length Scales** [Herman Lemmens](#) and Zhao Liu; Thermo Fisher Scientific, Netherlands

Imaging the microstructure of a battery cell at different length scales is important to understand the degradation processes through the battery cycle life. For example, investigating the formation of defects such as dendrites at the Li anode interface requires both high resolution imaging and large field of view. Ideally, imaging techniques cover the entire electrode thickness at submicron resolution with a method that preserves the sample interface. Here, we present an approach to probe the defects at the Li-metal battery interface. A coin cell has been sliced under cryo conditions with a laser inside the vacuum of the scanning electron microscope (SEM) chamber so a pristine surface is obtained and defect formation can be observed across the entire thickness of the cell.

In another example, transport properties for a thick NMC 811 cathode were obtained from focused ion beam (FIB) milling in combination with SEM. Because of the cathode thickness, an alternative to traditional Ga FIB milling was used. With a Xenon plasma beam, it was possible to obtain a 3D data set with more than 100  $\mu\text{m}$  field of view on a 70  $\mu\text{m}$  thick cathode. The microstructural characteristics extracted from such representative 3D volume help the understanding of the correlation between electrode microstructural evolution and performance deterioration.

#### 5:40 AM F.EN06.02.05

**Late News: Gaining a Better Understanding of Lithium-Ion Battery Functionality Through Scanning Electron Microscopy Analytical Studies** [Pawel Nowakowski](#)<sup>1</sup>, [Cecile Bonifacio](#)<sup>1</sup>, [Jean-Marie Doux](#)<sup>2</sup>, [Shirley Meng](#)<sup>2</sup>, [Mary Ray](#)<sup>1</sup> and [Paul Fischione](#)<sup>1</sup>; <sup>1</sup>E. A. Fischione Instruments, Inc., United States; <sup>2</sup>University of California, United States

All solid-state batteries (ASSB) promise high energy density, by enabling the use of Li metal anode, and safe operation, thanks to their non-flammable solid-state electrolyte. Degradation over the course of the ASSB lifecycle, however, remains a limiting issue for the technology, as the aging process constrains energy storage capabilities and performance. Better understanding of the degradation mechanisms is critical to improving ASSB functionality and performance, [1].

Scanning electron microscopy (SEM) analytical studies, such as energy dispersive X-ray spectroscopy (EDS) and electron backscatter diffraction (EBSD) analyses are important tools that give researchers the ability to characterize battery materials and understand their structures, as well as degradation. The role of the Li microstructure (grain size, crystallographic preferential orientation, etc.) on battery performance is not well understood; few reports on the microstructural characterization of lithium metal are to be found in the literature. In addition, further investigation is needed into the cathode/anode solid electrolyte interface, such as solid electrolyte decomposition, intermediate transition layer formation, and Li metal dendrite formation [2, 3].

To complete accurate and informative SEM analytical studies, the samples must be well-prepared and represent the native microstructure of study element without any oxidation, contamination and deformation or cracking induced by preparation. An artifact-free sample preparation technique is a critical key to better understand battery functionality and its ageing process. Preparing Li metal ASSB samples is particularly difficult because Li is highly sensitive to oxygen, nitrogen, water, and carbon dioxide; requiring Ar protective atmosphere. Lithium is also a very soft material and its crystallographic structure can be easily damaged by mechanical sample preparation techniques. The inherent characteristics of Li metal demand a controlled environment workflow from sample preparation through SEM analyses [4].

In this work we report on EBSD characterization of pure Li metal using a unique controlled environment workflow: argon broad ion beam milling, sample transfer to the SEM, and EBSD analyses. We present structural EBSD results on pure Li metal used as an anode in an ASSB, with special focus on texture and grain size. We will also present SEM imaging and EDS studies that document the interface layers formed during battery cycling.

#### References

[1] Abhik Banerjee, Xuefeng Wang, Chengcheng Fang, Erik A. Wu, and Ying Shirley Meng, *Interfaces and Interphases in All-Solid-State Batteries with Inorganic Solid Electrolytes*, Chemical Reviews 120 (14), 2020

- [2] Kaihui Nie, Yanshuai Hong, Jiliang Qiu, Qinghao Li, Xiqian Yu, Hong Li, and Liquan Chen, *Interfaces Between Cathode and Electrolyte in Solid State Lithium Batteries: Challenges and Perspectives*, *Frontiers in Chemistry*, Volume 6, 2018
- [3] Cheng Lin, Aihua Tang, Hao Mu, Wenwei Wang, and Chun Wang, *Aging Mechanisms of Electrode Materials in Lithium-Ion Batteries for Electric Vehicles*, *Journal of chemistry*, Volume 2015, 2015
- [4] Cecile Bonifacio, Pawel Nowakowski, Mary Ray, Paul Fischione, *Multi-length Scale Cryogenic Sample Preparation to Electron Microscopy of Battery Materials*, *Microscopy and Microanalyses*, 2020

#### 5:50 AM F.EN06.02.06

**Understanding the Interplay Between Li Insertion and Li Plating in Single Graphite Anode** Tao Gao<sup>1</sup>, Dimitrios Fraggedakis<sup>1</sup>, Supratim Das<sup>1</sup>, William C. Chueh<sup>2</sup>, Ju Li<sup>1</sup> and Martin Bazant<sup>1</sup>; <sup>1</sup>Massachusetts Institute of Technology, United States; <sup>2</sup>Stanford University, United States

The potential safety hazards of lithium ion batteries (LIBs), as well as their capacity fade and long charging time, are major challenges that currently prevent the widespread adoption of electric vehicles. These effects are strongly correlated with lithium plating, a parasitic reaction on graphite anodes that competes with lithium intercalation when LIBs are charged at high rates or under low temperature. Li plating is known for depletion of the lithium inventory, cell shorting, and thermal runaway.

Addressing Li plating problem relies on material engineering and battery operation optimization. The efficacy of these approaches lies in the fundamental understanding of Li plating mechanism. Despite Li ion battery has been invented for 30 years, a systematic understanding on the onset and growth of Li in graphite anode is still lacking. Thermodynamics criterion requires the voltage of graphite to be negative vs. Li metal for Li plating to happen. However, in practice graphite is usually able to tolerate certain degree of negative voltage without plating. Such discrepancy necessitates the incorporation of kinetic factors. Several kinetic mechanisms have been proposed, which include electrolyte transport limitation and solid diffusion limitation. However, neither of them are validated experimentally on graphite electrode.

In this work, we test these hypotheses and elucidate the mechanism of Li plating, by investigating the interplay between Li intercalation and Li plating on a single graphite particle, using in-situ optical microscopy coupled with electrochemical test. The results show Li plating happens when the surface of graphite saturates, which shuts down the intercalation reaction. The saturation can happen much earlier than full lithiation of graphite particle due to solid diffusion limitation, resulting in severe under-utilization. The physical picture was discussed by analyzing the energy landscape of the two competing reactions and their kinetics. A theory was proposed, followed by a 1D simulation of the dynamics of Li insertion and Li plating. The discovery sheds light on directions and guidelines of materials innovation or electrode design for reducing the risk of Li plating and extreme fast charging.

#### 6:00 AM \*F.EN06.02.07

**Pairing Lithium-Metal Anode with High-Nickel NMC and Sulfur Cathodes—Fundamental Understanding and Engineering Solutions** Arumugam Manthiram; The University of Texas at Austin, United States

Lithium-metal anode holds tremendous potential for enabling next generation of rechargeable batteries due to their high storage capacity (3,861 mAh g<sup>-1</sup>) and low reduction potential (-3.04 V vs SHE). When paired with a high-capacity cathode, such as high-nickel NMC or sulfur, lithium-metal anode can help deliver energy-dense storage systems with ~ 500 Wh kg<sup>-1</sup>. However, the poor efficiency associated with lithium plating and stripping severely limits the cycle life. For realizing practical viability, reversible lithium deposition needs to be achieved by stabilizing the lithium-electrolyte interphase (SEI) layer and mitigating the extreme volume changes accompanying the cycling.

The chemistry of the lithium-electrolyte interface is rendered distinct by the choice of the cathode in a full cell, *viz.*, high-nickel NMC or sulfur. This is not only due to the different electrolyte formulations used, but also due to the crossover of species between the cathode and anode. The characteristics of deposited lithium can fundamentally vary across different cathode systems, and unique strategies must be employed to stabilize lithium deposition in each case. Hence, an in-depth fundamental study is necessary to develop a thorough understanding of the lithium-electrolyte interfacial chemistry, while creative engineering solutions are necessary to achieve highly efficient lithium plating and stripping. This presentation will focus both on a fundamental understanding and offering engineering solutions.

When paired with a high-nickel NMC cathode, the lithium-metal anode is affected by transition-metal dissolution at the cathode and crossover to the anode. However, we find that during initial cycling, crossover of electrolyte decomposition products from the anode to the cathode is more severe and plays a more critical role. Not only does it alter/thicken the

cathode SEI layer, it also affects the anode itself as the lithium SEI components could continually dissolve. The magnitude of this crossover is expected to depend on the nickel content in the cathode.

When paired with a sulfur cathode, the lithium-metal anode is affected by polysulfide dissolution at the cathode and crossover to the anode. We use anode-free full cells, which contain no excess lithium at the anode, to investigate the dynamics of lithium deposition. With advanced surface characterization methodologies, *e.g.*, time-of-flight secondary ion spectrometry, we find that the depletion of cyclable lithium inventory is due to the formation of “dead” metallic lithium, which itself is caused by severe electrolyte decomposition on lithium-metal surface with cycling.

The presence of polysulfide intermediates is found to have an intrinsically stabilizing effect on lithium deposition in Li-S batteries. This motivates our strategies towards engineering further improvements in cycle life. With tellurium as a cathode additive, tellurium-substituted polysulfides are formed, which reduce on lithium surface to form  $\text{Li}_2\text{TeS}_3$  as a thin,  $\text{Li}^+$ -ion conducting SEI layer. This enables uniform deposition of lithium and mitigates electrolyte decomposition. A remarkable improvement in cyclability is achieved in energy-dense anode-free full cells and lean-electrolyte pouch cells. Similarly, using organosulfide molecules as electrolyte additives opens the possibility of favorably tuning the properties of lithium SEI layer by simply modifying the organic functional group.

The development of three-dimensional current collector matrices is also critical to achieving reversible lithium deposition. The highly conductive frameworks provide efficient electron/ion transport and guides a homogenous deposition of lithium, while the porous 3D architecture helps mitigate severe volume changes during cycling. The presentation will demonstrate various lithiophilic host materials that show considerable promise in improving the cyclability of lithium-metal anode when paired with both high-nickel NMC and sulfur cathodes.

#### SESSION F.EN06.03: Cathodes

On Demand Abstracts Available for Viewing Starting Saturday Morning, November 21, 2020  
F-EN06

##### 5:00 AM F.EN06.03.01

**Chemical Trends in the Lattice Thermal Conductivity of  $\text{Li}(\text{Ni}, \text{Mn}, \text{Co})\text{O}_2$  (NMC) Battery Cathodes** Hui Yang<sup>1,2</sup>, Christopher Savory<sup>3,2</sup>, Benjamin J. Morgan<sup>4,2</sup>, David O. Scanlon<sup>3,2,5</sup>, Jonathan Skelton<sup>6</sup> and Aron Walsh<sup>1,7,2</sup>; <sup>1</sup>Imperial College London, United Kingdom; <sup>2</sup>The Faraday Institution, United Kingdom; <sup>3</sup>University College London, United Kingdom; <sup>4</sup>University of Bath, United Kingdom; <sup>5</sup>Diamond House, United Kingdom; <sup>6</sup>University of Manchester, United Kingdom; <sup>7</sup>Yonsei University, Korea (the Republic of)

While the transport of ions and electrons in conventional Li-ion battery cathode materials is well understood, our knowledge of the phonon (heat) transport is still in its infancy. We present a first-principles theoretical investigation of the chemical trends in the phonon frequency dispersion, mode lifetimes, and thermal conductivity in the series of layered lithium transition-metal oxides  $\text{Li}(\text{Ni}_x\text{Mn}_y\text{Co}_z)\text{O}_2$  ( $x + y + z = 1$ ). The oxidation and spin states of the transition metal cations are found to strongly influence the structural dynamics. Calculations of the thermal conductivity show that  $\text{LiCoO}_2$  has highest average conductivity of  $45.9 \text{ W}\cdot\text{m}^{-1}\cdot\text{K}^{-1}$  at  $T = 300 \text{ K}$  and the largest anisotropy, followed by  $\text{LiMnO}_2$  with  $8.9 \text{ W}\cdot\text{m}^{-1}\cdot\text{K}^{-1}$ , and  $\text{LiNiO}_2$  with  $6.0 \text{ W}\cdot\text{m}^{-1}\cdot\text{K}^{-1}$ . The much lower thermal conductivity of  $\text{LiMnO}_2$  and  $\text{LiNiO}_2$  is found to be due to 1-2 orders of magnitude shorter phonon lifetimes. We further model the properties of binary and ternary transition metal combinations and show that the thermal conductivity of NMC is suppressed with decreasing Co content and increasing Ni/Mn content. The thermal conductivity of commercial NMC622 and NMC111 compositions are substantially larger than NMC811. These results serve as a guide to ongoing work on the design of multi-component battery electrodes with more effective thermal management.

[Ref 1] Yang, H., Yang, J.Y., Savory, C.N., Skelton, J.M., Morgan, B.J., Scanlon, D.O. and Walsh, A., *J. Phys. Chem. Lett.* 2019, 10, 18, 5552–5556

[Ref 2] Yang, H., Savory, C., Morgan, B., Scanlon, D., Skelton, J. and Walsh, A., Chemrxiv, 2020, <https://t.co/KNArzKhsdq>

##### 5:10 AM F.EN06.03.03

**Using High Entropy to Improve Capacity and Rate Capability in Cation-Disordered Rocksalt Cathodes** Zhengyan Lun<sup>1,2</sup>, Bin Ouyang<sup>1,2</sup>, Deok-Hwang Kwon<sup>1,2</sup>, Huiwen Ji<sup>2</sup> and Gerbrand Ceder<sup>1,2</sup>; <sup>1</sup>University of California, Berkeley, United

States; <sup>2</sup>Lawrence Berkeley National Laboratory, United States

The recent success of Li-excess cation-disordered rocksalt (DRX) cathodes is providing an avenue to develop high energy density cathodes with abundant and low-cost metals, such as Mn, Fe and Ti. As they have high energy density, these cathode materials are currently the most viable strategy to address the resource issues of Co / Ni that will arise as conventional layered-type Li-ion cathodes are scaled towards multiple TWh of annual production. In DRX cathodes, facile Li transport relies mostly on the so-called “0-TM” 3D percolation channel, in which the intermediate tetrahedral sites are coordinated only by Li (no transition metals, TMs). The Li migration barrier along this “0-TM” channel is significantly lower compared to that of “1-TM” channel, where the intermediate tetrahedral sites are coordinated by 3 Li and 1 TM. The complexity of DRX cathodes lies in the fact that in most cases, they present various types of cation short-range order (SRO), which influences the frequency and connectivity of “0-TM” channels, thus controls the capacity and rate capability of DRX cathodes. Monte Carlo simulations have suggested that the presence of SRO in DRX cathodes generally leads to reduced Li percolation, when compared to that of a random arrangement of TM species.

Inspired by the recent observations of nearly-random cation distribution in several high-entropy metal and oxide compounds, we have found that increasing the number of TM species in DRXs will improve Li transport properties by preventing the formation of a single dominant SRO type, resulting in improved capacity and high rate capability. We show that SRO in DRX cathodes systematically decreases as more TM components are added, and as a consequence, energy density and rate capability systematically increase. A DRX cathode with six TM species achieves 307 mAh g<sup>-1</sup> (955 Wh kg<sup>-1</sup>) at 20 mA g<sup>-1</sup> and retains more than 170 mAh g<sup>-1</sup> when cycling at 2,000 mA g<sup>-1</sup>. The high compositional flexibility of these materials can also enable the use of less pure precursor materials.

#### 5:20 AM F.EN06.03.05

**Enhanced Cycling Stability of Ni-Rich Cathode Material by Dry Coating Technique** Tianhang Chen and Donghai Wang; The Pennsylvania State University, United States

High nickel content cathodes (Ni >90%) are promising candidates for lithium ion batteries (LIBs) due to their high energy capacity and low cost. But they are still suffering from poor cycling stability and potential thermal run away since lattice structures would become unstable upon cycling. Incorporation of Al atom by dry coating into structure has been found to be beneficial to the electrochemical and thermal stability because Al doping not only can decrease the Li/Ni mixing ratio in the Li layer but also enhance the thermal resistance to oxygen evolution due to strong Al-O bonding. The Al doping by dry coating NCM (DC\_NCM\_Al(OH)<sub>3</sub> and DC\_NCM\_Al<sub>2</sub>O<sub>3</sub>) reserve 87.8% and 87.1 % capacity respectively after 200 cycles while NCM only remains 70.7 %. Additionally, DC\_NCM\_Al(OH)<sub>3</sub> at charged state exhibits an exothermic peak at 212.4 °C which is 10 °C higher than NCM. The Al doping NCM samples reveal improved properties for high nickel content cathode, which provides a strategy for next generation LIBs.

#### 5:30 AM F.EN06.03.06

**Concurrently Approaching Volumetric and Specific Capacity Limits of Lithium Battery Cathodes via Conformal Pickering Emulsion Graphene Coatings** Kyuyoung Park, Jin-Myoung Lim, Norman S. Luu, Julia R. Downing, Shay G. Wallace, Lindsay E. Chaney, Hocheon Yoo, Woo Jin Hyun, Hyeong-U Kim and Mark Hersam; Northwestern University, United States

To achieve the high energy densities demanded by emerging technologies, lithium-ion batteries (LIBs) require cathode electrodes possessing high volumetric and specific capacities<sup>1</sup>. While recent developments in Ni-rich cathode material composition have significantly increased the volumetric and specific capacities of cathode active materials<sup>2,3</sup>, the other inactive components, such as binders and carbon additives, still need to be minimized in order to approach theoretical volumetric and specific capacity limits of the entire cathode electrode. Towards this end, here we report conformal, ultrathin, and conductive graphene coatings on LIB active material particles using a scalable Pickering emulsion method<sup>4</sup>. Since this approach employs high-quality, liquid phase-exfoliated graphene that possesses exceptional electrical conductivity<sup>5</sup>, only 0.5 wt% graphene is required to achieve high electrochemical performance in electrodes. Furthermore, this minimal amount of conductive additive also allows the binder loading to be reduced to 0.8 wt%, even for industrially relevant active material areal loadings (~11 mg cm<sup>-2</sup>). Due to its exceptionally low inactive material loading, the resulting LiNi<sub>0.8</sub>Co<sub>0.15</sub>Al<sub>0.05</sub>O<sub>2</sub> (NCA) electrodes achieve specific and volumetric capacities that reach ~98% of the theoretical limits for NCA. The efficient electron conduction path from the graphene coating and the shortened lithium diffusion path due to a simplified electrode structure also imply superlative rate capability, while the conformal graphene coating mitigates electrochemical degradation mechanisms and consequently enhances cycle-life. Since this Pickering emulsion coating scheme is agnostic to the cathode material composition, it can be widely applied to other active material particles, thus providing a general pathway to theoretical specific and volumetric capacities in practical LIB electrodes.

1. Armand, M. & Tarascon, J. M. Building Better Batteries. *Nature* **451**, 652-657 (2008).
2. Liu, W. et al. Nickel-Rich Layered Lithium Transition-Metal Oxide for High-Energy Lithium-Ion Batteries. *Angew. Chem., Int. Ed.* **54**, 4440-4457 (2015).
3. Li, W., Erickson, E. M. & Manthiram, A. High-Nickel Layered Oxide Cathodes for Lithium-Based Automotive Batteries. *Nat. Energy* **5**, 26-34 (2020).
4. Park, K.-Y. et al. Concurrently Approaching Volumetric and Specific Capacity Limits of Lithium Battery Cathodes via Conformal Pickering Emulsion Graphene Coatings. *Adv. Energy Mater.* DOI: 10.1002/aenm.202001216 (2020).
5. Liang, Y. T. & Hersam, M. C. Highly Concentrated Graphene Solutions via Polymer Enhanced Solvent Exfoliation and Iterative Solvent Exchange. *J. Am. Chem. Soc.* **132**, 17661-17663 (2010).

**5:40 AM \*F.EN06.03.07**

**Building Ultra-Conformal Protective Layers on Both Secondary and Primary Particles of Layered Lithium Transition Metal Oxide Cathodes** Guiliang Xu and Khalil Amine; Argonne National Laboratory, United States

Nickel-rich layered lithium transition metal oxides are the most attractive cathode materials for the next generation lithium-ion batteries for automotive application. However, they suffer from crystal and interfacial structure instability under aggressive electrochemical and thermal driving force, leading to rapid performance degradation and severe safety concerns. In this talk, we reported a transformative approach by using an oxidative chemical vapour deposition technique to build a protective conductive polymer (PEDOT) skin on layered oxide cathode materials. The ultra-conformal PEDOT skin facilitates the transport of lithium ions and electrons, significantly suppresses the undesired layered to spinel/rock-salt phase transformation and the associated oxygen loss, mitigates intergranular and intragranular mechanical cracking, and effectively stabilizes cathode-electrolyte interface. This approach remarkably enhances the capacity and thermal stability under high-voltage operation. Building a protective skin at both secondary and primary particle levels of layered oxides offers a design strategy for the promising Ni-rich cathodes towards high-energy, long-life and safe lithium-ion batteries.

**5:55 AM F.EN06.03.09**

**Chemo-Mechanical Degradation in V<sub>2</sub>O<sub>5</sub> Thin-Film Cathodes of Li-Ion Batteries** Yuwei Zhang and Matt Pharr; Texas A&M University, United States

We have devised an approach to fabricate dense textured V<sub>2</sub>O<sub>5</sub> thin films, which allows us to scrutinize the root cause of capacity fade in V<sub>2</sub>O<sub>5</sub> cathodes of Li-ion batteries. Specifically, we performed in-situ measurements of stress of V<sub>2</sub>O<sub>5</sub> thin films during 50 electrochemical cycles. Surprisingly, electrochemical cycling appears to induce elastic and rate-independent deformation over a voltage range relevant to battery operation (4 - 2.8 V). However, the compressive stresses gradually increase with cycle number during the first few cycles, likely due to side reactions and/or residual Li left in the V<sub>2</sub>O<sub>5</sub>, even after delithiation (to 4 V). Further cycling leads to accumulated mechanical (e.g., fracture, delamination) and structural changes which ultimately result in severe capacity fade.

SESSION F.EN06.04: Liquid Electrolytes

On Demand Abstracts Available for Viewing Starting Saturday Morning, November 21, 2020

F-EN06

**5:00 AM F.EN06.04.01**

**Elimination of Fluorination—The Influence of Fluorine-Free Electrolytes on the Performance of Si-Based Li-Ion Batteries** Guiomar Hernández, Andrew J. Naylor, Yu-Chuan Chien, Daniel Brandell, Jonas Mindemark and Kristina Edstrom; Uppsala University, Sweden

One step towards more environmentally friendly and safer batteries is to eliminate fluorinated electrolytes, as they are susceptible to release toxic and corrosive compounds such as HF. Yet, fluorinated electrolytes are still dominating the research and market of lithium ion batteries.<sup>1</sup> Alternatively, replacing the state-of-the-art LiPF<sub>6</sub> with fluorine-free salt would

reduce cost, increase safety and decrease toxicity, both in the manufacturing and recycling processes.<sup>2</sup> In addition, additives able to form a stable solid-electrolyte interphase (SEI) are another common source of fluorine, for example fluoroethylene carbonate (FEC), which is particularly important for silicon-based electrodes as they suffer high volume changes upon cycling.<sup>3</sup> Despite this advantage of FEC, it has been also shown that it accelerates the degradation of the electrolyte containing LiPF<sub>6</sub> upon storage.<sup>4</sup>

Herein, we investigate the effects of electrolyte fluorination, from a highly fluorinated electrolyte based on the conventional LiPF<sub>6</sub> salt with FEC and vinylene carbonate (VC) as SEI-forming additives to a fluorine-free electrolyte based on lithium bis(oxalato)borate (LiBOB) salt and VC additive. These electrolytes were tested in full cells combining silicon-graphite composite electrodes with LiNi<sub>1/3</sub>Mn<sub>1/3</sub>Co<sub>1/3</sub>O<sub>2</sub> cathodes, and characterized by means of electrochemical testing and post-mortem analysis. Our results show that the SEI composition on the anode is very different, being F-rich in the fluorinated electrolyte and O-rich in the fluorine-free electrolyte. However, both electrolyte formulations are able to stabilise silicon-based electrodes and support long cycle life in full cells. Therefore, fluorine-free alternatives are good candidates for high-energy-density full cells opening new possibilities towards safer, more sustainable and less toxic batteries.<sup>5</sup>

<sup>1</sup> von Aspern, N.; Rösenthaller, G.-V.; Winter, M.; Cekic-Laskovic, I. Fluorine and Lithium: Ideal Partners for High-Performance Rechargeable Battery Electrolytes. *Angew. Chem. Int. Ed.* 2019, 58, 15978-16000.

<sup>2</sup> Xu, K. Nonaqueous Liquid Electrolytes for Lithium-Based Rechargeable Batteries. *Chem. Rev.* 2004, 104, 4303-4418.

<sup>3</sup> Etacheri, V.; Haik, O.; Goffer, Y.; Roberts, G. A.; Stefan, I. C.; Fasching, R.; Aurbach, D. Effect of Fluoroethylene Carbonate (FEC) on the Performance and Surface Chemistry of Si-Nanowire Li-Ion Battery Anodes. *Langmuir* 2012, 28, 965-976.

<sup>4</sup> Xu C.; Hernández G.; Abbrent S.; Kobera L.; Konefal R.; Brus J.; Edstrom K.; Brandell D.; Mindemark J. Unraveling and Mitigating the Storage Instability of Fluoroethylene Carbonate-Containing LiPF<sub>6</sub> Electrolytes To Stabilize Lithium Metal Anodes for High-Temperature Rechargeable Batteries. *ACS Appl. Energy Mater.* 2019, 2, 7, 4925-4935.

<sup>5</sup> Hernández G; Naylor A. J.; Chien Y-C.; Brandell D.; Mindemark J.; Edstrom K. Fluorine-Free Electrolytes on the Performance of LiNi<sub>1/3</sub>Mn<sub>1/3</sub>Co<sub>1/3</sub>O<sub>2</sub>/Silicon-Graphite Li-Ion Battery Cells. *ACS Sustain. Chem. Eng.* 2020, DOI 10.1021/acssuschemeng.0c01733.

#### 5:10 AM \*F.EN06.04.02

**Organosilicon Compounds Improve the Thermal and Electrochemical Stability of Lithium-Ion Batteries** Robert Hamers<sup>1</sup>, Sarah Guillot<sup>2</sup>, Monica Usrey<sup>2</sup>, Louis Morris<sup>1</sup> and Cesar Ortiz Ledon<sup>1</sup>; <sup>1</sup>University of Wisconsin-Madison, United States; <sup>2</sup>Silatronix, Inc., United States

Incorporation of organosilicon (OS) compounds in modest concentrations as low as several percent in conventional carbonate electrolytes lead to substantial improvements in the thermal and electrochemical stability of the resulting lithium ion batteries. We have been investigating the fundamental chemical degradation pathways of organosilicon compounds in an effort to understand the chemical and electrochemical origins of these remarkable properties. The combination of NMR spectroscopy, in situ FTIR, AFM, and XPS provides unique insights into how organosilicon electrolytes reduce or eliminate autocatalytic chemical pathways associated with PF<sub>6</sub> and its degradation products. OS compounds further alter the chemical nature of SEI layers on silicon, leading to improvements in overall performance. In this talk I will summarize some of our recent work characterizing organosilicon thermal stability and electrochemical stability against different materials, including silicon-based anodes and NMC-based cathodes.

#### 5:25 AM F.EN06.04.03

**Molecular Design for Electrolyte Solvents Enables Long-Cycling Anode-Free Lithium Metal Batteries** Zhiao Yu<sup>1</sup>, Hansen Wang<sup>1</sup>, Yi Cui<sup>1,2</sup> and Zhenan Bao<sup>1</sup>; <sup>1</sup>Stanford University, United States; <sup>2</sup>SLAC National Accelerator Laboratory, United States

Lithium (Li) ion batteries have made a great impact to society, recognized by the 2019 Nobel Prize in Chemistry. Albeit commercialized for decades, Li ion batteries are rapidly approaching their theoretical limit in energy density, thus motivating the revival of the Li metal chemistry. Nevertheless, the implementation of Li metal batteries is plagued by their poor cycle life. Uncontrollable reactions between Li metal and electrolytes form a chemically unstable and mechanically fragile solid-electrolyte interphase (SEI). The SEI easily cracks during cycling, leading to dendritic growth, “dead Li” formation and



irreversible Li inventory loss. By tuning the SEI structure and quality, electrolyte engineering is a critical and pragmatic approach. For a promising electrolyte, several key requirements are marked: (1) consistently high Coulombic efficiency (CE) to minimize Li loss, including that in the initial cycles; (2) functionality under lean electrolyte and limited-excess Li conditions for maximized energy density; (3) oxidative stability towards high-voltage cathodes; (4) moderate salt concentration for cost-effectiveness; (5) high boiling point and low flammability for safety and processability.

Several reports on electrolyte engineering improved the cyclability of Li metal batteries, such as additive optimization, solvent ratio modification, and liquified gas electrolytes. Particularly, the high concentration electrolytes (HCEs) and localized high concentration electrolytes (LHCEs) were acknowledged to be the most effective methods. Take the state-of-the-art version, LHCEs, as an example. The fluoro-diluents used in LHCEs were Li metal compatible yet hardly able to solvate  $\text{Li}^+$  ions by itself. As a consequence, small amount of unstable solvents were necessary for salt dissolution, reducing but not eliminating undesirable parasitic reactions. These side reactions with the solvent molecules led to low CE in the initial cycles. Therefore a detailed methodology of rational electrolyte design is still highly demanded.

In our work, we target new solvent molecules that not only dissolve Li salt but also stay compatible when confronted with both Li metal anodes and high-voltage cathodes. Thus we design a first-time synthesized liquid molecule, fluorinated 1,4-dimethoxybutane (FDMB), solely as the electrolyte solvent. It is paired with 1 molar lithium bis(fluorosulfonyl)imide (1 M LiFSI) in a single-salt, single-solvent formulation (1 M LiFSI/FDMB) to enable stable and high-energy-density Li metal batteries. Theoretical simulations show a unique  $\text{Li}^+$ -solvent interaction in 1 M LiFSI/FDMB and thus higher anion-solvent ratio in the  $\text{Li}^+$  solvation structure, endowing the electrolyte with both Li metal compatibility and high-voltage tolerance. Cryogenic transmission electron microscope of Li metal plated in 1 M LiFSI/FDMB reveals an ultrathin SEI (~6 nm), accompanied by a high CE (~99.52%) and fast activation (CE ramps up to >99% within 5 cycles) for Li metal anodes. The Li|NMC full cells with limited-excess Li retain 90% capacity after 420 cycles with an average CE of 99.98%. Industrial anode-free Cu|NMC 811 pouch cells achieve ~325 Wh  $\text{kg}^{-1}$  single-cell energy density while Cu|NMC532 ones show 80% capacity retention after 100 cycles, which is one of the best performing anode-free cells. Our rational design concept for electrolyte provides a promising path to high-energy, practical Li metal batteries with high cyclability and processability.

### 5:35 AM F.EN06.04.05

**Towards the Comprehension of Surface Species Formation in Nickel-rich Layered Materials and Their Reactivity Towards Electrolyte** Ana C. Martinez Maciel<sup>1,2,3</sup>, Sylvie Grugeon<sup>1,2</sup>, Dominique Cailieu<sup>4</sup>, Matthieu Courty<sup>1,2</sup>, Pierre Tran-Van<sup>3</sup> and Stéphane Laruelle<sup>1,2</sup>; <sup>1</sup>Laboratoire de Réactivité et de Chimie des Solides, UMR CNRS, Université de Picardie Jules Verne, France; <sup>2</sup>Réseau sur le Stockage Electrochimique de l'Énergie, CNRS RS2E, France; <sup>3</sup>Technocentre Renault, France; <sup>4</sup>Plate-Forme Analytique, Université de Picardie Jules Verne, France

Recently, layered oxides  $\text{LiNi}_{1-x-y}\text{Mn}_x\text{Co}_y\text{O}_2$  (NMC), have found wide use in the automotive industry as positive electrode materials for lithium-ion batteries, due to their high energy density given by the nickel content<sup>1</sup>. Unfortunately, their surface composition is readily compromised by the chemical reactivity towards  $\text{H}_2\text{O}$  and  $\text{CO}_2$ . The instability towards  $\text{H}_2\text{O}$  limits the aqueous processing of the electrodes<sup>2</sup> and the surface degradation towards  $\text{H}_2\text{O}$  and  $\text{CO}_2$  into surface species (typically  $\text{Li}_2\text{CO}_3$  and  $\text{LiOH}$ ) induces slurry gelation during the preparation of the electrodes<sup>3</sup>, increases the cell's impedance<sup>4</sup>, provokes early capacity fade<sup>5</sup> and heavier gassing is produced during battery operation<sup>6</sup>. Many research efforts have been devoted to demonstrating the negative consequences of  $\text{Li}_2\text{CO}_3$  and  $\text{LiOH}$  to the electrochemical performance of the battery. Nonetheless, the whole NMC surface degradation mechanism upon storage under  $\text{H}_2\text{O}/\text{CO}_2$  atmosphere is still controversial.

Therefore, in this work<sup>7</sup>, the complementary acid-base titration and inductively coupled plasma techniques were implemented as accurate methods to identify and quantify the amount of soluble species in four nickel-rich NMC: 532, 622, 811 and 901; before and after exposure under a specific  $\text{H}_2\text{O}/\text{CO}_2$  atmosphere. In addition to the typical  $\text{Li}_2\text{CO}_3$ , and  $\text{LiOH}$ , we unveiled the presence of lithium and sodium sulfate salts. Moreover, thanks to thermogravimetric analysis coupled to mass spectrometry of the as-received and exposed to  $\text{H}_2\text{O}/\text{CO}_2$  materials, we propose a novel NMC surface degradation mechanism that involves the formation of transition metal-based surface species. Lastly, the chemical reactivity of the surface species towards a commercial  $\text{LiPF}_6$ -based liquid electrolyte was studied through nuclear magnetic resonance (<sup>19</sup>F and <sup>31</sup>P NMR), at room and high temperature. In addition to discriminating between  $\text{LiOH}$  and  $\text{Li}_2\text{O}$  as surface species, these experiments evidenced the presence, as major decomposition product, of lithium difluorophosphate, well-known for its beneficial effect as electrolyte additive.

1. Myung, S. T., et al (2017). "Nickel-Rich Layered Cathode Materials for Automotive Lithium-Ion Batteries: Achievements and Perspectives." *Acs Energy Letters*, 2(1), 196-223.
2. Bichon, M., et al (2019). "Study of Immersion of  $\text{LiNi}_{0.5}\text{Mn}_{0.3}\text{Co}_{0.2}\text{O}_2$  Material in Water for Aqueous Processing of

- Positive Electrode for Li-Ion Batteries.” *Acs Applied Materials & Interfaces*, 11(20): 18331-18341.
3. Kim, D., et al (2012). “Positive electrode slurry composition for lithium secondary battery, lithium secondary battery comprising the same and method of making the lithium secondary battery.” Patent
4. Zhuang, G. V., et al (2004). “Li<sub>2</sub>CO<sub>3</sub> in LiNi<sub>0.8</sub>Co<sub>0.15</sub>Al<sub>0.05</sub>O<sub>2</sub> cathodes and its effects on capacity and power.” *Journal of Power Sources*, 134(2): 293-297.
5. Liu, H. S., et al (2006). “Investigation and improvement on the storage property of LiNi<sub>0.8</sub>Co<sub>0.2</sub>O<sub>2</sub> as a cathode material for lithium-ion batteries.” *Journal of Power Sources*, 162(1): 644-650.
6. Renfrew, S. E. and McCloskey, B. D. (2017). “Residual Lithium Carbonate Predominantly Accounts for First Cycle CO<sub>2</sub> and CO Outgassing of Li-Stoichiometric and Li-Rich Layered Transition-Metal Oxides.” *Journal of the American Chemical Society*, 139(49): 17853-17860.
7. Martinez, A. C., et al (2020). “High reactivity of the nickel-rich LiNi<sub>1-x-y</sub>Mn<sub>x</sub>Co<sub>y</sub>O<sub>2</sub> layered materials surface towards H<sub>2</sub>O/CO<sub>2</sub> atmosphere and LiPF<sub>6</sub>-based electrolyte.” *Journal of Power Sources*, 468, 228204.

SESSION F.EN06.05: Solid Electrolytes and Interfaces  
On Demand Abstracts Available for Viewing Starting Saturday Morning, November 21, 2020  
F-EN06

#### 5:00 AM \*F.EN06.05.01

**Ni-Rich Layered Cathodes for All-Solid-State Li Batteries—Effects of Microstructure and Solid Electrolyte** Yoon Jae Han, Sung Hoo Jung and Yoon Seok Jung; Hanyang University, Korea (the Republic of)

All-solid-state Li batteries (ASLBs) have been emerged as the enabler to achieve significantly enhanced safety and energy densities, as compared to conventional lithium-ion batteries (LIBs). Several classes of inorganic solid electrolyte (SE) materials have garnered much attention as they could be integrated with electrode active materials into ASLBs by a scalable process such as cold-pressing. Sulfides (or thiophosphates, e.g., Li<sub>6</sub>PS<sub>5</sub>Cl) and halides (e.g., Li<sub>3</sub>YCl<sub>6</sub>) satisfy critical features for scalable high-performance ASLBs; those are mechanically sinterability and high Li<sup>+</sup> conductivity. However, they show different comparative advantages in multiple aspects. For example, while halides are heavier than sulfides, they show superior electrochemical oxidation stability to sulfides.

As is the case for advanced LIBs based on liquid electrolytes, Ni-rich cathode materials are the key to the practical ASLB technologies. Unfortunately, they suffer from par below electrochemical performances in ASLBs, which are attributed to the interfacial instabilities in terms of both electrochemical and electrochemo-mechanical effects.

In this presentation, we report on our recent findings on the electrochemo-mechanical effects for Ni-rich layered cathode materials for ASLBs. Microstructural effects of NCM particles on the performance of ASLBs are revealed. Moreover, the performances of NCM using halide SEs are extensively compared. These results shed light on a design strategy for high-performance practical ASLBs.

#### References

- [1] K. H. Park, Q. Bai, D. H. Kim, D. Y. Oh, Y. Zhu, Y. Mo, Y. S. Jung, *Adv. Energy Mater.* **2018**, *8*, 1800035.  
[2] S. H. Jung, U.-H. Kim, J.-H. Kim, S. Jun, C. S. Yoon, Y. S. Jung, Y.-K. Sun, *Adv. Energy Mater.* **2020**, *10*, 1903360.

#### 5:15 AM F.EN06.05.02

**Advanced Polymers for High-Performance Lithium Batteries** Zhen Chen<sup>1</sup>, Cristina Iojoiu<sup>2</sup>, Elie Paillard<sup>3</sup>, Stefano Passerini<sup>1</sup> and Dominic Bresser<sup>1</sup>; <sup>1</sup>Karlsruhe Institute of Technology (KIT), Germany; <sup>2</sup>University Grenoble Alpes / CNRS, France; <sup>3</sup>Forschungszentrum Jülich GmbH, Germany

Polymers are playing already an important role for lithium batteries, serving as the main component for the separator and as binder to ensure the mechanical integrity of the electrodes. Recently, the use of polymer-based electrolytes has also gained an increasing momentum – not least due to the successful commercialization of lithium-metal polymer batteries employing poly(ethylene oxide) as ion conducting matrix.<sup>[1]</sup> Nonetheless, the need for adding a lithium salt in combination with the relatively low ionic mobility at ambient temperatures raises concerns about (reversed) charge carrier concentration gradients, rather low limiting current densities, and inhomogeneous lithium deposition at the negative electrode.<sup>[1-3]</sup> Single-ion conducting polymer electrolytes are considered beneficial in this regard – especially if the Li<sup>+</sup> transport occurs along well-defined conduction pathways.<sup>[2,3]</sup> The limited ionic conductivity of such systems, however, calls for alternative conduction mechanisms – e.g., employing molecular “vehicles” that facilitate Li<sup>+</sup> transport.<sup>[3-5]</sup>

Herein, the most recent findings in this field will be presented, covering fundamental insights about the charge transport mechanism, the potential safety of such systems, and their suitability for high-energy lithium-metal batteries incorporating Ni-rich  $\text{Li}[\text{Ni}_{1-x-y}\text{Mn}_x\text{Co}_y]\text{O}_2$  as active material for the positive electrode. Moreover, it will be shown that such single-ion conducting polymers can dramatically improve the interfacial stability at the cathode – also for hybrid systems.

## References

- [1] J. Kalkhoff, G. G. Eshetu, D. Bresser, S. Passerini, *ChemSusChem* **2015**, *8*, 2154–2175.
- [2] D. T. Hallinan, N. P. Balsara, *Annu. Rev. Mater. Res.* **2013**, *43*, 503–525.
- [3] D. Bresser, S. Lyonnard, C. Iojoiu, L. Picard, S. Passerini, *Mol. Syst. Des. Eng.* **2019**, *4*, 779–792.
- [4] H.-D. Nguyen, G.-T. Kim, J. Shi, E. Paillard, P. Judeinstein, S. Lyonnard, D. Bresser, C. Iojoiu, *Energy Environ. Sci.* **2018**, *11*, 3298–3309.
- [5] V. Bocharova, A. P. Sokolov, *Macromolecules* **2020**, DOI 10.1021/acs.macromol.9b02742.

### 5:25 AM F.EN06.05.03

**3D Printing of Thermally-Safe Composite Solid Polymer Electrolytes for Long Cycle Life Li Metal Batteries** Md Golam Rasul, Meng Cheng, Ramin Rojaee, Tolou Shokuhfar and Reza Shahbazian-Yassar; University of Illinois at Chicago, United States

With growing demand for energy storage technologies in emerging electric vehicles and flexible electronics, a combination of research on high-performance rechargeable batteries (i.e. enhanced thermal safety and longer cycle life) and smart manufacturing techniques (i. e. additive manufacturing) is becoming increasingly crucial. In order to face the challenges, research has been going on to improve batteries from three aspects: electrochemistry, material, and device architecture. New material candidates with improved properties are being tested for different battery components: electrode, electrolyte, and separator. While conventional electrolytes suffer from high flammability and parasitic reactions due to its liquid form and result early battery failure, solid polymer electrolytes using polymer materials are gaining attention to overcome these challenges (Zhao *et al.*, 2019). However, the main challenges associated with solid polymer electrolytes (SPEs), particularly for the so called “metal battery”, include finding SPEs that can: (i) offer fast  $\text{Li}^+$  ion transport at room temperature, (ii) accommodate volume changes at the anode by reversible deformation and high flexibility, (iii) suppress the Li dendrite growth by having mechanical rigidity, and (iv) increase battery reliability by reducing thermal runaway events. In this work, boron nitride nanosheets (BNNSs) incorporated SPEs (composite SPEs) were fabricated utilizing our lab-developed 3D printing technology. A robotic deposition system was used to extrude PVdF-based SPE inks onto electrode directly. This robotic deposition system is equipped with three-axis direction stage, control system, pneumatic extrusion dispenser, fine cylindrical nozzle, and self-designed heating block to facilitate printing of electrolytes continuously. This 3D printed composite SPE was further characterized, and performances were compared with SPE without BNNS by evaluating electrochemical, mechanical, and thermal properties. Electrochemical impedance spectroscopy study indicates 10 times improvement in ionic conductivity for composite SPE because of BNNSs addition. This increased  $\text{Li}^+$  ion conduction was observed because of the Lewis acidic characteristic of BNNS which facilitates to trap the anions in the electrolytes (Shim *et al.*, 2017). In addition, the Young’s modulus and yield strength are increased by 100 and 168 %, respectively, because of BNNS reinforcement. This improvement in mechanical properties may help to suppress Li dendrite growth as well as accommodation of volume changes (Monroe and Newman, 2005). Moreover, high thermal conductivity of BNNS is likely to enable homogenous heat distribution in composite SPEs. As a result, the hot-spot formation during parasitic thermal runaway events will be reduced, resulting in enhanced reliability of the battery. This increased mechanical robustness, homogenous heat distribution, and improved ionic conductivity will pave the way for longer battery cycle life.

### 5:35 AM F.EN06.05.04

**Nuclear Magnetic Resonance Investigation of Lithium-Ion Transport in a Highly Conducting Solid Polymer Electrolyte** Sahana Bhattacharyya<sup>1</sup>, Mounesha Garaga<sup>1</sup>, Matthew P. Widstrom<sup>2</sup>, Jesse Matthews<sup>2</sup>, Kyle Ludwig<sup>2</sup>, Chunsheng Wang<sup>2</sup>, Peter Kofinas<sup>2</sup> and Steven G. Greenbaum<sup>1</sup>; <sup>1</sup>City University of New York, United States; <sup>2</sup>University of Maryland, United States

Rechargeable battery technology awaits further advances to meet future demands for large scale and safe storage of energy from renewable but intermittent sources. Solid polymer electrolytes based on poly(ethylene oxide) (PEO) have been under investigation for some four decades as a safer alternative to flammable organic electrolytes.<sup>1</sup> It still lack sufficiently high ionic conductivity for practical use at ambient temperature.<sup>2</sup> Recent reports of high ionic conductivity and an expanded electrochemical window of aqueous electrolytes enabled by very high salt concentration ( $\sim 20\text{m}$ )<sup>3,4</sup> as well as earlier work on the “salt-in-polymer” concept<sup>5</sup> have inspired this investigation of a solid PEO-salt-water system, where the dissolved salt (LiTFSI) concentration approaches its solubility limit and in combination with water association succeeds in inhibiting

crystallization of the PEO matrix leading to higher conductivity. Room temperature ionic conductivity in these solid-like polymer electrolytes is about  $2 \text{ mS}\cdot\text{cm}^{-1}$ , which is sufficiently high for battery application.<sup>6</sup> We have further characterized the ion transport process by nuclear magnetic resonance (NMR) pulsed field gradient diffusion measurements over a wide range of temperature for  $^7\text{Li}$  and  $^{19}\text{F}$  as the cation and anion, respectively. The diffusion measurements in concert with electrochemical impedance spectroscopy show that the degree of salt ion dissociation in these electrolytes is also sufficiently high. It is found that the lithium transport number, which is related to the fraction of current carried by the Li ions, exceeds 0.6 for the whole temperature range, which is unusually high for polymer electrolytes.

#### References

1. M. B. Armand, J. M. Chabagno, M. J. Duclot, in International Conference on Fast Ion Transport in Solids, Electrodes, and Electrolytes., P. Vashishta, J. N. Mundy, G. K. Shenoy, Eds. (North Holland, Lake Geneva, Wisconsin, U.S.A., 1979), pp. 131.
2. M. Armand and J.-M. Tarascon, "Building Better Batteries," Nature, Vol. 451, 2008, pp. 652-657.
3. L. Suo, O. Borodin, T. Gao, M. Olguin, J. Ho, X. Fan, C. Luo, C. Wang, K. Xu, Science 2015, 350, 938-943.
4. O. Borodin, L. Suo, M. Gobet, E. Gobrogge, X. Ren, M. Olguin, M. S. Ding, M. Schroeder, A. von Cresce, J. Peng, A. Faraone, S. Munoz, J. Dura, S. Greenbaum, C. Wang, K. Xu, ACS Nano 11, 10462-10471 (2017).
5. C.A. Angell, C. Liu, E. Sanchez, Nature 362, 137-139 (1993).
6. S. Bhattacharyya, M. Garaga, S. Greenbaum, APS March Meeting 2019 abstract ID:E47.001

#### 5:45 AM F.EN06.05.05

**Understanding the Oxidative Decomposition of Polymer Electrolytes Through Electrochemical Method** Zhuo LI, Yineng Zhao and Wyatt Tenhaeff; University of Rochester, United States

Anodic stability of solid-state electrolyte in full-solid-state lithium ion batteries (SSLIBs) is attracting more attention recently as SSLIB is receiving increasing attention from both industry and academia. Yet neither the definition of electrochemical stability of solid-state electrolyte nor the determination of such stability has been thoroughly investigated. The most common characterization technique for oxidative stability of solid-state materials, linear sweep voltammetry (LSV), lacks validity and reproducibility while applied on solid-state systems, as its result is greatly affected by cell configuration, sample preparation and data processing method. For example, independent research groups have reported oxidation potentials spanning from 4.0 V–5.5 V vs.  $\text{Li}/\text{Li}^+$  for PEO electrolytes, 3.7 V–9.0 V vs.  $\text{Li}/\text{Li}^+$  for LLZO electrolytes and 2.1 V–4.0 V vs.  $\text{Li}/\text{Li}^+$  for LGPS electrolytes using LSV methods. In practice, cycling of PEO with cathodes having charge potentials above 4 V are usually unstable.

In this work, we revisited the open question of understanding the oxidative decomposition behavior of polymer electrolyte using electrochemical, spectroscopy and chromatographical tools. A capacity-based method was developed to replace current-based LSV method. A reversibility factor ( $R$ ), defined as the ratio between the Faradic (decomposition) charge versus non-Faradic (capacitive) charge during cycling, was established as a reliable reference for the degree of oxidative decomposition below certain cutoff potential. To reproduce the environment in solid-state cathode, a large amount of conductive additive was added into the polymer electrolyte sample and nuclear magnetic resonance (NMR) data suggests the sensitivity of the test is greatly improved. Using poly(ethylene oxide) (PEO) as sample material, the polymer was found gradually decomposing above 3.7 vs.  $\text{Li}/\text{Li}^+$  and reaches its practical stability limit around 4.0V vs.  $\text{Li}/\text{Li}^+$  with  $R$ -based test. The result was further confirmed with gel permeation chromatography (GPC), where the PEO sample was allowed to decompose at given voltage. Molecular weight-oxidation potential relation of the partially decomposed PEO shows good correlation with  $R$ -cutoff potential relation, providing direct support of the validity of the electrochemical test. The method is further verified with a nitrile-based, more oxidatively stable polymer electrolyte, hydrogenated butadiene nitrile rubber (HNBR), and the universality of such test for other polymer electrolytes was proved. HNBR was found decomposing above 3.9 V vs.  $\text{Li}/\text{Li}^+$  and reaches stability limit above 4.3 V vs.  $\text{Li}/\text{Li}^+$ .

#### 5:55 AM F.EN06.05.06

**Mixed Ionic-Electronic Conductor for All-Solid-State Lithium-Sulfur Batteries** Daiwei Wang, Shiyao Zheng and Donghai Wang; The Pennsylvania State University, United States

All-solid-state Lithium-Sulfur Battery (ASSLB) is one of the protagonists for next-generation energy storage system. The high theoretical capacity of sulfur, the nonflammable characteristics of solid electrolyte and the elimination of shuttle effect endow ASSLSBs with supreme safety, high energy density and long cycle life. However, due to the insulating nature of sulfur, the utilization of active material during cycling is usually low which leads to lower capacity and practical energy density. To resolve this issue, highly efficient ionic and electronic transportation framework needs to be constructed. In all-solid-state sulfur cathode, the weight of solid electrolyte is usually above 40 wt%. While serving as lithium ion conductor,

solid electrolytes generally possess low electronic conductivity ( $<10^{-8}$  mS cm<sup>-1</sup>) which may hinder electron transport in all-solid-state sulfur cathode. Therefore, to improve electronic transportation within sulfur cathode, we have prepared inorganic solid electrolytes with mixed ionic-electronic conductivity and controlled electronic conductivity for ASSLSBs. Specific capacity of the sulfur cathode could increase from below 900 mAh g<sup>-1</sup> to over 1300 mAh g<sup>-1</sup> (based on the weight of sulfur) at 0.1 C after employing the prepared mixed ionic-electronic conductive solid electrolyte. Besides, various aspects of the synthesized material and the fabricated sulfur cathode have also been investigated, including material structure and electrochemical evolution, cathode cycling stability, rate capability and etc.

#### 6:05 AM F.EN06.05.07

**Microstructural Heterogeneities and Interphase Effects on the Chemo-Mechanics of Thiophosphate Solid Electrolytes** Marm Dixit<sup>1</sup>, [Nikhilendra Singh](#)<sup>2</sup>, James Horwath<sup>3</sup>, Pavel Shevchenko<sup>4</sup>, Eric Stach<sup>3</sup>, Timothy Arthur<sup>2</sup> and Kelsey Hatzell<sup>1</sup>; <sup>1</sup>Vanderbilt University, United States; <sup>2</sup>Toyota Research Institute of North America, United States; <sup>3</sup>University of Pennsylvania, United States; <sup>4</sup>Argonne National Laboratory, United States

Advances in hybrid and electric vehicle technologies combined with a demand for green initiatives have motivated necessary diversification in energy storage research. To achieve customer expectations for hybrid and electric vehicles, new battery systems with higher energy densities, power densities and cycle life than the current state-of-art Lithium (Li)-ion battery are needed. Post Li-ion battery systems, especially those focused on the utilization of Li metal have recently come to the forefront of research. The ability to directly utilize Li metal anodes in rechargeable batteries presents itself as an ideal situation via the accessibility of a maximum possible theoretical specific capacity (3860 mAh/g) in comparison to commercially used anodes (e.g. graphite – 380 mAh/g). Hence, significant efforts in recent literature have targeted the development of robust Li metal anode systems.

One such system is Li-sulfur which has attracted attention due to its high theoretical capacity (1673 mAh/g) and potential low cost. However, this system is hindered by polysulfide dissolution and electrolyte decomposition at the Li metal anode. Among the various strategies which have been employed to overcome these hinderances, the use of solid-state electrolytes (inclusive of polymers, gels and conducting ceramics) stands out since the implementation of solid-state electrolytes can also serve as a mechanical barrier towards Li dendrite formation. However, solid-state electrolytes exhibit relatively lower ionic conductivities and also display poor interfacial stability towards Li metal anodes. While advances in solid-state electrolyte materials continue to improve their ionic conductivities, little is known about the interfacial interactions between sulfide-based solid-state electrolytes and Li metal. Hence, studies into understanding the interactions between Li metal and these solid-state electrolytes remains essential towards realizing all-solid-state Li battery technologies.

Here, we present a study into the chemo-mechanical transformations within lithium thiophosphates and at their solid-solid interfaces. Tandem analytical ex-situ and in-situ studies via X-ray tomography and transmission electron microscopy are used to reveal the interfacial interactions and failure modes between Li metal and lithium thiophosphates, the deposition and dissolution properties of Li metal from these electrolytes, and the effects of the deposition and dissolution properties on the bulk electrolyte structure. The presented studies allow for comparisons of Li deposition and dissolution properties below and above the critical current densities for each lithium thiophosphate electrolyte material and stand to help clarify interfacial, morphological and failure evolution mechanisms during Li cycling from them.

#### 6:15 AM F.EN06.05.08

**Designing Polymers for Stable Interphases in Lithium Metal Batteries** [Sanjuna Stalin](#) and Lynden Archer; Cornell University, United States

Reactive metal anodes like lithium are known to electrodeposit in the form of irregular morphological features on planar substrates. Formed during the earliest stages of deposition, these features are thought to seed non-planar, mossy structures that proliferate in the electrode spacing, hampering electrode reversibility. A growing body of work suggests that the mechanics, structure, ion transport properties, reductive stability, and interfacial energy of interphases formed spontaneously on the metal electrode play important, but differentiated roles in regulating nucleation, growth, and reversibility of these non-planar structures. Fundamental understanding of the formation mechanisms, mechanical stability, ion transport characteristics, and interfacial properties of solid-electrolyte interphases (SEI), though in its infancy is considered a requirement for progress.

Several approaches have been investigated to mitigate or, in rarer cases completely prevent the growth of lithium dendrites. These include salt additives to improve the properties of the SEI, concentrated electrolytes that change the solvation structure of the ions and resulting SEI formation, single ion conductors that prevent concentration gradients in the bulk electrolyte phase and high modulus electrolytes that prevent dendrite formation via mechanical pressure forces. Tailoring the lithium metal/electrolyte interface with polymer coatings that serve as a protective barrier against chemical and physical instabilities has been gaining a lot of attention in the past few years.

In this talk, we elucidate design rules for elastic interphases formed on any generic metal anode and utilize experiments based on Li metal anodes to evaluate their effectiveness in arresting the various instabilities (*e.g.* morphological, chemical, mechanical/orphaning, and hydrodynamic) known to lower lifetime and reversibility of metal anodes. By combining the experiments with a theoretical stability analysis of metal electrodeposition across elastic interphases, we find that interphase thickness, mechanics, ion transport and interfacial properties all play precise, differentiated roles in setting the optimal interphase design.

#### **6:25 AM F.EN06.05.09**

**Safety Considerations of Lithium Metal Anodes in Solid-State Batteries** Mihir D. Upadhye<sup>1</sup>, Alvaro Masias<sup>2,3</sup> and Jeff Sakamoto<sup>1,3</sup>; <sup>1</sup>University of Michigan, United States; <sup>2</sup>Ford Motor Company, United States; <sup>3</sup>University of Michigan, United States

The introduction of lithium-ion battery technology in 1991 has led to the prevalence of personal electronic devices and the burgeoning electric vehicle space. Advancements in energy density and safety of battery technology will enable further adoption of electric vehicles. Solid-state (SS) battery technology is a leading candidate for the next generation of energy storage in which the liquid electrolyte and polymer separators are replaced with a ceramic ionically conducting solid. While this technology replaces the flammable liquid electrolyte of lithium-based technology, the highly reactive lithium metal and brittle separator materials found in SS battery technology may, ostensibly, introduce other unknown considerations to safety.

Lithium metal is known to be reactive when exposed to water. With the potential application of SS battery technology in electric vehicles, an understanding of lithium metal water exposure in the context of battery architecture is necessary for the adoption of the technology. The reactivity of lithium metal in water has been assessed in various in-situ architectures in the context of existing international battery safety test standards.

SESSION F.EN06.06: Safety Devices and Mitigation of Failure Propagation  
On Demand Abstracts Available for Viewing Starting Saturday Morning, November 21, 2020  
F-EN06

#### **5:00 AM \*F.EN06.06.01**

**Understanding for Charge/Discharge Curves of Commercial Lithium-Ion Batteries** Yuhao Lu and Xiao Jie; NingDe Amperex Technology Limited, China

Lithium ion batteries (LIBs) are widely used for portable electronics and electric vehicles due to the favorable performance compared with other rechargeable batteries. However, their degradation deteriorate their service life remarkably. Fortunately, charge/discharge curves can provide quantitative information for understanding how such degradation correlates with usage conditions and environment of LIBs.

In general, the charge/discharge curves can be divided into two parts, i.e. the open circuit voltage (OCV) and the polarization in the cell. The OCV provides a thermodynamic fingerprint of the electrode which could be roughly estimated by charge/discharge the cell at very low C-rate. With regards to a commonly used 2430 coin cell, the difference between charge/discharge curve and theoretical OCV is less than 30mV at the full range of SOC when a 1/25C current rate is used. In this presentation, the changes in OCV during long cycles will be exhibited, which offers a quantified information on active material decay as well as the side reactions in the cell. The polarization of the cell is strongly affected by the electron and lithium ion transport inside the electrode microstructure. In this work, both the time-domain and the frequency-domain electrochemical methods were applied to the analysis to distinguish each process onto the polarization in the cell, i.e. the contact problem between the solid phases, the mass transport through the interface and in the solid phase of the electrodes, along with the slow electrochemical reactions. Furthermore, the thermodynamic fingerprints of the positive and negative materials have strongly relation with the polarization in the cell. These relations generally becomes very complex, and thus a mathematical modeling is also used to understand and explain the charge/discharge curve for LIB in detail. Overall, it is proposed that more collaborations could be needed between the academia and industry so that the lithium ion battery degradation could be fully investigated.

#### **5:15 AM \*F.EN06.06.02**

**Performance of High Energy and High Power Commercial Li-Ion Cells for Space Missions** Ratnakumar Bugga; California Institute of Technology, United States

Li-ion batteries are being widely used in planetary space missions, owing to their impressive performance characteristics, including high specific energy, long life, and the ability to operate over a wide temperature range. Historically, batteries with custom large-format Li-ion cells of 10-55 Ah have been used in various Mars missions, e.g., Mars Exploration Rovers (Spirit and Opportunity), Mars Curiosity Rover, Mars landers (Phoenix and InSight), Mars and Jupiter orbiters and the upcoming Mars 2020 Rover. However, in several other robotic and human space missions, e.g., Europa Clipper, Artemis missions to moon, and Portable Life Support System (PLSS) for Extra-Vehicular Activities, commercial 18650 Li-ion cells are being used due to their improved specific energies of ~250 Wh/kg (20-50% over custom cells), improved safety from built-in safety devices, modularity, and excellent uniformity, which obviate the need for cell-level control during charging. Several cell types with different chemistries and from different manufacturers are being evaluated at JPL. The cell chemistries differ mostly in cathodes, i.e., either lithium nickel cobalt aluminum oxide (NCA), Li-rich nickel manganese cobalt oxide (Ni-rich NMC) or blends with lithium manganese spinel oxide (LMO). Various performance tests, including cycle life at different depths of discharge, radiation tolerance and high-power characterization at different temperatures are being carried out in conjunction with Electrochemical Impedance Spectroscopy (EIS). In addition, destructive physical analysis of the cells have been performed to analyze the electrode materials, and correlate them with the performance characteristics. Finally, low temperature charge characterization studies have been carried out to ascertain the propensity of lithium plating as a function of charge current and temperature.

### 5:30 AM F.EN06.06.03

**Imaging Pristine Li-Ion Battery Separator Using Low Temperature SEM** Luyang Han<sup>1</sup>, Markus Boese<sup>1</sup>, Jianliu Huang<sup>2</sup>, Shuangwen Chen<sup>2</sup> and William Fadgen<sup>3</sup>; <sup>1</sup>Carl Zeiss Microscopy GmbH, Germany; <sup>2</sup>Carl Zeiss (Shanghai) Co., Ltd., China; <sup>3</sup>Carl Zeiss Microscopy, LLC, United States

Separators are an important component within a Li-ion battery cell. They need to mechanically separate anode and cathode within a cell while allowing maximum ionic conductivity of the Li-ion containing electrolyte. Commercially available separators are usually made from polyolefine membranes composed of pores in 10s to 100s of nanometers. The shape, size and distribution of porosity in the separator membrane is a key parameter influencing the performance of the Li-ion battery cell. Due to its small size, scanning electron microscopy is currently the preferred method to directly image and investigate the separators.

However, the separator membrane is highly insulating, and easily gets damaged by the electron beam. Typical SEM imaging condition usually causes significant shrinkage and melting of the porous structure, leading to the wrong measurement of pore size and distribution. In this contribution, we demonstrate a method to image the separator membrane at very low beam energy (< 1 kV) to reduce charging artifacts. Additionally, we use either a Peltier cooler or a liquid nitrogen cooled sample holder to stabilize the specimen against beam damage. The resulting images shows significantly different pore size distribution and surface morphology compared to typical SEM images obtained at room temperature. By optimizing the electron beam energy, scanning method and specimen temperature, an optimum strategy to image the separator membrane is developed to reveal its pristine surface morphology and pore structure.

### 5:40 AM \*F.EN06.06.04

**Thermal Conduction in Li-Ion Battery Materials** Ankur Jain; The University of Texas at Arlington, United States

Li-ion batteries offer excellent energy conversion rate and high energy storage density in electric vehicles, aircraft, consumer electronics and renewable energy storage. However, these batteries suffer from several safety related problems, as evidenced by recent product recalls and incidents of fires in electric cars and aircraft. Overheating due to poor thermal transport is at the heart of several of these challenges, and therefore, a fundamental understanding of heat transfer in Li-ion battery materials is critically needed. While Li-ion battery materials have been well optimized from the perspective of electrochemistry, the nature of thermal transport in these materials remains relatively less known.

This talk will summarize ongoing research on understanding and optimizing heat transfer in Li-ion battery materials through experiments and theoretical analysis. Measurement of orthotropic thermal conductivity of a Li-ion cell will be described. Measurements of thermal conductivity of the separator of a Li-ion cell will be discussed. Measurements that identify poor thermal transport across the cathode-separator interface as the fundamental root cause of the low thermal conductivity of Li ion cells will be discussed. A molecular bridging approach that reduces this rate-limiting thermal contact resistance by 4X through improved interfacial thermal transport will be discussed. This approach is expected to significantly enhance thermal conductivity of a Li-ion cell. More recent work on enhancement of thermal transport in Gel Polymer Electrolytes (GPEs) through inclusion of BN/Al<sub>2</sub>O<sub>3</sub> nano/microparticles will also be discussed. While this approach is shown to improve thermal

conduction in general, a careful optimization of thermal and ionic transport in GPEs will help fully utilize this promising class of materials for next-generation solid-state batteries. Related research on developing predictive models for onset of thermal runaway based on thermal properties of battery materials and kinetics of underlying electrochemical processes will also be discussed briefly.

#### 5:55 AM F.EN06.06.05

**Late News: Battery Calorimetric Analysis of Aging Effects on the Safety and Thermal Behavior of Cylindrical Lithium-Ion Cells** Carlos Ziebert, Dieter Freis, Zeming Lin, Nils Uhlmann and Hans Jürgen Seifert; Karlsruhe Institute of Technology, Germany

With increasing energy density safety and thermal management of Li-ion cells is becoming more and more important because the thermal runaway can cause an ignition or even explosion with simultaneous release of toxic gases. In order to prevent such hazards, extensive research is undertaken to determine the causes of thermal runaway, as well as the influencing factors. In the last nine years, we have established battery calorimetry as a versatile characterization technique, which allows advancements for the thermal management and the safety of batteries. With six adiabatic Accelerating Rate Calorimeters (ARC) of different sizes and two sensitive Tian-Calvet calorimeters combined with cyclers we operate Europe's largest battery calorimeter center. This enables the evaluation of thermodynamic, thermal and safety data on material, cell and pack level under quasiadiabatic and isoperibolic environments for both normal and abuse conditions (thermal, electrical, mechanical).

The primary purpose of this work was to determine the correlation between cell aging and the thermal runaway of commercial Sony VTC6 18650 cells with a nominal capacity of 3 Ah, a Li-containing graphite anode and a high-Ni  $\text{LiNi}_{0.9}\text{Co}_{0.075}\text{Al}_{0.025}\text{O}_2$  (NCA) cathode as determined by inductive coupled plasma optical emission spectroscopy (ICP-OES). Therefore, a comprehensive ageing study was performed with 116 cells.

First, fresh cells were stored in temperature chambers at different temperatures and states of charge and then characterized at fixed time intervals in order to study the influence of this storage on the performance (calendar ageing). Second, cells of the same type were aged in temperature chambers at different charge/discharge rates (cyclic aging) and comprehensively characterized every 100 cycles. The ageing procedure was stopped at a state-of-health (SOH) of 80%. Information on the causes of the aging was obtained using electrochemical impedance spectrometry (EIS), X-ray diffraction and measurement of the entropy changes using the potentiometric method, where the change in the open circuit voltage is monitored against the temperature. The change in entropy showed a capacity-dependent behavior. It was found that the cathode has no significant influence on the entropy changes and that the anode represents the dominating factor. This allows the determination of the loss of lithium inventory (LLI) in the anode and to correlate the LLI to the total capacity loss. The cathode only showed changes in the charge transfer resistance that was extracted from the EIS spectra.

After these characterizations, the cells were thermally abused using the Heat-Wait-Seek (HWS) test in an ARC. The cyclic aged cells showed increased exothermic reactions in the low temperature range. It is unclear whether these indicate lithium plating or decomposition of the SEI. The absence of these increases with calendar aging, in which plating can be ruled out, means that a larger SEI layer has a small influence on an increased temperature rate. Accordingly, it is assumed that the increase in cyclic aging in the low temperature range is due to a small amount of plating. The aged cells show a vent opening at higher temperatures than the fresh cells and minimal deviations in the temperature rates, which can be attributed to the lower capacity of the aged cells. Thus, it can be concluded that for these cells the safety level is not negatively affected when they reach a SOH of 80%.

The next step is to perform a similar analysis for cells aged until SOH 60% and 40% and to extract electrodes from the aged cells from which coin half cells can be prepared. These cells will then be studied using electrochemical impedance spectroscopy, CV measurements and both isothermal and adiabatic calorimetry.

#### 6:05 AM F.EN06.06.06

**Multi-Physics Modeling for Characterization of Latent Thermal Runaway** Kirsten B. Yapp<sup>1</sup>, Charles J. Patrissi<sup>2</sup>, Jacob L. Moyer<sup>2</sup>, Ryan E. Chamberlin<sup>2</sup>, Ugur Pasaogullari<sup>1</sup> and Wilson K. Chiu<sup>1</sup>; <sup>1</sup>University of Connecticut, United States; <sup>2</sup>Naval Undersea Warfare Center Newport, United States

Thermal and electrochemical behavior of a Li-ion battery throughout thermal runaway (TR) is investigated with a goal of understanding the conditions that cause this phenomena in an effort to improve battery safety testing. TR can be caused by multiple methods, but one that is nearly impossible to detect is one triggered by an latent event such as internal short circuit (ISC). This type of initiation mechanism has a low probability, but is still a severe risk when considering the safe use of Li-ion batteries because of the likelihood of catastrophic damage. During TR, the cell temperature increases which initiates and catalyses additional exothermic chemical reactions. These reactions become self sufficient, and if heat cannot be removed quickly enough, the cell fails and can result in ignition. The danger of a single cell TR is that it can propagate through an



entire battery pack because of the close packed arrangement of the cells.

Currently, research on alternative designs to prevent propagation as well as attempts to mitigate TR are being conducted. They are based on information gathered from studies that trigger TR through the use of external heaters which can affect the kinetics of the decomposition reactions in the trigger cell and surrounding cells and exacerbate the TR event and the propagation, respectively. It is clear that in order to improve upon the fidelity of Li-ion safety research, the TR method must be further characterized. This project aims to study the trigger mechanisms relating to ISC caused by point heat source through multi-physics modeling. The results will be applied in future investigations and development of a TR trigger device to be used in Li-ion safety testing.

Initially, the focus will be on thermal modeling to identify the dimensional constraints and power requirements for a local heat source to initiate TR. Specifically regarding heat generation results due to an ISC from anode active material to the positive current collector. Previous research in the field has determined acceptable values for initiating temperatures for electrochemical reactions in the solid electrolyte interface (SEI). These conditions are used as guidelines for the thermal models. The cell and heat source is studied as 1D, 2D, and/or 3D models. Cell layers are represented with accurate material properties, cell geometries for multiple electrode configurations (pouch and cylindrical), and will be paired with realistic cell voltage and impedance. The heat source size, shape, and power conditions will be varied in order to understand where the heat transfers throughout a Li-ion cell, and how long it takes for the temperature of the various components to reach initiation temperature for their respective electrochemical reactions. Simulations are adjusted accordingly until the hot spot results in TR while mimicking real world conditions within the cell. The results will give a more detailed understanding of how an ISC is formed and how it can lead to TR. The generic heat source will later be replaced with the properties of a resistive heating element to be used in the trigger device.

Characterization through simulation is not only convenient, but it also ensures safety during initial research. Thermal modeling will be paired with future electrochemical models for a more complete and accurate representation of a Li-ion cell throughout TR. Future work also includes experiments to further validate these findings. The knowledge gained from this research is vital for understanding the effects of geometry and power on spontaneous TR. Understanding what causes this phenomenon can lead to design innovations for tools meant to identify TR or prevent propagation and the development of mitigation techniques within Li-ion batteries.

#### **6:15 AM F.EN06.06.07**

**Advanced Single Cell Thermal Runaway Initiation Techniques** [Joshua Lamb](#) and Loraine Torres Castro; Sandia National Laboratories, United States

The evaluation of lithium ion battery safety has traditionally focused on the performance of single cells exposed to abusive conditions. As lithium ion batteries are fielded in increasingly large and complex systems, the system level safety performance is becoming of greater concern. Testing laboratories and battery end users have begun to consider the hazards associated with a localized thermal runaway event, a single cell or small group of cells, propagating to the bulk of a large battery system. Evaluating this propagating failure requires initiating thermal runaway of a single cell or group of cells and observing how that failure affects the surrounding system.

Ultimately, testing cell to cell propagation requires a method for initiating or simulating single cell runaway while adding a minimum of excess energy into the system. Traditionally single cell failure is initiated with standard battery abuse tests, such as overcharge, thermal ramp and nail penetration tests. However, nail penetration tests can be difficult to perform in fully developed battery systems while overcharge and thermal ramp add a significant amount of excess energy into the battery system. Recent work at Sandia has looked at non-traditional thermal runaway triggers that can be applied to off-the-shelf cells. Single cells were initiated using a fiber coupled laser to create a localized failure on a cell. The ability to initiate single cell failure in both pouch and cylindrical cells in multiple orientations is demonstrated. Limited cell to cell propagation initiated by the laser is performed as well, demonstrating the technique as a low energy initiation source for propagation testing.

Sandia National Laboratories is a multimission laboratory managed and operated by National Technology & Engineering Solutions of Sandia, LLC, a wholly owned subsidiary of Honeywell International Inc., for the U.S. Department of Energy's National Nuclear Security Administration under contract DE-NA0003525.

#### **6:25 AM \*F.EN06.06.08**

**Thermal Runaway Propagation Study on Lithium-ion Cells as Packaged for Transportation** [Judith Jeevarajan](#); Underwriters Laboratories, United States

Thermal runaway in lithium-based cells and batteries have been a significant concern during transportation. The ICAO had

set temporary restrictions on transportation to limit the SOC to 30% or less. In parallel, the ICAO commissioned the Society of Aerospace Engineers (SAE) to write a standard that would have test procedures that confirmed that li-based cells in the package as shipped will not become a fire hazard. The test procedure and the verification of test protocols have been looked into in this study. The results obtained as part of this test program will be presented.

SESSION F.EN06.07: Poster Session: Advancement of Lithium-Based High-Energy Density Batteries at Multiple Scales,  
Factoring in Safety  
On Demand Abstracts Available for Viewing Starting Saturday Morning, November 21, 2020  
5:00 AM - 8:00 AM  
F-EN06

#### **F.EN06.07.01**

**Phosphorus-Based Anode Materials via Electrostatic Spray Deposition for High-Performance Lithium-Ion Batteries** Amin Rabiei Baboukani<sup>1</sup>, Iman Khakpour<sup>1</sup>, Vadym Drozd<sup>2</sup> and Chunlei Wang<sup>1</sup>; <sup>1</sup>Florida International University, United States; <sup>2</sup>Center for the Study of Matter at Extreme Conditions (CeSMEC), United States

In the past few years, due to rapidly increased global demand for energy storage devices such as advanced electronics, electric vehicles (EVs), and implantable medical devices, it is essential to develop novel materials for energy storage technologies. Lithium-ion batteries (LIBs) have been the most popular and commercially available energy storage devices. However, anodes of LIBs still suffer poor theoretical capacity of graphite (372 mAh g<sup>-1</sup>). Recently, phosphorus as an anode material has attained much attention owing to its high theoretical capacity (2596 mAh/g) via Li<sub>3</sub>P alloying formation. White P (WP), black P (BP), and red P (RP) are the main three allotropes of solid phosphorus. WP is not stable in the air, flammable, and very toxic, which impose safety concerns for LIBs. BP is the most thermodynamically stable form of phosphorus with an orthorhombic crystal structure. However, the synthesis of BP via high-pressure and high-temperature process is expensive, which restricts its practical application. Compare to WP and BP, RP is non-toxic, low cost, eco-friendly, and easy to handle, making RP a promising anode for LIBs. Nevertheless, the application of RP in LIBs is obstructed by two serious issues: low electrical conductivity of RP (~ 10<sup>-14</sup> S cm<sup>-1</sup>), and huge volume change (more than 300 %) during lithiation and delithiation causing the pulverization of the active materials which leads to significant capacity fading, and poor cycling performance. Compositing phosphorous with carbonaceous materials and construing stable architecture are the two main methods that have been evaluated to resolve the issues and improve the electrochemical performance of P-based electrode materials. Moreover, the chemical bond of P to the conductive matrix could contribute to the integrity of the electrode during cycling. In this research, for the first time we developed a binder-free P-based anode materials with sulfurized polyacrylonitrile (SPAN) as functional polymer composite fabricated through ball-milling and electrostatic spray deposition (ESD) method. SPAN-based electrodes have shown attractive electrochemical performance such as good cycling life and Coulombic efficiency due to its chemical compatibility for energy storage devices. In addition, due to the low bonding energy of S-S (265 kJ mol<sup>-1</sup>) and its high reactivity to form additional chemical bonds with RP, the conductive SPAN could be an ideal composite to increase the conductivity and control the volume expansion of RP in LIBs. The electrochemical performance of the fabricated anode materials evaluated via electrochemical impedance spectroscopy, cyclic voltammetry, and galvanostatic charge/discharge tests. The RP-SPAN hybrid electrode exhibited excellent specific capacity up to 1605 mAh g<sup>-1</sup> at 0.1 A g<sup>-1</sup> at 100 cycles, which is one of the best reported performances among the RP-based composite electrode in LIBs. Moreover, a specific capacity of 320 mAh g<sup>-1</sup> was maintained at 3 A g<sup>-1</sup>. Due to the SEM images, the hybrid electrode still maintains its microstructural integrity without obvious degradation after cycling, indicating that the volume change didn't affect the structural stability. Our results show that the ESD method is an effective approach to prepare RP-based composite with favorable morphology and composition in order to buffer mechanical stress and alleviate crack formation during cycling. The RP-SPAN hybrid delivered high specific capacity, most likely due to the synergetic effect of chemical bonding and improved kinetics. The developed anode material and its material and electrochemical characterizations will be discussed in detail at the conference.

#### **F.EN06.07.03**

**Surface Modified Graphite Electrodes for Limiting Lithium Plating and Enabling Fast Charging of Li-Ion Batteries** Killian Tallman<sup>1</sup>, Bingjie Zhang<sup>1</sup>, Shan S. Yan<sup>2</sup>, Amy Marschilok<sup>1,2</sup>, Kenneth Takeuchi<sup>1</sup>, David Bock<sup>2</sup> and Esther Takeuchi<sup>1,2</sup>; <sup>1</sup>Stony Brook University, United States; <sup>2</sup>Brookhaven National Laboratory, United States

Lithium metal plating on graphite anodes has been identified as a mechanism contributing to diminished capacity retention of

Li-ion batteries under conditions of repeated fast charge. Due to mass transfer limitations, instead of lithium ion insertion in the graphite anode Li metal can deposit on the graphite anode surface when the electrode is highly polarized. The result is inactive Li metal which limits cell cycle life and raises risk of internal short-circuits due to dendrite growth. The objective of this research was to mitigate Li-plating during fast charging by increasing the overpotential of Li-deposition via interfacial surface modification. The hypothesis tested was that deposition of Cu or Ni metal on the surface of graphite electrodes can increase the Li nucleation overpotential due to crystalline mismatch and suppress Li-plating.

Thin metal films of Cu or Ni were deposited on graphite anodes. The films were characterized by a variety of methods including atomic force microscopy, scanning electron microscopy, X-ray photoelectron spectroscopy and X-ray absorption near edge structure spectroscopy. Lithium ion cells with the treated graphite anodes as well as control cells were assembled and evaluated using galvanostatic cycling. Benefit in capacity retention for the treated electrodes was demonstrated. Further, Li-plating was quantified over a series of experiments and supported the electrochemical results. The findings of this study establish that with rational design of an electrode interface, the overpotential for Li-deposition can be modulated, providing a new conceptual approach for reducing Li-plating on graphite anodes.

#### **F.EN06.07.04**

**Nanocomposite of SnO<sub>2</sub>/CeO<sub>2</sub> Nanostructured Electrode for Efficient Li-Ion Storage Application** Samuel Danquah, Messaoud Bahoura and Sangram K. Pradhan; Norfolk State University, United States

Cerium oxide (CeO<sub>2</sub>) nanocomposite material for Li-ion battery is synthesized using hydrothermal method. To fabricate a hybrid nanostructure electrode, CeO<sub>2</sub> is coated on tin oxide (SnO<sub>2</sub>) nanorods (NR), which is grown using a vapor-liquid-solid (VLS) technique on a steel substrate. The structure of SnO<sub>2</sub>/CeO<sub>2</sub> nanocomposite was confirmed by X-ray diffraction (XRD), field emission scanning electron microscopy (FESEM). The surface morphology of the hybrid nanostructure electrode confirms that, single-crystalline SnO<sub>2</sub> nanorods are grown vertically with spine-like structures, a few microns in length, as evident from FESEM. The electrochemical performance of SnO<sub>2</sub>/CeO<sub>2</sub> shows an enhanced charge storage capability. The coin cell shows improved capacity with a higher number of charging and discharging cycles. This SnO<sub>2</sub>/CeO<sub>2</sub> hybrid composite electrode shows better specific capacitance value as compared to the pristine SnO<sub>2</sub> electrode and pristine CeO<sub>2</sub> electrode.

#### **F.EN06.07.06**

**Nanoscale Three-Dimensional Imaging of Degradation in Composite Si-Containing Anodes** Zoey Huey<sup>1,2</sup>, Caleb Stetson<sup>1,2</sup>, Sang-Don Han<sup>1</sup>, Donal P. Finegan<sup>1</sup>, Yeyoung Ha<sup>1</sup>, Chun-Sheng Jiang<sup>1</sup>, Andrew Norman<sup>1</sup>, Steven DeCaluwe<sup>2</sup> and Mowafak Al-Jassim<sup>1</sup>; <sup>1</sup>National Renewable Energy Laboratory, United States; <sup>2</sup>Colorado School of Mines, United States

The use of silicon (Si) in the anodes of next-generation lithium ion batteries (LIBs) has the potential to dramatically improve electrochemical performance over current LIBs with graphite anodes, due to the higher specific capacity of silicon.<sup>1</sup> However, widespread implementation of Si-containing anodes is inhibited by issues such as significant volume expansion of Si during lithiation and an unstable solid-electrolyte interphase (SEI), resulting in unreliable performance and poor cycle life. Currently, composite anodes with both Si and graphite active materials are used to increase capacity and mitigate some of the limitations associated with Si. In composite electrodes with a heterogeneous distribution of components with varying electrical properties (including Si, graphite, conductive carbon additive, and binder), it is important to understand the local distribution of each component to correlate with electrochemical processes, particularly localized degradation and heterogeneous aging, and to optimize performance. The heterogeneous distribution of these components leads to localized lithiation, nonuniform SEI formation and material degradation, and complex electron transfer pathways, which all impact anode cycling and performance.

To investigate Si-containing composite anodes in the nanoscale, we employ scanning spreading resistance microscopy (SSRM), a form of scanning probe microscopy (SPM) that probes local electronic resistivities. By examining the contrast in intrinsic electronic resistivity between the anode components, separate phases can be distinguished and understood within the composite structure. Previous work has been conducted on composite Si-graphite electrodes using SSRM, as well as with X-ray tomography, to study degradation after cycling.<sup>2,3</sup> SSRM is able to measure composite electrode components over a wide range of relative intrinsic resistivities with nanometer-scale resolution and a smaller sampling volume than X-ray based methods, making it ideal for distinguishing anode components and determining their spatial positions. This work studies the effects of electrochemical cycling on component distribution and aging by comparing the electrical and structural evolution of composite Si-graphite electrodes before and after charge-discharge cycling. Additionally, we compare the resistivity maps to STEM-EDS and EELS results for both pristine and cycled electrodes to understand chemical changes that occur within the observed structure. By analyzing structural and chemical changes that occur during cycling, we identify degradation mechanisms and potential design improvements to increase capacity and cycle life next-generation composite anodes.

1. W. J. Zhang. A review of the electrochemical performance of alloy anodes for lithium-ion batteries *J. Power Sources* **196** 13–24 (2011)
2. S.H. Kim, Y.S. Kim, W.J. Baek, S. Heo, D.J. Yun, S. Han and H. Jung. Nanoscale Electrical Degradation of Silicon-Carbon Composite Anode Materials for Lithium-Ion Batteries *ACS Appl. Mater. Interfaces* **10** 24549–53 (2018)
3. O.O. Taiwo, M. Loveridge, S.D. Beattie, D.P. Finegan, R. Bhagat, D.J.L. Brett and P.R. Shearing. Investigation of cycling-induced microstructural degradation in silicon-based electrodes in lithium-ion batteries using X-ray nanotomography *Electrochim. Acta* **253** 85–92 (2017)

#### **F.EN06.07.07**

**Multiscale Modeling of Ni-Rich Cathode Materials—From Electrons, Ions, Atoms to Particles** Yugin Wu and Yue Qi; Michigan State University, United States

Ni-rich Li[Ni-Mn-Co]O<sub>2</sub> is a promising cathode material due to its high discharge capacity, high voltage and low cost, but its application is hindered by the poor thermal stability and low capacity retention. To guide the design of Ni-rich cathode materials, multiscale modeling analysis was used to determine its atomic structure, band structure, open-circuit voltage, and mechanical properties and to predict the critical size of Ni-rich cathode single particles that are mechanically stable. First, density functional theory (DFT) calculations were performed to identify the base structure of pure LiNiO<sub>2</sub> layered compounds based on three different space groups, namely Rm, C<sub>2</sub>/m, and P<sub>2</sub>/c. It was found the calculated band structures of the widely applied Rm structure of LiNiO<sub>2</sub> is metallic, contrary to the experimentally reported insulating behavior. P<sub>2</sub>/c structure, which allows a disproportionation of the oxidation state of Ni (Ni<sup>2+</sup> and Ni<sup>4+</sup>), is the most energetically stable and insulating layered structure of LiNiO<sub>2</sub>. Therefore, model structures representing Ni-rich NMC cathode materials were built by partially replacing Ni with Co or Mn in the base P<sub>2</sub>/c LiNiO<sub>2</sub> structure. The electronic structure of model Ni-rich NMC cathode shows that Ni tends to be Ni<sup>3+</sup> when neighboring with Co<sup>3+</sup>, while becoming Ni<sup>2+</sup> next to an Mn<sup>4+</sup>. Based on the model Ni-rich cathode structures, the elastic constants and fracture energy were also computed from DFT. The information served as input to a continuum diffusion induced stress model to predict when a crack starts to propagate and leads to the fracture of a single Ni-rich NMC particle. The predicted results show good agreement with single-particle observations.

#### **F.EN06.07.08**

**Enabling Lithium Metal Anode in Non-Flammable Phosphate Electrolyte with Electrochemically-Induced Chemical Reactions** Haochuan Zhang, Jingru Luo, Miao Qi, Haoyi Li and Qi Dong; Boston College, United States

Lithium metal anode holds great promise in the next-generation battery but it suffers from great challenges in efficiency and safety. Previous research has developed various methods to mitigate these issues but most of them are still based on traditional flammable electrolyte systems. Here we demonstrate that reversible Li plating/stripping process, which cannot be implemented in non-flammable phosphate electrolyte previously, can be realized by introducing oxygen as an additive in triethyl phosphate (TEP) electrolyte. The symmetric Li||Li cell can achieve more than 300 cycles at current density of 0.5 mA/cm<sup>2</sup> with O<sub>2</sub> existence. Mechanistic study reveals that the electrochemically induced chemical reactions between reactive O<sub>2</sub> species and TEP molecules alter the decomposition pathway of TEP. The possible products, Li<sub>3</sub>PO<sub>4</sub>/poly-phosphate thereby serve as beneficial SEI components to enable stable Li metal operation in non-flammable electrolyte. Demonstration of Li-O<sub>2</sub> and Li-ion battery also shows that it is promising to deploy phosphate-based electrolyte in future high-energy density batteries efficiently and safely.

#### **F.EN06.07.11**

**Late News: A New Method for Evaluating Li-Ion Battery Anode Materials Based on Surface Compositional and Structural Characterization of Li Thermal Diffusion** Jozef Ociepa, Paige Harford, Ryan Charlinski, Guenevere O'Hara and Bart Checinski; OCI Vacuum Microengineering Inc., Canada

There is a global effort to develop safer lithium-ion batteries with a high energy density and long lifetime. Material properties, their mutual interactions, and active interfaces are key factors in battery performance. Popular methods involve the mixing of different ingredients and development of a suitable fabrication process. Significant effort has been spent to understand the reaction mechanism of battery materials, but this is very challenging due to high system complexity. Different techniques have been developed to follow these reactions, and most significantly, the reactions between Li and electrode materials. Our team has developed a new method to characterize Li thermal diffusion and structural interaction on the surfaces of potential anode and cathode materials. This method is based on surface crystallographic and compositional characterization of deposited ultra-thin film of Li on potential single crystal anode material. For surface crystallography we

are using Low Energy Electron Diffraction (LEED) and for composition Auger Electron Spectroscopy (AES). This characterization monitors Li diffusion into the electrode surface and changes in surface crystalline structure and composition providing data on Li interaction with the crystalline anode material structure. This dynamic interaction of Li is monitored at the nanoscale level and gives the direct response how Li atoms interact with the substrate. The diffusion of evaporated Li on single crystals of HOPG, Si(111)-(211)-(100), SiC-6H, Diamond and LiNbO<sub>3</sub> have been performed. The results shows that HOPG is the excellent reference substrate for this method as Li diffuses at room temperature and surface crystallography of HOPG remains unchanged. The structural reaction of Li with Si is very strong causing LEED pattern to disappear and there is no Li diffusion at room temperature. The data for SiC-6H and LiNbO<sub>3</sub> shows better Li diffusional behavior than on Si but not as good as on HOPG. This method of using a single crystal substrate and basic surface characterization techniques is providing simple nanoscale access into the chemical reactions between Li and the substrate material that will result in better understanding of diffusional Li respond to high capacity anodes with new chemistry content.

#### **F.EN06.07.12**

**Late News: Structure and Electrochemistry of Transition Metal Substituted Lithium Vanadyl Phosphate for Lithium-Ion Batteries** Krystal J. Lee, Marc Francis V. Hidalgo, Yanxu Zhong, Mateusz Zuba, Natasha Chernova, Guangwen Zhou, Hao Liu and M.S. Whittingham; Binghamton University, United States

Li-ion intercalation compound enlisting multi-electron redox is a promising strategy to maximize the storage capacity of LIBs. Lithium vanadyl phosphate, LiVOPO<sub>4</sub>, is one such material that can intercalate up to two Li<sup>+</sup> ions per vanadium ion through the change in vanadium valence from V<sup>5+</sup> to V<sup>3+</sup>, which translates to a theoretical capacity of 305 mAh/g and an energy density above 900 Wh/kg. However, Li-ion intercalation in the high voltage region (V<sup>5+</sup>/V<sup>4+</sup>) is kinetically limited by the sluggish Li-ion diffusion, and thus impedes the use of LiVOPO<sub>4</sub> in practical applications. Transition metal substitution has been a technique used to enhance the performance of battery cathodes by changing its intrinsic properties and stabilizing the crystal structure. The goal of this work is to explore experimentally if substitution with chromium and niobium can enhance the electrochemical performance of LiVOPO<sub>4</sub>. X-ray diffraction and inductively coupled plasma atomic emission spectroscopy indicate the substituent is successfully incorporated into the structure. The effects of transition metal substitution on the crystal structure and the electrochemical performance of LiVOPO<sub>4</sub> will be discussed.

#### **F.EN06.07.13**

**Molybdenum Disulfide Anode of Lithium-Ion Battery for High Stability and Rate Capability** Chanho Park, Han S. Kang, Seung Won Lee, Hyeokjung Lee, Kyuho Lee and Cheolmin Park; Yonsei University, Korea (the Republic of)

Development of a lithium-ion battery (LIB) is of great interest with an anode based on transition metal dichalcogenide nanosheets due to their intrinsically high capacity. The stability of a LIB is, however, detrimental with the nanostructured MoS<sub>2</sub> anode resulting from the gradual decrease of electrical conductivity with time due to the re-stacking of the nanosheets. In this work, we present a novel MoS<sub>2</sub> anode with molecularly architecture graft polymer binder having functionalized groups, enabling the high stability of a LIB. The fluorinated graft polymer synthesized by one-step atomic transfer radical polymerization allows not only for exfoliating MoS<sub>2</sub> nanosheets in the liquid phase to guarantee the stable sheet-to-sheet separation by preventing re-aggregation but also for providing self-assembled ionic channels through which lithium ions in electrolyte readily reach close to the surface of the nanosheets. The electrochemical reduction of lithium ions efficiently occurs at the layered nanostructure of MoS<sub>2</sub> facilitated by the functionalized polymer binder, giving rise to a high-performance LIB with the high rate capability and stability. Our binary anode of MoS<sub>2</sub> nanosheets self-assembled with the graft polymer enables high cell capacity even without the requirement of conductive additives which are frequently employed for ensuring high conductivity and thus comparable cell capacity, making our approach one-step closer to commercial energy applications.

### **SYMPOSIUM F.EN07**

---

Innovative Materials and Cell Design, Processing and Manufacturing Strategies for Solid State Batteries  
November 21 - December 4, 2020

#### Symposium Organizers

Candace Chan, Arizona State Univ  
Hailong Chen, Georgia Institute of Technology  
Dina Fattakhova-Rohlfing, Universität Duisburg-Essen  
Jae Chul Kim, Stevens Institute of Technology

Symposium Support

**Bronze**  
Kleindiek Inc.

---

\* Invited Paper

SESSION F.EN07.08: Live Keynote I: Innovative Materials and Cell Design, Processing and Manufacturing Strategies for Solid State Batteries

Session Chairs: Candace Chan and Jae Chul Kim  
Wednesday Morning, December 2, 2020  
F.EN07

**11:30 AM \*F.EN07.02.01**

**Chemical and Mechanical Stability Issues at Electrolyte/Electrode Interfaces in Solid-State Batteries** Gerbrand Ceder<sup>1,2</sup>; <sup>1</sup>University of California, Berkeley, United States; <sup>2</sup>Lawrence Berkeley National Laboratory, United States

Stringent chemical and mechanical constraints apply to the interfaces in solid state batteries. They have to be (electro)chemically stable against the chosen electrode materials and applied potentials. In addition, they have to be tolerant to the various mechanical issues that occur in solid state batteries such as electrode swelling/shrinking, stress concentrations at current focusing areas etc. I will present the requirements for chemically stable interfaces between various cathode and electrolyte materials and discuss to what extent coatings can address chemical incompatibility. A repeated stripping and plating of a lithium metal anode presents significant challenges. I will present results from modeling to understand the interplay between current density, stress, and lithium growth through the electrolyte. Our results indicate that in good conductors the build-up of stress to the point that it fractures the electrolyte is unlikely, indicating that other mechanisms are responsible for lithium penetration through the solid electrolyte. We also find that conductivity of the solid electrolyte plays a central role in the mechanical reliability of a solid-state battery.

**12:30 PM \*F.EN07.01.01**

**All-Solid-State Batteries—Hype vs Reality** Y. Shirley Meng; University of California, San Diego, United States

All-solid-state batteries (ASSBs) have attracted enormous attention as one of the critical future technologies for safe and high energy batteries. With the emergence of many highly conductive solid electrolytes in recent years, the bottleneck is no longer Li-ion diffusion within the electrolyte. Instead, many ASSBs are limited by their low Coulombic efficiency, poor power performance, and short cycling life due to the high resistance at the interfaces within ASSBs. In this talk, I will highlight the complex characteristics of interphases, namely the composition, distribution, and electronic and ionic properties of the cathode–electrolyte and electrolyte–anode interfaces. We emphasize the significant role of chemo-mechanical behavior of the interfaces, especially when the ASSBs under constant stack pressure. Multiscale and multimodal characterization methods to explore, diagnose, and understand the dynamic and buried interfaces and interphases are essential to pave the pathway for practical high-energy ASSB.

SESSION F.EN07.09: Live Keynote II: Innovative Materials and Cell Design, Processing and Manufacturing Strategies for Solid State Batteries

Session Chairs: Candace Chan and Jae Chul Kim  
Thursday Morning, December 3, 2020  
F.EN07

**8:00 AM \*F.EN07.02.03**

## **From Bonding Interactions in Solid Electrolytes to Solvent-Influences on the Performance of Solid-State Batteries** Wolfgang Zeier; University of Muenster, Germany

The advent of solid-state batteries has spawned a recent increase in interest in lithium conducting solid electrolytes, especially in the lithium thiophosphates. However, many open questions remain when trying to optimize electrolytes and understand solid state battery chemistries.

In this presentation, we explore the influence of inductive effects in superionic conductors showing that in  $\text{Li}_{10}\text{GeP}_2\text{S}_{12}$ , these can strongly affect the ionic transport.

We further show a better understanding of the structure-transport properties of the novel lithium and sodium rare-earth halides that show promising ionic conductivities for their use in solid state batteries.

Lastly, we show how solvent treatment of the lithium argyrodite  $\text{Li}_6\text{PS}_5\text{Cl}$  affects battery performance despite having no influence on the structural stability, suggesting stronger influences of slurry processing than previously believed.

### **9:00 AM \*F.EN07.01.04**

**Towards a Fast Charging 4 V Class All-Solid-State Battery** Corsin Battaglia; Empa-Swiss Federal Laboratories for Materials Science and Technology, Switzerland

All-solid-state batteries combining an alkali metal anode and a high-voltage cathode have the potential to achieve high energy density. However, interface stability remains a major challenge. On the anode side, dendrite formation limits the maximum plating current density and prevents fast charging, while on the cathode side the limited oxidative stability of most solid electrolytes is a major challenge, especially when the battery is charged beyond 4 V.

Here we demonstrate that the critical current density for dendrite formation in the archetypical ceramic solid electrolyte  $\text{Na}\beta''$ -alumina is ten times higher than that measured on a garnet-type  $\text{Li}_7\text{La}_3\text{Zr}_2\text{O}_{12}$  electrolyte under equivalent conditions and reaches up to  $12 \text{ mA/cm}^2$  at room temperature [1]. Further, we show that above the melting temperature of sodium, a cumulative capacity of  $>10 \text{ Ah}$  of sodium can be plated and stripped at an enormous current density of  $1000 \text{ mA/cm}^2$  without dendrite formation [2].

On the cathode side, we have been developing hydroborate solid electrolytes reaching ionic conductivities  $>1 \text{ mS/cm}$  at room temperature [3]. We already demonstrated the integration of these electrolytes with a 3 V class cathode [4, 5], but recently managed to obtain stable cycling with a 4 V class cathode via a self-forming passivating interface [6]. Combined with their low gravimetric density  $<1.2 \text{ g/cm}^3$ , low toxicity, high thermal and chemical stability, stability vs lithium and sodium metal anodes, soft mechanical properties enabling cold pressing [4], compatibility with solution infiltration [7], and potential for low cost [8, 9], hydroborate electrolytes represent a promising option for the cathode side of a competitive future all-solid-state battery.

### **References:**

- [1] M.-C. Bay, M. Wang, R. Grissa, M. V. F. Heinz, J. Sakamoto, C. Battaglia, *Adv. Energy Mater.* 2019, 201902889
- [2] D. Landmann, G. Graeber, M. V. F. Heinz, S. Haussener, C. Battaglia, submitted
- [3] L. Duchêne, A. Remhof, H. Hagemann, C. Battaglia, *Energy Storage Mater.* 2020, 25, 782
- [4] L. Duchêne, R.-S. Kühnel, E. Stilp, E. Cuervo Reyes, A. Remhof, H. Hagemann, C. Battaglia, *Energy Environ. Science* 2017, 10, 2609
- [5] R. Asakura, L. Duchêne, R.-S. Kühnel, A. Remhof, C. Battaglia, *ACS Appl. Energy Mater.* 2019, 2, 6924
- [6] R. Asakura, D. Reber, L. Duchêne, A. Remhof, H. Hagemann, C. Battaglia, submitted
- [7] L. Duchêne, D. H. Kim, Y. B. Song, S. Jun, R. Moury, A. Remhof, H. Hagemann, Y. S. Jung, C. Battaglia, *Energy Storage Mater.*, 2020, 26, 543
- [8] A. Gigante, L. Duchêne, R. Moury, M. Pupier, A. Remhof, H. Hagemann, *ChemSusChem* 2019, 12, 4832
- [9] S. Payandeh, R. Asakura, P. Avramidou, D. Rentsch, Z. Lodziana, R. Cerny, A. Remhof, C. Battaglia, *Chem. Mater.* 2020, 32, 1101

SESSION F.EN07.10: Live Keynote III: Innovative Materials and Cell Design, Processing and Manufacturing Strategies for Solid State Batteries

Session Chairs: Candace Chan and Jae Chul Kim

Friday Morning, December 4, 2020

F.EN07

**11:30 AM \*F.EN07.01.02**

**Towards Solid-State Batteries for Electric Vehicles** Marca M. Doeff; Lawrence Berkeley National Laboratory, United States

All solid-state batteries with lithium anodes have the potential of outperforming lithium-ion batteries with respect to energy density, safety, and reliability. However, considerable challenges exist, particularly for ceramic-based electrolytes, with regards to their design for vehicle applications. The thin film configurations that currently exist have low practical energy densities, are difficult to scale, and require expensive vacuum technologies. To overcome these difficulties, we have been using a scalable freeze tape casting method to produce porous garnet scaffolds that can be co-sintered with thin, dense components to form bilayers. The scaffold is then infiltrated with active material and other components, and lithium is attached to the other side of the bilayer to form a cell. The use of a secondary soft electrolyte obviates the need for a co-sintering step, which carries with it the risk of adverse reactions between the active material and the garnet. Batteries prepared this way may be able to achieve specific energies in excess of 400 Wh/kg. We will discuss what still needs to be done to make this a reality.

SESSION F.EN07.01: New Developments in Solid State Batteries  
On Demand Abstracts Available for Viewing Starting Saturday Morning, November 21, 2020  
F-EN07

**5:00 AM \*F.EN07.01.01**

**All-Solid-State Batteries—Hype vs Reality** Y. Shirley Meng; University of California, San Diego, United States

All-solid-state batteries (ASSBs) have attracted enormous attention as one of the critical future technologies for safe and high energy batteries. With the emergence of many highly conductive solid electrolytes in recent years, the bottleneck is no longer Li-ion diffusion within the electrolyte. Instead, many ASSBs are limited by their low Coulombic efficiency, poor power performance, and short cycling life due to the high resistance at the interfaces within ASSBs. In this talk, I will highlight the complex characteristics of interphases, namely the composition, distribution, and electronic and ionic properties of the cathode–electrolyte and electrolyte–anode interfaces. We emphasize the significant role of chemo-mechanical behavior of the interfaces, especially when the ASSBs under constant stack pressure. Multiscale and multimodal characterization methods to explore, diagnose, and understand the dynamic and buried interfaces and interphases are essential to pave the pathway for practical high-energy ASSB.

**5:15 AM \*F.EN07.01.02**

**Towards Solid-State Batteries for Electric Vehicles** Marca M. Doeff; Lawrence Berkeley National Laboratory, United States

All solid-state batteries with lithium anodes have the potential of outperforming lithium-ion batteries with respect to energy density, safety, and reliability. However, considerable challenges exist, particularly for ceramic-based electrolytes, with regards to their design for vehicle applications. The thin film configurations that currently exist have low practical energy densities, are difficult to scale, and require expensive vacuum technologies. To overcome these difficulties, we have been using a scalable freeze tape casting method to produce porous garnet scaffolds that can be co-sintered with thin, dense components to form bilayers. The scaffold is then infiltrated with active material and other components, and lithium is attached to the other side of the bilayer to form a cell. The use of a secondary soft electrolyte obviates the need for a co-sintering step, which carries with it the risk of adverse reactions between the active material and the garnet. Batteries prepared this way may be able to achieve specific energies in excess of 400 Wh/kg. We will discuss what still needs to be done to make this a reality.

**5:30 AM \*F.EN07.01.03**

**Solid-State Lithium-Ion Battery with Mixed 2D and 3D Electrodes** David Ashby<sup>1</sup>, Christopher Choi<sup>2</sup>, Martin Edwards<sup>3</sup>, A. Talin<sup>1</sup>, Henry White<sup>3</sup> and Bruce S. Dunn<sup>2</sup>; <sup>1</sup>Sandia National Laboratories, United States; <sup>2</sup>University of California, Los Angeles, United States; <sup>3</sup>University of Utah, United States



It is well established that the miniaturization of batteries has not kept pace with the miniaturization of electronics. Three-dimensional (3D) batteries, which were developed with the intent of improving microbattery performance, have had limited success because of fabrication challenges and material constraints. Solid-state, 3D batteries have been particularly susceptible to these shortcomings, as conformal electrolytes for 3D configurations suffer from either having low conductivity or having interfacial reactions that lead to high electrolyte-electrode ionic resistances. In the work reported here, we overcome these solid electrolyte limitations by using an ionogel electrolyte, a subclass of solid electrolytes comprised of a room temperature ionic liquid electrolyte confined within an inorganic matrix. The high conductivity of the ionogel electrolyte ( $10^{-3}$  S cm<sup>-1</sup>) ensures sufficient ion transport for high power densities.

Rather than using a 3D geometry, we selected a different platform that not only demonstrates the benefit of a non-planar electrode configuration but also enables easier fabrication using established materials and processes. Specifically, we constructed a solid-state 2.5D battery consisting of a 3D LiFePO<sub>4</sub> (LFP) post array and a planar, Li anode separated by the ionogel electrolyte, which forms around the individual LFP posts and, while in the sol state, penetrates the 3D electrode array. The ability to process the ionogel as a liquid, which then gels to a macroscopic solid phase while maintaining the liquid-like behavior at the nanoscale, satisfies the conformality and wetting issues often required for complex electrode architectures. This 2.5D battery offers high areal energy densities from the post array while the high conductivity solid electrolyte enables high power densities (4 mWh cm<sup>-2</sup> at 2.8 mW cm<sup>-2</sup>). These values for the 2.5D solid-state microbattery exceed the energy and power densities of any 3D solid-state system. In addition, the battery exhibited minimal capacity loss when cycled at 0.5 mA cm<sup>-2</sup> over 50 cycles and complementary interfacial studies show that the 2.5D battery avoids the interface impedances which have limited other solid-state 3D battery systems. A multiphysics model derived for the 2.5D geometry provides guidance for achieving significantly higher energy and power densities.

**5:45 AM \*F.EN07.01.04**

**Towards a Fast Charging 4 V Class All-Solid-State Battery** Corsin Battaglia; Empa-Swiss Federal Laboratories for Materials Science and Technology, Switzerland

All-solid-state batteries combining an alkali metal anode and a high-voltage cathode have the potential to achieve high energy density. However, interface stability remains a major challenge. On the anode side, dendrite formation limits the maximum plating current density and prevents fast charging, while on the cathode side the limited oxidative stability of most solid electrolytes is a major challenge, especially when the battery is charged beyond 4 V.

Here we demonstrate that the critical current density for dendrite formation in the archetypical ceramic solid electrolyte Na $\beta$ -alumina is ten times higher than that measured on a garnet-type Li<sub>7</sub>La<sub>3</sub>Zr<sub>2</sub>O<sub>12</sub> electrolyte under equivalent conditions and reaches up to 12 mA/cm<sup>2</sup> at room temperature [1]. Further, we show that above the melting temperature of sodium, a cumulative capacity of >10 Ah of sodium can be plated and stripped at an enormous current density of 1000 mA/cm<sup>2</sup> without dendrite formation [2].

On the cathode side, we have been developing hydroborate solid electrolytes reaching ionic conductivities >1 mS/cm at room temperature [3]. We already demonstrated the integration of these electrolytes with a 3 V class cathode [4, 5], but recently managed to obtain stable cycling with a 4 V class cathode via a self-forming passivating interface [6]. Combined with their low gravimetric density <1.2 g/cm<sup>3</sup>, low toxicity, high thermal and chemical stability, stability vs lithium and sodium metal anodes, soft mechanical properties enabling cold pressing [4], compatibility with solution infiltration [7], and potential for low cost [8, 9], hydroborate electrolytes represent a promising option for the cathode side of a competitive future all-solid-state battery.

#### References:

- [1] M.-C. Bay, M. Wang, R. Grissa, M. V. F. Heinz, J. Sakamoto, C. Battaglia, *Adv. Energy Mater.* 2019, 201902889
- [2] D. Landmann, G. Graeber, M. V. F. Heinz, S. Haussener, C. Battaglia, submitted
- [3] L. Duchêne, A. Remhof, H. Hagemann, C. Battaglia, *Energy Storage Mater.* 2020, 25, 782
- [4] L. Duchêne, R.-S. Kühnel, E. Stilp, E. Cuervo Reyes, A. Remhof, H. Hagemann, C. Battaglia, *Energy Environ. Science* 2017, 10, 2609
- [5] R. Asakura, L. Duchêne, R.-S. Kühnel, A. Remhof, C. Battaglia, *ACS Appl. Energy Mater.* 2019, 2, 6924
- [6] R. Asakura, D. Reber, L. Duchêne, A. Remhof, H. Hagemann, C. Battaglia, submitted
- [7] L. Duchêne, D. H. Kim, Y. B. Song, S. Jun, R. Moury, A. Remhof, H. Hagemann, Y. S. Jung, C. Battaglia, *Energy Storage Mater.*, 2020, 26, 543
- [8] A. Gigante, L. Duchêne, R. Moury, M. Pupier, A. Remhof, H. Hagemann, *ChemSusChem* 2019, 12, 4832
- [9] S. Payandeh, R. Asakura, P. Avramidou, D. Rentsch, Z. Lodziana, R. Cerny, A. Remhof, C. Battaglia, *Chem. Mater.* 2020, 32, 1101

**6:00 AM \*F.EN07.01.05**

**Material Development and Manufacturing Strategies For Solid-State Batteries based on Sulfide Solid Electrolytes** Josh Buettner-Garrett; SolidPower, United States

Solid-state batteries have emerged as the most promising contender to displace conventional Li-ion batteries in applications such as electric vehicles with their potential for greater energy density and improved safety. In order to transition from hype to true disruptor however, significant performance, manufacturing, and cost advancements must still be demonstrated. The electrolyte is the most important component of a solid-state cell, and it must combine high conductivity with anode and cathode compatibility and allow for high-throughput cell production. Oftentimes, the highest conductivity sulfide electrolytes are compatible only with graphite or higher voltage LTO anodes which limits the energy density advantages of the solid-state cell. Likewise, most inorganic solid-state cells today require production methods such as high-temperature sintering or warm isostatic pressing that are not compatible with the Li-ion production infrastructure that has been critical in driving down costs in recent years.

Solid Power is addressing each of these challenges by combining its novel sulfide electrolytes with manufacturing that closely mirrors that of Li-ion mass production today. Solid Power has a truly all-solid material set based on electrolytes that deliver 2-9 mS/cm at room temperature with stability against both Li metal anodes and Ni-rich NMC cathodes. This presentation will cover key aspects of material design for solid-state cells with an emphasis on manufacturability. Solid Power's pilot roll-to-roll production line will be introduced along with performance of cells produced on the line. Solid Power is currently producing multi-layer pouch cells up to 20 Ah in capacity with an eye toward early electric vehicle qualification. The presentation will also include a discussion of low temperature performance, quick charge capability, and abuse testing.

SESSION F.EN07.02: Solid State Battery Interfaces

On Demand Abstracts Available for Viewing Starting Saturday Morning, November 21, 2020  
F-EN07

**5:00 AM \*F.EN07.02.01**

**Chemical and Mechanical Stability Issues at Electrolyte/Electrode Interfaces in Solid-State Batteries** Gerbrand Ceder<sup>1,2</sup>; <sup>1</sup>University of California, Berkeley, United States; <sup>2</sup>Lawrence Berkeley National Laboratory, United States

Stringent chemical and mechanical constraints apply to the interfaces in solid state batteries. They have to be (electro)chemically stable against the chosen electrode materials and applied potentials. In addition, they have to be tolerant to the various mechanical issues that occur in solid state batteries such as electrode swelling/shrinking, stress concentrations at current focusing areas etc. I will present the requirements for chemically stable interfaces between various cathode and electrolyte materials and discuss to what extent coatings can address chemical incompatibility. A repeated stripping and plating of a lithium metal anode presents significant challenges. I will present results from modeling to understand the interplay between current density, stress, and lithium growth through the electrolyte. Our results indicate that in good conductors the build-up of stress to the point that it fractures the electrolyte is unlikely, indicating that other mechanisms are responsible for lithium penetration through the solid electrolyte. We also find that conductivity of the solid electrolyte plays a central role in the mechanical reliability of a solid-state battery.

**5:15 AM \*F.EN07.02.03**

**From Bonding Interactions in Solid Electrolytes to Solvent-Influences on the Performance of Solid-State Batteries** Wolfgang Zeier; University of Muenster, Germany

The advent of solid-state batteries has spawned a recent increase in interest in lithium conducting solid electrolytes, especially in the lithium thiophosphates. However, many open questions remain when trying to optimize electrolytes and understand solid state battery chemistries.

In this presentation, we explore the influence of inductive effects in superionic conductors showing that in  $\text{Li}_{10}\text{GeP}_2\text{S}_{12}$ , these can strongly affect the ionic transport.

We further show a better understanding of the structure-transport properties of the novel lithium and sodium rare-earth halides that show promising ionic conductivities for their use in solid state batteries.

Lastly, we show how solvent treatment of the lithium argyrodite  $\text{Li}_6\text{PS}_5\text{Cl}$  affects battery performance despite having no

influence on the structural stability, suggesting stronger influences of slurry processing than previously believed.

#### 5:30 AM F.EN07.02.04

**Conformal Solid Electrolytes for Beyond Li-Ion Solid-State Batteries** [Ramsay B. Nuwayhid](#), Angelique J. Jarry, Alexander C. Kozen, Gary Rubloff and Keith E. Gregorczyk; University of Maryland, United States

We will discuss the development of Na-ion and K-ion conducting films using atomic layer deposition (ALD) and their progress towards nanoscale solid-state batteries (SSBs) based on more abundant alkali metals such as sodium and potassium. Building upon our achievement with 3D Li-ion SSBs<sup>1</sup>, the enabling feature of which was the development of a lithium phosphorus oxynitride (LiPON) solid-state electrolyte (SSE)<sup>2</sup>, we present two new solid electrolytes for Na-ion and K-ion batteries. The ALD process for these films can be generalized to involve the thermal reaction of the respective alkali *tert*-butoxide (XO<sup>t</sup>Bu, X = Li, Na, K) with diethylphosphoramidate (DEPA). The NaO<sup>t</sup>Bu-DEPA process produced a sodium phosphorus oxynitride (NaPON) film, analogous to its cousin LiPON. Surface analysis by X-ray photoelectron spectroscopy revealed that the NaPON (Na<sub>4</sub>PO<sub>3</sub>N) film closely resembled that of LiPON (Li<sub>2</sub>PO<sub>2</sub>N), containing similar atomic ratios (N/P = 1) and two nitrogen species (=N<sup>-</sup> and >N<sup>-</sup>), deeming their classification as phosphazenes.<sup>3</sup> However, the KO<sup>t</sup>Bu-DEPA process resulted in a potassium phosphate (KPO) film containing ~1% nitrogen and a considerable amount of carbon incorporation. Electrochemical analysis through electrochemical impedance spectroscopy (EIS) was employed to probe the materials ionic transport behavior. NaPON displayed an ionic conductivity of  $1.0 \times 10^{-7}$  S/cm at 25 °C and up to  $2.5 \times 10^{-6}$  S/cm at 80 °C, with an activation energy of 0.53 eV. The ionic conductivity and activation energy of NaPON are in close agreement with that of ALD LiPON and other ALD-fabricated Li-ion conductors. EIS measurements of KPO displayed a lower ionic conductivity of  $7.4 \times 10^{-9}$  S/cm at 25 °C, which is attributed to loss of nitrogen in the obtained structure. The NaPON and KPO ALD processes represent the first ALD synthesized Na-ion and K-ion conducting films. A holistic review of LiPON, NaPON, and KPO will be presented, ranging from their reaction mechanisms to their structure and ionic transport properties. Lastly, we will focus on the aim of obtaining a 3D Na-ion SSB enabled by the NaPON SSE. This includes consideration of the conformality of NaPON in nanoporous structures, electrochemical stability, and demonstration of planar Na-ion SSBs with thin-film electrodes.

1. Pearse, A.; Schmitt, T.; Sahadeo, E.; Stewart, D. M.; Kozen, A.; Gerasopoulos, K.; Talin, A. A.; Lee, S. B.; Rubloff, G. W.; Gregorczyk, K. E., Three-Dimensional Solid-State Lithium-Ion Batteries Fabricated by Conformal Vapor-Phase Chemistry. *ACS Nano* **2018**, *12* (5), 4286-4294.

2. Pearse, A. J.; Schmitt, T. E.; Fuller, E. J.; El-Gabaly, F.; Lin, C.-F.; Gerasopoulos, K.; Kozen, A. C.; Talin, A. A.; Rubloff, G.; Gregorczyk, K. E., Nanoscale Solid State Batteries Enabled by Thermal Atomic Layer Deposition of a Lithium Polyphosphazene Solid State Electrolyte. *Chemistry of Materials* **2017**, *29* (8), 3740-3753.

3. Nuwayhid, R. B.; Jarry, A.; Rubloff, G. W.; Gregorczyk, K. E., Atomic Layer Deposition of Sodium Phosphorus Oxynitride: A Conformal Solid-State Sodium-Ion Conductor. *ACS Applied Materials & Interfaces* **2020**, *12* (19), 21641-21650.

#### 5:40 AM F.EN07.02.05

**Reduction of Solid Electrolyte-Electrode Interfacial Impedance in Lithium-Ion Batteries Through a Buffer Layer** [Joseph Sullivan](#) and Arijit Bose; The University of Rhode Island, United States

Lithium ion batteries (LIBs) typically utilize organic liquid electrolytes, but their flammability often places limits on their use. Solid electrolytes may alleviate concerns regarding flammability, but the interfacial resistance between a solid electrolyte and an electrode is one major hindrance for their application. The introduction of a buffer layer at the electrode-electrolyte interface may reduce this resistance and improve battery performance. In this work, an acetonitrile containing buffer layer was introduced between a graphite anode and a PEO-LiTFSI electrolyte. This electrode was examined in a half-cell configuration. Impedance spectra for cells with and without the buffer layer were obtained at assembly and after three charge/discharge cycles. At assembly, the interfacial impedance of the cells with a buffer layer was reduced by 25% when compared to unbuffered cells, and it continued to decrease as the cells were cycled. Improved contact between the active material and electrolyte is a potential reason for the lowered interfacial impedance. The addition of a buffer layer shows promise towards the goal of making an all-solid LIB with acceptable electrochemical performance.

#### 5:50 AM F.EN07.02.06

**Substrate Strain Enhances the Reversible Cycling of Thin-Film Electrodes** Ananya Renuka Balakrishna and [Delin Zhang](#); University of Southern California, United States

Solid-state batteries have a potential to enhance energy density and offer greater safety when compared with the conventional

Li-ion batteries. However, a bottleneck with using a solid-state electrolyte lies in mechanically integrating the solid-state electrolyte with the active materials (electrodes). For example, inserting and extracting Li into electrode lattices expands electrode materials up to 10% in volume. These chemo-mechanical strains in the electrode induces misfit stresses at the electrode/electrolyte interfaces, which weaken the structural integrity and electrical conductivity of the battery material composite. In today's talk, we will show how epitaxial strains in thin-film electrodes can be engineered to deter delamination. We develop a continuum model to explore the interplay between phase-transformation microstructures and substrate strains in thin-film electrodes. We apply this model to the vanadium-oxide system, and show how tensile straining of electrodes deters delamination and enhances reversible cycling of electrode materials. We plot a “phase-diagram” for thin-film electrodes as a function of battery voltage and substrate strain—this plot identifies a narrow-range of electro-mechanical boundary conditions under which a thin-film electrode can be repeatedly cycled with minimum mechanical degradation. Broadly, our work provides a battery design framework to mechanically engineer electrodes, and to enhance battery safety and lifespan.

#### 6:00 AM F.EN07.02.07

**Effect of Gas Environment on Interfacial Degradation Between Al Doped  $\text{Li}_7\text{La}_3\text{Zr}_2\text{O}_{12}$  Electrolyte and  $\text{LiNi}_{0.6}\text{Mn}_{0.2}\text{Co}_{0.2}\text{O}_2$  Cathode** Younggyu Kim and Bilge Yildiz; Massachusetts Institute of Technology, United States

Conventional Li-ion batteries using liquid electrolytes suffer from inherent safety issues due to poor thermal stability of liquid electrolytes. Development of All-solid Li-ion Batteries by substituting liquid electrolytes to non-flammable solid electrolytes can solve this issue.  $\text{Li}_7\text{La}_3\text{Zr}_2\text{O}_{12}$  (LLZO) has been considered as a major candidate for making safe and high capacity cells due to its high ionic conductivity and chemical compatibility with Li anode. However, cathode side instability still needs to be overcome. Co-sintering is needed to gain good contact between cathode and LLZO, and to reduce contact resistances. However, this process leads to formation of detrimental Li-insulating interphases. Despite the computational studies on layered oxide cathode|LLZO predicting low chemical reactivity, many experimental studies including works from our group, show formation of detrimental secondary phases at the interface during sintering. Moreover, predicted decomposed phases do not match with experimental findings.

The discrepancy comes from the effect of gas environment, which was not addressed in former computational or experimental works. Recent works from our group addressed the detrimental role of the  $\text{CO}_2$  in the gas environment, on the interface stability of on  $\text{LiCoO}_2$ |LLZO,  $\text{LiNi}_{0.6}\text{Mn}_{0.2}\text{Co}_{0.2}\text{O}_2$ |LLZO interfacial stability.  $\text{Li}_2\text{CO}_3$  formed in both systems because of reaction with  $\text{CO}_2(\text{g})$  in ambient air. This is precursor to the formation of Li-deficient detrimental secondary phases such as  $\text{La}_2\text{Zr}_2\text{O}_7$  and La containing perovskite phases,  $\text{LaCoO}_3$ ,  $\text{La}(\text{Ni},\text{Co})\text{O}_3$ .

In this work, we systematically investigated effect of gas environment by annealing samples in pure  $\text{O}_2$ , humidified  $\text{O}_2$  ( $\text{O}_2$  with 2wt%  $\text{H}_2\text{O}$ ),  $\text{N}_2$ , and  $\text{CO}_2$  gas environments. Humidified  $\text{O}_2$  and  $\text{CO}_2$  environment were chosen to unravel effect of  $\text{H}_2\text{O}(\text{g})$  and  $\text{CO}_2(\text{g})$ . We chose  $\text{N}_2$  to investigate possibility of using it as a low-cost alternative for pure  $\text{O}_2$  environment. We deposited thin film (~100nm)  $\text{LiNi}_{0.6}\text{Mn}_{0.2}\text{Co}_{0.2}\text{O}_2$  on top of solid electrolyte by RF sputtering, and post-annealed samples to simulate the sintering process. The sample design placed interfacial region within detection depth of X-ray Absorption Spectroscopy. This thin film approach enabled us to detect the onset of interfacial degradation, even when formed secondary phases lack crystallinity. We correlated results from chemical characterization techniques (X-ray Absorption Spectroscopy, X-Ray Diffraction) with Electrochemical Impedance Spectroscopy to quantify the effect of interfacial degradation on cell performances.

The result showed that  $\text{O}_2$  environment enables the best stability, and actually improves the interface. Interfacial resistance decreased as annealing temperature increased in  $\text{O}_2$ , and interface remained chemically stable up to  $700^\circ\text{C}$ . Annealing in  $\text{N}_2$  environment also showed chemical stability up to  $700^\circ\text{C}$  as no secondary phases were observed. However, we could see slight reduction from the sample, showing that  $\text{N}_2$  environment is less favorable compared to pure  $\text{O}_2$ . We found that annealing at  $500^\circ\text{C}$  in humidified  $\text{O}_2$  led to hydration of the sample, causing interfacial resistance increase. However, we also observed interfacial resistance decrease along with dehydration at  $700^\circ\text{C}$ , showing that the detrimental effect of  $\text{H}_2\text{O}(\text{g})$  can be avoided with sufficiently high sintering temperature.  $\text{CO}_2$  environment was shown as most detrimental, as we observed total loss of cathode|electrolyte capacitance, together with major degradation products. This comparison concludes that avoiding  $\text{CO}_2$  is important for maintaining a well adhered cathode-LLZO interface that transfers Li ions fast.

We acknowledge funding from U.S. Army Research Office through Institute for Soldier Nanotechnologies. (Cooperative Agreement Number W911NF-18-2-0048)

#### 6:10 AM F.EN07.02.09

**Late News: Towards Enhanced Oxidative Stability for Na-Solid State Electrolytes via Halogenation—The Case of  $\text{Na}_4(\text{CB11H}_{12})_2\text{B}_{12}\text{Br}_{12}$**  Fabrizio Murgia<sup>1</sup>, Marc Nierstenhöfer<sup>2</sup>, Matteo Brighi<sup>1</sup>, Carsten Jenne<sup>2</sup> and Radovan Cerny<sup>1</sup>; <sup>1</sup>Université de Genève, Switzerland; <sup>2</sup>Bergische Universität Wuppertal, Germany

Seeking better performing solid-state electrolytes for post-Li batteries, complex hydride-based compounds have recently drawn attention thanks to several remarkable properties. They show chemical robustness and good thermal stability, but also superior oxidative stability and lower density with respect to oxides and sulphides.[1][2] Interestingly, such class of materials displays order-disorder phase transitions that dramatically increases the ionic conductivity, achieving superionic regime ( $\sigma > 1 \text{ mS cm}^{-1}$ ).[3] However, such rearrangement generally occurs far from room temperature (*rt*), thus limiting practical applications. Therefore, increasing the disorder in the structure to lower the phase transition towards ambient temperature is the key for further development. To do so, the combination of two different hydroborate salts can result in a new phase that decreases/suppresses the phase transition, achieving fast cation motion even at *rt*. [4]

Recently, electrochemical studies on a wide series of binary anion mixtures based on *closo*- and *carbacloso*-hydroborates pointed out that their oxidative stability is limited to the decomposition voltage of the less stable anion.[5] As an example, in the  $\text{Na}_4(\text{CB}_{11}\text{H}_{12})_2(\text{B}_{12}\text{H}_{12})$ , which shows the highest oxidative stability of the pool, the practical voltage window corresponds to the oxidation of the  $[\text{B}_{12}\text{H}_{12}]^{2-}$  cage.[6] It was already demonstrated that complete halogenation of a  $[\text{B}_{12}\text{H}_{12}]^{2-}$  leads to a framework less prone to the oxidation, thus potentially enhancing the overall electrochemical stability while employed in a solid-state conductor. On this basis, the novel phase  $\text{Na}_4(\text{CB}_{11}\text{H}_{12})_2\text{B}_{12}\text{Br}_{12}$  obtained by complete bromination of  $\text{Na}_2[\text{B}_{12}\text{H}_{12}]$  and subsequent solid-state high-energy ball-milling with  $\text{Na}[\text{CB}_{11}\text{H}_{12}]$  will be presented. DC conductivity at *rt* is found to be  $0.8 \text{ mS cm}^{-1}$ , while reaching  $2.2 \text{ mS cm}^{-1}$  at  $40^\circ\text{C}$ . Temperature-dependent electrochemical impedance spectroscopy reveals a non-Arrhenius behavior of the DC conductivity between  $-50^\circ\text{C}$  and  $150^\circ\text{C}$ , although without any conductivity jump due to order/disorder phase transition. Crystal structure analysis using temperature-dependent synchrotron powder diffraction will be also presented. The electrochemical characterization of the oxidative stability by means of slow-rate scan cyclic voltammetry evidenced a wide voltage window up to  $4.35 \text{ V vs. Na}^+/\text{Na}$ . Such improvement opens the gate to the use of high-voltage positive electrodes, such as  $\text{Na}_3\text{V}_2(\text{PO}_4)_2\text{F}_3$  (NVPF), thus achieving post-Li solid-state batteries with more competitive electrochemical performance.

[1] S. Kim, H. Oguchi, N. Toyama, T. Sato, S. Takagi, T. Otomo, D. Arunkumar, N. Kuwata, J. Kawamura, S. Orimo, *Nat. Commun.* 10 (2019) 1081.

[2] R. Asakura, L. Duchêne, R.S. Kühnel, A. Remhof, H. Hagemann, C. Battaglia, *ACS Appl. Energy Mater.* 2 (2019) 6924.

[3] W.S. Tang, M. Matsuo, H. Wu, V. Stavila, W. Zhou, A.A. Talin, A. V. Soloninin, R. V. Skoryunov, O.A. Babanova, A. V. Skripov, A. Unemoto, S.-I. Orimo, T.J. Udovic, *Adv. Energy Mater.* 6 (2016) 1502237.

[4] W.S. Tang, K. Yoshida, A. V. Soloninin, R. V. Skoryunov, O.A. Babanova, A. V. Skripov, M. Dimitrievska, V. Stavila, S. Orimo, T.J. Udovic, *ACS Energy Lett.* 1 (2016) 659.

[5] M. Brighi, F. Murgia, R. Cerny, *Cell Reports Phys. Sci.* 1 (2020) 100217.

[6] R.T. Boéré, J. Derendorf, C. Jenne, S. Kacprzak, M. Keßler, R. Riebau, S. Riedel, T.L. Roemmele, M. Rühle, H. Scherer, T. Vent-Schmidt, J. Warneke, S. Weber, *Chem. - A Eur. J.* 20 (2014) 4447.

#### 6:20 AM F.EN07.02.10

**Late News: Towards the Development of Air-Stable Li-La-Zirconate Based Solid Electrolyte Exhibiting Minimal Electrode/Electrolyte Interfacial Resistance for All-Solid-State Li-Ion Batteries** [Sushobhan Kobi](#), Amardeep Amardeep, Akhilesh Vyas, Parag Bhargava and Amartya Mukhopadhyay; Indian Institute of Technology Bombay, India

Despite being considered promising as a potential solid electrolyte for solid-state Li-ion batteries, Al-doped Li-La-Zirconate (LLZO) suffers from compositional/structural instability in the presence of moisture. In this regard, our prior work has indicated that the formation of  $\text{La}_2\text{Zr}_2\text{O}_7$  in the bulk (in addition to  $\text{Li}_2\text{CO}_3$  formation at surface) of Al-doped LLZO upon exposure to air leads to structural/mechanical instability and spontaneous cracking/disintegration due to the development of internal stresses [Kobi *et al.*; *J. Eur. Ceram. Soc.* 38 (2018) 4707]. This causes reduction in the Li-ion conductivity by at least  $\sim 3$  orders of magnitude within 3 weeks of exposure to air. In order to address this major problem, earth abundant Mg has been attempted as a dopant, fully or partially replacing the Al-dopant [Kobi *et al.*; *J. Electrochem. Soc.* 167 (2020) 120519, Amardeep *et al.*; *Scripta Mater.* 162 (2019) 214]. As has been realized, Mg-doping also allows stabilization of the desired cubic garnet phase at room temperature, leading to almost similar Li-ion conductivity as for Al-doped LLZO. More importantly, Mg-doping suppresses, in significant terms, the formation of deleterious phases and associated cracking upon long term exposure to air; thus causing no notable reduction in the Li-ion conductivity even after more than 3 weeks of air exposure. The outstanding air stability, concomitant absence of impurity phases at the surface and good Li-ion conductivity cast their influence also on the interfacial resistance at electrode/electrolyte interface. Thus, the optimized Al/Mg co-doped LLZO exhibits a very low area-specific resistance of  $\sim 18 \Omega \text{ cm}^2$ ; which is also among the lowest reported to-date, sans any additional surface/interfacial engineering.

#### 6:30 AM F.EN07.02.11

**Late News: An Investigation into Failure Mechanisms for a Novel Li-Ion Solid-State Electrolyte** [Tofunmi Ogunfunmi](#)<sup>1</sup>,

Nnaemeka Ebechidi<sup>2</sup>, Ridwan Ahmed<sup>1</sup>, Oluwaseun K. Oyewole<sup>1</sup>, John Obayemi<sup>1</sup> and Winston Soboyejo<sup>1,2,1</sup>; <sup>1</sup>Worcester Polytechnic Institute, United States; <sup>2</sup>African University of Science and Technology, Nigeria

Solid-state batteries are generally considered to be safer than their liquid-state counterparts due to their decreased potential for fire or short circuiting. The fabrication of solid-state batteries relies on the application of stack crimping pressure that increases the interfacial surface contacts between electrolytes and the electrodes. However, excessive compressive crimping stresses (that occur in cell assembly) can give rise to cracking phenomena that can degrade battery performance and lead to thermal runaway or failure. It is, therefore, important to develop an understanding of failure mechanisms in solid-state Li-ion electrolytes. In this paper, we use a combination of in-situ optical microscopy and Digital Imaging Correlation (strain mapping) techniques to study compressive deformation and cracking phenomena in a novel solid state Li-ion electrolyte. The stress states associated with the different stages of compressive deformation are also presented along with those due to charge-discharge cycles. The implications of the results are discussed for the material design of robust solid-state Li ion batteries.

SESSION F.EN07.03: Advanced Ceramic Processing for Solid State Batteries  
On Demand Abstracts Available for Viewing Starting Saturday Morning, November 21, 2020  
F-EN07

**5:00 AM \*F.EN07.03.01**

**Advancement of Low Temperature Ceramic Synthesis for Solid State Battery Components and Cells—A Personal Love Story** Jennifer Rupp; Massachusetts Institute of Technology, United States

Next generation of energy storage devices may largely benefit from fast and solid Li<sup>+</sup> ceramic electrolyte conductors to allow for safe and efficient batteries and fast data calculation. For those applications, the ability of Li-oxides to be processed as thin film structures and with high control over Lithiation and phases at low temperature is of essence to control conductivity. Through this presentation we review the field from a new angle, not only focused on the classics such as Li-ionic transport and electrochemical stability window for Li-solid state battery electrolytes, but focusing on opportunities and challenges routes in thermal and ceramic processing of the components and their assemblies with electrodes. Also, we will carefully review and give perspectives on the role of solid state battery ceramic strategies for the electrolyte on the electrode interfaces and towards charge transfer and vs. current densities. In other words, it will be a little ceramicist (own) love story on the good and the evil we can design by smart ceramic design at the interfaces originating by the very first choices made in the electrolyte ceramic structure and material design. In the second part of the talk we will discuss new opportunities on low temperature processing of solid state electrolyte ceramics that do not technically require “classic sintering” and avoid prior particle calcination; instead demonstrating opportunities to use liquid based direct densification routes and vacuum techniques to design solid electrolytes and grafting interfaces to new hybrid and solid state battery prototypes targeted at processing below 700C for all parts. Collectively, the insights on solid state energy storage provide evidence for the functionalities that those Li-solid state material designs can have for cost and mass manufacturable solid state and hybrid battery prototypes.

**References:**

1. A Low Ride on Processing Temperature for a Fast Li Conduction in Garnet Solid State Battery Films R Pfenninger, M. Struzik, I Garbayo, E Stilp, JLM Rupp, *Nature Energy*, 4, 475–483 2019, 2019
2. Lithium-Containing Thin Films JLM Rupp, R Pfenninger, M. Struzik, A Nanning, I Garbayo, *US 62/718,838* (2018)
3. Methods of Fabricating Thin Films Comprising Lithium-Containing Materials JLM Rupp, R Pfenninger, M. Struzik, A Nanning, I Garbayo, *US 62/718,842* (2018)
4. Glass-Type Polyamorphism in Li-Garnet Thin Film Solid State Battery Conductors I Garbayo, M Struzik, WJ Bowman, R Pfenninger, JLM Rupp, *Advanced Energy Materials*, 1702265 (2018)
5. Solid-state Electrolyte and Method of Manufacture Thereof. ZD Hood, Y Zhu, L Miara, JLM Rupp. *US 62/713,366* (2018)
6. Solution-Processed Solid-state Electrolyte and Method of Manufacture Thereof. Y Zhu, ZD Hood, L Miara, JLM Rupp *US 62/713,428* (2018)

**5:15 AM \*F.EN07.03.02**

**10 Seconds Ultrafast High Temperature Sintering (UHS) for High Performance Solid-State Electrolytes and Batteries** Liangbing Hu; University of Maryland, United States

We recently reported an ultrafast high temperature sintering (UHS) for solid state electrolytes (Science, 2020, May Cover). In this talk, I will discuss our progress in applying the UHS in the following various aspects for solid state batteries.

(1) *High-performance solid-state electrolyte*. The long sintering time of conventional syntheses can lead to Li loss in garnet SSEs caused by the evaporation of Li and the formation of secondary phases that lead to lower ionic conductivity. In contrast, the UHS technique enables us to tune the sintering time in units of seconds, which provides excellent control in terms of the Li content and grain growth. I will discuss our progress on applying UHS method to sintering various solid-state electrolyte, from compositions to microstructures. By programming the temperature and time (T-t), we can establish process diagrams to sinter porous vs. dense structures.

(2) *Printed thin film solid-state electrolyte*. I will talk about a solution-based printing process followed by rapid (~3 seconds) high-temperature (~1500 °C) reactive sintering for the fabrication of high-performance ceramic SSE films. The SSEs exhibit a dense, uniform structure and a superior ionic conductivity of up to 1 mS/cm, comparable to the bulk conductivity.

(3) Multilayer solid-state electrolyte and electrolyte-electrode co-sintering for solid state batteries. The rapid sintering also allows us to sintering multilayer solid-state electrolytes with significantly reduced interlayer diffusion.

A UMD spinoff, HighT-Tech LLC, is commercializing the above inventions ([www.highT-tech.com](http://www.highT-tech.com)).

### 5:30 AM F.EN07.03.03

**Ultrafast High-Temperature Sintering (UHS) Process for Solid State Electrolytes** Chengwei Wang and Liangbing Hu, University of Maryland, United States

Ceramic-based solid-state electrolytes (SSEs) are attractive materials for improving battery safety. To develop improved ceramic SSEs, computational predictions based on first principles methods can be a valuable tool in accelerating materials discovery. Experimental confirmation is essential after such predictions; however, materials screening rates are limited by the long processing time of conventional ceramic synthesis and sintering techniques, which are also prone to poor compositional control due to volatile element loss. To overcome these limitations in ceramic synthesis and processing, we report an ultrafast high-temperature sintering (UHS) process for the fabrication of ceramic materials by radiative heating that features a record-high temperature of up to 3,000 °C and an ultrafast heating rate of up to 100,000 °C/minute. The UHS method can directly sinter oxide precursors into solid, dense ceramics in seconds. Compared with previous fabrication techniques, the UHS process is >100–1000-times faster (e.g., reducing the sintering time from hours to ~10 s). As a result, we are able to achieve excellent compositional control of ceramics containing volatile components (e.g., Li in solid-state electrolytes), as well as prevent uncontrolled grain growth for outstanding material performance. Additionally, the UHS process provides excellent sintering at material interfaces with limited interdiffusion, which are essential for devices such as thin film batteries. Furthermore, this technique is compatible with 3D printing to produce novel ceramic structures and devices that are otherwise impossible to achieve by other rapid sintering methods. Finally, the UHS process is universal, allowing us to synthesize a wide range of new ceramic materials with novel composition and structure. This technique has the potential to transform and expand the discovery of ceramic compounds, with significant impacts for rapid materials screening and solid-state batteries.

### 5:40 AM F.EN07.03.05

**High Toughness Ceramic Nanocomposite Electrolytes** Christos E. Athanasiou, Mok Yun Jin, Cristina Ramirez, Nitin Padture and Brian Sheldon; Brown University, United States

The low fracture toughness of ceramic solid electrolytes can significantly limit battery performance and reliability. While small dimensions are generally needed for faster ion transport, these length scales also restrict the approaches that can be used to improve fracture resistance. Nanoscale reinforcements are thus a logical option for improving the fracture resistance of ceramic electrolytes. Reduced graphene oxide (rGO) and hexagonal boron nitride (hBN) have been successfully used to reinforce a variety of polymer and engineering ceramics, where significant changes in the elastic modulus and toughness have been obtained with relatively low volume fractions. In this talk, the reinforcement capability of small amounts of rGO and hBN added to oxide-based lithium-ion conductors will be discussed. Furthermore, a framework to assess the relevant toughening length scales and to provide guidelines for designing toughened solid electrolytes using nanomaterials will be presented.

### 5:50 AM F.EN07.03.06

**Thin-Film Microfabrication for High Performance 3D Solid-State Batteries** David M. Stewart, Haotian Wang, Victoria C. Ferrari, Keith E. Gregorczyk, Sangbok Lee and Gary Rubloff; University of Maryland, United States

Research from our Nanostructures for Electrical Energy Storage (NEES) Energy Frontier Research Center has shown that 3D architectures are key to enhanced performance in thin film batteries. As thin film processing and patterning have expanded to include battery materials, microfabrication is increasingly capable of creating high performance 3D solid state batteries (3D-SSBs). We have recently fabricated and studied two archetypal 3D-SSB designs: one employing multiple, coplanar battery layers and one using vertical channels of concentric batteries. Our experimental results validate the benefits of both 3D architectures for simultaneous high power and high energy.

Here we first summarize these results and highlight the distinctly different process sequences necessary for fabrication of the different 3D-SSBs. We then present new results from multiphysics modeling and simulation (COMSOL) that allow us to scale the energy and power metrics to different dimensions and configurations of the two designs. The electro-chemo-mechanical models also provide the basis for further examining the consequences of the 3D design. Calculations of the local stress distribution, Joule heating at high power, and transport properties at nano- and mesoscale will be shown. We find that although the physics is the same, the geometric differences play a large role in the ultimate performance of the 3D-SSBs.

These results indicate that 3D-SSBs may exceed the performance of conventional liquid electrolyte cells and also thin film solid-state batteries that use thick composite electrodes and sintered electrolytes, because thin film fabrication (1) enables designs optimized for simultaneous high power and energy and (2) minimizes excess and passive materials that do not contribute to performance. Results show that multilayer 3D thin film batteries can produce 2-3X higher energy density and 10X higher power density than conventional batteries. From these we share an emerging picture of cell design rules for further development of 3D-SSBs.

SESSION F.EN07.04: Polymer and Composite Electrolytes  
On Demand Abstracts Available for Viewing Starting Saturday Morning, November 21, 2020  
F-EN07

#### 5:00 AM \*F.EN07.04.01

**Polymer Electrolytes for Lithium-Ion and Future Emerging Battery Technologies** Julia Wellmann<sup>1</sup>, Junli Shi<sup>1</sup>, Tong Zhang<sup>1</sup>, Miaomiao Liang<sup>1</sup>, Ava Hosseinioun<sup>1</sup>, Balasubramanyian Rajagopalan<sup>1</sup>, Huu-Dat Nguyen<sup>2</sup>, Zhen Chen<sup>3</sup>, Dominik Steinle<sup>3</sup>, Xin He<sup>1</sup>, Jie Li<sup>4</sup>, Jean-Yves Sanchez<sup>5</sup>, Dominic Bresser<sup>3</sup>, Cristina Iojoiu<sup>2</sup> and Elie Paillard<sup>4</sup>; <sup>1</sup>Forschungszentrum Jülich GmbH, Germany; <sup>2</sup>Université Grenoble Alpes, France; <sup>3</sup>Karlsruhe Institute of Technology, Germany; <sup>4</sup>Politecnico di Milano, Italy; <sup>5</sup>University Carlos III de Madrid, Spain

Polymer gel electrolytes have been widely used in lithium-ion batteries since 1999, where they compete with liquid electrolytes. However, they do not fully qualify as solid-state electrolytes, since they are used in combination with separators and, despite common claims concerning safety, they are mostly used to improve the cohesion between battery elements and help the wetting of the separator onto which the polymers (usually PVDF-HFP) are coated. On the other hand, commercial lithium metal batteries use solvent-free (PEO-based) solid polymer electrolytes (SPEs) without any separator, but the operation temperature for automotive application of SPEs is limited to  $> 70^{\circ}\text{C}$  since the electrolyte is not sufficiently conductive at room temperature. Besides, solvent-free SPEs suffer from low anodic stability, which restricts the energy density of Li metal polymer batteries.

Research on SPEs has long been targeting single-ion conductors to prevent the establishment of concentration gradients and the resulting increase in electrolyte resistance and ultimately, the lithium depletion at metallic anodes, responsible for the fast growth of dendrites. However, until recently, these single-ion SPEs suffered from the same drawbacks as regular *salt-in-polymer* SPEs, with high operation temperatures and a limited anodic stability that prevents the use of high energy cathodes. On the other hand, studies on gel electrolytes are less clear regarding their aims, as they are often use unsubstantiated safety claims that are only fully valid for 'dry' SPEs.[1]

Thus, an overview of recent results on gel and polymer electrolytes for various types of batteries will be given. In particular, the use of non-fluorinated polymer matrixes such as crosslinked polymethacrylic acid (PMMA) to form gel electrolytes *in situ* for state-of-the-art lithium-ion batteries [2,3](or its fluorinated ionomeric version for forming crosslinked single-ion conductor gels) will be discussed. Besides, non-fluorinated and cheap ionomers such as lithium polyacrylate (LiPAA) were also proposed as *water-in-ionomer* electrolytes for high voltage aqueous lithium-ion batteries [4]. Finally, for next generation



lithium metal batteries, nanophase separated single-ion conductors membranes were easily processed from aromatic polyethersulfone block copolymers to allow high lithium plating current densities (*i.e.* 2 mA cm<sup>-2</sup> at 20°C) and to enable the operation of high voltage lithium metal battery down to 0°C. Finally, since PEO presents considerable advantages in terms of cathodic stability, especially critical for divalent cation batteries (*i.e.* Ca-metal) the strategies to allow for high voltage cathode operation in combination with PEO will be discussed as well.

#### Acknowledgments

The research has been partially done within the VIDICAT project, funded by the European Commission under GA n°829145 within the Horizon 2020 programme.

#### References

- [1] C. Iojoiu, E. Paillard, Polymer Electrolytes for Solid-State Lithium Batteries, in: S. Passerini, D. Bresser, A. Moretti, A. Varzi (Eds.), Encycloedia Electrochem. Sect. Batter., 2nd ed., Wiley-VCH Verlag, Weinheim, Germany, 2020: pp. XX–XX.
- [2] A. Hosseinioun, E. Paillard, In situ crosslinked PMMA gel electrolyte from a low viscosity precursor solution for cost-effective, long lasting and sustainable lithium-ion batteries, *J. Memb. Sci.* 594 (2020) 117456. doi:10.1016/j.memsci.2019.117456.
- [3] A. Hosseinioun, P. Nürnberg, M. Schönhoff, D. Diddens, E. Paillard, Improved lithium ion dynamics in crosslinked PMMA gel polymer electrolyte, *RSC Adv.* 9 (2019) 27574–27582. doi:10.1039/C9RA05917B.
- [4] X. He, B. Yan, X. Zhang, Z. Liu, D. Bresser, J. Wang, R. Wang, X. Cao, Y. Su, H. Jia, C.P. Grey, H. Frielinghaus, D.G. Truhlar, M. Winter, J. Li, E. Paillard, Fluorine-free water-in-ionomer electrolytes for sustainable lithium-ion batteries, *Nat. Commun.* 9 (2018) 5320. doi:10.1038/s41467-018-07331-6.

#### 5:15 AM \*F.EN07.04.02

**Long-Cycle-Life Solid-State Batteries with PVDF-Based Electrolytes** Liangliang Li, Xue Zhang, Chuanjiao Xue, Yang Shen and Cewen Nan; Tsinghua University, China

Solid-state lithium (Li) metal batteries based on solid polymer electrolytes are attracting a lot of interest due to good safety and high energy density. Among various polymer electrolytes, poly(vinylidene fluoride) (PVDF)-based electrolytes present higher ionic conductivity, large mechanical strength, and good electrochemical and thermal stability. In this talk, we will discuss the influence of (inorganic or organic) additives and residual solvent on the performance of the electrolytes as well as solid-state lithium metal batteries. A small amount of solvent [e.g., N,N-dimethylformamide (DMF)] is left in the electrolytes to bond with Li ions as Li-DMF complexes, not as free solvent, which could promote the Li-ion transport with the assistance of PVDF chains. Thus, by tuning the solvation effect and/or the synergistic effect with additives, the overall performance of the PVDF-based electrolytes including ionic conductivity, electrochemical stability window and stability against a Li anode can be significantly enhanced. With the fine-tuned PVDF-based electrolytes, the solid-state lithium metal batteries with a LiFeO<sub>4</sub> or LiCoO<sub>2</sub> cathode can possess a long cycle life of 1000 cycles and a high capacity retention at room temperature.

#### 5:30 AM F.EN07.04.03

**Pendent Polymer Electrolytes with Hydrocarbon Backbone and Li<sup>+</sup>-Conducting Side Chains** Yubin He, Nian Liu and Paul Kohl; Georgia Institute of Technology, United States

Solid polymer electrolytes (sPE) offer a pathway for safer, less flammable lithium batteries. However, developing a polymer that provides high Li<sup>+</sup> mobility as well electrochemical stability remains a challenge, because ion conductive functional units in the polymer main-chain (e.g., polycarbonate and polyether) usually suffer from poor electrochemical stability at high and low potentials. In the first part of this presentation, I will show our design and synthesis of an sPE with pendent carbonate on a hydrocarbon backbone, that has excellent conductivity and electrochemical stability simultaneously. This pendant polycarbonate is different from conventional polycarbonate electrolytes because the carbonate moiety is in the sidechain, which mitigates the stability problem of polycarbonate backbone while still providing high ionic conductivity when used with a plasticizer. Ionic conductivity as high as 1.1 mS/cm was obtained at 22°C. Stable lithium metal plating using and stripping using the sPE was observed for 1,200 hours and electrochemical stability up to 4.6 V vs Li<sup>+</sup>/Li has been demonstrated. The low interfacial resistance (<160 ohm cm<sup>2</sup> at 22°C) and reasonable ionic conductivity have enabled acceptable cycling performance in a Li-LiFePO<sub>4</sub> battery at 0.98 mA/cm<sup>2</sup> for 2,300 cycles. In the second part of this presentation, I will show our second-generation pendent polymer electrolyte with a block co-polymer structure, to enable facile tuning of the properties. This presentation is based on our recent publications:

1. Yubin He, Nian Liu, Paul Kohl. *Journal of the Electrochemical Society*, 2020, DOI: 10.1149/1945-7111/ab9759.
2. Yubin He, Nian Liu, Paul Kohl. *Journal of Power Sources*, under review

#### 5:40 AM F.EN07.04.04

**Ionic Conductivity Enhancement Induced by Crystallization Alignment in Polymer Electrolytes** Changhao Liu, Yangyang Wang, Jong Keum and Xi C. Chen; Oak Ridge National Laboratory, United States

Solid state electrolyte is the key component to enable the successful use of solid state lithium metal batteries. Poly(ethylene oxide) (PEO)-based solid polymer electrolyte is a promising candidate with advantages including flexibility, chemical stability, and compatibility with large-scale manufacturing<sup>1</sup>. However, PEO-based electrolytes have a relatively low room temperature conductivity, between  $10^{-9}$ - $10^{-5}$  S/cm, which is attributed to PEO crystallization<sup>1</sup>. The randomly oriented, non-conductive PEO crystalline lamellae increase the tortuosity of the conduction pathway and hinder ion transport in the amorphous phase<sup>2</sup>.

In this work, our objective is to improve the room-temperature ionic conductivity of PEO-based electrolytes by decreasing the tortuosity of the conduction pathway through alignment of the PEO crystalline phase. We use PEO/LiCF<sub>3</sub>SO<sub>3</sub> (EO to Li molar ratio is 16:1) as our model polymer electrolyte. In order to achieve alignment of the PEO crystalline phase, a hot-draw method is implemented for the first time to achieve the desired alignment of PEO lamellae. The polymer electrolyte film is heated to above PEO's melting temperature in N<sub>2</sub> environment followed by hot drawing till a desired strain is reached. The sample is then cooled down to room temperature to allow for crystallization with the strain maintained during the crystallization process. The hot-draw method enables a shape-stable membrane even after the tensile stress is released. Wide angle X-ray scattering (WAXS) experiments show that as the hot draw strain increases to 200%, the orientation of PEO's (120) and (032) planes are observed. As a result, the through-plane conductivity increases by over a factor of 2. The effect of hot draw strain, temperature, and crystallization rate will be discussed.

#### References

- (1) Zhao, Q.; Stalin, S.; Zhao, C.-Z.; Archer, L. A. Designing Solid-State Electrolytes for Safe, Energy-Dense Batteries. *Nat. Rev. Mater.* **2020**, *5* (3), 229–252. <https://doi.org/10.1038/s41578-019-0165-5>.
- (2) Cheng, S.; Smith, D. M.; Li, C. Y. Anisotropic Ion Transport in a Poly(Ethylene Oxide)–LiClO<sub>4</sub> Solid State Electrolyte Templated by Graphene Oxide. *Macromolecules* **2015**, *48* (13), 4503–4510. <https://doi.org/10.1021/acs.macromol.5b00972>.

#### 5:50 AM F.EN07.04.05

**Conditioning Hybrid Organic-Inorganic Solid Electrolytes for Improved Cation Mobility** Vazrik Keshishian and John Kieffer; University of Michigan, United States

Conventional lithium ion batteries that use liquid electrolytes are not very desirable due to lack of chemical stability, safety issues and cost of production. Solid state electrolytes (SSEs) not only have the potential to correct these drawbacks, but improve performance characteristics such as energy density and power density can also be improved. To simultaneously achieve high ionic conductivity and mechanical stiffness, a composite materials design approach for creating the novel SEEs is indicated. Here we report on our development of hybrid organic-inorganic electrolytes, in which a silica backbone is formed by sol-gel synthesis routes to provide a mechanically rigid backbone. The fluid in this nano-porous structure is subsequently replaced with polymer solutions. The polymer is grafted onto the backbone through reactive groups, and thus anchored into structure to establish the ion conducting phase. This unique approach allows us to decouple the influence of mechanical properties on ionic transport properties of materials and achieve both high elastic stiffness and ionic conductivity. Recently we discovered that the network structure of a gel-cast material can be further conditioned by influencing the structural evolution during drying, such as changing sample aspect ratio. This means of processing control appears to introduce a beneficial directionality in the structure that ensues. Here we will elucidate the structural developments that take place and how they lead to improved charge carrier mobility. Acknowledgment: NSF DMR-1610742

#### 6:00 AM F.EN07.04.06

**Solvent-Mediated Synthesis of Amorphous Li<sub>3</sub>PS<sub>4</sub>/PEO Composite Solid Electrolytes with High Li<sup>+</sup> Conductivity** Ethan C. Self<sup>1</sup>, Zachary Hood<sup>2</sup>, Teerth Brahmabhatt<sup>3</sup>, Frank M. Delnick<sup>1</sup>, Harry M. Meyer III<sup>1</sup>, Guang Yang<sup>1</sup>, Jennifer Rupp<sup>4</sup> and Jagjit Nanda<sup>1</sup>; <sup>1</sup>Oak Ridge National Laboratory, United States; <sup>2</sup>Argonne National Laboratory, United States; <sup>3</sup>The University of Tennessee, Knoxville, United States; <sup>4</sup>Massachusetts Institute of Technology, United States

A critical challenge for solid-state batteries (SSBs) is the development of solid electrolytes (SEs) with high Li<sup>+</sup> conductivity and good chemical/mechanical compatibility with Li metal anodes and high voltage cathodes. Crystalline  $\beta$ -Li<sub>3</sub>PS<sub>4</sub> (LPS) represents a promising SE candidate for next-generation SSBs due to its high ionic conductivity (e.g.,  $1.6 \times 10^{-4}$  S/cm at room temperature). However, a major bottleneck for this material is the lack of scalable processing methods to produce  $\beta$ -LPS films, which are typically fabricated using top-down approaches such as cold pressing. Furthermore, the nano-/polycrystalline structure of many LPS-based SEs leads to nonuniform current densities across the LPS/Li interface and Li

dendrite propagation during battery operation.

This presentation will discuss the synthesis and characterization of a new class of composite LPS/poly(ethylene oxide) (LPS/PEO) solid electrolytes which are completely amorphous and exhibit  $\text{Li}^+$  ionic conductivities up to  $1 \times 10^{-6}$  S/cm at room temperature. The presence of the PEO component facilitates the material's processability, and synthesis conditions can be tuned to suppress crystallization of the  $\beta$ -LPS phase at elevated temperature (140 – 200 °C). This presentation will describe how the structure (studied using cryo-TEM, vibrational spectroscopy, and neutron scattering) and composition of LPS/PEO composites impact their  $\text{Li}^+$  conductivity and viability for SSBs.

### Acknowledgements

This research is sponsored by the United States Department of Energy through the Office of Energy Efficiency and Renewable Energy (EERE) and Vehicle Technologies Office (VTO). A portion of this research was conducted at the Center for Nanophase Materials Sciences and Spallation Neutron Source, which are DOE Office of Science User Facilities.

SESSION F.EN07.05: Computational Modeling of Ionic Conductors  
On Demand Abstracts Available for Viewing Starting Saturday Morning, November 21, 2020  
F-EN07

### 5:00 AM \*F.EN07.05.01

**Data-Driven Discovery of New Materials for Solid-State Batteries** Yifei Mo; University of Maryland, United States

All-solid-state Li-ion battery based on solid electrolytes is a promising next-generation battery technology with high energy density, intrinsic safety, long cycle life, and wide operational temperatures. However, the lack of solid electrolyte materials that satisfy multiple requirements, such as high ionic conductivity, good stability, and interfacial compatibility with the electrode, are impeding the development of this new battery technology. To resolve these materials challenges, we develop and leverage an array of data-driven computation techniques including machine learning to discover and design novel solid-state Li-ion conductors as solid electrolytes for all-solid-state batteries. The data-driven approach enables rapid searching over a large materials space of tens of thousands of materials with highly diverse structures and chemistries. Dozens of novel solid-state conductors are discovered through our data-driven materials search. Our data-driven analyses provide unique insights into the fundamental understanding about solid-state Li-ion conductors beyond traditional physical mechanistic studies. Our study demonstrates a new paradigm of using machine learning techniques for materials discovery that overcome the data-scarcity challenges.

### 5:15 AM \*F.EN07.05.02

**Computational Materials Design for Solid-State Li and Na Ionic Conductors** Yan E. Wang<sup>1,2,3</sup>; <sup>1</sup>Samsung Research America, United States; <sup>2</sup>Massachusetts Institute of Technology, United States; <sup>3</sup>Lawrence Berkeley National Laboratory, United States

All-solid-state batteries are increasingly seen as essential for next-generation energy applications in consumer electronics and electric vehicles. Intense research effort has been devoted to designing safe, high energy density, long-life all-solid-state batteries. A major challenge has been to find solid electrolyte materials that can both support superionic conduction [1] and great interfacial stability against battery electrodes [2]. Sulfide-based solid-state electrolyte materials have demonstrated high ionic conductivity that exceeds the conductivity of liquid electrolytes. However, the stability of sulfides is rather limited and their instability and toxicity upon air or water exposure is a potential safety concern from battery industry's point of view. Oxide materials, on the other hand, have shown excellent air and electrochemical stability, but the ionic conductivity is generally lower than sulfide materials.

The ability of computational modeling based on density-functional-theory methods to accurately predict intrinsic properties of solid electrolyte materials has made modeling a critical tool for understanding the behavior of solid electrolytes and their integration in solid-state batteries [3]. Computational approaches have enabled the efficient design and discovery of new functional materials with desired properties, such as low cost, high alkali ionic conductivity, great phase and electrochemical stability, accelerating the development of all-solid-state batteries.

In this talk I will present recent findings in the physical and chemical design principles for solid-state electrolyte materials

with high ionic conductivity and stability with solid-state battery electrodes. More specifically, I will discuss crystallographic features in solid-state conductors which would enable fast ionic transport. I will also show progress of applying high-throughput screening in the computational design and discovery of lithium, sodium solid-state electrolytes and coating materials.

[1] Yan Wang *et al.*, “Design principles for solid-state lithium superionic conductors,” *Nature Materials* 14, 1026-1031, (2015).

[2] Y. Xiao, Y. Wang, S.-H. Bo, J. C. Kim, L. Miara, G. Ceder, “Understanding interface stability in solid-state batteries”, *Nature Review Materials* 5, 105-126 (2020).

[3] G. Ceder, S. Ong, Y. Wang, “Predictive modeling and design rules for solid electrolytes.” *MRS Bulletin*, 43(10), 746-751 (2018).

### 5:30 AM F.EN07.05.03

**Solid-State Chemistries Stable with High-Energy Cathodes for Lithium-Ion Batteries** Adelaide M. Nolan, Yunsheng Liu and Yifei Mo; University of Maryland, United States

The continued improvement in operating time and lifetime of electric vehicles and portable electronic devices require higher energy density in lithium ion batteries. The energy density of lithium-ion batteries can be increased by implementing high-voltage cathodes, but these cathodes are reactive and unstable during cycling with the electrolyte. To design coatings or solid electrolytes that can stabilize these cathodes, an understanding of how different chemistries interact with high-voltage cathodes is critically needed. We systematically evaluate the thermodynamic stability of a broad range of solid-state chemistries with common cathodes [1]. A materials trade-off is found in that materials stable with lithiated cathodes are often unstable with delithiated cathodes, which limits the possible choice of materials stable throughout the cycling voltage. These computational findings reaffirm previously demonstrated coating and solid electrolyte chemistries and suggest that several new chemistries, including lithium phosphates and lithium ternary fluorides, are promising solid-state chemistries stable with high-voltage cathodes. Our study provides guiding principles for designing coating and solid electrolyte materials with long-term stability with high-voltage cathodes for lithium-ion batteries.

[1] Nolan et al., *ACS Energy Lett.* 2019, 4, 2444–2451

### 5:40 AM F.EN07.05.04

**Accurate Machine-Learning Models for the Atomic-Scale Simulation of Doped LLZO Solid Electrolytes** Qian Wang<sup>1,2</sup>, Alexander Urban<sup>1</sup> and Nongnuch Artrith<sup>1</sup>; <sup>1</sup>Columbia University, United States; <sup>2</sup>Beijing University of Posts and Telecommunications, China

Cubic garnet structure  $\text{Li}_7\text{La}_3\text{Zr}_2\text{O}_{12}$  (LLZO) and doped LLZO show great promise as solid electrolytes for the next-generation solid-state Li-ion batteries due to their relatively high stabilities and bulk Li conductivities. The Li transport mechanism in the crystalline bulk structure of LLZO is well understood. However, the cell performance also depends critically on the Li transport in defected and non-crystalline LLZO phases that occur at grain boundaries or in the interphases near the electrodes. Characterizing Li transport in the narrow interphase regions is experimentally challenging, and the complex atomic structures of these phases also typically prevent first-principles modeling.

Here we develop a machine-learning (ML) model that enables the large-scale atomistic simulation of complex LLZO structures with near first-principles accuracy at a fraction of the computational cost. The model is based on an artificial neural network (ANN) potential trained on density-functional theory (DFT) reference data with an approach that we have previously developed [1-3], and it can be used to study the Li migration in crystalline and non-crystalline LLZO phases. The ANN potential has been constructed to describe defected LLZO and Al/Ga-doped LLZO compositions, since doping is needed to stabilize the cubic LLZO phase that exhibits good Li conductivity. The model is thoroughly validated by comparison with DFT calculations, confirming that our ANN potential is reliable for molecular dynamics simulations of complex LLZO structures with different Al/Ga dopant concentrations.

Our accurate and efficient LLZO ANN potential will form the basis of an extended ML approach for the modeling of grain boundaries, solid-electrolyte interphases, and cathode-electrolyte interphases in LLZO-based solid-state batteries.

[1] N. Artrith and A. Urban, *Comput. Mater. Sci.* **114** (2016) 135-150.

[2] N. Artrith, A. Urban, and G. Ceder, *Phys. Rev. B* **96** (2017) 014112.

[3] A. Cooper, J. Kästner, A. Urban, N. Artrith, *npj Comput. Mater.* **6** (2020) 54.

### 5:50 AM F.EN07.05.05

**Novel Solid-State Li-Ion Conductor by Computational Design and High-Throughput Screening** Wonseok Jeong<sup>1</sup>, Seungwu Han<sup>1</sup> and Youngho Kang<sup>2</sup>; <sup>1</sup>Seoul National University, Korea (the Republic of); <sup>2</sup>Incheon National University, Korea (the Republic of)

All-solid-state Li-ion batteries are receiving great attention because of various advantages such as enhanced safety, high energy density, and high durability. Up to date, several solid-state electrolytes (SSEs) including  $\text{Li}_{10}\text{GeP}_2\text{S}_{12}$ ,  $\text{Li}_7\text{La}_3\text{Zr}_2\text{O}_{12}$ , and  $\text{Li}_{1.3}\text{Al}_{0.3}\text{Ti}_{1.7}(\text{PO}_4)_3$  have been proposed from previous experiments or computational screening from publicly available materials databases. However, none of those SSEs are fully satisfactory due to insufficient ionic conductivity, chemical or mechanical instabilities.

In this work, using DFT calculations, we take one step further. Instead of simply exploring a pre-existing materials database, we carry out a large scale high-throughput screening of potential Li-ion conductors that can display the high ionic conductivity upon aliovalent substitution. Aliovalent substitution of the non-Li cation in Li compounds is known to enhance the ionic conductivity greatly, by enabling the diffusion of Li-ions to occur in a concerted manner.[1] Starting with 15,654 ternary compounds, we identify 436 materials to meet the various preliminary chemical, topological, and bandgap criteria. For these materials, we seek potential high-energy sites for extra Li ions that are introduced to compounds when an aliovalent substitution occurs, considering structural or local potential information. Then, we explicitly add Li-ions on the confirmed high-energy sites and evaluate their vibrational frequency to assess the smoothness of the potential energy surface (PES) on which the extra Li-ions will move. Based on several materials giving rise to low vibrational frequencies, i.e., smooth PES, we create the new crystal structures by substituting non-Li elements with lower valencies and adding extra Li-ions. Finally, we examine their Li-ion conductivities using ab-initio molecular dynamics simulations. As a result of the computational design and high-throughput screening, we suggest candidate SSEs, one of them are predicted to have high Li ionic conductivity of 19 mS/cm, the large bandgap of 6.8 eV, and the energy above hull as low as 9 meV/atom, which exceeds the performance of the state-of-the-art  $\text{Li}_{10}\text{GeP}_2\text{S}_{12}$ .

[1] Nat. Comm., 8, 1 (2017)

**6:00 AM F.EN07.05.06**

**Modeling the Electrical Double Layer at Solid-State Electrochemical Interfaces** Michael W. Swift<sup>1</sup>, James W. Swift<sup>2</sup> and Yue Qi<sup>1</sup>; <sup>1</sup>Michigan State University, United States; <sup>2</sup>Northern Arizona University, United States

Models of the electrical double-layer (EDL) at electrode/liquid-electrolyte interfaces no longer hold for all-solid-state electrochemistry. In this work, a new model for the EDL at a solid-state electrochemical interface based on the "Poisson-Fermi-Dirac equation" is formulated. By combining this model with density functional theory predictions, the interconnected electronic and ionic degrees of freedom in all-solid-state batteries, including the electronic band bending and defect concentration variation in the space-charge layer, are captured self-consistently. Along with a general mathematical solution, the EDL structure is presented in various materials that are thermodynamically stable in contact with a lithium metal anode: the solid electrolyte LLZO and the solid interlayer materials LiF,  $\text{Li}_2\text{O}$ , and  $\text{Li}_2\text{CO}_3$ . The model further predicts the optimum interlayer thicknesses to minimize the electrostatic barrier for lithium transport at relevant solid-state battery interfaces.

**6:10 AM F.EN07.05.07**

**Strain Effect on Li-Ion Conductivity of  $\beta\text{-Li}_3\text{PS}_4$  Assessed by *Ab Initio* Molecular Dynamics Study** Pjotr Zguns and Bilge Yildiz; Massachusetts Institute of Technology, United States

Electrochemo-mechanical strains are inherently present at electrode-electrolyte interfaces in solid-state Li-ion batteries. This originated from electrode expansion/contraction during battery charge/discharge, as well as volumetric changes due to interfacial reactions and electrolyte decomposition [1]. These strains reach ~3% (~10 GPa stresses) [1]. It is important to quantify how these strains affect Li-ion conduction, detrimental or beneficial, to understand their implication on battery performance. Here we investigate biaxial strain effect on Li-ion conductivity of bulk  $\beta\text{-Li}_3\text{PS}_4$ , sulfide solid-electrolyte, as a model system. We use Ab Initio Molecular Dynamics to quantify strain impact within elastic regime ( $\pm 2\%$ ). In response to biaxial strain, depending on the crystallographic-plane of strain ( $xy$ ,  $yz$ ,  $zx$ ) and temperature (550–650 K), Li-ion diffusivity can decrease or increase up to a factor of 2. Extrapolations to room temperature indicate that up to ~5-fold conductivity increase can be anticipated. This is comparable to impact of chemical doping and Li-off-stoichiometry in this material [2]. Atomistic mechanism behind the response of Li-ion diffusivity to strain is also being assessed, based on disorder and phonon modes [3].

[1] H.-K. Tian, A. Chakraborty, A.A. Talin, P. Eisenlohr and Y. Qi, Evaluation of The Electrochemo-Mechanically Induced Stress in All-Solid-State Li-Ion Batteries, *J. Electrochem. Soc.*, **167**, 090541, 2020

[2] N.J.J. de Klerk, E. van der Maas, and M. Wagemaker, Analysis of Diffusion in Solid-State Electrolytes through MD Simulations, Improvement of the Li-Ion Conductivity in  $\beta$ -Li<sub>3</sub>PS<sub>4</sub> as an Example, *ACS Appl. Energy Mater.*, **1**, 7, 3230–3242, 2018

[3] S. Muy, J.C. Bachman, L. Giordano, H.-H. Chang, D.L. Abernathy, D. Bansal, O. Delaire, S. Hori, R. Kanno, F. Maglia, S. Lupart, P. Lamph and Y. Shao-Horn, Tuning mobility and stability of lithium ion conductors based on lattice dynamics, *Energy Environ. Sci.*, **11**, 850-859, 2018

SESSION F.EN07.06: Materials for Solid State Batteries

On Demand Abstracts Available for Viewing Starting Saturday Morning, November 21, 2020

F-EN07

**5:00 AM \*F.EN07.06.01**

**Correlating Structure and Dynamics in Solid Electrolytes by NMR Spectroscopy** Sylvio Indris; Karlsruhe Institute of Technology, Germany

The correlation between structure and dynamics in different Li and Na solid electrolyte materials was investigated by a combination of different nuclear magnetic resonance (NMR) techniques, including magic-angle spinning NMR, temperature-dependent NMR lineshape analysis, NMR relaxometry, and field-gradient NMR. In that way, we are able to investigate the dynamics of Li or Na ions on different time scales from some nanoseconds to a few seconds, and thus we can observe the local hopping of these charge carriers as well as the long-range transport over several micrometers.

Some examples will be given for Li<sub>3</sub>PS<sub>4</sub>, Li<sub>6</sub>PS<sub>5</sub>Cl, Li<sub>0.29</sub>La<sub>0.57</sub>TiO<sub>3</sub>, and NASICON structures for Li and Na electrolytes [1-7]. The results of these NMR experiments are compared to those obtained by impedance spectroscopy and different diffraction techniques in order to obtain information about the diffusion pathways in these crystal structures and the energy landscapes probed by the mobile ions.

[1] H. Stöffler, T. Zinkevich, M. Yavuz, A.-L. Hansen, M. Knapp, J. Bednarčík, S. Randau, F. H. Richter, J. Janek, H. Ehrenberg, S. Indris, *J. Phys. Chem. C* **123**, 10280-10290 (2019).

[2] H. Stöffler, T. Zinkevich, M. Yavuz, A. Senyshyn, J. Kulisch, P. Hartmann, T. Adermann, S. Randau, F. Richter, J. Janek, S. Indris, H. Ehrenberg, *J. Phys. Chem. C* **122**, 15954-15965 (2018).

[3] M. Kaus, H. Stöffler, M. Yavuz, T. Zinkevich, M. Knapp, H. Ehrenberg, S. Indris, *J. Phys. Chem. C* **121**, 23370-23376 (2017).

[4] C. Dietrich, D. A. Weber, S. J. Sedlmaier, S. Indris, S. Culver, D. Walter, J. Janek, W. G. Zeier, *J. Mater. Chem. A* **5**, 18111-18119 (2017).

[5] T. Zinkevich, A. Fiedler, M. Guin, F. Tietz, O. Guillon, H. Ehrenberg, S. Indris, *Solid State Ionics* **348**, 115277 (2020).

[6] M. Kaus, M. Guin, M. Yavuz, M. Knapp, F. Tietz, O. Guillon, H. Ehrenberg, S. Indris, *J. Phys. Chem. C* **121**, 1449-1454 (2017).

[7] M. Guin, S. Indris, M. Kaus, H. Ehrenberg, F. Tietz, O. Guillon, *Solid State Ionics* **302**, 102-106 (2017).

**5:15 AM \*F.EN07.06.02**

**LGPS-Type Sulfide Solid Electrolytes** Ryoji Kanno, Satoshi Hori, Kouta Suzuki and Masaaki Hirayama; Tokyo Institute of Technology, Japan

All-solid-state is an ideal configuration of batteries. The solid electrolyte is a key technology for the development of all-solid-state batteries. Among the electrolytes proposed, the sulfide system is a candidate because of its high ionic conductivity. The LGPS (Li<sub>10</sub>GeP<sub>2</sub>S<sub>12</sub>) electrolyte exhibits a high bulk conductivity of over 10<sup>-2</sup> S cm<sup>-1</sup> at room temperature and is promising for applications requiring batteries with high power and energy densities [1]. Moreover, material variations of the LGPS electrolytes provided suitable combinations of the electrodes and the electrolyte. For example, the LGPS-group materials, such as Li<sub>9.54</sub>Si<sub>1.74</sub>P<sub>1.44</sub>S<sub>11.7</sub>Cl<sub>0.3</sub> and Li<sub>9.6</sub>P<sub>3</sub>S<sub>12</sub>, provided high power and high energy density to the all-solid-state cells [2]. These results derive from the intrinsic nature of the solid electrolytes, indicating the advantages of the all-solid-state devices over conventional electrochemical devices.

Systematic substitutions of the constituent elements were examined after the first report of Li<sub>10</sub>GeP<sub>2</sub>S<sub>12</sub>. The simplest substitution system was Si and Sn analogs. Solid solutions of the Ge-Si, Ge-Sn, and Si-Sn systems were examined. Among the substitution systems, the lithium tin-silicon system with Li<sub>10.35</sub>[Sn<sub>0.27</sub>Si<sub>1.08</sub>]P<sub>1.65</sub>S<sub>12</sub> showed high ionic conductivity which is comparable to the original LGPS material. On the other hand, the LGPS-type structure also appeared in the L-P-S ternary

system.  $\text{Li}_{9.6}\text{P}_3\text{S}_{12}$  with the LGPS-type showed high electrochemical stability which might be used for low potential ranges such as Li and carbon anode.

Partial substitution of the anion-site was studied for the halogen and oxygen systems. The oxygen and halogen substitution generally improved the electrochemical stabilities. The oxygen doped Li-P-S-O system showed higher electrochemical stability. Based on a wide composition range of the materials search, the LGPS materials were also found in the Li-A-P-S-X (A: Si, Ge, Sn, X: halogen) and Li-P-S-X (X: halogen) systems. For example,  $\text{Li}_{9.54}\text{Si}_{1.74}\text{P}_{1.44}\text{S}_{11.7}\text{Cl}_{0.3}$  showed the highest conductivity of  $25 \text{ mScm}^{-1}$  at room temperature. The halogen substitution systems of the L-P-S-X systems developed electrochemical stability.

The present study summarizes the materials varieties and formation ranges of the LGPS materials in these ternary and quaternary systems. In addition to the variety of the materials, the electrolyte-electrode combination which is another important parameter to achieve high battery characteristics is summarized. We also indicate the properties of the all-solid-state cells using these LGPS-type solid electrolytes with various anode and cathode systems.

## References

[1] N. Kamaya, K. Homma, Y. Yamakawa, M. Hirayama, R. Kanno, M. Yonemura, T. Kamiyama, Y. Kato, S. Hama, K. Kawamoto, A. Mitsui, *Nature Materials*, 10, 682 (2011).

[2] Y. Kato, S. Hori, T. Saito, K. Suzuki, M. Hirayama, A. Mitsui, M. Yonemura, H. Iba, R. Kanno, *Nature Energy*, 1, 201630, (2016).

<gdiv></gdiv>

## 5:30 AM \*F.EN07.06.04

**Understanding How Crystallographic Defects Govern the Charging Distribution in Solid Cathode Materials** Zhengrui Xu and Feng Lin; Virginia Tech, United States

Crystallographic defects exist in many redox active energy materials, e.g., battery and catalyst materials, which significantly alter their chemical properties for energy storage and conversion. In this presentation, we will address how these defects, e.g., grain boundaries and geometrically necessary dislocations, govern the charging distribution in solid layered oxide cathodes. The presentation will be divided into two sections, each addressing a specific defect type.

Architecting grain crystallographic orientation can modulate charge distribution and chemomechanical properties for enhancing the performance of polycrystalline battery materials. However, probing the interplay between charge distribution, grain crystallographic orientation, and performance remains a daunting challenge. Herein, we elucidate the spatially resolved charge distribution in lithium layered oxides with different grain crystallographic arrangements and establish a model to quantify their charge distributions. While the holistic “surface-to-bulk” charge distribution prevails in polycrystalline particles, the crystallographic orientation-guided redox reaction governs the charge distribution in the local charged nanodomains. Compared to the randomly oriented grains, the radially aligned grains exhibit a lower cell polarization and higher capacity retention upon battery cycling. The radially aligned grains create less tortuous lithium ion pathways, thus improving the charge homogeneity as statistically quantified from over 20 million nanodomains in polycrystalline particles. This study provides an improved understanding of the charge distribution and chemomechanical properties of polycrystalline battery materials.

Crystallographic defects, such as geometrically necessary dislocations, are reported to influence the redox reactions in battery particles through single-particle, multimodal, in situ synchrotron measurements. Through Laue X-ray microdiffraction, many crystallographic defects are spatially identified and statistically quantified from a large quantity of diffraction patterns in many layered oxide particles, including geometrically necessary dislocations, tilt boundaries, and mixed defects. The in situ and ex situ measurements, combining microdiffraction and X-ray spectroscopic imaging, reveal that  $\text{LiCoO}_2$  particles with a higher concentration of geometrically necessary dislocations provide deeper charging reactions, indicating that dislocations may facilitate redox reactions in layered oxides during initial charging. The present study illustrates that a precise control of crystallographic defects and their distribution can potentially promote and homogenize redox reactions in battery materials.

## 5:45 AM F.EN07.06.05

**LLZO: Al, Ta, Nb, W – Different Dopants and Their Effect on Microstructure and Lithium Diffusion** Charlotte A. Fritsch<sup>1</sup>, Anna-Lena Hansen<sup>1</sup>, Sylvio Indris<sup>1</sup>, Tatiana Zinkevich<sup>1</sup>, Michael Knapp<sup>1</sup>, Thomas Bergfeldt<sup>2</sup>, Volodymyr Baran<sup>3</sup> and Helmut Ehrenberg<sup>1</sup>; <sup>1</sup>Karlsruhe Institute of Technology, Germany; <sup>2</sup>Karlsruhe Institute of Technology, Germany; <sup>3</sup>Research Neutron Source FRM II, Germany

We investigated the influence of doping Al, Ta, Nb, W on structure and dynamics in LLZO. Using the dopants Nb or Ta yields cubic structured LLZO ( $\text{Li}_7\text{La}_3\text{Zr}_2\text{O}_{12}$ ) with highest ionic conductivities amongst this class of solid state electrolyte. In this study, we demonstrate that these dopants can cause a symmetry reduction in LLZO leading to its crystallization in a

different space group than usually considered: I-43d instead of Ia-3d. Neutron powder diffraction and  $^6\text{Li}$ -NMR are utilized to localize the Li atoms in these structures and the findings are compared to the structure of Al- and W-doped LLZO. The changes in the local structure arising from different occupations of the Li- and Zr-sites in each Al-, Nb-, Ta- or W-doped LLZO samples is evaluated with total scattering PDF analysis. The decrease of the crystal symmetry caused by Nb and Ta is supposed to have only minor influence on the bulk ionic conductivity. A 24-fold Li position splits into two 12-fold positions, so number and occupation of Li positions stays the same. To this end, impedance spectroscopic and temperature dependent  $^6\text{Li}$  NMR measurements are used to determine the Li ion conductivity. We provide evidence, that the structural differences indeed can be very well distinguished by diffraction and  $^6\text{Li}$  NMR. This enables us to deepen our understanding of the effect that doping / substitution has on the crystal lattice and thus the ionic conductivity.

#### 5:55 AM F.EN07.06.06

**Phase Behavior in NaSiCON Electrolytes and Electrodes** Zeyu Deng<sup>1</sup>, Sai Gautam Gopalakrishnan<sup>2</sup>, Christian Masquelier<sup>3</sup> and Pieremanuele Canepa<sup>1</sup>; <sup>1</sup>National University of Singapore, Singapore; <sup>2</sup>Princeton University, United States; <sup>3</sup>Universite de Picardie Jules Verne, France

The replacement of the presently used liquid electrolytes by a non-flammable solid electrolyte is an important avenue to create safer batteries. The Sodium Superionic CONductor (NaSiCON)  $\text{Na}_{1+x}\text{Zr}_2\text{Si}_x\text{P}_{3-x}\text{O}_{12}$  ( $0 < x < 3$ ) that displays high bulk ionic conductivity and good stability towards other NaSiCON-based electrodes is a good solid electrolyte in NaSiCON-based batteries. Despite the sizeable share of research on  $\text{Na}_{1+x}\text{Zr}_2\text{Si}_x\text{P}_{3-x}\text{O}_{12}$ , the structural and thermodynamic properties of NaSiCON require better understanding for more efficient synthesis and optimization as a solid electrolyte, which often follows chemical intuition. Here, we analyze the thermodynamic properties of the NaSiCON electrolyte by constructing the  $\text{Na}_{1+x}\text{Zr}_2\text{Si}_x\text{P}_{3-x}\text{O}_{12}$  phase diagram, based on density functional theory calculations, a cluster expansion framework, and Monte Carlo simulations. Specifically, we build the phase diagram as a function of temperature and composition ( $0 < x < 3$ ) for the high-temperature rhombohedral structure, which has been also observed in several positive electrode materials, such as  $\text{Na}_3\text{Ti}_2(\text{PO}_4)_3$ ,  $\text{Na}_3\text{V}_2(\text{PO}_4)_3$  and  $\text{Na}_3\text{Cr}_2(\text{PO}_4)_3$ . Through the phase diagram, we identify the concentration domains providing the highest  $\text{Na}^+$ -ion conductivity and previously unreported phase-separation behavior across three different single-phase regions. Further, we note the similarities in the phase behavior between  $\text{Na}_{1+x}\text{Zr}_2\text{Si}_x\text{P}_{3-x}\text{O}_{12}$  and other NaSiCON-based mono-transition metal electrodes and discuss the potential competition between thermodynamics and kinetics in experimentally observed phase separation. Our work is an important addition in understanding the thermodynamics of NaSiCON-based materials and in the development of inexpensive Na-ion batteries. From our results we propose that the addition of  $\text{SiO}_4^{4-}$  moieties to single-transition metal NaSiCON-phosphate-based electrodes will slow significantly the kinetics toward phase separation.

#### Reference

(1) Deng, Z.; Sai Gautam, G.; Kolli, S. K.; Chotard, J.-N.; Cheetham, A. K.; Masquelier, C.; Canepa, P.. Phase Behavior in Nasicon Electrolytes and Electrodes, 2020. <https://doi.org/10.26434/chemrxiv.12370334.v1>.

#### 6:05 AM F.EN07.06.07

**The Structure of the Amorphous Solid Electrolytes LiPON and LiSiPON** Andrew S. Westover<sup>1</sup>, Mordechai Kornbluth<sup>2</sup>, Jue Liu<sup>1</sup>, Nancy Dudney<sup>1</sup> and Andrew Kercher<sup>1</sup>; <sup>1</sup>Oak Ridge National Laboratory, United States; <sup>2</sup>Robert Bosch LLC., United States

The composition and structure of solid electrolytes are critical to their ability to enable the Li metal anode for high energy batteries. Perhaps the most successful solid electrolyte in terms of enabling the Li anode is the amorphous electrolyte lithium phosphorus oxynitride or LiPON. One of the most significant drawbacks of LiPON is the ionic conductivity is limited to  $\sim 3 \times 10^{-6}$  S/cm. Developing a solid electrolyte with the advantages of LiPON, but with higher ionic conductivity, could help improve solid-state Li metal batteries. There have been a few recent reports that Si-doped LiPON, or LiSiPON, can have an ionic conductivity of  $10^{-5}$  S/cm. In this work, we present a detailed modeling and experimental approach to characterize the structure of LiSiPON in comparison to that of LiPON. The first part of this work involves a careful look at ab-initio MD simulations of the materials. The addition of the Si increases the amount of O and N bridges between phosphate/silicate tetrahedra. These bridges have been linked to higher ionic conductivity in LiPON and could be the origin of the improved conductivity with Si doping. The second part of this work presents experimental neutron pair distribution functions. The first key result of the neutron scattering is the agreement between the experimental and simulated pair distribution functions. The neutron scattering also shows that both LiPON and LiSiPON have a pseudocrystalline repeating structure with a periodicity of  $\sim 2.3$  Å.



## 6:15 AM F.EN07.06.11

**Challenges for All-Solid-State-Batteries Based on Argyrodite-Type Solid Electrolyte** Xavier Randrema<sup>1,2</sup>, Mohamed Chakir<sup>1</sup>, Virginie Viallet<sup>2</sup> and Mathieu Morcrette<sup>2</sup>; <sup>1</sup>Renault, France; <sup>2</sup>Laboratoire de Réactivité et Chimie des Solides, France

The rapid growth of electric mobility is characterized by a strong interest of academic and industrial research laboratories on the so-called “All-Solid-State-Batteries”. Indeed, conventional commercialized batteries are based on liquid electrolyte composed by flammable compounds. The first target of solid-state technology is thus to solve concerns regarding safety issue for the more and more numerous users of electric vehicle. In addition, promising energy density ( $\text{Wh.kg}^{-1}$  and  $\text{Wh.l}^{-1}$ ) superior to conventional lithium-ion batteries are supposed thanks to the use of lithium metal as anode material ( $3860 \text{ mAh.g}^{-1}$ ). Solid electrolytes and particularly sulfide-based solid electrolyte have attracted attention because they present low temperature operation and a high ionic conductivity allowing fast charge application if lithium dendrites<sup>(1)</sup> can be solved. Among these, the  $\text{Li}_6\text{PS}_5\text{Cl}$  Argyrodite (space group ) discovered in 2008<sup>(2)</sup> is the subject of many recent studies due to its simplicity to obtain by mecano-synthesis<sup>(3)</sup> as well as a high ionic conductivity up to  $3 \text{ mS.cm}^{-1}$  at room temperature<sup>(4)</sup>. This material seems promising for its use in composite electrodes, but also in separator for all-solid-state-batteries made by dry or by wet process<sup>(5)</sup>. Nevertheless, intrinsic chemical instabilities<sup>(6)</sup> and decomposition reactions by contact with active material lead to electrochemical performances below expectations. Moreover, an industrial lock to solid-state technology development is the difficulty to produce those batteries on current Li-ion production lines based on slurry coating processes<sup>(7)</sup>.

In this work, we were first interested in the deep characterization of solid electrolyte only, to assess structure and ionic conductivity of the material. In a second time, the electrochemical stability of the phase was tested by galvanostatic cycle in order to verify the electrochemical window recently proposed by Wagemaker’s team. Then, all solid-state cells were assembled by dry mix to prove solid electrolyte viability in batteries. Finally, a wet process approach will be discussed in order to match with industrial prospects. First, a protocol of active material tuned with solid electrolyte will be introduced, showing intimate contacts between particles and enhanced  $\text{Li}^+$  percolation network. Secondly, preliminary results with slurry composed of tuned active material, carbon additive and binder coated on current collector using doctor-blade method will be presented. The goal of resulting all-solid-state cells is to give a concrete and practical example about solid-state technology in order to assess its industrial development possibility.

### References

- (1) J. Kasemchainan, S. Zekoll, D. Spencer Jolly, Z. Ning, G. O. Hartley, J. Marrow, and P. G. Bruce, *Nature Materials*, 18 (2019) 1105.
- (2) H-J. Deiseroth, S-T Kong, H. Eckert, J. Vannahme, C. Reiner, T. Zaiß, and M. Schlosser, *Angewandte Chemie*, 120 (2008) 767.
- (3) S. Boulineau, M. Courty, J-M. Tarascon, and V. Viallet, *Solid State Ionics*, 221 (2012) 1.
- (4) S. Wang, Y. Zhang, X. Zhang, T. Liu, Y-H. Lin, Y. Shen, L. Li, and C-W. Nan, *ACS Applied Materials Interfaces*, 10 (2018) 42279.
- (5) Y-J. Nam, D-Y. Oh, S-H. Jung, and Y-S. Jung, *Journal of Power Sources*, 375 (2018) 93.
- (6) T. Schwietert, V. Arszewska, C. Yu, C. Wang, A. Vasileiadis, N. de Klerk, J. Hageman, T. Hupfer, I. Kerkamm, Y. Xu, E. van der Maas, E. M. Kelder, S. Ganapathy, and M. Wagemaker, *Nature Materials*, (2020). (7) J. Schnell, T. Günthera, T. Knochea, C. Vieidera, L. Köhlera, A. Justa, M. Kellerb, S. Passerinib, G. Reinhart, *Journal of Power Sources*, 382 (2018) 160.

## 6:25 AM F.EN07.06.15

**Late News: Nido-Hydroborate Based Electrolytes for All-Solid-State Batteries** Seyedhosein Payandeh<sup>1</sup>, Ryo Asakura<sup>1,2</sup>, Daniel Rentsch<sup>1</sup>, Zbigniew Lodziana<sup>3</sup>, Petroula Avramidou<sup>1</sup>, Laurent Bigler<sup>4</sup>, Radovan Cerny<sup>2</sup>, Arndt Remhof<sup>1</sup> and Corsin Battaglia<sup>1</sup>; <sup>1</sup>Empa institute, Switzerland; <sup>2</sup>University of Geneva, Switzerland; <sup>3</sup>Polish Academy of Sciences, Poland; <sup>4</sup>University of Zurich, Switzerland

*Closo*-hydroborates and *carba-closo*-hydroborates recently emerged as a promising, yet costly class of solid electrolytes for all-solid-state batteries.[1-4] Here, we introduce *nido*-hydroborates,  $\text{MB}_{11}\text{H}_{14}$  ( $\text{M} = \text{Li}, \text{Na}$ ), with open cage-like structures as a new building block for solid electrolytes. We synthesized and purified  $\text{MB}_{11}\text{H}_{14}$  ( $\text{M} = \text{Li}, \text{Na}$ ) starting from  $\text{NaBH}_4$  as a cost-effective chemical feedstock.[5] Two-dimensional (2D) nuclear magnetic resonance combined with mass spectrometry techniques were used to analyze the structure of the new building blocks. High Li/Na ionic conductivity of up to  $> 1 \text{ mS/cm}$  at  $25^\circ\text{C}$  is achieved by combining *nido*- with *closo*/ *carba-closo*-hydroborates into cubic unit cells. Crystal structures are solved and refined using X-ray diffraction and density functional theory. Cyclic voltammetry reveals electrochemical stability of  $\sim 2.6 \text{ V}$  vs  $\text{Li}^+/\text{Li}$  or  $\text{Na}^+/\text{Na}$ , respectively. Galvanostatic cycling in symmetrical cells with lithium or sodium metal electrodes shows only a small overpotential increase after  $> 500$  cycles at  $50 \mu\text{A/cm}^2$ . These results demonstrate that despite

the thermodynamic instability of *nido*-hydroborates versus metallic anodes, stable interfaces are formed and the electrolytes were successfully employed in half cells using TiS<sub>2</sub> as cathode active material. Finally, we discuss routes to synthesize *carba-closo*-hydroborates from *nido*-hydroborate precursors by closing the cage with a carbon atom, opening a way for the cost-efficient synthesis of hydroborate-based solid-state electrolytes for Li/Na batteries.

[1] L. Duchêne, A. Remhof, H. Hagemann and C. Battaglia, *Energy Storage Mater.*, 2020, 25, 782–794.

[2] L. Duchêne, D. H. Kim, Y. B. Song, S. Jun, R. Moury, A. Remhof, H. Hagemann, Y. S. Jung and C. Battaglia, *Energy Storage Mater.*, 2020, 26, 543–549.

[3] F. Murgia, M. Brighi and R. Černý, *Electrochem. commun.*, 2019, 106, 106534.

[4] L. Duchêne, R.-S. Kühnel, E. Stilp, E. Cuervo Reyes, A. Remhof, H. Hagemann, C. Battaglia, *Energy Environ. Sci.*, 2017, 10, 2609–2615

[5] S. Payandeh, R. Asakura, P. Avramidou, D. Rentsch, Z. Lodziana, R. Cerny, A. Remhof and C. Battaglia, *Chem. Mater.*, 2020, 32, 1101–1110.

### 6:35 AM F.EN07.06.16

#### Late News: Charge Compensation and Ionic Conductivity in the (MgCoCuNiZn)<sub>1-x</sub>Li<sub>x</sub>O<sub>1</sub>- High Entropy

**Oxides** Nicolas Osenciat<sup>1</sup>, David Bérardan<sup>1</sup>, Diana Drago<sup>1</sup>, Brigitte Léridon<sup>2</sup>, Stéphane Holé<sup>2</sup>, Arun-Kumar Meena<sup>1</sup>, Sylvain Franger<sup>1</sup> and Nita Drago<sup>1</sup>; <sup>1</sup>Université Paris-Saclay, France; <sup>2</sup>École supérieure de physique et de chimie industrielles de la ville de Paris, France

A new class of materials has been discovered in 2015 [1], the high entropy oxides, which expand to ionic compounds the concept of High Entropy Alloys. The particularity of these materials is their stabilisation at high temperature by their entropy of configuration, that predominant in their total Gibbs Energy, given by Eq. (1):

$$(1) \Delta_r G = \Delta_r H - T \Delta_r S$$

To obtain an entropy-stabilized oxide, by maximizing their configurational entropy, we need to mix, at least, 5 binary oxides in equimolar proportions and heat them above a critical temperature (corresponding to  $\Delta_r G = 0$ ), followed by quenching to freeze the structure at room temperature. In these conditions, they form a solid metastable simple crystal structure where the cations are randomly dispersed on the cationic sublattice.

First studies, performed in our lab, have shown the large possibilities of composition by substituting cations or modulating their ratio from the initial formula (MgCoNiCuZn)O when keeping the charge balance between cations and anions (M<sup>2+</sup> and O<sup>2-</sup>) [2] and their very promising properties such as their colossal dielectric constant [2] and their alkali conductivity (Li<sup>+</sup> and Na<sup>+</sup>) [3]. These specificities make them promising candidates for solid-state electrolytes.

With the ambition to improve the ionic conductivity of Li<sup>+</sup> in these compounds, currently 1 mS.cm<sup>-1</sup> at room temperature in (MgCoNiCuZn)<sub>0.7</sub>Li<sub>0.3</sub>O [3], we have studied the (MgCoNiCuZn)<sub>1-x</sub>Li<sub>x</sub>O series to understand the charge compensation mechanisms that occur when Li<sup>+</sup> substitutes a 2+ element. Thanks to X-Ray Diffraction, coupled to thermogravimetric analysis and X-ray photoelectron spectroscopy, we found out that, for low fraction of Li<sup>+</sup>, compensation involves a partial oxidation of Co<sup>2+</sup> into Co<sup>3+</sup> and then, for large fractions of Li<sup>+</sup>, a combination of cobalt oxidation and a formation of oxygen vacancies [4].

[1] C.M. Rost et al., *Nature Communications*. 6, 8485, 2015

[2] D. Bérardan et al., *Physical Status Solidi RRL* 10, 328, 2016

[3] D. Bérardan et al., *Journal of Materials Chemistry A* 4, 9536, 2016

[4] N. Osenciat, et al.. *Journal of the American Ceramic Society*. 2019; 102: 6156– 6162

### 6:45 AM F.EN07.06.17

**Late News: Influence of Structural Distortion and Lattice Dynamics on Li-Ion Diffusion in Li<sub>3</sub>OCl<sub>1-x</sub>Br<sub>x</sub> Superionic Conductors** Ronghan Chen, Zhenming Xu and Hong Zhu; Shanghai Jiao Tong University, University of Michigan – Shanghai Jiao Tong University Joint Institute, China

The antiperovskite superionic conductors Li<sub>3</sub>OCl and Li<sub>3</sub>OBr show great differences in ionic conductivity. The more polarizable Li<sub>3</sub>OBr shows a lower ionic conductivity than Li<sub>3</sub>OCl, contradicting the idea that more polarizable framework is beneficial to achieving high ionic conductivity. In this work, we study the influence of substituting Cl with Br on the local

structure, lattice dynamics and Li ionic conductivity of  $\text{Li}_3\text{OCl}_{1-x}\text{Br}_x$ , based on first-principles calculations. We find that the incorporation of Br does soften the overall lattice stiffness of  $\text{Li}_3\text{OCl}_{1-x}\text{Br}_x$ , but the accompanied local structural distortion plays a dominant role on changing the activation energy for Li diffusion, which could increase the site energy as well as the Li ion vibration frequency. We suggest that the more distorted initial octahedral site and less distorted saddle trigonal-plane site lead to better ionic transport. In addition, the correlation between the activation energy and the pre-exponential factor of diffusivity extracted from Arrhenius plot of  $\text{Li}_3\text{OCl}_{1-x}\text{Br}_x$  is found to be nonlinear, which is due to the decreasing migration entropy with increasing activation energy.

#### 6:55 AM F.EN07.06.18

**Late News: Mixed-Anion Na-Hydroborates as New Class of Solid Electrolytes** Matteo Brighi, Fabrizio Murgia and Radovan Cerny; University of Geneva, Switzerland

Li- and Na-based hydroborates are known for their high ion dynamic, leading to liquid-like cation mobility after an order-disorder phase transition, suggesting their use as solid electrolytes for all-solid batteries.<sup>[1,2]</sup> However this transition takes place at elevated temperature, outside the typical operation range of a conventional battery.<sup>[3-5]</sup>

A systematic study on Na-based *closo*borates and carba-*closo*borates has been conducted by means of anion mixing, in order to stabilize room temperature Na-conducting phases, relying on increased structural disorder. The effect of such mixing is the suppression of any phase transition, leading to six novel Na-conductors with a Na-conductivity close to  $1 \text{ mS cm}^{-1}$  at room temperature.

Due to the three-dimensional aromatic nature of the boron cage, *closo*borates are among the more robust available polyanions;<sup>[6,7]</sup> the six presented phases are indeed thermodynamically stable in the investigated temperature range  $100 < T < 700 \text{ K}$ , while depending from the mixture the electrochemical stability window varies from 3 to 4.1 V *versus*  $\text{Na}^+/\text{Na}$ , allowing their implementation in high-voltage next generation solid-state batteries.<sup>[8]</sup>

The physical/electrochemical properties of this family will be presented, with particular remark to the non-Arrhenius conductivity behavior, arising from the ion-ion interaction. Their flexibility, in terms of operating voltage window, allowed also to check their compatibility towards different class of cathode materials such as  $\text{NaCrO}_2$ <sup>[9,10]</sup>,  $\text{Na}_2\text{Fe}_2(\text{SO}_4)_3$ <sup>[11]</sup> and  $\text{Na}_3\text{V}_2(\text{PO}_4)_2\text{F}_3$ .

#### References:

- [1] J. B. Varley, K. Kweon, P. Mehta, P. Shea, T. W. Heo, T. J. Udovic, V. Stavila, B. C. Wood, *ACS Energy Lett.* **2017**, *2*, 250.
- [2] K. E. Kweon, J. B. Varley, P. Shea, N. Adelstein, P. Mehta, T. W. Heo, T. J. Udovic, V. Stavila, B. C. Wood, *Chem. Mater.* **2017**, *29*, 9142.
- [3] T. J. Udovic, M. Matsuo, A. Unemoto, N. Verdal, V. Stavila, A. V. Skripov, J. J. Rush, H. Takamura, S. Orimo, *Chem. Commun.* **2014**, *50*, 3750.
- [4] T. J. Udovic, M. Matsuo, W. S. Tang, H. Wu, V. Stavila, A. V. Soloninin, R. V. Skoryunov, O. A. Babanova, A. V. Skripov, J. J. Rush, A. Unemoto, H. Takamura, S. I. Orimo, *Adv. Mater.* **2014**, *26*, 7622.
- [5] W. S. Tang, M. Matsuo, H. Wu, V. Stavila, W. Zhou, A. A. Talin, A. V. Soloninin, R. V. Skoryunov, O. A. Babanova, A. V. Skripov, *Adv. Energy Mater.* **2016**, *6*, 1502237.
- [6] J. Ichi Aihara, *J. Am. Chem. Soc.* **1978**, *100*, 3339.
- [7] R. J. Wiersema, M. F. Hawthorne, *Inorg. Chem.* **1973**, *12*, 785.
- [8] M. Brighi, Oral Contribution at *Swiss & Surrounding Battery days 2019*, Dübendorf (Switzerland)
- [9] L. Duchêne, R. S. Kühnel, E. Stimp, E. Cuervo Reyes, A. Remhof, H. Hagemann, C. Battaglia, *Energy Environ. Sci.* **2017**, *10*, 2609.
- [10] F. Murgia, M. Brighi, R. Černý, *Electrochem. commun.* **2019**, *106*, 106534.
- [11] M. Brighi, F. Murgia, R. Černý, *Cell Report Physical Science* **2020**, *1*, 100217

SESSION F.EN07.07: Poster Session: Innovative Materials and Cell Design, Processing and Manufacturing Strategies for Solid State Batteries

On Demand Abstracts Available for Viewing Starting Saturday Morning, November 21, 2020

5:00 AM - 8:00 AM

F-EN07

#### F.EN07.07.01

**Reducing of Grain Boundary Influences by Hybridization of Polyether /  $\text{Li}_{1.5}\text{Al}_{0.5}\text{Ge}_{1.5}(\text{PO}_4)_3$  for Li-Conductive Solid Electrolyte** Naamo Suzuki<sup>1</sup>, Kenta Fujii<sup>2</sup>, Koji Ohara<sup>3</sup> and Shiro Seki<sup>1</sup>; <sup>1</sup>Kogakuin University, Japan; <sup>2</sup>Yamaguchi University, Japan; <sup>3</sup>Japan Synchrotron Radiation Research Institute, Japan

### Introduction

Recently, rechargeable batteries are strongly desired as energy storage systems. In particular, Li-ion batteries have been realized for practical use from consumer use (e.g., smartphone, laptop computer) to large-scaled energy storage devices such as for in/output control of renewable energy and electric vehicle owing to their high-energy-density and cycle performances. However, safety will be the most important demands with the scale of batteries, and several ignition accidents have been reported. ‘Solvent-free’ all-solid-state batteries exhibit quite high safety and have high-energy-density due to realization of thin-film electrolyte layer without separators. Generally, solid electrolytes are mainly categorized to polymer and inorganic electrolytes. Polymer electrolyte have a sufficient self-standing property, formability of stable interface with electrode and mechanical properties. However, it exhibits relatively low ionic conductivity and Li cation transport number. On the other hand, inorganic electrolyte shows relatively high ionic conductivity, even though it have grain boundary (GB) and be easily broken by external force (e.g. dropping and expansion / contraction with charge-discharge processes). Therefore, in this study, we propose polymer / inorganic hybrid electrolyte for usage of both advantages. Hybrid electrolytes of P(EO/PO) network polymer and two-types of  $\text{Li}_{1.5}\text{Al}_{0.5}\text{Ge}_{1.5}(\text{PO}_4)_3$  (LAGP) presence/absence GB resistance were investigated for developing high-performance all-solid-state Li batteries.

### Experimental

All samples were prepared in a glove box under Ar atmosphere.  $\text{LiN}(\text{SO}_2\text{CF}_3)_2$ , rhombohedral (*r*, having GB resistances) and amorphous (*a*, not having GB resistances) LAGP (Toshima mfg.), DMPA (photo initiator) and acetonitrile (solvent) were dissolved into polyether-based macromonomer P(EO/PO) (TA-210, Dai-ichi Kogyo Seiyaku). Amount of hybridized LAGP(*a* or *r*) were 0~200 wt% with polymer electrolytes, respectively. Mixed samples were dried in vacuum for 12h to evaporate acetonitrile. Then the slurry was casted between two glass plates separated by spacers (0.5 mm) and radical polymerized by UV irradiation at 5 min. Then, ionic conductivity were measured by non-blocking electrode cells (Li metal / electrolyte / Li metal). In addition, molecular-level structures of prepared samples were analyzed by high-energy X-ray diffraction (HEXRD) at SPring-8 (BL04B2). LAGP-free polyether electrolyte, polyether/ LAGP(*a*)150wt% hybrid electrolyte and LAGP(*a*) powder were enclosed in a sample tube and HEXRD measurements were examined.

### Results and discussion

From the result of impedance measurement by blocking electrode systems, possibility of influence of GB may not appear when using an amorphous material was suggested. To compare the effects of GB, non-blocking electrode systems, clear differences between amorphous and rhombohedral were observed by the difference of frequency properties [1]. Impedance spectrum by non-blocking electrode systems of LAGP-free electrolyte and all amorphous LAGP systems showed two semicircular arcs. In both systems, high and low frequency components were assigned as bulk resistance and interfacial resistance with Li metal. On the other hand, rhombohedral LAGP systems showed ellipse behavior because GB resistance appears between the two resistance components. This result shows that amorphous LAGP obtain no GB resistance component into amorphous inorganic / polyether hybrid electrolyte. Also, the radial distribution function of three samples was calculated by HEXRD results. A periodic structure appeared in all electrolytes. Hybrid material of amorphous polymer and inorganic systems also could be measured. The results of this measurement will provide spectroscopic evidence supporting the elimination of GBs. Therefore, influence of GB by using amorphous inorganic electrolyte into polyether electrolyte were clarified.

[1] M. Kato, K. Hiraoka, S. Seki, *J. Electrochem. Soc.*, **167**, 070559 (2020).

### F.EN07.07.04

**Late News: Development of Ceramic Electrolytes for All-Solid-State Batteries** Andre Borchers, Magnus Rohde and Hans Jürgen Seifert; KIT, Germany

In contrast to Lithium, Sodium is abundant worldwide. Therefore, it is reasonable to investigate its potential as a substitute for Lithium in battery cells. In addition, solid electrolytes for Sodium-ions show promising characteristics for all-solid-state batteries. If such an electrolyte is made of a Sodium-ion conducting ceramic cells are not inflammable, do not tend to decompose and offer high mechanical strengths to stop dendrite growth. The cells are much safer and are able to operate at higher temperatures, if the solid electrolytes replace the liquid electrolyte and the separator.

For the design of all-solid-state batteries, the thermal properties of the used electrolytes need to be known accurately. As a promising solid electrolyte for sodium-ion cells,  $\text{Na}_3\text{Zr}_2(\text{SiO}_4)_2\text{PO}_4$ -powder with NASICON structure was synthesized by Sol-Gel-method using Sodium nitrate, Nitric acid, Ammonium dihydrogen phosphate, Tetraethyl orthosilicate and Zirconium

(IV) oxynitrate hydrate as precursor materials.

Subsequently, this powder material was sintered by Field Assisted Sintering Technology (FAST) and conventional sintering.

The sintered ceramic pellets were investigated with a focus on thermal properties such as heat capacity and phase transitions using differential scanning calorimetry and thermal conductivity using laser flash analysis. The ionic conductivity was measured by impedance spectroscopy. Stoichiometry of the samples was studied by ICP-OES.

SESSION F.LP05.06: Live Poster Session: Energy (F.EN04, F.EN07 and F.EN08)

Session Chairs: Candace Chan, Jae Chul Kim, Josef Matyas and Gleb Yushin

Thursday Afternoon, December 3, 2020

6:30 PM - 8:30 PM

F.EN04

#### **F.EN04.27.01**

##### **Structural Characterization of Solid-State Electrochemical Interfaces via Integrated Computation and Spectroscopy**

Deyu Lu<sup>1</sup>, Nongnuch Artrith<sup>2</sup>, Alexander Urban<sup>2</sup>, Shinjae Yoo<sup>1</sup> and Feng Wang<sup>1</sup>; <sup>1</sup>Brookhaven National Laboratory, United States; <sup>2</sup>Columbia University, United States

Solid-state batteries are attracting world-wide interest for their potential to enhance safety by eliminating the need for flammable liquid electrolytes and to increase the energy density by facilitating the use of Li metal anodes and high-capacity cathodes. When incorporated into real devices, the solid electrolyte interacts with Li anodes and cathodes to form a nanometer-thick amorphous/disordered interfacial layer known as the solid electrolyte interphase (SEI), which determines the resistivity and stability of the interfaces between the electrode and electrolyte. The inherent complexity and the dynamic evolution of the SEI cannot be handled directly with first-principles methods, such as density functional theory, because of the computational hurdle associated with the large system size (e.g., more than one thousand atoms) and time scale. In order to gain insights into the structural properties and the interfacial reactions at the SEI, an integrated approach that combines high-performance computing and machine learning tools with state-of-the-art synchrotron X-ray absorption/electron energy-loss spectroscopy, is developed to tackle the complex electrochemical interfaces. The approach and some recent results from the structural modeling and spectroscopy studies of the SEI at the LiTMO<sub>2</sub> (TM=Ni, Co, Mn) cathode/ Li<sub>7</sub>La<sub>3</sub>Zr<sub>2</sub>O<sub>12</sub> solid electrolyte interfaces will be presented.

#### **F.EN04.27.02**

**Realistic Modeling of AlCl<sub>4</sub> Intercalation in Strained Two-Dimensional Materials** Rizcky Tamarany<sup>1</sup>, Chan-Woo Lee<sup>1</sup>, Hana Yoon<sup>1</sup>, Chung-Yul Yoo<sup>2</sup> and Kanghoon Yim<sup>1</sup>; <sup>1</sup>Korea Institute of Energy Research, Korea (the Republic of); <sup>2</sup>Mokpo National University, Korea (the Republic of)

Graphite-based Al-ion battery has been attracted large attention due to its extremely fast charge/discharge rate and excellent cycle stability. However, the intercalation mechanism of AlCl<sub>4</sub> into graphite is still vague. The concern comes with the large size of the AlCl<sub>4</sub> molecule while the experimentally observed gallery height for graphite cathode is not large enough (~ 5.7 Å). In the past theoretical studies, the computational models mostly represent that the stable structure of intercalated AlCl<sub>4</sub> is the tetragonal form which resulted in a large expansion of the intercalation gallery to 8~9 Å. In those studies, researchers commonly considered thermodynamically stable structures that allow free expansions of electrode structures. In this study, we suggest that a strain effect in a realistic electrode structure governs the stable form of intercalating AlCl<sub>4</sub>. We have performed first-principles calculations to show a strain-structure relation of intercalated AlCl<sub>4</sub> in graphite and found that a planar-shape of AlCl<sub>4</sub> molecule is more probable in realistic conditions. Using the computational results, we made model energy for AlCl<sub>4</sub> intercalation at given structural conditions such as volume expansion rate and stage number of graphite electrode. The model energy shows good agreements with the experimental observations on the structure-engineered graphite electrodes. In addition, to examine new candidate materials for Al-ion cathode, we also conduct calculations on MoS<sub>2</sub> and MoS<sub>2</sub>/graphene hetero-structure for AlCl<sub>4</sub> intercalation. As a result, we believe our study provides a deeper understanding of the charging/discharging mechanism and a modeling rule to find more enhanced electrode materials in Al-ion batteries.

#### **F.EN04.27.04**

**Improved Cycle Lifetime of Lithium-Sulfur Battery by Polysulfide Entrapment Using a Surface Decorated Carbon Cloth** Saisaban Fahad and Akihiro Kushima; University of Central Florida, United States

Lithium sulfur batteries (LSBs) are attracting attention as a next generation energy storage device because of their high energy density, low cost, and environmental friendliness surpassing that of lithium ion batteries (LIBs). LIBs are considered insufficient for many applications such as grid energy storage and electric vehicles due to their high cost and low energy density. However, LSBs still have some problems that need to be overcome before they can be used commercially. The major problem that limits their capacity is the dissolution of long chain lithium polysulfide into the electrolyte which leads to a loss of active material and capacity decay during cycling. Here, we have developed a cost-effective method for the lithium polysulfide battery to achieve high performance by employing a nanostructured carbon black/ carbon cloth electrode that exhibits high electrical conductivity, good mechanical properties and high surface area. These benefits enable a high sulfur loading mass, capture the lithium polysulfide intermediate reaction products and avoid structural changes. As a result, this simple and novel design delivered a high specific discharge capacity exceeding 1350 mAh<sup>-1</sup> at 0.2 C and good capacity retention, providing a promising path towards practical lithium sulfur batteries.

#### **F.EN04.27.07**

**Enhanced Polysulfide Conversion Using 2D Alloy Catalyst in Li-S Batteries** Sanket D. Bhoyate<sup>1</sup>, Junyoung Kim<sup>1</sup>, Eunji Lee<sup>2</sup>, Eunho Lee<sup>1</sup>, Juhong Park<sup>1</sup>, Jeongyong Kim<sup>2</sup> and Wonbong Choi<sup>1</sup>; <sup>1</sup>University of North Texas, United States; <sup>2</sup>SKKU, Korea (the Republic of)

The lithium sulfur battery presents unique polysulfide chemistry to exhibit high theoretical capacity of 2,600 Wh/kg. However, the life cycle of Li-S battery is greatly affected due to unwanted shuttling of soluble lithium polysulfides (LiPSs) such as Li<sub>2</sub>S<sub>8</sub> and Li<sub>2</sub>S<sub>6</sub>, that corrodes the Li anode by forming an inactive sulfide layer. Previously, pristine 2D materials with polar surface were used as a catalyst in sulfur cathodes to overcome this issue by acting as polysulfide anchor and prevent shuttling effect. However, the concentration and weight loading of catalyst was high and lack the practical applicability in Li-S battery. To overcome this issue, we adopted novel strategy of synthesizing 2D alloys with very low concentration loading on carbon nanotube paper as a sulfur host cathode to efficiently catalyze the polysulfide reactions. The 2D alloy with mixed 2H-1T phase exhibited synergetic properties and showed high specific capacity of 1,228 mAh/g at 0.1 C and improved the cyclic stability to 400 cycles, as compared to 100 cycles for pristine cathode. The reduced shuttle effect and increased life cycle was due to accelerated transformation of the dissolved polysulfides to the insoluble LiPSs and back to sulfur. Our study shows novel approach with binder-free ultra-light weight catalytic cathodes for practical application of Li-S battery.

#### **F.EN04.27.10**

**Improvement of Specific Capacitance in Lithium Batteries by Three-Dimensional Carbon Networks** Valerio Dorvilien<sup>1</sup>, Carolina Rojas<sup>2</sup>, Neida Santacruz<sup>3</sup>, Cid Marie Calderon Rodriguez<sup>3</sup>, Omayra Ortiz Alicea<sup>3</sup>, Genesis M. Ferrer<sup>1</sup>, Frank Martinez-Henriquez<sup>1</sup>, Daniel Fontanez<sup>1</sup>, Frank Mendoza<sup>1</sup>, Carolina Rojas Michea<sup>4</sup>, Brad R. Weiner<sup>2</sup> and Gerardo Morell<sup>1</sup>; <sup>1</sup>University of Puerto Rico-Rio Piedras Campus, United States; <sup>2</sup>University of Puerto Rico, San Juan, Puerto Rico; <sup>3</sup>University of Puerto Rico, Rio Piedras Campus, Puerto Rico; <sup>4</sup>Universidad Autónoma de Chile, Chile

We propose a low cost and simple method to prepare three-dimensional (3D) carbon structures by Chemical Vapor Deposition (CVD) and characterized their structural and electrochemical properties. The 3D pore system were obtained using different zeolites (NaY, SBA-15, and ZMS-5) as solid template structures to assist in the synthesis of 3D carbon network structures. The carbon source consisted of radicals formed from the thermal decomposition of acetone, in a relatively facile and fast chemical deposition process. The 3D carbon network structures were characterized with X-ray diffraction, Raman spectroscopy, surface area measurement, scanning electron microscopy, and transmission electron microscopy. The carbon networks deposited in the pores consist of reduced graphene oxide and multiwalled carbon nanotubes; their size distribution correlates with the size of the pores of zeolites. The electrical conductivity and dispersed morphology of the 3Ds carbon network structures -based conductive electrode were examined by atomic force microscope (AFM), scanning electron microscope (SEM) and transmission electron microscope (TEM). Using the standard method we assembled the Lithium Ion Battery in the Ar-filled glove box, we used LiPF<sub>6</sub> with EC:DMC::1:2 ratio as the electrolyte, lithium foil as the counter electrode and the 3D carbon network material. The specific capacity and cycle-life stability of the 3Ds carbon network-based lithium ion battery was investigated by cyclic voltammetry analysis.

#### **F.EN04.27.11**

**3D Carbon-Coated MXene Architectures with High Capacity and Ultrafast Lithium/Sodium Storage** Peng Zhang, Qizhen Zhu and Bin Xu; Beijing University of Chemical Technology, China

MXene is a promising candidate for energy storage devices owing to its versatile characteristics. However, as 2D structured

material, layer restacking besides its surface oxidation is a serious issue. This re-stacking compromises significantly surface active sites, compelling the material to exhibit sluggish electro-kinetics behavior, and thus deterring the overall capacitive performance. Here, a tremella-like 3D architecture of carbon-coated Ti<sub>3</sub>C<sub>2</sub>T<sub>x</sub> MXene (T-MXene@C) is fabricated as an efficient anode material for lithium- (LIBs) and sodium-ion batteries (SIBs), respectively. The nanohybrid is synthesized via self-polymerization of dopamine over the surface of pristine Ti<sub>3</sub>C<sub>2</sub>T<sub>x</sub> MXene nanosheets succeeded by carbonization. The self-polymerization of dopamine in this case, facilitates the transformation of MXene sheets into 3D architectures where its post-carbonization subsequently forms a thin carbon layer over the structure, preserving the surface facets from oxidation and structural aggregation. The incursion of carbon layers within MXene not only contributes in provision of additional active area, but also enhances the structural durability of the material during charge/discharge process. Therefore, the T-MXene@C nanohybrid exhibits ultrahigh capacities, superior rate performance, and stable cyclability as anodes in both LIBs and SIBs. Moreover, the discussed strategy could be applied as general route to fabricate diverse MXene-based 3D structures with potential applications in many other areas.

#### F.EN04.27.12

**Tin Dioxide/Graphene/Graphene Oxide as Anode Material for Lithium-Ion Batteries** Valerio Dorvilien, Frank Martinez-Henriquez, Cid Marie Calderon Rodriguez, Daniel Fontanez, Genesis M. Ferrer, Omayra Ortiz Alicea, Frank Mendoza, Brad R. Weiner and Gerardo Morell; University of Puerto Rico-Rio Piedras Campus, United States

Graphene Oxide was synthesized using a Modified Hummer's Method. It is fairly known that SnO<sub>2</sub> is used as anode material for lithium-ion batteries applications due to their high specific capacity. Hence, we use a non-conventional synthesis route to obtain a final composite, G/GO/SnO<sub>2</sub>. G/GO, with its good surface-to-volume ratio, serves as a support and matrix for SnO<sub>2</sub> nanoparticles that buffers the huge volume changes the nanoparticles are used alone as anode for lithium ion batteries and then enhances its electrochemical properties. For the structural characterization of the synthesized material, scanning electron microscopy (SEM), energy dispersive spectroscopy (EDS) and Raman Spectroscopy were performed; showing a uniform distribution of the nanomaterial in the carbon matrix. Electrochemical analysis, such as charge/discharge profiles show that the composite can be used as anode in lithium ion batteries. In fact, at different current densities- 25, 75, 100, and 200 mA/g- the material deliver in the first cycle very high specific capacity-1808, 1253, 903, 886 mAhg<sup>-1</sup> respectively. After repeated cycling the composite is still offering reversible capacities over 400 mAhg<sup>-1</sup> for each current density, showing that G/GO is providing contact areas which results in more energy density at the interface electrode/electrolyte and that the SnO<sub>2</sub> provides additional ions to the EDL and the electrochemical process.

#### F.EN04.27.13

**Theoretical Intercalation Profiles of Layered NaMO<sub>2</sub> (M=Co, Ni, Fe) Cathodes—Learning from the Electronic Structure of LiMO<sub>2</sub>** Christopher Savory, Arthur B. Youd and David O. Scanlon; University College London, United Kingdom

Ab initio modelling can provide valuable insights into the electronic and structure behaviour of battery materials, including the prediction of sodium, potassium and magnesium cathodes.<sup>1,2</sup> Nevertheless, it is crucial that the accuracy of such ab initio calculations be established. The most common method to theoretically the strong correlation in the 3d valence electrons of transition metals is to use the addition of 'U' parameters to standard Density Functional Theory (DFT), enabling high throughput studies of Na-based materials;<sup>3</sup> however these parameters must be tuned to experimental measurements, and are highly sensitive to changes in oxidation state and composition - crucial properties during the intercalation of AMO<sub>2</sub> (A=Li, Na, K) layered cathodes.<sup>4,5</sup> Recent high-level quasiparticle self-consistent GW (QSGW) calculations performed on the layered LiMO<sub>2</sub> (M=Co, Ni, Mn) cathodes suggest that the charge transfer transition in LiMO<sub>2</sub> phases is underestimated, even when the inaccuracy of standard DFT at describing band gaps is accounted for, but it is well predicted by hybrid Density Functional Theory (DFT), which mixes exact exchange from Hartree-Fock theory.<sup>6</sup> In this study, we examine how electronic correlation is described in layered sodium cathode materials with various levels of theory. We calculate the electronic structures of NaCoO<sub>2</sub>, NaNiO<sub>2</sub> (in direct comparison to their Li counterparts) and ?-NaFeO<sub>2</sub> - ternaries typically alloyed to form stable and efficient sodium-based cathodes<sup>7</sup> -- using DFT+U, hybrid DFT (HSE06) and QSGW to establish a thorough comparison of the electronic properties at each level, and to establish that tuning is necessary to reproduce the valence electronic structure of such materials. We further demonstrate the practical impact of this theoretical description by calculating and comparing voltage intercalation profiles of these systems as a function of Na content, at both the DFT+U and hybrid DFT levels via a cluster expansion approach, in order to establish the most reliable comparison to experiment. We establish the necessity to use accurate, transferable methods to describe such systems, with an aim to inform ab initio studies on the future generation of first row transition metal-based cathodes. (1) Zhang, W.; Liu, Y.; Guo, Z. *Sci. Adv.* 2019, 5 (5), eaav7412. (2) Gao, Y.; Wang, Z.; Lu, G. J. *Mater. Chem. A* 2019, 7 (6), 2619. (3) Zhang, X.; Zhang, Z.; Yao, S.; Chen, A.; Zhao, X.; Zhou, Z. *npj Comput. Mater.* 2018, 4 (1), 13. (4) Urban, A.; Seo, D.-H.; Ceder, G. *npj Comput. Mater.* 2016, 2

(October 2015), 16002. (5) Zhou, F.; Cococcioni, M.; Marianetti, C. A.; Morgan, D.; Ceder, G. Phys. Rev. B - Condens. Matter Mater. Phys. 2004, 70 (23), 235121. (6) Savory, C. N.; Morgan, B.J., Walsh, A.; Scanlon, D. O. (in preparation) 2019 (7) Thorne, J. S.; Zheng, L.; Lee, C. L. D.; Dunlap, R. A.; Obrovac, M. N. ACS Appl. Mater. Interfaces 2018, 10 (26), 22013.

#### **F.EN04.27.16**

**Enhancement of Ionic Conductivity of Composite Electrolytes for All-Solid-State Lithium Rechargeable Batteries by Incorporating Gold Nanorods into a Polyethylene Oxide Matrix** Yifan Zhang, Nian Liu and John Zhang; Georgia Institute of Technology, United States

Solid state batteries have advantages such as safeness and high energy density. However, their conductivity at room temperature is low which limits their further commercialization. Gold nanorods can promote the Li ion transport by decreasing the crystallization of solid state electrolytes, and locally heat the electrolytes based on their photothermal conversion capability, providing a more efficient way to improve the performance of solid state batteries.

#### **F.EN04.27.17**

**Large-Scale Synthesis of Uniform and Extremely Small-Sized Cobalt Ferrite Nanoparticles as High-Performance Anode Materials for Lithium-Ion Batteries** Yifan Zhang, Nian Liu and John Zhang; Georgia Institute of Technology, United States

Spinel ferrites have emerged as an attracted class of materials that can find application in various fields, ranging from information storage, biomedical application to energy-related areas. As the anode in LIBs, spinel  $\text{CoFe}_2\text{O}_4$  attracts much attention because of its high theoretical specific capacity (916 mAh g<sup>-1</sup>). However, some issues impede its practical application such as drastic capacity fading and poor rate capability arising from an inherent low electronic conductivity, severe aggregation, and lithiation-induced volume expansion in the cycling process. Increasing surface-to-volume ratio could provide relatively short transport distance for lithium-ion diffusion and alleviate the volume expansion, which is one of the possible strategies to solve the above-mentioned problem. In this frame, an aminolytic method is described to synthesize ultra-small (<10 nm)  $\text{CoFe}_2\text{O}_4$  nanoparticles with good dispersion at a relatively low temperature without further annealing being required. Here, the 9.1 nm  $\text{CoFe}_2\text{O}_4$  nanoparticles synthesized by aminolytic method delivered a reversible specific capacity of 1238 mAh g<sup>-1</sup> after 100 cycles at a current density of 0.1C, a much better performance compared with  $\text{CoFe}_2\text{O}_4$  synthesized by traditional methods in previous reports. By adjusting the reaction temperature, 3.4 nm  $\text{CoFe}_2\text{O}_4$  nanoparticles could also be synthesized, delivering a slightly enhanced specific capacity (1343 mAh g<sup>-1</sup> after 100 cycles at 0.1C). For comparison, the  $\text{CoFe}_2\text{O}_4$  nanoparticles were also prepared by coprecipitation method and its electrochemical performance was studied in detail. It can be concluded that spinel  $\text{CoFe}_2\text{O}_4$  synthesized by aminolytic method is a promising anode for LIBs based on its superior lithium storage performance. Further, the aminolytic method can also be used to prepare other spinel materials in different fields. The systematically studied electrochemical performance of  $\text{CoFe}_2\text{O}_4$  nanoparticles is beneficial in the design of future anode materials for LIBs.

#### **F.EN04.27.23**

**$\text{Li}_2\text{S}_x$ -CNT Electrode with Lean Electrolyte for High-Energy-Density Li-S Battery** Yuichi Yoshie, Keisuke Hori and Suguru Noda; Waseda University, Japan

Sulfur is a promising active material because of a high theoretical capacity (1675 mA h g<sup>-1</sup>) and low cost. Nevertheless, practical applications of S electrode have been hindered by low S fraction in a cell. Excess Li in negative electrode, auxiliary materials such as heavy current collectors of metals, and large amount of electrolyte (Electrolyte/Sulfur ratio (E/S) > 7) have been used in previous works [1], which lowers energy density of the Li-S cells based on total mass/volume (including electrodes, separator and electrolyte). We previously demonstrated the high gravimetric and volumetric energy densities based on an electrode using self-supporting sponge-like paper of few wall carbon nanotubes (FWCNTs) as current collector. The unique properties of FWCNTs with high conductivity of ~100 S cm<sup>-1</sup> and high surface area of ~500 m<sup>2</sup> g<sup>-1</sup> enhanced the sulfur utilization; however, E/S ratio was still high [2]. In this work, we report the  $\text{Li}_2\text{S}_x$ -CNT (4?x?8) positive electrode that works effectively even with lean electrolyte. Self-supporting paper of FWCNTs was fabricated by dispersion and filtration. Then, three types of  $\text{Li}_2\text{S}_x$  (x = 4, 6, 8) in 1,2-dimethoxyethane (DME) solution were drop-casted on the papers and dried for 1 h to obtain the  $\text{Li}_2\text{S}_x$ -CNT electrodes. As a reference, the S-CNT electrode was also prepared by the S vapor deposition method [2]. The  $\text{Li}_2\text{S}_x$ -CNT and S-CNT (areal density of 2 mgS cm<sup>-2</sup> and 1 mgCNT cm<sup>-2</sup>) electrodes were evaluated by assembling 2032-type coin cell with Li foil (50 μm thick) as a negative electrode, a polyethylene separator, and an electrolyte of 1 M LiTFSI + 0.2 M LiNO<sub>3</sub> in 1:1 (v/v) DOL/DME. Although the S-CNT exhibited very small capacity, the  $\text{Li}_2\text{S}_6$ -CNT exhibited 1471 mA h g<sup>-1</sup> with lean electrolyte of E/S ratio of 3.2 μL mgS<sup>-1</sup>. Furthermore, the  $\text{Li}_2\text{S}_6$ -CNT achieved 526 W h kgcell<sup>-1</sup> based on the cell including positive and negative electrodes, separator, and electrolyte at second



discharge. The value is encouragingly high compared to the high-performance Li-ion battery of ~300 Wh/kg cell<sup>-1</sup> [1]. [1] M. Hagen et al., *Adv. Energy Mater.*, 5, 1401986 (2015). [2] K. Hori, et al., *J. Phys. Chem. C*, 123, 3951 (2019).

#### F.EN04.27.24

**Thin Li-Metal Negative Electrode Held in Self-Supporting Paper of Carbon Nanotubes for Stable, High Energy Density Rechargeable Batteries** Tomotaro Mae<sup>1</sup>, Keisuke Hori<sup>1</sup>, Yuki Yamada<sup>2</sup> and Suguru Noda<sup>1</sup>; <sup>1</sup>Waseda University, Japan; <sup>2</sup>The University of Tokyo, Japan

Li metal is a promising negative electrode because of its high theoretical capacity (3860 mAh/g) and low potential (3.04 V vs SHE). However, it has a serious safety problem of Li dendrite which penetrates a separator and causes short circuit [1]. Surface modification of Li foils by texture or additional layer have shown effective in suppressing the dendrite growth [2] [3], but many of such methods make the electrode too thick (several hundred μm), and excessive Li were used (5 times or more). In this work, we propose thin and light-weight electrode to achieve high gravimetric, volumetric and areal capacities. Self-supporting paper of few-wall carbon nanotubes (FWCNTs; areal mass of 0.3 mg/cm<sup>2</sup> and thickness of ~15 μm), having high conductivity of 40 S/cm and large specific surface area of ~500 m<sup>2</sup>/g, was used as non-metal 3D current collector. Cu nanoparticles (25 nm; 0.1-0.2 mg/cm<sup>2</sup>) were held in this 3D matrix as seeds for stable Li plating/stripping. The Cu-CNT film was prepared by dispersion and filtration [4]. 2032 coin cells of symmetrical configurations (Li-CNT//Li-CNT and Li-Cu-CNT//Li-Cu-CNT) were prepared by performing electrochemical pre-cycling of the Li foil (50 μm)/CNT//CNT and Li foil (50 μm)/Cu-CNT//Cu-CNT stacks with polypropylene separator (25 μm). Charge-discharge test was performed with an areal capacity of 4 mA h/cm<sup>2</sup> and current density of 0.4 mA/cm<sup>2</sup>. The former cell showed unstable plating/stripping behavior in several cycles due to micro-short circuits while the latter worked stably over 20 cycles with small excess (1.5-2 times of the areal capacity) in Li. The Cu nanoparticles working as the nucleation sites and mesopores in the FWCNT paper working as growth sites realized the stable operation of the cells. [1] L. Wang, et al., *Energy Storage Mater.* 14, 22 (2018). [2] Rodrigo V. Salvatierra, et al., *Adv. Mater.* 30, 50, (2018). [3] Y. Zhao, et al., *Nano energy.* 43, 368, (2018). [4] K. Hori, et al., *J. Phys. Chem. C* 123, 3951 (2019).

#### F.EN04.27.25

**A Versatile Crosslinked Solid Polymer Electrolyte for Lithium, Calcium, Aluminum and Sodium-Ion Conduction** Francielli Genier, Jiayue Wang, Tianyi Yao, Saeid Biria and Ian D. Hosein; Syracuse University, United States

The development of high-performance batteries is fundamental to meeting global energy demands, while also storing energy affordably and safely. An area of intense research in the battery field has been the replacement of the liquid or gel electrolyte with a solid polymer material, namely a solid polymer electrolyte (SPE). SPEs can allow the use of metal anodes due to its suppression of dendrite formation, which could thereby double the energy density, besides further addressing concerns over the volatility and flammability of liquid electrolytes. Crosslinked polymer electrolytes are quite attractive owing to their ability to enhance conductivity, while also retaining mechanical stability. 1 Studies on SPEs not only focus on different polymer systems, but also on improving the interaction of existing and new polymer networks to ions other than lithium-ion to achieve even less expensive and more efficient rechargeable batteries. Other univalent ions, in particular sodium cations, can be highlighted due to its wide availability and low cost comparing to lithium. Multivalent cations, such as Ca<sup>2+</sup> and Al<sup>3+</sup>, are also featured in SPE studies for their high energy density and mineral abundance. 2 In those studies, poly(ethylene oxide) (PEO) has been extensively employed as the electrolyte's backbone. However, polytetrahydrofuran (PTHF) has been reported as having a looser coordination with Li<sup>+</sup> than PEO, due to PTHF's fewer oxygen heteroatoms in its chain. 3 As a result, lower activation energy for ion motion is observed, leading to higher conductivity and transference numbers. In this work, we describe the synthesis of crosslinked SPEs for lithium, sodium, aluminum, and calcium conduction using a PTHF backbone. The SPEs were crosslinked through the photo-copolymerization of PTHF and 3,4-epoxycyclohexylmethyl 3,4-epoxycyclohexanecarboxylate. The crosslinked samples were evaluated for their ionic conductivity, thermal stability, amorphousness, and mechanical properties. Ionic conductivity of the order of 10<sup>-5</sup> - 10<sup>-4</sup> S/cm at room temperature was achieved, which is superior to some previously reported Ca, Na, and Al dry SPEs. 4,5 Thermogravimetric analysis of the electrolytes indicated that, within the operating temperature of a battery, all electrolytes were stable and showed minimal weight loss. Differential scanning calorimetry confirmed the amorphous feature of the polymer. The electrolytes also showed excellent mechanical stiffness and flexibility. Further electrochemical studies will be presented and discussed. This work represents a new route for cleaner and safer energy storage devices with the potential for a broad variety of applications. References 1. Placke, T., Kloepsch, R., Dühnen, S. & Winter, M. Lithium ion, lithium metal, and alternative rechargeable battery technologies: the odyssey for high energy density. *J. Solid State Electrochem.* 21, 1939-1964 (2017). 2. Xu, C. et al. Secondary batteries with multivalent ions for energy storage. *Nat. Publ. Gr.* 1-8 (2015). doi:10.1038/srep14120 3. Mackanic, D. G. et al. Crosslinked Poly ( tetrahydrofuran ) as a Loosely Coordinating Polymer Electrolyte. 1800703, 1-11 (2018). 4. Wang, J., Genier, F. S., Li, H., Biria, S. & Hosein, I. D. A Solid Polymer Electrolyte from Cross-Linked Polytetrahydrofuran

for Calcium Ion Conduction. ACS Appl. Polym. Mater. 1, 1837-1844 (2019). 5. Yao, T., Genier, F. S., Biria, S. & Hosein, I. D. A solid polymer electrolyte for aluminum ion conduction. Results Phys. 10, 529-531 (2018).

#### F.EN07.07.01

**Reducing of Grain Boundary Influences by Hybridization of Polyether /  $\text{Li}_{1.5}\text{Al}_{0.5}\text{Ge}_{1.5}(\text{PO}_4)_3$  for Li-Conductive Solid Electrolyte** Naamo Suzuki<sup>1</sup>, Kenta Fujii<sup>2</sup>, Koji Ohara<sup>3</sup> and Shiro Seki<sup>1</sup>; <sup>1</sup>Kogakuin University, Japan; <sup>2</sup>Yamaguchi University, Japan; <sup>3</sup>Japan Synchrotron Radiation Research Institute, Japan

#### Introduction

Recently, rechargeable batteries are strongly desired as energy storage systems. In particular, Li-ion batteries have been realized for practical use from consumer use (e.g., smartphone, laptop computer) to large-scaled energy storage devices such as for in/output control of renewable energy and electric vehicle owing to their high-energy-density and cycle performances. However, safety will be the most important demands with the scale of batteries, and several ignition accidents have been reported. 'Solvent-free' all-solid-state batteries exhibit quite high safety and have high-energy-density due to realization of thin-film electrolyte layer without separators. Generally, solid electrolytes are mainly categorized to polymer and inorganic electrolytes. Polymer electrolyte have a sufficient self-standing property, formability of stable interface with electrode and mechanical properties. However, it exhibits relatively low ionic conductivity and Li cation transport number. On the other hand, inorganic electrolyte shows relatively high ionic conductivity, even though it have grain boundary (GB) and be easily broken by external force (e.g. dropping and expansion / contraction with charge-discharge processes). Therefore, in this study, we propose polymer / inorganic hybrid electrolyte for usage of both advantages. Hybrid electrolytes of P(EO/PO) network polymer and two-types of  $\text{Li}_{1.5}\text{Al}_{0.5}\text{Ge}_{1.5}(\text{PO}_4)_3$  (LAGP) presence/absence GB resistance were investigated for developing high-performance all-solid-state Li batteries.

#### Experimental

All samples were prepared in a glove box under Ar atmosphere.  $\text{LiN}(\text{SO}_2\text{CF}_3)_2$ , rhombohedral (*r*, having GB resistances) and amorphous (*a*, not having GB resistances) LAGP (Toshima mfg.), DMPA (photo initiator) and acetonitrile (solvent) were dissolved into polyether-based macromonomer (P(EO/PO) (TA-210, Dai-ichi Kogyo Seiyaku)). Amount of hybridized LAGP(*a*) or (*r*) were 0~200 wt% with polymer electrolytes, respectively. Mixed samples were dried in vacuum for 12h to evaporate acetonitrile. Then the slurry was casted between two glass plates separated by spacers (0.5 mm) and radical polymerized by UV irradiation at 5 min. Then, ionic conductivity were measured by non-blocking electrode cells (Li metal / electrolyte / Li metal). In addition, molecular-level structures of prepared samples were analyzed by high-energy X-ray diffraction (HEXRD) at SPring-8 (BL04B2). LAGP-free polyether electrolyte, polyether/ LAGP(*a*)150wt% hybrid electrolyte and LAGP(*a*) powder were enclosed in a sample tube and HEXRD measurements were examined.

#### Results and discussion

From the result of impedance measurement by blocking electrode systems, possibility of influence of GB may not appear when using an amorphous material was suggested. To compare the effects of GB, non-blocking electrode systems, clear differences between amorphous and rhombohedral were observed by the difference of frequency properties [1]. Impedance spectrum by non-blocking electrode systems of LAGP-free electrolyte and all amorphous LAGP systems showed two semicircular arcs. In both systems, high and low frequency components were assigned as bulk resistance and interfacial resistance with Li metal. On the other hand, rhombohedral LAGP systems showed ellipse behavior because GB resistance appears between the two resistance components. This result shows that amorphous LAGP obtain no GB resistance component into amorphous inorganic / polyether hybrid electrolyte. Also, the radial distribution function of three samples was calculated by HEXRD results. A periodic structure appeared in all electrolytes. Hybrid material of amorphous polymer and inorganic systems also could be measured. The results of this measurement will provide spectroscopic evidence supporting the elimination of GBs. Therefore, influence of GB by using amorphous inorganic electrolyte into polyether electrolyte were clarified.

[1] M. Kato, K. Hiraoka, S. Seki, *J. Electrochem. Soc.*, **167**, 070559 (2020).

#### F.EN07.07.04

**Late News: Development of Ceramic Electrolytes for All-Solid-State Batteries** Andre Borchers, Magnus Rohde and Hans Jürgen Seifert; KIT, Germany

In contrast to Lithium, Sodium is abundant worldwide. Therefore, it is reasonable to investigate its potential as a substitute for Lithium in battery cells. In addition, solid electrolytes for Sodium-ions show promising characteristics for all-solid-state batteries. If such an electrolyte is made of a Sodium-ion conducting ceramic cells are not inflammable, do not tend to decompose and offer high mechanical strengths to stop dendrite growth. The cells are much safer and are able to operate at higher temperatures, if the solid electrolytes replace the liquid electrolyte and the separator.

For the design of all-solid-state batteries, the thermal properties of the used electrolytes need to be known accurately. As a promising solid electrolyte for sodium-ion cells,  $\text{Na}_3\text{Zr}_2(\text{SiO}_4)_2\text{PO}_4$ -powder with NASICON structure was synthesized by Sol-Gel-method using Sodium nitrate, Nitric acid, Ammonium dihydrogen phosphate, Tetraethyl orthosilicate and Zirconium (IV) oxynitrate hydrate as precursor materials.

Subsequently, this powder material was sintered by Field Assisted Sintering Technology (FAST) and conventional sintering.

The sintered ceramic pellets were investigated with a focus on thermal properties such as heat capacity and phase transitions using differential scanning calorimetry and thermal conductivity using laser flash analysis. The ionic conductivity was measured by impedance spectroscopy. Stoichiometry of the samples was studied by ICP-OES.

#### **F.EN08.07.01**

**A New Disposal Method for Radioactive Waste Using Chemically Adsorbed Monolayer** Teruyoshi Sasaki, Hiroto Funakoshi, Kazufumi Ogawa and Yoshifumi Suzuki; Kagawa University, Japan

Radioactive waste exists in the form of gas, liquid and solid. Among them, the disposal method of collecting radioactive waste, melted and solidifying it and burying it in the ground is common. However, in the current method, after the radioactive waste is collected, it is mixed with glass as it is to be melted and solidified, or it is mixed with cement and solidified, so that the volume of the waste becomes huge. Therefore, in this study, we investigated a process in which a chemically adsorbed monolayer having an imidazole group at the end was formed on a glass fiber, and only radioactive substances were adsorbed from a solution in which waste was dissolved, and then melted and solidified at once. As a result, we succeeded in adsorbing radioactive substances with high efficiency in solution. By using this method, if the melting point of the glass fiber is set low, the melted and solidifying process will be extremely simple, and it will be possible to manage the radioactive substances in the necessary minimum volume.

#### **F.EN08.07.02**

**Speciation by XANES of Copper Migrated into Compacted Bentonite Using Electromigration Techniques** Kazuya Idemitsu, Keisuke Yoshida, Yaohiro Inagaki and Tatsumi Arima; Kyushu University, Japan

Copper is a candidate for use as an overpack material in deep underground nuclear waste disposal. Copper, however, is susceptible to corrosion following closure of the repository and migration of the corrosion products through the buffer material may affect the migration of redox-sensitive radionuclides. Electromigration experiments were performed whereby a copper coupon, which was in contact with compacted bentonite, served as the working electrode and was held at a constant potential of +300 mV vs. Ag/AgCl electrode for up to 48 h. The chemical form of copper that migrated into the bentonite specimens were estimated by using Cu K-edge X-ray absorption near-edge structure (XANES) at Saga-Light Source, Japan. The results revealed that the oxidation state of Cu in the bentonite would be Cu(II) as shown the correlation between the amount of Cu migrated into bentonite and the corrosion current. On the other hand Cu(I) also observed on the copper coupon not in bentonite. Copper could corrode as Cu(II) then react with Cu metal and precipitate as  $\text{Cu}_2\text{O}$  on the copper metal.

#### **F.EN08.07.03**

**Effects of Chromium and Vanadium on the Sulfate Solubility of Sodium Aluminoborosilicate Glass** Natalie J. Smith-Gray<sup>1</sup>, Jason Lonergan<sup>2</sup> and John S. McCloy<sup>1,2</sup>; <sup>1</sup>Washington State University, United States; <sup>2</sup>Pacific Northwest National Laboratory, United States

In the composition space of interest for Hanford low-activity nuclear waste glass, the waste loading of some formulations is limited by the incorporation of sulfate into the glass (i.e., its solubility). Numerous studies have been undertaken to understand the mechanism of sulfate incorporation and its affect by various other additives. In particular, the model by Vienna et al (2014, J. Amer. Ceram. Soc. 97, 3135) identified elements which tend to raise or lower sulfate solubility in borosilicate glass. In the current experimental study, we focus on representative additives that purportedly decrease (chromium) or increase (vanadium) the sulfate solubility. A baseline aluminoborosilicate composition containing Ca and Na was melted with target composition of either i) 1 wt%  $\text{SO}_3$  and up to 2 wt%  $\text{Cr}_2\text{O}_3$  or ii) 2 wt%  $\text{SO}_3$  and up to 5 wt% percent  $\text{V}_2\text{O}_5$ . Thermal and physical properties were measured and structural analysis by Raman spectroscopy was performed to investigate changes in the glass structure with transition metal addition. Electron probe microanalysis was used to measure elemental compositions in melted glass for comparison with batched compositions. Increasing  $\text{Cr}_2\text{O}_3$  concentration caused saturation of Cr concentration within the glass and formation of crystalline eskolaite ( $\text{Cr}_2\text{O}_3$ ); glass transition temperature change was only dependent on the Cr which remained in glass, while measured density changes depended on both Cr in glass and eskolaite. No apparent change in sulfate solubility was observed, though not all the targeted sulfate was incorporated in

the glasses containing Cr. On the other hand, all the targeted V was incorporated into the glass, and as the concentration of  $V_2O_5$  increased, the glass transition temperature decreased. Again, not all of the batched sulfur was incorporated into the glass, but  $V_2O_5$  showed a weak tendency to increase the observed sulfur content in the glass. Some incorporation mechanisms to explain these trends are proposed.

#### F.EN08.07.04

##### Defect Evolution Measured by Raman Spectroscopy and EBSD in Rare-Earth Doped $UO_2$ Used Nuclear Fuel

Analogues Sam Karcher<sup>1</sup>, John S. McCloy<sup>1</sup>, Ritesh Mohun<sup>2</sup> and Claire L. Corkhill<sup>2</sup>; <sup>1</sup>Washington State University, United States; <sup>2</sup>The University of Sheffield, United Kingdom

Uranium dioxide prepared from depleted uranium is commonly used as an analogue to study used nuclear fuels. While actual used nuclear fuel is highly complex and contains a large number of fission products, synthetic analogues are often simplified by single species doping. Previous studies involving trivalent RE doped  $UO_2$  show reduced dissolution rates compared to undoped  $UO_2$ . When  $U^{IV}$  is replaced with a  $RE^{III}$  cation, defect clusters containing  $U^V$  resulting from local charge compensation form which can serve to limit ability to form  $U_3O_8$ . Uranyl ions  $(UO_2)^{2+}$ , which are allowed to form as a result of  $U^{VI}$  in  $U_3O_8$ , have a solubility much higher than stoichiometric  $UO_2$ . To predict the long-term stability of used nuclear fuel in oxidizing conditions it is necessary to understand the relationships between fuel chemistry, microstructure and environment.

Here, a series of  $UO_2$  pellets doped with Ce, Nd, Yb, Zr and Th at 1 at. % and 5 at. % were prepared via uranyl nitrate + RE-nitrate co-precipitation to ensure homogenous distribution of dopant ions before pelletizing and sintering at  $1700^\circ C$  in H-Ar reducing atmosphere. Defect signatures in the resulting near-stoichiometric  $(U,RE)O_{2+x}$  ceramic pellets were analyzed using Raman spectroscopy at multiple excitation wavelengths pre and post oxidation treatment. Through collaboration with the University of Sheffield, we have also obtained Raman data on our samples after irradiation with 1 MeV Kr ions at room temperature, fluence  $5 \times 10^{15}$  ions/cm<sup>2</sup> at the Dalton Cumbrian Facility. Deconvolution of Raman spectra reveals distinct signatures corresponding to defects such as interstitial or vacant oxygen sites or reduced lattice symmetry. The primary Raman peak observed in  $UO_2$  at  $445\text{ cm}^{-1}$  corresponds to the symmetric U-O stretching bond, and indicates the presence defects in the  $UO_2$  structure by losing intensity and broadening while shifting towards higher wavenumber. Thermogravimetric analysis up to  $900^\circ C$  in air show a delayed transition from  $UO_2$  to  $U_3O_8$  in the doped samples, the effect being greatest in Yb-doped  $UO_2$ . Using Raman mapping with in-situ heating we can track the evolution of defect bands during oxidation and correlate spectral features to the orientation, size and distribution of grains and grain boundaries measured by electron backscatter diffraction (EBSD).

### SYMPOSIUM F.EN08

---

Scientific Basis for Nuclear Waste Management  
November 21 - December 4, 2020

#### Symposium Organizers

Claire Corkhill, University of Sheffield  
Daniel Gregg, Australian Nuclear S&T Org  
Kazuya Idemitsu, Kyushu University  
Josef Matyas, Pacific Northwest National Laboratory

---

\* Invited Paper

SESSION F.EN08.08: Live Lightning/Flash I: Effects in Nuclear Waste Forms  
Session Chairs: Neil Hyatt and William Weber  
Wednesday Afternoon, December 2, 2020  
F.EN08

5:15 PM \*F.EN08.04.01

**Radiation Damage and Thermal Aging of Nuclear Waste Forms** William J. Weber; The University of Tennessee, United States

Self-radiation damage from the decay of radionuclides can affect microstructural evolution, phase stability, and thermodynamic properties in nuclear waste forms. The principal sources of radiation are beta-decay of the fission products and alpha-decay of the actinide elements. In general, beta-decay of the short-lived fission products leads to ionizing radiation that is the primary source of radiation and heat generation in high-level waste forms during the first 600 years of storage. Ionization can cause covalent and ionic bond rupture, valence changes, localized electronic excitations, and significant changes in ionic mobility; however, there is no evidence of significant long-term effects of fission product decay on the physical properties of nuclear waste forms. Because of the long half-lives of the actinides and their daughter products, alpha-decay is dominant over very long timescales. Alpha decay produces energetic alpha particles (4.5 to 5.5 MeV) and recoil nuclei (70 to 100 keV) that result in both radiation damage and the accumulation of helium. The evolution of radiation damage due to alpha-decay has been studied at ambient temperature using short-lived actinides, such as  $^{238}\text{Pu}$  and  $^{244}\text{Cm}$ , in many candidate glass and ceramic waste forms, and the early stages of evolution occur during the thermal period of the waste form. Ion beam irradiations of candidate ceramics are more frequently employed due to decreased costs, shorter irradiation timescales and the non-radioactive nature of the irradiated materials. Ion irradiations are performed over a wider range of irradiation conditions to implant helium, study radiation damage kinetics, understand the separate and combined effects of alpha particles and alpha recoils, and benchmark against alpha-decay damage due to short-lived actinides. At ion energies (keV to MeV) typically used to study alpha-decay damage in nuclear waste forms, the electronic and nuclear energy losses are both important, and the spatial coupling of electronic and nuclear energy loss can lead to reduced or enhanced damage production along the ion trajectory. While alpha particles are much less damaging than alpha recoils, the electronic energy loss from the alpha particles can also cause athermal annealing of alpha-recoil damage that can impact the evolution of radiation damage. Helium implantation studies have shown that helium bubbles form above a threshold helium concentration in candidate waste forms. Swift heavy ions (several hundred MeV to several GeV) have also been used to study radiation damage in nuclear waste forms; although the damage production mechanism and energy densities are substantially different from beta decay or alpha decay, large volumes are damaged.

5:21 PM OPEN DISCUSSION

5:27 PM F.EN08.04.03

**Characterising the Effect of Heavy-Ion Irradiation on the Microstructure of Ce-Doped Compounds** Ritesh Mohun<sup>1</sup>, Sebastian Lawson<sup>1</sup>, Theo Cordara<sup>1</sup>, Hannah Smith<sup>1</sup>, Clémence Gausse<sup>1</sup>, Max Cole<sup>1</sup>, John S. McCloy<sup>2</sup>, Marc Weber<sup>2</sup>, Sam Karcher<sup>2</sup>, Martin Stennett<sup>1</sup>, Neil Hyatt<sup>1</sup> and Claire L. Corkhill<sup>1</sup>; <sup>1</sup>The University of Sheffield, United Kingdom; <sup>2</sup>Washington State University, United States

In this study, we aimed to investigate the radiation effects in doped-fluorite structure ceramics.  $\text{CeO}_2$  was chosen as the host matrix because of its fluorite crystallographic (Fm-3m) structure, which consists of a simple cubic oxygen sub-lattice with the cation ions occupying alternate cube centres, similar to  $\text{UO}_2$ ,  $\text{PuO}_2$ , and  $\text{ThO}_2$ . The objective was first to quantify the defect chemistry/configurations when  $\text{CeO}_2$  is doped with trivalent yttrium at different concentrations, and then to study the atomistic changes when the solid solutions were irradiated with 3 MeV gold ion under two different fluence, corresponding to a damage level of 6 dpa and 33 dpa values respectively.

Initial X-ray diffraction measurements of the prepared samples showed a contraction of the unit cell with Y-content attributed to a certain long-range ordering of the anion vacancies with randomly distributed  $\text{Y}_2\text{O}_3$  micro-domains of 'C-type' structure which grows coherently within the fluorite matrix. This observation corroborates with Extended X-ray Absorption Fine Structure (EXAFs) analysis which indicated a change in the coordination number when the dopant is introduced in the  $\text{CeO}_2$ . On the other hand, Raman spectroscopy was used to quantify the presence of oxygen vacancy-type defects formed to compensate for the charge due to the substitution of  $\text{Ce}^{4+}$  with a trivalent dopant and the presence of reduced  $\text{Ce}^{3+}$ . In regards to the irradiated samples, the excellent radiation stability of Ce-based compounds was reported and it was observed that Au-incident ions tend to reduce  $\text{Ce}^{4+}$  to  $\text{Ce}^{3+}$ . In addition, Positron annihilation spectroscopy measurements showed that the lower irradiation fluence increases considerably the concentration of lattice damages close to the disorder saturation level, where all the implanted positrons are trapped and a further increase in the irradiation dose initiates a dynamic damage recovery. Relevant defect mechanisms for the two considered irradiation fluence studies were identified and will be detailed in this presentation.

### 5:33 PM F.EN08.04.05

**Effect of Ionizing Radiation on PuO<sub>2</sub> and Surrogate Oxide Materials Under Storage Condition** Luke Jones<sup>1</sup>, Darryl Messer<sup>1</sup>, Robin Orr<sup>2</sup>, Howard E. Sims<sup>2</sup>, Andrew B. Horn<sup>1</sup> and Simon M. Pimblott<sup>3</sup>; <sup>1</sup>University of Manchester, United Kingdom; <sup>2</sup>National Nuclear Laboratory, United Kingdom; <sup>3</sup>Idaho National Laboratory, United States

The stockpile of plutonium separated from used nuclear fuel amounts to many 100s of tonnes. The majority of this plutonium is stored as PuO<sub>2</sub> powder packaged in multi-can containers. The conditions during the packaging of reprocessed PuO<sub>2</sub> for long term storage are closely controlled to limit water uptake as radiolytic decomposition of any adsorbed water will lead to the formation of both a potentially flammable atmosphere containing molecular hydrogen as well as reactive oxygen species which may be incorporated into the oxide phase. Consequently, the safety case for the long-term storage of PuO<sub>2</sub> requires a complete understanding of the fundamental physical, chemical and materials degradation processes occurring at the water-oxide interface inside the storage canisters. This study investigates the effect of ionizing radiation on PuO<sub>2</sub> and various surrogate oxides under atmospheres potentially encountered in storage canisters.

To elucidate the effects of adsorbed water, samples of baked oxide powder were equilibrated in humidity chambers to attain a wide range of masses of water adsorbed onto the powder surface. In the case of PuO<sub>2</sub>, once the surface water on the oxide had equilibrated with the humid atmosphere, the samples were sealed into a glass vessel held at constant humidity with either an argon or a nitrogen over-gas and left for up to 3 months. Periodic sampling of the headspace was undertaken and the atmosphere above the oxide analyzed using gas chromatography. In the case of the surrogate oxides, once the oxides had adsorbed the maximum quantity of water, the samples were flame sealed under argon into a glass tube and Co-60 gamma irradiated. Prior to and after gamma irradiation, the oxide powders were characterized using a variety of different microscopy and spectroscopy methods. Following gamma irradiation, the headspace was analyzed using gas chromatography. For PuO<sub>2</sub>, the rate at which H<sub>2</sub> was produced increased with increasing water loading. This result contrasts with the experimental data in this study and from similar experiments in the literature utilizing UO<sub>2</sub>, CeO<sub>2</sub> and ZrO<sub>2</sub> which showed a higher rate of production for lower water coverages. There was no evidence of a steady state hydrogen concentration being reached in the PuO<sub>2</sub> experiments, an outcome opposite of that observed in storage canisters and in experiments performed by other groups in which the PuO<sub>2</sub> was not held under constant humidity. Radiolytic production of molecular oxygen was not observed.

Comparison of the properties of the surrogate oxide (ZrO<sub>2</sub>) powder prior to and post irradiation did not reveal any differences in stoichiometry, surface functionalization or the formation of oxygen-centered free radicals, so the location of the sibling oxidant to the evolved molecular hydrogen currently remains unanswered.

Parallel experimental and modeling studies considering the chemistry of PuO<sub>2</sub> and surrogate oxides in H<sub>2</sub>:O<sub>2</sub>:Ar atmospheres are ongoing. To perform the experiments, a bespoke manifold was designed and commissioned to mix various ratios of H<sub>2</sub>-O<sub>2</sub> and Ar gas. Gas chromatography was used to analyse post-irradiated samples. Experiments were performed in 10 ml volume 316 stainless steel canisters (with no degradable polymeric components). Experimental data will be presented showing the extent of recombination of H<sub>2</sub>-O<sub>2</sub> mixtures in Ar under <sup>60</sup>Co  $\gamma$  rays and accelerated He ion irradiation and the influence an oxide surface on this recombination: radiolytic reaction of H<sub>2</sub> with O<sub>2</sub> to form H<sub>2</sub>O is enhanced over what is expected from gas phase processes suggesting significant interfacial chemistry.

Acknowledgement: This work was supported by the Dalton Cumbrian Facility Project, a joint initiative of the University of Manchester and the Nuclear Decommissioning Authority, by the UK Engineering and Physical Sciences Research Council and by the US Department of Energy, Office of Nuclear Energy.

### 5:39 PM F.EN08.04.06

**Quantifying the Effects of Grain Boundary Areas on the Irradiation Behaviour of UO<sub>2</sub>** Ritesh Mohun, Sebastian Lawson, Daniel Bailey, Shikuan Sun, Clémence Gausse, Hannah Smith, Max Cole, Martin Stennett, Neil Hyatt and Claire L. Corkhill; The University of Sheffield, United Kingdom

Complex microstructural changes occur in nuclear fuels due to the extreme environments of intense irradiation and high temperature during in-reactor operations. Several theoretical and experimental works are currently in progress to determine the effect of crystalline defects which has a major influence on the behaviour of fission products, mainly in regards to rare gases, that may impact the life-span of the rod-type uranium fuel element. For instance, the nucleation of insoluble gas bubbles is thought to act as trapping sites for migrating vacancy-type defects, and further increase in the damage levels induces significant microstructural modifications. In this study, we aimed to investigate the specific role of microstructure on the radiation stability of nuclear fuels.

For this purpose, UO<sub>2</sub> pellets with different microstructures were initially prepared through the wet chemistry route and sintered at different temperatures. Scanning electron microscopy and X-ray diffraction characterisations were performed to quantify the grain size/boundaries areas and crystallinity of the pristine samples. Raman spectroscopy also proved useful and

allowed to investigate the effect of sintering temperature on the concentration of intrinsic lattice defects. The samples were then implanted with 1 MeV Krypton-ions at room temperature to induce irradiation damages in the matrix of the different grain-size  $\text{UO}_2$  pellets.

Post-irradiation measurements were carried to highlight the excellent radiation stability of fluorite-type nuclear fuels. However, it was observed that the  $\text{UO}_2$  microstructure has an important effect on the point defects produced by the displacement cascades induced by ionic implantation. In this presentation, an attempt is made to detail the mechanisms occurring near the defect-boundary interfaces in relation to radiation damage to highlight the precise role of grain boundaries modifying the defects behaviour and their subsequent evolution in fluorite structure relevant to nuclear fuels.

#### 5:45 PM F.EN08.04.07

**Assessment of Positrons for Defect Studies in  $\text{UO}_2$  and  $\text{CeO}_2$  Materials** Marc H. Weber<sup>1</sup>, Ritesh Mohun<sup>2</sup>, Sam Karcher<sup>1</sup>, Claire L. Corkhill<sup>2</sup> and John S. McCloy<sup>1</sup>; <sup>1</sup>Washington State University, United States; <sup>2</sup>The University of Sheffield, United Kingdom

The safe disposal and long-term isolation of spent mixed oxide nuclear fuel poses significant challenges. Uranium and plutonium oxides enriched with rare earth and lanthanide fission products and under constant irradiation with alpha particles and neutrons must be stored in geologic formations for thousands of years. A detailed understanding of the microstructure and chemistry is required to optimize processing designed to recover fissionable products from used fuel and to improve the safety and volume of radioactive waste. Cerium oxide (ceria) has been identified as a suitable non-radioactive substitute to study the microstructure and its evolution under long term irradiation.

A number of techniques have been applied to uranium and cerium oxides to investigate basic properties and point defects. These include neutron scattering, X-ray diffraction and Raman spectroscopy of as produced, irradiated and annealed materials. These are sensitive to structural properties (XRD, neutrons) and oxygen vacancies (Raman). Positron annihilation spectroscopies (PAS) are sensitive to neutral and negatively charged vacancy-like point defects and impurity-vacancy complexes. Positrons can provide depth resolved information about uranium or cerium vacancies to complement Raman data. PAS has been applied previously to  $\text{UO}_{2+x}$  to investigate the properties of nuclear fuels.[1,2,3] Virtually no PAS work exists on  $\text{CeO}_2$ , doped or undoped. Currently, PAS are being used to investigate rare earth and lanthanide doped cerium oxide. The work on uranium oxide by the group of MF Barthe[1,2] demonstrated the presence of significant concentrations of uranium vacancies or Schottky defects as well as the presence of negatively charged interstitial oxygen atoms in oxygen rich. They also investigated the effect of 1 MeV helium implantation and the interaction of the implanted helium with the formed vacancies during annealing. Xe bubbles and their thermal evolution could also be observed.[4]

In this presentation, the basics of positron annihilation spectroscopy will be presented. PAS work on undoped and doped cerium oxide will be shown and compared to results from uranium oxides. To simulate spent nuclear fuels, the samples were doped at different concentration with rare earth elements or yttrium, zirconium. Select samples were irradiated with heavy ions at different doses. Differences were observed depending on what simulated fission products are present. Preliminary results and literature searches show some correlation with Raman data.

**References:** [1] Barthe MF et al. EPJ Web of Conferences **115**, 03004 (2016), and references therein; [2] Barthe MF et al. Phys. Stat. Solidi **C4** 3627-3632 (2007); [3] Wiktor J Physical Review B **90**, 184101(2014); [4] Djourellov N. et al Journal of Nuclear Materials **432** 287-293 (2013)

**Acknowledgements:** MW, JM, and SK thank the Institute for Materials Research and U.S. Department of Energy Nuclear Energy University Program – Used Nuclear Fuel Disposition program, award # DE-NE0008689. JM thanks the US-UK Fulbright Commission, and JM and SK thank the S.Y. Chung Centenary Fellowship for support during the research period. RM and CC thank Engineering and Physical Sciences Research Council, under the UK-US Nuclear Energy University Programme (EP/R006075/1), an Early Career Research Fellowship awarded to CC (EP/N017870/1), and the MIDAS Facility, at the University of Sheffield, established with support from the UK Department of Energy and Climate Change.

SESSION F.EN08.09: Live Lightning/Flash II: Microstructural Investigations  
Session Chairs: Daniel Austin and Josef Matyas  
Wednesday Afternoon, December 2, 2020  
F.EN08

#### 6:00 PM F.EN08.06.02

**Secondary Phase Derived Uranium Oxy-Hydroxides as Potential Host Matrices for Anionic Fission Daughters** Gabriel Murphy, Philip Kegler, Andreas Wilden, Martina Klinkenberg and Evgeny Alekseev; Forschungszentrum Jülich GmbH,

## Germany

Layered uranium oxyhydroxide (LUOH) phases are important minerals which occur as weathering products of uraninite deposits and also importantly, are encountered during the paragenetic sequence of secondary phases that form during an accident scenario involving spent nuclear fuel (SNF) in the near-field (1). Understanding the structural-chemistry of these phases is of importance as via interaction mechanisms, they can potentially retard the transport of harmful fission daughters from SNF towards groundwater and the biosphere. Particularly it has been previously shown that the secondary LUOH phases, such as metaschoepite, uranophane and studite, can act to impede and retard the transport of fission daughters and SNF products such as  $\text{NpO}_2^+$ ,  $\text{Cs}^+$  and  $\text{Sr}^+$  (2,3). Chemically, the origin of these favourable interactions is predominantly due to favourable intercalation chemistry between cationic SNF species with that of anionic lattices of encountered phases. However in the case of anionic fission daughters, such as  $^{131}\text{I}$  and  $^{79}\text{Se}$ , these present considerable concern during release from SNF as the overwhelming majority of near-field SNF secondary phases and minerals possess anionic lattices, including LUOH phases, which are typically not expected to react and intercalate well with. Although some evidence is present for partial intercalation of anionic iodine into layered mineral structures through ionic exchange mechanisms in model system studies (4-6) the current consensus is the retention of anionic SNF release products in the near field is not proven and best considered in the far-field of SNF repository performance and accident scenario assessment. Layered double hydroxide (LDH) phases are considered prime candidate materials and minerals for the retention of these anionic phases and received considerable attention (7), however in the context of an accident scenario with SNF their occurrence is not certain. We have recently undertaken a comprehensive systematic investigation of actinide solid state systems relevant to SNF and nuclear waste management. In the course of our investigations we have examined the chemical interactions that may occur between the anionic fission daughter species, I and Se in different chemical forms with some potential LUOH phases associated with SNF. Using a combination of batch synthesis experiments and *in situ* exchange experiments, we provide evidence for the inclusion and retention of these anionic species in LUOH phases. Importantly, using single crystal X-ray diffraction we show the ability for anionic species to be incorporated into certain LUOH phases is a consequence of their respective topological arrangement of uranyl and hydroxyl groups. Furthermore, by considering the topology and structural chemistry of LUOH phases, it can allow for a predictive basis to be established towards which the relative interaction affinity between certain anionic fission daughter species and specific LUOH phases can be understood. The systematic experimental studies used in this investigation will be discussed in detail w.r.t potential interactions that occur between anionic fission daughters and LUOH derived secondary phases that occur during an accident scenario involving SNF.

### References:

- 1 P. C. Burns, R. C. Ewing, and A. Navrotsky, *Science* 335, 1184 (2012).
- 2 J. I. Friese, M. Douglas, E. C. Buck, S. B. Clark, and B. D. Hanson, *MRS Proceedings* 824, CC9.2, Cc9.2 (2004).
- 3 A. Espriu-Gascon, J. Giménez, I. Casas, and J. de Pablo, *Journal of Hazardous Materials* 353, 431 (2018).
- 4 S. Wu, S. Wang, A. Simonetti, F. Chen, and T. E. Albrecht-Schmitt, *Radiochim. Acta* 99, 573 (2011).
- 5 S. Wu, F. Chen, M. Kang, Y. Yang, and S. Dou, *Radiochim. Acta* 97, 459 (2009).
- 6 S. J. Wu, F. R. Chen, A. Simonetti, and T. E. Albrecht-Schmitt, *Environ. Sci. Technol.* 44, 3192 (2010).
- 7 N. Daniels et al., *Applied Clay Science* 176, 1 (2019).

### 6:06 PM F.EN08.06.03

**An Investigation into the Local Structure of  $\text{Ln}_2\text{TiO}_5$  Stuffed Pyrochlores Through XAS Analysis** Daniel A. Austin<sup>1</sup>, Martin Stennett<sup>1</sup>, Shikuan Sun<sup>1</sup>, Bruce Ravel<sup>2</sup> and Neil Hyatt<sup>1</sup>; <sup>1</sup>University of Sheffield, United Kingdom; <sup>2</sup>National Institute of Standards and Technology, United States

Stuffed pyrochlore ceramics, with the general stoichiometry  $\text{Ln}_2\text{TiO}_5$ , have received significant interest for application within the nuclear industry due to their high radiation tolerance, good thermal stability, and structural flexibility. These ceramics have been proposed as a potential wasteform for actinide wastes, for incorporation into inert matrix fuels (IMF), and as inclusion in oxide dispersion strengthened (ODS) steels. These materials can be viewed as derivatives of pyrochlore structured  $\text{Ln}_2\text{Ti}_2\text{O}_7$  phases and are often more conveniently written in the form  $\text{Ln}_2(\text{Ln}_{0.67}\text{Ti}_{1.33})\text{O}_{6.67}$ , where the pyrochlore B-site now contains mixed occupancy. These materials can adopt a variety of different crystal structures depending on the size of the lanthanide cation, and the temperature and pressure used during synthesis. The three reported crystal structures are orthorhombic (*Pnma*), hexagonal (*P6<sub>3</sub>/mmc*) and cubic defect-fluorite (*Fm-3m*). Compounds that are nominally assigned as defect-fluorite by X-ray diffraction have been probed by neutron diffraction (ND) and transmission electron microscopy (TEM) revealing features consistent with the presence of short range ordered regions with the (*Fd-3m*) cubic pyrochlore structure.



In this contribution we present a study probing the local structure of a series of  $\text{Ln}_2\text{TiO}_5$  ( $\text{Ln} = \text{La, Gd, Dy, Yb, Y}$ ) compounds. They were synthesised via a solid state synthesis route under different cooling regimes to prepare samples of identical chemistry but different short range ordering. Fabrication of high quality sintered specimens of  $\text{Ln}_2\text{TiO}_5$  phases is a particular challenge due to their refractory nature. Therefore, a systematic study of sintering parameters was undertaken to optimise the fabrication of sintered ceramic specimen. Characterisation of these materials was performed using techniques including XRD, SEM/EDX and XAS. Initial XAS results show that some of these materials do have a cubic pyrochlore-like local structure but show a deviation from the ideal coordination environment of cubic pyrochlore.

#### 6:12 PM F.EN08.06.04

##### **Chemical Bond Complexity in $\text{A}^{\text{III}}_6\text{B}^{\text{VI}}\text{O}_{12}$ Fluorite-Related Ternary Oxides** Maulik K. Patel<sup>1</sup>, Kurt E.

Sickafus<sup>2</sup> and Gianguido Baldinozzi<sup>3</sup>; <sup>1</sup>University of Liverpool, United Kingdom; <sup>2</sup>The University of Tennessee, Knoxville, United States; <sup>3</sup>Université Paris-Saclay, France

Oxides with generic stoichiometry  $\text{A}_7\text{O}_{12}$  occupy, in a generic phase diagram, an intermediate place between fluorite and bixbyite structure types. Their structure is derived from the ideal fluorite structure, and it is characterized by a more or less pronounced ordering of the O vacancies within the average fluorite sublattice. We believe that ternary oxides with this generic formula display some structural flexibility relevant to fission product stabilization in nuclear fuels and to the understanding of actinide waste forms as well. We would like to discuss the structural characteristics of the chemical bonds in these ternary systems consisting of trivalent and hexavalent cations studying the electron density using the tools of the quantum theory of atoms in molecules (Bader's AIM theory and ELF). Eventually, in these compounds with generic formula  $\text{A}^{\text{III}}_6\text{B}^{\text{VI}}\text{O}_{12}$ , the A cation can be either an actinide or a rare earth element, whereas the B cation can be either a transition metal (W, Mo) or hexavalent uranium. We believe that studying the characteristics of the polyhedron of the sevenfold coordinated A ion is particularly interesting: it is often described in the literature as a mono-capped trigonal prism, with bond lengths exhibiting an extremely large dispersion, ranging for instance from 2.19 to 2.70 Å in  $\text{Y}_6\text{WO}_{12}$ . We would discuss the implications of this large dispersion of distances on the chemical bond characteristics, compare DFT models with experiments on pristine and irradiated specimens, and discuss the competitive metastability of the oxygen deficient cubic fluorite phase that can be observed in some of these systems, as for instance  $\text{Y}_6\text{MoO}_{12}$ .

SESSION F.EN08.10: Live Lightning/Flash III: In Memory of Lou Vance and His Contribution to Development of Nuclear Waste

Session Chairs: Daniel Gregg and Josef Matyas

Thursday Morning, December 3, 2020

F.EN08

#### 11:30 AM F.EN08.01.01

**Remembering Eric (Lou) Vance (1942-2019)—A Pioneer in Nuclear Wasteforms** Daniel Gregg, Rifat Farzana, Pranesh Dayal, Rohan Holmes and Gerry Triani; Australian Nuclear Science and Technology Organisation, Australia

Dr Eric (Lou) Vance was a trailblazer in developing novel treatment solutions for intractable nuclear wastes, who spent 32 years at the Australian Nuclear Science & Technology Organisation (ANSTO) in Sydney. Largely known for his contributions to Synroc technology, Lou's experience spans multiple continents including time at Pennsylvania State University with McCarthy and Roy as well as time at the Atomic Energy of Canada Limited where he studied sphene glass-ceramics. In 1987 he was recruited to ANSTO to progress Synroc technology. Under Lou's leadership, the original Synroc titanate full ceramic formulations invented by Ringwood evolved into a waste treatment technology platform. This platform can be applied to produce glass, glass-ceramic and ceramic wasteforms via hot-isostatic pressing.

Lou's seminal contributions to the science of nuclear waste management are evident in his ~400 scientific articles in international journals/refereed conference proceedings and his co-authorship of 3 patents relating to Synroc. An entertaining and highly popular speaker, Lou was committed to attending two to three international conferences a year to showcase the Synroc technology and his innovative nuclear wasteform research. Lou was a steadfast member of the Scientific Basis for Nuclear Waste Management symposium for several decades and a highly enthusiastic mentor. In this paper, we celebrate the research career of the late Dr Vance and his substantial and essential contributions to the field of nuclear wasteform development and to the development of Synroc technology.

#### 11:36 AM F.EN08.01.02

**Iodine Waste Forms—Review and Contributions of Dr. Lou Vance** John S. McCloy<sup>1,2</sup>, Brian Riley<sup>2,1</sup> and Saehwa Chong<sup>2,1</sup>; <sup>1</sup>Washington State University, United States; <sup>2</sup>Pacific Northwest National Laboratory, United States

The capture and immobilization of long-lived radioactive iodine I-129 must be a priority for future nuclear fuel cycles involving reprocessing. This review summarizes work on waste forms for radioiodine, emphasizing the contributions of Dr. Lou Vance as well as recent work in other groups. As early as the 1980s, Dr. Vance recognized the need for iodine waste forms and was a leader in innovative waste form solutions for iodine and other volatile halides. His studies included immobilization in silicate minerals including zeolites and sodalite, encapsulation in metallic tin, partitioning in synroc mixed-phase ceramics, and consolidation of copper iodide. Here, we recognize his particular contributions to the understanding of iododolomite, and note some recent work by others following in his footsteps.

**11:42 AM F.EN08.01.03**

**Hot-Isostatic Pressing of Synroc-C—The Effect of Ti-Metal Additions** Daniel Gregg, Rifat Farzana, Pranesh Dayal, Zaynab Aly, Rohan Holmes and Gerry Triani; Australian Nuclear Science and Technology Organisation, Australia

Synroc-C, a multiphase ceramic wastefrom based on stable and leach resistant titanate minerals, was invented by Australian scientists in the late 1970s. The formulation was directed toward the immobilization of PUREX wastes from the reprocessing of nuclear fuels and was originally to be produced *via* hot-uniaxial pressing (HUPing). Although glass was chosen as the preferred technology during the “Atlanta shoot-out” in the US in 1981, this was ultimately because Synroc lacked the technical maturity of vitrification. However, given the enhanced performance properties of Synroc-C as a wastefrom, significant interest has been sustained in this Synroc formulation. The vast majority of work on Synroc-C has been undertaken following consolidation by HUP processing. There is very little reported on hot-isostatically pressed (HIPed) Synroc-C, where HIP canisters are filled with the calcined wastefrom material (waste + additives), evacuated and sealed. The HIP canister is then loaded into the HIP chamber and processed through the desired time-temperature-pressure profile to achieve a dense and consolidated wastefrom. The appropriate redox conditions within the HIP canister are vital to the formation of the correct phase composition and ultimately attaining a stable and leach resistant wastefrom.

In this study, we investigate the effect of Ti-metal addition on the phase formation, microstructural characteristics and durability of HIPed Synroc-C. Dense Synroc-C samples containing 20 wt.% simulated high level waste and with varying Ti-metal additions (0%, 2%, 4% and 8 wt.%) were prepared by HIPing in stainless steel HIP canisters. An investigation of microstructure, mineral phases and elemental distribution in the samples was carried out using quantitative X-ray diffraction and electron microscopic analyses. Results from durability tests are also discussed.

**11:48 AM F.EN08.01.04**

**Immobilisation Options for the Disposition of UK Plutonium** Neil Hyatt, Lewis Blackburn, Laura Gardner, Shikuan Sun, Martin Stennett and Claire L. Corkhill; University of Sheffield, United Kingdom

The UK holds the world’s largest inventory of separated plutonium under civil safeguards, projected to reach 140 tons at the end of reprocessing options. A significant fraction of this material requires immobilisation for disposal since it is unsuitable for reuse in MOX fuel, which is HM Government’s preferred policy for disposition. Additionally, should it not prove possible to implement the policy for plutonium reuse in MOX fuel an alternative immobilisation and disposal option will be required for the greater inventory. This presentation will review the current status of wastefrom engineering and process development for manufacture of zirconolite ceramic and glass-ceramic wastefroms for immobilisation of waste and inventory plutonium. We will demonstrate the development of Ce and U surrogate formulations, validated by targeted plutonium studies, with regard to phase assemblage and Pu / surrogate incorporation mechanism. The development of a novel containment system to enable hot isostatic pressing studies utilising U and Th surrogates will be presented, together with operational experience. The application of new, and potentially disruptive, wastefrom manufacture technology will also be discussed.

**11:54 AM F.EN08.01.05**

**Immobilization of Cesium and Iodine into Cs<sub>3</sub>Bi<sub>2</sub>I<sub>9</sub> Perovskite-Silica Composites and Core-Shell Waste Forms** Kun Yang and Jie Lian; Rensselaer Polytechnic Institute, United States

Cs<sub>3</sub>Bi<sub>2</sub>I<sub>9</sub>, a defect perovskite derivative, is a potential host phase to immobilize iodine and cesium with high waste loadings. In this work, two strategies are explored to form Cs<sub>3</sub>Bi<sub>2</sub>I<sub>9</sub>-silica composites and core-shell structures in order to improve chemical durability of waste form materials meanwhile maintaining high waste loadings. Cs<sub>3</sub>Bi<sub>2</sub>I<sub>9</sub> loadings as high as 70 wt.% were incorporated into a silica matrix to form silica-ceramic composites, and 20 wt.% Cs<sub>3</sub>Bi<sub>2</sub>I<sub>9</sub> was encapsulated into silica to form a core-shell structure at low temperatures and high pressure. Semi-dynamic leaching experiments indicated Cs

and I were incongruently released from waste form matrices depends on the bonding environment and surface passivating effect. A BiOI alteration layer formed during the surface reorganization, acting as a passivation layer to reduce the release of radionuclides. The long-term iodine release rate was low ( $30 \text{ mg m}^{-2} \text{ day}^{-1}$ ) for 70 wt.%  $\text{Cs}_3\text{Bi}_2\text{I}_9$ -silica composites leached in deionized water at  $90^\circ\text{C}$ , which can be further reduced to  $5 \times 10^{-3} \text{ mg m}^{-2} \text{ day}^{-1}$  for the 20 wt.% core-shell structure. This work highlights a robust way to immobilize the highly mobile radioactive nuclides and surface passivating mechanism through elemental transport across the liquid-solid interface for  $\text{Cs}_3\text{Bi}_2\text{I}_9$ .

#### 12:00 PM F.EN08.01.06

**Incorporation Mechanism of Sr and Ca in Geopolymer Cement Wasteforms** Brant Walkley<sup>1,1</sup>, Xinyuan Ke<sup>2,1</sup>, Ben Griffith<sup>3</sup>, Oday Hussein<sup>1</sup>, Susan Bernal<sup>4</sup>, John Hanna<sup>3</sup> and John Provis<sup>1</sup>; <sup>1</sup>The University of Sheffield, United Kingdom; <sup>2</sup>University of Bath, United Kingdom; <sup>3</sup>University of Warwick, United Kingdom; <sup>4</sup>University of Leeds, United Kingdom

Radioactive waste streams containing  $^{90}\text{Sr}$ , from nuclear power generation and environmental cleanup operations, are immobilised in the UK in blended Portland cement (PC) grouts to limit radionuclide leaching. Due to poor compatibility of certain wastes with PC, alternatives such as alkali aluminosilicate 'geopolymer' binders are being investigated. Here, we used multinuclear solid-state nuclear magnetic resonance (NMR) spectroscopy probing  $^{23}\text{Na}$ ,  $^{27}\text{Al}$ ,  $^{29}\text{Si}$  and  $^{39}\text{K}$  nuclei, including high-field (20.0 T) and cross polarisation experiments, along with X-ray diffraction experiments, to investigate the incorporation mechanism of  $\text{Sr}^{2+}$  and  $\text{Ca}^{2+}$  in geopolymer wasteforms formed by alkali-activation of metakaolin. The main reaction product identified in gels cured at both  $20^\circ\text{C}$  and  $80^\circ\text{C}$  is a fully polymerised Al-rich alkali aluminosilicate hydrate ((N,K)-A-S-H) gel comprising Al and Si in tetrahedral coordination, with Si in  $\text{Q}^4(4\text{Al})$  and  $\text{Q}^4(3\text{Al})$  sites, and  $\text{Na}^+$  and  $\text{K}^+$  balancing the negative charge resulting from  $\text{Al}^{3+}$  in tetrahedral coordination. Faujasite-Na and partially Sr-substituted zeolite Na-A form within the gels cured at  $80^\circ\text{C}$ . Incorporation of  $\text{Sr}^{2+}$  or  $\text{Ca}^{2+}$  displaces some  $\text{Na}^+$  and  $\text{K}^+$  from the charge-balancing sites, with a slight decrease in the Si/Al ratio of the (N,K)-A-S-H gel.  $\text{Ca}^{2+}$  and  $\text{Sr}^{2+}$  induce essentially the same structural changes in the gels. It was concluded that the disordered geopolymers can readily accommodate  $\text{Sr}^{2+}$  and  $\text{Ca}^{2+}$  into their aluminosilicate framework structure via substitution of the divalent alkaline earth cations for monovalent alkali cations in charge balancing sites. This indicates that geopolymer gels are excellent candidates for immobilisation of radioactive waste containing  $^{90}\text{Sr}$  and other alkaline earth radionuclides.

#### 12:06 PM \*F.EN08.01.07

**Development and Application of Colloidal Silica-Based Grouts for Waste Containment** Rebecca Lunn, M. Pedrotti, P. Bots, G. El Mountassir, A. Pegano and J. Renshaw; University of Strathclyde, United Kingdom

The UK's nuclear sites contain stored wastes in ponds and silos as well as large volumes of contaminated concrete and soil. During storage decommissioning and deconstruction operations, there are significant risks of radionuclide transport via groundwater and airborne particulate releases. Colloidal silica grout is a nano-particulate material that has the potential to reduce these risks very significantly. In order to utilize such nanoparticulate material as a barrier, we require a detailed understanding of the grout properties. These include its injectability, mechanical behaviour, hydraulic properties, durability and its impact on the geochemistry of radionuclides in the environment (e.g. fission products such as Sr and Cs). Over the past 5 years, experiments at Strathclyde have progressively investigated colloidal silica grout properties. Colloidal silica-grouted sand shows an increased stiffness and an enhanced peak friction angle, while still having a very low hydraulic conductivity ( $\sim 10^{-10}$  m/s), typical of intact clay. Even under drained conditions, the grout provides mechanical improvement to the soil and retains a very low hydraulic conductivity. The impact on radionuclide geochemistry has been investigated through combining leaching experiments with XAS analyses. These show that colloidal silica induces several competing effects on the mobility of Sr and Cs. First, cations within the colloidal silica gel compete with Sr and Cs for surface complexation sites. Second, an increased number of surface complexation sites is provided by the silica nanoparticles and finally, the elevated pH within the colloidal silica increases the surface complexation to clay minerals and the silica nanoparticles. Finally, experiments to investigate injectability and monitorability show that colloidal silica grout can be successfully injected in silty-sands, its gelling time can be accurately predicted in a full range of environmental conditions and the location of the subsurface barrier created can be accurately identified using Electrical Resistivity Tomography. Potential applications of colloidal silica on nuclear sites include inhibiting radionuclide migration from recently decommissioned structures during care and maintenance (e.g. silos and ponds from which wastes have already been retrieved); the development of primary or secondary barriers around existing radionuclide (or other) contaminated areas; and stabilisation of underground structures. Research work is continuing to improve the mechanical and chemical properties of colloidal silica grouts, such that they can be tailored to suit for individual nuclear site-based applications.

#### 12:12 PM F.EN08.01.08

**Utilizing Machine Learning in Nuclear Waste Management** Natalie J. Smith-Gray, Irmak Sargin, Scott Beckman and John S. McCloy; Washington State University, United States

Machine learning (ML) is a valuable tool that can be used, in combination with domain expertise, to provide insight into nuclear waste vitrification processes. This talk summarizes our preliminary efforts in using ML methods to address important problems facing the nuclear waste vitrification mission at the Hanford site in Washington State. Three case studies using ML modeling will be described: nepheline crystallization, refractory corrosion, and sulfate solubility. In Hanford high-level waste, nepheline crystallization can occur in melt compositions containing high Na and Al contents when glass cools slowly in the canister, partitioning radioactive components to a less-durable residual glass fraction. In low-activity waste compositions, which are generally higher in alkali and volatile components like sulfur and halides, different critical issues present. Firstly, the low solubility of sulfate in borosilicate glass has led to many studies to predict glass composition dependence of this property, such that excess sulfur is not volatilized or partitioned to an alkali molten salt phase during processing. Second, these glass compositions tend to be harsh on refractories, leading to concerns over corrosion and general degradation of melter ceramic components and premature failure. For these three cases, existing datasets were used along with ML techniques to investigate the datasets and create predictive models for the output properties of interest. For all these studies, data science was used to identify underlying trends and correlations which were then applied to create supervised learning models. As a result, it has become evident that ML is a powerful tool that can be utilized to provide insight into complex issues in nuclear waste management, here specifically focused on immobilization by vitrification.

**12:18 PM F.EN08.01.09**

**Machine Learning for Glass Wasteforms' Design and Performance** Mathieu Bauchy; University of California, Los Angeles, United States

Vitrification is a key process to turn high-level nuclear waste into durable glasses. However, the virtually infinite compositional envelope accessible to glass wasteforms renders traditional design methods based on empirical knowledge and trial-and-error poorly efficient. In addition, the complex, disordered atomic structure of glasses makes it challenging to develop some mechanistic models relating their composition to their properties and performance. Here, I will discuss how machine learning offers a promising alternative route to predict the properties of glass wasteforms and guide/accelerate the design of novel glasses with enhanced performance for nuclear waste immobilization applications.

**12:24 PM F.EN08.01.10**

**Developing High-Throughput Computational Methods to Discover Hierarchical Waste Forms** Matthew Christian, Vladislav Klepov, Kristen Pace, Gregory Morrison, Theodore Besmann and Hans-Conrad zur Loye; University of South Carolina, United States

The development of stable actinide and other radionuclide hierarchical waste-form materials offer potential advantages of greater efficiency/loading, lower leach rates, ease of processing for so-called legacy nuclear wastes. Current waste-form discovery relies heavily on experiments that may or may not be successful in producing a viable product. Computational crystal discovery has aided in the search for new materials for different applications through use of high-throughput algorithms. However, these approaches have not been adapted to actinide and lanthanide compounds due to additional corrections required to properly handle *f*-orbital-containing elements. This presentation will consider the challenges and possible solutions to creating high-throughput computational methods to aid in the experimental discovery of novel hierarchical waste forms and offer tangible examples.

**12:30 PM F.EN08.01.11**

**Thermodynamic Modelling of the Pd-Ru-Te-O for Nuclear High-Level Waste Immobilization** Stéphane Gosse<sup>1,2</sup>, C. Laurin<sup>3</sup>, E. Régnier<sup>3</sup>, A. Laplace<sup>3</sup> and S. Schuller<sup>3</sup>; <sup>1</sup>CEA, France; <sup>2</sup>Université Paris-Saclay, France; <sup>3</sup>Commissariat à l'Énergie Atomique – Centre de Marcoule, France

Pd and Ru are the main platinoid fission products formed during burnup of nuclear fuels. During fuel reprocessing, these element partly dissolve in nitric acid and they exhibit very low solubility into borosilicate glasses during the vitrification process. Due to their affinity towards tellurium from the fission product solution, palladium mainly precipitates under (Pd-Te) intermetallics [1] and ruthenium is likely to form hcp solid solutions [2]. The composition and microstructures of these phases are also sensitive to oxygen potential [3]; oxydation of ruthenium can lead to needle-shaped or polyhedral (Rh,Ru)O<sub>2</sub> oxide phases [4]. These precipitates can affect significantly the physico-chemical properties of the glass melt during melting in hot or cold crucible.

For decades, many studies were undertaken at CEA [5] to point out the high temperature interactions of the platinum group

metals (PGM) issuing from the calcinated waste. In parallel to these studies, a Calphad database is being developed to address the thermodynamics of such systems to provide an assessment of the PGMs in nuclear waste. This study presents the assessed binary systems. Some calculations are also performed to highlight how this flexible tool makes is used to predict the stability between metallic and oxide phases as a function of temperature and oxygen potential mainly driven by the glass.

[1] S. Gossé, C. Guéneau, *Intermetallics* 19 (2011) 621-629

[2] S. Gossé, N. Dupin, C. Guéneau, J.-C. Crivello, J.-M. Joubert, *J. Nuclear Mater* 474 (2016) 163-173

[3] S. Gossé, S. Bordier, C. Guéneau, E. Brackx, R. Domenger, J. Rogez, *J. Nuclear Mater* 500 (2018) 252-264

[4] R. Pflieger, L. Lefebvre, M. Malki, M. Allix, A. Grandjean, *J. Nuclear Mater* 389 (2009)

*J. Nuclear Mater*, Vol. 389, N°3

[5] O. Pinet, S. Mure, *Journal of Non-Crystalline Solids*, 355 (2009) 221-227

### 12:36 PM F.EN08.01.12

**Thermodynamic Assessment of Zn-Containing Hollandite as a Robust Waste Form** Juliano Schorne-Pinto<sup>1</sup>, Kyle Brinkman<sup>2</sup>, Jake Amoroso<sup>3</sup>, Scott Misture<sup>4</sup> and Theodore Besmann<sup>1</sup>; <sup>1</sup>University of South Carolina, United States; <sup>2</sup>Clemson University, United States; <sup>3</sup>Savannah River National Laboratory, United States; <sup>4</sup>Alfred University, United States

The hollandite phase is a potential nuclear waste form for alkaline-earth metals such as Cs and Ba by chemical incorporation into the crystalline lattice. The general hollandite formula is  $A_xB_8O_{16}$  with the A-site habitually occupied by large mono- or divalent cations (e.g., Ba, Sr, Na, K, Rb, Cs, Pb), and the B-site by small di-, tri-, or tetravalent cations (e.g., Ti, Al, Fe, Cr, Sc) and it crystallizes in a tetragonal or monoclinic structure depending on the composition. Recently, our group has developed a thermodynamic database to describe the BaO-Cs<sub>2</sub>O-TiO<sub>2</sub>-Cr<sub>2</sub>O<sub>3</sub>-Al<sub>2</sub>O<sub>3</sub>-Fe<sub>2</sub>O<sub>3</sub>-FeO-Ga<sub>2</sub>O<sub>3</sub> system based on the Calphad method, where the hollandite solid-solution was modeled using the Compound Energy Formalism (CEF). Recent findings show the impact of varying A-site Cs stoichiometry of Zn-containing hollandite compositions and related thermodynamic stability. This consequently improved the limited performance of the hollandite phase in a multi-phase composite called SYNROC. We here report on our efforts to include the Zn in our waste form thermodynamic database, modeling the phase equilibria of the complex hollandite-forming oxide waste system.

SESSION F.EN08.11: Live Lightning/Flash IV: Management of Volatile Fission Products

Session Chairs: Amanda Lines and John McCloy

Thursday Afternoon, December 3, 2020

F.EN08

### 1:00 PM \*F.EN08.03.01

**Multi-Column Evaluations for the Capture and Separation of Krypton and Xenon Using Mordenite Based Sorbents** Mitchell Greenhalgh, Amy Welty and Troy Garn; Idaho National Laboratory, United States

A multi-column adsorption system has been designed and installed to evaluate the independent capture and separation of xenon and krypton utilizing solid phase sorbents being developed by the DOE-NE Offgas Sigma team. The xenon and krypton are present in the offgas stream resulting from a used nuclear fuel reprocessing plant. The system is intended to provide greater operating flexibility and testing at a wide range of flow rates while maintaining desired pressure conditions. This system also allows for continuous analysis of effluent gas from each column. The system was set up by packing the first column with AgZ-PAN which has demonstrated a high selectivity for xenon over krypton at ambient temperatures. A second column was packed with HZ-PAN to capture the krypton. The AgZ-PAN column was maintained at ambient temperatures whereas the HZ-PAN column was maintained at 191K. A simulated offgas stream consisting of 1000 ppmv xenon and 150 ppmv krypton in a balance of air was introduced to the first column to capture the xenon and the resulting xenon free effluent was then routed into the second column for krypton capture. Flowrates of the feed stream were varied from 50-2000 scfm. The results of the multi-column testing demonstrated successful separation of xenon from krypton and indicated that increasing superficial velocity does not significantly impact sorbent capacity or initial breakthrough of the columns. This procedure, while not optimized, may be used to reduce the final waste volume of captured radioactive gas species emitted from a reprocessing facility.

### 1:06 PM OPEN SLOT

**1:12 PM F.EN08.03.03**

**The State-of-the-art Development of Mechanically and Chemically Robust Sorbent for Management of Iodine** Josef Matyas, James Amonette and Michael Sinnewell; Pacific Northwest National Laboratory, United States

New generation sorbents are being investigated for the removal and immobilization of radioiodine from the gas streams in a used nuclear fuel reprocessing facility. Silver-functionalized silica aerogel (Ag<sup>0</sup>-aerogel) exhibits high selectivity and sorption capacity for iodine. Moreover, a feasible consolidation of iodine-loaded Ag<sup>0</sup>-aerogel to a durable SiO<sub>2</sub>-based waste form is an attractive choice for sequestering radioiodine. Extended-duration testing of Ag<sup>0</sup>-aerogel in highly oxidizing reprocessing off-gas streams indicated fragmentation of granules into small particles. These particles were held up in the column without being carried-over into the off-gas system. However, production of small particles during sorption can lead to compaction of the sorbent, restricting the flow of gas through the column. Our study targeted development of mechanically and chemically stable Ag<sup>0</sup>-aerogel through optimized synthesis process, which included using a patent-pending technology treatment to strengthen the granules. The reinforced Ag<sup>0</sup>-aerogel with bulk density ~ 0.5 g/cm<sup>3</sup> went through rigorous testing at different off-gas streams followed by attrition testing with a vibratory sieve shaker. There were no fines generated even after 60 min exposure to shaking speeds of ~1800 revolutions per minute, with ~3 mm orbital shaker movement. The mechanically/chemically robust Ag<sup>0</sup>-aerogel retained high iodine sorption capacity of 400.5 ± 2.2 mg/g. The presentation will focus on various strategies that have been developed to improve the mechanical/chemical properties of Ag<sup>0</sup>-aerogel and conclude with a summary of highlights and a prognosis for future developments.

**1:18 PM \*F.EN08.03.04**

**On-Line Monitoring of Molten Salts to Characterize Chemical Composition** Amanda Lines, Shirmir Branch, Heather Felmy, Adan Medina, Hope Lackey, Gregg Lumetta and Samuel Bryan; Pacific Northwest National Laboratory, United States

Molten salt systems provide highly efficient heat transfer options without pressurization, making them a potentially valuable tool throughout the energy sector, including solar power and nuclear energy. Molten salt reactors are of particular interest due to the advancements they can offer to the nuclear field, such as improved safety. However, the chemical behavior of key species anticipated in molten salt reactors is not well understood. Tools are needed to monitor and characterize the chemical composition of molten salts to better understand the behavior of actinides, fission products, and corrosion products. Furthermore, these tools are needed to allow for molten salt process control and to support the maintenance of materials accountancy. Of the options available, optical spectroscopy enables powerful routes to characterize these systems *in situ*. Utilization of these tools allows for the fast and robust identification and quantification of many chemical species of interest to molten salt processing, reactor control, and corrosion characterization. Most importantly, optical spectroscopy can enable the analysis of oxidation state ratios and species complexation, which can significantly impact system performance and corrosion behavior. Optical spectroscopy-based monitoring can be leveraged in fundamental and applied research. For example, optical spectroscopy can be paired with electrochemistry in spectroelectrochemistry to provide a powerful route to fundamental characterization of redox behavior, speciation, and chemical behavior dependence on temperature. Optical spectroscopy can also be paired with chemometric analysis to enable real-time quantification of target analytes within salt melts. Complex salt systems containing many chemical species will exhibit complex spectral data, presenting signal interferences and band overlap, which can hinder accurate analysis. However, the application of chemometric analysis can enable accurate characterization of multicomponent streams to provide real-time, automated monitoring of a process stream or batch. Optical spectroscopy-based on-line monitoring enables fast and robust identification and quantification of many actinides, fission products, and corrosion products. Here we demonstrate the application of optical monitoring approaches to the characterization of chloride-based salt melts containing lanthanides and actinides.

SESSION F.EN08.12: Live Lightning/Flash V: Spent Nuclear Fuel and Glass Corrosion Research  
Session Chairs: Dirk Bosbach and Lena Evins  
Friday Morning, December 4, 2020  
F.EN08

**8:00 AM \*F.EN08.05.01**

**Overview of the SKB Spent Fuel Research Program over the Years—Knowledge Gained and Remaining Open Questions** Lena Z. Evins; Swedish Nuclear Fuel and Waste Management Co, Sweden

The Swedish strategy for spent nuclear fuel has, since around 1980, been direct geological disposal. Research about the properties and dissolution of spent fuel has been going on since then. An overview of this research program is given here with a focus on questions posed and answered along the way, ending with remaining open questions. At the beginning, some basic studies were performed to gain information about spent fuel as wasteform. Dissolution studies were at first mainly performed in contact with air, and often with aqueous solutions that mimicked the expected groundwater chemistry. However, complexities relating to precipitation of secondary phases indicated that simplified water compositions were preferred. Knowing that the radioactivity of the fuel caused radiolytic oxidation of uranium and thus controlled the dissolution rate, there were also attempts to achieve reducing conditions via bubbling a hydrogen/argon mixture in presence of a palladium-catalyst. The first attempts resulted in variable results, but notably, a reduction in apparent leach rate was observed for some experiments [1]. Later, possibilities to perform the leaching experiments in autoclaves, with controlled hydrogen atmosphere, allowed experimental conditions closer to the expected repository conditions. These experiments showed that hydrogen, during this type of experimental set-up, could suppress oxidative dissolution caused by radiolysis [2,3]. A new phase of research was thus started where the mechanistic explanation for the observed behaviour was sought. Experimental work, both with spent nuclear fuel and with analogue materials, was coupled with modelling efforts. At the time of the SR-Site safety assessment [4], which was a part of the license application submitted in 2011, a certain understanding had been reached, based on the effect of metallic particles in fuel. Still, questions remained and studies performed during the last decade (see for example [5]) can now be summarised to illustrate the knowledge gained, and remaining open questions. This summary is utilized in the next step in the licensing process: the application to start building the spent fuel repository, which is expected to be submitted within the next couple of years. In the coming decade the SKB research program will continue, with the goal to support the development of the safety assessment report, SAR, which will be submitted to the authorities as a part of the license application connected to start of trial operations.

During all these years, international collaboration has been a cornerstone of the SKB research program. This international collaboration has been carried out via European projects or bilateral agreements, and triggered the start-up of the Spent Fuel Workshops [6]. The research program has also been presented at this MRS symposium since the early 1980's.

[1] Forsyth R, 1983. The KBS UO<sub>2</sub> leaching program. Summary report 1983-02-01. KBS/SKBF Technical Report 83-26.

[2] Spahiu, K., Werme, L. and Eklund, U.B., 2000. The influence of near field hydrogen on actinide solubilities and spent fuel leaching. *Radiochimica Acta*, 88(9-11), pp.507-512.

[3] Werme, L.O., Spahiu, K., Johnson, L.H., Oversby, V.M., King, F., Grambow, B. and Shoesmith, D.W., 2004. Spent fuel performance under repository conditions: A model for use in SR-Can. SKB-TR-04-19. Swedish Nuclear Fuel and Waste Management Co.

[4] SKB, 2011. Long-term safety for the final repository for spent nuclear fuel at Forsmark. Main report of the SR-Site project. SKB TR-11-01, Swedish Nuclear Fuel and Waste Management Co.

[5] Barreiro Fidalgo, A., Kumagai, Y. and Jonsson, M., 2018. The role of surface-bound hydroxyl radicals in the reaction between H<sub>2</sub>O<sub>2</sub> and UO<sub>2</sub>. *Journal of Coordination Chemistry*, 71(11-13), pp.1799-1807.

[6] Werme LO, 1984. Proceedings of the third fuel workshop. KBS/SKBF Technical Report 83-76

### 8:06 AM F.EN08.05.3

**Understanding the Dissolution of Advanced Doped Nuclear Fuels for Geological Disposal** [Hannah Smith](#), Theo Cordara, Ritesh Mohun, Clémence Gausse, Max Cole, Martin Stennett, Neil Hyatt and Claire L. Corkhill; The University of Sheffield, United Kingdom

The addition of dopants, including chromium and aluminium, to uranium dioxide fuel results in the formation of larger grained microstructures, capable of higher fission gas retention and reduced swelling during operation within nuclear reactors. Despite their growing use by nuclear power plant operators, the long-term dissolution behaviour of spent doped fuels, when compared to typical spent fuel, is not yet well constrained. In a geological disposal facility, the release of radionuclides is known to be controlled by the oxidation of the UO<sub>2</sub> matrix and the subsequent dissolution of UO<sub>2</sub><sup>2+</sup> species, therefore any changes to the matrix from the addition of dopants could be expected to influence the dissolution kinetics and/or mechanisms.

We here present the results of an investigation of how the addition of Cr<sub>2</sub>O<sub>3</sub> to UO<sub>2</sub> fuel influences the crystal chemistry of UO<sub>2</sub> and its dissolution kinetics. Initial results, from experiments performed in air and a bicarbonate solution, show that the addition of Cr<sub>2</sub>O<sub>3</sub> reduces the normalised mass loss of uranium. The potential influencing factors that give rise to increased durability with Cr addition, e.g. defect concentration, Cr-oxidation state etc. are discussed.

### 8:12 AM \*F.EN08.05.04

**Physico-Chemical Phenomena Located at the Solid/Liquid Interface of Uranium-Based Oxide Materials** [Stephanie](#)

Szenknect<sup>1</sup>, Laurent Claparede<sup>2</sup>, Adel Mesbah<sup>3</sup>, Theo Cordara<sup>1</sup>, Thomas Dalger<sup>1</sup>, Solène Bertolotto<sup>4</sup>, Nicolas Clavier<sup>3</sup>, Renaud Podor<sup>3</sup> and Nicolas Dacheux<sup>2</sup>; <sup>1</sup>ICSM, CEA, France; <sup>2</sup>ICSM, UM, France; <sup>3</sup>ICSM, CNRS, France; <sup>4</sup>CEA, DEN, DMRC, France

The “back end” of the nuclear fuel cycle corresponds to the direct disposal or reprocessing of the spent nuclear fuel (SNF), and to the conditioning and disposal in an appropriate repository of the nuclear wastes. In most of these processes, the behavior of actinides and fission products is governed by dissolution reactions at solid/ liquid interface. The design of reprocessing process and of nuclear waste disposal strategy requires the determination of well constrained kinetic and thermodynamic data. The acquisition of reliable kinetic and thermodynamic data is a tough issue considering on the one hand, the complexity of SNF in terms of chemical composition and microstructure and on the other hand, the challenge posed by the manipulation of highly radioactive samples.

For several years, we developed and improved a methodology that aims to determine dissolution rates of uranium-based oxide materials and thermodynamic data of phases of interest for final disposal of spent fuel in deep-mined geological repositories. This methodology is based on the synthesis of model compounds with well defined composition and microstructure, on the measurement of macroscopic dissolution rates in controlled chemical and hydrodynamic conditions, and on the monitoring of the properties of the solid/ liquid interface at the microscopic scale. For that purpose, several surface characterization techniques were used and developed, such as 3D reconstruction of Environmental SEM images, AFM or Grazing Incidence-XRD. To illustrate the progress made beyond the state of the art by using this methodology, several examples have been selected among the studies that we reported in the literature. The selected examples deal either with the reprocessing of uranium based oxides in nitric acid conditions, or with the behavior of UO<sub>2</sub> in SNF under the weathering conditions of geologic disposal.

The mechanisms that control the kinetics of dissolution of U-based oxides in nitric acid solutions are illustrated through the study of samples showing different compositions and microstructures. The use of oriented UO<sub>2</sub> single crystals allowed to evidence the enhanced reactivity of the surface at defect sites during a first kinetic regime. The second kinetic step was attributed to a catalyzed dissolution mechanism involving species produced at the solid/ liquid interface during the first step. The key role of catalytic species in the strong increase of dissolution rate was demonstrated not only for UO<sub>2</sub> single crystals, but also for sintered pellets of (U, Th) mixed oxides and UO<sub>2</sub>-doped with platinum group metals. The monitoring of solid/ liquid interface by 3D-ESEM during uncatalyzed and catalyzed regimes revealed specific dissolution sites of enhanced reactivity and specific dissolution features related to UO<sub>2</sub> crystallographic orientation, which traduced a structural control of the topographic evolution of the material.

Most of the geologic sites under investigation for underground repositories are located in undisturbed clay-rich rock or granite, with silica-rich groundwaters, deep enough to have reducing conditions. Understanding the interaction of used fuel with the silicate-rich groundwaters is critical to evaluate the safety of different disposal strategies. For several years, we investigated the role of silicates in the mechanisms of UO<sub>2</sub> weathering. For the first time, we were able to show the formation of coffinite (USiO<sub>4</sub>) from UO<sub>2</sub> in the presence of solution saturated with respect to SiO<sub>2</sub>(am) under conditions typical of deep-mined geologic repositories for SNF. Through dedicated experiments, we have constrained the conditions of formation of coffinite in an Eh-pH diagram. Finally, we showed that coffinite precipitation could lower the uranium release from the UO<sub>2</sub> matrix of SNF through oxidative weathering in the presence of oxygen in the geological repository.

#### **8:18 AM F.EN08.05.05**

**Evaluating Divalent Cation (Zn, Ca, Mg) Behaviour During the Dissolution of Simulant UK High Level Waste Glass** Adam J. Fisher, Russell J. Hand and Claire L. Corkhill; University of Sheffield, United Kingdom

In an effort to incorporate high levels of Mo associated with the post-operational clean-out of high active liquor storage tanks at the Sellafield reprocessing facility in the UK, a modified version of the "MW" sodium aluminoborosilicate base glass has been adopted. The addition of Ca favours the formation of CaMoO<sub>4</sub>, while Zn infers improved viscosity. This new Ca/Zn MW base glass is currently being used to immobilise reprocessing wastes from oxide fuels and also magnox fuels, which contain a significant proportion of Mg. The divalent cations Ca<sup>2+</sup>, Zn<sup>2+</sup> and Mg<sup>2+</sup> are known to exert an influence on the durability of vitrified wastes, however the nature of their additive, or competitive effects are yet to be fully understood.

We here describe the results of a range of experiments that aim to elucidate the influence of divalent cations on the mechanisms and kinetics of glass dissolution. The addition of Zn to the glass was found to enhance durability in dilute, Si-undersaturated conditions, due to an increase in glass polymerisation with increasing Zn content, as determined by <sup>29</sup>Si MAS NMR. However, under conditions of Si-saturation, the presence of Zn prevented the formation of a passivating silica gel



layer, and promoted the formation of Zn-containing smectite clays, significantly enhancing the dissolution rate with increasing Zn content. Mg had a similar effect to Zn, which was additive, however glasses containing Ca generally showed lower dissolution rates, in agreement with other studies. The formation of Zn- and Mg-bearing silicates was concurrent with a significant increase in the dissolution rate, similar to Stage III "rate resumption" behaviour, which has previously only been associated with the formation of zeolites.

#### 8:24 AM \*F.EN08.05.06

**Fabrication of Unirradiated Advanced Fuel for Dissolution Studies Under Repository Conditions** M Nieves Rodríguez-Villagra<sup>1</sup>, Sergio Fernández<sup>1</sup>, Laura J. Bonales<sup>2</sup>, Abel Milena-Pérez<sup>1</sup>, Ana Nuñez<sup>1</sup>, Sofía Durán<sup>1</sup>, Laureano Anta<sup>1</sup>, Luis Gutierrez<sup>1</sup> and Joaquín Cobos<sup>3</sup>; <sup>1</sup>CIEMAT, Spain; <sup>2</sup>CSIC-INTA, Spain; <sup>3</sup>EBD-CSIC, Spain

Safety assessment of Spent Nuclear Fuel (SNF) disposal in a Deep Geological Repository (DGR) requires evidences of radionuclides release after groundwater eventually gets into a breached container and contacts the fuel. Within the frame of EU H2020 program into the DISCO project, the impact of additives (Cr, Cr/Al and Gd) is being investigated on the long term DGR dissolution performance and compared to conventional UO<sub>2</sub>. In particular, the effect of these dopants is studied on the long term matrix dissolution rate of the SNF, the so-called Advanced Tolerant Fuels (ATF), such as Cr<sub>2</sub>O<sub>3</sub>-doped UO<sub>2</sub>, and Cr<sub>2</sub>O<sub>3</sub>-Al<sub>2</sub>O<sub>3</sub>-doped UO<sub>2</sub> fuels.

ATF have demonstrated to reach higher burn-up than conventional UO<sub>2</sub> fuels because dopants provide enhanced safety against Pellet-Clad Interaction failure (PCI), higher density, enlarged grain size, lower fission gas release and higher creep rate. Besides, the difference between those ATF and standard UO<sub>2</sub> in thermo-physical properties is almost negligible [1-4]. However, the dopants influence upon the matrix leaching performance at long term under DGR conditions is still largely unknown when compared to traditional UO<sub>2</sub> SNF.

The combinatory effects of two uncertain parameters (dopants influence and H<sub>2</sub>) on UO<sub>2</sub> matrix leaching resistance are investigated. In the context of WP2 and WP4 of the DISCO project, UO<sub>2</sub>-based pellets doped with a nominal concentration of 0.06<sup>w</sup>‰Cr<sub>2</sub>O<sub>3</sub>, 0.05<sup>w</sup>‰Cr<sub>2</sub>O<sub>3</sub>-0.02<sup>w</sup>‰Al<sub>2</sub>O<sub>3</sub> and 4.5<sup>w</sup>‰Gd<sub>2</sub>O<sub>3</sub>, were systematically produced by homogenizing stoichiometric proportions of UO<sub>2</sub> and dopants, and carefully characterized in order to understand the effects of the addition of Cr- and/or Al-oxide into the fuel matrix dissolution behaviour. Gd-doped UO<sub>2</sub> was also included, as a burnable poison and a trivalent rare-earth dopants (RE<sup>III</sup>). The results are the basis for potential more complex systems which would correspond to irradiated doped fuels.

Previous studies suggest that RE<sup>III</sup> play an important role on the UO<sub>2</sub> oxidation, revealing that they prevent the fuel from a complete oxidation to U<sub>3</sub>O<sub>8</sub> [5], so in order to better understand the effect of trivalent RE<sup>III</sup>, a set of dissolution experiments is carried out. The presence of reducing species, such as H<sub>2</sub> (produced by anaerobic iron corrosion and radiolytically), affects the reactivity of UO<sub>2</sub>; hence, it must be considered in a long-term safety assessment. On the other hand, it is well known that HCO<sub>3</sub><sup>-</sup> (one of the key complexing constituents in the groundwater) is highly likely to influence fuel dissolution by enhancing the solubility of U<sup>VI</sup> thus preventing the secondary phase formation [6].

To experimentally evaluate the effect of additives (doped fuels) together with H<sub>2</sub>(g) and different leachants on UO<sub>2</sub> matrix dissolution rate, leaching experiments were performed under different representative aqueous systems. Prepared pellet/disks were characterized by means of XRD, Raman spectroscopy and SEM-EDX. In order to understand the effect of the presence/absence of HCO<sub>3</sub><sup>-</sup> that could be considered as relevant to those coming from the interaction of water between natural barriers (groundwater) and EBS (Engineering Barrier System), specific synthetic groundwater was used in the dissolution tests. Static leaching experiments of doped-UO<sub>2</sub> pellets were run in stainless steel autoclaves with reaction vessels made of PEEK autoclaves under a N<sub>2</sub>/4.7%<sup>v</sup>H<sub>2</sub> atmosphere. The U and dopants concentration released into the aqueous solution was quantified by ICP-MS. pH and redox measurements were also tracked during the experiments.

[1] Thomas, G.A. et al. (2013) LWR Fuel Performance Meeting. TopFuel 201.

[2] Gentet, G. et al. (2015) Top Fuel 2015 Conference Proceedings A0198, 170 – 176.

[3] Backman, K. et al. (2009) INIS-XA--1074. International Atomic Energy Agency (IAEA).

[4] "Technical Exchange Meeting: EnCore® Accident Tolerant Fuel ADOPT Fuel Pellets".

[5] Travis A. et al. (2020). J. Nucl. Mater. 530, 151959.

[6] Hossain, M.M. et al. (2006). J. Nucl. Mater., 358, (2-3), 202-208.

#### 8:30 AM F.EN08.05.07

**Investigation of Secondary Phases Formed During Long Term Aqueous Leaching of Spent Nuclear Fuel** Charlotta Askeljung<sup>1</sup>, Anders Puranen<sup>2</sup>, Olivia Roth<sup>1</sup>, Kyle Johnson<sup>1</sup>, Alexandre Barreiro Fidalgo<sup>1</sup>, Lena Z. Evins<sup>3</sup> and Kastriot Spahiu<sup>3</sup>; <sup>1</sup>Studsvik Nuclear AB, Sweden; <sup>2</sup>AB SVAFO, Sweden; <sup>3</sup>Swedish Nuclear Fuel and Waste Management Co, Sweden

For a future deep repository for spent nuclear fuel, the rate and mechanism for dissolution of fission products and actinides from spent fuel is a key parameter for the safety assessment of the disposal concept. Although the majority of the fuel to be

placed in the deep repository is expected to be intact at the time of disposal, some failed fuel rods will also be present. In a failed fuel rod, the uranium matrix may have been exposed to water in the reactor and during interim storage for several years or decades prior to disposal. This exposure can lead to oxidation of the matrix and the formation of secondary phases under conditions of low uranium solubility. Upon barrier failure and ground water exposure of the spent fuel in the deep repository, these pre-oxidized layers are expected to dissolve at a higher rate compared to unaffected  $\text{UO}_2$  and hence increase the rate of radionuclide release. For this reason, knowledge about the characteristics of failed fuel and its behavior under deep repository conditions is required for the evaluation of the long-term safety of geological repositories. The present work aims to add to this knowledge.

Although the behavior of spent nuclear fuel under deep repository conditions has been studied extensively, studies of failed fuel are, in this context, relatively scarce, in particular studies of failed fuel that has been exposed to water during decades of wet interim storage. However, at the Studsvik laboratory in Sweden, leaching tests of spent fuel have been performed since the 1980s. This provides an opportunity to investigate the effects of long term contact with water under aerated conditions, such as those occurring in a wet interim storage.

In this study, XRD investigations have been performed on the surfaces of two fuel pellet samples which have been exposed to leaching solutions (synthetic ground water and deionized water, respectively) for over 30 years. Furthermore, the fuel surfaces have been exposed to carbonate solutions in an effort to dissolve the oxidized phases formed during the extended leaching time. The aim is to characterize the fuel matrix alteration.

#### 8:36 AM F.EN08.05.08

##### **Preliminary Results of Dissolution Experiments with Cr-(Pu) Doped $\text{UO}_2$ in Reducing Conditions at SCK CEN** Christelle Cachoir, Thierry Mennecart and Karel Lemmens; SCK CEN, Belgium

The development of robust safety cases for geological disposal of spent fuel requires a solid understanding of its dissolution over very long time scale (up to a million years). While the dissolution of standard spent fuel has reached a good level of comprehension, the development of modern LWR fuels (Cr/Al-doped  $\text{UO}_2$  or MOX fuels) raises the question whether these fuels will behave similarly to standard fuels in geological repository conditions. Within the EU-DisCo project, systematic dissolution studies have been initiated with carefully prepared and characterized, simplified  $\text{UO}_2$ -based model materials to understand the matrix dissolution of these modern LWR fuels under geological repository relevant conditions. As DisCo partner SCK CEN has performed such dissolution tests to study the effect of Cr-doping on the  $\text{UO}_2$  matrix dissolution rate in reducing conditions. Tests were started on four model materials :  $\text{UO}_2$ , Cr- $\text{UO}_2$ , Pu- $\text{UO}_2$  and Pu/Cr- $\text{UO}_2$  with a density close to 94% of the theoretical density and average grain size around 10  $\mu\text{m}$  for  $\text{UO}_2$  and Pu- $\text{UO}_2$ , 35  $\mu\text{m}$  for Cr- $\text{UO}_2$  and 25  $\mu\text{m}$  for Pu/Cr- $\text{UO}_2$ . The Cr doped pellets contain 1600  $\mu\text{g}$   $\text{Cr}_2\text{O}_3$  per gram of  $\text{UO}_2$ , and the alpha doping level of the Pu-doped pellets ( $\sim 18$  MBq/g $\text{UO}_2$ ) is representative for a fuel age of 10,000 years. Static dissolution experiments with these model materials have been performed in autoclaves in two reference waters (synthetic young cementitious water at pH 13.5 and bicarbonate water at pH 9) under 10 bar  $\text{H}_2$  pressure and in presence of Pt/Pd catalyst. After a predissolution in 0.01 M NaCl solution for 3 weeks to remove the pre-oxidized UOX layer, samples were taken from the solution over a period up to 2 months. For the materials  $\text{UO}_2$  and Cr- $\text{UO}_2$ , the Cr-doping leads to lower uranium concentrations in solution, both in synthetic cementitious and in bicarbonate water. In the synthetic cementitious water, this effect is constant over the entire experiment, but the concentrations, increasing immediately after the replacement of the NaCl solution by the cementitious solution, remain high at  $\sim 10^{-7}$  M for  $\text{UO}_2$  and  $\sim 10^{-8}$  M for Cr- $\text{UO}_2$ . In bicarbonate water, the initial uranium concentrations (after replacement of the NaCl solution by the bicarbonate solution) are the same as for the cementitious water, but after 2 months, all concentrations are  $\sim 10^{-9}$  M. These preliminary results suggest that the Cr doping decreases the U release in solution, but the long-term effect depends on the leaching solution. Experiments with the Pu doped materials (Pu- $\text{UO}_2$  and Pu/Cr- $\text{UO}_2$ ) are now carried on to study the Cr-effect in combination with alpha-radiolysis of the solution.

#### 8:42 AM F.EN08.05.09

##### **Aqueous Leaching of Chromia-Doped $\text{UO}_2$ Spent Nuclear Fuel Under Oxidizing Conditions** Alexandre Barreiro Fidalgo<sup>1</sup>, Olivia Roth<sup>1</sup>, Lena Z. Evins<sup>2</sup> and Kastriot Spahiu<sup>2</sup>; <sup>1</sup>Studsvik Nuclear AB, Sweden; <sup>2</sup>SKB, Sweden

Programs for deep geological repositories are being developed in many countries to safely dispose of spent nuclear fuel. Therefore, understanding the behavior of spent nuclear fuel under relevant conditions is crucial for the safety assessment of these facilities. During the last decades, new types of nuclear fuel are being introduced in commercial reactors. To allow these new fuels in the spent fuel repository, it must be shown that they do not dissolve at a higher rate than standard fuel. Fuel additives such as chromium oxide ( $\text{Cr}_2\text{O}_3$ ) have an impact on the  $\text{UO}_2$  microstructure and therefore might affect properties

relevant to the safety assessment.

The main goal of this investigation is to understand the effects of Cr-doping on the instant release fraction of fission products and the matrix dissolution under oxidative conditions. A sample consisting of fuel fragments and separated cladding is leached in simplified groundwater under aerated conditions at Studsvik's Hot Cell Laboratory. The fuel used in this study was manufactured by AREVA and has been irradiated in a Swedish commercial pressurized water reactor (PWR) to a local burnup at the sampling position of ~59 MWd/kgU.

Data from the leaching experiments are presented and compared to other commercial fuels' leaching performance: Cr-doped fuel with lower doping levels (Advanced DOPed Pellet Technology, ADOPT) and standard UO<sub>2</sub> fuel.

#### 8:48 AM F.EN08.05.10

**UO<sub>2</sub>-Based Model Systems—Model Materials for Studying the Matrix Corrosion of Spent Modern Nuclear Fuels** Philip Kögler, Martina Klinkenberg, Andrey Bukaemskiy, Felix Brandt, Guido Deissmann and Dirk Bosbach; Forschungszentrum Jülich GmbH, Germany

The direct disposal of spent modern nuclear fuel (SNF) in a deep geological repository (DGR) requires an in-depth understanding of the long-term corrosion behavior of the SNF and the associated radionuclide source term. These are indispensable requirements for demonstrating the long-term safety of the DGR. Today's modern Cr- and Al-doped light water reactor (LWR) fuels have already successfully demonstrated their improved in-reactor performance, but it is still not known, whether the corrosion behavior of such fuels in a DGR is similar to conventional spent LWR-fuels. Due to the chemical and structural complexity of SNF and its high beta and gamma radiation field, experiments with SNF cannot unravel all of the various concurring dissolution mechanisms entirely. Thus within the EU-DisCo project single-effect dissolution studies are carried out with systematically produced and carefully characterized UO<sub>2</sub>-based model materials, to provide additional insights into the behavior of modern doped LWR-fuels under the post-closure conditions expected in a DGR, complementary to dedicated dissolution experiments with SNF.

Here, we present recent results on the dissolution behavior of tailor made UO<sub>2</sub> model materials in accelerated static batch experiments using H<sub>2</sub>O<sub>2</sub> as simulant for radiolytic oxidants, present in long-term disposal scenarios for SNF in failed container conditions due to the alpha-irradiation of water. In these dissolution experiments pure UO<sub>2</sub> reference pellets exhibiting different densities and grain sizes, as well as Cr-doped UO<sub>2</sub> pellets with various Cr-doping levels, produced using different doping methods having different grain sizes, were used. In addition, Nd-doped and industrially produced Cr- and Cr/ Nd-doped UO<sub>2</sub> pellets were used to determine the influence of these parameters on the dissolution rates. The dissolution experiments were performed under strictly controlled conditions with respect to exclusion of oxygen, temperature control, and exclusion of light. During the dissolution experiments, solutions were systematically sampled and the H<sub>2</sub>O<sub>2</sub> (UV-Vis) and the uranium (ICP-MS) concentrations were determined.

The initial dissolution rates of all materials were determined from the concentrations of dissolved U(VI) obtained within the first 24 hours of the experiments. In experiments with pure UO<sub>2</sub> reference pellets a clear linear dependence of the initial dissolution rates from the density of the pellets was observed, with higher initial dissolution rates at lower densities. No dependence on grain size was found. The initial dissolution rates of pure, Cr-doped, and Nd-doped UO<sub>2</sub> pellets fall into three groups: i) pure UO<sub>2</sub> pellets with the fastest dissolution rates, independent of the oxygen potential during sintering (and therefore the grain size), ii) Cr-doped UO<sub>2</sub> pellets, independent of doping method, doping level, and oxygen potential during sintering (grain size), and iii) Nd-doped UO<sub>2</sub> pellets with the lowest dissolution rates. The following initial dissolution rates were calculated for the different materials:

pure UO<sub>2</sub>:  $1.3 \pm 0.1 \cdot 10^{-6} \text{ mol/m}^2 \cdot \text{s}$

Cr-doped UO<sub>2</sub>:  $0.65 \pm 0.2 \cdot 10^{-6} \text{ mol/m}^2 \cdot \text{s}$

Nd-doped UO<sub>2</sub>:  $1.63 \pm 0.7 \cdot 10^{-7} \text{ mol/m}^2 \cdot \text{s}$

The slight difference between the dissolution rates of pure UO<sub>2</sub> and Cr-doped UO<sub>2</sub> pellets (i.e. factor 2) can partly be explained by the slightly lower density of pure UO<sub>2</sub> pellets compared to Cr-doped UO<sub>2</sub> pellets. A very strong influence of Nd, representative of fission lanthanides in SNF, on the dissolution rates in this type of experiments is clearly visible.

Although the density of the Nd-doped UO<sub>2</sub> pellets is similar to the Cr-doped pellets (i.e. 96-98% relative density), the initial dissolution rate is more than half an order of magnitude lower than for Cr-doped pellets. Overall, the results of this study indicate that the Cr-doping of modern nuclear fuels seems to have no significant effect on the corrosion behavior of UO<sub>2</sub>-based SNF.

#### 8:54 AM \*F.EN08.05.11

**Dissolution Kinetics of Metaluminous and Peralkaline Calcium Aluminosilicate Glass at 75°C, pH = 7.5: Rate Control**

**by Si-Content of Glass** Jon P. Icenhower, Hugh McMahon, Misty Riesbeck, Elzbieta Bakowska, Randall Youngman and Nicholas Smith; Corning, United States

The dissolution rates of six calcium aluminosilicate glasses were determined experimentally at  $\text{pH}(25\text{ }^\circ\text{C}) = 7.5$  and a temperature of  $75\text{ }^\circ\text{C}$  in a Single-Pass Flow-Through (SPFT) system. Glasses studied in this work can be categorized into two sets of three compositions each. In the first (metaluminous) set, the molar proportion of  $\text{CaO}$  to  $\text{Al}_2\text{O}_3$  remained the same (1:1), while  $\text{SiO}_2$  increased (40, 50 and 60 mol.%). The second (peralkaline) set was characterized by constant  $\text{Al}_2\text{O}_3$  (10 mol.%), with decreasing  $\text{CaO}$  and increasing  $\text{SiO}_2$  (40, 50 and 60 mol.%). Measurements of  $^{27}\text{Al}$  by MAS-NMR indicated a slight increase in  $\text{Al}^{[5]}$  at the expense of  $\text{Al}^{[4]}$  with decreasing Si concentration. One to four grams of powdered glass (300 to 425 mm diameter) were placed into 10 mL volume reactors with solution input through the bottom and effluent solution output through the top. Solutions were buffered by 0.05 M TRIS and flow-rates varied between  $\sim 38$  and 500 mL/d. A plot of the dissolution rate vs. flow-rate ( $q$ ) to surface area ( $S$ ) showed that all dissolution rates were maximized at  $q/S \approx 45 \times 10^8$  m/s. Dissolution rates were from 4.2, 1.5 and  $0.62 \times 10^{-7}$  mol/(m<sup>2</sup> sec) for the metaluminous and 1.0, 0.65 and  $0.50 \times 10^{-7}$  mol/(m<sup>2</sup> sec) in the peralkaline glasses, respectively. Interestingly, the data indicate that rates for the metaluminous trio are generally faster than those of the peralkaline set, which runs contrary to expectations. As a set of glasses, the  $\log_{10}$  rates [mol/(m<sup>2</sup> sec)] are inversely proportional to the fraction of Si in the glasses, forming a single array of values. These data indicate that rates are strongly tied to the Si content of glasses, and that other glass composition parameters— including Ca/Al (molar) ratio— exert a much weaker effect on dissolution rate in this medium.

#### 9:00 AM F.EN08.05.13

**Adsorption and Diffusion of Boron Isotopes in Aqueous Glass Dissolution** Thomas L. Gouët<sup>1</sup>, Rui Guo<sup>1,2</sup>, Sambuddha Misra<sup>1,3</sup>, Aleksey Sadekov<sup>4</sup>, Edward Tipper<sup>1</sup>, Madeleine Bohlin<sup>5</sup> and Ian Farnan<sup>1</sup>; <sup>1</sup>University of Cambridge, United Kingdom; <sup>2</sup>Tsinghua University, China; <sup>3</sup>Indian Institute of Science, India; <sup>4</sup>The University of Western Australia, Australia; <sup>5</sup>Uppsala University, Sweden

Predicting the release rates of radionuclides from nuclear waste glasses during aqueous dissolution within a disposal facility over geological timescales requires robust models of dissolution built upon an extensive understanding of glass dissolution mechanisms. However, many of the dissolution models presented in the past decade conflict regarding the mechanisms predicted to control dissolution. Whilst nanoscale post-process analyses of altered glasses have afforded insights into altered layer structures, these results highlight the need for an additional dimension to understand the mechanisms of glass dissolution beyond the conventionally employed techniques presented in the literature.

In a previous study, lithium isotope fingerprinting techniques were applied to the leachates of a simplified Magnox waste glass leached at  $90\text{ }^\circ\text{C}$ . It was shown that whilst dissolution was initially congruent, lithium isotopes leached incongruently through diffusive processes across a passivating altered layer component at longer durations. However, further evidence was required to rank the dissolution models presented in the literature. Here, boron isotope fingerprinting techniques were applied to the same Magnox glass to further understand its dissolution processes, understand how lithium and boron were leached and distinguish between dissolution models. Additionally, the same isotopic techniques were applied to leachates of an international benchmark glass composition to compare the dissolution processes of the two compositions and allow for interdiffusion models to be fitted to the results. Solution renewal experiments took place to further investigate the passivating nature of the altered layers and their role as a diffusive barrier to dissolution at long durations.

Boron isotopes leached from the Magnox glass were consistent with congruent models of dissolution in the initial stages of dissolution, but at later stages were consistent with diffusive isotopic fractionation across a passivating altered layer component about an incongruent dissolution front. Whilst boron isotopes in the leachates of International Simple Glass were consistent with diffusive, incongruent dissolution models throughout dissolution, boron isotopes in its solution renewal experiment were most consistent with congruent models of dissolution. As such, these isotopic methodologies demonstrate that no single dissolution model may be correct for all glass compositions and experimental conditions; providing an improved understanding of the mechanisms governing aqueous glass dissolution and supporting the idea of a model which unifies the mechanisms presented in the literature.

#### 9:06 AM F.EN08.06.05

**Chemical and Structural Investigations on Uranium Oxide Based Microparticles as Reference Materials for Analytical Measurements** Stefan Neumeier<sup>1</sup>, Philip Kegler<sup>1</sup>, Fabien Pointurier<sup>2</sup>, Anne-Laure Faure<sup>2</sup>, Kathy Dardenne<sup>3</sup>, Jörg Rothe<sup>3</sup>, Tonya Vitova<sup>3</sup>, Martina Klinkenberg<sup>1</sup>, Fabian Kreft<sup>1</sup>, Dirk Bosbach<sup>1</sup> and Irmgard Niemeyer<sup>1</sup>; <sup>1</sup>Forschungszentrum Jülich GmbH, Germany; <sup>2</sup>CEA, France; <sup>3</sup>Karlsruhe Institute of Technology, Germany

The analysis of individual micrometre- and submicrometre-sized particles collected by IAEA safeguards inspectors on swipe samples during in-field verification activities requires the implementation of a sustainable quality control system. This system

needs to be further advanced by developing mass spectrometric analytical measurements and of suitable reference materials. In this context pure and compound reference materials in microparticulate form such as U, Ln/U, Th/U and Pu/U microparticles are of special interest. For the design of these microparticulate reference materials, according to their required properties, the understanding of morphology, chemistry, and structure is essential.

To this end, the production of pure and neodymium doped uranium-oxide based microparticles utilising an aerosol-based particle production process which has been developed and established in the laboratories of Forschungszentrum Juelich since 2012 will be presented. This method allows for the generation of microparticles with monodisperse particle size distribution. SEM/EDX measurements confirmed the monodispersity of the produced microspheres as well as the incorporation of 15 mol% Nd into the compound particles. Additionally, results from *In-SEM*  $\mu$ -Raman (CEA, DAM) and U L<sub>3</sub>-edge XAFS measurements in U L<sub>α</sub> fluorescence yield detection mode (INE-Beamline @ KIT synchrotron radiation source) will be discussed pointing to the formation of U<sub>3</sub>O<sub>8</sub> microparticles for both compounds. The position and shape of the X-ray absorption spectrum is insignificantly affected by the incorporation of 15 mol% Nd, indicating the structural flexibility and stability of the U<sub>3</sub>O<sub>8</sub> microparticles. Additionally, a minor fraction of schoepite phase was identified by Raman measurements, which is most probably caused by ageing processes during storage under laboratory conditions. The first batch of U<sub>3</sub>O<sub>8</sub> microparticles produced in Juelich was successfully applied in an international laboratory exercise NUSIMEP9 organised by JRC-Geel and finally certified regarding the isotopic composition and the U amount per particle. These results demonstrate that the process established in Juelich allows for a very flexible and reliable preparation of reference materials for particle analysis methods applied in safeguards.

#### 9:12 AM F.EN08.06.06

##### **Nanostructured Uranium Oxide Thin Films Developed by Molecular Precursors Using Chemical Vapor**

**Deposition** Dennis Grödler, Lasse Jurgensen, Aida Raauf, Markus Zegke and Sanjay Mathur; Institute of Inorganic Chemistry, Germany

Advanced materials have been made using a variety of elements, however, uranium has not seen much impact. The common fear of working with “nuclear material” has prevented its chemical use, even though it has been known since 1911 to be an efficient catalyst in the widely applied Haber-Bosch process. A possible strategy to synthesize advanced materials based on uranium is the chemical vapor deposition (CVD). To date, only a few suitable uranium precursors have been reported. Here we report new volatile uranium(IV) complexes based on  $\beta$ -ketoenamine ligands, which have been structurally characterized and which can be synthesized via a simple salt metathesis. Functionalization of the N atom of the chelating ligand changes the coordination motif, and subsequent NMR studies offer a deeper insight into the coordination chemistry. Sterically demanding ligands (L) selectively lead to heteroleptic complexes of the form UCl<sub>2</sub>L<sub>2</sub> while an additional degree of freedom in the substituent allows for the isolation of homoleptic complex of the form UL<sub>4</sub> with significantly increased volatility. These are suitable candidates for CVD towards uranium oxide thin films. Uranium oxides with band-gap energies in a range of 1.8 – 2.7 eV coupled with their good electrical and catalytic properties mostly driven by facile valence dynamics of the uranium cations are promising electrode materials in photoelectrochemical water splitting reactions. We have been able to synthesize a variety of such ligands and present four novel uranium complexes which we are currently investigating with respect to the formation of novel uranium based thin film materials. Furthermore, using  $\beta$ -heteroarylthioketamine ligands leads to similar complexes that may be used as precursors for uranium sulfide thin films.

SESSION F.EN08.01: In Memory of Lou Vance and His Contribution to Development of Nuclear Waste Forms  
On Demand Abstracts Available for Viewing Starting Saturday Morning, November 21, 2020  
F-EN08

#### 5:00 AM F.EN08.01.01

**Remembering Eric (Lou) Vance (1942-2019)—A Pioneer in Nuclear Wasteforms** Daniel Gregg, Rifat Farzana, Pranesh Dayal, Rohan Holmes and Gerry Triani; Australian Nuclear Science and Technology Organisation, Australia

Dr Eric (Lou) Vance was a trailblazer in developing novel treatment solutions for intractable nuclear wastes, who spent 32 years at the Australian Nuclear Science & Technology Organisation (ANSTO) in Sydney. Largely known for his contributions to Synroc technology, Lou’s experience spans multiple continents including time at Pennsylvania State University with McCarthy and Roy as well as time at the Atomic Energy of Canada Limited where he studied sphen glass-ceramics. In 1987 he was recruited to ANSTO to progress Synroc technology. Under Lou’s leadership, the original Synroc titanate full ceramic formulations invented by Ringwood evolved into a waste treatment technology platform. This platform

can be applied to produce glass, glass-ceramic and ceramic wasteforms via hot-isostatic pressing. Lou's seminal contributions to the science of nuclear waste management are evident in his ~400 scientific articles in international journals/refereed conference proceedings and his co-authorship of 3 patents relating to Synroc. An entertaining and highly popular speaker, Lou was committed to attending two to three international conferences a year to showcase the Synroc technology and his innovative nuclear wasteform research. Lou was a steadfast member of the Scientific Basis for Nuclear Waste Management symposium for several decades and a highly enthusiastic mentor. In this paper, we celebrate the research career of the late Dr Vance and his substantial and essential contributions to the field of nuclear wasteform development and to the development of Synroc technology.

#### 5:10 AM F.EN08.01.02

**Iodine Waste Forms—Review and Contributions of Dr. Lou Vance** John S. McCloy<sup>1,2</sup>, Brian Riley<sup>2,1</sup> and Saehwa Chong<sup>2,1</sup>; <sup>1</sup>Washington State University, United States; <sup>2</sup>Pacific Northwest National Laboratory, United States

The capture and immobilization of long-lived radioactive iodine I-129 must be a priority for future nuclear fuel cycles involving reprocessing. This review summarizes work on waste forms for radioiodine, emphasizing the contributions of Dr. Lou Vance as well as recent work in other groups. As early as the 1980s, Dr. Vance recognized the need for iodine waste forms and was a leader in innovative waste form solutions for iodine and other volatile halides. His studies included immobilization in silicate minerals including zeolites and sodalite, encapsulation in metallic tin, partitioning in synroc mixed-phase ceramics, and consolidation of copper iodide. Here, we recognize his particular contributions to the understanding of iodosalite, and note some recent work by others following in his footsteps.

#### 5:20 AM F.EN08.01.03

**Hot-Isostatic Pressing of Synroc-C—The Effect of Ti-Metal Additions** Daniel Gregg, Rifat Farzana, Pranesh Dayal, Zaynab Aly, Rohan Holmes and Gerry Triani; Australian Nuclear Science and Technology Organisation, Australia

Synroc-C, a multiphase ceramic wasteform based on stable and leach resistant titanate minerals, was invented by Australian scientists in the late 1970s. The formulation was directed toward the immobilization of PUREX wastes from the reprocessing of nuclear fuels and was originally to be produced *via* hot-uniaxial pressing (HUPing). Although glass was chosen as the preferred technology during the “Atlanta shoot-out” in the US in 1981, this was ultimately because Synroc lacked the technical maturity of vitrification. However, given the enhanced performance properties of Synroc-C as a wasteform, significant interest has been sustained in this Synroc formulation. The vast majority of work on Synroc-C has been undertaken following consolidation by HUP processing. There is very little reported on hot-isostatically pressed (HIPed) Synroc-C, where HIP canisters are filled with the calcined wasteform material (waste + additives), evacuated and sealed. The HIP canister is then loaded into the HIP chamber and processed through the desired time-temperature-pressure profile to achieve a dense and consolidated wasteform. The appropriate redox conditions within the HIP canister are vital to the formation of the correct phase composition and ultimately attaining a stable and leach resistant wasteform. In this study, we investigate the effect of Ti-metal addition on the phase formation, microstructural characteristics and durability of HIPed Synroc-C. Dense Synroc-C samples containing 20 wt.% simulated high level waste and with varying Ti-metal additions (0%, 2%, 4% and 8 wt.%) were prepared by HIPing in stainless steel HIP canisters. An investigation of microstructure, mineral phases and elemental distribution in the samples was carried out using quantitative X-ray diffraction and electron microscopic analyses. Results from durability tests are also discussed.

#### 5:30 AM F.EN08.01.04

**Immobilisation Options for the Disposition of UK Plutonium** Neil Hyatt, Lewis Blackburn, Laura Gardner, Shikuan Sun, Martin Stennett and Claire L. Corkhill; University of Sheffield, United Kingdom

The UK holds the world's largest inventory of separated plutonium under civil safeguards, projected to reach 140 tons at the end of reprocessing options. A significant fraction of this material requires immobilisation for disposal since it is unsuitable for reuse in MOX fuel, which is HM Government's preferred policy for disposition. Additionally, should it not prove possible to implement the policy for plutonium reuse in MOX fuel an alternative immobilisation and disposal option will be required for the greater inventory. This presentation will review the current status of wasteform engineering and process development for manufacture of zirconolite ceramic and glass-ceramic wasteforms for immobilisation of waste and inventory plutonium. We will demonstrate the development of Ce and U surrogate formulations, validated by targeted plutonium studies, with regard to phase assemblage and Pu / surrogate incorporation mechanism. The development of a novel containment system to enable hot isostatic pressing studies utilising U and Th surrogates will be presented, together with operational experience. The application of new, and potentially disruptive, wasteform manufacture technology will also be discussed.

#### 5:40 AM F.EN08.01.06

##### **Immobilization of Cesium and Iodine into Cs<sub>3</sub>Bi<sub>2</sub>I<sub>9</sub> Perovskite-Silica Composites and Core-Shell Waste Forms** Kun Yang and Jie Lian; Rensselaer Polytechnic Institute, United States

Cs<sub>3</sub>Bi<sub>2</sub>I<sub>9</sub>, a defect perovskite derivative, is a potential host phase to immobilize iodine and cesium with high waste loadings. In this work, two strategies are explored to form Cs<sub>3</sub>Bi<sub>2</sub>I<sub>9</sub>-silica composites and core-shell structures in order to improve chemical durability of waste form materials meanwhile maintaining high waste loadings. Cs<sub>3</sub>Bi<sub>2</sub>I<sub>9</sub> loadings as high as 70 wt.% were incorporated into a silica matrix to form silica-ceramic composites, and 20 wt.% Cs<sub>3</sub>Bi<sub>2</sub>I<sub>9</sub> was encapsulated into silica to form a core-shell structure at low temperatures and high pressure. Semi-dynamic leaching experiments indicated Cs and I were incongruently released from waste form matrices depends on the bonding environment and surface passivating effect. A BiOI alteration layer formed during the surface reorganization, acting as a passivation layer to reduce the release of radionuclides. The long-term iodine release rate was low (30 mg m<sup>-2</sup> day<sup>-1</sup>) for 70 wt.% Cs<sub>3</sub>Bi<sub>2</sub>I<sub>9</sub>-silica composites leached in deionized water at 90 °C, which can be further reduced to 5×10<sup>-3</sup> mg m<sup>-2</sup> day<sup>-1</sup> for the 20 wt.% core-shell structure. This work highlights a robust way to immobilize the highly mobile radioactive nuclides and surface passivating mechanism through elemental transport across the liquid-solid interface for Cs<sub>3</sub>Bi<sub>2</sub>I<sub>9</sub>.

#### 5:50 AM F.EN08.01.07

##### **Incorporation Mechanism of Sr and Ca in Geopolymer Cement Wasteforms** Brant Walkley<sup>1,1</sup>, Xinyuan Ke<sup>2,1</sup>, Ben Griffith<sup>3</sup>, Oday Hussein<sup>1</sup>, Susan Bernal<sup>4</sup>, John Hanna<sup>3</sup> and John Provis<sup>1</sup>; <sup>1</sup>The University of Sheffield, United Kingdom; <sup>2</sup>University of Bath, United Kingdom; <sup>3</sup>University of Warwick, United Kingdom; <sup>4</sup>University of Leeds, United Kingdom

Radioactive waste streams containing <sup>90</sup>Sr, from nuclear power generation and environmental cleanup operations, are immobilised in the UK in blended Portland cement (PC) grouts to limit radionuclide leaching. Due to poor compatibility of certain wastes with PC, alternatives such as alkali aluminosilicate ‘geopolymer’ binders are being investigated. Here, we used multinuclear solid-state nuclear magnetic resonance (NMR) spectroscopy probing <sup>23</sup>Na, <sup>27</sup>Al, <sup>29</sup>Si and <sup>39</sup>K nuclei, including high-field (20.0 T) and cross polarisation experiments, along with X-ray diffraction experiments, to investigate the incorporation mechanism of Sr<sup>2+</sup> and Ca<sup>2+</sup> in geopolymer wasteforms formed by alkali-activation of metakaolin. The main reaction product identified in gels cured at both 20°C and 80°C is a fully polymerised Al-rich alkali aluminosilicate hydrate ((N,K)-A-S-H) gel comprising Al and Si in tetrahedral coordination, with Si in Q<sup>4</sup>(4Al) and Q<sup>4</sup>(3Al) sites, and Na<sup>+</sup> and K<sup>+</sup> balancing the negative charge resulting from Al<sup>3+</sup> in tetrahedral coordination. Faujasite-Na and partially Sr-substituted zeolite Na-A form within the gels cured at 80°C. Incorporation of Sr<sup>2+</sup> or Ca<sup>2+</sup> displaces some Na<sup>+</sup> and K<sup>+</sup> from the charge-balancing sites, with a slight decrease in the Si/Al ratio of the (N,K)-A-S-H gel. Ca<sup>2+</sup> and Sr<sup>2+</sup> induce essentially the same structural changes in the gels. It was concluded that the disordered geopolymers can readily accommodate Sr<sup>2+</sup> and Ca<sup>2+</sup> into their aluminosilicate framework structure via substitution of the divalent alkaline earth cations for monovalent alkali cations in charge balancing sites. This indicates that geopolymer gels are excellent candidates for immobilisation of radioactive waste containing <sup>90</sup>Sr and other alkaline earth radionuclides.

#### 6:00 AM \*F.EN08.01.08

##### **Development and Application of Colloidal Silica-Based Grouts for Waste Containment** Rebecca Lunn, M. Pedrotti, P. Bots, G. El Mountassir, A. Pegano and J. Renshaw; University of Strathclyde, United Kingdom

The UK’s nuclear sites contain stored wastes in ponds and silos as well as large volumes of contaminated concrete and soil. During storage decommissioning and deconstruction operations, there are significant risks of radionuclide transport via groundwater and airborne particulate releases. Colloidal silica grout is a nano-particulate material that has the potential to reduce these risks very significantly. In order to utilize such nanoparticulate material as a barrier, we require a detailed understanding of the grout properties. These include its injectability, mechanical behaviour, hydraulic properties, durability and its impact on the geochemistry of radionuclides in the environment (e.g. fission products such as Sr and Cs). Over the past 5 years, experiments at Strathclyde have progressively investigated colloidal silica grout properties. Colloidal silica-grouted sand shows an increased stiffness and an enhanced peak friction angle, while still having a very low hydraulic conductivity (~ 10<sup>-10</sup> m/s), typical of intact clay. Even under drained conditions, the grout provides mechanical improvement to the soil and retains a very low hydraulic conductivity. The impact on radionuclide geochemistry has been investigated through combining leaching experiments with XAS analyses. These show that colloidal silica induces several competing effects on the mobility of Sr and Cs. First, cations within the colloidal silica gel compete with Sr and Cs for surface complexation sites. Second, an increased number of surface complexation sites is provided by the silica nanoparticles and finally, the elevated pH within the colloidal silica increases the surface complexation to clay minerals and the silica

nanoparticles. Finally, experiments to investigate injectability and monitorability show that colloidal silica grout can be successfully injected in silty-sands, its gelling time can be accurately predicted in a full range of environmental conditions and the location of the subsurface barrier created can be accurately identified using Electrical Resistivity Tomography. Potential applications of colloidal silica on nuclear sites include inhibiting radionuclide migration from recently decommissioned structures during care and maintenance (e.g. silos and ponds from which wastes have already been retrieved); the development of primary or secondary barriers around existing radionuclide (or other) contaminated areas; and stabilisation of underground structures. Research work is continuing to improve the mechanical and chemical properties of colloidal silica grouts, such that they can be tailored to suit for individual nuclear site-based applications.

#### **6:15 AM F.EN08.01.09**

**Utilizing Machine Learning in Nuclear Waste Management** Natalie J. Smith-Gray, Irmak Sargin, Scott Beckman and John S. McCloy; Washington State University, United States

Machine learning (ML) is a valuable tool that can be used, in combination with domain expertise, to provide insight into nuclear waste vitrification processes. This talk summarizes our preliminary efforts in using ML methods to address important problems facing the nuclear waste vitrification mission at the Hanford site in Washington State. Three case studies using ML modeling will be described: nepheline crystallization, refractory corrosion, and sulfate solubility. In Hanford high-level waste, nepheline crystallization can occur in melt compositions containing high Na and Al contents when glass cools slowly in the canister, partitioning radioactive components to a less-durable residual glass fraction. In low-activity waste compositions, which are generally higher in alkali and volatile components like sulfur and halides, different critical issues present. Firstly, the low solubility of sulfate in borosilicate glass has led to many studies to predict glass composition dependence of this property, such that excess sulfur is not volatilized or partitioned to an alkali molten salt phase during processing. Second, these glass compositions tend to be harsh on refractories, leading to concerns over corrosion and general degradation of melter ceramic components and premature failure. For these three cases, existing datasets were used along with ML techniques to investigate the datasets and create predictive models for the output properties of interest. For all these studies, data science was used to identify underlying trends and correlations which were then applied to create supervised learning models. As a result, it has become evident that ML is a powerful tool that can be utilized to provide insight into complex issues in nuclear waste management, here specifically focused on immobilization by vitrification.

#### **6:25 AM F.EN08.01.10**

**Machine Learning for Glass Wasteforms' Design and Performance** Mathieu Bauchy; University of California, Los Angeles, United States

Vitrification is a key process to turn high-level nuclear waste into durable glasses. However, the virtually infinite compositional envelope accessible to glass wasteforms renders traditional design methods based on empirical knowledge and trial-and-error poorly efficient. In addition, the complex, disordered atomic structure of glasses makes it challenging to develop some mechanistic models relating their composition to their properties and performance. Here, I will discuss how machine learning offers a promising alternative route to predict the properties of glass wasteforms and guide/accelerate the design of novel glasses with enhanced performance for nuclear waste immobilization applications.

#### **6:35 AM F.EN08.01.11**

**Developing High-Throughput Computational Methods to Discover Hierarchical Waste Forms** Matthew Christian, Vladislav Klepov, Kristen Pace, Gregory Morrison, Theodore Besmann and Hans-Conrad zur Loye; University of South Carolina, United States

The development of stable actinide and other radionuclide hierarchical waste-form materials offer potential advantages of greater efficiency/loading, lower leach rates, ease of processing for so-called legacy nuclear wastes. Current waste-form discovery relies heavily on experiments that may or may not be successful in producing a viable product. Computational crystal discovery has aided in the search for new materials for different applications through use of high-throughput algorithms. However, these approaches have not been adapted to actinide and lanthanide compounds due to additional corrections required to properly handle *f*-orbital-containing elements. This presentation will consider the challenges and possible solutions to creating high-throughput computational methods to aide in the experimental discovery of novel hierarchical waste forms and offer tangible examples.

#### **6:45 AM F.EN08.01.12**

**Thermodynamic Modelling of the Pd-Ru-Te-O for Nuclear High-Level Waste Immobilization** Stéphane Gosse<sup>1,2</sup>, C. Laurin<sup>3</sup>, E. Régnier<sup>3</sup>, A. Laplace<sup>3</sup> and S. Schuller<sup>3</sup>; <sup>1</sup>CEA, France; <sup>2</sup>Université Paris-Saclay, France; <sup>3</sup>Commissariat à



Pd and Ru are the main platinoid fission products formed during burnup of nuclear fuels. During fuel reprocessing, these element partly dissolve in nitric acid and they exhibit very low solubility into borosilicate glasses during the vitrification process. Due to their affinity towards tellurium from the fission product solution, palladium mainly precipitates under (Pd-Te) intermetallics [1] and ruthenium is likely to form hcp solid solutions [2]. The composition and microstructures of these phases are also sensitive to oxygen potential [3]; oxydation of ruthenium can lead to needle-shaped or polyhedral (Rh,Ru)O<sub>2</sub> oxide phases [4]. These precipitates can affect significantly the physico-chemical properties of the glass melt during melting in hot or cold crucible.

For decades, many studies were undertaken at CEA [5] to point out the high temperature interactions of the platinum group metals (PGM) issuing from the calcinated waste. In parallel to these studies, a Calphad database is being developed to address the thermodynamics of such systems to provide an assessment of the PGMs in nuclear waste.

This study presents the assessed binary systems. Some calculations are also performed to highlight how this flexible tool makes is used to predict the stability between metallic and oxide phases as a function of temperature and oxygen potential mainly driven by the glass.

[1] S. Gossé, C. Guéneau, *Intermetallics* 19 (2011) 621-629

[2] S. Gossé, N. Dupin, C. Guéneau, J.-C. Crivello, J.-M. Joubert, *J. Nuclear Mater* 474 (2016) 163-173

[3] S. Gossé, S. Bordier, C. Guéneau, E. Brackx, R. Domenger, J. Rogez, *J. Nuclear Mater* 500 (2018) 252-264

[4] R. Pflieger, L. Lefebvre, M. Malki, M. Allix, A. Grandjean, *J. Nuclear Mater* 389 (2009)

*J. Nuclear Mater*, Vol. 389, N°3

[5] O. Pinet, S. Mure, *Journal of Non-Crystalline Solids*, 355 (2009) 221-227

#### 6:55 AM F.EN08.01.13

**Thermodynamic Assessment of Zn-Containing Hollandite as a Robust Waste Form** [Juliano Schorne-Pinto](#)<sup>1</sup>, Kyle Brinkman<sup>2</sup>, Jake Amoroso<sup>3</sup>, Scott Misture<sup>4</sup> and Theodore Besmann<sup>1</sup>; <sup>1</sup>University of South Carolina, United States; <sup>2</sup>Clemson University, United States; <sup>3</sup>Savannah River National Laboratory, United States; <sup>4</sup>Alfred University, United States

The hollandite phase is a potential nuclear waste form for alkaline-earth metals such as Cs and Ba by chemical incorporation into the crystalline lattice. The general hollandite formula is A<sub>x</sub>B<sub>8</sub>O<sub>16</sub> with the A-site habitually occupied by large mono- or divalent cations (e.g., Ba, Sr, Na, K, Rb, Cs, Pb), and the B-site by small di-, tri-, or tetravalent cations (e.g., Ti, Al, Fe, Cr, Sc) and it crystallizes in a tetragonal or monoclinic structure depending on the composition. Recently, our group has developed a thermodynamic database to describe the BaO-Cs<sub>2</sub>O-TiO<sub>2</sub>-Cr<sub>2</sub>O<sub>3</sub>-Al<sub>2</sub>O<sub>3</sub>-Fe<sub>2</sub>O<sub>3</sub>-FeO-Ga<sub>2</sub>O<sub>3</sub> system based on the Calphad method, where the hollandite solid-solution was modeled using the Compound Energy Formalism (CEF). Recent findings show the impact of varying A-site Cs stoichiometry of Zn-containing hollandite compositions and related thermodynamic stability. This consequently improved the limited performance of the hollandite phase in a multi-phase composite called SYNROC. We here report on our efforts to include the Zn in our waste form thermodynamic database, modeling the phase equilibria of the complex hollandite-forming oxide waste system.

SESSION F.EN08.02: Corrosion of Nuclear Fuel and Waste Containers  
On Demand Abstracts Available for Viewing Starting Saturday Morning, November 21, 2020  
F-EN08

#### 5:00 AM \*F.EN08.02.01

**An Overview of Corrosion Research on the Canadian Nuclear Waste Container** [Peter G. Keech](#)<sup>1</sup>, Wilfred J. Binns<sup>1</sup>, Mehran Behazin<sup>1</sup> and James J. Noel<sup>2</sup>; <sup>1</sup>NWMO, Canada; <sup>2</sup>University of Western Ontario, Canada

Canada's plan for the permanent storage of high level nuclear waste is to construct a Deep Geological Repository (DGR) at a depth of at least 500 m in a suitable host rock. The waste, which is composed almost entirely of CANDU fuel bundles, will be seal-welded into copper-coated steel "used fuel containers" (UFCs), which will be placed in bentonite clay within the DGR. Concurrent with site selection activities to find an informed, willing host community, the Nuclear Waste Management Organization (NWMO) is developing the UFC within a large technical and engineering program. The service life for the UFC is on the order of 1 million years, so research into container degradation, primarily via corrosion, is paramount to the success of the UFC development program. Research is done in partnership with many international waste management organizations, as well as through collaborations with national laboratories and academic research teams.

Overall, four types of corrosion comprise the total expected corrosion: oxic corrosion as a result of trapped oxygen during emplacement; radiation influenced corrosion owing to fuel decay; anoxic corrosion of copper and microbiologically-influenced corrosion. From these processes, some consideration must be made for non-uniform corrosion effects, and the service life must be supported by extensive modeling/simulation. This paper will provide experimental and modeling evidence for prediction of the long-term container corrosion performance, as well as outlining a path forward with respect to corrosion research as the Canadian program transitions through licensing activities and toward construction and operation.

5:15 AM \*F.EN08.02.02

**Long-Term Atmospheric Corrosion and Stress Corrosion Cracking of 304 Stainless Steel Used in Spent Nuclear Fuel Dry Storage Containers** Jenifer Locke<sup>1</sup>, Jay Srinivasan<sup>1</sup>, Alana Parey<sup>1,2</sup>, Gabriella Marino<sup>1</sup>, Benjamin Sutton<sup>1</sup>, Jianxiang Li<sup>1</sup>, Glenn Daehn<sup>1</sup>, Anupam Vivek<sup>1</sup>, Thodla Ramgopal<sup>3</sup>, Alexander Shapiro<sup>1,4</sup>, James Greigo<sup>2</sup>, Philip Noell<sup>2</sup>, Jason Taylor<sup>2</sup>, Charles Bryan<sup>2</sup>, Rebecca F. Schaller<sup>2</sup>, Eric Schindelholz<sup>1</sup> and Antonio Ramirez<sup>1</sup>; <sup>1</sup>The Ohio State University, United States; <sup>2</sup>Sandia National Laboratories, United States; <sup>3</sup>DNV-GL, United States; <sup>4</sup>Titanium Brazing Inc, United States

Welded austenitic stainless steels (SS) are used to construct canisters for the dry storage of spent nuclear fuel. Exposure to ambient marine environments can lead to salt deposition and brine deliquescence, which, at long storage times, may lead to localized corrosion and stress corrosion cracking (SCC). Studies on the effects of atmospheric relative humidity (RH), which determines electrolyte concentration and chemistry, on corrosion and SCC and the effectiveness of several SCC repair strategies are being conducted on SS304, a common material for canister construction.

Studies examining the effects of RH quantify the effect of electrolyte composition and exposure time (1 w to 2 y) on pitting corrosion. RH was found to play an influential role in determining pit density and morphology. Specifically, pit density is increased at the 40% RH compared to 76% RH, reaching a limiting pit density of roughly 6X higher. Additionally, at 76 % RH, pits displayed an ellipsoidal surface geometry with smooth facets at the pit base, whereas, at 40 % RH pits showed evidence of attack along distinct features that appear to be slip bands. Moreover, surface micro-cracks were found to emanate from pits at 40 % RH alone for all exposure times with no applied external load. As such, a hypothesis is presented for the effects of pit morphology and surface cracking at 40% RH based on synergistic electrochemical and microstructural causes. At low RH, high [Cl<sup>-</sup>], mass transport restriction due to precipitated salts at the surface, and preferential dissolution along slip bands results in a fissure-like pit geometry that serves as a stress concentrator. Together with residual stresses from surface grinding possibly forming strain-induced martensite, hydrogen embrittlement is possible to due to cathodic hydrogen generation. Studies are ongoing to confirm this theory. Furthermore, the effect of electrolyte chemistry and electrolyte droplet size are being conducted to determine the cause of the unique pit morphology produced under 40 % RH exposure.

A companion study to investigate the effect of pit morphology on SCC initiation under atmospheric exposure is examining tension samples printed with ASTM sea salt, pre-exposed at 40 and 76 % RH, producing pre-corrosion that will serve as crack initiation sites once loaded. After pre-exposure from 1 w to 2 y, samples are mechanically loaded (at 1.2 X the nominal yield strength) under the same atmospheric conditions. A preliminary investigation for 40 % RH (after 6 months of pre-exposure) show surface cracks after 6 months of mechanical loading. Finite element models are being developed to understand 3D stress concentration profiles around each pit morphology (i.e. 40 % vs 76 %).

A study is also underway to identify which of several candidate repair strategies are effective at repairing already present SCC and maintaining future atmospheric and SCC resistance. ASTM G-36 boiling MgCl<sub>2</sub> testing will be used to downselect between tungsten-arc welding, friction stir welding, vaporizing foil actuator welding, cold spray, and soldering for further research.

*This work is supported at The Ohio State University by Sandia National Laboratories (non-repair related research) and the Department of Energy [National Nuclear Security Administration] – Nuclear Energy University Program (DOE-NEUP) under Award Number DE-NE0008765 (repair related research). The views and opinions of authors expressed herein do not necessarily state or reflect those of the United States Government or any agency thereof. Sandia National Laboratories is a multimission laboratory managed and operated by National Technology and Engineering Solutions of Sandia LLC, a wholly owned subsidiary of Honeywell International Inc. for the U.S. Department of Energy's National Nuclear Security Administration under contract DE-NA0003525. SAND#2020-5962 A*

5:30 AM F.EN08.02.03

**Effect of Bentonite Dry Density on Corrosion of Embedded Copper** Claire Tully<sup>1</sup>, Dmitriy Zagidulin<sup>1</sup>, James J. Noel<sup>1,2</sup> and Wilfred J. Binns<sup>3</sup>; <sup>1</sup>The University of Western Ontario, Canada; <sup>2</sup>Surface Science Western, Canada; <sup>3</sup>Nuclear

The Nuclear Waste Management Organization plans to manage Canada's used nuclear fuel by isolating it underground within a multiple-barrier system, in a deep geological repository (DGR), in keeping with internationally accepted best practice.<sup>1</sup> In the proposed design, used fuel bundles will be sealed in copper-coated carbon steel used fuel containers (UFC), encased in blocks of highly compacted bentonite clay, and emplaced ~500 m below ground in the DGR. Any gaps between the rock walls and the bentonite blocks will then be filled with a bentonite gapfill material (GFM). Due to its physical and chemical properties, the bentonite will significantly limit the transport of reactive species to the UFCs. The high swelling pressure of bentonite can suppress the action of sulphate reducing bacteria (SRB) by decreasing the clay pore space and lowering water activity, which then limits microbially influenced corrosion of the UFC.<sup>2</sup>

The goal of this work is to investigate the effects of bentonite dry density, the presence of oxygen, and the evolution of environmental conditions on the corrosion of copper in contact with bentonite, and on SRB viability. We are conducting a series of experiments in bentonite-filled vessels exposed to ocean conditions (ocean modules, OM) and more controlled laboratory-based conditions (pressure cells, PC). The OM are porous vessels containing copper coupons embedded in GFM that has been compacted to various dry densities. The modules are then placed in the Pacific Ocean at depths of up to 2.6 km for months-to-years at a time, exposed to seawater, with hydrostatic pressures representative of potential DGR pressures. PC experiments contain copper coupons embedded in GFM and are pressurized to 100 bar with Type-1 water for varying durations up to 1 year. After exposure, copper coupons are analyzed by SEM, XPS, FIB, and AES, the water activity of the bentonite is assessed, and 16s RNA analysis used to determine the presence of SRB.

Two OMs, both with cold-spray ( $Cu_{cs}$ ) and wrought ( $Cu_w$ ) copper coupons, with GFM (dry density of 1.25 or 1.45 g/cm<sup>3</sup>) were exposed to seawater at a depth of 90 meters for 6 months. The surfaces of the copper coupons experienced non-uniform corrosion, possibly due to non-uniform wetting and subsequent swelling of the clay. The copper speciation in the surface corrosion products consisted of ~85 %  $Cu_2O$ , ~ 5 %  $Cu_2S$ , ~3 %  $CuCl$ , and ~ 3 %  $CuO$ .  $Cu_w$  had higher amounts of  $Cu_2O$  and lower amounts of  $Cu_2S$  at both GFM dry densities. Both the  $Cu_w$  and  $Cu_{cs}$  exposed to the higher density GFM had lower amounts of  $Cu_2S$  and higher amounts of  $Cu_2O$  on the surface. This may be the result of non-uniform swelling, decreased mobility of the sulphide or a decrease in the number of metabolically active SRBs, or a combination of those factors.<sup>2</sup> Mass loss measurements determined that  $Cu_{cs}$  had a higher corrosion rate than  $Cu_w$ ; however,  $Cu_w$  corrosion rates were less affected by the GFM density. Overall, the increase in bentonite dry density resulted in a decrease in copper corrosion rates, with the  $Cu_{cs}$  corrosion rate being decreased more significantly than that of  $Cu_w$ .

The experiments performed in PCs for 1 month duration provided similar results. Cross-sections of the film formed at the copper surface revealed the presence of copper, oxygen, and sulphur, unevenly distributed across the copper surface, accounting for the non-uniform corrosion observed. The corrosion rates were significantly higher than those in the OM experiments due to the higher oxygen concentration.

1. J. Noronha. Deep Geological Repository Conceptual Design Report Crystalline/Sedimentary Rock Environment, NWMO, Canada, APM-REP-00440-0015 R001, 2014.

2. S. Stroes-Gascoyne, C.J. Hamon, D. Priyanto, D. Jalique, C. Kohle, W. Evergen, A. Grigoryan, D. K. Kober, Microbial Analysis of a Highly Compacted Wyoming MX-80 Bentonite Plug Infused Under Pressure with Distilled Deionised Water over a Period of Almost Eight Years, NWMO, Canada, TR-2014-20, 2014.

#### 5:40 AM F.EN08.02.04

**Investigating the Corrosion of Natural Uranium Dioxide by Hydrogen Peroxide and Hydrogen** Martin Badley<sup>1</sup>, James J. Noel<sup>1,2</sup> and David W. Shoesmith<sup>1,2</sup>, <sup>1</sup>The University of Western Ontario, Canada; <sup>2</sup>Surface Science Western, Canada

The proposed plan for the long-term management of used nuclear fuel in Canada is to seal it in copper-coated steel containers (UFC) and emplace them in a deep geologic repository using a multi-barrier containment concept. While there is extensive literature providing confidence that UFCs will remain intact until fuel radiation levels decay to insignificant levels, it is judicious to investigate the consequences of container failure, when groundwater could come into contact with the fuel. The goal of this project is to investigate the effect of radiolytically produced oxidants on the corrosion/dissolution rates, and the influence of oxidant scavengers on the respective rates for fuel specimens that represent fuel used in Canada.

Within a failed UFC, water radiolysis could lead to the production of localized oxidizing conditions at the surface of the fuel, potentially leading to fuel corrosion and radionuclide release to the groundwater. The rate of such a process would be determined by the radiation dose rate from the fuel, and the reactivity of the fuel, which will be determined by its composition, in particular by the degree of non-stoichiometry and the concentration of fission products.<sup>1,2</sup> The corrosion rate at the fuel surface can be suppressed in the presence of oxidant scavengers produced at the steel-groundwater interface. These scavenging ions will consume radiolytically produced oxidants, largely through a catalytic reaction on noble metal particles.<sup>3</sup> For undoped  $UO_2$  (i.e., in the absence of fission products) the reactivity has been shown to be very dependent on the degree of non-stoichiometry ( $x$  in  $UO_{2+x}$ ), which can be estimated by electrical conductivity measurements.<sup>4</sup> Overall, specimen

conductivities are being measured by electrical impedance measurements. The reactivity of characterized specimens is subsequently being determined using either electrochemical measurements or analytical measurements of the amounts of H<sub>2</sub>O<sub>2</sub> consumed and U dissolved. Further, measurements of the oxidant scavenging properties of H<sub>2</sub> are being investigated in the absence of noble metal particles to observe the influence of localized non-stoichiometry. This research will work towards expanding the established model for the  $\alpha$ -radiolytic corrosion of used nuclear fuel.<sup>5</sup>

1. He, H.; Qin, Z.; Shoesmith, D. W., Characterizing the relationship between hyperstoichiometry, defect structure and local corrosion kinetics of uranium dioxide. *Electrochim. Acta* **2010**, *56* (1), 53-60.
2. Liu, N.; He, H.; Noël, J. J.; Shoesmith, D. W., The electrochemical study of Dy<sub>2</sub>O<sub>3</sub> doped UO<sub>2</sub> in slightly alkaline sodium carbonate/bicarbonate and phosphate solutions. *Electrochim. Acta* **2017**, *235*, 654-663.
3. Razdan, M.; Shoesmith, D. W., The influence of hydrogen peroxide and hydrogen on the corrosion of simulated spent nuclear fuel. *Faraday Discuss.* **2015**, *180* (0), 283-299.
4. Hyland, G. J.; Ralph, J., Electronic contributions to the high-temperature thermophysical properties of UO<sub>2+x</sub>: a critical analysis. *High Temp. - High Press.* **1983**, *15*, 179-190.
5. Wu, L.; Liu, N.; Qin, Z.; Shoesmith, D. W., Modeling the radiolytic corrosion of fractured nuclear fuel under permanent disposal conditions. *J. Electrochem. Soc.* **2014**, *161* (8), E3259-E3266.

#### 5:50 AM F.EN08.02.05

**Numerical Implementation of a Copper Corrosion Model for Used Fuel Containers Used in a Deep Geological Repository** Scott Briggs<sup>1</sup> and Fraser King<sup>2</sup>; <sup>1</sup>Nuclear Waste Management Organization, Canada; <sup>2</sup>Integrity Corrosion Consulting Ltd., Canada

The Nuclear Waste Management Organization is responsible for the implementation of Adaptive Phased Management (APM), Canada's plan for the long-term management of used nuclear fuel in a deep geological repository (DGR). Currently in the site selection process, NWMO is seeking partnership with an informed and willing community to host the DGR while technical research is on-going in support of APM. An integral part of isolating and containing the used nuclear fuel is the engineered barrier system which consists of the bentonite clay, a long-lived steel container (with copper coating) and a durable waste form (zircaloy cladding and high-density ceramic fuel pellet). The copper coating consists of a 3 mm copper layer on a steel container and in this current work, a copper corrosion model was developed to predict the long-term uniform corrosion behaviour. The current model builds on the work by King and Kolar (2006) by extending the previous 1D model to include 3D geometry effects. The model was developed in COMSOL Multiphysics using a finite-element approach including 1D and 3D implementations. A step-wise approach was used in the development of the model, starting with a simple reaction scheme and increasing mechanistic detail while ensuring numerical stability and careful validation against experimental results. The developed copper corrosion model predicts the corrosion potential along with environmental parameters (ex. [Cl<sup>-</sup>], [O<sub>2</sub>]), copper species concentrations and mass transfer rates which can be used to determine, mechanistically, the rate-controlling processes for both the anodic and cathodic reactions. Corrosion potentials can also be used to determine the likelihood of pitting corrosion in the DGR environment and the corrosion current density can be used to predict the rate of uniform corrosion.

#### References

King, F. and M. Kolar. 2006. Simulation of the consumption of oxygen in long-term *in situ* experiments and in the third case study repository using the copper corrosion model CCM UC.1.1. Ontario Power Generation, Nuclear Waste Management Division Report, 06819REP0130010084R00

SESSION F.EN08.03: Management of Volatile Fission Products  
On Demand Abstracts Available for Viewing Starting Saturday Morning, November 21, 2020  
F-EN08

#### 5:00 AM \*F.EN08.03.01

**Multi-Column Evaluations for the Capture and Separation of Krypton and Xenon Using Mordenite Based Sorbents** Mitchell Greenhalgh, Amy Welty and Troy Garn; Idaho National Laboratory, United States

A multi-column adsorption system has been designed and installed to evaluate the independent capture and separation of xenon and krypton utilizing solid phase sorbents being developed by the DOE-NE Offgas Sigma team. The xenon and

krypton are present in the offgas stream resulting from a used nuclear fuel reprocessing plant. The system is intended to provide greater operating flexibility and testing at a wide range of flow rates while maintaining desired pressure conditions. This system also allows for continuous analysis of effluent gas from each column. The system was set up by packing the first column with AgZ-PAN which has demonstrated a high selectivity for xenon over krypton at ambient temperatures. A second column was packed with HZ-PAN to capture the krypton. The AgZ-PAN column was maintained at ambient temperatures whereas the HZ-PAN column was maintained at 191K. A simulated offgas stream consisting of 1000 ppmv xenon and 150 ppmv krypton in a balance of air was introduced to the first column to capture the xenon and the resulting xenon free effluent was then routed into the second column for krypton capture. Flowrates of the feed stream were varied from 50-2000 sccm. The results of the multi-column testing demonstrated successful separation of xenon from krypton and indicated that increasing superficial velocity does not significantly impact sorbent capacity or initial breakthrough of the columns. This procedure, while not optimized, may be used to reduce the final waste volume of captured radioactive gas species emitted from a reprocessing facility.

#### 5:15 AM F.EN08.03.03

**The State-of-the-art Development of Mechanically and Chemically Robust Sorbent for Management of Iodine** Josef Matyas, James Amonette and Michael Sinnewell; Pacific Northwest National Laboratory, United States

New generation sorbents are being investigated for the removal and immobilization of radioiodine from the gas streams in a used nuclear fuel reprocessing facility. Silver-functionalized silica aerogel (Ag<sup>0</sup>-aerogel) exhibits high selectivity and sorption capacity for iodine. Moreover, a feasible consolidation of iodine-loaded Ag<sup>0</sup>-aerogel to a durable SiO<sub>2</sub>-based waste form is an attractive choice for sequestering radioiodine. Extended-duration testing of Ag<sup>0</sup>-aerogel in highly oxidizing reprocessing off-gas streams indicated fragmentation of granules into small particles. These particles were held up in the column without being carried-over into the off-gas system. However, production of small particles during sorption can lead to compaction of the sorbent, restricting the flow of gas through the column. Our study targeted development of mechanically and chemically stable Ag<sup>0</sup>-aerogel through optimized synthesis process, which included using a patent-pending technology treatment to strengthen the granules. The reinforced Ag<sup>0</sup>-aerogel with bulk density ~ 0.5 g/cm<sup>3</sup> went through rigorous testing at different off-gas streams followed by attrition testing with a vibratory sieve shaker. There were no fines generated even after 60 min exposure to shaking speeds of ~1800 revolutions per minute, with ~3 mm orbital shaker movement. The mechanically/chemically robust Ag<sup>0</sup>-aerogel retained high iodine sorption capacity of 400.5 ± 2.2 mg/g. The presentation will focus on various strategies that have been developed to improve the mechanical/chemical properties of Ag<sup>0</sup>-aerogel and conclude with a summary of highlights and a prognosis for future developments.

#### 5:25 AM \*F.EN08.03.04

**On-Line Monitoring of Molten Salts to Characterize Chemical Composition** Amanda Lines, Shirmir Branch, Heather Felmy, Adan Medina, Hope Lackey, Gregg Lumetta and Samuel Bryan; Pacific Northwest National Laboratory, United States

Molten salt systems provide highly efficient heat transfer options without pressurization, making them a potentially valuable tool throughout the energy sector, including solar power and nuclear energy. Molten salt reactors are of particular interest due to the advancements they can offer to the nuclear field, such as improved safety. However, the chemical behavior of key species anticipated in molten salt reactors is not well understood. Tools are needed to monitor and characterize the chemical composition of molten salts to better understand the behavior of actinides, fission products, and corrosion products. Furthermore, these tools are needed to allow for molten salt process control and to support the maintenance of materials accountancy. Of the options available, optical spectroscopy enables powerful routes to characterize these systems *in situ*. Utilization of these tools allows for the fast and robust identification and quantification of many chemical species of interest to molten salt processing, reactor control, and corrosion characterization. Most importantly, optical spectroscopy can enable the analysis of oxidation state ratios and species complexation, which can significantly impact system performance and corrosion behavior. Optical spectroscopy-based monitoring can be leveraged in fundamental and applied research. For example, optical spectroscopy can be paired with electrochemistry in spectroelectrochemistry to provide a powerful route to fundamental characterization of redox behavior, speciation, and chemical behavior dependence on temperature. Optical spectroscopy can also be paired with chemometric analysis to enable real-time quantification of target analytes within salt melts. Complex salt systems containing many chemical species will exhibit complex spectral data, presenting signal interferences and band overlap, which can hinder accurate analysis. However, the application of chemometric analysis can enable accurate characterization of multicomponent streams to provide real-time, automated monitoring of a process stream or batch. Optical spectroscopy-based on-line monitoring enables fast and robust identification and quantification of many actinides, fission products, and corrosion products. Here we demonstrate the application of optical monitoring approaches to

the characterization of chloride-based salt melts containing lanthanides and actinides.

SESSION F.EN08.04: Effects in Nuclear Waste Forms  
On Demand Abstracts Available for Viewing Starting Saturday Morning, November 21, 2020  
F-EN08

**5:00 AM \*F.EN08.04.01**

**Radiation Damage and Thermal Aging of Nuclear Waste Forms** William J. Weber; The University of Tennessee, United States

Self-radiation damage from the decay of radionuclides can affect microstructural evolution, phase stability, and thermodynamic properties in nuclear waste forms. The principal sources of radiation are beta-decay of the fission products and alpha-decay of the actinide elements. In general, beta-decay of the short-lived fission products leads to ionizing radiation that is the primary source of radiation and heat generation in high-level waste forms during the first 600 years of storage. Ionization can cause covalent and ionic bond rupture, valence changes, localized electronic excitations, and significant changes in ionic mobility; however, there is no evidence of significant long-term effects of fission product decay on the physical properties of nuclear waste forms. Because of the long half-lives of the actinides and their daughter products, alpha-decay is dominant over very long timescales. Alpha decay produces energetic alpha particles (4.5 to 5.5 MeV) and recoil nuclei (70 to 100 keV) that result in both radiation damage and the accumulation of helium. The evolution of radiation damage due to alpha-decay has been studied at ambient temperature using short-lived actinides, such as  $^{238}\text{Pu}$  and  $^{244}\text{Cm}$ , in many candidate glass and ceramic waste forms, and the early stages of evolution occur during the thermal period of the waste form. Ion beam irradiations of candidate ceramics are more frequently employed due to decreased costs, shorter irradiation timescales and the non-radioactive nature of the irradiated materials. Ion irradiations are performed over a wider range of irradiation conditions to implant helium, study radiation damage kinetics, understand the separate and combined effects of alpha particles and alpha recoils, and benchmark against alpha-decay damage due to short-lived actinides. At ion energies (keV to MeV) typically used to study alpha-decay damage in nuclear waste forms, the electronic and nuclear energy losses are both important, and the spatial coupling of electronic and nuclear energy loss can lead to reduced or enhanced damage production along the ion trajectory. While alpha particles are much less damaging than alpha recoils, the electronic energy loss from the alpha particles can also cause athermal annealing of alpha-recoil damage that can impact the evolution of radiation damage. Helium implantation studies have shown that helium bubbles form above a threshold helium concentration in candidate waste forms. Swift heavy ions (several hundred MeV to several GeV) have also been used to study radiation damage in nuclear waste forms; although the damage production mechanism and energy densities are substantially different from beta decay or alpha decay, large volumes are damaged.

**5:15 AM F.EN08.04.03**

**Characterising the Effect of Heavy-Ion Irradiation on the Microstructure of Ce-Doped Compounds** Ritesh Mohun<sup>1</sup>, Sebastian Lawson<sup>1</sup>, Theo Cordara<sup>1</sup>, Hannah Smith<sup>1</sup>, Clémence Gausse<sup>1</sup>, Max Cole<sup>1</sup>, John S. McCloy<sup>2</sup>, Marc Weber<sup>2</sup>, Sam Karcher<sup>2</sup>, Martin Stennett<sup>1</sup>, Neil Hyatt<sup>1</sup> and Claire L. Corkhill<sup>1</sup>; <sup>1</sup>The University of Sheffield, United Kingdom; <sup>2</sup>Washington State University, United States

In this study, we aimed to investigate the radiation effects in doped-fluorite structure ceramics.  $\text{CeO}_2$  was chosen as the host matrix because of its fluorite crystallographic (Fm-3m) structure, which consists of a simple cubic oxygen sub-lattice with the cation ions occupying alternate cube centres, similar to  $\text{UO}_2$ ,  $\text{PuO}_2$ , and  $\text{ThO}_2$ . The objective was first to quantify the defect chemistry/configurations when  $\text{CeO}_2$  is doped with trivalent yttrium at different concentrations, and then to study the atomistic changes when the solid solutions were irradiated with 3 MeV gold ion under two different fluence, corresponding to a damage level of 6 dpa and 33 dpa values respectively.

Initial X-ray diffraction measurements of the prepared samples showed a contraction of the unit cell with Y-content attributed to a certain long-range ordering of the anion vacancies with randomly distributed  $\text{Y}_2\text{O}_3$  micro-domains of 'C-type' structure which grows coherently within the fluorite matrix. This observation corroborates with Extended X-ray Absorption Fine Structure (EXAFs) analysis which indicated a change in the coordination number when the dopant is introduced in the  $\text{CeO}_2$ . On the other hand, Raman spectroscopy was used to quantify the presence of oxygen vacancy-type defects formed to compensate for the charge due to the substitution of  $\text{Ce}^{4+}$  with a trivalent dopant and the presence of reduced  $\text{Ce}^{3+}$ . In regards to the irradiated samples, the excellent radiation stability of Ce-based compounds was reported and it was observed that Au-incident ions tend to reduce  $\text{Ce}^{4+}$  to  $\text{Ce}^{3+}$ . In addition, Positron annihilation spectroscopy measurements

showed that the lower irradiation fluence increases considerably the concentration of lattice damages close to the disorder saturation level, where all the implanted positrons are trapped and a further increase in the irradiation dose initiates a dynamic damage recovery. Relevant defect mechanisms for the two considered irradiation fluence studies were identified and will be detailed in this presentation.

#### 5:25 AM F.EN08.04.04

**Structural Behavior of Ordered Mesoporous Silica Under Swift Heavy Ions and Electrons Irradiation** Jun Lin<sup>1</sup>, Xavier Deschanel<sup>1</sup>, Clara Grygiel<sup>2</sup>, Guillaume Toquer<sup>1</sup> and Sandrine Dourdain<sup>1</sup>; <sup>1</sup>ICSM, CEA, CNRS, ENSCM, Univ Montpellier, France; <sup>2</sup>CIMAP, CEA-CNRS, France

Ordered mesoporous silica still attracts considerable attention because of a myriad of industrial potential applications, such as catalysis, gas adsorption, electronics, optics, drug delivery and nuclear waste storage. More precisely concerning the latter example, alternative processes for the treatment of radioactive effluents containing actinides and fission products are developing. In this way, a precise knowledge of the damage induced in those materials, due to the radiation, is then required. Apart from radiation tolerance of mesoporous metallic foam already reported by Bringa *et al.*[1], other studies[2] have highlighted the collapse of the mesoporous network of silica-based materials induced by the ballistic radiation damage for an energy deposited close to a few  $10^{21}$  keV/cm<sup>3</sup>.

In this work, two kinds of samples have been irradiated to evaluate their dimensional effect in electronic regime. In one hand, thin films (~100 nm) of mesoporous silica deposited by dip-coating onto silicon wafer were irradiated at IRRSUD (GANIL) with ions having a stopping power in the 1-10 keV/nm range. In the second hand, pellets obtained by compaction of powders were irradiated at lower stopping power from  $10^{-3}$  keV/nm (2 MeV electrons, LSI) to 1 keV/nm (proton ~20 MeV, CEMHTI). These samples were analyzed before and after irradiation by X-ray reflectometry (thin films), nitrogen adsorption isotherm and small angle X-ray scattering measurements (pellets), electron microscopy (Scanning, Transmission) to investigate the evolution of the porous structure and also by spectroscopy (nuclear magnetic resonance, infra-red) to evaluate the evolution of the silica network. A mechanism is proposed to explain and describe the evolution of the mesoporous structure under irradiation.

#### References:

- [1] E.M.Bringa, J.D.Monk and A.Caro, Nano Lett, 12 (2012) 3351-5
- [2] L.Yu, S.Dourdain and C.Rey, Microporous and Mesoporous Materials, 251 (2017) 146-154

#### 5:35 AM F.EN08.04.05

**Effect of Ionizing Radiation on PuO<sub>2</sub> and Surrogate Oxide Materials Under Storage Condition** Luke Jones<sup>1</sup>, Darryl Messer<sup>1</sup>, Robin Orr<sup>2</sup>, Howard E. Sims<sup>2</sup>, Andrew B. Horn<sup>1</sup> and Simon M. Pimblott<sup>3</sup>; <sup>1</sup>University of Manchester, United Kingdom; <sup>2</sup>National Nuclear Laboratory, United Kingdom; <sup>3</sup>Idaho National Laboratory, United States

The stockpile of plutonium separated from used nuclear fuel amounts to many 100s of tonnes. The majority of this plutonium is stored as PuO<sub>2</sub> powder packaged in multi-can containers. The conditions during the packaging of reprocessed PuO<sub>2</sub> for long term storage are closely controlled to limit water uptake as radiolytic decomposition of any adsorbed water will lead to the formation of both a potentially flammable atmosphere containing molecular hydrogen as well as reactive oxygen species which may be incorporated into the oxide phase. Consequently, the safety case for the long-term storage of PuO<sub>2</sub> requires a complete understanding of the fundamental physical, chemical and materials degradation processes occurring at the water-oxide interface inside the storage canisters. This study investigates the effect of ionizing radiation on PuO<sub>2</sub> and various surrogate oxides under atmospheres potentially encountered in storage canisters.

To elucidate the effects of adsorbed water, samples of baked oxide powder were equilibrated in humidity chambers to attain a wide range of masses of water adsorbed onto the powder surface. In the case of PuO<sub>2</sub>, once the surface water on the oxide had equilibrated with the humid atmosphere, the samples were sealed into a glass vessel held at constant humidity with either an argon or a nitrogen over-gas and left for up to 3 months. Periodic sampling of the headspace was undertaken and the atmosphere above the oxide analyzed using gas chromatography. In the case of the surrogate oxides, once the oxides had adsorbed the maximum quantity of water, the samples were flame sealed under argon into a glass tube and Co-60 gamma irradiated. Prior to and after gamma irradiation, the oxide powders were characterized using a variety of different microscopy and spectroscopy methods. Following gamma irradiation, the headspace was analyzed using gas chromatography. For PuO<sub>2</sub>, the rate at which H<sub>2</sub> was produced increased with increasing water loading. This result contrasts with the experimental data in this study and from similar experiments in the literature utilizing UO<sub>2</sub>, CeO<sub>2</sub> and ZrO<sub>2</sub> which showed a higher rate of production for lower water coverages. There was no evidence of a steady state hydrogen concentration being reached in the

PuO<sub>2</sub> experiments, an outcome opposite of that observed in storage canisters and in experiments performed by other groups in which the PuO<sub>2</sub> was not held under constant humidity. Radiolytic production of molecular oxygen was not observed. Comparison of the properties of the surrogate oxide (ZrO<sub>2</sub>) powder prior to and post irradiation did not reveal any differences in stoichiometry, surface functionalization or the formation of oxygen-centered free radicals, so the location of the sibling oxidant to the evolved molecular hydrogen currently remains unanswered.

Parallel experimental and modeling studies considering the chemistry of PuO<sub>2</sub> and surrogate oxides in H<sub>2</sub>:O<sub>2</sub>:Ar atmospheres are ongoing. To perform the experiments, a bespoke manifold was designed and commissioned to mix various ratios of H<sub>2</sub>-O<sub>2</sub> and Ar gas. Gas chromatography was used to analyse post-irradiated samples. Experiments were performed in 10 ml volume 316 stainless steel canisters (with no degradable polymeric components). Experimental data will be presented showing the extent of recombination of H<sub>2</sub>-O<sub>2</sub> mixtures in Ar under <sup>60</sup>Co  $\gamma$  rays and accelerated He ion irradiation and the influence an oxide surface on this recombination: radiolytic reaction of H<sub>2</sub> with O<sub>2</sub> to form H<sub>2</sub>O is enhanced over what is expected from gas phase processes suggesting significant interfacial chemistry.

Acknowledgement: This work was supported by the Dalton Cumbrian Facility Project, a joint initiative of the University of Manchester and the Nuclear Decommissioning Authority, by the UK Engineering and Physical Sciences Research Council and by the US Department of Energy, Office of Nuclear Energy.

#### 5:45 AM F.EN08.04.06

**Quantifying the Effects of Grain Boundary Areas on the Irradiation Behaviour of UO<sub>2</sub>** Ritesh Mohun, Sebastian Lawson, Daniel Bailey, Shikuan Sun, Clémence Gausse, Hannah Smith, Max Cole, Martin Stennett, Neil Hyatt and Claire L. Corkhill; The University of Sheffield, United Kingdom

Complex microstructural changes occur in nuclear fuels due to the extreme environments of intense irradiation and high temperature during in-reactor operations. Several theoretical and experimental works are currently in progress to determine the effect of crystalline defects which has a major influence on the behaviour of fission products, mainly in regards to rare gases, that may impact the life-span of the rod-type uranium fuel element. For instance, the nucleation of insoluble gas bubbles is thought to act as trapping sites for migrating vacancy-type defects, and further increase in the damage levels induces significant microstructural modifications. In this study, we aimed to investigate the specific role of microstructure on the radiation stability of nuclear fuels.

For this purpose, UO<sub>2</sub> pellets with different microstructures were initially prepared through the wet chemistry route and sintered at different temperatures. Scanning electron microscopy and X-ray diffraction characterisations were performed to quantify the grain size/boundaries areas and crystallinity of the pristine samples. Raman spectroscopy also proved useful and allowed to investigate the effect of sintering temperature on the concentration of intrinsic lattice defects. The samples were then implanted with 1 MeV Krypton-ions at room temperature to induce irradiation damages in the matrix of the different grain-size UO<sub>2</sub> pellets.

Post-irradiation measurements were carried to highlight the excellent radiation stability of fluorite-type nuclear fuels. However, it was observed that the UO<sub>2</sub> microstructure has an important effect on the point defects produced by the displacement cascades induced by ionic implantation. In this presentation, an attempt is made to detail the mechanisms occurring near the defect-boundary interfaces in relation to radiation damage to highlight the precise role of grain boundaries modifying the defects behaviour and their subsequent evolution in fluorite structure relevant to nuclear fuels.

#### 5:55 AM F.EN08.04.07

**Assessment of Positrons for Defect Studies in UO<sub>2</sub> and CeO<sub>2</sub> Materials** Marc H. Weber<sup>1</sup>, Ritesh Mohun<sup>2</sup>, Sam Karcher<sup>1</sup>, Claire L. Corkhill<sup>2</sup> and John S. McCloy<sup>1</sup>; <sup>1</sup>Washington State University, United States; <sup>2</sup>The University of Sheffield, United Kingdom

The safe disposal and long-term isolation of spent mixed oxide nuclear fuel poses significant challenges. Uranium and plutonium oxides enriched with rare earth and lanthanide fission products and under constant irradiation with alpha particles and neutrons must be stored in geologic formations for thousands of years. A detailed understanding of the microstructure and chemistry is required to optimize processing designed to recover fissionable products from used fuel and to improve the safety and volume of radioactive waste. Cerium oxide (ceria) has been identified as a suitable non-radioactive substitute to study the microstructure and its evolution under long term irradiation.

A number of techniques have been applied to uranium and cerium oxides to investigate basic properties and point defects. These include neutron scattering, X-ray diffraction and Raman spectroscopy of as produced, irradiated and annealed materials. These are sensitive to structural properties (XRD, neutrons) and oxygen vacancies (Raman). Positron annihilation spectroscopies (PAS) are sensitive to neutral and negatively charged vacancy-like point defects and impurity-vacancy complexes. Positrons can provide depth resolved information about uranium or cerium vacancies to complement Raman data. PAS has been applied previously to UO<sub>2+x</sub> to investigate the properties of nuclear fuels.[1,2,3] Virtually no PAS work exists



on CeO<sub>2</sub>, doped or undoped. Currently, PAS are being used to investigate rare earth and lanthanide doped cerium oxide. The work on uranium oxide by the group of MF Barthe[1,2] demonstrated the presence of significant concentrations of uranium vacancies or Schottky defects as well as the presence of negatively charged interstitial oxygen atoms in oxygen rich. They also investigated the effect of 1 MeV helium implantation and the interaction of the implanted helium with the formed vacancies during annealing. Xe bubbles and their thermal evolution could also be observed.[4]

In this presentation, the basics of positron annihilation spectroscopy will be presented. PAS work on undoped and doped cerium oxide will be shown and compared to results from uranium oxides. To simulate spent nuclear fuels, the samples were doped at different concentration with rare earth elements or yttrium, zirconium. Select samples were irradiated with heavy ions at different doses. Differences were observed depending on what simulated fission products are present. Preliminary results and literature searches show some correlation with Raman data.

**References:** [1] Barthe MF et al. EPJ Web of Conferences **115**, 03004 (2016), and references therein; [2] Barthe MF et al. Phys. Stat. Solidi **C4** 3627-3632 (2007); [3] Wiktor J Physical Review B **90**, 184101(2014); [4] Djourelou N. et al Journal of Nuclear Materials **432** 287-293 (2013)

**Acknowledgements:** MW, JM, and SK thank the Institute for Materials Research and U.S. Department of Energy Nuclear Energy University Program – Used Nuclear Fuel Disposition program, award # DE-NE0008689. JM thanks the US-UK Fulbright Commission, and JM and SK thank the S.Y. Chung Centenary Fellowship for support during the research period. RM and CC thank Engineering and Physical Sciences Research Council, under the UK-US Nuclear Energy University Programme (EP/R006075/1), an Early Career Research Fellowship awarded to CC (EP/N017870/1), and the MIDAS Facility, at the University of Sheffield, established with support from the UK Department of Energy and Climate Change.

SESSION F.EN08.05: Spent Nuclear Fuel and Glass Corrosion Research  
On Demand Abstracts Available for Viewing Starting Saturday Morning, November 21, 2020  
F-EN08

#### 5:00 AM \*F.EN08.05.01

##### **Overview of the SKB Spent Fuel Research Program over the Years—Knowledge Gained and Remaining Open Questions** [Lena Z. Evins](#); Swedish Nuclear Fuel and Waste Management Co, Sweden

The Swedish strategy for spent nuclear fuel has, since around 1980, been direct geological disposal. Research about the properties and dissolution of spent fuel has been going on since then. An overview of this research program is given here with a focus on questions posed and answered along the way, ending with remaining open questions. At the beginning, some basic studies were performed to gain information about spent fuel as wasteform. Dissolution studies were at first mainly performed in contact with air, and often with aqueous solutions that mimicked the expected groundwater chemistry. However, complexities relating to precipitation of secondary phases indicated that simplified water compositions were preferred. Knowing that the radioactivity of the fuel caused radiolytic oxidation of uranium and thus controlled the dissolution rate, there were also attempts to achieve reducing conditions via bubbling a hydrogen/argon mixture in presence of a palladium-catalyst. The first attempts resulted in variable results, but notably, a reduction in apparent leach rate was observed for some experiments [1]. Later, possibilities to perform the leaching experiments in autoclaves, with controlled hydrogen atmosphere, allowed experimental conditions closer to the expected repository conditions. These experiments showed that hydrogen, during this type of experimental set-up, could suppress oxidative dissolution caused by radiolysis [2,3]. A new phase of research was thus started where the mechanistic explanation for the observed behaviour was sought. Experimental work, both with spent nuclear fuel and with analogue materials, was coupled with modelling efforts. At the time of the SR-Site safety assessment [4], which was a part of the license application submitted in 2011, a certain understanding had been reached, based on the effect of metallic particles in fuel. Still, questions remained and studies performed during the last decade (see for example [5]) can now be summarised to illustrate the knowledge gained, and remaining open questions. This summary is utilized in the next step in the licensing process: the application to start building the spent fuel repository, which is expected to be submitted within the next couple of years. In the coming decade the SKB research program will continue, with the goal to support the development of the safety assessment report, SAR, which will be submitted to the authorities as a part of the license application connected to start of trial operations.

During all these years, international collaboration has been a cornerstone of the SKB research program. This international collaboration has been carried out via European projects or bilateral agreements, and triggered the start-up of the Spent Fuel Workshops [6]. The research program has also been presented at this MRS symposium since the early 1980's.

[1] Forsyth R, 1983. The KBS UO<sub>2</sub> leaching program. Summary report 1983-02-01. KBS/SKBF Technical Report 83-26.

[2] Spahi, K., Werme, L. and Eklund, U.B., 2000. The influence of near field hydrogen on actinide solubilities and spent

fuel leaching. *Radiochimica Acta*, 88(9-11), pp.507-512.

[3] Werme, L.O., Spahiu, K., Johnson, L.H., Oversby, V.M., King, F., Grambow, B. and Shoesmith, D.W., 2004. Spent fuel performance under repository conditions: A model for use in SR-Can. SKB-TR-04-19. Swedish Nuclear Fuel and Waste Management Co.

[4] SKB, 2011. Long-term safety for the final repository for spent nuclear fuel at Forsmark. Main report of the SR-Site project. SKB TR-11-01, Swedish Nuclear Fuel and Waste Management Co.

[5] Barreiro Fidalgo, A., Kumagai, Y. and Jonsson, M., 2018. The role of surface-bound hydroxyl radicals in the reaction between H<sub>2</sub>O<sub>2</sub> and UO<sub>2</sub>. *Journal of Coordination Chemistry*, 71(11-13), pp.1799-1807.

[6] Werme LO, 1984. Proceedings of the third fuel workshop. KBS/SKBF Technical Report 83-76

### 5:15 AM F.EN08.05.03

**Understanding the Dissolution of Advanced Doped Nuclear Fuels for Geological Disposal** [Hannah Smith](#), Theo Cordara, Ritesh Mohun, Clémence Gausse, Max Cole, Martin Stennett, Neil Hyatt and Claire L. Corkhill; The University of Sheffield, United Kingdom

The addition of dopants, including chromium and aluminium, to uranium dioxide fuel results in the formation of larger grained microstructures, capable of higher fission gas retention and reduced swelling during operation within nuclear reactors. Despite their growing use by nuclear power plant operators, the long-term dissolution behaviour of spent doped fuels, when compared to typical spent fuel, is not yet well constrained. In a geological disposal facility, the release of radionuclides is known to be controlled by the oxidation of the UO<sub>2</sub> matrix and the subsequent dissolution of UO<sub>2</sub><sup>2+</sup> species, therefore any changes to the matrix from the addition of dopants could be expected to influence the dissolution kinetics and/or mechanisms.

We here present the results of an investigation of how the addition of Cr<sub>2</sub>O<sub>3</sub> to UO<sub>2</sub> fuel influences the crystal chemistry of UO<sub>2</sub> and its dissolution kinetics. Initial results, from experiments performed in air and a bicarbonate solution, show that the addition of Cr<sub>2</sub>O<sub>3</sub> reduces the normalised mass loss of uranium. The potential influencing factors that give rise to increased durability with Cr addition, e.g. defect concentration, Cr-oxidation state etc. are discussed.

### 5:25 AM \*F.EN08.05.04

**Physico-Chemical Phenomena Located at the Solid/Liquid Interface of Uranium-Based Oxide Materials** [Stephanie Szenknect](#)<sup>1</sup>, Laurent Claparede<sup>2</sup>, Adel Mesbah<sup>3</sup>, Theo Cordara<sup>1</sup>, Thomas Dalger<sup>1</sup>, Solène Bertolotto<sup>4</sup>, Nicolas Clavier<sup>3</sup>, Renaud Podor<sup>3</sup> and Nicolas Dacheux<sup>2</sup>; <sup>1</sup>ICSM, CEA, France; <sup>2</sup>ICSM, UM, France; <sup>3</sup>ICSM, CNRS, France; <sup>4</sup>CEA, DEN, DMRC, France

The “back end” of the nuclear fuel cycle corresponds to the direct disposal or reprocessing of the spent nuclear fuel (SNF), and to the conditioning and disposal in an appropriate repository of the nuclear wastes. In most of these processes, the behavior of actinides and fission products is governed by dissolution reactions at solid/ liquid interface. The design of reprocessing process and of nuclear waste disposal strategy requires the determination of well constrained kinetic and thermodynamic data. The acquisition of reliable kinetic and thermodynamic data is a tough issue considering on the one hand, the complexity of SNF in terms of chemical composition and microstructure and on the other hand, the challenge posed by the manipulation of highly radioactive samples.

For several years, we developed and improved a methodology that aims to determine dissolution rates of uranium-based oxide materials and thermodynamic data of phases of interest for final disposal of spent fuel in deep-mined geological repositories. This methodology is based on the synthesis of model compounds with well defined composition and microstructure, on the measurement of macroscopic dissolution rates in controlled chemical and hydrodynamic conditions, and on the monitoring of the properties of the solid/ liquid interface at the microscopic scale. For that purpose, several surface characterization techniques were used and developed, such as 3D reconstruction of Environmental SEM images, AFM or Grazing Incidence-XRD. To illustrate the progress made beyond the state of the art by using this methodology, several examples have been selected among the studies that we reported in the literature. The selected examples deal either with the reprocessing of uranium based oxides in nitric acid conditions, or with the behavior of UO<sub>2</sub> in SNF under the weathering conditions of geologic disposal.

The mechanisms that control the kinetics of dissolution of U-based oxides in nitric acid solutions are illustrated through the study of samples showing different compositions and microstructures. The use of oriented UO<sub>2</sub> single crystals allowed to evidence the enhanced reactivity of the surface at defect sites during a first kinetic regime. The second kinetic step was attributed to a catalyzed dissolution mechanism involving species produced at the solid/ liquid interface during the first step.

The key role of catalytic species in the strong increase of dissolution rate was demonstrated not only for UO<sub>2</sub> single crystals, but also for sintered pellets of (U, Th) mixed oxides and UO<sub>2</sub>-doped with platinum group metals. The monitoring of solid/liquid interface by 3D-ESEM during uncatalyzed and catalyzed regimes revealed specific dissolution sites of enhanced reactivity and specific dissolution features related to UO<sub>2</sub> crystallographic orientation, which traduced a structural control of the topographic evolution of the material.

Most of the geologic sites under investigation for underground repositories are located in undisturbed clay-rich rock or granite, with silica-rich groundwaters, deep enough to have reducing conditions. Understanding the interaction of used fuel with the silicate-rich groundwaters is critical to evaluate the safety of different disposal strategies. For several years, we investigated the role of silicates in the mechanisms of UO<sub>2</sub> weathering. For the first time, we were able to show the formation of coffinite (USiO<sub>4</sub>) from UO<sub>2</sub> in the presence of solution saturated with respect to SiO<sub>2</sub>(am) under conditions typical of deep-mined geologic repositories for SNF. Through dedicated experiments, we have constrained the conditions of formation of coffinite in an Eh-pH diagram. Finally, we showed that coffinite precipitation could lower the uranium release from the UO<sub>2</sub> matrix of SNF through oxidative weathering in the presence of oxygen in the geological repository.

#### 5:40 AM F.EN08.05.05

##### **Evaluating Divalent Cation (Zn, Ca, Mg) Behaviour During the Dissolution of Simulant UK High Level Waste Glass** Adam J. Fisher, Russell J. Hand and Claire L. Corkhill; University of Sheffield, United Kingdom

In an effort to incorporate high levels of Mo associated with the post-operational clean-out of high active liquor storage tanks at the Sellafield reprocessing facility in the UK, a modified version of the "MW" sodium aluminoborosilicate base glass has been adopted. The addition of Ca favours the formation of CaMoO<sub>4</sub>, while Zn infers improved viscosity. This new Ca/Zn MW base glass is currently being used to immobilise reprocessing wastes from oxide fuels and also magnox fuels, which contain a significant proportion of Mg. The divalent cations Ca<sup>2+</sup>, Zn<sup>2+</sup> and Mg<sup>2+</sup> are known to exert an influence on the durability of vitrified wastes, however the nature of their additive, or competitive effects are yet to be fully understood.

We here describe the results of a range of experiments that aim to elucidate the influence of divalent cations on the mechanisms and kinetics of glass dissolution. The addition of Zn to the glass was found to enhance durability in dilute, Si-undersaturated conditions, due to an increase in glass polymerisation with increasing Zn content, as determined by <sup>29</sup>Si MAS NMR. However, under conditions of Si-saturation, the presence of Zn prevented the formation of a passivating silica gel layer, and promoted the formation of Zn-containing smectite clays, significantly enhancing the dissolution rate with increasing Zn content. Mg had a similar effect to Zn, which was additive, however glasses containing Ca generally showed lower dissolution rates, in agreement with other studies. The formation of Zn- and Mg-bearing silicates was concurrent with a significant increase in the dissolution rate, similar to Stage III "rate resumption" behaviour, which has previously only been associated with the formation of zeolites.

#### 5:50 AM \*F.EN08.05.06

##### **Fabrication of Unirradiated Advanced Fuel for Dissolution Studies Under Repository Conditions** M Nieves Rodríguez-Villagra<sup>1</sup>, Sergio Fernández<sup>1</sup>, Laura J. Bonales<sup>2</sup>, Abel Milena-Pérez<sup>1</sup>, Ana Nuñez<sup>1</sup>, Sofia Durán<sup>1</sup>, Laureano Anta<sup>1</sup>, Luis Gutierrez<sup>1</sup> and Joaquín Cobos<sup>3</sup>; <sup>1</sup>CIEMAT, Spain; <sup>2</sup>CSIC-INTA, Spain; <sup>3</sup>EBD-CSIC, Spain

Safety assessment of Spent Nuclear Fuel (SNF) disposal in a Deep Geological Repository (DGR) requires evidences of radionuclides release after groundwater eventually gets into a breached container and contacts the fuel. Within the frame of EU H2020 program into the DISCO project, the impact of additives (Cr, Cr/Al and Gd) is being investigated on the long term DGR dissolution performance and compared to conventional UO<sub>2</sub>. In particular, the effect of these dopants is studied on the long term matrix dissolution rate of the SNF, the so-called Advanced Tolerant Fuels (ATF), such as Cr<sub>2</sub>O<sub>3</sub>-doped UO<sub>2</sub>, and Cr<sub>2</sub>O<sub>3</sub>-Al<sub>2</sub>O<sub>3</sub>-doped UO<sub>2</sub> fuels.

ATF have demonstrated to reach higher burn-up than conventional UO<sub>2</sub> fuels because dopants provide enhanced safety against Pellet-Clad Interaction failure (PCI), higher density, enlarged grain size, lower fission gas release and higher creep rate. Besides, the difference between those ATF and standard UO<sub>2</sub> in thermo-physical properties is almost negligible [1-4]. However, the dopants influence upon the matrix leaching performance at long term under DGR conditions is still largely unknown when compared to traditional UO<sub>2</sub> SNF.

The combinatory effects of two uncertain parameters (dopants influence and H<sub>2</sub>) on UO<sub>2</sub> matrix leaching resistance are investigated. In the context of WP2 and WP4 of the DISCO project, UO<sub>2</sub>-based pellets doped with a nominal concentration of 0.06<sup>w</sup>Cr<sub>2</sub>O<sub>3</sub>, 0.05<sup>w</sup>Cr<sub>2</sub>O<sub>3</sub>-0.02<sup>w</sup>Al<sub>2</sub>O<sub>3</sub> and 4.5<sup>w</sup>Gd<sub>2</sub>O<sub>3</sub>, were systematically produced by homogenizing stoichiometric proportions of UO<sub>2</sub> and dopants, and carefully characterized in order to understand the effects of the addition of Cr- and/or Al-oxide into the fuel matrix dissolution behaviour. Gd-doped UO<sub>2</sub> was also included, as a burnable poison and a trivalent

rare-earth dopants ( $RE^{III}$ ). The results are the basis for potential more complex systems which would correspond to irradiated doped fuels.

Previous studies suggest that  $RE^{III}$  play an important role on the  $UO_2$  oxidation, revealing that they prevent the fuel from a complete oxidation to  $U_3O_8$  [5], so in order to better understand the effect of trivalent  $RE^{III}$ , a set of dissolution experiments is carried out. The presence of reducing species, such as  $H_2$  (produced by anaerobic iron corrosion and radiolytically), affects the reactivity of  $UO_2$ ; hence, it must be considered in a long-term safety assessment. On the other hand, it is well known that  $HCO_3^-$  (one of the key complexing constituents in the groundwater) is highly likely to influence fuel dissolution by enhancing the solubility of  $U^{VI}$  thus preventing the secondary phase formation [6].

To experimentally evaluate the effect of additives (doped fuels) together with  $H_2(g)$  and different leachants on  $UO_2$  matrix dissolution rate, leaching experiments were performed under different representative aqueous systems. Prepared pellet/disks were characterized by means of XRD, Raman spectroscopy and SEM-EDX. In order to understand the effect of the presence/absence of  $HCO_3^-$  that could be considered as relevant to those coming from the interaction of water between natural barriers (groundwater) and EBS (Engineering Barrier System), specific synthetic groundwater was used in the dissolution tests. Static leaching experiments of doped- $UO_2$  pellets were run in stainless steel autoclaves with reaction vessels made of PEEK autoclaves under a  $N_2/4.7\%H_2$  atmosphere. The U and dopants concentration released into the aqueous solution was quantified by ICP-MS. pH and redox measurements were also tracked during the experiments.

[1] Thomas, G.A. et al. (2013) LWR Fuel Performance Meeting, TopFuel 201.

[2] Gentet, G. et al. (2015) Top Fuel 2015 Conference Proceedings A0198, 170 – 176.

[3] Backman, K. et al. (2009) INIS-XA--1074. International Atomic Energy Agency (IAEA).

[4] “Technical Exchange Meeting: EnCore® Accident Tolerant Fuel ADOPT Fuel Pellets”.

[5] Travis A. et al. (2020). J. Nucl. Mater. 530, 151959.

[6] Hossain, M.M. et al. (2006). J. Nucl. Mater., 358, (2-3), 202-208.

#### 6:05 AM F.EN08.05.07

**Investigation of Secondary Phases Formed During Long Term Aqueous Leaching of Spent Nuclear Fuel** Charlotta Askeljung<sup>1</sup>, Anders Puranen<sup>2</sup>, Olivia Roth<sup>1</sup>, Kyle Johnson<sup>1</sup>, Alexandre Barreiro Fidalgo<sup>1</sup>, Lena Z. Evins<sup>3</sup> and Kastriot Spahiu<sup>3</sup>; <sup>1</sup>Studsvik Nuclear AB, Sweden; <sup>2</sup>AB SVAFO, Sweden; <sup>3</sup>Swedish Nuclear Fuel and Waste Management Co, Sweden

For a future deep repository for spent nuclear fuel, the rate and mechanism for dissolution of fission products and actinides from spent fuel is a key parameter for the safety assessment of the disposal concept. Although the majority of the fuel to be placed in the deep repository is expected to be intact at the time of disposal, some failed fuel rods will also be present. In a failed fuel rod, the uranium matrix may have been exposed to water in the reactor and during interim storage for several years or decades prior to disposal. This exposure can lead to oxidation of the matrix and the formation of secondary phases under conditions of low uranium solubility. Upon barrier failure and ground water exposure of the spent fuel in the deep repository, these pre-oxidized layers are expected to dissolve at a higher rate compared to unaffected  $UO_2$  and hence increase the rate of radionuclide release. For this reason, knowledge about the characteristics of failed fuel and its behavior under deep repository conditions is required for the evaluation of the long-term safety of geological repositories. The present work aims to add to this knowledge.

Although the behavior of spent nuclear fuel under deep repository conditions has been studied extensively, studies of failed fuel are, in this context, relatively scarce, in particular studies of failed fuel that has been exposed to water during decades of wet interim storage. However, at the Studsvik laboratory in Sweden, leaching tests of spent fuel have been performed since the 1980s. This provides an opportunity to investigate the effects of long term contact with water under aerated conditions, such as those occurring in a wet interim storage.

In this study, XRD investigations have been performed on the surfaces of two fuel pellet samples which have been exposed to leaching solutions (synthetic ground water and deionized water, respectively) for over 30 years. Furthermore, the fuel surfaces have been exposed to carbonate solutions in an effort to dissolve the oxidized phases formed during the extended leaching time. The aim is to characterize the fuel matrix alteration.

#### 6:15 AM F.EN08.05.08

**Preliminary Results of Dissolution Experiments with Cr-(Pu) Doped  $UO_2$  in Reducing Conditions at SCK** CEN Christelle Cachoir, Thierry Mennecart and Karel Lemmens; SCK CEN, Belgium

The development of robust safety cases for geological disposal of spent fuel requires a solid understanding of its dissolution over very long time scale (up to a million years). While the dissolution of standard spent fuel has reached a good level of

comprehension, the development of modern LWR fuels (Cr/Al-doped  $\text{UO}_2$  or MOX fuels) raises the question whether these fuels will behave similarly to standard fuels in geological repository conditions. Within the EU-DisCo project, systematic dissolution studies have been initiated with carefully prepared and characterized, simplified  $\text{UO}_2$ -based model materials to understand the matrix dissolution of these modern LWR fuels under geological repository relevant conditions. As DisCo partner SCK CEN has performed such dissolution tests to study the effect of Cr-doping on the  $\text{UO}_2$  matrix dissolution rate in reducing conditions. Tests were started on four model materials :  $\text{UO}_2$ , Cr- $\text{UO}_2$ , Pu- $\text{UO}_2$  and Pu/Cr- $\text{UO}_2$  with a density close to 94% of the theoretical density and average grain size around 10  $\mu\text{m}$  for  $\text{UO}_2$  and Pu- $\text{UO}_2$ , 35  $\mu\text{m}$  for Cr- $\text{UO}_2$  and 25  $\mu\text{m}$  for Pu/Cr- $\text{UO}_2$ . The Cr doped pellets contain 1600  $\mu\text{g}$   $\text{Cr}_2\text{O}_3$  per gram of  $\text{UO}_2$ , and the alpha doping level of the Pu-doped pellets ( $\sim 18 \text{ MBq/gUO}_2$ ) is representative for a fuel age of 10,000 years. Static dissolution experiments with these model materials have been performed in autoclaves in two reference waters (synthetic young cementitious water at pH 13.5 and bicarbonate water at pH 9) under 10 bar  $\text{H}_2$  pressure and in presence of Pt/Pd catalyst. After a predissolution in 0.01 M NaCl solution for 3 weeks to remove the pre-oxidized UOX layer, samples were taken from the solution over a period up to 2 months. For the materials  $\text{UO}_2$  and Cr- $\text{UO}_2$ , the Cr-doping leads to lower uranium concentrations in solution, both in synthetic cementitious and in bicarbonate water. In the synthetic cementitious water, this effect is constant over the entire experiment, but the concentrations, increasing immediately after the replacement of the NaCl solution by the cementitious solution, remain high at  $\sim 10^{-7}$  M for  $\text{UO}_2$  and  $\sim 10^{-8}$  M for Cr- $\text{UO}_2$ . In bicarbonate water, the initial uranium concentrations (after replacement of the NaCl solution by the bicarbonate solution) are the same as for the cementitious water, but after 2 months, all concentrations are  $\sim 10^{-9}$  M. These preliminary results suggest that the Cr doping decreases the U release in solution, but the long-term effect depends on the leaching solution. Experiments with the Pu doped materials (Pu- $\text{UO}_2$  and Pu/Cr- $\text{UO}_2$ ) are now carried on to study the Cr-effect in combination with alpha-radiolysis of the solution.

#### 6:25 AM F.EN08.05.09

**Aqueous Leaching of Chromia-Doped  $\text{UO}_2$  Spent Nuclear Fuel Under Oxidizing Conditions** Alexandre Barreiro Fidalgo<sup>1</sup>, Olivia Roth<sup>1</sup>, Lena Z. Evins<sup>2</sup> and Kastriot Spahi<sup>2</sup>; <sup>1</sup>Studsvik Nuclear AB, Sweden; <sup>2</sup>SKB, Sweden

Programs for deep geological repositories are being developed in many countries to safely dispose of spent nuclear fuel. Therefore, understanding the behavior of spent nuclear fuel under relevant conditions is crucial for the safety assessment of these facilities. During the last decades, new types of nuclear fuel are being introduced in commercial reactors. To allow these new fuels in the spent fuel repository, it must be shown that they do not dissolve at a higher rate than standard fuel. Fuel additives such as chromium oxide ( $\text{Cr}_2\text{O}_3$ ) have an impact on the  $\text{UO}_2$  microstructure and therefore might affect properties relevant to the safety assessment.

The main goal of this investigation is to understand the effects of Cr-doping on the instant release fraction of fission products and the matrix dissolution under oxidative conditions. A sample consisting of fuel fragments and separated cladding is leached in simplified groundwater under aerated conditions at Studsvik's Hot Cell Laboratory. The fuel used in this study was manufactured by AREVA and has been irradiated in a Swedish commercial pressurized water reactor (PWR) to a local burnup at the sampling position of  $\sim 59 \text{ MWd/kgU}$ .

Data from the leaching experiments are presented and compared to other commercial fuels' leaching performance: Cr-doped fuel with lower doping levels (Advanced Doped Pellet Technology, ADOPT) and standard  $\text{UO}_2$  fuel.

#### 6:35 AM F.EN08.05.10

**$\text{UO}_2$ -Based Model Systems—Model Materials for Studying the Matrix Corrosion of Spent Modern Nuclear Fuels** Philip Kegler, Martina Klinkenberg, Andrey Bukaemskiy, Felix Brandt, Guido Deissmann and Dirk Bosbach; Forschungszentrum Jülich GmbH, Germany

The direct disposal of spent modern nuclear fuel (SNF) in a deep geological repository (DGR) requires an in-depth understanding of the long-term corrosion behavior of the SNF and the associated radionuclide source term. These are indispensable requirements for demonstrating the long-term safety of the DGR. Today's modern Cr- and Al-doped light water reactor (LWR) fuels have already successfully demonstrated their improved in-reactor performance, but it is still not known, whether the corrosion behavior of such fuels in a DGR is similar to conventional spent LWR-fuels. Due to the chemical and structural complexity of SNF and its high beta and gamma radiation field, experiments with SNF cannot unravel all of the various concurring dissolution mechanisms entirely. Thus within the EU-DisCo project single-effect dissolution studies are carried out with systematically produced and carefully characterized  $\text{UO}_2$ -based model materials, to provide additional insights into the behavior of modern doped LWR-fuels under the post-closure conditions expected in a DGR, complementary to dedicated dissolution experiments with SNF.

Here, we present recent results on the dissolution behavior of tailor made  $\text{UO}_2$  model materials in accelerated static batch

experiments using H<sub>2</sub>O<sub>2</sub> as simulant for radiolytic oxidants, present in long-term disposal scenarios for SNF in failed container conditions due to the alpha-irradiation of water. In these dissolution experiments pure UO<sub>2</sub> reference pellets exhibiting different densities and grain sizes, as well as Cr-doped UO<sub>2</sub> pellets with various Cr-doping levels, produced using different doping methods having different grain sizes, were used. In addition, Nd-doped and industrially produced Cr- and Cr/ Nd-doped UO<sub>2</sub> pellets were used to determine the influence of these parameters on the dissolution rates. The dissolution experiments were performed under strictly controlled conditions with respect to exclusion of oxygen, temperature control, and exclusion of light. During the dissolution experiments, solutions were systematically sampled and the H<sub>2</sub>O<sub>2</sub> (UV-Vis) and the uranium (ICP-MS) concentrations were determined.

The initial dissolution rates of all materials were determined from the concentrations of dissolved U(VI) obtained within the first 24 hours of the experiments. In experiments with pure UO<sub>2</sub> reference pellets a clear linear dependence of the initial dissolution rates from the density of the pellets was observed, with higher initial dissolution rates at lower densities. No dependence on grain size was found. The initial dissolution rates of pure, Cr-doped, and Nd-doped UO<sub>2</sub> pellets fall into three groups: i) pure UO<sub>2</sub> pellets with the fastest dissolution rates, independent of the oxygen potential during sintering (and therefore the grain size), ii) Cr-doped UO<sub>2</sub> pellets, independent of doping method, doping level, and oxygen potential during sintering (grain size), and iii) Nd-doped UO<sub>2</sub> pellets with the lowest dissolution rates. The following initial dissolution rates were calculated for the different materials:

pure UO<sub>2</sub>:  $1.3 \pm 0.1 \times 10^{-6}$  mol/m<sup>2</sup>\*s

Cr-doped UO<sub>2</sub>:  $0.65 \pm 0.2 \times 10^{-6}$  mol/m<sup>2</sup>\*s

Nd-doped UO<sub>2</sub>:  $1.63 \pm 0.7 \times 10^{-7}$  mol/m<sup>2</sup>\*s

The slight difference between the dissolution rates of pure UO<sub>2</sub> and Cr-doped UO<sub>2</sub> pellets (i.e. factor 2) can partly be explained by the slightly lower density of pure UO<sub>2</sub> pellets compared to Cr-doped UO<sub>2</sub> pellets. A very strong influence of Nd, representative of fission lanthanides in SNF, on the dissolution rates in this type of experiments is clearly visible.

Although the density of the Nd-doped UO<sub>2</sub> pellets is similar to the Cr-doped pellets (i.e. 96-98% relative density), the initial dissolution rate is more than half an order of magnitude lower than for Cr-doped pellets. Overall, the results of this study indicate that the Cr-doping of modern nuclear fuels seems to have no significant effect on the corrosion behavior of UO<sub>2</sub>-based SNF.

#### 6:45 AM \*F.EN08.05.11

**Dissolution Kinetics of Metaluminous and Peralkaline Calcium Aluminosilicate Glass at 75°C, pH = 7.5: Rate Control by Si-Content of Glass** Jon P. Icenhower, Hugh McMahon, Misty Riesbeck, Elzbieta Bakowska, Randall Youngman and Nicholas Smith; Corning, United States

The dissolution rates of six calcium aluminosilicate glasses were determined experimentally at pH(25 °C) = 7.5 and a temperature of 75 °C in a Single-Pass Flow-Through (SPFT) system. Glasses studied in this work can be categorized into two sets of three compositions each. In the first (metaluminous) set, the molar proportion of CaO to Al<sub>2</sub>O<sub>3</sub> remained the same (1:1), while SiO<sub>2</sub> increased (40, 50 and 60 mol.%). The second (peralkaline) set was characterized by constant Al<sub>2</sub>O<sub>3</sub> (10 mol.%), with decreasing CaO and increasing SiO<sub>2</sub> (40, 50 and 60 mol.%). Measurements of <sup>27</sup>Al by MAS-NMR indicated a slight increase in Al<sup>[5]</sup> at the expense of Al<sup>[4]</sup> with decreasing Si concentration. One to four grams of powdered glass (300 to 425 mm diameter) were placed into 10 mL volume reactors with solution input through the bottom and effluent solution output through the top. Solutions were buffered by 0.05 M TRIS and flow-rates varied between ~38 and 500 mL/d. A plot of the dissolution rate vs. flow-rate (*q*) to surface area (*S*) showed that all dissolution rates were maximized at  $q/S \approx 45 \times 10^8$  m/s. Dissolution rates were from 4.2, 1.5 and  $0.62 \times 10^{-7}$  mol/(m<sup>2</sup> sec) for the metaluminous and 1.0, 0.65 and  $0.50 \times 10^{-7}$  mol/(m<sup>2</sup> sec) in the peralkaline glasses, respectively. Interestingly, the data indicate that rates for the metaluminous trio are generally faster than those of the peralkaline set, which runs contrary to expectations. As a set of glasses, the log<sub>10</sub> rates [mol/(m<sup>2</sup> sec)] are inversely proportional to the fraction of Si in the glasses, forming a single array of values. These data indicate that rates are strongly tied to the Si content of glasses, and that other glass composition parameters— including Ca/Al (molar) ratio— exert a much weaker effect on dissolution rate in this medium.

#### 7:00 AM F.EN08.05.12

**Assessing the Effect of Radioactive Waste Glass Dissolution in an Updated Geological Disposal Facility Radionuclide Migration Model** Joseph Lillington<sup>1</sup>, Thomas L. Gout<sup>1</sup>, Tajudeen Iwalewa<sup>2</sup> and Ian Farnan<sup>1</sup>; <sup>1</sup>University of Cambridge, United Kingdom; <sup>2</sup>Harvard University, United States

The UK intends to ultimately dispose of its nuclear waste by storing it deep underground within a geological disposal facility (GDF). The planned setup is to vitrify high-level waste (HLW) within glass, encase this in a metal canister, and store this using a buffer within the host rock. Currently, there is no agreed site for a UK GDF, and therefore, accurate modelling is

required despite significant uncertainties in the modelling parameters. This study aims to build upon previous work that simulated HLW radionuclide migration within both clay and granite host rocks. Significant updates have been made to the original GoldSim Monte-Carlo models, including updating the HLW inventory, radionuclide sorption, diffusion, and solubility coefficients, canister degradation failure rates, number of waste canisters, granite/clay density, sensitivity analysis, and Monte-Carlo parameters. In addition, the effect of HLW dissolution has been examined by varying the source-terms used (initial dissolution, residual, and resumption rates) through variation on the original simplistic source-terms, and by coupling GoldSim with the analytical GRAAL model (via MATLAB). Results demonstrate that radionuclide migration behaviour is similar between the original and updated GoldSim models, despite cumulative activities being approximately one to two orders of magnitude lower in the upper part (crown) of the GDF. Variation on the original simplistic glass dissolution source terms has an understand but insignificant effect on GDF performance, with there being no substantial difference having used the original model glass dissolution rates versus those applied by the UK nuclear industry. Finally, radionuclide activities are strongly correlated with systematic modifications in analytical GRAAL model parameters through changes in glass degradation rates.

#### 7:10 AM F.EN08.05.13

**Adsorption and Diffusion of Boron Isotopes in Aqueous Glass Dissolution** Thomas L. Goût<sup>1</sup>, Rui Guo<sup>1,2</sup>, Sambuddha Misra<sup>1,3</sup>, Aleksey Sadekov<sup>4</sup>, Edward Tipper<sup>1</sup>, Madeleine Bohlin<sup>5</sup> and Ian Farnan<sup>1</sup>; <sup>1</sup>University of Cambridge, United Kingdom; <sup>2</sup>Tsinghua University, China; <sup>3</sup>Indian Institute of Science, India; <sup>4</sup>The University of Western Australia, Australia; <sup>5</sup>Uppsala University, Sweden

Predicting the release rates of radionuclides from nuclear waste glasses during aqueous dissolution within a disposal facility over geological timescales requires robust models of dissolution built upon an extensive understanding of glass dissolution mechanisms. However, many of the dissolution models presented in the past decade conflict regarding the mechanisms predicted to control dissolution. Whilst nanoscale post-process analyses of altered glasses have afforded insights into altered layer structures, these results highlight the need for an additional dimension to understand the mechanisms of glass dissolution beyond the conventionally employed techniques presented in the literature.

In a previous study, lithium isotope fingerprinting techniques were applied to the leachates of a simplified Magnox waste glass leached at 90 °C. It was shown that whilst dissolution was initially congruent, lithium isotopes leached incongruently through diffusive processes across a passivating altered layer component at longer durations. However, further evidence was required to rank the dissolution models presented in the literature. Here, boron isotope fingerprinting techniques were applied to the same Magnox glass to further understand its dissolution processes, understand how lithium and boron were leached and distinguish between dissolution models. Additionally, the same isotopic techniques were applied to leachates of an international benchmark glass composition to compare the dissolution processes of the two compositions and allow for interdiffusion models to be fitted to the results. Solution renewal experiments took place to further investigate the passivating nature of the altered layers and their role as a diffusive barrier to dissolution at long durations.

Boron isotopes leached from the Magnox glass were consistent with congruent models of dissolution in the initial stages of dissolution, but at later stages were consistent with diffusive isotopic fractionation across a passivating altered layer component about an incongruent dissolution front. Whilst boron isotopes in the leachates of International Simple Glass were consistent with diffusive, incongruent dissolution models throughout dissolution, boron isotopes in its solution renewal experiment were most consistent with congruent models of dissolution. As such, these isotopic methodologies demonstrate that no single dissolution model may be correct for all glass compositions and experimental conditions; providing an improved understanding of the mechanisms governing aqueous glass dissolution and supporting the idea of a model which unifies the mechanisms presented in the literature.

#### 7:20 AM F.EN08.05.15

**Late News: Using Data Analytics in Glass Property Prediction** Joseph Lillington<sup>1</sup>, Thomas L. Goût<sup>1</sup>, Mike Harrison<sup>2</sup> and Ian Farnan<sup>1</sup>; <sup>1</sup>University of Cambridge, United Kingdom; <sup>2</sup>National Nuclear Laboratory, United Kingdom

The rates of aqueous dissolution and radionuclide release from glasses used to immobilise high-level waste that will be disposed of within a geological disposal facility are strongly dependent on composition. Glasses are challenging to reliably fabricate because after liquid cooling, they are considered to be in non-thermodynamic equilibrium, and therefore their state variable, for example volume, cannot be predicted solely from temperature and composition, but also requires consideration of factors such as thermal history. Other material properties therefore prove valuable as descriptors of glass state, for example, glass viscosity or density. In addition, phase separation can occur depending on the glass composition, particularly with increased waste loadings. This study uses machine learning to predict glass viscosity, viscosity model fitting parameters, density, and phase separation, aiming to both predict glass properties and extract relevant compositional dependencies from the analytics. A series of algorithms have been applied both in isolation and in combination, for example, via voting or

stacking. Data has been provided by the nuclear industry or by making use of large-scale international datasets. Overall, results indicate that machine learning can be valuable either in accurately predicting the properties of nuclear waste glasses (viscosity, viscosity model fitting parameters, density, phase separation) or can be used to analyse the importance of different features either for determining particular properties directly or indirectly by correlating features and prediction errors.

SESSION F.EN08.06: Microstructural Investigations  
On Demand Abstracts Available for Viewing Starting Saturday Morning, November 21, 2020  
F-EN08

#### 5:00 AM F.EN08.06.02

**Secondary Phase Derived Uranium Oxy-Hydroxides as Potential Host Matrices for Anionic Fission Daughters** Gabriel Murphy, Philip Kegler, Andreas Wilden, Martina Klinkenberg and Evgeny Alekseev; Forschungszentrum Jülich GmbH, Germany

Layered uranium oxyhydroxide (LUOH) phases are important minerals which occur as weathering products of uraninite deposits and also importantly, are encountered during the paragenetic sequence of secondary phases that form during an accident scenario involving spent nuclear fuel (SNF) in the near-field (1). Understanding the structural-chemistry of these phases is of importance as via interaction mechanisms, they can potentially retard the transport of harmful fission daughters from SNF towards groundwater and the biosphere. Particularly it has been previously shown that the secondary LUOH phases, such as metaschoepite, uranophane and studite, can act to impede and retard the transport of fission daughters and SNF products such as  $\text{NpO}_2^+$ ,  $\text{Cs}^+$  and  $\text{Sr}^+$  (2,3). Chemically, the origin of these favourable interactions is predominantly due to favourable intercalation chemistry between cationic SNF species with that of anionic lattices of encountered phases. However in the case of anionic fission daughters, such as  $^{131}\text{I}$  and  $^{79}\text{Se}$ , these present considerable concern during release from SNF as the overwhelming majority of near-field SNF secondary phases and minerals possess anionic lattices, including LUOH phases, which are typically not expected to react and intercalate well with. Although some evidence is present for partial intercalation of anionic iodine into layered mineral structures through ionic exchange mechanisms in model system studies (4-6) the current consensus is the retention of anionic SNF release products in the near field is not proven and best considered in the far-field of SNF repository performance and accident scenario assessment. Layered double hydroxide (LDH) phases are considered prime candidate materials and minerals for the retention of these anionic phases and received considerable attention (7), however in the context of an accident scenario with SNF their occurrence is not certain. We have recently undertaken a comprehensive systematic investigation of actinide solid state systems relevant to SNF and nuclear waste management. In the course of our investigations we have examined the chemical interactions that may occur between the anionic fission daughter species, I and Se in different chemical forms with some potential LUOH phases associated with SNF. Using a combination of batch synthesis experiments and *in situ* exchange experiments, we provide evidence for the inclusion and retention of these anionic species in LUOH phases. Importantly, using single crystal X-ray diffraction we show the ability for anionic species to be incorporated into certain LUOH phases is a consequence of their respective topological arrangement of uranyl and hydroxyl groups. Furthermore, by considering the topology and structural chemistry of LUOH phases, it can allow for a predictive basis to be established towards which the relative interaction affinity between certain anionic fission daughter species and specific LUOH phases can be understood. The systematic experimental studies used in this investigation will be discussed in detail w.r.t potential interactions that occur between anionic fission daughters and LUOH derived secondary phases that occur during an accident scenario involving SNF.

#### References:

- 1 P. C. Burns, R. C. Ewing, and A. Navrotsky, *Science* 335, 1184 (2012).
- 2 J. I. Friese, M. Douglas, E. C. Buck, S. B. Clark, and B. D. Hanson, *MRS Proceedings* 824, CC9.2, Cc9.2 (2004).
- 3 A. Espriu-Gascon, J. Giménez, I. Casas, and J. de Pablo, *Journal of Hazardous Materials* 353, 431 (2018).
- 4 S. Wu, S. Wang, A. Simonetti, F. Chen, and T. E. Albrecht-Schmitt, *Radiochim. Acta* 99, 573 (2011).
- 5 S. Wu, F. Chen, M. Kang, Y. Yang, and S. Dou, *Radiochim. Acta* 97, 459 (2009).
- 6 S. J. Wu, F. R. Chen, A. Simonetti, and T. E. Albrecht-Schmitt, *Environ. Sci. Technol.* 44, 3192 (2010).
- 7 N. Daniels et al., *Applied Clay Science* 176, 1 (2019).

#### 5:10 AM F.EN08.06.03



**An Investigation into the Local Structure of Ln<sub>2</sub>TiO<sub>5</sub> Stuffed Pyrochlores Through XAS Analysis** [Daniel A. Austin](#)<sup>1</sup>, Martin Stennett<sup>1</sup>, Shikuan Sun<sup>1</sup>, Bruce Ravel<sup>2</sup> and Neil Hyatt<sup>1</sup>; <sup>1</sup>University of Sheffield, United Kingdom; <sup>2</sup>National Institute of Standards and Technology, United States

Stuffed pyrochlore ceramics, with the general stoichiometry Ln<sub>2</sub>TiO<sub>5</sub>, have received significant interest for application within the nuclear industry due to their high radiation tolerance, good thermal stability, and structural flexibility. These ceramics have been proposed as a potential wasteform for actinide wastes, for incorporation into inert matrix fuels (IMF), and as inclusion in oxide dispersion strengthened (ODS) steels. These materials can be viewed as derivatives of pyrochlore structured Ln<sub>2</sub>Ti<sub>2</sub>O<sub>7</sub> phases and are often more conveniently written in the form Ln<sub>2</sub>(Ln<sub>0.67</sub>Ti<sub>1.33</sub>)O<sub>6.67</sub>, where the pyrochlore B-site now contains mixed occupancy. These materials can adopt a variety of different crystal structures depending on the size of the lanthanide cation, and the temperature and pressure used during synthesis. The three reported crystal structures are orthorhombic (*Pnma*), hexagonal (*P6<sub>3</sub>/mmc*) and cubic defect-fluorite (*Fm-3m*). Compounds that are nominally assigned as defect-fluorite by X-ray diffraction have been probed by neutron diffraction (ND) and transmission electron microscopy (TEM) revealing features consistent with the presence of short range ordered regions with the (*Fd-3m*) cubic pyrochlore structure.

In this contribution we present a study probing the local structure of a series of Ln<sub>2</sub>TiO<sub>5</sub> (Ln = La, Gd, Dy, Yb, Y) compounds. They were synthesised via a solid state synthesis route under different cooling regimes to prepare samples of identical chemistry but different short range ordering. Fabrication of high quality sintered specimens of Ln<sub>2</sub>TiO<sub>5</sub> phases is a particular challenge due to their refractory nature. Therefore, a systematic study of sintering parameters was undertaken to optimise the fabrication of sintered ceramic specimen. Characterisation of these materials was performed using techniques including XRD, SEM/EDX and XAS. Initial XAS results show that some of these materials do have a cubic pyrochlore-like local structure but show a deviation from the ideal coordination environment of cubic pyrochlore.

#### 5:20 AM F.EN08.06.04

**Chemical Bond Complexity in A<sup>III</sup><sub>6</sub>B<sup>VI</sup>O<sub>12</sub> Fluorite-Related Ternary Oxides** Maulik K. Patel<sup>1</sup>, Kurt E.

Sickafus<sup>2</sup> and [Gianguido Baldinozzi](#)<sup>3</sup>; <sup>1</sup>University of Liverpool, United Kingdom; <sup>2</sup>The University of Tennessee, Knoxville, United States; <sup>3</sup>Université Paris-Saclay, France

Oxides with generic stoichiometry A<sub>7</sub>O<sub>12</sub> occupy, in a generic phase diagram, an intermediate place between fluorite and bixbyite structure types. Their structure is derived from the ideal fluorite structure, and it is characterized by a more or less pronounced ordering of the O vacancies within the average fluorite sublattice. We believe that ternary oxides with this generic formula display some structural flexibility relevant to fission product stabilization in nuclear fuels and to the understanding of actinide waste forms as well. We would like to discuss the structural characteristics of the chemical bonds in these ternary systems consisting of trivalent and hexavalent cations studying the electron density using the tools of the quantum theory of atoms in molecules (Bader's AIM theory and ELF). Eventually, in these compounds with generic formula A<sup>III</sup><sub>6</sub>B<sup>VI</sup>O<sub>12</sub>, the A cation can be either an actinide or a rare earth element, whereas the B cation can be either a transition metal (W, Mo) or hexavalent uranium. We believe that studying the characteristics of the polyhedron of the sevenfold coordinated A ion is particularly interesting: it is often described in the literature as a mono-capped trigonal prism, with bond lengths exhibiting an extremely large dispersion, ranging for instance from 2.19 to 2.70 Å in Y<sub>6</sub>WO<sub>12</sub>. We would discuss the implications of this large dispersion of distances on the chemical bond characteristics, compare DFT models with experiments on pristine and irradiated specimens, and discuss the competitive metastability of the oxygen deficient cubic fluorite phase that can be observed in some of these systems, as for instance Y<sub>6</sub>MoO<sub>12</sub>.

#### 5:30 AM F.EN08.06.05

**Chemical and Structural Investigations on Uranium Oxide Based Microparticles as Reference Materials for**

**Analytical Measurements** [Stefan Neumeier](#)<sup>1</sup>, Philip Kegler<sup>1</sup>, Fabien Pointurier<sup>2</sup>, Anne-Laure Faure<sup>2</sup>, Kathy Dardenne<sup>3</sup>, Jörg Rothe<sup>3</sup>, Tonya Vitova<sup>3</sup>, Martina Klinkenberg<sup>1</sup>, Fabian Kreft<sup>1</sup>, Dirk Bosbach<sup>1</sup> and Irmgard Niemeyer<sup>1</sup>; <sup>1</sup>Forschungszentrum Jülich GmbH, Germany; <sup>2</sup>CEA, France; <sup>3</sup>Karlsruhe Institute of Technology, Germany

The analysis of individual micrometre- and submicrometre-sized particles collected by IAEA safeguards inspectors on swipe samples during in-field verification activities requires the implementation of a sustainable quality control system. This system needs to be further advanced by developing mass spectrometric analytical measurements and of suitable reference materials. In this context pure and compound reference materials in microparticulate form such as U, Ln/U, Th/U and Pu/U microparticles are of special interest. For the design of these microparticulate reference materials, according to their required properties, the understanding of morphology, chemistry, and structure is essential. To this end, the production of pure and neodymium doped uranium-oxide based microparticles utilising an aerosol-based

particle production process which has been developed and established in the laboratories of Forschungszentrum Juelich since 2012 will be presented. This method allows for the generation of microparticles with monodisperse particle size distribution. SEM/EDX measurements confirmed the monodispersity of the produced microspheres as well as the incorporation of 15 mol% Nd into the compound particles. Additionally, results from *In-SEM*  $\mu$ -Raman (CEA, DAM) and U  $L_3$ -edge XAFS measurements in U  $L_{\alpha}$  fluorescence yield detection mode (INE-Beamline @ KIT synchrotron radiation source) will be discussed pointing to the formation of  $U_3O_8$  microparticles for both compounds. The position and shape of the X-ray absorption spectrum is insignificantly affected by the incorporation of 15 mol% Nd, indicating the structural flexibility and stability of the  $U_3O_8$  microparticles. Additionally, a minor fraction of schoepite phase was identified by Raman measurements, which is most probably caused by ageing processes during storage under laboratory conditions. The first batch of  $U_3O_8$  microparticles produced in Juelich was successfully applied in an international laboratory exercise NUSIMEP9 organised by JRC-Geel and finally certified regarding the isotopic composition and the U amount per particle. These results demonstrate that the process established in Juelich allows for a very flexible and reliable preparation of reference materials for particle analysis methods applied in safeguards.

#### 5:40 AM F.EN08.06.06

**Nanostructured Uranium Oxide Thin Films Developed by Molecular Precursors Using Chemical Vapor Deposition** Dennis Grödler, Lasse Jurgensen, Aida Raauf, Markus Zegke and Sanjay Mathur; Institute of Inorganic Chemistry, Germany

Advanced materials have been made using a variety of elements, however, uranium has not seen much impact. The common fear of working with “nuclear material” has prevented its chemical use, even though it has been known since 1911 to be an efficient catalyst in the widely applied Haber-Bosch process. A possible strategy to synthesize advanced materials based on uranium is the chemical vapor deposition (CVD). To date, only a few suitable uranium precursors have been reported. Here we report new volatile uranium(IV) complexes based on  $\beta$ -ketoenamine ligands, which have been structurally characterized and which can be synthesized via a simple salt metathesis. Functionalization of the N atom of the chelating ligand changes the coordination motif, and subsequent NMR studies offer a deeper insight into the coordination chemistry. Sterically demanding ligands (L) selectively lead to heteroleptic complexes of the form  $UCl_2L_2$  while an additional degree of freedom in the substituent allows for the isolation of homoleptic complex of the form  $UL_4$  with significantly increased volatility. These are suitable candidates for CVD towards uranium oxide thin films. Uranium oxides with band-gap energies in a range of 1.8 – 2.7 eV coupled with their good electrical and catalytic properties mostly driven by facile valence dynamics of the uranium cations are promising electrode materials in photoelectrochemical water splitting reactions. We have been able to synthesize a variety of such ligands and present four novel uranium complexes which we are currently investigating with respect to the formation of novel uranium based thin film materials. Furthermore, using  $\beta$ -heteroarylthioenamine ligands leads to similar complexes that may be used as precursors for uranium sulfide thin films.

SESSION F.EN08.07: Poster Session: Scientific Basis for Nuclear Waste Management  
On Demand Abstracts Available for Viewing Starting Saturday Morning, November 21, 2020  
5:00 AM - 8:00 AM  
F-EN08

#### F.EN08.07.01

**A New Disposal Method for Radioactive Waste Using Chemically Adsorbed Monolayer** Teruyoshi Sasaki, Hiroto Funakoshi, Kazufumi Ogawa and Yoshifumi Suzaki; Kagawa University, Japan

Radioactive waste exists in the form of gas, liquid and solid. Among them, the disposal method of collecting radioactive waste, melted and solidifying it and burying it in the ground is common. However, in the current method, after the radioactive waste is collected, it is mixed with glass as it is to be melted and solidified, or it is mixed with cement and solidified, so that the volume of the waste becomes huge. Therefore, in this study, we investigated a process in which a chemically adsorbed monolayer having an imidazole group at the end was formed on a glass fiber, and only radioactive substances were adsorbed from a solution in which waste was dissolved, and then melted and solidified at once. As a result, we succeeded in adsorbing radioactive substances with high efficiency in solution. By using this method, if the melting point of the glass fiber is set low, the melted and solidifying process will be extremely simple, and it will be possible to manage the radioactive substances in the necessary minimum volume.

#### **F.EN08.07.02**

**Speciation by XANES of Copper Migrated into Compacted Bentonite Using Electromigration Techniques** Kazuya Idemitsu, Keisuke Yoshida, Yaohiro Inagaki and Tatsumi Arima; Kyushu University, Japan

Copper is a candidate for use as an overpack material in deep underground nuclear waste disposal. Copper, however, is susceptible to corrosion following closure of the repository and migration of the corrosion products through the buffer material may affect the migration of redox-sensitive radionuclides. Electromigration experiments were performed whereby a copper coupon, which was in contact with compacted bentonite, served as the working electrode and was held at a constant potential of +300 mV vs. Ag/AgCl electrode for up to 48 h. The chemical form of copper that migrated into the bentonite specimens were estimated by using Cu K-edge X-ray absorption near-edge structure (XANES) at Saga-Light Source, Japan. The results revealed that the oxidation state of Cu in the bentonite would be Cu(II) as shown the correlation between the amount of Cu migrated into bentonite and the corrosion current. On the other hand Cu(I) also observed on the copper coupon not in bentonite. Copper could corrode as Cu(II) then react with Cu metal and precipitate as Cu<sub>2</sub>O on the copper metal.

#### **F.EN08.07.03**

**Effects of Chromium and Vanadium on the Sulfate Solubility of Sodium Aluminoborosilicate Glass** Natalie J. Smith-Gray<sup>1</sup>, Jason Lonergan<sup>2</sup> and John S. McCloy<sup>1,2</sup>; <sup>1</sup>Washington State University, United States; <sup>2</sup>Pacific Northwest National Laboratory, United States

In the composition space of interest for Hanford low-activity nuclear waste glass, the waste loading of some formulations is limited by the incorporation of sulfate into the glass (i.e., its solubility). Numerous studies have been undertaken to understand the mechanism of sulfate incorporation and its affect by various other additives. In particular, the model by Vienna et al (2014, J. Amer. Ceram. Soc. 97, 3135) identified elements which tend to raise or lower sulfate solubility in borosilicate glass. In the current experimental study, we focus on representative additives that purportedly decrease (chromium) or increase (vanadium) the sulfate solubility. A baseline aluminoborosilicate composition containing Ca and Na was melted with target composition of either i) 1 wt% SO<sub>3</sub> and up to 2 wt% Cr<sub>2</sub>O<sub>3</sub> or ii) 2 wt% SO<sub>3</sub> and up to 5 wt% percent V<sub>2</sub>O<sub>5</sub>. Thermal and physical properties were measured and structural analysis by Raman spectroscopy was performed to investigate changes in the glass structure with transition metal addition. Electron probe microanalysis was used to measure elemental compositions in melted glass for comparison with batched compositions. Increasing Cr<sub>2</sub>O<sub>3</sub> concentration caused saturation of Cr concentration within the glass and formation of crystalline eskolaite (Cr<sub>2</sub>O<sub>3</sub>); glass transition temperature change was only dependent on the Cr which remained in glass, while measured density changes depended on both Cr in glass and eskolaite. No apparent change in sulfate solubility was observed, though not all the targeted sulfate was incorporated in the glasses containing Cr. On the other hand, all the targeted V was incorporated into the glass, and as the concentration of V<sub>2</sub>O<sub>5</sub> increased, the glass transition temperature decreased. Again, not all of the batched sulfur was incorporated into the glass, but V<sub>2</sub>O<sub>5</sub> showed a weak tendency to increase the observed sulfur content in the glass. Some incorporation mechanisms to explain these trends are proposed.

#### **F.EN08.07.04**

**Defect Evolution Measured by Raman Spectroscopy and EBSD in Rare-Earth Doped UO<sub>2</sub> Used Nuclear Fuel Analogues** Sam Karcher<sup>1</sup>, John S. McCloy<sup>1</sup>, Ritesh Mohun<sup>2</sup> and Claire L. Corkhill<sup>2</sup>; <sup>1</sup>Washington State University, United States; <sup>2</sup>The University of Sheffield, United Kingdom

Uranium dioxide prepared from depleted uranium is commonly used as an analogue to study used nuclear fuels. While actual used nuclear fuel is highly complex and contains a large number of fission products, synthetic analogues are often simplified by single species doping. Previous studies involving trivalent RE doped UO<sub>2</sub> show reduced dissolution rates compared to undoped UO<sub>2</sub>. When U<sup>IV</sup> is replaced with a RE<sup>III</sup> cation, defect clusters containing U<sup>V</sup> resulting from local charge compensation form which can serve to limit ability to form U<sub>3</sub>O<sub>8</sub>. Uranyl ions (UO<sub>2</sub>)<sup>2+</sup>, which are allowed to form as a result of U<sup>VI</sup> in U<sub>3</sub>O<sub>8</sub>, have a solubility much higher than stoichiometric UO<sub>2</sub>. To predict the long-term stability of used nuclear fuel in oxidizing conditions it is necessary to understand the relationships between fuel chemistry, microstructure and environment.

Here, a series of UO<sub>2</sub> pellets doped with Ce, Nd, Yb, Zr and Th at 1 at. % and 5 at. % were prepared via uranyl nitrate + RE-nitrate co-precipitation to ensure homogenous distribution of dopant ions before pelletizing and sintering at 1700° C in H-Ar reducing atmosphere. Defect signatures in the resulting near-stoichiometric (U,RE)O<sub>2+x</sub> ceramic pellets were analyzed using Raman spectroscopy at multiple excitation wavelengths pre and post oxidation treatment. Through collaboration with the University of Sheffield, we have also obtained Raman data on our samples after irradiation with 1 MeV Kr ions at room temperature, fluence 5×10<sup>15</sup> ions/cm<sup>2</sup> at the Dalton Cumbrian Facility. Deconvolution of Raman spectra reveals distinct

signatures corresponding to defects such as interstitial or vacant oxygen sites or reduced lattice symmetry. The primary Raman peak observed in  $\text{UO}_2$  at  $445\text{ cm}^{-1}$  corresponds to the symmetric U-O stretching bond, and indicates the presence of defects in the  $\text{UO}_2$  structure by losing intensity and broadening while shifting towards higher wavenumber. Thermogravimetric analysis up to  $900^\circ\text{C}$  in air shows a delayed transition from  $\text{UO}_2$  to  $\text{U}_3\text{O}_8$  in the doped samples, the effect being greatest in Yb-doped  $\text{UO}_2$ . Using Raman mapping with in-situ heating we can track the evolution of defect bands during oxidation and correlate spectral features to the orientation, size and distribution of grains and grain boundaries measured by electron backscatter diffraction (EBSD).

## SYMPOSIUM F.EN09

---

Developing In Situ and Operando Methodology for Observation of Energy Conversion, Storage and Transport Processes in Materials and Devices  
November 21 - December 2, 2020

### Symposium Organizers

Lena Kourkoutis, Cornell University  
Katharine Page, The University of Tennessee, Knoxville  
Chengjun Sun, Argonne National Laboratory  
Markus Winterer, University of Duisburg-Essen

### Symposium Support

#### **Silver**

Carl Zeiss Microscopy, LLC  
University of Duisburg-Essen, CENIDE

---

\* Invited Paper

SESSION Tutorial F.EN09: Learning about In Situ and Operando Methods  
Session Chairs: Chi Chen, Peter Crozier, Matt Newville, Katharine Page and Markus Winterer  
Sunday Morning, November 29, 2020  
F.EN09

**8:00 AM \***

***In Situ and Operando TEM*** Peter A. Crozier; Arizona State University, United States

Instrumentation and applications of in situ microscopy will be reviewed with special emphasis on environmental transmission electron microscopy (ETEM). The importance of experimental design and control of artifacts is critical to obtain scientifically significant results. Applications of ETEM to metal supported catalysts, reducible oxide nanoparticles, nanotube/nanowire growth, and electron beam induced deposition will be illustrated.

**9:30 AM BREAK**

**9:45 AM \***

**X-Ray Absorption Spectroscopy** Matt Newville; The University of Chicago, United States

X-ray absorption spectroscopy (XAS) will be introduced, reviewing the fundamental physics that give unique information for chemical speciation from XANES and local atomic coordination from XAFS. Practical considerations for using XAS will be discussed, including recent instrumentation developments in analyzers and detectors to improve detection limits. Applications to fields including materials, energy, and geological sciences will be highlighted.

## 11:15 AM BREAK

### 11:30 AM

**High Throughput Quantitative *In Situ* Neutron Diffraction Study of Rechargeable Battery Materials** Jue Liu<sup>1</sup>, Zhijia Du<sup>1</sup>, Alex Chien<sup>1</sup> and Xianyang Wu<sup>1,2</sup>; <sup>1</sup>Oak Ridge National Laboratory, United States; <sup>2</sup>Purdue University, United States

The advantages of using neutron diffraction to characterize battery materials are well known. It is highly penetrating and non-destructive, making it an ideal tool to probe structure changes in large devices like Li/Na-ion batteries without disturbing the electrochemical reactions. In addition, the nuclear scattering lengths do not increase with atomic number but instead are isotope dependent and it is very sensitive to light elements (Li, C and O) which are key ingredients of Li/Na-ion battery materials. It is also capable of distinguishing adjacent 3d TM cations. Moreover, the nuclear scattering lengths do not decrease with momentum transfer (Q), making it more accurate to quantitatively determine the atomic environments of light elements such as oxygen. Despite these great advantages, neutron diffraction characterization of charged and discharged electrode materials, has remained somewhat limited. In this talk, I will discuss our recent progress on developing quantitative *in situ* neutron Bragg diffraction and total scattering characterization of battery materials. Two examples will be given: one on the *in situ* neutron total scattering investigation of the structural origin of thermal runaway of high energy battery cathode materials; the other on quantitative and high throughput *in situ* neutron diffraction study of battery materials during electrochemical cycling.

## 1:00 PM BREAK

### 1:15 PM \*

**The X-Ray Absorption Spectroscopy Database and Machine Learning** Chi Chen; University of California, San Diego, United States

Efforts at constructing the first-of-its-kind computed X-ray absorption spectroscopy database (XASdb), which contains over 500,000 spectra of over 100,000 materials. Machine learning (ML) models trained on this large dataset can be applied to the rapid identification of coordination environments from experimental XAS spectra.

SESSION F.EN09.12: Live Keynote I: Developing In Situ and Operando Methodology for Observation of Energy Conversion, Storage and Transport Processes in Materials and Devices

Session Chairs: Lena Kourkoutis, Katharine Page, Chengjun Sun and Markus Winterer

Tuesday Afternoon, December 1, 2020

F.EN09

### 1:45 PM \*F.EN09.01.01

***In Situ* Microscopy of Energy Materials with Electron and Photon Techniques** Gianluigi A. Botton<sup>1,2</sup>; <sup>1</sup>Canadian Light Source, Canada; <sup>2</sup>McMaster University, Canada

Electron microscopes have become very power tools to study the structure of materials at unprecedented resolution. From their invention, these tools have provided essential information on the structure and properties of the broadest range of materials used today in structural and functional applications. In-situ electron microscopy has evolved over the last few decades from dynamic experiments (heating, straining) to reaction in gases, and, more recently, even electrochemical experiments either in vacuum or in liquids. While the spatial resolution remains the first motivation for such in situ experiments in electron microscopy (so that even nucleation and early stages of growth of nanostructures formed during electrodeposition can be investigated), the flexibility and the more realistic environments remain the realm of synchrotron beam lines. Higher pressures, higher (or lower) temperatures, experiments in liquids and gases, can be carried out with exquisite spectroscopic resolution, penetrating power with diffraction techniques, in realistic and macroscopic samples and experimental conditions more suitable to represent operating conditions.

In this presentation, a comparison of the types of experiments that can be carried out with electron and photon techniques are discussed, in particular in the context of the nature of the samples, the time resolved sensitivity and the potential artefacts.

### 2:05 PM \*F.EN09.01.04

***In Situ* Scanning Transmission Electron Diffraction of Individual Electrically-Biased Phase Change Memory Ag-In-**

**Sb-Te Line Cells** Vadim Migunov<sup>1,2,3</sup>, Xuan Thang Vu<sup>2</sup>, Sebastian Walfort<sup>4</sup>, Karina Ruzaeva<sup>1</sup>, Benedikt Kersting<sup>5</sup>, Martin Salinga<sup>4</sup> and Rafal E. Dunin-Borkowski<sup>1</sup>; <sup>1</sup>Forschungszentrum Juelich, Germany; <sup>2</sup>RWTH Aachen University, Germany; <sup>3</sup>ABB AG, Germany; <sup>4</sup>University of Münster, Germany; <sup>5</sup>IBM Research-Zurich, Switzerland

As current memory technologies approach their fundamental limits, increasing demand for novel non-volatile memories is driving the development of new architectures, which are already showing their potential in high performance computing [1, 2]. As a result of their non-volatile nature, byte-addressability and fast response times, which are comparable to those of dynamic random-access memory, resistive-switching-based phase change materials (PCMs) are strong candidates for memory applications with reduced hardware cost and power consumption [3, 4].

The use of advanced transmission electron microscopy combined with *in situ* electrical biasing provides a powerful method for studying the local relationship between atomic structure and electrical properties in individual nanoscale memory elements, in order to identify the factors that affect their switching reproducibility and dynamics.

We have developed a multi-step lithographic procedure, which allows dedicated nanostructured line cells that contain PCM switching layers, electrical contacts and protective layers to be fabricated directly on electron-transparent silicon nitride membranes and used for switching experiments both outside and inside the transmission electron microscope. We used a special electrical setup to provide short (50 ns) electrical current pulses to individual line cells with sharp (approximately 3 ns) rising and falling edges. By using these pulses, PCM devices could be switched between crystalline low resistance and amorphous high resistance states inside a transmission electron microscope.

Even though each device consisted of several layers of different materials, resulting in a total thickness of between 200 and 300 nm, a fast pixelated direct electron detector could be used to record scanning electron diffraction patterns from amorphous/crystalline regions before and after successive switching cycles, while measuring the electric properties of the same devices. Newly-developed algorithms based on LiberTEM software [5] were used to follow the evolution of individual crystallites and to show that the switching mechanisms involved slow crystal growth or rapid recrystallization, depending on the details of the current pulses.

[1] K. Wu, F. Ober, S. Hamlin and D. Li, ArXiv:1708.02199 [Cs] (2017).

[2] Y. Zhang and S. Swanson, 31<sup>st</sup> Symposium MSST (IEEE, Santa Clara, CA, USA, 2015), pp. 1-10.

[3] T. Coughlin, IEEE Consumer Electronics Magazine 5, 133 (2016).

[4] S. Chhabra and Y. Solihin, 38<sup>th</sup> Annual ISCA (2011), pp. 177-188.

[5] A. Clausen et al. LiberTEM/LiberTEM: 0.5.0. (Zenodo, 2020). doi:10.5281/zenodo.3763313.

#### 2:25 PM \*F.EN09.02.01

**Synchrotron X-Ray Spectroscopy Analysis of Some Nanoalloys and Nanoclusters** Peng Zhang; Dalhousie University, Canada

Synchrotron X-ray absorption spectroscopy and associated techniques are useful tools for the element-specific analysis of the structure and properties of materials. In this talk, the application of such techniques in the study of some noble metal nanostructures toward catalytic applications will be presented. Materials of interest include nanoclusters, nanoalloys, and single-atomic-site catalysts. It will be demonstrated that the X-ray spectroscopy techniques, in association with other experimental and computational methods, can sensitively probe the structural and property changes of the catalysts induced by effects such as sample size, protecting ligands, and alloy bonding. The structural information revealed by the X-ray techniques is found useful to more thoroughly understand the structure-property relationships of the nanocatalysts.

#### 2:45 PM \*F.EN09.03.01

**Constant Wavelength *In Situ* Neutron Powder Diffraction for Rechargeable Batteries, Fuel Cells, Hydrogen Storage and Photovoltaics** Thomas C. Hansen; Institut Laue-Langevin, France

For the inspection of processes involving condensed matter, *in situ* neutron powder diffraction proves to be a versatile tool, giving insight into processes of technological pertinence. Only a few high-intensity powder diffractometers at intense neutron sources allow for this. D20 at Institut Laue-Langevin provides the highest available intensity in constant wavelength neutron powder diffraction. A stationary, curved linear position sensitive detector allows for *in-situ* diffraction studies down to a second and encourages the use of complex sample environments with inherently small sample sizes. D20 adapts to various levels of crystallographic complexity and rapidity of an observed phenomenon.

Rapid growth of the portable electronics market, as well as non-polluting ground transportation, needs portable energy

storage solutions with improved characteristics. One way to improve Li-ion batteries are solid electrolytes to overcome issues of liquid electrolytes in battery safety and high-voltage operation. Neutron diffraction determines the Li diffusion pathway in solid-state Li-ion conductors. Development of better electrode materials in terms of gravimetric and volumetric energy density, temperature operation range and cycling stability needs understanding of lithium (de)intercalation phenomena. *Operando* diffraction techniques are well suited here. Electrochemical cells based on a neutron-transparent (Ti,Zr) alloy combine good electrochemical properties and the ability to collect neutron diffraction patterns with reasonable statistics and no other Bragg peaks than those of the electrode material. This allows detailed structural determination of electrode materials by Rietveld refinement during operation.

Solid-oxide fuel cells convert chemical energy into electricity at higher efficiency than conventional methods, with less pollution. The anode (fuel electrode) must not alter at high temperature (thermal stability), not form nonconductive phases at interfaces (chemical stability) and not degrade upon reduction and oxidation cycles (redox stability). The state-of-the-art “cermet” of Ni and yttria-stabilized zirconia ceramic loses performance upon usage as its porosity is reduced by Ni agglomeration and as oxidation of Ni causes redox instability. Cermet deactivates through carbon coking and sulfur poisoning, making it unsuited for hydrocarbon fuels. Single-phase mixed ionic and electronic conductors provide microstructural stability and increase the electrode fraction accessible to oxide ions. Many of those oxides have been investigated successfully *in operando* at high temperature under oxidizing and reducing gas flow by neutron diffraction, following the crystal chemistry of oxide ions during the process.

Classical *in situ* work (thermo-diffractometry) has been done on the new photovoltaic materials,  $\text{MAPbI}_3$  and derivatives, and neutron diffraction turned out to be a perfect tool to screen the crystal chemistry of light organic atoms beside the heavy metal atoms over a wide range of temperatures.

Hydrogen is an attractive energy carrier for renewable energy sources due to its high energy density. Solid-state hydrogen storage provides higher storage capacities than compressed or liquefied hydrogen. Complex metal hydrides have high hydrogen storage capacities but suffer from poor kinetic and thermodynamic properties. Tuning the thermodynamics for dehydrogenation, in order to reduce the temperature at which hydrogen is evolved is achieved through the addition of a second phase, which will lead to the formation of a more stable product upon decomposition and thereby reducing the enthalpy for dehydrogenation. Neutron powder diffraction comes screens the crystal chemistry of the different phases *in situ* and localizes hydrogen in the structures.

### 3:05 PM \*F.EN09.06.01

#### **Advance Characterization Tools to Study and Develop Stable Anionic Redox for High-Energy Rechargeable Batteries** Minghao Zhang and Y. Shirley Meng; University of California, San Diego, United States

There is a growing consensus that the theoretical limit of one electron intercalation reactions will soon be reached. Recent discoveries on anion redox electrochemistry offer new opportunities and a possible paradigm shift in energy storage. By activating anion (e.g. oxygen, sulfur) for reversible electrochemical reactions, increased energy density has been demonstrated. In the past decade, the research community has made great progress on understanding key features of the anionic electrochemical activities and dynamic phenomena that govern the performance limitations including cycling voltage hysteresis and decay. However, the exact mechanism at molecular/atomic scales is still largely under-debate. The lack of conscience on the anionic redox mechanism which can be fueled by possible misinterpretation of experimental results. Of particular importance is determining what techniques provide accurate and reliable evidence for reversible bulk oxygen redox.

Compared with transition metal cations, oxygen anions are more challenging to be probed and quantified, which requires a multi-modal experimental approach with exceptional energy and spatial resolution combining computational modelling. Here, we advance: 1) from X-ray absorption spectroscopy to resonant inelastic X-ray scattering which shows a sharp feature with the corresponding excitation energy at 531 eV corresponding to the extra unoccupied electron orbitals of oxidized oxygen; 2) from neutron diffraction to neutron pair distribution function which is enormously valuable as a local probe that can reveal local distortions, when present along the oxygen redox reactions; 3) from X-ray diffraction to Bragg coherent diffraction imaging which will enable the direct observation of the strain dynamics with the exceptional sensitivity as small as 0.05% and phase evolution induced by the oxygen redox activity at nanoscale. It is through the in-depth understanding of electrochemical reactions mechanism at microscopic and macroscopic level during the operation of batteries; we can successfully formulate strategies to achieve reversible and stable anionic redox for next generation lithium-ion batteries.

### 3:25 PM \*F.EN09.03.04

#### **Advanced Neutron Characterisation of Rechargeable Battery Systems** Vanessa K. Peterson<sup>1,2</sup>; <sup>1</sup>Australian Nuclear Science and Technology Organisation, Australia; <sup>2</sup>University of Wollongong, Australia

The performance of functional materials central to energy devices, including rechargeable batteries, fuel cells, as well as gas

separation and storage technologies, is determined largely by atomic-scale materials structure and dynamic-function relations. Many energy materials function by undergoing change, such as compositional change in rechargeable battery electrodes that reversibly host charge-carrying ions and in gas storage and separation materials. Robust characterization methods that quantitatively and accurately capture these changes are essential to the strategic design of superior materials function, and consequently to improving energy device performance. Historically, a conflict existed between fast and detailed measurements of materials structure, particularly for measurements of materials within devices. This conflict was sometimes alleviated by using small model systems in which the material function was not representative of that in the corresponding commercially used device. Today, advanced characterization methods that capture material changes in detail while they are occurring is possible in whole devices under real-life operating conditions, as facilitated by advances in instrumentation.

This talk will give examples of in operando and in situ neutron measurements of energy materials used for rechargeable batteries capturing compositional change and/or non-equilibrium processes, with a focus on neutron powder diffraction using the high intensity neutron powder diffractometer Wombat at the Australian Centre for Neutron Scattering

SESSION F.EN09.13: Live Keynote II: Developing In Situ and Operando Methodology for Observation of Energy Conversion, Storage and Transport Process in Materials and Devices

Session Chairs: Lena Kourkoutis, Katharine Page, Chengjun Sun and Markus Winterer

Wednesday Morning, December 2, 2020

F.EN09

#### 8:00 AM \*F.EN09.05.01

##### **Novel Approaches for Electron Tomography to Investigate the Structure and Stability of Nanomaterials Under**

**Relevant Conditions** Sara Bals<sup>1,2</sup>, Wiebke Albrecht<sup>1,2</sup>, Hans Vanrompay<sup>1,2</sup>, Eva Bladt<sup>1,2</sup>, Alexander Skorikov<sup>1,2</sup>, Thomas Altantzis<sup>1,3</sup>, Jan Willem Buurlaeghe<sup>4</sup>, Daan Pelt<sup>4</sup>, Joost Batenburg<sup>5,4</sup> and Sandra Van Aert<sup>1,2</sup>; <sup>1</sup>EMAT-University of Antwerp, Belgium; <sup>2</sup>NANOLab Center of Excellence, University of Antwerp, Belgium; <sup>3</sup>ELCAT-University of Antwerp, Belgium; <sup>4</sup>CWI, Netherlands; <sup>5</sup>University of Leiden, Netherlands

Nanomaterials are important for a wide range of applications because of their unique properties, which are strongly connected to their three-dimensional (3D) structure. Electron tomography has therefore been used in an increasing number of studies. Most of these investigations resulted in 3D reconstructions with a resolution at the nanometer scale, but also atomic resolution was achieved in 3D.

In order to preserve the carefully designed morphologies and functionalities, understanding the stability of nanomaterials during application is crucial. It is hereby important to note that most electron tomography investigations have been performed at the conventional conditions of an electron microscope. An emerging challenge is therefore to fully understand the connection between the 3D structure and properties under more relevant conditions, including high temperatures as well as in the presence of liquids and gases. Therefore, innovative methodologies are required to track the fast 3D changes of nanomaterials that occur under such conditions.

Recently, we proposed an acquisition approach where a tilt series of 2D HAADF-STEM projection images is acquired within a few minutes. By continuously tilting the holder and simultaneously acquiring projection images while focusing and tracking the particle, we were able to reduce the total acquisition time for a tilt series by a factor of ten [1]. Moreover, a new approach was developed to compute high quality 2D virtual slices through nanoparticles in approximately 60 ms time. This technique drastically improves the efficiency of 3D characterization of nanomaterials by TEM. It enables explorative imaging and provides valuable information to dynamically adjust the acquisition parameters during an electron tomography experiment [2].

In this manner, we were able to study the 3D morphological evolution of anisotropic Au and AuPd nanoparticles as a function of both heating time and temperature [1,3]. Moreover, we measured the elemental diffusion dynamics of individual anisotropic Au-Ag nanoparticles in 3D [4]. We conclude that for a given composition, the shape of the nanoparticle does not influence the alloying process significantly. Based on our analysis, it is clear that interdiffusion of metals at the nanoscale is more complex than predicted by simple Fickian diffusion and that other factors such as surface diffusion need to be taken into account.



To quantify nanoparticle shape dynamics in a gaseous environment in 3D, HAADF-STEM images served as an input for atom counting procedures followed by 3D relaxation of the structure. In this manner, we characterized shape changes of a Pt nanoparticle in a gaseous environment. The conditions have been varied from vacuum to a 1 bar H<sub>2</sub> flow, followed by a 1 bar O<sub>2</sub> environment. To investigate the behaviour during cycling, we repeated the experiment several times using the same particle. We clearly observe morphology changes and we were even able to quantify the occurrence of the different surface facets [5].

## References

- [1] H. Vanrompay et al., *Nanoscale* **10** (2018), p. 22792
- [2] H. Vanrompay et al., *Particle and Particle System Characterization* (2020) in press
- [3] W. Albrecht et al., *ACS Nano* **13** (2019), p.6522
- [4] A. Skorikov et al., *ACS Nano* **13** (2019), p.13421
- [5] T. Altantzis et al., *Nano Letters* **19** (2019), p.477
- [6] This work was supported by the European Research Council (Grant 815128 REALNANO to SB, Grant 770887 PICOMETRICS to SVA and Grant 797153 SOPMEN to WA, Grant 823717 ESTEEM3). The authors acknowledge financial support from the Research Foundation Flanders (FWO, Belgium) through project fundings, a postdoctoral grant to EB and a doctoral grant to HV.

## 8:20 AM \*F.EN09.06.04

**Operando Characterization of Electrochemical Insertion into Hydrated and Solvated Metal Oxides** Veronica Augustyn; North Carolina State University, United States

Layered transition metal oxides that incorporate water or other solvents provide fundamental understanding of the effects of confinement on electrochemical ion transport and reactivity. They also tend to exhibit fast electrochemical ion insertion kinetics making them of interest for high power electrochemical energy storage. These materials are hybrids that consist of transition metal oxide layers separated by fluids that can be either ordered or disordered, and strongly or weakly bound to the oxide. Our group has investigated ion insertion into a range of hydrated and solvated metal oxides with *operando* characterization to connect structural changes to the electrochemical response. Since many of these materials exhibit fast kinetics (full charge/discharge in minutes), *operando* characterization techniques must have suitable temporal resolution to capture structural or chemical changes at these rates. This presentation will describe our use of three types of *operando* techniques to probe insertion kinetics at minute-to-second timescales: X-ray diffraction, atomic force microscopy, and electrochemical quartz crystal microbalance. It will also discuss how knowledge of the dynamics of ion insertion in these materials help us understand ion transport under confinement.

## 8:40 AM \*F.EN09.07.01

**Understanding Kinetic Limitations and Oxygen-Redox in Lithium Layered Transition-Metal Oxide Electrodes Through Operando X-Ray Scattering** Karena Chapman; Stony Brook University, United States

Chemical substitution of transition metal species is often used to tune the performance and cost of electrode materials. However, substitutions that improve one performance metric can be coupled to unintended consequences. This presentation will show how we have used operando X-ray scattering to understand kinetic limitations and O-redox in Li-layered transition metal oxide electrodes.

Substituted Li layered transition metal oxide (LTMO) electrodes such as Li<sub>x</sub>Ni<sub>y</sub>Mn<sub>z</sub>Co<sub>1-y-z</sub>O<sub>2</sub> (NMC) and Li<sub>x</sub>Ni<sub>y</sub>Co<sub>1-y-z</sub>Al<sub>z</sub>O<sub>2</sub> (NCA) show reduced first cycle Coulombic efficiency (90-87 % in standard cycling conditions) compared with archetypal Li<sub>x</sub>CoO<sub>2</sub> (LCO – ~98 % efficiency). We use operando x-ray diffraction (XRD) to demonstrate that the apparent first cycle capacity loss is a kinetic effect linked to limited Li mobility at  $x > 0.85$ , with near full capacity recovered and slow Li reinsertion during a potentiostatic hold following the galvanostatic charge–discharge cycle. The kinetic limitation manifests not only as the kinetic capacity loss during discharge, but as a subtle bimodal compositional distribution early in charge and, also, a dramatic increase of the charge–discharge voltage hysteresis at  $x > 0.85$ .

## 9:00 AM \*F.EN09.09.01

**Atomic Scale Dynamics of Oxide Island Growth During In Situ Oxidation of Copper** Judith C. Yang; University of Pittsburgh, United States

Understanding the structural changes at the atomic scale of nano-oxide formation via metal oxidation is critical for the rational design and control of oxides for a variety of technology-critical applications including heterogeneous catalysts,

sensors, and corrosion protection in extreme environments. Though classical oxidation theories, such as Cabrera-Mott, exist, little is known concerning the initial oxidation stages at the atomic scale. With the developments of in situ characterization tools, such as Environmental Transmission Electron Microscope (ETEM), we are now able to directly observe the structural changes during oxidation. In this work, we combine in situ ETEM with density functional theory (DFT) to fundamentally understand oxide island formation and growth at the atomic scale; Cu(001) was selected as the model metal system. As an example of this correlative approach, we recently observed a layer-by-layer growth of Cu<sub>2</sub>O island along Cu<sub>2</sub>O(110) plane, where our analysis of these growth dynamics suggests a diffusion limited monolayer growth process. DFT results supported these experimental observations of preferential growth along Cu<sub>2</sub>O(110) based on surface energies, diffusion barriers and adsorption energies simulations. We are currently investigating these critical surface reactions for binary alloys. Support for this research program is from NSF-DMR 1410055, 1508417, and 1410335.

**9:20 AM \*F.EN09.10.01**

**Sustainable Energy Materials—New Routes for *In Situ* Nanoscale Characterization and Their Correlation to Functionality** Stephan V. Roth; KTH Royal Institute of Technology, Sweden

The development of materials for sustainable energy conversion and storage requires new approaches on both the materials and process side. These approaches rely on the use of scattering techniques offering access to the molecular and nanoscale and exploiting both the virtues of X-rays and neutrons [1]. One crucial point is to observe the materials structural transformations in situ from the nano- to the microscale during materials' synthesis and subsequent device fabrication. These changes must be related to their (macroscopic) functionality. Preferentially the materials itself are sustainable, water-based, or biomaterials. To start with, we focus on wood-based biomaterials, such as cellulose and lignin. Introducing spray deposition as versatile process, ultrasmooth cellulose nanofibril films with controlled thickness are investigated [1,2]. Depending on their charge and roughness, the wettability can be controlled. This is crucial for optimizing the fabrication of hybrid materials, typical for energy conversion and storage. The tailoring of wettability is further pursued by surface functionalization of water-based latex colloids. These materials offer the possibility to tailor and fine-tune the wettability by tuning the core-shell colloid morphology in thin films, thus providing a facile template methodology for repellent surfaces of devices [3]. In materials synthesis, chemical modification of lignin affects the molecular network, aggregate stacking, and size of lignin thermosets. This in turn changes the macroscopic properties of the resulting thermoset [4]. Electronic properties manifest themselves for example in electrical conductivity changes and optical response. The electronic properties are governed by the nanoscale morphology. Imaging via scattering methods allows to extract the granular morphology up to and beyond the percolation threshold in situ during fabrication. At the same time, this analysis allows to predict the electrical behavior of hybrid composites and thus to optimized for example electrodes in such devices [5]. Silver nanowires offers electrical conductivity, mechanical flexibility as well as well high optical transparency when applied as meshes in top electrodes. Here, printing applications offer great potential for photovoltaics and flexible electronics. Two examples are presented: First, a tough composite for a 2D-printed film as top contact on a solar cell, and secondly a flexible composite applied for a 3D-printed flexible capacitor [6]. These examples highlight the advanced capabilities of scattering methods for in situ imaging of the nanoscale structure and for establishing the nanostructure-function relationship.

[1] C.J. Brett et al., *Macromolecules* 52, 4721 (2019)

[2] S. V. Roth, *J. Phys.: Condens. Matter* 28, 403003 (2016)

[3] J. Engström et al.: *Adv. Funct. Mater.*, 30, 1907720 (2020)

[4] M. E. Jawerth et al., *ACS ACS Appl. Polym. Mater.* 2, 668 (2020)

[5] M. Gensch et al., *ACS Appl. Mater. Interfaces* 11, 29416 (2019)

[6] T. E. Glier et al., *Scientific Reports* 9, 6465 (2019)

SESSION F.EN09.01: Advanced Microscopy Methods

On Demand Abstracts Available for Viewing Starting Saturday Morning, November 21, 2020

F-EN09

**5:00 AM \*F.EN09.01.01**

***In Situ* Microscopy of Energy Materials with Electron and Photon Techniques** Gianluigi A. Botton<sup>1,2</sup>; <sup>1</sup>Canadian Light Source, Canada; <sup>2</sup>McMaster University, Canada

Electron microscopes have become very power tools to study the structure of materials at unprecedented resolution. From their invention, these tools have provided essential information on the structure and properties of the broadest range of

materials used today in structural and functional applications. In-situ electron microscopy has evolved over the last few decades from dynamic experiments (heating, straining) to reaction in gases, and, more recently, even electrochemical experiments either in vacuum or in liquids. While the spatial resolution remains the first motivation for such in situ experiments in electron microscopy (so that even nucleation and early stages of growth of nanostructures formed during electrodeposition can be investigated), the flexibility and the more realistic environments remain the realm of synchrotron beam lines. Higher pressures, higher (or lower) temperatures, experiments in liquids and gases, can be carried out with exquisite spectroscopic resolution, penetrating power with diffraction techniques, in realistic and macroscopic samples and experimental conditions more suitable to represent operating conditions.

In this presentation, a comparison of the types of experiments that can be carried out with electron and photon techniques are discussed, in particular in the context of the nature of the samples, the time resolved sensitivity and the potential artefacts.

#### 5:15 AM F.EN09.01.02

**Operando Scanning Transmission Electron Microscopy of Li-O<sub>2</sub> Battery—*See and Believe*** Jihui Han<sup>1</sup>, Chen Hou<sup>2,1</sup>, Chuchu Yang<sup>1</sup>, Pan Liu<sup>2,1</sup>, Akihiko Hirata<sup>3,1</sup> and Mingwei Chen<sup>4,1</sup>; <sup>1</sup>Tohoku University, Japan; <sup>2</sup>Shanghai Jiao Tong University, China; <sup>3</sup>Waseda University, Japan; <sup>4</sup>Johns Hopkins University, United States

Rechargeable non-aqueous lithium-oxygen batteries with a large theoretical capacity are emerging as a high-energy electrochemical device for sustainable energy strategy. Although the fundamental electrochemical principle of lithium-oxygen batteries has been established for decades, the cathodic reaction kinetics, associated with the formation and decomposition of a solid Li<sub>2</sub>O<sub>2</sub> phase during charging and discharging, remains debating. Here we report direct visualization of the charge/discharge reactions on Au and RuO<sub>2</sub> cathodes in non-aqueous electrolytes with and without redox mediators using liquid-cell aberration-corrected scanning transmission electron microscopy (STEM) combining with synchronized electrochemical measurements. The real-time and real-space characterization by time-resolved quantitative STEM with ~1 nm spatial resolution reveals the electrochemical correspondence of discharge/charge overpotentials with the nucleation, growth and decomposition of Li<sub>2</sub>O<sub>2</sub> which are mediated by solid and liquid catalysts at constant current densities. The nano-scale operando observations unveil the underlying reaction pathways of lithium-oxygen batteries under different electrochemical conditions during round-trip discharging and charging and shed lights on the strategies in improving the performances of lithium-oxygen batteries by tailoring the cathodic reactions through cathode and electrolyte design.

#### 5:25 AM F.EN09.01.03

**Unveiling the Stable Nature of the Solid Electrolyte Interphase Between Lithium Metal and LiPON via Cryogenic Electron Microscopy** Diyi Cheng and Y. Shirley Meng; University of California, San Diego, United States

The solid electrolyte interphase (SEI) is regarded as the most complex but the least understood constituent in secondary batteries using liquid and solid electrolytes. The nanostructures of SEIs were recently reported to be equally important to the chemistry of SEIs for stabilizing Li metal in liquid electrolyte. However, the dearth of such knowledge in all-solid-state battery (ASSB) has hindered a complete understanding of how certain solid-state electrolytes, such as LiPON, manifest exemplary stability against Li metal. Characterizing such solid-solid interfaces is difficult due to the buried, highly reactive, and beam-sensitive nature of the constituents within. By employing cryogenic electron microscopy (cryo-EM), the interphase between Li metal and LiPON is successfully preserved and probed, revealing a multilayer mosaic SEI structure with concentration gradients of nitrogen and phosphorous, materializing as crystallites within an amorphous matrix. This unique SEI nanostructure is less than 80 nm and is shown stable and free of any organic lithium containing species or lithium fluoride components, in contrast to SEIs often found in state-of-the-art organic liquid electrolytes. Our findings reveal insights on the nanostructures and chemistry of such SEIs as a key component in lithium metal batteries to stabilize Li metal anode.

#### 5:35 AM \*F.EN09.01.04

**In Situ Scanning Transmission Electron Diffraction of Individual Electrically-Biased Phase Change Memory Ag-In-Sb-Te Line Cells** Vadim Migunov<sup>1,2,3</sup>, Xuan Thang Vu<sup>2</sup>, Sebastian Walfort<sup>4</sup>, Karina Ruzaeva<sup>1</sup>, Benedikt Kersting<sup>5</sup>, Martin Salanga<sup>4</sup> and Rafal E. Dunin-Borkowski<sup>1</sup>; <sup>1</sup>Forschungszentrum Juelich, Germany; <sup>2</sup>RWTH Aachen University, Germany; <sup>3</sup>ABB AG, Germany; <sup>4</sup>University of Münster, Germany; <sup>5</sup>IBM Research-Zurich, Switzerland

As current memory technologies approach their fundamental limits, increasing demand for novel non-volatile memories is driving the development of new architectures, which are already showing their potential in high performance computing [1, 2]. As a result of their non-volatile nature, byte-addressability and fast response times, which are comparable to those of dynamic random-access memory, resistive-switching-based phase change materials (PCMs) are strong candidates for memory applications with reduced hardware cost and power consumption [3, 4].

The use of advanced transmission electron microscopy combined with *in situ* electrical biasing provides a powerful method for studying the local relationship between atomic structure and electrical properties in individual nanoscale memory elements, in order to identify the factors that affect their switching reproducibility and dynamics.

We have developed a multi-step lithographic procedure, which allows dedicated nanostructured line cells that contain PCM switching layers, electrical contacts and protective layers to be fabricated directly on electron-transparent silicon nitride membranes and used for switching experiments both outside and inside the transmission electron microscope. We used a special electrical setup to provide short (50 ns) electrical current pulses to individual line cells with sharp (approximately 3 ns) rising and falling edges. By using these pulses, PCM devices could be switched between crystalline low resistance and amorphous high resistance states inside a transmission electron microscope.

Even though each device consisted of several layers of different materials, resulting in a total thickness of between 200 and 300 nm, a fast pixelated direct electron detector could be used to record scanning electron diffraction patterns from amorphous/crystalline regions before and after successive switching cycles, while measuring the electric properties of the same devices. Newly-developed algorithms based on LiberTEM software [5] were used to follow the evolution of individual crystallites and to show that the switching mechanisms involved slow crystal growth or rapid recrystallization, depending on the details of the current pulses.

[1] K. Wu, F. Ober, S. Hamlin and D. Li, ArXiv:1708.02199 [Cs] (2017).

[2] Y. Zhang and S. Swanson, 31<sup>st</sup> Symposium MSST (IEEE, Santa Clara, CA, USA, 2015), pp. 1-10.

[3] T. Coughlin, IEEE Consumer Electronics Magazine 5, 133 (2016).

[4] S. Chhabra and Y. Solihin, 38<sup>th</sup> Annual ISCA (2011), pp. 177-188.

[5] A. Clausen et al. LiberTEM/LiberTEM: 0.5.0. (Zenodo, 2020). doi:10.5281/zenodo.3763313.

#### 5:50 AM F.EN09.01.05

**Late News: Imaging Ionic Arrangements at Liquid-Solid Interfaces by Cryo-Electron Microscopy** [Haokun Li](#)<sup>1</sup>, J. Pedro de Souza<sup>2</sup>, Ze Zhang<sup>1</sup>, Joel Martis<sup>1</sup>, Kyle Sendgikowski<sup>3</sup>, John Cumings<sup>3</sup>, Martin Bazant<sup>2</sup> and Arun Majumdar<sup>1</sup>; <sup>1</sup>Stanford University, United States; <sup>2</sup>Massachusetts Institute of Technology, United States; <sup>3</sup>University of Maryland, United States

Electrically charged liquid-solid interfaces play a vital role in many electrochemical phenomena encountered in biology, energy, and the environment. At electrically charged interfaces, ions and solvent molecules rearrange to screen the surface charge, forming the electrical double layers. The ability to probe such systems with single-ion resolution is important to a basic understanding of their behaviors and the development of new ionic technologies. Although many techniques have been used to probe liquid-solid interfaces, it remains a challenge to acquire spatial information down to the single ion level. Here, using cryo-electron microscopy, we directly visualize individual ions and their distributions at electrically charged liquid-solid interfaces. We observe discrete layering of multivalent counterions, which arises from the finite ion size and the strong electrostatic interactions. In addition, correlated ion structures under extreme confinement are revealed, with the channel widths approaching the ion diameter (~1 nm). Our experiment opens up a new arena to study liquid-solid interfaces at the single ion level.

#### SESSION F.EN09.02: X-Ray Spectroscopy

On Demand Abstracts Available for Viewing Starting Saturday Morning, November 21, 2020

F-EN09

#### 5:00 AM \*F.EN09.02.01

**Synchrotron X-Ray Spectroscopy Analysis of Some Nanoalloys and Nanoclusters** [Peng Zhang](#); Dalhousie University, Canada

Synchrotron X-ray absorption spectroscopy and associated techniques are useful tools for the element-specific analysis of the structure and properties of materials. In this talk, the application of such techniques in the study of some noble metal nanostructures toward catalytic applications will be presented. Materials of interest include nanoclusters, nanoalloys, and single-atomic-site catalysts. It will be demonstrated that the X-ray spectroscopy techniques, in association with other experimental and computational methods, can sensitively probe the structural and property changes of the catalysts induced

by effects such as sample size, protecting ligands, and alloy bonding. The structural information revealed by the X-ray techniques is found useful to more thoroughly understand the structure-property relationships of the nanocatalysts.

#### 5:15 AM F.EN09.02.02

**In-Operando Study of Electrochemical Strain and Charge Storage Mechanisms in Defect-Engineered MnO<sub>2</sub> Nanosheet Electrodes** Madeleine N. Flint, Alec Ladonis, Peter Metz, Peng Gao, Robert Koch and Scott Misture; Alfred University, United States

MnO<sub>2</sub> nanosheets demonstrate an interesting response to reduction of Mn<sup>4+</sup> to Mn<sup>3+</sup>, where the Jahn-Teller distorted Mn<sup>3+</sup> is displaced out of the plane of the nanosheet forming a “surface Frenkel” defect. Atomic scale point defects enhance capacitance beyond 300F/g while lowering charge transfer resistance of δ-MnO<sub>2</sub> nanosheets by a factor of 10 and increasing cycle stability.

In-situ and in-operando X-ray total scattering and XRD was teamed with X-ray absorption spectroscopy, Raman spectroscopy, and related tools to probe the local atomic structure and defect chemistry during electrochemical cycling. The result is a description of the charging mechanism in high surface area MnO<sub>2</sub> nanosheet electrodes: reversible in-plane strains of up to 0.7% occurred during charging of nanosheets with little restacking, accompanied by Mn reduction. Bond distances obtained from Pair Distribution Functions correlated with the XRD where Mn-O and Mn-Mn bond lengths reversibly increased during charging. Raman spectra also demonstrate an increased number of Jahn-Teller distorted MnO<sub>6</sub> octahedra in the charged state.

Changes to the interlayer during electrochemical cycling were morphology dependent. Random assemblies of nanosheets with little sheet-to-sheet restacking showed only in-plane response, without changes in sheet-to-sheet distances. However, highly restacked nanosheets contract in the c direction on charging due to electrostatic changes to the interlayer. The results suggest that improved cycling stability is feasible using high-porosity, random assemblies of nanosheets and that the interlayer hydration is a key parameter in diffusion of the charging ions.

#### 5:25 AM F.EN09.02.03

**New Synchrotron Methods to Investigate the Breakdown of the Small-Polaron Hopping Model in Ternary Spinel** Anuj Bhargava<sup>1</sup>, Roni Eppstein<sup>2</sup>, Jiaxin Sun<sup>1</sup>, Michelle A. Smeaton<sup>1</sup>, Hanjong Paik<sup>1</sup>, Lena Kourkoutis<sup>1</sup>, Darrell Schlom<sup>1</sup>, Maytal Caspary Toroker<sup>2</sup> and Richard Robinson<sup>1</sup>; <sup>1</sup>Cornell University, United States; <sup>2</sup>Technion–Israel Institute of Technology, Israel

For the more than half a century the small polaron hopping model has been used to describe the electronic charge transport in semiconducting oxides. This model was originally developed for binary oxides, and despite its vast usage, the model's accuracy has not been rigorously tested for complex oxides (ternary and higher order oxides). Ternary spinel oxides are an important class of materials actively researched for applications in energy storage, catalysis, and data storage due to their exciting electrochemical, catalytic, and magnetic properties; and better understanding of charge transport in such systems can lead to higher performance devices. Previous experimental investigations of charge transport in ternary spinels are sparse and limited owing to the lack of accessible characterization techniques to correlate site occupation to properties, and also due to difficulties in achieving phase-pure ternary over a wide stoichiometric range. To overcome these challenges, we choose the Mn<sub>x</sub>Fe<sub>3-x</sub>O<sub>4</sub> system, which has exciting electrochemical and catalytic properties, and mixed oxidation states that enables us to examine the mechanisms of small polaron transport. We fabricate epitaxial and phase pure Mn<sub>x</sub>Fe<sub>3-x</sub>O<sub>4</sub> thin films over the complete ‘x’ range using molecular beam epitaxy (MBE); and use our recently developed method using x-ray emission spectroscopy (XES) to determine the site occupation of cations. Previously we have shown that XES is an accessible and a more accurate method than traditional methods such as x-ray absorption spectroscopy (XAS) in extracting cation site occupation. We find that in Mn<sub>x</sub>Fe<sub>3-x</sub>O<sub>4</sub>, polarons preferably localize at Mn octahedral sites and polaron hopping occurs only between like-elements (Fe to Fe and Mn to Mn), and as a result the conduction occurs along decoupled pathways formed by Mn and Fe cations. Since the role of cross-hopping and decoupled pathways have not been considered in the conventional polaron hopping model, we introduce new parameters in the conventional transport model. We test the validity of the new model on the Mn<sub>x</sub>Fe<sub>3-x</sub>O<sub>4</sub> system by comparing the concentration of charge carriers calculated using the conventional and the new model to the experimental conductivity trends. An excellent overlap of the new model with experimental trends confirms the precision of our augmented model and the limitation of the conventional model for ternary spinels. With this work, we use new synchrotron methods to provide a pragmatic tool for designing non-equilibrium oxides with enhanced performance with the aim to incorporate spinels in devices such as batteries, supercapacitors, and fuel cells.

#### 5:35 AM F.EN09.02.04

**Structural Characterization of Complex Catalysts for Heterogenous Oxidation** Jeremias Geiss and Markus Winterer; Universität Duisburg-Essen, Germany

Perovskite nanoparticles, composed of  $\text{LaCo}_x\text{Fe}_{1-x}\text{O}_3$ , are a promising heterogenous catalyst for oxidation reactions. As-synthesized nanocatalysts often exhibit a complex structure with a variety of defects. During operando experiments, the complexity of the structure increases by the addition of a boundary layer. Furthermore, the catalytic activity itself can result in structural changes. However, the understanding of the structure-activity relationship is critical to ultimately improve catalytic performance.

Due to their large surface to volume ration, the bulk as well as the surface of small nanoparticles can be probed by Extended X-Ray Absorption Fine Structure (EXAFS). Measurement at the different elemental absorption edges resolves the local structure around each atom type of the complex oxide.

The presentation is focused on the EXAFS measurements of  $\text{LaCo}_x\text{Fe}_{1-x}\text{O}_3$  nanoparticles at the Co-K, Fe-K and La-K edge to refine a mutual particle model by Reverse Monte Carlo (RMC) analysis.

Acknowledgements:

Funded by the Deutsche Forschungsgemeinschaft (DFG, German Research Foundation) – 388390466 – TRR 247.

**5:45 AM F.EN09.02.05**

**Revealing the Role of Point Defects in Nanostructured Catalyst Design with Ambient Pressure X-Ray Photoelectron Spectroscopy** Jiayue Wang<sup>1</sup>, Alexander K. Opitz<sup>2</sup> and Bilge Yildiz<sup>1</sup>; <sup>1</sup>Massachusetts Institute of Technology, United States; <sup>2</sup>Technische Universität Wien, Austria

A central theme in renewable energy technologies today is to design nanostructured catalysts towards desired reactions. Engineering the functional defects in materials is a key step in this direction. For this, we have to advance the understanding of the role of defect structures in the relevant properties of materials. Here we develop a generalizable experimental and analysis framework using ambient pressure X-ray spectroscopy (APXPS), density functional theory (DFT), and Monte Carlo (MC) calculations, to understand the role of point defects in catalyst generation under real working conditions.

A recent advance in materials for electrochemical energy and fuels conversion is to synthesize metal nanoparticles in a process termed “exsolution”. Unlike traditional nanoparticle infiltration techniques, the nanoparticle catalysts from exsolution are anchored in the parent oxide. This strong metal-oxide interaction makes the exsolved nanoparticles more resistant against particle agglomeration as compared to the infiltrated ones. In addition, the exsolved particles also open up the possibility of regeneration of catalysts. While being an exciting and promising pathway for generating stable oxide supported nanoparticles, rational control over the exsolved particles has yet to be achieved. In particular, it remains a big challenge to control the size and density of the exsolved nanoparticles.

In this work, we propose that point defect formation in the oxide lattice to be the fundamental knob to control exsolution, and demonstrate this approach in epitaxial  $\text{La}_{0.6}\text{Sr}_{0.4}\text{FeO}_3$  (LSF) thin films. By quantifying surface defect states with APXPS, we identify the initial oxygen vacancy ( $\text{V}_\text{O}$ ) formation and the following Schottky defect formation as the primary defect reactions in exsolution. Then, by tuning the formation energy of these two defects in LSF with biaxial lattice strain, we examined their impacts on metallic iron ( $\text{Fe}^0$ ) exsolution. As a result, the LSF surface with that has more of these point defects, also has the highest  $\text{Fe}^0$  concentration, the largest particle density, as well as the finest particle size. Finally, with the aid of DFT calculations and MC simulations, we suggest surface oxygen vacancy clusters to be the nucleation sites for the exsolved particles. These observations highlight the critical role of surface point defects in controlling the size and density of the nanoparticles.

SESSION F.EN09.03: Neutron Diffraction

On Demand Abstracts Available for Viewing Starting Saturday Morning, November 21, 2020

F-EN09

**5:00 AM \*F.EN09.03.01**

**Constant Wavelength *In Situ* Neutron Powder Diffraction for Rechargeable Batteries, Fuel Cells, Hydrogen Storage and Photovoltaics** Thomas C. Hansen; Institut Laue-Langevin, France

For the inspection of processes involving condensed matter, *in situ* neutron powder diffraction proves to be a versatile tool, giving insight into processes of technological pertinence. Only a few high-intensity powder diffractometers at intense neutron sources allow for this. D20 at Institut Laue-Langevin provides the highest available intensity in constant wavelength neutron powder diffraction. A stationary, curved linear position sensitive detector allows for *in-situ* diffraction studies down to a second and encourages the use of complex sample environments with inherently small sample sizes. D20 adapts to various levels of crystallographic complexity and rapidity of an observed phenomenon.

Rapid growth of the portable electronics market, as well as non-polluting ground transportation, needs portable energy storage solutions with improved characteristics. One way to improve Li-ion batteries are solid electrolytes to overcome issues of liquid electrolytes in battery safety and high-voltage operation. Neutron diffraction determines the Li diffusion pathway in solid-state Li-ion conductors. Development of better electrode materials in terms of gravimetric and volumetric energy density, temperature operation range and cycling stability needs understanding of lithium (de)intercalation phenomena. *Operando* diffraction techniques are well suited here. Electrochemical cells based on a neutron-transparent (Ti,Zr) alloy combine good electrochemical properties and the ability to collect neutron diffraction patterns with reasonable statistics and no other Bragg peaks than those of the electrode material. This allows detailed structural determination of electrode materials by Rietveld refinement during operation.

Solid-oxide fuel cells convert chemical energy into electricity at higher efficiency than conventional methods, with less pollution. The anode (fuel electrode) must not alter at high temperature (thermal stability), not form nonconductive phases at interfaces (chemical stability) and not degrade upon reduction and oxidation cycles (redox stability). The state-of-the-art “cermet” of Ni and yttria-stabilized zirconia ceramic loses performance upon usage as its porosity is reduced by Ni agglomeration and as oxidation of Ni causes redox instability. Cermet deactivates through carbon coking and sulfur poisoning, making it unsuited for hydrocarbon fuels. Single-phase mixed ionic and electronic conductors provide microstructural stability and increase the electrode fraction accessible to oxide ions. Many of those oxides have been investigated successfully *in operando* at high temperature under oxidizing and reducing gas flow by neutron diffraction, following the crystal chemistry of oxide ions during the process.

Classical *in situ* work (thermo-diffractometry) has been done on the new photovoltaic materials,  $\text{MaPbI}_3$  and derivatives, and neutron diffraction turned out to be a perfect tool to screen the crystal chemistry of light organic atoms beside the heavy metal atoms over a wide range of temperatures.

Hydrogen is an attractive energy carrier for renewable energy sources due to its high energy density. Solid-state hydrogen storage provides higher storage capacities than compressed or liquefied hydrogen. Complex metal hydrides have high hydrogen storage capacities but suffer from poor kinetic and thermodynamic properties. Tuning the thermodynamics for dehydrogenation, in order to reduce the temperature at which hydrogen is evolved is achieved through the addition of a second phase, which will lead to the formation of a more stable product upon decomposition and thereby reducing the enthalpy for dehydrogenation. Neutron powder diffraction comes screens the crystal chemistry of the different phases *in situ* and localizes hydrogen in the structures.

#### 5:15 AM \*F.EN09.03.04

**Advanced Neutron Characterisation of Rechargeable Battery Systems** [Vanessa K. Peterson](#)<sup>1,2</sup>; <sup>1</sup>Australian Nuclear Science and Technology Organisation, Australia; <sup>2</sup>University of Wollongong, Australia

The performance of functional materials central to energy devices, including rechargeable batteries, fuel cells, as well as gas separation and storage technologies, is determined largely by atomic-scale materials structure and dynamic-function relations. Many energy materials function by undergoing change, such as compositional change in rechargeable battery electrodes that reversibly host charge-carrying ions and in gas storage and separation materials. Robust characterization methods that quantitatively and accurately capture these changes are essential to the strategic design of superior materials function, and consequently to improving energy device performance. Historically, a conflict existed between fast and detailed measurements of materials structure, particularly for measurements of materials within devices. This conflict was sometimes alleviated by using small model systems in which the material function was not representative of that in the corresponding commercially used device. Today, advanced characterization methods that capture material changes in detail while they are occurring is possible in whole devices under real-life operating conditions, as facilitated by advances in instrumentation.

This talk will give examples of *in operando* and *in situ* neutron measurements of energy materials used for rechargeable batteries capturing compositional change and/or non-equilibrium processes, with a focus on neutron powder diffraction using the high intensity neutron powder diffractometer Wombat at the Australian Centre for Neutron Scattering

#### 5:30 AM F.EN09.03.05

**Late News: *Operando* Neutron Diffraction on All-Solid-State-Batteries Using a New Electrochemical Cell** [Cédric J. Barcha](#)<sup>1,2,3</sup>, [Xavier Randrema](#)<sup>1,2,3</sup>, [Théodosios Famprikis](#)<sup>1,3</sup>, [Tatiana Renzi](#)<sup>4,5,3</sup>, [Emmanuelle Suard](#)<sup>5</sup>, [Mohamed Chakir](#)<sup>2,3</sup>,

Nathalie Delpuech<sup>2,3</sup>, Jean-Noël Chotard<sup>1,3</sup>, Virginie Viallet<sup>1,3</sup>, Mathieu Morcrette<sup>1,3</sup>, Laurence Croguennec<sup>4,3</sup>, Vincent Seznec<sup>1,3</sup> and Christian Masquelier<sup>1,3</sup>; <sup>1</sup>Laboratoire de Réactivité et Chimie des Solides (LRCS), France; <sup>2</sup>Technocentre Renault (Groupe Renault), France; <sup>3</sup>Réseau sur le stockage électrochimique de l'énergie (RS2E), France; <sup>4</sup>Institut de Chimie de la Matière Condensée de Bordeaux (ICMCB), France; <sup>5</sup>Institut Laue-Langevin (ILL), France

The field of all-solid-state-batteries (ASSBs) is expected to potentially overcome associated issues of conventional LIBs and has recently attracted both industrial and academic attention <sup>(1)(2)</sup>. Indeed, by removing flammable liquid solvents, this technology may enable improved intrinsic safety at cell level and increased temperature stability, resulting in system level benefits compared with conventional LIBs based on liquid electrolytes. SEs should also allow the possibility to use lithium metal anode leading to an enhancement of the energy density. To develop the ASSB technology, it is mandatory to first understand the (de)lithiation mechanisms into/from active materials and investigate the stability of the solid electrolyte itself. Among in-situ techniques used to understand electrode materials, neutron diffraction (ND) is one of the most powerful due to its high penetration depth allowing simultaneous data collection from both electrodes.

Operando ND in Li-ion batteries has been widely used to determine lattice parameters, phase transitions, and detailed structural information such as Li position and content in anode and cathode materials <sup>(3)(4)(5)(6)</sup>, but also useful for commercial cell analysis <sup>(7)(8)(9)</sup>. In the long term, this tool could help the ASSB community with trending problems such as SE decomposition <sup>(10)</sup> or stability of crystalline coating on active materials <sup>(11)</sup>. A new operando electrochemical cell made of a Ti-Zr alloy completely transparent to neutrons was designed by the Institut Laue-Langevin, allowing operando neutron diffraction on the whole solid state battery, in a wide temperature range from -100°C to + 400 °C. The cell is completely airtight and offers the possibility of applying pressure. A first demonstration of the capabilities of the cell and of its limitations will be presented, using a solid-state battery based on a LiCoO<sub>2</sub> cathode, a Li<sub>4</sub>Ti<sub>5</sub>O<sub>12</sub> anode and Argyrodite Li<sub>6</sub>PS<sub>3</sub>Cl as the solid electrolyte. Temperature-controlled Li<sup>+</sup> extraction from LiCoO<sub>2</sub>, up to 150°C, made possible by the use of an ASSB, reveal new interesting phenomena. Over one electrochemical cycle, the structural integrity of the Argyrodite solid electrolyte appears to be maintained.

- (1) Yao, X., Huang, B., Yin, J., Peng, G., Huang, Z., Gao, C., Liu, D. & Xu, X. (2015). *Chinese Physics B*. 25,
- (2) Schnell, J., Knörzner, H., Imbsweiler, A. J. & Reinhart, G. (2020). *Energy Technology*. 1901237
- (3) Nazer, N. S., Yartys, V. A., Azib, T., Latroche, M., Cuevas, F., Forseth, S., Vie, P. J. S., Denys, R. V., Sørby, M. H., Hauback, B. C., Arnberg, L. & Henry, P. F. (2016). *J. Power Sources*. 326, 93–103.
- (4) Dong, B., Biendicho, J. J., Hull, S., Smith, R. I. & West, A. R. (2018). *J. Electrochem. Soc.* 165, A793–A801.
- (5) Bianchini, M., Leriche, J. B., Laborier, J.-L., Gendrin, L., Suard, E., Croguennec, L. & Masquelier, C. (2013). *J. Electrochem. Soc.* 160, A2176–A2183.
- (6) Rodriguez, M. A., Ingersoll, D., Vogel, S. C. & Williams, D. J. (2004). *Electrochem. Solid-State Lett.* 7, A8.
- (7) Taminato, S., Yonemura, M., Shiotani, S., Kamiyama, T., Torii, S., Nagao, M., Ishikawa, Y., Mori, K., Fukunaga, T., Onodera, Y., Naka, T., Morishima, M., Ukyo, Y., Adipranoto, D. S., Arai, H., Uchimoto, Y., Ogumi, Z., Suzuki, K., Hirayama, M. & Kanno, R. (2016). *Scientific Reports*. 6, 28843.
- (8) Shiotani, S., Naka, T., Morishima, M., Yonemura, M., Kamiyama, T., Ishikawa, Y., Ukyo, Y., Uchimoto, Y. & Ogumi, Z. (2016). *J. Power Sources*. 325, 404–409.
- (9) Bianchini, M., Fauth, F., Suard, E., Leriche, J.-B., Masquelier, C. & Croguennec, L. (2015). *Acta Crystallogr B Struct Sci Cryst Eng Mater*. 71, 688–701.
- (10) Tan, D. H. S., Wu, E. A., Nguyen, H., Chen, Z., Marple, M. A. T., Doux, J., Wang, X., Yang, H., Banerjee, A. & Meng, Y. S. (2019). *ACS Energy Letters*, 4, 2418–2427.
- (11) Xiao, Y., Miara, L. J., Wang, Y. & Ceder, G. (2019). *Joule* 2, 1–24.

SESSION F.EN09.04: Novel Microscopy Methods

On Demand Abstracts Available for Viewing Starting Saturday Morning, November 21, 2020

F-EN09

### 5:00 AM F.EN09.04.01

**Visualize and Quantify the Effect of Polymer Coatings on the Mechanical Behavior of LiCoO<sub>2</sub> Cathodes in Lithium-Ion Batteries** Laisuo Su<sup>1</sup>, Paul Choi<sup>1</sup>, Nathan Nakamura<sup>1</sup>, Harry Charalambous<sup>2</sup>, Shawn Litster<sup>1</sup>, Jan Ilavsky<sup>2</sup> and B. Reeja Jayan<sup>1</sup>; <sup>1</sup>Carnegie Mellon University, United States; <sup>2</sup>Argonne National Laboratory, United States



Surface engineering is the most effective method in regulating the chemo-mechanical interaction behavior of electrodes and further enhancing their electrochemical performance in lithium ion batteries (LIBs). Although extensive studies have been carried out to investigate the effect of coatings on the electrodes surface degradation, limited understanding have been obtained regarding how these coatings regulate the electrodes mechanical behavior. Here, for the first time, we combine in-operando synchrotron X-ray scattering technique and high-resolution transmission X-ray microscopy (TXM) technique to investigate the effect of a poly(3,4-ethylenedioxythiophene) (PEDOT) artificial coating on the electro-chemo-mechanical behavior of LiCoO<sub>2</sub>. TXM provides straightforward time-dependent images of LiCoO<sub>2</sub> particles, while X-ray scattering offers volume-averaged quantitative information of the LiCoO<sub>2</sub> electrodes during cycling. The complimentary of the two techniques is examined by an over-lithiation experiment of LiCoO<sub>2</sub> between 3.0 V – 0.5 V, during which LiCoO<sub>2</sub> particles/agglomerates crack and eventually pulverize. The two in-operando techniques are then applied to uncover the largely improved 4.5 V high-voltage cycling stability of LiCoO<sub>2</sub> from the PEDOT coating. The results suggest that the PEDOT coating not only alleviates LiCoO<sub>2</sub> surface deterioration and electrolyte decomposition, but also inhibits LiCoO<sub>2</sub> particles/agglomerates expansion during the cycling test. The understanding of the electro-chemo-mechanical behavior of battery electrodes will stimulate the development of advanced LIBs with fast charging ability and long cycle life.

#### 5:10 AM F.EN09.04.02

**Impact of Surface Adsorbates on Charge Carrier Transport in Metal-Oxides for Solar Water Splitting** Johanna Eichhorn<sup>1</sup>, Ian D. Sharp<sup>1</sup> and Francesca Maria Toma<sup>2</sup>; <sup>1</sup>Technische Universität München, Germany; <sup>2</sup>Lawrence Berkeley National Laboratory, United States

Photoelectrochemical water splitting is a promising route for efficient conversion of solar energy into chemical fuels. The chemical transformation of water into oxygen and hydrogen takes place at the photoelectrode surface. Consequently, the activity, efficiency, and reaction pathway are critically controlled by the material surface properties. Under operating conditions, surface properties depend on the surrounding environment, and may be altered in the course of the reaction. Thereby, absorption of molecules can modify the chemistry at the surface, for example by influencing the kinetics of reactants, products, or reaction intermediates, but they can also directly impact the electronic transport properties by acting as surface trap states. In this context, improved understanding of these complex surface interactions will aid the development of highly efficient light absorbers as well as the integration of effective passivation and catalyst layers for these materials.

Among different photoelectrode materials, bismuth vanadate (BiVO<sub>4</sub>) is one of the most actively investigated oxide semiconductors. Here, we employ photoconductive AFM under controlled *in-situ* conditions to gain insight into the relationship between surface interactions and interfacial charge transport characteristics in polycrystalline BiVO<sub>4</sub> thin films. We demonstrate that the low intrinsic bulk conductivity of BiVO<sub>4</sub> limits charge transport through the film, and that the transport mechanism can be attributed to space charge limited current in the presence of trap states. [1] By analyzing the space charge limited current in selective gas environments, we are able to quantify the impact of surface adsorbates on bulk transport properties. We find that surface adsorbed oxygen acts as a shallow trap state and accounts for 40% of the effective trap density in BiVO<sub>4</sub> thin films. [2] For humid environments, our results are consistent with the adsorption of water as an oriented dipole layer, which does not induce a surface charge transfer but partially inhibits the adsorption of oxygen at the surface. Disentangling the individual effects of oxygen and water on charge carrier trapping underpins the importance of trap state passivation for efficient transport of photogenerated charge carriers in BiVO<sub>4</sub>.

[1] Eichhorn *et al.*, *Nat. Commun.* **9**, 2597 (2018).

[2] Eichhorn *et al.*, *ACS Appl. Mater. Interfaces* **10**, 35129 (2018).

#### 5:20 AM F.EN09.04.03

**Nanosopic Operando Imaging-Guided Design of Photoelectrocatalysts for Energetically Efficient Water Decontamination** Xianwen Mao and Peng Chen; Cornell University, United States

Super-resolved fluorescence microscopy techniques have enabled significant advances in chemical and biological sciences. However, they can only interrogate entities that fluoresce — and most chemical or biological processes do not involve fluorescent species. Here we report ‘COMPEITS’ — a ‘COMPetition-Enabled Imaging Technique with Super-resolution’, that enables quantitative super-resolution imaging of nonfluorescent processes. It is based on the incorporation of competition into a single-molecule fluorescence detection scheme. We demonstrate COMPEITS by investigating a photoelectrocatalytic reaction; we map with nanometer precision a nonfluorescent surface reaction on single photocatalyst particles that is important for water decontamination. The sub-particle-level quantitative information of reactant adsorption affinities unambiguously decouples size and shape scaling laws on specific particle facets and uncovers surprising biphasic shape dependence, leading to catalyst design principles for optimal reactant adsorption efficacy. With its ability to provide

spatially-resolved information on the behaviors of unlabeled, nonfluorescent entities under operando conditions, COMPEITS can interrogate a variety of surface processes in fields ranging from heterogeneous catalysis and materials engineering to nanotechnology and energy sciences. (Reference: Mao et al. *Nature Chem.* **2019**, 11, 687-694)

#### 5:30 AM F.EN09.04.04

##### **Operando Characterization of Charge Extraction and Recombination Profiles in Solar Cells with Nanoscale Resolution** Tamir Yeshurun, Mor Fiegenbaum and Gideon Segev; Tel Aviv University, Israel

The next generation of solar energy conversion systems requires design and integration of new semiconductor materials. Detailed understanding of the opto-electronic properties of these materials, their driving forces and the loss mechanisms that limit device performance is essential to the development of high efficiency systems. However, these materials and systems are difficult to model and only few experimental methods are available for direct characterization of dominant loss processes under relevant operating conditions. To this end, empirical extraction of the spatial collection efficiency (SCE) and the spatial photon recycling efficiency (SPRE) are *operando*, analytical tools that provide functional depth profiles of the active regions in the device.

By coupling external quantum efficiency (EQE) measurements and optical modeling, SCE extraction allows quantifying charge transport properties and loss mechanisms across the device depth profile under real operating conditions with very few assumptions. Similar to SCE, combining optical modeling with wavelength dependent photoluminescence quantum yield (PLQY) measurements enables extracting the SPRE- the probability that an electron hole pair photogenerated at a specific point will contribute to photoluminescence from the device. In this contribution we will introduce the SPRE concept and will show a first demonstration of the SPRE extraction method applied to InP samples. Extracting the SPRE enables simple distinction between different losses such as surface recombination and self-absorption. The quantification of surface recombination losses makes this an excellent tool for characterizing the effect of surface passivation layers. Furthermore, since the PLQY is directly related to the obtainable photovoltage from the device, the SPRE also maps the contribution of different regions in the device to the photovoltage. As a result, combining the SPRE and SCE profiles at specific operating points provides detailed spatial information on charge extraction, contribution to the photovoltage, and discrimination between radiative and non-radiative recombination processes at the surface and in the bulk of the device.

#### SESSION F.EN09.05: Tomography

On Demand Abstracts Available for Viewing Starting Saturday Morning, November 21, 2020  
F-EN09

#### 5:00 AM \*F.EN09.05.01

##### **Novel Approaches for Electron Tomography to Investigate the Structure and Stability of Nanomaterials Under**

**Relevant Conditions** Sara Bals<sup>1,2</sup>, Wiebke Albrecht<sup>1,2</sup>, Hans Vanrompay<sup>1,2</sup>, Eva Bladt<sup>1,2</sup>, Alexander Skorikov<sup>1,2</sup>, Thomas Altantzis<sup>1,3</sup>, Jan Willem Buurlaeghe<sup>4</sup>, Daan Pelt<sup>4</sup>, Joost Batenburg<sup>5,4</sup> and Sandra Van Aert<sup>1,2</sup>; <sup>1</sup>EMAT-University of Antwerp, Belgium; <sup>2</sup>NANOLab Center of Excellence, University of Antwerp, Belgium; <sup>3</sup>ELCAT-University of Antwerp, Belgium; <sup>4</sup>CWI, Netherlands; <sup>5</sup>University of Leiden, Netherlands

Nanomaterials are important for a wide range of applications because of their unique properties, which are strongly connected to their three-dimensional (3D) structure. Electron tomography has therefore been used in an increasing number of studies. Most of these investigations resulted in 3D reconstructions with a resolution at the nanometer scale, but also atomic resolution was achieved in 3D.

In order to preserve the carefully designed morphologies and functionalities, understanding the stability of nanomaterials during application is crucial. It is hereby important to note that most electron tomography investigations have been performed at the conventional conditions of an electron microscope. An emerging challenge is therefore to fully understand the connection between the 3D structure and properties under more relevant conditions, including high temperatures as well as in the presence of liquids and gases. Therefore, innovative methodologies are required to track the fast 3D changes of nanomaterials that occur under such conditions.

Recently, we proposed an acquisition approach where a tilt series of 2D HAADF-STEM projection images is acquired within a few minutes. By continuously tilting the holder and simultaneously acquiring projection images while focusing and tracking the particle, we were able to reduce the total acquisition time for a tilt series by a factor of ten [1]. Moreover, a new

approach was developed to compute high quality 2D virtual slices through nanoparticles in approximately 60 ms time. This technique drastically improves the efficiency of 3D characterization of nanomaterials by TEM. It enables explorative imaging and provides valuable information to dynamically adjust the acquisition parameters during an electron tomography experiment [2].

In this manner, we were able to study the 3D morphological evolution of anisotropic Au and AuPd nanoparticles as a function of both heating time and temperature [1,3]. Moreover, we measured the elemental diffusion dynamics of individual anisotropic Au-Ag nanoparticles in 3D [4]. We conclude that for a given composition, the shape of the nanoparticle does not influence the alloying process significantly. Based on our analysis, it is clear that interdiffusion of metals at the nanoscale is more complex than predicted by simple Fickian diffusion and that other factors such as surface diffusion need to be taken into account.

To quantify nanoparticle shape dynamics in a gaseous environment in 3D, HAADF-STEM images served as an input for atom counting procedures followed by 3D relaxation of the structure. In this manner, we characterized shape changes of a Pt nanoparticle in a gaseous environment. The conditions have been varied from vacuum to a 1 bar H<sub>2</sub> flow, followed by a 1 bar O<sub>2</sub> environment. To investigate the behaviour during cycling, we repeated the experiment several times using the same particle. We clearly observe morphology changes and we were even able to quantify the occurrence of the different surface facets [5].

## References

[1] H. Vanrompay et al., *Nanoscale* **10** (2018), p. 22792

[2] H. Vanrompay et al., *Particle and Particle System Characterization* (2020) in press

[3] W. Albrecht et al., *ACS Nano* **13** (2019), p.6522

[4] A. Skorikov et al., *ACS Nano* **13** (2019), p.13421

[5] T. Altantzis et al., *Nano Letters* **19** (2019), p.477

[6] This work was supported by the European Research Council (Grant 815128 REALNANO to SB, Grant 770887 PICOMETRICS to SVA and Grant 797153 SOPMEN to WA, Grant 823717 ESTEEM3). The authors acknowledge financial support from the Research Foundation Flanders (FWO, Belgium) through project fundings, a postdoctoral grant to EB and a doctoral grant to HV.

## 5:15 AM F.EN09.05.02

**Lithium Plating Detection in Extremely Fast-Charged Lithium-Ion Batteries Using Simultaneous Neutron and X-Ray Imaging** Maha Yusuf<sup>1</sup>, Jacob M. LaManna<sup>2</sup>, Partha P. Paul<sup>3</sup>, Lambertus Hesselink<sup>1,1</sup>, Michael F. Toney<sup>3,4</sup> and Johanna Weker<sup>3</sup>; <sup>1</sup>Stanford University, United States; <sup>2</sup>National Institute of Standards and Technology, United States; <sup>3</sup>Stanford Synchrotron Radiation Light source, United States; <sup>4</sup>University of Colorado Boulder, United States

Lithium-ion batteries (LIBs) have profoundly advanced the development of electric vehicles (EVs). However, one of their remaining bottlenecks in the widespread deployment is the long charging time required for commercial LIBs. There is a global push towards extreme fast charging (XFC) to reduce charging times to 10-15 minutes.<sup>1</sup> But existing LIBs cannot achieve this goal without significantly reducing battery performance, mainly due to the loss of active lithium (Li). The lost Li either becomes “dead” from being electronically disconnected after plating on the anode or “inactive” because of the irreversible reaction of Li with the electrolyte to form a solid electrolyte interphase. Since Li plating is identified as one of the major degradation mechanisms from XFC in LIBs,<sup>2</sup> understanding its origin and characteristics is essential to developing designs to enable fast-charged batteries. Several studies have characterized Li plating using techniques such as cryo-electron microscopy, transmission electron microscopy, X-ray diffraction, and X-ray micro-computed tomography (CT) among others.<sup>3</sup> While valuable, these characterization techniques have limitations in terms of their sample preparation, spatial resolution, and imaging contrast required to distinguish between materials of similar atomic number (Z). In addition, due to the complex electrochemical reactions of Li plating, multiple methods for detecting Li metal and understanding the mechanistic details of Li plating are needed.

Here, we are using simultaneous neutron and X-ray-based dual-mode micro-computed tomography, a non-destructive imaging modality, to investigate the characteristics of Li plating during XFC in LIBs. Since X-rays and neutrons are sensitive to the electron and nuclear density of the material, respectively, dual-mode X-ray and neutron CT allows an easy segmentation of the different anode components such as Li, graphite, and pores. Higher energy X-rays are needed to get through the metallic components in batteries such as copper and aluminum. However, they do not have sufficient contrast to separate Li from graphite. Thus, neutrons are used due to their high sensitivity to lighter elements such as Li, especially <sup>6</sup>Li, and carbon.

We performed multi-modal imaging experiments at the Neutron and X-ray Tomography (NeXT)<sup>4</sup> system located on the BT-2 beamline at the National Institute of Standards and Technology Center for Neutron Research. We characterized pristine and cycled graphite anode strips containing plated lithium at different regions. For cycled anode strips, we disassembled the battery pouch cells and imaged the graphite anodes cycled under XFC conditions for 450 cycles at fully discharged condition. The spatial resolution achieved was ~10-15  $\mu\text{m}$ , thus providing sufficient resolution to pinpoint the location of Li plating within the anode thickness. With the dual-imaging datasets, we are now investigating a link between the spatial heterogeneity of Li plating and the local microstructure of the battery anode including porosity, tortuosity, and thickness. We want to investigate why and where Li plating occurs on the battery anode. Addressing these fundamental questions will inform improved battery designs, graphite anode architectures, and charging protocols that will reduce Li plating during XFC in LIBs.

#### References:

1. Liu, Y., Zhu, Y., & Cui, Y. (2019). Challenges and opportunities towards fast-charging battery materials. *Nature Energy*, 1.
2. Tomaszewska, A., Chu, Z., Feng, X., O'Kane, S., Liu, X., Chen, J., ... & Li, Y. (2019). Lithium-ion battery fast charging: A review. *eTransportation*, 1, 100011.
3. Liu, Qianqian, et al. "Understanding undesirable anode lithium plating issues in lithium-ion batteries." *RSC advances* 6.91 (2016): 88683-88700.
4. LaManna, J. M., Hussey, D. S., Baltic, E., & Jacobson, D. L. (2017). Neutron and X-ray Tomography (NeXT) system for simultaneous, dual modality tomography. *Review of Scientific Instruments*, 88(11), 113702.

#### 5:25 AM F.EN09.05.03

**Time Will Tell—Time-Dependent Material Characterization of Energy Devices** Robin White, Steve Kelly and William Harris; Carl Zeiss Microscopy, United States

Recent advances in laboratory-based X-ray microscopy (XRM) have led to the development of new opportunities for the visualization and characterization of a variety of energy materials. Through X-ray tomography, the process of reconstructing a volumetric data set from a series of 2D projection images, we can gain vital insight to the internal 3D structure of these types of materials over a range of relevant length scales spanning the millimeter to nanometer range. By combining 3D visualization through repeated identical location tomography scans at various temporal stages, powerful *in-situ* investigations of dynamic material properties can be obtained. This methodology is often termed as 4DCT (4-dimensional computed tomography) and is particularly well suited to study various dynamic and evolutionary processes in energy materials. The capability to incorporate a variety of *in situ* rigs within the flexible XRM architecture provides a multitude of possibilities for the direct observation of change in a sample's microstructure in response to a stimulus. This data can lead to improved understanding of material performance, degradation, or failure processes in a quantitative fashion. Recent advances and applications of XRM for energy materials will be presented, including *in situ* visualization of polymer electrolyte fuel cells and quantification of water distribution changes while monitoring cathode catalyst layer morphological changes, solid oxide fuel cells and temperature induced structural changes. Additional examples of imaging lithium ion batteries undergoing structural changes following charge cycles, combined with correlative post-mortem analysis are also discussed.

#### 5:35 AM F.EN09.05.04

**Cobalt Oxidation—An *In Situ* and *In Operando* Study by Atom Probe Tomography** Sten V. Lambeets<sup>1</sup>, Norbert Kruse<sup>2,1</sup> and Daniel Perea<sup>1</sup>; <sup>1</sup>Pacific Northwest National Laboratory, United States; <sup>2</sup>Washington State University, United States

Heterogeneous catalysis is a stone edge of chemical industry and "green chemistry". The sparse understanding of surface mechanisms at molecular scale impedes the development of new high-performance catalysts and requires the development of new tools and methodological approaches. Cobalt is capable to dissociate CO<sub>2</sub>, allowing further conversion to higher value compounds. Such mechanism will conduct to Co surface oxidation, which formation mechanism remains uncertain. In this work, we propose to investigate this process with Atom Probe Tomography and expose the Co to O<sub>2</sub>(g) by two different methods: one *in-situ* using an annex reactor chamber connected on APT; and one *in operando* by introducing O<sub>2</sub>(g) directly in APT analytic chamber during the ongoing analysis. After a cleaning process of the surface by field evaporation and surface imaging by FIM, the Co, shaped as a sharp needle, is transferred under UHV into a reactor chamber in which it is exposed to pure O<sub>2</sub>(g) at different temperatures and times. Oxidation is quenched on the APT cryogenic stage. Oxidation is revealed to be inhomogeneous and strongly influenced by surface structures. We detect local distribution of Co<sub>2</sub>O<sup>n+</sup> and CoO<sup>n+</sup> where

$\text{Co}_2\text{O}^{n+}$  is preferentially found deep in the Co volume, drawing the progression of the oxygen in the metal. *In operando* mode allows a real time direct observation of the surface oxidation. Surface composition is probed by applying periodic electric pulses, resulting into a virtual “reconstruction” representing a stack of the different surface composition states over time. As oxidation rate progressively increases while  $\text{P}(\text{O}_2)$  increases, starting from pure Co surface to successively an early and an advanced oxidation stage with  $\text{Co}_2\text{O}$  and  $\text{CoO}$  species. Inspired by the principles of the 1-D Atom Probe developed by Kruse *et al.*<sup>1</sup>, the influence of the electric potential, the pulses frequencies and how to study surface kinetics with an *in-operando* Atom Probe will be discussed.

<sup>1</sup>Kruse N., Abend G. and Block J.H., The kinetics of adsorption and thermal desorption of NO on stepped Pt single crystal surfaces, Journal of chemical Physics 88 (1987) 1307-1312

#### 5:45 AM F.EN09.05.06

**Late News: Operando Visualization of Thermal and Ion Transport Behaviors in Electrolytes During Electrochemical Device Operation Using Phase-Contrast X-Ray Imaging** Daiko Takamatsu, Akio Yoneyama, Shin Yabuuchi and Jyun Hayakawa; Hitachi, Ltd., Japan

A fundamental understanding of transport properties (e.g., ion transport, thermal transport, etc.) in electrolytes during battery operation is important for optimal operation and design of batteries especially for high-power applications such as vehicles. It is known that internal resistance of the lithium-ion batteries (LIBs) temporarily rises by repeating high-rate charge/discharge cycles and that it decreases by stopping the battery operation and rest. Because such a reversible resistance rise occurs only during the battery operation, this phenomenon is speculated to be related to the ion concentration distributions in the electrolyte. Such ion concentration distributions in the electrolyte have more serious effect on the performance of lead-acid batteries (LABs). The development of a vertical ion concentration gradient of sulfuric acid is called electrolyte stratification, which causes inhomogeneous current distribution in the vertical distribution of the electrodes by frequent charging-discharging, reducing the life of LABs. However, there are few techniques that can be used to quantitatively characterize ion concentration distribution that arise in electrolytes during the battery operation.

Phase-contrast X-ray imaging is a technique that can be used to visualize density differences by detecting the X-ray phase shift caused by an X-ray passing through a sample. The sensitivity of the phase-contrast X-ray imaging is about 1000 times higher than that of conventional X-ray absorption imaging in a hard X-ray region for light elements. Since the electrolytes of batteries are also composed of light elements, the phase-contrast X-ray imaging is expected to be effective in visualizing small density differences in an electrolyte during battery operation. We demonstrated that in situ phase-contrast X-ray imaging technique can quantitatively visualize ion concentration distributions that arise in electrolytes during battery operation (cf. LIBs [1], LABs [2]).

Another crucial concern about batteries used in high-power applications is the thermal management. It is known that temperature of the batteries temporarily rises by repeating high-rate charge/discharge cycles and such a temperature distribution causes inhomogeneous reaction distribution of batteries. Although there are several conventional temperature measurement methods, such as thermistors, resistive temperature detectors, thermocouples, infrared thermography, etc., these methods detect the temperature directory through physical contact or using infrared and visible light from the object, and therefore, the detectable depth is limited to a few mm from its surface. So, its inner temperature distribution cannot be measured in principle. We have successfully demonstrated that nondestructive observations of inner temperature and thermal flow in heated water by using phase-contrast X-ray imaging [3]. Recently, thermo-electrochemical cells (TECs), which generate electricity directly from low-grade heat, have attracted attention for the need to power sources of Internet-of-things (IoT) sensors. We have also performed operando visualization of ion and thermal transport behavior in electrolytes of TECs by phase-contrast X-ray imaging and succeeded in visualizing the convection generation behavior caused by the temperature gradient and ion gradient occurring in the electrolyte in real time.

In this presentation, we will show the quantitative evaluation of ion concentration distribution and thermal distribution (inner temperature gradient) in the electrolyte simultaneously during electrochemical device operation with high temporal (a few seconds) and spatial (a few microns) resolutions.

References: [1] J. Am. Chem. Soc., 140, 1608 (2018). [2] Chem. Commun., 56, 9553 (2020). [3] Sci. Rep., 8, 12674 (2018).

SESSION F.EN09.06: Synergy from Combining Methods

On Demand Abstracts Available for Viewing Starting Saturday Morning, November 21, 2020

F-EN09

#### 5:00 AM \*F.EN09.06.01

##### **Advance Characterization Tools to Study and Develop Stable Anionic Redox for High-Energy Rechargeable Batteries** Minghao Zhang and Y. Shirley Meng; University of California, San Diego, United States

There is a growing consensus that the theoretical limit of one electron intercalation reactions will soon be reached. Recent discoveries on anion redox electrochemistry offer new opportunities and a possible paradigm shift in energy storage. By activating anion (e.g. oxygen, sulfur) for reversible electrochemical reactions, increased energy density has been demonstrated. In the past decade, the research community has made great progress on understanding key features of the anionic electrochemical activities and dynamic phenomena that govern the performance limitations including cycling voltage hysteresis and decay. However, the exact mechanism at molecular/atomic scales is still largely under-debate. The lack of conscience on the anionic redox mechanism which can be fueled by possible misinterpretation of experimental results. Of particular importance is determining what techniques provide accurate and reliable evidence for reversible bulk oxygen redox.

Compared with transition metal cations, oxygen anions are more challenging to be probed and quantified, which requires a multi-modal experimental approach with exceptional energy and spatial resolution combining computational modelling. Here, we advance: 1) from X-ray absorption spectroscopy to resonant inelastic X-ray scattering which shows a sharp feature with the corresponding excitation energy at 531 eV corresponding to the extra unoccupied electron orbitals of oxidized oxygen; 2) from neutron diffraction to neutron pair distribution function which is enormously valuable as a local probe that can reveal local distortions, when present along the oxygen redox reactions; 3) from X-ray diffraction to Bragg coherent diffraction imaging which will enable the direct observation of the strain dynamics with the exceptional sensitivity as small as 0.05% and phase evolution induced by the oxygen redox activity at nanoscale. It is through the in-depth understanding of electrochemical reactions mechanism at microscopic and macroscopic level during the operation of batteries; we can successfully formulate strategies to achieve reversible and stable anionic redox for next generation lithium-ion batteries.

#### 5:15 AM F.EN09.06.02

##### **Investigating Solid-State Synthesis Reactions by *In Situ* Synchrotron X-Ray Diffraction and *Ab***

***Initio* Thermodynamics** Matteo Bianchini<sup>1,2</sup>, Jingyang Wang<sup>3</sup>, Raphael J. Clement<sup>4,3</sup>, Bin Ouyang<sup>5</sup>, Pascal Hartmann<sup>1</sup>, Torsten Brezesinski<sup>2</sup>, Jürgen Janek<sup>2,6</sup>, Wenhao Sun<sup>5,7</sup> and Gerbrand Ceder<sup>5,3</sup>; <sup>1</sup>BASF SE, Germany; <sup>2</sup>Karlsruhe Institute of Technology, Germany; <sup>3</sup>University of California, Berkeley, United States; <sup>4</sup>University of California, Santa Barbara, United States; <sup>5</sup>Lawrence Berkeley National Laboratory, United States; <sup>6</sup>Justus-Liebig-Universität Giessen, Germany; <sup>7</sup>University of Michigan, United States

In the synthesis of inorganic materials, reactions often yield non-equilibrium kinetic byproducts instead of the thermodynamic equilibrium phase [1]. Why is that? And why, on the other hand, compounds predicted as thermodynamically stable often cannot be synthesized experimentally? Understanding the competition between thermodynamics and kinetics is fundamental for answering these question and towards the rational synthesis of target materials [2]. In this presentation, we will highlight the use of in situ synchrotron x-ray diffraction to yield insights on the real time behavior of powder precursors during synthesis. We investigate the multistage crystallization pathways of the important two-layer (P2) sodium oxides  $\text{Na}_{0.67}\text{MO}_2$  (M = Co, Mn) [3]. We find a series of fast non-equilibrium phase transformations through metastable three-layer O3, O3' or P3 phases, before formation of the equilibrium two-layer P2 polymorph. A theoretical framework to rationalize the observed phase progression will be presented, demonstrating that even though P2 is the equilibrium phase that we target, the first phase to form will be the one with the most negative compositionally-unconstrained reaction energy from the powder precursors. In other words, the first phase to form is guided by thermodynamics and it does not necessarily have the composition corresponding to the overall precursor composition in the reaction vessel. Afterwards, the first phase may develop according to kinetic or thermodynamic arguments, depending on the system of choice. Further examples will be presented for industrially-relevant  $\text{LiNiO}_2$  and related compounds [4], where lithiation pathways can be instead more straightforward than sodiation ones; nonetheless, the high resolution of synchrotron XRD allows to observe detailed structural information revealing a complex behavior where metal vacancies play an important role. The insights we present constitutes a step forward towards unraveling the complex interplay between thermodynamics and kinetics during synthesis. Moreover, they can guide the choice of precursors and parameters towards the optimization of the solid-state synthesis of ceramic materials.

#### References:

- [1] M. Aykol et al., *Science Advances*, **2018**, 4(4), 148.
- [2] Z. Jiang et al., *Journal of Materials Chemistry C*, **2017**, 5(23), 5709-5717.
- [3] M. Bianchini, J. Wang et al., *Nature Materials*. **2020**, <https://doi.org/10.1038/s41563-020-0688-6>.
- [4] M. Bianchini et al., *Journal of Materials Chemistry A*, **2020**, 8(4), 1808-1820.

5:25 AM F.EN09.06.03

**Correlative *Operando* Structural, Chemical and Electrochemical Microscopy of Oxygen Evolving Electrocatalysts** J.T. Mefford; Stanford University, United States

The properties of emerging non-precious metal oxide electrocatalysts for the alkaline oxygen evolution reaction (OER,  $4\text{OH}^- \rightarrow \text{O}_2 + 2\text{H}_2\text{O} + 4\text{e}^-$ ) evolve dynamically with voltage during operation. While it is appreciated that the voltage-dependent behavior of the electrode may convert an inactive material into an active electrocatalyst or *vice versa* through bulk and surface ion-coupled electron transfer, the chemical and structural identity of the electrode in its active state cannot be directly extracted from the electrochemical data alone. Importantly, the active state of the electrocatalyst is generally a non-equilibrium state that can only be obtained at the voltages necessary to drive the OER. Thus, the accurate understanding of how material properties govern the kinetics of electron and ion transfer during the OER requires integrating electrochemical cells into advanced characterization methods to study reactivity during operation. Further, the sub-particle spatial heterogeneity of electrocatalysts during operation requires that these *operando* methods resolve the local chemical, physical, and electronic structure at the nanoscale and link these properties to the local electrochemical activity.

This talk will describe a suite of correlative *operando* microscopy techniques developed to study the OER on faceted Co (oxy)hydroxide nanoplatelets. Using *operando* Scanning X-Ray Transmission Microscopy (STXM) and Electrochemical Atomic Force Microscopy (EC-AFM), the local Co oxidation state and particle morphology are mapped across voltages spanning the bulk ion insertion reactions and OER regimes. These results are correlated to local electrochemical activity maps obtained through Scanning Electrochemical Cell Microscopy (SECCM) providing insight into where and why oxygen is evolved on the Co (oxy)hydroxide platelets. Combined with ensemble averaged bulk techniques including *operando* X-ray diffraction (XRD), UV-Vis spectroelectrochemistry, and Electrochemical Quartz Crystal Microbalance (EQCM), we provide a comprehensive description of the chemistry of an operating OER electrocatalyst. These experimental material properties and local reactivity measurements are integrated into a computational model that combines first principles thermodynamic adsorption energetics of OER surface intermediates and microkinetic modeling to derive the experimental electrochemical Tafel behavior. The results from our multi-modal correlative approach alter long standing assumptions about the OER-active properties of the Co (oxy)hydroxide system and provide an improved methodology towards developing predictive electrocatalytic theories based on material properties that govern reactivity away from open circuit conditions.

5:35 AM \*F.EN09.06.04

***Operando* Characterization of Electrochemical Insertion into Hydrated and Solvated Metal Oxides** Veronica Augustyn; North Carolina State University, United States

Layered transition metal oxides that incorporate water or other solvents provide fundamental understanding of the effects of confinement on electrochemical ion transport and reactivity. They also tend to exhibit fast electrochemical ion insertion kinetics making them of interest for high power electrochemical energy storage. These materials are hybrids that consist of transition metal oxide layers separated by fluids that can be either ordered or disordered, and strongly or weakly bound to the oxide. Our group has investigated ion insertion into a range of hydrated and solvated metal oxides with *operando* characterization to connect structural changes to the electrochemical response. Since many of these materials exhibit fast kinetics (full charge/discharge in minutes), *operando* characterization techniques must have suitable temporal resolution to capture structural or chemical changes at these rates. This presentation will describe our use of three types of *operando* techniques to probe insertion kinetics at minute-to-second timescales: X-ray diffraction, atomic force microscopy, and electrochemical quartz crystal microbalance. It will also discuss how knowledge of the dynamics of ion insertion in these materials help us understand ion transport under confinement.

5:50 AM F.EN09.06.05

**Late News: *Operando* Characterization of Low Temperature Surface Oxygenated Multicomponent Oxidation Catalysts** Shiyao Shan<sup>1</sup>, Shan Wang<sup>1</sup>, Jing Li<sup>1</sup>, Dominic Caracciolo<sup>1</sup>, Casey O'Brien<sup>2</sup>, Dat Tran<sup>2</sup>, Valeri Petkov<sup>3</sup>, Jin Luo<sup>1</sup> and Chuan-Jian Zhong<sup>1</sup>; <sup>1</sup>State University of New York at Binghamton, United States; <sup>2</sup>U.S. Army Research Laboratory, United States; <sup>3</sup>Central Michigan University, United States

Catalytic oxidation of air pollutants plays a major role in sustainable energy and environment fronts, e.g., fuel reforming and elimination of atmosphere emission exhaust. Recent interests in low temperature catalytic conversion of air pollutants are largely driven by increasingly-stringent environmental regulations. Understanding how surface atomic-scale active sites are created and stabilized on supported nanoalloy catalysts under reaction conditions is crucial for the understanding of catalytic

activity and stability which requires probing the dynamic structures in real time. However, little has been understood about the role of metal components in surface oxygenated highly active sites creation and stabilization in hydrocarbon and carbon monoxide oxidation. In this work, we will focus on recent findings in the investigation of oxygenated Pt (and/or Pd, Au) alloyed bi-/trimetallic catalysts for low temperature carbon monoxide and propane oxidation. The analysis of operando results on catalytic synergy from *in-situ/operando* characterization technique combining Diffuse Reflectance Infrared Fourier Transform Spectroscopy (DRIFTS), Synchrotron High-Energy X-ray Diffraction coupled with Pair Distribution Function analysis (HE-XRD/PDFs) and online mass spectrometer will be discussed. The results reveal largely-irregular oscillatory kinetics associated with the dynamic lattice expansion/shrinking, ordering/disordering, and formation of surface-oxygenated sites and intermediates. This work reveals new insights on catalyst design strategies into the catalytic reaction pathways and the structure-composition-activity correlation.

#### 6:00 AM F.EN09.06.06

**Late News: An *In Situ* Testing Platform for the Multi-Dimensional Diagnostic of Solid-State Li Batteries** Zheng Fan; University of Houston, United States

Global demand for high-performance energy storage systems has grown tremendously in recent years. The all-solid-state lithium-ion batteries (ASSLIBs) are promising for such storage solutions on account of the lithium metal anodes with high areal capacity and the solid-state electrolytes (SSEs) with critical safety.<sup>1</sup> However, the interfacial failure of the ASSLIBs poses a major hurdle towards the implementation of practical high-performance energy storage devices.<sup>2,3,4</sup> Time-resolved *in operando* techniques (*e.g.*, *in situ* microscopy, synchrotron X-ray tomography) are ideal for the direct and quantitative characterization of the interfacial deteriorations. However, the *in situ* analysis of solid-state batteries is still in its primary stage due to the difficulties in probing the buried interfacial layer. The specific causes of the high interfacial impedance and the lithium dendrite growth that deteriorates the battery in a few cycles remain nebulous.

To this end, we developed a multi-dimensional diagnostic platform that allows the direct probe of the chemical and spatial distribution on the interface while the cell operates. Parameters such as pressure and temperature, which have a strong influence on cell behavior, are also enabled by the platform. Moreover, the platform can be air-free transferred between analytical instruments like SEM, ToF-SIMS, and Raman, for a synergistic diagnose of the structural and chemical evolutions in the interfaces. A deeper understanding of interfaces and dendrites evolutions can be acquired by the testing platform, including (1) correlation between void formation and electrolyte decomposition, and (2) creeping mechanical properties of the lithium metal during the cell operations. These in-depth understandings will allow us to effectively optimize and enable further enhancements of solid-state Li batteries.

#### References

- [1] T. Famprikis and C Masquelier et al, Nat. Mater. 18, (2019) 1278-1291
- [2] K Park and J Goodenough et al, Chem. Mater. 28, (2016) 8051-8059
- [3] S Wang and A Manthiram et al, J. Am. Chem. Soc. 140 (2018) 250-257
- [4] Y Tian and G Ceder et al, Energy Environ. Sci. 10 (2017) 1150-1166

#### SESSION F.EN09.07: Dynamics and Kinetics

On Demand Abstracts Available for Viewing Starting Saturday Morning, November 21, 2020

F-EN09

#### 5:00 AM \*F.EN09.07.01

**Understanding Kinetic Limitations and Oxygen-Redox in Lithium Layered Transition-Metal Oxide Electrodes Through *Operando* X-Ray Scattering** Karena Chapman; Stony Brook University, United States

Chemical substitution of transition metal species is often used to tune the performance and cost of electrode materials. However, substitutions that improve one performance metric can be coupled to unintended consequences. This presentation will show how we have used operando X-ray scattering to understand kinetic limitations and O-redox in Li-layered transition metal oxide electrodes.

Substituted Li layered transition metal oxide (LTMO) electrodes such as  $\text{Li}_x\text{Ni}_y\text{Mn}_z\text{Co}_{1-y-z}\text{O}_2$  (NMC) and  $\text{Li}_x\text{Ni}_y\text{Co}_{1-y-z}\text{Al}_z\text{O}_2$  (NCA) show reduced first cycle Coulombic efficiency (90-87 % in standard cycling conditions) compared with archetypal  $\text{Li}_x\text{CoO}_2$  (LCO – ~98 % efficiency). We use operando x-ray diffraction (XRD) to demonstrate that the apparent



first cycle capacity loss is a kinetic effect linked to limited Li mobility at  $x > 0.85$ , with near full capacity recovered and slow Li reinsertion during a potentiostatic hold following the galvanostatic charge–discharge cycle. The kinetic limitation manifests not only as the kinetic capacity loss during discharge, but as a subtle bimodal compositional distribution early in charge and, also, a dramatic increase of the charge–discharge voltage hysteresis at  $x > 0.85$ .

#### 5:15 AM F.EN09.07.02

##### **Electrochromism as an *In Operando* Tool to Deconvolute Dynamic Charging Processes in Nanocrystal Li-Ion**

**Electrodes** Clayton J. Dahlgren<sup>1,2</sup>, Sungyeon Heo<sup>3,2</sup>, Youtian Zhang<sup>4</sup>, Lauren Reimnitz<sup>2</sup>, Daniel He<sup>2</sup>, Ming Tang<sup>4</sup> and Delia Milliron<sup>2</sup>; <sup>1</sup>University of California, Santa Barbara, United States; <sup>2</sup>The University of Texas at Austin, United States; <sup>3</sup>Princeton University, United States; <sup>4</sup>Rice University, United States

Li-ion insertion electrodes store and release charge through an assortment of reversible interactions, including surface capacitance, single-phase Li insertion and two-phase transformations. Several *in situ* and *in operando* characterization tools have been developed to deconvolute and quantify these processes to engineer better batteries. However, it is very difficult to resolve how batteries charge *in operando* at the time and length scales relevant to these processes simultaneously. Color is a simple, yet often overlooked, indicator of the convoluted processes that occur in electrodes. Indeed, electrochromism is commonly observed in many ion-insertion electrodes (e.g. graphite,  $\text{Li}_x\text{Ti}_5\text{O}_{12}$ ,  $\text{Li}_x\text{FePO}_4$  and  $\text{Li}_x\text{CoO}_2$ ). Transitions due to the band-gap (UV-visible), local defects (visible), electronic oscillations (near-IR) cause distinct features, which can be used to deconvolute charging processes. Coupled with electrochemistry, these measurements reveal rate-limiting processes and track the state-of-charge of independent charging transformations.

In this talk, we demonstrate how optical characterization of nanostructured  $\text{TiO}_2$  thin-film electrodes deconvolutes dynamic charging processes and reveals rate-limiting steps during (de)lithiation. Anatase  $\text{TiO}_2$  nanocrystal films, synthesized with nm-scale control of size and shape, are studied as a reliable model Li-ion anode that undergoes a distinct phase transformation between low- and high-Li content states. Using optical measurements during charge titration experiments, coupled with phase-field models of individual particles, we find that particle size systematically tunes the two-phase transformation potentials of nanocrystalline  $\text{TiO}_2$ . We demonstrate how the distribution of critical transformation potentials in an ensemble of particles changes non-equilibrium charging rates. These measurements yield an unexpected relationship between the initial state-of-charge and charging rates across a range of different nanocrystal particle morphologies. We conclude that neither Li diffusion nor phase propagation kinetics limit charging rates in this system. Rather, kinetics are limited by slow accumulation of Li in the particle ensemble *prior* to distinct crystalline transformations. More broadly, these results indicate a path forward to deconvolute non-equilibrium charging behavior in nanostructured systems through a combination of precise colloidal synthesis, first-principles modeling, and *in operando* resolution of dynamic processes with optical spectroscopy.

#### 5:25 AM F.EN09.07.03

**The Effect of Mechanical Strain on Lithium Staging in Graphene** Joshua Pondick<sup>1,2</sup>, Sajad Yazdani<sup>1,2</sup>, Milad Yarali<sup>1,2</sup>, Serrae N. Reed<sup>1,2</sup>, David Hynek<sup>1,2</sup> and Judy Cha<sup>1,2</sup>; <sup>1</sup>Yale University, United States; <sup>2</sup>Yale West Campus, United States

The development of next-generation electrodes for metal-ion batteries requires an understanding of intercalation dynamics in nanomaterials. Lithium intercalation into graphite is the foundation for the lithium-ion battery, and the thermodynamics of the lithiation of graphitic electrodes have been heavily investigated. Intercalated lithium undergoes structural ordering known as staging. Initially, lithium atoms are randomly distributed throughout the gaps between carbon sheets (Dilute Stage I), but increasing lithium concentration triggers a phase transition to ordered structures comprised of intercalated regions vertically separated by unintercalated regions. Lithium typically initiates staging by forming a Stage IV structure in graphite at a concentration around  $\text{LiC}_{24}$ , where the staging index indicates the number of graphene layers between the intercalant layers. This process is well-understood for bulk graphite; however, confinement effects become important at the nanoscale, which can significantly impact the electrochemistry of nanostructured electrodes.

Here, we show that small mechanical strain in graphene microflakes can significantly modulate the thermodynamics of lithium staging. We performed electrochemical lithium intercalation on nanodevices with mechanically exfoliated graphene microflakes and monitored the staging of intercalated lithium *in situ*. *In situ* Raman spectroscopy of graphene microflakes mechanically constrained at the edge during lithium intercalation reveals a thickness-dependent increase of up to 1.26 V in the electrochemical potential that induces lithium staging, marking a clear departure from the bulk behavior. Thus, we show that microscale mechanical strain significantly affects the formation of ordered lithium phases in graphene. While the induced mechanical strain energy increases with graphene thickness to the fourth power, its magnitude is small compared to the observed increase in electrochemical energy. We hypothesize that the mechanical strain increases a nucleation barrier for lithium staging, greatly delaying the formation of ordered lithium phases.

Our results suggest that electrode assembly can critically impact lithium staging dynamics important for cycling rates and

power generation for batteries. The observed effects of strain reach beyond energy storage. Strain engineering has been used to modify the local electronic band structure of two-dimensional (2D) nanomaterials for optoelectronics and catalysis, and our results indicate that strain can also be used to modulate the intercalation-induced phase transitions of 2D materials.

#### 5:35 AM F.EN09.07.04

***In Situ* Characterization of Single-Crystalline Oxide Materials During Electrocatalysis** Andrew Akbashev; Paul Scherrer Institut, Switzerland

*In situ* studies of model systems have always been central to fundamental electrochemistry as they provide precise potential-dependent quantities that can be used to assess theoretical models. In both fields of energy sciences and electrochemistry, structural evolution of electrocatalysts exposed to harsh oxidizing environment and the associated (electro)chemical pathways have remained rather mysterious. To gain the necessary insight, one has to employ not only a combination of advanced *in situ* characterization techniques, but also well-defined materials that can be directly modelled.

For example, some complex oxides demonstrated a high activity toward electrochemical water oxidation, and yet they are rarely used in precise *in situ* surface studies due to the difficulty in their controlled synthesis. The progress in the growth of epitaxial oxide films and superlattices (the area primarily being the realms of condensed matter physicists) has enabled us with a perfect tool to address some of the most pressing questions in the field of oxide electrocatalysis. A perfect control over the quality and composition of epitaxial films provides specimens that are ideally suited for precise *in situ* experiments. In this talk, I will discuss how model systems such as epitaxial films can be used for real-time observations of materials' evolution during electrocatalytic water splitting.

#### SESSION F.EN09.08: Operando Methods for Batteries

On Demand Abstracts Available for Viewing Starting Saturday Morning, November 21, 2020  
F-EN09

#### 5:00 AM F.EN09.08.02

**Quantification of Local and Global Degradation Mechanisms During Extreme Fast Charging in Lithium-Ion Batteries** Partha P. Paul<sup>1</sup>, Vivek Thampy<sup>1</sup>, Chuntian Cao<sup>1</sup>, Hans-Georg Steinrueck<sup>1,2</sup>, Andrew Jansen<sup>3</sup>, Alison Dunlop<sup>3</sup>, Tanvir Tanim<sup>4</sup>, Johanna Weker<sup>1</sup> and Michael F. Toney<sup>1</sup>; <sup>1</sup>Stanford Synchrotron Radiation Lightsource, United States; <sup>2</sup>Universität Paderborn, Germany; <sup>3</sup>Argonne National Laboratory, United States; <sup>4</sup>Idaho National Laboratory, United States

With the increasing demand for electric vehicles, there is an urgent need for Li-ion batteries (LIBs) with extreme fast charging (XFC) capabilities [1]. The need arises from making recharging times for commercial electric vehicles comparable to traditional refueling times. However, such XFC rates are associated with a drastic decrease in performance, as well as safety hazards. Current literature suggests that parasitic Li plating on the anode is the major factor contributing to decreasing battery capacity and therefore shortened battery life in LIBs [2]. Techniques used for understanding Li plating under *in situ* conditions have primarily involved two approaches. The first involves taking global measurements, averaged over the entire cell, to quantify the losses associated with lithium plating [3]. While such studies provide a good starting point, the lithium plating process is also known to be spatially heterogeneous across the cell. Therefore, other approaches probe the spatially heterogeneous nature of lithium plating across the cell, often using imaging based methods [1, 4]. There is a need to tie the two length scales together, in order to obtain a comprehensive picture of the origins and properties of lithium plating across the cell. In this work, high-energy X-ray diffraction (XRD) is presented as such a method, to bridge the two length scales. Firstly, XRD provides a way to quantify the amount of Li plating, as well as other loss mechanisms, and tie them to the global cell performance after XFC cycling. Second, XRD is an *in-situ* technique, allowing to characterize the entire battery in the fully assembled condition. Thus, local heterogeneities in the cathode and anode can be studied and correlated to heterogeneities in Li plating.

In this work, single layer pouch cells (3.5cm x 4cm, 3 mAh/cm<sup>2</sup>) with a porous graphite anode, NMC (LiNi<sub>x</sub>Mn<sub>y</sub>Co<sub>2</sub>O<sub>2</sub>) cathode and EC:MC (with LiPF<sub>6</sub> additive) electrolyte were charged at different rates within the XFC regime (4C-9C, 10-15 minutes charge) and characterized using *in-situ* XRD. The cells are all characterized after hundreds of cycles, in the fully discharged condition. At the local level, the characteristics of plated lithium crystallites such as the preferred crystallographic orientations and size of plated Li on graphite are revealed. Additionally, the regions with local lithium plating are correlated

with the local SOC (lithium occupancy) and loss of active surface area in the cathode and anode, in the discharged state. Finally, the capacity fade of the cycled cells is correlated to the amount of dead Li, with separated contributions from irreversibly plated Li, Li trapped in graphite as  $\text{Li}_x\text{C}$  (which cannot be reversibly extracted from the anode) and reaction of plated Li with the electrolyte. Based on this knowledge of the properties of lithium plating and the conditions that favor it, as well as its effect on overall battery performance, new approaches towards designing batteries can be realized, such that irreversible Li plating is minimized. This step will in turn help to guide the rational design of the next generation of XFC capable LIBs with a consistent and safe performance.

#### References:

- [1] T. R. Tanim, et al. Extreme fast charge challenges for lithium-ion battery: Variability and positive electrode issues. *Journal of The Electrochemical Society*, 166(10):A1926–A1938, 2019.
- [2] A. Tomaszewska, et al. Lithium-ion battery fast charging: A review. *eTransportation*, 1:100011, 2019.
- [3] L. Gold, et al. "Probing lithium-ion batteries' state-of-charge using ultrasonic transmission – Concept and laboratory testing," *Journal of Power Sources*, vol. 343, pp. 536-544, 2017.
- [4] F. Shi, et al. Strong texturing of lithium metal in batteries. *Proceedings of the National Academy of Sciences*, 114(46):12138–12143, 2017.

#### 5:10 AM F.EN09.08.03

**Understanding the Electrode-Electrolyte Interface of Polyethylene Oxide-Based Electrolyte for Lithium Secondary Batteries Using *Operando* Infrared Spectroscopy** Koki Yamada, Riho Matsuoka, Ryansu Sai, Yu Katayama and Hiromori Tsutsumi; Yamaguchi University, Japan

(Electro)chemical reaction at the electrode-electrolyte interface dramatically affects the performance of lithium secondary batteries, including cycle life and capacity<sup>1</sup>. Much effort has been made to reveal the (electro)chemical reaction at the electrode-electrolyte interface by using *operando* measurements, e.g., *operando* attenuated total reflection infrared (ATR-IR) spectroscopy, which successfully probes the surface reaction in liquid electrolyte<sup>2</sup>. Although solid polymer electrolyte (SPE) is considered as a next-generation electrolyte with flame retardancy and high mechanical stability<sup>3</sup>, its (electro)chemical reaction at the electrode-electrolyte interface is not well understood.

Here, we employed *operando* ATR-IR and various electrochemical measurements, including electrochemical impedance spectroscopy (EIS) and linear sweep voltammetry (LSV), to understand the surface reaction on model electrode surface in the SPE system. We selected the most widely used polymer electrolyte, polyethylene oxide (PEO)-based electrolyte with LiTFSAl<sup>4</sup>, as a target material. Cu nanofilm was used as a model electrode to achieve good S/N and avoid the undesirable reaction.

Linear sweep voltammetry (LSV) showed a small reduction current at *ca.* 2.0 V<sub>Li</sub> and *ca.* 1.0 V<sub>Li</sub>, which suggested the growth of the solid-electrolyte interphase (SEI) layer on the Cu electrode. The assignment was further supported by the EIS spectra, where we observed the increase in low-frequency semicircle during LSV, indicating the change in the charge transfer and SEI resistance. *Operando* ATR-IR spectra, obtained simultaneously with LSV, showed the voltage-dependent peaks at *ca.* 1000 cm<sup>-1</sup> and *ca.* 1200 cm<sup>-1</sup> along with the small reduction current, which corresponds to the vibration signals from SEI components. In this talk, we will discuss the formation mechanisms of the SEI and surface (electro)chemical reaction in the SPE system, based on the detailed analysis of *operando* ATR-IR spectra. Our findings will highlight the importance of the electrode-electrolyte interface in the SPE system, which enables the design of polymer electrolytes with superior cyclability and ion conductivity.

#### [Reference ]

1. An, S. J. *et al. Carbon N. Y.* **105**, 52–76 (2016).
2. Zhang, Y. *et al. Energy Environ. Sci.* **13**, 183–199 (2020).
3. Murata, K., Izuchi, S. & Yoshihisa, Y. *Electrochim. Acta* **45**, 1501–1508 (2000).
4. Mindemark, J., Lacey, M. J., Bowden, T. & Brandell, D. *Prog. Polym. Sci.* **81**, 114–143 (2018).

#### 5:20 AM F.EN09.08.04

**Using *In Situ* Neutron Reflectometry to Study Solid-Electrolyte Interphase Formation in aSi Anode Materials** Jim Browning<sup>1</sup>, Mathieu Doucet<sup>1</sup>, Gabriel Veith<sup>1</sup> and Katie Browning<sup>2</sup>; <sup>1</sup>Oak Ridge National Laboratory, United States; <sup>2</sup>Vanderbilt University, United States

A battery is comprised of a large number of interfaces, each of which are subject to reactions. The most important of these reactions being that occurring between the electrode and electrolyte – the so called solid-electrolyte interphase (SEI). Understanding the underlying mechanism that promotes the formation and dynamics of the SEI on battery electrode surfaces

is central to the development of better performing lithium-ion batteries. Neutron reflectometry (NR) is ideal for studying interfacial processes in battery materials, *in situ*. We have used NR to study SEI formation and growth on amorphous silicon (aSi) anodes. Silicon electrodes are of interest to battery researchers due to their large theoretical capacity ( $\text{Li}_{15}\text{Si}_4 - 3579 \text{ mAh g}^{-1}$ ) and low potential versus Li ( $< 0.4 \text{ V}$ ). In our work we have focused on investigating the amorphous silicon electrode surface with a standard battery electrolyte (1.2M  $\text{LiPF}_6$ -3:7 wt% ethylene carbonate (EC):dimethyl carbonate (DMC)). Combining NR with various *ex situ* complementary techniques we have determined the chemical reactivity of an aSi anode with electrolyte, the formation and growth of the SEI as a function of charge state, the formation and growth of the SEI with electrolyte additive as a function charge state and the role of binder material on SEI formation.

#### 5:30 AM F.EN09.08.05

**Insights into Ionic Fluxes at Electrode/Electrolyte Interface in Carbon-Based Electrochemical Capacitors with SPECS Technique and Electrochemical Dilatometry** Przemyslaw Galek<sup>1</sup>, Jakub Menzel<sup>1</sup>, Paulina Bujewska<sup>1</sup>, Scott Wilfred Donne<sup>2</sup> and Krzysztof Fic<sup>1</sup>; <sup>1</sup>Institute of Chemistry and Technical Electrochemistry, Poznan University of Technology, Poland; <sup>2</sup>University of Newcastle, Australia

It is often said that the highly developed surface area of electrode materials based on activated carbons (AC) ensures high capacitance, power and energy especially in electrochemical capacitors (EC). However, the real 'efficiency' of the surface exploited in charge storage remains often unknown. The unexploited potential of a highly developed AC surface comes often from a limited packing of electrolyte ions in carbon micropores, namely - relatively poor matching between pore and ion size. Only several techniques for effective specific surface area involvement in charge accumulation have been proposed recently. It turned out that the Step Potential Electrochemical Spectroscopy (SPECS) technique can be a useful tool for determining the real electrode/electrolyte interface surface during the operation of the device.

The SPECS technique allows for the comprehensive analysis of the total current output and evaluation of the capacitive, redox and other components. Together with the physicochemical data from nitrogen and  $\text{CO}_2$  adsorption techniques, we aim at the determination of the real surface area of AC used for charge accumulation in EC. SPECS measurements have been done in Swagelok<sup>®</sup> system equipped with reference electrode. Organic electrolyte 1-Ethyl-3-methylimidazolium bis(trifluoromethylsulfonyl)imide ( $\text{EMIM}^+\text{TFSI}^-$ ) was used as an electrolytic medium. The basis for choosing such an electrolyte was very small difference between cation and anion dimensions. The results will be supported by the recent findings from electrochemical dilatometry experiments. The tested materials include popular Kuraray YP-50F and Cabot BP-2000 with significant differences in pore distribution and structure.

Based on the knowledge gained to date, we assume that the efficiency of the interface 'exploitation' depends on many factors: pore size distribution, wettability of the electrode material by electrolyte, as well as the size of the ions. Thus, inappropriate selection of one of these parameters can aggravate the device performance, even if the excellent carbon material is applied as electrode component. The paper will provide the results from SPECS correlated with the physicochemical properties of carbon materials. It appears that the electrochemically accessible surface does not exceed 30% of the values estimated by  $\text{N}_2$  or  $\text{CO}_2$  adsorption.

#### 5:40 AM F.EN09.08.06

**Late News: Fundamental Study of Interfaces in All-Solid-State Batteries (ASSB) by Environmental Scanning Electron Microscopy (ESEM)** Neelam G. Yadav<sup>1</sup>, Xavier Randrema<sup>1,2</sup>, Alexis Maurel<sup>1</sup>, Jean Baptiste Chabert<sup>1</sup>, Arash Jamali<sup>3</sup>, Carine Davoisne<sup>1</sup> and Mathieu Morcrette<sup>1</sup>; <sup>1</sup>Reactivity and Chemistry of Solids Laboratory (LRCS) University of Picardy Jules, France; <sup>2</sup>Renault, France; <sup>3</sup>Plateforme de Microscopie Electronique (PME) University of Picardy Jules, Amiens (France), France

The interest in all solid-state batteries (ASSB) is widely known for two main things, one cited for its safety and the other its' ability to use the metallic anodes for enhancing the gravimetric energy density. In order to make solid state batteries a reality it's important <sup>1</sup> to understand the process responsible for failure in ASSB. **1.** During the cell assembly of all solid-state batteries, parameters such as pressure, temperature, preparation of the cathode composite<sup>2</sup>, etc. will influence the interface quality and in turn affect the battery cycling. **2.** Also, during battery operation, parameters such as the operating current density<sup>3</sup> and stack pressure influence battery cycling. They both (1&2) impact cycling performance leading to formation of new phases or interphases, the grains volumetric expansion inducing contact loss and crack formation, the possible dendrites formation leading to the battery short circuit. Among different techniques being used to understand the fundamentals of battery degradation, the scanning electron microscopy (SEM) offers a good compromise in terms of size and resolution of observation with the possibility to perform studies on the different types of interface with a good spatial resolution. By

combining the imaging with chemical analyses by X-ray energy dispersive spectroscopy (EDX), a complete survey of morphological and chemical modification induced at the interfaces is possible.

A home-made ASSB cell has been designed to perform in-situ and operando studies under real time in ESEM. To begin with, we studied the impact of current density ( $J$ ) for NMC-LPS-Li ASSB system, keeping other parameters of ASSB constant and relating cycling at different  $J$  to the battery degradation. This study has been carried out in two parts coupled with other techniques, ex-situ (SEM, XRD, Raman) and in-situ (SEM). The investigated ASSB system shows degradation of LPS at both interfaces, formation of voids, changes in LPS morphology depending on the cycling conditions. The plating and stripping of Li-metal was also investigated. These observations, along with other researches<sup>3</sup> aimed at improving the primary metal anode<sup>4</sup> or interface between metal anode and electrolyte<sup>5</sup> and understanding solid electrolyte<sup>6</sup> will help us to deal and design our future ASSB with improved performances. This kind of study will be further extended to understand other interesting ASSB system.

#### SESSION F.EN09.09: Electron Microscopy and Interfaces

On Demand Abstracts Available for Viewing Starting Saturday Morning, November 21, 2020

F-EN09

##### 5:00 AM \*F.EN09.09.01

**Atomic Scale Dynamics of Oxide Island Growth During *In Situ* Oxidation of Copper** Judith C. Yang; University of Pittsburgh, United States

Understanding the structural changes at the atomic scale of nano-oxide formation via metal oxidation is critical for the rational design and control of oxides for a variety of technology-critical applications including heterogeneous catalysts, sensors, and corrosion protection in extreme environments. Though classical oxidation theories, such as Cabrera-Mott, exist, little is known concerning the initial oxidation stages at the atomic scale. With the developments of in situ characterization tools, such as Environmental Transmission Electron Microscope (ETEM), we are now able to directly observe the structural changes during oxidation. In this work, we combine in situ ETEM with density functional theory (DFT) to fundamentally understand oxide island formation and growth at the atomic scale; Cu(001) was selected as the model metal system. As an example of this correlative approach, we recently observed a layer-by-layer growth of  $\text{Cu}_2\text{O}$  island along  $\text{Cu}_2\text{O}(110)$  plane, where our analysis of these growth dynamics suggests a diffusion limited monolayer growth process. DFT results supported these experimental observations of preferential growth along  $\text{Cu}_2\text{O}(110)$  based on surface energies, diffusion barriers and adsorption energies simulations. We are currently investigating these critical surface reactions for binary alloys. Support for this research program is from NSF-DMR 1410055, 1508417, and 1410335.

##### 5:15 AM F.EN09.09.02

**Probing Electrified Liquid-Solid Interfaces with Scanning Electron Microscopy** Hongxuan Guo<sup>1</sup>, Alexander Yulaev<sup>2</sup>, Evgheni Strelcov<sup>2</sup>, Alexander Tselev<sup>3</sup>, Christopher Arble<sup>2</sup>, Andras Vladar<sup>2</sup>, John Villarrubia<sup>2</sup> and Andrei A. Kolmakov<sup>2</sup>; <sup>1</sup>Southeast University Nanjing, China; <sup>2</sup>National Institute of Standards and Technology, United States; <sup>3</sup>University of Aveiro, Portugal

The processes related to the formation and dynamics of the electrical double layers (EDLs) at the solid-liquid electrolyte interfaces are crucial to numerous applications. However, EDLs formed in realistic interfaces are nanometer(s) thin. The shortage, therefore, exists in the experimental analytical tools capable of probing the concentration, composition, and potential profiles within nanometers thin EDLs with sufficient depth and spatial resolution. The escape depth of low energy electrons in liquids, on the other hand, is in the order of nanometer making electrons, and SEM in particular, to be a suitable probe for EDL. There is, however, an apparent experimental challenge to probe EDL with SEM due to ca. nine orders of magnitude pressure gap between the liquid sample and microscope chamber environments.

In our current communication, we report on a novel experimental approach to probe and image the electrical double layers (EDLs) at the electrified solid-liquid electrolyte interfaces using SEM. Our work resolves the “pressure gap” challenge using graphene as an electron-transparent vacuum separating membrane and demonstrates the sensitivity of the secondary electron yield from the electrified graphene-electrolyte interface to the interfacial processes such as electrolyte polarization and Faradaic processes. We developed finite element analysis models of the potential distribution near the interface and relay them with Monte Carlo simulations to explain the experimentally observed trends of bias-dependent SEM contrast [1]. The proposed method is most useful for studying electrochemical systems where laterally heterogeneous interfaces are present and high-resolution polarization mapping is required

## References

H. Guo et al. Probing Electrified Liquid-Solid Interfaces with Scanning Electron Microscopy arXiv:2006.04283

### 5:25 AM F.EN09.09.03

***In Situ* SEM and XRD Study of Redox Cycling in Transition Metal Oxide Regenerable Catalysts** Alec Ladonis, Scott Misture, Brendan Hill, M. Miller and K.D. McDevitt; Alfred University, United States

Selectively reducible oxides form the foundation of “regenerable” oxide-supported metal catalysts, where transition metals may be reduced from the oxide, then resorbed via oxidation to regenerate spent catalysts. We present in-situ studies of a model defective spinel catalyst under redox cycling conditions that mirror operation conditions for methane reforming and related reactions. Experiments show that these catalysts have excellent sulfur tolerance and high turnover frequencies for methane dry reforming. In-situ studies show that reduction causes crystallographically oriented surface cracking and complex surface structures decorated by metal nanoparticles assembled on crystal facets. In-situ XRD shows the spinel is completely regenerable during redox cycling, allowing for oxidative sulfur removal and metal oxide reincorporation. Microstructural development upon redox cycling is observed by in-situ HT-FESEM and is linked to improved catalytic performance upon redox cycling. Subsequent redox cycles create more surface roughness, as demonstrated by surface investigation after each redox cycle. The in-situ FESEM study even at high vacuum provides sufficient oxygen for reoxidation of the active metal particles, and agrees with calculated thermodynamic stability. Metal particle coarsening and migration is shown to be a function of temperature and the extent of faceting of the oxide, and re-oxidation is found to be a function of the ambient  $pO_2$ . Under high oxygen activity, the transition metal first oxidizes and then reacts with the defect spinel to regenerate the spinel, while at  $pO_2 < 200$  ppm full oxidation does not occur but instead the oxidation and resorption occur at the triple phase boundaries. Enhanced mass transport on the surfaces of the partially-reduced and defective spinel is likely a major contributor to the high catalytic activity and unusually high oxidative sulfur removal reaction.

### 5:35 AM F.EN09.09.04

**Investigation of the Photocorrosion of GaP, III-V Photoanode in Acid with *In Situ* UV/vis Spectroscopy** Sahar Pishgar and Joshua M. Spurgeon; University of Louisville, United States

Development of high efficiency and stable solar fuels production systems is one of the most promising routes to address the increasing energy demands and finite source of fossil fuels available around the world. Long-term stability of such systems has always been an obstacle for widespread implementation of solar fuels; hence, investigation of the mechanism of self-decomposition and corrosion of photoelectrodes under photoelectrochemical operation is of significant importance. In Striving to develop an in-situ photo-corrosion detection technique which is widely available in most labs we studied the photo-corrosion of GaP photoanodes, a promising III-V material for tandem top subcells, in strongly acidic condition via in-situ UV-Vis spectroscopy technique along with ex-situ SEM and XPS characterization to monitor the dissolved Ga and P species during photoelectrochemical reaction. The corrosion faradaic efficiency of n-GaP and p<sup>+</sup>-GaP was calculated as a function of applied bias and time and found to be very different in corrosion process. p<sup>+</sup>-GaP was uniformly dissolved across the active area, while n-GaP was etched in an anisotropic way with micropores formed on the surface of photoanode. Ultimately, a thin layer of TiO<sub>2</sub> protective layer was coated on n-GaP photoanodes to explore its consequences on corrosion mechanism which slowed the rate of GaP dissolution but also introduced a large charge-transfer resistance to the system.

SESSION F.EN09.10: In situ Observation of Materials Synthesis and Processing  
On Demand Abstracts Available for Viewing Starting Saturday Morning, November 21, 2020  
F-EN09

### 5:00 AM \*F.EN09.10.01

**Sustainable Energy Materials—New Routes for *In Situ* Nanoscale Characterization and Their Correlation to Functionality** Stephan V. Roth; KTH Royal Institute of Technology, Sweden

The development of materials for sustainable energy conversion and storage requires new approaches on both the materials and process side. These approaches rely on the use of scattering techniques offering access to the molecular and nanoscale and exploiting both the virtues of X-rays and neutrons [1]. One crucial point is to observe the materials structural

transformations in situ from the nano- to the microscale during materials' synthesis and subsequent device fabrication. These changes must be related to their (macroscopic) functionality. Preferentially the materials itself are sustainable, water-based, or biomaterials. To start with, we focus on wood-based biomaterials, such as cellulose and lignin. Introducing spray deposition as versatile process, ultrasmooth cellulose nanofibril films with controlled thickness are investigated [1,2]. Depending on their charge and roughness, the wettability can be controlled. This is crucial for optimizing the fabrication of hybrid materials, typical for energy conversion and storage. The tailoring of wettability is further pursued by surface functionalization of water-based latex colloids. These materials offer the possibility to tailor and fine-tune the wettability by tuning the core-shell colloid morphology in thin films, thus providing a facile template methodology for repellent surfaces of devices [3]. In materials synthesis, chemical modification of lignin affects the molecular network, aggregate stacking, and size of lignin thermosets. This in turn changes the macroscopic properties of the resulting thermoset [4]. Electronic properties manifest themselves for example in electrical conductivity changes and optical response. The electronic properties are governed by the nanoscale morphology. Imaging via scattering methods allows to extract the granular morphology up to and beyond the percolation threshold in situ during fabrication. At the same time, this analysis allows to predict the electrical behavior of hybrid composites and thus to optimized for example electrodes in such devices [5]. Silver nanowires offers electrical conductivity, mechanical flexibility as well as well high optical transparency when applied as meshes in top electrodes. Here, printing applications offer great potential for photovoltaics and flexible electronics. Two examples are presented: First, a tough composite for a 2D-printed film as top contact on a solar cell, and secondly a flexible composite applied for a 3D-printed flexible capacitor [6]. These examples highlight the advanced capabilities of scattering methods for in situ imaging of the nanoscale structure and for establishing the nanostructure-function relationship.

[1] C.J. Brett et al., *Macromolecules* 52, 4721 (2019)

[2] S. V. Roth, *J. Phys.: Condens. Matter* 28, 403003 (2016)

[3] J. Engström et al.: *Adv. Funct. Mater.*, 30, 1907720 (2020)

[4] M. E. Jawerth et al., *ACS ACS Appl. Polym. Mater.* 2, 668 (2020)

[5] M. Gensch et al., *ACS Appl. Mater. Interfaces* 11, 29416 (2019)

[6] T. E. Glier et al., *Scientific Reports* 9, 6465 (2019)

#### 5:15 AM F.EN09.10.02

***In Situ* R2R Spray Deposition of Flexible Nanocellulose/PEDOT:PSS-Based Supercapacitors Studied Using Surface Sensitive X-Ray Scattering** Calvin Brett<sup>1,2,1</sup>, Mehmet G. Say<sup>3</sup>, Isak Engquist<sup>3</sup>, Magnus Berggren<sup>3</sup>, Daniel Söderberg<sup>1,1</sup> and Stephan V. Roth<sup>2,1</sup>; <sup>1</sup>KTH Royal Institute of Technology, Sweden; <sup>2</sup>Deutsches Elektronen-Synchrotron, Germany; <sup>3</sup>Linköping University, Sweden

Large scale production of sustainable devices experiences a massive increase of attention over the last years. The global economy is initiating projects to minimize the use of fossil resources. However, it is yet unclear how sustainable bio-based devices perform and degrade under environmental influences and how we could improve possible drawbacks. We believe that wood-based cellulose is a key enabler for hierarchical bio-nanocomposites with unprecedented properties as lightweight, flexibility and durability [1]. Poly(3,4-ethylenedioxythiophene) polystyrene sulfonate (PEDOT:PSS) is nowadays widely used as high performance conductive polymer in the field of bioelectronics, solar cells, supercapacitors. Due to its water-solubility, it fulfils the sustainable approach of using less solvents to achieve environmentally friendly devices. The aim of this in situ spray deposition study was to correlate directly the inner morphology of the deposited thin films with its macro-scale physical properties. Herein we used spray deposition as industrial deposition technique on a roll-to-roll coater to fabricate large-scale films with unprecedented low surface roughness down to 2 nm [2-3]. The sprayed flexible and conductive bionanocomposite with thicknesses up to 30 µm are fabricated to provide high energy densities for battery and supercapacitor technologies. We investigated the effect of different layer formation parameters such as drying times, temperature and additives, in particular organization of PEDOT:PSS on CNF and film formation mechanism with spray coating method by means of surface sensitive X-ray scattering [2-4]. We thus achieved a better understanding of the morphology of such films and their electrochemical performance in order to create better energy storage and healthcare devices in the future.

#### References

[1] Mittal, N. et al. *ACS Nano* 12, 6378-6388 (2018)

[2] C. J. Brett et al., *Macromolecules* 52, 12, 4721-4728 (2019)

[3] W. Ohm et al., *J. Coat. Technol. Res.* 15, 759 (2018)

[4] J. Engström\*, C. J. Brett\* et al., *Adv. Funct. Mater.* 30, 1907720 (2020)

#### 5:25 AM F.EN09.10.03

***In Situ* Probing of Structure and Deagglomeration of SnO<sub>2</sub> Colloids via Small-Angle X-Ray Scattering** Viktor

Mackert and Markus Winterer; University of Duisburg-Essen, Germany

Nanoparticles are promising building blocks for materials in various energy applications i. e. fuel cells, batteries, photocatalysts. These materials are often produced by solution-based processing of colloidal nanoparticles. Detrimental in this process is the tendency of nanoparticles to agglomerate due to their high surface energy. Thus, agglomeration also influences for example catalytic properties and adsorption behavior of nanoparticles, as the effective specific surface area available is reduced. Nevertheless, it can be prevented by colloidal stabilization. However, before stabilization the agglomerates must be broken apart at best into individual (primary) nanoparticles. This can be achieved by energy input into the colloidal system. Ultrasonic deagglomeration is promising because, through ultrasonic cavitation, it generates high mechanical shear forces, shock waves and microjets that break down nanoparticle agglomerates.

In this context, it will be shown how synchrotron-based *in situ* small-angle X-ray scattering (SAXS) can be used to study the deagglomeration process in order to possibly produce tailor-made agglomerates on the nanoscale with respect to morphology and size. Therefore, the fractal structure and radii of gyration of differently sized SnO<sub>2</sub> nanocrystals synthesized in the gas phase are continuously monitored during sonication in a specifically designed X-ray transparent *in situ* cell as a function of time and energy input.

#### **Acknowledgement**

This research used resources of the Advanced Photon Source, a U.S. Department of Energy (DOE) Office of Science User Facility operated for the DOE Office of Science by Argonne National Laboratory under Contract No. DE-AC02-06CH11357.

#### **5:35 AM F.EN09.10.04**

**Pathways for *In Situ* X-Ray Absorption Investigation of the Chemical Vapor Synthesis Process** Oleksandr Levish and Markus Winterer; University of Duisburg Essen, Germany

Chemical vapor synthesis (CVS) is a technique enabling reproducible synthesis of narrow sized nanocrystals of high purity from the gas phase. By variation of essential synthesis parameters, such as the time-temperature (t-T) -profile, synthesis pressure and partial pressure of the reactants, different materials and morphologies can be created in the form of nanoparticles with the same synthesis assembly [1, 2]. One of the commonly used materials is iron. In combination with oxygen it can form a variety of compounds (e.g. FeO, Fe<sub>2</sub>O<sub>3</sub>) and phases (e.g.  $\alpha$ -Fe<sub>2</sub>O<sub>3</sub>,  $\gamma$ -Fe<sub>2</sub>O<sub>3</sub>) containing iron in different oxidation states and crystalline systems.

In order to design efficient and sustainable processes for the synthesis of tailored materials with desired properties and access to novel materials or morphologies, the synthesis process must be studied and understood in detail. This is enabled by providing an in-situ view of the synthesis process.

X-ray absorption spectroscopy (XAS) reveals the electronic properties of the material, its local structure and composition. We will present our ongoing study on the in-situ investigation of the CVS process using compounds containing iron and oxygen as model system. So far we studied the precursor and its vapor [3]. Furthermore, we describe the design of the mobile CVS reactor for in-situ investigation of the process with control over the t-T-profile. The parameter window for the reactor is defined based on investigations of iron oxide nanoparticles and evaluation of the reaction chamber with computational fluid dynamic simulations.

[1] Winterer, M., Discovering paths to optimized nanoparticle characteristics, Chem. Eng. Sci. 186, (2018).

[2] Levish, A. and Winterer, M., Nanoparticles generated by combining hot wall and microwave plasma chemical vapor synthesis, MRS Adv. 1-6, (2018).

[3] Levish, A. and Winterer, M., In situ cell for x-ray absorption spectroscopy of low volatility compound vapors, Rev. Sci. Instr. 91, (2020).

#### **Acknowledgment:**

This research was partially carried out at PETRA III at DESY (Hamburg, Germany), a member of the Helmholtz Association HGF, under Proposal No. I-20170647 and at the Diamond Light Source facilities at beamline I20 under Proposal No. 19229. We acknowledge the German Research Foundation (DFG) for funding through research unit FOR 2284 ‘Model-based scalable gas-phase synthesis of complex nanoparticles’ (Project No. WI-981/14).



### F.EN09.11.02

**High Efficiency Water Oxidation Through Oxide Bilayers with Electronically Coupled Phase Boundaries** [Aida Raauf](#), Dennis Grödler, Lasse Jurgensen and Sanjay Mathur; University of Cologne, Germany

New semiconductor metal oxides capable of driving water-splitting reactions by solar irradiation alone are required for sustainable hydrogen production. Whereas most metal oxides only marginally deliver the photochemical energy to split water molecules, uranium oxides are efficient photoelectrocatalysts due to their absorption properties ( $E_g \sim 2.0 - 2.6$  eV) and easy valence switching among uranium centers that additionally augment the photocatalytic efficiency. Although considered a scarce resource, the abundance of uranium compounds in the environment is manifested in the huge quantities of stored  $UF_6$  gas, produced as waste streams in the nuclear fuel enrichment process. Here we demonstrate that thin films of depleted uranium oxide ( $U_3O_8$ ) and their bilayers with hematite ( $\alpha-Fe_2O_3$ ) are high activity water oxidation catalysts due to electronically coupled phase boundaries. The electronic structure of uranium oxides showed an optimal band edge alignment in  $U_3O_8/Fe_2O_3$  bilayers (DFT calculations) resulting in improved charge-transfer at the heterojunction as supported by TAS and XAS measurements. The enhanced photocurrent density of the heterostructures with respect to well-known hematite offers unexplored potential of uranium oxide in artificial photosynthesis.

### F.EN09.11.03

**Enhanced Photocatalytic Oxygen Evolution Reaction—Surface Modification of the Multiferroics  $BiFeO_3$  Nanostructure Using  $IrO_2$  Nanoparticles** [Wegdan Ramadan](#)<sup>1</sup> and Detlef Bahnemann<sup>2,3,4</sup>; <sup>1</sup>Alexandria University, Egypt; <sup>2</sup>Institut für Technische Chemie, Leibniz Universität Hannover, Germany; <sup>3</sup>Saint-Petersburg State University, Laboratory “Photoactive Nanocomposite Materials”, Russian Federation; <sup>4</sup>Laboratorium für Nano- und Quantenengineering, Gottfried Wilhelm Leibniz Universität Hannover, Germany

$BiFeO_3$  (BFO) is a multiferroic that combines antiferromagnetic and ferroelectric order well above room temperature. It is narrow band gap semiconductor ( $\sim 2.2-2.7$  eV) hence, it can harvest significant amount of visible light. Combining such desired properties on simple ternary compound makes it easier to utilize in many different folds. However, the performance of BFO in the field of photocatalysis is still poor due to the fast recombination of the photogenerated charges which will negatively affect their performance. Here we report on the photocatalytic oxygen evolution reaction, OER, of  $BiFeO_3$  nanoparticles synthesized by sol gel. Oxygen evolution reaction is challenging because production of one molecule of gaseous oxygen,  $O_2$ , requires four holes (oxidize two molecules of water), and occurs on a time scale approximately 5 orders of magnitude slower than that required for  $H_2$  evolution. There are two important issues to address when photocatalysis intended for water redox reaction takes place; sacrificial agents to be used and the co-catalyst to be loaded on surface. For the former and in case of OER a sacrificial agent acts as an electron acceptor. Although many choices of sacrificial electron donor are available for water reduction to produce  $H_2$ , the choices are narrowing down to only few for sacrificial electron acceptors used for water oxidation to produce  $O_2$ .  $Ag^+$  and  $Fe^{3+}$  ions are commonly used for this purpose and to a lower extend sodium persulfate,  $Na_2S_2O_8$ . The redox potential of  $Ag^+$ ,  $Fe^{3+}$  and  $S_2O_8^{2-}$  at pH zero are 0.8 V, 0.77 V and 2.05 V, respectively. It is reported that both the quantum efficiency and the stability of the colloidal nanocrystals in solution improve with increasing redox potential of the scavenger. The higher redox potential leads to faster scavenging, which in turn increases quantum efficiency and stability of the catalyst since electron hole recombination and oxidation or reduction of the catalyst become less important. This finding is important for choosing hole/electron scavengers and for comparing efficiencies and stabilities for different photocatalytic nano systems. Hence the resolve to  $Na_2S_2O_8$  as electron scavenger. Mott Schottky measurements and the UV-Vis spectroscopy showed that the band positions of BFO, the conduction band and valence band lie at 0.46V and 2.69 V with respect to NHE, respectively. To enhance BFO photocatalytic OER,  $IrO_2$  nanoparticles as a co-catalyst were loaded on the surface using impregnation method. OER showed two folds enhancement upon loading with 2wt%  $IrO_2$ .  $IrO_2$  is one of the best catalysts for OER, unfortunately it is also one of the most expensive rare elements, so their applicability is limited by the high cost. Reducing  $IrO_2$  content onto the system should be an option to make its application feasible and cost effective and loading on  $IrO_2$  nanoparticles on the surface could be feasible solution. Scanning the loaded  $IrO_2$  content on BFO from 0.5 wt% up to 4 wt% showed a maximum of the evolved oxygen at 2wt % followed by a decrease in activity. XPS showed the 4f peaks of Ir, it shows symmetric two peaks at binding energies 64.9 and 61.87 eV corresponding to the 4f 5/2 and 4f 7/2 of Ir (IV) respectively. TEM indicated non uniform distribution of it on the surface.

Charge carrier lifetime and dynamics for pure BFO and IrO<sub>2</sub> loaded BFO have been studied by means of laser transient absorption spectroscopy, TAS, laser pulses of 20 ns and of  $\lambda = 540$  nm were used. 2wt.% IrO<sub>2</sub> loading showed the fastest decay of holes compared to other loading percentage indicating a significant role of the IrO<sub>2</sub> nanoparticles mediating the hole transfer process of the solar irradiated BFO system. This loading percentage corresponds to the observed highest OER. Band positions between BFO and IrO<sub>2</sub> favors the formation of heterojunction at the interface between IrO<sub>2</sub> and BiFeO<sub>3</sub> that enhances the separation of the photogenerated charges and the photocatalytic OER performance.

#### **F.EN09.11.05**

**Probing the Effects of Electrolyte Anions on the Adsorption of CO on Polycrystalline Cu Electrodes with Surface-Enhanced Infrared Absorption Spectroscopy** Vincent J. Ovalle and Matthias Waegle; Boston College, United States

On Cu electrodes, the electrochemical conversion of CO<sub>2</sub> to hydrocarbons occurs via surface-adsorbed CO. Understanding the molecular factors that determine the adsorption of CO on Cu under electrochemical conditions is therefore essential to improving the product selectivity of this electrocatalytic process. Previous studies probing the adsorption of CO on Cu electrodes have suggested that, at low overpotentials, CO likely competes with anions from the electrolyte for surface sites. However, prior work has not systematically explored the effects of anion concentration and identity on the coverage of CO on the electrode. In this work, we examine the impact of adsorbing and non-adsorbing anions (Cl<sup>-</sup>, SO<sub>4</sub><sup>2-</sup>, ClO<sub>4</sub><sup>-</sup>) at varying concentrations (10 mM and 1 M) on the adsorption and desorption of CO from polycrystalline Cu electrodes. Using surface-enhanced infrared absorption spectroscopy (SEIRAS), we observed the interplay between adsorbed CO and interfacial anions through the lens of the anion hydration shells, CO coverage, and CO stretch frequency under electrochemical conditions. In the presence of 10 mM anion, the potential dependent CO coverage and stretch frequency during a cyclic voltammogram (CV) is virtually independent of the anion identity. By contrast, at 1 M anion, the CO coverage and stretch frequency are distinctly dependent on the anion identity of the electrolyte. With weakly adsorbing and non-adsorbing anions (SO<sub>4</sub><sup>2-</sup> and ClO<sub>4</sub><sup>-</sup>), the CO saturation coverage is lowered by  $\approx 35\%$  compared to the corresponding 10 mM experiments. We attribute the lower coverage to quasi-specifically adsorbed anions that block adsorption sites. With 1 M Cl<sup>-</sup>, the CO saturation coverage is only lowered by  $\approx 12\%$  relative to the coverage in the presence of 10 mM Cl<sup>-</sup>. This moderate decrease is attributed to a decrease in the binding strength of CO to Cu in the presence of co-adsorbed Cl<sup>-</sup>, which is evidenced by the  $\sim 19$  cm<sup>-1</sup> blue shift in the CO stretch frequency. In contrast to all other electrolytes, there is no hysteresis in the adsorption/desorption profiles of CO in the presence of 1 M Cl<sup>-</sup>. This hysteresis between the forward and reverse scans in the CV is due to a CO-induced reversible reconstruction of the Cu electrode surface. In the presence of Cl<sup>-</sup>, this reconstruction is suppressed. We discuss our findings in the context of the effects of halides on the product selectivity of the CO<sub>2</sub> reduction reaction on Cu electrodes. Our study provides critical insight into the structure of the electric double layer and its evolution during the CO adsorption process.

#### **F.EN09.11.06**

**Identifying the Prevalent Surface Facets of Rough Cu Electrodes During CO Reduction Electrocatalysis** Charuni Gunathunge, Jingyi Li, Xiang Li, Julie Hong and Matthias M. Waegle; Boston College, United States

The surface morphology of rough Cu electrodes can profoundly affect the product selectivity and activity for the reduction of CO and CO<sub>2</sub> to hydrocarbons. Because of the scarcity of in situ methods for probing the atomic-level surface structure under electrochemical conditions, it is still debated how the atomic-level surface morphology gives rise to desirable catalytic activity and selectivity. In this work, we introduce a novel method for the determination of the prevalent surface facets on rough metal electrodes under electrochemical conditions. As model systems, we employed two types of rough Cu thin-film electrodes that are widely applied in surface-enhanced infrared absorption spectroscopy (SEIRAS). With differential electrochemical mass spectrometry (DEMS), we show that Cu films that are electrochemically deposited on Si-supported Au films (CuAu-Si) exhibit an onset potential for ethylene that is  $\sim 200 \pm 65$  mV more cathodic than the one of copper films (Cu-Si) that are electrolessly deposited onto Si crystals. With SEIRAS, we find that lineshapes of the CO stretch mode of surface-adsorbed CO exhibit greatly different potential-dependences for the two types of electrodes. Lineshape analysis reveals the presence of different prevalent terraces on these two types of electrodes. On the basis of this finding, we rationalize the higher overpotential for the formation of ethylene on the CuAu-Si film. We expect this novel methodology to be broadly applicable for the in situ surface characterization of rough metal electrodes. This structural information is critical for the development of rough metal electrodes with desirable catalytic characteristics.

#### **F.EN09.11.07**

**In Operando Study of the Role of Ni Nanoparticles and Their Coarsening on the Catalytic Activity of Solid Oxide Fuel Cell Anodes Using Distribution of Relaxation Times Analysis** Boshan Mo, Jillian Rix, Uday Pal, Srikanth Gopalan and Soumendhra Basu; Boston University, United States

Mitigating activation polarization and maintaining long-term stability in solid oxide fuel cell (SOFC) electrodes represent major challenges in improving their intermediate-temperature operation and applications. It has been shown that the infiltration of nanoparticle electrocatalysts increases the number of electrochemically active sites to decrease charge transfer polarization losses and improve performance. In this study, nickel and mixed ionic and electronic conducting (MIEC) phases were infiltrated into Ni-YSZ and Ni-doped YSZ anodes of symmetric cells, and their performances characterized in-operando using electrochemical impedance spectroscopy (EIS). The kinetics of various charge transfer processes are modeled by distribution of relaxation times (DRT) analysis of the EIS spectra, allowing for an understanding of the role of the nickel nanoparticles and the consequences of nickel coarsening on the catalytic activity of the anode.

#### F.EN09.11.09

**Electrochemomechanical Effects of Aqueous Cation Intercalation into Prussian Blue** [Saeed M. Saeed](#)<sup>1</sup>, Shelby Boyd<sup>1</sup>, Wan-Yu Tsai<sup>2</sup>, Ruocun Wang<sup>1</sup>, Nina Balke<sup>2</sup> and Veronica Augustyn<sup>1</sup>; <sup>1</sup>North Carolina State University, United States; <sup>2</sup>Oak Ridge National Laboratory, United States

Prussian blue ( $\text{Fe}_4[\text{Fe}(\text{CN}_6)]_3$ ) and its analogues are of interest as electrode materials for electrochemical energy storage. The open cubic framework of Prussian blue allows for long cycle life and reversible intercalation kinetics during cation insertion/extraction with capacities of up to 125 mAh/g in aqueous electrolytes. However, this performance is highly dependent on the electrolyte cation, and prior results indicate that a smaller hydrated cation radius leads to the best cyclability. The hypothesis guiding this study is that the cycling stability with smaller hydrated cations is tied to lower structural deformation of Prussian blue during electrochemical intercalation. In this study, we investigate the electrochemomechanics of Prussian blue due to the intercalation of three different aqueous cations,  $\text{K}^+$ ,  $\text{Na}^+$ , and  $\text{Li}^+$ . *Operando* atomic force microscopy (AFM) is used to measure the mechanical deformation of the electrode during electrochemical cycling as a function of electrolyte and cyclic voltammetry sweep rate. This technique confirms that the electrochemical stability as well as the local deformation of the Prussian blue is dependent on the hydrated cation radius, with smaller cations giving rise to larger deformation. The superior cycling stability seen during  $\text{K}^+$  insertion is commensurate with the high mechanical stability measured via *operando* AFM. This presentation will provide an understanding of the coupling between electrolyte cation size and electrochemomechanical response of a framework-type energy storage material.

#### F.EN09.11.10

**Metal-Organic Frameworks as Sacrificial Template—Novel Bimetallic Co-W-S Chalcogenide Confined in N, S Codoped Porous Carbon Matrix for Highly Stable Electrochemical Supercapacitors** [Aya M. Mohamed](#)<sup>1,2</sup>, Ahmed O. Abo El Naga<sup>3</sup>, Hanna B. Hassan<sup>1</sup>, Tamer Zaki<sup>3</sup> and Nageh K. Allam<sup>2</sup>; <sup>1</sup>Cairo University, Egypt; <sup>2</sup>American University in Cairo, Egypt; <sup>3</sup>Egyptian Petroleum Research Inst, Egypt

Transition metal dichalcogenides are gaining much interest in the energy storage sector due to the 2D nature and conductivity of the materials. However, single transition metal dichalcogenides are not stable, preventing their practical use in real devices. Herein, we demonstrate the synthesis of binary metal dichalcogenides (Co-W-S) via carbonization of (ZIF-67) metal organic framework encapsulated with phosphotungstic acid (PTA@ZIF-67). The morphology and surface functional groups of the as-synthesized Co-W-S composite are characterized via (FESEM), (HRTEM), and (FTIR). Furthermore, the crystal structure and the elemental composition of the fabricated Co-W-S composite are elucidated using (XRD) and (XPS) analyses. Upon testing its electrochemical performance as a supercapacitor electrode, the fabricated Co-W-S@N,S co-doped porous carbon (N,S-PC) shows exceptional specific capacitance ( $1929 \text{ Fg}^{-1}$  at  $5 \text{ mVs}^{-1}$ ). Furthermore, the constructed asymmetric supercapacitor device using Co-W-S@N,S-PC and activated carbon as positive and negative poles, respectively displays superior energy density and power density of  $32.9 \text{ Wh Kg}^{-1}$  and  $700.2 \text{ W kg}^{-1}$ , respectively with a high Columbic efficiency over 10000 charge/discharge cycles at  $10 \text{ A g}^{-1}$ .

#### F.EN09.11.11

**In Situ Raman Scattering of Photovoltaic Iron-Hydroxide Nanostructures in Dye-Sensitized Solar Cells** [Mikel Tucker](#), Kit Sze, Saroj Pramanik and Yucheng Lan; Morgan State University, United States

Iron hydroxide is a promising photovoltaic material because of its abundance on earth, chemical stability in aqueous media, and outstanding optical absorbance. Here, iron hydroxide nanostructures are synthesized by the atmospheric micro-plasma and characterized. The nanostructures are fabricated into dye-sensitized solar cells and their photovoltaic behaviors are measured. The *in-situ* Raman scattering of the integrated nanostructures is investigated under various experimental conditions. The *in-situ* investigation would enhance our understanding of the dynamic behaviors of the photovoltaic nanomaterial in solar cells.

#### F.EN09.11.12

**Operando Metrology with Photoelectron Spectroscopy and Organic Field-Effect Transistors for Interfacial Charge Transfers of Organic Semiconductor** Kyung-Geun Lim<sup>1</sup>, Jeong Won Kim<sup>1</sup> and Jaeyoon Baik<sup>2</sup>; <sup>1</sup>Korea Research Institution of Standards and Science (KRISS), Korea (the Republic of); <sup>2</sup>Pohang Accelerator Laboratory (PAL), Korea (the Republic of)

Many chemical transitions of organic semiconductors occur at the interface during device operations. Charges are transferred or accumulated at the interface between organic semiconductors and intimate functional materials as function of operating conditions. However, the kinetic materials properties at the interface of organic semiconductor are hardly observed with real-time operational transition. Operando metrology is used to analyze charge transfers at the interface of organic semiconductors by photoelectron spectroscopy during operating bottom gate top electrode p-type organic field-effect transistors (OFETs). The interfacial chemical potential shift of organic semiconductor is simultaneously compared according to electrical behaviors. The electronic activation in the nearest effective monolayers of organic semiconductors at the interface is explained to correlate with gating, doping, or transporting behaviors of OFETs. This operando metrology will shed a light on many veiled intermediate transitions during the operation of organic semiconductors.

#### F.EN09.11.13

**Fabrication of Nanoscale Multilayered Thin-Film Thermoelectric Materials and Devices** Lauren Williams, Rodricka Miller, Alandria Henderson and Zhigang Xiao; Alabama A&M University, United States

We report the growth of nanoscale multilayered thermoelectric thin films and the fabrication of integrated thermoelectric devices for high-efficiency energy conversion and solid-state cooling. Nano multilayered Bi<sub>2</sub>Te<sub>3</sub>/Sb<sub>2</sub>Te<sub>3</sub>, Sb/Sb<sub>2</sub>Te<sub>3</sub>, and Te/Bi<sub>2</sub>Te<sub>3</sub> thermoelectric thin-film materials were grown using the e-beam evaporation. The multilayered thin films were prepared with 100 to 300 layers, where each layer is about 3 to 5 nm thick. The effects of DC substrate bias on the growth of films such as the crystalline structures in the films were studied. Integrated thermoelectric devices with a high density of thermoelectric elements were fabricated with the nanoscale multilayered thin films using the clean room-based microfabrication techniques such as UV lithography. Plasma-enhanced atomic layer deposition (PE-ALD) was used to grow zirconium dioxide (ZrO<sub>2</sub>) as the insulation layer in the device fabrication. X-ray diffraction and high-resolution tunneling electron micrograph (HR-TEM) were used to analyze the nanoscale multilayered thin films. The fabricated device was cooled in liquid nitrogen or annealed at 150 °C for 30 min, respectively. HR-TEM was used to analyze the cross-section of the nanoscale multilayered thin films for the three cases: as-grown, after being cooled in the liquid nitrogen, and after being annealed, showing that the cooling made the multilayer structures to be sharper while the annealing made the multilayer structures to become weaker. The thermoelectric characteristics of the devices were measured and analyzed for the three cases of as fabricated, after being cooled, and after being annealed, respectively, showing that the integrated thermoelectric device had the highest efficiency of thermal-to-electrical energy conversion after being cooled in the liquid nitrogen.

#### F.EN09.11.14

**Late News: Correlating Cu-Based Catalyst Properties to Activity and Selectivity from Operando Studies of CO Electroreduction in a Gas-Fed Device** SooHong Lee<sup>1</sup>, Ian Sullivan<sup>2</sup>, Chengxiang Xiang<sup>2</sup> and Walter Drisdell<sup>1</sup>; <sup>1</sup>Lawrence Berkeley National Laboratory, United States; <sup>2</sup>California Institute of Technology, United States

Identifying the catalyst properties that determine catalyst activity and selectivity is of significant importance, as an understanding of the catalytic mechanism can provide a rational catalyst design principle for efficient energy devices. However, understanding the relationships between catalyst properties and performance remain challenges in general because of the co-existence of multiple factors that are irrelevant to the catalytic cycle, and the dynamic nature of the catalytic chemistry which is responsive to reaction rates. To investigate the complex dynamic catalyst structure, an *operando* characterization under realistic operation, particularly at electrochemical conditions approaching those used to evaluate and benchmark electrocatalysts, is needed. Here, we report a comprehensive study of catalyst properties that can determine the electrochemical CO reduction reaction (CORR) in a gas-fed cell. We first employed *operando* X-ray absorption spectroscopy (XAS) synchronized with simultaneous measurements of catalyst performance by gas chromatography (GC) to investigate the relationship between valence states of Cu-based catalysts and activity for ethylene (C<sub>2</sub>H<sub>4</sub>) production. By introducing an anodic oxidation process, which enhanced CORR performance, we demonstrated that the oxidation states do not correlate with the activity or selectivity of Cu-based catalysts. We also found that an increase in the number of active sites estimated by electrochemical surface area (ECSA) was not proportional to the C<sub>2</sub>H<sub>4</sub> yield, whereas hydrogen evolution reaction (HER) activity is positively correlated to the ECSA changes. Based on the post-mortem microscopic investigations of Cu-based catalysts, we suggest that the increased C<sub>2</sub>H<sub>4</sub> activity and selectivity may arise from a

morphological reconstruction that originates from the electrochemical oxidation-reduction process. The rapid reduction of the initial oxide structure into metallic Cu at the early stage of the CORR could generate a more active structure. This electrochemical oxidation-reduction process was used as a regeneration method that recovered the original catalyst activity and selectivity in the gas-fed cell without requiring cell disassembly.

#### F.EN09.11.15

**Late News: Determining the Effect of Local Heterogeneity on the Activity and Selectivity of Au<sub>1</sub>-xPd<sub>x</sub> Particles for the Hydrogenation of Alkynes with *In Situ* and *Ex Situ* Transmission Electron Microscopy** Alexandre Foucher and Eric Stach; University of Pennsylvania, United States

Heterogeneous catalysis plays a crucial role in the production of chemicals and requires the design of active and selective nanostructures. In situ transmission electron microscopy (TEM) can determine morphology or chemistry changes in novel catalysts during a chemical reaction. In this work, bimetallic Au<sub>1</sub>-xPd<sub>x</sub> particles supported on a raspberry colloid templated (RCT) silica support were studied under oxidative and reactive conditions with a temperature of up to 500 °C and a pressure of 1 bar. Pd is the minority component, representing no more than 25 weight percent of the total metallic loading, and the particles have an average size of 5.5 nm. The remarkable stability of this system, with limited particle migration and coalescence phenomena, was demonstrated. Sharp facets perpendicular to [100] and [111] directions are present when Pd's concentration is below four atomic percent. When the concentration of Pd exceeds four atomic percent, the particles have a spherical shape, and high-resolution spectroscopy revealed the presence of small Pd clusters on the surface of the as-prepared particles with an average size of 1-2 nm. In situ results combined with ex situ TEM and infrared spectroscopy show the growth of small Pd clusters on the nanoparticles' surface that explain changes in activity and selectivity observed after treating the sample with oxygen or hydrogen. These observations demonstrate how a combination of operando methods, aberration-corrected microscopy, and direct electron detection can be used to guide the design of future catalytic structures.

#### F.EN09.11.16

**Late News: Assessing the Durability and Composition of Pt-Based Ternary Nanoalloys in Proton Exchange Membrane Fuel Cells Using *In-Situ/Operando* High-Energy XRD Technique** Dominic Caracciolo, Shiyao Shan and Chuan-Jian Zhong; SUNY Binghamton, United States

Due to the rising demand for sustainable energy, there has been a global drive for developing clean energy from renewable sources (solar, wind, etc.) which will reduce our dependence on fossil fuels. Fuel cells represent an important vector in the development of clean and renewable energy, but major challenges for the mass commercialization of fuel cells are the high cost and poor durability of the catalysts at the cathode, which requires the prohibitive Pt as a catalyst to overcome the sluggish oxygen reduction reaction kinetics. This presentation will discuss recent results of our investigations of low-Pt binary and ternary nanoalloy electrocatalysts using different characterization techniques, including in operando synchrotron X-ray diffraction technique in standard electrochemical cells and proton exchange membrane fuel cells (PEMFC). The focus is to develop the fundamental understanding of the nanophase structures of the catalysts, which provide insights into the correlation between the durability and the composition of the nanoalloy catalysts in the PEMFCs.

#### F.EN09.11.17

**Late News: Self-Constructed MnCo<sub>2</sub>O<sub>4</sub> via Atomic Layer Deposition as an Efficient Bifunctional Catalyst for Zn-Air Battery** Arim Seong and Guntae Kim; Ulsan National Institute of Science and Technology, United States

The discovery of electrocatalysts for efficient oxygen reduction reaction (ORR) and oxygen evolution reaction (OER) is pivotal to the growth of a new generation of energy technologies. In this study, for the first time, we present an effective strategy for a nano-dispersed low amount of Co<sub>3</sub>O<sub>4</sub> materials (*i.e.*, 2.67 wt %) on La<sub>0.5</sub>Sr<sub>0.5</sub>MnO<sub>3-δ</sub> catalyst substrate for synthesizing an efficient bifunctional ORR/OER catalyst by utilizing an advanced ALD technique. Interestingly, the cation diffusion between LSM and Co<sub>3</sub>O<sub>4</sub> introduces a self-intercalated MnCo<sub>2</sub>O<sub>4</sub> spinel structure at the interface. The existence of MnCo<sub>2</sub>O<sub>4</sub> was assisted by TEM-EDS, XANES. Benefiting from the MnCo<sub>2</sub>O<sub>4</sub> interlayer, the LSM-20-Co catalyst exhibits excellent maximum power density (146.5 mW cm<sup>-2</sup>), specific capacity (755.0 mA gZn<sup>-1</sup>) and outstanding stability over 450mn without any increase of charge-discharge voltage gap. Consequently, the LSM-20-Co catalyst is an attractive bifunctional catalyst as an efficient air cathode catalyst for the alkaline metal-air system and provides insight into the rational design of a thin metal oxide with the ALD process.

## SYMPOSIUM F.FL01

---

Bioelectronic Materials for Neural Interfaces—Stimulation, Sensing, Power and Packaging  
November 21 - December 1, 2020

### Symposium Organizers

Polina Anikeeva, Massachusetts Institute of Technology  
Laura Poole-Warren, University of New South Wales  
Jonathan Rivnay, Northwestern University  
Jacob Robinson, Rice University

---

#### \* Invited Paper

SESSION F.FL01.08: Live Keynote I: Bioelectronic Materials for Neural Interfaces—Stimulation, Sensing, Power and Packaging

Session Chairs: Polina Anikeeva, Jonathan Rivnay and Jacob Robinson  
Sunday Morning, November 29, 2020  
F.FL01

#### 10:15 AM \*F.FL01.03.01

**Label-Free Optical Detection of Bioelectric Potentials Using Electrochromic Thin Films** Bianxiao Cui, Felix S. Alfonso, Yuecheng P. Zhou and Erica Liu; Stanford University, United States

Understanding how a network of interconnected neurons receives, stores, and processes information in the human brain is one of the outstanding scientific challenges of our time. The ability to reliably detect neuroelectric activities is essential to addressing this challenge. Optical recording using voltage-sensitive fluorescent probes has provided unprecedented flexibility for choosing regions of interest in recording neuronal activities. However, when recording at a high frame rate such as 500 to 1,000 Hz, fluorescence-based voltage sensors often suffer from photobleaching and phototoxicity, which limit the recording duration. Here, we report an approach called electrochromic optical recording (ECORE) that achieves label-free optical recording of spontaneous neuroelectrical activities. ECORE utilizes the electrochromism of poly(3,4-ethylenedioxythiophene) polystyrene sulfonate (PEDOT:PSS) thin films, whose optical absorption can be modulated by an applied voltage. Being based on optical reflection instead of fluorescence, ECORE offers the flexibility of an optical probe without suffering from photobleaching or phototoxicity. Using ECORE, we optically recorded spontaneous action potentials in cardiomyocytes, cultured hippocampal and dorsal root ganglion neurons, and brain slices. With minimal perturbation to cells, ECORE allows long-term optical recording over multiple days

SESSION F.FL01.09: Live Panel Discussion and Town Hall I: Trainee Panel I

Session Chairs: Polina Anikeeva, Jonathan Rivnay and Jacob Robinson  
Sunday Morning, November 29, 2020  
F.FL01

**11:15 AM PANEL DISCUSSION/TOWN HALL:**

**12:15 PM PANELIST: MELISSA TAN (STANFORD)**

**12:15 PM PANELIST: CSABA FORRO (STANFORD)**

**12:15 PM PANELIST: ALEXANDER BOYS (CAMBRIDGE)**

SESSION F.FL01.10: Live Keynote II: Bioelectronic Materials for Neural Interfaces—Stimulation, Sensing, Power and Packaging  
Session Chairs: Polina Anikeeva, Jonathan Rivnay and Jacob Robinson  
Monday Morning, November 30, 2020  
F.FL01

**8:00 AM \*F.FL01.01.04**

**Organic Materials and Devices for Neural Interfacing** George G. Malliaras; University of Cambridge, United Kingdom

One of the most important scientific and technological frontiers of our time is the interfacing of electronics with the human brain. This endeavour promises to help understand how the brain works and deliver new tools for diagnosis and treatment of pathologies including epilepsy and Parkinson's disease. Current solutions, however, are limited by the materials that are brought in contact with the tissue and transduce signals across the biotic/abiotic interface. Recent advances in organic electronics have made available materials with a unique combination of attractive properties, including mechanical flexibility, mixed ionic/electronic conduction, enhanced biocompatibility, and capability for drug delivery. I will present examples of novel devices for recording and stimulation of neurons and show that organic electronic materials offer tremendous opportunities to study the brain and treat its pathologies.

SESSION F.FL01.11: Live Panel Discussion and Town Hall II: Trainee Panel II  
Monday Morning, November 30, 2020  
F.FL01

**9:00 AM PANEL DISCUSSION/TOWN HALL:**

**10:00 AM PANELIST: GAURI BHAVE (RICE)**

**10:00 AM PANELIST: REEM RASHID (NORTHWESTERN)**

**10:00 AM PANELIST: ABDULELAH SALEH (KAUST)**

SESSION F.FL01.01: Device and Systems Towards Application and Translation  
On Demand Abstracts Available for Viewing Starting Saturday Morning, November 21, 2020  
F-FL01

**5:00 AM \*F.FL01.01.01**

**Translating Conformable Neural Interface Research Towards Clinical Reality** Giuseppe Schiavone, Florian Fallegger, Nicolas Vachicouras and Stephanie P. Lacour; Ecole Polytechnique Federale de Lausanne, Switzerland

The recent introduction of soft materials to design electrodes that conform and mimic neural tissue drives the development of neural interfaces with improved functionality and biointegration. While being used routinely in academic research, soft neural interfaces have not reached clinical translation, in part because scaling, reproducibility and reliability standards are yet to be established. Materials science and engineering is therefore at the core of translational research.

We propose a translational framework focused on electrode implants and based on systematic steps in design, manufacturing, in vitro biomimetic validation and in vivo functional evaluation to advance the technological readiness of soft neural interfaces. Geometrical scaling is driven by anatomy but also surgical handling and procedure. Systematic control of manufacturing processes guides reproducibility in terms of layout, electrical and electrochemical properties. Validation is first conducted in vitro using a multimodal platform that mimics the biological environment within which the interface is to be implanted, applies mechanical loading similar to those to be withstood in vivo, and enables electrochemical ageing and characterization. The shift from stiff to soft electrode materials requires adaptation of the models and characterization

methods to understand and predict electrode performance. Following iterations in characterization and manufacturing improvement, the soft neural interface is next evaluated in large animal models where therapeutic use may be implemented. Transition to medical grade materials and quality-controlled manufacturing are the next technological steps to implement and envision clinical evaluation of the soft neural interface.

This talk will illustrate this translational framework taking the example of the soft neurotechnology named e-dura – surface electrode arrays that mimic the natural dura mater and record or modulate neural activity in the central nervous system.

**5:15 AM \*F.FL01.01.02**

**Pushing the Limits of Intracortical Neural Recording** Chong Xie; Rice University, United States

The brain is a massively-interconnected and constantly-evolving network of specialized circuits, a systematic understanding of which requires an interface that functions at diverse spatial and temporal scales. Implanted electrodes provide a unique approach to decipher brain circuitry by allowing for time-resolved electrical detection of individual neuron activity. However, scalable and stable neural recording that can track and map a large ensemble of neurons across days, weeks and months remains challenging. We recently demonstrated that ultraflexible, cellular-dimensioned neural electrodes afford seamless integration with brain tissue and stable recording of individual neurons for over a year. Building upon this platform, I will also present our recent progress in further decreasing their form factors, and their massive scaling-up of channel count and density in behaving animals. I will finally discuss about our on-going efforts in applying these ultraflexible electrodes in fundamental and translational neurosciences.

**5:30 AM \*F.FL01.01.03**

**Translational Neuroelectronics** Dion Khodagholy; Columbia University, United States

As our understanding of the brain's physiology and pathology progresses, increasingly sophisticated technologies are required to advance discoveries in neuroscience and develop more effective approaches to treating brain disease. There is a tremendous need for advanced materials solutions at the biotic/abiotic interface to improve the spatiotemporal resolution of neuronal recording and stimulation. Organic electronic devices offer a unique approach to these challenges, due to their mixed ionic/electronic conduction, mechanical flexibility, enhanced biocompatibility, and capability for drug delivery. We designed, developed, and characterized conformable organic electronic devices in the form of electrodes, ion gated transistors, conformable batteries and ionic communication units to efficiently interface with the brain and acquire neurophysiological activity not previously accessible with recordings from the brain surface. These devices have facilitated large-scale rodent neurophysiology experiments and uncovered a novel oscillatory interaction. The biocompatibility of the devices allowed intra-operative recording from patients undergoing epilepsy and deep brain stimulation surgeries, highlighting the translational capacity of this class of neural interface devices. In parallel, we are developing the high-speed electronics and embedded acquisition and storage systems required to make high channel count, chronic neurophysiological recording from animals and human subjects possible. This multidisciplinary approach will enable the development of new devices based on organic electronics, with broad applicability to the understanding of physiologic and pathologic network activity, control of brain-machine interfaces, and therapeutic closed-loop devices.

**5:45 AM \*F.FL01.01.04**

**Organic Materials and Devices for Neural Interfacing** George G. Malliaras; University of Cambridge, United Kingdom

One of the most important scientific and technological frontiers of our time is the interfacing of electronics with the human brain. This endeavour promises to help understand how the brain works and deliver new tools for diagnosis and treatment of pathologies including epilepsy and Parkinson's disease. Current solutions, however, are limited by the materials that are brought in contact with the tissue and transduce signals across the biotic/abiotic interface. Recent advances in organic electronics have made available materials with a unique combination of attractive properties, including mechanical flexibility, mixed ionic/electronic conduction, enhanced biocompatibility, and capability for drug delivery. I will present examples of novel devices for recording and stimulation of neurons and show that organic electronic materials offer tremendous opportunities to study the brain and treat its pathologies.

**6:00 AM F.FL01.01.05**

**A Flexible, Transparent Microcoil Array for Precise Neuronal Stimulation** Vineeth Raghuram<sup>1,2,3</sup>, Aditya Datye<sup>2</sup>, Shelley Fried<sup>2,3,1</sup> and Brian Timko<sup>1</sup>; <sup>1</sup>Tufts University, United States; <sup>2</sup>Massachusetts General Hospital - Harvard Medical School, United States; <sup>3</sup>Boston VA Healthcare System, United States



The use of microcoils to magnetically stimulate neurons of the cortex has been shown to have several important advantages over conventional electrode-based stimulation. For example, the spatially asymmetric electric fields arising from microcoils can be used to activate specific populations of neurons [1] while avoiding others. This helps to confine activation to a focal region around the coil, and as a result, a microcoil-based approach may be an attractive platform where focal activation is critical, e.g. for next generation cortical visual prostheses that strive to restore high acuity vision. Initial studies have validated, using both computational and experimental approaches, the ability of a single microcoil to generate small, focal regions of activation [1], and the effects of varying coil shape/design on the both the spatial selectivity and strength of activation [2]. While devices that consist of a single microcoil may be useful in targeting a single, isolated region of the cortex, the ability to focally activate multiple cortical columns, or multiple layers within a single cortical column, either in synchrony or in temporally modulated intervals (interleaved), would be useful where the creation of multiple regions of neural activity is the goal, e.g. to elicit complex spatial patterns with a prosthesis. As a step towards this goal, we designed and fabricated an array of four individually accessible microcoils, each capable of activating a distinct region. Coils and interconnects were fabricated from copper and sandwiched between two layers of SU-8, which functioned as both conformable support substrate and passivation layer; the low young's modulus of SU-8 helped to minimize mechanical mismatch with brain tissue. Individual coils were V-shaped, a geometry previously shown to be effective in activating pyramidal neurons [2]. Inter-coil spacing was 250um, the approximate separation between adjacent cortical columns. Computational modeling of this design revealed that the magnitude of electric field gradients along the length of pyramidal neurons would be strongest along the edge and at the tip of the "V", thus increasing the likelihood of focal activation of neuronal processes located close to the tip while minimizing activation further away. Basic functionality of the array was confirmed by the measurement of electrical artifacts resulting from the passing of electrical current through individual coils. Use of a patch-clamp setup helped to prevent saturation of amplifiers and revealed that artifact shape was consistent with theoretical predictions. *In-vitro* experiments using GCaMP6 mice allowed the fluorescent response from neuronal populations to be measured in response to stimulation from individual coils; the transparency of SU8 allowed clear visualization of the fluorescent signals. As expected, activation from a single coil was largely confined to a focal region around the coil tip, thereby confirming functional performance of the coils. Future efforts will investigate the spatial activation patterns which result from the stimulation of multiple coils in the array.

[1] S. W. Lee, F. Fallegger, B. D. F. Casse, and S. I. Fried, "Implantable microcoils for intracortical magnetic stimulation," *Science Advances*, vol. 2, no. 12, p. e1600889, Dec. 2016, doi: 10.1126/sciadv.1600889.

[2] S. W. Lee, K. Thyagarajan, and S. Fried, "Micro-coil design influences the spatial extent of responses to intracortical magnetic stimulation," *IEEE Transactions on Biomedical Engineering*, pp. 1–1, 2018, doi: 10.1109/TBME.2018.2877713.

#### 6:10 AM F.FL01.01.06

**Implantable Cardiac Motion Sensor for *In Situ* Disease Diagnosis and Treatment** Jae Chul Hwang, Moohyun Kim and Jang-Ung Park; Yonsei University, Korea (the Republic of)

As a leading cause of death worldwide in recent years, cardiac disease needs continuous monitoring of cardiac activity for its prompt diagnosis and treatment. Pacemaker, a conventional technique for diagnosing and treating cardiac diseases such as arrhythmia, has adverse side effects at implantation sites such as infection and damage to blood vessels, and also causes discomfort in daily life due to its rigid and bulky form. Currently, with the emergence of soft bioelectronics that intimates 3D curvilinear bio tissues, various studies have been conducted to monitor the function of cardiac activities by attaching a device onto cardiac surface. Most recent soft electronic devices that detect cardiac functions are based on electrophysiology sensing such as electrocardiograms (ECGs). However, these devices that measure the electrical flow of cardiac surface as their sensing mechanism have limitations in implementing simultaneous electrical stimulation while sensing the electrical signal. This is due to the electrical interdependent between sensing and stimulation electrodes, resulting in unnecessary signal interferences in ECGs. Herein, we demonstrate an implantable and flexible cardiac motion sensor that can simultaneously detect cardiac beating rate and intensity, via pressure measurement of cardiac relaxation, and apply electrical pacing to modulate cardiac contractile function. This cardiac motion sensor consists of active-matrix arrays of pressure-sensitive Si transistors with air dielectric layers, and integrated platinum black electrodes for electrical stimulation. Also, an alginate-based hydrogel patch that is functionalized by multi-crosslinking moieties to enhance tissue adhesiveness and elastic modulus is reported. This hydrogel patch amplifies the pressure sensitivity of the motion sensor while securely fixing the motion sensor onto the epicardium surface without any surgical adjustment. Our results have shown that the flexible cardiac motion sensor is able to accurately detect cardiac mechanical activity such as systole and diastole, which are comparable with ECG trace during *in-vivo* trials using New Zealand White rabbits. Stimulation of synchronized electrical pulses to the left ventricle by our flexible cardiac motion sensor has modulated the cardiac beating frequency at a low threshold voltage while

simultaneously detecting changes in the beating frequency and intensity of the pressure signals without any signal noise. Our motion-sensing diagnostic tool specifically targets those associated with abnormal cardiac activities such as arrhythmia, cardiac hypertrophy, and dilated cardiomyopathy, etc. Thus, we envision that our demonstration will provide a new intuitive platform that enables the diagnosis and treatment of various cardiac diseases.

#### **6:20 AM F.FL01.01.07**

**Cardiac Organoid Pressure Mapping for Biomedical Modelling** Moohyun Kim, Jae Chul Hwang and Jang-Ung Park; Yonsei University, Korea (the Republic of)

Human stem cell derived organoids provide cellular models of human diseases without the need for in vivo trials, removing non-genetic pathological factors in disease modelling. Current physical modelling of myocardial infarction and drug cardiotoxicity in cardiac organoid is limited to optical image analysis. This method of analysis ranges from spatial proteomics to fluorescent imaging. However, diagnostic modelling of cardiac organoids requires a higher degree of precision and sensitivity in order to accurately measure beating frequency and intensity. In mechanically energetic cardiac organoids, actual collection and interpretation of raw physical data of organoid beating are important to better understand the contractility implication after drug screening. Herein, we introduce an innovative technology that analyzes the activity of cardiac organoid using a highly sensitive pressure sensor, which is fabricated from Si transistor with an air dielectric component. This device is integrated with electrical stimulating capability that can detect and modulate cardiac organoid beating simultaneously. This sophisticated active-matrix pressure array has a high spatial resolution, providing 2D tactile pressure mapping of cardiac organoid beating. Our novel device is capable of detecting real-time cardiac organoid physical functions, such as beating frequency and intensity, to model various cardiac conditions based directly on the organoids' mechanical parameter. The periodic beatings of cardiac organoids are converted from physical parameters into electrical signals within the pressure sensor. Our device innovatively replaces the conventional method of image analysis, where the organoid beating measurement is derived by dissecting video frames, for myocardial infarction and drug cardiotoxicity modelling.

SESSION F.FL01.02: Nano Materials for Neural Interfacing  
On Demand Abstracts Available for Viewing Starting Saturday Morning, November 21, 2020  
F-FL01

#### **5:00 AM \*F.FL01.02.01**

**Designing Soft-Hard Composites for Neural Interfaces** Bozhi Tian; University of Chicago, United States

Biointerface materials and devices can probe fundamental biological dynamics and improve the lives of human beings. However, the direct application of traditional rigid electronics onto soft tissues or cells can cause signal transduction and biocompatibility issues, partly due to the mechanical mismatch at the biointerfaces. One solution to this mismatch is the use of a soft-hard composite as a biomaterial; the hard components are stable, easy to control and provide the active functionalities, while the soft components promote compliant mechanical adhesion or active biointegration. Additionally, as substrates or encapsulation layers, the soft components can protect the high modulus electronic elements, and can facilitate mechanical operations (*e.g.*, stretching, bending, delivery, removal) of the entire composites. Advanced soft materials can also display dynamically responsive or even living behaviors currently lacking in rigid electronic systems. In this talk, I will discuss our recent efforts of designing different soft-hard composites for neural interface applications, such as *in vitro* and *in vivo* non-genetic neuromodulation. For example, dopant-modulated silicon membranes, when integrated with porous PDMS, can be implanted over the motor and somatosensory cortex regions and are capable of inducing limb motion in animals upon light stimulation. Silicon carbide-based devices can be produced directly with laser ablation from a PDMS substrate and were used for neural and cardiac modulation in flexible configurations. Besides using nonliving composites, our lab has also explored several living composites for neural and cardiac interfaces. These bio-hybrids hold great promise as minimally invasive interfaces to naturally occurring cells and tissues for cell-based therapeutics and control. Finally, we have started the initial effort in creating tissue-like materials for neural interfaces. For example, we recently found that granules-based hydrogel composites can be considered better analogs of biological tissues in terms of both the structure and the static and dynamic mechanical properties. I will end this talk by proposing new soft-hard components for future neural interfaces.

#### **5:15 AM F.FL01.02.02**

**Predictive Model of Piezoresistive Response of Conductive-Nanowire-Elastomer Composites** Csaba Forro<sup>1,2</sup>, Stephan

Ihle<sup>3</sup>, Sean Weaver<sup>3</sup>, Andreas Reichmuth<sup>3</sup>, Anne Bonnin<sup>3,4</sup>, Marco Stampanoni<sup>3,4</sup>, Klas Tybrandt<sup>5</sup> and János Vörös<sup>3</sup>; <sup>1</sup>Istituto Italiano di Tecnologia, Italy; <sup>2</sup>Stanford University, United States; <sup>3</sup>ETH Zürich, Switzerland; <sup>4</sup>Paul Scherrer Institut, Switzerland; <sup>5</sup>Linköping University, Sweden

Composites based on conductive nanowires embedded in elastomers are popular in a wide range of stretchable electronics applications where the requirements are either a stable (electrodes) or a highly increasing (strain sensors) electrical resistance upon strain. Despite the widespread use of such composites, their production protocol is not based on solid theoretical grounds but rather in empirical observations. There is a lack of a predictive framework for the piezoresistive quality of samples based on their production parameters. This is due to limitations in the methods for studying nanowire meshes, in particular the lack of knowledge on the spatial distribution of the nanowires and their rearrangement under strain. We overcame this hurdle by collecting 3D reconstructed X-ray tomographies of silver nanowires embedded in polydimethylsiloxane (PDMS) under variable deformations and obtained the missing structural information of the nanomaterial by unsupervised artificial intelligence image analysis<sup>1</sup>. This allowed us to reveal the precise assembly mechanisms of nanowire systems and derive a precise analytical formula for the piezoresistive response of the composites based on the nanowire material, the number of wires used, their aspect ratio, and the contact resistance between the wires<sup>2</sup>. We demonstrate a lower bound on the relative increase in resistance of the sample (gauge factor) –in particular, these systems cannot exhibit less than a 3-fold increase in their resistance when strained 100%. Finally to simulate the behavior of arbitrary samples in-silico and propose an exploratory design framework, we made an open-source simulation framework, validated by our experimental observations, which allows to simulate any arbitrary nanowire mesh and its piezoresistive behavior.

1. Ihle, S.J., Unsupervised data to content transformation with histogram-matching cycle-consistent generative adversarial networks. *Nat Mach Intell*, 461–470 (2019)

2. Forro et. al (in press). Visualizing and analyzing 3D metal nanowire networks for stretchable electronics, *Advanced Theory and Simulations*

#### **5:25 AM \*F.FL01.02.03**

**Modulating Neuronal Activity with Out-of-Plane Grown Three-Dimensional (3D) Fuzzy Graphene** Tzahi Cohen-Karni; Carnegie Mellon University, United States

The ability to modulate cellular electrophysiology is fundamental to the investigation of development, function, and disease. Currently, there is a need for remote, non-genetic, light-induced control of cellular activity in two-dimensional (2D) and three-dimensional (3D) platforms. Here, we report a breakthrough hybrid-nanomaterial for remote, non-genetic photothermal stimulation of 2D and 3D neural cellular systems. We combine one-dimensional (1D) nanowires (NWs) and 2D graphene flakes grown out-of-plane for highly controlled photothermal stimulation at subcellular precision without the need for genetic modification, with laser energies lower than hundred nanojoules, 1-2 orders of magnitude lower than Au-, C- and Si-based nanomaterials. Photothermal stimulation using NW-templated 3D fuzzy graphene (NT-3DFG) is flexible due to its broadband absorption and does not generate cellular stress. Therefore, it serves as a novel powerful toolset for studies of cell signaling within and between tissues and can enable new therapeutic interventions.

SESSION F.FL01.03: Optical Recording and Stimulation

On Demand Abstracts Available for Viewing Starting Saturday Morning, November 21, 2020

F-FL01

#### **5:00 AM \*F.FL01.03.01**

**Label-Free Optical Detection of Bioelectric Potentials Using Electrochromic Thin Films** Bianxiao Cui, Felix S. Alfonso, Yuecheng P. Zhou and Erica Liu; Stanford University, United States

Understanding how a network of interconnected neurons receives, stores, and processes information in the human brain is one of the outstanding scientific challenges of our time. The ability to reliably detect neuroelectric activities is essential to addressing this challenge. Optical recording using voltage-sensitive fluorescent probes has provided unprecedented flexibility for choosing regions of interest in recording neuronal activities. However, when recording at a high frame rate such as 500 to 1,000 Hz, fluorescence-based voltage sensors often suffer from photobleaching and phototoxicity, which limit the recording duration. Here, we report an approach called electrochromic optical recording (ECORE) that achieves label-free optical recording of spontaneous neuroelectrical activities. ECORE utilizes the electrochromism of poly(3,4-ethylenedioxythiophene) polystyrene sulfonate (PEDOT:PSS) thin films, whose optical absorption can be modulated by an

applied voltage. Being based on optical reflection instead of fluorescence, ECORE offers the flexibility of an optical probe without suffering from photobleaching or phototoxicity. Using ECORE, we optically recorded spontaneous action potentials in cardiomyocytes, cultured hippocampal and dorsal root ganglion neurons, and brain slices. With minimal perturbation to cells, ECORE allows long-term optical recording over multiple days

#### 5:15 AM F.FL01.03.02

**Highly-Integrated, Flexible Phototransistor Arrays Based on Three-Dimensional Soft Stimulation Electrodes for Vision Restoration of Live Mouse** Hyobeom Kim, Jiuk Jang and Jang-Ung Park; Yonsei University, Korea (the Republic of)

With the aging of global populations, there are emerging retinal disorder cases such as retinitis pigmentosa and macular degeneration. The patients lose their vision due to the damage in their photoreceptors; however, the ganglion cells, which transfer the signals from photoreceptors to the optic nerve, are well preserved in most cases. By stimulating the ganglion cells electrically, the sense of vision can be induced intentionally. Based on these principles, retinal prosthetic devices have been developed by combining photodetectors, such as cameras, and stimulating electrodes. Although there have been many studies of the retinal prosthesis that restore vision through electrical stimulus, several challenges remain to be solved. First, the resolution of the conventional retinal prosthesis is significantly lower than that of the actual vision. Second, the planar structure of stimulation electrodes leads to high impedance and high threshold current, resulting in interference between the surrounding pixels in electrical stimulation. Third, the integration of an optoelectronic array device, which detects the external light, and stimulation electrode for the in-vivo test is rarely reported.

Herein, we introduce highly-integrated, flexible phototransistor arrays based on three-dimensional (3D) stimulation electrodes for vision restoration of live mice. The phototransistor arrays allow the device to electrically stimulate the retina with high-resolution. Since we implemented the 3D structured stimulation electrodes instead of the planar, the device shows the much lower impedance, suggesting less interference between the surrounding pixels in electrical stimulation. These improvements enable the target cells of the retina to be accurately stimulated with the light intensity changes. Furthermore, these 3D stimulation electrodes are made of soft, self-healable material to prevent secondary damage to the retina and enable long-term operation. In-vitro and in-vivo animal trials have confirmed real-time array signals generated by retinal cells in electrical stimulation with the change in light intensity. We completed the verification of the biocompatibility and long-term stability of the device. We envision that retinal implants with the soft 3D stimulating electrode will provide a promising strategy to the biomedical field regarding retinal disorders soon.

#### 5:25 AM \*F.FL01.03.03

**Light Actuators for Cell Photo Stimulation** Giuglielmo Lanzani<sup>1,2</sup>; <sup>1</sup>Istituto Italiano di Tecnologia, Italy; <sup>2</sup>Politecnico di Milano, Italy

We develop and study non-genetic cell opto-stimulation techniques based on artificial light actuators that establish functional abiotic-biotic interfaces able to transduce a light signal into a biological stimulus. This talk reports on the state of our research regarding organic bio interfaces for inducing light sensitivity in cells, both in vitro and in vivo. Light actuators comes in different shapes: planar patches, nanoparticle, intramembrane probes. Their coupling mechanism is still far from being understood and attempts to shed light will be introduced. It seems that membrane modification is a crucial step in the photostimulation. Rescue vision in blind people is one of the most appealing practical outcome of this emerging technology, and recent achievements will be summoned.

#### 5:40 AM F.FL01.03.04

**Bacterial Proliferation Modulation by a Membrane-Targeted Amphiphilic Azobenzene** Giuseppe M. Paternò<sup>1</sup>, Gaia Bondelli<sup>1,2</sup>, Stefano Donini<sup>1</sup>, Vito Vurro<sup>1,2</sup>, Valentina Sesti<sup>2,1</sup>, Chiara Bertarelli<sup>2,1</sup> and Guglielmo Lanzani<sup>1,2</sup>; <sup>1</sup>Istituto Italiano di Tecnologia, Italy; <sup>2</sup>Politecnico di Milano, Italy

Optogenetics and covalent approaches to bio conjugation allow achieving large and effective cell photo-stimulation, yet these are invasive methods that might encounter severe limitations on the way towards clinical applications in photopharmacology.<sup>1</sup> The non-covalent affinity of photoresponsive molecules to biotargets represents an attractive alternative. In this context, we have recently proposed an amphiphilic azobenzene photochromic molecule (ZIAPIN2) whose selective dwelling in the plasma membrane enables modulation of the cell potential, remarkably permitting to evoke light-induced neuronal firing *in vitro* as well *in vivo*.<sup>2,3</sup>

Here, we show that the affinity of ZIAPIN2 to bacterial cell wall can be exploited to modulate bacterial proliferation. In

particular, we demonstrated that while in the dark proliferation is hindered, light illumination in the visible range leads to a total restoration of bacterial growth for both *Escherichia coli* (Gram (-)) and *Micrococcus Luteus* (Gram (+)). We preliminary attribute this effect to a light-triggered modification of the bacterial membrane potential brought about by ZIAPIN2 isomerization.

1. Zimmerman, J. F. & Tian, B. *ACS Nano* **12**, 4086–4095 (2018).

2. Paternò, G. M. *et al. Adv. Sci.* **7**, 1903241 (2020).

3. DiFrancesco, M. L. *et al. Nat. Nanotechnol.* **15**, 296–306 (2020).

#### 5:50 AM F.FL01.03.05

**Organic Printed Electronics Towards Opto-Stimulated Bio-Interfaces** Maxim Shkunov<sup>1</sup>, A.N. Solodukhin<sup>2</sup>, Pavlos Giannakou<sup>1</sup>, Leslie Askew<sup>1</sup>, D.O. Balakirev<sup>2</sup>, Y.N. Luponosov<sup>2</sup> and S.A. Ponomarenko<sup>2,3</sup>; <sup>1</sup>University of Surrey, United Kingdom; <sup>2</sup>Enikolopov Institute of Synthetic Polymeric Materials of the Russian Academy of Sciences, Russian Federation; <sup>3</sup>Lomonosov Moscow State University, Russian Federation

Opto-stimulation of semiconductor-biointerfaces provides efficient pathways towards eliciting neural activity through selective spectral excitation. In visual prosthesis, tri-colour excitation capability, is the key to restoring full-colour vision. Among organic semiconductor materials, donor–acceptor molecules have the most promising properties due to excellent light absorption, high stability and good solubility in organic solvents. Varying the donor and acceptor functionalities, allows fine tuning of the optical properties. These carbon based molecules bear intrinsic affinity to biological systems, and also demonstrate excellent photoresponses, electronic and ionic conductivity, and allow intimate interface with liquid bioenvironment.

We demonstrate tri-colour optoelectronic devices based on solution-processable conjugated donor-acceptor molecules with absorption in red, green and blue spectral regions, mimicking the absorption of human retinal cones. Photo-response is studied via interfacing with biological electrolyte solution and using long-pulse, narrow-band excitations, where both photo-voltage and photo-current responses show clear signatures of capacitive charging at the electrolyte/device interface.

We further explore ink-jet printing to reproduce individual photo-pixels with red, green and blue absorption characteristics, with small diameters of 35 to 45 microns.

We discuss the suitability of organic semiconductors for potential medical applications as retinal bio-engineered prosthesis for the restoration of human vision, and evaluate prospects of wider, colour-selective excitations of bio-interfaces.

#### 6:00 AM F.FL01.03.06

**Nanoengineered Bioelectronic Systems Using Semiconducting Polymers for All-Optical Control of Neuron Growth and Stimulation** Matthew Griffith<sup>1</sup>, Connor Sherwood<sup>2</sup>, Rafael Crovador<sup>2</sup>, Krishna Feron<sup>2</sup>, Julie Cairney<sup>1</sup>, Paul Dastoor<sup>2</sup>, Alan Brichta<sup>2</sup> and Rebecca Lim<sup>2</sup>; <sup>1</sup>The University of Sydney, Australia; <sup>2</sup>The University of Newcastle, Australia

Implantable neurostimulation devices play a key role in treating many serious injuries and diseases by providing a direct therapeutic link to the nervous system. This enables brain stimulation for treatment of Parkinson's disease and epilepsy, nerve guidance and regeneration to remedy spinal cord injury, and retinal prosthetic devices that could cure blindness.<sup>[1]</sup> To address such issues, new bioelectronic systems that can deliver electrical stimulation to nerve cells are required. Although silicon microelectronics and metal electrodes have been the historic gold standard for bioelectronic interfaces, their use in clinical practice is limited. The main obstacles to further translation of these devices include a low biocompatibility that reduces *in vivo* lifetimes,<sup>[2]</sup> a mechanical rigidity that is poorly matched with soft tissue, causing inflammation and ineffective electrical contact, and a requirement for costly external power supplies to deliver current.<sup>[3]</sup> These issues result in indiscriminate tissue activation, with a consequent lack of spatial selectivity.<sup>[4]</sup>

In this work, we report a strategy to simultaneously address these issues by combining soft carbon-based organic conductors and nanoscale science to build new bioelectrodes that allow optical neurostimulation without external power. Our approach creates bioelectronic interfaces from organic conductors that can be formed into customized nanoparticles with established solution-based chemistry methodologies. This approach enables the stimulating electrodes to be combined with targeted pharmaceutical factors in the fabrication procedure, which subsequently optimise connections to the neural network. We tune the optoelectronic properties of the organic conductors to cover standard red, green, and blue spectral regions, allowing spectrally selective platforms for neurostimulation. These conductors are turned into electroactive inks, and subsequently fabricated into pixelated arrays using inkjet printing. This approach establishes a new low-cost manufacturing methodology that is generally applicable to other organic materials and can be used for a variety of bioelectronic devices, creating a new manufacturing paradigm for biomedical technology.

We demonstrate both the anatomical and functional biocompatibility of neural tissue with our organic bioelectronic systems using immunolabelling with neuronal marker MAP2 and visualisation with epifluorescence microscopy to detect neurons cultured on the organic conductors. We demonstrate the controlled release of drugs from the organic conductive nanoparticles, aiding in precise spatial delivery of pharmaceutical factors. Finally, we employ whole-cell patch clamp electrophysiology recordings to demonstrate an exciting result; purely optical neurostimulation of dorsal root ganglion nerve cells. We demonstrate that the organic conductors can trigger changes in the nerve cell membrane potentials via a *capacitive coupling* mechanism, the efficacy of which can be improved by judicious selection of the device architecture. Importantly, capacitive neurostimulation does not require injection of current into biotic tissue to trigger changes in the membrane potentials. This means very confined stimulation is possible and therefore spatial selectivity is no longer limited by current spread and undesirable electrochemical reactivity is minimised.

#### References:

- [1] B. Zhu, S. C. Luo, H. Zhao, H. A. Lin, J. Sekine, A. Nakao, C. Chen, Y. Yamashita, H. H. Yu, *Nat. Commun.*, **2014**, *5*, 4523.
- [2] T. Someya, Z. Bao, G. G. Malliaras, *Nature*, **2016**, *540*, 379.
- [3] C. Liao, M. Zhang, M. Y. Yao, T. Hua, L. Li, F. Yan, *Adv. Mater.*, **2015**, *27*, 7493.
- [4] C. de Balthasar, S. Patel, A. Roy, R. Freda, S. Greenwald, A. Horsager, M. Mahadevappa, D. Yanai, M. J. McMahon, M. S. Humayun, R. J. Greenberg, J. D. Weiland, I. Fine, *Investig. Ophthalmology Vis. Sci.*, **2008**, *49*, 2303.

#### 6:10 AM F.FL01.03.07

***In Situ* Optical Quantification of Biological Electron Transfer Using Plasmonic Semiconductor Nanocrystals** Stephen Gibbs, Austin J. Graham, Camila Saez Cabezas, Yongdan Wang, Delia Milliron and Benjamin K. Keitz; The University of Texas at Austin, United States

Plasmonic semiconductor nanocrystals are more sensitive to electron transfer events than traditional plasmonic materials such as Au and Ag due to their lower free electron concentrations. Because the plasmon peak position and intensity depend on the free electron concentration, we can quantify electrons transferred to and from the semiconductor nanocrystals in real-time through simple spectroscopic measurements. Further, the surface of doped semiconductor nanocrystals can be functionalized with various ligands post-synthetically to customize solvent compatibility, ensure colloidal stability, and tune the interactions with other species in solution. Leveraging our ability to quantify the change in optical response with the aqueous biocompatibility of colloidal nanocrystal dispersions, we aimed to quantify redox activity from cell metabolism. Specifically, we quantified extracellular electron transfer (EET) rates from *Shewanella oneidensis*. EET is process by which electron flux from carbon metabolism is directed to metallic substrates in anaerobic environments. The utility of EET as a power source for microbial fuel cells, bioelectronics, and material synthesis has led to significant interest in quantification methods for microbial electron flux.

When dispersed together, plasmonic semiconductor nanocrystals serve as electron accepting substrates for *S. oneidensis*. We dispersed tin-doped indium oxide (ITO) nanocrystals with *S. oneidensis* in an aqueous buffer by stripping the nanocrystals of their native, hydrophobic ligands and wrapping them in a hydrophilic, random co-polymer. We used *in-situ* spectroscopy to track the plasmonic response of ITO in real-time and quantified kinetic EET rate constants from *S. oneidensis* on a per cell basis. Using this method, we distinguished EET rates of healthy cells from those starved of a carbon source. The consistent measurement of a steady-state electron transfer regime indicated that cellular respiration was primarily directed toward energy production via EET as opposed to growth. Lastly, we quantitatively differentiated electron flux from *S. oneidensis* strains that were genetically engineered to tune EET activity. The generated current ranged from 0.1 to 6.9 fA per cell, depending on expression levels of a key EET gene, *mtrC*. Overall, our results indicate that colloidal plasmonic semiconductor nanocrystals are a reliable sensing platform for probing metabolic activity in native biological environments. Looking forward, we aim to assess EET gene turn-on in real-time in response to environmental stimuli, enabling understanding of fundamental gene expression dynamics.

SESSION F.FL01.04: Organic Active Materials for Signal Transduction  
On Demand Abstracts Available for Viewing Starting Saturday Morning, November 21, 2020  
F-FL01

### 5:00 AM \*F.FL01.04.01

**Ion-Electron Coupling Defines the Principle of Operation in Organic Bioelectronic Devices** [Magnus Berggren](#);  
Linköping University, Sweden

The coupling of electronic charges and ions, in bioelectronic devices based on conjugated polymers, is unique and offers us a great opportunity to explore novel device concepts and also new science. The fundamental principles of charge accumulation and ion exchange in conjugated polymers, often referred to as doping, will be discussed. The dynamic control over doping can be achieved via electrochemical addressing and serves as the principle of operation in an array of organic electrochemical devices. Examples of such devices are the organic electronic sensors and actuators, devices that rely on *iontronic* electrode, transistor, conductor or diode configurations. Such devices and systems have then been applied to several biological and medical settings, targeting new biotech/med-tech tools, therapy and monitoring of physiology and neuronal functions.

### 5:15 AM \*F.FL01.04.02

**Electron Transporting Polymers for Metabolite Detection and Energy Conversion from Bodily Fluids** [Sahika Inal](#);  
King Abdullah University of Science and Technology (KAUST), Saudi Arabia

Being the primary energy source of mammalian cells, glucose is involved in numerous biological events. In this work, I will present an electronic platform based on an n-type conjugated polymer for detecting glucose as well as extraction of power from bodily fluids. We employ the n-type mixed (ionic and electronic) conductor in an accumulation mode organic electrochemical transistor (OECT). The polymer is engineered to have specific interactions with catalytic enzymes and requires no electron mediators to transduce enzymatic reactions. This micron-scale device detects glucose alongside lactate and shows excellent sensitivity and selectivity over five orders of magnitude wide detection range (1,2). When assembled as an enzymatic biofuel cell, the same polymer serves as the anode, converting the glucose metabolism in an aqueous medium into power (2). These devices can be fabricated on flexible substrates, paving the way for implantable self-powered metabolite sensing. While introducing these bioelectronic device concepts, I will touch upon approaches to further improve the performance of n-type mixed conductors.

1. Pappa et al Sci. Adv. **4**, 6, eaat0911 (2018)
2. Ohayon et al Nat. Mater. **19**, 456–463 (2020)

### 5:30 AM F.FL01.04.03

**Low-Impedance Electropolymerized Coatings on Microelectrodes for Higher Neuro-Transduction** [Anna Susloparova](#)<sup>1</sup>, Mahdi Ghazal<sup>1</sup>, David Guérin<sup>1</sup>, Sophie Halliez<sup>2</sup>, Yannick Coffinier<sup>1</sup>, Thomas Dargent<sup>1</sup>, Fabien Alibart<sup>1,3</sup> and Sébastien Pecqueur<sup>1</sup>; <sup>1</sup>Univ. Lille, CNRS, Centrale Lille, Univ. Polytechnique Hauts-de-France, UMR 8520 - IEMN, France; <sup>2</sup>Université de Lille, Univ. Lille, Inserm, CHU-Lille, Jean-Pierre Aubert Research Centre (JPArC, UMR - S 1172), France; <sup>3</sup>Université de Sherbrooke, Unité mixte internationale - Laboratoire Nanotechnologies & Nanosystèmes (UMI-LN2), Canada

Microelectrode arrays (MEAs) are widely used tools for investigating neural activity. To ensure the best sensitivity of the electronic devices to ionic signals and the lowest information loss, their electrochemical interface must be optimized by lowering their surface impedance, with materials that ensure the highest compatibility with the cells at the same time. Here, we show that by the electropolymerization of thiophene-derivatives, functionalized for higher cell biocompatibility and higher electrochemical performances, one can lower the microelectrodes' surface impedance by the control of the polymer morphology. The microelectrode structuring with bottom-up grown conducting polymers was monitored in-situ by voltage-ramped impedance spectroscopy upon electropolymerization to track its circuit-elements modification. Iterative impedance modeling over the growth confirmed the material's electrochemical dynamic to be controlled by the gradual modifications of specific discrete circuit elements at different frequency ranges, thanks to the surface electrodes microstructuring. More particularly, we systematically evidenced a monotonic change of the electrode charging from ideal capacitor to constant phase element dominated modes, due to the bulk charging of the conducting polymer. The evolution of the materials morphology screened by atomic force microscopy and electron microscopy has been confronted to the modification of the materials circuit element, and confirmed distinctive charging modes for the electrodes that are governed by their different texturing. In addition to the surface morphology, chemical tuning of the electrodeposited polymer has been performed and showed that a fine tuning of the polymer's glycolation promotes the decrease of the electrodes' electrochemical impedance down to -15% compared to the unglycolated polymers thanks to a right balance between ionic permeability and electronic performances.

Overall, lower impedance values than commercial MEAs have been systematically reached with performances comparable to spin-coated polymer electrodes', and with low performance dispersion over the whole population of electrodes in the MEAs. With the presented preliminary biocompatibility and stability tests, this study aims is to demonstrate that unusual microfabrication techniques derived from electrochemistry can provide unique features at the material level to match properties of future emerging bioelectronics technologies to the strong requirements of sensing involving biological materials with rich material chemistry and morphology.

#### 5:40 AM F.FL01.04.04

**Conducting Polymer Composites with DNA as Counterion for Bioelectronics** Serpil Tekoglu, Dominik Wielend, Clark Markus Scharber, Cigdem Yumusak and Niyazi Serdar Sariciftci; Johannes Kepler Universität Linz, Austria

Conductive polymers (CPs) are in the particular interest of bioelectronics as they combine the mechanical flexibility with the electrical and ionic conductivity. Poly(3,4-ethylenedioxythiophene):poly(styrene sulfonate) (PEDOT:PSS) has been widely studied as the most promising CP due to its conductivity, processability, and commercial availability.<sup>1</sup> However, the biocompatibility of this benchmark material for long-term applications is still under debate,<sup>2</sup> even though a recent study has demonstrated its stability in cell culture for up to four months.<sup>3</sup> Therefore, for interfacing electronics with biology, there is still a high demand for biocompatible devices and materials showing mixed electronic/ionic conductivity. Recently, PEDOT has been incorporated with biomolecule dopants, e.g., deoxyribonucleic acid (DNA), hyaluronic acid, dextran sulfonate, heparin, pectin, guar gum to modify the properties.<sup>4</sup> Among those, PEDOT:DNA has the main advantage of higher ionic conductivity with respect to PEDOT:PSS.<sup>5</sup>

In our work, we prepared PEDOT:DNA and polypyrrole:DNA aqueous dispersions by oxidative chemical polymerization. DNA was engaged as a stabilizer and dopant during the polymerization process of EDOT and pyrrole monomers. Different surfactants and secondary dopants were added into the dispersed solutions to support the thin-film processing using the spin-coating technique as well as to avoid the delamination of the films. Subsequently, we investigated the electrical, optical, and morphological properties of the biocomposite films. We fabricated organic electrochemical transistors (OECTs) involving conducting polymer biocomposites as the organic active layer and compared the transistor characteristics to PEDOT:PSS based OECTs.<sup>6</sup> Additionally, biocompatibility tests on the conductive films were carried out. The results showed that DNA-based conductive polymers can be considered as novel biocomposites for iontronics such as OECTs and biosensors.

1. Wen, Y.; Xu, J. Scientific Importance of Water-Processable PEDOT:PSS and Preparation, Challenge and New Application in Sensors of Its Film Electrode: A review. *J. Polym. Sci. A*, 55, 1121–1150 (2017).
2. Wei, B.; Liu, J.; Ouyang, L.; Kuo, C.-C.; Martin, D.C. Significant Enhancement of PEDOT Thin Film Adhesion to Inorganic Solid Substrates with EDOT-Acid. *ACS Appl. Mater. Interface*, 7, 15388-15394 (2015).
3. Dijk, G.; Rutz, A. L.; Malliaras, G. G.; Stability of PEDOT:PSS coated gold electrodes in cell culture conditions, *Adv. Mater. Technol.*, 1900662, (2019).
4. Mantione, D.; Del Agua, I.; Sanchez-Sanchez, A.; Mecerreyes, D. Poly(3,4-ethylenedioxythiophene) (PEDOT) Derivatives: Innovative Conductive Polymers for Bioelectronics. *Polymers*, 9, 354 (2017).
5. Ner, Y.; Invernale, M.A.; Grote, J.G.; Stuart, J.A.; Sotzing, A.G. Facile Chemical Synthesis of DNA-doped PEDOT. *Synthetic Metals*, Vol.160, Issue 5-6, 351-353 (2010).
6. Tekoglu, S.; Wielend, D.; Scharber, M. C.; Sariciftci, N. S.; Yumusak, Cigdem; Conductive Polymer-Based Nanocomposites Using Deoxyribonucleic Acid (DNA) as Counterion, *Adv. Mater. Technol.*, 1900699, (2019).

#### 5:50 AM F.FL01.04.05

**Peptide Based Biomaterials with Tunable Electron/Proton Conductivity** Nurit Ashkenasy; Ben Gurion University of the Negev, Israel

The emerging need for bioelectronic devices that interface with biological substances is accompanied by a growing need for biocompatible, biodegradable, conducting materials. Biomaterials, which are inherently biocompatible, biodegradable, are commonly considered to be "bad conductors". In order to overcome this challenge, our group is developing bio-inspired materials based on *de-novo* design of peptides that capture many of the features of proteins on one hand, and are optimized for electronic and/ or protonic conduction applications on the other hand. In this talk, I will demonstrate the use of *b*-sheet forming peptides for the development of conductive materials. Specifically, I will show that the sequence of the peptide can greatly influence the conductivity with sensitivity to even single sequence mutation. These effects are shown to originate both from the differences in the intrinsic ability of a specific amino acid to participate in the charge transport process, and also from their effects on the assembly of the structure, which in return affect the conductivity. Design concepts for improving



either electron<sup>1,2</sup> or proton<sup>3</sup> conductivity, or both,<sup>4</sup> will be presented. The structure function relationships we reveal can be used for the design of novel biocompatible organic bio-electronic devices.

## References

1. M. Amit, G. Cheng, I. W. Hamley, and N. Ashkenasy, "Conductance of amyloid  $\beta$  based peptide filaments: Structure-function relations". *Soft Matter*, **8**, 8690-8696, (2012).
2. D. Ivnitiski, M. Amit, O. Silberbush, Y. Atsmon-Raz, J. Nanda, R. Cohen-Luria, Y. Miller, G. Ashkenasy, and N. Ashkenasy, "Structure Polymorphism Strongly influences the conductivity of peptide fibrils" *Angewandte Chemie Int. Ed.*, **55**, 9988 (2016).
3. O. Silberbush, M. Amit, S. Roy and N. Ashkenasy "Significant enhancement of proton transport in bioinspired peptide fibrils by single acidic or basic amino acid mutation" *Adv. Func. Mat.* **27**, 1616-3028 (2017).
4. M. Amit, S. Appel, R. Cohen, G. Cheng, I. W. Hamley, and N. Ashkenasy, "Hybrid Proton and Electron Transport in Peptide Fibrils", *Adv. Func. Mat.* **24**, 5873-5880 (2014)

## 6:00 AM F.FL01.04.06

**Ions-Based High Bandwidth Communication for Implantable Bioelectronics** Zifang Zhao, Georgios Spyropoulos, Claudia Cea, Jennifer Gelinis and Dion Khodagholy; Columbia University, United States

Implanted devices such as pacemakers and brain stimulators are critical treatment modalities for certain patients. Establishing communication with implanted devices wirelessly remains a difficult task because biologic tissue absorbs most of the electromagnetic waves. Instead, we hypothesized that ions in biological tissue could serve as communicating carriers. The key parameters to achieve megahertz-bandwidth ionic communication with controllable propagation radius is unknown. Here, we describe the working principles of ionic communication (IC) and the effect of material and geometrical properties such as electrode area, material composition, ion type/concentration, and operating frequency on this process. For each of these properties, we performed electrochemical impedance spectroscopy (EIS) and a gain-bandwidth test. Using this approach, we were able to optimize the electrode design for different applications towards such as higher bandwidth or longer-range transmission. We then designed implantable transdermal IC electrodes with several MHz bandwidth. We used these devices to acquire high quality *in vivo* electrophysiological data from freely moving rats. The proposed working theory of IC and the resulting devices set the foundation for advanced biomedical implantable systems, such as brain-computer interfaces, that require a low consumption, high bandwidth wireless communication system.

## 6:10 AM F.FL01.04.07

**Late News: Probing the Impedance of a Biological Tissue with PEDOT:PSS Coated Metal Electrodes—Effect of Electrode Size on Sensing Efficiency** Dimitrios Koutsouras, Leona V. Lingstedt, Katharina Lieberth, Jonas Reinholz, Volker Mailänder, Paul W. Blom and Paschalis Gkoupidenis; Max Planck Institute for Polymer Research, Germany

PEDOT:PSS (Poly(3,4 ethylenedioxythiophene):polystyrene sulfonate) coated electrodes have been widely used to evaluate the integrity of cellular barriers. Nevertheless, an experimental and systematic study of the correlation between tissue integrity and impedance of the sensing device has not yet been conducted. In this work, with the use of impedance spectroscopy, we investigate the way that impedance ratio of the biological tissue to the recording device affects the recording ability of the latter. Various sized PEDOT:PSS coated electrodes are employed and the effect of their dimensions to their sensing ability is determined. A simple equivalent circuit is proposed to model the biotic/abiotic ensemble and an analytical expression of the total impedance as a function of frequency is extracted. The study results in a critical impedance ratio of the biological tissue to the sensor, which allows for efficient sensing of the tissue integrity. This work opens new pathways for the realization of improved impedance based biosensors with optimized sensitivity.

SESSION F.FL01.05: Transistors for Sensing

On Demand Abstracts Available for Viewing Starting Saturday Morning, November 21, 2020

F-FL01

## 5:00 AM F.FL01.05.01

**Effect of Channel Thickness on Noise in Organic Electrochemical Transistors** Anastasios Polyravas<sup>1</sup>, Nathan Schaefer<sup>2</sup>, Vincenzo F. Curto<sup>1</sup>, Andrea B. Calia<sup>2</sup>, Anton G. Brunet<sup>3,4</sup>, Jose A. Garrido<sup>2,5</sup> and George G. Malliaras<sup>1</sup>; <sup>1</sup>Electrical Engineering Division, Department of Engineering, University of Cambridge, 9 JJ Thomson Ave, Cambridge CB3 0FA,

United Kingdom, United Kingdom; <sup>2</sup>Catalan Institute of Nanoscience and Nanotechnology (ICN2), CSIC, Barcelona Institute of Science and Technology, Campus UAB, Bellaterra, Barcelona, Spain, Spain; <sup>3</sup>Institut de Microelectronica de Barcelona, IMB-CNM (CSIC), 08193, Bellaterra, Barcelona, Spain, Spain; <sup>4</sup>CIBER-BBN, Networking Center on Bioengineering, Biomaterials and Nanomedicine, Barcelona, Spain, Spain; <sup>5</sup>ICREA, Pg. Lluís Companys 23, 08010 Barcelona, Spain, Spain

Organic electrochemical transistors (OECTs) have been widely used as transducers in electrophysiology and other biosensing applications. Their identifying characteristic is a transconductance that increases with channel thickness, and this provides a facile mechanism to achieve high signal amplification. However, little is known about their noise behaviour. Here, we investigate noise and extract metrics for signal-to-noise ratio and limit of detection in OECTs with different channel thickness. These metrics are shown to improve as channel thickness increases, but the improvement is not proportional and tends to saturate for thicker channels. The results show that OECTs can be easily optimised to show not only high amplification, but also low noise.

#### 5:10 AM F.FL01.05.02

**Self-Aligned Laser-Cut OECTs for Biological Sensing** Reem B. Rashid and Jonathan Rivnay; Northwestern University, United States

Organic electrochemical transistors (OECTs) have gained popularity for biological sensing, for a variety of applications, ranging from neural signal recording to ion detection, due to their amplification capabilities. OECTs are three terminal devices where the organic semiconducting channel's bulk conductance is modulated via ionic/electronic interactions when operated in electrolyte. The main differences between OECTs and OFETs is the prevalence of bulk (as opposed to interfacial) charging and transport. As such, OECTs can take on smaller form factors, have high transconductance, and do not require the pristine interfaces that OFETs require which allows for more relaxed fabrication constraints. The same advantageous bulk charging, however, can result in parasitic capacitance when the mixed conductor/contact overlap in devices are large. In micro-OECT devices patterned photolithographically, these overlaps (which aid in layer-to-layer alignment) can account for >50% of the total measured device capacitance, slowing device response time.

In this work we simplify patterning and eliminate parasitic capacitance by fabricating OECTs with laser-cut channels and a self-aligning insulation. The self-aligning insulation is made of a hydrophobic coating that allows the semiconducting material to be "dragged and dropped" into the laser cut channel between the source and drain contacts, eliminating the need for photolithography, dry etching and a sacrificial insulation layer to pattern the organic material in the channel. The self-aligned OECTs showed one hundred percent yield and electronic properties (mobility and threshold voltage) similar to those fabricated with traditional methods. These self-aligned OECTs were also fabricated onto flexible substrates to show the applicability for biological applications.

This method of manufacturing was extended for use with vertical OECTs (vOECTs), by stacking another layer of gold contact to create a vertical channel between the source and drain contacts, which eliminates parasitic capacitance once again. Finally, we used these vOECTs to create simple circuits that allow for the possibility of simultaneous on-site amplification and signal processing, for applications such as differential and biochemical sensing, without increasing overall device footprint.

#### 5:20 AM F.FL01.05.03

**Post-Fabrication Optimization Technique of Organic Electrochemical Transistor (OECT) for Electrophysiology by Electropolymerization** Mahdi Ghazal<sup>1</sup>, Anna Susloparova<sup>1</sup>, Sophie Halliez<sup>2</sup>, Morvane Colin<sup>2</sup>, Luc Buée<sup>2</sup>, Yannick Coffinier<sup>1</sup>, Sébastien Pecqueur<sup>1</sup>, Thomas Dargent<sup>1</sup> and Fabien Alibart<sup>1,3</sup>; <sup>1</sup>Institut d'électronique de microélectronique et de nanotechnologie, France; <sup>2</sup>Jean-Pierre Aubert Research Centre, France; <sup>3</sup>Laboratoire Nanotechnologies and Nanosystemes, Canada

The recent progress in the extracellular microelectrode arrays (MEAs) have greatly improved our ability to probe cellular electrophysiological activities. Nevertheless, passive MEAs are subject to small signal-to-noise ratio and small potential detection.

Recently, organic electrochemical transistors (OECTs) have been identified as a promising device architecture to improve extracellular potentials recording in electroactive cells culture both in-vitro and in-vivo. In addition to unique properties of interest for electrophysiology such as biocompatibility, transparency and flexibility, OECTs operating principle is based on the transduction of ionic currents in the biological medium into electronic currents in the organic semiconductor (e.g. PEDOT:PSS) via electrochemical coupling. The transconductance represents an important figure of merit of OECTs and depends on geometrical and material parameters that rules largely OECTs performances for sensing electrophysiological

signals. However, as an organic electronic technology, larger device-property distributions are often encountered with respect to the one of metal- or inorganic-based technologies, inherent to the very nature of the soft organic materials involved in the OECTs transduction process.

Here, we explore the possibility to tune post-fabrication material and geometrical parameters of OECTs with electropolymerization of EDOT. We show that this strategy can be used to simultaneously improve OECT transconductance and its geometrical capacitance. The addressed OECT chips were micro-fabricated on a glass substrates with spin coated PEDOT:PSS. Electropolymerization of EDOT on top of spin-coated PEDOT:PSS was carried on with both fix voltage and ramp voltage techniques. A detail impedance analysis was performed during OECTs functionalization. DC electrical characterizations was used to correlate the transconductance and capacitance tuning due to electropolymerization and to assess device performances improvements. Scanning Electron Microscopy (SEM) was used to correlate morphological changes due to electropolymerization with the enhancement in the transconductance and capacitance of the OECTs. Finally, we performed bio-compatibility assessment between primary neural cells culture and the different possible monomers used for electropolymerization to evaluate the possibility to improve affinity between cultured neurons and electropolymerized materials.

The key novelty of this material engineering technique is to propose a promising method for tunable OECTs sensors development. For instance, this back-end-of-line tuning technique can reduce chip variability in terms of performance yield and bring OECTs technology to the next maturity level. Furthermore, such flexibility can enable matching the electrochemical impedance of the device to the one of the cells, and in the future promote exploratory sensing missions, merging brain-inspired information processing with neuro-sensing.

#### **5:30 AM F.FL01.05.04**

#### **Ultra-Low Power Neurotransmitter Sensor Using Aptamer Functionalized Deep Subthreshold Schottky-Barrier IGZO TFT** Abhijeet Barua, Ryan White and Rashmi Jha; University of Cincinnati, United States

Aptamer-based target biomolecule sensing is attracting much interest due to their excellent reception with high selectivity and specificity. The 3D structure coupled with the short strand length of aptamers enables detection within the Debye limit of ionic solutions [1]. Field effect transistors (FETs) offer an excellent platform to transduce and amplify the effective change in the charged aptamer morphology on target binding into electrical signals. However, these FETs need to be ultralow power and portable on flexible substrates for seamless integration with micro-probes or wearable devices. Amorphous oxide semiconductors such as InGaZnO (IGZO) demonstrate high mobility, low process complexity, good uniformity, stability in threshold voltage, and reduced leakage due to the wide bandgap [2]. Moreover, their low thermal budgets will allow them to be integrated heterogeneously on Si CMOS fabrication in Back End of Line (BEOL) processes. However, IGZO TFTs have been mostly studied at near threshold operations that require high bias voltages. Interestingly, recent reports have investigated Schottky barrier (SB) source and drain regions where the presence of two reverse biased Schottky diodes facilitate deep subthreshold operation due to gate-bias induced modulation of current injection or extraction at these terminals through the presence of a depletion region that impinges on the channel [3]. The diodes also enable early saturation of the transistor output curves and shield it from deleterious contact effects. Prior work has demonstrated SB formation in IGZO TFT with Ohmic metals such as Ti/Pt/Mo by modulating the vacancy concentration in IGZO via deposition under higher oxygen partial pressure [3], [4]. We report deep subthreshold SB IGZO TFTs by metal-IGZO contact engineering. Experimental verification of the deep subthreshold enabled ultra-low power operation with below unity switching voltages has been completed and almost infinite output resistance ( $\sim 10^{12}$  Ohms) and subsequent high intrinsic gain ( $>100$ ) have been derived. Stability tests in this regime have demonstrated extremely low drifts in device behavior. A model is under development for the behavior of the device in this subthreshold region, influenced by a reverse biased Schottky and a diffusion/drift behavior. The low-voltage operation is important for biosensors, where this would allow sensing within the electrochemical window ( $< 1V$ ) of the analyte solution, prevent local work function change of the electrodes, and enable stable bias stress operation to sample the analyte at regular intervals. We propose a platform of aptamer functionalized low power operation TFTs that can selectively and specifically detect physiological neurotransmitter (NT) concentrations in solutions to be used for diagnosis of mental disorders. Dopamine [2-(3,4-dihydroxyphenyl) ethylamine] is an important catecholamine NT that plays a crucial role in the central nervous, hormonal, renal and cardiovascular system and helps in the control of cognitive/motor and neuroendocrine functions. Imbalances in dopamine secretions can lead to neurological disorders such as post-traumatic stress disorder (PTSD), Parkinson's, Schizophrenia and Alzheimer's disease [1]. Therefore, preliminary tests have been conducted to evaluate TFTs for dopamine detection through a novel 'click chemistry' functionalization technique. This process incorporates the catalytic adhesion of an alkyne terminated molecule with an azide anchored aptamer which precludes the need for an intermediate molecular adhesion step. Hence, this would lead to a shorter overall bond length as well as lower steric hindrance. The aptamer was specifically synthesized for selectivity towards dopamine target and in vitro initial experiments with a lower limit of 10nM have been performed.

1. Science 2018 Oct 19;362(6412):319-324.
2. Appl. Phys. Lett. 92, 033502 (2008).
3. PNAS March 12, 2019 116 (11) 4843-4848.
4. Science 2016 Oct 21;354(6310):302-304.

#### 5:40 AM F.FL01.05.05

##### **Late News: Monitoring Reversible Tight Junction Modulation with a Current-Driven Organic Electrochemical Transistor**

**Katharina Lieberth**<sup>1</sup>, Maximilian Brückner<sup>1,2</sup>, Fabrizio Torricelli<sup>3</sup>, Volker Mailänder<sup>1,2</sup>, Paschalis Gkoupidenis<sup>1</sup> and Paul W. Blom<sup>1</sup>; <sup>1</sup>Max-Planck Institute for Polymer Research, Germany; <sup>2</sup>University Medical Center of the Johannes Gutenberg-University Mainz, Germany; <sup>3</sup>University of Brescia, Italy

Present characterization techniques for the tight junction modulation are either invasive, such as fluorescence marking<sup>[1]</sup>, or have low ion sensitivity, like trans-epithelial electrical resistance<sup>[2]</sup>. The organic electrochemical transistor (OECT) is able to operate in aqueous solutions at low voltages, so it is a biocompatible, label-free and low-cost ion-to-electron converter.<sup>[3]</sup> Therefore, OECTs are suited biosensors for drug delivery and related processes as cell barrier integrity.<sup>[4]</sup> The passage of nutrients and drugs into the blood is regulated by the barrier functionality of a cell layer. Hence, modulating the barrier functionality by external chemical agents like poly-L-lysine (PLL) is crucial for drug delivery.<sup>[5]</sup> The ability of a cell layer to impede the passage of ions through it and therefore to act as a barrier, can be assessed electrically by measuring the resistance across the cell layer. Here, we used an OECT in a current-driven configuration for the evaluation of reversible modulation of tight junctions in the epithelial colon carcinoma (Caco-2) cell line,<sup>[6]</sup> found in the small intestine, over time. Operating the OECT in current-driven configuration enhances the sensitivity,<sup>[7]</sup> required to study reversible ion permeability through tight junctions of Caco-2 cells. The reversible opening and closing of tight junctions was detected using the PLL at RT and under physiological conditions. Concentration and time dependent experiments resumed that the exposure to low and medium concentrations of PLL initiates reversible modulation, whereas a too high concentration induces an irreversible barrier disruption due to non-functional tight junction proteins. To support electrical measurements occluding-staining has been performed using immunofluorescence imaging. The results demonstrate the suitability of OECTs to *in-situ* monitor temporal barrier modulation and recovery, which can offer valuable information for drug delivery applications.

[1] M. Ramuz, A. Hama, M. Huerta, J. Rivnay, P. Leleux, R. M. Owens, *Adv. Mater.* **2014**, 7083.

[2] L. H. Jimison, S. A. Tria, D. Khodagholy, Gurfinkel M., E. Lanzarini, A. Hama, G. G. Malliaras, R. M. Owens, *Adv. Mater.* **2012**, 5919.

[3] J. Rivnay, P. Leleux, M. Sessolo, D. Khodagholy, T. Hervé, M. Fioocchi, G. G. Malliaras, *Advanced materials (Deerfield Beach, Fla.)* **2013**, 25, 7010.

[4] N. Y. Shim, D. A. Bernards, D. J. Macaya, J. A. DeFranco, M. Nikolou, R. M. Owens, G. G. Malliaras, *Sensors* **2009**, 9896.

[5] G.T.A. McEwan, M. A. Jepson, B. H. Hirst, N. L. Simmons, *Biochimica et Biophysica Acta* **1993**, 1148, 51.

[6] M. S. Balda, K. Matter, *Seminars in cell & developmental biology* **2000**, 11, 281.

[7] a) M. Ghittorelli, L. Lingstedt, P. Romele, N. I. Crăciun, Z.M. Kovács-Vajna, P.W.M. Blom, F. Torricelli, *Nature Communications* **2018**, 1441; b) L. V. Lingstedt, M. Ghittorelli, M. Brückner, J. Reinholz, N. I. Crăciun, F. Torricelli, V. Mailänder, P. Gkoupidenis, P. W. M. Blom, *Advanced healthcare materials* **2019**, 8, e1900128.

#### 5:50 AM F.FL01.05.06

##### **Late News: Operation Mechanism and Design Rules for Organic Electrochemical Transistors as Redox Chemical Transducers**

**Siew Ting Melissa Tan** and Alberto Salleo; Stanford University, United States

Organic Electrochemical Transistors (OECTs) have exhibited promising performance as transducers and amplifiers of low potentials due to their exceptional transconductance, enabled by the volumetric charging of Organic Mixed Ionic/Electronic Conductors (OMIECs) employed as the channel material. OECT performance in aqueous electrolytes as well as the OMIECs' redox activity has spurred a myriad of studies employing OECTs as chemical transducers. However, the OECT's large (potentiometrically derived) transconductance is not fully leveraged in common approaches that directly conduct chemical reactions amperometrically within the OECT electrolyte with direct charge transfer between the analyte and the OMIEC, which results in sub-unity transduction of gate to drain current. Hence, amperometric OECTs do not truly display current gains in the traditional sense, falling short of the expected transistor performance. We have demonstrated in our previous work an alternative device architecture that separates chemical transduction and amplification processes on two distinct electrochemical cells (*I*). This approach fully utilizes the OECT's large transconductance to achieve current gains of 10<sup>3</sup> and current modulations of four orders of magnitude. Furthermore, harvesting energy from the chemical reaction on the reaction cell renders the gate circuit self-powered. This simple yet overlooked transduction mechanism represents a general

approach enabling high-gain chemical OECT transducers.

In this current work, we investigate the device physics behind the different architectures and operation modes of the OECT as redox chemical sensors. Analyses reveal that in the amperometric operation of the OECT, approaches to optimize both chemical transduction and OECT operation are challenging at best, and even contradictory in some cases. Furthermore, conducting faradaic reactions at non-equilibrium conditions within the OECT result in complex effects arising from voltage-dependent redox reaction rates, spatially asymmetric voltage variations across the channel, and mass transport dependencies. In contrast, the operation of the RC-OECT at equilibrium conditions allows for a simple model to describe its operation, enabling straightforward optimization of its performance by materials selection and device design. Furthermore, the separation of chemical transduction and electronic amplification on two separate compartments allow for more feasible optimization of the individual components.

This study sheds light on the challenges faced by the conventional approach of conducting redox sensing reactions within the electrolyte of the OECT. Additionally, it suggests a promising alternative approach to simultaneously achieve chemical transduction and reap the full amplification capabilities of the OECT, including a simple model for understanding device operation. The RC-OECT's superior performance and predictability of device performance from fundamental materials properties will aid the future development of high-performance chemical sensors for early disease diagnosis.

I. S. T. M. Tan, A. Giovannitti, A. Melianas, M. Moser, B. L. Cotts, D. Singh, I. McCulloch, A. Salleo, Chemical to Electrical Transduction using Fuel Cell Powered Organic Electrochemical Transistors (2020), doi:10.26434/CHEMRXIV.12071136.V1.

SESSION F.FL01.06/SM05.05: Joint Session: Bioelectronics and Sensing  
On Demand Abstracts Available for Viewing Starting Saturday Morning, November 21, 2020  
F-FL01

**5:00 AM \*F.FL01.06/SM05.05.01**

**Electron Transporting Polymers for Biological Interfacing** Sahika Inal; King Abdullah University of Science and Technology (KAUST), Saudi Arabia

Fluidity, mobility, and resistivity are key characteristics of native membranes in our cells where cation channels regulate numerous molecular mechanisms (e.g., the excitation of neurons). Interfacing with biomimetic membranes via electronic devices promises to expand our understanding of the function of these membranes in disease states. The challenge is to form supported lipid bilayer (SLBs) on (semi)conducting films while sustaining high sensitivity and operational stability. In this talk, I will show the traits of n-type organic semiconductors for such biological interfaces. I will show the very first ion channel sensor based on an n-type, accumulation mode, microscale organic electrochemical transistor (OECT), which interfaces an SLB embedded with a pore-forming protein. The polymer is particularly sensitive to divalent cations, endowing the system with biomimetic properties. The side-chain engineering of semiconducting polymers prompts the development of next-generation bioelectronic hybrids where electron-transporting polymers establish bilateral electronic communication with living systems.

**5:15 AM \*F.FL01.06/SM05.05.02**

**Thin-Film Organic Electrochemical Devices for Applied Neural Control—Capacitive and Faradaic Effects** Eric Glowacki; Linköping University, Sweden

A great demand exists for minimally-invasive neuromodulation technologies to enable next-generation bioelectronic medicine. We report on our developments of ultrathin organic (opto)electronic devices for neurostimulation. All of these devices rely on far red/near infrared irradiation in the tissue transparency window to actuate nanoscale organic semiconductor components. Our flagship technology is the organic electrolytic photocapacitor (OEPC) – a device that mimics biphasic current-pulse neurostimulation and thus transduces an optical signal into directly-evoked action potentials in neurons. These devices are not only wireless, but also 100-1000 times thinner than most existing technologies. We will discuss chronic

implants capable of stimulating peripheral nerves (sciatic and vagus) when actuated from outside of the body using diode lasers. We have observed stable operation in rodent models for at least 100 days. As a different approach, we will report on favorable harnessing of DC electrochemistry effects, normally considered spurious and undesired. Specifically, we show how electrochemical generation of low doses of hydrogen peroxide can be used to reversibly stimulate M-type potassium channels, providing a novel method of controlling neural excitability.

#### 5:30 AM F.FL01.06/SM05.05.03

**Enhancement-Mode Ion-Based Transistors for *In Vivo* Electrophysiology and Real-Time Data Processing** Claudia Cea, Georgios Spyropoulos, Jennifer Gelinis and Dion Khodagholy; Columbia University, United States

Bioelectronic devices must have high speed and high performance to interact with the often rapid, low amplitude signals generated by neural tissue. They should also be capable of forming complementary logic and analog circuits to allow acquisition, processing and manipulation of a biological environment. However, the lack of readily available p-type polymers for use in enhancement mode transistors and their complicated synthesis significantly limits the investigation and application of such devices in bioelectronics. Here, we develop an enhancement mode ion-gated transistor (e-IGT) that functions based on a reversible redox reaction and hydrated ion reservoirs within the conducting polymer channel to enable long-term stable operation and shortened ion transit time. We combined a highly conductive poly(3, 4-ethylenedioxythiophene) doped with polystyrene sulfonate (PEDOT:PSS) and a reducing agent polyethylenimine (PEI) to enable doping of the polymer in an aqueous environment. The transistor operates as following: (1) the protonated PEI bonds with the PSS- and de-dopes the PEDOT:PSS chain resulting in an initial off-state of the transistor, (2) a subsequent application of negative gate voltage dopes the PEDOT:PSS switching the channel on. To determine an optimal transistor configuration and material composition, we microfabricated transistor arrays of varying geometrical parameters. The high-transconductance and high-speed of the e-IGTs resulted in a gain bandwidth product that is several orders of magnitude above other ion-based transistors. We used these transistors to acquire a wide range of electrophysiological signals, including *in vivo* recording of neural action potentials. Furthermore, we combined E-IGTs with d-IGTs to create a real-time non-linear rectifier to accurately detect epileptic discharges *in vivo*. In conclusion, E-IGTs offer a safe, reliable, and high performance building block for chronically implanted bioelectronics, with spatiotemporal resolution to the scale of individual neurons.

#### 5:40 AM F.FL01.06/SM05.05.04

**Organic Electrochemical Transistors Based on Electropolymerized Dendritic Structures** Kamila Janzakova<sup>1</sup>, Mahdi Ghazal<sup>1</sup>, Ankush Kumar<sup>1</sup>, Yannick Coffinier<sup>1</sup>, David Guérin<sup>1</sup>, Sébastien Pecqueur<sup>1</sup> and Fabien Alibart<sup>1,2</sup>; <sup>1</sup>University of Lille, France; <sup>2</sup>Laboratoire Nanotechnologies & Nanosystèmes (LN2), Canada

One of the neuromorphic engineering aims is using nanoelectronics' materials and devices to reproduce key features that are used by the brain for computing. Currently, neuromorphic engineering has explored standard silicon-based technologies (i.e. such as complementary metal-oxide-semiconductor) or more emerging material and devices (iono-electronic materials and resistive memory devices, for example). Most of these technologies are still bounded to a top down approach. However, brain computing largely rely on bottom-up processes. For instance, interconnectivity between cells and formation of communication pathway in neural networks result principally from bottom-up organization. Here, we show how dendritic growth of organic conductive polymers (PEDOT) can be used to mimic structural branching observed in neural network. Conducting-polymer based dendritic structures with different morphology are synthesized in a two-electrode setup by pulsed voltage-driven electropolymerization derived from state-of-the-art bipolar AC-electrochemical synthetic methods. We show how various AC signals can lead to a large variety of dendritic structures and PEDOT morphologies. In a second part, such dendritic structures are used to implement fonctionnal OECTs. More importantly, we focus on the transconductance and memory effects that can be obtained in such dendritic OECTs such as short tem plasticity. We report on the relationship between dendrites morphologies and STP time constant.

This work paves the way to new approaches for neuromorphic engineering, such as structural plasticity and neural network topology exploration.

#### 5:50 AM \*F.FL01.06/SM05.05.05

**Forming Input/Output (i/o) Interfaces with Excitable Cells And Tissue Using Nanocarbons** Tzahi Cohen-Karni; Carnegie Mellon University, United States

We focus on developing a new class of nanoscale materials and novel strategies for the investigation of biological entities at multiple length scales, from the molecular level to complex cellular networks. Our highly flexible bottom-up nanomaterials synthesis capabilities allow us to form unique hybrid-nanomaterials that can be used in various input/output bioelectrical interfaces. For example, we have developed several bioelectrical platforms based on graphene, a two-dimensional (2D)

atomically thin carbon allotrope. We have demonstrated recording of the electrical activity of excitable cells with graphene-based ultra-microelectrodes as small as the size of an axon ca. 2 μm in size. Using graphene-based hybrid-nanomaterials, we have formed remote, non-genetic bioelectrical interfaces with excitable cells and modulated cellular and network activity with high precision and low needed power. We have also developed a breakthrough bioelectrical interface, a 3D self-rolled biosensor arrays (3D-SR-BAs) of either active field effect transistors or passive microelectrodes to measure both cardiac and neural spheroids electrophysiology in 3D. Our approach enables electrophysiological investigation and monitoring of the complex signal transduction in 3D cellular assemblies toward an organ-on-an-electronic-chip (organ-on-e-chip) platform for tissue maturation investigations and development of drugs for disease treatment. In summary, the exceptional synthetic control and flexible assembly of nanomaterials provide powerful tools for fundamental studies and applications in life science and open up the potential to seamlessly merge either nanomaterials-based platforms or unique nanosensor geometries and topologies with cells, fusing nonliving and living systems together.

**6:05 AM \*F.FL01.06/SM05.05.06**

**High-Resolution Bioelectronic Interfaces Enabled by Nanoscale Soft Conductors** Flavia Vitale; University of Pennsylvania, United States

The rapid rise of bioelectronics has enabled a number of innovative approaches to treat neurological disorders, restore and repair lost functions, and modulate neural circuitry to control mood and behavior. The vast majority of bioelectronic interfaces, however, still rely on traditional noble metal and silicon materials, which are expensive to source and process and are intrinsically inadequate to address the mechanical, chemical, and electrical properties of excitable circuits in the body. To establish bioelectronic technologies as the clinical standard, significant innovations in materials and fabrication strategies are still required to achieve safety, softness, biocompatibility, and long-term stability. Nanostructured materials are uniquely positioned to address these challenges because they combine high electrical conductivity with intrinsically high mass-specific surface area and mechanical flexibility. Furthermore, they can interact with biological systems on a molecular scale and can be easily integrated within scalable solution-based processing, thus allowing easy modulation of their electronic and optical properties.

In this talk I will present the ongoing work in my lab to leverage the unique properties of nanostructured materials and engineer novel bioelectronic interfaces for sensing and stimulating neural and neuromuscular circuits. Specifically, I will describe the fundamental electronic, electrochemical, and mechanical properties of 2D transition metal carbides nanomaterials (a.k.a. MXenes) and how these translate into significant impedance and noise reduction when MXenes are integrated bioelectronic interfaces. Then, I will present *ad hoc*, scalable, rapid manufacturing processes developed in my lab to translate the exceptional material properties at the molecular scale into high-resolution, low impedance bioelectronic interfaces that are also compatible with clinical neuroimaging modalities, such as magnetic resonance imaging (MRI) and computerized tomography (CT). Finally, to illustrate the potential of MXene-based bioelectronics, I will present different examples of applications in both implantable and wearable interfaces.

**6:20 AM F.FL01.06/SM05.05.07**

**Late News: Spatiotemporal Response of Organic Electrochemical Transistors** Dimitrios Koutsouras<sup>1</sup>, Morteza Hassanpour Amiri<sup>1</sup>, Katharina Lieberth<sup>1</sup>, Kamal Asadi<sup>1</sup>, Fabrizio Torricelli<sup>2</sup>, Paul W. Blom<sup>1</sup> and Paschalis Gkoupidenis<sup>1</sup>; <sup>1</sup>Max Planck Institute for Polymer Research, Germany; <sup>2</sup>University of Brescia, Italy

Organic electrochemical transistors (OECTs) have recently attracted tremendous attention in the scientific community due to their unique set of features. Especially, the lack of an insulating layer that separates gate from channel, like in conventional field effect transistors, and their feature to support electrolyte gating open new pathways in the field of bioelectronics. In particular, they render the device ideal for measurements in the aqueous environments that dominate the biological world. Additionally, they provide extra possibilities in terms of the device architecture as the gating electrode can be patterned on the same plane as the conducting channel. In a set up like that, what is of extreme interest is the effect of the gate position with respect to the channel. In this work, the spatiotemporal response of a poly(3,4 ethylenedioxythiophene) polystyrene sulfonate (PEDOT:PSS) OECT is examined and its device physics is studied. This work opens new routes for exploiting the physics of multi terminal OECT devices in bioelectronics, sensing and neuromorphic electronics.

SESSION F.FL01.07: Poster Session: Bioelectronic Materials for Neural Interfaces—Stimulation, Sensing, Power and Packaging

On Demand Abstracts Available for Viewing Starting Saturday Morning, November 21, 2020

#### **F.FL01.07.04**

**Cost-Effective Manufacturing of a Bioelectronic Smart System Array (SiMBiT EU Project)** Fabrizio A. Viola and Mario Caironi; Istituto Italiano di Tecnologia - IIT, Italy

Digitizing biomarkers analysis by quantifying them at the single-molecule level is the new frontier for advancing the science of precision health. Such an occurrence will enormously enhance their ability of curing diseases by supporting better prognosis and permitting the application of precise treatment methods. The SiMBiT project will develop a bio-electronic smart system leveraging on an existing lab-based proof-of-concept that can perform single-molecule detection of both proteins and DNA bio-markers (pancreatic cancer precursors) in a minimal sample volume, with enhanced sensing capabilities. In its final shape, it comprises a 96-well plate with the electrolyte gated organic transistors (EG-TFTs) sensing array and the bio-functionalized gates module along with addressing and front-end electronics and an electronic plate reader. Here we present the activity of IIT group on SiMBiT project which is related to the fabrication, with large-area compatible processes such as printing, and optimization of the EG-TFT structure, which will be integrated in a 8x12 matrix. We will show the complete fabrication process and the electrical characterization of the EG-TFTs, together with the firsts sensing measurements which can show the high sensitivity and specificity of the devices, together with the high reproducibility and stability, which are fundamental for the development of a platform of biosensors.

#### **F.FL01.07.06**

**Towards Next-Generation Nerve Repair—Using Amorphous Ferromagnetic Microwires to Promote Nerve Regeneration** Xiaoyu Zhang<sup>1</sup>, Caroline Mills<sup>1</sup>, Yinying Hua<sup>1</sup>, Ryan Koppes<sup>1</sup>, Rafael Pérez del Real<sup>2</sup>, Manuel Vázquez Villalabeitia<sup>2</sup>, Abigail Koppes<sup>1</sup> and Laura Lewis<sup>1,1</sup>; <sup>1</sup>Northeastern University, United States; <sup>2</sup>Instituto de Ciencia de Materiales de Madrid, CSIC, Spain

Peripheral nervous system (PNS) injuries affect millions of people worldwide each year, and peripheral nerve repair remains challenging due to the limited functional recovery and the associated co-morbidities seen in current methods [i]. Modern nerve repair often relies on nerve regeneration, which has been reported to be sensitive to multiple external stimuli, including electromagnetic stimulus and topographical cue. Here we present encouraging results that neurite outgrowth of dorsal root ganglia (DRG) neurons is promoted by applied static magnetic field and, separately, also by topographical guidance from glass-coated magnetic microwires in their demagnetized state. These microwires (diameter ~ 20 microns), comprised of a metallic glass Fe(Co)SiB-based core coated with pyrex glass, possess an extraordinarily responsive magnetic character, with a saturation magnetization around 1.5 T of the metallic core, coercivity in the range of several A/m, and permeability up to around 10<sup>5</sup> [ii]. We hypothesize that employment of magnetized glass-coated microwires will significantly enhance nerve regeneration with combined applications of magnetic and topographical cues.

Magnetic stimulation was applied to DRG neurons using an apparatus developed with Ansys electromagnetic simulation software. This apparatus employed a pair of axially magnetized neodymium-iron-boron magnets joined by an electrical steel flux path to deliver a nominally uniform in-plane magnetic field  $\mu_0 H_{app} \sim 500$  G (0.05 T) to the cells. Topographical guidance was provided to these cells by a parallel assembly (1:5 mesh density) of glass-coated microwires in the absence of an applied magnetic field. As these magnetic microwires were in a demagnetized state, the cells were not subjected to a magnetic field. All cells were cultured for three consecutive days under controlled conditions in an incubator. Data derived from immunocytochemistry and image analysis with MATLAB revealed that the magnetic field application increased the overall neurite outgrowth volume by up to 152% compared to unstimulated controls. No directional guiding effect was observed from the applied magnetic field. However, the topographical cues from the aligned microwire assembly enhanced the directionality of neurite extension with an increase of 39% in average longest neurite length along the wires, but not in total outgrowth. Future investigations involve growing DRG neurons on magnetized glass-coated microwires meshes, providing combined magnetic and topographical stimuli.

**Acknowledgments:** This research was conducted under the auspices of Northeastern University, the Fulbright Scholar Program, and ICMM/CSIC, Spain.

#### **Reference:**

[i] Koppes, A.N., Zaccor, N.W., Rivet, C.J., Williams, L.A., Piselli, J.M., Gilbert, R.J. and Thompson, D.M., 2014. Neurite outgrowth on electrospun PLLA fibers is enhanced by exogenous electrical stimulation. *Journal of neural engineering*, 11(4), p.046002.



[ii] Vázquez, M., 2007. Advanced magnetic microwires, in Handbook of Magnetism and Advanced Magnetic Materials, Ed. S. Parkin & H. Kronmuller, John Wiley Vol 4, 2192-2222

#### **F.FL01.07.08**

**Late News: Multifunctional Nanomaterials for Surface Enhancement Raman Spectroscopic Detection of Cancer Biomarkers** Justine S. Gordon, Chuan-Jian Zhong and Shiyao Shan; SUNY Binghamton, United States

Cancer is one of the leading causes of death with approximately 7 million deaths each year. Although knowledge surrounding the prevention and treatment of cancer is increasing, there is a clear need of highly-sensitive techniques for early detection of cancer to increase the survival rate. This presentation describes recent findings of our investigations of multi-functional nanomaterials for Surface-enhanced Raman scattering (SERS) detection of cancer biomarkers. One important focus is the preparation of magnetic and plasmonic nanoparticles as the SERS probes with high sensitivity, high selectivity, and low detection limit. We have developed a dual-functional nanoprobe system for the SERS detection of the biomarkers. Results on the preparation of gold and core-shell nanoparticles with a magnetic core and plasmonic gold shell will be discussed, focusing on the control of size, composition, and surface properties. Tunable bio-conjugation of the nanoprobe with detection/capture antibodies for the detection of the cancer biomarker, e.g., carcinoembryonic antigen, has been demonstrated. Implications of the results for optimizing the magnetic-plasmonic properties and multiplexing detection of cancer biomarkers will also be discussed.

SESSION F.LP03.01: Live Poster Session: Flexible, Wearable Electronics, Textiles and Sensors (F.FL01 and F.FL02)  
Session Chairs: Polina Anikeeva and Jacob Robinson  
Tuesday Afternoon, December 1, 2020  
1:45 PM - 3:45 PM  
F.FL01

#### **F.FL01.07.04**

**Cost-Effective Manufacturing of a Bioelectronic Smart System Array (SiMBiT EU Project)** Fabrizio A. Viola and Mario Caironi; Istituto Italiano di Tecnologia - IIT, Italy

Digitizing biomarkers analysis by quantifying them at the single-molecule level is the new frontier for advancing the science of precision health. Such an occurrence will enormously enhance their ability of curing diseases by supporting better prognosis and permitting the application of precise treatment methods. The SiMBiT project will develop a bio-electronic smart system leveraging on an existing lab-based proof-of-concept that can perform single-molecule detection of both proteins and DNA bio-markers (pancreatic cancer precursors) in a minimal sample volume, with enhanced sensing capabilities. In its final shape, it comprises a 96-well plate with the electrolyte gated organic transistors (EG-TFTs) sensing array and the bio-functionalized gates module along with addressing and front-end electronics and an electronic plate reader. Here we present the activity of IIT group on SiMBiT project which is related to the fabrication, with large-area compatible processes such as printing, and optimization of the EG-TFT structure, which will be integrated in a 8x12 matrix. We will show the complete fabrication process and the electrical characterization of the EG-TFTs, together with the firsts sensing measurements which can show the high sensitivity and specificity of the devices, together with the high reproducibility and stability, which are fundamental for the development of a platform of biosensors.

#### **F.FL01.07.06**

**Towards Next-Generation Nerve Repair—Using Amorphous Ferromagnetic Microwires to Promote Nerve Regeneration** Xiaoyu Zhang<sup>1</sup>, Caroline Mills<sup>1</sup>, Yinying Hua<sup>1</sup>, Ryan Koppes<sup>1</sup>, Rafael Pérez del Real<sup>2</sup>, Manuel Vázquez Villalabeitia<sup>2</sup>, Abigail Koppes<sup>1</sup> and Laura Lewis<sup>1,1</sup>; <sup>1</sup>Northeastern University, United States; <sup>2</sup>Instituto de Ciencia de Materiales de Madrid, CSIC, Spain

Peripheral nervous system (PNS) injuries affect millions of people worldwide each year, and peripheral nerve repair remains challenging due to the limited functional recovery and the associated co-morbidities seen in current methods [i]. Modern nerve repair often relies on nerve regeneration, which has been reported to be sensitive to multiple external stimuli, including electromagnetic stimulus and topographical cue. Here we present encouraging results that neurite outgrowth of dorsal root ganglia (DRG) neurons is promoted by applied static magnetic field and, separately, also by topographical guidance from

glass-coated magnetic microwires in their demagnetized state. These microwires (diameter  $\sim 20$  microns), comprised of a metallic glass Fe(Co)SiB-based core coated with pyrex glass, possess an extraordinarily responsive magnetic character, with a saturation magnetization around 1.5 T of the metallic core, coercivity in the range of several A/m, and permeability up to around  $10^5$  [ii]. We hypothesize that employment of magnetized glass-coated microwires will significantly enhance nerve regeneration with combined applications of magnetic and topographical cues.

Magnetic stimulation was applied to DRG neurons using an apparatus developed with Ansys electromagnetic simulation software. This apparatus employed a pair of axially magnetized neodymium-iron-boron magnets joined by an electrical steel flux path to deliver a nominally uniform in-plane magnetic field  $\mu_0 H_{app} \sim 500$  G (0.05 T) to the cells. Topographical guidance was provided to these cells by a parallel assembly (1:5 mesh density) of glass-coated microwires in the absence of an applied magnetic field. As these magnetic microwires were in a demagnetized state, the cells were not subjected to a magnetic field. All cells were cultured for three consecutive days under controlled conditions in an incubator. Data derived from immunocytochemistry and image analysis with MATLAB revealed that the magnetic field application increased the overall neurite outgrowth volume by up to 152% compared to unstimulated controls. No directional guiding effect was observed from the applied magnetic field. However, the topographical cues from the aligned microwire assembly enhanced the directionality of neurite extension with an increase of 39% in average longest neurite length along the wires, but not in total outgrowth. Future investigations involve growing DRG neurons on magnetized glass-coated microwires meshes, providing combined magnetic and topographical stimuli.

Acknowledgments: This research was conducted under the auspices of Northeastern University, the Fulbright Scholar Program, and ICMM/CSIC, Spain.

#### Reference:

[i] Koppes, A.N., Zaccor, N.W., Rivet, C.J., Williams, L.A., Piselli, J.M., Gilbert, R.J. and Thompson, D.M., 2014. Neurite outgrowth on electrospun PLLA fibers is enhanced by exogenous electrical stimulation. *Journal of neural engineering*, 11(4), p.046002.

[ii] Vázquez, M., 2007. Advanced magnetic microwires, in *Handbook of Magnetism and Advanced Magnetic Materials*, Ed. S. Parkin & H. Kronmuller, John Wiley Vol 4, 2192-2222

#### **F.FL01.07.08**

**Late News: Multifunctional Nanomaterials for Surface Enhancement Raman Spectroscopic Detection of Cancer Biomarkers** Justine S. Gordon, Chuan-Jian Zhong and Shiyao Shan; SUNY Binghamton, United States

Cancer is one of the leading causes of death with approximately 7 million deaths each year. Although knowledge surrounding the prevention and treatment of cancer is increasing, there is a clear need of highly-sensitive techniques for early detection of cancer to increase the survival rate. This presentation describes recent findings of our investigations of multi-functional nanomaterials for Surface-enhanced Raman scattering (SERS) detection of cancer biomarkers. One important focus is the preparation of magnetic and plasmonic nanoparticles as the SERS probes with high sensitivity, high selectivity, and low detection limit. We have developed a dual-functional nanoprobe system for the SERS detection of the biomarkers. Results on the preparation of gold and core-shell nanoparticles with a magnetic core and plasmonic gold shell will be discussed, focusing on the control of size, composition, and surface properties. Tunable bio-conjugation of the nanoprobe with detection/capture antibodies for the detection of the cancer biomarker, e.g., carcinoembryonic antigen, has been demonstrated. Implications of the results for optimizing the magnetic-plasmonic properties and multiplexing detection of cancer biomarkers will also be discussed.

#### **F.FL02.09.01**

**Off-Stoichiometric-Thiol-ene Epoxy Polymers for Soft Implantable Electrode Array** Eleonora Borda, Marta Airaghi Leccardi and Diego Ghezzi; École Polytechnique Fédérale de Lausanne, Switzerland

Implantable electrode arrays have been widely used to treat neurological disorders such as Parkinson's disease, epilepsy, hearing loss, and chronic pain by applying electrical stimulation and/or recording neural activity. One of the main requirements for these devices is the ability to evoke minimal inflammatory tissue response to guarantee the long-term use of integrated functions. However, this can be limited by a mechanical mismatch between the implant, very stiff, and the tissue, very soft, inducing neural damages and leading to glial scar formation. So far, the most common materials used for fabrication of such neural interfaces are PI and PDMS. On one hand, thin-film microfabrication techniques allow the fabrication of flexible miniaturized and highly integrated stimulating or recording arrays in PI. However, the Young's modulus of PI is about a few GPa. On the other hand, PDMS because of its low Young's modulus (approximately 1 MPa)

and its elastic behaviour leads to less damage to the neural tissue, but it presents challenging steps in the microfabrication process, especially for the encapsulation of the active sites. Off-Stoichiometric-Thiol-ene Epoxy polymers (OSTE+) were developed firstly for rapid prototyping of microfluidic chips because they are less permeable to gas. OSTE+ materials are a good compromise between PI and PDMS. In fact, by adjusting the stoichiometry of the constituting monomers, the Young's modulus of OSTE+ can be decreased down to a few MPa at physiological temperature. The preparation of OSTE+ consists of two curing steps in which (1) thiol-ene photopolymerization allows to pattern the polymer surface and remove the non-polymerized areas before (2) thermal curing. Thus, it is possible to encapsulate the electrode array simply using photolithographic techniques. Taking advantage of these properties, we fabricated OSTE+ implantable multielectrode arrays with Pt serpentes in monolayer and bi-layer. The functional characteristics of these arrays have been tested by electrochemical characterization and recordings.

#### **F.FL02.09.02**

**Parylene-Based Double-Faced Electrode Array for Retinal Prosthesis** Namju Kim, Heewon Seo and Sohee Kim; Daegu Gyeongbuk Institute of Science & Technology, Korea (the Republic of)

Retinal prostheses require high-density electrode arrays to attain high spatial resolution in vision. However, the transmission lines panning out in the same layer with electrodes may hamper achieving high-density electrodes. Double-faced electrode arrays may circumvent this problem, in which the electrodes and bonding pads are arranged face-to-face and the transmission lines are absent. The electrodes can be connected with stimulation drivers such as photovoltaic cells directly through bonding pads. Here we present the fabrication of a flexible and transparent parylene-based double-faced electrode array and the method of integrating it with the stimulation driver IC.

#### **F.FL02.09.03**

**Transparent and Flexible Ultrathin Gold Microelectrode Arrays Using Layer-by-Layer Coated Polyelectrolytes for Electro-Optical Neural Interface** Woongki Hong, Yujin Hwang, Junil Kim, Hyuk-Jun Kwon, Jae Eun Jang and Hongki Kang; DGIST, Korea (the Republic of)

In recent years, neural interface technologies have been focused on flexible and transparent neural electrodes for high spatiotemporal resolution mapping of neuronal activities using electro-optical measurements. There had been several new material suggestions for the transparent, flexible neural electrodes such as ITO, graphene, conductive polymer, or patterned metal (nanowires, mesh patterns).[1, 2] However, these materials have shown several limitations such as high processing temperature, limited mechanical/electrical reliability, fabrication complexity and incompatibility with conventional microfabrication processes etc. To resolve these problems, in this work, we developed a flexible microelectrode array (MEA) using polymer-metal hybrid structures for high optical transparency and good electrical conductivity.

We used layer-by-layer assembly of polyelectrolytes as a nucleation inducing coating layer on transparent substrates (glass, polymer) to realize highly conductive vacuum deposited gold film at sub 10 nm thickness. We optimized the electrical and optical properties of the ultrathin gold electrodes, showing sheet resistance as low as  $7.24 \Omega/\text{sq}$  at 8 nm thickness and electrical conductivity of  $1.327 \times 10^6 \text{ S/m}$ . Despite the opaque characteristic of typical thick gold film, the ultrathin film of gold in this work still showed optical transparency of 77% at 550 nm, which is comparable to or better than most of transparent neural electrode materials. In addition, excellent mechanical stability is also demonstrated with bending radius down to 1 mm for at least 500 times of bending. We further measured the baseline noise properties of our ultrathin 40- $\mu\text{m}$  diameter gold MEA for *in vitro* neural recording setup. We have confirmed that it shows low RMS noise level of  $9.62 \pm 2.24 \mu\text{V}_{\text{rms}}$  ( $n=60$ , bandpass filtered in 200 Hz – 3.5 kHz). These results confirm that the polymer-metal hybrid structure based MEA we developed in this work can be used for simultaneous extracellular electrical neural recording and optical neural recording such as calcium imaging.

#### References

1. Jimbo, Y. *et al.* Ultraflexible Transparent Oxide/Metal/Oxide Stack Electrode with Low Sheet Resistance for Electrophysiological Measurements. *ACS Appl. Mater. Interfaces* **9**, 34744–34750 (2017).
2. Kshirsagar, P. *et al.* Transparent Graphene/PEDOT:PSS Microelectrodes for Electro- and Optophysiology. *Adv. Mater. Technol.* **4**, 1–7 (2019)

#### **F.FL02.09.04**

**Bioresorbable Endovascular Neural Interface for Minimally Invasive Neural Stimulation and Recording** Adele Fanelli, Laura Ferlauto and Diego Ghezzi; EPFL, Switzerland

Neural signal recording and direct stimulation of the brain have been widely used to mitigate neurological disorders, such as

epilepsy and Parkinson's disease. Current available techniques in this field commonly require invasive surgery potentially entailing both transient and permanent complications. A promising strategy designed to overcome these risks involves the exploitation of the cerebrovascular system as access route to the neural tissue. Cardiovascular stent technology, exceptionally designed for a minimally invasive procedure and maximum adherence to the vessel wall, represents an optimal scaffold for the recording/stimulating system. Moreover, given the versatility of this type of implant, peripheral nervous system could also be targeted for neural stimulation aimed at relieving intractable pain or supporting motor rehabilitation. Therefore, our goal is the development of a stent-inspired device, with electrodes embedded on its surface facing the vessel walls, for minimally invasive active and passive interaction with the surrounding neural tissue. In order to reduce the possibility of chronic local inflammation and delayed endothelialization, commonly occurring with metallic implants, our device has been fabricated using only biodegradable and biocompatible soft polymers such as poly- $\epsilon$ -caprolactone (PCL) and (3-glycidyloxypropyl)trimethoxysilane-doped poly(3,4-ethylenedioxythiophene) : poly(styrenesulfonate) (GOPS-doped PEDOT:PSS), for encapsulation and electrodes respectively. Electrochemical properties of the prototypes have been tested in both static and dynamic conditions, with the latter simulating the vascular environment and its pulsatile flow. Degradation analysis in vitro has been performed as well to define the device durability. The promising results open the doors to further investigation of the potentialities of this innovative device, able to replace invasive systems currently used for neural recording and stimulation. Its development will have a huge impact in the treatment of neuropathological conditions related to both central and peripheral nervous system.

#### **F.FL02.09.07**

**Enhanced Antioxidant Activity of Cerium Oxide Nanoparticles by Surface Modification and Their Potential Application for Mitigating Foreign Body Response in Implantation of Active Chronic Medical Devices** Yue Hu, Vicki L. Colvin and Vivian Ling; Brown University, United States

There are roughly 175,000 different medical devices in the US market. The global market for medical devices grows fast yearly, it reached nearly \$521.2 billion in 2017 and should reach \$674.5 billion by 2022, at a compound annual growth rate (CAGR) of 5.3% for the period of 2017-2022. Some relevant examples include joint replacements, cardiac pacemakers, hernia meshes, subcutaneous real-time glucose sensors, and neural recording devices. An important and growing subset of these devices termed here 'active' implants, require electrical contact to tissues. Their function demands that they have long-term electrical contact to host tissue; perhaps the most widely known example is cardiac pacemakers now found in over 235,000 people in the US alone. Important emerging disease treatments, however, also rely on active medical devices including subcutaneous glucose sensors and neural recording devices. In the case of glucose sensors, the real-time information can drive both dietary choices and mitigate Type 2 diabetes or be part of an automatic insulin delivery system that frees patients with Type 1 diabetes from self-administered insulin injections. In these cases, the implant must stay functional and non-changing in their tissue interactions for years.

Every medical device that is implanted in a person encounters the body's foreign body response (FBR) which in short results in the body physically walling off an object from its physiology. Initially discovered in the 1970s, this multi-stage process is initiated by the innate immune system upon the introduction of foreign material. After injury and implantation, FBR activated by blood/material interaction, followed by protein adsorption, immune cells adhesion, activation, and differentiation. The whole process undergoes acute inflammation, chronic inflammation, the generation of granulation tissue and end up with the fibrous encapsulation generated by FBGCs. Foreign body response (FBR) triggered by the implantation of medical devices limits the lifespan of devices.

One of the widely used solutions is to suppress the immune system response to medical devices. Reactive oxygen species (ROS) generated during the FBR process play a key role in immune responses to implantation. ROS are generally linked to aging, cancer, and nervous system diseases. Anti-inflammatories and antioxidants, such as nonsteroidal anti-inflammatory drugs (NSAIDs), dexamethasone, masitinib, and resveratrol have been combined with implantable devices in local delivery to fight against FBR. However, molecular antioxidants are facing several problems, such as short lifetime, instability in micro-environment, and ineffectiveness induced high doses, limiting the chronic efficiency of implanted devices.

Nanoparticles, well known with their high surface to volume ratios, are widely used in biomedical engineering these days. Cerium oxide nanoparticles exhibit recyclable antioxidant properties due to facile electron transfer between Cerium (III) and Cerium (IV). Recent studies reveal that ceria nanoparticles with diameters of 5 nm are non-toxic and efficient for quenching ROS in vivo. We developed a PEGylated polymeric ceria nanoparticle which is stable and biocompatible. We also observed that the antioxidant activity of cerium oxide nanoparticle is enhanced by this PEGylated surface modification which can be widely used in vivo to control the ROS levels at the implant site and relief FBR.

## SYMPOSIUM F.FL02

---

Advanced Neural Interfacing Materials, Devices and Microsystems  
November 21 - December 1, 2020

### Symposium Organizers

Mohammad Reza Abidian, University of Houston  
Hui Fang, Northeastern University  
Xiaoting Jia, Virginia Institute of Technology  
Sohee Kim, Daegu Gyeongbuk Institute of Science & Technology

---

\* Invited Paper

SESSION Tutorial F.FL02: Materials Advances for Neural Interfaces—Materials Meet the Mind  
Session Chair: Hui Fang  
Sunday Morning, November 29, 2020  
F.FL02

**10:00 AM \***

**Materials Advances for Neural Interfaces—Materials Meet the Mind** Guosong Hong; Stanford University, United States

The dichotomy between the materials world and the mental world has driven the curiosity of scientists to explore the wonders of the brain, as well as motivated the continued innovations of novel technologies based on advances in materials science and engineering to understand the brain. This tutorial introduces the basic principles of materials design and fabrication for probing the inner workings of the brain, discusses the fundamental challenges of state-of-the-art neurotechnologies, and explores the latest breakthroughs in materials-assisted neural interfaces. The tutorial will cover the following topics: understanding of the nervous system from a materials science perspective, physical, chemical and biological requirements of neural interfacing materials, materials for electrical/magnetic/optical/biochemical/thermal/acoustic neural interfaces and other materials as contrast agents for neuroimaging. After the tutorial, the attendees should be able to obtain a broad overview on how materials advances have been and will continue to be a main driving force to address pressing neuroscience challenges.

This tutorial will cover: Understanding Neuroscience Challenges with a Materials Science Perspective; Fundamental Requirements for Neural Interfacing Materials; Bidirectional Electrical Neural Interfaces; Bidirectional Optical Neural Interfaces; Bidirectional Biochemical Neural Interfaces and Materials for Neural Tissue Engineering; and Emerging Acoustic and Magnetic Neural Interfaces.

SESSION F.FL02.12: Live Keynote I: Advanced Neural Interfacing Materials, Devices and Microsystems  
Session Chairs: Hui Fang and Xiaoting Jia  
Monday Afternoon, November 30, 2020  
F.FL02

**7:30 PM \*F.FL02.08.01**

**Bioresorbable Materials in Temporary Implants for Neurostimulation, Sensing and Drug Delivery** John A. Rogers; Northwestern University, United States

Bioresorbable electronic materials serve as the basis for emerging classes of biomedical implants with operational lifetimes designed to match those of transient biological processes. These devices provide important functionality during a relevant timeframe and then naturally disappear within the body, thereby eliminating the need for surgical extraction. This talk presents our latest work in this area, with emphasis on materials aspects of (1) platforms for wireless neuromuscular electrical stimulation, with demonstrations of alleviated muscle atrophy resulting from denervation in rodent models via multiple

episodes of the distal nerve engagement and (2) devices for programmable release of drugs from multiple, independently addressable reservoirs, with illustrations in insulin and lidocaine delivery in animal models for control of blood glucose concentrations and pain responses, respectively.

**8:00 PM \*F.FL02.03.01**

**Magnetic Nanomaterials for Wireless Neuromodulation** [Polina Anikeeva](#); Massachusetts Institute of Technology, United States

Ion channels offer direct means to manipulating neural activity with specificity and temporal precision. The nanometer dimensions of these molecular machines inspire the design of neuromodulation tools operating at comparable spatial scales. In this talk I will discuss how magnetic nanotransducers based on synthetic magnetic materials can be applied to convert external weak magnetic fields into stimuli, such as heat, force, torque, pH change, and chemicals, commonly perceived by ion channels. I will illustrate the importance of magnetic properties in controlling magnetically-mediated neuronal modulation in the context of ion influxes and rodent behavior. This talk will also highlight opportunities offered by wireless magnetic modulation of cell function in neuroscience and beyond.

SESSION F.FL02.13: Live Panel Discussion I: Opportunities in Materials Innovation for Unmet Neural Interfacing Functionalities

Session Chairs: Hui Fang and Myung-Han Yoon

Monday Afternoon, November 30, 2020

F.FL02

**8:30 PM PANEL DISCUSSION—OPPORTUNITIES IN MATERIALS INNOVATION FOR UNMET FUNCTIONALITIES**

**8:32 PM PANELIST: MICHAEL MOORE**

**8:39 PM PANELIST: HYUNJOO LEE**

**8:46 PM PANELIST: LAN YIN**

**8:53 PM PANELIST: GUOSONG HONG**

**9:00 PM PANEL DISCUSSION—(Q&A) OPPORTUNITIES IN MATERIALS INNOVATION FOR UNMET FUNCTIONALITIES**

SESSION F.FL02.10: Live Keynote II: Advanced Neural Interfacing Materials, Devices and Microsystems

Session Chairs: Mohammad Reza Abidian, Hui Fang and Sohee Kim

Tuesday Afternoon, December 1, 2020

F.FL02

**7:30 PM \*F.FL02.01.01**

**High Channel Count Electrophysiology—Materials and Technology Toward “Whole Brain” Recording** [Timothy Harris](#)<sup>1,2</sup>; <sup>1</sup>HHMI Janelia Research Campus, United States; <sup>2</sup>Johns Hopkins University, United States

Application of more advanced microelectronics technologies over the past decade has increased routine extracellular recording capacity from dozens to thousands of neurons. The NIH BRAIN Initiative has catalyzed an explosion of innovative small area low noise analog circuit designs. A next generation of devices under development promises capacity of 10's to 100's of thousand neurons. I will review our work to develop high channel count devices, Neuropixels, and the pathway to an additional 10-50X capacity increase. Important materials innovation in recording electrodes, stress compensation layers, and circuit design are required to fuel this transformation of electrophysiology capability. This data volume has created

bottlenecks for analysis. Discuss the current state of current practice and the paths needed to convert the avalanche of data to neuroscience understanding. The scale of data is so much larger than historically typical that a complete alteration of analysis and visualization is required. Finally, I will open a discussion of limits, how do we understand when we have adequately sampled the relevant neural activity for each behavior. How can we estimate that needed sampling in advance?

**8:00 PM \*F.FL02.01.02**

**Nanoporous Materials for Neural Interfaces** Bozhi Tian; University of Chicago, United States

There is a pressing need for the development of novel materials-based tools that enable seamless biointerfaces across various spatiotemporal scales and can interrogate the nervous system with unprecedented resolution. Nanostructured materials have the potential of meeting the demands for next-generation devices given their small feature size, synthesis scalability, mechanical properties, and diverse signaling capabilities. Many forms of nanostructures, such as nanoparticles, nanowires/nanotubes, and nanomembranes, have been used for neural interfaces. They can enable electrical, optical, or magnetic interrogation of tissues, single cells, or even organelles.

In this talk, I will focus on nanoporous materials-based neural interfaces. The materials include nanoporous carbon membranes synthesized from micelle-enabled self-assembly, nanoporous silicon particles developed from nano-casting method, and nanoporous silicon membranes fabricated by wet chemical etching. They can deliver stimuli to cells and tissues through electrochemical, photothermal, and photoelectrochemical mechanisms. I will discuss the fundamentals and rationales of using the nanoporous structures for these studies, as well as diverse neural interface applications. Finally, I will discuss new materials and biological targets that could catalyze future advances.

SESSION F.FL02.11: Live Panel Discussion II: Challenges in Materials Innovation for Neurotechnology Transition  
Session Chairs: Hui Fang, Kip Ludwig and Xing Sheng  
Tuesday Afternoon, December 1, 2020  
F.FL02

**8:30 PM PANEL DISCUSSION—CHALLENGES IN MATERIALS INNOVATION FOR NEUROTECHNOLOGY TRANSLATION**

**8:32 PM PANELIST: NATHALIA PEIXOTO**

**8:39 PM PANELIST: JAMES WEILAND**

**8:46 PM PANELIST: DAVID MARTIN**

**8:53 PM PANELIST: JACOB ROBINSON**

**9:00 PM PANEL DISCUSSION—(Q&A) CHALLENGES IN MATERIALS INNOVATION FOR NEUROTECHNOLOGY TRANSLATION**

SESSION F.FL02.01: Electrical Neural Interfaces  
On Demand Abstracts Available for Viewing Starting Saturday Morning, November 21, 2020  
F-FL02

**5:00 AM \*F.FL02.01.01**

**High Channel Count Electrophysiology—Materials and Technology Toward “Whole Brain” Recording** Timothy Harris<sup>1,2</sup>; <sup>1</sup>HHMI Janelia Research Campus, United States; <sup>2</sup>Johns Hopkins University, United States

Application of more advanced microelectronics technologies over the past decade has increased routine extracellular recording capacity from dozens to thousands of neurons. The NIH BRAIN Initiative has catalyzed an explosion of innovative small area low noise analog circuit designs. A next generation of devices under development promises capacity of 10's to

100's of thousand neurons. I will review our work to develop high channel count devices, Neuropixels, and the pathway to an additional 10-50X capacity increase. Important materials innovation in recording electrodes, stress compensation layers, and circuit design are required to fuel this transformation of electrophysiology capability. This data volume has created bottlenecks for analysis. Discuss the current state of current practice and the paths needed to convert the avalanche of data to neuroscience understanding. The scale of data is so much larger than historically typical that a complete alteration of analysis and visualization is required. Finally, I will open a discussion of limits, how do we understand when we have adequately sampled the relevant neural activity for each behavior. How can we estimate that needed sampling in advance?

#### 5:15 AM F.FL02.01.02

**Ultra-Low Friction Neural Probe Implantation for Long-Term Recording in Large Scale Brains** Luizetta V. Elliott, Jialiang Lu, Doris Tsao and Julia R. Greer; California Institute of Technology, United States

Chronic reliability, and thus a reduced foreign body response, is key to realizing the promise of neural probe technology in applications such as brain-machine interfaces, connectome mapping and brain disorder investigations. A variety of flexible, low density probes with small footprints have been designed to minimize the foreign body response in mouse models. However, few are applicable to larger systems such as primate brains. Such implantations are challenging; probes must be inserted ~30cm into the brain, which could require ~100mN of force. Further, accurate targeting requires less than 2 degrees deflection and may involve repeated insertions during the up to 6 hour surgical procedure. Recent micro-scale characterization of insertion mechanics into brain tissue has demonstrated that, following an initial loading peak during tissue penetration, continued load increase is attributable to friction between the implant and the surrounding tissue. These forces often exceed the initial loading peak past 2mm of insertion, and are particularly relevant for large brain implantation. We therefore present a new strategy for reaching large brain targets with smaller probes: minimizing the coefficient of friction.

By minimizing the friction coefficient of the probe we can substantially decrease the insertion load and thus minimize the critical buckling load ( $P_{crit}$ ) required for successful implantation. Since for an Euler beam with one free end  $P_{crit} = \pi^2 EI / 4L^2$ , this enables probes with smaller cross-sectional areas (lower moment of inertia  $I$ ) and lower moduli  $E$  to be inserted to the target depth  $L$  without deflection due to buckling. To demonstrate this principle, we fabricated a carbon fiber/platinum insertion device with a muscle inspired polydopamine/ poly-2-methacryloyloxyethyl phosphorylcholine ultra low friction coating (previously reported coefficient of friction  $\mu=0.02$ ). We characterized the insertion properties of 84mm samples with a range of diameters (100-430 $\mu$ m) with and without the coating utilizing an agarose brain phantom model and a nm-precision stage. For probes with a 230 $\mu$ m diameter, we observed 1.4 +/- 0.5 degrees deflection in the coated samples compared to 6.2 +/- 0.3 in the control, indicating a surgically acceptable insertion accuracy at decreased cross-sectional area. We further characterized these insertion properties through MRI following a realistic surgery in porcine brain tissue.

These results suggest that incorporating a thin (<50nm) friction-reducing coating into a neural probe delivery device can enable an overall reduction in probe cross-sectional area, and therefore the expected dead zone during insertion. Such insertion devices could enable the translation of neural probe technologies from mouse brain models to complex primate systems by effectively delivering electrodes to target areas with minimal damage. In particular, we envision shape memory polymer based electrode deployment from the tip of this device, enabling long-term recording outside of any minimized dead or encapsulated zone.

#### 5:25 AM \*F.FL02.01.03

**3D Neural Microphysiological Systems—Opportunities for Materials Innovation** Michael J. Moore<sup>1,1,2</sup>; <sup>1</sup>Tulane University, United States; <sup>2</sup>AxoSim, Inc., United States

Microphysiological systems, also called organs-on-chips, are rapidly being adopted as advanced *in vitro* tools for modeling disease, development, and injury, and as high-throughput preclinical drug screening devices. Modeling the nervous system using such devices presents unique challenges owing to its complex hierarchical structure and organization, and its unique physiological role in information transmission and processing. Past designs of neural microphysiological systems based on microfabricated chip-based platforms and 3D neural organoids have limitations in their abilities to recapitulate appropriate cell-cell interactions, morphology, and functionality seen *in vivo*. Microfabricated platforms can provide specified tissue organization, but typically restrict cell biology to 2D configurations, which can alter cellular physiology. Conversely, self-assembling 3D neural organoids provide a more physiologically-relevant microenvironment but fail to represent macroscale tissue organization. Our laboratory has sought to advance neural organ-on-a-chip platforms that balance simplicity and complexity to recapitulate neural physiology for scientific discovery and drug screening. We developed and commercialized a 3D peripheral nerve-on-a-chip for drug screening that enables both physiological and histological evaluation in manners analogous to clinical evaluation. We have further developed relatively simple methods for assembling multiple neural tissue



types and shown the potential of this approach for modeling the transmission of physiological signals associated with pain. Recent efforts have been focused on the integration of these tissue systems with integrated microelectrode technology to enhance our ability to investigate the electrophysiological behavior of these model systems. In all of these endeavors, materials continue to serve as both enabling technologies and opportunities for innovation. Interestingly, these same model systems may serve as convenient platforms for testing novel neural interfacing materials and devices. In this presentation, I will highlight our advances in the development of neural microphysiological systems and discuss intersections with materials innovation.

**5:40 AM \*F.FL02.01.05**

**High-Performance Conducting Polymer-Based Direct Cellular and Tissue Interfaces for Electrical Stimulation and Recording** Myung-Han Yoon; Gwangju Institute of Science and Technology, Korea (the Republic of)

Due to the trade-off between their electrical/electrochemical performance and underwater stability, realizing polymerbased, high-performance direct cellular interfaces for electrical stimulation and recording has been very challenging. We developed conductive direct cellular interfaces based on a water-stable, high-performance poly(3,4-ethylenedioxythiophene):polystyrene sulfonate (PEDOT:PSS) film via solvent-assisted crystallization. The crystallized PEDOT:PSS exhibited excellent electrical/electrochemical characteristics, long-term underwater stability without dissolution/delamination, and good viability for primarily cultured neurons and cardiomyocytes over several weeks. Furthermore, the highly crystallized, nanofibrillar PEDOT:PSS networks enabled dramatically enlarged surface areas and electrochemical activities, which were successfully employed to modulate cardiomyocyte beating via direct electrical stimulation. Finally, the high-performance PEDOT:PSS was seamlessly incorporated into transparent microelectrode arrays and free-standing 3D fiber network-based interfaces for efficient, realtime recording of neuronal and cardiac tissue action potentials with a high signal fidelity. All these results demonstrate the strong potential of crystallized PEDOT:PSS as a crucial component for a variety of versatile bioelectronic interfaces.

**5:55 AM F.FL02.01.06**

**Human Brain Mapping with Multi-Thousand Channels Reveal Functional Boundaries and Oscillating Wave Patterns at Submillimeter Resolution** Youngbin Tchoe<sup>1</sup>, Andrew Bourhis<sup>1</sup>, Daniel Cleary<sup>2</sup>, Karen Tonsfeldt<sup>1</sup>, Brittany Stedelin<sup>3</sup>, Ahmed M. Raslan<sup>3</sup> and Shadi A. Dayeh<sup>1</sup>; <sup>1</sup>University of California, San Diego, Korea (the Republic of); <sup>2</sup>University of California, San Diego (UCSD), United States; <sup>3</sup>Oregon Health & Science University (OHSU), United States

Clinical mapping of electrophysiological activity in the human brain is routinely used for delineating margins between functional and pathological tissue, for therapeutic applications and for brain-machine interfaces. Trade-offs between spatial resolution and cortical coverage, specificity in recording and contact impedance, conformity/compliance to brain curvature/movement and complexity of grid designs often limit the scalability and the potential use of brain mapping electrodes. In this work, we developed a scalable manufacturing process to realize human-compatible electrocorticography surface grids with thousands of channels. The 7" long cortical electrodes together with our sterilizable compact connector overcome challenges associated with the required large separation between the sterile surgical field and the non-sterile acquisition electronics enabling reliable intraoperative recordings from patients undergoing neurosurgical resections. The electrode diameter and pitch were adjustable providing a spatial resolution from micrometer scale to millimeter scale. Pt nanorod electrodes were used as contact materials and demonstrated low impedances at frequencies of interest for brain activity mapping.

The spatiotemporal recording capability of the electrode is investigated first with anesthetized rat model undergoing whisker air-puff stimulations using high-density 32×32 array electrodes with 150µm pitch and 4.8mm×4.8mm coverage. The spatial mapping of stimulation evoked high gamma activity (HGA) measured from the electrode clearly distinguished functional boundaries of individual whisker barrels at 150µm resolution.

We recorded from awake patients undergoing tumor resection while performing motor tasks with our grid placed on the motor cortex. The geometry of the array included a 46×44 array with multiple 30µm diameter contacts and 1.8mm spacing extending over an area of 8cm×8cm. Motion sensors and an accelerometer were attached to a glove worn by patients who performed finger flexion/contraction tasks between thumb and the other four fingers. The motion signals were time-locked to the recordings using our custom-made intraoperative monitoring system. Both local field potentials and broadband HGA showed distinctive neural correlates of fine-motor movements for different fingers when compared to baseline. Furthermore, we recorded phase reversal boundaries during motor mapping to precisely localize the central sulcus in sub-mm scale resolution. These results with our high-density grids offer an unprecedented view of the functional organization and coordination of motor function over large brain regions in the human cortex.

6:05 AM F.FL02.01.07

**Scalable Penetrating Microwire Arrays with Flexible Substrate for Chronic Large Area Coverage Brain-Machine Interfaces** Sang Heon Lee<sup>1</sup>, Martin Thunemann<sup>2</sup>, Keundong Lee<sup>1</sup>, Youngbin Tchoe<sup>1</sup>, Farid Azzazy<sup>1</sup>, Anna Devor<sup>2</sup> and Shadi A. Dayeh<sup>1</sup>; <sup>1</sup>University of California, San Diego, United States; <sup>2</sup>Boston University, United States

We introduce sharp, needle-like Si-based neuronal probes on ultra-thin, biocompatible flexible substrates for penetrative, high-resolution, 3D mapping of brain activity. The flexible polyimide/parylene-C substrate carrier allows conformal adhesion to the cortical surface and embeds electrical leads for data streaming. We utilize optically transparent polyimide/parylene-C layer and Si substrates with conventional Si micromachining processes and double-side photolithography alignment in order to fabricate 3D Si micropillars on a flexible substrate. We report in this work two devices layouts. Device A consists of 32 individually-addressable, high aspect ratio pillars (wire-to-wire spacing of 400  $\mu\text{m}$ , 6 $\times$ 6 array, L=100  $\mu\text{m}$  and D=10  $\mu\text{m}$ ) on a sub-10 $\mu\text{m}$  thin flexible substrate. Electrode sensing sites at the tip of the pillars were engineered by coating Pt nanomesh structure which significantly increased the electrochemically active surface area of electrodes thus achieving sub-1M $\Omega$  electrochemical impedance in phosphate buffered solution (PBS). We demonstrated up to 196 days of reliable chronic implantation on mice and multimodal capabilities of the device with air puff stimulation-evoked activities from barrel cortex, optogenetically stimulated responses, and 2-photon intravascular imaging of the implant sites on the brain cortex. The scalability of this technology is shown by the preliminary recordings from Device B with 1024 microwire arrays (wire-to-wire spacing of 400  $\mu\text{m}$ , 32 $\times$ 32 array, L=200-300  $\mu\text{m}$  and sharp tips with sub-1  $\mu\text{m}$  diameter) which holds the potential for large-scale, higher fidelity recordings for brain-machine interfaces.

6:15 AM F.FL02.01.08

**Analysing the Cell-Electrode Interface—A State Space Time-Varying Model Towards 3D Geometrical Design Optimization** Ugo Bruno, Anna Mariano and Francesca Santoro; Istituto Italiano di Tecnologia, Italy

The whole-cell patch-clamp technique is probably the most commonly used technique to record neuronal electrical properties. Although this approach provides maximum achievable quality for intracellular recordings, it does not provide a sustainable method for simultaneous recordings and it inevitably leads to cell dialysis and loss of the intracellular machinery that may be essential for the expression of certain biological functions. Neuronal *in vitro* extracellular electrophysiology, instead, commonly relies on recording techniques which monitor neuronal activity by means of electrodes placed in close contact with the cells at their extracellular domain [1]. Since the interface scenario between cells and electrodes clearly affects the quality of recordings, this interaction is classically investigated applying equivalent electrical circuit models. Although conventional modelling approaches provide insights on the role of multiple interface parameters, they yet limit the studied systems in specific conditions, thus producing numerical results that are valid only for a fixed set of variables [2], ultimately impeding the understanding of the interface mechanical dynamics. However, systems theory [3], as already employed to analyse biological systems [4] or to study the cell-electrode interface in the frequency domain [5], promises to overcome these limits providing a modelling platform for multiparameter dynamic analysis. Moving from the base of classical electrical modelling frameworks to a novel interpretation of systems theory, a time-varying state-space model is presented, achieving a clear separation between non-linear spike-generation dynamics [6] and linear cell-electrode coupling, while also recovering interface dynamics. Here the systematic variation of multiple parameters allows to perform a simulated spike sorting and to follow a target recorded spike while changing the same coupling parameters over time. Hence, by screening different planar electrodes sizes, the recording detection limits for each specific situation are identified. Extending the approach to 3D electrodes, time-varying simulations are then exploited to highlight the effect of micro protrusions and shape-curvatures on the recorded signals. In this way, by continuously defining the electrical detection limits, a dynamic geometrical optimization is enabled during the electrodes 3D design.

[1] Fromherz P., Offenhauser A., Vetter T., Weis J., A neuron-silicon junction: a Retzius cell of the leech on an insulated-gate field-effect transistor, *Science*, 252, 1991.

[2] Martinoia S., Massobrio P., Bove M., Massobrio G., Cultured Neurons Coupled to Microelectrode Arrays: Circuit Models, Simulations and Experimental Data, *IEEE TRANSACTIONS ON BIOMEDICAL ENGINEERING*, 51, 2004.

[3] Magni L., Scattolini R., *Advanced and Multivariable control*, Pitagora, 2014.

[4] Izhikevich E.M., *Dynamical Systems in Neuroscience, The Geometry of Excitability and Bursting*, The MIT Press, 2007.

[5] Joye N., Schmid A., Leblebici Y., An Electrical Model of the Cell-Electrode Interface for High-density Microelectrode Arrays, 30th Annual International IEEE EMBS Conference, Vancouver, 2008.

[6] Hodgkin A. L., Huxley A. F., Propagation of electrical signals along giant nerve fibres, *Proc. R. Soc. Lond. B*, 140, 1952.

**5:00 AM \*F.FL02.02.01**

**Nanoporous Materials for Neural Interfaces** Bozhi Tian; University of Chicago, United States

There is a pressing need for the development of novel materials-based tools that enable seamless biointerfaces across various spatiotemporal scales and can interrogate the nervous system with unprecedented resolution. Nanostructured materials have the potential of meeting the demands for next-generation devices given their small feature size, synthesis scalability, mechanical properties, and diverse signaling capabilities. Many forms of nanostructures, such as nanoparticles, nanowires/nanotubes, and nanomembranes, have been used for neural interfaces. They can enable electrical, optical, or magnetic interrogation of tissues, single cells, or even organelles.

In this talk, I will focus on nanoporous materials-based neural interfaces. The materials include nanoporous carbon membranes synthesized from micelle-enabled self-assembly, nanoporous silicon particles developed from nano-casting method, and nanoporous silicon membranes fabricated by wet chemical etching. They can deliver stimuli to cells and tissues through electrochemical, photothermal, and photoelectrochemical mechanisms. I will discuss the fundamentals and rationales of using the nanoporous structures for these studies, as well as diverse neural interface applications. Finally, I will discuss new materials and biological targets that could catalyze future advances.

**5:15 AM \*F.FL02.02.02**

**Seeing the Sound—Mechanoluminescent Materials as a Deep-Tissue Light Source for Non-Invasive Optogenetics** Guosong Hong; Stanford University, United States

Optogenetics, which uses light to control neurons genetically modified with light-gated ion channels, is revolutionizing neuroscience research by the precise deconstruction of neural circuits with neuron-type specificity. However, the poor tissue penetration of visible light has limited the application of optogenetics due to invasive craniotomy and intracranial implantation of obtrusive optical fibers or light-emitting diodes (LEDs). Here, we present a new form of deep-tissue light source based on mechanoluminescence nanoparticles, which can be delivered intravenously, recharged during circulation, and turned on and off by brain-penetrant focused ultrasound with millisecond precision. With this circulation-delivered nanoscopic light source, we have achieved non-invasive ‘sono-optogenetic’ stimulation of Chr2-expressing neurons in the intact mouse brain, successfully evoking hindlimb motion that was synchronized with the ultrasound pulses. Our approach provides an ‘inside-out’ light source anywhere and anytime inside the body at will, and we envisage that it can be used for any application that needs a light source deep in the body, such as in organs (e.g., spinal cord, heart and lungs) that are usually refractory to fiber implantation.

**5:30 AM \*F.FL02.02.03**

**Mirroring Action Potentials—Non-Invasive and Accurate Recordings of Action Potentials** Francesco De Angelis; Istituto Italiano di Tecnologia, Italy

The recording of the action potentials in electrogenic cells plays a central role in many fields of research spanning from neuroscience to cardiology, cell biology and pharmacology. To this aim, many techniques have been developed both in research and in clinical applications. Broadly speaking they can be divided into two categories: direct electrical measurements performed with micro-electrodes (such as patch-clamp and multi-electrode arrays (MEAs)) and optical measurements collected from fluorescent reporters administered to the cell cultures. However, regardless of the field of application some fundamental needs are still not met. For instance, methods based on electrodes can provide very accurate measurements but they require inserting the electrode inside the cell by porating the cell membrane. Hence, they are very invasive, thus reporting on a perturbed system. Furthermore, only a limited number of cells can be investigated (few cells for patch-clamp, thousands for MEAs). Even in the latest generation CMOS –MEAs, that aims to monitor hundreds of thousands of cells, the distances between the electrodes remain large with respect to cell size thus providing fragmented information. The latter issue can be overcome with optical methods which can record a million points on multiple scales with no fragmentation. However, dyes are well known to be cyto-toxic. Even if nontoxic, fluorescent dyes may bind to membrane receptors altering the response of the cells to the administered treatment in unpredictable ways. These are serious issues in many applications, for example to investigate compound toxicity in pharmacology. In this regard, cardio-toxicity and brain-toxicity of potential drug-compounds account for 60% of rejection cases during trials. This massive rejection rate significantly contributes to making the drug development process extremely expensive (now exceeding 2 billion per drug on

average) and extremely long (13 years on average). This example, as with many others in neuroscience and cell biology, necessitates **the need for developing new technologies providing non-invasiveness and large spatial scalability combined with accurate monitoring. Namely, the possibility of measuring both shape and duration of the action potential with precision approaching the one achieved in patch-clamp (intracellular).**

**In this talk, we will show a radically new concept for monitoring action potentials in human cells that overcomes all of the mentioned limitations. It bases on the concept of “mirror charge” in classical electrodynamics:** electric charges placed in proximity of a conductor affect its spatial charge distribution thus generating mirror charges into the conductor itself. Hence, by monitoring the dynamics of the mirror charges one can monitor the dynamics of the “source charges” and the related electric potential, i.e. the action potential. The latter can be done by using charged dyes whose dynamics can be monitored by conventional optical methods. However, being the dyes placed in microfluidic chip, separated from the cell culture, the cells are subjected neither to dye contact, nor to direct light illumination, but are in a perfectly unperturbed physiological state. Remarkably, the optical signal perfectly resembles an action potential (AP) even without the need of cell membrane poration as for conventional electrical recording. We reported a set of experiments on human-derived cardiomyocytes that uniquely support our statements.

The working principle can be extended to other nanostructures such as Quantum Dot or plasmonic particles. More in general, this new approach based on “mirror or virtual cells” paves the way toward a new family of in-vitro bio-devices that can lay a new milestone in the field of electrophysiology. Such an innovative configuration could inspire a new disruptive class of electro-optical sensors or hybrid devices for optical computing.

**5:45 AM \*F.FL02.02.04**

**Listening to Molecules—Functional Optoacoustic Neuro-Tomography for Scalable Brain Recording** Daniel Razansky<sup>1,2</sup>; <sup>1</sup>ETH Zürich, Switzerland; <sup>2</sup>University of Zurich, Switzerland

Optoacoustic imaging is increasingly attracting the attention of the biomedical research community due to its excellent spatial and temporal resolution, centimeter scale penetration into living tissues, versatile endogenous and exogenous optical absorption contrast. State-of-the-art implementations of multi-spectral optoacoustic tomography are based on multi-wavelength excitation of tissues to visualize specific molecules within opaque tissues. As a result, the technique offers unmatched capacities for simultaneous visualization of structure (e.g., vascular anatomy, organ structure), function (total hemoglobin, oxygen saturation, blood flow, pH, metabolic rate of oxygen consumption), and molecular information (intrinsic bio-chromes, targeted agents, genetic reporters, sensors) from living tissues. Our recent work has established ultrafast functional optoacoustic neuro-tomography (FONT) technology to enable acquisition and visualization of spectroscopic information from the rodent brain at video rates. In this way, bulk changes in multiple hemodynamic parameters can be monitored non-invasively in whole mouse brains. We were also able to optoacoustically track neural dynamics using genetically encoded calcium indicators, thus overcoming the longstanding penetration barrier of optical microscopy in scattering brains. FONT captures hemodynamic responses and calcium fluxes as true three-dimensional information across the entire brain with 10 ms temporal and 100  $\mu\text{m}$  spatial resolution, thus enabling large-scale neural recording at penetration depths and spatio-temporal resolution scales not covered with the existing neuroimaging techniques. Several hybrid imaging solutions have further been developed to support concurrent acquisition of various combinations of functional optoacoustic, ultrasound and fluorescence data as well as concurrent ultrasound stimulation of the brain.

SESSION F.FL02.03: Magnetic Neural Interfaces

On Demand Abstracts Available for Viewing Starting Saturday Morning, November 21, 2020

F-FL02

**5:00 AM \*F.FL02.03.01**

**Magnetic Nanomaterials for Wireless Neuromodulation** Polina Anikeeva; Massachusetts Institute of Technology, United States

Ion channels offer direct means to manipulating neural activity with specificity and temporal precision. The nanometer dimensions of these molecular machines inspire the design of neuromodulation tools operating at comparable spatial scales. In this talk I will discuss how magnetic nanotransducers based on synthetic magnetic materials can be applied to convert

external weak magnetic fields into stimuli, such as heat, force, torque, pH change, and chemicals, commonly perceived by ion channels. I will illustrate the importance of magnetic properties in controlling magnetically-mediated neuronal modulation in the context of ion influxes and rodent behavior. This talk will also highlight opportunities offered by wireless magnetic modulation of cell function in neuroscience and beyond.

SESSION F.FL02.04: Novel Fabrication Approaches  
On Demand Abstracts Available for Viewing Starting Saturday Morning, November 21, 2020  
F-FL02

**5:00 AM F.FL02.04.01**

**Laser-Assisted Synthesis of Ceramics for Biointerface Studies** [Aleksander Prominski](#) and Bozhi Tian; The University of Chicago, United States

Ceramics find many applications in electronics, optics, energy storage, and medical implants. Synthesis of ceramic materials conventionally requires hours long processing time in a furnace. While this classic technique allows for large scale fabrication, it is not suitable for high throughput screenings necessary for efficient material discovery. New methods, such as flash sintering, rapid thermal annealing, and ultrafast high-temperature annealing, have been developed to address this issue. These methods rely on fast energy transfer to achieve uniform heating within the substrate, provide stable synthetic conditions, and speed up the processing time. However, all these approaches provide relatively standard synthetic conditions and do not enable new phases and structures.

Laser processing can enable new materials, increase research throughput, and allow for the instant prototyping of new devices. Here, we developed a modified laser processing to produce an intense photothermal effect over an elastic matrix, which allows the fast ceramics formation with a laser power as low as 10 mW. Out-of-equilibrium nature of the process and complex strain relaxation at the synthetic interface between the soft substrate and hard ceramic product create hierarchical anisotropic micro-structuring of the material on the scale from nano- to micrometers. Beyond understanding the fundamental principles of this laser-assisted synthesis, we have also explored their applications as diverse biointerfacing materials.

**5:10 AM \*F.FL02.04.03**

**Electrodeposition of Platinum-Iridium Alloy on Carbon Fiber Electrodes** [James Weiland](#), Elena della Valle, Cynthia Chestek and Elissa Welle; University of Michigan, United States

Next-generation brain-machine interfaces may use thin-film metals or non-metallic materials (e.g. carbon) for electrical connection to the brain. However, thin-films are not robust to electrical stimulation and carbon does not form a low impedance electrode interface with neural tissue. Thus, improving the electrical and mechanical stability of carbon fiber microelectrodes is a major challenge facing this promising technology. Surface roughening can improve interface properties, while maintaining small geometric area for targeted recording and stimulation of local neural populations. A platinum-iridium electrodeposition process has been developed for carbon fiber microelectrodes to improve the interfacial properties. We study the coating effect on impedance as well as morphology and composition of the deposited film. Carbon fiber electrodes (6.8 micron diameter) with parylene insulation and an exposed tip of approximately 10 microns were coated with a film of platinum-iridium. Accelerated soak test in a heated ( $T = 50$  degrees C) saline solution showed impedance variation of less than 8 % after 36 days (89 equivalent) of soaking. Compared to uncoated fibers, impedance modulus of carbon fibers coated with platinum-iridium was decreased (on average) by 96% at 10 Hz, 89% at 1 kHz, and 13% at 1 MHz, due to the high surface roughness of the platinum-iridium film. Loss of platinum-iridium film was noted in 3 of 43 electrodes after soaking. The small decrease in impedance at 1 MHz indicates that geometric area was maintained. SEM analysis confirmed that deposition was confined to the area with exposed carbon. Energy dispersive X-ray spectroscopy (EDS) quantified the percentages of platinum and iridium as  $\sim 70\%$  Pt,  $\sim 30\%$  Ir on the surface and the film appeared uniformly deposited. Focused ion beam was used to cut the coated microelectrode for cross sectional analysis. The film was about 400 nm thick and mostly continuous with some cracks. EDS was performed on the cross section using scanning transmission electron microscopy. As with the surface analysis, the cross-sectional analysis showed a homogeneous distribution of platinum and iridium with relative percentages similar to the surface measurements. Electrodeposition of platinum iridium is a feasible approach to decreasing the impedance of carbon fiber electrodes.

**5:25 AM \*F.FL02.04.04**

**Maleimide-Functionalized PEDOT Copolymers for Chemical and Biological Sensing** Samadhan Nagane, Peter Sitarik, Yuhang Wu, Michael Boeri, Quintin Baugh, Junghyun Lee, Shrirang S. Chhatre, Vivek Subramanian and David C. Martin; University of Delaware, United States

We continue to investigate the design, synthesis, and characterization of functionalized poly(3,4-ethylenedioxythiophene) (PEDOT) for use in a variety of applications including neural interfaces, as well as chemical and biological sensors. Here, we will present our recent results focused on maleimide-functionalized PEDOT variants that provide us a wide range of novel opportunities for post-polymerization modification with particular biomolecules. These copolymers can be precisely deposited onto electrodes using oxidative electrochemical deposition methods. Of particular current interest to us are the development of new materials that show specific responses to such biological and chemical agents as proteins, peptides, neurotransmitters, and opioids. We examine the morphology of our materials with optical and electron microscopy, as well as X-ray and electron diffraction. We examine the physical chemistry with UV-Vis, FTIR and Raman spectroscopy. Information about electrical transport is obtained by CV, electrochemical impedance spectroscopy, four-point probe, and transconductance measurements.

SESSION F.FL02.05: Minimally Invasive Neural Interfaces  
On Demand Abstracts Available for Viewing Starting Saturday Morning, November 21, 2020  
F-FL02

**5:00 AM \*F.FL02.05.01**

**Minimally Invasive Neuromodulation Through an In-Body Curing Injectable Electrode** Kip Ludwig<sup>1,2</sup>; <sup>1</sup>University of Wisconsin-Madison, United States; <sup>2</sup>Wisconsin Institute for Translational Neuroengineering, United States

Stimulation of the peripheral nervous system through implanted devices, often referred to as bioelectronic medicines, electroceuticals, or neuromodulation therapies, is increasingly being used to treat a variety of diverse conditions including FDA approvals for pain, overactive bladder, obesity, sleep apnea, migraine, essential tremor, and hypertension. Unfortunately, the availability of neuromodulation therapies is usually limited to patients that have failed conventional treatments. This is largely due to the need for invasive implantation procedures and resulting surgical risk. We have developed a minimally invasive method for stimulating the peripheral nervous system through a syringe-injectable electrode which is delivered as a pre-polymer composite material and cures *in vivo*, with the goals of reducing surgical risk, increasing the availability of neuromodulation therapies, and enabling the development of novel therapeutic strategies. This electrode, referred to as the Injectrode, can conform to complex target structures and is orders of magnitude less stiff compared to conventional neural stimulation electrodes.

This talk will cover our work developing the Injectrode, validating the material properties of the Injectrode, and our ongoing progress towards non-invasively interfacing with the Injectrode through a transcutaneous interface. This will include microscopic and electrochemical testing to assess the material properties most relevant to electrical stimulation of the nervous system mimicking FDA pre-clinical test requirements, as well as a comparison to clinical vagus nerve stimulation electrode. Dr. Ludwig will present a finite element model of the transcutaneous Injectrode concept, validated in a swine cadaver model, to investigate a method for non-invasively coupling to the Injectrode without use of an implantable pulse generator. Lastly, Dr. Ludwig will present feasibility studies in rats showing stimulation of complex peripheral nerve anatomy, comparisons to a clinical nerve cuff electrode, and *in vivo* non-invasive coupling to the Injectrode. The ability to deliver the Injectrode through a minimally invasive procedure - as well as non-invasively couple to it without the need for an implantable pulse generator - will lead to reduced surgical risk and the potential for fewer failure points. As such, this technology fits an unmet need for less invasive stimulation systems and could lead to novel and more widely applicable neuromodulation therapies.

**5:15 AM \*F.FL02.05.02**

**Biodegradable Materials and Devices for Neural Interfaces** Lan Yin and Liu Wang; Tsinghua University, China

Biodegradable devices represent an emerging type of electronics that can degrade in physiological environments and can therefore eliminate a second surgery for device retraction and minimize associated infection risks. Such devices could play a critical role in many therapeutic and diagnostic processes at neural interfaces, including promoting tissue regeneration, probing neurotransmitters, monitoring neural signals, etc. Herein, we introduce novel materials strategies and fabrication

schemes that enable a biodegradable and self-powered device for peripheral nerve regeneration. Successful nerve regrowth and motor functional recovery are realized in rodent models. Approaches detecting neurotransmitters and neural signals will also be discussed. These works will provide new insights for modulating and probing neural activities.

### 5:30 AM F.FL02.05.03

**Flexible CMOS Neuroelectrode Thread** Kyung Jin Seo<sup>1</sup>, Mackenna Hill<sup>2</sup>, Jonathan Viventi<sup>2</sup> and Hui Fang<sup>1</sup>; <sup>1</sup>Northeastern University, United States; <sup>2</sup>Duke University, United States

Techniques to study brain activities have been evolving tremendously, yet challenges remain in acquiring high throughput of simultaneous electrophysiological recordings. Here, we developed a soft neuroelectrode array that is on-site multiplexed. This novel array achieved up to 256 channels on a thin flexible substrate in only  $2.3 \times 0.3 \text{ mm}^2$  area, enabled by on-site multiplexing from Si thin film transistors, and with the electrode size of only  $238 \mu\text{m}^2$ , which is capable of measuring single-unit neuronal activity. The array showed high electrical performance of average SNR of  $\sim 71$  dB with over 91% yield. Mechanical bending test of 10,000 cycles proved great robustness of the device. We used 1 transistor current sensing method to reduce aliased white noise and multiplexer charge injection of the active electrodes. Acute auditory experiments in mice successfully validated in vivo use of this array. Together, these results demonstrate the promise of this on-site multiplexed, soft, penetrating neuroelectrode array for neuroscience and neural engineering.

## SESSION F.FL02.06: Neural Modulation

On Demand Abstracts Available for Viewing Starting Saturday Morning, November 21, 2020  
F-FL02

### 5:00 AM F.FL02.06.01

**High Density Subdural Spinal Cord Microelectrode Arrays for Neuromonitoring and Neuromodulation** Samantha Russman<sup>1</sup>, Daniel Cleary<sup>2,2</sup>, Andrew Bourhis<sup>2</sup>, Joel Martin<sup>2,2</sup>, Youngbin Tchoe<sup>2</sup>, Sang Heon Lee<sup>2</sup>, Joseph Ciacci<sup>2</sup> and Shadi Dayeh<sup>2</sup>; <sup>1</sup>University of California, San Diego, United States; <sup>2</sup>University of California San Diego, United States

Intraoperative neuromonitoring is a standard clinical practice in spinal cord surgeries as it is a detection method for neurological injury and helps limit postoperative impairments. Neuromonitoring is conducted by recording motor evoked potentials (MEPs) or somatosensory evoked potentials (SSEPs) via pulsed peripheral nerve or transcranial electrical stimulation (TES). These recordings are accomplished with electroencephalography (EEG) or electromyography (EMG), which require the use of large stimulation amplitudes (up to 1kV in TES and 60mA with peripheral nerve stimulation). Direct recordings from the spinal cord can reduce the stimulation thresholds required to detect neurological activity and provide another avenue for neural interface devices in the recovery from spinal cord injury. When performed with high channel count electrodes, direct recordings from the spinal cord can help to better localize pathologic spinal tissue. Standard clinical electrodes cannot provide intimate contact with spine and their spatial resolution is not suitable for these types of recordings.

Here we report and discuss the applicability of thin-film conformal and low impedance microelectrodes with hundreds of channels for neuromonitoring during spinal cord surgical resection and the potential translation of this technology to neuromodulation after spinal cord injury (SCI). We recorded from the pial surface of the spinal cord from patients undergoing an intramodular tumor resection during both transcranial and peripheral nerve stimulation. We recorded evoked potentials at subclinical threshold currents (as low as 4mA) for peripheral nerve stimulation compared to thresholds amplitudes (16mA) for clinical detection in these patients. The subdural placement permitted us to record activity that was otherwise missed with standard clinical and even high-density epidural electrodes. With the high channel count, we observed well-defined spatial variability depending on stimulus type: sensory versus motor and upper versus lower limb. Using these patterns, we investigated the applicability of our electrodes for neuromodulation after SCI via a brain-spine interface (BSI) by classifying sensory and motor events in the spinal cord. We took the first steps in performing such classification by using a supervised learning model to classify the applied stimulus type based on the spatiotemporal features of a single-trial recorded response. Taken together, these advances highlight the potential applicability of thin-film microelectrode arrays to transform neuromonitoring and to develop a soft subdural spinal cord implant for a BSI.

### 5:10 AM F.FL02.06.02

**Structured Metallic Glass-Based Multimaterial Fibers for Efficient Neural Stimulation and Recording** Wei Yan<sup>1,2</sup>, Nicholas D. James<sup>3</sup>, Inès Richard<sup>1</sup>, Güven Kurtuldu<sup>4</sup>, Giuseppe Schiavone<sup>5</sup>, Jordan Squair<sup>3</sup>, Reinis Ignatans<sup>6</sup>, Stephanie P.

Lacour<sup>5</sup>, Vasiliki Tileli<sup>6</sup>, Grégoire Courtine<sup>3</sup>, Jörg F. Löffler<sup>4</sup> and Fabien Sorin<sup>1</sup>; <sup>1</sup>École Polytechnique Fédérale de Lausanne, Switzerland; <sup>2</sup>Massachusetts Institute of Technology, United States; <sup>3</sup>École Polytechnique Fédérale de Lausanne, University Hospital of Vaud, and University of Lausanne, Switzerland; <sup>4</sup>Laboratory of Metal Physics and Technology, Department of Materials, ETH Zurich, Switzerland; <sup>5</sup>Bertarelli Foundation Chair in Neuroprosthetic Technology, Laboratory for Soft Bioelectronic Interfaces, Institute of Microengineering, Institute of Bioengineering, Centre for Neuroprosthetics, École Polytechnique Fédérale de Lausanne, Switzerland; <sup>6</sup>Institute of Materials, École Polytechnique Fédérale de Lausanne, Switzerland

Recent advances in techniques and methodologies for dissecting complex neural circuits are poised to unravel the function of neural networks and the underlying causes of neurological diseases<sup>1</sup>. Electrical stimulation of neural tissue and recording of neural activity play critical roles for our understanding of information transfer and processing within the nervous system. The traditional strategy for this purpose mainly exploits metal-based microwires that are mechanically and biologically incompatible with tissue. Recently, thermally-drawn multimaterial fibers that integrate electrodes and other modalities have emerged as promising tools for deciphering the neural circuitry in a unique way<sup>2-4</sup>. The development of in-fiber electrodes with low impedances, small feature sizes, arbitrary geometries and excellent electrochemical properties that allow for efficient both electrical stimulation and recording, however, remains challenging. Here we, for the first time, achieve such capability via thermal drawing of a peculiar material system — metallic glasses (MGs) — that is metallic yet exhibits disordered atomic-scale structure within a polymer matrix<sup>5</sup>. Thanks to the control over the interplay between fluid instabilities and crystallization dynamics, we are able to fabricate ultra-long MG electrodes spanning a wide size range from a few micrometers to around 40 nm. Designing the structures in a macroscopic scaled-up preform enables the fabrication of structured MGs with arbitrary transverse geometries previously unachievable. The electrochemical characterization reveal that these novel MG electrodes surpass in all accounts typical in-fiber electrodes including metallic or polymeric electrodes found in state-of-the-art fiber probes. The charge storage capacity is superior compared to typical metallic electrodes such as commercialized Pt and PtIr. The electrochemical stability is demonstrated by the long-term cyclic voltammetry and voltage transient cycles, is even on par with that of the state-of-art carbon nanotube and graphene fibers<sup>5</sup>. These merits can be attributed to the intrinsic microstructural homogeneity and isotropy of structured MGs. We demonstrate the unique applications of these fiber probes integrating multiple MG conductors embedded in a biocompatible polymer, and microfluidic channels for electrical stimulation and recording plus localized pharmacological manipulation in the deep brain of animals. Specifically, chronic experiments in rats show the ability to elicit robust behavioral responses when delivering electrical neurostimulation in deep structures, to record neuronal activity during unconstrained locomotion, and to deliver pharmacological agents to manipulate local circuits. Our MG probes are implantable, miniaturized and fully functional to form stable brain-machine interfaces in freely moving animals paving the way towards innovative long-term, multi-functional neuro-probes.

W.Y, N.J contributed equally.

1. Wei Yan, et al. Advanced Multimaterial Electronic and Optoelectronic Fibers and Textiles. *Advanced Materials* 31 (2019) 1802348.
2. Canales, A. et al. Multifunctional fibers for simultaneous optical, electrical and chemical interrogation of neural circuits in vivo. *Nat. Biotechnol.* 33, 277–284 (2015).
3. Guo, Y. et al. Polymer Composite with Carbon Nanofibers Aligned during Thermal Drawing as a Microelectrode for Chronic Neural Interfaces. *ACS Nano* 11, 6574–6585 (2017).
4. Frank, J. et al. Next-generation interfaces for studying neural function. *Nature Biotechnology* 37, 1013-1023 (2019).
5. Wei Yan, Inès Richard, Güven Kurtuldu, Niclolas James, Giuseppe Schiavone, Tung Nguyen-Dang, Tapajyoti Das Gupta, Yunpeng Qu, Jake Cao, Reinis Ignatans, Stéphanie P. Lacour, Vasiliki Tileli, Grégoire Courtine, Jörg F. Löffler, Fabien Sorin\*. Structured nanoscale metallic glasses fibers with extreme aspect ratios. *Nature Nanotechnology*. (In press, 2020).

### 5:20 AM \*F.FL02.06.03

**Miniaturized Ultrasound Transducers for Neuromodulation** Hyunjoo J. Lee; Korea Advanced Institute of Science and Technology, Korea (the Republic of)

Neuromodulation of the central nerve system (CNS) and periphery nerve system (PNS) is promising next-generation therapeutics for many neurological disorders. Direct physical stimulation such as electrical, magnetic, optical, and acoustic is an alternative approach to a pharmaceutical approach. Among various modalities, ultrasound is an attractive modality that offers distinct advantages, such as high spatial resolution, in-depth targeting, mature technology on beam-forming, and substantial data on biosafety of ultrasound on human. However, as neuromodulation based on ultrasound is in the early stage of development, further investigations on neuromodulation mechanism, therapeutic effects, and optimum neuromodulation protocols are still required. Thus, many new technological advancements such as miniaturized devices based on



microelectromechanical systems (MEMS) technology have been recently introduced for the specific purpose of neuromodulation. In this talk, these new neurotools which are essential to uncovering the fundamental mechanisms of ultrasound brain stimulation and essential to developing an effective therapeutic means for brain disorders will be discussed. Specifically, this talk will discuss the development of miniaturized ultrasound transducers for small animal experiments and also our research efforts to achieve higher spatial resolution. The functionalities and potential applications of our systems will also be discussed. This research was supported by the Brain Research Program through the National Research Foundation of Korea (NRF) funded by the Ministry of Science and ICT (2016M3C7A1904343).

**5:35 AM F.FL02.06.04**

**Establishing Electrochemical Safety Limits for Clinical Stimulation Using Depth and Strip Electrodes in the Pig Brain** Ritwik Vatsyayan, Daniel Cleary, Joel Martin and Shadi A. Dayeh; University of California, San Diego, United States

Clinically, the safety thresholds for electrical stimulation have long been empirically established by the Shannon's equation. The Shannon's equation models the charge injection needed to produce tissue damage but does not take into account the electrochemical safety limits for the stimulating electrodes. In this work, we investigated the electrochemical safety limits for bipolar current clamped electrical stimulation using Platinum based depth and strip macroelectrodes in pig cortical tissue. We contrasted these limits against those established by benchtop testing and investigated the observed differences. To characterize these limits, we first measured the tissue impedance using a 4-electrode setup. This allows us to isolate the electrode-tissue impedance, which can be subsequently modeled in terms of resistive and capacitive circuit elements and used to analyze the voltage drop across each. We subsequently performed cyclic voltammetry measurements to establish the water window both in saline and *in-vivo*. In bipolar stimulation, the electrochemical safety windows are larger than the traditionally established -0.6V and 0.8V and is dependent on the geometry of the electrode. We measured the voltage transients for both types of electrodes, using different current amplitude levels and pulse widths. This allows us to study the variation of the Charge Injection Capacity (CIC) for each individual electrode as a function of the pulse width. Our results show that the CIC is much lower in the brain, as compared to that calculated from benchtop testing. This is a consequence of the higher tissue-electrode impedance *in-vivo*. We developed basic circuit models that capture the complete electrochemical interface and can reproduce the experimental results with good accuracy. We compared these results with the clinical levels used for stimulation, especially those determined from the Shannon's equation, and found that the electrochemical safety limits established are lower than those used in clinical stimulation. These electrochemical limits are found to be lower than the reported tissue damage thresholds. We argue that the electrochemical limits and currents established experimentally in this study should therefore be considered the upper bounds for clinical stimulation.

SESSION F.FL02.07: Electrochemical Interfaces

On Demand Abstracts Available for Viewing Starting Saturday Morning, November 21, 2020

F-FL02

**5:00 AM \*F.FL02.07.01**

**Developing Next-Generation Coatings for Implantable Chemical and Electrical Interfaces for Neuromodulation** Nathalia Peixoto; George Mason University, United States

For the last several decades the neural engineering community has developed biocompatible interfaces for modulating the central and peripheral nervous systems. Related to such development there has been an enhanced design for reliability and robustness in implantable devices. The impacted areas range from retinal implants to electrode coatings. In this talk I will focus on those two devices and designs. From finite element modeling that leverages experimental results and merges electrochemical data (impedance and cyclic voltammetry) to device testing in chronically implanted animals, I will present results from our lab that show how materials can be combined in order to achieve impedance matching for applications in stimulation or recording of neural activity.

The sensorial prostheses designed for human use have gone through several design cycles. In this talk I will present a background of both epiretinal and subretinal designs for implants, and how materials were adapted for such objectives. Not only deep brain stimulators took advantage of platinum and iridium metal coatings, also retinal implants provided valuable experimental and modeling data to guide further designs. One critical example, which I will discuss in detail, is how the impedance of different layers of the retina makes it impossible to specify a single cell when stimulating using epiretinal or subretinal implants, and how the recording is impacted by this same feature of layered brain structure. I will discuss options to overcome such limitations based on engineering design. Novel combinations of materials designed to match Young's

modulus of the target tissue or to bio-dissolve over time after implantation.

The second topic to be discussed in detail is the effectiveness of coatings to enhance robustness and reliability of chemical, optical, and electrical implantable interfaces such as electrodes and sensors. For example, combining high surface area with several coating materials allow us to keep electrode micrometric size while increasing the charge delivery and guaranteeing biocompatibility of the device.

Finally, I will present possible future developments in engineered devices for immediate applications in biomedical engineering, specifically in combining multimodal sensors and hybrid systems with electronics embedded.

#### 5:15 AM F.FL02.07.02

**Electrochemical Characterization of Nanotube Coating on Silicon-Based Microelectrodes** [Nathaniel Keri](#), Ian Sands, Pejman Ghelich, Libo Zhou, Wuxia Zhang, Nicholas Nolta, Will Linthicum, Bryan D. Huey, Yupeng Chen and Martin Han; University of Connecticut, United States

Microelectrodes can treat injuries and disorders such Parkinson's disease through electrical stimulation, and can be used as powerful tools to help us learn more about neurological functions through neural recording. However, the foreign body response (FBR) can contribute to microelectrode failure over long implant durations. After insertion, glial cells eventually surround the implant, decreasing neural adhesion. The inflammatory environment may also inhibit neural function. As published previously, Janus base nanotubes (JBNTs) are synthetic molecules with a double ring mimicking DNA G<sup>A</sup>C bases and a lysine side chain. They present a potentially greater degree of biocompatibility than many microelectrode materials, eliciting fewer negative responses from the body. This project involves applying these nanotubes to the surfaces of microelectrodes, while avoiding negatively impacting the electrochemical properties of the microelectrode itself. Other chemical and medicinal coatings have also been shown to elicit positive physical responses but tend to disrupt the electrochemical properties of microelectrodes.

Initial tests of JBNTs have been conducted on developed microelectrodes. The microelectrodes have 2.5 mm long silicon shanks, gold/platinum/titanium traces, plasma-enhanced chemical vapor deposition (PECVD) silicon nitride and silicon dioxide insulation, and electrode sites with areas 2000-4000  $\mu\text{m}^2$  made of iridium. The microelectrodes were coated with RNTs through dipping, and SEM was used to examine the nanotube distribution on the electrode surfaces.

The tubes aggregated on the surfaces of the electrode sites, forming bundles around the edges. Electrochemical testing showed charge injection values remained largely unchanged, as did the impedances at 1 kHz. The cyclic voltammograms showed similarly consistent results, indicating the nanotubes did not contribute to a significant alteration of the microelectrodes' electrochemical characteristics. Additional electrochemical testing is ongoing, with electrodes of different sizes and materials. We expect that someday, JBNTs may be demonstrated as an important component of highly biocompatible, long-lasting neural microelectrodes.

#### 5:25 AM F.FL02.07.03

**Implantable Aptamer Field-Effect Transistor Neuroprobes Towards *In Vivo* Monitoring of Serotonin in Mice** [Chuanzhen Zhao](#), I-Wen Huang, Zhixin Xie, Kevin M. Cheung, Hanxiang Wu, Wenfei Liu, Nako Nakatsuka, Hongyan Yang, Yan Cao, Paul S. Weiss, Qibing Pei, Harold G. Monbouquette and Anne M. Andrews; University of California, Los Angeles, United States

Monitoring neurotransmitters *in vivo* necessitates sensors that approach the spatiotemporal resolution of neuronal communication, while differentiating similarly structured neurochemicals with high selectivity. We have developed biosensors based on aptamers, coupled to ultra-thin  $\text{In}_2\text{O}_3$  (~3-nm thick) field-effect transistors (FETs). These biosensors show high sensitivity and selectivity for serotonin and dopamine with femtomolar detection limits *in vitro*. To enable *in vivo* measurements, we miniaturized our sensor architecture to fabricate neuroprobes with arrays of aptamer-field-effect transistors. The initial prototype for an implantable microprobe is fabricated using micro-electro-mechanical systems (MEMS) technologies on silicon (150- $\mu\text{m}$  thick). Each neuroprobe has lithographically patterned interdigitated gold electrodes deposited atop ultrathin, semiconducting indium oxide channels, where the shank is of 150- $\mu\text{m}$  wide and 150- $\mu\text{m}$  thick. Functionalization of the exposed semiconducting surfaces with neurotransmitter-specific aptamers facilitated electronic neurotransmitter sensing. Reducing individual FET footprints leads to an increase in the numbers of independent transistors on a single neuroprobe for multi-site/multi-target detection capabilities. We characterized target sensitivity ranges, detection limits, and sensor stabilities *in vitro* prior to conducting *in vivo* measurements. We assessed the biofouling of neuroprobes using *ex vivo* measurements in brain tissue homogenates. We also fabricated flexible neuroprobes using polyimide as substrates instead of rigid Si to reduce immunological responses. Shuttle devices were used to assist the implantation of flexible polyimide neuroprobes. We are now working on shuttle-free flexible neuroprobes with temperature-responsive

polymers, which are hard at room temperature for implantation and soft in the brain after implantation. Implantable aptamer-field-effect transistor-neuroprobes, including additional designs on flexible polymers, will enable *in vivo* detection of neurotransmitters in the brain with high spatial resolution and selectivity.

**5:35 AM F.FL02.07.04**

**Development of a Microfluidic Neural Interface for Drug Delivery to the Brain** Yoo Na Kang and Sohee Kim; DGIST, Korea (the Republic of)

Implantable neural interfaces can record neural signals and electrically stimulate neurons. Several neural interfaces integrated with additional functions such as optical stimulation and drug delivery have been introduced recently. Among various neural electrodes, needle-type neural electrodes, for example, the Utah electrode arrays, have been widely used in non-human primate (NHP) and clinical studies. However, drug delivery function for the needle-type neural electrodes has not been implemented yet because of their structural characteristics. We previously developed a neural interface based on a flexible penetrating microelectrode array (FPMA), which is a needle-type neural electrodes array. Here, we propose a microfluidic flexible interconnection cable ( $\mu$ FIC), which is capable of delivering drugs to the FPMA, resulting in drugs delivered to the implant site. The neural signal recording was performed while delivering drugs to the brain *in vivo* experiments using the fabricated neural interface. The KCl-evoked excitation signals of neurons in the rat brain were recorded during the KCl solution delivery. Approximately 50% of the electrodes detected an elevation of the number of spikes and amplitude.

**5:45 AM F.FL02.07.05**

**Integrated Neural Implant with Transdermal Ionic Communication** Zifang Zhao, Georgios Spyropoulos, Claudia Cea, Jennifer Gelinis and Dion Khodagholy; Columbia University, United States

High-density neural interfaces are continuously progressing towards seamless integration of brain and electronics. As more effort has been dedicated to implantable devices, effective and non-invasive data communication between the implant and outside electronics becomes a critical unresolved issue. Although radio-frequency (RF)-based communication can provide a wireless link with high bandwidth, RF circuits suffer from high power consumption, complex rigid circuitry for signal transmission, and wave reflection that limit their capacity for prolonged use inside biological tissue. There is a tremendous need for a safe, low consumption, high-bandwidth wireless communication method for use in neural interface devices. Here we propose a fully integrated, conformable, high-channel count neural interface device equipped with a high-speed ionic communication (IC) link. We implanted the device in rodents and validated its performance in acquiring chronic *in vivo* electrophysiological data from freely moving animals without any tissue extruding components. To achieve this, we first designed a conformable ionic communication circuit for transmitting and receiving ion based signals. We then characterized the performance of this ion-based communication in terms of its bandwidth, depth of propagation, and capacity for parallel transmission at different operating frequencies. Next, we designed and tested IC transmitter and receiver pairs with various geometries to better understand the key parameters defining bandwidth and stability of the ionic link. Lastly, we were able to integrate the optimized configuration of each subsystem into a compact, fully implantable device. The proposed ionic communication scheme and the resulting devices demonstrate concrete steps toward a high performance, fully implanted neural interface system with prolonged effective operation time *in vivo*.

SESSION F.FL02.08: Multifunctional Neural Interfaces

On Demand Abstracts Available for Viewing Starting Saturday Morning, November 21, 2020  
F-FL02

**5:00 AM \*F.FL02.08.01**

**Bioresorbable Materials in Temporary Implants for Neurostimulation, Sensing and Drug Delivery** John A. Rogers; Northwestern University, United States

Bioresorbable electronic materials serve as the basis for emerging classes of biomedical implants with operational lifetimes designed to match those of transient biological processes. These devices provide important functionality during a relevant timeframe and then naturally disappear within the body, thereby eliminating the need for surgical extraction. This talk presents our latest work in this area, with emphasis on materials aspects of (1) platforms for wireless neuromuscular electrical stimulation, with demonstrations of alleviated muscle atrophy resulting from denervation in rodent models via multiple episodes of the distal nerve engagement and (2) devices for programmable release of drugs from multiple, independently

addressable reservoirs, with illustrations in insulin and lidocaine delivery in animal models for control of blood glucose concentrations and pain responses, respectively.

**5:15 AM \*F.FL02.08.02**

**Miniaturized Neural Implants Using Magnetic and Optical Biohybrids** Jacob Robinson; Rice University, United States

Neural interfaces promise to deliver more effective treatment for conditions affecting the brain and body by improving the specificity and timing of therapies. While miniaturization is key to improve biocompatibility and safe deployment of these technologies, we must also improve the specificity of devices that sense and actuate biological signals. In this talk, I will describe on-going work to co-design genetically engineered cells and miniature magnetic/optical devices. These biohybrid technologies combine the speed and programmability of electronics with the biochemical specificity of synthetic biology. Specifically, we will describe how magnetoelectric and magnetothermal biohybrids enable rapid and precise actuation of cell activity, while planar imaging devices combined with computational reconstruction algorithms enable high-resolution measurement of biological activity. Together these technologies can enable future minimally and minutely invasive links between the body and external electronic devices.

**5:30 AM F.FL02.08.04**

**The Windansea Probe—A Composite Surface/depth Electrophysiological Electrode and Multiphoton Interrogation for 3D Brain Mapping** Keundong Lee<sup>1,2</sup>, Martin Thunemann<sup>1</sup>, Lorraine A. Hossain<sup>1</sup>, Youngbin Tchoe<sup>1</sup>, Jihwan Lee<sup>1</sup>, Sang Heon Lee<sup>1</sup>, Yun Goo Ro<sup>1</sup>, Gyu-Chul Yi<sup>2</sup>, Anna Devor<sup>3</sup> and Shadi A. Dayeh<sup>1</sup>; <sup>1</sup>University of California, San Diego, United States; <sup>2</sup>Seoul National University, Korea (the Republic of); <sup>3</sup>Boston University, United States

One of the grand challenges in neuroscience is to understand how neuronal activity is orchestrated to produce function. Single modality technologies offer either high spatial or high temporal resolution and with varied degrees of coverage. Multimodal approaches that can probe the brain's activity from the surface, at depth, and with high spatiotemporal resolution are believed to yield results that may complete our understanding of behavior and function. We report the seamless integration of the electrical and optical modalities for comprehensive and interactive 3D probing and manipulation of cortical neuronal activity and optogenetic (OG) stimulation/inhibition. Our "Windansea" technology, named after the famous Windansea beach in La Jolla, will replace the current cranial glass windows providing measurements of the extracellular local field potential (LFP) and multiunit activity (MUA), as well as a see-through optical access. The Windansea allows us to obtain depth-resolved LFP/MUA information, which can be used for estimation of spiking and synaptic activity in specific cortical neuronal populations, while simultaneously sampling electrical neuronal activity from the cortical surface and implementing single/multiphoton optical imaging and optogenetic stimulation/inhibition in behaving animals.

We leveraged microelectromechanical systems (MEMS) surface micromachining techniques to develop the hybrid surface-depth electrode. The depth electrode can be maintained inside the cortex chronically and does not block optical access. Therefore, both the depth and surface electrodes are flush with the cortical surface: The integrated depth electrode in our device utilizes an inserter with a small neck-region (narrow-constriction) of SU8 that is sheared (thermally or mechanically) to separate the handle from the implanted portion of the depth electrode so that a chronic transparent cranial window can be placed on the cortical implant. The device was implanted chronically in mice for several weeks and we recorded electrophysiological signals and obtained single/multiphoton optical images in awake animals.

**5:40 AM F.FL02.08.05**

**Flexible and Transparent Sensor Materials Toward a Fully Implantable Brain-Measurement System** Tepei Araki<sup>1</sup>, Shusuke Yoshimoto<sup>1</sup>, Hiroki Hamanaka<sup>2</sup>, Yuki Noda<sup>1</sup>, Takafumi Uemura<sup>1</sup>, Toshikazu Nezu<sup>1</sup>, Shuichi Tsuruta<sup>1</sup>, Masayuki Hirata<sup>1</sup> and Tsuyoshi Sekitani<sup>1</sup>; <sup>1</sup>Osaka University, Japan; <sup>2</sup>National Institute of Information and Communications Technology, Japan

A telemetric methodology can be used for conducting efficient and effective preclinical research in small nonhuman primates during free movement. In this study, we propose a fully implantable brain-measurement system using stretchable components and a small measurement instrument that wirelessly records brain potentials, stimulates neural activities, and recharges its own battery. When the integrated system was fully implanted in a marmoset, simultaneous measurements of the cortical and local field potentials were successfully performed during free movements. Even after a month of the implantation, the marmoset remained in good health and displayed activity equivalent to the amount before implantation. The results confirm that the proposed system is minimally invasive.

A sheet-type stretchable electrode fabricated using Au/Au core/shell nanowire (AgNW/Au) was used to measure the

somatosensory-evoked potentials after a few months of implantation. Antithrombogenic polymer treatment was introduced in the electrode to stabilize the monitoring, thus preventing the growth of granulation tissues that could interrupt access to the targeted neuron [1]. Furthermore, the sheet-type stretchable electrode showed mechanical durability at 60% strain and optical transparency over 80%. The multifunction simultaneously realized an optogenetic stimulation and *in vivo* brain ECoG monitoring. The integrated system is equipped with a micro-LED light irradiation system and is compatible with the optogenetic stimulation, which could contribute to brain-machine interfaces with a feedback sensation for diagnoses and therapy of patients suffering from intractable diseases [2,3,4].

[1] J. M. Anderson, et al., *Semin. Immunol.*, 20 (2), 86–100, 2008.

[2] S. Royer et al., *Eur. J. Neurosci.*, 31 (12), 2279–91, 2010.

[3] A. L. Miguel et al., *Nat. Rev. Neurosci.*, 10 (7), 530–40, 2009.

[4] Dong-Wook Park et al., *Nature Comm.*, 5, 5258, 2014.

#### 5:50 AM F.FL02.08.06

**Stretchable, Fully Integrated Organic Circuits for Chronic *In Vivo* Monitoring of the Developing Brain** Claudia Cea, Georgios Spyropoulos, Jennifer Gelinis and Dion Khodagholi; Columbia University, United States

Investigation of neural circuits in the immature brain is critical to understand how brain functions emerge and can be disrupted. The developing brain undergoes significant structural and molecular changes postnatally, some of which are experience-dependent. Mice provide one of the most common and accessible methods to model the human brain and its disorders. However, longitudinal monitoring of high spatiotemporal resolution neural activity in small, fragile mouse pups as they develop from newborns to adults is currently not possible. Here, we propose a flexible, stretchable neural interface device that allows chronic *in vivo* acquisition of neurophysiologic signals during postnatal development. The high biocompatibility, conformability and ultralow thickness of the device allow it to be hosted in the body for a duration of at least 15 days without inducing tissue reactions. The probe is sufficiently flexible to match the low elastic modulus of the tissue and designed in a stretchable configuration to expand with the pup's growth via serpentine-shaped interconnects. An electrocorticography array (NeuroGrid) is placed on the cortical surface and each electrode is connected to a net of internal ion-gated organic electrochemical transistor (IGT)-based voltage amplifiers. The high speed and transconductance of the IGTs along with their independently gated activation create a scalable integrated circuit that amplifies and multiplexes the recorded signals. The interconnects elongate inside the subcutaneous space of the pup's back, and electrical contact pads placed on the back of the animal are sutured through the tissue to the backend electronics via conductive PEDOT:PSS fibers. This approach will enhance knowledge of brain development in health and disease.

#### 6:00 AM F.FL02.08.07

**Multifunctional Fiber-Based Probes as a Three-Dimensional Deep Brain Interface** Shan Jiang<sup>1</sup>, Dipan Patel<sup>2</sup>, Jongwoon Kim<sup>1</sup>, Shuo Yang<sup>1</sup>, Williams Mills III<sup>2,1</sup>, Yujing Zhang<sup>1</sup>, Kaiwen Wang<sup>1</sup>, Ziang Feng<sup>1</sup>, Sujith Vijayan<sup>1</sup>, Rebecca Cai<sup>1</sup>, Anbo Wang<sup>3</sup>, Yuanyuan Guo<sup>3</sup>, Ian Kimbrough<sup>1</sup>, Harald Sontheimer<sup>2,1</sup> and Xiaoting Jia<sup>1</sup>; <sup>1</sup>Virginia Tech, United States; <sup>2</sup>VTC Fralin Biomedical Research Institute, United States; <sup>3</sup>Tohoku University, Japan

Complex interactions between neurons in different brain regions have been studied using a variety of technologies including microwires, silicon-based multielectrode arrays, and electrode arrays with flexible substrates. Such technologies have been shown to provide high-resolution electrophysiological recordings with high signal-to-noise ratio. However, with single implantation, the physical properties of these devices limit their access to one, small brain region. To overcome this limitation, we developed a platform that provides three-dimensional coverage of brain tissue through multifunctional polymer fiber-based neural probes capable of interfacing simultaneously with neurons in multiple sites. A scaffold with helix hollow channels is employed to achieve the 3D expansion of the multifunctional fiber probes in the deep brain while a femtosecond laser micromachining technique is utilized to expose electrode recording sites, microfluidic channel openings, and waveguide windows along the single fiber branch. By using our 3D fiber probes, we have obtained chronic endogenous neural activities with single-unit resolution from the wild type mice and captured optically stimulated neural signals with chemical modulation from transgenic mice expressing channelrhodopsin-2demonstrate. Furthermore, varying electrographic brain activities from different brain regions of interest were detected by our customizable multisite 3D fiber-based neural probes in a mouse model of epilepsy, suggesting the potential of using these probes for the investigation of brain disorders such as epilepsy. Ultimately, we envision that this 3D multifunctional neural interface can bring new insights for deciphering complex brain functions and dynamics in the near future.

#### F.FL02.09.01

**Off-Stoichiometric-Thiol-ene Epoxy Polymers for Soft Implantable Electrode Array** Eleonora Borda, Marta Airaghi Leccardi and Diego Ghezzi; École Polytechnique Fédérale de Lausanne, Switzerland

Implantable electrode arrays have been widely used to treat neurological disorders such as Parkinson's disease, epilepsy, hearing loss, and chronic pain by applying electrical stimulation and/or recording neural activity. One of the main requirements for these devices is the ability to evoke minimal inflammatory tissue response to guarantee the long-term use of integrated functions. However, this can be limited by a mechanical mismatch between the implant, very stiff, and the tissue, very soft, inducing neural damages and leading to glial scar formation. So far, the most common materials used for fabrication of such neural interfaces are PI and PDMS. On one hand, thin-film microfabrication techniques allow the fabrication of flexible miniaturized and highly integrated stimulating or recording arrays in PI. However, the Young's modulus of PI is about a few GPa. On the other hand, PDMS because of its low Young's modulus (approximately 1 MPa) and its elastic behaviour leads to less damage to the neural tissue, but it presents challenging steps in the microfabrication process, especially for the encapsulation of the active sites. Off-Stoichiometric-Thiol-ene Epoxy polymers (OSTE+) were developed firstly for rapid prototyping of microfluidic chips because they are less permeable to gas. OSTE+ materials are a good compromise between PI and PDMS. In fact, by adjusting the stoichiometry of the constituting monomers, the Young's modulus of OSTE+ can be decreased down to a few MPa at physiological temperature. The preparation of OSTE+ consists of two curing steps in which (1) thiol-ene photopolymerization allows to pattern the polymer surface and remove the non-polymerized areas before (2) thermal curing. Thus, it is possible to encapsulate the electrode array simply using photolithographic techniques. Taking advantage of these properties, we fabricated OSTE+ implantable multielectrode arrays with Pt serpentine in monolayer and bi-layer. The functional characteristics of these arrays have been tested by electrochemical characterization and recordings.

#### F.FL02.09.02

**Parylene-Based Double-Faced Electrode Array for Retinal Prosthesis** Namju Kim, Heewon Seo and Sohee Kim; Daegu Gyeongbuk Institute of Science & Technology, Korea (the Republic of)

Retinal prostheses require high-density electrode arrays to attain high spatial resolution in vision. However, the transmission lines panning out in the same layer with electrodes may hamper achieving high-density electrodes. Double-faced electrode arrays may circumvent this problem, in which the electrodes and bonding pads are arranged face-to-face and the transmission lines are absent. The electrodes can be connected with stimulation drivers such as photovoltaic cells directly through bonding pads. Here we present the fabrication of a flexible and transparent parylene-based double-faced electrode array and the method of integrating it with the stimulation driver IC.

#### F.FL02.09.03

**Transparent and Flexible Ultrathin Gold Microelectrode Arrays Using Layer-by-Layer Coated Polyelectrolytes for Electro-Optical Neural Interface** Woongki Hong, Yujin Hwang, Junil Kim, Hyuk-Jun Kwon, Jae Eun Jang and Hongki Kang; DGIST, Korea (the Republic of)

In recent years, neural interface technologies have been focused on flexible and transparent neural electrodes for high spatiotemporal resolution mapping of neuronal activities using electro-optical measurements. There had been several new material suggestions for the transparent, flexible neural electrodes such as ITO, graphene, conductive polymer, or patterned metal (nanowires, mesh patterns). [1, 2] However, these materials have shown several limitations such as high processing temperature, limited mechanical/electrical reliability, fabrication complexity and incompatibility with conventional microfabrication processes etc. To resolve these problems, in this work, we developed a flexible microelectrode array (MEA) using polymer-metal hybrid structures for high optical transparency and good electrical conductivity. We used layer-by-layer assembly of polyelectrolytes as a nucleation inducing coating layer on transparent substrates (glass, polymer) to realize highly conductive vacuum deposited gold film at sub 10 nm thickness. We optimized the electrical and optical properties of the ultrathin gold electrodes, showing sheet resistance as low as 7.24  $\Omega$ /sq at 8 nm thickness and electrical conductivity of  $1.327 \times 10^6$  S/m. Despite the opaque characteristic of typical thick gold film, the ultrathin film of gold in this work still showed optical transparency of 77% at 550 nm, which is comparable to or better than most of

transparent neural electrode materials. In addition, excellent mechanical stability is also demonstrated with bending radius down to 1 mm for at least 500 times of bending. We further measured the baseline noise properties of our ultrathin 40- $\mu\text{m}$  diameter gold MEA for *in vitro* neural recording setup. We have confirmed that it shows low RMS noise level of  $9.62 \pm 2.24 \mu\text{V}_{\text{rms}}$  ( $n=60$ , bandpass filtered in 200 Hz – 3.5 kHz). These results confirm that the polymer-metal hybrid structure based MEA we developed in this work can be used for simultaneous extracellular electrical neural recording and optical neural recording such as calcium imaging.

#### References

1. Jimbo, Y. *et al.* Ultraflexible Transparent Oxide/Metal/Oxide Stack Electrode with Low Sheet Resistance for Electrophysiological Measurements. *ACS Appl. Mater. Interfaces* **9**, 34744–34750 (2017).
2. Kshirsagar, P. *et al.* Transparent Graphene/PEDOT:PSS Microelectrodes for Electro- and Optophysiology. *Adv. Mater. Technol.* **4**, 1–7 (2019)

#### F.FL02.09.04

**Bioresorbable Endovascular Neural Interface for Minimally Invasive Neural Stimulation and Recording** Adele Fanelli, Laura Ferlauto and Diego Ghezzi; EPFL, Switzerland

Neural signal recording and direct stimulation of the brain have been widely used to mitigate neurological disorders, such as epilepsy and Parkinson's disease. Current available techniques in this field commonly require invasive surgery potentially entailing both transient and permanent complications. A promising strategy designed to overcome these risks involves the exploitation of the cerebrovascular system as access route to the neural tissue. Cardiovascular stent technology, exceptionally designed for a minimally invasive procedure and maximum adherence to the vessel wall, represents an optimal scaffold for the recording/stimulating system. Moreover, given the versatility of this type of implant, peripheral nervous system could also be targeted for neural stimulation aimed at relieving intractable pain or supporting motor rehabilitation. Therefore, our goal is the development of a stent-inspired device, with electrodes embedded on its surface facing the vessel walls, for minimally invasive active and passive interaction with the surrounding neural tissue. In order to reduce the possibility of chronic local inflammation and delayed endothelialization, commonly occurring with metallic implants, our device has been fabricated using only biodegradable and biocompatible soft polymers such as poly- $\epsilon$ -caprolactone (PCL) and (3-glycidyloxypropyl)trimethoxysilane-doped poly(3,4-ethylenedioxythiophene) : poly(styrenesulfonate) (GOPS-doped PEDOT:PSS), for encapsulation and electrodes respectively. Electrochemical properties of the prototypes have been tested in both static and dynamic conditions, with the latter simulating the vascular environment and its pulsatile flow. Degradation analysis *in vitro* has been performed as well to define the device durability. The promising results open the doors to further investigation of the potentialities of this innovative device, able to replace invasive systems currently used for neural recording and stimulation. Its development will have a huge impact in the treatment of neuropathological conditions related to both central and peripheral nervous system.

#### F.FL02.09.07

**Enhanced Antioxidant Activity of Cerium Oxide Nanoparticles by Surface Modification and Their Potential Application for Mitigating Foreign Body Response in Implantation of Active Chronic Medical Devices** Yue Hu, Vicki L. Colvin and Vivian Ling; Brown University, United States

There are roughly 175,000 different medical devices in the US market. The global market for medical devices grows fast yearly, it reached nearly \$521.2 billion in 2017 and should reach \$674.5 billion by 2022, at a compound annual growth rate (CAGR) of 5.3% for the period of 2017-2022. Some relevant examples include joint replacements, cardiac pacemakers, hernia meshes, subcutaneous real-time glucose sensors, and neural recording devices. An important and growing subset of these devices termed here 'active' implants, require electrical contact to tissues. Their function demands that they have long-term electrical contact to host tissue; perhaps the most widely known example is cardiac pacemakers now found in over 235,000 people in the US alone. Important emerging disease treatments, however, also rely on active medical devices including subcutaneous glucose sensors and neural recording devices. In the case of glucose sensors, the real-time information can drive both dietary choices and mitigate Type 2 diabetes or be part of an automatic insulin delivery system that frees patients with Type 1 diabetes from self-administered insulin injections. In these cases, the implant must stay functional and non-changing in their tissue interactions for years.

Every medical device that is implanted in a person encounters the body's foreign body response (FBR) which in short results in the body physically walling off an object from its physiology. Initially discovered in the 1970s, this multi-stage process is initiated by the innate immune system upon the introduction of foreign material. After injury and implantation, FBR activated by blood/material interaction, followed by protein adsorption, immune cells adhesion, activation, and differentiation. The whole process undergoes acute inflammation, chronic inflammation, the generation of granulation tissue and end up with the

fibrous encapsulation generated by FBGCs. Foreign body response (FBR) triggered by the implantation of medical devices limits the lifespan of devices.

One of the widely used solutions is to suppress the immune system response to medical devices. Reactive oxygen species (ROS) generated during the FBR process play a key role in immune responses to implantation. ROS are generally linked to aging, cancer, and nervous system diseases. Anti-inflammatories and antioxidants, such as nonsteroidal anti-inflammatory drugs (NSAIDs), dexamethasone, masitinib, and resveratrol have been combined with implantable devices in local delivery to fight against FBR. However, molecular antioxidants are facing several problems, such as short lifetime, instability in micro-environment, and ineffectiveness induced high doses, limiting the chronic efficiency of implanted devices.

Nanoparticles, well known with their high surface to volume ratios, are widely used in biomedical engineering these days. Cerium oxide nanoparticles exhibit recyclable antioxidant properties due to facile electron transfer between Cerium (III) and Cerium (IV). Recent studies reveal that ceria nanoparticles with diameters of 5 nm are non-toxic and efficient for quenching ROS in vivo. We developed a PEGylated polymeric ceria nanoparticle which is stable and biocompatible. We also observed that the antioxidant activity of cerium oxide nanoparticle is enhanced by this PEGylated surface modification which can be widely used in vivo to control the ROS levels at the implant site and relief FBR.

### SYMPOSIUM F.FL03

---

Flexible, Wearable Electronics and Textiles  
November 21 - November 21, 2020

#### Symposium Organizers

Trisha Andrew, University of Massachusetts Amherst  
Wenlong Cheng, Monash University  
Jesse Jur, North Carolina State University  
Zijian Zheng, Hong Kong Polytechnic University

---

\* Invited Paper

SESSION F.FL03.01: Flexible Materials and Manufacturing—Printing for Flexible Electronics  
On Demand Abstracts Available for Viewing Starting Saturday Morning, November 21, 2020  
F-FL03

#### **5:00 AM \*F.FL03.01.01**

**Nanomaterials for Large Area Flexible Electronics and Small Area Ultra-Compact Microdevices** Oliver G. Schmidt; Leibniz IFW Dresden, Germany

Nanomaterials in the form of nanomembranes are thin, flexible, transferable and can be shaped into unique 3D micro and nanoarchitectures. This makes them attractive for various scientific disciplines ranging from «Electronic Soft-Wear» to «Microrobotic Hard-Ware». This talk explores the underlying science of nanomembranes and discusses the fascinating application potential of this particular class of nanomaterials ranging from integrated microelectronic skin [1] and self-assembled 3D microelectronics [2] to medical microbots [3] and the world's smallest self-propelled microelectronic systems [4].

[1] M. Kondo, M. Melzer, D. Karnaushenko, T. Uemura, S. Yoshimoto, M. Akiyama, Y. Noda, T. Araki, O. G. Schmidt, T. Sekitani, *Sci. Adv.* 6, eaay6094 (2020)

[2] D. Karnaushenko, T. Kang, V. K. Bandari, F. Zhu, O. G. Schmidt, *Adv. Mater.* 32, 1902994 (2020)

[3] M. Medina-Sánchez, O. G. Schmidt, *Nature* 545, 406 (2017)

[4] V. K. Bandari, Y. Nan, D. Karnaushenko, Y. Hong, B. Sun, F. Striggow, D. D. Karnaushenko, C. Becker, M. Faghieh, M. Medina-Sánchez, F. Zhu, O. G. Schmidt, *Nature Electron.* 3, 172 (2020)



5:15 AM F.FL03.01.02

**Flexible Inkjet-Printed Nanoparticle-Based Supercapacitors—Effect of Substrates, Printing and Materials** Maxim Shkunov and Pavlos Giannakou; University of Surrey, United Kingdom

Inkjet printing is highly promising fabrication technology for electronic devices, including energy storage systems, due to the fact that is an industrially mature, readily scalable, low-cost, digital, contactless and mask-free method with roll-to-roll capability, minimal processing steps and minute quantity of material waste. Solution-processing of nanomaterials in printed electronics via ink-jet allows for very efficient integration of different types of nanoparticles in electrochemical energy storage devices. However, it is important to address the challenges associated with the variation in printed layers properties and to investigate the effects of printing including substrates, materials, printing and processing on the electrochemical performance and response of the devices.

In this work, we have fabricated and characterised flexible, fully solution processed, co-planar, NiO-nanoparticle-based, micro-supercapacitors through inkjet printing. Cyclic voltammetry studies were performed to investigate the effect of substrate and printing resolution, different types of current collector silver inks, sintering temperatures and carbon residues in electrodes, different types of electrolytes, including liquid and gel electrolytes, binders and other organic compounds in electrolytes, and the effect of electrode gaps on the electrochemical response and capacitance of supercapacitors. The devices were prepared on flexible polyethylene terephthalate (PET), polyimide Kapton substrates and photographic paper. Two types of silver nanoparticle inks have been used as the current collectors in the devices. A NiO nanoparticle ink was developed and has been used in different concentrations as the active electrode material in the devices. Aqueous solutions of sodium hydroxide (NaOH), sodium nitrate (NaNO<sub>3</sub>), lithium hydroxide (LiOH), potassium hydroxide (KOH) and saturated magnesium perchlorate aqueous solution (SMPAS) have been used as electrolytes, either in liquid or gel form at different concentrations. The devices were scanned at voltage a window from 0 to 1 V, at scan rates from 10 to 1,500 mV/s. Capacitance has varied significantly depending on the substrate, printing resolution and the use of electrolyte and scan rate. Some of the highest capacitance values of 117 F/cm<sup>3</sup> at 10 mV/s were obtained on PET substrates. XPS measurements of carbon residues in active layers have been correlated with sintering temperatures and supercapacitors performance. Highly flexible, inkjet-printed supercapacitors, with a particular focus on wearable applications, are finally demonstrated as epidermal printable supercapacitor, water-transferred on the skin of a human subject, to potentially serve as the power source for wearable health systems.

We will discuss the summary of results on the effects of substrates, printing, sintering, choice of materials on microsupercapacitors performance and outline how these results can be extended to flexible electronics, realised through printing fabrication processes, including wearable devices, batteries and energy generation-and-storage systems.

5:25 AM F.FL03.01.04

**Printing Conformal 5G Antennas and Waveguides—A Material and Design Analysis** Bradley J. Pothier, Katherine Berry, Eric Brown, Edward Kingsley, Craig A. Armiento, Alkim Akyurtlu, Gary Walsh and Corey Shemelya; UMass Lowell, United States

With today's fast-paced research environment, a need is being established to bring new form-factors to new and existing technologies. One such technology RF antennas, systems and components. For this reason, it is beneficial to examine communication components and adapt their design paradigms for advanced manufacturing techniques; in this case to develop 5G antennas and waveguides in a flexible or 3D printed form factor. Our work at PERC has extended state-of-the-art printed electronic technologies beyond simple circuits, and into RF antennas and sub-systems; while also allowing IC integration with conformal/flexible designs. RF devices such as Bluetooth boards, conformal RF antennas, and planar phased array systems, have been fabricated using printed electronic technologies to allow everything from wireless external communications to phased array tracking systems [1,2].

This project investigates additively fabricated conformal 5G (6 GHz) antenna designs and their performance when printed on the conformal surfaces. Design factors such as antenna type, orientation, and RF properties are considered. Here we analyze waveguide designs such as grounded co-planar, co-planar, and microstrip for conformal single-layer and multi-layer designs. As such, we explore multiple printable material systems including: silver nano-inks, thin-flexible laminate boards, and Kapton polyimide films, in order to determine potential systems that satisfy both functionality and manufacturability requirements. Our initial designs utilize direct-write micro-pen dispensing systems in order to develop a tool-box for printed material systems which can then be applied to the Optomec 5X 5-axis direct-write system. All antenna designs (planar and conformal) are simulated in ANSYS HFSS to ensure printed, conformal layer thickness and feature sizes produce an optimal antenna response. Additionally, this work investigates potential antenna performance characteristics in relation to system longevity and durability. For example, the adhesion between printed layers to potential end-use conformal material systems, as well as the effectiveness of RF-transparent polymeric layers for ruggedization. As such, all designs are modeled to incorporate spray-coatable fluoropolymer coatings. This work describes problems that reside in conformal RF applications

such as retaining printing accuracy and compensating for the rounded shape and functional properties of the surface.

[1] C. Shemelya, L. Banuelos-Chacon, A. Melendez, C. Kief, D. Espalin, R. Wicker, G. Krijnen, E. MacDonald, "Multi-functional 3D printed and embedded sensors for satellite qualification structures," IEEE, SENSORS, Nov. 2015. 1-4.

[2] M. Haghzadeh, C. Armiento, A. Akyurtlu, "All-Printed Flexible Microwave Varactors and Phase Shifters Based on a Tunable BST/Polymer," IEEE Transactions on Microwave Theory and Techniques, 65 (6), 2030-2042, 2017.

#### 5:35 AM F.FL03.01.05

**The Large-Area Printing of Bending-Insensitive Pressure Sensors Achieved by Monodisperse Carbon Particles with Flower-Like Superstructures** Naoji Matsuhisa<sup>1,2,3</sup>, Stephen J. O'Neill<sup>2,4</sup>, Huaxin Gong<sup>2</sup>, Shucheng Chen<sup>2</sup>, Hanul Moon<sup>2,5</sup>, Hung-Chin Wu<sup>2</sup>, Xianfeng Chen<sup>4</sup>, Xiaodong Chen<sup>3</sup> and Zhenan Bao<sup>2</sup>; <sup>1</sup>Keio University, Japan; <sup>2</sup>Stanford University, United States; <sup>3</sup>Nanyang Technological University, Singapore; <sup>4</sup>The University of Edinburgh, United Kingdom; <sup>5</sup>Korea Advanced Institute of Science and Technology, Korea (the Republic of)

We demonstrate a bending-insensitive pressure sensor with extremely high sensitivity ( $2 \times 10^5$  kPa<sup>-1</sup>) by the simple blade coating of a composite containing carbon flowers. To date, highly sensitive pressure sensors have been fabricated by molding microstructures such as pyramids and domes. The printing of conductive particle-elastomer composites does not require any molds, and can simplify the fabrication. However, composite based pressure sensors have suffered from poor flexibility and large-area uniformity. This is because the percolation-based sensing mechanism can be easily influenced by the composite thickness, requiring a considerable thickness for high sensitivity. Our composite is made of an SEBS elastomer and monodisperse carbon particles, which have flower-like superstructures and can be synthesized at very low cost (carbon flowers) [1]. The unique structural properties of carbon flowers enable a contact-based pressure sensing mechanism to achieve extremely high sensitivity which is insensitive to the printed thickness. The active layer can be as thin as 13  $\mu$ m thickness, which to our knowledge is the thinnest among printed pressure sensors. The capability of pressure sensing was investigated under several bending radius down to 5.5 mm and showed consistent characteristics, although most previously reported pressure sensors have only been tested in a flat state after bending. Furthermore, we printed a pressure sensor over a substantial area (1 m  $\times$  2 cm), over which the sensors showed significantly uniform pressure sensing characteristics. This is achieved by the contact-based sensing mechanism that is robust against thickness variation across the large area printed composites. Our sensor demonstrates both high pressure sensing performance and high scale-ability, which is extremely suitable for applications in human-machine interfaces, healthcare, and Internet of Things (IoT).

[1] S. Chen, D. M. Koshy, Y. Tsao, R. Pfattner, X. Yan, D. Feng, Z. Bao, *J. Am. Chem. Soc.* **140**, 10297 (2018).

#### 5:45 AM F.FL03.01.06

**Digital 3D Printing for the Fabrication of Integrated Mechanical Sensors within Soft Personalized Wearables** Ryan van Dommelen<sup>1</sup>, Marco Riccardo Binelli<sup>2</sup>, Yannick Nagel<sup>3</sup>, Gilberto De Freitas Siqueira<sup>3</sup>, André R. Studart<sup>2</sup> and Danick Briand<sup>1</sup>; <sup>1</sup>École Polytechnique Fédérale de Lausanne, Switzerland; <sup>2</sup>ETH Zürich, Switzerland; <sup>3</sup>Empa—Swiss Federal Laboratories for Materials Science and Technology, Switzerland

The ultimate autonomous smart wearable device is one in which all parts are seamlessly integrated. One of main benefactors of these devices is the health sector. As currently the tools available for the evaluation of a patient's recovery are limited to either bulky stationary equipment, or non-customized wearable devices. Therefore, with the recent strong progress in the field of 3D printing it is now more than ever possible to 3D print completely customized objects on the fly. Especially due to the digital nature of the fabrication tools used, wherein the overall process is called digital manufacturing, it is possible to adapt a general device layout for a patient's needs. Especially of interest here is that these 3D printed, and custom-tailored devices could be worn to continuously monitor the gait and joint motions of a patient during recovery. Currently this is something that often can only be measured in a specialized room within an hospital. Furthermore, the usage of 3D printing tools allows for the fabrication of more complex geometries, and functional layers not possible to produce with more conventional methods. These advantages can be exploited to introduce smart features into other 3D printed objects as well.

One of the key challenges for the full exploitation of these technologies is the integration of the printing of functional layers within a repeatable process chain. The main bottleneck being currently that the range of 3D printable materials is often limited to either hard or non-flexible materials, let alone functional ones. Therefore, we have developed and are continuously improving an elastomeric material system that is fully printable using Direct Ink Writing (DIW). Our material system is created by making use of natural cellulose based fibers to be able print self-supporting soft structures. This system thus makes it an ideal candidate to produce truly three dimensional and fully soft wearable devices with a high degree of comfort. In parallel, we are exploiting the use of a custom made 5-axis multi-tool printing platform to be able to directly print multiple materials on curved surfaces. This platform is driven by software that allows for on the fly modifications to the input model,

which has resulted in a early stage approach towards personalization of our sensing devices. With the multi-tool capability, it allows us to perform all production step within the platform.

Accompanying this, we have so far investigated the fabrication of piezoresistive, capacitive and triboelectric mechanical sensors made from our materials system. These sensors have been tested in both ideal circumstances, using mechanical test benches to compress and bend the sensors, as well as by actual human motions. We will present their evaluation by means of simulated and non-simulated human motions. The simulated evaluations were performed using static compression tests, up to 1000 kPa, and dynamic compression tests, up to 2 Hz. The hysteresis characteristics of the sensors were also found using the mechanical test benches.

At this stage, we are exploiting these results to integrate the sensors into a wearable demonstrator. By using our 3D printing technologies, we also show that we can print structures in three dimensions to create geometries which are not possible or unfeasible with conventional technologies. This approach, which uses our material's inherent self-supporting ability, allows for the miniaturization of 3D printed structures. Using this we can create more compact sensors with improved responses, as well as enable multi-modal sensing. All these factors combined allow for the fabrication of truly novel fully 3D printed sensors. Since these sensors are produced in a completely digital fashion, they can be fully personalized for each person, while using the same printing infrastructure.

#### **5:55 AM F.FL03.01.08**

**Inkjet Printing Electronic Materials on Polymeric Platforms for Flexible and Wearable Electronics** Inhwan Kim, Ying Zhou and Jesse S. Jur; North Carolina State University, United States

Inkjet processing is a promising method for printed electronics for flexible and wearable electronics, allowing for nano- to micron-scale films with low temperature processing. In this work, we explore process engineering of inkjet printing electronic films and textiles (e-textiles) with the application of multi-layered conductive, dielectric, and semiconductor materials. Considering fluid characteristics and jetting parameters, electronic inks were formulated based on common inkjet processing conditions of low viscosity (<25cP) and 25-50 dyn/cm of surface tension. Particle-free reactive silver inks based on silver carboxylates ( $\text{Ag}^+ - \text{O}_2\text{C} - \text{R}_1$ ) and aqueous ammonia ligand ( $-\text{NH}_2 / -\text{NR}_2\text{H}$ ) was processed both on films and textiles. The quality of the patterns was able to be controlled by the drop spacing variation (5-200  $\mu\text{m}$ ) with consideration of a single drop size ( $\sim 50 \mu\text{m}$ ). After low-temperature annealing process (150°C), the low sheet resistance of  $<0.5 \Omega/\text{sq}$  was achieved by print resolution of 1693 dpi (15  $\mu\text{m}$  drop spacing) - 2540 dpi (10  $\mu\text{m}$  drop spacing) with only one print pass. The dielectric ink was formulated by the equal mass ratio of poly(4-vinylphenol) (PVP) and poly(melamine-co-formaldehyde) (PMF) in propylene glycol methyl ether acetate (PGMEA) solvent. Cross-linking process with UV and thermal annealing (150°C) after the inkjet process of the PVP/PMF dielectric ink as an insulator of the conductive silver layer. The inkjet processed reactive silver ink on the dielectric layer kept the dielectric layer compatible, showing potentials as the insulating materials for capacitors and transistors. In addition, p-type semiconductor ink with 6,13-bis(triisopropylsilylethynyl)-pentacene (TIPS-Pentacene) and polystyrene blend in tetralin was able to be inkjet printed on the flexible substrates to demonstrate the compatibility with the conductive and dielectric inks within the multi-layer device architecture via inkjet processing. Our study highlights viability of fully-inkjet processed flexible electronics in wearable technology applications.

#### **6:05 AM F.FL03.01.09**

**Printing of Dielectric Particle Enhanced Textiles for Antenna Designs** Ying Zhou<sup>1</sup>, Braden M. Li<sup>1</sup>, Chunxu Mao<sup>2</sup>, Yuhao Wu<sup>2</sup>, Inhwan Kim<sup>1</sup>, Henry Soewardiman<sup>1</sup>, Douglas Werner<sup>2</sup> and Jesse S. Jur<sup>1</sup>; <sup>1</sup>North Carolina State University, United States; <sup>2</sup>The Pennsylvania State University, United States

Printing methods are rapidly being developed for the improvement of fabrication efficiency in electronic devices, particularly in the field of electronic textiles (E-Textiles) of particular interest has been the formation of high efficiency antenna devices that provide a means for body area networking and data transfer. This work details a novel fabrication process for flexible textile antenna by a combination of the direct writing printing to enhance the dielectric properties of the textile. Using a direct write process, an ink consisting of a UV curable monomer with 4 wt.% 200 nm barium titanate nanoparticle loading is embedded within fabrics to enhance the dielectric constant of the naturally air porous textile architecture. This method is demonstrated to be universal for all kinds of the fabric, include nonwoven, woven, and knit fabric types. By controlling the spray parameters (time and translation speed) of the ink, the dielectric constant can be increases to 1.4 - 1.6 without significant blockage of the air gaps in the fabric. In this way, the flexibility and air permittivity of the fabric has minimal change. As a demonstration, the dielectric ink is applied to enhance the permittivity of a jersey knit fabric panel, allowing for a simplified manufacturing process for these traditionally complex e-textile systems. Combinations of nonwoven and knit layering through heat lamination is shown to provide the necessary structure for the antenna device with a conductive Ag

screen print active and ground layers with a conductivity of  $1.3 \times 10^6$  S/m. The methods explored are extended to a novel dual-port textile antenna aimed at 2.45 GHz with a low height profile and enhanced bandwidth for wearable applications, exhibiting a working bandwidth of 2.32 -2.45 GHz.

#### 6:15 AM F.FL03.01.10

**Thermoresistive Properties of Vapor Printed PEDOT-Cl Coated Fabrics** Linden K. Allison and Trisha L. Andrew; University of Massachusetts at Amherst, United States

Fabric-based circuits are an important component of developing wearables. Thermistors have proven to be a difficult factor to measure accurately using a fabric. Temperature sensing is an important part of health monitoring, as abnormalities could signal conditions such as fevers, infections, or heatstroke. Early detection of these temperature deviations can lead to more effective treatments. Currently, methods of monitoring body temperature are either invasive or inaccurate, since accurately measuring the temperature of the body's core is difficult to do from the surface of the skin. Additionally, temperature sensing could prove useful in other forms of health monitoring when paired with other types of sensors, such as humidity sensors. Herein, we demonstrate a technique to produce an all fabric, wearable thermistor. Using reactive vapor deposition (RVD) we produce a thermoresistive coating of PEDOT-Cl on a variety of commercially available fabrics. We show that the thermistive properties and sensitivities of the coatings can be tuned by using different weave porosities, fabric thicknesses, and fabric materials. We further explore the response of the PEDOT-Cl fabrics when subjected to varying humidity, or the hygro-resistivity, and how this can influence the thermo-resistivity of the coated fabrics. Additionally, we utilize these coatings to create a wearable device, capable of sensing body temperature. By measuring the temperature of several key locations on the body, the temperature of the core can be monitored. This work provides a platform to monitor body temperature in a non-invasive and comfortable way. We also use the PEDOT-Cl coated fabric to demonstrate how the thermo-resistive and hygro-resistive responses can be combined to measure breathing when incorporated into a face mask.

#### 6:25 AM F.FL03.01.11

**Continuous Pilot-Scale Production of High-Performance Multifunctional Paper Based Sensors for Internet of Things Applications** Sheila Goodman and Anthony Dichiaro; University of Washington, United States

The growing demand of wearable technology has caused a resurgence of paper-based flexible electronics, offering a biodegradable and low-cost alternative to petrochemical substrates. In this research, "smart" papers were produced from renewable pulp fibers using a pilot-scale web former operated at 4 m/min. The surface of bleached softwood fibers was modified *in situ* by electrically conductive carbon nanotubes pre-adsorbed with cellulose nanofibrils during the papermaking process. The interfacial properties were tailored based on a layer-by-layer nanoassembly method, enabling good retention and uniform distribution of nanofillers in the sheet even at high content (up to 15 wt%). The as-produced multifunctional smart papers were employed as an inexpensive and sustainable alternative for various chemical and physical resistive sensing applications. An Internet of Things (IoT) device was fabricated utilizing an affordable microcontroller and simple circuit to rapidly and reliably detect variations (temperature, pH, chemical presence) in aqueous media for over thirty response cycles, with a maximum relative resistance increase of ~12,000%. This device was able to detect the presence of small volumes of water, as low as 0.5  $\mu$ L, and the presence of water in organic solvents as low as 0.10 wt%, allowing for immediate signaling in circumstances where high water contents are intolerable. Electrical resistance changes remained stable and reversible in impure aqueous solutions, including tap water, and across a range of saline water concentrations which varied from 0.1 to 1 wt% NaCl. As-produced smart papers were successfully implemented as a piezoresistive device which demonstrated a wide sensitivity range (6 Pa~500 kPa) and low detection limit, with applications in gait and respiratory sensing. The versatility and efficacy of as-produced smart papers allows for a low-cost and biodegradable replacement for petrochemical substrates in multifunctional sensing applications.

#### 6:35 AM F.FL03.01.12

**Late News: Electrowetting Valves for Sweat-Based Microfluidics** Aditi Naik<sup>1</sup>, Brenda Warren<sup>1</sup>, Andrew Burns<sup>2</sup>, Ralf Lenigk<sup>2</sup>, Jeffrey Morse<sup>1</sup>, Azar Alizadeh<sup>2</sup> and James Watkins<sup>1</sup>; <sup>1</sup>University of Massachusetts Amherst, United States; <sup>2</sup>General Electric Global Research Center, United States

Skin-compatible microfluidic valving systems with on demand sweat capture are necessary to understand the temporal variation of chemical biomarkers. Here, we demonstrate solution-based electrowetting valves with rapid actuation integrated into a flexible microfluidic sweat collection patch. The valve is produced by inkjet-printing a pair of silver electrodes with spacings of 0.2 to 2 mm and modifying the downstream electrode with a hydrophobic self-assembled monolayer. To complete the valve, a microfluidic channel is fabricated from laser ablation of adhesive layers and pressed over the silver electrodes. Artificial perspiration is driven by capillary action within the channel until stopped by the electrowetting valve. A

low voltage is applied to the electrodes, altering the hydrophobic monolayer, and allowing the fluid front to continue through the microchannel. Statistical analysis demonstrates that applied voltage and not electrode spacing influences valve actuation time, with  $17 \pm 8$  s for 4 V and  $40 \pm 16$  s for 1 V. Inkjet-printing conditions were also optimized to achieve a valve fluid retention time of 9 hours. Using four electrowetting valves, an integrated wearable device is designed for artificial perspiration collection through valve actuation at distinct time points over 40 min. Finally, these inexpensive, user-friendly, and disposable electrowetting valves offer exciting opportunities for non-invasive point-of-care sweat monitoring.

#### 6:45 AM F.FL03.01.13

**Late News: 3D Patterned Electronic Paper from Nanocellulose and PEDOT:PSS** Makara Lay and Isak Engquist; Linköping University, Sweden

Printed electronic technology has become an important tool for the production of low-cost flexible electronic devices. However, due to the limited thickness of printed materials, they have a limited electric current capacity and cannot be used for applications that need high power.

This work aims to fabricate a 3D conductivity patterned paper from nanocellulose and PEDOT:PSS based materials using syringe injection and 3D printing methods. Unlike the usual concept of electronic papers, comprising conductive ink on a paper substrate, these 3D patterned papers integrate the conductor patterns in the bulk of paper, while non-conductive sections are used as support to form free-standing papers. Two different inks, non-conductive and conductive, were derived. The non-conductive ink consists of cellulose nanofiber (CNF), microfibrillated cellulose (MFC), glycerol, and alginate in different concentrations for syringe injection and 3D printing, respectively. CNF, PEDOT:PSS, glycerol, and ethylene glycol were used to prepare the conductive ink. Both inks were deposited on a substrate using syringe injection or 3D printing, creating 3D patterned papers that can be peeled off from the substrate. The patterned papers are flexible, conformable, wearable, and strong. The conductive parts show electrical conductivity of up to 202 S/cm, current capacity above 0.7 A, and the full patterned papers have a tensile strength of 25 MPa. The non-conductive sections have some ionic conductivity, making it possible to use the conductor patterns as electrodes, and the non-conductive patterns of the same paper as electrolyte for simple supercapacitor devices. This successful 3D patterning of electronic paper will pave the way for manufacture of paper-based power transistors, supercapacitors, wearable devices or smart packaging.

#### 6:55 AM F.FL03.01.14

**Printable, Flexible and Fully Tissue Equivalent X-Ray Detection Using Polymer Nanosensors with Ultralow Operating Bias and Tuneable Radiolucency** Matthew Griffith<sup>1</sup>, Jessie Posar<sup>2</sup>, Sophie Cottam<sup>3</sup>, Joshua Stamenkovic<sup>3</sup> and Marco Petasecca<sup>2</sup>; <sup>1</sup>The University of Sydney, Australia; <sup>2</sup>The University of Wollongong, Australia; <sup>3</sup>The University of Newcastle, Australia

Research interest in new materials for X-ray detection is rapidly growing, driven by demand from diverse applications such as medical imaging, radiotherapy, space exploration, security and defence, and personal wearable dosimeters.<sup>[1-2]</sup> Current detectors use inorganic semiconductors such as silicon, selenium or cadmium zinc telluride. However, X-ray detectors fabricated from these materials are expensive to manufacture, and cannot be easily fabricated into flexible sensors or large-area pixelated arrays.<sup>[4]</sup> Furthermore, these semiconductors are composed of heavier elements, which exhibit much stronger X-ray attenuation than the lighter elements in human tissue. Consequently, use of these materials for medically relevant dosimetry faces two major challenges:

1. Allowing X-rays through the detector without altering carefully calibrated beam intensity.
2. A requirement for complex and often unreliable calibrations to produce a response equivalent to the human body.

Here we report the development and characterisation of printable, flexible and fully tissue equivalent X-ray detectors fabricated from solution-processable organic conductors. The photodetectors are composed of donor polymer P3HT and two different acceptors: fullerene derivative PCBM and non-fullerene acceptor o-IDTBR. We show these organic electroactive inks are uniquely capable of both tissue equivalent X-ray attenuation and electrical conductivity. The non-fullerene acceptor material shows both higher charge carrier mobility and a greater radiation hardness, which we establish is due to greater crystallinity and improved nanoscale morphology using synchrotron-based scanning X-ray transmission microscopy. We systematically characterise the optical-to-electrical conversion efficiency of the photodetectors with a range of steady state and transient optoelectronic techniques, demonstrating that the photodetector performance of these nanoscale systems can be tuned to exhibit higher values than any other reported printable organic systems by varying the fabrication parameters.

X-ray nanosensors fabricated by coupling the photodetectors with a plastic scintillator can operate without the need for

external bias, a key feature of wearable electronics. The X-ray performance is shown to be energy independent between 50 keV and 6 MeV by testing with clinical orthovoltage or medical linear accelerators, providing versatile materials for use across a wide range of applications without additional calibrations. We show the X-ray detection sensitivity can be tuned to match that of state-of-the-art inorganic semiconductors or slightly reduced to provide almost completely radiolucent devices for wearable radiation dosimetry. The X-ray nanosensors were fabricated into pixelated arrays using inkjet printing to provide spatial resolution that matches state-of-the-art medical detectors. The organic nanosensors fabricated with o-IDTBR also exhibited remarkable temporal responses, detecting a pulsed X-ray source with microsecond resolution that was indistinguishable from a silicon PIN photodiode. Furthermore, the device exhibited excellent radiation hardness, withstanding a radiation dose that represents a 5-year working lifetime.

The new materials science and flexible devices we report here are an exciting breakthrough, providing the first stable, printable, flexible, and fully tissue equivalent X-ray detectors with functionality that is tuneable for optimized X-ray attenuation, or high radiolucency for applications such as radiotherapy, where simultaneous monitoring and transmission of the X-ray absorbed dose to the human body is a required.

#### References:

- [1] M. J. Griffith, S. Cottam, J. Stamenkovich, J. A. Posar, M. Petasecca, *Front. Phys.* **2020**, *8*, DOI: 10.3389/fphy.2020.00022.
- [2] B. Fraboni, A. Fraleoni-Morgera, N. Zaitseva, *Adv. Funct. Mater.* **2016**, *26*, 2276.
- [3] L. Basiricò, A. Ciavatti, T. Cramer, P. Cosseddu, A. Bonfiglio, B. Fraboni, *Nat. Commun.* **2016**, *7*, 13063.

SESSION F.FL03.02: Flexible Materials and Manufacturing—Liquid Metal and Composite Structures  
On Demand Abstracts Available for Viewing Starting Saturday Morning, November 21, 2020  
F-FL03

#### 5:00 AM F.FL03.02.01

**Fabrication of Orientation-Controlled Carbon-Nanotube/Polymer Composite Ribbon for Flexible Charge/Heat Conductors** Manish Pandey, Maireyee Bhattacharya, Naofumi Okamoto, Ryo Abe, Yuki Sekimoto, Yasuo Okajima, Kotaro Nishioka and Masakazu Nakamura; Nara Institute of Science and Technology, Japan

Carbon nanotubes (CNTs) possess tremendous potential applications owing to their excellent mechanical, electrical and thermal properties. Although isolated CNTs possess excellent anisotropic physical properties, their bulk ones are, in general, significantly restricted by the highly random networks. Therefore, bulk fabrication of aligned CNT films is expected to be important for many applications to get anisotropic and high thermal/electrical conductivity along the CNT orientation direction. Various attempts have been made in the past to increase the degree of CNT alignment to realize their theoretical properties using different methods such as cutting, electrophoresis, melt processing, using crowding effect, chemical vapor deposition, templated growth, solid spinning of CNT forest, magnetic field to induce alignment, flow coating, and mechanical stretching. However, few techniques are suitable for the fabrication of highly conducting and flexible strings. In this presentation, we report a novel method to fabricate ribbon-like films of CNT/polymer composite containing highly aligned CNT networks using a robotic dispenser [1]. This method can easily produce a uniform ribbon-like film with oriented CNTs along the drawing direction of the ribbon. We prepared 400–2000  $\mu\text{m}$  wide oriented ribbon of CNT/polymer films that can be used for roll-to-roll processing in length scale. CNTs were found to be aligned along the drawing direction as confirmed by polarized Raman mapping and scanning electron microscope images. Dependence of the electrical and thermal conductivities on the degree of CNT orientation will be also discussed.

- [1] M. Pandey, R. Abe, N. Okamoto, Y. Sekimoto, N. Kotaro, Y. Okajima, M. Nakamura, *Appl. Phys. Express* **13**, 065503 (2020).

#### 5:10 AM F.FL03.02.02

**Mechanically Robust Polymer-Perovskite Composite Solar Cells** Blake Finkenauer and Letian Dou; Purdue University, United States

Self-healing semiconducting materials have had limited successes due to the tradeoff between excellent electronic properties and suitable rheology properties. This is because high performance inorganic semiconductor materials have a crystalline

structure, unlike fluidic and amorphous polymers which use secondary bonding forces to heal. However, hybrid inorganic-organic halide perovskites are high performing semiconducting materials with crystal-liquid-like behaviors. Their fluidic crystal lattice features a large combination of secondary bonding interactions, giving perovskites their remarkable electronic properties, defect tolerance, and low formation energy. Here, we discuss our investigations in creating the first mechanically self-healing hybrid inorganic-organic halide perovskite semiconductor. A molecularly tailored self-healing polymer is coupled with fluidic methylammonium lead iodide perovskite to form bi-continuous composites capable of healing mechanical damage through synergistic grain growth and solid diffusion processes at slightly elevated temperatures. These self-healing composites are demonstrated in solar cell devices with power conversion efficiencies reaching ~10% with improved thermal and mechanical stability. This pioneer research showcases the concept of joining perovskite and organic materials to create a unique composite with first-of-its-kind functionalities.

### 5:20 AM F.FL03.02.03

**Polymer Nanocomposite Fabrication Using One Step *In Situ* Exfoliation of Two-Dimensional Layered Materials and Their Use as Flexible Multifunctional Sensors** [Ali Ashraf](#), Elizabeth Chang, Francis Farmer, Nikhil Jani, Suyeon Lee and Jennifer Lynch-Branzoi; Rutgers, The State University of New Jersey, United States

Polymer nanocomposites with two-dimensional (2D) nanofillers like graphene (Gr) and hexagonal boron nitride (hBN) have found widescale acceptance in healthcare, automotive, aerospace, energy storage, filtration, and military applications due to their exceptional mechanical, electrical, chemical, optical and thermal properties. However, the commercial use of this class of material is hindered due to problems with the nanomaterial fabrication and composite formation process-namely impurity incorporation, agglomeration, use of chemicals harmful to the environment, multi-step processes and cost. Here, we present one step innovative method to directly incorporate Gr and hBN to thermoplastic (polysulfone) and silicone elastomer (Ecoflex®, Dragon skin®) by in-situ exfoliation of bulk precursors (e.g. graphite) within the polymer. Unlike other conventional methods, this technique does not require use of solvents or harsh chemicals for preparation of nanomaterials, which additionally minimizes the probability of inadvertent impurity introduction during processing. Additionally, nanomaterials are exfoliated directly inside the polymer, providing pristine surface to form strong covalent bonds with the polymer matrix, resulting in significant material property enhancement<sup>1,2</sup>. These flexible smart materials have high conductivity of ~1.8 S/cm and were used as wearable health monitoring sensors (pulse, breathing, speech, muscle movement), mass sensors that can detect mass as small as ~3 mg, chemical sensors that can differentiate between droplets of solvents (acetone, hexane, ethanol, water), temperature sensors that can detect temperature in the range from 10-80 C (sensitivity factor of 12), and as strain sensors for structural health monitoring (gauge factor of 50 at 0.5% strain). Due to external stimuli (temperature, chemical infiltration-based swelling, strain), the distance between graphene flakes and the dimension of the polymer matrix changes, leading to change in electrical resistance path, which is utilized for sensing. The hBN nanomaterial was added as a second filler, which acts as an effective dispersion aid for Gr in the nanocomposite. The composite structure, bonding with nanomaterials and influence of fabrication parameters were investigated with scanning electron microscopy, X-ray photoelectron spectroscopy, differential scanning calorimetry, X-ray diffraction, tensile, flexural and impact testing, Raman spectroscopy and Rheometry. Moreover, mid infrared based thermography technique with micro scale imaging capability was utilized to determine the dispersion of nanomaterials within these composites<sup>3</sup>. Our one-step, in-situ, low cost process is compatible with manufacturing techniques like injection molding, 3D printing, screen printing, soft lithography, and therefore, has the potential to be a commercially viable production technique for flexible multifunctional sensors with high sensitivity.

1. Lynch-Branzoi, J. K.; Ashraf, A.; Tewatia, A.; Taghon, M.; Wooding, J.; Hendrix, J.; Kear, B. H.; Nosker, T. J., Shear exfoliation of graphite into graphene nanoflakes directly within polyetheretherketone and a spectroscopic study of this high modulus, lightweight nanocomposite. *Composites Part B: Engineering* **2020**, 107842.
2. Nosker, T.; Lynch, J.; Hendrix, J.; Kear, B.; Chiu, G.; Tse, S. In situ exfoliation method to fabricate a graphene-reinforced polymer matrix composite (G-PMC). Patent US9896565B2, 2018.
3. Ashraf, A.; Jani, N.; Farmer, F.; Lynch-Branzoi, J. K., Non-Destructive Investigation of Dispersion, Bonding, and Thermal Properties of Emerging Polymer Nanocomposites Using Close-Up Lens Assisted Infrared Thermography. *MRS Advances*, 1-8.

### 5:30 AM \*F.FL03.02.06

**High-Resolution 3D Printing of Liquid Metals for Wearable Electronics** [Jang-ung Park](#)<sup>1,2</sup>; <sup>1</sup>Yonsei University, Korea (the Republic of); <sup>2</sup>Institute for Basic Science (IBS), Korea (the Republic of)

Recent progress in optoelectronic devices for wearable electronics, bioelectronics, and soft robotics demands their outstanding physical deformability for versatile systems in daily life. However, the reliability of devices is often severely

restricted by concomitant failure, especially when excessive strains are applied beyond mechanical withstanding limits. Therefore the formation of stretchable interconnects with both high conductivity and high resolution is essential for providing conventional electronic systems an extra degree of deformability with high device integrity. This talk presents a high-resolution, reconfigurable 3D printing using liquid metal alloys and its application for wearable electronic devices with stretchable integrations. A minimum line-width of 2  $\mu\text{m}$  can be reliably formed using direct printing through a nozzle, and these printed patterns can be successively reconfigured into diverse free-standing 3D structures, while maintaining pristine resolutions. Furthermore, the high-resolution printing of 3D coil antennas and interconnects with wearable biosensors and displays represents substantial progress toward next-generation electronics.

#### 5:45 AM F.FL03.02.07

**Liquid Metal Inks for Stretchable Electronics** Christopher E. Tabor<sup>1</sup>, Carl Thrasher<sup>1</sup>, Michelle Yuen<sup>1</sup>, Zachary Farrell<sup>1,2</sup>, Nicholas J. Morris<sup>2,1</sup>, Alex E. Flynn<sup>1</sup> and Alexander Watson<sup>1,2</sup>; <sup>1</sup>Air Force, United States; <sup>2</sup>UES, Inc., United States

Low melting point metals and alloys such as those utilizing gallium and bismuth have garnered significant attention in flexible electronics due to their ability to provide highly repeatable electrical performance under elongation, compression, and other harsh mechanical conditions. While these properties have been demonstrated in the lab to impressive degrees, the ability to process these materials and package them in order take advantage of their highly attractive mechano-electronic properties within textiles has been limited due to difficulties of processing the bulk material and the need to retain the liquid in pre-defined areas. Through taking advantage of the increased implementation of additive manufacturing to develop wearable electronics, a printable liquid metal ink has been developed in our lab which fully sinters without the need for high temperatures, providing flexible and strain tolerant liquid electronics. The key enabler of this ink is our ability to chemically tether each particle to its neighbor, creating a polymerized Liquid Metal Network (poly-LMN). The polymerized network forms a self-supporting framework that retains the liquid ink as deposited until full encapsulation is performed, allowing for high definition features (<30  $\mu\text{m}$  linewidth) and the autonomous formation of an internal tortuous conductive path that provides strain insensitivity to the circuits up to at least 700% strain. Applications of poly-LMNs range from wearable power distribution, physically deformable antennas, and stretchable resistive heaters.

#### 6:00 AM F.FL03.02.08

**Microstructured Liquid Metal Transmission Lines for Sensing of Multimodal Deformations in Electronic Textiles** Andreas Leber, Chaoqun Dong, Rajasundar Chandran, Tapajyoti Dasgupta, Nicola Bartolomei and Fabien Sorin; Ecole Polytechnique de Federale Lausanne, Switzerland

The sensing of diverse deformations is an important functionality in soft electronics and wearable devices intended for use in health care, Internet-of-Things, or soft robotics. Current approaches usually rely on intricate arrays of sensors, which have no spatial resolution and cannot distinguish between different types of deformation. An alternative strategy toward distributed and multimodal sensing is electrical reflectometry in transmission lines. However, to create sensitive mechanical probes, the transmission lines must be built entirely with soft materials and feature a controlled microstructure over extended lengths. Here, we report the scalable fabrication of soft and stretchable transmission lines, composed of tens of liquid metal microchannel conductors meticulously arranged within an elastomer dielectric.[1] The interrogation with time-domain reflectometry converts the soft transmission lines into effective probes of deformation, enabling the detection of the mode, intensity, and location of multiple pressing and stretching events that are simultaneously applied. Additionally, the dynamically responsive line conductors yield a pressure sensitivity that is increased by a factor of 200 compared to conventional hard lines. Integrated within a larger fabric, an individual soft transmission line with a single interface port can decipher convoluted mechanical stimulation, bringing a new paradigm to sensing in functional textiles and robotic skins.

Reference:

[1] Leber, A. *et al.* Soft and stretchable liquid metal transmission lines as distributed probes of multimodal deformations. *Nat. Electron.* (2020). doi:10.1038/s41928-020-0415-y

#### 6:15 AM F.FL03.02.09

**Nanoscale Dewetting Based Direct Interconnection of Micro-LEDs (30  $\mu\text{m}$   $\times$  60  $\mu\text{m}$ ) for Flexible, Wearable Electronics** JuSeung Lee and Tae-il Kim; Sungkyunkwan University, Korea (the Republic of)

In the last few decades, the evolution of electronic devices has shown unprecedented progress, due to various discoveries of advanced materials, and improvements in fabrication technologies. Much more complicated tasks can be dealt with by miniaturized devices, such as smart wearable systems, which seemed impossible in the past. Electronic devices will become smaller and smaller in the future for multifunctionality, high performance, and power saving purposes, and will be densely



integrated and interconnected on limited areas. In particular, wearable devices that are deformable, and mountable on skin, need to be monolithically integrated on a single substrate for multifunctionality and miniaturization of devices. However, as electronic components, such as light emitting diodes (LEDs), transistors, and various sensors become smaller at microscale, there are some limitations on integrating them on the proper substrate by a general assembly method. Metal wiring, metal soldering, and anisotropic conductive film (ACF) are the most common integration method for electronics. However, metal wiring and metal soldering suffer from size limitation, significant reduction of the overall throughput yield, and poor mechanical stability. The ACF bonding requires high pressure of 2 – 5 MPa (20 -50 bar) and high temperature of 200 °C simultaneously for successful bonding. This process could be expected that the integration of a large number of microscale electronics needs significantly higher force to form electrical interconnect, which potentially raises assembly failure. Recently, research has been conducted to improve the fine pitch capability of interconnection by applying various methods, such as metal-coated polymer ball, multi-layered ACF and non-conductive film (NCF), sidewall insulation, and silver nanoparticle ink with eutectic gallium indium (EGaIn) liquid metal. But they still display multiple limitations such as size limitation and poor mechanical stability.

Here, we introduce a facile electrical interconnection method driven by selective dewetting of polymer adhesive that is applicable to a deterministic microelectronics assembly for flexible electronics. The interconnection system consists of polymer adhesive with nano-sized metal particles, or on protruding structured electrodes, so it can be used by a simple coating process, like spin-coating and jetting. As the stability and interfacial potential of thin polymer adhesive depend on the materials of substrate and adhesive, and the thickness of adhesive, the wettability and dewetting phenomenon of polymer adhesive could be controlled by modulating the condition of the coated polymer adhesive, and the size of nanoparticles (or morphology of the structured electrode). The minimum feature size for assembling microdevices is 30  $\mu\text{m}$   $\times$  60  $\mu\text{m}$  for microscale inorganic LED with 20  $\mu\text{m}$   $\times$  15  $\mu\text{m}$  electrode size and pitch. The transfer printing yield in terms of devices operation was ~99.9 %, so that thousands of micro LEDs can be printed at high throughput on a substrate with gold circuits. This interconnection of the microelectronics was strictly confirmed by harsh industrial levels under dramatic temperature change (-40 – 85 °C for 5 min, ramping rate: 25 °C/min) over 300 cycles, and high humidity and temperature environment (85 °C, 85 % relative humidity) for 300 hours. In addition, the theoretical calculation for the dewetting phenomenon is revealed.

#### 6:30 AM F.FL03.02.10

**Late News: Flexible Laser Scribed Graphene Dual-Function Integrated Device for Supercapacitor and Strain Sensor** Guangyuan Xu<sup>1,2</sup>, Fangshuai Chen<sup>3</sup>, Yanan Chen<sup>3</sup>, Yinji Ma<sup>1,2</sup> and Xue Feng<sup>1,2</sup>; <sup>1</sup>AML, Department of Engineering Mechanics, Tsinghua University, China; <sup>2</sup>Center for Flexible Electronics Technology, Tsinghua University, China; <sup>3</sup>Department of Material Science and Engineering, Tianjin University, China

An extensive range of nanocarbon, such as 0D fullerene, 1D carbon nanotubes and nanofibers, 2D graphene and graphene oxide, and 3D carbon aerogels have attracted significant attention from the scientific society. Because of its excellent properties and outstanding performance, nanocarbon has been demonstrated successfully in the application of fabricating electrodes towards wearable electrochemical energy storage and sensing devices. Graphene, being a well-studied and outstanding electrode material has already been evidenced by its performance for manufacturing supercapacitors and skin electronics. The direct laser writing was reported to be an innovative and efficient methodology that enabled to fabricate graphene electrode patterns within a single-step. Inspired by the dual-functions of piezoresistive and electrochemical properties offered by laser-scribed graphene (LSG), the LSG can be fabricated as the integrated flexible device with both functions of strain sensor and supercapacitor. In this work, we have demonstrated the LSG utilized in the integrated supercapacitor-sensor system for the first time. When two LSG electrodes were used as a supercapacitor, its current density was improved from 0.02 to 0.6 mA/cm<sup>2</sup> with the rising scan rate from 10 to 200 mV/s. The highest capacitance was calculated as 18 mF/cm<sup>2</sup> at the consistent current density at 0.02 mA/cm<sup>2</sup>. Also, the LSG supercapacitor showed excellent cycling stability after 5000 cycles. When the single electrode from the LSG supercapacitor was adopted as a strain sensor, the LSG electrode enabled to detect the phalangeal joint's motion by its resistance changes while bending up and down. The single LSG electrode could detect the strain signals simultaneously when charging and discharging the LSG supercapacitor. The integration strategy has permitted the possible promises for developing self-powered intelligent sensory, flexible, wearable, and healthcare electronics.

SESSION F.FL03.03: Flexible Materials and Manufacturing—Low Temperature Inorganic and Organic Materials  
On Demand Abstracts Available for Viewing Starting Saturday Morning, November 21, 2020

F-FL03

### 5:00 AM \*F.FL03.03.01

**Organic Optoelectronic Devices for Wearables** Hyeonwoo Lee, Taehyun Kim, Eungjun Kim, Junho Kim, Hanul Moon and Seunghyup Yoo; Korea Advanced Institute of Science and Technology, Korea (the Republic of)

Organic electronic devices are regarded as promising for wearables because the deposition of organic semiconductors is compatible with various substrates with a low thermal budget. This key benefit can allow for the realization of devices with versatile form factors such as flexible, foldable, and conformable devices that are considered desirable particularly for wearable applications. However, form factors are not the only advantage of organic electronic devices from the perspectives of wearable devices. Many of the organic semiconductors have rich optical properties, the strength of which has already been well recognized by the success of displays based on organic light-emitting diodes (OLEDs) and by the impressive progress recently made for organic solar cells. In this talk, we discuss what we can and what we need to do to unlock the full potential of organic optoelectronic technologies for wearable devices. The first part of the talk is dedicated to introducing some of our key efforts to make OLEDs ultra-flexible, stretchable, and more efficient. The second part then presents a case study where some of the inherent benefits of organic optoelectronic technologies are employed to realize organic wearable health-monitoring sensors with far less power consumption than that of conventional commercialized sensors with maximized photon utilization.

### 5:15 AM \*F.FL03.03.02

**Flexible Organic Solar Cells and Integrated Systems for Wearable Electronics** Kenjiro Fukuda<sup>1</sup>, Ruiyuan Liu<sup>1</sup>, Zhi Jiang<sup>1,2</sup>, Kilho Yu<sup>1</sup> and Takao Someya<sup>1,2</sup>; <sup>1</sup>RIKEN, Japan; <sup>2</sup>The University of Tokyo, Japan

The power conversion efficiency of organic solar cells has been significantly improved over the past decade. The certified power conversion efficiency (PCE) of single-junction organic solar cells exceeded 17%. In addition to a high PCE and excellent operational stability, good mechanical durability is also important to wearable/textile applications to ensure continuous operation under various moving conditions. It is possible to reduce the thickness of organic solar cells by using an extremely-thin (<10 um) polymer substrate. Owing to their extreme light-weight, improved bending stability, good conformability, and improved stretchability, these types of ultrathin solar cells cause minimal discomfort when integrated with textiles. Such ultrathin organic solar cells expand the applicability of flexible organic solar cells as power solutions for wearable electronics or for soft robots in the society of internet-of-things (IoT) in which numerous sensor devices need to be used. Recently, some integrated devices with these cells—such as conformable sensor systems—have been reported and used as power sources.

In this talk, we show our recent progress of flexible organic solar cells and integrated systems for wearable/textile electronics. First, we introduce how we improve the PCE and stability of ultra-thin organic solar cells [1]. Then the strategies to achieve good stability including air[2], high-temperature [3], water [4], and light illumination conditions [5][6] are discussed. Finally, we show some examples of integrated systems with charging devices [7], actuators [8], and sensors [9].

[1] W. Huang et al., *Joule* **2020**, *4*, 128.

[2] Z. Jiang et al., *Proc. Natl. Acad. Sci.* **2020**, *117*, 6391.

[3] X. Xu et al., *Proc. Natl. Acad. Sci.* **2018**, *115*, 4589.

[4] H. Jinno et al., *Nat. Energy* **2017**, *2*, 780.

[5] H. Kimura et al., *Adv. Mater.* **2019**, *31*, 1808033.

[6] M. Takakuwa et al., *Small Methods* **2020**, *4*, 1900762.

[7] R. Liu et al., *Adv. Energy Mater.* **2020**, *2000523*, 1.

[8] K. Yu et al., *Proc. IEEE* **2019**, *107*, 2137.

[9] S. Park et al., *Nature* **2018**, *561*, 516.

### 5:30 AM F.FL03.03.03

**Ultra-Stretchable Conductive Polymer Complex with Repeatable Autonomous Self-Healing Ability Towards Wearable Sensors** Yang Lu<sup>1,2</sup>, Ju-Won Jeon<sup>3</sup> and Evan K. Wujcik<sup>1</sup>; <sup>1</sup>The University of Alabama, United States; <sup>2</sup>Georgia Institute of Technology, United States; <sup>3</sup>Kookmin University, Korea (the Republic of)

Wearable strain sensors are essential for the realization of applications in the broad fields of remote healthcare monitoring, soft robots, immersive gaming, among many others. These flexible sensors should be comfortably adhered to skin and capable of monitoring human motions with high accuracy, as well as exhibiting excellent durability. However, it is

challenging to develop electronic materials that possess the properties of skin. The presented skin-like electronic material exhibits ultrahigh stretchability, repeatable autonomous self-healing ability, quadratic response to strain, and linear response to flexion bending. This conductive polymer system, under ambient conditions, synergistically constructs a regenerative dynamic polymer complex crosslinked by hydrogen bonds and electrostatic interactions, which enables these unique properties. Sensitive strain-responsive mechanisms owing to the homogenous and viscoelastic nature provide omnidirectional tensile strain and bending deformations. Furthermore, this material is scalable and simple to process in an environmentally-friendly manner, paving the way for the next generation wearable sensors.

#### 5:40 AM F.FL03.03.04

**Stretchable and Fully Conjugated Donor-Acceptor Terpolymers with High Performance and Elasticity** Jaewan Mun, Yuto Ochiai and Zhenan Bao; Stanford University, United States

Several strategies have been developed to impart stretchability to polymer semiconductors, which can be divided into two categories: 1) chemical structure modification, and 2) post-modification. However, altering chemical structures often results in reduced mobility, whereas post-modification of semiconducting polymers easily suffers from batch-to-batch variation. Here, a conjugated donor-acceptor terpolymer design is used to control microstructures of diketopyrrolopyrrole-based polymeric chains, which significantly improves stretchability of the polymers without any mobility and elasticity compromise. Analysis on the microstructures of the terpolymers confirms that they show well-maintained short-range ordered aggregates, while their crystallinity is significantly reduced. More importantly, the terpolymer films retain most of their ordered domains even under strain, which leads to record high mobility under strain. Fully stretchable transistors fabricated with our newly established semiconductor films exhibit one of the highest mobilities after repeated strain. All of the above results indicate that our simple molecular design is an effective way to achieve high-performance and stretchable semiconductors.

#### 5:50 AM F.FL03.03.06

**Intrinsically Stretchable Organic Light-Emitting Diodes for Next Generation Stretchable Displays** Jin-Hoon Kim and Jin-Woo Park; Yonsei University, Korea (the Republic of)

Stretchable electronics are emerging technologies that develop devices with the ability to conform to nonplanar and dynamic surfaces such as a human body. Especially, stretchable light emitting devices (s-LEDs) could be potentially applied to tactile displays and biomedical devices. Several approaches based on geometrical designs such as mechanical buckling and island interconnect have been used to fabricate s-LEDs. However, geometrical designs possess several limitations. For instance, s-LEDs based on mechanical buckling approaches have high surface roughness, which prevents conformal contact with human body. Also, s-LEDs based on mechanical buckling were only uni-axially stretchable, not bi-axially stretchable. Very complicating fabrication processes were required for s-LEDs based on island interconnect, also an areal density of s-LEDs was highly limited to be stretchable. Hence, a demand for s-LEDs consisting intrinsically stretchable (*is*-) constituent layers continues to increase. However, the researches of *is*-LEDs are still largely in its infancy. Most works related to *is*-LEDs were mainly focused on the development of the stretchable and transparent electrodes. Hence, development and in-depth investigation of other *is*-constituent layers have not been performed yet. In this work, we reported *is*-organic light emitting diodes (*is*-OLEDs) which constituent materials are all highly stretchable. To accomplish this objective, all constituent layers including anode, hole transport layer (HTL), emission layer (EML), electron transport layer (ETL), and cathode were carefully modified to be highly stretchable. For anode and cathode, hybrid materials between organic and low-dimensional inorganic nano-materials were used. To make HTL and EML mechanically stretchable, surfactant and polymer blending induced nano-structure modification method was applied. This unique method enabled realization of *is*-functional layers with superior mechanical and electrical properties. The resulting *is*-OLEDs can emit light when exposed to strains as large as 80%. The turn-on voltage is as low as 8 V, and the maximum luminance is 4500 cd×m<sup>-2</sup> on both the anode and cathode sides. It can also survive repeated stretching cycles up to 200 times, and small stretching to 50% is shown to significantly enhance its light-emitting efficiency. These results showed that the *is*-OLEDs superior mechanical stretchability compared to previously reported *is*-LEDs. Also, owing to the versatility of our approaches, *is*-OLEDs with various colors including red, green, and blue were successfully fabricated, which is essential in the realization of the stretchable displays. We expect that our works would be a milestone for development of *is*-optoelectronic devices by offering a general platform for *is*-optoelectronic devices.

#### 6:00 AM F.FL03.03.07

**Tuning Mechanical Properties of Polymer Semiconductor by Modulating Hydrogen Bonding Interactions** Yu Zheng<sup>1</sup>,

Minoru Ashizawa<sup>2</sup> and Zhenan Bao<sup>1</sup>; <sup>1</sup>Stanford University, United States; <sup>2</sup>Tokyo Institute of Technology, Japan

Polymer semiconductors have gathered much interest for their potential in next-generation deformable and wearable electronics applications. The optimum conjugated polymer film morphology for efficient charge transport consists of crystalline domains and effective inter-domain connections. Unfortunately, such a film morphology usually suffers from device failure under small strain deformation. Thus, it remains challenging to design polymer semiconductors that can maintain good electronic properties under mechanical strain.

The field of stretchable polymer semiconductor has witnessed rapid growth in recent years. Various strategies have been reported, including: (1) adding a secondary component and (2) molecular structural modification. The general design principle is to decrease the overall crystallinity of polymer semiconductor film, providing energy dissipation mechanisms from polymer conformation change during stretching. More design principles need to be investigated, to expand the tunability of polymer semiconductor mechanical properties and even imparting more functionalities.

Dynamic bonding has been widely incorporated into elastomers and hydrogels to enhance their mechanical properties. However, this strategy has not been used extensively to develop stretchable semiconductors. Our group reported that introducing 2,6-pyridine dicarboxamide (PDCA) H-bonding unit into a conjugated polymer backbone helped maintain its electrical performance under strain. The breakage of H-bonding between PDCA units was one of the mechanisms responsible. However, the structure-property relationship regarding H-bonding interactions and strain energy dissipation in polymer semiconductors needs to be further understood.

In this study, conjugation breakers (CBs) with different H-bonding chemistry and linker flexibility are designed. Two structural parameters need to be considered: (1) chemistry of H-bonding unit, and (2) linker between  $\pi$ -conjugated backbone and H-bonding unit. First, we choose urea, amide and urethane. They have structural similarities and can serve as fair comparisons in terms of H-bonding strength. Second, we use alkyl-chain or ether-chain as the linker. Choosing different linkers will influence the packing order of these H-bonding units, thus providing the possibility to tune H-bonding domain size and distribution.

After these H-bonding CBs are incorporated into a Diketopyrrolopyrrole (DPP)-based conjugated polymer backbone, the effects of H-bonding interactions on polymer semiconductor morphology, mechanical properties and electrical performance are systematically investigated. We observe that CBs with H-bonding self-association constant  $>0.7$  or denser packing tendency are able to induce higher polymer chain aggregation and crystallinity in as-casted thin film, resulting in higher modulus and crack on-set strain. Additionally, the rDoC (relative degree of crystallinity) of the stretched thin film with the highest crack on-set strain only suffers a small decrease, suggesting the main energy dissipation mechanism is the breakage of H-bonding interactions. By contrast, other less stretchable polymer films dissipate strain energy through the breakage of crystalline domains, indicated by drastic decrease in rDoC. Furthermore, we evaluate their electrical performance under mechanical strain in fully stretchable field-effect transistors. The polymer with the highest crack on-set strain has the least degradation in mobility as a function of strain. Overall, these observations suggest that we can aptly tune the mechanical properties in polymer semiconductors by modulating intermolecular interactions, such as H-bonding chemistry and linker flexibility. Such understanding provides molecular design guidelines for future stretchable semiconductors.

#### 6:10 AM F.FL03.03.09

**Fabrication Strategies for Large-Area, Flexible Magnetic Nanoparticle Arrays** Guinevere Strack<sup>1</sup>, Yassine Ait-El-Aoud<sup>2</sup>, Dennis Slafer<sup>3</sup>, Richard M. Osgood<sup>2</sup> and Alkim Akyurtlu<sup>1</sup>; <sup>1</sup>University of Massachusetts Lowell, United States; <sup>2</sup>US Army Combat Capabilities Development Command Soldier Center, United States; <sup>3</sup>MicroContinuum, Inc., United States

Two-dimensional metasurfaces comprised of ordered nanoparticle arrays can be tailored to obtain desired electromagnetic properties, which depend on the size, shape, composition, and spacing of the nanoparticles. Potential applications of these materials include active and lightweight textiles, e-textiles, smart fibers, signature management, power/energy harvesting, encryption, and identification capabilities. These ‘real world’ applications typically require magnetic nanoparticle (MNP) arrays on flexible substrates; therefore, there is a need for research that addresses the fabrication and performance of these materials in the context of flexible, wearable platforms.

Traditional fabrications strategies for MNP arrays require costly equipment and highly trained personnel. For example, e-beam lithography has been used to fabricate such arrays; however, this technique is not feasible for large-area samples. In addition, the majority of MNP arrays are fabricated on Si wafers, which provide an ideal, flat, surface, but do not readily translate to flexible platforms or roll-to-roll processes. In this presentation, we will discuss fabrication strategies for large-

area MNP arrays on flexible substrates, along with the resultant optical and magnetic properties. The fabrication strategies are based on nanosphere lithography (NSL) and nanoimprint lithography (NIL). In the NSL strategy, polystyrene spheres (PS) are packed in a monolayer on the selected substrate and used as a template to produce ordered particle arrays. The size and spacing of the MNP array can be controlled by the size of the PS beads and other fabrication parameters. Several NSL methods can be used to produce the MNP array—the method depends on the desired MNP array dimensions and the substrate material. In the NIL strategy, a 3D mold is used to form the desired pattern in a UV curable polymer on the selected substrate. Working NIL molds are made from a single master template using e-beam lithography, which enables formation of precise structures in a wide range of geometries with dimensions down to tens of nanometers. These patterns can be used to either contain MNPs or the patterns can be formed from MNPs. NIL techniques lend themselves to large-area, cost-effective manufacturing using roll-to-roll technology.

Understanding the optical and magnetic properties of MNP arrays enables future design strategies for flexible, wearable, multifunctional optical and electronic devices. For example, total integrated transmission and spectral scattering were measured using a spectrophotometer with an integrating sphere accessory to account for scattering characteristics of the nanostructured arrays on flexible substrates. Nanometric Co films and MNP arrays on Kapton were subjected to Superconducting Quantum Interference Device (SQUID) magnetometer measurements. Finally, obtained hysteresis loops (magnetic moment vs. applied magnetic field) were used to determine the saturation magnetization,  $M_s$ , and magnetic coercivity,  $H_c$ , of Co films and MNP arrays.

#### 6:20 AM F.FL03.03.11

**Late News: Three-Dimensional Optoelectronics Formed by Origami Transformation of a Plasticized Polymer Substrate** Gi-Gwan Kim, Yeongmin Kim, Seonggwang Yoo, Hun Soo Jang and Heungcho Ko; Gwangju Institute of Science and Technology, Korea (the Republic of)

The tremendous development of flexible electronics seems to pave a way to develop the three-dimensional optoelectronics, including hemispherical and polyhedral image sensors, and curved display system, which offers low optical aberration and wide field of view, from planar membrane-type electronics. Regarding optoelectronics, there are critical issues for 2D to 3D transformation. First, the devices require a transition of rigidity, soft for transformation, but rigid in the final shape. In the case of using membrane-type electronics, its flexibility allows the former but does not allow the latter, which naturally requires a supportive framework. Second, in order to minimize the optical path from or to the devices, the device layer should be placed on the top surface of the supportive framework; this effort naturally causes out of the neutral mechanical plane. In this case, during the deformation into either inward or outward curvature, the stress on the device naturally suffers from compressive or tensile tension. Third, in order to allow the pixel matrix design with common column and row connection lines, the Kirigami approach, which cuts off some areas, should be avoided. Fourth, removing the blind area is also important to enrich the visual information. The strategy uses the acrylonitrile-butadiene-styrene (ABS) framework that can support a membrane-type electronic layer and can undergo plasticized by using small molecules such as acetone and *N,N*-dimethylformamide (DMF). Sorption and desorption of the plasticizer in a controlled manner allows a dramatic decrease of elastic/hardening moduli of ABS by a thousand times of magnitude, with increased fracture strain up to 240%, which prevents mechanical failure from the deformation. Notably, a viscoplastic reflow of the ABS substrate can reduce stress/strain on the device layer, even in the case of placing the device layer on the top surface of the ABS substrate. Moreover, confining the plasticizing region within a microfluidic channel allows extreme folding of the ABS framework, and thereby a nondisruptive tucking-based origami to form a polyhedral optoelectronic device without cutting the connection lines. As an application, we demonstrate a tetrahedral image sensor for an omnidirectional camera<sup>[1]</sup> and double-sided/holographic/ hexahedral LED arrays.<sup>[2]</sup>

This work was supported by the National Research Foundation of Korea (NRF) grant funded by the Korea Government (MSIT) (No. 2018R1A2B2005067).

#### References

- [1] H. S. Jang, G.-G. Kim, S. H. Kang, Y. Kim, J. I. Yoo, S. Yoo, K.-K. Kim, C. Jung, and H. C. Ko, *Adv. Mater.*, **30**, 1907384 (2018).
- [2] G.-G. Kim, Y. Kim, S. Yoo, H. S. Jang, and H. C. Ko, *Adv. Mater. Technol.*, **5**, 2000010 (2020).

#### 6:30 AM F.FL03.03.12

**Late News: Vertically-Stacked Complementary Inverter Based on Oxide-TFTs on Flexible Polymeric Foil Substrate** Shu-Ming Hsu, Wei-Chen Lin, Hao-Lin Yang, Dung-Yue Su, Feng-Yu Tsai and I-Chun Cheng; National Taiwan University, Taiwan

With the increasing demand for wearable devices, realization of high-performance flexible electronic circuits becomes an important topic. Some oxide-semiconductor-based thin-film transistors (TFTs) have exhibited good operational stability and can be fabricated with a mass production compatible technology at low substrate temperatures. Therefore, they have been considered as potential candidates for flexible on-plastic circuits. Three-dimensional integrated circuit technology has been widely used in memories, image sensors, and logic circuits. The vertical integration of electrical components can enhance the device density. So far, only a few flexible oxide-TFT-based complementary inverters have been reported. In this work, we successfully demonstrate vertically-stacked complementary inverters by monolithically integrating n-type bottom-gated zinc oxide (ZnO) TFTs and p-type top-gated tin monoxide (SnO) TFTs on polyimide foil substrates. The ZnO TFT shows a linear field-effect mobility of  $0.6 \text{ cm}^2\text{V}^{-1}\text{s}^{-1}$ , subthreshold swing of  $0.31 \text{ Vdec}^{-1}$ , and on/off current ratio of  $>10^7$ . The corresponding values for the SnO TFT are  $0.7 \text{ cm}^2\text{V}^{-1}\text{s}^{-1}$ ,  $1.5 \text{ Vdec}^{-1}$ , and  $10^4$ , respectively. The vertically-stacked complementary inverter exhibits a static voltage gain of 36 V/V at a supply voltage of 10 V. To investigate the influence of mechanical strains on the electrical performance, the devices are evaluated when bent to various curvatures outwardly and inwardly. There is no significant change in the voltage gain and noise margins when the inverter is subjected to a tensile or a compressive strain. However, the stability against gate-bias stress for the SnO TFT deteriorates when a mechanical strain is applied, which may be mitigated by introducing an encapsulation layer to reduce the distance between the device and mechanical neutral plane.

SESSION F.FL03.04: Energy Harvesting for Wearables  
On Demand Abstracts Available for Viewing Starting Saturday Morning, November 21, 2020  
F-FL03

**5:00 AM \*F.FL03.04.01**

**Flexible Piezoelectric Devices for Energy Harvesting and Ultrasonic Imaging** Tianning Liu, Veronika Kovacova, Ajay Dangi, Sri-Rajasekhar Kothapalli, Kyusun Choi, Chris Rahn, Thomas Jackson and Susan E. Trolier-McKinstry; The Pennsylvania State University, United States

High quality piezoelectric thin films are typically crystallized at temperatures above  $500^\circ\text{C}$ , so integration in a flexible form factor can be challenging. In this work, two approaches will be described: films on metal foils for energy harvesting applications, and transferred films on polyimide substrates for ultrasound applications. For energy harvesters,  $\text{Pb}(\text{Zr},\text{Ti})\text{O}_3$  (PZT) and  $(\text{K},\text{Na})\text{NbO}_3$  (KNN) based harvesters using the piezoelectric compliant mechanism design, with resonances at 20, 40 and 70 Hz. Energy harvesting with the compliant design is more than twice as much efficient as for the simple cantilever beam. At 70Hz, the measured power densities corresponding to PZT and KNN are  $113.9$  and  $3.1 \mu\text{W}/\text{cm}^2$  respectively. The power density ratio between PZT and KNN is of the same magnitude as the ratio of their respective Figures of Merit. For ultrasound applications, PZT films were released from a high-temperature-compatible substrate by dissolution of a ZnO release layer. This enabled the design and fabrication of flexible ultrasonic transducers using  $1 \mu\text{m}$  thick PZT on  $5 \mu\text{m}$  thick polyimide substrates. The transducers were patterned single elements of PZT bar-resonators operating in width extension mode with center frequencies in the 8-80 MHz range. Pitch-catch was demonstrated with two  $100 \mu\text{m} \times 1000 \mu\text{m}$  neighboring elements respectively transmitting and receiving against an aluminum reflector at 1.5 cm distance. The element in receive detected a 0.2 mV pre-amplified signal for a driving frequency of 9.5 MHz.

**5:15 AM F.FL03.04.02**

**Ultrathin Stretchable Piezoelectric Generator with Ultrahigh Power Density** Heeyong A. Huh, Siyi Liu, Taewoo Ha and Nanshu Lu; The University of Texas at Austin, United States

Skin-conformable and mechanically imperceptible wearable electronics, a.k.a. epidermal electronics, is one of the trending fields in personal and biomedical device research. Although ultrathin, ultrasoft biometric sensors have been widely developed, most of them are dependent on rigid and bulky batteries for power, which is still limited in energy capacity. Wearable energy harvesters hence emerged as a non-depletable power source. However, ultrathin generators with ultrahigh power output are yet available. We introduce a stretchable and wearable piezoelectric generator made of  $28\text{-}\mu\text{m}$ -thick polyvinylidene fluoride (PVDF) serpentine ribbons. Through analytical and numerical modeling, the serpentine shape and electrode coverage has been optimized to yield a power density of  $0.24 \mu\text{W}/\text{cm}^2$  at 50% applied strain under a frequency of 0.5 Hz. The combined thinness, high stretchability, and high power density qualify our generator as one of the top wearable energy harvesters. We have applied this stretchable generator at the crook of the human arm as a wearable energy harvester.

We demonstrate that it was able to support the reading and storage of temperature every 10 minutes without battery. All the stored data can be read through an NFC-enabled cell phone whenever the cell phone approaches the e-tattoo.

#### 5:25 AM F.FL03.04.03

**Establish a Self-Sustainable Wearable Multi-Modular Bioenergy Microgrid System** Lu Yin, Kyeong Nam Kim, Jian Lyu and Joseph Wang; University of California, San Diego, United States

Despite the fast development of various energy harvesting and storage devices, their judicious integration into efficient, autonomous and sustainable wearable systems has not been widely explored. Here, we introduce the concept and design principles of microgrids to the world of wearable electronics by demonstrating the operation of a multi-module bioenergy microgrid system. Unlike earlier hybrid wearable energy systems, a bioenergy microgrid relies solely on human activities to work synergistically and autonomously, harvesting biochemical and biomechanical energy using energy harvesters such as sweat-based biofuel cells and triboelectric generators, and regulating the harvested energy via wearable energy storage modules such as batteries and supercapacitors. Through careful energy budgeting and performance pairing, the system can offer features like fast-booting, extended-harvesting, and smart energy management to efficiently power various wearable electronics. Implementing the “compatible form factors, commensurate performance and complementary functionality” design principles, the flexible, wearable bioenergy microgrid offers attractive prospects for the design and operation of efficient, sustainable and autonomous wearable systems.

#### 5:35 AM F.FL03.04.05

**Photonic Curing for High-Throughput Fabrication of Flexible Perovskite Solar Cells** Weijie Xu<sup>1</sup>, Robert Piper<sup>1</sup>, Trey Daunis<sup>1</sup>, Kurt Schroder<sup>2</sup> and Julia W. Hsu<sup>1</sup>; <sup>1</sup>The University of Texas at Dallas, United States; <sup>2</sup>Novacentrix, United States

Next-generation photovoltaics provide important energy sources for flexible devices. Among them, perovskite solar cells (PSCs) stand out for their high performance and low cost that is associated with solution processability. However, the critical bottleneck in commercializing PSCs is the processing speed. Thermal annealing is widely used in research labs as the post-deposition processing method for transport layers and active layers of PSCs. These minutes or even hours of processing time are incompatible with high-throughput manufacturing methods, e.g. roll-to-roll processes. At web speeds of 30 m/min, a typical 20 min annealing time would translate to an impractical 600-m-long oven. Additionally, thermal annealing is an equilibrium heating method, i.e. substrates and the surrounding environment are heated up together with the films, incurring large energy usage and inducing mechanical failure due to coefficient of thermal expansion mismatch between different layers. Consequently, eliminating thermal annealing steps is the key to achieve high-throughput, flexible PSCs. In this work, we have successfully utilized a pulsed light irradiation approach, photonic curing, to anneal both NiO and mixed cation perovskite (CsFAMA) films on Willow<sup>®</sup> Glass substrates. We substantially reduced the total processing time of p-i-n PSCs. The processing time for sol-gel NiO is below 0.5 ms, which is 10<sup>6</sup> times shorter than thermal annealing (0.5 ms vs. 45 min). The processing time for CsFAMA is 20 ms, which is a 10<sup>5</sup> reduction as well. The materials properties, including optical absorption, crystallinity, surface morphology, and work function, as well as device performance are compared between thermally annealed and photonic curing films. Successful fabrication of PSCs using photonic curing will establish it as a viable path forward to realizing high-throughput manufacturing of flexible PSCs.

#### 5:45 AM F.FL03.04.07

**3D Printed Flexible Triboelectric Nanogenerators—Functional Fibers and Stretchable Mechanosensors** Yuxin Tong, Ziang Feng, Jongwoon Kim, John Robertson, Xiaoting Jia and Blake N. Johnson; Virginia Tech, United States

Triboelectric generators and sensors have great potential as self-powered wearable devices for energy harvesting, biomedical monitoring, and recording human activity. Here, we report a process for 3D printing highly flexible functional fibers, stretchable membranes, meshes, and hollow 3D structures using elastomeric (silicone) metal (Cu)-core extrudates to produce triboelectric nanogenerators (TENGs). The triboelectric performance of single 3D-printed functional fibers and 3D-printed membranes is quantified by cyclic loading tests, which showed maximum power densities of 31.39 and 23.94 mW m<sup>-2</sup>, respectively. The utility of the flexible silicone-Cu TENG fibers and the 3D printing process is highlighted through various applications to wearable mechanosensors for organ and human activity monitoring. The use of machine learning algorithms for classification of sensor response is also discussed. Overall, this work expands the conductive and functional materials palette for 3D printing and encourages the use of 3D-printed triboelectric devices for self-powered sensing applications in biomanufacturing, medicine, and defense.

#### 5:55 AM F.FL03.04.08

**Triboelectric Nanogenerator for Self-Powered and Multi-Functional Tactile Sensors** Seung-Rok Kim and Jin-Woo Park;

Yonsei University, Korea (the Republic of)

With the rapid development of the multi-sensing electronic skin (E-skin) imitating human skin by converting the external stimuli into electrical signals, the needs for maintenance-free operation of E-skin have been triggered. To bridge the E-skin of the users and their surrounding environment, the sensors are core components with their functions, such as detecting the physiological signals of a person or noticing the hazardous surroundings. As the number of the sensors and the functions increases, the needs for the external power supply like batteries are still unsolved with the problems of recycling, health and environmental hazards, and miniaturization. Recently, to fabricate the power sources operating the many sensors light-weighted and miniaturized, various kinds of nanogenerators converting mechanical, chemical, thermal, or solar energy into electricity have been developed. Among those power generators, the triboelectric nanogenerators (TENGs) have attracted massive attention for scavenging the energy from the mechanical motions. By contact electrification and electrostatic induction at the interface of the TENG and the touching object, TENG has been used as a touch sensor. Using the impedance matching property of the TENG to the sensor (passive electric element), we could expect the self-powered sensing without any other power supply. In this study, we successfully fabricated the multifunctional tactile sensor using the gel polymer electrolyte capacitor. Additionally, we utilized electrospun P(VDF-TrFE) nanofibers for supplying enough energy to operate the multifunctional tactile sensor with recognizing the initiation of the touch. Embedding the nanofibers in the PDMS elastomer, we can fabricate an efficient, flexible, and transparent TENG. For sensing temperature and pressure in the single sensing component, we exploited P(VDF-TrFE-CTFE) relaxor nanofiber and temperature-responsive [EMIM][TFSI]/P(VDF-HFP) gel polymer electrolyte. Porous structure made by the relaxor nanofibers can induce the polarization and be the channels for the ion transfer. Those transferred ions are the factors for the capacitance increases by pressure and temperature stimulus. Our multifunctional tactile sensor showed the characteristic pressure response of the wide sensing range (0~100 kPa) with ~0.05 /kPa sensitivity and the temperature response of the high sensitivity up to 0.283 /°C compared with other wearable temperature sensors. The multifunctional sensor is integrated with the TENG expecting that sensor can transduce the generated signals at the outer touching surface depending on the pressure and the temperature. Using a self-powered multifunctional sensor, we could successfully map the pressure and the temperature at the same time without any extra power supplier.

#### 6:05 AM F.FL03.04.09

**Fabrication of Energy Harvesting Textiles Based on Fiber-Based Organic Photovoltaics** Siddhant Iyer, Nelaka Govinna, Zhiyu Xia, Lian Li, Claire Lepont, Ravi Morsukal, Jayant Kumar and Ramaswamy Nagarajan; University of Massachusetts Lowell, United States

Fiber-based organic photovoltaics (OPV) offer the advantages of low-cost, rapid fabrication, ease-of scale up, high flexibility and versatility of tailoring properties through molecular design of the active materials. We explore a solution-coating process to fabricate fiber-based OPV comprising of a working primary electrode (polished 316LVM stainless steel wire) coated with a titanium dioxide electron transport layer, followed by a nanostructured phenyl-C61/71-butyric acid methyl ester: Poly(3-hexylthiophene) (PC61BM:PC71BM:P3HT) active layer and a poly(3,4-ethylenedioxythiophene) polystyrene sulfonate (PEDOT:PSS) hole transport layer, which is wrapped around by a secondary counter electrode (silver-plated copper wire), for extraction of dissociated charge carriers. The device is encapsulated in an exfoliated mica (e-mica) reinforced modified epoxy based UV-curable cladding for imparting oxygen and moisture barrier properties. Individual wire specimens yielded a power conversion efficiency (PCE) of  $3.4 \pm 0.4\%$  and an output power density of  $\sim 1.5 \times 10^{-4}$  W/cm<sup>2</sup>. Multiple weaving configurations of the energy harvesting textiles based on fiber-based OPV was explored on a thread controller 2 (TC2) digital Jacquard loom to yield 10 × 10 in<sup>2</sup> OPV modules. The PCE, effective series resistance (Rser), fill factor (FF), open-circuit voltage (Voc), short-circuit current density (Jsc) and maximum power output of this energy harvesting textiles will be reported.

#### 6:15 AM F.FL03.04.10

**Late News: Study the Mechanical and Electrical Properties of Electrospun P(VDF-TrFE) and P(VDF-TrFE-CTFE) Nanofibers** Chia-Yin Ma<sup>1</sup>, Tu-Ngoc Lam<sup>1</sup>, Wen-Ching Ko<sup>2</sup>, Yi-Fan Chen<sup>3</sup>, Chung-Kai Chang<sup>4</sup>, Po-Han Hsiao<sup>1</sup> and E-Wen Huang<sup>1</sup>; <sup>1</sup>National Chiao Tung University, Taiwan; <sup>2</sup>Industrial Technology Research Institute, Taiwan; <sup>3</sup>National Central University, Taiwan; <sup>4</sup>National Synchrotron Radiation Research Center, Taiwan

P(VDF-TrFE) poly(vinylidene fluoride-trifluoroethylene) is a well-known piezoelectric electroactive polymer (EAP) with high crystallinity. If the third monomer (CTFE) is introduced to form P(VDF-TrFE-CTFE) poly(vinylidene fluoride-trifluoroethylene-chlorotrifluoroethylene), the ferroelectric domains will be fragmented into a relaxor ferroelectric domains which is nano polar region with high dielectric constant. In this study, we fabricated electrospun nanofibers of P(VDF-TrFE) and P(VDF-TrFE-CTFE). We conducted wide angle x-ray diffraction (WAXD) to study the impact of lattice structure and



crystallinity on the mechanical and piezoelectric properties. The mechanical and electrical properties of the copolymers and terpolymers were compared.

SESSION F.FL03.05: E-Textiles—Design Factors  
On Demand Abstracts Available for Viewing Starting Saturday Morning, November 21, 2020  
F-FL03

**5:00 AM \*F.FL03.05.01**

**Textiles and Functional Apparel Design for a Soft Wearable Robotic Glove** Diana Wagner, Diogo S. de Lucena, Kristin Nuckols, Christina Glover, Maxwell Herman, Cameron J. Hohimer, Will Moyo and Conor J. Walsh; Harvard University, United States

Soft wearable robotics is an emerging field which looks at methods of enabling functional, powered support to assist human movements using lightweight, low-profile, and flexible materials. Textiles hold great promise in establishing a platform to develop assistive devices that fit and feel like regular clothing. A diverse team of researchers in the Bidesign Lab at the Harvard School of Engineering and Applied Sciences are exploring the use of inflatable soft wearable robotics that leverage the functional properties inherent in textiles to provide mobility assistance for people with hand weakness through a soft robotic glove.

Hand weakness limits a person's ability to perform common activities of daily living such as eating, drinking and writing that can be the result of many conditions including stroke, ALS and spinal cord injury. For stroke survivors, hand function rehabilitation is one of the most important aspects to improve their quality of life and independence. Access to therapy is a key factor in a person's ability to perform rehabilitation exercises and recover motor function, however most stroke survivors do not receive the amount of therapy they need due to budget, time, and mobility constraints. Furthermore, achieving the high amount of repetitive hand movements required for successful rehabilitation is a major challenge in conventional methods of therapy.

The aim of our research is to show the viability of using a soft robotic glove to perform home-based hand rehabilitation for stroke survivors. The soft robotic glove facilitates high dosage repetitive stretching, active movement, and functional task training exercises through the use of comfortable, textile-based inflatable chambers that gently straighten and bend the fingers while an engaging digital interface guides the user through their exercises with motivating games.

Soft wearable robotic devices present a promising approach to hand rehabilitation due to their lightweight, compliant, and low-cost design. This talk will explore the development of the soft robotic glove through the lenses of functional apparel design and will present the human-centered design methods used in the collaborative development process.

**5:15 AM \*F.FL03.05.02**

**A Textile-Centric Approach to Wearable e-Textiles** Tricia B. Carmichael, Yunyun Wu and Sara Mechael; University of Windsor, Canada

The future of textiles is electronic, with new wearable devices integrated into "smart clothing" systems that will incorporate sensors to detect biometric data, light-emitting devices to display data, and integrated wiring and power sources. At present, e-textiles can be made by sewing discrete, rigid elements like light-emitting diodes (LEDs), optical fibers, or bulky "black box" battery packs into clothing, which reduces softness, stretchability, and wearability. The next generation of e-textiles are being made from functional materials seamlessly integrated into the textile itself, while maintaining softness and stretchability. The challenge with this integration is the porous, 3D structures of textiles that are obviously different from the flat and rigid surfaces conventionally used for device fabrication. Textiles present a non-planar surface for fabrication and readily absorb and wick solutions of functional inks. Approaches that planarize the textile surface using polymer layers lose the softness and stretchability of the original textile. In this presentation, we show that instead of masking textiles with planar polymer layers, the textile structure itself can be exploited to form the basis for a new, textile-centric design approach. As an example of this approach, we discuss how the open structure of a low-denier nylon and spandex ultrasheer fabric can be used as a framework for highly stretchable transparent electrodes in wearable and stretchable light-emitting devices. We furthermore discuss how the tufted structure of a velour fabric forms the basis for an architectural engineering approach to protect brittle functional materials from strain and demonstrate this approach by fabricating stretchable textile-based lithium-

ion batteries.

**5:30 AM \*F.FL03.05.03**

**Textile-Integrated Wearable Technologies—Best Practices, Applications and Open Challenges** Brad Holschuh; University of Minnesota, United States

This talk will focus on textile-integrated wearable technologies. I will discuss current best practices related to textile and garment integration of sensors, actuators, and circuitry, providing examples of work by the University of Minnesota Wearable Technology (WTL) Laboratory and other leading research institutions. I will highlight the specific advantages, challenges, and applications of garment-integration of these types of technologies, and will discuss future directions in this space where innovation can have significant impact, ranging from aerospace/military scenarios to medical, athletic, and commercial applications.

**5:45 AM \*F.FL03.05.04**

**Creating Smart Textiles** Shu Yang; University of Pennsylvania, United States

Wearable technology is poised to explode in the next decade. As flexible electronic devices have begun to be incorporated into clothing, there are pressing needs to turn responsive materials into fibers and yarns to create smart textiles that will respond to environmental changes and report personal health information.

Here, I will present our work on fabrication of polymer fibers and meter-long yarns with embedded chemical receptors and selective wettability. The yarns can be knitted, embroidered or weaved into various wearable fabric prototypes. By control of surface chemistry of the fibers, we demonstrate selective wettability of the yarns, which wicks aqueous solutions, and change colors in response to humidity, pH, and electrolytes. By selective embedding of functional yarns into different geometries, we create multi-sensors and “blooming” flowers that can respond to UV light intensity, temperatures, and electrical fields.

**6:00 AM \*F.FL03.05.05**

**Wearable Textile Electronics for Personalized Health Care** Jun Chen; University of California, Los Angeles, United States

**Abstract:**

There is nothing more personal than healthcare. Health care must move from its current reactive and disease-centric system to a personalized, predictive, preventative and participatory model with a focus on disease prevention and health promotion. As the world marches into the era of Internet of Things (IoT) and 5G wireless, technology renovation enables industry to offer a more individually tailored approach to healthcare with more successful health outcomes, higher quality and lower costs. However, empowering the utility of IoT enabled technology in personalized health care is still significantly challenged by the shortage of cost-effective and wearable biomedical devices to continuously provide real-time, patient-generated health data. Textiles have been concomitant and playing a vital role in the long history of human civilization. In this talk, I will introduce our current research on smart textiles for biomedical monitoring and personalized diagnosis, textile for therapy, and textile power generation as an energy solution for the future wearable medical devices.

**References**

1. G. Chen, Y. Li, M. Bick, **J. Chen\***. “Smart Textiles for Electricity Generation”, *Chemical Reviews*, 120, 8, 3668-3720 (2020)  
Front Main Cover.
2. Z. Zhou, K. Chen, X. Li, S. Zhang, Y. Wu, Y. Zhou, K. Meng, C. Sun, Q. He, W. Fan, E. Fan, Z. Lin, X. Tan, W. Deng, J. Yang\*, **J. Chen\***. “Sign-to-Speech Translation Using Machine-Learning-Assisted Stretchable Sensor Arrays”. *Nature Electronics*, in press (2020)
3. K. Meng, S. Zhao, Y. Zhou, Y. Wu, S. Zhang, Q. He, X. Wang, Z. Zhou, W. Fan, X. Tan, J. Yang, **J. Chen\***. “A Wireless Textile Based Sensor System for Self-Powered Personalized Health Care”. *Matter*, 2, 896-907 (2020) **Research Highlight by Prof. Trisha L. Andrew**: “The Future of Smart Textiles: User Interfaces and Health Monitors”. *Matter*, 2, 794-795(2020)
4. N. Zhang, F. Huang, S. Zhao, X. Lv, Y. Zhou, S. Xiang, S. Xu, Y. Li, G. Chen, C. Tao, Y. Nie, **J. Chen\***, and X. Fan\*. “Photo-Rechargeable Fabrics as Sustainable and Robust Power Sources for Wearable Bioelectronics”. *Matter*, 2, 1260-1269 (2020) **Research Highlight by Prof. Xiaodong Chen**: “Powering Body Area Sensor Networks”. *Matter*, 2, 1079-1090(2020)
5. Z. Zhou, S. Padgett, Z. Cai, G. Conta, Y. Wu, Q. He, S. Zhang, C. Sun, J. Liu, E. Fan, K. Meng, Z. Lin, C. Uy, J. Yang, **J. Chen\***. “Single-Layered Ultra-Soft Washable Smart Textiles for All-Around Ballistocardiograph, Respiration, and Posture

Monitoring during Sleep”. *Biosensors and Bioelectronics*, 155,112064 (2020)

6. J. Chen, Y. Huang, N. Zhang, H. Zou, R. Liu, C. Tao, X. Fan and Z. L. Wang. “Micro-Cable Structured Textile for Simultaneously Harvesting Solar and Mechanical Energy”, *Nature Energy*, 1, 16138 (2016)

7. Y. Peng, J. Chen, A. Y. Song, P. B. Catrysee, P.-C. Hsu, L. Cai, B. Liu, Y. Zhu, G. Zhou, D. S. Wu, H. R. Lee, S. Fan, and Y. Cui. “Nanoporous Polyethylene Microfibres for Large Scale Radiative Cooling Fabric”, *Nature Sustainability*, 1, 105 (2018) (Co-first author)

#### 6:15 AM F.FL03.05.06

**Influence of Textile-Based Armband Form Factors on Wearable ECG Monitoring Performance** Braden M. Li, Amanda Myers, Tashana J. Flewellin, Jacklyn L. Herzberg, Azin Saberi Bosari and Jesse S. Jur; North Carolina State University, United States

Wearable technologies exist in a variety of form factors to accommodate a broad range of health sensing applications. Textile-based form factors are among the most enticing because they enable the creation of large-area sensing networks with sensing modalities such as ECG, EMG, and EEG. But, multiple form factor design considerations need to be accounted for to ensure the full wearable system exhibits exceptional sensing ability. In this talk, we explore the key form factor design parameters affecting ECG sensing performance of an Electronic textile (E-textile) armband worn on the upper left arm. The E-textile armband is integrated with screen-printed dry electrodes arranged in a three-lead sensing configuration. We identify the optimal electrode location needed to achieve high-quality ECG signals at low measurement frequencies on the upper left arm, without sacrificing the practical assembly of the armband. Our analysis reveals that the armband diameter plays a crucial role in dictating contact pressure against the upper arm and the resulting ECG signal quality. We also develop a predictive contact pressure model based on the mechanics of thin-walled cylindrical pressure vessels. Our model provides a framework to predict the contact pressure and ECG signal quality as a function of armband diameter. The fundamental design principles discussed in this presentation lay the groundwork for creating future E-textile form factors that enable efficient sensing capabilities.

#### 6:25 AM F.FL03.05.07

**Extensible 3D Hierarchical Woven Materials** Widiyanto P. Moestopo<sup>1</sup>, Arturo J. Mateos<sup>1</sup>, Ritchie Fuller<sup>2</sup>, Julia R. Greer<sup>1</sup> and Carlos Portela<sup>3,1</sup>; <sup>1</sup>California Institute of Technology, United States; <sup>2</sup>Independent Artist, United States; <sup>3</sup>Massachusetts Institute of Technology, United States

Most architected materials to date have enabled properties such as extreme stiffness and strength, at levels unattainable independently by their constituent materials, with few works focusing on the compliant, extensible regime pertinent to flexible electronics. While exceptional mechanical properties such as extreme resilience and high deformability have been realized in many three-dimensional (3D) architected materials using beam-and-junction-based architectures, stress concentrations and constraints induced by the junctions limit their mechanical performance. Compliant architected materials that overcome these limitations, in combination with conductive components or constituent materials, could help enhance the performance of wearable electronics.

We present a new hierarchical design concept for flexible 3D architected materials in which fibers are interwoven to construct effective beams, such as the ones in classical monolithic-beam lattice architectures. Via in situ tension and compression experiments of additively manufactured polymeric woven and monolithic lattices at the microscale, we demonstrate the superior ability of woven architectures to achieve high tensile and compressive strains (>50%)—without failure events—via smooth reconfiguration of woven microfibers in the effective beams and junctions. Cyclic compression experiments reveal that woven lattices accrue less damage compared to lattices with monolithic beams. We employ numerical studies of woven beams with varying geometric parameters to present new design spaces for the development of architected materials with tailored compliance that is unachievable by similarly configured monolithic-beam architectures. This woven hierarchical design offers a pathway to make traditionally stiff and brittle materials more deformable by introducing a new building block for 3D architected materials, with complex nonlinear mechanics, applicable to flexible electronics applications.

SESSION F.FL03.06: Biosensing and Second-Skins I: Tactile Sensing and Human Motion  
On Demand Abstracts Available for Viewing Starting Saturday Morning, November 21, 2020  
F-FL03

#### 5:00 AM \*F.FL03.06.01

**Human-Interactive Sensing Displays with Field-Induced Electroluminescence** Cheolmin Park and Euihyuk Kim; Yonsei University, Korea (the Republic of)

Development of stimuli-interactive sensing display capable of spontaneously visualizing various external human sensible inputs has been of great interest and tremendous efforts are devoted to the visualization of nonvisible human senses such as touch, smell, taste, and sound. Field-induced electroluminescence under alternating current (AC) has been extensively studied and its unique device architecture in which an emitting layer is separated with an insulator from electrode offers a new platform for designing and developing emerging stimuli-interactive displays. In this presentation, we present 3 different types of interactive sensing displays. First, we demonstrate that simultaneous sensing and visualization of the conductive substance is achieved when the conductive object is coupled with the light emissive material layer on our novel parallel-type device. Second, a novel interactive skin display with epidermal stimuli electrode (ISDEE) is demonstrated, allowing for the simultaneous sensing and display of multiple epidermal stimuli on a single device. The ISDEE is directly mounted on human skin, which by itself serves as a field-responsive floating electrode of the display, allowing for displaying a variety of physiological skin factors, such as the temperature, sweat gland activity, and pressure. Finally, an interactive sensing memory platform is demonstrated, capable of sensing, monitoring, and storing the information of various liquids. Our platform utilizes sound arising from liquid-interactive ferroelectric actuation, which is dependent upon the polarity of the liquid, allowing for facile liquid sensing and identification. Moreover, our device successfully monitored the flow of a human serum liquid passing through channels and determined its velocity. Mechanically flexible and optically transparent tube-type LIFS AC devices allow for in situ analysis of the flow of a liquid in terms of sound.

#### 5:15 AM F.FL03.06.02

**A Bimodal Soft Electronic Skin for Tactile and Touchless Interaction in Real Time** Jin Ge<sup>1</sup>, Xu Wang<sup>1</sup>, Michael Drack<sup>2</sup>, Oleksii M. Volkov<sup>1</sup>, Mo Liang<sup>1</sup>, Gilbert Santiago Canon Bermudez<sup>1</sup>, Changan Wang<sup>1</sup>, Shengqiang Zhou<sup>1</sup>, Jürgen Fassbender<sup>1</sup>, Martin Kaltenbrunner<sup>2</sup> and Denys Makarov<sup>1</sup>; <sup>1</sup>Helmholtz-Zentrum Dresden-Rossendorf e.V., Germany; <sup>2</sup>Johannes Kepler University Linz, Austria

The transformative emergence of smart electronics, human-friendly robotics and supplemented or virtual reality will revolutionize the interplay with our surrounding. The complexity that is involved in the manipulation of objects in these emerging technologies is dramatically increased, which calls for electronic skins (e-skin) that can conduct tactile and touchless sensing events in a simultaneous and unambiguous way. Integrating multiple functions in a single sensing unit offers the most promising path towards simple, scalable and intuitive-to-use e-skin architectures. However, by now, this path has always been hindered by the confusing overlap of signals from different stimuli.

Here, we put forward the field of soft, flexible electronics by developing a compliant magnetic microelectromechanical platform (m-MEMS), which is able to transduce both tactile (via mechanical pressure) and touchless (via magnetic field) stimulations simultaneously and discriminate them in real time [1]. For the first time, the electric signals from tactile and touchless interactions are intrinsically separated into two different regions, allowing the m-MEMS, a single sensor unit, to unambiguously distinguish the two modes without knowing the signal history.

Owing to its intrinsic magnetic functionality, our complaint m-MEMS platform is able to discriminate magnetic vs. non-magnetic objects already upon touchless interaction. With this intrinsic selectivity, we address the long-standing problem in the field of touchless interaction – namely, the issue of interference with objects, which are irrelevant or even disturbing the interaction process. In addition, the interaction process is programmable. The sensitivity of the two interaction modes could be tuned by adjusting the magnetic field of the objects able to meet the requirements of different interaction tasks.

By using tactile and touchless sensing functions simultaneously, our m-MEMS e-skins enable complex interactions with a magnetically functionalized physical object that is supplemented with content data appearing in the virtual reality. We demonstrated data selection and manipulation with our m-MEMS e-skins leading to the realization of a multi-choice for augmented reality through three dimensional (3D) touch. Beyond the field of augmented reality, our m-MEMS will bring great benefits for healthcare, e.g. to ease surgery operations and manipulation of medical equipment, as well as for humanoid robots to overcome the challenging task of grasping.

[1] J. Ge, X. Wang, M. Drack, O. Volkov, M. Liang, G. S. Cañón Bermúdez, R. Illing, C. Wang, S. Zhou, J. Fassbender, M. Kaltenbrunner, and D. Makarov. *A bimodal soft electronic skin for tactile and touchless interaction in real time*. Nature Communications 10, 4405 (2019).

#### 5:25 AM F.FL03.06.04

**A Closed-Loop Tactile Sensor Array Using ZnO Thin-Film Transistors with Ultra-High Spatiotemporal Resolution** Hongseok Oh<sup>1</sup>, Gyuchul Yi<sup>2</sup>, Michael Yip<sup>1</sup> and Shadi A. Dayeh<sup>1</sup>; <sup>1</sup>University of California, San Diego, United States; <sup>2</sup>Seoul National University, Korea (the Republic of)

Closed-loop control system is critical in sophisticated object manipulations such as grasping and cracking a raw egg or flipping a note page, to avoid drop and slip. Human hands can perform such actions naturally even without watching the objects, because mechanoreceptors on hands can provide wide dynamic range tactile feedback on a variety of physical parameters such as shear forces to the brain for closed-loop control of hands. For robots to operate autonomously, similar tactile perception is needed to provide versatile manipulation of our everyday objects and fixtures. Furthermore, in majority of applications, a tactile sensitivity on flexible substrates is required for interaction with arbitrary geometries. Multiple modalities have been suggested so far to indirectly infer tactile information, but direct tactile sensation with shear force sensitivity is important for high fidelity haptic feedback. The challenges for achieving high spatiotemporal resolution with shear sensing ability can be addressed by employing tactile sensors which can perform both transducing forces and multiplexing signals [1]. This approach circumvents the tradeoffs for density and performance, since no additional driving element is required in construction of the array. Additional structural engineering can allow them to sense shear forces with high spatiotemporal resolution, which can lead to achieve human-level tactile perceptions for robotics. Still, manufacturing challenges remain in the realization of flexible multi-functional tactile sensors with desired density and shear-force sensation, because only scalable techniques are suitable for industrial applications.

Here, we report scalable flexible tactile sensor array with ultra-high spatiotemporal resolution including shear force sensation and real-time closed-loop grip adjustment for robotic android fingers and beyond [2]. We leveraged the flexible display technology and fabricated advanced dual-gated piezoelectric zinc oxide (ZnO) thin-film transistors (TFTs) on thin and flexible polyimide substrate. We attached a 3D Polydimethylsiloxane (PDMS) pillar array on the fabricated TFT arrays which exhibited excellent normal and shear force sensing over a broad range of forces, in both dry and wet environments. An individual ZnO TFT can intrinsically transduce the force and multiplex the signal, which allows integrating hundreds of elements with uniform sensitivity. The array composed of 256 TFTs achieved maximal spatial resolution of 100  $\mu\text{m}$  and maximal frame refresh rate of 100 Hz, which to the best of our knowledge is the highest spatiotemporal resolution reported to date. The TFTs were reliably operational under curved environments with bending radius of 5 mm, or after 10000 bending cycles. Closed-loop control of robotic fingers showed rapid slip-detection and grip adjustment using feedback exclusively from the tactile sensor array, enabling autonomous robotic tactile perception. Other novel applications such as water-proof operation and flow detection are also demonstrated.

[1] Vishniakou, Siarhei, Renjie Chen, Yun Goo Ro, Christopher J. Brennan, Cooper Levy, Edward T. Yu, and Shadi A. Dayeh. "Improved performance of zinc oxide thin film transistor pressure sensors and a demonstration of a commercial chip compatibility with the new force sensing technology." *Advanced Materials Technologies* 3, no. 3 (2018): 1700279.

[2] Hongseok Oh, Gyuchul Yi, Michael Yip and Shadi A. Dayeh, "Scalable Tactile Sensor Arrays on Flexible Substrates with High Spatiotemporal Resolution Enabling Slip and Grip for Closed-Loop Robotics", *submitted*.

**5:35 AM F.FL03.06.05**

**Wearable Kirigami-Based Sensor Patch for Rehabilitation of Shoulder Joint Injuries and Sports Performance**

**Analysis** Erin Evke, Amani Alkayyali, Rachel Menge, Alanson Sample and Max Shtein; University of Michigan–Ann Arbor, United States

Fitness activity trackers and health-monitoring devices are becoming increasingly prevalent in everyday life. Motion trackers constitute a class of wearable devices, with numerous applications, including physical therapy (PT) and analysis of sports performance, in which monitoring of the angular positions of joints can accelerate rehabilitation and improve performance. The shoulder joint is notoriously difficult to track, as it exhibits more degrees of freedom and greater articulation than most joints in the human body. Many traditional methods, as well as other wearable sensors used to record limb and shoulder movement remain quite limited in versatility or scalability.

We created a wearable patch from a flexible *kirigami* substrate, enabling a planar sheet with embedded circuits to conform to the three-dimensional shape of the shoulder. Upon deformation, the localization of stress near saddle-points in the kirigami structure is related to the degree of curvature, determined through finite-element modeling and experimental measurements, and assessed as a function of the sheet material and cut parameters. Strain gauges are strategically placed on the platform based on the stress distribution, creating a sensing device that corresponds to a standardized 19-camera motion tracking system, and can differentiate between many types of motion, including running, shrugging, arm circles, etc., in real time. The combination of electrical sensing elements and closed-shape kirigami structures demonstrated by this work enable a highly wearable, garment-integrable, inexpensive joint motion monitoring device that can be used for rehabilitation, athletic

training, feedback control for augmented mobility, robotics, and other applications.

#### 5:45 AM F.FL03.06.06

**Graphene Nanocomposite Kinesiology Tape for Human Motion Assessment** Yun-An Lin<sup>1</sup>, Yujin Park<sup>1</sup>, Long Wang<sup>1</sup>, Wei-Hung Chiang<sup>2</sup> and Kenneth J. Loh<sup>1,1</sup>; <sup>1</sup>University of California San Diego, United States; <sup>2</sup>National Taiwan University of Science and Technology, Taiwan

In recent years, wearable sensors have attracted considerable interest among the general public due to increased awareness in personal health. Technologies as such can be particularly beneficial to industries related to virtual reality, sports performance, military, and healthcare. However, most wearable sensors that are available today are still based on bulky, rigid, inconvenient, electronic devices. Furthermore, they are limited to discrete sensing at their instrumented locations. On the contrary, sensors in the form of patches are more conformable to the human body and are capable of distributed sensing. For this reason, the purpose of this study is to develop a flexible, skin-like sensor capable of continuous, real-time, human physiological monitoring. The approach was to integrate strain-sensitive graphene-based thin films with commercially available kinesiology tape (K-Tape) as the substrate. The strain and motion sensing properties of these Smart K-Tape were characterized using a load frame. Upon verifying their strain sensing properties, the wearable sensors were tested on individuals performing different activities and undergoing different types of movements. Data acquired from the wearable sensors were compared against post-processed recorded video of subjects performing different controlled motions. In addition, a network of these graphene-enhanced K-Tape could form a network of sensors for distributed motion monitoring. In general, repeatable and consistent sensing responses were obtained and confirmed, which demonstrated their potential applications for the development of next-generation human motion and physiological monitoring systems.

#### 5:55 AM F.FL03.06.08

**Computational Wrapping—A Universal Method Based on Computational Origami for Conformable and Wearable Devices** Yuki Lee<sup>1</sup>, Jyh-Ming Lien<sup>2</sup> and In-Suk Choi<sup>1</sup>; <sup>1</sup>Seoul National University, Korea (the Republic of); <sup>2</sup>George Mason University, United States

In this talk, we propose a novel method to make conformable devices on non-zero Gaussian surfaces, i.e. flexible devices that can be transformed into any complex 3-dimensional shape. We used computational polyhedral edge unfolding methods to obtain planar figures of arbitrary complex 3-dimensional shapes. It is well-known that 2-dimensional substrates cannot be attached on the non-zero surfaces without stretching, however, by computational approximation of 3-D surface and making it flat by algorithmic method, we could convert any 3-D shapes into a 2-D sheet. We can make devices having the programmed unfolded figures and return it to the original 3D shape. In this way, we could make electroluminescent lighting and primary battery which can conformably wrap diverse 3-D surfaces without failure. Shape programmable devices with computational wrapping design can cover anywhere on the 3-dimensional shapes including human skin and are able to be applied not only personalized wearable or skin attachable devices but also various industries, such as automotive design, clothing, and fashion accessories, medical services and so on.

#### 6:05 AM F.FL03.06.09

**Materials Selection Principles for Human Motion Detection via Textiles** S. Zohreh Homayounfar, Ali Kiaghadi, Deepak Ganesan and Trisha Andrew; University of Massachusetts, Amherst, United States

The advancement of smart apparels capable of tracking human physiological signals and body locomotion has a great potential to revolutionize human performance sensing and personalized health monitoring through transforming daily life clothing into sensors. Quantitative evaluation of kinetic parameters of individual gait along with physiological signals can be employed in games and sports, as well as in the diagnosis of many diseases such as Parkinson's, Multiple Sclerosis, and sleep disorders. Among different methodologies in developing wearable sensors such as inertial measurement units, textile-based electromechanical sensors encompass the majority of widely adopted applications. Electromechanical sensors fall into three major categories based on their active mechanisms: piezoelectric sensors, triboelectric sensors, and piezoresistive sensors. Recently, different combinations of materials and designs have been reported to develop wearable sensors, each of which provides a unique window into a slightly different range of motion sensitivity. For example, some human signals and motions lie in the small-scale range of pressures such as those of a subtle touch, arterial pulses, and sound vibrations, while the other body movements lie in medium to a large range of pressures, such as joint movements, and locomotion during sleep and intense activities. The ability to design an unobtrusive wearable sensor being highly responsive in the required range of signals calls for getting an insight into the difference between the three mechanisms of electromechanical sensing and their corresponding responses under certain conditions.

Here, we introduced a set of materials selection principles which gives researchers an in-depth insight into how to design a

wearable electromechanical sensor when it comes to acquiring data from a specific source of motion. In order to achieve this goal, we performed a set of purposefully designed experiments on three types of wash-stable fabric-based electromechanical sensors that had already been introduced by our lab, i.e., triboelectric sensor, piezoelectric sensor, and piezoionic sensor as a subset of piezoresistive ones. These experiments explored the effect of impact pressure, bending angle and speed, frequency, presence of a base pressure, response time, breathability, and having a multi-layer structure on the performance and sensitivity of each type of sensors. For an instance, it turned out that the triboelectric and piezoelectric sensors are a more reliable sensing element for dynamic pressures, such as joint movements, with the former being failed in the presence of a base pressure. Piezoresistive sensors are the ones with the ability to sense both static and dynamic pressures, as well as being responsive under a base pressure. However, piezoresistive one would not be a choice when it comes to bending applications. Upon this comprehensive comparison, we demonstrated a conclusive map that can provide the researchers with distinguishing features of these three types of sensors to be used in corresponding niche applications.

#### **6:15 AM F.FL03.06.10**

**Late News: Simulation and Fabrication of Pyramidal Microstructured PDMS Films for Capacitive Pressure Sensors** Michael Facchini-Rakovich and Manisha Gupta; University of Alberta, Canada

Capacitive pressure devices have been used for different applications such as wearable health sensors, soft-robotics, and prosthesis. These devices can be designed as parallel plate capacitors with an elastomer dielectric film like polydimethylsiloxane (PDMS). When different microstructures are added to these elastomer films then the pressure range and sensitivity can be tuned. Here, we conducted simulation for pyramidal microstructures as they spread the force evenly and can be repeatably fabricated. We introduce a simple finite-element-method simulation model for determining the capacitance and sensitivity of these microstructured films. The model sees the PDMS films as consisting of parallel and series capacitors, and volumetrically solves for the total capacitance. COMSOL Multiphysics is used to generate various geometries. Key parameters, such as pyramid spacing, width and height are seen to influence the performance of sensors. We studied these parameters from the 10 to 100  $\mu\text{m}$  range. We can modify the initial capacitance from 12.74 to 82.75 pF/cm<sup>2</sup>, and the sensitivity from 0.008 to 0.18 per kPa. As well, penetration into a lamination layer, and layer thicknesses are also studied. These are factors come into play during the moulding and bonding processes. Penetration was studied for 1 to 6  $\mu\text{m}$  range, and layer thicknesses from 7 to 105  $\mu\text{m}$ . These allow the control of capacitance from 12.15 to 27.9 pF/cm<sup>2</sup>, and sensitivity from 0.01 to 0.03 per kPa. Pyramidal structures can be fabricated via a moulding process of PDMS and bonding it to metalized plastic sheets. Moulds consist of square pyramidal arrays obtained by KOH etching of silicon wafers, and bonding can be performed by lamination to a thin PDMS layer. We will present the performance of devices in relation to these parameters and compare them with other mathematical models. Furthermore, we use the simulation to predict performance trends, and compare them with experimentally gathered data from fabricated devices. This simulation model may be used to predict the performance of new devices too by modifying the geometry. Doing so, devices can be tuned to obtain different ranges of pressure sensing and sensitivity for specialized applications. Ranging from monitoring pressure sores, with a necessary range up to 100kPa, to artificial skin with sensing below 1 kPa.

#### SESSION F.FL03.07: E-Textiles—Fiber-Based Processing

On Demand Abstracts Available for Viewing Starting Saturday Morning, November 21, 2020

F-FL03

#### **5:00 AM \*F.FL03.07.01**

**The Rise of Fiber Electronics** Huisheng Peng; Fudan University, China

**Abstract** : It is critically important to develop miniature electronic devices for a variety of emerging new fields, such as wearable facilities, smart textiles and internet of things. Here a novel family of energy and electronic devices with various functionalities, e.g., energy harvesting, energy storing, lighting, and sensing, in 1D fiber configuration are carefully discussed with unique and promising advantages such as lightweight and weaveable compared with the conventional planar architecture. The main efforts will be made to highlight the recent advance in the electrode material, device structure and property extension.

#### **5:15 AM \*F.FL03.07.02**

**Flexible Bioelectronics on a Thread** Sameer R. Sonkusale; Tufts University, United States

This talk will explore the new realm of using textile threads as an ultimate platform for flexible and stretchable bioelectronics. Threads offer unique advantages of universal availability, low cost, material diversity and simple textile-based processing. Interestingly, threads also provide an ideal platform for passive microfluidic sampling and delivery of analytes. In this talk, I will report reel-to-reel fabrication of functional smart threads for variety of sensing and electronics application. I will report on nanomaterial-infused smart threads for sensing physical activity and temperature. Nano-infused threads will be presented for sensing pH, glucose, lactate, ammonium and other chemical and biological biomarkers directly in biological fluids such as sweat or wound exudate. Colorimetric washable threads that can sense both ambient and dissolved gases will be shown. Beyond sensing and microfluidics, I will present our recent work on making super-thin transistors and electronics directly on threads. This new toolkit of highly flexible thread-based microfluidics, sensors, transistors and electronics makes it possible to realize smart surgical sutures and flexible smart bandages for chronic wounds. Our recent work on using threads for closed loop spatiotemporal dosage controlled drug delivery will also be presented.

**5:30 AM \*F.FL03.07.03**

**Fiber-Based Sensors for Electronic Textiles** Jordan Tabor, Ashish Kapoor and Tushar Ghosh; North Carolina State University, United States

Soft polymer-based wearable sensors as an integral part of textile structures have attracted considerable scientific and commercial interest recently because of their potential use in healthcare, security, and other areas. Electronic sensing capabilities can be integrated into textiles at fiber, yarn, or fabric level but unobtrusive integration of sensing capabilities while preserving all desirable textile qualities like comfort and flexibility can be better achieved by introducing the desired functions at the fiber level. In this research, we demonstrate a transformative sensing technology through the design of a multimodal and multifunctional woven sensor array by employing bicomponent fibers consisting of insulating and electrically conducting segments of unique cross-sectional shape, wherein each cross-over point in the woven fabric structure acts as a sensing pixel. To demonstrate the concept the fibers are initially fabricated using a benchtop coextrusion method. The insulating segments are formed using an ultraviolet curable poly(dimethylsiloxane) (PDMS) while the conducting segments are made from a conducting polymer composite containing PDMS and carbon black. The multimodal characteristic of the sensors is demonstrated through the measurement of capacitive and resistive responses while multifunctional capabilities are explored by measuring tactile (normal force), tensile, and shear deformations, as well as wetness and biopotential. As a potential biomedical application, these fiber-based sensing arrays are integrated into a prosthesis socket to monitor pressure within the inner socket environment of lower limb amputees. Also, a large channel sensor array is fabricated and its potential for contactless sensing of gestures is demonstrated as a potential textile-based human-machine interface. In order to demonstrate the scalability and commercial relevance of the concept, we have also fabricated the same sensory fiber using the tricomponent melt extrusion (TME) method. It is a process that involves the simultaneous extrusion of three distinct polymers to produce unique fiber shapes. Due to the complex nature of this process and the specialty equipment required, TME has rarely been utilized in research efforts and has not been explored for producing fiber-based sensors. So far in this ongoing research, we have extruded the sensory fibers of the desired shapes using the TME process and explored the influence of the shape control parameters such as flow-rate and fractional throughput. We have characterized the fibers for their morphological, mechanical, and electromechanical properties. Initial results indicate that the micron-scale fibers can be produced at speeds of >100 m/min thus providing a scalable and commercially relevant method of producing fiber-based sensors for wearable technology.

**5:45 AM F.FL03.07.04**

**Carbon Nanotube Yarn and Fabric for Wearable Electronic Textile Applications** Md. Milon Hossain<sup>1,2</sup>, Mostakima Lubna<sup>1</sup> and Philip Bradford<sup>1</sup>; <sup>1</sup>North Carolina State University, United States; <sup>2</sup>Khulna University of Engineering & Technology, Bangladesh

Individual carbon nanotubes (CNTs) have remarkable properties that are often hard to scale directly to macroscopic materials and devices. A tremendous effort has been made to assemble CNTs at the micro and macro scale in controlled methods to utilize their anisotropic material properties. Here we report a single-step method of assembling CNTs wrapped textile yarns for wearable electronic textile applications. The dry spinning method was used to fabricate CNT yarns from millimeter tall vertically aligned CNT arrays produced by the chemical vapor deposition method. Both pristine CNT and CNT wrapped textile yarns were produced and their structure-properties relationship were compared. This unique method of assembling CNTs with traditional textile yarns provides greater freedom to tailor the strength and conductivity of the yarns for desired applications. Surface morphology examination showed that CNTs were wrapped uniformly over the core textile yarn and have a similar diameter to those yarns suitable for producing highly flexible textile fabrics for body-worn applications. The CNT yarn showed very good mechanical properties and could withstand 1000 loading cycles at a 2% strain. The use of



polyurethane binder enhanced the mechanical stability of the CNT yarn and prevented the delamination and loss of CNTs from the core yarns during mechanical strain. The CNT yarn was knitted to produce a seamless 3D knitted structure for strain sensing and Joule heating applications. The produced knitted fabric could sense applied strain and successfully track the movement of the finger. When voltage was applied to the fabric, a highly stable heat was generated in seconds and the fabric can produce heat above skin temperature with as low as 3 volts applied. To realize the true potential of the CNT yarns for use in next-generation wearable electronics, the CNT yarn was subjected to an extensive wash durability study. It was found that the CNT yarn was extremely resistant to washing showing no significant changes in conductivity after 30 washing cycles. This yarn may also find uses in electromagnetic shielding and energy storage textile applications.

#### 5:55 AM F.FL03.07.05

**Nano-Structured Metallic Glass-Based Multimaterial Fiber Electronics** Wei Yan<sup>1,2</sup>, Inès Richard<sup>1</sup>, Güven Kurtuldu<sup>3</sup>, Nicholas D. James<sup>4</sup>, Giuseppe Schiavone<sup>5</sup>, Jordan Squair<sup>4</sup>, Tung Nguyen Dang<sup>1</sup>, Tapajyoti Gupta<sup>1</sup>, Yupeng Qu<sup>1</sup>, Jake Cao<sup>3</sup>, Reinis Ignatans<sup>6</sup>, Stephanie P. Lacour<sup>5</sup>, Vasiliki Tileli<sup>6</sup>, Grégoire Courtine<sup>4</sup>, Jörg F. Löffler<sup>3</sup> and Fabien Sorin<sup>1</sup>; <sup>1</sup>Laboratory of Photonic Materials and Fibre Devices (FIMAP), Institute of Materials, École Polytechnique Fédérale de Lausanne, Switzerland; <sup>2</sup>Research Laboratory of Electronics, Massachusetts Institute of Technology, United States; <sup>3</sup>Laboratory of Metal Physics and Technology, Department of Materials, ETH Zurich, Switzerland; <sup>4</sup>Defitech Center for Interventional Neurotherapies (NeuroRestore), Center for Neuroprosthetics and Brain Mind Institute, School of Life Sciences, École Polytechnique Fédérale de Lausanne, University Hospital of Vaud, and University of Lausanne, Switzerland; <sup>5</sup>Bertarelli Foundation Chair in Neuroprosthetic Technology, Laboratory for Soft Bioelectronic Interfaces, Institute of Microengineering, Institute of Bioengineering, Centre for Neuroprosthetics, École Polytechnique Fédérale de Lausanne, Switzerland; <sup>6</sup>Institute of Materials, École Polytechnique Fédérale de Lausanne, Switzerland

The integration of conducting architectures within thermally drawn thin and flexible fibers is emerging as a versatile platform for smart sensors and imaging systems, robotic surgery, biological and neural probes, and advanced textiles<sup>1-3</sup>. The fabrication of conductors with nanoscale feature sizes, large aspect ratios, complex transverse geometries and excellent conductivity within thermally-drawn fiber electronics, however, remain unresolved. Here we, for the first time, address this challenge via the thermal drawing of metallic glasses (MGs), a material system that is metallic yet with a disordered atomic structure compatible with controlled thermal deformation<sup>4</sup>. The high viscosity during drawing, combined with a viscous interface provided by a thermoplastic matrix surrounding MGs domains allows us to control fluid instabilities that are normally detrimental for molten crystalline metals. This fabrication strategy enables the production of ultra-long, highly uniform and well-ordered nanoscale MG domains with arbitrary cross-sectional geometries within flexible polymer fibers. In terms of integrating metallic electrodes within flexible fibers, catheters, capillaries or textiles, the figure of merit we can achieve, that can be defined as the ratio of the conductivity to feature sizes, significantly surpasses existing strategies. Beyond using MG components as electrodes, we further show that they can be monolithically integrated with other functional materials, forming novel all-in-fiber flexible devices and smart textiles. Specifically, optoelectronic fibers that integrate MG ribbons serving as highly conductive electrodes and a semiconducting selenium core serving as a photodetector are fabricated. The device exhibits a unique combination of excellent responsivity and sensitivity that compares favorably with other reported nanoscale planar devices. Moreover, the flexibility and form factor of the polymer cladding enable to weave the fiber into different types of textiles. Our work brings, for the first time, extreme miniaturization of highly conducting metal-based electrodes, paving the way towards the integration of more complex functionalities and devices in flexible electronics, fibers and fabrics.

W.Y and I.R contributed equally.

1. Wei Yan, Alexis Page, Tung Nguyen, Yunpeng Qu, Federica Sordo, Lei Wei, Fabien Sorin\*. Advanced Multimaterial Electronic and Optoelectronic Fibers and Textiles. *Advanced Materials* 31 (2019) 1802348.
2. Gabriel Loke#, Wei Yan#, Tural Khudiyev, Grace Noel, Yoel Fink\*. Recent progress and perspectives of thermally-drawn multimaterial fiber electronics. *Advanced Materials* 32 (2020) 1904911.
3. Wei Yan, Chaoqun Dong, Yuanzhuo Xiang, Shan Jiang, Andreas Leber, Gabriel Loke, Wenxin Xu, Chong Hou, Shifeng Zhou, Min Chen, Run Hu, Perry Shum Ping, Lei Wei, Xiaoting Jia, Fabien Sorin, Xiaoming Tao, Guangming Tao\* Thermally drawn advanced functional fibers: new frontier of flexible electronic devices. *Materials Today* (2020) <https://doi.org/10.1016/j.mattod.2019.11.006>
4. Wei Yan, Inès Richard, Güven Kurtuldu, Nicolas James, Giuseppe Schiavone, Tung Nguyen-Dang, Tapajyoti Das Gupta, Yunpeng Qu, Jake Cao, Reinis Ignatans, Stéphanie P. Lacour, Vasiliki Tileli, Grégoire Courtine, Jörg F. Löffler, Fabien Sorin\*. Structured nanoscale metallic glasses fibers with extreme aspect ratios. *Nature Nanotechnology*. (In press, 2020).

#### 6:05 AM F.FL03.07.06

**Full-Area Textile Displays with All Organic Light-Emitting Diode Fibers** Young Jin Song, Ha-Young Song and Sung-

Min Lee; Kookmin University, Korea (the Republic of)

As an emerging format of wearable electronics, the electronic textile (e-textile) display devices consisting on emitting fibers have been actively studied for substantiating ‘in-cloth’ information displays. Several technical issues have to be resolved to create fiber-based e-textile displays, such as high electroluminescence performance of luminescent fibers, solid passivation systems, and interconnectable configuration of pixel elements in fibers for the two-dimensional matrix-addressing. Recently, we successfully demonstrated a class of the e-textile displays by weaving interconnectable organic light-emitting diode (OLED) fibers with conductive fibers. This OLED e-textile display could be operated by the passive matrix addressing scheme due to perpendicularly aligned woven fiber network with interconnectable OLED fibers and conductive fibers that were served as scan and data lines, respectively. Moreover, it was reliably operated even in the water owing to the chemically/mechanically sturdy but electrically conductive passivation system formed on each OLED pixel. Despite the noticeable proof-of-concept, the reported devices could exploit a half area over the available entire textile area at the most due to the nature of woven network that OLED pixels placed alternately along the conductive fiber, which limited the imaging resolution. In this regard, here we present a strategy to achieve matrix-addressable e-textile OLED displays throughout the entire textile area by weaving only OLED fibers that can support the scan and data lines at the same time. To create the united functional fibers, phosphorescence OLED pixels are regularly deposited on the common indium tin oxide (ITO) electrode coated on one side of the rectangular-shaped polyimide (PI) fiber. The conductive metal bus electrode that can work as a data line in the matrix addressing scheme is thermally deposited on the opposite side of the PI fiber except the defined emitting spots. As the OLED pixels exist at every cross points of interlaced perpendicularly arranged OLED fibers, full-area OLED e-textile displays can be achieved, where high-resolution images are produced by the passive matrix addressing process.

**6:15 AM F.FL03.07.08**

**High-Throughput Cleanroom-Free Fabrication of Thread Based Transistors** Tanuj Kumar, Rachel E. Owyung and Sameer Sonkusale; Tufts University, United States

In the past few decades, applications such as wearable electronics, biosensing, and flexible displays have led to advances in flexible electronics.<sup>1,2</sup> Textile threads are a highly suitable substrate for truly flexible and biocompatible electronics. Recent works have demonstrated thread-based transistors (TBTs), but their methods were not scalable to manufacturing more than a few transistors.<sup>3,4</sup> To realize complex large-scale thread-based circuits for wearables, diagnostics, and flexible displays, a high throughput fabrication method of TBT is required.

In this work, we present a low-cost, high-throughput, and cleanroom-free fabrication process for ionogel gated, poly(3-hexylthiophene)-based organic TBTs. This lithography-inspired approach involves the use of a flexible Ecoflex “mask” that threads are pierced into, to fabricate the active channel area gap. Then, conductive carbon ink is painted or drop cast on to fully coat the exposed threads, and when dried, the threads are removed to reveal the active channel area of the transistor. Notably, the flexibility of the mask is paramount for easy insertion of threads when stretched and provides a tight seal around each thread when relaxed to inhibit electrode ink seepage.

In our preliminary experiments, we achieved a density of 1 TBT fabricated per cm<sup>2</sup> of Ecoflex mask; we demonstrate fabrication of close to 50 TBTs in a mask of approx. 50 cm<sup>2</sup>. After correcting for some geometrical variations from manual effort, we show consistent device performance among all TBTs with a threshold voltage of (1.48 ± 0.11) V, an operating region of 0 to -3V, and an ON/OFF ratio of the order of 10<sup>2</sup>. These results prove the feasibility of this new approach for batch fabrication of several TBTs which with automation, holds potential for even higher areal densities of fabricated TBTs and much tighter tolerances. What we have proposed will address the key bottleneck in scaling up threads as a substrate for very large-scale electronics on thread with applications in wearable devices, flexible displays, and diagnostic toolkits.

<sup>1</sup> A. Nathan, A. Ahnood, M.T. Cole, S. Lee, Y. Suzuki, P. Hiralal, F. Bonaccorso, T. Hasan, L. Garcia-Gancedo, A. Dyadyusha, et al. in *Proc. IEEE* (Institute of Electrical and Electronics Engineers Inc., 2012), pp. 1486–1517.

<sup>2</sup> J. Sheng, H.-J. Jeong, K.-L. Han, T. Hong, and J.-S. Park, *J. Inf. Disp.* **18**, 159 (2017).

<sup>3</sup> M. Hamedi, R. Forchheimer, and O. Inganäs, *Nat. Mater.* **6**, 357 (2007).

<sup>4</sup> R.E. Owyung, T. Terse-Thakoor, H. Rezaei Nejad, M.J. Panzer, and S.R. Sonkusale, *ACS Appl. Mater. Interfaces* **11**, 31096 (2019).

**6:25 AM F.FL03.07.10**

**Late News: The Effect of Cellulose Nanocrystals (CNCs) on the Conformation of Polyvinylidene Fluoride (PVDF) Nanocomposite Fibers and Triboelectricity of Textile Sensors** Jung-Eun Lee, Hyejin Ju, Ga-Hyeun Lee, Ji Hyun Kim and

Han Gi Chae; Ulsan National Institute of Science and Technology, Korea (the Republic of)

Polymers such as poly(vinylidene fluoride) (PVDF), and its copolymers with hexafluoropropylene (HFP), trifluoroethylene (TrFE) and chlorotrifluoroethylene (CTFE) are known to possess electroactive properties and have been studied for decades, enabling them one of the most promising candidates for wearable and smart textile applications. Nonetheless, the practical applications are still limited and are in the early stage of development because of poor mechanical integrity. Most of researches have focused on the form of film or electrospun mat (nanofiber) which showed weak mechanical properties to practically use. Since the high mechanical properties are the critical requirement to smart textiles because the resistance ability to external damage is related with the durability of textiles, the film and mat should be replaced with a stronger fibers. In the current study, PVDF and PVDF/cellulose nanocrystal (CNC) nanocomposite fibers were dry-jet wet spun at CNC concentrations of 0, 1, and 3 wt% with respect to the polymer. The high draw ratio (DR) of 8 and the interaction between PVDF matrix and CNC lead to superior mechanical properties and  $\beta$  phase fraction ( $F_\beta$ ), which is beneficial for practical application in smart textiles. The behavior of various conformation of PVDF were also analyzed according to DR and CNC contents. All fibers showed increase in tensile properties and  $F_\beta$  as the polymeric chains become extended with increasing DR. Among them, the highest 298.0 MPa of tensile strength, 3.3 GPa of tensile modulus, and 69.1% of  $F_\beta$  were exhibited in fibers with the addition of 1 wt% of CNCs at DR 8 based on their active interaction with PVDF. To demonstrate the use of these PVDF-based fibers in wearable devices, the triboelectric textile sensors were fabricated through a conventional weaving method based on their high mechanical integrity. They can detect a broad pressure range of 980 Pa to 98 kPa, enabling diverse pressure-sensor applications.

SESSION F.FL03.08: Biosensing and Second-Skins II: Biosensor Materials and Design  
On Demand Abstracts Available for Viewing Starting Saturday Morning, November 21, 2020  
F-FL03

**5:00 AM \*F.FL03.08.01**

**Skin-Interfaced Wearable Sweat Biosensors for Personalized Healthcare** Wei Gao; California Institute of Technology, United States

The rising research interest in personalized medicine promises to revolutionize traditional medical practices. This presents a tremendous opportunity for developing wearable devices toward predictive analytics and treatment. In this talk, I will introduce our recent advances in developing fully-integrated skin-interfaced flexible biosensors for non-invasive molecular analysis. Such wearable biosensors can continuously, selectively, and accurately measure a wide spectrum of sweat analytes including metabolites, electrolytes, hormones, drugs, and other small molecules. These devices also allow us to gain real-time insight into the sweat secretion and gland physiology. The clinical value of our wearable sensing platforms is evaluated through multiple human studies involving both healthy and patient populations toward physiological monitoring, disease diagnosis, and drug monitoring. This talk will also feature our very recent works on laser-engraved lab on the skin and biofuel-powered battery-free electronic skin toward metabolic/nutritional management as well as dynamic stress monitoring. These wearable and flexible devices could open the door to a wide range of personalized monitoring, diagnostic, and therapeutic applications.

**5:15 AM F.FL03.08.03**

**Highly Compliant and Printable Giant Magnetoresistive Sensors for Human-Interactive On-Skin Electronics** Minjeong Ha<sup>1</sup>, Gilbert Santiago Canon Bermudez<sup>1</sup>, Yevhen Zabala<sup>2</sup>, Jürgen Fassbender<sup>1</sup> and Denys Makarov<sup>1</sup>; <sup>1</sup>Helmholtz-Zentrum Dresden-Rossendorf, Germany; <sup>2</sup>Institute of Nuclear Physics PAN, Poland

The highly-compliant and skin-conformal magnetic field sensors have been of great interest for the human-interactive on-skin electronics capable of position recognition and tracking gesture. To design such on-skin electronics, solution-processable printing technologies are attractive way due to simple, cost-efficient, and highly adaptable to various materials. Here we report printable giant magnetoresistive (GMR) sensors on ultra-thin films that can naturally comply with the skin. Thanks to the strong interfacial bonding of triblock copolymer in GMR paste, the printed GMR microflakes could be firmly adhered to the any substrates with excellent mechanical stability under 16  $\mu\text{m}$  bending radius without any damage. The excellent percolation contacts among GMR microflakes coupled with 2<sup>nd</sup> antiferromagnetic maximum attribute the high sensitivity of 3  $\text{T}^{-1}$  in low magnetic field ranges of 0.88 mT on the bending curvature of 16  $\mu\text{m}$ , resulting in 3409 times higher figure of merits than current state-of-the-art printable magnetic field sensors. Since the fast quenching of binding matrix induced

random orientation of GMR microflakes rather than 2D stacks, the printed GMR sensors are omnidirectional magnetic field sensing capability regardless of angular change from 0 to 360° for freely locating GMR sensors on skin. With this performance, our printed GMR sensors on skin demonstrate a touchless control of virtual objects for the practical application in human-interactive wearable devices, artificial prosthetics, robotics, and internet of things.

#### 5:25 AM F.FL03.08.04

**Facilitating Hair Growth via Flexible Vertical Red  $\mu$ LED** Jaehee Lee and Keon Jae Lee; Korea Advanced Institute of Science and Technology, Korea (the Republic of)

A lot of people around the world have suffered from alopecia, which can lead to aesthetic issues, low self-esteem, and social anxiety. Therapeutic technology including thermal, electrical, pharmacological, and photo stimulation have been suggested to treat hair loss. Among them, laser stimulation to hair is a strong treatment, activating the proliferation of hair follicles without side effects. Particularly, periodically irradiating red light with a wavelength of 650nm in the hairless area can help efficient stimulation of hair follicles under the skin, because this light can penetrate deeper into the skin tissue than blue and green light with short wavelengths. However, this laser stimulation treatment has difficulty in high power consumption, large size, and spatiotemporal restriction. Recently, flexible micro-light-emitting diodes ( $\mu$ LEDs) have been a great attention for future biomedical devices, such as biosensors, pulse oximetry (SpO<sub>2</sub>) sensors, and optogenetic stimulators due to its high performance and outstanding stability. However, flexible  $\mu$ LEDs still have significant drawbacks in application to wearable phototherapeutic devices, such as high heat, low optical efficiency, and high energy consumption.

Herein, we report high-performance  $30 \times 30$  AlGaInP fVLEDs fabricated with transfer-free monolithic method for a wearable phototherapeutic device. Ultrathin flexible  $\mu$ LEDs were fabricated by vertically interconnecting top and bottom electrodes. The red f-VLED arrays were conformally attached on a human wrist with high irradiance of  $\sim 30$  mW mm<sup>-2</sup> and low forward voltage of  $\sim 2.8$  V. The red light with 650 nm wavelength deeply penetrate the skin and stimulate the hair follicles, which is located 2 mm under the skin. The thermal stability of the monolithic f-VLED was theoretically investigated by using finite element method (FEM) simulation and experimentally optimized by operating f-VLEDs on the skin. Mechanical stability of monolithic f-VLEDs was confirmed by harsh periodic bending/unbending motions, which is necessary for skin-attachable phototherapeutic devices. Finally, photostimulation in hairless region was performed to promote hair growth in a living depilated mouse via f-VLED array with thermal stability. Hair regrowth in the mice via f-VLED was verified by analyzing immunofluorescent and histological effects.

#### 5:35 AM F.FL03.08.05

**A Laser-Engraved Wearable Microneedle Array Based on Biopolymers Obtained from Food Residues** Elvira Fortunato; Universidade NOVA de Lisboa, Portugal

Although many delivery systems have been proposed to improve drug permeation through the skin, all of them suffer from several limitations. This drives a continuous search for innovative systems that can provide safe and effective transdermal drug delivery solutions. In line with this, microneedle arrays (MNs), a hybrid combination of hypodermic injections and transdermal patches, have been proposed. MNs consist of micro-scale needles that can pierce the skin by a simple, minimally invasive and painless route, enabling the transport of drugs and macromolecules into the human body. This study reports, for the first time, the use of a bio-based, biodegradable and biocompatible polymer, poly(3-hydroxybutyrate-co-3-hydroxyvalerate), P(3HB-co-3HV), for the fabrication of a biopolymer-based MNs patch. Molds of poly(dimethylsiloxane) (PDMS) were prepared by direct laser writing technology, a low-cost and mask-less technology, and used to produce biodegradable P(3HB-co-3HV) MNs by a thermosetting process. The best results were obtained with a laser power of 30 W at 0.15 m/s, with a spiral model as a pattern. The obtained MNs had a length of 0.69 mm and a diameter of 0.33 mm, ideal for painless penetration of the skin. Additionally, the produced MNs had good mechanical properties and the ability to successfully impregnate fluorescent dye (Rhodamine 6G). These features render P(3HB-co-3HV) a promising material for the development of novel MNs with improved functionality

#### 5:45 AM F.FL03.08.06

**Ultra-Low-Noise Organic Biosignal Amplifier with Flat Stamp Parallel Printed Electrodes** Takafumi Uemura<sup>1</sup>, Tomoharu Kimura<sup>2</sup>, Yayoi Shibafuji<sup>2</sup>, Takeshi Suyama<sup>2</sup>, Hiroyuki Ueno<sup>2</sup> and Tsuyoshi Sekitani<sup>1</sup>; <sup>1</sup>The Institute of Scientific and Industrial Research, Osaka University, Japan; <sup>2</sup>SCREEN Holdings Co., Ltd., Japan

The monitoring of microvolt-level biosignals such as electroencephalograms (EEG) requires the application of low-noise signal amplifier circuits, which, for single-use cases, must be fabricated for disposability using low-cost manufacturing techniques. In this study, we propose a scalable electrode printing process for organic transistors that can carry out precision measurement of EEG using a low-noise organic amplifier. In the transistor fabrication process, Ag electrodes are processed

via flat stamp parallel printing (FSPP), and fine-process optimization to minimize the charge-trapping effect enables a three-order reduction in transistor noise. The low-noise transistors were used to produce an organic pseudo-CMOS amplifier with a small noise level of 2.2  $\mu\text{Vp-p}$  at 10 Hz. The ultra-low-noise organic amplifier enables precision EEG monitoring in a close correlation with signals obtained using a commercialized measurement system.

Wearable biosensing equipment is a highly anticipated next-generation medical device technology for obtaining advanced personal healthcare and self-medication. A critical requirement for a wearable device is that it does not interfere with daily human activity, which means that it must be mechanically flexible and lightweight. Furthermore, to avoid motion-induced artificial noise and obtain higher-quality biosignals, the sensor device must be lightweight and remain in close contact with the surface of the human body. To meet these requirements, a number of sheet-type flexible biosensors have been recently developed [1-5]. A further requirement for wearable biosensor devices is disposability for single-use cases, which in turn requires the use of low-cost manufacturing processes. Also, the most critical circuit parameter in the development of biosignal detection circuits is transistor noise, which limits the minimum detectable signal level and quality of measurement. In this study, we demonstrate a low-noise printing process that minimizes transistor noise by optimizing the source-drain electrode stacking process. The device employs a bottom-contact, top-gate transistor structure in which source-drain silver electrodes are printed using the flat stamp parallel printing (FSPP) method. The FSPP is a type of reverse offset printing method that enables both the patterning of fine source-drain electrodes and a large-area biopotential input electrode. In the transistor stacking process, several improvements such as thinning the contact electrodes and insulator film and optimizing the chemical treatment process for the contact electrodes were conducted to evaluate their respective impacts on transistor noise. This process optimization resulted in improved mobility, reduced contact resistance, and reduced subthreshold slope and enabled the fabrication of a low-noise organic transistor,  $2.3 \times 10^{-11}/\text{Hz}$ , with improved transistor characteristics. Using the low-noise transistors, a pseudo-CMOS amplifier with an ultra-low output noise of 2.2  $\mu\text{Vp-p}$  at 10 Hz was successfully fabricated and enabled precision EEG monitoring. The scalable printing method for realizing low-noise organic amplifier is a useful fabrication method for a single-use daily personal healthcare system.

#### References

- [1] T. Someya et al., *Nature* 540, 379 (2016).
- [2] J. Heikenfeld et al., *Lab Chip* 18, 217 (2018).
- [3] W. Gao et al., *Acc. Chem. Res.* 52, 523 (2019).
- [4] M. L. Hammock et al., *Adv. Mater.* 25, 5997 (2013).
- [5] J. J. S. Norton et al., *Proc. Natl. Acad. Sci. USA* 112, 3920 (2015).

#### 5:55 AM F.FL03.08.08

**Fiber-Based Soft Electronic Sensors for Textile Electronics and *In Vivo* Bioelectronics** Jaehong Lee; Daegu Institute of Science and Technology (DGIST), Korea (the Republic of)

Electronic devices with stretchable and wearable features have been attracting a huge interest because of their potential applications in wearable electronics, electronic skins, biomedical engineering, and in-vivo bioelectronics. Among various types of soft and wearable electronic devices, textile electronics which combine conventional textiles and electronic devices is one of promising fields because clothes are essential at all times for all humans regardless of age or gender. However, conventional planar electronic devices have been limited to being woven into flexible textiles or integrated onto complex nonplanar substrates. Such limitation has hindered their use in textiles electronics or advanced wearable electronics.<sup>1</sup> In this regard, stretchable and wearable electronic devices in fiber (1D) form, which can be directly integrated into daily clothes or textiles without any inconsistency are greatly promising for future wearable electronics. In addition, the fiber-based electronic devices can successfully overcome practical limitations (e.g. structural mismatching, suturability, etc.) of previous planar soft electronics in *in-vivo* applications.<sup>2</sup>

In this talk, fiber-based (1D) soft pressure and strain sensors based on metallic nanomaterials, which can overcome the existing limitations of previous 2D electronic devices, are presented. The research starts with the development of stretchable conductive fibers with outstanding conductivity ( $>20,000$  S/m), stretchability ( $>450\%$ ) and stability over 10,000 stretching cycles using metallic nanoparticles.<sup>3</sup> Based on the conductive fibers, various fiber-based mechanical sensors such as pressure, strain, and multimodal sensors are fabricated for smart textile and wearable applications.<sup>3,4,5</sup> In addition to their successful demonstrations in wearable applications, this research is also focusing on considering practical issues in current implantable electronics which is important for clinical applications but have been barely considered so far.<sup>2</sup>

1. Recent advances in 1D stretchable electrodes and devices for textile and wearable electronics: materials, fabrications, and applications, Lee et al., *Advanced Materials*, 2020.

2. Suturable and solderless one dimensional strain sensors with wireless readout for biomedical applications, Lee et al., *Nature Electronics*, 2020, under revision

3. Conductive Fiber Based Ultrasensitive Textile Pressure Sensor for Wearable Electronics, Lee et al., *Advanced Materials*, 2015.
4. Highly Sensitive Multifilament Fiber Strain Sensors with Ultrabroad Sensing Range for Textile Electronics, Lee et al., *ACS NANO*, 2018.
5. Conductive Hierarchical Hairy Fibers for Highly Sensitive, Stretchable, and Water Resistant Multimodal Gesture Distinguishable Sensor, VR Applications, Choi et al., *Advanced Functional Materials*, 2019.

#### 6:05 AM \*F.FL03.08.09

**A Bioinspired Ion Channel for Wearable Electronic Skin** Joo Sung Kim, Vipin Amoli, Yoon Sun Chung, Yunah Kim, Hanbin Choi, Hyukmin Kweon and Do Hwan Kim; Hanyang University, Korea (the Republic of)

Creating artificial sensory skins that shows the tactile-sensing capability of human skin has been a big challenge in wearable skin electronics. In particular, biomimetics has emerged as a burgeoning area in the field of deformable tactile sensor skins that has led innovations in material designing and device structure manipulation with the aim of imitating sensing mechanism of human skin, intelligently.

In this talk, inspired by the sophisticated physiological ion dynamics of living cells, we describe a uniquely designed deformable ion channel consisting of artificial ions confined into well-designed hybrid interface. Novel bottom-up strategy employed here resulted into supramolecular polymer networks through non-covalent interactions between poroelastic artificial ions and viscoelastic polymer chains or through hydrogen-bonding triggered ion dynamics, which endows effective ion drift under mechanical stimuli, simultaneously. This design allows for high-performance synaptic plasticity as well as ultrasensitive mechano-transduction over a wide spectrum of pressure, which can serve next neuromorphic tactile platform for highly interactive human-machine interface.

#### 6:20 AM \*F.FL03.08.10

**Wearable Smart Sensor System** Youfan Hu; Peking University, China

The development of electronic devices that offer biointegration capabilities is of interest in various clinical and biological applications, where they could be used for monitoring, diagnosis and therapy. In general, an intimate interface is required between the device and the biological material, so the devices need to be built in a flexible form. At the same time, the increasing demand for portability restricts the allowable power dissipation of any device. Here we show several examples of wearable smart sensor systems for human body monitoring, including triboelectric nanogenerator-based self-powered sensors for respiratory and pulse monitoring, ultrasensitive flexible pressure sensors based on wrinkled microstructures for vocalization recognition, general 3D adjustable sensor platforms conformable to curved biological surface by utilizing kirigami art to extend 2D structures into 3D ones, and integrated smart sensor systems on ultrathin plastic foil with in-situ signal processing capability based on high-performance carbon nanotube complementary electronics. These cases show the great possibility of next-generation wearables for personal health care.

#### References:

- L. Xiang, F. Xia, H. Zhang, Y. D. Liu, F. Liu, X. L. Liang, Y. F. Hu\*, *Advanced Functional Materials*, 29, 1905518 (2019)
- X. W. Zeng, Z. X. Wang, H. Zhang, W. Yang, L. Xiang, Z. Z. Zhao, L.-M. Peng, Y. F. Hu\*, *ACS Applied Materials & Interfaces*, 11, 21218 (2019)
- Z. X. Liu, Z. Z. Zhao, X. W. Zeng, X. L. Fu\*, Y. F. Hu\*, *Nano Energy*, 59, 295 (2019)
- C. Yang, H. Zhang, Y. D. Liu, Z. L. Yu, X. D. Wei, Y. F. Hu\*, *Advanced Science*, 5, 1801070 (2018)
- H. Zhang, Y. D. Liu, C. Yang, L. Xiang, Y. F. Hu\*, L.-M. Peng\*, *Advanced Materials*, 30, 1805408 (2018)
- L. Xiang, H. Zhang, G. D. Dong, D. L. Zhong, J. Han, X. L. Liang, Z. Y. Zhang, L.-M. Peng, Y. F. Hu\*, *Nature Electronics*, 1, 237 (2018).
- H. Zhang, L. Xiang, Y. J. Yang, M. M. Xiao, J. Han, L. Ding, Z. Y. Zhang, Y. F. Hu\*, L.-M. Peng\*, *ACS Nano*, 12, 2773 (2018).
- Z. Z. Zhao, C. Yan, Z. X. Liu, X. L. Fu, L.-M. Peng, Y. F. Hu\*, Z. J. Zheng\*, *Advanced Materials*, 28, 10267 (2016).

#### 6:35 AM F.FL03.08.11

**Monitoring of Human Diseases with Smartphones Through Soft, Smart Contact Lenses** Eunkyung Cha and Jang-Ung Park; Yonsei University, Korea (the Republic of)

In order to diagnose and monitor the human disease, it is essential to continuously and periodically monitor the biomarker related to the disease. In a human body, eyes can act as sites that have the potential to provide various information about one's health condition including chemical and physical biomarkers. In particular, smart contact lenses have been studied as

the wearable medical device to diagnose and monitor diseases noninvasively, detecting biomarkers from the eyes. However, there has been no clear study regarding the correlation between the signals obtained from the eyes and the actual state of the disease. Smart contact lenses can have actual effects only when these two factors are established whether they are correlated. To address this problem, we studied the correlation of diseases using our smart contact lenses. One of the biomarkers that can be monitored by smart contact lenses is tear glucose level, which is related to diabetes. We fabricated the smart contact lens which includes electrochemical glucose sensor, antenna, and NFC chip, enabling its operation only with the smartphone. By applying this smart contact lens to the *in-vivo* test using live animals, we demonstrated that the tear glucose level is correlated with the blood glucose level. Accordingly, we verified that the smart contact lenses detecting tear glucose concentration can be used to diagnose and monitor diabetes. Another bio-signal that can be obtained from the eyes is the IOP (intraocular pressure), which can act as the indicator of glaucoma. To detect the IOP, we integrated the IOP sensor, transparent and stretchable antenna, and NFC chip onto the smart contact lens. We successfully measured human IOP with a smartphone by wearing this smart contact lens onto a human eye, presenting the feasibility of smart contact lens monitoring the state and progress of glaucoma.

#### 6:45 AM F.FL03.08.13

**Absorbent, Flexible and Transparent Substrate for Wearable Bioelectronic Devices** Dhruv R. Seshadri<sup>1,2</sup>, Christian A. Zorman<sup>1,2,1</sup> and Kath M. Bogie<sup>1,2,1</sup>; <sup>1</sup>Case Western Reserve University, United States; <sup>2</sup>Louis Stokes Cleveland Veterans Affairs Medical Center, United States

Epidermal electronics that conform to the irregular topography of the skin enable non-invasive monitoring and measurement of biomechanical, physiological, and biochemical parameters relevant to monitoring human health and performance. Materials such as polydimethyl siloxane (PDMS), polyethylene terephthalate (PET), and polyimide (PI) are routinely used as substrate materials; however, such materials are not absorbent thereby limiting their utility for applications that necessitate the wicking of large volume bodily fluids when placed on the open skin, such as for wound healing applications. Polyvinyl alcohol (PVA) has been routinely used as a sacrificial layer in fabricating epidermal electronics; however, its utility as a standalone material for substrates or flexible electrodes has not been extensively studied. The biocompatibility, relative ease of fabrication, cost, absorbing capabilities, and scalability render it an ideal material for wearable bioelectronic devices. The objective of this study was to develop an absorbent, flexible, transparent, and inexpensive substrate (herein referred to as *AFTIDerm*) for use in wearable bioelectronic applications that necessitate the aforementioned material properties. PVA solutions were created with varied glycerol concentrations (1 wt%, 3 wt%, 5 wt%, 7 wt%, and 10 wt%) and drop cast in 9 mm plastic dishes and cured overnight at room temperature for subsequent use. The absorbent capabilities of the substrate were assessed in phosphate buffer saline solution (PBS), pH 7.4 (mimicking a chronic wound environment), over a one-week period with samples assessed daily. An inverse relationship between the varied glycerol concentrations and percent mass increase was observed. The high variability among the 1% glycerol samples over the one-week period compared to the other glycerol concentrations (~ greater than 300% difference in mass increase over one week) suggest a potential percolation threshold at or below this level. The 5% glycerol samples demonstrated greatest stability (~120% mass increase) over the one-week period. Previous work by our group found that ~10% of individuals are sensitized to current commercial adhesives that are included in substrates today often resulting in erythema. Incorporation of silicone-based adhesives (compared to currently utilized acrylate-based adhesives) deposited in pre-defined geometries on the *AFTIDerm* substrate enable long-term adhesion to the skin without deleterious reaction. When placed over the wound in a porcine chronic wound model following a 4 mm biopsy, the 5% glycerol *AFTIDerm* substrate with the silicone adhesive absorbed exudate from the wound without swelling over a one-hour period. Mechanical stability of the *AFTIDerm* substrates was evaluated under cyclic loading over a strain range of 0 to 2.5% for 50 cycles. Data from each glycerol concentration suggest that the *AFTIDerm* substrates undergo a short burn-in period for less than 10 cycles before stabilizing. The 5% glycerol samples demonstrated the largest tensile stress of ~800 KPa over this duration with an increase in tensile stress noted over the initial burn in period, which was opposite to the decrease observed for the other PVA-glycerol samples. Overall, the measured tensile stress of the *AFTIDerm* substrate was significantly greater than that of Tegaderm™ (~50 KPa), which served as controls for all benchtop studies. Further elucidation of the mechanical properties of the PVA-glycerol substrate through pre-clinical and clinical testing will provide first-hand assessment of the utility of the *AFTIDerm* substrate for use in bioelectronic devices. Doping of the *AFTIDerm* substrate with conductive elements will assess the utility of the substrate as a platform for flexible electrode technologies.

#### 6:55 AM F.FL03.08.15

**Resettable Skin Interfaced Microfluidic Sweat Collection Devices with Chemesthetic Hydration Feedback** Jonathan Reeder; Northwestern University, United States

Recently introduced classes of thin, soft, skin-mounted microfluidic systems offer powerful capabilities for continuous, real-time monitoring of total sweat loss, sweat rate and sweat biomarkers. Although these technologies operate without the cost, complexity, size, and weight associated with active components or power sources, rehydration events can render previous measurements irrelevant and detection of anomalous physiological events, such as high sweat loss, requires user engagement to observe colorimetric responses. Here we address these limitations through monolithic systems of pinch valves and suction pumps for purging of sweat as a reset mechanism to coincide with hydration events, microstructural optics for reversible readout of sweat loss, and effervescent pumps and chemesthetic agents for automated delivery of sensory warnings of excessive sweat loss. Human subject trials demonstrate the ability of these systems to alert users to the potential for dehydration via skin sensations initiated by sweat-triggered ejection of menthol and capsaicin.

#### **7:05 AM F.FL03.08.16**

**A Printed Flexible Graphene Transistor-Based Biosensor for Real-Time Monitoring of Biomarkers** [Niazul I. Khan](#), MD Shaad Mahmud and Edward Song; University of New Hampshire, United States

Flexible and wearable electronics have become a rapidly emerging technology and are continuously finding new applications in the commercial world. The use of wearables has expanded far beyond being just a fashionable gadget and is now being recognized as a critically important and essential technology. In particular, the potential benefit it offers in the healthcare industry could revolutionize the field as it enables real-time continuous monitoring of biomarkers in a non-invasive manner without interrupting the user's daily activities. The use of nanomaterials in biosensors has shown to be very effective because of their high surface-to-volume ratio, enhanced reactivity, and in some cases, biocompatibility (Geim & Novoselov, 2007). Especially, 2D nanomaterials such as graphene show promising results in this regard. It not only offers highly sensitive detection of biomarkers due to its monolayer structure, exposing each carbon atom of the lattice to the sensing environment, but also provides flexibility in terms of its mechanical bendability which make them an unparalleled candidate for flexible wearable biosensors. As a result, its application as a channel material in field-effect transistors (FETs) offers numerous advantages in terms of mass-scale production, integration, power consumption as well as miniaturization. Graphene-based FETs (GFETs) have been shown by our group (Ghosh et al., 2018; Khan et al., 2020) and others (Wang et al., 2018; Zuccaro et al., 2015) to be effective in detecting biomarkers with high sensitivity. However, these devices developed for rigid substrates are not well-suited for the wearable platform requiring flexibility and stretchability. Recently, a flexible and stretchable GFET-based biosensor was developed for its potential use in wearable and implantable applications (Wang et al., 2019). However, the electrodes were deposited with metal evaporation and patterned with conventional photolithography and thus making the fabrication process expensive and complex. A viable alternative approach to manufacturing a wearable GFET device is the printing of conductive inks. The advantages of this method include rapid prototyping, low cost, and flexibility in the printed patterns among others. In this work, we investigate the feasibility of using a printed circuit board (PCB) printer with a polymer-based flexible substrate such as Kapton or polyethylene terephthalate (PET) film to develop a GFET biosensor. A Commercially available Voltera V-One PCB printer was used to pattern an electrode with conductive silver ink. A minimum feature size of 200  $\mu\text{m}$  was achieved. Afterwards, the fabricated flexible GFET device was used to monitor biomarkers commonly present in human sweat sample (such as Dermcidin, a breast cancer biomarker) to test its feasibility as a wearable sweat-based biosensor.

#### **References**

- Geim, A.K., Novoselov, K.S., 2007. *Nature Materials*. 6, 183–191.
- Ghosh, S., Khan, N.I., Tsavalas, J.G., Song, E., 2018. *Frontiers in Bioengineering and Biotechnology*. 6.
- Khan, N.I., Mousazadehkasin, M., Ghosh, S., Tsavalas, J.G., Song, E., 2020. *Analyst*.
- Wang, X., Zhu, Y., Olsen, T.R., Sun, N., Zhang, W., Pei, R., Lin, Q., 2018. *Electrochimica Acta* 290, 356–363.
- Wang, Z., Hao, Z., Yu, S., De Moraes, C.G., Suh, L.H., Zhao, X., Lin, Q., 2019. *Advanced Functional Materials*. 29, 1905202.
- Zuccaro, L., Tesauro, C., Kurkina, T., Fiorani, P., Yu, H.K., Knudsen, B.R., Kern, K., Desideri, A., Balasubramanian, K., 2015. *ACS Nano*. 9, 11166–11176.

#### **7:15 AM F.FL03.08.17**

**Breathable Dry Electrode Designs for Bioelectronic Sensing** [Amanda Myers](#), Elizabeth Cobarrubias and Jesse S. Jur; North Carolina State University, United States

The ongoing improvement of human health and increased accessibility to wearable electronics has created new garment-based platforms for continuous health monitoring. Additional innovation in sensor design for long-term use is necessary for these smart textiles to be comfortable and accurate. Wet electrodes traditionally used in biopotential monitoring cannot be used in these platforms due to a limited shelf life and the potential to cause skin irritation. Dry electrodes can be used in smart



textiles, but also face considerable comfort and sensing challenges such as breathability, application pressure, noisy bioelectronic signals, and motion artifact. This study investigates the effect of dry electrode design on bioelectronic signal quality. Dry electrodes were designed with varying surface areas and vacancies in the conductive ink and polyurethane layers to test moisture vapor transmission rate and application pressure and to correlate those effects to bioelectronic signal quality. Results showed that electrode design influenced its conformability where an increased number of holes increased the pressure exhibited. The increased number of vacancies also improved electrode breathability. Electrodes were sewn into an armband to evaluate electrocardiogram (ECG) sensing performance where the ECG signal to noise ratio was compared to the dry electrode surface area and vacancy designs. There is a notable trade-off between breathability, skin-electrode impedance, and ECG signal quality attributed to the electrode design. These results demonstrate that an optimal balance between electrode design and contact area can be achieved to realize increased user comfort while retaining desired biopotential electrode properties for potential long-term wearability of e-textiles.

#### 7:25 AM F.FL03.08.18

**Versatile Micro Nano Fibre Printing Technique Towards 3D Sensing Architectures and Bio-Interface Devices** Wenyu Wang, Yan Yan Shery Huang, Karim Ouarus, Alexandra Rutz and George G. Malliaras; University of Cambridge, United Kingdom

Fibrous structures and materials widely exist in nature and have played an important role in our daily life and industry. Thanks to the high aspect ratio, low bending stiffness, flexibility and transparency, fibres possess unique physical and optical properties that are usually inaccessible with conventional planer structures. Combining with functional materials and polymers, such as piezoelectric, conducting polymers and biocompatible materials, novel fibre-based devices and textiles could open up possibilities for emerging applications. Such prospects could range from transparent textile-based sensors to biointerfacing architectures. However, challenges largely remain with the current fibre fabrication techniques, in which the synthesised fibres are usually deposited to a surface substrate. Thus, the optomechanical properties of the planer substrates would largely compromise the advantageous properties of the fibres. Moreover, conventional fibre printing techniques usually suffer from inefficient functional material usage (*e.g.* blending functional material with passive polymer), and this could lead to an overall reduced performance in the final products.

Herein, we present two original fibre printing techniques, which are especially developed to efficiently print substrate-free functional fibres with different fibre dimensions and applications. First, the dynamic near field electrospinning is developed to fabricate *in situ* poled piezoelectric nanofiber mesh, with high visible light transparency (> 97%) and air permissiveness. Such suspended nanofiber mesh harnesses the physical merits of spider web in its high acoustic sensing ability and broad active bandwidth. Combined with piezoelectric polymers, such spider-web inspired acoustic sensor has a broad sensitivity bandwidth covering 200–5000 Hz at hearing safe sound pressure levels. Second, inflight fluidic fibre printing, which integrates conducting fibre production and fibre to circuit connection in a single step is developed to produce metallic (silver) or organic (PEDOT:PSS) fibres with 1-3  $\mu\text{m}$  diameter. Using PEDOT:PSS fibres as a cell-interfaced impedimetric sensor and a moisture sensor, we show that even a single fibre component can achieve complex functions or outperform conventional film-based devices. The capability to design suspended fibres and networks of homo-, hetero- cross-junctions, paves the way to applications including flow-permissive devices, and 3D optoelectronic and sensor architectures. Overall, we demonstrate the versatility and scalability of novel fibre printing methods that could pave way for the next-generation fibre-based devices that could fully harness the potential of the physical merits of fibres and the functional performances of advanced materials.

#### 7:35 AM F.FL03.08.19

**Late News: Thermal-Free, Wireless Patch-Type Tissue Oximeter with Radiative Cooling Structure** Minhyung Kang, Gil Ju Lee, Joon Hoon Lee, Min Seok Kim and Young Min Song; Gwangju Institute of Science and Technology, Korea (the Republic of)

For emerging skin-integrated electronics/optoelectronics, thermal management should be achieved for reliable signal acquisition as well as thermal comfort. However, the current layout of skin-integrated devices has limited their use to indoor settings, because of solar energy gain outdoors, particularly strongly in oximeters. Various approaches have been reported to release accumulated heat in the skin-integrated device, such as a thin metallic heat sink to dissipate the concentrated heat and a copper/paraffin bi-layer acting as a heat sink based on phase variation. However, metallic layers hinder wireless communication between the receiver and transmitter, and phase shift materials function irreversibly at high temperatures of  $\sim 50$  °C. In particular, in conventional wearable oximeter reported in the literature, since black encapsulation layer is adopted to block ambient light, using the conventional layout in outdoor environment considerably exacerbates device heating owing to solar energy absorption. Previous works could not provide an obvious solution for these challenges.

Here, we introduce a new platform of radiatively cooled wearable optoelectronics that is free from heat and light concerns, which enables assessing athletic performance in outdoor environments under direct sunlight. To maximize the radiative cooling performance, a nano-/micro-voids polymer (NMVP), a nonmetallic and flexible radiative cooler, is realized by applying bi-layer layout of two perforated polymers (*i.e.*, polymethylmethacrylate (PMMA) and styrene-ethylene-butylene-styrene (SEBS)), which are optically and mechanically optimized for wearable optoelectronics. The NMVP boasts near-unity reflectivity and emissivity in the solar spectrum and atmospheric window (*i.e.*, 8-13  $\mu\text{m}$ -wavelength) with flexible feature. As a result, the optimized NMVP exhibits sub-ambient cooling of 6 °C in daytime under various conditions such as scattered/overcast clouds, high humidity, and clear weather. Additionally, the integration of the optimum NMVP with the device enables maintaining temperature of ~ 34 °C on the skin under sunlight, whereas the normally used, black encapsulated device shows over 40 °C owing to solar absorption. The heated device exhibits an inaccurate tissue oxygen saturation ( $\text{StO}_2$ ) value of ~ 60 % compared with  $\text{StO}_2$  in a normal state (*i.e.*, ~ 80 %). However, our thermally protected device presents reliable  $\text{StO}_2$  of ~ 80%. This successful demonstration provides a potential of thermal management in wearable devices for outdoor applications.

**7:45 AM F.FL03.08.20**

**Late News: Wearable Humidity Sensor Based on Rhenium Disulfide ( $\text{ReS}_2$ ) for Respiration Monitoring** Vivek Adepu, Naveen Bokka and Parikshit Sahatiya; BITS-Pilani, Hyderabad Campus, India

Due to the immediate requirement of accurate control of humidity in various industries such as agricultural development, life and health, etc. the humidity sensors based on two-dimensional materials have provoked much attention because of their exceptional properties (*i.e.* high surface to volume ratio, large exposed surface area, tunable semiconducting properties, etc.)[1]. Rhenium disulfide ( $\text{ReS}_2$ ), being less explored transition metal di-chalcogenide (TMD) has unusual but exciting physicochemical properties[2]. Herein,  $\text{ReS}_2$  film was deposited on a flexible cellulose paper substrate using a vacuum filtration technique and was further applied as a humidity sensor. The 2D  $\text{ReS}_2$  humidity sensor demonstrated elevated sensitivity (~115%), faster response time (~15 seconds), and enhanced long-term stability[3]. In particular, the electropositivity of the transition metal plays a key role in humidity sensing. Compared to tungsten, molybdenum, and other well explored transition metals of TMDs rhenium has higher electropositivity, which indicates that  $\text{ReS}_2$  has more surface energy to capture water molecules and attach to the substrate[4]. The structural and compositional characterization of pristine  $\text{ReS}_2$  showed a hexagonal phase with the P63/mmc space group. Further, to demonstrate a real time application, the fabricated  $\text{ReS}_2$  humidity sensor was utilized as a respiration sensor to sense normal, slow, and fast breath patterns. The frequency and amplitude of the sensor current peaks were utilized to differentiate between various breath patterns which hold potential applications in non-invasive healthcare. The successful demonstration of scalable, cost-effective  $\text{ReS}_2$  based humidity sensor on flexible and decomposable cellulose paper offers exciting applications in flexible and wearable electronics.

#### References:

- [1] Y. Zhang, W. Zhang, Q. Li, C. Chen, and Z. Zhang, "Design and fabrication of a novel humidity sensor based on ionic covalent organic framework," *Sensors Actuators B Chem.*, vol. 324, p. 128733, 2020.
- [2] M. Rahman, K. Davey, and S.-Z. Qiao, "Advent of 2D Rhenium Disulfide ( $\text{ReS}_2$ ): Fundamentals to Applications," *Adv. Funct. Mater.*, vol. 27, no. 10, p. 1606129, 2017.
- [3] R. Bakiya Lakshmi and A. Vimala Juliet, "Effect of annealing on humidity sensing properties of Sm-doped  $\text{SnO}_2$  thin films," *J. Mater. Res. Technol.*, vol. 8, no. 6, pp. 5862–5866, 2019.
- [4] Y. Feng, S. Gong, E. Du, K. Yu, J. Ren, Z. Wang, and Z. Zhu, " $\text{TaS}_2$  nanosheet-based ultrafast response and flexible humidity sensor for multifunctional applications," *J. Mater. Chem. C*, vol. 7, no. 30, pp. 9284–9292, 2019.

SESSION F.FL03.09: Poster Session: Flexible, Wearable Electronics and Textiles  
On Demand Abstracts Available for Viewing Starting Saturday Morning, November 21, 2020  
5:00 AM - 8:00 AM  
F-FL03

**F.FL03.09.02**

**Developing of Ultraflexible Organic Photovoltaics with Reduced Angular Dependence** Masahito Takakuwa<sup>1,2</sup>, Kenjiro Fukuda<sup>2</sup>, Shinjiro Umezumi<sup>1</sup> and Takao Someya<sup>2</sup>; <sup>1</sup>Waseda University, Japan; <sup>2</sup>RIKEN, Japan

Ultraflexible OPVs are expected to be used as a flexible energy harvester for wearable devices such as wearable textiles. Wearable devices would be easily changed and deformed according to the movement of the body. Assuming such usage, angle of incident lights to ultraflexible OPV is always changing, and along with this, power conversion efficiency (PCE) of ultraflexible OPV is also changing. Thereby the suppression of angular dependence is important to get a stable power generation. One of the major reflection losses happened at the substrate surface, between air and a substrate because of the large difference of refractive index<sup>(1)</sup>. Therefore, controlling the surface reflection by fabricating nanostructure to substrate is one strategy to reduce the angular dependence. A previous work reported flexible OPVs with nanostructured substrate is exhibited 1.3 times less angular dependence than OPVs with flat substrate<sup>(1)</sup>. However, a 1- $\mu\text{m}$ -thick ultrathin substrate for ultraflexible OPV takes a susceptible to damage by conventional high energy patterning methods like laser carving method<sup>(2)</sup> so that it is hard fabrication process of nanopatterning to its.

This research shows the developed low energy patterning method for ultrathin substrate and the effect of reducing the angular dependence of the nanopatterning ultrathin substrate. Generally, ultrathin substrate is fabricated by evaporating the polymer materials onto glass applied fluorinated polymer. The fluorinated polymer is fabricated by spin coating as a decreasing the surface energy between the substrate and delaminating it easily. Therefore, we focus on the undried fluorinated polymer layer. Nanostructures are fabricated onto the low energy surface of the fluorinated polymer by optimizing the condition for the drying process of it like temperature and drying time with placing nanopatterned polydimethylsiloxane mold on undried fluorinated polymer. These nanostructures of fluorinated polymer layer are traced onto ultrathin substrate surface by evaporating the polymer materials onto nano patterned fluorinated polymer layer. Valid point of this method does not require the extra heating process or ultraviolet curing process for the nanopatterning. Therefore, the nanopatterned ultrathin substrate is fabricated with avoiding damage to it by this method. OPV with nano line patterns ultrathin substrate which has 760 nm of pitch and 100 nm of height was exhibited low angular dependence compare with OPV with flat ultrathin substrate. The performance of OPV was measured with changing incident light angle 0 degree to 70 degrees, every 10 degrees. For all angles >10 degrees, the difference of performance appears due to nanopattern ultrathin substrate, especially, maximum reduction of the angular dependence of 5.7% being observed at 50 degrees<sup>(3)</sup>. Furthermore, the surface reflection rate upon the ultraflexible OPV suppress due to the reduction of the light interference effect by using nanopatterned ultrathin substrates. As a result, ultraflexible OPV with nano patterned ultrathin substrates was exhibited higher short current density of 2.1% compared with ultraflexible OPV having flat ultrathin substrate<sup>(3)</sup>.

(1) J. Kettle, *et al. J.Phys.D: Appl. Phys.* **46**, 105102, 2013

(2) L. Müller Meskamp *et al. Adv. Mater.* **24**, 906 910, 2012

(3) M.Takakuwa, *et al. Small Methods*, **4**, 1900762, 2020

#### **F.FL03.09.03**

**Radiative Cooling Textiles for Personal Thermal Management** Yucan Peng, Jun Chen, Lili Cai, Po-Chun Hsu, Alex Song, Peter Catrysse, Shanhui Fan and Yi Cui; Stanford University, United States

Thermal comfort is essential for health and productivity. However, it consumes enormous energy to maintain thermal comfort through space heating and cooling, due to energy waste in the vast empty space of the entire building. Here, we propose the personal thermal management strategy focusing on temperature regulation of only the human body and its local environment, and present a passive personal thermal management textile system via engineering the thermal radiation property of textiles to reduce building energy consumption and improve the quality of human life.

#### **F.FL03.09.04**

**Wearable Biodiagnostics via Skin Volatile Emission Detection Using Colorimetric Sensors** Melissa Finnegan, Emer Duffy and Aoife Morrin; Dublin City University, Ireland

The focus of this research is to develop and apply new and existing soft responsive materials capable of responding to target biomarkers on the body emitted from the skin. One of the approaches being investigated is the use of responsive colorimetric dyes to track volatiles being emitted from the skin. Specifically, the acidity of the volatile emission is being assessed using pH-responsive dyes. Early evidence from the group has shown that the total volatile fatty acid emission (C8-C16) correlates well with skin surface pH as measured by a glass pH ion-selective electrode. This early study used a headspace-solid phase microextraction (HS-SPME) approach to sample the skin volatiles which were then analysed by GC-MS. This project aims to exploit this correlation of acidic volatile emissions with skin pH to develop a non-contact, skin pH sensor. Aldehyde emissions from the skin are also being examined.

A range of responsive colorimetric dye spots are being tested in this work to understand their response to the skin volatile

emission. pH, solvatochromic and metalloporphyrin dyes being used in the sensor array are immobilised as spots to flexible cellulose substrate. A sol-gel encapsulation matrix is used to allow the soluble dyes be converted into nanoporous pigments which are insoluble. The durability and stability of the dyes is improved by using this encapsulation method.<sup>1</sup> The response of each dye spot was recorded by imaging the sensor array before and after exposure to skin volatiles and the net colour response quantified. A host of different skin sampling methods have been examined including gauze sampling, swab sampling, tape stripping and also direct application on the skin incorporating a wire mesh spacer between the sensor array and the skin. This presentation will highlight some of the results from this research to date.

#### References:

(1) Lim, S. H.; Musto, C. J.; Park, E.; Zhong, W.; Suslick, K. S. A Colorimetric Sensor Array for Detection and Identification of Sugars. *Org. Lett.* **2008**, *10* (20), 4405–4408. <https://doi.org/10.1021/ol801459k>.

#### F.FL03.09.05

**Evaluation of a NaPc/TCNQ Complex Structure for Flexible Diode Applications** Leon Hamui; Universidad Anahuac, Mexico

This work is related to the progress on the implementation of sodium phthalocyanine for flexible organic diodes. A NaPc/TCNQ structure was deposited on TCO/PET for the electronic device and silver contacts were used to determine the optoelectronic properties. HV Thermal evaporation of small molecules and spin coating processes were used for device deposition. The Characterization of the electronic device was conducted using FTIR, AFM, UV-Vis, IV characteristics for chemical, structural, morphological, opto-electrical properties. FTIR measurements confirm an efficient transfer for the device to the PET flexible substrate with a smooth and homogeneous surface topography. A direct transition bandgap of 2.5 and 2 eV were obtained for different the NaPc deposited thicknesses. Diode type characteristics were obtained with threshold voltages of ~1.5 V and ~15 microAmps current across the device at 6 V. IV characteristics were measured with different incident led light colors showing a variation of the curves on the NaPc-TCNQ flexible device which gives evidence of the device and interfaces quality for diode applications.

#### F.FL03.09.06

**3D Printed Polymer-Based Multiferroic Nanocomposites for Electronics Application** Bedanga Sapkota and Vijaya K. Rangari; Tuskegee University, United States

Flexible polymer-based magnetoelectronics with an organized structure are most desirable in the field of memory, energy storage, sensing, and harvesting devices. In this work, we have developed flexible nickel ferrite (NiFe<sub>2</sub>O<sub>3</sub>)-PVDF nanocomposite films. The obtained composite films show excellent magnetoelectric coupling at room temperature, making them good candidates for improved ferroelectric devices. The nanocomposite films were prepared by the solution casting and 3D printing method, wherein the nickel ferrite nanoparticles with different weight percentage (5, 10, 15, 20, and 30%) were incorporated in the ferroelectric PVDF polymer matrices. The structural, morphological, mechanical, electrical, magnetic, and thermal properties of the nanocomposites were studied by X-ray diffraction, FTIR, scanning electron microscope, nanoindentation, DSC, TGA, and SQUID.

#### F.FL03.09.07

**Macro-Scale Graphene-Based Tactile Pressure Sensor Array Sheet** Seiji Wakabayashi<sup>1</sup>, Takayuki Arie<sup>1</sup>, Seiji Akita<sup>1</sup> and Kuni Takei<sup>1,2</sup>; <sup>1</sup>Osaka Prefecture University, Japan; <sup>2</sup>JST PRESTO, Japan

Macroscale flexible and stretchable pressure sensor enables to monitor pressure distribution on a variety of nonplanar objects such as infrastructure, vehicles, and humans if very thin flexible pressure sensor arrays can be realized. In fact, many types of flexible tactile pressure sensors have been studied. For the macroscale flexible sensor sheet, one important parameter is device cost. To realize economical sensor sheets, printing, transferring, and laser ablation methods have been widely proposed. As one of the potential economical process, this study proposes a simple and scalable fabrication process to form a very thin macroscale flexible tactile pressure sensor array.

Fabrication process is briefly explained. First, laser-induced graphene (LIG) was formed by exposing CO<sub>2</sub>-based laser over polyimide film. The LIG layer was then transferred into a polydimethylsiloxane (PDMS) elastomer film. In parallel, silver electrodes were screen-printed on a polyethylene terephthalate (PET) film. After the formations, PDMS and PET films were laminated. The total thickness of the device is ~300 μm. The sensing mechanism of tactile pressure is to measure contact resistance change between the LIG embedded in the PDMS and the silver electrodes on the PET films as a function of applied pressure.

Resistance change at an applied pressure was characterized. Due to the observation of contact area change between two

conductive materials, at low pressure range less than 30 kPa, resistance change is large while the resistance change gradually decreases by increasing the applied pressure. The maximum sensitivity is  $\sim 0.84$  %/kPa at 28.3 kPa, and the sensitivity at 566 kPa is  $\sim 0.1$  %/kPa. The response time is relative fast to be  $< 0.1$  s. Importantly, this sensitivity and response speed are independent with the device bending even under 1 cm curvature radius. After confirming the fundamental properties of very thin flexible tactile pressure sensor, uniformity, stability, and reliability were tested. The uniformity in terms of initial resistance and sensitivity at 56.6 kPa of the sensor are  $1062 \pm 62 \Omega$  and  $\sim 0.6 \pm 0.3$  %/kPa, respectively. The sensor can measure the pressure precisely more than 4500 cycles for a long time.

Finally, as a proof-of-concept, pressure distribution was measured by using an integrated  $4 \times 4$  array sheet. We confirmed that this sensor array sheet can monitor the finger position on a pen covered by the sensor sheet. Furthermore, by covering this sensor sheet surrounding a roller, pressure distribution of the roller under rolling onto a floor is successfully monitored in real time. These demonstrations depict that this very thin flexible sensor sheet can detect the pressure distribution regardless of the surface shape without changing the object shape drastically.

#### **F.FL03.09.08**

**Supercapacitive Polymer Hydrogel Electrode via Pure PEDOT:PSS Hydrogel Printed on Laser-Induced Graphene for DC Stimulation Applications** [Sebastian Shaner](#)<sup>1</sup>, Monsur Islam<sup>2</sup>, Jan Korvink<sup>2</sup> and Maria Asplund<sup>1</sup>; <sup>1</sup>Universität Freiburg, Germany; <sup>2</sup>Karlsruhe Institute of Technology, Germany

Bioelectronic interfaces rely on intimate contact with tissue to establish efficient signal exchange between electrodes and the biological target structure. Mechanically soft and ion conducting materials are beneficial in this context, in particular for semi-dry interfaces such as electrodes contacting skin. Typical natural (e.g. alginate, collagen, agar) and synthetic (e.g. polyacrylamide, polyethylene glycol, polyvinyl alcohol) hydrogels used for biomedical implementation are not inherently electronically and/or ionically conductive, wherefore development of conducting hydrogel systems is highly relevant. We demonstrate here how a supercapacitive polymer hydrogel whose network is entirely comprised of conducting polymer poly(3,4-ethylenedioxythiophene) polystyrene sulfonate (PEDOT:PSS) nanofibril interconnections can be combined with laser-induced graphene (LIG) on a flexible substrate (i.e. polyimide). This results in a bioelectronic interface which easily conform and connect to skin and can support both recording and electrical stimulation. The PEDOT:PSS hydrogel precursor can be printed (i.e. direct ink writing) or dip-coated onto laser pyrolyzed polyimide (e.g. Kapton) film. The LIG and PEDOT:PSS hydrogel electrode was shown to have a high charge storage capacity (up to  $1500$  mC/cm<sup>2</sup>), electrochemical stability (retains more than 85% of the original charge storage capacity over 500 cycles) and ability to deliver long term biologically-relevant electric fields (10-1000 mV/mm). In short, via affordable technology, we were able to make devices that outperform previous technology based on noble metals. Thereby we pave the way for disposable bioelectronics as well as DC stimulation of cells and tissues at levels relevant for regenerative therapy.

#### **F.FL03.09.10**

**Upcycling CDs into Soft Bioelectronics** [Matthew S. Brown](#), Louis Somma and Ahyeon Koh; SUNY Binghamton, United States

Soft bioelectronics are an emerging class of wearable electronics for point of care (POC) applications; however, fabrication processes for these stretchable devices have relied on time-consuming, expensive, and complicated microfabrication techniques. The required active materials (e.g., gold) present expensive deposition or complicated galvanization methods, for developing thin films of metals for stretchable electronics, which limits the transcendence of rapid, one-time devices. Of note, electronic CDs generate a large amount of electronic waste and contribute to the fast growing global problem of landfill waste. To solve critical challenges in the rapid fabrication of soft bioelectronics and environmental challenges, we have developed a fabrication method for upcycling gold compact discs into transient, fibrous, and permeable devices.

The reflect metal layer from compact discs (CDs) can be recycled for rapid, low cost development of thin gold films. Following the removal of the CD's protective layer, it can be easily cut to a feasible size for harvesting the gold layer. Utilizing water-soluble tape, the pickup at the optimal peel velocity highlighted the transfer efficacy, due to the stronger adhesion forces produced between the gold and tape rather than the gold and adhesive layer. Intricate patterns can be realized onto the gold film by laser engraving, capable of transforming the rigid constituent into fully flexible form factors. We present feature sizes of about  $700 \mu\text{m}$  that are contingent on the laser resolution with the drawback of sacrifice the gold's durability after patterning. Electrospinning synthetic polymers were further deposited onto the patterned gold film to increase durability and stretchability. With this fabrication method, a wide range of fibrous polymeric systems, including biodegradable and natural polymers, can apply to soft, mesh type bioelectronics. The mechanical and electrical properties of the developed bioelectronics have been systematically analyzed to confirm its conformality. Further, the devices were demonstrated in application as electrocardiography (ECG) electrodes.

#### **F.FL03.09.12**

**Development of Nanofiber-Based Sunscreen with a Portable Electrospinning System** Byeongjun Lee, Hyunwoo Lee, Chan Park, SungUk Hong, Hyunsuk Jung, HyongUk Kim, CheolJeong Park, JungMin Kim, YeonDo Jeong, Younghyeon Song, JeongBeom Kang, HaRan Lee, Jongwon Yoon and Seong Jin Cho; Chungnam National University (CNU), Korea (the Republic of)

Recently, as the harmfulness of ultraviolet rays (UV) is widely known, protecting skin from UV rays is attracted attention. However, the current use of liquid or stick sunscreen can cause skin problems due to the toxicity of chemicals and poor water resistance, it has a short durability, so there is inconvenienced to apply regularly. This study report a new type of sunscreen, nanofiber-based sunscreen, which is chemical-free, high water-resistance, dust resistance and gas breathability, and novel portable electrospinning system to apply it. The nanofiber-based sunscreen use biocompatible polymers and can be quickly applied by the portable electrospinning system. Nanofiber-based sunscreen consist of nanofiber-matrix structures, the fiber was solidified and chemically stable. Owing to its nature, the nanofibrous sunscreen does not dissolve in sweat or water and block micro dusts while allowing air and vapor to pass through. Also, skin trouble can be prevented due to the sterilizing effect of TiO<sub>2</sub> nanoparticles contained in nanofiber-based sunscreen. Due to its flexibility and stretchability, it can coated on skin conformably and be able to stretch and relaxed repeatedly along the skin without falling. Finally, the nanofiber-based sunscreen can be easily detached from skin without residue unlike liquid-type sunscreens. We believe our nanofiber-based sunscreen can be used in daily life and professional medical such as patients with organ transplants or skin diseases that are vulnerable to UV rays.

#### **F.FL03.09.13**

**Design of a Scalable, Flexible and Durable Thermoelectric Cooling Device for Wearable Applications** Zoe Rosenberg, Nathan Weiner, Hasan Shahariar, Jennifer Peavey, Amanda Myers and Jesse S. Jur; North Carolina State University, United States

There is growing interest in flexible thermoelectric cooling devices to provide personal thermal regulation to alleviate energy demands of current HVAC systems as well as to provide safety to workers in uncontrollable outdoor environments. Here we demonstrate flexible thermoelectric cooling devices, utilizing a foam substrate, that can be integrated into wearable products. Our flexible thermoelectric devices utilize commercially available materials and scalable processing techniques to improve the manufacturability. Thermoelectric legs were embedded in a foam substrate to provide flexibility, and kirigami-inspired cuts were patterned within the foam to mimic drape found in textile materials. In total, nine different configurations, three different fill factors, and three different kirigami cut patterns, were created and tested. The devices were assessed for thermal performance, mechanical durability, flexibility and drape. The results from this characterization show that adding kirigami patterns can increase the durability of the device, improve the flexibility, decrease the drape coefficient, and have <1% of impact on cooling performance at higher fill factors, reaching temperature differences up to  $4.39 \pm 0.17^\circ\text{C}$ . These thermoelectric cooling devices show great promise for the future of wearable cooling devices considering both the manufacturing scalability and its' familiar drape and feel, which will allow for easy integration of the devices into products.

#### **F.FL03.09.14**

**Reverse Engineering of E-Textile Products for Design and Material Evaluation** Caitlin Knowles, Amanda Myers and Jesse S. Jur; North Carolina State University, United States

E-textile design heavily relies on the human use case as well as factors such as price point and emphasis on sustainable material use. The e-textiles market is in its early years of commercial establishment, so there are few standards when it comes to material and design choices and product validation. This lack of standards makes designing new products difficult and when benchmarking against existing products, makes identifying areas for innovation challenging. This research examines the use of reverse engineering principles based on the disassembly, characterization, and analysis, of popular commercial e-textile products, allowing for both an analysis of the products disassembled and providing a framework of best practices for future designs. Using a reverse engineering framework, commercial products were evaluated based on their system block diagram and materials characterization, relating each to understanding the design criteria employed for their construction. Products with similar use cases are compared and evaluated for functionality, performance, and sustainability. This research ultimately provides a framework to better understand design criteria and material selection in order to improve future product designs.

### **F.FL03.09.15**

**Use Case Scenarios and Characterization Methods for Textile-Based Piezoelectric Energy Harvesting** Beomjun Ju, Braden M. Li and Jesse S. Jur; North Carolina State University, United States

Textile-based structures exhibit inherent properties such as flexibility, stretchability, breathability, and high durability under severe mechanical deformations. These properties make textiles an ideal platform to create conformable wearable electronics that rely on flexible circuitry. However, current wearable power supplies are not suitable for textile-based wearable platforms or smart textiles since they utilize functional materials that are rigid, heavy, and exhibit negative environmental impacts. Therefore, researchers have turned to harvesting energy resources from the human body that would have otherwise been wasted, as an alternative power supply solution for smart textiles.

In this work, we review the possible forms of harvestable mechanical energy from various human motions (i.e. Running, Bending Arms, etc) using piezoelectric polymers integrated into textile-based structures. Piezoelectric polymers such as polyvinylidene fluoride (PVDF) and poly(vinylidene fluoride-co-trifluoroethylene) (PVDF-TrFE) are ideal for smart textiles due to their high throughput, low-temperature processing capabilities and larger range of deformations compared to piezoelectric ceramics. We introduce the state of the art in textile-based piezoelectric energy harvesters using PVDF and PVDF-TrFE with regards to the hierarchical levels of textile structures (i.e. fiber -> yarn -> fabric). We categorize these textile energy harvesting devices as either *in-situ* or *ex-situ* based on their fabrication method and structural design of their electrodes. Then, we suggest standardized testing methods based on this in-situ/ex-situ classification system to accurately characterize energy output for various mechanical stimuli and working harvesting areas. Lastly, we create a framework based on the challenges and exciting opportunities for practical use case scenarios of these textile-based piezoelectric energy harvesters.

### **F.FL03.09.16**

**High Conductivity in Thin, Flexible and Stretchable Inter-Connect with Polymer Composite in a Sandwich Structure** Mayukh Nandy, Todd K. Houghton and Hongbin Yu; Arizona State University, United States

Flexible conducting materials has been in the forefront of a rapidly transforming electronic industry focusing on wearable devices for a variety of applications in our world today. Over the past few decades, bulky, rigid devices have been replaced with a surging demand for thin, flexible, light weight, ultra-portable yet high performance electronics. But the inter-connects available in the market today only satisfy a few of the desirable characteristics, making it necessary to compromise one feature over another. Materials like thin copper foils provide metallic conductivity but cannot be stretched or bent repeatedly over the lifetime of the product owing to bending fatigue and ultimately mechanical deformation leading to electrical failure. On the other hand, stretchable metal polymer composite structures previously explored by researchers in this industry failed to achieve high conductivity to compete with metal counterparts.

We present a method to prepare a thin, flexible, and stretchable inter-connect with much improved conductivity compared to what has been achieved before. It also satisfies most mechanical and electrical conditions desired in the wearable electronics industry today. The composite prepared with the widely available, low cost silicon-based organic polymer - Polydimethylsiloxane (PDMS) and Silver (Ag) is sandwiched between two cured PDMS layers. These two protective layers improve the mechanical stability of the inter-connect. The stretchability of the material is enhanced by over 100% by laser cutting it into a serpentine structure without compromising its electrical stability. The structure, less than 500 um thick, can be integrated into thin electronic packaging. The synthesis process of the composite material, along with their electrical, mechanical and corrosion resistive properties will be presented in detail.

### **F.FL03.09.17**

**Intrinsically Stretchable Biosensor Detecting Sweat Based Multi Analytes and ECG Using Ag Nanocomposite Electrode with Photo Patternable Ecoflex** Seungwan Kim<sup>1</sup>, Wonryung Lee<sup>2</sup>, Joohyuk Kang<sup>1</sup>, Injun Lee<sup>1</sup> and Byeong-Soo Bae<sup>1</sup>; <sup>1</sup>KAIST, Korea (the Republic of); <sup>2</sup>Korea Institute of Science and Technology, Korea (the Republic of)

Fusion of physical and chemical sensing onto a single platform cannot only provide information for physical parameter such as Electrocardiogram (ECG) but also offer more insightful and comprehensive chemical parameters from biofluids such as sweat [1]. From monitoring glucose and lactate level with ECG, biosensor could prevent the exerciser from hypoglycemic shock during intense exercise.

In this work, intrinsically stretchable electrode is fabricated to monitor biochemical and biophysical information using elastomeric composite comprised of Ag flake and photo-patterned Ecoflex [2,3]. Direct patterning of the Ecoflex benefits

from convenient fabrication process. Furthermore the encapsulation of Ecoflex improves the conductivity of Ag nanocomposite when it is stretched. That is induced by an efficient strain energy dissipation at an interface between the conductor and the encapsulation layer.

Since Ag electrode could be readily oxidized in biological circumstance and leach out the Ag ions to human tissue, the stretchable conductor consisting of Ag nanocomposite is limited to bioelectronics. To enhance the biocompatibility of Ag, the electrode is modified to form Pt and Au nanoparticles onto counter electrode and working electrode respectively by galvanic replacement process [4]. Various functional materials for multisensor are electrodeposited on to Au modified working electrodes. A pH sensor is performed via Polyaniline showing the 100mV/pH sensitivity stretched up to 50%. Glucose and Lactate sensors are operated *in vitro* showing 3nA  $\mu\text{M}^{-1}$ , 260nA  $\mu\text{M}^{-1}$  sensitivity respectively. Finally intrinsically stretchable multi biosensor *in vivo* are successfully monitoring a variation of analytes concentration of glucose and lactate in sweat before and after meal and exercise simultaneously with electrical signal.

[1] H. Lee, T. K. Choi, Y. B. Lee, H. R. Cho, R. Ghaffari, L. Wang, H. J. Choi, T. D. Chung, N. Lu, T. Hyeon, S. H. Choi and D.H. Kim, *Nature Nanotech.* **2016**, 11, 566-572

[2] S.H. Kim, S. Jung, I. S. Yoon, C. Lee, Y. Oh and J. M. Hong, *Adv.Mater.* **2018**, 30, 1800109

[3] A S. Bhagat, P. Jothimuthu and I. Papautsky, *Lap on a chip*, **2007**, 7, 1192-1197

[4] P. Won, J.J Park, T. Lee, I. Ha, S. Han, M. Choi, J. Lee, S. Hong, K.J. Cho, S.H. Ko, *Nano Lett.* **2019**, 19, 6087-6096

### F.FL03.09.18

**Methodology for Binary Detection Analysis of Inkjet Printed Optical Sensors for Chemical Detection** Li-lin Tay and John Hulse; National Res Council Canada, Canada

Development of sensors for early warning and protection against chemical and biological agents is a priority for front line first responders as well as military personnel. We have developed inkjet-printed surface enhanced Raman spectroscopy (SERS) sensors that is specifically designed to work with field portable Raman analyzers for the detection of chemical and biological agents. These SERS sensors are inkjet-printed on filter paper or fabric substrates. Ink formulation are carefully optimized colloidal silver or gold nanoparticle solutions synthesized in house. They are flexible, lightweight and provides point-of-sampling capabilities that other rigid planar SERS substrates lacks. These sensors can be integrated with the wearable gear of the first responders. These flexible and wearable sensors are designed for qualitative detection such as binary detection of either positive or negative presence of certain chemical/biological agent. Conventionally, performance of a SERS substrate is characterized by its enhancement factor which is defined as the ratio of the normalized SERS to normal Raman intensity. This is an inadequate measurand for a chemical/biological sensor. The performance of a chemical/biological sensor is best characterized by its sensitivity, probability of true positive detection, false positive rate and its response time. The sensors receiver operating characteristics (ROC) captures the performance trade-off between all these factors. It is meaningless to specify sensitivity without the confidence level of detection expressed as the probability of detection and the false positive rate. Although ROC has been used commonly for assessing chemical/biological sensors, it is not trivial to adapt it for SERS detection. In this presentation, we will present a new methodology developed specifically for the binary analysis of the SERS sensors using the receiver operating characteristic concept. This can be applied for all SERS sensors but we will focus its use with the printed SERS sensor.

### F.FL03.09.19

**ZnO Thin Film-Based Flexible Biosensor for the Continuous Monitoring of Glucose Levels in Sweat** Fahmida Alam, Shahrzad Forouzanfar, Ahmed H. Jalal and Nezhil Pala; Florida International University, United States

Diabetes is one of the significant causes of fatality throughout the world in the present day. The deficiency of insulin and hyperglycemia is caused by the metabolic disorder of diabetic patients. This disorder promotes high risks of kidney failure, heart attack, chronic liver diseases, and blindness. Thus, constricted day-to-day monitoring of glucose concentration is a demand for the diagnosis and treatment of diabetes. Also, fast, accurate and continuous monitoring of glucose concentration is of great importance. As a successful consumer product of wearable biosensors, it is important to demonstrate reliability, multiplexed functionality and ease-to-use noninvasive monitoring of glucose from the body fluids, such as sweat. Sweat is easy to analyze and is considered as one of the most widely used body fluids having significant medical information. However, the introduction of nanomaterials allows many new signal-transduction technologies results improved the sensitivity of different biosensors. ZnO thin film-based biosensors are promising to determine the glucose levels in sweat with better sensitivity, reliability, continuously, and in a noninvasive manner. ZnO itself has exclusive chemical and physical characteristics to enhance chemical stability in physiological environments. Moreover, it has highly catalytic activity, biocompatibility, and higher isoelectric point (IEP). ZnO nanoflakes (ZnO-NFs) exhibit several unique advantages compared to bulk materials. For example, polarized (0001) plane orientation enhances enzyme immobilization which improves sensing



performance. A high isoelectric point (9.5) of ZnO NFs enhances the immobilization of any biomolecules which eliminates the necessity of an additional binding layer. This elimination of additional layer and immobilization of enzyme offer a steady and shorter pathway for quick electron transportation increasing the electron transfer rate. A single step sonochemical approach was developed to synthesize a thin layer of ZnO-NFs virtually on any substrate. This technique is fast, catalyst-free, less expensive, and ecologically benign. The rate of reaction of the sonochemical approach is 100 times faster than conventional hydrothermal procedures, which enables a well-oriented growth on polyethylene terephthalate (PET) over an extensive range. The temperature for the process is low enough to permit the application of different materials, for example, fabrics, paper, and polymers.

In this study, an electrochemical glucose biosensor was fabricated by immobilization of glucose oxidase on ZnO nanoflakes with a thickness of 20nm, synthesized on Au-coated stretchable PET. The results demonstrated a fast response within 5s. The sensor was tested in the range of 10 pM – 20 mM, which covers the entire physiological range and capable of detecting as low as 1  $\mu$ M of the glucose concentration. The sensitivity of the sensor was determined by 4.53  $\mu$ A/decade/cm<sup>2</sup>. Moreover, the sensor performed repeatable characteristics having with average standard deviation (S.D.) of 0.14  $\mu$ A. Furthermore, in our experiment, the fabrication process is simple, and the thin film-based nano-biosensor provides excellent performance in stability, selectivity, sensitivity, and reproducibility.

#### **F.FL03.09.21**

##### **Copper-Coated Reduced Graphene Oxide Fiber Mesh-Polymer Composite Films for Electromagnetic Interference Shielding** Mingxin Li, Kun Yang and Jie Lian; Rensselaer Polytechnic Institute, United States

Expected to become mainstream in the electronics industry, flexible electronics still face major challenging issues. For polymeric-based flexible electronic substrates in particular, these challenges include a lack of electromagnetic shielding capability and poor heat dissipation. Here, we report a highly flexible and thermally conductive macroscopic polydimethylsiloxane (PDMS) polymer film embedded with a copper-coated reduced graphene oxide (rGO) fiber mesh. The rGO fibers are assembled into 3D fiber meshes and electroplated with micrometer-thick copper coatings, displaying excellent electrical and thermal conductivities. Oriented in the horizontal and perpendicular directions within the PDMS polymeric matrix, the fiber mesh serves as a highly electrically and thermally conductive backbone through the in-plane direction. Meanwhile, the fiber mesh also effectively shields electromagnetic interference in the X-band without causing thermal damage. The macroscopic film remains electrically insulated in the through-plane direction. Utilizing both the favorable thermal and electrical properties of the graphene fiber-based mesh and the flexibility of the PDMS matrix, our film may exhibit potential for flexible electronics applications such as wearable electronic thermal management and flexible microwave identification devices.

#### **F.FL03.09.24**

##### **Thermoelectric Ultrafine Fibers for Temperature Regulation and Power Generation** Elena Ewaldz, Morgan McLeroy and Blair Brettmann; Georgia Tech, United States

Thermoelectrics are materials consisting for an electron conductor (n-type) and a hole conductor (p-type) that are connected electrically in series and thermally in parallel. They work through both the Seebeck effect (power generation) and the Peltier effect (refrigeration). Through the Seebeck effect, a heat gradient causes current to flow generating electricity. Through the Peltier effect, a current flow generates a heat gradient leading to one side of the material being actively cooled. Traditionally inorganic materials are used that have a low natural abundance, high costs, and are rigid and brittle. Polymeric thermoelectrics or organic thermoelectrics (OTEs) overcome the limitations of conventional materials as they are low cost and flexible; though they typically have lower conductivity so they require enhanced designs such as high surface fibers. OTEs cannot readily be made into fibers as they are low molecular weight and have strong molecular interactions and high conductivity that alter fiber formation. In this work, we use electrospinning to prepare composite ultrafine fiber mats of organic based n- and p-type conductors enabling close contact between fibers. Electrospinning is a solution processing technology that creates nonwoven ultrafine fibers (diameter ~100nm-2 $\mu$ m). Ultrafine fibers have very high surface area allowing for many close contact points between fibers. PEDOT:PSS, a p-type conductor, is able to be electrospun with an insulating polymer at amounts up to 56wt%. NiETT, a n-type conductor, is made by forming a PVA-nickel salt complex through electrospinning then polymerizing the final fibers. These materials can then be layered to create a soft, flexible, wearable, electronic device.

#### **F.FL03.09.25**

##### **Controlled Light Scattering Over LWIR in Polyethylene Films** Yassine Ait-El-Aoud<sup>1,2</sup>, Ihsan Uluturk<sup>1</sup>, Elizabeth Welsh<sup>1</sup>,

Michael Okamoto<sup>1</sup>, Sean R. Dinneen<sup>1</sup>, Alkim Akyurtlu<sup>2</sup> and Richard M. Osgood<sup>1</sup>; <sup>1</sup>U.S. Army Combat Capabilities Development Command Soldier Center, United States; <sup>2</sup>University of Massachusetts Lowell, United States

Recently<sup>[1-3]</sup>, polyethylene (PE) has gained significant interest by the textile fiber/film industry and opened up new advanced textiles for personnel thermal management with simple structures and unique optical properties. Controlling these optical properties in the long wave infrared (LWIR) spectral range could have a strong effect on cooling and heating the body and per consequence it could be a solution to obtain a textile with enhanced radiative cooling/heating for passive releasing/trapping of human body heat and this is not found in conventional textiles. Moreover, PE is a durable polymer, scalable, cost-effective and lightweight materials.

In this study, we have demonstrated both the effect of polymer chain alignment and integration of inorganic particles into ultrahigh molecular weight polyethylene (UHMWPE) polymer on the optical properties of UHMWPE films. We have seen that the total transmittance of the films increases with higher the draw ratios while the scattered light can be controlled over LWIR by introducing a small percentage of inorganic particles where the forward scattering was found to be preferred over backward scattering. The high transparency of the films could be explained by the film thickness reduction on one side and the surface morphology of the film on the other side. In addition, the stretched films become thinner which allow more light comes through the film whereas the surface morphology of the films become one hand smoother and aligned and on other hand the films crystallinity increase significantly. Most importantly, we have seen that the intensity of the scattered light in the forward direction can be controlled by addition of additives into the pure UHMWPE film. The integration of inorganic nanoparticles into the pure UHMWPE polymer allows both the properties from inorganic nanoparticles (higher refractive index and higher forward scattering) and UHMWPE polymer (higher transparency) to be combined and enhanced the optical properties of films, particularly, in the LWIR regime. By preferentially scattering in the forward direction, these novel textile materials, in thin films, could release heat from an overheated body (eg. the human or warm equipment) better than if there is significant backscattering.

In this talk, the following will be presented and discussed : the fabrication process of highly oriented and transparent PE films, the heat-releasing data of PE films collected by a simulated device for skin temperature that operates at constant power output to produce the human skin temperature and lastly the controlled light scattering measurements in PE films over LWIR spectral range.

**Keywords:**

Polyethylene film, forward scattered light, backward scattered light, LWIR, UHMWPE, thermal management, thermal radiation, textiles.

**References:**

- [1] Svetlana V. Boriskina, "An ode to polyethylene", *MRS Energy & Sustainability: A Review Journal*, volume 6, E14, (2019).
- [2] Yi Cui et al. "Nanoporous polyethylene microfibrils for large-scale radiative cooling fabric", *Nature Sustainability*, volume 1, 105–112, (2018)
- [3] Yi Cui et al. "A dual-mode textile for human body radiative heating and cooling", *Science Advances*, Vol. 3, no. 11 (2017)

**F.FL03.09.26**

**Testing Mechanical Durability and Electrical Stability of Conducting Materials for Flexible and Stretchable Inter-Connects** Mayukh Nandy, Todd K. Houghton and Hongbin Yu; Arizona State University, United States

Over the past decades, foldable electronics have become a major area of research in the electronics industry. Our devices are getting smaller, more portable and the need for flexible electronics is booming for various applications. While a major part of the research is being performed on high performance flexible and foldable batteries, the longevity of the materials used as the interconnects has remained under-explored. The thin metal sheets available in the market today is an ideal choice for such applications owing to their high conductivity. Researchers have also explored conducting composite polymer interconnects for improved stretchability and flexibility despite their reduced conductivity. The lifetime and mechanical stability of these materials are most important before considering them for integration into flexible electronic packages.

In this paper, we propose testing methods and results for mechanical and electrical stability over extensive flexing and stretching cycles. The materials put into test are copper foils, copper coated polyimide (PI), aluminium coated Polyethylene terephthalate (PET) and conductive Silver (Ag) - Polydimethylsiloxane (PDMS) composite in a sandwich structure.

**F.FL03.09.28**

**Fabrication of Ni-Au Core-Shell Micro-Heater for Wearable Chemosensitive Sensor** Hak-Jong Choi, Soongeun Kwon, JaeJong Lee, Geehong Kim, Hyungjun Lim, Junhyoung Ahn and Kee-Bong Choi; Korea Institute of Machinery and Materials, Korea (the Republic of)

Nano-engineering is one of the most important technologies for development of the state-of-art electronics, healthcare device, and eco-friendly systems that provide the methods to control the extremely small size and properties of materials. In addition, nanostructured materials can serve the unique mechanical, electrical, and optical properties leading the advance of technology. Recently, there is an increasing demand for nano-engineering in various industry such as IoT sensor, smart grid, next-generation energy system, and self-diagnosis system to improve the performance and extend the functionality of that. However, nano-engineering process has not reached at a sufficient level to satisfy the design and suggestion. In this study, nanoimprint-assisted electroplating is suggested to fabricate metallic 3D nano/micro- structure applicable to various electronic and optoelectronic devices. Nano-engineering is one of the most important technologies for development of the state-of-art electronics, healthcare device, and eco-friendly systems that provide the methods to control the extremely small size and properties of materials. In addition, nanostructured materials can serve the unique mechanical, electrical, and optical properties leading the advance of technology. Recently, there is an increasing demand for nano-engineering in various industry such as IoT sensor, smart grid, next-generation energy system, and self-diagnosis system to improve the performance and extend the functionality of that. However, nano-engineering process has not reached at a sufficient level to satisfy the design and suggestion. In this study, nanoimprint-assisted electrodeposition and electroless deposition is suggested to fabricate Ni/Au core/shell micro-heater applicable to various sensor applications. In briefly, sacrificial template was fabricated by nanoimprint lithography. Then, Ni core was selectively deposited on conducting substrate. After that, template was removed and Au shell was coated by electroless plating to prevent oxidation problem during heating of the micro-heater. Finally, as-fabricated Ni/Au micro-heater was transferred on arbitrary substrate such as flexible polyimide film, PET film, and so on and characterized the heating performance.

#### **F.FL03.09.30**

**Laser Writing of Flexible Silicon Carbide-Based Devices for Bioelectronics** Aleksander Prominski, Vishnu Nair, Menahem Rotenberg and Bozhi Tian; The University of Chicago, United States

Laser-assisted production has increased in popularity due to their low cost and ease of use for general prototyping. In the context of materials science, laser-produced composites have the potential to increase the research throughput and enable unique complex phases. Recently, graphene-based conductive materials have been obtained in the process of laser ablation from the polyimide substrate and were efficiently applied for electrochemical biosensing. We sought to expand this synthetic framework with a platform that allows for the production of semiconductor-based structures and harness a plethora of electronic, electrochemical, photoelectrochemical, and photothermal properties for their application in bioelectronics.

Here, we show that laser writing can be used to synthesize semiconductor materials. We used polydimethylsiloxane (PDMS) as a precursor to silicon carbide (SiC) based materials. The doping and internal structure of the materials can be controlled with varying the processing parameters, which allowed us to synthesize both oxygen- and nitrogen-doped, glassy and crystalline materials, including rare SiC polytypes. A variety of doping levels and patterns create materials with tunable electronic properties. Synthesis of the material directly in the insulating elastomer matrix yields ready-to-use bioelectronic devices in which electrical and electrochemical properties can be used for cardiac pacing and muscle cell stimulation. Our results show the great potential for direct fabrication of semiconductor-based devices for tissue- and organ-modulation as well as building platforms for organoid research.

#### **F.FL03.09.31**

**An Artificial Cochlear Stimulation Model Using 3D Printing and Neural Network** Iek Man Lei<sup>1</sup>, Chen Jiang<sup>1</sup>, Chon Lok Lei<sup>2</sup>, Simone d. Rijk<sup>1</sup>, Yu Chuen Tam<sup>3</sup>, Manohar Bance<sup>1</sup> and Yan Yan Shery Huang<sup>1</sup>; <sup>1</sup>University of Cambridge, United Kingdom; <sup>2</sup>University of Oxford, United Kingdom; <sup>3</sup>Emmeline Centre for Hearing Implants, United Kingdom

Cochlear implants are widely recognised as a solution for patients with profound hearing loss. The implant restores auditory sensation by electrically stimulating nerve, remarkably improving patients' quality of life. Despite overall successful outcomes, the main problem with the present cochlear implants are their imprecise stimulation causing frequency dispersion and 'blurring' of the perceived sound. Traditional testing platforms, such as animals and cadavers, are impractical for studying the intra-cochlear potential distribution evoked by electrical stimuli. Animal models have different anatomy and electrical properties compared to human cochleae, and the limited availability of cadavers greatly restricts its popularity in cochlear research. It is also difficult to instrument them to measure electrical spread. Therefore, this study has developed a novel methodology that exploits 3D embedded printing and a neural network approach to create an artificial stimulation model of human cochleae for replicating the intra-cochlear potential distribution evoked by electrical stimuli.

We fabricated the model by embedded 3D printing a sacrificial cochlea-shaped structure inside a support bath. Our

fabrication method offers two key innovations – tuneable geometry and tuneable resistivity. With 3D embedded printing, our model can replicate the general geometric features of human cochleae and the large variation in the shape of human cochleae. By structuring a conductive network in the support bath, the resistivity of our model can be tuned over 2 orders of magnitude from 0.19 kΩcm to 22 KΩcm. This wide range of resistivity, which covers the reported resistivity of human cortical bone, cannot be replicated easily with the existing printable materials, such as thermoplastics and hydrogels.

To evaluate the ability of our model to replicate the physiological intra-cochlear potential distribution evoked by cochlear stimulation, we compared the electric field imaging (EFI) profile of our model and the patients' EFI profiles. EFI is a clinical method that measures how the intra-cochlear potential is distributed across the electrode array of a cochlear implant in patients' cochleae. Our results show that our model can replicate the mean intra-cochlear potential distribution in patients' cochleae. By fabricating a wide variety of models with different matrix resistivity and cochlear shapes, a dataset of EFIs is obtained. We then deployed a neural network (nn) approach to build a computational model that predicts the trend in the EFI resulting from different matrix resistivity and different cochlear shapes. Our nn model correctly predicts the EFIs within the dataset with over 85% accuracy. It can determine how fast the voltage decays in a particular cochlear shape and resistivity.

This study presents a simple workflow in modelling the intra-cochlear potential distribution evoked by electrical stimuli using 3D printing and neural network. Our model could potentially serve as a screening model for developing new cochlear implants, or a tool to predict patient-specific clinical outcome after cochlear implantation. Our methodology is general and can be readily adapted to other anatomical sites of electronic implants.

#### **F.FL03.09.32**

**Late News: Self-Signal Processing Pressure Sensor by Controlled Sensing Band and Its Response Curve** Chanho Jeong and Tae-il Kim; Sungkyunkwan University, Korea (the Republic of)

Resistive-type pressure sensor, which are mainly utilized in industry, are easy to manufacture and are not significantly affected by external electromagnetic fields, unlike capacitive type. However, the produced signal is not linear, and it is also difficult to measure a wide range of pressures using such a sensor. Therefore, before being utilized, the extracted nonlinear data from them need to be modified and re-processed for a specific target use. Here, we presented resistive-type pressure sensors whose response characteristic can be freely adjusted without the need of any additional computer processing. Five different types of introducing sensors performed different functions by the sensors themselves and they were manufactured by only modifying their electrodes: normal pressure sensor, linear pressure sensor, on/off switch sensor, high-pressure band sensor, and low-pressure band sensor. The operating mechanism of the sensor is the electron shortcut pathway in a designated electrode circuit from the contact area change of the deformed conductive elastomeric lenticular pattern. Sensors fundamental properties such as sensitivity and measurable range (~4 MPa) could be also controlled by selecting the polymer or controlling the electrode slope.

C. Jeong, J.S. Lee, B. Park, C.S. Hong, J.U. Kim and T.-i. Kim, *Adv. Mater.* 31,(36), 1902689

#### **F.FL03.09.36**

**Late News: Effects of Molecular Structures on Electrochemical Doping and UV-Vis/NIR Absorption in Thin Films of Conjugated Polymers** Onyu Bae, Taemin Kim, Yaena Na and Felix S. Kim; Chung-Ang University, Korea (the Republic of)

Conjugated polymers have been studied for developments of novel lighting devices, electronic components, and energy conversion and storage systems. The electronic energy levels and bandgaps of the conjugated polymers can be studied by photoelectron spectroscopies, electrochemical redox potentials, and UV-Vis-NIR absorption spectroscopies. In this work, we prepared thin films of polythiophene derivatives and investigated their electrochemical doping processes and UV-Vis-NIR absorption spectra. Polymer films were laminated with a gel electrolyte and electrodes and electrical potential was applied at the electrodes. Because the molecular structures of polymers govern their electronic and macroscale properties, we observed distinct spectral changes of the polymers caused by redox of the materials. The polymer films in a neutral state showed absorption in a visible range. When electrochemically activated, the absorption bands of pristine polymers decreased and strong NIR absorption bands evolved. We tried to link the observed spectral phenomena with performance of the electrochemical devices.

This work was supported by the research programs (2019M3F3A1A03079821 and 2019R1A2C1087234) through the National Research Foundation of Korea (NRF). This research was also funded in part and conducted under "the Competency Development Program for Industry Specialists" of the Korean Ministry of Trade, Industry and Energy (MOTIE), operated by Korea Institute for Advancement of Technology (KIAT), with the project No. P0012453, Next-generation Display Expert

Training Project for Innovation Process and Equipment, Materials Engineers.

#### **F.FL03.09.37**

**Late News: Electrospun Polyurethane-Polyvinylidene fluoride Nanofiber Webs Based Hybrid Pressure Sensor** Mohammad S. Reza, Kap Jin Kim and Hongdoo Kim; Kyung Hee Univ, Korea (the Republic of)

Recently, polymer-based pressure sensors have drawn much attention due to the importance of sensing device for soft robotics, wearable or/and health monitoring device etc. However, electrospun polyurethane (PU) nanofiber webs having very high amount of nano-sized open cell can be used as a piezo-capacitive sensor for monitoring both static and dynamic pressures due to excellent electrospinnability and very good elastic properties that has been reported in our previous study <sup>[1]</sup>. In contrast, electrospun Polyvinylidene fluoride (PVDF) exhibits high  $\beta$ -crystalline phase content and superior piezoelectricity <sup>[2]</sup>. Consequently, in this study, the mixture solution of PU and PVDF was electrospun under controlled compositions to obtain PU-PVDF hybrid nanofiber webs. Their physico-mechanical and piezo-responsive behaviors were investigated. When the dynamically changing force was applied to this hybrid sensor, dynamic pressure could be measured through the electric current generated by the orientational change of C-F dipoles in the PVDF part of the composite nanoweb as a function of time. When the static force was applied to this hybrid sensor, static pressure could be measured through the increasing capacitance value caused by the decreasing thickness of the composite nanoweb rather than the piezoelectric current. The piezoelectric and piezocapacitive properties of this hybrid sensor could be measured simultaneously using a piezoelectric amplifier and an LCR meter, respectively. Overall, 25~50 wt.% addition of PVDF in PU greatly enhanced the piezoelectric output signal as well as reduced pressure-capacitance hysteresis and higher capacitance change with the applied pressure due to the rubbery PU of this hybrid sensor. Moreover, AgNO<sub>3</sub>, which acts as a precursor of silver nano-particle (AgNP) formed in the electrospun PVDF nanoweb, was added into the PU-PVDF electrospun solution to get enhanced piezoelectric performance of the hybrid sensor caused by the preferential formation of  $\beta$ -phase of PVDF

#### **F.FL03.09.38**

**Late News: Chemical-Free Atomic Force Microscope Mechanical Bilayer Lithography—A Water Based Process to Fabricate Advanced Flexible Devices** Yu Shu and Harish Bhaskaran; University of Oxford, United Kingdom

Both polymer flexible substrates and two-dimensional materials (2DMs) have highly strict nanomanufacturing requirements that they should avoid using strong chemicals and minimize exposure to radiation damage. The current fabrication method for flexible 2DMS based devices mainly relies on transferring the devices prefabricated on rigid substrates by electron beam lithography or photolithography onto polymer substrates. This fabrication process is time-consuming and expensive, which restricts this method to a limited number of applications. Here, a water based technique, atomic force microscope mechanical bilayer lithography was proposed to improve this fabrication process by directly building devices on flexible substrates without introducing any hazardous chemicals during fabrication. It has been demonstrated to be suitable for both SiO<sub>2</sub>/Si and flexible polyethylene terephthalate (PET) substrates. The mechanical force applied on the AFM tip can be controlled flexibly without risk of substrate damage or pattern loss. It has also been proved to be effective to build MoS<sub>2</sub> photodetector on flexible PET substrates, which brings more opportunities to directly construct flexible 2DMs based devices.

#### **F.FL03.09.39**

**Late News: Sterically Stabilized Multilayer Graphene Nanoshells for Inkjet-Printed Resistors** Michael D. Orrill<sup>1</sup>, Dustin Abele<sup>2</sup>, Michael Wagner<sup>2</sup> and Saniya LeBlanc<sup>2</sup>; <sup>1</sup>NextFlex, United States; <sup>2</sup>The George Washington University, United States

Printable resistive materials are as important for printed electronic devices as highly conductive materials, but they are not investigated as widely, nor are they as commercially available. Of the few demonstrations of printed resistors, most require a variable component geometry to achieve different resistances. This requirement presents challenges for circuit layout as spare board space is often scarce and valuable.

Here we present ink synthesis and printing results for variable resistance patterns that are inkjet-printed with a novel and sustainable carbon nanomaterial—multilayer graphene nanoshells, the byproduct of a biofuel synthesis process from biomass<sup>1</sup>. The dispersed multilayer graphene nanoshells are stabilized with a surfactant (Triton X100). The optimal surfactant dosage achieves sufficient particle coverage without leading to agglomeration. Here, the optimal dosage is determined with a surface tension-based adsorption analysis technique, whose results suggest adsorption is driven primarily by hydrophobicity of the anchoring group in the surfactant molecule. The conformation of adsorbed surfactant molecules is explained by a geometric model. The difference in efficacy between sterically and electrostatically stabilized particles is demonstrated by comparing the energetic interparticle potentials between approaching particles stabilized by either mechanism.

Resistive patterns are inkjet-printed and electrically characterized. We find the resistivity of printed patterns can be varied by adjusting the solid-loading and the number of printed layers. We also discover that for few-printed layers, the presence of residual steric stabilizing material enhances the electrical conductivity of resistive patterns. This finding challenges the paradigm around the necessity of stabilizing material removal post-deposition and suggests some potential nascent and unique functionality for stabilizing materials. The multilayer graphene nanoshell inks demonstrated here present a promising new pathway toward practical and sustainable printed resistors that can achieve variable resistances within a constant areal footprint without a post-process.

<sup>1</sup> M. J. Wagner, J. Cox, T. McKinnon, K. Gneshin (George Washington University), "Hollow carbon nanosphere based secondary cell electrodes" *U.S. 8262942B2*, **2012**.

#### **F.FL03.09.40**

**Late News: Flexible Broadband (UV-Vis-NIR) Photodetector Based on All MoS<sub>2</sub> 0D/2D Mixed-Dimensional Unipolar Heterojunctions** Venkatarao Selamneni, Sankalp Koduvayur Ganeshan and Parikshit Sahatiya; Birla Institute of Technology and Science, Pilani, Hyderabad campus, India

With the recent advances in the field of electronic information technology, optoelectronic devices have become an indispensable part of the society and are widely used for various applications. Among them, photodetectors are extensively studied. Commercial photodetectors with active materials such as Germanium, Silicon, GaAs are rigid, which hinders their application in wearable electronics technology and further, these photodetectors are not responsive to a wide extend of electromagnetic range [1]. Hence, novel semiconductor materials which can easily be integrated with flexible substrates need to be researched for future flexible broadband photodetectors. In recent years, the research on two-dimensional (2D) materials and their heterostructures based photodetectors has tremendously increased, due to their tunable bandgap, high carrier mobility and high specific area for sufficient light harvesting [1-3]. Large number of reports published on MoS<sub>2</sub> based photodetectors [4], which shows the tremendous application prospects of MoS<sub>2</sub> in the next generation photodetectors. Pristine MoS<sub>2</sub> appears to show strong absorption in the NIR and visible region of the electromagnetic spectrum but not in UV locale [2,4]. The range of absorption of pristine MoS<sub>2</sub> in the electromagnetic spectra needs to be further increased which limits its applicability for far reaching applications. One of the possible ways to overcome this problem is by fabricating heterostructures with higher bandgap semiconducting materials such as quantum dots (QDs) [5]. QDs engineering the 2D materials by constructing 0D-2D heterostructures is an effective strategy to assist the dissociation of photogenerated electron-hole pairs by forming heterojunctions, along with increasing the range of absorption.

In this work, flexible broadband photodetector based on novel MoS<sub>2</sub>QDs/MoS<sub>2</sub> on a cellulose paper substrate was fabricated, wherein MoS<sub>2</sub> QDs and MoS<sub>2</sub> flakes were synthesized by one-pot hydrothermal method. The resultant MoS<sub>2</sub> flakes were deposited on paper substrate using facile and scalable vacuum filtration method and thereafter, MoS<sub>2</sub> QDs solution was drop-casted on MoS<sub>2</sub>/paper to form the unipolar heterostructures. Physico-chemical characterizations such as X-ray diffraction analysis, UV-vis spectroscopy, X-ray photoelectron spectroscopy, Transmission electron microscopy, Raman spectroscopy and photoluminescence spectroscopy reveals the formation, morphology and optical properties of MoS<sub>2</sub> and MoS<sub>2</sub> QDs with good stoichiometry.

The formation of heterostructures at the interface of MoS<sub>2</sub> QDs and MoS<sub>2</sub> flakes resulted in the improved responsivity and broadband photoresponse range from UV to NIR. The discretely decorated MoS<sub>2</sub>QDs on MoS<sub>2</sub> flakes not only enhances the sensitivity in the UV region but also create localized electric fields that help in the efficacious separation of the generated electrons and holes upon illumination of light. Further, the metal contacts for the device were taken from MoS<sub>2</sub> flakes, so as to reinforce the collection of the photogenerated carriers. The fabricated device exhibited good photodetection performance with a responsivity of 3.94 mA/W, 12.82 mA/W, and 7.55 mA/W and under NIR, visible, and UV light illumination, respectively. This work provides guidance for the development of large-area and flexible paper based broadband photodetectors using mixed dimensional 0D/2D heterojunctions that finds potential applications in the field of wearable electronics.

#### **References:**

1. M. Long, P. Wang, H. Fang, and W. Hu, *Adv. Funct. Mater.*, 2019, 29, 1803807.
2. P.T. Gomathi, P. Sahatiya, S. Badhulika, *Adv. Funct. Mater.*, 2017,27, 1701611.
3. V. Selamneni, N. Nerurkar, P. Sahatiya, *IEEE Sens. Lett.*, 2020, 4, 1-4.
4. H. S. Nalwa, *RSC Adv.*, 2020,10, 30529-30602.
5. H. Qiao, Z. Li, Z. Huang, X. Ren, J. Kang, M. Qiu, Y. Liu, X. Qi, J. Zhong, and H. Zhang, *Appl. Mater. Today*, 2020, 20, 100765.

#### **F.FL03.09.42**

**Late News: Wearable, Tactile Pressure Sensors Based on 1T MoS<sub>2</sub> Nanosheets Coated Porous Sponge for Real-Time Healthcare Monitoring and Human-Machine Interface Devices** Melih O. Cicek, Mustafa C. Gorur, Mete Batuhan Durukan and Husnu E. Unalan; Middle East Technical University, Turkey

Following their promising demonstration in various fields such as real-time healthcare monitoring, tactile information systems, gesture recognition and so on, there is an ever-increasing demand for flexible, lightweight and wearable sensors. To address this demand, various strain sensing mechanisms have been introduced and investigated. In this work, we fabricate a wearable tactile pressure sensor using a commercially available sponge decorated with conducting 1T phase of MoS<sub>2</sub> nanosheets and a very thin layer of elastomer. Solution based preparation of 1T phase of MoS<sub>2</sub> allowed scalable and cost-effective fabrication of the wearable tactile pressure sensors. MoS<sub>2</sub> nanosheets were decorated onto the sponge using a simple dip and dry method. Thanks to highly porous structure of the sponge, fabricated pressure sensors possessed high flexibility, favorable sensitivity ( $\sim 0.5 \text{ kPa}^{-1}$ ) and a wide working pressure range from 10 Pa to 100 kPa. A very thin layer of elastomer overcoat improved the stability of the sensors under cyclic compression and bending tests, while preserving its electromechanical properties. Finally, we demonstrated the use of tactile pressure sensors for real-time body motion monitoring and human-machine interface device. Results provided herein proves that the fabricated sensors hold strong potential as wearable sensors.

#### **F.FL03.09.43**

**Late News: Monolithic, Highly Sensitive, Parallel Plate Capacitive Sensors for Body-Motion Monitoring** Melih O. Cicek, Doga Doganay, Mete Batuhan Durukan and Husnu E. Unalan; Middle East Technical University, Turkey

Significant research efforts have been spent on capacitive pressure sensors due to recent developments in wearable electronics. However, the fabricated sensors still have some problems yet to be solved. Due to the additional electrode layers, most of the reported parallel plate capacitive pressure sensors suffer from excessive weight, lack of air permeability and washing stability, all of which are directly related with the user comfort. To overcome these issues, a parallel plate capacitive sensor with monolithic structure was demonstrated. In this work the monolithic capacitive pressure sensor was fabricated using 3-D masking technique, using a commercially available sponge with silver nanowire (Ag NW) electrode layers and a very thin protective layer of polydimethylsiloxane (PDMS). Finite-element analysis revealed the differences in deformation mechanisms between the classical parallel plate design and the monolithic design. More homogeneous stress distribution was obtained for the investigated monolithic system. Benefitting from these unique features, the developed monolithic capacitive sensors are light, have high sensitivity (up to  $1 \text{ kPa}^{-1}$ ), fast response/recovery times, very low-pressure sensing ability ( $< 1 \text{ Pa}$ ) and high mechanical stability. Finally, fabricated sensors were used to demonstrate real-time body motion monitoring.

#### **F.FL03.09.44**

**Late News: Printed and Nanostructured Breath Sensors** Guojun Shang, Shan Yan, Dong Dinh, Behnaz Malaei, Shan Wang, Shiyao Shan, Jin Luo, Mark Poliks, Susan Lu and Chuan-Jian Zhong; Binghamton University, The State University of New York, United States

There is a rising interest in the development of wearable sensors for monitoring human performance and health. One type of promising sensors is breath sensor that detects breath volatile organic compound (VOC) as biomarkers of certain diseases such as cancer and diabetes. However, a major challenge is the limited sensitivity and poor selectivity for many of the current breath sensors. This presentation describes recent results of an investigation of nanocomposite-structured materials as chemiresistor array sensing interfaces to enhance the sensitivity and selectivity of breath sensors. Results from both experimental testing and theoretical simulation of sensor arrays for detecting the VOCs will be discussed, revealing excellent agreement of the experimental data with the theoretical modeling. The fabrication of nanoparticle-printed chemiresistor devices on paper substrates and the formulation of the nanocomposites as printable sensing films will also be discussed. Implications of the findings for the design of advanced sensing materials and breath sensors will also be discussed.

#### **F.FL03.09.45**

**Late News: Surface-Mediated Interconnections of Nanoparticles Towards Multi-Functional Fibrous Sensors** Richard J. Robinson, Shan Yan, Shan Wang, Kevin Lee, Virginia Krause, Omar Lezcano, Serena Tycko and Chuan-Jian Zhong; State University of New York at Binghamton, United States

Fibrous materials serve as an intriguing class of 3D materials to meet the growing demands for flexible, foldable, biocompatible, biodegradable, disposable, inexpensive, and wearable sensors and the rising desires for higher sensitivity, greater miniaturization, lower cost, and better wearability. The use of such materials for the creation of a fibrous sensor

substrate that interfaces with a sensing film in 3D with the transducing electronics is however difficult by conventional photolithographic methods. This presentation will describe a highly effective pathway featuring surface-mediated interconnection of metal nanoclusters (NCs) and nanoparticles (NPs) in fibrous materials at ambient conditions for fabricating fibrous sensor substrates or platforms. Bimetallic gold-copper and silver-copper alloy NCs and NPs are used as a model system to demonstrate the semiconductive-to-metallic conductivity transition, quantized capacitive charging, and anisotropic conductivity characteristics. Upon coupling SMI of NCs/NPs as electrically conductive microelectrodes and surface-mediated assembly of the NCs/NPs as chemically sensitive interfaces, the fibrous chemiresistors function as sensitive and selective sensors for gaseous and vaporous analytes. This strategy has significant implications for manufacturing high-performance fibrous platforms to meet the growing demands of the advanced multifunctional sensors and biosensors.

## SYMPOSIUM F.MT01

---

Advanced In Situ Characterization of Materials Kinetics  
November 21 - December 3, 2020

### Symposium Organizers

Michael Behr, Dow Chemical  
Yu Han, King Abdullah University of Science and Technology  
Yuzi Liu, Argonne National Laboratory  
Yugang Sun, Temple University

### Symposium Support

**Platinum**  
Perkin Elmer

---

\* Invited Paper

SESSION Tutorial F.MT01: Advanced In Situ Characterization of Materials Kinetics (TEM and Synchrotron X-Ray)  
Session Chairs: Chengjun Sun, Huolin Xin and Hua Zhou  
Sunday Afternoon, November 29, 2020  
F.MT01

**12:30 PM \***

**Electron Microscopy** Huolin Xin; University of California, Irvine, United States

The instructor will introduce the most advanced analytical transmission electron microscopy and data science application in the field. The application of the advanced (S)TEM techniques will be discussed for solving materials problem in *operando* conditions. Deep learning is beginning to make major inroads within physics, chemistry and materials sciences and hold considerable promise for accelerating the discovery of new theories and materials. Prof. Xin will introduce deep convolutional neural networks and how they can be applied to the computer vision problems in transmission electron microscopy and tomographic imaging. At the end some perspectives on the future integration of analytical TEM characterization and spectroscopy techniques will be given.

**2:00 PM BREAK**

**2:15 PM \***

**Synchrotron X-Ray** Hua Zhou; Argonne National Laboratory, United States

The instructor will firstly guide the audience through a brief survey of the evolution of light sources from the earliest sealed tubes to electron storage rings and free-electron lasers, the global competition on modern synchrotrons and LINACs, and



pressing coherent X-ray techniques emerged from them. In the following, he will demonstrate a set of fresh science cases in the exploration of advanced multifunctional materials for information and energy applications enabled by applying these powerful X-ray toolkits, such as atomic mapping of an oxide heterostructure by phase retrieving coherent Bragg rods and structural motifs responsible for a strongly correlated perovskite fuel cell, and capturing field-driven material perturbations and defect flows in an emerging memristor device for neuromorphic computing.

### **3:45 PM BREAK**

### **4:00 PM \***

**Advanced X-Ray Spectroscopy Techniques** Chengjun Sun; Argonne National Laboratory, United States

The instructor will discuss the advanced X-ray spectroscopy techniques at APS, and their applications for investigating in the materials research. The in-situ/operando characterization on advanced battery materials, and other ex-situ characterization on various materials will be covered in this lecture too. In addition, the new opportunities with APS\_U and some future challenges will be discussed as well.

Moreover, the correlation between the electron microscopy and synchrotron x-ray characterizations will be briefly discussed as an open question to highlight the importance of multimodalities of materials characterization.

SESSION F.MT01.09: Live Panel Discussion: Advanced In Situ TEM for Material Science  
Session Chairs: Yuzi Liu and Yugang Sun  
Tuesday Morning, December 1, 2020  
F.MT01

### **8:00 AM PANEL DISCUSSION—ADVANCED TEM TECHNOLOGY: EVA OLSSON, MIAOFANG CHI AND RENU SHARMA**

### **9:00 AM PANEL DISCUSSION—LIQUID TEM AND BEYOND: HAIMEI ZHENG, JAMES DE YOREO, QIAN CHEN AND LIFEN WANG**

SESSION F.MT01.10: Live Keynote I: Ultrafast and Dynamic TEM for Materials/Emerging Process Study by Advanced In Situ Microscopy  
Session Chairs: Yuzi Liu and Yugang Sun  
Wednesday Afternoon, December 2, 2020  
F.MT01

### **5:15 PM \*F.MT01.02.10**

**MeV-UED—A Platform for *In Situ* Studies of Material** X.J. Wang; SLAC National Accelerator Laboratory, United States

MeV-UED has led to a new paradigm in ultrafast electron scattering: higher electron beam energy means stronger diffraction and significantly reduces space-charge effects hence leads to atomic spatial-temporal resolution [1-3]. Furthermore, MeV electrons experience less multiple-scattering, possess “real” flat Ewald-sphere and favourable sample environments; MeV-UED is a unique platform for *in situ* studies of material. MeV-UED has enabled broad scientific opportunities in material science and chemical dynamics, such as revealing the energy flow in superconductor [4] and atomic movie of light-induced structural distortion in the perovskites solar cell [5].

I will present two examples in capturing metastable states of functional material using MeV-UED: topological properties & charge density wave controlled by light [6-7]. Recently *in situ* characterization of transient state during the electrically-triggered insulator-metal transition was successfully realized at SLAC MeV-UED [8]. Future development of nano-probe at SLAC MeV-UED will open new window to probe metastable state and dynamics in spatially heterogeneous systems and in *in-situ* device geometries.

X.J. Wang *et al*, Phys. Rev. E , 54, No.4, R3121 -3124 (1996).  
P Zhu *et al*, New Journal of Physics 17 (6), 063004 (2014).  
S. Weathersby *et al*, Rev. Sci. Instrum. 2015, 86, 073702–073707.  
Tatiana Konstantinova *et al*, Sci. Adv. 2018;4:eaap7427, doi: 10.1126/sciadv.aap7427.  
Xiaoxi Wu *et al*, Sci. Adv. 3 e1602388 (2017) doi: 10.1126/sciadv.1602388.  
Edbert J. Sie *et al*, Nature 565,61–66(2019).  
A. Kogar *et al*, Nat. Phys.16, 159 (2019) doi: 10.1038/s41567-019-0705-3.  
SLAC MeV-UED: <https://lcls.slac.stanford.edu/instruments/mev-ued>.

#### 5:45 PM \*F.MT01.07.02

**Advances in *In Situ* and Ultrafast Electron Microscopy for Materials Characterization** [Ilke Arslan](#); Argonne National Laboratory, United States

With recent advances in in-situ microscopy, a new era in microscopy has arrived that allows for the dynamic imaging of materials under reaction conditions in the (scanning) transmission electron microscope. To better understand the structure/property relationships of materials, it is essential to get closer to the conditions in which the material will be used, such as high/low temperature, liquid environments, gas environments, or a combination thereof. Within these environments, moving beyond “real time” imaging to ultrafast imaging can provide yet another level of fundamental understanding of nanomaterials. Further, combining an in-situ or ex-situ experiment with electron tomography is a very powerful method for materials characterization as this provides the 3-D morphology of the (nano)materials under more relevant conditions. This talk will focus on newer developments such as in-situ heating in liquid, and the future of ultrafast transmission electron microscopy at the Center for Nanoscale Materials.

SESSION F.MT01.11: Live Keynote II: Emerging Process Study by Advanced In Situ Microscopy  
Session Chairs: Yuzi Liu and Yugang Sun  
Wednesday Afternoon, December 2, 2020  
F.MT01

#### 6:15 PM \*F.MT01.02.04

**Nanoscale Crystal Growth on van der Waals-Bonded Materials as Seen with *In Situ* Microscopy Techniques** [Frances M. Ross](#); Massachusetts Institute of Technology, United States

Two-dimensional materials provide exciting opportunities as substrates for the growth of three-dimensional nanocrystals. The difference in the nature of the bonding at the 3D nanocrystal / 2D material interface, compared to the situation for conventional epitaxy, is expected to generate interesting and potentially useful new growth modes and interfacial structures. It is well known that deposition of gold and other metals onto certain van der Waals-bonded materials produces faceted nanocrystals that can be aligned with the substrate lattice. Here we describe the use of several *in situ* microscopy techniques to explore the principles governing epitaxial growth in a broader range of nanocrystal / van der Waals substrate combinations. An unusual feature of the *in situ* experiments is that substrate preparation and materials deposition can be carried out under ultra high vacuum conditions in chambers that are connected to the microscope, while materials deposition is also possible while the sample is under observation within the microscope. These multiple capabilities are helpful in allowing flexibility and experimental robustness. Furthermore, for these particular experiments, a UHV environment (low  $10^{-10}$  Torr base pressure range) allows reactive materials such as niobium or germanium to be deposited and examined without oxidation. We will describe nanocrystal growth on suspended 2D materials using a UHV-TEM that has integrated capabilities for heating, laser cleaning, metal evaporation, and semiconductor chemical vapor deposition. Post-growth observation using scanning transmission electron microscopy yields atomic level compositional information as well as movies showing nanoparticle motion and annealing phenomena. We will also describe complementary measurements performed in a multi-probe, UHV *in situ* scanning tunneling microscope. This instrument provides opportunities to examine the atomic and electronic structure as well as to measure the transport properties of the nanocrystal / van der Waals material interface. We apply these techniques to evaluate nanocrystal morphology, orientation relation and interfacial structure and properties as a function of deposition parameters. We discuss strategies for morphological control and describe nanocrystal coalescence events and the patterning of the 2D substrate to control nucleation sites. We finally consider the formation of epitaxial alloy and heterostructure islands via sequential deposition. The eventual aim of the *in situ* experiments is to

understand the relationship between the interfacial structure and morphology in a nanocrystal / van der Waals-bonded material combination and the electronic properties that are required for its applications.

**6:45 PM \*F.MT01.04.02**

**Observation of Topological Transformations of Ferroelectric Vortices** Kai Du and He Tian; Zhejiang University, Chile

Topological structures based on controllable ferroelectric or ferromagnetic domain configurations offer the opportunity to develop microelectronic devices such as high-density memories. Despite the increasing experimental and theoretical insights into various domain structures (such as polar spirals, polar wave, polar vortex) over the past decade, manipulating the topological transformations of polar structures and comprehensively understanding its underlying mechanism remains lacking. We successfully developed a technique to realize domain structures modulation and take an atomic resolution observation simultaneously. This atomistic observation of dynamic evolution reveals the potential of modulating ferroelectric domain patterns in ferroelectric nano-devices. Here we systematically investigate the real-time topological transformations of polar structures in PbTiO<sub>3</sub>/SrTiO<sub>3</sub> multilayers at an atomic level. The procedure of vortex pair splitting and the transformation from polar vortex to polar wave and out-of-plane polarization are observed step by step. Furthermore, the redistribution of charge in various topological structures has been demonstrated under an external bias. These findings advance the current understanding of topological structures transformation manipulated by the external field and its origination in multilayers; it would ultimately enable the design of nanostructured materials to realize their potential applications in microelectronics.

#### References

- [1] Yadav, A. K. et al. Observation of polar Vortices in oxide superlattices. *Nature* 530, 198-201 (2016).
- [2] Tang, Y. L. et al. Observation of a periodic array of flux-closure quadrants in strained ferroelectric PbTiO<sub>3</sub> films. *Science* 348, 547-551 (2015).
- [3] Hong, Z. et al. Stability of Polar Vortex Lattice in Ferroelectric Superlattices. *Nano Lett.* 17, 2246-2252 (2017).
- [4] Li, S. et al. Periodic arrays of flux-closure domains in ferroelectric thin films with oxide electrodes. *Appl. Phys. Lett.* 111, 052901 (2017).
- [5] Rodriguez, B. J. et al. Vortex Polarization States in Nanoscale Ferroelectric Arrays. *Nano Lett.* 9, 1127-1131 (2009).
- [6] Wang, W. Y. et al. Large scale arrays of four-state vortex domains in BiFeO<sub>3</sub> thin film. *Appl. Phys. Lett.* 109, 202904 (2016).
- [7] Lu, L. et al. Topological Defects with Distinct Dipole Configurations in PbTiO<sub>3</sub>/SrTiO<sub>3</sub> Multilayer Films. *Phys. Rev. Lett.* 120, 177601 (2018).
- [8] Jia, C. L., Urban, K. W., Alexe, M., Hesse, D. & Vrejoiu, I. Direct Observation of Continuous Electric Dipole Rotation in Flux-Closure Domains in Ferroelectric Pb(Zr,Ti)O<sub>3</sub>. *Science* 331, 1420-1423 (2011).
- [9] Chen, W. J., Zheng, Y. & Wang, B. Vortex Domain Structure in Ferroelectric Nanoplatelets and Control of its Transformation by Mechanical Load. *Sci. Rep.* 2, 796 (2012).
- [10] Damodaran, A. R. et al. Phase coexistence and electric-field control of toroidal order in oxide superlattices. *Nat. Mater.* 16,1003-1009 (2017).

SESSION F.MT01.12: Live Town Hall: Advanced Synchrotron X-Ray for Materials Dynamics  
Session Chairs: Yuzi Liu and Hua Zhou  
Thursday Afternoon, December 3, 2020  
F.MT01

**3:00 PM OPERANDO SYNCHROTRON X-RAY STUDIES OF METAL ADDITIVE MANUFACTURING—TAO SUN**

**3:15 PM MULTI-SALE AND MULTI-MODAL X-RAY MICROSCOPY AND APPLICATIONS—XIANGHUI XIAO**

**3:30 PM DYNAMIC AND IN SITU CHARACTERIZATION USING X-RAY SYNCHROTRON SOURCES—MICHELLE MEJIA**

**3:45 PM \*F.MT01.03.11**

## **Interfacial Self-Assembly and Engineering of Hierarchically Structured Nanocrystals with Photocatalytic Activity** Hongyou Fan; Sandia National Laboratories, United States

Design and engineering of the size, shape, and chemistry of photoactive building blocks enable the fabrication of functional nanoparticles for applications in light harvesting, photocatalytic synthesis, water splitting, phototherapy, and photodegradation. Here, we report the synthesis of such nanoparticles through a surfactant-assisted interfacial self-assembly process using optically active porphyrin as a functional building block. The self-assembly process relies on specific interactions such as  $\pi$ - $\pi$  stacking and ligand coordination between individual porphyrin building blocks. Depending on the kinetic conditions, resulting structures exhibit well-defined one- to three-dimensional morphologies such as nanowires, nanooctahedra, and hierarchically ordered internal architectures. At the molecular level, porphyrins with well-defined size and chemistry possess unique optical and photocatalytic properties for potential synthesis of metallic structures. On the nanoscale, controlled assembly of macrocyclic monomers leads to formation of ordered nanostructures with precisely defined size, shape, and spatial monomer arrangement so as to facilitate intermolecular mass and energy transfer or delocalization for photocatalysis. Due to the hierarchical ordering of the porphyrins, the nanoparticles exhibit collective optical properties resulted from coupling of molecular porphyrins and photocatalytic activities such as photodegradation of methyl orange (MO) pollutants and hydrogen production. The capability of exerting rational control over dimension and morphology provides new opportunities for applications in sensing, nanoelectronics, and photocatalysis.

Sandia National Laboratories is a multimission laboratory managed and operated by National Technology and Engineering Solutions of Sandia, LLC., a wholly owned subsidiary of Honeywell International, Inc., for the U.S. Department of Energy's National Nuclear Security Administration under contract DE-NA0003525.

### **4:00 PM F.MT01.05.01**

***In Situ* X-Ray Investigation Underpins Roles of Water on Improving Crystallinity and Stability of Organohalide Perovskite** Hua Zhou<sup>1</sup>, Zhiyuan Ma<sup>1,2</sup>, Hsin-Hsiang Huang<sup>1,3</sup>, Wei Chen<sup>1,3</sup> and Zhang Jiang<sup>1</sup>; <sup>1</sup>Argonne National Laboratory, United States; <sup>2</sup>China University of Petroleum, China; <sup>3</sup>The University of Chicago, United States

Emerging organolead-halide-perovskite-based materials and devices have recently received tremendous attention due to their extraordinary photonic and optoelectronic performance and potential low production costs. Many physical and chemical properties beyond light harvests have erupted. Despite the rapid development of perovskite materials and devices, the impact of environmental factors on different stages of materials synthesis and device fabrication still remains unclear. Moisture or humidity is widely recognized as one of the major lethal factors in perovskite devices degrade or decompose after fabrication. However, recent reports have shown that moisture could be crucial to obtain high-performance perovskite films in a suitable moisture of ~35% relative humidity. Although a few attempts have been made to investigate the morphological evolution of organohalide perovskite films, a comprehensive understanding of the environmental influence in the process of thermal annealing is not achieved yet, as it is critically important to further improve the optoelectronic device performance.

By taking advantage of synchrotron-based grazing incident wide-angle x-ray scattering (GIWAXS), we *in situ* monitor the transformation of organohalide perovskites from precursors to final films upon thermal annealing at different relative humidity. *In situ* GIWAXS reveals the formation of crystalline perovskite materials over relevant time and moisture scales to decipher the effect of humidity on both phase transition and crystal structures during annealing. These *in situ* measurements demonstrate that moderate humidity accelerates the formation of organohalide perovskites and improves the orientation of the film, but more than 50% relative humidity retards the formation of perovskites and destructs their crystal structures. Furthermore, the highly orientated films obtained at optimized relative humidity are observed which could be attributed to the hydration of precursors. The beneficial influence of moisture content in the crystalline structure formation process on the operation stability of the resulting devices will also be discussed.

These findings clearly elucidate the influence of moisture environment in annealing process of organohalide perovskites and, in turn, allow us to correlate the improved performance of organohalide perovskite materials and devices to structural features in terms of environmental effects.

### **4:15 PM TOWN HALL DISCUSSION**

**5:00 AM \*F.MT01.01.01**

**Microscopic Kinetics of Crystallization in Graphene Nanocapillaries Revealed by *In Situ* TEM** Lifen Wang; Chinese Academy of Sciences, China

Graphene liquid cell was used for *in situ* electron microscopy because the single atom thickness, extraordinary mechanical strength and high conductivity of graphene allows the study of material in pristine stages with atomic resolution[1]. Using high-resolution transmission electron microscopy and electron energy loss spectroscopy, we show that BeO and NaCl follows unclassical crystallization process in graphene liquid cell. BeO in nature has a wurtzite structure and crystallizes in the sp<sup>2</sup>-coordinated, layered structure in liquid cells formed by sheets of graphene. We further reveal that the layered crystals can be thicker than the thermodynamically determined ultra-thin limit, beyond which the layered phase is energetically unfavored. The discovery counters a long-held dismissal and calls for a reevaluation of the possible existence of sp<sup>2</sup>-coordinated, layered polymorphs of octet compounds beyond the ultra-thin limit[2]. Sodium chloride has long been a classical crystallization model. Here we used time-resolved transmission electron microscopy to monitor crystallization of sodium chloride nanoparticles with atomic resolution in and out of graphene cell. The *in situ* observations, combined with large-scale reactive molecular dynamics simulations, reveal the details of the non-classical crystallization of sodium chloride nanoparticles via a nanoscale Wulff construction i. e. hexagon shape selection as they grow in a two dimensional confined system. Visualization of hexagon crystal growth strongly suggests the prominence of 2D confinement effect and allows us to quantify the effect on surface energy. Understanding the growth mechanism inside 2D confined system provides new revenue to rational design of nanomaterials with controlled properties.

**References:**

- [1] J. M. Yuk, J. Park, P. Ercius, K. Kim, D. J. Hellebusch, M. F. Crommie, J. Yong Lee, A. Zettl, A. P Alivisatos, *Science* 61-64 (2012): 336.  
[2] C. L. Freeman, F. Claeyssens, N. L. Allan, *Phys. Rev. Lett.* 066102 (2006): 96.

**5:15 AM F.MT01.01.02**

**Understanding Temperature-Dependent Nanoscale Electrochemistry Using Liquid Cell Transmission Electron Microscopy** Serin Lee<sup>1</sup>, Nicholas Schneider<sup>2</sup>, Kate Reidy<sup>1</sup>, Shu Fen Tan<sup>1</sup> and Frances M. Ross<sup>1</sup>; <sup>1</sup>Massachusetts Institute of Technology, United States; <sup>2</sup>Nicholas Schneider, United States

The technique of liquid cell transmission electron microscopy (LC-TEM) provides exciting information by applying the unique capabilities of electron microscopy to imaging and controlling nanoscale phenomena in liquid media. The liquid cell itself is a microfabricated enclosure that is hermetically sealed from the vacuum of the microscope and is filled with a liquid sandwiched between two electron-transparent membranes. LC-TEM provides a unique combination of spatial and temporal resolution for nanoscale liquid phase processes. However, a general limitation of LC-TEM has been the challenge of controlling and quantifying key aspects of the experimental conditions.

Here, we are particularly interested in processes that require simultaneous temperature and electrochemical control. These are important for designing batteries that must operate reliably over a range of environmental conditions or for understanding corrosion processes at elevated temperatures. We observe temperature-dependent electrochemistry using custom-fabricated microfabricated liquid cells that combine electrodes with an electrically isolated heater strip. Here we will discuss, using simulation tools, three key questions that must be understood in order to obtain quantitative information from these experiments.

We first calculate the spatial distribution of temperature in the liquid cell chip. Our setup controls temperature by Joule heating a Pt strip heater embedded within one of the electron transparent windows. We model the heater as an electrothermal system and solve for the temperature profile for a given potential difference, incorporating the temperature-dependent resistance change of the heater material. We also model two common experimental situations that can change the temperature and hence reaction kinetics within the imaged region: misalignment of the top and bottom chips and window bulging due to pressure differences. We show that the strip heater creates temperature gradients in three dimensions, discuss the dependence on experimental conditions, and propose changes in heater chip geometry to allow more precise temperature control. We next calculate the effect of the electron beam on the liquid (radiolysis) as a function of temperature. In TEM, radiolysis is modeled by including the rate at which incident electrons transfer energy to water and create radiolysis species and the subsequent diffusion and interactions of these species with each other and with other molecules present. All steps of this process are temperature-dependent, and we highlight the effects most relevant to our electrochemical experiments. We finally model the

temperature-dependent kinetics of an electrochemical reaction in the case where only part of the electrode is heated, as in our experiments. We focus in particular on Cu deposition under galvanostatic conditions, aiming to understand the role of spatially-dependent diffusion in determining how the deposited morphology evolves under simultaneous control of heat and electrochemical conditions. We are excited by the opportunities of LC-TEM in quantifying temperature-dependent electrochemical processes for a range of practical applications in energy storage, catalysis and corrosion.

#### 5:25 AM F.MT01.01.03

##### **Visualizing Ligand-Mediated Bimetallic Nanocrystal Formation Pathways with *In Situ* Liquid Phase Transmission Electron Microscopy** Synthesis Mei Wang and Taylor J. Woehl; University of Maryland, United States

Organic capping ligands play accompanying roles aside from controlling the size and shape of nanocrystals. For instance, heteronuclear ligand-metal complexes have been shown to facilitate alloying of colloidal bimetallic nanoparticles; however, the mechanism by which this occurs remains unclear. Here we utilize liquid-phase transmission electron microscopy (LP-TEM) to demonstrate the roles of metal thiolate complexes and thiol ligands in controlling the formation pathways of bimetallic AuCu nanoparticles. Direct visualization of AuCu nanocrystal under dose-rate controlled LP-TEM conditions shows that polyethylene glycol thiol (PEG-SH) capping ligands modulate the rates of inter-metal electron transfer and metal atom aggregation reactions by forming metal thiolate complexes and kinetically trapping random alloy structures *via* strong, rapid surface capping. Systematic LP-TEM experiments varying dose rate established imaging conditions that minimized electron beam induced nanoparticle aggregation and phase separation and produced alloyed bimetallic nanoparticles of similar structure to benchtop flask-based synthesis. Kinetic simulations of the reactions between ligands and electron beam produced radicals revealed that thiol functional groups were oxidized to disulfide groups and organic radicals. At sufficiently high levels of ligand oxidation (high electron beam fluxes), weak ligand capping by disulfide groups leads to nanoparticle aggregation and metal phase separation, while at low levels of capping ligand oxidation spherical alloyed nanocrystals are formed. Taken together, our results indicate that thiol ligands play a dual role in facilitating alloyed nanoparticle formation by confining metal species within metal-ligand precursor complexes, which promotes simultaneous chemical reduction of metal ions and minimizes inter-metal electron transfer reactions that cause phase separation, and strongly and rapidly capping nanoparticles to prevent phase separation during crystallization.

#### 5:35 AM F.MT01.01.04

##### **Graphene—A Promising Electrode Material in Liquid Cell Electrochemistry** Shu Fen Tan<sup>1</sup>, Kate Reidy<sup>1</sup>, Serin Lee<sup>1</sup>, Julian Klein<sup>1</sup>, Nicholas Schneider<sup>2</sup>, Haeyeon Lee<sup>1</sup> and Frances M. Ross<sup>1</sup>; <sup>1</sup>Massachusetts Institute of Technology, United States; <sup>2</sup>Renata Global, United States

Two-dimensional (2D) materials such as graphene and transition metal dichalcogenides (TMDs) are potential candidate materials for electrodes due to their exceptional intrinsic properties including their high specific surface area, high electrical charge mobility and good thermal conductivity and mechanical strength. Graphene in particular shows tuneable structures and electrocatalytic activity, excellent conductivity, good chemical resistance and mechanical flexibility, as well as the ease and low cost of production. Graphene-based composites have been explored as next generation electrode materials for electrical and optical devices, supercapacitors, organic electronics and dye-sensitized solar cells and graphene itself is considered a promising electrode material for applications ranging from photocatalysis and solar cell to optoelectronic devices. In electron microscopy, graphene is used in a different way: its remarkable mechanical and scavenging properties make it ideal for graphene liquid cells<sup>1</sup> where liquid is encapsulated between two graphene sheets for high-resolution imaging. However, the transfer method of graphene to fabricate high quality graphene liquid cells and the reproducibility of making liquid pockets with sufficient volume, exact chemical content and well-defined thickness are key experimental challenges with graphene liquid cells. Recent studies circumvent leakage issues by using a liquid cell that is a hybrid of SiN<sub>x</sub> and graphene to form leak-proof liquid confinement.<sup>2</sup> Furthermore, separating top and bottom graphene windows with a thin layer of hexagonal boron nitride (hBN) enables more control over liquid thickness and can provide a two-fold improvement in resolution<sup>3</sup> compared to conventional graphene liquid cells. Despite these and other advances in engineering 2D materials into liquid cell design, the full functionality associated with microfabricated liquid cells, such as addition of electrochemical, heating or flowing and mixing capabilities, are generally still absent.

Here we focus on the opportunities arising from the use of 2D materials in liquid cell electrochemistry. To establish whether 2D materials can indeed evolve into a reliable electrode material for both electroanalytical chemistry and electron microscopy, we need to develop a reproducible protocol in transferring 2D materials onto microfabricated liquid cell chips to achieve reliable electrical contact and mechanical robustness. We describe liquid cells equipped with 2D material electrodes and show results aimed at understanding the interplay of kinetics and thermodynamics during electrochemical deposition, measuring parameters such as the shape, size and epitaxy of electrochemically deposited nanoparticles. We discuss the effects of external parameters such as the thickness and nature of the 2D materials and the deposition potential and we

consider beam damage of these 2D materials. Exploring the possibility of 2D materials as electrode materials potentially opens up new opportunities for investigating a wide range of problems pertaining to energy storage and electrocatalysis.

1. Yuk, J. M.; Park, J.; Ercius, P.; Kim, K.; Hellebusch, D. J.; Crommie, M. F.; Lee, J. Y.; Zettl, A.; Alivisatos, A. P., High-Resolution EM of Colloidal Nanocrystal Growth Using Graphene Liquid Cells. *Science* **2012**, *336* (6077), 61-64.
2. Rasool, H.; Dunn, G.; Fathalizadeh, A.; Zettl, A., Graphene-sealed Si/SiN cavities for high-resolution in situ electron microscopy of nano-confined solutions (Phys. Status Solidi B 12/2016). *physica status solidi (b)* **2016**, *253* (12), 2544-2544.
3. Kelly, D. J.; Zhou, M.; Clark, N.; Hamer, M. J.; Lewis, E. A.; Rakowski, A. M.; Haigh, S. J.; Gorbachev, R. V., Nanometer Resolution Elemental Mapping in Graphene-Based TEM Liquid Cells. *Nano Letters* **2018**, *18* (2), 1168-1174.

#### 5:45 AM F.MT01.01.05

**Graphene Liquid Cell for High-Resolution *In Situ* S/TEM Imaging to Study Nucleation and Growth of Nanomaterials** Walid Dachraoui, Trond R. Henninen and Rolf Erni; Empa–Swiss Federal Laboratories for Materials Science and Technology, Switzerland

Understanding the chemical and the physical processes of nanomaterials (NMs) in liquid media is a crucial challenge and of fundamental interest to modern materials science, chemistry and biology [1]. For example, observing the initial steps of nucleation and the growth of solids is of highest importance for the development of novel materials. This requires techniques allowing the study of NMs in their liquid environments with the corresponding resolution necessary to observe the formation and evolution of clusters at atomic-scale. The most attractive and unique capabilities of a scanning/transmission electron microscope (S/TEM) is its high-resolution, enabling to study materials at the atomic-scale. Nevertheless, a key limitation of this technique is the need of high vacuum conditions to analyse samples. In recent years, a new frontier in the field of transmission electron microscopy has emerged to observe specimens in liquid environments instead of high-vacuum conditions, by separating the liquid sample from the vacuum column using thin impermeable/electron transparent membranes [2]. Recent advances in microfabrication technology has led to a number of commercially available liquid cell TEM holders, where the liquid cells are made of two micro-fabricated silicon nitride ( $\text{Si}_x\text{N}_{1-x}$ ) electron transparent thin films. The cell thickness can be controlled by spacers ranging from 50 nm to 5000 nm. Since the thickness of the encapsulating material is one aspect that negatively affects the resolution, the commercial cells are not optimized around achieving the highest spatial resolution including atomic resolution. Graphene-based liquid cell electron microscopy (GLC-EM) have demonstrated a better imaging resolution [3].

In this study, we optimized graphene-based liquid cells to realize in real time atomic-scale observations of nucleation and growth of gold (Au) nanoparticles in liquid mode, using high-spatial resolution S/TEM. The cell shows excellent imaging capabilities compared to conventional  $\text{Si}_x\text{N}_{1-x}$  liquid cells especially at higher-magnification. This work demonstrates that, using graphene to encapsulate small pockets of liquid, we were able to image and track in real time the very early stage of material growth at an interpretable atomic-scale resolution.

#### References:

- [1] Raymon R. Unoci, *Microsc. Microanal* 2015, 21.
- [2] Damien Alloyeau, Walid Dachraoui, Yasir Javed, Hannen Belkahla, Guillaume Wang, H el ene Lecoq, Souad Ammar, Ovidiu Ersen, Andreas Wisnet, Florence Gazeau, Christian Ricolleau, *Nano Letters* **2015**, *5*, 4, 2574-2581.
- [3] Astrid De Clercq, Walid Dachraoui, Olivier Margeat, Katrin Pelzer, Claude R. Henry, and Suzanne Giorgio, *J.Phys.Chem.Lett* **2014**, *5*, 2126–2130.
- [4] This project has received funding from the European Research Council (ERC) under the EU's Horizon 2020 research and innovation program (grant No. 681312).

#### 5:55 AM F.MT01.01.06

**From Atoms to Particles—Hetero- and Homogeneous Nucleation of Sub-nm Pt Clusters Observed at the Atomic Scale in Liquid** Trond R. Henninen, Debora Keller and Rolf Erni; Empa–Swiss Federal Laboratories for Materials Science and Technology, Switzerland

The formation of solid matter as modelled by the classical nucleation theory (CNT), assumes to be triggered by the generation of spherical nuclei. However, initially at sub-nm scale, non-spherical atomic clusters form with structures deviating from a bulk crystal. Understanding the atom-by-atom growth dynamics at this size, requires considering the individual atoms. Conventional liquid cell holders have enabled studying liquid systems in transmission electron microscopes, but are limited in spatial resolution by the thickness of the liquid and the encapsulating windows (in total 100-

1000 nm), making imaging at sub-nm resolution challenging. To further progress to atomic resolution, we use low vapour-pressure liquids, (glycerol or ionic liquids, such as 1-butyl-3-methyl imidazolium chloride).<sup>[1]</sup> The negligible vapour pressure makes such liquids directly vacuum compatible without windows, and enables atomic resolution in suspended nanofilms and supported nanodroplets (5-50 nm thickness). Furthermore, a melting point above room temperature enables adjusting the viscosity of the liquid, and thus reaction kinetics, by heating. In our liquid phase experiments, we can observe dispersed Pt atoms to nucleate into few-atom clusters, which further coalesce and grow into nanoparticles or disordered cluster agglomerates, or redissolve into the liquid. CNT tells us that the presence of a surface lowers the energy barrier of heterogeneous nucleation, compared to homogeneous nucleation in a liquid phase. In our liquid experiments, there is indeed a corresponding effect, where nucleation is rarely observed in the suspended liquid nanofilms, while easily observable at a high nucleation rate in the nanodroplets on a carbon surface. As the highly unstable sub-nm clusters nucleate and dissolve, increased stability is observed in clusters of ca 8-13 atoms, compared to smaller clusters. Indeed, nucleating clusters typically form directly into this size range, where various close-packed structures (such as fcc and icosahedral<sup>[2]</sup>) often can be observed. This indicates that the formation of close-packed, crystalline structures, already at the few-atomic scale, is an essential step of the nucleation process.

#### References:

[1] D. Keller, T. R. Henninen, R. Erni, *Micron* **2019**, *117*, 16.

[2] T. R. Henninen, M. Bon, F. Wang, D. Passerone, R. Erni, *Angew. Chemie Int. Ed.* **2019**, *2*.

[3] This project has received funding from the European Research Council (ERC) under the EU's Horizon 2020 research and innovation program (grant No. 681312)

SESSION F.MT01.02: Advanced In Situ TEM for Material Science  
On Demand Abstracts Available for Viewing Starting Saturday Morning, November 21, 2020  
F-MT01

#### 5:00 AM \*F.MT01.02.01

**Plasmonic Nanostructures for Room Temperature Catalysis** Renu Sharma and Wei-Chang Yang; National Institute of Standards and Technology, United States

In situ transmission electron microscopy (TEM) is now routinely used to measure the effect of external stimuli, such as temperature, gas or liquid environment, mechanical stress, etc., on the structure, chemistry, morphology and functioning of nanostructured materials. Here we employ in situ TEM to show that local surface plasmon resonance (LSP) energies can be used to initiate chemical reactions that mimics photocatalysis.

The energy barrier for most of the chemical reactions is overcome by heating the reactants in the presence of a suitable catalyst, where the thermal energy provided by heat helps in surpassing the barrier that has been reduced by the adsorption of the reactant molecules. In recent years, the localized surface plasmon (LSP) resonance energy has been used to replace the thermal energy to initiate reaction at low temperatures, even at room temperature.<sup>1,2</sup> As most of the plasmonic materials, Au, Ag or Al, are not generally catalytically active, i.e. do not adsorb most of the gas molecules, but have been successfully combined with active catalysts such as Pt, Ni, Ru, etc., for harvesting their LSP resonance energies for low temperature reactions. So far optical methods have been used to generate and measure the LSP resonance energies. However, the low spatial resolution, of the order of 100 nm, achievable by optical methods, does not provide sub-particle level distribution of coupling efficiency of different modes. On the other hand, high energy electrons not only excite all LSP modes simultaneously, but also provide high spatial resolution in the nanometer range to resolve their energy loss probability that indicates the location-specific efficiency of coupling to the LSP modes at certain resonance energies on the plasmonic nanoparticle. Therefore, we use a monochromated electron source in an environmental scanning-transmission electron microscope (ESTEM), combined with metallic nanoparticle boundary element method (MNPBEM) and density functional theory (DFT) simulations, to characterize various LSP modes and their coupling efficiency distribution within the shape- and size-controlled nanoparticles of Au and Al. We demonstrate that the knowledge gained from low-loss and core-loss EELS measurements can be used to design catalyst-plasmonic particle combination for selected chemical reactions.

1 Mukherjee, S. *et al.* Hot electrons do the impossible: plasmon-induced dissociation of H<sub>2</sub> on Au. *Nano letters* **13**, 240-247 (2012).

2 Yang, W.-C. D. W., Canhui; Fredin, Lisa A.; Lin, Pin Ann; Shimomoto, Lisa; Lezec, Henri J. and Sharma Renu Site-



selective CO disproportionation mediated by localized surface plasmon resonance excited by electron beam. *Nature materials* **18**, 614-619 (2019).

#### 5:15 AM \*F.MT01.02.02

**Probing Interfaces in Heterogeneous Catalysts via *In Situ* and 4D STEM** Miaofang Chi; Oak Ridge National Laboratory, United States

Interfaces in catalysts are inherently dynamic - they often form under vigorous synthesis conditions and dynamically adapt their structures down to atomic scale to the specific reaction conditions. Depending on the synthesis conditions and the phase of the reactant, the active interfaces include those between solid-gas, solid-liquid, and triple-phase interfaces of solid-gas-liquid. Hence, in order to understand the catalytic reaction mechanisms, not only their initial structural and chemical configurations matter, but also their evolution under reaction conditions have to be clearly elucidated. In this talk, I will present our recent studies on understanding the synthesis and reaction mechanisms of precious metal nanoparticle based heterogeneous catalysts, by using scanning transmission electron microscopy. Specifically, three examples will be given, including the understanding of the deposition and growth mechanisms of metal core-shell nanoparticles using *in situ* liquid cell electron microscopy, the probing of the dynamic evolutions of surface atomic structures of core-shell nanocubes via environmental cell STEM, and at last, the mapping of strong interactions between support and metal as a function of post-synthesis treatments using four-dimensional STEM.

**Acknowledgements:** research supported by the U.S. Department of Energy, Office of Science, Office of Basic Energy Sciences, Chemical Sciences, Geosciences, and Biosciences Division, and was performed at the Center for Nanophase Materials Sciences at Oak Ridge National Laboratory (ORNL), which is a DOE Office of Science User Facility.

#### 5:30 AM \*F.MT01.02.03

***In Situ*, Site Specific and High Spatial Precision Electron Microscopy Studies for Correlation of Atomic Structure to Properties** Eva M. Olsson; Chalmers Univ of Technology, Sweden

In situ electron microscopy allows us to reveal the correlation between local atomic structure and properties with high spatial resolution. The effect of electric fields, light, mechanical strain and temperature on both structure and properties can be imaged and studied using spectroscopy. The obtained knowledge is used to tune the properties of advanced materials and devices. Catalytic activity of metal nanoparticles and electrical properties of semiconducting nanowires are examples where the strain induced effects have a strong influence on the properties and performances. High resolution annular dark field (ADF) scanning transmission electron microscopy (STEM) imaging can provide high resolution (better than 1 Å) and high precision (better than 1 pm) information about the local atomic structure [1]. In situ and correlative microscopy can be used to perform spatially resolved electrical, mechanical and optical studies [2]. In addition, dynamic electric field induced changes on the atomic scale can be studied using in situ microscopy [3]. The precision of the measurement and the quantitative information enable important and theoretical modelling on the same material systems. New aspects of material properties and mechanisms, not obvious from measurements on the macro scale are revealed using in-situ electron microscopy where interfaces, surfaces, geometries and defects affect the material properties on the macro, micro, nano and atomic scale. The knowledge is crucial for the understanding of the mechanisms active on the nano- and atomic scale, the effect of atomic structure on the properties and also for the design of materials and devices with tailored properties.

#### References

- [1] T. Nilsson Pingel, M. Jørgensen, A.B. Yankovich, H. Grönbeck and E. Olsson, "Influence of atomic site-specific strain on catalytic activity of supported nanoparticles", *Nature Communications* **9** (2018) 149.
- [2] J. Holmér, L.J. Zeng, T. Kanne Nordqvist, J. Nygård, P. Krogstrup, L. De Knoop and E. Olsson, "An STM-SEM setup for characterizing photon and electron induced effects in single photovoltaic nanowires", *Nano Energy* **53** (2018) 175; Y.B. Yankovich, B. Munkhbat, D.G. Baranov, J. Cuadra, E. Olsén, H. Lourenco-Martins, H. Tizei, M. Kociak, E. Olsson and T. Shegai, "Visualising spatial variations of plasmon-exciton polaritons at the nanoscale using electron microscopy", *Nano Letters* **19** (2019) 8171.
- [3] L. de Knoop, M.J. Kuisma, J. Löfgren, K. Lodewijks, M. Thuvander, P. Erhart, A. Dmitriev and E. Olsson, Electric field controlled reversible order-disorder switching of a metal tip surface", *Phys. Rev. Mat.* **2** (2018) 085006.

5:45 AM \*F.MT01.02.04

**Nanoscale Crystal Growth on van der Waals-Bonded Materials as Seen with *In Situ* Microscopy Techniques** Frances M. Ross; Massachusetts Institute of Technology, United States

Two-dimensional materials provide exciting opportunities as substrates for the growth of three-dimensional nanocrystals. The difference in the nature of the bonding at the 3D nanocrystal / 2D material interface, compared to the situation for conventional epitaxy, is expected to generate interesting and potentially useful new growth modes and interfacial structures. It is well known that deposition of gold and other metals onto certain van der Waals-bonded materials produces faceted nanocrystals that can be aligned with the substrate lattice. Here we describe the use of several *in situ* microscopy techniques to explore the principles governing epitaxial growth in a broader range of nanocrystal / van der Waals substrate combinations. An unusual feature of the *in situ* experiments is that substrate preparation and materials deposition can be carried out under ultra high vacuum conditions in chambers that are connected to the microscope, while materials deposition is also possible while the sample is under observation within the microscope. These multiple capabilities are helpful in allowing flexibility and experimental robustness. Furthermore, for these particular experiments, a UHV environment (low  $10^{-10}$  Torr base pressure range) allows reactive materials such as niobium or germanium to be deposited and examined without oxidation. We will describe nanocrystal growth on suspended 2D materials using a UHV-TEM that has integrated capabilities for heating, laser cleaning, metal evaporation, and semiconductor chemical vapor deposition. Post-growth observation using scanning transmission electron microscopy yields atomic level compositional information as well as movies showing nanoparticle motion and annealing phenomena. We will also describe complementary measurements performed in a multi-probe, UHV *in situ* scanning tunneling microscope. This instrument provides opportunities to examine the atomic and electronic structure as well as to measure the transport properties of the nanocrystal / van der Waals material interface. We apply these techniques to evaluate nanocrystal morphology, orientation relation and interfacial structure and properties as a function of deposition parameters. We discuss strategies for morphological control and describe nanocrystal coalescence events and the patterning of the 2D substrate to control nucleation sites. We finally consider the formation of epitaxial alloy and heterostructure islands via sequential deposition. The eventual aim of the *in situ* experiments is to understand the relationship between the interfacial structure and morphology in a nanocrystal / van der Waals-bonded material combination and the electronic properties that are required for its applications.

6:00 AM \*F.MT01.02.05

**Investigating the Effects of Additives on Particle Nucleation and Assembly by Liquid Phase TEM** James J. De Yoreo<sup>1,2</sup>, Guomin Zhu<sup>2,1</sup>, Zhaoming Liu<sup>3,1</sup>, Maria Sushko<sup>1</sup>, Zhisen Zhang<sup>4</sup>, Benjamin Legg<sup>2,1</sup> and Ruikang Tang<sup>3</sup>; <sup>1</sup>Pacific Northwest National Laboratory, United States; <sup>2</sup>University of Washington, United States; <sup>3</sup>Zhejiang University, China; <sup>4</sup>Xiamen University, China

Due to a unique combination of spatial and temporal resolution, liquid phase (LP) TEM has provided new insights into poorly understood processes of particle nucleation and assembly. Here we describe the results of studies on metals, oxides, and carbonates aimed at understanding the effects of additives, both as surface-bound ligands and dopants, on nucleation pathways and particle assembly. Investigations into hematite (Hm) mesocrystal formation from a ferrihydrite (Fh) precursor show that, in the presence of oxalate, isolated Hm particles rarely form. However, when they do, new Hm particles then repeatedly nucleate about 2 nm away from the new surfaces and immediately undergo oriented attachment to the growing aggregates of coaligned particles. Because nucleation rates are statistically deterministic and direction-specific, the resulting mesocrystals exhibit a constant shape irrespective of size. Results on Au nanoparticle formation in the presence of citrate reveal a similar outcome and comparison to natural and synthetic systems suggests such interface-driven pathways are widespread. Classical DFT analyses indicate that, for both Hm and Au, the surface-bound organics create interfacial chemical gradients that result in enrichment of cation species about a nm from the surface, though in the case of Au the species and degree of enhancement is pH dependent. Investigations of calcite formation from amorphous calcium carbonate (ACC) precursors in the presence of additives reveal a very different outcome. When carboxyl-rich organics are added, ACC transforms to crystalline phases via dissolution-reprecipitation, but at slower rates than in pure solution. However, when Mg is added, ACC initially exhibits low electron contrast, which increases over time absent any change in particle morphology. Diffraction and spectroscopic analysis show that the ACC transforms to Mg-calcite accompanied by loss of structural water. In combination with molecular dynamics simulations, the results imply Mg brings excess water into ACC, inducing structural fluctuations that enable transformation without the need to nucleate a separate crystal. These results highlight the opportunity that LP-TEM provides for deciphering underlying mechanisms of particle nucleation and assembly.

6:15 AM \*F.MT01.02.06

**2D Nanostructure Formation and Defects Evolution Revealed by *In Situ* Liquid Cell Transmission Electron Microscopy** Haimei Zheng<sup>1,2</sup>; <sup>1</sup>Lawrence Berkeley National Laboratory, United States; <sup>2</sup>University of California, Berkeley,

United States

Two-dimensional (2D) materials have attracted significant attention due to their unique structure and properties. However, our understanding of their growth mechanisms, especially those in solution, is still limited. Using liquid cell transmission electron microscopy (TEM), we study the growth of 2D nanostructures and defects evolution with high spatial resolution in-situ. First, as an example, I will show the growth of 2D cobalt oxide and cobalt nickel oxide nanosheets. Our direct observation reveals that 3D nanoparticles are initially formed from the molecular precursor solution and they transform into 2D nanosheets. Ab initio calculations show that a small nanocrystal is dominated by positive edge energy, but when it grows to a certain size, the negative surface energy becomes dominant, driving the 3D nanocrystal transformation into a 2D structure. Uncovering these growth pathways, including the 3D-to-2D transition, provides opportunities for the future design and solution synthesis of novel materials. Second, I will also show the growth of 2D indium chloride nanostructures. The nucleation and growth of 2D nanosheets in solution are found through both classical and non-classical pathways. The growth kinetics at the low temperature is reduced compared to that at the room temperature. The fast growth induces high density of defects (e.g., nanotwins). In addition, our atomic structural analysis of the nanosheets and chemical mapping of the reaction front provides useful complementary information. These systematic studies allow us to develop an understanding of the growth mechanisms of  $\text{InCl}_3$  2D nanosheets and defect evolution. In conclusion, our development of high resolution liquid phase TEM opens opportunities for future study of many other nanomaterials growth and transformations.

**6:30 AM \*F.MT01.02.07**

**Machine-Learning Revealed Nanoparticle Dynamics from Liquid-Phase TEM Videos** Qian Chen; University of Illinois at Urbana-Champaign, United States

In this talk, I will present my group's recent in using our customized analysis framework based on a machine learning model based on convolutional neural network in extracting quantitative information from liquid-phase TEM videos. We apply this framework to three typical systems of colloidal nanoparticles, concerning their diffusion and interaction, reaction kinetics, and assembly dynamics, all resolved in real-time and real-space by liquid-phase TEM. A diversity of properties for differently shaped anisotropic nanoparticles are mapped, including the anisotropic interaction landscape of nanoprisms, curvature-dependent and staged etching profiles of nanorods, and an unexpected kinetic law of first-order chaining assembly of concave nanocubes. These systems represent properties at the nanoscale are otherwise experimentally inaccessible. Compared to the prevalent image segmentation methods, our method shows a superior capability to predict the position and shape boundary of nanoparticles from highly noisy and fluctuating background—a challenge common and sometimes inevitable in liquid-phase TEM videos. We expect our framework to push the potency of liquid-phase TEM to its full quantitative level, and to shed insights, in high throughput and statistically significant fashion, on the nanoscale dynamics of synthetic and biological nanomaterials.

**6:45 AM F.MT01.02.08**

**In Situ Imaging of Carbon-Coated Aluminum Nanoparticles via Low Energy Laser-Induced Heating in TEM** Chi-Chin Wu<sup>1</sup>, Trevor Clark<sup>2</sup>, Lily Giri<sup>1</sup>, Rose A. Pesce-Rodriguez<sup>1</sup> and Khalid Hattar<sup>2</sup>; <sup>1</sup>U.S. Army Research Laboratory, United States; <sup>2</sup>Sandia National Laboratories, United States

Metallic nanoparticles such as nano-aluminum (nAl) are promising candidates as energetic additives for improved combustion and detonation effects in explosive/propellant formulations because of the high heat of combustion for aluminum and potentially rapid burning of nAl enabled by the high surface area to volume ratio. Various carbon-coated core-shell nAl were produced via atmospheric dielectric barrier discharge plasmas using commercial nAl (40-60 nm avg. diameter). Preliminary ex-situ characterization via transmission electron microscopy (TEM) has discovered the formation of  $\gamma$ -alumina ( $\gamma\text{-Al}_2\text{O}_3$ ) crystallites that are both present in the organic coating and in the matrix of amorphous shell surrounding the Al core, presumably due to the phase transformation of the originally amorphous  $\text{Al}_2\text{O}_3$  ( $\alpha\text{-Al}_2\text{O}_3$ ) induced by the plasma process. This work aims to investigate in-situ the coupled effects of transformed  $\text{Al}_2\text{O}_3$  shell and organic coating on the dynamic behavior of nAl during heating experiments induced by a low-energy focused laser beam in TEM. The laser energy varied from ~1.5 W to 3 W with an incremental increase of 0.1 W every few minutes. The dynamic morphological and phase transformation during heating were investigated and captured through increasing numbers of hexagon-shaped  $\gamma\text{-Al}_2\text{O}_3$  crystals floating on molten Al cores at a lower threshold laser energy than the as-received commercial nAl. The results from this paper directly revealed the real-time interactions among Al,  $\alpha\text{-Al}_2\text{O}_3$ ,  $\gamma\text{-Al}_2\text{O}_3$ , and carbon-coating for enhancing fundamental understanding of nAl at high temperatures. This paper also underscores the significance of exploiting advanced in-situ materials characterization to enhance in-depth understanding of reactive nAl composites possessing plasma-altered surface modifications for optimal controls of synthesis conditions and resultant structural and chemical properties.

#### 6:55 AM F.MT01.02.09

**Probing Thermal Expansion Coefficient of SrTiO<sub>3</sub> Grain Boundaries by *In Situ* STEM-EELS** Kun-Yen Liao, Kiyou Shibata and Teruyasu Mizoguchi; The University of Tokyo, Japan

In nanocrystalline materials, smaller crystallite size and increasing grain boundary (GB) volume may result in different physical properties from those of the bulk. Thermal expansion coefficient (CTE), as one of the important factors for materials selection, has been investigated extensively in several nanocrystalline materials [1-3]. Conventional approaches include the measurement of bulk CTE with varied grain size as well as the determination of lattice constants by scattering methods. However, the inconsistency of experimental findings has left the question on whether GBs contribute to the enhancement of CTE. Direct determination of CTE near GBs may require the dedicated measurement of temperature and volume in nanometer scale and is still challenging issue for conventional methods due to the lack of spatial resolution.

In recent years, a nanoscale thermometry has been realized using valence electron energy loss spectroscopy (EELS) in scanning transmission electron microscope (STEM) [4]. Local temperature can be estimated by mapping the variation of plasmon energy. With this method, CTE of various 2-D materials has been successfully determined in nanoscale region with the support of theoretical calculation [5]. However, GBs contribution has not yet been discussed in the previous reports.

In this work, we attempt to probe the CTE of individual GBs by using in-situ valence EELS. Bicrystals of  $\Sigma 5$  and  $\Sigma 29$  strontium titanate (SrTiO<sub>3</sub>) GBs were investigated in a temperature range from 300 to 873K. The GB structure was analyzed by high angle annular dark field (HAADF) image. The plasmon energy was mapped near GBs in each temperature and compared with the density functional theory (DFT) calculation. By carefully monitoring the shift of plasmon energy, we achieved to obtain local CTE near selected GBs. The relationship between CTE and GB structure was further analyzed by molecular dynamics (MD) simulation. The details will be shown in my presentation.

[1] Klam, H. J., H. Hahn, and H. Gleiter. *Acta Metallurgica* 35.8 (1987).

[2] Szpunar, Barbara, et al. *Physical Review B* 60.14 (1999).

[3] Kuru, Y., et al. *Applied physics letters* 90.24 (2007).

[4] Mecklenburg, Matthew, et al. *Science* 347.6222 (2015).

[5] Hu, Xuan, et al. *Physical review letters* 120.5 (2018).

#### 7:05 AM F.MT01.02.10

***In Situ* High-Resolution Transmission Electron Microscope on Atomic Scaled Friction** Xiang Wang, Yang He and Scott X. Mao; University of Pittsburgh, United States

Observing atomic-friction and revealing the friction mechanism at the atomic-scale are significant to understand macro friction behaviors and control wastage induced by the friction between contacts in microdevices. Here, by designing the atomic-scale contacts under transmission electron microscopy (TEM) observation, the real-time atomic friction process is captured. Friction between single tungsten asperities shows a discrete stick-slip behavior and in-situ TEM experiment revealed that the accumulation and release of the strain energy during friction is an asynchronized process. This work paves a possible way to realize in-situ atomic-friction research and enriches the understanding of the atomic-friction.

SESSION F.MT01.03: Advanced Synchrotron X-Ray for Materials Dynamics  
On Demand Abstracts Available for Viewing Starting Saturday Morning, November 21, 2020  
F-MT01

#### 5:00 AM \*F.MT01.03.01

***Operando* Synchrotron X-Ray Studies of Metal Additive Manufacturing** Tao Sun<sup>1</sup>, Cang Zhao<sup>2</sup>, Niranjan Parab<sup>3</sup> and Sarah Wolff<sup>4</sup>; <sup>1</sup>University of Virginia, United States; <sup>2</sup>Tsinghua University, China; <sup>3</sup>Argonne National Laboratory, United States; <sup>4</sup>Texas A&M University, United States

Metal additive manufacturing (AM) refers to a group of disruptive technologies that build metallic three-dimensional objects by adding feedstock materials layer by layer based on computer models. AM not only unleashes the design freedom of engineers by allowing the build of geometrically complex parts, but also opens up tremendous opportunities for material

scientists to synthesize materials far-from-equilibrium and fabricate functionally graded architectures. While AM holds the promise for completely revolutionizing the way we make things, building defect-free metal products with precisely controlled material microstructures and part performance remains challenging. Indeed, substantial fundamental issues associated with metal AM still need to be addressed before it can reach its full potential, and many new research areas need to be explored.

At the Advanced Photon Source, we have been applying *operando* high-speed x-ray imaging and diffraction techniques to probe a variety of metal AM processes since 2016. The superior penetration power of high-energy x-rays and the extremely high photo fluxes afforded by the 3rd-generation synchrotron facility allows the quantitative characterization of dynamic structural evolution in bulk metallic materials with unprecedented spatial and temporal resolutions. Many highly transient phenomena that take place during the energy-matter interaction in metal AM were investigated, and the mechanisms responsible for different types of defects were identified.

In the presentation, I will give a brief overview of the *operando* synchrotron studies of metal AM performed by our team and other scientists around the world. These metal AM processes include laser powder bed fusion, directed energy deposition, and binder jetting. The strengths and limitations of different beamlines (i.e. source, detector) and *operando* AM systems will be elaborated. I will then introduce the new understanding gained from our synchrotron x-ray experiments, as well as their broad impact on the development of AM materials, technologies, and numerical models.

#### 5:15 AM \*F.MT01.03.02

**Multi-Scale and Multimodal X-Ray Microscopy and Applications** Xianghui Xiao and Xiaojing Huang; Brookhaven National Laboratory, United States

Interactions between x-ray and matters carry the matters' property information, e.g. chemical species, chemical states, electronic structures, morphological structures, etc. In a complex heterogeneous sample system that has a hierarchical structure, multi-modal and multi-scale characterizations are necessary to reveal the system's properties. Various x-ray microscopy and imaging techniques are valuable tools in such applications.

X-ray micro-imaging with synchrotron sources has been successfully applied to study dynamic systems of large volumes at high spatial and temporal resolutions. Compared to radiography, tomography is capable to provide structural information in three dimensions that is crucial in studying heterogeneous systems. However, with tomography, it is challenging to pursue temporal resolution as high as radiography. On the one hand, a tomography scan needs to take hundreds to thousands of radiography images of a sample. On the other hand, the sample needs to rotate during the image acquisition that may induce disturbances to the sample system due to unavoidable centrifugal force under rapid spinning. In this presentation, a recent development aiming to overcome these limitations will be presented.

At higher spatial resolution, it is possible to integrate multimodal techniques onto the same imaging/microscopy platform. Transmission X-ray Microscopes (TXM) have been widely used in energy storage material e.g. battery researches. One uniqueness of TXM is fast spectro-imaging capability at tens of nanometer spatial resolution that provides complex chemo-mechanical interaction information at a single electrode particle level in battery systems. Such information helps not only to understand the electrode materials' behaviors but also to improve battery electrode engineering designs to mitigate the potential damages under charge/discharge conditions.

Although TXM is capable to provide correlative spectro-morphological imaging capabilities, other scanning nano-probe techniques are needed to pursue even more modalities at higher sensitivity. At a state-of-art nanoprobe beamline, nano-diffraction, nano-fluorescence, and scanning imaging techniques can be integrated onto the same platform. Multimodal measurements with these techniques provide correlative structural information of the samples from different aspects. However, such measurements are slow, so it is not suitable for in situ and high throughput experiments. Combining TXM and nano-probe techniques overcomes each technique's limitations and provide deep insights into the measured system. Few examples of this approach will be discussed in the presentation.

#### 5:30 AM \*F.MT01.03.03

**Dynamic and *In Situ* Characterization Using X-Ray Synchrotron Sources** Michelle Mejia and Michael Behr; Dow, United States

High flux radiation sources where we have active research programs (APS, ALS, and NIST) enable the study of materials and material properties in non-ambient environments characteristic of their synthesis, processing conditions, and/or use in the field. The variety of sources allows for enhanced contrast mechanisms for the analysis of structure, composition, and phase behavior of a variety of systems across R&D from the atomic to near visible light scale. In-situ experiments, including thermal and mechanical, allow for in-depth understanding of mechanisms of energy transfer present in materials. This presentation will give an overview of the problem solving capabilities available to Dow as well as some case studies on in-

situ tensile/X-ray to examine energy absorbing mechanisms and in-situ DSC/X-ray to examine crystallization dynamics. Deformation and failure mechanisms of polyolefin blends are investigated by collecting X-ray scattering data during in-situ tensile experiments. By simultaneously collecting both WAXS and SAXS patterns during the tensile experiments various energy transfer mechanisms can be tracked/observed including changes in orientation, crystal breakup, microvoiding, and lamellar size and shape. It is the sequence, type, and magnitude of these mechanisms that dictate mechanical performance in a material. WAXS will reveal differences in orientation and crystallite size while SAXS will give insight into the presence of microvoiding as well as lamellar size and shape. By combining the X-ray data with the tensile data, we are able to track how the addition of propylene-based olefin block copolymer (P-OBC) compatibilizers of different composition to PE/PP blends affects the deformation mechanism present during strain.

Additionally, in-situ DSC/X-ray experiments were conducted in order to investigate the effect of P-OBC compatibilizers on the crystallization behavior of polyethylene. A change in temperature is observed in a static DSC experiment, however this test does not determine whether this change is caused by crystallization/nucleation of the P-OBC compatibilizer or microphase segregation of the P-OBC compatibilizer. In-situ experiments allows for this distinction and WAXS is used to track the crystallization and microphase segregation of these blends as a function of temperature.

#### 5:45 AM F.MT01.03.04

**Elucidating the Factors Governing the Cyclic Performance of MgO-Based Sorbents of CO<sub>2</sub> Using Time-Resolved *In Situ* XRD/PDF Techniques** Margarita Rekhtina, Maximilian Krödel, Paula M. Abdala and Christoph Müller; ETH Zürich, Switzerland

The development and deployment of technologies for CO<sub>2</sub> capture and storage (CCS) is key to limit the global warming below the 2 °C target (Paris Agreement). One of the CCS techniques considered is the post-combustion capture of carbon dioxide with solid sorbents. In particular, MgO-based sorbents are highly promising due to their abundance and low cost, as well as their intermediate operational temperature range of 200–450 °C and high theoretical uptake of 1.09 g<sub>CO<sub>2</sub></sub>/g<sub>MgO</sub>. However, an important disadvantage of MgO-based sorbents is their slow carbonation kinetics. To tackle this, promotion of MgO with molten salts, such as alkali metal nitrates, can drastically accelerate the rate of MgO carbonation. Nonetheless, it has been observed that over cyclic operation, the rate of CO<sub>2</sub> uptake in MgO-based sorbents can decrease considerably, leading to deactivation and representing a major issue for their industrial implementation. Thus, understanding the structural changes that occur during cyclic operation is crucial to advance sorbent design.

In this work, we use time-resolved (1 s) *in situ* synchrotron XRD to shed light onto the structural dynamics occurring during cyclic operation of MgO nanoparticles coated with NaNO<sub>3</sub> (MgO-NaNO<sub>3</sub>). The *in situ* XRD study allowed us to determine the structural evolution of the material in the kinetically controlled regime over ten consecutive cycles of carbonation (315 °C, CO<sub>2</sub>) and regeneration (450 °C, N<sub>2</sub>). The high signal to noise ratio and the time resolution of the collected data allowed us to obtain the detailed information of the crystalline phases and their transformation with time and cycle number. To quantitatively describe the phase composition of the sorbent parametric Rietveld analysis was performed, allowing to quantify the phase composition and its dynamics with time on CO<sub>2</sub> stream. This information enabled us to perform a kinetic analysis of the rate of MgCO<sub>3</sub> formation (via MgO+CO<sub>2</sub>→MgCO<sub>3</sub>). The NaNO<sub>3</sub> promoter is molten during the entire cyclic operation, and was probed using Pair Distribution Function analysis.

Furthermore, the data recorded revealed the formation of small quantities of a crystalline Na<sub>2</sub>CO<sub>3</sub> phase after the sorbent regeneration steps. We hypothesize that a partial decomposition of molten NaNO<sub>3</sub> into Na<sub>2</sub>O occurs during sorbent regeneration in N<sub>2</sub> (likely through NaNO<sub>3</sub>→NaNO<sub>2</sub>+0.5O<sub>2</sub> and subsequently 2NaNO<sub>2</sub>→Na<sub>2</sub>O+N<sub>2</sub>+1.5O<sub>2</sub>), followed by the reaction of Na<sub>2</sub>O with CO<sub>2</sub> in the carbonation step to form Na<sub>2</sub>CO<sub>3</sub>. Na<sub>2</sub>O is in an amorphous state or present as ionic species dissolved in the molten NaNO<sub>3</sub>. In the beginning of each carbonation cycle, Na<sub>2</sub>CO<sub>3</sub> rapidly (ca. 120 s) transformed into Na<sub>2</sub>Mg(CO<sub>3</sub>)<sub>2</sub>, while MgCO<sub>3</sub> starts to form only after ca. 15 min on CO<sub>2</sub> stream. The rate of MgCO<sub>3</sub> formation was described with an Avrami-Erofeev model. The presence of Na<sub>2</sub>Mg(CO<sub>3</sub>)<sub>2</sub> drastically enhanced the carbonation rate in each cycle, possibly by increasing the number of nucleation sites. Both the formation of Na<sub>2</sub>Mg(CO<sub>3</sub>)<sub>2</sub> and MgCO<sub>3</sub> has been found to be reversible during the regeneration step, but Na<sub>2</sub>CO<sub>3</sub> was not decomposed at any stage and its amount increased after each regeneration.

To conclude, we were able to show that the formation of Na<sub>2</sub>Mg(CO<sub>3</sub>)<sub>2</sub> via the decomposition of the promoter NaNO<sub>3</sub> enhances the carbonation rate and reduces the induction period for MgCO<sub>3</sub> formation. However, during cyclic operation the decomposition of the NaNO<sub>3</sub> promoter was found to be detrimental for the CO<sub>2</sub> capture performance of the sorbent.

#### 5:55 AM F.MT01.03.05

**Real-Time Coherent X-Ray Study of the Relationship Between Structure and Dynamics in Self-Organized Ion Beam Nanopatterning** Peco Myint<sup>1</sup>, Xiaozhi Zhang<sup>2</sup>, Yugang Zhang<sup>3</sup>, Lutz Wiegart<sup>3</sup>, Andrei Fluerașu<sup>3</sup>, Randall Headrick<sup>2</sup> and Karl Ludwig<sup>1,1</sup>; <sup>1</sup>Boston University, United States; <sup>2</sup>The University of Vermont, United States; <sup>3</sup>Brookhaven National

Laboratory, United States

Real-time coherent Grazing-Incidence Small-Angle X-ray Scattering was used to investigate the average kinetics and the fluctuation dynamics during self-organized nano-patterning of Silicon. Flat Silicon samples were bombarded by 1keV Ar<sup>+</sup> and Kr<sup>+</sup> at 65° polar angle, leading to the spontaneous formation of nanoscale ripples with 30 - 50 nm wavelengths. The temporal evolution of the average intensity shows the evolution of average kinetics, while the fluctuation dynamics is investigated by correlating speckles. At early times, the surface behavior can be understood within the framework of linear theory. The transition away from the linear theory behavior is observed in the dynamics through the intensity correlation function, which quickly evolves into a compressed exponential decay on length scales corresponding to the peak wavelength. On shorter length scales, the dynamics becomes stretched exponential in behavior. The correlation times are maximum at the ripple wavelengths while they are smaller at other wavelengths. This has notable similarities and differences with the phenomenon of de Gennes narrowing. Overall, this dynamics behavior is found to be consistent with the simulations of a nonlinear growth model by Harrison *et al.* (Phys. Rev. E, **96**, 032804). Following the formation of self-organized nano-ripples, they move across the surface. Homodyne X-ray alone cannot detect the motion, but because of the gradient of ion flux throughout the sample, there is a corresponding ripple velocity gradient that can be measured by cross correlating speckles and tracking their movements.

This work was supported by NSF grant DMR-1709380 (BU) and DOE grant DE- SC0017802 (UVM).

#### 6:05 AM F.MT01.03.06

**Theory-Guided *In Situ* X-Ray Absorption Spectroscopy Reveals Backbonding Contributions to Small Molecule Adsorption in a Cu<sup>I</sup>-Containing Metal-Organic Framework** Gregory Su<sup>1</sup>, Han Wang<sup>1</sup>, Brandon Barnett<sup>2,1</sup>, Jeffrey Long<sup>2,1</sup>, David Prendergast<sup>1</sup> and Walter Drisdell<sup>1</sup>; <sup>1</sup>Lawrence Berkeley National Laboratory, United States; <sup>2</sup>University of California, Berkeley, United States

Nanoporous metal-organic frameworks are promising materials for gas capture, separation, and storage due to their high surface area and tunable chemistry, allowing these frameworks to selectively adsorb small molecules. The metal-organic framework Cu<sup>I</sup>-MFU-4l, which contains coordinatively unsaturated Cu<sup>I</sup> centers, can engage in backbonding interactions with various small molecule guests, enabling distinct binding energies for different adsorbates. Understanding these fundamental electronic interactions is needed to design tailored frameworks with targeted adsorption properties. We use *in situ* near edge X-ray absorption fine structure spectroscopy coupled with theory to examine several gases expected to bind to the open Cu<sup>I</sup> sites in Cu<sup>I</sup>-MFU-4l via different electronic interactions, including  $\sigma$ -donation,  $\pi$ -backbonding, and formal electron transfer. We show that *in situ* Cu L-edge X-ray absorption spectroscopy of Cu<sup>I</sup>-MFU-4l in the presence of a gas can elucidate the  $\pi$ -backbonding contributions by directly probing excitations to unoccupied backbonding orbitals with Cu *d*-character, even for gases where other interactions, such as ligand-to-metal  $\sigma$ -donation, dominate. First-principles calculations based on time-dependent density functional theory reveal the backbonding molecular orbitals associated with these spectroscopic transitions. The energies of the transitions correlate with the energy levels of the isolated small molecule adsorbate, and the transition intensities are proportional to the binding energies of the guest molecules with Cu<sup>I</sup>-MFU-4l. This definitive probe of the molecular and electronic structure origins of backbonding between metal-organic frameworks with electron rich metal centers and small molecule guests provides guidelines for molecular-level design of solid-state sorbents for energy-efficient industrially relevant separations processes.

#### 6:15 AM F.MT01.03.07

***In Situ* Synchrotron Pair Distribution Function (PDF) Analysis to Monitor Synthetic Pathways Under Electromagnetic Excitation** B. Reejay Jayan<sup>1</sup>, Nathan Nakamura<sup>1</sup>, Laisuo Su<sup>1</sup>, Jianming Bai<sup>2</sup> and Sanjit Ghose<sup>2</sup>; <sup>1</sup>Carnegie Mellon University, United States; <sup>2</sup>Brookhaven National Laboratory, United States

We experimentally demonstrate that the application of external electromagnetic (EM) fields influence ceramic nanoparticle synthesis via distortions introduced in the local atomic structure. Such distortions do not occur during conventional hydrothermal synthesis. Prior studies show that EM fields can promote rapid, low-temperature synthesis and atomic structures not replicable using conventional hydrothermal routes. However, the mechanisms promoting these changes are not well understood, despite decades of scientific investigations. A critical limitation of prior studies was the inability to monitor structural changes while the EM field was applied, resulting in a lack of information about dynamic, field-driven changes in local atomic structure. We address this knowledge gap through a custom-designed microwave waveguide reactor (Gerling Applied Engineering) enabling in-situ synchrotron x-ray pair distribution function (PDF) analysis. This configuration (implemented in beamline 28-ID-2 at National Synchrotron Light Source II (NSLS-II), Brookhaven National Laboratory, USA) allows us to monitor EM field-induced changes in atomic structure in real-time during synthesis.

PDF analysis is an ideal tool for such in situ structural studies, as it can quantitatively characterize changes in the local atomic structure which serve as precursors to phase transitions and crystalline phase formation. PDF thus contrasts with x-ray diffraction (XRD), which is applicable to well ordered crystalline materials and is limited in characterizing systems with structural disorder or nanoscale features. Specifically, we find that the enhanced growth of crystalline rutile SnO<sub>2</sub> nanoparticles during EM field exposure is predated by structural reordering of the oxygen sub-lattice. In contrast, nanoparticles synthesized under conventional hydrothermal conditions exhibit no such structural changes and experience limited particle growth compared with EM field-assisted conditions. Our studies thus establish a clear difference in the phase formation mechanisms under EM fields, which would not be observable using conventionally used XRD techniques and *ex-situ* studies.

The lack of mechanistic insight into EM field-assisted processes has limited their widespread application. Our demonstration of a change in the synthetic pathway under EM field exposure holds important implications for materials design and inspires future work towards manipulating external fields for atomic-scale design of local structure in nanomaterials. Additionally, by revealing that applied fields influence individual sub-lattices before and during crystallization, we contribute significant knowledge towards fully understanding the mechanisms surrounding EM field-assisted phase formation. We believe this work will thus help guide the design of novel nanoparticles with altered local atomic structure, which will have a significant impact on materials for energy storage, catalysis, and advanced sensors.

#### 6:25 AM F.MT01.03.08

**Liquid-Solid and Vapor-Liquid Phase Transformations in Laser-Melted Ti- and Ni- Alloys—A Multi-Modal, *In Situ* Synchrotron Study** Rakesh R. Kamath<sup>1</sup>, Ryan Heldt<sup>1</sup>, Logan White<sup>1</sup>, David Garcia<sup>2</sup>, Rongxuan Wang<sup>2</sup>, Zhenyu Kong<sup>2</sup>, Kamel Fezzaa<sup>3</sup>, Tao Sun<sup>4,3</sup> and Hahn Choo<sup>1</sup>; <sup>1</sup>University of Tennessee Knoxville, United States; <sup>2</sup>Virginia Polytechnic Institute and State University, United States; <sup>3</sup>Argonne National Laboratory, United States; <sup>4</sup>University of Virginia, United States

The capability to tailor the grain and defect structure of the final product is critical in realizing the full potential of metal additive manufacturing (MAM) technologies. With regard to fusion-based MAM techniques, a fundamental knowledge of the ensuing phase transformations (vapor-liquid, liquid-solid and solid-solid) is critical to establish a correlation between MAM process parameters and the key physical variables governing the build microstructure. A wealth of fundamental solidification and applied welding literature points to the thermal gradient across the liquid-solid interface ( $G$ ) and the velocity of the liquid-solid interface ( $R$ ) as being the key physical variables in the liquid-to-solid phase transformation.

Ex-situ microstructural characterization of AM Ti-6Al-4V (Ti-64) builds produced using different melt strategies (and therefore, different  $G$  and  $R$ ) was performed using high-energy synchrotron x-ray diffraction (S-XRD). The analysis of the S-XRD patterns using Rietveld refinement revealed a distinct change in crystallographic texture type of the solidified  $\beta$ -BCC phase, preferred variant selection of daughter  $\alpha$ -HCP and a higher phase fraction of retained  $\beta$ -BCC compared to the Ti-64 powder used for the build. The crystallographic texture of  $\beta$ -BCC phase was observed to go from a cube texture in raster/line melt to a rotated cube/fiber-type texture in spot melts. Ex-situ synchrotron x-ray tomography on the Ti-64 builds revealed that the spot melt strategies result in higher porosity (both gas and lack of fusion defects) compared to the raster melts.

Motivated by the findings made in the ex-situ studies, the present in-situ studies used a laser-AM simulator (developed at beamline 32-ID-B, APS, Argonne National Laboratory) to mimic the unit processes of spot and line melt strategies on Ti-6Al-4V and IN-625 alloy plates, along with varying the relevant process parameters namely laser power, line scan speed, spot dwell time, and temporal and spatial intervals between two consecutive spot melts. In-situ dynamic synchrotron x-ray radiography was used in tandem with the laser-AM simulator to obtain the interface velocity ( $R$ ) of the liquid-solid interface with a state-of-the-art spatial resolution of 2  $\mu\text{m}$  and temporal resolution of a few  $\mu\text{s}$ . Simultaneous thermal imaging was performed on the top surface of the melts during the laser melting experiments to obtain the thermal gradient ( $G$ ) at the liquid-solid interface. Post-mortem, ex-situ SEM-EBSD characterization of the melt pools were used to correlate the measured  $G$  and  $R$  evolutions to the resulting microstructure, as well as indirectly estimating the thermal gradient ( $G$ ) for comparison to the in-situ experiments.

The in-situ x-ray radiographs were also used to observe the fluctuations in the vapor-liquid interface to study the conduction-to-keyhole transition and defect formation/mitigation mechanisms. Furthermore, the characteristics of the vapor-liquid interface, along with the liquid-solid interface, were used to validate/develop existing heat transfer models used to describe MAM.

#### 6:35 AM F.MT01.03.09



**Mapping of Elastic Stress and Density of Domain Variants in Bulk Twinned Materials by Dark-Field X-Ray Microscopy** Jan Schultheiß<sup>1,2</sup>, Lukas Porz<sup>2</sup>, Lalitha Kodumudi Venkataraman<sup>2</sup>, Marion Höfling<sup>2</sup>, Can Yildirim<sup>3</sup>, Philip Cook<sup>3</sup>, Carsten Detlefs<sup>3</sup>, Semen Gorfman<sup>4</sup>, Juergen W. Roedel<sup>2</sup> and Hugh Simons<sup>5</sup>; <sup>1</sup>NTNU Norwegian University of Science and Technology, Norway; <sup>2</sup>Technical University of Darmstadt, Germany; <sup>3</sup>European Synchrotron Radiation Facility, France; <sup>4</sup>Tel Aviv University, Israel; <sup>5</sup>Technical University of Denmark, Denmark

State-of-the art high-resolution in situ imaging techniques are limited to probing the surface of the material. This is an important drawback for the characterization of twinned materials as the strain state changes from biaxial at the surface to triaxial in the bulk, dramatically influencing the functional properties. One way around this is Dark-field X-Ray Microscopy, which allows to access structural information from the bulk. Its resolution, however, is determined by the optics of the lenses, which prohibits investigations on nano-sized domains common in complex twinned materials.

In this work, we overcome this limitation by using the full reciprocal-space intensity distribution, allowing to map nanosized domains highly localized in the bulk. Calculation of the local elastic stresses from measured raw data for a ferroelectric/ferroelastic (Ba,Ca)(Zr,Ti)O<sub>3</sub> model system as a function of the externally applied electric field demonstrates the power of our technique. We find that, for all electric fields, the local domain size is spatially coupled to the elastic stress. The electric field induced crystallographic texture narrows the distribution of the elastic stresses and reduces the mechanical elastic energies by 60%, while simultaneously increasing the domain size by 35%. The results pave the way towards in situ imaging of elasto-morphological correlations inside the bulk crucial for many scientific disciplines, ranging from complex oxides to other twinned systems, such as martensitic materials or high entropy alloys.

**6:45 AM F.MT01.03.11**

**In Situ X-Ray Investigation Underpins Roles of Water on Improving Crystallinity and Stability of Organohalide Perovskite** Hua Zhou<sup>1</sup>, Zhiyuan Ma<sup>1,2</sup>, Hsin-Hsiang Huang<sup>1,3</sup>, Wei Chen<sup>1,3</sup> and Zhang Jiang<sup>1</sup>; <sup>1</sup>Argonne National Laboratory, United States; <sup>2</sup>China University of Petroleum, China; <sup>3</sup>The University of Chicago, United States

Emerging organolead-halide-perovskite-based materials and devices have recently received tremendous attention due to their extraordinary photonic and optoelectronic performance and potential low production costs. Many physical and chemical properties beyond light harvests have erupted. Despite the rapid development of perovskite materials and devices, the impact of environmental factors on different stages of materials synthesis and device fabrication still remains unclear. Moisture or humidity is widely recognized as one of the major lethal factors in perovskite devices degrade or decompose after fabrication. However, recent reports have shown that moisture could be crucial to obtain high-performance perovskite films in a suitable moisture of ~35% relative humidity. Although a few attempts have been made to investigate the morphological evolution of organohalide perovskite films, a comprehensive understanding of the environmental influence in the process of thermal annealing is not achieved yet, as it is critically important to further improve the optoelectronic device performance.

By taking advantage of synchrotron-based grazing incident wide-angle x-ray scattering (GIWAXS), we *in situ* monitor the transformation of organohalide perovskites from precursors to final films upon thermal annealing at different relative humidity. *In situ* GIWAXS reveals the formation of crystalline perovskite materials over relevant time and moisture scales to decipher the effect of humidity on both phase transition and crystal structures during annealing. These *in situ* measurements demonstrate that moderate humidity accelerates the formation of organohalide perovskites and improves the orientation of the film, but more than 50% relative humidity retards the formation of perovskites and destructs their crystal structures. Furthermore, the highly orientated films obtained at optimized relative humidity are observed which could be attributed to the hydration of precursors. The beneficial influence of moisture content in the crystalline structure formation process on the operation stability of the resulting devices will also be discussed.

These findings clearly elucidate the influence of moisture environment in annealing process of organohalide perovskites and, in turn, allow us to correlate the improved performance of organohalide perovskite materials and devices to structural features in terms of environmental effects.

SESSION F.MT01.04: Emerging Process Study by advanced In Situ Microscopy  
On Demand Abstracts Available for Viewing Starting Saturday Morning, November 21, 2020  
F-MT01

**5:00 AM \*F.MT01.04.01**

**Magnetic Processes at the Nanoscale Observed Using *In Situ* Transmission Electron Microscopy** Amanda K. Petford-Long<sup>1,2</sup>, Frank Barrows<sup>2,1</sup>, Vuk Brajuskovic<sup>1</sup> and Charudatta Phatak<sup>1,2</sup>; <sup>1</sup>Argonne National Laboratory, United States; <sup>2</sup>Northwestern University, United States

Understanding the behavior of nanoscale magnetic structures relies on being able to understand the complex interplay of the energy terms that control this behavior at a local scale. The relative contribution of these energy terms can be modified by parameters such as geometric confinement, interfacial effects and interactions between adjacent magnetic nanostructures. In addition, it is important to be able to explore how a magnetic nanostructure responds to an external driving force, such as temperature, and electric or magnetic fields. Our approach is to use Lorentz transmission electron microscopy (LTEM) or electron holography combined with in-situ magnetizing, heating and biasing experiments to elucidate the micromagnetic behavior at the sub-micron scale in nanomagnetic structures. Quantitative analysis of the LTEM data is carried out using the transport of intensity equation (TIE) approach, which we have extended to allow us to visualize the magnetic structure in three dimensions. By comparing the phase reconstructions of the magnetic induction obtained experimentally with the results of micromagnetic simulations, we are able to gain a detailed understanding of the way in which the various energy terms contribute to the behavior that we observe. We are interested in both geometrically-confined structures, for example arrays of nanomagnets patterned on lattices (artificial spin ice (ASI) arrays), in addition to nanomagnetic structures such as skyrmions and other topological spin structures that we create in thin films.

Our recent interest in artificial spin ices has focused on ASIs patterned on quasicrystalline lattices, in which the lack of translational symmetry and the varying coordination number at the vertices at which the magnetic bars meet leads to a heterogeneous energy landscape and to varying magnetic frustration across the lattice, even in the ground state. Our reconstructed magnetic induction maps allow us to determine the local magnetization configuration and we can then calculate the energy at each vertex motif for each possible magnetic configuration from simulations and thus determine which vertices play the largest role in influencing magnetic frustration and thus behavior in response to magnetic fields and to changes in temperature. Applied to magnetic skyrmions we used in situ LTEM to observe skyrmions in a Co/Pt multilayer film as a function of applied magnetic field, and by combining with simulations we were able to determine the strength of the Dzyaloshinskii-Moriya interaction.

#### 5:15 AM \*F.MT01.04.02

**Observation of Topological Transformations of Ferroelectric Vortices** Kai Du and He Tian; Zhejiang University, Chile

Topological structures based on controllable ferroelectric or ferromagnetic domain configurations offer the opportunity to develop microelectronic devices such as high-density memories. Despite the increasing experimental and theoretical insights into various domain structures (such as polar spirals, polar wave, polar vortex) over the past decade, manipulating the topological transformations of polar structures and comprehensively understanding its underlying mechanism remains lacking. We successfully developed a technique to realize domain structures modulation and take an atomic resolution observation simultaneously. This atomistic observation of dynamic evolution reveals the potential of modulating ferroelectric domain patterns in ferroelectric nano-devices. Here we systematically investigate the real-time topological transformations of polar structures in PbTiO<sub>3</sub>/SrTiO<sub>3</sub> multilayers at an atomic level. The procedure of vortex pair splitting and the transformation from polar vortex to polar wave and out-of-plane polarization are observed step by step. Furthermore, the redistribution of charge in various topological structures has been demonstrated under an external bias. These findings advance the current understanding of topological structures transformation manipulated by the external field and its origination in multilayers; it would ultimately enable the design of nanostructured materials to realize their potential applications in microelectronics.

#### References

- [1] Yadav, A. K. et al. Observation of polar Vortices in oxide superlattices. *Nature* 530, 198-201 (2016).
- [2] Tang, Y. L. et al. Observation of a periodic array of flux-closure quadrants in strained ferroelectric PbTiO<sub>3</sub> films. *Science* 348, 547-551 (2015).
- [3] Hong, Z. et al. Stability of Polar Vortex Lattice in Ferroelectric Superlattices. *Nano Lett.* 17, 2246-2252 (2017).
- [4] Li, S. et al. Periodic arrays of flux-closure domains in ferroelectric thin films with oxide electrodes. *Appl. Phys. Lett.* 111, 052901 (2017).
- [5] Rodriguez, B. J. et al. Vortex Polarization States in Nanoscale Ferroelectric Arrays. *Nano Lett.* 9, 1127-1131 (2009).
- [6] Wang, W. Y. et al. Large scale arrays of four-state vortex domains in BiFeO<sub>3</sub> thin film. *Appl. Phys. Lett.* 109, 202904 (2016).
- [7] Lu, L. et al. Topological Defects with Distinct Dipole Configurations in PbTiO<sub>3</sub>/SrTiO<sub>3</sub> Multilayer Films. *Phys. Rev. Lett.* 120, 177601 (2018).

- [8] Jia, C. L., Urban, K. W., Alexe, M., Hesse, D. & Vrejoiu, I. Direct Observation of Continuous Electric Dipole Rotation in Flux-Closure Domains in Ferroelectric Pb(Zr,Ti)O<sub>3</sub>. *Science* 331, 1420-1423 (2011).
- [9] Chen, W. J., Zheng, Y. & Wang, B. Vortex Domain Structure in Ferroelectric Nanoplatelets and Control of its Transformation by Mechanical Load. *Sci. Rep.* 2, 796 (2012).
- [10] Damodaran, A. R. et al. Phase coexistence and electric-field control of toroidal order in oxide superlattices. *Nat. Mater.* 16,1003-1009 (2017).

### 5:30 AM F.MT01.04.04

**Voltage-Induced Periodic Domain Pattern in La-Doped BiFeO<sub>3</sub>** Marvin J. Müller<sup>1</sup>, Yen-Lin Huang<sup>2</sup>, Eric K. Parsonnet<sup>2</sup>, Ramamoorthy Ramesh<sup>2,2</sup>, Morgan Trassin<sup>1</sup> and Manfred Fiebig<sup>1</sup>; <sup>1</sup>ETH Zurich, Switzerland; <sup>2</sup>University of California, Berkeley, United States

The ability to switch magnetism through application of an electric field holds great promise to launch a new era of energy-efficient memory and logic devices.<sup>[1,2]</sup> Tremendous progress has been achieved with the integration of magnetoelectric BiFeO<sub>3</sub> thin films into oxide electronics architectures.<sup>[3,4]</sup> The remaining energy gap towards the coveted attojoule switching can be bridged by the refinement of materials properties such as reduced electric coercivity and lower polarization value. Bringing BiFeO<sub>3</sub> close to the ferroelectric-paraelectric phase boundary via high La doping has emerged as a promising approach.<sup>[5,6]</sup>

Here, we evaluate the prospects of highly-La-doped BiFeO<sub>3</sub> for technological applications. Using optical second harmonic generation microscopy, we directly access the polarization of the films once integrated in technology-relevant capacitor heterostructures. We find that La-doping results in a drastic deviation of the ferroelectric domain architecture from the prototypical BiFeO<sub>3</sub> domain configuration. This leads to the loss of the net in-plane polarization in the films in the pristine state. We show, however, that the application of out-of-plane electric fields leads to a spontaneous ordering of the La-doped BiFeO<sub>3</sub> domains. In particular, our results demonstrate the electric-field-induced emergence of the stripe-like domain pattern, key ingredient in the BiFeO<sub>3</sub>-based magnetoelectric switching. This suggests La-doped BiFeO<sub>3</sub> as an ideal candidate for integration into a new class of reduced-energy-consumption oxide memory and logic devices.

- [1] M. Bibes *et al.*, *Nat. Mater.* 7, 425 (2008).
- [2] M. Trassin, *J. Phys. Condens.* 28, 033001 (2016).
- [3] J. Heron *et al.*, *Nature* 516, 370 (2014).
- [4] S. Manipatruni *et al.*, *Nature* 565, 35 (2019).
- [5] Y.-L. Huang *et al.*, *Nat. Commun.* 11, 2836 (2020).
- [6] B. Prasad *et al.*, *Adv. Mater.* 2001943 (2020).

SESSION F.MT01.05: In Situ Study of Advanced Materials  
On Demand Abstracts Available for Viewing Starting Saturday Morning, November 21, 2020  
F-MT01

### 5:00 AM \*F.MT01.05.01

**Interfacial Self-Assembly and Engineering of Hierarchically Structured Nanocrystals with Photocatalytic Activity** Hongyou Fan; Sandia National Laboratories, United States

Design and engineering of the size, shape, and chemistry of photoactive building blocks enable the fabrication of functional nanoparticles for applications in light harvesting, photocatalytic synthesis, water splitting, phototherapy, and photodegradation. Here, we report the synthesis of such nanoparticles through a surfactant-assisted interfacial self-assembly process using optically active porphyrin as a functional building block. The self-assembly process relies on specific interactions such as  $\pi$ - $\pi$  stacking and ligand coordination between individual porphyrin building blocks. Depending on the kinetic conditions, resulting structures exhibit well-defined one- to three-dimensional morphologies such as nanowires, nanooctahedra, and hierarchically ordered internal architectures. At the molecular level, porphyrins with well-defined size and chemistry possess unique optical and photocatalytic properties for potential synthesis of metallic structures. On the nanoscale, controlled assembly of macrocyclic monomers leads to formation of ordered nanostructures with precisely defined size, shape, and spatial monomer arrangement so as to facilitate intermolecular mass and energy transfer or delocalization for photocatalysis. Due to the hierarchical ordering of the porphyrins, the nanoparticles exhibit collective optical properties resulted from coupling of molecular porphyrins and photocatalytic activities such as photodegradation of methyl orange (MO) pollutants and hydrogen production. The capability of exerting rational control over dimension and morphology

provides new opportunities for applications in sensing, nanoelectronics, and photocatalysis.

Sandia National Laboratories is a multimission laboratory managed and operated by National Technology and Engineering Solutions of Sandia, LLC., a wholly owned subsidiary of Honeywell International, Inc., for the U.S. Department of Energy's National Nuclear Security Administration under contract DE-NA0003525.

#### 5:15 AM F.MT01.05.02

**Amorphous Thin-Film Growth—Exploring Nanoscale Local Dynamics versus Average Kinetics** Chenyu Wang<sup>1</sup>, Christa Wagenbach<sup>1</sup>, Jeffrey G. Ulbrandt<sup>2</sup>, Meliha G. Rainville<sup>1</sup>, Suresh Narayanan<sup>3</sup>, Hua Zhou<sup>3</sup>, Randall Headrick<sup>2</sup> and Karl Ludwig<sup>1,1</sup>; <sup>1</sup>Boston University, United States; <sup>2</sup>The University of Vermont, United States; <sup>3</sup>Argonne National Laboratory, United States

X-ray photon correlation spectroscopy (XPCS) provides kinetics and dynamics information about condensed matter by characterizing fluctuations at nanoscales. We have used the technique to study the growth of amorphous WSi<sub>2</sub> on SiO<sub>2</sub> templates by sputter deposition at room temperature in order to explore the average kinetics and real-time dynamics as a function of pressure. It's known that, as a consequence of kinetic behavior, there is a transition from smooth to rough growth surfaces with increasing pressure. It's observed that the speckle-averaged X-ray scattering intensity doesn't change after the film reaches a kinetic steady-state. Four timescale parameters were determined for each of the three pressure conditions (16mTorr, 10mTorr and 8mTorr). Peaks are found in intensity vs. time curves, and the corresponding timescale parameters at the intensity peak for each wavenumber  $q_{//}$  represent the time when the local roughness is maximum at the length scale  $2\pi/q_{//}$ . Dynamic behavior is analyzed by means of two-time correlation functions at different  $q_{//}$  values. Most of the time parameters show  $q_{//}$  dependence. The time for local morphology to reach a steady state decreases most rapidly with  $q_{//}$ . Therefore, for high  $q_{//}$  regions (i.e. short length scales), it is found that a kinetic end point may be reached before the dynamic steady state is reached. In other words, in these regions, an average local structure is stabilized while processes of nanoscale deposition, relaxation and coarsening have not yet reached a dynamic equilibrium. The timescales for reaching dynamic and kinetic steady states, and the correlation time of surface structure in the final dynamic steady state all decrease as growth pressure and final surface roughness increase. This work was supported by the National Science Foundation (NSF) under Grant No. DMR-1709380 and by the U.S. Department of Energy (DOE) Office of Science under Grant No. DE-SC0017802.

#### 5:25 AM F.MT01.05.03

**Accelerated Solid-State Diffusion During Cation Exchange in Nanocrystals** Richard Robinson; Cornell University, United States

The phenomenology of solid-state transformations and diffusion at short length scales (where the interaction of point defects with free surfaces and interfaces is significant) remains poorly understood, is increasingly important for nanostructured devices that utilize the “nano properties” (quantum confinement, high surface-area-to-volume ratios, and short transport lengths), for applications utilizing nanoscale reactivity, and for understanding interfaces and defects responsible for mass transport through them. In this work, *via* in-situ synchrotron x-ray diffraction (XRD), we directly interrogate the structure and reaction kinetics of lead sulfide (PbS) nanocrystals transforming into cadmium sulfide (CdS) through cation exchange. The epitaxial relationship of zincblende CdS to rocksalt PbS breaks the overall symmetry of the core-shell nanocrystal without requiring the loss of unit cell symmetry, leading to anomalous peak shifts in the diffraction pattern. Conversion occurs in three stages: (1) surface exchange to form a metastable rocksalt CdS shell, (2) crystallization of this shell to zincblende, and (3) diffusive transport of ions through the completed shell. The interdiffusion coefficient,  $D$ , for ions diffusing through the shell follows the Arrhenius relationship with an activation energy of 160-180 kJ mol<sup>-1</sup>, which exceeds that observed in many other experiments in diffusion in nanoparticles and is similar to values measured in bulk solids, suggesting the barrier to exchange is dominated by the energies of point defect formation rather than surface-bound reactions. However, the magnitude of  $D$  is larger by four orders of magnitude or more compared to the slowest diffusing species in our system (self-diffusion of Cd in CdS). This surprising result suggests interdiffusion is enhanced in nanocrystals, and possible mechanisms include high concentrations of induced extrinsic defects and/or increase in the diffusive jump length through high-diffusivity paths. Cation exchange illustrates that the distinction between chemical diffusion in a potential gradient and diffusion at thermodynamic equilibrium has not been fully appreciated. Acceleration of interdiffusion in core-shell nanoparticles due to large chemical potential gradients will be important for understanding for nanoscale heterostructure formation and stability.

#### 5:35 AM F.MT01.05.04

**Suppressing Co-Crystallization of Halogenated Non-Fullerene Acceptors for Thermally Stable Ternary Solar**

Cells Sandra Hultmark; Chalmers University of Technology, Sweden

Solution-processed organic solar cells display inferior thermal stability largely because the nanostructure of the active layer blend changes upon heating. While photovoltaic blends based on non-fullerene acceptors such as indacenodithienothiophene-based ITIC derivatives are touted as more thermally stable than those based on fullerenes, they readily crystallize even far below their nominal glass transition temperature. We study two halogenated ITIC derivatives that readily co-crystallize upon mixing, which indicates that the use of an acceptor mixture alone does not guarantee the formation of a disordered mixture. The addition of the donor polymer to the acceptor mixture readily suppresses the crystallization which results in a fine-grained ternary blend with nanometer-sized domains that do not coarsen due to a high  $T_g \sim 200$  C. As a result, annealing at temperatures of up to 170 C does not markedly affect the photovoltaic performance of ternary devices, in contrast to binary devices that suffer from acceptor crystallization in the active layer. Our results indicate that the ternary approach enables the use of high-temperature processing protocols, which are needed for upscaling and high-throughput fabrication of organic solar cells.

5:45 AM F.MT01.05.05

**Grain Growth Suppression in Nanocrystalline Metal Oxides at High Temperatures via Excess Oxygen Content and Dimension Control** Gyu Rac Lee<sup>1</sup>, Hyeuk Jin Han<sup>2</sup>, Eugene Cho<sup>1</sup>, Judy Cha<sup>2</sup> and Yeon Sik Jung<sup>1</sup>; <sup>1</sup>Korea Advanced Institute of Science and Technology, Korea (the Republic of); <sup>2</sup>Yale university, United States

Nanoscale-engineered metal oxides have demonstrated improvement in device performance through enhancement in physical and chemical properties. Key factors in achieving the improved performances include high surface-to-volume ratios and high surface activities which are attributed to the decreased feature size by nanostructuring. Of the many variables that contribute to the performance enhancement, grain size is one feature, which plays an important role for improving the latent property of the material. For example, in catalyst and sensor applications, decrease in grain size increases the activity as a result of increased surface area. Furthermore, in sensors, decreasing the grain size to less than 10nm significantly increases sensitivity due to full depletion and accumulation of carriers in the sensing channels. Therefore, in terms of physical and chemical properties, nanostructures with nanosized grains can significantly improve the properties of high-performance devices. However, metal oxide devices commonly require an annealing process for crystallization and stabilization, which is usually accompanied by grain growth, particle agglomeration, and deformation of the nanostructure leading to degradation of device performance. Also, metal oxide nanostructures often operate at elevated temperatures and in chemically harsh environments, which induces structural change and gradual grain growth causing instability, sensor response and signal drift, and ultimately failure. Therefore, a strategy to maintain grain size and structure in metal oxide nanostructure during device operation is needed.

Here, we demonstrate a method to maintain grain size in crystalline metal oxide (i.e. tin oxide) nanowire through grain growth suppression by excess oxygen stoichiometry and nanoscale confinement control. Even at high annealing temperatures, grains with size below 10 nm retain their structural integrity and grain size. Grain growth dynamics and structural changes of the metal oxide nanowire during annealing were studied by in-situ and ex-situ TEM. Conditions such as temperature, nanowire diameter, annealing environment, and oxygen content were varied to understand the parameters needed for grain suppression. From the analysis, it was found that grain formation and growth are simultaneously affected by oxygen content in the nanowire and that suppression of grain growth occurs when the effect of oxygen inside the nanowire is maximized by controlling the diameter and stoichiometric oxygen ratio of the metal oxide nanowire. Grain growth suppression of nanosized grains in metal oxide nanowire provides an opportunity to fabricate structurally stable metal oxide nanostructures for high-performance gas sensor applications. By applying the parameters for grain suppression, a metal oxide nanostructure was fabricated by solvent-assisted nanotransfer printing. Consequently, the gas sensor built from the metal oxide nanowire accompanied by suppressed nanosized grains as the building block showed improved thermal and operation stability with high sensitivity toward ethanol gas. Our findings provide new insights into thermally stable nano-sized grains in metal oxide nanowire and suggest a novel material design for metal oxide based applications.

5:55 AM F.MT01.05.06

**The Nucleation and Crystallisation of Calcium Sulphate Phases** Stephen Yeandel<sup>1</sup>, Helen Freeman<sup>2</sup>, Rik Drummond-Brydson<sup>2</sup>, Colin Freeman<sup>1</sup> and John Harding<sup>1</sup>; <sup>1</sup>University of Sheffield, United Kingdom; <sup>2</sup>University of Leeds, United Kingdom

The calcium sulphate phases (anhydrite, bassanite and gypsum) are industrially important due to their widespread use in plaster and as a cement additive. The  $\text{CaSO}_4 \bullet x\text{H}_2\text{O}$  system displays easily reversible hydration/dehydration reactions between the different phases. In an aqueous environment it is known that bassanite ( $\text{CaSO}_4 \bullet \frac{1}{2}\text{H}_2\text{O}$ ) is formed first, before the thermodynamically more stable gypsum ( $\text{CaSO}_4 \bullet 2\text{H}_2\text{O}$ ). The bassanite then converts to gypsum, either by assembly into

elongated aggregates followed by transformation or by dissolution and reprecipitation<sup>1</sup>.

This work uses molecular dynamics simulations performed using the LAMMPS<sup>2</sup> code and the potential model of Byrne et al.<sup>3</sup> to explore the crystal growth of CaSO<sub>4</sub> phases. In our work we compute the aqueous surface energies for bassanite and gypsum which have been used to predict equilibrium morphologies which are in good agreement with previous studies<sup>4</sup>. Simulations of the assembly of bassanite nanoparticles in aqueous solution have been performed and compared with the recent work of Stawski *et al.*<sup>5</sup> The modelling studies are complemented by experimental liquid cell TEM studies of the bassanite to gypsum transformation. The implications for a non-classical mechanism of the crystallisation of calcium sulphates are discussed.

[1] Van Driessche, A.E.S., Benning, L.G., Rodriguez-Blanco, J.D., Ossorio, M., Bots, P. and Garcia-Ruiz, J.M., "The Role and Implications of Bassanite as a Stable Precursor Phase to Gypsum Precipitation" *Science* **336** (2012) 69-72

[2] Plimpton, S., "Fast Parallel Algorithms for Short-Range Molecular Dynamics" *J. Comput. Phys* **117** no. 1 (1995) 1-19

[3] Byrne, E.H., Raiteri, P. and Gale, J.D., "Computational insight into calcium-sulfate ion pair formation" *J. Phys. Chem. C* **121** (2017) 25956-25966

[4] Aquilano, D., et al. "Three study cases of growth morphology in minerals: Halite, calcite and gypsum" *Prog. Cryst. Growth Ch.* **62.2** (2016) 227-251

[5] Stawski, T.M., Freeman, H.M., Van Driessche, A.E.S., Hövelmann, J., Besselink, R., Wirth, R. and Benning, L.G., "Particle-mediated nucleation pathways are imprinted in the internal structure of calcium sulfate single crystals" *Cryst. Growth Des.* **19** (2019) 3714-3721

#### 6:05 AM F.MT01.05.07

**In Situ High Temperature Dynamics of Surface Residues and Monolayer MoS<sub>2</sub> on Graphene Surface** Heena Inani<sup>1</sup>, Dong Hoon Shin<sup>2</sup>, Jun Hee Choi<sup>2</sup>, Kimmo Mustonen<sup>1</sup>, Min Hee Kwon<sup>2</sup>, Clemens Mangler<sup>1</sup>, Hyunjeong Jeong<sup>2</sup>, Niall McEvoy<sup>3</sup>, Sang Wook Lee<sup>2</sup> and Jani Kotakoski<sup>1</sup>; <sup>1</sup>University of Vienna, Austria; <sup>2</sup>Ewha Womans University, Korea (the Republic of); <sup>3</sup>Trinity College, Ireland

Low-dimensional materials and their hetero-stacked systems have shown potential for various applications. Due to their atomically thin nature, atomic scale modifications are possible under external stimuli, e.g., heating and particle irradiation leading to nanofabrication techniques. Here, we show through atomic-resolution in situ scanning transmission electron microscopy (STEM) experiments, that Joule-heated suspended graphene can be used as an atomically thin and electron transparent high temperature "hot plate". In these experiments, we apply continuous voltage pulses through graphene while observing dynamical changes in surface contaminants on top of graphene [1], as well as drastic structural changes in a monolayer MoS<sub>2</sub> layer [2]. The highest temperatures of the graphene substrate were estimated to be above 2000 K. Specifically, we observe cleaning through evaporation of surface residues and hydrocarbon contaminants, as well as positional and rotational dynamics of residual particles on otherwise atomically clean graphene. In the MoS<sub>2</sub> structure, heating through the graphene substrate leads to increase in edge disorder and appearance of voids, accompanied by appearance of clusters on top of the edges. At the highest temperatures, the initially 2D MoS<sub>2</sub> structure breaks apart, and only independent 3D nanocrystals remain on graphene. The crystals have typically a hexagon-like shape with the 2H lattice. Our results show that graphene can be used as an efficient high-temperature substrate for in situ microscopy experiments and provide new insights into nanofabrication techniques for 2D materials for applications, for example, in catalysis.

[1] J.H. Choi, D.H. Shin, H. Inani, M.H. Kwon, K. Mustonen, C. Mangler, M. Park, H. Jeong, D.S. Lee, J. Kotakoski & S.W. Lee, *ACS Appl. Mater. Interfaces* (2020). DOI: 10.1021/acsami.0c02056

[2] H. Inani et al., to be submitted

#### 6:15 AM F.MT01.05.08

**Phase Transition-Driven Multiphysical Transformation of Vanadium Dioxide for Aerospace Applications** Latha Nataraj; Air Force Research Laboratory, United States

Vanadium dioxide (VO<sub>2</sub>) is a thermochromic material with thermally driven crystallographic transformation resulting in an insulator-to-metal transition [1]. The first-order monoclinic insulator phase to rutile metallic phase transition in VO<sub>2</sub> results in a fast reversible transition of

(i) electrical properties [1] - from electrically insulating properties at temperatures below the phase transition temperature (T<sub>c</sub>) of 68 °C to conductive properties at temperatures above T<sub>c</sub>,

(ii) optical properties [2]- from being transparent to infrared radiation (IR) below T<sub>c</sub> to reflecting IR above T<sub>c</sub>,

(iii) mechanical properties – with elastic anisotropy, significant increase in modulus along the transitioned rutile *c*-axis, and a pronounced phonon softening

(iv) magnetic properties [3] - from nonmagnetic below  $T_c$  to magnetic above  $T_c$ .

The electrical transition of VO<sub>2</sub> has potential applications in switching and sensing. VO<sub>2</sub> has also received renewed attention as a strongly correlated material for new ultrafast and microscopy techniques, ionic gating, and improved computational approaches. Our earlier work has exploited the magnetic and optical transitions for smart carbon fiber reinforced aerospace composites integrating them with micron-sized VO<sub>2</sub> particles [4]. In addition, mechanical actuation with large amplitude, fast response of ~10 ms, and long lifetime has been demonstrated combining the temperature dependent thermal expansion and actuation of vanadium dioxide (VO<sub>2</sub>) and the excellent electrical conductivity of carbon nanotube (CNT) thin films [5]. Practical mechanical actuation will be investigated via trade studies on the film thickness, displacement, and energy associated with two-dimensional shape change.

We present the dramatic multiphysical transformation of VO<sub>2</sub> resulting from the thermally driven crystallographic transformation. The challenging VO<sub>2</sub> film growth, structural characterization of the thin film, electrical transition, the in-situ thermo-mechanical response and theoretical underpinnings for VO<sub>2</sub>-based actuation for aerospace applications will be discussed.

## References

- [1] "Insulator-metal transition in substrate-independent VO<sub>2</sub> thin film for phase-change devices," Mohammad Taha et al, Sci Rep 7, 17899 (2017)
- [2] "Optical properties of VO<sub>2</sub> films at the phase transition: Influence of substrate and electronic correlations," Tobias Peterseim et al, Journal of Applied Physics 120, 075102 (2016)
- [3] "Understanding of metal-insulator transition in VO<sub>2</sub> based on experimental and theoretical investigations of magnetic features," R. Zhang et al, Sci Rrp, 17093 (2018)
- [4] "Vanadium Dioxide-Based Infrared Shielding for Aerospace Composites," by Latha Nataraj et al, ARL-TR 8958, 2020
- [5] "Flexible, All-Inorganic Actuators Based on Vanadium Dioxide and Carbon Nanotube Bimorphs," He Ma et al, Nano Lett. 2017, 17, 421-428

## 6:25 AM F.MT01.05.09

**TEM *In Situ* Investigation of Size Effects on the Mechanical Properties in Aerospace-Grade Epoxy** Raz Samira and Noa Lachman; Tel Aviv University, Israel

Epoxy polymers are often used as a base for composites in aviation and aerospace applications, owing to their light weight, good affinity to the fillers, excellent mechanical properties, and stability under chemical corrosion and high temperatures. Many studies previously demonstrated that reducing materials scales, such as thin films or nanotubes, provides significant increase in the mechanical properties compared to the bulk material. However, few studies have dealt with these size effects in epoxy resins, and none was able to validate a mechanism. We present here an in-situ flexural bending experiments of thin epoxy cantilevers (below 200 nm). A Picoindenter is combined within TEM in order to investigate size effects on the mechanical properties of epoxy. A real-time video of the fracture process is gathered with the corresponding mechanical data from force and displacement. Experiments show crack propagation within the elastic region until fracture, without a yield point. Furthermore, the nano-scale samples demonstrate a significant increase in the flexural strength and are impressively close to the theoretical strength of the material. The combination of mechanical measurements and morphological data enables deeper understanding of the mechanisms behind the mechanical behavior. This work can be further expanded towards potential application as thin inter-layer of matrix in reinforced composites or in MEMS applications.

## 6:35 AM F.MT01.05.10

**Sequential Interfacial Reactions Govern Phase Evolution in Solid-State Ceramic Synthesis** Wenhao Sun; University of Michigan, United States

Solid-state synthesis from powder precursors is the primary processing route to multicomponent ceramic materials. The black-box nature of the reaction vessel typically precludes an understanding of the solid-state reaction mechanisms that govern phase evolution, leading to trial-and-error approaches to synthesis. Here, we combine *ab initio* thermodynamics with *in situ* synchrotron X-ray scattering and TEM to build predictive theories for which non-equilibrium phases form during solid-state ceramic synthesis, and why. I will present examples from the ceramic synthesis of Na<sub>x</sub>MO<sub>2</sub> (M = Co, Mn) layered oxides [1] and also the classic high-temperature superconductor YBa<sub>2</sub>Cu<sub>3</sub>O<sub>6+x</sub> (YBCO) [2]. We derive an interfacial reaction model to predict the first-phase-to-form between two powder precursors, which can consume a large fraction of the reaction energy and can topotactically template structural transformations to other non-equilibrium intermediates. When there are three precursors, such as in Y<sub>2</sub>O<sub>3</sub> + BaO<sub>2</sub> + CuO --> YBCO, we show how sequential pairwise reactions dictate the

multi-step phase evolution process towards the target multicomponent ceramic. Our insights can help guide the choice of precursors and parameters employed in the solid-state synthesis of ceramic materials, and constitutes a step forward in unraveling the complex interplay between thermodynamics and kinetics during materials synthesis.

[1] M. Bianchini et al., "The interplay between thermodynamics and kinetics in the solid-state synthesis of layered oxides" *Nature Materials* 2020

[2] A. Miura et al., "Sequential pairwise reactions dictate phase evolution in the solid-state synthesis of  $\text{YBa}_2\text{Cu}_3\text{O}_{6+x}$ " (2020)

#### 6:45 AM F.MT01.05.11

**Electrically Driven Phase Changes in the Superionic Conductor  $\text{Cu}_{16}\text{Rb}_4\text{Cl}_{13}\text{I}_7$**  Baoming Wang<sup>1</sup>, Teodor Todorov<sup>2</sup>, Nicholas Schneider<sup>3</sup>, John Collins<sup>2</sup>, John Ott<sup>2</sup>, John Rozen<sup>2</sup> and Frances M. Ross<sup>1</sup>; <sup>1</sup>Massachusetts Institute of Technology, United States; <sup>2</sup>IBM T.J. Watson Research Center, United States; <sup>3</sup>Nicholas Schneider, United States

The highest room temperature conductivity of any solid electrolyte, 0.34 S/cm, was reported for the superionic conductor  $\text{Cu}_{16}\text{Rb}_4\text{Cl}_{13}\text{I}_7$  [1]. The crystal structure of this material has been determined using single-crystal X-ray diffraction [2] and neutron powder diffraction [3, 4], allowing models to be developed for the conduction pathways within the structure. Due to its high conductivity and insensitivity to air and humidity,  $\text{Cu}_{16}\text{Rb}_4\text{Cl}_{13}\text{I}_7$  is particularly interesting as a solid electrolyte for synaptic cells targeted for neuromorphic computing applications [5] and three-terminal, fast-switching memory elements have been developed. The operating principle of these devices is that a voltage applied to a control electrode causes  $\text{Cu}^+$  to migrate through the solid electrolyte and deposit onto a channel, changing its resistivity as measured using two read terminals. It is important to understand the physical phenomena that underlie copper ion transport in this material in order to optimize properties of the devices such as the on/off ratio and the reliability. We have therefore developed an experimental design for transmission electron microscopy (TEM) to bias devices based on solid electrolytes *in situ* while imaging the structural changes that take place during operation.

We fabricated electron-transparent thin film samples on commercial TEM window chips with a copper control electrode and various materials for a channel placed several hundred nm to one side. The chips are accommodated in a Hummingbird TEM holder with biasing capability. The entire active area of the device is visible and the structural changes both within the electrolyte and at the electrodes can be correlated with current flow. Movies recorded during these experiments show a variety of interlinked, dynamic phenomena. At the channel, copper is deposited as whiskers or nuclei, with morphology depending on the electrode material. Within the electrolyte, an unexpected structural modulation appears when the current density exceeds a certain threshold. Diffraction analysis reveals a phase transformation initiated at the electrode, converting the electrolyte from a polycrystalline structure to a nanocrystalline phase with different atomic spacings. A distinctive bright stripe becomes visible at the phase boundary with contrast that is consistent with the local reduction in ion concentration. We suggest that depletion of copper ions, initiated at the electrode, drives the conversion to a  $\text{CuRbClI}$  phase of different stoichiometry. Furthermore, we suggest that the lower ion conductivity of the new phase is responsible for the formation of the bright contrast: finite element and Monte Carlo simulations show that a drop in conductivity cause local depletion. The interlinked nature of the phase change, conductivity change, and ion concentration then alter the voltage and current flow at the next current pulse, allowing the structural modulation to propagate across the electrolyte in a series of bright stripes. We suggest that the insights achieved by TEM in terms of the structural stability and phase changes in the superionic conductor  $\text{Cu}_{16}\text{Rb}_4\text{Cl}_{13}\text{I}_7$  help to assess its capabilities as an electrolyte for neuromorphic devices and provide useful guidance for its other applications.

[1] Takahashi T., *Journal of The Electrochemical Society* 1979;126:1654.

[2] Geller S, Akridge JR, Wilber SA., *Physical Review B* 1979;19:5396-402.

[3] Kanno R, Ohno K, Kawamoto Y, Takeda Y, Yamamoto O, Kamiyama T, et al., *Journal of Solid State Chemistry* 1993;102:79-92.

[4] Oikawa K, Kamiyama T, Kanno R, Izumi F, Ikeda T, Chakoumakos BC., *Materials Science Forum* 2004;443-444:337-40.

[5] Teodor Todorov, Takashi Ando, Frances M Ross, John A. Ott, Jianshi Tang, Douglas Bishop, John Collins, Vijay Narayanan and John Rozen, *ECS Meeting Abstracts* 2019.

#### 6:55 AM F.MT01.05.12

***In Situ* Microscopy Analysis of Thermodynamic and Kinetic Contributions to Stability in Nanocrystalline Alloys** William S. Cunningham<sup>1</sup>, Wenbo Wang<sup>1</sup>, J. Sebastian Riano<sup>2</sup>, Sooyeon Hwang<sup>3</sup>, Andrea Hodge<sup>2,2</sup> and Jason R. Trelewicz<sup>1,1</sup>; <sup>1</sup>Stony Brook University, United States; <sup>2</sup>University of Southern California, United States; <sup>3</sup>Brookhaven National Laboratory, United States

Despite their intrinsic instabilities, nanocrystalline metals have demonstrated improved properties relative to their coarse-grained counterparts. Targeted doping of grain boundaries to offset their energetic penalty has been pursued as a



thermodynamic pathway for increasing thermal and mechanical stability. However, as recently demonstrated in a number of systems, notably Cu-Ta, dopant species thought to produce thermodynamically preferred nanocrystalline structures instead contain features such as small nanoprecipitates that act to inhibit grain boundary migration through kinetic pinning forces. In this study, we use thermodynamic nanostructure stability models to select a model system – Mo-Au – for exploring the interplay between thermodynamic and kinetic contributions to thermal stability in nanocrystalline alloys. A unique starting microstructure containing nano-metallic multilayers was employed and thermally aged through in situ electron microscopy experiments to access evolving segregation states. A combination of imaging and analytical electron microscopy was used to map solute segregation to different microstructural features and corresponding phase transitions as a function of temperature. Our results demonstrate the microstructure initially evolved through a phase transformation at lower homologous temperatures (< 600°C) where Au solute atoms cluster and segregate to the underlying grain structure, consistent with predictions from thermodynamic stability models. With increasing temperature, grain boundaries are shown to migrate and produce an increase in grain size, which was accompanied by intermittent pinning events from solute-rich regions. This regime transpired at temperatures where the microstructure thermodynamically phase separated, thus demonstrating kinetic contributions to stability at higher homologous temperatures.

#### 7:05 AM F.MT01.05.14

**Late News: *In Situ* Observation and Modelling of High Temperature Nanoparticle Evaporation** [James Horwath](#)<sup>1</sup>, Peter Voorhees<sup>2</sup> and Eric Stach<sup>1</sup>; <sup>1</sup>University of Pennsylvania, United States; <sup>2</sup>Northwestern University, United States

Understanding the evolution of systems of supported nanoparticles is vital to the field of industrial catalysis - high reaction temperatures and harsh conditions drive the degradation of small, highly active catalytic nanoparticles, thereby reducing activity. While research aimed to describe coarsening and degradation processes has been undertaken for decades, the difficulty of *in situ* observation and the analysis of *in situ* experimental data has inhibited the development of a theory which comprehensively describes the evolution of supported nanoparticles.

Here, we present the results of *in situ* Transmission Electron Microscopy (TEM) experiments studying the development of a model catalyst system, gold nanoparticles on a silicon nitride support, at high temperatures. After heating the system and annealing in vacuum we observe global mass loss through sublimation of the solid nanoparticles. Using deep learning to aid image analysis, we are able to observe nanoscale changes in sets of hundreds of nanoparticles with high spatial and temporal resolution. After compiling data describing size and shape change of these nanoparticles, we are able to study the evolution of both the entire system, to understand the fundamental behavior with respect the environmental conditions, and small groups of particles, to recognize and study short-range interactions and stochastic mass-exchange processes. With these data in hand we develop a theoretical model based on thermodynamics and kinetics which closely describes the evaporation and surface diffusion of gold nanoparticles leading to a degradation of the model catalyst. By imposing physical constraints on our model, we can relate parameters to individual physical properties of a catalyst material. Based on this, we will demonstrate how materials and processing methods can be chosen to develop supported catalysts which resist degradation, and how environmental factors impact the mechanisms by which nanoparticles interact and evolve.

#### SESSION F.MT01.06: Noval In Situ Techniques

On Demand Abstracts Available for Viewing Starting Saturday Morning, November 21, 2020  
F-MT01

#### 5:00 AM F.MT01.06.01

**Fabrication of Ferroelectric Thin-Film Specimen for *In Situ* Electrical Biasing S/TEM Studies by Focused Ion Beam** [Alexander Vogel](#)<sup>1,2</sup>, Martin Sarott<sup>2</sup>, Marco Campanini<sup>1</sup>, Manfred Fiebig<sup>2</sup>, Morgan Trassin<sup>2</sup> and Marta D.

Rossell<sup>1</sup>; <sup>1</sup>Empa–Swiss Federal Laboratories for Materials Science and Technology, Switzerland; <sup>2</sup>ETH Zürich, Switzerland

Piezoelectric actuators, sensors, dielectric capacitors and memory devices are examples of applications of ferroelectrics in modern life. In data storage applications, ferroelectricity presents a unique alternative to ferromagnetism as it allows for more energy efficient and faster devices. Commercially ferroelectrics have been hindered by major reliability issues [1,2] such as retention loss [3], imprint [4], and fatigue [5]. Overcoming these issues requires a deeper understanding of the microscopic mechanisms of domain wall kinetics, nucleation and the role of various types of defects, such as oxygen vacancies. Even so, at present, there is a lack of dynamical data on the ferroelectric switching process at the atomic scale, which impedes further development in this field.

In this work, we report on the fabrication by focused ion beam (FIB) of ferroelectric thin film specimens for in-situ electrical

biasing experiments inside the transmission electron microscope (TEM). The specimens were fabricated on commercial micro-electro-mechanical system (MEMS)-chips that allow for ferroelectric switching over large areas of the film under a uniform electric field in the absence of external strains. A plate capacitor geometry was adopted to mimic the environment of industrial applications for ferroelectric capacitors. The bottom electrode of the capacitor consists of a conductive substrate, such as Nb-doped SrTiO<sub>3</sub>, while Pt is used as the top electrode. The investigated ferroelectric thin films comprise Pb(Zr<sub>0.2</sub>Ti<sub>0.8</sub>)O<sub>3</sub> (PZT) and BiFeO<sub>3</sub> (BFO) grown by pulsed laser deposition.

The specimen geometry was optimized to prevent the mechanical failure of the electrodes caused by the strain induced by the piezoelectric response of the ferroelectric. This allowed for stable PZT thin film specimens, with a film thickness of 100 nm, up to a biasing voltage of 20 V. The investigation of the currents passing through the capacitor in response to the applied voltage revealed a Schottky-diode like behaviour. Typical currents in the reverse-bias direction were on the order of 100 nA at a biasing voltage of 5 V. A thermal breakdown of the lamella occurred once the leakage currents exceed 1 μA. The characterization of the ferroelectric thin films by dark-field (DF) TEM, differential-phase contrast scanning TEM (DPC-STEM) and high-resolution high-angle annular dark-field (HAADF) STEM imaging was performed using a FEI Titan Themis microscope equipped with a probe CEOS DCOR spherical aberration corrector operated at 300 kV. DF-TEM allows for tracking the in-plane or out-of-plane domain distribution in the ferroelectric film, while in DPC- and HAADF-STEM imaging, the ferroelectric polarization is mapped on the atomic scale by combining time series averaging [6], probe deconvolution and atomic column fitting [7].

Our results provide the path to prepare highly stable ferroelectric thin film capacitor specimens for in-situ S/TEM observations. This shall enable future studies on the dynamic processes in ferroelectric thin films under an applied bias voltage, which are crucial for the practical implementation of these materials in data storage devices [8].

[1] O. Auciello, J. F. Scott, and R. Ramesh, *Physics Today* 51 (1998), p. 22-27.

[2] W. L. Warren, D. Dimos, and R. M. Waser, *MRS Bulletin* 21 (1996), p. 40-45.

[3] A. Gruverman and M. Tanaka, *Journal of Applied Physics* 89 (2001), p. 1836.

[4] A. K. Tagantsev et al., *Journal of Applied Physics* 96 (2004), p. 6616-6623.

[5] A. K. Tagantsev et al., *Journal of Applied Physics* 90 (2001), p. 1387-1402.

[6] L. Jones et al., *Advanced Structural and Chemical Imaging* 1 (2015), p. 8.

[7] M. Nord et al., *Advanced Structural and Chemical Imaging* 3 (2017), p. 9.

[8] The authors gratefully acknowledge funding from the Swiss National Science Foundation under project number 175926.

#### 5:10 AM F.MT01.06.02

***In Situ* White-Light Interferometry for Early-Stage Uranium Oxidation and Hydride Characterization** Yaakov Idell, Wigbert Siekhaus, Kerri Blobaum and William McLean; Lawrence Livermore National Laboratory, United States

The corrosion of uranium by means of oxygen or hydrogen is a material degradation process that is a significant concern for long-term storage and disposal. Hydrogen can locally attack the uranium to form uranium hydride (UH<sub>3</sub>), which has been shown to increase brittleness of the uranium and to produce less desirable properties of tensile strength, hardness, and elongation. Corrosion of uranium by hydrogen has typically been characterized by an initiation time followed by pitting corrosion; however, variability in the UH<sub>3</sub> initiation time, thought to be correlated to thickness of the coherent uranium oxide (UO<sub>2</sub>) film, have made understanding of early-stage UH<sub>3</sub> growth quite difficult. We will introduce a novel characterization tool that can rapidly collect *in-situ* time-dependent 3-D spatial data using white-light interferometry and provides growth data for both the UO<sub>2</sub> film and UH<sub>3</sub> precipitates.

White-light interferometry is a non-destructive and non-contact optical surface profiling technique for materials characterization that offers μm-scale lateral and nm-scale vertical resolution. This optical profiling technique is based on interpreting a series of interferograms, a pattern of dark and bright lines, resulting from constructive and destructive interference caused by the optical path length difference between a beam interacting with a reference material and the sample of interest. The interferograms are individually processed using a frequency-domain analysis algorithm, which converts the vertical measurements interferometrically for each pixel in field of view creating a three-dimensional image of the sample surface.

The white-light interferometer is equipped with an environmental sample cell with flowing oxygen or hydrogen gas permitting *in-situ* heating experiments. Several experiments have been conducted at different temperatures ranging from 40 °C to 90 °C under oxygen and hydrogen gas flow will be presented. Because a single measurement requires less than ten seconds, the spatial data will display the effectiveness of this rapid novel characterization tool for early-stage time-dependent oxide thickness and UH<sub>3</sub> growth kinetics. Furthermore, activation energies of oxide film and UH<sub>3</sub> growth will be reported and compared to literature. The spatial data provides visual features that improve the current understanding of the early-stage

growth mechanisms for  $\text{UO}_2$  and  $\text{UH}_3$ .

Lawrence Livermore National Laboratory is operated by Lawrence Livermore National Security, LLC, for the U.S. Department of Energy, National Nuclear Security Administration under Contract DE-AC52-07NA27344.

#### 5:20 AM F.MT01.06.03

**Streamlining the Study of Materials Dynamics with an Integrated *In Situ* SEM Experimental Platform** William Harris<sup>1</sup>, Fang Zhou<sup>2</sup>, Luyang Han<sup>2</sup> and Hrishikesh Bale<sup>1</sup>; <sup>1</sup>Carl Zeiss Microscopy, United States; <sup>2</sup>Carl Zeiss Microscopy GmbH, Germany

Recent hardware and software advances are ushering in a new paradigm in materials characterization, in which the direct observation of dynamics is revealing exciting new connections between material microstructures and properties. By directly observing the same specimen as it undergoes change or is exposed to service conditions, the *in situ* experimental approach helps remove the ambiguity and sparse statistics often associated with interpreting disparate samples extracted from different stages of the materials lifecycle. Doing so properly requires that *in situ* observations must be made with appropriate length scales, time scales, and modalities to observe the relevant phenomena of interest.

As a ubiquitous materials characterization tool, scanning electron microscopy (SEM) offers prime opportunities for such *in situ* experiments, impacting a broad range of research fields. But to date, achieving such results in a coordinated fashion is not a simple feat. Performing *in situ* SEM experiments is in no way a trivial task, often involving manual coordination of hardware and software distributed across numerous platforms and vendors (electron imaging, analytics acquisition, *in situ* stage control). Beyond coordinating an experiment, further complications arise in data interpretation, with the challenge of correlating results in space and time originating from multiple data streams. These technical barriers serve to restrict access to these techniques to the elite super-users who are able to dedicate substantial time and resources to developing their instrumentation, expertise, and workflows.

This contribution will present a fully integrated solution to mitigate these problems, combining a tensile-compression stage, heating unit, dedicated high temperature detectors, EDS/EBSD sub-units, and processing tools controlled from a unified software environment. The user can prescribe automated runs with multiple ROI's, implement automated feature tracking and autofocus, and define different imaging conditions or EDS/EBSD acquisition per ROI and load. Furthermore, integrated digital image correlation (DIC) can be built into the workflows for rapid interpretation of localized strain evolution within samples. Examples will be presented including copper, steel, and nickel alloy systems. The implementation presented serves several purposes including: 1) facilitating difficult and complex *in situ* SEM experiments in a routine manner, 2) improving consistency and repeatability, allowing for more samples and increased statistics, and 3) doing so in such a way that it brings the power of this approach into the hands of the average researcher, where the focus can be shifted onto the materials science and engineering rather than heavily relying on microscopy expertise.

#### 5:30 AM F.MT01.06.04

**Structures of Point Defects in Ceramic Oxides During Microwave Radiation-Assisted Synthesis** Shuyan Zhang<sup>1</sup>, Shikhar Jha<sup>2</sup>, Jie Gong<sup>1</sup>, Nathan Nakamura<sup>1</sup>, Alan McGaughey<sup>1</sup> and B. Reeya Jayan<sup>1</sup>; <sup>1</sup>Carnegie Mellon University, United States; <sup>2</sup>Indian Institute of Technology Kanpur, India

Microwave radiation (MWR) is known to lower the temperatures required for crystallization of ceramic oxides by introducing changes in the local atomic structure. This structural disorder serves as a precursor to phase transitions and crystalline phase formation. To better understand these field-driven phenomena, structural changes during MWR-assisted synthesis of titanium dioxide ( $\text{TiO}_2$ ) were studied using *in situ* synchrotron X-ray diffraction (XRD) conducted at beamline 6-ID of the Advanced Photon Source at Argonne National Laboratory. We observed anisotropic expansion-contraction of the lattice parameters, which differs from the linear increase of lattice parameters with increasing temperature that is observed conventionally. Such anisotropy can be attributed to the structure becoming disordered under microwave exposure. Our Raman spectroscopy and X-ray photoemission spectroscopy experiments support such increased defect generation. We then applied molecular dynamics (MD) simulations to test the hypothesis that MWR-assisted synthesis leads to defect generation, such as the nucleation of vacancy-interstitial pairs. The second-moment tight-binding charge equilibrium (SMTB-Q) variable charge potential was used to model the  $\text{TiO}_2$  system. The mean square displacements (MSD) of the ions were calculated for different concentrations of titanium Frenkel defects, oxygen Frenkel defects, or oxygen vacancies to probe the influence of defects on atomic thermal vibration. The ionic translational mobility as the structures move toward equilibrium is enhanced as the defect concentration increases.

To more precisely understand the local disorder and defect structure under MWR, we combined MD simulations with pair distribution function (PDF) analysis, a powerful tool for studying atomic structures capable of quantitatively characterizing

both the long and short-range atomic order of a material. The X-ray PDF data of MWR-grown anatase TiO<sub>2</sub> and tetragonal zirconia dioxide (ZrO<sub>2</sub>) was collected at the National Synchrotron Light Source II (NSLS-II) at Brookhaven National Laboratory (BNL). The local order of the samples was characterized by a real space Rietveld refinement using the defected phases as structure models. The increase of the atomic displacement parameters (ADP) obtained from the refinement were consistent with the MSD calculation. The results strongly suggest the presence of point defects within MWR-grown TiO<sub>2</sub> and ZrO<sub>2</sub>. Utilizing *in situ* and *ex situ* characterization techniques and atomistic simulations, we provide evidence for the nonthermal field effect through defect generation. Our efforts to understand the fundamental mechanisms underlying electromagnetic field-assisted materials processing can help to realize low-temperature techniques to engineer ceramic and ceramic-polymer hybrid materials for energy storage, catalysis, and other electronics applications.

#### 5:40 AM F.MT01.06.06

**High-Throughput *In Situ* Tracking of Millisecond-Scale Metastable Phase Formation in Thin-Film Oxides** Aine Connolly<sup>1</sup>, Duncan Sutherland<sup>1</sup>, Katie Gann<sup>1</sup>, Max Amsler<sup>1,2</sup>, R. B. Van Dover<sup>1</sup> and Michael O. Thompson<sup>1</sup>; <sup>1</sup>Cornell University, United States; <sup>2</sup>University of Bern, Switzerland

Most analyses of high-speed materials transformations and kinetics are limited to comparisons before and after synthesis, and thus often forced to infer the materials' behavior during processing. Laser spike annealing, or LSA, is a powerful exploration technique that has been shown to form and trap a broad range of metastable phases in thin film oxide materials. With a small spatial footprint and wide temperature range within each anneal, lateral gradient LSA has been highly effective in high-throughput combinatorial studies. These transient thermally induced structural transformations can be characterized through a range of techniques including optical imaging, reflectance spectroscopy, and direct X-ray diffraction. Furthermore, the temporal evolution of materials phases can be probed during LSA scanning using spatially resolved techniques by displacing the probe with respect to the localized heat source. A single 2D image can capture the entire temporal evolution as well as, with lgLSA, the behavior as a function of peak temperature. Key events during the thermal cycle (nucleation, phase conversions) can thus be identified for further analysis.

We demonstrate the power of this technique to understand the formation and evolution of metastable phase transformations in thin-film Bi<sub>2</sub>O<sub>3</sub> and Ga<sub>2</sub>O<sub>3</sub>. In Bi<sub>2</sub>O<sub>3</sub>, as a function of dwell and temperature, the  $\delta$ ,  $\beta$  and  $\alpha$  phases can be formed; using the *in-situ* tracking, the evolution dynamics for these phases were observed. Similarly, in analyzing metastable phases of Ga<sub>2</sub>O<sub>3</sub>, we gain insight into the mechanisms that give rise to the nucleating phase  $\gamma$  and its subsequent evolution to the thermodynamically stable  $\beta$  phase. This approach can be adapted to take advantage of various analytic techniques, including synchrotron source X-ray diffraction.

#### 5:50 AM F.MT01.06.07

**A Machine Learning Approach to Materials Characterization** Xing Liu<sup>1</sup>, Christos E. Athanasiou<sup>1</sup>, Nitin Padture<sup>1</sup>, Brian Sheldon<sup>1</sup> and Huajian Gao<sup>1,2</sup>; <sup>1</sup>Brown University, United States; <sup>2</sup>Nanyang Technological University, Singapore

Analytical and empirical solutions to engineering problems are usually preferred because of their convenience in applications, especially in materials characterization. However, they are not always accessible in complex problems. A new class of solutions, based on machine learning (ML) models such as regression trees and neural networks (NNs), are proposed and their feasibility and value are demonstrated through the analysis of fracture toughness measurements including single cantilever and pillar indentation splitting methods. It is found that both solutions based on regression trees and NNs can provide accurate results for the specific problem, but NN-based solutions outperform regression-tree-based solutions in terms of their simplicity. This example demonstrates that ML solutions are a major improvement over analytical and empirical solutions in terms of both reliable functionality and rapid deployment. When analytical solutions are not available, the use of ML solutions can overcome the limitations of empirical solutions and substantially change the way that engineering problems are solved. This ML solution has been employed in our fracture toughness measurements of rGO-reinforced ceramic nanocomposites.

#### 6:00 AM F.MT01.06.08

***In Situ* Observation Thermoelastic Material Property Evolution in Ni-Based Concentrated Solid Solution Alloys Under Extreme Conditions** Cody A. Dennett; Idaho National Laboratory, United States

Directly observing the evolution of material performance *in situ* under extreme conditions remains a great challenge. Environments including high temperatures, high pressures, radiation fields, and others promote defect formation and microstructure evolution which may rapidly and drastically change the performance characteristics of metals and alloys. Emergent or transient behaviors in these conditions are often difficult or impossible to capture using property and microstructure characterization after the fact. In an effort to fill a gap in the ability to capture material performance

characteristics directly under extremes, transient grating spectroscopy (TGS), an all-optical photoacoustic methodology, has been implemented as an *in situ* diagnostic able to capture multi-property information while materials are exposed to the combined extremes of high temperature and ion beam bombardment. This non-destructive method returns elastic and thermal transport properties with second-scale time resolution. Here, recent work using this methodology to track the evolution of Ni-based solid-solution alloys using the *in situ* ion irradiation TGS (I<sup>3</sup>TGS) beamline will be described. Tracking material property evolution during long exposure times (hours) provides a clear indication of performance degradation due to irradiation-induced void swelling. On short timescales (seconds to minutes), observing rapid changes in thermoelastic properties as defect generation is initiated allows a unique window into bulk transient defect populations which are otherwise difficult to observe. This presentation will demonstrate the utility of this powerful new *in situ* technology as well as provide insight into the kinetic behavior of this interesting class of chemically-complex alloys under extremes.

**6:10 AM F.MT01.06.10**

***In Situ* Reflection High Energy Electron Diffraction in Atomic Layer Deposition for Monitoring Epitaxial Transformations** [Alexandra J. Howzen](#) and Nick C. Strandwitz; Lehigh University, United States

The maximum amount of thermal energy available during atomic layer deposition (ALD) is generally determined by the decomposition temperature of the precursors and also sets the maximum temperature in the “ALD window”. This maximum temperature in some cases limits the structural perfection and extent of crystallization in resulting films. Intermittent annealing during the film growth in between ALD chemical exposures has been explored previously and shown to increase density and quality of ALD films.<sup>1</sup> However, without direct monitoring of one or more of the physical properties of the films, it can be difficult to determine the nuances of film transformation, such as crystallization temperature, surface roughening, and dependence on gas ambient.

In this work we integrate reflection high energy electron diffraction (RHEED) into a home-built ALD system to monitor structural and morphological transformations during ALD growth and thermally-induced structural transformations. RHEED is a surface sensitive diffraction technique that utilizes high energy (> 10 keV) electrons at a glancing angle, and is most commonly utilized in molecular beam epitaxy and pulsed laser deposition systems. The relatively high pressures associated with ALD are incompatible with RHEED due to filament instability and resulting short electron mean free path within the chamber, necessitating either 1) differential pumping on the electron gun and a short path length between the electron gun and phosphor screen or 2) a pump down to high vacuum conditions. In addition to describing the system design, flow, and thermal modelling; we will show initial results of the deposition and annealing of ultrathin films (1-20 ALD cycles) focusing on transformations of polymorphic Ga<sub>2</sub>O<sub>3</sub>. The integration of RHEED with ALD offers a slow-motion picture of traditional epitaxial growth techniques by decoupling the deposition and crystallization steps with simultaneous monitoring of the surface structure.

<sup>1</sup> J.F. Conley, Y. Ono, and D.J. Tweet, Appl. Phys. Lett. **84**, 1913 (2004).

**6:20 AM F.MT01.06.11**

**Beyond the Thin-Film Limit, Extraction of Both Thickness and Optical Properties (n,k) with *In Situ* Ellipsometry to Monitor ALD Growth** [Florian Maudet](#)<sup>1</sup>, Soursih Banerjee<sup>1</sup>, Hanno Kroencke<sup>1</sup>, Veeresh Deshpande<sup>1</sup> and Catherine Dubourdieu<sup>1,2</sup>; <sup>1</sup>Helmholtz-Zentrum Berlin für Materialien und Energie, Germany; <sup>2</sup>Freie Universität Berlin, Germany

Spectroscopic ellipsometry (SE) is a powerful technique that is widely used to determine the thickness  $d$  of thin films as well as their dispersion law as a function of the wavelength  $\lambda$ , composed of the refractive index  $n(\lambda)$ , and of the extinction coefficient  $k(\lambda)$ . SE data interpretation relies on an optical model built to fit the measured  $\psi$  and  $\Delta$  values in order to extract  $n(\lambda)$ ,  $k(\lambda)$  and  $d$ . Given its sensitivity to small thickness variation, SE has also been applied *in situ* to monitor thin film growth in ALD reactors. However, in the case of very thin film ( $\sim 1\text{nm}$ ) the extraction of both optical properties and thickness is limited by the non-uniqueness of the solution (thickness,  $n$ ) that prevents from determining both values with precision. Thus, in an *in situ* ALD measurement, a model with fixed optical properties is usually applied and only thickness changes are considered. This is problematic as the different steps during the ALD growth cycles will obviously lead to different optical properties of the thin film that will incorrectly result as thickness variations on the model.

In order to address this issue, an expansion of the three-phase equation (air, thin film, substrate), was applied in the thin film limit ( $d \ll \lambda$ ) [1]. This expansion leads to a disambiguation of  $n$ ,  $k$  and  $d$  by measurements of the changes in the reflectance and in the complex reflectance ratio. By using this method, we were able to monitor the growth process of amorphous gallium oxide films and determine more reliably the thickness evolution than with classic interpretation of *in situ* ellipsometry. We were also able to evidence changes in the optical properties of the grown layer occurring during the different ALD cycles. We consequently evidenced the role of plasma exposure time in the minimization of absorbing defects

of the gallium oxide thin films.

[1] I.K. Kim, D.E. Aspnes, Analytic determination of  $n$ ,  $\kappa$ , and  $d$  of an absorbing film from polarimetric data in the thin-film limit, *J. Appl. Phys.* 101 (2007) 033109.

#### 6:30 AM F.MT01.06.12

##### **Late News: *In Situ* Characterization of the Thermal and Elastic Behavior of Rectifier Diodes Under Working**

**Conditions** Sara Román-Sánchez<sup>1</sup>, Aida Serrano<sup>1</sup>, Adolfo del Campo<sup>1</sup>, Israel Lorite<sup>2</sup>, José Francisco Fernández<sup>1</sup> and Alberto Moure<sup>1</sup>; <sup>1</sup>Institute of Ceramics and Glass, Spain; <sup>2</sup>SEG Automotive Germany GmbH, Germany

A widely extended application in semiconductor-based technology is the use of rectifier diodes in vehicles alternators to convert part of the mechanical energy into electrical energy. The most common failures in electric alternators are due to the electrochemical corrosion of the diodes or to damages as a consequence of the high current that circulates through diodes, which causes a significant temperature increase. This temperature increase is one of the system weakness, affecting directly to the device operation parameters. The diodes show a multicomponent nature since they are built up by different materials: epoxies to provide mechanical resistance, metals to evacuate the heat and a silicon semiconductor part. All of them have different physical characteristics and, therefore, different behavior, which is responsible of the appearance of diverse damaging phenomena such as the mechanical stress generation in the device.

The aim of this project is to understand what happens in the interfaces between the different materials of the device during its performance, mainly in the silicon interfaces, since it is the active part of the diode. For that, a study of several diodes currently used in automotive alternators has been carried out under certain working conditions which can lead to system failures, as well as to some phenomena allowing to understand their working mode. Some techniques such as confocal Raman microscopy and infrared thermography have allowed an *in operando* study of the diodes in forward biased and reverse biased conditions. The results show the device behavior at the interfaces, the generated stress in the different components and some system failure modes.

#### 6:40 AM F.MT01.06.13

##### **Late News: How Planar Nanowires Grow—Kinetic and *In Situ* Studies** Amnon Rothman<sup>1</sup>, Vladimir G. Dubrovskii<sup>2</sup>,

Anna E. Kossov<sup>1</sup>, Ifat Kaplan-Ashiri<sup>1</sup> and Ernesto Joselevich<sup>1</sup>; <sup>1</sup>Weizmann Institute of Science, Israel; <sup>2</sup>St. Petersburg State University, Russian Federation

The bottom-up assembly of nanowires facilitates control of their dimensions, structure, orientation and physical properties. Surface-guided growth of planar vapor-liquid-solid (VLS) nanowires has been shown to enable their assembly and alignment on substrates during growth, thus eliminating the need for additional post-growth processes. However, accurate control and understanding of the growth mechanism of the VLS planar nanowires were achieved only recently (PNAS **2020**, 117, 152). The new growth model presents two limiting regimes - either the Gibbs-Thompson effect controlling the growth of the thinner nanowires or surface-diffusion controlling the growth of thicker ones. Although the comprehensive growth model supported by post-growth and *ex-situ* characterization help understand the planar nanowire growth mechanism, it can only resolve the static morphology of the nanowire and is unable to provide a complete picture about the growth kinetics of the VLS growth. Recently, fundamental *in situ* studies of semiconductor nanowire growth using a transmission electron microscope (TEM) presented significant findings of the VLS growth kinetics. Unlike these studies whose precursor were supplied in the gas phase and therefore could be fed into the TEM chamber with no contamination issues, studying binary semiconductor nanowire as ZnSe and ZnS require solid-phase precursors. Here, we demonstrate the *in situ* observation of guided ZnSe and ZnS planar nanowires on sapphire substrate by environmental scanning electron microscope (ESEM). The ESEM chamber is used as a CVD system using solid-phase precursors, enabling the study of the nanowire growth mechanism. The study provides new insights during the nanowire growth process, such as nucleation and incubation times, the real growth rates, interaction between different nanowires and the evaluation of the final nanowire morphology. The experimental findings, combined with the suggested theoretical model, is an essential step in understanding the guided growth of planar nanowire phenomenon.

SESSION F.MT01.07: Ultrafast and Dynamic TEM for Materials Study  
On Demand Abstracts Available for Viewing Starting Saturday Morning, November 21, 2020  
F-MT01

### 5:00 AM \*F.MT01.07.01

**MeV-UED—A Platform for *In Situ* Studies of Material** X.J. Wang; SLAC National Accelerator Laboratory, United States

MeV-UED has led to a new paradigm in ultrafast electron scattering: higher electron beam energy means stronger diffraction and significantly reduces space-charge effects hence leads to atomic spatial-temporal resolution [1-3]. Furthermore, MeV electrons experience less multiple-scattering, possess “real” flat Ewald-sphere and favourable sample environments; MeV-UED is a unique platform for *in situ* studies of material. MeV-UED has enabled broad scientific opportunities in material science and chemical dynamics, such as revealing the energy flow in superconductor [4] and atomic movie of light-induced structural distortion in the perovskites solar cell [5].

I will present two examples in capturing metastable states of functional material using MeV-UED: topological properties & charge density wave controlled by light [6-7]. Recently *in situ* characterization of transient state during the electrically-triggered insulator-metal transition was successfully realized at SLAC MeV-UED [8]. Future development of nano-probe at SLAC MeV-UED will open new window to probe metastable state and dynamics in spatially heterogeneous systems and in *in-situ* device geometries.

X.J. Wang *et al*, Phys. Rev. E, 54, No.4, R3121 -3124 (1996).

P Zhu *et al*, New Journal of Physics 17 (6), 063004 (2014).

S. Weathersby *et al*, Rev. Sci. Instrum. 2015, 86, 073702–073707.

Tatiana Konstantinova *et al*, Sci. Adv. 2018;4:eap7427, doi: 10.1126/sciadv.aap7427.

Xiaoxi Wu *et al*, Sci. Adv. 3 e1602388 (2017) doi: 10.1126/sciadv.1602388.

Edbert J. Sie *et al*, Nature 565, 61–66 (2019).

A. Kogar *et al*, Nat. Phys. 16, 159 (2019) doi: 10.1038/s41567-019-0705-3.

SLAC MeV-UED: <https://lcls.slac.stanford.edu/instruments/mev-ued>.

### 5:15 AM \*F.MT01.07.02

**Advances in *In Situ* and Ultrafast Electron Microscopy for Materials Characterization** Ilke Arslan; Argonne National Laboratory, United States

With recent advances in in-situ microscopy, a new era in microscopy has arrived that allows for the dynamic imaging of materials under reaction conditions in the (scanning) transmission electron microscope. To better understand the structure/property relationships of materials, it is essential to get closer to the conditions in which the material will be used, such as high/low temperature, liquid environments, gas environments, or a combination thereof. Within these environments, moving beyond “real time” imaging to ultrafast imaging can provide yet another level of fundamental understanding of nanomaterials. Further, combining an in-situ or ex-situ experiment with electron tomography is a very powerful method for materials characterization as this provides the 3-D morphology of the (nano)materials under more relevant conditions. This talk will focus on newer developments such as in-situ heating in liquid, and the future of ultrafast transmission electron microscopy at the Center for Nanoscale Materials.

### 5:30 AM F.MT01.07.03

**Liquid-Liquid Phase Transitions and Dynamic Crystallization Phenomena in Phase-Change Materials Probed by Single Shot Femtosecond Electron Diffraction** Marc Zajac<sup>1</sup>, Thies Albert<sup>2</sup>, Aditya Sood<sup>3</sup>, Mianzhen Mo<sup>3</sup>, Peter Zalden<sup>4</sup>, Marius Milnikel<sup>2</sup>, Michael Kozina<sup>3</sup>, Xiaozhe Shen<sup>3</sup>, Daniel Krieg<sup>5</sup>, Duan Luo<sup>3</sup>, Anna Ziefuß<sup>2</sup>, Shuai Wei<sup>6</sup>, Peihao Sun<sup>3</sup>, Martin Jerman<sup>2</sup>, Antonowicz Jerzy<sup>7</sup>, Ryszard Sobierajski<sup>8</sup>, Jerome Hastings<sup>3</sup>, Matthias Wuttig<sup>6</sup>, Stephen Weathersby<sup>3</sup>, X.J. Wang<sup>3</sup>, Aaron Lindenberg<sup>1</sup> and Klaus Sokolowski-Tinten<sup>2</sup>; <sup>1</sup>Stanford University, United States; <sup>2</sup>Universität Duisburg-Essen, Germany; <sup>3</sup>SLAC National Accelerator Laboratory, United States; <sup>4</sup>European XFEL, Germany; <sup>5</sup>Technische Universität Dortmund, Germany; <sup>6</sup>RWTH Aachen University, Germany; <sup>7</sup>Polish Academy of Sciences, Poland; <sup>8</sup>Warsaw University of Technology, Poland

Phase change materials (PCMs) are semiconducting alloys that rapidly and reversibly switch between an amorphous (or glassy) state and a crystalline (or ordered) state via electrical and optical pulses. The two phases have optical and electrical properties that vary by orders of magnitude, which means that they can be used in rewritable optical data storage media and in fast, non-volatile memory devices. For these memory device applications, PCMs need to have fast (on the order of nanosecond) crystallization times in order to write data quickly, and they need to be able to quench into a room temperature stable glassy state, in order to enable long-term memory storage. These application specifications require a pronounced temperature dependence of the kinetic properties. Recent X-ray studies at LCLS on AIST and GeSb [1] have provided evidence for structural changes that occur in the super-cooled state, namely a Peierls-distortion-driven liquid-liquid phase

transition (LLPT), which governs the kinetic properties. It has been argued that a liquid-liquid phase transition is also responsible for the anomalous liquid-phase properties of water, silicon, and germanium. To understand the role that the liquid-liquid phase transition plays in these systems and to understand its “universality”, the single-pulse capabilities of the MeV Ultrafast Electron Diffraction (MeV-UED) instrument at the SLAC National Accelerator Laboratory were used to explore the transient structure and pair distribution function of laser-melt-quenched, strongly super-cooled PCMs, such as  $\text{Ge}_2\text{Sb}_2\text{Te}_5$  (GST),  $\text{Ag}_4\text{In}_3\text{Sb}_{67}\text{Te}_{26}$  (AIST),  $\text{Ge}_{15}\text{Sb}_{85}$ , and pure Sb at various thicknesses, as well as diamond-cubic structured semiconductors such as Ge and Si. Given the large momentum-transfer range of MeV-UED, the time-resolved pair-distribution functions are obtained at a high spatial resolution, which we use to explore interesting material dependent aspects of the liquid-liquid phase transitions.

## References

[1] Zalden et al., **364**, 6445 Science 2019

### 5:40 AM F.MT01.07.04

**Monitoring Energy Conversion in Photoexcited Gold Nanocrystals via Ultrafast Electron Diffraction** Burak Guzelturk<sup>1</sup>, James Utterback<sup>2</sup>, Igor Coropceanu<sup>3</sup>, Vladislav Kamysbayev<sup>3</sup>, Marc Zajac<sup>4</sup>, Nuri Yazdani<sup>5</sup>, Ben Cotts<sup>4</sup>, Suji Park<sup>4</sup>, Aditya Sood<sup>4</sup>, Ming-Fu Lin<sup>6</sup>, Alex Reid<sup>6</sup>, Xiaozhe Shen<sup>6</sup>, Stephen Weathersby<sup>6</sup>, Vanessa Wood<sup>5</sup>, Alberto Salleo<sup>4</sup>, X.J. Wang<sup>6</sup>, Dmitri Talapin<sup>3</sup>, Naomi Ginsberg<sup>2</sup> and Aaron Lindenberg<sup>4</sup>; <sup>1</sup>Argonne National Laboratory, United States; <sup>2</sup>University of California, Berkeley, United States; <sup>3</sup>The University of Chicago, United States; <sup>4</sup>Stanford University, United States; <sup>5</sup>ETH Zürich, Syrian Arab Republic; <sup>6</sup>SLAC National Accelerator Laboratory, United States

Gold nanocrystals exhibit attractive electronic, thermal and catalytic functionalities in response to light governed by dynamic energy conversion processes among photons, electrons and phonons. Although such processes have been typically investigated by optical methods, an understanding of the response of atomic structure following photoexcitation in nanocrystals has remained elusive to date. Here, we monitor energy conversion processes in gold nanocrystals from lattice point of view by resolving dynamic structural responses via femtosecond electron diffraction [1]. We uncover the effects of size and surface chemistry on the electron – phonon coupling and thermal relaxation. We show that smaller size leads to stronger electron – phonon coupling in these nanocrystals, which is associated with the reduced dielectric screening at the nanocrystal surfaces. In addition, we elucidate that surface ligands provide a tuning knob for the electron – phonon coupling. Particularly, thiol-based ligands slow down the cooling of hot carriers that are generated by surface plasmon polaritons. Overall, our findings provide new design principles to exploit dynamic energy conversion processes in gold nanocrystals in applications such as photocatalysis and thermoelectrics.

[1] B. Guzelturk et al. ACS Nano 14, 4792 (2020)

### 5:50 AM F.MT01.07.05

**In Situ Dynamics During Heating of Copper-Intercalated Bismuth Telluride Using Electron Microscopy** Pralav P. Shetty and Matthew T. McDowell; Georgia Institute of Technology, United States

Layered materials are characterized by strong covalent bonding within each layer, while the layers themselves are held together by weak van der Waals forces. These materials have received considerable attention owing to their compatibility with other materials, and exceptional electronic, optical, thermal, mechanical, and thermoelectric properties. The presence of a van der Waals gap between individual layers enables the intercalation of several species which can be used for tuning these properties. However, intercalation of species can also be an unintended consequence of diffusion from patterned contacts on the layered materials. In either scenario, the introduction of intercalant species into a layered material may lead to unanticipated structural and phase transformations. These transformations can be further exacerbated at elevated temperatures, yet little is understood about the high-temperature dynamics that occur in intercalated layered materials. Here, we use *in situ* transmission electron microscopy to investigate temperature-dependent structural evolution of  $\text{Bi}_2\text{Te}_3$ , a layered material with well-known application as a thermoelectric, when Cu is intercalated within the van der Waals gap. As temperature is increased, the initially disordered Cu undergoes local ordering within the van der Waals gap, which is followed by high-mobility boundary motion, polycrystal growth, and anisotropic sublimation behavior. As the temperature is raised further, layered  $\text{Cu}_2\text{Te}$  crystals nucleate and grow with a crystallographic relationship to the  $\text{Bi}_2\text{Te}_3$  lattice. The presence of Cu substantially alters both the transformation temperature of various phenomena, as well as the dynamic evolution of the crystals. These findings are consequential for the design of layered nanoscale devices and nanostructured systems where intercalants may intentionally or unintentionally alter the properties and stability of these systems.



#### F.MT01.08.01

**Probing the Structure of Oil-Water Mixtures in Porous Media Using Dielectric Spectroscopy** Abdullah AlShuaibi<sup>1,2</sup>, Amen Hammami<sup>1</sup> and Emmanuel Giannelis<sup>1</sup>; <sup>1</sup>Cornell University, United States; <sup>2</sup>King Faisal University, Saudi Arabia

Oil-water interactions play a critical role in wettability alteration and enhanced oil recovery (EOR). In this work, we study the dielectric response of oil-water mixtures in calcite and analyze the observed behavior in terms of structural ordering and fluctuation of charge carriers. In the presence of water, the dielectric response gives the rise to anomalous low-frequency dispersion (ALFD). Which follows two power-law regions, separated by a transition frequency ( $\omega_c$ ). The response is rationalized in terms of hopping transport. Additionally, we measured the dynamic dielectric response on untreated and aged calcite pressed pellets in partially saturated conditions using brines with different salinities and compositions. In the presence of oil, the dielectric dispersion and their corresponding transition frequency were shifted to lower frequencies and lower susceptibility values. This suggests less connectivity between water clusters in rocks, where the trapped oil is preventing direct contact between water and calcite grains. We also demonstrated that the power-law exponents can be used to understand the fractal structure of the inclusions. Whereas untreated calcite followed the predicted behavior of single fractal clusters, aged calcite followed that of percolation of many-clusters. Interestingly, aged calcite mixtures in various electrolytes fall between the two distinct behaviors, indicating a mixed contribution.

#### F.MT01.08.03

**Unraveling Shape Transformation of ZnO Nanostructures in Acid Solution by Correlative *In Situ* Microscopy** Fangyuan Liu, Xingxu Lu, Zichao Bian, Xiaohui Song, Guoan Zheng and Pu-Xian Gao; University of Connecticut, United States

Understanding of ZnO nanocrystal morphology evolution during wet chemical etching process is crucial for constructing nanoscale structures with desired physical and chemical properties [1,2]. However, the dynamic shape transformation in etching process is less revealed and understood so far, although it holds a key to control the surface exposure regularity of the etched ZnO nanostructures [3-5]. Here, we directly observe the reaction of ZnO rod-like structures in HCl solution using a combination of *in situ* liquid cell transmission electron microscopy (LC-TEM) and *in situ* optical microscopy. A crown-capped nanorod is captured as the intermediate structure. Microscopy images and calculations show that HCl attacks ZnO slowly to form a concave region of the crown base at each radial corner initially and exposes high index surfaces such as  $\{11-2k\}$ . The high atomic density and their semipolar nature of the high index planes of  $\{11-2k\}$  are suggested to be responsible for the stabilization in the concave crystal regions. Furthermore, when the new high index facets exposed outside during the etching, the surface energy and defects populate and lead to accelerating the etching rate of the crown cap. By using different acids with varied pH or temperature, the ZnO morphology can be readily controlled with different electronic and optical properties. These findings shed light on the understanding of wet chemical etching of ZnO and the future design of novel functional materials.

#### References

- [1] X. Ye *et al.*, *Science* **354**, 874 (2016)
- [2] P. Pal *et al.*, *Micro and Nano Systems Lett.* **3**, 6 (2015)
- [3] J. Wu *et al.*, *ACS Nano* **11**, 1696 (2017)
- [4] M. R. Hauwiller *et al.*, *Nano Lett.* **18**, 5731 (2018)
- [5] M. Sun *et al.*, *Small* 1906435 (2020)

#### F.MT01.08.05

**Ferroelectric Domain Switching in BFO/CFO Vertically Aligned Nanocomposites as a Function of Epitaxial Interface Proximity** Luis Ortiz<sup>1</sup>, Michael Martin<sup>1</sup>, Jingfeng Song<sup>2</sup>, Aiping Chen<sup>2</sup> and Bryan D. Huey<sup>1</sup>; <sup>1</sup>University of Connecticut, United States; <sup>2</sup>Los Alamos National Laboratory, United States

Self-assembled BiFeO<sub>3</sub>-CoFe<sub>2</sub>O<sub>4</sub> vertically aligned nanocomposites (VAN) are promising for their multiferroic functionality. In this work, we directly investigate interfacial-strain-controlled ferroelectric switching in the fully epitaxial BFO

nanostructures within a CFO matrix. By applying Tomographic Atomic Force Microscopy and its unique nanomachining capability, we achieved high fidelity PFM imaging sequences while minimizing imaging artifacts. This uniquely reveals interfacial strain effects on ferroelectric switching as a function of distance from the strained interface. Even a relatively low interfacial strain of 0.6% can significantly alter ferroelectric switching fields and especially domain nucleation behavior. Notably, ferroelectric domains along the BFO-CFO interfaces exhibit up to two times higher coercive voltages as well as diminished nucleation site densities. Such results from our new approach can provide critical insight into optimizing the properties of such laterally heterogeneous strain engineered functional materials systems.

#### **F.MT01.08.06**

**Late News: Effect of pH on the Shear Modulus of Anion Exchange Membranes** Amy Sharin<sup>1</sup>, Sohan Shetty<sup>2</sup>, Lindsay Wright<sup>3</sup>, Emily Zhang<sup>4</sup>, Aniket M. Raut<sup>5</sup> and Miriam H. Rafailovich<sup>5</sup>; <sup>1</sup>Lawrence High School, United States; <sup>2</sup>Half Hollow Hills High School East, United States; <sup>3</sup>Del Norte High School, United States; <sup>4</sup>General Douglas MacArthur High School, United States; <sup>5</sup>Stony Brook University, The State University of New York, United States

Anion exchange membranes (AEMs) are membranes with positively charged functional groups that enable the transport of anions and have been utilized for numerous purposes. AEMs may be used as membranes for hydrogen fuel cells, which have the potential for providing access to energy storage in hydrogen in an alkaline environment at lower operating temperatures with non-precious metals, which would dissolve in proton membranes and their solution. AEMs are also used in water filtration, including in the process of desalination whereby relatively fresh water is obtained from sea or wastewater by letting the water flow through the membrane. As more purposes are explored for AEMs it is important to determine and record their physical properties, such as shear modulus, that indicate qualities such as durability, strength, and ion conductivity for various uses and environments, such as changes in pH. A. Kisliuk et. al. determined that shear modulus specifically is correlated with increased barrier to ion conduction<sup>1</sup>. In this study, MTPN1-TMA membranes were soaked in potassium hydroxide solution of pH in the range of 8 to 14 for 1 hour before measuring shear modulus on an atomic force microscope. There were 6 trials conducted for each pH value and preliminary results reveal that the highest average shear modulus, 8.07, occurred at pH 9 and lowest average shear modulus, 1.84, occurred at pH 10. Changes in the measured shear modulus in response to the different pH environments could be due to changes in AEM surface roughness and the tendency for membranes to be hygroscopic when they are soaked in aqueous solution with KOH. Future characterizations of AEMs include zeta potential measurements, SEM, contact angle, and finally, shear modulus and durability measurements under other environmental conditions such as temperature and gas flow.

<sup>1</sup>Kisliuk, A et al. (2019). "Fundamental parameters governing ion conductivity in polymer electrolytes." *Electrochimica Acta*, Volume 299, Pages 191-196. <https://doi.org/10.1016/j.electacta.2018.12.143>

We gratefully acknowledge support from the Louis Morin Charitable Trust

SESSION F.LP05.07: Live Poster Session: Materials Theory, Characterization and Data Science (F.MT01, F.MT03, F.MT04, F.MT05 and F.MT06)

Session Chairs: Alexander Alexeev and Sanket Deshmukh

Thursday Afternoon, December 3, 2020

6:30 PM - 8:30 PM

F.MT01

#### **F.MT01.08.01**

**Probing the Structure of Oil-Water Mixtures in Porous Media Using Dielectric Spectroscopy** Abdullah AlShuaibi<sup>1,2</sup>, Amen Hammami<sup>1</sup> and Emmanuel Giannelis<sup>1</sup>; <sup>1</sup>Cornell University, United States; <sup>2</sup>King Faisal University, Saudi Arabia

Oil-water interactions play a critical role in wettability alteration and enhanced oil recovery (EOR). In this work, we study the dielectric response of oil-water mixtures in calcite and analyze the observed behavior in terms of structural ordering and fluctuation of charge carriers. In the presence of water, the dielectric response gives the rise to anomalous low-frequency dispersion (ALFD). Which follows two power-law regions, separated by a transition frequency ( $\omega_c$ ). The response is rationalized in terms of hopping transport. Additionally, we measured the dynamic dielectric response on untreated and aged calcite pressed pellets in partially saturated conditions using brines with different salinities and compositions. In the presence of oil, the dielectric dispersion and their corresponding transition frequency were shifted to lower frequencies and lower

susceptibility values. This suggests less connectivity between water clusters in rocks, where the trapped oil is preventing direct contact between water and calcite grains. We also demonstrated that the power-law exponents can be used to understand the fractal structure of the inclusions. Whereas untreated calcite followed the predicted behavior of single fractal clusters, aged calcite followed that of percolation of many-clusters. Interestingly, aged calcite mixtures in various electrolytes fall between the two distinct behaviors, indicating a mixed contribution.

#### F.MT01.08.03

##### **Unraveling Shape Transformation of ZnO Nanostructures in Acid Solution by Correlative *In***

***Situ* Microscopy** [Fangyuan Liu](#), Xingxu Lu, Zichao Bian, Xiaohui Song, Guoan Zheng and Pu-Xian Gao; University of Connecticut, United States

Understanding of ZnO nanocrystal morphology evolution during wet chemical etching process is crucial for constructing nanoscale structures with desired physical and chemical properties [1,2]. However, the dynamic shape transformation in etching process is less revealed and understood so far, although it holds a key to control the surface exposure regularity of the etched ZnO nanostructures [3-5]. Here, we directly observe the reaction of ZnO rod-like structures in HCl solution using a combination of *in situ* liquid cell transmission electron microscopy (LCTEM) and *in situ* optical microscopy. A crown-capped nanorod is captured as the intermediate structure. Microscopy images and calculations show that HCl attacks ZnO slowly to form a concave region of the crown base at each radial corner initially and exposes high index surfaces such as {11-2k}. The high atomic density and their semipolar nature of the high index planes of {11-2k} are suggested to be responsible for the stabilization in the concave crystal regions. Furthermore, when the new high index facets exposed outside during the etching, the surface energy and defects populate and lead to accelerating the etching rate of the crown cap. By using different acids with varied pH or temperature, the ZnO morphology can be readily controlled with different electronic and optical properties. These findings shed light on the understanding of wet chemical etching of ZnO and the future design of novel functional materials.

#### References

- [1] X. Ye *et al.*, *Science* **354**, 874 (2016)
- [2] P. Pal *et al.*, *Micro and Nano Systems Lett.* **3**, 6 (2015)
- [3] J. Wu *et al.*, *ACS Nano* **11**, 1696 (2017)
- [4] M. R. Hauwiller *et al.*, *Nano Lett.* **18**, 5731 (2018)
- [5] M. Sun *et al.*, *Small* 1906435 (2020)

#### F.MT01.08.05

##### **Ferroelectric Domain Switching in BFO/CFO Vertically Aligned Nanocomposites as a Function of Epitaxial Interface**

**Proximity** [Luis Ortiz](#)<sup>1</sup>, Michael Martin<sup>1</sup>, Jingfeng Song<sup>2</sup>, Aiping Chen<sup>2</sup> and Bryan D. Huey<sup>1</sup>; <sup>1</sup>University of Connecticut, United States; <sup>2</sup>Los Alamos National Laboratory, United States

Self-assembled BiFeO<sub>3</sub>-CoFe<sub>2</sub>O<sub>4</sub> vertically aligned nanocomposites (VAN) are promising for their multiferroic functionality. In this work, we directly investigate interfacial-strain-controlled ferroelectric switching in the fully epitaxial BFO nanostructures within a CFO matrix. By applying Tomographic Atomic Force Microscopy and its unique nanomachining capability, we achieved high fidelity PFM imaging sequences while minimizing imaging artifacts. This uniquely reveals interfacial strain effects on ferroelectric switching as a function of distance from the strained interface. Even a relatively low interfacial strain of 0.6% can significantly alter ferroelectric switching fields and especially domain nucleation behavior. Notably, ferroelectric domains along the BFO-CFO interfaces exhibit up to two times higher coercive voltages as well as diminished nucleation site densities. Such results from our new approach can provide critical insight into optimizing the properties of such laterally heterogeneous strain engineered functional materials systems.

#### F.MT01.08.06

##### **Late News: Effect of pH on the Shear Modulus of Anion Exchange Membranes**

Amy Sharin<sup>1</sup>, Sohan Shetty<sup>2</sup>, Lindsay Wright<sup>3</sup>, [Emily Zhang](#)<sup>4</sup>, Aniket M. Raut<sup>5</sup> and Miriam H. Rafailovich<sup>5</sup>; <sup>1</sup>Lawrence High School, United States; <sup>2</sup>Half Hollow Hills High School East, United States; <sup>3</sup>Del Norte High School, United States; <sup>4</sup>General Douglas MacArthur High School, United States; <sup>5</sup>Stony Brook University, The State University of New York, United States

Anion exchange membranes (AEMs) are membranes with positively charged functional groups that enable the transport of anions and have been utilized for numerous purposes. AEMs may be used as membranes for hydrogen fuel cells, which have the potential for providing access to energy storage in hydrogen in an alkaline environment at lower operating temperatures

with non-precious metals, which would dissolve in proton membranes and their solution. AEMs are also used in water filtration, including in the process of desalination whereby relatively fresh water is obtained from sea or wastewater by letting the water flow through the membrane. As more purposes are explored for AEMs it is important to determine and record their physical properties, such as shear modulus, that indicate qualities such as durability, strength, and ion conductivity for various uses and environments, such as changes in pH. A. Kisliuk et. al. determined that shear modulus specifically is correlated with increased barrier to ion conduction<sup>1</sup>. In this study, MTPN1-TMA membranes were soaked in potassium hydroxide solution of pH in the range of 8 to 14 for 1 hour before measuring shear modulus on an atomic force microscope. There were 6 trials conducted for each pH value and preliminary results reveal that the highest average shear modulus, 8.07, occurred at pH 9 and lowest average shear modulus, 1.84, occurred at pH 10. Changes in the measured shear modulus in response to the different pH environments could be due to changes in AEM surface roughness and the tendency for membranes to be hygroscopic when they are soaked in aqueous solution with KOH. Future characterizations of AEMs include zeta potential measurements, SEM, contact angle, and finally, shear modulus and durability measurements under other environmental conditions such as temperature and gas flow.

<sup>1</sup>Kisliuk, A et al. (2019). "Fundamental parameters governing ion conductivity in polymer electrolytes." *Electrochimica Acta*, Volume 299, Pages 191-196. <https://doi.org/10.1016/j.electacta.2018.12.143>

We gratefully acknowledge support from the Louis Morin Charitable Trust

### **F.MT03.08.01**

**3D Morphology of Double Gyroid and Double Diamond BCP Tubular Networks** [Edwin Thomas](#) and Xueyan Feng; Texas A&M University, United States

Block copolymers (BCPs) self assemble into a wide variety of periodic structures and elucidating their nano- and micro-structures has typically been accomplished by a combination of transmission electron microscopy and small angle xray scattering. Two of the more complex microdomain structures in BCPs are the double gyroid (DG) and double diamond (DD). We have developed a 3D reconstruction tool, slice and view scanning electron microscopy to create large volume tomograms of the DG and DD structures enabling detailed investigation of a host of supra- and sub- unit cell morphological characteristics. These include the nature of the curvature of the Interfacial dividing surface (IMDS), the length and angle distribution of the network struts as well as distortions of the cubic unit cells into triclinic variants. In addition to the periodic structure, we have discovered and classified various point, line and surface defects. Because the minority component in the DG and DD phases are 3D continuous networks, defects lead to changes in topology. We find loop and bridging defects in the networks, as well as dislocation defects and sharp, coherent twin grain boundaries and wide non-crystalline grain boundaries. Such defects generally occur during nucleation and growth of the phase and are important for order-order phase transformations as well as for mechanical and transport properties.

### **F.MT03.08.02**

**Multiscale Strain Mapping and Mechanical Properties Determinations of 2024 Aluminum Alloys Using Transmission Electron Microscopy Techniques** [Florent Ravoux](#), Humaira Zafar, Cyril Aubry and Dalaver H. Anjum; Khalifa University of Science and Technology, United Arab Emirates

Lightweight aluminum (Al) alloys reinforced with a second phase are widely used in aerospace industry. Nanometer scale precipitates distributed in an aluminum matrix considerably change the mechanical properties of these alloys. The degree of coherency of those precipitates, their density, and material properties (such as Young's modulus) considerably change the bulk mechanical behavior of the alloys. Therefore, investigation of their properties is of great interest for improving alloy characteristics.

The structure-property relationships between the precipitates and Al matrix are complex and often require advanced characterization techniques for their analysis. The formation of the precipitates results in the outbreak of internal stress fields due to the lattice mismatch between precipitates and Al matrix. Strain mapping techniques using Transmission Electron Microscope (TEM) are proven to be a powerful technique for investigating the mechanisms leading to the formation of stress fields. Commensurately, the technique of Electron Energy Loss Spectroscopy (EELS) provides a complementary information on the Young's modulus ( $Y_m$ ) through the analysis of the energies of bulk plasmons.

In this study, different TEM techniques are applied to characterize the influence of the Cu precipitates in an Al alloy. We focused on the characterization of a specific material namely 2024 Al alloy composed of Al-4.35 Cu-1.5 Mg-0.64 Mn-0.5 Si-0.5 Fe (wt.%). The samples are treated at 495°C followed by water quenching. Different aging processes are carried out to control and accelerate the formation of particular precipitates known as  $\theta''$ . Strain mapping techniques capable of generating results at different field of views are applied to get insights on the properties of  $\theta''$  precipitates. Specimens are prepared with a

standard lamella process using Focused Ion Beam (FIB) scanning electron microscope and TEM experiments are performed using aberration corrected microscope of model Titan 80-300 ST from Thermo-Fisher Scientific.

Geometric Phase Analysis (GPA) is applied to high resolution STEM images in order to determine the strain in Al matrix around the  $\theta''$  precipitates. This technique allows to determine at a very high spatial resolution the strain at the vicinity of the precipitates and their coherency. However, the field of view is limited to a 20 nm x 20 nm area. Nano beam diffraction (NBD) is used to determine strain at the microscale due to its higher field of view which allows to map mechanical deformation at the grain size scales. Due to the larger field of view (500 nm x 500 nm), this technique, combined with GPA, make the analysis of the strain inside grains possible and show the influence of the dislocations identified and localized with GPA.

Additionally, the determination of plasmon energies was carried out to evaluate the  $Y_m$  of the alloy at nanoscale. Moreover, the bulk modulus ( $B_m$ ), and shear modulus ( $G_m$ ) are established. Furthermore, the nano-indentation experiments and electron backscatter diffraction (EBSD) mappings are performed to correlate the bulk material properties to the nano and micro scale observations. In this way, a true structure property relationship of 2024 alloys has been investigated at bulk scales as well as at nanoscales.

In conclusion, the presented study shows that the employed techniques of TEM and EELS complement the results obtained by using the techniques of EBSD and nano indentation. Hence their combination enables to gather a deeper understanding of the strain relaxation mechanisms occurring in the alloy. This methodology resulted in the determination of a relation among (i) heat treatment, (ii) precipitates distribution and (iii) mechanical properties. In the end, the obtained results are used as inputs to propose a model for better prediction of mechanical properties of 2024 Al alloy.

#### **Acknowledgements:**

The work was funded by ADEK, Abu Dhabi, U.A.E. through the Project No. AARE19-131.

#### **F.MT03.08.03**

**Furthering the Resolution Limit of EBSD** Jakub Holzer<sup>1,2,3</sup>, Andrew Marshall<sup>4,3</sup>, Pavel Stejskal<sup>3</sup>, Chris Stephens<sup>3</sup> and Tomáš Vystavěl<sup>3</sup>; <sup>1</sup>Institute of Physics of Materials of CAS, Czechia; <sup>2</sup>Central European Institute of Technology of BUT, Czechia; <sup>3</sup>Thermo Fisher Scientific, Czechia; <sup>4</sup>The University of Surrey, United Kingdom

Electron Backscatter Diffraction (EBSD) has become an established crystallographic and microstructural characterization technique, particularly for metallurgical applications. The resolution of the technique is ultimately limited by the practical SEM probe size combined with the overlap of sampling interaction volumes. This spatial resolution is constrained further by the requirement to use high sample tilts to increase the diffraction contrast. As a result, certain applications often require the use of transmission Kikuchi diffraction, or other transmission electron microscopy (TEM) based techniques, which typically demand lengthy foil or lamellae preparation by focused ion beam. By utilizing an array of sensors capable of direct electron detection, mounted on a retractable arm around the microscope's objective pole piece, we are able gain several advantages compared to EBSD in a standard geometry. This tilt-free sample-to-detector geometry permits the collection of distortion free patterns from a well-defined area and the high sensitivity of the detector allows for pattern collection at lower incident electron energies. This enables a reduction of the sampling volume and has the potential for improved precision and physical spatial resolution with usable signal intensity. Here, we present an adapted methodology to determine the resolution of this tilt-free geometry together with the first experimental results on a molybdenum bi-crystal with a well-defined  $\Sigma 3$  boundary. By sampling perpendicular to the  $\Sigma 3$  boundary with 5nm step and evaluating the variation in the quality of the collected diffraction patterns, the physical resolution can be measured based on the full width at half maximum of the Gaussian curve fit of the pattern quality. Even with 5 nm step, the measured boundary on the indexed map is sharp. The EBSD results are further compared and validated by TEM measurements on lamellae prepared from the same specimen.

#### **F.MT03.08.06**

**Multimodal Characterization of Hybrid Nanocomposite Materials—The Case Study of the Oleophilic Hydrophobic Magnetic (OHM) Sponge for Oil Spill Remediation** Stephanie Ribet<sup>1</sup>, Vikas Nandwana<sup>1</sup>, Roberto dos Reis<sup>1</sup>, Tirzah Abbott<sup>2</sup>, Eric Roth<sup>2</sup> and Vinayak Dravid<sup>1,2</sup>; <sup>1</sup>Northwestern University, United States; <sup>2</sup>NUANCE Center, United States

There are significant intrinsic challenges to characterizing hybrid (hard-soft) materials due to the difference in properties between components of these structures. Nonetheless, establishing the structure-property relationships of these systems is an essential step in material design. Here we study the recently reported Oleophilic Hydrophobic Magnetic (OHM) sponge, a nanocomposite system that offers the ability to repeatedly adsorb 20-35 times its weight in oil. [1,2] The OHM sponge is synthesized by coating a polyurethane membrane with a nanocomposite, made of nanoparticles, such as  $Fe_3O_4$ , and graphite. In addition to the aforementioned challenge of distinguishing both the hard (nanocomposite) and soft (PU sponge) features,

this hierarchical material necessitates exploration at multiple length scales. Given the physically and chemically complex characteristics of this membrane, a correlative multimodal approach is needed to study the fundamental underpinnings contributing to the performance of this material. We apply a combination of SEM, S/TEM and Raman spectroscopy to probe the structure, morphology and chemistry of the OHM sponge including with *operando* techniques.

Preparing thin samples for electron microscopy of hybrid materials can be difficult due to the nonuniform mechanical properties of the system. Here, we embed the OHM sponge in resin at the sub-micron scale and use an ultramicrotome cross section approach to directly assess the nature of the coating. Scanning electron microscopy and spectroscopy techniques provide rich atomic and electronic information about the sponge both on the micro (SEM/Raman) and nano (S/TEM) scale. Using a combination of backscatter electron imaging (compositional contrast) and EDS, the spatial distribution of iron oxide nanoparticles can be explored. Additionally, by exploiting the distinct graphite  $sp^2$  ( $\pi$  bond) EELS edge and Raman spectral signature, we map the graphite distribution of the sponge, distinguishing it from the other carbon-based materials in the sample. This correlative approach is used to provide a complete assessment of the nature of this material and can be more broadly applied to other hybrid systems. Further, dynamic electron microscopy is a powerful tool to observe reactions as the progress in real time, and ESEM experiments, in particular, provide a pathway to characterize the solid-fluid interactions that contribute to the OHM sponge's performance.

The presentation will emphasize the holistic understanding of OHM sponge and other hierarchical, hybrid materials that can be attained through correlative and multimodal characterization methods.

[1] Nandwana, V. Ribet, S., et al., *Ind. Eng. Chem. Res.* 2020, 59, 23, 10945–10954.

[2] V. Dravid. US Patent 62/788,347, Filed: Jan 4, 2019.

#### **F.MT03.08.07**

**Nanoscale Nonlinear Optical Spectroscopy with Electron Beams** [Andrea Konecna](#)<sup>1</sup>, Valerio Di Giulio<sup>1</sup>, Vahagn Mkhitarian<sup>1</sup>, Claus Ropers<sup>2</sup> and Javier Garcia de Abajo<sup>1</sup>; <sup>1</sup>ICFO - The Institute of Photonic Sciences, Spain; <sup>2</sup>4th Physical Institute-Solids and Nanostructures, University of Gottingen, Germany

Electron energy loss spectroscopy (EELS) nowadays allows us to acquire information on excitations in nanostructures with high spatial and spectral resolution over a broad energy range covering vibrational, optical (valence-electron) and core-electron excitations [1, 2]. The possibility of nanoscale mapping of optical response beyond the diffraction limit has made EELS one of the leading techniques in characterization of nanophotonic structures. However, EEL spectra are typically dominated by linear optical response, as the nonlinear contributions are negligible due to weak interaction between electrons and sample, which prevents the use of EELS in studying the nanoscale behavior of nonlinear optical fields.

The interaction between electrons and optical excitations in a sample can be substantially increased if the sample is excited by external optical pumping. Such a scenario is possible in photon-induced near field electron microscopy (PINEM), where we can reach scattering probabilities of order unity, and obtain multiple energy quanta exchanges between the electron probe and the optical field [3, 4]. Additionally, high light intensities can also trigger substantial nonlinearities in the sample response, which should be reflected in measured PINEM spectra.

In our work [5], we suggest PINEM as a suitable technique for nanoscale mapping of nonlinear optical response. In particular, we show that the interaction of electrons with nonlinear optical fields introduces asymmetries in otherwise symmetric PINEM spectra, which we demonstrate on several realistic examples. First we focus on studying second-harmonic (SH) response of spherical gold nanoparticles. We show that the evanescent SH field, which cannot be probed by conventional nonlinear optical spectroscopies, gives rise to substantially asymmetric electron spectra under achievable illumination intensities. We further calculate SH field in gold nanorods and show that significant asymmetries in the PINEM spectra can be achieved for particular beam positions when the linear-field coupling is reduced. We envision that PINEM performed with variable illumination frequency and intensity could become a powerful technique for characterization of nonlinear optical response with unsurpassed combination of spatial and spectral resolution.

#### **References**

[1] P. E. Batson, N. Dellby, and O. L. Krivanek, *Nature* 418, 617 (2002).

[2] O. L. Krivanek, T. C. Lovejoy, N. Dellby, T. Aoki, R. W. Carpenter, P. Rez, E. Soignard, J. Zhu, P. E. Batson, M. J. Lagos, et al., *Nature* 514, 209 (2014).

[3] B. Barwick, D. J. Flannigan, and A. H. Zewail, *Nature* 462, 902 (2009).

[4] A. Feist, K. E. Echternkamp, J. Schauss, S. V. Yalunin, S. Schäfer, and C. Ropers, *Nature* 521, 200 (2015).

[5] A. Konečná, V. Di Giulio, V. Mkhitarian, C. Ropers, and F. J. García de Abajo, *ACS Photonics* 7, 1290 (2020).

#### **F.MT03.08.08**

##### **Observation of Crystal Grain Images by Using Multi-Segmented Back Scattered Electron Detector in Scanning Electron Microscope** Yusuke Sakuda, Takeshi Otsuka, Mayu Ishino and Hiroshi Onodera; JEOL Ltd., Japan

The characters of a material depend on the crystal grain size and grain boundaries. Therefore, evaluation of crystals from a viewpoint of crystallography is extremely important. Various methods by using Scanning Electron Microscope (SEM) have been extensively developed for the evaluation of crystals because samples can be handled in a bulk state and observed in the region of  $\mu\text{m}$  to  $\text{nm}$  order. One common method is the Electron Channeling Contrast (ECCI) method<sup>1</sup>, which allows to obtain an image contrast corresponding to crystal grain boundaries by using the intensity difference of Back Scattered Electrons (BSEs) emitted from a bulk sample. The other common method is the Electron Backscatter Diffraction (EBSD) pattern method<sup>2</sup>. The EBSD is possible to analyze crystal orientation distributions using diffraction patterns from a sample detected by a fluorescence screen. Those methods are quite useful for knowing grain distribution in the crystal as well. On the other hand, there are some issues in these methods of measuring a bulk sample. The ECCI is sometimes difficult to characterize the crystal structure and grain boundaries because it detects a mixture of BSEs originating from composition, channeling contrast and a diffraction pattern, while the EBSD has the limitation that a sample should be tilted significantly. Therefore, the lateral spatial resolution is about 100 nm in these methods and it would be difficult to analyze fine crystal structures and grain boundaries.

In order to improve the issues, we applied a multi-segmented BSE detector<sup>3</sup>. The detector is segmented to 16 parts located above a sample and detects BSEs. The method is similar to the ECCI method. However, in practice it is possible to detect only the diffraction patterns by using the new segmented detector. As a result, it is much more clearly separate the grain boundaries than with the ECCI method. The principle is that the diffraction patterns detected by 16 segments in each element are integrated to calculate the signal intensity distribution and display it as a grain boundary image. Because similar intensities can be obtained from the same diffraction pattern, the grains with similar signal intensities are evaluated as the same crystal orientation with high approximation. The Euclidean distance<sup>4</sup> was used to compare the signal intensities. We also tried to apply the decelerating method which is a SEM column technique for improving the electron probe diameter. In the decelerating method, incident electrons keep high energy when passing through an objective lens. Finally, the electron energy is reduced down just before the electron is landed to a sample. The method reduces the spherical aberration coefficient (Cs) and the chromatic aberration coefficient (Cc) related to the electron probe diameter and the spatial resolution can be improved<sup>5</sup>.

In this study, we will report that we tried to quickly acquire the grain boundary image with high spatial resolution using the multi-segmented BSE detector combined with the SEM-deceleration method.

#### References

- 1) Martin A. Crimp : *Microsc. res. technol.*, **69**, 374-381 (2006).
- 2) R. P. Goehner and J. R. Michael : *J. Res. Natl. Inst. Stand. Technol*, **101**, 301-308 (1996).
- 3) T. Otsuka, M. Hara, N. Erdman and S. Kitamura : *Proceedings of Microsc. Microanal.* **24**, 686 (2018).
- 4) M.M. Deza and E. Deza: *Encyclopedia of Distances*, (Springer Nature, Berlin, 2009) p. 94.
- 5) O. Terasaki, S. Asahina, Y. Sakuda, H. Takahashi, K. Tsutsumi, M. Kudo, R. W. Corkery and Y. Ma : *JEOL News*, **52**, 20 (2017).

#### **F.MT03.08.10**

##### **Thermal Expansion Coefficient of Silicon Nanoparticles with Nanometer Resolution** Bibash Sapkota, Prakash Parajuli, Serdar Ogut and Robert Klie; University of Illinois at Chicago, United States

With the size of electronic devices getting smaller and smaller, it has become important to understand thermal expansion coefficients and thermal properties in sub-nanometer scale [1-3]. However, traditional techniques, such as scanning thermal microscopy or Raman thermometry are limited in spatial resolution due to mechanical constraints or optical diffraction limit [1-3]. In the present work, we will utilize a novel approach of non-contact thermometry based on the combination of low-loss electron energy-loss spectroscopy (EELS) with first principles density functional theory (DFT) modeling to measure the thermal expansion coefficient (TEC) of materials with nano-meter resolution. The approach has been well-tested on 2D materials such as transition metal dichalcogenides (TMDs), graphene and MoS<sub>2</sub> by Hu et al [1]. In present work, we will extend the approach to Si nanoparticles to determine its TEC as a function of the temperature. In this contribution, we will also explore the effects of particle size, orientation and composition on the TEC, as well as the limits of measuring the local temperature using this approach.

References:

- [1] Hu et al., Phys. Rev. Lett. 120, 05590(2018)
- [2] Mecklenberg et al., Sci. 347, 6222(2015)
- [3] Mecklenberg et al., Phys. Rev. Applied 9, 014005(2018)
- [4] This work was supported by the National Science Foundation (DMR-18314061).

**F.MT03.08.11**

**Determination of Valence in Mn-Containing Oxides by Using Soft X-Ray Emission Spectroscopy (SXES) with Electron Microscopy** Yohei Kojima, Shunsuke Asahina, Shogo Koshiya, Takanori Murano and Hiroshi Onodera; JEOL Ltd., Japan

Mn-containing oxides are important materials that have been widely used for industrial applications such as battery, magnetic and superconducting materials. Therefore, a novel material of Mn-containing oxides has been remarkably investigated to improve their capability and quality. They have various physical properties because Mn usually has divalent, trivalent or tetravalent and each valence has different d-electron numbers in Mn-containing oxides. Thus, the determination of valence in Mn-containing oxide is a very important factor to know the characteristics of the material. As an analytical method for Mn valence, X-ray Absorption Fine Structure (XAFS) method is frequently performed in synchrotron radiation facilities [e.g. 1]. X-ray analysis in the synchrotron radiation facilities is quite powerful as it allows in-situ observation. However, it is difficult to conduct an analysis with a finer structure because the X-ray beam size is on the order of microns. For the chemical state analysis in a micro or nano-ordered structure, the method combining with Transmission Electron Microscopy (TEM) and Electron Energy-Loss Spectroscopy (EELS) is popular. Although this method has a high spatial resolution and high energy resolution, EELS cannot directly obtain information of the valence band associated with chemical bonding of the material. Recently, SXES that can be installed in Scanning Electron Microscope (SEM) and Electron Probe Micro-Analyzer (EPMA), has been developed for the chemical state analysis of a bulk with fine structures [2]. Soft X-ray means the X-ray with energies from 10 eV to a few keV, and includes the X-ray generated by electron transition from valence bands to inner-shell levels. Therefore, we can obtain chemical bonding information by spectral analysis of this X-ray. So far, we reported a valence analysis of Fe oxides by using SEM-SXES system and “Flank” method [3] suggested by Höfer et al. [4]. Flank method proceeds as below:

- 1) Calculating a spectrum difference between Fe<sup>2+</sup> endmember and Fe<sup>3+</sup> endmember.
- 2) Setting Flank positions of Fe L $\alpha$  and L $\beta$  at the maximum or minimum value position in the difference spectrum.
- 3) Taking the L $\beta$ /L $\alpha$  intensity ratio at the Flank position.

This method has higher resolution for valence than the conventional method of peak-intensity and area-intensity ratios. In this study, we attempt to apply this method for Mn-containing oxides.

MnO, Mn<sub>2</sub>O<sub>3</sub> and MnO<sub>2</sub> purchased from Hori Mineralogy Ltd. were used for samples. There is no element detected by SXES other than Mn and O. The SXES measurement was performed by using FE-SEM (JEOL JSM-7900F) equipped with SXES (SS-94040SXSER). The soft X-ray spectra were acquired at accelerating voltages of 10 kV, 5 kV and 2 kV with a beam current of 50 nA and acquired for 5 minutes.

In this study, we compared the intensity ratio of Mn L $\beta$ /L $\alpha$  calculated by the Flank method, peak-intensity ratio method and area-intensity ratio method. As a result, it is found that the Flank method has a higher energy resolution for the valence of Mn than the conventional peak-intensity ratio method and area-intensity ratio method for all accelerating voltages used in this study at 2, 5 and 10 kV. It is expected that this method will be widely applied to the valence analysis of Mn-containing oxides used in various industrial applications.

References:

- [1] Kobayashi et al., J. Mater. Chem., 14, 1843-1848 (2004).
- [2] Takahashi et al., IOP Conf. Ser.: Mater. Sci. Eng., 109, 012017 (2016).
- [3] Kojima, 12th Asia-Pacific Microscopy Conference Abstract (2020).
- [4] Höfer et al., Eur. J. Mineral., 6, 407-418 (1994).

**F.MT03.08.13**

**Late News: Using Direct Electron Detector Technologies to Determine Local Structure and Chemistry of Nanostructures** Alexandre Foucher and Eric Stach; University of Pennsylvania, United States

Direct electron detectors have revolutionized the field of structural biology and are beginning to find applications in materials science and nanoscience. Here, we show how these detectors can improve the ability of transmission electron microscopy to understand the physical and electronic structure of nanoparticles and thin films. These newly developed direct electron detection cameras reduce the signal-to-noise ratio compared to conventional CMOS / CCD cameras. In this study, electron



energy loss spectroscopy (EELS) spectra obtained from several materials systems - Ti<sub>2-x</sub>Nb<sub>x</sub>C MXenes, Mo<sub>4</sub>VAIC<sub>4</sub> MAX phase and CoPt nanoparticles - are quantified, and the improved signal quality with the direct detection system is demonstrated. We compared the effect of probe size, aperture size, camera length, and imaging filter aperture size on the signal-to-noise ratio. For nanoparticles and thin films, it was shown that probe size and camera length had the strongest influence on the signal intensity arising from inelastically scattered electrons. In contrast, imaging filter aperture size plays a minor role. The optimization of these parameters makes it possible to routinely perform valence-state analysis at an atomic level, with a resolution comparable to bulk approaches such as X-ray photoelectron spectroscopy or X-ray absorption spectroscopy (XAS). The increased Detected Quantum Efficiency (DQE) combined with a sub-pixel detection setting is also beneficial for recording diffraction patterns to perform electron pair-distribution function (ePDF) analysis from these same systems. The improvements in the quality of both spectral and scattering data can be expected to make transmission electron microscopy an even more powerful tool for characterizing nano materials.

#### **F.MT04.07.01**

**Synthesis of Si Block-Containing Gradient Block Copolymer with Increased Assembly Kinetics via Systematic Homopolymer Control for the Fabrication of a Perpendicular Lamellar Pattern** Yemin Park, Seung Won Song and Yeon Sik Jung; Korea Advanced Institute of Science and Technology, Korea (the Republic of)

The advancement in modern electronics has led to miniaturization of device and increase in demand for ultra-small and highly integrated device technology. Extreme ultraviolet lithography (EUV) has been utilized to meet the demand for patterning nano-elements of 20nm or less, however has issues regarding stochastic effects causing defects in the system. To resolve this issues, directed self-assembly of block copolymers has been considered as a promising candidate to aid EUV to develop of sub-10 nm patterns. To achieve the sub-10 nm pattern, block copolymers with high Flory-Huggins parameter ( $\chi$ ) is generally required for high quality pattern resolution. However, a few issues arise when using high  $\chi$  block copolymers. First, high  $\chi$  values generally lead to a large surface energy difference between the individual polymer blocks preventing formation of perpendicularly oriented lamellar patterns and reduce horizontal alignment of polymer blocks. Neutral brush layer coating on the substrate is an option to reduce the energy difference, but does not fully resolve the issue as it not only requires additional processes and cost but also cannot be applied on substrates with prefabricated patterns. Secondly, high  $\chi$  block copolymer has slower self-assembly kinetics, leading to increased defect occurrence and self-assembly time. Therefore, a deliberate design for block copolymers with moderately high  $\chi$  values as well as rapid kinetics is required for facile DSA of perpendicular patterns.

Here, we suggest a newly designed block copolymer that can achieve high  $\chi$  value while forming perpendicular lamellar pattern. The key to the block copolymer design is incorporating a gradient copolymer block with Si-containing block to promote universal perpendicular alignment of lamellar morphology without the need for additional surface treatment or neutral brush layer. The block copolymer was synthesized by reversible addition-fragmentation chain-transfer polymerization to form a styrene (S)/ 2,3,4,5,6-pentafluorostyrene (PFS) gradient with a Si-containing 4-(tert-butyl)dimethylsiloxy)-styrene (4BDSS) copolymer block (P(S-*g*-PFS)-*b*-P4BDSS). The styrene/ pentafluorostyrene gradient copolymer consists of gradual composition change from the block junction region to the tail, which creates surface energy difference enough to energetically drive perpendicular lamellae formation, well supported by a thermodynamic model. Furthermore, by mixing P4BDSS homopolymer block with the block copolymer, the kinetic factor can be increased to be greater than that of existing high  $\chi$  block copolymers to accelerate the self-assembly time and reduce the number of defect occurrence.

#### **F.MT04.07.05**

**Machine Learning Approach to Long Time Step Molecular Dynamics for Hard Sphere Systems** Ka Chun Chan; Karlsruhe Institute of Technology, Germany

Atomistic simulation techniques such as molecular dynamics (MD) provide an accurate and precise description of atomic motion, molecular structure and permit the prediction of the physical and chemical properties of molecular system. However, MD requires expensive computation of energy and force which leads to significant computational effort. This severely limits MD applications to biological system and soft matter physics on long time scales.

The usual MD time step is approximately 1/10 of the fastest frequency of the molecular system. In order to accelerate the MD computation, we propose a machine learning approach to propagate the molecular system instead of the usual MD time step. As a first step we developed a machine learning (ML) propagator for hard-sphere systems that propagates the molecular system with each atomic collision as a new time step. The proposed algorithm learns the time evolution of the atomic motion and the collision between atoms, such that the neural network are able to predict the system trajectory, identify the collided atomic pairs and correct the trajectory of the collided pairs for each collision time step. We will discuss the perspective of this newly ML propagator for the acceleration of MD simulations and further application to the molecular system with long time scales.

#### F.MT04.07.06

**Late News: High Throughput Prediction of Stress-Strain Curve of Thermoplastic Elastomer Model Block Copolymers by Combining Hierarchical Simulation and Deep Learning** Takeshi Aoyagi; National Institute of Advanced Industrial Science and Technology, Japan

Thermoplastic elastomer (TPE) is a typical industrial product, in which the microphase separation of block copolymer is utilized. The products can be seen in daily life, elastic fiber, film and adhesive for examples. The dynamic properties such as non-linear stress-strain (S-S) behavior are key issue to design such industrial products. The phase separated structure as well as a polymer chain structure affects the S-S behaviors. However, it is often the case that complicate metastable structures are observed in industrial products, and it is not simple to find the relation between such phase separated structures and S-S behaviors. To tackle the problem, we applied hierarchical simulation and deep learning technique. We chose ABA type triblock copolymers, where A blocks and B blocks form glassy domain and rubbery domain respectively, as a TPE model. Stress-strain curve of wide variety of volume fraction and phase separated structures were investigated by hierarchical simulation of self-consistent field theory and coarse-grained molecular dynamics. Furthermore, we applied 3D-convolutional neural network (3D-CNN) to make regression between the phase separated structures and S-S curves obtained by the coarse-grained molecular dynamics simulation. The predicted S-S curve of untrained structures using trained 3D-CNN showed good agreement with simulation, and high-throughput prediction could be realized comparing to the computationally intensive simulation.

This work was supported by a JSPS Grant-in-Aid for Scientific Research on Innovative Areas: “Discrete Geometric Analysis for Materials Design” [Grant Number 17H06464].

#### F.MT04.07.07

**Late News: AI-Guided Coarse-Graining for More Efficient Modeling of SARS-CoV-2 Spike Glycoprotein** Ziji Zhang<sup>1</sup>, David Zhang<sup>2</sup>, Aditya Narayanan<sup>3</sup>, Aditya Ramabadran<sup>4</sup>, Marcia Simon<sup>1</sup>, Miriam H. Rafailovich<sup>1</sup>, Yuefan Deng<sup>1</sup> and Peng Zhang<sup>1,1</sup>; <sup>1</sup>Stony Brook University, The State University of New York, United States; <sup>2</sup>Fremont High School, United States; <sup>3</sup>College Station High School, United States; <sup>4</sup>Lynbrook High School, United States

**Objectives:** The SARS-CoV-2 spike glycoprotein (S-protein), the presumed key receptor for binding to various material substrates, promotes the entry to host cells, and thereby causes infection. The binding dynamics of the S-protein to various substrates including organic, inorganic materials, and living cells is of great interest in biological science and clinical medicine. The all-atomic molecular dynamics (MD) simulations that are known to generate reliable results while mitigating potential biological risks for laboratory research are prohibitively expensive in computing time and resources.

**Methods:** We develop a coarse-grained (CG) model of the S-protein by intelligently learning the parameters from the corroborated *in vitro* and *in silico* data using DNNs on IBM’s supercomputer. The CG parameters are optimized with the protein in water to provide a medium that offered fluidity *in vivo*. The MD data produced by GROMACS, are fed to the DNN to predict the force field among the CG particles to be simulated in LAMMPS. The loss function that measures the discrepancy between MD values, NN prediction, and CGMD functions, is minimized during the learning process. CG models speed up the all-atomic model by coalescing atoms to form macromolecules and thereby forgoing the unnecessary calculations of the internal degrees of freedom. The CG force field is electro-free and the solvent is modeled using DPD at the mesoscopic scales. The interactions between the proteins, their surrounding solvent, and the surface they bind to are described by formulating a hybrid of the Morse-repulsive and the dissipative terms. Besides, AI is also used to predict the associated temporal scale parameters.

**Results:** The VMD model builder is used to construct two different CG models, shape-based coarse-graining (SBCG) and residue-based coarse-graining (RBCG), to the S-protein atomic data (PDB: 6VXX) which has 45,246 atoms, and evaluated their robustness with comparison to atomic-scale simulation. The nonbonded Lennard-Jones and bonded interaction parameters in the SBCG model, consisting of 355 beads with approximately 150 atoms per bead, were learned from the all-atom simulations. The bonded interaction parameters were tuned until the stiffness constants deviated less than 25% from those derived from the atomic-scale simulations. The RBCG model consists of 6498 beads, with approximately 7 atoms per bead, built with the RBCG 2007 topology file inside the Martini force field. We then solvated the model with Martini water and ionized the model with Na<sup>+</sup> and Cl<sup>-</sup> ions. After minimizing the CG system potentials, we successfully ran GPU-accelerated simulations with multiple runs to assess the impacts of the incrementally increasing timesteps to 14 fs. For verification and validation, the preliminary RMSD values were compared with the all-atomic simulations as the control, involving a single S-protein solvated in a water box with neutralizing ions at a temperature of 310K. The RMSD trends were converged which means our CG models have stable structures. Minimizing the differences of RMSD values by AI enables us

to obtain more accurate parameters for longer simulations.

**Discussions and Future Work:** Our CG model uses learned parameters from big data to accelerate the conventional all-atomic MD by 4~5 orders of magnitude, without significant loss of accuracy. As the first AI-guided multiscale CG model, it may help enable a thorough investigation of the binding dynamics of the S-protein at varied ambient conditions including temperature and pH values. The limitation of this work may be that depending on different research needs, this CG model could achieve protein chain level accuracy, but not the atomic level. Our AI-guided modeling methodology can be generalized conveniently to study a large collection of materials, *e.g.*, fibrinogen.

**Acknowledgment:** The project is supported by OVPR&IEDM COVID-19 Grant, SUNY-IBM Consortium Award and Garcia High School Program.

#### **F.MT04.07.09**

**Late News: Mesoscale Modeling of Controlled Erosion of Tetra-Arm Polyethylene Glycol Based Nanogels** Eric F. Miller, Vaibhav A. Palkar and Olga Kuksenok; Clemson University, United States

Controlled degradation of micro- and nanogels finds its use in several applications. For instance, in the healthcare field, drugs containing gel particles are utilized for drug delivery. Drug release from such gels can be controlled via degradation of the hydrogel network triggered by various external stimuli. A better understanding of the gel degradation process will aid in the development of such applications. Computational modeling of gel degradation allows one to capture the dynamics of the degradation process depending on the degradation rate constant, initial crosslink density, size of the nanogel particle, and polymer-solvent affinity. To this end, we have developed a Dissipative Particle Dynamic (DPD) approach to capture the degradation of tetra-arm polyethylene glycol based nanogels. These networks are of interest since they have near-ideal network structure thereby exhibiting superior mechanical strength prior to the controlled degradation. Within our simulation approach, we model bond breaking during degradation as a stochastic process. Our results allow us to identify two distinct stages of the nanogel degradation. During the first stage, the bonds breaking within the gel results in the decrease in the crosslink density within the bulk of the gel particle and small tetra-arm pieces breaking off the surface of the nanogel (surface erosion). During the second stage, bulk erosion and reverse gelation occurs. We characterize the transition between the two stages by focusing on the time evolution of the radius of gyration of the largest cluster and reduced degree of polymerization during the degradation process. We show that during the surface erosion, the radius of gyration of the largest cluster increases due to the effective decrease in the crosslink density being a major process, while during the second stage, this trend is reversed. We identify the effects of the gel size and an initial crosslink density on the crossover between the surface and bulk erosion. Our results represent a first mesoscale simulation study of a crossover between the surface and bulk erosion in gels.

#### **F.MT05.06.01**

**An Atom-Probe Tomography Study of High-Nickel Steel Weld Deposits with a Hierarchical Microstructure** Amir R. Farkoosh<sup>1</sup>, Daniel H. Bechetti<sup>2</sup>, Matthew F. Sinfield<sup>2</sup>, Jeffrey D. Farren<sup>2</sup> and David N. Seidman<sup>1,3</sup>; <sup>1</sup>Northwestern University, United States; <sup>2</sup>Carderock Division, Naval Surface Warfare Center, United States; <sup>3</sup>Northwestern University Center for Atom-Probe Tomography (NUCAPT), United States

Fabrication of steel structures requires joining by fusion welding. As requirements for weight and cost savings drive increased demand for advanced high-strength, high-toughness structural steels, the ability to balance mechanical performance and microstructural robustness of steels for the spectrum of welding processes poses a significant challenge. One aspect of this challenge is material responses to reheating during multi-pass welding. Thermal transients induce extensive microstructural changes in prior weld passes, whose nature and magnitude are highly dependent on the specifics of the chosen welding processes and the steel's composition. Herein, we present a new high-nickel steel, developed at the Naval Surface Warfare Center Carderock Division, which exhibits a positive response to the intrinsic heat treatment imposed during multi-pass welding processes. Because of the non-equilibrium solidification conditions, the weldments exhibit a hierarchical microstructure with several unique features, including: (i) cellular/dendritic substructure due to constitutional super-cooling; (ii) micro-segregation; (iii) high oxygen and hydrogen concentrations; and (iv) different amounts of lath martensite, and retained austenite across the fusion zone. Here, site-specific atom-probe tomography has become an essential tool that enables us to study the different regions of this hierarchical microstructure in great detail. The atom-probe tomography experiments are complemented by differential interference contrast optical microscopy, TEM, X-ray diffraction, and EBSD to study the microstructural features over hierarchical length scales. We have demonstrated that it is possible to produce a fine martensitic microstructure, which is reinforced by a high number density of V(N,C) nanoprecipitates, without post-weld heat treatments, leading to both high-strength and toughness. The presence of the V(N,C) nanoprecipitates has a twofold benefit: (i) provides dispersion strengthening; and (ii) removes nitrogen and diffusible hydrogen from the microstructure, which improves the ductility of the weldments and increases resistance against hydrogen embrittlement. The fundamental knowledge acquired in this study is also utilized to optimize the alloy system for the fabrication of structural components

through additive manufacturing processes.

#### **F.MT05.06.02**

**Dose Rate and Temperature Effect on the Alpha Prime Precipitation in Ion Irradiated Ultra-High Purity Fe-Cr Alloys** Yajie Zhao<sup>1</sup>, Arunodaya Bhattacharya<sup>2</sup>, Caleb Massey<sup>2</sup>, Pengcheng Zhu<sup>1</sup>, Cristelle Pareige<sup>3</sup>, Philip Edmondson<sup>2</sup>, Jean Henry<sup>4</sup> and Steven Zinkle<sup>1</sup>; <sup>1</sup>the University of Tennessee, United States; <sup>2</sup>Oak Ridge National Laboratory, United States; <sup>3</sup>Université et INSA de Rouen, France; <sup>4</sup>CEA, France

Cr-rich alpha prime ( $\alpha'$ ) precipitates are detrimental to the mechanical properties of FeCr based ferritic-martensitic steels. Understanding  $\alpha'$  precipitation under irradiation conditions is essential for the application of this steel in nuclear reactor environments. To study the effect of dose rate (ballistic dissolution) and irradiation temperature (radiation-enhanced diffusion) on  $\alpha'$  formation, ultra-high purity Fe-Cr alloys with 18 wt.% Cr (in either solid solution or thermally aged to form pre-existing  $\alpha'$  precipitates) were irradiated with 8 MeV Fe ions to a midrange ( $\sim 1$   $\mu\text{m}$ ) dose of 0.35-3.5 displacements per atom (dpa) between 300-450 °C at  $10^{-3}$ ,  $10^{-4}$  and  $10^{-5}$  dpa/s. Following irradiation, atom probe tomography (APT) was employed to characterize the number density, radius and Cr concentration of Cr-rich clusters. Homogeneously distributed  $\alpha'$  precipitates were revealed when radiation-enhanced diffusion dominates over ballistic dissolution ( $>300^\circ\text{C}$ ). All clusters are identified and quantified through the maximum separation method. The cluster Cr concentrations decrease as irradiation temperature decreases or dose rate increases. This is consistent with the less solute enrichment revealed by the proxigram across the iso-concentration interface. However, despite the irradiation conditions, all of the measured values are well below the equilibrium Cr concentration for  $\alpha'$  phase suggested by the phase diagram. The radius and number density of  $\alpha'$  clusters are similar and within statistical errors for different specimens. The segregation of Cr, C and N atoms to dislocation loops was also observed.

This research was sponsored by the Office of Fusion Energy Sciences, U.S. Department of Energy under contract DE-AC05-00OR22725 with UT-Battelle, LLC and grant # DE-SC0006661 with the University of Tennessee. The fabrication of the Fe-Cr binary alloys has been carried out within the framework of the EUROfusion Consortium and has received funding from the Euratom research and training program 2019–2020 under Grant Agreement No. 633053.

#### **F.MT05.06.03**

**High-Yield Cryo-APT Workflow Using a Low-Temperature Microgripper** Lorenz G. Lechner<sup>1</sup>, Andrew Smith<sup>2</sup> and Stephan Kleindiek<sup>2</sup>; <sup>1</sup>Kleindiek Inc., United States; <sup>2</sup>Kleindiek Nanotechnik, Germany

Focused-ion beam (FIB) target preparation is the gold standard for creating site-specific specimen for atom probe tomography (APT). However, FIB preparation can introduce artifacts, such as contamination, amorphization, and heating. One way to minimize sample damage is the usage of cryo-FIB. Cooling the specimen during FIB milling reduces heating related damage and limits the diffusion of Ga. Cryo-FIB sample preparation as part of a complete cryo-APT workflow enables the study of soft and unstable materials, e.g., organic solar cells or high-mobility hydrogen impurities. However, FIB lift-out preparation requires modifications to succeed at low temperatures. Conventional techniques for in-situ lift-out use beam induced deposition to temporarily attach the specimen to a manipulator and permanently mount the specimen on a sample support structure. These "soldering" techniques use metal-organic precursor gases injected into the microscope chamber and locally decomposed using the electron or ion beam. Unfortunately, these gas-phase deposition processes do not work at low temperatures because the precursors form thick condensates on all cold surfaces. Alternative techniques, like beam cured adhesives, are also not feasible at cryogenic temperature. Here, we demonstrate a gas-free cryo-liftout workflow using a low-temperature microgripper. The gripper assembly consists of a 3-axis micromanipulator equipped with an insulated gripper thermally anchored to the microscope's cold shield. Piezo motors position the system and actuate the gripper jaws with nanometer precision. The specimen is mounted inside the microscope on a cryo-stage. The region of interest is partially released from the bulk material using FIB cutting. The gripper grabs the specimen and — after a final release cut — maneuvers it onto a micro-post. After the specimen is attached to the post using redeposition welding, the gripper releases the specimen. In the last preparation step, annular FIB milling gives the sample its final shape.

In contrast to using conventional manipulation, there is no need to temporarily join the probe and specimen and subsequently cut them free. This simplification makes the process faster and more reliable, overall increasing its yield.

#### **F.MT05.06.05**

**Atom Probe-Aided Design of Additively Manufactured High-Temperature Aluminum Alloys** Richard A. Michi, Amit Shyam, Alex Plotkowski and Jonathan Poplawsky; Oak Ridge National Laboratory, United States

Conventional aluminum alloys cannot be utilized in the 250–450 °C temperature range due to a lack of microstructural stability, creating a technological gap currently filled by steels, titanium alloys, and Ni-base superalloys. Replacement of these materials with aluminum alloys has significant implications for the energy and transportation sectors (e.g., increased engine operating temperature and efficiency, lightweighting, cost reduction), but has yet to be achieved. In this talk, we will give examples of APT analysis aiding in the design of new generations of high-temperature, additively manufactured aluminum alloys specifically targeted for use in the 250–450 °C temperature range. In particular, we will show how APT analysis reveals Zr and Mn segregation to the coherent and semi-coherent interfaces of  $\theta'$  precipitates in a novel additively manufactured Al-Cu-Zr-Mn alloy, leading to thermal stability up to 350 °C. We will also discuss how the accurate measurement of matrix solute supersaturations facilitated by APT aid in the design of heat treatments for precipitation-strengthened alloys with thermally stable phases and the observations of refined, nanoscale microstructural features formed during the additive manufacturing process. APT was conducted at ORNL's Center for Nanophase Materials Sciences (CNMS), which is a U.S. DOE Office of Science User Facility.

#### **F.MT05.06.07**

#### **Tracking Coincident Pair Separation with Varying Concentration Reveals Insights on Nitride Field Evaporation** Olivia G. Licata and Baishakhi Mazumder; University at Buffalo, SUNY, United States

The unique ability of Atom probe tomography (APT) to study three-dimensional atomic distribution relies on the field evaporation of ions onto a position-sensitive detector. Multiple ion events reaching the detector within the same pulse period can result in compositional and spatial inaccuracies. Ideally, in APT analysis, acquisition parameters and conditions are modified so that the occurrence of multi-hit events is limited. Some material systems have a higher tendency for multi-hit events during field evaporation in APT, such as those containing boron, carbon, oxygen, nitrogen, and compound semiconductor materials. Under these unavoidable circumstances, these unique events have shown the potential to provide insight on field evaporation and material structure [1, 2]. Here, we define a metric by tracking the distance between coincident detector events within a heterostructure to gain insight on the unique evaporation behavior and crystallographic origin of nitride species. The distributions of pair distances are investigated for each species and region, to understand the influence of elemental composition on evaporated ion separation.

Al<sub>0.3</sub>Ga<sub>0.7</sub>N/AlN/GaN heterostructures, grown via molecular beam epitaxy (MBE) and metal-organic chemical vapor deposition (MOCVD), were utilized as test structures. Trends in mean and median pair separation distances were consistent between the two preparation methods. Additionally, individual pair species showed agreement within 0.2 nm in detector space. This finding allows for the distinction of Al-x and Ga-x events based on their pair separation. Interestingly, Al-x events show higher separation values than Ga-x events. This is in disagreement with the known lattice constants of Al-N and GaN. This result suggests that crystallographic spacing is not the dominant influence on pair separation. A more likely mechanism is related to the unique field evaporation of the species as well as characteristics of the surface field during acquisition. The crystallographic orientation upon evaporation may also play a role in the resulting pair separation. Distributions of pair separation distance were utilized to investigate variability in the spread of multi-hit events across heterostructure layers. The most prominent feature was the consistent bimodality of Al<sup>2+</sup>-N<sub>2</sub>, suggesting two separate evaporation phenomena. This unique behavior may originate from a combination of dissociation events and correlated events occurring for the same species.

This in-depth analysis presents a statistical protocol for interpreting multi-hit events from APT data. The reported findings help define species-specific evaporation trends within a compound semiconductor heterostructure in an aim to expand the application of APT to complex systems. Defining the relation between multi-hit events and structural chemistry will extend the current capabilities of APT to gain insight on atomic spacing that was previously unattainable without the aid of additional characterization methods. Furthermore, this methodology can be applied to other material systems to qualify the likelihood of correlation, potential dissociation trends, and crystallographic nature.

#### References

1. De Geuser, F., Gault, B., Bostel, A., & Vurpillot, F. (2007). Correlated field evaporation as seen by atom probe tomography. *Surface science*, 601(2), 536-543.
2. Müller, M., Saxey, D. W., Smith, G. D., & Gault, B. (2011). Some aspects of the field evaporation behaviour of GaSb. *Ultramicroscopy*, 111(6), 487-492.

### F.MT05.06.08

**Atom Probe Tomography and First Principal Calculation to Study N-Type Doping in  $(Al_xGa_{1-x})_2O_3$**  Jith Sarker, Ankit Sharma, Uttam Singiseti and Baishakhi Mazumder; University at Buffalo, The State University of New York, United States

Efficient n-type doping in ultra-wide bandgap  $(Al_xGa_{1-x})_2O_3$  is a key for the realization of high frequency transistors with theoretical performance limit. Group IV elements (Si, Sn and Ge) are being considered as efficient donors in  $(Al_xGa_{1-x})_2O_3$  as they are predicted to substitute in cation sites and contribute in conductivity [1]. First principal calculations by density functional theory (DFT) proposed that Si is the most promising candidate for achieving n-type conductivity in  $(Al_xGa_{1-x})_2O_3$  as it remains a shallow donor at the highest range of Al composition while other donors are likely to transform into deep level defects at high Al- $(Al_xGa_{1-x})_2O_3$  [1]. Incorporation of Si in  $(Al_xGa_{1-x})_2O_3$  has been reported experimentally. The dopant behavior in these films including dopant distribution, layer homogeneity, segregation/clustering with varying alloy composition is not reported so far. It has been reported for similar wide bandgap system, AlGaN that n-type doping introduces point defects such as cation vacancies ( $V_{Ga}$  and  $V_{Al}$ ). These defect sites act as charge trapping centers by interacting with dopants and forms complex defects ( $V_{Ga-Si_{Ga}}$  or  $V_{Al-Si_{Al}}$ ) [2]. This results in reduced carrier mobility at high doping regime and is termed as “compensating knee” [2]. Similar investigation on dopant behavior in  $(Al_xGa_{1-x})_2O_3$  is not reported yet. It is crucial to have in depth understanding of dopant interaction down to atomic level structural chemistry of  $(Al_xGa_{1-x})_2O_3$  films is pivotal to achieve excellent doping profile.

Atom probe tomography (APT) was employed to investigate the atomic level dopant behavior and dopant interaction in  $(Al_xGa_{1-x})_2O_3$  with varying Al content ( $x = 0.10-1.0$ ). APT reveals that at low Al content, Si distribution is homogeneous while some high Si density island-like regions appears at high Al content ( $x \approx 80\%$ ). The statistical radial distribution function (RDF) was used to understand the dopant interaction in by exploring the nearest neighbor chemistry in the bulk regions of each  $(Al_xGa_{1-x})_2O_3$  layer. RDF in layers with low Al contents ( $x = 10-20\%$ ) showed high Ga concentration in regions surrounding the Si atoms with Al concentration being very low, indicating Si is substituting in Ga sites. Ga concentration drops at the position of Si atoms implying the presence of  $V_{Ga}$ . This result indicates the potential  $V_{Ga-Si_{Ga}}$  defect complex formation. At high Al ( $x = 60-100\%$ ), high Al concentration was observed around Si atoms with Al concentration dropping at the location where Si atoms reside, indicating Al site occupancy with possible  $V_{Al-Si_{Al}}$  complexes. The initial interpretation of APT results coincided with what was observed in case of GaN, AlGaN and  $Ga_2O_3$  and would account for compensating effect in  $(Al_xGa_{1-x})_2O_3$ .

The information obtained from APT would provide a guide to the first principal DFT study of Si doped  $(Al_xGa_{1-x})_2O_3$ . DFT calculation will be performed to confirm the site specific substitution of dopants in  $(Al_xGa_{1-x})_2O_3$  at low and high Al content. DFT will confirm the vacancy, interstitial or vacancy-interstitial complex defects by evaluating the formation enthalpy of these defects and defect complexes at different Al contents that would explain carrier compensation in wide bandgap semiconductors.

We acknowledge Dr. Hongping Zhao’s group in Dept. of ECE at the Ohio State University for providing the samples.

[1] J. B. Varley *et al.*, Appl. Phys. Lett. **116**, 172104 (2020)

[2] J. S. Harris *et al.*, Appl. Phys. Lett. **112**, 152101 (2018)

### F.MT05.06.09

**APT Reveals the Synergistic Role of Mn and Zr/Ti in Producing  $\theta'$ /L1<sub>2</sub> Co-Precipitates in Al-Cu Alloys** Jonathan Poplawsky<sup>1</sup>, Brian Milligan<sup>2,1</sup>, Lawrence Allard<sup>1</sup>, Dongwon Shin<sup>1</sup>, Patrick Shower<sup>1</sup>, Matthew Chisholm<sup>1</sup> and Amit Shyam<sup>1</sup>; <sup>1</sup>Oak Ridge National Laboratory, United States; <sup>2</sup>Colorado School of Mines, United States

Typical AlCu-alloys used for automotive applications can only withstand temperatures up to 250 °C. Increasing this temperature will improve fuel efficiency. The presence of the  $\theta'$  ( $Al_2Cu$ ) precipitate in these alloys is critical for the alloy hardness; however,  $\theta'$  is a metastable precipitate that disappears (transforms) at higher temperatures, destroying the alloy properties. Recently, an affordable and castable Al-Cu alloy that retains  $\theta'$  and maintains its strength after a lengthy exposure to 350 °C was developed (> 200 Hrs). The addition of Mn in combination with Zr and their segregation to precipitate interfaces play a significant role in stabilizing the metastable  $\theta'$  precipitates, while adding Zr and Mn separately only improves the stability to 200 °C and 300 °C, respectively. A series of atom probe tomography (APT) and scanning transmission electron microscopy (STEM) experiments on Al-Cu-Mn-Zr/Ti-containing alloys subjected to long-term annealing (up to 2,100 h) in the critical temperature range, 300 °C and 350 °C, were performed to reveal how Mn and Zr work synergistically to stabilize the strengthening phase ( $\theta'$ ). The experimentally observed solute segregation to  $\theta'$  precipitate interfaces (APT) and atomic structure at the interfaces (STEM) were used to guide density functional theory (DFT) simulations to understand how Mn and Zr additions change the energetics of  $\theta'$  in an Al-matrix. The APT and STEM results reveal that Mn additions reduce interfacial energy, and thus, stabilize  $\theta'$  long enough for the slower diffusing Zr atoms to segregate to coherent  $\theta'$  interfaces that eventually create a  $\theta'$ /L1<sub>2</sub>-Al<sub>3</sub>(Zr<sub>x</sub>Ti<sub>1-x</sub>) co-precipitate structure. The co-precipitate is highly stable, is a key factor that governs microstructural stability beyond 300 °C. This study reveals how solute additions

with different stabilization mechanisms can work in concert to stabilize a desired microstructure, and the results provide insights that can be applied to other high-temperature alloy systems.

This research was supported by the DOE Office of Energy Efficiency and Renewable Energy, Vehicle Technologies Office, Propulsion Materials Program and the DOE Basic Energy Sciences, Materials Sciences and Engineering Division. APT was conducted at ORNL's Center for Nanophase Materials Sciences (CNMS), which is a US DOE Office of Science User Facility. The authors appreciate the support provided by the Oak Ridge Leadership Computing Facility at the ORNL. The authors thank Ray Unocic and Allen Haynes (ORNL) for reviewing the manuscript. The authors would also like to thank Dana McClurg for heat treatments and hardness measurements and James Burns for APT sample preparation and APT operation.

#### **F.MT05.06.10**

**Late News: Specimen Preparation of Environmentally Sensitive Materials for Compositional and Structural Analysis at the Atomic Scale by Correlative APT and TEM Studies** [Cecile Bonifacio](#)<sup>1</sup>, Daniel Perea<sup>2</sup>, Pawel Nowakowski<sup>1</sup> and Paul Fischione<sup>1</sup>; <sup>1</sup>E.A. Fischione Instruments, Inc., United States; <sup>2</sup>Pacific Northwest National Laboratory, United States

Atom probe tomography (APT) is a powerful characterization technique for obtaining three-dimensional structure and materials composition at the atomic scale and is complementary to transmission electron microscopy (TEM). In tandem, the two techniques provide detailed characterization of structure, composition, and chemistry. However, the full potential of both of these techniques is typically hindered by artifacts from specimen preparation (e.g., Ga implantation and amorphization) and environmental conditions that degrade the specimen's surface (e.g., surface oxidation). Dual beam FIB (DB-FIB), which is an efficient tool for removing a substantial amount of material and in situ electron beam imaging, allows more control when shaping the APT specimen tip and is typically used to prepare APT specimens. However, Ga-induced damage and amorphization from FIB milling can result in ambiguous results, especially for Al/Al alloys and Ga-containing materials. In fact, it was recently shown that amorphization due to the high energy Ga beam during FIB milling dramatically affected the shape of the mass spectrum due to tip heating during APT acquisitions in Si APT specimens. Studies such as this provoke this study of using low energy Ar ion milling post-FIB milling to obtain high-quality APT specimens. Low energy (< 1 keV) Ar ion milling has been shown to improve TEM specimen quality by removing amorphization and Ga implantation from FIB prepared specimens. We present a post-FIB specimen preparation of APT specimens under controlled environments using concentrated beam (< 1  $\mu\text{m}$ ), low energy Ar<sup>+</sup> milling for the removal of manufacturing damage, oxides and FIB-induced damage for TEM and APT analyses. This controlled environment is integrable to current APT environmentally controlled transfer system.

Al and Mg metals and their alloys were chosen as test specimens due to their highly oxidizing properties. The APT specimens were prepared in a FIB system using standard lift-out methods and annular milling. The APT specimen preparation workflow from FIB to an Ar<sup>+</sup> milling system using a FIB vacuum transfer system was interfaced with a glovebox in between transfers. For ease of specimen handling and transfer, the half-grid with the APT specimens was secured in the cartridge of a TEM vacuum transfer specimen holder that is compatible with the ion milling system. Ar<sup>+</sup> milling was performed by using a concentrated ion beam that is rastered longitudinally within a defined area on the APT specimen at decreasing milling energies. TEM, energy dispersive X-ray spectroscopy (EDS), and APT characterization were performed under controlled environments before and after ion milling to determine the removal of surface oxides and FIB-induced damage. Quantification of the removal of FIB-induced damage and the workflow's ability to prevent specimen oxidation and contamination will be presented.

#### **F.MT05.06.11**

**Late News: Atom Probe Tomography and Model-Free Methods for Analysis of Kinetics of a Binary Co-Sn Alloy** [Muna S. Khushaim](#)<sup>1</sup>, Fatimah Alahmari<sup>2</sup>, Delphine Chassaing<sup>3</sup> and Torben Boll<sup>3</sup>; <sup>1</sup>Taibahu University, Saudi Arabia; <sup>2</sup>Imam Abdulrahman bin Faisal University, Saudi Arabia; <sup>3</sup>Karlsruhe Institute of Technology, Germany

Recent studies of lithium-ion batteries suggest that the use of binary *CoSn* alloys as anodes should provide an improvement over currently used anode materials [1]. However, the implementation of *CoSn* alloys is challenging due to uncertainties regarding the phase transformations within this system. In order to understand these, we evaluate the compositions of different intermetallic compounds produced via the peritectic reactions, nucleate and grow within the microstructure of binary *Sn* -25 at.% *Co* by employing atom probe tomography (APT). Owing to its capability, APT with its exceptional capabilities of spatially resolution and quantitative chemical analyses is presented as a sophisticated analytical tool to elucidate the underlying process of the phase transition behaviour of different *Co-Sn* intermetallic compounds and the local structure of the solid solution. The APT results revealed the presence of *Co* clusters with  $(54.1 \pm 0.1)$  at.% *Co*,  $(23.34 \pm 0.3)$

at.% Co and  $(0.6 \pm 0.1)$  at.% Co in pure Sn phase [2], which is consistent with the equilibrium phase diagram that indicates there is limited solubility of Co in Sn (up to 0.6%) at a temperature of 1196 °C. This limited solubility of Co atoms induced the formation of different observed intermetallic phases that are CoSn and CoSn<sub>3</sub>. This study demonstrates the unique capabilities of APT to characterize a series of peritectic reactions within the binary Co-Sn alloy. Moreover, crystallization kinetics of the crystallization reactions in Co-Sn alloy system were investigated under non-isothermal as well as isothermal conditions. These investigations were performed by using of model -free (isoconversion) methods. The results show decreasing on the activation energy for the crystallization kinetics for CoSn and CoSn<sub>3</sub> phases with increasing temperature, which reveals the involvement of two processes of nucleation and diffusion during the crystallization of these intermetallic phases.

#### References

- [1] G. Mulas, S. Enzo, C. Bonatto Minella, E. Arca, C. Gerbaldi, N. Penazzi, S. Bodoardo, J. Hassoun and S. Panero, *Mechanochemical synthesis and electrochemical properties of nanostructured electrode materials for Li ion batteries*. Journal of Solid State Electrochemistry, 2009. 13(2): p. 239-243.
- [2] M. Khushaim, F. Alahmari, N. Kattan, D. Chassaing and T. Boll, Microstructural properties and peritectic reactions in a binary Co-Sn alloy by means of scanning electron microscopy and atom probe tomography, Mater. Res. Express 7 (2020) 086508

#### F.MT06.06.01

**Direct Correlation of Structure and Optical Properties of Defect Related Colour Centres in Hexagonal Boron Nitride** Soumya Sarkar, Sinu Mathew, Manohar Lal, T. Venky Venkatesan and Silvija Gradecak; National University of Singapore, Singapore

Hexagonal boron nitride (h-BN) has recently emerged as a prominent nanophotonic material due to observation of several unique optoelectronic phenomena such as natural hyperbolicity, strong second order non-linearities and robust deep UV emission. Specifically, its ultra wide bandgap ~ 6eV can host midgap defects that often exhibit intense room temperature quantum emission. Understanding the origin of such defect related emission is crucial to harness their technological potential. Here, we report controlled tailoring of defect states in hBN by focussed helium ions using a helium ion microscope and present a direct correlation of their structural and optical properties using a combination of Raman, photoluminescence (PL), cathodoluminescence (CL) and high resolution electron microscopy. We observe that while end of range defects cause an evolution of sp<sup>3</sup> phase in the otherwise sp<sup>2</sup> hBN leading to bright and previously unreported near infrared emission, near surface defects contribute to strong visible emitters often attributed to single photons. Our results provide a comprehensive overview of defect related colour centres in hBN across a wide spectral range that would serve as a platform to realize next generation quantum optoelectronic devices.

### SYMPOSIUM F.MT02

---

Multimodal, Functional and Smart Scanning Probe Microscopies for Characterization and Fabrication  
November 21 - December 2, 2020

#### Symposium Organizers

Neus Domingo Marimon, ICN2  
Ricardo Garcia, Consejo Superior de Investigaciones Cientificas  
Olga Ovchinnikova, Oak Ridge National Laboratory  
Roger Proksch, Asylum Research

---

\* Invited Paper

SESSION F.MT02.08: Live Panel Discussion: Multimodal, Functional and Smart Scanning Probe Microscopies for Characterization and Fabrication



Session Chair: Yongtao Liu  
Wednesday Morning, December 2, 2020  
F.MT02

**8:00 AM PANELISTS:**

**8:00 AM \*F.MT02.01.01**

**Practical Deep Learning in Scanning Probe Microscopy** Joshua Agar; Lehigh University, United States

**Deep learning (DL) has transformed tasks of computer vision and natural language processing. There has been significant interest in emulating this success in scanning probe microscopy and spectroscopies more broadly. While there has been a boon in DL theory developed to address non-scientific problems, and these have been applied in science, their success has been underwhelming. For DL to make transformative breakthroughs in science, it must address practical scientific challenges. For example, in scientific problems, symmetry, order, periodicity, and scale require consideration in ways not needed in conventional DL and solutions. Moreover, scientific problems require that the models are interpretable and parsimonious, rather than through randomness and multiplicity. In this presentation, we discuss progress on developing practical scientific theory and methodologies of deep learning to address challenges in scanning probe microscopy (SPM). We will discuss how computer vision models' scientific aptitude can be improved through the addition of symmetry awareness to enable the formation and search of latent spaces of image similarity. We will discuss how to build fully-unsupervised learning models capable of conducting spectral unmixing of noisy and complicated hyperspectral images commonly collected in multimodal SPM. We specifically highlight challenges and methodologies to control the structure, shape, and statistical distribution of the learned latent manifold, how to deal with long spectral sequences, and control sparsity. Furthermore, we will demonstrate how custom physics-informed regularizers can encourage parsimonious learning. Finally, we will conclude with how to deploy these models in practice. We will specifically highlight how to prune these models to fit on resource-constrained neural processing units for real-time deployment, where inference on the order of milliseconds is required.**

**8:08 AM \*F.MT02.01.02**

**Data Mining of Spatially Resolved Heterogeneous Electrical Conduction in Fuel Cells** Yunseok Kim; Sungkyunkwan University, Korea (the Republic of)

The electrodes of a polymer electrolyte membrane fuel cell (PEMFC) primarily contain a Pt/C catalyst and Nafion binder. Because these components play crucial roles in the redox reaction and proton transport, respectively, their distributions can directly affect the electrochemical reactivity, and thus, the device performance. Even though analyzing the component distribution is important to understand its electrochemical reactivity and improve the device performance, it is challenging to determine it for the PEMFC electrode. In this presentation, I will summarize our recent effort for visualizing the spatial distribution of the electrode components and their heterogeneous electrical properties using multidimensional current-voltage (I-V) spectroscopy combined with data mining. The electrical properties of the electrode components, i.e., the Pt/C catalyst and Nafion binder, were explored by I-V spectroscopy, and their electrical heterogeneity was spatially classified based on the shapes of the measured I-V curves by cluster analysis. These results imply that it is possible to get more insight on the data analysis in AFM even using a simple machine learning technique. Furthermore, the proposed method is expected to be applicable for investigating in detail not only the spatial properties of PEMFC electrodes, but also the properties of various material systems.

**8:16 AM \*F.MT02.02.02**

**Time Lapse Scanning Ion Conductance Microscopy (SICM) Combined with Super Resolution Optical Fluctuation Imaging (SOFI)** Georg Fantner, Samuel Mendes Leitao, Vytautas Navikas, Barney Drake and Aleksandra Radenovic; Ecole Polytechnique Federale de Lausanne, Switzerland

One of the key advantages many SPM techniques have for cell biology studies is their ability to non-destructively image cells in physiological environments. Using time lapse microscopy, it is then possible to observe how the cells change over time either during growth, development or due to drug treatments. For bacterial cells, time lapse atomic force microscopy (AFM) has been very helpful in understanding how cells grow, divide and react to antibiotic stresses. For soft mammalian cells however, long term time lapse using AFM is more difficult due to the complex and time varying force interaction between

the tip and the cell surface. For these cells, scanning ion conductance microscopy (SICM) would be better suited for time lapse experiments. Unfortunately, standard SICM instruments require 10s of minutes for good quality images, which is often too slow to follow important cell dynamics. In this talk I will describe a microscope we have developed for time resolved SICM imaging of mammalian cells that enables imaging durations of up to 48h with image acquisition times as low as 3 seconds. We have combined this SICM instrument with super-resolution optical fluctuation imaging (SOFI) to complement the morphological SICM data with biochemical fluorescence information. With this instrument we study cell growth, motility, macropinocytosis and cell differentiation.

#### 8:24 AM \*F.MT02.02.04

##### **Classification of Active Materials and Binder in a Composite Anode Using Multi-Modal Scanning Probe Microscopy** Seungbum Hong; Korea Advanced Institute of Science and Technology, Korea (the Republic of)

Here, we present a multimodal scanning probe microscopy study of a composite anode with a dispersed lithium silicon titanium phosphate (LSTP) lithium ion conductor for all-solid-state batteries. We used electro-chemical strain microscopy (ESM) and lateral force microscopy (LFM) to analyze the electromechanical response and friction force dependence as a function of the measurement parameters such as the tip loading force and AC drive voltage. We found that the sensitivities of friction force and ESM amplitude could be valid markers to identify each component in the composite anode. In addition, we visualized the distribution of active ionic sites of lithium ions in the region of LSTP and binder materials based on Pearson's correlation analysis between nanoscale ESM and LFM results. With the suggested technique, various components of composite electrodes can be directly visualized and distinguished in ambient conditions, with their properties being measured simultaneously. These methods will provide insights into the optimal conditions of composite electrodes and allow for developing next-generation all-solid-state batteries.

#### 8:32 AM \*F.MT02.03.01

##### **Mapping Nanoscale Viscoelasticity and Relaxation Times Underlying Growth and Shape of Multicellular Organisms Using Multifrequency AFM** Jacob Seifert, Casey Adam, Alba Piacenti and Sonia Contera; University of Oxford, United Kingdom

The dynamic shapes of biological tissues emerge from a complex interplay of physics, chemistry and genetics, which determines--at each temporal and spatial scale--the mechanical properties that eventually form the structures of living organisms. Shape and mechanical stability of living organisms rely on precise control in time and space of growth, which is achieved by dynamically tuning the mechanical (viscous and elastic) properties of their hierarchically built structures from the nanometer up.

It is now well-established that cellular behaviour (including stem cell differentiation) crucially depends on the mechanical properties of the cells' environment. Much attention has been directed towards the importance of the *stiffness* of the natural (extracellular matrix, ECM) or artificial matrices where cells grow, with the purpose of either understanding mechanotransduction, or controlling the behaviour of cells in tissue engineering. While stiffness (i.e. the capacity of a material to elastically store mechanical energy) has been the focus of most experimental research, neither cells nor matrices are elastic. Biological systems dissipate energy (i.e. they are viscous) and hence they do not respond to mechanical deformations instantaneously (like an ideal Hookean spring), but present different time responses at different spatial scales that characterise their responses to external stimuli.

Measuring viscoelasticity (especially at the nanoscale) has remained experimentally challenging [1,2]. In my talk I will present atomic force microscopy (AFM)-based techniques to measure and map the viscoelasticity of living tissues, cells, membranes, collagen, ECMs, and tissue engineering matrices across the spatial and temporal (from Hz to 100s of kHz) scales, and chirp-based spectroscopic techniques to assess viscoelasticity from Hz to 100s kHz at the nano and micro scale developed in my lab. I will also present tests for assessing which viscoelastic model better fits the experimental AFM results. Our results have uncovered that extracellular matrices of both living plants and tumours present an almost perfect linear viscoelastic behaviour that is key to understand their growth and shape. I will present our work showing how the growth and shape of the roots, leaves and hypocotyl of living *Arabidopsis thaliana* living plants are related to the nanoscale viscoelasticity of plant cell walls at the time scales probed by multifrequency AFM.

#### References:

- [1] "Multifrequency AFM reveals lipid membrane mechanical properties and the effect of cholesterol in modulating viscoelasticity" 2019. Z Al-Rekabi, S Contera; Proceedings of the National Academy of Sciences 115 (11), 2658-2663.
- [2] "Mapping nanomechanical properties of live cells using multi-harmonic atomic force microscopy" 2011 A Raman, S Trigueros, A Cartagena, APZ Stevenson, M Susilo, E Nauman, S Contera. Nature Nanotechnology 6 (12), 809.

8:40 AM \*F.MT02.03.02

**Thermal Scanning Probe Lithography and Å-Indentation for Manipulating and Characterizing 2D Materials** Elisa Riedo, Francesco Lavini, Filippo Cellini, Xiaorui Zheng, Annalisa Calò, Tengfei Cao, Edoardo Albisetti and Xiangyu Liu; New York University, United States

The ability to characterize and manipulate materials down to the atomic scale for tuning their mechanical and physical properties is the cornerstone of material science. Two-dimensional (2D) materials in particular are getting large attention because their extremely thin size gives rise to unique and groundbreaking properties.

Here we explore two different research topics. On one side we show how heat delivered by a scanning probe can be used for manipulating the electrical properties of 2D materials, and on the other side we present a recent scanning probe microscopy method to perform Å indentation experiments in supported 2D materials.

Among various novel materials, two-dimensional molybdenum disulfide ( $\text{MoS}_2$ ) is of particular interest due to its large band gap, low dielectric constant, and heavy carrier effective mass. Currently, a key issue in creating high performing field-effect transistors (FETs) based on  $\text{MoS}_2$  and other transition metal dichalcogenides (TMDC) films is the poor quality of the metal contacts fabricated on these atomic layers, and the difficulty to pattern dopants. Here, we report a strategy based on thermal scanning lithography (tSPL) to fabricate metal contacts on 2D materials with high reproducibility [1], and we demonstrate the integration of tSPL with a flow-through reactive gas cell to achieve nanoscale control of dopants in monolayer  $\text{MoS}_2$  [2]. The tSPL produced defects can present either p- or n-type doping on demand, depending on the used gasses, allowing the realization of field effect transistors, and p-n junctions with precise sub- $\mu\text{m}$  spatial control, and a rectification ratio of over  $10^4$ . Doping and defects formation are elucidated by means of X-Ray photoelectron spectroscopy, scanning transmission electron microscopy, and density functional theory. We find that p-type doping in  $\text{HCl}/\text{H}_2\text{O}$  atmosphere is related to the rearrangement of sulfur atoms, and the formation of protruding covalent S-S bonds on the surface. Alternatively, local heating  $\text{MoS}_2$  in  $\text{N}_2$  produces n-character.

Moreover, we report on the elastic properties of supported 2D graphene and h-BN films by the use of modulated Å-Indentation, a novel scanning probe microscopy (SPM)-based technique capable of achieving sub-Å indentation depths during force-indentation measurements [3, 4]. By using extremely small amplitude oscillations ( $\ll 1$  Å) at high frequency, we show how Å-Indentation enables non-destructive local accurate measurements of the contact stiffness and out-of-plane elastic moduli of ultra-thin ultra-stiff films, including CVD diamond films (thus even up to TPa range stiffness), as well as the transverse moduli of supported graphene and h-BN ( $< 1$  nm thickness) films. Å-Indentation thus obtains *in-situ* elasticity measurement combining superior resolution and indentation depths as small as 0.3 Å with AFM nanoscale topographical imaging. Thanks to this technique, we experimentally demonstrate that at room temperature and under localized indentation pressure, a single layer of graphene on top of a carbon interface layer (buffer layer), on SiC, exhibits a transverse stiffness superior to bulk diamond [3]. Extending the capabilities of the Å-indentation technique to the analysis of other 2D materials, these studies explore similar pressure-induced phase transition in hexagonal boron nitride (h-BN). We demonstrate that 2-layer h-BN flakes, on  $\text{SiO}_2$ , consistently exhibit a transverse elastic modulus almost two times larger than that of the bare substrate. This stiffening effect is observed only for flakes of thickness between 2 to 5 atomic layers, but not in single- nor multilayer ( $> 6$ -layer) h-BN, and is related to the conversion of h-BN to cubic BN (c-BN) induced by the pressure applied through the indenter.

1 Zheng et al. *Nature Electronics*, 2, 17–25 (2019)

2 Zheng et al. *Nature Communication*, (2020) <https://doi.org/10.1038/s41467-020-17241-1>

3 Gao et al. *Nature Nanotechnology* 13.2 (2018): 133

4 Cellini et al. *Scientific reports* 9.1 (2019): 4075

8:48 AM \*F.MT02.03.03

**Paddled Cantilever for AFM Beyond Topography** Hanna Cho; The Ohio State University, United States

Atomic Force Microscopy (AFM) is one of the most powerful and versatile tools to image and characterize materials with nanometer scale resolution, leading to the development of nano-/bio- science and technology. While AFM technology has advanced significantly by expanding its functionality beyond a nanoscale imaging tool, the majority of AFM users still find it difficult to employ the advanced techniques and interpret the data correctly due to artifacts. Such difficulties mainly originate from the complex dynamics of the AFM probe system, used as a mechanical transducer to deliver the tip-sample interaction force.

We address this issue by altering the AFM cantilever design. The current state of the art AFM probe is a single-body system, in the shape of a rectangular or triangular beam, which is not ideal for carrying more than one type of information. In

contrast, the new AFM probe, so-called paddled cantilever, is reshaped to have a two-field microcantilever design with a considerable dimensional discrepancy in the component part. By doing so, this mechanical transducer provides two discrete transduction channels such that they respond independently to the variations in surface topography and material properties/functionality. Thus, AFM users can effortlessly implement the advanced AFM schemes with minimal ambiguity, complications, and artifacts, by simply employing this new AFM probe.

Since the prototype device of paddled cantilever was first introduced, our team has taken effort to develop a batch fabrication process and, thus, have this advanced technology widely available for AFM users. The detailed dynamics of fabricated paddled cantilevers have been investigated by using the interferometric displacement sensor (IDS) with AFM to directly measure their deflection. The measured deflection along the whole cantilever revealed that the frequency of inner-paddle is not affected by the tip stiffness while its amplitude is proportional to the displacement input delivered through the tip. This is the basis how the paddled cantilever can provide two discrete transduction channels for functional AFM. A theoretical model based on a 2 degree-of-freedom system is also presented to understand the dynamic characteristics of paddled cantilever under various operational conditions. Because the design of paddled cantilever is simple to feasibly integrate into, and compatible with, current AFM probes and systems, this technology will easily extend the AFM functionality to characterize multi-physical properties beyond topography by providing a dual-channel mechanical transducer.

**8:56 AM \*F.MT02.04.01**

**Conductive Colloidal Scanning Probe Microscopy** Christine Kranz and Sven Daboss; Ulm University, Germany

Scanning electrochemical probe microscopy (SEPM) techniques such as scanning electrochemical microscopy (SECM) and in particular the hybrid techniques such as atomic force microscopy combined with scanning electrochemical microscopy (AFM-SECM) enable high resolution topographical imaging along with electrochemical information [1] but also electrochemical force spectroscopic measurements [2]. Recently, we introduced a new type of electrochemical scanning probe tip for combined AFM-SECM measurements providing instead of a conventional AFM tip, a conductive colloidal sphere attached to an otherwise insulated cantilever [3]. Such conductive spherical probes may consist of boron-doped diamond [4], a highly attractive electrode material, or may be electrochemically modified, e.g., functional polymers, suitable for force spectroscopic measurements such as adhesion measurements under potential control.

In this contribution, we present AFM-SECM measurements and electrochemical force spectroscopy using conductive colloidal AFM probes. Due to the spherical geometry and the low spring constant of the cantilever, these probes are highly suitable for mapping nanomechanical properties at soft samples, i.e. bacterial cells. Colloidal probes with BDD as spherical electrode can be used for various SPM experiments including conductive AFM given the physical and electrochemical inertness of BDD, for force spectroscopy under potential control providing information on electrified interfaces, and for AFM-SECM measurements. Notably, all these experiments can be performed with the same BDD-AFM-SECM probe. Colloidal probes can be modified with polymers i.e. polydopamine, which properties may be altered by applying potential to the spherical electrode. Single cell force spectroscopy on bacterial adhesion along with studies at electrified interfaces will be presented.

[1] A. Patel, C. Kranz, *Annu. Rev. Anal. Chem.* **2018**, *11*, 329.

[2] S. Daboss, J. Lin, M. Goddjehans, C. Kranz, **2020**, in press

[3] P. Knittel, H. Zhang, C. Kranz, G. G. Wallace, M. J. Higgins, *Nanoscale* **2016**, *8*, 4475.

[4] S. Daboss, P. Knittel, C. E. Nebel, C. Kranz, *Small* **2019**, *15*, 1902099.

**9:04 AM \*F.MT02.05.01**

**Nanoscale Ion Transport Dynamics—From Conjugated Polymers to Halide Perovskites Solar Cells** David S. Ginger<sup>1,2</sup>; <sup>1</sup>University of Washington, United States; <sup>2</sup>Pacific Northwest National Laboratory, United States

Imaging ion transport in nanostructure materials has applications in systems from neuromorphic computing, to electrochemical energy storage, and solar cells. We utilize multimodal imaging to probe transport phenomena in these systems. For instance, by combining nanoscale vibrational spectroscopy with structural imaging we can correlated local anion diffusion with structural phase transitions in conjugated polymer films being explored for neuromorphic computing and bioelectronics applications. We also combine similar IR imaging with time-resolved electrostatic force microscopy (trEFM) to uncover the dynamics of ion transport in various 3D and 2D halide perovskites of interest for applications in optoelectronics, especially solar cells, where ion transport can be a primary contributor to device aging and failure. This work bridges advances in scanning probe microscopy with tools from data science to better understand materials design rules for new applications.

### 9:12 AM \*F.MT02.06.01

**Tracking the Dynamics of Liquids and Solutes at Solid Nano-Interfaces** Luca Piantanida<sup>1,2</sup>, Amir F Payam<sup>1,3</sup>, Clodomiro Cafolla<sup>1</sup> and Kislon Voitchovsky<sup>1</sup>; <sup>1</sup>Durham University, United Kingdom; <sup>2</sup>Boise State University, United States; <sup>3</sup>Ulster University, United Kingdom

The molecular organisation and dynamics of liquids near the surface of solids underpins processes such as molecular exchanges, electrochemistry, nanofluidics, biomolecular function and lubrication. Depending on the local topographical and chemical properties of the solid, the behaviour of the interfacial liquid can vary significantly at the nanoscale, with consequences for interfacial processes. Scanning probe microscopies can derive local insights into the equilibrium organisation of interfacial liquids, often with sub-nanometre resolution. However, deriving quantitative information about the local liquid *dynamics* remains a considerable challenge.

Here we review some of our recent results obtained by combining high-resolution atomic force microscopy with highly localised rheological measurements to deduce quantitative information about the motion of liquids and dissolved molecules along immersed solids. We show that the dynamics is highly system-dependant and can be dominated by either the local configurational entropy or the interface or enthalpic interactions. We also describe a novel approach to quantify the preferred flow direction naturally adopted by liquids near walls, locally and with nanometre precision. The approach, based on AFM, combines a vertically oscillating tip with high frequency lateral oscillations to derive directional information about the interfacial liquid at each point of the system. To illustrate the method's capabilities, we investigate the dynamics of aqueous solutions containing different metal ions along the surface of a graphene oxide flake. We identify ion-specific flow dynamics that can be related to the well-established sieving properties of graphene oxide membranes.

### 9:20 AM \*F.MT02.06.02

**Using High-Speed, Molecularly-Resolved AFM and Fast Force Mapping to Investigate Nucleation and Solution Structure at Surfaces** James J. De Yoreo<sup>1,2</sup>, Benjamin Legg<sup>2,1</sup>, Elias Nakouzi<sup>1</sup>, Andrew G. Stack<sup>3</sup>, Sebastien Kerisit<sup>1</sup>, Christopher A. Mundy<sup>1,2</sup>, Gregory K. Schenter<sup>1</sup>, Jaehun Chun<sup>1</sup> and Kislon Voitchovsky<sup>4</sup>; <sup>1</sup>Pacific Northwest National Laboratory, United States; <sup>2</sup>University of Washington, United States; <sup>3</sup>Oak Ridge National Laboratory, United States; <sup>4</sup>Durham University, United Kingdom

Investigating nucleation from solutions is challenging, because it is a consequence of unstable density fluctuations, making the structures and events that must be probed both transient in nature and small in spatial extent. Moreover, when nucleation is heterogeneous, it is inherently linked to the structure and dynamics of the interfacial region between the bulk solution and the underlying substrate. Thus high-speed, molecularly resolved AFM combined with fast force mapping (FFM) provides a powerful and unrivalled combination to investigate nucleation from solution onto surfaces. Here I illustrate the deep level of fundamental insight into mechanisms of nucleation and the structure of the interfacial region made possible with these methods using results from investigations into nucleation of gibbsite ( $\text{Al}(\text{OH})_3$ ) on muscovite mica (001) and the structure of electrolyte solutions above mica and boehmite ( $\text{AlOOH}$ ) surfaces. In the case of gibbsite nucleation, we combine AFM observations of individual molecular adsorbates, transient clusters, and stable islands with Monte Carlo simulations to put together a coherent picture of surface speciation and nucleation. The results reveal a surface population of ions that is dominated by hydrolyzed species ( $\text{Al}(\text{OH})_2^+$  and  $\text{Al}(\text{OH})_2^{2+}$ ) even though  $\text{Al}^{3+}$  vastly dominates the bulk solution. These adsorbed ions evolve into subcritical clusters with increasing saturation state and temperature, constituting a population that decreases exponentially with size and exhibits dynamic fluctuations consistent with classical predictions. However, severe discrepancies with classical theory emerge when the values of key thermodynamic parameters are extracted from the AFM data. These discrepancies are resolved when the impact adsorbate charge on the capacitance of the mica-solution system is taken into account in calculating the work of cluster formation, but reveal a film formation process that occurs within a single phase region. Thus, the results imply that the gibbsite films constitutes a nanostructured 2D mesophase. To define the solution structure above boehmite and mica surfaces at lattice resolution, we developed a self-consistent scheme to decouple long-range tip-sample interactions from short-range solvation forces. In the case of boehmite, the results are benchmarked against molecular dynamics simulations that explicitly include the effects of the tip with different levels of approximation and systematically account for tip size, chemistry, and confinement effects. We find four laterally structured water layers within one nanometer of the surface, with the highest water densities at sites adjacent to hydroxyl groups. The findings reveal a complex relationship between site-specific chemistry, water density, and long-range particle interactions; and represent a major step forward towards quantitative data interpretation and widespread implementation of 3D FFM.

**5:00 AM \*F.MT02.01.01**

**Practical Deep Learning in Scanning Probe Microscopy** Joshua Agar; Lehigh University, United States

**Deep learning (DL) has transformed tasks of computer vision and natural language processing. There has been significant interest in emulating this success in scanning probe microscopy and spectroscopies more broadly. While there has been a boon in DL theory developed to address non-scientific problems, and these have been applied in science, their success has been underwhelming. For DL to make transformative breakthroughs in science, it must address practical scientific challenges. For example, in scientific problems, symmetry, order, periodicity, and scale require consideration in ways not needed in conventional DL and solutions. Moreover, scientific problems require that the models are interpretable and parsimonious, rather than through randomness and multiplicity. In this presentation, we discuss progress on developing practical scientific theory and methodologies of deep learning to address challenges in scanning probe microscopy (SPM). We will discuss how computer vision models' scientific aptitude can be improved through the addition of symmetry awareness to enable the formation and search of latent spaces of image similarity. We will discuss how to build fully-unsupervised learning models capable of conducting spectral unmixing of noisy and complicated hyperspectral images commonly collected in multimodal SPM. We specifically highlight challenges and methodologies to control the structure, shape, and statistical distribution of the learned latent manifold, how to deal with long spectral sequences, and control sparsity. Furthermore, we will demonstrate how custom physics-informed regularizers can encourage parsimonious learning. Finally, we will conclude with how to deploy these models in practice. We will specifically highlight how to prune these models to fit on resource-constrained neural processing units for real-time deployment, where inference on the order of milliseconds is required.**

**5:15 AM \*F.MT02.01.02**

**Data Mining of Spatially Resolved Heterogeneous Electrical Conduction in Fuel Cells** Yunseok Kim; Sungkyunkwan University, Korea (the Republic of)

The electrodes of a polymer electrolyte membrane fuel cell (PEMFC) primarily contain a Pt/C catalyst and Nafion binder. Because these components play crucial roles in the redox reaction and proton transport, respectively, their distributions can directly affect the electrochemical reactivity, and thus, the device performance. Even though analyzing the component distribution is important to understand its electrochemical reactivity and improve the device performance, it is challenging to determine it for the PEMFC electrode. In this presentation, I will summarize our recent effort for visualizing the spatial distribution of the electrode components and their heterogeneous electrical properties using multidimensional current-voltage (I-V) spectroscopy combined with data mining. The electrical properties of the electrode components, i.e., the Pt/C catalyst and Nafion binder, were explored by I-V spectroscopy, and their electrical heterogeneity was spatially classified based on the shapes of the measured I-V curves by cluster analysis. These results imply that it is possible to get more insight on the data analysis in AFM even using a simple machine learning technique. Furthermore, the proposed method is expected to be applicable for investigating in detail not only the spatial properties of PEMFC electrodes, but also the properties of various material systems.

**5:30 AM F.MT02.01.03**

**Machine Learning to Enhance Analysis of AFM Images** Dalia G. Yablon<sup>1</sup> and Ishita Chakraborty<sup>2</sup>; <sup>1</sup>SurfaceChar LLC, United States; <sup>2</sup>Stress Engineering, United States

Machine learning (ML) is permeating many areas of research including drug design, modeling, and materials design. In the realm of characterization, ML is only beginning to be integrated into experimentation and processing to improve the workflow. Here, the potential of ML to play a role in analysis of atomic force microscopy images is explored in two distinct applications.

The first area involves a classic application in ML of image recognition. A convolutional neural net was trained on AFM phase images of different polymer blends and achieved 100% accuracy in differentiating test data, compared with 94% accuracy with a less powerful traditional neural network. This study takes advantage of classic data augmentation methods to increase the sample size since the quantity of AFM images is limited by long acquisition times. The second application

involves using ML to conduct particle analysis in challenging AFM images where the background is varied and many of the particles are linked in a matrix phase. This study serves as an example of the ultimate customizable image analysis where the training of the model takes place on the specific class of challenging images. The hope is that this study serves as a building block for future, more powerful applications of the powerful ML tool in more challenging problems that will also be discussed including establishing structure-property relationships and autonomous operation of AFM.

#### 5:40 AM F.MT02.01.05

**Elucidating Bimodal Angular Dynamics of Protein Nanorods at Solid-Liquid Interfaces by High-Speed AFM and Machine Learning** Shuai Zhang<sup>1,2</sup>, Robbie Sadre<sup>3</sup>, Benjamin Legg<sup>1,2</sup>, Harley Pyles<sup>1</sup>, Talita P. Leite<sup>3</sup>, E. Wes Bethel<sup>3</sup>, David Baker<sup>1</sup>, Oliver Ruebel<sup>3</sup> and James J. De Yoreo<sup>2,1</sup>; <sup>1</sup>University of Washington, United States; <sup>2</sup>Pacific Northwest National Laboratory, United States; <sup>3</sup>Lawrence Berkeley National Laboratory, United States

Bio-macromolecules, including peptides, proteins, DNA and peptoids, self-assemble into bio-hybrid materials with two dimensional (2D) hierarchical architectures at solid-liquid interfaces, exhibiting relative epitaxial matching. While the structural details have been elucidated experimentally and rationalized through molecular simulations, in-situ characterizations of dynamics defining orientational selection of bio-macromolecular arrays at single molecular level with temporal resolution in second, are still limited.

In this presentation, we will report the most recent study of angular dynamics of individual protein nanorods<sup>1</sup> on (001) plane of muscovite mica by high-speed atomic force microscopy (HS-AFM) and machine learning (ML) based analysis. We quantitatively analyzed their free energy landscapes and elucidated the transition possibilities between various orientational states for a range of nanorod lengths and electrolytes. After comparing ML based analysis with standard physical models for nanorod dynamics in 2D, we found that the transitions between minima go through bimodal mechanisms. Unlike the in-plane Brownian motion between adjacent minima in the energetic barrier heights, the motion between more distant minima is analogous to Levy-flights, indicating the existence of a second high-energy angular motion for the proteins. This work provides the workflow for in-situ understanding biomacromolecular dynamics at solid-liquid interfaces and the insights for further improving the general approach of managing bio-macromolecular hierarchical architectures with high accuracy and efficiency.

1 Pyles, H., Zhang, S., De Yoreo, J. J. & Baker, D. Controlling protein assembly on inorganic crystals through designed protein interfaces. *Nature* **571**, 251-256, doi:10.1038/s41586-019-1361-6 (2019).

SESSION F.MT02.02: Multimodal SPM for Characterization and Fabrication  
On Demand Abstracts Available for Viewing Starting Saturday Morning, November 21, 2020  
F-MT02

#### 5:00 AM \*F.MT02.02.02

**Time Lapse Scanning Ion Conductance Microscopy (SICM) Combined with Super Resolution Optical Fluctuation Imaging (SOFI)** Georg Fantner, Samuel Mendes Leitao, Vytautas Navikas, Barney Drake and Aleksandra Radenovic; Ecole Polytechnique Federale de Lausanne, Switzerland

One of the key advantages many SPM techniques have for cell biology studies is their ability to non-destructively image cells in physiological environments. Using time lapse microscopy, it is then possible to observe how the cells change over time either during growth, development or due to drug treatments. For bacterial cells, time lapse atomic force microscopy (AFM) has been very helpful in understanding how cells grow, divide and react to antibiotic stresses. For soft mammalian cells however, long term time lapse using AFM is more difficult due to the complex and time varying force interaction between the tip and the cell surface. For these cells, scanning ion conductance microscopy (SICM) would be better suited for time lapse experiments. Unfortunately, standard SICM instruments require 10s of minutes for good quality images, which is often too slow to follow important cell dynamics. In this talk I will describe a microscope we have developed for time resolved SICM imaging of mammalian cells that enables imaging durations of up to 48h with image acquisition times as low as 3 seconds. We have combined this SICM instrument with super-resolution optical fluctuation imaging (SOFI) to complement the morphological SICM data with biochemical fluorescence information. With this instrument we study cell growth, motility, macropinocytosis and cell differentiation.

5:15 AM \*F.MT02.02.04

**Classification of Active Materials and Binder in a Composite Anode Using Multi-Modal Scanning Probe Microscopy** Seungbum Hong; Korea Advanced Institute of Science and Technology, Korea (the Republic of)

Here, we present a multimodal scanning probe microscopy study of a composite anode with a dispersed lithium silicon titanium phosphate (LSTP) lithium ion conductor for all-solid-state batteries. We used electro-chemical strain microscopy (ESM) and lateral force microscopy (LFM) to analyze the electromechanical response and friction force dependence as a function of the measurement parameters such as the tip loading force and AC drive voltage. We found that the sensitivities of friction force and ESM amplitude could be valid markers to identify each component in the composite anode. In addition, we visualized the distribution of active ionic sites of lithium ions in the region of LSTP and binder materials based on Pearson's correlation analysis between nanoscale ESM and LFM results. With the suggested technique, various components of composite electrodes can be directly visualized and distinguished in ambient conditions, with their properties being measured simultaneously. These methods will provide insights into the optimal conditions of composite electrodes and allow for developing next-generation all-solid-state batteries.

5:30 AM F.MT02.02.05

**Hyperspectral Image Analysis of Graphene Derivatives Using Tip-Enhanced Raman Spectroscopy** Chiung-Wei Huang<sup>1</sup>, Xiao You<sup>1,2</sup>, Kizhanipuram Vinodgopal<sup>3</sup> and Joanna M. Atkin<sup>1</sup>; <sup>1</sup>University of North Carolina, United States; <sup>2</sup>Texas A&M University, United States; <sup>3</sup>North Carolina Central University, United States

Interest in graphene has grown considerably in the last decade due to its unique optical and electrical properties. However, some potential applications of graphene, such as transistors, require a bandgap, which is challenging to generate in graphene. One strategy is to tune local electronic properties by chemical modification through oxidation and surface functionalization. Using transition metal complexes, a desirable energy gap can be opened up in graphene.

Understanding and thereby controlling the mechanism of functionalization is yet hampered by the high degree of structural and chemical disorder in graphene and graphene derivatives. Pure graphene contains inhomogeneous morphological defects such as grain boundaries, edges, and wrinkles. Engineering the electronic properties by surface modification can often lead to a larger degree of inhomogeneity in chemical composition, molecular structures, and the degree of sp<sup>2</sup> conjugation.

Since the number of molecules needed for chemical modification is low, macroscopic methods such as energy-dispersive X-ray spectroscopy or X-ray photoelectron spectroscopy lack the spatial and chemical sensitivity necessary to detect modifications in graphene.

In this work, we employ functional scanning probe microscopy (SPM) techniques that offer spatially resolved, chemically specific and quantitative information on chemically modified graphene derivatives.

Tip-enhanced Raman spectroscopy (TERS) is a powerful surface analysis technique that offers nanometer-resolved images with site-specific chemical fingerprints. We demonstrate nanoscale TERS mapping of structural and functional groups on graphene derivatives. We employ machine learning (ML) tools to extract information on chemical components and their spatial distribution from the hyperspectral TERS maps.

We validate the components resulted from ML-aided analysis by comparing the principal components with density functional theory (DFT) based calculation. The prediction of vibrational modes from DFT offers insights into understanding the site-specific derivative molecules and the bonding between molecules and graphene.

We further extend surface characterization by combining TERS with Kelvin probe force microscopy (KPFM) to locally examine the electrical properties. In conjunction with illumination, we employ KPFM to estimate the local conduction and valence band edge energies. This in situ measurement allows a direct correlation of local topography, chemical composition, and electronic properties.

These methods can be applied to correlated SPM data to obtain complex compositional information that is challenging to gain from any conventional method. By combining nanometer-resolved TERS and KPFM imaging, with computation-aided ML and analysis, we have offered a comprehensive view of chemical and spatial information and demonstrated a generally applicable approach for improving the accuracy of surface characterization. We expect this work to provide a more profound understanding of the molecular binding structures with guidance for optimizing graphene semiconductors and devices.

5:40 AM F.MT02.02.07

**Volume Production of Optical Transformer-Based Campanile Scanning Near-Field Probes Integrated on an AFM Cantilever** Keiko Munechika<sup>1</sup>, Khai Le<sup>1</sup>, Adam Legacy<sup>1</sup> and Stefano Cabrini<sup>2</sup>; <sup>1</sup>HighRI Optics, Inc, United States; <sup>2</sup>Lawrence Berkeley National Lab, United States

Near-field scanning optical microscopy (NSOM) has become one of the most crucial and powerful techniques to characterize



the chemical, physical, and biochemical properties of materials with nanometer-scale resolution in real-time. A key element for any NSOM systems that combine optical spectroscopy with scanning probe microscopy is the actual probe itself. An ideal NSOM probe provides a strong local electromagnetic field enhancement, efficient far-field to near-field coupling, nanoscale spatial resolution, background-free operation, and broadband photon-plasmon coupling to enable high spatial and temporal resolution. One of the most exciting optical probe architectures based on an optical transformer, “campanile,” was recently developed and has been successfully used for multidimensional spectroscopic imaging of nanostructures with nanoscale resolution, providing insights into novel optoelectronic process<sup>1</sup>. However, making such probes requires both the expertise and the facility, and reproducibility is a significant issue. The economic production of reasonable volumes of such probes is not possible. There is a critical need for the development of optical tip technology to yield high-performance and reliable near-field probes and to become available to the broader user community. The realization of such probes would impact nanoscale research at the same level that atomic force microscopes did when paving the way to modern nanoscale science. We present a wafer-scale realization of Campanile near-field scanning optical probes fabricated on an AFM platform. Figure 1 illustrates a 2D sketch and a scanning electron micrograph (SEM) image of an optical transformer on a cantilever. The figure shows the Boron Nitride flake sample and its topographical image taken by the Campanile AFM probe. Optical measurement results show a promising sign of probes’ functionality with a strong polarization dependence response, which is a tell-a-tale sign of a campanile. This work paves the way for low cost and volume manufacturing of near-field probes suitable for high-resolution hyperspectral imaging.

#### 5:50 AM F.MT02.02.08

**Probing Nanoscale Surface Phenomena by *In Situ* Near-Field Second Harmonic Generation Microscopy** Yoonsoo Rho<sup>1</sup>, Hee K. Park<sup>2</sup> and Costas Grigoropoulos<sup>1</sup>; <sup>1</sup>University of California, Berkeley, United States; <sup>2</sup>Laser Prisms LLC, United States

Accurate monitoring and control of surface chemical reaction by adsorbates on metal oxide semiconductors are of key interest in many electrochemical systems. These nanoscale surface chemistries are often probed by X-ray photon spectroscopy (XPS), scanning tunneling microscopy (STM), and tunneling electron microscopy (TEM) at high vacuum. However, these methods are not suitable for in-operando experiment under various gas environments and the use of energetic particles can potentially disturb the surface chemistry. In contrast, optical second harmonic generation (SHG) is a simple, non-invasive, vacuum-free, and sensitive probing method for surface chemistry. The intrinsic broken inversion symmetry of surface can induce SHG signals, which can be altered by changes in charge distribution at the surface, depending on the presence of chemical adsorbates. Integrated with tip-based scanning near-field optical microscopy (SNOM), optical SHG can interrogate various nanoscale surface phenomena and their dependence on the gas environment without complicated sample preparation.

Here, we demonstrate *in-situ* tip-based near-field SHG microscopy of chemical reactions at the surface of metal oxide nanowires, including titanium oxide (TiO<sub>2</sub>), zinc oxide (ZnO), and vanadium oxide (VO<sub>2</sub>). The nanoscale SHG can be amplified by local electric field enhancement by the tip-apex and provide surface chemical state with nanoscale resolution. Based on this method, we *in-situ* probed the reactions of oxygen and water vapor at the surface of TiO<sub>2</sub> and ZnO, depending on the local vacancy density and the occurrence of catalytic reaction at elevated temperature. In addition, strain effect on the local phase transition in VO<sub>2</sub> nanowires was probed on a mechanical clamped structure at controlled temperature. The correlated TEM inspection of these nanowires showed surface defects and phase state consonant with the near-field SHG imaging. We believe that the presented *in-situ* near-field SHG microscopy can provide powerful means for in-operando probe of various physicochemical phenomena.

#### 6:00 AM F.MT02.02.09

**Latest Advances in Nanoscale Chemical Imaging and Spectroscopy** Anirban Roy<sup>1</sup>, Honghua Yang<sup>1</sup>, Qichi Hu<sup>1</sup> and Curtis Marcott<sup>2</sup>; <sup>1</sup>Bruker Nano Surfaces, United States; <sup>2</sup>Light Light Solutions, United States

For the last few decades the rapid growth in the field of nanoscience and technology has led to the development of new characterization tools for nanoscale materials. Traditional IR and Raman spectroscopy and imaging offers excellent chemical insights; however, the spatial resolution is limited by the optical diffraction limit ( $\sim \lambda/2$ ). Although, recent Super-resolution microscopy techniques [1, 2] offer superior spatial resolution, they are primarily implemented in fluorescence imaging, hence needs external fluorophore tag for detection. Alternatively, high resolution multimodal imaging platforms offer unique combination of SPM and chemical spectroscopy/spectrometry, such as, IR, Raman and SIMS to probe nanoscale chemistry without external fluorophore. One of the above techniques, namely, nanoscale IR spectroscopy/imaging offers a “tag free” spectral detection by exploiting an AFM probe [3] to detect either photothermal expansion force (PTIR/AFM-IR) or near field scattered IR light (s-SNOM) with high spatial resolution beyond optical diffraction limit (2-5 nm).

Recent developments in PTIR/AFM-IR and s-SNOM technology have significantly augmented the speed and spatial resolution for chemical analysis. Exploiting different modalities in AFM, such as, contact, tapping and other heterodyne force detection modes (e.g., ultrasonic and/or acoustic force microscopy), we are able to acquire IR images at a specific absorption band simultaneously with sample topography and viscoelastic properties, providing a complete set of topographical, chemical and mechanical insights with ~10 nm spatial resolution. These high-resolution measurements are currently accompanied by high speed tunable lasers with broad spectral coverage ranging from 800-3600  $\text{cm}^{-1}$ , encompassing full capability of FTIR characterization for dimensions orders of magnitudes smaller than the optical diffraction limit. For example, Figure 1c shows topography and chemical map of PS-*b*-LDPE block copolymer on a silicon substrate. IR images at 1466/2920  $\text{cm}^{-1}$  and 1488/3032  $\text{cm}^{-1}$  highlight the distribution of low-density polyethylene (LDPE) and polystyrene (PS), respectively with feature sizes ~50 nm or smaller.

Along with high spatial resolution, high speed spectral acquisition enables acquiring hyperspectral data cube with large set of data. These high-volume data set opens up new avenues for machine learning algorithm for data processing and analysis, e.g., high resolution spectral map reconstruction using pan-sharpening algorithm [4].

In this presentation, we will highlight the technical background and applications of these emerging technologies in different fields, e.g., nanomaterials, life sciences, polymers, microelectronics etc.

[1] B Huang et al., *Annu. Rev. Biochem.*, **78** (2009), p. 993-1016

[2] T D Harris et al, *Appl. Spectrosc.*, **48** (1994), p. 14A-21A

[3] A Dazzi and C B Prater, *Chem. Rev.*, **117** (2016), p. 5146-5173

[4] N Borodinov et al., *npj Comput. Mater.*, **49** (2019), p. 1-9

#### **6:10 AM F.MT02.02.10**

**3D Ferroelectric Domain Wall Imaging by FIB and SPM** [Erik Roede](#)<sup>1</sup>, Aleksander B. Mosberg<sup>1</sup>, Donald M. Evans<sup>1</sup>, Theodor Secanell Holstad<sup>1</sup>, Zewu Yan<sup>2</sup>, Edith Bourret<sup>3</sup>, Antonius T. van Helvoort<sup>1</sup> and Dennis Meier<sup>1</sup>; <sup>1</sup>Norwegian University of Science and Technology, Norway; <sup>2</sup>ETH Zürich, Switzerland; <sup>3</sup>Lawrence Berkeley National Laboratory, United States

Charged ferroelectric domain walls are naturally occurring quasi-2D objects with a range of functional properties and potential technological applications. The hexagonal manganites ( $\text{RMnO}_3$ , R= Sc, Y, In, Dy to Lu) are an important model system for the study of domain walls, as these improper ferroelectrics naturally develop all orientations of 180° domain walls, including neutral and charged configurations. The charge state and properties are determined by the orientation and geometry of the domain wall, giving rise to rich electronic behavior. At the surface, the "projected" domain wall properties can readily be characterized, for example using scanning probe microscopy (SPM) and photoemission electron microscopy (PEEM), whereas mapping of their characteristics in three dimensions remains challenging.

In this work, I will discuss the use of focused ion beam (FIB) techniques for extending the surface information from SPM studies into 3D. As a first example case, I will discuss the use of FIB to prepare ferroelectric lamella samples with well-defined domain wall configurations determined via correlated microscopy techniques. In order to access the complete 3D information, surface SPM is combined with FIB tomography to image ferroelectric domain walls with nanoscale resolution and correlate the local sub-surface geometry with the measured properties at the surface. Understanding how the 3D geometry of the domain walls influences their local electronic response is an important step toward unlocking their full intrinsic functionality and application in nanoelectronics devices.

#### **6:20 AM F.MT02.02.11**

**The LaserFIB – Uniting High-Resolution Microscopy and Massive Material Ablation Sample Prep** Tobias Volkenandt, Fabián Pérez-Willard, Benjamin Tordoff and [Luyang Han](#); Carl Zeiss Microscopy GmbH, Germany

Modern materials research in combination with innovative fabrication and processing techniques enable development of increasingly complex materials and advanced components. Analyzing these new materials and understanding their microstructure requires sophisticated characterization tools. Focussed ion beam scanning electron microscopes (FIB-SEMs) are well established for sample analysis and preparation at the nano- to micro-scale in 2D, 3D or even 4D. However, when it came to sample modification and analysis at even larger scales up to millimeters FIB-SEMs were facing a challenge.

With the LaserFIB we present and introduce a new system to solve this challenge and bridge this gap. The LaserFIB features

a fs laser that has been integrated with a ZEISS Crossbeam. This combination enables high-resolution SEM imaging and FIB patterning as well as site-specific, large-scale sample structuring and preparation using the laser. All laser processing is done in a separate chamber extending the airlock to avoid damage and contamination of the components in the instrument's main chamber (Fig. 1). The massive material ablation by the laser is highly efficient in large volume bulk material removal and offers a way to gain access to deeply buried regions of interest (ROIs). Large cross-sections can be prepared in seconds and subsequently get analyzed by SEM leveraging all sorts of analytical techniques (e.g. EDS or EBSD). If needed the FIB allows to fine-polish the cross-section face for undisturbed imaging, however, it has been shown that details of the microstructure are already visible after laser polishing only and even suitable for e.g. EBSD analysis.

In this contribution we will introduce the new LaserFIB and explain the site-specific workflow in detail. Application examples covering different sample materials and applications will be shown. Among these are e.g. correlative sample preparation for X-ray nano-tomography, micro-mechanical testing and large-scale cross-sectioning.

#### 6:30 AM F.MT02.02.12

##### **Late News: Antiferromagnetic Spin Cycloidal Orders Imaged with a Commercial Scanning Nitrogen-Vacancy Magnetometer** Hai Zhong, Alexander Stark, Felipe Favaro and Patrick Maletinsky; Qnami AG, Switzerland

Antiferromagnetic thin films attract significant interest for future low-power spintronic devices. They are largely insensitive to external magnetic fields, exhibit domains with negligible cross-talk and can be switched at THz frequencies [1]. Furthermore, in multiferroics where antiferromagnetism can coexist with ferroelectricity, it is possible to control the magnetic state electrically - a particularly appealing feature for future device applications.

In this talk, we show how the Qnami ProteusQ™ -- a commercial room temperature scanning nitrogen-vacancy magnetometer (SNVM) -- can be used to quantitatively image antiferromagnetic spin textures with proven DC field sensitivity of  $\sim 2 \mu\text{T}/\sqrt{\text{Hz}}$ . We image the spin cycloid of a multiferroic bismuth ferrite ( $\text{BiFeO}_3$ ) thin film and extract a period of about 103 nm, indicative of a type II spin cycloid. [2] In addition, we take advantage of the quantitative nature of SNVM to extract an average magnetic moment density of  $0.08 \pm 0.02 \mu_{\text{B}}/\text{Fe}$  in the  $\text{BiFeO}_3$  film. These findings agree well with reported vibrating sample magnetometer results ( $M_{\text{S}} = 0.06 \mu_{\text{B}}/\text{Fe}$ ) on similar, strained  $\text{BiFeO}_3$  thin films. [3] Our results shed light on future design requirements for reconfigurable nanoscale spin textures in such multiferroic systems.

#### References:

- [1] V. Baltz, *et al.*, Rev. Mod. Phys. **90**, 015005 (2018)
- [2] A. Haykal, *et al.*, Nat. Commun. **11**, 1704 (2020)
- [3] W Eerenstein, *et al.*, Science **307**, 1203a (2005)

SESSION F.MT02.03: Nanomechanical and Viscoelastic Characterization with SPM  
On Demand Abstracts Available for Viewing Starting Saturday Morning, November 21, 2020  
F-MT02

#### 5:00 AM \*F.MT02.03.01

##### **Mapping Nanoscale Viscoelasticity and Relaxation Times Underlying Growth and Shape of Multicellular Organisms Using Multifrequency AFM** Jacob Seifert, Casey Adam, Alba Piacenti and Sonia Contera; University of Oxford, United Kingdom

The dynamic shapes of biological tissues emerge from a complex interplay of physics, chemistry and genetics, which determines--at each temporal and spatial scale--the mechanical properties that eventually form the structures of living organisms. Shape and mechanical stability of living organisms rely on precise control in time and space of growth, which is achieved by dynamically tuning the mechanical (viscous and elastic) properties of their hierarchically built structures from the nanometer up.

It is now well-established that cellular behaviour (including stem cell differentiation) crucially depends on the mechanical properties of the cells' environment. Much attention has been directed towards the importance of the *stiffness* of the natural (extracellular matrix, ECM) or artificial matrices where cells grow, with the purpose of either understanding mechanotransduction, or controlling the behaviour of cells in tissue engineering. While stiffness (i.e. the capacity of a material to elastically store mechanical energy) has been the focus of most experimental research, neither cells nor matrices are elastic. Biological systems dissipate energy (i.e. they are viscous) and hence they do not respond to mechanical

deformations instantaneously (like an ideal Hookean spring), but present different time responses at different spatial scales that characterise their responses to external stimuli.

Measuring viscoelasticity (especially at the nanoscale) has remained experimentally challenging [1,2]. In my talk I will present atomic force microscopy (AFM)-based techniques to measure and map the viscoelasticity of living tissues, cells, membranes, collagen, ECMs, and tissue engineering matrices across the spatial and temporal (from Hz to 100s of kHz) scales, and chirp-based spectroscopic techniques to assess viscoelasticity from Hz to 100s kHz at the nano and micro scale developed in my lab. I will also present tests for assessing which viscoelastic model better fits the experimental AFM results. Our results have uncovered that extracellular matrices of both living plants and tumours present an almost perfect linear viscoelastic behaviour that is key to understand their growth and shape. I will present our work showing how the growth and shape of the roots, leaves and hypocotyl of living *Arabidopsis thaliana* living plants are related to the nanoscale viscoelasticity of plant cell walls at the time scales probed by multifrequency AFM.

#### References:

- [1] “Multifrequency AFM reveals lipid membrane mechanical properties and the effect of cholesterol in modulating viscoelasticity” 2019. Z Al-Rekabi, S Contera; Proceedings of the National Academy of Sciences 115 (11), 2658-2663.
- [2] “Mapping nanomechanical properties of live cells using multi-harmonic atomic force microscopy” 2011 A Raman, S Trigueros, A Cartagena, APZ Stevenson, M Susilo, E Nauman, S Contera. Nature Nanotechnology 6 (12), 809.

#### 5:15 AM \*F.MT02.03.02

**Thermal Scanning Probe Lithography and Å-Indentation for Manipulating and Characterizing 2D Materials** Elisa Riedo, Francesco Lavini, Filippo Cellini, Xiaorui Zheng, Annalisa Calò, Tengfei Cao, Edoardo Albisetti and Xiangyu Liu; New York University, United States

The ability to characterize and manipulate materials down to the atomic scale for tuning their mechanical and physical properties is the cornerstone of material science. Two-dimensional (2D) materials in particular are getting large attention because their extremely thin size gives rise to unique and groundbreaking properties.

Here we explore two different research topics. On one side we show how heat delivered by a scanning probe can be used for manipulating the electrical properties of 2D materials, and on the other side we present a recent scanning probe microscopy method to perform Å indentation experiments in supported 2D materials.

Among various novel materials, two-dimensional molybdenum disulfide ( $\text{MoS}_2$ ) is of particular interest due to its large band gap, low dielectric constant, and heavy carrier effective mass. Currently, a key issue in creating high performing field-effect transistors (FETs) based on  $\text{MoS}_2$  and other transition metal dichalcogenides (TMDC) films is the poor quality of the metal contacts fabricated on these atomic layers, and the difficulty to pattern dopants. Here, we report a strategy based on thermal scanning lithography (tSPL) to fabricate metal contacts on 2D materials with high reproducibility [1], and we demonstrate the integration of tSPL with a flow-through reactive gas cell to achieve nanoscale control of dopants in monolayer  $\text{MoS}_2$  [2]. The tSPL produced defects can present either p- or n-type doping on demand, depending on the used gasses, allowing the realization of field effect transistors, and p-n junctions with precise sub- $\mu\text{m}$  spatial control, and a rectification ratio of over  $10^4$ . Doping and defects formation are elucidated by means of X-Ray photoelectron spectroscopy, scanning transmission electron microscopy, and density functional theory. We find that p-type doping in  $\text{HCl}/\text{H}_2\text{O}$  atmosphere is related to the rearrangement of sulfur atoms, and the formation of protruding covalent S-S bonds on the surface. Alternatively, local heating  $\text{MoS}_2$  in  $\text{N}_2$  produces n-character.

Moreover, we report on the elastic properties of supported 2D graphene and h-BN films by the use of modulated Å-Indentation, a novel scanning probe microscopy (SPM)-based technique capable of achieving sub-Å indentation depths during force-indentation measurements [3, 4]. By using extremely small amplitude oscillations ( $\ll 1$  Å) at high frequency, we show how Å-Indentation enables non-destructive local accurate measurements of the contact stiffness and out-of-plane elastic moduli of ultra-thin ultra-stiff films, including CVD diamond films (thus even up to TPa range stiffness), as well as the transverse moduli of supported graphene and h-BN ( $< 1$  nm thickness) films. Å-Indentation thus obtains *in-situ* elasticity measurement combining superior resolution and indentation depths as small as 0.3 Å with AFM nanoscale topographical imaging. Thanks to this technique, we experimentally demonstrate that at room temperature and under localized indentation pressure, a single layer of graphene on top of a carbon interface layer (buffer layer), on SiC, exhibits a transverse stiffness superior to bulk diamond [3]. Extending the capabilities of the Å-indentation technique to the analysis of other 2D materials, these studies explore similar pressure-induced phase transition in hexagonal boron nitride (h-BN). We demonstrate that 2-layer h-BN flakes, on  $\text{SiO}_2$ , consistently exhibit a transverse elastic modulus almost two times larger than that of the bare substrate. This stiffening effect is observed only for flakes of thickness between 2 to 5 atomic layers, but not in single- nor multilayer ( $> 6$ -layer) h-BN, and is related to the conversion of h-BN to cubic BN (c-BN) induced by the pressure applied through the indenter.

- 1 Zheng et al. *Nature Electronics*, 2, 17–25 (2019)  
2 Zheng et al. *Nature Communication*, (2020) <https://doi.org/10.1038/s41467-020-17241-1>  
3 Gao et al. *Nature Nanotechnology* 13.2 (2018): 133  
4 Cellini et al. *Scientific reports* 9.1 (2019): 4075

### 5:30 AM \*F.MT02.03.03

**Paddled Cantilever for AFM Beyond Topography** Hanna Cho; The Ohio State University, United States

Atomic Force Microscopy (AFM) is one of the most powerful and versatile tools to image and characterize materials with nanometer scale resolution, leading to the development of nano-/bio- science and technology. While AFM technology has advanced significantly by expanding its functionality beyond a nanoscale imaging tool, the majority of AFM users still find it difficult to employ the advanced techniques and interpret the data correctly due to artifacts. Such difficulties mainly originate from the complex dynamics of the AFM probe system, used as a mechanical transducer to deliver the tip-sample interaction force.

We address this issue by altering the AFM cantilever design. The current state of the art AFM probe is a single-body system, in the shape of a rectangular or triangular beam, which is not ideal for carrying more than one type of information. In contrast, the new AFM probe, so-called paddled cantilever, is reshaped to have a two-field microcantilever design with a considerable dimensional discrepancy in the component part. By doing so, this mechanical transducer provides two discrete transduction channels such that they respond independently to the variations in surface topography and material properties/functionality. Thus, AFM users can effortlessly implement the advanced AFM schemes with minimal ambiguity, complications, and artifacts, by simply employing this new AFM probe.

Since the prototype device of paddled cantilever was first introduced, our team has taken effort to develop a batch fabrication process and, thus, have this advanced technology widely available for AFM users. The detailed dynamics of fabricated paddled cantilevers have been investigated by using the interferometric displacement sensor (IDS) with AFM to directly measure their deflection. The measured deflection along the whole cantilever revealed that the frequency of inner-paddle is not affected by the tip stiffness while its amplitude is proportional to the displacement input delivered through the tip. This is the basis how the paddled cantilever can provide two discrete transduction channels for functional AFM. A theoretical model based on a 2 degree-of-freedom system is also presented to understand the dynamic characteristics of paddled cantilever under various operational conditions. Because the design of paddled cantilever is simple to feasibly integrate into, and compatible with, current AFM probes and systems, this technology will easily extend the AFM functionality to characterize multi-physical properties beyond topography by providing a dual-channel mechanical transducer.

### 5:45 AM F.MT02.03.04

**Detection of Defects in the Molecular Coating on Nanoparticles Using AFM Ringing Mode** Nadia Makarova<sup>1</sup>, Maxim Dokukin<sup>1,2,3</sup> and Igor Sokolov<sup>1,1,1</sup>; <sup>1</sup>Tufts University, United States; <sup>2</sup>NanoScience solutions Inc, United States; <sup>3</sup>Sarov Physics and Technology Institute, Russian Federation

A novel mode of AFM, FT-NanoDMA (Fourier transform dynamical mechanical analyzer), can be used to obtain information on the viscoelastic properties of individual cells. Compared to the recently introduced AFM-NanoDMA, FT-NanoDMA allows obtaining storage and loss modulus of multiple frequencies simultaneously. Also, the FT-NanoDMA design allows measuring the mechanics of biological cells, both fixed and alive, directly in a culture dish. Although it was demonstrated on the example of plant cells, the thick wall of those cells did not allow to resolve any features of the cell structure.

Here we demonstrate the ability of FT-NanoDMA to obtain high-resolution information on the viscoelastic properties of individual eukaryotic cells, which express a highly diverse distribution of its mechanical properties. Zebrafish melanoma cells and human osteoblast cells were studied. The storage, loss modulus and loss angle (the phase difference between the sample oscillation and the response of AFM cantilever) were simultaneously recorded for 9 different frequencies of oscillation ranging between 15 to 300 Hz. The obtained maps can be compared with a fluorescent optical image of the same cells. The results are discussed and different ways of visualizing these multidimensional data presented.

### 5:55 AM F.MT02.03.05

**Multidimensional Viscoelastic Tomography of Eukaryotic Cells with AFM FT-NanoDMA Mode** Nadia Makarova<sup>1</sup>, Maxim Dokukin<sup>1,2,3</sup> and Igor Sokolov<sup>1</sup>; <sup>1</sup>Tufts University, United States; <sup>2</sup>National Research Nuclear University MEPhI, Russian Federation; <sup>3</sup>NanoScience solutions Inc., United States

A novel mode of AFM, FT-NanoDMA (Fourier transform dynamical mechanical analyzer), can be used to obtain information on the viscoelastic properties of individual cells. Compared to the recently introduced AFM-NanoDMA, FT-NanoDMA allows obtaining storage and loss modulus of multiple frequencies simultaneously. Also, the FT-NanoDMA design allows measuring the mechanics of biological cells, both fixed and alive, directly in a culture dish. Although it was demonstrated on the example of plant cells, the thick wall of those cells didn't allow to resolve any features of the cell structure.

Here we demonstrate the ability of FT-NanoDMA to obtain high-resolution information on the viscoelastic properties of individual eukaryotic cells, which express a highly diverse distribution of its mechanical properties. Zebrafish melanoma cells and human osteoblast cells were studied. The storage, loss modulus and loss angle (the phase difference between the sample oscillation and the response of AFM cantilever) were simultaneously recorded for 9 different frequencies of oscillation ranging between 15 to 300 Hz. The obtained maps can be compared with a fluorescent optical image of the same cells. Using different load forces, we can probe mechanical properties at different indentation depth. This can bring a possibility to present a sort of tomography of cell mechanics. The excessive amount of data raises the problem of data visualization. The results are discussed and different ways of visualizing these multidimensional data are presented.

#### 6:05 AM F.MT02.03.06

**Mapping Nanomechanical Properties of Proteins and Polymers with Bimodal AFM** Simone Benaglia and Ricardo Garcia; Instituto de Ciencia de Materiales de Madrid, Spain

Fast, high-resolution mapping of the viscoelastic properties of soft matters, represents a major goal of atomic force microscopy (AFM) [1]. Bimodal AM-FM AFM is a suitable method for this purpose, since it allows the simultaneous acquisition of nanomechanical properties without losing in resolution and acquisition speed. This multifrequency configuration combines the robustness and simplicity of an amplitude modulation (AM) feedback in the first mode, with the sensitivity and a high signal-to-noise ratio of a frequency modulation (FM) feedback in the second mode. Finally, through the use of the appropriate contact mechanics model, it is possible to determine elastic and viscous properties of the analyzed sample [2].

Here we show how bimodal AM-FM is applied to extract the elastic properties of soft samples, such as proteins and polymers. Specifically, we characterize the elastic properties of a single protein in liquid, the 20S proteasome which in living organism plays a proteolytic role [3], and the elastic properties of a poly(styrene-block-methylmethacrylate) (PS-b-PMMA) copolymer sample [4].

[1] C. A. Amo, A. P. Perrino, A. F. Payam, and R. Garcia, ACS Nano 11, 8650 (2017).

[2] E. T. Herruzo, A. P. Perrino, and R. Garcia, Nat. Commun. 5, 3126 (2014).

[3] S. Benaglia, V. G. Gisbert, A.P. Perrino, C. A. Amo R. Garcia, Nat. Protoc. 13, 2890 (2018).

[4] S. Benaglia, C. A. Amo, R. Garcia, Nanoscale 11, 15289 (2019).

#### 6:15 AM F.MT02.03.07

**Physiologically Relevant Mechanics of Biodegradable Polyester Nanoparticles Using AFM** Nourin Alsharif, Behnaz Eshaghi, Bjoern Reinhard and Keith A. Brown; Boston University, United States

Despite the extensive use of biodegradable polyester nanoparticles for drug delivery, there is a lack of systematic studies that report the mechanics of these nanoparticles at physiologically relevant conditions. Given that nanoparticle mechanics have been reported to strongly influence nano-bio interactions, the accurate characterization of polymer nanoparticles is critical to understanding their behavior *in vivo*. Here, we use indentation experiments on poly(lactic acid) (PLA) and poly(lactide-co-glycolide) (PLGA) nanoparticles using atomic force microscopy (AFM) to identify their mechanical properties at different temperatures in both air and in water. While the particles are rigid at room temperature under dry conditions, their stiffness decreases by as much as 50 fold under physiological conditions (i.e. in water at 37 °C). Differential scanning calorimetry (DSC) confirms that this decrease in stiffness upon heating and immersion in water can be attributed to the phase transition of the nanoparticles from the glassy state to the rubbery state. This combination of AFM and DSC characterization allows us to determine the plasticizing effects of nanoscale size, polymer molecular weight, and immersion in water. Specifically, PLA and PLGA nanoparticles under 50 kDa molecular weight were found to exhibit glass transition temperatures below 37 °C in water, indicating that these biomedically-relevant nanoparticles will be rubbery in biological environments. Lastly, we investigate indentation experiments at elevated temperatures in air and find that insufficient AFM probe heating complicates the determination of nanoparticle temperature, thus preventing accurate recapitulation of the transition behavior for the nanoparticles. The artifacts observed while measuring particle mechanics in air further motivates nanoparticle mechanical characterization in water. Collectively, these experiments provide insight for experimentalists exploring the relationship between polymer nanoparticle mechanics and *in vivo* behavior, namely that thermoanalytical characterization can distinguish

whether the physiologically-relevant mechanical properties can be accurately estimated using bulk material characterization and help identify processes necessary for direct characterization of polymer nanoparticles.

#### 6:25 AM F.MT02.03.10

**Multiscale Characterization of Silk Nanofibrils—From Assembly Dynamics to Nanomechanics** Hui Sun and Benedetto Marelli; Massachusetts Institute of Technology, United States

Naturally occurring biopolymers are promising building blocks for a new generation of multifunctional materials that can work at the biotic-abiotic interface and better interact with the environment. Particularly, silk fibroin – a structural protein extracted from *Bombyx mori* silkworm cocoons, has attracted a lot of attention in the recent decades due to the potential use as technical material in a broad range of applications, encompassing drug delivery, regenerative medicine, food coating, printable sensors and optoelectronics etc. As more manufacturing methodologies with silk fibroin are being developed, a key question yet to be answered is how to endow silk fibroin-based bulk materials with complex nanoscale features. Unlike most of the current nanofabrication strategies that mainly focused on manipulation of nanostructures from the top-down perspective, we choose to approach this question by designing specific folding and assembly pathways of silk fibroin that result in highly ordered  $\beta$ -sheeted nanofibrils. Atomic force microscopy (AFM) in combination with a set of correlative optical, spectroscopy and X-ray scattering techniques are employed to probe the detailed mechanism of nanofibrils formation, from the driving forces for disorder-to-order transition to sequence-structure-property relationships across scales. In particular, high resolution nanomechanical data of silk fibroin at single fibril level in both dried and hydrated states are acquired by using AFM-based bimodal force microscopy and fast force mapping. Factors including silk fibroin molecular weight and crystallinity are found to directly correlate with the nanomechanical properties.

#### 6:35 AM F.MT02.03.11

**Probing Elastic and Viscoelastic Properties at Solid-Solid Interfaces Across Time and Temperature** Bede Pittenger, Sergey Osechinskiy, John Thornton, Sophie Loire and Thomas Mueller; Bruker, United States

The mechanical response of heterogeneous samples like polymer composites and thin films is controlled by the properties of the microstructure of the material. Since confinement effects and interphase formation can alter properties of the microphases, measurements on these samples must be localized at the nanometer scale to provide the needed property distribution. Mechanical properties of polymers are generally time dependent, so a full understanding requires measurements over a range of frequencies and temperatures as is provided (for bulk samples) by techniques such as dynamic mechanical analysis (DMA).

Atomic Force Microscopy (AFM) has the resolution and mechanical sensitivity to provide the needed local mechanical property information. However, previous AFM measurements of viscoelastic properties have suffered from some significant drawbacks. Contact resonance [1], for example, provides mechanical property maps at known frequencies, but the cantilever resonances are many orders of magnitude higher than DMA, making comparisons indirect at best. Intermittent contact methods like TappingMode [2], force volume, and PeakForce Tapping [3] face challenges in calculating intrinsic mechanical properties like storage and loss modulus (or tan delta) at well-defined frequencies due to the non-linear process of making and breaking contact.

A new mode called AFM-nDMA provides viscoelastic results which can be directly compared with bulk DMA. It provides spectra of storage and loss modulus across frequency and temperature allowing construction of master curves through Time Temperature Superposition [4]. These measurements are localized by the probe-sample contact, allowing observations to be co-located with high-resolution AFM imaging modes. This presentation will apply AFM-nDMA to investigate the mechanical properties of heterogeneous polymeric samples near interfaces between components and within microscopic domains. Time (and temperature) dependence of these properties will also be examined.

[1] U. Rabe, S. Amelio, E. Kester, V. Scherer, S. Hirsekorn, and W. Arnold, *Ultrasonics*, 2000, 38, 430.

[2] O. Sahin, C. Quate, O. Solgaard, and A. Atalar, *Phys. Rev. B*, 2004, 69, 1.

[3] B. Pittenger and D. G. Yablon, *Bruker App. Note* 149, 2017, doi: 10.13140/RG.2.2.15272.67844

[4] M. L. Williams, R. F. Landel, and J. D. Ferry, *J. Am. Chem. Soc.*, 1955, 77, 3701.

#### 6:45 AM F.MT02.03.12

**Topographic Lithography and Tomography with Atomic Force Microscopy** Will Linthicum, Jingfeng Song, Thomas Moran and Bryan D. Huey; University of Connecticut, United States

Tomographic Atomic Force Microscopy (AFM) uniquely enables volumetric mapping of nanoscale materials properties such as ferroelectricity, conductivity or photoconductivity. Based on alternating imaging and milling with the AFM probe itself,

this approach is effective for surface planarization to diminish topographic artifacts. It can also be extended for more complex surface patterning, such as fabricating smooth or stepped gradients in the remaining material thickness. Accordingly, the milling efficiency and conditions are compared for epitaxial monolithic thin films, multilayers, and polycrystalline samples, with the results demonstrating a coupling to bulk mechanical properties and also grain boundary energies. Such insight is beneficial to optimizing future AFM-based shape-engineered surfaces, which are valuable for follow-on investigations of thickness dependencies, subsurface structures, and other volumetric inhomogeneities.

SESSION F.MT02.04: Electrical Characterization with SPM  
On Demand Abstracts Available for Viewing Starting Saturday Morning, November 21, 2020  
F-MT02

**5:00 AM \*F.MT02.04.01**

**Conductive Colloidal Scanning Probe Microscopy** Christine Kranz and Sven Daboss; Ulm University, Germany

Scanning electrochemical probe microscopy (SEPM) techniques such as scanning electrochemical microscopy (SECM) and in particular the hybrid techniques such as atomic force microscopy combined with scanning electrochemical microscopy (AFM-SECM) enable high resolution topographical imaging along with electrochemical information [1] but also electrochemical force spectroscopic measurements [2]. Recently, we introduced a new type of electrochemical scanning probe tip for combined AFM-SECM measurements providing instead of a conventional AFM tip, a conductive colloidal sphere attached to an otherwise insulated cantilever [3]. Such conductive spherical probes may consist of boron-doped diamond [4], a highly attractive electrode material, or may be electrochemically modified, e.g., functional polymers, suitable for force spectroscopic measurements such as adhesion measurements under potential control.

In this contribution, we present AFM-SECM measurements and electrochemical force spectroscopy using conductive colloidal AFM probes. Due to the spherical geometry and the low spring constant of the cantilever, these probes are highly suitable for mapping nanomechanical properties at soft samples, i.e. bacterial cells. Colloidal probes with BDD as spherical electrode can be used for various SPM experiments including conductive AFM given the physical and electrochemical inertness of BDD, for force spectroscopy under potential control providing information on electrified interfaces, and for AFM-SECM measurements. Notably, all these experiments can be performed with the same BDD-AFM-SECM probe. Colloidal probes can be modified with polymers i.e. polydopamine, which properties may be altered by applying potential to the spherical electrode. Single cell force spectroscopy on bacterial adhesion along with studies at electrified interfaces will be presented.

[1] A. Patel, C. Kranz, *Annu. Rev. Anal. Chem.* **2018**, *11*, 329.

[2] S. Daboss, J. Lin, M. Goddjehans, C. Kranz, **2020**, in press

[3] P. Knittel, H. Zhang, C. Kranz, G. G. Wallace, M. J. Higgins, *Nanoscale* **2016**, *8*, 4475.

[4] S. Daboss, P. Knittel, C. E. Nebel, C. Kranz, *Small* **2019**, *15*, 1902099.

**5:15 AM F.MT02.04.02**

**Controlled Manipulation of Benzene Radicals Across Different Energy Landscapes** Omur E. Dagdeviren<sup>1</sup>, Chao Zhou<sup>1</sup>, Milica Todorovic<sup>2</sup>, Eric Altman<sup>1</sup> and Udo Schwarz<sup>1</sup>; <sup>1</sup>Yale University, United States; <sup>2</sup>Aalto University, Finland

The manipulation of single molecules has become possible with the continued development of scanning probe microscopy techniques. Thereby, the manipulation path can be chosen at will, and energy barriers between potential minima on that pathway can be quantified, as can the energy landscape around the molecule before and after manipulation. To explore the practicality of this novel pathway to catalysis research, we selected iodobenzene molecules on a Cu (100) surface as a model system. To this end, we first break the iodine atom from the benzene ring by applying a controlled bias voltage. A specific manipulation path is chosen and then the tip is moved at constant but continuously reduced heights while recording the oscillation amplitude  $A$  and phase  $\phi$  with the microscope operated in our recently developed tuned-oscillator (TO) detection scheme [1]. To preserve the accuracy of the recovered tip-sample interaction potentials and forces, we use oscillation amplitudes significantly larger than the decay length of the tip-sample interaction potential [2,3]. We then manipulated the benzene radical away from the iodine atom and measured the required energy barrier. With increasing distance from the iodine atom, the energy barrier required to move benzene radical decreases. Our experiments are disclosing the effect of local surface chemistry on controlled manipulation of molecules. For further insight, we also compared with computational results obtained using a Bayesian Optimization Structure Search (BOSS) protocol [4], a machine learning technique developed at



Aalto University that delivers the minimum energy pathways and entire energy landscapes with minimal computational effort.

#### References:

- [1] O. E. Dagdeviren et al., *Nanotechnology* **27**, 065703 (2016).
- [2] O. E. Dagdeviren et al., *Physical Review Applied* **9**, 044040 (2018).
- [3] O. E. Dagdeviren et al., *Review of Scientific Instruments* **90**, 033707 (2019).
- [4] M. Todorović et al., *NPJ Computational Materials* **5**, 35 (2019). <div id="UMS\_TOOLTIP" style="position: absolute; cursor: pointer; z-index: 2147483647; background-color: transparent; top: -100000px; left: -100000px; background-position: initial initial; background-repeat: initial initial;"> </div>

#### 5:25 AM F.MT02.04.03

**Characteristics of Charged Ferroelectric Domain Walls Under Alternating Voltages Frequencies** Jan Schultheiß<sup>1</sup>, Erik Lysne<sup>1</sup>, Jakob Schaab<sup>2</sup>, Edith Bourret<sup>3</sup>, Zewu Yan<sup>2,3</sup>, Lukas Puntigam<sup>4</sup>, Stephan Krohns<sup>4</sup>, Donald M. Evans<sup>1</sup> and Dennis Meier<sup>1</sup>; <sup>1</sup>NTNU Norwegian University of Science and Technology, Norway; <sup>2</sup>ETH Zurich, Switzerland; <sup>3</sup>Lawrence Berkeley National Laboratory, United States; <sup>4</sup>University of Augsburg, Germany

Ferroelectric domain walls are naturally occurring interfaces, separating regions with different orientation of the spontaneous polarization. The domain walls can have fundamentally different electronic properties than the surrounding domains. It is now established that the walls exhibit unusual electronic conduction under direct voltages (d.c.) and distinct vibrational modes under alternating voltages (a.c.) in the microwave regime. In contrast, very little is known about their behavior at low a.c. frequencies, where the walls respond adiabatically.

Here, we map the response of charged ferroelectric domain walls in the adiabatic regime under a.c. voltages in the kilo- and megahertz range. In our model material, ErMnO<sub>3</sub>, a.c.-cAFM conduction contrasts drop at significantly different frequencies for different types of domain walls. The characteristic frequencies at which the domain wall contrast vanishes is determined by the local polarization configuration of the adjacent domains. Extending the research on electronic transport mechanisms into the a.c. regime is an important step towards a better understand of the unusual conduction at ferroelectric domain walls and the future development of domain wall based nanoelectronic devices, such as filters, phase shifters, or tunable capacitors.

#### 5:35 AM F.MT02.04.05

**Tomographic Piezoresponse Force Microscopy for 3D Visualization and Analysis of Superlattice Dielectrics and Multiferroics** Thomas Moran<sup>1</sup>, Jingfeng Song<sup>1</sup>, Will Linthicum<sup>1</sup>, Keigo Suzuki<sup>2</sup>, Tadasu Hosokura<sup>2</sup>, Koji Murayama<sup>2</sup>, Erik Roede<sup>3</sup>, Dennis Meier<sup>3</sup> and Bryan D. Huey<sup>1</sup>; <sup>1</sup>University of Connecticut, United States; <sup>2</sup>Murata Manufacturing Co., Ltd., Japan; <sup>3</sup>Norwegian University of Science and Technology, Norway

Tomographic AFM (TAFM) extends atomic force microscopy beyond the measurement of surface properties and into the realm of three-dimensional analysis. For certain materials, the AFM tip can be used as a both a probe and a milling tool, measuring properties such as current or piezoresponse while simultaneously removing material from the surface. Instead of thousands of 2-D pixels, this yields datasets with millions of 3-D voxels, but all still with nanoscale resolution. The resulting tomographic reconstructions enable unprecedented visualization and analysis of heterogeneous materials, particularly those with isolated or networked sub-surface features, surface coatings, or vertical property gradients. This is especially applicable for 3-D mapping of thickness-dependent properties in functional materials including ferroelectric domain structures and interconnected conduction pathways. Examples are highlighted for both BTO/STO superlattices with multilayer chip capacitor applications, and also ferroelectric domain wall-based nanoelectronic devices such as single crystal ErMnO<sub>3</sub>.

#### 5:45 AM F.MT02.04.06

**Identifying Ferroelectric Polarization Switching in Ultra-Thin HZO Film with Scanning Capacitance Microscopy and Interferometric Piezo Force Microscopy** Haigang Zhang<sup>1</sup>, Keith Jones<sup>1</sup>, Ryan Wagner<sup>1</sup>, Suraj Cheema<sup>2</sup> and Roger Proksch<sup>1</sup>; <sup>1</sup>Asylum Research, Oxford Instruments, United States; <sup>2</sup>University of California, Berkeley, United States

Ferroelectric thin films epitaxially grown on silicon have attracted great interest for their potential application in energy-efficient electronics for their controllable ferroelectric polarization switching. As ferroelectric materials are made thinner, however, the ferroelectricity is usually suppressed, especially in the archetypal ferroelectric perovskite systems have so far proved unsuitable for thickness scaling and integration with modern semiconductor processes. Recently, Zr-doped HfO<sub>2</sub> grown by atomic layer deposition on silicon has been to be an exciting thin film ferroelectric material that is compatible with conventional Si processing[1, 2] However, such switching is not be easily demonstrated by conventional bulk-based characterization techniques due to the current leakage involved with such ultrathin films. Even though the conventional

scanning probe microscopy-based PFM has unique advantages in terms of nanoscale spatial resolution and ease of use, but is subject to crosstalk associated with long-range cantilever-sample electrostatic interactions which can be mistaken for localized piezoelectricity. We have developed and implemented an interferometric displacement sensor (IDS) that mitigates this problem.[3, 4] In addition, we have developed a new, high-sensitivity scanning capacitance microscopy (SCM) module. Recently, we have used these new approaches to study ferroelectricity in ultra-thin HZO films (1 nm).[2] We will discuss SCM and IDS butterfly loops that provide unambiguous evidence of localized ferroelectric behavior. Most importantly, both techniques eliminate the commonly observed artifacts thus provide conclusive evidence of polarization switching in this technologically relevant ultra-thin ferroelectric film grown on silicon.

[1] Chernikova, A. et al, "Ultrathin Hf<sub>0.5</sub>Zr<sub>0.5</sub>O<sub>2</sub> Ferroelectric Films on Si", ACS Appl. Mater. Interfaces 8, 7232–7237 (2016).

[2] S Cheema, et.al, "Enhanced ferroelectricity in ultrathin films grown directly on silicon." *Nature* **580**, 478–482 (2020).

[3] Labuda, A and R. Proksch "Quantitative measurements of electromechanical response with a combined optical beam and interferometric atomic force microscope", *Applied Physics Letters* 106, 253103 (2015).

[4] Collins, L. et.al, "Quantitative electromechanical atomic force microscopy." *ACS Nano* 13, 8055–8066 (2019).

#### 5:55 AM F.MT02.04.07

##### **Amplitude and Frequency Analysis for Open-Loop Sideband Frequency-Modulation Kelvin Probe Force Microscopy** Gheorghe Stan; National Institute of Standards and Technology, United States

In the last years new open-loop (OL) Kelvin probe force microscopy (KPFM) modes [1] were introduced to facilitate a faster and more accurate surface potential characterization at the nanoscale. Based on high-speed data capture, the OL KPFM modes observe the tip-sample electrostatic interaction in the time domain, which potentially can increase the temporal resolution by few orders of magnitude in comparison to common closed-loop (CL) KPFM implementations that rely on frequency domain detection [1, 2]. In this work, the high-speed digitization for open-loop sideband frequency-modulation (FM) KPFM is presented in terms of amplitude and frequency responses of the cantilever. In both cases, the tip-sample contact potential difference (CPD) is extracted from the time series analysis of the signals. This interpretation is demonstrated to be superior to the more common used analysis of the parabolic bias dependence of the OL KPFM signals. The OL sideband FM-KPFM amplitude and frequency responses were compared side-by-side to their CL AM-KPFM and CL FM-KPFM counterparts on materials of different surface potentials and subjected to various bias voltages. Notably, the OL sideband FM-KPFM frequency retains the tip-confinement sensitivity that is characteristic to the FM-KPFM based modes while the OL sideband FM-KPFM amplitude suffers from cantilever stray capacitive couplings much in the same way as the common CL AM-KPFM mode [3].

[1] L. Collins, A. Belianinov, S. Somnath, N. Balke, S. V. Kalinin, and S. Jesse, *Sci. Reports* **6**, 30557 (2016).

[2] L. Collins, M. Ahmadi, T. Wu, B. Hu, S. V. Kalinin, and S. Jesse, *ACS Nano* **11**, 8717 (2017).

[3] G. Stan, *Nanotechnology* in press (2020).

#### 6:05 AM F.MT02.04.08

##### **Late News: Photo-Sensitive Kelvin Probe Force Microscopy for Embedded Silicon-Oxide Interface**

**Characterization** Valentin Aubriet<sup>1,2,3</sup>, Benjamin Grevin<sup>4</sup>, Kristell Courouble<sup>2</sup>, Mickael Gros-Jean<sup>2</sup> and Lukasz Borowik<sup>1</sup>; <sup>1</sup>CEA-LETI, France; <sup>2</sup>STMICROELECTRONICS, France; <sup>3</sup>LTM (CEA-LETI/Minatec), France; <sup>4</sup>Univ. Grenoble Alpes, CNRS, CEA, INAC, SYMNES, France

Interfaces characterization is crucial for several types of devices like light emitting diodes, solar cells, photodetectors or transistors. In the particular case of photodetectors it is important to characterize such interfaces to see the impact of passivation, where defects present at the interfaces impact the dark current of the device. Moreover, such parameters like surface photovoltage (SPV) or carrier lifetime can reflect the influence of defects, even when embedded [L Borowik et al, *Nanotech.* (2010)].

For this particular purpose, we use heterodyne Kelvin Probe Force Microscopy (h-KPFM) [Yasuhiro Sugawara et al, *Appl. Phys. Lett.* (2012)] under illumination to characterize the silicon interfaces embedded under different types of oxides, specifically Al<sub>2</sub>O<sub>3</sub>, Al<sub>2</sub>O<sub>3</sub>/Ta<sub>2</sub>O<sub>5</sub>, HfO<sub>2</sub>, SiN, SiO<sub>2</sub>. In addition, we adopt a pump probe approach [Murawski, J. et al, *J. Appl. Phys.* (2015)] in order to time-resolve the photovoltage (tr-SPV). Besides of the capability to measure SPV, tr-SPV and charge carrier dynamics, the particularity of this setup is the analysis of these parameters as function of different illumination wavelengths and the possibility to perform in-depth dependent measurements.

In this work, we will present the developed experimental method using h-KPFM under frequency modulated and wavelength

dependent illumination in order to probe interfacial physical processes (i.e. the charge carrier dynamics and the influence of interface on surface photovoltage). Furthermore, we will correlate the h-KPFM results with additional interfacial characterization procedures (Corona Oxide Characterization Of Semiconductor method) [Marshall Wilson et al, AIP Conference Proceedings (2001)]. Finally, we will demonstrate the interest of a time-resolved approach (i.e. pump probe h-KPFM) for the characterization of embedded interfaces.

#### 6:15 AM F.MT02.04.09

**Electrical Characterization of Phase Change Random Access Memory (GST) by C-AFM in Ultra-High Vacuum** Mariam Ben Youssef<sup>1,2</sup>, Serge Blonkowski<sup>2</sup>, Olga Cueto<sup>2</sup>, Chiara Sabbione<sup>2</sup> and Martin Kogelschatz<sup>3,1,2</sup>; <sup>1</sup>LTM-CNRS, France; <sup>2</sup>CEA-LETI, France; <sup>3</sup>Université Grenoble Alpes, France

Ge<sub>2</sub>Sb<sub>2</sub>Te<sub>5</sub> (GST-225) is one of the most promising materials for use in phase change memory devices, which presents good scalability and high endurance. The operation of the PCM devices consists in switching between a high conductive (On) state and a low conductive (Off) state, which correspond respectively to the crystalline and amorphous phase. The switching from the OFF to the ON state (Set) is obtained by applying voltage pulses that heat the GST-225 material by Joule effect, leading to its crystallization. The switching from the ON state to the OFF state (Reset) is obtained by applying shorter pulses with higher voltages in order to quench the GST-225 and obtain the amorphous phase. For resistive memory cells the current necessary to obtain the phase change is in the order of several hundred of microamperes.

Conductive AFM (C-AFM) is widely used for the characterization of the electrical properties of materials at the nanometer scale. It allows in principle to obtain electrical information at nanometric scale while avoiding expensive lithographic processes. At present, the cyclability of writing and erasing process with C-AFM is limited by various practical factors, namely the high oxidation of the GST-225 in ambient conditions and the current limitation due to the tip degradation. For those reasons, successive Set and Reset steps were not observable, until now, on unpatterned samples by C-AFM. Those limitations can be overcome by using ultra-high vacuum in order to protect the GST-225 against oxidation and utilization of full diamond tips that resist to high current conditions.

In this work, we studied the electrical characteristics of phase change materials at nanometric scale by C-AFM under Ultra High Vacuum in pulse mode. We show that the used experimental configuration allows to cycle unpatterned GST-225 layers between the set and the reset state. We measured the resistive switching characteristics of GST-225 and reached 50 cycles. The experimental results will be compared to temperature and resulting crystalline fraction obtained by finite element simulation.

#### SESSION F.MT02.05: SPM for Perovskites Characterization

On Demand Abstracts Available for Viewing Starting Saturday Morning, November 21, 2020  
F-MT02

#### 5:00 AM \*F.MT02.05.01

**Nanoscale Ion Transport Dynamics—From Conjugated Polymers to Halide Perovskites Solar Cells** David S. Ginger<sup>1,2</sup>; <sup>1</sup>University of Washington, United States; <sup>2</sup>Pacific Northwest National Laboratory, United States

Imaging ion transport in nanostructure materials has applications in systems from neuromorphic computing, to electrochemical energy storage, and solar cells. We utilize multimodal imaging to probe transport phenomena in these systems. For instance, by combining nanoscale vibrational spectroscopy with structural imaging we can correlate local anion diffusion with structural phase transitions in conjugated polymer films being explored for neuromorphic computing and bioelectronics applications. We also combine similar IR imaging with time-resolved electrostatic force microscopy (trEFM) to uncover the dynamics of ion transport in various 3D and 2D halide perovskites of interest for applications in optoelectronics, especially solar cells, where ion transport can be a primary contributor to device aging and failure. This work bridges advances in scanning probe microscopy with tools from data science to better understand materials design rules for new applications.

#### 5:15 AM F.MT02.05.03

**Correlative Imaging of the Local Optoelectronic Properties within Single and Multijunction Halide Perovskite Solar Cells** Elizabeth Tennyson<sup>1</sup>, Kyle Frohna<sup>1</sup>, William Drake<sup>1</sup>, Florent Sahli<sup>2</sup>, Quentin Jeangros<sup>2</sup>, Christophe Ballif<sup>2</sup> and Samuel D. Stranks<sup>1,1</sup>; <sup>1</sup>University of Cambridge, United Kingdom; <sup>2</sup>École Polytechnique Fédérale de Lausanne, Photovoltaics and Thin-Film Electronics Laboratory, Switzerland

The functional properties of halide perovskite semiconductors at the micro and nanoscales are heterogeneous,<sup>1</sup> and there is a pressing need to understand how these properties (electrical, chemical, etc.) influence one another and affect overall photovoltaic (PV) performance. In this presentation, we begin by showing a variety of correlative microscopy methods that have been applied to perovskite solar cells to investigate the local electrical, chemical, and optical properties of single-junction devices.<sup>2-4</sup> For this, Kelvin probe force microscopy, nano-IR imaging, time-of-flight secondary ion mass spectroscopy depth profiling among other characterization techniques were implemented. These results reveal that the perovskite's (i) nanoscale voltage response depends on its chemical composition (ii) charge carrier dynamics depend on the incident photon energy (i.e. wavelength), and (iii) altered chemical properties due to the inclusion of potassium additives impact the electrical response in three dimensions.

Beyond single-junction perovskite PV, and a promising real-world application for this material class, is the multi-junction perovskite/c-Si solar cell. Not only are perovskites complex on their own, but when embedded within a textured heterojunction, the interactions between device architecture and material performance introduces new challenges. Commercial c-Si solar cells are etched to form micro-scale, randomly distributed pyramids on their front side, complicating the growth of the perovskite top cell. It is not well understood how the local light-matter interactions of the perovskite material behave when incorporated into this type of multijunction architecture. Therefore, we present optoelectronic microscopy measurements correlated with optical simulations of perovskite on textured c-Si solar cells. Through wide-field, hyperspectral photoluminescence (PL) imaging, we measure the photon out-coupling of the perovskite material and find both a spectral and spatial dependence on the geometrical patterning which dominates any grain-to-grain variation that is typically found in perovskite PL measurements.<sup>5</sup> Such heterogeneity reveals the importance of the underlying c-Si texture design, suggesting that tuning the surface morphology could lead to a homogenization of the perovskite's PL emission, which may boost the multi-junction solar cell efficiency.

(1) Tennyson, E. M.; Doherty, T. A. S.; Stranks, S. D. Heterogeneity at Multiple Length Scales in Halide Perovskite Semiconductors. *Nat Rev Mater* **2019**, 4 (9), 573–587 - **invited review, front cover**

(2) Tennyson, E. M.; Roose, B.; Garrett, J. L.; Gong, C.; Munday, J. N.; Abate, A.; Leite, M. S. Cesium-Incorporated Triple Cation Perovskites Deliver Fully Reversible and Stable Nanoscale Voltage Response. *ACS Nano* **2019**, 13 (2), 1538–1546 - **cover**

(3) Tennyson, E. M.; Howard, J. M.; Roose, B.; Garrett, J. L.; Munday, J. N.; Abate, A.; Leite, M. S. The Effects of Incident Photon Energy on the Time-Dependent Voltage Response of Lead Halide Perovskites. *Chem. Mater.* **2019**, 31 (21), 8969–8976 - **front cover**

(4) Tennyson, E. M.; Abdi-Jalebi, M.; Ji, K.; Garrett, J. L.; Gong, C.; Pawlicki, A., A.; Ovchinnikova, O., S.; Munday, J. N.; Stranks, S. D.; Leite, M. S. Correlated Electrical and Chemical Nanoscale Properties in Potassium-Passivated, Triple-Cation Perovskite Solar Cells. *Adv. Mater. Inter.* **2020** - **in press**

(5) Tennyson, E.M.; Frohna K.; Drake, W.K.; Sahli, F.; Yang, T. C.-Y.; Fu, F.; Werner, J.; Jeangros, Q.; Ballif, C.; Stranks, S.D. Multimodal Microscale Imaging of Textured Perovskite/c-Si Tandem Solar Cells - **in preparation**

#### 5:25 AM F.MT02.05.04

**Scanning Probe Studies of Transition Metal Perovskite Chalcogenides Under Illumination** Marudachalam Shanmugasundaram<sup>1</sup>, Boyang Zhao<sup>2</sup>, Fei Hou<sup>3</sup>, Shanyuan Niu<sup>4</sup>, Jan Seidel<sup>3</sup> and Jayakanth Ravichandran<sup>2</sup>; <sup>1</sup>HORIBA Instruments Inc, United States; <sup>2</sup>University of Southern California, United States; <sup>3</sup>University of New South Wales, Australia; <sup>4</sup>Stanford University, United States

The design, synthesis, and characterization of new semiconductor materials are important for the growth of electronics and energy solutions such as solar cells and fuel cells. Perovskite materials in particular are being investigated due to their compositional flexibility resulting from a wide range of stoichiometry in their design in contrast to conventional materials like silicon, thereby leading to a wide variety of optoelectronic properties. Some perovskites such as organic-inorganic lead halide perovskites and perovskite oxides are well-known for their power conversion efficiency and for their potential catalytic applications respectively. However, their respective toxicity / instability issues and the large energy gaps (>3 eV) pose serious challenges for their practical optoelectronic applications. Recently, transitional metal perovskite chalcogenides have emerged as a viable semiconductor that can address these issues (stability, abundance, toxicity, cost, and performance) as high performance photovoltaic materials, but a detailed understanding of their electronic and optical properties remains a key open question.

Here, we report the Scanning Probe Microscopy studies on the surfaces of single crystals of transition metal perovskite chalcogenides such as barium zirconium sulfide (BaZrS<sub>3</sub>, Ba<sub>3</sub>Zr<sub>2</sub>S<sub>7</sub>) using Kelvin Probe Force Microscopy (KPFM), and Raman and photoluminescence spectroscopy. Besides nominally undoped crystals, we also studied transitional metal doped

(Cr doping on Zr sites). While the nominally undoped BaZrS<sub>3</sub> has a bandgap of 1.8 eV, it shows strong photoluminescence at ~1.25 eV when a dopant such as chromium is introduced. KPFM was used to map the surface potential as well as electro-mechanical contrast proportional to capacitance. In addition, a precise optical coupling of the Raman microscope with the Scanning Probe Microscope allows surface potential changes to be mapped under dark and illuminated conditions. The surface potential of Ba<sub>3</sub>Zr<sub>2</sub>S<sub>7</sub> and Cr-doped BaZrS<sub>3</sub> changes dramatically in a reversible manner with laser illumination, highlighting the strong light-matter interaction and luminescent characteristics. It was found that this behavior is strongly dependent on the wavelength and laser power. The measured contact potential difference values provide indirect information on the evolution of work function during light illumination providing qualitative information on the quasi-Fermi level splitting induced by the photo-excitation. In summary, a unique combination of optical microscopy and scanning probe microscopy instrumentation were used to study optical, electronic, and photovoltaic properties of perovskite chalcogenides to evaluate their suitability for advanced photonic and energy applications.

#### 5:35 AM F.MT02.05.05

##### **Understanding the Chemo-Physical Interactions in Metal Halide Perovskites by Multimodal Imaging**

**Techniques** Yongtao Liu<sup>1,2</sup>, Anton Ievlev<sup>2</sup>, Nikolay Borodinov<sup>2</sup>, Liam Collins<sup>2</sup>, Stephen Jesse<sup>2</sup>, Kai Xiao<sup>2</sup>, Mahshid Ahmadi<sup>1</sup>, Bin Hu<sup>1</sup>, Sergei V. Kalinin<sup>2</sup> and Olga Ovchinnikova<sup>2</sup>; <sup>1</sup>The University of Tennessee, Knoxville, United States; <sup>2</sup>Oak Ridge National Laboratory, United States

Metal halide perovskites (MHPs) have shown promising applications in optoelectronic devices. Further improvement of MHPs devices toward commercialization necessitates a clear understanding of the factors impacting the functionality of MHPs. To date, ionic migration, ferroic behavior, structural distortion are mostly debated mechanisms credited with the functionality of MHPs. Given the interconnected nature of ionic states, ferroic properties, and structural distortion due to the screening effect and the compensation effect, the interactions among these properties can no longer be ignored. Here, in the combination of scanning probe microscopy (SPM) with other chemical and functional imaging techniques, as well as the machine learning approach, we have systematically investigated the ion migration, ferroic behavior, lattice strain, crystallographic orientation, and charge transport in MHPs and discovered a number of interesting phenomena. We have discovered the hysteretic ion migration—including intrinsic compositional ions (e.g. CH<sub>3</sub>NH<sub>3</sub><sup>+</sup>, I<sup>-</sup>) and decomposition chemical species (e.g. CH<sub>3</sub>NH<sub>3</sub><sup>+</sup> decomposition products)—in MHPs based devices by directly detecting ion migration by a newly developed time-resolved time-of-flight secondary ion mass spectrometry (tr-ToF-SIMS). Using time-resolved Kelvin probe force microscopy (tr-KPFM), we revealed how this hysteretic ion migration affects the local charge distribution in MHPs. We for the first time specified the contribution of CH<sub>3</sub>NH<sub>3</sub><sup>+</sup> and I<sup>-</sup> migration to the current-voltage hysteresis in an MHP device. In addition, we found that the CH<sub>3</sub>NH<sub>3</sub><sup>+</sup> migration is strongly coupled with a local lattice strain change and hence impacts the ferroic behavior of CH<sub>3</sub>NH<sub>3</sub>PbI<sub>3</sub>. Confocal photoluminescence microscopy study combining with piezoresponse force microscopy, electron backscatter diffraction, etc. directly unveiled the impact of chemical, strain, and ferroic properties on the charge recombination and transfer in MHPs. Altogether, our work offers a picture describing the interconnection of ionic, structural, ferroic, and optoelectronic properties of MHPs, which is expected to help to enhance the performance and the stability of MHPs-based optoelectronic devices.

#### SESSION F.MT02.06: SPM in Liquid Environment

On Demand Abstracts Available for Viewing Starting Saturday Morning, November 21, 2020  
F-MT02

#### 5:00 AM \*F.MT02.06.01

**Tracking the Dynamics of Liquids and Solutes at Solid Nano-Interfaces** Luca Piantanida<sup>1,2</sup>, Amir F Payam<sup>1,3</sup>, Clodomiro Cafolla<sup>1</sup> and Kislon Voitchovsky<sup>1</sup>; <sup>1</sup>Durham University, United Kingdom; <sup>2</sup>Boise State University, United States; <sup>3</sup>Ulster University, United Kingdom

The molecular organisation and dynamics of liquids near the surface of solids underpins processes such as molecular exchanges, electrochemistry, nanofluidics, biomolecular function and lubrication. Depending on the local topographical and chemical properties of the solid, the behaviour of the interfacing liquid can vary significantly at the nanoscale, with consequences for interfacial processes. Scanning probe microscopies can derive local insights into the equilibrium organisation of interfacial liquids, often with sub-nanometre resolution. However, deriving quantitative information about the local liquid *dynamics* remains a considerable challenge. Here we review some of our recent results obtained by combining high-resolution atomic force microscopy with highly

localised rheological measurements to deduce quantitative information about the motion of liquids and dissolved molecules along immersed solids. We show that the dynamics is highly system-dependant and can be dominated by either the local configurational entropy or the interface or enthalpic interactions. We also describe a novel approach to quantify the preferred flow direction naturally adopted by liquids near walls, locally and with nanometre precision. The approach, based on AFM, combines a vertically oscillating tip with high frequency lateral oscillations to derive directional information about the interfacial liquid at each point of the system. To illustrate the method's capabilities, we investigate the dynamics of aqueous solutions containing different metal ions along the surface of a graphene oxide flake. We identify ion-specific flow dynamics that can be related to the well-established sieving properties of graphene oxide membranes.

#### 5:15 AM \*F.MT02.06.02

**Using High-Speed, Molecularly-Resolved AFM and Fast Force Mapping to Investigate Nucleation and Solution Structure at Surfaces** James J. De Yoreo<sup>1,2</sup>, Benjamin Legg<sup>2,1</sup>, Elias Nakouzi<sup>1</sup>, Andrew G. Stack<sup>3</sup>, Sebastien Kerisit<sup>1</sup>, Christopher A. Mundy<sup>1,2</sup>, Gregory K. Schenter<sup>1</sup>, Jaehun Chun<sup>1</sup> and Kislon Voitchovsky<sup>4</sup>; <sup>1</sup>Pacific Northwest National Laboratory, United States; <sup>2</sup>University of Washington, United States; <sup>3</sup>Oak Ridge National Laboratory, United States; <sup>4</sup>Durham University, United Kingdom

Investigating nucleation from solutions is challenging, because it is a consequence of unstable density fluctuations, making the structures and events that must be probed both transient in nature and small in spatial extent. Moreover, when nucleation is heterogeneous, it is inherently linked to the structure and dynamics of the interfacial region between the bulk solution and the underlying substrate. Thus high-speed, molecularly resolved AFM combined with fast force mapping (FFM) provides a powerful and unrivalled combination to investigate nucleation from solution onto surfaces. Here I illustrate the deep level of fundamental insight into mechanisms of nucleation and the structure of the interfacial region made possible with these methods using results from investigations into nucleation of gibbsite ( $\text{Al}(\text{OH})_3$ ) on muscovite mica (001) and the structure of electrolyte solutions above mica and boehmite ( $\text{AlOOH}$ ) surfaces. In the case of gibbsite nucleation, we combine AFM observations of individual molecular adsorbates, transient clusters, and stable islands with Monte Carlo simulations to put together a coherent picture of surface speciation and nucleation. The results reveal a surface population of ions that is dominated by hydrolyzed species ( $\text{Al}(\text{OH})_2^+$  and  $\text{Al}(\text{OH})_2^{2+}$ ) even though  $\text{Al}^{3+}$  vastly dominates the bulk solution. These adsorbed ions evolve into subcritical clusters with increasing saturation state and temperature, constituting a population that decreases exponentially with size and exhibits dynamic fluctuations consistent with classical predictions. However, severe discrepancies with classical theory emerge when the values of key thermodynamic parameters are extracted from the AFM data. These discrepancies are resolved when the impact adsorbate charge on the capacitance of the mica-solution system is taken into account in calculating the work of cluster formation, but reveal a film formation process that occurs within a single phase region. Thus, the results imply that the gibbsite films constitutes a nanostructured 2D mesophase. To define the solution structure above boehmite and mica surfaces at lattice resolution, we developed a self-consistent scheme to decouple long-range tip-sample interactions from short-range solvation forces. In the case of boehmite, the results are benchmarked against molecular dynamics simulations that explicitly include the effects of the tip with different levels of approximation and systematically account for tip size, chemistry, and confinement effects. We find four laterally structured water layers within one nanometer of the surface, with the highest water densities at sites adjacent to hydroxyl groups. The findings reveal a complex relationship between site-specific chemistry, water density, and long-range particle interactions; and represent a major step forward towards quantitative data interpretation and widespread implementation of 3D FFM.

#### 5:30 AM F.MT02.06.03

**High-Speed Bimodal AFM Nanomechanical Mapping of Collagen Self-Assembly** Victor Gisbert<sup>1</sup>, Simone Benaglia<sup>1</sup>, Manuel Uhlig<sup>1</sup>, Roger Proksch<sup>2</sup> and Ricardo Garcia<sup>1</sup>; <sup>1</sup>Instituto de Ciencia de Materiales de Madrid (ICMM-CSIC), Spain; <sup>2</sup>Oxford Instruments-Asylum Research, United States

Collagen is the most abundant structural protein of the extracellular matrix. The assembly of collagen fibrils play relevant roles in a variety biological processes. The formation fibrils during the self-assembly process of collagen I have been studied by AFM [1,2]. Those studies lacked the time and mechanical properties resolution to clarify the mechanism of the earlier stages of collagen assembly and fibril structure formation. We have developed a high-speed bimodal AFM that combines the *ms* time resolution of high-speed AFM [3] with the nanomechanical force sensitivity of bimodal AFM [4,5]. High-speed bimodal AFM characterizes the earliest stages of the self-assembly of the collagen fibrils by proving time-resolved and high-spatial resolution maps of the evolution of the elasticity of the fibrils during the growth.

[1] F. Jiang, H. Hörber, J. Howard, D.J. Müller., J. Struct. Biol. **148**, 268–278 (2004).

[2] D.R. Stamov, E. Stock, C.M. Franz, T. Jähnke, H. Haschke, Ultramicroscopy **149**, 86–94 (2015).

[3] T. Ando. Nanotechnology **23**, 062001 ( 2012)

[4] S. Benaglia, V.G. Gisbert, A.P. Perrino, C.A. Amo, R. Garcia, Nat. Protoc. **13**, 2890 (2018)

[5] E.T. Herruzo, A.P. Perrino, R. Garcia, Nat. Commun. **5**, 3126 (2014).

#### 5:40 AM F.MT02.06.04

##### **Atomic-Scale Mapping of Hydrophobic Layers on MoS<sub>2</sub>, MoSe<sub>2</sub>, WS<sub>2</sub>, WSe<sub>2</sub> and Graphene Immersed in Water** Manuel R. Uhlig, Daniel Martin-Jimenez and Ricardo Garcia; ICMM CSIC, Spain

Solid-liquid interfaces are highly relevant for a number of phenomena in nature and technology. However, when it comes to hydrophobic surfaces, the structure of water in close proximity to the surface and its role in mediating interactions are not well understood. Two dimensional materials provide a variety of large and atomically flat surfaces that are mildly hydrophobic. We exploited the angstrom resolution capabilities of three-dimensional AFM [1,2] to image the interfacial water organization on MoS<sub>2</sub>, MoSe<sub>2</sub>, WS<sub>2</sub>, WSe<sub>2</sub> and graphene.

We demonstrate that these interfaces are characterized by layers of oscillating density within 2 nm above the solid surface (Fig. 1a). The distances between adjacent layers for MoS<sub>2</sub>, MoSe<sub>2</sub>, WS<sub>2</sub> and WSe<sub>2</sub> and graphene are  $\approx 0.50$  nm (Fig. 1b). This value is larger than the one predicted and measured for water density oscillations ( $\approx 0.30$  nm) [2,3]. The experiments indicate that on 2D material surfaces water molecules are expelled from the vicinity of the surface and replaced by several molecular-size hydrophobic solvation layers.

#### References:

[1] T. Fukuma, Y. Ueda, S. Yoshioka, and H. Asakawa, Phys. Rev. Lett. **104** (2010) 016101

[2] T. Fukuma, R. Garcia, ACS Nano **12** (2018) 11785

[3] D. Martin-Jimenez, R. Garcia, Nat. Comm. **7** (2016) 12164

[4] M. R. Uhlig, D. Martin-Jimenez, R. Garcia, Nat. Comm. **10** (2019) 2606

#### 5:50 AM F.MT02.06.05

##### **Closed-Loop Nanopatterning of Fluids with Scanning Probes** Verda Saygin, Bowen Xu, Sean Andersson and Keith A. Brown; Boston University, United States

High-throughput screening technologies such as microtiter plates enable chemists and biologists to simultaneously perform thousands of experiments in an automated fashion. While transformatively smaller than the vials used by the prior generation, the typical working volume for microtiter plates is in the range of microliters and there are still far too many compounds to study even with this degree of miniaturization. Scanning probe lithography (SPL) could provide a path to continuing this miniaturization in fluid handling as it encompasses approaches to pattern fluids with volumes at least  $10^9$  times smaller than what is achievable in microtiter plates. While the patterning of such sub-fL volumes has been demonstrated with various different materials over the years, to achieve controlled and reliable experimentation with SPL, it is crucial to have precise control over the size of features and amount of fluid that is transferred in real time. Here, we enable closed-loop control over the fluid written using SPL by combining a novel process for quantifying the fluid on a cantilever, the utilization of a tipless cantilever architecture, and a control strategy for adjusting writing parameters *in situ*. Specifically, we employ a two harmonic mode inertial sensing algorithm to reliably quantify the amount and location of fluid on the cantilever. Critically, sensing the mass of liquid on the cantilever before and after a fluid transfer event allows us to monitor the deposited amount with precision approaching the fL scale. This capability allows us to investigate the fundamental mechanisms and characteristics of fluid transport at this scale. Taking inspiration from experiments of fluid transfer between macroscopic parallel plates, we find that the fraction of the liquid that is transferred from the cantilever to the substrate is only a function of speed of the cantilever and surface energies of the substrates. Based on this discovery, we show that the amount of fluid that will be transferred can be predicted based on the amount of ink on the cantilever, hence it is possible to control the transferred amount by selecting writing parameters. With this insight in hand, we develop a closed-loop process for writing patterns with designed feature sizes. Given the versatility of scanning probes to characterize fluids once they are written, this work lays the foundation for multifunctional research systems in which chemical experiments are set up, performed, and evaluated at the nanometer scale.

#### 6:00 AM F.MT02.06.06

##### **Tip-Scanning AFM with Photothermal Excitation for Stable Operation in Liquid Environments** Christian Bippes, Jonathan Admas, Lukas Howald, Simon Fricker, Patrick Frederix and Dominik Ziegler; Nanosurf AG, Switzerland

AFM is a valuable tool for biologists and biophysicists to investigate structure, mechanics, and dynamics of biological

samples from single proteins or DNA molecules through lipid layers, protein matrices and hydrogels to whole cells or cellular assemblies. To preserve the physiological, hydrated state of these entities, most of these experiments are performed in an aqueous environment. Our newest instrument, the P6, is optimized to facilitate both high-resolution and large area measurements in any liquid environment. The fully motorized scan head includes a three-axis flexure-based tip scanner. Its proprietary design features an ultra-low-noise detection system with non-moving light sources. Moreover, the scan head is equipped with photothermal excitation (PTE). This is superior to the common piezo-acoustic excitation as it solely drives the cantilever without moving any other parts of the system, resulting in unparalleled excitation stability, especially in liquid operation. Textbook-like cantilever tuning results in high ease-of-use imaging and enables quantitative understanding of tip-sample interaction forces. The linear frequency response and high bandwidth of PTE enables multifrequency and high-speed applications. The instrument is compatible with any inverted optical microscope allowing for combined investigation of biological samples with AFM and various optical microscopy techniques, such as fluorescence imaging or super resolution imaging techniques. Apart from imaging, PTE also opens up new horizons for measurement modes and analysis techniques. PTE is, for instance, used to measure the mass of living cells at unprecedented time and mass resolution. [2] More advances in PTE-based techniques are to be expected soon.

Here, we show how we could overcome the engineering challenges posed by the different features of the scan head (full motorization, tip scanner and PTE) by employing a new opto-mechanic design. [1] This allowed building a stiff, large-range scanner that, in combination with sophisticated lowest noise-electronics and PTE, allows to routinely achieve high-resolution imaging in aqueous buffer solution, such as revealing the secondary structure of dsDNA.

[1] EP3450994A1

[2] D. Martinez-Martin et al. (2017) Nature 550: 500-5

#### **6:10 AM F.MT02.06.07**

**Simulating Electrochemical Environments at Metal-Liquid Interface** Yuhan Mei and Aaron Deskins; Worcester Polytechnic Institute, United States

Liquid-solid interfaces occur in many systems, such as batteries, catalysts, or in naturally occurring geochemical systems. Surface reactions may be strongly influenced by the presence of a liquid. In heterogenous catalysis, a solvation environment can be crucial in enabling surface certain reactions, such as oxidation reactions or electro catalysis reactions. The presence of the liquid-solid interface can speed up the reactions, increase the selectivity of products and open up new favorable reaction pathways. Therefore, it is important to understand the role of solvent in the liquid-solid interface surface reactions. For electrochemical systems, such as in batteries or electrocatalysts, the electrode potential can also have a significant impact on the chemisorption of molecules at metal surfaces as well as surface reactions. For instance, the electric field can affect the adsorption strength, the adsorption site and the intermolecular vibrational frequencies. Solvent and electrical field effects may both strongly influence surface reactivity. However, modeling efforts often ignore these two phenomena, or may not treat such phenomena appropriately. Methods to better describe electrochemical environments are still being developed and are an ongoing area of research. Herein, we modeled using density functional theory to simulate the ethanol oxidation reactions (EOR). We assessed how both the solvent and electrical fields influence important C-C and C-H bond scission reactions. Different solvation models exist for treating solvation. Implicit solvation models treat the solvent as a continuum and are generally “cheap” in terms of computational time. Explicit solvation models involve modeling the solvent molecules using density functional theory. Such calculations may be more computationally expensive, but in principle more accurate. Hybrid solvation models combine both the implicit and explicit approaches. We evaluated all three solvation models for describing surface chemistry on the Rh(111) surface, which is a typical catalyst for the EOR. Our results show that the reactions involving C-C and C-H scission are favorable in the presence of explicit water molecules due to intermolecular H bonding. However, the influence of hydrogen bond is negligible in the implicit solvation models. Thus, implicit models fail to properly describe solvent effects on ethanol oxidation. Our results do indicate that C-C and C-H bond scission becomes more favored when using a hybrid solvation model. The hybrid solvation model allows an efficient combination of both implicit and explicit solvation approaches. Field effects are also important in that they can have cause the adsorption energies of intermediates to fluctuate depending on the applied potential. The potential also can affect the energy barrier for bond breaking reactions. Our results assess the influence of the applied potential, and how modulating the potential may influence desired reactions. Overall, our work provides valuable insights on the effects of solvation and electric fields on surface chemistry in systems like batteries or electrocatalysts. We highlight a compelling approach to accurately and efficiently modeling electrochemical interfaces.

#### **6:20 AM F.MT02.06.08**

**Nanoscale Electrochemistry Study Using SECCM Option of Park Systems** Jiali Zhang, Byong Kim and Keibock Lee; Park Systems Inc., United States



Scanning electrochemical cell microscopy (SECCM) is a nanoelectrochemical scanning probe technique that creates a confined electrochemical cell (droplet) via meniscus contacting the surface by employing an electrolyte filled micropipette containing quasi-reference counter electrode (QRCE). [1] It is particularly useful to investigate the heterogeneity, or local electrochemical properties of the electrode surfaces by direct mapping the electroactivity with nanoscale resolution. In this study, the electrochemically reversible  $[\text{Ru}(\text{NH}_3)_6]^{3+/2+}$  electron transfer process at a highly ordered pyrolytic graphite (HOPG) surface was recorded using Park NX12 AFM system. A single barrel glass nanopipette with Ag/AgCl inserted as QRCE was utilized. Using previous successful experience in commercializing pipette-based electrochemical microscopy, [2] Park Systems' hardware and software enables localized nanoscopic cyclic voltammetry measurements conducted at each pixel each time the meniscus contacts the surface. Thus, a spatially resolved surface electroactivity mapping of HOPG at various scan rates were created with high-throughput at the micro-/nanoscale. The difference in electrochemical activity measured at the edge plane relative to the basal plane surface was shown.

This work demonstrates that Park Systems' commercial SECCM option is promising for quantitative electroanalysis at the nanoscale, with potential applications in energy storage (battery) studies and corrosion research.

[1] Gao, R., Edwards, M. A., Qiu, Y., Barman, K., & White, H. S. (2020). Visualization of Hydrogen Evolution at Individual Platinum Nanoparticles at a Buried Interface. *Journal of the American Chemical Society*.

[2] Shi, W., Goo, D., Jung, G., Pascual, G., Kim, B., & Lee, K. Simultaneous Topographical and Electrochemical Mapping using Scanning Ion Conductance Microscopy–Scanning Electrochemical Microscopy (SICM-SECM).

SESSION F.MT02.07: Poster Session: Multimodal, Functional and Smart Scanning Probe Microscopies for Characterization and Fabrication

On Demand Abstracts Available for Viewing Starting Saturday Morning, November 21, 2020

5:00 AM - 8:00 AM

F-MT02

#### **F.MT02.07.02**

**Measuring Steady-State and Time-Resolved Photoluminescence from a Positionable, Micrometer-Sized Observation Volume** Eugeny Ermilov, Volker Buschmann, Christian Oelsner, Frank Birke, Matthias Patting and Rainer Erdmann; PicoQuant GmBh, Germany

Over the years, luminescence spectroscopy has established itself as one of the fundamental methods for analyzing the photophysical properties of a variety of samples, ranging from simple organic molecules, complexes, luminescent proteins to semiconductors. The commonly used steady-state methods (i.e. excitation and emission spectroscopy) provide valuable insights into the photophysics of samples. However, such results give only a partial view of sample behaviors after photoexcitation. A further piece of the puzzle is often revealed by performing time-resolved luminescence spectroscopy. Studying luminescence lifetime data of materials is a very powerful analytical tool for spectroscopists and microscopists alike, as it provides insights into excited state dynamics of molecules, complexes, nanoparticles, or semiconductors. The fluorescence or phosphorescence lifetime is an intrinsic characteristic of luminescent species. It indicates how long species under consideration will remain in electronically excited states before returning to ground state. Each emitting species has a characteristic luminescence lifetime, that can be influenced by its environment.

A series of spectroscopic and microscopic methods based on luminescence lifetime have been developed and provide further information, which are not accessible by steady-state experiments. For example, with fluorescence lifetime imaging microscopy (FLIM), a very well established imaging method in life science, it is possible to gather lifetime information and spatial information as combination of a sample. This combined data can help to understand biochemical or physical processes by detecting changes in local environment such as pH, temperature, or ion concentration, and to identify molecular interactions or conformation changes via Förster Resonance Energy Transfer (FRET).

Time-resolved photoluminescence measurements are powerful tools in materials science also, e.g. for characterization of key parameters like charge carrier dynamics and mobility in semiconductors. Furthermore, combining spectral, spatial and lifetime information often provide a much better understanding of different dynamic processes occurring in luminescent samples.

Here we will demonstrate the performance of a spectrometer-microscope assembly for characterization and analysis of different materials in terms of lifetime, spectral and spatial resolution, as well as ability to measure long luminescence decays (in  $\mu\text{s}$  and  $\text{ms}$  time scales) using laser drivers with burst capabilities. The abilities of this multi-dimensional approach will be demonstrated with a series of examples reflecting a broad range of applications in materials science research.

### **F.MT02.07.03**

**Effect of Oxygen on the Electro-Thermal Properties of Gallium Doped ZnO Based Transparent Heater** Jasmine Beckford, Makhes K. Behera, Sangram K. Pradhan and Messaoud Bahoura; Norfolk State University, United States

There is growing interest in thin-film transparent heaters (TFTH) for optoelectronics, and a plethora of domestic usages such as smart windows, defrosters in automobiles and other applications. In this work, we present the growth and characterization of TFTH made of gallium doped zinc oxide (GZO). GZO thin films are deposited by pulsed laser deposition (PLD) with a varying range of oxygen (0-10 mTorr) on glass. Ga doped (5 atomic weight percentage) ZnO target was made in the laboratory using Ga<sub>2</sub>O<sub>3</sub> and ZnO powder. GZO is deposited on glass. Atomic force microscopy images reveal that the films are very smooth with excellent surface roughness. The temperature-dependent resistivity was measured using a linear four-probe technique and the sample showed low sheet resistance values. Our TFTH's exhibited high optical transparency value if (>85%) from transmission data. GZO transparency heaters showed a stable and reproducible Joule heating effect and the temperature reached easily 60°C by the application of low input (~8 V) voltage. This research funding may be beneficial for the potential use of GZO as transparent conducting oxide materials for possible applications in the emerging areas of low-cost power electronics, and flexible and wearable optoelectronic devices.

### **F.MT02.07.04**

**Visualization of Polarization Fatigue in PZT-5H of Piezoelectric Energy Harvester with Piezoresponse Force Microscopy** Seongmun Eom<sup>1</sup>, Jeongjae Ryu<sup>1</sup>, Jaegy Kim<sup>1</sup>, Seongwoo Cho<sup>1</sup>, Jiwon Yeom<sup>1</sup>, Eunnuri Cho<sup>1</sup> and Seungbum Hong<sup>1,2</sup>; <sup>1</sup>Korea Advanced Institute of Science and Technology, Korea (the Republic of); <sup>2</sup>KAIST Institute for NanoCentury, Korea (the Republic of)

Energy harvester converts wasted energy into usable electrical energy. Recently, with the rise of Internet of Things (IoT) technology, various types of sensors have been embedded into systems such as mobile and wearable devices, and unmanned equipment. Since it is difficult to supply all the energy required by many sensors with wired power systems, many studies have been conducted to overcome the issue of wired power through energy harvesting technology. Piezoelectric energy harvesters can generate the electrical energy to convert directly the applied strain energy from mechanical energy such as vibration. However, the major challenges of piezoelectric energy harvesters are the relatively low power yield and the degradation of the energy harvesting device due to fatigue caused by tens of millions of vibrations. Here we conducted the accelerated stressed cycle test in the low frequency range of 30 Hz band for a commercially available piezoelectric energy harvester, which is composed of a PZT-5H piezoelectric layer and a flexible substrate. Subsequently, we visualized the piezoelectric fatigue in microscopic region, and evaluated the degradation characteristics using piezoresponse force microscopy (PFM) to correlate the macroscopic fatigue with micron scale ferroelectric domain behavior.

### **F.MT02.07.05**

**Nanomechanical and Local Electrical Properties of Conjugated Polymer Thin Films Prepared Through Antisolvent Dripping and Electrochemical Doping** Krystal House, Hemanth Maddali and Deirdre O'Carroll; Rutgers, The State University of New Jersey, United States

Conjugated polymers have been extensively studied due to their tunable optical and electronic properties relevant to thin-film optoelectronic devices. Several techniques have been used to modify the electrical properties of these polymers, including solvent processing methods to enhance morphology, and molecular doping to enhance conductivity. Addition of a solvent in which the polymer has poor solubility (antisolvent) to the polymer solution prior to spin coating has been shown to improve the morphology of polymer thin films by promoting increased aggregation during solvent evaporation while spin coating. Here, we study the local physical and nanomechanical properties of several common conjugated polymer thin films prepared using an antisolvent dripping method in which the antisolvent is added during, rather than before, the spin coating process. This approach is expected to aid crystallization and produce uniform, stable, films.

Using atomic force microscopy (AFM), we establish a direct relation between the physical, mechanical, and electrical properties of conjugated polymer thin films prepared through antisolvent dripping and electrochemical doping. Phase imaging and fast force mapping (FFM) are used to visualize the nanoscale crystalline and amorphous domains. Additionally, in the case of doped conjugated polymer films, FFM and conductive AFM measurements (CAFM) have been combined for simultaneous measurement of topography, Young's modulus, and current. The combined FFM and CAFM technique splits the biased sample into a grid of points and records the deflection of the cantilever as a function of tip sample separation at each point, as well as the current measured through the sample by the tip, allowing for a direct comparison of mechanical and electrical properties at the nanoscale. The solvent used for the polymer precursor solution and antisolvent used during spin

coating were chosen based on Hansen solubility parameters (HSP). Using HSPs a list of good and poor solvents for the polymers were determined. Choosing a high-boiling-point, good solvent in the precursor solution ensures this solvent remains long enough during spin coating to allow for mixing with the poor solvent added during antisolvent dripping. This provides sufficient time for rearrangement of molecular chains to form a more ordered structure. In addition, for electrochemically doped conjugated polymer films, we find that higher dopant concentrations, and increased conductivity, occur in nanoscale crystalline domains compared to amorphous domains. Raman mapping and energy dispersive spectroscopy support the AFM findings at the micron scale. These results can be used to tune the morphology and resultant electrical properties of conjugated polymer films for use in electronic and optoelectronic devices.

#### **F.MT02.07.06**

**Vanishing Calibration Error with Magic Ratio AFM—Improving the Accuracy of Modulus Measurement Through Error Propagation Analysis** Richard J. Sheridan, David Collinson and L. Catherine Brinson; Duke University, United States

We present a new modality of force-curve-based AFM that eliminates systematic bias in the calculation of elastic modulus from cantilever spring constant calibration errors in force curve analysis. We show that the ratio between the probe deflection and substrate indentation has important implications for the uncertainty of modulus measurement when using generalized adhesive Hertzian indentation models. This error analysis codifies the widely understood rule-of-thumb tradeoff that must be made: if the cantilever deflection is much greater than the material indentation, bias due to error in cantilever calibration will be amplified, whereas if the cantilever deflection is much smaller than material indentation, photodetector noise will dominate. For example, attempts to measure the modulus of a stiff material with a very compliant probe result in a high indentation ratio and a large systematic error due to deflection sensitivity calibration. Our work reveals that, under the common calibration methods which involve the equipartition theorem, a special, “magic” indentation ratio appears between these limits with the ability to annihilate spring constant calibration error. In this presentation, the theory underlying the existence and error-nullifying properties of magic ratio indentation will be shown, followed by demonstrations on real data through custom analysis code and black-box commercial application routines. Caveats and limitations of magic ratio AFM will be discussed, as well as recommendations for users and manufacturers of AFM instruments. Additionally, opportunities for modulus measurement error mitigation with multi-modal and multi-functional methods will be surveyed.

#### **F.MT02.07.07**

**One Light Source Does It All—A Versatile Broadband IR Laser Source for Nanoscale IR Imaging and Spectroscopy** Honghua Yang, Qichi Hu and Anirban Roy; Bruker Nano Surfaces Division, United States

Nanoscale infrared spectroscopy and imaging techniques - AFM-IR and s-SNOM offer non-invasive material characterizations at the sub-diffraction limit. Recent development in AFM-IR and s-SNOM have significantly advanced the spatial resolution and detection sensitivity [1, 2]. However, the spectral range of the techniques are limited to 800-1900  $\text{cm}^{-1}$  and 2700-3600  $\text{cm}^{-1}$  which typically involves multiple laser sources. The demand for a versatile laser source that can provide wider tuning range and accommodates both AFM-IR and s-SNOM, therefore, motivates design and implementation of new light source and detection techniques.

In this presentation, we demonstrate a novel method of extending both AFM-IR and sSNOM to the full mid-IR range by coupling with a broadband laser source. Based on OPO/DFG tunable IR generation and seeded by a powerful fs pump laser, the novel broadband laser source delivers an ultra-broadband (6 octave) nano spectroscopy. For AFM-IR, a new modulation scheme is developed to modulate the broadband light at a repetition rate that matches one of the contact resonance frequencies of the AFM cantilever for resonance enhancement. The resulting spectrum is obtained by integration with an FTIR unit achieving 670 – 4000  $\text{cm}^{-1}$  with a typical 4  $\text{cm}^{-1}$  spectral resolution in a single laser shot. For s-SNOM measurements, the broadband laser operates in the quasi-cw mode, enabling both s-SNOM spectroscopy and imaging [3]. This versatile system sets a new standard in terms of flexibility and tuning range the for the two complementary nanoscale IR techniques.

In this context, we also highlight the laser performance and demonstrate its application on several representative samples which achieved promising new insights in the understanding of a multitude of different materials.

[1] A Dazzi and C B Prater, Chem. Rev., **117** (2016), p. 5146-5173

[2] E Muller et al., J. Phys. Chem. Lett., **6** (2015), p. 1275-1284

[3] J Yang et al., ACS Nano, **14** (2020), p. 1123–1132

## SYMPOSIUM F.MT03

---

Frontiers of Imaging and Spectroscopy in Electron Microscopy  
November 21 - December 4, 2020

### Symposium Organizers

Miaofang Chi, Oak Ridge National Laboratory  
Ryo Ishikawa, The University of Tokyo  
Robert Klie, Univ of Illinois-Chicago  
Quentin Ramasse, SuperSTEM Laboratory

---

\* Invited Paper

SESSION F.MT03.09: Live Keynote I: Frontiers of Imaging and Spectroscopy in Electron Microscopy  
Session Chairs: Miaofang Chi, Ryo Ishikawa and Quentin Ramasse  
Thursday Morning, December 3, 2020  
F.MT03

**8:00 AM \*F.MT03.01.04**

**Frontiers in Imaging Functional Behavior in Nanoscale Heterostructures Using Lorentz Transmission Electron Microscopy** [Charudatta Phatak](#); Argonne National Laboratory, United States

Confinement of magnetic structures geometrically as well as energetically, leads to novel and unexpected domain behavior. Lorentz transmission electron microscopy (LTEM) is ideally suited for quantitative analysis of magnetic domains and microstructure in functional nanoscale heterostructures. The current state of art LTEM enabled using aberration correctors allows for imaging down to sub-nanometer scale in field-free conditions. In this talk, the study of magnetic domain behavior in strongly interacting magnetic nanostructures namely artificial spin ices, curved 3D magnetic nanostructures, and functional materials that host skyrmions will be presented.

Artificial spin ice lattices consist of lithographically patterned arrays of interacting magnetic islands that exhibit magnetic frustration. We will present the results on emergence of magnetic excitations in such lattices which are topologically non-trivial as well as control of magnetic frustration and emergent ordering such as antiferromagnetic to ferromagnetic phase transition using lattice geometry. Furthermore, we will present a novel approach to understand such frustration behavior based on network topology that can be extended to use of graph neural networks to analyze and predict the behavior of spin ice lattices.

Topologically non-trivial spin textures such as skyrmions present unique opportunities to explore exciting fundamental phenomena, such as the topological Hall effect, as well as novel applications, such as skyrmion-based spintronics. The application of LTEM to visualize and understand the magnetic spin textures in multilayer  $[\text{Pt/Co}]_x$  thin films that can host skyrmions as well as controlled fabrication of skyrmions using Ga ion implantation will be discussed. In-situ magnetization reversal was used to understand the stability of the skyrmions.

Finally, we will also present a new approach based on machine learning for phase retrieval in LTEM that improves the achievable phase sensitivity and spatial resolution.

**8:30 AM \*F.MT03.03.03**

**Nanoscale Measurements of Vibrations, Dispersions and Emergent Phenomena Using Monochromated Electron Energy Loss Spectroscopy** [Jordan Hachtel](#); Oak Ridge National Laboratory, United States

Advances in electron monochromation have led to a sea change in electron energy loss spectroscopy (EELS) over the last 6 years. Modern monochromators scanning transmission electron microscopes (STEM) have improved EELS energy resolution by an order of magnitude (from ~50 meV down to < 5 meV). This new level of energy resolution enables direct access to a

host of new phenomena, such as phonons, vibrational modes, infrared optical excitations, and low-lying states in the electronic structure. Moreover, it also presents many new opportunities to probe difficult and complex systems by exploiting novel interactions between the electron beam and these ultra-low energy excitations. As a result, monochromated EELS is a highly versatile tool that can be applied to a wide range of different disciplines and materials systems and deliver exciting results.

In this talk, I will focus on three different materials systems where monochromated EELS presents a unique opportunity to provide new insights into important topics: biological, optical, and quantum materials. In terms of biological materials, I will demonstrate how we can the efficient long-range coupling of vibrational modes to the electron beam, to provide in depth spectroscopic analysis of ultra-beam sensitive biological materials. Furthermore, I will demonstrate how we can use the combine the natively high spatial and spectral resolution of monochromated EELS with various flavors of momentum-resolution to probe the dispersions of infrared quasiparticles directly at the nanoscale. Lastly, I will discuss how we can apply this technique to coupled networks of colloidal nanoparticles to examine emergent properties in quantum systems.

This work was performed at the Center for Nanophase Materials Sciences, which is a DOE Office of Science User Facility. This research was conducted, in part, using instrumentation within ORNL's Materials Characterization Core provided by UT-Battelle, LLC, under Contract No. DE-AC05-00OR22725 with the DOE, and sponsored by the Laboratory Directed Research and Development Program of Oak Ridge National Laboratory, managed by UT-Battelle, LLC, for the U.S. Department of Energy.

## 9:00 AM OPEN DISCUSSION

## 9:15 AM BREAK

## 9:30 AM \*F.MT03.03.01

**Monochromated STEM EELS of Phononic and Photonic Excitations** Kartik Venkatraman, Qianlang Liu, Barnaby D. Levin and Peter A. Crozier; Arizona State University, United States

The enhanced energy resolution of recently developed monochromators now make it possible to use electron energy-loss spectroscopy (EELS) in the scanning transmission electron microscope (STEM) to probe materials systems in new ways. This powerful spectroscopic capability combined with the small focused electron probe opens the door to explore photonic and phononic/vibrational excitations with high spatial resolution [1-3]. Here we describe recent advances leading to nanoscale and atomic resolution vibrational spectroscopy and novel approaches to probe guided photonic modes in dielectric particles. The fast electron in the electron microscope can excite vibrational modes in materials either through dipole interactions (similar to IR absorption spectroscopy) or impact scattering (similar to inelastic neutron scattering). The spatial localization of these two scattering mechanisms is very different. Impact scattering typically involves higher momentum transfers yielding a spatially localized spectral signal. In a crystal, high momentum transfer interactions are associated with exciting the short wavelength phonon modes at the Brillouin zone boundaries (BZB). Efficient excitation of these modes requires experimental conditions that favor Bragg scattering from the associated Miller planes. This can be easily accomplished in the conventional STEM EELS geometry by tilting the crystal into a suitable zone axis orientation and using a probe convergence angle that spans the Bragg angle associated with the BZB of interest. This convergence angle also permits a small probe to be formed which enables resolution of the associated Miller plane spacing. We have used this approach to demonstrate nanoscale and atomic resolution on a sample of Si, SiO<sub>2</sub> and BN [1]. EELS can also be employed to explore the characteristic photonic modes present in dielectric nanoparticles since the electron beam can provide a source of virtual photons to illuminate the object. We have explored the variation in photonic modes for high refractive index oxide particles such as TiO<sub>2</sub>, Ta<sub>2</sub>O<sub>5</sub> and CeO<sub>2</sub> [2]. The modes show up as peaks in the bandgap region of the spectrum. The energies of the modes are determined not only by the particle shape and size but also due to coupling between adjacent particles. Coupling between phonons and IR photons can give rise to phonon polaritons [3,4]. Polariton characteristics are also influenced by sample geometry, and so the polaritonic modes can be manipulated by changing the sample shape/size. Here we use STEM EELS to demonstrate variations in the polaritonic response on patterned SiO<sub>2</sub> thin films.

## References:

- [1] K. Venkatraman et al., Nature Physics 15 (2019) 1237-1241.
- [2] Q. Liu et al., Phys. Rev. B 99 16 (2019) 165102.
- [3] K. Venkatraman et al., Microscopy 67 (2018) i14 - 23.
- [4] A. Konečná et al., Phys. Rev. B 98 20 (2018) 205409.
- [5] The support from US National Science Foundation CHE-1508667 and U.S. DOE (DE-SC0004954), the use of (S)TEM at

Eyring Materials Center at Arizona State University is gratefully acknowledged.

SESSION F.MT03.10: Live Keynote II: Frontiers of Imaging and Spectroscopy in Electron Microscopy  
Session Chairs: Miaofang Chi and Robert Klie  
Friday Afternoon, December 4, 2020  
F.MT03

**1:45 PM \*F.MT03.03.01**

**Materials Science Applications of Four Dimensional–Scanning Transmission Electron Microscopy (4D-STEM)** Colin Ophus; Lawrence Berkeley National Laboratory, United States

Traditional scanning transmission electron microscopy (STEM) detectors are large, monolithic regions that integrate a subset of the transmitted electron beam signal scattered from each electron probe position. These STEM imaging experiments record only 1-5 values per probe position, throwing away most of the diffracted signal information. With the introduction of extremely high speed direct electron detectors, we can now record a full image (2D data) of the diffracted electron probe scanned over the sample (2D grid of positions), producing a four-dimensional dataset we refer to as a 4D-STEM experiment. These diffraction images of the electron probe are extremely rich in atomic-scale information, such as the sample structure, orientation, composition, phonon spectra, defect structure and more. The spacing between adjacent STEM probes can be varied from below one Angstrom to hundreds of micrometers, allowing us to probe the functional length scale of materials and devices.

In this talk, I will discuss how 4D-STEM can be used to measure various properties important to materials science. I will show several examples of nanobeam electron diffraction used to measure sample structure, orientation and strain, for samples ranging from metallurgical alloys to conductive polymers. I will also show how 4D-STEM can enable phase contrast imaging methods. Finally, I will also show how the scattering matrix (S-matrix) formalism can be used both to numerically invert sample structure under conditions of multiple scattering of the electron beam, and also for very fast simulation of large 4D-STEM datasets. I will show an updated version of Prismatic, our open source simulation code that includes GUIs for easy application.

**2:15 PM \*F.MT03.02.02**

**Imaging Chemical Reactions in Solution Using Distributed Electron Microscopy** Joseph P. Patterson; University of California, Irvine, United States

Imaging chemical reactions in solution is essential for the understanding complex mechanisms involved in nanomaterial synthesis. Liquid phase electron microscopy (LP-EM) is an emerging technique capable of directly monitoring morphological changes of materials in solution with a unique combination of temporal and spatial resolution. LP-EM has been used to study the reaction mechanisms such as metal nanoparticle formation, polymer self-assembly, wet etching of semiconducting materials, growth of metal–organic frameworks, nucleation of calcium carbonate and Li electrodeposition. These studies provided an unprecedented insight into nanoscale reaction mechanisms that have significantly improved our understanding of nanomaterial synthesis. The primary challenge for the field of LP-EM is understanding the role that the electron beam plays in the observed mechanism. It is common to perform control experiments to establish a critical dose limit with which a process can be observed. A consequence of having to work below a critical dose limit is that LP-EM has mostly been used to monitor reactions over a period of seconds to minutes, despite the fact that many reactions take place over hours to days. Furthermore, even after a critical dose has been established, it is impossible to completely rule out the role of the electron beam using LP-EM experiments alone. Consequently, it is essential to study reaction mechanisms using multiple imaging modalities. Cryo-EM can also provide direct high-resolution information on reaction mechanisms in solution. The advantage of cryo-EM is that electron beam effects are well understood and, using appropriately low doses, are insignificant. The disadvantage of cryo-EM is that it is impossible to know the history or future of any individual particle being imaged. Consequently, the data on reaction mechanisms has to be presented by selecting images that the user determines to be representative of the process occurring in solution. For simple processes that evolve homogeneously, it is possible to determine a mechanism with high confidence using cryo-EM alone. However, for complex processes that evolve heterogeneously, the confidence with which mechanisms can be determined by cryo-EM alone is low. Here, a simple process is defined as a process with a single step or single pathway and a complex process is defined as a process with multiple steps or multiple pathways. A homogenous evolution is characterized by a process where only one particle state is observed at each

sampled time point, while a heterogeneous evolution is characterized by a process where multiple states are observed at each sampled time point. Consequently, cryo-EM is limited in its ability to resolve complex heterogeneous processes. Despite the obvious benefits of combining LP-EM and cryo-EM, most studies using these techniques have been only conducted with a single EM modality. Here we discuss the application of distributed electron microscopy for studying reaction mechanisms in solution. The term distributed is used because the data required to understand the mechanism is shared between multiple imaging modalities and sample preparation methods. The strength of this approach is that our proposed hypothesis is consistent with data taken from experiments with complementary benefits and limitations.

#### **2:45 PM \*F.MT03.02.01**

**Crystal Growth via Oriented Attachment—5-Fold Twin Formation** [Dongsheng Li](#)<sup>1</sup>, Miao song<sup>1</sup>, Gang Zhou<sup>2</sup> and Ning Lu<sup>3</sup>; <sup>1</sup>Pacific Northwest National Laboratory, United States; <sup>2</sup>Institute of Metal Research, Chinese Academy of Sciences, China; <sup>3</sup>University of Michigan, United States

Oriented attachments are recognized as a common pathway for crystal growth in both natural and synthetic systems, leading interface free or twin related structures. The occurrence of 5-fold twinned nanoparticles leads to unique properties. However, nearly 200 years after their discovery, the formation mechanism is still ambiguous. Using in situ high-resolution transmission electron microscopy combined with molecular dynamics simulations, we demonstrate that 5-fold twinning occurs via repeated oriented attachment of ~3 nm Au nanoparticles. These oriented attachment events create high-energy grain boundaries, which accumulate strain during atomic rearrangements and consequently decompose via nucleation and growth of a special class of twins whose net strain is zero, inducing the 5-fold twin structures. The results provide a quantitative understanding of the 5-fold twinning process; this knowledge provides guidance for interpreting and controlling twin structures and morphologies of a wide range of materials.

#### **3:15 PM \*F.MT03.06.01**

**Mapping Structure and Composition of Intact Li-Metal Anodes after Cycling** [Katherine L. Jungjohann](#)<sup>1</sup>, Katharine Harrison<sup>1</sup>, Daniel Long<sup>1</sup>, Renae Gannon<sup>2</sup>, Laura Merrill<sup>1</sup>, Subrahmanyam Goriparti<sup>1</sup> and Steven Randolph<sup>3</sup>; <sup>1</sup>Sandia National Laboratories, United States; <sup>2</sup>University of Oregon, United States; <sup>3</sup>Thermo Fisher Scientific, United States

The electrolyte 2.8 M lithium bis(fluorosulfonyl)imide (LiFSI) in dimethoxyethane (DME) has demonstrated good cycling behavior and stable Li morphology upon plating and stripping for high-capacity Li batteries, which is thought to be due to the formation of a stable solid-electrolyte interphase (SEI) layer for good ionic transport. Characterization of this SEI layer on lithium metal has been limited, due to the air-sensitivity and beam sensitivity of these materials, as well as the incompatibility of the electrolyte with the high vacuum environment necessary for nanoscale characterization with electron microscopy techniques. New cryogenic stages and transfer tools have enabled the characterization of frozen solid-liquid interfaces for lithium metal structures. Here, we used cryogenic focused ion beam (FIB) and ultrashort pulse laser ablation to create a cross-section of the lithium metal anode in contact with the electrolyte at various plating/stripping cycles to understand the morphological evolution of the lithium and SEI. Additionally, with cryo-FIB we utilized lift-out procedures under cryogenic temperatures for extraction of a lamella sample for investigation using scanning/transmission electron microscopy with energy dispersive x-ray spectroscopy and electron energy loss spectroscopy. The nanoscale chemical maps have allowed for a greater understanding of the SEI components and how they redistribute with reaction to the lithium metal over the course of many cycles. These results present a step towards visualization of the intact battery stack. We have determined a failure mechanism beyond short circuiting of the lithium metal anodes, due to reaction of the lithium with this LiFSI in DME chemistry.

This work was funded by Sandia National Laboratories' Laboratory Directed Research and Development program. It was performed, in part, at the Center for Integrated Nanotechnologies, an Office of Science User Facility operated for the U.S. Department of Energy (DOE) Office of Science. Sandia National Laboratories is a multi-mission laboratory managed and operated by National Technology and Engineering Solutions of Sandia, LLC., a wholly owned subsidiary of Honeywell International, Inc., for the U.S. DOE's National Nuclear Security Administration under contract DE-NA-0003525. The views expressed in the article do not necessarily represent the views of the U.S. DOE or the United States Government.

SESSION F.MT03.01: 4D STEM Imaging and Electron Holography  
On Demand Abstracts Available for Viewing Starting Saturday Morning, November 21, 2020  
F-MT03

### 5:00 AM \*F.MT03.01.01

#### **Materials Science Applications of Four Dimensional–Scanning Transmission Electron Microscopy (4D-STEM)** Colin Ophus; Lawrence Berkeley National Laboratory, United States

Traditional scanning transmission electron microscopy (STEM) detectors are large, monolithic regions that integrate a subset of the transmitted electron beam signal scattered from each electron probe position. These STEM imaging experiments record only 1-5 values per probe position, throwing away most of the diffracted signal information. With the introduction of extremely high speed direct electron detectors, we can now record a full image (2D data) of the diffracted electron probe scanned over the sample (2D grid of positions), producing a four-dimensional dataset we refer to as a 4D-STEM experiment. These diffraction images of the electron probe are extremely rich in atomic-scale information, such as the sample structure, orientation, composition, phonon spectra, defect structure and more. The spacing between adjacent STEM probes can be varied from below one Angstrom to hundreds of micrometers, allowing us to probe the functional length scale of materials and devices.

In this talk, I will discuss how 4D-STEM can be used to measure various properties important to materials science. I will show several examples of nanobeam electron diffraction used to measure sample structure, orientation and strain, for samples ranging from metallurgical alloys to conductive polymers. I will also show how 4D-STEM can enable phase contrast imaging methods. Finally, I will also show how the scattering matrix (S-matrix) formalism can be used both to numerically invert sample structure under conditions of multiple scattering of the electron beam, and also for very fast simulation of large 4D-STEM datasets. I will show an updated version of Prismatic, our open source simulation code that includes GUIs for easy application.

### 5:15 AM \*F.MT03.01.02

#### **Maximizing the Information Provided by High-Resolution EELS and Zero-Loss Filtered 4D-STEM Using a Hybrid Pixel Direct Detector with High Dynamic Range** Christoph T. Koch<sup>1</sup>, Benedikt Haas<sup>1</sup>, Alberto Eljarrat<sup>1</sup>, Wouter Van den Broek<sup>1</sup>, Marcel Schloz<sup>1</sup>, Johannes Müller<sup>1</sup>, Holm Kirmse<sup>1</sup>, Thomas C. Pekin<sup>1</sup>, Tracy Lovejoy<sup>2</sup> and Ondrej Krivanek<sup>2,1</sup>; <sup>1</sup>Humboldt University of Berlin, Germany; <sup>2</sup>Nion Company, United States

Recent progress in aberration correction and monochromation in the scanning transmission electron microscope (STEM) has enabled a wide range of new experiments that greatly enhance the depth of information becoming accessible in materials characterization. Direct detection of electron diffraction patterns and spectra became available just at the right time to push the limits of detectability and resolution of these electron optically advanced instruments even further and make experimental data fully quantifiable, to the point, where the match of simulations and experiment is ultimately only limited by counting statistics.

We will report on the recent development of advanced data reconstruction algorithms for recovering the dielectric function from relativistic EELS spectra [1], a versatile ptychography reconstruction algorithm that includes various regularization options [2], and other ways to process 4D-STEM data [3]. We will present results obtained by applying these algorithms to data having been recorded using a monochromated STEM (Nion HERMES microscope operating between 30 ... 200 kV, EELS-resolution < 6 meV, spatial resolution < 0.07 nm) [4] equipped with a Dectris ELA hybrid pixel detector [5] that combines true single electron sensitivity, high speed (> 5000 fps for 514 x 1030 pixels at reduced bit depth, and 2250 full fps at 16 bit) and nearly perfect point spread function (1.3 pixels in integration mode) with the capacity for a high dynamic range (> 10<sup>7</sup>). Being able to detect spectra and (zero-loss filtered) diffraction patterns without read-out noise greatly increases the level at which these reconstruction algorithms can extract the underlying dielectric function, local crystal structure or maps of the electrostatic potential.

Example applications that will be presented include the extraction of IR-dispersion information from high-resolution EELS of plasmonic nanostructures and a comparison of various data processing algorithms (ptychography, center-of-mass, etc.) applied to (zero-loss filtered) 4D-STEM data.

[1] A. Eljarrat and C.T. Koch, *Ultramicroscopy* 206 (2019) 112825

[2] M. Schloz, T.C. Pekin, Z. Chen, W. Van den Broek, D.A. Muller, C.T. Koch, arxiv :2005.01530

[3] B. Haas, M. Schloz, J. Müller, A. Mittelberger, O.L. Krivanek, L. Jones, W. Van den Broek, D. Cooper, J.-L. Rouvière, and C.T. Koch, *EMC Abstract* (2020)

[4] O.L. Krivanek, N. Dellby, J.A. Hachtel, J.-C. Idrobo, M.T. Hotz, B. Plotkin-Swing, N.J. Bacon, A.L. Bleloch, G.J. Corbin, M.V. Hoffman, C.E. Meyer, T.C. Lovejoy, *Ultramicroscopy* 203 (2019) 60-67

[5] T.C. Lovejoy, B. Plotkin-Swing, N. Dellby, C.E. Meyer, A. Mittelberger, A. Eljarrat, B. Haas, C. Koch, J. Müller and



**5:30 AM \*F.MT03.01.03**

**Exploiting Dynamical Scattering in 4D-STEM to Reveal Challenging Material Structures** [Joanne Etheridge](#)<sup>1</sup>, [Wei Chao](#)<sup>1</sup>, [Espen Drath Bøjesen](#)<sup>2</sup>, [Bryan Esser](#)<sup>1</sup>, [Matus Kranak](#)<sup>3</sup>, [Weilun Li](#)<sup>1</sup>, [Timothy Petersen](#)<sup>1</sup> and [Changlin Zheng](#)<sup>4</sup>; <sup>1</sup>Monash University, Australia; <sup>2</sup>Aarhus University, Denmark; <sup>3</sup>Quantum Detectors Ltd, United Kingdom; <sup>4</sup>Fudan University, China

Convergent beam electron diffraction (CBED) provides a two-dimensional map of the intensity of scattered beams as a function of angle of incidence. Imprinted on the CBED pattern is a historical record of the multiple interactions of the electron wavefield as it is scattered within the specimen, making the pattern acutely sensitive to the specimen structure.

For more than half a century, this sensitivity has been exploited to determine crystal symmetries, refine crystal structures and measure bonding charge density distributions, to name just a few examples [1,2].

Today, with the advent of new, high speed, high dynamic range detectors, it is possible to read out the whole CBED pattern at each position of an electron beam as it is raster scanned across a specimen (often called “4D-STEM”) [3]. This delivers an unprecedented wealth of specimen information buried in terabytes of data! How can we decode this data to extract the specimen information we want? Various schemes, including ptychography and differential phase contrast, have been demonstrated successfully with fast detectors. These various approaches have enabled enhanced image resolution, mapping of electric and magnetic fields, strain, polarisation domains and octahedral tilts (for a review, see [3]).

In this paper, we will discuss some approaches that exploit the power and sensitivity of dynamical electron scattering that underpins 4D-STEM, to provide alternative imaging contrast mechanisms and interpretative schemes that can reveal targeted specimen information. We illustrate these with applications to metallic nanoparticles, beam-sensitive functional perovskites and semiconducting nanostructures.

[1] Zuo J.M. and Spence J.C.H. (1992) *Electron Microdiffraction* Springer. ISBN 978-1-4899-2353-0

[2] Tanaka M. (1997) *Convergent-Beam Electron Diffraction*. In: Dorset D.L., Hovmöller S., Zou X. (eds) *Electron Crystallography*. ISBN 978-94-015-8971-0

[3] Ophus C. (2019) *Microscopy and Microanalysis* **25**, 563–582.

**5:45 AM \*F.MT03.01.04**

**Frontiers in Imaging Functional Behavior in Nanoscale Heterostructures Using Lorentz Transmission Electron Microscopy** [Charudatta Phatak](#); Argonne National Laboratory, United States

Confinement of magnetic structures geometrically as well as energetically, leads to novel and unexpected domain behavior. Lorentz transmission electron microscopy (LTEM) is ideally suited for quantitative analysis of magnetic domains and microstructure in functional nanoscale heterostructures. The current state of art LTEM enabled using aberration correctors allows for imaging down to sub-nanometer scale in field-free conditions. In this talk, the study of magnetic domain behavior in strongly interacting magnetic nanostructures namely artificial spin ices, curved 3D magnetic nanostructures, and functional materials that host skyrmions will be presented.

Artificial spin ice lattices consist of lithographically patterned arrays of interacting magnetic islands that exhibit magnetic frustration. We will present the results on emergence of magnetic excitations in such lattices which are topologically non-trivial as well as control of magnetic frustration and emergent ordering such as antiferromagnetic to ferromagnetic phase transition using lattice geometry. Furthermore, we will present a novel approach to understand such frustration behavior based on network topology that can be extended to use of graph neural networks to analyze and predict the behavior of spin ice lattices.

Topologically non-trivial spin textures such as skyrmions present unique opportunities to explore exciting fundamental phenomena, such as the topological Hall effect, as well as novel applications, such as skyrmion-based spintronics. The application of LTEM to visualize and understand the magnetic spin textures in multilayer [Pt/Co]<sub>x</sub> thin films that can host skyrmions as well as controlled fabrication of skyrmions using Ga ion implantation will be discussed. In-situ magnetization reversal was used to understand the stability of the skyrmions.

Finally, we will also present a new approach based on machine learning for phase retrieval in LTEM that improves the achievable phase sensitivity and spatial resolution.

### 6:00 AM F.MT03.01.05

**Tracking the Layered-to-Rock Salt Phase Transition in LiNiO<sub>2</sub> by 4D STEM** Anuj Pokle<sup>1</sup>, Shamail Ahmed<sup>1</sup>, Matteo Bianchini<sup>2</sup>, Manveer Singh Munde<sup>1</sup>, Pascal Hartmann<sup>2</sup>, Torsten Brezesinski<sup>2</sup>, Andreas Beyer<sup>1</sup>, Jürgen Janek<sup>2</sup> and Kerstin Volz<sup>1</sup>; <sup>1</sup>Philipps-Universität Marburg, Germany; <sup>2</sup>Karlsruhe Institute of Technology (KIT), Germany

The layered oxide cathode materials are promising candidates for high energy density lithium-ion batteries (LIB). However, the Ni-rich layered compounds, especially the end member LiNiO<sub>2</sub> (LNO), suffer from stoichiometric challenges (Li/Ni ratios) and instability issues leading to structural degradation [1,2]. It is challenging to synthesize LNO without defects, which further results in severe capacity loss during electrochemical cycling. The phase transition structure/ mechanism is widely under debate, and obtaining a thorough insight is crucial for enhancing the cathode material performance. Directly visualizing the structure at the atomic scale can give us further insight, nonetheless detecting the light elements in energy materials is not trivial.

All the major studies over imaging lithium are carried out on free-standing single-crystalline nanoparticles [3]. However, the real cathode active materials (CAMs) are polycrystalline particles composed of densely packed primary particles/nanocrystals. This poses challenges in sample preparation to achieve the optimum thickness parameters to visualize lithium. In this report, we have investigated the phase transformed region using aberration-corrected scanning transmission electron microscopy (AC-STEM) combined with the pixelated detector (pnCCD). Selecting specific regions in the convergent beam electron diffraction (CBED) patterns and calculating the so-called virtual enhanced ABF (eABF) images is shown to enhance the contrast of the lighter elements even in the thicker sample of ~ 95 nm [4-6]. Moreover, to verify the dependency of this technique at various thicknesses, final gradational thinning of the focused ion beam (FIB) prepared lamellae is carried out by focused low energy Ar-ion NanoMill. Ultimately, we apply the HAADF (high angle annular dark field), ABF, and eABF imaging techniques simultaneously to image the entire layered-to-rock salt phase transition region.

Interestingly, we have been able to access the phase transformed region in between the layered and the rock-salt structure by collecting four-dimensional datasets (4D STEM). This has enabled us to atomically track Ni as well as the light elements, especially lithium and oxygen. The analysis of the layered-to-rock salt phase transition region suggests that there is no sharp interface, as previously assumed. Instead, the transformation appears to take place gradually [1]. The current findings warrant a re-examination of commonly assumed models on this important class of energy materials. Moreover, our results shine a light on the phase transformation mechanism at high spatial resolution and can influence the future design for stabilizing LNO against structural transitions.

#### References:

- [1] S. Ahmed, M. Bianchini, A. Pokle et al. Visualization of Light Elements using 4D STEM: The Layered-to-Rock Salt Phase Transition in LiNiO<sub>2</sub> Cathode Material. *Advanced Energy Materials* **n/a**, 2001026.
- [2] M. Bianchini, M. Roca Ayats, P. Hartmann, T. Brezesinski, J. Janek, There and Back Again—The Journey of LiNiO<sub>2</sub> as a Cathode Active Material, *Angewandte Chemie International Edition*. 58 (2019)10434–10458. <https://doi.org/10.1002/anie.201812472>.
- [3] Y. Oshima, S. Lee, K. Takayanagi, Visualization of lithium ions by annular bright field imaging, *Microscopy (Oxf)*. 66 (2017) 15–24. <https://doi.org/10.1093/jmicro/dfw098>.
- [4] S.D. Findlay, Y. Kohno, L.A. Cardamone, Y. Ikuhara, N. Shibata, Enhanced light element imaging in atomic resolution scanning transmission electron microscopy, *Ultramicroscopy*. 136 (2014) 31–41. <https://doi.org/10.1016/j.ultramic.2013.07.019>.
- [5] M. Ohtsuka, T. Yamazaki, Y. Kotaka, I. Hashimoto, K. Watanabe, Imaging of light and heavy atomic columns by spherical aberration corrected middle-angle bright-field STEM, *Ultramicroscopy*. 120 (2012) 48–55. <https://doi.org/10.1016/j.ultramic.2012.06.006>.
- [6] Rose, H., *Phase Contrast in Scanning Transmission Electron Microscopy*, *Optik* 1974, 39, 416–436. (1974).

### 6:10 AM F.MT03.01.06

**Expanding the Dimensions of a Small, Two-Dimensional Diffraction Detector** Xi Chen<sup>1</sup>, Matthew Hauwiller<sup>1</sup>, Abinash Kumar<sup>1</sup>, Aubrey Penn<sup>2</sup> and James M. LeBeau<sup>1</sup>; <sup>1</sup>Massachusetts Institute of Technology, United States; <sup>2</sup>North Carolina State University, United States

4D STEM has gained popularity in recent years and is now widely applied to the quantitative phase and orientation mapping[1], strain mapping[2], electromagnetic field measurements[3], and ptychographic reconstructions[4]. The realization of routine 4D STEM is closely related to the development of new detectors. Direct electron detectors, for example, have

overcome the limitations faced by CCD and indirect CMOS sensors, providing much higher dynamic range and frame rate, while maintaining single-electron sensitivity. In some cases, e.g. the hybrid pixel array detectors, these detectors are limited in size. (Medipix3 has 256x256 pixels [5], the EMPAD has 128x128 pixels [6]). Therefore, it is of great value to be able to expand the effective size of a small detector.

In this presentation, we demonstrate a method to increase the effective size of a small detector by capturing and combining sub-regions of reciprocal space. We will highlight how to script the microscope to shift the diffraction pattern across the detector. Taking control of the diffraction shift also allows more flexibility in practical application. For example, this technique can be used to capture only certain segments of reciprocal space to save time and storage. It is possible to acquire along an annulus of the diffracted intensity to avoid the central beam and capture only high angle diffuse scattering. In this case, the diffraction pattern can be shifted in a ring pattern instead of a normal grid pattern. Furthermore, we will show how this technique expands a small detector's application space. Electrons all the way out to the objective lens bore can be captured with a high sampling rate. Limitations and challenges of acquiring such data will also be discussed.

As for reconstruction, we will highlight our automated routine to accurately and precisely align the data post-acquisition. We will also examine the challenges associated with reconstructing the datasets, including rotating the pattern shift axes and lens hysteresis. Consistency of the alignment will also be discussed. We also explore the accuracy of the reconstruction as a function of pattern exposure time and sub-pattern overlap to help guide experimental parameters. Finally, we will also show that being able to capture the Bragg peak intensities at the same time as diffuse scattering provides opportunities for quantitative diffraction analysis.

#### References:

- [1] Funderberger et al., *Ultramicroscopy* **96** (2003), P127-137
- [2] Muller et al., *Appl. Phys. Lett.* **101**(2012), P212110
- [3] Ryll et al., *Journal of Instrumentation* **11**(2016), P04006
- [4] Lupini et al., *Microsc. Microanal* **21**(2015), P1219-1220
- [5] MW Tate et al., *Microsc. Microanal* **22** (2016), P237
- [6] Mir et al., *Ultramicroscopy* **182**(2017), P 44-53
- [7] We acknowledge support for this work from the Air Force Office of Scientific Research (FA9550-17-1-0225. This work was performed in part at the Analytical Instrumentation Facility (AIF) at North Carolina State University, which is supported by the State of North Carolina and the National Science Foundation (award number ECCS-1542015). The AIF is a member of the North Carolina Research Triangle Nanotechnology Network (RTNN), a site in the National Nanotechnology Coordinated Infrastructure (NNCI).

#### 6:20 AM F.MT03.01.07

**Correlation Between Structural Heterogeneity with Ductility and Glass Forming Ability in Metallic Glasses Using 4D Scanning Transmission Electron Microscopy** Soohyun Im<sup>1</sup>, Pengyang Zhao<sup>2</sup>, Geun Hee Yoo<sup>3</sup>, Gabriel Calderon<sup>1</sup>, Mehrdad Abbasi Gharacheh<sup>1</sup>, Olivia G. Licata<sup>4</sup>, Baishakhi Mazumder<sup>4</sup>, Eun Soo Park<sup>3</sup>, Yunzhi Wang<sup>1</sup> and Jinwoo Hwang<sup>1</sup>; <sup>1</sup>The Ohio State University, United States; <sup>2</sup>Shanghai Jiao Tong University, China; <sup>3</sup>Seoul National University, Korea (the Republic of); <sup>4</sup>University of Buffalo-SUNY, United States

We determine the correlation between the structural heterogeneity and unprecedented detailed parameters of medium range ordering (MRO) using 4-dimensional scanning transmission electron microscopy (4-D STEM). The details of MRO constitute nano-scaled structural heterogeneity, such as the type, size, and fraction of MRO structures, which are directly correlated with the important properties, including the ductility and glass forming ability of Zr-Cu-Co-Al metallic glasses. In this study, the quantitative analyses of the data are enabled by our 4-D STEM using the new-generation Electron Microscopy Pixel Array Detector (EMPAD). This new detector can not only support high dynamic range, which is necessary for the quantification, but also take nanodiffraction patterns continuously throughout a large sample area with oversampling. Thus, it allows us to obtain the statistically reliable information on the structural heterogeneity at the nanoscale. We confirm the fact that the important properties of Zr-Cu-Co-Al MGs and Ti-Zr-Ni-Be MGs are directly related to the determined MRO parameters. In the Zr-based MG system, the smaller and more diverse MRO types result in high ductility, and more structurally frustrated MRO type relates to the higher glass forming ability. In the case of Ti-based MGs, the addition of Be in Ti-Zr-Ni can break down icosahedral-MRO structure, which is our hypothesis based on the angular correlation analysis.

**5:00 AM \*F.MT03.02.01**

**Crystal Growth via Oriented Attachment—5-Fold Twin Formation** Dongsheng Li<sup>1</sup>, Miao song<sup>1</sup>, Gang Zhou<sup>2</sup> and Ning Lu<sup>3</sup>; <sup>1</sup>Pacific Northwest National Laboratory, United States; <sup>2</sup>Institute of Metal Research, Chinese Academy of Sciences, China; <sup>3</sup>University of Michigan, United States

Oriented attachments are recognized as a common pathway for crystal growth in both natural and synthetic systems, leading interface free or twin related structures. The occurrence of 5-fold twinned nanoparticles leads to unique properties. However, nearly 200 years after their discovery, the formation mechanism is still ambiguous. Using in situ high-resolution transmission electron microscopy combined with molecular dynamics simulations, we demonstrate that 5-fold twinning occurs via repeated oriented attachment of ~3 nm Au nanoparticles. These oriented attachment events create high-energy grain boundaries, which accumulate strain during atomic rearrangements and consequently decompose via nucleation and growth of a special class of twins whose net strain is zero, inducing the 5-fold twin structures. The results provide a quantitative understanding of the 5-fold twinning process; this knowledge provides guidance for interpreting and controlling twin structures and morphologies of a wide range of materials.

**5:15 AM \*F.MT03.02.02**

**Imaging Chemical Reactions in Solution Using Distributed Electron Microcopy** Joseph P. Patterson; University of California, Irvine, United States

Imaging chemical reactions in solution is essential for the understanding complex mechanisms involved in nanomaterial synthesis. Liquid phase electron microscopy (LP-EM) is an emerging technique capable of directly monitoring morphological changes of materials in solution with a unique combination of temporal and spatial resolution. LP-EM has been used to study the reaction mechanisms such as metal nanoparticle formation, polymer self-assembly, wet etching of semiconducting materials, growth of metal-organic frameworks, nucleation of calcium carbonate and Li electrodeposition. These studies provided an unprecedented insight into nanoscale reaction mechanisms that have significantly improved our understanding of nanomaterial synthesis. The primary challenge for the field of LP-EM is understanding the role that the electron beam plays in the observed mechanism. It is common to perform control experiments to establish a critical dose limit with which a process can be observed. A consequence of having to work below a critical dose limit is that LP-EM has mostly been used to monitor reactions over a period of seconds to minutes, despite the fact that many reactions take place over hours to days. Furthermore, even after a critical dose has been established, it is impossible to completely rule out the role of the electron beam using LP-EM experiments alone. Consequently, it is essential to study reaction mechanisms using multiple imaging modalities. Cryo-EM can also provide direct high-resolution information on reaction mechanisms in solution. The advantage of cryo-EM is that electron beam effects are well understood and, using appropriately low doses, are insignificant. The disadvantage of cryo-EM is that it is impossible to know the history or future of any individual particle being imaged. Consequently, the data on reaction mechanisms has to be presented by selecting images that the user determines to be representative of the process occurring in solution. For simple processes that evolve homogeneously, it is possible to determine a mechanism with high confidence using cryo-EM alone. However, for complex processes that evolve heterogeneously, the confidence with which mechanisms can be determined by cryo-EM alone is low. Here, a simple process is defined as a process with a single step or single pathway and a complex process is defined as a process with multiple steps or multiple pathways. A homogenous evolution is characterized by a process where only one particle state is observed at each sampled time point, while a heterogeneous evolution is characterized by a process where multiple states are observed at each sampled time point. Consequently, cryo-EM is limited in its ability to resolve complex heterogeneous processes. Despite the obvious benefits of combining LP-EM and cryo-EM, most studies using these techniques have been only conducted with a single EM modality. Here we discuss the application of distributed electron microcopy for studying reaction mechanisms in solution. The term distributed is used because the data required to understand the mechanism is shared between multiple imaging modalities and sample preparation methods. The strength of this approach is that our proposed hypothesis is consistent with data taken from experiments with complementary benefits and limitations.

**5:30 AM \*F.MT03.02.03**

**“Live” Visualization of Catalysts at Atomic-Resolution** Stig Helveg; Center for Visualizing Catalytic Processes (VISION), Department of Physics, Technical University of Denmark, Denmark

Electron microscopy has progressed extraordinarily to become a powerful tool for studying nanostructured catalysts at the atomic-scale. Advances in electron optics and detection have made atomic-resolution electron microscopy capable of resolving the three-dimensional surface structure of the complex catalytic nanomaterials. In parallel, the introduction of differentially pumped electron microscopes and micro-electro-mechanical-system devices has enabled *in situ* observations of catalysts during the exposure to gasses at pressures of up to atmospheric levels and temperatures of up to several hundred centigrade as well as *operando* studies by concurrent measurements of catalytic functionality. While these developments build a foundation for time-resolved observations of catalysts at the atomic-scale, such observations are challenged by electron-beam-induced alterations of the catalysts and mass-transport phenomena in the fluid phase. In this contribution, I will outline electron microscopy advances addressing the chemical relevance of atomic-scale visualizations. Moreover, I will showcase these “live” visualizations for exploring the dynamical and functional behavior of complex catalytic nanomaterials.

#### 5:45 AM F.MT03.02.04

**Investigating the Effect of *In Situ* Heating on the Morphology and Composition of Temperature-Responsive Polymers by Using Energy-Filtered Transmission Electron Microscopy** [Dalaver H. Anjum](#)<sup>1</sup>, Rahul Shevate<sup>2,3</sup> and Klaus-Viktor Peinemann<sup>2</sup>; <sup>1</sup>Khalifa University, United Arab Emirates; <sup>2</sup>King Abdullah University of Science & Technology (KAUST), Saudi Arabia; <sup>3</sup>University of Houston, United States

Transmission electron microscopy (TEM) is a powerful materials' characterization technique for investigating their structure and properties at nanoscale dimensions. It has become an indispensable tool in the present era of nanoscience and nanotechnology. In this study, we employed the energy-filtered TEM (EFTEM) mode to investigate the effect of in-situ heating on the thin-layers of a stimuli-responsive (temperature) poly(N-isopropylacrylamide) (pNIPAm) which has been covalently attached to hollow titania (TiO<sub>2</sub>) nanowires. The temperature-responsive behavior was characterized by observing the morphology and composition of samples as a result of heating. The pNIPAm has the swelling to shrinking transition temperature defined as lower critical solution temperature (LCST) of ~32 °C at standard conditions. We characterized the morphology and composition of the samples below and above the phase transition temperature of the pNIPAm by applying in-situ heating inside TEM. The EFTEM imaging and elemental mapping were applied at room temperature to determine the conformity of the pNIPAm layer and the elemental distributions of all elements present in samples. In the analysis, the elemental distribution of the element carbon (C) was attributed to the presence of the pNIPAm layer in the samples. The TiO<sub>2</sub> nanowires regions in the samples were identified by the overlapping of generated titanium (Ti) and oxygen (O) elemental maps. The EFTEM analysis was then repeated at the same sample regions by applying incremental in-situ heating, during which the temperature of samples was increased from ambient (23 °C) to high (100 °C) temperature with an interval of 10 °C. The acquired results revealed that the phase transition temperature of the pNIPAm came out to be 95 °C inside the TEM, which was higher than the expected value. Similarly, during the cooling of samples inside the TEM, the pNIPAm did not revert to the original morphology once the samples reached room temperature. However, the pNIPAm was found to recover the morphology by cooling the samples in standard atmospheric conditions. In conclusion, our findings show that the pNIPAm may exhibit a different swelling to shrinking behavior inside the TEM than under standard atmospheric conditions. The discrepancy is believed to be due to the rate of heat transfer between the surrounding environment and the samples and the relative humidity at ambient conditions, which evidently play a critical role for the pNIPAm transition from swelling to shrinking as well as from shrinking to swelling phase.

#### 5:55 AM F.MT03.02.05

**Insights into the Real-Time Structural Dynamics of Liquid-Vapor Interface at Nanometer Resolution by *In Situ* TEM** [Amy Ren](#)<sup>1,2</sup>, David Lu<sup>1,3</sup> and Gang Ren<sup>1</sup>; <sup>1</sup>Lawrence Berkeley National Laboratory, United States; <sup>2</sup>University of California Santa Babra, United States; <sup>3</sup>Brown University, United States

Visualization of the dynamic structure of the liquid, essential for studying the virus and cell activity, has remained elusive for decades due to lack of an effective tool for direct visualization beyond micrometer resolution. Here, we designed a simple liquid-cell for encapsulating the liquid state of sodium for transmission electron microscopic (TEM) observation. The real-time dynamic structure of the liquid-vapor interface was imaged and videoed by TEM on the sample of electron irradiated sodium chloride (NaCl) crystals, a well-studied sample with low melting temperature and quantum super-shells of clusters. The nanometer resolution images exhibit the fine structures of the capillary waves, composed of three zones of structures and features, i.e. flexible nanoscale fibers, nanoparticles/clusters, and a low-pressure area that sucks the nanoparticles from the liquid to the interface. Although the phenomenon was observed based on irradiated NaCl crystals, the similarity of the phenomenon to predictions suggest our first-time videos of the dynamic structure might be useful in validating long-debated theoretical models of the liquid-vapor interface. By implemented the technique to biology, we imaged virus and cell in wet for insights into the 3D structure of the intermediates of viral infection cell.

### 6:05 AM F.MT03.02.06

**Electron Microscopy Study of Nanoparticles During Electrocatalytic Reactions** Jinglong Guo<sup>1</sup>, Xue Rui<sup>1</sup>, Dongyoung Chung<sup>2</sup>, Pietro Papa Lopes<sup>2</sup> and Robert Klie<sup>1</sup>; <sup>1</sup>University of Illinois at Chicago, United States; <sup>2</sup>Argonne National Laboratory, United States

The oxygen evolution reaction (OER) plays an important role in energy conversion and storage applications, such as metal-air electrochemical cells and the production of hydrogen from water electrolysis. Metal oxide nanoparticles acting as high-quality electro-catalysts allows for anionic redox of oxygen at the particle surface. [1] However, this reaction may lead to considerable dissolution and degradation of the nanoparticle catalyst. Perovskite oxides have been previously demonstrated that, by enhancing the hybridization between the O 2p and transition metal 3d orbitals, the OER activity can be enhanced significantly. [2] KOH electrolyte with Fe impurities have been found to significantly increase the activity of Ni-based perovskite oxides electrocatalysts. [3] In this contribution, we evaluate the role of Fe impurities together with Sr-doping on LaCoO<sub>3</sub> based materials on the activity and stability for OER in alkaline electrolyte using combination of scanning transmission electron microscopy (STEM) imaging, electron energy loss spectrum (EELS) and energy dispersive x-ray spectroscopy (EDXS). Our analysis is conducted on the same particles on pristine and after cycling (Identical-Location TEM; ILTEM), which enables us to track the effect of electrochemical cycling on the particles. In addition to the La<sub>1-x</sub>Sr<sub>x</sub>CoO<sub>3</sub> catalysts, we also studied MnWO particles decorated with Ir catalyst nanoparticles using the ILTEM approach. From the comparison of the same particles on pristine and after cycling, the dissolution of the Ir nanoparticle on the surface of MnWO particles was observed. The results will be combined with first principal calculation to show the effect of surface composition and structural evolution during activity of OER.

References:

- [1] E Fabbri et al., Nature Materials **16** (2017), p. 925.
- [2] JT Mefford et al., Nat Commun **7** (2016), p. 11053.
- [3] L Trotochaud et al., Journal of the American Chemical Society **136** (2014), p. 6744.

SESSION F.MT03.03: Vibrational, Phonon and Core-Loss EELS  
On Demand Abstracts Available for Viewing Starting Saturday Morning, November 21, 2020  
F-MT03

### 5:00 AM \*F.MT03.03.01

**Monochromated STEM EELS of Phononic and Photonic Excitations** Kartik Venkatraman, Qianlang Liu, Barnaby D. Levin and Peter A. Crozier; Arizona State University, United States

The enhanced energy resolution of recently developed monochromators now make it possible to use electron energy-loss spectroscopy (EELS) in the scanning transmission electron microscope (STEM) to probe materials systems in new ways. This powerful spectroscopic capability combined with the small focused electron probe opens the door to explore photonic and phononic/vibrational excitations with high spatial resolution [1-3]. Here we describe recent advances leading to nanoscale and atomic resolution vibrational spectroscopy and novel approaches to probe guided photonic modes in dielectric particles. The fast electron in the electron microscope can excite vibrational modes in materials either through dipole interactions (similar to IR absorption spectroscopy) or impact scattering (similar to inelastic neutron scattering). The spatial localization of these two scattering mechanisms is very different. Impact scattering typically involves higher momentum transfers yielding a spatially localized spectral signal. In a crystal, high momentum transfer interactions are associated with exciting the short wavelength phonon modes at the Brillouin zone boundaries (BZB). Efficient excitation of these modes requires experimental conditions that favor Bragg scattering from the associated Miller planes. This can be easily accomplished in the conventional STEM EELS geometry by tilting the crystal into a suitable zone axis orientation and using a probe convergence angle that spans the Bragg angle associated with the BZB of interest. This convergence angle also permits a small probe to be formed which enables resolution of the associated Miller plane spacing. We have used this approach to demonstrate nanoscale and atomic resolution on a sample of Si, SiO<sub>2</sub> and BN [1]. EELS can also be employed to explore the characteristic photonic modes present in dielectric nanoparticles since the electron beam can provide a source of virtual photons to illuminate the object. We have explored the variation in photonic modes for high refractive index oxide particles such as TiO<sub>2</sub>, Ta<sub>2</sub>O<sub>5</sub> and CeO<sub>2</sub> [2]. The modes show up as peaks in the bandgap region of the spectrum. The energies of the modes are determined not only by the particle shape and size but also due to coupling between adjacent particles.

Coupling between phonons and IR photons can give rise to phonon polaritons [3,4]. Polariton characteristics are also influenced by sample geometry, and so the polaritonic modes can be manipulated by changing the sample shape/size. Here we use STEM EELS to demonstrate variations in the polaritonic response on patterned SiO<sub>2</sub> thin films.

#### References:

- [1] K. Venkatraman et al., Nature Physics 15 (2019) 1237-1241.
- [2] Q. Liu et al., Phys. Rev. B 99 16 (2019) 165102.
- [3] K. Venkatraman et al., Microscopy 67 (2018) i14 - 23.
- [4] A. Konečná et al., Phys. Rev. B 98 20 (2018) 205409.
- [5] The support from US National Science Foundation CHE-1508667 and U.S. DOE (DE-SC0004954), the use of (S)TEM at Eyring Materials Center at Arizona State University is gratefully acknowledged.

#### 5:15 AM \*F.MT03.03.03

##### **Nanoscale Measurements of Vibrations, Dispersions and Emergent Phenomena Using Monochromated Electron Energy Loss Spectroscopy Jordan Hachtel; Oak Ridge National Laboratory, United States**

Advances in electron monochromation have led to a sea change in electron energy loss spectroscopy (EELS) over the last 6 years. Modern monochromators scanning transmission electron microscopes (STEM) have improved EELS energy resolution by an order of magnitude (from ~50 meV down to < 5 meV). This new level of energy resolution enables direct access to a host of new phenomena, such as phonons, vibrational modes, infrared optical excitations, and low-lying states in the electronic structure. Moreover, it also presents many new opportunities to probe difficult and complex systems by exploiting novel interactions between the electron beam and these ultra-low energy excitations. As a result, monochromated EELS is a highly versatile tool that can be applied to a wide range of different disciplines and materials systems and deliver exciting results.

In this talk, I will focus on three different materials systems where monochromated EELS presents a unique opportunity to provide new insights into important topics: biological, optical, and quantum materials. In terms of biological materials, I will demonstrate how we can the efficient long-range coupling of vibrational modes to the electron beam, to provide in depth spectroscopic analysis of ultra-beam sensitive biological materials. Furthermore, I will demonstrate how we can use the combine the natively high spatial and spectral resolution of monochromated EELS with various flavors of momentum-resolution to probe the dispersions of infrared quasiparticles directly at the nanoscale. Lastly, I will discuss how we can apply this technique to coupled networks of colloidal nanoparticles to examine emergent properties in quantum systems.

This work was performed at the Center for Nanophase Materials Sciences, which is a DOE Office of Science User Facility. This research was conducted, in part, using instrumentation within ORNL's Materials Characterization Core provided by UT-Battelle, LLC, under Contract No. DE-AC05-00OR22725 with the DOE, and sponsored by the Laboratory Directed Research and Development Program of Oak Ridge National Laboratory, managed by UT-Battelle, LLC, for the U.S. Department of Energy.

#### 5:30 AM \*F.MT03.03.04

**Vibrational EELS in the STEM at Single Atom Sensitivity Fredrik S. Hage<sup>1,2</sup>, G. Radtke<sup>3</sup>, Demie Kepaptsoglou<sup>1,4</sup>, M. Lazzeri<sup>3</sup>, L.J. Allen<sup>4,5</sup> and Quentin Ramasse<sup>1,6</sup>; <sup>1</sup>SuperSTEM Laboratory, SciTech Daresbury Campus, United Kingdom; <sup>2</sup>University of Oxford, United Kingdom; <sup>3</sup>Sorbonne Université, MuséumNational d'Histoire Naturelle, UMR CNRS 7590, Institut de Minéralogie, de Physique des Matériaux et de Cosmochimie, France; <sup>4</sup>The University of Melbourne, Australia; <sup>5</sup>Ernst Ruska-Centre for Microscopy and Spectroscopy with Electrons, Forschungszentrum Jülich, Germany; <sup>6</sup>University of Leeds, United Kingdom**

Vibrational electron energy loss spectroscopy (EELS) in the scanning transmission electron microscope (STEM) has over the recent years emerged as a versatile tool for characterizing molecular to bulk or surface vibrational modes in a wide range of materials systems, at the nanoscale [1]. The possibility of going beyond the nanoscale, reaching atomic resolution, has been discussed extensively in the community. We recently demonstrated such a capability using a so-called dark-field (DF) experimental geometry, suppressing the relative spectral contribution of elastic and delocalized inelastic *dipole* scattering by phonons, favoring instead beam electrons having undergone localized *impact* phonon scattering [2]. This approach allows for acquiring phonon structure images using the acoustic and/ or optical phonon EEL peaks [2] and, is equally applicable to polar [2] and non-polar materials [3]. Moreover, these results verify experimentally that annular dark field (ADF) Z-contrast imaging is based on beam electrons being scattered inelastically by phonons, in agreement with the quantum excitation of phonons model [2]. As a next step, we applied this methodology to probe the vibrational response of a single tri-valent

substitutional Si atom in a single layer of suspended graphene. Spatially resolved EEL spectra show a characteristic vibrational signature associated with the Si impurity, localized to the defect atom itself. This is rationalized by means of density functional theory (DFT) calculations, attributing the measured response to the Si atom inducing pseudo-localized phonon modes: i.e. defect modes hybridizing with the graphene bulk continuum, setting up resonant states [3]. Possible applications of the demonstrated atomic resolution and single atom sensitivity, as well as practical aspects of the experimental approach, will be discussed.

[1] O. L. Krivanek et al., *Ultramicroscopy* **203** (2019) p. 60–67.

[2] F. S. Hage et al., *PRL* **122** (2019) 016103.

[3] F. S. Hage et al., *Science* **367** (2020) p. 1124–1127.

#### **5:45 AM \*F.MT03.03.05**

**Tailored Nanoscale Plasmon-Enhanced Vibrational Electron Spectroscopy** Luiz H. Galvao Tizei; CNRS, France

Atomic vibrations and phonons are an excellent source of information on nanomaterials that we can access through a variety of methods including Raman scattering, infrared spectroscopy, and electron energy-loss spectroscopy (EELS). In the presence of a plasmon local field, vibrations are strongly modified and, in particular, their dipolar strengths are highly enhanced, thus rendering Raman scattering and infrared spectroscopy extremely sensitive techniques.

In this contribution [1], we experimentally demonstrate that the interaction between a relativistic electron and vibrational modes in nanostructures is fundamentally modified in the presence of plasmons. This could be observed due to the current developments in electron optics, making possible the generation of sub-nanometer wide sub-10 meV electron beams with 60 keV primary energy. We finely tune the energy of surface plasmons in metallic micrometer-long Ag nanowires in the vicinity of hexagonal boron nitride flakes, making it possible to monitor and disentangle both strong phonon–plasmon coupling and plasmon-driven phonon enhancement at the nanometer scale. Because of the near-field character of the electron beam–phonon interaction, optically inactive phonon modes are also observed. Besides increasing our understanding of phonon physics, our results hold great potential for investigating sensing mechanisms and chemistry in complex nanomaterials down to the molecular level.

The strong coupling limit is reached between surface plasmons and phonon modes as the largest coupling constant,  $g$ , reached was 52 meV and the full width at half maximum of the two coupled excitations were 23 and 19 meV. The signature of strong coupling is observed along the whole nanowires, including for nanowire regions far away from any h-BN (point to the coherence of the coupled modes along the nanowire). The spatial dependence at nanometer scale of these modes will be described.

More interestingly, the presence of plasmons modify the way fast electrons couple to bulk modes of h-BN, leading to enhancement of their signal and the observation of usually “dark modes”. As an example, the ZO-phonon mode of hBN, usually not observed for electron beams perpendicularly incident on an h-BN flake, can be observed when close to metallic nanowires. We will describe how this enhanced signature changes as a function of the distance of the electron probe to the nanowire surface, varying in the tens-of-nanometers scale. Experiments have been performed with the ChromaTEM microscope (TEMPOS project, ANR-10-EQPX-50), a modified Nion HERMES200 operated at 60 kV. The electron beam was set to have an energy spread in the 6-10 meV range and a nanometer size. Experiments are under way to achieve similar enhancement in molecular systems.

If time allows, recent nano-optics experiments using ChromaTEM will be discussed.

#### **6:00 AM \*F.MT03.03.06**

**Nanoscale Optical and Vibrational Spectroscopy of Low-Dimensional Materials in Electron Microscope** Ryosuke Senga; AIST, Japan

The excitations of quasiparticles govern the physical properties of low-dimensional materials. Furthermore, assessing the irregular stacking sequences and behaviours at imperfect sections (such as boundaries and edges) is undoubtedly important to understand the performance of nanodevices. However, such local information has usually been averaged in conventional inelastic scattering techniques using x-ray, neutron, and light sources because of their diffraction limit. We demonstrate the nanoscale optical and vibrational spectroscopy of 1D or 2D materials by using a monochromatic electron source mounted in a transmission electron microscope (TEM).

All experiments were performed using a TEM (JEOL TripleC#2 at 30–60 kV) equipped with a Schottky field emission gun, a double Wien filter monochromator, and delta correctors. The energy resolution was set to a value less than 50 meV and allowed to access the quasiparticle excitations (i.e. phonon, exciton, and plasmon) of low-dimensional materials by electron energy-loss spectroscopy (EELS). The EEL spectra were collected using a GATAN GIF quantum spectrometer designed for



low-voltage operations.

The spatial and momentum resolutions in electron microscopes balance each other and can be finely tuned with magnetic/electrostatic lenses. For instance, an atomically thin probe can be formed with an integration of a large momentum space. This allows us to extract local information from single defects. We have successfully measured the optical gap transitions from a defect of an individual semiconducting carbon nanotube [1,2]. Recently, atomically localized vibrational spectroscopic techniques have also been developed [3,4].

In contrast, an electron probe consisting of a parallel beam has a higher momentum resolution and provides dispersions of quasiparticle excitations. The EEL spectra are collected from each momentum transfer ( $q$ ) by a pinhole aperture or a  $q$ -slit in a diffraction plane. Using this method, we have obtained phonon dispersions of graphene and h-BN from a single layer. Interestingly, the inelastically scattered electrons by phonon excitations provide sufficient signals at a large  $q$  even in the second and third Brillouin zone. Such signal enhancement due to a charge modulation at a large  $q$  helps draw a phonon dispersion curve of graphene even from a single layer. In addition, the spatial resolution of this method (a few to a few tens of nanometres, depending on its momentum resolution) is more advantageous than other dispersion measurement techniques such as inelastic x-ray spectroscopy. By maintaining the momentum resolution better than  $\pm 0.2 \text{ \AA}^{-1}$ , each vibrational mode can be assigned at a region of a few tens of nanometres. Therefore, the propagation of each phonon mode at defects such as edges in graphene has been unambiguously visualized [5]. Such local spectroscopy with a large flexibility could help unravel the defect physics of quantum matters.

#### References

- [1] R. Senga, T. Pichler and K. Suenaga Nano Letters **16** (2016), 3661.
- [2] R. Senga et al., Nano Letters **18** (2018), 3920.
- [3] F. Hage et al., Phys. Rev. Lett. **122** (2019), 016103
- [4] K. Venkatraman et al., Nature Physics **15** (2019), 1237
- [5] R. Senga et al., Nature **573** (2019), 247

#### 6:15 AM F.MT03.03.07

**Improving the Resolution of Polymer EELS by Exploiting the Beam-Induced Chemistry** Robert Colby, Yu Fan and Donald Carpenter; ExxonMobil Research and Engineering Company, United States

Electron energy loss spectroscopy (EELS) can be used to identify polymers and similar organics, but is limited by the rate at which materials damage when probed with  $\sim 100$  kV electrons. Any modern scanning transmission electron microscope (STEM) is routinely capable of producing a sub-nanometer probe, but the fluence rate (electrons/nm<sup>2</sup> s) needed to achieve enough signal at this level of resolution cannot be tolerated by most organics, even at low temperatures. Many polymers show signs of damage well below 10 electrons/Å<sup>2</sup>, a threshold frequently identified for studying organic material. Even with ongoing detector improvements, “damage-free” EELS fine structure mapping of polymers with nanometer-sized pixels does not seem conventionally attainable. However, the ways in which an electron beam modifies a given polymer—and the resulting changes that can be observed with EELS—are arguably even more unique than the initial EELS fine structure.

The type and extent of beam-induced chemistry for a given polymer depends on at least dose, dose-rate, sample temperature, and vacuum conditions. These dependencies provide opportunities to exploit beam damage as a means for polymer chemistry identification. Beam-induced chemistry significantly precedes substantial mass loss and/or sample distortion in many polymers, particularly at cryogenic temperatures. The simplest option is to probe the fluence dependence by recording a series of STEM-EELS maps with a fixed current and temperature. These 4D fluence-dependent EELS maps can be collected with total fluences normally considered too high for accurate polymer identification, while at lower fluence rates, enabling spatial higher resolution mapping. This will be demonstrated for model polymer blends for  $< 20$  nm pixels, using a spectrometer with a CCD-based EELS detector.

Many studies have unintentionally mapped damaged polymers, and/or specifically measured damage evolution with EELS, but resolving and using the beam-induced evolution of sample chemistry to improve mapping is novel. Ultimately, spatial resolution is still limited by beam-induced changes: e.g., the rate of mass loss and the diffusion of generated radicals and gases. While application to polymer EELS will be shown, the approach is quite generic to materials with a measurable chemical evolution preceding significant sample morphology change.

#### 6:25 AM F.MT03.03.08

**Isotope Effect in the Vibrational Modes of hBN Flakes** Fadil Iyikanat<sup>1</sup>, Andrea Konecna<sup>1</sup> and F. Javier Garcia de Abajo<sup>1,2</sup>; <sup>1</sup>ICFO-Institut de Ciències Fòniques, Spain; <sup>2</sup>ICREA-Institució Catalana de Recerca i Estudis Avançats, Spain

In this study, we perform first-principles calculations to investigate the effect of isotopic substitutions in the vibrational modes of hBN flakes. Using density functional theory calculations the ground state atomic configuration and the dynamical matrix of hBN flake are obtained. The eigenmodes and eigenfrequencies are calculated by diagonalization of the dynamical matrix. Using semiclassical formalism, the interaction between a focused electron beam and vibrations is described. We employ this approach to predict the effect of isotopes on the spatially-resolved electron energy-loss spectra (EELS) of hBN flakes.

#### 6:35 AM F.MT03.03.09

**Spontaneous and Stimulated Electron-Photon Interactions in Nanoscale Plasmonic Near Fields** [Matthias Liebtrau](#)<sup>1</sup>, Murat Sivis<sup>2</sup>, Armin Feist<sup>2</sup>, Hugo Lourenco-Martins<sup>2</sup>, Nicolas Pazos-Perez<sup>3</sup>, Ramon A. Alvarez-Puebla<sup>3,4</sup>, Javier Garcia de Abajo<sup>5</sup>, Albert Polman<sup>1</sup> and Claus Ropers<sup>2</sup>; <sup>1</sup>AMOLF, Netherlands; <sup>2</sup>University of Goettingen, Germany; <sup>3</sup>Universitat Rovira i Virgili, Spain; <sup>4</sup>Catalan Institution for Research and Advanced Studies, Spain; <sup>5</sup>ICFO–The Institute of Photonic Sciences, Spain

We study spontaneous and stimulated interactions between high-energy electrons and photons in nanoscale plasmonic near fields using Electron Energy Loss Spectroscopy (EELS), Cathodoluminescence (CL) spectroscopy and Photon-Induced Near-field Electron Microscopy (PINEM) in a Scanning (Transmission) Electron Microscope (S(T)EM). In recent years, EELS, CL and PINEM have enabled tremendous advances in probing (resonant) optical materials excitations with extreme spatial, temporal and energy resolution [1,2]. In EELS and CL, the time-varying evanescent electric field of the swift electrons serves as an ultra-broadband excitation source that can couple to a wide range of optical modes in a material [3]. The energy transfer during this interaction is a *spontaneous* process, resulting in a characteristic electron energy loss (EELS) and the subsequent emission of light (CL). Conversely, in PINEM, the electrons interact with an intense laser-driven near-field, giving rise to both electron energy-gain and -loss transitions by *stimulated* absorption and emission of photons at an energy determined by the laser frequency [4,5].

We demonstrate spatially-resolved EELS, CL and PINEM measurements of highly-localized dipolar optical fields at the sharp tip apexes of a chemically-synthesized Au nanostar [6]. We highlight similarities and differences between the measured EELS, CL and PINEM distributions, and discuss the role of the underlying excitation mechanisms driven either by the electron itself (EELS and CL) or the external laser (PINEM). Supported by electromagnetic boundary element method calculations for a simplified model geometry, we show that in the limit of a single isolated tip mode, spatial variations in the spontaneous and stimulated electron-photon interactions are purely determined by the modal electric near field profile, irrespective of the excitation source.

The interaction strength between free electrons and localized optical fields scales with the Fourier amplitude of the electric near field component along the electron trajectory at a single spatial frequency that is determined by the electron velocity [3,7,8]. As a consequence, the measured EELS, CL and PINEM distributions depend on the initial electron energy, with the maximum interaction strength shifting towards smaller electron energies for increasing field confinement. In general, the full three-dimensional (3D) reconstruction of an electric near-field distribution is therefore only possible by extensive tomographic measurements at multiple electron energies. Yet, using PINEM we show that for an axially-symmetric tip, we can determine the laser-induced surface charge density profile along the tip contour and thus obtain the desired 3D near-field distribution from a single measurement at a fixed electron energy and incident angle.

#### References:

- [1] A. Losquin and T. T. A. Lummen, *Front. Phys.* **12**, 127301 (2017).
- [2] A. Polman, M. Kociak, and F. J. Garcia de Abajo, *Nature Mater.* **18**, 1558-1171 (2019).
- [3] F. J. Garcia de Abajo, *Rev. Mod. Phys.* **82**, 209-275 (2010).
- [4] B. Barwick, D. J. Flannigan, and A. H. Zewail, *Nature* **462**, 902-906 (2009).
- [5] A. Feist, K. E. Echternkamp, J. Schauss, S. V. Yalunin, S. Schaefer, and C. Ropers, *Nature* **521**, 200-203 (2015).
- [6] N. Pazos-Perez, L. Guerrini, and R. A. Alvarez-Puebla, *ACS Omega* **3**, 17173-17179 (2016).
- [7] A. Losquin and M. Kociak, *ACS Photonics* **2**, 1619-1627 (2015).
- [8] F. J. Garcia de Abajo and M. Kociak, *New J. Phys.* **10**, 073035 (2008).

SESSION F.MT03.04: 3D Electron Microscopy

On Demand Abstracts Available for Viewing Starting Saturday Morning, November 21, 2020  
F-MT03

## 5:00 AM \*F.MT03.04.01

### Strategies for Quantifying the 3D Atomic Structure and the Dynamics of Nanomaterials Using Model-Based

**STEM** Sandra Van Aert<sup>1</sup>, Annick De Backer<sup>1</sup>, Annelies De wael<sup>1</sup>, Jarmo Fatermans<sup>1</sup>, Ece Arslan Irmak<sup>1</sup>, Thomas Friedrich<sup>1</sup>, Ivan Lobato<sup>1</sup>, Lewys Jones<sup>2</sup>, Arjan den Dekker<sup>3</sup>, Peter Nellist<sup>4</sup> and Sara Bals<sup>1</sup>; <sup>1</sup>EMAT, NANOLab Center of Excellence, University of Antwerp, Belgium; <sup>2</sup>CRANN & School of Physics, Trinity College Dublin, University of Dublin, Ireland; <sup>3</sup>imec-Vision Lab, University of Antwerp, Belgium; <sup>4</sup>Department of Materials, University of Oxford, United Kingdom

Quantitative 3D characterization at high resolution is often required in order to fully exploit structure–property relations of nanomaterials. In recent years, the resolution of electron tomography has reached the atomic scale. However, for a successful 3D reconstruction using electron tomography multiple exposures are required, which is not always feasible when studying, e.g., radiation-sensitive nanostructures. In order to overcome these limitations, an alternative method can be used where the 3D atomic structure is reconstructed from atom counts obtained from a single ADF STEM projection image. These atom counts can be used to create an initial atomic model which serves as an input for an energy minimization to obtain a relaxed 3D reconstruction of a nanostructure [1].

To count atoms with single-atom sensitivity, a minimally required electron dose is necessary, while on the other hand the risk of knock-on damage, induced by the high energy electrons, puts an upper limit on the tolerable dose. An important challenge is therefore to develop experimental strategies to optimize the electron dose by balancing atom-counting fidelity versus the risk of knock-on damage. To achieve this goal, a statistical framework combined with physics-based modelling of the dose-dependent processes is proposed and experimentally verified. This model enables an investigator to theoretically predict, in advance of an experimental measurement, the electron dose resulting in an unambiguous quantification of nanostructures in their native state with the highest attainable precision [2].

For beam-sensitive materials, where the optimal electron dose can be low, the images will exhibit a limited signal-to-noise ratio and additionally, they will show a very weak contrast in the presence of light elements. In order to reliably detect the presence or absence of atomic columns and even single atoms, the maximum *a posteriori* (MAP) probability rule is proposed as a model-order selection method in which a Bayesian framework is used [3]. By using MAP selection, the probabilities for an increasing number of atomic columns present in an experimental image can be calculated. This method therefore allows us to predict the most probable atomic structure. In addition, in recent work we investigated the use and potential benefit of deep convolutional neural networks to restore low dose, scan noise distorted ADF STEM images.

Our method for atom-counting opens up new opportunities to measure variations of the 3D atomic structure of nanoparticles under the flow of a selected gas [4]. *In situ* experiments clearly demonstrate that many questions in materials science require a quantification of the material's dynamics from a series of sequentially recorded images. However, the standard approach for atom-counting, where each frame is analyzed individually, does not take advantage of the time aspect available in a series of ADF STEM images. We therefore extended the atom-counting method using the so-called factorial hidden Markov model. This new method is very promising for revealing atomic scale dynamics [5]. In conclusion, new developments in the field of quantitative STEM will be presented enabling one to reliably quantify dynamic structural changes resulting from adatom dynamics, surface diffusion, beam effects or during *in situ* experiments.

## References

- [1] A De Backer et al., *Nanoscale* **9** (2017), p. 8791.
- [2] S. Van Aert et al., *Physical Review Letters* **122** (2019), 066101.
- [3] J. Fatermans et al., *Physical Review Letters* **121** (2018), 056101.
- [4] T. Altantzis et al., *Nano Letters* **19** (2019), p. 477.
- [5] A. De wael et al., *Physical Review Letters* **124** (2020), 106105.
- [6] This work was supported by the European Research Council (Grant 770887 PICOMETRICS to SVA and Grant 815128 REALNANO to SB, Grant 823717 ESTEEM3). The authors acknowledge financial support from the Research Foundation Flanders (FWO, Belgium) through project fundings, a postdoctoral grant to ADB and a doctoral grant to ADw.

## 5:15 AM \*F.MT03.04.02

**Three-Dimensional Charge Density, Electric Field and Electrostatic Potential Mapping of an Electrically-Biased Needle Using Off-Axis Electron Holography** Fengshan Zheng<sup>1</sup>, Vadim Migunov<sup>1,2</sup>, Jan Caron<sup>1</sup>, Hongchu Du<sup>1,2</sup>, Giulio Pozzi<sup>1,3</sup> and Rafal E. Dunin-Borkowski<sup>1</sup>; <sup>1</sup>Forschungszentrum Juelich, Germany; <sup>2</sup>RWTH Aachen University,

Germany; <sup>3</sup>University of Bologna, Italy

The electrical properties of nanoscale electronic devices, such as *p-n* junctions, transistors and light-emitting diodes, are affected strongly by the presence of defects, dopants, interfaces and surfaces [1]. Just as the performance of field emitters is influenced by geometrical factors such as their shape, curvature and crystallographic orientation [2], in atom probe tomography the shape, chemistry and defects in a needle-shaped specimen can affect the trajectories of field-evaporated ions and the fidelity of the reconstruction of the three-dimensional (3D) atomic positions [3], while tip-enhanced catalytic efficiency is influenced by the shape and species of the tip [4]. A knowledge of the 3D charge density, electric field and electrostatic potential inside and around such nanostructures is therefore required.

Off-axis electron holography provides direct access to the projected electrostatic potential within and around a specimen in the transmission electron microscope (TEM) [5]. Here, we combine off-axis electron holography with electron tomography and a model-based iterative reconstruction algorithm [6] to determine the 3D charge density, electric field and electrostatic potential within and around an electrically-biased C fibre needle. The needle was prepared using a standard focused ion beam preparation procedure. A Nanofactory holder was used for electrical biasing. A  $\mu\text{m}$ -sized Au tip was used as a counter-electrode at a distance of 4.5  $\mu\text{m}$  from the needle. The diameter of the apex of the needle was  $\sim 60$  nm and its length was  $\sim 2.5$   $\mu\text{m}$ . Two tomographic tilt series of off-axis electron holographic phase images were acquired between  $-52^\circ$  and  $+48^\circ$  with a tilt increment of  $4^\circ$ . One series was acquired without an electrical bias applied to the needle. This dataset includes only the mean inner potential contribution to the phase. It was used to reconstruct the 3D morphology of the needle and to subtract the mean inner potential contribution to the phase from a second dataset recorded with an electrical bias of 40 V applied to the needle.

The reconstructed 3D charge density in the needle reveals that the charge density is greatest at the apex and has a maximum value of  $2.94 \times 10^{18} \text{ cm}^{-3}$ . 2D slices extracted from the 3D reconstruction show that the charge density distribution is asymmetrical. The majority of the charge is found to be located close to the surface of the needle. A region with a locally increased charge density may be associated with damage by Ga bombardment during sample preparation. The 3D electric field and 3D electrostatic potential are calculated from the reconstructed 3D charge density on the assumption that image charges are defined by the counter-electrode. The strength of the electric field is greatest close to the apex of the needle and has a maximum value of  $\sim 0.25$  GV/m [7].

#### References:

- [1] S.M. Sze, *Semiconductor devices: physics and technology*, Wiley, 2008.
- [2] H. Zhang, *et al.*, *Nat. Nanotech.* 11 (2016) 273.
- [3] F. Vurpillot, *et al.*, *Ultramicroscopy*. 159 (2015) 202.
- [4] Y. Su, *et al.*, *Nat. Nanotech.* 11 (2016) 609.
- [5] H. Lichte, *et al.*, *Rep. Prog. Phys.* 71 (2007) 016102.
- [6] F. Zheng, *et al.*, *J. Elec. Spec. Rel. Phenom.* 2020, *in press*.
- [7] The authors acknowledge the European Union for funding through the Marie Curie Initial Training Network Grant No. 606988 under FP7-PEOPLE-2013-ITN).

#### 5:30 AM F.MT03.04.03

**3D Characterization of Supported Catalysts Using Dual Axis Electron Tomography** Jessi van der Hoeven, Stephan Kraemer, Tanya Shirman, David Bell, Cynthia Friend and Joanna Aizenberg; Harvard University, United States

Supported metal catalysts, consisting of finely dispersed metal nanoparticles on high-surface-area supports, are key players in chemical industry. The interplay between the metal and supporting oxide is an important parameter in modulating the properties of heterogeneous catalysts. To gain fundamental understanding, and therefore increase our control over these metal-support interactions, 3D visualization with nano-scale precision is crucial.

Here, we achieve a quantitative 3D characterization of the local environment of metal nanoparticles embedded in a metal oxide support using dual axis electron tomography. Specifically, we studied raspberry colloid templated (RCT) catalysts – a porous silica support with partially embedded  $\text{Au}_{97}\text{Pd}_3$  and Au nanoparticles in the pore walls [1] – which are active hydrogenation and oxidation catalysts [2][3]. By performing the tomography analysis over two perpendicular tilt axes, we minimized the missing wedge artifacts around the metal particles, allowing the assessment of the particle shape and geometrical confinement of 400 individual nanoparticles. We complemented the electron tomography analysis with a wet-chemical approach relying on metal overgrowth, to visualize the chemical accessibility of nanoparticles within the support. A combination of silver overgrowth on embedded Au nanoparticles and aberration-corrected high-angle annular dark-field

scanning transmission electron microscopy (HAADF-STEM) imaging, and Energy Dispersive X-ray spectroscopy (EDX) mapping unveiled that although the particles were substantially embedded in the silica support they were exposed to the pore network and are readily accessible through the interconnected micropores of the silica matrix in the RCT catalyst. Altogether our work provides a general approach to probe the geometrical confinement and chemical accessibility of a statistically relevant number of metal nanoparticles in supported catalysts in three dimensions and with nano-scale precision.

[1] E. Shirman, T. Shirman, A. V. Shneidman, A. Grinthal, K. R. Phillips, H. Whelan, E. Bulger, M. Abramovitch, J. Patil, R. Nevarez, J. Aizenberg, *Adv. Funct. Mat.*, **28**, 1704559 (2018).

[2] M. Luneau, E. Guan, W. Chen, A. C. Foucher, N. Marcella, T. Shirman, D. M. A. Verbart, J. Aizenberg, M. Aizenberg, E. A. Stach, R.J. Madix, A. I. Frenkel, Cynthia M. Friend, *Commun Chem* **3**, 46 (2020).

[3] M. Luneau, T. Shirman, A. Filie, J. Timoshenko, W. Chen, A. Trimpalis, M. Flytzani-Stephanopoulos, E. Kaxiras, A. Frenkel, J. Aizenberg, C. M. Friend and R. J. Madix, *Chem. Mat.* **31**, 5759 (2019).

#### 5:40 AM F.MT03.04.04

**Nanoscale Photogrammetry—Correlation of 3D Representations with SIMS in a Single Instrument** Alexander D. Ost, Jean-Nicolas Audinot and Tom Wirtz; Luxembourg Institute of Science and Technology (LIST), Luxembourg

The trend in miniaturisation of devices is increasing the need for characterisation techniques that are capable of investigating objects in 3D at nanoscale with both structural and chemical information. Microscopy and spectroscopy are correlated together to overcome the boundaries of each technique and to go beyond the limitations of microscopy in data treatment. In this context, we have coupled a Zeiss Orion NanoFab Helium Ion Microscope (HIM) with a specifically designed Secondary Ion Mass Spectrometry (SIMS) system in order to add analytical capabilities to the microscope [1]. In the standard HIM mode, the instrument provides secondary electron (SE) images with a sub-nm lateral resolution. These ultra-high resolution SE images can be correlated in 2D with sub-20 nm resolution SIMS images to combine the nanoscale structure and composition information for a deeper understanding of the investigated samples [2].

This two-dimensional correlative microscopy approach has been extended to three dimensions by creating 3D SE–SIMS representations of nanomaterials to give a more extensive view on the analysed objects [3]. Therefore, photogrammetry is used i.e. the sample stage is tilted and SE images are taken at a specific pattern of rotation angles with a He<sup>+</sup> primary beam around the region of interest (ROI). The 2D SE images are implemented into a photogrammetry software to obtain a 3D SE model observable at all possible angles and magnifications. The SIMS images of the ROI are acquired in-situ at normal incidence with a Ne<sup>+</sup> primary beam and projected then onto the 3D photogrammetry representation using correspondence points and by overlaying both image textures. The result displays SE and SIMS information together throughout the 4D reconstruction enhancing specimen visualisation and data interpretation.

In this presentation, we will show step-by-step the workflow of 4D reconstruction for real case studies in nanomaterials applications to illustrate the potential of this method for a variety of many other fields.

The authors gratefully acknowledge support by the National Research Fund Luxembourg (FNR) under grant no INTER/DFG/17/11779689.

[1] T. Wirtz, O. De Castro, J. Audinot, and P. Philipp, “Imaging and Analytics on the Helium Ion Microscope,” *Annu. Rev. Anal. Chem.*, vol. 12, no. 1, pp. 523–543, 2019.

[2] F. Vollnhals *et al.*, “Correlative Microscopy Combining Secondary Ion Mass Spectrometry and Electron Microscopy: Comparison of Intensity-Hue-Saturation and Laplacian Pyramid Methods for Image Fusion,” *Anal. Chem.*, vol. 89, no. 20, pp. 10702–10710, 2017.

[3] F. Vollnhals and T. Wirtz, “Correlative Microscopy in 3D: Helium Ion Microscopy-Based Photogrammetric Topography Reconstruction Combined with in situ Secondary Ion Mass Spectrometry,” *Anal. Chem.*, vol. 90, pp. 11989–11995, 2018.

SESSION F.MT03.05: Instrumentation and Technique Development of Electron Microscopy  
On Demand Abstracts Available for Viewing Starting Saturday Morning, November 21, 2020  
F-MT03

#### 5:00 AM \*F.MT03.05.01

**abTEM—*Ab Initio* Transmission Electron Microscopy Image Simulations** Toma Susi and Jacob Madsen; University of Vienna, Austria

Transmission electron microscopy (TEM) is a powerful tool for studying the properties of materials down to the atomic level. In many cases, the quantitative interpretation of images requires simulations based on atomistic structure models. Image simulation for TEM has typically relied on the independent atom model (IAM) that neglects bonding effects, which are measurable and important for understanding many systems. The rearrangement of charge due to bonding is directly detectable in HRTEM images and can be crucial for the interpretation of small differences in the atomic contrast [1]. Moreover, the recent rise in popularity of the four-dimensional (4D) scanning TEM has been partially due to promises of unprecedented sensitivity to electromagnetic fields [2]; however, such data call for rigorous theoretical interpretation through simulations.

Since all electrons and the nuclear cores contribute to the scattering potential, simulations that go beyond the IAM have relied on computationally highly demanding all-electron calculations. We have developed a method to generate *ab initio* electrostatic potentials when describing the core electrons by projector functions. Combined with an interface to quantitative image simulations, this implementation enables an easy and fast means to model electron scattering. By comparing simulated transmission electron microscopy images and diffraction patterns to experimental data, we can show an accuracy equivalent to earlier all-electron calculations at a much lower computational cost [3].

We have now implemented this method in a freely available open-source program based on Python, dubbed “abTEM” for *ab initio* Transmission Electron Microscopy. abTEM integrates directly with two popular open-source Python codes: the Atomic Simulation Environment (ASE) [4] for setting up atomistic models, and GPAW for calculating electrostatic potentials based on the real-space projector-augmented wave implementation of density functional theory [5]. A highly efficient first-principles description of van der Waals interactions can be included via the libvdwxc library [6].

abTEM is designed for accuracy and includes up to the second-order expansion of the multislice solution of the high-energy Schrödinger equation and uses the correct integration of the sub-slicing of the three-dimensional potential [7]. Due to integration with ASE, it is straightforward to model temperature in the frozen phonon approximation using realistic configurations from molecular dynamics simulations. abTEM works as a standard full-featured multislice simulation program, and we have additionally implemented features for speeding up simulations at some cost to accuracy.

We demonstrate the capabilities of our method by modeling twisted bilayer graphene, which has recently received considerable attention due to its extraordinary and highly tunable properties [8]. This system requires on the order of a thousand atoms to represent in simulations, which, to our knowledge, is the largest system ever to be used in a quantitative electron microscopy image simulation that includes an accurate representation of bonding effects. The differences are subtle due to the large contribution of the cores; hence a great deal of care needs to be taken when extracting charge rearrangements solely based on (S)TEM measurements.

More information about abTEM is available online [9].

#### References:

- [1] S. Kurasch, Beilstein J. Nanotechnol. 2, 394 (2011)
- [2] C. Ophus, Microsc. and Microanalysis 25, 563 (2017)
- [3] T. Susi et al., Ultramicroscopy 197, 16 (2019)
- [4] A.H. Larsen et al., J. Phys: Condens. Matter 29, 273002 (2017)
- [5] J.J. Mortensen et al., Phys. Rev. B 71, 035109 (2005)
- [6] A.H. Larsen et al., Model. Simul. Mater. Sci. Eng. 25, 065004 (2017)
- [7] I. Lobato and D. van Dyck, Ultramicroscopy 156, 9 (2015)
- [8] M. Yankowitz et al., Science 363, 1059 (2018)
- [9] <https://github.com/jacobma/abTEM>

The work was supported by the European Research Council (ERC) Grant No. 756277-ATMEN.

**5:15 AM \*F.MT03.05.02**

**Development of Magnetic-Field-Free Atomic Resolution STEM** Naoya Shibata<sup>1,2</sup>; <sup>1</sup>The University of Tokyo,

Japan; <sup>2</sup>JFCC-NSRL, Japan

Aberration-corrected scanning transmission electron microscopy (STEM) is a powerful technique to directly observe atomic-scale structures and chemistry inside materials and devices. In the state-of-the-art STEM, a probe size of less than 0.5 Å in diameter has been experimentally realized. By combining with new elaborate STEM detectors, we can not only image single atoms, but can also image electric field distribution of atoms through differential phase contrast (DPC) imaging techniques. It then becomes tempting to observe magnetic fields at very high resolution, which should strongly correlate with the properties of magnetic materials and devices. However, high spatial resolution observation of magnetic materials is essentially very difficult, because high magnetic fields (~2T) are always exerted on samples inside the magnetic objective lens. In recent years, we have developed a new magnetic objective lens system that realizes a magnetic field free environment at the sample position. Using this new objective lens system combined with the state-of-the-art higher order aberration corrector, atom-resolved imaging in a magnetic field free environment has been achieved. The details of this magnetic-field-free STEM and the material application results will be presented in the talk.

### 5:30 AM \*F.MT03.05.03

**Ultra-Fast Nano-Optic with a High Brightness Transmission Electron Microscope** Sophie Meuret<sup>1</sup>, Yves Auad<sup>2</sup>, Luiz Tizei<sup>2</sup>, Huan-Cheng Chang<sup>3</sup>, Florent Houdellier<sup>1</sup>, Mathieu Kociak<sup>2</sup> and Arnaud Arbouet<sup>1</sup>; <sup>1</sup>CEMES/CNRS, Netherlands; <sup>2</sup>Laboratoire de Physique des Solides, France; <sup>3</sup>Institute of Atomic and Molecular Sciences, Taiwan

Nanoscale properties rule the emission and absorption of light by nano-structures, for example the shape of metallic nanoparticles or the atomic design of semiconductor heterostructures. To overcome the diffraction limit of light ( $\approx 400$  nm) one of the best techniques is electron microscopy. Indeed, the electron beam probes nano-object with sub-nanometer resolution. Both Cathodoluminescence (CL) and electron energy loss spectroscopy (EELS) study the optical properties of nanostructures. They probe, for example, the luminescence properties for CL [1] and the local density of state for EELS [2]. Time-resolved electron microscopy is emerging since a decade, expanding the possibilities of these two techniques. In this presentation, we will use a unique time-resolved transmission electron microscope based on a cold-FEG electron gun [3]. This technology allows, among other things, to reach a spatial resolution of 1 nanometer in pulsed mode. We will discuss the latest results of electron energy gain spectroscopy and the acquisition of the first cathodoluminescence decay traces in a transmission electron microscope.

**Electron energy gain spectroscopy** is the study of the coupling of a fast-electron with the near field created by the interaction of light with the nanostructure [4]. The group of Zewail in Caltech did the first experimental study in 2009 [5] followed by a few groups [6]. In this presentation, we will discuss electron gain spectroscopy using the first cold-FEG transmission electron gun [7]. **This unique TEM allows the highest spatial resolution and highest brightness, leading to a spatial resolution of 1 nm and a strong interaction between the electron beam and the near field.**

The development of time-resolved Cathodoluminescence (TR-CL) enabled the measurement of the lifetime of excited states in semiconductors with a sub-wavelength spatial resolution. It was used for example to measure the influence of stacking faults on the GaN exciton [12]. Recently, the first pump-probe cathodoluminescence experiment using diamond revealed the effect of electron excitation on the nitrogen vacancy color center [15]. These results demonstrate that TR-CL is essential to study the correlation between semiconductor optical and structural properties (composition, defects, strain...). **While all these pioneering studies were done using a scanning electron microscope, the improvement of the spatial resolution and the combination with other electron-based spectroscopies offered by transmission electron microscopes will be a step forward for TR-CL.** In this presentation, we will discuss the first time-resolved cathodoluminescence experiments within a transmission electron microscope.

- [1] L. F. Zagonel *et al.*, *Nano Lett.*, vol. 11, pp. 568, 2011.
- [2] A. Losquin *et al.*, *Nano-Letters*, vol. 15, pp. 1229, 2015.
- [3] F. Houdellier *et al.*, *Ultramicroscopy*, vol. 186, pp. 128, 2018.
- [4] F. J. G. de Abajo *et al.*, *Phys. Rev. Lett.*, vol. 100, 106804, 2008.
- [5] B. Barwick *et al.*, *Nature*, vol. 462, no. 7275, pp. 902, 2009.
- [6] A. Feist *et al.*, *Nature*, vol. 521, no. 7551, pp. 200, 2015.
- [7] F. Houdellier, *et al.*, *Ultramicroscopy*, vol. 186, pp. 128, 2018.
- [8] B. G. Yacobi *et al.*, Springer, 1990.
- [9] L. F. Zagonel *et al.*, *Nano Lett.*, vol. 11, pp. 568, Feb. 2011.
- [10] L. H. G. Tizei *et al.*, *Phys. Rev. Lett.*, vol. 110, p. 153604, 2013.
- [11] S. Meuret *et al.*, *Phys. Rev. Lett.*, vol. 114, no. 19, 2015.
- [12] P. Corfdir *et al.*, *J. Appl. Phys.*, vol. 105, 043102, 2009.

[13] R. J. Moerland et al, *Opt. Express*, vol. 24, 24760, 2016.

[14] X. Fu et al. *ACS Nano*, vol. 8, 3412, 2014.

[15] M. Solà-Garcia et al, *ACS Photonics* 7, 232 (2020).

#### 5:45 AM F.MT03.05.04

**Quantum Effects in the Interaction of Optical Excitations and Fast Electrons** Valerio Di Giulio<sup>1</sup>, Mathieu Kociak<sup>2</sup> and Javier Garcia de Abajo<sup>1,3</sup>, <sup>1</sup>ICFO, Spain; <sup>2</sup>Université Paris Sud XI, France; <sup>3</sup>ICREA, Spain

Electrons, used as probes in electron microscopes, are of primal importance to measure material properties with unequalled combined spatial and energy resolution. For instance, inelastically scattered electrons can be collected and energetically separated in order to obtain spectra as a function of their energy loss or, with the same purpose, the radiated light can be collected in the far field and filtered in polarization and frequency. In particular, electron energy loss spectroscopy (EELS) can be considered the richest source of information as it carries the influence from the surface-sustained modes as well as from the bulk response of the system. Additionally, the synchronization of femtosecond laser illumination with electron pulses at the sample opens the routes to study the ultrafast dynamics of nanostructured materials and their influence on optical near-fields. The evanescent components, produced by the excitations in the material, efficiently overcomes the unavoidable energy-momentum mismatch between free photons and free electrons yielding appreciable light-electron couplings. This strong interaction leads to multiple exchanges of quanta between the electron and the optical field, accompanied by a complex sub-fs dynamics. Based on this principle, photon-induced near-field electron microscopy (PINEM) is performed by analysing the resulting multiple gain and loss features in the electron spectra. PINEM experiments have so far relied on coherent light sources (i.e., lasers), for which the measured spectra are well reproduced by assuming sample bosonic excitations that are coherently populated with a large number of quanta. The probability of each electron spectral peaks associated with a net exchange of  $l$  quanta is then simply given by squared Bessel function. Additionally, this technique, performed with coherent light, has been combined with an electron free propagation of few millimeters to yield a temporal compression of the electron density of the order of attoseconds. Despite the numerous results obtained in this context, different aspects of the interaction between free electrons and confined light remain unexplored. For instance, the effects induced by the replacement of the coherent laser pulses with a quantum light source on electron spectra, are expected to show interesting physics significantly departing from the one previously studied.

In this work, we use quantum-optics methods in order to describe the quantum nature of the optical field and to understand how the resulting electron spectra strongly depend on the statistics of the sample excitations and their population, whose autocorrelation functions are directly retrieved from the ratios of electron gain intensities. In particular, in the limit of highly populated mode, we recover the usual results of classical PINEM for Fock and coherent states but we find a significant difference in the distribution of the gain and loss peaks of electron spectra in the case of thermal state. Furthermore, we study the role of quantum states of light, e.g. squeezed states, in shaping the longitudinal part of the electron wave function after a macroscopic propagation distance observing a faster compression of the electron density for light states with low phase uncertainty.

In conclusion, we consider this work of fundamental importance in the understanding of quantum many bodies excitations and their statistics as well as in the ability of tailoring the electron wave function via the use of light.

#### 5:55 AM F.MT03.05.05

**Electron Beam Aberration Correction Using Optical Near Fields** Andrea Konecna and Javier Garcia de Abajo; ICFO, Spain

Over last decades, electron microscopy has become very powerful and versatile technique for nano- or atomic-scale imaging and spectroscopy [1]. Major advancements and outstanding capabilities have been made possible thanks better spatial and temporal control over the amplitude and phase of the wave function that characterizes the fast electrons used as sample probes. Control over the beam shape is commonly achieved by means of complex arrangements of magneto- and electrostatic electron lenses that enable sub-Ångstrom focusing and beam scanning, as well as correcting aberrations of electron optics. The phase of the electron wave function can be additionally modified by introducing static phase plates.

We envision an alternative to traditional electron-optics elements emerging by using optically-driven phase plates and enabling dynamical shaping of electron-beam wave functions both in space and time. This approach capitalizes recent experimental demonstrations of wave function control through optical near fields [2-4]. The electron-light interaction can in principle allow us to generate arbitrary electron beam shapes; as an application with high potential for improving the resolution of electron microscopes, we employ it here to correct for aberrations of standard electro- or magneto-static lenses



used in current setups.

We demonstrate aberration correction via the interaction of the electron wave function with suitably profiled optical fields. We illustrate this concept by focusing on primary spherical aberration, which due to rotational invariance typically requires complex and expensive aberration correctors. Our work suggests that an optical corrector can help to significantly improve the focal spot and beam profile over the aberrated configuration, and that it can be in principle used to eliminate any undesired beam distortions in both standard and ultrafast (scanning) transmission electron microscopy. Optical aberration correctors could offer better versatility and compactness with respect to traditional corrector designs, and we foresee that they could open a new era of electron microscopy both in aberration correction and in the generation of on-demand electron beams.

- [1] P. E. Batson, N. Dellby, and O. L. Krivanek, *Nature* 418, 617 (2002).
- [2] B. Barwick, D. J. Flannigan, and A. H. Zewail, *Nature* 462, 902 (2009).
- [3] A. Feist, K. E. Echternkamp, J. Schauss, S. V. Yalunin, S. Schäfer, and C. Ropers, *Nature* 521, 200 (2015).
- [4] G. M. Vanacore, et al., *Nat. Mater.* 18, 573 (2019).

#### 6:05 AM F.MT03.05.06

**Photon Emission Dynamics in Cathodoluminescence Induced by Picosecond Electron Pulses** Magda Sola-Garcia<sup>1</sup>, Marnix Vreugdenhil<sup>1</sup>, Kelly W. Mauser<sup>1</sup>, Sophie Meuret<sup>2</sup> and Albert Polman<sup>1</sup>; <sup>1</sup>AMOLF, Netherlands; <sup>2</sup>CEMES-CNRS, France

Ultrafast electron microscopy allows for the study of nanoscale material dynamics at picosecond time resolution. Electron pulses are typically generated using pulsed-laser induced photoemission from the electron cathode, and often multiple electrons are emitted within a single picosecond pulse. Here we study the dynamics of photon emission after excitation by dense collision cascades generated with controlled electron pulse densities. We use an ultrafast SEM cathodoluminescence (CL) microscope equipped with a pump-probe configuration, which enables a direct comparison between electron and light excitation.

Our pump-probe SEM-CL microscope is based on a 1-30 keV SEM equipped with a Schottky field-emission electron cathode. We use 250-femtosecond laser pulses at a wavelength of 258 nm to excite the W/ZrO electron cathode at a repetition rate from 200 kHz up to 25 MHz and create picosecond electron pulses by photoemission. By tuning the laser power we vary the average number of electrons per pulse from less than 1 up to 500. We record  $g^{(2)}(\tau)$  autocorrelation statistics of the CL emission at a wavelength of 450 nm from InGaN/GaN quantum wells using a Hanbury-Brown and Twiss interferometer with 70 ps temporal resolution.

Previous work using continuous and ns-pulsed electron beams has shown that strong bunching ( $g^{(2)}(0)$  up to 150) of CL photons can occur when exciting a sample with high-energy electrons, due to the fact that a single collision cascade can generate multiple CL photons [1,2]. Here, we extend this method to study bunching after excitation with ps electron pulses created using photoemission. We find that  $g^{(2)}(0)-1$  decreases inversely proportional to the number of electrons per pulse, similar to the trend with electron current found in previous work. We introduce an analytical and a statistical model to describe the bunching process and reproduce the measured dependence of  $g^{(2)}(\tau)$  on electron density in the ps pulses. Further analysis shows how the number of excitations/photons generated in each collision cascade can be derived from the data. The results suggest that despite the very high density of collision cascades, non-linear effects do not play a role in the plasmon generation, carrier diffusion and carrier recombination effects that follow electron impact on the InGaN/GaN quantum wells. Next, we use the SEM-CL microscope in pump-probe configuration, by sending part of the femtosecond laser into the SEM chamber. We use this to further study the dynamics of carrier generation and recombination in electron and laser-excited semiconductors [3]. We probe the decay dynamics of bandgap emission in GaAs and CZTS ( $\text{Cu}_2\text{ZnSnS}_4$ ) upon ps electron excitation (at 5-30 keV) and 250 fs laser excitation ( $\lambda=345$  and 517 nm). We study the variations in carrier decay dynamics as a function of laser power and electron pulse density, to deduce the contribution of the different radiative and non-radiative decay mechanisms in each case. These results allow us to compare carrier densities in dense collision cascades and optically excited volumes in these semiconductors.

Finally, we combine CL and PL measurements to perform pump-probe spectroscopy, in which we use a delay stage to control the time between arrival of electron and laser pulses on the sample. We use the electron as a pump and the laser as a probe, and vice versa, aiming to probe non-linear effects in the evolution of dense electron cascades generated by picosecond electron pulses.

- [1] S. Meuret, L. H. G. Tizei, T. Cazimajou, R. Bourrellier, H. C. Change, F. Treussart, and M. Kociak. *Phys. Rev. Lett* **114**, 197404 (2015)
- [2] S. Meuret, T. Coenen, H. Zeijlemaker, M. Latzel, S. Christiansen, S. Conesa-Boj, and A. Polman, *Phys. Rev. B* **96**,

035308 (2017)

[3] M. Solà-Garcia, S. Meuret, T. Coenen, and A. Polman, ACS Photonics 7(1), 232-240 (2020)

SESSION F.MT03.06: Materials Characterization

On Demand Abstracts Available for Viewing Starting Saturday Morning, November 21, 2020

F-MT03

**5:00 AM \*F.MT03.06.01**

**Mapping Structure and Composition of Intact Li-Metal Anodes after Cycling** Katherine L. Jungjohann<sup>1</sup>, Katharine Harrison<sup>1</sup>, Daniel Long<sup>1</sup>, Renae Gannon<sup>2</sup>, Laura Merrill<sup>1</sup>, Subrahmanyam Goriparti<sup>1</sup> and Steven Randolph<sup>3</sup>; <sup>1</sup>Sandia National Laboratories, United States; <sup>2</sup>University of Oregon, United States; <sup>3</sup>Thermo Fisher Scientific, United States

The electrolyte 2.8 M lithium bis(fluorosulfonyl)imide (LiFSI) in dimethoxyethane (DME) has demonstrated good cycling behavior and stable Li morphology upon plating and stripping for high-capacity Li batteries, which is thought to be due to the formation of a stable solid-electrolyte interphase (SEI) layer for good ionic transport. Characterization of this SEI layer on lithium metal has been limited, due to the air-sensitivity and beam sensitivity of these materials, as well as the incompatibility of the electrolyte with the high vacuum environment necessary for nanoscale characterization with electron microscopy techniques. New cryogenic stages and transfer tools have enabled the characterization of frozen solid-liquid interfaces for lithium metal structures. Here, we used cryogenic focused ion beam (FIB) and ultrashort pulse laser ablation to create a cross-section of the lithium metal anode in contact with the electrolyte at various plating/stripping cycles to understand the morphological evolution of the lithium and SEI. Additionally, with cryo-FIB we utilized lift-out procedures under cryogenic temperatures for extraction of a lamella sample for investigation using scanning/transmission electron microscopy with energy dispersive x-ray spectroscopy and electron energy loss spectroscopy. The nanoscale chemical maps have allowed for a greater understanding of the SEI components and how they redistribute with reaction to the lithium metal over the course of many cycles. These results present a step towards visualization of the intact battery stack. We have determined a failure mechanism beyond short circuiting of the lithium metal anodes, due to reaction of the lithium with this LiFSI in DME chemistry.

This work was funded by Sandia National Laboratories' Laboratory Directed Research and Development program. It was performed, in part, at the Center for Integrated Nanotechnologies, an Office of Science User Facility operated for the U.S. Department of Energy (DOE) Office of Science. Sandia National Laboratories is a multi-mission laboratory managed and operated by National Technology and Engineering Solutions of Sandia, LLC., a wholly owned subsidiary of Honeywell International, Inc., for the U.S. DOE's National Nuclear Security Administration under contract DE-NA-0003525. The views expressed in the article do not necessarily represent the views of the U.S. DOE or the United States Government.

**5:15 AM F.MT03.06.02**

**Identifying High-Temperature Superconductivity at Complex Oxide Interfaces** Y. Eren Suyolcu<sup>1,2</sup>, Gennady Logvenov<sup>1</sup> and Peter A. van Aken<sup>1</sup>; <sup>1</sup>Max Planck Institute for Solid State Research, Germany; <sup>2</sup>Cornell University, United States

Transition metal oxide heterostructures host many novel functionalities and have stimulated large interest due to the possibilities of tailoring the functionalities at the atomic layer scale. It is the complex interactions at the interfaces of epitaxial oxide systems that contribute to intriguing physical effects induced by the local variation of electronic and ionic species. In this work, we focus on high-temperature superconductivity (HTSC)[1] of La<sub>2</sub>CuO<sub>4</sub>-based iso-structural and non-iso-structural systems. In particular, we fabricate (i) La<sub>1.6</sub>A<sub>0.4</sub>CuO<sub>4</sub>-La<sub>2</sub>CuO<sub>4</sub> (A = Ca, Sr, Ba) metallic-insulating (M-I) bilayers [2] and (ii) (La,Sr)<sub>2</sub>CuO<sub>4</sub>-SrMnO<sub>3</sub>-LaMnO<sub>3</sub>-La<sub>2</sub>CuO<sub>4</sub> multilayers [3] using atomic-layer-by-layer oxide molecular beam epitaxy (ALL-Oxide MBE) [4].

In order to correlate local structure and superconducting properties, we extensively probe the interfaces using aberration-corrected analytical scanning transmission electron microscopy (STEM) techniques including high-angle annular dark-field (HAADF) and annular bright-field (ABF) imaging, electron energy-loss spectroscopy (EELS), and energy-dispersive X-ray spectroscopy (EDXS). For the atomic-resolution analyses, a JEOL JEM-ARM200F STEM equipped with a cold field-emission electron source, a probe C<sub>s</sub>-corrector (DCOR, CEOS GmbH), a Gatan GIF Quantum ERS spectrometer and a large solid-angle JEOL Centurio SDD-type EDXS detector was used. STEM imaging and EELS were performed at probe semi-convergence angles of 20 mrad and 28 mrad, respectively. The collection angles for HAADF and ABF images were 75-310 mrad and 11-23 mrad, respectively. O-O picker tool [5] software has been utilized for STEM image quantification.

The choice of the dopant substantially influences the superconducting mechanisms as a consequence of the dopant distribution near the nominal M–I bilayers interfaces. In the case of Sr- and Ca-doping, sharp interfaces induce striking interface effects, *i.e.* electronic redistribution. Differently, for Ba-doped bilayer, HTSC is attributed to “classical” homogeneous doping determined by cationic intermixing.[6] Moreover, we demonstrate that sharper Sr-doped  $\text{La}_2\text{CuO}_4$  interfaces can be achieved by the heteroepitaxial contacts with manganite layers. The dopant distribution in  $\text{La}_2\text{CuO}_4$  is affected by the elemental intermixing at the first atomic monolayer of the interfacial  $\text{LaMnO}_3$  contact. Different superconducting behavior (interface vs filamentary) at the two different interface systems are correlated with the interface sharpness and will be discussed in detail.

#### References

- [1] A. Gozar, G. Logvenov, L. F. Kourkoutis, A. T. Bollinger, L. A. Giannuzzi, D. A. Muller, I. Bozovic, *Nature* 2008, 455, 782.
- [2] Y. E. Suyolcu, Y. Wang, F. Baiutti, A. Al-Temimy, G. Gregori, G. Cristiani, W. Sigle, J. Maier, P. A. van Aken, G. Logvenov, *Sci. Rep.* 2017, 7, 453.
- [3] G. Kim, Y. Khaydukov, M. Bluschke, Y. E. Suyolcu, G. Cristiani, K. Son, C. Dietl, T. Keller, E. Weschke, P. A. van Aken, G. Logvenov, B. Keimer, *Phys. Rev. Mater.* 2019, 3, 084420.
- [4] Y. E. Suyolcu, G. Cristiani, P. A. van Aken, G. Logvenov, *J. Supercond. Nov. Magn.* 2020, 33, 107.
- [5] Y. Wang, U. Salzberger, W. Sigle, Y. Eren Suyolcu, P. A. van Aken, *Ultramicroscopy* 2016, 168, 46.
- [6] Y. E. Suyolcu, Y. Wang, W. Sigle, F. Baiutti, G. Cristiani, G. Logvenov, J. Maier, P. A. van Aken, *Adv. Mater. Interfaces* 2017, 4, 1700737.

#### 5:25 AM F.MT03.06.03

**Imaging and Quantification of Topological Charges in  $\text{BiFeO}_3$  Domain Walls** [Marco Campanini](#)<sup>1</sup>, Elzbieta Gradauskaite<sup>2</sup>, Morgan Trassin<sup>2</sup>, Di Yi<sup>3</sup>, Pu Yu<sup>3</sup>, Ramamoorthy Ramesh<sup>4</sup>, Rolf Erni<sup>1</sup> and Marta D. Rossell<sup>1</sup>; <sup>1</sup>Empa, Switzerland; <sup>2</sup>ETHZ, Switzerland; <sup>3</sup>Tsinghua University, China; <sup>4</sup>University of California, United States

Domain walls (DWs) in ferroelectrics constitute the two-dimensional (2D) boundary region between domains characterized by different values of the order parameter, *i.e.* the ferroelectric polarization. One of the most striking properties of DWs is their ability to carry a bound charge, due to the screening by the free carriers of the material. In ferroelectric oxides, such charged DWs behave as 2D conductive pathways embedded in an insulating matrix. This special feature has raised a vast interest in conductive DWs for their potential use in future nanoelectronics. In particular, as the DWs in ferroelectric oxides are often movable under an external electric field, [1,2] they represent a very promising element for novel rewritable circuitry.

Deepening our knowledge about the charge screening processes is of fundamental relevance to achieve a complete understanding of their conduction properties. However, the lack of experimental techniques that are directly sensitive to the localized charges with sub-nanometer resolution makes the identification and the quantification of the screening charges a challenging problem.

In this study, we perform an atomic-scale study of the origin of the enhanced conductivity in charged  $109^\circ$  tail-to-tail (T-T) domain walls in the archetype multiferroic  $\text{BiFeO}_3$  (BFO), by combining state-of-the-art scanning probe techniques – such as piezo-response force microscopy (PFM) and conductive atomic force microscopy (cAFM) – with differential phase-contrast (DPC) scanning transmission electron microscopy (STEM). [3]

Our study was conducted on the heterostructure  $\text{BiFeO}_3$  (120 nm)/ $\text{La}_{0.7}\text{Sr}_{0.3}\text{MnO}_3$  (5 nm)/ $\text{SrRuO}_3$  (1 nm)/ $\text{SrTiO}_3$  grown by pulsed laser deposition. The ferroelectric domain pattern observed by PFM displays the typical contrast of  $71^\circ$  DWs with head-to-tail DWs, which are oriented along the main directions of the cubic substrate. Interestingly, strongly charged T-T DWs are generated at the merging points of  $71^\circ$  stripes with different orientations. Thanks to their topologically charged state, these charged DWs display enhanced conductivity.

The analysis of the atomic displacements from high-resolution high-angle annular dark-field (HAADF) STEM demonstrates that the charged T-T domain wall presents a mixed Ising-Néel structure and is composed of a strained core with a lateral thickness of 6-8 unit cells. The charged-state of the DW was initially assessed by computing the density of bound charge ( $\rho_B$ ) starting from the polarization maps. In particular, we image a distribution of positive charges mostly localized at the DW, with localized maxima separated a few nanometers from each other. The  $\rho_B$  reaches a maximum value of 1 oxygen vacancy ( $\text{O}_v$ ) every 4 unit cells.

In order to directly image the topological charges at the DW, we employ the differential-DPC (dDPC) imaging technique. The differential form of DPC – thanks to its enhanced sensitivity to low Z species – has been recently been proven to be effective for imaging light elements, such as N, [4] Li, [5] and O. [6] By using dDPC, we successfully image the O columns in the BFO layer and thus map the  $\text{O}_v$  distribution along the DW core.

Our results elucidate the nature of the conductive DWs in BFO, providing new insights about their structure and charge

screening phenomena. In particular, combining atomic displacement mapping and dDPC-STEM imaging we can image and quantify the local charges that are responsible for their high conductivity. This work paves the way for future studies about the structure-properties relationship in such charged DWs.

[1] T. Rojac et al., *Adv. Funct. Mater.* 25, 2099, 2015.

[2] J. C. Agar et al., *Nat. Mater.* 15, 549, 2016.

[3] M. Campanini et al., *Nanoscale* 12, 9186, 2020.

[4] E. Yücelen et al., *Sci. Rep.* 8, 2676, 2018.

[5] A. Carlsson et al., *Microsc. Microanal.* 24, 122, 2018.

[6] S. Findlay et al., *Microsc. Microanal.* 25, 1732, 2019.

[7] The authors acknowledge funding from the Swiss National Science Foundation (project Nr. 200021\_175926).

#### 5:35 AM F.MT03.06.04

**Competition Between Doping and the Polar Instability in a Ferroelectric Superconductor** [Salva Salmani-Rezaie](#)<sup>1</sup>, Kaveh Ahadi<sup>2,1</sup> and Susanne Stemmer<sup>1</sup>; <sup>1</sup>University of California, Santa Barbara, United States; <sup>2</sup>North Carolina State University, United States

The competition between polar distortions and the mobile charge carriers is a problem of longstanding interest to the development of a quantum theory of ferroelectricity. It is also a key issue for polar superconductors, which are a promising route to unconventional Cooper pairing.

SrTiO<sub>3</sub> is an incipient ferroelectric in unstrained, stoichiometric form, but easily becomes ferroelectric when subjected to small perturbations, including chemical substitution or applied stress. Ferroelectricity precedes superconductivity in doped, strained SrTiO<sub>3</sub>, suggesting a complex relationship between two instabilities. Using an atomic-resolution scanning transmission electron microscope, we show atomic-scale evidence of the interplay between itinerant electrons and the correlated polar distortions above Curie temperature.

The undoped, strained SrTiO<sub>3</sub> films show correlated polar nanodomains above Curie temperature, suggesting an order-disorder type ferroelectric phase transition. We observe a systematic suppression of the correlated polar distortions, i.e. nanodomains, and ferroelectricity with introducing Sm dopants. The itinerant electrons screen polar distortions and disrupt nanodomains above Curie temperature. Increasing the dopant density, strain field of the dopants overlap and randomize the polar distortions. The results provide direct evidence that the long-range Coulomb interactions, already present in the paraelectric phase, are driving the ferroelectric transition and are becoming increasingly short-ranged with doping. Moreover, we show that the disorder caused by the dopant atoms themselves presents a second contribution to the destabilization of the ferroelectric state. This disorder completely destroys the nanodomains at high dopant concentrations, thereby. The results thus provide evidence for two distinct mechanisms that suppress the polar transition with doping and the presence of both competing and collaborative microscopic interactions in a ferroelectric superconductor. We also observe an inverse relationship between the critical temperature of superconductivity and the magnitude of polar distortions. Understanding the nature of ferroelectric transition and its interplay with itinerant electrons is of interest for testing the different proposed theoretical models for superconductivity in SrTiO<sub>3</sub>.

#### 5:45 AM F.MT03.06.06

**Toward Precision Manipulation of Materials in the Transmission Electron Microscope** [Cassandra Pate](#)<sup>1</sup>, Joshua Agar<sup>2</sup> and Mitra L. Taheri<sup>1</sup>; <sup>1</sup>Johns Hopkins University, United States; <sup>2</sup>Lehigh University, United States

Realization of precision, close-loop processes requires an integrated suite of integrated hardware [1], software [2] and modeling [3], and materials synthesis/optimization. With spatio-temporal control, deterministic synthesis can be achieved in quantum devices, patterned assemblies, and tailored additive manufacturing of materials. Real time processing multidimensional (hyperspectral) data signals benefit from machine learning approaches presenting an opportunity for implementation of a feedback loop for manufacturing of critical technologies, from quantum computers to 3D printed turbine blades. In order to probe specific phenomena, stimulus and detection must be linked; without real time “learning,” key events are left undetected due to temporal resolution limits or failed temporal triggering alignments. Novel detector designs enable manufacturing processes to be viewed “in operando” at high acquisition speeds (upwards of 4000 fps). The combination of machine learning with these detectors makes automation for atomic-scale manipulation a realistic goal. Here we present the application of machine learning techniques to hyperspectral data to demonstrate a framework for understanding rapidly evolving phenomena using convolutional neural networks trained on >10,000 spectra collected at 400 frames per second during an electron beam manipulation of complex oxide structures. We extend these studies to despite very noisy data collected at 400 fps. unsupervised learning via feature extraction instead of comparing to known labels, which enables the analysis of situations when otherwise inaccessible transformations or metastable states occur. These techniques provide the ability to precisely and predictively tune complex materials toward. To that end, we will highlight extension of these

techniques to surface termination manipulation in 2D materials.

#### 5:55 AM F.MT03.06.07

##### **Excited State Pathways for Electron Beam Induced Point Defect Manipulation in Graphene**

**Nanomaterials** Panchapakesan Ganesh<sup>1</sup>, David B. Lingerfelt<sup>1</sup>, Tao Yu<sup>2</sup>, Jacek Jakowski<sup>1</sup> and Bobby Sumpter<sup>1</sup>; <sup>1</sup>Oak Ridge National Laboratory, United States; <sup>2</sup>University of North Dakota, United States

The use of scanning transmission electron microscopes to manipulate substitutional defects in graphene has recently been demonstrated and modeled using ground state molecular dynamics, but the role of electronic excitations induced through inelastic electron scattering in promoting these transformations has so-far remained unexplored. In this work[1,2,3] we probe the effects of electronic excitations on the structural dynamics of localized-defects induced by an electron-beam (a point-charge perturbation), such as substitutional Si/P in graphene quantum-dots as well as the recently observed mobile Si-C<sub>3</sub> defects in graphene nanoflakes. Particularly, the ground and excited state potential energy barriers for the structural transformations are evaluated using time-dependent density functional theory and reveal that the barriers for such localized structural transformations can be effectively lowered upon excitation to the defect-centered excited state through an electronically nonadiabatic pathway. Optically bright excited states in which the barrier is decreased are identified in the low energy region of the electronic spectrum, suggesting that photoexcitation can modulate the reactivity of defects in graphene under electron beam irradiation. Implications of this discovery on directing localized nanoscale transformations using electron-beams will be further discussed, especially in quantum-materials.

[1] “Understanding Beam Induced Electronic Excitations in Materials”, David B. Lingerfelt, P. Ganesh, Jacek Jakowski, Bobby G Sumpter, *J. Chem. Theory Comput.*, 16, 2, 1200–1214 (2020)

[2] “Electronically Nonadiabatic Structural Transformations Promoted by Electron Beams”, David B. Lingerfelt, P. Ganesh, Jacek Jakowski, Bobby G Sumpter, *Advanced Functional Materials*, 1901901, (2019)

[3] “Localized Electronic Excitations in Silicon-Doped Graphene and their Role in Defect Diffusion”, David B. Lingerfelt, Tao Yu, P. Ganesh, Jacek Jakowski and Bobby G. Sumpter (under review)

SESSION F.MT03.07: Cryogenic and Beam-Sensitive Electron Microscopy  
On Demand Abstracts Available for Viewing Starting Saturday Morning, November 21, 2020  
F-MT03

#### 5:00 AM F.MT03.07.01

**Imaging Polymer Crystallinity with STEM** Hui Luo, Hazel Assender and Peter Nellist; University of Oxford, United Kingdom

The spatial atomic structure of PEN is accessible for the first time with ptychographic reconstruction under low dosage illumination.

##### **Introduction**

Organic crystalline structures have been determined by diffraction methods that only generate average structural information from the characterization region. However, crystal structure and orientation in polymers, which depends on e.g. temperature, interfacial interactions and strain, will vary locally. To resolve the detailed microstructure, high resolution imaging is required.

In a case study of annealed thin films of polyethylene naphthalate (PEN) [1], crystalline domains were found to vary with the depth from a surface. We use PEN as a model system to demonstrate high resolution imaging of polymer crystals. High resolution imaging of polymers is limited by the low contrast generated by light elements and beam damage from the high-intensity illumination that is used to get sufficient resolution. Low dose imaging techniques applied here have proved very helpful to acquire data from the pristine structure before it is significantly altered by radiolysis.

##### **Ptychography**

A thin polymer specimen can be treated as a weak phase object. When the electron probe scans through a thin specimen consisting of light elements, the amplitude is not expected to change significantly, while the phase contrast will offer more useful information.

Ptychography [2] is a dose efficient imaging technique with phase retrieval capacity by making use of a 4D STEM dataset. It has these advantages: i) Phase can be retrieved by Wigner-Distribution Deconvolution, and lens aberration can be corrected

in post-acquisition computation. ii) Depth information can be obtained with optical sectioning, from the 4D dataset recorded in only one scan. This is very useful for beam sensitive materials. iii) Equipped with a fast-pixelated detector, the dataset recorded in low dose illumination can be adjusted to give sufficient signal for reconstruction.

### **High resolution image of PEN with discrepancy from XRD**

Figure. 1 shows a ptychographic image of a grain in PEN. Many of the spatial frequencies present in the image, such as the (200) spacing, agree with previous models derived from X-ray diffraction studies. Noticeable in Figure. 1, however, there are some details between the (200) planes that are not predicted from the previous model. This information can only be uncovered by direct imaging.

This technique will enable the study of crystallography and defects of soft matter, hence assist us understand the property-structure relation of synthetic polymers at atomic level, and potentially the structure of natural macromolecules, e.g. protein, DNA, RNA.

### **Reference**

[1] Shinotsuka, K. & Assender, H. In situ AFM study of near-surface crystallization in PET and PEN. *J. Appl. Polym. Sci.* 133, (2016).

[2] Yang, H. et al. Simultaneous atomic-resolution electron ptychography and Z-contrast imaging of light and heavy elements in complex nanostructures. *Nat. Commun.* 7, 12532 (2016).

### **5:10 AM F.MT03.07.02**

**Graphene Encapsulation Sample Platform for Imaging and Analysis of Biological Cells** Christopher Arble<sup>1</sup>, Hongxuan Guo<sup>2</sup>, Alessia Matruglio<sup>3</sup>, Lisa Vaccari<sup>4</sup> and Andrei A. Kolmakov<sup>1</sup>; <sup>1</sup>NIST, United States; <sup>2</sup>Southeast University, China; <sup>3</sup>University College London, United Kingdom; <sup>4</sup>Elettra Sincrotrone Trieste, Italy

Label-free spectroscopy and microscopy of live cells offers the capability to examine in-vivo conditions of cellular functions and structure providing valuable insight into biomolecular components of cells [1]. The physicochemical insulation of a samples' biologically relevant environment and instrumentation is critical for the proper understanding of underlying processes and reactions for label-free investigations. The recent development of two dimensional (2D) materials, i.e. graphene, makes it possible to isolate the sample environment from UHV conditions using these materials as molecularly impermeable, electron transparent membranes [2]. The latter opens the application of vacuum-based analytical techniques such as soft x-rays and electrons for in vivo cellular studies. Herein we report the design and fabrication of graphene encapsulated liquid cell platform designed to be suitable for in-situ studies of hydrated biological samples. The encapsulation with graphene allows the sample to be intimately confined and have its interstitial fluid environment preserved while becoming suitable to be studied with multiple analytical techniques [3]. This approach reduces the parasitic adsorption and scattering of the surrounding matrix while still providing nourishment to the cells for an enhanced lifetime [4]. The platform consists of an array of Si<sub>3</sub>N<sub>4</sub> windows on which the samples are deposited allowing for combinatorial batch analysis. The platform has a small cross-section with photon and electrons making it compatible with a wide range of spectroscopies and microscopies. Implementation of sample immobilization with a biocompatible patternable hydrogel media allows for an extended lifetime of realistic conditions and potentially extended cellular lifetimes under measurement. Preliminary results into the viability of graphene encapsulation for biological samples were conducted with fluorescence optical, SEM, and FTIR microscopies.

### **References:**

1. C. W. Freudiger et al, *Science*, **322** (2008) p. 1857-1861.
2. A. Kolmakov et al, *Nature Nanotechnology* **6** (2011) p. 651.
3. A. Yulaev et al, *Advanced Materials Interfaces*, **4**, (2016) p.1600734
4. A. Matruglio et al, *Journal of Instrumentation*, **13**, 05 (2018), p. C05016

### **5:20 AM F.MT03.07.04**

**Investigating Solution-Processed Optoelectronic Materials with Cryo-EM** Nikita Dutta, Nakita K. Noel and Craig Arnold; Princeton University, United States

Solution processing is a common first step in optoelectronic device fabrication, as it is a low-cost method with considerable flexibility. While it has been observed in several systems that solution chemistry affects both the morphology and properties of the deposited material, the manner in which these effects arise is rarely well understood; this is due in large part to the experimental difficulty of characterizing materials in solution. Here we demonstrate how cryo-electron microscopy (cryo-EM) can be used to overcome this challenge, sharing results from two technologically relevant systems: chalcogenide glasses and lead-halide perovskites. We show multiple cryo-EM methods, including single particle analysis, and discuss how an informed choice of method can reveal unique information about each material. Our results shine a light into the black box of solution processing, ultimately enabling better control over film morphology and optoelectronic performance.

#### 5:30 AM F.MT03.07.05

##### **Characterizing the Mesoscale Organization of Beam-Sensitive Organic Semiconductors Using Low-Dose**

**Transmission Electron Microscopy** Camila Cendra<sup>1</sup>, Christopher J Takacs<sup>2</sup> and Alberto Salleo<sup>1</sup>; <sup>1</sup>Stanford University, United States; <sup>2</sup>SLAC National Accelerator Laboratory, United States

Electronic and ionic transport in semiconducting polymers depends strongly on both molecular structure and mesoscale morphology. Transmission electron microscopy (TEM) studies of semiconducting polymers have proven to be challenging due to their inherent beam sensitivity and the interconnectedness of the physical processes occurring at various length scales. The complex, often hierarchical, internal structure of these molecular systems requires characterization tools that allow us to correlate structure from the nanoscale through the mesoscale all the way to their macroscopic properties. We leverage advances in high-resolution TEM (HRTEM) hardware, such as ultra-sensitive detectors and the use of cryogenic temperatures, and parallel computing data analytics tools to characterize the mesoscale organization of semiconducting polymers across areas similar in size to electronic devices ( $\sim 10 \mu\text{m}^2$ ). The vast amount of data acquired from HRTEM imaging enables a statistical approach, which is necessary given the inherently disordered nature of semicrystalline materials.

We directly image the structure of a series of semicrystalline conjugated polymers using a fast read-out direct detector to record dose-fractionated exposure series (i.e., “movies”). The dose-fractionated exposure series are then analyzed using Fourier space image processing techniques and computer-based corrections for beam-induced specimen motion. The structure is spatially resolved through mapping of the alkyl (100) or backbone (001) spacing reflections, revealing the rich, peculiar nature of the nanoscale organization of semiconducting polymers. Through analysis of the local orientational correlations, we provide insights into the mesoscale organization of these materials. In addition, constructed orientation maps and director field lines with nanoscale resolution ( $\sim 3 - 5 \text{ nm}$ ) allow us to visualize the alignment of molecular chains and understand electronic connectivity. The results show how beam-sensitive organic materials can be visualized and characterized at the nanoscale level using low-dose HRTEM to uncover their long and short-range organization, which is essential for understanding their macroscopic functional properties.

#### 5:40 AM F.MT03.07.06

**Understanding Order in Disordered Organic Semiconductors** Christopher J. Takacs; SLAC National Laboratory, United States

Organic semiconductors are of interest for a variety of applications such as biocompatible electronic devices, transistors, batteries, and solar cells. The morphology and self-assembly of these materials strongly influence charge and ion transport. While our fundamental understanding of structure-function relationships has improved greatly in recent years, significant questions remain about the nature of order at the nanoscale, the role of mesoscale organization, and its connection to the device transport properties. Here I discuss recent work examining the structure of a high-mobility semiconducting polymer previously thought to be amorphous. Thin-film synchrotron scattering, x-ray free-electron laser nano-diffraction, cryo-EM, and 4D-STEM are combined to demonstrate a rich, hierarchical organization with significant local fluctuations in molecular packing and signs of homoepitaxial order. These results combined with molecular modeling suggest a range of intra- and inter-molecular defects that break translational order but allow good long-range electronic coupling necessary for high mobility. This case highlights the need to develop and apply new high-resolution structural probes in heterogeneous systems to self-consistently understand structure in disordered materials.

#### 5:50 AM F.MT03.07.07

##### **Continuously Variable Temperature Cryo-STEM: Atomic-Resolution from 100 K to Room Temperature and**

**Beyond** Elisabeth Bianco, Berit Goodge, Ismail El Baggari, Noah Schnitzer and Lena Kourkoutis; Cornell University, United States

Sub-Ångström-resolution STEM has become a routine tool to study radiation-hard inorganic crystals, but only recently has it been achieved at cryogenic temperatures. This advancement has provided the capability to capture exotic electronic states, such as charge ordering [1-3]. However, precisely tracking the emergence of low-temperature states requires high-resolution and precision STEM across a broad range of temperatures, cryogenic and intermediate, which remains a serious challenge. Here, we demonstrate a new side-entry, dual-tilt cryogenic holder (HennyZ) that combines liquid nitrogen cooling with fast, local heating *via* a 6-pin MEMS device. This enables intermediate temperature studies at atomic resolution and the flexibility for more complex experiments, such as coupling with *in situ* biasing [4]. Sub-Å resolution is enabled by consistently low drift rates of 0.3-0.4 Å/s in the full temperature range from ~100-1000 K. Furthermore, the local heating in this continuously variable temperature (CVT) cryo-STEM approach allows the temperature to be cycled repeatedly and rapidly within a single experiment, affording novel dynamic studies. Understanding structural changes in materials at the atomic scale and at temperatures where they occur is critical for manipulating quantum states. We demonstrate CVT cryo-STEM as an effective local probe for revealing unexpected structural phenomena, such as metastable intermediate phases, in Nb<sub>3</sub>Br<sub>8</sub>—a 2D magnetic material [5,6].

#### References:

- [1] I. El Baggari, *et al.*, Proc. Natl. Acad. Sci. U.S.A. **115** (2018), p. 1445.
- [2] B.H. Savitzky, *et al.*, Ultramic. **191** (2018), p. 56.
- [3] A.M. Minor, *et al.*, MRS Bull. **44** (2019), p. 961.
- [4] B.H. Goodge, *et al.*, Microsc. Microanal. First View (2020).
- [5] C. Pasco, *et al.*, ACS Nano **13** (2019), p. 9457.
- [6] This work is supported by PARADIM, an NSF-MIP (DMR-1539918), and NSF DMR 1429155 & DMR-1719875.

SESSION F.MT03.08: Poster Session: Frontiers of Imaging and Spectroscopy in Electron Microscopy  
On Demand Abstracts Available for Viewing Starting Saturday Morning, November 21, 2020  
5:00 AM - 8:00 AM  
F-MT03

#### **F.MT03.08.01**

**3D Morphology of Double Gyroid and Double Diamond BCP Tubular Networks** Edwin Thomas and Xueyan Feng; Texas A&M University, United States

Block copolymers (BCPs) self assemble into a wide variety of periodic structures and elucidating their nano- and micro-structures has typically been accomplished by a combination of transmission electron microscopy and small angle x-ray scattering. Two of the more complex microdomain structures in BCPs are the double gyroid (DG) and double diamond (DD). We have developed a 3D reconstruction tool, slice and view scanning electron microscopy to create large volume tomograms of the DG and DD structures enabling detailed investigation of a host of supra- and sub- unit cell morphological characteristics. These include the nature of the curvature of the Interfacial dividing surface (IMDS), the length and angle distribution of the network struts as well as distortions of the cubic unit cells into triclinic variants. In addition to the periodic structure, we have discovered and classified various point, line and surface defects. Because the minority component in the DG and DD phases are 3D continuous networks, defects lead to changes in topology. We find loop and bridging defects in the networks, as well as dislocation defects and sharp, coherent twin grain boundaries and wide non-crystalline grain boundaries. Such defects generally occur during nucleation and growth of the phase and are important for order-order phase transformations as well as for mechanical and transport properties.

#### **F.MT03.08.02**

**Multiscale Strain Mapping and Mechanical Properties Determinations of 2024 Aluminum Alloys Using Transmission Electron Microscopy Techniques** Florent Ravaux, Humaira Zafar, Cyril Aubry and Dalaver H. Anjum; Khalifa University of Science and Technology, United Arab Emirates

Lightweight aluminum (Al) alloys reinforced with a second phase are widely used in aerospace industry. Nanometer scale precipitates distributed in an aluminum matrix considerably change the mechanical properties of these alloys. The degree of coherency of those precipitates, their density, and material properties (such as Young's modulus) considerably change the bulk mechanical behavior of the alloys. Therefore, investigation of their properties is of great interest for improving alloy



characteristics.

The structure-property relationships between the precipitates and Al matrix are complex and often require advanced characterization techniques for their analysis. The formation of the precipitates results in the outbreak of internal stress fields due to the lattice mismatch between precipitates and Al matrix. Strain mapping techniques using Transmission Electron Microscope (TEM) are proven to be a powerful technique for investigating the mechanisms leading to the formation of stress fields. Commensurately, the technique of Electron Energy Loss Spectroscopy (EELS) provides a complementary information on the Young's modulus ( $Y_m$ ) through the analysis of the energies of bulk plasmons.

In this study, different TEM techniques are applied to characterize the influence of the Cu precipitates in an Al alloy. We focused on the characterization of a specific material namely 2024 Al alloy composed of Al-4.35 Cu-1.5 Mg-0.64 Mn-0.5 Si-0.5 Fe (wt.%). The samples are treated at 495°C followed by water quenching. Different aging processes are carried out to control and accelerate the formation of particular precipitates known as  $\theta''$ . Strain mapping techniques capable of generating results at different field of views are applied to get insights on the properties of  $\theta''$  precipitates. Specimens are prepared with a standard lamella process using Focused Ion Beam (FIB) scanning electron microscope and TEM experiments are performed using aberration corrected microscope of model Titan 80-300 ST from Thermo-Fisher Scientific.

Geometric Phase Analysis (GPA) is applied to high resolution STEM images in order to determine the strain in Al matrix around the  $\theta''$  precipitates. This technique allows to determine at a very high spatial resolution the strain at the vicinity of the precipitates and their coherency. However, the field of view is limited to a 20 nm x 20 nm area. Nano beam diffraction (NBD) is used to determine strain at the microscale due to its higher field of view which allows to map mechanical deformation at the grain size scales. Due to the larger field of view (500 nm x 500 nm), this technique, combined with GPA, make the analysis of the strain inside grains possible and show the influence of the dislocations identified and localized with GPA.

Additionally, the determination of plasmon energies was carried out to evaluate the  $Y_m$  of the alloy at nanoscale. Moreover, the bulk modulus ( $B_m$ ), and shear modulus ( $G_m$ ) are established. Furthermore, the nano-indentation experiments and electron backscatter diffraction (EBSD) mappings are performed to correlate the bulk material properties to the nano and micro scale observations. In this way, a true structure property relationship of 2024 alloys has been investigated at bulk scales as well as at nanoscales.

In conclusion, the presented study shows that the employed techniques of TEM and EELS complement the results obtained by using the techniques of EBSD and nano indentation. Hence their combination enables to gather a deeper understanding of the strain relaxation mechanisms occurring in the alloy. This methodology resulted in the determination of a relation among (i) heat treatment, (ii) precipitates distribution and (iii) mechanical properties. In the end, the obtained results are used as inputs to propose a model for better prediction of mechanical properties of 2024 Al alloy.

#### **Acknowledgements:**

The work was funded by ADEK, Abu Dhabi, U.A.E. through the Project No. AARE19-131.

#### **F.MT03.08.03**

**Furthering the Resolution Limit of EBSD** [Jakub Holzer](#)<sup>1,2,3</sup>, Andrew Marshall<sup>4,3</sup>, Pavel Stejskal<sup>3</sup>, Chris Stephens<sup>3</sup> and Tomáš Vystavěl<sup>3</sup>; <sup>1</sup>Institute of Physics of Materials of CAS, Czechia; <sup>2</sup>Central European Institute of Technology of BUT, Czechia; <sup>3</sup>Thermo Fisher Scientific, Czechia; <sup>4</sup>The University of Surrey, United Kingdom

Electron Backscatter Diffraction (EBSD) has become an established crystallographic and microstructural characterization technique, particularly for metallurgical applications. The resolution of the technique is ultimately limited by the practical SEM probe size combined with the overlap of sampling interaction volumes. This spatial resolution is constrained further by the requirement to use high sample tilts to increase the diffraction contrast. As a result, certain applications often require the use of transmission Kikuchi diffraction, or other transmission electron microscopy (TEM) based techniques, which typically demand lengthy foil or lamellae preparation by focused ion beam. By utilizing an array of sensors capable of direct electron detection, mounted on a retractable arm around the microscope's objective pole piece, we are able gain several advantages compared to EBSD in a standard geometry. This tilt-free sample-to-detector geometry permits the collection of distortion free patterns from a well-defined area and the high sensitivity of the detector allows for pattern collection at lower incident electron energies. This enables a reduction of the sampling volume and has the potential for improved precision and physical spatial resolution with usable signal intensity. Here, we present an adapted methodology to determine the resolution of this tilt-free geometry together with the first experimental results on a molybdenum bi-crystal with a well-defined  $\Sigma 3$  boundary. By sampling perpendicular to the  $\Sigma 3$  boundary with 5nm step and evaluating the variation in the quality of the collected diffraction patterns, the physical resolution can be measured based on the full width at half maximum of the Gaussian curve fit of the pattern quality. Even with 5 nm step, the measured boundary on the indexed map is sharp. The EBSD results are further compared and validated by TEM measurements on lamellae prepared from the same specimen.

### F.MT03.08.06

**Multimodal Characterization of Hybrid Nanocomposite Materials—The Case Study of the Oleophilic Hydrophobic Magnetic (OHM) Sponge for Oil Spill Remediation** [Stephanie Ribet](#)<sup>1</sup>, Vikas Nandwana<sup>1</sup>, Roberto dos Reis<sup>1</sup>, Tirzah Abbott<sup>2</sup>, Eric Roth<sup>2</sup> and Vinayak Dravid<sup>1,2</sup>; <sup>1</sup>Northwestern University, United States; <sup>2</sup>NUANCE Center, United States

There are significant intrinsic challenges to characterizing hybrid (hard-soft) materials due to the difference in properties between components of these structures. Nonetheless, establishing the structure-property relationships of these systems is an essential step in material design. Here we study the recently reported Oleophilic Hydrophobic Magnetic (OHM) sponge, a nanocomposite system that offers the ability to repeatedly adsorb 20-35 times its weight in oil. [1,2] The OHM sponge is synthesized by coating a polyurethane membrane with a nanocomposite, made of nanoparticles, such as Fe<sub>3</sub>O<sub>4</sub>, and graphite. In addition to the aforementioned challenge of distinguishing both the hard (nanocomposite) and soft (PU sponge) features, this hierarchical material necessitates exploration at multiple length scales. Given the physically and chemically complex characteristics of this membrane, a correlative multimodal approach is needed to study the fundamental underpinnings contributing to the performance of this material. We apply a combination of SEM, S/TEM and Raman spectroscopy to probe the structure, morphology and chemistry of the OHM sponge including with *operando* techniques.

Preparing thin samples for electron microscopy of hybrid materials can be difficult due to the nonuniform mechanical properties of the system. Here, we embed the OHM sponge in resin at the sub-micron scale and use an ultramicrotome cross section approach to directly assess the nature of the coating. Scanning electron microscopy and spectroscopy techniques provide rich atomic and electronic information about the sponge both on the micro (SEM/Raman) and nano (S/TEM) scale. Using a combination of backscatter electron imaging (compositional contrast) and EDS, the spatial distribution of iron oxide nanoparticles can be explored. Additionally, by exploiting the distinct graphite sp<sup>2</sup> ( $\pi$  bond) EELS edge and Raman spectral signature, we map the graphite distribution of the sponge, distinguishing it from the other carbon-based materials in the sample. This correlative approach is used to provide a complete assessment of the nature of this material and can be more broadly be applied to other hybrid systems. Further, dynamic electron microscopy is a powerful tool to observe reactions as the progress in real time, and ESEM experiments, in particular, provide a pathway to characterize the solid-fluid interactions that contribute to the OHM sponge's performance.

The presentation will emphasize the holistic understanding of OHM sponge and other hierarchical, hybrid materials that can be attained through correlative and multimodal characterization methods.

[1] Nandwana, V. Ribet, S., et al., *Ind. Eng. Chem. Res.* 2020, 59, 23, 10945–10954.

[2] V. Dravid. US Patent 62/788,347, Filed: Jan 4, 2019.

### F.MT03.08.07

**Nanoscale Nonlinear Optical Spectroscopy with Electron Beams** [Andrea Konecna](#)<sup>1</sup>, Valerio Di Giulio<sup>1</sup>, Vahagn Mkhitarian<sup>1</sup>, Claus Ropers<sup>2</sup> and Javier Garcia de Abajo<sup>1</sup>; <sup>1</sup>ICFO - The Institute of Photonic Sciences, Spain; <sup>2</sup>4th Physical Institute-Solids and Nanostructures, University of Gottingen, Germany

Electron energy loss spectroscopy (EELS) nowadays allows us to acquire information on excitations in nanostructures with high spatial and spectral resolution over a broad energy range covering vibrational, optical (valence-electron) and core-electron excitations [1, 2]. The possibility of nanoscale mapping of optical response beyond the diffraction limit has made EELS one of the leading techniques in characterization of nanophotonic structures. However, EEL spectra are typically dominated by linear optical response, as the nonlinear contributions are negligible due to weak interaction between electrons and sample, which prevents the use of EELS in studying the nanoscale behavior of nonlinear optical fields.

The interaction between electrons and optical excitations in a sample can be substantially increased if the sample is excited by external optical pumping. Such a scenario is possible in photon-induced near field electron microscopy (PINEM), where we can reach scattering probabilities of order unity, and obtain multiple energy quanta exchanges between the electron probe and the optical field [3, 4]. Additionally, high light intensities can also trigger substantial nonlinearities in the sample response, which should be reflected in measured PINEM spectra.

In our work [5], we suggest PINEM as a suitable technique for nanoscale mapping of nonlinear optical response. In particular, we show that the interaction of electrons with nonlinear optical fields introduces asymmetries in otherwise symmetric PINEM spectra, which we demonstrate on several realistic examples. First we focus on studying second-harmonic (SH) response of spherical gold nanoparticles. We show that the evanescent SH field, which cannot be probed by

conventional nonlinear optical spectroscopies, gives rise to substantially asymmetric electron spectra under achievable illumination intensities. We further calculate SH field in gold nanorods and show that significant asymmetries in the PINEM spectra can be achieved for particular beam positions when the linear-field coupling is reduced. We envision that PINEM performed with variable illumination frequency and intensity could become a powerful technique for characterization of nonlinear optical response with unsurpassed combination of spatial and spectral resolution.

## References

- [1] P. E. Batson, N. Dellby, and O. L. Krivanek, *Nature* 418, 617 (2002).
- [2] O. L. Krivanek, T. C. Lovejoy, N. Dellby, T. Aoki, R. W. Carpenter, P. Rez, E. Soignard, J. Zhu, P. E. Batson, M. J. Lagos, et al., *Nature* 514, 209 (2014).
- [3] B. Barwick, D. J. Flannigan, and A. H. Zewail, *Nature* 462, 902 (2009).
- [4] A. Feist, K. E. Echternkamp, J. Schauss, S. V. Yalunin, S. Schäfer, and C. Ropers, *Nature* 521, 200 (2015).
- [5] A. Konečná, V. Di Giulio, V. Mkhitarian, C. Ropers, and F. J. García de Abajo, *ACS Photonics* 7, 1290 (2020).

## F.MT03.08.08

### Observation of Crystal Grain Images by Using Multi-Segmented Back Scattered Electron Detector in Scanning Electron Microscope Yusuke Sakuda, Takeshi Otsuka, Mayu Ishino and Hiroshi Onodera; JEOL Ltd., Japan

The characters of a material depend on the crystal grain size and grain boundaries. Therefore, evaluation of crystals from a viewpoint of crystallography is extremely important. Various methods by using Scanning Electron Microscope (SEM) have been extensively developed for the evaluation of crystals because samples can be handled in a bulk state and observed in the region of  $\mu\text{m}$  to nm order. One common method is the Electron Channeling Contrast (ECCI) method<sup>1</sup>, which allows to obtain an image contrast corresponding to crystal grain boundaries by using the intensity difference of Back Scattered Electrons (BSEs) emitted from a bulk sample. The other common method is the Electron Backscatter Diffraction (EBSD) pattern method<sup>2</sup>. The EBSD is possible to analyze crystal orientation distributions using diffraction patterns from a sample detected by a fluorescence screen. Those methods are quite useful for knowing grain distribution in the crystal as well. On the other hand, there are some issues in these methods of measuring a bulk sample. The ECCI is sometimes difficult to characterize the crystal structure and grain boundaries because it detects a mixture of BSEs originating from composition, channeling contrast and a diffraction pattern, while the EBSD has the limitation that a sample should be tilted significantly. Therefore, the lateral spatial resolution is about 100 nm in these methods and it would be difficult to analyze fine crystal structures and grain boundaries.

In order to improve the issues, we applied a multi-segmented BSE detector<sup>3</sup>. The detector is segmented to 16 parts located above a sample and detects BSEs. The method is similar to the ECCI method. However, in practice it is possible to detect only the diffraction patterns by using the new segmented detector. As a result, it is much more clearly separate the grain boundaries than with the ECCI method. The principle is that the diffraction patterns detected by 16 segments in each element are integrated to calculate the signal intensity distribution and display it as a grain boundary image. Because similar intensities can be obtained from the same diffraction pattern, the grains with similar signal intensities are evaluated as the same crystal orientation with high approximation. The Euclidean distance<sup>4</sup> was used to compare the signal intensities. We also tried to apply the decelerating method which is a SEM column technique for improving the electron probe diameter. In the decelerating method, incident electrons keep high energy when passing through an objective lens. Finally, the electron energy is reduced down just before the electron is landed to a sample. The method reduces the spherical aberration coefficient (Cs) and the chromatic aberration coefficient (Cc) related to the electron probe diameter and the spatial resolution can be improved<sup>5</sup>.

In this study, we will report that we tried to quickly acquire the grain boundary image with high spatial resolution using the multi-segmented BSE detector combined with the SEM-deceleration method.

## References

- 1) Martin A. Crimp : *Microsc. res. technol.*, **69**, 374-381 (2006).
- 2) R. P. Goehner and J. R. Michael : *J. Res. Natl. Inst. Stand. Technol*, **101**, 301-308 (1996).
- 3) T. Otsuka, M. Hara, N. Erdman and S. Kitamura : *Proceedings of Microsc. Microanal.* **24**, 686 (2018).
- 4) M.M. Deza and E. Deza: *Encyclopedia of Distances*, (Springer Nature, Berlin, 2009) p. 94.
- 5) O. Terasaki, S. Asahina, Y. Sakuda, H. Takahashi, K. Tsutsumi, M. Kudo, R. W. Corkery and Y. Ma : *JEOL News*, **52**, 20 (2017).

## F.MT03.08.10

### Thermal Expansion Coefficient of Silicon Nanoparticles with Nanometer Resolution Bibash Sapkota, Prakash Parajuli, Serdar Ogut and Robert Klie; University of Illinois at Chicago, United States

With the size of electronic devices getting smaller and smaller, it has become important to understand thermal expansion coefficients and thermal properties in sub-nanometer scale [1-3]. However, traditional techniques, such as scanning thermal microscopy or Raman thermometry are limited in spatial resolution due to mechanical constraints or optical diffraction limit [1-3]. In the present work, we will utilize a novel approach of non-contact thermometry based on the combination of low-loss electron energy-loss spectroscopy (EELS) with first principles density functional theory (DFT) modeling to measure the thermal expansion coefficient (TEC) of materials with nano-meter resolution. The approach has been well-tested on 2D materials such as transition metal dichalcogenides (TMDs), graphene and MoS<sub>2</sub> by Hu et al [1]. In present work, we will extend the approach to Si nanoparticles to determine its TEC as a function of the temperature. In this contribution, we will also explore the effects of particle size, orientation and composition on the TEC, as well as the limits of measuring the local temperature using this approach.

#### References:

- [1] Hu et al., Phys. Rev. Lett. 120, 05590(2018)
- [2] Mecklenberg et al., Sci. 347, 6222(2015)
- [3] Mecklenberg et al., Phys. Rev. Applied 9, 014005(2018)
- [4] This work was supported by the National Science Foundation (DMR-18314061).

#### F.MT03.08.11

**Determination of Valence in Mn-Containing Oxides by Using Soft X-Ray Emission Spectroscopy (SXES) with Electron Microscopy** Yohei Kojima, Shunsuke Asahina, Shogo Koshiya, Takanori Murano and Hiroshi Onodera; JEOL Ltd., Japan

Mn-containing oxides are important materials that have been widely used for industrial applications such as battery, magnetic and superconducting materials. Therefore, a novel material of Mn-containing oxides has been remarkably investigated to improve their capability and quality. They have various physical properties because Mn usually has divalent, trivalent or tetravalent and each valence has different d-electron numbers in Mn-containing oxides. Thus, the determination of valence in Mn-containing oxide is a very important factor to know the characteristics of the material. As an analytical method for Mn valence, X-ray Absorption Fine Structure (XAFS) method is frequently performed in synchrotron radiation facilities [e.g. 1]. X-ray analysis in the synchrotron radiation facilities is quite powerful as it allows in-situ observation. However, it is difficult to conduct an analysis with a finer structure because the X-ray beam size is on the order of microns. For the chemical state analysis in a micro or nano-ordered structure, the method combining with Transmission Electron Microscopy (TEM) and Electron Energy-Loss Spectroscopy (EELS) is popular. Although this method has a high spatial resolution and high energy resolution, EELS cannot directly obtain information of the valence band associated with chemical bonding of the material. Recently, SXES that can be installed in Scanning Electron Microscope (SEM) and Electron Probe Micro-Analyzer (EPMA), has been developed for the chemical state analysis of a bulk with fine structures [2]. Soft X-ray means the X-ray with energies from 10 eV to a few keV, and includes the X-ray generated by electron transition from valence bands to inner-shell levels. Therefore, we can obtain chemical bonding information by spectral analysis of this X-ray. So far, we reported a valence analysis of Fe oxides by using SEM-SXES system and “Flank” method [3] suggested by Höfer et al. [4]. Flank method proceeds as below:

- 1) Calculating a spectrum difference between Fe<sup>2+</sup> endmember and Fe<sup>3+</sup> endmember.
- 2) Setting Flank positions of Fe L $\alpha$  and L $\beta$  at the maximum or minimum value position in the difference spectrum.
- 3) Taking the L $\beta$ /L $\alpha$  intensity ratio at the Flank position.

This method has higher resolution for valence than the conventional method of peak-intensity and area-intensity ratios. In this study, we attempt to apply this method for Mn-containing oxides.

MnO, Mn<sub>2</sub>O<sub>3</sub> and MnO<sub>2</sub> purchased from Hori Mineralogy Ltd. were used for samples. There is no element detected by SXES other than Mn and O. The SXES measurement was performed by using FE-SEM (JEOL JSM-7900F) equipped with SXES (SS-94040XSER). The soft X-ray spectra were acquired at accelerating voltages of 10 kV, 5 kV and 2 kV with a beam current of 50 nA and acquired for 5 minutes.

In this study, we compared the intensity ratio of Mn L $\beta$ /L $\alpha$  calculated by the Flank method, peak-intensity ratio method and area-intensity ratio method. As a result, it is found that the Flank method has a higher energy resolution for the valence of Mn than the conventional peak-intensity ratio method and area-intensity ratio method for all accelerating voltages used in this study at 2, 5 and 10 kV. It is expected that this method will be widely applied to the valence analysis of Mn-containing oxides used in various industrial applications.

#### References:

- [1] Kobayashi et al., J. Mater. Chem., 14, 1843-1848 (2004).

- [2] Takahashi et al., IOP Conf. Ser.: Mater. Sci. Eng., 109, 012017 (2016).  
[3] Kojima, 12th Asia-Pacific Microscopy Conference Abstract (2020).  
[4] Höfer et al., Eur. J. Mineral., 6, 407-418 (1994).

### **F.MT03.08.13**

**Late News: Using Direct Electron Detector Technologies to Determine Local Structure and Chemistry of Nanostructures** Alexandre Foucher and Eric Stach; University of Pennsylvania, United States

Direct electron detectors have revolutionized the field of structural biology and are beginning to find applications in materials science and nanoscience. Here, we show how these detectors can improve the ability of transmission electron microscopy to understand the physical and electronic structure of nanoparticles and thin films. These newly developed direct electron detection cameras reduce the signal-to-noise ratio compared to conventional CMOS / CCD cameras. In this study, electron energy loss spectroscopy (EELS) spectra obtained from several materials systems - Ti<sub>2-x</sub>Nb<sub>x</sub>C MXenes, Mo<sub>4</sub>VAlC<sub>4</sub> MAX phase and CoPt nanoparticles - are quantified, and the improved signal quality with the direct detection system is demonstrated. We compared the effect of probe size, aperture size, camera length, and imaging filter aperture size on the signal-to-noise ratio. For nanoparticles and thin films, it was shown that probe size and camera length had the strongest influence on the signal intensity arising from inelastically scattered electrons. In contrast, imaging filter aperture size plays a minor role. The optimization of these parameters makes it possible to routinely perform valence-state analysis at an atomic level, with a resolution comparable to bulk approaches such as X-ray photoelectron spectroscopy or X-ray absorption spectroscopy (XAS). The increased Detected Quantum Efficiency (DQE) combined with a sub-pixel detection setting is also beneficial for recording diffraction patterns to perform electron pair-distribution function (ePDF) analysis from these same systems. The improvements in the quality of both spectral and scattering data can be expected to make transmission electron microscopy an even more powerful tool for characterizing nano materials.

## **SYMPOSIUM F.MT04**

---

Using Machine Learning and Multiscale Modeling to Study Soft Materials and Interfaces  
November 21 - December 3, 2020

### Symposium Organizers

Alexander Alexeev, Georgia Institute of Technology  
Sanket Deshmukh, Virginia Tech  
Anne-Virginie Salsac, Université de Technologie de Compiègne  
Emanuela Zaccarelli, Consiglio Nazionale delle Ricerche

### Symposium Support

**Silver**  
Lam Research

---

\* Invited Paper

SESSION F.MT04.08: Live Keynote I: Using Machine Learning and Multiscale Modeling to Study Soft Materials and Interfaces

Session Chairs: Sanket Deshmukh and Emanuela Zaccarelli  
Wednesday Morning, December 2, 2020  
F.MT04

### **11:30 AM \*F.MT04.01.01**

**Coarse-Grained Modeling of Solid Polymer Electrolytes and Ion Conduction** Lisa M. Hall; The Ohio State University, United States

Using solvent-free solid polymer electrolytes in batteries would reduce concerns about flammability and potentially decrease weight and cost, especially if their ion conductivity can be improved. Strategies to improve ion conduction in ion containing polymer materials include using bulky anions or using a high dielectric constant polymer. These both effectively decrease the strength of Coulomb interactions between ions at contact and can reduce ion agglomeration, which can improve conductivity. However, strong ion-polymer interactions can slow ion motion, and size asymmetry between ions may increase preferential solvation of cations versus the larger anions, lowering the transference number  $t_+$  (fraction of conductivity contributed by the cation). We study these effects using coarse-grained molecular dynamics (MD) simulations which include a  $1/r^4$  potential to capture size-dependent ion-monomer and ion-ion solvation effects. This is the same form as the interaction between an ion and an induced dipole. For block copolymer systems, we have also been guided by theoretical calculations to show the effects of macroscopic phase behavior. From MD, we calculate conductivity from ion mobilities in an external electric field, which improves accuracy versus the typical use of fluctuation dissipation relationships. We assess the impacts of ion size and polymer dielectric strength, including polymer dielectric strength contrast for block copolymer systems, on ion correlations, diffusion, and conductivity.

11:45 AM .

11:46 AM \*F.MT04.01.02

**Molecular Modeling Discloses a Protein-Like Dynamical Transition in Non-Biological Macromolecules** Letizia Tavagnacco; Sapienza University of Rome, Italy

Proteins are known to undergo a dynamical transition at low temperature, typically between 220 and 240 K. This transition consists in a steep enhancement of the protein atomic mobility which is related to the onset of anharmonic motions. At the same temperature proteins start to be biologically active and thus a full understanding of the molecular origin of this phenomenon is of particular relevance. While the protein dynamical transition always occurs in aqueous environment, with the protein confinement preventing the onset of ice crystallization, the role of water is still a controversial issue.

Here we focus on the low temperature behavior of a non-biological macromolecule, i.e. poly(N-isopropylacrylamide), commonly known as PNIPAM. This polymer is mostly exploited for its thermo-responsive nature, but it is also of interest because of its affinity with proteins in terms of energy landscape and amphiphilic chemical composition. Depending on the specific synthesis protocol, different PNIPAM based molecular architecture can be originated, such as linear chains or microgels, i.e. polymer network particles with a colloidal size. In this talk I will discuss two studies on the low temperature behavior of this synthetic soft material where atomistic molecular dynamics simulations are combined to elastic incoherent neutron scattering experiments.

In the first part I will provide a description of the evidences of the occurrence of a low temperature dynamical transition in PNIPAM microgels, akin to that observed in proteins [1,2]. This study is based on a nanoscale model of a microgel network in water, which quantitatively reproduces neutron scattering experiments. By correlating the information extracted from the analysis of the polymer relaxations times, water self-diffusion coefficients and hydrogen bonding interactions I will show that water-polymer coupling plays a driving role in the phenomenon.

In the second part, I will report the observation of a low temperature dynamical transition also in PNIPAM linear chains, which suggest a wide generality of the phenomenon, independently on the macromolecular architecture [3]. I will also show that simulations allow to identify the specific motions underlying the onset of the transition.

References

[1] Zanatta M. et al. "Evidence of a low-temperature dynamical transition in concentrated microgels" *Science advances* 2018, 4, eaat5895.

[2] Tavagnacco L. et al. "Water-polymer coupling induces a dynamical transition in microgels" *The journal of physical chemistry letters*, 2019, 10, 870-876.

[3] Tavagnacco L. et al. "The dynamical transition of hydrated polymer chains" in preparation.

12:01 PM OPEN DISCUSSION

12:18 PM \*F.MT04.03.01

**Multiscale, Multiphysics Modeling of Rigid Polyurethane Foams** Valeriy V. Ginzburg<sup>1</sup>, Huikuan Chao<sup>1</sup>, Irfan Khan<sup>1</sup>, Steven Arturo<sup>1</sup>, Jerome Claracq<sup>2</sup>, Asjad Shafi<sup>1</sup>, Weijun Zhou<sup>1</sup>, Mirella Coroneo<sup>3</sup>, Kshitish Patankar<sup>1</sup>, Michael Desanker<sup>1</sup>, Quan Yuan<sup>1</sup>, Chi-Wei Tsang<sup>1</sup> and Paul Gillis<sup>1</sup>; <sup>1</sup>Dow Chemical Co, United States; <sup>2</sup>Dow Benelux B.V., Netherlands; <sup>3</sup>DOW ITALIA S.R.L., Italy

Rigid polyurethane (PU) foams play crucial role in improving energy efficiency of our homes, offices, and appliances. The preparation of an insulating rigid PU panel is a complex physico-chemical process that includes several concurrent reactions (blowing and gelling), polymer molecular weight build-up, gelation and vitrification, bubble nucleation and growth, Ostwald ripening and coalescence; these phenomena take place as the reacting fluid is pushed into a mold and must occupy the space there without leaving any voids or other imperfections. Designing this process – from selecting the right formulation components (surfactants, catalysts, polyols, isocyanates, etc.) to optimizing the mold geometry – is a complex task requiring multiple and expensive trials. We describe a new multiscale modeling framework aiming to predict the foam flow into the mold and the final foam properties as a function of the formulation. The modeling tool has been validated in several experimental tests and is being utilized to help design new rigid PU foam formulations to better satisfy customer needs.

**12:33 PM .**

**12:34 PM \*F.MT04.03.02**

**Molecular Latent Space Simulators** Hythem Sidky<sup>1</sup>, Wei Chen<sup>2</sup> and [Andrew Ferguson](#)<sup>1</sup>; <sup>1</sup>The University of Chicago, United States; <sup>2</sup>University of Illinois at Urbana-Champaign, United States

Molecular dynamics (MD) is a powerful approach to probe molecular-level mechanisms, thermodynamics, and kinetics, but is limited to millisecond time scales even on the world's fastest supercomputers. We have developed molecular latent space simulators (LSS) to break this time scale barrier by learning highly efficient and accurate surrogate dynamical models of the long-time molecular dynamics. The LSS comprises three back-to-back deep learning networks with specialized architectures that are trained over modest MD training data to (i) learn an encoding of a molecular system into a low latent space, (ii) construct a low-dimensional dynamic propagator in this space, and (iii) generatively decode molecular configurations to produce a synthetic molecular trajectory. The trained LSS is then deployed to generate novel ultra-long molecular trajectories at six orders of magnitude lower cost than MD. The low-cost of these synthetic trajectories enable resolution of rare thermodynamic states and kinetic transitions with arbitrarily low statistical uncertainties. In an application to Trp-cage mini-protein, we generate millisecond trajectories in just minutes of wall clock time, demonstrate excellent agreement with the structure, thermodynamics, and kinetics of the MD calculations, and resolve stabilities and rates with 10-fold higher accuracy.

**12:49 PM .**

**12:50 PM \*F.MT04.04.01**

**Soft and Biological Materials Design via Cyber-Enabled Computational Methods** [Meenakshi Dutt](#); Rutgers, The State University of New Jersey, United States

There has been a recent surge in interest in soft and biological materials due to their potential applications in diverse areas including biomedicine, energy and nanoelectronics. The chemical diversity in the building blocks/sequences of the molecules constituting these materials yield an enormous molecular parameter space. A fundamental understanding of the impact of chemical block/sequence on the structure-activity relation of these soft and biological materials will accelerate their development and use, thereby accelerating the advancement of diverse disciplines.

Cyber-enabled computational methods, which integrate molecular simulations with analytical techniques, advanced computing and sampling tools, are used to study and develop new soft and biological materials with desired sequence/block-structure-activity properties in a more time- and cost-efficient way. The extended spatiotemporal scales connecting molecules to materials is addressed via the use of coarse-grained representations of the molecular species. The dynamics underlying the formation of the materials is resolved via the classical Molecular Dynamics simulation technique.

SESSION F.MT04.09: Live Keynote II: Using Machine Learning and Multiscale Modeling to Study Soft Materials and Interfaces

Session Chairs: Alexander Alexeev and Sanket Deshmukh

Thursday Afternoon, December 3, 2020

F.MT04

**3:00 PM \*F.MT04.04.02**

**Curvature and De-Mixing in Asymmetric Bilayers—Effect of Protein Inclusions** Shikha Prakash and [Durba Sengupta](#);

National Chemical Laboratory, India

Topology and curvature changes in cellular membranes, especially in response to protein inclusions is important for a variety of cellular functions. Continuum elastic models such as the Helfrich model is able to describe several membrane elastic properties, but specific lipid-protein interactions (and feedback effects) are usually missing from these models. Here, we use coarse-grain molecular dynamics simulations to analyse the molecular-level mechanistic properties of a series of bilayers together with caveolin-1 as a protein inclusion. We show that in asymmetric, multi-component bilayers, differential stress between the two leaflets exists and may lead to non-additive curvature effects. The differential bilayer stress and the area mismatch cannot always be compensated directly in these systems. Binding of caveolin-1 can lead to a lipid clustering and de-mixing of multi-component bilayers. We show that the de-mixing is dependent both on specific protein-lipid interactions, as well as curvature-dependent lipid sorting. Our work is an important step in understanding mechanical properties of complex asymmetric bilayers and the role of protein inclusions.

References:

Krishna & Sengupta, 2019, Biophys. J.

Krishna et al., 2020, J. Phys. Chem. B

3:15 PM .

3:16 PM \*F.MT04.04.03

**Tuning the LCST-Like Transition of Elastin-Like-Peptide (ELP) and Conjugates of ELP to Collagen-Like-Peptide (CLP) Using ELP Sequence and Composition** [Arthi Jayaraman](#) and Phillip Taylor; University of Delaware, United States

Peptide based biomaterials have garnered significant attention due to their ability to respond to external stimuli such as heat, light, and pH, thus allowing for controllable release of therapeutics for drug delivery applications and tunable mechanical and chemical properties for tissue engineering and *in vitro* cell culture applications. In this talk, I will present our recent work involving atomistic and coarse-grained molecular dynamics (MD) simulation studies of thermoresponsive polypeptides, specifically elastin-like peptides (ELP) and elastin-like peptide – collagen-like peptide (ELP-CLP) bioconjugates. ELPs are polypeptides that mimic the extracellular matrix protein, elastin, and are composed of repeat units of (VPGXG), where V, P, and G, are valine, proline, and glycine, respectively. The fourth residue, X, is termed the guest residue and can be any amino acid besides proline. Aqueous solutions of ELPs undergo a lower critical solution temperature (LCST)-like phase transition, wherein ELPs remain soluble below the transition temperature,  $T_t$ , and insoluble above  $T_t$ . We have focused our recent computational work on understanding the impact of substitution of F with Tyrosine (Y) and Tryptophan (W) guest residues and the sequence of these substitutions on the  $T_t$  of short ELPs in free state and when ELPs are conjugated to CLPs. Through a combination of atomistic and coarse-grained MD simulations we have described the molecular interactions that drive the observed shifts in the transition temperatures in our experimental collaborator's lab.

3:31 PM .

3:32 PM \*F.MT04.05.01

**Interpretable Machine Learning for Structure/Property Relationships of Graphene Oxide Nanomaterials** [Amanda Barnard](#)<sup>1</sup>, Benyamin Motevalli<sup>2</sup> and Bronwyn L. Fox<sup>3</sup>; <sup>1</sup>The Australian National University, Australia; <sup>2</sup>CSIRO, Australia; <sup>3</sup>Swinburne University of Technology, Australia

Materials informatics, and the associated field of nanoinformatics, offer a plethora of new approaches to solving existing challenges in (nano)materials design. These enabling technologies leverage over 50 years of innovation in theoretical computer science on machine learning algorithms, and an even longer history of research in statistics to underpin the essential preliminary data science. Provided sufficient appropriate data is available to describe the material or system, new insights can be gained that would be otherwise obscured using conventional experimental or computational methods. Hidden structure/property relationships we can use to inform further research and materials development. Extracting useful insights (such as structure/property relationships) from data analytics and machine learning is however more complicated than simply gathering data and training models, since not all methods are interpretable, and interpretability is essential for decision making. Correlation is also different to causation, and so the importance relationships identified using many machine learning methods are not always actionable. In this presentation we will discuss the importance of accuracy, generalizability and interpretability, and demonstrate the advantages of combining a series of different machine learning methods to uncover



useful relationships between the properties, structure and processing conditions of graphene oxide nanoflakes.

**3:47 PM .**

**3:48 PM \*F.MT04.05.03**

**AI Guided Materials Discovery and Design** Subramanian Sankaranarayanan<sup>1,2</sup>; <sup>1</sup>Argonne National Laboratory, United States; <sup>2</sup>University of Illinois at Chicago, United States

The ever-increasing power of modern supercomputers, along with the availability of highly scalable atomistic simulation codes, has begun to revolutionize predictive modeling of materials. Molecular dynamics (MD), in particular, has led to breakthrough advances in diverse fields, including tribology, energy storage, catalysis, sensing. Furthermore, recent integration of MD simulations with X-ray characterization has demonstrated promise in real-time 3-D atomistic characterization of materials. The popularity of MD is driven by its applicability at disparate length/time-scales, ranging from *ab initio* MD (hundreds of atoms and tens of picoseconds) to all-atom classical MD (millions of atoms and tens of nanoseconds), and coarse-grained (CG) models (microns and tens of micro-seconds). Nevertheless, a substantial gap persists between AIMD, which is highly accurate but restricted to extremely small sizes, and those based on classical force fields (atomistic and CG) with limited accuracy but access to larger length/time scales. The accuracy and predictive power of classical MD is dictated by the empirical force fields, and their capability to capture the relevant physics. In this talk, we will present some of our recent work on the use of machine learning (ML) to seamlessly bridge the electronic, atomistic and mesoscopic scales for materials modeling. Our automated ML framework aims to bridge the significant gulf that exists between the handful of research groups that develop new interatomic potential models (often requiring several years of effort) and the increasingly large user community from academia and industry that applies these models. Our ML approach has showed marked success in developing force fields for a wide range of materials from metals, oxides, nitrides, hetero-interfaces to two-dimensional (2-D) materials and even water (arguably the most difficult system to capture from a molecular perspective). This talk will also briefly discuss our ongoing efforts to integrate such cheap yet accurate atomistic models with (a) AI techniques to perform inverse design and construct metastable phase diagrams of materials (b) Deep learning to improve spatiotemporal resolutions of ultrafast X-ray imaging.

**4:03 PM .**

**4:04 PM \*F.MT04.05.04**

**Hiding in a Fluid—Autonomously Revealing Hidden Local Structures in Colloidal Systems** Laura Filion; University of Utrecht, Netherlands

Developments in machine learning have opened the door to a new generation of methods for studying phase transitions, due to their ability to efficiently and autonomously identify complex patterns in many-body systems. Applications of machine learning techniques in statistical physics vary from locating phase transitions in spin systems to pinpointing weak spots in colloidal glasses. The rapid emergence of machine learning applications in both statistical mechanics and materials science demonstrates that these techniques are destined to become an important tool for soft matter physics.

One problem this tool seems ideally suited to solve, both experimentally and in simulations, is the identification of different (crystalline) phases – even on the level of a single particle. For example, when we use either experiments or simulations to look at crystallization at the microscopic level, it is always a challenge to determine which particles are part of the fluid, and which ones have already crystallized. In this talk I will describe how machine learning techniques can automatically figure this out for us, even if we do not know in advance what crystal structure to look for. We will also examine how such methods might reveal new structural insights in “purely” disordered systems like glasses.

**4:19 PM .**

**4:20 PM \*F.MT04.06.02**

**Self-Directed Self-Assembly** Alfredo Alexander-Katz and Hejin Huang; Massachusetts Institute of Technology, United States

Block copolymer (BCP) self-assembly, and in particular directed self-assembly (DSA), has provided a powerful route to fabricate complex thin film structures at small length scales. Despite DSAs success in fabricating various 2D patterns, fabrication of complex 3D nanostructures remains a challenge. Here, we will introduce a novel method, which we call Self-

Directed Self-Assembly, and demonstrate how it can be leveraged to assemble 3D designer nanostructures using block copolymers. In particular we will demonstrate that uniform and non-uniform multilayer nanostructures can be obtained through stacking two or more "orthogonal" block copolymers. Finally, by introducing a patterned substrate to the first layer and performing multilayer stacking, we will demonstrate how to propagate information upwards in the film. Different complex multilayer structures will be shown, and at the end we will present an outlook on exciting new computational and artificial intelligence avenues of research in this field.

**4:35 PM .**

SESSION F.MT04.01: Soft Polymeric Materials  
On Demand Abstracts Available for Viewing Starting Saturday Morning, November 21, 2020  
F-MT04

**5:00 AM \*F.MT04.01.01**

**Coarse-Grained Modeling of Solid Polymer Electrolytes and Ion Conduction** [Lisa M. Hall](#); The Ohio State University, United States

Using solvent-free solid polymer electrolytes in batteries would reduce concerns about flammability and potentially decrease weight and cost, especially if their ion conductivity can be improved. Strategies to improve ion conduction in ion containing polymer materials include using bulky anions or using a high dielectric constant polymer. These both effectively decrease the strength of Coulomb interactions between ions at contact and can reduce ion agglomeration, which can improve conductivity. However, strong ion-polymer interactions can slow ion motion, and size asymmetry between ions may increase preferential solvation of cations versus the larger anions, lowering the transference number  $t_+$  (fraction of conductivity contributed by the cation). We study these effects using coarse-grained molecular dynamics (MD) simulations which include a  $1/r^4$  potential to capture size-dependent ion-monomer and ion-ion solvation effects. This is the same form as the interaction between an ion and an induced dipole. For block copolymer systems, we have also been guided by theoretical calculations to show the effects of macroscopic phase behavior. From MD, we calculate conductivity from ion mobilities in an external electric field, which improves accuracy versus the typical use of fluctuation dissipation relationships. We assess the impacts of ion size and polymer dielectric strength, including polymer dielectric strength contrast for block copolymer systems, on ion correlations, diffusion, and conductivity.

**5:15 AM \*F.MT04.01.02**

**Molecular Modeling Discloses a Protein-Like Dynamical Transition in Non-Biological Macromolecules** [Letizia Tavagnacco](#); Sapienza University of Rome, Italy

Proteins are known to undergo a dynamical transition at low temperature, typically between 220 and 240 K. This transition consists in a steep enhancement of the protein atomic mobility which is related to the onset of anharmonic motions. At the same temperature proteins start to be biologically active and thus a full understanding of the molecular origin of this phenomenon is of particular relevance. While the protein dynamical transition always occurs in aqueous environment, with the protein confinement preventing the onset of ice crystallization, the role of water is still a controversial issue.

Here we focus on the low temperature behavior of a non-biological macromolecule, i.e. poly(N-isopropylacrylamide), commonly known as PNIPAM. This polymer is mostly exploited for its thermo-responsive nature, but it is also of interest because of its affinity with proteins in terms of energy landscape and amphiphilic chemical composition. Depending on the specific synthesis protocol, different PNIPAM based molecular architecture can be originated, such as linear chains or microgels, i.e. polymer network particles with a colloidal size. In this talk I will discuss two studies on the low temperature behavior of this synthetic soft material where atomistic molecular dynamics simulations are combined to elastic incoherent neutron scattering experiments.

In the first part I will provide a description of the evidences of the occurrence of a low temperature dynamical transition in PNIPAM microgels, akin to that observed in proteins [1,2]. This study is based on a nanoscale model of a microgel network in water, which quantitatively reproduces neutron scattering experiments. By correlating the information extracted from the analysis of the polymer relaxations times, water self-diffusion coefficients and hydrogen bonding interactions I will show that water-polymer coupling plays a driving role in the phenomenon.

In the second part, I will report the observation of a low temperature dynamical transition also in PNIPAM linear chains, which suggest a wide generality of the phenomenon, independently on the macromolecular architecture [3]. I will also show

that simulations allow to identify the specific motions underlying the onset of the transition.

#### References

- [1] Zanatta M. et al. "Evidence of a low-temperature dynamical transition in concentrated microgels" *Science advances* 2018, 4, eaat5895.
- [2] Tavagnacco L. et al. "Water-polymer coupling induces a dynamical transition in microgels" *The journal of physical chemistry letters*, 2019, 10, 870-876.
- [3] Tavagnacco L. et al. "The dynamical transition of hydrated polymer chains" in preparation.

#### 5:45 AM F.MT04.01.04

**Simulating Hydrodynamic Interactions in Topologically Complex Polymers** [Phillip Rauscher](#), Stuart Rowan and Juan de Pablo; The University of Chicago, United States

Over the last few decades, a great deal of attention has been given to topologically linked ring polymers by both the physics and chemistry communities. However, the dynamics of such systems remain largely unstudied. Indeed, these systems represent a major theoretical challenge as they are typically subject to both topological and hydrodynamic interactions, which make the equations of motion intractable. We circumvent this difficulty by considering the dynamics of linked rings with pre-averaged hydrodynamic interactions in the spirit of the Zimm model and demonstrate that the symmetries of the rings lead to a hydrodynamic decoupling of the internal ring relaxations. In other words, the hydrodynamic interactions occur only at the ring center-of-mass level. This decoupling dramatically simplifies the problem and actually holds for any averaging procedure, even for non-Gaussian polymers and non-equilibrium conditions. We use this result to design efficient algorithms for Brownian dynamics simulations which offer enormous computational speed-ups and use these methods to study the dynamics of catenated polymers.

#### 5:55 AM F.MT04.01.06

**Atomistic Resolution of the Effects of Charge Density on Polyelectrolyte Brush Microstructure via Molecular Dynamics Simulations** [Harnoor S. Sachar](#), Turash H. Pail, Bhargav S. Chava and Siddhartha Das; University of Maryland, United States

Polyelectrolyte (PE) brushes are formed when charge-bearing polymer molecules are grafted to a substrate in close vicinity of each other. PE brushes have been at the forefront of soft materials research for quite some time due to a plethora of applications ranging from ion sensing, emulsion stabilization, nanofluidic energy conversion to drug delivery and oil recovery. The most intriguing properties of PE brushes stem from their responsiveness to external stimuli such as the solvent quality, pH and bulk salt concentration. We use an all-atom Molecular Dynamics (MD) framework to study the effects of varying charge density on the microstructure of densely grafted planar polyacrylic acid (PAA) brushes. Such a variation in the PE charge density due to changes in the degree of ionization of the weakly acidic/basic PE functional groups is typically brought by a variation in the pH of the surrounding medium. We investigate the properties of the PE molecules such as brush height and chain mobility along with the local structure and distribution of the counterions and water molecules within the brushes. Our results uncover several non-intuitive phenomena such as a grafting density dependent non-monotonic variation in the static dielectric constant of water molecules within the brushes with the degree of ionization. Moreover, we observe a remarkable increase in the species storage capacity of the brushes with the degree of ionization as characterized by an enhancement in the number density of both counterions and water molecules trapped within the PE layer. Our results shall help answer fundamental questions regarding the behaviour of weak PE brushes which is vital to improve the efficiency of several PE brush-based devices such as nanomechanical gates, nanofluidic diodes, current rectifiers, etc.

#### 6:05 AM F.MT04.01.07

**Atomistically Resolved Electroosmotic Transport in Polyelectrolyte Brush Grafted Nanochannels** Turash H. Pail, Harnoor S. Sachar, Parth Desai and [Siddhartha Das](#); University of Maryland, United States

Polyelectrolyte (PE) brush grafted systems have been used in a plethora of applications for their responsiveness to different stimuli. Here, we have used all-atom molecular dynamics (MD) calculations to study PE brush grafted nanochannels with added salt and their response to external electric fields generating electroosmotic (EOS) transport. We have discovered that nanoconfinement creates an overscreening effect inside PE brush layer, which implies a presence of excessive counterions ( $\text{Na}^+$ ) inside negatively PE brush layer. As a result, in low electric fields the overall EOS flow of the solvent water is dictated by the motion of the excess cations present in the brush-free bulk. Along with a higher concentration of cations in the bulk, higher velocity of cations than counterions in these applied electric fields also helps the solvent to move with cations.

Therefore, we find a fascinating scenario where the EOS flow is coion-dictated, while EOS flow has always been known to be counterion-dictated. On the other hand, for a larger electric field, the PE brush height reduces significantly and excludes some overscreening-inducing counterions into the brush-free bulk, which ensures parity in the number of coions and counterions in the bulk. Similar concentration and velocity of coions and counterions in the bulk in this electric field are overwhelmed by the larger residence time of water molecules inside the first solvation shell of counterions which ultimately results in a counterion dominated solvent flow in the direction of the applied electric field. Therefore, we encounter another highly surprising situation where the direction of the nanochannel EOS transport could be switched by merely changing the magnitude of the applied electric field.

**Acknowledgement:** This work has been supported by the U.S. Department of Energy Office of Science grant DE-SC0017741.

#### 6:15 AM F.MT04.01.08

**Multiscale Modeling of Polymer Nanocomposite Interphase** Boran Ma, Yilong Zhou, Gaurav Arya and L. Catherine Brinson; Duke University, United States

Multiphase polymer systems, including polymer nanocomposites (PNC), have a wide range of current and potential uses due to extraordinary tailorability of a variety of physical properties with small composition or processing changes. However, the details of the polymer physics controlling these changes is poorly understood. Modeling the interphase region in PNCs is crucial for achieving both better understanding of underlying physics and rational design of functional PNCs. Properties of the interphase region depend on that of the polymer matrix, nanoscale reinforcements, and surface chemistry in addition to microstructural characteristics of the distribution of nanoparticles in the PNCs. However, identifying the local property profile and the length scale of the interphase remains challenging. In this work, we establish a multiscale modeling framework to study the role that microstructure plays in determining bulk mechanical and viscoelastic properties of PNCs, bridging simulations at molecular and continuum level. Sensitivity of the structure--property relationship is also discussed.

#### 6:25 AM F.MT04.01.09

**High-Throughput Screening for Separation of H<sub>2</sub> and CH<sub>4</sub> in Functionalized IRMOF-1 Type Metal-Organic Frameworks Membranes** Fangxi Wang, Abhishek T. Sose, Samrendra Singh and Sanket A. Deshmukh; Virginia Tech, United States

**The microporous material Metal-Organic Frameworks (MOFs) show great potential in gas separation. Among them, Zinc-based isoreticular metal-organic frameworks (IRMOFs) share similar primitive cubic (pcu) topology with different linkers. Consequently, gas adsorption properties are different which is promising for gas separation. By decorating linkers with appropriate functional groups, its interaction with a particular gas molecule can be tuned to improve its selectivity and/or permeability. In this study, we have generated hypothetical MOFs by using different linkers and functionalizing them with urea, acetamides, CH<sub>3</sub>, and CF<sub>3</sub>. Several thousand structures were then used to perform the separation of H<sub>2</sub>/CH<sub>4</sub> gas mixtures using non-equilibrium molecular dynamics (NEMD) simulations. Results show that the permeability of both H<sub>2</sub> and CH<sub>4</sub> decreases in the presence of functional groups compared to bare MOFs. The permeabilities of both gases are close to zero when the linkers which are perpendicular to the external force are fully saturated with the urea and acetamide groups. When the functional groups are located at the linkers which are parallel to the external force, the selectivity increases.**

#### 6:35 AM F.MT04.01.10

**Thermal Gradient Driven Transport in Brush Functionalized Nanochannels** Vishal Sankar Sivasankar, Harnoor S. Sachar, Sai Ankit Etha and Siddhartha Das; University of Maryland, United States

Liquid and ion transport in nanofluidic systems have wide applications in ionic sensing, energy generation, bio-medicine, and the development of biomimetic systems. In this study, we analyze liquid transport by applying thermal gradient in a nanochannel functionalized with backbone charged pH-responsive polyelectrolytes (PE) brushes which is modeled using recently developed Augmented Strong Stretching theory (SST). We find that grafting nanochannels with charged polyelectrolyte brushes leads to enhanced thermoosmotic (TOS) fluid flow when compared to the bare nanochannels, as opposed to the general understanding that the polymer/PE brushes retard the flow owing to increase in drag due to the brushes. This is due to the fact that the PE brush induced localization of the Electric Double Layer (EDL) charge density away from the nanochannel walls results in a larger background flow for the migration of these ions. We quantify the electric field induced due to TOS flow and analyze its three components: ionic, osmotic, and thermal components. For various chosen parameters, we witness that the TOS velocity is greater in magnitude for the nanochannels grafted with backbone charged PE

brushes when compared to the bare nanochannels or the nanochannels grafted with PE brushes with charge only at the end away from the wall.

#### 6:45 AM F.MT04.01.11

**Three-Dimensional Constitutive Model for Shear Thickening Gel and Its Applications** Jinsu Kim, Yeonsong Kim and Woong-Ryeol Yu; Seoul National University, United States

There are few researches for constitutive modeling of shear thickening materials, though it is essential to predict their shear stiffening behavior, understand the mechanism of rate-dependent stiffness, and design new absorption devices. In this study, the constitutive model of shear thickening gels (STG) was developed by assuming STG consisting of soft and hard segments, the volume fraction of which are dependent on the shear rates. As such, two different rheological models were used for the soft and hard segments. The parameters of each rheological model were determined by carrying out the lap shear and pulling-out tests of STG. Finally, the developed constitutive model was validated by simulating the impact behavior of multi-layered sandwich composites including STG and polymer films and comparing the results with experiments.

#### 6:55 AM F.MT04.01.12

**Molecular Mechanism of Gas Separation Through Polymer-Metal Organic Framework (MOF) MMMs** Abhishek T. Sose, Fangxi Wang and Sanket A. Deshmukh; Virginia Tech, United States

The need to develop environmentally friendly and energy efficient technology for gas separations can be fulfilled by polymer Mixed Matrix Membranes (MMMs) with Metal organic frameworks (MOFs). Gas separations via selective transport in MMMs have shown to enhance selectivity and permeability. In these MMMs, polymers, MOFs and the polymer-MOF interface are known to play an important role in determining the gas separation mechanism. However, fundamental understanding of the parameters determining the compatibility of the polymer-MOF interface and its effect on the separation mechanism is yet to be developed due to limitations of experimental characterization methods. In this study, we have performed all-atom molecular dynamics (MD) simulation of a model polymer-MOF MMMs of polystyrene (PS) and polyacrylic acids (PAA) polymers with IRMOF-1 and HKUST as fillers. We have also studied separation of complex gas mixtures such as CH<sub>4</sub>/H<sub>2</sub> and N<sub>2</sub>/CO<sub>2</sub> through these polymer-MOF MMMs performed using microsecond long all-atom nonequilibrium molecular dynamics (NEMD) simulations. Their simulation trajectories were analyzed in order to determine the effect of polymer rigidity and hydrophilicity, polymer chain length, and MOF geometry on their selectivity and permeability.

#### 7:05 AM F.MT04.01.14

**Late News: Meso Scale Modelling of Crystallizing Polymer Films—From Processing to Imaging** Balaji Sessa Sarath Pokuri<sup>1</sup>, Kiran Vaddi<sup>2</sup>, Saurabh Kumar<sup>1</sup>, Guoyan Zhang<sup>3</sup>, Enrique Gomez<sup>3</sup>, Olga Wodo<sup>2</sup> and Baskar Ganapathysubramanian<sup>1</sup>; <sup>1</sup>Iowa State University, United States; <sup>2</sup>State University of New York at Buffalo, United States; <sup>3</sup>The Pennsylvania State University, United States

Active layer morphology plays a critical role in the performance of organic electronics. For most high performing material systems, the process of morphology formation involves simultaneous phase separation and crystallization of the acceptor layer materials. In order to fully understand the influence of processing conditions on the device performance, it becomes important to understand the formation of morphology under state-of-the-art device manufacturing techniques like solvents, co-solvents, additives and substrate induced phase separation. In this work, we first propose a meso-scale modeling framework to account for the effects of crystallization in solvent evaporation induced phase separation processes. This proposed framework has the capability to (a) be extensible to multiple crystallizing components, and (b) use experimentally measurable parameters like heat of crystallization and energy barrier of crystallization. We then demonstrate this multi-phase, multi-physics finite element framework for modeling crystallization and phase separation to a current high performing material system like PM6-Y6. PM6-Y6 system has been shown by several recent studies to have interesting crystallization-phase separation behavior, as well as a very high power conversion efficiency. Using this material system, we investigate the effect of evaporating conditions on the active layer morphology. Furthermore, we integrate this framework with virtual instruments to create an end-to-end platform for in-silico in-situ morphology characterization - quantification tool.

SESSION F.MT04.02: Colloidal Materials and Interfaces and Nano  
On Demand Abstracts Available for Viewing Starting Saturday Morning, November 21, 2020  
F-MT04

#### 5:00 AM F.MT04.02.02

**Exploring Behavior of Compressed Microgel Suspensions Using Mesoscale Simulations** [Svetoslav Nikolov](#)<sup>1</sup>, Alberto Fernandez-Nieves<sup>1,2,3</sup> and Alexander Alexeev<sup>1,2</sup>; <sup>1</sup>Georgia Institute of Technology, United States; <sup>2</sup>University of Barcelona, Spain; <sup>3</sup>ICREA-Institutio Catalana de Recerca i Estudis Avancats, Spain

Microgels are highly compressible colloids that can swell and deswell by absorbing or expelling solvent from their interior. As such, suspensions of microgel particles can be concentrated far more than a suspension comprised of hard colloids. This leads to unusual mechanical properties of microgel suspensions including a drastic difference between the bulk and shear moduli. Microgels in compressed suspension can respond to compression in a variety of ways such as interpenetration, deformation, and shrinking. Previous experiments have offered insightful, but somewhat conflicting accounts of the behavior of individual microgels in compressed suspensions. We employ a mesoscale computational model to probe the mechanics and behavior of compressed microgel suspensions. We consider monodisperse microgels a viscous solvent and investigate the effects microgel architecture, the packing fractions, and solvent conditions on the suspension bulk modulus and the behavior of individual microgels. We use two methods to change the suspension packing fraction. In the first method, the suspension is volumetrically compressed, whereas in the second method the solvent quality is changed to induce microgel swelling and deswelling. We find that above random close packing microgels predominantly change the shape and mildly shrink. Microgel interpenetration remains relatively small and comparable to the mean distance between crosslinks. At higher packing fractions, microgels solely shrink. We find that the mechanics of suspension is defined by the bulk modulus of a single microgel. This result holds for microgels with different architectures, and insensitive to the method used to alter the suspension packing fraction even as the suspension undergoes colloidal gelation. Thus, the single-microgel bulk modulus established the correct mechanical measure for compressed microgel suspensions.

#### 5:10 AM F.MT04.02.04

**Development of Non-Bonded Interaction Parameters Between Molybdenum Disulfide and Water** [Abhishek T. Sose](#), Samrendra Singh, Preeya Achari and Sanket A. Deshmukh; Virginia Tech, United States

Molybdenum disulfide ( $\text{MoS}_2$ ) is becoming increasingly popular as a substrate due to its more suitable electronic properties, higher signal-to-noise ratio, and increased biological compatibility as compared to graphene. Moreover, water is ubiquitous and most materials will inevitably come into contact with it. Consequently, understanding the structure of water at the  $\text{MoS}_2$ -water interface is imperative in determining the level of performance of  $\text{MoS}_2$  devices in industrial and nanofluidic applications. Using experimental techniques, however, to understand interactions at the molecular level is too difficult using modern technologies. We have developed non-bonded FF parameters between an  $\text{MoS}_2$  sheet and water molecules, which are represented by 12-6 Lennard-Jones (LJ) potential. The FF parameters were optimized to reproduce the macroscopic contact angle of water of  $\sim 69^\circ$  on the  $\text{MoS}_2$  sheet, which falls within the experimentally reported range of  $65^\circ$  to  $75^\circ$ . The  $\text{MoS}_2$  sheet was represented by Stillinger-Weber (SW) potential. Three widely used water models, namely, SPC, SPC/E, and SPC/Fw, were used to model water. In order to validate the accuracy of the optimized FF parameters, the interaction energy of a single water molecule in its preferential orientation placed above a sheet of  $\text{MoS}_2$  was calculated and compared to values reported in the existing literature. The structure of water at the  $\text{MoS}_2$ -water interface was also analyzed to validate the resulting parameters; specifically, the Z-density profile, average hydrogen bonds per molecule, and the angle made by the O-H vector with the normal to the  $\text{MoS}_2$  sheet were calculated and studied.

#### 5:20 AM F.MT04.02.05

**Computational Modeling of MDI Additives in SBS-Modified Asphalt** [Jocelyn Ting](#), Eesha Khare, Kai Jin and Markus Buehler; Massachusetts Institute of Technology, United States

Asphalt, used for roads and pavements, is an important building material that must endure a wide range of temperatures for many years. Asphalt originates from crude oil and contains millions of distinct organic molecules whose interactions contribute to the mechanical properties of the mixture. The study of this ubiquitous and complex material is essential in order to make its components more sustainable as well as improve durability to reduce the frequency of replacement. The effects of additives on asphalt have been extensively studied empirically, and several molecular models have arisen for the purpose of predicting interactions computationally. However, due to the chemical complexity of the system, there is still a large effort to improve current molecular models to understand interactions between different organic components within asphalt. In this study we firstly validate and refine the SARA (saturates, aromatics, resins, and asphaltenes) model [1] of asphalt in conjunction with experimental results. Secondly, we will use the improved model to describe the impact of additives on asphalt performance. Here we show a multistep process in which we utilize xTB, a semi-empirical tight binding program [2]

to optimize molecular geometry, DFT for chemical property calculation, and molecular dynamics for large scale mechanical properties. We discuss how this approach of modeling complex molecular systems such as asphalt enables the rapid evaluation of several theoretical model compounds. We then use these results to propose potential additives for the improved sustainability and performance of asphalt.

**References:**

[1] Martín-Martínez, F.; J., Fini; E. H.; Buehler, M. J. *RSC Advances* **2015**, 5(1), 753-759.

[2] Bannwarth, C.; Ehlert; S.; Grimme, S. *Journal of chemical theory and computation* **2019**, 15, (3), 1652-1671.

**5:30 AM F.MT04.02.06**

**Temperature and Humidity Triggered Framework Heterogeneity and Disorder and Its Impact on Catalytic Activity of 2D Metal-Organic Frameworks** Mohammad Reza Momeni Taheri, Zeyu Zhang and Farnaz A. Shakib; New Jersey Institute of Technology, United States

Effects of framework deformation due to temperature and solvent (water) effects on the redox-active Co transition metal sites present in layered 2D conductive Co<sub>3</sub>(HTTP)<sub>2</sub> metal-organic framework is studied in details. By combining classical molecular dynamics simulations with accurate and flexible ab initio parameterized force fields and ab initio periodic and cluster electronic structure calculations we show that including framework flexibility and solvent effects lead to higher reactivity for the oxidative dehydrogenation of propane to propene and hydrogen compared to the case that these effects are ignored in the conventional static electronic structure calculations.

SESSION F.MT04.03: Computational Methods and Models  
On Demand Abstracts Available for Viewing Starting Saturday Morning, November 21, 2020  
F-MT04

**5:00 AM \*F.MT04.03.01**

**Multiscale, Multiphysics Modeling of Rigid Polyurethane Foams** Valeriy V. Ginzburg<sup>1</sup>, Huikuan Chao<sup>1</sup>, Irfan Khan<sup>1</sup>, Steven Arturo<sup>1</sup>, Jerome Claracq<sup>2</sup>, Asjad Shafi<sup>1</sup>, Weijun Zhou<sup>1</sup>, Mirella Coroneo<sup>3</sup>, Kshitish Patankar<sup>1</sup>, Michael Desanker<sup>1</sup>, Quan Yuan<sup>1</sup>, Chi-Wei Tsang<sup>1</sup> and Paul Gillis<sup>1</sup>; <sup>1</sup>Dow Chemical Co, United States; <sup>2</sup>Dow Benelux B.V., Netherlands; <sup>3</sup>DOW ITALIA S.R.L., Italy

Rigid polyurethane (PU) foams play crucial role in improving energy efficiency of our homes, offices, and appliances. The preparation of an insulating rigid PU panel is a complex physico-chemical process that includes several concurrent reactions (blowing and gelling), polymer molecular weight build-up, gelation and vitrification, bubble nucleation and growth, Ostwald ripening and coalescence; these phenomena take place as the reacting fluid is pushed into a mold and must occupy the space there without leaving any voids or other imperfections. Designing this process – from selecting the right formulation components (surfactants, catalysts, polyols, isocyanates, etc.) to optimizing the mold geometry – is a complex task requiring multiple and expensive trials. We describe a new multiscale modeling framework aiming to predict the foam flow into the mold and the final foam properties as a function of the formulation. The modeling tool has been validated in several experimental tests and is being utilized to help design new rigid PU foam formulations to better satisfy customer needs.

**5:15 AM \*F.MT04.03.02**

**Molecular Latent Space Simulators** Hythem Sidky<sup>1</sup>, Wei Chen<sup>2</sup> and Andrew Ferguson<sup>1</sup>; <sup>1</sup>The University of Chicago, United States; <sup>2</sup>University of Illinois at Urbana-Champaign, United States

Molecular dynamics (MD) is a powerful approach to probe molecular-level mechanisms, thermodynamics, and kinetics, but is limited to millisecond time scales even on the world's fastest supercomputers. We have developed molecular latent space simulators (LSS) to break this time scale barrier by learning highly efficient and accurate surrogate dynamical models of the long-time molecular dynamics. The LSS comprises three back-to-back deep learning networks with specialized architectures that are trained over modest MD training data to (i) learn an encoding of a molecular system into a slow latent space, (ii) construct a low-dimensional dynamic propagator in this space, and (iii) generatively decode molecular configurations to produce a synthetic molecular trajectory. The trained LSS is then deployed to generate novel ultra-long molecular trajectories at six orders of magnitude lower cost than MD. The low-cost of these synthetic trajectories enable resolution of rare thermodynamic states and kinetic transitions with arbitrarily low statistical uncertainties. In an application to Trp-cage mini-protein, we generate millisecond trajectories in just minutes of wall clock time, demonstrate excellent agreement with the

structure, thermodynamics, and kinetics of the MD calculations, and resolve stabilities and rates with 10-fold higher accuracy.

#### **5:30 AM F.MT04.03.03**

**Accuracy of Classical Potentials for Polyethylene Structures Away from Equilibrium** Keara Frawley, Lihua Chen, Huan Tran, Naresh Thadhani and Rampi Ramprasad; Georgia Institute of Technology, United States

Realistic simulations of polymers require a large number of atoms due to the anisotropic nature of their morphology. Although density functional theory (DFT) is considered highly accurate, it is too computationally expensive to handle large systems. Classical potentials used for molecular dynamics studies are trained on experimental or quantum mechanical equilibrium structures, and their accuracy away from equilibrium is not well known. This work is a comparative study of two widely used classical potentials—Optimized Potentials for Liquid Simulations (OPLS) and the reactive force-field (ReaxFF)—with respect to DFT. Their performance for polyethylene (PE), a simple model polymer, is benchmarked by comparing the classical energies, forces, and stresses against DFT.

The equilibrium crystal structure of PE is orthorhombic. In situations away from equilibrium, PE undergoes a phase transition to monoclinic. This work focuses on variations of these two crystal structures, along with some amorphous structures, to model realistic PE morphology. The energy resulting from the classical potentials is highly accurate when compared to DFT results. Force, an atomistic property, is not as easily captured, but stress, a bulk property, can also be accurately captured by classical potentials.

Additionally, a pressure-temperature phase diagram for PE is computed using OPLS and ReaxFF. ReaxFF performs better at high temperatures than OPLS when compared to experimental results. Although the classical potentials do not perfectly capture the DFT and experimental behavior, the results are close enough to justify their use when large system sizes are required. Consequently, these results will be used for shock simulations involving far from equilibrium structures.

#### **5:40 AM F.MT04.03.04**

**Photocycloreversions within Confined Environments of Single Polymer Chains** Modan Liu<sup>1</sup>, Wolfgang Wenzel<sup>1</sup> and Hendrik Frisch<sup>2</sup>; <sup>1</sup>Karlsruhe Institute of Technology, Germany; <sup>2</sup>Queensland University of Technology, Australia

Folding single polymer chains into nanoparticles mimics the natural process of folding peptides into proteins, whilst for single chain nanoparticles (SCNP), the combinatorial possibilities in polymeric components, precise control over intramolecular crosslinks, and tailored functionalization of the synthetic nanoparticle expand potentials beyond natural mechanism. Light-gated reversible photocycloaddition reactions allow bonds to form and break within the SCNP for controlled folding via gauging irradiation wavelengths.

Here we developed a holistic coarse-grained molecular dynamics model of photocycloaddition reactions within the confined environment of single polymer chains, which grants real-time monitoring capabilities in the degree of intramolecular crosslinking and morphology of the polymer coil. It is revealed that in the confined environment, cycloaddition and cycloreversion reactions lost orthogonal addressibility, when both shorter and longer wavelength irradiations induce SCNP folding. Separated in timescales between bond recombination and diffusion, their collective effect results in wavelength-gated photostationary states where degree of crosslinking and polymer chain compaction converge both from simulation and experiment.

The developed model of single-chain polymer folding serves as a blueprint in understanding the quantitative structure-property relationship and control of photostationary states within polymer networks.

#### **5:50 AM F.MT04.03.05**

**Multi-Scale Modelling and Decision Making in Industrial Applications of Soft Materials Using FORCE** Frank Longford, Sean Parsons and Petr Kungurtsev; Enthought, United Kingdom

Industrial applications of soft materials need to consider a whole range of additional factors in combination to scientific knowledge provided by modelling techniques alone. A proposed technical solution may fail if it turns out not to be economically viable. Therefore, it is vital to factor business logic into an organization's decision making process when designing and producing new products.

The Formulations and Computational Engineering (FORCE) project, implemented within the EU Horizon 2020 program (<https://www.the-force-project.eu>), aims to bring materials modelling to the heart of business decision making via creation of Business Decision Support Systems (BDSS). By doing so, industries will be able to make more knowledgeable decisions based not only on existing legacy data, but also on new data generated by state of the art multi-scale and multi-physics materials modelling. Development of the FORCE BDSS and Workflow Manager has been closely aligned to activities of the



European Materials Modelling Council (EMMC) and also builds on the SimPhoNy framework (<https://www.simphony-project.eu>) for multi-scale modelling in materials science.

The FORCE BDSS provides three key features:

- A **library** containing wrappers for state-of-the-art MCO algorithms
- A **platform** for designing and running MCO calculations on arbitrary systems
- A **framework** for integrating existing modelling and experimental pipelines together via a common universal data typing system

The interoperability of data between both modelling software and physical domains is placed at the core of our FORCE BDSS, which we demonstrate as the FORCE Workflow Manager GUI, available at <https://github.com/force-h2020>. This software provides an integrated framework that connects simulation models of varying complexity, experimental data sets and commercially relevant information together as a 'Workflow' pipeline construct. Consequently, users are able to select from a wide variety of parameters and key performance indicators (KPI) that can be used to identify the optimal trade off when making a business decision. For example, a set of KPIs may include material properties such as tensile strength or viscosity, but also component cost and availability. An integrated set of multi-criteria optimization (MCO) algorithms will then identify optimal outcomes to consider, typically by mapping out a Pareto frontier.

We report on an example use case targeting the industrial application of micelles that has been investigated using the software. By doing so, we demonstrate how the BDSS may be used to design simple pipelines that optimize chemical formulations by performing and processing molecular dynamics simulations. Our example MCO includes conflicting KPI goals that aim to yield the highest quality product under typical business constraints. Therefore we do not expect to be able to identify an optimal solution, but by exploring the Pareto frontier we attempt to locate the best set of trade offs that could be made for any given scenario.

Finally, we describe how the FORCE BDSS is not restricted as a modelling framework, but rather can be integrated into both data science and experimental laboratory pipelines. Future use cases aim to include Workflow constructs working with legacy datasets and containing a combination of simulation, machine learning and wet lab operations. By doing so, we open up the potential for machine learning and multi-scale modelling to be truly incorporated within an organization's R&D.

#### 6:00 AM F.MT04.03.06

**En-to-End Differentiable Molecular Simulations for Control and Learning** Wujie Wang<sup>1</sup>, [Simon Axelrod](#)<sup>1,2</sup> and Rafael Gomez-Bombarelli<sup>1</sup>; <sup>1</sup>Massachusetts Institute of Technology, United States; <sup>2</sup>Harvard University, United States

Molecular dynamics simulations use statistical mechanics at the atomistic scale to enable both the elucidation of fundamental mechanisms and the engineering of matter for desired tasks. The behavior of molecular systems at the microscale is typically simulated with differential equations parameterized by a Hamiltonian, or energy function. The Hamiltonian describes the state of the system and its interactions with the environment. In order to derive predictive microscopic models, one wishes to infer a molecular Hamiltonian that agrees with observed macroscopic quantities. Recent advances in automatic differentiation provide possibilities for the optimization and control of complex Hamiltonians with analytical gradients. From the perspective of engineering, one wishes to control the Hamiltonian to achieve desired simulation outcomes and structures, as in self-assembly and optical control, to then realize systems with the desired Hamiltonian in the lab. In both cases, the goal is to modify the Hamiltonian such that emergent properties of the simulated system match a given target. We demonstrate how this can be achieved using differentiable simulations where bulk target observables and simulation outcomes can be analytically differentiated with respect to Hamiltonians, opening up new routes for parameterizing Hamiltonians to infer macroscopic models and develop control protocols.

#### 6:10 AM F.MT04.03.07

**REACTER—A Heuristic Method for Reactive Molecular Dynamics** [Jacob Gissinger](#), Benjamin D. Jensen and Kristopher E. Wise; NASA Langley Research Center, United States

REACTER ([www.react.org](http://www.react.org)) is a heuristic protocol that enables the simulation of complex reactions using atomistic molecular dynamics (MD) with a fixed-valence force field. Incorporating reactions into classical MD with this approach allows modeling of reactive systems over greatly-increased time scales, enabling systems to be modeled with MD that would not otherwise be feasible. One or more competing multi-step reactions or series of reactions can be invoked simultaneously. Special treatment can be applied to neighboring atoms to relax high energy configurations while the simulation progresses.

The original version of REACTER, which was implemented in the open-source LAMMPS simulation package as *fix bond/react*, was only available for serial simulations. This work describes the expansion of *fix bond/react* for use in parallel simulations, as well as the addition of various new options, including deletion of reaction by-products, reversible reactions, and custom reaction constraints. These new capabilities are demonstrated through large-scale simulations (200,000+ atoms) of the polymerization of polystyrene and nylon 6,6. The morphologies of both polymers are analyzed after reaching >99% extent of polymerization. Finally, the newly-added reversible reactions feature is demonstrated by rupturing these highly-entangled systems under uniaxial strain by defining a chain scission reaction.

#### 6:20 AM F.MT04.03.08

**A High-Throughput Multi-Scale Infrastructure for Automating Materials Science Computations** Rasha Atwi, Matthew Bliss and Nav Nidhi Rajput; Tufts University, United States

In this talk, I will present our group's effort to build a high-throughput infrastructure for the automated execution of materials science computations and analysis. This work is an extension of open-source Python packages that have been developed in Materials Project [1]: (1) *pymatgen* [2] for structure representation and input/output files generation and handling, (2) *FireWorks* [3] for managing workflows over computing resources, and (3) *Custodian* [4] for monitoring inevitable errors during the simulations and applying on-the-fly fixes. In our work, we benefit from these three libraries to build well-tested workflows for speeding up the prediction and screening of materials properties relevant to various applications with a focus on battery systems. At the backend, the infrastructure interfaces with the Gaussian [5] software which enables electronic structure calculations of chemical systems, and LAMMPS [6] open-source code for molecular dynamics (MD) simulations. In addition to its ability to handle the generation of input/data files and parsing of output files from the mentioned computational software, the infrastructure allows management of the collected data and storing it in MongoDB [7], a NoSQL database program using JSON-like documents with flexible schema. Examples of implemented Gaussian-based workflows include the calculation of electrostatic partial charges, NMR chemical shift, binding energy, ionization potential, electron affinity, and bond dissociation energy. Each derived property is saved in its own collection with auxiliary information like molecular metadata (smiles representation, chemical formula, ...), which makes it easy to query and data-mine structure-property relationships. The user can tune the calculations by overriding default workflow parameters, for example, the functional and basis set, by-passing selected steps, or packing many jobs over multiple nodes for supercomputing resources. LAMMPS workflows allow the execution of MD simulations in different ensembles and analysis of the dumped trajectories for various dynamical and structural properties. The infrastructure enables coupling first-principles calculations with classical MD simulations to address chemical and physical phenomena occurring in a given system at different length and time scales. This approach aids in the development of databases required for training machine-learning models to accelerate the design and screening of materials with optimized properties for various materials science applications.

1. Jain, A., et al., *Commentary: The Materials Project: A materials genome approach to accelerating materials innovation*. *Apl Materials*, 2013. **1**(1): p. 011002.
2. Ong, S.P., et al., *Python Materials Genomics (pymatgen): A robust, open-source python library for materials analysis*. *Computational Materials Science*, 2013. **68**: p. 314-319.
3. Jain, A., et al., *FireWorks: a dynamic workflow system designed for high-throughput applications*. *Concurrency and Computation: Practice and Experience*, 2015. **27**(17): p. 5037-5059.
4. Custodian. <<https://github.com/materialsproject/custodian>>.
5. Frisch, M.J., et al., *Gaussian 16 Rev. C.01*. 2016: Wallingford, CT.
6. Plimpton, S., *Fast parallel algorithms for short-range molecular dynamics*. 1993, Sandia National Labs., Albuquerque, NM (United States).
7. MongoDB Inc., M., 2014.

#### 6:30 AM F.MT04.03.09

**Chemical Potential Differences in Small Systems** Vilde Bråten<sup>1</sup>, Øivind Wilhelmsen<sup>1,2</sup> and Sondre Kvalvåg Schnell<sup>1</sup>; <sup>1</sup>Norwegian University of Science and Technology, Norway; <sup>2</sup>Sintef, Norway

Free energy and other related properties are not averages of functions of the phase space coordinates of the system, which means that they can not be calculated directly from the simulation trajectory. Under this category we find the chemical potential, which can be calculated with the Widom [4] particle insertion method. One drawback of this method is that it becomes very inefficient and often fails at higher densities. We propose a new method which utilizes the size and shape dependency of small systems to extract chemical potential differences from molecular dynamics simulation trajectories. The method is based on the difference in behavior of small and large systems, which can be summarized by the surface area to volume ratio. Since this ratio is much larger for small systems, the surface effects become much more significant, and the

properties can no longer be directly compared to thermodynamic properties of macroscopic systems [1]. The Small System Method (SSM) [2], exploits the size dependency of these properties, and uses properties calculated for small systems to obtain the value of the same property for a macroscopic system. The small systems are created by placing small non-periodic subsystems at random positions inside a larger periodic reservoir. From statistical mechanics, the fluctuations in number of particles is coupled to different properties of the systems, like compressibility, heat capacity, partial molar volume and enthalpy. By combining SSM with the Overlapping Distribution Method originally developed by Bennett [3] we can also obtain values for chemical potential, pressure and free energy in the small systems. As with the previously mentioned properties, these can be extrapolated to the thermodynamic limit in order to obtain the macroscopic value of the properties. The method works well for a range of different densities, which makes it a promising alternative to the Widom [4] particle insertion method.

[1] Hill TL. Thermodynamics of Small Systems. J Chem Phys. 1962;36(12):3182–3197.

[2] Schnell SK, Vlugt TJH, Simon JM, Bedeaux D, Kjelstrup S. Thermodynamics of a small system in a  $\mu$ T-reservoir. Chem Phys Lett. 2011;504(4):199 – 201.

[3] Bennett CH. Efficient estimation of free energy differences from Monte Carlo data. J Comput Phys. 1976;22(2):245-268

[4] WidomB. Some Topics in the Theory of Fluids. J Chem Phys. 1963;39(11):2808–2812.

SESSION F.MT04.04: Biological and Bioinspired Materials  
On Demand Abstracts Available for Viewing Starting Saturday Morning, November 21, 2020  
F-MT04

#### **5:00 AM \*F.MT04.04.01**

**Soft and Biological Materials Design via Cyber-Enabled Computational Methods** Meenakshi Dutt; Rutgers, The State University of New Jersey, United States

There has been a recent surge in interest in soft and biological materials due to their potential applications in diverse areas including biomedicine, energy and nanoelectronics. The chemical diversity in the building blocks/sequences of the molecules constituting these materials yield an enormous molecular parameter space. A fundamental understanding of the impact of chemical block/sequence on the structure-activity relation of these soft and biological materials will accelerate their development and use, thereby accelerating the advancement of diverse disciplines.

Cyber-enabled computational methods, which integrate molecular simulations with analytical techniques, advanced computing and sampling tools, are used to study and develop new soft and biological materials with desired sequence/block-structure-activity properties in a more time- and cost-efficient way. The extended spatiotemporal scales connecting molecules to materials is addressed via the use of coarse-grained representations of the molecular species. The dynamics underlying the formation of the materials is resolved via the classical Molecular Dynamics simulation technique.

#### **5:15 AM \*F.MT04.04.02**

**Curvature and De-Mixing in Asymmetric Bilayers—Effect of Protein Inclusions** Shikha Prakash and Durba Sengupta; National Chemical Laboratory, India

Topology and curvature changes in cellular membranes, especially in response to protein inclusions is important for a variety of cellular functions. Continuum elastic models such as the Helfrich model is able to describe several membrane elastic properties, but specific lipid-protein interactions (and feedback effects) are usually missing from these models. Here, we use coarse-grain molecular dynamics simulations to analyse the molecular-level mechanistic properties of a series of bilayers together with caveolin-1 as a protein inclusion. We show that in asymmetric, multi-component bilayers, differential stress between the two leaflets exists and may lead to non-additive curvature effects. The differential bilayer stress and the area mismatch cannot always be compensated directly in these systems. Binding of caveolin-1 can lead to a lipid clustering and de-mixing of multi-component bilayers. We show that the de-mixing is dependent both on specific protein-lipid interactions, as well as curvature-dependent lipid sorting. Our work is an important step in understanding mechanical properties of complex asymmetric bilayers and the role of protein inclusions.

References:

Krishna & Sengupta, 2019, Biophys. J.

**5:30 AM \*F.MT04.04.03**

**Tuning the LCST-Like Transition of Elastin-Like-Peptide (ELP) and Conjugates of ELP to Collagen-Like-Peptide (CLP) Using ELP Sequence and Composition** Arthi Jayaraman and Phillip Taylor; University of Delaware, United States

Peptide based biomaterials have garnered significant attention due to their ability to respond to external stimuli such as heat, light, and pH, thus allowing for controllable release of therapeutics for drug delivery applications and tunable mechanical and chemical properties for tissue engineering and *in vitro* cell culture applications. In this talk, I will present our recent work involving atomistic and coarse-grained molecular dynamics (MD) simulation studies of thermoresponsive polypeptides, specifically elastin-like peptides (ELP) and elastin-like peptide – collagen-like peptide (ELP-CLP) bioconjugates. ELPs are polypeptides that mimic the extracellular matrix protein, elastin, and are composed of repeat units of (VPGXG), where V, P, and G, are valine, proline, and glycine, respectively. The fourth residue, X, is termed the guest residue and can be any amino acid besides proline. Aqueous solutions of ELPs undergo a lower critical solution temperature (LCST)-like phase transition, wherein ELPs remain soluble below the transition temperature,  $T_i$ , and insoluble above  $T_i$ . We have focused our recent computational work on understanding the impact of substitution of F with Tyrosine (Y) and Tryptophan (W) guest residues and the sequence of these substitutions on the  $T_i$  of short ELPs in free state and when ELPs are conjugated to CLPs. Through a combination of atomistic and coarse-grained MD simulations we have described the molecular interactions that drive the observed shifts in the transition temperatures in our experimental collaborator's lab.

**5:45 AM F.MT04.04.04**

**Melanin-Based Materials as Biocompatible Mixed Conductors** Micaela Matta and Alessandro Troisi; University of Liverpool, United Kingdom

Eumelanin is an amorphous insoluble pigment present in both mammals and invertebrates. This natural material consists of amorphous aggregates of DHI (5,6-dihydroxyindole) and DHICA (5,6-dihydroxyindole-2-carboxylic acid) oligomers, interacting via  $\pi$ - $\pi$  stacking and hydrogen bonding.<sup>1</sup> Synthetic melanins are usually obtained using either DHICA or DHI and present a lower degree of structural disorder. Due to their dual protonic and electronic conductivity<sup>2,3</sup> and intrinsic biocompatibility, melanins are being investigated for energy storage/production<sup>4</sup> and as composite materials for biomedical applications.<sup>5</sup>

We present a systematic study of the electronic structure and conformational space of DHICA oligomers, characterized by a linear polymeric structure and strong antioxidant properties. Our computational insight not only fits well within existing experimental evidence, but can also predict the charge transport landscape in the bulk polymer.<sup>6</sup> We then use molecular dynamics simulations to study the fiber-like structures formed by this material, and investigate its morphology dependent properties.

Finally, we describe our approach towards the simulation of realistic DHI melanin aggregates using a combination of experimental evidence, chemical kinetics and molecular dynamics.

1. d'Ischia, M.; Wakamatsu, K.; Cicoira, F.; Di Mauro, E.; Garcia-Borron, J. C.; Commo, S.; Galván, I.; Ghanem, G.; Kenzo, K.; Meredith, P.; et al. *Pigment Cell Melanoma Res.* **2015**, *28* (5), 520–544.
2. Migliaccio, L.; Manini, P.; Altamura, D.; Giannini, C.; Tassini, P.; Maglione, M. G.; Minarini, C.; Pezzella, A. *Front. Chem.* **2019**, *7* (March), 1–8.
3. Wünsche, J.; Deng, Y.; Kumar, P.; Di Mauro, E.; Josberger, E.; Sayago, J.; Pezzella, A.; Soavi, F.; Cicoira, F.; Rolandi, M.; et al. *Chem. Mater.* **2015**, *27* (2), 436–442.
4. Kumar, P.; Di Mauro, E.; Zhang, S.; Pezzella, A.; Soavi, F.; Santato, C.; Cicoira, F. *J. Mater. Chem. C* **2016**, *4* (40), 9516–9525.
5. Migliaccio, L.; Altamura, D.; Scattarella, F.; Giannini, C.; Manini, P.; Gesuele, F.; Maglione, M. G.; Tassini, P.; Pezzella, A. *Adv. Electron. Mater.* **2019**, *5* (3), 1–8.
6. Matta, M.; Pezzella, A.; Troisi, A. *J. Phys. Chem. Lett.* **2020**, *11*, 3, 1045–1051.

**5:55 AM F.MT04.04.05**

**Structure-Mechanical Behavior Relation for the Facet Capsule Ligament via Multiscale Modeling** Jacob Merson and Catalin Picu; Rensselaer Polytechnic Institute, United States

Hierarchical multiscale modeling is used in this work to model collagen based biotissues, with direct application to the

mechanics of the facet capsule ligament (FCL) of the spine. The biomaterial is modeled in the continuum sense using finite elements, whose constitutive description is provided by representative volume elements (RVEs) containing discrete representation of the underlying network. This technique offers a mechanism to predict the macroscopic properties of biological structures from the properties of the constituent fibers. A requirement of the hierarchical multiscale scheme is that RVEs at each material point must be much smaller than the corresponding continuum scale element. In fibrous materials, this can be problematic due to large size effects in three dimensions. Generalized boundary conditions are developed to mitigate the size effect and reduce the required size of the RVEs, therefore enabling larger multiscale models with increased macroscale geometry resolution. Predictions of the mechanical behavior of the FCL which account for the fiber-scale, microscale and ligament-scale collagen architecture are presented.

#### 6:05 AM F.MT04.04.06

**Quantum Multifractality in Thermal Conduction Across Random Interfaces** [Taishan Zhu](#)<sup>1,1</sup>, Giuseppe Romano<sup>1</sup>, Martin Ostoj-Starzewski<sup>2</sup> and Jeffrey C. Grossman<sup>1</sup>; <sup>1</sup>Massachusetts Institute of Technology, United States; <sup>2</sup>University of Illinois at Urbana-Champaign, United States

Self-affine morphology of random interfaces governs material functionalities across tribological, geological, (opto-)electrical and biological applications. However, the knowledge of how energy carriers or generally classical/quantum waves interact with structural irregularity is still incomplete. In this work, we study vibrational energy transport through random interfaces exhibiting different correlation functionals on the two-dimensional hexagonal lattice. We show that random interfaces are Cantor-composites populated on geometrical fractals, thus multifractals, and calculate their quantized conductance using atomistic approaches. The interfacial conductance increases when disorder enhances, and we obtain a universal scaling law. This scaling law contains self-similarity for mass perturbation, and exponential scaling of structural irregularity quantified by Hausdorff dimension. We resolve the modal characteristics by atomic Green's function, wavepacket simulation, and molecular dynamics, and ascribe the disorder-induced enhancement of conductance to the increased harmonic transmission of transverse and flexural modes, augmented by anharmonic interactions near interfaces. The multifractal nature and Cantor-composite picture may be extendable to charge and photon transport across random interfaces.

#### SESSION F.MT04.05: Machine Learning

On Demand Abstracts Available for Viewing Starting Saturday Morning, November 21, 2020  
F-MT04

#### 5:00 AM \*F.MT04.05.01

**Interpretable Machine Learning for Structure/Property Relationships of Graphene Oxide Nanomaterials** [Amanda Barnard](#)<sup>1</sup>, Benyamin Motevalli<sup>2</sup> and Bronwyn L. Fox<sup>3</sup>; <sup>1</sup>The Australian National University, Australia; <sup>2</sup>CSIRO, Australia; <sup>3</sup>Swinburne University of Technology, Australia

Materials informatics, and the associated field of nanoinformatics, offer a plethora of new approaches to solving existing challenges in (nano)materials design. These enabling technologies leverage over 50 years of innovation in theoretical computer science on machine learning algorithms, and an even longer history of research in statistics to underpin the essential preliminary data science. Provided sufficient appropriate data is available to describe the material or system, new insights can be gained that would be otherwise obscured using conventional experimental or computational methods. Hidden structure/property relationships we can use to inform further research and materials development. Extracting useful insights (such as structure/property relationships) from data analytics and machine learning is however more complicated than simply gathering data and training models, since not all methods are interpretable, and interpretability is essential for decision making. Correlation is also different to causation, and so the importance relationships identified using many machine learning methods are not always actionable. In this presentation we will discuss the importance of accuracy, generalizability and interpretability, and demonstrate the advantages of combining a series of different machine learning methods to uncover useful relationships between the properties, structure and processing conditions of graphene oxide nanoflakes.

#### 5:15 AM \*F.MT04.05.03

**AI Guided Materials Discovery and Design** [Subramanian Sankaranarayanan](#)<sup>1,2</sup>; <sup>1</sup>Argonne National Laboratory, United States; <sup>2</sup>University of Illinois at Chicago, United States

The ever-increasing power of modern supercomputers, along with the availability of highly scalable atomistic simulation

codes, has begun to revolutionize predictive modeling of materials. Molecular dynamics (MD), in particular, has led to breakthrough advances in diverse fields, including tribology, energy storage, catalysis, sensing. Furthermore, recent integration of MD simulations with X-ray characterization has demonstrated promise in real-time 3-D atomistic characterization of materials. The popularity of MD is driven by its applicability at disparate length/time-scales, ranging from *ab initio* MD (hundreds of atoms and tens of picoseconds) to all-atom classical MD (millions of atoms and tens of nanoseconds), and coarse-grained (CG) models (microns and tens of micro-seconds). Nevertheless, a substantial gap persists between AIMD, which is highly accurate but restricted to extremely small sizes, and those based on classical force fields (atomistic and CG) with limited accuracy but access to larger length/time scales. The accuracy and predictive power of classical MD is dictated by the empirical force fields, and their capability to capture the relevant physics. In this talk, we will present some of our recent work on the use of machine learning (ML) to seamlessly bridge the electronic, atomistic and mesoscopic scales for materials modeling. Our automated ML framework aims to bridge the significant gulf that exists between the handful of research groups that develop new interatomic potential models (often requiring several years of effort) and the increasingly large user community from academia and industry that applies these models. Our ML approach has showed marked success in developing force fields for a wide range of materials from metals, oxides, nitrides, hetero-interfaces to two-dimensional (2-D) materials and even water (arguably the most difficult system to capture from a molecular perspective). This talk will also briefly discuss our ongoing efforts to integrate such cheap yet accurate atomistic models with (a) AI techniques to perform inverse design and construct metastable phase diagrams of materials (b) Deep learning to improve spatiotemporal resolutions of ultrafast X-ray imaging.

#### 5:30 AM \*F.MT04.05.04

**Hiding in a Fluid—Autonomously Revealing Hidden Local Structures in Colloidal Systems** [Laura Filion](#); University of Utrecht, Netherlands

Developments in machine learning have opened the door to a new generation of methods for studying phase transitions, due to their ability to efficiently and autonomously identify complex patterns in many-body systems. Applications of machine learning techniques in statistical physics vary from locating phase transitions in spin systems to pinpointing weak spots in colloidal glasses. The rapid emergence of machine learning applications in both statistical mechanics and materials science demonstrates that these techniques are destined to become an important tool for soft matter physics.

One problem this tool seems ideally suited to solve, both experimentally and in simulations, is the identification of different (crystalline) phases – even on the level of a single particle. For example, when we use either experiments or simulations to look at crystallization at the microscopic level, it is always a challenge to determine which particles are part of the fluid, and which ones have already crystallized. In this talk I will describe how machine learning techniques can automatically figure this out for us, even if we do not know in advance what crystal structure to look for. We will also examine how such methods might reveal new structural insights in “purely” disordered systems like glasses.

#### 5:45 AM F.MT04.05.06

**Multi-Resolution Convolutional Neural Networks for Inverse Problems** [Feng Wang](#)<sup>1,2</sup>, Alberto Eljarrat<sup>2</sup>, Johannes Müller<sup>2</sup>, Trond R. Henninen<sup>1</sup>, Rolf Erni<sup>1</sup> and Christoph T. Koch<sup>2</sup>; <sup>1</sup>EMPA, Switzerland; <sup>2</sup>Institut für Physik, Germany

Inverse problems in image processing, phase imaging, and computer vision often share the same structure of mapping input image(s) to output image(s) but are usually solved by different application-specific algorithms. Deep convolutional neural networks have shown great potential for highly variable tasks across many image-based domains, but sometimes can be challenging to train due to their internal non-linearity. We propose a novel, fast-converging neural network architecture capable of solving generic image(s)-to-image(s) inverse problems relevant to a diverse set of domains. We show this approach is useful in recovering wavefronts from direct intensity measurements, imaging objects from diffusely reflected images, and denoising scanning transmission electron microscopy images, just by using different training datasets. These successful applications demonstrate the proposed network to be an ideal candidate solving general inverse problems falling into the category of image(s)-to-image(s) translation.

#### 5:55 AM F.MT04.05.07

**Understanding Nanoscale Adhesion via Machine Learning on Topology-Adhesion Correlated Data** [Yijie Jiang](#)<sup>1</sup>, Nava Raj Khatri<sup>1</sup> and Xin Ji<sup>2</sup>; <sup>1</sup>University of North Texas, United States; <sup>2</sup>Thomas Jefferson University Hospital, United States

Adhesion is a ubiquitous phenomenon that exists between every pair of surfaces. As an interfacial force, adhesion becomes dominant at nanoscale compared with body forces. Nanoscale adhesion is critical for applications such as the design of

nanoscale devices, MEMS, and nanofabrication. Local roughness at the nano- and atomic-scales significantly influence the adhesion and can reduce the adhesion by more than one order of magnitude than that predicted by classic idealized models. Statistical parameters, such as root mean square (rms) roughness, are proposed to develop new adhesion models and characterize nanoscale adhesion properties. Although the roughness is simplified into a statistical parameter in this way, it is inevitable to lose a lot of useful details of topological data. Here, we use machine learning to characterize interfacial adhesion properties based on nanoscale topology-adhesion correlated data. We perform high frequency quantitative nanoscale mechanical mapping (QNM) by AFM to simultaneously acquire topology at sub-nm resolution and adhesion at nanoscale at the interface between an AFM tip and a nominally flat surface. The adhesion varies over 20 folds (7.57 nN to 166.4 nN) due to nanoscale roughness. Local adhesion data is used as target and topological data at this and nearby locations (in-plane radius of 0.5 to 8 nm) is used as features. We use several machine learning methods to analyze the data, among which support vector regression (SVR) with radial basis function (RBF) kernel has the optimal performance. The prediction of the testing set (40% training and 60% testing data set) reaches  $r^2$  more than 0.97. Based on the results of machine learning, we develop an interfacial mechanics model that establishes the relationship between detailed local topology and adhesion. This model can be generalized for different materials and interfaces to understand nanoscale adhesion and the effect of roughness.

#### 6:05 AM F.MT04.05.09

**Frequency-Dependent Dielectric Constant Prediction of Polymers Using Machine Learning** [Lihua Chen](#) and Rampi Ramprasad; Georgia Institute of Technology, United States

The dielectric constant ( $\epsilon$ ) is a critical parameter utilized in the design of polymeric dielectrics for energy storage capacitors, microelectronic devices, and high-voltage insulations. However, agile discovery of polymer dielectrics with desirable  $\epsilon$  remains a challenge, especially for high-energy, high-temperature applications. To aid accelerated polymer dielectrics discovery, we have developed a machine-learning (ML)-based model to instantly and accurately predict the frequency-dependent  $\epsilon$  of polymers with the frequency range spanning 15 orders of magnitude. Our model is trained using a dataset of 1210 experimentally measured  $\epsilon$  values at different frequencies, an advanced polymer fingerprinting scheme and the Gaussian process regression algorithm. The developed ML model is utilized to predict the  $\epsilon$  of synthesizable 11,000 candidate polymers across the frequency range 60–10<sup>15</sup> Hz, with the correct inverse  $\epsilon$  vs. frequency trend recovered throughout. Furthermore, using  $\epsilon$  and another previously studied key design property (glass transition temperature,  $T_g$ ) as screening criteria, we propose five representative polymers with desired  $\epsilon$  and  $T_g$  for capacitors and microelectronic applications. This work demonstrates the use of surrogate ML models to successfully and rapidly discover polymers satisfying single or multiple property requirements for specific applications.

#### 6:15 AM F.MT04.05.11

**Phase Separation of Binary Mixture from a Data-Driven Approach** [Joydeep Munshi](#) and Ganesh Balasubramanian; Lehigh University, United States

Phase segregation of binary mixture has many applications including their popular application to investigate the evolution bulk heterojunction morphology (BHJ) from solvent evaporation of ternary mixture consisting of donor, acceptor and solvent molecules. Typically, macroscopic time evolution of phase separation is modeled computationally using system of coupled partial differential equations (PDE). Spontaneous separation of initially dispersed binary mixture is predominantly approximated by Cahn-Hilliard equations. However, the numerical simulations using physics-driven PDE equations are iterated through a computationally expensive scheme until the final steady-state decomposition is achieved. On the other hand, deep learning techniques enabled great progress in the area of computer vision applied to microstructure evolution. We employ convolutional neural network (CNN) to predict phase segregation by sampling final decomposition of binary mixture purely based on observations from coarse-grained molecular dynamics simulations. Our deep learning approach can learn and predict non-linear physical phenomenon such as phase separation without any knowledge of the underlying atomic interactions between the constituent materials. The ability to infer phase segregation phenomena is potentially appealing for the rational microstructure design given several solution processing conditions, the initially dispersed microstructure consisting of the constituent materials and their interaction parameters.

#### 6:25 AM F.MT04.05.12

**Prediction of Defect Locations in Graphene Using Machine Learning** [Bowen Zheng](#) and Grace Gu; UC Berkeley, United States

The presence of defects in two-dimensional (2D) materials, such as graphene, can deteriorate the properties, performances, and functionalities of graphene-based devices. The prior knowledge of defect information in graphene such as the defect type, size, and density allows us to make predictions of properties of graphene. Nevertheless, the detection of unknown defects

with an atomic-resolution probe such as transmission electron microscope is technically demanding and involves complex sample preparations. An alternative perspective arises when the thermal vibration of graphene sheets is examined. Because the absence or the substitution of an atom alters the boundary condition of adjacent oscillators, defective regions exhibit different vibrational properties compared to the pristine counterpart. However, the relation between defects and thermal vibration properties cannot be modeled explicitly. Here, we develop a machine learning-based approach to predict the unknown defect locations by thermal vibration topographies of graphene sheets, which overcomes the implicit relation between defect contents and vibration properties. Based on a kernel ridge regression model, two prediction strategies are developed, an atom-based method constructing data by atom indices, and a domain-based method constructing data by domain discretization. Trained by hundreds of thousands of vibrational energy distributions computed by molecular dynamics simulation, both methods can detect unknown graphene defects with a high accuracy. While the atom-based method is capable to predict a single-atom vacancy, the domain-based method can predict an unknown number of defects with an arbitrary distribution. The proposed data-driven strategy may also shed light on the defect detection in 2D materials of a broad variety.

#### 6:35 AM F.MT04.05.13

**Polymer Property Prediction and Design Through Multi-Task Learning** Christopher B. Kuenneth, Lihua Chen, Huan Tran, Chiho Kim, Arunkumar Rajan and Rampi Ramprasad; Georgia Institute of Technology, United States

Polymers are an important and diverse class of materials that span a huge chemical and property space. Machine learning methods have been recently successfully deployed to explore this space, revealing previously unidentified and novel polymers. The training of machine learning models requires a numerical representation of polymers, commonly termed fingerprints, as inputs which are “mapped” to the polymer properties as outputs. Single-task machine learning models learn the mapping between fingerprints and individual properties, one at a time. In contrast, multi-task algorithms learn the mapping of the chemical structure to multiple properties simultaneously. The effectiveness of this multi-task approach is because cross-property correlations, when present, are exploited implicitly. In this work, we benchmark two neural network based multi-task models against two single-task models for 27 different polymer properties. All models are trained on a polymer database containing ~8,000 polymers encompassing ~16,000 property points. The multi-task models demonstrate superiority over the single-task models, specifically for correlated polymer properties. An interpretability analysis of the multi-task model has also been performed that allow for the extraction of structure-property design rules.

#### 6:45 AM F.MT04.05.14

**Probing the Complexity of Coarse Grained Potentials with Gaussian Process Regression** Blake Duschatko, Jonathan Vandermause, Nicola Molinari and Boris Kozinsky; Harvard University, United States

Recent advances in machine learning have inspired the development of novel coarse grained molecular dynamics techniques wherein large length and time scale systems can be made more computationally tractable. Such regimes are essential for studying the dynamics soft materials, protein folding, and other complex processes that, in most cases, cannot be treated with current fully atomistic methods. In these schemes, where degrees of freedom in the all-atom picture are integrated out, one of the primary challenges lies in the construction of a free energy surface.

While the learned effective potential can be constructed on a variety of different physical bases, we consider those potentials that preserve the statistical mechanical properties of the atomistic system [1]. It is well known that the coarse graining process can induce complexity in the coarse grained potential that is not present in the all-atom case. In this work, we demonstrate the applicability of Gaussian processes for determining the optimal complexity of the free energy surface. This knowledge is crucial in designing models that are both computationally efficient and capture the essential physics of the problem.

In addition, we show the utility of active learning in the context of coarse graining. Recent efforts have shown that force field construction for ab initio molecular dynamics with Gaussian process regression [2] is amenable to active learning frameworks, and we demonstrate how this idea is transferable to coarse grained potentials. In this setting, we address the issue of “fine graining,” wherein an atomic representation of a given latent space despite the dramatic loss of information may be desirable.

[1] W. G. Noid, Jih-Wei Chu, Gary S. Ayton, Vinod Krishna, Sergei Izvekov, Gregory A. Voth, Avisek Das and Hans C. Andersen. “The multiscale coarse-graining method. I. A rigorous bridge between atomistic and coarse-grained models,” J. Chem. Phys. 128, 244114 (2008).

[2] Jonathan Vandermause, Steven B Torrissi, Simon Batzner, Alexie M Kolpak, and Boris Kozinsky. Submitted. “On-the-Fly



Bayesian Active Learning of Interpretable Force-Fields for Atomistic Rare Events,” npj Computational Materials 6 (2020).

#### 6:55 AM F.MT04.05.15

**Accelerated Discovery of Dielectric Polymer Materials Using Graph Attention Neural Networks** [Pankaj Rajak](#)<sup>1</sup>, Ankit Mishra<sup>2</sup>, Ekin Dogus Cubuk<sup>3</sup>, Ajinkya Deshmukh<sup>4</sup>, Yang Cao<sup>4</sup>, Greg Sotzing<sup>4</sup>, Rajiv Kalia<sup>2</sup>, Aiichiro Nakano<sup>2</sup>, Rampi Ramprasad<sup>5</sup> and Priya Vashishta<sup>2</sup>; <sup>1</sup>Argonne National Laboratory, United States; <sup>2</sup>University of Southern California, United States; <sup>3</sup>Google Inc, United States; <sup>4</sup>University of Connecticut, United States; <sup>5</sup>Georgia Institute of Technology, United States

Polynorbornene (PNB) is an important amorphous polymer system, which has potential applications as a high energy density polymer due to its high breakdown strength with low dielectric loss and high thermal stability. Moreover, electrical properties of PNB can be significantly enhanced by incorporation of defects or synthesis with controlled crystallinity by hydrogenation reaction. However, this process is challenging, since it involves experimental synthesis and characterization of combinatorially large number of polymer systems to identify potential candidates. Here, we propose a deep learning-based graph neural network (GNN) model with attention mechanism that can identify polymer systems capable of exhibiting increased energy and power density. The GNN model is trained to predict dielectric constant for a polymer, where the training data for the high-frequency dielectric constant of PNB polymers are computed via ab-initio molecular dynamics simulation. The attention mechanism in our GNN model provides key insight about the functional groups and their spatial location inside the polymer chain that contributes the most in its dielectric properties. Our model can significantly aid experimental synthesis of potentially new dielectric polymer materials, which is otherwise difficult using simplistic statistical procedures.

\*This work was supported by the Office of Naval Research through a Multi-University Research Initiative (MURI) under grant number (N00014-17-1-2656).

#### 7:05 AM F.MT04.05.16

**Tensor-Field Molecular Dynamics—An Uncertainty-Aware, Scalable and Accurate Deep Learning Model of Interatomic Force-Fields for Reactive Dynamics Simulations** [Simon L. Batzner](#)<sup>1,2</sup>, Lixin Sun<sup>1</sup>, Tess Smidt<sup>3</sup> and Boris Kozinsky<sup>1</sup>; <sup>1</sup>Harvard University, United States; <sup>2</sup>Massachusetts Institute of Technology, United States; <sup>3</sup>Lawrence Berkeley National Laboratory, United States

Deep Learning has great promise for accelerating Molecular-Dynamics simulations by learning complex representations of atomistic data. We present Tensor-Field Molecular Dynamics, an SE(3)-equivariant Graph-Neural Network that leverages rotationally equivariant graph convolutions to operate on geometric tensors (rather than only scalar values) to learn energies and forces of atomic systems. We demonstrate state-of-the-art performance on a diverse series of systems, including molecules, complex surface reactions, solvated polymers, extended systems, and water. In addition, we show that our proposed methods generalizes well from very small training data sets, which challenges the common belief that deep neural networks require massive training sets for accurate predictions. We then analyze a series of resulting Molecular Dynamics Simulations and compare thermodynamic and kinetic properties to the original ab-initio simulations. Finally, quantifying uncertainty of model prediction is critical for reliable long dynamics simulations. We outline a scalable method to obtain predictive uncertainty estimates of energies and forces from Tensor-Field models and present results on several different systems.

#### 7:15 AM F.MT04.05.17

**Machine Learning and Multiscale Modeling Based Prediction of Electronic Properties of PEDOT:PSS** Salvador León<sup>1</sup>, Patrick Reiser<sup>2</sup>, Loïc M. Roch<sup>3</sup>, Alán Aspuru-Guzik<sup>4</sup> and [Pascal Friederich](#)<sup>2,2</sup>; <sup>1</sup>Universidad Politécnica de Madrid, Spain; <sup>2</sup>Karlsruhe Institute of Technology, Germany; <sup>3</sup>ChemOS, Switzerland; <sup>4</sup>University of Toronto, Canada

Many organic electronics applications such as organic solar cells or thermoelectric generators rely on PEDOT:PSS as a conductive polymer that is printable and transparent. It was found that doping PEDOT:PSS with sorbitol enhances the conductivity through morphological changes. However, the microscopic mechanism is not well understood. We combine multiscale modeling techniques with machine learning to investigate changes in morphological and electronic properties of PEDOT:PSS when doped with sorbitol. We find that sorbitol improves the alignment of PEDOT oligomers, leading to a reduction of energy disorder and an increase in electronic couplings between PEDOT chains. The high accuracy ( $r^2 > 0.9$ ) and speedup of energy level predictions of neural networks compared to density functional theory enables us to analyze HOMO energies of PEDOT oligomers as a function of time which was computationally infeasible without machine learning. We find a surprisingly low degree of static energy disorder compared to other organic semiconductors. This finding might help to better understand the microscopic origin of the high charge carrier mobility of PEDOT:PSS in general and potentially

help to design new conductive polymers.[1]

We will furthermore show how the same machine learning approach can be applied to other organic semiconductors to evaluate static and dynamic energy disorder on an level of detail that was previously impossible due to the large computational cost of quantum mechanical calculations.

[1] The influence of sorbitol doping on aggregation and electronic properties of PEDOT:PSS: a theoretical study, Pascal Friederich, Salvador Leon, Jose Dario Perea Ospina, Loic Roch and Alan Aspuru-Guzik, Machine Learning: Science and Technology, 2020

#### 7:25 AM F.MT04.05.18

**Predicting the Long-Time Creep Dynamics of Colloidal Gels from Their Static Structure by Machine Learning** Han Liu and Mathieu Bauchy; University of California, Los Angeles, United States

the relationship, if any, between the structure and creep dynamics of gels remains elusive. Here, based on accelerated molecular dynamics simulations and classification-based machine learning, we show that the propensity of a gel to exhibit long-time creep is encoded in its static, unloaded structure. We extract a local, non-intuitive structural descriptor (“softness”) that is strongly correlated with the dynamics of the gel particles—wherein the macroscopic creep rate exhibits an exponential dependence on the average softness. We find that creep results in a decrease in softness in the gel structure, which, in turn, explains the gradual decay of the creep rate over time.

#### 7:35 AM F.MT04.05.19

**Physics-Guided Machine Learning Model of Lithium-Ion Battery Systems Involving Multiple Physics, Scales and Phases** Juner Zhu, Wei Li, Tomasz Wierzbicki and Martin Bazant; Massachusetts Institute of Technology, United States

Energy storage systems such as lithium-ion batteries (LIB) are ubiquitous in modern society with particular applications from consumer electronics to electric vehicles. One of the most fundamental challenges of studying and modeling the energy storage systems stems from the high dimensionality of the system, known as the *curse of dimensionality* (a great number of variables or degrees of freedom). For a commercial liquid-electrolyte battery cell, a comprehensive theoretical characterization of the LIB system should incorporate all the governing equations of the mechanics of the solid phases (electrodes, separator, and current collectors) and the liquid phase (electrolyte), the electrochemistry that involves mass transfer process of lithium ions, kinetics (rate of the reactions), and thermodynamics of materials, as well as the heat transfer processes over the electrodes and the whole battery cell. The complexity of the system increases exponentially considering that each of the governing equations has its own initial and boundary conditions that depend on the external loads and charge-discharge battery cycling behavior. Analytically solving such a system is almost impossible, and the real-world applicability of the existing so-called multi-physics numerical models based on the finite element method is usually hurt by the harsh conditions for convergence. Here, we use physics-guided machine learning algorithms to solve the coupled partial differential equations (PDE) of energy storage systems, and in this study, we demonstrate the applicability of the developed tool by using it to solve the poro-plasticity behavior of the battery, which involves Drucker-Prager/cap plasticity of the solid phase, Darcy’s law of the liquid phase, as well as the continuity equations. A neural network taking the spatial coordinates as the input and the displacement and stress of the solid phase and the velocity and pressure of the liquid phase as the output is constructed to approximate the exact solution. The prediction of the overall mechanical response is compared with the experimental data as validation. At last, a simplified battery electrochemistry model based on the multiphase porous electrode theory (MPET) is incorporated into the poro-plasticity framework, and the overall model is implemented by designing neural networks to reflect the multiple physics.

#### 7:45 AM F.MT04.05.21

**Late News: High-Throughput Exploration of Materials-Phase Diagram Maps in Multi-Component Organic Blends** Kiran Vaddi<sup>1</sup>, Balaji Sessa Sarath Pokuri<sup>2</sup>, Baskar Ganapathysubramanian<sup>2</sup> and Olga Wodo<sup>1</sup>; <sup>1</sup>University at Buffalo, United States; <sup>2</sup>Iowa State University of Science and Technology, United States

Organic thin films made of conjugated polymers and/or small molecules have captured the interest of the organic electronics industry due to their wide range of alterable properties (e.g., the color of light emission and solubility in organic solvents). High-performing devices have recently been designed with a multicomponent material system (as opposed to initial studies that focused on binary blends). This reaffirmed the need for a holistic approach to materials design beyond binary blends used to understand the mixing behavior and morphology formation during the fabrication of multicomponent organic thin films.

In this talk, we present a thermodynamics-based framework to identify the suitable solvents for a given electron-donor and accepting material with good performance as organic solar cells (OSC). We present high throughput exploration and construction of a material-phase diagram map that captures thermodynamics characteristics and facilitates understanding of the multicomponent solution's mixing behavior. Our analysis pipeline consists of (i) a physics based model to determine phase diagrams of multicomponent mixtures using the convex hull method; and (ii) high throughput analysis of a large set of phase diagrams using dimensionality reduction coupled with the clustering. To illustrate our pipeline, we derive the design rules for a few material systems typically used in OSC and compare it to the solubility sphere design rules.

SESSION F.MT04.06: Self-Assembly in Soft Materials  
On Demand Abstracts Available for Viewing Starting Saturday Morning, November 21, 2020  
F-MT04

**5:00 AM \*F.MT04.06.02**

**Self-Directed Self-Assembly** Alfredo Alexander-Katz and Hejin Huang; Massachusetts Institute of Technology, United States

Block copolymer (BCP) self-assembly, and in particular directed self-assembly (DSA), has provided a powerful route to fabricate complex thin film structures at small length scales. Despite DSAs success in fabricating various 2D patterns, fabrication of complex 3D nanostructures remains a challenge. Here, we will introduce a novel method, which we call Self-Directed Self-Assembly, and demonstrate how it can be leveraged to assemble 3D designer nanostructures using block copolymers. In particular we will demonstrate that uniform and non-uniform multilayer nanostructures can be obtained through stacking two or more "orthogonal" block copolymers. Finally, by introducing a patterned substrate to the first layer and performing multilayer stacking, we will demonstrate how to propagate information upwards in the film. Different complex multilayer structures will be shown, and at the end we will present an outlook on exciting new computational and artificial intelligence avenues of research in this field.

**5:15 AM F.MT04.06.03**

**Multifarious Assemblies Designed Through Linker-Mediated Interaction of Colloidal Particles** James Stahley and Mehdi Zanjani; Miami University, United States

DNA-mediated assembly of colloidal particles can be utilized to produce a variety of structures which may have desirable phononic, photonic, or electronic transport properties. Recent developments in linker-mediated assembly processes allow for interactions to be coordinated between many different types of colloidal particles more easily and with fewer unique sequences than direct hybridization. However, the dynamics of programmed self-assembly become increasingly more complex when coordinating interactions between three or more distinct interacting elements. In such cases particle pairs with similar binding energies are allowed to interact unpredictably, and enthalpically degenerate binding sites will be noticeably more present while numerous secondary phases may also result from the self-assembly process. Therefore, it is necessary to develop procedures for predicting feasible superstructure geometries for these systems before they can be implemented in material design.

Here we investigate the formation of multi-component ordered structures through self-assembly of spherically symmetrical colloidal particles of different sizes with a variety of interaction matrices. We utilize Molecular Dynamics (MD) and Brownian Dynamics (BD) simulations to study the growth behavior of systems with different types of interacting elements and predict the formation and stability of target structures. Our results provide direct guidelines for designing multifarious colloidal structures with three or more types of building blocks. We also study phononic spectrum of various ternary structures in order to identify the influence of key structural parameters on phonon bandgap frequencies and ranges. Overall, this study provides new directions for future experimental work to target formation of multi-component colloidal superstructures beyond the well-established binary symmetries studied in the past.

**5:25 AM F.MT04.06.04**

**Advances in DPD Simulations for Block Copolymer Self-Assembly** Hejin Huang and Alfredo Alexander-Katz; Massachusetts Institute of Technology, United States

Dissipative particle dynamics (DPD) has demonstrated excellent capabilities in describing the assembly and dynamics of

soft-matter systems in the past. Its intuitive representation and ease of use has been important to many areas, and in particular to self-assembly of block copolymers (BCPs). However, DPD in its original implementation to block copolymers is unable to capture accurately the different entropies for block copolymers at interfaces, which leads to erroneous qualitative results for BCP thin films. We have recently re-parameterized the DPD force field to yield accurate results in a multitude of thin film conditions. Here we present some of the unanticipated consequences of such new parametrization that appears to predict much better experimental results for phase transitions in BCPs than the traditional field theoretic methods. In particular we will introduce results from different densities to show how the order-disorder transition converges to a universal value similar to the experimental value, how the order-disorder transition is affected by polymer length, and finally how one can combine directly evolutionary algorithms to predict grapho and chemo epitaxial templates for desired thin film morphologies. Our results indicate that for typical copolymers with molecular weights below  $\sim 10^5$  g/mol, the order disorder transition occurs at a universal value of  $\chi N$ . Furthermore, our results clarify the role of entropic elasticity in the order-disorder transition. Simple scaling arguments demonstrate that SCFT and its corrections will fail to capture the correct order disorder temperature in the short to medium length copolymers. Our work should be useful to understand how experimentally relevant BCPs self assemble in different conditions as well as introduce the audience to new advances in the DPD technique that allow it to rival any field theoretic method, especially considering that DPD is a much more intuitive platform which is easier to implement and that it has a smaller computational footprint.

#### 5:35 AM F.MT04.06.05

**Design of Porous Materials by Self-Assembly of Isotropically DNA-Functionalized Particles** Runfang Mao and Jeetain Mittal; lehigh university, United States

The formation of porous structures such as diamond by bottom-up assembly remains one of the significant open challenges in colloidal systems. The interest in these materials with functional architectures stems from their broad potential applicability in diverse fields such as catalysis, separations, and photonics. The recently proposed approaches based on “DNA-functionalized particles” (DFPs) show promising results in the synthesis of low-coordination open structures such as diamond lattices in nanoparticle assemblies [1,2]. However, the underlying design approach in most of these cases is usually too complex to be scalable. In this work, for the first time, we demonstrate using multi-scale molecular simulations that low-coordination lattices (e.g., honeycomb in two-dimensional (2D) and diamond in three-dimensional (3D) systems) can be formed using simple isotropic functionalization of nanoparticles with DNA. The strength of our approach lies in its simplicity and potential ease with which the proposed design scheme can be implemented in the laboratory experiments.

[1] Wang, Yifan, et al. "Colloidal crystals with diamond symmetry at optical lengthscales." *Nature communications* 8.1 (2017): 1-8.

[2] Liu, Wenyan, et al. "Diamond family of nanoparticle superlattices." *Science* 351.6273 (2016): 582-586.

SESSION F.MT04.07: Poster Session: Using Machine Learning and Multiscale Modeling to Study Soft Materials and Interfaces

On Demand Abstracts Available for Viewing Starting Saturday Morning, November 21, 2020

5:00 AM - 8:00 AM

F-MT04

#### F.MT04.07.01

**Synthesis of Si Block-Containing Gradient Block Copolymer with Increased Assembly Kinetics via Systematic Homopolymer Control for the Fabrication of a Perpendicular Lamellar Pattern** Yemin Park, Seung Won Song and Yeon Sik Jung; Korea Advanced Institute of Science and Technology, Korea (the Republic of)

The advancement in modern electronics has led to miniaturization of device and increase in demand for ultra-small and highly integrated device technology. Extreme ultraviolet lithography (EUV) has been utilized to meet the demand for patterning nano-elements of 20nm or less, however has issues regarding stochastic effects causing defects in the system. To resolve this issues, directed self-assembly of block copolymers has been considered as a promising candidate to aid EUV to develop of sub-10 nm patterns. To achieve the sub-10 nm pattern, block copolymers with high Flory-Huggins parameter ( $\chi$ ) is generally required for high quality pattern resolution. However, a few issues arise when using high  $\chi$  block copolymers. First, high  $\chi$  values generally lead to a large surface energy difference between the individual polymer blocks preventing formation of perpendicularly oriented lamellar patterns and reduce horizontal alignment of polymer blocks. Neutral brush

layer coating on the substrate is an option to reduce the energy difference, but does not fully resolve the issue as it not only requires additional processes and cost but also cannot be applied on substrates with prefabricated patterns. Secondly, high  $\chi$  block copolymer has slower self-assembly kinetics, leading to increased defect occurrence and self-assembly time. Therefore, a deliberate design for block copolymers with moderately high  $\chi$  values as well as rapid kinetics is required for facile DSA of perpendicular patterns.

Here, we suggest a newly designed block copolymer that can achieve high  $\chi$  value while forming perpendicular lamellar pattern. The key to the block copolymer design is incorporating a gradient copolymer block with Si-containing block to promote universal perpendicular alignment of lamellar morphology without the need for additional surface treatment or neutral brush layer. The block copolymer was synthesized by reversible addition-fragmentation chain-transfer polymerization to form a styrene (S)/ 2,3,4,5,6-pentafluorostyrene (PFS) gradient with a Si-containing 4-(tert-butyldimethylsiloxy)-styrene (4BDSS) copolymer block (P(S-*g*-PFS)-*b*-P4BDSS). The styrene/ pentafluorostyrene gradient copolymer consists of gradual composition change from the block junction region to the tail, which creates surface energy difference enough to energetically drive perpendicular lamellae formation, well supported by a thermodynamic model. Furthermore, by mixing P4BDSS homopolymer block with the block copolymer, the kinetic factor can be increased to be greater than that of existing high  $\chi$  block copolymers to accelerate the self-assembly time and reduce the number of defect occurrence.

#### **F.MT04.07.05**

**Machine Learning Approach to Long Time Step Molecular Dynamics for Hard Sphere Systems** Ka Chun Chan; Karlsruhe Institute of Technology, Germany

Atomistic simulation techniques such as molecular dynamics (MD) provide an accurate and precise description of atomic motion, molecular structure and permit the prediction of the physical and chemical properties of molecular system. However, MD requires expensive computation of energy and force which leads to significant computational effort. This severely limits MD applications to biological system and soft matter physics on long time scales.

The usual MD time step is approximately 1/10 of the fastest frequency of the molecular system. In order to accelerate the MD computation, we propose a machine learning approach to propagate the molecular system instead of the usual MD time step. As a first step we developed a machine learning (ML) propagator for hard-sphere systems that propagates the molecular system with each atomic collision as a new time step. The proposed algorithm learns the time evolution of the atomic motion and the collision between atoms, such that the neural network are able to predict the system trajectory, identify the collided atomic pairs and correct the trajectory of the collided pairs for each collision time step. We will discuss the perspective of this newly ML propagator for the acceleration of MD simulations and further application to the molecular system with long time scales.

#### **F.MT04.07.06**

**Late News: High Throughput Prediction of Stress-Strain Curve of Thermoplastic Elastomer Model Block Copolymers by Combining Hierarchical Simulation and Deep Learning** Takeshi Aoyagi; National Institute of Advanced Industrial Science and Technology, Japan

Thermoplastic elastomer (TPE) is a typical industrial product, in which the microphase separation of block copolymer is utilized. The products can be seen in daily life, elastic fiber, film and adhesive for examples. The dynamic properties such as non-linear stress-strain (S-S) behavior are key issue to design such industrial products. The phase separated structure as well as a polymer chain structure affects the S-S behaviors. However, it is often the case that complicate metastable structures are observed in industrial products, and it is not simple to find the relation between such phase separated structures and S-S behaviors. To tackle the problem, we applied hierarchical simulation and deep learning technique. We chose ABA type triblock copolymers, where A blocks and B blocks form glassy domain and rubbery domain respectively, as a TPE model. Stress-strain curve of wide variety of volume fraction and phase separated structures were investigated by hierarchical simulation of self-consistent field theory and coarse-grained molecular dynamics. Furthermore, we applied 3D-convolutional neural network (3D-CNN) to make regression between the phase separated structures and S-S curves obtained by the coarse-grained molecular dynamics simulation. The predicted S-S curve of untrained structures using trained 3D-CNN showed good agreement with simulation, and high-throughput prediction could be realized comparing to the computationally intensive simulation.

This work was supported by a JSPS Grant-in-Aid for Scientific Research on Innovative Areas: “Discrete Geometric Analysis for Materials Design” [Grant Number 17H06464].

#### **F.MT04.07.07**

**Late News: AI-Guided Coarse-Graining for More Efficient Modeling of SARS-CoV-2 Spike Glycoprotein** Ziji Zhang<sup>1</sup>, David Zhang<sup>2</sup>, Aditya Narayanan<sup>3</sup>, Aditya Ramabadrana<sup>4</sup>, Marcia Simon<sup>1</sup>, Miriam H. Rafailovich<sup>1</sup>, Yuefan Deng<sup>1</sup> and Peng Zhang<sup>1,1</sup>; <sup>1</sup>Stony Brook University, The State University of New York, United States; <sup>2</sup>Fremont High School, United States; <sup>3</sup>College Station High School, United States; <sup>4</sup>Lynbrook High School, United States

**Objectives:** The SARS-CoV-2 spike glycoprotein (S-protein), the presumed key receptor for binding to various material substrates, promotes the entry to host cells, and thereby causes infection. The binding dynamics of the S-protein to various substrates including organic, inorganic materials, and living cells is of great interest in biological science and clinical medicine. The all-atomic molecular dynamics (MD) simulations that are known to generate reliable results while mitigating potential biological risks for laboratory research are prohibitively expensive in computing time and resources.

**Methods:** We develop a coarse-grained (CG) model of the S-protein by intelligently learning the parameters from the corroborated *in vitro* and *in silico* data using DNNs on IBM's supercomputer. The CG parameters are optimized with the protein in water to provide a medium that offered fluidity *in vivo*. The MD data produced by GROMACS, are fed to the DNN to predict the force field among the CG particles to be simulated in LAMMPS. The loss function that measures the discrepancy between MD values, NN prediction, and CGMD functions, is minimized during the learning process. CG models speed up the all-atomic model by coalescing atoms to form macromolecules and thereby forgoing the unnecessary calculations of the internal degrees of freedom. The CG force field is electro-free and the solvent is modeled using DPD at the mesoscopic scales. The interactions between the proteins, their surrounding solvent, and the surface they bind to are described by formulating a hybrid of the Morse-repulsive and the dissipative terms. Besides, AI is also used to predict the associated temporal scale parameters.

**Results:** The VMD model builder is used to construct two different CG models, shape-based coarse-graining (SBCG) and residue-based coarse-graining (RBCG), to the S-protein atomic data (PDB: 6VXX) which has 45,246 atoms, and evaluated their robustness with comparison to atomic-scale simulation. The nonbonded Lennard-Jones and bonded interaction parameters in the SBCG model, consisting of 355 beads with approximately 150 atoms per bead, were learned from the all-atom simulations. The bonded interaction parameters were tuned until the stiffness constants deviated less than 25% from those derived from the atomic-scale simulations. The RBCG model consists of 6498 beads, with approximately 7 atoms per bead, built with the RBCG 2007 topology file inside the Martini force field. We then solvated the model with Martini water and ionized the model with Na<sup>+</sup> and Cl<sup>-</sup> ions. After minimizing the CG system potentials, we successfully ran GPU-accelerated simulations with multiple runs to assess the impacts of the incrementally increasing timesteps to 14 fs. For verification and validation, the preliminary RMSD values were compared with the all-atomic simulations as the control, involving a single S-protein solvated in a water box with neutralizing ions at a temperature of 310K. The RMSD trends were converged which means our CG models have stable structures. Minimizing the differences of RMSD values by AI enables us to obtain more accurate parameters for longer simulations.

**Discussions and Future Work:** Our CG model uses learned parameters from big data to accelerate the conventional all-atomic MD by 4~5 orders of magnitude, without significant loss of accuracy. As the first AI-guided multiscale CG model, it may help enable a thorough investigation of the binding dynamics of the S-protein at varied ambient conditions including temperature and pH values. The limitation of this work may be that depending on different research needs, this CG model could achieve protein chain level accuracy, but not the atomic level. Our AI-guided modeling methodology can be generalized conveniently to study a large collection of materials, *e.g.*, fibrinogen.

**Acknowledgment:** The project is supported by OVPR&IEDM COVID-19 Grant, SUNY-IBM Consortium Award and Garcia High School Program.

#### **F.MT04.07.09**

**Late News: Mesoscale Modeling of Controlled Erosion of Tetra-Arm Polyethylene Glycol Based Nanogels** Eric F. Miller, Vaibhav A. Palkar and Olga Kuksenok; Clemson University, United States

Controlled degradation of micro- and nanogels finds its use in several applications. For instance, in the healthcare field, drugs containing gel particles are utilized for drug delivery. Drug release from such gels can be controlled via degradation of the hydrogel network triggered by various external stimuli. A better understanding of the gel degradation process will aid in the development of such applications. Computational modeling of gel degradation allows one to capture the dynamics of the degradation process depending on the degradation rate constant, initial crosslink density, size of the nanogel particle, and polymer-solvent affinity. To this end, we have developed a Dissipative Particle Dynamic (DPD) approach to capture the degradation of tetra-arm polyethylene glycol based nanogels. These networks are of interest since they have near-ideal network structure thereby exhibiting superior mechanical strength prior to the controlled degradation. Within our simulation approach, we model bond breaking during degradation as a stochastic process. Our results allow us to identify two distinct stages of the nanogel degradation. During the first stage, the bonds breaking within the gel results in the decrease in the crosslink density within the bulk of the gel particle and small tetra-arm pieces breaking off the surface of the nanogel (surface

erosion). During the second stage, bulk erosion and reverse gelation occurs. We characterize the transition between the two stages by focusing on the time evolution of the radius of gyration of the largest cluster and reduced degree of polymerization during the degradation process. We show that during the surface erosion, the radius of gyration of the largest cluster increases due to the effective decrease in the crosslink density being a major process, while during the second stage, this trend is reversed. We identify the effects of the gel size and an initial crosslink density on the crossover between the surface and bulk erosion. Our results represent a first mesoscale simulation study of a crossover between the surface and bulk erosion in gels.

## SYMPOSIUM F.MT05

---

Advancing Materials Characterization Through Atom Probe Tomography  
November 21 - December 3, 2020

### Symposium Organizers

Mukesh Bachhav, Idaho National Laboratory  
Baishakhi Mazumder, University at Buffalo, The State University of New York  
Jonathan Poplawsky, Oak Ridge National Laboratory  
Jae Bok Seol, Gyeongsang National University

### Symposium Support

**Bronze**  
CAMECA Instruments, Inc.  
Thermo Fisher Scientific

---

\* Invited Paper

SESSION F.MT05.07: Live Lightning/Flash I: Advancing Materials Characterization Through Atom Probe Tomography  
Session Chairs: Jonathan Poplawsky and Jae Bok Seol  
Wednesday Afternoon, December 2, 2020  
F.MT05

### 7:30 PM \*F.MT05.01.03

**Automation Advancements in Atom Probe Tomography** Katherine Rice, Brian Geiser, Timothy Payne, Gard Groth, Edward Oltman and Daniel Lenz; CAMECA Instruments, Inc., United States

CAMECA's recent innovations in the areas of automated acquisition, reconstruction, and data analysis have greatly increased the throughput and utilization of the Local Electrode Atom Probe™ [1]. These advances position the commercial atom probe as a process monitoring tool for nanoscale devices, providing routine characterization for suitable applications for the microelectronics industry.

CAMECA's Chain Acquisition module enables atom probe data to be acquired from multiple samples, without user intervention, using a recipe-based architecture [2]. Image processing technology is used to do automatic alignment of specimens on a microtip coupon, enabling the user to build a list of specimens that can be analyzed according to individual experimental plans. Live calibration and automated ranging can be performed as the instrument is acquiring data, enabling both accurate charge state ratios and reduced user input to mass spectrum assignments. Automated local electrode testing can be performed between analyses, preventing a compromised electrode from affecting the quality of planned experiments, keeping a record of the electrode condition over time, and notifying a user when an electrode may have decreased in quality. The experimental conditions can also be dynamically changed with CAMECA's Scripted Acquisition module. Triggers can be defined to modify acquisition conditions in response to composition, background level, number of ions, or a variety of other experimental outputs. Scripted Acquisition can be used in conjunction with Chain Acquisition to further increase throughput; for example, the acquisition can be stopped after the region of interest is collected and automatically begin acquisition from the next specimen in the chain. This decreases acquisition overall time and increases the value of the dataset by only

collecting the necessary volumes. Project management allows scripts to easily be shared between users so that repeatable experiments can be conducted in laboratories around the world. In addition to automated acquisitions, CAMECA's Atom Probe (AP) Suite enables recipe-based reconstructions and analysis. Reconstructions are completed automatically via user-entered parameters, so that the data is ready for review shortly after collection. Automated reconstruction parameters can also be selected from a pre-existing list of experiment recipes. Further automated analysis can be queued with application of standard or custom analysis recipes applied to the finished reconstructions. This allows the analyst to repeatably extract the most important information from a dataset without manually applying the analysis steps. Together, these advances have made it faster and easier to collect data and reduce the experience requirements for new users to successfully collect and analyze data with atom probe tomography and reduce time-to-knowledge in the experimental process.

#### References

1. Larson, D. J. et al. Local Electrode Atom Probe Tomography (Springer Publishing, 2013).
2. Reinhard, D. A. et al. Atom Probe Tomography Productivity Enhancements. *Microscopy and Microanalysis* 25, 522–523 (2019).

#### 7:40 PM \*F.MT05.01.02

**Navigating the Forest Through the Trees via Machine Learning—Detecting Morphology from Atom Probe Images** Krishna Rajan; University at Buffalo, The State University of New York, United States

A paradox in APT is that while on the one hand, it provides an unprecedented level of imaging resolution in three dimensions, it is very difficult to obtain an accurate perspective of morphology or shape outlined by atoms of similar chemistry and microstructure. Hence, unlike scattering techniques such as electron microscopy, interfaces appear diffuse, not sharp. This, in turn, makes it challenging to visualize and quantitatively interpret the microstructure at the “meso” scale, where one is interested in the shape and form of the interfaces and their associated chemical gradients. In this presentation we provide an overview of the computational and machine learning approaches to characterize interface chemistry and morphology directly from atom probe images.

#### 7:50 PM F.MT05.01.04

**Cluster Analysis Using Machine Learning and Spatial Statistics** Galen B. Vincent, Andrew P. Proudian and Jeremy D. Zimmerman; Colorado School of Mines, United States

Clustering of atoms and molecules significantly impacts material properties and is therefore important to characterize accurately. In this work, we use machine learning and spatial statistics to quantify clustering behavior in simulated and experimental APT data. We base our technique on Ripley's K-function analysis,  $K(r)$ , which is a sensitive measure of spatial correlation (e.g. clustering). We use features from the  $K(r)$  analysis to train a Bayesian regularized neural network (BRNN) to extract radius metrics, intra-cluster density, and background density.

For our test case, training data was simulated for a fixed solute density with clusters of various mean radius, radius variance, intra-particle density, background density, and number of particles. The system was verified on a set of similarly generated data sets, with over 90% of the BRNN-based estimates falling within 10% of the true radius values. Comparing the accuracy of our model against values obtained from the maximum separation algorithm (MSA) in our simulated APT data, we find that the MSA algorithm exhibits large variations based on user-defined inputs while the BRNN model quantifies morphologies accurately. We also apply this analysis to an experimental APT reconstruction with MgZn clusters in a 7000 series aluminum alloy, easily extracting cluster parameters from real APT data.

#### 8:00 PM \*F.MT05.02.03

**Using a Laser-Pulsed Atom Probe Instrument for Thermal Processing** David R. Diercks, Akansha Singh, Rajesh Jha, cristian ciobanu and Aaron Stebner; Colorado School of Mines, United States

Heat treatment of materials to improve performance has been employed for thousands of years. Control of the final size, composition, and distribution of the material's phases is of paramount importance and can be influenced by small changes in initial compositions, temperature, and annealing time. Therefore, knowing what occurs at the earliest stages of the



transformation process would shed insight into how to modify the materials for better control of their properties. It has been only within the last one hundred years that the characterization technologies for probing the nanometer-scale mechanisms behind the improved material performance resulting from heat treatments have been developed. While these tools have immensely expanded our understanding of materials and the mechanisms acting on them during thermal processing, there are still aspects that remain challenging to evaluate. In particular, sensitive quantitative compositional measurement with the combination of nano-scale spatial resolution and fractions of a second temporal resolution would provide needed insights into the earliest steps in diffusional processes.

Presented here is a demonstration of how the laser in a laser-pulsed atom probe instrument has been used to thermally induce crystallization and subsequently probe the resulting material structure for a Fe-Si-Nb-Cu-B alloy. Methods of estimating the laser induced temperature profile, determining the cumulative annealing time, and evaluating the resultant three-dimensional nanoscale crystallization are explored. Correlated transmission electron microscopy imaging and diffraction are used to supplement the atom probe results. The distribution of copper-rich cluster sizes and cluster densities measured by atom probe tomography are compared with Thermo-Calc modeling results. Through this example, advantages and limitations of using the atom probe as a processing tool are evaluated.

#### **8:10 PM \*F.MT05.02.01**

**Measuring Nanosized Void Chemistry at High Accuracy Using Atom Probe Tomography** Xing Wang<sup>1,2</sup>, Constantinos Hatzoglou<sup>3,4</sup>, Yanwen Zhang<sup>2,5</sup>, Baptiste Gault<sup>6,7</sup>, Karren More<sup>2</sup>, Francois Vurpillot<sup>3</sup> and Jonathan Poplawsky<sup>2</sup>; <sup>1</sup>The Pennsylvania State University, United States; <sup>2</sup>Oak Ridge National Laboratory, United States; <sup>3</sup>Normandie Université, France; <sup>4</sup>Norwegian University of Science and Technology, Norway; <sup>5</sup>The University of Tennessee, Knoxville, United States; <sup>6</sup>Max-Planck-Institut für Eisenforschung, Germany; <sup>7</sup>Imperial College London, United Kingdom

Nanosized voids, including pores and bubbles, are a common type of defects that can either improve or degrade the material properties. Voids are essentially empty cavities. Accurate measurement of the material chemistry around voids is important for understanding the void-material interactions. Atom probe tomography (APT) is a promising technique for this task because of its capability to reconstruct 3D positions of elements in materials with a high spatial resolution and chemical sensitivity. However, there has been a knowledge gap regarding how voids are imaged using APT. By performing a correlative scanning transmission electron microscopy (STEM) and APT analysis on void-containing materials, we demonstrated that voids could lead to obvious aberrations in APT reconstructions. Specifically, the local atomic density near voids in an APT dataset can either increase or decrease compared to the matrix. Field evaporation simulations combined with experiments revealed the physical mechanisms for these aberrations and identified the key factors that determined the nature of the aberrations. Based on this study, a general approach for quantifying elemental concentrations near voids using APT has been proposed that has higher accuracy than traditional STEM-based techniques. This approach has been applied to characterize elemental segregations near bubbles in medium and high-entropy alloys (HEAs). The accurate APT measurement shows that in Ni-based HEAs, both Cr and Fe become depleted near bubbles, but Cr depletes more, indicating higher vacancy mobility via Cr. This finding is consistent with the defect energies calculated based on density functional theory and explains the faster bubble growth rate in Ni-based HEAs containing Cr.

#### **Acknowledgment**

This work was supported by the Energy Dissipation to Defect Evolution (EDDE) Center, an Energy Frontier Research Center funded by the U.S. Department of Energy (DOE), Office of Science, Basic Energy Sciences under contract number DE-AC05-00OR22725. Electron microscopy and APT were conducted at Oak Ridge National Laboratory's Center for Nanophase Materials Sciences (CNMS), which is a U.S. DOE Office of Science User Facility. We acknowledge the financial support of the Region Normandie-FEDER and ANR / EMC3 Labex, DYNAMITE project and support from Semiconductor Research Corporation (SRC) under task ID 2679.001 for the field evaporation simulation.

#### **8:19 PM BREAK**

#### **8:24 PM \*F.MT05.02.02**

**Atom Probe Tomography Using a Wavelength-Tunable Femtosecond-Pulsed Coherent Extreme Ultraviolet Light** Ann Chiramonti-Debay<sup>1</sup>, Luis Miaja<sup>1</sup>, Benjamin W. Caplins<sup>1</sup>, David R. Diercks<sup>2</sup>, Brian P. Gorman<sup>2</sup> and Norman A. Sanford<sup>1</sup>; <sup>1</sup>National Institute of Standards and Technology, United States; <sup>2</sup>Colorado School of Mines, United States

Atom probe tomography (APT) is a powerful tool for 3D materials characterization due to its desirable combination of high spatial resolution and high analytical sensitivity. In state-of-the-art laser-pulsed APT, a near ultraviolet (NUV) laser ( $E \approx 3.5$  eV to 3.6 eV;  $\lambda \approx 355$  nm to 343 nm) incident on the specimen provides the thermal energy to overcome the activation barrier

for field ion evaporation. NUV laser-pulsed APT has been used to successfully analyze a wide range of materials including metals, semiconductors, insulators, biological materials, and even liquids. However, the data quality is often degraded due to artifacts from the thermal pulsing mechanism. These various artifacts manifest in the form of increased uncertainty in the quantification of specimen composition from the time-of-flight mass spectrometry measurement.

Photon energies in the extreme ultraviolet region of the electromagnetic spectrum ( $E \approx 10$  eV to 100 eV;  $\lambda \approx 124$  nm to 12 nm) are significantly higher than those in the near ultraviolet and as such, have the potential to trigger entirely new ionization and desorption mechanisms that are not possible with the much lower photon energies in the NUV band. These include various athermal ionization pathways and/or highly local heating that is entirely unlike that achieved using NUV sources.

Initial results from the world's first EUV (41.85 eV;  $\lambda = 29.6$  nm) radiation-pulsed atom probe microscope will be presented. This instrument uses wavelength-tunable femtosecond-pulsed coherent EUV radiation from phase-matched high harmonic generation in a hollow-core capillary waveguide. EUV radiation-pulsed field ion emission in a variety of materials types will be discussed with respect to the quality of the mass spectrometry data and compared to results obtained using NUV sources. Specifically, the measured composition, time-independent background, time-delayed evaporation, charge state ratios, and multiple hit counts will be compared and related.

This project was made possible with material support from CAMECA Instruments through a Cooperative Research and Development Agreement.

#### 8:34 PM F.MT05.02.04

**Surface Dynamics Studies at the Nanoscale by Atom Probe Microscopy—Oxygen Atoms Tracking on Rh, Pt and PtRh Surfaces During  $H_2+O_2$  Reaction** Sten V. Lambeets<sup>1</sup>, Thierry Visart de Bocarmé<sup>2</sup>, Sylwia Owczarek<sup>3</sup>, Norbert Kruse<sup>4,1</sup> and Daniel Perea<sup>1</sup>; <sup>1</sup>Pacific Northwest National Laboratory, United States; <sup>2</sup>Université Libre de Bruxelles, Belgium; <sup>3</sup>University of Wrocław, Poland; <sup>4</sup>Washington State University, United States

Metallic surfaces undergo a series of surface and subsurface structural and chemical transformations that drastically change their surface and mechanical properties. Understanding such dynamics from a fundamental science standpoint is particularly important in the case of heterogeneous catalysis, as such fundamental understanding is needed to build rational links between chemical/structural surface properties and the desired catalytic performance. This work addresses the dynamics of  $O_2$  hydrogenation over rhodium (Rh), platinum (Pt) and PtRh alloy (10% wt Rh) revealed with Field Emission/Ion Microscopy (FIM/FEM). A comparative study is conducted with the use of other oxygen carrier gases:  $N_2O$ , CO and  $CO_2$ . Finally, Atom Probe Tomography (APT) is used to map the path of the oxygen atoms on and through the Rh surface. FIM and FEM are capable to image the apex of sharp needles with nanometric lateral resolution. At the nanoscale, this apex is in the form of a hemisphere with a variety of exposed atomic planes and facets that can be simultaneously probed. Morphology of such sample mimicks a single metal nanoparticle by its size and shape. FEM exhibits image contrast which is mainly determined by crystallographic plane-dependent variations of the work function. Local brightness variations on video-FEM is used to probe dynamic surface reactions<sup>1</sup>. The APT in turn provides a 3D atom-by-atom map of the entire apex volume with near atomic scale spatial resolution and part per million chemical sensitivity. By mapping the 3D distribution of Rh oxide and the morphology of the oxide/metal interface within the bulk after a controlled  $O_2(g)$  exposure, APT is used to explore the nature of oxygen atom penetration in the bulk.

Crystallographically-dependent chemical and structural dynamics of Rh and Pt surface oxidation during an ongoing oxygen exposure is directly observed with FIM/FEM. Focusing on Rh, we observe a mechanism of inter-facet cooperation between Rh{012} and Rh{113} crystallographic surface facets. Clean Rh surface (i.e. no oxide) exhibits bright contrast over {012} facets while {113} facets remain dark. However, upon exposure to oxygen originating from  $O_2$ ,  $N_2$ , or  $CO_2$ , we observe simultaneously, an increase brightness over the {113} facets and a decrease in brightness over the {012} facets. This tells us that dissociative adsorption of  $O_{ads}$  occurs on the {012} and is followed by oxygen penetration into the subsurface through the {113}. Similar dynamics are observed on Pt and PtRh with exposure to other oxygen carrier gases of  $N_2O$  and  $CO_2$ . Additionally, the addition of  $H_2$  recovers the original FEM pattern reflecting the reaction between  $H_{ads}$  and  $O_{ads}$ . This mechanism of inter-facet cooperation leads to a unique distribution of oxygen atoms within the bulk, which can be directly observed by APT. Following a 600s exposure of  $O_2$  ( $2.0 \times 10^{-2}$  Pa) at 700K of a pristine Rh needle (i.e. no native surface oxide), APT analysis reveals an anisotropic distribution of Rh oxides ( $RhO_x$ ) and the complex morphology of the oxide/metal interface reflecting a specific crystallographic dependence<sup>2</sup>. An enhanced density of  $RhO_x^{n+}$  ( $x = 1$  or  $2$  and  $n = 1$  or  $2$ ) species are found both under the (111) central plane and along only one of the two three-fold symmetric crystal zones comprising the {113} facets. An iso-density surface of the APT reconstruction reveals a central accumulation of  $RhO_x$  species along the [111] direction, connected to the {113} vicinal facets. In summary, we conclude  $O_{ads}$  occurs on the

{012} and is followed by oxygen penetration into the subsurface through the {113} towards the [111]. The combination of FEM and APT analysis delivers new insight into the Rh oxide formation and offers exciting perspectives leading a better and more fundamental understanding of the heterogenous catalysis as well as corrosion dynamics.

<sup>1</sup>Lambeets, S.V. et al. , *J.Phys. Chem. C* 121, 16238 (2017)

<sup>2</sup>Lambeets, S.V. et al. , *J.Phys. Chem. Lett.* 11, 3144 (2020)

#### 8:44 PM F.MT05.06.05

**Atom Probe-Aided Design of Additively Manufactured High-Temperature Aluminum Alloys** Richard A. Michi, Amit Shyam, Alex Plotkowski and Jonathan Poplawsky; Oak Ridge National Laboratory, United States

Conventional aluminum alloys cannot be utilized in the 250–450 °C temperature range due to a lack of microstructural stability, creating a technological gap currently filled by steels, titanium alloys, and Ni-base superalloys. Replacement of these materials with aluminum alloys has significant implications for the energy and transportation sectors (e.g., increased engine operating temperature and efficiency, lightweighting, cost reduction), but has yet to be achieved. In this talk, we will give examples of APT analysis aiding in the design of new generations of high-temperature, additively manufactured aluminum alloys specifically targeted for use in the 250–450 °C temperature range. In particular, we will show how APT analysis reveals Zr and Mn segregation to the coherent and semi-coherent interfaces of  $\theta'$  precipitates in a novel additively manufactured Al-Cu-Zr-Mn alloy, leading to thermal stability up to 350 °C. We will also discuss how the accurate measurement of matrix solute supersaturations facilitated by APT aid in the design of heat treatments for precipitation-strengthened alloys with thermally stable phases and the observations of refined, nanoscale microstructural features formed during the additive manufacturing process. APT was conducted at ORNL's Center for Nanophase Materials Sciences (CNMS), which is a U.S. DOE Office of Science User Facility.

#### 8:54 PM F.MT05.03.05

**Atomic-Level Investigation of Preferential Impurity Segregation to Grain Boundaries in Y-TZP Through a Graph-Based Structure** Olivia G. Licata<sup>1</sup>, Parth Desai<sup>1</sup>, Olga Wodo<sup>1</sup>, Jonathan Poplawsky<sup>2</sup> and Baishakhi Mazumder<sup>1</sup>; <sup>1</sup>University at Buffalo, SUNY, United States; <sup>2</sup>Oak Ridge National Laboratory, United States

Yttria-stabilized tetragonal zirconia polycrystal (Y-TZP) is of great interest due to its superior corrosion, wear-resistance, and high flexural strength. Y-TZP exhibits a unique toughening mechanism when a stimulus is applied, in which it transforms from tetragonal (t) to monoclinic (m) phase. Over time, this transformation can lead to an aging phenomenon known as low-temperature degradation (LTD)[1]. The aging process is influenced by microstructural features, such as porosity, impurities, grain size, and stabilizer content. These features are also interlinked with one another, making the route for process optimization less clear. Grain boundaries (GBs) are thought to serve as the nucleation site for t-m transformation as well as the path for transformation propagation [2,3]. In an attempt to strengthen the GBs and limit LTD, commercial processing methods have introduced dopants and varying stabilizers to the zirconia microstructure. For every pair of yttria ions in Y-TZP, one oxygen vacancy is introduced (to neutralize the excess charge of  $Y^{3+}$ )[4]. The annihilation of oxygen vacancies is widely accepted as the root cause of hydrothermal aging in Y-TZP; however, the underlying mechanism and its connection to the destabilization of the tetragonal phase is not fully understood. In this work, we will combine atomic-level insights on chemical distribution from atom probe tomography (APT) with graph-based materials representation to quantify the extent of elemental heterogeneity influence on microstructural features linked with the t-m transformation.

APT analysis was performed on a set of commercial 3Y-TZP ceramics (3 mol.%  $Y_2O_3$ ), revealing trace levels of Aluminum (Al), Hafnium (Hf), and Silicon (Si), which were introduced in the raw material and during processing steps. The three-dimensional atom maps from APT demonstrated Y-rich GBs, with a limited number of GBs exhibiting preferential segregation of Al impurities, as well. Concentration profiles taken perpendicularly across the GBs indicated 5 at.% Y and 2 at.% Al within the GB and ~1.5 at.% Y throughout the matrix. APT analysis provides the three-dimensional positions and chemical identity for each atom. The positional data from regions of interest were converted to a graph representation, allowing for the definition and extraction of descriptors to understand the underlying physical phenomena. For example, the nearest neighbor distance between ions of the same species was used to define a descriptor that helps identify the number and distribution of phases present within the sample. Another descriptor was based on the shortest path consisting of Al to help assess the propensity of diffusion. These methods were further extended to understand the likelihood of an O vacancy in a particular region.

Our combined approach utilizes rigorous materials characterization techniques and informatics to quantify critical variations in microstructure related to the t-m transformation. Through graph-based representation, we define new metrics to correlate the microstructure with potential routes for degradation. These understandings will aid in the improved design and processing of zirconia-based ceramics to limit the susceptibility to LTD aging while maintaining their valuable mechanical properties. Our method enhances the capabilities of APT data to quantify the underlying phenomena of material degradation.

#### References:

1. Chevalier, J. *et al.*, *Acta Biomaterialia*, **7**(7), 2986-2993 (2011).
2. Mecartney, M. L., & Rühle, M., *Acta metallurgica*, **37**(7), 1859-1863 (1989).
3. Chevalier, J., *Biomaterials*, **27**(4), 535-543 (2006).
4. Krishnamurthy R., *et al.*, *Journal of the American Ceramic Society* **87**(10), 1821-1830 (2004).
5. Acknowledgement: APT was conducted at ORNL's Center for Nanophase Materials Sciences (CNMS), which is a U.S. DOE Office of Science User Facility.

#### 9:04 PM \*F.MT05.05.01

**Exploring New Science Domains with Atom Probe Tomography Enabled by an Environmental Transfer Hub** Daniel Perea; Pacific Northwest National Laboratory, United States

It is well known that environmental exposure of materials can lead to alteration, such as for example, the formation of an unintended surface oxide layer, that in some cases can affect the intended analysis. To prevent unwanted morphological or chemical alteration of specimens prior to analysis, control of the specimen environment during transfer between instruments is required for specimens sensitive to air or thermal exposure. At PNNL, we have developed a suite of hardware and experimental protocols for the preparation and handling of environmentally sensitive materials centered around the combination of a unique environmental transfer hub chamber, modified specimen suitcase device, and modified cryo FIB/SEM capabilities. The hub chamber design also allows the connection of ancillary tools, such as a gas phase reactor chamber for controlled surface reaction studies and UHV specimen transfer. The ability to prepare, manipulate, and transfer specimens under either cryogenic or vacuum conditions provides a means to uniquely apply APT analysis to address new science domains in biological, nuclear, and catalytic materials. Here I will describe in detail the design of our system and our developed workflows focusing on specific examples of APT analysis applied to *temperature sensitive* material systems requiring cryo specimen preparation and transfer, as well as *air sensitive* materials systems requiring vacuum or inert vacuum transfer.

#### 9:14 PM F.MT05.05.03

**Cryogenic Atom Probe Tomography for Hydrogen Characterisation in Steel Microstructures** Eason Chen and Julie Cairney; The University of Sydney, Australia

The presence of hydrogen in steels can lead to catastrophic embrittlement/early-fracture. This is a serious issue for hydrogen transportation and storage. However, consensus has not been reached on the exact mechanism of hydrogen embrittlement, mainly due to the difficulty to provide direct evidence of the hydrogen-materials interactions that underpins the hypotheses [1]. In addition, a proposed solution to hydrogen embrittlement by using steels that contain hydrogen traps such as carbide precipitates [2], is limited in its effectiveness, due to the inability to directly observe the proposed hydrogen trapping at microstructural features.

As such, we used atom probe to study the hydrogen distribution at key features, including dislocations [3], grain boundaries [3], and both incoherent [3] and coherent [4] carbide precipitates in BCC/BCT iron matrix. To enable these studies, we charged the sample with deuterium (a hydrogen isotope) to avoid ambiguity from background hydrogen, and utilised a cryogenic sample transfer protocol to allow sufficient signal to be retained for observations. These efforts lead to the confirmations of: i) hydrogen enrichment at dislocations, providing a concrete validation of the hydrogen-enhanced dislocation mobility theory of embrittlement; ii) hydrogen enrichment at grain boundaries, underpinning the hydrogen-enhanced grain boundary decohesion theory; iii) the hydrogen at the interface between large, incoherent precipitates and the surrounding steel matrix, settling a long-standing debate around whether hydrogen trapping is an interfacial effect; and iv) the hydrogen at the interior of small, coherent carbides, suggesting hydrogen can internalise into carbides under certain conditions.

#### Reference:

- [1] I. M. Robertson, et al. *Metall. Mater. Trans. A* **46a**(6), 2323-2341 (2015)
- [2] H. K. D. H. Bhadeshia, *ISIJ Int.* **56**, 24-36 (2016)

- [3] Y.-S. Chen et al., *Science* **367**, 171-175 (2020)  
[4] Y.-S. Chen et al., *Science* **355**, 1196-1199 (2017)

## 9:23 PM CLOSING SUMMARY

SESSION F.MT05.08: Live Lightning/Flash II: Advancing Materials Characterization Through Atom Probe Tomography  
Session Chairs: Baishakhi Mazumder and Jonathan Poplawsky  
Thursday Morning, December 3, 2020  
F.MT05

### 11:30 AM \*F.MT05.01.01

**The Quest for Nanometric Clouds and Clusters in Modern Engineered Materials** Stephan Gerstl<sup>1,2</sup>, Robin Schäublin<sup>1,2</sup>, Lijuan Cui<sup>3</sup>, Yong Dai<sup>3</sup>, Severin Küchler<sup>2</sup>, Vladimir Vojtech<sup>2</sup>, Leonardo Pierobon<sup>2</sup> and Jörg F. Löffler<sup>2</sup>; <sup>1</sup>ETH Zurich, Switzerland; <sup>2</sup>ETH Zürich, Switzerland; <sup>3</sup>Paul Scherrer Institut, Switzerland

In this contribution, we review and demonstrate various methods by which we push our characterization limits to better understand nanometric features in the smallest – possibly the most influential – features in nanostructurally engineered materials. Oxide dispersion strengthening of steels for example and, more generally, materials relying on multi-phase strengthening, precipitation hardening, and cluster-strengthening all require an initial catalytic core for the formation of the desired precipitates or mesoscale phases. There is thus a thrust in looking for these pre-precipitation clusters and nano-clouds, which occur in a wide variety of materials research projects. For their analysis we take advantage of correlative techniques between Atom Probe Tomography (APT), Transmission Electron Microscopy, and electron backscatter diffraction, some in combination with modeling & simulation and others utilizing our original cryo-transfer enabling developments.

We will first focus on FeCr alloys, which model ferritic steels relevant for the fusion community. Here we find intriguing details in the cluster and interfacial chemistry in its  $\alpha/\alpha'$  decomposed high-purity binary system [1]. We applied multiple analysis methods to determine their precipitate core compositions, as their structurally coherent boundaries have often shown to be relatively broad compared to other matrix/precipitate systems.

In the field of ferritic steels for advanced nuclear facilities, the nascent irradiation induced clustering and precipitation of nuclear transmutation byproducts is generally investigated to better understand the alloys' evolution of mechanical properties over extended lifetimes and thus irradiation doses. In our near-atomic-scale study we are able to identify the isotopic specificity and thus the particular ions of interest that influence the steel's mechanical properties.

Focusing on SmCo high-temperature supermagnets, we are able to determine the geometry, packing density and local chemistry between Zr-rich nano-platelets and Cu-rich cells, which prove to strongly influence the magnetic properties, such as coercivity [2]. Among these phases, even the finest clustering features may have a strong impact on the macroscopic magnetic properties. With respect to light metals, we show results of room-temperature ('natural') aging of Al alloys, where we have also investigated further alloy classes in Al and Mg that require specimens to remain at cryogenic temperatures from after their creation – to focused ion beam sharpening of the APT tips – to transferring them to the atom probe and enable interrogating their arrested nanostructures [3,4,5].

These examples demonstrate the impact of near-atomic to nano-scale analyses not only to better understand the initial 'gatherings' of atoms (nano-clouds) within a structure, but to stress the continued need for pushing boundaries of highest-resolution characterization methods, the correlation amongst each other, and deploying cryo-vacuum transfer methods.

[1] S. Küchler, V. Vojtech, S.S.A. Gerstl, R.E. Schäublin, J.F. Löffler, submitted to Acta Mater.

[2] L. Pierobon, András Kovács, R.E. Schäublin, S. S. A. Gerstl, J. Caron, U. Wyss, R.E. Dunin-Borkowski, J.F. Löffler, M. Charilaou, arXiv:1901.01922, 2019

[3] S. Pogatscher,<sup>1,2</sup> H. Antrekowitsch,<sup>2</sup> M. Werinos,<sup>2</sup> F. Moszner,<sup>1</sup> S. S. A. Gerstl,<sup>3</sup> M. F. Francis,<sup>4</sup> W. A. Curtin,<sup>4</sup> J. F. Löffler,<sup>1</sup> and P. J. Uggowitzer, Phys. Rev. Letters 112 (2014) 225701

[4] M. Cihova, R.E. Schäublin, L.B. Hauser, S.S.A. Gerstl, C. Simson, P.J. Uggowitzer, J.F. Löffler, Acta Mater. 158 (2018) 214-229.

[5] R.E. Schäublin, M. Becker, M. Cihova, S.S.A. Gerstl, D. Deiana, C. Hébert, S. Pogatscher, P.J. Uggowitzer and J.F. Löffler, submitted to Acta Mater.

### 11:40 AM .

11:41 AM F.MT05.01.06

**Local Uncertainty and Confidence Envelopes in Atom Probe Tomographic Reconstructions** Andrew P. Proudian and Jeremy D. Zimmerman; Colorado School of Mines, United States

A unique advantage of APT is its ability to provide precise mass information (*i.e.*  $< 1$  Da) over volumes of thousands of cubic nanometers with a three-dimensional spatial resolution of  $< 1$  nm. This resolution completely depends on the reconstruction process used to convert the raw data into its final form for analysis: the method must be accurate yet fast enough to work on a typical APT dataset containing millions of ions. Any assessment of spatial signal (*e.g.* clustering) in APT relies on the fidelity of the reconstruction.

Currently, the vast majority of reconstructions fundamentally rely on point-projection. This method is fast but suffers from spatial resolution inaccuracies—such as ions being placed unphysically close or unphysical voids or variations in the sample shape—because of its assumptions about both the sample geometry and ion trajectories. Furthermore, current reconstruction techniques and analyses derived from them do not have an associated uncertainty because they usually generate only a single, user-directed reconstruction. This makes it laborious to compare different sets of inputs even though it is known that these parameters can cause the reconstructions to vary substantially even when constrained by other knowledge of the sample (*e.g.* TEM). As a result, APT experiments generally base conclusions off of a single reconstruction without stating a statistical confidence.

We have developed a reconstruction method that provides a solution envelope, increasing confidence in the conclusions drawn from the data regardless of the exact solution. This method does so without needing measurements of the sample other than APT. We explicitly account for the lower x-y resolution of APT by shifting points in x & y, which incorporates this uncertainty into subsequent analyses. This adjustment is determined by solving the well-studied Assignment and Exact Cover Problems for slices of data in detector space; this process can also constrain the reconstruction to maintain density and minimum particle spacing. We may then use the resultant solution sets to determine the robustness of the morphological signal as compared to a null hypothesis of random labeling using the tools of spatial statistics.

We evaluate this method using simulated APT data containing small (0.7 nm diameter) clusters of boron in a random close packed (RCP) matrix of silicon, a system in which there is an approximately 2:1 evaporation field difference that leads to chromatic aberrations. A conventional reconstruction completely loses the clustering signal ( $p = 0.224$ ), even when optimized to minimize the positioning error with the known input pattern. In comparison, our method still recovers a clear clustering signature across the ensemble of reconstruction solutions ( $p < 0.001$ ). These results demonstrate that this reconstruction method can significantly improve the accuracy of reconstructions and increase confidence in any morphological conclusions.

11:52 AM \*F.MT05.03.01

**Nanoscale Visualization of Carbon Deposits and Magnesium Clusters in Zeolites Active in the Methanol-to-Olefins Process** Sophie H. van Vreeswijk<sup>1</sup>, Jonathan Poplawsky<sup>2</sup>, Irina Yarulina<sup>3</sup> and Bert M. Weckhuysen<sup>1</sup>; <sup>1</sup>Utrecht University, Netherlands; <sup>2</sup>Center for Nanophase Materials Sciences, United States; <sup>3</sup>BASF Corporation, Netherlands

In the methanol-to-hydrocarbons (MTH) process, methanol is converted to more valuable products, such as olefins and aromatics, using zeolite or zeotype catalysts. Methanol can be obtained from conventional as well as from more renewable sources, such as biomass, carbon containing waste and CO<sub>2</sub>, which explains the great commercial interest of this catalytic process. [1][2] The exact end-product of the process is determined by the zeolite pore structure and the number and nature of the acidic active sites. A key step in this MTH mechanism is the formation of a so-called hydrocarbon pool in which olefins and aromatic compounds function as activating and deactivating reaction intermediates. [3] Most of the unmodified proton form zeolites are extensively studied for their performance and deactivation in the MTH process. However, protons can be exchanged by other cations, which can drastically influence catalytic performance. [3] These influences on the catalytic behaviour are nonetheless not well understood.

In this work, magnesium was introduced in the chabazite structure SSZ-13 to (partially) replace the protons in the zeolite framework. This resulted in differences in both catalytic performance as well as catalyst deactivation. Using *operando* UV-Vis spectroscopy and *operando* X-ray diffraction, differences between reaction intermediates and catalyst characteristics can be linked to the catalytic performance.

Zeolites are notoriously difficult to study at the nano-scale, because of their instability under *e.g.* electron beams. [4] Atom probe tomography (APT) is uniquely positioned among all tomographic techniques; it can provide 3D chemical information

with sub-nm resolution, making it the only technique capable of finding nanometre scale relationships in these materials, and especially for studying elements that offer no significant z-contrast differences (e.g. Al and Si). With this technique we were able to visualize magnesium clusters, obtain information about the distribution of the magnesium with respect to the aluminium, as well as the correlation between magnesium and coke molecules after the MTH process.

To conclude, in this work both *operando* as well as APT studies on (un)-modified zeolites are described to be able to contribute to the unravelling of the MTH mechanism in the presence of e.g. Mg.

## References

- [1] Ji, Y.; Deimund, et al. *ACS Catal.* 2015, 5, 4456–4465.
- [2] Vogt, C.; et al. *Nat. Catal.* 2019, 2, 188–197.
- [3] Yarulina, I.; et al. *Nat. Catal.* 2018, 1, 398–411
- [4] Schmidt, J. E.; et al. *Angew. Chem. Int. Ed.* 2018, 57, 10422–10435

### 12:03 PM F.MT05.03.08

#### Stacking Order Dependent Elemental Diffusion Between STO/LMO/LASO Layers Revealed by Atom Probe Tomography Jith Sarker<sup>1,2</sup>, Wei Guo<sup>2</sup>, Manual Roldan<sup>3</sup>, Hans Christen<sup>2</sup>, Baishakhi Mazumder<sup>1</sup> and Jonathan

Poplawsky<sup>2</sup>; <sup>1</sup>University at Buffalo-SUNY, United States; <sup>2</sup>Oak Ridge National Laboratory, United States; <sup>3</sup>Arizona State University, United States

Perovskite metal oxides (ABO<sub>3</sub>) are highly promising for artificial superlattice fabrications due to their exceptional physical properties and chemical stabilities. Among perovskite metal oxide superlattice, SrTiO<sub>3</sub> (STO) and LaMnO<sub>3</sub> (LMO) based heterostructures has gained significant attention due to enhanced magnetic properties compared to bulk LMO, which is desirable for spintronic devices. Previous scanning transmission electron microscopy (STEM) results demonstrated that the oxygen octahedral rotation (the angle between Mn-O-Mn bonding) at the STO/LMO interface plays a vital role in tuning the magnetic moments in the LMO/STO superlattice. Diffusion of elements across these interfaces can also play a role in the magnetic properties; however, diffusion across these interfaces has not been well documented. STEM has been heavily used to study these materials because it is ideal for observing interfacial structure, but a small amount of interfacial elemental diffusion is difficult to quantify using analytical STEM techniques, such as electron energy loss spectroscopy (EELS). Atom probe tomography (APT) is a good candidate for quantifying the chemistry through these interfaces because it is a sub-nm resolution technique with a maximum sensitivity of ~10 ppm. To this end, APT was employed to map the interfacial chemistry of the STO/LMO superlattice structure. Two different superlattice structures were tested to isolate the top and bottom STO/LMO interfaces. STO/LMO/LASO (5x) and LASO/LMO/STO (5x) superstructures were grown by atomic layer deposition (ALD) on STO substrates to isolate LMO grown on top of STO (LMO→STO) and STO grown on top of LMO (STO→LMO). The saturation magnetic moment per Mn ion was significantly higher for LMO→STO ( $M_S \sim 1.67 \mu_B$  per Mn ion) compared to STO→LMO ( $M_S \sim 1.23 \mu_B$  per Mn ion). Other samples grown in the same manner showed the same behavior. The APT results reveal differences in interfacial elemental diffusion that can explain the observed differences in magnetic behavior. In this presentation, the impact of growth order on elemental diffusion using ALD and how elemental diffusion influences magnetic properties will be discussed. This study provides a direct insight on how changes in interfacial structure and chemistry of LMO/STO superlattice can modify the subsequent magnetic functionalities when the growth sequence is reversed. This information is crucial for understand the ALD growth technique of complex oxides and how to optimize ferromagnetism in future spintronic devices. APT was conducted at ORNL's Center for Nanophase Materials Sciences (CNMS), which is a U.S. DOE Office of Science User Facility.

### 12:14 PM \*F.MT05.04.02

#### Alloying for Corrosion Resistance—The Effect of Manganese and Silicon on a Polycrystalline Nickel-Based Superalloy Stella Pedrazzini; Imperial College London, United Kingdom

Nickel superalloys are employed in the hottest part of jet engines and industrial gas turbines for power generation. In these harsh environments, sulphur contamination can occur in-service, causing reductions in the predicted component lifetime. Our work uses environmental exposures and state of the art characterisation to explore the effect of low-level silicon (0.5 wt%) and manganese (1 wt%) additions on the sulphidation and type-2 hot corrosion response of a polycrystalline nickel superalloy.

Silicon was added promote formation of a compact dual-layer chromia-alumina scale that reduced oxidation rate in long-term experiments. The silicon-containing alloy was more resistant to hot corrosion from coupled NaCl + SO<sub>x</sub> exposure.

Manganese improved oxidation resistance by creating MnCr<sub>2</sub>O<sub>4</sub>, which reduced the oxidation rate but did not change the oxide scale morphology. The presence of Mn (a known sulphur scavenger) proved less effective than silicon, reducing the sulphidation and corrosion damage extent but not the overall depth.

## 12:24 PM BREAK

### 12:29 PM \*F.MT05.04.01

**ODS Steels—The Ideal Case to Study Biases Occurring During APT Analysis of Nanoparticles** Constantinos Hatzoglou<sup>1,2</sup>, Bertrand Radiguet<sup>1</sup>, Gerald Da Costa<sup>1</sup>, philippe Pareige<sup>1</sup> and Francois Vurpillot<sup>1</sup>; <sup>1</sup>Groupe de Physique des Materiaux (GPM), France; <sup>2</sup>Norwegian University of Science and Technology (NTNU), Norway

Oxide Dispersion Strengthened (ODS) steels are promising candidates for future nuclear reactors, partly due to the fine and dense dispersion of the nanoparticles they contain. Until now, there was no consensus as to the nature of the nanoparticles, because their analysis pushed the techniques to their limits and in consequence, introduced some artefacts.

Atom probe tomography (APT) analysis of an ODS steel reveal a dense dispersion ( $10^{23}$ – $10^{24}$  m<sup>-3</sup>) of small ( $\approx 2$  nm) nanoparticles enriched in Y, Ti and O. There are also numerous evidences of APT artefacts: high amount of matrix atoms in the particles (*i.e.* Fe and Cr), reconstructed morphology variations and so atomic density fluctuations, all depending of particles size. It appears that the current understanding of APT artefacts cannot explain all these observations. According to field evaporation simulations, composition and morphological biases result from a cross-over of ions trajectories. It then appears that the particles are pures in Y, Ti and O and therefore all the Fe and Cr atoms, observed in the particles (> 80 at.%), are coming for trajectories aberrations. This conclusion is supported by an analytical model (CCC), that can be applied to other materials, and by complementary experimental analysis (TEM measurements on extractive replica). Moreover, the proportion of Fe and Cr, artificially introduced in the particles, provides the composition of the Cr rich shell around the particles.

From this observation, a literature review shows a significant dispersion of the APT measurement in Y, Ti and O in the particles (considering only those elements), which makes precise characterization difficult. Several factors may be at the origin of this dispersion: the ODS steel (14YWT, MA957, 12YWT, MKCR...), the particles size, the data treatment protocol (and so the user), the APT used (ECOWATAP, LAWATAP, LEAP...) and its analysis conditions (pulse type, pulse fraction, temperature...). One of the objectives is to understand this measurement dispersion by limiting itself to the influence of the APT used. To do this, selected ODS steels was analyzed on different APT, available to the Material Physics Group and to the Norwegian University of Science and Technology and the data was processed by a single user with a quasi-automatic data treatment protocol.

### 12:40 PM \*F.MT05.04.03

**Atom Probe Tomography for Steel Product Development** Rosalia Rementeria; ArcelorMittal Global R&D, Spain

When it comes to structures, steel has an ability like no other material to provide outstanding and versatile combinations of strength and toughness, but also to boast with durability and cost efficiency. The properties of steel, as in most structural materials, are attainable by selection of the composition and adjustment of thermomechanical sequence and heat treatment. The migration and final distribution of solute atoms into the iron lattice and its inherent defects determines the performance of the end product. Atom probe tomography (APT) allows to image and quantify nano-scale phenomena relevant to steel metallurgy that have been known to exist for long but could not be directly observed, such as the first stages of tempering in carbon steels or solute decoration of dislocations, the so-known as Cottrell atmospheres. From the viewpoint of the properties, APT helps to understand in deep detail the mechanisms leading to precipitation strengthening, improved ductility, grain boundary pinning, toughness maximization or deterioration and grain boundary embrittlement, among others. Steel is fun to play with due to its infinite combinations of interstitial and substitutional alloying elements, the various equilibrium and non-equilibrium reactions of the matrix and its complex and sometimes abundant lattice defect substructure. We will review here application cases of APT in steel product development carried out by ArcelorMittal in collaboration with leading institutions.



## 1:02 PM F.MT05.05.04

**Correlative Microscopy of Stress Corrosion Cracking Using Atom Probe Tomography and High Speed Atomic Force Microscopy** Tomas Martin<sup>1</sup>, Stacy Moore<sup>1</sup>, Robert Burrows<sup>2</sup>, Loren Picco<sup>3,1</sup> and Oliver Payton<sup>1</sup>; <sup>1</sup>University of Bristol, United Kingdom; <sup>2</sup>National Nuclear Laboratory, United Kingdom; <sup>3</sup>Virginia Commonwealth University, United States

Stress corrosion cracking (SCC) is an important degradation mechanism in a number of key engineering applications, including water-cooled nuclear reactors. The mechanism behind SCC requires a susceptible material, a local stress and a corrosive environment, but the local behaviour and chemistry at the crack tip is complex and still not fully understood. For improved understanding of the SCC mechanism, it is necessary to better characterise the mechanical behaviour of the material during the formation of cracks, as well as the local chemistry at the crack tip. Atom probe tomography (APT) has been used previously to image the chemical composition of the grain boundary ahead of a crack tip in SUS316 stainless steel, showing that segregation of Ni plays an important role in sensitising the grain boundary to corrosive attack [1]. The high-speed atomic force microscope (HS-AFM) is a contact mode form of atomic force microscopy that can image the topography of surfaces at frames-per-second acquisition rates, enabling live images of chemical processes. Recent work with HS-AFM has observed real-time formation of cracks in 20Cr-25Ni-Nb stabilised stainless steel [2] and AISI Type 304 stainless steel [3] in a corrosive solution known to accelerate SCC. The ability to watch a grain boundary corrode and crack at video frame rates is a powerful tool to link SCC behaviour to the underlying mechanisms behind the process. In this study, the atomic-scale chemical characterisation capability of APT is utilised on crack tips of a sensitised AISI type 304 stainless steel that was observed cracking in an in-situ HS-AFM experiment in an aggressive thiosulphate solution. An APT liftout was obtained from a region close to the crack tip using a specimen preparation method adapted from that used to lift out site-specific grain boundaries in silicon [4]. This preparation method was able to site the crack interface routinely within the APT region of interest, and APT data of the metal-oxide interface showed is a depletion of Cr and Ni enrichment at the boundary, with a thin porous oxide rich in sodium. This was confirmed by focused ion beam cross-sectioning showing large voids at grain boundaries below the surface with a thin Na-rich oxide only at the edges of the voids, indicating a cracking mechanism dominated by the stress. The preparation process will be detailed, as well as correlative data between the two techniques to further the understanding of SCC behaviour in steels.

[1] M. Meisnar, M.P. Moody & S. Lozano-Perez, Atom probe tomography of stress corrosion crack tips in SUS316 stainless steel, *Corrosion Science* 98, pp 661-671, 2015

[2] S. Moore et al, A study of dynamic nanoscale corrosion initiation events using HS-AFM, *Faraday Discussions*, 210, 2018

[3] A Laferrere et al, In situ imaging of corrosion processes in nuclear fuel cladding, *Corros. Eng., Sci. Technol.*, 52, 596 — 604, 2017

[4] C Lotharukpong et al, Specimen preparation methods for elemental characterisation of grain boundaries and isolated dislocations in multicrystalline silicon using atom probe tomography, *Materials Characterisation*, 131, pp 472-479, 2017

## 1:12 PM CLOSING SUMMARY

SESSION F.MT05.01: Data Analysis, Algorithms and Reconstructions  
On Demand Abstracts Available for Viewing Starting Saturday Morning, November 21, 2020  
F-MT05

## 5:00 AM \*F.MT05.01.01

**The Quest for Nanometric Clouds and Clusters in Modern Engineered Materials** Stephan Gerstl<sup>1,2</sup>, Robin Schäublin<sup>1,2</sup>, Lijuan Cui<sup>3</sup>, Yong Dai<sup>3</sup>, Severin Kuchler<sup>2</sup>, Vladimir Vojtech<sup>2</sup>, Leonardo Pierobon<sup>2</sup> and Jörg F. Löffler<sup>2</sup>; <sup>1</sup>ETH Zurich, Switzerland; <sup>2</sup>ETH Zürich, Switzerland; <sup>3</sup>Paul Scherrer Institut, Switzerland

In this contribution, we review and demonstrate various methods by which we push our characterization limits to better understand nanometric features in the smallest – possibly the most influential – features in nanostructurally engineered materials. Oxide dispersion strengthening of steels for example and, more generally, materials relying on multi-phase strengthening, precipitation hardening, and cluster-strengthening all require an initial catalytic core for the formation of the desired precipitates or mesoscale phases. There is thus a thrust in looking for these pre-precipitation clusters and nano-clouds, which occur in a wide variety of materials research projects. For their analysis we take advantage of correlative techniques between Atom Probe Tomography (APT), Transmission Electron Microscopy, and electron backscatter diffraction, some in

combination with modeling & simulation and others utilizing our original cryo-transfer enabling developments. We will first focus on FeCr alloys, which model ferritic steels relevant for the fusion community. Here we find intriguing details in the cluster and interfacial chemistry in its  $\alpha/\alpha'$  decomposed high-purity binary system [1]. We applied multiple analysis methods to determine their precipitate core compositions, as their structurally coherent boundaries have often shown to be relatively broad compared to other matrix/precipitate systems.

In the field of ferritic steels for advanced nuclear facilities, the nascent irradiation induced clustering and precipitation of nuclear transmutation byproducts is generally investigated to better understand the alloys' evolution of mechanical properties over extended lifetimes and thus irradiation doses. In our near-atomic-scale study we are able to identify the isotopic specificity and thus the particular ions of interest that influence the steel's mechanical properties.

Focusing on SmCo high-temperature supermagnets, we are able to determine the geometry, packing density and local chemistry between Zr-rich nano-platelets and Cu-rich cells, which prove to strongly influence the magnetic properties, such as coercivity [2]. Among these phases, even the finest clustering features may have a strong impact on the macroscopic magnetic properties. With respect to light metals, we show results of room-temperature ('natural') aging of Al alloys, where we have also investigated further alloy classes in Al and Mg that require specimens to remain at cryogenic temperatures from after their creation – to focused ion beam sharpening of the APT tips – to transferring them to the atom probe and enable interrogating their arrested nanostructures [3,4,5].

These examples demonstrate the impact of near-atomic to nano-scale analyses not only to better understand the initial 'gatherings' of atoms (nano-clouds) within a structure, but to stress the continued need for pushing boundaries of highest-resolution characterization methods, the correlation amongst each other, and deploying cryo-vacuum transfer methods.

[1] S. Küchler, V. Vojtech, S.S.A. Gerstl, R.E. Schäublin, J.F. Löffler, submitted to Acta Mater.

[2] L. Pierobon, András Kovács, R.E. Schäublin, S. S. A. Gerstl, J. Caron, U. Wyss, R.E. Dunin-Borkowski, J.F. Löffler, M. Charilaou, arXiv:1901.01922, 2019

[3] S. Pogatscher,1,2 H. Antrekowitsch,2 M. Werinos,2 F. Moszner,1 S. S. A. Gerstl,3 M. F. Francis,4 W. A. Curtin,4 J. F. Löffler,1 and P. J. Uggowitzer, Phys. Rev. Letters 112 (2014) 225701

[4] M. Cihova, R.E. Schäublin, L.B. Hauser, S.S.A. Gerstl, C. Simson, P.J. Uggowitzer, J.F. Löffler, Acta Mater. 158 (2018) 214-229.

[5] R.E. Schäublin, M. Becker, M. Cihova, S.S.A. Gerstl, D. Deiana, C. Hébert, S. Pogatscher, P.J. Uggowitzer and J.F. Löffler, submitted to Acta Mater.

### 5:15 AM \*F.MT05.01.02

#### **Navigating the Forest Through the Trees via Machine Learning—Detecting Morphology from Atom Probe Images** Krishna Rajan; University at Buffalo, The State University of New York, United States

A paradox in APT is that while on the one hand, it provides an unprecedented level of imaging resolution in three dimensions, it is very difficult to obtain an accurate perspective of morphology or shape outlined by atoms of similar chemistry and microstructure. Hence, unlike scattering techniques such as electron microscopy, interfaces appear diffuse, not sharp. This, in turn, makes it challenging to visualize and quantitatively interpret the microstructure at the "meso" scale, where one is interested in the shape and form of the interfaces and their associated chemical gradients. In this presentation we provide an overview of the computational and machine learning approaches to characterize interface chemistry and morphology directly from atom probe images.

### 5:30 AM \*F.MT05.01.03

#### **Automation Advancements in Atom Probe Tomography** Katherine Rice, Brian Geiser, Timothy Payne, Gard Groth, Edward Oltman and Daniel Lenz; CAMECA Instruments, Inc., United States

CAMECA's recent innovations in the areas of automated acquisition, reconstruction, and data analysis have greatly increased the throughput and utilization of the Local Electrode Atom Probe™ [1]. These advances position the commercial atom probe as a process monitoring tool for nanoscale devices, providing routine characterization for suitable applications for the microelectronics industry.

CAMECA's Chain Acquisition module enables atom probe data to be acquired from multiple samples, without user intervention, using a recipe-based architecture [2]. Image processing technology is used to do automatic alignment of specimens on a microtip coupon, enabling the user to build a list of specimens that can be analyzed according to individual experimental plans. Live calibration and automated ranging can be performed as the instrument is acquiring data, enabling both accurate charge state ratios and reduced user input to mass spectrum assignments. Automated local electrode testing can be performed between analyses, preventing a compromised electrode from affecting the quality of planned experiments, keeping a record of the electrode condition over time, and notifying a user when an electrode may have decreased in quality.

The experimental conditions can also be dynamically changed with CAMECA's Scripted Acquisition module. Triggers can be defined to modify acquisition conditions in response to composition, background level, number of ions, or a variety of other experimental outputs. Scripted Acquisition can be used in conjunction with Chain Acquisition to further increase throughput; for example, the acquisition can be stopped after the region of interest is collected and automatically begin acquisition from the next specimen in the chain. This decreases acquisition overall time and increases the value of the dataset by only collecting the necessary volumes. Project management allows scripts to easily be shared between users so that repeatable experiments can be conducted in laboratories around the world.

In addition to automated acquisitions, CAMECA's Atom Probe (AP) Suite enables recipe-based reconstructions and analysis. Reconstructions are completed automatically via user-entered parameters, so that the data is ready for review shortly after collection. Automated reconstruction parameters can also be selected from a pre-existing list of experiment recipes. Further automated analysis can be queued with application of standard or custom analysis recipes applied to the finished reconstructions. This allows the analyst to repeatably extract the most important information from a dataset without manually applying the analysis steps. Together, these advances have made it faster and easier to collect data and reduce the experience requirements for new users to successfully collect and analyze data with atom probe tomography and reduce time-to-knowledge in the experimental process.

#### References

1. Larson, D. J. et al. Local Electrode Atom Probe Tomography (Springer Publishing, 2013).
2. Reinhard, D. A. et al. Atom Probe Tomography Productivity Enhancements. *Microscopy and Microanalysis* 25, 522–523 (2019).

#### 5:45 AM F.MT05.01.04

**Cluster Analysis Using Machine Learning and Spatial Statistics** Galen B. Vincent, Andrew P. Proudian and Jeremy D. Zimmerman; Colorado School of Mines, United States

Clustering of atoms and molecules significantly impacts material properties and is therefore important to characterize accurately. In this work, we use machine learning and spatial statistics to quantify clustering behavior in simulated and experimental APT data. We base our technique on Ripley's K-function analysis,  $K(r)$ , which is a sensitive measure of spatial correlation (e.g. clustering). We use features from the  $K(r)$  analysis to train a Bayesian regularized neural network (BRNN) to extract radius metrics, intra-cluster density, and background density.

For our test case, training data was simulated for a fixed solute density with clusters of various mean radius, radius variance, intra-particle density, background density, and number of particles. The system was verified on a set of similarly generated data sets, with over 90% of the BRNN-based estimates falling within 10% of the true radius values. Comparing the accuracy of our model against values obtained from the maximum separation algorithm (MSA) in our simulated APT data, we find that the MSA algorithm exhibits large variations based on user-defined inputs while the BRNN model quantifies morphologies accurately. We also apply this analysis to an experimental APT reconstruction with MgZn clusters in a 7000 series aluminum alloy, easily extracting cluster parameters from real APT data.

#### 5:55 AM F.MT05.01.06

**Local Uncertainty and Confidence Envelopes in Atom Probe Tomographic Reconstructions** Andrew P. Proudian and Jeremy D. Zimmerman; Colorado School of Mines, United States

A unique advantage of APT is its ability to provide precise mass information (*i.e.*  $< 1$  Da) over volumes of thousands of cubic nanometers with a three-dimensional spatial resolution of  $< 1$  nm. This resolution completely depends on the reconstruction process used to convert the raw data into its final form for analysis: the method must be accurate yet fast enough to work on a typical APT dataset containing millions of ions. Any assessment of spatial signal (e.g. clustering) in APT relies on the fidelity of the reconstruction.

Currently, the vast majority of reconstructions fundamentally rely on point-projection. This method is fast but suffers from spatial resolution inaccuracies—such as ions being placed unphysically close or unphysical voids or variations in the sample shape—because of its assumptions about both the sample geometry and ion trajectories. Furthermore, current reconstruction techniques and analyses derived from them do not have an associated uncertainty because they usually generate only a single, user-directed reconstruction. This makes it laborious to compare different sets of inputs even though it is known that these parameters can cause the reconstructions to vary substantially even when constrained by other knowledge of the sample (e.g. TEM). As a result, APT experiments generally base conclusions off of a single reconstruction without stating a

statistical confidence.

We have developed a reconstruction method that provides a solution envelope, increasing confidence in the conclusions drawn from the data regardless of the exact solution. This method does so without needing measurements of the sample other than APT. We explicitly account for the lower x-y resolution of APT by shifting points in x & y, which incorporates this uncertainty into subsequent analyses. This adjustment is determined by solving the well-studied Assignment and Exact Cover Problems for slices of data in detector space; this process can also constrain the reconstruction to maintain density and minimum particle spacing. We may then use the resultant solution sets to determine the robustness of the morphological signal as compared to a null hypothesis of random labeling using the tools of spatial statistics.

We evaluate this method using simulated APT data containing small (0.7 nm diameter) clusters of boron in a random close packed (RCP) matrix of silicon, a system in which there is an approximately 2:1 evaporation field difference that leads to chromatic aberrations. A conventional reconstruction completely loses the clustering signal ( $p = 0.224$ ), even when optimized to minimize the positioning error with the known input pattern. In comparison, our method still recovers a clear clustering signature across the ensemble of reconstruction solutions ( $p < 0.001$ ). These results demonstrate that this reconstruction method can significantly improve the accuracy of reconstructions and increase confidence in any morphological conclusions.

SESSION F.MT05.02: Field/Laser/Tip Interactions  
On Demand Abstracts Available for Viewing Starting Saturday Morning, November 21, 2020  
F-MT05

#### 5:00 AM \*F.MT05.02.01

**Measuring Nanosized Void Chemistry at High Accuracy Using Atom Probe Tomography** [Xing Wang](#)<sup>1,2</sup>, Constantinos Hatzoglou<sup>3,4</sup>, Yanwen Zhang<sup>2,5</sup>, Baptiste Gault<sup>6,7</sup>, Karren More<sup>2</sup>, Francois Vurpillot<sup>3</sup> and Jonathan Poplawsky<sup>2</sup>; <sup>1</sup>The Pennsylvania State University, United States; <sup>2</sup>Oak Ridge National Laboratory, United States; <sup>3</sup>Normandie Université, France; <sup>4</sup>Norwegian University of Science and Technology, Norway; <sup>5</sup>The University of Tennessee, Knoxville, United States; <sup>6</sup>Max-Planck-Institut für Eisenforschung, Germany; <sup>7</sup>Imperial College London, United Kingdom

Nanosized voids, including pores and bubbles, are a common type of defects that can either improve or degrade the material properties. Voids are essentially empty cavities. Accurate measurement of the material chemistry around voids is important for understanding the void-material interactions. Atom probe tomography (APT) is a promising technique for this task because of its capability to reconstruct 3D positions of elements in materials with a high spatial resolution and chemical sensitivity. However, there has been a knowledge gap regarding how voids are imaged using APT. By performing a correlative scanning transmission electron microscopy (STEM) and APT analysis on void-containing materials, we demonstrated that voids could lead to obvious aberrations in APT reconstructions. Specifically, the local atomic density near voids in an APT dataset can either increase or decrease compared to the matrix. Field evaporation simulations combined with experiments revealed the physical mechanisms for these aberrations and identified the key factors that determined the nature of the aberrations. Based on this study, a general approach for quantifying elemental concentrations near voids using APT has been proposed that has higher accuracy than traditional STEM-based techniques. This approach has been applied to characterize elemental segregations near bubbles in medium and high-entropy alloys (HEAs). The accurate APT measurement shows that in Ni-based HEAs, both Cr and Fe become depleted near bubbles, but Cr depletes more, indicating higher vacancy mobility via Cr. This finding is consistent with the defect energies calculated based on density functional theory and explains the faster bubble growth rate in Ni-based HEAs containing Cr.

#### Acknowledgment

This work was supported by the Energy Dissipation to Defect Evolution (EDDE) Center, an Energy Frontier Research Center funded by the U.S. Department of Energy (DOE), Office of Science, Basic Energy Sciences under contract number DE-AC05-00OR22725. Electron microscopy and APT were conducted at Oak Ridge National Laboratory's Center for Nanophase Materials Sciences (CNMS), which is a U.S. DOE Office of Science User Facility. We acknowledge the financial support of the Region Normandie-FEDER and ANR / EMC3 Labex, DYNAMITE project and support from Semiconductor Research Corporation (SRC) under task ID 2679.001 for the field evaporation simulation.

#### 5:15 AM \*F.MT05.02.02

**Atom Probe Tomography Using a Wavelength-Tunable Femtosecond-Pulsed Coherent Extreme Ultraviolet Light** [Ann](#)

Chiaromonti-Debay<sup>1</sup>, Luis Miaja<sup>1</sup>, Benjamin W. Caplins<sup>1</sup>, David R. Diercks<sup>2</sup>, Brian P. Gorman<sup>2</sup> and Norman A. Sanford<sup>1</sup>; <sup>1</sup>National Institute of Standards and Technology, United States; <sup>2</sup>Colorado School of Mines, United States

Atom probe tomography (APT) is a powerful tool for 3D materials characterization due to its desirable combination of high spatial resolution and high analytical sensitivity. In state-of-the-art laser-pulsed APT, a near ultraviolet (NUV) laser ( $E \approx 3.5$  eV to 3.6 eV;  $\lambda \approx 355$  nm to 343 nm) incident on the specimen provides the thermal energy to overcome the activation barrier for field ion evaporation. NUV laser-pulsed APT has been used to successfully analyze a wide range of materials including metals, semiconductors, insulators, biological materials, and even liquids. However, the data quality is often degraded due to artifacts from the thermal pulsing mechanism. These various artifacts manifest in the form of increased uncertainty in the quantification of specimen composition from the time-of-flight mass spectrometry measurement.

Photon energies in the extreme ultraviolet region of the electromagnetic spectrum ( $E \approx 10$  eV to 100 eV;  $\lambda \approx 124$  nm to 12 nm) are significantly higher than those in the near ultraviolet and as such, have the potential to trigger entirely new ionization and desorption mechanisms that are not possible with the much lower photon energies in the NUV band. These include various athermal ionization pathways and/or highly local heating that is entirely unlike that achieved using NUV sources.

Initial results from the world's first EUV (41.85 eV;  $\lambda = 29.6$  nm) radiation-pulsed atom probe microscope will be presented. This instrument uses wavelength-tunable femtosecond-pulsed coherent EUV radiation from phase-matched high harmonic generation in a hollow-core capillary waveguide. EUV radiation-pulsed field ion emission in a variety of materials types will be discussed with respect to the quality of the mass spectrometry data and compared to results obtained using NUV sources. Specifically, the measured composition, time-independent background, time-delayed evaporation, charge state ratios, and multiple hit counts will be compared and related.

This project was made possible with material support from CAMECA Instruments through a Cooperative Research and Development Agreement.

#### **5:30 AM \*F.MT05.02.03**

**Using a Laser-Pulsed Atom Probe Instrument for Thermal Processing** David R. Diercks, Akansha Singh, Rajesh Jha, cristian ciobanu and Aaron Stebner; Colorado School of Mines, United States

Heat treatment of materials to improve performance has been employed for thousands of years. Control of the final size, composition, and distribution of the material's phases is of paramount importance and can be influenced by small changes in initial compositions, temperature, and annealing time. Therefore, knowing what occurs at the earliest stages of the transformation process would shed insight into how to modify the materials for better control of their properties. It has been only within the last one hundred years that the characterization technologies for probing the nanometer-scale mechanisms behind the improved material performance resulting from heat treatments have been developed. While these tools have immensely expanded our understanding of materials and the mechanisms acting on them during thermal processing, there are still aspects that remain challenging to evaluate. In particular, sensitive quantitative compositional measurement with the combination of nano-scale spatial resolution and fractions of a second temporal resolution would provide needed insights into the earliest steps in diffusional processes.

Presented here is a demonstration of how the laser in a laser-pulsed atom probe instrument has been used to thermally induce crystallization and subsequently probe the resulting material structure for a Fe-Si-Nb-Cu-B alloy. Methods of estimating the laser induced temperature profile, determining the cumulative annealing time, and evaluating the resultant three-dimensional nanoscale crystallization are explored. Correlated transmission electron microscopy imaging and diffraction are used to supplement the atom probe results. The distribution of copper-rich cluster sizes and cluster densities measured by atom probe tomography are compared with Thermo-Calc modeling results. Through this example, advantages and limitations of using the atom probe as a processing tool are evaluated.

#### **5:45 AM F.MT05.02.04**

**Surface Dynamics Studies at the Nanoscale by Atom Probe Microscopy—Oxygen Atoms Tracking on Rh, Pt and PtRh Surfaces During H<sub>2</sub>+O<sub>2</sub> Reaction** Sten V. Lambeets<sup>1</sup>, Thierry Visart de Bocarmé<sup>2</sup>, Sylwia Owczarek<sup>3</sup>, Norbert Kruse<sup>4,1</sup> and Daniel Perea<sup>1</sup>; <sup>1</sup>Pacific Northwest National Laboratory, United States; <sup>2</sup>Université Libre de Bruxelles, Belgium; <sup>3</sup>University of Wrocław, Poland; <sup>4</sup>Washington State University, United States

Metallic surfaces undergo a series of surface and subsurface structural and chemical transformations that drastically change their surface and mechanical properties. Understanding such dynamics from a fundamental science standpoint is particularly

important in the case of heterogeneous catalysis, as such fundamental understanding is needed to build rational links between chemical/structural surface properties and the desired catalytic performance. This work addresses the dynamics of O<sub>2</sub> hydrogenation over rhodium (Rh), platinum (Pt) and PtRh alloy (10% wt Rh) revealed with Field Emission/Ion Microscopy (FIM/FEM). A comparative study is conducted with the use of other oxygen carrier gases: N<sub>2</sub>O, CO and CO<sub>2</sub>. Finally, Atom Probe Tomography (APT) is used to map the path of the oxygen atoms on and through the Rh surface. FIM and FEM are capable to image the apex of sharp needles with nanometric lateral resolution. At the nanoscale, this apex is in the form of a hemisphere with a variety of exposed atomic planes and facets that can be simultaneously probed. Morphology of such sample mimicks a single metal nanoparticle by its size and shape. FEM exhibits image contrast which is mainly determined by crystallographic plane-dependent variations of the work function. Local brightness variations on video-FEM is used to probe dynamic surface reactions<sup>1</sup>. The APT in turn provides a 3D atom-by-atom map of the entire apex volume with near atomic scale spatial resolution and part per million chemical sensitivity. By mapping the 3D distribution of Rh oxide and the morphology of the oxide/metal interface within the bulk after a controlled O<sub>2</sub>(g) exposure, APT is used to explore the nature of oxygen atom penetration in the bulk.

Crystallographically-dependent chemical and structural dynamics of Rh and Pt surface oxidation during an ongoing oxygen exposure is directly observed with FIM/FEM. Focusing on Rh, we observe a mechanism of inter-facet cooperation between Rh{012} and Rh{113} crystallographic surface facets. Clean Rh surface (i.e. no oxide) exhibits bright contrast over {012} facets while {113} facets remain dark. However, upon exposure to oxygen originating from O<sub>2</sub>, N<sub>2</sub>, or CO<sub>2</sub>, we observe simultaneously, an increase brightness over the {113} facets and a decrease in brightness over the {012} facets. This tells us that dissociative adsorption of O<sub>ads</sub> occurs on the {012} and is followed by oxygen penetration into the subsurface through the {113}. Similar dynamics are observed on Pt and PtRh with exposure to other oxygen carrier gases of N<sub>2</sub>O and CO<sub>2</sub>.

Additionally, the addition of H<sub>2</sub> recovers the original FEM pattern reflecting the reaction between H<sub>ads</sub> and O<sub>ads</sub>. This mechanism of inter-facet cooperation leads to a unique distribution of oxygen atoms within the bulk, which can be directly observed by APT. Following a 600s exposure of O<sub>2</sub> (2.0×10<sup>-2</sup>Pa) at 700K of a pristine Rh needle (i.e. no native surface oxide), APT analysis reveals an anisotropic distribution of Rh oxides (RhO<sub>x</sub>) and the complex morphology of the oxide/metal interface reflecting a specific crystallographic dependence<sup>2</sup>. An enhanced density of RhO<sub>x</sub><sup>n+</sup> (x = 1 or 2 and n = 1 or 2) species are found both under the (111) central plane and along only one of the two three-fold symmetric crystal zones comprising the {113} facets. An iso-density surface of the APT reconstruction reveals a central accumulation of RhO<sub>x</sub> species along the [111] direction, connected to the {113} vicinal facets. In summary, we conclude O<sub>ads</sub> occurs on the {012} and is followed by oxygen penetration into the subsurface through the {113} towards the [111].

The combination of FEM and APT analysis delivers new insight into the Rh oxide formation and offers exciting perspectives leading a better and more fundamental understanding of the heterogenous catalysis as well as corrosion dynamics.

<sup>1</sup>Lambeets, S.V. et al. , *J.Phys. Chem. C* 121, 16238 (2017)

<sup>2</sup>Lambeets, S.V. et al. , *J.Phys. Chem. Lett.* 11, 3144 (2020)

### 5:55 AM F.MT05.02.05

**Estimating Evaporation Fields and Specific Heats with Atom Probe Tomography** [Andrew P. Proudian](#) and Jeremy D. Zimmerman; Colorado School of Mines, United States

Estimations of evaporation field values in atom probe tomography are sparse in the literature despite their importance in the reconstruction and data analysis process. This work describes a method for estimating the zero-barrier evaporation field (ZBEF) using a straightforward measurement series of voltage versus laser pulse energy at a constant evaporation rate. This estimate depends on the sample radius of curvature and its specific heat. If a similar measurement is made of the voltage versus base temperature for a given evaporation rate, direct extraction of the material's specific heat can be made, leaving only the sample radius of curvature as an input parameter.

The method is applied to extract ZBEF in a previously published voltage versus laser pulse energy dataset for CdTe (18.07(87) V/nm).[1] Furthermore, using the published voltage versus base temperature sweep of CdTe permits extraction of a specific heat (11.27(254) J/K/mol @ 23.1 K) in good agreement with the literature (11.14 J/K/mol @ 22.17 K).[2] This method is then applied to a number of organic small molecules to understand how ZBEF depends on molecular properties.

[1] Diercks & Gorman, *J. Phys. Chem. C*, 119(35), 20623–20631 (2015).

[2] Birch, *J. Phys. C*, 8(13), 2043–2047 (1975).

**5:00 AM \*F.MT05.03.01**

**Nanoscale Visualization of Carbon Deposits and Magnesium Clusters in Zeolites Active in the Methanol-to-Olefins Process** Sophie H. van Vreeswijk<sup>1</sup>, Jonathan Poplawsky<sup>2</sup>, Irina Yarulina<sup>3</sup> and Bert M. Weckhuysen<sup>1</sup>; <sup>1</sup>Utrecht University, Netherlands; <sup>2</sup>Center for Nanophase Materials Sciences, United States; <sup>3</sup>BASF Corporation, Netherlands

In the methanol-to-hydrocarbons (MTH) process, methanol is converted to more valuable products, such as olefins and aromatics, using zeolite or zeotype catalysts. Methanol can be obtained from conventional as well as from more renewable sources, such as biomass, carbon containing waste and CO<sub>2</sub>, which explains the great commercial interest of this catalytic process. [1][2] The exact end-product of the process is determined by the zeolite pore structure and the number and nature of the acidic active sites. A key step in this MTH mechanism is the formation of a so-called hydrocarbon pool in which olefins and aromatic compounds function as activating and deactivating reaction intermediates. [3] Most of the unmodified proton form zeolites are extensively studied for their performance and deactivation in the MTH process. However, protons can be exchanged by other cations, which can drastically influence catalytic performance. [3] These influences on the catalytic behaviour are nonetheless not well understood.

In this work, magnesium was introduced in the chabazite structure SSZ-13 to (partially) replace the protons in the zeolite framework. This resulted in differences in both catalytic performance as well as catalyst deactivation. Using *operando* UV-Vis spectroscopy and *operando* X-ray diffraction, differences between reaction intermediates and catalyst characteristics can be linked to the catalytic performance.

Zeolites are notoriously difficult to study at the nano-scale, because of their instability under e.g. electron beams. [4] Atom probe tomography (APT) is uniquely positioned among all tomographic techniques; it can provide 3D chemical information with sub-nm resolution, making it the only technique capable of finding nanometre scale relationships in these materials, and especially for studying elements that offer no significant z-contrast differences (e.g. Al and Si). With this technique we were able to visualize magnesium clusters, obtain information about the distribution of the magnesium with respect to the aluminium, as well as the correlation between magnesium and coke molecules after the MTH process.

To conclude, in this work both *operando* as well as APT studies on (un)-modified zeolites are described to be able to contribute to the unravelling of the MTH mechanism in the presence of e.g. Mg.

**References**

- [1] Ji, Y.; Deimund, et al. *ACS Catal.* 2015, 5, 4456–4465.
- [2] Vogt, C.; et al. *Nat. Catal.* 2019, 2, 188–197.
- [3] Yarulina, I.; et al. *Nat. Catal.* 2018, 1, 398–411
- [4] Schmidt, J. E.; et al. *Angew. Chem. Int. Ed.* 2018, 57, 10422–10435

**5:15 AM F.MT05.03.05**

**Atomic-Level Investigation of Preferential Impurity Segregation to Grain Boundaries in Y-TZP Through a Graph-Based Structure** Olivia G. Licata<sup>1</sup>, Parth Desai<sup>1</sup>, Olga Wodo<sup>1</sup>, Jonathan Poplawsky<sup>2</sup> and Baishakhi Mazumder<sup>1</sup>; <sup>1</sup>University at Buffalo, SUNY, United States; <sup>2</sup>Oak Ridge National Laboratory, United States

Yttria-stabilized tetragonal zirconia polycrystal (Y-TZP) is of great interest due to its superior corrosion, wear-resistance, and high flexural strength. Y-TZP exhibits a unique toughening mechanism when a stimulus is applied, in which it transforms from tetragonal (t) to monoclinic (m) phase. Over time, this transformation can lead to an aging phenomenon known as low-temperature degradation (LTD)[1]. The aging process is influenced by microstructural features, such as porosity, impurities, grain size, and stabilizer content. These features are also interlinked with one another, making the route for process optimization less clear. Grain boundaries (GBs) are thought to serve as the nucleation site for t-m transformation as well as the path for transformation propagation [2,3]. In an attempt to strengthen the GBs and limit LTD, commercial processing methods have introduced dopants and varying stabilizers to the zirconia microstructure. For every pair of yttria ions in Y-TZP, one oxygen vacancy is introduced (to neutralize the excess charge of Y<sup>3+</sup>)[4]. The annihilation of oxygen vacancies is widely accepted as the root cause of hydrothermal aging in Y-TZP; however, the underlying mechanism and its connection to the destabilization of the tetragonal phase is not fully understood. In this work, we will combine atomic-level insights on

chemical distribution from atom probe tomography (APT) with graph-based materials representation to quantify the extent of elemental heterogeneity influence on microstructural features linked with the t-m transformation.

APT analysis was performed on a set of commercial 3Y-TZP ceramics (3 mol.%  $Y_2O_3$ ), revealing trace levels of Aluminum (Al), Hafnium (Hf), and Silicon (Si), which were introduced in the raw material and during processing steps. The three-dimensional atom maps from APT demonstrated Y-rich GBs, with a limited number of GBs exhibiting preferential segregation of Al impurities, as well. Concentration profiles taken perpendicularly across the GBs indicated 5 at.% Y and 2 at.% Al within the GB and  $\sim 1.5$  at.% Y throughout the matrix. APT analysis provides the three-dimensional positions and chemical identity for each atom. The positional data from regions of interest were converted to a graph representation, allowing for the definition and extraction of descriptors to understand the underlying physical phenomena. For example, the nearest neighbor distance between ions of the same species was used to define a descriptor that helps identify the number and distribution of phases present within the sample. Another descriptor was based on the shortest path consisting of Al to help assess the propensity of diffusion. These methods were further extended to understand the likelihood of an O vacancy in a particular region.

Our combined approach utilizes rigorous materials characterization techniques and informatics to quantify critical variations in microstructure related to the t-m transformation. Through graph-based representation, we define new metrics to correlate the microstructure with potential routes for degradation. These understandings will aid in the improved design and processing of zirconia-based ceramics to limit the susceptibility to LTD aging while maintaining their valuable mechanical properties. Our method enhances the capabilities of APT data to quantify the underlying phenomena of material degradation.

#### References:

1. Chevalier, J. *et al.*, *Acta Biomaterialia*, **7**(7), 2986-2993 (2011).
2. Mecartney, M. L., & Rühle, M., *Acta metallurgica*, **37**(7), 1859-1863 (1989).
3. Chevalier, J., *Biomaterials*, **27**(4), 535-543 (2006).
4. Krishnamurthy R., *et al.*, *Journal of the American Ceramic Society* **87**(10), 1821-1830 (2004).
5. Acknowledgement: APT was conducted at ORNL's Center for Nanophase Materials Sciences (CNMS), which is a U.S. DOE Office of Science User Facility.

#### 5:25 AM F.MT05.03.06

**Quantification of Carbon in Implanted Silicon Using Atom Probe Tomography** Paul Dumas<sup>1,2</sup>, Sébastien Duguay<sup>2</sup>, Julien Borrel<sup>1</sup>, Fanny Hilario<sup>1</sup> and Didier Blavette<sup>2</sup>; <sup>1</sup>STMICROELECTRONICS, France; <sup>2</sup>GPM ROUEN, France

Quantification of carbon in materials using Atom Probe Tomography (APT) is a common issue. Large underestimation in the carbon content is often observed [1,2]. One well known reason arises from multiple events that occur when several ions strike the detector nearly simultaneously and close to each other. When this happens, a part of ions may be lost due to the so-called electronic “dead time” and “dead zone” existing between each hit. This phenomenon is very likely when analyzing carbon because the high electric field needed to induce its evaporation promotes correlated departures of carbon ions at the tip surface. Dissociation of molecular ions during their flight from the tip to the detector is another source of carbon multiple events.

Carbon biases can also arise from mass-to-charge ratio overlaps in APT mass spectra. For example,  $(^{12}C^{12}C)^{2+}$  and  $^{12}C^+$  ions are overlapped as they share the same mass-to-charge ratio (12 Da). In this case, the proportion of each overlapped ion is needed to make a correct quantification. These quantities can sometimes be derived using isotopes abundance. In the above example, the true number of  $(^{12}C^{12}C)^{2+}$  counts at 12 Da can be derived from  $(^{12}C^{13}C)^{2+}$  counts at 12.5 Da. However, since the stable isotope  $^{13}C$  only account for 1.07% of the total carbon amount, ions containing  $^{13}C$  are not systematically detected. This issue arises in materials containing a low amount of carbon (less than 1%), for instance in the matrix of steels or in semiconductors.

The overlap issue faced in materials containing a low carbon content was addressed in this study using  $(^{12}C)^+$  and  $(^{13}C)^+$  implanted in equal proportion. Doses, energies and tilts used to introduce  $(^{12}C)^+$  and  $(^{13}C)^+$  in a 300 mm silicon wafer were  $1 \pm 0.01 \times 10^{15} \text{ cm}^{-2}$ , 30 keV and  $3^\circ$  respectively. The wafer was then annealed to restore silicon crystallinity (750°C for 5 hours). Carbon solubility in silicon being very low ( $\sim 2$  ppb at 750°C) compared to the implanted content ( $\sim 0.2$  at. %), carbon clusters were found by APT. Most peaks were indeed related to molecular ions originating from these clusters. Statistics was successfully used to identify these peaks and quantify the contribution of molecular ions to the carbon content.

Carbon quantification using APT was found more accurate using low electric fields conditions (high laser powers applied at



the tip surface). This was attributed to the hindering of molecular ion dissociation at low electric fields. Furthermore, the atomic fraction of carbon in clusters was found close to that of the expected SiC phase, only when using low electric field conditions (high laser power). This gives a mean number of trapped self-interstitials per carbon atom close to one, in agreement with other studies [3,4].

[1] Thuvander, Mattias, et al. "Quantitative atom probe analysis of carbides." *Ultramicroscopy* 111.6 (2011): 604-608.

[2] Estivill, Robert, et al. "Quantitative analysis of Si/SiGeC superlattices using atom probe tomography". *Ultramicroscopy* 159 (2015): 223-231.

[3] Cristiano et al. "Interstitial trapping efficiency of c+ implanted into preamorphised silicon—control of EOR defects." *Nuclear Instruments and Methods in Physics Research Section B: Beam Interactions with Materials and Atoms* 127 (1997): 22-26.

[4] Cacciato et al. "Dislocation formation and B transient diffusion in C coimplanted Si." *Journal of applied physics* 79.5 (1996): 2314-2325.

### 5:35 AM F.MT05.03.08

#### **Stacking Order Dependent Elemental Diffusion Between STO/LMO/LASO Layers Revealed by Atom Probe Tomography** Jith Sarker<sup>1,2</sup>, Wei Guo<sup>2</sup>, Manual Roldan<sup>3</sup>, Hans Christen<sup>2</sup>, Baishakhi Mazumder<sup>1</sup> and Jonathan

Poplawsky<sup>2</sup>; <sup>1</sup>University at Buffalo-SUNY, United States; <sup>2</sup>Oak Ridge National Laboratory, United States; <sup>3</sup>Arizona State University, United States

Perovskite metal oxides (ABO<sub>3</sub>) are highly promising for artificial superlattice fabrications due to their exceptional physical properties and chemical stabilities. Among perovskite metal oxide superlattice, SrTiO<sub>3</sub> (STO) and LaMnO<sub>3</sub> (LMO) based heterostructures has gained significant attention due to enhanced magnetic properties compared to bulk LMO, which is desirable for spintronic devices. Previous scanning transmission electron microscopy (STEM) results demonstrated that the oxygen octahedral rotation (the angle between Mn-O-Mn bonding) at the STO/LMO interface plays a vital role in tuning the magnetic moments in the LMO/STO superlattice. Diffusion of elements across these interfaces can also play a role in the magnetic properties; however, diffusion across these interfaces has not been well documented. STEM has been heavily used to study these materials because it is ideal for observing interfacial structure, but a small amount of interfacial elemental diffusion is difficult to quantify using analytical STEM techniques, such as electron energy loss spectroscopy (EELS). Atom probe tomography (APT) is a good candidate for quantifying the chemistry through these interfaces because it is a sub-nm resolution technique with a maximum sensitivity of ~10 ppm. To this end, APT was employed to map the interfacial chemistry of the STO/LMO superlattice structure. Two different superlattice structures were tested to isolate the top and bottom STO/LMO interfaces. STO/LMO/LASO (5x) and LASO/LMO/STO (5x) superstructures were grown by atomic layer deposition (ALD) on STO substrates to isolate LMO grown on top of STO (LMO→STO) and STO grown on top of LMO (STO→LMO). The saturation magnetic moment per Mn ion was significantly higher for LMO→STO ( $M_S \sim 1.67 \mu_B$  per Mn ion) compared to STO→LMO ( $M_S \sim 1.23 \mu_B$  per Mn ion). Other samples grown in the same manner showed the same behavior. The APT results reveal differences in interfacial elemental diffusion that can explain the observed differences in magnetic behavior. In this presentation, the impact of growth order on elemental diffusion using ALD and how elemental diffusion influences magnetic properties will be discussed. This study provides a direct insight on how changes in interfacial structure and chemistry of LMO/STO superlattice can modify the subsequent magnetic functionalities when the growth sequence is reversed. This information is crucial for understand the ALD growth technique of complex oxides and how to optimize ferromagnetism in future spintronic devices. APT was conducted at ORNL's Center for Nanophase Materials Sciences (CNMS), which is a U.S. DOE Office of Science User Facility.

SESSION F.MT05.04: Structural Materials

On Demand Abstracts Available for Viewing Starting Saturday Morning, November 21, 2020

F-MT05

### 5:00 AM \*F.MT05.04.01

#### **ODS Steels—The Ideal Case to Study Biases Occurring During APT Analysis of Nanoparticles** Constantinos

Hatzoglou<sup>1,2</sup>, Bertrand Radigue<sup>1</sup>, Gerald Da Costa<sup>1</sup>, philippe Pareige<sup>1</sup> and Francois Vurpillot<sup>1</sup>; <sup>1</sup>Groupe de Physique des Materiaux (GPM), France; <sup>2</sup>Norwegian University of Science and Technology (NTNU), Norway

Oxide Dispersion Strengthened (ODS) steels are promising candidates for future nuclear reactors, partly due to the fine and

dense dispersion of the nanoparticles they contain. Until now, there was no consensus as to the nature of the nanoparticles, because their analysis pushed the techniques to their limits and in consequence, introduced some artefacts. Atom probe tomography (APT) analysis of an ODS steel reveal a dense dispersion ( $10^{23}$ – $10^{24}$  m<sup>-3</sup>) of small ( $\approx 2$  nm) nanoparticles enriched in Y, Ti and O. There are also numerous evidences of APT artefacts: high amount of matrix atoms in the particles (*i.e.* Fe and Cr), reconstructed morphology variations and so atomic density fluctuations, all depending of particles size. It appears that the current understanding of APT artefacts cannot explain all these observations. According to field evaporation simulations, composition and morphological biases result from a cross-over of ions trajectories. It then appears that the particles are pures in Y, Ti and O and therefore all the Fe and Cr atoms, observed in the particles (> 80 at.%), are coming for trajectories aberrations. This conclusion is supported by an analytical model (CCC), that can be applied to other materials, and by complementary experimental analysis (TEM measurements on extractive replica). Moreover, the proportion of Fe and Cr, artificially introduced in the particles, provides the composition of the Cr rich shell around the particles.

From this observation, a literature review shows a significant dispersion of the APT measurement in Y, Ti and O in the particles (considering only those elements), which makes precise characterization difficult. Several factors may be at the origin of this dispersion: the ODS steel (14YWT, MA957, 12YWT, MKCR...), the particles size, the data treatment protocol (and so the user), the APT used (ECOWATAP, LAWATAP, LEAP...) and its analysis conditions (pulse type, pulse fraction, temperature...). One of the objectives is to understand this measurement dispersion by limiting itself to the influence of the APT used. To do this, selected ODS steels was analyzed on different APT, available to the Material Physics Group and to the Norwegian University of Science and Technology and the data was processed by a single user with a quasi-automatic data treatment protocol.

#### 5:15 AM \*F.MT05.04.02

##### **Alloying for Corrosion Resistance—The Effect of Manganese and Silicon on a Polycrystalline Nickel-Based Superalloy** Stella Pedrazzini; Imperial College London, United Kingdom

Nickel superalloys are employed in the hottest part of jet engines and industrial gas turbines for power generation. In these harsh environments, sulphur contamination can occur in-service, causing reductions in the predicted component lifetime. Our work uses environmental exposures and state of the art characterisation to explore the effect of low-level silicon (0.5 wt%) and manganese (1 wt%) additions on the sulphidation and type-2 hot corrosion response of a polycrystalline nickel superalloy.

Silicon was added promote formation of a compact dual-layer chromia-alumina scale that reduced oxidation rate in long-term experiments. The silicon-containing alloy was more resistant to hot corrosion from coupled NaCl + SO<sub>x</sub> exposure.

Manganese improved oxidation resistance by creating MnCr<sub>2</sub>O<sub>4</sub>, which reduced the oxidation rate but did not change the oxide scale morphology. The presence of Mn (a known sulphur scavenger) proved less effective than silicon, reducing the sulphidation and corrosion damage extent but not the overall depth.

#### 5:30 AM \*F.MT05.04.03

##### **Atom Probe Tomography for Steel Product Development** Rosalia Rementeria; ArcelorMittal Global R&D, Spain

When it comes to structures, steel has an ability like no other material to provide outstanding and versatile combinations of strength and toughness, but also to boast with durability and cost efficiency. The properties of steel, as in most structural materials, are attainable by selection of the composition and adjustment of thermomechanical sequence and heat treatment. The migration and final distribution of solute atoms into the iron lattice and its inherent defects determines the performance of the end product. Atom probe tomography (APT) allows to image and quantify nano-scale phenomena relevant to steel metallurgy that have been known to exist for long but could not be directly observed, such as the first stages of tempering in carbon steels or solute decoration of dislocations, the so-known as Cottrell atmospheres. From the viewpoint of the properties, APT helps to understand in deep detail the mechanisms leading to precipitation strengthening, improved ductility, grain boundary pinning, toughness maximization or deterioration and grain boundary embrittlement, among others. Steel is fun to play with due to its infinite combinations of interstitial and substitutional alloying elements, the various equilibrium and non-equilibrium reactions of the matrix and its complex and sometimes abundant lattice defect substructure. We will review here application cases of APT in steel product development carried out by ArcelorMittal in collaboration with leading institutions.

#### 5:45 AM \*F.MT05.04.04

##### **Improving the Strength of Grain Boundaries in Molybdenum by Segregation Engineering** S. Jakob<sup>1</sup>, K. Leitner<sup>1,2</sup>, A.

Lorich<sup>3</sup>, W. Knabl<sup>3</sup>, Helmut Clemens<sup>1</sup> and V. Maier-Kiener; <sup>1</sup>Montanuniversitaet Leoben, Austria; <sup>2</sup>voestalpine BÖHLER Edelstahl GmbH, Austria; <sup>3</sup>Plansee SE, Austria

Combining mechanical properties with chemical information on the nanometer scale have become a key approach in recent characterization techniques of metals and their alloys. The application of advanced high-resolution characterization techniques such as local electrode atom probe tomography enables a detailed investigation of the material's interfaces on an atomic level. Molybdenum has advantageous structural as well as functional properties leading to a broad range of applications. As a structural material, however, the application of technically pure molybdenum at low temperatures is limited because of its tendency for brittle intergranular failure. The direct correlation of strength and ductility with segregation content at the boundaries significantly helps to understand the intergranular fracture of molybdenum. The deliberate introduction of cohesion enhancing elements lead to a change in fracture mode, a lower brittle-to-ductile transition temperature and a higher ductility of the material. In this work, the site-specific preparation of the region of interest for atom probe measurement is performed using focused ions and so-called transmission Kikuchi diffraction. The grain boundaries of molybdenum alloys, which are showing a fracture mode change, are analyzed and compared to pure molybdenum. An outlook for improved ductility of molybdenum focusing on segregated elements is given.

SESSION F.MT05.05: Technique Development  
On Demand Abstracts Available for Viewing Starting Saturday Morning, November 21, 2020  
F-MT05

**5:00 AM \*F.MT05.05.01**

**Exploring New Science Domains with Atom Probe Tomography Enabled by an Environmental Transfer Hub** Daniel Perea; Pacific Northwest National Laboratory, United States

It is well known that environmental exposure of materials can lead to alteration, such as for example, the formation of an unintended surface oxide layer, that in some cases can affect the intended analysis. To prevent unwanted morphological or chemical alteration of specimens prior to analysis, control of the specimen environment during transfer between instruments is required for specimens sensitive to air or thermal exposure. At PNNL, we have developed a suite of hardware and experimental protocols for the preparation and handling of environmentally sensitive materials centered around the combination of a unique environmental transfer hub chamber, modified specimen suitcase device, and modified cryo FIB/SEM capabilities. The hub chamber design also allows the connection of ancillary tools, such as a gas phase reactor chamber for controlled surface reaction studies and UHV specimen transfer. The ability to prepare, manipulate, and transfer specimens under either cryogenic or vacuum conditions provides a means to uniquely apply APT analysis to address new science domains in biological, nuclear, and catalytic materials. Here I will describe in detail the design of our system and our developed workflows focusing on specific examples of APT analysis applied to *temperature sensitive* material systems requiring cryo specimen preparation and transfer, as well as *air sensitive* materials systems requiring vacuum or inert vacuum transfer.

**5:15 AM F.MT05.05.03**

**Cryogenic Atom Probe Tomography for Hydrogen Characterisation in Steel Microstructures** Eason Chen and Julie Cairney; The University of Sydney, Australia

The presence of hydrogen in steels can lead to catastrophic embrittlement/early-fracture. This is a serious issue for hydrogen transportation and storage. However, consensus has not been reached on the exact mechanism of hydrogen embrittlement, mainly due to the difficulty to provide direct evidence of the hydrogen-materials interactions that underpins the hypotheses [1]. In addition, a proposed solution to hydrogen embrittlement by using steels that contain hydrogen traps such as carbide precipitates [2], is limited in its effectiveness, due to the inability to directly observe the proposed hydrogen trapping at microstructural features.

As such, we used atom probe to study the hydrogen distribution at key features, including dislocations [3], grain boundaries [3], and both incoherent [3] and coherent [4] carbide precipitates in BCC/BCT iron matrix. To enable these studies, we charged the sample with deuterium (a hydrogen isotope) to avoid ambiguity from background hydrogen, and utilised a cryogenic sample transfer protocol to allow sufficient signal to be retained for observations. These efforts lead to the confirmations of: i) hydrogen enrichment at dislocations, providing a concrete validation of the hydrogen-enhanced

dislocation mobility theory of embrittlement; ii) hydrogen enrichment at grain boundaries, underpinning the hydrogen-enhanced grain boundary decohesion theory; iii) the hydrogen at the interface between large, incoherent precipitates and the surrounding steel matrix, settling a long-standing debate around whether hydrogen trapping is an interfacial effect; and iv) the hydrogen at the interior of small, coherent carbides, suggesting hydrogen can internalise into carbides under certain conditions.

Reference:

[1] I. M. Robertson, et al. *Metall. Mater. Trans. A* **46a**(6), 2323-2341 (2015)

[2] H. K. D. H. Bhadeshia, *ISIJ Int.* **56**, 24-36 (2016)

[3] Y.-S. Chen et al., *Science* **367**, 171-175 (2020)

[4] Y.-S. Chen et al., *Science* **355**, 1196-1199 (2017)

#### 5:25 AM F.MT05.05.04

**Correlative Microscopy of Stress Corrosion Cracking Using Atom Probe Tomography and High Speed Atomic Force Microscopy** Tomas Martin<sup>1</sup>, Stacy Moore<sup>1</sup>, Robert Burrows<sup>2</sup>, Loren Picco<sup>3,1</sup> and Oliver Payton<sup>1</sup>; <sup>1</sup>University of Bristol, United Kingdom; <sup>2</sup>National Nuclear Laboratory, United Kingdom; <sup>3</sup>Virginia Commonwealth University, United States

Stress corrosion cracking (SCC) is an important degradation mechanism in a number of key engineering applications, including water-cooled nuclear reactors. The mechanism behind SCC requires a susceptible material, a local stress and a corrosive environment, but the local behaviour and chemistry at the crack tip is complex and still not fully understood. For improved understanding of the SCC mechanism, it is necessary to better characterise the mechanical behaviour of the material during the formation of cracks, as well as the local chemistry at the crack tip. Atom probe tomography (APT) has been used previously to image the chemical composition of the grain boundary ahead of a crack tip in SUS316 stainless steel, showing that segregation of Ni plays an important role in sensitising the grain boundary to corrosive attack [1]. The high-speed atomic force microscope (HS-AFM) is a contact mode form of atomic force microscopy that can image the topography of surfaces at frames-per-second acquisition rates, enabling live images of chemical processes. Recent work with HS-AFM has observed real-time formation of cracks in 20Cr-25Ni-Nb stabilised stainless steel [2] and AISI Type 304 stainless steel [3] in a corrosive solution known to accelerate SCC. The ability to watch a grain boundary corrode and crack at video frame rates is a powerful tool to link SCC behaviour to the underlying mechanisms behind the process. In this study, the atomic-scale chemical characterisation capability of APT is utilised on crack tips of a sensitised AISI type 304 stainless steel that was observed cracking in an in-situ HS-AFM experiment in an aggressive thiosulphate solution. An APT liftout was obtained from a region close to the crack tip using a specimen preparation method adapted from that used to lift out site-specific grain boundaries in silicon [4]. This preparation method was able to site the crack interface routinely within the APT region of interest, and APT data of the metal-oxide interface showed is a depletion of Cr and Ni enrichment at the boundary, with a thin porous oxide rich in sodium. This was confirmed by focused ion beam cross-sectioning showing large voids at grain boundaries below the surface with a thin Na-rich oxide only at the edges of the voids, indicating a cracking mechanism dominated by the stress. The preparation process will be detailed, as well as correlative data between the two techniques to further the understanding of SCC behaviour in steels.

[1] M. Meisnar, M.P. Moody & S. Lozano-Perez, Atom probe tomography of stress corrosion crack tips in SUS316 stainless steel, *Corrosion Science* 98, pp 661-671, 2015

[2] S. Moore et al, A study of dynamic nanoscale corrosion initiation events using HS-AFM, *Faraday Discussions*, 210, 2018

[3] A Laferrere et al, In situ imaging of corrosion processes in nuclear fuel cladding, *Corros. Eng., Sci. Technol.*, 52, 596 — 604, 2017

[4] C Lotharukpong et al, Specimen preparation methods for elemental characterisation of grain boundaries and isolated dislocations in multicrystalline silicon using atom probe tomography, *Materials Characterisation*, 131, pp 472-479, 2017

SESSION F.MT05.06: Poster Session: Advancing Materials Characterization Through Atom Probe Tomography  
On Demand Abstracts Available for Viewing Starting Saturday Morning, November 21, 2020

5:00 AM - 8:00 AM

F-MT05

#### F.MT05.06.01

**An Atom-Probe Tomography Study of High-Nickel Steel Weld Deposits with a Hierarchical Microstructure** Amir R. Farkoosh<sup>1</sup>, Daniel H. Bechetti<sup>2</sup>, Matthew F. Sinfield<sup>2</sup>, Jeffrey D. Farren<sup>2</sup> and David N. Seidman<sup>1,3</sup>; <sup>1</sup>Northwestern University,

United States; <sup>2</sup>Carderock Division, Naval Surface Warfare Center, United States; <sup>3</sup>Northwestern University Center for Atom-Probe Tomography (NUCAPT), United States

Fabrication of steel structures requires joining by fusion welding. As requirements for weight and cost savings drive increased demand for advanced high-strength, high-toughness structural steels, the ability to balance mechanical performance and microstructural robustness of steels for the spectrum of welding processes poses a significant challenge. One aspect of this challenge is material responses to reheating during multi-pass welding. Thermal transients induce extensive microstructural changes in prior weld passes, whose nature and magnitude are highly dependent on the specifics of the chosen welding processes and the steel's composition. Herein, we present a new high-nickel steel, developed at the Naval Surface Warfare Center Carderock Division, which exhibits a positive response to the intrinsic heat treatment imposed during multi-pass welding processes. Because of the non-equilibrium solidification conditions, the weldments exhibit a hierarchical microstructure with several unique features, including: (i) cellular/dendritic substructure due to constitutional super-cooling; (ii) micro-segregation; (iii) high oxygen and hydrogen concentrations; and (iv) different amounts of lath martensite, and retained austenite across the fusion zone. Here, site-specific atom-probe tomography has become an essential tool that enables us to study the different regions of this hierarchical microstructure in great detail. The atom-probe tomography experiments are complemented by differential interference contrast optical microscopy, TEM, X-ray diffraction, and EBSD to study the microstructural features over hierarchical length scales. We have demonstrated that it is possible to produce a fine martensitic microstructure, which is reinforced by a high number density of V(N,C) nanoprecipitates, without post-weld heat treatments, leading to both high-strength and toughness. The presence of the V(N,C) nanoprecipitates has a twofold benefit: (i) provides dispersion strengthening; and (ii) removes nitrogen and diffusible hydrogen from the microstructure, which improves the ductility of the weldments and increases resistance against hydrogen embrittlement. The fundamental knowledge acquired in this study is also utilized to optimize the alloy system for the fabrication of structural components through additive manufacturing processes.

#### **F.MT05.06.02**

**Dose Rate and Temperature Effect on the Alpha Prime Precipitation in Ion Irradiated Ultra-High Purity Fe-Cr Alloys** Yajie Zhao<sup>1</sup>, Arunodaya Bhattacharya<sup>2</sup>, Caleb Massey<sup>2</sup>, Pengcheng Zhu<sup>1</sup>, Cristelle Pareige<sup>3</sup>, Philip Edmondson<sup>2</sup>, Jean Henry<sup>4</sup> and Steven Zinkle<sup>1</sup>; <sup>1</sup>the University of Tennessee, United States; <sup>2</sup>Oak Ridge National Laboratory, United States; <sup>3</sup>Université et INSA de Rouen, France; <sup>4</sup>CEA, France

Cr-rich alpha prime ( $\alpha'$ ) precipitates are detrimental to the mechanical properties of FeCr based ferritic-martensitic steels. Understanding  $\alpha'$  precipitation under irradiation conditions is essential for the application of this steel in nuclear reactor environments. To study the effect of dose rate (ballistic dissolution) and irradiation temperature (radiation-enhanced diffusion) on  $\alpha'$  formation, ultra-high purity Fe-Cr alloys with 18 wt.% Cr (in either solid solution or thermally aged to form pre-existing  $\alpha'$  precipitates) were irradiated with 8 MeV Fe ions to a midrange ( $\sim 1$   $\mu\text{m}$ ) dose of 0.35-3.5 displacements per atom (dpa) between 300-450 °C at  $10^{-3}$ ,  $10^{-4}$  and  $10^{-5}$  dpa/s. Following irradiation, atom probe tomography (APT) was employed to characterize the number density, radius and Cr concentration of Cr-rich clusters. Homogeneously distributed  $\alpha'$  precipitates were revealed when radiation-enhanced diffusion dominates over ballistic dissolution ( $>300^\circ\text{C}$ ). All clusters are identified and quantified through the maximum separation method. The cluster Cr concentrations decrease as irradiation temperature decreases or dose rate increases. This is consistent with the less solute enrichment revealed by the proxigram across the iso-concentration interface. However, despite the irradiation conditions, all of the measured values are well below the equilibrium Cr concentration for  $\alpha'$  phase suggested by the phase diagram. The radius and number density of  $\alpha'$  clusters are similar and within statistical errors for different specimens. The segregation of Cr, C and N atoms to dislocation loops was also observed.

This research was sponsored by the Office of Fusion Energy Sciences, U.S. Department of Energy under contract DE-AC05-00OR22725 with UT-Battelle, LLC and grant # DE-SC0006661 with the University of Tennessee. The fabrication of the Fe-Cr binary alloys has been carried out within the framework of the EUROfusion Consortium and has received funding from the Euratom research and training program 2019–2020 under Grant Agreement No. 633053.

#### **F.MT05.06.03**

**High-Yield Cryo-APT Workflow Using a Low-Temperature Microgripper** Lorenz G. Lechner<sup>1</sup>, Andrew Smith<sup>2</sup> and Stephan Kleindiek<sup>2</sup>; <sup>1</sup>Kleindiek Inc., United States; <sup>2</sup>Kleindiek Nanotechnik, Germany

Focused-ion beam (FIB) target preparation is the gold standard for creating site-specific specimen for atom probe tomography (APT). However, FIB preparation can introduce artifacts, such as contamination, amorphization, and heating. One way to minimize sample damage is the usage of cryo-FIB. Cooling the specimen during FIB milling reduces heating

related damage and limits the diffusion of Ga. Cryo-FIB sample preparation as part of a complete cryo-APT workflow enables the study of soft and unstable materials, e.g., organic solar cells or high-mobility hydrogen impurities. However, FIB lift-out preparation requires modifications to succeed at low temperatures. Conventional techniques for in-situ lift-out use beam induced deposition to temporarily attach the specimen to a manipulator and permanently mount the specimen on a sample support structure. These "soldering" techniques use metal-organic precursor gases injected into the microscope chamber and locally decomposed using the electron or ion beam. Unfortunately, these gas-phase deposition processes do not work at low temperatures because the precursors form thick condensates on all cold surfaces. Alternative techniques, like beam cured adhesives, are also not feasible at cryogenic temperature.

Here, we demonstrate a gas-free cryo-liftout workflow using a low-temperature microgripper. The gripper assembly consists of a 3-axis micromanipulator equipped with an insulated gripper thermally anchored to the microscope's cold shield. Piezo motors position the system and actuate the gripper jaws with nanometer precision. The specimen is mounted inside the microscope on a cryo-stage. The region of interest is partially released from the bulk material using FIB cutting. The gripper grabs the specimen and — after a final release cut — maneuvers it onto a micro-post. After the specimen is attached to the post using redeposition welding, the gripper releases the specimen. In the last preparation step, annular FIB milling gives the sample its final shape.

In contrast to using conventional manipulation, there is no need to temporarily join the probe and specimen and subsequently cut them free. This simplification makes the process faster and more reliable, overall increasing its yield.

#### **F.MT05.06.05**

**Atom Probe-Aided Design of Additively Manufactured High-Temperature Aluminum Alloys** Richard A. Michi, Amit Shyam, Alex Plotkowski and Jonathan Poplawsky; Oak Ridge National Laboratory, United States

Conventional aluminum alloys cannot be utilized in the 250–450 °C temperature range due to a lack of microstructural stability, creating a technological gap currently filled by steels, titanium alloys, and Ni-base superalloys. Replacement of these materials with aluminum alloys has significant implications for the energy and transportation sectors (e.g., increased engine operating temperature and efficiency, lightweighting, cost reduction), but has yet to be achieved. In this talk, we will give examples of APT analysis aiding in the design of new generations of high-temperature, additively manufactured aluminum alloys specifically targeted for use in the 250–450 °C temperature range. In particular, we will show how APT analysis reveals Zr and Mn segregation to the coherent and semi-coherent interfaces of  $\theta'$  precipitates in a novel additively manufactured Al-Cu-Zr-Mn alloy, leading to thermal stability up to 350 °C. We will also discuss how the accurate measurement of matrix solute supersaturations facilitated by APT aid in the design of heat treatments for precipitation-strengthened alloys with thermally stable phases and the observations of refined, nanoscale microstructural features formed during the additive manufacturing process. APT was conducted at ORNL's Center for Nanophase Materials Sciences (CNMS), which is a U.S. DOE Office of Science User Facility.

#### **F.MT05.06.07**

**Tracking Coincident Pair Separation with Varying Concentration Reveals Insights on Nitride Field Evaporation** Olivia G. Licata and Baishakhi Mazumder; University at Buffalo, SUNY, United States

The unique ability of Atom probe tomography (APT) to study three-dimensional atomic distribution relies on the field evaporation of ions onto a position-sensitive detector. Multiple ion events reaching the detector within the same pulse period can result in compositional and spatial inaccuracies. Ideally, in APT analysis, acquisition parameters and conditions are modified so that the occurrence of multi-hit events is limited. Some material systems have a higher tendency for multi-hit events during field evaporation in APT, such as those containing boron, carbon, oxygen, nitrogen, and compound semiconductor materials. Under these unavoidable circumstances, these unique events have shown the potential to provide insight on field evaporation and material structure [1, 2]. Here, we define a metric by tracking the distance between coincident detector events within a heterostructure to gain insight on the unique evaporation behavior and crystallographic origin of nitride species. The distributions of pair distances are investigated for each species and region, to understand the influence of elemental composition on evaporated ion separation.

Al<sub>0.3</sub>Ga<sub>0.7</sub>N/AlN/GaN heterostructures, grown via molecular beam epitaxy (MBE) and metal-organic chemical vapor deposition (MOCVD), were utilized as test structures. Trends in mean and median pair separation distances were consistent between the two preparation methods. Additionally, individual pair species showed agreement within 0.2 nm in detector space. This finding allows for the distinction of Al-x and Ga-x events based on their pair separation. Interestingly, Al-x events show higher separation values than Ga-x events. This is in disagreement with the known lattice constants of Al-N and GaN. This result suggests that crystallographic spacing is not the dominant influence on pair separation. A more likely mechanism is related to the unique field evaporation of the species as well as characteristics of the surface field during

acquisition. The crystallographic orientation upon evaporation may also play a role in the resulting pair separation. Distributions of pair separation distance were utilized to investigate variability in the spread of multi-hit events across heterostructure layers. The most prominent feature was the consistent bimodality of  $\text{Al}^{2+}\text{-N}_2$ , suggesting two separate evaporation phenomena. This unique behavior may originate from a combination of dissociation events and correlated events occurring for the same species.

This in-depth analysis presents a statistical protocol for interpreting multi-hit events from APT data. The reported findings help define species-specific evaporation trends within a compound semiconductor heterostructure in an aim to expand the application of APT to complex systems. Defining the relation between multi-hit events and structural chemistry will extend the current capabilities of APT to gain insight on atomic spacing that was previously unattainable without the aid of additional characterization methods. Furthermore, this methodology can be applied to other material systems to qualify the likelihood of correlation, potential dissociation trends, and crystallographic nature.

## References

1. De Geuser, F., Gault, B., Bostel, A., & Vurpillot, F. (2007). Correlated field evaporation as seen by atom probe tomography. *Surface science*, 601(2), 536-543.
2. Müller, M., Saxey, D. W., Smith, G. D., & Gault, B. (2011). Some aspects of the field evaporation behaviour of GaSb. *Ultramicroscopy*, 111(6), 487-492.

### F.MT05.06.08

**Atom Probe Tomography and First Principal Calculation to Study N-Type Doping in  $(\text{Al}_x\text{Ga}_{1-x})_2\text{O}_3$**  Jith Sarker, Ankit Sharma, Uttam Singiseti and Baishakhi Mazumder; University at Buffalo, The State University of New York, United States

Efficient n-type doping in ultra-wide bandgap  $(\text{Al}_x\text{Ga}_{1-x})_2\text{O}_3$  is a key for the realization of high frequency transistors with theoretical performance limit. Group IV elements (Si, Sn and Ge) are being considered as efficient donors in  $(\text{Al}_x\text{Ga}_{1-x})_2\text{O}_3$  as they are predicted to substitute in cation sites and contribute in conductivity [1]. First principal calculations by density functional theory (DFT) proposed that Si is the most promising candidate for achieving n-type conductivity in  $(\text{Al}_x\text{Ga}_{1-x})_2\text{O}_3$  as it remains a shallow donor at the highest range of Al composition while other donors are likely to transform into deep level defects at high Al- $(\text{Al}_x\text{Ga}_{1-x})_2\text{O}_3$  [1]. Incorporation of Si in  $(\text{Al}_x\text{Ga}_{1-x})_2\text{O}_3$  has been reported experimentally. The dopant behavior in these films including dopant distribution, layer homogeneity, segregation/clustering with varying alloy composition is not reported so far. It has been reported for similar wide bandgap system, AlGaN that n-type doping introduces point defects such as cation vacancies ( $V_{\text{Ga}}$  and  $V_{\text{Al}}$ ). These defect sites act as charge trapping centers by interacting with dopants and forms complex defects ( $V_{\text{Ga}}\text{-Si}_{\text{Ga}}$  or  $V_{\text{Al}}\text{-Si}_{\text{Al}}$ ) [2]. This results in reduced carrier mobility at high doping regime and is termed as “compensating knee” [2]. Similar investigation on dopant behavior in  $(\text{Al}_x\text{Ga}_{1-x})_2\text{O}_3$  is not reported yet. It is crucial to have in depth understanding of dopant interaction down to atomic level structural chemistry of  $(\text{Al}_x\text{Ga}_{1-x})_2\text{O}_3$  films is pivotal to achieve excellent doping profile.

Atom probe tomography (APT) was employed to investigate the atomic level dopant behavior and dopant interaction in  $(\text{Al}_x\text{Ga}_{1-x})_2\text{O}_3$  with varying Al content ( $x = 0.10\text{-}1.0$ ). APT reveals that at low Al content, Si distribution is homogeneous while some high Si density island-like regions appears at high Al content ( $x80\%$ ). The statistical radial distribution function (RDF) was used to understand the dopant interaction in by exploring the nearest neighbor chemistry in the bulk regions of each  $(\text{Al}_x\text{Ga}_{1-x})_2\text{O}_3$  layer. RDF in layers with low Al contents ( $x = 10\text{-}20\%$ ) showed high Ga concentration in regions surrounding the Si atoms with Al concentration being very low, indicating Si is substituting in Ga sites. Ga concentration drops at the position of Si atoms implying the presence of  $V_{\text{Ga}}$ . This result indicates the potential  $V_{\text{Ga}}\text{-Si}_{\text{Ga}}$  defect complex formation. At high Al ( $x = 60\text{-}100\%$ ), high Al concentration was observed around Si atoms with Al concentration dropping at the location where Si atoms reside, indicating Al site occupancy with possible  $V_{\text{Al}}\text{-Si}_{\text{Al}}$  complexes. The initial interpretation of APT results coincided with what was observed in case of GaN, AlGaN and  $\text{Ga}_2\text{O}_3$  and would account for compensating effect in  $(\text{Al}_x\text{Ga}_{1-x})_2\text{O}_3$ .

The information obtained from APT would provide a guide to the first principal DFT study of Si doped  $(\text{Al}_x\text{Ga}_{1-x})_2\text{O}_3$ . DFT calculation will be performed to confirm the site specific substitution of dopants in  $(\text{Al}_x\text{Ga}_{1-x})_2\text{O}_3$  at low and high Al content. DFT will confirm the vacancy, interstitial or vacancy-interstitial complex defects by evaluating the formation enthalpy of these defects and defect complexes at different Al contents that would explain carrier compensation in wide bandgap semiconductors.

We acknowledge Dr. Hongping Zhao's group in Dept. of ECE at the Ohio State University for providing the samples.

[1] J. B. Varley *et. al.*, *Appl. Phys. Lett.* **116**, 172104 (2020)

[2] J. S. Harris *et. al.*, Appl. Phys. Lett. **112**, 152101 (2018)

#### F.MT05.06.09

**APT Reveals the Synergistic Role of Mn and Zr/Ti in Producing  $\theta'$ /L1<sub>2</sub> Co-Precipitates in Al-Cu Alloys** Jonathan Poplawsky<sup>1</sup>, Brian Milligan<sup>2,1</sup>, Lawrence Allard<sup>1</sup>, Dongwon Shin<sup>1</sup>, Patrick Shower<sup>1</sup>, Matthew Chisholm<sup>1</sup> and Amit Shyam<sup>1</sup>; <sup>1</sup>Oak Ridge National Laboratory, United States; <sup>2</sup>Colorado School of Mines, United States

Typical AlCu-alloys used for automotive applications can only withstand temperatures up to 250 °C. Increasing this temperature will improve fuel efficiency. The presence of the  $\theta'$  (Al<sub>2</sub>Cu) precipitate in these alloys is critical for the alloy hardness; however,  $\theta'$  is a metastable precipitate that disappears (transforms) at higher temperatures, destroying the alloy properties. Recently, an affordable and castable Al-Cu alloy that retains  $\theta'$  and maintains its strength after a lengthy exposure to 350 °C was developed (> 200 Hrs). The addition of Mn in combination with Zr and their segregation to precipitate interfaces play a significant role in stabilizing the metastable  $\theta'$  precipitates, while adding Zr and Mn separately only improves the stability to 200 °C and 300 °C, respectively. A series of atom probe tomography (APT) and scanning transmission electron microscopy (STEM) experiments on Al-Cu-Mn-Zr/Ti-containing alloys subjected to long-term annealing (up to 2,100 h) in the critical temperature range, 300 °C and 350 °C, were performed to reveal how Mn and Zr work synergistically to stabilize the strengthening phase ( $\theta'$ ). The experimentally observed solute segregation to  $\theta'$  precipitate interfaces (APT) and atomic structure at the interfaces (STEM) were used to guide density functional theory (DFT) simulations to understand how Mn and Zr additions change the energetics of  $\theta'$  in an Al-matrix. The APT and STEM results reveal that Mn additions reduce interfacial energy, and thus, stabilize  $\theta'$  long enough for the slower diffusing Zr atoms to segregate to coherent  $\theta'$  interfaces that eventually create a  $\theta'$ /L1<sub>2</sub>-Al<sub>3</sub>(Zr<sub>x</sub>Ti<sub>1-x</sub>) co-precipitate structure. The co-precipitate is highly stable, is a key factor that governs microstructural stability beyond 300 °C. This study reveals how solute additions with different stabilization mechanisms can work in concert to stabilize a desired microstructure, and the results provide insights that can be applied to other high-temperature alloy systems.

This research was supported by the DOE Office of Energy Efficiency and Renewable Energy, Vehicle Technologies Office, Propulsion Materials Program and the DOE Basic Energy Sciences, Materials Sciences and Engineering Division. APT was conducted at ORNL's Center for Nanophase Materials Sciences (CNMS), which is a US DOE Office of Science User Facility. The authors appreciate the support provided by the Oak Ridge Leadership Computing Facility at the ORNL. The authors thank Ray Unocic and Allen Haynes (ORNL) for reviewing the manuscript. The authors would also like to thank Dana McClurg for heat treatments and hardness measurements and James Burns for APT sample preparation and APT operation.

#### F.MT05.06.10

**Late News: Specimen Preparation of Environmentally Sensitive Materials for Compositional and Structural Analysis at the Atomic Scale by Correlative APT and TEM Studies** Cecile Bonifacio<sup>1</sup>, Daniel Perea<sup>2</sup>, Pawel Nowakowski<sup>1</sup> and Paul Fischione<sup>1</sup>; <sup>1</sup>E.A. Fischione Instruments, Inc., United States; <sup>2</sup>Pacific Northwest National Laboratory, United States

Atom probe tomography (APT) is a powerful characterization technique for obtaining three-dimensional structure and materials composition at the atomic scale and is complementary to transmission electron microscopy (TEM). In tandem, the two techniques provide detailed characterization of structure, composition, and chemistry. However, the full potential of both of these techniques is typically hindered by artifacts from specimen preparation (e.g., Ga implantation and amorphization) and environmental conditions that degrade the specimen's surface (e.g., surface oxidation). Dual beam FIB (DB-FIB), which is an efficient tool for removing a substantial amount of material and in situ electron beam imaging, allows more control when shaping the APT specimen tip and is typically used to prepare APT specimens. However, Ga-induced damage and amorphization from FIB milling can result in ambiguous results, especially for Al/Al alloys and Ga-containing materials. In fact, it was recently shown that amorphization due to the high energy Ga beam during FIB milling dramatically affected the shape of the mass spectrum due to tip heating during APT acquisitions in Si APT specimens. Studies such as this provoke this study of using low energy Ar ion milling post-FIB milling to obtain high-quality APT specimens. Low energy (< 1 keV) Ar ion milling has been shown to improve TEM specimen quality by removing amorphization and Ga implantation from FIB prepared specimens. We present a post-FIB specimen preparation of APT specimens under controlled environments using concentrated beam (< 1  $\mu$ m), low energy Ar<sup>+</sup> milling for the removal of manufacturing damage, oxides and FIB-induced damage for TEM and APT analyses. This controlled environment is integrable to current APT environmentally controlled transfer system.

Al and Mg metals and their alloys were chosen as test specimens due to their highly oxidizing properties. The APT specimens were prepared in a FIB system using standard lift-out methods and annular milling. The APT specimen



preparation workflow from FIB to an Ar<sup>+</sup> milling system using a FIB vacuum transfer system was interfaced with a glovebox in between transfers. For ease of specimen handling and transfer, the half-grid with the APT specimens was secured in the cartridge of a TEM vacuum transfer specimen holder that is compatible with the ion milling system. Ar<sup>+</sup> milling was performed by using a concentrated ion beam that is rastered longitudinally within a defined area on the APT specimen at decreasing milling energies. TEM, energy dispersive X-ray spectroscopy (EDS), and APT characterization were performed under controlled environments before and after ion milling to determine the removal of surface oxides and FIB-induced damage. Quantification of the removal of FIB-induced damage and the workflow's ability to prevent specimen oxidation and contamination will be presented.

#### F.MT05.06.11

**Late News: Atom Probe Tomography and Model-Free Methods for Analysis of Kinetics of a Binary Co-Sn Alloy** Muna S. Khushaim<sup>1</sup>, Fatimah Alahmari<sup>2</sup>, Delphine Chassaing<sup>3</sup> and Torben Boll<sup>3</sup>; <sup>1</sup>Taibahu University, Saudi Arabia; <sup>2</sup>Imam Abdulrahman bin Faisal University, Saudi Arabia; <sup>3</sup>Karlsruhe Institute of Technology, Germany

Recent studies of lithium-ion batteries suggest that the use of binary *CoSn* alloys as anodes should provide an improvement over currently used anode materials [1]. However, the implementation of *CoSn* alloys is challenging due to uncertainties regarding the phase transformations within this system. In order to understand these, we evaluate the compositions of different intermetallic compounds produced via the peritectic reactions, nucleate and grow within the microstructure of binary *Sn* -25 at.% *Co* by employing atom probe tomography (APT). Owing to its capability, APT with its exceptional capabilities of spatially resolution and quantitative chemical analyses is presented as a sophisticated analytical tool to elucidate the underlying process of the phase transition behaviour of different *Co-Sn* intermetallic compounds and the local structure of the solid solution. The APT results revealed the presence of *Co* clusters with  $(54.1 \pm 0.1)$  at.% *Co*,  $(23.34 \pm 0.3)$  at.% *Co* and  $(0.6 \pm 0.1)$  at.% *Co* in pure *Sn* phase [2], which is consistent with the equilibrium phase diagram that indicates there is limited solubility of *Co* in *Sn* (up to 0.6%) at a temperature of 1196 °C. This limited solubility of *Co* atoms induced the formation of different observed intermetallic phases that are *CoSn* and *CoSn*<sub>3</sub>. This study demonstrates the unique capabilities of APT to characterize a series of peritectic reactions within the binary *Co-Sn* alloy. Moreover, crystallization kinetics of the crystallization reactions in *Co-Sn* alloy system were investigated under non-isothermal as well as isothermal conditions. These investigations were performed by using of model -free (isoconversion) methods. The results show decreasing on the activation energy for the crystallization kinetics for *CoSn* and *CoSn*<sub>3</sub> phases with increasing temperature, which reveals the involvement of two processes of nucleation and diffusion during the crystallization of these intermetallic phases.

#### References

- [1] G. Mulas, S. Enzo, C. Bonatto Minella, E. Arca, C. Gerbaldi, N. Penazzi, S. Bodoardo, J. Hassoun and S. Panero, *Mechanochemical synthesis and electrochemical properties of nanostructured electrode materials for Li ion batteries*. Journal of Solid State Electrochemistry, 2009. 13(2): p. 239-243.
- [2] M. Khushaim, F. Alahmari, N. Kattan, D. Chassaing and T. Boll, Microstructural properties and peritectic reactions in a binary Co-Sn alloy by means of scanning electron microscopy and atom probe tomography, Mater. Res. Express 7 (2020) 086508

### SYMPOSIUM F.MT06

---

Strain and Defect-Driven Transport Properties in van der Waals Solids  
November 21 - December 2, 2020

#### Symposium Organizers

Tianshu Lai, Sun Yat-sen University  
SungWoo Nam, University of Illinois at Urbana-Champaign  
Michael Pettes, Los Alamos National Laboratory  
Yaguo Wang, The University of Texas at Austin

\* Invited Paper

SESSION Tutorial F.MT06: Strain Generation and Characterization van der Waals Materials  
Session Chairs: James Hone, Jung-Fu Lin, SungWoo Nam, Yaguo Wang and Yong Zhu  
Sunday Afternoon, November 29, 2020  
F.MT06

**2:45 PM \***

**Stretching 2D Materials—Freestanding or on a Stretchable Substrate** Yong Zhu; North Carolina State University, United States

2D materials are predicted to possess outstanding mechanical and electromechanical properties. It is of great interest to measure the elastic properties, fracture properties, and multiphysical properties (e.g., elastic strain engineering) of 2D materials. Mechanical testing of 2D materials is, however, challenging. Several mechanical testing methods of 2D materials have emerged recently such as indentation or pressurization induced stretching, stretching using a micro-device, and stretching through shear stress transfer from a substrate or matrix. This tutorial will provide a brief overview of these materials and related testing results.

**3:45 PM BREAK**

**4:00 PM \***

**Compressive Strain Tuning of 2D Material Properties in a High Pressure** Jung-Fu Lin; The University of Texas at Austin, United States

This tutorial will show how to use compressive strain in a diamond anvil cell to tune physical properties of 2D transition metal dichalcogenides, graphene, and their heterostructures. The use of soft, inert pressure medium in a diamond cell can produce hydrostatic pressure and strain rate up to 10-20%. Such a compressive strain can significantly shorten the interlayer van der Waals bonds of 2D materials. When coupled with time-resolved laser spectroscopy and physical property measurement systems, electronic, optical, thermal transport properties of 2D materials can be effectively tuned, resulting in semiconductor-metal transition, enhanced thermal conductivity, direct-indirect band gap transition, charge transfer, and carrier density and mobility change.

**5:00 PM BREAK**

**5:15 PM \***

**Modeling and Testing the Mechanical Behavior of Single-Crystal and Polycrystalline Graphene** James Hone; Columbia University, United States

This tutorial will review the following topics: (1). Experimental methods for mechanical testing of graphene and 2D materials using nano-indentation. (2). Non-linear finite element modeling based on ab initio calculations at large strain. (3). Mechanical testing of polycrystalline graphene and grain boundaries. (4). Detailed multiscale modeling of failure in polycrystalline graphene. In particular, we construct a multiscale model using a cohesive zone element at the grain boundaries, and use this model to establish a relationship between the failure load and the grain boundary distance. This allows us to calculate a semi-analytical probability density function (PDF) to allow for direct comparison with experiments.

SESSION F.MT06.07/EL04.20: Joint Session Live Keynote and Panel Discussion: Quantum Phenomena in Atomically Thin Materials  
Session Chairs: SungWoo Nam and Yaguo Wang  
Tuesday Afternoon, December 1, 2020  
F.MT06

**1:45 PM \*F.MT06.03/EL04.13.01**

## **Interlayer Excitons in van der Waals Heterostructures** Philip Kim; Harvard University, United States

A pair of electron and hole across the interface of semiconductor heterostructure can form a bound quantum state of the interlayer exciton. In a coupled interface between atomically thin van der Waals layers (vdW), the Coulomb interaction of the interlayer exciton increases further. In this presentation, we will discuss observing interlayer exciton formation in semiconducting transition metal dichalcogenide (TMDC) layers. Unlike conventional semiconductor heterostructures, charge transport in of the devices is found to critically depend on the interlayer charge transport, electron-hole recombination process mediated by tunneling across the interface. We demonstrate the enhanced electronic, optoelectronic performances in the vdW heterostructures, tuned by applying gate voltages, suggesting that these a few atom thick interfaces may provide a fundamental platform to realize novel physical phenomena. Furthermore, complete experimental control of density, displacement and magnetic fields in our graphene double layer system enables us to explore the rich phase diagram of several superfluid exciton phases with the different internal quantum degrees of freedom.

**2:15 PM \*F.MT06.03/EL04.13.02**

## **Tunable Quantum Transport High Mobility 2D Materials** Jeanie Lau; The Ohio State University, United States

One of the most alluring features of 2D materials is their tunability, as their carrier density, effective mass, band gap, and electronic phases can be tuned in situ by external parameters such as electric field, magnetic field and strain. Here we will present transport studies of high quality 2D materials. For instance, we demonstrate large tunable SOC and zero-field spin-splitting in atomically thin InSe with unprecedented mobility. From beating patterns in quantum oscillations, we establish that the SOC parameter  $a$  is thickness-dependent; it can be continuously modulated over a large range by an out-of-plane electric field, achieving zero-field splitting tunable between 0 and 20 meV. Surprisingly,  $a$  could be enhanced by an order of magnitude in some devices, suggesting that SOC can be further manipulated by variations in interlayer spacing induced by stacking and/or electrostatic compression. Our work highlights the extraordinary tunability of SOC in 2D materials, which can be harnessed for *in operando* spintronic and topological devices and applications.

**2:35 PM BREAK**

**2:45 PM \*F.MT06.03/EL04.13.03**

## **Electron Interactions in 2D Materials—Correlated Multi-Particle Excitations and Optical Field Driven ARPES** Steven G. Louie<sup>1,2</sup>; <sup>1</sup>University of California, Berkeley, United States; <sup>2</sup>Lawrence Berkeley National Laboratory, United States

Many-electron interaction effects dominate many spectroscopic properties of reduced-dimensional systems, leading often to manifestation of novel phenomena not seen in the bulk. In this talk, I present some of our recent work on electron interaction effects in atomically thin quasi 2D materials: (1) strongly bounded correlated multi-particle excitations, such as trions and bi-excitons, in quasi 1D and 2D materials; (2) giant excitonic effects in shift currents, a nonlinear optical phenomenon, in non-centrosymmetric quasi 2D semiconductors; and (3) excitons and band renormalization in optical field driven angle-resolved photoemission spectroscopy (ARPES). Studies of these novel phenomena are made possible because of newly developed theoretical methods which incorporate higher-order many-electron correlation effects from first principles, using an interacting Green's function approach.

**3:05 PM PANEL DISCUSSION**

SESSION F.MT06.08: Live Lightning/Flash: Strain and Defect-Driven Transport Properties in van der Waals Solids  
Session Chairs: Feng He, Michael Pettes and Yaguo Wang  
Wednesday Morning, December 2, 2020  
F.MT06

**8:00 AM \*F.MT06.01.01**

## **Quantum Confined-Photon Emission in Layered Materials** Andrea C. Ferrari; University of Cambridge, United Kingdom

Layered Materials (LMs) have potential for quantum technologies, as scalable sources of single photon emitters (SPEs)[1,2].

LM heterostructures can be built with tuneable properties depending on the constituent materials and their relative crystallographic orientation[3,4]. Quantum emitters in LMs hold potential in terms of scalability, miniaturization, integration. Generation of quantum emission from the recombination of indirect excitons in heterostructures made of different LMs is a path with enormous potential. I will discuss how LM combinations can be used to generate SPEs and confinement of interlayer excitons[5].

- 1.C. Palacios-Berraquero et al., Nat. Commun. 8, 15093 (2017)
- 2.C. Palacios-Berraquero, et al., Nat. Commun. 7, 12978 (2016)
- 3.P. Rivera et al., Nat. Nanotech. 13,1004 (2018)
- 4.M. Barbone et al. Nat. Commun 9, 3721 (2018)
5. A. R. P. Montblanch et al. arxiv:2005.02416 (2020)

#### 8:06 AM \*F.MT06.01.02

##### **Moire Superpotentials and Quantum Calligraphy of Single Photon Emitters in van der Waals Heterostructures** Berend T. Jonker; Naval Research Laboratory, United States

Single photon emitters (SPEs), or quantum emitters, are key components in a wide range of nascent quantum-based technologies. A solid state host offers many advantages for realization of a functional system, but creation and placement of SPEs are difficult to control. We describe here a novel paradigm for encoding strain into 2D materials to create and deterministically place SPEs in arbitrary locations with nanometer-scale precision [1]. We demonstrate the direct writing of SPEs in 2D semiconductors based on a materials platform consisting of a WSe<sub>2</sub> monolayer on a deformable substrate using an atomic force microscope nano-indentation process. This quantum calligraphy allows deterministic placement and real time design of arbitrary patterns of SPEs for facile coupling with photonic waveguides, cavities and plasmonic structures.

The weak interlayer bonding in van der Waals heterostructures (vdWh) enables one to rotate the layers at arbitrary azimuthal angles. For transition metal dichalcogenide vdWh, twist angle has been treated solely through the use of rigid-lattice moiré patterns. No atomic reconstruction has been observed to date, although reconstruction can be expected to have a significant impact on all measured properties, and its existence will fundamentally change our understanding of such systems. Here we demonstrate via conductive AFM and TEM that vdWh of MoSe<sub>2</sub>/WSe<sub>2</sub> and MoS<sub>2</sub>/WS<sub>2</sub> undergo significant atomic level reconstruction at twist angles  $\leq 1^\circ$  leading to discrete commensurate domains divided by narrow domain walls [2], rather than a smoothly varying rigid-lattice moiré pattern as has been assumed in prior work. We show that this occurs because the energy gained from adopting low energy vertical stacking configurations is larger than the accompanying strain energy [3]. Such reconstruction impacts both the local conductivity and the optical properties.

[1] M.R. Rosenberger et al, *ACS Nano* **13**, 904 (2019). DOI: 10.1021/acsnano.8b08730

[2] M.R. Rosenberger et al, *ACS Nano* **14**, 4550 (2020). <https://dx.doi.org/10.1021/acsnano.0c00088>

[3] M. Phillips and C.S. Hellberg, ArXiv 190902495 Cond-Mat (2019)

\*Work done in collaboration with Matthew R. Rosenberger, Hsun-Jen Chuang, Madeleine Phillips, Kathleen M. McCreary, and C. Stephen Hellberg of the *Naval Research Laboratory*, Washington DC, and Chandriker Kavir Dass and Joshua R. Hendrickson of the *Air Force Research Laboratory*, Wright-Patterson AFB, OH.

† This work was supported by AFOSR and core programs at NRL.

#### 8:18 AM \*F.MT06.01.04

##### **Understanding Tunability in the Electronic and Optical Response of Two-Dimensional Materials with Defects by Computational Analysis** Ruth Pachter and Jie Jiang; Air Force Research Laboratory, United States

The ability to tune the electronic and optical properties of 2D materials by induced defects has wide-ranging applications. For example, patterned graphene surfaces can be used for biosensing, while strained 2D transition metal dichalcogenides (TMDs) could enable the control of excitons for quantum emitters. Here, we first report on electronic band structure calculations of periodically patterned graphene, which can be fabricated using electron-beam chemistry with radiolyzed water (Islam, et al. *Carbon* **2020**, *166*, 446-455). Analysis of the effects of alternating strips in the graphene surface, which are pristine or with epoxide defects, illustrate electronic confinement in the graphene ribbon, which leads to one-dimensional quasi-metallic or semiconducting response, dependent on the strip's width. Electron transport calculations demonstrate electron

transmission along the graphene strip direction, minimized in the direction perpendicular to edges terminated by oxygen atoms, while intrinsic current-voltage ( $I$ - $V$ ) characteristics indicate comparable performance to graphene nanoribbons with perfect edges. The electron transport in a device setting with gold electrodes shows improved conductivity in comparison to a graphene-based device. Next, in an effort to move towards controlled emission properties, such as for single-photon emission applications, we consider strained 2D WSe<sub>2</sub> monolayers with varying wrinkle structures. The tunability we demonstrate in the optical response of the mechanically deformed nanostructures is described in detail. Our results on exciton tunability by wrinkle structure could motivate experimental fabrication.

**8:24 AM \*F.MT06.02.01**

**Weakened Interlayer Interaction of Incommensurate Graphene as a Key Factor for Superior Lithium Intercalation** [Tereza Paronyan](#); HeXalayer, LLC, United States

Carbon/graphite-based energy storage devices, such as lithium-ion batteries (LIBs), are the most reliable energy storage devices for portable electronics, electric vehicles (EV) and electric grid storage due to their high-power density, stability, low cost, and safety. Despite the wide use of LIBs, the graphitic anode has limited capacity (372 mAh.g<sup>-1</sup>) due to the limited rate of lithium diffusion within the commensurately stacked layered structure.

Here we discuss the unique superior capacity of Lithium intercalation of multilayered graphene structures, named as an Incommensurate Multilayer Graphene (IMLG), that consists of closely packed rotated graphene layers. In-plane and out-plane features of graphene are studied by Raman spectroscopy, High-Resolution Transmission Electron Microscopy (HRTEM), and X-ray Diffraction. The commensurate-incommensurate transition of layered graphene is analyzed by Raman spectroscopy and the range of the key parameters is discussed as a significant for efficient Lithium intercalation.

The structural and binding features of graphene anode before and after Lithium insertion is studied, and a new lithium intercalation model is considered. We revealed that weakened interplanar Van der Waals interaction as it occurs within rotated graphene layers enables easy and full penetration of lithium, followed by flexible adjustment of layers for stable and reversible stable cycling without affecting graphene in-plane features. Superior Lithium intercalation provides reversible and stable long-term charge/ discharge of IMLG anodes reaching up over 1500 mAh.g<sup>-1</sup> capacity of LiBs.

Our recent development of IMLG confirms the feasibility of the synthesis technique which allows us the development of high energy density and powerful lightweight secondary batteries in the nearest future.

**8:30 AM \*F.MT06.02.03**

**Piezoelectricity and Exotic Nonlinearities in Monolayer TMDC Resonators** [Horacio Espinosa](#), Shiva Nathamgari and Siyan Dong; Northwestern University, United States

Monolayer transition metal dichalcogenides (TMDCs), with the general chemical formula MX<sub>2</sub> (M = Mo or W and X = S, Se and Te), are a class of 2D materials that have been predicted to be piezoelectric using Density Functional Theory (DFT) calculations. In addition, some of the TMDCs possess certain advantages in monolayer form – such as a direct bandgap and better Q-factors – over graphene. Here, we present resonance and piezoelectric measurements on monolayer transition metal dichalcogenides (TMDCs) using cavity-interferometry. We also demonstrate that TMDCs are promising candidates for Nanoelectromechanical Systems (NEMS) due to their low mass and intrinsic piezoelectricity.

Cavity-interferometry refers to a displacement transduction technique in nanoelectromechanical systems (NEMS). Most fabrication protocols for NEMS naturally render an optical cavity where the NEMS structure and the underlying substrate constitute the two mirrors. The modulation in the cavity depth due to the motion of the NEMS translates to intensity variations of the reflected light from the optical cavity, which can be measured on an appropriate detector. By optimizing the cavity depth, wavelength of the probe laser and the back-end electronics, exquisite displacement sensitivity (sub picometer/Hz<sup>1/2</sup>) can easily be achieved [1].

Device fabrication is challenging; hence, we explored various fabrication methods for creation of suspended 2D material devices and established working protocols for both exfoliated and chemical vapor grown TMDCs. We also developed a new transfer method driven by water wettability to facilitate fabrication efforts. To perform device characterization, we developed an integrated in-vacuum Raman/Interferometer setup [1]. By exploiting the cavity formed between suspended 2D TMDC “bridges” and underneath substrates, resonance frequencies of various modes were characterized including exotic line shapes arising due to 1:1 internal resonance coupling in the nonlinear regime. Using a combined experimental-computational approach and the measured shift of fundamental resonance frequencies, induced by applied bias, we extracted piezoelectric

properties of monolayer WS<sub>2</sub> and MoS<sub>2</sub>. The exfoliated samples display piezoelectric coefficients that are in good agreement with DFT predictions. By contrast, CVD grown monolayers, exhibit a 10-fold reduction in piezoelectricity, likely due to the existence of atomic defects such as vacancies.

Additionally, by driving resonance in the nonlinear regime, we revealed internal resonance pairs in monolayer WS<sub>2</sub>. Discovery of Hopf bifurcations linearly varying with driving forces inspired novel sensing modality with ultrahigh force sensitivity (aN) at room temperature [2]. Our efforts in fabricating and experimenting on suspended 2D TMDC devices will support further development in applying 2D materials to sensors and NEMS applications.

[1] S. S. P. Nathamgari, S. Dong, E. Hosseinian, L. J. Lauhon and H. D. Espinosa, "An Experimental Setup for Combined In-Vacuo Raman Spectroscopy and Cavity-Interferometry Measurements on TMDC Nano-resonators" *Experimental Mechanics*, Vol. 59, p. 349-359, 2019.

[2] S. S. P. Nathamgari, S. Dong, L. Medina, N. Moldovan, D. Rosenmann, R. Divan, D. Lopez, L. J. Lauhon and H. D. Espinosa, "Nonlinear Mode Coupling and One-to-One Internal Resonances in a Monolayer WS<sub>2</sub> Nanoresonator" *Nano Letters*, Vol. 19, No. 6, p. 4052-4059, 2019.

#### 8:35 AM \*F.MT06.02.04

**Single Photon Emitters Using Strained Low-Dimensional Materials** Hong Gyu Park; Korea University, Korea (the Republic of)

The quantum confinement in atomically-thin transition metal dichalcogenides (TMDCs) has been investigated for single photon emission based on naturally or artificially occurring defects. In particular, the precise control of the position of a single photon emitter by applying mechanical strains to the TMDC is feasible. Strains have been induced in TMDCs using various nanostructures including dielectric pillars, nanobubbles, optical waveguide, metal nanogaps, and metal nanoparticles. However, polarization control and integration with a high-quality (Q) cavity to increase the Purcell factor remain elusive in TMDC-based single photon sources.

In this talk, I will present the deterministic control of both the position and polarization of single photon emitters in atomically thin WSe<sub>2</sub> placed on a nanogap array. Manipulation of the band structure by a local strain gradient generates a potential well at the nanogap site, and position-controlled single photon emission is subsequently achieved. Additionally, directional elongations of the potential well, which are tuned by changing the nanogap size, allow polarization-controlled single photon emission. Moreover, single photons with a  $g^{(2)}$  of  $\sim 0.1$  are generated at 4-20 K. To take a full advantage of such deterministic control of the position and polarization of single photon emitters, the emitters are integrated with one-dimensional photonic crystal cavities. Therefore, this approach is a unique way to develop next-generation, deterministic, controllable single photon emitters based on TMDC materials, which outperform the present single photon sources with random occurrence and uncontrolled polarization properties.

#### 8:41 AM \*F.MT06.02.07

**2D Material Based Electronics Under High Mechanical Strain** Jong-Hyun Ahn; Yonsei University, Korea (the Republic of)

Rapid advances in synthesis of graphene and 2D materials, and fabrication methods for functional devices enable sophisticated types of functionality and their application to various emerging electronics, such as flexible, wearable and optoelectronic applications, that cannot be addressed with conventional materials. In this talk, I present that graphene and 2D materials can play critical roles in this context, through demonstrations of complex, mechanically assembled electronic and optoelectronic devices for flexible and wearable applications. Specifically, the mechanics of graphene and MoS<sub>2</sub> can yield various devices in distinct, engineered flexible geometries that cannot be easily reproduced with conventional materials and/or conventional device layouts. Examples of devices include touch, tactile sensors and wearable OLED display.

#### 8:47 AM \*F.MT06.04.03

**Defect and Strain Engineering of Two-Dimensional Materials** Jun Lou; Rice University, United States

Two-dimensional (2D) materials, such as Graphene, hBN and MoS<sub>2</sub>, are promising candidates in a number of advanced functional and structural applications, owing to their exceptional electrical, thermal and mechanical properties. To better meet

the requirements of practical applications, property modification and regulation are oftentimes desired. Defect and strain engineering strategies are powerful tools to modulate electronic, optoelectronic and other functional properties of 2D semiconductors.

In this talk, we will report our efforts to employ such strategies to tune functional properties of 2D semiconductors. We first demonstrated how substrate interfacial chemistry can be utilized to tailor the physical properties of single-crystalline molybdenum disulfide ( $\text{MoS}_2$ ) monolayers. We use self-assembled monolayers with a variety of end termination chemistries to functionalize substrates and systematically study their influence on the physical properties of  $\text{MoS}_2$ . Our data shows that combined interface-related effects of charge transfer, built-in molecular polarities, varied densities of defects, and remote interfacial phonons strongly modify the electrical and optical properties of  $\text{MoS}_2$ . Tunable friction behavior of the heterostructure of monolayer  $\text{MoS}_2$  and different self-assembled organic molecules (SAMs) were also demonstrated, which was attributed to the charge transfer from SAMs to  $\text{MoS}_2$  influencing the electron concentration and thus the carrier-mediated friction in  $\text{MoS}_2$ . In another example, we systematically characterize chemical vapor deposition (CVD)-grown  $\text{MoS}_2$  by photoluminescence spectroscopy and mapping and demonstrate non-uniform strain in single-crystalline monolayer  $\text{MoS}_2$  and strain-induced bandgap engineering. We further modified our CVD process to create a Janus  $\text{SMoSe}$  monolayer and demonstrated high basal plane hydrogen evolution reaction (HER) activity in such samples and DFT calculation implies that the activity originates from the synergistic effect of the intrinsic defects and structural strain inherent in the Janus structure.

**8:52 AM \***

**Conformal, Area-Specific and Switchable Graphene Nanowrinkles** Teri W. Odom; Northwestern University, United States

Selective patterning and functionalization of graphene can produce spatially-defined properties. Buckling or wrinkling of graphene on polymeric substrates enables a direct approach to tune the physical properties without lithographic steps, and the resulting curvature of the wrinkles can control local chemical reactivity. However, most buckling methods have been limited by the range of wavelength tunability, only global control of the wrinkled patterns, and delamination and cracks in the graphene. This talk will describe a scalable approach to achieve area-specific reactivity and patterning of conformal graphene wrinkles. We will discuss how a fluoropolymer layer sandwiched between graphene and different polymer substrates can facilitate crack-free and switchable graphene nanostructures. Such patterned areas with different curvatures show different reactivities based on a plasma fluorination reaction. Our approach for large-area, fine control over graphene wrinkle topographies has prospects for other two-dimensional electronic materials and optoelectronics and plasmonics applications.

**8:57 AM BREAK**

**9:04 AM \*F.MT06.04.01**

**Chemical Properties and Applications of 2D TMDCs Mediated by Defects** Qing Hua Wang; Arizona State University, United States

The two-dimensional transition metal dichalcogenides (2D TMDCs) tend to have basal planes that are chemically relatively inert. Many approaches and reaction schemes have been demonstrated to modify the chemical nature of TMDCs, resulting in new chemical properties and applications. This talk will highlight our recent work on the chemical properties of 2D TMDCs mediated by point defects and edges, which subsequently enable applications in water treatment and antimicrobial treatment. We have shown robust and versatile covalent functionalization of materials across the metal chalcogenides including  $\text{MoS}_2$ ,  $\text{MoSe}_2$ ,  $\text{WS}_2$ ,  $\text{WSe}_2$ ,  $\text{Bi}_2\text{S}_3$ , and  $\text{Sb}_2\text{S}_3$  using aryl diazonium salts. The reaction mechanism is initiated at point defect sites and edges, but propagates across the chalcogenide surfaces in a chain-like step growth. We have also shown the ability for  $\text{MoS}_2$  to remove Pb contamination from water via a reaction with the surface sites to form sulfate precipitates. The reaction mechanism is again initiated at defect sites in the  $\text{MoS}_2$ . Finally, we have used single stranded DNA to encapsulate  $\text{MoSe}_2$  nanosheets and shown their broad-spectrum antimicrobial properties against multidrug resistant bacteria. The choice of ssDNA sequence influences the conformal coating, and the ability for the edges of  $\text{MoSe}_2$  to cut through bacterial cell membranes.

**9:10 AM \*F.MT06.04.02**

**Chemical Trends of Deep Levels in van der Waals Semiconductors** Penghong Ci<sup>1</sup>, Xuezheng Tian<sup>2</sup>, Jun Kang<sup>3</sup>, Sefaattin (Sef) Tongay<sup>4</sup>, Wladek Walukiewicz<sup>1</sup>, Jianwei (John) Miao<sup>2</sup>, Oscar Dubon<sup>1</sup> and Junqiao Wu<sup>1</sup>; <sup>1</sup>University of California, Berkeley, United States; <sup>2</sup>University of California, Los Angeles, United States; <sup>3</sup>Beijing Computational Science Research Center, China; <sup>4</sup>Arizona State University, United States

Properties of semiconductors are largely defined by crystal imperfections including native defects. Van der Waals (vdW) semiconductors, a newly emerged class of materials, are no exception: defects exist even in the purest materials and strongly affect their electrical, optical, magnetic, catalytic and sensing properties. However, unlike conventional semiconductors where energy levels of defects are well documented, they are experimentally unknown in even the best studied vdW semiconductors, impeding the understanding and utilization of these materials. We directly evaluate deep levels and their chemical trends in the bandgap of MoS<sub>2</sub>, WS<sub>2</sub> and their alloys by transient spectroscopic study. One of the deep levels is found to follow the conduction band minimum of each host, attributed to the native sulfur vacancy. A switchable, DX center-like deep level has also been identified, whose energy lines up instead on a fixed level across different host materials, which explains the chemical trend of native electron density in the hosts as well as a persistent photoconductivity up to 400K.

#### 9:15 AM \*F.MT06.04.04

**Emerging Electron Microscopy Techniques for 2D Materials** [Kayla Nguyen](#), Edmund Han, Chia-Hao Lee, Jeffrey Huang and Pinshane Y. Huang; University of Illinois at Urbana-Champaign, United States

The study of atomic-monolayer materials has been extremely popular within the last decade due to the emergence of a family of two-dimensional (2D) materials with expansive mechanical, electrical and magnetic properties. Subtle changes in these 2D materials at the atomic length scales, ranging from strain fields and dislocations, have large effects for tuning the electronic and mechanical properties, especially when used in real devices. Electron microscopy can provide the insight needed to visualize these effects [1-2]. Recent advancements in detector technology have already pushed the limits of resolution using 2D bilayer molybdenum disulfide using ptychographic reconstruction [3-4]. In my talk, I will discuss ways electron microscopy can provide opportunities for sensitive strain and magnetic measurements of 2D materials, with an emphasis on emerging techniques provided by the electron microscope pixel array detector (EMPAD), a state-of-the-art, high-dynamic range and high-speed electron diffraction detector.

[1] Lee, CH et al, *Nanoletters*, 20 (5), 3369–3377 (2020).

[2] Han, E et al, *Nature Materials*, 19 (3), 305-309 (2019).

[3] Tate, MW et al, *Microscopy and Microanalysis*, 22 (1), 237-249 (2016).

[4] Jiang, Y et al, *Nature*, 559 (7714), 343-349 (2018).

#### 9:21 AM \*F.MT06.05.02

**Exotic Spin Transport in Two-Dimensional Materials** Stephan Roche<sup>1,2</sup> and [Jose H. Garcia Aguilar](#)<sup>1</sup>; <sup>1</sup>Catalan Institute of Nanoscience and Nanotechnology, Spain; <sup>2</sup>ICREA--Institució Catalana de Recerca i Estudis Avançats, Spain

The field of spin transport in two-dimensional has flourished in the past couple of years. Some remarkable features are the reports of large charge-to-spin in graphene-based heterostructures [1], the discovery of the quantum spin Hall effect [2], and ultra-clean spin transport measurements within the ballistic regime [3]. In this talk, we will present predictions on diffusive and ballistic spin transport in different two-dimensional materials. Using complementary large-scale numerical transport methods, we developed a theory showing that contacts have a dramatic effect on the spin transport in systems with a size comparable to the spin relaxation length, leading to underestimating the latter [4]. We then apply this theory and bulk transport methods to unveil the role of broken symmetries in the spin transport of transition metal dichalcogenides in their 1T' and 1Td structural phases, showing they can promote an unconventional spin transport regimen. We believe our predictions will lead to a better understanding of the recent measurements of the quantum spin Hall effect in WTe<sub>2</sub> and will help optimize experimental setups for its harvesting.

[1] Nat. Mater. 19, 170–175 (2020).

[2] Science 359,6371, pp. 76-79, (2018).

[3] Phys. Rev. Lett. 124, 177701 (2020).

[4] Phys. Rev. Lett. 124, 196602 (2020).

#### 9:27 AM \*F.MT06.05.01

**Study of Thermal and Magnetic Transport in Functional Materials Enabled by Ultrafast Optical Metrology** [Xiaoqia Wang](#); University of Minnesota Twin Cities, United States

Transport phenomena play an important role in designing and engineering materials with tailored functionalities. Thermal conductivity and spin precession damping, as basic transport properties of materials, can provide a wealth of information on



the fundamental scattering processes of phonons and magnons with structural defects and interface imperfection. In this talk, I will share our group's recent progress on utilizing time-resolved magneto-optical Kerr effect (TR-MOKE) metrology to study the thermal and magnetic properties of functionalized materials spanning a wide range of applications. This will include: (1) revealing the 3D anisotropic thermal transport in black phosphorus, as the next-generation of "wonder materials" for the semiconductor industry; (2) developing low-damping and high-thermal stability materials with perpendicular magnetic anisotropy for spintronic applications; and (3) manipulating spin precession using optically launched acoustic strains via a strong magnon-phonon coupling at ultra-high frequencies (~60 GHz). The structure-property relationships of functional materials revealed by the ultrafast pump-probe technique open up opportunities of tailoring material properties by structural engineering at the atomic and molecular levels. Ultimately, such an understanding can be leveraged to guide the design and optimization of materials, as promising building blocks for high-performance electronics, thermal management, hard-disk data storage, and magnetoacoustic devices.

**9:33 AM \*F.MT06.05.03**

**Strain Induced Tuning of Physical Properties of Materials** Abhishek K. Singh; Indian Institute of Science, India

Tuning physical properties of materials by applying strain opens up wide range of applications. In this presentation, sensitivity of these properties on application of strain will be illustrated for the case of TMDs. Using first principles calculations, the effect of normal compressive (NC), bi-axial compressive (BC), and bi-axial tensile (BT) strain on the electronic properties of few layered MoS<sub>2</sub> has been investigated. Regardless of the type of strain, a reversible semiconductor-to-metal transition is observed MoS<sub>2</sub>. The effect of strain as a function of number of layers on the transport properties is investigated. It is found that the 3L and 2L-MoS<sub>2</sub> emerge as the most efficient thermoelectric materials under NC and BT strain, respectively. The study was further extended to semi-metallic TMD TiS<sub>2</sub>, which has been in focus due to its application in energy storage and thermoelectric materials. Upon application of uniform biaxial strain, TiS<sub>2</sub> transforms from semi-metal to semiconducting phase. The transport calculations show three-fold enhancement in thermopower for both *p*- and *n*-type doped TiS<sub>2</sub>. Further, the effect of strain on thermal conductivity of bulk MoS<sub>2</sub> is explored, wherein an increase of cross-plane thermal conductivity from 3.5 to about 25 W/m-K. The giant enhancement arises from the increase in interlayer interaction on application of strain and decrease in phonon lifetimes due to the unbundling effect along the cross-plane direction. The concepts proposed from our studies can be extended to other semiconducting and metallic TMDs.

References:

Semiconductor-metal transition in semiconducting bilayer sheets of transition-metal dichalcogenides, Phys. Rev. B, **86**, 075454 (2012)

Pressure-induced semiconducting to metallic transition in multilayered molybdenum disulphide, Nat. Commun., **5**, 3731 (2014)

Effect of strain on electronic and thermoelectric properties of few layers to bulk MoS<sub>2</sub>, Nanotechnology, **25**, 465701 (2014)

Strain-induced electronic phase transition and strong enhancement of thermopower of TiS<sub>2</sub>, Phys. Rev. B, **90**, 174301 (2014)

Thermal Conductivity Enhancement in MoS<sub>2</sub> under Extreme Strain, Phys. Rev. Lett., **122**, 155901 (2019)

**9:39 AM \*F.MT06.05.04**

**Towards Room-Temperature Magnetic Semiconductors in van der Waals Layered Materials** Seok Joon Yun, Jinbao Jiang, Dinh Loc Duong and Young Hee Lee; Sungkyunkwan University, Korea (the Republic of)

The ferromagnetic state in van der Waals two-dimensional (2D) materials has been reported recently in the monolayer limit. Intrinsic CrI<sub>3</sub> and CrGeTe<sub>3</sub> semiconductors reveal ferromagnetism but the T<sub>c</sub> is still low below 60K. In contrast, monolayer VSe<sub>2</sub> is ferromagnetic metal with T<sub>c</sub> above room temperature but incapable of controlling its carrier density. Moreover, the long-range ferromagnetic order in doped diluted chalcogenide semiconductors has not been demonstrated at room temperature. The key research target is to realize the long-range order ferromagnetism, T<sub>c</sub> over room temperature, and semiconductor with gate tunability. Here, Ferromagnetic order is manifested using magnetic force microscopy up to 360K, while retaining high on/off current ratio of ~10<sup>5</sup> at 0.1% V-doping concentration. The V-substitution to W sites keep a V-V separation distance of 5 nm without V-V aggregation, scrutinized by high-resolution scanning transmission-electron-microscopy. More importantly, the ferromagnetic order is clearly modulated by applying a back gate. We also observe a ferromagnetic hysteresis loop together with oscillatory behavior at room temperature in diluted V-doped WSe<sub>2</sub>, while maintaining the semiconducting characteristic of WSe<sub>2</sub> with a high on/off current ratio of five orders of magnitude. Our findings open new opportunities for using two-dimensional transition metal dichalcogenides for future spintronics.

9:45 AM \*F.MT06.05.07

**Phonons in van der Waals Solids for Thermal Management Devices** Sina Najmaei; US Army Research Lab, United States

Active thermal management devices often lack the efficacy and energy efficiency of electronic switches. This is mainly because of the bosonic nature of phonons and the type of interactions they have with external forces. As a result, discovery of materials with unique vibrational properties that provide better control of thermal carriers is necessary. Our research shows that the phonons in group IVB transition metal dichalcogenides such as hafnium disulfide have distinct characteristics and provide remarkable mechanism for control of thermal carriers. This is caused by the intermixing of van der Waals forces and covalent bonds in the material structure combined with their highly anisotropic bond properties. In this talk we present our results on vibrational and thermal transport properties of a member of this group, hafnium disulfide ( $\text{HfS}_2$ ). The highly asymmetric bond properties in  $\text{HfS}_2$  dominate the structure and vibrational properties of this material. We explore the physics of  $\text{HfS}_2$  by developing a comprehensive computational model to study its phonon behavior, anharmonic properties, and phonon transport characteristics. Our findings demonstrate a unique phonon behavior in the material where the absence of a phonon-gap between the acoustic and optical branches grant a more prominent and unique role to the optical modes of  $\text{HfS}_2$ . As a result  $\text{HfS}_2$  has a low thermal conductivity, ranging between 0.3-5W/mK. In addition only one acoustic phonon branch, the ZA branch, contributes up to 80% to the thermal transport of the material in both out-of-plane and in-plane crystal orientations. Our experiments confirm and support the theory and add further insight into an anomalous behavior in the optical modes. Our quasi-harmonic model reveals a structural phase transformation at around room temperature that leads to unique anharmonicity, discernible in the experimental results of the zone center out-of-plane optical mode. This unique phase transformation contributes to both changes in the phonon decay properties and thermal transport behavior. The structural phase transformation combined with the constricted ZA branch phonon carriers and the distinct scattering physics in optical branches of  $\text{HfS}_2$  provide unique means for control of thermal transport. We explore a few strategies for control of thermal properties in  $\text{HfS}_2$  based on fundamental vibrational properties of the material. We demonstrate that a successful approach for dynamic control of thermal conductivity is the control of van der Waals gap properties. We demonstrate that through intercalation and modification of these gaps a 4-fold control of cross-plane thermal conductivity in hafnium disulfide from  $0.35\text{Wm}^{-1}\text{K}^{-1}$  to  $1.45\text{Wm}^{-1}\text{K}^{-1}$  is achievable. We also demonstrate that an out-of-plane strain can be used to make thermal regulators based on  $\text{HfS}_2$ . This research unveils a unique class of 2D layers with vibrational properties suitable for development of thermal management devices

9:51 AM F.MT06.05.05

**Thermal Conductivities of 2D  $\text{MoS}_2$  Under Mechanical Strains** Annie Xian Zhang; Stevens Institute of Technology, United States

In recent years, transition metal dichalcogenides become emergent thermoelectric materials with potential wide spread in wearable electronics applications. Considering the extensive applications of transition metal dichalcogenides, many research efforts have been paid and good progresses have been made. So far, all of the researches in this field focus on the electrical properties of them. It has not been reported about the transition metal dichalcogenides' thermal transport properties under mechanical strains. Due to their potential applications, it is of significance to discover the thermal transport properties of transition metal dichalcogenides at large mechanical strains, and thus develop the novel thermoelectric platforms which can sustain the extreme environments in wearable electronics.

In this work, we demonstrate using Raman optothermal technique to measure the thermal conductivities of two dimensional (2D)  $\text{MoS}_2$ . We first utilize more direct measurements of the optical absorption, and then by comparing the response of the samples using different laser spot sizes, we are able to measure the thermal conductivities of the 2D  $\text{MoS}_2$ . Then thermal conductivities at large mechanical strains are obtained providing more scientific merits.

The Raman optothermal technique has been the most successful method for measurement of thermal conductivity of 2D materials, and was used to measure the 2D materials at large mechanical strains for the first time in this work. In this technique, a laser is focused at the center of a thin film and used to measure the peak position of a Raman-active mode. As the laser power is increased, the sample is heated which enables red-shift Raman mode due to thermal softening. Another comparison experiment is conducted by placing the samples on a heating platform and monitor the change of Raman-active mode peak position shift. Combining these two sections of experiments provide us the thermal modeling can then be used to extract the thermal conductivity from the measured shift rate. We have used a refined version of the optothermal Raman technique to study thermal conductivity of 2D  $\text{MoS}_2$ , at large mechanical strains. It is the first thermal measurement on 2D

materials at large mechanical strains. This work also addresses several important issues in the measurement of thermal conductivity of 2D materials at large strains using Raman spectroscopy.

In conclusion, we have used Raman optothermal technique to study thermal transport properties of 2D MoS<sub>2</sub> at large mechanical strains. This work addresses several important issues in the measurement of thermal conductivity of the 2D materials MoS<sub>2</sub> using Raman spectroscopy. We derive the thermal conductivity values at large mechanical strains. These results are of significance to discover the thermal transport properties of 2D transition metal dichalcogenides at large mechanical strains, and thus develop the efficient 2D thermoelectric materials which can sustain the large mechanical strains and in turn to use strains to tune their thermal properties.

#### 9:56 AM F.MT06.06.02

**Late News: Controlling Defects in Continuous 2D GaS Films for High-Performance Electronic and Optoelectronic Devices** Yang Lu<sup>1</sup> and Jamie Warner<sup>2</sup>; <sup>1</sup>University of Oxford, United Kingdom; <sup>2</sup>The University of Texas at Austin, United States

A chemical vapor deposition method is developed for thickness-controlled (one to four layers), uniform, and continuous films of both defective gallium(II) sulfide (GaS): GaS<sub>0.87</sub> and stoichiometric GaS. The unique degradation mechanism of GaS<sub>0.87</sub> with XPS and HAADF-STEM is studied, and it is found that the poor stability and weak optical signal from GaS are strongly related to photo-induced oxidation at defects. Photodetectors based on the two materials are fabricated with short response time (<66 ms), excellent UV photoresponsivity. An enhanced stability of the stoichiometric GaS is demonstrated under laser and strong UV light, and by controlling defects in GaS, the photoresponse range can be changed from vis-to-UV to UV-discriminating.

Besides the role in degradation mechanism, defects in GaS<sub>0.87</sub> also contributed to the formation of a new band sitting within its bandgap, which is confirmed by cathodoluminescence results. As a result, controlling defects in GaS turns the band alignment of the bilayer GaS-WS<sub>2</sub> van der Waals heterostructure from type I to type II. XPS and KPFM characterization demonstrates that the defect band can facilitate the charge transfer from WS<sub>2</sub> to GaS. Devices based on the type-II heterojunction further show that the defect band greatly assisted the carrier transport by lowering the contact resistance, and also demonstrate superior photodetector properties with a large linear dynamic range (>73 dB) at a R of 13 A/W for green light.

[1] Lu, Y., Chen, J., Chen, T., Shu, Y., Chang, R.-J., Sheng, Y., Shautsova, V., Mkhize, N., Holdway, P., Bhaskaran, H., Warner, J. H., Controlling Defects in Continuous 2D GaS Films for High-Performance Wavelength-Tunable UV-Discriminating Photodetectors. *Adv. Mater.* 2020, 32, 1906958.

[2] Lu, Y., Warner, J. H., et al., Transition of type-I to type-II heterojunction in monolayer GaS-WS<sub>2</sub>. In preparation.

#### SESSION F.MT06.01: Emerging Phenomena

On Demand Abstracts Available for Viewing Starting Saturday Morning, November 21, 2020  
F-MT06

#### 5:00 AM \*F.MT06.01.01

**Quantum Confined-Photon Emission in Layered Materials** Andrea C. Ferrari; University of Cambridge, United Kingdom

Layered Materials (LMs) have potential for quantum technologies, as scalable sources of single photon emitters (SPEs)[1,2]. LM heterostructures can be built with tuneable properties depending on the constituent materials and their relative crystallographic orientation[3,4]. Quantum emitters in LMs hold potential in terms of scalability, miniaturization, integration. Generation of quantum emission from the recombination of indirect excitons in heterostructures made of different LMs is a path with enormous potential. I will discuss how LM combinations can be used to generate SPEs and confinement of interlayer excitons[5].

1.C. Palacios-Berraquero et al., *Nat. Commun.* 8, 15093 (2017)

2.C. Palacios-Berraquero, et al., *Nat. Commun.* 7, 12978 (2016)

3.P. Rivera et al., *Nat. Nanotech.* 13,1004 (2018)

4.M. Barbone et al. *Nat. Commun* 9, 3721 (2018)

5. A. R. P. Montblanch et al. arxiv:2005.02416 (2020)

**5:15 AM \*F.MT06.01.02**

**Moire Superpotentials and Quantum Calligraphy of Single Photon Emitters in van der Waals Heterostructures** Berend T. Jonker; Naval Research Laboratory, United States

Single photon emitters (SPEs), or quantum emitters, are key components in a wide range of nascent quantum-based technologies. A solid state host offers many advantages for realization of a functional system, but creation and placement of SPEs are difficult to control. We describe here a novel paradigm for encoding strain into 2D materials to create and deterministically place SPEs in arbitrary locations with nanometer-scale precision [1]. We demonstrate the direct writing of SPEs in 2D semiconductors based on a materials platform consisting of a WSe<sub>2</sub> monolayer on a deformable substrate using an atomic force microscope nano-indentation process. This quantum calligraphy allows deterministic placement and real time design of arbitrary patterns of SPEs for facile coupling with photonic waveguides, cavities and plasmonic structures.

The weak interlayer bonding in van der Waals heterostructures (vdWh) enables one to rotate the layers at arbitrary azimuthal angles. For transition metal dichalcogenide vdWh, twist angle has been treated solely through the use of rigid-lattice moiré patterns. No atomic reconstruction has been observed to date, although reconstruction can be expected to have a significant impact on all measured properties, and its existence will fundamentally change our understanding of such systems. Here we demonstrate via conductive AFM and TEM that vdWh of MoSe<sub>2</sub>/WSe<sub>2</sub> and MoS<sub>2</sub>/WS<sub>2</sub> undergo significant atomic level reconstruction at twist angles  $\leq 1^\circ$  leading to discrete commensurate domains divided by narrow domain walls [2], rather than a smoothly varying rigid-lattice moiré pattern as has been assumed in prior work. We show that this occurs because the energy gained from adopting low energy vertical stacking configurations is larger than the accompanying strain energy [3]. Such reconstruction impacts both the local conductivity and the optical properties.

[1] M.R. Rosenberger et al, *ACS Nano* **13**, 904 (2019). DOI: 10.1021/acsnano.8b08730

[2] M.R. Rosenberger et al, *ACS Nano* **14**, 4550 (2020). <https://dx.doi.org/10.1021/acsnano.0c00088>

[3] M. Phillips and C.S. Hellberg, ArXiv 190902495 Cond-Mat (2019)

\*Work done in collaboration with Matthew R. Rosenberger, Hsun-Jen Chuang, Madeleine Phillips, Kathleen M. McCreary, and C. Stephen Hellberg of the *Naval Research Laboratory*, Washington DC, and Chandriker Kavir Dass and Joshua R. Hendrickson of the *Air Force Research Laboratory*, Wright-Patterson AFB, OH.

† This work was supported by AFOSR and core programs at NRL.

**5:30 AM \*F.MT06.01.04**

**Understanding Tunability in the Electronic and Optical Response of Two-Dimensional Materials with Defects by Computational Analysis** Ruth Pachter and Jie Jiang; Air Force Research Laboratory, United States

The ability to tune the electronic and optical properties of 2D materials by induced defects has wide-ranging applications. For example, patterned graphene surfaces can be used for biosensing, while strained 2D transition metal dichalcogenides (TMDs) could enable the control of excitons for quantum emitters. Here, we first report on electronic band structure calculations of periodically patterned graphene, which can be fabricated using electron-beam chemistry with radiolyzed water (Islam, et al. *Carbon* **2020**, *166*, 446-455). Analysis of the effects of alternating strips in the graphene surface, which are pristine or with epoxide defects, illustrate electronic confinement in the graphene ribbon, which leads to one-dimensional quasi-metallic or semiconducting response, dependent on the strip's width. Electron transport calculations demonstrate electron transmission along the graphene strip direction, minimized in the direction perpendicular to edges terminated by oxygen atoms, while intrinsic current-voltage (*I-V*) characteristics indicate comparable performance to graphene nanoribbons with perfect edges. The electron transport in a device setting with gold electrodes shows improved conductivity in comparison to a graphene-based device. Next, in an effort to move towards controlled emission properties, such as for single-photon emission applications, we consider strained 2D WSe<sub>2</sub> monolayers with varying wrinkle structures. The tunability we demonstrate in the optical response of the mechanically deformed nanostructures is described in detail. Our results on exciton tunability by wrinkle structure could motivate experimental fabrication.

**5:45 AM F.MT06.01.05**

**Visualizing Twisted Bilayer Graphene in Momentum- and Real-Space—Flat Electronic Band and Moiré**

**Lattices** Iqbal B. Utama<sup>1</sup>, Roland Koch<sup>2</sup>, Kyunghoon Lee<sup>1</sup>, Nicolas Leconte<sup>3</sup>, Hongyuan Li<sup>1</sup>, Sihan Zhao<sup>1</sup>, Lili Jiang<sup>1</sup>, Jiayi Zhu<sup>1</sup>, Kenji Watanabe<sup>4</sup>, Takashi Taniguchi<sup>4</sup>, Paul Ashby<sup>5</sup>, Alexander Weber-Bargioni<sup>5</sup>, Alex Zettl<sup>1</sup>, Chris Jozwiak<sup>2</sup>, Jeil

Jung<sup>3</sup>, Eli Rotenberg<sup>2</sup>, Aaron Bostwick<sup>2</sup> and Feng Wang<sup>1</sup>; <sup>1</sup>University of California, Berkeley, United States; <sup>2</sup>Advanced Light Source, United States; <sup>3</sup>University of Seoul, Korea (the Republic of); <sup>4</sup>National Institute for Materials Science, Japan; <sup>5</sup>Molecular Foundry, United States

Stacking two-dimensional layers with slightly different lattice vectors produces a new periodic structure known as moiré lattices. As one of such moiré system, twisted bilayer graphene (tBLG) has been predicted to host a moiré miniband with flat dispersion if the layers are stacked at the 'magic angles'. Recently, magic angle tBLG was reported to exhibit correlated transport phenomena, where the presence of the flat miniband in the system is thought to be essential. Although STM and compressibility measurements in tBLG have found a van Hove singularity consistent with the presence of the flat band, a direct observation of the flat dispersion in the momentum-space of such a moiré miniband in tBLG is still lacking. Here, we report the visualization of this flat moiré miniband by using angle-resolved photoemission spectroscopy with nanoscale resolution (nanoARPES) [1]. Meanwhile, we probed the real-space structure of the moiré lattice with scanning microwave impedance microscopy (sMIM), where the sub-5 nm spatial resolution has also allowed us to image the strain-related inhomogeneity and defect structures in various graphene-based moiré lattices [2]. Our measurements demonstrate the existence of the flat moiré band near the charge neutrality for tBLG close to the magic angle at room temperature.

[1] **MIB Utama\***, RJ Koch\*, K. Lee\*, et al. Nature Physics 2020 (in press), ArXiv:1912.00587

[2] K. Lee\*, **MIB Utama\***, S Kahn\*, et al, ArXiv:2006.04000 (2020)

**5:55 AM F.MT06.01.06**

**Ab Initio Strain-Dependent Valley Dynamics in Monolayer Transition Metal Dichalcogenides** Christopher J. Ciccarino, Chitraleema Chakraborty and Prineha Narang; Harvard University, United States

Two-dimensional transition metal dichalcogenides (TMDCs) have unique optoelectronic properties in part because of their spin- and valley-selective carrier dynamics at the band edges. However, limited valley coherence times represent a major challenge for application. Here we comprehensively investigate electron-phonon interactions at valleys in both the valence and conduction band edges using a first-principles, spin-resolved approach. We capture the effects of strain by introducing  $\pm 2\%$  biaxial strain to each of the four monolayer TMDCs (MoS<sub>2</sub>, MoSe<sub>2</sub>, WS<sub>2</sub> and WSe<sub>2</sub>) studied. We find that the strength of the spin-orbit splitting is strongly sensitive to strain for tungsten-based monolayers relative to molybdenum-based compounds. Additionally, our results show that the direct nature of the bandgap of monolayer TMDCs is sensitive to less than 1% compressive strain. Our results detail the relevant mode- and wavevector-resolved electron-phonon processes responsible for scattering involving valley states, which we find to be highly tunable by strain. Most notably, we find up to an order of magnitude increase in conduction-band lifetimes under tensile strain. Overall we find significant potential in engineering valley dynamics and optoelectronic properties of monolayer TMDCs through the use of applied strain.

**6:05 AM F.MT06.01.07**

**Temperature-Resolved Observations and Predictions of Phonon-Mediated Hydrodynamic Flow of Electrons in WTe<sub>2</sub>** George Varnavides<sup>1,2</sup>, Uri Vool<sup>1</sup>, Yaxian Wang<sup>1</sup>, Assaf Hamo<sup>1</sup>, Polina Anikeeva<sup>2,2</sup>, Amir Yacoby<sup>1</sup> and Prineha Narang<sup>1</sup>; <sup>1</sup>Harvard University, United States; <sup>2</sup>Massachusetts Institute of Technology, United States

Recent measurements of spatially-resolved current flows have revealed that electrons in condensed matter can behave hydrodynamically, exhibiting classical fluid phenomena such as vortices and Poiseuille flow<sup>1,2,3</sup>. This occurs when microscopic scattering processes conserve momentum over time- and length-scales significantly exceeding those of the experimental probe<sup>4</sup>. In contrast with graphene, where the hydrodynamic regime persists well into room-temperature, other materials exhibit hydrodynamic flow only within a finite low-temperature window, and as such require temperature-resolved measurements. Here, we report direct observation of temperature-dependent electron hydrodynamic flow in the van der Waals solid WTe<sub>2</sub>, via measurements of the associated stray magnetic field using nitrogen vacancy echo magnetometry. At low-enough temperatures the onset of ballistic flow competes with the hydrodynamic regime, eventually resulting in a flat current profile.

In this work, we predict temperature-resolved lifetimes for various electron scattering mechanisms in WTe<sub>2</sub> from first principles<sup>5</sup>. We use our ab initio microscopic lifetimes as inputs to the electronic Boltzmann transport equation<sup>6</sup>, capturing the non-monotonic behavior in the experimental data. This provides a quantitative estimate for the electron interaction length in WTe<sub>2</sub>, which seems to be robust against a wide range of impurity concentrations. We find that these results cannot be explained using a direct Coulomb effect alone and that the major contributing momentum-conserving process is a Frohlich-like phonon-mediated electron interaction. We then investigate the effect of strain on the hydrodynamic regime in WTe<sub>2</sub>, concluding both the temperature-window and the magnitude of the hydrodynamic flow vary.

- <sup>1</sup> Ella, L., Rozen, A., Birkbeck, J. et al. *Nat. Nanotechnol.* 14, 480–487 (2019)
- <sup>2</sup> Sulpizio, J.A., Ella, L., Rozen, A. et al. *Nature* 576, 75–79 (2019)
- <sup>3</sup> Ku, M.J.H., Zhou, T.X., Li Q. et al. arXiv:1905.10791 (2019)
- <sup>4</sup> Varnavides G., Jermyn A.S., Anikeeva P. et al. arXiv:2002.08976 (2020)
- <sup>5</sup> Coulter J., Sundaraman R., Narang P., *Phys. Rev. B* 98, 115130 (2018)
- <sup>6</sup> de Jong M.J.M., Molenkamp L.W. *Phys. Rev. B* 51, 13389 (1995)

#### 6:15 AM F.MT06.01.08

**Dynamical Modulation of Defect-Phonon Coupling in Transition Metal Dichalcogenides** Chitrалеema Chakraborty, Christopher J. Ciccarino and Prineha Narang; Harvard University, United States

The formation of atomic defects is unavoidable in 2D materials with currently available growth techniques <sup>1</sup>. Nevertheless, there is a myriad of functionalities in modern optoelectronic and nanophotonic devices that leverage quantum defects including the recent demonstration of single photon emitters in 2D materials <sup>2,3</sup>. In parallel, advances in atomic-resolution imaging techniques provide new opportunities to directly create, manipulate and characterize defects down to the atomic scale in low-dimensional materials <sup>4</sup>. Therefore, we present theoretical calculations and analysis of optically active quantum defects in 2D materials. We study the electron-phonon interactions <sup>5,6</sup> of electronic transitions in defects and quantify their optical efficiency by calculating the Huang-Rhys factor. This presents a pathway for maximizing the optical efficiency of designer defect and provides a deterministic choice for defect creation at the atomic scale using scanning probe techniques <sup>2</sup>.

[1] D. Edelberg, et al, *Nano Lett.* 19, 7, (2019)

[2] O. Dyke et al, *Nat. Mat.*, 4, 497, (2019)

[3] C. Chakraborty, L. Kinnischtzke, K. Goodfellow, R. Beams, and N. Vamivakas, *Nat. Nano.* 10, 507 (2015)

[4] G. Grosso, H. Moon, B. Lienhard, S. Ali, D. K. Efetov, M. M. Furchi, P. Jarillo-Herrero, M. J. Ford, I. Aharonovich, and D. Englund, *Nat. Comm.* 8, 705, (2017)

[5] C. J. Ciccarino, T. Christensen, R. Sundaraman, and P. Narang, *Nano Lett.* 18, 5709, (2018)

[6] C. J. Ciccarino, C. Chakraborty, D. Englund, and P. Narang, *Far. Disc.* 214, 175, (2018)

SESSION F.MT06.02: Novel Devices Enabled by Strain or Defect  
On Demand Abstracts Available for Viewing Starting Saturday Morning, November 21, 2020  
F-MT06

#### 5:00 AM \*F.MT06.02.01

**Weakened Interlayer Interaction of Incommensurate Graphene as a Key Factor for Superior Lithium Intercalation** Tereza Paronyan; HeXalayer, LLC, United States

Carbon/graphite-based energy storage devices, such as lithium-ion batteries (LIBs), are the most reliable energy storage devices for portable electronics, electric vehicles (EV) and electric grid storage due to their high-power density, stability, low cost, and safety. Despite the wide use of LIBs, the graphitic anode has limited capacity ( $372 \text{ mAh.g}^{-1}$ ) due to the limited rate of lithium diffusion within the commensurately stacked layered structure.

Here we discuss the unique superior capacity of Lithium intercalation of multilayered graphene structures, named as an Incommensurate Multilayer Graphene (IMLG), that consists of closely packed rotated graphene layers. In-plane and out-plane features of graphene are studied by Raman spectroscopy, High-Resolution Transmission Electron Microscopy (HRTEM), and X-ray Diffraction. The commensurate-incommensurate transition of layered graphene is analyzed by Raman spectroscopy and the range of the key parameters is discussed as a significant for efficient Lithium intercalation.

The structural and binding features of graphene anode before and after Lithium insertion is studied, and a new lithium intercalation model is considered. We revealed that weakened interplanar Van der Waals interaction as it occurs within rotated graphene layers enables easy and full penetration of lithium, followed by flexible adjustment of layers for stable and reversible stable cycling without affecting graphene in-plane features. Superior Lithium intercalation provides reversible and

stable long-term charge/ discharge of IMLG anodes reaching up over 1500 mAh.g<sup>-1</sup> capacity of LiBs. Our recent development of IMLG confirms the feasibility of the synthesis technique which allows us the development of high energy density and powerful lightweight secondary batteries in the nearest future.

#### 5:15 AM \*F.MT06.02.03

**Piezoelectricity and Exotic Nonlinearities in Monolayer TMDC Resonators** Horacio Espinosa, Shiva Nathamgari and Siyan Dong; Northwestern University, United States

Monolayer transition metal dichalcogenides (TMDCs), with the general chemical formula MX<sub>2</sub> (M = Mo or W and X = S, Se and Te), are a class of 2D materials that have been predicted to be piezoelectric using Density Functional Theory (DFT) calculations. In addition, some of the TMDCs possess certain advantages in monolayer form – such as a direct bandgap and better Q-factors – over graphene. Here, we present resonance and piezoelectric measurements on monolayer transition metal dichalcogenides (TMDCs) using cavity-interferometry. We also demonstrate that TMDCs are promising candidates for Nanoelectromechanical Systems (NEMS) due to their low mass and intrinsic piezoelectricity.

Cavity-interferometry refers to a displacement transduction technique in nanoelectromechanical systems (NEMS). Most fabrication protocols for NEMS naturally render an optical cavity where the NEMS structure and the underlying substrate constitute the two mirrors. The modulation in the cavity depth due to the motion of the NEMS translates to intensity variations of the reflected light from the optical cavity, which can be measured on an appropriate detector. By optimizing the cavity depth, wavelength of the probe laser and the back-end electronics, exquisite displacement sensitivity (sub picometer/Hz<sup>1/2</sup>) can easily be achieved [1].

Device fabrication is challenging; hence, we explored various fabrication methods for creation of suspended 2D material devices and established working protocols for both exfoliated and chemical vapor grown TMDCs. We also developed a new transfer method driven by water wettability to facilitate fabrication efforts. To perform device characterization, we developed an integrated in-vacuum Raman/Interferometer setup [1]. By exploiting the cavity formed between suspended 2D TMDC “bridges” and underneath substrates, resonance frequencies of various modes were characterized including exotic line shapes arising due to 1:1 internal resonance coupling in the nonlinear regime. Using a combined experimental-computational approach and the measured shift of fundamental resonance frequencies, induced by applied bias, we extracted piezoelectric properties of monolayer WS<sub>2</sub> and MoS<sub>2</sub>. The exfoliated samples display piezoelectric coefficients that are in good agreement with DFT predictions. By contrast, CVD grown monolayers, exhibit a 10-fold reduction in piezoelectricity, likely due to the existence of atomic defects such as vacancies.

Additionally, by driving resonance in the nonlinear regime, we revealed internal resonance pairs in monolayer WS<sub>2</sub>. Discovery of Hopf bifurcations linearly varying with driving forces inspired novel sensing modality with ultrahigh force sensitivity (aN) at room temperature [2]. Our efforts in fabricating and experimenting on suspended 2D TMDC devices will support further development in applying 2D materials to sensors and NEMS applications.

[1] S. S. P. Nathamgari, S. Dong, E. Hosseinian, L. J. Lauhon and H. D. Espinosa, "An Experimental Setup for Combined In-Vacuo Raman Spectroscopy and Cavity-Interferometry Measurements on TMDC Nano-resonators" *Experimental Mechanics*, Vol. 59, p. 349-359, 2019.

[2] S. S. P. Nathamgari, S. Dong, L. Medina, N. Moldovan, D. Rosenmann, R. Divan, D. Lopez, L. J. Lauhon and H. D. Espinosa, "Nonlinear Mode Coupling and One-to-One Internal Resonances in a Monolayer WS<sub>2</sub> Nanoresonator" *Nano Letters*, Vol. 19, No. 6, p. 4052-4059, 2019.

#### 5:30 AM \*F.MT06.02.04

**Single Photon Emitters Using Strained Low-Dimensional Materials** Hong Gyu Park; Korea University, Korea (the Republic of)

The quantum confinement in atomically-thin transition metal dichalcogenides (TMDCs) has been investigated for single photon emission based on naturally or artificially occurring defects. In particular, the precise control of the position of a single photon emitter by applying mechanical strains to the TMDC is feasible. Strains have been induced in TMDCs using various nanostructures including dielectric pillars, nanobubbles, optical waveguide, metal nanogaps, and metal nanoparticles. However, polarization control and integration with a high-quality (Q) cavity to increase the Purcell factor remain elusive in TMDC-based single photon sources.

In this talk, I will present the deterministic control of both the position and polarization of single photon emitters in atomically thin  $\text{WSe}_2$  placed on a nanogap array. Manipulation of the band structure by a local strain gradient generates a potential well at the nanogap site, and position-controlled single photon emission is subsequently achieved. Additionally, directional elongations of the potential well, which are tuned by changing the nanogap size, allow polarization-controlled single photon emission. Moreover, single photons with a  $g^{(2)}$  of  $\sim 0.1$  are generated at 4-20 K. To take a full advantage of such deterministic control of the position and polarization of single photon emitters, the emitters are integrated with one-dimensional photonic crystal cavities. Therefore, this approach is a unique way to develop next-generation, deterministic, controllable single photon emitters based on TMDC materials, which outperform the present single photon sources with random occurrence and uncontrolled polarization properties.

**5:45 AM \*F.MT06.02.07**

**2D Material Based Electronics Under High Mechanical Strain** Jong-Hyun Ahn; Yonsei University, Korea (the Republic of)

Rapid advances in synthesis of graphene and 2D materials, and fabrication methods for functional devices enable sophisticated types of functionality and their application to various emerging electronics, such as flexible, wearable and optoelectronic applications, that cannot be addressed with conventional materials. In this talk, I present that graphene and 2D materials can play critical roles in this context, through demonstrations of complex, mechanically assembled electronic and optoelectronic devices for flexible and wearable applications. Specifically, the mechanics of graphene and  $\text{MoS}_2$  can yield various devices in distinct, engineered flexible geometries that cannot be easily reproduced with conventional materials and/or conventional device layouts. Examples of devices include touch, tactile sensors and wearable OLED display.

SESSION F.MT06.03/F.EL04.13: Joint Session: Quantum Phenomena in Atomically Thin Materials  
On Demand Abstracts Available for Viewing Starting Saturday Morning, November 21, 2020  
F-MT06

**5:00 AM \*F.MT06.03/F.EL04.13.01**

**Interlayer Excitons in van der Waals Heterostructures** Philip Kim; Harvard University, United States

A pair of electron and hole across the interface of semiconductor heterostructure can form a bound quantum state of the interlayer exciton. In a coupled interface between atomically thin van der Waals layers (vdW), the Coulomb interaction of the interlayer exciton increases further. In this presentation, we will discuss observing interlayer exciton formation in semiconducting transition metal dichalcogenide (TMDC) layers. Unlike conventional semiconductor heterostructures, charge transport in of the devices is found to critically depend on the interlayer charge transport, electron-hole recombination process mediated by tunneling across the interface. We demonstrate the enhanced electronic, optoelectronic performances in the vdW heterostructures, tuned by applying gate voltages, suggesting that these a few atom thick interfaces may provide a fundamental platform to realize novel physical phenomena. Furthermore, complete experimental control of density, displacement and magnetic fields in our graphene double layer system enables us to explore the rich phase diagram of several superfluid exciton phases with the different internal quantum degrees of freedom.

**5:15 AM \*F.MT06.03/F.EL04.13.02**

**Tunable Quantum Transport High Mobility 2D Materials** Jeanie Lau; The Ohio State University, United States

One of the most alluring features of 2D materials is their tunability, as their carrier density, effective mass, band gap, and electronic phases can be tuned in situ by external parameters such as electric field, magnetic field and strain. Here we will present transport studies of high quality 2D materials. For instance, we demonstrate large tunable SOC and zero-field spin-splitting in atomically thin InSe with unprecedented mobility. From beating patterns in quantum oscillations, we establish that the SOC parameter  $a$  is thickness-dependent; it can be continuously modulated over a large range by an out-of-plane electric field, achieving zero-field splitting tunable between 0 and 20 meV. Surprisingly,  $a$  could be enhanced by an order of magnitude in some devices, suggesting that SOC can be further manipulated by variations in interlayer spacing induced by stacking and/or electrostatic compression. Our work highlights the extraordinary tunability of SOC in 2D materials, which can be harnessed for *in operando* spintronic and topological devices and applications.



**5:30 AM \*F.MT06.03/F.EL04.13.03**

**Electron Interactions in 2D Materials—Correlated Multi-Particle Excitations and Optical Field Driven ARPES** Steven G. Louie<sup>1,2</sup>; <sup>1</sup>University of California, Berkeley, United States; <sup>2</sup>Lawrence Berkeley National Laboratory, United States

Many-electron interaction effects dominate many spectroscopic properties of reduced-dimensional systems, leading often to manifestation of novel phenomena not seen in the bulk. In this talk, I present some of our recent work on electron interaction effects in atomically thin quasi 2D materials: (1) strongly bounded correlated multi-particle excitations, such as trions and bi-excitons, in quasi 1D and 2D materials; (2) giant excitonic effects in shift currents, a nonlinear optical phenomenon, in non-centrosymmetric quasi 2D semiconductors; and (3) excitons and band renormalization in optical field driven angle-resolved photoemission spectroscopy (ARPES). Studies of these novel phenomena are made possible because of newly developed theoretical methods which incorporate higher-order many-electron correlation effects from first principles, using an interacting Green's function approach.

**5:45 AM \*F.MT06.03/F.EL04.13.04**

**Quantum Anomalous Hall Effect in Intrinsic Magnetic Topological Insulator  $\text{MnBi}_2\text{Te}_4$**  Yuanbo Zhang; Fudan University, China

In a magnetic topological insulator, nontrivial band topology conspires with magnetic order to produce exotic states of matter that are best exemplified by quantum anomalous Hall (QAH) insulators and axion insulators. Up till now, such magnetic topological insulators are obtained by doping topological insulators with magnetic atoms. The random magnetic dopants, however, inevitably introduce disorders that hinder further exploration of topological quantum effects in the material. We resolve this dilemma by probing quantum transport in  $\text{MnBi}_2\text{Te}_4$  thin flake—a topological insulator with intrinsic magnetic order. In this layered van der Waals crystal, the ferromagnetic layers couple anti-parallel to each other, so bulk  $\text{MnBi}_2\text{Te}_4$  is an antiferromagnet. Atomically thin  $\text{MnBi}_2\text{Te}_4$ , however, becomes ferromagnetic when the sample has odd number of septuple layers (a septuple layer represents a single structural unit in the out-of-plane direction). We observe zero-field QAH effect in a five-septuple-layer specimen; an external magnetic field further enhance the QAH quantization by forcing all layers to align ferromagnetically.  $\text{MnBi}_2\text{Te}_4$  therefore becomes the first intrinsic magnetic topological insulator exhibiting QAH effect.

**6:00 AM \*F.MT06.03/F.EL04.13.05**

**THz-Driven Irreversible Topological Phase Transition in Monolayer  $\text{MoTe}_2$**  Keith A. Nelson; Massachusetts Institute of Technology, United States

The availability of intense tabletop terahertz-frequency pulses and simple field-enhancement structures that enable peak electric fields of tens of MV/cm have led to demonstrations of highly nonlinear THz-induced responses from a wide variety of materials. THz-driven electronic, magnetic, and structural phase transitions and domain switching have illustrated novel possibilities for control over collective properties and dynamics. In experiments on single-layer and few-layer  $\text{MoTe}_2$ , we have found that irradiation with just one sufficiently strong THz pulse induces an irreversible phase transition [1]. The initial, noncentrosymmetric 2H phase disappears, as shown by the disappearance of characteristic Raman lines and second harmonic generation. After further THz irradiation, the topological insulator phase appears, revealed by its distinct Raman spectrum. Single-shot measurements of the  $\text{MoTe}_2$  evolution as a function of time after THz irradiation reveal complex dynamics over many-picosecond time scales. Theoretical calculations show that the transition is induced through THz-induced liberation of carriers which stabilize the new phase and reduce the energy barrier between the two phases. The result illustrates the prospects for THz control over complex multiphase landscapes in quantum materials.

[1] “Terahertz-driven irreversible topological phase transition in two-dimensional  $\text{MoTe}_2$ ,” J. Shi, Y.-Q. Bie, W. Chen, S. Fang, J. Han, Z. Cao, T. Taniguchi, K. Watanabe, V. Bulović, E. Kaxiras, P. Jarillo-Herrero, and K. A. Nelson, *arXiv:1901.13609* (2019).

**6:15 AM \*F.MT06.03/F.EL04.13.06**

**Conformal, Area-Specific and Switchable Graphene Nanowrinkles** Teri W. Odom; Northwestern University, United States

Selective patterning and functionalization of graphene can produce spatially-defined properties. Buckling or wrinkling of graphene on polymeric substrates enables a direct approach to tune the physical properties without lithographic steps, and the resulting curvature of the wrinkles can control local chemical reactivity. However, most buckling methods have been limited

by the range of wavelength tunability, only global control of the wrinkled patterns, and delamination and cracks in the graphene. This talk will describe a scalable approach to achieve area-specific reactivity and patterning of conformal graphene wrinkles. We will discuss how a fluoropolymer layer sandwiched between graphene and different polymer substrates can facilitate crack-free and switchable graphene nanostructures. Such patterned areas with different curvatures show different reactivities based on a plasma fluorination reaction. Our approach for large-area, fine control over graphene wrinkle topographies has prospects for other two-dimensional electronic materials and optoelectronics and plasmonics applications.

SESSION F.MT06.04: Synthesis and Characterization  
On Demand Abstracts Available for Viewing Starting Saturday Morning, November 21, 2020  
F-MT06

**5:00 AM \*F.MT06.04.01**

**Chemical Properties and Applications of 2D TMDCs Mediated by Defects** Qing Hua Wang; Arizona State University, United States

The two-dimensional transition metal dichalcogenides (2D TMDCs) tend to have basal planes that are chemically relatively inert. Many approaches and reaction schemes have been demonstrated to modify the chemical nature of TMDCs, resulting in new chemical properties and applications. This talk will highlight our recent work on the chemical properties of 2D TMDCs mediated by point defects and edges, which subsequently enable applications in water treatment and antimicrobial treatment. We have shown robust and versatile covalent functionalization of materials across the metal chalcogenides including MoS<sub>2</sub>, MoSe<sub>2</sub>, WS<sub>2</sub>, WSe<sub>2</sub>, Bi<sub>2</sub>S<sub>3</sub>, and Sb<sub>2</sub>S<sub>3</sub> using aryl diazonium salts. The reaction mechanism is initiated at point defect sites and edges, but propagates across the chalcogenide surfaces in a chain-like step growth. We have also shown the ability for MoS<sub>2</sub> to remove Pb contamination from water via a reaction with the surface sites to form sulfate precipitates. The reaction mechanism is again initiated at defect sites in the MoS<sub>2</sub>. Finally, we have used single stranded DNA to encapsulate MoSe<sub>2</sub> nanosheets and shown their broad-spectrum antimicrobial properties against multidrug resistant bacteria. The choice of ssDNA sequence influences the conformal coating, and the ability for the edges of MoSe<sub>2</sub> to cut through bacterial cell membranes.

**5:15 AM \*F.MT06.04.02**

**Chemical Trends of Deep Levels in van der Waals Semiconductors** Penghong Ci<sup>1</sup>, Xuezheng Tian<sup>2</sup>, Jun Kang<sup>3</sup>, Sefaattin (Sef) Tongay<sup>4</sup>, Wladek Walukiewicz<sup>1</sup>, Jianwei (John) Miao<sup>2</sup>, Oscar Dubon<sup>1</sup> and Junqiao Wu<sup>1</sup>; <sup>1</sup>University of California, Berkeley, United States; <sup>2</sup>University of California, Los Angeles, United States; <sup>3</sup>Beijing Computational Science Research Center, China; <sup>4</sup>Arizona State University, United States

Properties of semiconductors are largely defined by crystal imperfections including native defects. Van der Waals (vdW) semiconductors, a newly emerged class of materials, are no exception: defects exist even in the purest materials and strongly affect their electrical, optical, magnetic, catalytic and sensing properties. However, unlike conventional semiconductors where energy levels of defects are well documented, they are experimentally unknown in even the best studied vdW semiconductors, impeding the understanding and utilization of these materials. We directly evaluate deep levels and their chemical trends in the bandgap of MoS<sub>2</sub>, WS<sub>2</sub> and their alloys by transient spectroscopic study. One of the deep levels is found to follow the conduction band minimum of each host, attributed to the native sulfur vacancy. A switchable, DX center-like deep level has also been identified, whose energy lines up instead on a fixed level across different host materials, which explains the chemical trend of native electron density in the hosts as well as a persistent photoconductivity up to 400K.

**5:30 AM \*F.MT06.04.03**

**Defect and Strain Engineering of Two-Dimensional Materials** Jun Lou; Rice University, United States

Two-dimensional (2D) materials, such as Graphene, hBN and MoS<sub>2</sub>, are promising candidates in a number of advanced functional and structural applications, owing to their exceptional electrical, thermal and mechanical properties. To better meet the requirements of practical applications, property modification and regulation are oftentimes desired. Defect and strain engineering strategies are powerful tools to modulate electronic, optoelectronic and other functional properties of 2D semiconductors.

In this talk, we will report our efforts to employ such strategies to tune functional properties of 2D semiconductors. We first demonstrated how substrate interfacial chemistry can be utilized to tailor the physical properties of single-crystalline

molybdenum disulphide (MoS<sub>2</sub>) monolayers. We use self-assembled monolayers with a variety of end termination chemistries to functionalize substrates and systematically study their influence on the physical properties of MoS<sub>2</sub>. Our data shows that combined interface-related effects of charge transfer, built-in molecular polarities, varied densities of defects, and remote interfacial phonons strongly modify the electrical and optical properties of MoS<sub>2</sub>. Tunable friction behavior of the heterostructure of monolayer MoS<sub>2</sub> and different self-assembled organic molecules (SAMs) were also demonstrated, which was attributed to the charge transfer from SAMs to MoS<sub>2</sub> influencing the electron concentration and thus the carrier-mediated friction in MoS<sub>2</sub>. In another example, we systematically characterize chemical vapor deposition (CVD)-grown MoS<sub>2</sub> by photoluminescence spectroscopy and mapping and demonstrate non-uniform strain in single-crystalline monolayer MoS<sub>2</sub> and strain-induced bandgap engineering. We further modified our CVD process to create a Janus SMOSe monolayer and demonstrated high basal plane hydrogen evolution reaction (HER) activity in such samples and DFT calculation implies that the activity originates from the synergistic effect of the intrinsic defects and structural strain inherent in the Janus structure.

#### 5:45 AM \*F.MT06.04.04

**Emerging Electron Microscopy Techniques for 2D Materials** [Kayla Nguyen](#), Edmund Han, Chia-Hao Lee, Jeffrey Huang and Pinshane Y. Huang; University of Illinois at Urbana-Champaign, United States

The study of atomic-monolayer materials has been extremely popular within the last decade due to the emergence of a family of two-dimensional (2D) materials with expansive mechanical, electrical and magnetic properties. Subtle changes in these 2D materials at the atomic length scales, ranging from strain fields and dislocations, have large effects for tuning the electronic and mechanical properties, especially when used in real devices. Electron microscopy can provide the insight needed to visualize these effects [1-2]. Recent advancements in detector technology have already pushed the limits of resolution using 2D bilayer molybdenum disulfide using ptychographic reconstruction [3-4]. In my talk, I will discuss ways electron microscopy can provide opportunities for sensitive strain and magnetic measurements of 2D materials, with an emphasis on emerging techniques provided by the electron microscope pixel array detector (EMPAD), a state-of-the-art, high-dynamic range and high-speed electron diffraction detector.

[1] Lee, CH et al, *Nanoletters*, 20 (5), 3369–3377 (2020).

[2] Han, E et al, *Nature Materials*, 19 (3), 305-309 (2019).

[3] Tate, MW et al, *Microscopy and Microanalysis*, 22 (1), 237-249 (2016).

[4] Jiang, Y et al, *Nature*, 559 (7714), 343-349 (2018).

#### 6:00 AM F.MT06.04.06

**Quantifying Peak Profile Analysis of 2D Tellurium Nanostructures by 4D-STEM** [Alejandra Londono-Calderon](#)<sup>1</sup>, Darrick Williams<sup>1</sup>, Colin Ophus<sup>2</sup> and Michael Pettes<sup>1</sup>; <sup>1</sup>Los Alamos National Laboratory, United States; <sup>2</sup>Lawrence Berkeley National Laboratory, United States

Tellurium nanostructures are promising candidates for functional electronic and optical nanomaterials. The anisotropic helical crystal structure of trigonal tellurium (t-Te) and the weak van der Waals stacking of its layers; allows the formation of a variety of 1D nanostructures such as nanowires and nanobelts. A kinematically driven growth can promote the formation of 2D tellurium known as tellurene. This recent realization of 2D tellurium has allowed scientists to demonstrate an air-stable mono-elemental van der Waals material with remarkable potential for applications in electronics and optoelectronics. The chiral-chain structure of ultrathin Te allows controllable electronic and optical properties due to the non-monotonic carrier mobility and an increase in electronic band-gap as the thickness is reduced. Scalable and accurate production of 2D Te-based functional devices will require detailed knowledge of structural defects and strain field distributions that can be linked to transport properties.

Standard HRTEM images provide localized crystallographic information, which usually leaves out larger-scale structural components. Precise quantification of lattice parameters and additional structural features is often not fully captured in this type of analysis. Modern single electron detectors allow the rapid collection of 2D diffraction patterns of a 2D set of probe positions in the so-called 4D Scanning Transmission Electron Microscopy (4D-STEM). 4D-STEM provides a remarkable tool for structural analysis across many length scales, and enables extracting the crystalline structure, orientation, virtual images, and strain information at the nanometer scale.

In this presentation, we will demonstrate a new microwave-assisted synthesis method for 1D and 2D tellurium nanostructures and the analysis of the micro/nanostructure using conventional XRD and the new 4D-STEM technique. Fast collection of nano beam electron diffraction (NBED) patterns of beam sensitive Te nanowires and flakes was performed using a Gatan K3 direct electron detector, and these data sets were used to perform peak profile analysis over the thousands of NBED patterns to quantify the nanostructure of 1D and 2D Te including chirality and grain boundary analysis.

**6:10 AM F.MT06.04.07**

**Ultra-High-Resolution Imaging of Moiré Lattices and Superstructures under Ambient Conditions** [Kyunghoon Lee](#)<sup>1,2,3</sup>, Iqbal Bakti Utama<sup>2</sup>, Salman Kahn<sup>2</sup>, Appalakondaiah Samudrala<sup>4</sup>, Nicolas Leconte<sup>4</sup>, Birui Yang<sup>2</sup>, Shuopei Wang<sup>5</sup>, Kenji Watanabe<sup>6</sup>, Takashi Taniguchi<sup>6</sup>, Guangyu Zhang<sup>5</sup>, Alexander Weber-Bargioni<sup>1</sup>, Michael Crommie<sup>2,1,3</sup>, Paul Ashby<sup>1</sup>, Jeil Jung<sup>4</sup>, Feng Wang<sup>2,1,3</sup> and Alex Zettl<sup>2,1,3</sup>; <sup>1</sup>Lawrence Berkeley National Laboratory, United States; <sup>2</sup>University of California, Berkeley, United States; <sup>3</sup>Kavli Energy NanoScience Institute, United States; <sup>4</sup>University of Seoul, Korea (the Republic of); <sup>5</sup>Institute of Physics, Chinese Academy of Sciences, China; <sup>6</sup>National Institute for Materials Science, Japan

A moiré lattice is produced by stacking lattice-mismatched 2D materials or by introducing misalignment. The moiré lattices generate the periodic potential that can strongly modify the electronic properties of the constituent 2D layers. In addition, superstructures of moiré lattices can emerge from multiple misaligned lattice vectors or inhomogeneous strain distribution, which offers an extra degree of freedom in engineering electronic band structure. Thus, a high-resolution imaging moiré lattices and superstructures is critical to correlate the moiré structure with the resulting material behavior. Here we report the versatility of ultra-high-resolution implementation of scanning impedance microwave microscopy (sMIM) in imaging the moiré superlattices in various graphitic systems at ambient conditions. We show that an ultra-high spatial resolution better than 5 nm can be achieved although the scanning probe tip has a gross radius of ~100 nm. The high sensitivity of sMIM allows the imaging of the intricate nanostructural details in the superlattice. Furthermore, the imaging capability of sMIM enables the characterization of various composite moiré designs, including the super-moiré pattern and Kagome-like superlattice.

## SESSION F.MT06.05: Transport Properties

On Demand Abstracts Available for Viewing Starting Saturday Morning, November 21, 2020

F-MT06

**5:00 AM \*F.MT06.05.01**

**Study of Thermal and Magnetic Transport in Functional Materials Enabled by Ultrafast Optical Metrology** [Xiaojia Wang](#); University of Minnesota Twin Cities, United States

Transport phenomena play an important role in designing and engineering materials with tailored functionalities. Thermal conductivity and spin precession damping, as basic transport properties of materials, can provide a wealth of information on the fundamental scattering processes of phonons and magnons with structural defects and interface imperfection. In this talk, I will share our group's recent progress on utilizing time-resolved magneto-optical Kerr effect (TR-MOKE) metrology to study the thermal and magnetic properties of functionalized materials spanning a wide range of applications. This will include: (1) revealing the 3D anisotropic thermal transport in black phosphorus, as the next-generation of "wonder materials" for the semiconductor industry; (2) developing low-damping and high-thermal stability materials with perpendicular magnetic anisotropy for spintronic applications; and (3) manipulating spin precession using optically launched acoustic strains via a strong magnon-phonon coupling at ultra-high frequencies (~60 GHz). The structure-property relationships of functional materials revealed by the ultrafast pump-probe technique open up opportunities of tailoring material properties by structural engineering at the atomic and molecular levels. Ultimately, such an understanding can be leveraged to guide the design and optimization of materials, as promising building blocks for high-performance electronics, thermal management, hard-disk data storage, and magnetoacoustic devices.

**5:15 AM \*F.MT06.05.02**

**Exotic Spin Transport in Two-Dimensional Materials** [Stephan Roche](#)<sup>1,2</sup> and [Jose H. Garcia Aguilar](#)<sup>1</sup>; <sup>1</sup>Catalan Institute of Nanoscience and Nanotechnology, Spain; <sup>2</sup>ICREA--Institutió Catalana de Recerca i Estudis Avançats, Spain

The field of spin transport in two-dimensional has flourished in the past couple of years. Some remarkable features are the reports of large charge-to-spin in graphene-based heterostructures [1], the discovery of the quantum spin Hall effect [2], and ultra-clean spin transport measurements within the ballistic regime [3]. In this talk, we will present predictions on diffusive and ballistic spin transport in different two-dimensional materials. Using complementary large-scale numerical transport methods, we developed a theory showing that contacts have a dramatic effect on the spin transport in systems with a size comparable to the spin relaxation length, leading to underestimating the latter [4]. We then apply this theory and bulk transport methods to unveil the role of broken symmetries in the spin transport of transition metal dichalcogenides in their 1T' and 1Td structural phases, showing they can promote an unconventional spin transport regimen. We believe our predictions

will lead to a better understanding of the recent measurements of the quantum spin Hall effect in WTe<sub>2</sub> and will help optimize experimental setups for its harvesting.

- [1] Nat. Mater. 19, 170–175 (2020).
- [2] Science 359,6371, pp. 76-79, (2018).
- [3] Phys. Rev. Lett. 124, 177701 (2020).
- [4] Phys. Rev. Lett. 124, 196602 (2020).

#### 5:30 AM \*F.MT06.05.03

**Strain Induced Tuning of Physical Properties of Materials** [Abhishek K. Singh](#); Indian Institute of Science, India

Tuning physical properties of materials by applying strain opens up wide range of applications. In this presentation, sensitivity of these properties on application of strain will be illustrated for the case of TMDs. Using first principles calculations, the effect of normal compressive (NC), bi-axial compressive (BC), and bi-axial tensile (BT) strain on the electronic properties of few layered MoS<sub>2</sub> has been investigated. Regardless of the type of strain, a reversible semiconductor-to-metal transition is observed MoS<sub>2</sub>. The effect of strain as a function of number of layers on the transport properties is investigated. It is found that the 3L and 2L-MoS<sub>2</sub> emerge as the most efficient thermoelectric materials under NC and BT strain, respectively. The study was further extended to semi-metallic TMD TiS<sub>2</sub>, which has been in focus due to its application in energy storage and thermoelectric materials. Upon application of uniform biaxial strain, TiS<sub>2</sub> transforms from semi-metal to semiconducting phase. The transport calculations show three-fold enhancement in thermopower for both *p*- and *n*-type doped TiS<sub>2</sub>. Further, the effect of strain on thermal conductivity of bulk MoS<sub>2</sub> is explored, wherein an increase of cross-plane thermal conductivity from 3.5 to about 25 W/m-K. The giant enhancement arises from the increase in interlayer interaction on application of strain and decrease in phonon lifetimes due to the unbundling effect along the cross-plane direction. The concepts proposed from our studies can be extended to other semiconducting and metallic TMDs.

#### References:

- Semiconductor-metal transition in semiconducting bilayer sheets of transition-metal dichalcogenides, Phys. Rev. B, **86**, 075454 (2012)
- Pressure-induced semiconducting to metallic transition in multilayered molybdenum disulphide, Nat. Commun., **5**, 3731 (2014)
- Effect of strain on electronic and thermoelectric properties of few layers to bulk MoS<sub>2</sub>, Nanotechnology, **25**, 465701 (2014)
- Strain-induced electronic phase transition and strong enhancement of thermopower of TiS<sub>2</sub>, Phys. Rev. B, **90**, 174301 (2014)
- Thermal Conductivity Enhancement in MoS<sub>2</sub> under Extreme Strain, Phys. Rev. Lett., **122**, 155901 (2019)

#### 5:45 AM \*F.MT06.05.04

**Towards Room-Temperature Magnetic Semiconductors in van der Waals Layered Materials** Seok Joon Yun, Jinbao Jiang, Dinh Loc Duong and [Young Hee Lee](#); Sungkyunkwan University, Korea (the Republic of)

The ferromagnetic state in van der Waals two-dimensional (2D) materials has been reported recently in the monolayer limit. Intrinsic CrI<sub>3</sub> and CrGeTe<sub>3</sub> semiconductors reveal ferromagnetism but the T<sub>c</sub> is still low below 60K. In contrast, monolayer VSe<sub>2</sub> is ferromagnetic metal with T<sub>c</sub> above room temperature but incapable of controlling its carrier density. Moreover, the long-range ferromagnetic order in doped diluted chalcogenide semiconductors has not been demonstrated at room temperature. The key research target is to realize the long-range order ferromagnetism, T<sub>c</sub> over room temperature, and semiconductor with gate tunability. Here, Ferromagnetic order is manifested using magnetic force microscopy up to 360K, while retaining high on/off current ratio of ~10<sup>5</sup> at 0.1% V-doping concentration. The V-substitution to W sites keep a V-V separation distance of 5 nm without V-V aggregation, scrutinized by high-resolution scanning transmission-electron-microscopy. More importantly, the ferromagnetic order is clearly modulated by applying a back gate. We also observe a ferromagnetic hysteresis loop together with oscillatory behavior at room temperature in diluted V-doped WSe<sub>2</sub>, while maintaining the semiconducting characteristic of WSe<sub>2</sub> with a high on/off current ratio of five orders of magnitude. Our findings open new opportunities for using two-dimensional transition metal dichalcogenides for future spintronics.

#### 6:00 AM F.MT06.05.05

**Thermal Conductivities of 2D MoS<sub>2</sub> Under Mechanical Strains** [Annie Xian Zhang](#); Stevens Institute of Technology, United States

In recent years, transition metal dichalcogenides become emergent thermoelectric materials with potential wide spread in

wearable electronics applications. Considering the extensive applications of transition metal dichalcogenides, many research efforts have been paid and good progresses have been made. So far, all of the researches in this field focus on the electrical properties of them. It has not been reported about the transition metal dichalcogenides' thermal transport properties under mechanical strains. Due to their potential applications, it is of significance to discover the thermal transport properties of transition metal dichalcogenides at large mechanical strains, and thus develop the novel thermoelectric platforms which can sustain the extreme environments in wearable electronics.

In this work, we demonstrate using Raman optothermal technique to measure the thermal conductivities of two dimensional (2D) MoS<sub>2</sub>. We first utilize more direct measurements of the optical absorption, and then by comparing the response of the samples using different laser spot sizes, we are able to measure the thermal conductivities of the 2D MoS<sub>2</sub>. Then thermal conductivities at large mechanical strains are obtained providing more scientific merits.

The Raman optothermal technique has been the most successful method for measurement of thermal conductivity of 2D materials, and was used to measure the 2D materials at large mechanical strains for the first time in this work. In this technique, a laser is focused at the center of a thin film and used to measure the peak position of a Raman-active mode. As the laser power is increased, the sample is heated which enables red-shift Raman mode due to thermal softening. Another comparison experiment is conducted by placing the samples on a heating platform and monitor the change of Raman-active mode peak position shift. Combining these two sections of experiments provide us the thermal modeling can then be used to extract the thermal conductivity from the measured shift rate. We have used a refined version of the optothermal Raman technique to study thermal conductivity of 2D MoS<sub>2</sub>, at large mechanical strains. It is the first thermal measurement on 2D materials at large mechanical strains. This work also addresses several important issues in the measurement of thermal conductivity of 2D materials at large strains using Raman spectroscopy.

In conclusion, we have used Raman optothermal technique to study thermal transport properties of 2D MoS<sub>2</sub> at large mechanical strains. This work addresses several important issues in the measurement of thermal conductivity of the 2D materials MoS<sub>2</sub> using Raman spectroscopy. We derive the thermal conductivity values at large mechanical strains. These results are of significance to discover the thermal transport properties of 2D transition metal dichalcogenides at large mechanical strains, and thus develop the efficient 2D thermoelectric materials which can sustain the large mechanical strains and in turn to use strains to tune their thermal properties.

#### **6:10 AM F.MT06.05.06**

**Strain-Induced Effects on Transport in 2D Materials** Jennifer Coulter and Boris Kozinsky; Harvard University, United States

Understanding the influence of strain on transport properties, such as piezoresistive effects, is important for device applications of 2D materials. Accurate predictions of transport in materials depend on detailed knowledge of electron-phonon interactions, calculations of which have only recently become feasible due to algorithmic improvements. In particular, we can now apply the Electron-Phonon Averaged approximation to reduce the cost of such calculations and automate the prediction of resistivity with respect to variations in strain. Using first-principles electron-phonon calculations, we explore the specific mechanisms underlying piezoresistive effects in systems such as graphene and transition metal dichalcogenides, and provide additional understanding of how to manipulate these effects for practical use.

#### **6:20 AM \*F.MT06.05.07**

**Phonons in van der Waals Solids for Thermal Management Devices** Sina Najmaei; US Army Research Lab, United States

Active thermal management devices often lack the efficacy and energy efficiency of electronic switches. This is mainly because of the bosonic nature of phonons and the type of interactions they have with external forces. As a result, discovery of materials with unique vibrational properties that provide better control of thermal carriers is necessary. Our research shows that the phonons in group IVB transition metal dichalcogenides such as hafnium disulfide have distinct characteristics and provide remarkable mechanism for control of thermal careers. This is caused by the intermixing of van der Waals forces and covalent bonds in the material structure combined with their highly anisotropic bond properties. In this talk we present our results on vibrational and thermal transport properties of a member of this group, hafnium disulfide (HfS<sub>2</sub>). The highly asymmetric bond properties in HfS<sub>2</sub> dominate the structure and vibrational properties of this material. We explore the physics of HfS<sub>2</sub> by developing a comprehensive computational model to study its phonon behavior, anharmonic properties, and phonon transport characteristics. Our findings demonstrate a unique phonon behavior in the material where the absence of a phonon-gap between the acoustic and optical branches grant a more prominent and unique role to the optical modes of HfS<sub>2</sub>.

As a result HfS<sub>2</sub> has a low thermal conductivity, ranging between 0.3-5W/mK. In addition only one acoustic phonon branch, the ZA branch, contributes up to 80% to the thermal transport of the material in both out-of-plane and in-plane crystal orientations. Our experiments confirm and support the theory and add further insight into an anomalous behavior in the optical modes. Our quasi-harmonic model reveals a structural phase transformation at around room temperature that leads to unique anharmonicity, discernible in the experimental results of the zone center out-of-plane optical mode. This unique phase transformation contributes to both changes in the phonon decay properties and thermal transport behavior. The structural phase transformation combined with the constricted ZA branch phonon carriers and the distinct scattering physics in optical branches of HfS<sub>2</sub> provide unique means for control of thermal transport. We explore a few strategies for control of thermal properties in HfS<sub>2</sub> based on fundamental vibrational properties of the material. We demonstrate that a successful approach for dynamic control of thermal conductivity is the control of van der Waals gap properties. We demonstrate that through intercalation and modification of these gaps a 4-fold control of cross-plane thermal conductivity in hafnium disulfide from 0.35Wm<sup>-1</sup>K<sup>-1</sup> to 1.45Wm<sup>-1</sup>K<sup>-1</sup> is achievable. We also demonstrate that an out-of-plane strain can be used to make thermal regulators based on HfS<sub>2</sub>. This research unveils a unique class of 2D layers with vibrational properties suitable for development of thermal management devices

SESSION F.MT06.06: Poster Session: Strain and Defect-Driven Transport Properties in van der Waals Solids  
On Demand Abstracts Available for Viewing Starting Saturday Morning, November 21, 2020  
5:00 AM - 8:00 AM  
F-MT06

#### **F.MT06.06.01**

**Direct Correlation of Structure and Optical Properties of Defect Related Colour Centres in Hexagonal Boron Nitride** Soumya Sarkar, Sinu Mathew, Manohar Lal, T. Venky Venkatesan and Silvija Gradecak; National University of Singapore, Singapore

Hexagonal boron nitride (h-BN) has recently emerged as a prominent nanophotonic material due to observation of several unique optoelectronic phenomena such as natural hyperbolicity, strong second order non-linearities and robust deep UV emission. Specifically, its ultra wide bandgap ~ 6eV can host midgap defects that often exhibit intense room temperature quantum emission. Understanding the origin of such defect related emission is crucial to harness their technological potential. Here, we report controlled tailoring of defect states in hBN by focussed helium ions using a helium ion microscope and present a direct correlation of their structural and optical properties using a combination of Raman, photoluminescence (PL), cathodoluminescence (CL) and high resolution electron microscopy. We observe that while end of range defects cause an evolution of sp<sup>3</sup> phase in the otherwise sp<sup>2</sup> hBN leading to bright and previously unreported near infrared emission, near surface defects contribute to strong visible emitters often attributed to single photons. Our results provide a comprehensive overview of defect related colour centres in hBN across a wide spectral range that would serve as a platform to realize next generation quantum optoelectronic devices.

#### **F.MT06.06.02**

**Late News: Controlling Defects in Continuous 2D GaS Films for High-Performance Electronic and Optoelectronic Devices** Yang Lu<sup>1</sup> and Jamie Warner<sup>2</sup>; <sup>1</sup>University of Oxford, United Kingdom; <sup>2</sup>The University of Texas at Austin, United States

A chemical vapor deposition method is developed for thickness-controlled (one to four layers), uniform, and continuous films of both defective gallium(II) sulfide (GaS): GaS<sub>0.87</sub> and stoichiometric GaS. The unique degradation mechanism of GaS<sub>0.87</sub> with XPS and HAADF-STEM is studied, and it is found that the poor stability and weak optical signal from GaS are strongly related to photo-induced oxidation at defects. Photodetectors based on the two materials are fabricated with short response time (<66 ms), excellent UV photoresponsivity. An enhanced stability of the stoichiometric GaS is demonstrated under laser and strong UV light, and by controlling defects in GaS, the photoresponse range can be changed from vis-to-UV to UV-discriminating.

Besides the role in degradation mechanism, defects in GaS<sub>0.87</sub> also contributed to the formation of a new band sitting within its bandgap, which is confirmed by cathodoluminescence results. As a result, controlling defects in GaS turns the band alignment of the bilayer GaS-WS<sub>2</sub> van der Waals heterostructure from type I to type II. XPS and KPFM characterization demonstrates that the defect band can facilitate the charge transfer from WS<sub>2</sub> to GaS. Devices based on the type-II

heterojunction further show that the defect band greatly assisted the carrier transport by lowering the contact resistance, and also demonstrate superior photodetector properties with a large linear dynamic range (>73 dB) at a R of 13 A/W for green light.

[1] Lu, Y., Chen, J., Chen, T., Shu, Y., Chang, R.-J., Sheng, Y., Shautsova, V., Mkhize, N., Holdway, P., Bhaskaran, H., Warner, J. H., Controlling Defects in Continuous 2D GaS Films for High-Performance Wavelength-Tunable UV-Discriminating Photodetectors. *Adv. Mater.* 2020, 32, 1906958.

[2] Lu, Y., Warner, J. H., et al., Transition of type-I to type-II heterojunction in monolayer GaS-WS<sub>2</sub>. In preparation.

## SYMPOSIUM F.MT07

---

Data Science and Automation to Accelerate Materials Development and Discovery  
November 21 - November 21, 2020

### Symposium Organizers

Kristen Brosnan, Superior Technical Ceramics  
Keith Brown, Boston University  
Tonio Buonassisi, Massachusetts Institute of Technology  
Kedar Hippalgaonkar, Nanyang Technological University

---

\* Invited Paper

SESSION F.MT07.01: AI-Ready Data for Materials Science  
On Demand Abstracts Available for Viewing Starting Saturday Morning, November 21, 2020  
F-MT07

### 5:00 AM \*F.MT07.01.01

**FAIR Data Infrastructures Towards New Horizons for Materials Research** [Claudia Draxl](#)<sup>1,2</sup>; <sup>1</sup>Humboldt-Universität zu Berlin, Germany; <sup>2</sup>Fritz-Haber-Institut Berlin, Germany

Novel approaches of Artificial Intelligence (AI) can find patterns and correlations in data that cannot be obtained from individual calculations or experiments and not even from high-throughput studies. In fact, data-driven research is adding a new research paradigm to the scientific landscape. For a real breakthrough, *Open Data* and sharing, as well as an efficient data infrastructure is key [1]. In other words, for shaping this forth paradigm and contributing to the development or discovery of improved and novel materials, data must be what is now called FAIR - Findable, Accessible, Interoperable, and Reusable [2].

The NOMAD Laboratory [3,4] is a living example for such infrastructure in computational materials science, comprising the NOMAD *Repository* (raw data) and its *Archive* (normalized, i.e. code-independent data). The NOMAD *Encyclopedia* is a web-based public platform that visualizes the results of this vast amount of calculations. The NOMAD Analytics Toolkit provides a collection of examples and tools to demonstrate how materials data can be turned into knowledge by AI approaches (e.g. [5,6]). I will give a guided tour through this data lab and discuss successes and challenges [7] ahead of us for exploiting the whole wealth of materials data – including experiment and sample synthesis.

[1] C. Draxl and M. Scheffler, *Big-Data-Driven Materials Science and its FAIR Data Infrastructure*, Invited Perspective in Handbook Andreoni W., Yip S. (eds) Handbook of Materials Modeling. Springer, Cham (2019).

[2] M. D. Wilkinson et al., The FAIR Guiding Principles for scientific data management and stewardship, *Sci Data* 3, 160018 (2016).

[3] The NOMAD Laboratory, <https://nomad-coe.eu/>, including metadata and various software for parsing, analysis, and



visualization.

[4] C. Draxl and M. Scheffler, NOMAD: The FAIR Concept for Big-Data-Driven Materials Science, *MRS Bulletin* 43, 676 (2018).

[5] L. M. Ghiringhelli, J. Vybiral, S. V. Levchenko, C. Draxl, and M. Scheffler, *Big Data of Materials Science - Critical Role of the Descriptor*, *Phys. Rev. Lett.* 114, 105503 (2015).

[6] L. M. Ghiringhelli, J. Vybiral, E. Ahmetcik, R. Ouyang, S. V. Levchenko, C. Draxl, and M. Scheffler, *Learning physical descriptors for materials science by compressed sensing*, *New J. Phys.* 19, 023017 (2017).

[7] C. Draxl and M. Scheffler, *The NOMAD Laboratory: From Data Sharing to Artificial Intelligence*, *J. Phys. Mater.* 2, 036001 (2019).

#### 5:15 AM F.MT07.01.02

**The Perovskite Database Project—How Do We Get Experimentalists to Share All Their Data in a Form Useful for Others?** Tor J. Jacobsson<sup>1,2</sup> and Eva Unger<sup>1</sup>; <sup>1</sup>Helmholtz-Zentrum Berlin für Materialien und Energie, Germany; <sup>2</sup>Uppsala University, Sweden

Lead halide perovskites have in the last decade gained a large interest as a promising solar cell material and the number of published papers has now surpassed 15000. The sheer amount of papers makes it increasingly difficult to keep track of the field, and the lack of standards for describing, reporting, and sharing device data is something that seriously limit the pace of discovery. To deal with those problems, we have initiated the Perovskite Database Project where we aim at collecting all past and future perovskite device data in one place in a standardised machine-readable format. The project includes a web app, interactive graphics enabling anyone to explore and learn from the data, open source code, and mechanisms for collecting new data. The project is scheduled to go online during the autumn of 2020. In this talk we will discuss challenges and insights gained during this project including: how to motivate volunteers to gather previously published data, how do we get a sufficiently large part of a research community to share all their new data, how to organise data in a way that is simple to collect and robust to reporting errors, how do we ensure that the data is useful for as many as possible, and what can we really do with the data once we have it?

#### 5:25 AM F.MT07.01.03

**Accuracy, Uncertainty, Inspectability—Learning with Compositionally-Restricted Attention-Based Networks** Steven K. Kauwe<sup>1</sup>, Anthony Y. Wang<sup>2</sup> and Taylor D. Sparks<sup>1</sup>; <sup>1</sup>The University of Utah, United States; <sup>2</sup>Technische Universität Berlin, Germany

The materials science community has established that data-driven modeling, based on chemical composition, generates accurate and actionable results. Tools for performing this task have evolved from simple statistical methods to large endeavors containing complex neural-networks with millions of parameters. With each successive work, we have seen a marked improvement in property predictions with a trend towards raw model accuracy. However, model performance often includes additional considerations such as uncertainty quantification or interpretability.

In this talk, I will present our new model architecture, the Compositionally-Restricted Attention-Based Network (CrabNet). CrabNet generates high-fidelity predictions based on the self-attention mechanism, a fundamental component of the transformer architecture which revolutionized natural language processing. The transformer encoder uses self-attention to encode the context-dependent behavior for the components within a system. In physical environments, elements contribute differently to a material's property based on the materials system itself. For example, boron behaving as an electrical dopant in one system while behaving as a mechanical strengthening bond modification in another. CrabNet's ability to potentially capture this type of context-dependent behavior allows for highly accurate model predictions.

CrabNet does not stop there. Our modeling approach uses a robust loss function and model ensembling techniques to provide uncertainty values along with the property predictions. Importantly, we achieve this with a model architecture that generates simple and inspectable self-attention maps. These attention maps govern the learned material property by representing element importance and interactions. The visualization and analysis of these attention maps are available during training and inference periods.

As a result, CrabNet provides property prediction, uncertainty estimation, and the governing element interactions for every prediction. We expect that the ideas and capabilities of CrabNet will encourage additional research and discussion around the uses and benefits of our community's maturing data-driven approaches.

#### 5:35 AM F.MT07.01.04

**Late News: Uncertainty-aware microstructural database to accelerate data consolidation in organic electronics** Christopher W. Hong<sup>1</sup>, Snigdha Motadaka<sup>2</sup>, Boris Glavic<sup>1</sup>, Oliver Kennedy<sup>2</sup> and Olga Wodo<sup>3</sup>; <sup>1</sup>Illinois Institute of Technology, United States; <sup>2</sup>University at Buffalo, The State University of New York, United States; <sup>3</sup>State University of New York at Buffalo, United States

Stimulated by the Materials Genome Initiative (MGI), more databases with materials and materials properties are becoming publicly available. Among them, the databases are the Materials Project and the Harvard Clean Energy Project. Databases at the next scale - microstructure - are relatively less explored and consist of various application-specific and sparse datasets. This is because, among others, microstructural datasets are relatively expensive to obtain due to the high cost of sample preparation, limitations of imaging instruments, simulation cost, and individual labs' capabilities to generate a large volume of data. This limits machine learning's applicability and necessitates some form of data consolidation between various labs with the following challenges:

(i) data consolidation is hindered by the inherently diverse nature of materials data (as most data repositories focus on a specific subset of materials data) but also lab effects (e.g., different protocols of data processing or sample preparation);  
(ii) microstructural data is sparse and noisy data due to incomplete observations or imprecise measurements.

In this talk, we present the microstructural database build on the principles of probabilistic and incomplete databases. Unlike a classic database, the probabilistic database can deal with uncertain, incomplete information-missing values or uncertain information (value of an attribute represented as probability density function over the set of possible value instead of a single value). They inherently handle problems that emerge from data integration from various sources that are diverse and often incompatible. We show two frameworks: vizier and mimic that are used to integrate and store the datasets, respectively.

To demonstrate our database's effectiveness, we showcase the integration of three data sets generated through three projects aimed to improve the efficiency of organic solar cells. In each project, the microstructures were analyzed to predict the solar cell efficiencies. However, the microstructures were annotated with a different set of descriptors. Moreover, different types of microstructures were analyzed (i.e., dendritic, spinodal, and wavy). We illustrate how the integrated, although incomplete, data is used to impute the missing data in the respective datasets. Finally, we showcase the framework's capabilities to mark database entry or imputed values in conflict with other entries or violating the physics-based constraints.

**5:45 AM F.MT07.01.05**

**Late News: Data Automation and Data Intelligence for Data-Driven R&D** Max Petersen and Rob Brown; Dotmatics, United States

Data-driven R&D, especially machine learning (ML) and artificial intelligence (AI), are receiving lots of attention as avenues to accelerate new product development and to avoid/supplement costly lab experimentation. The pre-requisite for all these approaches is of course the availability of reliable high-quality data. However in real-life AI/ML projects an excess of time is spent aggregating and curating data, leading inevitably to dirty datasets and poor prediction results. Sadly, the IT infrastructure required to automate the provision of clean and properly contextualized data is often an afterthought.

This presentation gives an overview on our recent progress on an R&D IT infrastructure that solves the data provisioning problem in process-driven R&D. We will focus on three key areas: the automation of instrument data acquisition and their mass storage, combined querying across semantic and highly structured data, and the application of graph searching across chemistry experiments for reaction pathway mapping.

Managing instrument data is challenging not only because of their volume, but also because of their variability in data formats. Commonly, R&D IT systems capture incomplete data, e.g. by only saving processed files, or by placing them in inaccessible data silos where they can only provide limited use to data science efforts. We will discuss our approach that retains the full information content of all instrument data generated, while at the same time providing a framework to automate data processing and streamline lab operations.

Scientific data are notorious difficult to deal with in data modeling contexts. This is because of the combination of highly structured data, e.g. structure-property relationships, and unstructured semantic data that is generated as part of analyses, observations, conclusions, etc. Here, we will discuss an approach to embed semantic technologies into our scientific data platform to solve this complex problem.

Finally, we will discuss an application of graph technologies to mining reaction data that allows analysis of reaction pathways that span a multitude of experiments. This functionality is useful to compile information for patent submissions, or to optimize and discover synthetic routes based on existing IP.

**5:00 AM \*F.MT07.02.01**

**FAIR Digital Object Framework and High Throughput Experiment** Zachary T. Trautt<sup>1</sup>, Raymond L. Plante<sup>1</sup>, Gretchen Greene<sup>1</sup>, Jason R. Hattrick-Simpers<sup>1</sup>, Brian L. DeCost<sup>1</sup>, Gilad Kusne<sup>1</sup> and Andriy Zakutayev<sup>2</sup>; <sup>1</sup>National Institute of Standards and Technology, United States; <sup>2</sup>National Renewable Energy Laboratory, United States

With the increasing use of data-driven methodologies, concerns around data discovery, data access, and data interoperability have come to the forefront. Beginning in August 2019, communities have convened to work towards convergence of three complementary visions: (1) Digital Object Architecture, (2) Linked Data and Semantic Web, (3) FAIR Data Principles. This convergence has established the FAIR Digital Object Framework. This talk will overview these developments, summarize work within the NIST Material Measurement Laboratory to support adoption of the FAIR Digital Object Framework within the materials science and engineering community, and provide practical examples of how researchers can leverage these developments.

**5:15 AM F.MT07.02.02**

**Automated Prediction of Crystal Lattice Parameters from Powder Diffraction Data** Sathya R. Chitturi<sup>1,2</sup>, Daniel Ratner<sup>1,2</sup>, Kevin Stone<sup>1,2</sup>, Richard Walroth<sup>1,2</sup>, Vivek Thampy<sup>1,2</sup>, Mike Dunne<sup>1,2</sup> and Christopher Tassone<sup>1,2</sup>; <sup>1</sup>SLAC National Accelerator Laboratory, United States; <sup>2</sup>Stanford University, United States

X-ray powder diffraction (powder XRD) is an important experimental characterization technique used to determine crystal structure. Current powder XRD analysis involves several time-consuming and error-prone human intervention steps including peak identification and indexing. In this work, we use one-dimensional Convolutional Neural Networks (1D CNNs) to perform the task of lattice parameter prediction, a critical step in the analysis pipeline.

We train independent regression models for each of the six crystal systems in order to take advantage of specific symmetry constraints on the lattice parameters. We perform simulations based on allowed Bragg angles for each crystal system in order to quantify best-case performance under conditions of perfect information. We show that, with sufficient data, it is possible to meet arbitrarily low mean percentage error (MPE) thresholds. Furthermore, the amount of data needed for perfect prediction scales directly with the number of independent lattice parameters in each crystal system. We also present results for simulated data based on the Cambridge Structural Database (CSD), containing over one million unique entries which span a very wide range of lattice parameter space. We achieve an MPE value of less than 10% for the cubic crystal system and MPE values of less than 20% for all other crystal systems. Validation of these results is performed in GSASII using standard refinement procedures.

This analysis builds on previous works focusing on classification tasks such as crystal system and space group prediction from powder XRD data. We hope that our results will further the eventual goal of high-throughput, real-time crystal structure analysis.

**5:25 AM F.MT07.02.03**

**Accelerating Structural Investigation in InGaO<sub>3</sub>(ZnO)<sub>m</sub> Using Rapid and Cost-Effective Optical Pre-Screening** Vidit Gupta<sup>1</sup>, Aine Connolly<sup>1</sup>, Duncan Sutherland<sup>1</sup>, Max Amsler<sup>1,2</sup>, Sebastian Ament<sup>1</sup>, R. B. Van Dover<sup>1</sup> and Michael O. Thompson<sup>1</sup>; <sup>1</sup>Cornell University, United States; <sup>2</sup>University of Bern, Switzerland

We have investigated structural transformations in the InGaO<sub>3</sub>(ZnO)<sub>m</sub> (IGZO) homologous series using optical and X-ray techniques. Following thermal processing via lateral gradient Laser Spike Annealing (lgLSA), structural transformation kinetics were observed as a function of composition ( $1 < m < 12$ ), processing time (250 us - 10 ms), and peak temperature (500-1400°C). The high dimensionality of this composition and processing space dictates the use of automation in both sample generation and data analysis. Two complementary high-throughput and low-cost spatially resolved optical techniques were initially used to identify optical transitions that correlate strongly with structural transformations. As these samples are thin transparent films, the optical techniques are sensitive to extremely small changes in the optical path length due to physical

thickness and optical index (phase) variations. This ability to efficiently prescreen the experimental phase space enabled automated and accelerated determination of structural transformations (if any) associated with these optically determined boundaries using X-ray diffraction. We propose a model for structural evolution along this IGZO pseudo-binary based on the ordering of In-O and (Ga,Zn)-O layers.

#### 5:35 AM F.MT07.02.04

**Image Similarity Latent Manifolds for Materials Microscopy** Tri N. Nguyen, Yichen Guo and Joshua Agar; Lehigh University, United States

Instruments of scientific discovery (e.g., electron microscopes, scanning probe microscopes, and others) acquire vast collections of images that contain physical insight. Humans, however, struggle to search and draw correlations from enormous databases of images; thus, only a small fraction of the data collected is translated into knowledge. Researchers need an analytical toolbox that can create an image similarity latent manifold and allow visual interaction in an informative, comprehensive, and intuitive way. Here, we develop machine learning algorithms to create image similarity projections using a dataset of 25,000 piezoresponse force microscopy images. We implement a variety of pre-trained convolutional neural networks optimized on the ImageNet dataset to extract latent features of size [1x1x4096]. We extend this concept by updating the pre-trained model by classifying wallpaper group symmetries to create physics-informed latent representations. We use manifold learning techniques [e.g., t-Distributed Stochastic Neighbor Embedding (t-SNE) and Uniform Manifold Approximation and Projection (UMAP)] to generate interpretable 2D projections of these features. We demonstrate how this tool can be used for recursive image similarity searching and exploration accelerating discovery of trends in materials microscopy. Our algorithms are capable of identifying microstructure in diverse microscopy images across length scales. We will discuss how this concept can be integrated with structured scientific databases containing images and metadata as well as interactive graphical user interfaces to enable the rapid extraction of actionable information from materials microscopy data. While we demonstrate the aptitude of this approach on piezoresponse force microscopy images, this approach is amenable to other forms of microscopy and imaging techniques.

#### 5:45 AM F.MT07.02.05

**Combining Experiment, Physics-Based Modeling and Bayesian Inference to Enhance Voltammetric Characterization** Alexis M. Fenton Jr. and Fikile Brushett; Massachusetts Institute of Technology, United States

Voltammetry is a ubiquitous electroanalytical technique used for qualitative and quantitative characterization of redox-active species for a range of purposes (e.g., materials development, detection).<sup>1,2</sup> For dilute electrolyte solutions, known fundamental relationships, based on the mathematical treatment of reaction-transport processes, can be used to discern key physical and electrochemical properties of deterministically prepared electrolytes.<sup>1,3</sup> Further, voltammetry may be readily performed *in-situ* or *in-operando*, making it a minimally invasive and rapid diagnostic technique. However, many studies seek to track the chemical evolution of redox-active species in non-deterministically generated electrolytes, often by identifying the chemical by-products of this evolution.<sup>4,5</sup> Voltammetric methods alone are inadequate to uniquely identify compounds, as multiple species may have similar electrochemical properties; as a result, electrolyte characterization also includes suites of *ex-situ* techniques (e.g., mass spectrometry, UV-Vis spectroscopy). Advanced labeling protocols – potentially involving machine learning (ML) methods – may enable voltammetry to uniquely identify more compounds, which, in turn, may streamline characterization workflows. Indeed, ML methods have already been shown to enhance voltammetric capabilities,<sup>6,7</sup> but, to our knowledge, no studies have combined ML methods and electrochemical descriptors to identify compounds.

In this presentation, we describe a framework to identify solution-phase redox couples using experimental voltammetry, electrochemical descriptors from physics-based simulations, and Bayesian inference. This protocol references a library of candidate compounds comprised of molecular property sets (e.g., diffusion coefficient, redox potential) and compares it to experimental data to characterize the electrolyte being examined. The compound identities and the associated probabilities are then reported, enabling targeted follow-up experiments. We discuss the development and the validation of this protocol using a model set of redox-active molecules, demonstrating viability and motivating further development. We also explore possible expansions of this Bayesian framework, and we conclude by discussing potential applications (e.g., electrolytes for energy storage technologies). As a result, this protocol may extend the capabilities of voltammetric analysis, thereby accelerating the materials development pipeline for systems involving redox-active compounds.

Acknowledgements: This work was funded by the National Science Foundation under Award Number 1805566.

References:

1. Kwabi, D. G. *et al.* Alkaline Quinone Flow Battery with Long Lifetime at pH 12. *Joule* **2**, 1894–1906 (2018).
2. Komorsky-Lovrić, Š., Vukašinović, N. & Penovski, R. Voltammetric determination of microparticles of some local anesthetics and antithusics immobilized on the graphite electrode. *Electroanalysis* **15**, 544–547 (2003).
3. Northrop, P. W. C. & Cole, J. V. A Pulse Voltammetry Analysis Toolkit for Battery and Fuel Cell Material. *ECS Trans.* **85**, 23–42 (2018).
4. Goulet, M. & Aziz, M. J. Flow Battery Molecular Reactant Stability Determined by Symmetric Cell Cycling Methods. *J. Electrochem. Soc.* **165**, 1466–1477 (2018).
5. Day, R. P. *et al.* Differential thermal analysis of Li-Ion cells as an effective probe of liquid electrolyte evolution during aging. *J. Electrochem. Soc.* **162**, A2577–A2581 (2015).
6. Ye, J. J., Lin, C. H. & Huang, X. J. Analyzing the anodic stripping square wave voltammetry of heavy metal ions via machine learning: Information beyond a single voltammetric peak. *J. Electroanal. Chem.* 113934 (2020).
7. Li, J., Kennedy, G. F., Gundry, L., Bond, A. M. & Zhang, J. Application of Bayesian Inference in Fourier-Transformed Alternating Current Voltammetry for Electrode Kinetic Mechanism Distinction. *Anal. Chem.* **91**, 5303–5309 (2019).

#### SESSION F.MT07.03: Constitutive Modeling

On Demand Abstracts Available for Viewing Starting Saturday Morning, November 21, 2020  
F-MT07

##### 5:00 AM \*F.MT07.03.01

**Scientific AI in Materials Science—Reproducibility, Trusting Archival Data and Single Scalar Labels** Jason R. Hattrick-Simpers<sup>1</sup>, Brian L. DeCost<sup>1</sup>, Zachary T. Trautt<sup>1</sup>, Gilad Kusne<sup>1</sup>, Eva Campo<sup>2</sup> and Martin L. Green<sup>1</sup>; <sup>1</sup>National Institute of Standards and Technology, United States; <sup>2</sup>National Science Foundation, United States

Scientists are increasingly turning to the power of artificial intelligence (AI) to increase the rate of knowledge extraction, provide insight into new materials and discover unexpected correlations. In some cases, robust AIs have even been coupled with experimental (or theoretical) automation to generate autonomous scientific platforms capable of planning and executing experimental designs without human intervention. With the excitement around AI rapidly increasing it is time to begin thinking about the bursting of the AI bubble and what are the actions we can take as a community to mitigate its severity. Here scientific-AI and the opportunities and paths forward for creating a sustainable and scalable paradigm within materials science will be discussed. Of particular note will be issues with the reproducibility of AI model results, the use of archival data to build models, and the common usage of single scalar labels to summarize data sets. We will show building the same model using the same data set using a different implementation of the same algorithm does not result in statistically identical results. Next we will discuss the importance of preserving a record of primary data underlying archival labels, by highlighting the impact of using a fuzzy metric to classify the state of a material. Finally, we will discuss the issue of labeling uncertainty with the idea that an AI will not always be presented with pristine data for evaluation and make recommendations for possible methods to capture disagreement between experts in the literature.

##### 5:15 AM F.MT07.03.02

**Neural Network Approach for Predicting Organic Molecular Properties from Core-Loss Spectroscopy** Kakeru Kikumasa<sup>1</sup>, Shin Kiyohara<sup>2</sup>, Kiyou Shibata<sup>1</sup> and Teruyasu Mizoguchi<sup>1</sup>; <sup>1</sup>The University of Tokyo, Japan; <sup>2</sup>Tokyo Institute of Technology, Japan

Core-loss spectroscopy observed by electron, electron energy loss spectroscopy (EELS), and X-ray, X-ray adsorption spectroscopy (XAS), are analytical techniques used for wide variety of materials, including battery, catalysis, and functional oxides. In particular, electron energy loss near edge structure (ELNES) and x-ray adsorption near edge structure (XANES) correspond to the electronic transition from a core orbital to conduction bands and contain various information on local atomic structures and electronic states.

In general, ELNES/XANES spectra of target samples are interpreted through comparison with reference spectra which are often obtained with time-consuming theoretical calculations. However, the interpretation of these spectra is very difficult because of the ambiguous relationship between the spectral features and the properties of target materials. Moreover, up to tens of spectra can be obtained in an experiment due to time-resolved and/or space resolved observation by high performance experimental equipment. For these reasons, individual interpretation of the spectra by the conventional approaches is becoming unrealistic.

In recent years, machine learning (ML) approaches, which can overcome obstacles to handling multidimensional big-data,

have spread in materials science. ML has been applied to spectroscopic data including ELNES/XANES spectra and succeeded in predicting local chemical environment and properties including bond length, bond angle and Mulliken charge [1]. However, few studies have attempted to utilize ML on carbon-K edge ELNES/XANES spectra of functional organic molecules for investigating local chemical properties.

In this research, ML was applied to carbon-K edge dataset generated by theoretical calculations. A neural network model was adopted to extract information about properties of organic molecules from carbon-K edges. Moreover, we added some data about molecules as input data to improve the accuracy of prediction.

Input data of neural network was composed of 240-dimensional vector data of spectral intensities, which were referred to range of 24 eV in 0.1 eV steps. For output data, several molecular properties were selected. Hyperparameters, including the number of hidden layers, the number of neurons and the weight decay parameter, were tuned through cross validation. To construct the carbon-K edge dataset, 7,941 structural data of organic molecules were extracted from the QM9 database [2,3]. Carbon-K edges were calculated from these data by a first principle pseudopotential method using CASTEP code [4].

Several properties such as HOMO-LUMO gap were successfully predicted, whereas the regression accuracy of internal energy remained at a low level. Careful investigation suggested that it was difficult to accurately predict the extensive properties when only spectral data was used as the input data. We found that the prediction accuracy of these extensive properties could be drastically improved using additional input data about molecules.

In summary, we clarified that carbon-K edges contained sufficient information on organic molecular properties. Our neural network model enables fast, accurate, and direct prediction of molecular properties from ELNES/XANES, which contributes to a new way to investigate materials properties beyond the conventional comparison approach.

- [1] S. Kiyohara *et al.*, *J. Phys. Mater.*, **2** (2019) 024003,
- [2] L. Ruddigkeit *et al.*, *J. Chem. Inf. Model.*, **52** (2012), 2864-2875,
- [3] R. Ramakrishnan *et al.*, *Scientific Data*, **1** (2012), 140022,
- [4] M. D. Segall *et al.*, *J. Phys. Condens. Matter.*, **24** (2002), 2717-2744.

#### 5:25 AM F.MT07.03.03

**Assessing the Predictive Power of the Pauling Rules Using Modern Data Analysis** Janine George, David Waroquiers, Davide Di Stefano, Guido Petretto, Gian-Marco Rignanese and Geoffroy Hautier; Université catholique de Louvain, Belgium

Materials scientists are trying to accelerate the discovery of new materials, for example, by using high-throughput computations and machine learning. Chemical heuristics such as the Pauling rules<sup>[1]</sup> have long served as the only guide for experimentalists to discover and understand new materials. The Pauling rules promised to be a structure-stability relationship that could accelerate the discovery of stable materials. They relate the coordination environments and their connections to the stability of materials. Despite being a corner-stone of solid-state chemistry and materials science, the Pauling rules have not been systematically and statistically evaluated. Here, we will present such a systematic assessment using modern informatics tools and a recently developed code which automatically detects coordination environments and their connections.<sup>[2]</sup> Using a database of 5000 known oxides, we will report on the quality of the different Pauling rules and provide a general assessment of their predictive power.<sup>[3]</sup> Our work shows how traditional empirical rules can now be tested and challenged using modern tools of data analysis and available structural databases.

#### References:

- [1] L. Pauling, *J. Am. Chem. Soc.* **1929**, *51*, 1010.
- [2] D. Waroquiers, J. George, M. Horton, S. Schenk, K. Persson, G.-M. Rignanese, X. Gonze, G. Hautier, *ChemRxiv Preprint* **2019**, DOI 10.26434/chemrxiv.11294480.v1.
- [3] J. George, D. Waroquiers, D. Di Stefano, G. Petretto, G. Rignanese, G. Hautier, *Angew. Chem. Int. Ed.* **2020**, *59*, 7569–7575.

#### Acknowledgements:

J.G. acknowledges funding from the European Union's Horizon 2020 research and innovation programme under the Marie Skłodowska-Curie grant agreement No 837910.

#### 5:35 AM F.MT07.03.04

**A Bayesian Approach to Quantify the Single-Crystal Elastic Constants in a Polycrystalline  $\beta$  Metastable Titanium Alloy** Ravi raj purohit Purushottam Raj Purohit<sup>1,1</sup>, Thiebaud Richeton<sup>1,1</sup>, Lionel Germain<sup>1,1</sup>, Stephane Berbenni<sup>1,1</sup>, Nathalie

Gey<sup>1,1</sup> and Olivier Castelnau<sup>2</sup>; <sup>1</sup>Université de Lorraine, France; <sup>2</sup>Arts et Métiers ParisTech/ CNRS 8006, France

The identification of single-crystal elastic constants (SEC) of a high strength near- $\beta$  titanium alloy, used in aeronautical applications, has been investigated with a Bayesian approach. The literature on the identified SEC of the cubic  $\beta$  phase in the Ti-alloys shows no substantial agreement, with anisotropic index (Zener ratio) extending from 1.6 to 8 [1]. The directional elastic moduli (DEM) from the X-ray diffraction (XRD) analysis are often used to identify the SEC following the method of Kröner (inverse identification) [2,3]. However, several studies [3,4] have reported that the DEM for Ti-alloy can be insensitive to the bulk modulus, thus resulting in several possible SECs that satisfy the lattice strain evolution. This is addressed by evaluating the SEC at a fixed bulk modulus. In the current study, the high energy XRD and elastic self-consistent modeling [5,6] is revisited with a Bayesian framework and applied to a near- $\beta$  Ti-10V-2Fe-3Al alloy in its as-forged state (dual phase: 15% of primary hexagonal  $\alpha_p$  nodules embedded in a cubic  $\beta$  matrix). The effect of each phase elastic anisotropy was systematically investigated along with different parameters of the micro-mechanical model and also the biases introduced by the XRD data on the identification of the SEC of the  $\beta$  phase. The grain aspect ratio in the self-consistent model, which is often simplified in the literature was found to be the most significant parameter affecting the identification of SEC. The grain shape should therefore be taken into account in the micro-mechanical model when identifying the SEC from diffraction data.

#### Reference:

1. S. Lhadi, S. Berbenni, N. Gey, T. Richteton, L. Germain, Micromechanical modeling of the effect of elastic and plastic anisotropies on the mechanical behavior of  $\beta$ -Ti alloys, *Int. J. Plast.*, Vol. 109 (2018), 88-107
2. Matthies, S., H. G. Priesmeyer, and M. R. Daymond, On the diffractive determination of single-crystal elastic constants using polycrystalline samples. *J. Appl. Cryst* 34.5 (2001): 585-601.
3. Cho, J. R., D. Dye, K. T. Conlon, M. R. Daymond, and R. C. Reed. "Intergranular strain accumulation in a near-alpha titanium alloy during plastic deformation." *Acta materialia* 50, no. 19 (2002): 4847-4864.
4. Obbard, E. G., Y. L. Hao, R. J. Talling, S. J. Li, Y. W. Zhang, D. Dye, and R. Yang. The effect of oxygen on  $\alpha$  "martensite and superelasticity in Ti-24Nb-4Zr-8Sn. *Acta materialia* 59, no. 1 (2011): 112-125.
5. Meng, Q, Qing L, Shun G, Yongqi Z, and Xinqing Z. Effect of thermo-mechanical treatment on mechanical and elastic properties of Ti-36Nb-5Zr alloy. *Progress in Natural Science: Materials International* 25, no. 3 (2015): 229-235.
6. Faurie D., O. Castelnau, R. Brenner, P.O. Renault, E. Le Bourhis, P. Goudeau, In situ diffraction strain analysis of elastically deformed polycrystalline thin films, and micromechanical interpretation, *J. Appl. Cryst.*, 42 (2009), p.1073-1084.
7. C. Mareau, S. Berbenni, An affine formulation for the self-consistent modeling of elasto-viscoplastic heterogeneous materials based on the translated field method, *Int.J. Plast.*, 64 (2015) 134-150

#### 5:45 AM F.MT07.03.05

**Automatic Generation of Computational Reaction Networks for Unbiased Exploration of Chemical Pathways** Evan W. Spotte-Smith<sup>1,2</sup>, Samuel M. Blau<sup>1</sup>, Xiaowei Xie<sup>1,2</sup>, Brandon Wood<sup>1</sup>, Hetal Patel<sup>1,2</sup>, Shyam Dwaraknath<sup>1</sup> and Kristin A. Persson<sup>1,2</sup>; <sup>1</sup>Lawrence Berkeley National Laboratory, United States; <sup>2</sup>University of California, Berkeley, United States

Reaction networks, graph-based representations of the reactions occurring between chemical species, have long served as tools for the identification of chemical pathways and for the study of chemical dynamics. In recent years, high-throughput first-principles calculations have been used to generate computational reaction networks (CRNs) consisting of hundreds of molecules and thousands of chemical reactions. However, the systems thus far considered in CRN literature have been limited by insufficient automation. Specifically, automating calculations involving complex chemistries (ions, open-shell molecules, metal-coordinated molecules, solvated molecules, etc.) remains a challenge.

Here, we present a computational framework for the automatic generation of massive CRNs based on density functional theory (DFT) calculations. Using a robust and accurate level of theory and automated error handling, we have achieved a 95% success rate for DFT calculations of electrochemically relevant molecules. Using graph theory, we can generate CRNs consisting of all possible elementary reactions between the chemical species that we have studied without the use of complex pre-defined mechanisms. Our framework can also automatically identify optimal reaction pathways in massive CRNs based on reaction thermodynamics or energy barriers. As a demonstration of these automated tools, we present a CRN for the formation of the solid-electrolyte interphase in Li-ion batteries consisting of over 8,000 species and over 100,000 chemical reactions, the largest CRN based on reaction thermodynamics yet reported. Using shortest path algorithms, we have recovered critical pathways for electrolyte decomposition in a fully automated fashion, indicating the power of unbiased pathway detection for enhancing chemical understanding.

#### 5:55 AM \*F.MT07.03.06

**Microscope is a Laboratory—Supervised and Unsupervised Automated Experiment in Scanning Probe and Electron Microscopy** Sergei V. Kalinin, Maxim Ziatdinov, Kyle Kelly, Ondrej Dyck, Stephen Jesse, Andrew Lupini and Rama Vasudevan; Oak Ridge National Laboratory, United States

Discovery, optimization, and design of novel materials is the primary challenge facing civilization in the XXI century. The transition from simple functionalities in structural, optical, and semiconductor materials to complex intertwined functionalities in batteries, fuel cells, information technology and sensor devices renders the classical paradigm of serendipitous discovery and sequential optimization impractical and necessitates alternative pathways for materials discovery and optimization. One, actively explored at present, paradigm is automated experimentation and guided or combinatorial synthesis combined with rapid throughput characterization. However, a second pathway can be developed based on modern imaging tools including scanning probes and electron microscopy that allow us to not only visualize and probe functionalities of materials on the nanometer and atomic scales, but also to introduce controllable modifications in materials. Effectively, we aim to discover the defined mesoscopic and atomic structures and probe their functional properties, establish the pathways towards controllable creation of these structures, and ideally extend these towards macroscopic assemblies. Here, we discuss possible strategies towards autonomous experimentation (AE) in STEM and SPM. We demonstrate the examples of Bayesian optimization-based workflows for AE SPM and STEM using prior data sets, and discuss the development of the acquisition and pathfinder functions. We further discuss opportunities for the development of self-training AE workflows in microscopy, where the features of interest are unknown a-priori and are discovered during the experiment. The experimental realization of these concepts is demonstrated for ferroelectric domain manipulation and electron-beam induced chemical reactions.

**6:10 AM F.MT07.03.08**

**Contrasting Error Cancellation in *Ab Initio* and Machine Learning Predictions of Thermodynamic Stability** Christopher Bartel<sup>1</sup>, Amalie Trewartha<sup>1</sup>, Qi Wang<sup>2</sup>, Alexander Dunn<sup>2,1</sup>, Anubhav Jain<sup>2</sup> and Gerbrand Ceder<sup>1,2</sup>; <sup>1</sup>University of California, Berkeley, United States; <sup>2</sup>Lawrence Berkeley National Laboratory, United States

The realization of autonomous materials discovery depends critically on the ability to predict whether a given material will be synthesizable. This problem is generally addressed *in silico* by calculating the thermodynamic stability of candidate materials using density functional theory (DFT). There have been many recent claims that this step can be greatly accelerated using machine learning instead of DFT to predict the formation energy of inorganic solids. However, thermodynamic stability is ultimately dictated by relative formation energies between chemically similar competing phases, and not by the absolute formation energy of any single compound. It is therefore essential to assess how well these machine learning predictions of intrinsic thermodynamic quantities generalize to the problem of relative materials stability. In this work, we systematically probe this question by testing a diverse set of materials representations and learning algorithms on a variety of problems that simulate real applications of materials discovery. Our findings emphasize the value of including structure in materials representations and suggest that error cancellation plays a critical role in the prediction of thermodynamic stability.

**6:20 AM F.MT07.03.09**

**Automated Calculation and Convergence of Defect Transport Tensors** Thomas D. Swinburne<sup>1</sup> and Danny Perez<sup>2</sup>; <sup>1</sup>CNRS / CINaM, France; <sup>2</sup>Los Alamos National Laboratory, United States

Defect transport is a key process in materials science and catalysis, but as migration mechanisms are often too complex to enumerate a priori, calculation of transport tensors typically have no measure of convergence and require significant end user intervention. These two bottlenecks prevent high-throughput implementations essential to propagate model-form uncertainty from interatomic interactions to predictive simulations. In order to address these issues, we extend a massively parallel accelerated sampling scheme[1], autonomously controlled by Bayesian estimators of statewise sampling completeness, to build atomistic kinetic Monte Carlo models on a state space irreducible under exchange and space group symmetries. Focusing on isolated defects, we derive analytic expressions for defect transport tensors and provide a convergence metric by calculating the Kullback-Leiber divergence across the ensemble of diffusion processes consistent with the sampling uncertainty. The autonomy and efficacy of the method is demonstrated on surface trimers in tungsten and hexa-interstitials in magnesium oxide, both of which exhibit complex, correlated migration mechanisms[2].

[1] Swinburne & Perez, Phys. Rev. Mat, 2018

[2] Swinburne & Perez, arXiv:2003.07752, 2020

**6:30 AM F.MT07.03.10**

**Machine-Learning Approaches to Elucidate Structure-Property Relationships in 2D Materials** Siyu I. Tian<sup>1</sup>, Alexandra Carvalho<sup>2</sup>, Zekun Ren<sup>1</sup>, Mohammed AlEzzi<sup>2</sup>, Antonio H. Castro Neto<sup>2</sup>, Kostya S. Novoselov<sup>2</sup> and Tonio Buonassisi<sup>1,3</sup>; <sup>1</sup>Singapore-MIT Alliance for Research and Technology, Singapore; <sup>2</sup>National University of Singapore,



Singapore; <sup>3</sup>Massachusetts Institute of Technology, United States

Over the past decade, the family of 2D crystals increased dramatically, with 2D materials now covering a huge range of properties: metallic, semiconducting, ferromagnetic, superconducting... As the field attempts to engineer materials properties by design, an outstanding challenge is to develop high-accuracy predictive models that reversibly connect material structure with their properties. Herein, we adapt the recently-proposed Fourier Transform of Crystal Properties (FTCP) framework [1] to 2D materials, toward generating an invertible crystallographic representation of 2D materials suitable for materials search and inverse design tasks. When we train on ~2000 2D materials in the publicly available 2D MatPedia database, we can predict simple ground-state properties such as formation energy with mean average errors of 281 meV/atom. When a transfer-learning approach is employed, whereby ~51,000 3D materials from MaterialsProject are used, the mean average error of formation energy predictions improves to 209 meV/atom. We believe this framework presents a promising approach to predict certain ground-state properties of 2D materials, and may potentially extend to other properties in the near future.

[1] D. Ren *et al.*, <https://arxiv.org/abs/2005.07609>

#### SESSION F.MT07.04: Data Mining

On Demand Abstracts Available for Viewing Starting Saturday Morning, November 21, 2020

F-MT07

##### 5:00 AM \*F.MT07.04.01

**Jump Planner for Autonomous Materials Discovery** Chiwoo Park<sup>1</sup>, Peihua Qiu<sup>2</sup>, Jennifer Carpena-Núñez<sup>3</sup>, Rahul Rao<sup>3</sup>, Michael Susner<sup>3</sup> and Benji Maruyama<sup>3</sup>; <sup>1</sup>Florida State University, United States; <sup>2</sup>University of Florida, United States; <sup>3</sup>Air Force Research Laboratory, United States

We propose an autonomous AI planner that recommends the next experiments based on the outcomes of all past experiments with the goal of materials discovery in accelerated paces. We are particularly interested in accelerating an experimental campaign for mapping out an unknown relation of experimental conditions to the experimental outcomes of interest, e.g. resulting material properties and kinetic rates of reaction. The relation often has discontinuities in that there are abrupt changes in the experimental outcomes for a small change in the experimental conditions over some boundary regions such as boundaries of reaction equilibrium or chemical regime changes. In such cases, many conventional experimental planners, exploiting the continuity and smoothness of the relation, cannot be applicable. We propose a jump planner to optimize the experimental planning under discontinuities of the underlying relation to discover. Its application will be illustrated with carbon nanotube growth experiments with various catalysts.

##### 5:15 AM F.MT07.04.02

**Autonomous Discovery of Materials for Intercalation Electrodes** Felix Tim Bølle, Tejs Vegge, Juan Maria Garcia Lastra and Ivano E. Castellí; Technical University of Denmark, Denmark

The development of automated computational tools is required to accelerate the discovery of novel battery materials. In this work, we design and implement a workflow, based on Density Functional Theory calculations, to autonomously identify materials to be used as intercalation electrodes in batteries. The materials selection is based on thermodynamic and kinetic descriptors, such as adsorption energies and diffusion barriers. A substantial acceleration for the calculations of the kinetic properties is obtained thanks to the recent implementation of the Nudged Elastic Bands (NEB) method, which takes into consideration the symmetries of the system to reduce the number of images to calculate. We have applied this workflow to discover new cathode materials for Mg batteries, where two of these materials display a threefold increase in the potential of the Chevrel phase, the state of the art cathode in commercial prototype Mg batteries. In addition to the discovery of new materials, the dataset produced with this workflow has been used to train a machine-learning algorithm to accelerate and generalize the discovery of electrodes, beyond Mg-ion batteries.

##### 5:25 AM F.MT07.04.03

**Largest Possible Mobility of Molecular Semiconductors and Strategies to Achieve It** Tahereh Nematiamram, Daniele Padula, Alessandro Troisi and Alessandro Landi; University of Liverpool, United Kingdom

A large database of known molecular semiconductors is used to define a plausible physical limit to the charge carrier mobility achievable within this materials class. From a detailed study of the desirable properties in a large dataset, it is possible to establish whether such properties can be optimized independently and what would be a reasonably achievable optimum for each of them. All relevant parameters are computed from a set of almost five thousand known molecular semiconductors, finding that the best known materials are not ideal with respect to all properties. These parameters in decreasing order of importance are the molecular area, the nonlocal electron-phonon coupling, the 2D nature of transport, the local electron-phonon coupling, and the highest transfer integral. It is also found that the key properties related to the charge transport are either uncorrelated or “constructively” correlated (i.e., they improve together) concluding that a tenfold increase in mobility is within reach in a statistical sense, on the basis of the available data. It is demonstrated that high throughput screenings, when coupled with physical models of transport produce both specific target materials and a more general physical understanding of the materials space.

#### 5:35 AM F.MT07.04.04

**Crystal Synthesis Prediction Using Deep Learning** [Ali Davari](#) and Sara Kadkhodaei; University of Illinois at Chicago, United States

Predicting the synthesizability of hypothetical crystals has proven to be challenging due to the wide range of parameters that govern the crystalline materials synthesis. In this work, we convert the atomic structures of known synthesized or observed crystals in databases into three-dimensional pixel-wise images color-coded by chemical species and electronegativity and use them to train a deep-network convolutional autoencoder (CAE). We extract the latent features of synthesizability hidden in structural and chemical arrangements of crystalline materials embedded in the auto-encoder. The accurate classification of materials into synthesizable crystals vs. crystal anomalies based on these features across a broad range of crystal structure types and chemical compositions confirms the validity of our model.

#### 5:45 AM F.MT07.04.05

**Physically Informed Deep Learning for Accelerated Photosensitizer Discovery** [Jiali Li](#), Shidang Xu, Pengfei Cai, Xiaoli Liu, Bin Liu and Xiaonan Wang; National University of Singapore, Singapore

Photodynamic therapy is arising as a non-invasive treatment modality for cancer and other diseases. One of the key factors to determine the therapeutic function is the efficiency of photosensitizers (PSs). According to the latest studies, reducing the energy gap ( $\Delta E_{ST}$ ) between the lowest excited singlet state ( $S_1$ ) and lowest excited triplet state ( $T_1$ ) was an effective approach to yield highly efficient PSs, and  $\Delta E_{ST}$  could be fine-tuned through precise molecular donor-acceptor engineering. There is a growing literature where small families of small- $\Delta E_{ST}$  PS compounds are explored experimentally, or purely computationally at a slightly broader scale. Here, we report a large-scale data-driven search for novel PSs, with a special focus on red PS. This work comprehensively integrates computational quantum chemistry, machine learning, organic synthesis, and nanoagent fabrication and testing.

By providing the list of commonly used donors, acceptors and bridges, there is a chemical design space of more than 7 million possible PSs. Such a vast search space can hardly be explored by chemical intuitions or Edison's approaches. Even performing quantum calculations of this vast space can take infeasibly long time. A data-driven approach by screening the  $\Delta E_{ST}$  of 7 million PSs with a well-trained deep learning model provides a possible solution. Herein, we have created a high-throughput quantum calculation toolset for the construction of a novel dataset of 10k PSs with  $\Delta E_{ST}$  information. This training dataset contains representative donors, acceptors and bridges with both Donor-Acceptor and Donor-Acceptor-Donor structures. A molecular graph convolutional neural network with molecular structure as features is trained on this dataset. In combination with a high-throughput PS generator, we could efficiently predict the  $\Delta E_{ST}$  of possible PSs within the chemically intuited design framework. In order to further improve the performance of the predictive model, we have also employed a transfer learning approach. In addition to this physically informed design model, we utilize a motif-based hierarchical encoder-decoder (hgraph2graph) as another deep learning method for the direct generation of possible PS candidates. These two approaches will be compared with results discussions. Furthermore, the experimental validation of chosen PSs with low  $\Delta E_{ST}$  is conducted and presented. Finally, the potentials and limitations of this work will be discussed.

SESSION F.MT07.05: Materials Representations

On Demand Abstracts Available for Viewing Starting Saturday Morning, November 21, 2020

F-MT07

5:00 AM \*F.MT07.05.01

**Machine Learning of Experimental Databases for Predictions and Discovery of Novel Functional Materials** Ichiro Takeuchi; University of Maryland, United States

Combinatorial experimentation has become a well-established technique to explore new compounds with enhanced physical properties in a variety of functional materials fields. High-throughput experiments are particularly effective when designs and layouts of combinatorial libraries are guided by predictions. With the advent of high-throughput computational screening, it is now possible to come up with a large list of possible new compounds quickly. In many areas of functional and quantum materials, however, it remains a formidable challenge to make accurate predictions through computational means. When properly curated experimental databases are available, it is also possible to mine such databases in order to identify trends among known materials compositions and make predictions of new materials. As an example, we have previously developed machine learning models of superconductors based on the SuperCon database within MatNavi (NIMS, Japan) which contains over 29,000 experimental entries. Although SuperCon lacks structural property information, random forest regression was able to build models, which can decipher key distinctions between different families of superconductors. In many materials areas, such an approach is unfortunately hampered by the lack of sufficiently large experimental databases with very few exceptions. I will discuss our recent work where we have combined structural property predictions using ICSD with compositional information in order to identify trends in materials discoveries and make predictions based on clustering of known compounds through neural network. This work is carried out in collaboration with Valentin Stanev, Haotong Liang, and A. Gilad Kusne, and is funded by NIST.

5:15 AM F.MT07.05.03

**Platform for Polymer Inverse-Design by Graph Generative Algorithms** Seiji Takeda<sup>1</sup>, Toshiyuki Hama<sup>1</sup>, Hsianghan Hsu<sup>1</sup>, Victoria Piunova<sup>2</sup>, Dmitry Zubarev<sup>2</sup>, Daniel Sanders<sup>2</sup> and Daiju Nakano<sup>1</sup>; <sup>1</sup>IBM Research - Tokyo, Japan; <sup>2</sup>IBM Almaden Research Center, United States

### 1. Introduction

Designing “tailored” material that possesses desired characteristics is a long-awaited technology. Especially molecular design is important across broad industrial domains. It is to solve a complex combinatorial problem in terms of molecule’s atomistic configuration patterns, that significantly exceeds  $10^{60}$ . In this extra-vast parameter space, human SMEs (Subject-Matter-Experts) can only explore around a tiny space by trial-and-error relying on their experience and knowledge. To accelerate their design speed and expand the structural variety of molecules, AI can play a key role. Several AI molecular design tools and algorithms exist [1,2], but following issues in practical use are unaddressed; (1) deep learning - based methods rely on extremely large amount of material data, (2) models are black box, therefore hard to tune for chemists, (3) customization for specific material domains is not supported, (4) a certain level of IT skill is required to use. To address those issues, we developed a platform for small organic molecules [3]. In this paper, we exhibit customization of the tool for polymer domains and demonstrate to design new acrylic polymers having specific Tg (glass transition temperature).

### 2. Method

The fundamental workflow of our tool consists of sequential 5 steps; (1) data input, (2) feature encoding, (3) property prediction, (4) solution search, and (5) structure generation. First, a data set listing pairs of chemical structures and target properties is input as a training dataset. Structures are encoded to a set of feature vectors, by which a regression model to predict target properties is built. After the model is built, a user inputs target property values. The system performs the solution search to identify candidate feature vectors that satisfy the target property values. Finally, the feature vectors are decoded to concrete molecular structures by improved McKay’s Canonical Costruction Path algorithm, that builds up a molecular graph by connecting atoms and substructures indicated in the feature vector. That process is called “inverse-design”; to solve a model inversely starting from target properties.

We further customized the tool for polymer domain; first, the tool identifies monomer’s main chain and extract only side chain structures as a part to design. Second, structure generation algorithm is reinforced by structural constraints to avoid chemically unrealistic structures.

### 3. Results

To demonstrate inverse-design of polymers, from PolyInfo we extracted acrylic polymer data consisting of 378 pairs of SMILES and Tg. Side chain structures are extracted from the acrylic main chain, and encoded to about 50 dimensional feature vectors, in which each element represents a number of substructures. Regressions were carried out on the feature vectors to predict Tg. The best regression model exhibited determination coefficient  $R^2 \sim 0.68$  corresponding to RMSE  $\sim 30$  C°. Inverse-design was carried out on the model targeting Tg  $\sim 150$  C°. Running several hours, more than 100 structures were generated, that is significant acceleration in design speed compared with typical SMEs. The generated structures were

reviewed by a polymer SME for screening, and some of the candidates were successfully synthesized in the lab.

#### **Platform in Service**

The above platform is running on the cloud of IBM. They are provided as-a-service to our client companies for research purpose. Two interfaces; Python-based command line interface and GUI-based web application are provided to cover broad range of user's IT-skills. In the presentation, we will also demonstrate the web application.

#### **Reference**

- [1] R.G.Bombarelli, et al. "Automatic chemical design using a data-driven continuous representation of molecules", 2018
- [2] G.B.Goh, et al. "Using Rule-Based Labels for Weak Supervised Learning: A ChemNet for Transferable Chemical Property Prediction", 2018
- [3] S.Takeda, et al. "Molecular Inverse-Design Platform for Material Industries", 2020

#### **5:25 AM F.MT07.05.04**

##### **Navigating Chemical Composition Spaces Using Gaussian Processes and Representation Learning Jens S.**

Hummelshoej, Muratahan Aykol, Joseph H. Montoya, Linda Hung and Santosh Suram; Toyota Research Institute, United States

Rapid experimentation and discovery of materials has typically centered around high throughput screening of materials in high-dimensional composition settings. Machine learning assisted selection of composition spaces is expected to significantly accelerate the experimental materials discovery process. To achieve this, frameworks that enable learning across composition spaces are necessary. A central aspect of such a framework is digital representation of compositions that are tuned for the composition-property mapping task of interest. While generic descriptors of elements exist we show that a framework that learns these representations for a specific task significantly outperforms generic representations.

Specifically, in this talk we present methodologies to learn composable digital representations of the chemical elements that enable learning about composition-property relationships across composition spaces. We demonstrate these methodologies by predicting formation energy, band gap in compositional spaces that cannot be interpolated from the training composition spaces. We also demonstrate that digital representations learned from simulation data can be transferred to predict experimental data.

Further, we demonstrate large scale predictions of formation energy by combining digital representation of elements, physical constraints into a Gaussian process framework. We demonstrate that using physical constraints and clustering based on covariances we can address the scalability limitations of Gaussian processes, allowing their deployment for large scale discovery applications. Finally, this work provides a framework to accelerate extrapolative exploration of composition spaces for materials discovery.

#### **5:35 AM F.MT07.05.05**

**Machine Learning Based Design of Transition Metal Catalysts** Gabriel dos Passos Gomes<sup>1</sup>, David Balcells<sup>2</sup>, Alán Aspuru-Guzik<sup>1</sup> and Pascal Friederich<sup>3,3</sup>; <sup>1</sup>University of Toronto, Canada; <sup>2</sup>University of Oslo, Norway; <sup>3</sup>Karlsruhe Institute of Technology, Germany

Homogeneous catalysis using transition metal complexes is ubiquitously used for organic synthesis, as well as technologically relevant in applications such as water splitting and CO<sub>2</sub> reduction. Automatic selection and optimization of catalysts also plays a very important role for automated and autonomous experimental synthesis platforms. The key steps underlying homogeneous catalysis require a specific combination of electronic and steric effects from the ligands bound to the metal center. Finding the optimal combination of catalysts and ligands is a challenging task due to the exceedingly large number of possibilities and the non-trivial ligand–ligand interactions. We show how quantum mechanical calculations and machine learning (ML) methods can be combined to enable the prediction of reactivity within large chemical spaces containing thousands of complexes. We illustrate our approach using the classic examples of the Vaska's complex [1] as well as a gold catalyzed cyclization reaction. We compare multiple different machine learning methods based on their accuracy, interpretability as well as their ability to learn from small amounts of data. In contrast to experiments and calculations requiring several days to be completed, the ML models were trained and used on a laptop on a time-scale of minutes.

[1] Pascal Friederich, Gabriel dos Passos Gomes, Riccardo De Bin, Alán Aspuru-Guzik and David Balcells, Chemical Science, 11, 4584-4601, 2020. DOI: 10.1039/D0SC00445F

#### **5:45 AM \*F.MT07.05.06**

**Accelerating Materials Discovery Using Autonomous Experimentation** R. B. Van Dover<sup>1</sup>, Michael O. Thompson<sup>1</sup>, Carla

Gomes<sup>1</sup>, Bart Selman<sup>1</sup>, John Gregoire<sup>2</sup> and Max Amsler<sup>1</sup>; <sup>1</sup>Cornell University, United States; <sup>2</sup>California Institute of Technology, United States

High throughput combinatorial methods have accelerated searches for new materials, but most remain constrained by experimental limitations and human decisions. We are developing fully autonomous methods that enable discovery of functional materials, especially non-equilibrium materials that have yet to be synthesized by traditional techniques. To achieve this goal, we use a hierarchy of closed-loop processing/characterization agents (systems) to identify and execute an experimental strategy that optimizes the deployment of experimental resources (time, money, and access). This results in extremely efficient exploration of broad composition and processing spaces leading to the rapid and autonomous discovery of new metastable phases.

At the experimental level, we employ lateral-gradient Laser Spike Annealing to process amorphous thin film composition-spread libraries prepared on standard Si wafers. A variety of optical and X-diffraction (XRD) techniques are used to identify regions in the high-dimensional space {composition fractions { $x_i$ }, temperature T, dwell/quench time, t} that are associated with distinct crystal structures and/or microstructures. While optical characterization alone cannot label crystal structures or crystallographic texture, these low cost optical techniques are very sensitive and can rapidly identify transitions that provide valuable prior knowledge for structural XRD studies, either asynchronously through subsequent follow-up autonomous investigations at synchrotron sources, or synchronously in a fully coupled autonomous experimental loop. Intelligent exploration of the high-dimensional space requires effective active learning—using the results of initial and accumulated characterization of the phase space to decide the next [{ $x_i$ }, T, t] condition to be explored. This involves real-time interaction of the experiments with a community of AI-based agents that must: (a) interpret optical or XRD patterns to create a model of the evolving “processing phase diagram,” (b) identify the conditions that, when characterized, are most likely to decrease uncertainty in the boundaries of this map, (c) direct automated equipment to execute the chosen processing, and (d) complete the loop by managing and controlling optical or XRD characterization. To tackle this challenge, we employ various Gaussian Process (GP) models with carefully designed kernels that capture subtleties of the physics associated with the transformations.

This approach enables us to identify regions with distinct structures. To determine the particular crystal structure(s) associated with each region, we apply novel computational techniques that we have developed and that have proven to be highly effective at automated crystal structure phase mapping. Example results from several systems will be used to demonstrate the current state of these agents and the overall process.

As these methods are fully realized, we will achieve the key goals of:

- \* developing a methodology for real-time closed-loop autonomous synthesis/process/characterization experiments using active learning
- \* identifying opportunities and demonstrating examples where state-of-the-art AI methods offer unique advantages for scientific experimentation
- \* creating new materials with superior functional properties, and advancing our understanding of the fundamentals of phase transformation in rapid-thermal-processed materials.

#### 6:00 AM F.MT07.05.07

**Automatic Cyclometalated Iridium(III) Complex Design Using a Data-Driven Fragmentation Representation of Molecules** Hsianghan Hsu<sup>1</sup>, Seiji Takeda<sup>1</sup>, Toshiyuki Hama<sup>1</sup>, Jed Pitera<sup>2</sup> and Daiju Nakano<sup>1</sup>; <sup>1</sup>IBM Research - Tokyo, Japan; <sup>2</sup>IBM Almaden Research Center, United States

Data is a resource to drive discovery, fueled by multiple factors such as new funding, open source, and AI. Inspired by demands from the materials industry, an inverse design solver accompanied with an end-to-end AI-based tool for small organic molecule design is developed. Our published studies show good correspondence between predicted properties and calculated values [1]. In this report, we extend the scope of our tool, ensuring that the newly generated ligands form optimized Ir(III) complex structures, and finally perform validation through DFT simulations confirming energy gaps large enough to blue light LED material candidates.

Cyclometalated Ir(III) complexes are a well-established class of metal-organic compounds with attractive photophysical properties [2]. The design of the ligands around the Ir ion dominates the performance. By using open data sets and reliable models, a vast number of ligand candidates can be generated. However, considering the complexity of the three-fold symmetric structure, it is still difficult to effectively calculate representative characteristics even when subject matter expert insight is included. An automatic, high throughput workflow is discussed in the followings.

Initial searches extracted 1400 samples with CIE 1931 color coordinates and SMILES information. For deep blue emission the target values are (0.15, 0.12). This corresponds to a calculated energy gap larger than 2.5 eV according to experience. Multiple fused rings in the ligands leads to encode features with atom count, ring count, substructures, and fingerprints. In the prediction step, the hyper-parameters are further optimized by exhaustive grid search algorithm. The model with highest cross validation score is input to estimate new features and ligand generation.

In parallel, another framework is established to inherit the generated results. Newly generated ligands are converted to 3D structures and optimized by force field. Although the tris-heteroleptic Ir(III) complex is the more general use case, the detail of dealing with tris-homoleptic ones is described here. The two coordinating ions (A and B) to Ir ion are identified by a rule-based algorithm with more than 90 % accuracy. The three ligands coordinates are put in a 3D space without interference and Ir ion is located at the origin. The atom and bonding information are updated and do 2nd structure optimization. Because the ligand structures are optimized prior to the attachment, the degrees of freedom can be reduced to only three for the purpose of finding energy in global minimum. Three ligands are rotated simultaneously along the vector sum of Ir-A and Ir-B. By using genetic algorithm with many enough iterations, the angle combination with the lowest total energy is obtained. Finally, the hydrogen atoms are attached and ready for DFT simulation.

The workflow is validated by reproducing the numbers in [3]. There are 100 samples with tabulated values of LUMO, HOMO, dipole moment, S1, and T1 wavelength. Different software and parameters (G98 vs. GAMESS) are used. The results show good correspondence with R-square scores: 0.98, 0.98, 0.74, 0.71, and 0.89. With this framework, we can validate the newly generated ligands also have large enough band gap energy such as c1cnc2ccn3cc(C4CCCC4)nc3c2c1 (4.20 eV), c1ccc2c(c1)ncn1c3ccccc3nc21 (3.64 eV).

The framework is capable of forming facial and meridional coordination geometries by adjusting the fitness in the optimization algorithm. Multiple dockerized packages provide such workflow automation. The potential of the developed tool is still increasing by adapting the customization for other functional materials.

[1] S. Takeda, et al. "Molecular Inverse-Design Platform for Material Industries", Proc. of KDD (2020)

[2] Z. Wu, et al, "Novel Design of Iridium Phosphors with Pyridinylphosphinate Ligands for High-Efficiency Blue Organic Light-emitting Diodes", Scientific Reports (2016)

[3] D. B. Knowles, U.S. Patent 2008/0297033A1

#### 6:10 AM F.MT07.05.08

**Extracting Relevant Features For Understanding and Predicting Metal-Insulator Materials from Machine Learning Models** [Alexandru Georgescu](#)<sup>1</sup>, Aubrey R. Toland<sup>2</sup>, Peiwen Ren<sup>1</sup>, Nicholas Wagner<sup>1</sup>, Elsa Olivetti<sup>2</sup> and James Rondinelli<sup>1</sup>; <sup>1</sup>Northwestern University, United States; <sup>2</sup>Massachusetts Institute of Technology, United States

Metal-insulator transition (MIT) compounds are both of high technological interest, with potential applications to low-power computation and transistors, glass coatings and of broad general scientific interest, as the metal-insulator transition is due to a rich interplay of complex electronic and atomic degrees of freedom. This interplay makes it difficult for high-throughput, first-principles approaches to find potential MIT candidates, while machine-learning approaches can be difficult to implement and understand due to the limited number of known MIT compounds. In this work we show that, using a gradient boosted decision tree, we can nonetheless obtain a surprisingly strong model to predict which materials may or may not exhibit thermally driven MITs. By comparing a model in which the most important features of the materials are extracted automatically, to one in which they are added gradually and physically informed using domain knowledge, we extract novel insights into the physics of metal-insulator transition materials, as well as into how best to search for improved MIT material candidates.

**Acknowledgement:** This work was supported in part by the National Science Foundation (NSF) under award number DMR-1729303. The information, data, or work presented herein was also funded in part by the Advanced Research Projects Agency-Energy (ARPA-E), U.S. Department of Energy, under Award Number DE-AR0001209. The views and opinions of authors expressed herein do not necessarily state or reflect those of the United States Government or any agency thereof.

#### 6:20 AM F.MT07.05.09

**Inferring Physical Laws of Material Degradation in Perovskite Solar Cells Using Machine Learning** [Richa R. Naik](#),

Armi Tiihonen, Shijing Sun, Zhe Liu and Tonio Buonassisi; Massachusetts Institute of Technology, United States

To date, most applications of machine learning (ML) in materials science have focused on process optimization and improving engineering parameters of merit. Inferring physical laws directly from data has a great potential to accelerate materials research by allowing us to extract generalizable scientific information from the data. In this study, we explore the use of ML algorithms to study perovskite degradation, with the aim of gaining knowledge of the underlying degradation mechanisms. The environmental instability of halide perovskite materials hinders the commercialization of perovskite solar cells. The degradation mechanisms are still not fully understood due to the complexity of degradation phenomena. The functional space of feasible physics equations capturing these mechanisms is enormous [1]. Furthermore, experimental data is noisy and often sparse, making inference of quantitative analytic descriptions even more challenging.

We show a case study of perovskite degradation to infer physical laws from data and we interpret them in the context of proposed theoretical degradation pathways for perovskites [1]. We analyze simulated datasets for the degradation of perovskites under heat and continue to experimental data: Methylammonium lead iodide (MAPI) films subjected to degradation in our in-house environmental chamber at various temperatures, low humidity, and 0.15 sun illumination. We monitor their degradation using an optical camera extracting color versus time, capturing the transition from black MAPI to yellow lead iodide (PbI<sub>2</sub>). Utilizing experimental and modeled data, we conduct a systematic study modeling degradation processes using a (1) traditional regression approach, (2) fitting parameters to partial differential equations (PDEs), and finally shifting to (3) symbolic regression of PDEs [2, 3, 4].

We find that the regression approaches extract variables of interest with relative errors as low as 2%, even with 5% Gaussian noise superimposed upon the simulated datasets. However, this requires knowledge of the equation form. We demonstrate that sparse regression [2] identifies the underlying equation from noiseless data with errors less than 10%. We have PDE extraction calculations underway, with preliminary results, governing physical laws for MAPI degradation using a genetic programming algorithm for symbolic regression [3]. We examine three data-driven algorithms for learning differential equations and find that they are generally challenged to fit exponential equations (common to many materials-science problems) and handle noise. We conclude that the study of materials degradation can be rendered more quantitative, by including inference of physical laws of degradation, using regression and potentially ML-based PDE extraction techniques. We also opine about the gap that exists between ML-based tools today and common materials science challenges.

[1] Smecca, Emanuele, et al. "Stability of solution-processed MAPbI<sub>3</sub> and FAPbI<sub>3</sub> layers." *Physical Chemistry Chemical Physics* 18.19 (2016): 13413-13422

[2] Rudy, Samuel H., et al. "Data-driven discovery of partial differential equations." *Science Advances* 3.4 (2017): e1602614.

[3] Atkinson, Steven, et al. "Data-driven discovery of free-form governing differential equations." arXiv preprint arXiv:1910.05117 (2019).

[4] Willard, Jared, et al. "Integrating physics-based modeling with machine learning: A survey." arXiv preprint arXiv:2003.04919 (2020).

**6:30 AM \*F.MT07.05.10**

**Learning to Electrodeposit Corrosion-Resistant Alloy Coatings Through Autonomous Electrochemical Experimentation** Brian L. DeCost<sup>1</sup>, Howie Joress<sup>1</sup>, Bruce Ravel<sup>1</sup>, Suchismita Sarker<sup>2</sup>, Apurva Mehta<sup>2</sup>, Najlaa Hassan<sup>1</sup>, Trevor Braun<sup>1</sup> and Jason R. Hatrick-Simpers<sup>1</sup>; <sup>1</sup>National Institute of Standards and Technology, United States; <sup>2</sup>SLAC National Accelerator Laboratory, United States

Autonomous laboratory systems continually learn by adaptively planning and executing campaigns of physical and/or in silico experiments to achieve a scientific or engineering goal without requiring direct human intervention. The current research community is demonstrating new opportunities in accelerated materials synthesis, evaluation, and optimization, but major challenges remain for application of robotic systems for broader scientific discovery in materials and chemistry. Foremost, current AI systems used in robotic science applications make and test predictions, but lack the mechanistic modeling components needed for formulating and evaluating scientific hypotheses that explain these predictions in terms of generalizable physical principles. Furthermore, learning to reliably synthesize materials, and reconciling multiple structure and property data streams make it difficult to comprehensively explore complex and multiscale structures that determine the performance of engineering materials.

This talk will focus on technical and methodological aspects of building AI agents that drive closed-loop synthesis and characterization platforms and deploying them for scientific discovery. We explore these issues using an autonomous scanning droplet cell (ASDC) platform designed for on-demand alloy electrodeposition and real-time electrochemical characterization. Our initial studies seek to jointly optimize electrochemical deposition of binary ZnNi alloys while maximizing their corrosion resistance properties. We present exploratory research incorporating mechanistic transport models into the Gaussian Process modeling framework we use for surrogate modeling and active selection of experiments. We also discuss the challenge of disentangling the effects of chemistry, crystal structure, and microstructure on material properties, focusing on corrosion resistance within a ternary NbTiTa refractory alloy system that we have characterized with a multimodal X-ray diffraction and corrosion study.

As the materials community surmounts the challenge of incorporating mechanistic modeling components into our machine learning systems, automated materials synthesis and characterization platforms offer much more than black-box optimization of engineering materials: they offer the potential to develop and deploy new algorithms for generating and testing scientific hypotheses.

#### 6:45 AM F.MT07.05.11

**Late News: Representations for Data-Driven Material Discovery** [Kiran Vaddi](#) and Olga Wodo; University at Buffalo, United States

Representations play a crucial role in building predictive models using data driven approaches. In this work we present a representation based approach to high-throughput experimental data analysis of X-ray diffraction (XRD) and Cyclic Voltammetry (CV)--where the input is systematically swept and the response is collected for all the materials screened. A common data representation in above cases is to use the output as an n-dimensional vector with discrete inputs as corresponding dimensions/components. In this talk, we present a couple of other representations namely a metric space and a function space representation with a goal to encode known physical knowledge. We evaluate the representations in two different case studies with applications involving material discovery and cyclic voltammetry. Our first case study involves using a metric space representation where topology of the sampled data is captured using a physics based metric. Metric space representation presented in this talk is an automated way of computing distance measure and achieves comparable accuracy to computationally complex, expert defined distance measures. A second case study involves a function space representation tailored for CV data analytics. We use covariance functions of Gaussian process (GP) as basis functions to encode the two dimensional CV curve onto a vector space represented by the basis functions. We show that the GP based methodology presented here is analogous to using images with each pixel represented using a Gaussian distribution thus allowing us to use well developed image analysis techniques for downstream analysis. We present two case studies of function space representations 1) iterative design of experiments to identify materials with fast kinetics in an electro-chemical environment with application to catalyst discovery of oxygen reduction and evolution reaction 2) iterative identification of an optimal mechanism from a set of postulated mechanisms by combining experiments with a physics based model. Approaches presented here will also highlight the importance of building a physics based representation of data for downstream analysis.

#### 6:55 AM F.MT07.05.13

**Topology-Driven Completion of Chemical Data** [Dmitry Zubarev](#) and Petar Ristoski; IBM Research - Almaden, United States

Efficient discovery of novel functional materials strongly relies on development of the exploration strategies in the chemical space. In this contribution we are describing an approach that helps to identify lacunae in the existing data and complete the missing pieces in a targeted manner. The proposed approach consists of 2 main steps.

Step 1: We perform topological data analysis on the set of molecules. Molecular set is treated as a point cloud with pair-wise distances defined using standard chemoinformatic approaches. We apply the Mapper algorithm [1] to produce a simplified description of the data in a form of a graph  $G=(C,E)$ , where  $C$  is a set of clusters represented as nodes, and  $E$  is the set of all edges. Each node in the graph represents a cluster of molecules, and an edge between 2 clusters indicates that the clusters overlap. Mapper graph directly visualizes such aspects of the data shape as holes and branches (loops and flares on the Mapper graph, respectively), which indicate that there is missing data. Our task, therefore, is to generate new molecules that fill out the loops (elimination of the branches can be done in a similar fashion). First, we search for the scaffolds in the dataset that are most promising for the molecule generation. Operationally, we prioritize scaffolds found in small clusters along big loops on the Mapper graph. For each cluster we identify the smallest (in terms of hops) loop  $l$  using the Dijkstra's algorithm [2], then we calculate the length of the cycle  $w_l$ , which is the sum of the length of each edge in the loop. For each



molecule in each cluster we calculate the Bemis-Murcko scaffolds  $S = \{s_1, s_2, \dots, s_n\}$ . For each scaffold  $s$  we introduce the generative potential  $g_s = \sum_{c_s} \text{mean}(|C|) w_{lc} / |c_l|$  where  $c_s$  are all the clusters where the scaffold appears, and the  $w_{lc}$  is the length of the cycle for that cluster. A high  $g_s$  value indicates that the scaffold appears in small clusters with large cycle length, meaning they are part of bigger loops, and have a higher potential for generating novel molecules. We normalize the  $g_s$  values between 0 and 1.

Step 2: To generate novel molecules that complete loops on Mapper graph we adapt an existing graph-generative model for scaffold-based molecular design, using variational autoencoders (VAE). Here, the input scaffold is extended by sequentially adding atoms and bonds, i.e., the generation is conditioned on the existing scaffolds, making sure that all generated molecules contain the input scaffold. We modify the standard VAE loss function to take in consideration the generative potential of the scaffolds:  $L = (1 - g_s) (L_r + L_{KM} + \alpha (g_s - g_{sn}))$ , where  $\alpha$  is a hyperparameter between 0 and 1,  $g_{sn}$  is the generative potential of the scaffold of the newly generated molecule,  $L_r$  is the reconstruction error of the input  $s$  and generated scaffold  $s_n$  and  $L_{KL}$  is the Kullback-Leibler divergence between the prior and approximate posterior distribution. With this loss function we reduce the influence of the scaffolds with low generative potential and penalize the model when it generates molecules with low generative potential  $g_{sn}$ . To calculate the  $g_{sn}$  of a new scaffold, we include the newly generated molecule in the Mapper analysis after each iteration.

We will discuss the application and performance of the described approach to the exploration of the space of photo-acid generators.

- [1] Gurjeet, S., Mémoli, F., & Carlsson, G. E. "Topological methods for the analysis of high dimensional data sets and 3d object recognition." SPBG (2007).
- [2] Dijkstra, Edsger W. "A note on two problems in connexion with graphs." *Numerische mathematik* 1.1 (1959): 269-271.
- [3] Lim, J., Hwang, S. Y., Moon, S., Kim, S., & Kim, W. Y. "Scaffold-based molecular design with a graph generative model." *Chemical Science* (2020)

#### 7:05 AM F.MT07.05.14

#### **Molecule Representation Governs Predictive Accuracy—Case Study on Predicting Minimum Inhibitory**

**Concentration of Large Molecules** Armi Tiihonen<sup>1</sup>, Sarah J. Cox-Vazquez<sup>2</sup>, Harry Q. Liang<sup>1</sup>, Zekun Ren<sup>3</sup>, Noor Titan Putri Hartono<sup>1</sup>, Shijing Sun<sup>1</sup>, Guillermo Bazan<sup>2</sup> and Tonio Buonassisi<sup>1</sup>; <sup>1</sup>Massachusetts Institute of Technology, United States; <sup>2</sup>National University of Singapore, Singapore; <sup>3</sup>Singapore-MIT Alliance for Research and Technology, Singapore

Much progress in molecular property prediction has been made by generating and curating datasets, and developing machine-learning (ML) models. However, to increase predictive accuracy of machine-learning-driven research, combining these two with improved data representations (which capture the structural and chemical features relevant for property prediction) remains an outstanding challenge. This is especially true for large, non-rigid molecules containing more than 30 atoms. Proper data representation maximizes the probability that an ML algorithm will successfully infer correlations between molecular structure and chemistry and output properties of interest.

There are a multitude of successful molecule representations in literature [1-2], but a remaining limitation especially in understanding large molecules is the ability to efficiently capture both chemistry and three-dimensional (3D) structure. Molecular fingerprint sets can be designed as a combination of features reflecting the 3D structure and chemistry of the molecule but may have a limited generalizability. SMILES strings provide a straightforward method for mapping the molecular structure into 1D, and graph representations develop the idea further to capture bonds between the molecules, albeit using a dimensionless representation.

We investigate molecule representations from the viewpoint of capturing both chemistry and 3D structure. We show a case study of predicting antibiotic potential of large (20–100 carbon atoms) antibiotic molecule candidates via an experimentally measured indicator, minimum inhibitory concentration. Our consistent investigation involves comparison of different representations ranging from chemistry only to ones attempting to integrate 1D – 3D structure (chemistry-only and structure-capturing features downselected automatically from a set of 5000 potential features, SMILES, and molecular bond graph with combinations of the previous ones), compared in traditional and complex models (including random forest regression and directed message passing neural network [3]).

We demonstrate the power of improving model predictions by focusing on optimum representation, show that representation can be tuned utilizing models with faster ramp up time, and find that structure-capturing representation improves predictive accuracy especially when the data consists of large, non-rigid molecules. Our systematic case study highlights the importance

of data representation when optimizing for predictive accuracy.

References:

- [1] Elton, Daniel C., Zois Boukouvalas, Mark D. Fuge, and Peter W. Chung. "Deep learning for molecular design - a review of the state of the art." *Molecular Systems Design & Engineering* 4, no. 4 (2019): 828-849.
- [2] Schwalbe-Koda, Daniel, and Rafael Gómez-Bombarelli. "Generative models for automatic chemical design." In *Machine Learning Meets Quantum Physics*, pp. 445-467. Springer, Cham, 2020.
- [3] Yang, Kevin, Kyle Swanson, Wengong Jin, Connor Coley, Philipp Eiden, Hua Gao, Angel Guzman-Perez et al. "Analyzing learned molecular representations for property prediction." *Journal of chemical information and modeling* 59, no. 8 (2019): 3370-3388.

SESSION F.MT07.06: Material Design

On Demand Abstracts Available for Viewing Starting Saturday Morning, November 21, 2020

F-MT07

**5:00 AM \*F.MT07.06.01**

**Active Learning Guided Online Materials Synthesis and Full-Map Understanding** Xiaonan Wang; National University of Singapore, Singapore

The rapid development of deep learning enabled artificial intelligence (AI) has brought new opportunities to accelerate conventional experimental design in materials science. The discovery of high-dimensional synthesis recipes that yield desired material properties used to be costly and time-consuming, while advances in machine learning (ML) driven high-throughput experiments are able to rapidly achieve optimal conditions to produce the target materials. I will introduce our recently developed online active learning approaches that can effectively guide experiments and achieve full-map understanding of the design space.

The first case study demonstrates a two-step active learning framework that combines Bayesian Optimization (BO) and Deep Neural Network (DNN) in a loop with a high-throughput microfluidic platform, to optimize the synthesis of silver nanoparticles with the desired absorbance spectrum. In Step I, the optimization process is accelerated by the offline introduction of DNN after a few runs of targeted sampling through BO with a Gaussian Process. In step II, the DNN is allowed to sample the parameter space using grid optimization to test its regression function. The fully trained DNN can then predict absorbance spectra around the target and possibly optimize the synthesis towards a new target.

The second case study further extends the active learning method to a hierarchical AI framework, which is tested for strain sensor material synthesis. The challenge to obtain customized sensing devices with designated working windows comes from the complex and unclear structure-composition-property relationships that are hard to predict and pre-design. A feasibility classifier using support vector machine (SVM) is first constructed as the screening layer towards the material design. An active machine learning loop is then designed to perform full-map exploring and learning by sampling the "most informative" data points to perform explorations. Besides, comprehensive algorithm optimization is performed for better AI prediction performance. The framework enables a full-map understanding to the system and provides new insights and principles for sensor design.

Moreover, we have developed a series of interpretation and visualization approaches to understand "black-box" ML models and make them more favoured by domain experts to extract knowledge of complex systems that embed a huge amount of hidden information. Although promising opportunities are identified, many challenges exist in this highly interdisciplinary field, such as construction of valuable and open datasets, in-depth understandings of descriptors, lack of standard algorithms workflow and fully autonomous experimental platforms, which will be briefly discussed as future directions.

**5:15 AM F.MT07.06.02**

**Meta-Reinforcement Learning as the Driver of Data Acquisition in Autonomous Polymer Discovery** Sarathkrishna Swaminathan, Chinyere Agunwa, Victoria Piunova, Krystelle Lioni, Daniel Sanders and Dmitry Zubarev; IBM Research, United States

Discovery and development of polymer materials is strongly driven by experimental data acquisition. Polymer materials have

to be prepared and characterized in order to be patentable. The immediate outcome of the polymerization reaction can be transformed into multiple materials with strikingly different properties by means of formulation and processing. Potential for IP development increases sharply as the polymerization product evolves via formulation and processing into the final material. Experimental data acquisition, therefore, unfolds under conditions of delayed rewards on incredibly rich landscapes shaped by access to multiple experimental degrees of freedom that can be both continuous (concentration, temperature, radiation, time) and categorical (monomers, catalysts, initiators, solvents) [1,2].

In the presented contribution, we report results of the ongoing effort in the development of an end-to-end reinforcement learning (RL) approach to the experimental data acquisition in the polymer material domain. The application is the development of a simple spin-on-glass. It starts with the acquisition of initial experimental data, proceeds to training a RL agent to search for the experimental settings (generating experimental hypothesis) that produce materials with desired properties, then to applying a trained RL agent to design the experimental plan, and finally to executing the experimental plan using the existing robotic platform. We identify and discuss the following factors that we are systematically addressing:

- Direct access to the lab equipment during the training phase is impractical; given the complexity of the polymer synthesis and processing, therefore, the most viable option is to prepare a surrogate model of the system and use it to set up the RL environment. The optimal choice of the surrogate as well as handling the uncertainties deserves systematic investigation.
- The task of materials discovery often comprises a search for multiple promising solutions, both search and enumeration, but not necessarily global optimization. The search task can be learned in the narrow context of the specific experimental project (cf. navigation of one specific maze); a significantly stronger result is to train a RL agent to navigate experimental landscapes *as such* (cf. learning general strategies of maze navigation). This brings meta-learning to the top of the priority list [3].
- RL is notoriously data-greedy; meta-learning further amplifies the need for abundant and diverse training data. Therefore, data augmentation is necessary, particularly around creating families of the surrogate models. The specifics of the data augmentation, that leads to optimal performance, needs careful observation.
- As is generally the case with RL, the reward system plays a big role. One possible (and informative) approach is to develop reward systems that mimic effective “rewards” and “penalties” for human researchers solving similar data acquisition tasks.

On the artificial intelligence angle, we describe the specifics of the implementation (OpenAI Gym based environment, and RL algorithms) and discuss obtained performance metrics and approaches to the diagnostics of the RL agent behavior.

1. Li, H. et al. “Tuning the Molecular Weight Distribution from Atom Transfer Radical Polymerization Using Deep Reinforcement Learning” *Mol. Syst. Des. Eng.*, 2018.
2. Zhou, Z. et al. “Optimizing Chemical Reactions with Deep Reinforcement Learning” *ACS Cent. Sci.* 2017.
3. Kobbe, K. et al. “Quantifying Generalization in Reinforcement Learning” *PMLR 97*, 2019.

### 5:25 AM F.MT07.06.03

**Model-Based Reinforcement Learning for Predictive Synthesis of MoS<sub>2</sub>** Pankaj Rajak<sup>1</sup>, Aravind Krishnamoorthy<sup>2</sup>, Ankit Mishra<sup>2</sup>, Ye Luo<sup>1</sup>, Rajiv Kalia<sup>2</sup>, Aiichiro Nakano<sup>2</sup> and Priya Vashishta<sup>2</sup>; <sup>1</sup>Argonne National Laboratory, United States; <sup>2</sup>University of Southern California, United States

Scalable synthesis of two-dimensional (2D) materials is a major bottleneck to more widespread adoption of layered material-based devices. Chemical vapor deposition (CVD) has emerged as a viable method for large-scale synthesis of 2D materials. However, neither experiment nor theory has been able to decipher mechanisms and selection rules for different growth scenarios or make predictions of optimized growth parameters. Here, we have designed a workflow using model-based reinforcement learning (RL) and neural autoregressive density estimator (NADE-CVD) to generate the optimal synthesis condition for the prototypical two-dimensional semiconductor, monolayer MoS<sub>2</sub> with high 2H-phase fraction in minimum time from MoO<sub>3</sub> crystal. Here, the NADE-CVD models the probability density function of CVD-synthesis and is trained using 15,000 reactive molecular dynamics (RMD) simulation trajectories each for 20 ns of MoS<sub>2</sub>. After training, NADE-CVD serves as a dynamics model of CVD-synthesis and interacts with the RL agent. Using the reward singles from the dynamics model, the RL agent is able to propose synthesis conditions (such as temperature profile and S<sub>2</sub>, H<sub>2</sub> and H<sub>2</sub>S partial pressures) and their dependencies among each other that generates MoS<sub>2</sub> crystal with maximum 2H phase fraction quickly, thus paving the way toward rational design of CVD synthesis techniques for MoS<sub>2</sub> and other layered materials.

This work was supported as part of the Computational Materials Sciences Program funded by the U.S. Department of Energy, Office of Science, Basic Energy Sciences, under Award Number DE-SC0014607. Simulations were performed at the Argonne Leadership Computing Facility under the DOE INCITE program and Aurora Early Science programs and at the Center for High Performance Computing of the University of Southern California.

**5:35 AM F.MT07.06.04**

**Accelerating Inverse Design of Conjoined Photovoltaic and Thermoelectric Generator Systems via Physics-Driven Machine Learning** Aleks Siemenn, Tonio Buonassisi and Zhe Liu; Massachusetts Institute of Technology, United States

Humanity is accumulating magnitudes of data for many discrete components — but how do we best utilize these data to improve complex systems? The world of “big data” begins to intersect “systems engineering.” In this contribution, we contemplate a model system — conjoined photovoltaic and thermoelectric generators (PV+TEG) — which has tens of design variables and corresponding response curves [1]. However, with such voluminous design and response data (in machine-learning parlance, “vast state space”), it is unclear how we can inversely map the response data back to our design variables to improve system energy yield under a given set of operating conditions. Therefore, to leverage the supply of big data coming from our simulated and experimental systems such as PV+TEG, we propose a framework for system optimization via supervised surrogate models (*e.g.*, neural networks) and model-free optimization (Bayesian optimization, BO), which combines the advantages of embedded physics domain knowledge and adaptability to complex action-responses outside the model.

Conducting system optimization using this framework promotes high-throughput iterative design cycles for faster rates of learning [2]. There is great importance in optimizing new or existing systems using high-throughput iterative design because by informing a new design based on learning data trends rather than experimentally building a new system each iteration, significant savings are seen in time, energy, and material costs [2]. In the example of solar energy, photovoltaics and thermoelectric modules are both well-established technologies individually, however, by drilling down to the design components of each device, the thermoelectric module can be better optimized to improve the energy yield of a photovoltaic device, in turn, requiring a smaller area to generate the same power. The working principle of this system improvement framework is that: (1) physics-driven models establish the fundamental relationship between PV+TEG design variables and response outputs; (2) experimental response curves provide ground-truth relationships for a narrow band of design variables and outputs; (3) physics-fusion neural networks combine simulated and experimental response data to build robust inferences of feasible PV+TEG designs [3]; (4) the manifold of PV+TEG design variables is searched by BO to generate operational system designs that maximize energy yield. We demonstrate that with large volumes of operational system data, neural networks and Bayesian optimization are used to accelerate the convergence on optimal photovoltaic and thermoelectric generator designs by 10x relative to the state of the art Multiphysics simulation while allowing more parameter customization [4]. By reducing design time, fiber laser-powered gallium arsenide PV+TEGs will be explored in a gamut of small-scale applications to maximize energy transmission efficiency.

References:

- [1] H. Hashim, J. J. Bomphrey, and G. Min, “Model for geometry optimisation of thermoelectric devices in a hybrid PV/TE system,” *Renew. Energy*, vol. 87, pp. 458–463, 2016, doi: 10.1016/j.renene.2015.10.029.
- [2] A. T. D. Perera, P. U. Wickramasinghe, V. M. Nik, and J. L. Scartezini, “Machine learning methods to assist energy system optimization,” *Appl. Energy*, vol. 243, pp. 191–205, 2019, doi: 10.1016/j.apenergy.2019.03.202.
- [3] Y. Ba, G. Zhao, and A. Kadambi, “Blending Diverse Physical Priors with Neural Networks,” no. 1, pp. 1–15, 2019.
- [4] Z. Ren *et al.*, “Embedding physics domain knowledge into a Bayesian network enables layer-by-layer process innovation for photovoltaics,” *npj Comput. Mater.*, vol. 6, no. 1, pp. 1–9, 2020, doi: 10.1038/s41524-020-0277-x.

**5:45 AM F.MT07.06.05**

**Inverse Design of Nanoporous Crystalline Reticular Materials with Deep Generative Models** Zhenpeng Yao<sup>1,2</sup>, Benjamín Sánchez-Lengeling<sup>1</sup>, N. Scott Bobbitt<sup>3</sup>, Benjamin Bucior<sup>3</sup>, Tom Woo<sup>4</sup>, Omar Farha<sup>3</sup>, Randall Snurr<sup>3</sup> and Alán Aspuru-Guzik<sup>1,2</sup>; <sup>1</sup>Harvard University, United States; <sup>2</sup>University of Toronto, Canada; <sup>3</sup>Northwestern University, United States; <sup>4</sup>University of Ottawa, Canada

Reticular frameworks are crystalline porous materials that form *via* the self-assembly of molecular building blocks (*i.e.*, nodes and linkers) in different topologies. Many of them have high internal surface areas and other desirable properties for gas storage, separation, and other applications. The notable variety of the possible building blocks and the diverse ways they can be assembled endow reticular frameworks with a near-infinite combinatorial design space, making reticular chemistry both promising and challenging for prospective materials design. Here, we propose an automated nanoporous materials

discovery platform powered by a supramolecular variational autoencoder (SmVAE) for the generative design of reticular materials with desired functions. We demonstrate the automated design process with a class of metal-organic framework (MOF) structures and the goal of separating CO<sub>2</sub> from natural gas or flue gas. Our model exhibits high fidelity in capturing structural features and reconstructing MOF structures. We show that the autoencoder has a promising optimization capability when jointly trained with multiple top adsorbent candidates identified for superior gas separation. MOFs discovered here are strongly competitive against some of the best-performing MOFs/zeolites ever reported. This platform lays the groundwork for the design of reticular frameworks for desired applications.

SESSION F.MT07.07: Science of Optimization  
On Demand Abstracts Available for Viewing Starting Saturday Morning, November 21, 2020  
F-MT07

**5:00 AM \*F.MT07.07.01**

**AMANDA—An Autonomous Materials and Device Application Platform for the Laboratory of the Future and the Next Generation Materials Research** Christoph J. Brabec<sup>1,2</sup>; <sup>1</sup>FAU, Germany; <sup>2</sup>Forschungszentrum Jülich GmbH, Germany

The development of high performance, stable solar cell materials poses a multi-objective optimization problem in a considerable multidimensional parameter space. Solving it requires reproducible, user independent laboratory work and intelligent preselection of conducted experiments. However, research on organic photovoltaics (OPV) is a field where manual routines are still predominant, although other domains like pharmacy have long used robotics and automation.

To better utilize automation in materials science, we introduce AMANDA (Autonomous Materials and Device Application Platform), a generic software framework for distributed materials research and its research line LineOne (L1), a robotic facility for the production and characterization of solution processed solar cells.

We integrated pipetting and transport robots with spin coating and evaporation units as well as characterization tools like spectrometers and electrical measurements into LineOne. With this setup, the AMANDA Platform automatically produces and measures OPV cells without human interaction while it is capable of rapidly screening large materials and processing parameter spaces in a combinatorial approach at high precision. The current hardware configuration is fully scalable and allows the high throughput screening of up to 270 variations per day on LineOne. The output comprises the complete fabrication of solar cells, full characterization and comprehensive documentation of all applied process steps as well as compiled results for each individual solar cell. We demonstrate the capabilities of AMANDA by the process development for OPV solar cells based on PM6:Y6 with 13.7% efficiency when processed in air and through the detailed investigations of the impact of subtle process parameters, like solution concentration and volume of solution deposited for spin coating, on film quality and performance.

**5:15 AM F.MT07.07.02**

**An Automated Formulation System to Accelerate Development of Printed Thin-Film Materials** Kane L. Scipioni<sup>1</sup>, Amir H. Khalighi<sup>1</sup>, Kuya Takami<sup>1</sup>, James A. Corson<sup>1</sup>, Colin J. McNeece<sup>1</sup>, Michael C. Heiber<sup>1</sup>, Christopher L. Farrow<sup>1</sup>, Roger T. Bonnecaze<sup>2</sup> and Eric Jones<sup>1</sup>; <sup>1</sup>Enthought, United States; <sup>2</sup>The University of Texas at Austin, United States

Formulation chemistry is big business for a wide variety of industries, where formulated fluids cover a market worth hundreds of billions of dollars per year. Formulations for printing applications represent one of many components of this market and include a diverse range of products from consumer inks to advanced electronic materials. Industrial ink formulations can be extremely complex with a wide range of specifically selected components to impart multifunctionality on the final dry film. Film materials have important requirements for optical, electrical, and mechanical properties as well as longer-term chemical, temperature, and UV stability. In addition, formulations must meet specific surface tension and viscosity criteria to be printable. Meeting these complex requirements requires optimization over many dimensions. In our experience working with various specialty chemical companies, we have observed that, most often, these formulation optimization experiments are still performed using slow, labor-intensive workflows. This dramatically limits what can be explored given realistic budget constraints.

In recent years, advances in machine learning together with greater accessibility of robotic automation tools have enabled a new paradigm of accelerated materials development using autonomous research systems. In the printed electronics space, several exemplary autonomous research systems have been recently created.<sup>1,2</sup> However, these systems have been designed to create thin films by spin-coating or drop-casting, which are less applicable to large-area, high-throughput industrial

manufacturing processes. Previous systems have also used robotic pipetting to measure out different formulations in a slow batch-based process.

To tackle real industry problems with our clients, we have developed a modular automated system for rapid flow-based microfluidic formulation, fluid characterization, inkjet printing, and film characterization. As opposed to the methods used in previous autonomous systems, inkjet printing is a key enabling additive manufacturing technology that is mature and widely used for high volume manufacturing. The system includes multiple characterization modes along the workflow, including shear-rate-dependent viscosity, complex jetting behavior, and final film quality. Where possible, we have also been developing low-cost hardware modules to help alleviate the sticker shock that often occurs when new automated systems are proposed to business units with tight R&D budgets.

In our first case study, the system was able to improve upon an existing manual process used to develop polymer films for display applications. The legacy process took around 35 person-hours per recipe, including slow ink formulation, printing, characterization, and cleaning. The new system reduced that worker time to almost zero and features automated cleaning, freeing up skilled researchers' time to work on other tasks. The system now takes about 15 minutes to investigate each recipe with minimal human interaction and is also able to rapidly map out the multidimensional printability window. One of the key enablers of this was the inkjet stroboscopic imaging setup. There is a wealth of information in the dynamic shape of jetted droplets which correlates strongly with the viscoelasticity, surface chemistry, and microstructure of the fluid. We are currently implementing an experiment planning and scheduling system that can execute various strategies for hierarchical optimization. With this in place, the system will not simply maximize sample throughput but also focus on performing experiments where the likelihood of knowledge gain is the highest.

1. Langner, S. *et al.* Beyond Ternary OPV: High-Throughput Experimentation and Self-Driving Laboratories Optimize Multicomponent Systems. *Adv. Mater.* **32**, 1907801 (2020).
2. MacLeod, B. P. *et al.* Self-driving laboratory for accelerated discovery of thin-film materials. *Sci. Adv.* **6**, eaaz8867 (2020).

#### 5:25 AM F.MT07.07.03

**Applications and Development of an Autonomous Alloy Electrochemical Deposition and Corrosion Platform** Howie Joross<sup>1</sup>, Brian L. DeCost<sup>1</sup>, Bruce Ravel<sup>1,2</sup>, Suchismita Sarker<sup>3</sup>, Najlaa Hassan<sup>1</sup>, Trevor Braun<sup>1</sup>, Apurva Mehta<sup>3</sup> and Jason R. Hattrick-Simpers<sup>1</sup>; <sup>1</sup>National Institute of Standards and Technology, United States; <sup>2</sup>Brookhaven National Laboratory, United States; <sup>3</sup>SLAC National Accelerator Laboratory, United States

We present our work on the development and application of a mesofluidic electrochemical deposition and analysis platform. Our scanning droplet cell (SDC), coupled with a bank of syringe pumps is capable of serial electrodeposition and electrochemical corrosion measurements on millimeter scale areas. We have also demonstrated integration of our platform into the 6-BM end-station at NSLS-II to add in situ x-ray fluorescence and diffraction capabilities. In addition to describing this platform in detail, we will present two validation studies: In the first we use this system for serial corrosion measurements of sputtered combinatorial thin-film metallic glass and high-entropy alloy libraries. Second, we will discuss our on-going efforts to combine synthesis and characterization, controlled by an autonomous AI agent. In this work we look at the effect of electrodeposition processing parameters for Ni-Zn plating, such as solution concentration and bias, on alloy corrosion resistance, composition, and structure. Our goal here is to experimentally generate a machine learning based model to describe optimal deposition conditions for an arbitrary alloy composition in its most corrosion resistant state and describe the corrosion behavior of that alloy. In this way, we hope that this system can transcend simple optimization and can begin to decouple the interplay of deposition, structure, and corrosion resistance in order to generate new knowledge.

#### 5:35 AM F.MT07.07.05

**Accessing Creativity and Institutional Knowledge of Polymer Chemists via Expert-in-the-Loop AI—Case of Acrylic Polymer Design** Victoria Piunova<sup>1</sup>, Dmitry Zubarev<sup>1</sup>, Petar Ristoski<sup>1</sup>, Anna Lisa Gentile<sup>1</sup>, Linda Kato<sup>1</sup>, Seiji Takeda<sup>2</sup>, Toshiyuki Hama<sup>2</sup>, Hsianghan Hsu<sup>2</sup>, Daiju Nakano<sup>2</sup>, Daniel Gruhl<sup>1</sup>, Seteve Welch<sup>1</sup> and Daniel Sanders<sup>1</sup>; <sup>1</sup>IBM Almaden Research Center, United States; <sup>2</sup>IBM Tokyo Research Laboratory, Japan

With ever increasing demand of the modern world for the materials with advanced properties, we are facing the pressure to accelerate the discovery through a paradigmatic shift. One of the major practical bottlenecks – actionability bottleneck - is majority of the computationally generated hypotheses fail to transition to the experimental phase. In this case, the target properties are expected to meet project requirements, but the candidates fail to satisfy broader project-specific constraints. The most problematic constraints represent institutional knowledge, broadly defined. Institutional knowledge is not systematically captured in publications, but rather carried by subject matter experts (SMEs). This explains fundamental

difficulty of capturing institutional knowledge, introducing it into the training phase of statistical modeling, and propagating into the hypothesis generation phase.

This contribution addresses resolution of the actionability bottleneck via capture and instantiation of SME's creativity and institutional knowledge in the form of AI models. This is accomplished using a two-tiered expert-in-the-loop (EITL) approach [1,2]. Specifically, we considered monomer design for acrylic polymers. The first tier of EITL AI included training a discriminator that was reproducing SME's decision-making in the adjudication of the candidate monomers. The candidate monomers were generated using recently developed system for molecular inverse-design [3]. The SME – a polymer chemist responsible for the polymerization experiments – accepted or rejected the candidates as they answered the question: “Is it practical to synthesize this monomer?” The question, as discussed with the SME, implied subjective assessment of the synthetic accessibility, expected behavior during polymerization, and novelty. The second tier of EITL AI leveraged the adjudication results and the trained discriminator to train a generative model producing monomer candidates that were likely to be accepted by the SME. We trained 2 sequential neural network models and 3 generative adversarial networks (GANs); generative models were refined via separate adjudication of their output until acceptable performance was reached. At this point the generative form of EITL AI combined implicit models of SME's knowledge and creativity as both these components informed the adjudication processes.

The trained generative component of EITL AI was queried by the SME to identify candidates for the experimental phase. The generated structures were evaluated on the basis of novelty and synthetic complexity. Selected structures were additionally assessed based on the following criteria:

- the ease of synthesis or commercial availability for the monomer precursor
- the number of transformations, their difficulty, commercial availability and price of starting materials and reagents
- the ease of polymerizable handle installation on the monomer precursor
- the ability of the obtained monomer to be polymerized in a free radical polymerization process

Five monomers were selected to produce acrylic polymers. Performance metrics of the AI models, experimental procedures, and polymer characterization results will be discussed along with existing challenges and potential extensions.

#### 5:45 AM \*F.MT07.07.06

**Robot-Accelerated, Data-Enabled Investigation into Metal Halide Perovskite Reaction Networks** Zhi Li<sup>1</sup>, Jakob Dahl<sup>2,1</sup>, Mansoor Ani N. Nellikkal<sup>3</sup>, Joshua Schrier<sup>4</sup>, Alexander Norquist<sup>3</sup> and Emory Chan<sup>1</sup>; <sup>1</sup>Lawrence Berkeley National Laboratory, United States; <sup>2</sup>University of California, Berkeley, United States; <sup>3</sup>Haverford College, United States; <sup>4</sup>Fordham University, United States

We present the development of high-throughput, data-enabled strategies for understanding the crystallization and chemical transformations of metal halide perovskites in the form of macroscopic single crystals and nanocrystals. These approaches combine robotic synthesis workflows developed at the Molecular Foundry with data-driven approaches that can predict crystallization outcomes and elucidate reaction networks. We will first discuss our Robot-Accelerated Perovskite Investigation and Discovery (RAPID) workflow, which we used to rapidly identify and optimize synthesis conditions for the formation of high quality single crystals via inverse temperature crystallization (ITC). A total of 8172 metal halide perovskite synthesis reactions were performed using 45 organic ammonium cations. Robotic screening increased the number of metal halide perovskite materials accessible by an ITC synthesis route by more than five-fold and resulted in the formation of two new phases. The resulting dataset enabled the construction and evaluation of machine learning models that were able to predict the formation of a diverse range of crystal compositions and morphologies with >85% accuracy after only 100 reactions. We used the same robotic apparatus to systematically explore the reaction networks that produce cesium lead bromide nanocrystals. Deploying automated spectroscopy and a custom deconvolution algorithm to extract the relative populations of each reaction product (i.e. molecular clusters, nanoplatelets, and nanocubes), we generated phase maps of the high-dimensional Cs-Pb-Br synthetic space. Based on these maps, we attempted chemical transformations from each of the as-synthesized products to all other species. The resulting transformation data revealed a dynamic equilibrium between species and allowed us to construct chemical reaction network that provides a holistic view of this weakly reversible system. This work demonstrates the concept that combining high throughput experimentation, machine learning, and data-enabled approaches accelerates and enhances the study of metal halide perovskite crystallization, and that this approach is generalizable across different synthetic routes, materials, and their length scales.

#### 6:00 AM F.MT07.07.07

**A Framework Enabling AI-Assisted High-Throughput Experimentation** Linda Hung<sup>1</sup>, Brian Rohr<sup>1</sup>, John Gregoire<sup>2</sup>, Li Cheng Kao<sup>3</sup>, Jens S. Hummelshøj<sup>1</sup>, Wenhui Li<sup>3</sup>, Junko Yano<sup>3</sup>, Steven Torrisi<sup>4</sup> and Santosh Suram<sup>1</sup>; <sup>1</sup>Toyota Research Institute, United States; <sup>2</sup>California Institute of Technology, United States; <sup>3</sup>Lawrence Berkeley National Laboratory, United States

States; <sup>4</sup>Harvard University, United States

The acceleration of high-throughput experimental discovery involves several recurring challenges such as data ingestion, visualization, analysis, and recommendation. In this talk, we describe how the ACE (AI-assisted Catalyst Experimentation) framework addresses these challenges and enables scientists to improve decision-making in high-throughput experimentation.

We highlight the following aspects of our framework:

1. **Data Ingestion:** We describe an experimental database schema that has minimal built-in assumptions, follows FAIR principles, and is expected to generalize to a wide variety of scientific applications using one of the largest experimental datasets as an example.<sup>1</sup>
2. **Data Visualization:** Scientists can easily navigate the database by using a domain specific language as part of the UI. These queries are bolstered with visual aids about metadata. In addition, the UI automatically provides a set of useful visualizations for dataset statistics, trends, and details of individual samples and processes.
3. **Analysis:** Analysis of materials characterization data remains one of the critical bottlenecks for high-throughput experimental materials discovery. We present specific examples for AI-assisted analysis of X-ray spectroscopy to demonstrate the capabilities of our framework to address this bottleneck.
4. **Recommendation:** The current recommendation capabilities of our framework include a) sequential recommendation for accelerated discovery within a composition space, b) recommendation of composition spaces for experiments using representation learning. We demonstrate these capabilities for learning formation energy, band gap, and catalytic properties. We also show human and machine benchmarks for sequential learning within a specific composition space.

These components that make up ACE are designed to be modular and generalizable; and aim to provide foundational infrastructure for accelerated adoption of machine learning for diverse high-throughput experimental applications.

References:

1. Soedarmadji, E. et al. Tracking materials science data lineage to manage millions of materials experiments and analyses. *npj Comput Mater* 5, 79 (2019).

### **6:10 AM F.MT07.07.08**

**Benchmarking the Performance of Bayesian Optimization Across Multiple Experimental Domains** [Harry Q. Liang<sup>1</sup>](#), Aldair E. Gongora<sup>2</sup>, Zekun Ren<sup>3</sup>, Zhe Liu<sup>1</sup>, Armi Tiihonen<sup>1</sup>, Shijing Sun<sup>1</sup>, Flore C. Mekki-Berrada<sup>4</sup>, Saif A. Khan<sup>4</sup>, Daniil Bash<sup>5</sup>, Kedar Hippalgaonkar<sup>5</sup>, Keith A. Brown<sup>2</sup>, John W. Fisher<sup>1</sup> and Tonio Buonassisi<sup>1</sup>; <sup>1</sup>Massachusetts Institute of Technology, United States; <sup>2</sup>Boston University, United States; <sup>3</sup>Singapore-MIT Alliance for Research and Technology, Singapore; <sup>4</sup>National University of Singapore, Singapore; <sup>5</sup>Agency for Science, Technology and Research (A\*STAR), Singapore

High-throughput autonomous research has recently emerged as the new frontier of accelerated materials discovery. This success has sparked efforts to improve not only lab automation infrastructure but also optimization algorithms. In materials optimization campaigns, sequential learning approaches such as Bayesian Optimization (BO) have gained great popularity due to their ability to improve parameters of merit with fewer number of experiment cycles in comparison to brute-force approaches. Previous attempts to quantitatively evaluate the acceleration of research through sequential learning have been limited to specific materials systems [1]. Therefore, two open questions that remain are: (a) how does performance of BO in sequential learning approaches vary across multiple experimental domains and manifold complexities. (b) how we could improve upon current optimization algorithms and attend to the needs of a broader materials science community.

In this work, we benchmark the performance of sequential learning approaches within the BO framework across four experimental domains. Each focusing on a different materials system, four experimental datasets with varying sizes, dimensionalities and dataset manifold complexities are used to build representations of ground truths, where we draw from these to simulate optimization campaigns. We compare the performance of BO algorithms employing one of three surrogate models and five myopic acquisition functions. The performance of each surrogate model and acquisition function pair is benchmarked against random acquisition, and further quantified via learning rate metrics designed to measure different research objectives.



It is observed that BO consistently reduces the number of experiment cycles necessary to reach superior materials response by factors of 5 to 15 across all experimental systems. Random forest surrogate model paired with a lower confidence bound acquisition function of balanced mean and standard deviation shows higher-ranking performance for research tasks such as finding any or all of the candidates with top 5% response. Interestingly, in the case of surrogate models, random forests outclass gaussian processes in optimization tasks when using the same acquisition functions across all datasets, likely due to their nature of making fewer structural assumptions about manifold landscapes. In addition, we further explore the benefits of utilizing look-ahead decision policies as an alternative to the traditional myopic acquisition functions in the BO framework. Complementary to our findings, our benchmarking effort has yielded many useful insights on how experimentalists interested in novel materials systems could select the most suitable BO methods prior to embarking on an optimization campaign. These can be utilized by a broader materials science community in further progressing the field of autonomous research.

[1] Rohr, B., Stein, H.S., Guevarra, D., Wang, Y., Haber, J.A., Aykol, M., Suram, S.K. and Gregoire, J.M., 2020. Benchmarking the acceleration of materials discovery by sequential learning. *Chemical Science*, 11(10), pp.2696-2706.

6:20 AM F.MT07.07.09

**Reassessing High-Dimensional Optimization Strategies Using Interpretable Machine Learning For Perovskite Solar Cell Manufacturing** Zhe Liu<sup>1</sup>, Nicholas Rolston<sup>2</sup>, Zekun Ren<sup>3</sup>, Felipe Oviedo<sup>1</sup>, Harry Q. Liang<sup>1</sup>, Reinhold H. Dauskardt<sup>2</sup> and Tonio Buonassisi<sup>1,3</sup>; <sup>1</sup>Massachusetts Institute of Technology, United States; <sup>2</sup>Stanford University, United States; <sup>3</sup>Singapore-MIT Alliance for Research and Technology, Singapore

Developing novel scalable fabrication processes for perovskite PV devices involves optimizing many process variables, which is challenging for human intuition alone to solve the problem efficiently. Autonomous high-throughput experimentation has recently demonstrated a very encouraging outcome to aid rapid materials development<sup>1-3</sup>. Preliminary success has also been demonstrated by introducing machine learning (ML) in the loop to guide the experiments<sup>4</sup> for developing a fabrication process. However, the black-box nature of machine learning is a key limitation that hinders wide adoption in physical science research<sup>5</sup>. Although ML is a powerful statistical tool to navigate and optimize in a high-dimensional space, rigorously-trained materials scientists are not able to easily understand the decisions made by ML algorithms. Due to this lack of model interpretability, researchers usually find it difficult to intellectually engage with ML-driven optimization.

In this work, we investigate how we can work cooperatively with an ML algorithm and maximize the acceleration of the optimization process. To do so, we revisit a historical dataset of perovskite devices with open-air spray deposition, and then adopt commonly used sequential learning methods to navigate the process optimization of perovskite solar cells. Based on this case study, we find three generalizable points to better utilize machine learning tools for materials research. **First, initial sampling is crucial to ensure rapid optimization.** We compare different initial sampling methods, *e.g.*, chronological, random, and Latin hypercube sequences, and find the initialization method plays an important role to facilitate the subsequent optimization. Without a good initial design of experiments guided by domain knowledge, the acceleration benefits with an ML algorithm is very limited. **Second, the acquisition and objective functions need to be tuned for different research objectives of optimizing device performance or building a predictive regression model.** By assigning different weights to “exploitation” and “exploration”, we evaluate the optimization outcomes for various acquisition functions with different regression models. Echoing previous findings by Rohr *et al.*<sup>6</sup>, we also observe that acceleration in building a predictive model is not necessarily easy with sequential learning algorithms, but it could significantly accelerate the process optimization of device efficiency (where up to 2x acceleration could be found). **Third, the algorithm interpretability allows researchers to engage with the ML model and avoid mistakes.** At each step, our framework helps visualize how sampling decisions are made by the ML algorithm: whether an acquisition decision is influenced more by the predicted mean or the predicted uncertainty, whether it favors exploration in the unsampled regions or exploitation in the known regions, or which process variable has the highest impact on the decision. We envision the impact of this work as a human-in-loop machine-learning platform where researchers can understand the framework of ML and utilize ML algorithms to accelerate the research of novel materials.

Reference:

1. Stein, H. S. & Gregoire, J. M. Progress and prospects for accelerating materials science with automated and autonomous workflows. *Chem. Sci.* **10**, 9640–9649 (2019).
2. MacLeod, B. P. *et al.* Self-driving laboratory for accelerated discovery of thin-film materials. *Sci. Adv.* **6**, eaaz8867 (2020).
3. Li, Z. *et al.* Robot-Accelerated Perovskite Investigation and Discovery (RAPID): 1. Inverse Temperature Crystallization. (2019) chemrxiv.10013090.v1.

4. Attia, P. M. *et al.* Closed-loop optimization of fast-charging protocols for batteries with machine learning. *Nature* **578**, 397–402 (2020).
5. Towards trustable machine learning. *Nat. Biomed. Eng.* **2**, 709–710 (2018).
6. Rohr, B. *et al.* Benchmarking the acceleration of materials discovery by sequential learning. *Chem. Sci.* **11**, 2696–2706 (2020).

### 6:30 AM \*F.MT07.07.10

#### Accelerated Quantum Dot Development in Flow—Convergence of Flow Chemistry, Colloidal Synthesis and Machine Learning Milad Abolhasani; North Carolina State University, United States

Metal halide perovskite quantum dots (QDs) have recently emerged as an exciting class of semiconducting materials, outperforming conventional II-VI, IV-VI, and III-V semiconductor nanocrystals in QD-based optoelectronic devices.<sup>1</sup> Despite the substantial improvement in performance of perovskite QD-based optoelectronic devices over the past five years, two major obstacles hinder their development: **(i)** Edisonian (trial and error)-based QD synthesis, discovery, and optimization methods, and **(ii)** poor size dispersity of batch-synthesized colloidal nanocrystals, resulting in surface trap states. Existing material development strategies very often fail to overcome the demands of colloidal QDs' vast colloidal synthesis and processing universe, resulting in time- and cost-intensive QD development efforts.

Recent advances in machine learning (ML),<sup>2</sup> including deep neural networks (DNNs) and reinforcement learning algorithms, provide an exciting opportunity for reshaping the synthesis and development of perovskite QDs, through the machine-based direction of a high-throughput QD synthesis bot. Capitalizing on the recent progress of ML-based optimization algorithms, *smart* QD manufacturing strategies relying on DNNs trained on experimentally measured QD properties can be envisioned to accelerate the discovery, synthesis, and manufacturing of metal halide perovskite QDs with application-guided optoelectronic properties.

In this talk, I will present an *Artificial Chemist*,<sup>3</sup> a modular intelligent fluidic microprocessor<sup>4</sup> capable of autonomous synthesis, optimization, and end-to-end manufacturing of colloidal QDs for direct utilization in high-performance and low-cost optoelectronic devices. The Artificial Chemist can rapidly and efficiently **(i)** explore the massive parameter space of colloidal perovskite QDs, **(ii)** learn their synthesis and processing schemes, **(iii)** identify the composition and relevant synthesis route(s) of perovskite QDs to achieve specific optoelectronic properties, and **(iv)** continuously manufacture the rapidly optimized perovskite QDs at a fraction of time/cost of batch techniques. The reconfigurable Artificial Chemist technology utilizes a multimodal *in-situ* material diagnostic probe (absorption/photoluminescence (PL) spectroscopy) in conjunction with a real-time, ensemble DNN adaptive sampling algorithm to enable simultaneous optimization of PL quantum yield and emission linewidth of colloidal QDs for any desired peak emission energy. The Artificial Chemist technology can be readily adapted for accelerated development and autonomous end-to-end manufacturing of other solution-processed nanomaterials.

#### References

1. (a) Hazarika, A., *et al.*, *ACS Nano* **2018**, *12* (10), 10327-10337; (b) Sanehira, E. M., *et al.*, *Sci. Adv.* **2017**, *3* (10); (c) Swarnkar, A., *et al.*, *Science* **2016**, *354* (6308), 92-95; (d) Yoon, H. C., *et al.*, *ACS Applied Materials & Interfaces* **2016**, *8* (28), 18189-18200; (e) Lu, M., *et al.*, *Advanced Functional Materials* **0** (0), 1902008.
2. (a) LeCun, Y., *et al.*, *Nature* **2015**, *521*, 436; (b) Le, T. C.; Winkler, D. A., *Chem. Rev.* **2016**, *116* (10), 6107-6132.
3. Epps, R. W., *et al.*, *Advanced Materials* **2020**, (in press), 2001626.  
<https://doi.org/10.1002/adma.202001626>
4. (a) Abdel-Latif, K., *et al.*, *Advanced Functional Materials* **2019**, *29* (23), 1900712; (b) Epps, R. W., *et al.*, *Lab Chip* **2017**, *17* (23), 4040-4047.

### 6:45 AM F.MT07.07.11

#### Using Quantified Uncertainty to Guide Efficient Phase Diagram Determination via Sequential Learning Theresa Davey<sup>1</sup>, Brandon J. Bocklund<sup>2</sup>, Zi-Kui Liu<sup>2</sup> and Ying Chen<sup>1</sup>; <sup>1</sup>Tohoku University, Japan; <sup>2</sup>The Pennsylvania State University, United States

Phase diagrams are a fundamental tool in materials design, but thorough experimental determination is challenging, expensive, and time consuming. Phase diagrams calculated entirely from first-principles may reduce time and expense, providing information at the prediction stage. Our previous work demonstrated a methodology to obtain a first-principles only CALPHAD-type solid phase diagram reproducing all major features, with little or no prior knowledge of the system [1]. This can guide reduced experiments needed for database validation.

Considering the quantified uncertainty of the first-principles phase diagram using PDUQ [2] and ESPEI [3], a sequential

learning approach is taken to systematically add thermodynamic and phase boundary data in regions of highest uncertainty. This simulates how the first-principles only phase diagram can most efficiently guide experimental investigation towards a thorough understanding of a materials system. This convergence towards a target phase diagram will be quantified and compared to the chronological introduction of experimental data.

[1] T. Davey et al., CALPHAD XLVIII, June 2019.

[2] N. Paulson et al., Acta Mater. 174 (2019) 9–15.

[3] B. Bocklund et al., MRS Commun. (2019) 1-10.

#### **6:55 AM F.MT07.07.12**

**A Unified Bayesian Approach to Learning Many-Body Potentials** Jonathan Vandermause and Boris Kozinsky; Harvard University, United States

A number of competing frameworks for learning interatomic potentials have been proposed in the last decade, including Gaussian Approximation Potentials (GAP), Spectral Neighbor Analysis Potentials (SNAP), and the Atomic Cluster Expansion (ACE). We here present a Bayesian approach that unites these three frameworks, allowing uncertainty estimates on many-body energies, forces, and stresses to be rigorously computed. We first show how a multi-species generalization of the 3-body ACE descriptor can be used to define an efficient many-body kernel similar to the Smooth Overlap of Atomic Positions kernel used in GAP models. We use this kernel to construct Gaussian process (GP) models of the potential energy surface, and show that uncertainties derived from the predictive posterior distribution of the GP correlate with true model error on independent test sets. Mean predictions of the GP are shown to be linear in an integer power of the descriptor, eliminating the expensive loop over training points required in GP regression and establishing a connection to the SNAP framework. The resulting linear models are implemented in the molecular dynamics program LAMMPS, and shown to achieve competitive performance for a range of molecular and extended systems.

The predictive uncertainties of our Gaussian process models open the door to automated training during molecular dynamics simulations, allowing a wide range of material compositions to be explored in a closed-loop fashion. In this approach, training structures are selected with active learning by making calls to density functional theory only when the predictive uncertainty on a force component exceeds a threshold value. We apply this on-the-fly molecular dynamics method to the shape memory alloy nitinol, and show that we accurately capture the martensite/austenite phase transition that occurs in this material at ambient pressure. Guided by model uncertainties, we systematically expand the training set to examine the effects of dopants, defects, and nonequiatomic compositions on the martensitic transition temperature.

#### **7:05 AM F.MT07.07.14**

**Automated Workflows for Surface Generation and 0D and 2D Structural and Electronic Optimisation and Analysis via WASP@N and SAINT** Helen Duncan and Scott Woodley; University College London, United Kingdom

Automating materials calculations to populate a searchable and curated web-accessible database is non-trivial problem. Moreover, we are interested in enabling the model creation, initialisation of simulations and control of the workflow (as well as the content of the database) from a webpage interface which unfortunately leads to an additional conflict between increasing the desirable accessibility/functionality whilst maintaining security to prevent malicious cyber-attacks. Over a period of 10 years we have developed and implemented a combined hardware (housing the webserver, database and dedicated compute node) and software solution to handle such workflows. To date, we have applied our approach to assisting two different communities: those interested in research based on the atomic structure of clusters, or small sized nanoparticles; and those interested in simulations of surfaces and their reactivity with probe molecules. The former is part of the WASP@N project, whereas the latter is part of the UK's Materials Chemistry HEC Consortium's SAINT project. Both offer access to a database of their respective models, which users can also contribute, and include useful tools for analysis via their web-interfaces.

WASP@N (Web-Assisted Structure Prediction at the Nanoscale) was developed to support the dissemination and comparison of atomic configurations found from global optimisation studies of energy landscapes, which can subsequently be used as models for further studies (their electronic and physical properties or their interaction with other media). All uploaded structures are automatically optimised using the FHI-aims electronic structure code and hyperlinks – based on either composition, energy, and connectivity – that users can follow are created between both the original and refined structures and other entries in the database (all uploaded structures are also linked via DOI to their original publication).

SAINT (The Surface and Interface Toolkit) was developed to support researchers' day-to-day surface simulations, by

providing tools for generating surface models and enabling automatic calculation of surface energies using the CRYSTAL electronic structure code. SAINT offers fully relaxed surface models for a range of metal oxides and maps of their reactivity to three probe molecules; the ability to generate surfaces and then download input files for a range of different DFT and IP codes; and a method of dissemination of published surface models.

Here we will first discuss our insights into hardware and software solutions for such automation and database population along with the need to balance security of the data with ease of accessibility and how this can be applied to other databases and automation. Next, we will demonstrate a case-study using SAINT to produce reactivity maps of non-polar surfaces for a range of compounds with respect to three probe molecules, and how this information can streamline simulations of surfaces with more complex reaction species.

SESSION F.MT07.08: Machine Learning in Theory and First Principles  
On Demand Abstracts Available for Viewing Starting Saturday Morning, November 21, 2020  
F-MT07

**5:00 AM \*F.MT07.08.01**

**Applying Automated Process Analytical Technology to Challenges in Material Synthesis** Jason Hein; University of British Columbia, Canada

Optimizing multicomponent chemical processes is a challenge which lends itself well to automation due to the large number of experiments usually required. In addition to classic high throughput and Design of Experiment methodologies, the application of online analytical tools provides real-time feedback and therefore acute control over the chemistry in question. This approach enables fundamental insights to be translated into practical application at an unprecedented pace, particularly when coupled to machine learning capabilities. Herein we present two examples of automated process analytical technology designed to resolve bottlenecks in materials R&D and chemical manufacturing.

The supply of specific, high-performance molecular conductors is critical to the development of organic photovoltaic devices. Unfortunately, the gold-standard molecule used almost ubiquitously (Spiro-OMeTAD) is notoriously expensive as its synthesis remains underdeveloped. To address this challenge, we have developed a range of automated tools capable of formulating reactions, taking samples, and performing online HPLC analysis. Our versatile platforms are also compatible with air sensitive chemistry occurring in an inert atmosphere. We use these tools to generate temporal reaction profiles and rapidly optimize the synthesis of key materials such as Spiro-OMeTAD.

As a second case study, we apply advanced crystallization methodologies inspired by the pharmaceutical industry to access battery-grade lithium carbonate from waste brines. The dynamic nature of crystallization requires the continuous assessment of sample purity and the corresponding manipulation of crystallization parameters. Our suite of process analytical technology provides comprehensive data on sample composition (IC, FTIR), turbidity (computer vision), and crystal growth (microscopy) to enable feedback control and consistently isolate high-purity product.

**5:15 AM F.MT07.08.02**

**Transferable Nonlocal Exchange Density Functionals via Machine Learning** Kyle W. Bystrom and Boris Kozinsky; Harvard University, United States

Due to its computational efficiency compared to other quantum mechanical methods, semi-local density functional theory (DFT) is a popular tool for simulating large, complex systems like surfaces, interfaces, point defects, and battery cathode materials. However, the complex electronic structure of these systems cannot be described accurately by the approximate exchange-correlation (XC) functionals used in semi-local DFT. More accurate methods, such as exact exchange and post-Hartree Fock, are prohibitively expensive for large systems. To remedy this problem, we introduce nonlocal exchange density functionals that are fit via machine learning (ML) and can be computed more efficiently than the exact exchange energy. We build on work in both analytical and ML functionals to perform feature engineering that enables the use of lightweight, smooth, and transferable machine learning models. We explore how Gaussian Processes can be used to construct uncertainty estimates of the exchange energy and assess the performance of different kernels. To construct large training

databases, we also develop code to evaluate the exchange energy density on real-space grids. To benchmark this new class of functionals, we implement the functional derivatives to find the exchange potential and use it in self-consistent field calculations on a diverse set of small molecules.

#### 5:25 AM F.MT07.08.03

**Quantifying Uncertainty in High-Throughput Density Functional Theory** Vinay Hegde<sup>1</sup>, Christopher K. Borg<sup>1</sup>, Zachary del Rosario<sup>1,2</sup>, Yoolhee Kim<sup>1</sup>, Maxwell Hutchinson<sup>1</sup>, Erin Antono<sup>1</sup>, Julia Ling<sup>1</sup>, Paul Saxe<sup>3</sup>, James E. Saal<sup>1</sup> and Bryce Meredig<sup>1</sup>; <sup>1</sup>Citrine Informatics, United States; <sup>2</sup>Olin College of Engineering, United States; <sup>3</sup>Virginia Tech, United States

The completely automated nature of high-throughput density functional theory (HT-DFT) creates unique challenges, such as how to choose DFT parameters and post-processing techniques that work across all materials classes, and strike an effective balance between computational cost and accuracy. These challenges have been tackled in different ways by the several large HT-DFT databases that have emerged so far. However, the effect of the different approaches on the calculated materials properties is as yet unclear. Here, we quantify the uncertainty in the HT-DFT properties resulting from such different-yet-reasonable parameter choices, by consolidating three large HT-DFT databases: Automatic-FLOW (AFLOW), Materials Project, and the Open Quantum Materials Database (OQMD), onto a common data platform and analyzing comparable records. Overall, we find the variance in reported properties between HT-DFT databases to be comparable to that between DFT and experiment. We identify the underlying physical factors responsible for some of the larger discrepancies, and outline paths toward further standardization of HT-DFT.

#### 5:35 AM F.MT07.08.04

**Two-Tier Machine Learning Acceleration of Molecular Dynamics with Enhanced Sampling—Predicting Reaction Rates of Hydrogenation Reactions on Metal Catalysts** Lixin Sun, Simon L. Batzner, Steven B. Torrisi, Yu Xie, Jin Soo Lim, Jonathan Vandermause and Boris Kozinsky; Harvard University, United States

Aldehydes, in particular formaldehyde (CH<sub>2</sub>O), are key precursors of many important chemical compounds. Cu-based catalysts are attractive for its production since they allow anhydrous alcohol dehydrogenation that does not need expensive distillation and produces a valuable byproduct, H<sub>2</sub>.

However, the fundamental mechanism of alcohol dehydrogenation on Cu is not yet fully understood. Static DFT calculations fail to predict the nonlinear dependency of the dehydrogenation reaction rates on the size of the alkoxy molecule [1]. To address this problem, we use molecular dynamics to directly model the dehydrogenation process on the Cu(110) surface, which can capture the dynamical effects that are missed in static DFT calculations.

But due to the slow reaction rates, it is prohibitive to directly compute these reactions with *ab initio* molecular dynamics. Therefore, we use a two-step approach to accelerate molecular dynamics simulations. First, DFT force calculations are replaced by machine learning force fields. We train two different models, Tensor-Field neural networks and mapped Gaussian processes[2]. Both models can reach near DFT level accuracy at much lower computational cost. Second, we use nonlinear dimensionality reduction to learn reaction coordinates and employ them to explore the free energy landscape around the reaction path, speeding up sampling of rare transition events and obtaining reaction rates from free energy barriers.

[1] Chen, W.; Cubuk, E. D.; Montemore, M. M.; Reece, C.; Madix, R. J.; Friend, C. M.; Kaxiras, E. A Comparative Ab Initio Study of Anhydrous Dehydrogenation of Linear-Chain Alcohols on Cu(110). *J. Phys. Chem. C* **2018**, *122* (14), 7806–7815.

[2] Vandermause, J.; Torrisi, S. B.; Batzner, S.; Xie, Y.; Sun, L.; Kolpak, A. M.; Kozinsky, B. On-the-Fly Active Learning of Interpretable Bayesian Force Fields for Atomistic Rare Events. *npj Computational Materials* **2020**, *6* (1), 1–11.

#### 5:45 AM F.MT07.08.05

**Late News: End-to-End Automatic Differentiation for Experimentally-Informed Molecular Dynamics** Wujie Wang, Simon Axelrod and Rafael Gomez-Bombarelli; Massachusetts Institute of Technology, United States

Molecular dynamics simulations use statistical mechanics at the atomistic scale to enable both the elucidation of fundamental mechanisms and the engineering of matter for desired tasks. The behavior of molecular systems at the microscale is typically simulated with differential equations parameterized by a Hamiltonian, or energy function. The Hamiltonian describes the state of the system and its interactions with the environment. In order to derive predictive microscopic models, one wishes to infer a molecular Hamiltonian that agrees with observed macroscopic quantities. From the perspective of engineering, one wishes to control the Hamiltonian to achieve desired simulation outcomes and structures, as in self-assembly and optical

control, to then realize systems with the desired Hamiltonian in the lab. In both cases, the goal is to modify the Hamiltonian such that emergent properties of the simulated system match a given target. We demonstrate how this can be achieved using differentiable simulations where bulk target observables and simulation outcomes can be analytically differentiated with respect to Hamiltonians, opening up new routes for parameterizing Hamiltonians to infer macroscopic models and develop control protocols.

#### 5:55 AM \*F.MT07.08.06

**Autonomous Materials Discovery with Boundless Objective-Free Exploration** Koji Tsuda; The University of Tokyo, Japan

Materials chemists develop chemical compounds to meet often conflicting demands of industrial applications. This process may not be properly modeled by black-box optimization because the target property is not well defined in some cases. Herein, we propose a new algorithm for automated materials discovery called BoundLess Objective-free eXploration (BLOX) that uses a novel criterion based on kernel-based Stein discrepancy in the property space. Unlike other objective-free exploration methods, a boundary for the materials properties is not needed; hence, BLOX is suitable for open-ended scientific endeavors. We demonstrate the effectiveness of BLOX by finding light-absorbing molecules from a drug database. Our goal is to minimize the number of density functional theory calculations required to discover out-of-trend compounds in the intensity–wavelength property space. Using absorption spectroscopy, we experimentally verified that eight compounds identified as outstanding exhibit the expected optical properties. Our results show that BLOX is useful for chemical repurposing, and we expect this search method to have numerous applications in various scientific disciplines.

#### 6:10 AM F.MT07.08.07

**Accelerated Search and Optimization of Uniform Pseudo-Magnetic Fields and Magnetic Edges in Strained Monolayer Graphene Using Artificial Intelligence** Stefan Sorescu<sup>1</sup>, Jason Inirio<sup>1</sup>, Zhuofa Chen<sup>1</sup>, Mounika Vutukuru<sup>1</sup>, Paul Hanakata<sup>2</sup> and Anna Swan<sup>1</sup>; <sup>1</sup>Boston University, United States; <sup>2</sup>Harvard University, United States

Pseudo-magnetic fields (PMFs) in graphene are an intriguing strain-emergent phenomenon that lead to exciting physics such as Landau level quantization and zero-field quantum Hall effect. PMFs have been demonstrated experimentally first on small nanostructures such as nanobubbles [1]. Experimentally, generating uniform PMF of sufficiently large magnitude is of interest. However, as the strength of the generated PMF is inversely related to the size of the strained region, only small dimensions of graphene have been explored for this purpose. Of more technological interest are larger structures with engineered PMFs [2].

In this work, we are interested in the strain-induced uniform PMF and PMF-zero edges in various geometries in the scale of micrometers. From finite element simulations of strained graphene shapes with varying PMF distributions, we utilize a variational autoencoder that learns the pseudo-magnetic field emergent from geometric images. Our aim is to discover hitherto novel geometries by learning over the geometry-PMF possibility space (a generative approach). We further analyze geometries that will have optimal, robust PMF-zero edges under uniaxial strain via advanced graphing theory algorithms. Finally, we train an auxiliary neural network to rapidly classify large batch, simulated images of strained graphene to arrive at optimally strained graphene geometries that would produce well-defined pseudo-Landau levels for use in advanced electronic devices, such as transistors.

[1] N. Levy et al., “Strain-induced pseudo-magnetic fields greater than 300 Tesla in Graphene nanobubbles,” *Science*, vol. 329, no. July, pp. 544–547, 2010, doi: 10.1126/science.1191700.

[2] S. Zhu, J. A. Stroscio, and T. Li, “Programmable Extreme Pseudomagnetic Fields in Graphene by a Uniaxial Stretch,” *Phys. Rev. Lett.*, vol. 115, no. 24, p. 245501, Dec. 2015, doi: 10.1103/PhysRevLett.115.245501.

#### 6:20 AM F.MT07.08.08

**Efficient Uncertainty Estimation of Neural Network Potentials with Atomic-Level Resolution Enabled by Replica Ensemble** Wonseok Jeong, Dongsun Yoo, Kyuhyun Lee, Jisu Jung and Seungwu Han; Seoul National Univ, Korea (the Republic of)

Neural network potentials (NNPs) are gaining much attention as they enable fast atomic simulations for a wide range of systems while maintaining the accuracy of density functional theory calculations. Since NNP is constructed by machine learning on training data, its prediction uncertainty increases drastically as atomic environments deviate from training points. Therefore, it is essential to monitor the uncertainty level during the simulations to judge the soundness of the results. In this presentation, we present an uncertainty estimator based on the replica ensemble in which NNPs are trained over atomic

energies of a reference NNP that drives the target simulations. The replica ensemble is trained efficiently and its standard deviation provides atomic-resolution uncertainties. We apply this method to a silicidation process of Ni deposited on Si(001) and confirm that the replica ensemble can spatially and temporally trace simulation errors at the atomic resolution, which in turn guides on augmenting the training set. The refined NNP completes a 3.6-ns molecular dynamics simulation without any noticeable defects. The efficient and atomic-resolution uncertainty indicator suggested in this presentation will contribute to achieving reliable NNP simulations.

#### 6:30 AM F.MT07.08.09

**Machine Learning as a Solution to the Electronic Structure Problem** Beatriz Gonzalez del Rio, Christopher B. Kuenneth, Huan Tran and Rampi Ramprasad; Georgia Institute of Technology, United States

An essential component of materials research is the use of simulations based on density functional theory (DFT), which imposes severe limitations on the size of the system under study. A promising development in recent years is the use of machine learning (ML) methodologies to train surrogate models with DFT data to predict quantum-accurate results for larger systems. Many successful ML models have been created to predict higher-level DFT results such as the total potential energy and atomic forces, and initial steps have been taken to create deep-learning based ML methodologies that can predict fundamental DFT outputs such as the charge density, wave functions and corresponding energy levels [1]. Here, we explore the applicability of this latter methodology using convolutional and recurrent neural networks to learn and predict the electronic charge density and the density of states of carbon, for a large variety of allotropes spanning from metallic to insulating behavior. Further improvements to the speed, accuracy and versatility of this DFT-emulation methodology will also be presented.

[1] A. Chandrasekaran, D. Kamal, R. Batra, C. Kim, L. Chen, and R. Ramprasad, *Npj Comput. Mater.* 5, 22 (2019)

#### 6:40 AM F.MT07.08.10

**Prediction on Electron Density of States in Metal Nanoclusters by Atomic Configuration via Machine Learning** Kiyou Shibata and Teruyasu Mizoguchi; The University of Tokyo, Japan

For understanding and design of functional materials, density of states (DOS) is an important property. DOS hosts an essential information on various materials properties such as stability, thermal property, magnetism and catalytic activities [1]. The DOS projected on orbitals, so-called projected DOS (proDOS), provides site-specific properties and is closely related to the local physical property and chemical activity. The DOS is also used for understanding experimental data such as core-loss spectroscopy and X-ray photoelectron spectroscopy. Generally, the DOS and proDOS is obtained by a first-principles calculation, which requires a high computational cost. If a lower-cost computational method can alternate the first-principles calculation, search for new functional materials and extraction of information from huge experimental data can be accelerated.

In recent years, Materials Informatics, a combination of materials science and informatics methods, has been attracting great attention as a way for realizing the search for substances that exhibit excellent physical properties and the extraction of information from experimental data. In principle, the DOS is a quantity that is uniquely determined by an atomic arrangement, although its distribution drastically changes in various ways by a splitting and a shift of states due to a formation of bonded/anti-bonded states according to the atomic arrangement. Regarding the application of informatics on DOS, predictions on DOS of bulk crystals and surface using principal component analysis have been reported [2], which focuses on the composition dependence of alloys with a certain specific structure and the plane orientation dependence of surface DOS. From the viewpoint of atomic coordinates, however, the machine learning prediction on DOS has not been investigated well so far. In this research, we have tried to predict the DOS of metal nanoclusters from their atomic arrangements using the machine learning.

The nanocluster structures composed of several metal atoms were randomly sampled with a constraint on an interatomic distance. The first-principles calculation was performed using VASP code [3] for the generated atomic arrangements without a structural relaxation by PAW method with a planewave cutoff energy of 500 eV and a generalized gradient approximation with considering a spin polarization. Each ProDOS data for the analysis was extracted as two 64-dimensional vectors for each spin up and down, 128-dimensional vectors in total. In order to predict ProDOS, we first trained a variational auto-encoder (VAE) to extract features of ProDOS as latent vectors.

The trained VAE reproduces ProDOS to the extent that the physical property values, such as a d-band center, are roughly reproduced. Interestingly, we found that latent variables are one-dimensionally distributed as a function of interatomic

distance in the latent variable space. We then trained another neural network for regression of the encoded latent vectors by atomic configurations. The predicted ProDOS obtained by decoding predicted latent vector from atomic configurations with the trained VAE shows good agreement of the calculated ProDOS.

In summary, we constructed the combination of the VAE and the neural network in order to predict the ProDOS of the metal nanoclusters. In the presentation, we will show examples of the ProDOS prediction performance, the model details, the distribution of the VAE latent variables, the generalization performance, and the examples of the diatomic molecules composed of different atoms.

#### Reference

- [1] B. Hammer and J.K. Nørskov, *Adv. Catal* **45** (2000) 71,
- [2] B. C. Yeo, D. Kim, C. Kim & S. S. Han, *Sci. Rep.* **9** (2019) 5879,
- [3] G. Kresse and J. Furthmüller, *Comput. Mater. Sci.* **6** (1996) 15.

### SESSION F.MT07.09: Transfer Learning

On Demand Abstracts Available for Viewing Starting Saturday Morning, November 21, 2020  
F-MT07

#### 5:00 AM \*F.MT07.09.01

**Real-Time Control and Analysis in Autonomous Materials Synthesis** [Kristofer G. Reyes](#)<sup>1</sup>, Soojung Baek<sup>1</sup>, Kevin Yager<sup>2</sup>, Frank Alexander<sup>2</sup>, Jennifer Carpena<sup>3</sup>, Rahul Rao<sup>3</sup> and Benji Maruyama<sup>3</sup>; <sup>1</sup>University at Buffalo, The State University of New York, United States; <sup>2</sup>Brookhaven National Laboratory, United States; <sup>3</sup>Air Force Research Laboratory, United States

Many current autonomous materials platforms employ Bayesian optimization or active learning techniques, in which synthesis and processing parameters are sequentially considered in a search for the growth conditions that optimize some material response. While these techniques optimize within a closed-loop framework, each experiment done considers the input parameter settings as fixed and treats the synthesis and characterization of the material as a black-box, with input parameters ultimately yielding characterized output properties. We can, however, take advantage of the ability to perform in-situ characterization to provide yet another level of control in the search for optimized parameters by allowing strategically selected changes to real-time-controllable parameters such as temperature or gas flow rates within an experiment. In this talk, we describe the modeling framework and decision-making policies needed to take advantage of real-time control and characterization currently available in many autonomous materials platforms. We provide examples of how such a system can be used to dynamically control and optimize synthesis pathways in chemical kinetics, and show how to overcome hurdles in characterization resolution associated to in-situ measurements.

#### 5:15 AM F.MT07.09.02

**An Autonomous Experimentation System with Multiple Information Sources** [Aldair E. Gongora](#)<sup>1</sup>, Emily Whiting<sup>1</sup>, Patrick Riley<sup>2</sup>, Kristofer G. Reyes<sup>3</sup>, Elise F. Morgan<sup>1</sup> and Keith A. Brown<sup>1</sup>; <sup>1</sup>Boston University, United States; <sup>2</sup>Google, United States; <sup>3</sup>University at Buffalo, The State University of New York, United States

By combining automated experimentation and active learning, autonomous experimentation systems have accelerated the pace of research in fields such as materials science, chemistry, biology, and mechanics. While advancements in automated experimentation such as robotic platforms can increase the throughput of experiments to further accelerate the pace of research, an alternative path to accelerating learning is to utilize multiple information sources, with varying predictive power and cost, to evaluate the property of interest in the active learning loop. For example, a property of interest can be evaluated via a computational model or experimental measurement. This is particularly salient in the field of mechanics where both computational tools such as finite element analysis (FEA) and experimental characterization such as mechanical testing offer measurements of mechanical properties with varying fidelity. While imperfect and limited to mechanical properties that can be reasonably predicted, FEA encompasses useful information that can be utilized to explore vast design spaces for optimal designs. Conversely, for properties that cannot be reliably simulated, such as toughness, autonomous experimentation systems have emerged to efficiently search the design space for high-performing structures.<sup>1</sup> An open question that remains, however, is how to accelerate learning by utilizing multiple information sources available to an autonomous experimentation system.



In this work, we present a multi-information source optimization (MISO) framework for autonomous experimentation systems by incorporating simulated mechanical responses from FEA in the learning campaign. In this way, the learning campaigns become physics-informed instead of proceeding as a strictly black-box approach. We evaluate this MISO approach by simulating physics-informed learning campaigns and compare the resulting performance to that of black-box learning campaigns. From this study, we observed that including physics-based simulations, in our case FEA, leads to a decrease in both the number of experiments and time necessary to find optimal mechanical designs. Additionally, we evaluate the utility of these approaches in autonomous experimental campaigns. The development of this MISO framework by combining machine learning, physics-based simulations, and physical experimentation presents an approach for incorporating and leveraging numerous information sources available to accelerate research.

1. A. E. Gongora, B. Xu, W. Perry, C. Okoye, P. Riley, K. G. Reyes, E. F. Morgan, K. A. Brown “A Bayesian Experimental Autonomous Researcher for Mechanical Design” *Sci. Adv.* **2020**

**5:25 AM F.MT07.09.04**

**Combining Synthetic and Experimental Data in Multi-Fidelity Machine Learning Models to Accelerate Glass Discovery** Kai Yang and Mathieu Bauchy; University of California, Los Angeles, United States

Developing novel glasses with new, improved properties and functionalities is key to address some of the Grand Challenges facing our society. Although machine learning offers a unique opportunity to accelerate the discovery of novel glasses with exotic functionalities, it faces the “curse of dimensionality.” This is especially significant for glass discovery, since glasses can virtually accommodate the entire periodic table, which, in turn, results in highly dimensional models. Such high dimensionality must be matched with high numbers of glass property data, which is presently lacking. Here, to address this issue, we present a new machine learning pipeline that simultaneously leverages experimental and simulation-based (synthetic) data by means of multi-fidelity Gaussian process regression (GPR) models. We show that our hybrid model systematically outperforms models relying solely on experimental data.

SESSION F.MT07.10: Poster Session: Data Science and Automation to Accelerate Materials Development and Discovery  
On Demand Abstracts Available for Viewing Starting Saturday Morning, November 21, 2020  
5:00 AM - 8:00 AM  
F-MT07

**F.MT07.10.01**

**Optimization of Multiple Physical Properties by Machine Learning Incorporating the Concept of Deviation Value** Kokin Nakajin<sup>1,2</sup>, Takuya Minami<sup>1</sup>, Toshio Fujita<sup>1,2</sup>, Masaaki Kawata<sup>3</sup>, Katsumi Murofushi<sup>1</sup>, Hiroshi Uchida<sup>1</sup>, Kazuhiro Omori<sup>1</sup> and Yoshishige Okuno<sup>1</sup>; <sup>1</sup>Showa Denko, Japan; <sup>2</sup>Research Association of High-Throughput Design and Development for Advanced Functional Materials(ADMAT), Japan; <sup>3</sup>National Institute of Advanced Industrial Science and Technology (AIST), Japan

Machine learning (ML) [1,2] has become popular method in materials design, and came to be used in various fields nowadays, especially in metal material [3,4] and organic material [5]. Actually, so far it was reported that ML have the effect of shorting the lead time of product development. By contrast, at the development site, there are multiple required characteristics. Because there is a trade-off relationship for multiple characteristics, it is difficult to achieve all of them in same time.

Therefore, researchers will conduct experiments on the combinations of various ingredients and their compound ratios, and search for the optimal synthesis method by trial and error. However, it is not easy to find out optimum conditions breaking the trade-off from an enormous number of combinations, even if you use existing ML.

In this study, we verified the effectiveness of machine learning in developing thermosetting transparent flexible films. The thin films were obtained by cross-linking the pre-polymers synthesized by using the mixture of three diol ingredients and a single isocyanate ingredient. Here, we explored the optimum experimental conditions for maximizing transparency, elongation, and elastic modulus.

The predictive model was trained using 27 data obtained by the experimentalist. The hydroxyl values and Extended-connectivity fingerprints (ECFP) of pre-polymers were employed as the explanatory variables X [6,7], and the film properties were used as the objective variables y. The ECFP of each pre-polymers was calculated by summing up the ECFPs of all ingredients with weighted by mixing ratio.

We compared the number of trials required for improving the performance of thin films between that performed by the experimentalist and that by machine learning. As a result, the predictive model successfully found the high-performance films by a lower number of trials compared to the experimentalist.

Additionally, we also report the results by the above model applying Bayesian optimization.

\* This work was supported by a grant from the New Energy and Industrial Technology Development Organization (NEDO) of Japan (JPNP16010).

- [1] K. Rajan. *Materials Today*, 8, 38 (2005)
- [2] A. Jain, et al., *APL Materials*, 1, 011002 (2013)
- [3] A. Agrawal, et al., *Integr. Mater. Innovation* 3, 1-19 (2014)
- [4] Frang Ren, et al., *Science Advances* 4 4 1566 (2018)
- [5] R. Gomez-Bombarelli. et al., *Nature Materials*, 15, 1120-1127 (2016)
- [6] T. Minami, et al., *MRS Advances*, 3(49), 2975 (2018)
- [7] T. Minami, et al., *MRS Advances*, 4(19), 1125 (2019)

### **F.MT07.10.03**

**Charting Lattice Thermal Conductivity of Inorganic Crystals** [Taishan Zhu](#)<sup>1,1</sup>, Sheng Gong<sup>1</sup>, Tian Xie<sup>1</sup>, Prashun Gorai<sup>2</sup> and Jeffrey C. Grossman<sup>1</sup>; <sup>1</sup>Massachusetts Institute of Technology, United States; <sup>2</sup>Colorado School of Mines, United States

Thermal conductivity is a fundamental material property but challenging to predict, with less than 5% out of about  $10^5$  synthesized inorganic materials being documented. In this work, we extract the structural chemistry that governs lattice thermal conductivity, by combining graph neural networks and random forest approaches. We show that both mean and variation of unit-cell configurational properties, such as atomic volume and bond length, are the most important features, followed by mass and elemental electronegativity. We chart the structural chemistry of lattice thermal conductivity into extended van-Arkel triangles, and predict the thermal conductivity of all known inorganic materials in the Inorganic Crystal Structure Database (stoichiometric). For the latter, we develop a transfer learning framework extendable for other applications.

### **F.MT07.10.05**

**Authoring Interactive and Extensible Visualizations from a Materials Knowledge Graph** [Michael Deagen](#)<sup>1</sup>, James P. McCusker<sup>2</sup>, Sam Stouffer<sup>2</sup>, Tolulomo Fateye<sup>3</sup>, Linda S. Schadler<sup>1</sup> and L. Catherine Brinson<sup>3</sup>; <sup>1</sup>The University of Vermont, United States; <sup>2</sup>Rensselaer Polytechnic Institute, United States; <sup>3</sup>Duke University, United States

Effective data visualization accelerates the analysis and communication of data-driven science by enabling humans to interpret, comprehend, and form hypotheses around complex datasets. A large number of high-quality data visualization tools have emerged in recent years, however the adoption of proprietary formats or stand-alone software can hinder interoperability in the pursuit of FAIR data principles. We have developed a visualization authoring tool for the NanoMine knowledge graph (KG) database that combines the query language for RDF data (SPARQL) with a high-level specification for transforming raw data into interactive charts (Vega-Lite). This combination of open-source tools provides a glimpse into the broad collection of experimental materials data curated from the polymer nanocomposites literature into the NanoMine KG. Charts created using this tool are saved to the KG along with provenance information and made accessible via a Gallery on the NanoMine website. The Gallery allows visitors and new users to assess the available data in NanoMine, while advanced users can use the source code (SPARQL query, Vega-Lite spec) behind these charts as inspiration for their own contributions to the Gallery. The reusability of charts created with this approach allows a community of users to learn, build upon examples, and realize the rich expressiveness of SPARQL and Vega-Lite. Together, this data visualization authoring tool provides an interoperable, reusable, and extensible mechanism for users of NanoMine to inspect data quality, perform their own analyses, and pursue new research questions.

### **F.MT07.10.06**

**Data-Driven Thermoelectric Modelings—Prospects and Current Challenges** [Mamadou T. Mbaye](#), Sangram K. Pradhan and Messaoud Bahoura; Norfolk State University, United States

Recent advancements in computing technologies coupled with the need to make sense of large amounts of raw data have renewed much interest in data-driven materials properties modeling and prediction. Traditional materials science research relies heavily on experimental data to gauge the properties of materials. However, this paradigm is purely based on trial and

error and ongoing research can take decades to discover new materials. Data-driven modeling tools such as machine learning and its proven libraries can help speed up the materials discovery process through the implementation of powerful algorithms on readily available materials datasets mined from the ever-increasing privately and government-funded materials databases. In this work, we applied various machine learning models on tens of hundreds of thermoelectric compounds obtained from Density Functional Theory (DFT) calculation results. In our preliminary analysis, we made use of pymatgen and the powerful materials science library matminer to add and explore key materials features that have the propensity to accurately predict our achievable target output. We evaluated the accuracy and performance of our models with K-Fold cross-validation estimators and identified the most important descriptors for our materials. Finally, we reviewed the current state-of-the-art in data-driven materials research, its prospects, and current challenges.

#### **F.MT07.10.09**

**Inverse Design of Colossal Permittivity Materials with Crystal Graph Convolutional Neural Networks** Dillon C. Yost, Sheng Gong, Tian Xie and Jeffrey C. Grossman; Massachusetts Institute of Technology, United States

Colossal permittivity dielectric materials exhibit great potential as essential building blocks for future electronic devices and energy storage applications. Recent research has demonstrated that a giant dielectric constant could be achieved for certain materials with perovskite-like crystal structure (e.g.  $\text{CaCu}_3\text{Ti}_4\text{O}_{12}$ ) or by co-doping the transition metal oxides (e.g. In and Nb doped in  $\text{TiO}_2$ ). This opens up tremendous opportunities for inventing and tailoring materials with desired dielectric properties, while it also comes with significant challenges including a gigantic high-dimensional materials design space and unclear colossal permittivity mechanisms. Here, we leverage first-principles calculations and deep learning via the crystal graph convolutional neural network (CGCNN) method to predict and understand dielectric properties of a diverse array of materials. In doing so, we greatly accelerate the exploration and screening of candidate materials for colossal permittivity, and we clarify some of the complex relationships between dielectric properties and material structure and composition.

#### **F.MT07.10.10**

**Automated Cluster Analysis of 2-Dimensional X-Ray Diffraction for Composition Spread Oxide Thin Film Fabricated by Combinatorial Synthesis, Aiming to Visual Information-Guided Material Discovery** Akihiro Yamashita<sup>1,2</sup>, Takahiro Nagata<sup>2</sup>, Shinjiro Yagyu<sup>2</sup>, Toru Asahi<sup>1</sup> and Toyohiro Chikyow<sup>2</sup>; <sup>1</sup>Waseda University, Japan; <sup>2</sup>National Institute for Materials Science, Japan

Data-driven material research can radically shorten time to discover new materials compared to traditional methods. However, collecting and classifying materials data is time consuming. A number of researchers focus on automation methods, however automated analysis of 2-dimensional X-ray diffraction (2D-XRD), which contains various information on structure and is beneficial to thin film research, is not well researched compared to conventional 1D-XRD. We consider automated cluster analysis of 2D-XRD with non-negative matrix factorization (NMF) and also visualization method with variational autoencoder (VAE). In this work, we analyzed 2D-XRD of  $(\text{Ga}_x\text{In}_{1-x})_2\text{O}_3$  composition spread film fabricated on various crystal growth conditions.

For X-ray diffraction (XRD) data, which is the basic analysis method for structural analysis, identification of each peak in a XRD data and classifying each XRD data into some group are essential to understand the correlation between crystal structures and physical properties, but tough work. NMF is already reported to separate XRD dataset into clusters and, consequently, identifying few XRD patterns which are characteristic to each cluster is enough to understand the cluster analysis result [1]. However, the reported XRD data is from one composition spread film, so the cluster analysis result is based on the effects of composition differences on the crystal structure. Effects of crystal growth conditions such as substrates, growth temperatures, and reactive gases on cluster analysis result are still unknown. Also, for thin films, properties such as high oriented, mosaicity, and grained structures affect physical properties, which can be identified by 2D-XRD. Therefore, we have applied NMF to 2D-XRD, and as a case study, the 2D-XRD data of  $(\text{Ga}_x\text{In}_{1-x})_2\text{O}_3$  composition spread samples fabricated by pulsed laser deposition varying composition ratio, substrate, oxygen partial pressure, and substrate temperature were analyzed. We confirmed that NMF can automatically separate the 2D-XRD data into some clusters corresponding to single crystalline, oriented polycrystalline, grained structures, etc. In addition, we applied VAE for converting differences among 2D-XRD data into a graphical image according to physical properties and growth conditions. VAE can convert input data into latent variables following some probability distribution, so differences in the input data is represented as the different positions in the distribution. Analyzing relationships among probability distribution of converted 2D-XRD data, cluster analysis result from NMF, and physical condition will guide us to improved fabrication process based on the obtained graphical image.

[1] C. J. Long, D. Bunker, X. Li, V. L. Karen, and I. Takeuchi, Review of Scientific Instruments **80**, 103902 (2009)

#### **F.MT07.10.12**

**Machine Learning Materials Properties for Small Datasets** Pierre-Paul De Breuck, Geoffroy Hautier and Gian-Marco Rignanese; Université catholique de Louvain, Belgium

In order to make accurate predictions of crystalline materials properties, current machine-learning approaches generally require large amounts of data. However, in practice, problems that could benefit from machine learning are intrinsically slow and thus small in data size. In this work, a novel all-round framework is presented which relies on a feedforward neural network and the selection of a limited set of physically-meaningful and property-relevant descriptors. Moreover, it enables the prediction of multiple properties, such as temperature or pressure curves, by using a novel tree-like architecture. This does slightly improve accuracy by taking advantage of information stored across different properties, known as joint transfer learning.

Next to being faster in terms of training time, this approach is shown to outperform current graph-network models on small datasets.

Furthermore, excellent accuracy is found when using the composition only, very helpful for identifying experimental candidates. In particular, the vibrational entropy at 305K of crystals is predicted with a mean absolute error of 0.01 meV/K/atom (four times lower than previous studies).

Finally, next to improving prediction performances, the selection algorithm highlights the most important features and thus helps understanding the underlying physics.

#### **F.MT07.10.14**

**Development of All-Atom and Coarse-Grained Embedded Atom Method Potentials for Gold Using Particle Swarm Optimization** Gaurav Anand, Troy Gustke, Abhishek T. Sose, Soumil Joshi, Fangxi Wang and Sanket A. Deshmukh; Virginia Tech, United States

New embedded atom method (EAM) potentials have been developed to describe the interatomic interaction for face-centered cubic (FCC) gold represented by all-atom and coarse-grained (CG) models using particle swarm optimization (PSO) algorithm. These EAM potentials show good physical properties such as lattice constant, bulk modulus, and elastic constant, in agreement with the experimental and computational data. The reliability of each EAM potential is assessed using Gaussian Process (GP) regression and Bayesian statistical framework. The GP model predicted quantities of interest (QOI) such as surface energies, density, and vacancy formation energy, show good consistency with QOI obtained from molecular dynamics simulation, which indicates the GP model is good to reduce the computational cost significantly. Further, the GP model is used to develop 10,000 data points for the Bayesian framework. The Bayesian analysis shows that this EAM can predicate the physical properties with a high confidence level. The above optimization framework will be extended to develop the interatomic potentials for other metals and their alloys in a more efficient way.

#### **F.MT07.10.15**

**Mechanical Characterization of Ceramic Nanocomposites via Multi-Fidelity Neural Networks** Christos E. Athanasiou, Xing Liu, Lu Lu, Nitin Padture, Huajian Gao and Brian Sheldon; Brown University, United States

Nanocomposites are at the forefront of materials research as they could meet the challenges and growing needs of diverse strategic fields from energy storage to transportation to advanced manufacturing. The investigation of the mechanical properties of such materials requires the combination of novel experimental microscale testing combined with labor/time-intensive finite element computations. In this talk, we will present a new approach for ceramic nanocomposite materials characterization based on the latest developments in deep learning. Specifically, we will discuss how multi-fidelity deep learning can significantly accelerate fracture toughness characterizations at small scales, without the need for large finite element-generated datasets. The predictive capabilities of this method will be accessed by direct comparisons with single-fidelity machine learning.

#### **F.MT07.10.16**

**Adaptive Spectral Graph Convolutional Neural Network in Crystal Property Prediction** Jiali Li<sup>1</sup>, Lingtong Chen<sup>2</sup>, Zekun Ren<sup>3</sup>, Xiaoli Liu<sup>1</sup>, Qian Xie<sup>4</sup> and Xiaonan Wang<sup>1</sup>; <sup>1</sup>National University of Singapore, Singapore; <sup>2</sup>University of Southern California, United States; <sup>3</sup>Singapore MIT Alliance for Research and Technology, Singapore; <sup>4</sup>Anhui University of Technology, China

Machine Learning (ML) has been more and more widely used in accelerating the design of new materials due to its close accuracy and less computational cost in predicting material properties compared to simulation methods. However, existing ML methods for designing crystalline materials are usually not flexible to handle different crystal types or hard to interpret

because of the arbitrary size. Although there are more generalized models such as Crystal Graph Convolutional Neural Networks (CGCNN) that utilize graph CNN to encode the structure of a crystal, they are over-localized and impossible to learn beyond the bond connectivity. Here we show a stronger and more adaptive framework, based on spectral convolutional neural network, which is not only capable for arbitrary crystal structure but also learns a unique graph representation based on both global and local topology of each crystal.

First a crystal graph is produced based on the cif file of the crystal similar to CGCNN, and each node is encoded with its atomic properties such as electronegativity, covalent radius, etc. The connectivity is determined based on the distance between each atom. The graph Laplacian  $L$  is then obtained by performing graph Fourier transformation on the crystal graph. The transformation process can be decomposed by a complete set of eigenvectors  $U$  and the eigenvalue matrix  $LAMBDA(\lambda)$ , which represents the topology of the graph. The spectral filter  $g_\theta(\lambda)$  generates a customized convolution kernel on the graph in space which can be formulated by:

$$g_\theta(\lambda) = \sum_{k=0}^{k-1} \theta_k \lambda^k$$

Where  $k$  can be interpreted as the number of convolutions in space.

However, this graph convolution cannot exploit the topological property of the graph. It is possible that the disconnected nodes have larger correlation than those connected nodes. To achieve the capability to learn from the geometric structure, we adapted a new spectral filter from Li et al.<sup>1</sup> which takes a non-Euclidean metric so that it learns a residual graph apart from the intrinsic crystal graph by making a correction on the original graph Laplacian  $L$ :

$$L_{\text{new}} = L + \alpha L_{\text{res}}$$

The overall intrinsic plus residue graph is trained with the spectral graph convoluted neural network to predict chemical properties of crystal and results are compared with various existing models. The proposed method has achieved better prediction accuracy especially in larger crystals with more than 4 elements.

Further work has been done by encoding the momentum space feature of the crystal with a graph of reciprocal lattice. Both graphs in real space and momentum space are trained with spectral graph convoluted neural network, but with their own parameters. The outcomes are concatenated and used to make predictions with a neural network. The results are further improved than the model with only the real space graph trained.

[1] Li, R., Wang, S., Zhu, F. and Huang, J., 2018, April. Adaptive graph convolutional neural networks. In Thirty-second AAAI conference on artificial intelligence.

#### **F.MT07.10.17**

**Computational Structure Prediction for Discovery of Novel Crystalline Phases** [Lauren McRae](#) and Scott Warren; University of North Carolina Chapel Hill, United States

Many next-generation technologies rely on increasing the capacity of batteries. Although lithium-ion batteries have attracted the most attention, batteries that shuttle anions like fluoride remain relatively unexplored. Anion shuttle batteries may offer high capacity to enable next-generation technologies and may be made from abundant materials. The promise of anion shuttle batteries warrants a comprehensive investigation of phase-space to discover new materials that can intercalate anions. In the past, materials discovery was done exclusively through experiment, often tedious and time-consuming work. Within the past 20 years, many methods have been developed to explore phase-space more efficiently by computationally predicting structures and calculating properties. With the goal of predicting new materials for anion intercalation, we have developed a computational method of rapid stable and metastable structure prediction using known chemical intuition rules and well-established structure prediction methods. This method uses an evolutionary algorithm to predict complete phase diagrams combined with density functional theory calculations to optimize each predicted structure and obtain an accurate energy. Stable and metastable phases of similar chemical systems can then be predicted based on the calculated phase diagram, with similarity of systems quantified using a previously published measure of atomic similarity. Using this method, we can rapidly predict novel, synthesizable structures that have desirable properties for various applications, including next-generation batteries.

#### **F.MT07.10.18**

**Tackling Data Scarcity in Materials Research—Augmentation of Training Data for Classification of X-Ray Diffraction (XRD) Patterns** [Shreyaa Raghavan](#), Zhe Liu and Tonio Buonassisi; Massachusetts Institute of Technology,

United States

When applying deep learning in material characterization tasks, generating and manually labeling experimental data can be expensive and time-consuming [1]. Especially, this is not an option when large amounts of data are necessary to obtain accurate results from a machine learning model. For this reason, the idea of training deep learning models with simulated data is appealing to tackle data scarcity, particularly when the simulation data can be generated easily and cheaply. A recent study about XRD pattern classification [2] found that the simulated XRD patterns provide some but a limited improvement on accuracy due to the differences between simulated data and experimental data. To close this gap, we explore a Generative Adversarial Network (GAN) [3] to augment the simulated XRD patterns with “realistic” features from experimental data, so that the training of the highly-accurate classifier can be completed with the simulation data only. The GAN consists of a refiner network and a discriminative network with an adversarial loss, where the refiner network reintroduces those realistic features, and the discriminative network penalizes large changes between the original simulated data and the refined data. To avoid the instability of two competing networks in the refined XRD patterns, the discriminative network in our study uses a history of the refined patterns rather than only ones from the current batch. By doing this, our GAN model has a longer-term memory to prevent the refiner network from reintroducing errors. First, we are building and testing this GAN model for data augmentation with 2000 simulated data with labels and 88 unlabeled experimental data, generated following the protocol established in Ref. [2]. Second, we will compare the prediction accuracy of classifying the space groups of the XRD patterns with the model training model using three types of training data: the original simulation data only, the original simulation and experimental data, and the refined simulation data. Third, following the protocol established in Ref. [2], we will adopt the class activation map (CAM) method to identify and understand the root causes of classification error when trained by different training datasets. We envision the method is generalizable to tackle the data scarcity in materials research, where large labeled experimental datasets are not readily available, and further accelerate many characterization tasks with machine learning.

References:

[1] Christopher Bowles et al. Gan augmentation: Augmenting training data using generative adversarial networks. ArXiv, abs/1810.10863, 2018.

[2] Oviedo, F., Ren, Z., Sun, S. *et al.* Fast and interpretable classification of small X-ray diffraction datasets using data augmentation and deep neural networks. *npj Comput Mater* 5, 60 (2019). <https://doi.org/10.1038/s41524-019-0196-x>

[3] A. Shrivastava, T. Pfister, O. Tuzel, J. Susskind, W. Wang, and R. Webb. Learning from simulated and unsupervised images through adversarial training. arXiv preprint arXiv:1612.07828, 2016.

#### **F.MT07.10.19**

**Monte Carlo Simulations of Materials with Autoregressive Generative Models** James K. Damewood, Daniel Schwalbe Koda and Rafael Gomez-Bombarelli; Massachusetts Institute of Technology, United States

Monte Carlo simulation is a standard tool for the investigation of the thermodynamic properties of materials. However, the usage of these methods in a high-throughput framework is limited by the efficiency of the current algorithms. The problem becomes even more challenging when considering the difficulty of modeling the multi-component systems at the forefront of many materials disciplines. Recent advances in autoregressive generative models have introduced new sampling methods to optimize the simulation of spin systems through Neural Markov Chain Monte Carlo (NMCMC) and Neural Importance Sampling (NIS). We will demonstrate the applicability of these methods to the study of lattice models in materials science. In particular, we will present the performance of these approaches on benchmark systems, including Copper-Gold and Nickel-Gold. Furthermore, we will discuss results when extending the model’s possible state-space beyond two components. Finally, we will evaluate the potential for using these machine learning led simulations in high-throughput screening platforms for perovskites.

#### **F.MT07.10.20**

**Boltzmann Sigmoidal Modeling Analysis of Patterned GaAsSbN Nanowires** Sean Johnson, Rabin Pokharel, Michael Lowe, Hirandeep Kuchoor, Surya Nalamati and Shanthi Iyer; North Carolina A&T State University, United States

The first reports of the application of the Boltzmann Sigmoidal model on pitch-dependency in patterned nanowires (NWs) of dilute nitride GaAsSbN on p-Si (111) substrates by self-catalyzed plasma-assisted molecular beam epitaxy are presented in this study. Sizeable bandgap tuning of ~75 meV, as ascertained from 4K photoluminescence (PL), over a pitch length variation of 200 nm to 1200 nm has been demonstrated. Axial and radial growth rates reveal a logistic sigmoidal growth

trend with respect to pitch, which differs from those commonly observed in other patterned non-nitride III-V NWs. Sigmoidal modeling offers additional insight into the shift of the PL spectral arising from differences in Sb and N incorporation from pitch induced variation in secondary fluxes. Results signal that sigmoidal fitting can be a valuable tool to ascertain optimal pitch length for patterned NW arrays of dilute nitrides, and other highly mismatched alloys.

This work is financially supported by National Science Foundation (Award No. 1649517) and through the Title III HGBI PhD Fellowship. This work was performed at Joint School of Nanoscience and Nanoengineering, a member of the South eastern Nanotechnology Infrastructure Corridor (SENIC). The authors acknowledge the use of the Shared Materials Instrumentation Facility (SMIF) at Duke University.

#### **F.MT07.10.21**

**Accelerating Materials Development and Discovery via the Signac Data Management Framework** [Brandon L. Butler](#), Bradley Dice, Vyas Ramasubramani, Carl Simon Adorf and Sharon C. Glotzer; University of Michigan, United States

High-throughput data generation and analysis via automation and applications of machine learning offer incredible potential for accelerating materials discovery and development, especially if used in conjunction with well-managed computational workflows. The open-source *signac* data management framework\* ([signac.io](http://signac.io)) enables researchers to maintain well-formed, reusable data spaces from early exploration through automated production runs and analysis on platforms ranging from laptops to supercomputers. This is achieved through a transparent data and workflow model combined with a simple and unobtrusive programmatic interface. The framework is application-agnostic, and has been applied in molecular simulations, quantum chemistry, photonics, computational fluid dynamics, machine learning, graph mining, and even organizing experimental data. Recently, the framework has been extended significantly with the addition of FlowGroups and aggregation to *signac*'s workflow model. We have added the ability to group operations on the data space for larger throughput on computer clusters and multiple independent resource specifications allowing for different resource requests on different computing platforms. In addition, we generalized operations from working with individual data points to operating on arbitrary subsets of an arbitrarily large data space. In this presentation, we show examples of applications of these new additions to *signac* that demonstrate the efficacy and versatility of *signac* in materials discovery and development.

\*The *signac* framework is a NumFOCUS affiliated project.

#### **F.MT07.10.22**

**Self-Supervised Graph Representation Learning for Cell-Penetrating Peptides** [Ting-Chi Liu](#), Wei-Han Hui, Chia-Ching Chou and Shu-Wei Chang; National Taiwan University, Taiwan

Scientists have used deep learning algorithms to accelerate drug screening and design in the past few years. For example, transforming the organic compound structure into SMILES notation and leveraging the n-gram model have been used to compute the embedding for the downstream task. Most of these models are based on heavily hand-craft rules to preprocess the training data, and it remains challenging to encode the molecular property. In order to solve these problems, we propose a self-supervised method to learn the molecular representation from the molecular graph directly. We develop a novel approach to encode the information of bond rather than the node and use this embedding for membrane penetrating predictions. The self-supervised graph representation learning method is used to learn the molecular representation both hierarchically and as a whole, to understand the influence of the molecular size. Our model is evaluated with membrane-penetrating peptide database and our results show that this model can successfully predict the cell-penetrating peptides with less human heuristics.

#### **F.MT07.10.23**

**Excitonic Effects in Absorption Spectra of Carbon Dioxide Reduction Photocatalysts** [Tathagata Biswas](#); Arizona State University, United States

We study the quasiparticle bandstructure and excitonic properties of 52 materials, which were recently shortlisted for their potential as a catalyst for CO photo-reduction through rigorous firstprinciples computation-based screening strategy. Many body perturbation theory within GW approximation has been used to explore the electronic structure of these materials. To inspect the excitonic effects we use state-of-the-art Bethe-Salpeter formalism. A high-throughput computational workflow using the "atomate" package was used to perform the GW-BSE calculations and analyze the results. We validate our results with 10 previously studied (using both theoretical and experimental methods) materials found in literature and report the results for 42 promising unexplored materials. In addition to providing a more accurate quasiparticle description of the

electronic structure, our study further investigates the suitability of these materials in applications such as CO photo-reduction, efficient solar cells, etc. by examining their absorption spectra and excitonic properties.

#### **F.MT07.10.24**

**Prediction of Change of DOS Associated with Bond Formation Using Machine Learning** Eiki Suzuki, Kiyou Shibata and Teruyasu Mizoguchi; The University of Tokyo, Japan

The density of states (DOS) is a diagram to describe the electronic structure of the material and provides direct information on chemical bonding and materials properties. For example, electronic and photonic properties are mainly correlated to the DOS profiles around bandgap, and catalytic activity is also known to be correlated to the DOS profile of d-band[1]. The DOS is usually obtained by a density functional theory (DFT) simulations which are often time-consuming, especially in a large system. Machine learning (ML) methodologies have been used to create alternative models to predict some DFT outputs for overcoming this problem[2]. Besides, while a bond formation is a fundamental phenomenon in materials and molecules, changes in the orbital interactions and DOS profiles accompanying the bond formation are often complicated.

In this study, we have predicted the changes in DOS using ML techniques. Artificial neural network models have been developed to predict DOS of the atom combined system using DOS of the corresponding isolated system as inputs. We obtained successful results including prediction of gradual change of DOS with respect to bond distance.

First, the DOS database has been created by DFT computations on isolated atoms, diatomic molecules, and single-atom-adsorbed graphene and ethylene with various bond distances using various elements from H to Kr. Second, the ML models based on the artificial neural network has been developed and trained. Finally, the prediction of DOS has been demonstrated for unseen test species on each database.

All the first-principles DFT calculations are performed with the Vienna Ab-initio Simulation Package (VASP)[3] under the generalized gradient approximation (GGA) of Perdew-Burke-Ernzerhof (PBE). Ion cores are modeled with projector augmented wave (PAW) potentials. Semi-core orbital is included in valence. Cut-off energy of 500 eV is used. Spin polarization is considered. SCAN + rVV10[4] is used for considering van der Waals forces. All the structures and the cells are fixed and only electronic relaxation is performed.

For each system, a feedforward neural network model has been developed for DOS prediction. DOS of isolated atoms or adatom is used as input data and DOS of corresponding diatomic molecules or adsorbed systems is used as output data. The DOS of diatomic molecules is also used as input data only for adsorbed systems. The size of the dataset is 14750, 5694, and 2670 sets for diatomic molecules, adsorbed graphene, and adatom-ethylene system respectively. Each dataset is separated into 8:2 for train data and test data. Note that species used in the train data is not included in the test data. Mean squared error (MSE) is used as a loss function.

The DOS prediction for diatomic molecules which are the unseen test species have shown good agreement with calculated DOS. The prediction model reproduces change in shapes with respect to the bond distance. For instance, in the case of O-O molecule, characteristic changes in the DOS profile depending on the bond length would be predicted sufficiently. Main peaks appear around -14 eV in the most stable model with the bond distance of 1.2Å which is shifted to -10 eV in models with larger bond distance, and then it becomes a double-peak feature in the 4.0Å model. On the other hand, the accurate predictions for the adsorbed graphene and ethylene have achieved only when the DOS of the diatomic molecule (calculated) is served as the additional inputs for the prediction model. We are going to present the details in my presentation.

[Reference]

[1] B. Hammer and J.K.Nørskov, Adv. Catal. **45**, 71 (2000).

[2] A. Chandrasekaran, D. Kamal, R. Batra et al., npj Comput. Mater. **5**, 22 (2019).

[3] G. Kresse and J. Furthmüller, Comput. Mater. Sci. **6**, 15 (1996).

[4] H. Peng et al., Phys. Rev. X **6**, 041005 (2016).

#### **F.MT07.10.25**

**Data-Driven Approach to the Prediction of Mechanical Properties in Carbon Fiber Reinforced Composites** Vade Shah, Steven Zadourian, Charles Yang, Zilan Zhang and Grace Gu; University of California, Berkeley, United States

For decades, fiber-reinforced composite materials have been integral to the aerospace, automotive, and military industries due to their lightweight properties. Fiber-reinforced composite manufacturing process involves the curing of the matrix material, which is typically a resin, polymer, or ceramic. The curing process is dependent on several factors, including humidity, temperature, and cycle time, altogether referred to as the curing environment. Curing environments are known to have a significant impact on the mechanical properties, such as modulus and strength, of the final product. While many studies have focused on predicting the mechanical properties of composites, the curing environment is usually not considered. In this work, a data-driven method is applied to various uni-directional carbon fiber laminates to investigate the effects of curing environments on mechanical properties such as longitudinal/transversal strength and modulus. We have conducted statistical



and exploratory data analyses to identify trends, using data from the National Center for Advanced Materials Performance (NCAMP). Results show that high curing temperatures can yield stronger composites, and that the variability in material property values may be resistant to temperature for some resins but not all. Additionally, using machine learning techniques, we develop and compare regressive models considering varying curing environments to predict the strength and modulus of these materials in both longitudinal and transverse directions. This work establishes a statistical framework to analyze complex empirical data for both inference and insight for optimal designs.

#### **F.MT07.10.26**

**Late News: Inverse Design of Potential Singlet Fission Molecules Using a Transfer Learning Based Approach** [Akshay Subramanian](#), Utkarsh Saha, Tejasvini Sharma, Naveen Tailor and Soumitra Satapathi; Indian Institute of Technology Roorkee, India

Singlet fission has emerged as one of the most exciting phenomena known to improve the efficiencies of different types of solar cells and has found uses in diverse optoelectronic applications. The number of discovered singlet fission molecules is however limited, since molecules have to satisfy certain energy conditions in order to make the phenomenon possible. Recent advances in drug and molecular design have made use of state of the art Deep Learning models for inverse design that have enabled the prediction of drugs by optimizing targeted properties of interest.

These techniques have been particularly helpful in uncovering information from large datasets and using the learned information to generate new structures. However, unlike the field of drug discovery, we seldom encounter large datasets linking structures to properties in the field of materials science.

In our work, we tackle this scarcity of materials data with a transfer learning approach and demonstrate the utility of the inverse design approach to the design of singlet fission molecules.

Our approach is based on a deep generative model (Variational Autoencoder (VAE)) which has been inspired from Gomez-Bombarelli et al.'s work on de novo drug design. We attempt to extend the utility of their approach to Materials Science datasets (singlet fission in our case) that are often small in size.

We initially pre-train the VAE on an unsupervised task of SMILES string reconstruction on a large database (ChEMBL) of drug molecules. This pre-training allows the model to learn basic SMILES string grammar and the resulting trained weights can serve as a good initialization for the subsequent fine-tuning task on the singlet fission dataset. This can be thought of as similar to the common approach used in Computer Vision of pre-training models on the large ImageNet dataset and subsequently fine-tuning on various downstream tasks. This pre-training approach has been shown to remarkably improve the performance on downstream tasks, especially when the downstream datasets are small.

An important condition for the Singlet Fission phenomenon to occur is  $E(S1) - 2 \times E(T1) \geq 0$ . This condition ensures that Singlet Fission can proceed without the need for external thermal activation. So, we use  $E(S1) - 2 \times E(T1)$  as the targeted property to optimize in our fine-tuning task. We fine-tune the pre-trained VAE model and an MLP (Multilayer Perceptron) regression head jointly on SMILES string reconstruction and property ( $E(S1) - 2 \times E(T1)$ ) regression tasks, on the Singlet Fission dataset. This guides the model to learn a latent (encoded) representation that segregates molecules based on the value of  $E(S1) - 2 \times E(T1)$ . We were then able to predict potential optimized molecules by performing targeted sampling from this learned latent space.

A second important condition for Singlet Fission to occur is  $E(T2) - 2 \times E(T1) \geq 0$ . This is to ensure that the generated triplet excitons do not annihilate each other immediately after their formation. We model this condition by training an MLP on the prediction of  $E(T2) - 2 \times E(T1)$ . We apply this trained model to the previously sampled molecules and eliminate the ones with negative valued predictions. Finally, we were left with four molecules that could potentially show Singlet Fission properties.

Our work demonstrates the formulation of a transfer learning based inverse design framework that can significantly minimize the efforts involved in the computational screening of molecules by allowing targeted traversal of a boundless search space. This approach can easily be extended to many classes of materials though we demonstrate its utility only to Singlet Fission molecules.

#### **F.MT07.10.27**

**Late News: Multigenerational Crumpling of 2D Materials for Anticounterfeiting Patterns with Deep Learning Authentication** [Lin Jing](#) and Po-Yen Chen; National University of Singapore, Singapore

Physical unclonable function (PUF) is a cornerstone of anticounterfeiting. However, conventional PUF key-based secure tags encounter several bottlenecks, such as complicated manufacturing, specialized and tedious readout, long authentication time, and insufficient stability. To address these challenges, we utilize various two-dimensional materials (2DMs), including  $Ti_3C_2T_x$  MXene and graphene oxide, to construct multigenerational microstructures as PUF anticounterfeiting patterns. Two intermediate treatments, cation intercalation and moisture-induced lubrication, are introduced in between sequential substrate

contractions to *in situ* engineer the multiscale patterns in a transfer-free and scalable fashion. To accelerate the authentication, a deep learning (DL)-facilitated software is developed to pre-categorize the hierarchical topographies with classifiable features. Afterwards, the search-and-compare is conducted within a smaller database to shorten the overall authentication time. The synergy between 2DM tags and DL-facilitated authentication software enables a reliable and environmentally stable anticounterfeiting technology, *DeepKey*, showing superior encoding capacity ( $>10^{144,494}$ ) and short authentication time (~3.5 minutes). Our 2DM anticounterfeiting tag is finally integrated with QR codes to provide two-layer information security.

#### F.MT07.10.28

**Late News: Matching Optimal Physical Descriptors of Two-Layer Materials in Search of High Interfacial Thermal Conductance Using Gaussian Process Regression** [Ainur Koshkinbayeva](#), Azat Abdullaev and Zhandos Utegulov; Nazarbayev University, Kazakhstan

Prediction of the highest or lowest interfacial thermal conductance (ITC) across dissimilar materials is of high technological importance for effective heat management in nuclear and fusion reactors [1], thermal barrier coatings, nanoelectronics and thermoelectric devices [2]. It might take several decades to discover new materials using traditional methods such as physics-based modeling and testing of the pilot samples. In contrast, newly emerging and dynamically developing machine learning algorithms allow to accelerate this process by minimizing the trial-failure routine thanks to an availability of large number of measurement and simulation data generated over the years of active materials research. Today's industry requires much higher rates of materials improvement in thermal and mechanical properties. In this regard, the application of machine learning algorithms allows to discover high-performance materials and interfaces with sufficient accuracy at the lowest consumption of materials and time to discovery.

In this work we present an application of Gaussian Process Regression (GPR) method applied to earlier published experimental reports of ITCs measured across various *metal-nonmetal* and *nonmetal-nonmetal* two-layer interfaces. The following physical descriptors of both, the film and the substrate, were considered: thermal conductivity  $k$ , Debye temperature  $\theta_D$ , longitudinal sound velocity  $v_l$ , melting temperature  $T_m$ , mass density  $\rho$ , Young's modulus  $E$ , molar volume  $V_\mu$ . These parameters of the corresponding films and substrates were found to be substantially affecting the resulting ITC across them [3, 4].

Pearson correlation coefficient map was built to evaluate the linear correlation of different physical descriptors with the corresponding ITC value. The analysis based on the given data set showed that such film parameters as  $v_l$ ,  $E$  and  $\theta_D$  have the strongest correlation with the ITC.

The values of  $G$  of two-layered structures fell in the range of 1.5 to 1500 W/m<sup>2</sup>K. The tendency of the parameter's ratio for the 5 cases of  $G$  values were compared. The results show that the ITC is maximum if the ratios of the film and the substrate descriptors are in the range of 0.7 - 1.7. Moreover, we see that *matching* of  $v_l$ ,  $k$ ,  $T_m$  and  $V_\mu$  between films and substrates is of critical importance to maximize ITC values.

#### *Acknowledgements*

Funding support is acknowledged from grant AP05130446 and state-targeted program # BR05236454 by Kazakhstan Ministry of Education & Science and FDCR grant # 110119FD4501 by Nazarbayev University.

#### References

- [1] M. Khafizov, V. Chauhan, Y. Wang, F. Riyad, N. Hang, D.H. Hurley, Investigation of thermal transport in composites and ion beam irradiated materials for nuclear energy applications, *J. Mater. Res.* 32 (1), 204–216 (2016).
- [2] T. Zhan, L. Fang, and Y. Xu, Prediction of thermal boundary resistance by the machine learning method, *Nature Scientific Reports* 7, 7109 (2017).
- [3] Y.-J. Wu, T. Zhan, Zh. Hou, L. Fang, and Y. Xu, Physical and chemical descriptors for predicting interfacial thermal resistance, *Nature Scientific Data* 7, 36 (2020).
- [4] Ruxandra M. Costescu, Marcel A. Wall, and David G. Cahill, Thermal conductance of epitaxial interfaces, *Phys. Rev. B* 67, 054302 (2003).

#### F.MT07.10.29

**Late News: Improving the Performance of Machine-Learning Models for the Prediction of AxA(1-x)BX<sub>3</sub> Perovskite Bandgaps** [Heesoo Park](#)<sup>1</sup>, Raghvendra Mall<sup>2</sup>, Adnan Ali<sup>1</sup>, Halima Bensmail<sup>2</sup>, Stefano Sanvito<sup>3</sup> and Fadwa El Mellouhi<sup>1</sup>; <sup>1</sup>Qatar Environment and Energy Research Institute, Hamad Bin Khalifa University, Qatar; <sup>2</sup>Qatar Computing Research Institute, Hamad Bin Khalifa University, Qatar; <sup>3</sup>School of Physics, AMBER and CRANN Institute, Trinity College, Dublin, Ireland

Machine-learning-inspired computational approaches have accelerated the chemical composition space exploration hence motivating experimental laboratories to adopt this strategy for novel materials discovery. In this work, we build an extensive

dataset based on density functional theory calculations using 2x2x2 supercells of halide and chalcogenide mixed cation Perovskites ( ) with varying ratios of A/A'-cations mixture to account for the local distortions in the BX<sub>6</sub> octahedra. An automated workflow is employed to handle the DFT calculation, followed by the extraction of relevant physical properties and target features from the converged and verified density functional calculations (DFT) calculations. Subsequently, the dataset is built, curated and prepared using the chemical and structural features of the perovskites. This dataset is divided into two datasets sampled randomly: training and test dataset. Subsequently, this procedure is followed by a series of machine learning training based on a 5-fold cross-validation for each hyper-parameter combination to select the best hyper-parameters set until the model is optimized using the training dataset.

Here, we report the details of building a highly accurate predictor for halide and chalcogenide mixed cation Perovskites ( ) bandgaps that takes into account the subtle structural and octahedral deformation a perovskite structure might experience upon mixing the organic cations. A high level of accuracy could be achieved with a careful investigation of the input features [1]. Our analysis emphasizes how important the feature selection stands for constructing the predictive model as we challenge the robustness of our machine learning predictor in a lab validation setup.

A model-to-lab validation is undertaken by synthesizing mixed-cation MA<sub>x</sub>DMA<sub>(1-x)</sub>PbI<sub>3</sub> perovskite thin films while varying the DMA concentration over a broad range, namely, for (1 - x)=0.0, 0.005, 0.01, 0.02, 0.05, 0.1, and 0.15. We find that the incorporation of DMA at concentrations of 5, 10, and 15 mol % results in non-perovskites in agreement with earlier findings. This indicates that beyond 2 mol % the local strain of DMA on MAPbI<sub>3</sub>, due to its size, is too large to be accommodated within the perovskite structure. The experimental bandgaps of MA<sub>x</sub>DMA<sub>(1-x)</sub>PbI<sub>3</sub> thin films, as measured by UV-vis spectrophotometer analysis feature systematic bandgap increase with the DMA concentration, with modest variations of the order of 0.02 eV, which are expected given the small concentration range explored. Hence, the observed bandgap increase upon DMA doping is related to small local distortions of the PbI<sub>6</sub> octahedra and not to volumetric effects. Reverting back to our perovskite band gap predictor that have trained and tested over a limited number of DFT calculations for cation concentrations requiring moderate-sized supercells, the model enables to map the bandgap of mixed-cation hybrid perovskites over a broad range of chemical and structural compositions not accessible by DFT. In this presentation, we will discuss not only the performances of our model but also the machine-learning training procedure to obtain a robust machine learning model.

#### **Acknowledgements:**

This work is sponsored by the Qatar National Research Fund (QNRF) through the National Priorities Research Program (NPRP8-090-2-047 & NPRP12S-0209-190063) and by the Qatar Environment and Energy Research Institute (FE). Computational resources have been provided by the research computing group at Texas A&M University at Qatar. We are grateful to QEERI core labs for the XRD and SEM characterizations.

[1] Park et al. "Importance of Structural Deformation Features in the Prediction of Hybrid Perovskite Bandgaps" *Comput. Mater. Sci.*, **2020**, *184*, 109858 <https://doi.org/10.1016/j.commatsci.2020.109858>

#### **F.MT07.10.30**

**Late News: Data-Driven Discovery of the Functional Form of the Superconducting Critical Temperature** Stephen R. Xie, Yundi Quan, Gregory R. Stewart, James J. Hamlin, Peter J. Hirschfeld and Richard G. Hennig; University of Florida, United States

Predicting the critical temperature T<sub>c</sub> of superconductors is a notoriously difficult task, even for electron-phonon systems. We build on earlier efforts by McMillan and Allen and Dynes [1] to model T<sub>c</sub> from various measures of the phonon spectrum and the electron-phonon interaction by using machine learning algorithms. Specifically, we use symbolic regression implemented in the Sure Independence and Sparsifying Operator (SISSO) method [2] to identify a new, physically interpretable equation for T<sub>c</sub> as a function of a small number of physical quantities. We show that our model [3], trained using the relatively small T<sub>c</sub> < 10K data tested by Allen and Dynes, improves upon the Allen-Dynes fit and can reasonably generalize to superconducting materials with higher T<sub>c</sub> such as H3S. We find that recently-discovered superconducting systems with a more two-dimensional electron-phonon coupling are outliers in both the Allen-Dynes equation and our analytical expression, suggesting a need for a descriptor that also characterizes Fermi surface properties. Furthermore, we explore the use of variational autoencoders and Eliashberg theory to augment the data. By incorporating physical insights and constraints into a data-driven approach, we demonstrate that machine-learning methods can identify the relevant physical quantities and obtain predictive equations using small but high-quality datasets.

[1] P. B. Allen and R. C. Dynes, *Phys. Rev. B* **12**, 905 (1975).

[2] R. Ouyang, S. Curtarolo, E. Ahmetcik, M. Scheffler, and L. M. Ghiringhelli, *Phys. Rev. Materials* **2**, 083802(2018).

[3] S. R. Xie, G. R. Stewart, J. J. Hamlin, P. J. Hirschfeld, and R. G. Hennig, *Phys. Rev. B* **100**, 174513 (2019).

## SYMPOSIUM F.NM01

---

Nanophotonics—Emerging Hybrid Platforms, Materials and Functions  
November 21 - December 4, 2020

### Symposium Organizers

Hatice Altug, École Polytechnique Fédérale de Lausanne  
Viktoriia Babicheva, University of New Mexico  
Artur Davoyan, University of California, Los Angeles  
Philip Hon, Northrop Grumman Corporation

---

\* Invited Paper

SESSION Tutorial F.NM01: Emergent Nanophotonic Platforms and Functions  
Session Chairs: Andrea Alù, Artur Davoyan, Jennifer Dionne, Nader Engheta and Din-Ping Tsai  
Sunday Morning, November 29, 2020  
F.NM01

**8:00 AM \***

**Exotic Light-Matter Interactions in Metamaterials with Broken Symmetries** [Andrea Alù](#); City University of New York, United States

In this tutorial, I will overview emerging sub-fields of electromagnetics and nano-optics showing how suitably tailored meta-atoms and suitable arrangements of them open exciting venues to realize new phenomena and devices for light, radio-waves and sound. In particular, I discuss venues in which broken symmetries play a pivotal role in establishing emerging physical properties in metamaterials, from geometrical asymmetries and generalized forms of chirality, to time-reversal symmetry and parity-time symmetry. The opportunities offered by hybrid metamaterials combining classical photonic material platforms with 2D and quantum materials with exotic lattice symmetries will also be discussed. Our work shows how these concepts can provide interesting tools to largely break Lorentz reciprocity and realize isolation without the need of magnetic bias, based on broken time-reversal symmetry induced by mechanical motion, spatio-temporal modulation and/or nonlinearities. I also discuss how broken symmetries in space and space-time can open the opportunity to induce topological order in metamaterials. In the talk, I will also discuss the impact of these concepts from basic science to practical technology, from classical waves to quantum phenomena.

**9:30 AM BREAK**

**9:45 AM \***

**Optical Meta-Devices—Advances and Applications** [Din P. Tsai](#); The Hong Kong Polytechnic University, Hong Kong

Metasurfaces, the 2D counterpart of artificial metamaterials, have attracted much attention because of their exceptional ability to manipulate the electromagnetic wave such as amplitude, phase, polarization, propagation direction, and so on. Different from conventional optical components, meta-devices based on the metasurface optics are truly flat and compact and exhibit superior novel performance. Recent progress in the developments of optical meta-devices will be discussed. First, the working principle and characteristics of optical meta-devices are explored. Then, it is described how the dispersion aberration in optical meta-devices can be used or eliminated to make them suitable for being employed in a range of applications that are difficult or impossible for traditional optical components. In addition, various optical meta-devices based applications are introduced, including imaging, high spectral resolution spectroscopy, and multiplex color routing, etc. Introduction and review of the reconfigurable and tunable optical meta-devices is also included. This talk will be concluded by addressing the future prospects of novel optical meta-devices.

## 11:15 AM BREAK

### 11:30 AM \*

**Near-Zero-Index Material Platforms and Dispersion Engineering** [Nader Engheta](#); University of Pennsylvania, United States

Materials are often used to manipulate and control photons. As such they play major roles in all aspects of nanophotonics. Metamaterials -- specially engineered material structures -- have enabled scientists and technologists to engineer desired dispersion and to construct platforms with unconventional material parameters, thus providing exciting opportunities to manipulate light-matter interaction in unconventional ways that exhibit unprecedented physics and technology for optical devices and components. One such platform is the near-zero-index metamaterials. In such structures, the effective relative permittivity and/or relative permeability is designed to be near zero at operating frequencies, causing the effective refractive index to be near zero. Consequently, in such epsilon-near-zero (ENZ), mu-near-zero (MNZ), and/or near-zero-index (NZI) structures the wavelength is “stretched”, and therefore the phase distribution is effectively uniform throughout this volume. This leads to a variety of unique features including supercoupling, photonic doping, photonic surface states, electric levitation, extreme quantum optics, thermal beaming, and giant nonlinearity, just to name a few. In this tutorial, I will present an overview of some of the fundamental principles and unique physics of wave interaction with such near-zero-index structures and their engineered dispersion. I will then discuss some of the applications of such platforms in photonics and microwave technologies. Possible future directions of research in this field will also be forecasted.

## 1:00 PM BREAK

### 1:15 PM \*

**Hybrid Nanophotonic Platforms to Control Chiral Light-Matter Interactions** [Jennifer A. Dionne](#); Stanford University, United States

Chirality in Nature can be found across all length scales. At the molecular scale, the spatial dissymmetry in the atomic arrangements of pairs of mirror-image molecules, known as enantiomers, gives rise to fascinating and often critical differences in chemical and physical properties. With increasing hierarchical complexity, protein function, cell communication, and organism health rely on enantioselective interactions between molecules with selective handedness. For example, neurodegenerative and neuropsychiatric disorders including Alzheimer’s and Parkinson’s diseases have been linked to distortion of chiral-molecular structure. Moreover, d-amino acids have become increasingly recognized as potential biomarkers, necessitating comprehensive analytical methods for diagnosis that are capable of distinguishing l- from d-forms and quantifying trace concentrations of d-amino acids. Correspondingly, many pharmaceuticals and agrochemicals consist of chiral molecules that target particular enantioselective pathways. Yet, despite the importance of molecular chirality, it remains challenging to sense and to separate chiral compounds. Chiral-optical spectroscopies are designed to analyze the purity of chiral samples, but they are often insensitive to the trace enantiomeric excess that might be present in a patient sample, such as blood, urine, or sputum, or pharmaceutical product. Similarly, existing separation schemes to enable enantiopure solutions of chiral products are inefficient or costly. Consequently, most pharmaceuticals or agrochemicals are sold as racemic mixtures, with reduced efficacy and potential deleterious impacts.

Recent advances in nanophotonics lay the foundation toward highly sensitive and efficient chiral detection and separation methods. In this Tutorial, we highlight efforts of our lab and the broader community to leverage nanoscale chiral light-matter interactions to detect, characterize, and separate enantiomers, potentially down to the single molecule level. Notably, certain resonant nanostructures can significantly enhance circular dichroism for improved chiral sensing and spectroscopy as well as high-yield enantioselective photochemistry. We first describe how achiral metallic and dielectric nanostructures can be utilized to increase the local optical chirality density by engineering the coupling between electric and magnetic optical resonances. While plasmonic nanoparticles locally enhance the optical chirality density, high-index dielectric nanoparticles can enable large-volume and uniform-sign enhancements in the optical chirality density. By overlapping these electric and magnetic resonances, local chiral fields can be enhanced by several orders of magnitude. We show how these design rules can enable high-sensitivity circular dichroism as well as high-yield enantioselective photochemistry. We also show how hybrid nanophotonic platforms can enable structure-sensitive vibrational IR and Raman spectroscopy. The Tutorial will describe both computational and experimental approaches, including methods to sense the structure of molecular monolayers and dynamically detect the structural transformations of chiral molecules. Finally, we discuss future challenges and opportunities spanning fundamental research to technology translation.

SESSION F.NM01.11: Live Lightning/Flash I: Emergent Nanophotonic Systems and Effects  
Session Chairs: Hatice Altug and Artur Davoyan  
Wednesday Morning, December 2, 2020  
F.NM01

**8:00 AM INTRODUCTION AND ANNOUNCEMENTS**

**8:12 AM \*F.NM01.04.02**

**Atomic Layer Deposited VO<sub>2</sub> Thin Films Towards Modulated Infrared Optoelectronic Devices** V. D. Wheeler<sup>1</sup>, Chase Ellis<sup>1</sup>, Marc Currie<sup>1</sup>, J.R. Avila<sup>2</sup>, Michael A. Meeker<sup>1</sup>, Joshua D. Caldwell<sup>3</sup> and Joseph Tischler<sup>1</sup>; <sup>1</sup>U.S. Naval Research Laboratory, United States; <sup>2</sup>ASEE Postdoctoral Fellow, United States; <sup>3</sup>Vanderbilt University, United States

VO<sub>2</sub> is a phase change material that undergoes a first order crystalline phase transition at a critical temperature ( $T_c = 68^\circ\text{C}$ ), resulting in significant changes in intrinsic electrical and optical properties, especially in the infrared. Optical changes with this phase transition are of particular interest as passive and active components of optoelectronic devices, specifically for thermal regulation and modulated signaling. Realizing this type of device often requires the integration of thin, conformal VO<sub>2</sub> films with complex, non-planar structures (like metamaterials). Thus, atomic layer deposition (ALD) is the ideal deposition method in these cases.

Traditional metal-based plasmonic materials suffer from high optical losses, which has promoted research towards alternative low-loss materials that can support plasmonic-like effects. One such approach employs phonon-mediated collective-charge oscillations (surface phonon polaritons, SPhPs) that are supported by nanostructured polar dielectric materials (SiC, AlN, etc), which inherently are low-loss. Geometric design of the nanostructures enables spectral tuning of resonant features between the longitudinal and transverse optical phonons of the polar material, typically in the infrared regions. However, the spectral position and amplitude of these resonances remain fixed after fabrication. Integrating phase change materials with these structures provides a way to achieve active modulation of resonances.

In this work, we will discuss the ALD process optimization and characterization of thin VO<sub>2</sub> films itself and subsequent integration into different optoelectronic structures for active modulation. In particular we will present a case study where nanopillar arrays were etched into SiC and AlN to create narrowband resonances in the long-wave infrared region. These structures were subsequently coated with ALD VO<sub>2</sub> films with different thicknesses (8-75nm). As-deposited VO<sub>2</sub> films are highly conformal and amorphous, and cause the resonances to shift and broaden due to the different dielectric environment. However, after annealing the films at 525°C in  $6 \times 10^{-5}$  Torr, the VO<sub>2</sub> films crystallize resulting in sharper resonances and spectral locations close to the initial uncoated structures. Temperature-dependence reflectance and emission measurements show that by heating through the VO<sub>2</sub> transition temperature, the amplitude of the resonances can be modulated. Full signal modulation (ie. on/off) requires at least a 16nm VO<sub>2</sub> film. This work shows the ability to actively tune surface phonon polariton resonances using ALD phase change materials.

**8:20 AM BREAK**

**8:28 AM F.NM01.07.05**

**Photonic Designs for Laser Driven Propulsion** Ho-Ting Tung and Artur Davoyan; University of California, Los Angeles, United States

In this work we examine principles of laser propulsion for spaceflight in the solar system. We discuss regimes of laser operation, system requirements on acceleration distance and sail-craft dimensions and weight. We show that with laser propulsion small satellites may be injected into various trajectories on a path to other planets. We show that travel times to planets may be as small as one month. We analyze spacecraft trajectory for various laser illumination regimes. Lastly, we discuss sail-craft materials and photonic design. We show that with a proper choice of low-loss materials and photonic engineering highly reflective sails may be crafted to ensure efficient momentum transfer. We further study pathways for radiative heat dissipation to ensure sustainable spacecraft operation and propulsion. We discuss several specific design concepts and demonstrate the feasibility and promise of such laser propulsion with today's technology. Our work shows that laser propulsion may offer an alternative for fast transit time and high velocity missions beyond the reach of conventional chemical rockets and plasma engines.

**8:36 AM \*F.NM01.05.06**

**Miniature Optical Systems Based on Cascaded Metasurfaces** Andrew McClung, Mahdad Mansouree, Sarath Samudrala, Mahsa Torfeh, Babak Mirzapourbeinekalaye and Amir Arbabi; University of Massachusetts Amherst, United States

Miniaturized optical systems with planar form factors and low power consumption have many applications in consumer electronics, imaging and spectral sensing systems, and as integral parts of medical and industrial equipment. Flat optical devices based on dielectric metasurfaces introduce a new approach for the realization of such systems at low cost using conventional nanofabrication techniques. In this talk, I will present an overview of our work on the development of various high-performance optical dielectric metasurface components and systems. In particular, I will discuss multi-layer dielectric metasurfaces that enable complete control of wavefront at multiple wavelengths. I will present an on-chip integration platform enabled by vertical or lateral integration of multiple metasurfaces and active optoelectronic components such as laser arrays and image sensors. I will also introduce a novel technique for engineering chromatic dispersion by cascading and discuss various optical systems implemented in this platform and a single-snapshot multispectral imager.

**8:44 AM \*F.NM01.11.07**

**Manipulating Light and Matter at the Nanoscale for Next Generation Solar Energy Conversion Devices** Esther Alarcon-Llado; AMOLF, Netherlands

Introducing thin, light-weight and high efficiency photovoltaics will ensure solar cells to be integrated in urban landscapes, small gadgets or even in space. While thinning down of absorber materials is a good strategy to overcome these restrictions, it comes down to the expense of poor light absorption. By contrast, nano-structuring is an effective approach to tackle flexibility, material and weight reduction without compromising absorption through the exploiting of their strong interactions with light.

In this talk I will describe the power of semiconductor nanostructures to capture and trap sunlight, enabling a wide range of new solar cells designs. First, I will introduce the wave guiding effects in semiconductor nanowires. The absorption cross-section in semiconductor nanowires can reach up to x100 their geometrical footprint, so that nanowire arrays can reach to the same absorption as in bulk films with a small fraction (< 3%) of the material. We have seen experimental evidence for the strong extinction in vertically standing GaAs and InAs nanowires, using 3D confocal fluorescence microscopy. We observe how light is perturbed up to few microns away from the nanowires for a broad range of wavelengths. We demonstrate that by probing ordered arrays with this method, the effective absorption coefficient and cross-section can be obtained without the need of a transparent substrate. Because of the absorption cross-section in nanowires is ruled by the efficient incoupling of light to the waveguide modes, absorption is relatively narrow-band (~50 nm) with the central wavelength depending on the nanowire diameter. The coloured appearance in sparse arrays are actually the perfect framework to generate a new class of semi-transparent photovoltaics, that can be used as windows and other urban spaces. We find that the multi-mode absorption in the arrays, result into higher absorbance as compared to the thin film counterpart with the same average visible transparency. Second, I will show that the diffractive power of nanowire arrays can be modulated by the wavelength-selective 1D wave guiding in the nanowires. Using the tailored structural properties in the array, we show that a nanowire array can serve as both solar cell and light in-coupler to a thin film cell underneath. The dual waveguiding effects in GaAs nanowire-Si thin film tandem architectures give rise to a 4-fold light absorption increase in the Si ultrathin bottom cell. This is a significant light trapping scheme that is obtained “for free” when using a nanostructured top cell. As a final remark, I will touch upon emerging fabrication methods for nanostructured semiconductor and conducting metamaterials. In particular, electrochemical deposition is a convenient growth method that allows for control over the growth conditions through combinations of solvents, additives, and pH, in addition to conventional parameters such as heat and pressure. By combining scalable imprint lithography with electrochemical deposition, we demonstrate large-area plasmonic lattices of In,Ga metals that can be electrochemically transformed to dielectric (In,Ga)As.

*References*

- [1] R. Frederiksen, G. Tutuncuoglu, F. Matteini, K. L. Martinez, A. Fontcuberta, and E. Alarcon-Llado, “Visual Understanding of Light Absorption and Waveguiding in Standing Nanowires with 3D Fluorescence Confocal Microscopy,” *ACS Photonics* 2017.
- [2] N. Tavakoli, E. Alarcon-Llado, "Combining 1D and 2D waveguiding in an ultrathin GaAs NW/Si tandem solar cell", *Optics Express* 2019
- [3] Valenti, M. et al. "Grain size control of crystalline III–V semiconductors at ambient conditions using electrochemically mediated growth", *J. Mat. Chem. A* 2020

**8:52 AM \*F.NM01.03.02**

**Linear and Nonlinear Conducting Oxide Epsilon-Near-Zero Nanophotonics** Sudip Gurung<sup>1</sup>, Jingyi Yang<sup>1</sup>, Aleksei Anopchenko<sup>1</sup>, Khant Minn<sup>1</sup> and Ho Wai (Howard) Lee<sup>1,2</sup>; <sup>1</sup>Baylor University, United States; <sup>2</sup>University of California,

Irvine, United States

The optical response of epsilon-near-zero (ENZ) materials has been a topic of significant interest in the last few years as the electromagnetic field inside media with near-zero permittivity has been shown to exhibit unique optical properties, including strong electromagnetic wave confinement, non-reciprocal magneto-optical effects, and abnormal nonlinearity.

This talk will review our recent development on the linear and nonlinear properties of conducting oxide epsilon-near-zero materials [1-6]. I will present a method to engineer the nonlinear refraction coefficients and the nonlinear absorption coefficients of Al-doped zinc oxide (AZO) ENZ thin films synthesized by atomic layer deposition (ALD) technique. Our results suggest that ENZ nonlinear refraction and nonlinear absorption properties of AZO films are enhanced by excitation of the ENZ modes and can be engineered by changing the mode-strengths via control over either the excitation angles or by ALD engineering of material dispersion/ film thickness. Measured values as large  $n_2^{(\text{eff})} \sim 10^{-9}$  mm<sup>2</sup>/W and  $\beta_2^{(\text{eff})} \sim 10^{-5}$  mm/W are obtained along with approximately an order of magnitude tunability.

In addition, I will also discuss the first experimental demonstration of optically confined ENZ resonance excitation in a side-polished optical fiber waveguide uniformly coated with AZO nanolayer. We observed a transmission resonance dip in the ENZ regime with on and off resonance difference of ~20 dB in an ENZ-optical fiber with a 30 nm-thick AZO layer, which is attributed to the coupling between the fundamental mode of the optical fiber and ENZ mode supported by the ultrathin AZO film. We also demonstrate the active nonlinear optical and electrical control of the hybrid ENZ resonances in the AZO ENZ optical fibers. The ENZ-optical fiber provides a unique excitation platform of hybrid ENZ resonance with relatively long light-interaction length and eases the complexity of optical configuration without required sophisticated prism/grating coupling, which has potential applications in nonlinear and quantum zero index photonics, in-fiber optical sensing, lasers, and dispersion control.

This work was supported in part by the National Science Foundation (grant number: 1752295), Air Force Office of Scientific Research (AFOSR, Award number: FA9550-19-1-0274; FA2386-18-1-4099), and Defense Advanced Research Projects Agency (grant number N66001-17-1-4047).

#### Reference:

- (1) A. Anopchenko, L. Tao, C. Arndt, H. W. Lee, "Field-effect tunable and broadband Epsilon-near-zero perfect absorbers with deep subwavelength thickness," *ACS Photonics* 5, 2631 (2018).
- (2) A. Anopchenko, S. Gurung, L. Tao, C. Arndt, H. W. Lee, "Atomic Layer Deposition of Ultra-thin and smooth Al-doped ZnO for Zero-Index Photonics," *Materials Research Express*, 5, 014012 (2018).
- (3) S. Gurung, A. Anopchenko, S. Bej, J. Joyner, J. Myers, J. Frantz, H. W. Lee, "Atomic layer engineering of epsilon-near-zero ultrathin films with controllable field enhancement," Accepted in *Advanced Materials Interfaces* (2020).
- (4) K. Minn, A. Anopchenko, J. Yang, H. W. Lee, "Excitation of epsilon-near-zero resonance in ultra-thin indium tin oxide shell embedded nanostructured optical fiber," *Nature Scientific Reports* 8, 2342 (2018).
- (5) J. Yang, K. Minn, A. Anopchenko, S. Gurung, H. W. Lee, "Coupling to Epsilon-near-Zero Mode on Ultrathin Atomic Layer Deposited Conducting Oxide Film in Optical Fiber", submitted (2020).
- (6) A. Anopchenko, S. Gurung, S. Bej, H. W. Lee, "Field Enhancement of Epsilon-near-Zero Modes in Realistic Ultra-Thin Absorbing Films," submitted (2020).

#### 9:00 AM \*F.NM01.09.03

##### **Designing Tunable Phase-Change Material Based Metasurfaces Using Multiphysics Simulations** Dmitry N. Chigrin<sup>1,2</sup>; <sup>1</sup>DWI–Leibniz Institute for Interactive Materials, Germany; <sup>2</sup>RWTH Aachen University, Germany

Tunable metasurfaces allow to control the phase, amplitude and propagation direction of electromagnetic waves. Integrating phase-change materials into metasurface design provide an opportunity to control metamaterial properties at the meta-atom length scale. This could enable full reprogrammability and post-fabrication adjustments of adaptive metasurfaces. A state of phase change material near a meta-atom can be switched by a local deposition of heat using optical, electrical pulses or hot scanning probes. Resulting phase transition process is intrinsically non-stationary and inhomogeneous. The phase transition from crystalline to amorphous state is accompanied by the drastic change of the material properties leading to time-varying and position-dependent refractive index, conductivity, absorption rate and heat conduction. In order to describe local phase transition in metamaterials, a self-consistent numerical treatment of electromagnetic, carrier transport, heat transfer and phase transition processes becomes of primary importance. Understanding the phase transition process at the meta-atom length scale is essential for a purposeful design of programmable adaptive metasurfaces. Here, we report on a self-consistent multiphysics description of a local phase transition in metasurfaces. The developed model is applied to analyse local phase



transition in different metasurfaces under the application of different mechanism of the local heat deposition.

**9:08 AM \*F.NM01.07.02**

**Metamaterial Computing Machines** Nader Engheta; University of Pennsylvania, United States

Metamaterials and metasurfaces have offered exciting platforms for engineering light-matter interaction that can provide desired functionalities. Over the past several years, numerous features and exciting applications of metastructures have been explored and developed. One of the interesting possibilities in using metamaterials is the development of “metamaterial computing machines”, which we have been exploring in my group. In such paradigm, structures are designed in order to perform mathematical operations when waves propagate through them. Effectively, materials become computing machines. We have been investigating various scenarios in which metastructures can solve integral and differential equations and can invert matrices as incoming waves interact with them. In addition to using materials platform for this purpose, we have also investigated how collections of the Mach-Zehnder interferometers (MZIs) can provide another platform for solving equations and doing mathematics with light. In this talk, I will discuss some of our ongoing research projects on this topic and will present an overview of our most recent results.

SESSION F.NM01.12: Live Keynote I: Nature Photonics Editorial—Writing and Submitting Your Papers  
Session Chairs: Hatice Altug and Artur Davoyan  
Wednesday Morning, December 2, 2020  
F.NM01

**9:20 AM \*F.NM01.01.01**

**Writing and Submitting Your Papers** Rachel Won; Nature Photonics, United Kingdom

This talk introduces you to all the existing and new journals in the family of *Nature*. It covers the detailed information and guidelines on scientific manuscript preparation and submission. Tips for writing a good abstract and a good paper will be provided. Editorial and peer-review processes will be discussed.

SESSION F.NM01.13: Live Panel Discussion I: Emergent Photonic Materials and Methods  
Session Chairs: Artur Davoyan and Philip Hon  
Thursday Afternoon, December 3, 2020  
F.NM01

**3:00 PM PANELIST: BOUBACAR KANTE, ALBERT POLMAN, KAI-MEI FU AND AUGUSTINE URBAS**

SESSION F.NM01.14: Live Lightning/Flash II: Materials for Advanced nanophotonic Devices  
Session Chairs: Artur Davoyan and Philip Hon  
Thursday Afternoon, December 3, 2020  
F.NM01

**4:00 PM \*F.NM01.03.04**

**Lattice Resonances in Arrays of Metallic Nanostructures** Alejandro Manjavacas; The University of New Mexico, United States

Periodic arrays are an exceptionally interesting arrangement for plasmonic nanostructures due to their ability to support strong collective lattice resonances, which arise from the coherent multiple scattering enabled by the array periodicity. Thanks to these exceptional properties, periodic arrays are being exploited in a wide variety of applications, including ultrasensitive biosensing, nanoscale light emission, and color printing, to cite a few. In this talk, we will discuss the response

of arrays with multi-particle unit cells using an analytical approach based on plasmon hybridization, which provides a simple and efficient way to design periodic arrays with engineered properties [1]. We will pay particular attention to bipartite arrays and show how, depending on the relative position of the particles within the unit cell, these systems can support super- or subradiant lattice resonances [2]. We will also discuss how the interplay between the response of the individual constituents and the collective interaction determines the ultimate limits of the field enhancement provided by a periodic array [3]. We will finish by addressing the effect that the presence of edges as well as disorder have on the response of these systems [4].

[1] Baur, S.; Sanders, S.; Manjavacas, A. ACS Nano 2018, 12, 1618.

[2] Cuartero-Gonzalez, A.; Sanders, S.; Zundel, L.; Fernandez-Dominguez, A. I.; Manjavacas, A.; submitted 2020.

[3] Manjavacas, A.; Zundel, L.; Sanders, S. ACS Nano 2019, 13, 10682.

[4] Zundel, L.; Manjavacas, A. J. Phys: Photonics 2019, 1, 015004.

#### 4:08 PM F.NM01.02.02

**Functional Metasurfaces for Rapid, Colorimetric Cancer Tissue Diagnostics** [Lisa V. Poulikakos](#)<sup>1,2</sup>, Mark Lawrence<sup>1</sup>, David R. Barton<sup>1</sup>, Stefanie S. Jeffrey<sup>1</sup> and Jennifer A. Dionne<sup>1</sup>; <sup>1</sup>Stanford University, United States; <sup>2</sup>UC San Diego, United States

Hundreds of thousands of patients in the United States are diagnosed with cancer annually. While the accurate determination of disease stage is closely linked to the probability of patient survival, current diagnostic technology presents patients and physicians with trade-offs between duration, precision and cost. Here, we present an all-optical, label-free technology for quantitative, real-time cancer tissue diagnostics on a single, clinically-compatible chip. Periodically-arranged sub-wavelength dielectric nanostructures, known as metasurfaces, are patterned into dielectric layers on glass microscope coverslips, where biopsied tumor tissue sections can be deposited following routine clinical procedure. Specifically, our technique maps the anisotropy and orientation of collagen fibers, a quantitative marker of cancer stage in tissue, onto metasurface structural color.

We pattern a sub-wavelength rectangular lattice of rhombohedral perturbations into stacked layers of silicon nitride (215 nm) and silicon dioxide (75 nm), where  $< 10$  nm bandwidth guided-mode resonances yield a high-purity chromaticity in reflectance, with a polarization-sensitive colorimetric response. With full-field numerical simulations, we demonstrate how selective tuning of the guided-mode resonances maps the orientation angle of collagen fibers onto blue-to-green chromaticity, while changes in refractive index are separately mapped onto red-to-green chromaticity as the sensing medium varies from air to biological tissue. For the example case of breast cancer diagnostics, where the presence and orientation of collagen fibers at the tumor margin can distinguish early-stage from metastasized disease, we quantify the performance of our metasurface via the 1976 CIE Lab color discrimination. We find that our metasurface outperforms polarized light microscopy by unambiguously mapping tissue orientation onto structural color at higher color discrimination values, while enabling the distinction of orientation angles which otherwise yield an identical response. This improved performance is attributed to engineered symmetry-breaking of the metasurface geometry by Stokes parameter analysis of the metasurface-reflected fields. Finally, we experimentally characterize the anisotropic optical properties of planar sheets of ordered synthetic collagen scaffolds using both conventional polarimetry and our metasurface device. Working at the interface of nanoscale optics and medicine, our colorimetric metasurface platform has the potential to set a new benchmark for rapid, quantitative and cost-effective cancer tissue diagnostics.

#### 4:15 PM \*F.NM01.05.05

**Straintronics and ITO-Photonics—Advances in Heterogeneous Opto-Electronic Devices** [Volker J. Sorger](#); George Washington University, United States

Here I discuss our recent demonstrations of ITO-based opto-electronic devices and introduce the concept of 'Strainoptronics'. The presentation includes the following concepts: 1) Here we demonstrate a spectrally broadband, gigahertz-fast Mach-Zehnder interferometric modulator exhibiting a miniscule  $V\pi$  L of 95 V- $\mu$ m, deploying a subwavelength short electrostatically tunable plasmonic phase shifter based on heterogeneously integrated indium tin oxide thin films into silicon photonics. This GHz-fast broadband integrated modulator bears relevance since ITO is a foundry-compatible material. Unlike the crystal-orientation-sensitive LN, ITO optoelectronics is synergistic to enhancing electrostatics known from transistor technology. 2) Strain-engineered high-responsivity MoTe<sub>2</sub> photodetector for silicon photonic integrated circuits In integrated photonics, specific wavelengths such as 1,550 nm are preferred due to low-loss transmission and the availability of optical

gain in this spectral region. For chip-based photodetectors, two-dimensional materials bear scientifically and technologically relevant properties such as electrostatic tunability and strong light–matter interactions. However, no efficient photodetector in the telecommunication C-band has been realized with two-dimensional transition metal dichalcogenide materials due to their large optical bandgaps. Here we demonstrate a MoTe<sub>2</sub>-based photodetector featuring a strong photoresponse (responsivity 0.5 A/W) operating at 1,550 nm in silicon photonics enabled by strain engineering the two-dimensional material. Non-planarized waveguide structures show a bandgap modulation of 0.2 eV, resulting in a large photoresponse in an otherwise photoinactive medium when unstrained. Unlike graphene-based photodetectors that rely on a gapless band structure, this photodetector shows an approximately 100-fold reduction in dark current, enabling an efficient noise-equivalent power of 90 pW/Hz<sup>0.5</sup>. Such a strain-engineered integrated photodetector provides new opportunities for integrated optoelectronic systems.

4:23 PM \*F.NM01.05.08

**2.5D Photonics as Engines of Information Manipulation** Rajesh Menon; The University of Utah, United States

Micro- and nanostructures have been widely applied to enhance the performance of optical components and systems. Structures whose characteristic dimensions are greater than the wavelength of interest,  $l$ , can effectively manipulate the **scalar** properties of light, while nanostructures with dimensions  $\ll l/2$  can manipulate the **vector** properties of light. By restricting the photonic functionality to a thin plane (i.e., 2.5D photonics), it's possible to create very thin lightweight imaging lenses,<sup>1</sup> spectrum-splitting solar concentrators,<sup>2</sup> and integrated-photonics devices.<sup>3</sup> In this presentation, we will highlight examples of each such device that overcome limitations of conventional implementations (if they exist at all). For example, flat multi-level diffractive lenses (MDLs) have recently shown achromatic bandwidth,<sup>4,5</sup> depth-of-focus<sup>6</sup> and efficient high-numerical aperture focusing<sup>7</sup> far better than their conventional counterparts, all while reducing weight and thickness by several orders of magnitude.

Computational techniques, such as nonlinear optimization, coupled with electromagnetics modeling can drive the *inverse design* of novel optical and photonic components and systems. When guided by manufacturing constraints, such techniques can result in highly practical, low-cost, ultra-compact (on the order of  $l \times l$ ) and multi-functional integrated-photonics components, such as polarization beam-splitters,<sup>3</sup> wavelength splitters,<sup>8</sup> couplers,<sup>9</sup> waveguide bends,<sup>10</sup> etc. We'll also describe a nanophotonic cloak that enables two devices to be placed closer together than is otherwise feasible, leading to an increase in integration density.<sup>11</sup>

When coupled with advanced machine-learning or linear-algebraic methods, 2.5D photonics can engines of information manipulation, enabling highly non-intuitive forms of optical systems such as photography with no lenses<sup>12,13</sup> or microscopy with only a surgical needle<sup>14,15</sup> or multi-spectral imaging with a diffractive element.<sup>16</sup>

#### References:

- S. Banerji, *et al.*, *PNAS*, 116(43) 21375 (2019).
- P. Wang, *et al.*, *Prog. Photovolt.* 23(9) 1073 (2015).
- B. Shen, *et al.*, *Nat. Photon.* 9, 378 (2015).
- M. Meem, *et al.*, arXiv:2004.13476 (2020).
- M. Meem, *et al.*, arXiv:2001.03684 (2020).
- S. Banerji, *et al.*, *Optica* 7(3) 214-2017 (2020)
- M. Meem, *et al.*, *Optica* 7(3) 252-253 (2020).
- A. Y. Piggott, *et al.*, *Nat. Photon.* 9, 374 (2015).
- B. Shen, *et al.*, *Opt. Exp.* 22(22) 27175 (2014).
- B. Shen, *et al.*, *Opt. Lett.* 40(24) 5750 (2015).
- B. Shen, *et al.*, *Nat. Commun.* 7, 13126 (2016).
- G. Kim & R. Menon, *Opt. Exp.* 26(18), 22826 (2018).
- G. Kim, *et al.*, *Appl. Opt.* 56(23) 6450 (2017).
- G. Kim, *et al.*, *Sci. Rep.* 7, 44791 (2017).
- G. Kim, *et al.*, *Appl. Phys. Lett.* 106, 261111 (2015).
- P. Wang & R. Menon, *Optica*, 2(11) 933 (2015).

SESSION F.NM01.15: Live Keynote II: Optical Nano-Kirigami  
Session Chairs: Artur Davoyan and Philip Hon

Thursday Afternoon, December 3, 2020  
F.NM01

**4:30 PM \*F.NM01.07.01**

**Optical Nano-Kirigami** Nicholas Fang<sup>1</sup>, Huifeng Du<sup>1</sup>, Xinhao Li<sup>1</sup>, Zhiguang Liu<sup>1</sup>, Jiafang Li<sup>2</sup> and Ling Lu<sup>3</sup>; <sup>1</sup>Massachusetts Institute of Technology, United States; <sup>2</sup>Beijing Institute of Technology, China; <sup>3</sup>Chinese Academy of Sciences, China

Recently, exciting new physics of plasmonics has inspired a series of key explorations to manipulate, store and control the flow of information and energy at unprecedented dimensions. For example, analogous to the familiar description of optical energy and linear momentum, non-local symmetry transformations of photons lead to new degrees of freedoms with respect to optical spin and optical helicities that are controllable at sub-wavelength scales thanks to the emerging nanohelical structures and networks. In this talk I will introduce versatile 3D shape transformations of nanoscale structures by deliberate engineering of the topography-guided stress equilibrium of gold nanostructures. By using the topography-guided stress equilibrium, rich 3D shape transformation such as buckling, rotation, and twisting of nanostructures is precisely achieved, which can be predicted by our mechanical modeling. Benefiting from the nanoscale 3D twisting features, giant optical chirality is achieved in an intuitively designed 3D pinwheel-like structure, in strong contrast to the achiral 2D precursor without nano-kirigami. High-contrast cross-polarized diffractions are successfully observed in both linear and radial configurations, resulting from constant phase difference between the pinwheel structures of opposite handedness. We further demonstrate an on-chip and electromechanically reconfigurable nano-kirigami with optical functionalities. The nano-electromechanical system is built on a CMOS-compatible Au/SiO<sub>2</sub>/Si substrate and operated via attractive electrostatic forces between the top gold nanostructure and bottom silicon substrate. Large-range nano-kirigami like 3D deformations are clearly observed and reversibly engineered, with scalable pitch size down to 0.975 μm. The demonstrated nano-kirigami, as well as the exotic 3D nanostructures, could be adopted in broad nanofabrication platforms and could open up new possibilities for the exploration of functional micro-/nanophotonic and mechanical devices. Nanoscale control of optical spin and optical helicities with nano-kirigami are promising for numerous technological applications, such as chiral molecular sensing, separation and synthesis, super resolution imaging, nanorobotics, and ultrathin broadband optical components for chiral light.

SESSION F.NM01.16: Live Panel Discussion II: Future Materials for Advanced Devices and Applications  
Session Chairs: Viktoriia Babicheva and Artur Davoyan  
Friday Afternoon, December 4, 2020  
F.NM01

**6:30 PM PANELIST: HARRY ATWATER, JENNIFER DIONNE, IGAL BRENER AND ARKA MAJUMDAR**

SESSION F.NM01.17: Live Lightning/Flash III: Novel Approaches to the Design of Functional Materials  
Session Chairs: Viktoriia Babicheva and Artur Davoyan  
Friday Afternoon, December 4, 2020  
F.NM01

**7:30 PM \*F.NM01.07.03**

**Advanced Optimization Algorithms for Nanophotonic Design at the Device and System Level** Katherine T. Fountaine<sup>1,2</sup>, Prachi Thureja<sup>2</sup>, Yury Tokpanov<sup>2</sup>, Dagny Fleischman<sup>2</sup> and Harry Atwater<sup>2</sup>; <sup>1</sup>Northrop Grumman Aerospace Systems, United States; <sup>2</sup>California Institute of Technology, United States

Nanophotonic design spaces are often highly nonlinear; the large number of parameters (both geometric and material properties) will result in an exceptionally complex and high dimensionality design space that renders an exhaustive parameter sweep computationally insurmountable. Additionally, the design of a full nanophotonic device involves optimization at multiple levels, including material selection/design, device design, and system level design. In this talk, I will discuss multiple optimization frameworks for different design problems, including device level design for multispectral filters and

phase modulation devices and system level design for beamsteering devices and other active metasurfaces. At the device level, we have (1) employed NOMAD (non-linear optimization using mesh adaptive direct search), a hybrid (global +local), derivative free optimization method, and (2) developed a new Bayesian optimization algorithm, MF-MI-Greedy, which uses multiple levels of fidelity, to optimize various nanophotonic structures including dielectric metasurfaces and multispectral filters. At the system level, we have (1) developed a new iterative genetic algorithm and (2) employed neural nets to optimize antenna arrays of active metasurfaces with non-ideal phase and amplitude characteristics. These studies suggest that selection of the correct optimization algorithm at a given design level can significantly reduce computational time for design and improve overall device performance.

7:38 PM \*F.NM01.08.04

### Investigating and Controlling the Opto-Electronic/Valleytronic/Spintronic Properties of van der Waals

**Nanomaterials/Heterostructures/Metastructures** Nai-Chang Yeh, Wei-Hsiang Lin, Chen-Chih Hsu, Duxing Hao, Deepan Kishore Kumar and Chia-Shuo Li; California Institute of Technology, United States

Thin layers of van der Waals (vdW) materials, ranging from insulators to semiconductors, semi-metals and superconductors, exhibit novel optical, electronic, orbital, magnetic, topological and superconducting properties. Varying the interfacial stacking order of vdW homo/heterostructures further yields Moiré bands and new physical phenomena. Nanoscale strain-engineering of vdW materials (*e.g.*, graphene, transition-metal dichalcogenides, TMDs) can induce novel quantum/topological phenomena, such as giant pseudo-magnetic fields (PMF) and flat bands associated with quantized Landau levels in monolayer graphene, and strain-dependent energy gaps and exciton lifetimes for monolayer 2H-phase TMDs. Quantum confinement due to reduced spatial dimensions and broken symmetry is known to induce new quantum states that are non-existent in the bulk. Spin-orbit coupling of light by optical vortices (*a.k.a.* twisted light, Laguerre-Gaussian beam) and plasmonic vortices produces photons with nontrivial spin/orbital-angular-momentum, which can impart integer and fractional *topological charges* onto condensed matter and atomic/molecular systems through light-matter interactions. Therefore, investigating and controlling the light-matter interactions in vdW nanomaterials/heterostructures/metastructures represents a pathway to explore new quantum phenomena and to advance opto-electronic/valleytronic/spintronic applications.

We employ scalable CVD and PECVD fabrication techniques to synthesize a variety of vdW nanomaterials and their heterostructures, including monolayer and bilayer graphene,<sup>[1-3]</sup> quasi one-dimensional (1D) graphene nanostripes,<sup>[1,4]</sup> h-BN,<sup>[5]</sup> and monolayer-to-multilayer TMDs  $\text{MX}_2$  and  $\text{MX}_{2-y}\text{X}'_y$  ( $\text{M} = \text{Mo}, \text{W}$ ;  $\text{X}, \text{X}' = \text{S}, \text{Se}, \text{Te}$ ;  $0 \leq y \leq 2$ ).<sup>[6]</sup> We investigate their properties by means of spatially resolved and polarization-dependent photoluminescence (PL), time-resolved PL (TRPL), Raman spectroscopy, x-ray photoelectron spectroscopy (XPS), Kelvin-probe force microscopy, conductive atomic force microscopy (c-AFM), scanning tunneling microscopy/spectroscopy (STM/STS).<sup>[6,7]</sup> We perform nanoscale strain engineering on monolayer graphene to control the strain-dependent PMF and electronic correlation, and to achieve valley/spin polarization;<sup>[7]</sup> and on TMDs to control the energy gaps and exciton lifetimes. We develop plasmonic vortices on TMDs by metasurfaces together with circularly polarized light to control the light-matter interaction and valley/spin polarization in TMD and the topological charge. Our approach leads to various interesting findings, including: valley splitting, quantum oscillations, spontaneous symmetry breaking and spin polarization, quantum valley-Hall and quantum anomalous-Hall effects in valley Hall transistors based on nanoscale strain-engineered monolayer graphene;<sup>[7]</sup> exceedingly long and temperature independent optically excited carrier lifetimes ( $\sim 10$  ns) as well as broadband (from IR to UV) photoluminescence in quasi-1D graphene nanostripes; much enhanced valley polarization in monolayer  $\text{WS}_2$  by combining plasmonic vortices with circularly polarized light; and compositional dependent opto-electronic/valleytronic properties in  $\text{WS}_{2-y}\text{Te}_y$  ( $0 < y < 2$ ). Based on these experimental findings, we discuss potential applications of van der Waals nanomaterials/heterostructures/metastructures to opto-electronic/valleytronic/spintronic devices.

### References:

- [1] N.-C. Yeh *et al.*, *Nanotechnology* **30**, 162001 (2019).
- [2] D. A. Boyd *et al.*, *Nat. Commun.* **6**, 6620 (2015).
- [3] Y.-C. Chen *et al.*, *Carbon* **156**, 212-224 (2020).
- [4] C.-C. Hsu *et al.*, *Carbon* **129**, 527 (2018).
- [5] W.-H. Lin *et al.*, *Chem. Mat.* **29**, 4700 (2017).
- [6] W.-H. Lin *et al.*, *ACS Nano* **14**, 1350-1359 (2020).
- [7] C.-C. Hsu *et al.*, *Sci. Adv.* **129**, 527 (2018).

**7:46 PM \*F.NM01.09.01**

**Dynamically Switchable Photonics Based on Alloyed Metal Hydrides** Jeremy N. Munday; University of California, Davis, United States

The ability to control the optical properties of photonic materials on demand is essential for the operation of a variety of devices ranging from active color filters and routers to switchable mirrors and sensors. Here we will present our latest work on actively controllable photonic devices using alloyed metal hydrides. Using our recently developed apparatus for *in situ* measurements of optical and mechanical response upon hydrogenation, we first show how pure metal hydrides containing Pd, Mg, Zr, Ti, and V can be used as tunable photonic elements throughout the visible and near-infrared [1]. A number of devices will be shown including structures that have five orders of magnitude change in reflectivity, as well as planar systems for physical encryption and counterfeit detection. Second, we will show how alloying can not only improve cyclability, but also lead to higher hydrogen fractions than previously obtained as a result of film stresses and microstructuring [2]. These results have led to new insights in the dynamic behavior of metal-hydrides and will help in the design of next-generation hydrogen sensors and tunable photonic devices.

[1] Kevin J. Palm, Joseph B. Murray, Tarun C. Narayan, and Jeremy N. Munday, "Dynamic Optical Properties of Metal Hydrides," *ACS Photonics*, **5**, 4677–4686 (2018)

[2] KJ Palm, JB Murray, JP McClure, MS Leite, JN Munday, "In Situ Optical and Stress Characterization of Alloyed Pd<sub>x</sub>Au<sub>1-x</sub> Hydrides" *ACS applied materials & interfaces* **11**, 45057-45067 (2019)

**7:53 PM \*F.NM01.09.02**

**Approaches for Tuning of Chalcogenide Glass Dielectric Metasurfaces** Jesse Frantz<sup>1</sup>, Jason D. Myers<sup>1</sup>, Robel Y. Bekele<sup>2</sup>, Anthony Clabeau<sup>2</sup>, Vinh Nguyen<sup>1</sup>, Jiannan Gao<sup>3</sup>, Mikhail Shalaev<sup>3</sup>, Natalia Litchinitser<sup>3</sup> and Jas Sanghera<sup>1</sup>; <sup>1</sup>U.S. Naval Research Laboratory, United States; <sup>2</sup>University Research Foundation, United States; <sup>3</sup>Duke University, United States

Chalcogenide glasses have recently received attention for their potential use in dielectric metasurfaces for several reasons: They typically possess high linear refractive indexes, enabling high index contrast devices; some compositions exhibit exceptionally high optical nonlinearity ( $n_2 > 1000\times$  that of silica) making them good candidates for nonlinear devices; they have wide transmission windows spanning from the visible through the longwave infrared; and some compositions undergo a structural phase transition, enabling devices with switching based on phase-change. We discuss a variety of approaches to achieve tunability in chalcogenide glass metasurfaces from our work and that of others. We review recent progress on the use of the Kerr nonlinearity in As<sub>2</sub>S<sub>3</sub> films to achieve power-dependent behavior and the application of this effect for the manipulation of orbital angular momentum. We discuss the design and realization of chalcogenide-based photonic quasicrystals enabling simultaneous phase matching of an arbitrary number of nonlinear optical processes in a single engineered nanostructure. We discuss recent observations that a permanent index change can be induced in As<sub>2</sub>Se<sub>3</sub> via thermal tuning and the use of this effect to achieve permanent one-way tuning of the optical resonance of a metasurface. We discuss work being done by a variety of groups on phase-change chalcogenide materials such as germanium-antimony-telluride and gallium-lanthanum-sulfide in order to realize switchable metasurfaces. Finally, we discuss future prospects for the use of chalcogenide glass metasurfaces for applications that require tuning of the optical response.

SESSION F.NM01.18: Live Keynote III: Advanced Meta-Optics Platforms

Session Chairs: Viktoriia Babicheva and Artur Davoyan

Friday Afternoon, December 4, 2020

F.NM01

**8:00 PM \*F.NM01.05.02**

**Volumetric Meta-Optics for Novel Device Functionalities** Andrei Faraon; California Institute of Technology, United States

Three-dimensional elements, with refractive index distribution structured at subwavelength scale, provide an expansive optical design space that can be harnessed for demonstrating multifunctional free-space optical devices. We present 3D dielectric elements, designed to be placed on top of the pixels of image sensors, that sort and focus light based on its color and polarization with efficiency significantly surpassing 2D absorptive and diffractive filters. The devices are designed via iterative gradient-based optimization to account for multiple target functions while ensuring compatibility with existing

nanofabrication processes, and they are experimentally validated using a scaled device that operates at microwave frequencies. This approach combines arbitrary functions into a single compact element, even where there is no known equivalent in bulk optics, enabling novel integrated photonic applications. We further discuss capabilities enabled by volumetric meta-optical devices for compact on-chip polarimetry and discuss implementations using multi-layer nanofabrication.

SESSION F.NM01.01: Special Talk by Rachel Won—Insights from the Editor  
On Demand Abstracts Available for Viewing Starting Saturday Morning, November 21, 2020  
F-NM01

**5:00 AM \*F.NM01.01.01**

**Writing and Submitting Your Papers** [Rachel Won](#); Nature Photonics, United Kingdom

This talk introduces you to all the existing and new journals in the family of *Nature*. It covers the detailed information and guidelines on scientific manuscript preparation and submission. Tips for writing a good abstract and a good paper will be provided. Editorial and peer-review processes will be discussed.

SESSION F.NM01.02: Advanced Biophotonic Systems, Platforms and Applications  
On Demand Abstracts Available for Viewing Starting Saturday Morning, November 21, 2020  
F-NM01

**5:00 AM \*F.NM01.02.01**

**Emerging Nanophotonic Platforms for Infectious Disease Diagnostics—Re-Imagining the Conventional Microbiology Toolkit** [Jennifer A. Dionne](#), Jack Hu, Jefferson Dixon, John M. Abendroth, Loza Tadesse, Amr Saleh, Mark Lawrence, Michelle Solomon and Fareeha Safir; Stanford University, United States

We present our research controlling light at the nanoscale for infectious disease diagnostics, including detecting bacteria at low concentration, sensing COVID antibodies and antigens, and visualizing in-vivo inter-cellular forces. First, we combine Raman spectroscopy and deep learning to accurately classify bacteria by both species and antibiotic resistance in a single step. We design a convolutional neural network (CNN) for spectral data and train it to identify 30 of the most common bacterial strains from single-cell Raman spectra, achieving antibiotic treatment identification accuracies exceeding 99% and species identification accuracies similar to leading mass spectrometry identification techniques. Our combined Raman-CNN system represents a proof-of-concept for rapid, culture-free identification of bacterial isolates and antibiotic resistance.

Second, we describe resonant nanophotonic surfaces, known as “metasurfaces” that enable multiplexed detection of SARS-CoV-2 antibodies and antigens. Our metasurfaces utilize guided mode resonances excited in high refractive index nanostructures. The high quality factor (“high-Q”) modes ( $Q > 1000$ ) produce a large amplification of the electromagnetic field intensities near the nanostructures that increase the response to minute refractive index changes from targeted binding of an antibody; simultaneously, the optical signal is beam-steered for multiplexed detection. We describe how this platform can be manufactured at scale for portable, low-cost assays.

Finally, we introduce a new class of *in vivo* optical probes to monitor biological forces with high spatial and temporal resolution. Our design is based on upconverting nanoparticles that, when excited in the near-infrared, emit light of a different color and intensity in response to nano-to-microNewton forces. The nanoparticles are sub-30nm in size, do not bleach or photoblink, and can enable deep tissue imaging with minimal tissue autofluorescence. We present the design, synthesis, and characterization of these nanoparticles both in vitro and in vivo, focusing on the forces generated by the roundworm *C. elegans* as it feeds and digests its bacterial food. Chronic cytotoxicity assays are used to confirm biocompatibility. Our force measurements are coupled with electrical measurements of muscle contractions in both wild-type and mutant animals, providing insight into the interplay between mechanical, electrical, and chemical signaling *in vivo*.

### 5:15 AM F.NM01.02.02

**Functional Metasurfaces for Rapid, Colorimetric Cancer Tissue Diagnostics** [Lisa V. Poulikakos](#)<sup>1,2</sup>, Mark Lawrence<sup>1</sup>, David R. Barton<sup>1</sup>, Stefanie S. Jeffrey<sup>1</sup> and Jennifer A. Dionne<sup>1</sup>; <sup>1</sup>Stanford University, United States; <sup>2</sup>UC San Diego, United States

Hundreds of thousands of patients in the United States are diagnosed with cancer annually. While the accurate determination of disease stage is closely linked to the probability of patient survival, current diagnostic technology presents patients and physicians with trade-offs between duration, precision and cost. Here, we present an all-optical, label-free technology for quantitative, real-time cancer tissue diagnostics on a single, clinically-compatible chip. Periodically-arranged sub-wavelength dielectric nanostructures, known as metasurfaces, are patterned into dielectric layers on glass microscope coverslips, where biopsied tumor tissue sections can be deposited following routine clinical procedure. Specifically, our technique maps the anisotropy and orientation of collagen fibers, a quantitative marker of cancer stage in tissue, onto metasurface structural color.

We pattern a sub-wavelength rectangular lattice of rhombohedral perturbations into stacked layers of silicon nitride (215 nm) and silicon dioxide (75 nm), where  $< 10$  nm bandwidth guided-mode resonances yield a high-purity chromaticity in reflectance, with a polarization-sensitive colorimetric response. With full-field numerical simulations, we demonstrate how selective tuning of the guided-mode resonances maps the orientation angle of collagen fibers onto blue-to-green chromaticity, while changes in refractive index are separately mapped onto red-to-green chromaticity as the sensing medium varies from air to biological tissue. For the example case of breast cancer diagnostics, where the presence and orientation of collagen fibers at the tumor margin can distinguish early-stage from metastasized disease, we quantify the performance of our metasurface via the 1976 CIE Lab color discrimination. We find that our metasurface outperforms polarized light microscopy by unambiguously mapping tissue orientation onto structural color at higher color discrimination values, while enabling the distinction of orientation angles which otherwise yield an identical response. This improved performance is attributed to engineered symmetry-breaking of the metasurface geometry by Stokes parameter analysis of the metasurface-reflected fields. Finally, we experimentally characterize the anisotropic optical properties of planar sheets of ordered synthetic collagen scaffolds using both conventional polarimetry and our metasurface device. Working at the interface of nanoscale optics and medicine, our colorimetric metasurface platform has the potential to set a new benchmark for rapid, quantitative and cost-effective cancer tissue diagnostics.

### 5:25 AM F.NM01.02.03

**Xanthommatin Biophotonics—Fundamental Optical Properties and Squid Skin Optics** [Richard M. Osgood](#)<sup>1</sup>, Sean R. Dinneen<sup>1</sup>, Zhuangsheng Lin<sup>2</sup>, Camille Martin<sup>2</sup>, Amrita Kumar<sup>2</sup>, Leila Deravi<sup>2</sup>, Yassine Ait-El-Aoud<sup>1</sup>, Steven Kooi<sup>3</sup>, Elizabeth Welsh<sup>1</sup>, Michael Okamoto<sup>1</sup> and Ihsan Uluturk<sup>1</sup>; <sup>1</sup>US Army CCDC-SC, United States; <sup>2</sup>Northeastern University, United States; <sup>3</sup>Massachusetts Institute of Technology, United States

Biomaterials are of increasing interest for photonics applications, including for biophotonics. The size of bioparticles used for nanophotonics can be similar to that of plasmonic nanoparticles; e.g., in the range of 50-500 nm. Some virus simulants scatter light and have been detected by highly sensitive photonic crystals.

Cephalopods are known to have important coloration and camouflage properties. The chromatophores in squid skin can change shape and influence light scattering and color; they are responsible for the bulk color changes (red, yellow, brown) observed in cephalopods. Underneath the chromatophore lie iridocyte cells, multilayered Bragg reflectors that reflect color and can cause iridescence. The chromatophore contains xanthommatin (Xa) pigments confined in nanostructured granules with sizes in the range 300-600 nm and achieves both pancake-like, expanded states and spherical, punctate state. The diameters of these granules are well-sized, and perhaps optimized for nanophotonic scattering of visible light, especially blue-green wavelengths; not absorption. Recently, researchers have succeeded in mimicking chromatophore color and in particular, the light scattering (diameter  $\sim 500$  nm) granules within them, using artificial materials and chemically-synthesized Xa[1]. These novel material platforms can be used for more efficient control of light at the nanoscale.

In the past, our group has discovered that the Xa pigment in cephalopod chromatophores has a very high refractive index ( $n < 1.92$ ), using fixed-wavelength refractometry (589 nm) and cavity ring-down spectrometry [2]. The latter experiment required drying aerosols. Here we report comprehensive broadband ellipsometric measurements of broadband (300 nm – 3200 nm) optical indices ( $n$  and absorption coefficient  $k$ ) of Xa pigment, using a novel method for extracting natural Xa pigment from the squid's chromatophores and forming smooth, high-quality films. These measurements give a more complete description



of Xa's fundamental optical properties, than previously known. We report a new short wave infrared absorption resonance and its possible origin. These important findings will assist in the design of new lightweight optical components, such as lenses, that can change in response to external stimuli and perhaps even image underwater. Most lenses are designed for a broad spectrum of light, where it is essential to know  $(n, k)$  across the entire wavelength range of interest, in order to predict optical system performance.

In this presentation, with a more advanced and quantitative understanding of squid skin optics, we improve on earlier results, that made important breakthroughs but did not have experimental optical constants, to extract scattering and absorption parameters. We use a 4-flux optical model (specular and diffuse light) of the chromatophore, optically coupled to the iridocyte. Armed with fundamental values of  $n$  and  $k$ , we employ direct experimental data for Xa to better quantitatively assess the optical response (e.g. scattering, reflectivity, transmission, and absorption) of the combined chromatophore-iridocyte optics.

These fundamental findings are important and will aid in the control of nanoscale light, using the novel Xa biomaterial, which can enable new scattering and coloration functionalities due to its unusually high  $n$ . Such a high-index material, which may be possible to synthesize in an environmentally-friendly way, may enable new designs of lightweight optical systems that can adapt and change shape, perhaps with an electrical trigger, and may aid in underwater detection or imaging. We discuss possible new designs and new nanophotonic systems, using the interesting Xa biomaterial.

[1] Adv. Opt. Mat. 6 1701369 2018.

[2] J. Phys. Chem. Lett. 8 313 2017.

#### 5:35 AM F.NM01.02.04

**Surface Plasmon Enhanced Shortwave Infrared Fluorescence for *In Vivo* Imaging of Ovarian Cancer** Shengnan Huang, Ching-Wei Lin, Jifa Qi, Archana M. Iyer, Yanpu He, Yingzhong Li, Neelkanth Bardhan, Darrell Irvine, Paula T. Hammond and Angela Belcher; Massachusetts Institute of Technology, United States

Shortwave infrared (SWIR, 900-1700nm) enables *in vivo* imaging with high spatial resolution and penetration depth due to the reduced photon scattering and suppressed tissue autofluorescence at long wavelengths. Recently, small organic SWIR dyes have drawn great interest because SWIR dyes have excellent biocompatibility as compared to their inorganic counterparts. However, the application of SWIR dyes for *in vivo* imaging is hampered by their low quantum yield and photostability. To resolve these issues, in this work, the SWIR dyes are placed in close proximity to gold nanorod (AuNR) for surface plasmon enhanced SWIR fluorescence. The plasmon enhancement is optimized by varying the dye-to-AuNR number ratio and a maximum enhancement factor of  $\sim 45$ -fold is achieved. In addition, it is found that the highest dye-to-AuNR number ratio gives the maximum emission on the weight basis and this ratio is used for synthesizing the plasmon enhanced SWIR imaging probes. The outmost surface of the imaging probes is modified with different ligands. Their effect on the targeting capability and intratumor distribution of the imaging probes is investigated and compared in two orthotopic ovarian cancer models. Lastly, it is demonstrated that the plasmon enhanced SWIR imaging probes are able to detect submillimeter-sized ovarian cancer nodules, making them excellent candidates for real-time fluorescence imaging-guided surgery.

#### 5:45 AM F.NM01.02.06

**High Quality Factor Metasurfaces for SARS-CoV-2 Antibody Detection** Jack Hu, Jefferson Dixon, Mark Lawrence, John M. Abendroth, Lisa V. Poulidakos, Fareeha Safir, Stefanie S. Jeffrey, Scott Boyd and Jennifer A. Dionne; Stanford University, United States

As of June 1st 2020, COVID-19 has impacted 213 countries with over 6 million cases globally. Antibody tests identify individuals who have been infected with SARS-CoV-2 and have developed an immune response; they also identify individuals with anti-SARS-CoV-2 antibodies who are potential donors of convalescent plasma. However, current serologic antibody tests are either qualitative or slow, are unable to correlate viral loads to antibody type and level, and do not offer real-time information about antibody-antigen binding on-rates, off-rates, or affinity constants. Here, we design and fabricate high quality factor (Q) silicon metasurfaces to sensitively detect SARS-CoV-2 antibodies and monitor antigen-antibody interaction dynamics at the few-protein level. Our metasurfaces utilize guided mode resonances excited in high refractive index nanostructures. The high Q modes ( $Q > 1000$ ) produce a large amplification of the electromagnetic field intensities near the nanostructures that increase the response to minute refractive index changes from targeted binding of an antibody. Using a Si-on-Sapphire platform, we fabricate biperiodic array metasurfaces with quality factors exceeding 2500. Next, we functionalize our metasurfaces with the spike receptor-binding domain (RBD) to bind with IgM, IgG, and IgA, and their

subtypes. Importantly, our zwitterionic and PEGylated matrix functionalization minimizes non-specific adsorption and enables oriented antibody attachment. On dried samples, transmission spectroscopy reveals metasurface resonant shifts exceeding the resonant full-width-half-max with varied antibody concentrations from clinical samples. A fluidic platform also allows real-time interrogation of metasurface resonant shifts as the serological samples are introduced. We describe how this platform can be manufactured at scale for portable, low-cost assays, and also how it can be modified to enable point-of-care antigen testing.

SESSION F.NM01.03: Dispersion Engineered Materials and Metamaterials  
On Demand Abstracts Available for Viewing Starting Saturday Morning, November 21, 2020  
F-NM01

**5:00 AM \*F.NM01.03.01**

**Nonlinear and Hyperbolic Metasurfaces and Applications** Augustine Urbas; AFRL, United States

Efforts to examine large optical nonlinear response in structured and novel electromagnetic materials are ongoing. This work is partly motivated by the promise of leveraging structural resonances or regions of exotic materials response, such as the epsilon near zero or ENZ regime to amplify the underlying nonlinear response of component materials. This nonlinear response can in turn be leveraged to explore new device response when incorporated into metasurfaces and metamaterial structures. The mechanisms for this nonlinear response are varied and span the range of traditional nonlinear materials. Leveraging such resonances or narrow response regimes however, leads to limitations in the band width of the response as has been reported previously. In this presentation, we will explore the use of multilayered structures composing so-called hyperbolic metamaterials as nonlinear media with large and broad band optical response. Such structures have been proposed as nonlinear materials as well as for a variety of other applications. We examine the spectrally and temporally-resolved response of multilayer Arsenide semiconductor materials which are constructed to possess hyperbolic metamaterial properties. By controlling the composition and doping of the materials, and then examining their response during optical excitation of free carriers, we can examine the material, structure, and optical effects on the nonlinear response. To analyze ultrafast changes in carrier concentration we use a pump-probe experiment. Pump and probe laser pulses are 85 fs in duration and their center wavelength can be tuned separately with an optical parametric amplifier (OPA) and difference frequency generator (DFG) in either path. Typical wavelengths used were 1300 nm for the pump and 4, 5, or 5.5  $\mu\text{m}$  for the probe. The differential intensity measurements were taken by appropriately positioned detectors to record  $\Delta R/R$  for reflection or  $\Delta T/T$  for transmission. We have explored the photo-induced change in optical properties of a multilayer semiconductor system constructed so as to generate hyperbolic dispersion under photoexcitation using pump-probe spectroscopy. The response shows characteristic wavelength and polarization dependent features that support the emergence of hyperbolic dispersion at pump excitation that induce sufficient photoinduced carrier responses. This response can serve as a basis for highly nonlinear systems and as a material from which highly nonlinear metasurfaces can be made.

**5:15 AM \*F.NM01.03.02**

**Linear and Nonlinear Conducting Oxide Epsilon-Near-Zero Nanophotonics** Sudip Gurung<sup>1</sup>, Jingyi Yang<sup>1</sup>, Aleksei Anopchenko<sup>1</sup>, Khant Minn<sup>1</sup> and Ho Wai (Howard) Lee<sup>1,2</sup>; <sup>1</sup>Baylor University, United States; <sup>2</sup>University of California, Irvine, United States

The optical response of epsilon-near-zero (ENZ) materials has been a topic of significant interest in the last few years as the electromagnetic field inside media with near-zero permittivity has been shown to exhibit unique optical properties, including strong electromagnetic wave confinement, non-reciprocal magneto-optical effects, and abnormal nonlinearity.

This talk will review our recent development on the linear and nonlinear properties of conducting oxide epsilon-near-zero materials [1-6]. I will present a method to engineer the nonlinear refraction coefficients and the nonlinear absorption coefficients of Al-doped zinc oxide (AZO) ENZ thin films synthesized by atomic layer deposition (ALD) technique. Our results suggest that ENZ nonlinear refraction and nonlinear absorption properties of AZO films are enhanced by excitation of the ENZ modes and can be engineered by changing the mode-strengths via control over either the excitation angles or by ALD engineering of material dispersion/ film thickness. Measured values as large  $n_2^{(\text{eff})} \approx 10^{-9} \text{ mm}^2/\text{W}$  and  $\beta_2^{(\text{eff})} \approx 10^{-5} \text{ mm/W}$  are obtained along with approximately an order of magnitude tunability.

In addition, I will also discuss the first experimental demonstration of optically confined ENZ resonance excitation in a side-

polished optical fiber waveguide uniformly coated with AZO nanolayer. We observed a transmission resonance dip in the ENZ regime with on and off resonance difference of ~20 dB in an ENZ-optical fiber with a 30 nm-thick AZO layer, which is attributed to the coupling between the fundamental mode of the optical fiber and ENZ mode supported by the ultrathin AZO film. We also demonstrate the active nonlinear optical and electrical control of the hybrid ENZ resonances in the AZO ENZ optical fibers. The ENZ-optical fiber provides a unique excitation platform of hybrid ENZ resonance with relatively long light-interaction length and eases the complexity of optical configuration without required sophisticated prism/grating coupling, which has potential applications in nonlinear and quantum zero index photonics, in-fiber optical sensing, lasers, and dispersion control.

This work was supported in part by the National Science Foundation (grant number: 1752295), Air Force Office of Scientific Research (AFOSR, Award number: FA9550-19-1-0274; FA2386-18-1-4099), and Defense Advanced Research Projects Agency (grant number N66001-17-1-4047).

#### Reference:

- (1)A. Anopchenko, L. Tao, C. Arndt, H. W. Lee, "Field-effect tunable and broadband Epsilon-near-zero perfect absorbers with deep subwavelength thickness," *ACS Photonics* 5, 2631 (2018).
- (2)A. Anopchenko, S. Gurung, L. Tao, C. Arndt, H. W. Lee, "Atomic Layer Deposition of Ultra-thin and smooth Al-doped ZnO for Zero-Index Photonics", *Materials Research Express*, 5, 014012 (2018).
- (3)S. Gurung, A. Anopchenko, S. Bej, J. Joyner, J. Myers, J. Frantz, H. W. Lee, "Atomic layer engineering of epsilon-near-zero ultrathin films with controllable field enhancement," Accepted in *Advanced Materials Interfaces* (2020).
- (4)K. Minn, A. Anopchenko, J. Yang, H. W. Lee, "Excitation of epsilon-near-zero resonance in ultra-thin indium tin oxide shell embedded nanostructured optical fiber," *Nature Scientific Reports* 8, 2342 (2018).
- (5)J. Yang, K. Minn, A. Anopchenko, S. Gurung, H. W. Lee, "Coupling to Epsilon-near-Zero Mode on Ultrathin Atomic Layer Deposited Conducting Oxide Film in Optical Fiber", submitted (2020).
- (6)A. Anopchenko, S. Gurung, S. Bej, H. W. Lee, "Field Enhancement of Epsilon-near-Zero Modes in Realistic Ultra-Thin Absorbing Films," submitted (2020).

#### 5:45 AM \*F.NM01.03.04

**Lattice Resonances in Arrays of Metallic Nanostructures** Alejandro Manjavacas; The University of New Mexico, United States

Periodic arrays are an exceptionally interesting arrangement for plasmonic nanostructures due to their ability to support strong collective lattice resonances, which arise from the coherent multiple scattering enabled by the array periodicity. Thanks to these exceptional properties, periodic arrays are being exploited in a wide variety of applications, including ultrasensitive biosensing, nanoscale light emission, and color printing, to cite a few. In this talk, we will discuss the response of arrays with multi-particle unit cells using an analytical approach based on plasmon hybridization, which provides a simple and efficient way to design periodic arrays with engineered properties [1]. We will pay particular attention to bipartite arrays and show how, depending on the relative position of the particles within the unit cell, these systems can support super- or subradiant lattice resonances [2]. We will also discuss how the interplay between the response of the individual constituents and the collective interaction determines the ultimate limits of the field enhancement provided by a periodic array [3]. We will finish by addressing the effect that the presence of edges as well as disorder have on the response of these systems [4].

[1] Baur, S.; Sanders, S.; Manjavacas, A. *ACS Nano* 2018, 12, 1618.

[2] Cuartero-Gonzalez, A.; Sanders, S.; Zundel, L.; Fernandez-Dominguez, A. I.; Manjavacas, A.; submitted 2020.

[3] Manjavacas, A.; Zundel, L.; Sanders, S. *ACS Nano* 2019, 13, 10682.

[4] Zundel, L.; Manjavacas, A. *J. Phys: Photonics* 2019, 1, 015004.

#### 6:00 AM \*F.NM01.03.05

**Absorption, Nonparabolicity and the Origins of Extreme Nonlinearity in Epsilon-Near-Zero Materials** Nathaniel Kinsey<sup>1</sup>, Ray Secondo<sup>1</sup> and Jacob Khurgin<sup>2</sup>; <sup>1</sup>Virginia Commonwealth University, United States; <sup>2</sup>Johns Hopkins University, United States

Optical researchers have long sought to develop materials and systems that enable more efficient nonlinear processes. From semiconductors, polymers, organize, and metamaterials, many promising materials, and approaches have been investigated, yet the primary platforms for nonlinear phenomena remain bulk crystals and optical fiber. A new entry into the area of nonlinear materials is epsilon-near-zero materials. In the past few years, these films have been shown to enhance various nonlinear processes from extreme refractive index tuning, phase conjugation, harmonic generation, and adiabatic frequency

shifts in films with a thickness on the order of the wavelength due to unique intrinsic and extrinsic enhancement of the nonlinear response. Despite a variety of experimental successes, the theory of the effect has largely lagged behind. Here we outline a theoretical approach to describing extreme nonlinear index tuning in Drude epsilon-near-zero materials such as transparent conducting oxides. Our approach provides an analytical description suited to estimate the order of magnitude of the nonlinearity given basic properties, as well as a full numerical approach capable of predicting the strength, dispersion, and intensity dependence of the nonlinearity for multiple materials without fitting parameters. We utilize this model to investigate the impact of loss on the nonlinear response and develop a figure of merit to evaluate the performance of up-and-coming material platforms. Ultimately we believe our approach will aid the development and optimization of the promising epsilon-near-zero platform for both free-space and on-chip nonlinear applications.

#### 6:15 AM F.NM01.03.06

**Mie-Resonant Three-Dimensional Metacrystals** [Seokhyoung Kim](#)<sup>1</sup>, Cindy Zheng<sup>1</sup>, George C. Schatz<sup>1</sup>, Koray Aydin<sup>1</sup>, Kyoung-Ho Kim<sup>2</sup> and Chad Mirkin<sup>1</sup>; <sup>1</sup>Northwestern University, United States; <sup>2</sup>Chungbuk National University, Korea (the Republic of)

Optical metamaterials are engineered structures that exhibit electromagnetic properties not found in naturally occurring materials. These structures, which can exhibit properties including near-zero or negative refractive indices, very large electric permittivities, and negative permeabilities, may enable new cloaking, metatronic nanocircuitry, and optical computing technologies. While there have been significant advances in the design and fabrication of two-dimensional (2D) metasurfaces, planar structures create nontrivial angular and polarization sensitivities, making omnidirectional operation impossible. Although three-dimensional (3D), isotropic metamaterials have been proposed, including ones that exhibit unnaturally high refraction, they have yet to be made. Here, we report the use of DNA-mediated programmable assembly to prepare isotropic 3D metacrystals from oligonucleotide-modified Au nanocubes. We use finite-element modeling to show such structures could have an effective index as large as  $\sim 8$  in the mid-infrared, far greater than that of natural materials, and for the first time, experimentally observe multipolar Mie resonances in 3D metacrystals with well-formed habits. Specifically, we synthesized cubic superlattices with effective indices of  $\sim 4.7$ , comparable to the previous record in the optical regime for 2D metasurfaces. These sub-micron cube-shaped metacrystals exhibit mid-infrared Mie resonances, which were characterized by synchrotron infrared microspectroscopy.

SESSION F.NM01.04: Emergent Optoelectronic Materials and Platforms  
On Demand Abstracts Available for Viewing Starting Saturday Morning, November 21, 2020  
F-NM01

#### 5:00 AM \*F.NM01.04.01

**Aluminum Plasmonics** [Naomi Halas](#); Rice University, United States

While the noble/coinage metals have dominated chemistry research in nanomaterials that support surface plasmons, more recently the quest for sustainable and inexpensive plasmonic media has begun to focus on Aluminum. The nucleation and growth chemistry of Aluminum is unique, however, and few lessons learned from aqueous-based metal nanoparticle nucleation and growth apply to this metal. Aluminum nanocrystal growth is catalyst-driven, and the nucleation event is also strongly influenced by solvent molecules that complex with the catalyst-alane precursor. Studies of this system has led us to discover paths toward size and shape control dependent on the catalyst properties. With both size and shape dependence come new properties, which include new roles as optical antennas in plasmonic photocatalyst complexes. We show that for reactions that are driven by a hot electron mechanism, there is a strong dependence of reaction rate upon nanoparticle shape, for particles with the same plasmon resonant energy.

#### 5:15 AM \*F.NM01.04.02

**Atomic Layer Deposited VO<sub>2</sub> Thin Films Towards Modulated Infrared Optoelectronic Devices** [V. D. Wheeler](#)<sup>1</sup>, Chase Ellis<sup>1</sup>, Marc Currie<sup>1</sup>, J.R. Avila<sup>2</sup>, Michael A. Meeker<sup>1</sup>, Joshua D. Caldwell<sup>3</sup> and Joseph Tischler<sup>1</sup>; <sup>1</sup>U.S. Naval Research Laboratory, United States; <sup>2</sup>ASEE Postdoctoral Fellow, United States; <sup>3</sup>Vanderbilt University, United States

VO<sub>2</sub> is a phase change material that undergoes a first order crystalline phase transition at a critical temperature ( $T_c = 68^\circ\text{C}$ ), resulting in significant changes in intrinsic electrical and optical properties, especially in the infrared. Optical changes with

this phase transition are of particular interest as passive and active components of optoelectronic devices, specifically for thermal regulation and modulated signaling. Realizing this type of device often requires the integration of thin, conformal VO<sub>2</sub> films with complex, non-planar structures (like metamaterials). Thus, atomic layer deposition (ALD) is the ideal deposition method in these cases.

Traditional metal-based plasmonic materials suffer from high optical losses, which has promoted research towards alternative low-loss materials that can support plasmonic-like effects. One such approach employs phonon-mediated collective-charge oscillations (surface phonon polaritons, SPhPs) that are supported by nanostructured polar dielectric materials (SiC, AlN, etc), which inherently are low-loss. Geometric design of the nanostructures enables spectral tuning of resonant features between the longitudinal and transverse optical phonons of the polar material, typically in the infrared regions. However, the spectral position and amplitude of these resonances remain fixed after fabrication. Integrating phase change materials with these structures provides a way to achieve active modulation of resonances.

In this work, we will discuss the ALD process optimization and characterization of thin VO<sub>2</sub> films itself and subsequent integration into different optoelectronic structures for active modulation. In particular we will present a case study where nanopillar arrays were etched into SiC and AlN to create narrowband resonances in the long-wave infrared region. These structures were subsequently coated with ALD VO<sub>2</sub> films with different thicknesses (8-75nm). As-deposited VO<sub>2</sub> films are highly conformal and amorphous, and cause the resonances to shift and broaden due to the different dielectric environment. However, after annealing the films at 525°C in 6x10<sup>-5</sup> Torr, the VO<sub>2</sub> films crystallize resulting in sharper resonances and spectral locations close to the initial uncoated structures. Temperature-dependence reflectance and emission measurements show that by heating through the VO<sub>2</sub> transition temperature, the amplitude of the resonances can be modulated. Full signal modulation (ie. on/off) requires at least a 16nm VO<sub>2</sub> film. This work shows the ability to actively tune surface phonon polariton resonances using ALD phase change materials.

#### 5:30 AM F.NM01.04.04

**Wurtzite Gallium Phosphide Structures for Photonic Applications** Bruno da Silva<sup>1</sup>, Odilon D. Couto Jr<sup>1</sup>, Carlos A. Senna<sup>2</sup>, Braulio S. Archanjo<sup>2</sup>, Fernando Iikawa<sup>1</sup> and Monica A. Cotta<sup>1</sup>; <sup>1</sup>University of Campinas, Brazil; <sup>2</sup>National Institute of Metrology, Quality and Technology, Brazil

Wurtzite Gallium Phosphide (GaP) nanowires have been intensively studied due to the possibility of finding a new direct band gap material in the green spectral range. However, recent works have suggested a pseudodirect band gap instead. Here, we investigate the optical properties of Au-catalyzed GaP nanowires, obtained by chemical beam epitaxy and nanoparticle crawling-assisted vapor-liquid-solid growth. We discuss how this phenomenon impacts nanowire morphology, and leads to the formation of an asymmetric GaP nanostructure. Using large volume (micron-sized) GaP structures in the wurtzite phase, we were able to carry out absorption measurements to elucidate the exact value of the fundamental band gap, excitonic emissions and valence band splitting energies of the wurtzite phase. Our data indicates the existence of a dipole forbidden (pseudo-direct) band gap at low temperature at (2.19 +/- 0.02) eV. We also discuss how to control the incorporation of unintentional impurities and its effect on the luminescence of this material. Furthermore, we show that high densities of large volume, wurtzite GaP structures (up to 40micra in length and over 2micra in diameter), with sidewalls presenting roughness in nanometer scale, can easily be obtained with our nanoparticle crawling-assisted growth method for antireflective coating in device applications.

#### 5:40 AM F.NM01.04.05

**Physical Properties and Formation of Zinc Oxide Nano-Scaled Using Natural Extract from Dry Corn Husk (Zea Mays) via Green Chemistry Assisted by Spin Coating Technique** Moussa Bakayoko<sup>1,2,3</sup>, Balla Diop Ngom<sup>2</sup>, Papa D. Tall<sup>2</sup>, Malik Maaza<sup>3,1</sup> and Ibrahima Ngom<sup>1,2,3</sup>; <sup>1</sup>University Of South Africa, South Africa; <sup>2</sup>Université Cheikh Anta Diop de Dakar, Senegal; <sup>3</sup>iThemba Laboratory for Accelerator Based Science, South Africa

Biosynthesis, as an alternative method, sparked an attractive attention in the research world due to its biocompatibility concerning production potential antibacterial agents. However, compared to chemical and physical methods, the main drawback associated with the biological synthesis is the inability to get the size and / or shape desired nanoparticles with a good yield.

In order to overcome this granulometry problem associated with a biological approach, this research work consisted, first step, to synthesize zinc oxide nanoparticles (ZnO NPs), by an entirely ecological chemistry process, simple and profitable using the extract from the dry husk of corn (Zea mays) as an effective chemical reducing agent without the addition of any standard acid or basic component. The physical properties such as structure, size, morphology and elementary composition, as well as the optical properties of the bio-synthesized nanoparticles were determined using the following different characterization techniques: High resolution scanning electron microscopy (HR -MEB), high resolution transmission electron

microscopy (HR-MET), X-ray diffraction (DRX), energy dispersive X-ray spectroscopy, Fourier transform infrared spectroscopy and Raman scattering, UV-Visible spectroscopy, as well as photoluminescence (PL) spectroscopy.

In a second step, we therefore synthesized zinc oxide nanofilms (ZnO NFs) in a biological approach assisted by spin coating technique, and thus studied its main physical properties using the same investigation techniques as mentioned above through a comparative study with the properties of bio-synthesized ZnO nanoparticles (ZnO NPs).

After investigation, the results show that the size of ZnO nanoparticles has been reduced by 20%, thus suggesting that the spin coating technique is an appropriate high quality method for improving the biosynthesis process of oxide-based nanomaterials, by overcoming the size phenomenon linked to this biological approach.

#### 5:50 AM F.NM01.04.07

**N-Doping of Quantum Dots by Lithium-Ion Intercalation** Woo Je Chang, Kyu-Young Park, Yizhou Zhu, Christopher Wolverton, Mark Hersam and Emily Weiss; Northwestern University, United States

The electronic and optical properties of colloidal quantum dots (QDs) are significantly affected by impurities and doping. Crucial to efficient electronic doping of QDs is suitable charge compensation, but current compensation methods based on surface chemical modification and substitutional impurities have limited controllability and feasibility, respectively. Here, we describe an electronic *n*-type doping method where charge compensation is achieved with Li<sup>+</sup> ions occupying interstitial sites. By controlling the electrochemical potential, Li<sup>+</sup> ions are intercalated into CdSe QDs, allowing compositional control of Li<sub>x</sub>CdSe,  $x \leq 0.3$ . At high lithiation levels, the Fermi energy is shifted into the QD conduction band, resulting in *n*-type degenerate doping characteristics, including bleaching of the band edge optical absorption, activation of intraband transitions, and blue-shifting of the photoluminescence spectrum. By reversing the sweep of the electrochemical potential, the original optical features of undoped QDs are partially recovered, indicating the reversibility of Li<sup>+</sup> ion intercalation. Overall, this work establishes electrochemical interstitial doping as a reversible method for tuning the optical properties of colloidal QDs.

#### 6:00 AM F.NM01.04.08

**High Plasmonic Quality Titanium Nitride Films Grown on MgO-Buffered Si (001)** Kai Ding<sup>1</sup>, Dhruv Fomra<sup>1</sup>, Alexander Kvit<sup>2</sup>, Hadis Morkoç<sup>1</sup>, Nathaniel Kinsey<sup>1</sup>, Ümit Özgür<sup>1</sup> and Vitaliy Avrutin<sup>1</sup>; <sup>1</sup>Virginia Commonwealth University, United States; <sup>2</sup>University of Wisconsin–Madison, United States

Titanium nitride (TiN) thin films on Si are very attractive for TiN-based integrated plasmonic devices. However, the heretofore reported TiN films on highly coveted Si substrates typically exhibited only moderate plasmonic properties due in large part to substantial defect densities caused by the large lattice mismatch between Si and TiN (21.9%). Therefore, smaller lattice mismatched substrates such as sapphire and bulk MgO have been more commonly used. In this work, we report a comparative study on the structural and optical properties of TiN thin films grown by atomic layer deposition on different substrate materials including Si (001), MgO-buffered Si (001), c-sapphire, and bulk MgO (001). High-resolution X-ray diffraction (XRD), high-resolution scanning transmission electron microscopy (STEM), and variable angle spectroscopic ellipsometry were used to characterize the TiN films on these substrates. We observed that the TiN films grown on Si (001), MgO-buffered Si (001), and bulk MgO (001) substrates are all (001)-oriented possessing four-fold in-plane symmetry, while the films grown on c-sapphire substrate exhibit (111) orientation with six-fold in-plane symmetry. Insertion of a thin (~10 nm) MgO buffer led the intensity of XRD reflections from the TiN films grown on Si (001) to increase significantly, and cube-on-cube epitaxial growth was confirmed by high-angle annular dark-field imaging analysis of STEM. To characterize the plasmonic quality of the TiN films grown on different substrates, we used the traditional figure of merit (FOM) that equals to  $-\epsilon''/\epsilon'$ , which quantifies the tradeoff between dielectric losses ( $\epsilon''$ ) and metallicity ( $\epsilon'$ ). The peak FOM values are 2.4, 2.7, 2.8, and 2.9 for TiN films grown on Si (001), c-sapphire, MgO-buffered Si (001), and bulk MgO (001), respectively. As a result of the improved crystalline quality, use of a thin MgO buffer layer enhances the plasmonic quality of TiN films on Si (001) nearly to the level of TiN on bulk MgO (001) substrate. This thin MgO interlayer makes TiN thin films on MgO-buffered Si (001) an attractive material for applications in integrated plasmonic devices such as modulators and resonators based on the silicon platform.

#### 6:10 AM F.NM01.04.11

**Titanium Nitride for Plasmonic and Metamaterial Applications** Amber N. Reed, Hadley Smith, Zachary Biegler, Krishnamurthy Mahalingam, Kurt Eyink and Augustine Urbas; Air Force Research Laboratory, United States

Titanium nitride (TiN) is a promising material for plasmonic and metamaterials due to its temperature stability, chemical stability, low surface energy, mechanical robustness, and zero-crossover wavelength in the visible region. In this work we demonstrate the reactive magnetron sputtering of heteroepitaxial TiN on (0001)-Al<sub>2</sub>O<sub>3</sub>, (001)-MgO and (0001)-LiNbO<sub>3</sub> substrates. Additionally, we demonstrate the incorporation of TiN in metal-dielectric stacks. We discuss the effect of

substrate material and deposition conditions on the TiN growth, stoichiometry and crystallinity. Coupled x-ray diffraction (XRD) show high quality epitaxial TiN growth on all three substrates. Pendellosung fringes on the (111)-TiN diffraction peak for the coupled XRD of TiN on c-plane sapphire and LiNbO<sub>3</sub> and the (001)-TiN diffraction peak on MgO indicate uniform d-spacing and a pristine interface. Further structural characterization, however, reveals differences in crystal defects, strain and surface morphology based on substrate crystal structure and lattice mismatch. A 6-fold symmetry is seen in the pole figure XRD of the TiN grown on sapphire, indicating the presence of stacking faults. These domains, which are also evident in atomic force microscopy (AFM) of the TiN surface, are attributed to different stacking within the TiN domains. Cross-hatching features similar to those on the bare MgO substrate seen in the AFM of the TiN surface. X-ray photoelectron spectroscopy was used to investigate compositional differences between films grown with different deposition conditions. The real ( $\epsilon_1$ ) and imaginary ( $\epsilon_2$ ) permittivity for TiN was measured using variable angle spectroscopic ellipsometry. The TiN behaves metallic on all substrates for wavelengths above 470-490 nm. We calculate a quality factor (QLSPR =  $-\epsilon_1/\epsilon_2$ ) of 3.34, 3.9 and 4.2 for TiN on LiNbO<sub>3</sub>, MgO and Al<sub>2</sub>O<sub>3</sub> respectively, for a wavelength of 1550 nm.

#### 6:20 AM F.NM01.04.12

**Modulating the Phase Transition in VO<sub>2</sub> Nanoparticles Produced by Solid-State Dewetting** Samuel T. White, James R. Taylor, Thomas Folland, Joshua D. Caldwell and Richard F. Haglund; Vanderbilt University, United States

Phase-change materials (PCMs) can introduce reconfigurable behavior into metamaterials and optical devices that otherwise have fixed properties. Vanadium dioxide (VO<sub>2</sub>) is outstanding among PCMs due to its near-room-temperature transition ( $T_c \sim 68^\circ\text{C}$ ), sharp change in optical properties, and ultrafast (tens of femtoseconds) switching speeds. It has served as the active material in passive thermal control coatings, ultrafast photonic modulators, tunable ring resonators, and reconfigurable hyperbolic metamaterials. Many avenues for tailoring the optical properties and transition behavior of thin-film VO<sub>2</sub> have been explored—doping, strain, and defects being among the most prominent—but adjusting  $T_c$  without loss of contrast between the metal and insulating phases remains a challenge. Tungsten doping, for example, can reduce  $T_c$ ; but heavy doping severely reduces the contrast and degrades the sharpness of the transition, before  $T_c$  is even below room temperature.

In contrast to thin films, VO<sub>2</sub> nanoparticles, doped with tungsten and embedded in a silica matrix, can achieve  $T_c \sim -25^\circ\text{C}$  without significant loss of contrast (1). Here, we investigate the formation of self-assembled VO<sub>2</sub> nanoparticles by solid-state dewetting of VO<sub>2</sub> thin films, and study how the phase transition behavior of those nanoparticles depends on particle size, W-doping, and silica encapsulation. Nanoparticle formation by solid-state dewetting, much simpler and faster than lithographic techniques, is driven by surface energies and statistical mechanics of particle aggregation. The resulting nanoparticles are remarkably consistent across different film deposition techniques (pulsed laser deposition, atomic layer deposition, RF sputtering, and vapor transport); a comparison of results on silicon shows that the average nanoparticle radius is directly proportional (slope  $\approx 2.8$ ) to the initial film thickness, regardless of the deposition method. We show how this size dependence, as well as the nanoparticle size distribution, can be predicted with a simple model.

The effect of nanoparticle size on hysteresis in the metal-insulator transition has been studied previously, usually by measuring large groups of particles in aggregate and considering the average particle size. By employing scattering-type scanning near-field optical microscopy, we observe the phase transition in individual nanoparticles with increased sensitivity, spatial resolution, and temperature resolution (across the region of strong correlation) relative to previous work (2).

Simultaneously investigating multiple individual nanoparticles allows us to observe precise size and shape effects and to understand the degree of intrinsic particle-to-particle variation. Finally, by comparing the effects of W-doping and SiO<sub>2</sub>-encapsulation on these nanoparticles and on corresponding thin films, we elucidate how particle-size effects, strain resulting from encapsulation, and/or a synergistic combination of the two can lead to greater tunability of  $T_c$  without loss of switching contrast. Together, these results represent an advancement in our understanding of how VO<sub>2</sub> nanoparticles form via solid-state dewetting and in our ability to tailor their size, shape,  $T_c$ , and hysteretic behavior to suit the needs of individual applications, thus further increasing the versatility of VO<sub>2</sub> as an active component for “smart” optical devices.

1. Lopez R, Haynes TE, Boatner LA, Feldman LC, Haglund RF. 2002. Temperature-controlled surface plasmon resonance in VO<sub>2</sub> nanorods. *Opt. Lett.* 27:1327-9

2. Donev EU, Lopez R, Feldman LC, Haglund RF. 2009. Confocal Raman Microscopy across the Metal-Insulator Transition of Single Vanadium Dioxide Nanoparticles. *Nano Lett.* 9:702-6

#### 6:30 AM F.NM01.04.13

**Dual-Mode Infrared Absorption by Segregating Dopants within Plasmonic Semiconductor Nanocrystals** Stephen Gibbs<sup>1</sup>, Christopher Dean<sup>1</sup>, Joey Saad<sup>1</sup>, Bharat Tandon<sup>1</sup>, Corey Staller<sup>1</sup>, Ankit Agrawal<sup>2</sup> and Delia Milliron<sup>1</sup>; <sup>1</sup>University of Texas at Austin, United States; <sup>2</sup>Lawrence Berkeley National Laboratory, United States

Degenerately doped metal oxides derive a high free charge carrier population from charge-compensated defects. Spatial

control of the dopant distribution within each nanocrystal allows tuning of the potential energy landscape for charge carriers in a way not possible for conventional metals. Here, we employ a slow-addition approach to nanocrystal synthesis that enables control of radial distribution of substitutional tin dopants within an indium oxide lattice. When dopants are segregated either to the core or surface of spherical indium oxide nanocrystals, the potential established by space-charge build up at the interface between indium oxide and tin-doped indium oxide prevents charge carriers from distributing homogeneously throughout the nanocrystal. The doped region maintains a higher carrier concentration than the undoped region. The dielectric permittivity then varies radially, resulting in two distinct spectral modes in the plasmonic optical response. Spectra reported previously for spherical plasmonic semiconductor nanocrystals have shown hints of this dual-mode response, but the reason for its appearance has remained largely uninvestigated. We developed a simple model employing a core-shell Maxwell-Garnett effective medium approximation that can reliably fit dual-mode spectra and can explain the evolution of the secondary mode in our dopant-segregated system.

Two sample series were synthesized and investigated: one with an undoped core and doped shell of increasing thickness and another with a doped core and undoped shell of increasing thickness. After shell growth of sufficient thickness, a second absorption mode manifested in both series. The effective medium model allowed us to extract intrinsic material properties, in particular the carrier concentration of both the core and the shell, that supported the experimentally observed trends in both series. Lastly, we proved that the sensitivity of the plasmonic response to the surrounding refractive index depends on dopant distribution, underlining the impact that intra-nanocrystal carrier distribution can have on the interaction between plasmonic nanocrystals and their environment.

SESSION F.NM01.05: Integrated Nanophotonic Architectures and Metasurfaces  
On Demand Abstracts Available for Viewing Starting Saturday Morning, November 21, 2020  
F-NM01

**5:00 AM \*F.NM01.05.01**

**Hybrid Photonic Devices Based on Gallium Phosphide and Diamond** Kai-Mei Fu; University of Washington, United States

Solid-state defect qubit systems with viable spin-photon interfaces show promise for single-photon generation, metrology and quantum information applications. Photon collection efficiency presents a major challenge for efficient utilization of defect qubits in high refractive index host materials like diamond and silicon carbide. Here we present a flexible inverse-design optimization framework that can reconcile a broad range of design constraints and generate planar dielectric photonic structures operating near the theoretical limit. Our optimized device utilizes a hybrid gallium phosphide (GaP) on diamond structure for photoluminescence (PL) extraction from synthesized NV centers in diamond. The enhancement is fairly insensitive to spatial localization and efficiently extracts photons from all dipole orientations. Additionally, we constrain patterning to the GaP layer, to minimize perturbations of the NV environment due to diamond etching. We fabricate the optimized device and observe efficient PL extraction from shallow (~100 nm) single NVs and near-surface (<100 nm) NV ensembles created by nitrogen ion implantation and annealing. These versatile devices exhibit a broadband PL enhancement for wavelengths in the measured range of 575 nm to 800 nm. We measure up to fourteen fold enhancement of free-space PL collection rate from device coupled NVs over non-device NVs and quantify the effect of fabrication and device integration on defect charge state and spectral stability. We expect such inverse-design hybrid devices will enable realization of scalable arrays of single-photon emitters, rapid characterization of new quantum emitters, high sensitivity metrology and efficient heralded entanglement schemes.

**5:15 AM \*F.NM01.05.02**

**Volumetric Meta-Optics for Novel Device Functionalities** Andrei Faraon; California Institute of Technology, United States

Three-dimensional elements, with refractive index distribution structured at subwavelength scale, provide an expansive optical design space that can be harnessed for demonstrating multifunctional free-space optical devices. We present 3D dielectric elements, designed to be placed on top of the pixels of image sensors, that sort and focus light based on its color and polarization with efficiency significantly surpassing 2D absorptive and diffractive filters. The devices are designed via iterative gradient-based optimization to account for multiple target functions while ensuring compatibility with existing nanofabrication processes, and they are experimentally validated using a scaled device that operates at microwave



frequencies. This approach combines arbitrary functions into a single compact element, even where there is no known equivalent in bulk optics, enabling novel integrated photonic applications. We further discuss capabilities enabled by volumetric meta-optical devices for compact on-chip polarimetry and discuss implementations using multi-layer nanofabrication.

### **5:30 AM \*F.NM01.05.03**

**Van der Waals Material Integrated Nanophotonics** Arka Majumdar; University of Washington, United States

Atomically thin van der Waals (vdW) materials have generated strong interest in the community due to its unusual physical properties and possibility of creating high-performance devices. However, the ultrathin nature of these materials limits the achievable light-matter interaction. One promising way to increase such interaction is via nanophotonic confinement of light. In fact, researchers have demonstrated various nanophotonic devices using such vdW materials, including optically pumped lasing, second harmonic generation, cavity enhanced electroluminescence, and exciton-polaritons. In this talk, I will explore the possibility of going to quantum optical regime using this material system integrated with nanophotonic resonators. I will discuss the role of exciton-phonon interaction in the cavity photoluminescence spectrum and present a quantum optical model of the coupled system in presence of the phonons. I will then report the observation of the exciton-polaritons using transition metal dichalcogenides (TMD) coupled with a metasurface structure. This hybrid light-matter system can be used to reach single photon nonlinear regime via further engineering the nanophotonic structure and patterning the TMD material.

### **5:45 AM \*F.NM01.05.04**

**Ultrafast Semiconductor Dielectric Metasurfaces** Igal Brener; Sandia National Laboratories and Center for Integrated Nanotechnologies, United States

Resonant dielectric metasurfaces offer unparalleled degrees of freedom to design flat-optics and study fundamental aspects of light-matter interaction, due to the freedom to use optical resonances of electrical and magnetic character and different symmetries, extremely low loss when operating below the semiconductor band gap, and controlled coupling and interactions between the meta-atoms. Additionally, transient sub-picosecond behavior can be imparted to the metasurface using optical pumping and controlling of carrier dynamics and decay. In this talk I will overview some of our work based on such metasurfaces made from III-V semiconductors. In particular, I will focus on ultrafast switching and diffraction, transient frequency conversion and perfect absorbing metasurfaces for THz emission and detection.

### **6:00 AM \*F.NM01.05.05**

**Straintronics and ITO-Photonics—Advances in Heterogeneous Opto-Electronic Devices** Volker J. Sorger; George Washington University, United States

Here I discuss our recent demonstrations of ITO-based opto-electronic devices and introduce the concept of 'Strainoptronics'. The presentation includes the following concepts: 1) Here we demonstrate a spectrally broadband, gigahertz-fast Mach-Zehnder interferometric modulator exhibiting a miniscule  $V\pi$  L of 95 V- $\mu$ m, deploying a subwavelength short electrostatically tunable plasmonic phase shifter based on heterogeneously integrated indium tin oxide thin films into silicon photonics. This GHz-fast broadband integrated modulator bears relevance since ITO is a foundry-compatible material. Unlike the crystal-orientation-sensitive LN, ITO optoelectronics is synergistic to enhancing electrostatics known from transistor technology. 2) Strain-engineered high-responsivity MoTe<sub>2</sub> photodetector for silicon photonic integrated circuits In integrated photonics, specific wavelengths such as 1,550 nm are preferred due to low-loss transmission and the availability of optical gain in this spectral region. For chip-based photodetectors, two-dimensional materials bear scientifically and technologically relevant properties such as electrostatic tunability and strong light-matter interactions. However, no efficient photodetector in the telecommunication C-band has been realized with two-dimensional transition metal dichalcogenide materials due to their large optical bandgaps. Here we demonstrate a MoTe<sub>2</sub>-based photodetector featuring a strong photoresponse (responsivity 0.5 A/W) operating at 1,550 nm in silicon photonics enabled by strain engineering the two-dimensional material. Non-planarized waveguide structures show a bandgap modulation of 0.2 eV, resulting in a large photoresponse in an otherwise photoinactive medium when unstrained. Unlike graphene-based photodetectors that rely on a gapless band structure, this photodetector shows an approximately 100-fold reduction in dark current, enabling an efficient noise-equivalent power of 90 pW/Hz<sup>0.5</sup>. Such a strain-engineered integrated photodetector provides new opportunities for integrated optoelectronic systems.

**6:15 AM \*F.NM01.05.06**

**Miniature Optical Systems Based on Cascaded Metasurfaces** Andrew McClung, Mahdad Mansouree, Sarath Samudrala, Mahsa Torfeh, Babak Mirzapourbeinekalaye and Amir Arbabi; University of Massachusetts Amherst, United States

Miniaturized optical systems with planar form factors and low power consumption have many applications in consumer electronics, imaging and spectral sensing systems, and as integral parts of medical and industrial equipment. Flat optical devices based on dielectric metasurfaces introduce a new approach for the realization of such systems at low cost using conventional nanofabrication techniques. In this talk, I will present an overview of our work on the development of various high-performance optical dielectric metasurface components and systems. In particular, I will discuss multi-layer dielectric metasurfaces that enable complete control of wavefront at multiple wavelengths. I will present an on-chip integration platform enabled by vertical or lateral integration of multiple metasurfaces and active optoelectronic components such as laser arrays and image sensors. I will also introduce a novel technique for engineering chromatic dispersion by cascading and discuss various optical systems implemented in this platform and a single-snapshot multispectral imager.

**6:30 AM \*F.NM01.05.07**

**Optical Meta Devices—Eyes to the Future** Din-Ping Tsai, Mu-Ku Chen and Yongfeng Wu; The Hong Kong Polytechnic University, Hong Kong

The novel property of optical metasurface which consist of nano-antenna made by artificial nanostructures, has attracted a lot of attention lately. Nano-antenna at the interface can behave like secondary radiation sources after interactions of the incident electromagnetic wave. Various optical devices based on the specific designs of meta-surfaces are called optical meta-devices. The great advantages of meta-devices are their new properties, lighter weight, small size, high efficiency, better performance, broadband operation, lower energy consumption, and CMOS compatibility for mass production. Given the demands of photonics, many optical meta-devices for the applications of controlling of the incident light are developed, such as for beam deflection and reflection, polarization control and analysis, meta-holography, second-harmonic generation, meta-laser, tunability, imaging, absorption, color display, focusing of light, multiplexer of colour routing and light-field sensing, etc. Considering the flexibility, the metasurface with integrated functionalities may be promising for multi-focusing microscopy, high-dimension quantum technology, hyperspectral microscopy, micro robotic vision, automobile sensing, virtual and augmented reality (VR and AR), drones, and miniature personal security systems [1-7].

**References**

1. S. M. Wang, P. C. Wu, V.-C. Su, Y.-C. Lai, C. H. Chu, J.-W. Chen, S.-H. Lu, J. Chen, B. B. Xu, C.-H. Kuan, T. Li, S. N. Zhu and D. P. Tsai, *Nature Comm.* 8, 187 (2017).
2. B. H. Chen, P. C. Wu, V.-C. Su, Y.-C. Lai, C. H. Chu, I. C. Lee, J.-W. Chen, Y. H. Chen, Y.-C. Lan, C.-H. Kuan and D. P. Tsai, *Nano Lett.* 17, 6345 (2017).
3. S. M. Wang, P. C. Wu, V.-C. Su, Y.-C. Lai, M.-K. Chen, H. Y. Kuo, B. H. Chen, Y. H. Chen, T.-T. Huang, J.-H. Wang, R.-M. Lin, C.-H. Kuan, T. Li, Z. Wang, S. Zhu and D. P. Tsai, *Nature Nanotechnology* 13, 227 (2018).
4. V.-C. Su, C. H. Chu, G. Sun and D. P. Tsai, *Optics Express* 26, 13148 (2018).
5. M. L. Tseng, H.H. Hsiao, C. H. Chu, M. K. Chen, G. Sun, A.Q. Liu and D. P. Tsai, *Adv. Optical Mater.* 6, 1800554 (2018).
6. R. J. Lin, V.-C. Su, S. M. Wang, M. K. Chen, T. L. Chung, Y. H. Chen, H. Y. Kuo, J. W. Chen, J. Chen, Y. T. Huang, J.H. Wang, C. H. Chu, P. C. Wu, T. Li, Z. Wang S. Zhu and D. P. Tsai, *Nature Nanotechnology*, 14, 227 (2019).
7. W. Yang, S. Xiao, Q. Song, Y. Liu, Y. Wu, S. Wang, J. Yu, J. Han, and D. P. Tsai, "All-dielectric metasurface for high-performance structural color," *Nature Communications* 11, 1864 (2020).

**6:45 AM \*F.NM01.05.08**

**2.5D Photonics as Engines of Information Manipulation** Rajesh Menon; The University of Utah, United States

Micro- and nanostructures have been widely applied to enhance the performance of optical components and systems. Structures whose characteristic dimensions are greater than the wavelength of interest,  $l$ , can effectively manipulate the **scalar** properties of light, while nanostructures with dimensions  $\ll l/2$  can manipulate the **vector** properties of light. By restricting the photonic functionality to a thin plane (i.e., 2.5D photonics), it's possible to create very thin lightweight imaging lenses,<sup>1</sup> spectrum-splitting solar concentrators,<sup>2</sup> and integrated-photonics devices.<sup>3</sup> In this presentation, we will highlight examples of each such device that overcome limitations of conventional implementations (if they exist at all). For example, flat multi-level diffractive lenses (MDLs) have recently shown achromatic bandwidth,<sup>4,5</sup> depth-of-focus<sup>6</sup> and efficient high-numerical aperture focusing<sup>7</sup> far better than their conventional counterparts, all while reducing weight and thickness by several orders of magnitude.

Computational techniques, such as nonlinear optimization, coupled with electromagnetics modeling can drive the *inverse*

design of novel optical and photonic components and systems. When guided by manufacturing constraints, such techniques can result in highly practical, low-cost, ultra-compact (on the order of  $1 \times 1$ ) and multi-functional integrated-photonics components, such as polarization beam-splitters,<sup>3</sup> wavelength splitters,<sup>8</sup> couplers,<sup>9</sup> waveguide bends,<sup>10</sup> etc. We'll also describe a nanophotonic cloak that enables two devices to be placed closer together than is otherwise feasible, leading to an increase in integration density.<sup>11</sup>

When coupled with advanced machine-learning or linear-algebraic methods, 2.5D photonics can engines of information manipulation, enabling highly non-intuitive forms of optical systems such as photography with no lenses<sup>12,13</sup> or microscopy with only a surgical needle<sup>14,15</sup> or multi-spectral imaging with a diffractive element.<sup>16</sup>

#### References:

- S. Banerji, *et al.*, *PNAS*, 116(43) 21375 (2019).  
P. Wang, *et al.*, *Prog. Photovolt.* 23(9) 1073 (2015).  
B. Shen, *et al.*, *Nat. Photon.* 9, 378 (2015).  
M. Meem, *et al.*, arXiv:2004.13476 (2020).  
M. Meem, *et al.*, arXiv:2001.03684 (2020).  
S. Banerji, *et al.*, *Optica* 7(3) 214-2017 (2020)  
M. Meem, *et al.*, *Optica* 7(3) 252-253 (2020).  
A. Y. Piggott, *et al.*, *Nat. Photon.* 9, 374 (2015).  
B. Shen, *et al.*, *Opt. Exp.* 22(22) 27175 (2014).  
B. Shen, *et al.*, *Opt. Lett.* 40(24) 5750 (2015).  
B. Shen, *et al.*, *Nat. Commun.* 7, 13126 (2016).  
G. Kim & R. Menon, *Opt. Exp.* 26(18), 22826 (2018).  
G. Kim, *et al.*, *Appl. Opt.* 56(23) 6450 (2017).  
G. Kim, *et al.*, *Sci. Rep.* 7, 44791 (2017).  
G. Kim, *et al.*, *Appl. Phys. Lett.* 106, 261111 (2015).  
P. Wang & R. Menon, *Optica*, 2(11) 933 (2015).

#### 7:00 AM F.NM01.05.09

**Nonlinear Photonic CMOS Technology for Optoelectronics Integration and Sub-7nm ULSI and ASIC—Is Hybrid Approach or Hybrid Silicon Laser Still Necessary?** James Pan<sup>1,2</sup>; <sup>1</sup>Advanced Enterprise and License Company, United States; <sup>2</sup>Northrop Grumman Corporation, United States

A photonic MOSFET includes a low resistance laser or LED in the MOSFET drain region, and a photon sensor or avalanche photo diode (APD) in the well region. MOSFET, laser and APD are fabricated as one integral device. When a voltage is applied to the MOSFET gate, and a voltage is applied to the drain, both MOSFET and laser are on. Light emitted from the laser is absorbed by the APD or photon sensor in the channel / well region right next to the laser, and a light current is triggered. The large light current flows into the drain to contribute to the total output drain current. When the MOSFET is turned off, both laser and APD are switched to off immediately. Photonic CMOS includes a photonic NMOSFET and a photonic PMOSFET.

There are two approaches to fabricate photonic CMOS transistors: (1) The MOS transistor is built in a silicon wafer. Lasing semiconductor films (III-V or II-VI) are selectively deposited in the drain region with low temperature selective CVD or epitaxy. (2) A thin silicon film is deposited on a GaAs (or GaN) substrate. CMOS is built in this thin Si layer. In the drain region, the Si layer is selectively etched with RIE (Reactive Ion Etch or "Dry Etch"). Lasing semiconductor films are selectively deposited on the opened GaAs substrate. Photon sensors or APD are fabricated in the substrate prior to the CMOS process. The process integration is simplified and low cost - compatible to the existing sub-7nm advanced CMOS process flow, including FINFETs.

Nonlinear optical materials are fabricated in the CMOS isolation regions, or buried oxide (BOX) for silicon on insulator (SOI), and in the optical waveguides connected with the photonic CMOS. The nonlinear feature enables the photonic CMOS for laser communications, and optical computing. When an external IR laser beam reaches a photonic CMOS, it is converted to a higher frequency light, and processed by the built-in photon sensor or APD in the photonic CMOS. The may also be laser communications among the photonic CMOS transistors.

Since silicon is an indirect bandgap material and can not emit light, a hybrid platform, or hybrid silicon laser, needs to rely on lasers in GaAs, GaN or other II-VI materials bonded or fabricated with silicon. The bonding process often comes with higher resistance, lower speed, and additional costs (due to the system on chip configuration and more expensive packages).

Forming a substrate with both Si and GaAs (InP, GaN..etc.) results in complicated process integration, and is not compatible to advanced CMOS ULSI or ASIC. If a laser is built with GaAs, then connected with a nearby silicon circuit, the process is quite sophisticated and performance may be compromised.

For high power lasers, the hybrid approach could cause more instability and vulnerable to temperature variations.

All such issues can be bypassed or resolved with the photonic CMOS technology. Lasing films are selectively deposited in the drain regions of CMOSFETs. CMOS and lasers are combined for higher speed, drive current, and better performance.

In this paper we would like to present I-V characteristics of photonic CMOS, and the effects of laser quantum efficiency and photon sensor absorption rate on the photon CMOS performance. We will also show several process integration schemes for nonlinear optical effects. Other potential products with photonic CMOS, such as new SRAM, circuit designs, and CMOS imaging applications will be discussed.

SESSION F.NM01.06: Light-Assisted Chemistry  
On Demand Abstracts Available for Viewing Starting Saturday Morning, November 21, 2020  
F-NM01

#### **5:00 AM F.NM01.06.01**

**Enhancing Methanol Production by Photothermal Desorption in Solid-Gas Phase CO<sub>2</sub> Hydrogenation** Siyuan Zhu, Peter Novello and Jie Liu; Duke University, United States

Currently, burning fossil fuels all over the world causes excessive emission of CO<sub>2</sub> accelerating climate change and causing detrimental harm to the environment. The capture of CO<sub>2</sub> and converting it into a high-value fuel has the potential to close the carbon cycle and mitigate harm to the climate in the future. Methanol is widely used in the chemical industry for producing chemicals, such as olefins, formaldehyde, methyl tert-butyl ether, and acetic acid. The reaction which produces methanol by CO<sub>2</sub> hydrogenation favors strict reaction conditions, like low temperature and high pressure. By using indium oxide as catalyst under ambient atmosphere, we found there is the fastest reaction rate at 250C with limited methanol desorption and the fastest methanol desorption at 500C with limited methanol production. Here, we design a two temperature processes for CO<sub>2</sub> hydrogenation reaction to produce methanol by shifting temperature between 250C and 500C. Indium oxide can absorb light from a blue LED efficiently, and allows quick temperature flip from these two temperatures. When using a blue LED to increase the temperature from 250C to 500C, the temperature increases more rapidly with the help of photothermal effect than pure heating, which can save about 1 min in the total desorption process. The study of these two temperature processes and using light as a heating source are investigating the energy efficiency between the pure heating process and the light plus heating process to optimize the energy input in the chemical reaction.

#### **5:10 AM F.NM01.06.05**

**Hot Carrier Photophysics and Thermoplasmonic Response of Water-Soluble Plasmonic HfN Nanocrystals** Sven Askes and Erik Garnett; AMOLF, Netherlands

Plasmonic nanostructures feature extraordinary absorption cross sections, highly tunable optical responses, and capability of concentrating the excitation energy in subwavelength volumes. They are furthermore attractive for driving sustainable photochemistry such as selective CO<sub>2</sub>-reduction and N<sub>2</sub>-fixation under mild conditions due to the presence of an active catalytic surface and the participation of hot electrons and/or phonons upon light excitation. Although Au and Ag nanoparticles have a strong visible range plasmonic response, they are relatively unstable in high-demanding photocatalytic environments due to thermal deformation and oxidation (for Ag). In contrast, the metallic refractory material hafnium nitride (HfN) offers a desirable combination of a visible range plasmonic response, high chemical inertness, catalytically active surface, and an extremely high melting point. Although the merits are clear, the synthesis of nanostructured HfN and the detailed photophysical characterization are still relatively unexplored.

In our work we use ultrafast transient absorption to characterize the photophysical behavior of crystalline, water-soluble HfN nanoparticles with a plasmonic response around 550 nm. We find that the ultrafast response is distinctly different from the noble metals due to the extremely short lifetime of plasmonic hot electrons in HfN. Using a dual-parabolic two-step model, we completely justify the response at short and longer timescales, and predict a phonon outburst directly after pulsed light

excitation. Our results reveal that HfN is highly promising for thermoplasmonic and photocatalytic applications, where material robustness is essential.

SESSION F.NM01.07: New Device Concepts, Architectures and Applications  
On Demand Abstracts Available for Viewing Starting Saturday Morning, November 21, 2020  
F-NM01

**5:00 AM \*F.NM01.07.01**

**Optical Nano-Kirigami** [Nicholas Fang](#)<sup>1</sup>, [Huifeng Du](#)<sup>1</sup>, [Xinhao Li](#)<sup>1</sup>, [Zhiguang Liu](#)<sup>1</sup>, [Jiafang Li](#)<sup>2</sup> and [Ling Lu](#)<sup>3</sup>; <sup>1</sup>Massachusetts Institute of Technology, United States; <sup>2</sup>Beijing Institute of Technology, China; <sup>3</sup>Chinese Academy of Sciences, China

Recently, exciting new physics of plasmonics has inspired a series of key explorations to manipulate, store and control the flow of information and energy at unprecedented dimensions. For example, analogous to the familiar description of optical energy and linear momentum, non-local symmetry transformations of photons lead to new degrees of freedoms with respect to optical spin and optical helicities that are controllable at sub-wavelength scales thanks to the emerging nanohelical structures and networks. In this talk I will introduce versatile 3D shape transformations of nanoscale structures by deliberate engineering of the topography-guided stress equilibrium of gold nanostructures. By using the topography-guided stress equilibrium, rich 3D shape transformation such as buckling, rotation, and twisting of nanostructures is precisely achieved, which can be predicted by our mechanical modeling. Benefiting from the nanoscale 3D twisting features, giant optical chirality is achieved in an intuitively designed 3D pinwheel-like structure, in strong contrast to the achiral 2D precursor without nano-kirigami. High-contrast cross-polarized diffractions are successfully observed in both linear and radial configurations, resulting from constant phase difference between the pinwheel structures of opposite handedness. We further demonstrate an on-chip and electromechanically reconfigurable nano-kirigami with optical functionalities. The nano-electromechanical system is built on a CMOS-compatible Au/SiO<sub>2</sub>/Si substrate and operated via attractive electrostatic forces between the top gold nanostructure and bottom silicon substrate. Large-range nano-kirigami like 3D deformations are clearly observed and reversibly engineered, with scalable pitch size down to 0.975  $\mu\text{m}$ . The demonstrated nano-kirigami, as well as the exotic 3D nanostructures, could be adopted in broad nanofabrication platforms and could open up new possibilities for the exploration of functional micro-/nanophotonic and mechanical devices. Nanoscale control of optical spin and optical helicities with nano-kirigami are promising for numerous technological applications, such as chiral molecular sensing, separation and synthesis, super resolution imaging, nanorobotics, and ultrathin broadband optical components for chiral light.

**5:15 AM \*F.NM01.07.02**

**Metamaterial Computing Machines** [Nader Engheta](#); University of Pennsylvania, United States

Metamaterials and metasurfaces have offered exciting platforms for engineering light-matter interaction that can provide desired functionalities. Over the past several years, numerous features and exciting applications of metastructures have been explored and developed. One of the interesting possibilities in using metamaterials is the development of “metamaterial computing machines”, which we have been exploring in my group. In such paradigm, structures are designed in order to perform mathematical operations when waves propagate through them. Effectively, materials become computing machines. We have been investigating various scenarios in which metastructures can solve integral and differential equations and can invert matrices as incoming waves interact with them. In addition to using materials platform for this purpose, we have also investigating how collections of the Mach-Zehnder interferometers (MZIs) can provide another platform for solving equations and doing mathematics with light. In this talk, I will discuss some of our ongoing research projects on this topic and will present an overview of our most recent results.

**5:30 AM \*F.NM01.07.03**

**Advanced Optimization Algorithms for Nanophotonic Design at the Device and System Level** [Katherine T. Fountaine](#)<sup>1,2</sup>, [Prachi Thureja](#)<sup>2</sup>, [Yury Tokpanov](#)<sup>2</sup>, [Dagny Fleischman](#)<sup>2</sup> and [Harry Atwater](#)<sup>2</sup>; <sup>1</sup>Northrop Grumman Aerospace Systems, United States; <sup>2</sup>California Institute of Technology, United States

Nanophotonic design spaces are often highly nonlinear; the large number of parameters (both geometric and material properties) will result in an exceptionally complex and high dimensionality design space that renders an exhaustive parameter sweep computationally insurmountable. Additionally, the design of a full nanophotonic device involves optimization at

multiple levels, including material selection/design, device design, and system level design. In this talk, I will discuss multiple optimization frameworks for different design problems, including device level design for multispectral filters and phase modulation devices and system level design for beamsteering devices and other active metasurfaces. At the device level, we have (1) employed NOMAD (non-linear optimization using mesh adaptive direct search), a hybrid (global +local), derivative free optimization method, and (2) developed a new Bayesian optimization algorithm, MF-MI-Greedy, which uses multiple levels of fidelity, to optimize various nanophotonic structures including dielectric metasurfaces and multispectral filters. At the system level, we have (1) developed a new iterative genetic algorithm and (2) employed neural nets to optimize antenna arrays of active metasurfaces with non-ideal phase and amplitude characteristics. These studies suggest that selection of the correct optimization algorithm at a given design level can significantly reduce computational time for design and improve overall device performance.

**5:45 AM \*F.NM01.07.04**

**Manipulating Light and Matter at the Nanoscale for Next Generation Solar Energy Conversion Devices** Esther Alarcon-Llado; AMOLF, Netherlands

Introducing thin, light-weight and high efficiency photovoltaics will ensure solar cells to be integrated in urban landscapes, small gadgets or even in space. While thinning down of absorber materials is a good strategy to overcome these restrictions, it comes down to the expense of poor light absorption. By contrast, nano-structuring is an effective approach to tackle flexibility, material and weight reduction without compromising absorption through the exploiting of their strong interactions with light.

In this talk I will describe the power of semiconductor nanostructures to capture and trap sunlight, enabling a wide range of new solar cells designs. First, I will introduce the wave guiding effects in semiconductor nanowires. The absorption cross-section in semiconductor nanowires can reach up to x100 their geometrical footprint, so that nanowire arrays can reach to the same absorption as in bulk films with a small fraction (< 3%) of the material. We have seen experimental evidence for the strong extinction in vertically standing GaAs and InAs nanowires, using 3D confocal fluorescence microscopy. We observe how light is perturbed up to few microns away from the nanowires for a broad range of wavelengths. We demonstrate that by probing ordered arrays with this method, the effective absorption coefficient and cross-section can be obtained without the need of a transparent substrate. Because of the absorption cross-section in nanowires is ruled by the efficient incoupling of light to the waveguide modes, absorption is relatively narrow-band (~50 nm) with the central wavelength depending on the nanowire diameter. The coloured appearance in sparse arrays are actually the perfect framework to generate a new class of semi-transparent photovoltaics, that can be used as windows and other urban spaces. We find that the multi-mode absorption in the arrays, result into higher absorbance as compared to the thin film counterpart with the same average visible transparency. Second, I will show that the diffractive power of nanowire arrays can be modulated by the wavelength-selective 1D wave guiding in the nanowires. Using the tailored structural properties in the array, we show that a nanowire array can serve as both solar cell and light in-coupler to a thin film cell underneath. The dual waveguiding effects in GaAs nanowire-Si thin film tandem architectures give rise to a 4-fold light absorption increase in the Si ultrathin bottom cell. This is a significant light trapping scheme that is obtained “for free” when using a nanostructured top cell. As a final remark, I will touch upon emerging fabrication methods for nanostructured semiconductor and conducting metamaterials. In particular, electrochemical deposition is a convenient growth method that allows for control over the growth conditions through combinations of solvents, additives, and pH, in addition to conventional parameters such as heat and pressure. By combining scalable imprint lithography with electrochemical deposition, we demonstrate large-area plasmonic lattices of In,Ga metals that can be electrochemically transformed to dielectric (In,Ga)As.

*References*

- [1] R. Frederiksen, G. Tutuncuoglu, F. Matteini, K. L. Martinez, A. Fontcuberta, and E. Alarcon-Llado, “Visual Understanding of Light Absorption and Waveguiding in Standing Nanowires with 3D Fluorescence Confocal Microscopy,” *ACS Photonics* 2017.
- [2] N. Tavakoli, E. Alarcon-Llado, "Combining 1D and 2D waveguiding in an ultrathin GaAs NW/Si tandem solar cell", *Optics Express* 2019
- [3] Valenti, M. et al. "Grain size control of crystalline III–V semiconductors at ambient conditions using electrochemically mediated growth", *J. Mat. Chem. A* 2020

**6:00 AM F.NM01.07.05**

**Photonic Designs for Laser Driven Propulsion** Ho-Ting Tung and Artur Davoyan; University of California, Los Angeles, United States

In this work we examine principles of laser propulsion for spaceflight in the solar system. We discuss regimes of laser operation, system requirements on acceleration distance and sail-craft dimensions and weight. We show that with laser

propulsion small satellites may be injected into various trajectories on a path to other planets. We show that travel times to planets may be as small as one month. We analyze spacecraft trajectory for various laser illumination regimes. Lastly, we discuss sail-craft materials and photonic design. We show that with a proper choice of low-loss materials and photonic engineering highly reflective sails may be crafted to ensure efficient momentum transfer. We further study pathways for radiative heat dissipation to ensure sustainable spacecraft operation and propulsion. We discuss several specific design concepts and demonstrate the feasibility and promise of such laser propulsion with today's technology. Our work shows that laser propulsion may offer an alternative for fast transit time and high velocity missions beyond the reach of conventional chemical rockets and plasma engines.

#### 6:10 AM F.NM01.07.06

**Inverse Designed Metagratings for Far-Field Integral Equations Solving** Andrea Cordaro<sup>1</sup>, Brian Edwards<sup>2</sup>, Vahid Nikkha<sup>2</sup>, Andrea Alù<sup>3</sup>, Albert Polman<sup>1</sup> and Nader Engheta<sup>2</sup>; <sup>1</sup>AMOLF, Netherlands; <sup>2</sup>University of Pennsylvania, United States; <sup>3</sup>The City University of New York, United States

As we approach the physical speed and power consumption limits of standard microelectronics processors, new strategies for computing are required. Among the different explored routes, analog optical computing has gained significant attention for its capability to process large amounts of data at negligible energy per bit and high speeds. Moreover, recent advances in nanofabrication techniques have enabled unprecedented control over light propagation and manipulation via subwavelength thickness metasurfaces. This, in turn, opens entirely new avenues in the field of optical analog computing.

Here, we propose a metasurface-based platform for analog computing that solves the Fredholm integral equation of the second kind for free-space radiation

$$\Phi(x) = I_0(x) + \int_a^b K(x,t)\Phi(t)dt \quad (1)$$

where  $\Phi(x)$  is the unknown solution of Eq.(1),  $K(x,t)$  is a function of two variables that acts as the kernel of the integral operator, and  $I_0(x)$  is an arbitrary input function. When the kernel of such an integral equation does not match that of an integral transform for which we have an inversion formula (e.g. Fourier transform) and is not separable, the last resort to solve Eq. (1) is to exploit the Neumann series. The latter is a successive approximation method: the initial guess  $\Phi_0(x) = I_0(x)$  is fed into the integral in Eq. (1) obtaining a second approximation  $\Phi_1(x)$ . By repeating this procedure iteratively, our guess  $\Phi_n(x)$  approaches the solution  $\Phi(x)$  as  $n \rightarrow \infty$ .

Following the same reasoning, it is possible to physically implement this method in an analog fashion by means of a metasurface coupled to a feedback system. In fact, Eq. (1) can be discretized by sampling its terms over  $N$  points in the interval  $[a, b]$  thus being equivalent to an  $N \times N$  matrix equation. Next, it is possible to think of the  $N$  sampling points as  $N$  physical modes addressing the system and to consider the integral operator as a scattering matrix which performs matrix multiplication between sets of these modes. In our proposed scheme, the modes are the discrete diffraction channels characterizing a 2D metagrating, determined by its periodicity, while the discretized integral operator is given by the metasurface scattering matrix  $S$ . An arbitrary discretized input  $I_0(x)$  (where  $x$  is a vector of length  $N$ ) is multiplied by the metasurface  $S$ -matrix upon reflection and it is fed back by a semi-transparent mirror for the next iteration. Intuitively, this system performs an analog Neumann series.

The core requirement of this procedure is the possibility of designing a metasurface that has a prescribed  $S$ -matrix. To this end, we optimize the metagrating unit cell by means of the adjoint method. In order to prove the generality of this method, we choose a random passive and reciprocal  $S$ -matrix with  $N=3$  as our objective. The resulting optimized unit cell consists of a complex silicon nanostructure on a sapphire substrate. The unit cell is embedded in a  $\text{SiO}_2$  superstrate capped on top by a silver semi-transparent mirror. The design wavelength is  $\approx 710$  nm while the unit cell is 825 nm wide and 415 nm deep. These dimensions are chosen such that only 3 diffraction order exists in the superstrate (where the Neumann series is performed) while 3 plus 4 extra “dump” channels diffraction order are present in the substrate to act as energy dumps in the case of a non-unitary kernel. The optimized metagrating can approximate rather well the desired  $S$ -matrix achieving a figure of merit  $\text{FOM} = \sum_{i,j} |S_{ij} - S_{\text{opt},ij}|^2$ , where  $S_{\text{opt},ij}$  is the simulated optimized  $S$ -matrix and  $S_{ij}$  is the prescribed one.

Next, we compared the simulated response of the entire structure (including the mirror) to the ideal solution of Eq. (1) showing a nice agreement. At the conference, we will show our experimental progress and optical measurements.

#### 6:20 AM F.NM01.07.08

**Guided-Mode Resonator Devices for Quantitative Phase-Contrast Imaging** Anqi Ji<sup>1</sup>, Jung-Hwan Song<sup>1</sup>, Qitong Li<sup>1</sup>, Pieter Kik<sup>2</sup>, David A. Miller<sup>1</sup> and Mark L. Brongersma<sup>1</sup>; <sup>1</sup>Stanford University, United States; <sup>2</sup>University of Central Florida, United States

Phase-contrast imaging is an optical method invented by Nobel Laureate Frits Zernike to visualize unstained living cells. As cells are highly transparent, their structural information is hidden in the phase profile of the transmitted light field, where different micro-organisms inside the cell induce different amounts of phase delay. The underlying key principle of the phase-

contrast technique is to interfere the light scattered by a specimen with reduced,  $\pi/2$  phase-retarded unscattered light (DC component). As a result, the original phase undulation of the electric field is transformed into an enhanced amplitude modulation and thus the contrast in the image is maximized. Conventionally, phase-contrast imaging is achieved with a set of bulky Fourier optics components for filtering and selective phase retarding elements, limiting its use in certain applications. Due to the physical diffraction by these elements, conventional phase-contrast suffers from a limited range of enhancement and various artifacts, including halos and shade-off.

Here, we propose to replace the bulky optics in conventional phase contrast imaging by nanopatterned cover slip that can conveniently be inserted into any bright field microscope to achieve phase-contrast imaging. The cover slip is patterned with a 1 mm-by-1 mm area of a visually transparent guided-mode resonance structure. More specifically, we fabricated a 90-nm-thick, 210-nm-wide  $\text{Si}_3\text{N}_4$  gratings on top of 136-nm-thick  $\text{Si}_3\text{N}_4$  slab waveguide with a lattice constant of 390 nm. The structure can be used to perform phase-contrast microscopy by interfacing the normally-incident planewave to the guided-mode resonance at a 630 nm illumination wavelength. The DC incident light incurs a 98% amplitude reduction and a  $\pi/2$  phase pickup while the scattered, non-DC Fourier components of the scattered light from a specimen pass through with near-unity transmission. We deposit the  $\text{Si}_3\text{N}_4$  waveguide on an amorphous quartz substrate by plasma-enhanced chemical vapor deposition (PECVD) and pattern the grating with electron beam lithography and reactive ion etching (RIE). We characterize the optical dispersion properties of the fabricated samples and verify the phase contrast imaging capability with various phase objects such as cells, nanofabricated samples and 2D material flakes. We observe a 10 fold contrast enhancement for a wide range of objects with reduced artifacts as compared to Zernike's method. We expect this opens a promising avenue for compact, quantitative, and high-accuracy phase-contrast microscopy.

#### 6:30 AM F.NM01.07.09

**Meta-Sails for Stable Beam-Riding—Local Manipulation of Optical Forces** Mohammad Mahdi Salary and Hossein Mosallaei; Northeastern University, United States

Light can exert an optical force upon its interaction with an object due to the momentum exchange between massless photons and the object. The optical force has been harnessed for a variety of applications including trapping, accelerating and binding microscopic particles as well as pressurizing thin-films and two-dimensional materials. It has also been envisioned as a propulsion mechanism for space applications, leading to the advent of light sailing technology. Light sails gain momentum from the radiation pressure due to illumination from a light source - the Sun or laser beams - to provide the thrust for driving satellites in an orbit or driving spacecrafts in certain trajectories without reliance on reaction mass thus allowing for continuous acceleration and greater longevity. In this talk, we will demonstrate how photonic metasurfaces can be used as light sails offering an unprecedented control over motion degrees of freedom via local manipulation of optical forces and torques through anomalous reflection and refraction. We will present a comprehensive modeling of motion dynamics of large-area meta-sails consisting of graded pattern nanostructured metasurfaces by linking the macroscopic optical response evaluated via a ray tracing approach based on the generalized Snell's law to the mechanical response governed by Newton-Euler equations, through Maxwell's stress tensor method. We will discuss the required conditions for the stability of a meta-sail riding on a high-power laser beam toward achieving relativistic velocities for deep space exploration and interstellar voyage, in terms of phase gradient and center of mass location. We will show an all-dielectric metasurface design featuring ultralow areal density while offering a high reflectivity and wide phase agility in a broad bandwidth which enables efficient acceleration with sustainable beam-riding stability for target relativistic velocities up to 20% speed of light despite relativistic Doppler broadening. In particular, we will discuss how the chromatic dispersion of the metasurface affects the stability and acceleration due to the relativistic Doppler shift in the frame of the accelerating meta-sail. We will present the estimated motion trajectories of the meta-sail driven by a 100 GW laser beam reaching to 20% speed of light in less than 12 minutes and illustrate that the Doppler-induced effects can be used for damping the amplitude of bounded oscillations through an engineered chromatic dispersion to yield a radiative loss in the reflection channel, toward minimizing the residual motion of the meta-sail and achieving a high-precision trajectory en route to a far destination.

#### 6:40 AM F.NM01.07.10

**Nanowire Devices Add Another Dimension to Terahertz Spectroscopy and Imaging** Kun Peng<sup>1</sup>, Dimitars Jevtics<sup>2</sup>, Fanlu Zhang<sup>3</sup>, Sabrina Sterzl<sup>1</sup>, Djamshid A. Damry<sup>1</sup>, Mathias U. Rothmann<sup>1</sup>, Benoit Guilhabert<sup>2</sup>, Michael Strain<sup>2</sup>, H. Hoe Tan<sup>3,3</sup>, Laura Herz<sup>1</sup>, Lan Fu<sup>3,3</sup>, Martin Dawson<sup>2</sup>, Antonio Hurtado<sup>2</sup>, Chennupati Jagadish<sup>3,3</sup> and Michael Johnston<sup>1</sup>; <sup>1</sup>University of Oxford, United Kingdom; <sup>2</sup>University of Strathclyde, United Kingdom; <sup>3</sup>The Australian National University, Australia

The terahertz (THz) band of the electromagnetic spectrum falls in the region between microwaves and infrared, spanning from 0.1 to 30 THz. This is an information-rich frequency regime, where many molecular vibration/rotation modes and collective excitations occur in materials, providing THz "fingerprints". Hence, THz spectroscopy and imaging are considered



powerful tools for materials characterization and identification [1], being particularly beneficial to the biomedical field (e.g. diagnostics) and defense (e.g. security screening) due to their ionization-free nature and transparency to non-conducting materials. Furthermore, pulsed THz spectroscopy and imaging are particularly powerful for studying dynamic processes in materials with femtosecond time resolution. To date, the vast majority of THz pulsed systems are based on generation of single-cycle linearly polarized THz pulses, with a detection technique that can only measure one polarization component over one real-time scan. This is problematic when exploring complex material systems (e.g. birefringent materials) with anisotropic properties that could be affected by surface topography, crystal structure, stress and magnetic fields. In this work, we have designed, fabricated and characterized polarization-sensitive THz detectors based on orthogonally-crossed semiconductor nanowire networks [2], and realized a single monolithic device that allows simultaneous measurements of the orthogonal components of the electric field of THz pulses without crosstalk. This device architecture is inspired by our previous findings [3] that both single semiconductor nanowires and bow-tie THz antenna exhibit extremely high polarization selectivity to THz radiation. Single-crystal indium phosphide nanowires were used as the active material, grown by selective area epitaxy in a metalorganic chemical vapor deposition system, and were fabricated with a double-bowtie electrode (antenna) geometry design. A nanoscale 'Transfer Print' technique was developed [4], enabling rapid and accurate integration of nanowires onto the devices with well-defined location and orientation. The fabricated nanowire devices were incorporated into a THz time-domain spectroscopy system for performance tests. Moreover, the capabilities of the detector in metamaterials and birefringent materials analysis were demonstrated. Our nanowire detectors are derived from photoconductive antennas, and thus share the same operating mechanism and data analysis technique, which are the most popular detector type employed in many custom-made and commercial THz pulsed systems, suggesting an ease of direct implementation in both scientific and industrial settings. This detector type can be miniaturized down to the nanoscale size for on-chip THz spectroscopic and imaging applications.

#### Reference

- [1] S. S. Dhillon et al., *Journal of Physics D: Applied Physics* 50, 043001 (2017).
- [2] K. Peng et al., *Science* 368, 510-513 (2020).
- [3] K. Peng et al., *Nano Letters* 16, 4925-4931 (2016).
- [4] B. Guilhabert et al., *ACS Nano* 10, 3951-3958 (2016).

#### 6:50 AM F.NM01.07.11

**Mid-Infrared Molecular Sensing Using Mie Antennas on a Mirror** Kan Yao, Jie Fang and Yuebing Zheng; University of Texas at Austin, United States

Mid-infrared (MIR) spectroscopy is a powerful technique for sensing through identifying the vibrational fingerprints of the analyte molecules. However, due to the large mismatch between the nanometric sizes of the molecules and the wavelengths of MIR light, a sufficient amount of samples is a necessity to produce long enough optical paths so that signals from the intrinsically weak light-molecule interactions can accumulate to the sensitivity threshold of the detectors. Conventional characterization techniques, such as Fourier-transform infrared (FTIR) spectrometers, require either samples with a thickness of at least some hundreds of nanometers or complex apparatus, such as attenuated total reflection (ATR) accessories. As a consequence, high-sensitivity identification of molecules with minute samples is still a challenge in MIR spectroscopy. Nanophotonic resonators offer unprecedented opportunities to boost the optical fields at the subwavelength scale. Coupling the analyte molecules with resonant building blocks has been proven an effective approach to enhance light-molecule interactions. However, as the wavelength extends to the MIR region, plasmonic resonances gradually fade out and become less intense compared with in the visible region, making them not ideal candidates for sensing purposes. Here, taking advantage of the high-quality silicon microspheres as lossless Mie resonators, we exploit the possibility of using high-index dielectric antennas for enhanced molecular sensing.

High-index dielectric particles are well-known for their capability to support Mie resonances. For example, spheres sized a few hundreds of nanometers can scatter visible light in a highly directional manner due to the interference between electric and magnetic dipole modes. By using FTIR microspectroscopy, we manage to characterize infrared optical properties of single silicon microspheres and identify the first 14 modes, from magnetic dipole up to the electric 128-pole, with the help of Mie theory. Then, to get the optima conditions for the sensing purpose, we study the evolution of the resonance modes when the particles are placed on a mirror, i.e., at different locations of a standing wave. It is found that at MIR wavelengths, the fundamental magnetic and electric dipole modes, which spectrally overlap the molecular vibrations, can be selectively enhanced by altering the design of the substrate. We demonstrate ultra-sensitive measurements of sub-10 nm Poly(methyl methacrylate) (PMMA) under different conditions, evidenced by the pronounced spectral feature corresponding to the C=O bond vibration near  $1722\text{ cm}^{-1}$ . In comparison, measurements in the absence of the Si antennas or an optimized spacer do not record any meaningful sensing signals. Our results provide a possible solution to high-sensitivity MIR molecular sensing based on a miniaturized photonic platform with minute analytes.

7:00 AM F.NM01.07.12

**Late News: Mie Resonances in High-Index Nanoparticle Arrays for Control of Coherent Light States** Vahid Karimi and Viktoriia Babicheva; The University of New Mexico, United States

The ultra-thin optical structures of high-refractive-index materials, such as semiconductors and III-V compounds, can be used for control of light at the subwavelength scale [1]. We envision that metasurfaces with Mie resonances have a high potential in being utilized for control of coherent light states. The integration of light-emitting devices, such as VCSELs and VeCSELs, and dielectric metasurfaces has been shown as a viable technique to solve the issues of an arbitrary beam-shaping light-emitting device with programmable controllability as well as laser profiles and self-collimation [2]. The monolithic approach based on direct sculpturing of emitting surfaces into metasurfaces provides an authentic new degree of freedom of beam-shaping VCSELs without compromising the device performance.

Nanopillar metasurface at the back-side surface of a bare VCSEL is used as polarization insensitive meta-atoms, and each nanopillar works as an independent nanoscale resonator with a low-quality factor. The larger the effective refractive index, the more drastic change in the transmitted phase delay can be induced. Simultaneously, the bigger diameter of nanopillars, the better the transverse confinement of light is achieved. The integrated III-V compound metasurface operates as a passive element shaping the laser beam at the emission surface rather than adjusting the laser cavity. Programmable laser emission is controlled by the metasurface properties with the employment of arbitrary beam profiles.

We examine the scattering properties as well as reflection, transmission, and absorption of various high-index nanopillar supporting Mie resonances. We also analyze the effect of the thickness of the intermediate layer between the nanopillars and oxide substrate. We report on the scattering features of the metasurface illuminated normally from either substrate or superstrate side. We demonstrate that adding the high-index intermediate layer can shift desired resonances along the spectrum.

[1] H. Ahmed and V.E. Babicheva, "Nanostructured Tungsten Disulfide WS<sub>2</sub> as Mie Scatterers and Nanoantennas," MRS Advances 5, 1819-1826 (2020).

[2] Y.-Y. Xie, et al., "Metasurface-integrated vertical cavity surface-emitting lasers for programmable directional lasing emissions," Nat. Nanotechnology 15, 125-130 (2020).

SESSION F.NM01.08: Novel Physical Phenomena and Quantum Systems

On Demand Abstracts Available for Viewing Starting Saturday Morning, November 21, 2020

F-NM01

5:00 AM \*F.NM01.08.01

**Progress on Topological Light Sources and Sensors** Boubacar Kante<sup>1,2</sup>; <sup>1</sup>University of California, Berkeley, United States; <sup>2</sup>Lawrence Berkeley National Laboratory, United States

Topology plays a fundamental role in contemporary physics and enables new information processing schemes and wave device physics with built-in robustness. Recently, significant efforts have been devoted to transposing topological principles to bosonic systems. In the first part of this talk, I will discuss our invention of the first topological laser, a non-reciprocal light source capable of coupling stimulated emission to selected waveguide output in a controllable manner. I will also discuss unique optical devices based on this platform. In the second part of the talk, I will discuss our recently proposed scheme to systematically implement singularities known as exceptional points in passive plasmonics. I will discuss the new scheme and how we overcame current immuno-assay nano sensing record with plasmons by more than two orders of magnitude.

5:15 AM \*F.NM01.08.02

**Holography, Quantum Correlations and Extreme Near Fields in Optical Metasurfaces** Albert Polman; AMOLF, Netherlands

We use cathodoluminescence imaging spectroscopy (CL) as a powerful tool to characterize optical metasurfaces at deep-subwavelength spatial resolution.[1] In CL, a 5-30 keV electron beam is raster-scanned over the surface while the emitted radiation in the optical and near-infrared spectral range is detected. In the coherent excitation mode the electron beam passing through the metasurface creates a femtosecond electric field oscillation that couples strongly to polarizable electrons in the material, providing a spectrally broadband nanoscale probe of the local optical density of states.

We use CL to image localized modes of resonant plasmonic and dielectric nanostructures and reconstruct their scattering wavefronts using CL holography. We determine the phase and amplitude of wavefronts scattered by single-crystalline Au nanocubes and nanoholes, and derive from that the dominant scattering dipoles.[2] We discuss how the electron wavepacket may collapse as it generates a coherent superposition of surface plasmon polaritons and plasmonic transition dipole radiation that interfere in the far field.

We correlate CL data with photon-induced near-field electron microscopy (PINEM) of plasmonic nanotips in Au nanostars. As shown before,[3] strong plasmonic near fields can dress the high-energy electron energy spectrum into a ladder of coherent harmonics, shaping the electron quantum wavepacket. We will show that this enables probing of the plasmon charge distribution and the corresponding near-field intensity of plasmonic nanotips at the true nanoscale. We introduce how specially tailored optical metasurfaces enable entirely new ways to shape electron wavepackets in space and time.

[1] Polman, A., Kociak, M. & García de Abajo, F.J. Electron-beam spectroscopy for nanophotonics, *Nature Mater.* **18**, 1158 (2019)

[2] Schilder, N., Agrawal, H., Garnett, E.C. & Polman, A. Phase-resolved surface plasmon scattering probed by cathodoluminescence holography, *ACS Photonics*, <https://doi.org/10.1021/acsp Photonics.0c00209> (2020)

[3] Feist, A., Echternkamp, K.E., Schauss, J., Yalunin, S.V., Schafer, S. & Ropers, C. Quantum coherent optical phase modulation in an ultrafast transmission electron microscope, *Nature* **521**, 200 (2015).

### 5:30 AM \*F.NM01.08.03

#### **Plasmonic, Photonic and Excitonic States Interfaces—Time-Modulated Flat Optics and Time-Resolved Measurements** Harry Atwater; California Institute of Technology, United States

Plasmonic, photonic and excitonic states at interfaces govern the optical response of tunable nanophotonic structures such as active metasurfaces, photodetectors and photocatalysts. I will discuss how we can harness plasmonic and excitonic states at interfaces to enable power-efficient phase modulation of active metasurfaces and discuss implications for time-modulated flat optics. Specifically, I will discuss avenues for increasing the power density and power efficiency of plasmonic conducting oxide metasurfaces for temporal phase and amplitude modulation and requirements for time-modulated photonic applications, such as multi-frequency generation and realization of non-reciprocal metasurfaces. I will also report on how time-resolved measurements of plasmonic and excitonic states at interfaces can yield insights about fundamental light-matter interactions in these systems. Specifically, I will discuss i) how electron-hole correlations affect the dynamics of hot carrier relaxation in plasmonic Au/GaN photodetectors and photocatalysts and ii) how time-resolved measurements of excitons generation inform our understanding of carrier dynamics and transport in transition metal dichalcogenides such as WS<sub>2</sub> and MoS<sub>2</sub>.

### 5:45 AM \*F.NM01.08.04

#### **Plasmonics in Topological Insulator Thin Films and Multilayers** Stephanie Law; University of Delaware, United States

Topological insulators (TIs) are materials with a bulk bandgap crossed by surface states that exhibit linear dispersion and spin-momentum locking. Electrons occupying these surface states have low mass and large Fermi velocity, while the spin-momentum locking leads to a reduction in scattering, since a change in momentum requires a spin flip. Among other interesting properties, two-dimensional Dirac plasmons can be excited from these surface electrons. These plasmons are expected to exhibit resonances in the terahertz (THz), a frequency range of interest for chemical identification, imaging, and communication. The TI plasmons should inherit the unusual properties of their constituent electrons: the excitations should be two-dimensional and massless, similar to those found in graphene. Unlike graphene, TI plasmons should also exhibit spin-momentum locking, leading to a reduction in scattering and an increased plasmon lifetime.

In this talk, I will describe our efforts to excite localized plasmon polaritons in TI nanoribbons, propagating plasmon polaritons in TI thin films, and complex plasmon phonon polariton modes in TI multilayer stacks. In thin films, a plasmon can be excited on the top and bottom of the film simultaneously. These plasmons couple to each other, resulting in an acoustic and optical mode. When the film is etched into stripes, we can excite localized plasmon polaritons. By changing the stripe width and film thickness, we can map out the dispersion of these modes, demonstrating extraordinarily high mode indices and long plasmon lifetimes. We can also apply a metallic grating to an unpatterned TI thin film and couple into propagating plasmon polariton modes. I will discuss our efforts to map the propagating plasmon polariton dispersion by changing the grating parameters. Finally, using molecular beam epitaxy, we can grow stacks comprising alternating layers of TI material and trivially-insulating band insulator material. These stacks house multiple topological surface states, and the plasmons residing in these states can couple to one another and to the phonons in the system. The multilayers thus contain complex coupled plasmon phonon polariton modes. We can understand the properties of these modes by changing the

various structural parameters in these films. By growing a stack comprising many alternating TI/trivial insulator layers, we can move toward creating a THz Dirac metamaterial.

**6:00 AM \*F.NM01.08.05**

**Investigating and Controlling the Opto-Electronic/Valleytronic/Spintronic Properties of van der Waals Nanomaterials/Heterostructures/Metastructures** Nai-Chang Yeh, Wei-Hsiang Lin, Chen-Chih Hsu, Duxing Hao, Deepan Kishore Kumar and Chia-Shuo Li; California Institute of Technology, United States

Thin layers of van der Waals (vdW) materials, ranging from insulators to semiconductors, semi-metals and superconductors, exhibit novel optical, electronic, orbital, magnetic, topological and superconducting properties. Varying the interfacial stacking order of vdW homo/heterostructures further yields Moiré bands and new physical phenomena. Nanoscale strain-engineering of vdW materials (*e.g.*, graphene, transition-metal dichalcogenides, TMDs) can induce novel quantum/topological phenomena, such as giant pseudo-magnetic fields (PMF) and flat bands associated with quantized Landau levels in monolayer graphene, and strain-dependent energy gaps and exciton lifetimes for monolayer 2H-phase TMDs. Quantum confinement due to reduced spatial dimensions and broken symmetry is known to induce new quantum states that are non-existent in the bulk. Spin-orbit coupling of light by optical vortices (*a.k.a.* twisted light, Laguerre-Gaussian beam) and plasmonic vortices produces photons with nontrivial spin/orbital-angular-momentum, which can impart integer and fractional *topological charges* onto condensed matter and atomic/molecular systems through light-matter interactions. Therefore, investigating and controlling the light-matter interactions in vdW nanomaterials/heterostructures/metastructures represents a pathway to explore new quantum phenomena and to advance opto-electronic/valleytronic/spintronic applications.

We employ scalable CVD and PECVD fabrication techniques to synthesize a variety of vdW nanomaterials and their heterostructures, including monolayer and bilayer graphene,<sup>[1-3]</sup> quasi one-dimensional (1D) graphene nanostripes,<sup>[1,4]</sup> h-BN,<sup>[5]</sup> and monolayer-to-multilayer TMDs  $MX_2$  and  $MX_{2-y}X'_y$  ( $M = Mo, W$ ;  $X, X' = S, Se, Te$ ;  $0 \leq y \leq 2$ ).<sup>[6]</sup> We investigate their properties by means of spatially resolved and polarization-dependent photoluminescence (PL), time-resolved PL (TRPL), Raman spectroscopy, x-ray photoelectron spectroscopy (XPS), Kelvin-probe force microscopy, conductive atomic force microscopy (c-AFM), scanning tunneling microscopy/spectroscopy (STM/STS).<sup>[6,7]</sup> We perform nanoscale strain engineering on monolayer graphene to control the strain-dependent PMF and electronic correlation, and to achieve valley/spin polarization;<sup>[7]</sup> and on TMDs to control the energy gaps and exciton lifetimes. We develop plasmonic vortices on TMDs by metasurfaces together with circularly polarized light to control the light-matter interaction and valley/spin polarization in TMD and the topological charge. Our approach leads to various interesting findings, including: valley splitting, quantum oscillations, spontaneous symmetry breaking and spin polarization, quantum valley-Hall and quantum anomalous-Hall effects in valley Hall transistors based on nanoscale strain-engineered monolayer graphene;<sup>[7]</sup> exceedingly long and temperature independent optically excited carrier lifetimes ( $\sim 10$  ns) as well as broadband (from IR to UV) photoluminescence in quasi-1D graphene nanostripes; much enhanced valley polarization in monolayer  $WS_2$  by combining plasmonic vortices with circularly polarized light; and compositional dependent opto-electronic/valleytronic properties in  $WS_{2-y}Te_y$  ( $0 < y < 2$ ). Based on these experimental findings, we discuss potential applications of van der Waals nanomaterials/heterostructures/metastructures to opto-electronic/valleytronic/spintronic devices.

#### References:

- [1] N.-C. Yeh *et al.*, *Nanotechnology* **30**, 162001 (2019).
- [2] D. A. Boyd *et al.*, *Nat. Commun.* **6**, 6620 (2015).
- [3] Y.-C. Chen *et al.*, *Carbon* **156**, 212-224 (2020).
- [4] C.-C. Hsu *et al.*, *Carbon* **129**, 527 (2018).
- [5] W.-H. Lin *et al.*, *Chem. Mat.* **29**, 4700 (2017).
- [6] W.-H. Lin *et al.*, *ACS Nano* **14**, 1350-1359 (2020).
- [7] C.-C. Hsu *et al.*, *Sci. Adv.* **129**, 527 (2018).

**6:15 AM F.NM01.08.07**

**Dipole-Coupled Defect Pairs as Deterministic Entangled Photon Pair Sources** Derek Wang, Tomas Neuman and Prineha Narang; Harvard University, United States

Non-classical states of light are important resources for scalable quantum technologies, such as quantum information processing, networking, and metrology. Entangled photon pairs, in particular, have applications in solid-state quantum repeaters, a crucial component of long-distance quantum networking that overcomes transmission loss by leveraging the effects of entanglement swapping and quantum teleportation. Despite the diverse applications for such non-classical states of

light, methods for generating them deterministically remain limited. Here, we propose a scheme to deterministically generate entangled photon pairs from dipole-coupled pairs of defects in solid-state materials [1], which already have wide applicability in quantum technologies as quantum memories because they combine the favorable coherence and nonclassical emission properties of isolated atoms with the scalability and stability of solid-state technologies. Based on this scheme, we predict spectroscopic signatures and quantify the entanglement with physically realizable system parameters. We find that the entanglement measures of the emitted photons are robust to relative differences in frequency between the intermediate states. Importantly, the Bell state fidelity can be optimized by e.g. tuning the defect transition dipole moments. A defect-based entangled photon pair source would offer numerous advantages including flexible on-chip photonic integration and tunable emission properties via external fields, electromagnetic environments, and defect selection.

[1] Wang, D., Neuman, T., & Narang, P., arxiv:2004.13725 (2020).

#### 6:25 AM F.NM01.08.08

**Electrons Generate Broadband Vortex Light Beams Using Chiral Plasmonic Metasurfaces** Nika van Nielen<sup>1</sup>, Mario Hentschel<sup>2</sup>, Nick Schilder<sup>1</sup>, Harald Giessen<sup>2</sup>, Albert Polman<sup>1</sup> and Nahid Talebi<sup>3</sup>; <sup>1</sup>Center for Nanophotonics, AMOLF, Netherlands; <sup>2</sup>4th Physics Institute and Research Center SCoPE, University of Stuttgart, Germany; <sup>3</sup>Institute of Experimental and Applied Physics, Christian Albrechts University, Germany

Vortex beams of light have recently attracted great attention because of their ability to sensitively probe symmetries and topologies of materials. At the same time, electron beams are known to excite special states of light, for example by the generation of transition radiation (TR) or surface plasmon polaritons (SPPs). Here we bring together these two worlds, and present a plasmonic optical metasurface which under excitation with 30 keV electrons generates a collimated light beam with well-defined orbital angular momentum in the visible-near-infrared spectral range.

We fabricate spiral-shaped geometries composed of arrays of holes in a 40-nm Au film on a Si<sub>3</sub>N<sub>4</sub> membrane by Au<sup>++</sup> focused ion beam milling. We excite the spiral geometries with 30 keV electrons almost at the center and collect the coherent cathodoluminescence and observe clear light vortex beams in the far field. We fabricate spiral arrays with left- and right-handed geometries and different winding numbers and find that the angular momentum of the generated TE- and TM-polarized Laguerre-Gauss-like light beams matches the number of spiral arms in our structure. Finite-difference-time-domain (FDTD) simulations are used to determine the evolution of electric and magnetic field components over time and space, and provide detailed insights in the interference effects that lead to the build of the vortex beams over time.

We describe the observation of the vortex CL beams with well-defined topological charge by a model in which 30 keV electrons create: (1) TR at the point of impact and (2) SPPs that travel over the metal surface and scatter out by generating magnetic dipoles in the plasmonic holes. Interference of these two scattering contributions in the far field then leads to the vortex beams. Propagation of SPPs along the spiral shaped hole arrays contributes strongly to the creation of the vortex beam. In our geometries, the diameter of the holes was varied from 50-200 nm along the spirals, which enabled the creation of vortex beams over a broad spectral range from 380-900 nm.

The generation of electron-beam induced light beams with tailored topology, spectrum, and temporal profile enables femtosecond pump-probe spectroscopy in which material excitations are created by electron excitation and probed with tailored light pulses that arrive at well-defined times.

#### 6:35 AM F.NM01.08.09

**Highly Directional Light Emission from Perovskite Nanocrystals by Dielectric Nanolenses** Julia van der Burgt and Erik C. Garnett; Amolf institute, Netherlands

On macroscopic scale, solar cell efficiency can be increased with concentrating lenses, that focus the sunlight on the cell. An equivalent effect can be achieved with nanostructures that make the light emitted by the solar cell directive towards the sun, while eliminating some of the drawbacks of macroscopic concentration. We have developed an evolutionary algorithm to design dielectric nanostructures for directional emission, leading to structures with a directivity as high as 306. In our previous work<sup>[1]</sup> the experimentally achieved value was significantly lower than the modeled directivity, due to several limiting factors. In this work we overcome these limitations, by using a newly build measurement setup and a specially designed material system. By combining a Fourier microscope with an integrating sphere, we are able to measure emission into the full  $4\pi$  solid angle, which allows us to measure full directivity. The predicted directivity is calculated for a point source at the center of the nanolens. In the experiment the point source is resembled by small clusters of emitting particles, which are placed in an ordered array to facilitate the proper alignment. This is achieved with a recently developed technique of direct patterning of CsPbBr<sub>3</sub> perovskite nanocrystals by e-beam lithography, by which the ligands of the nanocrystals are directly crosslinked upon exposure. Subsequently the dielectric nanolenses are fabricated on top of the clusters by 2-photon lithography.

[1] Johlin, E.; Mann, S. A.; Kasture, S.; Koenderink, A. F.; Garnett, E. C. Broadband highly directive 3D nanophotonic lenses. *Nature Communications* 2018, 9, 1-7.

#### 6:45 AM F.NM01.08.11

**Confinement of Light in Monolayers of Oxide Perovskites** Dominik M. Juraschek and Prineha Narang; Harvard University, United States

The confinement of electromagnetic radiation in hybrid modes of light and collective excitations in solids (polaritons) promises to open new ways of dynamical control of matter, such as manipulation of radiative electronic transitions and of redistribution of vibrational energy. Two-dimensional (2D) materials have become the primary platform for polaritonic applications, where hexagonal boron nitride is the gold standard for exhibiting 2D phonon polaritons that confine light to volumes several orders of magnitude smaller than in free space [1,2].

Here, we show that phonon polaritons in the recently synthesized monolayers of oxide perovskites [3] can keep up with the benchmarks set by hexagonal boron nitride and confine electromagnetic radiation to extremely small volumes in the technologically important low mid-infrared and terahertz spectral regions. Specifically, we use a combination of first-principles calculations and microscopic phenomenological modeling to compute polaritonic figures of merit, such as the confinement and propagation quality factors of monolayers of SrTiO<sub>3</sub>, KTaO<sub>3</sub>, and LiNbO<sub>3</sub>. Our results combined with the extraordinary tunability of oxides suggest that monolayers of oxide perovskites will become an emergent platform for 2D phonon polaritonics in the near future.

[1] Siyuan et al., *Adv. Mater.* 1806603 (2019)

[2] Rivera, Christensen, and Narang, *Nano Lett.* 19, 2653 (2019)

[3] Dianxiang et al., *Nature* 570, 87 (2019)

[4] Juraschek and Narang, in preparation (2020)

#### 6:55 AM F.NM01.08.13

**On-Demand Directivity Modulations of the Excitation and Emission of Nanoemitters Using a Subwavelength Mie Antenna** Jie Fang, Mingsong Wang, Kan Yao and Yuebing Zheng; The University of Texas at Austin, United States

Effective control over the emission properties is of great importance to nanoemitters in order to realize optimized functionalities and to reduce undesired losses. However, challenges exist in both efficiency and integration when extra optical components are coupled at the nanometer scale. High-index dielectric nanoantennas hold particular promise to tackle these challenges, owing to their multipolar Mie resonances and low material loss. Uniquely, the mutual interference of the size-dependent magnetic and electric modes can lead to effective directivity modulation of the far-field radiation pattern. Since coupling with nanoantennas can significantly modify the emission properties of emitters via Purcell effect and sophisticated interference, positioning such dielectric resonators in the near field of a nanoemitter is also a potential route for directional emission. Moreover, a combination of the directivity modulations of both excitation and emission can provide more degrees of freedom to tune the emission properties in total.

Here, we propose a universal platform for dipole nanoemitters, based on single lossless hydrogenated amorphous Si nanospheres (a-SiNS:H), to modulate the directivity of both the excitation and emission at visible wavelengths. Thanks to its truly subwavelength nature, a-SiNS:H can strongly modify the emission of coupled emitters and make the radiation pattern highly directional. As a zero-dimensional (0D) structure, it also provides high spatial resolution so that multiple functions can be realized under an ultra-compact design, which fits well with the compactness of nanoemitters. Specifically, rigorous analytical theory for dipole-sphere hybrids is derived, along with numerical simulations, to predict the performance under a variety of conditions. Controllable forward-to-backward intensity (F/B) ratios as predicted by theory are experimentally proved with 125 samples of 532 nm laser excitation and 635 nm exciton emission from a monolayer WS<sub>2</sub>. Moreover, flexible emission property engineering is demonstrated for different nanoemitters (e.g. WS<sub>2</sub> and MoS<sub>2</sub>) and excitation wavelengths, thanks to the facile sphere size control.

In the derivation, we consider an a-SiNS:H coupled with an electric dipole emitter, which is oriented tangential to the surface of a-SiNS:H and positioned out of it by a small distance, mimicking the exciton emission from the monolayer of transition-metal dichalcogenides (TMDs). Following a similar procedure as in the standard Lorenz-Mie theory, we expand the incident field, i.e., the exciton emission, and the scattered field, by vector spherical harmonics. The derived analytical solution in the form of expanded spherical harmonics then allows fast computation of the far-field optical properties for information to guide the directivity modulation. Also, it helps to understand the role of each resonance in constituting the total scattering and determining the directivity.

To demonstrate the controllable F/B ratios experimentally, we modify our microscope system to effectively separate the directivity modulations of the excitation and emission. A CVD-grown monolayer WS<sub>2</sub> is used as the nanoemitter. The comparison of the modulated emission (excitation) in the forward and backward directions is always made with fixed excitation (emission) conditions. The F/B ratio can be up to 2.5 and down to 0.5.

Finally, the proposed a-SiNS:H-based platform enables us to achieve the desired emission properties, such as enhanced/suppressed emission in the forward/backward direction. More importantly, the same a-SiNS:H-nanoemitter hybrid can perform different functions by tuning the excitation wavelengths with rational designs. This gives us two degrees of freedom, i.e., the a-SiNS:H size and excitation wavelength, to fit the wanted performances for any nanoemitters, leading to potential applications in ultra-compact and multiplexed integrated photonics.

#### 7:05 AM F.NM01.08.14

**Late News: Liquid Crystal Cavities as a Platform for Engineering of Spin-Orbit Optical Interaction** Katarzyna Rechcinska<sup>1</sup>, Mateusz Król<sup>1</sup>, Rafal Mazur<sup>2</sup>, Przemyslaw Morawiak<sup>2</sup>, Karolina Lempicka<sup>1</sup>, Rafal Mirek<sup>1</sup>, Przemyslaw Kula<sup>2</sup>, Wiktor Piecek<sup>2</sup>, Michal Matuszewski<sup>3</sup>, Witold Bardyszewski<sup>1</sup>, Pavlos G. Lagoudakis<sup>4</sup>, Barbara Pietka<sup>1</sup> and Jacek Szczytko<sup>1</sup>; <sup>1</sup>University of Warsaw, Poland; <sup>2</sup>Military University of Technology, Poland; <sup>3</sup>Polish Academy of Sciences, Poland; <sup>4</sup>University of Southampton, United Kingdom

Spin-orbit optical interactions in photonic systems exploit the analogy between the quantum mechanical description of electronic spin-orbit system and synthetic Hamiltonians derived for propagation of electromagnetic waves in dedicated spatial structures. In the presented work a two-dimensional system – a thin optical cavity filled with liquid crystal – was created, in which trapped photons have unusual properties. It was found that during the modification of the properties of the cavity by external voltage, they behaved like quasiparticles endowed with a magnetic moment, that is "spin", under the influence of an artificial magnetic field. We show that for the liquid crystal cavity different regimes can be obtained. First this unique system allows for tunability of TE-TM splitting and shows giant values of this splitting. One of the most interesting phenomena directly dependent on the TE-TM splitting in a cavity is the optical spin Hall effect. We show that thanks to the novel design and the unique possibility to tune the splitting even for zero incidence angle, we are able to observe typical for normal cavities quadrupole spin textures as well as never reported before patterns resembling: dipole, spin doughnuts and whirls [1]. Secondly, we investigate an artificial Rashba-Dresselhaus spin-orbit interaction (SOI) and synthetic magnetic field (Zeeman-like term) [2]. With the ability to manipulate the effective refractive indices for different polarizations of light it is possible to tune the energy splitting between cavity modes. When two linearly polarized modes of different parity are brought into resonance theoretical analysis of birefringent electromagnetic waveguide results in SOI effects of light, in the form of  $H_{RD} = -2a\sigma_z k_y$ , where  $\sigma_z$  is the Pauli matrix describing polarization (spin) of light and  $k_y$  is light's direction of propagation. The new photonic system perfectly imitates electronic properties and leads to many surprising physical effects. It allows to control the spin state of photon making a new building block for the novel optoelectronic devices e.g., optical neural networks and performing neuromorphic calculations. It can be integrated with light emitters (like various dopants: quantum dots, dyes, thin layers of transition metal dichalcogenides) for room-temperature strong light-matter coupling and lasing. While, engineering of spin-orbit synthetic Hamiltonians in cavities opens the way to photonic emulators of quantum Hamiltonians with internal degrees of freedom.

#### References:

- [1] K. Lekenta et al., Tunable optical spin Hall effect in a liquid crystal microcavity. *Light Sci. Appl.* 7, 74 (2018),
- [2] K. Rechcinska et al., Engineering spin-orbit synthetic Hamiltonians in liquid-crystal optical cavities. *Science* 366, 727 (2019).

SESSION F.NM01.09: Tunable and Nonlinear Photonic Materials and Devices  
On Demand Abstracts Available for Viewing Starting Saturday Morning, November 21, 2020  
F-NM01

#### 5:00 AM \*F.NM01.09.01

**Dynamically Switchable Photonics Based on Alloyed Metal Hydrides** Jeremy N. Munday; University of California, Davis, United States

The ability to control the optical properties of photonic materials on demand is essential for the operation of a variety of devices ranging from active color filters and routers to switchable mirrors and sensors. Here we will present our latest work

on actively controllable photonic devices using alloyed metal hydrides. Using our recently developed apparatus for *in situ* measurements of optical and mechanical response upon hydrogenation, we first show how pure metal hydrides containing Pd, Mg, Zr, Ti, and V can be used as tunable photonic elements throughout the visible and near-infrared [1]. A number of devices will be shown including structures that have five orders of magnitude change in reflectivity, as well as planar systems for physical encryption and counterfeit detection. Second, we will show how alloying can not only improve cyclability, but also lead to higher hydrogen fractions than previously obtained as a result of film stresses and microstructuring [2]. These results have led to new insights in the dynamic behavior of metal-hydrides and will help in the design of next-generation hydrogen sensors and tunable photonic devices.

[1] Kevin J. Palm, Joseph B. Murray, Tarun C. Narayan, and Jeremy N. Munday, "Dynamic Optical Properties of Metal Hydrides," *ACS Photonics*, **5**, 4677–4686 (2018)

[2] KJ Palm, JB Murray, JP McClure, MS Leite, JN Munday, "In Situ Optical and Stress Characterization of Alloyed Pd<sub>x</sub>Au<sub>1-x</sub> Hydrides" *ACS applied materials & interfaces* **11**, 45057-45067 (2019)

#### 5:15 AM \*F.NM01.09.02

**Approaches for Tuning of Chalcogenide Glass Dielectric Metasurfaces** Jesse Frantz<sup>1</sup>, Jason D. Myers<sup>1</sup>, Robel Y. Bekele<sup>2</sup>, Anthony Clabeau<sup>2</sup>, Vinh Nguyen<sup>1</sup>, Jiannan Gao<sup>3</sup>, Mikhail Shalaev<sup>3</sup>, Natalia Litchinitser<sup>3</sup> and Jas Sanghera<sup>1</sup>; <sup>1</sup>U.S. Naval Research Laboratory, United States; <sup>2</sup>University Research Foundation, United States; <sup>3</sup>Duke University, United States

Chalcogenide glasses have recently received attention for their potential use in dielectric metasurfaces for several reasons: They typically possess high linear refractive indexes, enabling high index contrast devices; some compositions exhibit exceptionally high optical nonlinearity ( $n_2 > 1000\times$  that of silica) making them good candidates for nonlinear devices; they have wide transmission windows spanning from the visible through the longwave infrared; and some compositions undergo a structural phase transition, enabling devices with switching based on phase-change. We discuss a variety of approaches to achieve tunability in chalcogenide glass metasurfaces from our work and that of others. We review recent progress on the use of the Kerr nonlinearity in As<sub>2</sub>S<sub>3</sub> films to achieve power-dependent behavior and the application of this effect for the manipulation of orbital angular momentum. We discuss the design and realization of chalcogenide-based photonic quasicrystals enabling simultaneous phase matching of an arbitrary number of nonlinear optical processes in a single engineered nanostructure. We discuss recent observations that a permanent index change can be induced in As<sub>2</sub>Se<sub>3</sub> via thermal tuning and the use of this effect to achieve permanent one-way tuning of the optical resonance of a metasurface. We discuss work being done by a variety of groups on phase-change chalcogenide materials such as germanium-antimony-telluride and gallium-lanthanum-sulfide in order to realize switchable metasurfaces. Finally, we discuss future prospects for the use of chalcogenide glass metasurfaces for applications that require tuning of the optical response.

#### 5:30 AM \*F.NM01.09.03

**Designing Tunable Phase-Change Material Based Metasurfaces Using Multiphysics Simulations** Dmitry N. Chigrin<sup>1,2</sup>; <sup>1</sup>DWI–Leibniz Institute for Interactive Materials, Germany; <sup>2</sup>RWTH Aachen University, Germany

Tunable metasurfaces allow to control the phase, amplitude and propagation direction of electromagnetic waves. Integrating phase-change materials into metasurface design provide an opportunity to control metamaterial properties at the meta-atom length scale. This could enable full reprogrammability and post-fabrication adjustments of adaptive metasurfaces. A state of phase change material near a meta-atom can be switched by a local deposition of heat using optical, electrical pulses or hot scanning probes. Resulting phase transition process is intrinsically non-stationary and inhomogeneous. The phase transition from crystalline to amorphous state is accompanied by the drastic change of the material properties leading to time-varying and position-dependent refractive index, conductivity, absorption rate and heat conduction. In order to describe local phase transition in metamaterials, a self-consistent numerical treatment of electromagnetic, carrier transport, heat transfer and phase transition processes becomes of primary importance. Understanding the phase transition process at the meta-atom length scale is essential for a purposeful design of programmable adaptive metasurfaces. Here, we report on a self-consistent multiphysics description of a local phase transition in metasurfaces. The developed model is applied to analyse local phase transition in different metasurfaces under the application of different mechanism of the local heat deposition.

#### 5:45 AM F.NM01.09.04

**Nonlinear Metasurfaces—New Frontiers in Nonlinear Optics** Igal Brener; Sandia National Laboratories and Center for Integrated Nanotechnologies, United States

While metasurfaces are on the path to revolutionize the way we realize passive optical components, they have the same potential to affect the field of nonlinear optics. The interplay between relaxation of phase matching, control over microscopic



optical fields and ability to manipulate far-fields make nonlinear metasurfaces a new paradigm for this field. Metasurfaces can become nonlinear in different ways: they can be made from nonlinear optical materials or can be fabricated on top of such materials. In this tutorial I will cover the evolution of nonlinear metasurfaces starting from all metallic, metallic on different nonlinear materials, to dielectric and then using engineered nonlinearities using heterostructures of different materials.

#### 5:55 AM \*F.NM01.09.05

**Light with a Phase Transition for Tunable Nanophotonics** Guru V. Naik; Rice University, United States

Among many emerging technologies, energy and display are two essential technologies that can revolutionize our current society. Tunable nanophotonics holds the key to both these emerging technologies. While tunable meta-devices enable 3D displays and such other display applications, tunable thermal emitters enable efficient energy conversion. Phase transition phenomena that arise from the collective behavior of materials enables both these classes of nanophotonic devices. While an electronic phase transition leads to a huge optical tunability, an optical one results in highly selective thermal emitters necessary for efficient energy conversion. Here, we demonstrate tunable nanophotonic devices based on strong correlations in 1T-TaS<sub>2</sub> and frequency-selective thermal emitters based on non-Hermitian nanophotonics.

Optical systems with losses such as thermal emitters require non-Hermitian physics to describe them. Such a non-Hermitian description of thermal emitters allows new powerful design tools such as phase, symmetry, topology. Here, we demonstrate an optical phase transition in a hybrid plasmonic-photonic system exhibiting passive parity-time symmetry. We employ localized dielectric resonances in an array of silicon disks forming a quasi-bound state in-continuum for dielectric resonance. A tungsten bottom plane serves as a plasmonic resonator. The electric dipolar resonance in the silicon resonator is coupled to its image in the tungsten and exhibits passive parity-time symmetry. The thickness of the MgF<sub>2</sub> spacer controls the coupling between the two resonators. Using this hybrid plasmonic-photonic system, we show that the best of both plasmonic and dielectric resonances, i.e., high spectral selectivity and near-unity emissivity can be achieved. Further, we elicit the role of symmetry and topology on the spatial and spectral selectivity of the thermal radiation in this system.

Another type of phase transition arising from the collective behavior of electrons in solids results in a large optical tunability. In general, the speed and magnitude of optical tunability trade-off with each other. For example, MEMS devices are slow but highly tunable, while nonlinear materials are ultrafast but possess tiny tunability. However, a large tunability and a moderately fast response are simultaneously possible in strongly correlated materials exhibiting phase transition due to their collective behavior. 1T-TaS<sub>2</sub> is one such strongly correlated material that exhibits an electronic phase transition above room temperature. Previous studies have shown that many stimuli can tune the electrical properties of 1T-TaS<sub>2</sub>. However, optical properties remained less explored. Here, we demonstrate that a unity-order index tunability at room temperature is possible in 1T-TaS<sub>2</sub> shows just by shining low-intensity incoherent white light. Upon incoherent illumination of intensity less than 1000 mW/cm<sup>2</sup>, the c-axis permittivity of this material was observed to change by unity order. We show that the tunability arises from the change in stacking order of charge density wave-domains across layers of this material. The observed tunability has a sub-microsecond response time allowing a few MHz speed. Thus, 1T-TaS<sub>2</sub> is promising for tunable nanophotonic devices. We demonstrate an optically tunable meta-grating device that could potentially revolutionize the emerging display and imaging technologies.

#### 6:10 AM F.NM01.09.06

**A Comprehensive Active Photonic Platform Driven by Liquids** Qitong Li, Jorik Van de Groep, Adam White, Jung-Hwan Song, Scott Longwell, Polly Fordyce, Stephen Quake and Mark L. Brongersma; Stanford University, United States

Starting from the 1970s, great efforts have been made to miniaturize bulky optical devices. The progress accelerated significantly over the last decade due to the emerging field of metasurfaces. These planar nanophotonic devices, made from judiciously-engineered, subwavelength-thick optical nano-resonators, are capable of controlling the amplitude, phase, and spectral properties of light waves with subwavelength resolution. Some progress has also been made to create active metasurfaces, but it remains challenging to create large-scale devices that offer repeatable and fast dynamic manipulation of the light field. Dynamic tuning is challenging, as the semiconductors and noble metals used in metasurfaces generally display weak electrorefractive and electroabsorptive effects. On the other hand, materials which show larger tunability often only support low-quality optical resonances and/or are not chemically stable.

Here, we demonstrate a comprehensive active photonic platform that affords facile tuning of silicon (Si) nano-resonators by altering their isotropic dielectric environment with microfluidics. We show this platform enables broadband amplitude

control, full-color spectral control, and precise manipulation of geometric phase elements. The tunability, speed and robustness meet the requirements of various display and phased array applications. Specifically, we show that the integration of a nanophotonic device with a microfluidic cavity can provide on-demand control over the refractive index ( $n=1-1.7$ ) of the environment of the nanoresonators in a metasurface by flowing different liquids in real time.

The observed, broad tunability of our metasurfaces results from the strong dispersion of the resonances with the refractive-index of the surrounding medium. This dispersion allows us to manipulate the interference of the scattered light from the Si nano-resonators. By summing up the scattering contribution from all the excited multipoles with the same symmetry, the optical response of a Si nano-resonator array can be modeled as two effective optical planar cavities with symmetric and anti-symmetric radiation profiles. Because of the different electric field distribution inside the nanoresonators, the two cavities show different dispersion with the refractive index of surrounding medium. An intuitive temporal coupled mode theory is applied to calculate the reflection and polarization conversion (diffraction) efficiency spectra and they agree well with full-field simulations.

To show of our platform and design concept, we experimentally demonstrate both a broadband ( $\sim 100$  nm) large amplitude modulation and full-color spectral tuning (from blue to red, reflection peak shifts from 480 nm to 580 nm) for individual pixels. We stress that these numbers are measured under un-polarized white light illumination. A digital number display controlled by microfluidic circuitry is also fabricated and characterized to verify the possible use of these elements for display applications. We also demonstrate that a geometric phase metasurface can be turned “on” and “off” actively, leading to new applications such as temporal beam tapping. What’s more, multiplexing different resonator arrays enables the opportunity to switch the function of a metasurface phased array. For example, an achromatic active lens that can select which color of light be focused is demonstrated. We show that the dielectric environment can be programmed up to 20 Hz, satisfying a number of vision-related applications.

Altogether, these results demonstrate an unprecedented comprehensive active photonic platform driven by liquids. They can lead to many practical applications, ranging from temporal beam focusing, steering, to real-time holography. The successful integration of nanophotonics with mature microfluidic cavity technologies further paves the way towards actively controlled nanophotonic displays and phased arrays.

#### **6:20 AM F.NM01.09.07**

**Optical Nanomanipulation and Reconfigurable Assembly of Colloidal Nanostructures** Jingang Li and Yuebing Zheng; The University of Texas at Austin, United States

Subwavelength nanostructures with tunable compositions and geometries show favorable optical functionalities for the implementation of nanophotonic devices. Diverse colloidal particles are appealing building blocks to construct these functional nanostructures. So far, many optical techniques have been developed to manipulate, assemble, and print colloidal particles from aqueous solutions into desired configurations on solid substrates. However, these techniques operated in liquid environments usually suffer from pattern collapses, Brownian motion of nanoparticles, and challenges on reconfigurable assembly.

Here, we present an all-optical technique, termed optothermally-gated photon nudging (OPN), for the versatile manipulation and dynamic patterning of a variety of colloidal particles on a solid substrate at nanoscale accuracy. OPN takes advantage of a thin surfactant layer to optothermally modulate the particle-substrate interaction, which enables the manipulation of colloidal particles on substrates with optical scattering forces. Along with in situ optical spectroscopy, this non-invasive and contactless nanomanipulation technique provides a powerful platform to design active optical devices and study the coupling between colloidal structures. We further demonstrated the assembly of active dielectric chiral nanostructures on a solid surface, where the chiroptical responses are tailored on-demand via manipulating the silicon nanoparticle. The optical chirality originates from the coupling between the optical resonances of the silicon nanoparticle and the silicon nanowire, which is supported by both numerical simulations and coupled mode theory analysis. Our technique not only provides insights into designing functional nanomaterials but also kindles new strategies to develop adaptive devices for photonic and electronic applications.

#### **6:30 AM F.NM01.09.08**

**Modulation of Ultrafast Electron Transport Through Photoswitchable Ligands on Quantum Dots** Christopher Eckdahl, Suyog Padgaonkar, Jakub Sowa, Dana Westmoreland, Tamar Seideman, Mark Hersam, Julia Kalow and Emily Weiss; Northwestern University, United States

Surface functionalization with photoswitches, organic molecules that reversibly change their conformations in response to light, introduces photoresponsivity to otherwise static nanomaterials. A promising class of nanomaterials for optoelectronics is mixed-dimensional heterojunctions (MDHJs) between quantum dots (QDs) and monolayered semiconductors such as molybdenum disulfide (MoS<sub>2</sub>). I have developed ligands that can be used to introduce photoresponsivity to such materials through surface functionalization. The class of photoswitches I will discuss, fulgides, switch between twisted, non-conjugated states and planar, conjugated states on picosecond time scales. I designed and synthesized a fulgide QD ligand that can extract electrons from photoexcited QDs in one state but not the other (Figure 1). This photoswitchable charge extraction enables reversible control of QD photoluminescence, with possible applications in all-optical memory. I synthesized derivatives of these photoswitchable ligands that can functionalize MoS<sub>2</sub> monolayers and thereby serve as bridging ligands in MoS<sub>2</sub>-QD MDHJs. In this role, the photoswitches could be used to modulate charge transfer in mixed-dimensional heterojunctions and thus enable reconfigurable optoelectronic devices.

#### 6:40 AM F.NM01.09.09

**Late News: Nanoscale Topological Corner States of Light for Nonlinear Optics** [Sergey Kruk](#)<sup>1,2</sup>, Wenlong Gao<sup>1</sup>, Duk-Yong Choi<sup>2</sup>, Thomas Zentgraf<sup>1</sup>, Shuang Zhang<sup>3</sup> and Yuri Kivshar<sup>2</sup>; <sup>1</sup>Universität Paderborn, Germany; <sup>2</sup>Australian National University, Australia; <sup>3</sup>University of Birmingham, United Kingdom

Topological states of light have attracted a lot of attention recently due to the existence of counter-intuitive nontrivial boundary effects arising from bulk properties of optical systems. The corresponding edge states, having their origin in topological properties of a bulk, are protected from perturbations and defects, and therefore they are promising for a wide range of applications in photonic circuitries. Conventionally, the bulk-boundary correspondence relates an n-dimensional bulk to a (n-1)-dimensional boundary state [1]. Recently the bulk-boundary correspondence was generalized to describe higher-order effects such that an n-dimensional bulk defines its (n-m)-dimensional imbedded boundary states. Prominent examples are 0D topological corner states of light in 2D structures [2-4] realized so far at the micrometre scales. Such corner states, due to their tight confinement in all directions, provide a novel route towards facilitating light-matter interactions in novel type of topological cavities. However, the current systems supporting the corner states employ building blocks that are an order of magnitude larger compared to the wavelength of light, which cannot be used for applications in nanophotonics. Here we bring topological corner states of light to the nanoscale and employ them for enhancing nonlinear optical processes. Specifically, we design topologically nontrivial 2D dielectric metasurfaces with C<sub>6</sub>-symmetric honeycomb lattices supporting both 1D edge states and 0D corner states. We observe topology-driven nonlinear light generation from the nanoscopic corner states and compare topological and trivial localisation of light.

In the past, judiciously designed high-index dielectric nanostructures supporting both electric and magnetic Mie resonances have been successfully employed for conventional forms of bulk-boundary correspondence, such as 1D states in 2D structures [5] and 0D states in 1D structures [6]. Here we observe 0D corner states in a 2D nanophotonic topological insulator. In our system, nontrivial topology arises from topological insulator geometry of periodic photonic structures, and the corner states emerge in a cascaded process in which first a bandgap is opened in a spectrum of 2D bulk modes which is bridged by 1D topological edge modes; second, a mini bandgap is opened in 1D modes hosting 0D corner states. We realize this concept experimentally using resonant dielectric metasurfaces on a metal substrate. The metasurfaces consist of two arrays of silicon nanopillars hexamers —expanded and shrunken hexamers, characterized by distinct topological invariants. We fabricate our sample with standard EBL and employ a nonlinear imaging to excite a broad sample area with a short pulse, high peak power tuneable laser and detect nonlinear third-harmonic signal generated by Si hexamers. We observe experimentally 2D bulk modes, 1D edge states, and 0D corner states at different wavelengths. We study several types of topologically nontrivial corner states and compare them to trivial light localisations. Miniaturization of topological corner states to the nanoscale paves the way towards their on-chip applications in compact classical and quantum nanophotonic cavities.

[1] L. Lu et al., “Topological photonics,” *Nat. Photon.*, 8, 821, 2014.

[2] J. Noh et al., “Topological protection of photonic mid-gap defect modes,” *Nat. Photon.* 12, 408 2018.

[3] A. El Hassan et al., “Corner states of light in photonic waveguides,” *Nat. Photon*, 13, 697 2019.

[4] S. Mittal et al., “Photonic quadrupole topological phases,” *Nat. Photon.*13, 692 2019.

[5] D. Smirnova et al., “Third-harmonic generation in photonic topological metasurfaces,” *Phys. Rev. Lett.* 123, 103901, 2019.

[6] S. Kruk et al., “Nonlinear light generation in topological nanostructures,” *Nat. Nanotech.* 14, 126 2019.

#### 6:50 AM F.NM01.09.10

**Late News: Size-Controlled Synthesis of Second Harmonic Active Lithium Niobate Nanocrystals Through Solution-**

**Phase Methods** Rana Faryad Ali and Byron Gates; Simon Fraser University, Canada

We advanced the development of solution-phase approaches for the preparation of lithium niobate (LiNbO<sub>3</sub>) nanoparticles with an average, tunable size from 7 to 100 nm. This solution-phase process results in the formation of crystalline, uniform nanoparticles of LiNbO<sub>3</sub> at a reaction temperature of 220 °C with an optimal reaction time of as short as 30 h. Advantages of these methods include the preparation of single-crystalline LiNbO<sub>3</sub> nanoparticles without the need for further heat treatment or without the need for using an inert reaction atmosphere. The growth of these nanoparticles began with a controlled agglomeration of nuclei formed during a solvolysis step. The reactions subsequently underwent the processes of condensation, aggregation, and Ostwald ripening, which remained the dominant process during further growth of the nanoparticles. These processes did produce single-crystalline nanoparticles of LiNbO<sub>3</sub>, suggesting an oriented attachment process. Average dimensions of the nanoparticles were tuned from 7 to ~100 nm by either increasing the reaction time or changing the concentration of the lithium salts used in the solvothermal process. The nanoparticles were also confirmed to be optically active for second harmonic generation (SHG). These particles could enable further development of SHG based microscopy techniques.

SESSION F.NM01.10: Poster Session: Nanophotonics—Emerging Hybrid Platforms, Materials and Functions  
On Demand Abstracts Available for Viewing Starting Saturday Morning, November 21, 2020  
5:00 AM - 8:00 AM  
F-NM01

#### **F.NM01.10.01**

**A General Phase Function of Micro/Nanoparticle Composites** Junxin Wang, Annica Nilsson and Gunnar Niklasson; Uppsala University, Sweden

Light scattering from particles show unique angular scattering patterns, which are strongly dependent on the particle size to incident wavelength ratio and the refractive index contrast between host medium and the particles. Multiple scattering becomes important when the particle concentration increases, which complicates the angular scattering distributions. In many cases, empirical phase functions have to be applied. A novel empirical phase function was introduced to describe the angle-dependent distribution of scattered light from a collection of micro/nanoparticles inside a thin layer. Angular dependence of light scattering from a polymer host containing sub-micron dielectric and metallic particles was measured. The method gives an excellent approximation to the angular effects of multiple scattering arising from aggregation, non-spherical shape and surface roughness. In addition, it is also a good approximation in the single scattering regime, since it closely reproduces scattering phase functions of particles in the Rayleigh, Mie and geometrical optics regimes. The feasibility of our approach was demonstrated by its ability to fit experimental data on the forward and backward scattering profiles of plasmonic and dielectric submicron particle composite layers. The robust and wide applicability of our method is expected to attract a board interest from researchers in physics and materials science.

#### **F.NM01.10.02**

**Arylazopyrazole-Fused PDMS Composites as Solid-State Photo-Switchable Materials** Ikemefuna Uba, Demetris Geddis, Kesete Ghebreyessus and Uwe Hommerich; Hampton University, United States

Arylazopyrazoles (AAP) show significant potential as a new family of molecular photoswitches owing to their efficient reversible trans-to-cis photoisomerization behavior and the high thermal stability of their metastable cis-isomer. Herein, we report on the design and synthesis of new arylazopyrazole based molecular switches with different spacer length and functional (OH, COOH) groups. The new AAPs were used for the fabrication of solid-state photoswitchable polydimethylsiloxane (PDMS) based composite films. The thin films were prepared by using PDMS as a polymer matrix and different concentrations of AAPs as chromophores at room temperature *via* spin-coating. The photoswitching behavior of the PDMS-AAP blend films and the neat AAP samples induced by irradiation with specific wavelength of light were investigated. We found that the as prepared PDMS-AAP blend films showed rapid and near-quantitative reversible trans-to-cis isomerization rates upon alternating irradiation with UV ( $\lambda = 365$  nm) and green ( $\lambda = 525$  nm) light which is comparable to the isomerization behavior of the neat AAP chromophores in solution. This indicates that the excellent photoswitching properties of AAPs are preserved in the PDMS-AAP composite films. Additionally, the as prepared PDMS-AAP films in the cis-form possess outstanding thermal stability and long-term optical stability. The results also show that the optical properties of the PDMS-AAP composite films can be tuned by using different ratios of the AAP chromophores and exposure to UV

irradiation. This methodology provides a new approach for exploring the fabrication of polymers with solid-state photoswitching functionality. The effect of concentration of the AAPs on the reversible *trans*-to-*cis* isomerization processes of the PDMS-AAP composite films will be discussed in this presentation.

#### **F.NM01.10.09**

**Late News: Fabrication of a Fine-Pattern Flexible Nanowire Photodetector by Shadow Mask** Mustafa A. Yildirim and Kasif Teker; Marmara University, Turkey

Recently, ultraviolet photodetectors (UVPDs) have been used on large scale applications such as environmental monitoring, flame detection, space communication, biomedical applications, pharmaceutical, and chemical analysis. Besides, advances in internet technologies such as the internet of things (IoT) endorse the integration of sensors more rapidly in every aspect of our lives. This trend demands the fabrication of smaller, lighter, less complicated, and low power devices. Therefore, designing low cost, self-powered, highly sensitive, flexible UVPD nanodevices are becoming a hot research area for near future optoelectronics. Silicon carbide (SiC), a wide bandgap semiconductor, is an excellent contender to fulfill those expectations. In addition to having characteristics of one-dimensional nanostructure such as high surface to volume ratio, high crystalline quality, SiC nanowires also possess superior material attributes like high breakdown voltage, high thermal conductivity, high drift velocity, excellent chemical and physical stability. In this study, we propose a very cost-effective, flexible, self-powered single SiC nanowire ultraviolet photodetector (SiCNW-UVPD) fabricated on a polyvinylchloride (PVC) substrate.

The self-powered flexible SiCNW-UVPD was fabricated via a commercially available transmission electron microscopy (TEM) grid (physical mask) and a sputter coater system. Gold (Au) electrodes of 110  $\mu\text{m}$  x 110  $\mu\text{m}$  and a gap of 4  $\mu\text{m}$  were successfully achieved without the use of complicated and expensive methods like photolithography. Two-probe photocurrent-time (I-t) and I-V measurements were performed to reveal photoresponse characteristics such as the photo-to-dark current ratio (PDCR), sensitivity, and responsivity under 254 nm wavelength UV light at 0 V bias. A shallow dark current around 0.087 pA and a good PDCR value of 18 are obtained. Moreover, sensitivity and responsivity values are calculated as 1756 and 170 mA/W, respectively. In addition, the specific detectivity calculations, the effect of bias, and vigorous bending test results are discussed as well. Our work provides the following unique advantages: (i) to the best of our knowledge, the first demonstration of a single SiC nanowire PD on a flexible substrate with great performance, (ii) a very cost-effective fabrication method and readily applicable to any substrate, (iii) exhibiting high sensitivity and responsivity values under UV light at 0 V bias. Therefore, our SiCNW-UVPD device presents an opportunity for low-cost, easy to fabricate, self-powered photodetectors for upcoming future technologies such as wearable sensors, electronic skins, and the internet of things.

#### **F.NM01.10.10**

**Late News: Combined, Localized Plasmonic Heating and Temperature Measurement in Nanocomposite Hydrogels** Wei Yu, Olivier Deschaume, Stijn Jookan, Pengfei Zhang, Jolan Wellens, Fanglei Guo, Christ Glorieux and Carmen Bartic; KU Leuven, Belgium

As scaffold materials for tissue engineering applications, hydrogels can mimic many important functions of extracellular matrices found in living tissues. Local temperature gradients can greatly impact the bioactivity of the matrix and cellular processes such as adhesion, migration and differentiation [1,2], while the knowledge of local temperature is essential understanding and modulating the cell properties and their responses. Various methods have been developed and applied for thermal measurements at the nano- and micro-scales, relevant to living tissues, such as infrared thermography [3], micro-thermocouples [4], AFM with thermocouple [5] and fluorescence-based thermography [6]. However, only a limited number of successful applications have been reported regarding three-dimensional localized temperature measurements as the first three methods can only be applied in two-dimensional cases [3-5]. In this contribution, we report a versatile platform to realize localized, simultaneous heating and temperature readout in both two and three dimensions. Localized heating was implemented in hydrogels by functionalizing them with gold nanorods (GNR) with high absorption around 785 nm, while the local temperature is reported by the incorporated Rhodamine B (RhB)-loaded silica particles or quantum dots. For these thermal nano-probe, the fluorescence intensity decreases when temperature increases. In combination with the nanomaterials, a versatile optical stimulation and readout platform was developed. We demonstrate that plasmonic NIR heating could lead to localized, up to 10 degrees temperature changes in hydrogel-based cellular matrices that can be monitored in situ by fluorescent nanoprobe, both in 2D and 3D.

Funding: This research was funded by the KU Leuven C1 projects, grant numbers C14/16/063 OPTIPROBE, C14/18/061 and the FWO research grant, grant number G0947.17N.

References:

- [1] F. Rico et. al Biophys. J., 2010, 99, 1387-1396
- [2] A.A. Khalili et.al Int J Mol Sci, 2015, 16(8), 18149–18184
- [3] C.W. Meyer et.al Front. Phys., 2017, 8
- [4] F. Yang et.al Sci Rep 2017, 7, 1721
- [5] J. Rho et.al RSC Adv., 2018,8, 27616-27622
- [6] K.Okabe et.al Pflugers Arch - Eur J Physiol 2018, 470, 717–731

**SYMPOSIUM F.NM02**

---

Advanced Linear/Nonlinear, Tunable and Quantum Materials for Metasurfaces, Metamaterials and Plasmonics  
November 21 - December 4, 2020

Symposium Organizers

Viktoriia Babicheva, University of New Mexico  
Igal Brener, Sandia National Laboratories  
Patrice Genevet, Centre National de la Recherche Scientifique  
Ho Wai (Howard) Lee, University of California, Irvine  
Dangyuan Lei, Chinese University of Hong Kong

Symposium Support

**Bronze**  
ACS Photonics | ACS Publications

---

\* Invited Paper

SESSION Tutorial F.NM02: Optical Metasurfaces—Materials, Designs, and Advanced Applications  
Session Chairs: Harry Atwater, Viktoriia Babicheva, Igal Brener, Mark Brongersma, Jonathan Fan and Ho Wai (Howard) Lee  
Sunday Afternoon, November 29, 2020  
F.NM02

**12:30 PM \***

**Creating Metasurfaces and Metadevices with Mie Resonators** Mark L. Brongersma; Stanford University, United States

Semiconductor nanostructures are at the heart of electronic devices and systems. When properly sized and shaped, they can also support optical, Mie-type resonances that are capable of boosting light-matter interaction over bulk materials. By combining their desirable electronic and optical properties, it is possible to create new optoelectronic functionalities. In this tutorial talk, I will start with a discussion of the basic properties of Mie resonators and show how they have been harnessed to create a large variety of passive metasurfaces. One of the key application areas for passive metasurfaces is the realization of flat optical components that can replace more bulky traditional counterparts (e.g. lenses and gratings). One of the next frontiers is to realize active flat optics capable of dynamically shaping optical wavefronts to e.g. tune the focal length of a lens or to actively steer laser beams. I will illustrate different approaches to achieve such active functions. Another area of interest that I will highlight is the development of Mie-resonant antennas and metasurfaces that enable real-time measurement of the wavelength, polarization state, angle of incidence and angular momentum of light.

**2:00 PM BREAK**

**2:15 PM \***

**Nonlinear Metasurfaces—New Frontiers in Nonlinear Optics** Igal Brener; Sandia National Laboratories, United States

While metasurfaces are on the path to revolutionize the way we realize passive optical components, they have the same potential to affect the field of nonlinear optics. The interplay between relaxation of phase matching, control over microscopic optical fields and ability to manipulate far-fields make nonlinear metasurfaces a new paradigm for this field. Metasurfaces can become nonlinear in different ways: they can be made from nonlinear optical materials or can be fabricated on with or on top of such materials. In this tutorial I will cover the evolution of nonlinear metasurfaces starting from all metallic, metallic on different nonlinear materials, to dielectric and then using engineered nonlinearities using heterostructures of different materials.

### **3:45 PM BREAK**

#### **4:00 PM \***

**Electrically Tunable Metasurfaces for Control of Absorption, Emission and Scattering** [Harry Atwater](#); California Institute of Technology, United States

Progress in understanding resonant subwavelength optical structures has fueled a worldwide explosion of interest in both fundamental processes and nanophotonic devices for imaging, sensing, solar energy conversion and thermal radiation control. For most nanophotonic materials, the optical properties are encoded and fixed permanently into the nanoscale structure at the time of fabrication. Achieving electronic tunability of the optical properties is an emerging opportunity to bring metamaterials and metasurfaces to life as dynamic objects composed of tunable nanoscale resonators and antennas. Gated field effect tuning of the carrier density in conducting oxides and twodimensional materials enables the optical dispersion of individual structures to be altered from dielectric to plasmonic, yielding active nano-antenna arrays with electrically tunable absorption, radiative emission and scattering properties.

### **5:30 PM BREAK**

#### **5:45 PM \***

**Optimization and Machine Learning for Metasurface Design** [Jonathan Fan](#); Stanford University, United States

Inverse design, in which the design process is performed through iterative optimization, has the potential to push metasurface performance to the physical limits of composite materials engineering. In this tutorial, we will discuss a range of state-of-the-art numerical optimization methods for metasurface design. We will introduce the objective-first and adjoint variables methods, which are gradient-based optimization concepts that can produce high performance freeform geometries. We will also provide an overview of machine learning techniques as applied to electromagnetics problems and show how generative neural networks can be harnessed as an effective global optimizer for photonic devices.

SESSION F.NM02.09: Live Keynote I: Advanced Linear/Nonlinear, Tunable and Quantum Materials for Metasurfaces, Metamaterials and Plasmonics I

Session Chairs: Ho Wai (Howard) Lee and Jingyi Yang

Tuesday Afternoon, December 1, 2020

F.NM02

#### **1:45 PM \*F.NM02.04.25**

**Plasmonic, Photonic and Excitonic States Interfaces—Time-Modulated Flat Optics and Time-Resolved Measurements** [Harry Atwater](#); California Institute of Technology, United States

Plasmonic, photonic and excitonic states at interfaces govern the optical response of tunable nanophotonic structures such as active metasurfaces, photodetectors and photocatalysts. I will discuss how we can harness plasmonic and excitonic states at interfaces to enable power-efficient phase modulation of active metasurfaces and discuss implications for time-modulated flat optics. Specifically, I will discuss avenues for increasing the power density and power efficiency of plasmonic conducting oxide metasurfaces for temporal phase and amplitude modulation and requirements for time-modulated photonic applications, such as multi-frequency generation and realization of non-reciprocal metasurfaces. I will also report on how time-resolved measurements of plasmonic and excitonic states at interfaces can yield insights about fundamental light-matter interactions in these systems. Specifically, I will discuss i) how electron-hole correlations affect the dynamics of hot carrier

relaxation in plasmonic Au/GaN photodetectors and photocatalysts and ii) how time-resolved measurements of excitons generation inform our understanding of carrier dynamics and transport in transition metal dichalcogenides such as WS<sub>2</sub> and MoS<sub>2</sub>.

**2:15 PM \*F.NM02.04.19**

**Dynamic 2D Quantum Metasurfaces** Mark L. Brongersma; Stanford University, United States

Since the development of diffractive optical elements in the 1970s, major research efforts have focused on replacing bulky optical components by thinner, planar counterparts. The more recent advent of nanophotonic metasurfaces has further accelerated the development of flat optics through the realization that resonant optical antenna elements can be utilized to facilitate local control over the light scattering amplitude and phase. In this presentation, I will highlight recent efforts to realize electrically-tunable metasurfaces employing nanomechanics, electrical gating, microfluidics, and phase change materials. I will pay particular attention to the opportunity of realizing dynamic metasurfaces from atomically-thin semiconductors. Such elements are capable of active wavefront manipulation for optical beam steering and dynamic holography. I will illustrate how the proposed optical elements can be fabricated by scalable fabrication technologies, opening the door to many commercial applications.

**2:45 PM \*F.NM02.04.16**

**Kerr Metasurfaces Enabled by Metallic Quantum Wells** Zhaowei Liu; University of California, San Diego, United States

Optical metasurfaces have emerged as promising candidates for multi-functional devices. Dynamically reconfigurable metasurfaces have been introduced by employing phase-change materials and/or by applying voltage, heat, or strain. While existing metasurfaces exhibit appealing properties, they don't express any significant nonlinear effects due to the negligible nonlinear responses from the typical materials used to build the metasurface. In this work, we propose and experimentally demonstrate one kind of Kerr metasurfaces that shows strong intensity-dependent responses. The Kerr metasurface is composed of a top layer of gold antennas, a dielectric spacer, and a ground layer of metallic quantum wells (MQWs) made by TiN/Al<sub>2</sub>O<sub>3</sub> multilayer stack. Due to the large Kerr nonlinearity supported by the MQWs, the effective optical properties of the MQWs can change gradually from metallic to dielectric with increasing of the input intensity, leading to dramatic modifications of the metasurface responses. This opens up new routes for tunable metasurface applications in the fields of nonlinear optics and extremely fast meta-optics.

**3:15 PM \*F.NM02.09.04**

**Wave-Matter Interaction in Spatiotemporal Metastructures** Nader Engheta; University of Pennsylvania, United States

Manipulation of waves is mostly achieved by materials with spatial inhomogeneities. However, exploiting the dimension of time, in addition to the three dimensions of space, for variation of material parameters can bring additional functionalities in such tailoring and sculpting the wave. The spatiotemporal metastructures in which the material parameters are engineered with spatial and/or temporal inhomogeneities exhibit special features that enrich the functionality of light-matter interaction. In my group, we are investigating a variety of scenarios in which such four-dimensional (4D) spatiotemporal material platforms can be exploited. These scenarios include 4D materials that provide us with temporal aiming, temporal anisotropy, anti-reflection temporal coatings, frozen waves, phase conjugation, asymmetric diffusion, temporal effective medium methods, etc. In this talk, I will give an overview of our most recent results in this area

SESSION F.NM02.10: Live Keynote II: Advanced Linear/Nonlinear, Tunable and Quantum Materials for Metasurfaces, Metamaterials and Plasmonics II

Session Chairs: Igal Brener and Ho Wai (Howard) Lee

Wednesday Afternoon, December 2, 2020

F.NM02

**7:30 PM \*F.NM02.04.17**

**Soft Metamaterials—From Isotropy to Quantum Interaction** Sui Yang and Xiang Zhang; University of California, Berkeley, United States

Metamaterials are artificially engineered structures designed to shape electromagnetic responses not found in nature



including superlensing, cloaking and communications. They traditionally comprise an array of fabricated subwavelength anisotropic structures on a planar geometry, which inevitably limit their responses in certain directions. We explore a novel type of soft metamaterial to overcome such limitations, in which building blocks and overall configurations that can be freely tailored, even after formation. In particular, we explored the complex soft metamaterial nanoarchitectures with tailored symmetries that achieved isotropic negative index at the optical frequency. Moreover, we expand such soft metamaterial design that created the first Casimir quantum trap in solution by manipulating electromagnetic waves from quantum fluctuations. These results provide new insights that facilitate and expand novel metamaterial design and applications.

#### 8:00 PM \*F.NM02.04.01

**Artificial Chirality Evolution in Micro-/Nano-Scale 3D Plasmonic Metamaterials** [Junsuk Rho](#)<sup>1,2</sup>; <sup>1</sup>Pohang University of Science and Technology (POSTECH), Korea (the Republic of); <sup>2</sup>Pohang University of Science and Technology, Korea (the Republic of)

Plasmonic chiral metamaterials has attracted significant attention as it provides a new route to intriguing optical properties such as negative refractive index, light polarization filters, and phase modulation. However, the fabrication regarding with limited resolution in conventional synthesis and complexity of asymmetric synthesis pose a major hindrance for further development. In this study, a new class of three dimensional chiral plasmonic nanostructures was successfully fabricated using molecular shape modifiers and crystallographic control of nanoparticle. Previously, we developed three-dimensional chiral metamaterials based on photolithography overlay and electron-beam lithography overlay for terahertz and near-infrared, respectively. We found scaling down them further to visible frequency is extremely difficult. As an alternative solution, we discovered a novel system that characteristic of molecule is transformed into distinctive gold nanoparticle shape. On the basis of this system, chirality transfer between molecular modifier and gold surface allow us to achieve numerous chiral morphologies of gold nanoparticle, named plasmonic helicoids. Particularly, enantiospecific interaction of molecule and high index plane plays pivotal role to provide asymmetric structuring process on the gold surface, forming distinct chiral morphology in single nanoparticle level. One of the representative shapes of helicoid structure showed gammadion-like structure, consisting of four highly curved arms of increasing width, in all six faces of cubic geometry. The unprecedented chiral morphology of plasmonic helicoid has remarkable optical activity (dissymmetry factor  $\sim 0.2$  at 622 nm) even in a randomly dispersed solution, substantiated by direct visualization of macroscopic color transformation. Changes in molecular recognition and growth parameter led to different morphological evolution, and structural alterations provided a straightforward means of tailoring optical response, such as optical activity, handedness, and resonance wavelength. Also, our aqueous phase synthesis is readily scalable without losing exquisite chiral structure at nanoscale. In these aspects, our approach, chirality evolution in single nanoparticle, provides a truly new paradigm and valuable insight for chiral metamaterial fabrication. Such unique fabrication technique will provide the opportunity to achieve the significant step making metamaterials from science to technology. References 1. S. Zhang et al., Phys. Rev. Lett. 102, 023901 (2009) 2. S. Zhang et al., Nat. Commun. 3, 942 (2012) 3. G. Yoon et al., Sci. Rep. 7, 6668 (2017) 4. J. Mun et al., Opt. Lett. 43, 2856-2859 (2018) 5. M. Kim et al., Opt. Express 26, 14051-14057 (2018) 6. H. Lee et al., Nature 556, 360-365 (2018) (with News and Views Article, Nature 556, 313-314 (2018)) 7. J. Mun et al., Nanophotonics 8, 941-948 (2019) 8. H. Lee et al., Nature Commun. (in revision) 9. J. Mun et al., Light: Sci. Appl. (in review)

#### 8:30 PM \*F.NM02.04.09

**Metamaterials Defined by Connectivity** [C.T. Chan](#); The Hong Kong University of Science and Technology, Hong Kong

We report on the study of some metamaterials whose properties, including dispersions and topological characteristics, are determined by the connectivity of a network rather than the resonance of individual resonators.

Metamaterials are described using effective medium theories in the long-wavelength limit in the sense that their optical properties can be described using local permittivity and permeability tensors. We will see that some metallic structures cannot be described using such a language. Their properties depends on the network connectivity, where braiding can create effective sythetic gauge fields that induce shift in momentum space. The consequence is that such materials can have their index ellipsoids centered not at  $k=0$ , and they can possess multiple index ellipsoids centered at arbitrary nonzero  $k$ -points. The number of modes that are allowed at zero frequency can be described by Betti numbers. Such systems differ from conventional metamaterials because the functionality does not come from the resonances of individual resonators and as such, their functionalities tend to be broadband.

We will also discuss network structures that have non-trivial topology in momentum space and these materials can couple orbital angular momenta with the wave vector. The topological character originates from the connectivity of the network and goes beyond typical space group descriptions. Such systems can exhibit angular momentum-dependent one-way edge states,

and their properties can be described using local Chern numbers. Such systems can also be used to realize other interesting topological systems such as high order topological insulators and topological Anderson insulators, and topological systems in which the topological order cannot be described by integers.

**9:00 PM \*F.NM02.04.02**

**Electrically Reconfigurable Metasurface for Spatial Light Modulation** Junghyun Park, Byung Gil Jeong, Sun Il Kim, Duhyun Lee, Kyoungho Ha and Hyuck Choo; Samsung Advanced Institute of Technology, Korea (the Republic of)

We have demonstrated an ultrafast, ultra-compact, and all-solid-state metaphotonic spatial light modulator (M-SLM) which can dynamically shape light in reflection. The M-SLM is an array of electrically controlled plasmonic nanostrip cavities, and it can continuously adjust the phase of reflected light from 0 to 360 degrees and, at the same time, independently modulate the amplitude over its full range. The fabricated M-SLM contains 50 active pixels and measures 250×250 μm<sup>2</sup> in dimensions. By tuning the voltages applied to the M-SLM, we have demonstrated beam steering and beam splitting with a steering angle up to 8°, the side mode suppression ratio of +2.7 dB (the highest value reported in the field), and the deflection efficiency up to 48%. The experimentally measured modulation speed marks 5.6 MHz while the energy consumption per pixel is calculated to be as low as 354 pJ per switching. Accomplishing arbitrary light manipulation using active metaphotonics has remained challenging, especially due to coupling between the phase and amplitude during modulation which resulted in unwanted background noises. To overcome this limitation, we have delved into the fundamental modeling of the light wave and observed that it would require minimum two variables, for example, the real and imaginary coefficients, to properly express the phase and amplitude of the light wave. Based on this observation, we developed the two-control-parameter algorithm and translated the concept into the hardware design. In the array of the designed M-SLM, each plasmonic nanostrip cavity is a stacked double-gated structure with an indium-tin-oxide layer as an active intermediate channel, which allows an application of two independent control voltages to the top and bottom gate metals. We have also performed extensive numerical investigation and confirmed that the highly versatile light-manipulating capability of the designed M-SLM, including arbitrary phase and amplitude modulation, originates from the superposition of the effects generated by the voltages applied independently to the top and bottom metals. To our knowledge, the M-SLM is the first all-solid-state, electrically controlled metasurface that accomplishes the 360-degree full phase sweep and independent amplitude modulation. Unlike previously reported work, our M-SLM does not involve the use of slow, temperature-sensitive liquid crystals, stiction- and-vibration-prone micro-electromechanical systems (MEMS), or an array of pre-fabricated size-varying structures to achieve phase changes. The M-SLMs extremely low power consumption, ultrafast modulation speed, ultra-compact form factor, outstanding predicted reliability, and the use of standard IC-fabrication processes promises wide adaptation and proliferation of the ultrafast and extremely power-efficient SLMs for 3-dimensional real-time holographic display, light detection and ranging (LiDAR), and wearable display for virtual reality. We look forward to sharing and discussing the details of our M-SLM design philosophy, hardware design & fabrication, and testing results with the audience at the MRS 2020 Spring.

SESSION F.NM02.11: Live Keynote III: Advanced Linear/Nonlinear, Tunable and Quantum Materials for Metasurfaces, Metamaterials and Plasmonics III

Session Chairs: Viktoriia Babicheva and Ho Wai (Howard) Lee

Thursday Morning, December 3, 2020

F.NM02

**11:30 AM \*F.NM02.04.22**

**Metasurfaces for Holography and Light Harvesting—New Approaches with Orbital Angular Moment Modes and Tailored Disorder** Stefan A. Maier<sup>1,2</sup>, Haoran Ren<sup>1</sup> and Changxu Liu<sup>1</sup>; <sup>1</sup>LMU Munich, Germany; <sup>2</sup>Imperial College London, United Kingdom

Metasurfaces significantly widen the parameter space for control over light, mainly via the many ways phase control can be achieved and varied within the plane of the surface. Here, we take a closer look on how to further widen these possibilities via introducing elements such as control over amplitude and phase simultaneously, i.e. the complex amplitude of the impinging light field, and secondly via disorder.

As a first application, we examine the use of beams of higher orbital angular momentum coupled to metasurfaces in a context of holography. We demonstrate the design and implementation of metasurface phase holograms with strong orbital angular momentum selectivity, based on nanostructured gallium nitride. This opens up a new degree of multiplexing, allowing

lensless reconstruction of distinct holographic images in each orbital angular momentum channel. We further show how metasurfaces with additional variation in the height of the underpinning nanostructures allow for complete control over the complex amplitude of the impinging wave. We demonstrate that this significantly reduces cross talk between different orbital angular momentum coding channels, enabling up to 200 independent orthogonal image frames for realistic parameters. The second application is in a context of energy harvesting. Based on a disordered array of plasmonic nanoresonators, we show how deterministic coupling of this effective photonic layer to an external cavity can lead to two different regimes of operation — broadband absorption and narrow-band reflection. As an example, we demonstrate the use of such coupled disordered-layer / cavity systems for colour generation.

**12:00 PM \*F.NM02.01.06**

**Coherent Coupling of a Quantum Emitter and a Plasmonic Nanoantenna** Vahid Sandoghdar; Max Planck Institute for the Science of Light, Germany

Plasmonic antennas are capable of enhancing the coupling of light and matter due to their strong electric field confinement. At room temperature, where dephasing is the dominant contribution to the linewidth of a solid-state emitter, studies of plasmonic coupling have usually concerned incoherent interactions, e.g. a Purcell enhancement [1]. At low temperatures, however, the resonant coherent scattering from the emitter becomes significant and another regime of plasmonic interactions can be observed: here, not only the plasmonic particle changes the interaction of the emitter with light, but the emitter can influence the scattering properties of the plasmonic particle. In an extreme case, a single molecule can fully suppress scattering from a (much larger) plasmonic particle, rendering it effectively transparent [2]. In this presentation, I discuss an experiment, where a single organic molecule partially cloaks a large gold nanoparticle [3].

It has recently been reported that a nanogap antenna formed by a gold nanoparticle separated from a metallic substrate by a thin dielectric gap can achieve ultra-strong enhancement, even at room temperature [4]. When the enhanced emission rate is fast enough to compete with the room temperature dephasing and the plasmon losses rates, the emitter starts to interact coherently with the plasmon mode, bringing the system into the strong coupling regime. In this presentation, we also demonstrate a significant enhancement of a single quantum dot coupled to a plasmonic nanogap antenna. We observe an ultrashort fluorescence lifetime less than 38 ps limited by the instrumental response function. Moreover, by controlling the position of the quantum dot with respect to the nanogap antenna, we can tune the system from the weak coupling to the strong coupling regime leading to spectral splitting in the fluorescence spectra [5].

[1] K. Matsuzaki, *et al.*, *Sci. Rep* **7**, 42307 (2017).

[2] X-W. Chen, V., Sandoghdar, M., Agio, *Phys. Rev. Lett.*, **110**, 153605 (2013).

[3] J. Zirkelbach, *et al.*, *Phys. Rev. Lett.* under review (2020); arXiv:2004.08156

[4] R. Chikkaraddy, *et al.*, *Nature* **535**, 127 (2016).

[5] Liu, *et al.*, *in preparation*.

**12:30 PM \*F.NM02.04.24**

**Vortical Reflection and Spiraling Fermi Arcs with Weyl Metamaterials** Shuang Zhang; Univ of Birmingham, United Kingdom

Weyl points are linear band crossings at discrete points in the momentum space, corresponding to three-dimensional (3D) extensions of the two-dimensional (2D) Dirac nodes, and functioning as monopoles of Berry flux with topological charges defined by the Chern numbers. In photonics, Weyl points have been realized in systems with broken inversion symmetry such as photonic crystals and metamaterials, with broken time reversal symmetry such as magnetized plasma and in synthetic dimensions. As a key signature of Weyl systems, Fermi arcs that connect between the projections of Weyl points of opposite topological charges have been observed. However, the manifestation of the topological nature of Weyl points in their interaction with free space radiations remain obscure in both quantum and classical systems. Scatterings and transport in Weyl semimetals have caught growing attention in both condensed matter and classical physics. In condensed matter systems, the chiral zero modes and the associated magnetoresistance and chiral magnetic effects underlie some highly unusual scattering and transport properties of Weyl semimetals. It has also been proposed that Weyl semimetals may have handedness dependent Imbert–Fedorov shift within the bulk Weyl material. Electrical conductance is usually measured in the experiments, which has contribution from both the bulk Weyl nodes and the fermi arcs. However, it is generally difficult to perform momentum resolved scattering and transport studies, since the leads that transport the electrons to the Weyl semimetals, by their nature, cannot control the momentum of the input electrons. Therefore, previous attempts to associate the topology to scattering matrix mostly remain theoretical.

In this work, vortical phase profile in the momentum space is demonstrated for elliptically polarized electromagnetic waves reflected by a photonic Weyl system, which represents a key signature of the topological nature of the Weyl points and could lead to alignment-free phase plates for vortex beams generation. The nontrivial topology of Chern insulator can not only be revealed by the number of surface states, but also by the scattering matrix  $S$ , i.e. the total winding number in  $2\pi$  of the phase of the eigenvalues of the scattering matrix. It has been rigorously proven that the topological classification of the Hamiltonian and the scattering matrix are equivalent. The scattering matrix method however, are more accessible for investigation in photonics with the readily available optical components from visible to microwave wavelengths to perform the angle resolved measurements.

We further discover a novel type of spiraling guided mode in a hybrid waveguide system formed by the Weyl metamaterial and a metal plate, enabled by the vortical phase profile in the momentum space. we demonstrate that the fermi arcs possessing arbitrary number of windings around the projected Weyl points can be realized in a photonic Weyl semimetal-waveguide hybrid system, revealing a new intriguing physical properties of photonic Weyl systems. The metamaterial-waveguide hybrid system is formed by an air layer sandwiched between a metallic ground plane and an ideal Weyl metamaterial. In such a system, the surface arc states exponentially decay into the Weyl metamaterial, while forming waveguide modes in the thin air layer between the Weyl metamaterial and the confining metallic plate. By measuring the electromagnetic field distribution inside the waveguide, we are able to visualize the Fermi arc's iso-frequency contour in the momentum space through Fourier transformation, and demonstrate the windings of the Fermi arcs in the vicinity of the Weyl frequency.

**1:00 PM \*F.NM02.04.23**

**Dielectric Nano-Structures Functionalized Optical Fibers—A Novel Pathway Towards Single-Fiber Optical Trapping and Boosting In-Coupling Efficiencies** Markus Schmidt<sup>1,2,3</sup>, Malte Plidschun<sup>1,3</sup>, Henrik Schneidewind<sup>1</sup>, Uwe Huebner<sup>1</sup>, Matthias Zeisberger<sup>1</sup>, Torsten Wieduwilt<sup>1</sup>, Jisoo Kim<sup>1,3</sup>, Ronny Foerster<sup>1</sup>, Oleh Yermakov<sup>4</sup>, Yuri Kivshar<sup>4,5</sup>, Andrey Bogdanov<sup>4</sup>, Haoran Ren<sup>6</sup> and Stefan A. Maier<sup>6</sup>; <sup>1</sup>Leibniz Institute of Photonic Technology, Germany; <sup>2</sup>Otto Schott Institute of Materials Research, Germany; <sup>3</sup>Abbe Center of Photonics and Faculty of Physics, Germany; <sup>4</sup>ITMO University, Russian Federation; <sup>5</sup>The Australian National University, Australia; <sup>6</sup>Ludwig Maximilian University of Munich, Germany

The interfacing of nano-structures or meta-surfaces with optical fibers represents a promising approach to unlock novel types of functionalities within a multitude of fields including biophotonics, quantum technologies or optical sensing. Here commonly used top-down implementation strategies are hard to employ in case fiber end-faces are considered due to the intrinsic mismatch of the fiber geometry with wafer-based fabrication technology.

Within this presentation, we would like to report on two implementation pathways to circumvent the mentioned bottleneck, namely (i) 3D nano-printing and (ii) modified electron-beam lithography. Both approaches allow for the implementation of sophisticated nano-structures on the end-face of optical fibers leading to significant performance improvements compared to fibers with unstructured end faces. These improvements are shown here on the examples of (i) optical trapping using only one single-mode fiber via the integration of dielectric meta-surfaces and (ii) boosting in-coupling efficiencies into fibers at almost grazing incidence via dielectric ring-type nano-structures .

(i) A tight focus of light plays an essential role in a vast number of applications including optical imaging, optical manipulation, material processing, biophotonics, microscopy and quantum technology. Here optical fibers show fundamental limitations due to the divergence of light emerging from the fiber facet which for instance has limited the use of single fibers within optical trapping, demanding numerical apertures  $>0.8$ . In this presentation we show that 3D nano-printing via direct laser writing allows for the integration of ultra-high numerical aperture meta-lenses on the facet of single-mode fibers that include beam expansion sections. Record-high numerical apertures of up to 0.9 and diffraction-limited spots have been reached. The capabilities of this device have been demonstrated by optically trapping microbeads and biologically relevant bacteria (*E. coli*) for the first time with one single-mode fiber, solving a serious limiting factor within fiber optics research.

(ii) Optical fibers are particularly difficult to use within the context of wafer-based implementation technologies due to the large aspect ratios of fibers, being complementary to wafers. Using an additional planarization step prior to nano-fabrication we open up a novel pathway to implement dielectric nano-structures onto the end-face of optical fibers via electron-beam based technology. Here, we show that by integrating dielectric gratings consisting of concentric rings located on the core of single-mode fibers, in-coupling efficiencies can be increased by more than four orders of magnitude at almost grazing incidence compared to fibers with unstructured end faces. Specifically, application relevant in-coupling efficiencies of several percent at angles of more than  $75^\circ$  have been reached, suggesting a clear pathway to solve one serious bottleneck of optical fibers which has imposed limitations on applications of optical fibers.

SESSION F.NM02.12: Live Keynote IV: Advanced Linear/Nonlinear, Tunable and Quantum Materials for Metasurfaces,  
Metamaterials and Plasmonics IV  
Session Chairs: Ho Wai (Howard) Lee and Jingyi Yang  
Friday Afternoon, December 4, 2020  
F.NM02

**4:00 PM \*F.NM02.04.27**

**Remote Structuring of Near-Field Landscapes** Federico Capasso<sup>1</sup>, Vincent Ginis<sup>1,2</sup>, Marco Piccardo<sup>1,3</sup> and Michele Tamagnone<sup>1</sup>; <sup>1</sup>Harvard University, United States; <sup>2</sup>Vrije Universiteit Brussel, Belgium; <sup>3</sup>Istituto Italiano di Tecnologia, Italy

The electromagnetic near-field enables subwavelength applications such as near-field microscopy and nanoparticle manipulation. Present methods to structure the near-field rely on optical antenna theory, involving nanostructures that locally convert propagating waves into confined near-field patterns. We develop a theory of remote rather than local near-field shaping, based on cascaded mode conversion and interference of counterpropagating guided waves with different propagation constants. We demonstrate how to structure at will the longitudinal and transverse variation of the near-field, allowing for distributions beyond the conventional monotonic decay of the evanescent field. We provide an experimental realization that confirms our theory. Our method applies to fields with arbitrary polarization states and mode profiles, providing a new path towards unprecedented three-dimensional control of the near-field.

**4:30 PM \*F.NM02.04.21**

**High Quality Factor Phase-Gradient Metasurfaces** Jennifer A. Dionne, Mark Lawrence, David R. Barton, Dixon Jefferson, Elissa Klopfer and Sahil Dagli; Stanford University, United States

High quality factor (“High Q”) cavities have revolutionized information processing, communications, sensing, and nonlinear optics by increasing photon storage times and significantly enhancing light-matter interactions. However, when the size of dielectric cavities is reduced to the nanoscale, resonant modes start to resemble point sources, scattering an incident wave in many different directions. While this scattering has been leveraged to create remarkable metasurfaces that precisely control the phase, amplitude, and polarization of light in an ultrathin footprint, metasurfaces generally exhibit high radiative loss rates and thus low Q-factors. Indeed, to date, resonant features in the far-field transmission of metasurfaces have Q-factors on the order of ten.

Here, we describe a general strategy for generating high quality factor resonances in a phase gradient metasurface. Resonances are created by including subtle structural changes in individual resonators to weakly couple free-space light into otherwise bound modes. We experimentally demonstrate control over the quality factor and resonant wavelengths in this scheme, achieving record metasurface Q’s greater than 2500. We also show via simulations that Q-factors can exceed millions. We highlight this scheme’s general applicability by designing and fabricating metasurfaces that act as beamsteerers to different angles, beam splitters, and lenses. We also show how this platform can be integrated with electro-optic materials for low-power metasurface modulation. Finally, we describe applications of high-Q metasurfaces spanning i) free-space optical sensors of COVID-19 antigens and antibodies; ii) all-optical magnetic switching; and iii) an all-optical self-isolating laser.

**5:00 PM \*F.NM02.01.10**

**Plasmonic Nanoantennas and Their Applications** Pierre Berini; University of Ottawa, Canada

Nanometallic structures, such as resonant plasmonic nanoantennas, are useful for the conversion of light to surface plasmon-polaritons (SPPs) localized to ultra-small volumes [1]. Such structures can provide highly enhanced fields, strong confinement, high surface sensitivity, and can double as a device electrode for applying voltages or passing currents to active regions in optoelectronic devices. Here we review some of their many applications, in the areas of plasmon-enhanced nonlinear optics [2-5] and optoelectronics [6-9].

In nonlinear optics, plasmon enhancement can be applied to the pump [2], or to the nonlinear emission [3-5], through spectral alignment. An advantage of the former is that all nonlinear processes involving the pump are enhanced, but a disadvantage is that the pump, typically of high intensity, can damage the nanostructures. Nonetheless, such enhancement was exploited in high-harmonic generation via re-collision radiation in Si [2], where a 10x enhancement was observed for all harmonics emitted up to the 9<sup>th</sup>. Alternatively, exploiting the latter is advantageous because the structures are resonant with the nonlinear emission which is typically weak, and non-resonant with the pump so are less susceptible to damage. Such enhancement was

exploited in Raman scattering experiments [3-5], where the nanoantennas were spectrally-aligned with the Stokes wavelengths of graphene. Under this scenario, single-antenna scattering cross-section enhancements of over 500× were observed [5].

In optoelectronics, plasmon enhancement can be exploited to improve the performance of, *e.g.*, electro-optic modulators [6], photodetectors [7,8], and beam-steering devices [9]. A key requirement is for the plasmonic enhancement to overlap strongly with the active region of the device, which requires that the nanostructure also operate as a device electrode. Such a structure consists of an array of Au nanoantennas contacted perpendicularly by electrical contact lines. The contact lines may be aligned on the nanoantennas such that they are minimally invasive optically. Structures such as these are very promising for beam steering, as each row can be routed to an individual contact such that a 1D phase gradient is applied over the array [9]. Nanostructures that consist of holes in a metal film are also of significant interest [10], especially arrangements of nanoholes (*e.g.*, heptamers), which can be fabricated via focussed ion beam milling because they exhibit interesting and useful Fano resonances [11].

## References

- [1] Bharadwaj, P., Deutsch, B., Novotny, L., *Adv. Opt. Photonics* 1, 438-483, 2009
- [2] Vampa, G., Ghamsari, B. G., Siadat Mousavi, S., Hammond, T. J., Olivieri, A., Lisicka-Skrek, E., Naumov, A., Villeneuve, D. M., Staudte, A., Berini, P., Corkum, P. B., *Nature Physics* 13, 659, 2017
- [3] Ghamsari, B. G., Olivieri, A., Variola, F., Berini, P., *Nanophotonics* 3, 363, 2014
- [4] Ghamsari, B. G., Olivieri, A., Variola, F., Berini, P., *Phys. Rev. B* 91, 201408, 2015
- [5] Al-Shehab, M., Ghamsari, B. G., Berini, P., *J. Opt. Soc. Am. B*, 36, F49, 2019
- [6] Olivieri, A., Chen, C., Hassan, S., Lisicka-Skrzek, E., Tait, R. N., Berini, P., *Nano Letters* 15, 2304-2311, 2015
- [7] Alavirad, M., Olivieri, A., Roy, L., Berini, P., *Optics Express* 24, 22544-22554, 2016
- [8] Alavirad, M., Olivieri, A., Roy, L., Berini, P., *Chin. Opt. Lett.* 16, 050007, 2018
- [9] Calà Lesina, A., Goodwill, D., Bernier, E., Ramunno, L., Berini, P., *IEEE J. Sel. Top. Quant. Electr.*, DOI: 10.1109/JSTQE.2020.2991386
- [10] Gordon, R., Brolo, A. G., McKinnon, A., Rajora, A., Leathem, B., Kavanagh, K. L., *Phys. Rev. Lett.* 92, 037401, 2004
- [11] Hahn, C., Hajebifard, A., Berini, P., *Nanophotonics* 9, 393-399, 2020

## 5:30 PM \*F.NM02.04.11

**Scalable Light-Matter Interactions in Nanoparticle Lattices** Teri W. Odom; Northwestern University, United States

Rationally assembled nanostructures exhibit distinct physical and chemical properties beyond their individual units. This talk will describe fundamentals and applications of metal nanoparticle lattices that show long-range diffractive interactions when the lattice spacing is close to the wavelength of incident light. These collective excitations are known as surface lattice resonances (SLRs) or lattice plasmons. We will discuss advances in nanofabrication techniques that have enabled the patterning of a wide range nanoparticle materials over macroscale ( $> \text{in}^2$ ) areas and with units that are highly uniform in size, shape, and crystallinity. Such patterned substrates support SLRs with wavelengths that approach the theoretical limit. We will also describe how different lattice symmetries can result in band-edge modes at high symmetry points in reciprocal space. The confined electromagnetic fields of SLRs can manipulate processes such as exciton-plasmon coupling, nanolasing, and imaging via tunable, flat optics.

## SESSION F.NM02.01: Plasmonics

On Demand Abstracts Available for Viewing Starting Saturday Morning, November 21, 2020

F-NM02

## 5:00 AM \*F.NM02.01.01

**Perovskite-Based Plasmonic Nanolasers** Yu-Jung Lu<sup>1,2,3</sup>; <sup>1</sup>Academia Sinica, Taiwan; <sup>2</sup>National Taiwan University, Taiwan; <sup>3</sup>California Institute of Technology, United States

Nanolasers with plasmonic mode confinement represent a critical area of photonics, as new scientific phenomena such as low power consumption and fast switching are accessible because of the accompanying very small mode volumes and laser thresholds. That will be beneficial for its application in future on-chip ultracompact integrated circuits for imaging, data storage, quantum information technology, and optical communication. While plasmonic nanolasers are well established, with demonstrations in several gain materials and cavity geometries, notably missing among this important family of photonic

devices is an upconverting nanolaser.

In this study, we demonstrate the first known example of a subwavelength plasmonic upconverting nanolaser. This organo-lead trihalide perovskite based plasmonic upconverting nanolaser, realized via a two-photon nonlinear optical pumping process, features a record-small mode volume ( $\sim 0.06 \lambda^3$ ) and an ultralow lasing threshold ( $10 \mu\text{Jcm}^{-2}$ ). In addition, we observed temporal coherence of the emission, which is an important feature of lasing. This result was made possible by replacing the conventional noble metal plasmonic cavity structure with one composed of titanium nitride, whose material properties can be tailored during the fabrication processes to co-optimize the pump photon absorption and the upconverted photon emission rate. Moreover, the results show a very close agreement between the experiment and modeling, which provides detailed insight into the novel working mechanism of a plasmonic upconverting nanolaser. In addition, we demonstrate a continuous wave lasing from single lead halide perovskite ( $\text{CsPbBr}_3$ ) quantum dot integrated with plasmonic nanocavity with undetectable threshold (power density lower than  $90 \text{ mWcm}^{-2}$ ) and ultra-sharp single mode lasing (linewidth of 1.4 nm) under a cryogenic temperature at 4 K. We will discuss the outlook for perovskite-based plasmonic nanolasers as well as quantum-dot based plasmonic nanolasers as robust on-chip light sources for bio-imaging, optical communication applications.

#### 5:15 AM \*F.NM02.01.02

**Ultralow-Threshold Lasing from Single Quantum Dot in a Gap Plasmon Nanocavity** Yu-Jung Lu; Academia Sinica, Taiwan

One of the main obstacles limiting potential applications of semiconductor nanolasers is the high threshold carrier density required for lasing, which makes them difficult to realize electrically driven lasing and integrate into optoelectronic devices. Organo-lead halide perovskite materials have recently received considerable attention for achieving an economic and tunable diode laser, owing to the use of solution-processable materials and the exceptional optical attributes of long carrier lifetimes and diffusion lengths, high fluorescence quantum yields, wavelength tunability and high optical gain coefficients ( $> 10^4 \text{ cm}^{-1}$ ). However, reducing the volume of such lasers to the nanoscale is the challenge nanophotonics, with potential applications in arrays of ultra-compact lasers on a chip. In this work, we demonstrate a continuous wave lasing from single lead halide perovskite ( $\text{CsPbBr}_3$ ) quantum dot integrated with plasmonic nanocavity with undetectable threshold (power density lower than  $90 \text{ mWcm}^{-2}$ ) and ultra-sharp single mode lasing (linewidth of 1.4 nm) under a cryogenic temperature at 4 K. In our design, a silver nano-cube was placed on a gold substrate, with a single  $\text{CsPbBr}_3$  quantum dot placed in between. By finite-difference time-domain simulation method to calculate the electric field distribution of the designed structure, we theoretically observed a strong localized optical confinement, plasmonic gap mode, formed between the silver nanocube and the gold substrate acts as plasmonic nanocavity and contributes a large Purcell enhancement (Purcell factor  $\sim 200$ ) which can be determined via time-resolved photoluminescence measurement. In order to avoid quenching effect, a 6 nm  $\text{Al}_2\text{O}_3$  spacer was used to separate the quantum dot and the gold substrate, and the silver nano-cube was covered by 1 nm Polyvinylpyrrolidone to isolate the emitter. In order to measure the lasing threshold, the temperature dependent light-in-light-out curve was performed and we observed a very small lasing threshold (power density lower than  $188 \text{ mWcm}^{-2}$ ) at 80 K. We will also discuss the outlook for lead halide perovskite plasmonic nanolasers in applications including, on-chip coherent light sources for of bio-imaging, optical communication applications.

#### 5:30 AM \*F.NM02.01.03

**Excited States at Metal-Semiconductor Interfaces—Carrier Transport and Selective Photoelectrocatalysis** Harry Atwater; California Institute of Technology, United States

Harvesting non-equilibrium carriers at semiconductor-metal interfaces offers an opportunity to modify the rates and pathways for photochemical reactions at the nanoscale. The carrier generation, transport and interface dynamics can be addressed with a combination of first-principles theory for carrier excitation and relaxation, observation of carrier dynamics via hot-carrier photocurrent spectroscopy, ultrafast transient absorption spectroscopy, and photoelectrochemical measurements that assess current transport, product yield and selectivity. We use as an example the gold/gallium nitride interface and compare results of theory to excited carrier transport, transient absorption and photocatalysis measurements. We also report the first known example of photoexcited hot hole injection at a metal-p-type wide bandgap semiconductor interface. Despite the presence of an interfacial Schottky barrier to hot-hole injection of more than 1 eV across the Au/p-GaN heterojunction, plasmonic Au/p-GaN photocathodes exhibit photoelectrochemical properties consistent with the injection of hot holes from Au nanoparticles into p-GaN upon plasmon excitation. The incident photon-electron conversion efficiency spectrum for the plasmonic photocathodes faithfully follows the surface plasmon resonance absorption spectrum of the Au nanoparticles, and a sustained photovoltage during plasmon excitation of plasmon-induced hot-hole capture and conversion, using a gold/p-type gallium nitride (Au/p-GaN) interface conditions tailored for studying photoelectrochemical  $\text{CO}_2$  reduction. Whereas the Au/p-GaN structure has an interfacial Schottky barrier to hot-hole injection of more than 1 eV, the Au/p-NiO has an approximately zero

Schottky barrier height. Taken together, our results offer experimental validation of photoexcited hot holes in high-barrier Au/p-GaN structures and also in low-barrier structures, such as Au/NiO. These results, together with other recent advances, form an outlook for the use of photoexcited carriers as a tool for enhancing chemical product selectivity in photon-driven catalytic processes.

**5:45 AM \*F.NM02.01.05**

**Recent Progress in Plasmonic Nanolasers** Cun-Zheng Ning<sup>1,2</sup>; <sup>1</sup>Tsinghua University, China; <sup>2</sup>Arizona State University, United States

Great progress has been made in the last 10+ years since the first demonstrations of plasmonic nanolasers or spasers. This talk intends to present more recent progress and points to certain existing problems that remain unresolved.

**6:00 AM \*F.NM02.01.06**

**Coherent Coupling of a Quantum Emitter and a Plasmonic Nanoantenna** Vahid Sandoghdar; Max Planck Institute for the Science of Light, Germany

Plasmonic antennas are capable of enhancing the coupling of light and matter due to their strong electric field confinement. At room temperature, where dephasing is the dominant contribution to the linewidth of a solid-state emitter, studies of plasmonic coupling have usually concerned incoherent interactions, e.g. a Purcell enhancement [1]. At low temperatures, however, the resonant coherent scattering from the emitter becomes significant and another regime of plasmonic interactions can be observed: here, not only the plasmonic particle changes the interaction of the emitter with light, but the emitter can influence the scattering properties of the plasmonic particle. In an extreme case, a single molecule can fully suppress scattering from a (much larger) plasmonic particle, rendering it effectively transparent [2]. In this presentation, I discuss an experiment, where a single organic molecule partially cloaks a large gold nanoparticle [3].

It has recently been reported that a nanogap antenna formed by a gold nanoparticle separated from a metallic substrate by a thin dielectric gap can achieve ultra-strong enhancement, even at room temperature [4]. When the enhanced emission rate is fast enough to compete with the room temperature dephasing and the plasmon losses rates, the emitter starts to interact coherently with the plasmon mode, bringing the system into the strong coupling regime. In this presentation, we also demonstrate a significant enhancement of a single quantum dot coupled to a plasmonic nanogap antenna. We observe an ultrashort fluorescence lifetime less than 38 ps limited by the instrumental response function. Moreover, by controlling the position of the quantum dot with respect to the nanogap antenna, we can tune the system from the weak coupling to the strong coupling regime leading to spectral splitting in the fluorescence spectra [5].

[1] K. Matsuzaki, *et al.*, *Sci. Rep* **7**, 42307 (2017).

[2] X-W. Chen, V., Sandoghdar, M., Agio, *Phys. Rev. Lett.*, **110**, 153605 (2013).

[3] J. Zirkelbach, *et al.*, *Phys. Rev. Lett.* under review (2020); arXiv:2004.08156

[4] R. Chikkaraddy, *et al.*, *Nature* **535**, 127 (2016).

[5] Liu, *et al.*, *in preparation*.

**6:15 AM \*F.NM02.01.07**

**Nonlinear Optics with Hot Carriers** Wenshan Cai; Georgia Institute of Technology, United States

In nanostructured metals, the coherent coupling of electromagnetic radiations to plasmons creates a nonequilibrium distribution of electrons at an elevated temperature, which is termed hot electrons. The dynamics of such hot carriers has been widely employed for various applications, ranging from the detection of sub-bandgap photons in semiconductors to the production of hydrogen gas via photocatalytic processes.

The generation, transfer, and relaxation of hot carriers also provide a novel route to nonlinear optical effects. For example, the optical Kerr nonlinearity of plasmonic metals provides enticing prospects for developing reconfigurable and ultracompact all-optical modulators. Although enhanced nonlinear responses of metals are known to enable the optical control of light, the intrinsically slow relaxation dynamics of photoexcited carriers, primarily governed by electron-phonon interactions, impedes sub-picosecond modulation speeds. In this talk, we present femtosecond all-optical modulation in plasmonic systems via the activation of relaxation pathways for hot-electrons at the interface of metals and electron acceptor materials. We show that the relaxation kinetics and the optical nonlinearity can be tuned by leveraging the spectral response of the plasmonic system in the linear regime. Our findings introduce a generic scheme for achieving sub-picosecond modulation speeds in plasmonic



systems, suitable for the ultrafast control of the intensity, polarization, and phase of light upon exchange of energetic hot carriers.

The dynamics of hot carriers in hybrid plasmonic system is further exploited for the creation of optically induced second-order nonlinear materials. Second-order optical processes are pivotal to the active modulation and wave mixing of light waves. The inversion symmetry in most materials, however, prevents achieving a bulk  $\chi^2$  effect, thereby limiting the portfolio of second-order nonlinear materials. We propose and demonstrate ultrafast conversion of a statically-passive dielectric to a transient second-order nonlinear medium upon the generation and transfer of plasmonically induced hot electrons. Triggered by an optical switching signal, the amorphous dielectric with vanishing intrinsic  $\chi^2$  develops dynamically tunable second-order nonlinear responses, which can be leveraged to address the critical need for all-optical control of second-order nonlinearities in nanophotonic systems. The methodology developed here can be readily extended to any electron reservoir/acceptor pairs, enabling a new class of “material-by-design” for second-order nonlinear optical effects.

#### 6:30 AM \*F.NM02.01.10

##### **Plasmonic Nanoantennas and Their Applications** Pierre Berini; University of Ottawa, Canada

Nanometallic structures, such as resonant plasmonic nanoantennas, are useful for the conversion of light to surface plasmon-polaritons (SPPs) localized to ultra-small volumes [1]. Such structures can provide highly enhanced fields, strong confinement, high surface sensitivity, and can double as a device electrode for applying voltages or passing currents to active regions in optoelectronic devices. Here we review some of their many applications, in the areas of plasmon-enhanced nonlinear optics [2-5] and optoelectronics [6-9].

In nonlinear optics, plasmon enhancement can be applied to the pump [2], or to the nonlinear emission [3-5], through spectral alignment. An advantage of the former is that all nonlinear processes involving the pump are enhanced, but a disadvantage is that the pump, typically of high intensity, can damage the nanostructures. Nonetheless, such enhancement was exploited in high-harmonic generation via re-collision radiation in Si [2], where a 10x enhancement was observed for all harmonics emitted up to the 9<sup>th</sup>. Alternatively, exploiting the latter is advantageous because the structures are resonant with the nonlinear emission which is typically weak, and non-resonant with the pump so are less susceptible to damage. Such enhancement was exploited in Raman scattering experiments [3-5], where the nanoantennas were spectrally-aligned with the Stokes wavelengths of graphene. Under this scenario, single-antenna scattering cross-section enhancements of over 500 $\times$  were observed [5].

In optoelectronics, plasmon enhancement can be exploited to improve the performance of, e.g., electro-optic modulators [6], photodetectors [7,8], and beam-steering devices [9]. A key requirement is for the plasmonic enhancement to overlap strongly with the active region of the device, which requires that the nanostructure also operate as a device electrode. Such a structure consists of an array of Au nanoantennas contacted perpendicularly by electrical contact lines. The contact lines may be aligned on the nanoantennas such that they are minimally invasive optically. Structures such as these are very promising for beam steering, as each row can be routed to an individual contact such that a 1D phase gradient is applied over the array [9]. Nanostructures that consist of holes in a metal film are also of significant interest [10], especially arrangements of nanoholes (e.g., heptamers), which can be fabricated via focussed ion beam milling because they exhibit interesting and useful Fano resonances [11].

#### References

- [1] Bharadwaj, P., Deutsch, B., Novotny, L., *Adv. Opt. Photonics* 1, 438-483, 2009
- [2] Vampa, G., Ghamsari, B. G., Siadat Mousavi, S., Hammond, T. J., Olivieri, A., Lisicka-Skrek, E., Naumov, A., Villeneuve, D. M., Staudte, A., Berini, P., Corkum, P. B., *Nature Physics* 13, 659, 2017
- [3] Ghamsari, B. G., Olivieri, A., Variola, F., Berini, P., *Nanophotonics* 3, 363, 2014
- [4] Ghamsari, B. G., Olivieri, A., Variola, F., Berini, P., *Phys. Rev. B* 91, 201408, 2015
- [5] Al-Shehab, M., Ghamsari, B. G., Berini, P., *J. Opt. Soc. Am. B*, 36, F49, 2019
- [6] Olivieri, A., Chen, C., Hassan, S., Lisicka-Skrzek, E., Tait, R. N., Berini, P., *Nano Letters* 15, 2304-2311, 2015
- [7] Alavirad, M., Olivieri, A., Roy, L., Berini, P., *Optics Express* 24, 22544-22554, 2016
- [8] Alavirad, M., Olivieri, A., Roy, L., Berini, P., *Chin. Opt. Lett.* 16, 050007, 2018
- [9] Calà Lesina, A., Goodwill, D., Bernier, E., Ramunno, L., Berini, P., *IEEE J. Sel. Top. Quant. Electr.*, DOI: 10.1109/JSTQE.2020.2991386
- [10] Gordon, R., Brolo, A. G., McKinnon, A., Rajora, A., Leathem, B., Kavanagh, K. L., *Phys. Rev. Lett.* 92, 037401, 2004
- [11] Hahn, C., Hajebifard, A., Berini, P., *Nanophotonics* 9, 393-399, 2020

#### 6:45 AM F.NM02.01.14

##### **Plasmonics in Coupled Topological Insulator Heterostructures** Zhengtianye Wang, Vishnuvardhan Mambakkam, Theresa

Ginley, Yuying Zhang, Greeshma Chandan, Chaoying Ni and Stephanie Law; University of Delaware, United States

Topological insulators (TI) are a class of quantum materials that exhibit metallic surface states and bulk insulating states. Electrons occupying these surface states are 2D massless, linear dispersed, and spin-momentum locked Dirac Fermions. The optical transitions among these surface states, for example Dirac plasmon polariton, are in the hardly accessed far-IR and THz spectral ranges by traditional semiconductors. In TI thin film, Dirac plasmons are excited simultaneously on the top and bottom surfaces. They are electrostatically coupled and generate an optical mode and an acoustic mode. Only the former can be observed in optical measurements because of a non-zero dipole. In addition, for the 3D TI  $\text{Bi}_2\text{Se}_3$ , the continuum plasmon state interacts with discrete bulk phonon states, namely the  $\alpha$  phonon at 2THz and the  $\beta$  phonon at 4THz, giving rise to plasmon-phonon polariton modes. These unique properties enable TI a promising platform for far-IR sensing, security screening, and other optoelectronic devices that function in the THz.

Similar to the two surfaces coupling in a single layer TI film, the multiple surfaces introduced by stacking alternating TI and band insulator (BI) layers will also couple and produce additional plasmon modes. The optical responses are expected to be dependent on the structural parameters and bulk properties of both the TI and BI material. To create multiple topological edge states, we stack  $\text{Bi}_2\text{Se}_3$  with  $(\text{Bi}_{0.5}\text{In}_{0.5})_2\text{Se}_3$  (BIS), which is topologically trivial band insulator. It has the same van der Waals structure and close lattice constant to  $\text{Bi}_2\text{Se}_3$ . We build a five layer structure comprising BIS / $\text{Bi}_2\text{Se}_3$ /BIS/ $\text{Bi}_2\text{Se}_3$ /BIS on a c-plane sapphire substrate via molecular beam epitaxy (MBE) and explored the plasmonic polariton coupling of such layered TI heterostructures by varying the structural parameters: spacer BIS thickness and  $\text{Bi}_2\text{Se}_3$  thickness. To excite localized surface plasmons polariton, the films were patterned into periodic microribbon arrays. The wavevector of the polariton is defined by  $q=\pi/a$ ,  $a$  is the width of a microribbon, so we can map out the dispersion by measuring polariton frequencies in films with different microribbon widths.

An asymmetric Fano lineshape extinction curve is observed in the FTIR measurement due to the plasmon hybridization with both  $\alpha$  phonon and  $\beta$  phonon. Three plasmon-phonon polariton modes are generated: two of them ( $\omega_l$  for lower frequency,  $\omega_h$  for higher frequency) show visible peaks in the range of 2-8THz where detector is sensitive and the sapphire substrate is transparent; the other one is pushed below 2THz due to the Fano-resonance. With increasing wavevector,  $\omega_l$  and  $\omega_h$  both blue shift, in accordance with the dispersion predicted by transfer matrix (T-matrix) modelling. Fixing the wavevector, when the BIS spacer thickness  $d_s < 50\text{nm}$ ,  $\omega_l$  blueshifts and  $\omega_h$  redshifts, which is not captured by T-matrix modelling; when  $d_s > 50\text{nm}$ , they both stay nearly constant, agree well with modelling. With increasing  $\text{Bi}_2\text{Se}_3$  thickness  $d_{\text{TI}}$ ,  $\omega_l$  always blueshifts while  $\omega_h$  shows a redshift. All the modes shifts can be explained within the frame of plasmon-phonon hybridization except the behavior for thin  $d_s$ . These changes can only be explained by the quantum correlation of the surface states across the band insulator layer, or in other words, coupling of two  $\text{Bi}_2\text{Se}_3$  layer. This has revealed that the Dirac surface states can also couple across a topologically trivial band insulator even though the spin-orbit coupling strength is weak inside the bulk. A thorough understanding of how these surface states in multilayer TIs are coupled will provide a deep insight to the many-body interaction in low-dimensional strong spin-orbit coupling systems.

6:55 AM F.NM02.01.15

**All-Optical Manipulation of Magnetization Enhanced by Surface Plasmons** Feng Cheng, [Chuangtang Wang](#), Zhaoxian Su, Xinjun Wang, Ziqiang Cai, Nian Sun and Yongmin Liu; Northeastern University, United States

Plasmonic nanostructures enable to confine light into deep subwavelength scales and at the same time significantly increase the local field intensity. They have been utilized to increase the device performances in a variety of applications, such as plasmon-enhanced energy harvesting, magneto-plasmonics and heat-assisted magnetic recording (HAMR). In the HAMR technique, the plasmonic nanoantenna first locally heat up the recording media within a data bit. Then an external magnetic field (generated by electric currents) is applied to write data within that heated area. This technique can boost the recording areal density to the petabyte per meter square level<sup>1,2</sup>. On the other hand, recent research work has demonstrated the control of magnetization by femtosecond ( $10^{-15}$  s) lasers, paving the way towards all-optical recording with the writing speed three orders of magnitude higher than that of the current magnetic data storage technologies. In all-optical recording, laser is utilized to directly record data on the magnetic media, and the external magnetic field is no longer needed. The phenomenon was firstly found in rare-earth transition-metal (RE-TM) ferrimagnetic alloys, and later demonstrated in ferromagnetic thin films<sup>3-5</sup>.

Combining plasmonics with all-optical recording is of great research interest, which can potentially be developed into a magnetic recording technique with low power, high intensity and ultrafast speed. Such plasmonic-enhancement effect in all-optical recording has been demonstrated in the RE-TM materials<sup>6</sup>. People have been pursuing similar enhancement effects in ferromagnetic thin films, but no experimental demonstrations were reported so far. In this talk, we will present the experimental observation of the plasmon-enhanced all-optical magnetic manipulation in ferromagnetic thin films<sup>7</sup>. We have integrated the gold nanoislands on top of the Co/Pt thin films (with a  $\text{SiO}_2$  separation layer). The gold nanoislands were

fabricated by annealing a thin film of gold layer under appropriate temperature and time. We have measured the minimum laser power required for magnetic manipulation under the on- and off-resonance conditions, and have observed an 18.5% decrease in the threshold power. The full-wave simulations indicated an averaged 14.6% field enhancement of the electric field intensity in the Co/Pt thin films, which quantitatively explains the observed reduction in the threshold. Our research findings demonstrate the possibility to achieve all-optical magnetic recording with low energy consumption, low cost, and high areal density by integrating plasmonic nanostructures with magnetic media.

## References

1. Challener, W. A., et al. "Heat-assisted magnetic recording by a near-field transducer with efficient optical energy transfer." *Nature photonics* 3.4 (2009): 220-224.
2. Stipe, Barry C., et al. "Magnetic recording at 1.5 Pb m<sup>-2</sup> using an integrated plasmonic antenna." *Nature photonics* 4.7 (2010): 484-488.
3. Stanciu, C. D., et al. "All-optical magnetic recording with circularly polarized light." *Physical review letters* 99.4 (2007): 047601.
4. Lambert, Charles-Henri, et al. "All-optical control of ferromagnetic thin films and nanostructures." *Science* 345.6202 (2014): 1337-1340.
5. Mangin, Stéphane, et al. "Engineered materials for all-optical helicity-dependent magnetic switching." *Nature materials* 13.3 (2014): 286-292.
6. Liu, Tian-Min, et al. "Nanoscale confinement of all-optical magnetic switching in TbFeCo-competition with nanoscale heterogeneity." *Nano letters* 15.10 (2015): 6862-6868.
7. Cheng, Feng, et al. "Plasmon-Enhanced All-Optical Manipulation of Magnetization." *Nano letters* (2020), submitted.

## 7:05 AM F.NM02.01.17

**Dynamics of Strongly Coupled Singlet Fission Molecules in Optical Microcavity** [Bin Liu](#)<sup>1</sup>, Vinod Menon<sup>1,2</sup> and Matthew Sfeir<sup>2,2</sup>; <sup>1</sup>The City College of New York, United States; <sup>2</sup>The City University of New York, United States

We use transient optical spectroscopy to study a molecular singlet fission system that is strongly coupled to an optical microcavity to probe the interconversion of exciton-polaritons, singlet excitons, and triplet excitons. We find that transient spectra in the optical microcavity are influenced by modifications of the exciton-photon coupling conditions in addition to the population dynamics of "reservoir" or uncoupled molecular excited states. For example, though our exciton-polaritons themselves are short-lived (< 1ps), weak interactions with long-lived molecular excited states give rise to exciton-polariton emission signatures that persist for the lifetime of the singlet exciton (~ 50 ps). Similarly, we observe long-lived transient signals corresponding to optical transitions of the exciton-polariton, even in the absence of a real polariton population. Following singlet fission, polariton transient features persist for > 10us, consistent with the excited state lifetimes of dark triplet excitons. We conclude that in addition to the usual singlet fission population dynamics, microcavity transient spectra reveal information pertaining to the dynamics of (1) exciton-polaritons populated via direct excitation, (2) exciton-polaritons populated via scattering from "reservoir" states, and (3) transient modification of the exciton-polariton transition energies due to changes in the population of molecular excited states.

## 7:15 AM F.NM02.01.18

**Evanescence Field Polarization for Giant Chiroptical Modulation from Achiral Gold Half-Rings—Theoretical Insight from Simulations** [Luca Bursi](#); Department of Physics, University of North Texas, United States

Metal nanoantennas have been under intense investigation due to their strong light-matter interactions and significant polarization sensitivities determined by their nano-structure. For applications seeking to realize on-chip polarization-discriminating nanoantennas, efficient energy conversion from surface waves to far-field radiation is desirable. However, the response of individual nanoantennas to the particular polarization states achievable in surface waves, such as evanescent fields, has not yet been thoroughly studied. Here, we report the giant modulation of the visible light scattering predicted from gold half-ring, pinwheel, and other nanoantennas excited through total internal reflection of left- and right-handed circularly polarized light, by exploiting the distinct polarization properties of surface evanescent waves<sup>1</sup>. This result provides a fundamentally different mechanism for chiroptical responses requiring a phase delay between transverse and longitudinal electric field oscillations, not found in free-space light<sup>2</sup>. Specifically, we focus on the insight provided by theory, and in particular by the electromagnetic simulations, performed with COMSOL Multiphysics software, of the systems of interest and aspects of their chiroptical response. References (1) Smith, K.W.; et al. *ACS Nano* 2018, 12, 11657-11663. (2) McCarthy, L.A.; et al. submitted.

7:25 AM F.NM02.01.19

**Dynamic Organic Plasmonics from Conductive Polymer Nanoantennas** Shangzhi Chen and Magnus Jonsson; Linköping University, Sweden

Metal nanostructures are key elements in nanooptics due to their strong resonant interaction with light through plasmonic charge oscillations<sup>1</sup>. Their ability to shape light at the nanoscale have made them critical in a multitude of areas, including biosensing, energy conversion and ultrathin flat metaoptics. Yet another dimension of avenues is foreseen for dynamic nanoantennas<sup>2</sup>, ranging from tuneable metalenses for miniaturized medical devices to adaptable windows that control radiation flows in and out of buildings. However, enabling nano-optical antennas to be dynamically controllable remains highly challenging and particularly so for traditional metals with fixed permittivity<sup>1</sup>. Here, I will present our recent work that introduces conductive polymers as a new class of redox-tuneable plasmonic materials<sup>3</sup>. We show that nanodisks of highly conductive polymers can provide clear optical extinction peaks via excitation of dipolar localised surface plasmon resonances. The resonances redshift with increasing nanodisk aspect ratio, in agreement with simulations and calculations based on dipolar polarizability theory. We furthermore demonstrate complete and reversible switching of the optical response of the organic nanoantennas by chemical tuning of their redox state, which modulates the permittivity between plasmonic and dielectric regimes. Our results show that conductive polymer nanostructures can act as redox-tuneable plasmonic nanoantennas, based on polaronic charge carriers rather than electrons or holes as in conventional metals. Future research may investigate different polymers and geometries and explore their use in various applications. References 1 Maier, S. A. Plasmonics: Fundamentals and Applications. (Springer Science & Business Media, 2007). 2 Shaltout, A. M., Shalaev, V. M. & Brongersma, M. L. Spatiotemporal light control with active metasurfaces. *Science* 364, eaat3100 (2019). 3 Chen, S., Kang, E. S. H., Shiran Chaharsoughi, M., Stanishev, V., Kuhne, P., Sun, H., Wang, C., Fahlman, M., Fabiano, S., Darakchieva, V., & Jonsson, M. P. arXiv: 1907.11453 (2019).

7:35 AM F.NM02.01.21

**Understanding the Physics of Interaction Between Surface Plasmons and Dielectric Matters in Ag/ZnO Nanorod System Using STEM-EELS** Jaeyeon Jo and Miyoung Kim; Seoul National University, Korea (the Republic of)

Localized Surface Plasmons (LSPs) of metal nanoparticles have a distinguished characteristic, confining the electromagnetic fields on the nanometer length scale. This feature fascinates many researchers who are interested in surface-enhance Raman spectroscopy, biosensing, and nano-optics. Recently, the interaction between LSPs and dielectric matter as well as the LSPs themselves have drawn attentions from many people due to its unique energy dispersion and potential applications. However, the fundamental process in plasmon-matter interaction is not well understood. The clear understanding the physics of the phenomena is essential for tailoring them to specific applications, which can be achieved by correlating measurements with theoretical simulations. In this study, a silver nanoparticle on a ZnO nanorod is used as a model system, in which the plasmon-exciton strong coupling was reported [1]. For characterization, Scanning Transmission Electron Microscopy (STEM) – monochromated Electron Energy Loss Spectroscopy (EELS) approach is chosen to investigate the spatial distributions of plasmonic or plasmon-matter coupled modes. In addition, Cathodoluminescence (CL) measurement in a STEM mode was also employed for complementary information on electronic structures. We discuss the differences in EEL spectra in the Ag/ZnO nanorod system compared to the spectrum of a single silver nanoparticle. Boundary Element Method (BEM) simulations are performed for more correct theoretical interpretation of EEL spectra with MNPBEM developed by Hohenester, Ulrich [2]. Various factors such as distorted shape of a silver nanoparticle, symmetry breaking of dielectric environment, and plasmon-exciton coupling are considered to find the origin of the differences. The work will help to figure out the fundamental principle for light-matter interaction. It also highlights the power of STEM-EELS and STEM-CL for studying plasmonics. [1] Wei, Jiak, et al. *Nano letters* 15.9 (2015): 5926-5931. [2] Hohenester, Ulrich. *Computer Physics Communications* 185.3 (2014): 1177-1187.

7:45 AM F.NM02.01.24

**Universal Metric for Plasmonicity of Excitations at the Nanoscale** Luca Bursi<sup>1,1,2</sup>, Runmin Zhang<sup>1,1</sup>, Kyle D. Chapkin<sup>1,1</sup>, Naomi Halas<sup>1,1,1</sup> and Peter J. Nordland<sup>1,1,1</sup>; <sup>1</sup>Rice University, United States; <sup>2</sup>University of North Texas, United States

A promising trend in plasmonics involves shrinking the size of plasmon-supporting structures down to a few nanometers, thus enabling control over light-matter interaction at extreme-subwavelength scales. In this limit, quantum mechanical effects, such as nonlocal screening and size quantization, strongly affect the plasmonic response, rendering it substantially different from classical predictions. For very small clusters and molecules, collective plasmonic modes are hard to distinguish from other excitations such as single-electron transitions or photonic modes. Using rigorous quantum mechanical computational techniques for a wide variety of physical systems, we describe how an optical resonance of a nanostructure can be quantitatively classified as either plasmonic or nonplasmonic. More precisely, we define a universal metric for such

classification, the generalized plasmonicity index<sup>1</sup> (GPI), which can be straightforwardly implemented in any computational electronic-structure method or classical electromagnetic approach to discriminate plasmons from single-particle excitations and photonic modes. The GPI relates to experimentally accessible quantities and it is equivalent—at resonance—to the Q-factor of the corresponding harmonic oscillator. Using the GPI, we investigate the plasmonicity of optical resonances in a wide range of systems including: classification and characterization of features in single and hybrid classical systems; the emergence of plasmonic behavior in small jellium spheres as the size and the number of electrons increase; atomic-scale metallic clusters as a function of the number of atoms; and nanostructured graphene as a function of size and doping down to the molecular plasmons in polycyclic aromatic hydrocarbons (PAHs). Further, the GPI identifies molecular plasmonic excitations of selected charged PAHs, in the visible region of the spectrum, whose excited-state lifetime dynamics is then studied<sup>2</sup>. The GPI metric deepens our fundamental understanding of what is a plasmon down to the molecular limit of plasmon-supporting nanostructures and provides a rigorous foundation for their further development based on molecular plasmonics. References (1) Zhang, R.; et al. ACS Nano 2017, 11, 7321–7335. (2) Chapkin, K.D.; et al. Proc. Natl. Acad. Sci. USA 2018, 115, 9134–9139.

#### 7:55 AM F.NM02.01.25

**Plasmonic Lattices Enable Engineering of Quantum Dot Lasing** Jun Guan<sup>1</sup>, Laxmi K. Sagar<sup>2</sup>, Ran Li<sup>1</sup>, Danqing Wang<sup>1</sup>, Golam Bappi<sup>2</sup>, Nicolas E. Watkins<sup>1</sup>, Marc R. Bourgeois<sup>1</sup>, Larissa Levina<sup>2</sup>, Fengjia Fan<sup>2</sup>, Sjoerd Hoogland<sup>2</sup>, Oleksandr Voznyy<sup>2</sup>, Joao Martins de Pina<sup>2</sup>, Richard D. Schaller<sup>1</sup>, George C. Schatz<sup>1</sup>, Edward H. Sargent<sup>2</sup> and Teri W. Odom<sup>1</sup>; <sup>1</sup>Northwestern University, United States; <sup>2</sup>University of Toronto, Canada

Colloidal quantum dots (QDs) are attractive gain materials for coherent light sources because of their bright photoluminescence, size-controlled color tunability, and solution processability. Engineering directionality of QD lasing is important for applications in remote sensing, laser projection, and on-chip optical network. This talk describes how the emission angle of a QD nanolaser can be manipulated by leveraging the high-symmetry points in plasmonic nanoparticle lattices. We built nanolasers by conformally coating CdSe-CdS core-shell QDs on two-dimensional square arrays of Ag nanoparticles. With waveguide-surface lattice resonances (W-SLRs) near the  $\Delta$  point in the Brillouin zone as optical feedback, we realized lasing emission at off-normal emission angles. Varying the periodicity of the plasmonic lattices enables other high-symmetry points ( $\Gamma$  or  $M$ ) of the lattice to overlap with the QD gain, which facilitates controllable lasing direction. We also increased the thickness of the QD film to access higher order W-SLR modes with additional avoided crossings in the band structure, thereby expanding the selection of cavity modes for any desired lasing emission angle.

#### 8:05 AM F.NM02.01.26

**Extraordinarily Large Permittivity Modulation in Undoped Zinc Oxide for Ultrafast Dynamic Nanophotonics** Soham Saha, Aavek Dutta, Clayton DeVault, Benjamin Diroll, Zhaxylyk Kudyshev, Xiaohui Xu, Richard D. Schaller, Vladimir Shalaev, Alexander Kildishev and Alexandra Boltasseva; Purdue University, United States

Active modulation of a material's permittivity makes it possible to control the phase, amplitude, and polarization of light interacting with the material. The ideal material for tunable nanophotonics would exhibit large optical changes and fast response times, in addition to being compatible with industrial fabrication techniques [1].

Extraordinary optical phenomena like ultrafast reflection modulation [2], extraordinary enhancements of nonlinearities [3], and broadband frequency shifts [4] have been demonstrated with doped conducting oxides. Thus, the ultrafast time-scales of optical modulation make it a promising avenue to study optical non-reciprocity [5], control topology protection [6], and implement photonic time-crystals [7]. Yet the effect of optical pumping on their permittivities tuning limits, optical losses, and their effective carrier masses remain largely unexplored.

In this work, we demonstrate unity-order permittivity changes in low, loss, undoped zinc oxide films, induced by optically generated free-carriers. Because of this permittivity modulation, metal-backed ZnO films demonstrate broadband reflectance modulation up to 70% at the telecommunication wavelengths, with picosecond-scale relaxation times. The epsilon near zero points can be dynamically tuned from 8.5 microns down to 1.6 microns with an optical pump, with picosecond-scale relaxation times. The modulation can be selectively enhanced at specific wavelengths by designing hybrid plasmonic resonators while maintaining the picosecond switching times. The modulation is limited by the increasing effective mass of the photoexcited carriers, saturable absorption of the material at the pump wavelength, and the increased Drude damping of the photoexcited electrons.

This work provides insights into the free-carrier-assisted permittivity modulation in zinc oxide, and demonstrates reflectivity modulation of both lithography-free and patterned nanostructures, with large modulation depth and picosecond response

times. The techniques employed in this work can be used to study doped conducting oxides employed in optically switched nanophotonic devices and will facilitate the realization of active devices for beam-steering, polarizers, and spatial light modulators.

#### References:

- [1] S. M. Choudhury, D. Wang, K. Chaudhuri, C. Devault, A. V. Kildishev, A. Boltasseva, and V. M. Shalaev, *Nanophotonics* **7**, 959 (2018).
- [2] M. Clerici, N. Kinsey, C. DeVault, J. Kim, E. G. Carnemolla, L. Caspani, A. Shaltout, D. Faccio, V. Shalaev, A. Boltasseva, and M. Ferrera, *Nat. Commun.* **8**, 15829 (2017).
- [3] M. Z. Alam, I. De Leon, and R. W. Boyd, *Science* **352**, 795 (2016).
- [4] V. Bruno, S. Vezzoli, C. DeVault, E. Carnemolla, M. Ferrera, A. Boltasseva, V. M. Shalaev, D. Faccio, and M. Clerici, *Appl. Sci.* **10**, 1318 (2020).
- [5] A. M. Shaltout, V. M. Shalaev, and M. L. Brongersma, *Science* (80-. ). **364**, eaat3100 (2019).
- [6] Z. A. Kudyshev, A. V. Kildishev, A. Boltasseva, and V. M. Shalaev, *ACS Photonics* **6**, 1922 (2019).
- [7] E. Lustig, Y. Sharabi, and M. Segev, *Optica* **5**, 1390 (2018).

#### 8:15 AM F.NM02.01.27

**Non-Fading Plasmonic Color Printing on Semicontinuous Metal Films** Sarah N. Chowdhury<sup>1</sup>, Piotr Nyga<sup>1,2</sup>, Zhaxylyk Kudyshev<sup>1</sup>, Alexander Kildishev<sup>1</sup>, Vladimir Shalaev<sup>1</sup> and Alexandra Boltasseva<sup>1</sup>; <sup>1</sup>Purdue University, United States; <sup>2</sup>Military University of Technology, Poland

With sixteen million colors available in the realm of natural and artificial palette, we are still yearning for new shades of colors. Common approaches to achieve a wide color range involve synthetic dyes that expel toxic chemicals that are not only non-biodegradable and carcinogenic, but also are capable of altering the physical and chemical properties of soil, deteriorating water bodies and causing harm to the environment. With a growing demand for higher resolution and shrinking of the ink-jets, current color printing technologies generate ultrasmall particles that cause adverse health effects such as cardio-pulmonary ailments and complex disorders in cellular processes.

Recently, plasmonic colors have emerged as a no-fade, environmentally-friendly alternative for artificial dyes. Their color filtering effects are a consequence of the resonant coupling of light and free electrons in metal nanoparticles, known as surface plasmons that confine light at the nanoscale and lead to the enhancement of the local electromagnetic field. Semicontinuous metal films (SMF), which are randomly distributed metal nanoparticles at the near-percolation regime, can offer both plasmonic sub-wavelength color resolution and large-scale, low-cost fabrication. Random, fractal-type island SMFs are comprised of nanoparticles of diverse sizes and shapes resonating at different wavelengths. When illuminated with high-intensity laser light, thermal effects modify nanoparticles in SMFs, leading to variations in the optical response, and hence, generation of different colors.

In this work, we demonstrate a wide range of plasmonic colors generated by a silver SMF on a silver mirror with a dielectric spacer (SMF/M). This structure utilizes the so-called gap-plasmon modes and generates colors in the reflection mode. The thickness of Ag SMF layer is varied, and the dependence on a dielectric overcoating layer to increase the stability of Ag SMF is analyzed. An ultrafast Ti:Sapphire femtosecond laser (1 kHz, 80 fs, 800 nm, linear polarization) is used to structurally modify the Ag nanoparticles for respective color generation through varying the laser parameters. We obtain intricate artistic designs with the in-house built laser scanning setup.

The proposed approach offers the possibility of producing CMYK colors in an easy and less expensive manner compared to commonly used e-beam lithography. Potentially, SMF-based coloring can be applied to flexible substrates. In addition to color printing and arts, the demonstrated sub-micrometer resolution technique could pave the way to security and optical data storage applications while successfully addressing the challenges of scalability and toxicity across multiple technologies.

#### 8:25 AM F.NM02.01.28

**Highly Anisotropic Tungsten Bronze Nanocrystals for Tunable NIR-Plasmonic Absorption and Scattering** Yannis Cheref<sup>1</sup>, Louise Dugas<sup>1</sup>, Capucine Cleret de Langavant<sup>1</sup>, Florian Lochon<sup>2</sup>, Axel Laborieux<sup>1</sup>, Eric Larquet<sup>1</sup>, Alexandre Baron<sup>2</sup>, Thierry Gacoin<sup>1</sup> and Jongwook Kim<sup>1</sup>; <sup>1</sup>Ecole Polytechnique - CNRS, France; <sup>2</sup>Centre de Recherche Paul Pascal - CNRS, France

The study of doped semiconductor nanocrystals exhibiting localized surface plasmon resonances (LSPR) has been growing over the last decade, with the main interest being their intrinsic tunability through dopant concentration. Among these

materials, degenerately doped metal oxide nanocrystals are of particular interest because of their ability to absorb light in the near-infrared (NIR) range while remaining non-absorbing at visible frequencies. These properties open many opportunities for applications in the fields of solar shielding, laser optics, and biomedical treatments [1].

Hexagonal tungsten bronzes (HTB) have a unique NIR-LSPR property originating from their highly anisotropic crystal phase. It was shown that the crystalline anisotropy of HTB nanocrystals influences the LSPR ‘band-splitting’ in conjunction with the effect of shape anisotropy. This results in a double peak feature of isotropically shaped particles and a band overlap for elongated particles [2]. However, synthesis of HTB nanocrystals with a good control over both their crystalline structure and their morphology has been challenging. Specifically, high aspect ratio HTB rods have not been reported, however producing them could confirm the theorized ‘bands-crossover’ effect and the polarization selectivity of the absorbance.

We investigated the limitations of the previous chloride-salt-based synthetic process and found them to be linked to a competitive precipitation of alkaline chloride salt. Using alternative reactants, we achieved synthesis of highly anisotropic HTB nanorods, with aspect ratios up to 6.5 and lengths up to 100 nm. Extending the tunability of the particles’ aspect ratio also extended the LSPR tunability further in the NIR range. We present a full LSPR band dynamics where particles grow from strongly colored HTB platelets to long HTB rods invisible to the eye. Furthermore, control of the particle size allowed us to measure LSPR light scattering for the first time in doped semiconductor nanoparticles, despite carrier densities in these materials being lower than in the well-studied noble metal nanoparticles. These experimental measurements are supported by numerical simulations based a finite-element model and using an anisotropic Drude-Lorentz dispersion for the dielectric constant of HTB. Our simulations are in good agreement with the experimental measurements. These findings extend our insight into LSPR phenomena, allowing for tunable dual-band NIR absorbers and scatterers.

[1] Kriegel, I., Scotognella, F., & Manna, L. (2017). Plasmonic doped semiconductor nanocrystals: Properties, fabrication, applications and perspectives. *Physics Reports*, 674, 1-52.

[2] Kim, J., Agrawal, A., Krieg, F., Bergerud, A., & Milliron, D. J. (2016). The interplay of shape and crystalline anisotropies in plasmonic semiconductor nanocrystals. *Nano letters*, 16(6), 3879-3884.

**8:35 AM F.NM02.01.29**

**Tin Oxide Nanowire Networks Decorated with Plasmonic Rhodium Nanopyramids and Thermochromic VO<sub>2</sub> Particles for Enhanced Gas Detection** David Graf, Sanjay Mathur and Michael Frank; University of Cologne, Germany

The high surface-to-volume ratio as well as the typically high crystallinity and directional charge carrier transport of metal oxide NWs are beneficial for the use in chemo-resistive gas sensors. Semiconducting n-type SnO<sub>2</sub> nanowire networks have been site-selective deposited on gas sensor platforms by chemical vapor deposition approach based on a gold catalyst-mediated vapor-liquid-solid (VLS) growth mechanism. The selective detection of target gas molecules in a complex gaseous composition is quite challenging. We improved the lack of selectivity toward gaseous species through surface decoration with metal oxides (VO<sub>2</sub>) and noble metals (Rh) nanoparticles by a second CVD step. For this approach, we developed novel molecular precursors based on designed multidentate organic ligands in order to tailor the gas-phase conversion into targeted nanoobjects with defined size and shape. An enhanced gas detection capability towards reducing gases and oxidizing gases were demonstrated, due to electronic and chemical sensitization via spill-over effects. Moreover, optical reflectance spectroscopy revealed plasmonic resonance absorption in visible (465 nm) and UV (350) region resulted from the gold catalyst on the tip on the SnO<sub>2</sub> nanowire and distinctive rhodium nanopyramids. In addition, surface decoration with thermochromic VO<sub>2</sub> exhibits a plasmon resonance absorbance in the near-infrared region. The potential as a multimodal optical sensor towards adsorbed complex chemical species will be discussed.

**8:45 AM F.NM02.01.30**

**Hybridization of Plasmonic Resonances in Nanorod Polygons Revealed by High-Resolution Electron Energy Loss Spectroscopy** Grace Pakeltis<sup>1</sup>, David Garfinkel<sup>1</sup>, Siamak Khorasani<sup>2</sup>, Robyn Collette<sup>1</sup>, Juan C. Idrobo<sup>3</sup>, David Masiello<sup>2</sup> and Philip D. Rack<sup>1,3</sup>; <sup>1</sup>The University of Tennessee, Knoxville, United States; <sup>2</sup>University of Washington, United States; <sup>3</sup>Oak Ridge National Laboratory, United States

The search for metamaterials that support negative permittivity and permeability towards the visible frequency has led to the exploration of various architectures that support coupled plasmonic responses. While standard split ring resonators (SRR) have been extensively studied and shown to be extendable to near infrared frequencies, pushing to higher frequencies is challenging. Thus ring-like structures of nanoparticles and nanorods have become a viable solution for higher frequency

applications. While coupled nanosphere assemblies have been more extensively studied for their unique optical and magnetic properties, rods have stronger polarizability and plasmon resonances. High-aspect-ratio nanorods, in particular, provide an additional route for engineering plasmonic responses, however, have not been studied as extensively as spherical nanoparticles. Although studies on individual nanoparticle/nanorod arrangements have been studied, a comprehensive investigation on the geometric effects on the hybridization of plasmonic nanorods is still lacking. In this study, the hybridization of the electric and magnetic dipoles for a series of polygons were lithographically patterned, where the number of edges ( $n=3-6$ ), gap length, and edge length were studied. High-resolution EELS spectrum images were measured, and the combined spectra and spectrum images clearly reveal the nature of the various resonance modes that are active. Electron discrete dipole approximation simulations were performed to clarify the resultant consequent electric and magnetic field distributions. This work elucidates the hybridization trends of arranged polygons to provide the opportunity for negative permeability and permittivity.

#### 8:55 AM F.NM02.01.32

**Metal Optoelectronics—Hot Carrier Devices Using Novel Materials and Substrates** Jeremy N. Munday; University of California, Davis, United States

High conductivity metals have long been the material of choice for traditional electronics, and over the past two decades low-loss metals have led to many novel optical devices and structures as a result of plasmonic confinement. As these fields merge, metal optoelectronics using hot carrier effects may pave the way for new device architectures with improved flexibility, frequency response, and ultrafast time-dynamics. In this presentation, we will discuss our recent work building hot electron photodetectors for NIR detection using Si and metal oxides [1], improved response using nanoscale metal alloys [2], and time-resolved ultrafast detection via pump-probe techniques exploiting surface plasmon excitation [3]. Further, we will show how the incorporation of index near zero (INZ) substrates can lead to nearly 100% absorption in thin metal films, providing a new platform for hot electron devices [4]. We will conclude with an outlook and discuss future possibilities with these novel material systems.

[1] Kim et al, "Interfacial Defect-Mediated Near-Infrared Silicon Photodetection with Metal Oxides," *ACS Appl. Mater. Interfaces*, **11**, 47516–47524 (2019)

[2] Krayer et al, "Enhanced near-infrared photoresponse from nanoscale AgAu alloyed films," *ACS Photonics* (in press)

[3] Memarzadeh et al, "Surface plasmon assisted control of hot-electron relaxation time," *Optica* (in press)

[4] Krayer et al, "Optoelectronic devices on index-near-zero substrates," *ACS Photonics*, **6**, 2238-2244 (2019)

#### 9:05 AM F.NM02.01.33

**Optothermal Generation and Manipulation of Plasmons** Eduardo Brioso Dias<sup>1</sup>, Renwen Yu<sup>1</sup> and F. Javier Garcia de Abajo<sup>1,2</sup>; <sup>1</sup>ICFO—The Institute of Photonic Sciences, Spain; <sup>2</sup>ICREA - Institució Catalana de Recerca i Estudis Avançats, Spain

Nanoscale photothermal effects enable important applications in cancer therapy, imaging, and catalysis. They also induce substantial changes in the optical response experienced by probing light, thus suggesting their application in all-optical modulation. These important applications have been extensively investigated in conducting materials due to the substantial enhancement produced in the strength of nanoscale photothermal processes as a result of the excitation of their collective electron oscillations, known as plasmons. In this work [1], we theoretically investigate the thermal control of plasmons assisted by light absorption in graphene, thin metals and graphene/metal hybrid films.

Graphene displays stronger photothermal effects than noble metals. A small amount of heat deposited on graphene electrons causes large temperature variations and changes in its optical response because the electronic heat capacity of this material is remarkably small. On the other hand, because plasmon resonances are deep subwavelength excitations, extra momentum is required to couple external light into them. Recently, an alternative route to excite graphene plasmons has been proposed [2], where two interfering optical pump beams create a periodic spatial temperature profile in graphene to assist the coupling of a probe beam to plasmons. Here, we further demonstrate that not only graphene plasmons but also metal plasmons or even sub-wavelength acoustic plasmons can be excited using this approach. We assume a periodic pattern of electron temperature created by the optical grating pump only inside the graphene sheet with a modulated temperature range extending from 300 to 8000 K. Due to the strong temperature dependence of the graphene conductivity, this is spatially modulated and serves as an effective grating.

Lateral patterning of the structures considered above directly enables light coupling to their plasmons. We study the thermo-



optical properties of these types of structures by considering a thin metal grating placed underneath a graphene sheet. We first investigate metal-like plasmons occurring at a higher energy and supported primarily by the metal. Importantly, we consider graphene doped to some Fermi level  $E_F$  and choose a silver grating period such that the plasmon energy is slightly smaller than  $2E_F$ , so that a large modulation is expected by thermally activating interband transitions. At room temperature,  $2\mu \approx 2E_F$  is above the plasmon energy, so we have well-defined modes observed in the reflection spectrum of the patterned 1-nm silver film. However, when graphene electrons are heated to a high temperature via ultrafast optical pumping, the chemical potential can be reduced, enabling Landau damping of the plasmon, whose quality factor strongly drops. The observed dip in peak reflectance is observed also for graphene acoustic plasmons and even for metal plasmons in the absence of graphene, although in these cases the effect is due to the increasing of the electronic inelastic damping. Depending on the material composition and thickness, this modulation effect can be as strong as  $>70\%$ .

The remarkably small electronic heat capacity of atomically thin systems, such as graphene and few-atomic-layer noble metal films, allows us to elevate their electron temperature via ultrafast optical pumping in such a way that their optical responses are dramatically modified with moderate pump intensities below the damage threshold. We have shown that the addition of a noble metal film in close proximity to graphene enables similar levels of modulation  $>70\%$  to be reached over a wider spectral range extending down to the visible domain.

[1] E.J.C. Dias et al. Thermal manipulation of plasmons in atomically thin films. *Light. Sci. Appl.* 9, 87 (2020).

[2] R. Yu et al. Photothermal engineering of graphene plasmons. *Phys. Rev. Lett.* 121, 057404 (2018).

#### 9:15 AM F.NM02.01.35

**Broad Infrared Spectrum Accessibility Through Plasmonic Coupling in In:CdO Thin Films** [Angela Cleri](#)<sup>1</sup>, Joshua Nolen<sup>2</sup>, Joshua D. Caldwell<sup>2</sup>, Evan Runnerstrom<sup>3</sup> and Jon-Paul Maria<sup>1</sup>; <sup>1</sup>The Pennsylvania State University, United States; <sup>2</sup>Vanderbilt University, United States; <sup>3</sup>U.S. Army Research Office—Materials Science Division, United States

Cadmium oxide (CdO) is one of the most promising material systems for low-loss infrared (IR) plasmonics. Through reactive co-sputtering using high power impulse magnetron sputtering (HiPIMS) and radio frequency (RF) sputtering, doped CdO demonstrates high mobility films with tunable carrier concentrations across a range corresponding to plasmonic light-matter interactions coupling to wavelengths spanning the mid-IR and reaching into the near-IR. Specifically, indium-doped CdO (In:CdO) yields carrier densities ranging between  $2 \times 10^{19} \text{ cm}^{-3}$  and  $5 \times 10^{20} \text{ cm}^{-3}$  while maintaining mobilities between 300-400  $\text{cm}^2/\text{Vs}$  across this range, thus allowing for the widest accessibility of the IR spectrum ( $1650\text{-}5325 \text{ cm}^{-1}$ ) of a single plasmonic material grown by sputtering.

Fully accessing the spectrum of plasmonic applications, including surface plasmon oscillations, epsilon-near-zero (ENZ) modes, and strong coupling phenomena requires that one maintains these appealing transport properties over a film thickness range spanning a few tens to a few thousands of nanometers. Extensive CdO fabrication experiments using high-power impulse magnetron sputtering reveal a strong dependence of carrier density and mobility on film thickness when thickness drops below 100 nm, a particularly significant range for ENZ modes. We attribute this behavior to well-reported surface charge accumulation and depletion layers caused by Fermi level pinning. In this presentation, we demonstrate the reversal between surface charge accumulation and depletion in In:CdO. Further, we show how these surface effects can influence optical properties, i.e. perfect absorber ENZ modes, and how they can be controlled by suppressing acceptor defect formation and sandwiching ENZ layers between unintentionally doped CdO to eliminate interfacial defects.

#### 9:25 AM F.NM02.01.36

**Doped Conjugated Polymers for Infrared Plasmonics** [Hemanth Maddali](#) and Deirdre O'Carroll; Rutgers, The State University of New Jersey, United States

Plasmonic materials have garnered a lot of interest due to their ability to confine light below the diffraction limit which enables applications in energy harvesting, light localization and detection, and for environmental sensing in the mid-infrared. The vast majority of plasmonic materials used at visible and infrared wavelengths are either metals or doped inorganic semiconductors. Most metals exhibit their plasma frequency in the UV or visible wavelength regions and both localized plasmon resonances and surface plasmon polaritons can be supported at wavelengths spanning from the UV to near infrared (IR). Inorganic semiconductor compounds cannot support visible-wavelength plasmonic modes; however, they can exhibit strong plasmonic behavior in the infrared if their conductivity is high enough. Many of these inorganic compounds are expensive and involve high processing and fabrication costs that make devices that include these materials very expensive. Doped organic semiconductors, such as conjugated polymers, could act as cheaper and more versatile IR plasmonic materials that enable advancement of IR localization and sensing. Numerous studies have shown that highly-doped conjugated polymer

materials such as polyacetylene, polypyrrole and polythiophene can exhibit conductivities ranging from ~100 S/cm to 10,000 S/cm. In that conductivity range, a plasmonic response could be observed at mid-IR wavelengths because highly-doped polymers can exhibit metal-like behavior. However, very few studies have demonstrated plasmonic responses in the IR region for highly-doped conjugated polymers.

In this study, we investigate the use of doped conjugated polymers as potential IR plasmonic materials. Drude model calculations were performed to estimate the theoretical conductivity that is required for a material to exhibit a plasma frequency in the mid-IR region. A correlation was established between plasma frequency and the conductivity of the thin films was established using the calculations. Poly(3,4-ethylenedioxythiophene):polystyrene sulfonate (PEDOT:PSS) thin films were doped multiple times with para-toulenesulfonic acid (PTSA) in dimethyl sulfoxide (DMSO). These doped films were then treated with sulfuric acid to further increase the conductivity of the PEDOT:PSS films. IR reflectivity measurements will be performed across mid-IR wavelengths to check for a non-linear increase in reflectivity from the highly doped PEDOT:PSS films. This is expected to provide evidence for the occurrence of a plasma frequency in the IR region. Subsequently, the surface of the PEDOT:PSS will be imprinted with gratings using nano imprinting lithography. These gratings will then be excited at a range of incident angles to investigate if surface plasmon polaritons can be launched on the doped polymer films.

### 9:35 AM \*F.NM02.01.38

**Phonon Sculpting—Infrared Functionality via Vibration** Thomas Beechem<sup>1</sup>, Eric Hoglund<sup>2</sup>, Thomas Folland<sup>3</sup>, Amun Jarzembki<sup>1</sup>, Joshua Shank<sup>1</sup>, Sean Smith<sup>1</sup>, Elizabeth Paisley<sup>1</sup>, Chris Saltonstall<sup>1</sup>, James Howe<sup>2</sup>, Joseph R. Matson<sup>3</sup>, Roman Engel-Herbert<sup>4</sup>, Jon Ihlefeld<sup>2</sup>, Jason G. Valentine<sup>3</sup>, Patrick Hopkins<sup>2</sup> and Joshua D. Caldwell<sup>3</sup>; <sup>1</sup>Sandia National Laboratories, United States; <sup>2</sup>University of Virginia, United States; <sup>3</sup>Vanderbilt University, United States; <sup>4</sup>The Pennsylvania State University, United States

The optical phonons of many oxides manifest through atomic oscillations at infrared frequencies. Often polar, these oscillations create electric fields that themselves have infrared frequencies. When exposed to IR-photons, the electromagnetic and vibration-induced fields can be of similar energy and momentum causing interactions that dominate the material's infrared properties within the Reststrahlen band bounded by the transverse- and longitudinal-optical phonon modes. Thus, by controlling, modifying, and even creating "designer" polar phonons, a route is opened to induce infrared phenomena. Here, the infrared properties of composite oxides composed of lamellar combinations of common dielectrics and ferroelectrics—MgO/CaO and SrTiO<sub>3</sub>/CaTiO<sub>3</sub> specifically—are examined to this end. Using a suite of vibrational spectroscopies in combination with materials modelling, the optical response of these "Reststrahlen laminates" extends beyond just a summation of the constituents. The resulting optical properties are examined in light of "synthetic" phonon dispersions that emerge with the variations in periodicity implicit in lamellar structures. Together, the work suggests a means of creating arbitrary infrared materials via composite phonon responses. This work was performed, in part, at the Center for Integrated Nanotechnologies, an Office of Science User Facility operated for the U.S. Department of Energy (DOE) Office of Science. Sandia National Laboratories is a multimission laboratory managed and operated by National Technology & Engineering Solutions of Sandia, LLC, a wholly owned subsidiary of Honeywell International, Inc., for the U.S. DOE's National Nuclear Security Administration under contract DE-NA-0003525. The views expressed in the article do not necessarily represent the views of the U.S. DOE or the United States Government.

SESSION F.NM02.02: Surface-Enhanced Raman Spectroscopy (SERS) and Alternative Plasmonic Materials  
On Demand Abstracts Available for Viewing Starting Saturday Morning, November 21, 2020  
F-NM02

### 5:00 AM \*F.NM02.02.01

**Surface-Enhanced Raman Scattering on Colloidal Au Nanobipyramids** Hui Wang; University of South Carolina, United States

Au nanobipyramids are anisotropic nanostructures with tunable plasmon resonance frequencies and well-defined electromagnetic hot spots, both of which are highly desired for quantitative surface-enhanced Raman spectroscopy (SERS). Here I will talk about how to fine-tune the plasmon resonance frequencies and fine-tailor the tip sharpness to achieve the optimal SERS enhancements on colloidal Au nanobipyramids. Taking full advantage of their wide plasmon tuning range and narrow plasmon bandwidths, we were able to systematically tune the longitudinal plasmon resonance frequency of Au nanobipyramids with respect to the excitation laser wavelength and the Raman scattering frequency of the molecular

adsorbates. We found that the highest SERS enhancements were achieved when the plasmon resonance energies of the nanobipyramids matched the energies of the inelastic scattering photons rather than those of the excitation photons. We also discovered that the tip sharpness of Au nanobipyramids could be tailored in a highly controllable manner through plasmon hot electron-driven photocorrosion, which allowed us to establish a detailed correlation between the surface curvature at the nanobipyramid tips and the Raman enhancements.

**5:15 AM \*F.NM02.02.02**

**Towards Applications of Plasma-Synthesized Plasmonic TiN Nanoparticles as an Alternative to Gold and Silver** Lorenzo Mangolini, Carla Berrospe Rodríguez, Alejandro Alvarez Barragan and Giorgio Nava; University of California, Riverside, United States

The great capacity of plasmonic nanoparticles to efficiently absorb, scatter and emit light has recently garnered attention for application of these materials in plasmon-based photocatalysts, solar cells and thermo emitters. Particularly, gold and silver have been used to successfully drive hydrogen dissociation and CO oxidation reactions by injecting hot electrons into molecules adsorbed to their surface. However, due to the low thermal stability and the high cost of both materials, the need of studying alternative plasmonic materials, that potentially will expand the field towards more cost-effective applications, has been growing in the last years. Titanium nitride (TiN) is a conductive ceramic with high hardness and bulk melting point (2930 °C). Its plasmon resonance located in the visible-NIR region, low cost (relative to gold and silver), and the well-understood properties as a thin film in the semiconductor industry, make it a strong alternative to plasmonic metals. The present work encompasses a comprehensive study of the plasma-based synthesis of TiN nanocrystals and highlights its potential as a high-temperature-resistant photothermal absorber. TiN particles were synthesized via a scalable, modular, non-thermal plasma method. Titanium and nitrogen precursors were transported into a RF frequency plasma where TiN particles nucleate and grow. Platinum nanoparticles were subsequently deposited on the TiN by photo-induced reduction of an aqueous solution of chloroplatinic acid (H<sub>2</sub>PtCl<sub>6</sub>). The reduction of the precursor metal was driven by electron hole pair generation via plasmon decay. The addition of methanol as a hole scavenger increased the electron lifetime, obtaining metallic platinum. This reaction occurred at temperatures below 40°C under visible light illumination. In addition, a novel TiN@SiO<sub>x</sub>N<sub>y</sub> core-shell structure was produced by taking advantage of the modular capabilities of the non-thermal plasma synthesis method. The synthesized core shell particles displayed a 60% higher plasmon peak in the extinction coefficient with respect to the uncoated TiN particles. To probe the potential of these heterostructures, core-shell and uncoated TiN particles were deposited on SiO<sub>x</sub> substrates by coupling the plasma reactor with a nozzle. This simple modification enables to deposit a thin film by jet impaction method. The absorptivity (1 - reflectivity) of both samples were measured under vacuum conditions, demonstrating the high temperature resistance of TiN@SiO<sub>x</sub>N<sub>y</sub> core-shell films, as their optical properties at 700 °C remained stable. This simple experiment demonstrates the stark promise of this material as an alternative to gold and silver nanoparticles.

**5:30 AM F.NM02.02.05**

**Controlling Optical Properties of TiN Epitaxial Films by Tuning Their Stoichiometry** Ragini Mishra<sup>1</sup>, Ching-Wen Chang<sup>2</sup>, Zih-Ho Song<sup>1</sup>, Chang-Wei Cheng<sup>1</sup>, Khant Minn<sup>3</sup>, Ho Wai (Howard) Lee<sup>3</sup> and Shangjr Gwo<sup>1</sup>; <sup>1</sup>National Tsing Hua University, Taiwan; <sup>2</sup>Academia Sinica, Taiwan; <sup>3</sup>Baylor University, United States

Recently developed plasmonic metasurface approach contributes an extraordinary way to manipulate the light-matter interaction at nanoscale, which plays a vital role in various fields such as biological and chemical sensors, surface enhanced Raman spectroscopy (SERS), nonlinear optics, and manipulation of quantum states. Titanium nitride is a promising material due to excellent plasmonic properties from visible to near-infrared. In this work, epitaxial TiN (111) thin films were grown on c-sapphire via plasma-assisted molecular beam epitaxy technique (PAMBE) under ultra-high vacuum conditions. By tuning stoichiometry of TiN via controlling nitrogen flux from lower nitrogen flux to nitrogen rich condition, the spotty reflection high-energy electron diffraction (RHEED) pattern became streakier, indicating a change in surface morphology. The smooth stoichiometric TiN provides excellent optical properties which can replace gold as a plasmonic material platform. The dielectric functions of TiN have been determined via Drude-Lorentz oscillator model fitting and ellipsometry measurement. It also reveals the plasmonic frequency has a blue shift from 2.6 eV (475 nm) to 2.7 eV (452 nm). Therefore, not only can replace TiN for gold in visible to near-infrared regions, but also TiN outperforms gold in the short wavelength region (<500 nm). XRD omega scan indicated the full width at half maximum is ~200 arcsec and the high-resolution atomic image revealed TiN crystalline arrangement. Furthermore, the epitaxial relationships of TiN and sapphire are determined to be TiN (111)|| sapphire (0001), TiN (1-10)|| sapphire (10-10) and TiN (11-2)|| sapphire (11-20). Reference: 1. W. P. Guo et al., Titanium Nitride Epitaxial Film as a Plasmonic Material Platform: Alternative to Gold, ACS Photonics 6, 1848-1854 (2019). 2. R. P. Sugavaneshwar et al., Fabrication of Highly Metallic TiN Films by Pulsed Laser Deposition Method for Plasmonic Applications, ACS Photonics 5, 814-819 (2018).

**5:40 AM F.NM02.02.06**

**Bifunctional Nanocrystals for Catalyzing and Reporting on Chemical Reactions** [Shi Shi](#) and Dong Qin; Georgia Institute of Technology, United States

Bifunctional nanocrystals with integrated plasmonic and catalytic activities embrace great promise for monitoring chemical reactions by in situ surface-enhanced Raman spectroscopy (SERS). In this talk, I first introduce two distinctive strategies to achieve dual functionality. The first strategy involves the fabrication of Ag-based bimetallic nanostructures with an integrated SERS activity from Ag and catalytic activity from the platinum group metals such as Pt or Pd. The second strategy relies on tuning the passivation of Ag surface with an isocyanide molecule for revitalizing the catalytic activity of Ag toward hydrogenation reaction. Next, I use the reduction of 4-nitrothiophenol as a model system to evaluate the capabilities of these two different types of bifunctional nanocrystals for monitoring catalytic reactions and elucidating reaction mechanisms.

**5:50 AM F.NM02.02.07**

**Studying the Properties of Active Metamaterials Using Infrared Photoreflectance** [Thomas Folland](#)<sup>1</sup>, V. D. Wheeler<sup>2</sup> and Joshua D. Caldwell; <sup>1</sup>Vanderbilt University, United States; <sup>2</sup>U.S. Naval Research Laboratory, United States

Active meta-materials offer an appealing way to create high speed modulators in the mid- and far- infrared which cannot be realized with currently available technology. This kind of device typically relies on a material with optical properties which change upon application of an electric and/or optical field, resulting in changes to their refractive index and/or loss. Whilst conventional characterization techniques (such as FTIR) are capable of accurately characterizing large changes in the properties of an active metamaterial, measuring small absolute changes is often problematic. This is particularly important for understanding the properties of devices which are functioning off-resonance, or trying to determine changes to any weak resonances in the spectral response. In this paper, we describe how the use of photoreflectance implemented in a FTIR microscope acts as a powerful tool to understand the properties of active metamaterials in the infrared with high dynamic range. In particular, we study the modulated behaviour of VO<sub>2</sub> films and coatings integrated onto SiC nano resonator arrays. Photoreflectance is a technique which was originally used to study semiconductor quantum wells in the visible to near infrared, capable of measuring optically dark transitions. It is based on using a modulated pump laser to modulate the optical constants of a material, and then using a lock-in amplifier to monitor the corresponding change in sample reflectance. Here, we extend this technique to FTIR microscopy using broadband cooled MCT detectors, providing modulated information across an extremely broad spectral range. Our approach is an expansion of earlier implementations in the mid-infrared, where we use a combination of amplitude modulated step-scan spectroscopy and visible pump lasers, in order to build a photoreflectance system. In order to characterize the properties of our photoreflectance system we study films of vanadium dioxide (VO<sub>2</sub>), a correlated oxide with a volatile metal-insulator phase transition near room temperature. VO<sub>2</sub> acts as an exemplary material for such studies, as when fully switched it shows an extremely large change in its optical properties across the mid-infrared, and has been widely integrated into metamaterials. First, we consider thin (35nm) planar films of VO<sub>2</sub> in order to determine the sensitivity of the photoreflectance technique. By fully undergoing the MIT in VO<sub>2</sub> we can observe the change in optical properties using both conventional FTIR microscopy, as well as photoreflectance. However, with photoreflectance we are able to characterize much smaller changes in the optical properties, in particular close to the phonon energies of VO<sub>2</sub>. Furthermore, we are able to probe the spectral regions close to the optical phonons of the film. To implement these studies for studying metamaterial devices, we then study silicon carbide nanopillars which are conformally coated with a layer of VO<sub>2</sub>. We are able to quantify the change in device response across the full Reststrahlen band, and the modulation speed of the device, which would normally be extremely difficult without infrared lasers. We envision that this technique could act as a platform to understanding the coupling of metamaterials to active materials, including those with small changes in optical constants such as in piezoelectric materials.

**6:00 AM F.NM02.02.09**

**All-Gas Phase Plasma Synthesis of Plasmonic Zirconium Nitride for Advanced Photochemistry Applications** [Chris Rudnicki](#), Stephen Exarhos, Alejandro Alvarez Barragan and Lorenzo Mangolini; University of California, Riverside, United States

Plasmonic nanomaterials absorb light extremely well due to a localized surface plasmon resonance (LSPR) that is correlated with the density of free charge carriers in nanomaterials. Plasmonic nanomaterials have received interest in a broad variety of fields, such as photocatalysis, photochemistry, photovoltaics, biophotonics, spectroscopy, sensing, and wave-guiding. We present a novel technique for the synthesis of plasmonic zirconium nitride (ZrN) nanoparticles using a scalable non-thermal plasma process.<sup>1</sup> Cost, production concerns and most importantly high thermal stability motivate the search for plasmonic materials alternative to gold and silver, like Group IV transition metal-nitrides such as TiN<sub>2</sub> the relatively unexplored ZrN.

Our ZrN nanoparticles display a plasmonic peak around 620 nm and from XRD and TEM we infer the crystallinity of the particles to be a cubic rock salt structure and a tunable size distribution below 10 nm. To prevent oxidation and the subsequent loss of plasmonic effect, we developed a modular non-thermal plasma system that coats the particles with amorphous silicon nitride in flight. This coating acts as an oxygen-sink when the material is exposed to atmosphere and yields blue-shifted and increased-intensity absorption. An attractive application of these plasmonic particles is the reduction of metals like platinum and chromium (VI) species in water which are extremely toxic.<sup>3</sup> Here we have provided evidence of plasmon driven photo catalytic activity within visible wavelengths to reduce Platinum in solution.<sup>4</sup> An aqueous solution of ZrN, methanol, and chloroplatinic acid (H<sub>2</sub>PtCl<sub>6</sub>) was illuminated using a monochromator set to various wavelengths in the visible regime. Energy dispersive X-ray spectroscopy (EDS) was then used to determine the ratio of reduced platinum to zirconium at a given wavelength. A similar method was used to reduce Chromium (VI) in water. [1] S. Exarhos, A. Alvarez Barragan, E. Aytan, A. A. Balandin, and L. Mangolini, "Plasmonic Core-shell Zirconium Nitride-Silicon Oxynitride Nanoparticles," ACS Energy Lett., no. September, p. acsenergylett.8b01478, 2018. [2] A. Alvarez Barragan, N. V. Ilawe, L. Zhong, B. M. Wong, and L. Mangolini, "A Non-Thermal Plasma Route to Plasmonic TiN Nanoparticles," J. Phys. Chem. C, vol. 121, no. 4, pp. 2316–2322, 2017. [3] M. Valari, A. Antoniadis, D. Mantzavinos, and I. Poullos, "Photocatalytic reduction of Cr(VI) over titania suspensions," Catal. Today, vol. 252, pp. 190–194, 2015. [4] A. Alvarez Barragan et al., "Photochemistry of Plasmonic Titanium Nitride Nanocrystals," J. Phys. Chem. C, p. acs.jpcc.9b06257, 2019.

### 6:10 AM F.NM02.02.13

**Undoped Organic Semiconductor Films for Surface Enhanced Raman Spectroscopy Application** Antonio Facchetti<sup>1,2</sup>; <sup>1</sup>Northwestern University, United States; <sup>2</sup>Flexterra Inc., United States

Organic small molecules comprising  $\pi$ -conjugated moieties and functional groups have been the subject of considerable applications in organic opto-electronics, however,  $\pi$ -conjugated small molecules have yet to play a significant role as substrate for Surface Enhanced Raman Spectroscopy (SERS) studies. Very recently we demonstrated that metal-free nanostructured semiconductor films based on a  $\pi$ -conjugated small molecule, (DFH-4T diperfulorohexyl-quaterthiophene), could be SERS-active with a remarkable enhancement factor (EF) surpassing 10<sup>3</sup>.<sup>13</sup> Prompted by this breakthrough, we questioned whether molecular engineering of the SERS-active organic semiconductors, and thus the corresponding optoelectronic properties and solid-state microstructure/morphology, can be tuned to further advance Raman enhancement performance. Here we report that a fluoroarene-modified oligothiophene, (DFP-4T, diperfluorophenyl-quaterthiophene) semiconductor, which includes an electron-rich quaterthiophene  $\pi$ -core similar to that of DFH-4T but end-capped with  $\pi$ -electron-deficient perfluorophenyl (-C<sub>6</sub>F<sub>5</sub>) units. Thus, this molecule employs a quite different design approach as compared with DFH-4T, wherein the  $\pi$ -insulating perfluoroalkyl substituents present in DFH-4T are removed and replaced with -C<sub>6</sub>F<sub>5</sub> substituents leads to a fully  $\pi$ -conjugated backbone featuring small intramolecular torsions. Hydrophobic and nanostructured DFP-4T films prepared via PVD are found to exhibit unprecedented EF values of >10<sup>5</sup>, indicating that the SERS performance of metal-free organic semiconductor films now approach those of the current plasmonic metal and inorganic semiconducting platforms. Furthermore, a very low detection limit of 10<sup>-9</sup> M is demonstrated for methylene blue (MB) as the probe molecule.

SESSION F.NM02.03: Advances in the Colloidal Synthesis of Plasmonic Nanostructures  
On Demand Abstracts Available for Viewing Starting Saturday Morning, November 21, 2020  
F-NM02

### 5:00 AM \*F.NM02.03.02

**Chirality, Complexity and Criticality in Inorganic Nanostructures** Nicholas Kotov; University of Michigan, United States

The early observation of strong circular dichroism for individual nanoparticles (NPs) and their assemblies have developed into a rapidly expanding field of chiral inorganic nanostructures. They encompass a large family of mirror-asymmetric constructs from metals, semiconductors, ceramics, and nanocarbons with multiple chiral geometries with characteristic scales from Ångströms to microns. Versatility in dimensions and polarizability of the inorganic materials enables their multiscale engineering to attain a broad range of optical and chemical properties. These capabilities as chiral materials enabled their fast technological translation for biosensing and optoelectronics, which, in turn, opened new venues for scientific inquiry into the unifying role chirality at the interface of materials science, biology, chemistry, and physics. This talk will address (1) the origin of the uniquely high values of optical anisotropy; (2) mechanisms of chirality transfer in inorganic materials; and (3)

differences/similarities with chiral supramolecular, liquid crystal, and biological assemblies. Special attention will be given to the relationship between chirality and complexity traced over a large family of nano-, meso-, and microscale particles. Strict enumeration of complexity was accomplished by developing graph theory methods to describe NPs assemblies resulting in phase diagrams relating chirality and complexity. Non-uniform rise of complexity depending on temperature and enantiomeric excess in the system was examined in relationship with the phase transition between different hierarchical assemblies. The highest complexity was observed when high chirality coincided with the triple critical point in the phase diagram. If time permits, emerging venues for practical realizations of chiral inorganic nanoassemblies related to circular polarization spectroscopy in terahertz spectral window with chiroplasmonic kirigami composites will be introduced and discussed in relation to long-standing questions intermolecular interactions of chiral supramolecules.

#### 5:15 AM F.NM02.03.06

**A Nanoscale Plasmonic Reactor—Light-Driven Synthesis of Individual Core@Shell Nanoparticles** [Rifat Kamarudheen](#), Gayatri Kumari, Guillaume Baffou and Andrea Baldi; Dutch Institute for Fundamental Energy Research, Netherlands

Light is an efficient tool to activate and control a wide range of chemical reactions, from heterogeneous photocatalysis, to molecular switching, and pharmaceutical drug production. The advent of nanophotonics has further advanced these fields by allowing to focus, control and steer light at the nanoscale. In particular, the use of localised surface plasmon resonances, which are light-driven oscillations of free electrons in metal nanoparticles, is currently being explored to drive chemical processes such as nanoparticle syntheses, photocatalytic reactions, and nanolithographic patterning. These plasmon resonances can activate chemical reactions thanks to non-equilibrium "hot" charge carriers, near-field enhancement of the electromagnetic fields, and nanoscale temperature gradients.<sup>1</sup> The relative contribution of these different mechanisms is often quite difficult to disentangle due to the complex light propagation, poorly-understood quantum mechanical charge carrier generation and ejection, and complicated macroscopic and microscopic heat dissipation in irradiated reaction vessels.<sup>2</sup> Single nanoparticle studies can be used to elucidate the mechanism at play, as parameters such as illumination intensity, light polarization, and sample and illumination geometry can be accurately controlled.<sup>3</sup> So far, however, it has been challenging to control the synthesis of individual nanostructures with desired chemical compositions and controlled morphologies. Here, we show how we can selectively use plasmonic photothermal heating to activate and control the synthesis of individual Au@semiconductor core@shell nanoparticles.<sup>4</sup> Under plasmon excitation of individual gold nanoparticles in a reactive flow cell, we activate the formation of conformal metal oxide and metal sulfide shells with growth rates that scale with the nanoparticle surface temperature. Given the large spectral sensitivity of plasmon resonances to the nanoparticle morphology, the shell growth reaction is self-limited in nature and can be monitored in-situ by tracking the photoluminescence spectra of the growing plasmonic nanostructure under laser irradiation. We demonstrate the versatility of plasmonic heating as a chemical activation mechanism by synthesizing CeO<sub>2</sub>, ZnO and ZnS shells on gold nanoparticles of different sizes and shapes. The use of light as a tool to activate and control chemical reactions at the nanoscale can lead to the synthesis of shape- and size-controlled hierarchical nanostructures which are inaccessible with classical colloidal synthetic methods, with potential applications in nanolithography, catalysis, energy conversion, and photonic devices. <sup>1</sup> M.L. Brongersma, N.J. Halas, and P. Nordlander, *10, 25* (2015). <sup>2</sup> R. Kamarudheen, G.W. Castellanos, L.P.J. Kamp, H.J.H. Clercx, and A. Baldi, *ACS Nano* **12**, 8447 (2018). <sup>3</sup> J. Olson, S. Dominguez-Medina, A. Hoggard, L.-Y. Wang, W.-S. Chang, and S. Link, *Chem. Soc. Rev.* **44**, 40 (2015). <sup>4</sup> R.Kamarudheen, G. Kumari, G. Baffou, and A.Baldi (submitted)

#### 5:25 AM F.NM02.03.07

**Enabling Spatially-Selective Photochemical Transformations with Plasmonics** [Katherine Sytwu](#), Michal Vadal, Fariah Hayee, Alan Dai, Dixon Jefferson and Jennifer A. Dionne; Stanford University, United States

Plasmons have emerged as one solution to optically control chemistry at the nanoscale. Plasmonic photocatalysts have not only demonstrated increased reactivity, product selectivity, and new reaction pathways for heterogeneous catalysis, but also nanolocalized chemistry. However, in plasmonic photocatalytic systems, the overall reactivity is dictated by both the regions of localized enhanced electromagnetic fields ("hot spots") and regions of high innate chemical reactivity (i.e. undercoordinated sites), which often coincide. To gain a systematic understanding of the influence of light on chemical reactions, one needs to be able to decouple the optical response from the surface chemistry preferred in the dark. Here, we spatially separate the electromagnetic hot spot from the catalytically favorable sites to demonstrate how plasmons can modify a reaction. As a proof of concept, we visualize the dehydrogenation of Pd nanorods coupled to Au nanobars in a cross-bar geometry. We use electron-beam lithography to pattern 75 nm wide Au nanobars onto a Si<sub>3</sub>N<sub>4</sub> membrane, followed by the deposition of a 2.5 nm SiO<sub>2</sub> spacer layer. Colloidally synthesized Pd nanorods of median length 450 nm are then dropcast on top. This geometry supports a strong gap plasmon mode between the Au nanobar and the Pd nanorod, creating an electromagnetic hot spot that is localized to the center of the Pd nanorod and well separated from the catalytically more favorable Pd tips. Using a light-coupled environmental transmission electron microscope, we track the plasmon-induced

dehydrogenation of individual Pd nanorods with sub-particle, nanometer-scale resolution. We map the nucleation site of the new phase as a function of hydrogen pressure, illumination power, and wavelength. Without illumination, the Pd nanorods dehydrogenate from their tips. In contrast, upon resonant illumination (around 640nm), the Pd nanorods nucleate their new phase in the middle of the nanorod near the plasmonic hot spot. We confirm this behavior across six Au-Pd antenna-reactor systems for H<sub>2</sub> pressures spanning 49Pa-89Pa. By varying the illumination wavelength, we further confirm that this induced phase transition depends on exciting the gap plasmon resonance as no phase transition happens with off-resonance illumination. Our direct visualization of a plasmon-driven, spatially-selective reaction demonstrates optical control of reactive sites, an important result towards designing next-generation, multifunctional photocatalysts.

#### 5:35 AM F.NM02.03.08

**Lanthanide-Doped Nanophosphors for Multiplexed Spectral Imaging of Complex Biological Interactions** Dayne F. Swearey, Stefan Fischer and Jennifer A. Dionne; Stanford University, United States

Immunogold staining is the current standard for characterizing cellular ultra-structures using the sub-nanometer resolution afforded within an electron microscope. However, despite nearly 50 years of use, immunogold staining only yields binary information based on image contrast between the heavy gold atoms and carbonaceous cellular structures and therefore cannot provide multiplexed imaging capabilities. This limit restricts the potential of immunogold staining when imaging critical biological phenomena such as protein-protein interactions or to map the extensive ensemble of transmembrane proteins across a cell's surface. Here, we report on the development of a library of small, electron-beam stable, and bright cathodoluminescent nanophosphors based on an alkaline-earth rare-earth fluoride host lattice. The base composition of each nanophosphor is BaYF<sub>5</sub>, where the Y<sup>3+</sup> cations can be substituted with lanthanide cations (Ln<sup>3+</sup>) between 0 and 100% doping to act as optical emitters with distinct spectral emissions under electron beam excitation. The nanophosphors were colloiddally synthesized using a strategy based on the thermal decomposition of mixed metal trifluoroacetate salts in a solvent system composed of oleic acid, octadecene, and oleylamine, which resulted in the nucleation of a narrow size distribution of 5 nm cores. Following a series of subsequent shelling steps, the nanophosphors were grown systematically until cubic nanoparticles with median edge lengths of 20 nm and 25 wt% loading of Ln<sup>3+</sup> are incorporated into the nanophosphor where Ln<sup>3+</sup> = Ce, Pr, Nd, Sm, Eu, Tb, Dy, Ho, Er, Tm, or Yb. These nanophosphors result in distinct and narrow spectral emissions that are characteristic of the atomic identity of the lanthanide dopant. Using an optically coupled scanning transmission electron microscope, ensemble cathodoluminescent spectra were obtained for eleven distinct nanophosphors using a focused electron beam at low currents (<100 pA) and short acquisition times (greater than or equal to 10 seconds). Focusing on the brightest nanophosphors, dozens of single nanoparticle cathodoluminescence spectra were obtained for three BaY<sub>0.75</sub>Ln<sub>0.25</sub>F<sub>5</sub> species, where Ln<sup>3+</sup> = Ho, Tb, Er. Each of these nanophosphors produce distinct cathodoluminescent spectra with maximum spectral emission at l<sub>Er</sub>= 675 nm, l<sub>Ho</sub>= 635 nm, and l<sub>Tb</sub>= 555 nm. The distinct emission of each nanophosphor allows for the realization of multiplexed spectrum imaging, and line scan analysis on samples containing both BaY<sub>0.75</sub>Tb<sub>0.25</sub>F<sub>5</sub> and BaY<sub>0.75</sub>Ho<sub>0.25</sub>F<sub>5</sub> opening the door to true nanoscale multiplexed imaging based on optical signatures from lanthanides. Through future work on surface modification, individual cathodoluminescent nanophosphors can be selectively attached to specific proteins of interest using similar chemistry pioneered through 50 years of immunogold staining research. This development opens the possibility for multiplexed imaging of biomolecules at the single-molecule level within the cellular ultra-structure, providing insight into the distribution and expression of proteins within cells at the high resolution afforded by electron microscopes.

#### 5:45 AM F.NM02.03.09

**Synthesis of Gold Nanostructures and Applications from Photonics to Photocatalysis** Stephane Parola, Denis Chateau, Anthony Desert, Frederic Lerouge and Frederic Chaput; Chemistry Laboratory, Ecole Normale Supérieure de Lyon, France

Among the various studied shapes of gold nanoparticles, nanobipyramids are one of the most interesting ones. Their anisotropic structure enables the tuning of their LSPR even further than gold nanorods, with higher local electric field enhancement, and their morphology (aspect-ratio, roughness, size, etc.) can be controlled with more freedom. We developed in our lab a high yield process to make such nanostructures, in the classic submillimolar concentration range. While this process was very efficient, its low concentration makes the production of concentrated solutions quite cumbersome and generates lots of waste. Therefore, we developed a new versatile process enabling the direct preparation of gold nanobipyramids and several other pentatwinned nanostructures at concentrations range between 15 and 30 mM (3 to 6g per liter). This novel synthesis has nearly quantitative yields, while allowing an easy tuning of LSPR wavelength. A specific influence of the nature of the reducing agent on the morphology has been observed, and this can be further controlled or enhanced by varying experimental conditions (surfactant, temperature, co-reagents). Those breakthroughs open further uses for gold pentatwinned nanostructures by simplifying their preparation at gram scale and tuning their morphology for specific uses. In order to illustrate the potentialities of such gold nanostructures, we will show our recent investigations on their use

for optical applications. We developed an easy and general gold surface modification by a functional thiolated silicon polymer. In addition to be an alternative to the use of surfactants or long-chain polymers in order to provide efficient colloidal stabilization in a wide range of solvent, this surface modification allows us to prepare homogeneous hybrid materials like gold-doped sol-gel silica. Association with various photoactive compounds have been explored and enhancement for example of photocatalytic properties of TiO<sub>2</sub> or non-linear optical absorption of dye-doped glasses. Finally, we will present our current efforts regarding core-shell AuBP@SiO<sub>2</sub> NPs for enhanced photocatalysis based on singlet oxygen generation.

#### 5:55 AM F.NM02.03.11

**Hydrophobicity Modification of an Au Nanowire Substrate for the Collection and Detection of Low-Concentration Analytes via Surface-Enhanced Raman Spectroscopy** Minjoon Kim and Yeon Sik Jung; Korea Advanced Institute of Science and Technology, Korea (the Republic of)

Detection of trace amount molecules is crucial for analytical studies and inspection of environmental contaminants. Of many detection systems, surface-enhanced Raman spectroscopy (SERS) stands out as an outstanding option not only for its rapid process but also for its non-destructive properties and molecular-specific signals. Previous studies have reported up to attomolar concentration detection via SERS by utilizing “hot spots” produced from diverse nanostructures and fabrication methods. “Hot spots” are regions with localized surface plasmon resonance (LSPR) formed between nanostructured gaps that significantly enhance the Raman signal of analytes. Yet, despite advances in fabricating noble metal nanostructures with high-signal enhancement factors, trace-amount detection remains problematic as the delivery of adequate amounts of analytes to the proximity of “hot spots” is required for sufficient enhancement effects. Therefore, a platform to gather enough target molecules within the vicinity of “hot spots” is important for trace-amount molecule detection.

Here, we introduce a hydrophobic Au nanowire substrate with a hydrophilic center for the collection and detection of low-concentration analytes. The hydrophilic center acts as a concentrating point during the evaporation of highly-dilute analyte solutions and allows easy location of the measurement point during direct Raman spectroscopy. The SERS substrate is fabricated via solvent-assisted nanotransfer printing (S-nTP) to form the highly dense Au nanowire surface. The center is then selectively coated with a thin layer of SiO<sub>2</sub> to provide hydrophilicity while the surrounding area is subsequently functionalized with 1H,1H,2H,2H-Perfluorodecanethiol (PFDT) to amplify the hydrophobicity of the remaining Au nanowires. When an analyte solution is dropped and dried on the substrate, the solution is guided towards the hydrophilic center with minimum liquid contact line pinning on the hydrophobic surroundings. As a result, Raman measurements at the hydrophilic area show clear spectra of the dye and pollutant molecules up to attomolar concentrations compared to non-functionalized Au nanowire substrates with analytes spread over the entire surface.

SESSION F.NM02.04: Metamaterials, Metasurfaces and Nanoantenna  
On Demand Abstracts Available for Viewing Starting Saturday Morning, November 21, 2020  
F-NM02

#### 5:00 AM \*F.NM02.04.01

**Artificial Chirality Evolution in Micro-/Nano-Scale 3D Plasmonic Metamaterials** Junsuk Rho<sup>1,2</sup>; <sup>1</sup>Pohang University of Science and Technology (POSTECH), Korea (the Republic of); <sup>2</sup>Pohang University of Science and Technology, Korea (the Republic of)

Plasmonic chiral metamaterials has attracted significant attention as it provides a new route to intriguing optical properties such as negative refractive index, light polarization filters, and phase modulation. However, the fabrication regarding with limited resolution in conventional synthesis and complexity of asymmetric synthesis pose a major hindrance for further development. In this study, a new class of three dimensional chiral plasmonic nanostructures was successfully fabricated using molecular shape modifiers and crystallographic control of nanoparticle. Previously, we developed three-dimensional chiral metamaterials based on photolithography overlay and electron-beam lithography overlay for terahertz and near-infrared, respectively. We found scaling down them further to visible frequency is extremely difficult. As an alternative solution, we discovered a novel system that characteristic of molecule is transformed into distinctive gold nanoparticle shape. On the basis of this system, chirality transfer between molecular modifier and gold surface allow us to achieve numerous chiral morphologies of gold nanoparticle, named plasmonic helicoids. Particularly, enantiospecific interaction of molecule and high index plane plays pivotal role to provide asymmetric structuring process on the gold surface, forming distinct chiral morphology in single nanoparticle level. One of the representative shapes of helicoid structure showed gammadion-like



structure, consisting of four highly curved arms of increasing width, in all six faces of cubic geometry. The unprecedented chiral morphology of plasmonic helicoid has remarkable optical activity (dissymmetry factor  $\sim 0.2$  at 622 nm) even in a randomly dispersed solution, substantiated by direct visualization of macroscopic color transformation. Changes in molecular recognition and growth parameter led to different morphological evolution, and structural alterations provided a straightforward means of tailoring optical response, such as optical activity, handedness, and resonance wavelength. Also, our aqueous phase synthesis is readily scalable without losing exquisite chiral structure at nanoscale. In these aspects, our approach, chirality evolution in single nanoparticle, provides a truly new paradigm and valuable insight for chiral metamaterial fabrication. Such unique fabrication technique will provide the opportunity to achieve the significant step making metamaterials from science to technology. References 1. S. Zhang et al., Phys. Rev. Lett. 102, 023901 (2009) 2. S. Zhang et al., Nat. Commun. 3, 942 (2012) 3. G. Yoon et al., Sci. Rep. 7, 6668 (2017) 4. J. Mun et al., Opt. Lett. 43, 2856-2859 (2018) 5. M. Kim et al., Opt. Express 26, 14051-14057 (2018) 6. H. Lee et al., Nature 556, 360-365 (2018) (with News and Views Article, Nature 556, 313-314 (2018)) 7. J. Mun et al., Nanophotonics 8, 941-948 (2019) 8. H. Lee et al., Nature Commun. (in revision) 9. J. Mun et al., Light: Sci. Appl. (in review)

#### 5:15 AM \*F.NM02.04.02

**Electrically Reconfigurable Metasurface for Spatial Light Modulation** Junghyun Park, Byung Gil Jeong, Sun Il Kim, Duhyun Lee, Kyoungho Ha and Hyuck Choo; Samsung Advanced Institute of Technology, Korea (the Republic of)

We have demonstrated an ultrafast, ultra-compact, and all-solid-state metaphotonic spatial light modulator (M-SLM) which can dynamically shape light in reflection. The M-SLM is an array of electrically controlled plasmonic nanostrip cavities, and it can continuously adjust the phase of reflected light from 0 to 360 degrees and, at the same time, independently modulate the amplitude over its full range. The fabricated M-SLM contains 50 active pixels and measures  $250 \times 250 \mu\text{m}^2$  in dimensions. By tuning the voltages applied to the M-SLM, we have demonstrated beam steering and beam splitting with a steering angle up to  $8^\circ$ , the side mode suppression ratio of +2.7 dB (the highest value reported in the field), and the deflection efficiency up to 48%. The experimentally measured modulation speed marks 5.6 MHz while the energy consumption per pixel is calculated to be as low as 354 pJ per switching. Accomplishing arbitrary light manipulation using active metaphotonics has remained challenging, especially due to coupling between the phase and amplitude during modulation which resulted in unwanted background noises. To overcome this limitation, we have delved into the fundamental modeling of the light wave and observed that it would require minimum two variables, for example, the real and imaginary coefficients, to properly express the phase and amplitude of the light wave. Based on this observation, we developed the two-control-parameter algorithm and translated the concept into the hardware design. In the array of the designed M-SLM, each plasmonic nanostrip cavity is a stacked double-gated structure with an indium-tin-oxide layer as an active intermediate channel, which allows an application of two independent control voltages to the top and bottom gate metals. We have also performed extensive numerical investigation and confirmed that the highly versatile light-manipulating capability of the designed M-SLM, including arbitrary phase and amplitude modulation, originates from the superposition of the effects generated by the voltages applied independently to the top and bottom metals. To our knowledge, the M-SLM is the first all-solid-state, electrically controlled metasurface that accomplishes the 360-degree full phase sweep and independent amplitude modulation. Unlike previously reported work, our M-SLM does not involve the use of slow, temperature-sensitive liquid crystals, stiction- and-vibration-prone micro-electromechanical systems (MEMS), or an array of pre-fabricated size-varying structures to achieve phase changes. The M-SLMs extremely low power consumption, ultrafast modulation speed, ultra-compact form factor, outstanding predicted reliability, and the use of standard IC-fabrication processes promises wide adaptation and proliferation of the ultrafast and extremely power-efficient SLMs for 3-dimensional real-time holographic display, light detection and ranging (LiDAR), and wearable display for virtual reality. We look forward to sharing and discussing the details of our M-SLM design philosophy, hardware design & fabrication, and testing results with the audience at the MRS 2020 Spring.

#### 5:30 AM \*F.NM02.04.03

**Extreme Nonlinear Optics in Epsilon-Near-Zero Materials** Yuanmu Yang; Tsinghua University, China

In this talk, I will present our recent efforts to drastically enhance the efficiency of high-harmonic generation (HHG) and broadband terahertz (THz) generation in ultra-thin transparent conducting oxide films leveraging the epsilon-near-zero (ENZ) effect. HHG has been used to generate extreme ultra-violet (EUV) light sources to probe fast electron dynamics in the attosecond time scale. While traditionally observed in rare-gas atoms, HHG has also recently been reported in solids with reduced threshold pump field. Here, we use the ENZ effect to greatly boost the efficiency of the HHG process in solids. We report high-harmonic emission up to the 9th order directly from a low-loss, solid-state ENZ medium: indium-doped cadmium oxide, with an excitation intensity at the GW  $\text{cm}^{-2}$  level. Furthermore, the observed HHG signal exhibits a pronounced spectral red-shift as well as linewidth broadening, resulting from the photo-induced electron heating and the consequent time-

dependent resonant frequency of the ENZ film. THz technology has undergone much development in the past few decades, yet it still remains a grand challenge to realize THz sources on an integrated platform. The intensity and spectral bandwidth of typical nonlinear THz sources are limited by the phase matching condition in the nonlinear medium. Here, we demonstrate broadband THz emission, both in transmission and reflection configurations, from a commercially available 10-nm-thick indium tin oxide (ITO) film, leveraging the ENZ effect in ITO. The bandwidth of the THz signal generated from the ultrathin ITO film is unrestricted by the phase matching condition.

**5:45 AM \*F.NM02.04.04**

**Tunable Chiral Optical Properties in Semiconductor Nanocrystals and Metamaterials** Vivian Ferry; University of Minnesota, United States

Optical nanomaterials offer the ability to bend, twist, guide, and confine light in nanoscale dimensions. Among these materials, chiral nanostructures particularly show promise for applications ranging from polarization manipulation to 3D displays, sensing, and spin-selective transport. Compared to their molecular counterparts, chiral nanomaterials exhibit orders of magnitude stronger dissymmetry factors, but have only been realized in a limited set of materials systems. We have recently demonstrated different strategies to tune and manipulate the polarization response of chiral metamaterials that combine metallic nanostructures, dielectric materials, and semiconductor nanocrystals. By controlling the refractive index of the dielectric components in different architectures, we show that the sign of the circular dichroism can be reversed, and the polarization and directionality of the outcoupled luminescence from nearby nanocrystals can be controlled. To create light-emitting metamaterials, it is additionally useful to create nanostructured elements comprised entirely of photoluminescent materials. We have recently developed patterning methods to transform semiconductor nanocrystals into patterned nanocrystal solids, realizing lateral feature sizes as small as 30 nm and heights in excess of 100 nm without degradation of the photoluminescence. We show that by designing the shape of the nanocrystal solid at this length scale and controlling connectivity between the nanocrystals, the refractive index and nanostructure absorptivity can be tailored. This work points to new strategies to design dynamically tunable metamaterials and control nanoscale light-matter interactions.

**6:00 AM \*F.NM02.04.05**

**Reststrahlen-Band Photonics—Extreme Infrared Light Control with Semiconductors** Stavroula Foteinopoulou; University of New Mexico, United States

Heteropolar or polar covalent semiconductors can have their opposite-phase transverse phonon vibrations activated by an impinging infrared (IR) light beam. Thus, strong coupling occurs between the incoming light and the matter vibrations resulting in a hybrid mode known as phonon polariton (PhP). This hybrid PhP mode has a frequency gap in its photonic dispersion, typically referred to as the reststrahlen band, which signifies a regime of forbidden light propagation inside the material; hence bulk PhP materials are near-perfect reflectors. This is why PhP materials have been largely overlooked as the material of choice to control the flow of infrared light for modern photonic applications. However, in the recent years there has been a heightened attention around PhP materials which now are prominent candidate materials for infrared photonics. PhP materials owe this recent growing interest to the versatile photonic responses within and around the reststrahlen band which include plasmonic-like responses similar to those of noble metals in the visible spectrum as well as epsilon-near-zero (ENZ) responses. In this talk, we discuss how to bring judiciously together material patterning and PhP photonic responses for extreme light control in the mid- and far-IR. We present paradigm PhP-based systems exhibiting unconventional infrared effects such as uni-directional, almost all-forward, thermal emission and ultrathin near-perfect PhP absorbers. These effects can have a vast applications range such as for bolometric detectors, high-intensity one-way THz/infrared sources, or thermal-management devices.

**6:15 AM \*F.NM02.04.06**

**Nonlinear Dielectric Metasurfaces—Towards High Efficiency and Full Spatial Phase Control** Thomas Zentgraf; Paderborn University, Germany

For efficient nonlinear processes, the engineering of the nonlinear optical properties of the used materials becomes an important task. The most well-known technique for spatially engineering nonlinear optical properties is the quasi-phase-matching scheme for second-order processes like second-harmonic generation. However, the widely used technique of periodic polling of natural crystals only provides a binary state for the nonlinear material polarization, which is equivalent to a discrete phase change of  $\pi$  of the nonlinear polarization. The continuous tailoring of the phase of the nonlinear susceptibility can greatly enhance the flexibility in the design and reduce parasitic effects, like the generation of other undesired frequency components.

Metasurfaces have the potential to address some of the issues with the continuous phase tailoring in nonlinear processes. In

the linear optical regime, they have shown great promise for tailoring the wavefronts of beams for a large variety of applications, ranging from lenses for imaging and vector beam generation to optical holography. For that different concepts were used to address the issue of tailoring the spatial phase and amplitude. One promising concept is the Pancharatnam-Berry phase that appears for a polarization conversion of the light. However, this concept is not directly transferable to nonlinear metasurfaces, where each meta-atom performs also a nonlinear optical process, like a harmonic generation. The reason is the coupling of different spatial field components through the nonlinear susceptibility tensor, which complicates the design and can give even rise to different phase factors at the same time. Furthermore, the optimization for a particular phase factor might counteract the goal for high conversion efficiency.

Here, we will discuss the concepts of enhancing nonlinear processes with simultaneously engineering the phase for the manipulation of third-harmonic generation from metasurfaces and the arising restrictions for symmetry and geometry of meta-atoms. We theoretically and experimentally studied the nonlinear geometric-phases associated with the THG process occurring in silicon metasurfaces. The THG process involves the wave coupling among the different components of the fundamental field excited inside the dielectric nanoresonators. This gives rise to different geometric-phases carried by the THG signal. We show that the dielectric nanofin structures with various in-plane rotational symmetries generate circularly polarized TH signals carrying the geometric-phases as predicted by the selection rule for nonlinear processes. However, additional phase terms can arise due to the complexity of the mode field inside the nanoresonators. The experiment results agree with our theoretical model.

Furthermore, by tailoring the geometry of high index resonators can result in the excitation of a particular magnetic dipole or higher-order modes that result in relatively strong fields and high conversion efficiencies. We analyze how such modes can be used for tailoring the nonlinear phase utilizing the Pancharatnam-Berry phase approach. By using the recently introduced concept of bound states in the continuum in nanoresonators, we demonstrate that a relatively high conversion efficiency can be obtained for a third-harmonic generation while preserving the spatial phase control possibility using the geometrical phase effect. Controlling the properties of nonlinear metamaterials has fundamental significance in nonlinear optics and for tailored nonlinearities, as such materials provide a further degree of freedom in the design of nonlinear materials.

#### **6:30 AM \*F.NM02.04.08**

**Wave-Matter Interaction in Spatiotemporal Metastructures** [Nader Engheta](#); University of Pennsylvania, United States

Manipulation of waves is mostly achieved by materials with spatial inhomogeneities. However, exploiting the dimension of time, in addition to the three dimensions of space, for variation of material parameters can bring additional functionalities in such tailoring and sculpting the wave. The spatiotemporal metastructures in which the material parameters are engineered with spatial and/or temporal inhomogeneities exhibit special features that enrich the functionality of light-matter interaction. In my group, we are investigating a variety of scenarios in which such four-dimensional (4D) spatiotemporal material platforms can be exploited. These scenarios include 4D materials that provide us with temporal aiming, temporal anisotropy, anti-reflection temporal coatings, frozen waves, phase conjugation, asymmetric diffusion, temporal effective medium methods, etc. In this talk, I will give an overview of our most recent results in this area

#### **6:45 AM \*F.NM02.04.09**

**Metamaterials Defined by Connectivity** [C.T. Chan](#); The Hong Kong University of Science and Technology, Hong Kong

We report on the study of some metamaterials whose properties, including dispersions and topological characteristics, are determined by the connectivity of a network rather than the resonance of individual resonators.

Metamaterials are described using effective medium theories in the long-wavelength limit in the sense that their optical properties can be described using local permittivity and permeability tensors. We will see that some metallic structures cannot be described using such a language. Their properties depends on the network connectivity, where braiding can create effective sythetic gauge fields that induce shift in momentum space. The consequence is that such materials can have their index ellipsoids centered not at  $k=0$ , and they can possess multiple index ellipsoids centered at arbitrary nonzero  $k$ -points. The number of modes that are allowed at zero frequency can be described by Betti numbers. Such systems differ from conventional metamaterials because the functionality does not come from the resonances of individual resonators and as such, their functionalities tend to be broadband.

We will also discuss network structures that have non-trivial topology in momentum space and these materials can couple orbital angular momenta with the wave vector. The topological character originates from the connectivity of the network and goes beyond typical space group descriptions. Such systems can exhibit angular momentum-dependent one-way edge states, and their properties can be described using local Chern numbers. Such systems can also be used to realize other interesting topological systems such as high order topological insulators and topological Anderson insulators, and topological systems in

which the topological order cannot be described by integers.

**7:00 AM \*F.NM02.04.11**

**Scalable Light-Matter Interactions in Nanoparticle Lattices** Teri W. Odom; Northwestern University, United States

Rationally assembled nanostructures exhibit distinct physical and chemical properties beyond their individual units. This talk will describe fundamentals and applications of metal nanoparticle lattices that show long-range diffractive interactions when the lattice spacing is close to the wavelength of incident light. These collective excitations are known as surface lattice resonances (SLRs) or lattice plasmons. We will discuss advances in nanofabrication techniques that have enabled the patterning of a wide range nanoparticle materials over macroscale ( $> \text{in}^2$ ) areas and with units that are highly uniform in size, shape, and crystallinity. Such patterned substrates support SLRs with wavelengths that approach the theoretical limit. We will also describe how different lattice symmetries can result in band-edge modes at high symmetry points in reciprocal space. The confined electromagnetic fields of SLRs can manipulate processes such as exciton-plasmon coupling, nanolasing, and imaging via tunable, flat optics.

**7:15 AM \*F.NM02.04.12**

**Flexible Holographic Metasurfaces** Andrea Di Falco; University of St Andrews, United Kingdom

Optical metasurfaces [1] can be fabricated in flexible substrates [2,3]. Flexibility brings additional advantages to MSs respect to their rigid counterpart, in terms of scalability, conformability, and tunability [4-7]. When metasurfaces are used as supports to encode computer generated holograms, flexibility allows to harness the shape and topology of the target substrate as an additional degree of freedom to encode the holographic information [8,9].

Here we show that this platform can be scaled from the visible to the mm-wave range. This in turn opens the way to the exploitation of flexible holographic metasurfaces for a large number of applications, from security holograms that display the correct image only when the substrate has a determined shape, to the possibility to interface the metamaterials technology to biophotonics systems or to create holographic patches to retrofit existing antennas infrastructures for telecommunication applications [10].

**References**

- [1] N. Yu, P. Genevet, M. A. Kats, F. Aieta, J. Tetienne, F. Capasso, Z. Gaburro, *Science* **334**, 333 (2011).
- [2] A. Di Falco, M. Ploschner, and T. F. Krauss, *New J. Phys.* **12**, 113006 (2010).
- [3] A. Di Falco, Y. Zhao, and A. Alú, *Appl. Phys. Lett.* **99**, 163110 (2011).
- [4] X. Li, C. Rizza, S. A. Schulz, A. Ciattoni, A. Di Falco, *APL Photonics* **4**, 056107 (2019).
- [5] S. Song, X. Ma, M. Pu, X. Li, K. Liu, P. Gao, Z. Zhao, Y. Wang, C. Wang, X. Luo, *Advanced Optical Materials* **5**, 1600829 (2017).
- [6] S. M. Kamali, A. Arbabi, E. Arbabi, Y. Horie, A. Faraon, *Nature Comm.* **7**, 11618 (2016).
- [7] S. C. Malek, H. S. Ee, R. Agarwal, *Nano Letters* **17**, 3641 (2017).
- [8] J. Burch, D. Wen, X. Chen, and A. Di Falco, *Sci. Rep.* **7**, 501 (2017).
- [9] J. Burch and A. Di Falco, *ACS Photonics* **5**, 1762 (2018).
- [10] J. Burch *et al.* *Appl. Phys. Lett.* **115**, 021104 (2019).

**7:30 AM \*F.NM02.04.13**

**Tunable and Time Modulated Active Metasurfaces** Mohammad Mahdi Salary, Seyedali Forouzmard, Raana Sabri, Hooman Barati Sedeh and Hossein Mosallaei; Northeastern University, United States

Realization of active optical metasurfaces capable of tunable phase modulation of light in response to variations in an external stimulus has recently stimulated a great interest in nanophotonics community as it can pave the way toward achieving flat ultrathin optical components offering reprogrammable functions with real-time control. In this talk, we will give an overview of our works on realization of active metasurfaces with robust voltage-controlled phase response. We will demonstrate that the integration of electro-optical tuning mechanisms based on free-carrier and quantum-confined effects into the constituent building blocks of metasurfaces can be exploited for achieving wide phase tuning in reflection and transmission modes. We will discuss the routes toward attaining optimal tunable performance based on field effect modulation of carrier density in degenerately doped semiconductors such as indium-tin-oxide. We will also explore novel photonic design paradigms based on extreme light-matter interactions for enhancing the tunability of optical response arising from the weak electro-refractions due to double carrier injection in p-i-n junctions and carrier accumulation in p-n junctions of moderately doped semiconductors, as well as quantum-confined Stark effect in multi-quantum well structures by

leveraging high- $Q$  resonant modes such as cavity modes, guided mode resonances, and quasi-bound states in the continuum. As the next frontier of active metasurfaces, we will examine time-modulated optical metasurfaces which render a four-dimensional design space and give rise to a myriad of novel physical phenomena through generation of higher-order frequency harmonics. We will illustrate that the phase of higher-order frequency harmonics generated by a time-modulated metasurface can be tuned with uniform amplitude via a non-resonant dispersionless geometric phase shift induced by the modulation phase delay. This dispersionless phase elevates time-modulated metasurfaces beyond their quasi-static counterparts relying on resonant phase delays in terms of dynamic wavefront engineering capabilities in that it increases the functionality bandwidth and minimizes spurious spatial scattering by providing access to the full phase span ( $2\pi$ ) with uniform amplitude. Moreover, we will show that frequency conversion operations in space-time gradient metasurfaces can break the time-reversal symmetry and lift the Lorentz reciprocity constraint. We will highlight the required conditions toward achieving strong nonreciprocal responses and will demonstrate high- $Q$  time-modulated metasurfaces can serve as free-space optical isolators by providing access to the non-adiabatic modulation regime with small electro-optical modulation frequencies.

**7:45 AM \*F.NM02.04.14**

**Machine-Learning-Assisted Photonics** Alexandra Boltasseva, [Zhaxylyk Kudyshev](#), Alexander Kildishev and Vladimir Shalaev; Purdue University, United States

**Abstract:**

Discovering novel, unconventional optical designs in combination with advanced machine-learning assisted data analysis techniques can uniquely enable new phenomena and breakthrough advances in many areas including on-chip circuitry, imaging, sensing, energy, and quantum information technology. Topology optimization, which has previously revolutionized aerospace and mechanical engineering by providing non-intuitive solutions to highly constrained material distribution problems, has recently emerged as a powerful architect for advanced photonic design. Compared to other inverse-design approaches that require extreme computation power to undertake a comprehensive search within a large parameter space, topology optimization can expand the design space while improving the computational efficiency. This talk will highlight our most recent findings on 1) merging topology optimization with artificial-intelligence-assisted algorithms and 2) integrating machine-learning based analysis with photonic design and quantum optical measurements. Particularly, we will discuss our studies on implementing deep-learning assisted topology optimization for advanced metasurface design development, focusing on highly efficient thermal emitter/absorber development for thermal-photovoltaics applications. We will outline our recent work on merging topology optimization technique with quantum device design for achieving ultrafast single-photon source that offers efficient on-chip integration. Finally, we will outline our recent works on implementing a novel convolutional neural network-based technique for real-time material defect metrology at the quantum level that outperforms all existing approaches in terms of speed and fidelity. This new method rapidly extracts the values of the single-photon autocorrelation function at zero delays from sparse data and ensures one order speed up on solving “bad”/“good” emitter classification problem in comparison with conventional techniques.

**References:**

- [1] Zh. Kudyshev, A. V. Kildishev, V. M. Shalaev, A. Boltasseva, Machine-learning-assisted metasurface design for high-efficiency thermal emitter optimization, *Applied Physics Reviews*, 7, 021407 (2020); <https://doi.org/10.1063/1.5134792>
- [2] Zh. A. Kudyshev, S. Bogdanov, T. Isacson, A. V. Kildishev, A. Boltasseva, V. M. Shalaev, Rapid classification of quantum sources enabled by machine learning, arXiv preprint at <https://arxiv.org/abs/1908.08577> (2019)

**8:00 AM \*F.NM02.04.15**

**Recent Advances in Mid-Infrared Graphene Plasmonics: Electrically Tunable Metasurface for Complex Amplitude Modulation** [Min Seok Jang](#); Korea Advanced Institute of Science and Technology, Korea (the Republic of)

The use of reconfigurable metasurfaces to dynamically control the complex amplitude modulation of scattered light has stimulated the interest of the research community. Despite an extensive cumulative body of knowledge in metasurfaces, insights and observations for the most intriguing possibilities have remained elusive due to the lack of design methodology. All proposed designs thus far can only control the optical phase over a fraction of a wavelength, and, furthermore, they are highly inefficient, and couple the phase and amplitude of the scattered light. In short, the current strategies offer very low prospects of creating a transformative optical device. This fundamental problem poses severe performance limitations – particularly for applications relying on accurate spatiotemporal complex field modulation, which includes dynamic holography, high-resolution imaging, optical tweezing, and optical information processing.

Tunable plasmonic modes offered by graphene provide new opportunities to create electro-optically active devices with novel characteristics that have thus far been impossible to be realized by using conventional media. In this talk, we present a new strategy for dynamically controlling the local complex amplitude of light. We devise “metamolecules” consisting of a pair of subwavelength graphene plasmonic metaatoms. Independent tuning of the two metaatoms secures the complete control of both amplitude and phase of light. Our proposed metasurface allows for  $2\pi$  phase shift as well as large amplitude modulation including perfect absorption. The capabilities of the proposed metasurface were proven by demonstrating active beam steering and holographic wavefront reconstruction with an unprecedented figure-of-merit. Our proposed metamolecule represents a conceptual advancement to metasurface design, allowing for complete amplitude and phase control of light, and should find its application in active thermal engineering and real-time hologram systems beyond the mid-infrared.

**8:15 AM \*F.NM02.04.16**

**Kerr Metasurfaces Enabled by Metallic Quantum Wells** [Zhaowei Liu](#); University of California, San Diego, United States

Optical metasurfaces have emerged as promising candidates for multi-functional devices. Dynamically reconfigurable metasurfaces have been introduced by employing phase-change materials and/or by applying voltage, heat, or strain. While existing metasurfaces exhibit appealing properties, they don't express any significant nonlinear effects due to the negligible nonlinear responses from the typical materials used to build the metasurface. In this work, we propose and experimentally demonstrate one kind of Kerr metasurfaces that shows strong intensity-dependent responses. The Kerr metasurface is composed of a top layer of gold antennas, a dielectric spacer, and a ground layer of metallic quantum wells (MQWs) made by TiN/Al<sub>2</sub>O<sub>3</sub> multilayer stack. Due to the large Kerr nonlinearity supported by the MQWs, the effective optical properties of the MQWs can change gradually from metallic to dielectric with increasing of the input intensity, leading to dramatic modifications of the metasurface responses. This opens up new routes for tunable metasurface applications in the fields of nonlinear optics and extremely fast meta-optics.

**8:30 AM \*F.NM02.04.17**

**Soft Metamaterials—From Isotropicity to Quantum Interaction** [Sui Yang](#) and Xiang Zhang; University of California, Berkeley, United States

Metamaterials are artificially engineered structures designed to shape electromagnetic responses not found in nature including superlensing, cloaking and communications. They traditionally comprise an array of fabricated subwavelength anisotropic structures on a planar geometry, which inevitably limit their responses in certain directions. We explore a novel type of soft metamaterial to overcome such limitations, in which building blocks and overall configurations that can be freely tailored, even after formation. In particular, we explored the complex soft metamaterial nanoarchitectures with tailored symmetries that achieved isotropic negative index at the optical frequency. Moreover, we expand such soft metamaterial design that created the first Casimir quantum trap in solution by manipulating electromagnetic waves from quantum fluctuations. These results provide new insights that facilitate and expand novel metamaterial design and applications.

**8:45 AM \*F.NM02.04.18**

**Tunable Flat Optoelectronics** [Jinghua Teng](#); Institute of Materials Research and Engineering (IMRE), A\*STAR, Singapore

Metasurfaces and flat optics with sub-wavelength structures fabricated on a thin film have shown their strong power in light manipulation and potentials in compact optical device applications. Metasurfaces normally are constructed by sub-wavelength meta-atoms such as disks or pillars spatially arranged according to the design and the function of the device. Meta-optics having a flat surface with meta-atoms embedded within the film would facilitate multi-layer integration for an optical system and ease the electrical control layout for active devices besides the benefits of robustness. Tunable flat optoelectronics allowing dynamic control of the light wave is highly desirable to increase the functionality and flexibility of the optical device and system design. On the other hand, the emergence of two-dimensional (2D) transition metal dichalcogenides (TMDCs) semiconductors offer great opportunities for optoelectronic applications for their strong quantum confinement and the easiness in forming heterostructures enabled by the out-of-plane van der Waals bonding. The intriguing exciton characters in 2D TMDCs and their heterostructures render new dimensions to realize tunable flat optoelectronic devices operable at a wide spectral range from ultra-violet (UV) to mid-far-infrared (IR).

In this talk I will introduce several of our work on tunable flat optoelectronics including programmable flat optics through continuously reversible refractive index change in the phase change materials GST by laser pulse writing, electrical and thermal tuning of terahertz response and complete reflection suppression in an atomically smooth Si metasurface produced by CMOS compatible process, and the gate tunable absorption in TDMC heterostructures by manipulating the interlayer excitons for room temperature high responsivity mid-far IR photodetection, and the 2D flat lens made on 10 nm thick

TMDCs for sub-diffraction limit focusing and imaging at 450 nm wavelength.

**9:00 AM \*F.NM02.04.19**

**Dynamic 2D Quantum Metasurfaces** [Mark L. Brongersma](#); Stanford University, United States

Since the development of diffractive optical elements in the 1970s, major research efforts have focused on replacing bulky optical components by thinner, planar counterparts. The more recent advent of nanophotonic metasurfaces has further accelerated the development of flat optics through the realization that resonant optical antenna elements can be utilized to facilitate local control over the light scattering amplitude and phase. In this presentation, I will highlight recent efforts to realize electrically-tunable metasurfaces employing nanomechanics, electrical gating, microfluidics, and phase change materials. I will pay particular attention to the opportunity of realizing dynamic metasurfaces from atomically-thin semiconductors. Such elements are capable of active wavefront manipulation for optical beam steering and dynamic holography. I will illustrate how the proposed optical elements can be fabricated by scalable fabrication technologies, opening the door to many commercial applications.

**9:15 AM \*F.NM02.04.21**

**High Quality Factor Phase-Gradient Metasurfaces** [Jennifer A. Dionne](#), Mark Lawrence, David R. Barton, Dixon Jefferson, Elissa Klopfer and Sahil Dagli; Stanford University, United States

High quality factor (“High Q”) cavities have revolutionized information processing, communications, sensing, and nonlinear optics by increasing photon storage times and significantly enhancing light-matter interactions. However, when the size of dielectric cavities is reduced to the nanoscale, resonant modes start to resemble point sources, scattering an incident wave in many different directions. While this scattering has been leveraged to create remarkable metasurfaces that precisely control the phase, amplitude, and polarization of light in an ultrathin footprint, metasurfaces generally exhibit high radiative loss rates and thus low Q-factors. Indeed, to date, resonant features in the far-field transmission of metasurfaces have Q-factors on the order of ten.

Here, we describe a general strategy for generating high quality factor resonances in a phase gradient metasurface. Resonances are created by including subtle structural changes in individual resonators to weakly couple free-space light into otherwise bound modes. We experimentally demonstrate control over the quality factor and resonant wavelengths in this scheme, achieving record metasurface Q’s greater than 2500. We also show via simulations that Q-factors can exceed millions. We highlight this scheme’s general applicability by designing and fabricating metasurfaces that act as beamsteerers to different angles, beam splitters, and lenses. We also show how this platform can be integrated with electro-optic materials for low-power metasurface modulation. Finally, we describe applications of high-Q metasurfaces spanning i) free-space optical sensors of COVID-19 antigens and antibodies; ii) all-optical magnetic switching; and iii) an all-optical self-isolating laser.

**9:30 AM \*F.NM02.04.22**

**Metasurfaces for Holography and Light Harvesting—New Approaches with Orbital Angular Moment Modes and Tailored Disorder** [Stefan A. Maier](#)<sup>1,2</sup>, Haoran Ren<sup>1</sup> and Changxu Liu<sup>1</sup>; <sup>1</sup>LMU Munich, Germany; <sup>2</sup>Imperial College London, United Kingdom

Metasurfaces significantly widen the parameter space for control over light, mainly via the many ways phase control can be achieved and varied within the plane of the surface. Here, we take a closer look on how to further widen these possibilities via introducing elements such as control over amplitude and phase simultaneously, i.e. the complex amplitude of the impinging light field, and secondly via disorder.

As a first application, we examine the use of beams of higher orbital angular momentum coupled to metasurfaces in a context of holography. We demonstrate the design and implementation of metasurface phase holograms with strong orbital angular momentum selectivity, based on nanostructured gallium nitride. This opens up a new degree of multiplexing, allowing lensless reconstruction of distinct holographic images in each orbital angular momentum channel. We further show how metasurfaces with additional variation in the height of the underpinning nanostructures allow for complete control over the complex amplitude of the impinging wave. We demonstrate that this significantly reduces cross talk between different orbital angular momentum coding channels, enabling up to 200 independent orthogonal image frames for realistic parameters. The second application is in a context of energy harvesting. Based on a disordered array of plasmonic nanoresonators, we show how deterministic coupling of this effective photonic layer to an external cavity can lead to two different regimes of operation — broadband absorption and narrow-band reflection. As an example, we demonstrate the use of such coupled disordered-layer / cavity systems for colour generation.

9:45 AM \*F.NM02.04.23

**Dielectric Nano-Structures Functionalized Optical Fibers—A Novel Pathway Towards Single-Fiber Optical Trapping and Boosting In-Coupling Efficiencies** Markus Schmidt<sup>1,2,3</sup>, Malte Plidschun<sup>1,3</sup>, Henrik Schneidewind<sup>1</sup>, Uwe Huebner<sup>1</sup>, Matthias Zeisberger<sup>1</sup>, Torsten Wieduwilt<sup>1</sup>, Jisoo Kim<sup>1,3</sup>, Ronny Foerster<sup>1</sup>, Oleh Yermakov<sup>4</sup>, Yuri Kivshar<sup>4,5</sup>, Andrey Bogdanov<sup>4</sup>, Haoran Ren<sup>6</sup> and Stefan A. Maier<sup>6</sup>; <sup>1</sup>Leibniz Institute of Photonic Technology, Germany; <sup>2</sup>Otto Schott Institute of Materials Research, Germany; <sup>3</sup>Abbe Center of Photonics and Faculty of Physics, Germany; <sup>4</sup>ITMO University, Russian Federation; <sup>5</sup>The Australian National University, Australia; <sup>6</sup>Ludwig Maximilian University of Munich, Germany

The interfacing of nano-structures or meta-surfaces with optical fibers represents a promising approach to unlock novel types of functionalities within a multitude of fields including biophotonics, quantum technologies or optical sensing. Here commonly used top-down implementation strategies are hard to employ in case fiber end-faces are considered due to the intrinsic mismatch of the fiber geometry with wafer-based fabrication technology.

Within this presentation, we would like to report on two implementation pathways to circumvent the mentioned bottleneck, namely (i) 3D nano-printing and (ii) modified electron-beam lithography. Both approaches allow for the implementation of sophisticated nano-structures on the end-face of optical fibers leading to significant performance improvements compared to fibers with unstructured end faces. These improvements are shown here on the examples of (i) optical trapping using only one single-mode fiber via the integration of dielectric meta-surfaces and (ii) boosting in-coupling efficiencies into fibers at almost grazing incidence via dielectric ring-type nano-structures .

(i) A tight focus of light plays an essential role in a vast number of applications including optical imaging, optical manipulation, material processing, biophotonics, microscopy and quantum technology. Here optical fibers show fundamental limitations due to the divergence of light emerging from the fiber facet which for instance has limited the use of single fibers within optical trapping, demanding numerical apertures  $>0.8$ . In this presentation we show that 3D nano-printing via direct laser writing allows for the integration of ultra-high numerical aperture meta-lenses on the facet of single-mode fibers that include beam expansion sections. Record-high numerical apertures of up to 0.9 and diffraction-limited spots have been reached. The capabilities of this device have been demonstrated by optically trapping microbeads and biologically relevant bacteria (*E. coli*) for the first time with one single-mode fiber, solving a serious limiting factor within fiber optics research.

(ii) Optical fibers are particularly difficult to use within the context of wafer-based implementation technologies due to the large aspect ratios of fibers, being complementary to wafers. Using an additional planarization step prior to nano-fabrication we open up a novel pathway to implement dielectric nano-structures onto the end-face of optical fibers via electron-beam based technology. Here, we show that by integrating dielectric gratings consisting of concentric rings located on the core of single-mode fibers, in-coupling efficiencies can be increased by more than four orders of magnitude at almost grazing incidence compared to fibers with unstructured end faces. Specifically, application relevant in-coupling efficiencies of several percent at angles of more than  $75^\circ$  have been reached, suggesting a clear pathway to solve one serious bottleneck of optical fibers which has imposed limitations on applications of optical fibers.

10:00 AM \*F.NM02.04.24

**Vortical Reflection and Spiraling Fermi Arcs with Weyl Metamaterials** Shuang Zhang; Univ of Birmingham, United Kingdom

Weyl points are linear band crossings at discrete points in the momentum space, corresponding to three-dimensional (3D) extensions of the two-dimensional (2D) Dirac nodes, and functioning as monopoles of Berry flux with topological charges defined by the Chern numbers. In photonics, Weyl points have been realized in systems with broken inversion symmetry such as photonic crystals and metamaterials, with broken time reversal symmetry such as magnetized plasma and in synthetic dimensions. As a key signature of Weyl systems, Fermi arcs that connect between the projections of Weyl points of opposite topological charges have been observed. However, the manifestation of the topological nature of Weyl points in their interaction with free space radiations remain obscure in both quantum and classical systems.

Scatterings and transport in Weyl semimetals have caught growing attention in both condensed matter and classical physics. In condensed matter systems, the chiral zero modes and the associated magnetoresistance and chiral magnetic effects underlie some highly unusual scattering and transport properties of Weyl semimetals. It has also been proposed that Weyl semimetals may have handedness dependent Imbert–Fedorov shift within the bulk Weyl material. Electrical conductance is usually measured in the experiments, which has contribution from both the bulk Weyl nodes and the fermi arcs. However, it is generally difficult to perform momentum resolved scattering and transport studies, since the leads that transport the electrons to the Weyl semimetals, by their nature, cannot control the momentum of the input electrons. Therefore, previous attempts to associate the topology to scattering matrix mostly remain theoretical.



In this work, vortical phase profile in the momentum space is demonstrated for elliptically polarized electromagnetic waves reflected by a photonic Weyl system, which represents a key signature of the topological nature of the Weyl points and could lead to alignment-free phase plates for vortex beams generation. The nontrivial topology of Chern insulator can not only be revealed by the number of surface states, but also by the scattering matrix  $S$ , i.e. the total winding number in  $2\pi$  of the phase of the eigenvalues of the scattering matrix. It has been rigorously proven that the topological classification of the Hamiltonian and the scattering matrix are equivalent. The scattering matrix method however, are more accessible for investigation in photonics with the readily available optical components from visible to microwave wavelengths to perform the angle resolved measurements.

We further discover a novel type of spiraling guided mode in a hybrid waveguide system formed by the Weyl metamaterial and a metal plate, enabled by the vortical phase profile in the momentum space. we demonstrate that the fermi arcs possessing arbitrary number of windings around the projected Weyl points can be realized in a photonic Weyl semimetal-waveguide hybrid system, revealing a new intriguing physical properties of photonic Weyl systems. The metamaterial-waveguide hybrid system is formed by an air layer sandwiched between a metallic ground plane and an ideal Weyl metamaterial. In such a system, the surface arc states exponentially decay into the Weyl metamaterial, while forming waveguide modes in the thin air layer between the Weyl metamaterial and the confining metallic plate. By measuring the electromagnetic field distribution inside the waveguide, we are able to visualize the Fermi arc's iso-frequency contour in the momentum space through Fourier transformation, and demonstrate the windings of the Fermi arcs in the vicinity of the Weyl frequency.

**10:15 AM \*F.NM02.04.25**

**Plasmonic, Photonic and Excitonic States Interfaces—Time-Modulated Flat Optics and Time-Resolved Measurements** [Harry Atwater](#); California Institute of Technology, United States

Plasmonic, photonic and excitonic states at interfaces govern the optical response of tunable nanophotonic structures such as active metasurfaces, photodetectors and photocatalysts. I will discuss how we can harness plasmonic and excitonic states at interfaces to enable power-efficient phase modulation of active metasurfaces and discuss implications for time-modulated flat optics. Specifically, I will discuss avenues for increasing the power density and power efficiency of plasmonic conducting oxide metasurfaces for temporal phase and amplitude modulation and requirements for time-modulated photonic applications, such as multi-frequency generation and realization of non-reciprocal metasurfaces. I will also report on how time-resolved measurements of plasmonic and excitonic states at interfaces can yield insights about fundamental light-matter interactions in these systems. Specifically, I will discuss i) how electron-hole correlations affect the dynamics of hot carrier relaxation in plasmonic Au/GaN photodetectors and photocatalysts and ii) how time-resolved measurements of excitons generation inform our understanding of carrier dynamics and transport in transition metal dichalcogenides such as WS<sub>2</sub> and MoS<sub>2</sub>.

**10:30 AM \*F.NM02.04.26**

**Multi-Objective and Robust Global Optimization of Nanophotonic Devices** [Jonathan Fan](#); Stanford University, United States

Inverse design algorithms enable metasurfaces and other nanophotonic devices to achieve new functionalities and high efficiencies. We will discuss recent advances in inverse algorithms based on global topology optimization networks (GLONets), in which global optimization is framed as the training of a generative neural network. We will show how reparameterization methods, in which device layouts are recast in a latent space, can be used to strictly enforce design constraints such as minimum feature size and robustness to fabrication imperfections. We will also show how multi-objective problems, such as those involving the selection of materials from a materials database, can be solved using GLONets. We apply these concepts to a range of devices, from metasurfaces and thin film stacks to grating couplers, showing how GLONets can produce nanophotonic devices operating near the physical limits of structured media.

**10:45 AM \*F.NM02.04.27**

**Remote Structuring of Near-Field Landscapes** Federico Capasso<sup>1</sup>, [Vincent Ginis](#)<sup>1,2</sup>, Marco Piccardo<sup>1,3</sup> and Michele Tamagnone<sup>1</sup>; <sup>1</sup>Harvard University, United States; <sup>2</sup>Vrije Universiteit Brussel, Belgium; <sup>3</sup>Istituto Italiano di Tecnologia, Italy

The electromagnetic near-field enables subwavelength applications such as near-field microscopy and nanoparticle manipulation. Present methods to structure the near-field rely on optical antenna theory, involving nanostructures that locally convert propagating waves into confined near-field patterns. We develop a theory of remote rather than local near-field shaping, based on cascaded mode conversion and interference of counterpropagating guided waves with different propagation constants. We demonstrate how to structure at will the longitudinal and transverse variation of the near-field, allowing for

distributions beyond the conventional monotonic decay of the evanescent field. We provide an experimental realization that confirms our theory. Our method applies to fields with arbitrary polarization states and mode profiles, providing a new path towards unprecedented three-dimensional control of the near-field.

**11:00 AM \*F.NM02.04.28**

**Novel Insights on the Field Enhancements and Time Dynamics in All-Dielectric Antennas Through Their Quasinormal Modes** Rémi Colom<sup>1</sup>, Brian Stout<sup>2</sup> and Nicolas Bonod<sup>2</sup>; <sup>1</sup>Zuse Institute, Germany; <sup>2</sup>Aix Marseille Univ, CNRS, Centrale Marseille, Institut Fresnel, France

All-dielectric nanostructures composed of high refractive index host Mie resonances that yield resonant light scattering and enhanced internal field [1-4]. Mie resonances result from the existence of complex eigen-frequencies. In the framework of the multipolar theory, the Mie scattering coefficients have an infinite set of complex eigen-frequencies. The scattering matrix can be expanded with respect to the eigen-frequencies of the nanostructure [5,6] which allows to calculate the internal and scattered fields with respect to the eigen-frequencies of the cavity. A thorough convergence analysis shows that the convergence is faster for the internal field and that the field can almost be fully retrieved by taking into account a very limited number of eigen-frequencies [6]. This theoretical framework turns out to be of high interest to explain the formation of anapoles that correspond to non-radiating current distributions [7]. Anapoles have attracted a strong interest to enhance light matter interactions in subwavelength dielectric nanostructures with applications in second and third harmonic generation or enhanced Raman signal [8]. Anapoles can be well identified in the spectrum of the dipolar and electric Mie coefficient as a strong dip that closely follows a peak. It turns out that the anapole is spectrally close to the maximum of the electric dipolar polarizability. Two eigen-frequencies can be found in this spectral range, with a common real part and a large and a weak imaginary part. In other words, two modes associated with high and small quality (Q) factors will influence the optical response. The low Q-mode does not influence the internal field that only results from the high Q-mode. However, the low Q-mode contributes to the external field. The external field is the result of an interference between three terms: the fields associated with the low and high Q-modes plus a non resonant term. Depending on the phase of these terms, the external field can feature a maximum or a minimum. The important result is that neither the maximum nor the minimum correspond to the real parts of the poles, due to the contribution of the non resonant term. As a result, the spectral location of the anapole does not correspond to the maximum of the internal field that is given by the real part of the high Q-mode [7]. In a second step, a Fourier transform of the modal scattering matrix (S- or T- matrix) provides a time dependant scattering matrix. The impulse response function (IRF) of the S-matrix can be found by considering an incoming field described by a Dirac distribution. This modal IRF allows us to retrieve the outgoing field when the Mie scatterer is excited by any kind of pulse. A case of special interest is the case of a causal sinusoidal excitation field, consisting of a sinusoidal excitation behind a Heaviside. The sharp excitation in the time domain of the dielectric cavity yields a transient field. Once the sharp excitation is over and the excitation driven exclusively by the sinusoidal field, the transient regime vanishes and is replaced by a permanent regime. The modal analysis of this problem reveals that the eigen-modes of the cavity contribute only to the response of the cavity during the transient regime, and not during the permanent regime [9]. This study shows that how quasinormal modes turn out to be excellent tools to unveil the complex time dynamics of dielectric cavities.

**11:15 AM \*F.NM02.04.29**

**Shaping Microwaves with Tunable Metasurfaces—From Concepts to Applications** Geoffroy Lerosey; Greenerwave, France

Electromagnetic waves are essential to our lives, due to the information they carry, be it through the sense of vision in the visible domain or in our everyday wireless communications within the lower frequency range of the microwaves. Controlling them dynamically is hence of paramount interest. Several approaches have been proposed in the past, using large numbers of independently controlled sources, such as in the concept of phased arrays originally used in radars and now in massive MIMO. Yet these systems are extremely complex and costly, especially for large apertures containing high number of sources, if not impossible to design for instance in the optical domain. In this domain, a paradigm shift has been proposed 10 years ago with the introduction of wavefront shaping, where one does not control the emission of waves, but rather their reflections [1]. This is achieved using large arrays of tunable reflectors, namely spatial light modulators, that are based on micrometric liquid crystal cells or movable micro-mirrors. Due to its simplicity and versatility, wavefront shaping has recently opened avenues for applications, from imaging inside scattering media to communicating with multimode fibers [2]. In this talk I will show that the concept of wavefront shaping can be transposed to the microwave domain using tunable metasurfaces that are controlled by real time electronics. Starting from conventional approaches to beamforming in the radiofrequency domain such as phased array or time reversal, I will first discuss the drastic hardware simplifications that

allow the use of tunable metasurfaces alongside algorithms inspired from wavefront shaping [3]. To do so I will introduce the concept of spatial and temporal degrees of freedom that are levers to the physicist to control the propagation of waves. This will allow me to connect the various concepts introduced before.

Further, I will briefly introduce various applications we develop at Greenerwave using wavefront shaping in the radiofrequency domain, from the low frequency of RFID to the millimeter wave range. More specifically, I will first demonstrate how any box such as a fridge or a cabinet can be made smart using wavefront shaping of microwaves, ensuring error-free RFID detection at very low power and cost. Then, I will focus on the millimeter wave range and prove that a leaky cavity dressed with a tunable metasurface can turn a simple electromagnetic dipole into a dynamically reconfigurable antenna whose properties are unique, paving the way to low cost and fully electronically steerable antennas for 5G and satellite applications. Finally, I will explain how the concept can also turn a cheap detect and avoid system into a powerful imaging device. This tool is an ideal complement to cameras and lidars that are currently used in the context of autonomous vehicles, notably in difficult weather conditions.

[1] Focusing coherent light through opaque strongly scattering media. I.M. Vellekoop and A.P. Mosk. *Optics Letters* 32, 2309-2311 (2007).

[2] Controlling waves in space and time for imaging and focusing in complex media. A.P. Mosk, A. Lagendijk, G. Lerosey and M. Fink. *Nature Photonics* 6, 283-292 (2012)

[3] Shaping complex microwave fields in reverberating media with binary tunable metasurfaces. N. Kaina, M. Dupré, G. Lerosey and M. Fink. *Scientific Reports* 4, 6693 (2014).

### 11:30 AM F.NM02.04.30

**A Janus Radiative Cooler for Migrating the High Temperature of the Automobile** Seyeon Heo, Gil Ju Lee, Do Hyeon Kim, Yeong Jae Kim and Min Seok Kim; Gwangju Institute of Science and Technology, Korea (the Republic of)

As car is one the most important transportation for each individual, cooling private vehicles has highly demanded. In particular, the extreme temperature can develop in stationary automobile under the greenhouse effect, when the windows are transparent for incoming solar radiation but opaque for outgoing long-wave thermal radiation. The temperature inside the cabin tremendously increased to approach 60 °C, which is causing human discomfort and car aging problem. Current car cooling methods mostly rely on vapor compression and fluid-cooled systems. However, 28.4% of the total vehicle power is consumed for space cooling and place enormous stress on fuels consumption and CO<sub>2</sub> emission. Passive cooling strategy, which is sustainable alternatives to active cooling technologies, can release heat without energy consumption or pollutant emission.

Recently reported passive radiative coolers have shown outstanding sub-ambient cooling during the daytime. Those coolers are attached on exterior materials, roof, or human skin to draw heat from the periphery through conduction and convection. However, this attractive solution has explicit limitation in thermally sealed space (e.g., stationary automobiles). Since most of conventional radiative coolers only consider emissivity of the side exposed to the sky, they cannot thermally access to inside of the enclosure. Emissivity of the inner side could open the path to inside of the enclosure and allow the trapped heat to escape by increasing the inner radiation flux. Accordingly, strategic design of emission spectra on both sides of the cooler is vital for releasing the trapped heat.

Here, we propose a *Janus* cooler that acts as a selective emitter on the top side and a broadband emitter on the bottom side. This design effectively draws heat from enclosure because the bottom side can absorb thermal input in a broad spectral range while the top side emits heat to space without disturbing ambient radiation. We first design a *Janus* cooler comprising of an Ag-polydimethylsiloxane layer on micro-patterned quartz substrate. The induced spoof surface plasmon polariton helps overcome inherent emissivity loss of the polymer, and creates near-ideal selective and broadband emission on the separate sides. Next, we demonstrated several modification methods to improve adaptability as a car roof, such as scalability and mechanical strength, while maintain its optical properties. Consequently, we obtain large-scaled *Janus* cooler with affordability by replacing quartz substrate to PMMA and PDMS and high elastic modulus and scratch resistance by using harder material.

Last, we theoretically and experimentally demonstrate the remarkable cooling performances of *Janus* cooler for enclosures. We numerically solved the steady-state heat transfer model of enclosed space to estimate the impact of emissivity of each layer on cooling. The *Janus* cooler was more effective in drawing heat away as compared to materials with no emissivity and one-directional emissivity. Using *Janus* bi-directional emission characteristics, the *Janus* cooler lowered the temperature of a radiative object inside an enclosure by ~4 °C compared to the Conventional radiative cooler in experiments simulating a stationary automobile environment. The significance of the *Janus* cooler for migrating the high temperature of the automobile is illuminating the importance of emissivity of the substrate itself meanwhile designing the selective emitter in an

interpretive way. With the superior ability to passively cool the enclosure, this advanced design leads to comfortability and cost effectiveness in unconscious way, which are critical demands for situation where heat entrance is present and exit is absent.

#### 11:40 AM F.NM02.04.31

**Late News: Asymmetric Light Generation in Nonlinear Metasurfaces** Sergey Kruk<sup>1,2</sup>, Lei Wang<sup>2</sup>, Basudeb Sain<sup>1</sup>, Dong Zhaogang<sup>3</sup>, Joel Yang<sup>4,3</sup>, Thomas Zentgraf<sup>1</sup> and Yuri Kivshar<sup>2</sup>; <sup>1</sup>Universität Paderborn, Germany; <sup>2</sup>Australian National University, Australia; <sup>3</sup>A\*Star, Singapore; <sup>4</sup>Singapore University of Technology and Design, Singapore

Recent studies of nanoresonators with strong confinement of light opened the way towards efficient nonlinear processes at the subwavelength scales [1]. All-dielectric nanostructures are particularly promising to enhance the efficiency of nonlinear processes. Such nanostructures can support nontrivial optical modes, including optically induced magnetic dipole resonances, higher-order multipoles, and composite resonances [2]. High field enhancements at the magnetic dipole modes and composite resonances increase the efficiency of nonlinear processes by orders of magnitude. Being assembled in 2D layouts such nanoresonators may form ultra-thin flat optical components – metasurfaces – in which the nonlinear response enables functionalities beyond their linear counterparts. [3]

Here we demonstrate experimentally a novel class of nonlinear metasurfaces with an asymmetric response. We fabricate translucent dielectric metasurfaces that generate images in transmission at third-harmonic frequency. Compared to conventional holograms, such metasurfaces generate completely independent images being illuminated from the opposite sides.

We employ cylindrical dielectric nanoresonators as our building blocks for the metasurface. The resonators consist of two layers of materials with different optical constants: Si and SiN, which introduce asymmetry in the direction normal to the metasurface. The resonators further support two Mie resonances – electric and magnetic dipoles overlapped spectrally. Asymmetric bi-layer design leads to magneto-electric coupling between the two dipole modes, where the coupling constant (positive or negative) depends on the direction of excitation as well as on the resonator geometry. In the linear optics regime, such bi-layer nanoresonators demonstrate identical forward-scattering for the illumination from both sites. However, for the two illumination cases, the near-field distributions are drastically different due to positive/negative magneto-electric coupling between the two Mie resonances hosted within the resonators. For high intensities of light, the nonlinearities of the constituent dielectric materials start playing a role, whereas the different near-field distributions lead to different nonlinear changes of the material parameters when the transmitter and receiver positions are exchanged. Such changes generally have small effects on the light scattering at the fundamental frequency in particular for low-loss materials as well as within the approximations of perturbative nonlinearities and the nondepleted pump approximation. These processes however lead to a striking contrast in the efficiency of the nonlinear generation of optical harmonics.

We employ a set of four dissimilar resonators that allows us to assemble metasurfaces generating independent images for two opposite directions of excitation due to asymmetry in the nonlinear light generation. We fabricate such metasurfaces with standard electron-beam lithography and conduct their optical diagnostics with a tuneable short-pulse laser system.

We discuss connections between asymmetric third-harmonic generation in our metasurfaces and nonlinearity-induced optical nonreciprocity [4]. We believe that the ability to engineer optical interactions at the subwavelength scale beyond the electric dipole type to induce a strong artificial magnetic response and strong magnetoelectric coupling pave the way towards optical nonreciprocity at the nanoscale.

[1] K. Koshelev et al., “Subwavelength dielectric resonators for nonlinear nanophotonics.,” *Science* 367, 288, 2020.

[2] S. Kruk and Y. S. Kivshar, “Functional Meta-Optics and Nanophotonics Govern by Mie Resonances,” *ACS Photonics* 4, 2638, 2017.

[3] G. Li, “Nonlinear photonic metasurfaces,” *Nat. Rev. Mater.* 2, 17010, 2017.

[4] C. Caloz, “What is Nonreciprocity? Part II,” arXiv:1804.00238, 2018.

#### 11:50 AM F.NM02.04.32

**Atomic Layer Engineering of Al-Doped Zinc Oxide Thin Films with Controllable Epsilon-near-Zero Optical Nonlinearity** Sudip Gurung<sup>1</sup>, Subhajit Bej<sup>1</sup>, Zhenhuan Yi<sup>2</sup> and Ho Wai (Howard) Lee<sup>1</sup>; <sup>1</sup>Baylor University, United States; <sup>2</sup>Texas A&M University, United States

Giant Kerr-type optical nonlinearity of transparent conducting oxide (TCO) thin films in their epsilon-near-zero (ENZ)

region (i.e. the region where the real part of their dielectric permittivity approaches zero), have been reported recently [1,2,3]. Under excitations of plasmon-polariton modes near the ENZ wavelength ( $\lambda_{ENZ}$ ), effective nonlinear optical properties of these films can be further boosted. Due to ultra-fast response time of these nonlinear processes, the ENZ TCO films could open distinct functionalities to the path to revolutionary nanoscale nonlinear optics and ultrafast on-chip optical applications. In this work, we present a method to engineer the nonlinear refraction coefficients ( $n_2$ ) and the nonlinear absorption coefficients ( $\alpha$ ) of Al-doped zinc oxide (AZO) ENZ thin films synthesized by atomic layer deposition (ALD) technique. To engineer the effective nonlinear optical properties, we first design the linear absorption and electric field intensity enhancement (FIE) associated with ENZ modes in these AZO nanolayers via control over the ENZ wavelengths and optical losses by ALD deposition parameters such as dopant ratio and number of macro cycles. The dopant ratio determines the material dispersion and ENZ wavelength whereas the macro cycle regulates the film thickness. Since the optical Kerr nonlinearity has cubic dependence on the electric field confined inside the TCO films, the controllable and enhanced FIE of the ENZ mode could lead to an enhancement of the ENZ nonlinearity. AZO thin films with ENZ wavelengths varying between 1400-1600 nm and thicknesses ranging from 55 to 205 nm are fabricated via ALD technique to examine the ENZ nonlinearity [4]. The nonlinear optical properties of the fabricated films are measured using Z-scan and degenerate pump-probe spectroscopy techniques with linearly polarized femto-second laser pulses (pulse duration  $\sim 70$  fs, repetition rate 1 KHz, peak wavelength  $\lambda_p$  tunable between 1200-1600 nm). Experiments are performed for normal and oblique incidences of TE/ TM polarized light pulses and for different pulse peak wavelengths ( $\lambda_p = \lambda_{ENZ}$ ,  $\lambda_p > \lambda_{ENZ}$ , and  $\lambda_p < \lambda_{ENZ}$ ). Wavelength and angular dependence of  $n_2$  and  $\alpha$  values of the films are evaluated upon fitting the close and open-aperture Z-scan data. Results suggest that ENZ nonlinear refraction and nonlinear absorption properties of AZO films are enhanced by excitation of the ENZ modes and can be engineered by changing the mode-strengths via control over either the excitation angles or by ALD engineering of material dispersion/ film thickness. Measured values as large as  $n_2^{(eff)} \sim 10^{-9}$  mm<sup>2</sup>/Watt and  $\alpha^{(eff)} \sim 10^{-5}$  mm/Watt are obtained along with approximately an order of magnitude tunability. The temporal dynamics of the nonlinear processes are also measured. The rise and fall-times of the nonlinear processes are evaluated to be sub-picosecond. We believe that giant ultra-fast Kerr nonlinearity of these ALD AZO films in their ENZ region and their controllability will be important for efficient all-optical signal processing. [1] a) M. Z. Alam, I. De Leon, R. W. Boyd, Science 2016, 352, 795; b) L. Caspani, R. Kaipurath, M. Clerici, M. Ferrera, T. Roger, J. Kim, N. Kinsey, M. Pietrzyk, A. Di Falco, V. M. Shalaev, Physical review letters 2016, 116, 233901; c) M. Clerici, N. Kinsey, C. DeVault, J. Kim, E. G. Carnemolla, L. Caspani, A. Shaltout, D. Faccio, V. Shalaev, A. Boltasseva, Nature communications 2017, 8, 15829. [2] A. Anopchenko, S. Gurung, L. Tao, C. Arndt, H. W. H. Lee, Materials Research Express 2018, 5, 014012. (This work is supported in part by the Young Faculty Award Program from Defense Advanced Research Projects Agency (grant number N66001-17-1-4047) and Robert A. Welch Foundation (Award number: AA-1956-20180324)

#### 12:00 PM F.NM02.04.33

**Phonon-Polaritons in Calcite Nanostructures** Daniel Ratchford, Vanessa M. Breslin, Alexander J. Giles, Adam Dunkelberger and Jeffrey C. Owrutsky; U.S. Naval Research Laboratory, United States

Nanophotonics has incredible potential for developing new mid-infrared technologies for applications including free-space communications and spectroscopic-based sensing. Phonon-polaritons, electromagnetic modes of a polar material resulting from the coupling of light with optical phonons, are a particularly promising area of mid-infrared nanophotonic research because these modes can enhance light-matter interactions through their ability to concentrate light to nanoscale dimensions. We report on the confinement of phonon-polaritons in calcite, a ubiquitous polar material. We fabricated calcite nanopillars with varying aspect ratio using focused ion beam etching. In the mid-infrared reflection spectra of the nanopillars, we observe multiple phonon-polariton modes with frequencies that depend on the aspect ratio. The modes are supported in the spectral region where calcite's permittivity is hyperbolic, i.e., where the principal components of the permittivity tensor have opposite sign, and the modes are identified as volume-confined modes. Our interpretation of the modes as aspect-ratio dependent volume modes is reinforced by the good agreement with FDTD simulations. The results demonstrate the basic properties of phonon-polaritons in calcite and highlight the material's potential for developing mid-infrared nanophotonic devices.

#### 12:10 PM F.NM02.04.34

**Tunable Indium Tin Oxide for Metamaterial Perfect Absorbers and Nonlinear Devices** Evan M. Smith<sup>1</sup>, Joshua Hendrickson<sup>2</sup>, Justin W. Cleary<sup>2</sup>, Kevin Leedy<sup>2</sup>, Junpeng Guo<sup>3</sup> and Shivashankar Vangala<sup>2</sup>; <sup>1</sup>KBR, United States; <sup>2</sup>Air Force Research Laboratory, United States; <sup>3</sup>The University of Alabama, United States

Indium tin oxide (ITO) has become a very useful plasmonic and nonlinear material for NIR and MWIR applications in that it has highly tunable electric and optical properties, and has exhibited strong optical nonlinearity. In particular, ITO exhibits interesting properties at and around its epsilon-near-zero (ENZ) wavelength. We present here the detailed process parameters of a high temperature reactive sputter process to finely tune the ENZ wavelength throughout the NIR up to the MIR

spectrum. Films are characterized by spectroscopic ellipsometry, X-ray diffraction and energy dispersive spectroscopy. Electrical characterization is also reported. Films are designed to be integrated into a NIR perfect absorber that exhibits second harmonic generation.

#### 12:20 PM F.NM02.04.36

**Optical Fourier Surfaces** Nolan Lassaline<sup>1</sup>, Raphael Brechbühler<sup>1</sup>, Sander Vonk<sup>2,1</sup>, Korneel Ridderbeek<sup>3</sup>, Korneel Spieser<sup>4</sup>, Samuel Bisig<sup>4</sup>, Boris le Feber<sup>1</sup>, Freddy Rabouw<sup>2</sup> and David J. Norris<sup>1</sup>; <sup>1</sup>ETH Zurich, Switzerland; <sup>2</sup>Utrecht University, Netherlands; <sup>3</sup>Helmholtz Pioneer Campus, Germany; <sup>4</sup>Heidelberg Instruments Nano/SwissLitho, Switzerland

Gratings and holograms are patterned surfaces that tailor optical signals by diffraction. Despite their long history, variants with remarkable functionalities continue to be discovered. Further advances could exploit Fourier optics, which specifies the surface pattern that generates a desired diffracted output through its Fourier transform. To shape the optical wavefront, the ideal surface profile should contain a precise sum of sinusoidal waves, each with a well-defined amplitude, spatial frequency, and phase. However, because fabrication techniques typically yield profiles with at most a few depth levels, complex "wavy" surfaces cannot be obtained, limiting the straightforward mathematical design and implementation of sophisticated diffractive optics. Here we present a simple yet powerful approach to eliminate this design-fabrication mismatch by demonstrating optical surfaces that contain an arbitrary number of specified sinusoids. We combine thermal scanning-probe lithography and templating to create periodic and aperiodic surface patterns with continuous depth control and sub-wavelength spatial resolution. Multicomponent linear gratings allow precise manipulation of electromagnetic signals through Fourier-spectrum engineering. Consequently, we immediately resolve an important problem in photonics by creating a single-layer grating that simultaneously couples red, green, and blue light at the same angle of incidence. More broadly, we analytically design and accurately replicate intricate two-dimensional moiré patterns, quasicrystals, and holograms, demonstrating a variety of previously impossible diffractive surfaces. Therefore, this approach provides instant benefit for optical devices (biosensors, lasers, metasurfaces, and modulators) and emerging topics in photonics (topological structures, transformation optics, and valleytronics).

#### 12:30 PM F.NM02.04.37

**Anticounterfeiting Visible Metaholograms Multiplexed with Spin, Direction and Wavelength** Inki Kim<sup>1</sup>, Muhammad A. Ansari<sup>2</sup>, Muhammad Q. Mehmood<sup>2</sup> and Junsuk Rho<sup>1,1</sup>; <sup>1</sup>Pohang University of Science and Technology, Korea (the Republic of); <sup>2</sup>Information Technology University of the Punjab, Pakistan

Computer-generated holography (CHG) involves iterative numerical algorithms to obtain the phase and/or amplitude profiles needed to physically realize holograms. Metasurfaces consist of arrays of subwavelength nanoresonators that can control the wavefront of light in a desired way. They recently proved themselves to be an effective platform for CGH by surpassing the quality of traditional holograms in terms of image resolution and field-of-view. These metasurface holograms showed prospects not only in imaging and display but also in security applications [1]. In particular, applying metaholograms to anticounterfeiting applications requires not only the technology of encoding multiple pieces of information, but also the manufacturability of highly efficient devices. To meet these complex needs, we have implemented a highly efficient metahologram based on hydrogenated amorphous silicon (a-Si:H) [2]. Compared to well-known titanium dioxide (TiO<sub>2</sub>) and gallium nitride (GaN)-based metasurfaces, a-Si:H metasurfaces offer easier nanofabrication thanks to a low aspect ratio of 3~5 (cf. TiO<sub>2</sub>/GaN: 10~15) and is more suitable for mass production using CMOS fabrication methods. In this abstract, I will discuss our efforts in realizing multifunctional a-Si:H metaholograms that can encode multiple pieces of information in a monolayer device for anticounterfeiting applications. First, I will present a spin-multiplexed visible metahologram [3]. A straightforward method for encoding multiple pieces of information in a single metahologram device is using polarization. To obtain significant birefringence for the control and reversal of photon spin, two sets of nanorods are designed, and depending on their orientation, they imprint inverted spin photons along their corresponding geometrical phase. As a result, this allows switching between two different images by simply flipping the handedness of the circularly polarized light on the transmission-type metahologram with 61% diffraction efficiency. Second, I will introduce a direction-multiplexed visible metahologram [4]. This approach is to multiplex two distinct pieces of information onto a monolayer metahologram operating in the forward and backward directions depending on the direction of light incident on the device. Particularly, in this part we will reveal underlying physics of high transmission efficiency (around 75%), which is the antiferromagnetic resonances in the a-Si:H nanorod. Finally, I will propose a wavelength-multiplexed visible/NIR metahologram. The device consists of a-Si:H and gold (Au) metasurfaces in a monolayer device, which is fabricated by the electron beam lithography overlay process. The a-Si:H metasurfaces generate a visible hologram and the Au metasurfaces produce a NIR hologram simultaneously with low crosstalk. I believe our efforts for making a multiplexed metahologram will lead to pragmatic anticounterfeiting applications. [1] I. Kim et al., ACS Photonics 5, 3876-3895 (2018) [2] I. Kim\* et al., ACS Nano 11, 9382-9389 (2017) [3] I. Kim\* et al., Laser and Photonics Reviews 13, 1900065 (2019) [4] I. Kim\* et al., Nanoscale Horizons

(2019) (DOI:10.1039/c9nh00460b)

**12:40 PM F.NM02.04.39**

**All-Optical Control of Magnetism in Ferromagnetic Thin Films with Silicon Metasurfaces** John M. Abendroth<sup>1</sup>, Michelle Solomon<sup>1</sup>, Mohammed S. El Hadri<sup>2</sup>, David R. Barton<sup>1</sup>, Eric E. Fullerton<sup>2</sup> and Jennifer A. Dionne<sup>1</sup>; <sup>1</sup>Stanford University, United States; <sup>2</sup>University of California, San Diego, United States

Controlling magnetism and spin as a state variable in devices for high-performance computing has received increased attention as an energy-efficient alternative to processing and storing data with electric charge. This approach circumvents increasing power requirements that accompany Moore's Law scaling of transistors. Deterministic reversal of ferromagnetic domains using circularly polarized, ultrafast light pulses arising from magnetic circular dichroism promises an all-optical approach towards high-performance data storage, non-volatile memory technologies, and quantum computation. However, domain-size criteria have limited helicity-dependent switching in ferromagnetic films, placing restraints on available materials and film thicknesses/coercivities in devices for deterministic magnetization reversal with light. Moreover, using light to control magnetization for high-density recording requires reduction of the size of optically switched areas below the diffraction limit. Here, we show how metasurfaces can locally confine, tune, and enhance these magneto-optical effects, leading to more precise control over magnetic ordering for energy-efficient memory and logic architectures. Metasurfaces amplify both electric and magnetic field strengths while preserving the complex phase angle between them. In particular, periodic nanoscale dielectric disks can enhance the electromagnetic density of chirality,  $C$ , controlling magnetic circular dichroism in ferromagnetic films. We fabricated Si nanodisk arrays via sputter deposition and electron-beam lithography on ferromagnetic [Pt (0.7 nm)/Co (0.6 nm)] $N$  multilayers, where  $N = 1, 2$ , or  $3$ . The Co/Pt films are designed to exhibit perpendicular magnetic anisotropy, with the easy-axis of magnetization out-of-plane. The radii of the Si nanoantennas are varied between 130-190 nm in 5 nm increments, supporting electric and magnetic resonances that overlap and cross with increasing radius; transmission measurements confirm spectral overlap at wavelengths spanning 700-1000 nm depending on Si disk radius. Magnetic circular dichroism of the films, detected by asymmetry in transmission and reflection, is measured using left- and right-handed circularly polarized light for substrates magnetized parallel vs antiparallel to the direction of light propagation at normal incidence. Increasing disk radii modulates the magnetic circular dichroism of the Co/Pt multilayer films with local maxima and minima of increasing amplitude as  $N$  is increased from 1 to 3. We find a maximum enhancement of transmission asymmetry of 2x over unpatterned films, correlating with overlap of electric and magnetic dipole resonances as predicted by full-field electromagnetic simulations. To deconvolute near-field enhancements from Fabry-Pérot cavity effects, we vary the separation distance between the ferromagnetic metal layers and Si disks using an SiO<sub>2</sub> spacer region with thickness of 0, 30, and 100 nm. This modulation and enhancement in magnetic circular dichroism is translatable to diverse materials including metamagnetic films, chiral magnetic nanostructures, and single-molecule magnets, and can be utilized directly in the design of waveguide magneto-optical modulators and non-reciprocal device elements. Our presentation will also describe ultrafast magnetization dynamics for Co/Pt films patterned with Si metasurfaces showing how they can enhance all-optical control over magnetic domain switching.

**12:50 PM F.NM02.04.40**

**Elucidating the Design of Nanophotonic Materials with Interpretable Convolutional Neural Networks** Aaswath P. Raman; University of California, Los Angeles, United States

Reaching the true potential of nanophotonic materials devices requires the arbitrary control of spectral and angular selectivity in the absorption and emission of electromagnetic waves. To this end, previously investigated design methods for nanophotonic structures and have encompassed both conventional inverse-optimization approaches as well as nascent machine-learning (ML) strategies. However, inverse-optimization processes are computationally-intensive, and image generation-based ML design techniques which can facilitate the generation of complex geometries require exhaustive investigation to produce stable results. Moreover, the possibility of using machine learning approaches to enable forward design (that is, to effectively function as an electromagnetic simulator) has largely been unexplored. Here, we demonstrate that stable and well-established deep learning architectures such as convolutional neural networks (CNN) can effectively enable "forward design" and thereby replicate the functionality of a traditional numerical electromagnetics solver, for a limited class of nanophotonic structure. We then show that the same networks can also be utilized for "inverse design" by leveraging neural network interpretability and visualization methods. To illustrate this capability, we trained a CNN model with 10,000 images of selective mid-infrared thermal emitters and their corresponding absorption spectra. The trained CNN established the relationships between nanophotonic structures and their responses, then predicted the responses of new and unknown designs with over 95% accuracy. After training the CNN, we applied the Shapley Additive Explanations (SHAP) algorithm to the model to determine features that made positive or negative contributions towards specific spectral points, thereby informing which features to create or eliminate in order to meet a target spectrum. These explanations, for the first

time, allow us to systematically understand the underlying physical relationship between a given nanophotonic structure and its electromagnetic response. We demonstrate a concrete example of the CNN and SHAP algorithms recovering a previously known analytical relationship between the length of a metal-insulator-metal metamaterial resonator and its resonance wavelength. We also show how this approach can yield insights into why more complex, optimized designs are able to perform well, for instance in terms of their spectral peaks or shapes of their electromagnetic modes. Furthermore, using this strategy, we show that a starting electromagnetic metasurface design can be selectively manipulated to create or remove spectral peaks, thus demonstrating that inverse design can be achieved by exposing the valuable information that is hidden within a neural network. More broadly, our results highlight that emerging approaches to opening the 'black box' of neural networks can yield real physical insights into the relationship between a given nanophotonic structure and its electromagnetic response. Deep learning approaches such as the one we implement can thus enable physics discovery and elucidate the design of broad classes of nanophotonic materials and devices.

**1:00 PM F.NM02.04.42**

**Non-Hermitian Selective Thermal Emitters Using Hybrid Metal-Semiconductor Resonators** Gururaj Naik; Rice University, United States

Thermal emitters always have absorption losses and hence are open systems. Open systems are non-Hermitian and are best described by non-Hermitian physics. Here, we develop a non-Hermitian description of resonant thermal emitters and thereby take advantage of absorption loss in the system. Further, the non-Hermitian description provides new design tools such as symmetry, phase, and topology to control the properties of thermal emission. We demonstrate such a thermal emitter using coupled plasmonic and photonic resonators. A lossless silicon photonic resonator is coupled to a lossy tungsten plasmonic resonator via a spacer. As the spacer thickness is increased, the thermal emission from the device held at 1000 K exhibits a transition from PT-symmetric to symmetry-broken phase through an exceptional point. The thermal emission from the device breaks the trade-off between emission brightness and spectral selectivity and simultaneously achieves both. Further, we show that the internal phase of resonators is a powerful tool to control the thermal emission from this device. Overall, this work is an unorthodox approach towards designing not only thermal but also other nanophotonic light sources.

**1:10 PM F.NM02.04.43**

**Full and Grey-Scale Structural Colors Using Array of Engineered Mie-Resonators** Jaehyuck Jang and Junsuk Rho; Pohang University of Science and Technology, Korea (the Republic of)

Mie-resonators scatter when its size is comparable to the wavelength of the incident light. The scattering modes of Mie-resonator are determined by its size and refractive index. The nanostructures composed of high index material such as silicon can have multipole scattering modes in visible regime. When Mie-scatterers are arrayed, the scattering response can be greatly amplified; the subwavelength arrays of the resonators are called metasurfaces. To properly design metasurface, the hybridization of radiation mode of scatterer and lattice effect, i.e. guided-mode resonance (GMR), must be understood. Nevertheless, the exact mechanism behind the scattering response of metasurface has not been fully addressed so far. A precise understanding of the scattering mechanism may enable to design metasurface as spectral filters, i.e. metasurface structural coloration [1-3].

Herein, we would like to provide the scattering mechanisms behind the hybridization between individual scattering mode and lattice effect, and use them to realize full and grey-scale structural coloration by silicon-based metasurface [4]. The array of silicon resonators play three roles: (i) Diffraction grating for momentum matching to allow lattice coupling, (ii) waveguide of laterally propagating light through lattice, (iii) outcoupler which determines radiation modes to free-space. Through multipole expansion and RCWA simulation, we have successfully verified our design method to modulate bandwidth of lattice coupling and resonant peaks of radiation. For experimental demonstration, we chose two types of silicon for metasurface: silicon(P25) and (P45). Silicon(P25) has a higher refractive index and extinction coefficient than silicon(P45) so that radiation modes coupled to lattice differ from each other under the same geometry. As an application, silicon(P25)- and (P45)-based metasurface has been utilized for full and grey-scale structural colors, respectively. We believe that a solid understanding of the coupling between individual Mie resonators and the lattice resonances can be a strong basis for designing all-dielectric structural colors for applications in advanced imaging, ultrahigh-definition television (UHDTV), and other display technologies.

[1] Kim, I.+; Yoon, G.+; Jang, J.+; Genevet, P.; Nam, K. T.; Rho, J. Outfitting Next Generation Displays with Optical Metasurfaces. *ACS Photonics* **2018**, *5*, 3876–3895.

[2] Jang, J.+; Jeong, H.; Hu, G.; Qiu, C.-W.; Nam, K. T.; Rho, J. Kerker-Conditioned Dynamic Cryptographic Nanoprints. *Adv. Opt. Mater.* **2018**, *7*, 1801070.

[3] Kim, M.+; Kim, I.+; Jang, J.+; Lee, D.; Nam, K. T.; Rho, J. Active Color Control in a Metasurface by Polarization



Rotation. *Appl. Sci.* **2018**, *8*.

[4] [Jang, J.+; Badloe, T.+; Yang, Y.+; Lee, T.; Mun, J.; Rho, J.](#) Full and grey-scale structural coltration using engineered silicon metasurface. (submitted)

#### 1:20 PM F.NM02.04.44

**Wavefront Shaping and Modulation with High-Q Electro-Optic Metasurfaces** [David R. Barton](#), Mark Lawrence and Jennifer A. Dionne; Stanford University, United States

Metasurfaces sculpt the phase, amplitude, and polarization of light at subwavelength scales, allowing for unprecedented control of the far field. For applications spanning LIDAR, LiFi, and AR/VR, it is imperative that metasurfaces be reconfigurable, for example able to steer light to particular directions, change their focal lengths, and otherwise react to their environment. However, the subwavelength size of metasurface constituents makes modulation and reconfigurable designs challenging to realize, as the interaction of light and matter is generally very weak. Here, we introduce an electro-optic scheme for reconfigurable and modulatable metasurfaces. Using Lithium Niobate (LNO) as part of the nanoantenna design, we utilize an electric field to change the refractive index, which modifies the phase gradient response. While the electro-optic effect is generally quite weak ( $r_{33} \sim 30$  pm/V), we employ high quality factor resonances to increase the environmental sensitivity of the diffraction, significantly reducing the required DC electric field strength. We provide designs in the near infrared based on 1 dimensional arrays of 600 nm tall silicon nanobars on top of a 200 nm layer Lithium Niobate. A design consisting of bar widths of 175 nm, 236 nm, and 350 nm repeated every 1.8 microns leads to beamsteering metasurfaces with 70% diffraction efficiency of 1400 nm light into the +1<sup>st</sup> diffraction order. Subtle periodic perturbations in the form of grooves into the largest bar couples normally incident light into guided mode resonances. On resonance, at wavelengths near 1400 nm, the beamsteering efficiency drops from 70% to less than 7%, with an increase in the -1<sup>st</sup> diffraction intensity (~20%). In addition to this strong contrast (~10 dB), light is trapped within the silicon bar and leaks into the LNO layer. We capitalize on both of these effects to create an efficient electro-optically tunable metasurface with an applied DC electric field. We show with full-field electromagnetic simulations that applying a DC electric field modifies the refractive index of the LNO, shifting the spectral position of the guided mode resonance. At 1400nm, this manifests in the far field as an obvious change in the diffraction spectrum from beamsteering in the +1<sup>st</sup> order to the -1<sup>st</sup> order with an applied electric field. Using full device simulations we show that, due to strong modal overlap with the electro-optic material and the high quality factor of the guided resonance, electrically tunable beamsteering and beamsplitting metasurfaces can be achieved with low (less than 15V) operating voltages. Via preliminary simulations, we also demonstrate methods to push this dynamic metasurface design principle to visible wavelengths using lithium niobate, rather than silicon, as the metasurface element. Our work shows the broad applicability of high-Q resonant LNO-based metasurfaces as reconfigurable optical devices, for applications spanning ultra-compact LIDAR, efficient and dynamic focusing elements for ultrathin cameras and displays, and dynamic manipulation of light at the nanoscale.

#### 1:30 PM F.NM02.04.45

**Roll-to-Roll Fabrication of Dielectric Metasurfaces** [Joon-Suh Park](#)<sup>1</sup>, Xinghui Yin<sup>1</sup>, Karl K. Stensvad<sup>2,2</sup>, Robert L. Brott<sup>2,2</sup>, Martin B. Wolk<sup>2,2</sup>, James M. Nelson<sup>2,2</sup> and Federico Capasso<sup>1</sup>; <sup>1</sup>Harvard University, United States; <sup>2</sup>3M, United States

In recent years, the idea of using structures of subwavelength scale has led to the birth of what is now called “Flat Optics” or “Metasurfaces.” Metasurfaces locally impart phase shifts, amplitude modulations, and polarization changes to the outgoing light, and therefore achieve the resulting wavefront that performs one or more optical functions. As the metasurfaces can be as thin as the wavelengths with which they interact while achieving near-ideal optical functionalities, the reduction of volume and weight compared to those of the traditional refractive optical elements poses a great advantage in applications where footprint and payload are of concern.

Many experimental demonstrations of metasurfaces were designed to work in the visible or near-infrared wavelengths and therefore were required to use optically transparent materials. Their structure dimensions range from tens to hundreds of nanometers and require high-resolution lithography techniques such as electron beam lithography. When such fabrication methods limited size scalability and mass-producibility, other widely used CMOS compatible, wafer-based fabrication techniques, such as deep-ultraviolet (DUV) lithography and nano-imprint lithography (NIL), were also introduced as promising approaches.

In this presentation, we depart from the conventional wafer-based approaches and instead use roll-to-roll (R2R) fabrication methods to realize optically functional metasurfaces. As demonstrated by the many film manufacturing industries, R2R methods provide scalability in size, and throughput, while reducing the per-unit cost for large volume applications. An example of an industrial R2R film format would be rolls of film with lengths on the order of 1 km.

However, the transition from the wafer-based approach to a R2R compatible process has introduced a pair of challenges to overcome. First, as the R2R fabricated products are wound into rolls of film, free-standing nanostructures are undesirable for

reasons related to robustness and integration. We therefore design metasurfaces comprising high-refractive index nanostructures embedded in an optically transparent, low-refractive index material for process and end use compatibility. Second, embedding the nanostructures comes at a cost: The overall height of the nanostructures needs to be increased from that of the free-standing metasurface elements to compensate for the refractive index contrast loss and to achieve the same optical functionality. This requires a departure from direct replication techniques of NIL, which have intrinsic limitations on aspect-ratio.

Successful implementation of a R2R process to fabricate a metasurface requires careful reconsideration of the optical design step. The optical design not only needs to consider the optical properties of the constituting materials, but also constraints arising due to process demands, such as sidewall draft angles. In this presentation, we discuss both design and fabrication strategies to create embedded metasurfaces using a R2R process and also show resulting fabricated examples. In detail, we present a R2R fabricated, TiO<sub>2</sub>-based embedded metasurface with optical functionality in the visible spectral region. We believe that the presented method paves the way to industrial-scale production of metasurfaces.

#### 1:40 PM F.NM02.04.46

**Dynamic Manipulation of Hybridized Epsilon-Near-Zero Resonances in Optical Fibers** Jingyi Yang<sup>1</sup>, Khant Minn<sup>1</sup>, Aleksei Anopchenko<sup>1</sup> and Ho Wai (Howard) Lee<sup>1,2</sup>; <sup>1</sup>Baylor University, United States; <sup>2</sup>University of California, Irvine, United States

Optical fiber is a well-established waveguiding technology that has been employed in a wide variety of applications such as data communications, spectroscopy, and imaging, remote sensing, surgeries, seismic activity monitoring, etc. However, the defining attributes of an optical fiber (for instance, mode intensity and propagation loss) are fixed after drawing fabrication due to the dielectric properties of the constituent materials. Zero-index photonics, with vanishing permittivity (epsilon) and permeability values, have been studied for unique and extreme optical properties [1]. Ultrathin epsilon-near-zero (ENZ—the real part of permittivity approaches zero) layer can support plasmon polariton mode with enhanced and highly confined optical field [2]. Recent studies on ultrathin transparent conducting oxide (TCO) ENZ films have reported various optical applications such as enhanced nonlinearity [3, 4] and electrically tunable meta-devices [5, 6] among others.

In this work, we demonstrate for the first time the active nonlinear optical and electrical control of hybrid ENZ resonances in thin aluminum-doped zinc oxide (AZO) film integrated onto D-shaped optical fiber. The AZO film is deposited on the polished side of the fiber via atomic layer deposition (ALD) and possesses ENZ property in the near-infrared regime. The guided core mode of unpolished fiber is launched at the input. At the D-shaped portion of the fiber, the evanescent optical field interacts with the AZO layer on the polished side, coupling to the ENZ mode in the ultrathin film which can be detected at the output as a dip in the transmission. Meanwhile, a pump beam from an ultrafast femtosecond laser at the ENZ wavelength is incident on the AZO film from the air. The enhanced pump field due to the ENZ effect inside the AZO layer induces enhanced Kerr nonlinearity, leading to the modulation of complex refractive index and the shift in the ENZ resonance of the coupled fiber mode which is detected at the output as modulated transmission. As a result, the polarization-dependent propagation loss of AZO-coated fiber can be tuned with modulation strength of ~3.5 dB/mm near the ENZ wavelengths with the fs laser intensity of 150 GW/cm<sup>2</sup>. On the other hand, due to the tunable optical properties of the AZO film, the mode propagating in the ENZ optical fiber can be dynamically manipulated by introducing the AZO-HfO<sub>2</sub>-Au gate structure and applying bias. Our preliminary results show that the transmission dip of the hybridized epsilon-near-zero resonance redshifts ~20 nm with an applied bias of 5 V. The dynamic control of optical fiber modes by hybridization with ENZ resonance offers an alternative way of manipulating the ENZ property and functionality of optical fiber, which can find applications in tunable attenuator, polarization-controller, and other active optical fiber devices.

This work was supported in part by the Air Force Office of Scientific Research (AFOSR, Award number: FA9550-19-1-0274), Defense Advanced Research Projects Agency (grant number N66001-17-1-4047), and Robert A. Welch Foundation (Award number: AA-1956-20180324).

#### References

1. Liberal, I.; Engheta, N. *Nature Photonics*, 11(3), 149 (2017).
2. Campione, Salvatore, Igal Brener, and Francois Marquier. *Physical Review B* 91.12, 121408 (2015).
3. Alam, M. Z.; Schulz, S. A.; Upham, J.; De Leon, I.; Boyd, R. W. *Nature Photonics*, 12, (2), 79 (2018).
4. Kinsey, N., DeVault, C., Kim, J., Ferrera, M., Shalaev, V. M., & Boltasseva, A. *Optica*, 2, (7), 616-622 (2015).
5. Huang, Y.-W.; Lee, H. W. H.; Sokhoyan, R.; Pala, R. A.; Thyagarajan, K.; Han, S.; Tsai, D. P.; Atwater, H. A. *Nano Letter*, 16, (9), 5319-5325 (2016).
6. Anopchenko, A.; Tao, L.; Arndt, C.; Lee, H. W. H. *ACS Photonics*, 5, (7), 2631-2637 (2018).

#### 1:50 PM F.NM02.04.47

**Light Driven Space Exploration** Artur Davoyan; University of California, Los Angeles, United States

At present deep space exploration is limited by transit time and overall mission costs. Conventional spacecraft make use of chemical or electric engines, which have fundamental limitations on the possible speed one can achieve. Light driven propulsion offers a conceptually different approach to space travel. Without a need to carry propellant and power on board, spacecraft propelled by the forces of radiation pressure can attain very high velocities, potentially close to relativistic speeds. In this talk we will discuss our recent work on solar and laser driven spacecraft propulsion.

Specifically we will discuss the use of high power laser radiation for space exploration within our solar system. We outline key dynamical equations and solve for possible trajectories. We show that with realistic systems parameters month long planetary missions are possible. We then discuss laser requirements, such as power and aperture. And show that relatively moderate power lasers (~1MW) may be utilized. Next we also study materials and photonic designs. We analyze a tradeoff between mass, reflectance and a need for a radiative cooling. Finally, suggest a range of materials and designs that can yield a desired performance.

In the talk, we will also touch upon the use of solar radiation pressure to propel a spacecraft. We show that solar sails with high area-to-mass ratio may be propelled to >30 AU/year velocities (i.e., more than 8 times faster than the Voyager – fastest space probe we've ever built). Achieving such velocities will pave the way to a new era of affordable and scalable deep space exploration. At the same time such velocities are achieved by a very close perihelion slingshot, where the spacecraft may face extreme conditions. We perform a feasibility study. Specifically, outline conditions needed for maximizing excess velocity and, hence, minimizing mission time, while at the same time ensuring spacecraft durability over the course of the mission. Our estimates show that sails based missions with >30 AU/year are feasible.

#### 2:00 PM F.NM02.04.48

**Enhanced Photoluminescence of MoS<sub>2</sub> Monolayers on Epsilon-Near-Zero TiN Films** Aleksei Anopchenko<sup>1</sup>, Khant Minn<sup>1</sup>, Ching-Wen Chang<sup>2</sup>, Yu-Jung Lu<sup>3,4</sup>, Shangjr Gwo<sup>2,3</sup> and Ho Wai (Howard) Lee<sup>1,5</sup>; <sup>1</sup>Baylor University, United States; <sup>2</sup>National Tsing-Hua University, Taiwan; <sup>3</sup>Academia Sinica, Taiwan; <sup>4</sup>National Taiwan University, Taiwan; <sup>5</sup>University of California, United States

We present a study of room-temperature photoluminescence (PL) of MoS<sub>2</sub> monolayer flakes on TiN thin films. The TiN films of several thicknesses are grown on sapphire substrates by molecular beam epitaxy (MBE) [1] and magnetron sputtering [2]. The permittivity and thickness of TiN films are obtained by spectroscopic ellipsometry that shows the presence of a region of near-zero permittivity (ENZ) in visible wavelengths. Monolayer MoS<sub>2</sub> flakes, grown on silicon substrates using chemical vapor deposition, are transferred onto TiN and sapphire substrates using the dry-stamping method [3]. Before transferring MoS<sub>2</sub> monolayers, the TiN films were coated by a thin layer of aluminum oxide (Al<sub>2</sub>O<sub>3</sub> spacer) using atomic layer deposition to avoid PL quenching due to metallic TiN.

PL spectra are obtained using a confocal laser scanning microscope with 405, 445, 488 and 561 nm excitation wavelengths. PL signal has neutral A- and B-exciton peaks and charged A<sup>-</sup> trion peak. The observed PL is stronger for the MoS<sub>2</sub> monolayers on TiN than sapphire substrates for all used excitation wavelengths. The PL enhancement factors are measured as the ratio of areas under the PL peaks for TiN and sapphire substrates and calculated using a luminescence modelling method based on the dyadic Green's functions [4-6]. A good agreement is observed between measured and calculated enhancements. For small Al<sub>2</sub>O<sub>3</sub> spacer thickness, the PL enhancement has the maximum at the excitation wavelength that matches the ENZ wavelength of TiN films. An 8-fold PL enhancement is observed for a thicker spacer due to a positioning of MoS<sub>2</sub> monolayer in the anti-node of the standing wave above the TiN film. Larger PL enhancements are reported for MBE-grown than sputtered TiN films because of the lower optical losses of single-crystalline TiN films. We also calculated absorptance and electric field intensity enhancement in MoS<sub>2</sub> monolayer as a function of the excitation wavelength. The increase in absorptance and field enhancement around the ENZ wavelength of TiN films is observed. Thus, the ENZ substrate enhances absorption and electric field of light excitation in MoS<sub>2</sub> monolayer and hence enhances its spontaneous emission. This study will enrich the fundamental understanding of spontaneous emission on ENZ substrates that might find applications for the development of advanced nanophotonic light sources.

This work was supported in part by the AFOSR-AOARD (Award number: FA2386-18-1-4099), Robert A. Welch Foundation (Award number: AA-1956-20180324), and the Ministry of Science and Technology in Taiwan (Grant No.: MOST 107-2923-M-007-004-MY3).

1. W.-P. Guo, R. Mishra, C.-W. Cheng, B.-H. Wu, L.-J. Chen, M.-T. Lin, and S. Gwo, "Titanium nitride epitaxial films as a plasmonic material platform: Alternative to gold," *ACS Photonics* **6**, 1848-1854 (2019).
2. Y.-J. Lu, R. Sokhoyan, W.-H. Cheng, G. Kafaie Shirmanesh, A. R. Davoyan, R. A. Pala, K. Thyagarajan, and H. A. Atwater, "Dynamically controlled Purcell enhancement of visible spontaneous emission in a gated plasmonic heterostructure," *Nat. Commun.* **8**, 1631 (2017).

3. A. Castellanos-Gomez, M. Buscema, R. Molenaar, V. Singh, L. Janssen, H. S. J. van der Zant, and G. A. Steele, "Deterministic transfer of two-dimensional materials by all-dry viscoelastic stamping," *2D Mater.* **1**, 011002 (2014).
4. N. Danz, R. Waldhausl, A. Brauer, and R. Kowarschik, "Dipole lifetime in stratified media," *J. Opt. Soc. Am. B-Opt. Phys.* **19**, 412-419 (2002).
5. K. A. Neyts, "Simulation of light emission from thin-film microcavities," *J. Opt. Soc. Am. A* **15**, 962-971 (1998).
6. W. Lukosz and R. E. Kunz, "Light emission by magnetic and electric dipoles close to a plane interface. I. Total radiated power," *J. Opt. Soc. Am.* **67**, 1607-1615 (1977).

## 2:10 PM F.NM02.04.49

**Al:ZnO with Enhanced Doping Efficiency by Atomic Layer Deposition as a Platform for Near-Zero-Index Photonics** Dhruv Fomra, Kai Ding, Vitaliy Avrutin, Ümit Özgür and Nathaniel Kinsey; Virginia Commonwealth University, United States

In the last two decades, several technological breakthroughs have been closely linked to material discovery and development. Just as development of gallium nitride, high purity silica, and high-k dielectrics provided the foundation for the progress in solid state lighting, optical fibers, and integrated circuits, near-zero-index materials (NZI) have great potential to drive advancements in nanophotonics, nonlinear optics, and quantum optics. In addition to exhibiting enhanced light-matter interaction due to slow light effects, these materials offer excellent electrical and optical tunability. Due to these unique properties, NZI materials have already led to demonstrations of dynamic metamaterials, ultrafast photonic modulators, and extreme all-optical processes. Among a wide range of NZI materials explored for these applications, Al doped ZnO, which has a vanishing index in the telecommunication bands, is particularly attractive combining high electrical conductivity and transparency in the visible range, well-established ZnO fabrication technology, high solubility limits of Al, and the abundance of Zn in nature. To realize the potential of ZnO as a material platform for NZI photonics, there is a need for scalable deposition methods yielding high-quality material. Atomic layer deposition (ALD) is a versatile technique due to its ability to provide conformal, uniform, and pin-hole free thin films with sub-nanometre thickness control over large area at low deposition temperatures. However, NZI films grown by ALD have typically suffered from poor optical quality, exhibiting reduced free-carrier density and higher loss when compared to those grown by other methods.

In this work, we overcome the limitations impeding the deposition of high quality ZnO:Al by improving the doping efficiency (ratio of electron concentration to total Al content in the matrix) of the ALD method from 13% commonly reported in literature to 54%. As a result, we demonstrate films with low losses ( $\epsilon'' < 0.35$ ), high conductivity ( $\rho \sim 2.8 \times 10^{-4} \Omega\text{-cm}$ ) and sufficiently high carrier density ( $8.5 \times 10^{20} \text{ cm}^{-3}$ ) to enable Al doped ZnO films with NZI regions tunable across both O and C telecommunication bands, for the first time. This significant material improvement became possible by moving away from the conventional ALD process of depositing doped films in a "digital" manner, wherein one dopant layer of  $\text{AlO}_x$  is incorporated periodically into the ZnO matrix and Al:ZnO is formed by the out-diffusion of Al into ZnO. Intuitively, such a process is very inefficient and leads to the creation of an inhomogeneous film where dopant atoms do not contribute to the free carrier density, but rather form clusters that increase carrier scattering and reduce the metallicity. However, moving away from the surface saturation condition during the Al precursor pulse, which is characteristic of the conventional ALD approach, leads to enhanced Al incorporation in each dosing cycle. This has been realized by utilizing  $\text{H}_2\text{O}/\text{DEZ}/\text{TMA}$  pulse sequence to increase competition between Zn and Al precursors (diethyl zinc, DEZ, and trimethyl aluminium, TMA) for the surface sites, thus reducing the amount of Al precursor supplied in each pulse to decrease surface coverage of Al precursor, and by concurrently increasing the substrate temperature to lower the density of OH groups on the surface, which act as active sites. Such growth conditions allowed us to incorporate the dopant cycle 4x more frequently in the growth process (every 0.5 nm, as opposed to every 2 nm for conventional ALD) and ensure a more uniform distribution of Al throughout the film, simultaneously increasing the doping efficiency and reducing density of clusters. Furthermore, this process provides a pathway to improve the electrical and optical properties of other emerging doped binary semiconductors such as doped GaN, CdO, and  $\text{Ga}_2\text{O}_3$  grown using ALD.

## 2:20 PM F.NM02.04.50

**Plasmonic Modes and Spasing in Metaphotonic Nanostructures** Viktorii Babicheva; University of New Mexico, United States

Plasmonic nanostructures can significantly enhance electric and magnetic fields at nanoscale dimensions. Fields localized at nanosized plasmonic nanostructures can be several orders of magnitude higher than the incident light field, and this field enhancement strongly affects light-matter interaction processes in plasmonic nanostructures. Here, we study field enhancement in nanoparticle clusters and periodic arrays and analyze surface plasmon amplification by stimulated emission (spaser) in such nanostructures. We consider both sphere and disk plasmonic nanoparticles and employ full-wave numerical simulations for modeling field enhancement. Planar optical elements with efficient light control at the nanoscale can be

designed based on transdimensional photonic lattices that include three-dimensional-engineered nanoantennas supporting multipole Mie resonances and arranged in the two-dimensional arrays to harness collective effects in the nanostructure. Periodic arrays of nanoparticles have gained special attention because of extraordinary lattice resonances in proximity to the wavelength of diffraction, the so-called wavelength of Rayleigh anomaly. Using full-wave modeling, we numerically observe plasmonic modes with even and odd field distributions in nanoparticle clusters and identify spatial regions with nodes and anti-nodes of the field enhancement. We use quantum density matrix (optical Bloch) equations for the spaser, calculate the plasmon amplification, and show its correspondence to the total mode characteristics. Because of the strong field enhancement in the plasmonic nanostructures, amplification of plasmons in nanoparticle clusters and periodic arrays is more efficient than ones in the proximity to a single nanoparticle and can be used as an ultra-compact light source in optical devices and medical applications. Acknowledgment. This material is based upon work supported by the Air Force Office of Scientific Research under Grant No. FA9550-19-1-0032.

SESSION F.NM02.05: Plasmonic/Nanophotonic Sensing and Spectroscopy  
On Demand Abstracts Available for Viewing Starting Saturday Morning, November 21, 2020  
F-NM02

#### 5:00 AM F.NM02.05.01

**Color Tuning with Nanoparticle Decorated TiO<sub>2</sub> Electrospun Fibers in Electrochromic Applications** Cavit Eyovge;  
University of Twente, Netherlands

Titanium dioxide (TiO<sub>2</sub>) has attracted a lot of attention in plenty of applications varying from batteries, photo/electrocatalysis to optoelectronics and sensors. Although there are many different procedures for synthesizing sound TiO<sub>2</sub> layers, methods leading to one dimensional (1D) structures are of interest due to having superior properties. Electrospinning is one of those methods to synthesize 1D mesoporous TiO<sub>2</sub> fibers. Having the advantages of high surface area and ease of functionalization, those fibers can be quite beneficial in optoelectronic applications. Here in this study, nanoparticle (NP) decorated TiO<sub>2</sub> fibers were formed with a modified electrospinning method and used as an active layer in an electrochromic (EC) device. A coaxial nozzle was used to form a core/shell type of TiO<sub>2</sub>/NP fibers. Structural and morphological properties were characterized by various techniques, such as scanning electron microscopy (SEM), transmission electron microscopy (TEM) and x-ray diffraction (XRD). Fibers of 198.66±21.47 nm average diameter were confirmed to have the anatase phase of TiO<sub>2</sub>. The effects of different NPs such as silver (Ag), gold (Au) and copper(II) oxide (CuO), on optical properties were also investigated. The ultraviolet/visible/near-infrared spectroscopy (UV/Vis/NIR) revealed that depending on the absorption wavelength of the decorative NPs used, it is possible to tune the band gap of TiO<sub>2</sub>/NP final composite structure. Governing effects of the composite structures on electrochemical properties were evaluated in half-cell configuration in which EC layers were cycled in between ±3V. It was observed that the color attained can also be altered with different NPs. For instance, Ag shows a black-brown color while Au yields dark blue and CuO leads to a dark green color under negative bias. In addition, fast switching times below 10 seconds were possible in each TiO<sub>2</sub>/NP configuration. This is attributed to the faster kinetics of electrospun fibers in redox reactions.

#### 5:10 AM F.NM02.05.02

**Surface Plasmon Polaritons for Energy-Tunable Hot Carriers and Electrochemical Probing of Strong Coupling** Blake S. Simpkins<sup>1</sup>, Wonmi Ahn<sup>2</sup>, Jeremy H. Pietron<sup>3</sup> and Igor Vurgaftman<sup>1</sup>; <sup>1</sup>U.S. Naval Research Laboratory, United States; <sup>2</sup>Excet, United States; <sup>3</sup>Lawrence Livermore National Laboratory, United States

We use surface plasmon polaritons (SPPs) as the foundation for examining two important phenomena. First, SPPs were used to generate energy-tunable hot carriers that can be injected into semiconductors or molecular systems, opening a new pathway to drive photo-induced chemical reactions. [1] Unlike metal nanoparticles that suffer from resonance inhomogeneity and limited spectral tunability, metal films support SPPs that are homogeneous in-plane and accessible by simply tuning an illumination angle in a broad spectral range. We measured light-induced electrochemical currents of a metal/semiconductor heterofilm (Ag/TiO<sub>2</sub>) and a bare metal film (Au) interfaced with a sodium hydroxide:methanol solution. We observed plasmonic electrochemical currents and extracted a strong photon-energy dependence of the photon-to-carrier conversion efficiency. This phenomenon was described using a Schottky transport model. Secondly, we examined strong optical coupling between the SPP mode and a thin molecular dye film. The dye, methylene blue (MB), is redox active enabling examination of the electrochemical response under strong coupling conditions. Our results demonstrate full modulation of the Rabi splitting, a diffusion-limited redox process, and imaging of molecular adsorption/desorption on the metal surface. All of

these results have important implications for chemistries enhanced or enabled by light-matter interactions. [1] Ahn, W., Vurgaftman, I., Pietron, J. J., Pehrsson, P. E., and Simpkins, B. S. "Energy-Tunable Photocatalysis by Hot Carriers Generated by Surface Plasmon Polaritons" *J. Mater. Chem. A.*, 2019, 7, 7015-7024.

#### 5:20 AM F.NM02.05.03

**Delineating Photothermal and Photoexcitation Effects in the Photoelectrodeposition of Cuprous Oxide** James Lowe and Robert Coridan; University of Arkansas, United States

Cuprous oxide (Cu<sub>2</sub>O) is an earth-abundant, p-type semiconductor of interest to photovoltaic and photoelectrochemical applications. Cu<sub>2</sub>O can be synthesized directly into its semiconducting phase by electrodeposition, rather than requiring a high-temperature calcining step as is necessary for most other electrodeposited metal oxides. As a result, Cu<sub>2</sub>O electrodeposition rates can be enhanced by illumination during growth. In recent work, we showed that photoelectrodeposition forms a composite of Cu<sub>2</sub>O doped by Cu nanocrystals throughout, resulting in a black film with high absorptivity across the visible spectrum. Continued growth is enhanced even for illumination with energies smaller than the band gap of Cu<sub>2</sub>O due to the sensitivity of the Cu<sub>2</sub>O electrodeposition to local temperatures at the electrode-electrolyte interface. Here, we describe experiments to discriminate the local photothermal and photoelectrochemical effects in the photoelectrodeposition of Cu<sub>2</sub>O. Identifying the role of each effect will lead to more robust control over the composition and structure of Cu<sub>2</sub>O-based interfacial heterostructures. In addition to standard spectroscopic and electrochemical characterization, we will describe novel experiments that use in situ high-speed microscopy to unveil the complex interplay between light and heat on the electrodeposition of Cu<sub>2</sub>O.

#### 5:30 AM F.NM02.05.04

**Discerning Between All Possible Activation Mechanisms in Plasmon-Driven Nanoparticle Syntheses** Rifat Kamarudheen, Guus Aalbers, Ruben Hamans and Andrea Baldi; Dutch Institute for Fundamental Energy Research, Netherlands

Noble metal nanoparticles find applications in a wide range of fields, from (photo)catalysis, to bioimaging, and surface enhanced Raman spectroscopy. One of the most striking characteristics of these nanoparticles is that they can sustain localized surface plasmon resonances (LSPRs), light-driven oscillations of conduction electrons that give rise to strong scattering and absorption of light. These LSPRs can be used to activate a wide range of chemical and physical processes at the metal surface. For example, plasmon resonances have been used to perform the light-driven synthesis of hierarchical metal nanoparticles in solution with high yields and precise morphologies.<sup>1,2</sup> The growth of these nanostructures can be linked to the decay of LSPRs via several different mechanisms: 1) plasmonic enhancement of the electromagnetic field at the nanoparticle surface that activates photosensitive precursors, 2) photothermal heating that accelerates kinetically limited reactions following the Arrhenius law, and 3) plasmonically-generated (inraband) and photo-generated (interband) electrons and holes that can catalyze redox reactions. In most plasmon-driven chemical reactions, however, these mechanisms are challenging to disentangle and typically occur simultaneously. Furthermore, the relative weight of their contributions is heavily dependent on the illumination and sample geometries.<sup>3</sup> For these reasons, it would be ideal to develop a plasmon-driven process in which all the possible activation mechanisms can be assessed independently. Here, we develop a plasmon-assisted synthesis of Au@Ag core@shell nanorods in which interband "hot" holes are the only driving force of the reactions. Using a combination of extinction spectroscopy, transmission electron microscopy, thermal characterization, and finite-difference time-domain (FDTD) simulations, we can unequivocally exclude any effects due to photothermal heating, near-field enhancement, and intraband electrons and holes. In our experiments, we compare the growth rate of Ag shells while exciting either the transverse or the longitudinal resonances of Au nanorods using 532 nm and 730 nm continuous wave lasers, respectively. The laser powers in the two cases are modulated to obtain the same total amount of absorbed optical power in the solution and therefore the same magnitude of photothermal effects. We find that the Ag shell growth rate under 730 nm irradiation equals the one in the dark and therefore shows no plasmonic enhancement. On the contrary, the rate is strongly enhanced under 532 nm irradiation, although such enhancement slowly decreases and becomes negligible as the Ag shell approaches ~5 nm in thickness. The striking rate disparity under identical total absorbed power demonstrates the non-thermal nature of the enhancement mechanism. Furthermore, using FDTD we show that the intensity of the scattered electromagnetic fields at the nanorod surface increases with increasing Ag shell thickness. Near-field enhancements cannot therefore explain the observed time evolution of the reaction rate when using 532 nm light. Finally, the absence of any enhancement rate under 730 nm irradiation, which corresponds to an energy just below the interband transition of gold, shows that d-band "hot" holes in gold are the main responsible for the effects observed under 532 nm irradiation. Strikingly, these holes have typical mean free paths of a few nanometers, corresponding to the Ag shell thickness at which plasmon-driven effects are quenched. Understanding the mechanism of plasmon-activated chemistry at the surface of metal nanoparticles is of paramount importance for a wide range of applications, from the rational design of novel light-assisted

nanoparticle syntheses to the development of plasmonic nanostructures for catalytic and therapeutic purposes. 1. Jin, R. et al. *Science* 294, 1901–1903 (2001) 2. Zhai, Y. et al. *Nat. Mater.* 15, 889–895 (2016) 3. Kamarudheen, R. et al. *ACS Nano* 12, 8447–8455 (2018)

#### 5:40 AM F.NM02.05.05

**Nanometer-Resolution Electron Spectroscopy of Plasmonic Nanostructures in Reactive Liquid Environments** Alan Dai, Michal Vadal and Jennifer A. Dionne; Stanford University, United States

Sustainable and industrial photochemical and photocatalytic reactions, including artificial photosynthesis, organic synthesis, and pollutant degradation, require nanoparticle catalysts in liquid environments for physically significant reactivity. Plasmonic nanostructures have emerged as materials which promise enhanced efficiency and selectivity at milder conditions compared to traditional metal catalysts. However, developing more efficient plasmon catalysts requires investigating them at the single and sub-particle level, monitoring their properties at particular spatial and temporal coordinates throughout a reaction. This approach both prevents the averaging of plasmonic responses across an ensemble of particles as well as enables the capture of variations in plasmonic and catalytic behavior across and within a single particle. In-situ transmission electron microscopy (TEM) has seen recent use in vacuum and gaseous environments to obtain real-time information of plasmonic nanostructures and monitor plasmon-driven reactions at sub-particle spatial and millisecond time resolution. Here, we bring these techniques to aqueous- and organic-phase environments via in-situ liquid TEM. We perform combined scanning TEM and monochromated electron energy loss spectroscopy (EELS) on a model system of individual Au nanoparticles, measuring and comparing their plasmon resonance energies for distinct chemical environments. We use a variety of particle shapes ranging from 30–100 nm in size, synthesized both through colloidal (reduction of AuCl<sub>4</sub> in CTAB solution) and lithographic (e-beam lithography and metal lift-off) methods onto a specially designed liquid cell chip. Two such chips are used to enclose a small pocket of liquid for stable imaging and spectroscopy in the TEM. Selecting particles located in thinner regions of liquid (< 100 nm thick), we demonstrate that plasmon resonances can be measured with sub-second total acquisition times while maintaining sufficient signal-to-noise ratios, circumventing the dominant liquid background signal and without any interfering electron-induced side reactions. Furthermore, we observe that enough spectral resolution is maintained to differentiate resonances corresponding to spatially dependent visible modes in each shape of particle. For example, across colloidal synthesized Au rods bound to a SiN membrane, we measure longitudinal and transverse resonances which normally lie at 700-900 nm and 500-600 nm in vacuum but experience a 30-50 nm and 5-10 nm redshift, respectively, in water. Likewise, for lithographically fabricated triangular prisms we map edge and tip modes around 490 and 520 nm, respectively, in vacuum, and we observe a similar redshift to that of the rods when immersed in water. These trends quantitatively agree with calculated results from BEM methods for the geometries examined. We then change the solvent in the liquid cell via flow tubing, showing that Au particles experience a shift in plasmon resonance arising from the refractive index change of varying liquid environments vs. vacuum, agreeing with simulations. This work provides the foundation for in-situ TEM characterization of plasmonic catalysts for critical reactions in solution such as biosynthesis and water splitting.

#### 5:50 AM F.NM02.05.06

**Ultrafast Carrier Dynamics of GaAs by mid-IR Pump-Probe Spectroscopy** Roisul H. Galib, John A. Tomko, David Olson, Ashutosh Giri, John Gaskins and Patrick Hopkins; University of Virginia, United States

Ultrafast laser spectroscopy is a versatile technique that is commonly used to both understand and manipulate carrier scattering mechanisms in semiconductors. We report the observation of excited carrier relaxation times in GaAs using optical pump mid IR probe spectroscopy. We find a sharp change in relaxation times occurs at the intervalley transitions of GaAs. Our results also show the relaxation times becomes faster with increasing photoexcitation fluence. These results provide direct evidence that excited carrier decay at greatly different rates based on their energy relative to the conduction band minimum. These findings provide additional insight into the energy-dependent nature and rate of phonon emission during electronic relaxation.

#### 6:00 AM F.NM02.05.08

**Orientation Sensing from Optical Microscopy Images by Deep-Learning** Jingtian Hu<sup>1</sup>, Tingting Liu<sup>1</sup>, Priscilla Choo<sup>1</sup>, Shengjie Wang<sup>2</sup>, Thaddeus Reese<sup>1</sup>, Alex Sample<sup>1</sup> and Teri W. Odom<sup>1</sup>; <sup>1</sup>Northwestern University, United States; <sup>2</sup>University of Washington, United States

Automated particle-tracking techniques are important for studying biological processes ranging from tissue deformation to cellular uptake. Existing tracking methods, however, only focus on visualizing the translational motion but not rotational motion, which can also provide critical information on cellular activities such as membrane protein diffusion. The development of next-generation particle-tracking platforms that can characterize rotational dynamics requires concurrent

advances in imaging strategies and computational analyses.

This presentation reports a deep-learning rotation-tracking platform based on 3D nanoparticle imaging probes and differential interference contrast (DIC) microscopy. We obtained libraries of DIC images at each sampled nanoparticle structure and orientation for training the prediction models based on convolutional networks. These models predicted the in-plane orientation of gold nanorods based on simulated and measured DIC images with an accuracy only limited by the inherent resolution of the technique. Using low-symmetry gold nanostars as imaging probes, the method could resolve particle rotations in the full 0-360° range by accounting for DIC patterns at multiple wavelengths simultaneously. This deep-learning method could make consistent orientation predictions that are insensitive to varying imaging backgrounds. Finally, we demonstrated the simultaneous prediction of in-plane and out-of-plane orientations from a 3D nanostar by analysis of DIC images collected at multiple wavelengths.

#### **6:10 AM F.NM02.05.09**

**Phase-Resolved Surface Plasmon Scattering Probed by Cathodoluminescence Holography** Nick Schilder, Harshal Agrawal, Erik C. Garnett and Albert Polman; AMOLF, Netherlands

We introduce cathodoluminescence holography to directly retrieve the phase of light scattered from nanoscale objects. We use 30-keV electrons to coherently excite with a nanoscale spatial precision surface plasmon polaritons (SPP) that subsequently scatter from either nanoholes made in a Ag film or single-crystalline Ag nanocubes. We use transition radiation excited at the electron impact position as a broadband reference to create a far-field interference pattern that is collected in both angular and spectral domain. From the holography data we directly resolve the SPP dispersion and probe the phase of resonant coupling of SPPs to individual nanoscatterers. From the far-field wave fronts we derive the full basis of scattering dipoles using a modal decomposition analysis and unravel the relative strength and phase of all SPP-excited dipolar modes. We also show that scattering from a SPP off a helical nanoaperture leads to chiral light in the farfield. We observe experimentally a topological charge of -1. Cathodoluminescence holography takes advantage of the nanoscale electron excitation source and can find a broad range of applications to probe surface wave scattering by individual nanoscatterers.

#### **6:20 AM F.NM02.05.10**

**Plasmonic Surfaces as Optical Components for Infrared Sensing and Imaging** Jyotirmoy Mandal and Aaswath P. Raman; University of California, Los Angeles, United States

In recent years, infrared (IR) optical systems have been increasingly used in imaging and sensing applications, as evidenced by a surge in demand for infrared sensors during the COVID-19 pandemic. However, cost and ease of fabrication of germanium-based optical elements used in IR systems remains a major barrier to widespread adoption, particularly in low-resource settings.

In this talk, we will demonstrate spectrally selective plasmonic surfaces as scalable and low-cost IR optical components that absorb ultraviolet-to-shortwavelength IR radiation, while showing a specular behavior in the longer infrared wavelengths. These surfaces can be conveniently manufactured at large scales, and alone or in combination with other materials, used as reflective or transmissive IR optical components.

The talk will present FDTD simulation results that validate the concept, and present experimental demonstration of the optical capability (selectivity, specularity and integrability into optical systems) using a specific plasmonic design. Since the fabrication, physical operation and application of our designs span different fields, a short, interdisciplinary overview of related challenges and opportunities will also be presented.

*Acknowledgments: Jyotirmoy Mandal was supported by Schmidt Science Fellows, in partnership with the Rhodes Trust.*

SESSION F.NM02.06: Low-Dimensional Photonics

On Demand Abstracts Available for Viewing Starting Saturday Morning, November 21, 2020  
F-NM02

#### **5:00 AM F.NM02.06.02**

**Enhancing Graphene's Plasmonic Tunability via Its Dielectric Environment** Amun Jarzembki, Michael Goldflam and Thomas Beechem; Sandia National Laboratories, United States



Graphene's high mobility, linear band structure, and two-dimensional density of states result in tunable optical properties within the infrared (IR) that present new opportunities for dynamic multifunctional detectors and filters. Being atomically thin, however, necessitates field confinement to achieve practical utility. Graphene plasmons serve this purpose by both concentrating the electric field while "carrying" the tunability, which is dependent upon the charge concentration within graphene. In addition to graphene's electronic properties, its surrounding optical environment has a profound effect on the plasmonic response. Thus, design of the dielectric layers used to facilitate the electrostatic doping of graphene- required for active tunability- is of critical importance. Recognizing this fact, we examine here how dielectric layers can be chosen to enhance the spectral tunability of graphene plasmonic devices. To this end, the tunability of graphene's plasmonic dispersion is quantified relative to the dielectric atop of which it sits by solving for poles in the imaginary part of the reflection coefficient in a multilayer model. By solving for the dispersion at varying Fermi-levels (i.e., charge concentrations), the extent of tunability is quantified. Tunability varies appreciably between several materials typically employed in graphene plasmonic devices-HfO<sub>2</sub>, SiO<sub>2</sub>, and Al<sub>2</sub>O<sub>3</sub>. The causes for this material variation are then examined by assessing the dependence of tuning relative to parameters making up the transverse-optical longitudinal-optical (TOLO) dielectric function, which typically describes the optical properties of the dielectrics employed. Paths are highlighted by which synthetic multilayer oxides can be designed to enhance tuning in graphene devices beyond that presently attainable.

Acknowledgements: Sandia National Laboratories is a multi-mission laboratory managed and operated by the National Technology & Engineering Solutions of Sandia, LLC, a wholly owned subsidiary of Honeywell International Inc., for the U.S. Department of Energy's National Nuclear Security Administration under contract No. DE-NA0003525.

#### 5:10 AM F.NM02.06.05

**Non-Reciprocal Electrodynamics and Axion Field in Weyl Semimetal Co<sub>3</sub>Sn<sub>2</sub>S<sub>2</sub>** Dennis M. Nenko<sup>1,2</sup>, Christina Garcia<sup>1</sup>, Claudia Felser<sup>2</sup> and Prineha Narang<sup>1</sup>; <sup>1</sup>Harvard University, United States; <sup>2</sup>Max Planck Institute for Chemical Physics of Solids, Germany

Co<sub>3</sub>Sn<sub>2</sub>S<sub>2</sub> is an ideal Weyl semimetal in its magnetic phase [1]. Its ground state is antiferromagnetic and electromagnetic fields can induce a phase transition between the two states [2]. Using ab-initio tools, we analyse the axion field [3] and the linear and non-linear optical responses in the two phases of this time-reversal breaking compound. Our calculations include both electron-electron scattering events, as well as interactions with phonons [4]. We discuss how the phases can be distinguished from each other by their optical and electrical response, how the axion field in the Weyl semimetal state provide a way to realise non-reciprocal thermal emitters [5] and finally, present results on the shift-current generation and second-harmonic emission.

[1] Liu et al., Nature physics 14, 1125 (2018)

[2] Soh et al., Phys. Rev. B 100, 201102(R) (2019)

[3] Nenko et al., Nat. Rev. Phys. (under review, 2020)

[4] Garcia et al., Phys. Rev. Res. 2, 013073 (2020)

[5] Zhao et al., Nano Lett. 20, 1923 (2020)

#### 5:20 AM F.NM02.06.06

**Origin of Energy Blueshift in a Tunable Microcavity with 2D-Perovskite Based on Free-Standing Thin Films** Karolina Lempicka<sup>1</sup>, Magdalena Furman<sup>1</sup>, Marcin Muszynski<sup>1</sup>, Mateusz Król<sup>1</sup>, Adam Wincukiewicz<sup>1</sup>, Katarzyna Rechcinska<sup>1</sup>, Rafal Mazur<sup>2</sup>, Maria Kaminska<sup>1</sup>, Wiktor Piecek<sup>2</sup>, Pawel W. Majewski<sup>1</sup>, Jacek Szczytko<sup>1</sup> and Barbara Pietka<sup>1</sup>; <sup>1</sup>University of Warsaw, Poland; <sup>2</sup>Military University of Technology, Poland

Recently, interest in organic-inorganic perovskites has increased due to their application in photovoltaics, photonics and optoelectronics. They have also been used as a strong light emitters in the microcavities, due to the possibility of obtaining strong light-matter coupling regime, and the occurrence of coherent macroscopic effects, such as Bose-Einstein condensation of exciton-polaritons. Compared with multi quantum wells heterostructures produced by epitaxial growth of inorganic semiconductors, 2D perovskites displays stronger dielectric confinement in the inorganic layers, whereas excitons in such materials are characterized by a higher binding energy and exhibits strong nonlinearities. It indicates that the devices based on polaritons in 2D perovskites layers can work stable at the room temperature.

Optical and electronic properties of perovskites can be easily tuned by changing the thickness, which makes them an ideal system for the investigation of strong light-matter coupling phenomena. In this direction, we studied the unusual photoluminescence (PL) behavior in function of temperature of a 2D-layered perovskite-type semiconductor, (C<sub>6</sub>H<sub>5</sub>(CH<sub>2</sub>)<sub>2</sub>NH<sub>3</sub>)<sub>2</sub>PbI<sub>4</sub> deposited on a dielectric

mirror prepared from a solution using spin-coating technique as well as free-standing layers of 2D-perovskite with substrate from solution P2611:NMP. The low-temperature ( $< 110$  K) photoluminescence of 2D perovskite reveals two distinct emission peaks. Furthermore the bandgap exhibits an unusual blueshift (about 7 nm) with increasing temperature from 4.5 to 295 K. The temperature-driven additional photoluminescence peak can be attributed to the presence of molecularly disordered domains.

We demonstrate a strong light-matter coupling regime between the excitonic resonance in 2D-perovskite and cavity photon in an open, tunable microcavity at room temperature. Exciton-polaritons in this material are expected to show unusually strong non-linear effects due to significant third order Kerr nonlinearity. At strong excitation conditions (up to 1 mW) we observe emission blueshift up to 8 meV from polariton mode. We demonstrate that this blue-shift can be attributed to the non-linear polariton interaction and the change of exciton-photon interaction strength. Exploring emission characteristics of a 2D-perovskites in wide range of temperatures and under strong light-matter coupling conditions provides a lot of important information regarding the performance of a light-emitting device, solar cell based on perovskites and physics phenomena related to non-linear effects observed previously only at cryogenic temperatures.

#### SESSION F.NM02.07: Nanophotonic Devices

On Demand Abstracts Available for Viewing Starting Saturday Morning, November 21, 2020  
F-NM02

##### 5:00 AM F.NM02.07.01

**A Refractive-Index-Controllable Si Nanoparticle-Polymer Composite Material for Terahertz-Range Optical Devices and Anti-Reflective Coating Application** Junshi Soeda<sup>1</sup>, Yoichi Kawada<sup>2</sup>, Hiroshi Satozono<sup>2</sup>, Hironori Takahashi<sup>2</sup>, Masayuki Chokai<sup>1</sup> and Yoshinori Ikeda<sup>1</sup>; <sup>1</sup>Teijin Limited, Japan; <sup>2</sup>Hamamatsu Photonics K.K., Japan

Owing to advancements in related technologies over the last few decades, terahertz waves possess the potential to be utilized in fields related to imaging, non-destructive testing, analysis, and next-generation telecommunication, among others. Optical elements are also currently being explored as tools that can extend the applicability of terahertz (THz) waves. One obstacle in the development of THz optical elements is that there are fewer feasible materials that have different refractive indices in THz frequencies than there are such materials in other frequency ranges. Specifically, the options for transparent optical materials are limited to polymethylpentene, other olefin-based polymers, and highly resistive silicon.

In this study, we developed a highly transparent composite material composed of polymer and silicon nanoparticles (SiNPs) for THz optics; the refractive index can be controlled by varying the fraction of SiNPs in the composite. We also demonstrated its applicability as an anti-reflection (AR) coating for Si optical elements prone to reflection loss due to the large discrepancy between the refractive indices of Si and air.

Highly pure SiNPs with a typical diameter of 100 nm were employed to control the refractive index of the composite. The SiNPs were fabricated via a laser pyrolysis method. This method entails laser irradiation to decompose semiconductor-grade monosilane gas; hence, the SiNPs have extremely low metal impurity (i.e., on the order of ppb) and consequently, high resistivity. The utilization of highly resistive Si creates favorable conditions for THz waves as it allows for the composite material to be transmitted without absorption. Furthermore, the problem of wave scattering is eliminated, as the typical diameter of the SiNPs is smaller than the wavelength of THz waves by a factor of 1000.

We first characterized the basic optical properties of the SiNPs and its composite with a polymer chosen for present study. THz-wave transmission was characterized via THz time-domain spectroscopy of the SiNP films deposited on highly resistive Si (HR-Si) wafers. The transmission spectrum was observed to be in agreement with the spectrum calculated from the thickness, porosity of the film, and refractive index of Si; this indicated that the THz waves were not significantly absorbed or scattered by the film.

The refractive indices of the SiNP-polymer composites were also evaluated from the transmission spectrum of the composite films on HR-Si. The refractive index was controlled between 1.52 and 1.95 under a Si-content range of approximately 0–30 vol%.

Subsequently, for demonstration, we designed and fabricated bilayer AR coatings to apply to the Si plates. The SiNP-polymer composite layer ( $n = 1.95$ ) and polymer layer ( $n = 1.52$ ) were stacked on both sides of the Si plates. The amplitude transmittance of the Si plates with AR coatings exceeded 90%, with a bandwidth of 0.8 THz at around 1 THz, whereas in the case of Si plates without AR coatings, the transmittance was expected to be 70%.

In conclusion, we developed a novel refractive-index-controllable SiNP/polymer composite material for THz-range optics. The SiNPs demonstrated negligible absorbance and scattering of THz waves, confirming their suitability for THz-range

optics applications. Additionally, the refractive index of the composite was controlled between 1.52 and 1.95. This range addresses several existing limitations regarding THz-range optical element designs. Furthermore, the AR coating developed using the proposed composite material successfully increased the transmittance of THz waves through Si. Thus, the proposed composite material can be applied in the design of various types of THz-range optical elements and has the potential to be used for developing optical elements with higher functionality.

#### 5:10 AM F.NM02.07.03

**ITO-Based Epsilon-Near-Zero Photonics—From Modulators to Optical Limiters** Volker J. Sorger, Mario Miscuglio, Yaliang Gui and Rubab Amin; George Washington University, United States

The material class of transparent conductive oxides features a variety of properties that are interesting and useful for optical and opto-electronic applications. ITO belonging to this class has shown to be either processed (Gui et al, Nat. Sci. Rep. 2019), or electro-statically-biased (Sorger et al., Nanoph. 2012) into the ENZ regime. Here, I review our latest work including; (1) ITO ENZ material deposition control, (1) the first ITO-based phase-shifters in silicon photonics with  $V_{pL}=0.5V$ -mm (Amin et al, APL 2018) and  $0.06V$ -mm performance (Amin et al, arXiv 1907.11131 2019), (2) electro-optic nonlinear activation function in feed-forward photonic neural networks (Amin et al, APL Mat. 2019), (3), optical-phase array in silicon-ITO photonics for GHz-fast beam steering, (4) a metatronic circuit board towards an analog photonic computer for PDEs, and (5) strong nonlinearity in ENZ ITO showing  $\sim 10$ dB of optical limiting.

#### 5:20 AM F.NM02.07.04

**Spray-Deposited Metal-Chalcogenide Photoconductors and Photodiodes for Low Cost Infrared Imagers** Tommy O. Boykin II<sup>1</sup>, Nagendra Dhakal<sup>1</sup>, Javaneh Boroumand<sup>1</sup>, F. Javier Gonzalez<sup>1</sup>, Isaiah Oladeji<sup>2</sup>, Pedro Figueiredo<sup>2</sup>, Stephen Neshul<sup>3</sup> and Robert Peale<sup>1</sup>; <sup>1</sup>University of Central Florida, United States; <sup>2</sup>Truventic, LLC, United States; <sup>3</sup>iCRco, United States

Low cost, light-weight, low-power, large-format, room-temperature, mid-wave infrared (MWIR) detectors are needed for drones, unmanned aerial systems (UAS), unmanned aerial vehicles (UAV), and other reduced-scale aircraft. An opportunity, suggested by direct-read X-radiography systems, is the use of thin-film transistor (TFT) array as read-out integrated circuit (ROIC) for low-cost sensors deposited directly and unpatterned onto this ROIC. TFTs have already been thoroughly optimized for power, weight, large-format and cost by the flat panel display industry. We present experimental investigation of aqueous-spray-deposited, mid-wave-IR, metal-chalcogenide photoconductors and heterojunction photodiodes for this application. Measured responsivity, detectivity  $D^*$ , and photoresponse spectra are reported for ternary PbSSe photoconductors and PbS/CdS photodiodes.

#### 5:30 AM F.NM02.07.05

**Vertically Heterogeneous n-Doped CdO Films as a Platform for Infrared Nano-Photonics—Mode Coupling and Hyperbolicity** Joshua Nolen<sup>1</sup>, Angela Cleri<sup>2</sup>, Thomas Folland<sup>1</sup>, Evan Runnerstrom<sup>3,4</sup>, Kyle P. Kelley<sup>5,4</sup>, Mingze He<sup>1</sup>, Simone De Liberato<sup>6</sup>, Nader Engheta<sup>7</sup>, Jon-Paul Maria<sup>2</sup> and Joshua D. Caldwell<sup>1</sup>; <sup>1</sup>Vanderbilt University, United States; <sup>2</sup>The Pennsylvania State University, United States; <sup>3</sup>U.S. Army Research Office—Materials Science Division, United States; <sup>4</sup>North Carolina State University, United States; <sup>5</sup>Oak Ridge National Laboratory, United States; <sup>6</sup>University of Southampton, United Kingdom; <sup>7</sup>University of Pennsylvania, United States

Doped transparent conducting oxides (TCOs) have recently found utility as potential alternative plasmonic materials. One highly promising TCO which has been demonstrated to exhibit broad tunability while maintaining exceptionally low optical losses is highly-doped CdO. This is due to CdO possessing both a low effective mass (ranging from 0.12-0.26 in epitaxially-grown films with carrier densities ranging from  $10^{19}$ - $10^{20}$  cm<sup>-3</sup>) as well as electronic mobilities extending upwards to 500 cm<sup>2</sup>/V-s with carrier densities ranging from  $10^{19}$  to  $10^{20}$  cm<sup>-3</sup>. Unique to this material is a range of carrier densities where increasing values result in increasing mobilities. Due to the low optical losses and broadly tunable plasma wavelength, CdO has been shown to support, carrier tunable surface plasmon polaritons (SPP) and epsilon-near-zero (ENZ) modes throughout the mid-infrared (MIR). These ENZ modes are associated with extreme electric field confinement, enabling control over light-matter interactions such as resonant perfect absorption and strong nonlinear interactions. Here we show how vertically heterogeneous films of doped CdO can be leveraged to create different nanophotonic phenomena across the infrared. Careful control over the carrier density during film growth has opened the door to achieving multilayer homoepitaxial CdO films. Despite the homogeneity of the crystal structure, the elevated carrier density and carrier density dependent changes to Fermi energy and effective mass confine carriers to their constitutive layers. Owing to this material's low carrier diffusivity multilayer stacks composed of deeply subwavelength thickness CdO films, each supporting ENZ modes at different frequencies, exhibit multifrequency absorption/emission. Further, prior work has shown that epitaxially-grown bilayer stacks

of CdO, with bottom and top layers supporting SPP and ENZ modes respectively, exhibit strong coupling between the ENZ and SPP modes. The combined ENZ-SPP dispersion of these bilayer films displays a prominent anti-crossing with a separation that is dependent on both the spectral and spatial overlap of the modes. Here we have extended our focus to trilayer CdO films, where an unintentionally-doped ( $N_d \sim 1 \times 10^{19} \text{ cm}^{-3}$ , much less than  $N_d$  of the SPP or ENZ layers) CdO film is grown between the SPP and ENZ layers. The spacer layer thickness modifies the spatial overlap of the constituent electric fields as well as alters the effective index of the region above the SPP layer, decreasing the degree of spectral splitting and shifting the anti-crossing position to higher momentum. The strong carrier confinement in doped CdO also allows for the engineering of extreme anisotropy in multilayer CdO films. By growing CdO layers of subwavelength thickness and alternating carrier densities (low-doped acting as a dielectric layer, high-doped as a metallic layer) hyperbolic metamaterials can be realized in a fully plasmonic, homoepitaxial system. In these metamaterials, the sign of the in- and out-of-plane components of the dielectric function are opposite in sign. This leads to an open hyperbolic dispersion relation which allows for the propagation of high-momentum, and therefore highly-confined, optical modes. Through careful control over the carrier densities and thicknesses of the CdO layers, tunable hyperbolic resonances can be supported throughout the MIR, allowing for the potential realization of next generation emission devices and subwavelength imaging.

#### 5:40 AM F.NM02.07.06

**Ultra-Short-Period Undulators for the Next Generation X-Ray Free Electron Lasers** Derya Berkin Gurel<sup>1</sup>, Omer Polat<sup>1</sup>, Nilay Gunduz Akdogan<sup>2</sup> and Ozan Akdogan<sup>1</sup>; <sup>1</sup>Bahcesehir University, Turkey; <sup>2</sup>Piri Reis University, Turkey

There is a growing interest on the compact XFELs to be used in applications such as medical science (surgery, fat removal), material science and military. In order to build a compact XFEL, constructing an undulator with sub-millimeter period ( $\lambda_u$ ) is mandatory. Many problems arise due to miniaturization of undulators; such as keeping the magnetic field high while still having a considerable gap to minimize beam scraping. In this work, RADIA program has been employed for the modeling of sub millimeter period undulators ( $20 \mu\text{m} < \lambda_u < 400 \mu\text{m}$ ) with three different magnet configuration; namely Up-Down ( $\uparrow\downarrow\uparrow\downarrow\dots$ ), Halbach (Wiggler) ( $\uparrow\rightarrow\downarrow\leftarrow\uparrow\dots$ ) and Hybrid ( $\rightarrow\uparrow\leftarrow\downarrow\rightarrow\dots$ ). Effects of sub-millimeter undulator period and gap on the magnetic field pattern of the undulator have been discussed. This work was supported by TUBITAK project: 118F319

#### 5:50 AM F.NM02.07.08

**Super Mossian Nanophotonic Demonstrated with Iron Pyrite** Chloe F. Doiron and Gururaj Naik; Rice University, United States

All dielectric nanophotonics has opened new pathways for engineering optical metamaterials, enabling a wide range of optical devices including perfect reflectors, magnetic mirrors, and flat optics. One method to decrease the size of nanophotonic resonators and increase the quality factor of resonances is to use materials with larger refractive index. However, it is commonly stated that the bandgap and refractive index of semiconductors are related to a constant through the empirical rule  $n^4 \times E_g \approx 95 \text{ eV}$  referred to as the Moss rule. From this rule, it is expected that any increase in refractive index comes at the cost of decreased bandgap. Because of the corresponding increase in optical losses, this is detrimental to optical devices operating in the sub-bandgap region. While the constant of 95 eV works for a variety of materials, this constant only works for materials with similar band structures. Here, we experimentally demonstrate iron pyrite (FeS<sub>2</sub>) as a high index material platform for nanophotonics with refractive index greater than 4.5 in the mid-IR. This high refractive index is obtained with a bandgap of 0.95 eV, resulting in FeS<sub>2</sub> surpassing the common form of the Moss rule by over 40%, making iron pyrite a super Mossian optical material. Furthermore, we will present experimental results of an optical bound state in the continuum (BIC) in nanoscale FeS<sub>2</sub> resonators showing the potential for high index super Mossian materials in nanophotonics. Finally, we will conclude with a discussion on the electronic and optical properties to screen for to aid in the identification of additional super Mossian materials.

#### 6:00 AM F.NM02.07.09

**Optical Isolation in III-Nitride Photonics** Ganapathi Subramania<sup>1</sup>, Keshab Sapkota<sup>1</sup>, Nicholas Karl<sup>1</sup>, Adam Backer<sup>1</sup>, George Wang<sup>1</sup>, Igal Brener<sup>1</sup>, Zachary Meinelt<sup>2</sup> and Daniel Feezell<sup>2</sup>; <sup>1</sup>Sandia National Laboratories, United States; <sup>2</sup>The University of New Mexico, United States

III-Nitride based nanostructures can be designed to create photonic crystals or metamaterials that operate in the visible frequency regime. Nanophotonic devices that are important for many applications like solid-state lighting and quantum information science and flat optics can be enabled using such structures. A key issue in creating optical nanostructures in III-nitrides has been in creating optical isolation from the high refractive index GaN growth template due to a lack of compatible natural low index materials. In silicon photonics this is mitigated by using silicon-on-insulator substrate that provide a low

index silicon oxide cladding, while in III-V semiconductors such as GaAs this is achieved by oxidation of high Al content AlGaAs buffer layer. While there are some examples in III-nitrides such as observation of low threshold lasing in nanowire array geometry photonic crystals [1], achieving simple optical isolation for membrane PhC, metasurfaces and VCSEL structure has been a challenge. A recent work [2] has demonstrated electrochemically etched nanoporous layers can provide lower index isolation. Here we will discuss achieving optical isolation in III-nitride nanophotonic devices using electrochemical/ photo-electrochemical [3] etching techniques. We will describe the fabrication of GaN nanowire array with optical isolation and present optical response to demonstrate the effectiveness of this approach.

Sandia National Laboratories is managed and operated by NTESS under DOE NNSA contract DE-NA0003525..

[1] Wright, J. B.; Liu, S.; Wang, G. T.; Li, Q.; Benz, A.; Koleske, D. D.; Lu, P.; Xu, H.; Lester, L.; Luk, T. S.; Brener, I.; Subramania, G., Multi-Colour Nanowire Photonic Crystal Laser Pixels. *Sci. Rep.* **2013**, 3, 2982.

[2] Mishkat-Ul-Masabih, S.; Luk, T. S.; Rishinaramangalam, A.; Monavarian, M.; Nami, M.; Feezell, D., Nanoporous distributed Bragg reflectors on free-standing nonpolar m-plane GaN. *Applied Physics Letters* **2018**, 112 (4), 041109.

[3] Anderson, P. D.; Fischer, A. J.; Koleske, D. D.; Gunning, B. P.; Subramania, G., III-nitride photonic crystal emitters by selective photoelectrochemical etching of heterogeneous quantum well structures. *Optical Materials Express* **2018**, 8 (11), 3543-3550.

#### 6:10 AM F.NM02.07.10

**Electromechanically Tunable Metaphotonic Color-Imaging Devices** Min Ho Lee<sup>1</sup>, Sung-Min Lee<sup>2</sup> and Kyung Cheol Choi<sup>1</sup>; <sup>1</sup>Korea Advanced Institute of Science and Technology, Korea (the Republic of); <sup>2</sup>Kookmin university, Korea (the Republic of)

Metaphotonic materials and systems can create unusual optical properties through the interaction between light and artificial nanostructures. Such unusual properties can allow color imaging devices over the diffraction limit level (~100,000 dpi) that cannot be simply implemented with conventional imaging technology. Although these ultra-high resolution imaging technologies have shown substantial potential for applications that handle static images, such as color filters and printing, the feasible options for dynamic imaging technology using passive metaphotonic elements have not been fully demonstrated, impeding their application in active display devices.

Motivated by these issues, we introduce electrically controllable active color imaging metaphotonic devices consisting of metal/insulator/metal nanodisk stacks; the resonance modes of these stacks can be reversibly changed by structure deformation. To achieve the function of electrically driven mechanical deformation, disk elements of inconsistent size are designed, and electric potential is applied between the upper and lower metal disks, where the large upper metal disk can be bent by columbic force of induced reciprocal charges. The tunable gap between the stacked metal disks provokes resonance mode change, thereby resulting in variation of the transmission/reflection spectra. The fabricated metaphotonic nanodisk stacks exhibited a reasonable shift in reflectance spectra when sufficient electrical voltage was applied, which demonstrated the feasibility of sub-wavelength imaging technology for application in display devices.

SESSION F.NM02.08: Poster Session: Advanced Linear/Nonlinear, Tunable and Quantum Materials for Metasurfaces, Metamaterials and Plasmonics

On Demand Abstracts Available for Viewing Starting Saturday Morning, November 21, 2020

5:00 AM - 8:00 AM

F-NM02

#### F.NM02.08.01

**Optical and Electrical Properties of Organic Semiconductor Thin Films on Aperiodic Plasmonic Metasurfaces** Zhongkai Cheng, Nasir Javed and Deirdre O'Carroll; Rutgers, The State University of New Jersey, United States

Metal electrodes are playing an increasingly important role in controlling photon absorption and in promoting optimal light management in thin-film semiconductor devices. For organic optoelectronics devices, it is challenging to control the surface of the metal electrode to promote good light management because metal electrode deposition is used as the last step in the conventional device fabrication approach. However, an inverted fabrication approach that builds the device on top of a metal electrode, makes it possible to control the morphology of the metal surface, independently of the organic semiconductor active layer, to achieve a variety of photonic and plasmonic behavior useful for optoelectronic devices. Silver (Ag) is one of

the most suitable metals for fabrication of nanostructured electrodes with plasmonic behavior (i.e., plasmonic electrodes) because of its low parasitic absorption loss and high reflectivity.

In this work, we study the physical and optical characteristics of Ag nanoparticle (AgNP) aperiodic plasmonic metasurfaces. Then, we investigate the photonic and electrical behavior of the AgNP plasmonic metasurfaces when interfaced with thin films of the organic semiconducting polymer, poly(9,9-dioctylfluorene-alt-benzothiadiazole) (F8BT), using the inverted fabrication approach. The luminescence quantum yield of F8BT thin films increases from 29% on planar silver up to 66% on AgNP metasurfaces due to the Purcell Effect and the improved extraction of emission coupled to surface plasmon polariton (SPP) modes. In particular, we show that plasmonic enhancement can overcome ohmic losses associated with metals and metal-induced exciton quenching. According to the current-voltage characteristics of F8BT hole-only devices with and without plasmonic metasurfaces, we conclude that AgNP plasmonic metasurfaces have comparable electrical behavior to planar metal electrodes while having superior light management capability.

#### **F.NM02.08.05**

**All Plasmonic Nanophotonic Device Displaying Passive PT-Symmetry** Frank Yang, Chloe F. Doiron and Gururaj Naik; Rice University, United States

In quantum mechanics, Hamiltonians exhibiting real eigenvalues are often Hermitian. However, non-Hermitian systems that respect parity-time (PT) symmetry can also possess real eigenvalues. PT-symmetric Hamiltonians display unconventional behavior, such as the coalescence of eigenmodes at exceptional points. This unconventional behavior allows optical devices to take advantage of symmetry, topology, and phase, enabling new functionalities in ultra-sensitive sensing and lasing. There are two approaches to satisfying PT-symmetry in optics: active and passive. Active PT-symmetry requires a system with balanced optical gain and loss. Because of the difficulty of adding gain in nanophotonic systems, passive PT-symmetry is an ideal method for demonstrating PT-symmetry at the nanoscale. In comparison, passive PT-symmetry requires both nearly zero and large optical losses. While plasmonics has enabled many new optical devices, there have been no demonstrations of PT-symmetry in all plasmonic systems due to the large optical losses of plasmonic materials, which limit loss asymmetry. Here we will present an experimental demonstration of an all plasmonic system demonstrating passive PT-symmetry. To achieve this, we engineer a coupled plasmonic antenna system exhibiting large loss asymmetry. The system undergoes a PT phase transition as the coupling, or separation, between the antennas is varied. At high coupling, the system is in a PT-symmetric phase with two resonant absorption peaks. With decreased coupling, the peaks coalesce at the exceptional point. Further decreasing the coupling results in an optical phase transition to a broken PT-symmetric phase with a single resonant absorption peak. Using our nanophotonic PT-symmetric system, we will conclude with a discussion on guidelines for implementing PT-symmetry in nanophotonic devices.

#### **F.NM02.08.07**

**Unity Order Index Tunability at Room Temperature in 1T-TaS<sub>2</sub>—A Strongly Correlated Material** Weijian Li, Ming Yi, Kevin Kelly, Gururaj Naik and Frank Yang; Rice University, United States

Strongly correlated materials could greatly respond to a stimulus due to their collective behavior. Thus, strongly correlated materials are well studied in the past for their tunable properties, especially electrical and thermal. However, their optical properties remain to be explored. In this work, we study the optical properties of 1T-TaS<sub>2</sub>, a quasi-2D material supporting charge density waves (CDW). 1T-TaS<sub>2</sub> is the only material to exhibit a nearly commensurate CDW phase at room temperature and its electrical and thermal properties are shown to exhibit a large change with temperature, DC and AC biases, pressure, and light. Here, we study the optical properties of 1T-TaS<sub>2</sub> under DC and AC biases, different intensities of optical illumination, and at different temperatures. Under all these conditions, we observe a unity-order change in the refractive index of thin films of 1T-TaS<sub>2</sub>. We hypothesize that the stacking of CDWs in this material changes with stimulus resulting in its optical constants to change. ARPES and STM measurements are underway to verify the hypothesis. Our discovery of the large tunability of optical constants of 1T-TaS<sub>2</sub> presents opportunities in studying light-matter interaction in strongly correlated materials and its application to nanophotonic devices.

#### **F.NM02.08.08**

**A Novel Approach to Tailor the Band Structure of Metal-Organic Framework Nanocrystals in One-Dimensional Periodic Array for Light Induced Energy Transfer Applications** Sujoy Saha, Joseph Sarobin and Hemali Rathnayake; JSNN, University of North Carolina, United States

The study of band structures of different types of Metal-Organic Frameworks (MOFs) is indispensable for the advancement

of nanoelectronics. We designed a novel approach to predict and tailor the band structure of MOFs nanocrystals in a one-dimensional periodic array through the variation of structural and materials parameters. From the Bloch condition of the Schrodinger equation, we could predict the amplitude of potentials,  $\phi$  and  $\psi$  for periodically arranged MOFs only in one-dimension using experimental values of dielectric constant, absorption and emission peaks of MOFs. Predicting energy band structures of the one-dimensional array of an isorecticular MOF, IRMOF-8A using a theoretical method combined with experimental values of dielectric constants and amplitude of potentials provide insight into electronic band energy to tailor optoelectronic properties of MOFs and understanding their energy transfer capabilities with respect to the different ligand type. The dielectric constants of three different IRMOFs synthesized from the same metal precursor ( $Zn^{2+}$ ) and three different organic ligands with varying conjugation length were predicted from this novel approach. Band gap depends on the amplitude of potentials, which is a function of the conjugation length of the ligand and its dielectric constant. Thus, the effective conjugation length of the ligand in MOFs have a significant impact on the jumps between two allowed bands in energy band structures of the 1-D array of MOFs. This design method can widely applicable for predicting band energy for any designed MOFs and serves as a versatile tool to tailor and predict the electronic properties of MOFs with different ligand units.

#### **F.NM02.08.09**

**Hybrid Plasmonic Nanostructures for Biomolecular Sensing** [Debadrita Paria](#)<sup>1</sup>, Chi Zhang<sup>1</sup>, Steve Semancik<sup>2</sup> and Ishan Barman<sup>1</sup>; <sup>1</sup>Johns Hopkins University, United States; <sup>2</sup>National Institute of Standards and Technology, United States

Metal nanostructures are well known for various ultra-sensitive spectroscopic applications because of their ability to concentrate and enhance the local electromagnetic field due to a phenomenon called localized surface plasmon resonance (LSPR). The intense light localization, also known as "hotspot", becomes more pronounced near a narrow plasmonic gap. In this work, we report tailored hybrid metal nanostructures for LSPR sensing and surface enhanced Raman spectroscopy (SERS) of serum albumin. Using a combination of physical vapor deposition and thermal annealing, different hybrid metal nanostructure configurations have been fabricated, which create well defined arrangements of hotspots. The hybrid metal nanostructures have multiple resonance peaks, which demonstrate the capability of the identification of ultra-low differences in refractive index (0.001) when combined with machine learning algorithms. A detailed FEA simulation of these plasmonic nanostructures provides a quantitative estimate and the spatial distribution of hotspot closely match our experimental observations. The simulations also help us understand the various interactions between the nanostructures via their near field. Finally, these structures also show potential for sensitive label-free SERS detection. Overall, our study explores an integrated multimodal biosensing platform featuring LSPR combined with machine learning and surface enhanced Raman spectroscopy (SERS) for quantitative determination of concentration and molecular fingerprinting.

#### **F.NM02.08.11**

**Optical Properties of Random Nanoparticle Films Made of Spheres with an Overlapping Electric and Magnetic Dipole Response** [Parker Wray](#) and Harry Atwater; California Institute of Technology, United States

We investigate theoretically the unidirectional optical scattering properties of random monolayer particle films composed of dielectric particles that support overlapping electric and magnetic dipoles. The particle films exhibit dramatic reflection and transmission behavior which are manifest in the forward-to-backward scattering ratio of the nanoparticle building block. We also show that these films do not exhibit polarization dependent scattering and lack a traditional Brewster's angle. Our theoretical analysis uses a generalized version of Mie theory, which accounts for particle coupling effects, and was validated by full-wave simulations. For fill fractions up to 40% the average scattering response of an embedded particle is shown to accurately predict the behavior of the random film, and the overlap of the electric and magnetic dipole resonances are found to be robust to effects of particle coupling. Continuing research will extend this analysis to multi-layer particle films. This work indicates potential for the design of optical filters and anti-reflective coatings using single materials, without the need for self-assembly.

#### **F.NM02.08.12**

**Imaging Single Particle Enhanced Upconversion Luminescence from  $NaYF_4:Yb^{3+},Tm^{3+}$  Nanoparticles on Plasmonic Substrates** [Anahita Haghizadeh](#)<sup>1</sup>, Aravind Baride<sup>2</sup>, Stanley May<sup>2</sup> and Steve Smith<sup>1</sup>; <sup>1</sup>South Dakota School of Mines and Technology, United States; <sup>2</sup>University of South Dakota, United States

We use single particle spectroscopic imaging and statistical analysis to assess the plasmonic enhancement of NIR-to-visible upconversion luminescence (UCL) from single  $\gamma$ - $NaYF_4:Yb^{3+}:Tm^{3+}$  upconverting nanoparticles (UCNPs) supported on substrates consisting of random arrangements of Ag nanowires (NW) and Au nano-cavity arrays. We measure both apparent luminescence enhancement, which is power dependent due to the nonlinear kinetics of energy transfer upconversion (ETU),

and the excitation enhancement, defined as the ratio of the excitation intensity needed to produce a given UCL emission, divided by the equivalent power needed to produce the same emission on the plasmonic substrate<sup>1</sup>. By examining the effects at the single particle level, and accumulating a statistical sampling of single particle emitters, both on and off the plasmonic substrates studied, we can eliminate the effects of particle fluctuations on the apparent UCL emission enhancement and map out the statistical distribution of excitation and luminescence enhancement on the plasmonic substrates. The distributions obtained are reproduced by Finite Difference Time Domain (FDTD) calculations of the fields near the plasmonic substrate, assuming the variations are due to variations in UCNPs coupling to the plasmonic substrate based on an exponential decay with distance. We compare these results to statistical analysis of ensemble measurements made of Er<sup>3+</sup> doped UCNPs supported on random Ag NW substrates<sup>2</sup> and both wide field and confocal spectroscopic imaging of single UCNPs on and off the plasmonic substrates. (1) Fisher, J.; Zhao, B.; Lin, C.; Berry, M. T.; May, P. S.; Smith, S. Spectroscopic Imaging and Power Dependence of NIR to Visible Upconversion Luminescence from NaYF<sub>4</sub>:Yb<sup>3+</sup>,Er<sup>3+</sup> Nanoparticles on Nano-Cavity Arrays. *J. Phys. Chem. C* 2015, 119, 24976–24982. (2) Hor, A.; Luu, Q.; May, P.; Berry, M.; Smith, S. Non-Linear Density Dependent Upconversion Luminescence Enhancement of ?-NaYF<sub>4</sub>: Yb<sup>3+</sup> : Er<sup>3+</sup> Nanoparticles on Random Ag Nanowire Aggregates. *MRS Adv.* 2016, 1, 2677–2682.

#### F.NM02.08.14

##### **Full Factorial Experimental Optimization of Gold Nanostructures Fabrication by Solid-State Dewetting for**

**SERS** Siarhei Zavatski<sup>1,2</sup>, Hanna V. Bandarenka<sup>3,2</sup> and Olivier J. Martin<sup>1</sup>; <sup>1</sup>Ecole Polytechnique Federale de Lausanne, Switzerland; <sup>2</sup>Belarusian State University of Informatics and Radioelectronics, Belarus; <sup>3</sup>Arizona State University, United States

The optimization of nanostructures for a specific application is a rather complex task, often akin to shooting in the dark with the hope of hitting the right target, viz. the best performing nanostructure. This difficulty stems from the usually large number of experimental parameters that can be changed in a nanotechnology process. This is the case for example in the fabrication of plasmonic nanostructures for surface enhanced Raman scattering (SERS): the choice of metal, its thickness, the shape of the nanostructures as well as their distribution on the substrate are all parameters that determine the overall Raman enhancement. Even for a relatively simple design, exploring all possible combinations of parameters is a prohibitive task both in terms of nanofabrication time and costs. In that contribution, we focus on the large scale fabrication of plasmonic nanostructures using solid-state dewetting and demonstrate how a full factorial design technique can efficiently optimize the process. In that approach, a target response for optimization and two specific values for the  $n$  fabrication parameters are first chosen, leading to an initial set of  $2n$  experiments [1]. Here, as experimental parameters we consider the gold film thickness, the annealing temperature and time, and the heating rate; with the objective of maximizing the intensity of the SERS signal, specifically the 1363 cm<sup>-1</sup> vibrational band of Rhodamine 6G. The corresponding 16 experiments provide a model of the dependency of the Raman enhancement on the four experimental parameters considered here. In the classical optimization procedure by full factorial design, this dependency is chosen linear. The set of experimental parameters that is obtained in this first fit of linear model does not necessarily lead to the strongest Raman enhancement and another set of experiments may be required. However, the full factorial approach also provides the direction in the parameter space in which one needs to move these parameters to reach a better solution. After such a solution is found, the linear model may need to be refined using second order functions to clarify the optimum region. This is usually done with the central composite experimental design [2]. The optimization process for the fabricated samples is documented in detail by studying the morphology and optical properties of each sample by scanning electron microscopy and UV-Vis spectroscopy. The gold nanostructures we fabricated this way have typical dimensions in the 50 nm range, which is in good agreement with data reported in the literature [3]. Furthermore, the optimized plasmonic substrate can be used to identify non-resonant bioorganic macromolecules such as bovine serum albumin. This work reveals an effective approach to optimize nanofabrication processes for large-scale and cost-effective production of uniform and highly sensitive SERS substrates. [1] Leardi, R. *Analytica chimica acta* 2009, 652(1-2), 161-172. [2] Box, G. E., & Wilson, K. B. *J. R. Stat. Soc. Series B Stat. Methodol.* 1951, 13(1), 1-38. [3] Krug et al. *J. Am. Chem. Soc.* 1999, 121, 9208-14.

#### F.NM02.08.15

**Planar Nanophotonic Structures for Intensity-Based Readout Refractive Index Sensing of Dissolved Methane** Morgan Blevins<sup>1,2,3</sup>, Anna Michel<sup>1</sup> and Svetlana Boriskina<sup>2</sup>; <sup>1</sup>Woods Hole Oceanographic Institute, United States; <sup>2</sup>Massachusetts Institute of Technology, United States; <sup>3</sup>MIT-WHOI Joint Program, United States

As global temperatures rise, permafrost in the Arctic is thawing, stimulating increased release of methane, a key greenhouse gas. Accurate measurements of the dissolved methane concentration in seawater and freshwater are important for finding and quantifying the release of natural seabed and Arctic methane seeps to better understand how these sources are contributing to increasing global methane levels. In surface waters, the methane concentration can be as low as 3-10 nM (atmospheric



equilibrium) while concentrations as high as 800-1000 nM are found in methane saturated deep seawater and near thawing permafrost. To measure the concentration of dissolved methane, changes in the refractive index (RI) of polymers functionalized to selectively trap methane molecules can be measured via an optical readout mechanism. However, the range of the RI change is very narrow, from 1.41198 to 1.41358 for atmospheric to saturated methane concentration levels ranging from 0 nM to 300 nM, which requires the use of highly sensitive optical sensors. This paper analyzes and compares three simple and low-cost planar nanophotonic and plasmonic structures as optical transducers for measuring refractive index change of polydimethylsiloxane (PDMS) polymer films doped with cryptophane-A molecules, which selectively trap methane. These structures include (i) a Bragg reflector with a defect layer, (ii) a hybrid plasmonic-photonic multi-layer stack that supports a Tamm plasmon mode, and (iii) a hybrid plasmonic-photonic stack that acts as a magnetic mirror, and can be used in a simple intensity-based measurement scheme with low cost light sources and detectors. Through numerical simulations, we evaluate the sensitivity of the proposed structures in both the angular-resonant-mode shift readout mode and in the reflectance intensity readout mode and compare them to the standard surface-plasmon-polariton-mode Spreeta sensor as a reference. Our results show that the planar Bragg reflector with a defect layer exhibits the largest intensity response and is the most promising design for a low cost and robust photonic chip for dissolved methane sensing. A practical implementation of this chip with a simple intensity-based measurement scheme is proposed. Integration of this planar structure into a small, portable, and low-cost dissolved methane sensor offers a way to make climate monitoring more widespread and accessible to researchers. The structures evaluated here all show promise for other chemical and biological sensing applications that require monitoring very small RI changes. Significantly, each structure has been designed to support resonant modes in both s and p polarizations, which allows enhanced sensitivity by calculating the ratio of the spectral responses of orthogonal polarizations, similar to the complex reflectance ratio measured with ellipsometry. Importantly, the response in both polarizations only needs to be monitored in the reflectance intensity readout mode, avoiding the use of expensive and large ellipsometry equipment.

#### **F.NM02.08.16**

**Identifying Plasmon-Like Excited States in Bare and Ligand-Protected Metal Nanoclusters** Rebecca Gieseking; Brandeis University, United States

Noble metal nanoclusters containing dozens to hundreds of metal atoms are of great interest because of their unique optical properties. Classical electrodynamics fails to describe the optical properties of clusters smaller than a few nm, so quantum mechanical models are needed to describe these clusters. However, it is challenging to identify which features of the computed excited states indicate plasmon-like character, particularly in a way that is generalizable to the ligand-protected clusters that are commonly studied in experiments. We present an analytical method to identify plasmon-like excited states using three quantifiable indicators that must be considered in combination: (1) large superatomic character, (2) large collectivity among single-particle excitations, and (3) large additivity of contributions of these single-particle excitations to the transition dipole moment. Visualizing these three indicators on a single plot enables rapid classification of hundreds of excited states into plasmon-like, collective, single-particle, or interband categories, or as intermediate between these categories. This method is used to identify excited states with plasmon-like character in both bare and ligand-protected Ag clusters at the TDDFT level. Using these three nearly orthogonal indicators in combination provides more information than any one criterion can provide.

#### **F.NM02.08.18**

**Stable Dispersion of Titanium Nitride Nanoparticles** Idalis Hernandez, Eric Bartlett, Sanchari Chowdhury and Michaelann Tartis; New Mexico Tech, United States

Alternative plasmonic titanium nitride nanoparticles (TiN) are attractive photothermal agents because of their ability to strongly absorb a broad spectrum of light ranging from visible to near-infrared and convert that into heat. Additional advantages of low cost and stability of these refractory nanomaterials make them attractive for different applications ranging from photothermal cancer therapy to solar energy mediated catalytic reactions. In this work, we are developing a method to obtain a stable and monodispersed TiN nanoparticles solutions, which is an important prerequisite for most of their applications. Moreover, our goal is to optimize a solution based coating method to obtain a uniform well dispersed thin film of TiN nanoparticles on the substrate, which will be useful for their application in the device. However, preventing aggregation of TiN nanoparticles in a solvent has been a challenge. We have optimized protocols based on ultra-probe sonication and centrifugation, to obtain relatively monodisperse and stable TiN nanoparticles in an aqueous solution. We have applied our method to commercially available polydisperse TiN nanoparticles of average size 80nm and 20 nm. Using the optimized method we were able to decrease the polydispersity index (PDI), the measure of the distribution of nanoparticles in a solution, from 0.351 to 0.18 indicating a significantly more monodispersed solution. Moreover, we used a sol-gel based method for incorporating nanoparticles in transparent silica gels. There was no aggregation of the TiN

nanoparticles observed during the sol-gel transition. UV-Vis spectroscopy and dynamic light scattering method confirm that incorporating TiN nanoparticles in silica gel preserved both of their optical properties and the dispersibility as in the original solution. The nanoparticles stay stable in the solution for several days. A biocompatible silica coating on TiN nanoparticles can be useful for drug delivery and photothermal therapy. In summary, we are developing a simple commercially viable method to efficiently disperse and stabilize titanium nanoparticles in solution and subsequently coating them on the substrate which can easily be applied for large scale applications.

#### **F.NM02.08.19**

**Confined Nucleation of ErAs NPs in Er:InAs QDs to Fabricate Nanoparticle Quantum Dot Hybrids** Kurt Eyink, Yuanchang Zhang, Albert M. Hilton and Krishnamurthy Mahalingam; Air Force Research Laboratory, United States

Directed assembly has been the subject of extensive research over the years due to the desire to grow structures at specific locations. This is accomplished by increasing the probability of nucleation at the desired location. Mechanisms such as reduction of the diffusion of species, reduction of the strain to lower the bulk free energy to reduce the critical nuclei size, or a lowering of the surface energy which also reduces the critical nuclei size have previously been used. In all these cases, nucleation of the desired phase occurs directly on the substrate. Here we propose and demonstrate a scheme for directed assembly in which we confined the nucleation of the desired material to the region of a nanostructure formed on the surface. We accomplish this through the use of a dilute alloy containing the desired material and subsequent removal of the major constituent of the alloy inducing nucleation at some point after the dilute species exceeds its solubility limit. In particular, we use this approach to control the nucleation of ErAs nanoparticles from Er:InAs quantum dots by evaporation of InAs. We studied ErAs NP formation from InAs QD nominally doped to concentration of 1.25% and 2.5% on GaAs (001). The Er:InAs quantum dots were grown using normal conditions for the growth of undoped InAs and produced similar quantum dot densities (near 100/square micron). We explain these observed results in terms of normal nucleation and growth given the mesoscopic concentration of Er atoms expected in the InAs QD. A comparison of the undoped and Er-doped InAs quantum dots before and after InAs evaporation show the number of the ErAs nanoparticles is less than the original quantum dot density showing nanoparticles do not form in every quantum dot and suggests a critical number of Er atoms needed for nucleation. We have used our confined nucleation process in conjunction with normal direct assembly processes for InAs QDs to produce hybrid structures composed of InAs QDs and ErAs NP. We have formed vertically stacked Er:InAs QD over undoped InAs QDs to form ErAs NP over InAs QDs. We have formed Er:InAs quantum dots formed in ErAs divots to form ErAs nanoparticle clusters and have used Er:InAs to place ErAs in patterned surface. Transmission electron microscopy of these structures show that at times multiple nucleation sites are possible in the structure and suggest the potential of forming rich hybrid structures using this approach.

#### **F.NM02.08.21**

**Optical Parameters of Bioinspired Sub-Monolayer Nanoparticle Arrays** Sean R. Dinneen<sup>1</sup>, Richard M. Osgood<sup>1</sup>, Zhuangsheng Lin<sup>2</sup>, Camille Martin<sup>2</sup>, Michael Okamoto<sup>1</sup>, Ihsan Uluturk<sup>1</sup> and Leila Deravi<sup>2</sup>; <sup>1</sup>Combat Capabilities Development Command Soldier Center, United States; <sup>2</sup>Northeastern University, United States

Cephalopods have the ability to take advantage of pigmented and structural coloration when camouflaging, signaling, or otherwise communicating through their adaptive coloration. The chromatophore, which is the actuating organ responsible for pigmented color within cephalopods, is populated with 500-600 nm diameter particles composed of pigment and protein called pigment granules. The pigment, identified as xanthommatin, has been found to have a uniquely high refractive index and contributes highly to the scattering of light with broadband optical properties. Developing metamaterials out of synthetic pigment granules, where the particle periodicity is smaller than the wavelengths of light with which they interact, was the next logical choice for us to not only further our understanding of the complex photonic system of cephalopods, but to explore its application in adaptable optical systems and possibly chemical sensing.

In this work, we aim to leverage our knowledge of biomaterials (namely the biopigment xanthommatin) to generate sub-monolayers of synthetically made pigment granules. Xanthommatin is encapsulated within polystyrene-co-maleic anhydride (PSMA) nanoparticles with good physical retention while maintaining its coloration. Sub-monolayer arrays are prepared via Chumanov-style roll-coating on substrates within a vial containing the solution of particles, and are physically characterized by scanning electron microscopy. We then show the arrays' optical properties measured by integrating sphere spectrophotometry and broadband multi-angle ellipsometry. Depending on the spacings of the particles, the arrays will resonate at certain wavelengths within the visible. Our updated models, taking into account the particle's refractive index and contribution from the pigment, will show a dependence of spacing and material on wavelength resonance. With the pigment as a functional feature within the particles, we explore the retained chemical properties (such as absorption changes with pH) with the possible inclusion of chemical sensing.

### **F.NM02.08.22**

**Spatial Inhomogeneity of Optical Binding in Many-Body Systems** Fei Han; Clarkson University, United States

Optical matter can be formed by electrodynamic interactions of metal nanoparticles in an optical field. This light-mediated self-organization of nanoparticles offers a route to study mesoscale electrodynamic interactions in many-body systems. By controlling the intensity, phase, and polarization of light, the optical field can be tailored to assemble stable optical matter with up to 101 nanoparticles. Here we report that the spatial inhomogeneity of circularly polarized optical binding in a many-particle system. The spatial stability of self-organized nanoparticles is strongly influenced by the laser intensity and polarization state. In particular, the nanoparticles in the central area of an optical matter array are more stable than those on the edge. Moreover, larger arrays are self-protected from fluctuation-induced instability by incorporation more nanoparticle constituents. This study provides important information about the spatial inhomogeneity of optical binding interactions in mesoscale nanoparticle arrays.

SESSION F.LP06.03: Live Poster Session: Nanomaterials and Quantum Materials (F.NM01, F.NM02, F.NM05 and F.NM06)

Session Chairs: Kasra Sardashti and Javad Shabani

Friday Morning, December 4, 2020

11:30 AM - 1:30 PM

F.NM01

### **F.NM01.10.01**

**A General Phase Function of Micro/Nanoparticle Composites** Junxin Wang, Annica Nilsson and Gunnar Niklasson; Uppsala University, Sweden

Light scattering from particles show unique angular scattering patterns, which are strongly dependent on the particle size to incident wavelength ratio and the refractive index contrast between host medium and the particles. Multiple scattering becomes important when the particle concentration increases, which complicates the angular scattering distributions. In many cases, empirical phase functions have to be applied. A novel empirical phase function was introduced to describe the angle-dependent distribution of scattered light from a collection of micro/nanoparticles inside a thin layer. Angular dependence of light scattering from a polymer host containing sub-micron dielectric and metallic particles was measured. The method gives an excellent approximation to the angular effects of multiple scattering arising from aggregation, non-spherical shape and surface roughness. In addition, it is also a good approximation in the single scattering regime, since it closely reproduces scattering phase functions of particles in the Rayleigh, Mie and geometrical optics regimes. The feasibility of our approach was demonstrated by its ability to fit experimental data on the forward and backward scattering profiles of plasmonic and dielectric submicron particle composite layers. The robust and wide applicability of our method is expected to attract a board interest from researchers in physics and materials science.

### **F.NM01.10.02**

**Arylazopyrazole-Fused PDMS Composites as Solid-State Photo-Switchable Materials** Ikemefuna Uba, Demetris Geddis, Kesete Ghebreyessus and Uwe Hommerich; Hampton University, United States

Arylazopyrazoles (AAP) show significant potential as a new family of molecular photoswitches owing to their efficient reversible trans-to-cis photoisomerization behavior and the high thermal stability of their metastable cis-isomer. Herein, we report on the design and synthesis of new arylazopyrazole based molecular switches with different spacer length and functional (OH, COOH) groups. The new AAPs were used for the fabrication of solid-state photoswitchable polydimethylsiloxane (PDMS) based composite films. The thin films were prepared by using PDMS as a polymer matrix and different concentrations of AAPs as chromophores at room temperature *via* spin-coating. The photoswitching behavior of the PDMS-AAP blend films and the neat AAP samples induced by irradiation with specific wavelength of light were investigated. We found that the as prepared PDMS-AAP blend films showed rapid and near-quantitative reversible trans-to-cis isomerization rates upon alternating irradiation with UV ( $\lambda = 365$  nm) and green ( $\lambda = 525$  nm) light which is comparable to the isomerization behavior of the neat AAP chromophores in solution. This indicates that the excellent photoswitching properties of AAPs are preserved in the PDMS-AAP composite films. Additionally, the as prepared PDMS-AAP films in the cis-form possess outstanding thermal stability and long-term optical stability. The results also show that the optical properties

of the PDMS-AAP composite films can be tuned by using different ratios of the AAP chromophores and exposure to UV irradiation. This methodology provides a new approach for exploring the fabrication of polymers with solid-state photoswitching functionality. The effect of concentration of the AAPs on the reversible *trans*-to-*cis* isomerization processes of the PDMS-AAP composite films will be discussed in this presentation.

#### F.NM01.10.09

**Late News: Fabrication of a Fine-Pattern Flexible Nanowire Photodetector by Shadow Mask** Mustafa A. Yildirim and Kasif Teker; Marmara University, Turkey

Recently, ultraviolet photodetectors (UVPDs) have been used on large scale applications such as environmental monitoring, flame detection, space communication, biomedical applications, pharmaceutical, and chemical analysis. Besides, advances in internet technologies such as the internet of things (IoT) endorse the integration of sensors more rapidly in every aspect of our lives. This trend demands the fabrication of smaller, lighter, less complicated, and low power devices. Therefore, designing low cost, self-powered, highly sensitive, flexible UVPD nanodevices are becoming a hot research area for near future optoelectronics. Silicon carbide (SiC), a wide bandgap semiconductor, is an excellent contender to fulfill those expectations. In addition to having characteristics of one-dimensional nanostructure such as high surface to volume ratio, high crystalline quality, SiC nanowires also possess superior material attributes like high breakdown voltage, high thermal conductivity, high drift velocity, excellent chemical and physical stability. In this study, we propose a very cost-effective, flexible, self-powered single SiC nanowire ultraviolet photodetector (SiCNW-UVPD) fabricated on a polyvinylchloride (PVC) substrate.

The self-powered flexible SiCNW-UVPD was fabricated via a commercially available transmission electron microscopy (TEM) grid (physical mask) and a sputter coater system. Gold (Au) electrodes of 110  $\mu\text{m}$  x 110  $\mu\text{m}$  and a gap of 4  $\mu\text{m}$  were successfully achieved without the use of complicated and expensive methods like photolithography. Two-probe photocurrent-time (I-t) and I-V measurements were performed to reveal photoresponse characteristics such as the photo-to-dark current ratio (PDCR), sensitivity, and responsivity under 254 nm wavelength UV light at 0 V bias. A shallow dark current around 0.087 pA and a good PDCR value of 18 are obtained. Moreover, sensitivity and responsivity values are calculated as 1756 and 170 mA/W, respectively. In addition, the specific detectivity calculations, the effect of bias, and vigorous bending test results are discussed as well. Our work provides the following unique advantages: (i) to the best of our knowledge, the first demonstration of a single SiC nanowire PD on a flexible substrate with great performance, (ii) a very cost-effective fabrication method and readily applicable to any substrate, (iii) exhibiting high sensitivity and responsivity values under UV light at 0 V bias. Therefore, our SiCNW-UVPD device presents an opportunity for low-cost, easy to fabricate, self-powered photodetectors for upcoming future technologies such as wearable sensors, electronic skins, and the internet of things.

#### F.NM01.10.10

**Late News: Combined, Localized Plasmonic Heating and Temperature Measurement in Nanocomposite Hydrogels** Wei Yu, Olivier Deschaume, Stijn Jookan, Pengfei Zhang, Jolan Wellens, Fanglei Guo, Christ Glorieux and Carmen Bartic; KU Leuven, Belgium

As scaffold materials for tissue engineering applications, hydrogels can mimic many important functions of extracellular matrices found in living tissues. Local temperature gradients can greatly impact the bioactivity of the matrix and cellular processes such as adhesion, migration and differentiation [1,2], while the knowledge of local temperature is essential understanding and modulating the cell properties and their responses. Various methods have been developed and applied for thermal measurements at the nano- and micro-scales, relevant to living tissues, such as infrared thermography [3], micro-thermocouples [4], AFM with thermocouple [5] and fluorescence-based thermography [6]. However, only a limited number of successful applications have been reported regarding three-dimensional localized temperature measurements as the first three methods can only be applied in two-dimensional cases [3-5]. In this contribution, we report a versatile platform to realize localized, simultaneous heating and temperature readout in both two and three dimensions. Localized heating was implemented in hydrogels by functionalizing them with gold nanorods (GNR) with high absorption around 785 nm, while the local temperature is reported by the incorporated Rhodamine B (RhB)-loaded silica particles or quantum dots. For these thermal nano-probe, the fluorescence intensity decreases when temperature increases. In combination with the nanomaterials, a versatile optical stimulation and readout platform was developed. We demonstrate that plasmonic NIR heating could lead to localized, up to 10 degrees temperature changes in hydrogel-based cellular matrices that can be monitored in situ by fluorescent nanoprob, both in 2D and 3D.

**Funding:** This research was funded by the KU Leuven C1 projects, grant numbers C14/16/063 OPTIPROBE, C14/18/061 and the FWO research grant, grant number G0947.17N.

#### References:

- [1] F. Rico et. al Biophys. J., 2010, 99, 1387-1396
- [2] A.A. Khalili et.al Int J Mol Sci, 2015, 16(8), 18149–18184
- [3] C.W. Meyer et.al Front. Phys., 2017, 8
- [4] F. Yang et.al Sci Rep 2017, 7, 1721
- [5] J. Rho et.al RSC Adv., 2018,8, 27616-27622
- [6] K.Okabe et.al Pflugers Arch - Eur J Physiol 2018, 470, 717–731

#### **F.NM02.08.01**

**Optical and Electrical Properties of Organic Semiconductor Thin Films on Aperiodic Plasmonic Metasurfaces** Zhongkai Cheng, Nasir Javed and Deirdre O'Carroll; Rutgers, The State University of New Jersey, United States

Metal electrodes are playing an increasingly important role in controlling photon absorption and in promoting optimal light management in thin-film semiconductor devices. For organic optoelectronics devices, it is challenging to control the surface of the metal electrode to promote good light management because metal electrode deposition is used as the last step in the conventional device fabrication approach. However, an inverted fabrication approach that builds the device on top of a metal electrode, makes it possible to control the morphology of the metal surface, independently of the organic semiconductor active layer, to achieve a variety of photonic and plasmonic behavior useful for optoelectronic devices. Silver (Ag) is one of the most suitable metals for fabrication of nanostructured electrodes with plasmonic behavior (i.e., plasmonic electrodes) because of its low parasitic absorption loss and high reflectivity.

In this work, we study the physical and optical characteristics of Ag nanoparticle (AgNP) aperiodic plasmonic metasurfaces. Then, we investigate the photonic and electrical behavior of the AgNP plasmonic metasurfaces when interfaced with thin films of the organic semiconducting polymer, poly(9,9-dioctylfluorene-alt-benzothiadiazole) (F8BT), using the inverted fabrication approach. The luminescence quantum yield of F8BT thin films increases from 29% on planar silver up to 66% on AgNP metasurfaces due to the Purcell Effect and the improved extraction of emission coupled to surface plasmon polariton (SPP) modes. In particular, we show that plasmonic enhancement can overcome ohmic losses associated with metals and metal-induced exciton quenching. According to the current-voltage characteristics of F8BT hole-only devices with and without plasmonic metasurfaces, we conclude that AgNP plasmonic metasurfaces have comparable electrical behavior to planar metal electrodes while having superior light management capability.

#### **F.NM02.08.05**

**All Plasmonic Nanophotonic Device Displaying Passive PT-Symmetry** Frank Yang, Chloe F. Doiron and Gururaj Naik; Rice University, United States

In quantum mechanics, Hamiltonians exhibiting real eigenvalues are often Hermitian. However, non-Hermitian systems that respect parity-time (PT) symmetry can also possess real eigenvalues. PT-symmetric Hamiltonians display unconventional behavior, such as the coalescence of eigenmodes at exceptional points. This unconventional behavior allows optical devices to take advantage of symmetry, topology, and phase, enabling new functionalities in ultra-sensitive sensing and lasing. There are two approaches to satisfying PT-symmetry in optics: active and passive. Active PT-symmetry requires a system with balanced optical gain and loss. Because of the difficulty of adding gain in nanophotonic systems, passive PT-symmetry is an ideal method for demonstrating PT-symmetry at the nanoscale. In comparison, passive PT-symmetry requires both nearly zero and large optical losses. While plasmonics has enabled many new optical devices, there have been no demonstrations of PT-symmetry in all plasmonic systems due to the large optical losses of plasmonic materials, which limit loss asymmetry. Here we will present an experimental demonstration of an all plasmonic system demonstrating passive PT-symmetry. To achieve this, we engineer a coupled plasmonic antenna system exhibiting large loss asymmetry. The system undergoes a PT phase transition as the coupling, or separation, between the antennas is varied. At high coupling, the system is in a PT-symmetric phase with two resonant absorption peaks. With decreased coupling, the peaks coalesce at the exceptional point. Further decreasing the coupling results in an optical phase transition to a broken PT-symmetric phase with a single resonant absorption peak. Using our nanophotonic PT-symmetric system, we will conclude with a discussion on guidelines for implementing PT-symmetry in nanophotonic devices.

#### **F.NM02.08.07**

**Unity Order Index Tunability at Room Temperature in 1T-TaS<sub>2</sub>—A Strongly Correlated Material** Weijian Li, Ming

Yi, Kevin Kelly, Gururaj Naik and Frank Yang; Rice University, United States

Strongly correlated materials could greatly respond to a stimulus due to their collective behavior. Thus, strongly correlated materials are well studied in the past for their tunable properties, especially electrical and thermal. However, their optical properties remain to be explored. In this work, we study the optical properties of 1T-TaS<sub>2</sub>, a quasi-2D material supporting charge density waves (CDW). 1T-TaS<sub>2</sub> is the only material to exhibit a nearly commensurate CDW phase at room temperature and its electrical and thermal properties are shown to exhibit a large change with temperature, DC and AC biases, pressure, and light. Here, we study the optical properties of 1T-TaS<sub>2</sub> under DC and AC biases, different intensities of optical illumination, and at different temperatures. Under all these conditions, we observe a unity-order change in the refractive index of thin films of 1T-TaS<sub>2</sub>. We hypothesize that the stacking of CDWs in this material changes with stimulus resulting in its optical constants to change. ARPES and STM measurements are underway to verify the hypothesis. Our discovery of the large tunability of optical constants of 1T-TaS<sub>2</sub> presents opportunities in studying light-matter interaction in strongly correlated materials and its application to nanophotonic devices.

#### **F.NM02.08.08**

**A Novel Approach to Tailor the Band Structure of Metal-Organic Framework Nanocrystals in One-Dimensional Periodic Array for Light Induced Energy Transfer Applications** Sujoy Saha, Joseph Sarobin and Hemali Rathnayake; JSNN, University of North Carolina, United States

The study of band structures of different types of Metal-Organic Frameworks (MOFs) is indispensable for the advancement of nanoelectronics. We designed a novel approach to predict and tailor the band structure of MOFs nanocrystals in a one-dimensional periodic array through the variation of structural and materials parameters. From the Bloch condition of the Schrodinger equation, we could predict the amplitude of potentials,  $\phi$  and  $\chi$  for periodically arranged MOFs only in one-dimension using experimental values of dielectric constant, absorption and emission peaks of MOFs. Predicting energy band structures of the one-dimensional array of an isorecticular MOF, IRMOF-8A using a theoretical method combined with experimental values of dielectric constants and amplitude of potentials provide insight into electronic band energy to tailor optoelectronic properties of MOFs and understanding their energy transfer capabilities with respect to the different ligand type. The dielectric constants of three different IRMOFs synthesized from the same metal precursor (Zn<sup>2+</sup>) and three different organic ligands with varying conjugation length were predicted from this novel approach. Band gap depends on the amplitude of potentials, which is a function of the conjugation length of the ligand and its dielectric constant. Thus, the effective conjugation length of the ligand in MOFs have a significant impact on the jumps between two allowed bands in energy band structures of the 1-D array of MOFs. This design method can widely applicable for predicting band energy for any designed MOFs and serves as a versatile tool to tailor and predict the electronic properties of MOFs with different ligand units.

#### **F.NM02.08.09**

**Hybrid Plasmonic Nanostructures for Biomolecular Sensing** Debadrita Paria<sup>1</sup>, Chi Zhang<sup>1</sup>, Steve Semancik<sup>2</sup> and Ishan Barman<sup>1</sup>; <sup>1</sup>Johns Hopkins University, United States; <sup>2</sup>National Institute of Standards and Technology, United States

Metal nanostructures are well known for various ultra-sensitive spectroscopic applications because of their ability to concentrate and enhance the local electromagnetic field due to a phenomenon called localized surface plasmon resonance (LSPR). The intense light localization, also known as "hotspot", becomes more pronounced near a narrow plasmonic gap. In this work, we report tailored hybrid metal nanostructures for LSPR sensing and surface enhanced Raman spectroscopy (SERS) of serum albumin. Using a combination of physical vapor deposition and thermal annealing, different hybrid metal nanostructure configurations have been fabricated, which create well defined arrangements of hotspots. The hybrid metal nanostructures have multiple resonance peaks, which demonstrate the capability of the identification of ultra-low differences in refractive index (0.001) when combined with machine learning algorithms. A detailed FEA simulation of these plasmonic nanostructures provides a quantitative estimate and the spatial distribution of hotspot closely match our experimental observations. The simulations also help us understand the various interactions between the nanostructures via their near field. Finally, these structures also show potential for sensitive label-free SERS detection. Overall, our study explores an integrated multimodal biosensing platform featuring LSPR combined with machine learning and surface enhanced Raman spectroscopy (SERS) for quantitative determination of concentration and molecular fingerprinting.

#### **F.NM02.08.11**

**Optical Properties of Random Nanoparticle Films Made of Spheres with an Overlapping Electric and Magnetic Dipole Response** Parker Wray and Harry Atwater; California Institute of Technology, United States

We investigate theoretically the unidirectional optical scattering properties of random monolayer particle films composed of dielectric particles that support overlapping electric and magnetic dipoles. The particle films exhibit dramatic reflection and transmission behavior which are manifest in the forward-to-backward scattering ratio of the nanoparticle building block. We also show that these films do not exhibit polarization dependent scattering and lack a traditional Brewster's angle. Our theoretical analysis uses a generalized version of Mie theory, which accounts for particle coupling effects, and was validated by full-wave simulations. For fill fractions up to 40% the average scattering response of an embedded particle is shown to accurately predict the behavior of the random film, and the overlap of the electric and magnetic dipole resonances are found to be robust to effects of particle coupling. Continuing research will extend this analysis to multi-layer particle films. This work indicates potential for the design of optical filters and anti-reflective coatings using single materials, without the need for self-assembly.

#### **F.NM02.08.12**

**Imaging Single Particle Enhanced Upconversion Luminescence from NaYF<sub>4</sub>:Yb<sup>3+</sup>,Tm<sup>3+</sup> Nanoparticles on Plasmonic Substrates** [Anahita Haghizadeh](#)<sup>1</sup>, Aravind Baride<sup>2</sup>, Stanley May<sup>2</sup> and Steve Smith<sup>1</sup>; <sup>1</sup>South Dakota School of Mines and Technology, United States; <sup>2</sup>University of South Dakota, United States

We use single particle spectroscopic imaging and statistical analysis to assess the plasmonic enhancement of NIR-to-visible upconversion luminescence (UCL) from single  $\lambda$ -NaYF<sub>4</sub>:Yb<sup>3+</sup>:Tm<sup>3+</sup> upconverting nanoparticles (UCNPs) supported on substrates consisting of random arrangements of Ag nanowires (NW) and Au nano-cavity arrays. We measure both apparent luminescence enhancement, which is power dependent due to the nonlinear kinetics of energy transfer upconversion (ETU), and the excitation enhancement, defined as the ratio of the excitation intensity needed to produce a given UCL emission, divided by the equivalent power needed to produce the same emission on the plasmonic substrate<sup>1</sup>. By examining the effects at the single particle level, and accumulating a statistical sampling of single particle emitters, both on and off the plasmonic substrates studied, we can eliminate the effects of particle fluctuations on the apparent UCL emission enhancement and map out the statistical distribution of excitation and luminescence enhancement on the plasmonic substrates. The distributions obtained are reproduced by Finite Difference Time Domain (FDTD) calculations of the fields near the plasmonic substrate, assuming the variations are due to variations in UCNP coupling to the plasmonic substrate based on an exponential decay with distance. We compare these results to statistical analysis of ensemble measurements made of Er<sup>3+</sup> doped UCNPs supported on random Ag NW substrates<sup>2</sup> and both wide field and confocal spectroscopic imaging of single UCNPs on and off the plasmonic substrates. (1) Fisher, J.; Zhao, B.; Lin, C.; Berry, M. T.; May, P. S.; Smith, S. Spectroscopic Imaging and Power Dependence of NIR to Visible Upconversion Luminescence from NaYF<sub>4</sub>:Yb<sup>3+</sup>,Er<sup>3+</sup> Nanoparticles on Nano-Cavity Arrays. *J. Phys. Chem. C* 2015, 119, 24976–24982. (2) Hor, A.; Luu, Q.; May, P.; Berry, M.; Smith, S. Non-Linear Density Dependent Upconversion Luminescence Enhancement of  $\lambda$ -NaYF<sub>4</sub>: Yb<sup>3+</sup> : Er<sup>3+</sup> Nanoparticles on Random Ag Nanowire Aggregates. *MRS Adv.* 2016, 1, 2677–2682.

#### **F.NM02.08.14**

**Full Factorial Experimental Optimization of Gold Nanostructures Fabrication by Solid-State Dewetting for**

**SERS** [Siarhei Zavatski](#)<sup>1,2</sup>, Hanna V. Bandarenka<sup>3,2</sup> and Olivier J. Martin<sup>1</sup>; <sup>1</sup>Ecole Polytechnique Federale de Lausanne, Switzerland; <sup>2</sup>Belarusian State University of Informatics and Radioelectronics, Belarus; <sup>3</sup>Arizona State University, United States

The optimization of nanostructures for a specific application is a rather complex task, often akin to shooting in the dark with the hope of hitting the right target, viz. the best performing nanostructure. This difficulty stems from the usually large number of experimental parameters that can be changed in a nanotechnology process. This is the case for example in the fabrication of plasmonic nanostructures for surface enhanced Raman scattering (SERS): the choice of metal, its thickness, the shape of the nanostructures as well as their distribution on the substrate are all parameters that determine the overall Raman enhancement. Even for a relatively simple design, exploring all possible combinations of parameters is a prohibitive task both in terms of nanofabrication time and costs. In that contribution, we focus on the large scale fabrication of plasmonic nanostructures using solid-state dewetting and demonstrate how a full factorial design technique can efficiently optimize the process. In that approach, a target response for optimization and two specific values for the  $n$  fabrication parameters are first chosen, leading to an initial set of  $2n$  experiments [1]. Here, as experimental parameters we consider the gold film thickness, the annealing temperature and time, and the heating rate; with the objective of maximizing the intensity of the SERS signal, specifically the 1363 cm<sup>-1</sup> vibrational band of Rhodamine 6G. The corresponding 16 experiments provide a model of the dependency of the Raman enhancement on the four experimental parameters considered here. In the classical optimization procedure by full factorial design, this dependency is chosen linear. The set of experimental parameters that is obtained in this first fit of linear model does not necessarily lead to the strongest Raman enhancement and another set of experiments may be required. However, the full factorial approach also provides the direction in the parameter space in which one needs

to move these parameters to reach a better solution. After such a solution is found, the linear model may need to be refined using second order functions to clarify the optimum region. This is usually done with the central composite experimental design [2]. The optimization process for the fabricated samples is documented in detail by studying the morphology and optical properties of each sample by scanning electron microscopy and UV-Vis spectroscopy. The gold nanostructures we fabricated this way have typical dimensions in the 50 nm range, which is in good agreement with data reported in the literature [3]. Furthermore, the optimized plasmonic substrate can be used to identify non-resonant bioorganic macromolecules such as bovine serum albumin. This work reveals an effective approach to optimize nanofabrication processes for large-scale and cost-effective production of uniform and highly sensitive SERS substrates. [1] Leardi, R. *Analytica chimica acta* 2009, 652(1-2), 161-172. [2] Box, G. E., & Wilson, K. B. *J. R. Stat. Soc. Series B Stat. Methodol.* 1951, 13(1), 1-38. [3] Krug et al. *J. Am. Chem. Soc.* 1999, 121, 9208-14.

#### **F.NM02.08.15**

**Planar Nanophotonic Structures for Intensity-Based Readout Refractive Index Sensing of Dissolved Methane** Morgan Blevins<sup>1,2,3</sup>, Anna Michel<sup>1</sup> and Svetlana Boriskina<sup>2</sup>; <sup>1</sup>Woods Hole Oceanographic Institute, United States; <sup>2</sup>Massachusetts Institute of Technology, United States; <sup>3</sup>MIT-WHOI Joint Program, United States

As global temperatures rise, permafrost in the Arctic is thawing, stimulating increased release of methane, a key greenhouse gas. Accurate measurements of the dissolved methane concentration in seawater and freshwater are important for finding and quantifying the release of natural seabed and Arctic methane seeps to better understand how these sources are contributing to increasing global methane levels. In surface waters, the methane concentration can be as low as 3-10 nM (atmospheric equilibrium) while concentrations as high as 800-1000 nM are found in methane saturated deep seawater and near thawing permafrost. To measure the concentration of dissolved methane, changes in the refractive index (RI) of polymers functionalized to selectively trap methane molecules can be measured via an optical readout mechanism. However, the range of the RI change is very narrow, from 1.41198 to 1.41358 for atmospheric to saturated methane concentration levels ranging from 0 nM to 300 nM, which requires the use of highly sensitive optical sensors. This paper analyzes and compares three simple and low-cost planar nanophotonic and plasmonic structures as optical transducers for measuring refractive index change of polydimethylsiloxane (PDMS) polymer films doped with cryptophane-A molecules, which selectively trap methane. These structures include (i) a Bragg reflector with a defect layer, (ii) a hybrid plasmonic-photonic multi-layer stack that supports a Tamm plasmon mode, and (iii) a hybrid plasmonic-photonic stack that acts as a magnetic mirror, and can be used in a simple intensity-based measurement scheme with low cost light sources and detectors. Through numerical simulations, we evaluate the sensitivity of the proposed structures in both the angular-resonant-mode shift readout mode and in the reflectance intensity readout mode and compare them to the standard surface-plasmon-polariton-mode Spreeta sensor as a reference. Our results show that the planar Bragg reflector with a defect layer exhibits the largest intensity response and is the most promising design for a low cost and robust photonic chip for dissolved methane sensing. A practical implementation of this chip with a simple intensity-based measurement scheme is proposed. Integration of this planar structure into a small, portable, and low-cost dissolved methane sensor offers a way to make climate monitoring more widespread and accessible to researchers. The structures evaluated here all show promise for other chemical and biological sensing applications that require monitoring very small RI changes. Significantly, each structure has been designed to support resonant modes in both s and p polarizations, which allows enhanced sensitivity by calculating the ratio of the spectral responses of orthogonal polarizations, similar to the complex reflectance ratio measured with ellipsometry. Importantly, the response in both polarizations only needs to be monitored in the reflectance intensity readout mode, avoiding the use of expensive and large ellipsometry equipment.

#### **F.NM02.08.16**

**Identifying Plasmon-Like Excited States in Bare and Ligand-Protected Metal Nanoclusters** Rebecca Gieseck; Brandeis University, United States

Noble metal nanoclusters containing dozens to hundreds of metal atoms are of great interest because of their unique optical properties. Classical electrodynamics fails to describe the optical properties of clusters smaller than a few nm, so quantum mechanical models are needed to describe these clusters. However, it is challenging to identify which features of the computed excited states indicate plasmon-like character, particularly in a way that is generalizable to the ligand-protected clusters that are commonly studied in experiments. We present an analytical method to identify plasmon-like excited states using three quantifiable indicators that must be considered in combination: (1) large superatomic character, (2) large collectivity among single-particle excitations, and (3) large additivity of contributions of these single-particle excitations to the transition dipole moment. Visualizing these three indicators on a single plot enables rapid classification of hundreds of excited states into plasmon-like, collective, single-particle, or interband categories, or as intermediate between these categories. This method is used to identify excited states with plasmon-like character in both bare and ligand-protected Ag



clusters at the TDDFT level. Using these three nearly orthogonal indicators in combination provides more information than any one criterion can provide.

#### **F.NM02.08.18**

**Stable Dispersion of Titanium Nitride Nanoparticles** Idalis Hernandez, Eric Bartlett, Sanchari Chowdhury and Michaelann Tartis; New Mexico Tech, United States

Alternative plasmonic titanium nitride nanoparticles (TiN) are attractive photothermal agents because of their ability to strongly absorb a broad spectrum of light ranging from visible to near-infrared and convert that into heat. Additional advantages of low cost and stability of these refractory nanomaterials make them attractive for different applications ranging from photothermal cancer therapy to solar energy mediated catalytic reactions. In this work, we are developing a method to obtain a stable and monodispersed TiN nanoparticles solutions, which is an important prerequisite for most of their applications. Moreover, our goal is to optimize a solution based coating method to obtain a uniform well dispersed thin film of TiN nanoparticles on the substrate, which will be useful for their application in the device. However, preventing aggregation of TiN nanoparticles in a solvent has been a challenge. We have optimized protocols based on ultra-probe sonication and centrifugation, to obtain relatively monodisperse and stable TiN nanoparticles in an aqueous solution. We have applied our method to commercially available polydisperse TiN nanoparticles of average size 80nm and 20 nm. Using the optimized method we were able to decrease the polydispersity index (PDI), the measure of the distribution of nanoparticles in a solution, from 0.351 to 0.18 indicating a significantly more monodispersed solution. Moreover, we used a sol-gel based method for incorporating nanoparticles in transparent silica gels. There was no aggregation of the TiN nanoparticles observed during the sol-gel transition. UV-Vis spectroscopy and dynamic light scattering method confirm that incorporating TiN nanoparticles in silica gel preserved both of their optical properties and the dispersibility as in the original solution. The nanoparticles stay stable in the solution for several days. A biocompatible silica coating on TiN nanoparticles can be useful for drug delivery and photothermal therapy. In summary, we are developing a simple commercially viable method to efficiently disperse and stabilize titanium nanoparticles in solution and subsequently coating them on the substrate which can easily be applied for large scale applications.

#### **F.NM02.08.19**

**Confined Nucleation of ErAs NPs in Er:InAs QDs to Fabricate Nanoparticle Quantum Dot Hybrids** Kurt Eyink, Yuanchang Zhang, Albert M. Hilton and Krishnamurthy Mahalingam; Air Force Research Laboratory, United States

Directed assembly has been the subject of extensive research over the years due to the desire to grow structures at specific locations. This is accomplished by increasing the probability of nucleation at the desired location. Mechanisms such as reduction of the diffusion of species, reduction of the strain to lower the bulk free energy to reduce the critical nuclei size, or a lowering of the surface energy which also reduces the critical nuclei size have previously been used. In all these cases, nucleation of the desired phase occurs directly on the substrate. Here we propose and demonstrate a scheme for directed assembly in which we confined the nucleation of the desired material to the region of a nanostructure formed on the surface. We accomplish this through the use of a dilute alloy containing the desired material and subsequent removal of the major constituent of the alloy inducing nucleation at some point after the dilute species exceeds its solubility limit. In particular, we use this approach to control the nucleation of ErAs nanoparticles from Er:InAs quantum dots by evaporation of InAs. We studied ErAs NP formation from InAs QD nominally doped to concentration of 1.25% and 2.5% on GaAs (001). The Er:InAs quantum dots were grown using normal conditions for the growth of undoped InAs and produced similar quantum dot densities (near 100/square micron). We explain these observed results in terms of normal nucleation and growth given the mesoscopic concentration of Er atoms expected in the InAs QD. A comparison of the undoped and Er-doped InAs quantum dots before and after InAs evaporation show the number of the ErAs nanoparticles is less than the original quantum dot density showing nanoparticle do not form in every quantum dot and suggests a critical number of Er atoms needed for nucleation. We have used our confined nucleation process in conjunction with normal direct assembly processes for InAs QDs to produce hybrid structures composed of InAs QDs and ErAs NP. We have formed vertically stacked Er:InAs QD over undoped InAs QDs to form ErAs NP over InAs QDs. We have formed Er:InAs quantum dots formed in ErAs divots to form ErAs nanoparticle clusters and have used Er:InAs to place ErAs in patterned surface. Transmission electron microscopy of these structures show that at times multiple nucleation sites are possible in the structure and suggest the potential of forming rich hybrid structures using this approach.

#### **F.NM02.08.21**

**Optical Parameters of Bioinspired Sub-Monolayer Nanoparticle Arrays** Sean R. Dinneen<sup>1</sup>, Richard M. Osgood<sup>1</sup>, Zhuangsheng Lin<sup>2</sup>, Camille Martin<sup>2</sup>, Michael Okamoto<sup>1</sup>, Ihsan Uluturk<sup>1</sup> and Leila Deravi<sup>2</sup>; <sup>1</sup>Combat Capabilities Development Command Soldier Center, United States; <sup>2</sup>Northeastern University, United States

Cephalopods have the ability to take advantage of pigmented and structural coloration when camouflaging, signaling, or otherwise communicating through their adaptive coloration. The chromatophore, which is the actuating organ responsible for pigmented color within cephalopods, is populated with 500-600 nm diameter particles composed of pigment and protein called pigment granules. The pigment, identified as xanthommatin, has been found to have a uniquely high refractive index and contributes highly to the scattering of light with broadband optical properties. Developing metamaterials out of synthetic pigment granules, where the particle periodicity is smaller than the wavelengths of light with which they interact, was the next logical choice for us to not only further our understanding of the complex photonic system of cephalopods, but to explore its application in adaptable optical systems and possibly chemical sensing.

In this work, we aim to leverage our knowledge of biomaterials (namely the biopigment xanthommatin) to generate sub-monolayers of synthetically made pigment granules. Xanthommatin is encapsulated within polystyrene-co-maleic anhydride (PSMA) nanoparticles with good physical retention while maintaining its coloration. Sub-monolayer arrays are prepared via Chumanov-style roll-coating on substrates within a vial containing the solution of particles, and are physically characterized by scanning electron microscopy. We then show the arrays' optical properties measured by integrating sphere spectrophotometry and broadband multi-angle ellipsometry. Depending on the spacings of the particles, the arrays will resonate at certain wavelengths within the visible. Our updated models, taking into account the particle's refractive index and contribution from the pigment, will show a dependence of spacing and material on wavelength resonance. With the pigment as a functional feature within the particles, we explore the retained chemical properties (such as absorption changes with pH) with the possible inclusion of chemical sensing.

#### **F.NM02.08.22**

**Spatial Inhomogeneity of Optical Binding in Many-Body Systems** Fei Han; Clarkson University, United States

Optical matter can be formed by electrodynamic interactions of metal nanoparticles in an optical field. This light-mediated self-organization of nanoparticles offers a route to study mesoscale electrodynamic interactions in many-body systems. By controlling the intensity, phase, and polarization of light, the optical field can be tailored to assemble stable optical matter with up to 101 nanoparticles. Here we report that the spatial inhomogeneity of circularly polarized optical binding in a many-particle system. The spatial stability of self-organized nanoparticles is strongly influenced by the laser intensity and polarization state. In particular, the nanoparticles in the central area of an optical matter array are more stable than those on the edge. Moreover, larger arrays are self-protected from fluctuation-induced instability by incorporation more nanoparticle constituents. This study provides important information about the spatial inhomogeneity of optical binding interactions in mesoscale nanoparticle arrays.

#### **F.NM05.07.01**

**Observation of Strong Electron-Phonon and Electron-Photon Interactions in Topological Weyl Semimetals** Kunyan Zhang<sup>1</sup>, Tong Wang<sup>2</sup>, Xiaoqi Pang<sup>2</sup>, Fei Han<sup>3</sup>, Nguyen Tuan Hung<sup>2</sup>, Ahmad R. Nugraha<sup>2,4</sup>, Mingda Li<sup>3</sup>, Riichiro Saito<sup>2</sup> and Shengxi Huang<sup>1</sup>; <sup>1</sup>The Pennsylvania State University, United States; <sup>2</sup>Tohoku University, Japan; <sup>3</sup>Massachusetts Institute of Technology, United States; <sup>4</sup>Indonesian Institute of Sciences, Indonesia

Electron-phonon interaction plays an important role in the electronic properties of topological materials by affecting the dispersion and lifetime of phonon and electronic states. For example, Kohn anomaly describes the phonon softening phenomenon when the dielectric screening from conducting electrons in a metal is disrupted. Another evidence of strong electron-phonon interaction is Fano resonance, the interference between discrete and continuous states, featured by an asymmetric Breit-Wigner-Fano lineshape. In this work, we present the anisotropic Kohn anomaly and Fano resonance in a type-II Weyl semimetal candidate LaAlSi by polarized Raman spectroscopy. The B<sub>1</sub> phonon mode in our Raman spectra shows excitation-wavelength-dependent phonon-softening and lineshape asymmetry. In type-I Weyl semimetal TaP, abnormal symmetry breaking of another B<sub>1</sub> mode in polarized Raman spectroscopy has been observed, attributed to the quantum interference of degenerate carrier pockets with different symmetries. The experimental observations combined with density-functional theory (DFT) calculations provide valuable insights into microscopy scattering pathways and transport properties of the type-II Weyl semimetal candidate LaAlSi and type-I Weyl semimetal TaP.

#### **F.NM05.07.02**

**1.5  $\mu\text{m}$  Telecom-Wavelength Single Photon Source of InAs/InP Quantum Dot via Strain-Controlled Growth** Youngho Ko<sup>1</sup>, Mireu Lee<sup>1,2</sup>, Hosung Kim<sup>1</sup>, Won Seok Han<sup>1</sup>, Je-Hyung Kim<sup>2</sup> and Jung Jin Ju<sup>1</sup>; <sup>1</sup>Electronics and Telecommunications Research Institute, Korea (the Republic of); <sup>2</sup>Ulsan National Institute of Science and Technology, Korea (the Republic of)

Owing to the rapid development of quantum information technology including quantum communication, quantum sensor, and quantum computer, realization of quantum light source, an essential element for the photonic quantum information applications, have been required. There have been numerous efforts to obtain single photon sources as a quantum light source by using various solid-state material platforms including semiconductor quantum dots (QDs), defect-based color centers in diamond and SiC, QDs in two-dimensional material of WS<sub>2</sub> and WSe<sub>2</sub>, and etc. III-V semiconductor QDs have been widely considered as a promising platform for the single photon source due to their various advantages of high generation efficiency of single photon, wavelength tunability, and favourable integration with various semiconductor-based photonic circuits. Single photon emission in 1.5 μm telecom-wavelength range was quite important because of compatible with quantum communication and photonic integrated circuits of silicon photonics. However, single photon emission in telecom-wavelength range was still challenge. InAs QDs are normally grown by Stranski–Krastanov growth mode with molecular-beam epitaxy or metal organic chemical vapor deposition (MOCVD). Because the diameter and height of the self-assemble InAs QDs are determined by strain originated from lattice mismatch with host materials, it was difficult to obtain telecom-wavelength single photon emission from InAs/GaAs or InAs/InP QDs. In this study, we obtained 1.5 μm telecom-wavelength single photon emission from InP-based InAs QDs by using strain-controlled layer of InAlGaAs. The single photon source was fabricated with circular bragg grating structure to obtain high collection efficiency of single photon emission. Moreover, we proposed integrated single photon devices to realize integrated quantum light source with photonic integrated circuits. For the strain control during the growth of InAs QDs, tensile-strained InAlGaAs layers as a host material were grown on the InP substrate. The InAs QDs were grown by Stranski–Krastanov growth mode in MOCVD. lattice-mismatched InAlGaAs on InP showed 0.74 % tensile strain with InP, which was characterized by x-ray diffraction measurement. We monitored the structural properties of InAs QDs by atomic force microscopy and transmission electron microscopy with changing the strain-controlled layers of InAlGaAs, InGaAs, and InP and with changing the thickness of strain-controlled layers. To optimize the size and density of the QD, InAs samples were grown with various growth condition including the temperature, growth rate, and the III/V ratio. We found that the size of InAs QDs were strongly dependent on the density and As flow was critical for emission efficiency of QD and wetting layer. Through systematic study, we could obtain low enough density of InAs QD from 10<sup>7</sup> /cm<sup>2</sup> to 10<sup>9</sup> /cm<sup>2</sup> for fabrication of single photon emitter. We carried out the micro-photoluminescence measurement at 3.4 K for optical analysis of QDs. The single QD emission peak was exhibited from 1.5 to 1.6 μm wavelength. The second-order correlation function was measured for single photon analysis through Hanbury-Brown Twiss experiment. We designed circular bragg grating structures with InAs/InAlGaAs QD for collection efficiency and Purcell enhancement of cavity. Optical simulation of the QD in cavity was performed by finite-difference time domain simulation. The collection efficiency of the circular bragg grating structure was more than 80 % to objective lens of NA 0.7. We also designed the integrated single photon source with Si photonic circuit. InAlGaAs waveguide was designed as the nano tapered waveguide and SiO<sub>2</sub> interlayer was adopted to efficiently couple the single photon emission with Si waveguide. The QD-based telecom-wavelength single photon source of high collection efficiency and integrated single photon source could provide a solution for on-chip quantum photonic devices.

#### **F.NM06.11.02**

**Optical Control of Spin Transfer in Hybrid Perovskites-TMDC Heterostructures** [Anna Stadlbauer](#)<sup>1</sup>, Lissa Eyre<sup>1</sup>, Jonathan Zerhoch<sup>1</sup>, Sean A. Bourelle<sup>2</sup> and Felix Deschler<sup>1</sup>; <sup>1</sup>Walter Schottky Institute - Technical University of Munich, Germany; <sup>2</sup>University of Cambridge, United Kingdom

It is a fundamental question how material properties of heterostructures can control spin transfer. This work investigates how spin can be transferred in a heterosystem of a hybrid metal-halide perovskite and a 2D material, with focus on transition metal dichalcogenide (TMDC) layers. Metal halide perovskites and TMDC have already been combined in type II heterostructure devices such as photodetectors [1,2]. However, spin transfer has not yet been reported to the best of our knowledge, which would open up opportunities for optical control in spintronics applications.

Following our study of spin-exciton interactions and spin depolarization times in hybrid perovskites, we aim to investigate how the properties of the heterostructures control spin transfer. The most suitable 2D materials for this approach are semiconducting TMDCs due to their reported controllable valley degree of freedom [3,4]. To benefit from the coupling between spins and valleys in TMD layers, the components in the investigated heterosystem require not only a suitable combination of bandgaps and appropriate band alignment but also positions in k-space that fulfill the optical selection rules [3].

We analyze the obtained heterostructures with ultrafast time resolved photoluminescence spectroscopy, circularly polarized transient absorption spectroscopy and Faraday rotation to resolve the excitation and spin dynamics.

From our fundamental insights into the spin transfer in TMDC-perovskite-heterosystems, we anticipate to discover avenues

and design guidelines for application of our for emerging spintronic technologies.

- [1] Ma, C. et al., *Adv. Mater.* **2016**, 28, 3683–3689
- [2] Shi et al., *Chem. Soc. Rev.*, **2018**, 47, 6046
- [3] Mak, K. et al. *Nature Photonics*, **2018**, 12, 451-460
- [4] Ciccarino, C., et al. *Nano Lett.*, **2018**, 18, 57809-5715

### SYMPOSIUM F.NM03

---

Nanotubes, Graphene and Related Nanostructures  
November 21 - December 4, 2020

#### Symposium Organizers

Jeffrey Fagan, National Institute of Standards and Technology  
Tanja Kallio, Aalto University  
Naoyuki Matsumoto, National Institute of Advanced Industrial Science and Technology  
Yoke Khin Yap, Michigan Technological University

---

\* Invited Paper

SESSION F.NM03.10: Live Panel Discussion I: Synthesis and Chirality Control  
Session Chairs: Jeffrey Fagan and Yoke Khin Yap  
Thursday Morning, December 3, 2020  
F.NM03

**8:00 AM INTRODUCTION AND ANNOUNCEMENTS**

**8:05 AM INDUSTRIALIZATION OF VERTICALLY-ALIGNED CARBON NANOTUBES—DON FUTABA**

**8:15 AM CORRELATION BETWEEN RAMAN SPECTROSCOPY AND TRANSMISSION ELECTRON MICROSCOPY—ADAM BOIES**

**8:25 AM BREAK**

**8:30 AM TRANSFORMING CNT MASS PRODUCTION-CHALLENGES AND OPPORTUNITIES—ANNICK LOISEAU**

**8:40 AM IN SITU TEM STUDIES ON NANOTUBES AND 2D MATERIALS—XUEDONG BAI**

**8:50 AM CLOSING SUMMARY**

SESSION F.NM03.11: Live Panel Discussion II: Emerging Electronic and Energy Applications  
Session Chairs: Jeffrey Fagan and Yoke Khin Yap  
Thursday Morning, December 3, 2020  
F.NM03

**8:55 AM INTRODUCTION AND ANNOUNCEMENTS**

**9:00 AM HOW TO DESIGN NANOMATERIALS FOR THERMOELECTRIC AND PHOTOVOLTAIC APPLICATIONS THROUGH AB-INITIO AND MACHINE LEARNING TOOLS—SWAPAN PATI**

**9:10 AM ORGANIC PASSIVATION LAYERS FOR CNT:SI PHOTOVOLTAICS—BEN FLAVEL**

**9:20 AM BREAK**

**9:25 AM ONE-DIMENSIONAL VAN DER WAALS HETEROSTRUCTURES—SHIGEO MARUYAMA**

**9:35 AM NOVEL ELECTRONICS OF ATOMIC CHAINS INSIDE NANOTUBES—PEIDE YE**

**9:45 AM NANOCARBON FIELD-EFFECT TRANSISTORS AS BIOSENSORS—DELPHINE BOUILLY**

**9:55 AM CLOSING SUMMARY**

SESSION F.NM03.12: Live Panel Discussion III: Emerging Biological and Chemical Applications  
Session Chairs: Jeffrey Fagan and Yoke Khin Yap  
Friday Afternoon, December 4, 2020  
F.NM03

**4:00 PM INTRODUCTION AND ANNOUNCEMENTS**

**4:05 PM SIMPLE APPROACHES TO SOLVE COMPLEX BIOLOGICAL QUESTIONS—NAZMIYE YAPICI**

**4:15 PM DNA/CARBON NANOTUBE INTERACTIONS AT THE SHORT DNA OLIGOMER LIMIT—MING ZHENG**

**4:25 PM BREAK**

**4:30 PM SPINTRONICS IN FUNCTIONALIZED NANOTUBES—RANJIT PATI**

**4:40 PM EMERGING APPLICATIONS OF BORON NITRIDE NANOTUBES AS NANOSUBSTRATES—YOKE KHIN YAP**

**4:50 PM CLOSING SUMMARY**

SESSION F.NM03.13: Live Panel Discussion IV: Novel Processing and Characterization  
Session Chairs: Jeffrey Fagan and Yoke Khin Yap  
Friday Afternoon, December 4, 2020  
F.NM03

**4:55 PM INTRODUCTION AND ANNOUNCEMENTS**

**5:00 PM EXFOLIATION YIELD AND THE TOPOLOGICAL SURFACE STATES—SARAH HAIGH**

**5:10 PM IN-SITU MANIPULATION OF MATERIALS IN VIENNA—TOMA SUSI**

**5:20 PM CHARACTERIZATION OF LOW DIMENSIONAL SYSTEMS-CHALLENGES AND OPPORTUNITIES—NEDJMA BENDIAB**

**5:30 PM BREAK**

**5:35 PM ALIGNMENT OF CARBON NANOTUBE FILMS—WILLIAM RICE**

**5:45 PM ENDOHEDRAL CONTROL FOR SWCNT PROPERTY MODULATION—JEFFREY FAGAN**

**5:55 PM CLOSING SUMMARY**

SESSION F.NM03.01: Controlled Synthesis

On Demand Abstracts Available for Viewing Starting Saturday Morning, November 21, 2020  
F-NM03

**5:00 AM \*F.NM03.01.01**

**Our Efforts on Industrializing Carbon Nanotubes** Don Futaba, Shunsuke Sakurai, Guohai Chen and Takashi tsuji; National Institute of Advanced Industrial Science and Technology, Japan

In the nearly 30 years since the elucidation of the carbon nanotube structure, the reality of mainstream commercial applications, such as touch panels, sealing materials, high performance power sources, etc. are now in the foreseeable future. However, to realize this vision, the practical developmental obstacles need to be resolved. This is precisely the work which is undertaken by the CNT-Application Research Center, AIST. Over the past 15 years, our Center has been working in collaboration with academia and industry to support the establishment of a carbon nanotube industry in Japan by addressing the various stages of research spanning discovery, development, application, scale-up, and commercialization for the general top vital to the development of applications, such as synthesis, processing, and evaluation. In this way, our center works to bring scientific discoveries and bring them to society.

This presentation will provide an overview of our recent progress in the synthesis and application of highly efficient synthesis of millimeter-scale, vertically-aligned single-walled carbon nanotubes using the water-assisted “Super-growth” CVD. In one section of my presentation, I will describe our efforts toward the economical mass-production of single-walled carbon nanotubes (SWCNT). I will then present our progress on the development of commercial applications, and finally I will present some of our work in developing the new technology for the synthetic control of SWCNTs.

**5:15 AM \*F.NM03.01.02**

**Chiral Carbon Nanotube Control via Size Resolved Solid Catalysts** Adam Boies, Xiao Zhang, Brian Graves and Michael De Volder; University of Cambridge, United Kingdom

**Single-walled carbon nanotubes (SWCNTs) with controlled chirality possess superior performance in many sensor and electronic applications. However, direct growth of SWCNTs with a narrow chirality distribution is still challenging. Recently, catalysts that remain solid state during growth have renewed the possibility to achieve chirality controlled through direct growth. To facilitate scaled-up SWCNT production and clarify the mechanism behind chirality selection, we show the synthesis of high melting point metal nanoparticles with near monodisperse sizes in the range of 1 to 5 nm using a continuous, gas-phase synthesis process. Random and aligned SWCNTs with a narrow range of chiralities are grown on substrates. Chiral angles of  $19\pm 5^\circ$  are particularly prevalent with their abundance reaching over 93%. We attribute the mechanism to the extension of growth time afforded to fast growing chiralities. The solid catalysts are also shown to be effective via floating catalyst growth. The facile production of chirality-controlled SWCNTs increases their availability for broad academic and industrial applications.**

**5:30 AM F.NM03.01.03**

**Conversion of Waste Plastic into CNTs Using Stainless Steel Catalyst—An Optimization Approach to Maximize the Yield** Aidin Panahi, Xiao Sun, Di Chang and Yiannis Levendis; Northeastern University, United States

As a result of China’s recent ban on the import of most plastic waste, the US and other industrialized countries that have been exporting their plastic waste to China for recycling will need to find new ways to handle the disposal of their waste as much of it is already starting to pile up in landfills. In research conducted at Northeastern University, plastic wastes have been thermally recycled by pyrolytic gasification to carbon nanotubes (CNTs) and gaseous fuel. To achieve this conversion, a

laboratory-scale pyrolytic gasifier was fed with waste plastics including (polyethylene, polypropylene, polyethylene terephthalate, polystyrene, etc.) in an inert N<sub>2</sub> or He or Ar or CO<sub>2</sub> atmospheres with different flow rates (0.1-2 l/min). The plastic wastes were gasified in an electrically heated reactor at 600-800 °C. Under these conditions, the polymer pyrolyzed into a gaseous mixture of hydrocarbons and hydrogen. The pyrolyzate mixture was then conducted into a separate reactor where it was used as a carbon precursor for chemical vapor deposition process to synthesize carbon nanoparticles. The second reactor was set at temperatures in the range of 800-1000 °C. The catalytic substrate used for the nanoparticle growth consisted of different grades of stainless steel mesh (SS-304, SS-316 and SS-316L). The wire cloths were used either as-received or upon chemical etching by acid wash and/or heat-treatment in air, nitrogen or helium at 800 °C followed by rapid air quenching. In those cases, the yields were determined by the mass of the product relative to the mass of feedstock and ranged from 1% to 30%. With the purpose of purification and sorting, the catalysts and the produced CNTs were investigated from synthesis, structure and property characterization by the use of SEM, TEM, AFM, TEM+EDX, HAADF, and TGA. Results showed that the catalyst type, composition and pre-treatment, carrier gas and flowrate as well as the type of waste plastic, are all influential on the yields and physical characteristics of the synthesized CNTs.

#### 5:40 AM F.NM03.01.05

**Diffusion Inhibitors in Catalyst Particles for Growth of Ultra-Long Carbon Nanotubes** Michael J. Bronikowski; University of Tampa, United States

This report presents recent results from studies of growth of Carbon Nanotubes (CNTs) by CVD using metal catalyst particles doped with heavy refractory metals. In such growth, the heavy metal acts as a diffusion inhibitor to prevent erosion and Ostwald ripening of the catalyst particles, extending the lifetime of these particles in the CVD environment and thus allowing the growth of longer carbon nanotubes than would normally result. This effect has been demonstrated in several of our recent studies. Here, we report extension of our results to new reactive systems utilizing new catalyst/inhibitor combinations and new carbon feedstock gases. Implications for the growth of ultra-long (tens of cm or more) CNTs will be discussed.

#### 5:50 AM F.NM03.01.06

**Large Area, High-Density SWCNT Forests with Remarkably Invariant Structural Properties Over a Wide Range of Synthesis Conditions** Sei Jin Park, Eric Meshot, Kathleen Moyer, Steven F. Buchsbaum, Melinda Jue, Kuang Jen Wu and Francesco Fornasiero; Lawrence Livermore National Laboratory, United States

Driven by the exceptional thermal, electrical, optical, mechanical and fluidic properties of single-walled carbon nanotubes (SWCNT), commercial use of vertically aligned “forests” are on the horizon for applications<sup>1</sup> ranging from optical absorbers and thermal interfaces to selective membranes and advanced fabrics.<sup>2,3</sup> Large-area SWCNT forests with high densities and small diameters are especially important for many applications, yet they are conspicuously absent from the literature due to synthesis challenges.

Here, we demonstrate synthesis of high-density ( $> 10^{12}$  CNTs/cm<sup>2</sup>), small-diameter (~ 2 nm) SWCNT forests with structural characteristics that remain uniform over large areas (up to 6-in. diameter)<sup>4</sup> and, surprisingly, largely unchanged over a wide range of synthesis conditions. We also find that our growth regime enables a record-high carbon conversion efficiency and a stable mass kinetics, both of which are invariant with catalyst type (Fe vs Fe/Mo mixes). To identify the limiting steps in the SWCNT growth kinetics and the factors contributing to the process robustness, we determine the dependence of the reaction rate and carbon conversion efficiency on broad ranges of synthesis parameters. Effects of catalyst area (from  $1 \times 1$  cm<sup>2</sup> to 6-in wafers), growth pressure (20-790 mbar), gas composition (30-fold acetylene partial pressure, hydrogen-argon ratio), and flowrates (8-fold variation) are presented. The observed growth rate trends can be explained quantitatively with a simple kinetic model in which bulk diffusion of acetylene in gas phase is the limiting step in CNT production and hydrocarbon byproduct formation becomes dominant at high hydrogen partial pressure.

Our demonstration of such robust and reproducible growth of high-density forests over a wide range of synthesis conditions provides valuable insights for future scale-up efforts of SWCNT forest production, which are key for widespread adoption of advanced CNT technologies.

1. R. Rao et al., *ACS Nano*, 12 (2018) 11756.
2. N. Bui, E. R. Meshot, S. Kim, J. Peña, P. W. Gibson, K. J. Wu, F. Fornasiero, *Adv. Mater.*, 28 (2016) 5871.
3. Y. Li, C. Chen, E. R. Meshot, S. F. Buchsbaum, M. Herbert, R. Zhu, O. Kulikov, B. McDonald, N. Bui, M. L. Jue, S. Park, C. Valdez, S. Hok, C. J. Doona, K. J. Wu, T. M. Swager, F. Fornasiero, *Adv. Funct. Mater.*, (2020) 2000258.
4. E. R. Meshot, S. Park, S. F. Buchsbaum, M. L. Jue, T. R. Kuykendall, E. Schaible, L. B. Bayu Aji, S. Kucheyev, K. J. Wu, F. Fornasiero, *Carbon*, 159 (2020) 236-246.

This work was performed under the auspices of the U.S. Department of Energy by Lawrence Livermore National Laboratory under Contract DE-AC52-07NA27344. LLNL-ABS-797268

#### 6:00 AM F.NM03.01.07

**Origin of Catalysts for the Synthesis of Boron Nitride Nanotubes** Sambhawana Sharma<sup>1</sup>, Siqi Zhang<sup>1</sup>, Rodney Oakley<sup>2</sup>, Dongyan Zhang<sup>1</sup> and Yoke Khin Yap<sup>1</sup>; <sup>1</sup>Michigan Technological University, United States; <sup>2</sup>StabiLuX Biosciences Inc., United States

#### Abstract

Boron Nitride Nanotubes (BNNTs) have been of great interest due to their electrically insulating, optically transparent, and biocompatible properties. As we have demonstrated, these properties make BNNTs attractive nanomaterials for novel electronic<sup>1-3</sup> and biomedical<sup>4</sup> applications. All these applications require high-quality and high-purity BNNTs. One promising approach is by the use of catalytic chemical vapor deposition (CCVD), where the synthesis of BNNTs are well controlled by the use of catalyst<sup>5-6</sup>. Therefore, understanding the catalytic behavior and growth mechanism will enable better control of the quality and purity of BNNTs.

Here we describe the discovery of a new compound  $Mg_x(SiO_2)_y$ , as the original catalyst for the growth of BNNTs. Based on the growth-vapor trapping (GVT) approach, we have demonstrated the growth of high-quality BNNTs in a regular tube furnace often used for the synthesis of carbon nanotubes, graphene, and many other two-dimensional (2D) materials.<sup>5-6</sup> Such CCVD approach enable the growth of BNNTs using the boron oxide chemistry without involving dangerous and corrosive materials. We found that MgO powders are the effective “catalyst” for our synthesis. However, our results suggest that MgO will work well only on Si substrates, not on other inert substrates. Detailed experiments and analysis suggest that  $Mg_x(SiO_2)_y$  is the actual catalyst responsible for the growth of high-quality BNNTs. We further compare the synthesis of BNNTs using various Magnesium based compounds, some of which favor the growth of BNNTs in very small tube diameters. A detailed study of these results will be presented at the meeting.

#### Acknowledgment

We acknowledge the support from National Science Foundation (Awards numbers 1521057 and 1738466).

#### References

- <sup>1</sup>Bhandari, S., et al, “Two-dimensional gold quantum dots with tunable bandgaps”. *ACS Nano*, 13(4), 4347 (2019).
- <sup>2</sup>Qin, J. K., et al, “Raman response and transport properties of tellurium atomic chains encapsulated in nanotubes”. *Nature Electronics*, 3(3), 141 (2020).
- <sup>3</sup>Lee, C. H., et al, “Room Temperature Tunneling Behavior of Boron Nitride Nanotubes Functionalized with Gold Quantum Dots”. *Advanced Materials*, 25(33), 4544 (2013).
- <sup>4</sup>Yap, Y. K. Zhang, D. Yapici, N. B, “High-Brightness Fluorophores,” US Patent Application US20180296705A1.
- <sup>5</sup>Lee, C. H., et al, “Effective growth of boron nitride nanotubes by thermal chemical vapor deposition”. *Nanotechnology*, 19(45), 455605 2008.
- <sup>6</sup>(Review) Jiesheng Wang, Chee Huei Lee and Yoke Khin Yap, “Recent advancements in boron nitride nanotubes,” *Nanoscale* 2, 2028 (2010).

#### 6:10 AM F.NM03.01.08

**Late News: Fullerene Nanopottery—Precise Dimerization of Hollow Compartments** Fei Han<sup>1</sup> and Hongyu Chen<sup>2</sup>; <sup>1</sup>Nanyang Technological University, Singapore; <sup>2</sup>Nanjing Tech University, China

Pottery brings the dawn of manufacturing in human history. With it, one can readily design, build, and assemble hollow containers with tailored shapes for various applications. However, this important concept has yet to be emulated in nanoscience. We report a facile synthetic methodology: Nanopottery, where hollow fullerene compartments with tailored shapes and precise stoichiometry can be readily created and assembled via the manipulation of their liquid template, advancing from isolated hollow units to multi-compartment vessels.<sup>1</sup>

Precisely controlled docking, merging, and welding of hollow nano-/micro-structures are essential in constructing sophisticated hollow systems, in ways similar to the building of plumbing and biosystems. To this end, regioselectivity during the processes is an important milestone demanding new tools.

We bring steric effect, a powerful regioselective method in organic reactions, to nanoscale for the precise assembly of fullerene nanobowls, reaching dimers of 93.6% purity in one-step. To the best of our knowledge, the dimerization sets a new record of the highest purity sample before purification. *m*-xylene liquid nanodroplets that template the growth of bowls can be readily docked and merged, producing the dimers and tetramers. The regioselectivity is controlled by steric



hindrance, *i.e.*, the relative size of the exposed liquid droplets vs. the hemispherical shell, so that the docking process can be readily modulated to govern the stoichiometry. The mechanism is studied in detail and further supported by geometrical models. We believe that the development of new regioselective tools and the understanding in docking and welding hollow structures would expand the horizon of nanoscience, opening new possibilities for designing sophisticated hollow nano-systems.<sup>2</sup>

Reference:

1. Fei Han and Hongyu Chen\* et al. "On demand synthesis of hollow fullerene nanostructures." Nat. Commun., 2019, 10, 1548.
2. Fei Han and Hongyu Chen\* et al. "Precise dimerization of hollow fullerene compartments." J. Am. Chem. Soc., 2020, Just accepted (DOI 10.1021/jacs.0c06190).

SESSION F.NM03.02: Chiral Sorting and Characterization  
On Demand Abstracts Available for Viewing Starting Saturday Morning, November 21, 2020  
F-NM03

**5:00 AM \*F.NM03.02.01**

**DNA/Carbon Nanotube Interactions at the Short DNA Oligomer Limit** Ming Zheng; National Institute of Standards and Technology, United States

DNA-carbon nanotube (DNA-CNT) hybrids are useful constructs for CNT sorting and biosensing applications. Historically, shorter sequences (~ 10 to 12 mers) are found to give rise to better separation outcome. Even though it is known that sequences shorter than 10 mers leads to less stable dispersions, the length limit has never been explored systematically in terms of dispersion stability and separability. We have recently combined experimental and machine learning guided search to explore short ( $N \geq 5$ ) DNA sequence space in a non-biased manner. In this talk, I will present our new CNT resolving sequences identified through this work, and their utility in chiral sensing of small molecules.

**5:15 AM \*F.NM03.02.02**

**Comparing Resonant Raman Spectroscopy and Atomic Resolution Transmission Electron Microscopy for SWCNT Sample Characterization** Alice Castan<sup>1</sup>, Salomé Forel<sup>2</sup>, Frédéric Fossard<sup>1</sup>, Dmitri Levshov<sup>2</sup>, Wim Wenseleers<sup>2</sup>, Sofie Cambré<sup>2</sup> and Annick Loiseau<sup>1</sup>; <sup>1</sup>LEM, CNRS-ONERA, France; <sup>2</sup>University of Antwerpen, Belgium

Having access to SWCNTs samples enriched in certain structures is a fundamental goal in order to exploit their properties within the scope of specific applications. One way to produce such samples is to achieve structurally selective growth of SWCNTs. Aside from the obvious scientific challenges related to this very active research field, being able to precisely and accurately assess the composition of a growth sample is a key point for understanding the phenomena underlying growth selectivity.

A widely used characterization methodology for assessing the selectivity of CVD grown SWCNT on flat substrates is based on resonant Raman spectroscopy mappings using a set of discrete laser lines. In this work we thoroughly investigate the reliability of this methodology through cross-characterizations with other techniques on specifically chirality- and/or diameter-sorted samples. By comparing, first, Raman results with atomic resolution transmission electron microscopy statistical analyses, we evidence significant discrepancies between the two techniques. Further comparison with photoluminescence and optical absorption measurements shows that the observed discrepancies clearly stem from the chirality-dependence of SWCNT Raman cross-sections and the patchy vision offered by the use of only a few discrete excitation wavelengths, allowing us to propose some insights for a more reliable methodology.

**5:30 AM F.NM03.02.03**

**Precise Synthetic Control of  $sp^3$  Defects for Tunable Light Emission from Semiconducting Carbon Nanotubes** Felix J. Berger<sup>1</sup>, Simon Settele<sup>1</sup>, Sebastian Lindenthal<sup>1</sup>, Nicolas F. Zorn<sup>1</sup>, Abdurrahman Ali El Yumin<sup>1</sup>, Jesus Alejandro de Sousa<sup>2</sup>, Nuria Crivillers<sup>2</sup> and Jana Zaumseil<sup>1</sup>; <sup>1</sup>Heidelberg University, Germany; <sup>2</sup>Institut de Ciencia de Materials de Barcelona, Spain

Narrowband emission in the near-infrared and electrical generation of excitons make long, polymer-sorted semiconducting single-walled carbon nanotubes (SWNTs) desirable materials for light-emitting devices. Their successful functionalization with  $sp^3$  defects acting as luminescent exciton traps (ACS Nano 2019, 13, 9259) has emerged as a powerful route to accomplish red-shifted emission with increased efficiency and even single-photon emission at room temperature. Since the

emission properties of individual defects depend crucially on their binding configuration to the SWNT lattice and the nature of the attached functional group, they can be tuned over a certain energy range. Here, we present functionalization strategies enabling precise control of the defect binding configuration and thus emission wavelength and lifetime in polymer-wrapped (6,5) and (7,5) SWNTs. Electroluminescence from the introduced defects is readily achieved by incorporating such tailored SWNTs into a light-emitting field-effect transistor structure. To add further functionality, we have created  $sp^3$  defects bearing stable organic radicals. These paramagnetic and redox-active moieties respond to magnetic and electric fields and thereby allow for unprecedented control of the electronic structure at the defect site.

#### 5:40 AM F.NM03.02.05

**Liquid-Vapor Phase Transition of Water in Individual Single-Walled Carbon Nanotubes** Matthias Kuehne<sup>1</sup>, Samuel Faucher<sup>1</sup>, Mohan Teja Dronadula<sup>2</sup>, Mohammad Heiranian<sup>2</sup>, Narayana Aluru<sup>2</sup> and Michael Strano<sup>1</sup>; <sup>1</sup>Massachusetts Institute of Technology, United States; <sup>2</sup>University of Illinois at Urbana-Champaign, United States

The thermodynamic properties of fluids confined within nanometer-sized pores greatly differ from the ones of their bulk form. In particular, as the pore size becomes comparable to the size of the fluid's constituent molecules, the continuum assumption breaks down and peculiar size-dependent physicochemical behavior emerges. Here, we use Raman spectroscopy to probe the liquid-vapor phase transition of water inside individual, free-standing single-walled carbon nanotubes of different diameters. We report controlled and reversible vaporization of the nanoconfined water by varying the laser power of the Raman excitation laser. The Raman G band serves as built-in thermometer of the local nanotube temperature. We show that our measurements can be described by a diffusive heat transfer model, which allows extraction of the diameter-dependent phase transition temperature based on the characteristic redshift of the nanotube's radial breathing mode upon vaporization. We further perform all-atom molecular dynamics simulations to computationally corroborate our experimental results and to elucidate the underlying molecular behavior of water in these single-digit nanopores. Our results shed new insights on the physicochemistry of nanoconfined fluids, and will inform ongoing efforts in the field towards establishing a unified force field for water.

#### SESSION F.NM03.03: Theoretical Study

On Demand Abstracts Available for Viewing Starting Saturday Morning, November 21, 2020

F-NM03

#### 5:00 AM \*F.NM03.03.01

**Spin Filtering with Fluorinated Boron Nitride Nanotube** Ranjit Pati; Michigan Technological University, United States

Spin filtering, which is an important prerequisite for spin logic, involves the selective transmission of spin-polarized carriers. A perfect spin filter allows all majority (or minority) spin carriers to pass through a *channel* while blocking the minority (or majority) carriers. Since the discovery of magnetism in polymerized  $C_{60}$ , the search for a novel low-dimensional metal-free material that would exhibit magnetism at a higher temperature with excellent spin filtering property has been intensively pursued. In this talk, I will give an example of a spin filter comprised of a metal-free fluorinated single-wall boron nitride nanotube (F-BNNT) coupled to non-magnetic electrodes to elucidate the physics of spin filtering. Upon functionalization with fluorine, BNNT is found to display long-range ferromagnetic ordering of spins that is stable at a temperature much above the room temperature. The quantum transport approach is adopted to model the spin filter. Spin filter efficiency as high as 99.8% is found in a model F-BNNT junction.

#### 5:15 AM \*F.NM03.03.02

**Computational Modeling of Nanomaterials for Their Applications in Transistors and Layered Anodes** Swapan K. Pati; Jawaharlal Nehru Centre for Advanced Scientific Research, India

In recent years, many nanosystems, namely, carbon nanotube (CNT), graphene, BN sheet, metal dichalcogenides (MDC), borocarbonitride (BCN), black phosphorus (BP) etc. have been shown to exhibit many fold benefits for applications in a number of fields, namely, absorbates, chemical sensors, field effect transistors, solar cells, rechargeable battery, to name a few. In fact, recent experimental advancements on the control over the structural aspects of nanomaterials has enabled material scientists to tailor the material properties with improved reliability and functionality. We have been modeling these materials for their applications in electronic charge transport, as Li/Na/Mg Anode and various electronic and optical sensing

behaviors. We have derived relaxation time formulation from complete Boltzmann transport equation and obtained all the parameters from ab-initio density functional theory. Using this formalism, we have calculated charge carrier mobilities of a few BN-modified graphene layers and bilayer systems. We have shown that leading carrier transport in BCN layers can be changed from electrons to holes with high mobility values through change in surface topology [1]. We have computed mobility values for trilayer phosphorene and bilayer MoS<sub>2</sub> polytypes. The microscopic reason behind the carrier anisotropy and variation in terms of polytypes have been obtained [2,3]. In the case of rechargeable battery, we have looked at the potential of using Boron-sheet, BCN layer and BP as anode materials for Li, Na and Mg ion rechargeable battery and supercapacitors [4-6]. If time permits, I shall discuss Born-Oppenheimer Molecular Dynamics (BOMD) and DFT studies on trapping of BPA (Bisphenol A) with solvent [7], gaseous pollutants [8], DDT [9] on MDC, doped graphene and doped CNT respectively. We also have shown that it is possible to tune the interlayer coupling dynamically by signing light on the superlattices of graphene and BN sheet [10].

1. S. Banerjee and S K Pati, "Criticality of Surface Topology for Charge-carrier Transport Characteristics in Two-Dimensional Borocarbonitrides: Design Principle of an Efficient Electronic Material", *Nanoscale* **6**, 13430 (2014).
2. S. Banerjee and S K Pati, "Charge Transport Anisotropy in Black Phosphorus: Critical dependence on the number of layers", *Phys. Chem. Chem. Phys.* **18**, 16345 (2016).
3. S. Banerjee, J. Park, C. S. Hwang, J -H Choi, S -C Lee and S K Pati, "Polytypism regulates the transport property: A computational study on bilayer MoS<sub>2</sub>", *Phys. Chem. Chem. Phys.* **19**, 21282 (2017).
4. S. Banerjee, G. Periyasamy and S K Pati, "Possible application of 2D-Boron sheets as Anode Material in Lithium Ion Battery: A DFT and AIMD study", *J. Mater. Chem. A* **2**, 3856 (2014).
5. S. Banerjee, S. Neihial and S K Pati, "First-principles Design of a Borocarbonitride based Anode for Superior Performance in Sodium-ion Battery and Capacitor", *J. Mater. Chem. A* **4**, 5517 (2016).
6. S. Banerjee and S K Pati, "Anodic performance of Black Phosphorus in Magnesium-ion Battery: The Significance of Mg-P Bond synergy", *Chem. Commun.* **52**, 8381 (2016).
7. S. Banerjee and S K Pati, "Surface Mediated Extraction and Photo-response Modulation of Bisphenol A derivatives: A Computational Study", *ACS Appl. Mater. Interfaces* **7**, 23893 (2015).
8. D. Ghosh and S. K Pati, "Trapping of gaseous pollutants on defective N-doped graphene", *Phys. Chem. Chem. Phys.* **19**, 636 (2017).
9. A. Bandyopadhyay, D. Ghosh and S K Pati, "Sensing and Trapping Hazardous Insecticides by Single Walled Carbon Nanotubes", *Phys. Chem. Chem. Phys.* (revision, 2017).
10. P. Kumar et. al, "Laser Shock Tuning Dynamic Interlayer Coupling in Graphene-Boron Nitride Moire' Superlattices", *Nano Lett.* **19**, 283 (2019).

#### SESSION F.NM03.04: Biological Application

On Demand Abstracts Available for Viewing Starting Saturday Morning, November 21, 2020  
F-NM03

##### 5:00 AM F.NM03.04.01

**Ultra-High Brightness Fluorophores Based on Nanotubes** Yoke Khin Yap<sup>1</sup>, Nazmiye Yapici<sup>2</sup>, Rodney Oakley<sup>2</sup>, Xiuling Liu<sup>1</sup>, Steve Tokarz<sup>2</sup> and Dongyan Zhang<sup>1</sup>; <sup>1</sup>Michigan Technological University, United States; <sup>2</sup>StabiLux Biosciences, United States

We have developed a new nanotube technology for producing a series of dyes with ultra-high fluorescent brightness for biomedical application [1]. The brightness of our dyes is widely tunable, up to 1000 times brighter than any known dyes. Based on this technology, we have synthesized three types of new dyes NovoLux<sup>®</sup> 488 (488/515 nm), NovoLux<sup>®</sup> 560<sup>®</sup> (560/580 nm), and NovoLux 640<sup>®</sup> (640/660 nm). The design, synthesis, antibody conjugation, and extinction coefficient data of these new dyes will be presented in the meeting.

Organic dyes, and fluorescent proteins are widely used for biomedical application such as fluorescent microscopy and flow cytometry. Conventional organic dyes are not as bright as protein dyes such as PE (extinction coefficient,  $\epsilon = 2.5 \times 10^6 \text{ M}^{-1} \text{ cm}^{-1}$ ; quantum yield, QY= 0.8) and APC ( $\epsilon = 7.0 \times 10^5 \text{ M}^{-1} \text{ cm}^{-1}$ , QY=0.68). Our new platform dye technology allows us to synthesize ultra-high brightness dyes with extinction coefficient as high as  $10^{10} \text{ M}^{-1} \text{ cm}^{-1}$  [1]. Our dyes are constructed by three components: DSPE-PEG(5000)Amine, 1,2-distearoyl-sn-glycero-3-phosphoethanolamine-N-[amino(polyethylene glycol)-5000] as the polymeric linkers, carbon nanotubes (CNTs) and boron nitride nanotubes (BNNTs) as the nanocarriers,

and organic dyes as the fluorescent elements. DSPE-PEG (5000) Amine are *used as the linkers to conjugate organic dye molecules and antibody on CNTs or BNNTs*. BNNTs are chosen because they are electrically insulating and optically transparent (band gap of 6eV) [2-4]. BNNTs also offer defect-free surfaces with fully coordinated hexagonal boron nitride (h-BN) network that allow simple pi-pi conjugation of polymer linkers. Because of these unique properties, hundreds of organic dyes can be self-assembled on the surfaces of BNNTs through the DSPE-PEG linkers without quenching. This contributes to the high extinction coefficient and high-brightness of our dyes. Details of the design, synthesis, antibody conjugation, and extinction coefficient data of these new dyes will be presented in the meeting.

- [1] Y. K. Yap, D. Zhang, N. B. Yapici, "High-Brightness Fluorophores," US Patent Application US20180296705A1.  
[2] (Review) J. Wang, C. H. Lee, Y. K. Yap, "Recent Advancement in Boron Nitride Nanotubes," *Nanoscale* **2**, 2028 (2010)  
[3] C. H. Lee, et al, *Advanced Materials* **25**, 2544 (2013).  
[4] J. K. Qin, et al, *Nature Electronics*, 3(3), 141 (2020).

NovoLux® 488 and NovoLux® 640 are developed under the support of National Science Foundation (IIP 1521057, IIP 1738466). NovoLux® 560 is developed under the support of M-TRAC for Life Sciences Innovation Hub co-managed by the University of Michigan and the Michigan Economic Development Corporation (MEDC). We acknowledge supports from the Michigan Corporate Relations Network (MCRN) Small Company Innovation Program (SCIP), The Michigan Emerging Technologies Fund (ETF).

#### 5:10 AM \*F.NM03.04.02

**Ultra-High Brightness Dyes with Tunable Brightness for Flow Cytometry** Nazmiye Yapici<sup>1,2</sup>, Rodney Oakley<sup>1</sup>, Xiuling Liu<sup>2</sup>, Dongyan Zhang<sup>2</sup> and Yoke Khin Yap<sup>2</sup>; <sup>1</sup>Stabilux Biosciences, Inc., United States; <sup>2</sup>Michigan Technological University, United States

We have developed a platform technology which allow us to synthesize new dyes with ultra-high brightness for flow cytometry applications. Our unique technology allows us tuning brightness to desired levels (10X to 1000X brighter than commercial dyes) for detection of undetectable by achieving femtomole detection level.

Brightness of dyes are defined by multiplication of quantum yield (QY) and extinction coefficient of a dye. The known brightest commercial dyes are PE and APC with extinction coefficients  $2.5 \times 10^6 \text{ M}^{-1} \text{ cm}^{-1}$  (QY=0.8) and  $7.0 \times 10^5 \text{ M}^{-1} \text{ cm}^{-1}$  (QY=0.7), respectively. To date, we have developed ultra-high brightness fluorescent dyes in three colors: NovoLux® 488, NovoLux® 560 and NovoLux® 640. For one of our NovoLux 488 samples, the extinction coefficient is  $7 \times 10^7 \text{ M}^{-1} \text{ cm}^{-1}$  (QY= 0.5). This is brighter than FITC dye by 897X (extinction coefficient of FITC is  $7.8 \times 10^4 \text{ M}^{-1} \text{ cm}^{-1}$  QY=0.5). This make NovoLux 488 the brightest dye in the 488 channels. On the other hand, one of our NovoLux 560 samples offers an extinction coefficient of  $3 \times 10^7 \text{ M}^{-1} \text{ cm}^{-1}$  (QY=0.3), which resulted in 400X enhancement of conventional rhodamine B (extinction coefficient of  $7.5 \times 10^4 \text{ M}^{-1} \text{ cm}^{-1}$ , QY=0.3). Furthermore, NovoLux 560 is more photostable than rhodamine B and 6X brighter than PE. Finally, we have developed NovoLux 640 as the photostable and brighter dye option in the 640 channel. One of our NovoLux 640 sample offers an extinction coefficient of  $4 \times 10^7 \text{ M}^{-1} \text{ cm}^{-1}$  (QY=0.11). This NovoLux 640 sample is 110X brighter than Cy5.5 dye (extinction coefficient  $2 \times 10^5$ , QY=0.2). Furthermore, NovoLux 640 is more photostable than Cy5.5 and 8X brighter than APC.

As mentioned, the fluorescent brightness of NovoLux dyes can be tuned for desired brightness to meet various sample needs. The extinction coefficient of NovoLux dyes can be as high as  $1 \times 10^{10} \text{ M}^{-1} \text{ cm}^{-1}$  [1]. This unique property allow increase in signal to noise ratio, thus results in detection of rare antigens. The spectral properties, tunability, and application of NovoLux dyes in flow cytometry will be presented during the meeting.

- [1] Y. K. Yap, D. Zhang, N. B. Yapici, "High-Brightness Fluorophores," US Patent Application US20180296705A1.  
NovoLux 488 and NovoLux 640 are developed under the support of National Science Foundation (IIP 1738466) STTR Phase I and II awards. NovoLux 560 is developed under the support of M-TRAC for Life Sciences Innovation Hub co-managed by the University of Michigan and the Michigan Economic Development Corporation (MEDC). We acknowledge supports from the Michigan Corporate Relations Network (MCRN) Small Company Innovation Program (SCIP), The Michigan Emerging Technologies Fund (ETF).

#### 5:25 AM F.NM03.04.04

**Toxicological and Immunological Response Towards Carbon Nanomaterials—Hollow Carbon Spheres vs Graphene and Carbon Nanotubes** Isabel Gessner<sup>1</sup>, Sourav Mukherjee<sup>2</sup>, Fernando T. Andón<sup>2</sup>, Tim Ludwig<sup>1</sup>, Michael Wilhelm<sup>1</sup>, Bengt Fadeel<sup>2</sup> and Sanjay Mathur<sup>1</sup>; <sup>1</sup>University of Cologne, Germany; <sup>2</sup>Karolinska Institutet, Sweden

Carbon-based nanomaterials including low dimensional hollow carbon spheres (HCS) as well as graphene (GO) and carbon

nanotubes (CNTs) have found increasing application in various fields of our research and everyday life, being even considered as carriers for therapeutics and as intracellular imaging units. However, when it comes to medicinal applications of nanomaterials, toxicity remains a key issue. Approval of new therapeutic tools requires a detailed understanding of material-cell interactions starting with interactions with the first line of defense in our body, the immune system. We therefore synthesized HCS and GO nanosheets and evaluated their cytotoxic potential in comparison to single-walled CNTs (SWCNTs) towards human-monocyte derived macrophages. Besides electron microscopic evaluation of nanomaterial uptake and intracellular distribution, the formation of reactive oxygen species (ROS) and secretion of pro-inflammatory cytokines and chemokines was investigated revealing significant differences between carbon-based materials. Moreover, receptor line specific assays as well as by computational data were performed to analyze the roll of toll-like receptors (TLRs) in immunological nanomaterial sensing.

5:35 AM \*F.NM03.04.05

**Late News: The 'Chemistry' in Chemical Vapour Deposition CNT Growth—Insight from Molecular Simulations** Alister Page; The University of Newcastle, Australia, Australia

Over the last few decades, catalytic chemical vapor deposition (CVD) has matured as a synthetic technique for producing carbon nanotubes (CNTs) and graphene. The general mechanism of graphene and CNT formation during CVD is now well established [1]; nucleation and growth begin with the precipitation/aggregation of carbon atoms on a catalyst surface to form extended carbon chains, which quickly combine and oligomerise to form “islands” of  $sp^2$ -hybridized carbon. Larger nanostructures then form *via* the coalescence of these structures on the catalyst surface, which are stabilised through strong carbon-catalyst  $\sigma$ -bonding.

However, by and large this picture of nucleation has been developed by considering the chemistry of carbon by itself, when, in reality, there are many other chemical species present in a CVD reaction chamber. In this lecture I will discuss our recent work that shows the influence of such species on the nucleation and growth mechanisms of carbon nanomaterials during CVD (e.g.  $H_2$  [2,3],  $H_2O$  [4],  $NH_3$  [5], acetonitrile [6] etc.). I will also discuss how they influence catalyst formation and CNT nucleation during floating-catalyst CVD with ferrocene precursors [7]. Our simulations demonstrate how each of these parameters can potentially be exploited towards controlling growth. Importantly, we show that chemical etchants play key roles regarding growth control and kinetics, despite being overlooked in popular growth models to date.

[1] B. McLean et al., *Phys. Chem. Chem. Phys.* **19**, 26466-26494 (2017).

[2] I. Mitchell et al., *Carbon* **128**, 215 (2018).

[3] A. Saeed et al., *Adv. Func. Mater.*, (2020) DOI: 10.1002/adfm.202005016

[4] Hussein, A. et al., *Nanoscale*. **12**, 12263-12267 (2020).

[5] C. A. Eveleens et al., *Nanoscale* **9**, 1727 (2017).

[6] C. A. Eveleens et al., *Carbon* **146**, 535-541 (2019).

[7] B. McLean et al., *J. Appl. Phys.* (submitted)

SESSION F.NM03.05: Characterization

On Demand Abstracts Available for Viewing Starting Saturday Morning, November 21, 2020  
F-NM03

5:00 AM \*F.NM03.05.01

**Understanding Deformation and Exfoliation as a Route to Improved Exfoliation Yield and Topological Surface States** Sarah J. Haigh<sup>1</sup>, Zheling Li<sup>1</sup>, Aidan Rooney<sup>1</sup>, Yaping Yang<sup>1</sup>, Robert Young<sup>1</sup>, Feng Ding<sup>2</sup> and Artem Mishchenko<sup>1</sup>; <sup>1</sup>University of Manchester, United Kingdom; <sup>2</sup>Ulsan National Institute of Science and Technology (UNIST), Korea (the Republic of)

Scanning Transmission Electron Microscopy (STEM) is a key technique for probing the local defect microstructure of 2D materials and their parent crystals at the atomic scale. By combining STEM with electron energy loss spectroscopy and energy dispersive X-ray spectroscopy the local chemistry can also be investigated. Here we demonstrate the use of STEM imaging and analysis to investigate the microstructure of mechanically deformed and liquid phase exfoliated 2D van der Waals materials (graphite, boron nitride,  $MoSe_2$ ).

We find that at the atomic scale the bending behaviour, and types of microstructural defect that result, can be predicted from

just the bend angle and thickness of the materials.[1] In particular, we find that above a critical thickness the deformed materials exhibit numerous twin boundaries and for large bend angles these can contain nanoscale regions of local delamination. Such microstructural features are proposed to be important in determining how easily the material can be thinned by mechanical or liquid phase exfoliation.[1] Recent work has extended these studies to consider the microstructure of liquid exfoliated 2D van der Waals materials at the early stages of processing.[2] We demonstrate that during ultrasonic liquid phase exfoliation, the transition from graphite flakes to graphene takes place in three distinct stages. Firstly, sonication leads to the rupture of large flakes and the formation of kink band striations on the flake surfaces, primarily along zig-zag directions. Secondly, cracks form along these striations, and together with intercalation of solvent, lead to the unzipping and peeling off of thin graphite strips that in the final stage are exfoliated into graphene.[2] We anticipate that the findings will be of great value in the quest to optimize the lateral dimensions, thickness and yield of graphene and other 2D materials for various applications.

Furthermore, we demonstrate that in deformed graphite, zigzag kink bands (and associated twin boundaries) induce local stacking faults. Thus, the Raman signature of zigzag kink bands in graphite can be used to determine crystallographic directions. A sequence of ideal zigzag twin boundaries produces a region of crystal with a complex and highly unfavourable stacking sequence AABBC.[1] We find that by peeling along specific crystallographic direction mechanical exfoliation can be used to induce large areas of thermodynamically unfavourable rhombohedral (ABC) stacking in graphite. then perform directional encapsulation of ABC-rich graphite crystallites with hexagonal boron nitride (hBN). Encapsulation with hexagonal boron nitride, which is introduced parallel to the graphite zigzag edges, preserves ABC stacking, while encapsulation along the armchair edges transforms the stacking to ABA. [3] The ability to create and preserve ABC stacking has recently been used to reveal an abundance of exotic interaction-induced physics including topological surface states in this material. [4]

#### References

- [1] A. P. Rooney et al. Anomalous twin boundaries in two dimensional materials, Nature Communications (2018) 9, 3597
- [2] Z. Li et al Mechanisms of Liquid Phase Exfoliation for the Production of Graphene, ACS Nano, Article ASAP, 2020, 10.1021/acsnano.0c03916
- [3] Y. Yang et al. Stacking Order in Graphite Films Controlled by van der Waals Technology, Nano Lett. 2019, 19, 12, 8526–8532
- [4] Y. Shi et al Electronic phase separation in topological surface states of rhombohedral graphite, arXiv:1911.04565

#### 5:30 AM \*F.NM03.05.02

***In Situ* TEM Studies on 2D Materials** Xuedong Bai; Chinese Academy of Sciences, China

Two-dimensional (2D) materials show a variety of promising properties, and characterizing their structural properties is fundamental for basic research and practical applications. In-situ transmission electron microscopy (TEM) method is powerful in a way that it can directly correlate the atomic structure with physical and chemical properties. By using the in-situ TEM technique, the physical and chemical properties of nanomaterials have been investigated. In this presentation, we will report our progress on studies of electrochemical properties and phase transition mechanism of carbon nanostructures and 2D layered transition metal dichalcogenides (TMDs) by alkali metal storage. And the epitaxial growth of large-scale single crystal hBN monolayer will be also included.

#### 6:00 AM \*F.NM03.05.03

**Defects and Interlayer Coupling in van der Waals Heterostructures** Nedjma Bendiab<sup>1</sup>, G. Nayak<sup>1</sup>, Simone Lisi<sup>1</sup>, D. Kalita<sup>1,2</sup>, M. Lazzeri<sup>3</sup>, J. Renard<sup>1</sup>, V. Bouchiat<sup>1</sup>, J. Coraux<sup>1</sup> and L. Marty<sup>1</sup>; <sup>1</sup>Univ. Grenoble Alpes, CNRS, Grenoble INP, Institut NEEL, France; <sup>2</sup>Sorbonne Université, MNHN, UMR CNRS, France; <sup>3</sup>CEA, INAC-PHELIQS, France

Van der Waals heterostructures give access to a wide variety of new phenomena that emerge due to the combination of layered materials with different properties. One of the key engineers the properties of 2D materials could be in the ability to alter their structure in a controllable way. Different methods are possible: functionalization, intercalation, inducing defects etc. Whatever the chosen method the consequences is a strong modification of their structure and thus on their electronic and vibrational properties. All these effects can be probed efficiently by optical phonons. Up to now various methods have been used as argon bombardment, electron beam irradiation, graphene oxidation, ..ect.

In this work we will try to unravel the structural modification induced by defects in the case of graphene and MoS<sub>2</sub>. In the case of few- and single-layer MoS<sub>2</sub> hosting substantial defects densities, these defects are thought to influence the doping level, the crystal structure, and the binding of electron–hole pairs. We disentangle the concomitant spectroscopic expression

of all three effects and identify to what extent they are intrinsic to the material or extrinsic to it, i.e., related to its local. We discover a defect-bound state having a low binding energy of 20 meV that does not appear sensitive to strain and doping, unlike charged excitons. Conversely, the defect does not significantly dope or strain MoS<sub>2</sub> [1].

We also show here that due to an enhanced interaction cross section in such structure, made of molybdenum disulphide and boron nitride, electron-hole pairs can be generated by incident electrons and give rise to cathodoluminescence. Using Raman spectroscopy and photoluminescence, we show that low energy electron beam irradiation can nevertheless cause irreversible structural damages in molybdenum disulphide. A correlation between molybdenum disulphide/boron nitride coupling and the defect creation is established. Our work demonstrates that cathodoluminescence is powerful tool images the electronic properties in van der Waals heterostructures at the nanometer scale.

In the case of graphene, we report the observation of an intense anomalous peak in the Raman spectrum in specific growth conditions that cannot be attribute to structural defects. In fact, bombardment with an electron beam demonstrates that this new peak is clearly distinct from the well-studied D' peak appearing as defects are created in graphene [3].

[1] S. Dubey, et al, *ACS Nano*, **2017**, *11* (11), pp 11206–11216

[2] G. Nayak et al, *Phys. Rev. Materials* **3**, 114001 (2019)

[3] D. Kalita et al, submitted to PRB.

### 6:30 AM \*F.NM03.05.04

#### Electron-Beam Manipulation of Covalently Bound Lattice Impurities Toma Susi; University of Vienna, Austria

Covalently bound impurity atoms in crystal lattices can be manipulated using the atomically focused electron probe of an aberration-corrected scanning transmission electron microscope. This has unveiled new perspectives for top-down atomic engineering, with the potential to surpass existing techniques in both versatility and capabilities. Such advances have been made possible by developments in electron optics and instrument stability, and the incorporation of impurity elements using techniques such as ion implantation [1].

The first system where this potential was realized was incidental silicon impurities in single-layer graphene. Elastic backscattering of an energetic probe electron from a moving C nucleus [2] causes the Si to *directly exchange* places with one neighboring C atom via an out-of-plane displacement [3], and such dynamics can be controlled by directing the focused electron beam at the desired atom [4,5]. Recent experiments have demonstrated greatly improved control [6], with a manipulation rate already nearly on par with any atomically precise atom manipulation technique. Such manipulation is also possible in large-diameter single-walled carbon nanotubes [7].

Besides Si impurities, P dopants in graphene can be manipulated with an electron beam [8], but at least for the out-of-plane displacement mechanism, it seems there are physical limits on what is feasible since significantly heavier Ge impurities cannot be thus manipulated [9]. The curious replacement of irradiated impurities by carbon atoms has also emerged as a practical hurdle for the further scaling of the technique. However, there are many possible lattice impurity atoms whose atomic dynamics under electron irradiation have been observed, including N and B [10], though their manipulation has not yet been demonstrated.

Even more excitingly, the electron-beam manipulation of Bi dopants in bulk silicon was recently reported [11], although the precise mechanism remained unclear. We have applied our established *ab initio* modeling methodology [12] to address this question, revealing a novel type of mechanism we call *indirect exchange*. Contrary to the process in graphene, the primary knock-on atom does not end up as a neighbor of the impurity, but as a next-nearest neighbor, displacing another silicon atom during the dynamics. It is thus clear that electron-beam manipulation of lattice impurities has opened an exciting new frontier for materials science and nanotechnology.

#### References:

[1] T. Susi *et al.*, *2D Mater.* **4**, 021013 (2017)

[2] T. Susi, J.C. Meyer, J. Kotakoski, *Nat. Rev. Phys.* **1**, 397 (2019)

[3] T. Susi *et al.*, *Phys. Rev. Lett.* **113**, 115501 (2014)

[4] T. Susi *et al.*, *Ultramicroscopy* **180**, 163 (2017)

[5] O. Dyck *et al.*, *Appl. Phys. Lett.* **111**, 113104 (2017)

[6] M. Tripathi *et al.*, *Nano Lett.* **18**, 5319 (2018)

[7] K. Mustonen *et al.*, *Adv. Func. Mat.* **29**, 1901327 (2019)

[8] C. Su *et al.*, *Sci. Adv.* **5**:eaav2252 (2019)

- [9] M. Tripathi *et al.*, ACS Nano 12, 4641 (2018)  
[10] T. Susi *et al.*, 2D Mater. 4, 042004 (2017)  
[11] B. Hudak *et al.*, ACS Nano 12, 5873 (2018)  
[12] T. Susi *et al.*, Nature Communications 7, 13040 (2016)

#### 7:00 AM F.NM03.05.05

**Vertically Oriented Graphene Edges as a Tuneable Support to Preferentially Align Metal Electrocatalysts for Energy Conversion Reactions** Constantine Tsounis<sup>1</sup>, Nicholas Bedford<sup>1</sup>, Rose Amal<sup>1</sup> and Zhaojun Han<sup>1,2</sup>; <sup>1</sup>UNSW Sydney, Australia; <sup>2</sup>CSIRO, Australia

Engineering the metal-carbon hetero-interface has become an increasingly important route toward achieving cost effective and high performing electrocatalysts. In general, these interfaces can alter the valence states of metal electrocatalysts, changing the adsorbate energy of intermediates, and thus the reaction kinetics. The unique properties of graphene edge sites, such as the high available density of states and extended unpaired  $\pi$ -bonding, make it a promising candidate to tune the electronic properties of metal catalysts. Yet to date, understanding and leveraging graphene edge-metal catalysts for improved electrocatalytic performance remains largely elusive.

We demonstrate an efficient yet tuneable method to synthesize graphene edge planes at scale by combining plasma-enhanced chemical vapor deposition (PECVD) methods with a post-treatment Ar plasma. PECVD results in the growth of vertically aligned graphene (VG), with high surface area, an open and interconnected 3D structure, good mechanical stability, and high conductivity, on a range of substrates such as metal foams, foils, and carbon fibers. On the other hand, the Ar plasma post-treatment acts to induce branching of the graphene edges, rearranging carbon atoms under the plasma induced electric field, systematically increasing their exposed surface. By employing this method, it becomes possible to synthesize carbon-based electrocatalytic supports with desirable properties and edge-states, at large scale.

To demonstrate a specific application which exploits the exposed edge planes of VG, we employed this combined PECVD method with Ar plasma post-treatment to synthesize edge-rich VG (er-VG), and used it as a support for electrodeposited Ni-Fe hydroxides in the oxygen evolution reaction (OER). The hybrid Ni-Fe/er-VG catalyst exhibits excellent OER performance with a mass current of 4051 A g<sup>-1</sup> (at overpotential  $\eta$  = 300 mV) and turnover frequency (TOF) of 4.8 s<sup>-1</sup> ( $\eta$  = 400 mV), outperforming Ni-Fe deposited on pristine VG and other metal foam supports.

To understand how the edges were able to influence the valence state properties of the deposited metal, angle-dependent X-ray absorption spectroscopy was used to show that the edge-rich VG support can preferentially template Fe-O units with a specific valence orbital alignment interacting with the unoccupied density of states on the graphene edges. This graphene edge-metal interaction was shown to facilitate the formation of undersaturated and strained Fe-sites with high valence states, while promoting the formation of redox-activated Ni species, thus improving OER performance.

These findings open new opportunities in rationally designing the graphene edge-metal interface in electrocatalysts for various energy conversion and chemical synthesis reactions.

#### 7:10 AM F.NM03.05.06

**Fast Ion Diffusion in Carbon Nanotube Channels** Steven F. Buchsbaum, Melinda Jue, Chiatay Chen, Sei Jin Park, April Sawvel, Eric Meshot, Edmund Y. Lau, Tuan Anh Pham, Kuang Jen Wu and Francesco Fornasiero; Lawrence Livermore National Laboratory, United States

Many simulations and experiments have investigated pressure-driven fluid flow in carbon nanotubes (CNTs) and demonstrated enormous transport rates through these channels. Comparatively little attention has been given so far to concentration-driven transport<sup>1,2</sup> in CNTs despite its importance in a large variety of fields. While several studies assumed bulk/hindered diffusion for small molecules through nm-wide CNTs, other simulations have predicted self-diffusion coefficients several times larger than in the bulk. These large uncertainties in the magnitude of the diffusion rates through CNTs have hampered their full exploitation in nanofluidic devices.<sup>3</sup>

To obtain a precise quantification of the diffusive flow in CNTs, we have fabricated membranes with a large but known number of single-walled carbon nanotubes (SWCNT) as fluid transport pathways. Contrary to previous membrane systems, this platform enables us to minimize uncertainties in the calculation of the per-pore flow rate. A series of stringent control experiments confirms that these membranes are defect free and that transport occurs only through SWCNTs. Once corrected for the boundary layer resistance at the membrane/fluid interface, our measurements reveal that the transport diffusivity of



small ions in single-walled carbon nanotubes is more than one order of magnitude faster than in the bulk.<sup>4</sup> This flow enhancement scales with the ion free energy of transfer from bulk solutions to a nanoconfined, lower-dielectric environment. Together with indicating that CNT membranes could enable dialysis processes with unprecedented efficiency, these results have important implications for a broad range of applications such as energy storage/harvesting and chemical separation/detection, where ion permeation through nanoporous carbon materials is key.

## References

1. Y. Li, C. Chen, E. R. Meshot, S. F. Buchsbaum, M. Herbert, R. Zhu, O. Kulikov, B McDonald, N. Bui, M. L. Jue, S. J. Park, C. Valdez, S. Hok, C. J. Doona, K. J. Wu, T. M. Swager, F. Fornasiero, *Adv. Funct. Mater* (2020)
2. N. Bui, E. R. Meshot, S. Kim, J. Peña, P. W. Gibson, K. J. Wu, F. Fornasiero, *Adv. Mater.*, 28 (2016) 5871.
3. S. Guo, E. R. Meshot, T. Kuykendall, S. Cabrini, F. Fornasiero, *Adv. Mater.* 28 (2015), 5871.
4. S. Buchsbaum, M. L. Jue, C. Chen, E. R. Meshot, S. J. Park, A. Sawvel, E. Lau, T. A. Pham, K. J. Wu, F. Fornasiero, *under review* (2020)

### SESSION F.NM03.06: Thin Film Application

On Demand Abstracts Available for Viewing Starting Saturday Morning, November 21, 2020  
F-NM03

#### 5:00 AM \*F.NM03.06.02

**Tailoring Electronic Structure of SWCNTs for Transparent and Conductive Film Applications** Albert Nasibulin<sup>1,2</sup>; <sup>1</sup>Skolkovo Institute of Science and Technology, Russian Federation; <sup>2</sup>Aalto University, Finland

Single-walled carbon nanotubes (SWCNTs) are among the strongest candidates for the replacement of commonly used transparent and conductive films (TCFs) based on doped metal oxides, such as indium tin oxide. SWCNTs possess unique multifunctional nature, which is based on their outstanding combination of mechanical strength and flexibility, chemical stability, exceptional electrical conductivity and optical properties. However, to fully utilize these properties in modern transparent electrode applications, SWCNT-based TCFs have to demonstrate the optoelectronic performance at the level of high-end ITO-based TCFs. This has not been achieved for SWCNT films yet and as a result limit their practical usage.

Using gold chloride as the most effective dopant for the SWCNTs, we improve their optoelectrical characteristics by optimizing the doping solvent and conditions. We examined various solvents to push the optoelectrical performance of the TCFs based on SWCNTs. As a result, we obtained the sheet resistance as low as 40  $\Omega$ /sq at the transmittance of 90% (at 550 nm) using 15 mM HAuCl<sub>4</sub> solution. This optoelectrical performance is better than that of ITO on PET substrates and satisfy most of the requirements for modern applications and relatively stable without additional protection over two years storing under ambient conditions.

We propose a few interesting novel methods for SWCNT doping: aerosol doping and dip-coating methods will be discussed.

The effect of the presence of catalyst particles on the optoelectronic properties of the SWCNT films is also investigated.

Also, we propose a novel approach to enhance optoelectronic performance of SWCNTs using ionic liquid. The method provides fine and reversible tuning of optoelectrical properties of SWCNT films over a wide range of parameters. Using imidazolium-based ionic liquid with a wide electrochemical window (BMIM-PF<sub>6</sub>), we achieved the film sheet resistance as low as 53  $\Omega$ /sq at the 90% transmittance, thereby shifting the SWCNT Fermi level up to 1.4 eV. We believe the results to promote collateral research of adjustable tuning of the electronic structure of carbon nanomaterials as promising components for future electronics, electrochromic devices, and ionotronics.

Although carbon nanotubes have been already demonstrated to be a promising material for bolometric photodetectors, the sensitivity enhancement while maintaining the speed of operation remains a great challenge. Here, we present a holey carbon nanotube network, designed to improve the temperature coefficient of resistance for highly sensitive ultra-fast broadband bolometers. Treatment of carbon nanotube films with low frequency oxygen plasma allows fine tuning of electronic properties of the material. The temperature coefficient of resistance of our films is much greater than reported values for

pristine carbon nanotubes, up to  $-2.8\% \text{ K}^{-1}$  at liquid nitrogen temperature. The bolometer prototypes made of the treated films demonstrate high sensitivity in a wide IR range, short response time, smooth spectral characteristics and low noise level.

And finally, we develop a novel transparent p-type flexible electrode based on SWCNTs combined with poly(3,4-ethylenedioxythiophene) polystyrene sulfonate (PEDOT:PSS), molybdenum oxide and SWCNT fibers. We achieved a record equivalent sheet resistance of  $17 \Omega/\text{sq}$  with a transmittance of 90% at 550 nm and a high degree of flexibility. We demonstrate that our solar cells based on the proposed electrode and hydrogenated amorphous silicon (a-Si:H) yield an outstanding short-circuit current density of  $J_{sc} = 15.03 \text{ mA}/\text{cm}^2$  and a record power conversion efficiency of  $\text{PCE} = 8.8\%$  for SWCNTs/a-Si:H hybrid solar cells.

This work was supported by the Russian Science Foundation (Project identifier: 17-19-01787) and RFBR (project number: 20-03-00804).

#### 5:15 AM F.NM03.06.03

**Selectivity, Ion Transport and Osmotic Power Generation in Boron Nitride and Carbon Nanotube Membranes** Semih Cetindag<sup>1</sup>, Aaditya Pendse<sup>2</sup>, Richard Castellano<sup>1</sup>, Joshua Yi<sup>1</sup>, Robert F. Praino<sup>3</sup>, Sangil Kim<sup>2</sup> and Jerry Shan<sup>1</sup>; <sup>1</sup>Rutgers, The State University of New Jersey, United States; <sup>2</sup>University of Illinois, Chicago, United States; <sup>3</sup>Chasm Advanced Materials, United States

Carbon nanotube (CNT) membranes are known to have enhanced transport of fluids, including water vapor, gases, and liquids. They are not known for having enhanced ion transport or being ion-selective, unless their pores are sub-nanometer in diameter or their tips/surfaces are functionalized. On the other hand, recent experiments with single  $\sim 30\text{-}80\text{nm}$ -diameter boron-nitride nanotubes (BNNTs) have reported large surface charge in aqueous solution, and ion selectivity for diameters beyond the well-known Donnan exclusion that is typical of separation membranes. When placed in a salt-concentration gradient, the single BNNT generated electrical power from the Gibbs free energy of mixing at power densities up to  $4,000 \text{ W}/\text{m}^2$  when extrapolated to macroscopic membranes. However, no such macroscopic BNNT membranes have ever been fabricated, and their performance at large scales and pore densities has been unknown.

Here, we describe the scalable fabrication of the first macroscopic, vertically aligned- (VA-) BNNT membranes with pore densities of  $10^7$  open-BNNTs/ $\text{cm}^2$ , and report their remarkable osmotic-power-generation performance. We make comparison to vertically aligned carbon-nanotube membranes fabricated by the same solution-based technique, which have similar atomically perfect, 1D (but uncharged) pores. We find that that the fast, selective ion transport in 3 and 12 nm-diameter BNNT pores arises from enhanced diffusio-osmotic transport of concentrated cations next to the negatively charged surface, coupled with the deformation or removal of hydration shells around the ions. Due to nanoscale confinement and surface charge in their pores, the BNNT membranes were highly cation-selective, generating an open circuit potential of 295mV and a short circuit current of  $20\mu\text{A}$ , even for 1M solution for which the Debye length is smaller than the nanotube radius. In comparison, CNT membranes with the same 3 nm-diameter pores showed no selectivity and generated negligible osmotic power. The BNNT pores showed fast cation transport rates under a concentration gradient, exceeding the rate of bulk diffusion by at least  $21\times$  for  $\text{Li}^+$ . This ultrafast, selective cation transport in BNNT pores generated osmotic power via reverse electrodialysis at extraordinary power densities of  $14,000 \text{ W}/\text{m}^2$  of open pore area for 1M:1mM LiCl solutions at pH 11. With surface-dominated transport, novel ion-selective membranes with 1D BNNT pores overcome the traditional trade-off between selectivity and transport rates in polymeric membranes, and may enable harvesting of blue energy, as well as efficient desalination and other separations, via a fundamentally different mechanism than conventional systems.

#### 5:25 AM F.NM03.06.04

**Molybdenum Disulfide Quantum Dot-Sensitized Zinc Oxide Thin-Film Solar Cells** Jeff Kabel<sup>1</sup>, Amit Acharya<sup>1</sup>, Mingxiao Ye<sup>2,1</sup>, Dongyan Zhang<sup>1</sup> and Yoke Khin Yap<sup>1</sup>; <sup>1</sup>Michigan Technological University, United States; <sup>2</sup>The University of Texas at Dallas, United States

Thin-film solar cells show promise for light-weight, low-cost, large area, flexible devices. Unlike competing materials, zinc oxide (ZnO) and molybdenum trioxide ( $\text{MoO}_3$ ) are relatively abundant, environmentally stable, and have been proven effective for use in quantum dot-sensitized solar cells. The surfaces of nanostructures are often dominated with dangling bonds capable of trapping charges and limiting effective charge transport after electron-hole separation. Thus, it is anticipated that quantum dot-sensitized ZnO solar cells will be more efficient than devices constructed with traditional ZnO nanostructures. Molybdenum disulfide ( $\text{MoS}_2$ ) has attractive features, including its semiconducting nature and indirect-to-direct band gap transition when cleaved from bulk to monolayer.  $\text{MoS}_2$  quantum dots have been shown to have broad absorption bands, potentially making them invaluable for QD-sensitized photovoltaic devices. In this work, we use

conventional thin film technology to fabricate MoS<sub>2</sub> QD-Sensitized ZnO thin film solar cells.

A top-down approach was employed to convert bulk MoS<sub>2</sub> powder into QDs via sonication and solvothermal methods. The MoS<sub>2</sub> QDs absorb a wide spectrum of white, ranging from 320 nm to 520 nm, and fluoresce wavelengths ranging from 385 nm to 569 nm. This broad absorption wavelength contains the peak of the solar radiation spectrum, which enables effective photoelectron production in our device. Additionally, the QDs were found to exhibit fluorescence dependent on the excitation wavelength, enabling the production of excitons from a wider range of solar wavelengths.

Morphological characterization of the produced MoS<sub>2</sub> QDs was carried out using transmission electron microscopy (TEM) and atomic force microscopy (AFM), and statistical analysis of the lateral dimension and thickness was conducted. The MoS<sub>2</sub> QDs range from 2 – 40 nm in dimension. The devices were fabricated by depositing ZnO, MoS<sub>2</sub> QDs, MoO<sub>3</sub>, and Au respectively onto commercial indium tin oxide (ITO) glass using pulsed laser deposition (PLD). Fluorometry measurements were conducted following each deposition to obtain the fluorescence spectra. The current-voltage characteristics of the devices were measured under the illumination of a solar simulator, and the fill factor and power conversion efficiency (PCE) were calculated. A detailed discussion of the results of optimized devices will be had during the presentation.

#### 5:35 AM F.NM03.06.05

**Morphology and Structure Optimization of Freestanding Reduced Graphene Oxide Films as Highly Conductive and Flexible Electrodes** Tim Ludwig, Minyeong Je, Heechae Choi, Michael Wilhelm and Sanjay Mathur; University of Cologne, Germany

Lithium-ion-batteries (LIBs) are one of many applications that is expected to benefit from mechanical strength, high surface area and electrical conductivity of graphene when incorporated into electrode materials. For the integration in commercial LIBs, it is important to develop simple, cost effective and scalable methods for the production of graphene-like structures. Here we report on a green and simple wet chemical synthesis for the controlled formation of freestanding paper-like structures of regularly arranged graphene oxide (GO) flakes, using GO as starting material. As obtained structures were mechanically stable, scalable to mass production and could be used as flexible electrode materials in LIBs. Besides superior mechanical properties, rGO films led to increased volumetric energy densities due to the reduction in weight, making use of a current collector and the preparation of a battery slurry obsolete.

Moreover, morphology and structure of the material was significantly influenced by pre-reduction and vapor treatment of the films leading to enhanced electrical conductivities and lithium storage capacities. Especially in terms of defects and interlayer distances the results confirm the subtle interplay of chemical treatments and electronic properties of graphene oxide materials, which was additionally proven by DFT calculations.

In terms of cathode materials, freestanding rGO films served as a highly conductive backbone for lithium sulfide/rGO-composites, in which the active material was well-distributed within the carbon matrix. This prevents the agglomeration of lithium sulfide, buffers the volume change during cycling and offers a good accessibility for charge carriers.

Our results demonstrate the integration of freestanding and flexible rGO films into LIB half-cells highlighting their exceptional versatility and high application potential.

#### 5:45 AM F.NM03.06.06

**Porous Organo-Heterostructure Based Reduced Graphene Oxide Materials for Hydrogen Storage** Feng Yan and Petra Rudolf; University of Groningen, Netherlands

Hydrogen is a promising sustainable alternative to conventional fuels that can push forward the energy transition because of its prominent advantages such as high energy density (142 MJ kg<sup>-1</sup>), great variety of potential sources, light weight, and low environmental impact, while the storage remains a formidable scientific challenge. Magnesium hydride, with its inherently high gravimetric and volumetric density (7.6 wt.% & 110 g L<sup>-1</sup>), presents a compelling platform for hydrogen storage, however, two major impediments hindered its practical utilization: the sluggish hydrogen kinetics of uptake and release process and high temperature operation.

Herein, a novel porous heterostructure material with high specific surface area and narrow pore size distribution was synthesized by sol-gel reaction of Graphene Oxide and an organosilicon precursor, followed by MgH<sub>2</sub> particle (d < 5nm) grown in the framework. The material was characterized with BET, SEM, XRD and TEM and shows remarkable crosslinked layered structure with narrow interlayer distance. Studies of hydrogen storage properties showed that hydrogen released at low temperature (110 °C) and centred at 350 °C with kinetics dependent to some extent on the particle size.

**5:00 AM \*F.NM03.07.01**

**Device Applications of One-Dimensional Van der Waals Hetero-Nanotubes** Shigeo Maruyama; The University of Tokyo, Japan

We have synthesized a new coaxial nanotube structure, in which mono- or few-layer hexagonal boron nitride nanotube (BNNT) seamlessly wrap around a single-walled carbon nanotube (SWCNT); SWCNT@BNNT [1]. We named these as one-dimensional van der Waals hetero-nanotubes, because we found no correlation between chiral angle of inner SWCNT and outer BNNT for 'double-walled' SWCNT@BNNT. We have further developed the 1D coating CVD of transition metal dichalcogenide nanotubes (TMD-NT), such as MoS<sub>2</sub> nanotubes [1]. These nanotubes can be labelled as SWCNT@BNNT@MoS<sub>2</sub>. Because BNNT is thermally more stable than SWCNT, we can remove SWCNT from SWCNT@BNNT by the gentle oxidation process. Hence, we can produce BNNT with inner diameter determined by the original SWCNT. Then, the MoS<sub>2</sub> CVD can result BNNT@MoS<sub>2</sub>. These hetero-nanotubes are characterized by HR-TEM, STEM-EELS, absorption, Raman and photoluminescence (PL) spectroscopy. We found the bright PL from MoS<sub>2</sub> nanotubes for BNNT@MoS<sub>2</sub>. From DFT calculations, we expect that the K point direct band gap for 2D MoS<sub>2</sub> should appear for MoS<sub>2</sub> nanotubes with larger diameter such as 3-4 nm. The PL from MoS<sub>2</sub> was quenched by inner SWCNT (metallic or small band-gap semiconductor) in the hetero-nanotube, SWCNT@BNNT@MoS<sub>2</sub>. So far, the coating growth can be efficiently performed for vertically aligned array of SWCNT, suspended SWCNTs between pillars, zeolite based bulk sample and dry-deposited random network films. For field effect transistor (FET) devices, we need to start from suspended SWCNTs. We will demonstrate the growth of suspended hetero-nanotubes between pillars and the transfer to Si/SiO<sub>2</sub> substrate for device characterizations.

Reference:

[1] R. Xiang, T. Inoue, Y. Zheng, A. Kumamoto, Y. Qian, Y. Sato, M. Liu, D. Tang, D. Gokhale, J. Guo, K. Hisama, S. Yotsumoto, T. Ogamoto, H. Arai, Y. Kobayashi, H. Zhang, B. Hou, A. Anissimov, M. Maruyama, Y. Miyata, S. Okada, S. Chiashi, Y. Li, E. I. Kauppinen, Y. Ikuhara, K. Suenaga, S. Maruyama, *Science* **367**, 537-542 (2020).

**5:15 AM \*F.NM03.07.02**

**Raman Response and Transport Properties of Tellurium Atomic Chains Encapsulated in Nanotubes** Peide P. Ye; Purdue University, United States

Tellurium can form nanowires of helical atomic chains. With their unique one-dimensional van der Waals structure, these nanowires are expected to show physical and electronic properties that are remarkably different from those of bulk tellurium. Here, we show that few-chain and single-chain van der Waals tellurium nanowires can be isolated using carbon nanotube and boron nitride nanotube encapsulation. With this approach, the number of atomic chains can be controlled by the inner diameter of the nanotube. The Raman response of the structures suggests that the interaction between a single-atomic tellurium chain and a carbon nanotube is weak, and that the inter-chain interaction becomes stronger as the number of chains increases. Compared with bare tellurium nanowires on SiO<sub>2</sub>, nanowires encapsulated in boron nitride nanotubes exhibit a dramatically enhanced current-carrying capacity, with a current density of  $1.5 \times 10^8$  A cm<sup>-2</sup> that exceeds that of most semiconducting nanowires. We also use our tellurium nanowires encapsulated in boron nitride nanotubes to create field-effect transistors with a diameter of only 2 nm. The work is in close collaborations with the research teams of Profs. Moon J. Kim, Wenzhuo Wu, Xianfan Xu, Hai-Yan Wang, Li Yang, Yoke Khin Yap.

**5:30 AM \*F.NM03.07.03**

**Surface Functionalization of Nanocarbon Field-Effect Transistors Using Diazonium Chemistry** Delphine Bouilly, Claudia Marcela Bazan, Anouk Béraud and Amira Bencherif; Université de Montréal, Canada

In field-effect transistors made of atomically-thin nanomaterials such as carbon nanotubes or graphene, functionalization of the nanocarbon surface is necessary to control its interaction with surrounding media, especially for applications as chemical or biosensors. Aryldiazonium salts are a common approach to form covalent adducts on nanocarbon materials, but controlling the density and position of grafts is a challenge. In this presentation, I will describe the recent development of approaches based on nanolithography and electrochemistry to control the distribution of aryldiazonium-based adducts on nanocarbon materials. I will discuss differences between carbon nanotubes and graphene, as well as applications of such functionalized

field-effect transistors for biosensing and single-molecule experiments.

**5:45 AM \*F.NM03.07.04**

**Nafion/CNT Passivated Charge Selective Contacts for Silicon Photovoltaics** Ben Flavel; Karlsruhe Institute of Technology, Germany

In the past, the application of carbon nanotube-silicon solar cell technology to industry has been limited by the use of a metallic frame to define the active area in the middle of a silicon wafer. In our work, we use industry standard device geometries with a front- and back-junction design which allow for the entire wafer to be used as the active area. These are enabled by the use of an intermixed Nafion layer which simultaneously acts a passivation, antireflective and physical blocking layer as well as a nanotube dopant. This leads to the formation of a hybrid nanotube/Nafion passivated charge selective contact (PCSC) and solar cells with active areas of 1 – 16 cm<sup>2</sup> are fabricated. Record maximum power conversion efficiencies of 15.2% and 18.9% are reported for front- and back-junction devices for 1 cm<sup>2</sup> and 3 cm<sup>2</sup> active areas, respectively. By placing the nanotube film on the rear of the device in a back-junction architecture many of the design related challenges for carbon nanotube silicon solar cells are addressed and their future application to industrialized processes are discussed.

Additionally, traditional silicon solar cells extract holes and achieve interface passivation with the use of a boron dopant and dielectric thin films such as silicon oxide or hydrogenated amorphous silicon. Without these two key components, few technologies have realized power conversion efficiencies above 20%. We now develop a carbon nanotube/Nafion ink that can be spin coated directly onto a silicon wafer to serve simultaneously as a hole extraction layer, but also to passivate interfacial defects. This enables a low-cost fabrication process that is absent of vacuum equipment and high-temperatures. Power conversion efficiencies of 21.4% on an device area of 4.8 cm<sup>2</sup> and 20% on an industrial size (245.71 cm<sup>2</sup>) wafer are obtained.

[1] D. D. Tune, N. Mallik, H. Fornasier, B. S. Flavel, *Adv. Energy Mater.* 10, 2020, 1903261. DOI: 10.1002/aenm.201903261

[2] J. Chen, D. D. Tune, K. Ge, H. Li, B. S. Flavel, *Adv. Funct. Mater.* 2020, 2000484. DOI: 10.1002/adfm.202000484

[3] J. Chen, L. Wan, H. Li, J. Yan, J. Ma, B. Sun, F. Li, B. S. Flavel, *Adv. Funct. Mater.* 2020, just accepted manuscript. DOI: 10.1002/adfm.202004476

**6:00 AM F.NM03.07.07**

**Radio Frequency Heating of Carbon Nanomaterial-Based Structures—Universal Patterns and Application to Electronic Circuit Characterization** Muhammad Anas<sup>1</sup>, Mazin Mustafa<sup>1</sup>, Daniel Carey<sup>1</sup>, Lee Moores<sup>2</sup> and Micah Green<sup>1</sup>; <sup>1</sup>Texas A&M University, United States; <sup>2</sup>U.S. Army Engineer Research and Development Center, United States

Our group has recently demonstrated low frequency (1-200 MHz) and low power (<100 W) radio frequency (RF) heating of carbon nanomaterial-loaded structures such as thin films and polymer nanocomposites using an array of contact and non-contact applicators. These heating techniques have opened up routes for faster and efficient composite manufacturing, 3D printing, and fiber processing. It is known that electrical conductivity is required for RF heating of carbon-based nanomaterials. However, it is not well understood how RF heating rates vary with conductivity and if the pattern is generalizable for all types of RF susceptor-loaded structures. In this work, we use experiments and simulations to explore the universal patterns observed between RF heating rates and in-plane electrical conductivity for different nanomaterial-loaded thin films. We also show existence of similar patterns in chirality-sorted nanomaterial films, and finally we show a novel RF heating-based high-throughput quality screening technique for carbon nanotube circuits.

We synthesize multi-walled carbon nanotube (MWCNT) films, laser-induced graphene (LIG) films, and carbon nanofiber-polyamide (CNF-PA) composites of varying electrical conductivity by changing sprayed film thickness, laser parameters, and CNF content, respectively. We use a coplanar strip fringing-field applicator to assess RF heating behavior of nanomaterials in the frequency range of 1-200 MHz and at power of 2 W. This applicator allows for non-contact capacitive coupling of RF fields with the sample and heat it as high as 70°C/s at 2 W.

We find that for each of the nanomaterials tested, the highest heating rate observed across all frequencies is non-monotonically related with the in-plane electrical conductivity. This relationship has a distinguished maximum at approximately the same DC in-plane electrical conductivity (in the range of 0.1-0.2 mS) for all nanomaterials. We find that the point of maximum heating rate is closely associated with the percolation threshold. It is because at percolation a conductive network is formed and if the conductivity is increased further, reflections of RF fields lead to decrease in heat rates. This is also confirmed by our assessment of RF heating behavior of sorted and purified metallic (m-) and semi-conducting (s-) single-walled carbon nanotubes (SWCNTs). We find that 98% pure m-SWCNT film reflect RF fields and

heat at a highest rate of 2 °C/s compared to 100% pure s-SWCNT film's highest heating rate of 26 °C/s. We also find that the presence of impurities in the m-SWCNT film increases its heating rate to 10 °C/s due to disruption of the conductive network. These findings could make RF heating a promising metric for evaluating m-SWCNT film purity.

Finally, we apply the conductivity dependent RF heating behavior to demonstrate a reliable and high-throughput screening method for screen-printed MWCNT circuits. We show that large amounts of circuits can be simultaneously scanned over a fringing-field applicator which allows for rapid screening based on the uniformity of thermal response and the heating temperature observed using a thermal camera. This method is ideal for faster production of CNT circuits and replaces previous time-consuming quality metrics such as 2-point probe and 4-point probe measurements. It provides a tenfold increase in speed, allowing for real-time monitoring of circuits as they are produced. The scanning method is more reliable than the traditional metric in screening-out faulty circuits and can also be employed at various stages of the circuit manufacturing process.

#### 6:10 AM F.NM03.07.08

##### **Excess Polymer in Single-Walled Carbon Nanotube Field-Effect Transistors—Does It Really Need to be Removed**

**Prior to Fabrication** [Nicole Rice](#)<sup>1</sup>, Brendan Mirka<sup>1</sup>, Phillip Williams<sup>1</sup>, Mathieu Tousignant<sup>1</sup>, William J. Bodnaryk<sup>2</sup>, Darryl Fong<sup>2</sup>, Alex Adronov<sup>2</sup> and Benoit Lessard<sup>1</sup>; <sup>1</sup>University of Ottawa, Canada; <sup>2</sup>McMaster University, Canada

Single-walled carbon nanotubes (SWNTs) are promising nanomaterials for incorporation into solution-processed organic electronic devices (OEDs). As-synthesized SWNTs are insoluble and comprised of a mixture of metallic and semiconducting SWNTs (sc-SWNTs), necessitating dispersal and purification before integration into OEDs. Refinement of conjugated polymer extraction techniques has allowed for the isolation of sc-SWNTs from metallic in a reproducible and scalable manner, affording highly-soluble dispersions of sc-SWNTs for potential integration into inexpensive solution-processing techniques. Furthermore, the availability of ultrapure sc-SWNT materials has facilitated the production of field-effect transistors (FETs) with very high charge carrier mobilities and good on-off ratios, outperforming most organic semiconducting small molecules and polymers.

Despite the plethora of high-quality polymer-sorted sc-SWNT dispersions reported in the literature, the realization of commercial OED applications has not yet been achieved. This is partially attributed to the prohibitive time and materials costs associated with purifying sc-SWNTs. Current protocols for dispersing sc-SWNTs with conjugated polymers typically involve three broad steps: (1) dispersion of bulk SWNT material with the conjugated polymer, (2) removal of non-dispersed carbonaceous materials, and (3) removal of excess polymer through filtration or centrifugation. While the first two steps are relatively facile and can be performed on large scales, the final step of removal of excess polymer is laborious and resource-intensive. However, removal of excess polymer is viewed as essential for preparing high-performing FETs, as the conjugated polymer has much lower performance compared to SWNTs.

In this study, we performed the first systematic investigation of the effect of excess polymer during device fabrication on SWNT FET performance. Large numbers of replicate FET devices were characterized using several metrics, including mobility, threshold voltage, on/off ratios and hysteresis. Two different conjugated polymers were investigated at three different SWNT concentrations, with varying ratios of excess polymer added. Extensive analysis of the polymer-sorted sc-SWNT films through Raman spectroscopy and atomic force microscopy (AFM) showed that below a threshold amount of excess polymer, a simple rinsing step was sufficient to remove all unbound polymer from the substrate surface. The volume of solvent required for this rinsing step was substantially lower than that required for filtration or centrifugation; additionally, many literature procedures for sc-SWNT FET device fabrication already incorporate similar solvent rinses. Most importantly, at higher SWNT concentrations, the presence of excess polymer during device fabrication resulted in moderately improved device performance in both mobility and on/off ratios, with preeminent devices achieved from the original dispersions (before removal of excess polymer) for both polymer systems. Analysis of AFM images of these polymer-sorted sc-SWNT films with a novel Machine Learning algorithm showed that improved device performance could be attributed to more even sc-SWNT films and reduced bundling. Our results have important implications in the development of SWNT inks for commercial printing applications, as the presence of excess polymer can both increase the stability of the inks, as well as improve viscosity.

#### 6:20 AM F.NM03.07.09

##### **Late News: Electronic Properties of Bottom-Up Synthesized 17- and 13-Atom-Wide Graphene Nanoribbons**

[Junichi Yamaguchi](#)<sup>1</sup>, Hironobu Hayashi<sup>2</sup>, Hideyuki Jippo<sup>1</sup>, Akitoshi Shiotari<sup>3</sup>, Manabu Ohtomo<sup>1</sup>, Mitsuhiro Sakakura<sup>2</sup>, Nao Hieda<sup>2</sup>, Naoki Aratani<sup>2</sup>, Mari Ohfuchi<sup>1</sup>, Yoshiaki Sugimoto<sup>3</sup>, Hiroko Yamada<sup>2</sup> and Shintaro Sato<sup>1</sup>; <sup>1</sup>Fujitsu Laboratories Ltd. and Fujitsu Ltd., Japan; <sup>2</sup>Nara Institute of Science and Technology, Japan; <sup>3</sup>The University of Tokyo, Japan

Graphene nanoribbons (GNRs) exhibit unique electronic and magnetic properties that do not appear in two-dimensional graphene. These properties can emerge from the structural boundary conditions imposed by the atomically precise width and

edge structure of GNRs. For instance, armchair-edged GNRs (AGNRs) show sizable gapped electronic states established by the quantum confinement and edge effects. In graphene-based electronics, AGNRs with finite bandgaps at room temperature have attracted much attention for their potential reliability as semiconducting channels for field-effect transistors (FETs). For fabricating atomically precise GNRs, a bottom-up synthesis technique has recently been demonstrated via on-surface-assisted polymerization and subsequent cyclodehydrogenation of precursor monomers on metal substrates [1]. The bottom-up synthesis of *N*-AGNRs (where *N* is the number of carbon atom pairs across the ribbon) has been widely conducted because the bandgap of AGNRs can be tuned by changing their width. According to first-principles calculations using many-body perturbation theory (*GW* approximation) for freestanding *N*-AGNRs, the quasiparticle gap is predicted to be 3.80 eV for *N* = 7, 2.16 eV for *N* = 9, and 2.25 eV for *N* = 13 [2]. Previous studies on FETs using bottom-up AGNRs with widths of *N* = 7, 9, and 13 presented their electrical transport characteristics [3, 4]. However, in such GNR-based FETs, the intrinsic transport properties of AGNRs were obscured by a large Schottky barrier resistance between the AGNRs and metal contacts due to the large bandgaps in the above AGNRs, substantially exceeding 1 eV. These transport characteristics can be improved with wider AGNRs, as they are expected to have lower Schottky barriers arising from their small bandgap features. In our presentation, we show the bottom-up synthesis of well-structured 17-AGNRs and 13-AGNRs on Au(111) by using 1,2-bis-(2-anthracenyl)-3,6-dibromobenzene and 1,2-bis-(2-naphthalenyl)-3,6-dibromobenzene, respectively [5]. To systematically control the width of these AGNR, in the precursor monomers, either two anthracene or naphthalene units were attached at the *ortho*-positions of *p*-dibromobenzene. Characterization of the atomic and electronic structures of the 17- and 13-AGNRs on Au(111) was carried out by combining scanning tunneling microscopy and spectroscopy (STM/STS) and non-contact atomic force microscopy (nc-AFM). In both AGNRs, STM and nc-AFM observations revealed their widths and armchair-edged structures at atomic precision. In the *GW* calculations, the quasiparticle gap for freestanding 17- and 13-AGNRs is predicted to be 0.63 and 2.25 eV, and their values are corrected as 0.20 and 1.29 eV considering the image-charge effects from the metal substrates [6]. By STS measurements, we revealed that the experimental gap is 0.19±0.03 and 1.34±0.03 eV for the 17- and 13-AGNRs on Au(111), which is consistent with the accordingly corrected quasiparticle gaps predicted from the *GW* calculations. For more detailed discussions on the electronic band dispersions of the 17- and 13-AGNRs, we carried out Fourier-transformed STS (FT-STs) measurements. We found that the FT-STs provides the electronic band dispersions, which reasonably match the simply rigid-shifted *GW* quasiparticle bands in both AGNRs. As far as we know, the bottom-up synthesis of 17-AGNRs is the first demonstration of GNRs having a bandgap smaller than 1 eV in a controlled manner, which will pave the way for the development of GNR-based electronic devices. This work was supported by CREST JST (no. JPMJCR15F1) and MEXT/JSPS KAKENHI grant nos. 26105004, 16H02286, 18K14190, and 18H01807.

- [1] J. Cai *et al.*, Nature **466**, 470 (2010).
- [2] L. Yang *et al.*, Phys. Rev. Lett. **99**, 186801 (2007).
- [3] P. B. Bennett *et al.*, Appl. Phys. Lett. **103**, 253114 (2013).
- [4] J. P. Llinas *et al.*, Nat. Commun. **8**, 633 (2017).
- [5] J. Yamaguchi *et al.*, Commun Mater **1**, 36 (2020).
- [6] O. Deniz *et al.*, Nano Lett. **17**, 2197 (2017).

SESSION F.NM03.08: Processing

On Demand Abstracts Available for Viewing Starting Saturday Morning, November 21, 2020  
F-NM03

#### 5:00 AM \*F.NM03.08.01

**Global Alignment of Solution-Based Single-Wall Carbon Nanotube Films via Machine-Vision Controlled Filtration** William Rice<sup>1,2</sup>, Joshua Walker<sup>1</sup>, Jeffrey Fagan<sup>3</sup>, Adam Biacchi<sup>3</sup>, Valerie Kuehl<sup>1</sup>, Thomas A. Searles<sup>4</sup> and Angela Hight Walker<sup>3</sup>; <sup>1</sup>University of Wyoming, United States; <sup>2</sup>Charles Stark Draper Laboratory, United States; <sup>3</sup>National Institute of Standards and Technology, United States; <sup>4</sup>Howard University, United States

Over the past decade, substantial progress has been made in the chemical control of single-wall carbon nanotubes (SWCNTs). Large, horizontally aligned films can now be created out of post-processed SWCNT solutions, which has led to advances in SWCNT physics, including the observation of intersubband plasmons, hyperbolic thermal emission, ultrastrong exciton-polariton coupling, nanotube quantum wells, and directional nanotube optoelectronics. Here, we use machine-vision automation to simultaneously produce globally aligned SWCNT films using pressure-driven filtration. Feedback control enables filtration to occur with a constant flow rate that not only improves the nematic ordering of the SWCNT films, but

also provides the ability to align a wide range of SWCNT types and on a variety of nanoporous membranes using the same filtration parameters. Using polarized optical spectroscopy, we show that under standard implementation meniscus combing produces a two-dimensional radial SWCNT alignment on one side of the film. After we flatten the meniscus through silanation, spatially resolved nematicity maps on both sides of the SWCNT film reveal global alignment across the entire structure. From experiments changing ionic strength and membrane charging, we provide evidence that the SWCNT alignment mechanism stems not from pre-existing membrane grooving, but from membrane charging.

#### 5:15 AM F.NM03.08.02

**Inner and Outer Side Doping of Single-Walled Carbon Nanotubes** Anastasia E. Goldt<sup>1</sup>, Mikhail Bulavskiy<sup>1</sup>, Orysia Zaremba<sup>1</sup>, Alexey P. Tsapenko<sup>1,2</sup>, Konstantin V. Larionov<sup>3</sup>, Zakhar I. Popov<sup>3</sup>, Kimmo Mustonen<sup>4</sup>, Pavel Sorokin<sup>3</sup>, Fedor Fedorov<sup>2</sup> and Albert Nasibulin<sup>1,2</sup>; <sup>1</sup>Skolkovo Institute of Science and Technology, Russian Federation; <sup>2</sup>Aalto University, Finland; <sup>3</sup>National University of Science and Technology "MISIS", Russian Federation; <sup>4</sup>University of Vienna, Austria

Transparent conducting films are now in limelight of modern electronics driven by the expanding field of flexible devices that include displays, touch screens, solar cells, *etc.* Beside high transparency and good conductivity, such applications require rather good flexibility of materials to be preferably made under cost-effective fabrication protocols. As a result, the dominance of classical TCF material, indium tin oxide, is being impugned by alternatives like Ag nanowires mesh, PEDOT:PSS, graphene, reduced graphene oxide and single-walled carbon nanotubes (SWCNTs).

Here, we developed a novel easy strategy of simultaneous outer- and inner-surface SWCNT doping with H<sub>2</sub>AuCl<sub>4</sub> ethanol solution for efficient optoelectrical performance enhancement. Application of the proposed strategy allowed us to obtain transparent conductive SWCNT films with a record equivalent sheet resistance value of  $31 \pm 4 \Omega/\text{sq}$  at the annealing temperature of 400°C. We also showed that enhancement of optoelectrical properties of thermally treated SWCNT films should be attributed to the cap's removal during the annealing, thus providing feasible penetration of dopant solution into the inner SWCNT cavity under capillary forces. Electrochemical investigation of doping process confirmed more efficient *p*-doping of annealed SWCNTs in comparison to pristine. Besides, the origin of these differences was proposed to be switch of doping species from [AuCl<sub>4</sub>]<sup>-</sup> to stronger electron-accepting [AuCl<sub>2</sub>]<sup>-</sup>. DFT-calculations of SWCNT doping proved more significant Fermi-level downshift in case of simultaneous doping from outside and inside of nanotube confirming stronger doping. Based on UV-vis-nIR and Raman spectroscopies we have established that caps' removal process starts from 300 °C annealing, while comparing the equivalent sheet resistances of doped films we found the optimal treatment temperature range to be 300 - 400 °C. The reliability of conclusions was confirmed by the results consistency of UV-vis-nIR and Raman spectroscopies, TEM imaging, electrochemical measurements and DFT-calculations.

The experimental part of the research was supported by the Russian Science Foundation (No. 17-19-01787).

#### 5:25 AM F.NM03.08.03

**Ultrahigh Thermoelectric Power Factors of Ultrahigh Conductivity Carbon Nanotube Fibers** Natsumi Komatsu<sup>1</sup>, Yota Ichinose<sup>2</sup>, Oliver S. Dewey<sup>1</sup>, Lauren W. Taylor<sup>1</sup>, Mitchell Trafford<sup>1</sup>, Yohei Yomogida<sup>2</sup>, Matteo Pasquali<sup>1</sup>, Kazuhiro Yanagi<sup>2</sup> and Junichiro Kono<sup>1</sup>; <sup>1</sup>Rice University, United States; <sup>2</sup>Tokyo Metropolitan University, Japan

Because of the rapid growth of integrated wireless sensor networks (WSNs), for diverse applications from health to environmental monitoring, recharge-free, safe, and flexible power sources are in urgent demand. Thermoelectric (TE) generators based on macroscopic, neat assemblies of carbon nanotubes are strong candidates due to their superb electrical, thermal, and mechanical properties, combining the advantages of inorganic and organic TE materials (1). Here we report an ultrahigh value of thermoelectric power factor at room temperature ( $14 \pm 5 \text{ mWm}^{-1}\text{K}^{-2}$ ) for carbon nanotube fibers with an ultrahigh electrical conductivity ( $>10^7 \text{ Sm}^{-1}$ ). These fibers are also flexible, strong, and refractory at the same time (2). By combining these unique properties, we fabricated a wearable power generator. Through temperature and magnetic field dependent electrical conductivity measurements, we found that electrical transport in the fiber is highly metallic, showing small quantum corrections at the lowest temperatures ( $< \sim 40\text{K}$ ). Our theoretical simulations, combined with Fermi-energy-dependent experiments through doping and gating, show that the observed ultrahigh power factor is a consequence of simultaneously enhanced conductivity and Seebeck coefficient when the Fermi energy is near a van Hove singularity in the electronic density of states of carbon nanotubes.

Reference:

1. J. L. Blackburn, A. J. Ferguson, C. Cho, and J. C. Grunlan, Carbon-Nanotube-Based Thermoelectric Materials and Devices. *Adv. Mater.* **30**, 1704386 (2018).
2. N. Behabtu, C. C. Young, D. E. Tsentalovich, O. Kleinerman, X. Wang, A. W. K. Ma, E. A. Bengio, R. F. ter Waarbeek, J.



J. de Jong, R. E. Hoogerwerf, S. B. Fairchild, J. B. Ferguson, B. Maruyama, J. Kono, Y. Talmon, Y. Cohen, M. J. Otto, and M. Pasquali, Strong, Light, Multifunctional Fibers of Carbon Nanotubes with Ultrahigh Conductivity. *Science*. **339**, 182 (2013).

#### 5:35 AM F.NM03.08.04

**Carbon Nanotube-Cu Through-Si-via Interposer with Cu-Level Electrical Conductivity but Si-Comparable Coefficient of Thermal Expansion** Guohai Chen, Rajyashree Sundaram, Asuko Sekiguchi, Kenji Hata and Don Futaba; National Institute of Advanced Industrial Science and Technology (AIST), Japan

In microelectronic packaging, an interposer is an intermediate substrate acting as a bridge connecting the nanometer-level I/Os at the die to the micrometer-level package at the substrate. A through-silicon-via (TSV) interposer is very common one with copper filled inside the via as interconnections. As electronic devices continue miniaturization, the significantly increased heat generation inside the miniature devices deteriorates their lifetime/reliability, generally caused by delamination or break at the interface due to the non-uniform strain distribution induced by the mismatch of the coefficient of thermal expansion (CTE) between Si and copper. Therefore, the demands for interposer materials with high electrical conductivity but low CTE are growing. Here we demonstrate a fabrication/application feasibility of carbon nanotube-copper (CNT-Cu) composite using as interposer utilizing its superior electrical and thermal properties. The CNT-Cu composite showed a Cu-level electrical conductivity ( $\sim 2.5 \times 10^5$  S/cm) and Si-comparable CTE ( $\sim 7$  ppm/K). The CTE mismatch between CNT-Cu and Si was greatly reduced, only 1/5 of that between Cu and Si. Finally, we demonstrated several applications of CNT-Cu TSV interposer. The CNT-Cu TSV interposer may be one of potential candidates in microelectronic packaging.

#### 5:45 AM F.NM03.08.05

**Synthesis and Properties of Nanocomposites of Graphene Nanoribbons and Nanosheets Formed in Metals by an Electrocharging Assisted Process** Lourdes G. Salamanca-Riba<sup>1</sup>, Xiaoxiao Ge<sup>1</sup>, Christopher Klingshirn<sup>1</sup>, Madeline Morales<sup>1,2</sup>, Oded Rabin<sup>1,1</sup>, Manfred Wuttig<sup>1</sup>, Christopher Shumeyko<sup>2</sup>, Daniel P. Cole<sup>2</sup> and Shenjia Zhang<sup>3</sup>; <sup>1</sup>University of Maryland, United States; <sup>2</sup>U.S. Army Research Laboratory, United States; <sup>3</sup>General Cable, United States

Composites consisting of a metal matrix with embedded carbon nanostructures, such as graphene and carbon nanotubes, can have properties that take advantage of the excellent charge carrier mobility, thermal conductivity and mechanical strength of the carbon nanostructures and the high density of electrons in the metal. The combination of the composites' high mechanical strength with high electrical and/or thermal conductivities make them unique candidates in applications such as high power transmission lines, interconnects, heat exchangers, motors, photovoltaic cells and transparent electrodes, among others. Metal/nanocarbon composites made by chemical vapor deposition, friction stir, ball milling, and plasma spraying have yielded materials with enhanced hardness and tensile strength but unimproved electrical and thermal conductivities. We use an electrocharging assisted process to produce composites, which consists of the application of a high DC current to a mixture of liquid metal and particles of activated carbon. The high current density transforms the activated carbon particles from amorphous to crystalline graphitic nanoribbons in the liquid metal. Upon solidification of the metal the nanoribbons self-assemble with an epitaxial relation with the metal. We have used Al 1350 and activated carbon particles of <100 nm and obtained samples with global electrical conductivities more than 5% higher than the parent alloy as well as enhanced local stiffness, measured by nanoindentation. The conductivity enhancement is correlated with increasing crystallite size and concentration of the produced graphene nanoribbons. Molecular dynamic simulations of nanoindentation tests into the nanocarbon metal composite show how the graphene nanoribbons impede dislocation motion and increase hardness with little to no impact on elastic properties. Conductive AFM shows an increase in the local conductivity from these samples compared to the parent aluminum alloy.

Supported by DOE EERE Award EE0008313 and the Army Research Laboratory under Cooperative Agreement W911NF-19-2-0291.

#### 5:55 AM F.NM03.08.06

**Late News: High Aspect Ratio Pt Single-Walled Carbon Nanotube Composite Electrocatalysts for Sustainable Hydrogen Economy** Olli Sorsa<sup>1</sup>, Hua Jiang<sup>1</sup>, Kari Laasonen<sup>1</sup>, Toma Susi<sup>2</sup>, Rachel Backhouse<sup>3</sup> and Tanja M. Kallio<sup>1</sup>; <sup>1</sup>Aalto University, Finland; <sup>2</sup>University of Vienna, Austria; <sup>3</sup>ITM Power, United Kingdom

Based on the IEA energy outlook [1], both solar and wind based energy supply will increase by more than one decade by the year 2040. This development lays foundation for the hydrogen economy concept where hydrogen serves as an energy carrier. Hydrogen utilization requires, however, introduction of efficient, durable and economically feasible electrochemical conversion technologies for converting electrical energy into hydrogen bond energy and *vice versa*. Electrochemical water splitting electrolyzers and fuel cells based on low-temperature membrane technologies can meet these expectations if their

key components, such as electrocatalysts for hydrogen reactions, can be improved to meet the sustainability and cost requirements. Today scarce platinum group metals (PGMs) are utilized to electrocatalyze the hydrogen evolution and oxidation reactions met in electrolyzers and fuel cells, respectively. In addition to PGM availability and cost issues, these electrocatalysts suffer from inadequate durability.

Here, utilization of high aspect ratio electrocatalyst comprising of Pt nanowire (PtNW) and particles on single-walled carbon nanotubes (SWNTs) is suggested as low PGM electrocatalyst [2]. SWNTs have several beneficial properties needed for electrochemical applications: In addition to high conductivity and good chemical and electrochemical durability, they have appropriate properties for fabricating 3D electrodes needed for efficient mass transfer during the reactions.

The feasibility of composite Pt/SWNT electrocatalysts is verified in a single cell laboratory-scale polymer electrolyte electrolyzer. In terms of activity, even with one tenth of Pt mass loading at the cathode ( $0.02 \text{ mg}_{\text{Pt}} \text{ cm}^{-2}$ ), this catalyst accomplishes close to the level of the state-of-the-art Pt/C. The high activity is attributed to favorable PtNW interaction with the SWNTs as well as exposed PtNW edge-sites which adsorb hydrogen optimally and help to alleviate repulsive interactions on the nanowire surface. In addition, the metallic nature of Pt, morphological effects and enhanced surface wetting contribute positively to the performance.

The stability and durability are confirmed with 8,000 h of chronopotentiometry measurements and 10,000 potential cycles in the electrolyzer. These are combined with in-situ electrochemical and post-mortem analysis to investigate the durability of the electrocatalyst and aging mechanisms. Overall, the Pt/SWNT compares favorably to the reference Pt/C.

[1] Annon., World Energy Outlook. Part B. Special focus on renewable energy. IEA 2016.

[2] T. Rajala, T. Kallio, Ultra-low Pt electrocatalyst, Invention disclosure has been filed to Aalto University with nr. IPID2180 27.6.2018.

[3] T. Rajala, R. Kronberg, R. Backhouse, M. E. M. Buan, M. Tripathi, A. Zitolo, H. Jiang, K. Laasonen, T. Susi, F. Jaouen, T. Kallio, A platinum nanowire electrocatalyst on single-walled carbon nanotubes to drive hydrogen evolution, Applied Catalysis B: Environmental 265 (2020) 118582.

SESSION F.NM03.09: Poster Session: Nanotubes, Graphene and Related Nanostructures  
On Demand Abstracts Available for Viewing Starting Saturday Morning, November 21, 2020  
5:00 AM - 8:00 AM  
F-NM03

#### **F.NM03.09.04**

**Transparent, Transferrable and Flexible Pseudocapacitors from Ternary PEDOT/V<sub>2</sub>O<sub>5</sub>/ Graphene with Record Durability in Organic Electrolytes** [Sanju Gupta](#)<sup>1,2</sup>; <sup>1</sup>CCNY-CUNY, United States; <sup>2</sup>WKU, United States

Transparent conductive electrodes (TCEs) are of enormous significance to the continued growth of optoelectronic devices and the emergence of flexible and wearable electronics in the foreseeable future. Versatile and tunable TCEs, featuring not only high optical transmittance but also intriguing features of electrochemical energy-storage capability, flexibility, and transferability, remain a significant challenge. Here we strategically develop a graphene-conjugated V<sub>2</sub>O<sub>5</sub>/poly(3,4-ethylene dioxithiophene (from hereon, V<sub>2</sub>O<sub>5</sub>/PEDOT) hybrid, serving as an easily transferable, transparent, capacitive active electrode films. The constructed electrodes exhibit a high areal capacitance of 50-60 mF cm<sup>-2</sup> at optical transparency of > 60 percent with a record durability over thousands of cycles. As demonstrated by experimental results, both the kinetic blocking of the PEDOT layer and the anchoring capability of graphene upon soluble vanadium ions from V<sub>2</sub>O<sub>5</sub> nanoribbons/nanotubes contribute synergistically to the unusual electrochemical stability and electroactivity shown using scanning electrochemical microscopy. Transparent symmetric and asymmetric solid-state supercapacitors made of the as-fabricated pseudocapacitive TCEs deliver a broad voltage window of 1.4 V or higher under two different electrolytes (aqueous LiCl and organic gel made from LiCl and polyvinyl alcohol) demonstrate highest power and energy density that outperforms all the previously reported transparent devices (< 0.1 microWatt h cm<sup>-2</sup>).

#### **F.NM03.09.07**

**Thermal Diode Based on Polyethylene Nanofiber** [Xiao Luo](#) and Sheng Shen; Carnegie Mellon University, United States

Thermal diode is a two-terminal device which rectifies heat flow. For its non-linear nature, interest in thermal diode has been growing for more than 15 years. Thermal diodes have been numerically and experimentally realized with bulk as well as nanomaterial. Among them, phase transition material can realize high rectification with relatively narrower temperature bias.

Current optimization studies of phase transition junction thermal diode consider phase transition as a step function of temperature, while in some cases phase transition could happen in a temperature range in the same magnitude with temperature bias. In this study we simulated and optimized the thermal diode based on our recently experimentally realized phase transition of polyethylene nanofiber with a finite temperature range of phase transition.

There is a phase transition within polyethylene nanofiber with high degree of crystallinity: crystalline structure shifts from orthorhombic to hexagonal cell with a sharp decrease of thermal conductivity within about 5K temperature range at around 430 ~ 450K[1]. E-beam irradiation can alter the phase transition behavior. Phase transition retains with a lower critical temperature if irradiation is weak, while phase transition disappears if irradiation is strong[2]. Thus, heavily-irradiated-pristine (HI-P) and lightly-irradiated-pristine (LI-P) junction diode can be fabricated by partially irradiating the PE nanofiber with different exposure time. HI-P junction can rectify heat flow in one certain direction, while LI-P junction can rectify heat flow in both directions under different working temperature.

Calculation based on finite temperature range of phase transition shows a smooth heat flow curve with a better match with experimental data. Calculation based on step-function phase transition gives a limit of rectification value but tends to overestimate the rectification performance under small temperature bias. Optimization formula derived from step-function model can still be used for estimating optimized length fraction of e-beam irradiation despite the range of temperature bias, as maximum rectification value always occurs when interface temperature difference is zero. Specifically, a proper value of thermal conductance value is required for LI-P junction such that rectification performances in both directions can be optimized with one single length fraction of irradiation.

[1] R. Shrestha, Y. Luan, S. Shin, T. Zhang, X. Luo, J.S. Lundh, W. Gong, M.R. Bockstaller, S. Choi, T. Luo, R. Chen, K. Hippalgaonkar, S. Shen, High-contrast and reversible polymer thermal regulator by structural phase transition, *Sci. Adv.* 5 (2019) eaax3777. <https://doi.org/10.1126/sciadv.aax3777>.

[2] Unpublished.

#### **F.NM03.09.09**

**A GFET Nitrile Sensor Using a Graphene-Binding Fusion Protein** Abubaker A. Mohamed<sup>1,1</sup>, Mirano Tsukiiwa<sup>2</sup>, Hironaga Noguchi<sup>2</sup>, Takumi Komikawa<sup>2</sup>, Chen Chen<sup>2</sup>, Qadri E. Mubarak<sup>1</sup>, Rachel Heath<sup>1,1</sup>, Masayoshi Tanaka<sup>2</sup>, Mina Okuchi<sup>2</sup>, Samuel de Visser<sup>1,1</sup>, Yuhei Hayamizu<sup>2</sup> and Christopher F. Blanford<sup>1,1</sup>; <sup>1</sup>University of Manchester, United Kingdom; <sup>2</sup>Tokyo Institute of Technology, Japan

A bottleneck in the development of enzyme-based graphene field effect transistors is the protein immobilization method used. Non-specific adsorption of protein on graphene is undesirable as it hinders access to the enzyme's active site whilst also changing the natural conformation of proteins by having surface residues bind to the graphene surface. Proteins require specific 3D conformation to be functional and so label-free immobilisation methods is preferred as it increases sensing capabilities of biosensors by maintaining proteins catalytic activity upon immobilization.

Here, a bi-functional self-assembling and graphene-binding peptide was fused to a QueF nitrile reductase protein to create a fusion protein for nitrile detection. The peptide was derived from silk protein fibroin and is capable of forming stable antiparallel  $\beta$ -sheet structure on graphene (1) and so is used to guide protein immobilization. Incorporating this tag into various proteins for enhancing biosensing applications offers a new and effective platform for enzyme-based graphene field effect transistors.

QueF nitrile reductase was chosen because it is the only known enzyme capable of NADPH-mediate nitrile to amine reduction (2). Surface topology of the fusion protein functionalized graphene was observed by atomic force microscopy and showed that both oligopeptide and the fusion protein incorporating it formed a monolayer with six-fold symmetry.

The QueF fusion protein sensing capabilities was first assessed on its natural nitrile substrate which upon immobilisation on graphene field effect transistor showed a 1.4-fold increase in binding affinity compared the wild-type protein which did not incorporate the peptide tag.

Fusion protein was also used to create an agricultural biosensor through the detection on benzyl cyanide. Benzyl cyanide is a chemical distress signal produced by plants and detection of this compound could therefore be used to provide means for crop monitoring and pesticide administration. The fusion protein showed a 3.3-fold increase in response to benzyl cyanide when compared to the wild-type protein. Work here provides a novel immobilisation method for enzyme based graphene field effect transistor biosensing.

(1) Li, P.; Sakuma, K.; Tsuchiya, S.; Sun, L.; Hayamizu, Y. Fibroin-like Peptides Self-Assembling on Two-Dimensional Materials as a Molecular Scaffold for Potential Biosensing. *ACS Appl. Mater. Interfaces* **2019**, *11* (23), 20670–20677. <https://doi.org/10.1021/acsami.9b04079>.

(2) Moeller, K.; Nguyen, G. S.; Hollmann, F.; Hanefeld, U. Expression and Characterization of the Nitrile Reductase QueF from *E. Coli*. *Enzyme Microb. Technol.* **2013**, *52* (3), 129–133. <https://doi.org/10.1016/j.enzmictec.2012.12.003>.

#### F.NM03.09.13

**Fullerene C<sub>76</sub>—An Plored Superior Electrode Material with Wide Operating Potential Window for High Performance Supercapacitors** Nageh K. Allam, Basant A. Ali and Ahmed Biby; American University in Cairo, Egypt

Carbon materials have widely been used to enhance the performance of a plethora of supercapacitor electrode materials. In this regard, it is crucial to identify carbon materials that function over a wide pH range while enjoying a wide potential window. Herein, the DFT calculations were used to elucidate the electronic performance of C<sub>76</sub> and the C<sub>76</sub>/electrolyte interface. The electronic investigation revealed the nature of the conductivity and charge storage mechanism of C<sub>76</sub> based on the bandgap and quantum capacitance calculations. Also, the electrochemical and electronic properties of fullerene C<sub>76</sub> have been extensively investigated over a wide pH range; acidic H<sub>2</sub>SO<sub>4</sub>, basic KOH, and neutral Na<sub>2</sub>SO<sub>4</sub>. The results showed a promising performance in the three electrolytes. Moreover, C<sub>76</sub> electrodes exhibited a potential window of 1.9 V in Na<sub>2</sub>SO<sub>4</sub> electrolyte, resulting in capacitances of 171 F/g and 142 F/g at a scan rate of 1 mV/s in the positive and negative potential windows, respectively. The material showed a pseudocapacitance performance of 65% in Na<sub>2</sub>SO<sub>4</sub> electrolyte in the positive potential window. We believe higher fullerenes provide a new class of materials for developing versatile supercapacitor devices for efficient energy storage

#### F.NM03.09.14

**In Situ Formation of Graphene Stabilizes Zero-Valent Copper Nanoparticles and Significantly Enhances the Efficiency of Photocatalytic Water Splitting** Nageh K. Allam; American University in Cairo, Egypt

There is a growing need for new techniques to synthesize metallic copper nanoparticles due to their remarkable use in many advanced technologies. Herein, a novel method to synthesize stable and non-agglomerated zero-valent copper nanoparticles (ZVCNPs) via the in-situ formation of reduced graphene oxide (rGO) during the electrospinning process in the presence of polyvinylpyrrolidone (PVP) as a carbon source is presented. X-ray diffraction (XRD), Raman spectroscopy, electron paramagnetic resonance (EPR), transmission electron microscopy (TEM), and x-ray photoelectron spectroscopy (XPS) techniques were used to investigate the morphology, structure, and composition of the fabricated materials. The synthesized ZVCNPs were coupled with TiO<sub>2</sub> nanofibers and rGO to form an efficient photoactive material to photocatalytically produce hydrogen via water splitting, resulting in 344% increase in the hydrogen yield compared to that of TiO<sub>2</sub> nanofibers. The density functional theory (DFT) calculations showed that the ZVCNPs enhance the charge transfer and lower the energy needed for photocatalytic water splitting. This study suggests a novel method for metallic copper stabilization and illustrates the effect of metallic copper as a catalyst for the in-situ formation of rGO.

#### F.NM03.09.15

**Topology Influence of Hydroxyl and Epoxide Functional Groups on the Mechanical and Fracture Behavior of Graphene Domain** Akarsh Verma<sup>1</sup> and Avinash Parashar<sup>2</sup>; <sup>1</sup>University of Petroleum and Energy Studies, India; <sup>2</sup>Indian Institute of Technology Roorkee, India

Aim of this article is to study the effects of hydroxyl functional group with different coverage percentages on the mechanical strength and fracture toughness of graphene. The hydroxyl functional group forms the backbone of intrinsic atomic structure of graphene oxide (GO).

Molecular dynamics based simulations were performed in conjunction with reactive force field (ReaxFF) parameters to capture the mechanical properties and Mode-I fracture toughness of functionalized graphene. Moreover, these simulations helped in concluding that spatial distribution and concentration of hydroxyl functional group significantly affects the fracture morphology of graphene nanosheet. Room temperature (300 K) was used for the simulations and virial stress components were evaluated for predicting the stress tensor.

In contrast to literature investigations, here the atomistic simulations have predicted a transition in the failure morphology of hydroxyl functionalised graphene from brittle to ductile as a function of its spatial distribution on graphene sheet. This transition in failure morphology from brittle to ductile was gradual in nature and was observed at lower percentage coverage

of graphene in the range of 25-50%. Failure morphologies depict that hydroxyl groups tend to boost the ductility through atomic chains and elongated rings formation at lower percentage coverage.

As the graphene nanosheet is highly brittle in nature, so the authors have evaluated the fracture toughness of graphene with the help of Griffith's criteria. We then functionalized the graphene sheet (with an pre-crack) with epoxide functional group and observed that a chemical epoxide-to-ether chemical transformation enhanced the fracture toughness value by 25%, as compared to the pristine graphene.

From this investigation, we concluded that spatial distribution and concentration of functional groups significantly affects the mechanical and fracture behavior of oxide functionalized graphene nanosheet.

#### **F.NM03.09.16**

**Anomalous Characteristics of Functionalized Grain Boundaries in Graphene—A Nano-Mechanics Study** [Akarsh Verma](#)<sup>1</sup> and Avinash Parashar<sup>2</sup>; <sup>1</sup>University of Petroleum and Energy Studies, India; <sup>2</sup>Indian Institute of Technology Roorkee, India

Enduring an ultrahigh mechanical strength and thermal conductivity, pristine two-dimensional graphene is still a hypothetical concept in the scientific community. Fabrication techniques for this quantum confined two-dimensional nanomaterial in the experimental environment induce various defects in its polycrystalline domain such as the atomic level grain boundaries (GB). Various computational techniques such as the molecular dynamics and density functional theory have unravelled complex mechanisms operating in the presence of these boundary phases to tune graphene's mechanical, fracture and thermal properties.

Molecular dynamics-based simulations were performed in conjunction with reactive force field (ReaxFF) parameters to capture the mechanical properties of functionalized GB in graphene. Room temperature (300 K) was used for the simulations and virial stress components were evaluated for predicting the stress tensor.

Herein this article, the authors have predicted certain spatial configurations of epoxide functionalized bicrystalline graphene, which could dilute its catastrophic brittle nature and transform it into stable ductile behavior. Altering of failure path and epoxide-to-ether chemical transformations were the chief mechanisms behind the enhanced plasticity for functionalized graphene. Due to brittle nature of graphene, it was expected that failure of graphene would tend to take place from the GB, but in contrast, we found that the failure started from the interior of crystal. This tailoring of failure path induced plasticity in the domain and acted as an energy dissipation mechanism.

The present work provided new insights into the mechanical behavior of bicrystalline GO and predicts plasticity in epoxide functionalized sandwich structure. This persisting ductility of epoxide rich configurations would enable GO to absorb more energy prior to failure and amplified toughness as well, leading to improved structural integrity.

#### **F.NM03.09.18**

**Atomistic Simulations to Explore the Water Interaction Mechanism Through a Defective 2D h-BN Nanosheet—Reactive Forcefield Development and Molecular Dynamics Study** [Akarsh Verma](#)<sup>1,2</sup>, Weiwei Zhang<sup>1</sup> and Adri v. Duin<sup>1</sup>; <sup>1</sup>The Pennsylvania State University, United States; <sup>2</sup>University of Petroleum and Energy Studies, India

Desalination corresponds to supplying of potable water from oceans and seas, which can dissolve the water scarcity problem for human consumption, agriculture use and energy needs. Conversion of earth's 97% salty water into a fresh source is still an ambiguous challenge for the research community. Moreover, conducting costly and time consuming commercial experimental techniques such as reverse osmosis and thermal desalination have consistently proved to be a brain storming challenge for the scientists. So, in order to rectify this problem, herein the authors have performed molecular dynamics simulations to investigate the transport of water molecules through artificially created pores on the honeycomb lattice domain of two-dimensional hexagonal Boron Nitride (h-BN) nanosheet. Initially, a reactive force field (ReaxFF) was developed that had water parameters in conjunction with vacancy defects data for monolayer h-BN derived from the density functional theory incorporated in it. We then checked the structural stability of an h-BN monolayer (both pristine and defected) at different temperatures (300, 500 and 800 K) and ensembles (NVT and NPT); thus, predicting that the developed ReaxFF showed a minimal out-of-plane displacement. From the interaction point of view, we revealed that the water molecules tend to accumulate (droplet formation) and form sharp contact angles (hydrophobic nature) with h-BN. Furthermore, on compressing water molecules by applying external pressure on h-BN nanosheet the water molecules tend to arrange themselves in a layered structure. Finally, we investigated the water dissociation mechanism on a defected h-BN nanosheet,

and noticed that the water molecule dissociates into hydroxyl group and hydrogen atom thereby getting attached to boron and nitrogen vacancy edge atoms, respectively (Relative energy barriers with respect to initial configurations were 0.395 and - 2.18 eV). These outcomes on h-BN nanosheet may prove to be valuable for designing of 2D nanodevices/nanomembranes for water desalination purpose.

#### F.NM03.09.19

**Synthesis and Functionalization of Carbon Nanospheres in One Step by APCVD** Gerardo Patiño Guillén<sup>1</sup>, Alan Arceta Lozano<sup>1</sup>, Jessica A. Falcón Montes<sup>1</sup>, Esmeralda García Díaz<sup>2</sup>, Jorge Noé Díaz de León<sup>3</sup>, Rafael Vázquez Duhalt<sup>3</sup>, Miguel A. Méndez Rojas<sup>1</sup> and Jessica R. Campos Delgado<sup>1</sup>; <sup>1</sup>Universidad de las Américas Puebla, Mexico; <sup>2</sup>Benemérita Universidad Autónoma de Puebla, Mexico; <sup>3</sup>Universidad Nacional Autónoma de México, Mexico

A one-step synthesis/functionalization of carbon nanospheres (CNS) is presented. The synthesis was carried out *via* the APCVD method using toluene and ethanol (0wt%- 5wt% ethanol) as precursors. Different weight percentages of ethanol were implemented in order to evaluate their effect on the CNS's solubility in water, size distribution, morphology, surface area and surface chemistry. Since this method is a one-step *in situ* functionalization (with oxygen-containing groups), there's no need of a post-treatment to functionalize the sample or the use aggressive chemical reactants that could significantly modify the nanomaterial. Characterization techniques implemented for this study included FT-IR, SEM, EDX, XPS, Raman spectroscopy, BET and solubility tests. Results indicated that CNS possess higher water solubility when a 3 wt% ethanol solution is implemented for the synthesis. It was also demonstrated that higher ethanol concentrations decrease CNS's diameter and induce polydispersion. Finally the increased solubility and stability of the functionalized CNS are highlighted, envisaging applications in the biomedical field where hydrophilicity and availability of functional groups are mandatory.

#### F.NM03.09.21

**Precision Defect Engineering of Graphene for Applications Using Electron-Beam Chemistry with Radiolyzed Water** Michael A. Susner<sup>1,2</sup>, Ahmad Islam<sup>1</sup>, Rahul Rao<sup>1</sup>, Jennifer Carpena-Núñez<sup>1,2</sup>, San-Hui Chi<sup>1,2</sup> and Benji Maruyama<sup>1</sup>; <sup>1</sup>Air Force Research Laboratory, United States; <sup>2</sup>UES, Inc., United States

Defect engineering of graphene is attractive for a wide range of applications. Here, we present a mask-less, resist-free, and fully reversible process to engineer defects in graphene using electron-beam (e-beam) chemistry with radiolyzed water. This process was performed inside a variable pressure scanning electron microscope by generating radiolysis products using reactions between the e-beam and water vapor, which in turn reacted with the graphene at the location of the probe. These reactions enabled controlled chemistry on the graphene surface at a resolution of ~ 60 nm and hence created defects in precise locations defined by the e-beam. Detailed characterization and theoretical analyses suggested the presence of sp<sup>3</sup>-type defects, the density of which was tuned by varying the e-beam dose. In addition, these sp<sup>3</sup>-type defects were cycled in and out of graphene by alternating e-beam chemistry and thermal annealing. We present initial results showing the ability to manipulate the plasmonic response in graphene through the creation of quickly patterned nanoribbons.

#### F.NM03.09.23

**Synthesis, Reversible Insulator-Metal Transition as Well as High Conductivity and Ampacity of Cobalt Oxide Based Misfit Nanotubes** Kankona S. Roy; Indian Institute of Technology Bombay, India

Misfit layered compounds (MLCs) consist of two alternating sub-lattices with different lattice constants at least in one of the directions. One can selectively alter one of the sub-lattices without affecting the other that can tune both the physical and electronic properties. Among them, calcium cobaltite (Ca<sub>3</sub>Co<sub>4</sub>O<sub>9</sub>, CCO)<sup>1</sup> and strontium cobaltite (Sr<sub>3</sub>Co<sub>4</sub>O<sub>9</sub>, SCO)<sup>2</sup> are gaining interest as potential thermoelectric materials. Bringing them to low-dimensions could further enhance their thermoelectric properties. However, synthesizing them in a one-dimensional structure is extremely difficult. Recently, we have synthesized calcium deficient cobalt oxide-based misfit nanotube<sup>3,4</sup> from the bulk starting material. However, the yield of these nanotubes is rather low. Besides, the physical and electrical properties of these nanotubes have not been explored yet. Here, we present the synthesis of 1D nanotubes (NT) from oxide misfit compounds with a very high yield (80%) by a combination of solid-state and solution-based synthesis. We have also studied their electrical properties on individual nanotube level by patterning with electron beam lithography.

All the synthesized nanotubes are thoroughly characterized by a combination of X-ray diffraction pattern (XRD), scanning electron microscope (SEM), high-resolution scanning transmission electron microscopy (HRSTEM), electron diffraction (ED) and X-ray photoelectron spectroscopy (XPS). It is found that the crystal structure varies in the case of nanotubes from the bulk starting material. Absorption studies show the bandgap of 2.7 eV and 1.7 eV in case of CCO and SCO NTs, respectively. We have fabricated source-drain channels on individual nanotubes by electron beam lithography to find out

their electronic properties. In the case of CCO nanotubes, it is found that the nanotubes are of p-type semiconductor with a high charge carrier concentration of  $7.05 \times 10^{19}$  per  $\text{cm}^3$ , which suggest that these NTs are promising conducting materials. The current-carrying capacity of these nanotubes is around  $6.5 \times 10^5$  A/ $\text{cm}^2$  (for an individual nanotube). But surprisingly, in the case of SCO nanotube, it shows a very high current carrying capacity of  $0.88 \times 10^8$  A/ $\text{cm}^2$  for a single NT. These values are close to the reported  $\text{WS}_2$  NTs having the highest current carrying capacity (ampacity) of  $2.4 \times 10^8$  A/ $\text{cm}^2$  among the inorganic nanotubes.<sup>5</sup> Temperature dependent resistivity measurements show that both the nanotubes are semiconducting in nature. However, we have observed a voltage-induced semiconductor to metal transition in the case of SCO NTs. We have observed the four-probe resistance for the SCO nanotube to be 10 k $\Omega$  which is lowest among the existing oxide-based inorganic nanotubes. We believe electronic properties can be further tuned by changing the chemical composition between Ca/Co and Sr/Co. These results demonstrate that the high conductivity of these nanotubes could be a potential building block for future thermoelectric devices and interconnects.

## References

- Yuzuru Miyazaki, *Solid State Ion.* **2004**, *172*, 463–467.  
Jakub D. Baran, Demie Kepaptsoglou, Marco Molinari, Nuth Kulwongwit, Feridoon Azough, Robert Freer, Quentin M. Ramasse, and Stephen C. Parker, *Chem. Mater.* **2016**, *28*, 7470–7478.  
Leela S. Panchakarla, Luc Lajaunie, Ashwin Ramasubramaniam, Raul Arenal, Reshef Tenne, *ACS Nano.* **2016**, *10*, 6248–6256.  
Luc Lajaunie, Ashwin Ramasubramaniam, Leela S. Panchakarla, Raul Arenal, *Appl. Phys. Lett.* **2018**, *113*.  
Roi Levi, Ora Bitton, Gregory Leitun, Reshef Tenne, Ernesto Joselevich, *Nano Lett.* **2013**, *13*, 3736–3741.

### F.NM03.09.24

**Getting Pristine Graphene-Like Behaving rGO—What Really Matters** Mohammed Sedki<sup>1</sup>, Pegah S. Mirabedini<sup>1</sup>, Kenta Nakama<sup>2</sup>, Garrett Stephens<sup>3</sup>, Michael Groves<sup>3</sup>, Mahesh R. Neupane<sup>4</sup> and Ashok Mulchandani<sup>1</sup>; <sup>1</sup>University of California, Riverside, United States; <sup>2</sup>Tokyo University of Agriculture and Technology, Japan; <sup>3</sup>California State University, Fullerton, United States; <sup>4</sup>U. S. Army Research Laboratory, United States

Chemically synthesized graphene or reduced graphene oxide (rGO) is very promising for many applications from coatings and fillers to electronics, as it is economic, easy to prepare and scale up, and has unique properties. Despite the huge expansion of GO/rGO market, there is a clear lack of experimental and computational studies on getting high quality GO and rGO nanosheets/thin films. This caused a huge variation in the reported properties of GO/rGO, with a majority of low quality and low competency in electronic applications. In this work, a detailed experimental study of the factors affecting GO/rGO properties, supported by Density Functional Theory (DFT) calculations, is introduced to help prepare pristine graphene-like rGO. In addition, the impact of lateral sheet size on GO/rGO properties, as one of the factors addressed in this work, was studied using DFT calculations and experimental measurements for the first time, to the best of our knowledge. Field-effect transistor (FET) was used to study and optimize rGO. The optimized rGO-FET device showed the lowest resistance ( $200 \pm 20 \Omega$ ) and the highest charge carrier mobilities ( $53279$  and  $39891 \text{ cm}^2/\text{V}\cdot\text{s}$  for holes and electrons, respectively) reported. Furthermore, FET characteristic curve of rGO-FET showed the ambipolar behavior of high-quality graphene, with Dirac point around zero. In addition, the optical band gap of rGO nanosheets ( $0.4 \text{ eV}$ ) prepared in this work is the smallest reported, so far. These results highlight the importance of this study for both researchers and companies aiming at using rGO as an alternative for graphene obtained by liquid phase exfoliation or chemical vapor deposition.

### F.NM03.09.26

**Electronic Functionality Encoded Laser-Induced Graphene for Paper Electronics** Hyunjin Park, Minsu Kim, Byoung Gak Kim and Yun Ho Kim; Korea Research Institute of Chemical Technology, Korea (the Republic of)

Laser-induced graphene (LIG) has been utilized as a non-metallic conductor for the development of various electronics due to its facile, direct, and scalable synthesis process. Here, the graphitization degree of LIG is simply controlled by adjusting the lasing conditions to encode different electronic functionalities such as resistance and capacitance on commercially available papers. The effect of lasing conditions including the number of lasing scans and the lasing power on the graphitization degree of paper-derived LIG is systematically investigated by evaluating the optical, chemical, and electrical properties. The paper-derived LIG with various lasing conditions exhibits a relatively wide sheet resistance range of  $61.5$  to  $9140 \Omega \text{ sq}^{-1}$ . The corresponding LIG is used to fabricate resistors and capacitors, and the different electronic functionality encoding is successfully demonstrated by monolithically fabricating non-volatile read-only memory and resistor-capacitor circuits and verifying the electrical performance of the fabricated devices. This work presents a practical approach to develop paper electronics for cost-effective and environmentally-friendly manufacturing.

### F.NM03.09.27

#### **Robust Microscale Superlubricity Under Airborne Contaminants** Kunqi Wang; Tsinghua University, China

Structural superlubricity, which results from the incommensurability of directly contacted crystalline surfaces, achieves ultralow friction and inspires disruptive innovations in applications across length scales. It is a common belief that this phenomenon requires the contact interface being ultra-clean, ensured by either a clean environment or self-cleaning of the contact. However, in this paper, the observation of robust superlubricity with a contaminant-rich interface is reported. After intentionally introducing airborne contaminants into microscale superlubric graphite contacts, we surprisingly find that two important features of structural superlubricity are well preserved: the nearly-zero friction coefficient and the drastic commensurate/incommensurate anisotropy of frictional force. Moreover, contaminants are found to reduce the friction of a commensurate contact, but increase the friction of an incommensurate contact, which leads to the decrease of anisotropy ratio in friction as the contaminant concentration increases. Molecular dynamics simulations reveal the different roles of the third bodies in commensurate and incommensurate contacts. Our results encourage explorations of structural superlubricity in contaminant-rich environments that practical devices could be facing.

### F.NM03.09.28

#### **Revealing Structure–Activity Links in Hydrazine Oxidation—Doping and Nanostructure in Carbide–Carbon Electrocatalysts** Tomer Burshtein<sup>1</sup>, Eliyahu Farber<sup>1</sup>, Kasinath Ojha<sup>2</sup> and David Eisenberg<sup>1</sup>; <sup>1</sup>Technion–Israel Institute of Technology, Israel; <sup>2</sup>Leiden University, Netherlands

The oxidation of hydrazine ( $N_2H_4$ ) is an important challenge in electrocatalysis, with applications in direct hydrazine fuel cells and in medical and environmental sensing. Interest in alternative, nitrogen-based fuels for fuel cells was rekindled by recent advances in alkaline membranes, and by the surfacing of challenges in the transportation of hydrogen. Direct hydrazine fuel cells promise high theoretical voltage (1.56 V with  $O_2$ ), clean emissions, and improved fuel transportability. We now report a multi-doped carbide–carbon composite with excellent hydrazine electro-oxidation (HzOR) activity in alkaline pH. While iron carbide containing materials are well known catalysts for several applications (e.g. oxygen reduction), our N-doped,  $Fe_3C$ -embedded carbons provide the first examples of a carbide-based HzOR catalyst. Multi-doping was thought to enhance reactivity (possibly through cooperation of  $M=Cu/Zn, Fe$ , and edge N atoms), possibly by pore-etching, layers exfoliation or graphitization promotion, thus modulating surface area, mass transfer and conductivity. To prepare the composites, we designed tunable multi-doped precursors: an organometallic structure combining iron with either copper, zinc, or iron, to investigate the effect of molybdenum-doping reported earlier. Pyrolysis and washing of the fore mentioned precursors yielded HzOR-active composites of  $Fe_3C$  nanoparticles and a hierarchically porous, partially graphitic N-doped carbon (NC). Thorough characterization by voltammetry and by a broad range of spectroscopic and microscopic methods revealed that the activity is ordered as: Cu-derived NC > Zn-derived NC > Fe-derived NC. While the catalysts had similar compositions, their nanostructure varied: both Zn- and Cu-doping induced the formation of micropores and small mesopores (5–13 nm diameter). The dopant-induced active site exposure (affecting micropore volume) and improved material flow (linked to mesopore volume) contributed to enhanced HzOR electroactivity. Furthermore, the intimate mixing of the metals in the precursor is hypothesized to homogenize and enhance the doping effect, as the structure enhancing metal ions ( $Zn^{2+}$  or  $Cu^{2+}$ ) exposed the nearby catalytic  $Fe_3C$  sites. Acid washing of the pyrolyzed carbon was crucial for producing microporosity in the Cu-based carbon, but had little effect on the Zn-derived one. This revealed the importance of micropores and small mesopores for HzOR electrocatalysis, and the different nanostructuring mechanisms of the two dopants: while  $Zn_{(g)}$  boils during pyrolysis and thus etches micropores into the carbon,  $Cu_{(s)}$  diffuses and spreads throughout, making exfoliation by acid reaction more efficient. Further work in our group is dedicated to the catalytic activity of pure phase  $Fe_3C$ , and its modification by other dopants.

[Burshtein et al., *J. Mater. Chem. A*, **2019**, doi: 10.1039/C9TA03357B]

### F.NM03.09.30

#### **Synthesis of Flexible 3D Electrodes of TiN Nanotube Arrays Using Atomic Layer Deposition** Seokjung Yun<sup>1</sup>, Sang-Joon Kim<sup>2</sup>, Jaesung Youn<sup>1</sup>, Hoon Kim<sup>1</sup>, Jeongjae Ryu<sup>1</sup>, Changdeuck Bae<sup>3</sup>, Kwangsoo No<sup>1</sup> and Seungbum Hong<sup>1,4</sup>; <sup>1</sup>Korea Advanced Institute of Science and Technology, Korea (the Republic of); <sup>2</sup>Korea Research Institute of Chemical Technology, Korea (the Republic of); <sup>3</sup>Sungkyunkwan University, Korea (the Republic of); <sup>4</sup>KAIST Institute for NanoCentury (KINC), Korea (the Republic of)

Flexible nanoscale electrode can be used in many applications such as electrochemical energy storage, electrocatalysts and solid memory devices by providing higher density faradaic reaction sites. Although many processing techniques have been used to produce nano-structured electrodes on flexible substrates, prior ones lack the mechanical stability. Here, the mechanical properties and flexibility of the TiN nanotube array on the Pt substrate were improved using a Ti interlayer as an



adhesion promoter. Highly aligned TiN nanotube array was fabricated on a Pt substrate using an anodized aluminum oxide (AAO) template and atomic layer deposition (ALD) system. We show that with the use of a Ti interlayer as adhesion promoter between the TiN nanotube arrays and Pt substrate, the TiN nanotube arrays could perfectly attach to the Pt substrate without delamination and faceted phenomena. Peeling was not observed even when the bending test was performed at a high curvature (radius of curvature, -2 mm). In addition, reliable and uniform contact the nanotube and the substrate evidenced by conducting atomic force microscopy (C-AFM) analysis proved the excellent local transport properties of our electrodes. Furthermore, the mechanical bending test results attest to the excellent flexibility for use in flexible electronic devices. We envision that our 3D electrodes will be implemented as embedded electrodes in semiconductors as well as flexible plastic substrates.

### F.NM03.09.31

#### Single Step Reduction and PEGylation of Nanographene Oxide for Drug Delivery and Photothermal Cancer

**Therapy** Raquel Costa-Almeida<sup>1,2</sup>, Diana Bogas<sup>3</sup>, Cristiana Couto<sup>3</sup>, Lúcia Timochenco<sup>3</sup>, Filipa A. Silva<sup>1,2</sup>, José R.

Fernandes<sup>4</sup>, Inês C. Gonçalves<sup>1,2</sup>, Fernão D. Magalhães<sup>3</sup> and Artur Moreira Pinto<sup>1,2,3</sup>; <sup>1</sup>Instituto de Investigação e Inovação em Saúde, Universidade do Porto, Portugal; <sup>2</sup>INEB - Instituto de Engenharia Biomédica, Portugal; <sup>3</sup>LEPABE, Faculdade de Engenharia, Universidade do Porto, Portugal; <sup>4</sup>CQVR – Centro de Química Vila Real, Universidade de Trás-os-Montes e Alto Douro, Portugal

Cancer is the second leading cause of death worldwide. Current treatments frequently rely on surgical resection, radiotherapy, and high-dose chemotherapy, with unsatisfactory outcomes and side effects. Thus, there is a great need for novel and more effective strategies. Photothermal therapy (PTT), a non-invasive alternative based on near-infrared (NIR) light energy conversion into heat, results in hyperthermia (39-47 °C) and induces higher nanoparticle/drug uptake due to increased membrane permeability and tumor cell apoptosis. Nanomaterials, like graphene-based materials (GBM), hold potential as photothermal absorbers to enhance PTT selectivity within the target tumor tissue toward achieving therapeutic temperatures using less total light energy, minimizing damage to the healthy surrounding tissue [1]. This study explored GBM and GBM loaded with 5-fluorouracil (5-FU), an anti-cancer drug, as platforms for combined chemo-photothermal therapy.

Nanographene oxide (GOn) was produced through the modified Hummer's method [2] followed by ultrasonication in a custom-built industrial grade system. Following a one-step procedure, GOn was thermally reduced and non-covalent functionalized with poly(ethylene) glycol (PEG) to obtain stable aqueous dispersions (rGOn-PEG) [3]. GOn and rGOn-PEG (0.25 mg/mL) were mixed with 5-FU at a drug concentration varying between 0.25-5 mg/mL. GBM aqueous dispersions were irradiated with a LED source of 812.8±29.9nm (150 mW/cm<sup>2</sup>) and temperature recorded using a thermocouple. The effect of GBM and NIR irradiation was evaluated by resazurin cell viability assay using a human skin carcinoma cell line (A431 cells, ATCC).

Reduction and PEGylation of GOn were confirmed by chemical characterization through FTIR, XPS and UV-vis spectroscopy, as well as thermal analysis by TGA. GOn and rGOn-PEG were obtained with mean lateral dimensions of 287 nm and 521 nm, respectively as determined by TEM. GOn and rGOn-PEG dispersions showed colloidal stability with zeta potential values around -25.6±0.8 mV and -10.2±0.3 mV (pH=7), respectively. Loading capacity of 5-FU on GBM reached 5.8±0.8 mg 5-FU/mg GOn and 3.6±1.2 mg 5-FU/mg rGOn-PEG by simple molecular physisorption. NIR irradiation increased rGOn-PEG temperature to 47 °C after 30 min, which is within temperature ranges of hyperthermia. rGOn-PEG in combination with NIR reduced A431 cells viability, in opposition to rGOn-PEG alone.

This study demonstrated the successful non-covalent functionalization and reduction of nanographene oxide, rendering a material with potential to be further explored for combined chemotherapy and PTT for cancer treatment.

*Acknowledgements:* This work was financed by FEDER - Fundo Europeu de Desenvolvimento Regional funds through the COMPETE 2020 - Operacional Programme for Competitiveness and Internationalisation (POCI), Portugal 2020, and by Portuguese funds through FCT/MCTES in the framework of the projects POCI-01-0145-FEDER-031143; POCI-01-0145-FEDER-006939; POCI-01-0145-FEDER-007274; PTDC/BTM-MAT/31143/2017, and Unidade de Investigação UID/EQU/00511/2019 - Laboratório de Engenharia de Processos, Ambiente, Biotecnologia e Energia – LEPABE.

#### REFERENCES:

- [1] Doughty ACV *et al.*, *Materials*, 2019, 12.
- [2] Pinto AM *et al.*, *Carbon*, 2015, 99:318.
- [3] Chen J *et al.*, *Biomaterials*, 2014, 35: 4986.

### F.NM03.09.32

#### Investigation of a Catalyst Ink Dispersion and Three-Dimensional Analysis of Catalyst Layer in Polymer Electrolyte Membrane Fuel Cells Dan Wu, Samindi M. Jayawickrama and Tsuyohiko Fujigaya; Kyushu University, Japan

Carbon-based supports have been widely used to support Pt catalysts in polymer electrolyte fuel cells (PEMFCs) [1]. In our group, we developed polybenzimidazole (PBI)-wrapping onto carbon support that successfully achieved higher cell performance [2].

In this study, we present a dispersion investigation of the catalyst ink using PBI-wrapped catalyst (CB/PBI/Pt) and non-wrapped (CB/Pt) catalyst with a wide range of ionomer: carbon ratio (I/C). The effects of ink parameters, which include carbon black structure, and ionomer concentration, on the ink microstructure of catalyst ink were studied using visual study in combination with dynamic light scattering (DLS). Heterogeneous porous structure of the catalyst layer in PEMFCs is a significantly important parameter because it strongly determines the gas diffusion properties of the catalyst layer. And the connectivity of the network structure is largely depended on the structure of the catalyst agglomerations as well as the homogeneity of the ionomer on the carbon supporting materials. Therefore, we used scanning electron microscopy combined with focused ion beam (FIB-SEM) to visualize the nano-scale pore structure of the catalyst layer. Post-processing of a series of two-dimensional images reconstructed the three-dimensional pore-space of the catalyst layer.

We found that the catalyst ink of CB/PBI/Pt remained as a very stable dispersion in the range of I/C = 0.2~1.4, whereas for CB/Pt, the catalyst ink easily forms aggregation at high I/C (>0.6). The FIB-SEM images of CB/Pt catalyst layer with optimum I/C = 0.6 and CB/PBI/Pt catalyst layer with optimum I/C = 0.2 was analyzed. It is found that the CB/Pt catalyst layer has isolated large pores with the porosity of 0.55, while CB/PBI/Pt catalyst layer shows a uniform porous structure with the porosity of 0.7. It is reported that the presence of isolated pores increases the O<sub>2</sub> transport resistance in the catalyst layer, resulting in lower fuel cell performance [3,4]. Therefore, we concluded that the dispersion stability of catalyst ink is enhanced by PBI wrapping onto the CB surface, thus ensuring a better porous structure of the catalyst layer in PEMFCs. Furthermore, the particle-particle interactions in catalyst ink will be discussed in the presentation.

## References

- [1] Xin, L.; Yang, F., Polybenzimidazole (PBI) Functionalized Nanographene as Highly Stable Catalyst Support for Polymer Electrolyte Membrane Fuel Cells (PEMFCs). *J. J. Electrochem. Soc.* 2016, 163, 10.
- [2] T. Fujigaya, et al., Improved Durability of Electrocatalyst Based on Coating of Carbon Black with Polybenzimidazole and their Application in Polymer Electrolyte Fuel Cells. *J. ACS Appl. Mater. Interfaces* 2016, 8, 23, 14494–14502.
- [3] Inoue, G.; Kawase, M., Effect of porous structure of catalyst layer on effective oxygen diffusion coefficient in polymer electrolyte fuel cell. *J. Power Sources* 2016, 327, 1-10.
- [4] Inoue, G.; Yokoyama, K.; Ooyama, J.; Terao, T.; Tokunaga, T.; Kubo, N.; Kawase, M., Theoretical examination of effective oxygen diffusion coefficient and electrical conductivity of polymer electrolyte fuel cell porous components. *J. Power Sources* 2016, 327, 610-621.

## **F.NM03.09.33**

### **Monitoring of Adsorption Behavior of Serum Albumin onto the Fatty Acid-Modified Single-Walled Carbon**

**Nanotube** Kenta Nakamura, Yoshiaki Niidome, Yukiko Nagai, Tanaka Naoki, Tomohiro Shiraki, Takeshi Mori, Yoshiki Katayama and Tsuyohiko Fujigaya; Kyushu University, Japan

Single-walled carbon nanotube (SWNT) are attracting increasing attentions in biological applications because of their unique thermal, physical and optical properties. To use SWNT for in vivo applications, SWNT need to be biocompatible. Up to date, coating of SWNT with biocompatible materials especially polyethylene glycol (PEG) has been investigated due to its stealth property. However, it was pointed that the PEG-modified materials are rapidly excreted from the blood due to an immune reaction when they are repeatedly administered, which is known as accelerated blood clearance (ABC) phenomenon. To avoid such a problem, serum albumin (SA) attracts recent attention as an alternative material of PEG since SA is a blood protein derived from a living body. However, since the adsorption coefficient of SA onto SWNT surface is lower than that of the other proteins, the increase of the adsorption to avoid the risk of the replacement might be necessary. Therefore, in this study, we introduced fatty acid onto the surface of SWNT to improve the binding of SA by utilizing the strong binding between SA and fatty acid, where the introduction of the fatty acid was carried out by the radical grafting of the fatty acid derivative onto the SWNT sidewall. Here, the adsorption behavior was monitored by monitoring of the unique red-shifted and brighter photoemission (PL) generated from the grafting site compared to that of the non-functionalized SWNT.

## **F.NM03.09.35**

**A Novel Route for Controlling and Improving the Texture of Porous Structures Through Dual Growth of Alumina Nanoparticles and Carbon Nanotubes Using Explosion Process of Solid Fuel** Osama Saber and Adil Alshoabi; King Faisal University, Saudi Arabia

Micro- and meso-porous structures of alumina have attracted attention for their potential use in different applications. In this research, a novel and facile route was introduced for dual growth of alumina nanoparticles and carbon nanotubes together to fabricate nanocomposites at low temperature 250°C through explosive processes of solid fuel. In this trend, series of alumina species with and without carbon nanotubes were prepared and characterized by X-ray diffraction, Raman spectra and transmission electron microscopy. The surface properties of the alumina-CNT nanocomposites were characterized and compared with the prepared nanoparticles of alumina by adsorption-desorption system. The specific surface area of the prepared alumina-CNT nanocomposites was increased from 257.9 to 307.7 m<sup>2</sup>/g and 314.8 m<sup>2</sup>/g with growing CNTs inside the porous structure of alumina. These increments were observed because of the dual growth of nanoparticles and nanotubes by which new micropores inside their nanocomposites were created. When the source of CNTs was changed from ethanol to methanol, pure mesoporous structure with narrow pore size distribution was observed for the alumina-CNT nanocomposite. In addition, the surface area and the total pore volume increased to be 324.9 m<sup>2</sup>/g and 0.673 cm<sup>3</sup>/g; respectively. The detonation technique of an explosive solid has been used for the first time to improve and control the porous structure of alumina through dual growth of CNTs and alumina at low temperature to meet the special requirements of the markets of catalysis and water purification.

#### **F.NM03.09.37**

**Failure Behavior and Mechanisms in Dense Highly Aligned Brittle Nanowire Structures** Rebecca Gallivan and Julia R. Greer; California Institute of Technology, United States

Nanowires have become an increasingly prevalent nanomaterials in composites and devices. In both surface coatings and mechanically coupled sensing applications, arrays and other complex geometries provide numerous design advantages, such as pixel like features. However, little investigation has been done regarding the mechanical behavior of these micron sized structures. With contact and load bearing applications, both the failure behavior and the underlying failure mechanisms are critical for robust device design. Though in-situ microcompression experiments on highly aligned dense bundles of single crystalline zinc oxide (ZnO) nanowires we investigate these types of structures to build a model for better understanding structural failure.

The ZnO nanowires are formed through hydrothermal growth from an aqueous zinc nitrate solution with hexamethylenetetramine (HMTA) and electrolysis conditions to promote fast growing high aspect ratio nanowires. 2µm and 4µm diameter bundles with individual nanowires of approximately 300nm in diameter and 4µm tall were investigated. These structures provides a range of 10-130 nanowires per bundle and thus probes an order of magnitude in scale. Experiments show two regimes of failure in the nanowire bundles: localized non-catastrophic events and global structural failure. No size dependence is observed in either regime and failure stress ranges from 0.3-1.3GPa and 0.83-2.20GPa respectively. Localized failure corresponds to interfacial splitting between nanowires and can be modeled using a mode I double cantilever beam tests. Analysis of this mechanism provides insight to the flaw size and failure initiation in the structures. Ultimate global failure can be modeled by coupling the accumulation of local failure from interfacial splitting to specific failure parameters of the nanowire material. Utilizing Weibull statistics and experimental results, we demonstrate the validity of this technique for analyzing flaw distribution and predicting the expected failure stress range of the bundle structures. The technique shows the sensitivity of failure behavior to degree of alignment, flaw size, interfacial interactions of constituents, and structural surface effects. Through analysis of behavior in this specific system, we develop insight to broader fundamental mechanisms for local failure and statistical techniques for assessing and predicting failure behavior of highly aligned structures.

#### **F.NM03.09.38**

**Relationship Between the Dispersibility of Carbon Nanotubes and the Properties of Their Polymer Nanocomposites** Taiyo Shimizu, Ryoichi Kishi, Kazufumi Kobashi, Takahiro Morimoto, Toshiya Okazaki, Takeo Yamada and Kenji Hata; National Institute of Advanced Industrial Science and Technology (AIST), Japan

Polymer materials with superior properties have been more and more widely used in our daily life. As compared to metals, light weight and good-processability are particularly beneficial properties of polymer materials. However, there are also several properties of polymers which are required to be improved, e.g. mechanical, electrical and thermal properties, and thus a plenty of research to improve these properties have been conducted so far. Improving these properties can realize the extension of applicable fields of polymer materials.

In order to improve objective properties of polymers, incorporation of appropriate kinds of fillers into polymer matrix is frequently adopted. For instance, carbon nanotubes (CNTs) are one of the most prominent fillers with superior properties such as high mechanical strength and electrical conductivities. Nanocomposite materials with CNTs have been widely explored and various kinds of nanocomposites possessing improved properties have been fabricated so far. However,

addition of substantial amount of nanofillers, not limited to CNTs, is required in most cases, and thus the inherent properties of polymer matrix, such as good-processability, tend to be degraded. These kinds of nanofillers are basically aggregated in a pristine form, and are required to be dispersed properly in their nanocomposites, in order to extract their potential as a filler. In this presentation, we will describe the relationship between the dispersibility of CNTs and the resultant properties of their nanocomposites. As an example, the thermal stability of CNT nanocomposite will be focused on. We successfully fabricated the CNT/silicone rubber nanocomposites with high thermal stability achieved by well-dispersed single-walled CNTs. The temperature at 5 % weight loss ( $T_{d,5\%}$ ) of silicone rubber, obtained from thermogravimetric analysis, was increased by incorporation of low amount of CNTs. Remarkably, we found that the degree of increase in the  $T_{d,5\%}$  depends on the dispersion process of CNTs, and appropriate dispersion process can realize higher increase in the temperature than that of the CNT dispersion process only by stirring. This phenomenon is considered to be originated from the homogeneity in the distributions of CNTs in nanocomposites, which has been ascertained by analytical techniques. We also confirmed that the CNT/silicone rubber nanocomposites fabricated by appropriate dispersion process can retain rubbery elasticity after a thermal aging test, while pristine silicone rubber was embrittled soon after the onset of the test. These results indicate that appropriately dispersed CNTs can impart thermal stability in both short- and long-term to silicone matrix only by small amount of loading. Our findings indicate that appropriate dispersion of CNTs can enhance the effectiveness of incorporation of CNT to matrix, and we believe that these kinds of approach can be applicable to a broad range of matrix, not limited to polymers.

### F.NM03.09.39

#### **Elucidation of Adsorption Behavior of Polybenzimidazole on Carbon Material Surface by Adsorption Isotherm Measurement** Nana Kayo<sup>1</sup> and Tsuyohiko Fujigaya<sup>1,2,1</sup>; <sup>1</sup>Kyushu University, Japan; <sup>2</sup>WPI-I2CNER, Japan

In polymer electrolyte fuel cells (PEFC), a composite of carbon black (CB) with platinum particles (Pt) is widely used as an electrode catalyst after mixing with acidic electrolyte. However, low platinum utilization efficiency because of the uneven distribution of acid electrolyte on the CB surface that caused the insufficient protons transport was the issue [1]. We reported that improvement of platinum utilization efficiency and power density by coating of polybenzimidazole (PBI) onto CB surface prior to the platinum loading [2], in which the distribution of the electrolyte become uniform by the coating of PBI. However, its coating homogeneity of PBI onto CB has not been clarified yet.

In this study, the adsorption state of PBI on CB was studied by estimating the adsorption isotherm and the interaction acting between the carbon materials and PBI was investigated.

From the adsorption isotherm of PBI on CB, it was revealed that PBI adsorption reached adsorption equilibrium from a low concentration, suggesting that PBI was adsorbed in a monolayer on the carbon materials efficiently. In addition, the PBI coverage at the coating concentration of 0.50 mg/mL, used for coating, calculated from the Langmuir equation showed as high as 99.9%. Therefore, we concluded PBI uniformly coats CB. Also, based on the calculation of thermodynamic parameters, it was found that  $\Delta H$  and  $\Delta S$  were 14 kJ/mol, and 0.11 kJ/mol, respectively. The temperature dependence of the isotherm revealed that this adsorption process was entropy driven since the PBI adsorption amount increased with increasing the temperature. The adsorption behavior and interaction of PBI with other carbon materials will be discussed in the presentation.

#### References

[1] S. Jayawickrama *et al.*, *Electrochim. Acta.* **2019**, *312*, 349.

[2] T. Fujigaya, *et al.*, *ACS Appl. Mater. Interfaces* **2011**, *8*, 14494.

### F.NM03.09.40

#### **Combined Theoretical and Experimental Study of All-Carbon Transistors** Ali D. Özdemir, Artem Fediai, Feliks Pyatkov, Pramit Barua, Ralph Krupke and Wolfgang Wenzel; Institute of Nanotechnology, Karlsruhe Institute of Technology, Germany

Low-dimensional all-carbon nanostructures are promising candidates for future flexible and transparent transistors, as well as light-emitters [Pyatkov *et al.*, *Nature Photonics* **10**, 420–427 (2016)]. Carbon nanotube field-effect transistors with graphene electrodes offer high thermal stability and allow for ultra-flat devices able to carry high current densities. Understanding quantum transport in such systems is essential for device manufacturing. However, conventional simulation methods are limited to local contacts with an overlap width of only a few angstroms, and first-principle quantum transport calculations in systems with realistic contact geometries remained unfeasible. Simulation methods for extended CNT/metal contacts were presented in prior theoretical studies [Fediai *et al.*, *Nanoscale*, **8**, 10240 (2016)]. Here, we report quantum transport calculations based on the non-equilibrium Green function formalism and density functional theory, which are capable of treating ~100nm long CNT/graphene overlap regions and electrostatic gating at a pure ab-initio level. These calculations are

compared with experiments where graphene electrodes were fabricated and dielectrophoretically bridged with single semiconducting CNTs followed by an electrical characterization over a wide temperature range. The simulation results are in agreement with the experimental data and the fabricated devices exhibit ambipolar behavior, consistent with the theory. Due to large CNT/graphene spacing and small CNT/graphene overlap, only a fraction of the quantum conductance can be achieved for the on-state conductivity. A remarkable feature of the all-carbon transistor with graphene electrodes is electrostatically induced doping of the carbon-system in the contact regions caused by the gate electrode. This is made possible by the low density of states in graphene near the K-point. We hope that this newly developed and verified simulation approach will accelerate progress in fabrication as well as the understanding of advanced all-carbon devices.

#### **F.NM03.09.41**

**Plasma Treated Single-Walled Carbon Nanotubes Decorated by RuO<sub>x</sub> Nanoparticles for High Performance Hydrogen Evolution Reaction** Fedor Fedorov<sup>1</sup>, Daniel Settapani<sup>2</sup>, Marthe Buan<sup>2</sup>, Jani Sainio<sup>2</sup>, Farhan S.M. Ali<sup>2</sup>, Daniil Ilatovskii<sup>1</sup>, Tanja M. Kallio<sup>2</sup> and Albert Nasibulin<sup>1,2</sup>; <sup>1</sup>Skolkovo Institute of Science and Technology, Russian Federation; <sup>2</sup>Aalto University, Finland

The constant and growing need in new catalysts for hydrogen evolution reaction is triggered by increasing energy demands and promises of its eco-friendliness combined with large gravimetric storage capacity. Carbon nanotubes are also known to be quite promising for hydrogen (and oxygen) evolution reaction and are characterized by large specific surface area, excellent conductivity, and rather good durability.

We report a cathode material based on plasma-treated single-walled carbon nanotubes decorated by RuO<sub>x</sub> nanoparticles using atomic layer deposition (ALD). We have examined cathode performance towards hydrogen evolution reaction by tailoring material wettability, conductivity yielded by plasma-treatment, and the catalyst loading [1]. We discuss that nucleation of particles is facilitated by the appearance of carboxylic and hydroxyl groups triggered by oxygen plasma action. The best performance is associated with samples containing RuO<sub>x</sub> particles of 4-5 nm, which show hydrogen evolution onset potential to be about -5 mV (vs. RHE) in 0.5 M H<sub>2</sub>SO<sub>4</sub> measured at a current density of -1 mA cm<sup>-2</sup> and Tafel slope of 47.5 mV/dec. The material possesses stable performance at -10 mA cm<sup>-2</sup> with a potential of about -160 mV.

The reported study was funded by RFBR, project number 20-03-00804

[1] Fedor Fedorov, Daniel Settapani, Marthe Emelie Melandsø Buan, Jani Sainio, Farhan S.M. Ali, Daniil Ilatovskii, Tanja Kallio, Albert G. Nasibulin (2020) *ChemElectroChem* <https://doi.org/10.1002/celec.202000528>.

#### **F.NM03.09.44**

**Synthesis of Cu<sub>x</sub>S/Graphene Aerogel for Photocatalytic Reduction of CO<sub>2</sub>** Feng Wang and Liejin Guo; Xi'an Jiaotong University, China

Using solar energy to convert CO<sub>2</sub> into hydrocarbon fuel is a promising technique for harvesting solar energy storage and reducing carbon dioxide. Recently, Graphene-based semiconductor composites have been a topic of great interest, especially in the field of photocatalysis. Graphene has the advantages of high surface area, excellent conductivity, and anticorrosion capacity, which can overcome the limitations of traditional photocatalysts. Thus, graphene-based material can be a feasible photocatalyst for photocatalytic CO<sub>2</sub> reduction. Besides, as an environment-friendly and earth abundant material, Cu<sub>x</sub>S has considered as a good candidate for photocatalytic reactions, due to its unique optical, electronic, physical and chemical properties. Herein, we report the photocatalytic reduction of CO<sub>2</sub> using Cu<sub>x</sub>S/graphene aerogel as the photocatalyst, which was prepared by hydrothermal method. The as prepared Cu<sub>x</sub>S/graphene aerogel exhibited pretty good activity for photocatalytic reduction of CO<sub>2</sub>. C<sub>2</sub> products (ethanol, acetate) are main products. In this composite photocatalyst, graphene aerogel not only serves as a 3 dimensional support for Cu<sub>x</sub>S, but also transfers the photo generated charges. Moreover, density functional theory calculations were performed to reveal the chemical reactions and the charge transfer between Cu<sub>x</sub>S and graphene. Also, the study of Cu<sub>x</sub>S/graphene aerogels photocatalyst presents useful information for efficient photocatalytic CO<sub>2</sub> reduction without noble-metals.

#### **F.NM03.09.45**

**Graphene Encapsulated Nanoscale Vacuum Channel Transistors** Girish Rughoobur and Akintunde I. Akinwande; Massachusetts Institute of Technology, United States

There is a growing need for devices that operate at THz frequencies, and with the end Moore's device scaling law approaching, alternatives to solid-state transistors need to be explored. The inherent limitation of solid-state transistors such

as the metal-oxide semiconductor field-effect transistor (MOSFET) is the semiconductor channel, which not only causes carrier scattering, velocity saturation of carriers due to optical phonon scattering, but is also susceptible to high temperature and radiation effects. Current research attempts to mitigate these negative effects focus on using wide bandgap semiconductor channels. In contrast, the use of ‘empty-space’, which can be regarded as the ultimate wide bandgap material, as the device channel could overcome these limitations. This is because in vacuum, there is no carrier scattering (ballistic transport), avalanche breakdown or thermal generation. The absence of any atoms further enhances the tolerance to high temperature as the channel retains its properties. Nanotechnology and nanofabrication has enabled the realization of nanoscale vacuum channel transistors (NVCTs) that could potentially surpass solid state devices of equivalent channel length owing to ballistic transport of electrons, shorter transit time and higher intrinsic breakdown field. Hence, transistors with a vacuum channels could have very high Johnson figure of merit ( $J_{\text{FoM}} = E_{\text{BDVsat}}/2\pi$ ) of  $\sim 10^{14}$  V/s, even exceeding ultra-wide bandgap materials such as AlGaN and diamond.

We report the demonstration of NVCTs based on gated vertical silicon field emission arrays with two self-aligned gates. The two gates are separated by an oxide with thickness of 350 nm. A first gate with aperture diameter of 360 nm is used to extract electrons from a sharp emitter tip (radius < 7 nm) and the second gate, with aperture diameter of 570 nm, is used to focus the electron in to a vacuum channel. The emitter tips density is  $10^8$  emitters/cm<sup>2</sup>. NVCTs with such electron sources are highly sensitive to barrier variations caused by surface adsorption of molecules on the tip in poor vacuum environment. Here we demonstrate the nano-encapsulation of the electron source for operation in poor vacuum, using several layers of graphene, which are transparent to electrons but impermeable to the larger gas atoms in a poor vacuum. This device architecture with two self-aligned gates also enables the application of a different voltage bias on the graphene and hence controlling the energy of the electrons in the channel, while reducing the encapsulation volume significantly. We demonstrate turn-on voltages below 10 V and operation in poor vacuum and at atmospheric pressure. This device architecture is highly promising to realize empty space electronics capable of functioning at higher power and harsher conditions (high radiation and high temperature, such as in space and in nuclear reactors) transcending the performance of solid state electronics.

#### **F.NM03.09.46**

**Oil Dynamic Shell Surrounding Fullerenes** [Aaron Morelos-Gomez](#)<sup>1</sup>, Kunio Kondo<sup>2</sup>, Hiroshi Ushiyama<sup>3</sup>, Kazuhiro Omori<sup>2</sup>, Ryuji Monden<sup>2</sup>, Yu Gao<sup>2</sup>, Masumi Kuritani<sup>2</sup>, Taiki Yokokawa<sup>1</sup>, Rodolfo Cruz-Silva<sup>1</sup>, Syogo Tejima<sup>3</sup>, Mauricio Terrones<sup>4</sup> and Morinobu Endo<sup>1</sup>; <sup>1</sup>Shinshu University, Japan; <sup>2</sup>Showa Denko K.K., Japan; <sup>3</sup>Research Organization for Information Science & Technology, Japan; <sup>4</sup>The Pennsylvania State University, United States

Given the increase in technology development the need for more energy efficient devices is required. In mechanical systems a large amount of energy is lost due to friction between sliding surfaces. For this reason, the creation of effective lubricants is needed. Transition metal disulfides such as WS<sub>2</sub> and MoS<sub>2</sub> fulleroids have been used as oil additives. However, disulfides are prone to oxidation and release of sulphide compounds under heat and may corrode metal surfaces creating metal sulphides. Carbon materials can exhibit higher chemical inertness and therefore exhibit longer lubrication lifetime under heat than transition metal disulfides. Among carbon materials; graphene, carbon nanotubes and fullerenes have been added into oil to decrease friction between two metal surfaces. Unfortunately, the molecular interaction between carbon nanomaterials and lubricants has not been fully understood. We studied the molecular interactions between fullerenes and mineral oil, known as “nano oil”, by ultraviolet Raman spectroscopy and molecular dynamics simulations. The results indicate that aromatic molecules help to disperse individual C<sub>60/70</sub> molecules from aggregates whereas the alkane molecules help to stabilize fullerenes by forming a dynamic shell structure around them. Our findings demonstrate that fullerenes can be used as high-performance additives for effective lubrication.

#### **F.NM03.09.51**

**Computational Geometry-Centric Evaluation for Electrical Conductivity Variation of Thin-Film Conducting Nanocomposites** [Jungmin Lee](#)<sup>1</sup>, Yesol Yun<sup>2</sup>, Sang Hyun Lee<sup>2</sup> and Jinyoung Hwang<sup>1</sup>; <sup>1</sup>Korea Aerospace University, Korea (the Republic of); <sup>2</sup>Korea University, Korea (the Republic of)

Hybrid carbon nanotube (CNT) composites consisting of multiple types of fillers have been developed to provide enhanced characteristics as compared to CNT single-filler composites. The incorporation of secondary fillers, such as silica, CaCO<sub>3</sub>, and BaSO<sub>4</sub>, yields remarkably improved mechanical strength and stiffness of the CNT composite and electrical conductivity of the hybrid composite network under the control based on geometry and content of the constituent particulate fillers. In particular, higher electrical conductivity can be attained with the addition of micro-scale secondary fillers to the CNT composite network, while the addition of nano-scale particulate fillers incurs lowering the electrical conductivity of the nanocomposite network. Such electrical conductivity transition is attributed to distinct variations in the network topology caused by the excluded volume originating from the loading of secondary fillers with different scales. Micro-silica

composites result in dense clusters of CNTs, thereby forming CNT conducting paths, while densely-dispersed nano-size fillers cause severely twisted CNTs, reducing forming a conducting network. In this work, Monte-Carlo simulation is first conducted for the estimation of the electrical conductivity of the CNT network of hybrid composites. To obtain a realistic model, flexible CNTs are modeled as long thin cylindrical objects with many joints interconnected in a row. In addition, to take the resistance of the conducting CNTs into account, individual joints are considered to be tiny lumped resistor elements. A computational characterization approach based on numerical linear algebra technique is applied under various size and concentration configurations of composite components, and the corresponding electrical conductivity of the network is derived. The computational results exhibit that the ratio of the average diameter of the particulate filler to the nanotube length governs the tendency of the electrical conductivity variation, as compared to the change of filler contents only affecting the degree of the conductivity change. As the ratio of the silica diameter to the CNT length increases, the ratio of the conductivity without ( $\sigma_0$ ) and with ( $\sigma$ ) the secondary particulate fillers, i.e.  $\sigma/\sigma_0$ , increases from the value less than one to the value more than one. This indicates that the impact of the second fillers on the electrical conductivity of the composites shows a transition. By contrast, if the geometric configuration of the fillers is almost fixed, the degree of the conductivity variation increases as the silica content increases, while decreasing for the increasing CNT content. The electrical behaviors of hybrid composites can be simply characterized by the combination of computational geometry centric notions such as Voronoi tessellations and Swiss cheese model along with their associated percolation theory. In the developed model, the CNT dispersed around particulate fillers indicating effective conducting paths can be classified with tessellations from Voronoi cells. The conductance of each effective path is designated by local conductance determined from the density of CNTs in the local region. The reliability of the model is validated based on comparison with the numerical results obtained from the MC simulation. The developed approach achieves, as compared to the MC simulation, remarkable computing cost reduction. Therefore, the combined computational framework enables to provides a novel strategy to estimate for the electrical conductivity of the hybrid composites under the external deformation such as bending, stretching, and patterning, and it is a viable model for the design of the hybrid composites at hand.

#### F.NM03.09.53

**Investigation of the Growth Mechanism for Hierarchical Polymer/Carbon Nanotube Nanohybrid Shish-Kebab Structures to Enable High-Performance Printable Thin-Film Transistors** Kevin Schnittker and Joseph B. Andrews; University of Wisconsin-Madison, United States

Aerosol jet printing has gained a considerable amount of attention as a method to additively fabricate electronic device. In part, this is due to the compatibility with a wide range of ink viscosities (1-1000 cps) and the ability to print on non-planar surfaces. One elusive material for aerosol jet printed active electronics is a high-performance semiconducting ink with low-variability. One potential promising ink would be a combination of high-mobility carbon nanotubes (CNTs) with highly uniform semiconducting polymers. However, CNTs fully encapsulated by semiconducting polymers have not shown noteworthy improvement. One method to capture both positive attributes of CNTs and semiconducting polymers is through a hierarchical nanostructured composite. The conjugated polymer regioregular poly(3-hexylthiophene) (P3HT) has the ability to self-assemble and form periodic crystals on CNTs due to  $\pi$ - $\pi$  interactions. These structures, coined nano-hybrid shish kababs (NHSKs), may directly improves charge carrier transport in printed thin-film electronic devices.

The objective of this project is to fabricate a novel semiconducting ink that consists of P3HT/CNT NHSKs. In developing this ink, we investigated the P3HT shish kabab crystallization and kinetic growth on (6,5) chirality SWNTs. This was done by manipulating the P3HT-SWNT concentrations, the solvent concentration, and crystallization temperature. The P3HT fibril shape, size, and period were found to be correlated to the above parameters. The morphology and purity/concentration were measured using atomic force microscopy (AFM) and ultra-violet/visible spectroscopy.

NHSKs were fabricated via a 6:1 P3HT to SWNT mass concentration solution mixed in 70°C anisole solution. The P3HT supramolecular structures were found to be  $32\pm 3.7$  nm wide and  $269\pm 11.4$  nm long. At higher mass ratios (40:1 P3HT to SWNT), full encapsulation was observed with little periodicity. In conclusion, this work investigates the growth mechanisms of P3HT polymer crystals on single chirality CNTs for semiconducting ink applications. Next steps include the manipulation of the solution to increase printability and the fabrication of NHSK-based thin-film transistors.

#### F.NM03.09.54

**Enhanced Heat Transfer of Functionalized Graphene Nanoplatelets in Nanofluids for Energy Conversion and Storage of Solar Power Plants** Michael Wilhelm<sup>1</sup>, Tim Ludwig<sup>1</sup>, Thomas Fischer<sup>1</sup>, Dileep Singh<sup>2</sup> and Sanjay Mathur<sup>1</sup>; <sup>1</sup>University of Cologne, Germany; <sup>2</sup>Argonne National Laboratory, United States

The unique thermal conductivity of graphene makes it one of the most promising materials for next generation heat transfer applications that, given the increasing demand for energy supply from sustainable energy sources such as concentrated solar power, has emerged as key technology. The incorporation of graphene and graphene-like nanomaterials into conventional

heat transfer fluids has been shown to significantly improve their thermal transport properties. Due to their cost-efficient carbon-based starting material, its high surface area and sheet-like structure, graphene nanoplatelets (GNPs) are suitable for colloidal thermal conductive fluids demonstrating enhanced heat transfer efficiencies.

In this work, hydrophobic graphene nanoplatelets were used as starting material and surface functionalized by acid treatments to synthesize highly stable, exfoliated, surfactant-free and highly concentrated (4 wt.%) graphene nanofluids maintaining high thermal conductivity. Characterization by SEM, XPS, XRD, Raman and FT-IR spectroscopy revealed a significant influence of shape, reaction period, acid volume and temperature on the resulting thermal conductivity values of the nanofluids relative to the carrier fluid. After 14h of measurement in a dormant system, thermal conductivities up to 0.586 W/m\*K (base fluid: 0.391 W/m\*K) were measured. In combination with a low viscosity of 6.39 cP the overall efficiency of the functionalized particles could be increased to 77 % in comparison to the base fluid. The combination of both low viscosity and high thermal conductivity, even after 14h in a standing system, demonstrate the extraordinary properties of surface functionalized graphene nanoplatelets prepared in this work in comparison to other nanofluidic systems.

#### **F.NM03.09.57**

**Modeling the Effective Electrical Conductivity of Nanocarbon-Metal Composites Made by the Electrocharging Assisted Process** Christopher Klingshirn<sup>1</sup>, Andrew Palughi<sup>2</sup>, Xiaoxiao Ge<sup>1</sup>, Madeline Morales<sup>1</sup>, Jessica Ye<sup>1</sup>, Christopher Shumeyko<sup>3</sup>, Tahir Cagin<sup>2</sup> and Lourdes G. Salamanca-Riba<sup>1</sup>; <sup>1</sup>University of Maryland, United States; <sup>2</sup>Texas A&M University, United States; <sup>3</sup>U.S. Army Research Laboratory, United States

Robust materials with high conductivity are essential to electronic devices and systems. Nanocarbon-metal composites have the potential to improve upon the electrical conductivity of established metals and alloys such as Al and Cu by incorporating carbon nanostructures known for their superior electrical properties. During the fabrication of novel nanocarbon-metal composites called covetics, direct electric current applied to a metal melt containing a dispersion of carbon source material is believed to ionize carbon atoms and lead to the formation of nanoscale graphitic ribbons and chains that ultimately incorporate within the metal lattice upon solidification. The electrical conductivity of the resulting composites is consistently greater than the original alloy, but the magnitude of conductivity enhancement varies significantly from sample to sample, and the theoretical upper limit of conductivity enhancement in these systems remains unclear.

This work combines fundamental assumptions about the nature of covetics, specifically a tightly bound metal-carbon interface, with a simple effective-medium model to estimate the bulk conductivity of ideal Al and Cu covetics with randomly distributed graphene nanoribbons (GNRs). Density-functional theory estimates of charge transfer at the graphene-metal interface, local electrical conductivity measurements, and transmission electron microscopy investigation of the interface region provide inputs to the model. The implications of quantum confinement in narrow GNRs are also explored. We use the model to project a range of performance-enhancement goals for the covetics fabrication community and find the potential for conductivity improvements on the order of 10% under ideal conditions, however fabrication challenges remain before these gains may be realized on an industrial scale.

This work is supported by the U.S. Department of Energy under Award No. DE-EE0008313.

#### **F.NM03.09.59**

**Carbon Nanotube Embedded Vertical Aligned PVDF Membraned with High Mechanical Properties for PRO Membrane Application** Juran Noh, Mehdi Habibollahzadeh, Choongho Yu and Ahmed Abdel-Wahab; Texas A&M University at Qatar, Qatar

Water desalination has been a critical issue for reserving the freshwater for human survival, further civilization, industry development. Pressure retarded osmosis (PRO) is desalination technology emerging from the osmosis phenomenon; water flux through the membrane, excluding undesired macromolecules or ions with applying pressure. Thus, a high water permittable membrane with stronger mechanical strength to bear in high water pressure should be developed for a high-performance PRO desalination process. High mechanical strength and water permittivity could be a trade-off relationship based on thickness and porosity. Thus, vertical oriented polyvinylidene fluoride (PVDF) membrane with 3D connected carbon nanotube (CNT) is presented. Vertical pores made of hydrophobic polyvinyl fluoride (PVDF) and hydrophilic metal-organic framework (MOF) decorated on the surface improve their water permeability and salt rejection. The CNT embedded structure in the vertically aligned membrane improves mechanical strength along the in-plane direction. This work presents CNT additives can significantly improve the mechanical properties of water desalination membranes by smartly designing the morphology of the substrate and properly inserting functional materials in the active layer.



### F.NM03.09.60

#### Near Infrared Photoluminescence Properties of Locally Functionalized Single-Walled Carbon Nanotubes with Proximal Modification Sites [Aoki Haruka](#), Yu Boda, Tanaka Naoki, Tsuyohiko Fujigaya and Tomohiro Shiraki; Kyushu University, Japan

Single-walled carbon nanotubes (SWNTs) have attractive optical properties based on their unique one-dimensional nano structures. Especially, semiconducting SWNTs emits photoluminescence (PL) originating from the  $E_{11}$  emission of photogenerated exciton in the near infrared regions (900-1600 nm), which can be applied for bioimaging and telecom devices. Compared to such  $E_{11}$  PL, redshifted and brighter  $E_{11}^*$  PL have been recently reported by the  $sp^3$  carbon defect doping to the crystalline  $sp^2$  carbon lattice of SWNTs. The resultant SWNTs are locally functionalized SWNTs (lf-SWNTs) [1] that have the doped sites with narrower bandgaps and exciton trapping features. We have reported proximal modification using bis-aryldiazonium salts (bADs). The lf-SWNTs modified with bADs (lf-SWNT-bA) showed largely redshifted PL ( $E_{11}^{2*}$ ) than  $E_{11}^*$  PL [2] and were found to show sensitive  $E_{11}^{2*}$  PL property changed depending on the chemical structures of bAD, in which the  $E_{11}^{2*}$  PL wavelengths were shifted with strong dependence of methylene spacer lengths and connected positions in the bADs [3]. Therefore, proximal modification is useful approach for remarkable PL property modulation of the lf-SWNTs compared to typical mono-aryl functionalized lf-SWNTs.

In this study, we newly synthesize modifiers having multiple reactive groups for structural changes of the proximal modification sites of lf-SWNTs. The SWNTs (CoMoCAT, (6,5) chirality-rich) were solubilized in  $D_2O$  containing sodium dodecyl sulfate by sonication and separated by ultracentrifugation. A tris-aryldiazonium salt (tAD) having three aryldiazonium groups was mixed with the solubilized SWNTs for local chemical functionalization. After the chemical modification, multiple PL peaks appeared over typical  $E_{11}^*$  regions (>1200 nm). The NIR absorption and Raman scattering measurements supported the local chemical functionalization of the modifiers on the SWNTs, in which small absorbance changes at 980 nm and the increase of D-band intensity due to the defect introduction were observed, respectively. In addition, the reaction conditions such as solution concentrations were found to show significant influence on such new longer wavelength PL generation. The detail results including chemical structure effects of the modifiers and the reaction condition dependency will be discussed at the meeting.

In this study, we newly synthesize modifiers having multiple reactive groups for structural changes of the proximal modification sites of lf-SWNTs.

The SWNTs (CoMoCAT, (6,5) chirality-rich) were solubilized in  $D_2O$  containing sodium dodecyl sulfate by sonication and separated by ultracentrifugation. A tris-aryldiazonium salt (tAD) having three aryldiazonium groups was mixed with the solubilized SWNTs for local chemical functionalization. After the chemical modification, multiple PL peaks appeared over typical  $E_{11}^*$  regions (>1200 nm). The NIR absorption and Raman scattering measurements supported the local chemical functionalization of the modifiers on the SWNTs, in which small absorbance changes at 980 nm and the increase of D-band intensity due to the defect introduction were observed, respectively. In addition, the reaction conditions such as solution concentrations were found to show significant influence on such new longer wavelength PL generation. The detail results including chemical structure effects of the modifiers and the reaction condition dependency will be discussed at the meeting.

#### References

- [1] Y. Piao, B. Meany, L. R. Powell, N. Valley, H. Kwon, G. C. Schatz, Y. Wang, *Nat. Chem.* **2013**, *5*, 840.
- [2] T. Shiraki, T. Shiraishi, G. Juhasz, N. Nakashima, *Sci. Rep.* **2016**, *6*, 28393.
- [3] T. Shiraki, B. Yu, T. Shiraishi, T. Shiga, T. Fujigaya, *Chem. Lett.* **2019**, *48*, 791.

### F.NM03.09.61

#### Isopropanol-Assisted Hot Lamination for Facile Synthesis of Large-Area Atomically Thin Graphene

Membranes [Peifu Cheng](#)<sup>1</sup>, Nicole K. Moehring<sup>1</sup>, Andrew Naclerio<sup>1</sup>, Mattigan Kelly<sup>1</sup>, Dahsong Lee<sup>1</sup>, Juan C. Idrobo<sup>2</sup> and Piran Ravichandran Kidambi<sup>1</sup>; <sup>1</sup>Vanderbilt University, United States; <sup>2</sup>Oak Ridge National Laboratory, United States

Atomically thin graphene membrane has been considered as an ideal candidate for next-generation membrane-based technologies. While catalytic chemical vapor deposition (CVD) has been demonstrated to be an economical and versatile way of enabling the commercial production of high-quality graphene, CVD graphene has to be transferred from the growth substrate onto a porous support substrate to provide mechanical stability for membrane applications. However, commonly used polymer scaffold methods typically leave polymer residues detrimental to membrane performance, while transfers without sacrificial polymers suffer from low transfer yield leading to high membrane leakage. Hence, high-yield transfer of clean large-area graphene onto appropriately porous supports using scalable processes for membrane applications remains elusive. In this work, we systematically investigate the factors influencing the transfer of CVD graphene from a Cu foil onto a model polycarbonate track etch (PCTE) support for fabricating large-area atomically thin membranes via manual compression, mechanical press and scalable lamination approaches. Particularly, we report on a novel roll-to-roll manufacturing compatible isopropanol-assisted hot lamination that allows for facile, clean and scalable transfer of centimeter-scale graphene onto model PCTE supports with coverage  $\geq 99.2\%$  without compromising support porosity, which is one of the best values reported to this date for centimeter-scale atomically thin membranes. The remaining 0.8% of leakage is attributed to defects (>50 nm) primarily along wrinkles formed during CVD growth. Furthermore, water-assisted oxidation effectively detaches CVD graphene from the Cu foil and helps graphene transfer, but significantly damages (~10%) graphene along wrinkles. Finally, fully functional centimeter-scale atomically thin membranes are demonstrated. Our work provides a facile and effective method for the fabrication of atomically thin graphene membranes and can help on the progress towards the practical application of graphene membrane technologies relevant to gas separation, nanofiltration, desalination, ionic/molecular transport, energy and biomedical fields and beyond.

### F.NM03.09.63

**Effect of Orientation of Graphene Upon Dielectric and Electrical Characteristics of PBAT-PLA-Graphene Composites** Radha Perumal Ramasamy<sup>1</sup>, Xianghao Zuo<sup>2</sup>, Yiwei Fang<sup>2</sup> and Miriam H. Rafailovich<sup>2</sup>; <sup>1</sup>Anna University, India; <sup>2</sup>Stony Brook University, United States

Graphene has several fascinating characteristics such as high thermal and electrical conductivity. Graphene polymer composites is usually made using molding. To enhance the application of graphene in nanocomposites controlling its alignment is important as graphene has different conductivity along and perpendicular to its surface. The orientation of graphene in polymeric materials is a challenging task. Recently 3D printing has been used for aligning graphene in composites. In this research varying amounts of graphene (grade H5 – XG Sciences) was mixed with PBAT-PLA mixture and molded. Also 3D printed PBAT-PLA-graphene composites were made. The dielectric measurements were made by placing the composites between two brass electrodes of diameter 1cm. The dielectric measurements were made using Wayne-kerr- 6500p LCR meter. The frequency was varied from 100 to 10<sup>6</sup> Hz. The measurements were made at room temperature (22 °C). The samples had cuboid shapes. The measurements were made along height and depth of the samples. The height corresponded to the direction of application of pressure during molding and the depth corresponded to the direction perpendicular to the direction of application of pressure and parallel the surface of the samples. The following observations were made. (A) The dielectric constant for 3D printed samples (along height) was less than dielectric constant for 3D printed samples (along depth) which was less than dielectric constant for molded samples (along height). (B) The dielectric constant for molded samples (along depth) was less than dielectric constant for molded samples (along height). (C) Along depth, for molded samples the dielectric constant becomes negative for 20% graphene containing samples indicating percolation. (D) The electrical conductivity for 3D printed samples (along height) was less than conductivity for molded samples (along height) and (E) Electrical conductivity for 3D printed samples (along depth) was less than electrical conductivity for molded samples (along depth). The observed variations in dielectric and electrical characteristics are attributed to the orientation of graphene in the composites.

### F.NM03.09.64

**Modification of P-Plasmon Energy in Single Walled Carbon Nanotube Induced by the Interaction Between Carbon Nanotube and Gold Nanoparticles** Masahide Shima<sup>1</sup>, Hiroki Kato<sup>1</sup>, Noriaki Endo<sup>1</sup>, Eiji Okunishi<sup>1</sup>, Masaki Tanemura<sup>2</sup> and Yoshikazu Homma<sup>3</sup>; <sup>1</sup>JEOL Ltd., Japan; <sup>2</sup>Nagoya Institute of Technology, Japan; <sup>3</sup>Tokyo University of Science, Japan

Graphene, which is an atomic layer carbon with the honeycomb structure, has several interesting properties, such as high optical transparency, high electrical and thermal conductivities. Graphene possesses also unusual properties in plasmon, such as the confinement, long lifetime, and long propagation distances of plasmons. Due to the tunability of plasmon, graphene is promising for the plasmon-based application, such as THz technologies and gas sensors. For the device application, the investigation of interaction between graphene and metal is also essential, because the graphene-metal contacts are unavoidable of every graphene-based device, and the electronic properties of graphene strongly depends on the substrate. It is known that the plasmon in free standing graphene show the different properties from those supported by substrate. It is also known that the properties of plasmon in graphene depend on the materials used for substrate, which is important for graphene plasmonics. On the other hand, the interaction between the substrate and graphene is not fully understood. Especially in nanoscale structures, it is not well known how plasmons in graphene are affected by the metal substrate. In this study, p-plasmon in single-walled carbon nanotube (SWCNT) with and without the deposition of gold nanoparticles (Au NPs) was investigated using TEM-EELS (Transmission Electron Microscopy – Electron Energy Loss Spectroscopy) method as the first step to elucidate the effect of the gold substrate on p-plasmon in honeycomb structured carbon. The plasmons show the linear dispersion in monolayer graphene-metal interface similar to that in SWCNT-metal interfaces, and the controllability of Au NPs in shape and size is much higher on SWCNTs than on graphene. So, the investigation using SWCNT-Au NPs system would be the simplified model system for the honeycomb structured nanocarbon on metal substrates.

The solution of SWCNTs dispersed in an organic solvent, was dropped on the a microgrid for TEM. Then gold nanoparticles were vapor-deposited thereon. In order to avoid the contamination during TEM-EELS measurement, the microgrid thus prepared was pre-heated for 10 min in 1x 10<sup>-5</sup> Pa. TEM observation and EELS measurement performed using JEM-F200 (JEOL) and GIF Quantum (Gatan), respectively. The accelerating voltage for the TEM observation and EELS measurement was 80 kV for preventing sample damage. The energy resolution of zero loss peak was below 0.5 eV.

On the microgrid, various types of SWCNTs with and without Au NPs were recognized such as isolated, bundled, and cross-linked ones. The peak shift in the energy loss spectra of p-plasmon was biggest for the bundled SWCNTs without Au NP. The peak shift increased for an isolated SWCNT with an Au NP, and was highest for SWCNTs sandwiching a Au NPs. These results showed the plasmon energy can be controlled by the configuration of SWCNTs and Au NPs.

#### **F.NM03.09.66**

##### **Why Aren't Nano Carbon Based Composites Rise Up to Their Theoretical Potential and How Can We Get Them Closer?** Noa Lachman; Tel Aviv University, Israel

Carbon Nanotubes (CNT) and graphene are considered highly promising nanomaterials for composite reinforcement. The nanoscale dimensions of the carbon structures provide ultra-high surface-to-volume ratio, nearly defect-free structure, and their exceptional properties: mechanical (1TPa – five times the value for steel), thermal conductivity (2000-6000 Wm<sup>-1</sup>K<sup>-1</sup> – four to ten times the value for silver) and electrical conductivity (roughly equivalent to copper) makes them highly useful in very many applications. However, these same scale and properties complicate the processing and fabrication of polymer based nanocomposites: high surface-to-volume means that even in small filler concentrations composite process-affecting properties as melt viscosity, heat transfer and other characteristics will drastically change. Morphology control, and thus post-processing behavior prediction, are also challenging – as dispersion and orientation are applied indirectly in the process, and different mechanisms are dominant at different length-scales. Therefore, transferring the exquisite properties of the CNT and graphene to the composite level have been proven less than ideal, as the measured mechanical, electrical and thermal properties of the nanocomposites are usually lower than predicted by rule-of-mixture calculations.

In this talk, various approaches for carbon nanocomposite fabrications, both “top-down” and “bottom-up”, will be presented in case-studies. A few of the major issues inhibiting nanocarbon based composites from achieving their true potential will be highlighted. Effects of different fabrication techniques, including 3D printing, on the morphology of nanocomposites and the resultant behavior will be discussed, and possible solutions to the aforementioned issues will be presented. The new methods can provide better control for improved planning and designing of nano carbon based composites.

#### **F.NM03.09.67**

##### **Flexible Devices Based on Polyurethane and Reduced Graphene Oxide Composites for Applications in Tactile Sensing** Flavio A. Borges<sup>1</sup>, Monica A. Cotta<sup>1</sup>, Cecilia d. Silva<sup>2</sup>, Talita Mazon<sup>3</sup>, Joao H. Clerici<sup>1</sup> and Daniel M.

Ugarte<sup>1</sup>; <sup>1</sup>University of Campinas, Brazil; <sup>2</sup>MackGraphe – Graphene and Nanomaterials Research Center, Brazil; <sup>3</sup>Institute of Information Technology Renato Archer, Brazil

New opportunities have been created along with the advances of the wearable device technology. For pressure sensing and transduction in soft objects like human skin, direct contact between sensor and target area is necessary; therefore, sensor flexibility is a very important parameter for the viability of the sensing device.

In this work, we report on the development of a sensing system that translates the electric signals of low cost composites based on polyurethane (PU) and reduced graphene oxide (r-GO) fabricated in-house. The graphene oxide (GO) is deposited by dispersion in PU foam. The GO reduction is carried out by immersion in ascorbic acid. Different commercial foams were tested and sample heights could be reduced to 1mm with electrical resistance range of 1-100 kΩ for a 90% compression. Electrical resistances were measured in function of the applied force and an exponential character was identified. With the force range which the foams endure and the calibration curve obtained for the samples, a rigid device was developed by integrating an Arduino system to the sensors so that responses could be obtained via a graphical interface, adapted to visual feedback.

The foam shows great conformity with surfaces; flexible contacts, printed in Kapton film using conductive paint, are used to obtain the flexible device. We thus expect to have a flexible sensor integrated to a functioning system fully prepared to neurological rehabilitation applications.

#### **F.NM03.09.68**

##### **Transition Metal Chalcogenide Nanostructures for High Energy Density Supercapacitors** Harish Singh and Manashi Nath; Missouri University of Science and Technology, United States

Electrochemical capacitors (ECs) or supercapacitors (SCs) are considered to be most promising energy storage devices and have received great attention because of their excellent electrochemical performance with high output power, short discharging time and long-term cycle stability. Transition metal chalcogenides (especially selenides and tellurides) have recently attracted considerable attention for electrochemical applications mainly due to better electronic conductivity, facile charge transfer, redox tunability, and chemical stability. In the current project, transition metal telluride-based nanostructure composites were studied for supercapacitor applications. The nickel telluride nanostructures were grown directly on Nickel foam by hydrothermal method as well as electrodeposition process without addition of any binder to the catalyst. The capacitor performance was measured in a three-electrode system with the nickel-telluride electrode as the anode. A specific capacitance of 1826 F/g was achieved at a current density of 1 A/g. The composite electrode maintained cyclic stability of

more than 90 % at a higher current density of 10 A/g after 1000 cycles. Also, more than 80 % current density retention achieved at higher current density of 20 A/g. Moreover, doping effect on the transition metal site on the supercapacitor performance was also illustrated in this work. Doping in the transition metal site had a positive influence on the supercapacitor activity since, it led to lattice distortion, electronic structure modification as well as helped to tune the surface redox behavior. Also, combining different carbon-based materials (carbon nanotubes, activated carbons and graphene) with the active nickel telluride nanostructures enhanced specific capacitance and overall cyclic stability by increasing the active surface area and porosity of the composite. In this presentation we will discuss the supercapacitor performance of these telluride nanostructures as well as the effect of transition metal doping and carbon nanostructure additives, and explain how the chemistry of transition metal chalcogenides influences their electrochemical functionality and potential as future energy storage devices.

#### F.NM03.09.71

**Nanopores in Multilayer Hexagonal Boron Nitride** Mehmet Dogan<sup>1,2</sup>, S. Matt Gilbert<sup>1,2,3</sup>, Thang Pham<sup>1,2,3</sup>, Brian Shevitski<sup>1,2,3</sup>, Peter Ercius<sup>2</sup>, Shaul Aloni<sup>2</sup>, Alex Zettl<sup>1,2,3</sup> and Marvin L. Cohen<sup>1,2</sup>; <sup>1</sup>University of California, Berkeley, United States; <sup>2</sup>Lawrence Berkeley National Laboratory, United States; <sup>3</sup>Kavli Energy NanoScience Institute, United States

Controlling the size and shape of nanopores in two-dimensional materials is a key challenge in applications such as DNA sequencing, sieving, and quantum emission in artificial atoms. In single-layer hexagonal boron nitride (*h*-BN), under a high-energy electron beam with certain properties, triangular pores are formed whose edges are entirely made up of nitrogen atoms. This allows fabrication of triangular pores at will with matching orientation throughout the two-dimensional material. However, in multilayer *h*-BN, which is usually in the AA' stacking, neighboring sheets are rotated by 60° with respect to each other, which causes triangular pores in consecutive layers to be misaligned. Here, we investigate experimentally and theoretically triangular vacancies in (unconventional) Bernal-stacked *h*-BN (AB-*h*-BN) formed using a high-energy electron beam. Due to the geometric configuration of AB-*h*-BN, triangular pores in different layers are aligned, and their sizes are controlled by the duration of the electron irradiation. Interlayer covalent bonding at the edge of the pore is not favored, as opposed to what occurs in the more common AA'-stacked BN. A variety of monolayer, concentric and bilayer pores in bilayer AB-*h*-BN are observed in high-resolution transmission electron microscopy and characterized using *ab initio* simulations. Bilayer pores in AB-*h*-BN are commonly formed, and grow without breaking the bilayer character. Nanopores in AB-*h*-BN exhibit a wide range of electronic properties, ranging from half-metallic to non-magnetic and magnetic semiconducting. Therefore, because of the controllability of the pore size, the electronic structure is also highly controllable in these systems, and can potentially be tuned for particular applications.

#### F.NM03.09.72

**Enhanced Mechanical Properties of Polymer-Matrix Nanocomposites Reinforced with Graphene Synthesized in Atmospheric Plasmas** Albert Dato, Jacob Knego, Nicole Subler, Taylor Sloop, Chance Bisquera and Kevin Nakahara; Harvey Mudd College, United States

Graphene can be synthesized in the gas phase using atmospheric plasmas. Gas-phase-synthesized graphene (GSG) is pure and highly ordered. Additionally, GSG contains graphitic nanocrystals that provide the two-dimensional material with significant mechanical stability and enable GSG sheets to resist deformation. GSG is also more environmentally friendly to produce than graphene that is obtained from graphite. These unique features make GSG a promising filler material for fabricating high-strength multifunctional nanocomposites that have a wide range of applications, such as automobiles, aircraft, and wind turbines.

Here we present the results of an investigation into epoxy-matrix nanocomposites reinforced with GSG. We show that as-synthesized GSG effectively disperses in epoxy resins and resists aggregation indefinitely. We report that incorporating a relatively low loading of GSG into epoxy (0.1 wt%) results in nanocomposites that exhibit significant increases in both strength and strain at break. In contrast, epoxy-matrix nanocomposites that were filled with 0.1 wt% graphene nanoplatelets had enhanced strength but diminished strain at break. Scanning electron microscopy images of nanocomposite fracture surfaces will be presented, which indicate much higher matrix reinforcement by GSG relative to graphene nanoplatelets. These results indicate that (1) GSG could overcome the challenges of contemporary graphene-based nanocomposites and (2) unique strengthening mechanisms exist in polymers reinforced with GSG.

#### F.NM03.09.73

**Metal-Free, Highly Conductive Protein Carbon Nanotube Dispersions and Their Films for Biological Applications** Ankarao Kalluri and Vijaya Kumar Challa; University of Connecticut, United States

A simple and facile method to produce highly concentrated ( $> 5$  mg/ml) and high-quality multi-walled carbon nanotube (MWCNT) dispersions by ordinary benchtop magnetic stirrer is reported here. Exfoliation and debundling of the MWCNTs were possible by stirring in the presence of a protein, driving the adsorption of the protein onto the nanotube surfaces. High concentrations of the debundled nanotubes were obtained (6 mg/ml) after stirring for 5 days, and these are much higher than other reports in the literature. The bioCNT aqueous dispersions are stable up to 6 months, which is important for storage and practical applications. We also fabricated the facile, inexpensive, highly conductive and flexible CNT paper (Bucky paper) by vacuum filtration of the dispersion through an ordinary filter, which composed of self-assembled, randomly oriented, and highly packed CNTs. These metal-free CNT films were flexible and showed a high electrical conductivity of  $> 1000$  S/cm than expected. These biological CNT dispersions used as conductive ink on cellulose paper, which can be used in printed and flexible electronics, bio-electrochemical sensors, bio-supercapacitor electrode applications. Therefore, inexpensive, highly concentrated biological CNT dispersions prepared by a simple method of stirring provides new opportunities for a wider range of CNT applications.

#### **F.NM03.09.74**

**Sub-Nanometer Carbon-Nanotube Membranes with Anomalously Enhanced Water-Vapor Flux** Da-Chi Yang<sup>1</sup>, Richard Castellano<sup>1</sup>, Melinda Jue<sup>2</sup>, Ricardo P. Silvy<sup>3</sup>, Robert F. Praino<sup>3</sup>, Francesco Fornasiero<sup>2</sup> and Jerry Shan<sup>1</sup>; <sup>1</sup>Rutgers, The State University of New Jersey, United States; <sup>2</sup>Lawrence Livermore National Laboratory, United States; <sup>3</sup>Chasm Advanced Materials, Inc., United States

Fluid transport through the inner cores of carbon nanotubes (CNTs) is known to occur at extraordinary rates, exceeding classical predictions by several orders of magnitude, especially for very-small-diameter nanotubes. However, macroscopic, vertically aligned- (VA-) CNT membranes with sub-nanometer pores have not been previously fabricated due to the difficulty in growing aligned forests of such small CNTs. Here, we report the scalable, solution-based fabrication of the first macroscopic membranes with VA-CNTs of sub-nanometer diameter, and the first water-vapor transport measurements for such membranes. Membranes were fabricated from CNT powder using electric-field alignment and electrophoretic concentration of suspended nanotubes, followed by solvent replacement with a liquid prepolymer and UV curing. The single-wall nanotubes are grown in bulk by chemical-vapor deposition with a specialized catalyst, tuned to produce long, 0.8 nm diameter CNTs. After etching to open CNT pores, the membranes filter out dye solution and demonstrate sublinear conductance scaling with salt concentration at low concentrations. These observations indicate that our fabrication process produces defect-free membranes with CNT pores as the primary trans-membrane pathway. Based on KCl-conductance estimates for the total open pore area in the membranes, the concentration-driven water-vapor permeability is enhanced by many orders of magnitude, well above values reported in literature for larger-diameter VA-CNT membranes. Interestingly, the enhancement in concentration-driven water-vapor transport appears to considerably exceed the enhancement present in the pressure-driven flux of dry nitrogen gas in the pores. Additionally, due to the size of the CNT pores, and the charge present on carboxyl groups at the CNT tips, the membranes demonstrate cation selectivity in KCl solution. Coupled with the enhanced flux of liquid water, such membranes could increase the energy efficiency of membrane-based desalination techniques. These findings present new opportunities to scalably fabricate VA-CNT membranes with sub-nanometer pores and study their fundamental transport properties, with possible applications in breathable and protective garments as well as desalination technologies.

#### **F.NM03.09.75**

**Growth Pressure Dependence of Graphene Direct Growth on A-Plane Sapphire Using Metal-Catalyst-Free Low-Pressure CVD** Yuki Ueda, Takahiro Maruyama and Shigeya Naritsuka; Meijo University, Japan

Graphene direct growth on sapphire by metal-catalyst-free chemical vapor deposition (CVD) has attracted much attention as the method to avoid the transfer process [1]. The transfer process not only damages but also deteriorates the graphene. Recently, we reported a graphene direct growth on r-plane sapphire using metal-catalyst-free low-pressure CVD where the graphene grows very fast and quite uniformly comparing to that on c-plane sapphire [2]. However, there are many unknown parts in the growth mechanism. In this report, we focused on a-plane sapphire as a substrate, which is often used in horizontally-aligned growth of carbon nanotubes [3]. The growth pressure was systematically changed in metal-catalyst-free low-pressure CVD to reveal the growth mechanism.

Graphene was directly grown on a-plane sapphire using low-pressure CVD without using a metal catalyst. A mixture gas of N<sub>2</sub>, H<sub>2</sub>, and 3-Hexyne was flown in a reaction chamber at a constant flow rate of 1000 sccm. The growth temperature, H<sub>2</sub>, and 3-Hexyne partial pressures were fixed at 1250 °C, 500 Pa, and 0.3 Pa while the growth pressure was systematically changed from 5 kPa to 50 kPa.

Raman measurements show that graphene was only grown below 17 kPa and all the grown graphene was smooth and uniform with mono-layer-thick. At the same time, the D/G ratio decreased with decreasing the growth pressure. To

investigate the reason, the early stages of growth were studied between 5 kPa and 15 kPa. Consequently, AFM study showed that the density of graphene islands on the sample grown at 5 kPa was approximately 3 times lower than that of the sample grown at 15 kPa. On the contrary, the growth rate of graphene at 5 kPa was much faster than that at 15 kPa. A high growth rate usually means a high supersaturation, and, therefore, a high nucleation rate. In our case, however, the nucleation rate was slow at low growth pressure. This inconsistency suggests the existence of a special mechanism, which controls the nucleation. From the AFM study, the most graphene islands were found at the step edges of the sapphire substrate. At a low growth pressure, the thermal decomposition of the sapphire surface is enhanced and nucleation sites, in other words, surface steps are destroyed at the same time. This brings the difficulty to the graphene nucleation at the step edges even with a higher supersaturation at a low pressure. Consequently, excellent smooth monolayer graphene with a small D/G ratio of less than 0.2 was successfully obtained on a-plane sapphire at 5 kPa with forming larger grains.

Acknowledgement: This work was supported in part by JSPS KAKENHI Grant Numbers 15H03558 and 26105002.

#### Reference

- [1] M. A. Fanton et al., ACS Nano 5, 8062 (2011).
- [2] Y. Ueda et al., Appl. Phys. Lett. 115, 013103 (2019).
- [3] N. Ishigami et al., J. Am. Chem. Soc. 130, 9918 (2008).

#### F.NM03.09.76

**Partially Reduced Graphene Oxide Enhancement of Thrombin Activation of Fibrinogen Clots** Rebecca Isseroff<sup>1</sup>, Juyi Li<sup>1</sup>, Jonathan Lederer<sup>2</sup>, Nava Schein<sup>1</sup>, Abraham Balsam<sup>1</sup> and Miriam H. Rafailovich<sup>1</sup>; <sup>1</sup>Stony Brook University, The State University of New York, United States; <sup>2</sup>Columbia University, United States

Partially reduced graphene oxide (pRGO) has been found to enhance the enzymatic activity of microbial transglutaminase on the cross-linking of gelatin. To determine if this is a more general phenomenon in modification of enzymatic activity, we tested whether it has an effect on thrombin's ability to clot fibrinogen, an easily quantifiable effect to measure.

Three ml of 10 mg/ml fibrinogen solution in PBS were tested with 8  $\mu$  thrombin/ml as a control. Upon adding thrombin, rheometry was used to measure the clotting time as well as the clot modulus. Sharp increases in modulus, shorter clotting times, and stronger clots would indicate enhancement of thrombin, whereas slow increases in modulus, longer clotting time, and weaker clots would indicate inhibition of the enzyme. Test samples included 0.5 ml of 1 mg GO/ml PBS in the fibrinogen mixture, and 0.5 ml of 1 mg pRGO/ml PBS added to the fibrinogen. The pRGO solution produced a clot with an elastic modulus four times greater than the control, and 1.5 times greater than the clot with GO. Different concentrations of pRGO in PBS were then added to fibrinogen solutions and tested. Increasing pRGO concentrations increased the maximum elastic modulus and decreased the clotting time. The elastic moduli were found to be logarithmic, as the logarithmic trendlines had relatively high R<sup>2</sup> values. Higher concentrations of pRGO had higher coefficients, indicating shorter clotting times. Results suggest further future study of partially reduced graphene oxide as a modifier of enzymatic activity.

#### F.NM03.09.77

**Interactions Between Graphene Oxide and Pyrrole Towards Understanding the Electro-Polymerized Substrates—A Molecular Dynamics Study** Todd M. Richards and Isaac Macwan; Fairfield University, United States

Graphene Oxide, an oxidized form of graphene, a carbon allotrope, has many applications including the formation of conductive films for use in flexible electronics and chemical sensors, nanofiltration membranes, and even as a replacement for tin-oxide in batteries. One of the pressing issues with carbon allotropes in general and graphene oxide in particular, however, is that they cannot form freestanding films on their own, instead they rely on a secondary reactant to help aid in the synthesis of such films. To synthesize such nanocomposite substrates, cyclic voltammetry is a very commonly used technique, where an electrolyte containing a monomer to be electro-polymerized is used along with the nanoparticles. Electro-polymerized substrates consisting of GO and Polypyrrole (Ppy), an organic polymer created by polymerizing pyrrole, have drawn much attention owing to their applications in solid state supercapacitors, biosensing, tissue engineering, and artificial muscle studies. It has been proven theoretically and experimentally that Ppy and GO do interact and exhibit improvement in conductivity and thermal stability compared to pure Ppy and GO, but there is still very little information on the interactions at the molecular level between GO and pyrrole monomers especially during the synthesis of such nanocomposites. This work deals with the study of interactions at the interface of GO and pyrrole in order to better understand the evolution of polypyrrole over the surface of graphene oxide during the formation of these films. The system is

modeled using Visual Molecular Dynamics (VMD) and all-atom simulations are carried out using Nanoscale Molecular Dynamics (NAMD) at ten different temperatures based on the peak currents and scan-rate through the Randles-Sevcik equation. Each simulation is carried out for 100ns, thereby looking into a total of one microsecond long window of interactions between GO and 50 pyrrole monomers as the polypyrrole film is evolved over the surface of GO. Stability of the GO/Ppy nanocomposite is quantified through RMSD (Root Mean Square Deviation), conformational energies and center of mass deviations. Interaction energies are calculated to understand the role of non-bonding interactions such as Van der Waals and electrostatics between the monomers and between monomers and GO. It is anticipated that pyrrole monomers form dimers in the bulk of the solution, trimers when near the surface of GO, and tetramers when adsorbed on the surface of the GO. Based on these results, a potential mechanism is proposed on the way monomers interact with the nanoparticles during electro-polymerization and the role of such interactions in synthesizing carbon-based free-standing films.

#### **F.NM03.09.78**

##### **Development of Planar-Type Thermoelectric Device Using Carbon Nanotube Sheet for Wearable**

**Application** [Tsuyohiko Fujigaya](#)<sup>1,2,3</sup>, Ryohei Yamaguchi<sup>1</sup> and Naoki Tanaka<sup>1</sup>; <sup>1</sup>Kyushu University, Japan; <sup>2</sup>Center for Molecular System, Kyushu University, Japan; <sup>3</sup>International Institute for Carbon-Neutral Energy Research, Kyushu University, Japan

Single-walled carbon nanotube (SWNT) is ideal materials for thermoelectric conversion because of their high Seebeck coefficient and electrical conductivity. Development of the wearable thermoelectric device using SWNTs is now investigated by taking advantage of their film toughness and flexibility. Up to date,  $\pi$ -shape structure has been proposed for the SWNT thermoelectric sheet. However, this structure needs to attach on a skin vertically and not preferable for the wearable application. Therefore, we proposed a new planar-type structure, in which the sheet can attach on the skin surface and preferable as a wearable device. Since sequential repeating of p-type and n-type properties are necessary for the devices, in this study, we investigated the patterned doping of p-type SWNT sheet into n-type. We found that the deposition of benzimidazole derivatives successfully turned un-masked area into n-type, giving a repeating of p and n-type structure. Detail characterization of the n-doping were carried out by Raman spectroscopy, X-ray photoelectron spectroscopy and Seebeck Coefficient measurements. Device performance of the thermoelectric sheet will be introduced in the presentation.

#### **F.NM03.09.79**

**Fabrication and Characterization of PbTiO<sub>3</sub> Multi-Layered Truss Structure** [Hyunji Kim](#), Kisun Kim, Hoon Kim, Seokjung Yun, Gun Park, Seokwoo Jeon and Seungbum Hong; Korea Advanced Institute of Science and Technology, Korea (the Republic of)

Future society will enjoy augmented reality, haptic displays, intelligent cars, and robots in everyday life. Those devices require tactile enhancement which would be improved by high piezoelectric coefficient and strain limit. PbTiO<sub>3</sub> is one of the piezoelectric materials which has high piezoelectric coefficient, low price and wide application but at the expense of low elastic strain limit. In this work, we applied nanoscale truss structure to enhance the elastic stress limit while maintaining the high piezoelectric coefficient of PbTiO<sub>3</sub>. Fabricating PbTiO<sub>3</sub> in multi-layered truss structure around 20~30 nm, we expect to improve both piezoelectric coefficient and strain limit up to 300% respectively. We deposited 8 nm PbTiO<sub>3</sub> layer 3 times on the Nickel template and after deposition of multilayers, Nickel template was removed. Each layer of PbTiO<sub>3</sub> was formed by depositing TiO<sub>2</sub> using atomic layered deposition (ALD) and PbO gas reaction in the tube furnace. The crystallinity of each PbTiO<sub>3</sub> layer was confirmed by XRD. We expect multi-layered PbTiO<sub>3</sub> to show 100% higher piezoelectric coefficient than single-layered PbTiO<sub>3</sub> showing better crystallinity.<sup>[1]</sup> After measuring the crystallinity, thickness was measured by TEM. By measuring the deposition thickness according to the distance, we will set thickness of single-layered PbTiO<sub>3</sub> to 8 nm. This will be a significant experiment in that it stacks nano layers of targeted thickness. Also, our approach will provide insight into making piezoelectric materials that have both high piezoelectric coefficient and strain limit, and realize various tactile applications.

<sup>[1]</sup> M.Park *et al.*, Appl. Phys. Lett.**94**, 092901(2009)

#### **F.NM03.09.80**

**Layer-by-Layer Self-Assembly PEI/MWCNT-COOH Nano-Porous Coating for Enhanced Heat Transfer Characteristics of Heat Dissipation Devices** [Jaemin Lee](#), Daehyeon Kyeong, Ji heon Kim and Wonjoon Choi; Korea University, Korea (the Republic of)

With the development of AI, 5G, and autonomous vehicles, higher performance electronic devices are required for more data

collection and data processing. In addition, as electronic devices are gradually downsized and thinned, the amount of heat generated per unit area also increases exponentially, so conventional heat dissipation devices (e.g. Heat sink, Heat pipe and Vapor chamber) cannot satisfy these heat generation and electronic device manufacturing conditions. In order to improve the performance of these heat dissipating devices, many studies have improved heat transfer performance through various coating methods such as CVD, PVD, ALD and Spray coating. However, these coating methods are not suitable for heat sinks with complex shapes or heat pipes with a thin tube structure because they require special process conditions such as high temperature or vacuum, and the process cost is large or greatly affected by the shape and size of substrate.

The Layer-by-Layer (LbL) coating method is a solution-based technique which is a self-assembled coating using electrostatic force through the difference in zeta potential between positive and negative solution. Since the LbL coating method is based on a solution-based processing, it can be coated to the complex structures regardless of the size or shape of the substrate. This characteristic enables the direct applications to a heat sink within fin structures or a tubular heat pipe within an inner micro porous structure.

Herein, we present multi-functional LbL PEI/MWCNT-COOH nano-porous coatings based on a solution processing to improve the heat transfer characteristics of heat sinks and heat pipes. To investigate the direct correlation of the nano-porous coatings and the heat transfer characteristics, the LbL PEI/MWCNT coatings were prepared as bare, 10-bi, 20-bi, and 30-bi layers. The change in thickness and surface morphologies of LbL coatings was precisely analyzed through FIB and SEM image analysis, while the surface area and pore size distribution according to the number of LbL coatings was examined using BET surface area analysis. Furthermore, the wettability of the PEI/MWCNT coating was measured to confirm the capillary rise, which is one of the important factors to determine the heat transfer performances of the devices.

Through the natural convection test of the LbL coated heat sinks, it was confirmed that the enhanced thermal performances could be obtained due to increasing the porosity and surface area of the LbL coating. As the porosity and surface area was optimized in the number of coatings, the overall thermal performances including heat transfer coefficients were significantly improved up to 11% for 30 bi-layers coated heat sink due to the increase in the surface area, in comparison with that of the bare heat sink. Furthermore, the LbL functional coating layers could highly improve the heat transfer characteristics of the heat pipes, as well. Because a nano-micro sized bi-porous structure appeared in the microporous-sintered heat pipe with the LbL coating layers, such bi-porous structure could strengthen capillary wicking, fluid transportation, and superhydrophilicity as well as increasing surface area, thereby improving heat transfer efficiency and thermal resistance up to 14.3% in a 10 bi-layers coated heat pipe.

The PEI/MWCNT LbL nano-porous coating, which was used for the heat dissipation devices (i.e. heat sink and heat pipe) could show the enhanced heat transfer characteristics, while the fabricate process was based on the only simple and low-cost LbL coating technology. This multi-functional and thin PEI/MWCNT LbL nano-porous coating not only improved the performance of the conventional heat dissipation device, but also is expected the design trend of miniaturization, thinning, and lightweight electronic equipment.

#### **F.NM03.09.81**

**Dielectrophoresis (DEP)-Aligned Semiconducting Carbon Nanotubes for Fabricating Electronic Devices** Abram Jones, Lauren Williams, Brandon Whitaker, Rodricka Miller, Jhamaree Elam, Qunying Yuan and Zhigang Xiao; Alabama A&M University, United States

We report the deposition and alignment of semiconducting carbon nanotubes with the alternating electric field-directed dielectrophoresis (DEP) method and the fabrication of carbon nanotube-based electronic devices with the DEP-aligned semiconducting carbon nanotubes (CNTs). Semiconducting carbon nanotubes, which were dispersed ultrasonically in the *n*-methyl pyrrolidone (NMP) solution, were deposited and aligned onto a pair of gold electrodes using the dielectrophoresis method. The excellent alignment of carbon nanotubes was achieved by optimizing the AC voltage, frequency, and deposition time of the applied AC signal. The DEP-aligned tubes were further fabricated into carbon nanotube field-transistors (CNTFETs) and CNTFET-based electronic devices such as CNT-based inverters using the microfabrication techniques. Plasma-enhanced atomic layer deposition (PE-ALD) was used to grow hafnium dioxide (HfO<sub>2</sub>) as the high-*k* gate oxide in the fabrication of CNTFETs. The aligned carbon nanotubes and fabricated devices were imaged using the scanning electron microscope (SEM), and the electrical properties were measured from the fabricated devices using the semiconductor analyzer. About 70% yield was obtained from the semiconducting carbon nanotube-based CNTFETs, and the fabricated CNTFETs and CNT-based inverters demonstrated excellent current (*I*) – voltage (*V*) curves and transfer characteristics.

#### **F.NM03.09.82**



**Inertial Sensor Based on Energy Harvesting Carbon Nanotube Yarn** Ji Hwan Moon and Seon Jeong Kim; Hanyang University, Korea (the Republic of)

Inertial sensors are devices that can monitor inertial movements like linear acceleration and angular motions, in various applications such as industrial and human monitoring. For wearable and portable applications, inertial sensors are better to be self-powered and miniaturized. Here, we developed a self-powered inertial sensor with various applications having high accuracy based on carbon nanotube (CNT) yarn. Our inertial sensor can sense and monitor inertial movements without any external power by harvesting the mechanical energy to electric energy by the coiled CNT yarn. For applications, the sensor can monitor practical kinds of inertial movements, such as impact energy, vibrations, tilting, and body motions such as walking, running, jump and squatting motions. These results suggest that the self-powered inertial sensor shows the advantages of portable and wearable application in industrial and human motion monitoring system.

<gdiv></gdiv><gdiv></gdiv>

**F.NM03.09.83**

**Formation of Nanosheets via Unfurling of Vanadate Nanoscrolls from Bulk Vanadium Oxide** Md Shahidul Islam Khan<sup>1</sup> and John B. Wiley<sup>1,2</sup>; <sup>1</sup>The University of New Orleans, United States; <sup>2</sup>Advanced Materials Research Institute, United States

Vanadium oxide materials are renowned for their catalytic properties, super-capacitance, chemical sensing, and high energy density cathodic properties. A two-step synthesis method was applied to obtain 2D structures of vanadium oxide ( $V_2O_5$ ) or vanadate ( $V_{2-x}O_{5-x}$ ) nanosheets from bulk  $V_2O_5$  where the first step involved the formation of vanadate nanoscrolls, 1D structures, that resulted from the dissociation of layered vanadium oxide. In the second step, the nanoscrolls were unfurled to obtain nanosheets, 2D materials. This latter step can be performed using a wet chemical process or annealing treatment. During the wet chemical process, vanadate nanoscrolls turn into thin-layered vanadate nanosheets, and with the annealing process, thin-layered vanadium oxide nanosheets are produced. The formation of these different types of nanosheets was confirmed by X-ray diffraction. Nanosheets obtained from the wet process showed the presence of organic groups that were detected using FTIR and Raman spectroscopy. Both the vanadate and vanadium oxide nanosheets were single or multilayered but only the latter one possesses irregular hexagonal shape which was confirmed through TEM.

**F.NM03.09.84**

**Self-Assembly of Tetra-Peptides on Surfaces of Two-Dimensional Materials** Wei Luo, CHEN CHEN and Yuhei Hayamizu; Tokyo Institute of Technology, Japan

As the novel “bottom-up” strategy for fabricating nanomaterials, molecular self-assembly has attracted considerable attention worldwide. On one hand, two-dimensional (2D) materials such as graphite and molybdenum disulfide ( $MoS_2$ ) have been demonstrated as the platform for this self-assembly due to their unique electrical, optical properties, and atomically flat surfaces, etc. [1,2]. On the other hand, amphiphilic peptides with both of the hydrophobic and hydrophilic nature also have already been used as ideal building blocks for forming various sophisticated self-assembling materials with certain applications. Therefore, in order to functionalize the 2D material surface by peptides self-assembly, it is necessary for a deliberate understanding of the interaction between biomolecules and 2D substrate materials [3].

Molecular dynamics (MD) simulation provides insight into the molecular-scale structure detail of interface. Several works have been done on solid surface to understand the role of peptides, like on Au (111) for self-assembly [4] or on calcite for biomineralization [5]. More recently, peptides on graphene [6] or  $MoS_2$  [7] have been studied because of the atomically flat surface and some progress in experiments exhibiting the molecular resolution morphology. From these, aromatic amino and charged amino acids are considered to have a meaningful interaction with those surfaces. Although the peptide-peptide interaction is also important for surface self-assembly of peptides, the understanding for both interpeptides and peptide-surface interactions are still limited.

In this work, we aim to utilize computational approaches to understand the molecular mechanism. For this purpose, we started with a tetrapeptide consisting of aromatic and charged amino acids, where these amino acids may play a role for the self-assembly. We performed the molecular dynamics simulation (MD) starting with single tetrapeptide on graphene surface. From this calculation, we obtained the most stable tetrapeptide structure on graphene surface. Analyses of center-of-mass distance between peptide and graphene surface, angle change of aromatic rings, and free energy distribution revealed that the balance between interpeptide and peptide-surface is a key to have a well assembled peptides on surface. Furthermore, information about binding process for tetrapeptide on 2D surface was also obtained. This work can be a foundation for building a conformation-property relation of amphiphilic tetrapeptide self-assembly on 2D material surfaces.

**Reference:**

- [1] Li P, Sakuma K, Tsuchiya S, et al. ACS applied materials & interfaces, 2019.  
[2] Chen J, Zhu E, Liu J, et al. Science, 2018, 362(6419): 1135-1139.  
[3] Qiu F, Chen Y, Tang C, et al. International journal of nanomedicine, 2018, 13: 5003.  
[4] Braun, R, Sarikaya, M, Schulten, K, Journal of Biomaterials Science, Polymer Edition, 2002, 12, 747-757.  
[5] Mingjun Yand, P. Mark Rodger, John H. Harding & S.L.S, Molecular Simulation, 2009, 35:7, 547-553.  
[6] Hughes, Z E; Walsh, T R, Journal of Materials Chemistry B, 2015, 3, 3211–3221.  
[7] Huang C, Libo L, Tao Z, et al, J. Phys. Chem. C 2018, 122, 4, 2070–2080.

#### **F.NM03.09.85**

**Formation of Various Cross-Linked Gel Layer Around Single-Walled Carbon Nanotubes** Tsuyohiko Fujigaya<sup>1,2,3</sup> and Yukiko Nagai<sup>1</sup>; <sup>1</sup>Kyushu University, Japan; <sup>2</sup>Center for Molecular System, Kyushu University, Japan; <sup>3</sup>International Institute for Carbon-Neutral Energy Research, Kyushu University, Japan

Single-walled carbon nanotubes (SWNTs) have unique near-infrared (NIR) absorption and NIR photoemission that are attractive for in vivo biological applications such as photothermal cancer treatment and imaging. Therefore, a smart functionalization strategy for SWNTs to create biocompatible surfaces and introduce various ligands to target cancer cells without losing their unique optical properties of the SWNTs is strongly required. We developed novel coating technique of SWNTs inspired by emulsion polymerization method, in which the micelle dispersion of SWNT was used for free radical polymerization. In the dispersion, polymerization takes place in the surfactant micelle having SWNT in the core. Thus the SWNTs were coated by polymer layer. When the cross-linker was added, the SWNTs were coated by gel layer, offering the highly stable coating of SWNT

We have revealed the requirement for the formation of the thin cross-linked polymer-wrapped SWNTs, in which the use of monomers that can undergo polymerization inside the micelles was important. In our study, such hybrids were formed when using various monomers in aqueous SDS dispersions of the SWNTs in the presence of APS and BIS as the initiator and cross-linker, respectively in high yield (>75%) except acryl amide and hydroxymethyl methacrylate. The present study provides useful insight into preparing many polymer-SWNT hybrids with designed functions due to the wide availability of the monomers.

#### **F.NM03.09.86**

**Investigation of Electrocharging-Assisted Fabrication Parameters for Nanocarbon-Al Composites with Improved Electrical Conductivity and Tensile Strength** Madeline Morales<sup>1,2</sup>, Xiaoxiao Ge<sup>1</sup>, Christopher Klingshirn<sup>1</sup>, Christopher Shumeyko<sup>2</sup>, Daniel P. Cole<sup>3</sup> and Lourdes G. Salamanca-Riba<sup>1</sup>; <sup>1</sup>University of Maryland, United States; <sup>2</sup>US CCDC Army Research Laboratory, Vehicle Technology Directorate, United States; <sup>3</sup>US CCDC Army Research Laboratory, Army Research Office, United States

Nanocarbon-metal composites are sought after for their excellent mechanical, electrical and thermal properties. Electrocharging-assisted processing of a novel class of materials, called “covetics,” presents a practical option for macroscale production of nanocarbon-metal composites. This process incorporates carbon on the order of several weight percent in metals such as Al and Cu where carbon solubility is in the low ppm range. Increased tensile strength and electrical conductivity have been measured in Al covetics; however, there is limited understanding of the electrocharging-assisted process and subsequently high variability in measured properties among trials. It has been found that under the influence of a high direct current applied to the molten metal, the activated carbon precursor is converted to sp<sup>2</sup> graphitic carbon with increased crystallite size, as measured by the Tuinstra-Koenig relation for Raman spectra. Electrical conductivity is also enhanced in areas that show increased graphitic carbon crystallite size. A series of experiments varying applied current have been carried out to understand the effect of current density on carbon crystallization rate and size of reaction volume within the Al-1350 melt where carbon crystallization occurs. Local electromechanical behavior is measured by nanoindentation and AFM to gain insight into the structure-property relationship at the nanoscale, which can be used to further inform optimization of the electrocharging-assisted process.

Funded by DOE-EERE grant DE-EE0008313. Sponsored by the Army Research Laboratory under Cooperative Agreement W911NF-19-2-0291.

#### **F.NM03.09.87**

**Direct *In Situ* Observation of Toughening and Fatigue Behavior in Alumina/Graphene Nanocomposites** Qizhong Wang<sup>1</sup>, Cristina Ramirez<sup>2</sup> and Nitin Padture<sup>1</sup>; <sup>1</sup>Brown University, United States; <sup>2</sup>Instituto de Cerámica y Vidrio, Spain

There is growing interest in using 2D graphene-related reinforcements to toughen brittle ceramics in nanocomposites. However, there is a lack of fundamental understanding of the toughening mechanisms and microstructural effects in such nanocomposites. To address this paucity, fully-dense nanocomposites of aluminum oxide ( $\text{Al}_2\text{O}_3$ ) matrix and reduced graphene-oxide (rGO) reinforcements (~5 vol%) of different average-thicknesses and orientations are fabricated and characterized. The interactions between stably propagating cracks and rGO in the  $\text{Al}_2\text{O}_3$ /rGO nanocomposites are observed *in situ* inside a scanning electron microscope (SEM). Toughening by pullout of thick rGO in the crack-tip wake in the cross-section orientation is found to be the most effective, which is consistent with the highest fracture toughness ( $K_{IC} \sim 6.7 \text{ MPa}\cdot\text{m}^{0.5}$ ) measured in those  $\text{Al}_2\text{O}_3$ /rGO nanocomposites. Interestingly, while achieving stable crack growth for flat punch compression of notched samples, we found that upon unloading and reloading, the intact rGO crack-bridges appear to crinkle and uncrinkle without a remnant crease, respectively, which is a unique deformation property of multi-layer graphene-like materials. Information extracted accompanied by the Raman spectroscopy studies has permitted to have a deeper understanding of the fatigue resistance mechanisms in this novel material. This is unlike conventional ceramic composites toughened by fibers or whiskers which have poor cyclic fatigue resistance due to the degradation of the crack-wake bridging and pointing to a possible new cyclic-fatigue resistance mechanism in the nanocomposites. The results from this study have implications for the creation of high-toughness, fatigue-resistant, and wear-resistant graphene-reinforced ceramic nanocomposites of the future.

#### **F.NM03.09.89**

**Effects of Electrical Image Forces on Salt Dissolved in Water** Jeffrey B. Sokoloff<sup>1,2</sup> and Andy Lau<sup>2</sup>; <sup>1</sup>Northeastern University, United States; <sup>2</sup>Florida Atlantic University, United States

Onsager and Samara have shown that electrical image charge forces acting on ions dissolved in water can explain the observed increase of the surface tension due to the presence of dissolved ions. Electrical image charge forces at the interface of a salt solution and air are repulsive, but at the interface between the salt solution and a dielectric of higher dielectric constant than that of the solution or a metal, in contrast, the force is attractive. It has also recently been shown that electrical image forces may play a role in the attraction of ions to the electrodes in capacitive desalination, and to play an important role in the freezing of a confined room temperature ionic liquid. Here, the effect of electrical image forces on the distribution of salt ions in a solution that is in contact with a metallic or dielectric surface is considered. It is shown that in the case of either a metallic or dielectric surface, the salt ion concentration near the surface can be very large, raising the possibility that this could result in precipitation of the salt. In fact, solidification of ionic liquids near a metallic surface with which they are in contact has been observed. Concentration of ions near a metallic surface could be used to desalinate salt water by pushing the salt water between an array of parallel plates of a conducting material. Graphene would be an excellent coating for these plates because the friction between flowing water and graphene is known to be extremely small. In order to support our prediction of a high ionic concentration near metallic and dielectric surfaces, we have performed a variational calculation of the grand canonical partition function to lowest order in the ion density, which is the Debye-Huckel approximation. This calculation supports our conclusion. Our calculation also confirms the concentration dependence of the surface tension found by Onsager and Samarasa in the small salt concentration limit.

#### **F.NM03.09.90**

**Detection of Limonene Using Graphene Field Effect Transistor Modified by Self-Assembling Peptide** Chishu Homma<sup>1</sup>, Hironaga Noguchi<sup>1</sup>, Yoshiaki Sugizaki<sup>2</sup>, Atsunobu Isobayashi<sup>2</sup> and Yuhei Hayamizu<sup>1</sup>; <sup>1</sup>Tokyo Institute of Technology, Japan; <sup>2</sup>Toshiba Corporation, Japan

Graphene, a representative two-dimensional material, has excellent electronic properties due to its high mobility and specific surface area. Biosensors based on graphene field-effect transistor (GFET) are expected to be applied in various fields such as medical diagnosis, environmental monitoring, and security management. A number of studies on biosensors using GFET have been carried out so far. The surface functionalization with probe molecules is crucial, which gives a high affinity to the target molecule. In this process, covalent bonding and  $\pi$ - $\pi$  interaction have been used to immobilize probe molecules to the surface. However, there are two disadvantages with these detection methods. Firstly, chemical modifications may degrade inherent electronic properties of graphene. Secondly, random adsorption of probe molecules on the surface may result in loss of the probe activity. These lead to a decrease in sensitivity as a sensor.

So far, there have been various demonstration of GFET biosensors reported. The target of the biosensors have been living cells, virus, DNA, and proteins. There is a still challenge here to detect relatively small molecules. These small molecules have low molecular weight and generally do not have a polarization. GFET-based biosensors have a drawback for these small molecules, because the detection mechanism depends on the Coulombic interaction between trapped molecules and graphene. In addition, most of the small molecules are volatile and insoluble. Therefore, in aqueous solutions, it is very difficult to detect volatile molecules dissolved in small amounts. This is also one of the challenges for biosensors.

To solve these problems, we suggest an alternative surface modification method using peptide self-assembly. Peptides are known to recognize crystalline structures of inorganic material surfaces and form uniform structures through interactions among molecules [1]. These peptides are physically adsorbed to the surface. Thus, the surface can be modified without losing their intrinsic electronic properties. These self-assembly of peptides has been demonstrated on gold, boron nitride (BN), transition metal chalcogenides, and graphene in previous studies. The self-assembly of peptides have potential as a scaffold domain for biosensors [2]. In this study, we aimed to develop a new technique to detect an odor molecule, which is relatively small and volatile. For this sake, we utilized rationally designed peptides as a molecular scaffold [3] and probe peptides on graphene surface. Then, we performed odor sensing with limonene, a representative molecule for the smell of lemons. We successfully detected limonene with high sensitivity. We also found that the sensitivity to limonene was altered by the amino acid sequence of the probe domain.

This work was supported by the Cabinet Office (CAO), Cross-ministerial Strategic Innovation Promotion Program (SIP), “An intelligent knowledge processing infrastructure, integrating physical and virtual domains” (funding agency: NEDO).

[1] Y. Hayamizu, C. So, S. Dag et al.; *Scientific Reports*, 2016, 6, 1-9

[2] D. Khatayevich, T. Page, C. Gresswell et al.; *Small*, 2014, 10, 8, 1505-1513

[3] P. Li, K. Sakuma, S. Tsuchiya et al. *ACS Appl. Mater. Interfaces*, 2019, 11, 20670–20677

#### **F.NM03.09.91**

##### **Direct Measurements of Tensile Properties and Current-Carrying Capacity of 14 cm-Tall Few-Walled CNT**

**Forest Tatsuhiro Hayashi<sup>1</sup>**, Takayuki Nakano<sup>1</sup>, Hisashi Sugime<sup>2</sup>, Suguru Noda<sup>2,2</sup> and Yoku Inoue<sup>1</sup>; <sup>1</sup>Shizuoka University, Japan; <sup>2</sup>Waseda University, Japan

We have clarified the tensile properties and electron transport capacity properties of macro-sized continuous crystal few-walled CNT forests, which have a height of 14 cm. The present CNT is the highest forest ever reported. The CNT was grown by a CVD method using a Fe-Gd catalyst on Al oxide support [1]. The crystal structures of CNT were evaluated by SEM, TEM, and Raman measurements. Then, the bundle taken out from the CNT forest was converted to a cylindrical structure to define a cross-sectional area and weight density. The cylindrical specimens were tailored by passing through a pinhole with a diameter of 30-100  $\mu\text{m}$ . The reshaped CNT bundle enables to measure tensile tests and electrical measurements by the conventional methods for macroscale specimen. From tensile measurements, it was found that the nominal tensile strength and Young's modulus of the individual CNT were 0.59 GPa and 48 GPa, respectively. This nominal tensile property was obtained by using the entire cross-sectional area, including the inner hole space of the tubular structure for calculation. These results are comparable with reported values, which were measured on various types of CNT by the microscopic methods, and it is lower than theoretical values. The difference between the theoretical and the experimental results is because the present extremely long bundle includes a large number of crystal defects. Also, bundling of millions of CNTs induces further weakening of tensile properties compared to those of micro-sized single CNTs. As for the electrical properties, conductivity and the current-carrying capacity, ampacity, were 140 S/cm and 6700 A/cm<sup>2</sup>, respectively. These properties were improved significantly by heat treatment at 2800°C in Ar, up to 340 S/cm and 8800 A/cm<sup>2</sup>, respectively. These results correspond to the specific conductivity of 1560 S\*cm<sup>2</sup>/g and ampacity per CNT of 5.2×10<sup>4</sup> A/cm<sup>2</sup>. The ampacity of our CNT was as high as that of commercially available Cu wire (5.8×10<sup>4</sup> A/cm<sup>2</sup>).

[1] Hisashi Sugime, Toshihiro Sato, Rei Nakagawa, Cinzia Cepek, and Suguru Noda, *ACS Nano* **13**, 13208-13216, 2019.

#### **F.NM03.09.92**

##### **Copper Oxide Nanocrystals Catalyzed Growth of Nanospheres, Solid and Hollow Carbon Spheres in Thermally Stressed Jet A-1** Pooja Sharma Parihar; Indian Institute of Science, India

Aviation turbine fuel, Jet A-1 contains trace metals that catalyze carbonaceous nanostructures formation and their transformation to carbon spheres in the liquid phase at low temperature (190 °C) by flask tests. Thermal stressing of Jet A-1 produced nanospheres, solid and hollow carbon spheres in this work, which is consistent and continuation of a previous study [1]. Focus of the current study is to identify the trace metallic compounds that catalyze the growth of spherical nanoparticles and carbon spheres in thermally stressed Jet A-1. In the previous study [1], however, the formation of carbon spheres by self-assembly was observed, and their characterization was conducted. Heteroatoms and trace metals are precursors to the deposit formation in the thermally stressed jet fuel [2, 3]. The presence of trace metals and heteroatoms in the Jet A-1 deposits is validated by transmission electron microscopy (TEM), energy dispersive x-ray spectroscopy (EDS), scanning transmission electron microscopy (STEM) and high-angle annular dark-field (HAADF), and high-resolution transmission electron microscopic (HRTEM) micrographs. Heteroatomic species were also recorded by Fourier transform infrared (FTIR) spectroscopy. Trace metal copper oxide nanocrystals (CuO and Cu<sub>2</sub>O) were identified by HRTEM and selected area electron diffraction (SAED) analysis. TEM EDS spectra provided the ratio of Cu and O; Cu to O ratio approximately 1:1 and 2:1.

Indexing of the polycrystalline SAED pattern generated the d-values corresponding with copper oxides nanoparticles. Copper oxides nanocrystals as constituents of spherical particles were confirmed by comparing the measured d-values and calculated Miller indices (h k l) for copper oxides with i) ICSD database and, ii) simulated diffraction pattern of the Cu<sub>2</sub>O, CuO by Crystal Maker software. Furthermore, structure elucidation of Fe and S nanocrystals is in progress and can suggest the effect of trace metal catalysts on the spherical nanoparticles, and carbon spheres formation in the thermally stressed kerosene type fuel.

Keywords: Jet A-1, copper oxide, trace metals, carbon spheres, nanostructures

#### References

1. P. Sharma et al, Formation of hollow and solid carbon spheres in thermally stressed jet fuel in the low temperature autoxidation regime, Chem. Engg. Sci, 206(2009), 335-347.
2. Robert N. Hazlett, Thermal Oxidative Stability of Aviation Turbine Fuels, ASTM, 1991.
3. P. Sharma, Spectroscopic analysis of Jet A-1 heteroatomic components, Chem. Engg. Sci, 207(2009), 588-599.

#### F.NM03.09.118

**Late News: Carbon Nanotube Field-Effect Transistor Model for a Wide Temperature Range** Junsung Park and Michael Shur; Rensselaer Polytechnic Institute, United States

The carbon nanotube field-effect transistor (CNT FET) has been intensively studied due to the high mobility and large current carrying capacity, thus considered as a promising material for nano-scale electronics. For the commercialization of the CNT FETs, the accurate and reliable model is an essential requirement. Especially, transport characteristics of the CNT FETs at high temperature (>300K) is crucially important since the CNT FETs typically operate at elevated temperature. We now report on an improved compact model of the CNT FET. The model is based on the unified charge control model (UCCM) suitable for implementation in standard computer-aided design (CAD) environment such as SPICE. The model accurately describes the current-voltage characteristics for all operation regimes over a wide range of temperatures from 295 to 523K. The model accounts for the temperature and bias effects on the threshold voltage and mobility as the key metrics impacting the CNT FET's performance. It reproduces the mobility, subthreshold swing, on- and off-state current, and threshold voltage behavior as functions of the operating temperature. The model is validated by comparison with the experimental data for the CNT FET reported earlier. The model applications include the device design, characterization, large scale simulation, and parameter extraction of the CNT-based devices and integrated circuits.

#### F.NM03.09.119

**Late News: Laser Peening Enhances Tribological Resistance of Electrodeposited Cr Coatings Reinforced with Yttria Stabilized Zirconia and Carbon Nanotubes** Pragya Tripathi, Kantesh Balani and Janakarajan Ramkumar; Indian Institute of Technology, India

Laser shock peening is performed on chromium based electrochemical coatings consisting of 3 mol% yttria stabilized zirconia nanoparticles (YSZ) and carbon nanotubes (CNT) as reinforcements, deposited on steel substrate as a suitable strategy to further enhance mechanical and tribological properties of protective coatings. Coated Cr has shown an increased hardness after laser peening from ~8 GPa to ~9.4 GPa, whereas, upto 26 GPa hardness is obtained for Cr-YSZ-CNT coating. Increased hardness might be accredited to high compressive stresses, ranging up to ~1757 MPa, induced as a result of laser peening. Synergistically reinforced with YSZ and CNT after laser peening treatment, minimum wear rate of  $\sim 1.8 \times 10^{-5}$  mm<sup>3</sup>/Nm by fretting wear test is recorded in the Cr matrix, which is concomitant with maximum dislocation density of  $\sim 3.0 \times 10^{16}$  m<sup>-2</sup>. An overall improvement in mechanical and tribological properties i.e. low wear constant of the order of 10<sup>-6</sup> is achieved, out of which Cr-YSZ-CNT outperformed the other coating systems. Addition of YSZ strengthens the Cr matrix, whereas, multi-functionality of CNT provides with lubrication along with matrix strengthening as well as bridging effect to crack propagation. Therefore, synergistic effect of two reinforcements (YSZ, CNT) in Cr matrix combined with the laser peening treatment lead to superior properties of the coating (Cr-YSZ-CNT) capable enough of limiting the problems of wear and erosion.

#### F.NM03.09.95

**Self-Assembled Peptides for Suppression of Non-Specific Binding of Biomolecules on Graphene** Mirano Tsukiiwa, Yasuaki Nakata, Hironaga Noguchi, Chishu Homma and Yuhei Hayamizu; Tokyo Institute of Technology, Japan

Graphene is suitable for an active layer for biosensors with high-sensitivity because of their fascinating electrical properties with atomically-flat surface and high specific surface area. Biomolecular immobilization on the active layer of biosensing devices is of vital importance for the functionality, such as sensing with biomolecular probes and protecting from unnecessary unspecific adsorption of biomolecules. However, the immobilization by chemical bonding will introduce atomic defects for graphene, which influences its intrinsic properties to some extent. Self-assembled peptide can be a good candidate. Specific peptides spontaneously form ordered structures through non-covalent intermolecular interactions on the surface of graphene without losing the intrinsic electrical properties of the materials.[1][2][3] On the other hand, non-specific adsorption of biomolecule causes a background noise and decrease the sensing ability of a bio-probe. Therefore, the suppression of nonspecific adsorption is an important issue for the realization of high-performance biosensors. To solve these problems, in this research, we designed new self-assembled peptides and evaluated their performance, aiming at construction of surfaces with the anti-fouling property. The designed peptides consisted of three main domains. (1) antifouling domain: hydrophilic and zwitterionic, which is effective in reducing protein non-specific adsorption. The hydrophilic groups are known to form a hydration layer and create a physical energy barrier that prevents adsorption. (2) Peptide-to-peptide interaction domain: inspired by fibroin, a protein of silk thread. The repetitive sequences of glycine (G) and alanine (A) are introduced. Here we expect the formation of a strong and stable peptide monolayer derived from the  $\beta$ -sheet structure.[2] (3) Anchoring domain: electrons in tyrosine are expected to help to have a stacking of the aromatic ring with the surface of two-dimensional materials. The aqueous solution was placed on the surface of graphite to form a self-assembled film of peptides. The surface structure of these samples was characterized using atomic force microscopy (AFM). We found that peptides had a tendency coverage with increasing concentration. The peptide structure had a six-fold symmetry, which is same as one of underlying graphene lattice. The hydrophilic properties of the peptide film were characterized using contact angle measurements. Furthermore, the antifouling performance was evaluated by AFM and graphene field effect transistors (GFETs). It showed that the adsorption of proteins was greatly inhibited. The peptide offer to be a new molecular scaffold for sensitive graphene biosensors.

## Reference

- [1] Hayamizu, Yuhei, et al. "Bioelectronic interfaces by spontaneously organized peptides on 2D atomic single layer materials." *Scientific reports* 6 (2016): 33778.
- [2] Li, Peiying, et al. "Fibroin-like peptides self-assembling on two-dimensional materials as a molecular scaffold for potential biosensing." *ACS applied materials & interfaces* 11.23 (2019): 20670-20677.
- [3] Sun, Linhao, et al. "Water stability of self-assembled peptide nanostructures for sequential formation of two-dimensional interstitial patterns on layered materials." *RSC advances* 6.99 (2016): 96889-96897.

## F.NM03.09.109

**Late News: Application of Starch-Derived Graphene Quantum Dot Embedded Carbon Aerogel as Efficient Catalyst in Proton Exchange Membrane Fuel Cell** [Eric J. Kim](#) and Sunil Sharma; Stony Brook University, The State University of New York, United States

Proton Exchange Membrane Fuel Cells (PEMFC) are considered to be one of the most promising clean energy sources to mitigate the global crisis of climate change and air pollution. However, its dependence on expensive catalyst materials with low durability, such as platinum, prevent this technology from being widely commercialized. In this study, we present the application of a metal-free starch-derived graphene quantum dot (GQD) supported on highly porous carbon aerogel (GQD/CA) in PEMFC to overcome these technical barriers. Structural, morphological, and crystalline features of GQDs and GQD/CA are analyzed using HRTEM, TEM, AFM, and XRD. Further electrochemical characteristics are investigated using cyclic voltammetry (CV), CO-stripping, ORR polarization, and fuel cell testing. Additionally, the durability of the catalyst is measured using the DOE2020 accelerated stress test (AST). The TEM imaging shows the small size and uniformity of GQDs, which allows for an even distribution of GQDs onto the support and a higher electrochemical surface area (ECSA). The presence of functional groups on GQD is shown to improve ORR performance by up to 10 times compared to platinum. In addition, the structural integrity of both GQD and CA create a synergistic effect to prevent the agglomeration of particles during AST. As a result, compared to a commercial standard catalyst, platinum supported on carbon black (Pt/CB), GQD/CA shows significantly higher electrocatalytic activity, with up to 220% increase in ECSA and 1432% increase in peak power density. After 30,000 cycles of AST testing, GQD/CA is shown to retain 92.9% of its ECSA, 97.1 % of its specific activity, and 98.4% of its mass activity. Thus, GQD/CA is demonstrated to be a highly efficient, durable, and economical catalyst for PEMFCs to mitigate the ever-present effects of climate change and air pollution.

## F.NM03.09.120

**Late News: Graphene-Protein Adhesion Interactions are Influenced by Substrate Properties** Eleanor L. Brightbill, Katherine Young, Hilena F. Gezahagne, Decarle S. Jin, Bryce Hitchcock and Eric M. Vogel; Georgia Institute of Technology, United States

A wealth of studies utilizing graphene to sense biomolecules (such as glucose, DNA, Concanavalin A) across different sensing modalities (such as surface plasmon resonance, redox, field effect transistor) have been published due to graphene's unique properties including high surface area and conductivity. However, in any sensor device where graphene interacts with a biofluid, the graphene must be supported by some underlying substrate. Moreover, previous studies indicate that the substrate can influence graphene's properties, where substrate hydrophilicity can affect graphene's water contact angle and substrate polarity can affect the success of epitaxial growth through a graphene layer. Despite this, little to no work has been completed describing how the substrate support effects the graphene-biological solution interaction.

In this study, *ex situ* protein adsorption is measured via ellipsometry and X-ray photoelectron spectroscopy (XPS) of model small (Lysozyme), medium (Bovine Serum Albumin, BSA), and large (Fibrinogen) proteins on substrates with a variety of hydrophobicity and surface polarity with and without a transferred graphene monolayer. Additionally, we investigate the *in situ* adhesion of lysozyme on Si and Au substrates with and without transferred graphene via quartz crystal microbalance with dissipation (QCM-D) to monitor kinetic differences in attachment. Fully coalesced graphene was synthesized via Chemical Vapor Deposition and transferred onto various substrates using a wet transfer process and PMMA scaffold.

*Ex-situ* ellipsometry and XPS results reveal that the impact of the substrate on protein attachment to graphene depends on the protein studied. The largest model protein, Fibrinogen, shows a similar level of attachment across all 4 substrates regardless of the presence of graphene. Lysozyme, the smallest model protein, shows a difference in adsorption only when a graphene monolayer is added to non-polar substrates. The adsorption of BSA, the intermediate size protein, is influenced strongly by substrate hydrophilicity, where less adsorption is observed on more hydrophilic substrates with or without the presence of graphene. Overall, a more hydrophobic substrate leads to a larger amount of adsorption to graphene.

*In-situ* QCM-D results show that not only the equilibrium attachment, but also the kinetics of interaction, can be affected by the substrate. Modeling the attachment of lysozyme to graphene on Au and Si substrates indicates that the appropriate kinetic model may be determined by the substrate even in cases where differences in absolute adsorption are observed, further indicating that support substrates have a significant effect on protein adsorption behavior to graphene.

This work indicates that the substrate of a graphene-based biosensor is an important but currently overlooked parameter when understanding and optimizing the performance of the device. The *ex-situ* ellipsometry and XPS analysis of protein attachment indicates that the substrate can have a profound impact on protein-graphene interactions, to the extent that twice the BSA attachment to graphene is observed when graphene is supported by TaN rather than Si. The level of non-selective protein adsorption on graphene can be independently engineered through modifying the support substrate without directly modifying the graphene itself.

#### **F.NM03.09.97**

**Nonlocal and Nonlinear Optical Response in Guided Nanoribbon Plasmons** Alvaro Rodriguez Echarrri<sup>1</sup>, Javier Garcia de Abajo<sup>1,2</sup> and Joel Cox<sup>3,4</sup>; <sup>1</sup>ICFO - The institute of Photonic Sciences, Spain; <sup>2</sup>ICREA – Institució Catalana de Recerca i Estudis Avançats, Spain; <sup>3</sup>Center for Nano Optics, University of Southern Denmark, Denmark; <sup>4</sup>Danish Institute for Advanced Study, University of Southern Denmark, Denmark

Electrically-doped graphene supports highly-confined and actively-tunable plasmons that exhibit lower losses than their conventional noble metal counterparts, positioning the atomically-thin carbon layer as an ideal active ingredient in nanophotonic devices. These appealing properties are maintained in nanostructured graphene, which is emerging as a promising candidate for the excitation and guiding of propagating plasmons in future optoelectronic circuitry. Here we employ realistic quantum-mechanical simulations to describe the nonlocal optical response associated with highly-confined propagating plasmons in graphene nanoribbons, accounting for quantum finite-size and edge-termination effects in their electronic band structure. In addition to strong nonlocal effects manifesting in the linear dynamics of plasmons moving in the direction of transverse symmetry, we observe a stronger dependence on quantum finite-size effects in the nonlinear optical response, which involves additional transitions among the quantized electronic Bloch states. We further explore the breaking of inversion symmetry that occurs for optical excitation with large in-plane optical momenta along the transverse direction of the ribbon and reveal that even-ordered nonlinear optical processes such as a second-harmonic generation can occur with remarkably-high efficiency when enhanced by plasmonic resonances. These findings suggest possibilities to exploit the active tunability of graphene to engineer interactions among individual quantized propagating plasmons supported by 1-D

nanoribbons.

#### **F.NM03.09.93**

#### **Structural Analyses of Single Walled Carbon Nanotubes Obtained by Highdensity Plasma Chemical Vapor Deposition** Ronaldo D. Mansano and Ana Paula M. Mansano; University of São Paulo, Brazil

Carbon nanotubes have been an important subject of many recent studies owing to their possible potential applications in nano-scale technologies. Carbon nanotubes can be described as fiber like structures consisting of concentric graphite sheets nested along their long axis and extending to several micrometers. Single-walled carbon nanotubes (SWNTs) can be either metallic or semiconductors depending on the diameter and chirality. All the synthetic methods can be roughly categorized into three groups: the carbon arc-discharge method, laser vaporization of a graphite electrode and chemical methods. In this work, carbon nanotubes were obtained by chemical vapor deposition using high-density plasma processes. Structural studies of carbon nanotubes have relied heavily on Raman spectroscopy. Raman spectroscopy is an analytical technique largely used for characterization of different carbon based materials, either graphite-like or diamond-like. The great versatility of carbon materials rises from the strong dependence of their physical properties on the ratio of  $sp^2$  (graphite-like) to  $sp^3$  (diamond-like bonds). Raman spectroscopy of carbon nanotubes has attracted a lot of attention in recent years, both theoretically and experimentally. Theoretically, it is possible to predict morphological characteristics such as the diameter of the tubes or their conductance properties, especially of single wall carbon nanotubes. Experimentally, it is a powerful method for determining the degree of structural ordering or presence of contaminants [3]. In the Raman spectra of graphite and SWCNTs, there are many features that can be identified with specific phonon modes and with specific Raman scattering processes that contribute to each feature. The Raman spectra of SWCNTs can provide us much information about the exceptional 1D properties of carbon materials, such as their phonon structure and their electronic structure, as well as information about sample imperfections (defects). Raman spectra provide much general information about the structure and properties of SWNTs. The Radial Breathing Mode (RBM) is a unique phonon mode, appearing only in carbon nanotubes and its observation in the Raman spectrum provides direct evidence that a sample contains SWNTs. The RBM is a bond-stretching out-of-plane phonon mode for which all the carbon atoms move coherently in the radial direction, and whose frequency  $\omega_{RBM}$  is about  $100-500\text{ cm}^{-1}$ .

The results obtained with the Raman spectroscopy have been compared with the results obtained by Fourier Transformed Infrared (FTIR) spectroscopy, and by Scanning Electronic Microscopy (SEM). The results obtained by these technical analyzes confirm the deposition of single-walled carbon nanotubes with metallic features by high-density plasma chemical vapor deposition.

The results obtained in this work, show the possibility to obtain higher aligned single-walled carbon nanotubes deposited at room temperature by HDPCVD. In this way, it was necessary the increase of the surface energy, that promotes the nano-structuration of the carbon materials, using diamond powder as a seed. It was observed the presence of carbon nanotubes and other kinds of nano-structures of carbon. The results obtained by SEM, Raman spectroscopy and Fourier Transformed Infrared spectroscopy FTIR, improved the carbon nanotubes bundles and “islands” of amorphous carbon materials and, due the different of surface energy promoted by the precursor.

#### **F.NM03.09.110**

#### **Late News: A Green Graphene-Based Ink for Artworks—Toward a Green Chemistry in Synthesis of**

**Graphene** Sepidar Sayyar, Jo Law, Agnieszka Golda, Helen McGregor, Aaron Burton and Gordon Wallace; University of Wollongong, Australia

Climate change is a major threat to the future of our planet and its inhabitants, and there is no doubt that human activities have been the dominant contributor. Scientists can play an important role in mitigating these contributing factors by utilising green approaches in manufacturing and developing eco-friendly materials in different fields. This work presents how our interdisciplinary collaborative research team, consisting of contemporary artists, a materials scientist, and a climate scientist, promote environmental sustainability through the development of ‘green’ materials and techniques. The aim of the project is to develop a graphene-based ink through a green chemistry/engineering approach and use the ink to create conductive screen-printed e-textile artworks that communicate climate science. Graphene is a unique two-dimensional carbon structure with excellent electrical, thermal and mechanical properties that make it ideal candidate for a variety of applications<sup>1,2</sup>. However, converting graphene to a processable material involves hazardous chemical reactions using toxic materials<sup>3</sup>. We developed a graphene-based ink without using any hazardous or toxic chemicals through a facile mechanical exfoliation method. The viscosity of the ink is easily tunable owing to its thermos-sensitive nature, which makes it a suitable material for screen-printing. The ink is used to screen-print electrically conductive patterns for the e-textile art works. The results of the phase 1 of the project were exhibited at the Museum of Applied Arts and Science in Sydney and attracted over 26,000 visitors. Preliminary experiments demonstrated that this material is a suitable candidate for developing sustainable sewable smart



electronics.

#### **F.NM03.09.94**

**Hydrophobic Properties of Nano-Structured Carbon Films Obtained with Alumina Ceramic Powder** Ronaldo D. Mansano, Ana Paula M. Mansano and Nelson Ordonez; University of São Paulo, Brazil

In this work, we have obtained nano-structured carbon films using ceramic powder (alumina) as seed and pure methane plasmas. The nano-structured carbon films were obtained using a high density plasma chemical vapour deposition system. The present study demonstrates the creation of hydrophobic surface using the nano-scale roughness inherent in high-aligned carbon nanotubes forest, when we used alumina as precursor material. The hydrophobic properties of the nano-structured carbon films were analyzed by Atomic Force Microscope (AFM), Scanning Electron Microscope (SEM) and Contact Angle Measurements (drop shape method), and the structural properties of the nano-films were analyzed by Far-FTIR. The high-density plasma chemical vapour deposition (HDPCVD) system uses a new conception on plasma generation: a planar coil coupled in a RF system and an electrostatic shield for plasma densification. In this mode, are obtained high-density plasmas and for the ion acceleration we have used another RF system on planar configuration. The substrates used to deposit the films were 75 mm diameter silicon wafers, 380  $\mu\text{m}$  thick and orientation (100). They were submitted to a Piranha clean, followed by a diluted HF dip, before the modification of the surface. The alumina ceramic powder presence promotes the increase of the surface energy of the silicon wafers. In this case, nano-structures are formed. Before the films deposition, alumina ceramic powder was deposited on the silicon wafers by spinner (1000 rpm, 30 sec.). The alumina powder dispersion was made in acid solution. We have used different final deposition times (30 min, 1h, 2h, 3h, 4h and 5h). After preparation of the sample, the DLC films were deposited. The parameters of the DLC films depositions were: 15 mTorr, 250 W (coil power, RF, 13.56 MHz, remote plasma), 40 sccm (methane).

The hydrophobic properties of the nano-structured carbon films were analyzed by Atomic Force Microscope (AFM), Scanning Electron Microscope (SEM) and Contact Angle Measurements (drop shape method), and the structural properties of the nano-films were analyzed by Far-FTIR. High-density plasma is quite for the growth of good quality nano-structured carbon films. But the properties of these films are largely dependent on the deposition conditions. The roughness of the nano-structured carbon films is important, in this situation, because it is affected by surface topography and the hydrophobic properties of these nano-materials.

The surface morphologies of the nano-structured carbon films obtained with alumina powder varied with the final time of deposition process. When the final time is increased, the atoms fill the holes and are accumulated around the islands (formed by the filled holes) and the roughness decreases. This effect promotes the reduction of the surface energy and the hydrophobicity of these films increases too. For longer deposition time, the atoms cover every nano-islands and the spaces between one island and another, forming a continuous film (for deposition time of 4 hours, the roughness was 40 nm). In this way, we noticed that the contact angle measurements showed that nano-structured carbon films obtained using alumina as precursor materials obtained for longer deposition time, showed more super hydrophobicity effect

#### **F.NM03.09.101**

**Single-Walled Carbon Nanotube Growth from Ir Catalysts by Alcohol Gas Source Method** Takahiro Maruyama, Takuya Okada, Takahiro Saida and Shigeya Naritsuka; Meijo University, Japan

Single-walled carbon nanotubes (SWCNTs) have been anticipated for applications in a lot of future nanodevices. However, there still remain several problems for realizing the SWCNT devices, and one of the most significant issues is high-yield growth of semiconducting SWCNTs. So far, to grow SWCNTs with high-yield,  $\text{Al}_2\text{O}_3$  buffer layers are widely used, because they prevent migration of catalysts on the substrate surface at growth temperature and aggregation of catalyst particles are suppressed [1]. In this study, we attempted to grow SWCNTs using Ir catalysts without  $\text{Al}_2\text{O}_3$  buffer layers, which have never been used as catalysts in SWCNT growth.

After deposition of Ir catalysts on  $\text{SiO}_2/\text{Si}$  substrates, SWCNT growth was carried out using alcohol gas source method in a high vacuum [2]. Growth Temperature and growth time were set at 800°C and 1 h, respectively. The ethanol pressure was varied between  $1 \times 10^{-3}$  and  $1 \times 10^{-1}$  Pa. The grown SWCNTs were characterized by FE-SEM, TEM and Raman spectroscopy. SEM and Raman results showed that, as the ethanol pressure increased, the SWCNT yield became higher and the SWCNT diameter became narrower. When the ethanol pressure was  $1 \times 10^{-1}$  Pa, high-density vertically aligned SWCNTs were grown, whose lengths were about 2  $\mu\text{m}$ . Raman measurement showed that SWCNT diameter were distributed between 0.8 and 1.1 nm. Our results indicated that Ir catalysts are effective to obtain high-density vertically aligned and small diameter SWCNTs using no  $\text{Al}_2\text{O}_3$  buffer layers.

[1] K. Hata et al. Science 306 (2004) 1362.

[2] T. Maruyama et al. Carbon 116 (2017) 128.

### F.NM03.09.121

**Late News: Electrochemical Cathodic Exfoliation of Graphite into Graphene in Aqueous Solutions of Alkali Metal Salts** Md Habibullah Dalal, Chong-Yong Lee and Gordon Wallace; University Wollongong, Australia

Electrochemical exfoliation has emerged as a green, effective and scalable route to mass production of graphene.[1] The use of reductive cathodic exfoliation of graphite, offers a direct production of high quality and low defect graphene.[2] However, cathodic exfoliation protocols reported to date use organic solvents in which often requires extended intercalation time, and post-treatment to further exfoliate the intercalated graphene layers.[3] In contrast, the employment of environmentally friendly aqueous-based electrolytes, coupling with a shorter exfoliation period would be attractive features of any new protocol. Here, we demonstrate for the first time, efficient cathodic electrochemical exfoliation of graphite to graphene in aqueous electrolytes using common and inexpensive alkali-metal salts such as KCl. The key to exfoliate graphite successfully in aqueous electrolyte is applying a sufficiently high voltage, and a high salt concentration which facilitates hydrated cationic intercalation, and promotes hydrogen evolution to exfoliate the graphene. The cathodic exfoliated graphene produced using KCl electrolyte exhibits a low defect density ( $I_D/I_G$  of 0.06, a C/O ratio of 57.8), high graphite exfoliation yield (>80%) in short time (< 10 mins for 1 cm<sup>2</sup> electrodes) and the highly conductive 6 to 7 layers graphene sheets served as an excellent support materials for electrocatalytic reactions. This environment-benign aqueous-based cathodic electrochemical graphite exfoliation approach opens a new opportunity in large-scale and low cost production of high quality graphene.

#### References

- [1] S. Yang, M. R. Lohe, K. Müllen and X. Feng, *Adv. Mater.*, 29 (2016) 6213-6221.
- [2] A. M. Abdelkader, A. J. Cooper, R. A. W. Dryfe and I. A. Kinloch, *Nanoscale*, 16 (2015) 6944-6956.
- [3] A. J. Cooper, N. R. Wilson, I. A. Kinloch and R. A. W. Dryfe, *Carbon*, 66 (2014) 340-350.

### F.NM03.09.111

**Late News: Multibit Optoelectronic Memory Using Graphene/Diamond (carbon sp<sup>2</sup>-sp<sup>3</sup>) Heterojunctions** Kenji Ueda, Y. Mizuno and Y. Ito; Nagoya University, Japan

Recently, interfaces between graphene and diamond (carbon sp<sup>2</sup>-sp<sup>3</sup> interfaces) has attracted much attention because the carbon sp<sup>2</sup>-sp<sup>3</sup> interfaces become sources of various interesting physical phenomena and novel functions. Although there are many interesting theoretical predictions on the interfaces, experimental results regarding the electronic properties of such interfaces have rarely been reported. More recently, we found that vertically aligned graphene (carbon nanowalls: CNW)/diamond heterojunctions, that is, C sp<sup>2</sup>-sp<sup>3</sup> interfaces became photo-controllable memristors [1], which are optically controllable memory-resistors with nonvolatile memory and switching functions. One of the most important application of the photo-controllable memristors is thought to be optoelectronic memory, which possess both photo-sensing and data storage function.

In this study, we show the CNW/diamond heterojunctions can be used as multibit optoelectronic memories, where light information stores as multilevel resistance in nonvolatile manner [2].

CNW were formed on B-doped diamond semiconductors in-situ by using microwave plasma CVD apparatus [1, 3]. Junctions using the CNW/diamond heterostructures were fabricated (area: 40-160 μm φ) and their current-voltage (*I-V*) characteristics were measured at room temperature in air, with or without photo-irradiation by using visible LED.

In the Raman spectrum of the CNW on diamond, four major peaks, which are characteristic of vertically aligned graphene, were observed: G, 2D, D' and D peaks, in addition to the diamond related peak (Dia.) at 1332 cm<sup>-1</sup>. A SEM image of the CNW/diamond surface showed numerous wall-like structures, which also suggested formation of CNW on diamond. The transmission electron microscope (TEM) image of the interface of the CNW/diamond bilayers indicates that CNW with good crystallinity and clear interfaces were formed on the diamond semiconductors. These Raman, SEM and TEM results suggest CNW/diamond heterostructures with sharp interfaces were successfully formed. The CNW/diamond junctions exhibited hysteretic I-V behaviors. The resistance of the junctions was changed to low or high resistance states by the light irradiation with bias voltage application and the resistance states was maintained in nonvolatile manner. The mechanism for the photoconductive change is considered to be originated from oxidation-reduction of the CNW and/or CNW-diamond interfaces through the movement of oxygen ions by bias with photo-irradiation. The CNW/diamond junctions also show apparent response to optical pulses. The output current, that is, conductivity was increased (or decreased) step-by-step in proportion to the number of optical pulses under positive (or negative) bias. The number of levels and heights of the current steps can be controlled by changing optical pulse intensity, pulse width, bias voltage, etc. To determine the relationship between output current and applied pulse numbers precisely, multiple (~10) optical pulses (38 μW/cm<sup>2</sup>, 30 ms, 1 Hz) were

applied to the junctions. The output current, that is, conductance increased linearly from 2 nA to 142 nA in response to the total optical pulse numbers from 1 to 10. The linear relationship between the number of optical pulses ( $n$ ) and the output current [ $I(n)$  (nA)] can be expressed as " $I(n) = 14.26 * n + 2.27$ ". Application of one optical pulse induces current increase of  $\sim 14$  nA. This means that the junctions are also used as optical computing-memory devices with arithmetic functions such as counting, addition, and subtraction. These results indicate the CNW/diamond heterojunctions are capable of multibit optoelectronic devices, where light information is stored as multilevel resistance in nonvolatile manner and the stored information is processed immediately.

Ref.:

- [1] K. Ueda et al., J. Mater. Res. 34 (2019) 626.
- [2] K. Ueda et al., Appl. Phys. Lett. 117 (2020) 092103.
- [3] K. Ueda et al., Dia. Rel. Mater., 38 (2013) 41.

#### **F.NM03.09.122**

**Late News: Nanoporous Free-Standing SWCNT Films** [Radovan Kukobat](#), Dragana Stevic and Katsumi Kaneko; Shinshu University, Japan

Nanoporous free-standing SWCNT films are essential for understanding porosity of these films which should be promising for catalyst supports and supercapacitors. The SWCNTs form networks of randomly distributed SWCNTs, giving materials such as transparent thin films and free-standing films. The transparent thin films of SWCNTs form two dimensional porous networks of randomly oriented SWCNTs whose pore sizes vary from micropores to mesopores, according to the SEM and TEM observation. On the other hand, porosity of the free-standing SWCNT films is not straightforward because the micropores and mesopores are hidden in the three-dimensional structures of these films. We use nitrogen adsorption at 77 K to characterize porosity of the free-standing SWCNT films. The nitrogen adsorption isotherm shows a prominent hysteresis loop over the wide relative pressure range of  $\sim 10^{-3}$  to  $\sim 1$ , which we assigned to the presence of ultramicropores of  $< 0.7$  nm. These ultramicropores were open during ultrasonication treatment of the SWCNTs prior to the free-standing film fabrication. The ultramicropores are evidenced as defects on SWCNTs using Raman spectroscopy. The D- and G-band ratio increases from pristine SWCNTs of 0.04 to SWCNTs of free-standing films of 0.11. The surface area increases from pristine SWCNTs of 320 and 280  $\text{m}^2/\text{g}$  (BET and  $\alpha_s$ ) to free-standing SWCNT film of 605 and 590  $\text{m}^2/\text{g}$  (BET and  $\alpha_s$ ). Micropore volume increases from pristine SWCNTs to free-standing SWCNT film from 0.06 to 0.18  $\text{cm}^3/\text{g}$ , respectively. High surface area of the free-standing SWCNT films is assigned to the ultramicropores. Also, the free-standing SWCNT film is composed of mesopores created by entangling of SWCNTs in the network as observed with SEM and TEM. Understanding porosity of the free-standing SWCNT films is important for developing the SWCNT electrodes of desired porosity and surface area for the electrochemical applications.

#### **F.NM03.09.105**

**Organophilicity of Graphene Oxide for Enhanced Wettability of ZnO Nanowires** Pavan Emani<sup>1</sup>, Hisham A. Maddah<sup>1</sup>, Arjun Rangoonwala<sup>1</sup>, Songwei Che<sup>1</sup>, Dieter Gruen<sup>2</sup>, Vikas Berry<sup>1</sup> and [Sanjay K. Behura](#)<sup>1</sup>; <sup>1</sup>University of Illinois at Chicago, United States; <sup>2</sup>Dimerond Technologies, United States

Interfacing two-dimensional graphene oxide (2D GO) platelets with one-dimensional zinc oxide nanowires (1D ZnO) would create mixed-dimensional heterostructures suitable for modern optoelectronic devices. However, there remains a lack in understanding of interfacial chemistry and wettability in GO-on-ZnO heterostructures. Here, we propose a hydroxyl-based dissociation-exchange mechanism to understand interfacial interactions responsible for GO adsorption onto ZnO hydrophobic substrates. The proposed mechanism would allow us to overcome the poor wettability of the super-hydrophobic ZnO surface (with contact angle  $140.5^\circ$ ) to GO, from the dispersion of GO suspension with various organic media prior to drop-casting of GO on the ZnO. The addition of different classes of organics into the relatively high pH GO suspension with a volumetric ratio of 1:3 (organic-to-GO) is believed to introduce free radicals (OH and COOH), which consequently result in enhancing adhesion (chemisorption) between ZnO nanowires and GO platelets. The wettability study shows as high as 75% reduction in contact angle ( $\theta = 35.5^\circ$ ) when the GO suspension is mixed with alcohols (e.g. ethanol) prior to interfacing ZnO nanowires. The proposed method brings forth a scalable tool for developing graphene-coated-ZnO heterojunctions for photovoltaics, photocatalysis, biosensors, and UV detectors.

#### **F.NM03.09.112**

**Late News: Preparation of Large Surface Area Nanocarbon from Cellulose Nanocrystals and Its Carbonization Mechanism** [Jung-Eun Lee](#), Hyejin Ju, Min Jeong Kim, Ga-Hyeun Lee and Han Gi Chae; Ulsan National Institute of Science and Technology, Korea (the Republic of)

In the recent time, the biomass-derived carbon materials have attracted attention for application to energy storage and battery devices based on the abundant resources, low cost, and sustainability of precursors. Among them, cellulose nanocrystal (CNC), which can be obtained from the removal of amorphous region of cellulose materials by acid hydrolysis, is regarded as promising carbon precursor. Its high crystallinity (54-88%) compared to other conventional cellulose causes high mechanical integrity, high thermal stability, and the formation of more developed carbon crystallites after carbonization. Although it is prerequisite to thoroughly define the carbonization mechanism of CNC for use in a variety of applications, however, there is still an insufficient research. In particular, only speculations have been reported about the interesting phenomenon that the CNC often shows a graphitic phase at a low carbonization temperature of 1000 °C, unlike carbonized cellulose. Therefore, in the current study, we dried the CNCs by spray-freeze-drying method and carbonized them in the range of 1000-2500 °C. They showed interconnected fibrillar morphology and large surface area of 265.2 m<sup>2</sup>/g after carbonization at 2500 °C, which is favorable to use as a carbon nanofiller, purification, or catalyst support. In addition, the different behavior between amorphous and crystalline region of cellulose materials was thoroughly analyzed based on HRTEM, Raman, WAXD, and MD simulation results. The current study will not only open the new application of CNC-based nanocarbons but provide in-depth mechanism of carbonization of cellulosic materials.

#### F.NM03.09.123

##### **Late News: Effects of Water and Different Solutes on Carbon-Nanotube Low-Voltage Field-Effect**

**Transistors** Raphael Pfattner<sup>1,2</sup>, Amir M. Foudeh<sup>1</sup>, Shiheng Lu<sup>1,3</sup>, Nicola S. Kubzdela<sup>1</sup>, Theodore Gao<sup>1</sup>, Ting Lei<sup>1,4</sup> and Zhenan Bao<sup>1</sup>; <sup>1</sup>Stanford University, United States; <sup>2</sup>Materials Science Institute of Barcelona (ICMAB-CSIC), Spain; <sup>3</sup>Duke University, United States; <sup>4</sup>Peking University, China

Semiconducting single-walled carbon nanotubes (swCNTs) are a promising class of materials for emerging applications. In particular, they are demonstrated to possess excellent biosensing capabilities, and are poised to address existing challenges in sensor reliability, sensitivity, and selectivity.<sup>[1,2]</sup> Functionalized and pristine individual CNTs have shown high sensitivity and selectivity down to the single molecule level.<sup>[3,4]</sup> However, single CNT devices are challenging to make and characterize compared to CNT networks which add further complexity due to inter-CNT contacts. Such systems may not be as sensitive or selective compared to single CNT devices, but may be a cost-effective alternative for particular environments. Here, we report on the characteristics of single-walled carbon nanotube (swCNT) networks exposed directly to aqueous solutions containing different solutes.<sup>[1]</sup> This was made possible by employing a solid-state dielectric poly(vinylidene fluoride-co-hexafluoropropylene) (ePVDF-HFP), which has been demonstrated to be compatible with swCNTs and also enables low-voltage field-effect transistor (FET) operation.<sup>[5,6]</sup>

These devices exhibit small device-to-device variation as well as high current output at low voltages (<0.5 V), making them compatible with most physiological liquids. Using this platform, the swCNT devices are directly exposed to aqueous solutions containing different solutes to characterize their effects on FET current-voltage (FET I-V) characteristics. Clear deviation from ideal characteristics is observed when swCNTs are directly contacted by water.

Such changes are attributed to strong interactions between water molecules and sp<sup>2</sup>-hybridized carbon structures. Selective response to Hg<sup>2+</sup> is discussed along with reversible pH effect using two distinct device geometries. Additionally, the influence of aqueous ammonium/ammonia in direct contact with the swCNTs is investigated. Understanding the FET I-V characteristics of low-voltage swCNT FETs may provide insights for future development of stable, reliable, and selective biosensor systems.

[1] A. M. Foudeh, R. Pfattner, S. Lu, N. S. Kubzdela, T. Z. Gao, T. Lei, Z. Bao, *Small* 2020, 16, 2002875.

[2] V. Schroeder, S. Savagatrup, M. He, S. Lin, T. M. Swager, *Chem. Rev.*, 2019, 119, 599.

[3] S. Sorgenfrei, C.-Y. Chiu, R. L. Gonzalez, Y.-J. Yu, P. Kim, C. Nuckolls, K. L. Shepard, *Nat. Nanotechnol.*, 2011, 6, 126.

[4] J. Chaste, A. Eichler, J. Moser, G. Ceballos, R. Rurali, A. Bachtold, *Nat. Nanotechnol.*, 2012, 7, 301.

[5] C. Wang, W.-Y. Lee, D. Kong, R. Pfattner, G. Schweicher, R. Nakajima, C. Lu, J. Mei, T. H. Lee, H.-C. Wu, J. Lopez, Y. Diao, X. Gu, S. Himmelberger, W. Niu, J. R. Matthews, M. He, A. Salleo, Y. Nishi, Z. Bao, *Sci. Rep.*, 2015, 5, 17849.

[6] R. Pfattner, A. M. Foudeh, C. Liong, L. Bettinson, A. C. Hinckley, D. Kong, Z. Bao, *Adv. Electron. Mater.*, 2018, 4, 1700326.

#### F.NM03.09.113

##### **Late News: Effect of Cellulose Nanocrystal(CNC) on Polyacrylonitrile(PAN) Polymer Chain Structure in the**

**PAN/CNC Fibers Prepared Through an *In Situ* Polymerization** Hyejin Ju, Jung-Eun Lee, Min Jeong Kim and Han Gi Chae; Ulsan National Institute of Science and Technology, Korea (the Republic of)

In-situ polymerization of polyacrylonitrile (PAN) polymer in the presence of cellulose nanocrystal (CNC) is conducted to produce CNC reinforced PAN nanocomposite fibers for high-performance carbon fiber. Cellulose is the most abundant organic material available on earth, therefore it can be an environmentally sustainable resource for producing carbon materials and carbon fiber. Also, CNC is useful for the reinforcing agent in nanocomposite materials due to its excellent properties such as high crystallinity and mechanical properties.

In the current study, there are two main effects 1) CNC into the nanocomposite fiber and 2) the impact of in-situ polymerization. We have conducted the thorough characterizations of CNC dispersion and radical polymerization of PAN polymer in the presence of about 1.5 wt% CNC. In-situ PAN/CNC nanocomposite fiber was produced by the dry-jet wet spinning method right after the polymerization was terminated.

From the mechanical and crystal orientation measurement, CNC is able to affect improving polymer chain orientation through interaction between PAN and hydroxyl groups of CNC. Furthermore, as the in-situ PAN/CNC nanocomposite solution is used directly without any removing PAN polymer with low molecular weight, it is supposed that they can act as plasticizers during the fiber spinning and affect the polymer chain structure transition during the heat-treatment process. Besides, using thermal analyses, the heat treatment conditions of precursor fiber have been set for manufacturing CNC reinforced high-performance carbon fiber. And the evolution of the structure from polymer chain to the graphite form during the stabilization and carbonization in the presence of CNC has been investigated.

#### **F.NM03.09.124**

**Late News: Bifacial Float Transfer of Multilayer Graphene** Joseph Andrade<sup>1</sup>, Jan Folkson<sup>1</sup>, Mohamed Boukhicha<sup>2</sup>, Amanda Carr<sup>1</sup> and Matthew Eisaman<sup>1</sup>; <sup>1</sup>Stony Brook University, The State University of New York, United States; <sup>2</sup>Brookhaven National Laboratory, United States

We present a method for graphene transfer we refer to as “bifacial transfer” that allows transfer of multilayer chemical vapor deposition (CVD) graphene from both sides of a native metal substrate, such as an as-received nickel catalyst. In traditional transfer methods, the graphene on the “non-preferred” side, i.e. the bottom of the substrate, is removed with oxygen plasma before removal of the metal catalyst in etchant solution. Although this treatment prevents undesired aggregation of the graphene films, it fails to utilize both sides of CVD-grown graphene. Our bifacial transfer method reduces the cost of multilayer graphene by allowing the transfer of graphene from both sides of the substrate. After hot-press lamination to a polymer film and a temporary metal etching step, the graphitic films separate cleanly at the air-liquid interface due to an oxide interlayer. We characterize this separation layer and compare the quality of graphene transferred from both sides onto target glass and polymer substrates. The results of optical microscopy, confocal Raman spectroscopy, atomic force microscopy (AFM), and electronic transport measurements suggest that the quality of the multilayer graphene on the “non-preferred” side does not differ significantly from that of the “preferred” side. This method will allow more efficient and cost-effective use of graphene by doubling the usable graphene per area of growth substrate, and by eliminating the need for intermediate sacrificial transfer substrates such as poly(methyl methacrylate), PMMA.

#### **F.NM03.09.114**

**Late News: A Thin, Flexible, Highly Sensitive Ultrasonic Sensor Based on Polydopamine@Hybrid Carbon Nanofillers/Polyvinylidene Fluoride Nanocomposites** Zengsheng Weng and Fangxin Zou; Hong Kong Polytechnic University, Hong Kong

Sensors that are thin and flexible and are yet highly sensitive to small deformations have become considerably crucial to a number of high-value-added applications such as wearable electronics, human machine interface, and condition monitoring of high-stake engineering structures. In recent years, these sensors have been undergoing rapid advancement owing to the development of low-dimensional nanomaterials. In particular, by optimizing the synthesis process, it is even possible to fabricate nanocomposite strain sensors that can be used to probe high-frequency, microscopic vibrations generated by ultrasonic waves. In fact, ultrasonic wave is one of the most widely used diagnostic means for *in situ* assessments of structural integrity.

The tunnelling effect and the piezoresistive effect are the main physics principles that allow nanocomposite strain sensors to acquire ultrasonic waves. When a sensor is impinged by ultrasonic waves, the conductive nanofillers inside the sensor will undergo high-frequency micro-vibrations. Such vibrations will cause the inherent electrical resistances of the nanofillers to fluctuate and the distances between adjacent nanofillers to vary, eventually resulting in changes in the overall electrical resistance of the sensor. However, the sensitivity of the existing nanocomposite strain sensors to ultrasonic waves is still far from satisfactory.

There are two main reasons behind the limited sensitivity. One is that the agglomeration of nanofillers or the poor capacitive compatibility between nanofillers and polymer matrices results in poor dispersion of nanofillers inside nanocomposite structures. The other is the lack of effective tunnelling nodes who is not conducive to the tunneling effect.

In this work, we fabricated a highly sensitive nanocomposite sensor for acquiring high-frequency micro-vibrations generated by ultrasonic waves, from polydopamine(PDA)-coated hybrid carbon nanofillers. First, multi-walled carbon nanotubes (MWCNTs) were coated by 10s nm thick viscous PDA to improve their compatibility with polyvinylidene fluoride (PVDF) substrates. The PDA nanolayers on MWCNTs do not only act as a dispersed phase that reduces the entanglement of MWCNTs, but also serves as the buffer layers between MWCNTs and PVDF matrices, helping to improve the responsiveness of the sensors to ultrasonic waves. Compared to uncoated MWCNTs, the use of 15 wt.% PDA-coated MWCNTs led to a 40% increase in sensitivity. Then, one-dimensional PDA@MWCNTs were mixed with two-dimensional single-layer graphene to enhance the geometric contact between nanofillers. Compared with the use of nanofillers of a single dimensionality, the mixing of nanofillers of different dimensionalities can effectively increase the number of tunneling nodes within a unit volume in a nanostructure. As the mass fraction of graphene within the hybrid nanofillers expanded from 33% to 66%, the sensitivity of the proposed sensor improved by approximately 120%, surpassing that of pure graphene sensors, which had been reported to possess the highest sensitivity to ultrasonic waves. The superior sensitivity of the proposed sensor, which actually utilizes a lower graphene content, was shown to be derived from the synergy between the two types of nanofillers which are of different dimensionalities.

Overall, we put forward new strategy for optimizing the sensitivity of nanocomposite strain sensors to high-frequency micro-vibrations. The feasibility of the idea has been validated by a series of experiments that encompass both material characterizations and measurements of ultrasonic signals.

#### **F.NM03.09.115**

**Late News: Enhanced Heavy Metals Removal Using a New Buckypaper Membrane Containing MWCNTs and Two Biopolymers—Chitosan and Carrageenan** Sara S. Alnasser, Afnan Alharbi, Ahmed Alshahrani and Bandar alOtaibi; KACST, Saudi Arabia

Due to the current global water crisis, wastewater treatment requires considerable attention and development. Dissolved heavy metals in water trigger serious alerts and can have lethal effects on various components of the environment including water resources, soil, plants, animals, and can also be threatening the health of human beings. In this study, we addressed the issue by introducing novel Buckypaper membranes that were fabricated using a combination of biopolymers (i.e., chitosan and carrageenan) and multi-walled carbon nanotubes (MWCNTs). Three dispersions of MWCNTs with chitosan, carrageenan, and chitosan-carrageenan with 0.1% v/w were prepared using vacuum filtration. The removal of six heavy metals (i.e., cobalt, nickel, copper, cadmium, barium, and lead) was investigated in this study. The water permeability and the removal of heavy metals were evaluated using a dead-end (DE) filtration system. Heavy metals removal was studied at pH 7 and under a range of varying applied pressures (1 to 6 bar). At an applied pressure of 1 bar, the removal of lead and copper by the MWCNTs/carrageenan membrane reached 99% and 88%, respectively. However, MWCNTs/carrageenan membrane was found to be fragile. Nevertheless, adding chitosan to carrageenan had significantly improved the mechanical strength of the membrane while sustain the excellent removal properties of the heavy metals. That is, MWCNT/chitosan-carrageenan membrane significantly exceeds MWCNTs/carrageenan membrane in tensile strength, tensile strain and young's modules by 400%, 17%, and 6%, respectively. On the other hand, the MWCNTs/chitosan membrane showed a high water permeate flux that reached up to 200 L/h.m<sup>2</sup>. Also, the electrical conductivity of all membranes varied from 37 S/CM to 57 S/CM. Additional characterization techniques on the three membranes were conducted in this study as well.

#### **F.NM03.09.127**

**Late News: Oil Fly Ash-Derived Carbon Nanostructures for Flexible Supercapacitors** Nuha A. Alhebshi<sup>1</sup>, Haneen S. Alshaikheid<sup>1</sup>, Numan Salah<sup>1</sup> and Husam Alshareef<sup>2</sup>; <sup>1</sup>King Abdulaziz University, Saudi Arabia; <sup>2</sup>King Abdullah University of Science and Technology (KAUST), Saudi Arabia

A variety of innovative designs of wearable electronics require to be powered by energy storage devices such as supercapacitors based on flexible electrodes. One of the current challenges that would delay the implementations of supercapacitors is the high cost of the electrode materials. In this research, Abundant oil fly ash is obtained from a power plant in Jeddah, Saudi Arabia, as a source for the synthesis of carbon nanostructures by sonication (JSON) and carbon nanotubes (CNTs) by chemical vapor deposition [1,2]. These CNTs have diameters around 30-40 nm, few micrometers lengths, and clear zigzagged structures, which are mostly different than the commercial CNTs, as characterized by high resolution transmission electron microscope. To utilize the promising properties of CNTs in a practical application, flexible supercapacitor electrodes of CNTs have been fabricated on carbon cloth as a current collector in addition to H<sub>2</sub>SO<sub>4</sub> electrolyte, then tested and compared with JSON electrode in terms of cyclic voltammetry, galvanostatic charging-discharging and electrochemical impedance spectroscopy. Interestingly, CNTs electrode exhibits maximum areal and gravimetric capacitances of 77 mF/cm<sup>2</sup> and 55 F/g, respectively, which are one order of magnitude higher than those of JSON electrode. This improvement can be attributed to the smaller size and hence the larger surface area of CNTs than JSON.

Moreover, CNTs electrode shows exceedingly small equivalent series resistance and charge transfer resistance ascribing to the good contact of the electrode active materials within the carbon cloth substrate and the electrolyte. In addition, the vertical impedance line in the low frequency range of Nyquist plots indicates an excellent electrolyte ion diffusion into the electrode due to the porosity of CNTs. The successful fabrication of such flexible supercapacitors based on affordable and scalable CNTs would facilitate their cost-effective manufacturing.

#### ACKNOWLEDGMENT

This joint project was co-funded by King Abdulaziz University (KAU), Jeddah, and King Abdullah University of Science and Technology (KAUST), Thuwal, under grant number "JP-19-002". The authors, therefore, acknowledge with thanks KAU & KAUST for their technical and financial support.

#### REFERENCES

- [1] N. A. Salah, *Method of forming carbon nanotubes from carbon-rich fly ash*. US patent Number: 8,609,189 B2 (2013).
- [2] N. Salah, A. A. Al-ghamdi, A. Memic, S. S. Habib, Z. H. Khan, *Formation of carbon nanotubes from carbon rich fly ash: growth parameters and mechanism*. Mater. Manuf. Process 31, 146–156 (2016).

#### F.NM03.09.116

**Late News: Multifunctional MoS<sub>2</sub>-Supported Nanocomposites for Water Decontamination** Kfir Shapira and Ines Zucker; Tel-Aviv University, Israel

Pollution of drinking water sources by a variety of inorganic compounds has created a need to develop more efficacious removal technologies to ensure contaminant-free and clean water. Conventional methods for water decontamination involve physicochemical separation and chemical oxidation. Yet, physicochemical separation lacks pollutant selectivity and produces toxic waste streams,<sup>1</sup> while chemical oxidation requires intensive energy and chemical inputs and may form transformation byproducts.<sup>2</sup>

Nanotechnology-based approaches are increasingly explored as an alternative for decontamination methods. Many new technologies leverage the reactive and tunable properties of nanomaterials for increased cost-efficiency, selectivity toward priority pollutants and energy/chemical sustainability.<sup>3</sup> Through manipulation of material size, morphology, and chemical structure, nanomaterials can have exceptional adsorptive and catalytic properties for water decontamination.

Molybdenum disulfide (MoS<sub>2</sub>) nanosheets stand out as a promising advanced-material for water decontamination. MoS<sub>2</sub> act as an efficient and selective adsorbent for the removal of heavy metal ions (e.g., Hg<sup>2+</sup> and Ag<sup>+</sup>) through strong Lewis acid and base soft-soft interactions with sulfur atoms in MoS<sub>2</sub>. Affixing MoS<sub>2</sub> nanosheets onto a platform is essential minimize risk of nanomaterial release into the environment. In the context of nano-assisted water treatment technologies, affixing nanomaterials onto *active* platforms such as granular activated carbon media may enable multifunctional decontamination. Activated carbon is the predominant adsorbent used widely in water treatment today, due to its high affinity for organic pollutant adsorption, but lack affinity to inorganics. MoS<sub>2</sub> affixed onto activated carbon, enhances overall decontamination performance by enabling simultaneous adsorption of organic and inorganic pollutants.

In this research, we examined the tunable water decontamination capabilities of MoS<sub>2</sub> nanosheets grown on activated carbon (MoS<sub>2</sub>@AC) in a hydrothermal method for the adsorption of organic (methylene blue) and inorganic (mercury) contamination from water. In a batch experiments, we demonstrated the high mercuric adsorption potential of MoS<sub>2</sub>@AC (~2000 mg Hg/g MoS<sub>2</sub>) in the absence and presence methylene blue. Furthermore, methylene blue was removed in similar rates by MoS<sub>2</sub>@AC and pristine AC. These results suggest that while MoS<sub>2</sub> is active and enable the removal of mercury, its presence does not interrupt the activated carbon activity. Moreover, we will investigate the practical application of this nanocomposite by evaluating the effect of background ions on the mercuric adsorption capacity. We also assess the nanomaterial leaching during operation in various conditions to demonstrate the reuse capabilities and to assure safe and durable use. Overall, results from this study provide a proof-of-concept for water treatment enhancement by 2D nanomaterials.

#### Bibliography

1. Drewes, J. E., Reinhard, M. & Fox, P. Comparing microfiltration-reverse osmosis and soil-aquifer treatment for indirect potable reuse of water. *Water Res.* **37**, 3612–21 (2003).
2. Hübner, U., von Gunten, U. & Jekel, M. Evaluation of the persistence of transformation products from ozonation of trace organic compounds – A critical review. *Water Res.* **68**, 150–170 (2015).
3. Bhaduri, B. *et al.* Dual functionality of an Ag-Fe<sub>3</sub>O<sub>4</sub>-carbon nanotube composite material: Catalytic reduction and antibacterial activity. *J. Environ. Chem. Eng.* **6**, 4103–4113 (2018).

#### F.NM03.09.128

**Late News: Ethylene Glycol Removal Characteristics of 2D Nanoporous h-BN Sheets —Computational Predictions** Nirmalay Barua<sup>1</sup>, Ingrid Padilla Espinosa<sup>2,1</sup> and Ram Mohan<sup>1</sup>; <sup>1</sup>North Carolina A&T State University, United

States; <sup>2</sup>University of California, Merced, United States

Hexagonal boron nitride (h-BN) is a new material with potential for applications in electronic devices, tribology, and separation membranes. Limited theoretical and experimental researches have been conducted to explore their efficiency as a desalination membrane. With the recent advancement of their controlled synthesis, researchers have become more interested in exploiting their interaction with organic materials. The purpose of this work is to explore the efficiency and potential of porous h-BN as a separation membrane for ethylene glycol (EG) removal from water. Very few experiments have been previously conducted to assess the capability of porous h-BN for EG or other organic pollutants removal. However, no prior theoretical or computational work that studies the molecular interactions between EG and h-BN has been reported. In this work, a methodological approach to simulate the atomic interactions of h-BN and EG in different pore configurations is proposed and investigated using classical molecular dynamics. Our results exhibit that nanometer-scale pores in single layer h-BN can effectively reject approximately 90% of EG from EG contaminated water. We also report the removal performance of the freestanding porous h-BN sheet as a function of pore diameter and applied pressure.

#### **F.NM03.09.129**

**Late News: Ionicity-Dependent Separation Property of Graphene Oxide Membrane** Mutsuki Oikawa<sup>1</sup>, Haruka Takeuchi<sup>2</sup>, Zheng-Ming Wang<sup>3</sup> and Setsuko Koura<sup>1</sup>; <sup>1</sup>Chiba Institute of Technology, Japan; <sup>2</sup>Kyoto University, Japan; <sup>3</sup>AIST, Japan

Graphene oxide membrane (GO-M) has recently attracted a great interest because of its potential applications for desalination and for removal of organic matter. The carbon-based GO-M is excellent in chemical resistance, anti-fouling effect, low cost, and so forth as compared to polymer or ceramics membranes. It is known that GO has polar oxygen functional groups and is negatively charged in water, which makes it possible to remove ionic species in water. It has been reported that GO-M shows selective separability toward some neutral solvent molecules. However, its ionicity-based separation property has not yet been sufficiently understood. In this research, we focused on surface charging property of GO-M and examined its separation behaviors toward inorganic ions and organic dyes of different charging properties. It was found that the separation or permeation of inorganic cations by GO-M is dependent on the ionic type and charge number. The rejection ratio can be accounted for by the strength of their electrostatic interaction with the GO surface. GO-M shows good rejection toward anionic dyes but great adsorption toward neutral and cationic dyes, resulting in the blockade of membrane path.

#### **F.NM03.09.131**

**Late News: Atomistic Study of the Influence of Oxide Shell Layers on the Material Properties of Aluminum Nanowires** Hoang Thien Luu<sup>1</sup>, Yudi Rosandi<sup>2</sup>, Herbert M. Urbassek<sup>3</sup> and Nina Gunkelmann<sup>1</sup>; <sup>1</sup>Clausthal University of Technology, Germany; <sup>2</sup>Universitas Padjadjaran, Indonesia; <sup>3</sup>University of Kaiserslautern, Germany

For materials with high oxygen affinity, oxide layers will significantly change the material properties. At aluminum surfaces, an oxide layer may form in seconds, even under vacuum conditions. Recent studies show that thin amorphous oxide shell layers on aluminum surfaces significantly change the responses of the material. However, the relations between the thickness of the oxidized layer, the temperature and the mechanical response of nanowires have not been investigated intensively. In this study, we use a ReaxFF potential to analyze the influences of oxide shell layers on the material responses of the nanowires under uniaxial loading at different strain rates. We conduct simulations within a wide range of strain rates and temperatures varying between 10K and 500K. The Al-O interface leads to an increased defect nucleation rate at the oxide interface preventing localized deformation.

SESSION F.LP05.04: Live Poster Session I: Nanomaterials and Quantum Materials I (F.NM03)

Session Chairs: Jeffrey Fagan and Tanja Kallio

Thursday Morning, December 3, 2020

11:30 AM - 1:30 PM

F.NM03

#### **F.NM03.09.04**

**Transparent, Transferrable and Flexible Pseudocapacitors from Ternary PEDOT/V<sub>2</sub>O<sub>5</sub>/ Graphene with Record Durability in Organic Electrolytes** Sanju Gupta<sup>1,2</sup>; <sup>1</sup>CCNY-CUNY, United States; <sup>2</sup>WKU, United States



Transparent conductive electrodes (TCEs) are of enormous significance to the continued growth of optoelectronic devices and the emergence of flexible and wearable electronics in the foreseeable future. Versatile and tunable TCEs, featuring not only high optical transmittance but also intriguing features of electrochemical energy-storage capability, flexibility, and transferability, remain a significant challenge. Here we strategically develop a graphene-conjugated V2O5/poly(3,4-ethylene dioxythiophene (from hereon, V2O5/PEDOT) hybrid, serving as an easily transferable, transparent, capacitive active electrode films. The constructed electrodes exhibit a high areal capacitance of 50-60 mF cm<sup>-2</sup> at optical transparency of > 60 percent with a record durability over thousands of cycles. As demonstrated by experimental results, both the kinetic blocking of the PEDOT layer and the anchoring capability of graphene upon soluble vanadium ions from V2O5 nanoribbons/nanotubes contribute synergistically to the unusual electrochemical stability and electroactivity shown using scanning electrochemical microscopy. Transparent symmetric and asymmetric solid-state supercapacitors made of the as-fabricated pseudocapacitive TCEs deliver a broad voltage window of 1.4 V or higher under two different electrolytes (aqueous LiCl and organic gel made from LiCl and polyvinyl alcohol) demonstrate highest power and energy density that outperforms all the previously reported transparent devices (< 0.1 microWatt h cm<sup>-2</sup>).

#### F.NM03.09.07

**Thermal Diode Based on Polyethylene Nanofiber** Xiao Luo and Sheng Shen; Carnegie Mellon University, United States

Thermal diode is a two-terminal device which rectifies heat flow. For its non-linear nature, interest in thermal diode has been growing for more than 15 years. Thermal diodes have been numerically and experimentally realized with bulk as well as nanomaterial. Among them, phase transition material can realize high rectification with relatively narrower temperature bias. Current optimization studies of phase transition junction thermal diode consider phase transition as a step function of temperature, while in some cases phase transition could happen in a temperature range in the same magnitude with temperature bias. In this study we simulated and optimized the thermal diode based on our recently experimentally realized phase transition of polyethylene nanofiber with a finite temperature range of phase transition.

There is a phase transition within polyethylene nanofiber with high degree of crystallinity: crystalline structure shifts from orthorhombic to hexagonal cell with a sharp decrease of thermal conductivity within about 5K temperature range at around 430 ~ 450K[1]. E-beam irradiation can alter the phase transition behavior. Phase transition retains with a lower critical temperature if irradiation is weak, while phase transition disappears if irradiation is strong[2]. Thus, heavily-irradiated-pristine (HI-P) and lightly-irradiated-pristine (LI-P) junction diode can be fabricated by partially irradiating the PE nanofiber with different exposure time. HI-P junction can rectify heat flow in one certain direction, while LI-P junction can rectify heat flow in both directions under different working temperature.

Calculation based on finite temperature range of phase transition shows a smooth heat flow curve with a better match with experimental data. Calculation based on step-function phase transition gives a limit of rectification value but tends to overestimate the rectification performance under small temperature bias. Optimization formula derived from step-function model can still be used for estimating optimized length fraction of e-beam irradiation despite the range of temperature bias, as maximum rectification value always occurs when interface temperature difference is zero. Specifically, a proper value of thermal conductance value is required for LI-P junction such that rectification performances in both directions can be optimized with one single length fraction of irradiation.

[1] R. Shrestha, Y. Luan, S. Shin, T. Zhang, X. Luo, J.S. Lundh, W. Gong, M.R. Bockstaller, S. Choi, T. Luo, R. Chen, K. Hippalgaonkar, S. Shen, High-contrast and reversible polymer thermal regulator by structural phase transition, *Sci. Adv.* 5 (2019) eaax3777. <https://doi.org/10.1126/sciadv.aax3777>.

[2] Unpublished.

#### F.NM03.09.09

**A GFET Nitrile Sensor Using a Graphene-Binding Fusion Protein** Abubaker A. Mohamed<sup>1,1</sup>, Mirano Tsukiiwa<sup>2</sup>, Hironaga Noguchi<sup>2</sup>, Takumi Komikawa<sup>2</sup>, Chen Chen<sup>2</sup>, Qadri E. Mubarak<sup>1</sup>, Rachel Heath<sup>1,1</sup>, Masayoshi Tanaka<sup>2</sup>, Mina Okuchi<sup>2</sup>, Samuel de Visser<sup>1,1</sup>, Yuhei Hayamizu<sup>2</sup> and Christopher F. Blanford<sup>1,1</sup>; <sup>1</sup>University of Manchester, United Kingdom; <sup>2</sup>Tokyo Institute of Technology, Japan

A bottleneck in the development of enzyme-based graphene field effect transistors is the protein immobilization method used. Non-specific adsorption of protein on graphene is undesirable as it hinders access to the enzyme's active site whilst also changing the natural conformation of proteins by having surface residues bind to the graphene surface. Proteins require specific 3D conformation to be functional and so label-free immobilisation methods is preferred as it increases sensing capabilities of biosensors by maintaining proteins catalytic activity upon immobilization.

Here, a bi-functional self-assembling and graphene-binding peptide was fused to a QueF nitrile reductase protein to create a fusion protein for nitrile detection. The peptide was derived from silk protein fibroin and is capable of forming stable antiparallel  $\beta$ -sheet structure on graphene (1) and so is used to guide protein immobilization. Incorporating this tag into various proteins for enhancing biosensing applications offers a new and effective platform for enzyme-based graphene field effect transistors.

QueF nitrile reductase was chosen because it is the only known enzyme capable of NADPH-mediate nitrile to amine reduction (2). Surface topology of the fusion protein functionalized graphene was observed by atomic force microscopy and showed that both oligopeptide and the fusion protein incorporating it formed a monolayer with six-fold symmetry.

The QueF fusion protein sensing capabilities was first assessed on its natural nitrile substrate which upon immobilisation on graphene field effect transistor showed a 1.4-fold increase in binding affinity compared the wild-type protein which did not incorporate the peptide tag.

Fusion protein was also used to create an agricultural biosensor through the detection on benzyl cyanide. Benzyl cyanide is a chemical distress signal produced by plants and detection of this compound could therefore be used to provide means for crop monitoring and pesticide administration. The fusion protein showed a 3.3-fold increase in response to benzyl cyanide when compared to the wild-type protein. Work here provides a novel immobilisation method for enzyme based graphene field effect transistor biosensing.

(1) Li, P.; Sakuma, K.; Tsuchiya, S.; Sun, L.; Hayamizu, Y. Fibroin-like Peptides Self-Assembling on Two-Dimensional Materials as a Molecular Scaffold for Potential Biosensing. *ACS Appl. Mater. Interfaces* **2019**, *11* (23), 20670–20677. <https://doi.org/10.1021/acsami.9b04079>.

(2) Moeller, K.; Nguyen, G. S.; Hollmann, F.; Hanefeld, U. Expression and Characterization of the Nitrile Reductase QueF from *E. Coli*. *Enzyme Microb. Technol.* **2013**, *52* (3), 129–133. <https://doi.org/10.1016/j.enzmictec.2012.12.003>.

#### **F.NM03.09.13**

**Fullerene C<sub>76</sub>—An Ploed Superior Electrode Material with Wide Operating Potential Window for High Performance Supercapacitors** Nageh K. Allam, Basant A. Ali and Ahmed Biby; American University in Cairo, Egypt

Carbon materials have widely been used to enhance the performance of a plethora of supercapacitor electrode materials. In this regard, it is crucial to identify carbon materials that function over a wide pH range while enjoying a wide potential window. Herein, the DFT calculations were used to elucidate the electronic performance of C<sub>76</sub> and the C<sub>76</sub>/electrolyte interface. The electronic investigation revealed the nature of the conductivity and charge storage mechanism of C<sub>76</sub> based on the bandgap and quantum capacitance calculations. Also, the electrochemical and electronic properties of fullerene C<sub>76</sub> have been extensively investigated over a wide pH range; acidic H<sub>2</sub>SO<sub>4</sub>, basic KOH, and neutral Na<sub>2</sub>SO<sub>4</sub>. The results showed a promising performance in the three electrolytes. Moreover, C<sub>76</sub> electrodes exhibited a potential window of 1.9 V in Na<sub>2</sub>SO<sub>4</sub> electrolyte, resulting in capacitances of 171 F/g and 142 F/g at a scan rate of 1 mV/s in the positive and negative potential windows, respectively. The material showed a pseudocapacitance performance of 65% in Na<sub>2</sub>SO<sub>4</sub> electrolyte in the positive potential window. We believe higher fullerenes provide a new class of materials for developing versatile supercapacitor devices for efficient energy storage

#### **F.NM03.09.14**

**In Situ Formation of Graphene Stabilizes Zero-Valent Copper Nanoparticles and Significantly Enhances the Efficiency of Photocatalytic Water Splitting** Nageh K. Allam; American University in Cairo, Egypt

There is a growing need for new techniques to synthesize metallic copper nanoparticles due to their remarkable use in many advanced technologies. Herein, a novel method to synthesize stable and non-agglomerated zero-valent copper nanoparticles (ZVCNPs) via the in-situ formation of reduced graphene oxide (rGO) during the electrospinning process in the presence of polyvinylpyrrolidone (PVP) as a carbon source is presented. X-ray diffraction (XRD), Raman spectroscopy, electron paramagnetic resonance (EPR), transmission electron microscopy (TEM), and x-ray photoelectron spectroscopy (XPS) techniques were used to investigate the morphology, structure, and composition of the fabricated materials. The synthesized ZVCNPs were coupled with TiO<sub>2</sub> nanofibers and rGO to form an efficient photoactive material to photocatalytically produce hydrogen via water splitting, resulting in 344% increase in the hydrogen yield compared to that of TiO<sub>2</sub> nanofibers. The density functional theory (DFT) calculations showed that the ZVCNPs enhance the charge transfer and lower the energy needed for photocatalytic water splitting. This study suggests a novel method for metallic copper stabilization and illustrates

the effect of metallic copper as a catalyst for the in-situ formation of rGO.

#### **F.NM03.0915**

**Topology Influence of Hydroxyl and Epoxide Functional Groups on the Mechanical and Fracture Behavior of Graphene Domain** Akarsh Verma<sup>1</sup> and Avinash Parashar<sup>2</sup>; <sup>1</sup>University of Petroleum and Energy Studies, India; <sup>2</sup>Indian Institute of Technology Roorkee, India

Aim of this article is to study the effects of hydroxyl functional group with different coverage percentages on the mechanical strength and fracture toughness of graphene. The hydroxyl functional group forms the backbone of intrinsic atomic structure of graphene oxide (GO).

Molecular dynamics based simulations were performed in conjunction with reactive force field (ReaxFF) parameters to capture the mechanical properties and Mode-I fracture toughness of functionalized graphene. Moreover, these simulations helped in concluding that spatial distribution and concentration of hydroxyl functional group significantly affects the fracture morphology of graphene nanosheet. Room temperature (300 K) was used for the simulations and virial stress components were evaluated for predicting the stress tensor.

In contrast to literature investigations, here the atomistic simulations have predicted a transition in the failure morphology of hydroxyl functionalised graphene from brittle to ductile as a function of its spatial distribution on graphene sheet. This transition in failure morphology from brittle to ductile was gradual in nature and was observed at lower percentage coverage of graphene in the range of 25-50%. Failure morphologies depict that hydroxyl groups tend to boost the ductility through atomic chains and elongated rings formation at lower percentage coverage.

As the graphene nanosheet is highly brittle in nature, so the authors have evaluated the fracture toughness of graphene with the help of Griffith's criteria. We then functionalized the graphene sheet (with an pre-crack) with epoxide functional group and observed that a chemical epoxide-to-ether chemical transformation enhanced the fracture toughness value by 25%, as compared to the pristine graphene.

From this investigation, we concluded that spatial distribution and concentration of functional groups significantly affects the mechanical and fracture behavior of oxide functionalized graphene nanosheet.

#### **F.NM03.09.16**

**Anomalous Characteristics of Functionalized Grain Boundaries in Graphene—A Nano-Mechanics Study** Akarsh Verma<sup>1</sup> and Avinash Parashar<sup>2</sup>; <sup>1</sup>University of Petroleum and Energy Studies, India; <sup>2</sup>Indian Institute of Technology Roorkee, India

Enduring an ultrahigh mechanical strength and thermal conductivity, pristine two-dimensional graphene is still a hypothetical concept in the scientific community. Fabrication techniques for this quantum confined two-dimensional nanomaterial in the experimental environment induce various defects in its polycrystalline domain such as the atomic level grain boundaries (GB). Various computational techniques such as the molecular dynamics and density functional theory have unravelled complex mechanisms operating in the presence of these boundary phases to tune graphene's mechanical, fracture and thermal properties.

Molecular dynamics-based simulations were performed in conjunction with reactive force field (ReaxFF) parameters to capture the mechanical properties of functionalized GB in graphene. Room temperature (300 K) was used for the simulations and virial stress components were evaluated for predicting the stress tensor.

Herein this article, the authors have predicted certain spatial configurations of epoxide functionalized bicrystalline graphene, which could dilute its catastrophic brittle nature and transform it into stable ductile behavior. Altering of failure path and epoxide-to-ether chemical transformations were the chief mechanisms behind the enhanced plasticity for functionalized graphene. Due to brittle nature of graphene, it was expected that failure of graphene would tend to take place from the GB, but in contrast, we found that the failure started from the interior of crystal. This tailoring of failure path induced plasticity in the domain and acted as an energy dissipation mechanism.

The present work provided new insights into the mechanical behavior of bicrystalline GO and predicts plasticity in epoxide functionalized sandwich structure. This persisting ductility of epoxide rich configurations would enable GO to absorb more energy prior to failure and amplified toughness as well, leading to improved structural integrity.

### F.NM03.09.18

**Atomistic Simulations to Explore the Water Interaction Mechanism Through a Defective 2D h-BN Nanosheet—Reactive Forcefield Development and Molecular Dynamics Study** Akarsh Verma<sup>1,2</sup>, Weiwei Zhang<sup>1</sup> and Adri v. Duin<sup>1</sup>; <sup>1</sup>The Pennsylvania State University, United States; <sup>2</sup>University of Petroleum and Energy Studies, India

Desalination corresponds to supplying of potable water from oceans and seas, which can dissolve the water scarcity problem for human consumption, agriculture use and energy needs. Conversion of earth's 97% salty water into a fresh source is still an ambiguous challenge for the research community. Moreover, conducting costly and time consuming commercial experimental techniques such as reverse osmosis and thermal desalination have consistently proved to be a brain storming challenge for the scientists. So, in order to rectify this problem, herein the authors have performed molecular dynamics simulations to investigate the transport of water molecules through artificially created pores on the honeycomb lattice domain of two-dimensional hexagonal Boron Nitride (h-BN) nanosheet. Initially, a reactive force field (ReaxFF) was developed that had water parameters in conjunction with vacancy defects data for monolayer h-BN derived from the density functional theory incorporated in it. We then checked the structural stability of an h-BN monolayer (both pristine and defected) at different temperatures (300, 500 and 800 K) and ensembles (NVT and NPT); thus, predicting that the developed ReaxFF showed a minimal out-of-plane displacement. From the interaction point of view, we revealed that the water molecules tend to accumulate (droplet formation) and form sharp contact angles (hydrophobic nature) with h-BN. Furthermore, on compressing water molecules by applying external pressure on h-BN nanosheet the water molecules tend to arrange themselves in a layered structure. Finally, we investigated the water dissociation mechanism on a defected h-BN nanosheet, and noticed that the water molecule dissociates into hydroxyl group and hydrogen atom thereby getting attached to boron and nitrogen vacancy edge atoms, respectively (Relative energy barriers with respect to initial configurations were 0.395 and - 2.18 eV). These outcomes on h-BN nanosheet may prove to be valuable for designing of 2D nanodevices/nanomembranes for water desalination purpose.

### F.NM03.09.19

**Synthesis and Functionalization of Carbon Nanospheres in One Step by APCVD** Gerardo Patiño Guillén<sup>1</sup>, Alan Arceta Lozano<sup>1</sup>, Jessica A. Falcón Montes<sup>1</sup>, Esmeralda García Díaz<sup>2</sup>, Jorge Noé Díaz de León<sup>3</sup>, Rafael Vázquez Duhalt<sup>3</sup>, Miguel A. Méndez Rojas<sup>1</sup> and Jessica R. Campos Delgado<sup>1</sup>; <sup>1</sup>Universidad de las Américas Puebla, Mexico; <sup>2</sup>Benemérita Universidad Autónoma de Puebla, Mexico; <sup>3</sup>Universidad Nacional Autónoma de México, Mexico

A one-step synthesis/functionalization of carbon nanospheres (CNS) is presented. The synthesis was carried out *via* the APCVD method using toluene and ethanol (0wt%- 5wt% ethanol) as precursors. Different weight percentages of ethanol were implemented in order to evaluate their effect on the CNS's solubility in water, size distribution, morphology, surface area and surface chemistry. Since this method is a one-step *in situ* functionalization (with oxygen-containing groups), there's no need of a post-treatment to functionalize the sample or the use aggressive chemical reactants that could significantly modify the nanomaterial. Characterization techniques implemented for this study included FT-IR, SEM, EDX, XPS, Raman spectroscopy, BET and solubility tests. Results indicated that CNS possess higher water solubility when a 3 wt% ethanol solution is implemented for the synthesis. It was also demonstrated that higher ethanol concentrations decrease CNS's diameter and induce polydispersion. Finally the increased solubility and stability of the functionalized CNS are highlighted, envisaging applications in the biomedical field where hydrophilicity and availability of functional groups are mandatory.

### F.NM03.09.21

**Precision Defect Engineering of Graphene for Applications Using Electron-Beam Chemistry with Radiolyzed Water** Michael A. Susner<sup>1,2</sup>, Ahmad Islam<sup>1</sup>, Rahul Rao<sup>1</sup>, Jennifer Carpena-Núñez<sup>1,2</sup>, San-Hui Chi<sup>1,2</sup> and Benji Maruyama<sup>1</sup>; <sup>1</sup>Air Force Research Laboratory, United States; <sup>2</sup>UES, Inc., United States

Defect engineering of graphene is attractive for a wide range of applications. Here, we present a mask-less, resist-free, and fully reversible process to engineer defects in graphene using electron-beam (e-beam) chemistry with radiolyzed water. This process was performed inside a variable pressure scanning electron microscope by generating radiolysis products using reactions between the e-beam and water vapor, which in turn reacted with the graphene at the location of the probe. These reactions enabled controlled chemistry on the graphene surface at a resolution of ~ 60 nm and hence created defects in precise locations defined by the e-beam. Detailed characterization and theoretical analyses suggested the presence of sp<sup>3</sup>-type defects, the density of which was tuned by varying the e-beam dose. In addition, these sp<sup>3</sup>-type defects were cycled in and out of graphene by alternating e-beam chemistry and thermal annealing. We present initial results showing the ability to manipulate the plasmonic response in graphene through the creation of quickly patterned nanoribbons.

### F.NM03.09.23

#### **Synthesis, Reversible Insulator-Metal Transition as Well as High Conductivity and Ampacity of Cobalt Oxide Based Misfit Nanotubes** Kankona S. Roy; Indian Institute of Technology Bombay, India

Misfit layered compounds (MLCs) consist of two alternating sub-lattices with different lattice constants at least in one of the directions. One can selectively alter one of the sub-lattices without affecting the other that can tune both the physical and electronic properties. Among them, calcium cobaltite ( $\text{Ca}_3\text{Co}_4\text{O}_9$ , CCO)<sup>1</sup> and strontium cobaltite ( $\text{Sr}_3\text{Co}_4\text{O}_9$ , SCO)<sup>2</sup> are gained interest as potential thermoelectric materials. Bringing them to low-dimensions could further enhance their thermoelectric properties. However, synthesizing them in a one-dimensional structure is extremely difficult. Recently, we have synthesized calcium deficient cobalt oxide-based misfit nanotube<sup>3,4</sup> from the bulk starting material. However, the yield of these nanotubes is rather low. Besides, the physical and electrical properties of these nanotubes have not been explored yet. Here, we present the synthesis of 1D nanotubes (NT) from oxide misfit compounds with a very high yield (80%) by a combination of solid-state and solution-based synthesis. We have also studied their electrical properties on individual nanotube level by patterning with electron beam lithography.

All the synthesized nanotubes are thoroughly characterized by a combination of X-ray diffraction pattern (XRD), scanning electron microscope (SEM), high-resolution scanning transmission electron microscopy (HRSTEM), electron diffraction (ED) and X-ray photoelectron spectroscopy (XPS). It is found that the crystal structure varies in the case of nanotubes from the bulk starting material. Absorption studies show the bandgap of 2.7 eV and 1.7 eV in case of CCO and SCO NTs, respectively. We have fabricated source-drain channels on individual nanotubes by electron beam lithography to find out their electronic properties. In the case of CCO nanotubes, it is found that the nanotubes are of p-type semiconductor with a high charge carrier concentration of  $7.05 \times 10^{19}$  per  $\text{cm}^3$ , which suggest that these NTs are promising conducting materials. The current-carrying capacity of these nanotubes is around  $6.5 \times 10^5$  A/ $\text{cm}^2$  (for an individual nanotube). But surprisingly, in the case of SCO nanotube, it shows a very high current carrying capacity of  $0.88 \times 10^8$  A/ $\text{cm}^2$  for a single NT. These values are close to the reported  $\text{WS}_2$  NTs having the highest current carrying capacity (ampacity) of  $2.4 \times 10^8$  A/ $\text{cm}^2$  among the inorganic nanotubes.<sup>5</sup> Temperature dependent resistivity measurements show that both the nanotubes are semiconducting in nature. However, we have observed a voltage-induced semiconductor to metal transition in the case of SCO NTs. We have observed the four-probe resistance for the SCO nanotube to be 10 k $\Omega$  which is lowest among the existing oxide-based inorganic nanotubes. We believe electronic properties can be further tuned by changing the chemical composition between Ca/Co and Sr/Co. These results demonstrate that the high conductivity of these nanotubes could be a potential building block for future thermoelectric devices and interconnects.

#### **References**

- Yuzuru Miyazaki, Solid State Ion. **2004**, 172, 463–467.  
Jakub D. Baran, Demie Kepaptsoglou, Marco Molinari, Nuth Kulwongwit, Feridoon Azough, Robert Freer, Quentin M. Ramasse, and Stephen C. Parker, Chem. Mater. **2016**, 28, 7470–7478.  
Leela S. Panchakarla, Luc Lajaunie, Ashwin Ramasubramaniam, Raul Arenal, Reshef Tenne, ACS Nano. **2016**, 10, 6248–6256.  
Luc Lajaunie, Ashwin Ramasubramaniam, Leela S. Panchakarla, Raul Arenal, Appl. Phys. Lett. **2018**, 113.  
Roi Levi, Ora Bitton, Gregory Leitius, Reshef Tenne, Ernesto Joselevich, Nano Lett. **2013**, 13, 3736–3741.

### F.NM03.09.24

#### **Getting Pristine Graphene-Like Behaving rGO—What Really Matters** Mohammed Sedki<sup>1</sup>, Pegah S. Mirabedini<sup>1</sup>, Kenta Nakama<sup>2</sup>, Garrett Stephens<sup>3</sup>, Michael Groves<sup>3</sup>, Mahesh R. Neupane<sup>4</sup> and Ashok Mulchandani<sup>1</sup>; <sup>1</sup>University of California, Riverside, United States; <sup>2</sup>Tokyo University of Agriculture and Technology, Japan; <sup>3</sup>California State University, Fullerton, United States; <sup>4</sup>U. S. Army Research Laboratory, United States

Chemically synthesized graphene or reduced graphene oxide (rGO) is very promising for many applications from coatings and fillers to electronics, as it is economic, easy to prepare and scale up, and has unique properties. Despite the huge expansion of GO/rGO market, there is a clear lack of experimental and computational studies on getting high quality GO and rGO nanosheets/thin films. This caused a huge variation in the reported properties of GO/rGO, with a majority of low quality and low competency in electronic applications. In this work, a detailed experimental study of the factors affecting GO/rGO properties, supported by Density Functional Theory (DFT) calculations, is introduced to help prepare pristine graphene-like rGO. In addition, the impact of lateral sheet size on GO/rGO properties, as one of the factors addressed in this work, was studied using DFT calculations and experimental measurements for the first time, to the best of our knowledge. Field-effect transistor (FET) was used to study and optimize rGO. The optimized rGO-FET device showed the lowest resistance ( $200 \pm 20$   $\Omega$ ) and the highest charge carrier mobilities (53279 and 39891  $\text{cm}^2/\text{V}\cdot\text{s}$  for holes and electrons, respectively) reported.

Furthermore, FET characteristic curve of rGO-FET showed the ambipolar behavior of high-quality graphene, with Dirac point around zero. In addition, the optical band gap of rGO nanosheets (0.4 eV) prepared in this work is the smallest reported, so far. These results highlight the importance of this study for both researchers and companies aiming at using rGO as an alternative for graphene obtained by liquid phase exfoliation or chemical vapor deposition.

#### **F.NM03.09.26**

**Electronic Functionality Encoded Laser-Induced Graphene for Paper Electronics** Hyunjin Park, Minsu Kim, Byoung Gak Kim and Yun Ho Kim; Korea Research Institute of Chemical Technology, Korea (the Republic of)

Laser-induced graphene (LIG) has been utilized as a non-metallic conductor for the development of various electronics due to its facile, direct, and scalable synthesis process. Here, the graphitization degree of LIG is simply controlled by adjusting the lasing conditions to encode different electronic functionalities such as resistance and capacitance on commercially available papers. The effect of lasing conditions including the number of lasing scans and the lasing power on the graphitization degree of paper-derived LIG is systematically investigated by evaluating the optical, chemical, and electrical properties. The paper-derived LIG with various lasing conditions exhibits a relatively wide sheet resistance range of 61.5 to 9140  $\Omega$  sq<sup>-1</sup>. The corresponding LIG is used to fabricate resistors and capacitors, and the different electronic functionality encoding is successfully demonstrated by monolithically fabricating non-volatile read-only memory and resistor-capacitor circuits and verifying the electrical performance of the fabricated devices. This work presents a practical approach to develop paper electronics for cost-effective and environmentally-friendly manufacturing.

#### **F.NM03.09.27**

**Robust Microscale Superlubricity Under Airborne Contaminants** Kunqi Wang; Tsinghua University, China

Structural superlubricity, which results from the incommensurability of directly contacted crystalline surfaces, achieves ultralow friction and inspires disruptive innovations in applications across length scales. It is a common belief that this phenomenon requires the contact interface being ultra-clean, ensured by either a clean environment or self-cleaning of the contact. However, in this paper, the observation of robust superlubricity with a contaminant-rich interface is reported. After intentionally introducing airborne contaminants into microscale superlubric graphite contacts, we surprisingly find that two important features of structural superlubricity are well preserved: the nearly-zero friction coefficient and the drastic commensurate/incommensurate anisotropy of frictional force. Moreover, contaminants are found to reduce the friction of a commensurate contact, but increase the friction of an incommensurate contact, which leads to the decrease of anisotropy ratio in friction as the contaminant concentration increases. Molecular dynamics simulations reveal the different roles of the third bodies in commensurate and incommensurate contacts. Our results encourage explorations of structural superlubricity in contaminant-rich environments that practical devices could be facing.

#### **F.NM03.09.28**

**Revealing Structure–Activity Links in Hydrazine Oxidation—Doping and Nanostructure in Carbide–Carbon Electrocatalysts** Tomer Burshtein<sup>1</sup>, Eliyahu Farber<sup>1</sup>, Kasinath Ojha<sup>2</sup> and David Eisenberg<sup>1</sup>; <sup>1</sup>Technion–Israel Institute of Technology, Israel; <sup>2</sup>Leiden University, Netherlands

The oxidation of hydrazine (N<sub>2</sub>H<sub>4</sub>) is an important challenge in electrocatalysis, with applications in direct hydrazine fuel cells and in medical and environmental sensing. Interest in alternative, nitrogen-based fuels for fuel cells was rekindled by recent advances in alkaline membranes, and by the surfacing of challenges in the transportation of hydrogen. Direct hydrazine fuel cells promise high theoretical voltage (1.56 V with O<sub>2</sub>), clean emissions, and improved fuel transportability. We now report a multi-doped carbide–carbon composite with excellent hydrazine electro-oxidation (HzOR) activity in alkaline pH. While iron carbide containing materials are well known catalysts for several applications (e.g. oxygen reduction), our N-doped, Fe<sub>3</sub>C-embedded carbons provide the first examples of a carbide-based HzOR catalyst. Multi-doping was thought to enhance reactivity (possibly through cooperation of M=Cu/ Zn, Fe, and edge N atoms), possibly by pore-etching, layers exfoliation or graphitization promotion, thus modulating surface area, mass transfer and conductivity. To prepare the composites, we designed tunable multi-doped precursors: an organometallic structure combining iron with either copper, zinc, or iron, to investigate the effect of molybdenum-doping reported earlier. Pyrolysis and washing of the fore mentioned precursors yielded HzOR-active composites of Fe<sub>3</sub>C nanoparticles and a hierarchically porous, partially graphitic N-doped carbon (NC). Thorough characterization by voltammetry and by a broad range of spectroscopic and microscopic methods revealed that the activity is ordered as: Cu-derived NC > Zn-derived NC > Fe-derived NC. While the catalysts had similar compositions, their nanostructure varied: both Zn- and Cu-doping induced the formation of micropores and small mesopores (5–13 nm diameter). The dopant-induced active site exposure (affecting micropore volume) and improved material flow (linked to mesopore volume) contributed to enhanced HzOR electroactivity. Furthermore, the

intimate mixing of the metals in the precursor is hypothesized to homogenize and enhance the doping effect, as the structure enhancing metal ions ( $Zn^{2+}$  or  $Cu^{2+}$ ) exposed the nearby catalytic  $Fe_3C$  sites. Acid washing of the pyrolyzed carbon was crucial for producing microporosity in the Cu-based carbon, but had little effect on the Zn-derived one. This revealed the importance of micropores and small mesopores for HzOR electrocatalysis, and the different nanostructuring mechanisms of the two dopants: while  $Zn_{(g)}$  boils during pyrolysis and thus etches micropores into the carbon,  $Cu_{(s)}$  diffuses and spreads throughout, making exfoliation by acid reaction more efficient. Further work in our group is dedicated to the catalytic activity of pure phase  $Fe_3C$ , and its modification by other dopants.

[Burshtein et al., *J. Mater. Chem. A*, **2019**, doi: 10.1039/C9TA03357B]

### F.NM03.09.30

**Synthesis of Flexible 3D Electrodes of TiN Nanotube Arrays Using Atomic Layer Deposition** Seokjung Yun<sup>1</sup>, Sang-Joon Kim<sup>2</sup>, Jaesung Youn<sup>1</sup>, Hoon Kim<sup>1</sup>, Jeongjae Ryu<sup>1</sup>, Changdeuck Bae<sup>3</sup>, Kwangsoo No<sup>1</sup> and Seungbum Hong<sup>1,4</sup>; <sup>1</sup>Korea Advanced Institute of Science and Technology, Korea (the Republic of); <sup>2</sup>Korea Research Institute of Chemical Technology, Korea (the Republic of); <sup>3</sup>Sungkyunkwan University, Korea (the Republic of); <sup>4</sup>KAIST Institute for NanoCentury (KINC), Korea (the Republic of)

Flexible nanoscale electrode can be used in many applications such as electrochemical energy storage, electrocatalysts and solid memory devices by providing higher density faradaic reaction sites. Although many processing techniques have been used to produce nano-structured electrodes on flexible substrates, prior ones lack the mechanical stability. Here, the mechanical properties and flexibility of the TiN nanotube array on the Pt substrate were improved using a Ti interlayer as an adhesion promoter. Highly aligned TiN nanotube array was fabricated on a Pt substrate using an anodized aluminum oxide (AAO) template and atomic layer deposition (ALD) system. We show that with the use of a Ti interlayer as adhesion promoter between the TiN nanotube arrays and Pt substrate, the TiN nanotube arrays could perfectly attach to the Pt substrate without delamination and faceted phenomena. Peeling was not observed even when the bending test was performed at a high curvature (radius of curvature, -2 mm). In addition, reliable and uniform contact the nanotube and the substrate evidenced by conducting atomic force microscopy (C-AFM) analysis proved the excellent local transport properties of our electrodes. Furthermore, the mechanical bending test results attest to the excellent flexibility for use in flexible electronic devices. We envision that our 3D electrodes will be implemented as embedded electrodes in semiconductors as well as flexible plastic substrates.

### F.NM03.09.31

**Single Step Reduction and PEGylation of Nanographene Oxide for Drug Delivery and Photothermal Cancer Therapy** Raquel Costa-Almeida<sup>1,2</sup>, Diana Bogas<sup>3</sup>, Cristiana Couto<sup>3</sup>, Licinia Timochenco<sup>3</sup>, Filipa A. Silva<sup>1,2</sup>, José R. Fernandes<sup>4</sup>, Inês C. Gonçalves<sup>1,2</sup>, Fernão D. Magalhães<sup>3</sup> and Artur Moreira Pinto<sup>1,2,3</sup>; <sup>1</sup>Instituto de Investigação e Inovação em Saúde, Universidade do Porto, Portugal; <sup>2</sup>INEB - Instituto de Engenharia Biomédica, Portugal; <sup>3</sup>LEPABE, Faculdade de Engenharia, Universidade do Porto, Portugal; <sup>4</sup>CQVR – Centro de Química Vila Real, Universidade de Trás-os-Montes e Alto Douro, Portugal

Cancer is the second leading cause of death worldwide. Current treatments frequently rely on surgical resection, radiotherapy, and high-dose chemotherapy, with unsatisfactory outcomes and side effects. Thus, there is a great need for novel and more effective strategies. Photothermal therapy (PTT), a non-invasive alternative based on near-infrared (NIR) light energy conversion into heat, results in hyperthermia (39-47 °C) and induces higher nanoparticle/drug uptake due to increased membrane permeability and tumor cell apoptosis. Nanomaterials, like graphene-based materials (GBM), hold potential as photothermal absorbers to enhance PTT selectivity within the target tumor tissue toward achieving therapeutic temperatures using less total light energy, minimizing damage to the healthy surrounding tissue [1]. This study explored GBM and GBM loaded with 5-fluorouracil (5-FU), an anti-cancer drug, as platforms for combined chemo-photothermal therapy. Nanographene oxide (GOn) was produced through the modified Hummer's method [2] followed by ultrasonication in a custom-built industrial grade system. Following a one-step procedure, GOn was thermally reduced and non-covalent functionalized with poly(ethylene) glycol (PEG) to obtain stable aqueous dispersions (rGOn-PEG) [3]. GOn and rGOn-PEG (0.25 mg/mL) were mixed with 5-FU at a drug concentration varying between 0.25-5 mg/mL. GBM aqueous dispersions were irradiated with a LED source of  $812.8 \pm 29.9$  nm (150 mW/cm<sup>2</sup>) and temperature recorded using a thermocouple. The effect of GBM and NIR irradiation was evaluated by resazurin cell viability assay using a human skin carcinoma cell line (A431 cells, ATCC).

Reduction and PEGylation of GOn were confirmed by chemical characterization through FTIR, XPS and UV-vis spectroscopy, as well as thermal analysis by TGA. GOn and rGOn-PEG were obtained with mean lateral dimensions of 287 nm and 521 nm, respectively as determined by TEM. GOn and rGOn-PEG dispersions showed colloidal stability with zeta potential values around  $-25.6 \pm 0.8$  mV and  $-10.2 \pm 0.3$  mV (pH=7), respectively. Loading capacity of 5-FU on GBM reached

5.8±0.8 mg 5-FU/mg GOn and 3.6±1.2 mg 5-FU/mg rGOn-PEG by simple molecular physisorption. NIR irradiation increased rGOn-PEG temperature to 47 °C after 30 min, which is within temperature ranges of hyperthermia. rGOn-PEG in combination with NIR reduced A431 cells viability, in opposition to rGOn-PEG alone.

This study demonstrated the successful non-covalent functionalization and reduction of nanographene oxide, rendering a material with potential to be further explored for combined chemotherapy and PTT for cancer treatment.

*Acknowledgements:* This work was financed by FEDER - Fundo Europeu de Desenvolvimento Regional funds through the COMPETE 2020 - Operacional Programme for Competitiveness and Internationalisation (POCI), Portugal 2020, and by Portuguese funds through FCT/MCTES in the framework of the projects POCI-01-0145-FEDER-031143; POCI-01-0145-FEDER-006939; POCI-01-0145-FEDER-007274; PTDC/BTM-MAT/31143/2017, and Unidade de Investigação UID/EQU/00511/2019 - Laboratório de Engenharia de Processos, Ambiente, Biotecnologia e Energia – LEPABE.

#### REFERENCES:

- [1] Doughty ACV *et al.*, *Materials*, 2019, 12.
- [2] Pinto AM *et al.*, *Carbon*, 2015, 99:318.
- [3] Chen J *et al.*, *Biomaterials*, 2014, 35: 4986.

#### F.NM03.09.32

##### **Investigation of a Catalyst Ink Dispersion and Three-Dimensional Analysis of Catalyst Layer in Polymer Electrolyte Membrane Fuel Cells** Dan Wu, Samindi M. Jayawickrama and Tsuyohiko Fujigaya; Kyushu University, Japan

Carbon-based supports have been widely used to support Pt catalysts in polymer electrolyte fuel cells (PEMFCs) [1]. In our group, we developed polybenzimidazole (PBI)-wrapping onto carbon support that successfully achieved higher cell performance [2].

In this study, we present a dispersion investigation of the catalyst ink using PBI-wrapped catalyst (CB/PBI/Pt) and non-wrapped (CB/Pt) catalyst with a wide range of ionomer: carbon ratio (I/C). The effects of ink parameters, which include carbon black structure, and ionomer concentration, on the ink microstructure of catalyst ink were studied using visual study in combination with dynamic light scattering (DLS). Heterogeneous porous structure of the catalyst layer in PEMFCs is a significantly important parameter because it strongly determines the gas diffusion properties of the catalyst layer. And the connectivity of the network structure is largely depended on the structure of the catalyst agglomerations as well as the homogeneity of the ionomer on the carbon supporting materials. Therefore, we used scanning electron microscopy combined with focused ion beam (FIB-SEM) to visualize the nano-scale pore structure of the catalyst layer. Post-processing of a series of two-dimensional images reconstructed the three-dimensional pore-space of the catalyst layer.

We found that the catalyst ink of CB/PBI/Pt remained as a very stable dispersion in the range of I/C = 0.2~1.4, whereas for CB/Pt, the catalyst ink easily forms aggregation at high I/C (>0.6). The FIB-SEM images of CB/Pt catalyst layer with optimum I/C = 0.6 and CB/PBI/Pt catalyst layer with optimum I/C = 0.2 was analyzed. It is found that the CB/Pt catalyst layer has isolated large pores with the porosity of 0.55, while CB/PBI/Pt catalyst layer shows a uniform porous structure with the porosity of 0.7. It is reported that the presence of isolated pores increases the O<sub>2</sub> transport resistance in the catalyst layer, resulting in lower fuel cell performance [3,4]. Therefore, we concluded that the dispersion stability of catalyst ink is enhanced by PBI wrapping onto the CB surface, thus ensuring a better porous structure of the catalyst layer in PEMFCs. Furthermore, the particle-particle interactions in catalyst ink will be discussed in the presentation.

#### References

- [1] Xin, L.; Yang, F., Polybenzimidazole (PBI) Functionalized Nanographene as Highly Stable Catalyst Support for Polymer Electrolyte Membrane Fuel Cells (PEMFCs). *J. J. Electrochem. Soc.* 2016, 163, 10.
- [2] T. Fujigaya, et al., Improved Durability of Electrocatalyst Based on Coating of Carbon Black with Polybenzimidazole and their Application in Polymer Electrolyte Fuel Cells. *J. ACS Appl. Mater. Interfaces* 2016, 8, 23, 14494–14502.
- [3] Inoue, G.; Kawase, M., Effect of porous structure of catalyst layer on effective oxygen diffusion coefficient in polymer electrolyte fuel cell. *J. Power Sources* 2016, 327, 1-10.
- [4] Inoue, G.; Yokoyama, K.; Ooyama, J.; Terao, T.; Tokunaga, T.; Kubo, N.; Kawase, M., Theoretical examination of effective oxygen diffusion coefficient and electrical conductivity of polymer electrolyte fuel cell porous components. *J. Power Sources* 2016, 327, 610-621.

#### F.NM03.09.33

##### **Monitoring of Adsorption Behavior of Serum Albumin onto the Fatty Acid-Modified Single-Walled Carbon**



**Nanotube** Kenta Nakamura, Yoshiaki Niidome, Yukiko Nagai, Tanaka Naoki, Tomohiro Shiraki, Takeshi Mori, Yoshiki Katayama and Tsuyohiko Fujigaya; Kyushu University, Japan

Single-walled carbon nanotube (SWNT) are attracting increasing attentions in biological applications because of their unique thermal, physical and optical properties. To use SWNT for in vivo applications, SWNT need to be biocompatible. Up to date, coating of SWNT with biocompatible materials especially polyethylene glycol (PEG) has been investigated due to its stealth property. However, it was pointed that the PEG-modified materials are rapidly excreted from the blood due to an immune reaction when they are repeatedly administered, which is known as accelerated blood clearance (ABC) phenomenon. To avoid such a problem, serum albumin (SA) attracts recent attention as an alternative material of PEG since SA is a blood protein derived from a living body. However, since the adsorption coefficient of SA onto SWNT surface is lower than that of the other proteins, the increase of the adsorption to avoid the risk of the replacement might be necessary. Therefore, in this study, we introduced fatty acid onto the surface of SWNT to improve the binding of SA by utilizing the strong binding between SA and fatty acid, where the introduction of the fatty acid was carried out by the radical grafting of the fatty acid derivative onto the SWNT sidewall. Here, the adsorption behavior was monitored by monitoring of the unique red-shifted and brighter photoemission (PL) generated from the grafting site compared to that of the non-functionalized SWNT.

#### **F.NM03.09.35**

**A Novel Route for Controlling and Improving the Texture of Porous Structures Through Dual Growth of Alumina Nanoparticles and Carbon Nanotubes Using Explosion Process of Solid Fuel** Osama Saber and Adil Alshoaibi; King Faisal University, Saudi Arabia

Micro- and meso-porous structures of alumina have attracted attention for their potential use in different applications. In this research, a novel and facile route was introduced for dual growth of alumina nanoparticles and carbon nanotubes together to fabricate nanocomposites at low temperature 250°C through explosive processes of solid fuel. In this trend, series of alumina species with and without carbon nanotubes were prepared and characterized by X-ray diffraction, Raman spectra and transmission electron microscopy. The surface properties of the alumina-CNT nanocomposites were characterized and compared with the prepared nanoparticles of alumina by adsorption-desorption system. The specific surface area of the prepared alumina-CNT nanocomposites was increased from 257.9 to 307.7 m<sup>2</sup>/g and 314.8 m<sup>2</sup>/g with growing CNTs inside the porous structure of alumina. These increments were observed because of the dual growth of nanoparticles and nanotubes by which new micropores inside their nanocomposites were created. When the source of CNTs was changed from ethanol to methanol, pure mesoporous structure with narrow pore size distribution was observed for the alumina-CNT nanocomposite. In addition, the surface area and the total pore volume increased to be 324.9 m<sup>2</sup>/g and 0.673 cm<sup>3</sup>/g; respectively. The detonation technique of an explosive solid has been used for the first time to improve and control the porous structure of alumina through dual growth of CNTs and alumina at low temperature to meet the special requirements of the markets of catalysis and water purification.

#### **F.NM03.09.37**

**Failure Behavior and Mechanisms in Dense Highly Aligned Brittle Nanowire Structures** Rebecca Gallivan and Julia R. Greer; California Institute of Technology, United States

Nanowires have become an increasingly prevalent nanomaterials in composites and devices. In both surface coatings and mechanically coupled sensing applications, arrays and other complex geometries provide numerous design advantages, such as pixel like features. However, little investigation has been done regarding the mechanical behavior of these micron sized structures. With contact and load bearing applications, both the failure behavior and the underlying failure mechanisms are critical for robust device design. Though in-situ microcompression experiments on highly aligned dense bundles of single crystalline zinc oxide (ZnO) nanowires we investigate these types of structures to build a model for better understanding structural failure.

The ZnO nanowires are formed through hydrothermal growth from an aqueous zinc nitrate solution with hexamethylenetetramine (HMTA) and electrolysis conditions to promote fast growing high aspect ratio nanowires. 2µm and 4µm diameter bundles with individual nanowires of approximately 300nm in diameter and 4µm tall were investigated. These structures provides a range of 10-130 nanowires per bundle and thus probes an order of magnitude in scale. Experiments show two regimes of failure in the nanowire bundles: localized non-catastrophic events and global structural failure. No size dependence is observed in either regime and failure stress ranges from 0.3-1.3GPa and 0.83-2.20GPa respectively. Localized failure corresponds to interfacial splitting between nanowires and can be modeled using a mode I double cantilever beam tests. Analysis of this mechanism provides insight to the flaw size and failure initiation in the structures. Ultimate global failure can be modeled by coupling the accumulation of local failure from interfacial splitting to specific failure parameters of

the nanowire material. Utilizing Weibull statistics and experimental results, we demonstrate the validity of this technique for analyzing flaw distribution and predicting the expected failure stress range of the bundle structures. The technique shows the sensitivity of failure behavior to degree of alignment, flaw size, interfacial interactions of constituents, and structural surface effects. Through analysis of behavior in this specific system, we develop insight to broader fundamental mechanisms for local failure and statistical techniques for assessing and predicting failure behavior of highly aligned structures.

#### F.NM03.09.38

##### **Relationship Between the Dispersibility of Carbon Nanotubes and the Properties of Their Polymer**

**Nanocomposites** Taiyo Shimizu, Ryoichi Kishi, Kazufumi Kobashi, Takahiro Morimoto, Toshiya Okazaki, Takeo Yamada and Kenji Hata; National Institute of Advanced Industrial Science and Technology (AIST), Japan

Polymer materials with superior properties have been more and more widely used in our daily life. As compared to metals, light weight and good-processability are particularly beneficial properties of polymer materials. However, there are also several properties of polymers which are required to be improved, e.g. mechanical, electrical and thermal properties, and thus a plenty of research to improve these properties have been conducted so far. Improving these properties can realize the extension of applicable fields of polymer materials.

In order to improve objective properties of polymers, incorporation of appropriate kinds of fillers into polymer matrix is frequently adopted. For instance, carbon nanotubes (CNTs) are one of the most prominent fillers with superior properties such as high mechanical strength and electrical conductivities. Nanocomposite materials with CNTs have been widely explored and various kinds of nanocomposites possessing improved properties have been fabricated so far. However, addition of substantial amount of nanofillers, not limited to CNTs, is required in most cases, and thus the inherent properties of polymer matrix, such as good-processability, tend to be degraded. These kinds of nanofillers are basically aggregated in a pristine form, and are required to be dispersed properly in their nanocomposites, in order to extract their potential as a filler. In this presentation, we will describe the relationship between the dispersibility of CNTs and the resultant properties of their nanocomposites. As an example, the thermal stability of CNT nanocomposite will be focused on. We successfully fabricated the CNT/silicone rubber nanocomposites with high thermal stability achieved by well-dispersed single-walled CNTs. The temperature at 5 % weight loss ( $T_{d,5\%}$ ) of silicone rubber, obtained from thermogravimetric analysis, was increased by incorporation of low amount of CNTs. Remarkably, we found that the degree of increase in the  $T_{d,5\%}$  depends on the dispersion process of CNTs, and appropriate dispersion process can realize higher increase in the temperature than that of the CNT dispersion process only by stirring. This phenomenon is considered to be originated from the homogeneity in the distributions of CNTs in nanocomposites, which has been ascertained by analytical techniques. We also confirmed that the CNT/silicone rubber nanocomposites fabricated by appropriate dispersion process can retain rubbery elasticity after a thermal aging test, while pristine silicone rubber was embrittled soon after the onset of the test. These results indicate that appropriately dispersed CNTs can impart thermal stability in both short- and long-term to silicone matrix only by small amount of loading. Our findings indicate that appropriate dispersion of CNTs can enhance the effectiveness of incorporation of CNT to matrix, and we believe that these kinds of approach can be applicable to a broad range of matrix, not limited to polymers.

#### F.NM03.09.39

##### **Elucidation of Adsorption Behavior of Polybenzimidazole on Carbon Material Surface by Adsorption Isotherm**

**Measurement** Nana Kayo<sup>1</sup> and Tsuyohiko Fujigaya<sup>1,2,†</sup>; <sup>1</sup>Kyushu University, Japan; <sup>2</sup>WPI-I2CNER, Japan

In polymer electrolyte fuel cells (PEFC), a composite of carbon black (CB) with platinum particles (Pt) is widely used as an electrode catalyst after mixing with acidic electrolyte. However, low platinum utilization efficiency because of the uneven distribution of acid electrolyte on the CB surface that caused the insufficient protons transport was the issue [1]. We reported that improvement of platinum utilization efficiency and power density by coating of polybenzimidazole (PBI) onto CB surface prior to the platinum loading [2], in which the distribution of the electrolyte become uniform by the coating of PBI. However, its coating homogeneity of PBI onto CB has not been clarified yet.

In this study, the adsorption state of PBI on CB was studied by estimating the adsorption isotherm and the interaction acting between the carbon materials and PBI was investigated.

From the adsorption isotherm of PBI on CB, it was revealed that PBI adsorption reached adsorption equilibrium from a low concentration, suggesting that PBI was adsorbed in a monolayer on the carbon materials efficiently. In addition, the PBI coverage at the coating concentration of 0.50 mg/mL, used for coating, calculated from the Langmuir equation showed as high as 99.9%. Therefore, we concluded PBI uniformly coats CB. Also, based on the calculation of thermodynamic parameters, it was found that  $\Delta H$  and  $\Delta S$  were 14 kJ/mol, and 0.11 kJ/mol, respectively. The temperature dependence of the isotherm revealed that this adsorption process was entropy driven since the PBI adsorption amount increased with increasing the temperature. The adsorption behavior and interaction of PBI with other carbon materials will be discussed in the

presentation.

#### References

- [1] S. Jayawickrama *et al.*, *Electrochim. Acta.* **2019**, *312*, 349.  
[2] T. Fujigaya, *et al.*, *ACS Appl. Mater. Interfaces* **2011**, *8*, 14494.

#### F.NM03.09.40

**Combined Theoretical and Experimental Study of All-Carbon Transistors** Ali D. Özdemir, Artem Fediai, Feliks Pyatkov, Pramit Barua, Ralph Krupke and Wolfgang Wenzel; Institute of Nanotechnology, Karlsruhe Institute of Technology, Germany

Low-dimensional all-carbon nanostructures are promising candidates for future flexible and transparent transistors, as well as light-emitters [Pyatkov *et al.*, *Nature Photonics* **10**, 420–427 (2016)]. Carbon nanotube field-effect transistors with graphene electrodes offer high thermal stability and allow for ultra-flat devices able to carry high current densities. Understanding quantum transport in such systems is essential for device manufacturing. However, conventional simulation methods are limited to local contacts with an overlap width of only a few angstroms, and first-principle quantum transport calculations in systems with realistic contact geometries remained unfeasible. Simulation methods for extended CNT/metal contacts were presented in prior theoretical studies [Fediai *et al.*, *Nanoscale*, **8**, 10240 (2016)]. Here, we report quantum transport calculations based on the non-equilibrium Green function formalism and density functional theory, which are capable of treating ~100nm long CNT/graphene overlap regions and electrostatic gating at a pure ab-initio level. These calculations are compared with experiments where graphene electrodes were fabricated and dielectrophoretically bridged with single semiconducting CNTs followed by an electrical characterization over a wide temperature range. The simulation results are in agreement with the experimental data and the fabricated devices exhibit ambipolar behavior, consistent with the theory. Due to large CNT/graphene spacing and small CNT/graphene overlap, only a fraction of the quantum conductance can be achieved for the on-state conductivity. A remarkable feature of the all-carbon transistor with graphene electrodes is electrostatically induced doping of the carbon-system in the contact regions caused by the gate electrode. This is made possible by the low density of states in graphene near the K-point. We hope that this newly developed and verified simulation approach will accelerate progress in fabrication as well as the understanding of advanced all-carbon devices.

#### F.NM03.09.41

**Plasma Treated Single-Walled Carbon Nanotubes Decorated by RuO<sub>x</sub> Nanoparticles for High Performance Hydrogen Evolution Reaction** Fedor Fedorov<sup>1</sup>, Daniel Settapani<sup>2</sup>, Marthe Buan<sup>2</sup>, Jani Sainio<sup>2</sup>, Farhan S.M. Ali<sup>2</sup>, Daniil Ilatovskii<sup>1</sup>, Tanja M. Kallio<sup>2</sup> and Albert Nasibulin<sup>1,2</sup>; <sup>1</sup>Skolkovo Institute of Science and Technology, Russian Federation; <sup>2</sup>Aalto University, Finland

The constant and growing need in new catalysts for hydrogen evolution reaction is triggered by increasing energy demands and promises of its eco-friendliness combined with large gravimetric storage capacity. Carbon nanotubes are also known to be quite promising for hydrogen (and oxygen) evolution reaction and are characterized by large specific surface area, excellent conductivity, and rather good durability.

We report a cathode material based on plasma-treated single-walled carbon nanotubes decorated by RuO<sub>x</sub> nanoparticles using atomic layer deposition (ALD). We have examined cathode performance towards hydrogen evolution reaction by tailoring material wettability, conductivity yielded by plasma-treatment, and the catalyst loading [1]. We discuss that nucleation of particles is facilitated by the appearance of carboxylic and hydroxyl groups triggered by oxygen plasma action. The best performance is associated with samples containing RuO<sub>x</sub> particles of 4-5 nm, which show hydrogen evolution onset potential to be about -5 mV (*vs.* RHE) in 0.5 M H<sub>2</sub>SO<sub>4</sub> measured at a current density of -1 mA cm<sup>-2</sup> and Tafel slope of 47.5 mV/dec. The material possesses stable performance at -10 mA cm<sup>-2</sup> with a potential of about -160 mV.

The reported study was funded by RFBR, project number 20-03-00804

- [1] Fedor Fedorov, Daniel Settapani, Marthe Emelie Melandsø Buan, Jani Sainio, Farhan S.M. Ali, Daniil Ilatovskii, Tanja Kallio, Albert G. Nasibulin (2020) *ChemElectroChem* <https://doi.org/10.1002/celec.202000528>.

#### F.NM03.09.44

**Synthesis of Cu<sub>x</sub>S/Graphene Aerogel for Photocatalytic Reduction of CO<sub>2</sub>** Feng Wang and Liejin Guo; Xi'an Jiaotong University, China

Using solar energy to convert CO<sub>2</sub> into hydrocarbon fuel is a promising technique for harvesting solar energy storage and reducing carbon dioxide. Recently, Graphene-based semiconductor composites have been a topic of great interest, especially in the field of photocatalysis. Graphene has the advantages of high surface area, excellent conductivity, and anticorrosion capacity, which can overcome the limitations of traditional photocatalysts. Thus, graphene-based material can be a feasible photocatalyst for photocatalytic CO<sub>2</sub> reduction. Besides, as an environment-friendly and earth abundant material, Cu<sub>x</sub>S has considered as a good candidate for photocatalytic reactions, due to its unique optical, electronic, physical and chemical properties. Herein, we report the photocatalytic reduction of CO<sub>2</sub> using Cu<sub>x</sub>S/graphene aerogel as the photocatalyst, which was prepared by hydrothermal method. The as prepared Cu<sub>x</sub>S/graphene aerogel exhibited pretty good activity for photocatalytic reduction of CO<sub>2</sub>. C<sub>2</sub> products (ethanol, acetate) are main products. In this composite photocatalyst, graphene aerogel not only serves as a 3 dimensional support for Cu<sub>x</sub>S, but also transfers the photo generated charges. Moreover, density functional theory calculations were performed to reveal the chemical reactions and the charge transfer between Cu<sub>x</sub>S and graphene. Also, the study of Cu<sub>x</sub>S/graphene aerogels photocatalyst presents useful information for efficient photocatalytic CO<sub>2</sub> reduction without noble-metals.

#### F.NM03.09.45

**Graphene Encapsulated Nanoscale Vacuum Channel Transistors** [Girish Rughoobur](#) and Akintunde I. Akinwande; Massachusetts Institute of Technology, United States

There is a growing need for devices that operate at THz frequencies, and with the end Moore's device scaling law approaching, alternatives to solid-state transistors need to be explored. The inherent limitation of solid-state transistors such as the metal-oxide semiconductor field-effect transistor (MOSFET) is the semiconductor channel, which not only causes carrier scattering, velocity saturation of carriers due to optical phonon scattering, but is also susceptible to high temperature and radiation effects. Current research attempts to mitigate these negative effects focus on using wide bandgap semiconductor channels. In contrast, the use of 'empty-space', which can be regarded as the ultimate wide bandgap material, as the device channel could overcome these limitations. This is because in vacuum, there is no carrier scattering (ballistic transport), avalanche breakdown or thermal generation. The absence of any atoms further enhances the tolerance to high temperature as the channel retains its properties. Nanotechnology and nanofabrication has enabled the realization of nanoscale vacuum channel transistors (NVCTs) that could potentially surpass solid state devices of equivalent channel length owing to ballistic transport of electrons, shorter transit time and higher intrinsic breakdown field. Hence, transistors with a vacuum channels could have very high Johnson figure of merit ( $J_{FOM} = E_{BD}V_{sat}/2\pi$ ) of  $\sim 10^{14}$  V/s, even exceeding ultra-wide bandgap materials such as AlGaN and diamond.

We report the demonstration of NVCTs based on gated vertical silicon field emission arrays with two self-aligned gates. The two gates are separated by an oxide with thickness of 350 nm. A first gate with aperture diameter of 360 nm is used to extract electrons from a sharp emitter tip (radius < 7 nm) and the second gate, with aperture diameter of 570 nm, is used to focus the electron in to a vacuum channel. The emitter tips density is 10<sup>8</sup> emitters/cm<sup>2</sup>. NVCTs with such electron sources are highly sensitive to barrier variations caused by surface adsorption of molecules on the tip in poor vacuum environment. Here we demonstrate the nano-encapsulation of the electron source for operation in poor vacuum, using several layers of graphene, which are transparent to electrons but impermeable to the larger gas atoms in a poor vacuum. This device architecture with two self-aligned gates also enables the application of a different voltage bias on the graphene and hence controlling the energy of the electrons in the channel, while reducing the encapsulation volume significantly. We demonstrate turn-on voltages below 10 V and operation in poor vacuum and at atmospheric pressure. This device architecture is highly promising to realize empty space electronics capable of functioning at higher power and harsher conditions (high radiation and high temperature, such as in space and in nuclear reactors) transcending the performance of solid state electronics.

#### F.NM03.09.46

**Oil Dynamic Shell Surrounding Fullerenes** [Aaron Morelos-Gomez](#)<sup>1</sup>, Kunio Kondo<sup>2</sup>, Hiroshi Ushiyama<sup>3</sup>, Kazuhiro Omori<sup>2</sup>, Ryuji Monden<sup>2</sup>, Yu Gao<sup>2</sup>, Masumi Kuritani<sup>2</sup>, Taiki Yokokawa<sup>1</sup>, Rodolfo Cruz-Silva<sup>1</sup>, Syogo Tejima<sup>3</sup>, Mauricio Terrones<sup>4</sup> and Morinobu Endo<sup>1</sup>; <sup>1</sup>Shinshu University, Japan; <sup>2</sup>Showa Denko K.K., Japan; <sup>3</sup>Research Organization for Information Science & Technology, Japan; <sup>4</sup>The Pennsylvania State University, United States

Given the increase in technology development the need for more energy efficient devices is required. In mechanical systems a large amount of energy is lost due to friction between sliding surfaces. For this reason, the creation of effective lubricants is needed. Transition metal disulfides such as WS<sub>2</sub> and MoS<sub>2</sub> fulleroids have been used as oil additives. However, disulfides are prone to oxidation and release of sulphide compounds under heat and may corrode metal surfaces creating metal sulphides. Carbon materials can exhibit higher chemical inertness and therefore exhibit longer lubrication lifetime under heat than transition metal disulfides. Among carbon materials; graphene, carbon nanotubes and fullerenes have been added into oil to

decrease friction between two metal surfaces. Unfortunately, the molecular interaction between carbon nanomaterials and lubricants has not been fully understood. We studied the molecular interactions between fullerenes and mineral oil, known as “nano oil”, by ultraviolet Raman spectroscopy and molecular dynamics simulations. The results indicate that aromatic molecules help to disperse individual  $C_{60/70}$  molecules from aggregates whereas the alkane molecules help to stabilize fullerenes by forming a dynamic shell structure around them. Our findings demonstrate that fullerenes can be used as high-performance additives for effective lubrication.

#### **F.NM03.09.51**

**Computational Geometry-Centric Evaluation for Electrical Conductivity Variation of Thin-Film Conducting Nanocomposites** Jungmin Lee<sup>1</sup>, Yesol Yun<sup>2</sup>, Sang Hyun Lee<sup>2</sup> and Jinyoung Hwang<sup>1</sup>; <sup>1</sup>Korea Aerospace University, Korea (the Republic of); <sup>2</sup>Korea University, Korea (the Republic of)

Hybrid carbon nanotube (CNT) composites consisting of multiple types of fillers have been developed to provide enhanced characteristics as compared to CNT single-filler composites. The incorporation of secondary fillers, such as silica,  $CaCO_3$ , and  $BaSO_4$ , yields remarkably improved mechanical strength and stiffness of the CNT composite and electrical conductivity of the hybrid composite network under the control based on geometry and content of the constituent particulate fillers. In particular, higher electrical conductivity can be attained with the addition of micro-scale secondary fillers to the CNT composite network, while the addition of nano-scale particulate fillers incurs lowering the electrical conductivity of the nanocomposite network. Such electrical conductivity transition is attributed to distinct variations in the network topology caused by the excluded volume originating from the loading of secondary fillers with different scales. Micro-silica composites result in dense clusters of CNTs, thereby forming CNT conducting paths, while densely-dispersed nano-size fillers cause severely twisted CNTs, reducing forming a conducting network.

In this work, Monte-Carlo simulation is first conducted for the estimation of the electrical conductivity of the CNT network of hybrid composites. To obtain a realistic model, flexible CNTs are modeled as long thin cylindrical objects with many joints interconnected in a row. In addition, to take the resistance of the conducting CNTs into account, individual joints are considered to be tiny lumped resistor elements. A computational characterization approach based on numerical linear algebra technique is applied under various size and concentration configurations of composite components, and the corresponding electrical conductivity of the network is derived. The computational results exhibit that the ratio of the average diameter of the particulate filler to the nanotube length governs the tendency of the electrical conductivity variation, as compared to the change of filler contents only affecting the degree of the conductivity change. As the ratio of the silica diameter to the CNT length increases, the ratio of the conductivity without ( $\sigma_0$ ) and with ( $\sigma$ ) the secondary particulate fillers, i.e.  $\sigma/\sigma_0$ , increases from the value less than one to the value more than one. This indicates that the impact of the second fillers on the electrical conductivity of the composites shows a transition. By contrast, if the geometric configuration of the fillers is almost fixed, the degree of the conductivity variation increases as the silica content increases, while decreasing for the increasing CNT content. The electrical behaviors of hybrid composites can be simply characterized by the combination of computational geometry centric notions such as Voronoi tessellations and Swiss cheese model along with their associated percolation theory. In the developed model, the CNT dispersed around particulate fillers indicating effective conducting paths can be classified with tessellations from Voronoi cells. The conductance of each effective path is designated by local conductance determined from the density of CNTs in the local region. The reliability of the model is validated based on comparison with the numerical results obtained from the MC simulation. The developed approach achieves, as compared to the MC simulation, remarkable computing cost reduction. Therefore, the combined computational framework enables to provides a novel strategy to estimate for the electrical conductivity of the hybrid composites under the external deformation such as bending, stretching, and patterning, and it is a viable model for the design of the hybrid composites at hand.

#### **F.NM03.09.53**

**Investigation of the Growth Mechanism for Hierarchical Polymer/Carbon Nanotube Nanohybrid Shish-Kebab Structures to Enable High-Performance Printable Thin-Film Transistors** Kevin Schnittker and Joseph B. Andrews; University of Wisconsin-Madison, United States

Aerosol jet printing has gained a considerable amount of attention as a method to additively fabricate electronic device. In part, this is due to the compatibility with a wide range of ink viscosities (1-1000 cps) and the ability to print on non-planar surfaces. One elusive material for aerosol jet printed active electronics is a high-performance semiconducting ink with low-variability. One potential promising ink would be a combination of high-mobility carbon nanotubes (CNTs) with highly uniform semiconducting polymers. However, CNTs fully encapsulated by semiconducting polymers have not shown noteworthy improvement. One method to capture both positive attributes of CNTs and semiconducting polymers is through a hierarchical nanostructured composite. The conjugated polymer regioregular poly(3-hexylthiophene) (P3HT) has the ability to self-assemble and form periodic crystals on CNTs due to  $\pi$ - $\pi$  interactions. These structures, coined nano-hybrid shish

nanoribbons (NHSKs), may directly improve charge carrier transport in printed thin-film electronic devices. The objective of this project is to fabricate a novel semiconducting ink that consists of P3HT/CNT NHSKs. In developing this ink, we investigated the P3HT shish nanoribbon crystallization and kinetic growth on (6,5) chirality SWNTs. This was done by manipulating the P3HT-SWNT concentrations, the solvent concentration, and crystallization temperature. The P3HT nanoribbon shape, size, and period were found to be correlated to the above parameters. The morphology and purity/concentration were measured using atomic force microscopy (AFM) and ultra-violet/visible spectroscopy. NHSKs were fabricated via a 6:1 P3HT to SWNT mass concentration solution mixed in 70°C anisole solution. The P3HT supramolecular structures were found to be  $32 \pm 3.7$  nm wide and  $269 \pm 11.4$  nm long. At higher mass ratios (40:1 P3HT to SWNT), full encapsulation was observed with little periodicity. In conclusion, this work investigates the growth mechanisms of P3HT polymer crystals on single chirality CNTs for semiconducting ink applications. Next steps include the manipulation of the solution to increase printability and the fabrication of NHSK-based thin-film transistors.

#### **F.NM03.09.54**

**Enhanced Heat Transfer of Functionalized Graphene Nanoplatelets in Nanofluids for Energy Conversion and Storage of Solar Power Plants** Michael Wilhelm<sup>1</sup>, Tim Ludwig<sup>1</sup>, Thomas Fischer<sup>1</sup>, Dileep Singh<sup>2</sup> and Sanjay Mathur<sup>1</sup>; <sup>1</sup>University of Cologne, Germany; <sup>2</sup>Argonne National Laboratory, United States

The unique thermal conductivity of graphene makes it one of the most promising materials for next generation heat transfer applications that, given the increasing demand for energy supply from sustainable energy sources such as concentrated solar power, has emerged as key technology. The incorporation of graphene and graphene-like nanomaterials into conventional heat transfer fluids has been shown to significantly improve their thermal transport properties. Due to their cost-efficient carbon-based starting material, its high surface area and sheet-like structure, graphene nanoplatelets (GNPs) are suitable for colloidal thermal conductive fluids demonstrating enhanced heat transfer efficiencies. In this work, hydrophobic graphene nanoplatelets were used as starting material and surface functionalized by acid treatments to synthesize highly stable, exfoliated, surfactant-free and highly concentrated (4 wt.%) graphene nanofluids maintaining high thermal conductivity. Characterization by SEM, XPS, XRD, Raman and FT-IR spectroscopy revealed a significant influence of shape, reaction period, acid volume and temperature on the resulting thermal conductivity values of the nanofluids relative to the carrier fluid. After 14h of measurement in a dormant system, thermal conductivities up to 0.586 W/m\*K (base fluid: 0.391 W/m\*K) were measured. In combination with a low viscosity of 6.39 cP the overall efficiency of the functionalized particles could be increased to 77 % in comparison to the base fluid. The combination of both low viscosity and high thermal conductivity, even after 14h in a standing system, demonstrate the extraordinary properties of surface functionalized graphene nanoplatelets prepared in this work in comparison to other nanofluidic systems.

#### **F.NM03.09.57**

**Modeling the Effective Electrical Conductivity of Nanocarbon-Metal Composites Made by the Electrocharging Assisted Process** Christopher Klingshirn<sup>1</sup>, Andrew Palughi<sup>2</sup>, Xiaoxiao Ge<sup>1</sup>, Madeline Morales<sup>1</sup>, Jessica Ye<sup>1</sup>, Christopher Shumeyko<sup>3</sup>, Tahir Cagin<sup>2</sup> and Lourdes G. Salamanca-Riba<sup>1</sup>; <sup>1</sup>University of Maryland, United States; <sup>2</sup>Texas A&M University, United States; <sup>3</sup>U.S. Army Research Laboratory, United States

Robust materials with high conductivity are essential to electronic devices and systems. Nanocarbon-metal composites have the potential to improve upon the electrical conductivity of established metals and alloys such as Al and Cu by incorporating carbon nanostructures known for their superior electrical properties. During the fabrication of novel nanocarbon-metal composites called covetics, direct electric current applied to a metal melt containing a dispersion of carbon source material is believed to ionize carbon atoms and lead to the formation of nanoscale graphitic ribbons and chains that ultimately incorporate within the metal lattice upon solidification. The electrical conductivity of the resulting composites is consistently greater than the original alloy, but the magnitude of conductivity enhancement varies significantly from sample to sample, and the theoretical upper limit of conductivity enhancement in these systems remains unclear.

This work combines fundamental assumptions about the nature of covetics, specifically a tightly bound metal-carbon interface, with a simple effective-medium model to estimate the bulk conductivity of ideal Al and Cu covetics with randomly distributed graphene nanoribbons (GNRs). Density-functional theory estimates of charge transfer at the graphene-metal interface, local electrical conductivity measurements, and transmission electron microscopy investigation of the interface region provide inputs to the model. The implications of quantum confinement in narrow GNRs are also explored. We use the model to project a range of performance-enhancement goals for the covetics fabrication community and find the potential for conductivity improvements on the order of 10% under ideal conditions, however fabrication challenges remain before these gains may be realized on an industrial scale.

This work is supported by the U.S. Department of Energy under Award No. DE-EE0008313.

#### **F.NM03.09.59**

**Carbon Nanotube Embedded Vertical Aligned PVDF Membranes with High Mechanical Properties for PRO Membrane Application** Juran Noh, Mehdi Habibollahzadeh, Choongho Yu and Ahmed Abdel-Wahab; Texas A&M University at Qatar, Qatar

Water desalination has been a critical issue for reserving the freshwater for human survival, further civilization, industry development. Pressure retarded osmosis (PRO) is desalination technology emerging from the osmosis phenomenon; water flux through the membrane, excluding undesired macromolecules or ions with applying pressure. Thus, a high water permittable membrane with stronger mechanical strength to bear in high water pressure should be developed for a high-performance PRO desalination process. High mechanical strength and water permittivity could be a trade-off relationship based on thickness and porosity. Thus, vertical oriented polyvinylidene fluoride (PVDF) membrane with 3D connected carbon nanotube (CNT) is presented. Vertical pores made of hydrophobic polyvinyl fluoride (PVDF) and hydrophilic metal-organic framework (MOF) decorated on the surface improve their water permeability and salt rejection. The CNT embedded structure in the vertically aligned membrane improves mechanical strength along the in-plane direction. This work presents CNT additives can significantly improve the mechanical properties of water desalination membranes by smartly designing the morphology of the substrate and properly inserting functional materials in the active layer.

#### **F.NM03.09.61**

**Isopropanol-Assisted Hot Lamination for Facile Synthesis of Large-Area Atomically Thin Graphene Membranes** Peifu Cheng<sup>1</sup>, Nicole K. Moehring<sup>1</sup>, Andrew Naclerio<sup>1</sup>, Mattigan Kelly<sup>1</sup>, Dahsong Lee<sup>1</sup>, Juan C. Idrobo<sup>2</sup> and Piran Ravichandran Kidambi<sup>1</sup>; <sup>1</sup>Vanderbilt University, United States; <sup>2</sup>Oak Ridge National Laboratory, United States

Atomically thin graphene membrane has been considered as an ideal candidate for next-generation membrane-based technologies. While catalytic chemical vapor deposition (CVD) has been demonstrated to be an economical and versatile way of enabling the commercial production of high-quality graphene, CVD graphene has to be transferred from the growth substrate onto a porous support substrate to provide mechanical stability for membrane applications. However, commonly used polymer scaffold methods typically leave polymer residues detrimental to membrane performance, while transfers without sacrificial polymers suffer from low transfer yield leading to high membrane leakage. Hence, high-yield transfer of clean large-area graphene onto appropriately porous supports using scalable processes for membrane applications remains elusive. In this work, we systematically investigate the factors influencing the transfer of CVD graphene from a Cu foil onto a model polycarbonate track etch (PCTE) support for fabricating large-area atomically thin membranes via manual compression, mechanical press and scalable lamination approaches. Particularly, we report on a novel roll-to-roll manufacturing compatible isopropanol-assisted hot lamination that allows for facile, clean and scalable transfer of centimeter-scale graphene onto model PCTE supports with coverage  $\geq 99.2\%$  without compromising support porosity, which is one of the best values reported to this date for centimeter-scale atomically thin membranes. The remaining 0.8% of leakage is attributed to defects ( $>50$  nm) primarily along wrinkles formed during CVD growth. Furthermore, water-assisted oxidation effectively detaches CVD graphene from the Cu foil and helps graphene transfer, but significantly damages ( $\sim 10\%$ ) graphene along wrinkles. Finally, fully functional centimeter-scale atomically thin membranes are demonstrated. Our work provides a facile and effective method for the fabrication of atomically thin graphene membranes and can help on the progress towards the practical application of graphene membrane technologies relevant to gas separation, nanofiltration, desalination, ionic/molecular transport, energy and biomedical fields and beyond.

#### **F.NM03.09.63**

**Effect of Orientation of Graphene Upon Dielectric and Electrical Characteristics of PBAT-PLA-Graphene Composites** Radha Perumal Ramasamy<sup>1</sup>, Xianghao Zuo<sup>2</sup>, Yiwei Fang<sup>2</sup> and Miriam H. Rafailovich<sup>2</sup>; <sup>1</sup>Anna University, India; <sup>2</sup>Stony Brook University, United States

Graphene has several fascinating characteristics such as high thermal and electrical conductivity. Graphene polymer composites is usually made using molding. To enhance the application of graphene in nanocomposites controlling its alignment is important as graphene has different conductivity along and perpendicular to its surface. The orientation of graphene in polymeric materials is a challenging task. Recently 3D printing has been used for aligning graphene in composites. In this research varying amounts of graphene (grade H5 – XG Sciences) was mixed with PBAT-PLA mixture and molded. Also 3D printed PBAT-PLA-graphene composites were made. The dielectric measurements were made by

placing the composites between two brass electrodes of diameter 1cm. The dielectric measurements were made using Waynekerr- 6500p LCR meter. The frequency was varied from 100 to  $10^6$  Hz. The measurements were made at room temperature (22 °C). The samples had cuboid shapes. The measurements were made along height and depth of the samples. The height corresponded to the direction of application of pressure during molding and the depth corresponded to the direction perpendicular to the direction of application of pressure and parallel the surface of the samples. The following observations were made. (A) The dielectric constant for 3D printed samples (along height) was less than dielectric constant for 3D printed samples (along depth) which was less than dielectric constant for molded samples (along height). (B) The dielectric constant for molded samples (along depth) was less than dielectric constant for molded samples (along height). (C) Along depth, for molded samples the dielectric constant becomes negative for 20% graphene containing samples indicating percolation. (D) The electrical conductivity for 3D printed samples (along height) was less than conductivity for molded samples (along height) and (E) Electrical conductivity for 3D printed samples (along depth) was less than electrical conductivity for molded samples (along depth). The observed variations in dielectric and electrical characteristics are attributed to the orientation of graphene in the composites.

#### **F.NM03.08.66**

**Why Aren't Nano Carbon Based Composites Rise Up to Their Theoretical Potential and How Can We Get Them Closer?** Noa Lachman; Tel Aviv University, Israel

Carbon Nanotubes (CNT) and graphene are considered highly promising nanomaterials for composite reinforcement. The nanoscale dimensions of the carbon structures provide ultra-high surface-to-volume ratio, nearly defect-free structure, and their exceptional properties: mechanical (1TPa – five times the value for steel), thermal conductivity (2000-6000 Wm<sup>-1</sup>K<sup>-1</sup> – four to ten times the value for silver) and electrical conductivity (roughly equivalent to copper) makes them highly useful in very many applications. However, these same scale and properties complicate the processing and fabrication of polymer based nanocomposites: high surface-to-volume means that even in small filler concentrations composite process-affecting properties as melt viscosity, heat transfer and other characteristics will drastically change. Morphology control, and thus post-processing behavior prediction, are also challenging – as dispersion and orientation are applied indirectly in the process, and different mechanisms are dominant at different length-scales. Therefore, transferring the exquisite properties of the CNT and graphene to the composite level have been proven less than ideal, as the measured mechanical, electrical and thermal properties of the nanocomposites are usually lower than predicted by rule-of-mixture calculations. In this talk, various approaches for carbon nanocomposite fabrications, both “top-down” and “bottom-up”, will be presented in case-studies. A few of the major issues inhibiting nanocarbon based composites from achieving their true potential will be highlighted. Effects of different fabrication techniques, including 3D printing, on the morphology of nanocomposites and the resultant behavior will be discussed, and possible solutions to the aforementioned issues will be presented. The new methods can provide better control for improved planning and designing of nano carbon based composites.

#### **F.NM03.09.67**

**Flexible Devices Based on Polyurethane and Reduced Graphene Oxide Composites for Applications in Tactile Sensing** Flavio A. Borges<sup>1</sup>, Monica A. Cotta<sup>1</sup>, Cecilia d. Silva<sup>2</sup>, Talita Mazon<sup>3</sup>, Joao H. Clerici<sup>1</sup> and Daniel M.

Ugarte<sup>1</sup>; <sup>1</sup>University of Campinas, Brazil; <sup>2</sup>MackGraphe – Graphene and Nanomaterials Research Center, Brazil; <sup>3</sup>Institute of Information Technology Renato Archer, Brazil

New opportunities have been created along with the advances of the wearable device technology. For pressure sensing and transduction in soft objects like human skin, direct contact between sensor and target area is necessary; therefore, sensor flexibility is a very important parameter for the viability of the sensing device.

In this work, we report on the development of a sensing system that translates the electric signals of low cost composites based on polyurethane (PU) and reduced graphene oxide (r-GO) fabricated in-house. The graphene oxide (GO) is deposited by dispersion in PU foam. The GO reduction is carried out by immersion in ascorbic acid. Different commercial foams were tested and sample heights could be reduced to 1mm with electrical resistance range of 1-100 kΩ for a 90% compression. Electrical resistances were measured in function of the applied force and an exponential character was identified. With the force range which the foams endure and the calibration curve obtained for the samples, a rigid device was developed by integrating an Arduino system to the sensors so that responses could be obtained via a graphical interface, adapted to visual feedback.

The foam shows great conformity with surfaces; flexible contacts, printed in Kapton film using conductive paint, are used to obtain the flexible device. We thus expect to have a flexible sensor integrated to a functioning system fully prepared to neurological rehabilitation applications.



SESSION F.LP06.07: Live Poster Session II: Nanomaterials and Quantum Materials II (F.NM03)

Session Chairs: Jeffrey Fagan and Yoke Khin Yap

Friday Afternoon, December 4, 2020

6:30 PM - 8:30 PM

F.NM03

### F.NM03.09.68

**Transition Metal Chalcogenide Nanostructures for High Energy Density Supercapacitors** Harish Singh and Manashi Nath; Missouri University of Science and Technology, United States

Electrochemical capacitors (ECs) or supercapacitors (SCs) are considered to be most promising energy storage devices and have received great attention because of their excellent electrochemical performance with high output power, short discharging time and long-term cycle stability. Transition metal chalcogenides (especially selenides and tellurides) have recently attracted considerable attention for electrochemical applications mainly due to better electronic conductivity, facile charge transfer, redox tunability, and chemical stability. In the current project, transition metal telluride-based nanostructure composites were studied for supercapacitor applications. The nickel telluride nanostructures were grown directly on Nickel foam by hydrothermal method as well as electrodeposition process without addition of any binder to the catalyst. The capacitor performance was measured in a three-electrode system with the nickel-telluride electrode as the anode. A specific capacitance of 1826 F/g was achieved at a current density of 1 A/g. The composite electrode maintained cyclic stability of more than 90 % at a higher current density of 10 A/g after 1000 cycles. Also, more than 80 % current density retention achieved at higher current density of 20 A/g. Moreover, doping effect on the transition metal site on the supercapacitor performance was also illustrated in this work. Doping in the transition metal site had a positive influence on the supercapacitor activity since, it led to lattice distortion, electronic structure modification as well as helped to tune the surface redox behavior. Also, combining different carbon-based materials (carbon nanotubes, activated carbons and graphene) with the active nickel telluride nanostructures enhanced specific capacitance and overall cyclic stability by increasing the active surface area and porosity of the composite. In this presentation we will discuss the supercapacitor performance of these telluride nanostructures as well as the effect of transition metal doping and carbon nanostructure additives, and explain how the chemistry of transition metal chalcogenides influences their electrochemical functionality and potential as future energy storage devices.

### F.NM03.09.71

**Nanopores in Multilayer Hexagonal Boron Nitride** Mehmet Dogan<sup>1,2</sup>, S. Matt Gilbert<sup>1,2,3</sup>, Thang Pham<sup>1,2,3</sup>, Brian Shevitski<sup>1,2,3</sup>, Peter Ercius<sup>2</sup>, Shaul Aloni<sup>2</sup>, Alex Zettl<sup>1,2,3</sup> and Marvin L. Cohen<sup>1,2</sup>; <sup>1</sup>University of California, Berkeley, United States; <sup>2</sup>Lawrence Berkeley National Laboratory, United States; <sup>3</sup>Kavli Energy NanoScience Institute, United States

Controlling the size and shape of nanopores in two-dimensional materials is a key challenge in applications such as DNA sequencing, sieving, and quantum emission in artificial atoms. In single-layer hexagonal boron nitride (*h*-BN), under a high-energy electron beam with certain properties, triangular pores are formed whose edges are entirely made up of nitrogen atoms. This allows fabrication of triangular pores at will with matching orientation throughout the two-dimensional material. However, in multilayer *h*-BN, which is usually in the AA' stacking, neighboring sheets are rotated by 60° with respect to each other, which causes triangular pores in consecutive layers to be misaligned. Here, we investigate experimentally and theoretically triangular vacancies in (unconventional) Bernal-stacked *h*-BN (AB-*h*-BN) formed using a high-energy electron beam. Due to the geometric configuration of AB-*h*-BN, triangular pores in different layers are aligned, and their sizes are controlled by the duration of the electron irradiation. Interlayer covalent bonding at the edge of the pore is not favored, as opposed to what occurs in the more common AA'-stacked BN. A variety of monolayer, concentric and bilayer pores in bilayer AB-*h*-BN are observed in high-resolution transmission electron microscopy and characterized using *ab initio* simulations. Bilayer pores in AB-*h*-BN are commonly formed, and grow without breaking the bilayer character. Nanopores in AB-*h*-BN exhibit a wide range of electronic properties, ranging from half-metallic to non-magnetic and magnetic semiconducting. Therefore, because of the controllability of the pore size, the electronic structure is also highly controllable in these systems, and can potentially be tuned for particular applications.

### F.NM03.09.72

**Enhanced Mechanical Properties of Polymer-Matrix Nanocomposites Reinforced with Graphene Synthesized in**

**Atmospheric Plasmas** Albert Dato, Jacob Knego, Nicole Subler, Taylor Sloop, Chance Bisquera and Kevin Nakahara; Harvey Mudd College, United States

Graphene can be synthesized in the gas phase using atmospheric plasmas. Gas-phase-synthesized graphene (GSG) is pure and highly ordered. Additionally, GSG contains graphitic nanocrystals that provide the two-dimensional material with significant mechanical stability and enable GSG sheets to resist deformation. GSG is also more environmentally friendly to produce than graphene that is obtained from graphite. These unique features make GSG a promising filler material for fabricating high-strength multifunctional nanocomposites that have a wide range of applications, such as automobiles, aircraft, and wind turbines.

Here we present the results of an investigation into epoxy-matrix nanocomposites reinforced with GSG. We show that as-synthesized GSG effectively disperses in epoxy resins and resists aggregation indefinitely. We report that incorporating a relatively low loading of GSG into epoxy (0.1 wt%) results in nanocomposites that exhibit significant increases in both strength and strain at break. In contrast, epoxy-matrix nanocomposites that were filled with 0.1 wt% graphene nanoplatelets had enhanced strength but diminished strain at break. Scanning electron microscopy images of nanocomposite fracture surfaces will be presented, which indicate much higher matrix reinforcement by GSG relative to graphene nanoplatelets. These results indicate that (1) GSG could overcome the challenges of contemporary graphene-based nanocomposites and (2) unique strengthening mechanisms exist in polymers reinforced with GSG.

#### **F.NM03.09.73**

**Metal-Free, Highly Conductive Protein Carbon Nanotube Dispersions and Their Films for Biological Applications** Ankarao Kalluri and Vijaya Kumar Challa; University of Connecticut, United States

A simple and facile method to produce highly concentrated ( $> 5$  mg/ml) and high-quality multi-walled carbon nanotube (MWCNT) dispersions by ordinary benchtop magnetic stirrer is reported here. Exfoliation and debundling of the MWCNTs were possible by stirring in the presence of a protein, driving the adsorption of the protein onto the nanotube surfaces. High concentrations of the debundled nanotubes were obtained (6 mg/ml) after stirring for 5 days, and these are much higher than other reports in the literature. The bioCNT aqueous dispersions are stable up to 6 months, which is important for storage and practical applications. We also fabricated the facile, inexpensive, highly conductive and flexible CNT paper (Bucky paper) by vacuum filtration of the dispersion through an ordinary filter, which composed of self-assembled, randomly oriented, and highly packed CNTs. These metal-free CNT films were flexible and showed a high electrical conductivity of  $> 1000$  S/cm than expected. These biological CNT dispersions used as conductive ink on cellulose paper, which can be used in printed and flexible electronics, bio-electrochemical sensors, bio-supercapacitor electrode applications. Therefore, inexpensive, highly concentrated biological CNT dispersions prepared by a simple method of stirring provides new opportunities for a wider range of CNT applications.

#### **F.NM03.09.74**

**Sub-Nanometer Carbon-Nanotube Membranes with Anomalously Enhanced Water-Vapor Flux** Da-Chi Yang<sup>1</sup>, Richard Castellano<sup>1</sup>, Melinda Jue<sup>2</sup>, Ricardo P. Silvy<sup>3</sup>, Robert F. Praino<sup>3</sup>, Francesco Fornasiero<sup>2</sup> and Jerry Shan<sup>1</sup>; <sup>1</sup>Rutgers, The State University of New Jersey, United States; <sup>2</sup>Lawrence Livermore National Laboratory, United States; <sup>3</sup>Chasm Advanced Materials, Inc., United States

Fluid transport through the inner cores of carbon nanotubes (CNTs) is known to occur at extraordinary rates, exceeding classical predictions by several orders of magnitude, especially for very-small-diameter nanotubes. However, macroscopic, vertically aligned- (VA-) CNT membranes with sub-nanometer pores have not been previously fabricated due to the difficulty in growing aligned forests of such small CNTs. Here, we report the scalable, solution-based fabrication of the first macroscopic membranes with VA-CNTs of sub-nanometer diameter, and the first water-vapor transport measurements for such membranes. Membranes were fabricated from CNT powder using electric-field alignment and electrophoretic concentration of suspended nanotubes, followed by solvent replacement with a liquid prepolymer and UV curing. The single-wall nanotubes are grown in bulk by chemical-vapor deposition with a specialized catalyst, tuned to produce long, 0.8 nm diameter CNTs. After etching to open CNT pores, the membranes filter out dye solution and demonstrate sublinear conductance scaling with salt concentration at low concentrations. These observations indicate that our fabrication process produces defect-free membranes with CNT pores as the primary trans-membrane pathway. Based on KCl-conductance estimates for the total open pore area in the membranes, the concentration-driven water-vapor permeability is enhanced by many orders of magnitude, well above values reported in literature for larger-diameter VA-CNT membranes. Interestingly, the enhancement in concentration-driven water-vapor transport appears to considerably exceed the enhancement present in the pressure-driven flux of dry nitrogen gas in the pores. Additionally, due to the size of the CNT pores, and the charge

present on carboxyl groups at the CNT tips, the membranes demonstrate cation selectivity in KCl solution. Coupled with the enhanced flux of liquid water, such membranes could increase the energy efficiency of membrane-based desalination techniques. These findings present new opportunities to scalably fabricate VA-CNT membranes with sub-nanometer pores and study their fundamental transport properties, with possible applications in breathable and protective garments as well as desalination technologies.

#### F.NM03.09.75

##### **Growth Pressure Dependence of Graphene Direct Growth on A-Plane Sapphire Using Metal-Catalyst-Free Low-Pressure CVD** Yuki Ueda, Takahiro Maruyama and Shigeya Naritsuka; Meijo University, Japan

Graphene direct growth on sapphire by metal-catalyst-free chemical vapor deposition (CVD) has attracted much attention as the method to avoid the transfer process [1]. The transfer process not only damages but also deteriorates the graphene. Recently, we reported a graphene direct growth on r-plane sapphire using metal-catalyst-free low-pressure CVD where the graphene grows very fast and quite uniformly comparing to that on c-plane sapphire [2]. However, there are many unknown parts in the growth mechanism. In this report, we focused on a-plane sapphire as a substrate, which is often used in horizontally-aligned growth of carbon nanotubes [3]. The growth pressure was systematically changed in metal-catalyst-free low-pressure CVD to reveal the growth mechanism.

Graphene was directly grown on a-plane sapphire using low-pressure CVD without using a metal catalyst. A mixture gas of N<sub>2</sub>, H<sub>2</sub>, and 3-Hexyne was flown in a reaction chamber at a constant flow rate of 1000 sccm. The growth temperature, H<sub>2</sub>, and 3-Hexyne partial pressures were fixed at 1250 °C, 500 Pa, and 0.3 Pa while the growth pressure was systematically changed from 5 kPa to 50 kPa.

Raman measurements show that graphene was only grown below 17 kPa and all the grown graphene was smooth and uniform with mono-layer-thick. At the same time, the D/G ratio decreased with decreasing the growth pressure. To investigate the reason, the early stages of growth were studied between 5 kPa and 15 kPa. Consequently, AFM study showed that the density of graphene islands on the sample grown at 5 kPa was approximately 3 times lower than that of the sample grown at 15 kPa. On the contrary, the growth rate of graphene at 5 kPa was much faster than that at 15 kPa. A high growth rate usually means a high supersaturation, and, therefore, a high nucleation rate. In our case, however, the nucleation rate was slow at low growth pressure. This inconsistency suggests the existence of a special mechanism, which controls the nucleation. From the AFM study, the most graphene islands were found at the step edges of the sapphire substrate. At a low growth pressure, the thermal decomposition of the sapphire surface is enhanced and nucleation sites, in other words, surface steps are destroyed at the same time. This brings the difficulty to the graphene nucleation at the step edges even with a higher supersaturation at a low pressure. Consequently, excellent smooth monolayer graphene with a small D/G ratio of less than 0.2 was successfully obtained on a-plane sapphire at 5 kPa with forming larger grains.

Acknowledgement: This work was supported in part by JSPS KAKENHI Grant Numbers 15H03558 and 26105002.

#### Reference

- [1] M. A. Fanton et al., ACS Nano 5, 8062 (2011).
- [2] Y. Ueda et al., Appl. Phys. Lett. 115, 013103 (2019).
- [3] N. Ishigami et al., J. Am. Chem. Soc. 130, 9918 (2008).

#### F.NM03.09.76

##### **Partially Reduced Graphene Oxide Enhancement of Thrombin Activation of Fibrinogen Clots** Rebecca Isseroff<sup>1</sup>, Juyi Li<sup>1</sup>, Jonathan Lederer<sup>2</sup>, Nava Schein<sup>1</sup>, Abraham Balsam<sup>1</sup> and Miriam H. Rafailovich<sup>1</sup>; <sup>1</sup>Stony Brook University, The State University of New York, United States; <sup>2</sup>Columbia University, United States

Partially reduced graphene oxide (pRGO) has been found to enhance the enzymatic activity of microbial transglutaminase on the cross-linking of gelatin. To determine if this is a more general phenomenon in modification of enzymatic activity, we tested whether it has an effect on thrombin's ability to clot fibrinogen, an easily quantifiable effect to measure.

Three ml of 10 mg/ml fibrinogen solution in PBS were tested with 8 μ thrombin/ml as a control. Upon adding thrombin, rheometry was used to measure the clotting time as well as the clot modulus. Sharp increases in modulus, shorter clotting times, and stronger clots would indicate enhancement of thrombin, whereas slow increases in modulus, longer clotting time, and weaker clots would indicate inhibition of the enzyme. Test samples included 0.5 ml of 1 mg GO/ml PBS in the fibrinogen mixture, and 0.5 ml of 1 mg pRGO/ml PBS added to the fibrinogen. The pRGO solution produced a clot with an elastic modulus four times greater than the control, and 1.5 times greater than the clot with GO. Different concentrations of

pRGO in PBS were then added to fibrinogen solutions and tested. Increasing pRGO concentrations increased the maximum elastic modulus and decreased the clotting time. The elastic moduli were found to be logarithmic, as the logarithmic trendlines had relatively high  $R^2$  values. Higher concentrations of pRGO had higher coefficients, indicating shorter clotting times. Results suggest further future study of partially reduced graphene oxide as a modifier of enzymatic activity.

#### **F.NM03.09.77**

#### **Interactions Between Graphene Oxide and Pyrrole Towards Understanding the Electro-Polymerized Substrates—A Molecular Dynamics Study** Todd M. Richards and Isaac Macwan; Fairfield University, United States

Graphene Oxide, an oxidized form of graphene, a carbon allotrope, has many applications including the formation of conductive films for use in flexible electronics and chemical sensors, nanofiltration membranes, and even as a replacement for tin-oxide in batteries. One of the pressing issues with carbon allotropes in general and graphene oxide in particular, however, is that they cannot form freestanding films on their own, instead they rely on a secondary reactant to help aid in the synthesis of such films. To synthesize such nanocomposite substrates, cyclic voltammetry is a very commonly used technique, where an electrolyte containing a monomer to be electro-polymerized is used along with the nanoparticles. Electro-polymerized substrates consisting of GO and Polypyrrole (Ppy), an organic polymer created by polymerizing pyrrole, have drawn much attention owing to their applications in solid state supercapacitors, biosensing, tissue engineering, and artificial muscle studies. It has been proven theoretically and experimentally that Ppy and GO do interact and exhibit improvement in conductivity and thermal stability compared to pure Ppy and GO, but there is still very little information on the interactions at the molecular level between GO and pyrrole monomers especially during the synthesis of such nanocomposites. This work deals with the study of interactions at the interface of GO and pyrrole in order to better understand the evolution of polypyrrole over the surface of graphene oxide during the formation of these films. The system is modeled using Visual Molecular Dynamics (VMD) and all-atom simulations are carried out using Nanoscale Molecular Dynamics (NAMD) at ten different temperatures based on the peak currents and scan-rate through the Randles-Sevcik equation. Each simulation is carried out for 100ns, thereby looking into a total of one microsecond long window of interactions between GO and 50 pyrrole monomers as the polypyrrole film is evolved over the surface of GO. Stability of the GO/Ppy nanocomposite is quantified through RMSD (Root Mean Square Deviation), conformational energies and center of mass deviations. Interaction energies are calculated to understand the role of non-bonding interactions such as Van der Waals and electrostatics between the monomers and between monomers and GO. It is anticipated that pyrrole monomers form dimers in the bulk of the solution, trimers when near the surface of GO, and tetramers when adsorbed on the surface of the GO. Based on these results, a potential mechanism is proposed on the way monomers interact with the nanoparticles during electro-polymerization and the role of such interactions in synthesizing carbon-based free-standing films.

#### **F.NM03.09.78**

#### **Development of Planar-Type Thermoelectric Device Using Carbon Nanotube Sheet for Wearable**

**Application** Tsuyohiko Fujigaya<sup>1,2,3</sup>, Ryohei Yamaguchi<sup>1</sup> and Naoki Tanaka<sup>1</sup>; <sup>1</sup>Kyushu University, Japan; <sup>2</sup>Center for Molecular System, Kyushu University, Japan; <sup>3</sup>International Institute for Carbon-Neutral Energy Research, Kyushu University, Japan

Single-walled carbon nanotube (SWNT) is ideal materials for thermoelectric conversion because of their high Seebeck coefficient and electrical conductivity. Development of the wearable thermoelectric device using SWNTs is now investigated by taking advantage of their film toughness and flexibility. Up to date,  $\pi$ -shape structure has been proposed for the SWNT thermoelectric sheet. However, this structure needs to attach on a skin vertically and not preferable for the wearable application. Therefore, we proposed a new planar-type structure, in which the sheet can attach on the skin surface and preferable as a wearable device. Since sequential repeating of p-type and n-type properties are necessary for the devices, in this study, we investigated the patterned doping of p-type SWNT sheet into n-type. We found that the deposition of benzimidazole derivatives successfully turned un-masked area into n-type, giving a repeating of p and n-type structure. Detail characterization of the n-doping were carried out by Raman spectroscopy, X-ray photoelectron spectroscopy and Seebeck Coefficient measurements. Device performance of the thermoelectric sheet will be introduced in the presentation.

#### **F.NM03.09.79**

**Fabrication and Characterization of PbTiO<sub>3</sub> Multi-Layered Truss Structure** Hyunji Kim, Kisun Kim, Hoon Kim, Seokjung Yun, Gun Park, Seokwoo Jeon and Seungbum Hong; Korea Advanced Institute of Science and Technology, Korea (the Republic of)

Future society will enjoy augmented reality, haptic displays, intelligent cars, and robots in everyday life. Those devices

require tactile enhancement which would be improved by high piezoelectric coefficient and strain limit.  $\text{PbTiO}_3$  is one of the piezoelectric materials which has high piezoelectric coefficient, low price and wide application but at the expense of low elastic strain limit. In this work, we applied nanoscale truss structure to enhance the elastic stress limit while maintaining the high piezoelectric coefficient of  $\text{PbTiO}_3$ . Fabricating  $\text{PbTiO}_3$  in multi-layered truss structure around 20–30 nm, we expect to improve both piezoelectric coefficient and strain limit up to 300% respectively. We deposited 8 nm  $\text{PbTiO}_3$  layer 3 times on the Nickel template and after deposition of multilayers, Nickel template was removed. Each layer of  $\text{PbTiO}_3$  was formed by depositing  $\text{TiO}_2$  using atomic layered deposition (ALD) and  $\text{PbO}$  gas reaction in the tube furnace. The crystallinity of each  $\text{PbTiO}_3$  layer was confirmed by XRD. We expect multi-layered  $\text{PbTiO}_3$  to show 100% higher piezoelectric coefficient than single-layered  $\text{PbTiO}_3$  showing better crystallinity.<sup>[1]</sup> After measuring the crystallinity, thickness was measured by TEM. By measuring the deposition thickness according to the distance, we will set thickness of single-layered  $\text{PbTiO}_3$  to 8 nm. This will be a significant experiment in that it stacks nano layers of targeted thickness. Also, our approach will provide insight into making piezoelectric materials that have both high piezoelectric coefficient and strain limit, and realize various tactile applications.

<sup>[1]</sup> M.Park *et al.*, Appl. Phys, Lett.**94**, 092901(2009)

### **F.NM03.09.80**

**Layer-by-Layer Self-Assembly PEI/MWCNT-COOH Nano-Porous Coating for Enhanced Heat Transfer Characteristics of Heat Dissipation Devices** Jaemin Lee, Daehyeon Kyeong, Ji heon Kim and Wonjoon Choi; Korea University, Korea (the Republic of)

With the development of AI, 5G, and autonomous vehicles, higher performance electronic devices are required for more data collection and data processing. In addition, as electronic devices are gradually downsized and thinned, the amount of heat generated per unit area also increases exponentially, so conventional heat dissipation devices (e.g. Heat sink, Heat pipe and Vapor chamber) cannot satisfy these heat generation and electronic device manufacturing conditions. In order to improve the performance of these heat dissipating devices, many studies have improved heat transfer performance through various coating methods such as CVD, PVD, ALD and Spray coating. However, these coating methods are not suitable for heat sinks with complex shapes or heat pipes with a thin tube structure because they require special process conditions such as high temperature or vacuum, and the process cost is large or greatly affected by the shape and size of substrate.

The Layer-by-Layer (LbL) coating method is a solution-based technique which is a self-assembled coating using electrostatic force through the difference in zeta potential between positive and negative solution. Since the LbL coating method is based on a solution-based processing, it can be coated to the complex structures regardless of the size or shape of the substrate. This characteristic enables the direct applications to a heat sink within fin structures or a tubular heat pipe within an inner micro porous structure.

Herein, we present multi-functional LbL PEI/MWCNT-COOH nano-porous coatings based on a solution processing to improve the heat transfer characteristics of heat sinks and heat pipes. To investigate the direct correlation of the nano-porous coatings and the heat transfer characteristics, the LbL PEI/MWCNT coatings were prepared as bare, 10-bi, 20-bi, and 30-bi layers. The change in thickness and surface morphologies of LbL coatings was precisely analyzed through FIB and SEM image analysis, while the surface area and pore size distribution according to the number of LbL coatings was examined using BET surface area analysis. Furthermore, the wettability of the PEI/MWCNT coating was measured to confirm the capillary rise, which is one of the important factors to determine the heat transfer performances of the devices.

Through the natural convection test of the LbL coated heat sinks, it was confirmed that the enhanced thermal performances could be obtained due to increasing the porosity and surface area of the LbL coating. As the porosity and surface area was optimized in the number of coatings, the overall thermal performances including heat transfer coefficients were significantly improved up to 11% for 30 bi-layers coated heat sink due to the increase in the surface area, in comparison with that of the bare heat sink. Furthermore, the LbL functional coating layers could highly improve the heat transfer characteristics of the heat pipes, as well. Because a nano-micro sized bi-porous structure appeared in the microporous-sintered heat pipe with the LbL coating layers, such bi-porous structure could strengthen capillary wicking, fluid transportation, and superhydrophilicity as well as increasing surface area, thereby improving heat transfer efficiency and thermal resistance up to 14.3% in a 10 bi-layers coated heat pipe.

The PEI/MWCNT LbL nano-porous coating, which was used for the heat dissipation devices (i.e. heat sink and heat pipe) could show the enhanced heat transfer characteristics, while the fabricate process was based on the only simple and low-cost

LbL coating technology. This multi-functional and thin PEI/MWCNT LbL nano-porous coating not only improved the performance of the conventional heat dissipation device, but also is expected the design trend of miniaturization, thinning, and lightweight electronic equipment.

#### **F.NM03.09.81**

**Dielectrophoresis (DEP)-Aligned Semiconducting Carbon Nanotubes for Fabricating Electronic Devices** Abram Jones, Lauren Williams, Brandon Whitaker, Rodricka Miller, Jhamaree Elam, Qunying Yuan and Zhigang Xiao; Alabama A&M University, United States

We report the deposition and alignment of semiconducting carbon nanotubes with the alternating electric field-directed dielectrophoresis (DEP) method and the fabrication of carbon nanotube-based electronic devices with the DEP-aligned semiconducting carbon nanotubes (CNTs). Semiconducting carbon nanotubes, which were dispersed ultrasonically in the *n*-methyl pyrrolidone (NMP) solution, were deposited and aligned onto a pair of gold electrodes using the dielectrophoresis method. The excellent alignment of carbon nanotubes was achieved by optimizing the AC voltage, frequency, and deposition time of the applied AC signal. The DEP-aligned tubes were further fabricated into carbon nanotube field-transistors (CNTFETs) and CNTFET-based electronic devices such as CNT-based inverters using the microfabrication techniques. Plasma-enhanced atomic layer deposition (PE-ALD) was used to grow hafnium dioxide (HfO<sub>2</sub>) as the high-*k* gate oxide in the fabrication of CNTFETs. The aligned carbon nanotubes and fabricated devices were imaged using the scanning electron microscope (SEM), and the electrical properties were measured from the fabricated devices using the semiconductor analyzer. About 70% yield was obtained from the semiconducting carbon nanotube-based CNTFETs, and the fabricated CNTFETs and CNT-based inverters demonstrated excellent current (*I*) – voltage (*V*) curves and transfer characteristics.

#### **F.NM03.09.82**

**Inertial Sensor Based on Energy Harvesting Carbon Nanotube Yarn** Ji Hwan Moon and Seon Jeong Kim; Hanyang University, Korea (the Republic of)

Inertial sensors are devices that can monitor inertial movements like linear acceleration and angular motions, in various applications such as industrial and human monitoring. For wearable and portable applications, inertial sensors are better to be self-powered and miniaturized. Here, we developed a self-powered inertial sensor with various applications having high accuracy based on carbon nanotube (CNT) yarn. Our inertial sensor can sense and monitor inertial movements without any external power by harvesting the mechanical energy to electric energy by the coiled CNT yarn. For applications, the sensor can monitor practical kinds of inertial movements, such as impact energy, vibrations, tilting, and body motions such as walking, running, jump and squatting motions. These results suggest that the self-powered inertial sensor shows the advantages of portable and wearable application in industrial and human motion monitoring system.

<gdiv></gdiv><gdiv></gdiv>

#### **F.NM03.09.83**

**Formation of Nanosheets via Unfurling of Vanadate Nanoscrolls from Bulk Vanadium Oxide** Md Shahidul Islam Khan<sup>1</sup> and John B. Wiley<sup>1,2</sup>; <sup>1</sup>The University of New Orleans, United States; <sup>2</sup>Advanced Materials Research Institute, United States

Vanadium oxide materials are renowned for their catalytic properties, super-capacitance, chemical sensing, and high energy density cathodic properties. A two-step synthesis method was applied to obtain 2D structures of vanadium oxide (V<sub>2</sub>O<sub>5</sub>) or vanadate (V<sub>2-x</sub>O<sub>5-x</sub>) nanosheets from bulk V<sub>2</sub>O<sub>5</sub> where the first step involved the formation of vanadate nanoscrolls, 1D structures, that resulted from the dissociation of layered vanadium oxide. In the second step, the nanoscrolls were unfurled to obtain nanosheets, 2D materials. This latter step can be performed using a wet chemical process or annealing treatment. During the wet chemical process, vanadate nanoscrolls turn into thin-layered vanadate nanosheets, and with the annealing process, thin-layered vanadium oxide nanosheets are produced. The formation of these different types of nanosheets was confirmed by X-ray diffraction. Nanosheets obtained from the wet process showed the presence of organic groups that were detected using FTIR and Raman spectroscopy. Both the vanadate and vanadium oxide nanosheets were single or multilayered but only the latter one possesses irregular hexagonal shape which was confirmed through TEM.

#### **F.NM03.09.84**

**Self-Assembly of Tetra-Peptides on Surfaces of Two-Dimensional Materials** Wei Luo, CHEN CHEN and Yuhei Hayamizu; Tokyo Institute of Technology, Japan

As the novel “bottom-up” strategy for fabricating nanomaterials, molecular self-assembly has attracted considerable attention worldwide. On one hand, two-dimensional (2D) materials such as graphite and molybdenum disulfide (MoS<sub>2</sub>) have been demonstrated as the platform for this self-assembly due to their unique electrical, optical properties, and atomically flat surfaces, etc. [1,2]. On the other hand, amphiphilic peptides with both of the hydrophobic and hydrophilic nature also have already been used as ideal building blocks for forming various sophisticated self-assembling materials with certain applications. Therefore, in order to functionalize the 2D material surface by peptides self-assembly, it is necessary for a deliberate understanding of the interaction between biomolecules and 2D substrate materials [3].

Molecular dynamics (MD) simulation provides insight into the molecular-scale structure detail of interface. Several works have been done on solid surface to understand the role of peptides, like on Au (111) for self-assembly [4] or on calcite for biomineralization [5]. More recently, peptides on graphene [6] or MoS<sub>2</sub> [7] have been studied because of the atomically flat surface and some progress in experiments exhibiting the molecular resolution morphology. From these, aromatic amino and charged amino acids are considered to have a meaningful interaction with those surfaces. Although the peptide-peptide interaction is also important for surface self-assembly of peptides, the understanding for both interpeptides and peptide-surface interactions are still limited.

In this work, we aim to utilize computational approaches to understand the molecular mechanism. For this purpose, we started with a tetrapeptide consisting of aromatic and charged amino acids, where these amino acids may play a role for the self-assembly. We performed the molecular dynamics simulation (MD) starting with single tetrapeptide on graphene surface. From this calculation, we obtained the most stable tetrapeptide structure on graphene surface. Analyses of center-of-mass distance between peptide and graphene surface, angle change of aromatic rings, and free energy distribution revealed that the balance between interpeptide and peptide-surface is a key to have a well assembled peptides on surface. Furthermore, information about binding process for tetrapeptide on 2D surface was also obtained. This work can be a foundation for building a conformation-property relation of amphiphilic tetrapeptide self-assembly on 2D material surfaces.

#### Reference:

- [1] Li P, Sakuma K, Tsuchiya S, et al. ACS applied materials & interfaces, 2019.
- [2] Chen J, Zhu E, Liu J, et al. Science, 2018, 362(6419): 1135-1139.
- [3] Qiu F, Chen Y, Tang C, et al. International journal of nanomedicine, 2018, 13: 5003.
- [4] Braun, R, Sarikaya, M, Schulten, K, Journal of Biomaterials Science, Polymer Edition, 2002, 12, 747-757.
- [5] Mingjun Yand, P. Mark Rodger, John H. Harding & S.L.S, Molecular Simulation, 2009, 35:7, 547-553.
- [6] Hughes, Z E; Walsh, T R, Journal of Materials Chemistry B, 2015, 3, 3211–3221.
- [7] Huang C, Libo L, Tao Z, et al, J. Phys. Chem. C 2018, 122, 4, 2070–2080.

#### F.NM03.09.85

**Formation of Various Cross-Linked Gel Layer Around Single-Walled Carbon Nanotubes** Tsuyohiko Fujigaya<sup>1,2,3</sup> and Yukiko Nagai<sup>1</sup>; <sup>1</sup>Kyushu University, Japan; <sup>2</sup>Center for Molecular System, Kyushu University, Japan; <sup>3</sup>International Institute for Carbon-Neutral Energy Research, Kyushu University, Japan

Single-walled carbon nanotubes (SWNTs) have unique near-infrared (NIR) absorption and NIR photoemission that are attractive for in vivo biological applications such as photothermal cancer treatment and imaging. Therefore, a smart functionalization strategy for SWNTs to create biocompatible surfaces and introduce various ligands to target cancer cells without losing their unique optical properties of the SWNTs is strongly required. We developed novel coating technique of SWNTs inspired by emulsion polymerization method, in which the micelle dispersion of SWNT was used for free radical polymerization. In the dispersion, polymerization takes place in the surfactant micelle having SWNT in the core. Thus the SWNTs were coated by polymer layer. When the cross-linker was added, the SWNTs were coated by gel layer, offering the highly stable coating of SWNT

We have revealed the requirement for the formation of the thin cross-linked polymer-wrapped SWNTs, in which the use of monomers that can undergo polymerization inside the micelles was important. In our study, such hybrids were formed when using various monomers in aqueous SDS dispersions of the SWNTs in the presence of APS and BIS as the initiator and cross-linker, respectively in high yeild (>75%) except acryl amide and hydroxymethyl methacrylate. The present study provides useful insight into preparing many polymer-SWNT hybrids with designed functions due to the wide availability of the monomers.

#### F.NM03.09.86

**Investigation of Electrocharging-Assisted Fabrication Parameters for Nanocarbon-Al Composites with Improved Electrical Conductivity and Tensile Strength** Madeline Morales<sup>1,2</sup>, Xiaoxiao Ge<sup>1</sup>, Christopher Klingshirn<sup>1</sup>, Christopher Shumeyko<sup>2</sup>, Daniel P. Cole<sup>3</sup> and Lourdes G. Salamanca-Riba<sup>1</sup>; <sup>1</sup>University of Maryland, United States; <sup>2</sup>US CCDC Army Research Laboratory, Vehicle Technology Directorate, United States; <sup>3</sup>US CCDC Army Research Laboratory, Army

Research Office, United States

Nanocarbon-metal composites are sought after for their excellent mechanical, electrical and thermal properties. Electrocharging-assisted processing of a novel class of materials, called “covetics,” presents a practical option for macroscale production of nanocarbon-metal composites. This process incorporates carbon on the order of several weight percent in metals such as Al and Cu where carbon solubility is in the low ppm range. Increased tensile strength and electrical conductivity have been measured in Al covetics; however, there is limited understanding of the electrocharging-assisted process and subsequently high variability in measured properties among trials. It has been found that under the influence of a high direct current applied to the molten metal, the activated carbon precursor is converted to  $sp^2$  graphitic carbon with increased crystallite size, as measured by the Tuinstra-Koenig relation for Raman spectra. Electrical conductivity is also enhanced in areas that show increased graphitic carbon crystallite size. A series of experiments varying applied current have been carried out to understand the effect of current density on carbon crystallization rate and size of reaction volume within the Al-1350 melt where carbon crystallization occurs. Local electromechanical behavior is measured by nanoindentation and AFM to gain insight into the structure-property relationship at the nanoscale, which can be used to further inform optimization of the electrocharging-assisted process.

Funded by DOE-EERE grant DE-EE0008313. Sponsored by the Army Research Laboratory under Cooperative Agreement W911NF-19-2-0291.

#### **F.NM03.09.87**

**Direct *In Situ* Observation of Toughening and Fatigue Behavior in Alumina/Graphene Nanocomposites** Qizhong Wang<sup>1</sup>, Cristina Ramirez<sup>2</sup> and Nitin Padture<sup>1</sup>; <sup>1</sup>Brown University, United States; <sup>2</sup>Instituto de Cerámica y Vidrio, Spain

There is growing interest in using 2D graphene-related reinforcements to toughen brittle ceramics in nanocomposites. However, there is a lack of fundamental understanding of the toughening mechanisms and microstructural effects in such nanocomposites. To address this paucity, fully-dense nanocomposites of aluminum oxide ( $Al_2O_3$ ) matrix and reduced graphene-oxide (rGO) reinforcements (~5 vol%) of different average-thicknesses and orientations are fabricated and characterized. The interactions between stably propagating cracks and rGO in the  $Al_2O_3$ /rGO nanocomposites are observed *in situ* inside a scanning electron microscope (SEM). Toughening by pullout of thick rGO in the crack-tip wake in the cross-section orientation is found to be the most effective, which is consistent with the highest fracture toughness ( $K_{IC} \sim 6.7$  MPa.m<sup>0.5</sup>) measured in those  $Al_2O_3$ /rGO nanocomposites. Interestingly, while achieving stable crack growth for flat punch compression of notched samples, we found that upon unloading and reloading, the intact rGO crack-bridges appear to crinkle and uncrinkle without a remnant crease, respectively, which is a unique deformation property of multi-layer graphene-like materials. Information extracted accompanied by the Raman spectroscopy studies has permitted to have a deeper understanding of the fatigue resistance mechanisms in this novel material. This is unlike conventional ceramic composites toughened by fibers or whiskers which have poor cyclic fatigue resistance due to the degradation of the crack-wake bridging and pointing to a possible new cyclic-fatigue resistance mechanism in the nanocomposites. The results from this study have implications for the creation of high-toughness, fatigue-resistant, and wear-resistant graphene-reinforced ceramic nanocomposites of the future.

#### **F.NM03.09.89**

**Effects of Electrical Image Forces on Salt Dissolved in Water** Jeffrey B. Sokoloff<sup>1,2</sup> and Andy Lau<sup>2</sup>; <sup>1</sup>Northeastern University, United States; <sup>2</sup>Florida Atlantic University, United States

Onsager and Samara have shown that electrical image charge forces acting on ions dissolved in water can explain the observed increase of the surface tension due to the presence of dissolved ions. Electrical image charge forces at the interface of a salt solution and air are repulsive, but at the interface between the salt solution and a dielectric of higher dielectric constant than that of the solution or a metal, in contrast, the force is attractive. It has also recently been shown that electrical image forces may play a role in the attraction of ions to the electrodes in capacitive desalination, and to play an important role in the freezing of a confined room temperature ionic liquid. Here, the effect of electrical image forces on the distribution of salt ions in a solution that is in contact with a metallic or dielectric surface is considered. It is shown that in the case of either a metallic or dielectric surface, the salt ion concentration near the surface can be very large, raising the possibility that this could result in precipitation of the salt. In fact, solidification of ionic liquids near a metallic surface with which they are in contact has been observed. Concentration of ions near a metallic surface could be used to desalinate salt water by pushing the salt water between an array of parallel plates of a conducting material. Graphene would be an excellent coating for these plates because the friction between flowing water and graphene is known to be extremely small. In order to support our prediction of a high ionic concentration near metallic and dielectric surfaces, we have performed a variational calculation of



the grand canonical partition function to lowest order in the ion density, which is the Debye-Huckel approximation. This calculation supports our conclusion. Our calculation also confirms the concentration dependence of the surface tension found by Onsager and Samarasa in the small salt concentration limit.

#### F.NM03.09.90

**Detection of Limonene Using Graphene Field Effect Transistor Modified by Self-Assembling Peptide** Chishu Homma<sup>1</sup>, Hironaga Noguchi<sup>1</sup>, Yoshiaki Sugizaki<sup>2</sup>, Atsunobu Isobayashi<sup>2</sup> and Yuhei Hayamizu<sup>1</sup>; <sup>1</sup>Tokyo Institute of Technology, Japan; <sup>2</sup>Toshiba Corporation, Japan

Graphene, a representative two-dimensional material, has excellent electronic properties due to its high mobility and specific surface area. Biosensors based on graphene field-effect transistor (GFET) are expected to be applied in various fields such as medical diagnosis, environmental monitoring, and security management. A number of studies on biosensors using GFET have been carried out so far. The surface functionalization with probe molecules is crucial, which gives a high affinity to the target molecule. In this process, covalent bonding and  $\pi$ - $\pi$  interaction have been used to immobilize probe molecules to the surface. However, there are two disadvantages with these detection methods. Firstly, chemical modifications may degrade inherent electronic properties of graphene. Secondly, random adsorption of probe molecules on the surface may result in loss of the probe activity. These lead to a decrease in sensitivity as a sensor.

So far, there have been various demonstration of GFET biosensors reported. The target of the biosensors have been living cells, virus, DNA, and proteins. There is a still challenge here to detect relatively small molecules. These small molecules have low molecular weight and generally do not have a polarization. GFET-based biosensors have a drawback for these small molecules, because the detection mechanism depends on the Coulombic interaction between trapped molecules and graphene. In addition, most of the small molecules are volatile and insoluble. Therefore, in aqueous solutions, it is very difficult to detect volatile molecules dissolved in small amounts. This is also one of the challenges for biosensors.

To solve these problems, we suggest an alternative surface modification method using peptide self-assembly. Peptides are known to recognize crystalline structures of inorganic material surfaces and form uniform structures through interactions among molecules [1]. These peptides are physically adsorbed to the surface. Thus, the surface can be modified without losing their intrinsic electronic properties. These self-assembly of peptides has been demonstrated on gold, boron nitride (BN), transition metal chalcogenides, and graphene in previous studies. The self-assembly of peptides have potential as a scaffold domain for biosensors [2]. In this study, we aimed to develop a new technique to detect an odor molecule, which is relatively small and volatile. For this sake, we utilized rationally designed peptides as a molecular scaffold [3] and probe peptides on graphene surface. Then, we performed odor sensing with limonene, a representative molecule for the smell of lemons. We successfully detected limonene with high sensitivity. We also found that the sensitivity to limonene was altered by the amino acid sequence of the probe domain.

This work was supported by the Cabinet Office (CAO), Cross-ministerial Strategic Innovation Promotion Program (SIP), “An intelligent knowledge processing infrastructure, integrating physical and virtual domains” (funding agency: NEDO).

[1] Y. Hayamizu, C. So, S. Dag et al.; *Scientific Reports*, 2016, 6, 1-9

[2] D. Khatayevich, T. Page, C. Gresswell et al.; *Small*, 2014, 10, 8, 1505-1513

[3] P. Li, K. Sakuma, S. Tsuchiya et al. *ACS Appl. Mater. Interfaces*, 2019, 11, 20670–20677

#### F.NM03.09.91

**Direct Measurements of Tensile Properties and Current-Carrying Capacity of 14 cm-Tall Few-Walled CNT Forest** Tatsuhiko Hayashi<sup>1</sup>, Takayuki Nakano<sup>1</sup>, Hisashi Sugime<sup>2</sup>, Suguru Noda<sup>2,2</sup> and Yoku Inoue<sup>1</sup>; <sup>1</sup>Shizuoka University, Japan; <sup>2</sup>Waseda University, Japan

We have clarified the tensile properties and electron transport capacity properties of macro-sized continuous crystal few-walled CNT forests, which have a height of 14 cm. The present CNT is the highest forest ever reported. The CNT was grown by a CVD method using a Fe-Gd catalyst on Al oxide support [1]. The crystal structures of CNT were evaluated by SEM, TEM, and Raman measurements. Then, the bundle taken out from the CNT forest was converted to a cylindrical structure to define a cross-sectional area and weight density. The cylindrical specimens were tailored by passing through a pinhole with a diameter of 30-100  $\mu\text{m}$ . The reshaped CNT bundle enables to measure tensile tests and electrical measurements by the conventional methods for macroscale specimen. From tensile measurements, it was found that the nominal tensile strength and Young's modulus of the individual CNT were 0.59 GPa and 48 GPa, respectively. This nominal tensile property was obtained by using the entire cross-sectional area, including the inner hole space of the tubular structure for calculation. These results are comparable with reported values, which were measured on various types of CNT by the microscopic methods, and it is lower than theoretical values. The difference between the theoretical and the experimental results is because the present extremely long bundle includes a large number of crystal defects. Also, bundling of millions of CNTs induces further

weakening of tensile properties compared to those of micro-sized single CNTs. As for the electrical properties, conductivity and the current-carrying capacity, ampacity, were 140 S/cm and 6700 A/cm<sup>2</sup>, respectively. These properties were improved significantly by heat treatment at 2800°C in Ar, up to 340 S/cm and 8800 A/cm<sup>2</sup>, respectively. These results correspond to the specific conductivity of 1560 S\*cm<sup>2</sup>/g and ampacity per CNT of 5.2×10<sup>4</sup> A/cm<sup>2</sup>. The ampacity of our CNT was as high as that of commercially available Cu wire (5.8×10<sup>4</sup> A/cm<sup>2</sup>).

[1] Hisashi Sugime, Toshihiro Sato, Rei Nakagawa, Cinzia Cepek, and Suguru Noda, ACS Nano **13**, 13208-13216, 2019.

#### **F.NM03.09.92**

#### **Copper Oxide Nanocrystals Catalyzed Growth of Nanospheres, Solid and Hollow Carbon Spheres in Thermally Stressed Jet A-1** Pooja Sharma Parihar; Indian Institute of Science, India

Aviation turbine fuel, Jet A-1 contains trace metals that catalyze carbonaceous nanostructures formation and their transformation to carbon spheres in the liquid phase at low temperature (190 °C) by flask tests. Thermal stressing of Jet A-1 produced nanospheres, solid and hollow carbon spheres in this work, which is consistent and continuation of a previous study [1]. Focus of the current study is to identify the trace metallic compounds that catalyze the growth of spherical nanoparticles and carbon spheres in thermally stressed Jet A-1. In the previous study [1], however, the formation of carbon spheres by self-assembly was observed, and their characterization was conducted. Heteroatoms and trace metals are precursors to the deposit formation in the thermally stressed jet fuel [2, 3]. The presence of trace metals and heteroatoms in the Jet A-1 deposits is validated by transmission electron microscopy (TEM), energy dispersive x-ray spectroscopy (EDS), scanning transmission electron microscopy (STEM) and high-angle annular dark-field (HAADF), and high-resolution transmission electron microscopic (HRTEM) micrographs. Heteroatomic species were also recorded by Fourier transform infrared (FTIR) spectroscopy. Trace metal copper oxide nanocrystals (CuO and Cu<sub>2</sub>O) were identified by HRTEM and selected area electron diffraction (SAED) analysis. TEM EDS spectra provided the ratio of Cu and O; Cu to O ratio approximately 1:1 and 2:1. Indexing of the polycrystalline SAED pattern generated the d-values corresponding with copper oxides nanoparticles. Copper oxides nanocrystals as constituents of spherical particles were confirmed by comparing the measured d-values and calculated Miller indices (h k l) for copper oxides with i) ICSD database and, ii) simulated diffraction pattern of the Cu<sub>2</sub>O, CuO by Crystal Maker software. Furthermore, structure elucidation of Fe and S nanocrystals is in progress and can suggest the effect of trace metal catalysts on the spherical nanoparticles, and carbon spheres formation in the thermally stressed kerosene type fuel.

Keywords: Jet A-1, copper oxide, trace metals, carbon spheres, nanostructures

#### References

1. P. Sharma et al, Formation of hollow and solid carbon spheres in thermally stressed jet fuel in the low temperature autoxidation regime, Chem. Engg. Sci, 206(2009), 335-347.
2. Robert N. Hazlett, Thermal Oxidative Stability of Aviation Turbine Fuels, ASTM, 1991.
3. P. Sharma, Spectroscopic analysis of Jet A-1 heteroatomic components, Chem. Engg. Sci, 207(2009), 588-599.

#### **F.NM03.09.93**

#### **Structural Analyses of Single Walled Carbon Nanotubes Obtained by Highdensity Plasma Chemical Vapor Deposition** Ronaldo D. Mansano and Ana Paula M. Mansano; University of São Paolo, Brazil

Carbon nanotubes have been an important subject of many recent studies owing to their possible potential applications in nano-scale technologies. Carbon nanotubes can be described as fiber like structures consisting of concentric graphite sheets nested along their long axis and extending to several micrometers. Single-walled carbon nanotubes (SWNTs) can be either metallic or semiconductors depending on the diameter and chirality . All the synthetic methods can be roughly categorized into three groups: the carbon arc-discharge method, laser vaporization of a graphite electrode and chemical methods . In this work, carbon nanotubes were obtained by chemical vapor deposition using high-density plasma processes. Structural studies of carbon nanotubes have relied heavily on Raman spectroscopy. Raman spectroscopy is an analytical technique largely used for characterization of different carbon based materials, either graphite-like or diamond-like. The great versatility of carbon materials rises from the strong dependence of their physical properties on the ratio of sp<sup>2</sup> (graphite-like) to sp<sup>3</sup> (diamond-like bonds). Raman spectroscopy of carbon nanotubes has attracted a lot of attention in recent years, both theoretically and experimentally. Theoretically, it is possible to predict morphological characteristics such as the diameter of the tubes or their conductance properties, especially of single wall carbon nanotubes. Experimentally, it is a powerful method for determining

the degree of structural ordering or presence of contaminants [3]. In the Raman spectra of graphite and SWCNTs, there are many features that can be identified with specific phonon modes and with specific Raman scattering processes that contribute to each feature. The Raman spectra of SWCNTs can provide us much information about the exceptional 1D properties of carbon materials, such as their phonon structure and their electronic structure, as well as information about sample imperfections (defects). Raman spectra provide much general information about the structure and properties of SWNTs. The Radial Breathing Mode (RBM) is a unique phonon mode, appearing only in carbon nanotubes and its observation in the Raman spectrum provides direct evidence that a sample contains SWNTs. The RBM is a bond-stretching out-of-plane phonon mode for which all the carbon atoms move coherently in the radial direction, and whose frequency  $\omega_{\text{RBM}}$  is about 100-500  $\text{cm}^{-1}$ .

The results obtained with the Raman spectroscopy have been compared with the results obtained by Fourier Transformed Infrared (FTIR) spectroscopy, and by Scanning Electronic Microscopy (SEM). The results obtained by these technical analyzes confirm the deposition of single-walled carbon nanotubes with metallic features by high-density plasma chemical vapor deposition.

The results obtained in this work, show the possibility to obtain higher aligned single-walled carbon nanotubes deposited at room temperature by HDPCVD. In this way, it was necessary the increase of the surface energy, that promotes the nano-structuration of the carbon materials, using diamond powder as a seed. It was observed the presence of carbon nanotubes and other kinds of nano-structures of carbon. The results obtained by SEM, Raman spectroscopy and Fourier Transformed Infrared spectroscopy FTIR, compared the carbon nanotubes bundles and "islands" of amorphous carbon materials and, due the different of surface energy promoted by the precursor.

#### **F.NM03.09.94**

**Hydrophobic Properties of Nano-Structured Carbon Films Obtained with Alumina Ceramic Powder** Ronaldo D. Mansano, Ana Paula M. Mansano and Nelson Ordonez; University of São Paulo, Brazil

In this work, we have obtained nano-structured carbon films using ceramic powder (alumina) as seed and pure methane plasmas. The nano-structured carbon films were obtained using a high density plasma chemical vapour deposition system. The present study demonstrates the creation of hydrophobic surface using the nano-scale roughness inherent in high-aligned carbon nanotubes forest, when we used alumina as precursor material. The hydrophobic properties of the nano-structured carbon films were analyzed by Atomic Force Microscope (AFM), Scanning Electron Microscope (SEM) and Contact Angle Measurements (drop shape method), and the structural properties of the nano-films were analyzed by Far-FTIR.

The high-density plasma chemical vapour deposition (HDPCVD) system uses a new conception on plasma generation: a planar coil coupled in a RF system and an electrostatic shield for plasma densification. In this mode, are obtained high-density plasmas and for the ion acceleration we have used another RF system on planar configuration. The substrates used to deposit the films were 75 mm diameter silicon wafers, 380  $\mu\text{m}$  thick and orientation (100). They were submitted to a Piranha clean, followed by a diluted HF dip, before the modification of the surface. The alumina ceramic powder presence promotes the increase of the surface energy of the silicon wafers. In this case, nano-structures are formed. Before the films deposition, alumina ceramic powder was deposited on the silicon wafers by spinner (1000 rpm, 30 sec.). The alumina powder dispersion was made in acid solution. We have used different final deposition times (30 min, 1h, 2h, 3h, 4h and 5h). After preparation of the sample, the DLC films were deposited. The parameters of the DLC films depositions were: 15 mTorr, 250 W (coil power, RF, 13.56 MHz, remote plasma), 40 sccm (methane).

The hydrophobic properties of the nano-structured carbon films were analyzed by Atomic Force Microscope (AFM), Scanning Electron Microscope (SEM) and Contact Angle Measurements (drop shape method), and the structural properties of the nano-films were analyzed by Far-FTIR. High-density plasma is quite for the growth of good quality nano-structured carbon films. But the properties of these films are largely dependent on the deposition conditions. The roughness of the nano-structured carbon films is important, in this situation, because it is affected by surface topography and the hydrophobic properties of these nano-materials.

The surface morphologies of the nano-structured carbon films obtained with alumina powder varied with the final time of deposition process. When the final time is increased, the atoms fill the holes and are accumulated around the islands (formed by the filled holes) and the roughness decreases. This effect promotes the reduction of the surface energy and the hydrophobicity of these films increases too. For longer deposition time, the atoms cover every nano-islands and the spaces between one island and another, forming a continuous film (for deposition time of 4 hours, the roughness was 40 nm). In this way, we noticed that the contact angle measurements showed that nano-structured carbon films obtained using alumina as precursor materials obtained for longer deposition time, showed more super hydrophobicity effect

#### **F.NM03.09.95**

**Self-Assembled Peptides for Suppression of Non-Specific Binding of Biomolecules on Graphene** Mirano Tsukiiwa,

Yasuaki Nakata, Hironaga Noguchi, Chishu Homma and Yuhei Hayamizu; Tokyo Institute of Technology, Japan

Graphene is suitable for an active layer for biosensors with high-sensitivity because of their fascinating electrical properties with atomically-flat surface and high specific surface area. Biomolecular immobilization on the active layer of biosensing devices is of vital importance for the functionality, such as sensing with biomolecular probes and protecting from unnecessary unspecific adsorption of biomolecules. However, the immobilization by chemical bonding will introduce atomic defects for graphene, which influences its intrinsic properties to some extent. Self-assembled peptide can be a good candidate. Specific peptides spontaneously form ordered structures through non-covalent intermolecular interactions on the surface of graphene without losing the intrinsic electrical properties of the materials.[1][2][3] On the other hand, non-specific adsorption of biomolecule causes a background noise and decrease the sensing ability of a bio-probe. Therefore, the suppression of nonspecific adsorption is an important issue for the realization of high-performance biosensors. To solve these problems, in this research, we designed new self-assembled peptides and evaluated their performance, aiming at construction of surfaces with the anti-fouling property. The designed peptides consisted of three main domains. (1) antifouling domain: hydrophilic and zwitterionic, which is effective in reducing protein non-specific adsorption. The hydrophilic groups are known to form a hydration layer and create a physical energy barrier that prevents adsorption. (2) Peptide-to-peptide interaction domain: inspired by fibroin, a protein of silk thread. The repetitive sequences of glycine (G) and alanine (A) are introduced. Here we expect the formation of a strong and stable peptide monolayer derived from the  $\beta$ -sheet structure.[2] (3) Anchoring domain: electrons in tyrosine are expected to help to have a stacking of the aromatic ring with the surface of two-dimensional materials. The aqueous solution was placed on the surface of graphite to form a self-assembled film of peptides. The surface structure of these samples was characterized using atomic force microscopy (AFM). We found that peptides had a tendency coverage with increasing concentration. The peptide structure had a six-fold symmetry, which is same as one of underlying graphene lattice. The hydrophilic properties of the peptide film were characterized using contact angle measurements. Furthermore, the antifouling performance was evaluated by AFM and graphene field effect transistors (GFETs). It showed that the adsorption of proteins was greatly inhibited. The peptide offer to be a new molecular scaffold for sensitive graphene biosensors.

## Reference

- [1] Hayamizu, Yuhei, et al. "Bioelectronic interfaces by spontaneously organized peptides on 2D atomic single layer materials." *Scientific reports* 6 (2016): 33778.
- [2] Li, Peiying, et al. "Fibroin-like peptides self-assembling on two-dimensional materials as a molecular scaffold for potential biosensing." *ACS applied materials & interfaces* 11.23 (2019): 20670-20677.
- [3] Sun, Linhao, et al. "Water stability of self-assembled peptide nanostructures for sequential formation of two-dimensional interstitial patterns on layered materials." *RSC advances* 6.99 (2016): 96889-96897.

## F.NM03.09.97

**Nonlocal and Nonlinear Optical Response in Guided Nanoribbon Plasmons** [Alvaro Rodriguez Echarrí](#)<sup>1</sup>, Javier Garcia de Abajo<sup>1,2</sup> and Joel Cox<sup>3,4</sup>; <sup>1</sup>ICFO - The institute of Photonic Sciences, Spain; <sup>2</sup>ICREA – Institució Catalana de Recerca i Estudis Avançats, Spain; <sup>3</sup>Center for Nano Optics, University of Southern Denmark, Denmark; <sup>4</sup>Danish Institute for Advanced Study, University of Southern Denmark, Denmark

Electrically-doped graphene supports highly-confined and actively-tunable plasmons that exhibit lower losses than their conventional noble metal counterparts, positioning the atomically-thin carbon layer as an ideal active ingredient in nanophotonic devices. These appealing properties are maintained in nanostructured graphene, which is emerging as a promising candidate for the excitation and guiding of propagating plasmons in future optoelectronic circuitry. Here we employ realistic quantum-mechanical simulations to describe the nonlocal optical response associated with highly-confined propagating plasmons in graphene nanoribbons, accounting for quantum finite-size and edge-termination effects in their electronic band structure. In addition to strong nonlocal effects manifesting in the linear dynamics of plasmons moving in the direction of transverse symmetry, we observe a stronger dependence on quantum finite-size effects in the nonlinear optical response, which involves additional transitions among the quantized electronic Bloch states. We further explore the breaking of inversion symmetry that occurs for optical excitation with large in-plane optical momenta along the transverse direction of the ribbon and reveal that even-ordered nonlinear optical processes such as a second-harmonic generation can occur with remarkably-high efficiency when enhanced by plasmonic resonances. These findings suggest possibilities to exploit the active tunability of graphene to engineer interactions among individual quantized propagating plasmons supported by 1-D nanoribbons.

## F.NM03.09.101

**Single-Walled Carbon Nanotube Growth from Ir Catalysts by Alcohol Gas Source Method** Takahiro Maruyama, Takuya Okada, Takahiro Saida and Shigeya Naritsuka; Meijo University, Japan

Single-walled carbon nanotubes (SWCNTs) have been anticipated for applications in a lot of future nanodevices. However, there still remain several problems for realizing the SWCNT devices, and one of the most significant issues is high-yield growth of semiconducting SWCNTs. So far, to grow SWCNTs with high-yield, Al<sub>2</sub>O<sub>3</sub> buffer layers are widely used, because they prevent migration of catalysts on the substrate surface at growth temperature and aggregation of catalyst particles are suppressed [1]. In this study, we attempted to grow SWCNTs using Ir catalysts without Al<sub>2</sub>O<sub>3</sub> buffer layers, which have never been used as catalysts in SWCNT growth.

After deposition of Ir catalysts on SiO<sub>2</sub>/Si substrates, SWCNT growth was carried out using alcohol gas source method in a high vacuum [2]. Growth Temperature and growth time were set at 800°C and 1 h, respectively. The ethanol pressure was varied between 1×10<sup>-3</sup> and 1×10<sup>-1</sup> Pa. The grown SWCNTs were characterized by FE-SEM, TEM and Raman spectroscopy. SEM and Raman results showed that, as the ethanol pressure increased, the SWCNT yield became higher and the SWCNT diameter became narrower. When the ethanol pressure was 1×10<sup>-1</sup> Pa, high-density vertically aligned SWCNTs were grown, whose lengths were about 2 μm. Raman measurement showed that SWCNT diameter were distributed between 0.8 and 1.1 nm. Our results indicated that Ir catalysts are effective to obtain high-density vertically aligned and small diameter SWCNTs using no Al<sub>2</sub>O<sub>3</sub> buffer layers.

[1] K. Hata et al. Science 306 (2004) 1362.

[2] T. Maruyama et al. Carbon 116 (2017) 128.

**F.NM03.09.105**

**Organophilicity of Graphene Oxide for Enhanced Wettability of ZnO Nanowires** Pavan Emani<sup>1</sup>, Hisham A. Maddah<sup>1</sup>, Arjun Rangoonwala<sup>1</sup>, Songwei Che<sup>1</sup>, Dieter Gruen<sup>2</sup>, Vikas Berry<sup>1</sup> and Sanjay K. Behura<sup>1</sup>; <sup>1</sup>University of Illinois at Chicago, United States; <sup>2</sup>Dimerond Technologies, United States

Interfacing two-dimensional graphene oxide (2D GO) platelets with one-dimensional zinc oxide nanowires (1D ZnO) would create mixed-dimensional heterostructures suitable for modern optoelectronic devices. However, there remains a lack in understanding of interfacial chemistry and wettability in GO-on-ZnO heterostructures. Here, we propose a hydroxyl-based dissociation-exchange mechanism to understand interfacial interactions responsible for GO adsorption onto ZnO hydrophobic substrates. The proposed mechanism would allow us to overcome the poor wettability of the super-hydrophobic ZnO surface (with contact angle 140.5°) to GO, from the dispersion of GO suspension with various organic media prior to drop-casting of GO on the ZnO. The addition of different classes of organics into the relatively high pH GO suspension with a volumetric ratio of 1:3 (organic-to-GO) is believed to introduce free radicals (OH and COOH), which consequently result in enhancing adhesion (chemisorption) between ZnO nanowires and GO platelets. The wettability study shows as high as 75% reduction in contact angle ( $\theta = 35.5^\circ$ ) when the GO suspension is mixed with alcohols (e.g. ethanol) prior to interfacing ZnO nanowires. The proposed method brings forth a scalable tool for developing graphene-coated-ZnO heterojunctions for photovoltaics, photocatalysis, biosensors, and UV detectors.

**F.NM03.09.109**

**Late News: Application of Starch-Derived Graphene Quantum Dot Embedded Carbon Aerogel as Efficient Catalyst in Proton Exchange Membrane Fuel Cell** Eric J. Kim and Sunil Sharma; Stony Brook University, The State University of New York, United States

Proton Exchange Membrane Fuel Cells (PEMFC) are considered to be one of the most promising clean energy sources to mitigate the global crisis of climate change and air pollution. However, its dependence on expensive catalyst materials with low durability, such as platinum, prevent this technology from being widely commercialized. In this study, we present the application of a metal-free starch-derived graphene quantum dot (GQD) supported on highly porous carbon aerogel (GQD/CA) in PEMFC to overcome these technical barriers. Structural, morphological, and crystalline features of GQDs and GQD/CA are analyzed using HRTEM, TEM, AFM, and XRD. Further electrochemical characteristics are investigated using cyclic voltammetry (CV), CO-stripping, ORR polarization, and fuel cell testing. Additionally, the durability of the catalyst is measured using the DOE2020 accelerated stress test (AST). The TEM imaging shows the small size and uniformity of GQDs, which allows for an even distribution of GQDs onto the support and a higher electrochemical surface area (ECSA). The presence of functional groups on GQD is shown to improve ORR performance by up to 10 times compared to platinum. In addition, the structural integrity of both GQD and CA create a synergistic effect to prevent the agglomeration of particles during AST. As a result, compared to a commercial standard catalyst, platinum supported on carbon black (Pt/CB), GQD/CA shows significantly higher electrocatalytic activity, with up to 220% increase in ECSA and 1432% increase in peak power density. After 30,000 cycles of AST testing, GQD/CA is shown to retain 92.9% of its ECSA, 97.1 % of its specific activity,

and 98.4% of its mass activity. Thus, GQD/CA is demonstrated to be a highly efficient, durable, and economical catalyst for PEMFCs to mitigate the ever-present effects of climate change and air pollution.

#### F.NM03.09.110

##### **Late News: A Green Graphene-Based Ink for Artworks—Toward a Green Chemistry in Synthesis of**

**Graphene** Sepidar Sayyar, Jo Law, Agnieszka Golda, Helen McGregor, Aaron Burton and Gordon Wallace; University of Wollongong, Australia

Climate change is a major threat to the future of our planet and its inhabitants, and there is no doubt that human activities have been the dominant contributor. Scientists can play an important role in mitigating these contributing factors by utilising green approaches in manufacturing and developing eco-friendly materials in different fields. This work presents how our interdisciplinary collaborative research team, consisting of contemporary artists, a materials scientist, and a climate scientist, promote environmental sustainability through the development of 'green' materials and techniques. The aim of the project is to develop a graphene-based ink through a green chemistry/engineering approach and use the ink to create conductive screen-printed e-textile artworks that communicate climate science. Graphene is a unique two-dimensional carbon structure with excellent electrical, thermal and mechanical properties that make it ideal candidate for a variety of applications<sup>1,2</sup>. However, converting graphene to a processable material involves hazardous chemical reactions using toxic materials<sup>3</sup>. We developed a graphene-based ink without using any hazardous or toxic chemicals through a facile mechanical exfoliation method. The viscosity of the ink is easily tunable owing to its thermos-sensitive nature, which makes it a suitable material for screen-printing. The ink is used to screen-print electrically conductive patterns for the e-textile art works. The results of the phase 1 of the project were exhibited at the Museum of Applied Arts and Science in Sydney and attracted over 26,000 visitors. Preliminary experiments demonstrated that this material is a suitable candidate for developing sustainable sewable smart electronics.

#### F.NM03.09.111

**Late News: Multibit Optoelectronic Memory Using Graphene/Diamond (carbon sp<sup>2</sup>-sp<sup>3</sup>) Heterojunctions** Kenji Ueda, Y. Mizuno and Y. Ito; Nagoya University, Japan

Recently, interfaces between graphene and diamond (carbon sp<sup>2</sup>-sp<sup>3</sup> interfaces) has attracted much attention because the carbon sp<sup>2</sup>-sp<sup>3</sup> interfaces become sources of various interesting physical phenomena and novel functions. Although there are many interesting theoretical predictions on the interfaces, experimental results regarding the electronic properties of such interfaces have rarely been reported. More recently, we found that vertically aligned graphene (carbon nanowalls: CNW)/diamond heterojunctions, that is, C sp<sup>2</sup>-sp<sup>3</sup> interfaces became photo-controllable memristors [1], which are optically controllable memory-resistors with nonvolatile memory and switching functions. One of the most important application of the photo-controllable memristors is thought to be optoelectronic memory, which possess both photo-sensing and data storage function.

In this study, we show the CNW/diamond heterojunctions can be used as multibit optoelectronic memories, where light information stores as multilevel resistance in nonvolatile manner [2].

CNW were formed on B-doped diamond semiconductors in-situ by using microwave plasma CVD apparatus [1, 3]. Junctions using the CNW/diamond heterostructures were fabricated (area: 40-160 μm φ) and their current-voltage (*I-V*) characteristics were measured at room temperature in air, with or without photo-irradiation by using visible LED.

In the Raman spectrum of the CNW on diamond, four major peaks, which are characteristic of vertically aligned graphene, were observed: G, 2D, D' and D peaks, in addition to the diamond related peak (Dia.) at 1332 cm<sup>-1</sup>. A SEM image of the CNW/diamond surface showed numerous wall-like structures, which also suggested formation of CNW on diamond. The transmission electron microscope (TEM) image of the interface of the CNW/diamond bilayers indicates that CNW with good crystallinity and clear interfaces were formed on the diamond semiconductors. These Raman, SEM and TEM results suggest CNW/diamond heterostructures with sharp interfaces were successfully formed. The CNW/diamond junctions exhibited hysteretic I-V behaviors. The resistance of the junctions was changed to low or high resistance states by the light irradiation with bias voltage application and the resistance states was maintained in nonvolatile manner. The mechanism for the photoconductive change is considered to be originated from oxidation-reduction of the CNW and/or CNW-diamond interfaces through the movement of oxygen ions by bias with photo-irradiation. The CNW/diamond junctions also show apparent response to optical pulses. The output current, that is, conductivity was increased (or decreased) step-by-step in proportion to the number of optical pulses under positive (or negative) bias. The number of levels and heights of the current steps can be controlled by changing optical pulse intensity, pulse width, bias voltage, etc. To determine the relationship between output current and applied pulse numbers precisely, multiple (~10) optical pulses (38 μW/cm<sup>2</sup>, 30 ms, 1 Hz) were applied to the junctions. The output current, that is, conductance increased linearly from 2 nA to 142 nA in response to the total optical pulse numbers from 1 to 10. The linear relationship between the number of optical pulses (*n*) and the output

current [ $I(n)$  (nA)] can be expressed as " $I(n) = 14.26 * n + 2.27$ ". Application of one optical pulse induces current increase of  $\sim 14$  nA. This means that the junctions are also used as optical computing-memory devices with arithmetic functions such as counting, addition, and subtraction. These results indicate the CNW/diamond heterojunctions are capable of multibit optoelectronic devices, where light information is stored as multilevel resistance in nonvolatile manner and the stored information is processed immediately.

Ref.:

[1] K. Ueda et al., J. Mater. Res. 34 (2019) 626.

[2] K. Ueda et al., Appl. Phys. Lett. 117 (2020) 092103.

[3] K. Ueda et al., Dia. Rel. Mater., 38 (2013) 41.

#### F.NM03.09.112

##### **Late News: Preparation of Large Surface Area Nanocarbon from Cellulose Nanocrystals and Its Carbonization**

**Mechanism** Jung-Eun Lee, Hyejin Ju, Min Jeong Kim, Ga-Hyeun Lee and Han Gi Chae; Ulsan National Institute of Science and Technology, Korea (the Republic of)

In the recent time, the biomass-derived carbon materials have attracted attention for application to energy storage and battery devices based on the abundant resources, low cost, and sustainability of precursors. Among them, cellulose nanocrystal (CNC), which can be obtained from the removal of amorphous region of cellulose materials by acid hydrolysis, is regarded as promising carbon precursor. Its high crystallinity (54-88%) compared to other conventional cellulose causes high mechanical integrity, high thermal stability, and the formation of more developed carbon crystallites after carbonization. Although it is prerequisite to thoroughly define the carbonization mechanism of CNC for use in a variety of applications, however, there is still an insufficient research. In particular, only speculations have been reported about the interesting phenomenon that the CNC often shows a graphitic phase at a low carbonization temperature of 1000 °C, unlike carbonized cellulose. Therefore, in the current study, we dried the CNCs by spray-freeze-drying method and carbonized them in the range of 1000-2500 °C. They showed interconnected fibrillar morphology and large surface area of 265.2 m<sup>2</sup>/g after carbonization at 2500 °C, which is favorable to use as a carbon nanofiller, purification, or catalyst support. In addition, the different behavior between amorphous and crystalline region of cellulose materials was thoroughly analyzed based on HRTEM, Raman, WAXD, and MD simulation results. The current study will not only open the new application of CNC-based nanocarbons but provide in-depth mechanism of carbonization of cellulosic materials.

#### F.NM03.09.113

##### **Late News: Effect of Cellulose Nanocrystal(CNC) on Polyacrylonitrile(PAN) Polymer Chain Structure in the**

**PAN/CNC Fibers Prepared Through an *In Situ* Polymerization** Hyejin Ju, Jung-Eun Lee, Min Jeong Kim and Han Gi Chae; Ulsan National Institute of Science and Technology, Korea (the Republic of)

In-situ polymerization of polyacrylonitrile (PAN) polymer in the presence of cellulose nanocrystal (CNC) is conducted to produce CNC reinforced PAN nanocomposite fibers for high-performance carbon fiber. Cellulose is the most abundant organic material available on earth, therefore it can be an environmentally sustainable resource for producing carbon materials and carbon fiber. Also, CNC is useful for the reinforcing agent in nanocomposite materials due to its excellent properties such as high crystallinity and mechanical properties.

In the current study, there are two main effects 1) CNC into the nanocomposite fiber and 2) the impact of in-situ polymerization. We have conducted the thorough characterizations of CNC dispersion and radical polymerization of PAN polymer in the presence of about 1.5 wt% CNC. In-situ PAN/CNC nanocomposite fiber was produced by the dry-jet wet spinning method right after the polymerization was terminated.

From the mechanical and crystal orientation measurement, CNC is able to affect improving polymer chain orientation through interaction between PAN and hydroxyl groups of CNC. Furthermore, as the in-situ PAN/CNC nanocomposite solution is used directly without any removing PAN polymer with low molecular weight, it is supposed that they can act as plasticizers during the fiber spinning and affect the polymer chain structure transition during the heat-treatment process. Besides, using thermal analyses, the heat treatment conditions of precursor fiber have been set for manufacturing CNC reinforced high-performance carbon fiber. And the evolution of the structure from polymer chain to the graphite form during the stabilization and carbonization in the presence of CNC has been investigated.

#### F.NM03.09.114

##### **Late News: A Thin, Flexible, Highly Sensitive Ultrasonic Sensor Based on Polydopamine@Hybrid Carbon**

**Nanofillers/Polyvinylidene Fluoride Nanocomposites** Zengsheng Weng and Fangxin Zou; Hong Kong Polytechnic University, Hong Kong

Sensors that are thin and flexible and are yet highly sensitive to small deformations have become considerably crucial to a number of high-value-added applications such as wearable electronics, human machine interface, and condition monitoring of high-stake engineering structures. In recent years, these sensors have been undergoing rapid advancement owing to the development of low-dimensional nanomaterials. In particular, by optimizing the synthesis process, it is even possible to fabricate nanocomposite strain sensors that can be used to probe high-frequency, microscopic vibrations generated by ultrasonic waves. In fact, ultrasonic wave is one of the most widely used diagnostic means for *in situ* assessments of structural integrity.

The tunnelling effect and the piezoresistive effect are the main physics principles that allow nanocomposite strain sensors to acquire ultrasonic waves. When a sensor is impinged by ultrasonic waves, the conductive nanofillers inside the sensor will undergo high-frequency micro-vibrations. Such vibrations will cause the inherent electrical resistances of the nanofillers to fluctuate and the distances between adjacent nanofillers to vary, eventually resulting in changes in the overall electrical resistance of the sensor. However, the sensitivity of the existing nanocomposite strain sensors to ultrasonic waves is still far from satisfactory.

There are two main reasons behind the limited sensitivity. One is that the agglomeration of nanofillers or the poor capacitive compatibility between nanofillers and polymer matrices results in poor dispersion of nanofillers inside nanocomposite structures. The other is the lack of effective tunnelling nodes who is not conducive to the tunneling effect.

In this work, we fabricated a highly sensitive nanocomposite sensor for acquiring high-frequency micro-vibrations generated by ultrasonic waves, from polydopamine(PDA)-coated hybrid carbon nanofillers. First, multi-walled carbon nanotubes (MWCNTs) were coated by 10s nm thick viscous PDA to improve their compatibility with polyvinylidene fluoride (PVDF) substrates. The PDA nanolayers on MWCNTs do not only act as a dispersed phase that reduces the entanglement of MWCNTs, but also serves as the buffer layers between MWCNTs and PVDF matrices, helping to improve the responsiveness of the sensors to ultrasonic waves. Compared to uncoated MWCNTs, the use of 15 wt.% PDA-coated MWCNTs led to a 40% increase in sensitivity. Then, one-dimensional PDA@MWCNTs were mixed with two-dimensional single-layer graphene to enhance the geometric contact between nanofillers. Compared with the use of nanofillers of a single dimensionality, the mixing of nanofillers of different dimensionalities can effectively increase the number of tunneling nodes within a unit volume in a nanostructure. As the mass fraction of graphene within the hybrid nanofillers expanded from 33% to 66%, the sensitivity of the proposed sensor improved by approximately 120%, surpassing that of pure graphene sensors, which had been reported to possess the highest sensitivity to ultrasonic waves. The superior sensitivity of the proposed sensor, which actually utilizes a lower graphene content, was shown to be derived from the synergy between the two types of nanofillers which are of different dimensionalities.

Overall, we put forward new strategy for optimizing the sensitivity of nanocomposite strain sensors to high-frequency micro-vibrations. The feasibility of the idea has been validated by a series of experiments that encompass both material characterizations and measurements of ultrasonic signals.

#### **F.NM03.09.115**

**Late News: Enhanced Heavy Metals Removal Using a New Buckypaper Membrane Containing MWCNTs and Two Biopolymers—Chitosan and Carrageenan** Sara S. Alnasser, Afnan Alharbi, Ahmed Alshahrani and Bandar alOtaibi; KACST, Saudi Arabia

Due to the current global water crisis, wastewater treatment requires considerable attention and development. Dissolved heavy metals in water trigger serious alerts and can have lethal effects on various components of the environment including water resources, soil, plants, animals, and can also be threatening the health of human beings. In this study, we addressed the issue by introducing novel Buckypaper membranes that were fabricated using a combination of biopolymers (i.e., chitosan and carrageenan) and multi-walled carbon nanotubes (MWCNTs). Three dispersions of MWCNTs with chitosan, carrageenan, and chitosan-carrageenan with 0.1% v/w were prepared using vacuum filtration. The removal of six heavy metals (i.e., cobalt, nickel, copper, cadmium, barium, and lead) was investigated in this study. The water permeability and the removal of heavy metals were evaluated using a dead-end (DE) filtration system. Heavy metals removal was studied at pH 7 and under a range of varying applied pressures (1 to 6 bar). At an applied pressure of 1 bar, the removal of lead and copper by the MWCNTs/carrageenan membrane reached 99% and 88%, respectively. However, MWCNTs/carrageenan membrane was found to be fragile. Nevertheless, adding chitosan to carrageenan had significantly improved the mechanical strength of the membrane while sustain the excellent removal properties of the heavy metals. That is, MWCNT/chitosan-carrageenan membrane significantly exceeds MWCNTs/carrageenan membrane in tensile strength, tensile strain and young's modules by 400%, 17%, and 6%, respectively. On the other hand, the MWCNTs/chitosan membrane showed a high water permeate flux that reached up to 200 L/h.m<sup>2</sup>. Also, the electrical conductivity of all membranes varied from 37 S/CM to 57 S/CM. Additional characterization techniques on the three membranes were conducted in this study as well.



### F.NM03.09.116

**Late News: Multifunctional MoS<sub>2</sub>-Supported Nanocomposites for Water Decontamination** Kfir Shapira and Ines Zucker; Tel-Aviv University, Israel

Pollution of drinking water sources by a variety of inorganic compounds has created a need to develop more efficacious removal technologies to ensure contaminant-free and clean water. Conventional methods for water decontamination involve physicochemical separation and chemical oxidation. Yet, physicochemical separation lacks pollutant selectivity and produces toxic waste streams,<sup>1</sup> while chemical oxidation requires intensive energy and chemical inputs and may form transformation byproducts.<sup>2</sup>

Nanotechnology-based approaches are increasingly explored as an alternative for decontamination methods. Many new technologies leverage the reactive and tunable properties of nanomaterials for increased cost-efficiency, selectivity toward priority pollutants and energy/chemical sustainability.<sup>3</sup> Through manipulation of material size, morphology, and chemical structure, nanomaterials can have exceptional adsorptive and catalytic properties for water decontamination.

Molybdenum disulfide (MoS<sub>2</sub>) nanosheets stand out as a promising advanced-material for water decontamination. MoS<sub>2</sub> act as an efficient and selective adsorbent for the removal of heavy metal ions (e.g., Hg<sup>2+</sup> and Ag<sup>+</sup>) through strong Lewis acid and base soft-soft interactions with sulfur atoms in MoS<sub>2</sub>. Affixing MoS<sub>2</sub> nanosheets onto a platform is essential minimize risk of nanomaterial release into the environment. In the context of nano-assisted water treatment technologies, affixing nanomaterials onto *active* platforms such as granular activated carbon media may enable multifunctional decontamination. Activated carbon is the predominant adsorbent used widely in water treatment today, due to its high affinity for organic pollutant adsorption, but lack affinity to inorganics. MoS<sub>2</sub> affixed onto activated carbon, enhances overall decontamination performance by enabling simultaneous adsorption of organic and inorganic pollutants.

In this research, we examined the tunable water decontamination capabilities of MoS<sub>2</sub> nanosheets grown on activated carbon (MoS<sub>2</sub>@AC) in a hydrothermal method for the adsorption of organic (methylene blue) and inorganic (mercury) contamination from water. In a batch experiments, we demonstrated the high mercuric adsorption potential of MoS<sub>2</sub>@AC (~2000 mg Hg/g MoS<sub>2</sub>) in the absence and presence methylene blue. Furthermore, methylene blue was removed in similar rates by MoS<sub>2</sub>@AC and pristine AC. These results suggest that while MoS<sub>2</sub> is active and enable the removal of mercury, its presence does not interrupt the activated carbon activity. Moreover, we will investigate the practical application of this nanocomposite by evaluating the effect of background ions on the mercuric adsorption capacity. We also assess the nanomaterial leaching during operation in various conditions to demonstrate the reuse capabilities and to assure safe and durable use. Overall, results from this study provide a proof-of-concept for water treatment enhancement by 2D nanomaterials.

#### Bibliography

1. Drewes, J. E., Reinhard, M. & Fox, P. Comparing microfiltration-reverse osmosis and soil-aquifer treatment for indirect potable reuse of water. *Water Res.* **37**, 3612–21 (2003).
2. Hübner, U., von Gunten, U. & Jekel, M. Evaluation of the persistence of transformation products from ozonation of trace organic compounds – A critical review. *Water Res.* **68**, 150–170 (2015).
3. Bhaduri, B. *et al.* Dual functionality of an Ag-Fe<sub>3</sub>O<sub>4</sub>-carbon nanotube composite material: Catalytic reduction and antibacterial activity. *J. Environ. Chem. Eng.* **6**, 4103–4113 (2018).

### F.NM03.09.118

**Late News: Carbon Nanotube Field-Effect Transistor Model for a Wide Temperature Range** Junsung Park and Michael Shur; Rensselaer Polytechnic Institute, United States

The carbon nanotube field-effect transistor (CNT FET) has been intensively studied due to the high mobility and large current carrying capacity, thus considered as a promising material for nano-scale electronics. For the commercialization of the CNT FETs, the accurate and reliable model is an essential requirement. Especially, transport characteristics of the CNT FETs at high temperature (>300K) is crucially important since the CNT FETs typically operate at elevated temperature. We now report on an improved compact model of the CNT FET. The model is based on the unified charge control model (UCCM) suitable for implementation in standard computer-aided design (CAD) environment such as SPICE. The model accurately describes the current-voltage characteristics for all operation regimes over a wide range of temperatures from 295 to 523K. The model accounts for the temperature and bias effects on the threshold voltage and mobility as the key metrics impacting the CNT FET's performance. It reproduces the mobility, subthreshold swing, on- and off-state current, and threshold voltage behavior as functions of the operating temperature. The model is validated by comparison with the experimental data for the CNT FET reported earlier. The model applications include the device design, characterization, large scale simulation, and parameter extraction of the CNT-based devices and integrated circuits.

### F.NM03.09.119

**Late News: Laser Peening Enhances Tribological Resistance of Electrodeposited Cr Coatings Reinforced with Yttria Stabilized Zirconia and Carbon Nanotubes** Pragya Tripathi, Kantesh Balani and Janakarajan Ramkumar; Indian Institute of Technology, India

Laser shock peening is performed on chromium based electrochemical coatings consisting of 3 mol% yttria stabilized zirconia nanoparticles (YSZ) and carbon nanotubes (CNT) as reinforcements, deposited on steel substrate as a suitable strategy to further enhance mechanical and tribological properties of protective coatings. Coated Cr has shown an increased hardness after laser peening from  $\sim 8$  GPa to  $\sim 9.4$  GPa, whereas, upto 26 GPa hardness is obtained for Cr-YSZ-CNT coating. Increased hardness might be accredited to high compressive stresses, ranging up to  $\sim 1757$  MPa, induced as a result of laser peening. Synergistically reinforced with YSZ and CNT after laser peening treatment, minimum wear rate of  $\sim 1.8 \times 10^{-5}$  mm<sup>3</sup>/Nm by fretting wear test is recorded in the Cr matrix, which is concomitant with maximum dislocation density of  $\sim 3.0 \times 10^{16}$  m<sup>-2</sup>. An overall improvement in mechanical and tribological properties i.e. low wear constant of the order of  $10^{-6}$  is achieved, out of which Cr-YSZ-CNT outperformed the other coating systems. Addition of YSZ strengthens the Cr matrix, whereas, multi-functionality of CNT provides with lubrication along with matrix strengthening as well as bridging effect to crack propagation. Therefore, synergistic effect of two reinforcements (YSZ, CNT) in Cr matrix combined with the laser peening treatment lead to superior properties of the coating (Cr-YSZ-CNT) capable enough of limiting the problems of wear and erosion.

### F.NM03.09.120

**Late News: Graphene-Protein Adhesion Interactions are Influenced by Substrate Properties** Eleanor L. Brightbill, Katherine Young, Hilena F. Gezahagne, Decarle S. Jin, Bryce Hitchcock and Eric M. Vogel; Georgia Institute of Technology, United States

A wealth of studies utilizing graphene to sense biomolecules (such as glucose, DNA, Concanavalin A) across different sensing modalities (such as surface plasmon resonance, redox, field effect transistor) have been published due to graphene's unique properties including high surface area and conductivity. However, in any sensor device where graphene interacts with a biofluid, the graphene must be supported by some underlying substrate. Moreover, previous studies indicate that the substrate can influence graphene's properties, where substrate hydrophilicity can affect graphene's water contact angle and substrate polarity can affect the success of epitaxial growth through a graphene layer. Despite this, little to no work has been completed describing how the substrate support effects the graphene-biological solution interaction.

In this study, *ex situ* protein adsorption is measured via ellipsometry and X-ray photoelectron spectroscopy (XPS) of model small (Lysozyme), medium (Bovine Serum Albumin, BSA), and large (Fibrinogen) proteins on substrates with a variety of hydrophobicity and surface polarity with and without a transferred graphene monolayer. Additionally, we investigate the *in situ* adhesion of lysozyme on Si and Au substrates with and without transferred graphene via quartz crystal microbalance with dissipation (QCM-D) to monitor kinetic differences in attachment. Fully coalesced graphene was synthesized via Chemical Vapor Deposition and transferred onto various substrates using a wet transfer process and PMMA scaffold.

*Ex-situ* ellipsometry and XPS results reveal that the impact of the substrate on protein attachment to graphene depends on the protein studied. The largest model protein, Fibrinogen, shows a similar level of attachment across all 4 substrates regardless of the presence of graphene. Lysozyme, the smallest model protein, shows a difference in adsorption only when a graphene monolayer is added to non-polar substrates. The adsorption of BSA, the intermediate size protein, is influenced strongly by substrate hydrophilicity, where less adsorption is observed on more hydrophilic substrates with or without the presence of graphene. Overall, a more hydrophobic substrate leads to a larger amount of adsorption to graphene.

*In-situ* QCM-D results show that not only the equilibrium attachment, but also the kinetics of interaction, can be affected by the substrate. Modeling the attachment of lysozyme to graphene on Au and Si substrates indicates that the appropriate kinetic model may be determined by the substrate even in cases where differences in absolute adsorption are observed, further indicating that support substrates have a significant effect on protein adsorption behavior to graphene.

This work indicates that the substrate of a graphene-based biosensor is an important but currently overlooked parameter when understanding and optimizing the performance of the device. The *ex-situ* ellipsometry and XPS analysis of protein attachment indicates that the substrate can have a profound impact on protein-graphene interactions, to the extent that twice the BSA attachment to graphene is observed when graphene is supported by TaN rather than Si. The level of non-selective protein adsorption on graphene can be independently engineered through modifying the support substrate without directly modifying the graphene itself.

### F.NM03.09.121

**Late News: Electrochemical Cathodic Exfoliation of Graphite into Graphene in Aqueous Solutions of Alkali Metal Salts** Md Habibullah Dalal, Chong-Yong Lee and Gordon Wallace; University Wollongong, Australia

Electrochemical exfoliation has emerged as a green, effective and scalable route to mass production of graphene.[1] The use of reductive cathodic exfoliation of graphite, offers a direct production of high quality and low defect graphene.[2] However, cathodic exfoliation protocols reported to date use organic solvents in which often requires extended intercalation time, and post-treatment to further exfoliate the intercalated graphene layers.[3] In contrast, the employment of environmentally friendly aqueous-based electrolytes, coupling with a shorter exfoliation period would be attractive features of any new protocol. Here, we demonstrate for the first time, efficient cathodic electrochemical exfoliation of graphite to graphene in aqueous electrolytes using common and inexpensive alkali-metal salts such as KCl. The key to exfoliate graphite successfully in aqueous electrolyte is applying a sufficiently high voltage, and a high salt concentration which facilitates hydrated cationic intercalation, and promotes hydrogen evolution to exfoliate the graphene. The cathodic exfoliated graphene produced using KCl electrolyte exhibits a low defect density ( $I_D/I_G$  of 0.06, a C/O ratio of 57.8), high graphite exfoliation yield (>80%) in short time (< 10 mins for 1 cm<sup>2</sup> electrodes) and the highly conductive 6 to 7 layers graphene sheets served as an excellent support materials for electrocatalytic reactions. This environment-benign aqueous-based cathodic electrochemical graphite exfoliation approach opens a new opportunity in large-scale and low cost production of high quality graphene.

#### References

- [1] S. Yang, M. R. Lohe, K. Müllen and X. Feng, *Adv. Mater.*, 29 (2016) 6213-6221.
- [2] A. M. Abdelkader, A. J. Cooper, R. A. W. Dryfe and I. A. Kinloch, *Nanoscale*, 16 (2015) 6944-6956.
- [3] A. J. Cooper, N. R. Wilson, I. A. Kinloch and R. A. W. Dryfe, *Carbon*, 66 (2014) 340-350.

### F.NM03.09.122

**Late News: Nanoporous Free-Standing SWCNT Films** Radovan Kukobat, Dragana Stevic and Katsumi Kaneko; Shinshu University, Japan

Nanoporous free-standing SWCNT films are essential for understanding porosity of these films which should be promising for catalyst supports and supercapacitors. The SWCNTs form networks of randomly distributed SWCNTs, giving materials such as transparent thin films and free-standing films. The transparent thin films of SWCNTs form two dimensional porous networks of randomly oriented SWCNTs whose pore sizes vary from micropores to mesopores, according to the SEM and TEM observation. On the other hand, porosity of the free-standing SWCNT films is not straightforward because the micropores and mesopores are hidden in the three-dimensional structures of these films. We use nitrogen adsorption at 77 K to characterize porosity of the free-standing SWCNT films. The nitrogen adsorption isotherm shows a prominent hysteresis loop over the wide relative pressure range of  $\sim 10^{-3}$  to  $\sim 1$ , which we assigned to the presence of ultramicropores of < 0.7 nm. These ultramicropores were open during ultrasonication treatment of the SWCNTs prior to the free-standing film fabrication. The ultramicropores are evidenced as defects on SWCNTs using Raman spectroscopy. The D- and G-band ratio increases from pristine SWCNTs of 0.04 to SWCNTs of free-standing films of 0.11. The surface area increases from pristine SWCNTs of 320 and 280 m<sup>2</sup>/g (BET and *as*) to free-standing SWCNT film of 605 and 590 m<sup>2</sup>/g (BET and *as*). Micropore volume increases from pristine SWCNTs to free-standing SWCNT film from 0.06 to 0.18 cm<sup>3</sup>/g, respectively. High surface area of the free-standing SWCNT films is assigned to the ultramicropores. Also, the free-standing SWCNT film is composed of mesopores created by entangling of SWCNTs in the network as observed with SEM and TEM. Understanding porosity of the free-standing SWCNT films is important for developing the SWCNT electrodes of desired porosity and surface area for the electrochemical applications.

### F.NM03.09.123

**Late News: Effects of Water and Different Solutes on Carbon-Nanotube Low-Voltage Field-Effect Transistors** Raphael Pfattner<sup>1,2</sup>, Amir M. Foudeh<sup>1</sup>, Shiheng Lu<sup>1,3</sup>, Nicola S. Kubzdela<sup>1</sup>, Theodore Gao<sup>1</sup>, Ting Lei<sup>1,4</sup> and Zhenan Bao<sup>1</sup>; <sup>1</sup>Stanford University, United States; <sup>2</sup>Materials Science Institute of Barcelona (ICMAB-CSIC), Spain; <sup>3</sup>Duke University, United States; <sup>4</sup>Peking University, China

Semiconducting single-walled carbon nanotubes (swCNTs) are a promising class of materials for emerging applications. In particular, they are demonstrated to possess excellent biosensing capabilities, and are poised to address existing challenges in sensor reliability, sensitivity, and selectivity.<sup>[1,2]</sup> Functionalized and pristine individual CNTs have shown high sensitivity and

selectivity down to the single molecule level.<sup>[3,4]</sup> However, single CNT devices are challenging to make and characterize compared to CNT networks which add further complexity due to inter-CNT contacts. Such systems may not be as sensitive or selective compared to single CNT devices, but may be a cost-effective alternative for particular environments.

Here, we report on the characteristics of single-walled carbon nanotube (swCNT) networks exposed directly to aqueous solutions containing different solutes.<sup>[1]</sup> This was made possible by employing a solid-state dielectric poly(vinylidene fluoride-co-hexafluoropropylene) (ePVDF-HFP), which has been demonstrated to be compatible with swCNTs and also enables low-voltage field-effect transistor (FET) operation.<sup>[5,6]</sup>

These devices exhibit small device-to-device variation as well as high current output at low voltages (<0.5 V), making them compatible with most physiological liquids. Using this platform, the swCNT devices are directly exposed to aqueous solutions containing different solutes to characterize their effects on FET current–voltage (FET I–V) characteristics. Clear deviation from ideal characteristics is observed when swCNTs are directly contacted by water.

Such changes are attributed to strong interactions between water molecules and sp<sup>2</sup>-hybridized carbon structures. Selective response to Hg<sup>2+</sup> is discussed along with reversible pH effect using two distinct device geometries. Additionally, the influence of aqueous ammonium/ammonia in direct contact with the swCNTs is investigated. Understanding the FET I–V characteristics of low-voltage swCNT FETs may provide insights for future development of stable, reliable, and selective biosensor systems.

[1] A. M. Foudeh, R. Pfattner, S. Lu, N. S. Kubzdelo, T. Z. Gao, T. Lei, Z. Bao, *Small* 2020, 16, 2002875.

[2] V. Schroeder, S. Savagatrup, M. He, S. Lin, T. M. Swager, *Chem. Rev.*, 2019, 119, 599.

[3] S. Sorgenfrei, C.-Y. Chiu, R. L. Gonzalez, Y.-J. Yu, P. Kim, C. Nuckolls, K. L. Shepard, *Nat. Nanotechnol.*, 2011, 6, 126.

[4] J. Chaste, A. Eichler, J. Moser, G. Ceballos, R. Rurali, A. Bachtold, *Nat. Nanotechnol.*, 2012, 7, 301.

[5] C. Wang, W.-Y. Lee, D. Kong, R. Pfattner, G. Schweicher, R. Nakajima, C. Lu, J. Mei, T. H. Lee, H.-C. Wu, J. Lopez, Y. Diao, X. Gu, S. Himmelberger, W. Niu, J. R. Matthews, M. He, A. Salleo, Y. Nishi, Z. Bao, *Sci. Rep.*, 2015, 5, 17849.

[6] R. Pfattner, A. M. Foudeh, C. Liong, L. Bettinson, A. C. Hinckley, D. Kong, Z. Bao, *Adv. Electron. Mater.*, 2018, 4, 1700326.

#### F.NM03.09.124

**Late News: Bifacial Float Transfer of Multilayer Graphene** [Joseph Andrade](#)<sup>1</sup>, Jan Folkson<sup>1</sup>, Mohamed Boukhicha<sup>2</sup>, Amanda Carr<sup>1</sup> and Matthew Eisaman<sup>1</sup>; <sup>1</sup>Stony Brook University, The State University of New York, United States; <sup>2</sup>Brookhaven National Laboratory, United States

We present a method for graphene transfer we refer to as “bifacial transfer” that allows transfer of multilayer chemical vapor deposition (CVD) graphene from both sides of a native metal substrate, such as an as-received nickel catalyst. In traditional transfer methods, the graphene on the “non-preferred” side, i.e. the bottom of the substrate, is removed with oxygen plasma before removal of the metal catalyst in etchant solution. Although this treatment prevents undesired aggregation of the graphene films, it fails to utilize both sides of CVD-grown graphene. Our bifacial transfer method reduces the cost of multilayer graphene by allowing the transfer of graphene from both sides of the substrate. After hot-press lamination to a polymer film and a temporary metal etching step, the graphitic films separate cleanly at the air-liquid interface due to an oxide interlayer. We characterize this separation layer and compare the quality of graphene transferred from both sides onto target glass and polymer substrates. The results of optical microscopy, confocal Raman spectroscopy, atomic force microscopy (AFM), and electronic transport measurements suggest that the quality of the multilayer graphene on the “non-preferred” side does not differ significantly from that of the “preferred” side. This method will allow more efficient and cost-effective use of graphene by doubling the usable graphene per area of growth substrate, and by eliminating the need for intermediate sacrificial transfer substrates such as poly(methyl methacrylate), PMMA.

#### F.NM03.09.127

**Late News: Oil Fly Ash-Derived Carbon Nanostructures for Flexible Supercapacitors** Nuha A. Alhebshi<sup>1</sup>, [Haneen S. Alshaikeid](#)<sup>1</sup>, Numan Salah<sup>1</sup> and Husam Alshareef<sup>2</sup>; <sup>1</sup>King Abdulaziz University, Saudi Arabia; <sup>2</sup>King Abdullah University of Science and Technology (KAUST), Saudi Arabia

A variety of innovative designs of wearable electronics require to be powered by energy storage devices such as supercapacitors based on flexible electrodes. One of the current challenges that would delay the implementations of supercapacitors is the high cost of the electrode materials. In this research, Abundant oil fly ash is obtained from a power plant in Jeddah, Saudi Arabia, as a source for the synthesis of carbon nanostructures by sonication (JSON) and carbon nanotubes (CNTs) by chemical vapor deposition [1,2]. These CNTs have diameters around 30-40 nm, few micrometers lengths, and clear zigzagged structures, which are mostly different than the commercial CNTs, as characterized by high

resolution transmission electron microscope. To utilize the promising properties of CNTs in a practical application, flexible supercapacitor electrodes of CNTs have been fabricated on carbon cloth as a current collector in addition to H<sub>2</sub>SO<sub>4</sub> electrolyte, then tested and compared with JSON electrode in terms of cyclic voltammetry, galvanostatic charging-discharging and electrochemical impedance spectroscopy. Interestingly, CNTs electrode exhibits maximum areal and gravimetric capacitances of 77 mF/cm<sup>2</sup> and 55 F/g, respectively, which are one order of magnitude higher than those of JSON electrode. This improvement can be attributed to the smaller size and hence the larger surface area of CNTs than JSON. Moreover, CNTs electrode shows exceedingly small equivalent series resistance and charge transfer resistance ascribing to the good contact of the electrode active materials within the carbon cloth substrate and the electrolyte. In addition, the vertical impedance line in the low frequency range of Nyquist plots indicates an excellent electrolyte ion diffusion into the electrode due to the porosity of CNTs. The successful fabrication of such flexible supercapacitors based on affordable and scalable CNTs would facilitate their cost-effective manufacturing.

#### ACKNOWLEDGMENT

This joint project was co-funded by King Abdulaziz University (KAU), Jeddah, and King Abdullah University of Science and Technology (KAUST), Thuwal, under grant number "JP-19-002". The authors, therefore, acknowledge with thanks KAU & KAUST for their technical and financial support.

#### REFERENCES

- [1] N. A. Salah, *Method of forming carbon nanotubes from carbon-rich fly ash*. US patent Number: 8,609,189 B2 (2013).
- [2] N. Salah, A. A. Al-ghamdi, A. Memic, S. S. Habib, Z. H. Khan, *Formation of carbon nanotubes from carbon rich fly ash: growth parameters and mechanism*. Mater. Manuf. Process 31, 146–156 (2016).

#### F.NM03.09.128

**Late News: Ethylene Glycol Removal Characteristics of 2D Nanoporous h-BN Sheets —Computational Predictions** Nirmalay Barua<sup>1</sup>, Ingrid Padilla Espinosa<sup>2,1</sup> and Ram Mohan<sup>1</sup>; <sup>1</sup>North Carolina A&T State University, United States; <sup>2</sup>University of California, Merced, United States

Hexagonal boron nitride (h-BN) is a new material with potential for applications in electronic devices, tribology, and separation membranes. Limited theoretical and experimental researches have been conducted to explore their efficiency as a desalination membrane. With the recent advancement of their controlled synthesis, researchers have become more interested in exploiting their interaction with organic materials. The purpose of this work is to explore the efficiency and potential of porous h-BN as a separation membrane for ethylene glycol (EG) removal from water. Very few experiments have been previously conducted to assess the capability of porous h-BN for EG or other organic pollutants removal. However, no prior theoretical or computational work that studies the molecular interactions between EG and h-BN has been reported. In this work, a methodological approach to simulate the atomic interactions of h-BN and EG in different pore configurations is proposed and investigated using classical molecular dynamics. Our results exhibit that nanometer-scale pores in single layer h-BN can effectively reject approximately 90% of EG from EG contaminated water. We also report the removal performance of the freestanding porous h-BN sheet as a function of pore diameter and applied pressure.

#### F.NM03.09.129

**Late News: Ionicity-Dependent Separation Property of Graphene Oxide Membrane** Mutsuki Oikawa<sup>1</sup>, Haruka Takeuchi<sup>2</sup>, Zheng-Ming Wang<sup>3</sup> and Setsuko Koura<sup>1</sup>; <sup>1</sup>Chiba Institute of Technology, Japan; <sup>2</sup>Kyoto University, Japan; <sup>3</sup>AIST, Japan

Graphene oxide membrane (GO-M) has recently attracted a great interest because of its potential applications for desalination and for removal of organic matter. The carbon-based GO-M is excellent in chemical resistance, anti-fouling effect, low cost, and so forth as compared to polymer or ceramics membranes. It is known that GO has polar oxygen functional groups and is negatively charged in water, which makes it possible to remove ionic species in water. It has been reported that GO-M shows selective separability toward some neutral solvent molecules. However, its ionicity-based separation property has not yet been sufficiently understood. In this research, we focused on surface charging property of GO-M and examined its separation behaviors toward inorganic ions and organic dyes of different charging properties. It was found that the separation or permeation of inorganic cations by GO-M is dependent on the ionic type and charge number. The rejection ratio can be accounted for by the strength of their electrostatic interaction with the GO surface. GO-M shows good rejection toward anionic dyes but great adsorption toward neutral and cationic dyes, resulting in the blockade of membrane path.

#### F.NM03.09.131

**Late News: Atomistic Study of the Influence of Oxide Shell Layers on the Material Properties of Aluminum Nanowires** Hoang Thien Luu<sup>1</sup>, Yudi Rosandi<sup>2</sup>, Herbert M. Urbassek<sup>3</sup> and Nina Gunkelmann<sup>1</sup>; <sup>1</sup>Clausthal University of Technology, Germany; <sup>2</sup>Universitas Padjadjaran, Indonesia; <sup>3</sup>University of Kaiserslautern, Germany

For materials with high oxygen affinity, oxide layers will significantly change the material properties. At aluminum surfaces, an oxide layer may form in seconds, even under vacuum conditions. Recent studies show that thin amorphous oxide shell layers on aluminum surfaces significantly change the responses of the material. However, the relations between the thickness of the oxidized layer, the temperature and the mechanical response of nanowires have not been investigated intensively. In this study, we use a ReaxFF potential to analyze the influences of oxide shell layers on the material responses of the nanowires under uniaxial loading at different strain rates. We conduct simulations within a wide range of strain rates and temperatures varying between 10K and 500K. The Al-O interface leads to an increased defect nucleation rate at the oxide interface preventing localized deformation.

## SYMPOSIUM F.NM04

---

Material Systems for Manipulating and Controlling Magnetic Skyrmions  
November 21 - December 4, 2020

### Symposium Organizers

Geoffrey Beach, Massachusetts Institute of Technology  
Markus Garst, Karlsruhe Institute of Technology  
Oleg Tretiakov, University of New South Wales  
Xiuzhen Yu, RIKEN

---

\* Invited Paper

SESSION F.NM04.04: Live Keynote I: Material Systems for Manipulating and Controlling Magnetic Skyrmions  
Session Chairs: Markus Garst and Oleg Tretiakov  
Thursday Afternoon, December 3, 2020  
F.NM04

## 6:30 PM INTRODUCTION AND ANNOUNCEMENTS

### 6:35 PM \*F.NM04.01.03

**Skyrmions in Thin-Film Heterostructures** Kang L. Wang<sup>1</sup>, Hao Wu<sup>1</sup>, Ying Ying Wu<sup>1</sup>, Arvin Razavi<sup>1</sup> and Alexander Grutter<sup>2</sup>; <sup>1</sup>University of California, Los Angeles, United States; <sup>2</sup>National Institute of Standards and Technology, United States

Magnetic skyrmions are swirling topological spin textures in either non-centrosymmetric magnetic bulk compounds or thin films resulted from broken inversion symmetry. Their presence is the result of the balance among the Dzyaloshinskii–Moriya interaction, the Heisenberg exchange interaction, magnetic anisotropy, and the Zeeman energy and was first demonstrated in cryogenic temperatures. Skyrmions behave as particles, which can be created, annihilated, and manipulated and can be as small as a few nanometers by careful design of material structures. The study of skyrmions is of great interest as they may be a strong candidate for high density and energy-efficient information storage and processing. In this talk, we will briefly review the requirements for the presence and the establishment of the phase diagram of skyrmions in various thin films. Particularly we will discuss the room-temperature skyrmion phase diagram as affected by DMI, anisotropy, and the Zeeman energy. Because of the interest in applications in logics and memories, there is an increased interest in using electric means, current or voltage, to create and manipulate skyrmions in ferromagnetic and antiferromagnetic thin-film materials platforms. For room-temperature skyrmions, nonuniform current in geometric restrictions was used to create and move skyrmions. We will describe the use of magneto-transport and the Kerr effect to study and image skyrmions, followed by the discussion on the use of neutron scattering, X-ray magnetic dichroism, and others to study the interface magnetism of heterostructures and to understand their creation and annihilation by torques of different origins. The materials platforms to be discussed include

ferromagnetic and antiferromagnetic (AFM) materials. The use of metallic CoFeB/MgO/heavy metal (Ta, W, etc.) was used to demonstrate and image skyrmions. Other examples include topological insulator/AFM (MnTe) heterostructures, which will be described to show the use of the induced exchange bias via interface proximity effect for controlling the topological charge number via field cooling. Structures consisting of antiferromagnetic (AFM) and ferri-magnetic materials (FRM) offer the speed advantage to THz for information propagation in the form of spin and skyrmion current. In this area, we will discuss the exchange coupling of the two sub-lattices of FRM and AFM as revealed from x-ray dichroism and neutron scattering. In particular, the use of insulator heterostructures will be discussed, which have the advantage of having no electrical charge current. The voltage control of perpendicular anisotropy will be discussed to show the creation and annihilation of skyrmions and their dynamics without the use of an applied magnetic field. Lastly, we will discuss the recent progress of 2D materials for skyrmionics and in general for spintronics as 2D materials make possible a wider choice of materials available to experiments. In addition, the 2-D van der Waals gap may offer different interaction characteristics for their presence as well as creation and manipulations under current and voltage drives. The study of skyrmions and anti-skyrmions in analogy with the creation and annihilation of particles and antiparticle may provide a condensed matter platform for studying the particle counterparts.

Supported by ARO, NSF, and DOE.

## 7:25 PM BREAK

### 7:30 PM \*F.NM04.01.01

**Microwave Resonances of Magnetic Skyrmions in Multilayers** Christos Panagopoulos; Nanyang Technological University, Singapore

We report a magnetic resonance study of the chiral multilayer Ir/Fe/Co/Pt hosting Néel skyrmions at room temperature. Employing in-plane ac fields, experiments reveal two distinct resonances of the skyrmion phase with frequencies between 6-12 GHz. Complementary micromagnetic simulations indicate that both resonances exhibit a counterclockwise rotation of the net magnetic dipole moment. Whereas the magnon probability distribution for the lower-frequency resonance is well localized to the skyrmion core, it extends over the inter-skyrmion area for the resonance with higher frequency. The properties of both modes depend sensitively on the interlayer distance due to the dipolar coupling between ferromagnetic layers. Our work reveals the tunability of the resonance response of skyrmions in magnetic architectures over a broadband frequency range, a promising avenue towards tailored microwave applications based on room temperature topological spintronics.

### 7:55 PM \*F.NM04.02.06

**Structures and Dynamics of Spin Textures with Boundaries** Naoto Nagaosa<sup>1,2</sup>, Wataru Koshibae<sup>2</sup> and Jan Masell<sup>2</sup>; <sup>1</sup>University of Tokyo, Japan; <sup>2</sup>RIKEN Center for Emergent Matter Science (CEMS), Japan

Structures and dynamics of spin textures in magnets are the subject of extensive studies, which is a crucial issue also for applications. The structures and their motion in the bulk are rather well understood, but the influence of the boundaries is less studied. In this talk I would focus on the effects of boundaries such as surfaces and edges as revealed by theoretical analysis. It includes (i) the skyrmion string in a thin film with associated topological defects, and (ii) the helix with boundaries. In the former case with an out-of-plane magnetic field, a step edge on the thin film substantially affects the motion of a skyrmion string, leading to its splitting and annihilation. These processes are understood by introducing two types of topological indices, i.e., the bulk monopole number and the surface skyrmion number. For an in-plane magnetic field, on the other hand, several kinds of topological defects are found to appear, which is consistent with the experimental observations. Recently, the helix structure was proposed to show inductance under an ac current. Therefore, the nonlinear dynamics of the helix are an important issue, which we have investigated both by numerical simulations and analytical calculations. It turns out that the role of the boundary is crucial to determine the direction of the wavevector of the helix: There is a 90° difference between periodic boundary condition and open boundary condition, revealing the vital role of the boundary.

## 8:20 PM CLOSING SUMMARY

SESSION F.NM04.05: Live Keynote II: Material Systems for Manipulating and Controlling Magnetic Skyrmions  
Session Chairs: Markus Garst and Oleg Tretiakov

## 11:30 AM INTRODUCTION AND ANNOUNCEMENTS

### 11:35 AM \*F.NM04.02.05

**Chiral Non Collinear Spin Textures** Stuart S. Parkin; Max Planck Institute of Microstructure Physics, Germany

Magnetic non-collinear spin textures that have chiral structures are of great current interest. The same type of Dzyaloshinskii-Moriya (DMI) vector exchange interactions that stabilize chiral Néel domain walls in magnetic multilayers<sup>1-3</sup> results in the formation of topological spin textures in bulk compounds. We recently discovered magnetic *antiskyrmions* in a tetragonal inverse Heusler compound  $\text{Mn}_{1.4}\text{Pt}_{0.9}\text{Pd}_{0.1}\text{Sn}$  using Lorentz transmission electron microscopy (LTEM)<sup>4</sup>. Unlike skyrmions in B20 compounds, that have been extensively studied, the size of the anti-skyrmion can be tuned by varying the thickness of the host material allowing for sizes varying from nanometer to microns in the same material<sup>5</sup>. This is due to long range magneto-dipole interactions that are important in this compound that has a complex DMI interaction with a symmetry that follows the  $D_{2d}$  symmetry of its crystalline structure. The same symmetry ensures that anti-skyrmions are robust to temperature and magnetic field<sup>6</sup>. The magnetic dipole-dipole interactions also allow for the formation of metastable “elliptical skyrmions” in this same material<sup>7</sup>. These have Bloch-like boundaries that we can directly observe using LTEM. Finally, we discuss our recent discovery of novel Néel like skyrmions in a metallic compound that exist almost to room temperature and that are also tunable in size<sup>8</sup>. Chiral spin textures in ferro-, ferri- and anti-ferrimagnetic materials and thin film heterostructures are of fundamental interest with potential for spintronic applications especially Racetrack Memory.

1. Yang, S.-H., Ryu, K.-S. & Parkin, S. S. P. Domain-wall velocities of up to  $750 \text{ ms}^{-1}$  driven by exchange-coupling torque in synthetic antiferromagnets. *Nat. Nano.* **10**, 221-226, (2015).
2. Yang, S.-H., Garg, C. & Parkin, S. Chiral Exchange Drag and Chirality Oscillations in Synthetic Antiferromagnets *Nat. Phys.* **15**, 543–548, (2019).
3. Bläsing, R. *et al.* Exchange coupling torque in ferrimagnetic Co/Gd bilayer maximized near angular momentum compensation temperature. *Nat. Commun.* **9**, 4984, (2018).
4. Nayak, A. K. *et al.* Magnetic antiskyrmions above room temperature in tetragonal Heusler materials. *Nature* **548**, 561-566, (2017).
5. Ma, T. *et al.* Tunable Magnetic Antiskyrmion Size and Helical Period from Nanometers to Micrometers in a  $D_{2d}$  Heusler Compound. *Adv. Mater.*, 2002043, (2020).
6. Saha, R. *et al.* Intrinsic stability of magnetic anti-skyrmions in the tetragonal inverse Heusler compound  $\text{Mn}_{1.4}\text{Pt}_{0.9}\text{Pd}_{0.1}\text{Sn}$  *Nat. Commun.* **10**, 5305, (2019).
7. Jena, J. *et al.* Elliptical Bloch skyrmion chiral twins in an antiskyrmion system. *Nat. Commun.* **11**, 1115, (2020).
8. Srivastava, A. K. *et al.* Observation of Robust Néel Skyrmions in Metallic PtMnGa. *Adv. Mater.* **32**, 1904327, (2020).

### 12:00 PM \*F.NM04.01.02

**Skyrmions in Chiral Magnetic Multilayers** Katharina Zeissler<sup>1</sup>, Simone Finizio<sup>2</sup>, Kowsar Shahbazi<sup>1</sup>, Jamie Massey<sup>1</sup>, Fatma Al Ma'mari<sup>1</sup>, Alexandra Huxtable<sup>1</sup>, David Bracher<sup>2</sup>, Armin Kleibert<sup>2</sup>, Sebastian Wintz<sup>2</sup>, Sina Mayr<sup>2</sup>, Teresa Weßels<sup>3</sup>, Alexandr Sadovnikov<sup>4</sup>, Mark Rosamond<sup>1</sup>, Edmund Linfield<sup>1</sup>, Thomas Moore<sup>1</sup>, Joerg Raabe<sup>2</sup>, Gavin Burnell<sup>1</sup> and Christopher Marrows<sup>1</sup>; <sup>1</sup>University of Leeds, United Kingdom; <sup>2</sup>Paul Scherrer Institut, Switzerland; <sup>3</sup>Forschungszentrum Jülich GmbH, Germany; <sup>4</sup>Saratov State University, Russian Federation

Magnetic skyrmions are topologically-nontrivial spin textures with particle-like properties [1]. Their size, topological stability, and mobility suggest their use in future generations of spintronic devices, the prototype of which is the skyrmion racetrack [2]. To realise a racetrack requires three basic operations: the nucleation (writing), propagation (manipulation), and detection (reading) of a skyrmion, all by electrical means. Here we show that all three are experimental feasible at room temperature in Pt/Co/Ir or Pt/CoB/Ir multilayers in which the different heavy metals above and below the magnetic layer break inversion symmetry and induce chirality by means of the Dzyaloshinskii-Moriya interaction, defining the structure of Néel skyrmion spin textures [3]. We show deterministic nucleation on nanosecond timescales using an electrical point contact on top of the multilayer [4], current-driven propagation along a wire in which the skyrmions are channelled by defects in the multilayer [5], and their detection by means of the Hall effect that reveals an unexpectedly large contribution to the Hall signal that correlates with the topological winding number [6].

[1] N. Nagaosa & Y. Tokura, *Nat. Nanotech.* **8**, 899 (2013).

[2] A. Fert et al. *Nature Nanotech.* **8**, 152 (2013).



- [3] K. Zeissler et al. *Sci. Rep.* **7**, 15125 (2017).  
[4] S. Finizio et al., *Nano Lett.* **19**, 7246 (2019).  
[5] K. Zeissler et al., *Nature Comm.* **11**, 428 (2020)  
[6] K. Zeissler et al. *Nature Nanotech.* **13**, 1161 (2018).

## 12:25 PM BREAK

### 12:30 PM \*F.NM04.02.04

**Magnetic Skyrmions and Hopfions in Three-Dimensional Chiral Magnets** Jiadong Zang; University of New Hampshire, United States

In this talk, various three-dimensional (3D) topological spin textures in magnets without inversion symmetry will be introduced. The first part of the talk features the recent observation of target skyrmions in chiral magnet nanodisks through theory-experiment collaborations. Two types of zero-field target skyrmions are confirmed, and Bloch points are identified during topological transition between different types of target skyrmions. The spectrum of collective spin wave modes in target skyrmions also reveal the 3D nature of spin excitations.

Second part of the talk introduces a very recent work on hopfions in chiral magnetic nanodisk. This is one of the first experimentally feasible prediction on magnetic hopfions. The hopfion in this setup is confirmed by analyzing the linking between any two equal-spin loops and calculating the Hopf invariant. Another topological configuration, the pairing between monopole and anti-monopole, is also identified in the same system. Transition from this state to hopfion, being identical to sphere-torus topological deformation, can be achieved by an external magnetic field. Dynamics of hopfions will also be discussed.

This work is supported by the U.S. Department of Energy (DOE), Office of Science, Basic Energy Sciences (BES) under Award No. de-sc0020221.

### 12:55 PM \*F.NM04.03.02

**Skyrmions—A Playground for Non-Conventional Computing and Phase Transitions in 2D** Mathias Klauui; Johannes Gutenberg University Mainz, Germany

In our information-everywhere society IT is a major player for energy consumption. Novel spintronic devices can play a role in the quest for GreenIT if they are stable and can transport and manipulate spin with low power. Devices have been proposed, where switching by energy-efficient approaches, such as spin-polarized currents is used [1], Firstly, to obtain ultimate stability of states, topological spin structures that emerge due to the Dzyaloshinskii-Moriya interaction (DMI) at structurally asymmetric interfaces, such as chiral domain walls and skyrmions with enhanced topological protection can be used [2-5]. We have investigated in detail their dynamics and find that it is governed by the topology of their spin structures [2]. By designing the materials, we can even obtain a skyrmion lattice phase as the ground state [3].

Secondly, for ultimately efficient spin manipulation, we use spin-orbit torques, that can transfer more than 1hbar per electron by transferring not only spin but also orbital angular momentum. We combine ultimately stable skyrmions with spin orbit torques into a skyrmion racetrack device [3-5], where the real time imaging of the trajectories allows us to quantify the novel skyrmion Hall effect [5,6].

Beyond conventional memory, we furthermore use spin-orbit torque induced skyrmion dynamics for non-conventional stochastic computing applications, where we have developed a skyrmion reshuffler device [6]. Here we use thermal skyrmion motion to implement a key component for stochastic computing [6]. Such thermal skyrmion diffusion can also be controlled by symmetry breaking [7] and this is useful for token – based Brownian computing.

Finally the thermal dynamics of skyrmion quasi-particles lends itself to exploiting this system for the study of phases and phase transitions in 2D. We have studied the transition of skyrmion arrangements from the liquid phase across the hexatic phase unique to 2D systems into the solid phase [8]. These transitions occur in a wide range of skyrmions systems [8,9], thus showing that skyrmions have evolved from an object of study themselves and are now being understood controlled sufficiently well for use as model systems to study exciting statistical physics in 2D.

- [1] Reviews G. Finocchio et al., *J. Phys. D: Appl. Phys.* **49**, 423001 (2016); K. Everschor-Sitte et al., *J. Appl. Phys.* **124**, 240901 (2018).  
[2] F. Büttner et al., *Nature Phys.* **11**, 225 (2015).  
[3] S. Woo et al, *Nature Mater.* **15**, 501 (2016).

- [4] K. Litzius et al., *Nature Phys.* **13**, 170 (2017).  
 [5] K. Litzius et al., *Nature Electron.* **3**, 30 (2020).  
 [6] J. Zazvorka et al., *Nature Nano.* **14**, 658 (2019).  
 [7] N. Kerber et al., arxiv:2004.07976  
 [8] J. Zazvorka et al., arxiv:2004.09244  
 [9] P. Huang et al., arxiv:1807.08352 (*Nature Nano.* (2020)); M. Kläui, *News&Views, Nature Nano.* (2020).

## 1:20 PM CLOSING SUMMARY

SESSION F.NM04.01: Skyrmions in Magnetic Thin Films and Multilayers  
 On Demand Abstracts Available for Viewing Starting Saturday Morning, November 21, 2020  
 F-NM04

### 5:00 AM \*F.NM04.01.01

**Microwave Resonances of Magnetic Skyrmions in Multilayers** Christos Panagopoulos; Nanyang Technological University, Singapore

We report a magnetic resonance study of the chiral multilayer Ir/Fe/Co/Pt hosting Néel skyrmions at room temperature. Employing in-plane ac fields, experiments reveal two distinct resonances of the skyrmion phase with frequencies between 6-12 GHz. Complementary micromagnetic simulations indicate that both resonances exhibit a counterclockwise rotation of the net magnetic dipole moment. Whereas the magnon probability distribution for the lower-frequency resonance is well localized to the skyrmion core, it extends over the inter-skyrmion area for the resonance with higher frequency. The properties of both modes depend sensitively on the interlayer distance due to the dipolar coupling between ferromagnetic layers. Our work reveals the tunability of the resonance response of skyrmions in magnetic architectures over a broadband frequency range, a promising avenue towards tailored microwave applications based on room temperature topological spintronics.

### 5:15 AM \*F.NM04.01.02

**Skyrmions in Chiral Magnetic Multilayers** Katharina Zeissler<sup>1</sup>, Simone Finizio<sup>2</sup>, Kowsar Shahbazi<sup>1</sup>, Jamie Massey<sup>1</sup>, Fatma Al Ma'mari<sup>1</sup>, Alexandra Huxtable<sup>1</sup>, David Bracher<sup>2</sup>, Armin Kleibert<sup>2</sup>, Sebastian Wintz<sup>2</sup>, Sina Mayr<sup>2</sup>, Teresa Weßels<sup>3</sup>, Alexandr Sadovnikov<sup>4</sup>, Mark Rosamond<sup>1</sup>, Edmund Linfield<sup>1</sup>, Thomas Moore<sup>1</sup>, Joerg Raabe<sup>2</sup>, Gavin Burnell<sup>1</sup> and Christopher Marrows<sup>1</sup>; <sup>1</sup>University of Leeds, United Kingdom; <sup>2</sup>Paul Scherrer Institut, Switzerland; <sup>3</sup>Forschungszentrum Jülich GmbH, Germany; <sup>4</sup>Saratov State University, Russian Federation

Magnetic skyrmions are topologically-nontrivial spin textures with particle-like properties [1]. Their size, topological stability, and mobility suggest their use in future generations of spintronic devices, the prototype of which is the skyrmion racetrack [2]. To realise a racetrack requires three basic operations: the nucleation (writing), propagation (manipulation), and detection (reading) of a skyrmion, all by electrical means. Here we show that all three are experimentally feasible at room temperature in Pt/Co/Ir or Pt/CoB/Ir multilayers in which the different heavy metals above and below the magnetic layer break inversion symmetry and induce chirality by means of the Dzyaloshinskii-Moriya interaction, defining the structure of Néel skyrmion spin textures [3]. We show deterministic nucleation on nanosecond timescales using an electrical point contact on top of the multilayer [4], current-driven propagation along a wire in which the skyrmions are channelled by defects in the multilayer [5], and their detection by means of the Hall effect that reveals an unexpectedly large contribution to the Hall signal that correlates with the topological winding number [6].

- [1] N. Nagaosa & Y. Tokura, *Nat. Nanotech.* **8**, 899 (2013).  
 [2] A. Fert et al. *Nature Nanotech.* **8**, 152 (2013).  
 [3] K. Zeissler et al. *Sci. Rep.* **7**, 15125 (2017).  
 [4] S. Finizio et al., *Nano Lett.* **19**, 7246 (2019).  
 [5] K. Zeissler et al., *Nature Comm.* **11**, 428 (2020)  
 [6] K. Zeissler et al. *Nature Nanotech.* **13**, 1161 (2018).

### 5:30 AM \*F.NM04.01.03

**Skyrmions in Thin-Film Heterostructures** Kang L. Wang<sup>1</sup>, Hao Wu<sup>1</sup>, Ying Ying Wu<sup>1</sup>, Arvin Razavi<sup>1</sup> and Alexander

Grutter<sup>2</sup>; <sup>1</sup>University of California, Los Angeles, United States; <sup>2</sup>National Institute of Standards and Technology, United States

Magnetic skyrmions are swirling topological spin textures in either non-centrosymmetric magnetic bulk compounds or thin films resulted from broken inversion symmetry. Their presence is the result of the balance among the Dzyaloshinskii–Moriya interaction, the Heisenberg exchange interaction, magnetic anisotropy, and the Zeeman energy and was first demonstrated in cryogenic temperatures. Skyrmions behave as particles, which can be created, annihilated, and manipulated and can be as small as a few nanometers by careful design of material structures. The study of skyrmions is of great interest as they may be a strong candidate for high density and energy-efficient information storage and processing. In this talk, we will briefly review the requirements for the presence and the establishment of the phase diagram of skyrmions in various thin films. Particularly we will discuss the room-temperature skyrmion phase diagram as affected by DMI, anisotropy, and the Zeeman energy. Because of the interest in applications in logics and memories, there is an increased interest in using electric means, current or voltage, to create and manipulate skyrmions in ferromagnetic and antiferromagnetic thin-film materials platforms. For room-temperature skyrmions, nonuniform current in geometric restrictions was used to create and move skyrmions. We will describe the use of magneto-transport and the Kerr effect to study and image skyrmions, followed by the discussion on the use of neutron scattering, X-ray magnetic dichroism, and others to study the interface magnetism of heterostructures and to understand their creation and annihilation by torques of different origins. The materials platforms to be discussed include ferromagnetic and antiferromagnetic (AFM) materials. The use of metallic CoFeB/MgO/heavy metal (Ta, W, etc.) was used to demonstrate and image skyrmions. Other examples include topological insulator/AFM (MnTe) heterostructures, which will be described to show the use of the induced exchange bias via interface proximity effect for controlling the topological charge number via field cooling. Structures consisting of antiferromagnetic (AFM) and ferri-magnetic materials (FRM) offer the speed advantage to THz for information propagation in the form of spin and skyrmion current. In this area, we will discuss the exchange coupling of the two sub-lattices of FRM and AFM as revealed from x-ray dichroism and neutron scattering. In particular, the use of insulator heterostructures will be discussed, which have the advantage of having no electrical charge current. The voltage control of perpendicular anisotropy will be discussed to show the creation and annihilation of skyrmions and their dynamics without the use of an applied magnetic field. Lastly, we will discuss the recent progress of 2D materials for skyrmionics and in general for spintronics as 2D materials make possible a wider choice of materials available to experiments. In addition, the 2-D van der Waals gap may offer different interaction characteristics for their presence as well as creation and manipulations under current and voltage drives. The study of skyrmions and anti-skyrmions in analogy with the creation and annihilation of particles and antiparticle may provide a condensed matter platform for studying the particle counterparts.

Supported by ARO, NSF, and DOE.

#### 5:45 AM \*F.NM04.01.04

**Magnetic Spin Textures in Thin-Film Heterostructures** Suzanne G. te Velthuis; Argonne National Laboratory, United States

Topologically protected chiral spin textures, such as magnetic skyrmions, that exhibit quasi-particle like behavior have been envisioned to enable low-power information technologies, and consequently have engaged considerable the interest of the scientific community in recent years [1]. To this end, inversion asymmetric multilayers consisting of ferromagnetic and heavy metal layers have been explored and have been shown to host chiral domain walls and stabilize magnetic skyrmions due to interfacial Dzyaloshinskii-Moriya interactions. The controlled generation and manipulation of these spin structures is key to harnessing their potential in applications. We have shown that diverging electric charge currents can locally generate skyrmions. The diverging currents can be created by making use of geometric constrictions [2,3], and from nonmagnetic conducting point contacts [4]. Due to spin orbit torques at the interfaces, the spin textures can also be manipulated by charge currents. Magnetic skyrmions have been shown to exhibit a transverse motion relative to the current direction, i.e., the skyrmion Hall effect [5]. This effect arises due to the non-trivial topological charge of the skyrmions and is the analogue of the ordinary Hall effect for electrical charges in the presence of a magnetic field. The skyrmion Hall effect should vanish for antiferromagnetic skyrmions because of the cancelation of opposite topological charges and likewise for ferrimagnets at the compensation temperature. To explore this idea, we have investigated the current driven motion in artificially ferrimagnetic multilayers consisting of Co and Gd. We have studied the temperature dependence of the motion from room temperature down to temperatures below the compensation point of around 100 K and find a dependency of the skyrmion Hall angle and domain wall speed on the applied temperature.

[1] W. Jiang, *et al.*, Physics Reports **704**, 1 (2017).

[2] W. Jiang, *et al.*, Science **349**, 283 (2015).

[3] O. Heinonen, *et al.*, Phys. Rev. B **93**, 094407 (2016).

[4] Z. Wang, *et al.*, Phys. Rev. B **100**, 184426 (2019).

[5] W. Jiang, *et al.*, Nature Phys. **13**, 162 (2017).

#### 6:00 AM \*F.NM04.01.05

**Manipulation of Magnetic Skyrmion for Future Electronic Application** Joonyeon Chang<sup>1</sup>, Kyung Mee Song<sup>1</sup> and Seonghoon Woo<sup>2</sup>; <sup>1</sup>KIST, United States; <sup>2</sup>IBM T.J. Watson Research Center, United States

Most magnetic materials show collinear magnetic ordering due to the large exchange interaction between neighbouring magnetic moments. If provided the Dzyaloshinskii-Moriya interaction (DMI) is strong enough to overcome the exchange interaction, magnetic spins tend to align in a non-collinear manner with fixed homochirality. In any structures where the broken inversion symmetry leads to sufficiently large DMI, non-trivial small cylindrical swirling spin structures, called magnetic skyrmions can be energetically stable. Magnetic skyrmions are topologically protected spin textures that have nanoscale dimensions and can be manipulated by an electric current. These properties make the structures potential information carriers in data storage, processing and transmission devices.

The room temperature stabilization of magnetic skyrmions and their current pulse-induced displacement on nano-tracks has been reported in magnetic heterostructures. While such current controlled skyrmion motion is applicable to an actual device scheme, the deterministic writing and deleting of a single isolated magnetic skyrmion is required for fully functional skyrmionic devices.

In order to utilize skyrmion for any electrical electronic devices, we have studied current driven dynamics of skyrmions and inhibition of the skyrmion Hall effect which is detrimental to application. [1~3] We have shown that the current-induced creation, motion, detection and deletion of skyrmions at room temperature can be used to store information as well as to mimic the potentiation and depression behaviours of biological synapses. In particular, the accumulation and dissipation of magnetic skyrmions in ferrimagnetic multilayers can be controlled with electrical pulses to represent the variations in the synaptic weights. [4]

In this talk, I will briefly introduce current induced dynamics of skyrmions and discuss about future application of skyrmions in terms of non-volatile memory and synapse devices for neuromorphic computing.

#### 6:15 AM F.NM04.01.06

**Controlling Dzyaloshinskii-Moriya Interaction in Ferrimagnetic GdCo—A First Principles Calculation** Md Golam Morshed<sup>1</sup>, Khoong Hong Khoo<sup>2</sup>, Yassine Quessab<sup>3</sup>, Robert Laskowski<sup>2</sup>, Prasanna Balachandran<sup>1,1</sup>, Andrew D. Kent<sup>3</sup> and Avik W. Ghosh<sup>1,1</sup>; <sup>1</sup>University of Virginia, United States; <sup>2</sup>Institute of High Performance Computing, Agency for Science, Technology and Research, Singapore; <sup>3</sup>New York University, United States

Magnetic skyrmions are topological spin textures with potential applications in next-generation memory and logic. Controlling the inversion symmetry breaking interfacial Dzyaloshinskii-Moriya Interaction (DMI) is the key to stabilizing skyrmions in magnetic multilayers. We investigate the DMI of compensated ferrimagnetic GdCo alloy using Density Functional Theory (DFT), and explain the impact of Tungsten (W) alloying in a Pt/GdCo/Pt<sub>1-x</sub>W<sub>x</sub> structure. We find that a small amount of W (~10%) is sufficient to give rise to a non-zero DMI by breaking the inversion symmetry of Pt/GdCo/Pt. We also find that the DMI increases as a function of W composition (x), but saturates at higher W composition, in agreement with experiment. We show that the vanishing of spin-orbit coupling (SOC) energy to the adjacent metal layers of the top interface and the simultaneous constancy of the bottom interface is responsible for such saturating behavior of the DMI. Additionally, we investigate Pt/GdCo/X, where X = Ta, W, Ir to demonstrate the effect of capping layer heavy metals on the DMI. Our results predict that W in the capping layer favors a higher value of the DMI than Ta and Ir. Our results open up exciting combinatorial possibilities for controlling the DMI in ferrimagnets to nucleate and manipulate ultrasmall high-speed skyrmions.

#### 6:25 AM F.NM04.01.07

**Experimental Observation of Exchange-Driven Chiral Effects in Parabolic Nanostripes** Oleksii M. Volkov, Denys Makarov and Jürgen Fassbender; Helmholtz-Zentrum Dresden-Rossendorf, Germany

Broken magnetic symmetry is a key aspect in condensed matter physics and in particular in magnetism. It results in the appearance of chiral effects, e.g. topological Hall effect [1] and non-collinear magnetic textures including chiral domain walls and skyrmions [2,3]. These chiral structures are in the heart of novel concepts for magnonics [4], antiferromagnetic spintronics [5], spin-orbitronics [6] and oxitronics [7].

The main origin of the chiral symmetry breaking and thus for the magnetochiral effects in magnetic materials is associated to an antisymmetric exchange interaction, the intrinsic Dzyaloshinskii-Moriya interaction (DMI). At present, tailoring of DMI is done rather conventionally by optimizing materials, either doping a bulk single crystal or adjusting interface properties of

thin films and multilayers. A viable alternative to the conventional material screening approach can be the exploration of the interplay between geometry and topology. This interplay is of fundamental interest throughout many disciplines in condensed matter physics, including thin layers of superconductors [8] and superfluids [9], nematic liquid crystals [10], cell membranes [11], semiconductors [12]. In the emergent field of curvilinear magnetism chiral effects are associated to the geometrically broken inversion symmetries [13]. Those appear in curvilinear architectures of even conventional materials. There are numerous exciting theoretical predictions of exchange and magnetostatically-driven curvature effects, which do not rely on any specific modification of the intrinsic magnetic properties, but allow to create non-collinear magnetic textures in a controlled manner by tailoring local curvatures and shapes [14,15]. Until now the predicted chiral effects due to curvatures remained a neat theoretical abstraction.

Here, we demonstrate the very first experimental confirmation of the existence of the curvature-induced chiral interaction with exchange origin in a conventional soft ferromagnetic material [16]. It is experimentally explored the theoretical predictions, that the magnetisation reversal of flat parabolic stripes shows a two step process. At the first switching event, a domain wall pinned by the curvature induced exchange-driven DMI is expelled leading to a magnetisation state homogeneous along the parabola's long axis. Measuring the depinning field enables to quantify the effective exchange-driven DMI interaction constant. The magnitude of the effect can be tuned by the parabola's curvature. It is found that the strength of the exchange-induced DMI interaction for the experimentally realised geometries is remarkably strong, namely  $\approx 0.4$  mJ/m<sup>2</sup>, compared the surface induced DMI. The presented study legitimates the predictive power of full-scale micromagnetic simulations to design the properties of ferromagnets through their geometry, thus stabilising chiral textures.

- [1] N. Nagaosa, et al., Nature Nanotech. 8, 899 (2013)
- [2] U. K. Röbber, et al., Nature 442, 797 (2006)
- [3] A. Fert, et al., Nature Rev. Mat. 2, 17031 (2017)
- [4] A. V. Chumak, et al., Nature Physics 11, 453 (2015)
- [5] T. Jungwirth, et al., Nature Nanotech. 11, 231 (2016)
- [6] I. M. Miron, et al., Nature 476, 189 (2011)
- [7] V. Garcia, et al., Nature 460, 81 (2009)
- [8] J. Tempere, et al., Phys. Rev. B 79, 134516 (2009)
- [9] H. Kuratsuji, Phys. Rev. E 85, 031150 (2012)
- [10] T. Lopez-Leon, et al., Nature Physics 7, 391 (2011)
- [11] H. T. McMahon, et al., Nature 438, 590 (2005)
- [12] C. Ortix, Phys. Rev. B 91, 245412 (2015)
- [13] Y. Gaididei, et al., Phys. Rev. Lett. 112, 257203 (2014)
- [14] J. A. Otálora, et al., Phys. Rev. Lett. 117, 227203 (2016)
- [15] V. P. Kravchuk, et al., Phys. Rev. Lett. 120, 067201 (2018)
- [16] O. M. Volkov, et al., Phys. Rev. Lett. 123, 077201 (2019)

### 6:35 AM F.NM04.01.08

**Design of Giant DMI and Its Microscopic Origin in Magnetic Bilayers** Priyamvada Jadaun, Leonard Register and Sanjay Banerjee; UT Austin, United States

Magnetic skyrmions are compact spin textures that show remarkably unique, particle-like properties. They are widely regarded as promising candidates for emergent magnetic devices as they are small in size and easily maneuverable. The Dzyaloshinskii-Moriya interaction (DMI) is often critical to the generation and manipulation of skyrmions. However, there has been a fundamental lack of understanding of the microscopic origin of DMI or the mechanisms by which DMI stabilizes skyrmions in magnetic bilayers. Little has been known of the material parameters that determine the value of DMI. This knowledge is critical for rational design of skyrmion-hosting materials and further development of skyrmion technology. Here we investigate DMI in a series of magnetic bilayers using first principles methods. We present a new theoretical model that explains the microscopic origin of DMI in magnetic bilayers. We demonstrate that the value of DMI depends on two material parameters, interfacial hybridization and orbital contributions of the heavy metal. Using these parameters, we explain experimentally observed DMI trends. We also report four new materials systems predicted to have giant DMI and can be expected to outperform the best materials known so far, and new designs for magnetic multilayers. Our results provide a new understanding of DMI, discover highly promising materials and suggest pathways for the controlled generation of skyrmions.

**5:00 AM \*F.NM04.02.01**

**Advances in X-Ray Spectromicroscopies to Study Novel Topological Spin Textures** Peter Fischer<sup>1,2</sup>; <sup>1</sup>Lawrence Berkeley National Lab, United States; <sup>2</sup>University of California, Santa Cruz, United States

Microscopic spin textures and their dynamics are key to understand and control the properties, behavior and functionalities of novel magnetic materials. Of particular interest are topological systems, as they hold the promise to improve speed, size and energy efficiency of future spin driven technologies. Advanced characterization tools that provide magnetic sensitivity to spin textures at high spatial resolution, ultimately at buried interfaces and in all three dimensions [1], and at high temporal resolution to capture the spin dynamics across scales, are therefore of large scientific interest.

Magnetic soft X-ray spectro-microscopies [2] provide unique characterization opportunities to study the statics and dynamics of spin textures in magnetic materials combining X-ray magnetic circular dichroism (X-MCD) as element specific, quantifiable magnetic contrast mechanism with spatial and temporal resolutions down to fundamental magnetic length, time, and energy scales.

Current developments of x-ray sources aim to increase dramatically the coherence of x-rays opening the path to new approaches and characterization tools, such as ptychography [3] or x-ray photo-correlation spectroscopy (XPCS) [4] that allow unprecedented studies of nanoscale heterogeneity, complexity, and fluctuations.

I will review recent results studying the static properties and dynamic behavior of magnetic skyrmion [5,6] textures with potential application to novel magnetic logic and storage devices, as well as first results from target skyrmions that are seen as precursors for hopfions [7]. An unexpected and drastic change of the correlation times in nanoscale spin fluctuations near phase boundaries, i.e., in the skyrmion phase, and near the boundary with the stripe phase of a multilayered Fe/Gd system [4] was observed in an XPCS study at LCLS with a novel 2-pulse scheme.

**Acknowledgement**

This work was supported by the U.S. Department of Energy, Office of Science, Office of Basic Energy Sciences, Materials Sciences and Engineering Division Contract No. DE-AC02-05-CH1123 in the Non-Equilibrium Magnetic Materials Program (MSMAG).

- [1] P. Fischer, et al. APL Materials 8 010701 (2020)
- [2] P. Fischer and H. Ohldag, Report on Progress in Physics 78 094501 (2015)
- [3] X. Shi, et al, Appl Phys Letter 108, 094103 (2016)
- [4] M. H. Seaberg, et al, Phys Rev Lett 119 067403 (2017)
- [5] S. Woo, et al., Nature Materials 15 501 (2016)
- [6] N. Kent, et al., Appl Phys Lett 115 112404 (2019)
- [7] P. Sutcliffe, P. Journal of Physics A: Mathematical and Theoretical 51, 375401 (2018)

**5:15 AM \*F.NM04.02.03**

**Three-Dimensional Skyrmionic Networks in Chiral Magnets and Liquid Crystals** Andrey Leonov; Hiroshima University, Japan

Chiral skyrmions [1] are particle-like topological solitons with complex non-coplanar spin structures stabilized in noncentrosymmetric magnetic materials by specific Dzyaloshinskii-Moriya interaction (DMI). Being surrounded by the homogeneously magnetized state, skyrmions represent ensembles of weakly *repulsive axisymmetric particles* [2] oriented along the field. With the onset of the conical phase, skyrmions become non-axisymmetric and due to the attractive interaction tend to produce multi-skyrmion bound states - clusters [3]. Both types of skyrmions were observed experimentally in PdFe/Ir(111) bilayers with induced DMI [2] and in thin ( $\approx 70$  nm) single-crystal samples of  $\text{Cu}_2\text{OSeO}_3$  [3]. Moreover, the attracting skyrmions were predicted to underlie precursor phenomena (e.g., A-phase in B20 magnets) and to have prospects of being used in spintronics as *an effective alternative* to the common axisymmetric skyrmions [4]. Prototypes of spintronic devices based on the crossover of skyrmion-skyrmion interaction and low spin currents required to set skyrmions into motion were suggested in Ref. [4]. Note that the cross-section of isolated skyrmions within the conical phase has the typical structure of bimerons introduced in Ref. [5] and shown to develop an anisotropic character of skyrmion-skyrmion interaction in lacunar spinels  $\text{GaV}_4\text{Se}_8$  with the  $C_{3v}$  symmetry and easy-plane uniaxial anisotropy.

Skyrmions may also become oblique with respect to the field. In particular, in  $\text{Cu}_2\text{OSeO}_3$  due to the competing exchange and

cubic anisotropies [6], the conical phase tilts away from the field direction and thus underlies the deviation of skyrmions. As a result, attracting oblique skyrmions may potentially form *extended networks* in which their axes are not parallel to each other as in previously reported skyrmion clusters. Skyrmion networks with *mutually orthogonal isolated skyrmions* [7] were directly visualized in thin layers of chiral liquid crystals. We used chiral nematics as a model system for probing the skyrmion behavior due to the similarity of phenomenological models for both condensed-matter systems, chiral magnets and liquid crystals.

Thus, in the present abstract *by experimental and theoretical means*, I will introduce different classes of oblique non-axisymmetric skyrmions and elucidate the principles of their meshing into a large diversity of extended three-dimensional *skyrmionic networks* in chiral magnets and liquid crystals.

[1] U. K. Röbner *et al.*, *J. of Phys.: Conf. Ser.* **303**, 012105 (2011); H. Wilhelm *et al.*, *Phys. Rev. Lett.* **107**, 127203 (2011).

[2] A. O. Leonov *et al.*, *New J. of Phys.* **18**, 065003 (2016).

[3] A. O. Leonov *et al.*, *J. Phys.: Condens. Matter* **28**, 35LT01 (2016); J. Loudon *et al.*, *Phys. Rev. B* **97**, 134403 (2018).

[4] A. Leonov *et al.*, *Appl. Phys. Lett.* **109**, 172404 (2016); A. Leonov, M. Mostovoy, *Nat. Commun.* **8**, 14394 (2017).

[5] A. O. Leonov and I. Kézsmárki, *Phys. Rev. B*, **96**, 014423 (2017).

[6] F. Qian *et al.*, *Science Advances*, **4**: eaat7323 (2018); L. J. Bannenberg, *et al.*, *npj Quantum Materials*, **4**, 11 (2019).

[7] H. R. O. Sohn *et al.*, *Phys. Rev. B*, **100**, 104401 (2019).

#### 5:30 AM \*F.NM04.02.04

**Magnetic Skyrmions and Hopfions in Three-Dimensional Chiral Magnets** Jiadong Zang; University of New Hampshire, United States

In this talk, various three-dimensional (3D) topological spin textures in magnets without inversion symmetry will be introduced. The first part of the talk features the recent observation of target skyrmions in chiral magnet nanodisks through theory-experiment collaborations. Two types of zero-field target skyrmions are confirmed, and Bloch points are identified during topological transition between different types of target skyrmions. The spectrum of collective spin wave modes in target skyrmions also reveal the 3D nature of spin excitations.

Second part of the talk introduces a very recent work on hopfions in chiral magnetic nanodisk. This is one of the first experimentally feasible prediction on magnetic hopfions. The hopfion in this setup is confirmed by analyzing the linking between any two equal-spin loops and calculating the Hopf invariant. Another topological configuration, the pairing between monopole and anti-monopole, is also identified in the same system. Transition from this state to hopfion, being identical to sphere-torus topological deformation, can be achieved by an external magnetic field. Dynamics of hopfions will also be discussed.

This work is supported by the U.S. Department of Energy (DOE), Office of Science, Basic Energy Sciences (BES) under Award No. de-sc0020221.

#### 5:45 AM \*F.NM04.02.05

**Chiral Non Collinear Spin Textures** Stuart S. Parkin; Max Planck Institute of Microstructure Physics, Germany

Magnetic non-collinear spin textures that have chiral structures are of great current interest. The same type of Dzyaloshinskii-Moriya (DMI) vector exchange interactions that stabilize chiral Néel domain walls in magnetic multilayers<sup>1-3</sup> results in the formation of topological spin textures in bulk compounds. We recently discovered magnetic *antiskyrmions* in a tetragonal inverse Heusler compound  $Mn_{1.4}Pt_{0.9}Pd_{0.1}Sn$  using Lorentz transmission electron microscopy (LTEM)<sup>4</sup>. Unlike skyrmions in B20 compounds, that have been extensively studied, the size of the anti-skyrmion can be tuned by varying the thickness of the host material allowing for sizes varying from nanometer to microns in the same material<sup>5</sup>. This is due to long range magneto-dipole interactions that are important in this compound that has a complex DMI interaction with a symmetry that follows the  $D_{2d}$  symmetry of its crystalline structure. The same symmetry ensures that anti-skyrmions are robust to temperature and magnetic field<sup>6</sup>. The magnetic dipole-dipole interactions also allow for the formation of metastable “elliptical skyrmions” in this same material<sup>7</sup>. These have Bloch-like boundaries that we can directly observe using LTEM. Finally, we discuss our recent discovery of novel Néel like skyrmions in a metallic compound that exist almost to room temperature and that are also tunable in size<sup>8</sup>. Chiral spin textures in ferro-, ferri- and anti-ferrimagnetic materials and thin film heterostructures are of fundamental interest with potential for spintronic applications especially Racetrack Memory.

1. Yang, S.-H., Ryu, K.-S. & Parkin, S. S. P. Domain-wall velocities of up to 750 ms<sup>-1</sup> driven by exchange-coupling torque in synthetic antiferromagnets. *Nat. Nano.* **10**, 221-226, (2015).

2. Yang, S.-H., Garg, C. & Parkin, S. Chiral Exchange Drag and Chirality Oscillations in Synthetic Antiferromagnets *Nat. Phys.* **15**, 543-548, (2019).

3. Bläsing, R. *et al.* Exchange coupling torque in ferrimagnetic Co/Gd bilayer maximized near angular momentum compensation temperature. *Nat. Commun.* **9**, 4984, (2018).
4. Nayak, A. K. *et al.* Magnetic antiskyrmions above room temperature in tetragonal Heusler materials. *Nature* **548**, 561-566, (2017).
5. Ma, T. *et al.* Tunable Magnetic Antiskyrmion Size and Helical Period from Nanometers to Micrometers in a  $D_{2d}$  Heusler Compound. *Adv. Mater.*, 2002043, (2020).
6. Saha, R. *et al.* Intrinsic stability of magnetic anti-skyrmions in the tetragonal inverse Heusler compound  $Mn_{1.4}Pt_{0.9}Pd_{0.1}Sn$  *Nat. Commun.* **10**, 5305, (2019).
7. Jena, J. *et al.* Elliptical Bloch skyrmion chiral twins in an antiskyrmion system. *Nat. Commun.* **11**, 1115, (2020).
8. Srivastava, A. K. *et al.* Observation of Robust Néel Skyrmions in Metallic PtMnGa. *Adv. Mater.* **32**, 1904327, (2020).

#### 6:00 AM \*F.NM04.02.06

**Structures and Dynamics of Spin Textures with Boundaries** Naoto Nagaosa<sup>1,2</sup>, Wataru Koshibae<sup>2</sup> and Jan Masell<sup>2</sup>; <sup>1</sup>University of Tokyo, Japan; <sup>2</sup>RIKEN Center for Emergent Matter Science (CEMS), Japan

Structures and dynamics of spin textures in magnets are the subject of extensive studies, which is a crucial issue also for applications. The structures and their motion in the bulk are rather well understood, but the influence of the boundaries is less studied. In this talk I would focus on the effects of boundaries such as surfaces and edges as revealed by theoretical analysis. It includes (i) the skyrmion string in a thin film with associated topological defects, and (ii) the helix with boundaries. In the former case with an out-of-plane magnetic field, a step edge on the thin film substantially affects the motion of a skyrmion string, leading to its splitting and annihilation. These processes are understood by introducing two types of topological indices, i.e., the bulk monopole number and the surface skyrmion number. For an in-plane magnetic field, on the other hand, several kinds of topological defects are found to appear, which is consistent with the experimental observations. Recently, the helix structure was proposed to show inductance under an ac current. Therefore, the nonlinear dynamics of the helix are an important issue, which we have investigated both by numerical simulations and analytical calculations. It turns out that the role of the boundary is crucial to determine the direction of the wavevector of the helix: There is a 90° difference between periodic boundary condition and open boundary condition, revealing the vital role of the boundary.

#### 6:15 AM F.NM04.02.07

**Anomalous Magnetic Response at Topological Defects in FeGe** Mariia Stepanova<sup>1,2</sup>, Erik Lysne<sup>1,2</sup>, Peggy Schoenher<sup>3,4</sup>, Jan Masell<sup>5</sup>, Laura Köhler<sup>6,7</sup>, Achim Rosch<sup>8</sup>, Naoya Kanazawa<sup>9</sup>, Yoshinori Tokura<sup>5,9</sup>, Markus Garst<sup>6,7</sup>, Alireza Qaiumzadeh<sup>1,2</sup>, Arne Brataas<sup>1,2</sup> and Dennis Meier<sup>1,2</sup>; <sup>1</sup>Norwegian University of Science and Technology, Norway; <sup>2</sup>Center for Quantum Spintronics, NTNU, Norway; <sup>3</sup>ETH Zurich, Switzerland; <sup>4</sup>UNSW Sydney, Australia; <sup>5</sup>RIKEN, Japan; <sup>6</sup>Technische Universität Dresden, Germany; <sup>7</sup>Karlsruhe Institute of Technology, Germany; <sup>8</sup>Universität zu Köln, Germany; <sup>9</sup>University of Tokyo, Japan

The lamellar morphology of chiral spin textures is analogous to liquid crystals and biological systems. Analogous to cholesteric liquid crystals, chiral magnets possess a periodic layered structure and form a wide variety different types of non-trivial topological defects. Using magnetic force microscopy (MFM) on the near-room temperature helimagnet FeGe we resolve 1D and 2D topological defects, including disclinations and dislocations with nonzero topological winding number, as well as three fundamental types of helimagnetic domain walls. Interestingly, in addition to their non-trivial structure, all topological defects in FeGe exhibit an unusual magnetic response in MFM, which is not observed in regions with perfect lamellar-like order. This magnetic signature is reminiscent of the so-called “lines of flare” in cholesteric liquid crystals, suggesting local variations in magnetic susceptibility. We investigate the origin of the magnetic signature of the topological defects and discuss the possibilities to utilize the local MFM response as read-out signal in spintronics devices.

#### 6:25 AM F.NM04.02.08

**Topological Half-Skyrmions and Bimerons in an Antiferromagnetic Insulator at Room Temperature** Hariom Jani<sup>1</sup>, Jheng-Cyuan Lin<sup>2</sup>, Jiahao Chen<sup>2</sup>, Jack Harrison<sup>2</sup>, Francesco Maccherozzi<sup>3</sup>, Jonathon Schäd<sup>4</sup>, Saurav Prakash<sup>1</sup>, CHANG-BEOM EOM<sup>4,4</sup>, Ariando Ariando<sup>1</sup>, T. Venky Venkatesan<sup>1</sup> and Paolo G Radaelli<sup>2</sup>; <sup>1</sup>National University of Singapore, Singapore; <sup>2</sup>University of Oxford, United Kingdom; <sup>3</sup>Diamond Light Source, United Kingdom; <sup>4</sup>University of Wisconsin–Madison, United States

In the quest for post-CMOS technologies, ferromagnetic domain walls and topological skyrmions have shown great promise as elements in spintronic racetrack devices. Recently, attention has been shifted to antiferromagnetic (AFM) analogues, as they are anticipated to demonstrate relativistic dynamics, fast motion without transverse deflection and size scaling. Despite this, experimental implementations in natural antiferromagnetic systems at room temperature are yet to emerge. Here, we



demonstrate a family of topological antiferromagnetic spin-textures in  $\alpha$ -Fe<sub>2</sub>O<sub>3</sub> – an earth-abundant oxide insulator – capped with a Pt over-layer. By varying temperature and doping, we stabilize exotic AFM merons-antimerons (half-skyrmions), and AFM bimerons, which can be erased by magnetic fields and re-generated by temperature cycling. Controlled by current-based spin-torques from the heavy-metal over-layer, these AFM textures could emerge as prime candidates for low-energy antiferromagnetic spintronics.

SESSION F.NM04.03: Static and Dynamic Properties of Magnetic Skyrmion  
On Demand Abstracts Available for Viewing Starting Saturday Morning, November 21, 2020  
F-NM04

#### 5:00 AM \*F.NM04.03.01

**Skyrmions in Centrosymmetric Magnets** Shinichiro Seki; The University of Tokyo, Japan

Magnetic skyrmion, i.e., a topologically stable swirling spin configuration, has recently attracted attention as a particle-like object potentially suitable for the design of high-density information bits. Previous observations of skyrmions have mostly focused on noncentrosymmetric systems, where Dzyaloshinskii-Moriya interaction plays an important role[1,2]. On the other hand, recent theoretical studies suggest that skyrmions can be stabilized even in centrosymmetric systems by considering different microscopic mechanisms. For example, geometrical frustration of short-range exchange interactions on triangular lattice is predicted to stabilize a hexagonal lattice of skyrmions[3]. Another potential mechanism is the RKKY and four-spin interactions mediated by itinerant electrons, which is expected to favor a skyrmion lattice state for highly-symmetric (such as hexagonal or tetragonal) crystal lattice systems[4].

In this talk, I overview the recent experimental discovery of skyrmions in centrosymmetric systems[5-7]. In particular, we focus on the case of centrosymmetric tetragonal magnet GdRu<sub>2</sub>Si<sub>2</sub>, where the square lattice of skyrmions with extremely small diameter (1.9nm, i.e. the smallest value ever reported for single-component bulk materials) has been observed[7]. Our results demonstrate that skyrmions can be stabilized even without geometrically frustrated lattice nor inversion symmetry breaking, and suggest that rare-earth intermetallics with highly-symmetric crystal lattice may ubiquitously host nanometric skyrmions of exotic origins.

[1] S. Muhlbauer *et al.*, *Science* **323**, 915 (2009).

[2] S. Seki *et al.*, *Science* **336**, 198 (2012).

[3] A. O. Leonov *et al.*, *Nature Comm.* **6**, 8275 (2015).

[4] S. Hayami *et al.*, *Phys. Rev. B* **95**, 224424 (2017).

[5] R. Takagi, S. Seki *et al.*, *Science Advances* **4**, 3402 (2018).

[6] T. Kurumaji *et al.*, *Science* **365**, 6456 (2019).

[7] N. D. Khanh, S. Seki *et al.*, *Nature Nanotechnology* (2020). <https://doi.org/10.1038/s41565-020-0684-7>

#### 5:15 AM \*F.NM04.03.02

**Skyrmions—A Playground for Non-Conventional Computing and Phase Transitions in 2D** Mathias Klauui; Johannes Gutenberg University Mainz, Germany

In our information-everywhere society IT is a major player for energy consumption. Novel spintronic devices can play a role in the quest for GreenIT if they are stable and can transport and manipulate spin with low power. Devices have been proposed, where switching by energy-efficient approaches, such as spin-polarized currents is used [1],

Firstly, to obtain ultimate stability of states, topological spin structures that emerge due to the Dzyaloshinskii-Moriya interaction (DMI) at structurally asymmetric interfaces, such as chiral domain walls and skyrmions with enhanced topological protection can be used [2-5]. We have investigated in detail their dynamics and find that it is governed by the topology of their spin structures [2]. By designing the materials, we can even obtain a skyrmion lattice phase as the ground state [3].

Secondly, for ultimately efficient spin manipulation, we use spin-orbit torques, that can transfer more than 1hbar per electron by transferring not only spin but also orbital angular momentum. We combine ultimately stable skyrmions with spin orbit torques into a skyrmion racetrack device [3-5], where the real time imaging of the trajectories allows us to quantify the novel skyrmion Hall effect [5,6].

Beyond conventional memory, we furthermore use spin-orbit torque induced skyrmion dynamics for non-conventional stochastic computing applications, where we have developed a skyrmion reshuffler device [6]. Here we use thermal skyrmion

motion to implement a key component for stochastic computing [6]. Such thermal skyrmion diffusion can also be controlled by symmetry breaking [7] and this is useful for token – based Brownian computing. Finally the thermal dynamics of skyrmion quasi-particles lends itself to exploiting this system for the study of phases and phase transitions in 2D. We have studied the transition of skyrmion arrangements from the liquid phase across the hexatic phase unique to 2D systems into the solid phase [8]. These transitions occur in a wide range of skyrmions systems [8,9], thus showing that skyrmions have evolved from an object of study themselves and are now being understood controlled sufficiently well for use as model systems to study exciting statistical physics in 2D.

[1] Reviews G. Finocchio et al., J. Phys. D: Appl. Phys. **49**, 423001 (2016); K. Everschor-Sitte et al., J. Appl. Phys. **124**, 240901 (2018).

[2] F. Büttner et al., Nature Phys. **11**, 225 (2015).

[3] S. Woo et al, Nature Mater. **15**, 501 (2016).

[4] K. Litzius et al., Nature Phys. **13**, 170 (2017).

[5] K. Litzius et al., Nature Electron. **3**, 30 (2020).

[6] J. Zazvorka et al., Nature Nano. **14**, 658 (2019).

[7] N. Kerber et al., arxiv:2004.07976

[8] J. Zazvorka et al., arxiv:2004.09244

[9] P. Huang et al., arxiv:1807.08352 (Nature Nano. (2020)); M. Kläui, News&Views, Nature Nano. (2020).

### 5:30 AM \*F.NM04.03.03

#### **Detection and Transformation of Confined Magnetic Skyrmions in Metal Silicide and Germanide Nanostructures** Song Jin; University of Wisconsin--Madison, United States

Skyrmions are novel topologically stable spin vortices that show promise for next-generation magnetic storage due to their nanoscale domains to enable high information storage density and their low threshold for current-driven motion to enable ultralow energy consumption. One-dimensional (1D) nanowires are ideal hosts for skyrmions since they not only serve as a natural platform for magnetic racetrack memory devices but also can stabilize skyrmions. We have developed synthetic methods for nanowires (and nanoplates) of non-centrosymmetric cubic B20 monosilicides (MnSi, FeSi, CoSi) and monogermanides (FeGe) and their alloys (such as  $\text{Fe}_x\text{Co}_{1-x}\text{Si}$  and  $\text{Fe}_{1-x}\text{Co}_x\text{Ge}$ ), many of which display exotic helimagnetic and skyrmion magnetic phases with domain sizes from 10 to 230 nm. Collaborating with several groups, we have used Lorentz TEM, off-axis electron holography (EH), magnetotransport measurements to confirm that magnetic skyrmion phases are stable over a larger magnetic field-temperature range in these nanostructures compared to bulk crystals and thin films. Magnetoresistance (MR) measurements revealed the critical magnetic fields for the transitions between different magnetic spin structures at different temperatures. Topological Hall effect (THE) measurements of MnSi nanowires and  $\text{Fe}_{1-x}\text{Co}_x\text{Ge}$  ( $x < 0.1$ ) nanoplates further confirmed the extended skyrmion stability, for example, in FeGe nanowires and  $\text{Fe}_{1-x}\text{Co}_x\text{Ge}$  ( $x < 0.1$ ) nanoplates with skyrmions stable up to about 280 K. We have further demonstrated the current-driven motion of skyrmions in this extended skyrmion phase region in MnSi nanowires. Correlating real space magnetic imaging with the magnetotransport measurements reveals previously unexplored transformation of skyrmion strings and other magnetic ordering due to nanoscale confinements. These results open up the exploration of nanowires as an attractive platform for investigating skyrmion physics in 1D systems and exploiting skyrmions in magnetic storage concepts.

### 5:45 AM \*F.NM04.03.04

#### **Thermal Effects on the Skyrmion Dynamics** Wanjun Jiang; Tsinghua University, China

Skyrmions are particle-like topological spin textures stabilized by the Dzyaloshinskii-Moriya interaction, which have recently stimulated great interests in spintronics community. The dynamics of which have been frequently studied via using magnetic fields and current-induced spin torques. On the other hand, a comprehensive understanding of thermal effects, including random thermal fluctuation and directional thermal currents, on the dynamics of skyrmions are not fully established yet.

In this talk, I will first discuss our recent experimental observation of the thermal fluctuation-induced random walk of a single isolated Néel-type magnetic skyrmion in an interfacially asymmetric Ta/CoFeB/TaO<sub>x</sub> multilayer. In particular, an intriguing topology dependent Brownian gyromotion behavior of skyrmions has been identified. The onset of Brownian gyromotion of a single skyrmion induced by the thermal effects, including a nonlinear temperature-dependent diffusion coefficient and topology-dependent gyromotion are further formulated based on the stochastic Thiele equation.

Subsequently, I will discuss the thermal generation, manipulation and detection of nanoscale skyrmions, which were made in microstructured devices made of different multilayers – [Ta/CoFeB/MgO]<sub>15</sub>, [Pt/CoFeB/MgO/Ta]<sub>15</sub> and

[Pt/Co/Ta]<sub>15</sub> integrated with on-chip heaters, by using a full-field soft X-ray microscopy. In particular, the thermal generation of densely packed skyrmions at the device edge, together with the unidirectional diffusion of skyrmions from the hot region towards the cold region were experimentally observed. These thermally generated skyrmions can be further electrically detected by measuring the accompanied anomalous Nernst voltages. These results could open another exciting avenue for enabling skyrmionics, and promote interdisciplinary studies among spin caloritronics, magnonics and skyrmionics.

[1] W. Jiang, et al., *Science*, 349, 283 (2015).

[2] W. Jiang, et al., *Nature Physics*, 13, 162 (2017).

[3] W. Jiang, et al., *Physics Reports*, 704, 1-49 (2017).

[4] J. Zázvorka et al. *Nature Nanotechnology* **14**, 658-661 (2019).

[5] L. Zhao, et al., *Phys. Rev. Letts.* In press, arXiv:1901.08206 (2019).

[6] Z. Wang, et al., arXiv:2005.07441(2019).

#### 6:00 AM F.NM04.03.06

**Stabilization of Skyrmion States by a Gradient of Curvature in Ferromagnetic Shells** Oleksandr Pylypovskyi<sup>1,2</sup>, Denys Makarov<sup>1</sup>, Volodymyr Kravchuk<sup>3,4</sup>, Avadh Saxena<sup>5</sup> and Denis Sheka<sup>2</sup>; <sup>1</sup>Helmholtz-Zentrum Dresden-Rossendorf e.V., Ukraine; <sup>2</sup>Taras Shevchenko National University of Kyiv, Ukraine; <sup>3</sup>Karlsruhe Institute of Technology, Germany; <sup>4</sup>Bogolyubov Institute for Theoretical Physics of National Academy of Sciences of Ukraine, Ukraine; <sup>5</sup>Los Alamos National Laboratory, United States

Skyrmions represent a class of chiral magnetic textures with unique properties relevant for spintronic and spin-orbitronic applications [1]. Geometrical curvature can be used as an efficient mean to tailor chiral and anisotropic responses of thin ferromagnetic shells [2-4]. This was recently confirmed by quantifying the strength of the Dzyaloshinskii-Moriya interaction (DMI) in curved nanostripes [5]. Furthermore, there are numerous predictions of the stabilization of curvature-driven of small-radius skyrmions in spherical shells [6] and an appearance of skyrmion lattices as the ground state in intrinsically chiral curvilinear thin films [7].

Here, we demonstrate a new pathway of stabilizing Neel skyrmion and skyrmionium states relying on the gradient of curvature using a magnetic thin film hosting a circular nanoindentation [8]. These skyrmion states can be formed in a material even without an intrinsic DMI. We propose a physical picture of this effect, which is related to the pinning of a chiral magnetic domain wall at the bend of a nanoindentation. Geometry of the film is described by two principal curvatures  $k_1(r)$ , describing film geometry in radial direction, and  $k_2(r)$  inversely proportional to the distance from origin. In this respect, the spatial inhomogeneity of the curvature-induced DMI governing by  $k_1(r)$  is responsible for the stabilization of the skyrmion state. The lateral dimensions of the stabilized chiral magnetic textures are varied in a broad range by engineering the size of the nanoindentation. We describe the stability condition of skyrmion states. Furthermore, on the fundamental side, we put forth a general analytical framework allowing us to map a complex problem of the description of a magnetic texture at a surface of revolution to a standard planar problem with modified constants of DMI and magnetic anisotropy. In this respect, our model predicts a new mechanism of pinning of magnetic domain walls in planar ferromagnetic films with intrinsic DMI on inhomogeneities of the DMI.

[1] A. Fert, N. Reyren, V. Cros, *Nat. Rev. Mater.*, Vol. 2, 17031 (2017)

[2] R. Streubel, P. Fischer, F. Kronast et al., *J. Phys. D: Appl. Phys.* Vol. 49, 363001 (2016)

[3] O. Pylypovskyi, V. Kravchuk, D. Sheka et al., *Phys. Rev. Lett.* Vol. 114, 197204 (2015)

[4] Y. Gaididei, A. Goussev, V. Kravchuk et al., *J. Phys. A: Mat. and Theor.* Vol. 50, 385401 (2017)

[5] Volkov, Kakay, Kronast et al., *Phys. Rev. Lett.* Vol. 123, 077201 (2019)

[6] V. Kravchuk, U. K. Röbner, O. M. Volkov et al., *Phys. Rev. B.* 94, 144402 (2016)

[7] V. Kravchuk, D. Sheka, A. Kákay et al., *Phys. Rev. Lett.* Vol. 120, 067201 (2018)

[8] O. Pylypovskyi, D. Makarov, V. Kravchuk et al., *Phys. Rev. Appl.* Vol. 10, 064057 (2018)

#### 6:10 AM F.NM04.03.07

**Topological Transformation of Magnetic Skyrmion Strings in Nanostructures of Cubic B20 Materials** Nitish Mathur<sup>1</sup>, Fehmi Yasin<sup>2</sup>, Matthew J. Stolt<sup>1</sup>, Wensen Wei<sup>3</sup>, Haifeng Du<sup>3</sup>, Mingliang Tian<sup>3</sup>, Xiuzhen Yu<sup>2</sup> and Song Jin<sup>1</sup>; <sup>1</sup>University of Wisconsin-Madison, United States; <sup>2</sup>RIKEN Center for Emergent Matter Science, Japan; <sup>3</sup>High Magnetic Field Laboratory, Chinese Academy of Science, China

Magnetic skyrmions are topological spin textures that have shown promise due to their potential applications in high density

and energy efficient memory nanodevices. Chiral helimagnets with the non-centrosymmetric cubic B20 crystal structure host Bloch-type skyrmions due to the antisymmetric spin exchange interaction known as the Dzyaloshinskii-Moriya interaction (DMI). Although magnetic skyrmions are depicted as two-dimensional spin texture in bulk crystals, in reality, they possess a three-dimensional structure of skyrmions that looks like elongated strings extending throughout the thickness of the sample. In geometrically confined nanostructures, such as FeGe nanowires or nanoplates, these skyrmion strings (SkS) are stabilized over large range of temperature and magnetic field. We have developed “bottom-up” chemical vapor deposition (CVD) synthetic techniques to synthesize single-crystal FeGe nanowires and  $\text{Fe}_{1-x}\text{Co}_x\text{Ge}$  ( $x < 0.1$ ) nanoplates. We have observed increased sensitivity of magnetotransport measurements towards magnetic phase transitions in FeGe nanostructures when the applied magnetic field is parallel to the current, which could be mapped to the transformations of conical and helimagnetic spin textures to/from SkS. We further implemented Lorentz TEM imaging technique on nanostructures with applied magnetic field perpendicular to the observation direction to visualize the topological transformations of SkS to helical/conical spin states in real space. These Lorentz TEM imaging in correlation with the magnetotransport measurements reveal previously unexplored transformation of skyrmion strings due to nanoscale confinements.

#### 6:20 AM F.NM04.03.08

**Mechanism of Structural and Chemical Control Over Skyrmion Phases in Lacunar Spinels** Daniil A. Kitchaev, Emily C. Schueller and Anton Van der Ven; University of California, Santa Barbara, United States

The formation of magnetic skyrmions is intrinsically controlled by the coupling between magnetic interactions and the underlying crystal structure, meaning that skyrmion phase stability is particularly sensitive to chemical variations, structural transitions and mechanical deformation. The  $\text{GaM}_4\text{X}_8$  ( $M=\text{V}/\text{Mo}$ ,  $X=\text{S}/\text{Se}$ ) lacunar spinels are a versatile class of model materials for studying these couplings as they exhibit a variety of skyrmionic phase diagrams across several structures and chemistries. First, we use electronic-structure calculations and generalized cluster expansions to derive a universal magnetic phase diagram for materials in this space, and argue that reported variations in skyrmion stability are quantitatively explained by structurally- and chemically-induced changes to magnetocrystalline anisotropy[1]. In particular, skyrmion stability across all temperatures below  $T_c$  reported in some of these materials is a direct consequence of minimal uniaxial anisotropy. Second, we combine experimental and first-principles computational analysis to demonstrate that subtle variations in the structural evolution of  $\text{GaMo}_4\text{Se}_8$  lead to dramatic changes in magnetic behavior, switching from skyrmion host to ferromagnet[2] and corresponding to a giant effective magnetostructural coupling. Our results reveal specific materials design strategies for engineering robust skyrmion-host materials, and controlling skyrmion behavior through mechanical means.

[1] Kitchaev, D. A., Schueller, E. C., and Van der Ven, A. *Physical Review B*, 101(5), 054409. (2020).

[2] Schueller, E. C., Kitchaev, D. A., Zuo, J. L., Bocarsly, J. D., Cooley, J. A., Van der Ven, A., Wilson S. D., and Seshadri, R. *Physical Review Materials*, 4(6), 064402. (2020).

### SYMPOSIUM F.NM05

---

Emerging Materials for Quantum Information Technologies  
November 21 - December 4, 2020

#### Symposium Organizers

Mei-Yin Chou, Academia Sinica  
Peter Krogstrup, University of Copenhagen  
Tzu-Ming Lu, Sandia National Laboratories  
Javad Shabani, New York University

---

\* Invited Paper

SESSION F.NM05.08: Live Keynote I: Emerging Materials for Quantum Information Technologies  
Session Chairs: Peter Krogstrup and Javad Shabani

Wednesday Morning, December 2, 2020  
F.NM05

**11:30 AM \*F.NM05.04.02**

**Andreev Bound States and Majorana Fermions in Helical 1D Systems** [Jelena Klinovaja](#); University of Basel, Switzerland

In my talk, I will discuss low-dimensional condensed matter systems, in which topological properties could be engineered per demand. Majorana fermions can emerge in hybrid systems with proximity-induced superconducting pairing. I will present our numerical and analytical studies of such geometries with proximity effects [1-3]. In the second part of the talk, I will discuss an analytical model of a Rashba nanowire that is partially covered by and coupled to a thin superconducting layer, where the uncovered region of the nanowire forms a quantum dot [4,5]. Even if there is no topological superconducting phase possible, there is a trivial Andreev bound state that becomes pinned exponentially close to zero energy as a function of magnetic field strength when the length of the quantum dot is tuned with respect to its spin-orbit length such that a resonance condition of Fabry-Perot type is satisfied. In this case, the Andreev bound state remains pinned near zero energy for Zeeman energies that exceed the characteristic spacing between Andreev bound state levels but that are smaller than the spin-orbit energy of the quantum dot. Importantly, as the pinning of the Andreev bound state depends only on properties of the quantum dot, this behavior is unrelated to topological superconductivity.

References

- [1] C. Reeg, D. Loss, and J. Klinovaja, Phys. Rev. B **97**, 165425 (2018).
- [2] C. Reeg, D. Loss, and J. Klinovaja, Phys. Rev. B **96**, 125426 (2017).
- [3] C. Reeg, J. Klinovaja, and D. Loss, Phys. Rev. B **96**, 081301 (2017).
- [4] C. Reeg, O. Dmytruk, D. Chevallier, D. Loss, and J. Klinovaja, Phys. Rev. B **98**, 245407 (2018).
- [5] O. Dmytruk, D. Chevallier, D. Loss, and J. Klinovaja, Phys. Rev. B **98**, 165403 (2018).

**12:00 PM \*F.NM05.04.03**

**Materials Considerations for Majorana Based Quantum Computations** [Jay Sau](#); University of Maryland, United States

Majorana modes are one of the most promising candidates for the creation of topological qubits in the long term. While evidence for Majorana modes has been obtained for Majorana modes in several systems such as semiconductor nanowires, semiconductor 2DEGs, iron-based superconductors, topological insulators as well as iron atom chains to name a few, evidence for a qubit degree of freedom is elusive. I will begin by reviewing what it means experimentally to observe a qubit. Following this we will discuss the central device challenge in this regard i.e. quasiparticle poisoning. I will then describe potential material dependence of this phenomena as well as how quasiparticle poisoning can manifest in various experiments related to topological superconductivity. Specifically, we will discuss how the observation of quantized conductance into a zero-bias conductance peak associated with a Majorana over a range of tunneling provides some bounds on quasiparticle poisoning times. The measurement of Coulomb blockade transport, which has been observed only for a limited number of superconductors can provide more precise information on such bounds.

**12:30 PM \*F.NM05.04.05**

**Topological Superconductivity in Superconductor–Semiconductor Heterostructures** [Roman Lutchyn](#); University of California, Santa Barbara, United States

Superconductor–semiconductor heterostructures represent a versatile platform for realizing Majorana zero-energy modes. In this talk, I will explain how to engineer topological superconductivity at the interface of a conventional (s-wave) superconductor and a semiconductor with spin-orbit interaction. I will discuss state-of-the-art numerical approaches for modeling realistic devices which take into account proximity-induced superconductivity, orbital and Zeeman effect of an applied magnetic field, spin-orbit coupling as well as the electrostatic environment on equal footing. Finally, I will review recent materials science progress in growing superconductor–semiconductor heterostructures and discuss promising new directions.

**1:00 PM \*F.NM05.04.04**

**Materials Science, Physics and Engineering of Topological Quantum Circuits** [Sergey Frolov](#); University of Pittsburgh, United States

With Quantum Supremacy upon us, and with major tech companies investing in quantum computing, one may wonder how

much room is left there for academic research? The answer is: more than ever! Our existing qubits are great, but it is difficult to see them carrying us beyond the modern era of noisy intermediate-scale quantum processors, and ushering in the truly scalable, fault tolerant and commercially viable computers. Most likely, a qubit and its couplings, gates will once more need to be re-thought from the ground up - from the atomic first-principles level to the device architecture level. At the same time, the progress we made in quantum control and engineering is so huge that these methods have themselves become mature tools of science. They can be applied beyond quantum computing - to understand the basic questions of quantum dynamics and to probe exotic matter.

One solution may come from studying topological superconductivity. This is an interesting state most notable for spurring Majorana zero modes. Those modes can be both investigated as some of the first non-Abelian excitations, and they can be used in quantum circuits for storing and protecting quantum information. Majorana research has posed many basic materials questions of how to engineer the precise structures that possess intrinsic fault tolerance through topological protection. In my work I have developed new materials and devices for unambiguous observation of robust Majorana modes. I have worked on establishing clear criteria (signatures) of Majorana modes and how to tell them apart from other excitations that may be present in the same devices. It is exciting to apply modern quantum probes, developed based on transmon and spin qubits, to these systems in search for new exotic quantum matter. And perhaps solving some of the big challenges facing quantum computing at the same time.

SESSION F.NM05.09: Live Keynote II: Emerging Materials for Quantum Information Technologies  
Session Chairs: Mei-Yin Chou and Tzu-Ming Lu  
Thursday Morning, December 3, 2020  
F.NM05

#### 8:00 AM \*F.NM05.01.01

**Atomic Qubits in Silicon** Michelle Y. Simmons<sup>1,2</sup>; <sup>1</sup>University of New South Wales, Australia; <sup>2</sup>Silicon Quantum Computing Pty Ltd, Australia

Atom qubits in silicon have demonstrated extremely long electron and nuclear spin coherence times [1,2] making silicon a promising semiconductor material for spin-based quantum information. The two-level spin state of single electrons bound to shallow phosphorus donors in silicon provide well defined, reproducible qubits [3] with low gate densities. An important challenge in these systems is the realisation of an architecture, where we can position donors within a crystalline environment with <20nm separation, individually address each donor, manipulate the electron spins using ESR techniques, read-out their spin states and perform both single and two qubit gates.

We have pioneered a unique strategy to build a scalable quantum computer in silicon atom by atom. We use scanning tunneling microscope lithography and ultra-high vacuum crystal growth to precisely position individual P donors in Si [4] aligned with nanoscale precision to local control gates [5] necessary to initialize, manipulate, and read-out the spin states [6-8].

During this talk I will focus on demonstrating fast, high fidelity single-shot spin read-out [9], ESR control of precisely-positioned P donors in Si [10] and our recent results of demonstrating a fast (~ns) two-qubit SWAP gate [11,12]. We have also published a 3D architecture for implementation of error correction using the surface code [13]. With important advances in control at the atomic-scale, I will attempt to highlight the benefits of single atom qubits in silicon.

#### References

- [1] K. Saeedi *et al.*, Science 342, 130 (2013).
- [2] J. T. Muhonen *et al.*, Nature Nanotechnology 9, 986 (2014).
- [3] B.E. Kane, Nature 393, 133 (1998).
- [4] M. Fuechsle *et al.*, Nature Nanotechnology 7, 242 (2012).
- [5] B. Weber *et al.*, Science 335, 6064 (2012).
- [6] H. Buch *et al.*, Nature Communications 4, 2017 (2013).
- [7] B. Weber *et al.*, Nature Nanotechnology 9, 430 (2014).
- [8] T. F. Watson *et al.*, Science Advances 3, e1602811 (2017).
- [9] D. Keith *et al.*, Physical Review X 9, 041003 (2019)

- [10] S. Hile *et al.*, *Science Advances* 4, eaaq1459 (2018).  
[11] M.A. Broome *et al.*, *Nature Communications* 9, 980 (2018).  
[12] S. Gorman, Y. He *et al.*, *Nature* 571, 371 (2019).  
[13] C. Hill *et al.*, *Science Advances* 1, e1500707 (2015).

**8:24 AM \*F.NM05.06.03**

**Effects of Coulomb Interactions in Silicon Quantum Dots** Susan Coppersmith<sup>1,2</sup>; <sup>1</sup>University of New South Wales, Australia; <sup>2</sup>University of Wisconsin–Madison, United States

Silicon is an attractive materials platform for developing large-scale quantum computers because of its compatibility with classical silicon electronics and its potential for scalability. Recent progress towards quantum computing in silicon has been impressive, but better understanding of the materials will enable improved controllability and predictability of qubit devices.

This talk will discuss some of the fundamental physics and materials science challenges that arise, focussing on the nontrivial interplay between Coulomb interactions and the valley degree of freedom in silicon quantum dots containing more than one electron. Prospects for further development will also be discussed.

**8:48 AM \*F.NM05.06.04**

**Exchange Control of Three Spins in Si Triple Quantum Dots** Seigo Tarucha; RIKEN, Japan

High-fidelity quantum operations of single and two spins as well as readout and initialization have recently been demonstrated for Si quantum dots. Among them exchange control between spins is an ingredient of quantum entanglement for implementing quantum algorithms, but the demonstration of entanglement has been limited to two-qubit entanglement mainly due to difficulties in controlling exchange couplings in a multi-qubit array. We use a triple quantum dot equipped with a micro-magnet to control exchange couplings in two or three spin systems. We first measure the single qubit fidelity for three spins in the (1,1,1) charge state and obtain the values of 99.4 to 99.9 % for three spins. Then we use two spins to study exchange control of two qubits or singlet-triplet qubit drive. We use a resonant drive technique of the exchange interaction at the qubit frequency and obtained the fidelity of 99.6% thanks to the symmetric operation and a large micro-magnet Zeeman field gradient. Finally we use three spins to implement three-qubit entanglement. We precisely control exchange couplings between three spins and generate GHZ state. The GHZ state generation protocol will be useful to encode and decode a logical state for the bit-flip quantum error correction code.

**9:12 AM \*F.NM05.06.01**

**Quantum Computing with Semiconductors—Spins Inside** Lieven Vandersypen; TU Delft, Netherlands

Quantum computation has captivated the minds of many for almost two decades. For much of that time, it was seen mostly as an extremely interesting scientific problem. In the last few years, we have entered a new phase as the belief has grown that a large-scale quantum computer can actually be built. Quantum bits encoded in the spin state of individual electrons in silicon quantum dot arrays, have emerged as a highly promising direction [1]. In this talk, I will present our vision of a large-scale spin-based quantum processor, and ongoing work to realize this vision.

First, we created local registers of spin qubits with sufficient control that we can program arbitrary sequences of operations. We show the creation of each of the Bell states with fidelities of 85-90% and the implementation of the four instances of the Deutsch-Jozsa and the Grover algorithms on two qubits [2].

Second, we have explored coherent coupling of spin qubits at a distance via two routes. In the first approach, the electron spins remain in place and are coupled via an intermediary degree of freedom. After showing this principle with an ancillary quantum dot as a coupler [3], we recently observed strong coupling of a single spin to a single microwave photon in a superconducting resonator [4]. In the second approach, spins are shuttled along a quantum dot array, preserving both the spin projection [5] and spin phase [6].

Third, in close collaboration with Intel, we have fabricated and measured quantum dots using all-optical lithography on 300 mm wafer, using industry-standard processing [7]. Qubit measurements are now underway. We expect that this industrial approach to nanofabrication will be critical for achieving the extremely high yield necessary for devices containing hundreds or thousands of qubits. Furthermore, we anticipate that the device stability and charge noise levels will eventually outperform those of devices made in university-style cleanrooms.

When combined, the progress along these various fronts can lead the way to scalable networks of high-fidelity spin qubit registers for computation and simulation.

- [1] L.M.K. Vandersypen, H. Bluhm, J.S. Clarke, A.S. Dzurak, R. Ishihara, A. Morello, D.J. Reilly, L.R. Schreiber, M. Veldhorst, Interfacing spin qubits in quantum dots and donors – hot, dense and coherent, *npj Quantum Information* 3, 34 (2017).
- [2] T. F. Watson, S. G. J. Philips, E. Kawakami, D. R. Ward, P. Scarlino, M. Veldhorst, D. E. Savage, M. G. Lagally, Mark Friesen, S. N. Coppersmith, M. A. Eriksson, L. M. K. Vandersypen, A programmable two-qubit quantum processor in silicon, *Nature* 555, 633-637 (2018)
- [3] T.A. Baart, T. Fujita, C. Reichl, W. Wegscheider, L.M.K. Vandersypen, Coherent spin-exchange via a quantum mediator, *Nature Nanotechnology*, 12, 26 (2017)
- [4] N. Samkharadze, G. Zheng, N. Kalhor, D. Brousse, A. Sammak, U. C. Mendes, A. Blais, G. Scappucci, L. M. K. Vandersypen, Strong spin-photon coupling in silicon, *Science* 359, 1123-1127 (2018)
- [5] T. A. Baart, M. Shafiei, T. Fujita, C. Reichl, W. Wegscheider, L. M. K. Vandersypen, Single-Spin CCD, *Nature Nanotechnology* 11, 330 (2016)
- [6] T. Fujita, T. A. Baart, C. Reichl, W. Wegscheider, L. M. K. Vandersypen, Coherent shuttle of electron-spin states, *npj Quantum Information* 3, 22 (2017)
- [7] R. Pillarisetty, H.C. George, T.F. Watson, L. Lampert, N. Thomas, S. Bojarski, P. Amin, R. Caudillo, E. Henry, N. Kashani, P. Keys, R. Kotlyar, F. Luthi, D. Michalak, K. Millard, J. Roberts, J. Torres, O. Zietz, T. Krähenmann, A.-M. Zwerver, M. Veldhorst, G. Scappucci, L.M.K. Vandersypen, and J.S. Clarke, 2019 IEEE IEDM San Francisco, pp. 31.5.1-31.5.4.

#### 9:36 AM \*F.NM05.06.02

**Si/SiGe Heterostructures for Quantum Information Science** [Clayton A. Jackson](#); HRL Laboratories, United States

Quantum information and computing are at the forefront of computer science, but their implementation relies on the identification and development of a suitable materials system. One such candidate is Si/SiGe. Much progress has been made in Si/SiGe heterostructures grown on metamorphic SiGe substrates as hosts to lithographically defined quantum dots. In this presentation we focus on the general structure and requirements of SiGe quantum dot heterostructures, the demands imposed by necessary dot performance, and advances in characterization methods for these materials.

SESSION F.NM05.10: Live Keynote III: Emerging Materials for Quantum Information Technologies  
Session Chairs: Tzu-Ming Lu and Javad Shabani  
Friday Afternoon, December 4, 2020  
F.NM05

#### 1:45 PM \*F.NM05.02.01

**Engineering Semiconductors for Spin-Based Quantum Technologies** Christopher Anderson, Alexandre Bourassa, Kevin Miao and [David Awschalom](#); University of Chicago, United States

Silicon carbide (SiC) is a technologically mature semiconductor material that is host to a variety of different solid-state spin defects. These spin qubits not only boast long coherences but also a natural spin-photon interface that can mediate entanglement at a distance. However, as for any solid-state quantum technology, issues of charge noise and magnetic fluctuations are prevalent. In this talk, we present recent advances in minimizing and controlling these sources of noise.

We first discuss our ability to mitigate charge noise in commercial SiC electronic devices [1]. Surprisingly, the integration of single spins into these devices results in THz-scale tunability of a single divacancy spin's optical interface while simultaneously eliminating spectral diffusion and blinking. This results in an electrically-tunable single photon source that can be tuned over 40,000 linewidths, constituting a near-ideal spin-photon interface at wafer scales near the telecommunications band.

We then describe the control and optimization of the nuclear spin environment for these spin qubits [2]. In general, nuclear spins are both a cause of decoherence and a valuable resource for electron spins in the solid-state. While isotopic purification



removes noise, it also reduces the availability of nuclear spin quantum memories that are vital to many quantum technologies. Guided by *ab-initio* theory, we strike this balance and find an optimal isotopic concentration that maximizes the number of available quantum memories. Experimentally, we demonstrate extended coherences and the first entanglement and control of single nuclear spins in silicon carbide through isotopic engineering.

The elimination of electrical noise combined with finely tuning the nuclear environment results in a material platform for quantum technology that combines a stable spin-photon interface with an electron spin that can leverage entanglement with local nuclear spin qubit clusters. We show that this electron spin state has long coherence times ( $T_2 > 2.3$  ms,  $T_2^* > 370$   $\mu$ s), state-of-the-art control fidelities ( $> 99.984\%$ ), and displays readout and initialization contrast exceeding 99%, providing an exciting pathway toward scalable quantum information technologies in the solid-state.

This work was done in collaboration with Mykyta Onizhuk, He Ma, Gary Wolfowicz, Peter Mintun, Alex Crook, Hiroshi Abe, Jawad Ul Hassan, Nguyen Son, Takeshi Ohshima and Giulia Galli.

[1] C. P. Anderson\*, A. Bourassa\*, K. C. Miao, G. Wolfowicz, P. J. Mintun, A. L. Crook, H. Abe, J. U. Hassan, N. T. Son, T. Ohshima, D. D. Awschalom, "Electrical and optical control of single spins integrated in scalable semiconductor devices," *Science* **336**, 6470, 1225-1230 (2019)

[2] A. Bourassa\*, C. P. Anderson\*, K. C. Miao, M. Onizhuk, H. Ma, A. Crook, H. Abe, J. Ul-Hassan, T. Ohshima, N. T. Son, G. Galli, D. D. Awschalom, "Entanglement and control of single quantum memories in isotopically engineered silicon carbide," *arXiv* 2005.07602 (2020)

## 2:15 PM \*F.NM05.02.03

**Scalable Quantum Networks with Artificial Atoms** [Dirk R. Englund](#); Massachusetts Institute of Technology, United States

The central challenge in building quantum computers and long-range quantum networks is distributing entanglement across multiple individually-controllable quantum memories. While proof-of-concept experiments are possible with today's optical components, scaling these systems to tens, hundreds, or thousands of individually controllable quantum memories requires very-large-scale integration of electronic and photonic circuits.

Diamond color centers (CC) have emerged as leading solid state "artificial atom" qubits, having recently surpassed the entanglement-to-decoherence threshold for deterministic delivery of quantum entanglement[1] as well as the first demonstration of "useful" quantum-memory-enhanced communication beating any direct-transmission optical channel[2]. A central challenge now lies in the development of quantum information processing architectures to improve entanglement rates, reduce decoherence, and to scale systems for applications ranging from quantum repeaters to general-purpose quantum computers.

To answer this challenge, we are developing photonic integrated circuits (PICs) with integrated quantum memories based on diamond CCs. In particular, this talk discusses our recent demonstration of a PIC with 128 waveguide-integrated silicon vacancy (SiV) and germanium vacancy (GeV) color centers[3].

Secondly, this talk will review recent advances on spin and optical properties of recently discovered tin-vacancy (SnV) CCs which have significantly larger ground state orbital splitting than the lighter Group IV-vacancy complexes. We observe that even at modest temperatures near  $\sim 4$ K, the SnV possesses the essential attributes for a spin-photon interface: optical transitions approaching the lifetime limit and a long-lived electronic spin state[4].

The talk will finish with an outlook on resource-performance analyses for large-scale quantum repeaters [3,5,6], modular quantum computers[7,8], and coherent interfaces to phonons and microwave photons[9].

[1] P. C. Humphreys, N. Kalb, J. P. J. Morits, R. N. Schouten, R. F. L. Vermeulen, D. J. Twitchen, M. Markham, and R. Hanson, *Nature* **558**, 268 (2018).

[2] M. K. Bhaskar, R. Riedinger, B. Machielse, D. S. Levonian, C. T. Nguyen, E. N. Knall, H. Park, D. Englund, M. Lončar, D. D. Sukachev, and M. D. Lukin, *arXiv [quant-Ph]* (2019).

[3] N. H. Wan, T.-J. Lu, K. C. Chen, M. P. Walsh, M. E. Trusheim, L. De Santis, E. A. Bersin, I. B. Harris, S. L. Mouradian, I. R. Christen, E. S. Bielejec, and D. Englund, *arXiv [quant-Ph]* (2019); to appear in *Nature* (2020)

[4] M. E. Trusheim, B. Pingault, N. H. Wan, M. Gündoğan, L. De Santis, R. Debroux, D. Gangloff, C. Purser, K. C. Chen, M. Walsh, J. J. Rose, J. N. Becker, B. Lienhard, E. Bersin, I. Paradeisanos, G. Wang, D. Lyzwa, A. R.-P. Montblanch, G. Malladi, H. Bakhru, A. C. Ferrari, I. A. Walmsley, M. Atatüre, and D. Englund, *Phys. Rev. Lett.* **124**, 023602 (2020).

[5] Y. Lee, E. Bersin, A. Dahlberg, S. Wehner, and D. Englund, *arXiv [quant-Ph]* (2020).

[6] K. C. Chen, E. Bersin, and D. Englund, *arXiv [quant-Ph]* (2020).

[7] H. Choi, D. Zhu, Y. Yoon, and D. Englund, *Phys. Rev. Lett.* **122**, 183602 (2019).

[8] H. Choi, M. Pant, S. Guha, and D. Englund, *Npj Quantum Information* 5, 104 (2019).

[9] T. Neuman, M. Eichenfield, M. Trusheim, L. Hackett, P. Narang, and D. Englund, arXiv [quant-Ph] (2020).

#### 2:45 PM \*F.NM05.03.04

**Coherent Control of a Hybrid Superconducting Circuit Made with van der Waals Heterostructures** William Oliver and I-Jan Wang; Massachusetts Institute of Technology, United States

In this talk, we present the demonstration of a superconducting transmon qubit realized using a graphene-based weak-link junction. The graphene is encapsulated by hexagonal Boron Nitride (hBN), forming a van der Waals heterostructure. Applying a voltage to a backgate in proximity to the weak-link junction enables voltage tunability of the qubit frequency. We present the coherent control of this qubit, and discuss the promise and the challenges of building superconducting qubits with such van der Waals heterostructures.

#### 3:15 PM \*F.NM05.03.01

**Quantum Computing with Superconducting Circuits** Ryan T. Gordon; IBM Research, United States

Quantum computing has made tremendous progress in recent years, including both experimental advances and hardware developments. Quantum processors have scaled significantly in size, as measured by the number of quantum bits (qubits) connected on a chip, with devices incorporating 10's of qubits available today. An example of a publicly available quantum system is the IBM Q Experience ([www.research.ibm.com/ibm-q](http://www.research.ibm.com/ibm-q)). While the goal of fault-tolerant universal quantum computing is still some time away, early applications and demonstrations can be implemented on smaller scale near-term quantum systems. Among the different hardware implementations, Josephson-junction-based superconducting quantum circuits are a promising technology to scale quantum processors. Together with increasing the number of qubits, other metrics need to evolve and improve as well, such as qubit quality, hardware integration, and system level performance. In this talk, I will review the current status and discuss some of the remaining challenges.

### SESSION F.NM05.01: Atomic Precision Fabrication

On Demand Abstracts Available for Viewing Starting Saturday Morning, November 21, 2020  
F-NM05

#### 5:00 AM \*F.NM05.01.01

**Atomic Qubits in Silicon** Michelle Y. Simmons<sup>1,2</sup>; <sup>1</sup>University of New South Wales, Australia; <sup>2</sup>Silicon Quantum Computing Pty Ltd, Australia

Atom qubits in silicon have demonstrated extremely long electron and nuclear spin coherence times [1,2] making silicon a promising semiconductor material for spin-based quantum information. The two-level spin state of single electrons bound to shallow phosphorus donors in silicon provide well defined, reproducible qubits [3] with low gate densities. An important challenge in these systems is the realisation of an architecture, where we can position donors within a crystalline environment with <20nm separation, individually address each donor, manipulate the electron spins using ESR techniques, read-out their spin states and perform both single and two qubit gates.

We have pioneered a unique strategy to build a scalable quantum computer in silicon atom by atom. We use scanning tunneling microscope lithography and ultra-high vacuum crystal growth to precisely position individual P donors in Si [4] aligned with nanoscale precision to local control gates [5] necessary to initialize, manipulate, and read-out the spin states [6-8].

During this talk I will focus on demonstrating fast, high fidelity single-shot spin read-out [9], ESR control of precisely-positioned P donors in Si [10] and our recent results of demonstrating a fast (~ns) two-qubit SWAP gate [11,12]. We have also published a 3D architecture for implementation of error correction using the surface code [13]. With important advances in control at the atomic-scale, I will attempt to highlight the benefits of single atom qubits in silicon.

#### References

[1] K. Saeedi *et al.*, *Science* 342, 130 (2013).

- [2] J. T. Muhonen *et al.*, Nature Nanotechnology 9, 986 (2014).
- [3] B.E. Kane, Nature 393, 133 (1998).
- [4] M. Fuechsle *et al.*, Nature Nanotechnology 7, 242 (2012).
- [5] B. Weber *et al.*, Science 335, 6064 (2012).
- [6] H. Buch *et al.*, Nature Communications 4, 2017 (2013).
- [7] B. Weber *et al.*, Nature Nanotechnology 9, 430 (2014).
- [8] T. F. Watson *et al.*, Science Advances 3, e1602811 (2017).
- [9] D. Keith *et al.*, Physical Review X 9, 041003 (2019)
- [10] S. Hile *et al.*, Science Advances 4, eaaq1459 (2018).
- [11] M.A. Broome *et al.*, Nature Communications 9, 980 (2018).
- [12] S. Gorman, Y. He *et al.*, Nature 571, 371 (2019).
- [13] C. Hill *et al.*, Science Advances 1, e1500707 (2015).

### 5:15 AM F.NM05.01.02

**A Multiscale Model of the Reaction Pathway for P-Type Doping Using Diborane on Si(100)-2x1** Quinn Campbell, Jeffrey A. Ivie, Scott W. Schmucker, Andrew Baczewski and Shashank Misra; Sandia National Laboratories, United States

Diborane ( $B_2H_6$ ) is a promising precursor molecule for atomic precision p-type doping of silicon that has recently been experimentally demonstrated on the Si (100) surface [Škeren, et al., 2019]. We use first principles density functional theory (DFT) calculations to determine the reaction pathway of diborane dissociating into incorporated boron at the silicon surface. We show that diborane must overcome an energy barrier to even adsorb onto the bare silicon surface, explaining the low sticking coefficient seen in previous studies. Heating can be used to increase the initial adsorption rate. From there, the diborane has a roughly half chance of splitting into two  $BH_3$  particles or merely losing hydrogen to form a boron dimer such as  $B_2H_4$ . Dimers of boron are likely electrically inactive, thus making it crucial that the diborane split for final incorporation of an electrically active acceptor. The dissociation process proceeds with high energy barriers, necessitating the use of high temperatures for incorporation. Using the barriers calculated from DFT, we parameterize a Kinetic Monte Carlo model, predicting incorporation statistics of diborane as a function of initial depassivation geometry, dose pressure, and anneal temperature. Finally, we present a theoretical comparison of diborane to other potential acceptor precursor molecules.

Sandia National Laboratories is a multimission laboratory managed and operated by National Technology and Engineering Solutions of Sandia, LLC., a wholly owned subsidiary of Honeywell International, Inc., for the U.S. Department of Energy's National Nuclear Security Administration under contract DE-NA-0003525. This paper describes objective technical results and analysis. Any subjective views or opinions that might be expressed in the paper do not necessarily represent the views of the U.S. Department of Energy or the United States Government.

### 5:25 AM F.NM05.01.03

**Low-Temperature Processing for Atomically Precise Dopant Incorporation with CMOS Integration** Scott W. Schmucker, Evan M. Anderson, Esther Frederick, Jeffrey A. Ivie, Ezra Bussman, DeAnna Campbell, Lisa A. Tracy, Tzu-Ming Lu, Ping Lu, George Wang, Daniel Ward and Shashank Misra; Sandia National Laboratories, United States

Scanning tunneling microscopy and hydrogen depassivation lithography (HDL) have enabled tip-defined placement of dopant atoms in Si for Atomic Precision Advanced Manufacturing (APAM) [1-2] of conventional and quantum electronic devices. Although it affords greater placement accuracy than ion implantation, APAM has historically required high-temperature processing incompatible with microelectronics fabrication workflows. Recent process developments have reduced the thermal budget for APAM sample prep, the highest temperature step of the process, to temperatures comparable to activation for ion implantation. Reduced temperature prep opens the door to integrating APAM near the end of front-end-of-line (FEOL) fabrication thereby integrating atomic-scale dopant placement with conventional microelectronic processes. Further reducing the thermal budget for key parts of the APAM process flow – sample preparation, hydrogen termination, dopant incorporation, and silicon capping – may open the door to adding dopants during back-end-of-line (BEOL) fabrication for the first time.

Here, we discuss techniques for FEOL and BEOL APAM integration of donor and acceptor dopants in Silicon. We demonstrate room-temperature Si(100) hydrogen passivation without compromising HDL and reduced-temperature Si encapsulation without significantly compromising electron transport. In an effort to reduce surface preparation temperatures and achieve BEOL CMOS compatibility, we explore both wet chemical and ion beam processes for low-temperature Si(100) 2x1 preparation and discuss the limitations of each. Thermal budget considerations explored here are one of the key challenges which must be addressed to enable APAM integration. We conclude that hydrogen passivation, HDL, dopant

introduction, and Si encapsulation can be made compatible with BEOL integration. Future challenges remain for sample cleaning, but preliminary results are encouraging and suggest, with continued development, the possibility of APAM BEOL CMOS integration.

This work was supported by the Laboratory Directed Research and Development Program at Sandia National Laboratories, and was performed, in part, at the Center for Integrated Nanotechnologies, a U.S. DOE, Office of Basic Energy Sciences user facility. Sandia National Laboratories is managed and operated by National Technology and Engineering Solutions of Sandia, LLC., a wholly owned subsidiary of Honeywell International, Inc., for the U.S. Department of Energy under contract DE-NA-0003525. The views expressed do not necessarily represent the views of the U.S. DOE or the United States Government.

[1] D.R. Ward et al., Appl. Phys. Lett. 111, 193101 (2017)

[2] D.R. Ward et al., EDFA Magazine 22, 1 (2020)

#### 5:35 AM F.NM05.01.04

**Atomically Precise P-Type Doping Using Alanes** Wiley P. Kirk<sup>1,2</sup>, Eduardo Maldonado<sup>1</sup>, Jeffery Murphy<sup>1,2</sup> and Jean-Francois Veyan<sup>3</sup>; <sup>1</sup>3D Epitaxial Technologies, United States; <sup>2</sup>The University of Texas at Arlington, United States; <sup>3</sup>The University of Texas at Dallas, United States

Recently, new devices for future classical and quantum computation technologies have been demonstrated using scanning tunneling microscopy (STM) and hydrogen depassivation lithography (HDL) to position phosphorous or arsenic atoms as donors in silicon with atomic-scale precision.[1,2] Although precursors such as phosphine (PH<sub>3</sub>) and arsine (AsH<sub>3</sub>) serve satisfactorily as gaseous sources for donors, the potential counterpart acceptor precursors such as diborane (B<sub>2</sub>H<sub>6</sub>) and alane (aluminum hydride, AlH<sub>3</sub>) as sources have proven to be more challenging when combined with the aforesaid atomic-scale STM-HDL technology. In particular, alanes are energetically stable only at temperatures  $T \leq 120$  K. On the other hand, recent DFT calculations [3] show a stable route exists for AlH<sub>3</sub> dissociation and Al incorporation (following selective surface hydrogen desorption by STM). Moreover, the DFT results show the overall process of AlH<sub>3</sub> surface interactions on Si parallels PH<sub>3</sub>; hence, atomically precise acceptor doping should be possible using alanes. With these constraints in mind, we have developed a new type of low-temperature alane precursor source that provides p-type dopants that are compatible with atomic-scale fabrication techniques. Specifically, infrared data from fast Fourier transform spectroscopy, examining alane formation and specie type, will be presented as a function of temperature. In addition, electronic transport characteristics from van der Pauw and Hall effect measurements as a function of temperature are planned for presentation.

#### REFERENCES

1. Schofield, S. R.; Curson, N. J.; Simmons, M. Y.; Rueß, F. J.; Hallam, T.; Oberbeck, L.; Clark, R. G. *Atomically Precise Placement of Single Dopants in Si*. Phys. Rev. Lett. **91**, 136104 (2003).
2. Stock, Taylor J. Z.; Warschkow, Oliver; Constantinou, Procopios C.; Li, Juerong; Fearn, Sarah; Crane, Eleanor; Hofmann, Emily V. S.; Kölker, Alexander; McKenzie, David R.; Schofield, Steven R.; Curson, Neil J., *Atomic-Scale Patterning of Arsenic in Silicon by Scanning Tunneling Microscopy*, ACS Nano, **14**(3), 3316-3327 (2020).
3. Smith, Richard; Bowler, David, R., *Reaction paths of alane dissociation on the Si(001) surface*, Journal of Physics: Condensed Matter **30**(10), 105002 (2018).

#### 5:45 AM F.NM05.01.05

**Solving the Puzzle of Al Atom Density on Delta-Doped Si (100)** Ke Tang<sup>1,2</sup>, Hyun Soo Kim<sup>1,2</sup>, Aruna Ramanayaka<sup>1</sup> and Joshua M. Pomeroy<sup>1</sup>; <sup>1</sup>National Institute of Standards and Technology, United States; <sup>2</sup>University of Maryland, United States

Efforts to grow Si (100) with a supersaturated Al delta layer in pursuit of a superconducting phase are hampered by an ambiguity in the surface Al atom density as measured by STM (scanning tunneling microscopy). An apparent consensus for decades has been that Al tends to form surface dimers, which can appear as single sphere in positive bias, in 2 x 2 structure at low temperature and saturates at 0.5 monolayer ( $3.4 \times 10^{14}$  cm<sup>-2</sup>) before Al cluster formation (monolayer is in reference to Si(100) site density). However, our recent SIMS (secondary ion mass spectroscopy) analysis shows that the 2D number density of Al on Si (100) is actually 0.25 monolayer ( $1.7 \times 10^{14}$  cm<sup>-2</sup>), half of the prior STM density, indicating the possibility of another Al phase on Si (100) surface. In addition, mesa etched hall bar devices fabricated find p-type carriers with consistent densities  $\approx 1.5 \times 10^{14}$  cm<sup>-2</sup> and mobility of  $\approx 20$  cm<sup>2</sup>/V s. Developing a complete phase diagram of the surface doping will enable optimal Al dosing above the expected superconducting critical density of 4 at. % with a minimum number of mixed Al clusters in the doped lattice.

#### 5:55 AM F.NM05.01.06

**Triethyl Aluminium—A Precursor for Atomically-Precise Acceptor Dopant Placement** James H. Owen, Robin Santini and John Randall; Zyvex Labs, United States

The fabrication of n-type dopant-based devices such as the ‘single atom transistor’ [1] and 2D Quantum Metamaterials[2] uses STM lithography to create patterns of reactive Si dangling bonds with a background of passive H-terminated Si. Phosphine (PH<sub>3</sub>) is used as a precursor molecule for the P dopant atoms adsorbing extremely selectively onto the bare Si atoms which make up the device pattern. For p-type dopants, the Group III equivalents of phosphine, the alanes, are thought to react on the surface in a similar way [3], but are not stable at room temperature. Diborane has a very low sticking coefficient onto bare Si, forcing the use of very large doses to achieve a good density of B dopants[4]. Here we are exploring alkyl dopant sources, including Trimethyl Al, Triethyl Al and Tri-isobutyl Al, which are widely used in III-V CVD reactors. Recently, we have focused on Triethyl Al, as it has a much higher sticking coefficient than Tri-isobutyl Al and is preferred over Trimethyl Al for lower carbon contamination of the grown films. On Si, ethylene is known to desorb from the clean Si surface at about 400°C, which promises a lower carbon incorporation rate.

We have conducted adsorption and selectivity experiments with Triethyl Al on bare and H-terminated Si(001) surfaces. At room temperature, we find that the sticking coefficient of the molecule is low even on the bare Si(001) surface. There is no apparent adsorption on the H-terminated surface. However, we find that patterns drawn on the H-terminated surface after a TEAL dose will slowly fill with adsorbates over time, indicating the presence on the surface of mobile molecules, which are weakly bound and invisible to the STM. By performing the adsorption at elevated temperatures, we were able to remove these mobile molecules, and at the same time, the reaction of the bare surface to these molecules was greatly increased. After adsorption, the ethyl groups were driven off the surface, and the Al atoms incorporated into the surface, using a high-temperature anneal to around 400°C. This recipe was used to create delta layers of Al, which were then buried using the same process as used to bury P delta layers [1]. SIMS data of these delta layers show good confinement of Al to the delta layer. We continue to refine the adsorption and annealing process to increase the peak concentration of the Al in the delta layer, minimise segregation into the overgrowth, as well as to further reduce the amount of carbon trapped at the delta layer. Considering the bigger picture, if a suitable process can be found for Triethyl Al, this process is likely to be compatible with other standard CVD dopant precursors, such as TriEthyl Ga, and similar precursors for other elements, such as Zn or Er, which would greatly broaden the applicability of the atomically-precise dopant placement process.

1: M. Fuechsle, J. A. Miwa, S. Mahapatra, H. Ryu, S. Lee, O. Warschkow, L. C. L. Hollenberg, G. Klimeck, and M. Y. Simmons Nat Nano 7 242-246 (2012)

2: <https://www.zyvexlabs.com/2d-workshop/workshop-overview/>

3: R. Smith and D.R. Bowler, J. Phys. Condens. Matter 30, 105002 (2018).

4: T. Skeren, S. Koster, B. Douhard, C. Fleischmann and A. Fuhrer, Arxiv: 1912.06188 (2019)

**6:05 AM F.NM05.01.07**

**Feedback Controlled Lithography for Atomically Perfect Quantum Devices and Materials in Si** Jonathan Wyrick<sup>1</sup>, Xiqiao Wang<sup>1</sup>, Ranjit Kashid<sup>1</sup>, Pradeep Namboodiri<sup>1</sup>, Fan Fei<sup>2,2</sup> and Richard Silver<sup>1</sup>; <sup>1</sup>National Institute of Standards and Technology, United States; <sup>2</sup>University of Maryland, United States

In recent years it has become possible to construct near-atomically perfect phosphorus-based structures, 2D materials and quantum devices, embedded in silicon using STM bottom-up fabrication. If this technology can be developed to a sufficient degree of accuracy and reproducibility, it will have very clear applications for quantum computing and quantum information architectures in addition to realizing the promise of scaling electronics to the atomic limit. In the current implementation of the bottom-up fabrication technique, the STM is used to generate regions of clean silicon by selective removal of H atoms from a hydrogen terminated Si (100) surface. This is followed by introduction of phosphine (PH<sub>3</sub>) gas which chemically bonds only to depassivated sites. Subsequent thermal processing allows for reactions to take place in which P atoms substitutionally replace Si surface atoms so that spacings between electronic components (defined by P) are controlled to within a few lattice sites. Individual components can be scaled down to the point that they are composed of few P atom clusters. However, to date, deterministic control over the number of P atoms incorporated at a site has not been achieved in a reliable manner. Results from previous studies have found that for targeted single-atom sites, there is approximately a 20% chance of failure to incorporate any atoms (i.e. the site is left empty).

In this talk, we detail our progress towards achieving true single atom per site control. We write patterns intended for single P atom incorporation using feedback controlled lithography (FCL) so that adsorption sites are atomically identical. In a subset of patterned sites, we investigate STM-based manipulation of the deposited phosphine species. These results are combined with a density functional theory analysis in which precise adsorption configurations and reaction products can be identified via STM image simulation to gain insights into the chemistry of phosphine adsorption at FCL-tailored sites. We find that for

perfectly patterned structures, sub-nanometer precision in placement of individual P atoms is achieved and that there is evidence of the presence of the P atoms after the thermal processing step in which P is incorporated. While technically demanding, these results suggest a path to fabricate devices with absolute certainty in the number of P atoms comprising key components, enabling precision control over their electronic structure and, therefore, quantum properties.

#### 6:15 AM F.NM05.01.08

**Quantum Transport and Hubbard Physics in a 3×3 Artificial Lattice of Few-Donor Quantum Dots** Xiqiao Wang<sup>1,2</sup>, Fan Fei<sup>1,2</sup>, Jonathan Wyrick<sup>1</sup>, Ranjit Kashid<sup>1</sup>, Pradeep Namboodiri<sup>1</sup>, Emily Townsend<sup>1</sup>, Albert Rigosi<sup>1</sup>, Garnett Bryant<sup>1</sup> and Richard Silver<sup>1</sup>; <sup>1</sup>National Institute of Standards and Technology, United States; <sup>2</sup>University of Maryland, United States

Donor-based quantum materials in silicon are a promising candidate for scalable solid-state quantum computing and analog quantum simulation. Central to the scalability and performance of this quantum materials system is the precision control and physical understanding of materials properties at the atomic scale. Recent advances in atomically precise fabrication in silicon using scanning tunneling microscopy (STM) have demonstrated success in atomic-scale control of tunneling and atom-by-atom construction of single and few-donor quantum devices, enabling donor-based quantum meta-materials and high-fidelity two-qubit gates. In this presentation, we demonstrate the construction of a 3×3 artificial square lattice using precision patterned few-donor quantum dots. We probe the resonant quantum transport and Hubbard properties of the donor-array towards the possibilities of using the donor-based artificial lattice as a Hubbard quantum simulator.

The Hubbard model has been one of the primary models for capturing the essential physics and materials properties in condensed matter and emerging quantum systems. Due to its natural long-range Coulomb interactions, accessible low-temperatures, and atomic-scale nature, an artificial lattice of donor clusters made of one or multiple donor atoms in silicon is advantageous in simulating Hubbard many-body problems, especially in strong interaction regimes. In this presentation, we focus on the atomic-scale fabrication and low-temperature transport characterization of an STM-patterned 3×3 array of few-donor quantum dots. By embedding the dot-array system in the electrostatic environment of the real transport device and solving the extended Hubbard model, we analyze the Coulomb blockade and quantum transport features through the donor array. We estimate the microscopic structure and tunnel coupling of individual quantum dots at each artificial lattice site by measuring single-electron tunneling spectroscopy through single and few-donor quantum dots with atomically defined tunnel gaps. Combining experimental and simulated results, we evaluate the potential impact of disorder and atomic-scale imperfection in the donor array on single-electron transport and the possibility of using quantum transport as a sensitive probe for understanding Hubbard physics in donor-based quantum materials systems.

#### 6:25 AM F.NM05.01.09

**B- and Al-Doped Delta Layers in Si Using Halogen-Based Precursors** Sungha Baek<sup>1</sup>, Azadeh Farzandeh<sup>1</sup>, Matthew S. Radue<sup>2</sup>, Quinn Campbell<sup>3</sup>, Kevin J. Dwyer<sup>1</sup>, Andrew Baczewski<sup>3</sup>, Yifei Mo<sup>1</sup>, Shashank Misra<sup>3</sup> and Robert E. Butera<sup>1,2</sup>; <sup>1</sup>University of Maryland, United States; <sup>2</sup>Laboratory for Physical Sciences, United States; <sup>3</sup>Sandia National Laboratories, United States

The technology required to fabricate atomic-scale quantum devices in silicon has advanced significantly over the past decade to produce a variety of dopant-based devices, including qubits, atomic wires, tunnel junctions, and single electron transistors. Nearly all such devices made to date have been phosphorous-based and achieved through the careful control of the reaction PH<sub>3</sub> with the silicon surface. While the PH<sub>3</sub>/Si system has been well studied, little progress has been made towards the realization of analogous acceptor-based devices. With the promise of hole-based qubits with extremely long coherence times and strong coupling to electric fields, along with the potential to achieve superconductivity in Si, there are tremendous opportunities to advance Si-based quantum computing upon the identification of an ideal gaseous precursor. Here, we present results on the use of BCl<sub>3</sub> and AlCl<sub>3</sub> as dopant precursors for the formation of acceptor-doped, delta layers in silicon. Surface reactions were studied with scanning tunneling microscopy (STM), X-ray photoelectron spectroscopy (XPS), secondary ion mass spectroscopy (SIMS), and density functional theory (DFT) calculations to elucidate the reaction pathways for B and Al dopants leading towards dopant incorporation into the Si surface. SIMS measurements confirm B and Al concentrations in excess of 10<sup>20</sup> cm<sup>-3</sup>. These results provide a major step in the further development of atomic-scale quantum devices in Si. SNL is managed and operated by NTESS under DOE NNSA contract DE-NA0003525.

SESSION F.NM05.02: Dots, Defects and Color Centers

On Demand Abstracts Available for Viewing Starting Saturday Morning, November 21, 2020  
F-NM05

### 5:00 AM \*F.NM05.02.01

**Engineering Semiconductors for Spin-Based Quantum Technologies** Christopher Anderson, Alexandre Bourassa, Kevin Miao and David Awschalom; University of Chicago, United States

Silicon carbide (SiC) is a technologically mature semiconductor material that is host to a variety of different solid-state spin defects. These spin qubits not only boast long coherences but also a natural spin-photon interface that can mediate entanglement at a distance. However, as for any solid-state quantum technology, issues of charge noise and magnetic fluctuations are prevalent. In this talk, we present recent advances in minimizing and controlling these sources of noise.

We first discuss our ability to mitigate charge noise in commercial SiC electronic devices [1]. Surprisingly, the integration of single spins into these devices results in THz-scale tunability of a single divacancy spin's optical interface while simultaneously eliminating spectral diffusion and blinking. This results in an electrically-tunable single photon source that can be tuned over 40,000 linewidths, constituting a near-ideal spin-photon interface at wafers scales near the telecommunications band.

We then describe the control and optimization of the nuclear spin environment for these spin qubits [2]. In general, nuclear spins are both a cause of decoherence and a valuable resource for electron spins in the solid-state. While isotopic purification removes noise, it also reduces the availability of nuclear spin quantum memories that are vital to many quantum technologies. Guided by *ab-initio* theory, we strike this balance and find an optimal isotopic concentration that maximizes the number of available quantum memories. Experimentally, we demonstrate extended coherences and the first entanglement and control of single nuclear spins in silicon carbide through isotopic engineering.

The elimination of electrical noise combined with finely tuning the nuclear environment results in a material platform for quantum technology that combines a stable spin-photon interface with an electron spin that can leverage entanglement with local nuclear spin qubit clusters. We show that this electron spin state has long coherence times ( $T_2 > 2.3$  ms,  $T_2^* > 370$   $\mu$ s), state-of-the-art control fidelities ( $> 99.984\%$ ), and displays readout and initialization contrast exceeding 99%, providing an exciting pathway toward scalable quantum information technologies in the solid-state.

This work was done in collaboration with Mykyta Onizhuk, He Ma, Gary Wolfowicz, Peter Mintun, Alex Crook, Hiroshi Abe, Jawad Ul Hassan, Nguyen Son, Takeshi Ohshima and Giulia Galli.

[1] C. P. Anderson\*, A. Bourassa\*, K. C. Miao, G. Wolfowicz, P. J. Mintun, A. L. Crook, H. Abe, J. U. Hassan, N. T. Son, T. Ohshima, D. D. Awschalom, "Electrical and optical control of single spins integrated in scalable semiconductor devices," *Science* **336**, 6470, 1225-1230 (2019)

[2] A. Bourassa\*, C. P. Anderson\*, K. C. Miao, M. Onizhuk, H. Ma, A. Crook, H. Abe, J. Ul-Hassan, T. Ohshima, N. T. Son, G. Galli, D. D. Awschalom, "Entanglement and control of single quantum memories in isotopically engineered silicon carbide," *arXiv* 2005.07602 (2020)

### 5:15 AM \*F.NM05.02.02

**Correlating Surface Spectroscopy with Qubit Measurements to Systematically Eliminate Sources of Noise** Nathalie P. de Leon; Princeton University, United States

The nitrogen vacancy (NV) center in diamond exhibits spin-dependent fluorescence and long spin coherence times under ambient conditions, enabling applications in quantum information processing and sensing. NV centers near the surface can have strong interactions with external materials and spins, enabling new forms of nanoscale spectroscopy. However, NV spin coherence degrades within 100 nanometers of the surface, suggesting that diamond surfaces are plagued with ubiquitous defects. Prior work on characterizing near-surface noise has primarily relied on using NV centers themselves as probes; while this has the advantage of exquisite sensitivity, it provides only indirect information about the origin of the noise. I will describe our recent efforts to use X-ray and photoelectron spectroscopies, diffraction techniques, and morphology characterization to understand sources of noise at the diamond surface. By correlating this spectroscopic data with single spin measurements, we have been able to devise new surface processing and termination techniques to stabilize shallow NV centers within 5 nm of the surface with coherence times exceeding 100 ms [1]. Specifically, we are able to demonstrate reversible and reproducible control over the top layer of atoms. These highly coherent, shallow NV centers will provide a

platform for sensing and imaging down to the scale of single atoms.

In fact, many platforms for quantum technologies are limited by noise and loss arising from uncontrolled defects at surfaces and interfaces, including superconducting qubits, trapped ions, and semiconductor quantum dots. Our approach for correlating surface spectroscopy techniques with single qubit measurements to realize directed improvements is generally applicable to many systems, and I will describe our recent efforts to tackle noise and microwave losses in superconducting qubits. Building large, useful quantum systems based on transmon qubits will require significant improvements in qubit relaxation and coherence times, which are orders of magnitude shorter than limits imposed by bulk properties of the constituent materials. This indicates that relaxation likely originates from uncontrolled surfaces, interfaces, and contaminants. Previous efforts to improve qubit lifetimes have focused primarily on designs that minimize contributions from surfaces. However, significant improvements in the lifetime of two-dimensional transmon qubits have remained elusive for several years. We have fabricated two-dimensional transmon qubits that have both lifetimes and coherence times with dynamical decoupling exceeding 0.3 milliseconds by replacing niobium with tantalum in the device [2]. We have observed increased lifetimes for many devices, indicating that these material improvements are robust, paving the way for higher gate fidelities in multi-qubit processors.

#### References

1. S. Sangtawasin, B. L. Dwyer, S. Srinivasan, J. J. Allred, L. V. H. Rodgers, K. De Greve, A. Stacey, N. Dentschuk, K. M. O'Donnell, D. Hu, D. A. Evans, C. Jaye, D. A. Fischer, M. L. Markham, D. J. Twitchen, H. Park, M. D. Lukin, N. P. de Leon, "Origins of diamond surface noise probed by correlating single spin measurements with surface spectroscopy," *Physical Review X* 9, 031052 (2019).
2. A. P. M. Place, L. V. H. Rodgers, P. Mundada, B. M. Smitham, M. Fitzpatrick, Z. Leng, A. Premkumar, J. Bryon, S. Sussman, G. Cheng, T. Madhavan, H. K. Babla, B. Jaeck, A. Gyenis, N. Yao, R. J. Cava, N. P. de Leon, A. A. Houck, "New material platform for superconducting transmon qubits with coherence times exceeding 0.3 milliseconds," arXiv:2003.00024.

#### 5:30 AM \*F.NM05.02.03

**Scalable Quantum Networks with Artificial Atoms** Dirk R. Englund; Massachusetts Institute of Technology, United States

The central challenge in building quantum computers and long-range quantum networks is distributing entanglement across multiple individually-controllable quantum memories. While proof-of-concept experiments are possible with today's optical components, scaling these systems to tens, hundreds, or thousands of individually controllable quantum memories requires very-large-scale integration of electronic and photonic circuits.

Diamond color centers (CC) have emerged as leading solid state "artificial atom" qubits, having recently surpassed the entanglement-to-decoherence threshold for deterministic delivery of quantum entanglement[1] as well as the first demonstration of "useful" quantum-memory-enhanced communication beating any direct-transmission optical channel[2]. A central challenge now lies in the development of quantum information processing architectures to improve entanglement rates, reduce decoherence, and to scale systems for applications ranging from quantum repeaters to general-purpose quantum computers.

To answer this challenge, we are developing photonic integrated circuits (PICs) with integrated quantum memories based on diamond CCs. In particular, this talk discusses our recent demonstration of a PIC with 128 waveguide-integrated silicon vacancy (SiV) and germanium vacancy (GeV) color centers[3].

Secondly, this talk will review recent advances on spin and optical properties of recently discovered tin-vacancy (SnV) CCs which have significantly larger ground state orbital splitting than the lighter Group IV-vacancy complexes. We observe that even at modest temperatures near ~ 4K, the SnV possesses the essential attributes for a spin-photon interface: optical transitions approaching the lifetime limit and a long-lived electronic spin state[4].

The talk will finish with an outlook on resource-performance analyses for large-scale quantum repeaters [3,5,6], modular quantum computers[7,8], and coherent interfaces to phonons and microwave photons[9].

[1] P. C. Humphreys, N. Kalb, J. P. J. Morits, R. N. Schouten, R. F. L. Vermeulen, D. J. Twitchen, M. Markham, and R. Hanson, *Nature* 558, 268 (2018).

[2] M. K. Bhaskar, R. Riedinger, B. Machielse, D. S. Levonian, C. T. Nguyen, E. N. Knall, H. Park, D. Englund, M. Lončar, D. D. Sukachev, and M. D. Lukin, arXiv [quant-Ph] (2019).

[3] N. H. Wan, T.-J. Lu, K. C. Chen, M. P. Walsh, M. E. Trusheim, L. De Santis, E. A. Bersin, I. B. Harris, S. L. Mouradian, I. R. Christen, E. S. Bielejec, and D. Englund, arXiv [quant-Ph] (2019); to appear in *Nature* (2020)

[4] M. E. Trusheim, B. Pingault, N. H. Wan, M. Gündoğan, L. De Santis, R. Debroux, D. Gangloff, C. Purser, K. C. Chen, M. Walsh, J. J. Rose, J. N. Becker, B. Lienhard, E. Bersin, I. Paradeisanos, G. Wang, D. Lyzwa, A. R.-P. Montblanch, G. Malladi, H. Bakhru, A. C. Ferrari, I. A. Walmsley, M. Atatüre, and D. Englund, *Phys. Rev. Lett.* 124, 023602 (2020).

[5] Y. Lee, E. Bersin, A. Dahlberg, S. Wehner, and D. Englund, arXiv [quant-Ph] (2020).



- [6] K. C. Chen, E. Bersin, and D. Englund, arXiv [quant-Ph] (2020).  
[7] H. Choi, D. Zhu, Y. Yoon, and D. Englund, Phys. Rev. Lett. 122, 183602 (2019).  
[8] H. Choi, M. Pant, S. Guha, and D. Englund, Npj Quantum Information 5, 104 (2019).  
[9] T. Neuman, M. Eichenfield, M. Trusheim, L. Hackett, P. Narang, and D. Englund, arXiv [quant-Ph] (2020).

#### 5:45 AM F.NM05.02.05

**Hybridized Defects in 2D Materials as Artificial Molecules** Derek Wang<sup>1</sup>, Christopher J. Ciccarino<sup>1</sup>, Johannes Flick<sup>2</sup> and Prineha Narang<sup>1</sup>; <sup>1</sup>Harvard University, United States; <sup>2</sup>Flatiron Institute, United States

The optical and electronic properties of defects in solid-state materials can be tuned with external fields, as well as with sculpted electromagnetic environments, such as cavities and waveguides. Here, we add to this toolbox by computationally demonstrating that defects, often described as “artificial atoms,” become “artificial molecules” when placed within a few unit cells of each other. Specifically in monolayer hexagonal boron nitride, we observe dissociation curves and hybridization of defect orbitals into bonding and antibonding orbitals, as well as changes in frequency and intensity of dipole-allowed transitions. We calculate the energetics of *cis* and *trans* analogs of paired out-of-plane defects and find that paired in-plane defects interact more strongly than out-of-plane ones. We envision leveraging this chemical degree of freedom to more precisely engineer defects as quantum memories and quantum emitters for quantum information applications.

#### 5:55 AM F.NM05.02.06

**Growth and Direct Observation of SiV Centers in Ultrasmall Nanodiamonds** Shuo Li<sup>1,2</sup>, Daniel Angell<sup>2</sup>, Hye Ryoung Lee<sup>2,1</sup> and Nicholas Melosh<sup>1,2</sup>; <sup>1</sup>SLAC National Accelerator Laboratory, United States; <sup>2</sup>Stanford University, United States

Single photon emitters (SPEs) in solids have emerged as promising candidates for various applications such as quantum technology, nanophotonics and biological imaging. Silicon-vacancy color centers in diamond exhibit high-brightness, stable photo-stability and room-temperature quantum emission, but the precise localization, controllable formation, and direct observation of SiV centers within nanometer scale still remain elusive. Here, we use grow ultrasmall high-quality nanodiamonds using plasma-enhanced vapor deposition (PECVD) from molecular diamondoids as seedings, and incorporated SiV centers during growth. We directly observe SiV emission from 20 nm nanodiamond particles using a combination of cathodoluminescence (CL) and cryogenic transmission electron diffraction (cryo-TEM). Our results provide the controlled growth and direct observation of stable SiV emission in nanometer-scale CVD grown nanodiamonds. These findings are important for fundamental understanding of color center formation mechanism and stability in nanoscale, and are promising for the realization of precise localization of color centers for various quantum applications.

#### 6:05 AM F.NM05.02.07

**Strong Spin-Orbit Quenching in Group IV Neutral Defects in Diamond via the Product Jahn-Teller Effect** Christopher J. Ciccarino<sup>1</sup>, Johannes Flick<sup>2</sup>, Isaac Harris<sup>1,3</sup>, Matthew Trusheim<sup>1</sup>, Dirk R. Englund<sup>3</sup> and Prineha Narang<sup>1</sup>; <sup>1</sup>Harvard University, United States; <sup>2</sup>Flatiron Institute, United States; <sup>3</sup>Massachusetts Institute of Technology, United States

Defects in diamond are leading solid-state candidates for a range of quantum technologies. Recent research has focused on identifying new color centers with properties that reach beyond the limitations of the well-known nitrogen-vacancy (NV<sup>-</sup>) center. Group IV-vacancy centers have been a primary focus due to their symmetry-protected optical transitions and long-lived spin degree of freedom. A detailed understanding of the electronic structure of these emitters is paramount to their use in spin-photon systems. Here we detail the ground- and excited-state properties of the neutral group IV color centers using first principles methods. In particular, we capture the product Jahn-Teller (pJT) effect [1] resulting from the simultaneous Jahn-Teller interactions in two defect orbitals. The significant pJT effects found suggest the excited state is a coupled electron-phonon (vibronic) system, which can have important implications on electronic observables. In particular, we present a nonperturbative approach to capturing the effective spin-orbit splitting [2], which we find to be significantly quenched as a result of this pJT interaction. The lowest optically-active <sup>3</sup>E<sub>u</sub> states are weakly spin-split into ms-resolved states. Our spin-resolved level structure predictions will be useful in understanding the finer details of the SiV<sup>0</sup> as well as provide additional fingerprints for experimental identification of the other group IV neutral emitters.

- [1] Harris, I., Ciccarino, C.J., Flick, J., Englund, D.R., and Narang, P., arXiv:1907.12548 (2019).  
[2] Ciccarino, C.J., Flick, J., Harris, I., Trusheim, M.E., Englund, D.R. and Narang, P., arXiv:2001.07743 (2020).

#### 6:15 AM F.NM05.02.09

**Late News: Dangling Bonds in Hexagonal Boron Nitride for Quantum Information Science** Mark Turiansky<sup>1</sup>, Audrius Alkauskas<sup>2</sup>, Lee Bassett<sup>3</sup> and Chris G. Van de Walle<sup>1</sup>; <sup>1</sup>University of California, Santa Barbara, United States; <sup>2</sup>Center for

Physical Sciences and Technology (FTMC), Lithuania; <sup>3</sup>University of Pennsylvania, United States

Hexagonal boron nitride has been found to host single-photon emitters across a range of energies. Among the observed emitters is a group in the visible spectrum, known as the 2 eV emitters, that are notoriously heterogeneous. Extensive experimental efforts have uncovered a wealth of interesting properties; most notably, the 2 eV emitters are highly desirable for quantum information applications, having minimal coupling to phonons and spin-dependent transitions. Despite these efforts, the microscopic origin of the emitters is the subject of intense debate. We propose that boron dangling bonds are the source of the observed emission. We apply first-principles calculations, based on density functional theory with a hybrid functional, to characterize the properties of these dangling bonds and demonstrate that they provide a consistent understanding of the experimental observations. In the negative charge state, the boron dangling bond is occupied with two electrons. Excitation of one electron into a localized  $p_z$  state results in optical emission with a zero-phonon line of 2.06 eV. The transition is linearly polarized, and the coupling to phonons is characterized by a Huang-Rhys factor of 2.3. Proximity of the states to the conduction band allows for an indirect excitation mechanism for sufficiently large energies. This unique feature explains the misalignment of the absorptive and emissive dipole observed in experiment. While the ground state is a singlet state, we predict the existence of a metastable triplet state, which allows for spin-dependent transitions. All of these features are in line with experimental observations, indicating that boron dangling bonds are the likely origin of the observed emission.

SESSION F.NM05.03: Materials for Superconducting Quantum Systems  
On Demand Abstracts Available for Viewing Starting Saturday Morning, November 21, 2020  
F-NM05

**5:00 AM \*F.NM05.03.01**

**Quantum Computing with Superconducting Circuits** Ryan T. Gordon; IBM Research, United States

Quantum computing has made tremendous progress in recent years, including both experimental advances and hardware developments. Quantum processors have scaled significantly in size, as measured by the number of quantum bits (qubits) connected on a chip, with devices incorporating 10's of qubits available today. An example of a publicly available quantum system is the IBM Q Experience ([www.research.ibm.com/ibm-q](http://www.research.ibm.com/ibm-q)). While the goal of fault-tolerant universal quantum computing is still some time away, early applications and demonstrations can be implemented on smaller scale near-term quantum systems. Among the different hardware implementations, Josephson-junction-based superconducting quantum circuits are a promising technology to scale quantum processors. Together with increasing the number of qubits, other metrics need to evolve and improve as well, such as qubit quality, hardware integration, and system level performance. In this talk, I will review the current status and discuss some of the remaining challenges.

**5:15 AM \*F.NM05.03.03**

**Materials Loss Measurements Using Superconducting Microwave Resonators** Corey Rae McRae<sup>1</sup> and Josh Mutus<sup>2</sup>; <sup>1</sup>University of Colorado Boulder, United States; <sup>2</sup>Google, United States

Two level system (TLS) loss in dielectric materials and interfaces remains at the forefront of materials research in quantum information science. The identification of low loss fabrication techniques, materials, and thin film dielectrics is critical to achieving scalable architectures for superconducting quantum computing. Superconducting microwave resonators provide a convenient qubit proxy for assessing loss performance and studying loss mechanisms such as TLS loss, non-equilibrium quasiparticles, and magnetic flux vortices. In this talk, an overview of design considerations for accurate resonator loss measurements will be given, summarizing techniques that have been evolving for over two decades, and will conclude with recommendations for future measurements in this field.

**5:30 AM \*F.NM05.03.04**

**Coherent Control of a Hybrid Superconducting Circuit Made with van der Waals Heterostructures** William Oliver and I-Jan Wang; Massachusetts Institute of Technology, United States

In this talk, we present the demonstration of a superconducting transmon qubit realized using a graphene-based weak-link junction. The graphene is encapsulated by hexagonal Boron Nitride (hBN), forming a van der Waals heterostructure.

Applying a voltage to a backgate in proximity to the weak-link junction enables voltage tunability of the qubit frequency. We present the coherent control of this qubit, and discuss the promise and the challenges if building superconducting qubits with such van der Waals heterostructures.

#### 5:45 AM F.NM05.03.05

**Characterization of the Structure and Superconducting Properties of Plasma Assisted Molecular Beam Epitaxy Grown  $\text{Nb}_x\text{Ti}_{1-x}\text{N}$  Alloy Thin Films** Austin Thomas<sup>1,2</sup>, Alan Kramer<sup>1</sup> and Christopher Richardson<sup>1,2</sup>; <sup>1</sup>Laboratory for Physical Sciences, United States; <sup>2</sup>University of Maryland, United States

Several niobium titanium nitride ternary superconducting alloys were grown to assess the superconducting properties of an alloy which can be tuned to grow pseudomorphically with an insulating layer. The goal is to engineer a superconductor that may decrease charge noise and has improved critical current across the interface of a Josephson junction. This alloy can be paired with wide-bandgap nitrides to create an oxygen-free heterostructure.  $\text{Nb}_x\text{Ti}_{1-x}\text{N}$  thin films were grown using plasma assisted molecular beam epitaxy on C-plane sapphire substrates, across the compositional range  $0 \leq x \leq 1$ . Sample topography is verified using reflection high energy electron diffraction and ex-situ atomic force microscopy. The surface exhibits a river-rock-type topography across the compositional range with RMS roughness values under one nanometer. The structure is analyzed using x-ray diffraction and Rutherford backscattering spectroscopy, which shows the change in composition causes a corresponding change in lattice constants. All films are completely relaxed, and consistent with an abrupt metamorphic growth mode. Variations in the alloy phase and corresponding superconducting properties will be discussed.

#### 5:55 AM F.NM05.03.07

**Synthesis and Characterization of AlN and TiN for All Nitride Josephson Junctions** Alan R. Kramer, Ashish Alexander, Austin M. Thomas and Christopher Richardson; University of Maryland, United States

The non-linear building blocks of superconducting qubits are Josephson Junctions (JJs). The current state-of-the-art is qubits fabricated with JJs that are made from Al/AlOx/Al using the double-angle evaporation and oxidation method. The need to fabricate higher quality, lower loss, and more uniform superconducting devices motivates this work to focus on making epitaxial Josephson junction heterostructures using transition metal nitride superconductors and a wide-bandgap nitride dielectric on a low-loss substrate.

Aluminum nitride and Titanium nitride are two foundation materials in the construction of an all nitride JJ. We use plasma assisted molecular beam epitaxy (PAMBE) with varying metal-nitrogen growth flux ratios from nitrogen rich to metal rich growth conditions. The optimization of both epitaxial materials is guided by characterization of the bulk by x-ray diffraction (XRD), chemical profile using energy dispersive x-ray spectroscopy (EDX), 'near' surface structure using electron backscatter diffraction (EBSD) and surface topography via atomic force microscopy (AFM).

Superconducting TiN epitaxial growth parameters and their correlation to structure are reported along with temperature dependent resistivity and critical temperature. Superconducting microwave loss is a key parameter for quantum information applications, and will be explored for all films and correlated to structure using coplanar waveguide resonators.

#### 6:05 AM F.NM05.03.08

**Improved Surface Quality of *A*-Axis  $\text{YBa}_2\text{Cu}_3\text{O}_{7-\delta}$  Thin Films** Y. Eren Suyolcu<sup>1</sup>, Jiaxan Sun<sup>1</sup>, Jürgen Schubert<sup>2</sup> and Darrell Schlom<sup>1,3</sup>; <sup>1</sup>Cornell University, United States; <sup>2</sup>Peter Gruenberg Institute (PGI-9) and JARA-Fundamentals of Future Information Technology, Germany; <sup>3</sup>Kavli Institute at Cornell for Nanoscale Science, United States

Due to the significantly longer superconducting coherence length along the *a*-axis of  $\text{YBa}_2\text{Cu}_3\text{O}_{7-\delta}$  (YBCO) than along the *c*-axis, the growth of *a*-axis YBCO films is important for Josephson junctions, provided they can be made sufficiently smooth.[1] The necessity for smoothness is so Josephson junctions, regardless of their position on the wafer, have the same thickness of the tunnel barrier.[2,3] With the goal of making smoother *a*-axis YBCO films, we utilize ozone-assisted molecular beam epitaxy (MBE) to grow *a*-axis YBCO films and perform comprehensive structural, morphological, and electrical characterization. The *a*-axis films are grown on (100)  $\text{LaAlO}_3$  substrates. The structural quality and *a*-axis content of the samples is examined using four-circle x-ray diffraction (XRD). The morphology of the film surfaces is assessed by atomic force microscopy (AFM). Leveraging a new temperature-ramping model, we achieve high structural quality and improved surface roughness of *a*-axis YBCO films. *In-situ* reflection high-energy electron diffraction (RHEED) substantiates the gradually improved crystallinity during the temperature ramping. *Ex-situ* XRD measurements prove the films to have >99% *a*-axis content, while AFM measurements reveal improved surface quality with a root-mean-square (rms) roughness of < 2 nm. Resistivity vs. temperature measurements exhibit the onset of the superconducting transition at  $T_c \sim 87$  K.

## References

- [1] J. B. Barner, C. T. Rogers, A. Inam, R. Ramesh, S. Bersey, Appl. Phys. Lett. 1991, 59, 742.
- [2] Z. Trajanovic, I. Takeuchi, P. A. Warburton, C. J. Lobb, T. Venkatesan, Appl. Phys. Lett. 1995, 66, 1536.
- [3] I. Takeuchi, P. A. Warburton, Z. Trajanovic, C. J. Lobb, Z. W. Dong, T. Venkatesan, M. A. Bari, W. E. Booij, E. J. Tarte, M. G. Blamire, Appl. Phys. Lett. 1996, 69, 112.

## 6:15 AM F.NM05.03.10

**Influence of Al Thickness on Tunneling Spectra of Nb/Al Based N/I/S Tunnel Junction** Zachary Barcikowski<sup>1,2</sup> and J.M. Pomeroy<sup>2</sup>; <sup>1</sup>University of Maryland, United States; <sup>2</sup>National Institute of Standards and Technology, United States

A metallic bilayer system can behave like two materials when thick, but in the thin film limit may exhibit properties that are a hybrid of the individual layers or dominated by one. As an example, the Nb/Al bilayer, in conjunction with AlO<sub>x</sub>, is a widely utilized material stack for quantum computing, where in the thin film limit (<100 nm) the Al superconducting properties are strongly perturbed by the proximity of the Nb. Each metal individually has liabilities: when used separately in tunnel junction devices, Al's lower T<sub>c</sub> requires lower operation temperatures but Nb oxides introduce a range of problematic features including magnetic scattering and dissipation. By choosing an appropriate Al thin film thickness on Nb, it may be possible to mitigate both to get 1) the higher Nb T<sub>c</sub> and 2) better AlO<sub>x</sub> tunnel barrier. We have fabricated a series of Nb/Al/AlO<sub>x</sub>/normal metal tunnel junctions while varying the Al thin film thickness in order to investigate the tunnel junction properties with changing Al thickness. The normalized sub-gap conductance in tunneling spectra is found to strongly vary as a function of Al thickness, with sub-gap conductance exceeding normal state conductance in some cases, which is typically attributed to Andreev reflection. Tunnel junction spectra are well modeled within the Blonder-Tinkham-Klapwijk (BTK) theory and we discuss trends between BTK barrier strength Z and the apparent superconducting gap as the Al thin film thickness varies. Additionally, we will present temperature dependent tunneling spectra measured between 4 K and , and discuss the analysis of the data within the BTK theory.

## SESSION F.NM05.04: Materials for Topological Quantum Systems

On Demand Abstracts Available for Viewing Starting Saturday Morning, November 21, 2020

F-NM05

## 5:00 AM \*F.NM05.04.01

**Compound Semiconductor Nanowire Networks** Anna Fontcuberta i Morral; EPFL, Switzerland

Nanowires are filamentary crystals with a tailored diameter ranging from few to ~100 nm. The reduced dimensions and longitudinal morphology of these nanowires results in interesting optical and electrical properties and provides a great potential for many applications, including sensing, quantum computing and all those that involve photonics [1]. In all these potential applications, the deterministic positioning of nanowires and associated branches on a substrate is key. In this talk we will present our strategy to obtain III-V nanowire networks in an organized fashion on a device substrate. We will consider different shapes of the nanostructure connections as well as strategies to increase the carrier mobility in views of ballistic 1D transport. We will address the growth and the optical and electronic properties as well as perspectives for quantum technology applications [2-4].

## References:

- [1] L. Güniat, P. Caroff, A. Fontcuberta i Morral, Chem. Revs. 119, 8958 (2019)
- [2] G. Tütüncüoğlu et al, Nanoscale 7, 19453 (2015)
- [3] M. Friedl et al Nano Lett. 18, 2666 (2018)
- [4] M. Fried. et al Nano Lett. 20, 3577 (2020)

## 5:15 AM \*F.NM05.04.02

**Andreev Bound States and Majorana Fermions in Helical 1D Systems** Jelena Klinovaja; University of Basel, Switzerland

In my talk, I will discuss low-dimensional condensed matter systems, in which topological properties could be engineered per demand. Majorana fermions can emerge in hybrid systems with proximity-induced superconducting pairing. I will present our numerical and analytical studies of such geometries with proximity effects [1-3]. In the second part of the talk, I will discuss an analytical model of a Rashba nanowire that is partially covered by and coupled to a thin superconducting layer, where the uncovered region of the nanowire forms a quantum dot [4,5]. Even if there is no topological superconducting phase possible, there is a trivial Andreev bound state that becomes pinned exponentially close to zero energy as a function of magnetic field strength when the length of the quantum dot is tuned with respect to its spin-orbit length such that a resonance condition of Fabry-Perot type is satisfied. In this case, the Andreev bound state remains pinned near zero energy for Zeeman energies that exceed the characteristic spacing between Andreev bound state levels but that are smaller than the spin-orbit energy of the quantum dot. Importantly, as the pinning of the Andreev bound state depends only on properties of the quantum dot, this behavior is unrelated to topological superconductivity.

References

- [1] C. Reeg, D. Loss, and J. Klinovaja, Phys. Rev. B **97**, 165425 (2018).
- [2] C. Reeg, D. Loss, and J. Klinovaja, Phys. Rev. B **96**, 125426 (2017).
- [3] C. Reeg, J. Klinovaja, and D. Loss, Phys. Rev. B **96**, 081301 (2017).
- [4] C. Reeg, O. Dmytruk, D. Chevallier, D. Loss, and J. Klinovaja, Phys. Rev. B **98**, 245407 (2018).
- [5] O. Dmytruk, D. Chevallier, D. Loss, and J. Klinovaja, Phys. Rev. B **98**, 165403 (2018).

**5:30 AM \*F.NM05.04.03**

**Materials Considerations for Majorana Based Quantum Computations** Jay Sau; University of Maryland, United States

Majorana modes are one of the most promising candidates for the creation of topological qubits in the long term. While evidence for Majorana modes has been obtained for Majorana modes in several systems such as semiconductor nanowires, semiconductor 2DEGs, iron-based superconductors, topological insulators as well as iron atom chains to name a few, evidence for a qubit degree of freedom is elusive. I will begin by reviewing what it means experimentally to observe a qubit. Following this we will discuss the central device challenge in this regard i.e. quasiparticle poisoning. I will then describe potential material dependence of this phenomena as well as how quasiparticle poisoning can manifest in various experiments related to topological superconductivity. Specifically, we will discuss how the observation of quantized conductance into a zero-bias conductance peak associated with a Majorana over a range of tunneling provides some bounds on quasiparticle poisoning times. The measurement of Coulomb blockade transport, which has been observed only for a limited number of superconductors can provide more precise information on such bounds.

**5:45 AM \*F.NM05.04.04**

**Materials Science, Physics and Engineering of Topological Quantum Circuits** Sergey Froloy; University of Pittsburgh, United States

With Quantum Supremacy upon us, and with major tech companies investing in quantum computing, one may wonder how much room is left there for academic research? The answer is: more than ever! Our existing qubits are great, but it is difficult to see them carrying us beyond the modern era of noisy intermediate-scale quantum processors, and ushering in the truly scalable, fault tolerant and commercially viable computers. Most likely, a qubit and its couplings, gates will once more need to be re-thought from the ground up - from the atomic first-principles level to the device architecture level. At the same time, the progress we made in quantum control and engineering is so huge that these methods have themselves become mature tools of science. They can be applied beyond quantum computing - to understand the basic questions of quantum dynamics and to probe exotic matter.

One solution may come from studying topological superconductivity. This is an interesting state most notable for spurring Majorana zero modes. Those modes can be both investigated as some of the first non-Abelian excitations, and they can be used in quantum circuits for storing and protecting quantum information. Majorana research has posed many basic materials questions of how to engineer the precise structures that possess intrinsic fault tolerance through topological protection. In my work I have developed new materials and devices for unambiguous observation of robust Majorana modes. I have worked on establishing clear criteria (signatures) of Majorana modes and how to tell them apart from other excitations that may be present in the same devices. It is exciting to apply modern quantum probes, developed based on transmon and spin qubits, to these systems in search for new exotic quantum matter. And perhaps solving some of the big challenges facing quantum computing at the same time.

**6:00 AM \*F.NM05.04.05**

**Topological Superconductivity in Superconductor–Semiconductor Heterostructures** [Roman Lutchyn](#); University of California, Santa Barbara, United States

Superconductor–semiconductor heterostructures represent a versatile platform for realizing Majorana zero-energy modes. In this talk, I will explain how to engineer topological superconductivity at the interface of a conventional (s-wave) superconductor and a semiconductor with spin-orbit interaction. I will discuss state-of-the-art numerical approaches for modeling realistic devices which take into account proximity-induced superconductivity, orbital and Zeeman effect of an applied magnetic field, spin-orbit coupling as well as the electrostatic environment on equal footing. Finally, I will review recent materials science progress in growing superconductor–semiconductor heterostructures and discuss promising new directions.

**6:15 AM F.NM05.04.06**

**Synthesis and Size Effects on Resistivity of Topological Metal MoP Nanostructures** [Hyeuk Jin Han](#), David Hynek, Zishan Wu, Lei Wang, Pengzi Liu, Joshua Pondick, Sajad Yazdani, John Woods, Milad Yarali, Yujun Xie, Hailiang Wang and Judy Cha; Yale University, United States

Nanoscale topological materials can enhance the contributions of the topologically protected surface states to transport signals by increasing their surface to volume ratios. For potential applications in quantum computing, and low-power electronics that exploit the topological properties, fundamental studies of electronic phases of nanoscale topological materials are critical. Recently, molybdenum phosphide (MoP) was discovered as a triple-point topological semi-metal with excellent transport properties of bulk resistivity of  $8.2 \mu\Omega\cdot\text{cm}$  and carrier density of  $1.1 \times 10^{23} \text{ cm}^{-3}$  at room temperature (Kumar et al., Nat.comm., 2019). Due to the topological protection predicted to suppress electron scattering at the surface, MoP may preserve its low resistivity values at the nanoscale, which may rival the line resistance of current Cu interconnects. Here, we report the synthesis and transport properties of MoP nanostructures, which were obtained by the direct conversion of MoO<sub>3</sub> nanostructures. We observe that the initial size of the MoO<sub>3</sub> nanostructure critically determines the crystalline quality of the converted MoP nanostructures. Large MoO<sub>3</sub> flakes lead to porous MoP flakes, while narrow MoO<sub>3</sub> nanowires lead to MoP nanowires without pores. The size-dependent porosity observed in the MoP nanostructures is attributed to volume changes during the conversion reaction and nanoscale confinement effects. Notably, MoO<sub>3</sub> nanowires with diameters less than 10 nm were converted to single-crystalline MoP nanowires. Because of their porous nature, the resistivity values of the MoP nanoflake were higher than the reported values of MoP bulk crystals. However, despite the high porosity, the residual resistance ratio was  $\sim 2$ , and the temperature-dependent resistivity curves did not show any strong surface or grain-boundary scattering. The simple synthesis strategy opens opportunities to study the nature of topological surface states in MoP, which could be sensitive to the overall morphology and dimensions of the nanostructure, and to explore their feasibility as nanoscale interconnects.

**6:25 AM F.NM05.04.08**

**Remote Doping of InGaAs Nanowire Branches** [Didem Dede](#)<sup>1</sup>, Martin Friedl<sup>1</sup>, Kristopher Cerveny<sup>2</sup>, Chunyi Huang<sup>3</sup>, Nicholas P. Morgan<sup>1</sup>, Wonjong Kim<sup>1</sup>, Lucas Guniat<sup>1</sup>, Akshay Balgarkashi<sup>1</sup>, Jean-Baptiste Ieran<sup>1</sup>, Valerio Piazza<sup>1</sup>, Mohammad Samani<sup>2</sup>, Megan Hill<sup>3</sup>, Jaime Segura<sup>4</sup>, Lincoln J. Lauhon<sup>3</sup>, Dominik Zumbuhl<sup>2</sup> and Anna Fontcuberta i Morral<sup>1</sup>; <sup>1</sup>École Polytechnique Fédérale de Lausanne, Switzerland; <sup>2</sup>Universität Basel, Switzerland; <sup>3</sup>Northwestern University, United States; <sup>4</sup>European Synchrotron Radiation Facility, France

III-V semiconductor nanowires (NWs) have been the building blocks of many different research areas including photonics, solar cells, energy storage, and recently, quantum computing.<sup>1,2</sup> In particular, the fast-growing field of topological quantum computing has brought great attention to In-based NWs, thanks to the core properties of these materials including high electron mobility, large Landé g-factor, and high spin-orbit coupling. The most common growth technique for these NWs results in the formation of free-standing, vertical structures which require transfer onto a host substrate for further characterization, and this hinders their scalability for industrial applications. To overcome this limitation and to achieve high-quality NW junctions, selected area epitaxy (SAE) of horizontal NW networks has been proposed as a more scalable approach. Recently, SAE of InAs NWs has been demonstrated on GaAs substrates.<sup>3,4</sup> To decrease the number of detrimental defects, nanomembranes or buffer layers have been used as templates. Thanks to the defect-free nature of these GaAs nanomembranes, NWs with high crystal-quality have been obtained. However, the attempt to grow pure InAs NWs on (111)B GaAs membranes resulted in the formation of intermixed InGaAs NWs with low In content ( $\sim 20\%$ ).<sup>4</sup> Even though these NWs were shown to have quasi-1D transport, their electrical and transport properties were insufficient for quantum applications, leaving much room for improvement.

Herein, we present remotely doped InGaAs NW branches to enhance the properties of these structures.<sup>5</sup> Remote doping, or so-called modulation doping, has been commonly used in different material platforms to enhance mobility by suppressing ionized impurity scattering. In our growths, silicon dopants are introduced close to the interface during the membrane growth stage. The location of these dopants was later confirmed by atom-probe tomography. By using this information in our finite element analysis, we demonstrate that the electrons are localized in the wire segment thanks to the band alignment of GaAs and InGaAs. Moreover, by investigating the InAs growth window while changing In and As flux, we achieved In concentrations of up to 50% in our NWs. Finally, transport and electrical properties of these Y-junctions are characterized under magnetic field at low temperatures. Together with reduced donor scattering, the increase in the In content results in enhanced mobility and large electron mean free paths. Additionally, these NWs exhibit weak anti-localization, which is the hallmark of strong spin-orbit interaction. All these improvements make these NWs promising for future applications in topological quantum computing.

## References

- <sup>1</sup>E. Garnett et al, *Chem. Rev.* **119** (2019)
- <sup>2</sup>H.Zhang et al, *Nat. Commun.* **10** (2019)
- <sup>3</sup>F. Krizek et al, *Phys. Rev. Mat.* **2** (2018)
- <sup>4</sup>M. Friedl et al, *Nano Lett.* **18** (2018)
- <sup>5</sup>M. Friedl et al, *Nano Lett.* **20** (2020)

**Acknowledgements:** Funding from Swiss National Science Foundation, NCCR QSIT

## 6:35 AM F.NM05.04.10

**Hybrid-Interfaces in Topological Quantum Materials** Panchapakesan Ganesh and Anh Pham; Oak Ridge National Laboratory, United States

Two dimensional magnetic topological materials, such as magnetic topological insulators and magnetic Weyl semimetals, represent a novel platform exhibiting the quantum anomalous Hall effect (QAHE). To realize the quantum anomalous Hall state, the material system needs to break time reversal symmetry while maintaining a nontrivial 2D bulk gap protected by a nonzero Chern number. One pathway is to realize *hybrid-interfaces* between different quantum materials to achieve this synergy. The scientific objective is the rational design of quantum materials and control over their properties by exploiting low dimensionality at heterointerfaces.

In this talk, I will focus on our recent works[1,2,3], employing a combination of density functional Theory (DFT) and k.p model Hamiltonian calculations, to design synthesizable hybrid-interfaces where QAHE can potentially be realized. By systematically investigating such magnetically doped topological insulating materials, we reveal that interfaces between Cr-doped Sb<sub>2</sub>Te<sub>3</sub> and the antiferromagnetic insulator Cr<sub>2</sub>O<sub>3</sub> are ideal for realizing functional QAHE since the system consists of a large bulk insulating gap with the Fermi level pinned inside a bulk gap due to a type-I band offset, while the dopants at the interface of the TI layer exhibit robust ferromagnetism. We also screened viable vdW-bonded hybrid-interfaces, and discovered that exploiting the unique ‘buried’ topology in CrI<sub>3</sub> is a good strategy, which can be achieved by interfacing it with elemental layers of antimonene, so as to induce a semimetallic transition in CrI<sub>3</sub> through a charge transfer process. Progress in our ongoing effort in simulating topological heterogeneities, such as step-edges, at interfaces of intrinsic magnetic topological materials, such as MnBi<sub>2</sub>Te<sub>4</sub>, using real-space DFT-methods that allow few-thousand electrons, will also be presented.

- [1] “Realizing gapped surface states in magnetic topological insulator MnBi<sub>2-x</sub>Sb<sub>x</sub>Te<sub>4</sub>”, Wonhee Ko et. al., arXiv:2003.00180 (2020)
- [2] “Designing Magnetic Topological van der Waals Heterostructure”, Anh Pham and P. Ganesh, arXiv:2003.05840 (2020)
- [3] “Quantum material topology via defect engineering”, Anh Pham and P. Ganesh, Phys. Rev. B 100, 241110(R) (2020)

SESSION F.NM05.05: Novel Materials and Characterizations  
On Demand Abstracts Available for Viewing Starting Saturday Morning, November 21, 2020  
F-NM05

**5:00 AM \*F.NM05.05.02**

**Exploring Quantum Systems via Scanning Transmission Electron Microscopy—Machine Learning and Artificial Intelligence Based Workflows** [Sergei V. Kalinin](#), Ondrej Dyck, Stephen Jesse, Rama Vasudevan, Christopher Nelson, Matthew Chisholm, Andrew Lupini and Maxim Ziatdinov; Oak Ridge National Laboratory, United States

The emergence of quantum information systems necessitates the development of the tools and workflows capable of probing quantum functionalities on the atomic scale and connecting them to the local structures. Recent advances in Scanning Transmission Electron Microscopy have allowed the direct visualization of materials structures with picometer-scale precision, as well as collection of high-veracity information on local electronic, plasmonic, and vibrational properties via Electron Energy Loss Spectroscopy (EELS). However, the interpretation of these data sets even on the exploratory level of identification of the repeatable units, site symmetries, and outliers remains largely driven by human operator and limited to a priori defined models. Notably, the nature of the STEM data sets, as affected by observational biases and limited to small number of materials, limits the applicability of the classical correlation-based machine learning methods. However, the analysis of such data can be performed assuming the parsimony of structural descriptors and generative mechanisms and adopting the Bayesian analysis frameworks. In this presentation, I will illustrate several applications of the machine learning based workflows based on rotationally invariant and conditional variational autoencoders for the elucidation of the local structures and structure-breaking distortions in 2D materials and ferroelectric oxides. The Bayesian nature of these methods can also be used to extend these to the analysis of the causal relationships between the physical and chemical degrees of freedom. Ultimately, we seek to answer the questions such as whether electronic instability due to the average Fermi level guides the development of the local atomic structure, or frozen atomic disorder drives the emergence of the local structural distortions, whether the nucleation spot of phase transition can be predicted based on observations before the transition, and what is the driving forces controlling the emergence of unique functionalities of morphotropic materials and ferroelectric relaxors. The unique aspect of Bayesian methods is their potential to quantify uncertainty, and harnessing this for automated experimentation is discussed on example of ferroelectric domain patterning and atomic fabrication via electron beams.

**5:15 AM \*F.NM05.05.03**

**From Materials to Quantum Devices and Back Again** [Giulia Galli](#); University of Chicago, United States

We discuss computational strategies to predict materials with desired characteristics for quantum sensing and quantum computations, and the impact that quantum computers may have in revolutionizing materials simulations [1] and hence materials design and innovation.

[1] Quantum simulations of materials on near-term quantum computers, He Ma, Marco Govoni, Giulia Galli, npj, Comp. Mat. 2020 (in press)

**5:30 AM F.NM05.05.05**

**Electric-Field Manipulation of Spins in Dilute Magnetic Ferroelectrics** [Katherine Inzani](#)<sup>1</sup>, Weichaun Huang<sup>2</sup>, Junjie Liu<sup>3</sup>, Sujit Das<sup>2</sup>, Valentin V. Laguta<sup>4</sup>, Ruchira Chatterjee<sup>1</sup>, Evan Sheridan<sup>1</sup>, Arzhang Ardavan<sup>3</sup>, Ramamoorthy Ramesh<sup>2,1</sup> and Sinead Griffin<sup>1</sup>; <sup>1</sup>Lawrence Berkeley National Laboratory, United States; <sup>2</sup>University of California, Berkeley, United States; <sup>3</sup>University of Oxford, United Kingdom; <sup>4</sup>The Czech Academy of Sciences, Czechia

As a pathway to quantum computing, spins in multiferroic materials offer novel routes of manipulation due to their coupled electrical and magnetic properties. In order to control individual spins as in defect-based qubits, we explore ferroelectric materials with magnetic dopants. Using Fe<sup>3+</sup>-doped PbTiO<sub>3</sub> as a model system, we present a combined first-principles and electron paramagnetic resonance study of the spin-orbit coupling effect in dilute magnetic ferroelectrics. We show that the spins in the Fe<sup>3+</sup> ion are strongly aligned perpendicular to the ferroelectric polar axis and follow manipulation by an electric field. First principles modelling indicates the atomic scale effects of lattice modification on qubit switching parameters by way of strain and defect complexes, in excellent agreement with experimental observations. These results demonstrate the manipulation of spins by electric field and the possibility to tailor spin control by the atomic environment.

**5:40 AM F.NM05.05.07**

**Uncovering Electron Scattering in Goniopolar Metal NaSn<sub>2</sub>As<sub>2</sub> from First Principles** [Yaxian Wang](#) and Prineha Narang; Harvard University, United States



**Electron scattering on a non-trivial Fermi surface topology plays an important role in electron transport, thus giving rise to exotic phenomena such as violation of Wiedemann Franz law, hydrodynamic electron flow, unusual phonon decay etc. Recent experimental discoveries in axis-dependent conduction polarity, or goniopolarity, have observed that the charge carriers can conduct like either electrons or holes depending on the crystallographic direction they travel along in layered compounds such as NaSn2As2 and PdCoO2, the latter of which also features hydrodynamic electron flow.**

**In this talk, we present an ab initio study of electron scattering in such systems. Taking NaSn2As2 as an example, we study different microscopic scattering mechanisms from ab initio and present the electron-phonon scattering time distribution on its Fermi surface in momentum space, the anisotropy of which is proposed to be the origin of the axis-dependent conduction polarity. Further, we obtain the overall anisotropic lifetime tensors in real space at different electron chemical potentials and temperatures and discuss how they contribute to the macroscopic thermopower. While we find that the contribution of the in-plane and cross plane lifetimes exhibits a similar trend, the concave portion of the Fermi surface alters the electron motion significantly in the presence of a magnetic field, thus flipping the conduction polarity as measured via the Hall effect. Our calculations and analysis of NaSn2As2 also suggests the strong possibility of hydrodynamic electron flow in the system. These results together have implications for electron lifetimes in a broad class of new quantum materials and provide key, general insights into electron scattering on open Fermi surfaces.**

**5:50 AM F.NM05.05.08**

**2D-Ordered Nanodomains in Doped Rutile VO<sub>2</sub> Driven by Structural Geometric Frustration** Jared M. Allred<sup>1</sup>, Matthew Davenport<sup>1</sup>, Tyra Douglas<sup>1</sup>, Top B. Rawot Chhetri<sup>1</sup>, Stephan Rosenkranz<sup>2</sup>, Ray Osborn<sup>2</sup> and Matthew J. Krogstad<sup>2</sup>; <sup>1</sup>University of Alabama, United States; <sup>2</sup>Argonne National Laboratory, United States

The rutile crystal structure is a classic crystal structure type that is an important platform for potential device application, including solar cells (TiO<sub>2</sub>) and ultrafast optical switches (VO<sub>2</sub>). Open d-shell systems such as VO<sub>2</sub> usually undergo a structural distortion that is strongly coupled to changes in the electronic properties. Using single crystal total x-ray scattering and the 3D- $\Delta$ PDF method, we discovered a new manifestation of structural order in rutile characterized by a loss of displacement coherence in one dimension but not the other two, resulting in the formation of nanoscopically ordered domains of size  $\sim 50 \times 50 \times 5$  Å. The loss of dimensionality is attributed to geometric frustration of strongly interacting atomic displacements, since the long- and short-range axes are crystallographically equivalent.

**6:00 AM F.NM05.05.09**

**Imaging Phonon-Mediated Hydrodynamic Flow in WTe<sub>2</sub> with Cryogenic Quantum Magnetometry** Uri Vool<sup>1</sup>, Assaf Hamo<sup>1</sup>, George Varnavides<sup>1</sup>, Yaxian Wang<sup>1</sup>, Tony Zhou<sup>1</sup>, Nitesh Kumar<sup>2</sup>, Johannes Gooth<sup>2</sup>, Claudia Felser<sup>2</sup>, Prineha Narang<sup>1</sup> and Amir Yacoby<sup>1</sup>; <sup>1</sup>Harvard University, United States; <sup>2</sup>Max Planck institute for chemical physics in solids, Germany

Tungsten ditelluride (WTe<sub>2</sub>) is a layered semimetal with many unique features. It is a Type-II Weyl semimetal candidate(1), exhibits large magnetoresistance(2), and superconductivity under strain(3). To gain insight into the electron-electron and electron-phonon interactions in WTe<sub>2</sub>, we study the spatial structure of current flowing through a WTe<sub>2</sub> flake. Significant electron-electron scattering can lead to hydrodynamic effects in electron flow(4), which have been imaged in graphene(5,6). We adapt these techniques to study the nature of interactions in WTe<sub>2</sub>.

We study the current profile in WTe<sub>2</sub> by imaging the local magnetic field above it using a nitrogen-vacancy (NV) center in a diamond scanning tip. Using coherent quantum sensing, we obtain magnetic field resolution of  $\sim 10$  nT and spatial resolution of  $\sim 100$  nm. The current pattern we observe differs substantially from the flat profile of a normal metal, and indicates correlated flow through the semimetal. The pattern also shows significant temperature dependence, with hydrodynamic effects increasing as the system is cooled and peaking at  $\sim 20$  K. At lower temperatures the current profile becomes flatter, likely due to a competition between hydrodynamic and ballistic effects.

We compare our results to an ab initio calculation of electron scattering mechanisms, which are used to extract a current profile using the electronic Boltzmann transport equation. These calculations show quantitative agreement with our measurement, capturing the non-monotonic temperature dependence. This comparison allows us to quantitatively extract the strength of electron-electron interactions in our material. Furthermore, this strong interaction cannot be explained by a direct Coulomb effect, and is mostly phonon-mediated electron-electron interaction. This surprising result opens a path for hydrodynamic flow and strong interactions even in high-density materials with significant screening of Coulomb interactions.

- 1 Soluyanov, A. et al. Nature 527 (2015)
- 2 Ali, M. et al. Nature 514 (2014)
- 3 Kang, D. et al. Nat. Comm. 6 (2015)
- 4 Levitov, L. and Falkovich. G., Nat. Phys 12 (2016)
- 5 Sulpizio, J. et al. Nature 576(2019)
- 6 Ku, M. et al. arXiv:1905.10791 (2019)

#### 6:10 AM F.NM05.05.10

**Late News: Potential of Rare-Earth Doped Sesquioxide Thin Films Grown by Chemical Vapour Deposition as a Material Platform for Quantum Technologies** Nao Harada<sup>1</sup>, Alban Ferrier<sup>1</sup>, Diana Serrano<sup>1</sup>, Emrick Briand<sup>2</sup>, Romain Bachelet<sup>3</sup>, Ian Vickridge<sup>2</sup>, Jean-Jacques Ganem<sup>2</sup>, Philippe Goldner<sup>1</sup> and Alexandre Tallaire<sup>1</sup>; <sup>1</sup>IRCP CNRS, France; <sup>2</sup>INSP, France; <sup>3</sup>INL, France

Harnessing rare-earth (RE) ions outstanding optical coherent properties for quantum information technologies has attracted a lot of attention recently, in the race for exploiting emerging solid-state quantum-grade systems. Indeed, REs offer a wide tunability of their ultra-narrow optical transitions, including the useful telecom-band wavelength. While macroscopic bulk oxide crystals (such as  $\text{Y}_2\text{SiO}_5$ ) are usually the preferred host material for RE ions, the development of a silicon-compatible thin film platform would greatly facilitate post-processing, up-scalability as well as interfacing with other systems in a hybrid design. In this work, we focus on the synthesis of nanoscale Eu-doped  $\text{Y}_2\text{O}_3$  thin films on silicon wafers using a modified version of Chemical Vapour Deposition (CVD) based on direct liquid injection (DLI-CVD) of the precursors. This approach improves the control of the composition and purity of the films by alleviating the issue of low volatility of heavy RE elements. We successfully obtained films in the full Eu composition range, with a strong-(111) texture that crystallized in the bixbyite cubic phase. We probed the  $^5\text{D}_0 - ^7\text{F}_2$  transition lifetime following resonant excitation of the  $^7\text{F}_0 - ^5\text{D}_2$  level and found values of the order of 1 ms for the lowest Eu concentrations. Inhomogeneous linewidths as narrow as 50 GHz were also measured. Finally, using spectral hole burning (SHB) spectroscopy we successfully burned a spectral hole in a 200 nm-thin film with a 2 % Eu doping with an estimated homogeneous linewidth of 11 MHz. These values are still at least an order of magnitude higher than those reported for bulk single crystals indicating that additional decoherence mechanisms exist in our nanometric films. Further improvements of the crystalline quality and purity of the films is thus desired so that the full potential of such CVD-grown thin films is unleashed for integrated quantum information processing devices.

#### 6:20 AM F.NM05.05.11

**Late News: Tuning the Particle Size and Photoluminescence in Phase-Pure CdSe Quantum Dots Synthesized Through Novel Solution-Growth Technique** Naveen Narasimhachar Joshi<sup>1,2</sup> and Muttanagoud Kalasad<sup>3</sup>; <sup>1</sup>Indian Institute of Technology Kharagpur, India; <sup>2</sup>Indian Institute of Science, India; <sup>3</sup>Davangere University, India

In the present work, we show that the *in situ* growth of highly oriented cadmium selenide quantum dots can be explored to alter and tune the emission intensity of the particles. As such, the impact of particle size and distribution on the band emission is studied. Monodispersed cadmium selenide quantum dots (CdSe QDs) were prepared through non-coordinating solvent route, using cadmium oxide (CdO) and selenium (Se) as precursor materials and oleic acid as a capping molecule. The as-synthesized particles were found to be highly stable, with narrow size distribution and good homogeneity. No precipitate was observed for several months. X-ray diffraction (XRD) and transmission electron microscopy (TEM) measurements confirm the formation of (Wurtzite structure) phase-pure CdSe QDs with a diameter tunable between 4 and 6 nm. The particle size is controlled by varying the precursor concentration, reaction time and temperature, without the need for post-synthesis heat treatment techniques. This work was performed without the use of pyrophoric precursors and the reported method represents a basic concept for the preparation of small nanoparticles in general [1]. The smaller sized quantum dots exhibit a strong band emission and are more easily tuned because of their larger surface-area-to-volume ratio [2]. Results demonstrate that the emission wavelength of CdSe QDs vary as a function of particle size, exhibiting high photoluminescence quantum yield (QY) ( $\approx 62\%$ ). This finding reveals the fluorescence property of CdSe QDs that offers new opportunities for future applications of quantum sources as emerging light emitting materials [3].

#### References:

- [1] Pu, Y., Cai, F., Wang, D., Wang, J.X. and Chen, J.F., 2018. Colloidal synthesis of semiconductor quantum dots toward large-scale production: a review. *Industrial & Engineering Chemistry Research*, 57(6), pp.1790-1802.
- [2] Shang, Y. and Ning, Z., 2017. Colloidal quantum-dots surface and device structure engineering for high-performance light-emitting diodes. *National Science Review*, 4(2), pp.170-183.

[3] Jiang, Y., Cho, S.Y. and Shim, M., 2018. Light-emitting diodes of colloidal quantum dots and nanorod heterostructures for future emissive displays. *Journal of Materials Chemistry C*, 6(11), pp.2618-2634.

### 6:30 AM F.NM05.05.12

**Late News: *In Situ* Formation and Conductance of Spin 1/2 Coordination Complexes** Masha Kamenetska; Boston University, United States

Electronic and spin states in single coordination complexes containing a paramagnetic center are a promising material platform for use in Quantum Information Science (QIS).<sup>1,2</sup> Such molecules can display a high degree of molecular anisotropy that can be tuned synthetically either by the choice of the metal ion center or through the ligand field of the complex, making them attractive as potential qubits. However, metal-containing complexes have recently been observed to fragment on gold surfaces, impeding the use of these molecules for QIS applications.<sup>3</sup> Here, we demonstrate the *in situ* assembly of coordination complexes between the tip and substrate of our scanning tunneling microscope break junction (STM-BJ) setup. Our measurements and density functional theory (DFT) calculations point to the formation of an open-shell structure where a single gold atom coordinates to the nitrogen atoms of imidazolate ligands; this structure bridges the metal electrodes with at least ~1.5 eV of binding energy per bond. We measure a reproducible conductance signature of this coordination complex, which suggests that a selective binding mechanism results in repeatable junction geometries.<sup>4</sup> This *in situ* formation of stable spin ½ single molecule junctions with a robust electronic signature at room temperature points to potential applications of these nanoscale materials in QIS.

(1) Wasielewski, M. R.; Forbes, M. D. E.; Frank, N. L.; Kowalski, K.; Scholes, G. D.; Yuen-Zhou, J.; Baldo, M. A.; Freedman, D. E.; Goldsmith, R. H.; Goodson, T.; et al. Exploiting Chemistry and Molecular Systems for Quantum Information Science. *Nat. Rev. Chem.* **2020**, 1–15. <https://doi.org/10.1038/s41570-020-0200-5>.

(2) Atzori, M.; Sessoli, R. The Second Quantum Revolution: Role and Challenges of Molecular Chemistry. *Journal of the American Chemical Society*. American Chemical Society July 24, 2019, pp 11339–11352. <https://doi.org/10.1021/jacs.9b00984>.

(3) Knaak, T.; González, C.; Dappe, Y. J.; Harzmann, G. D.; Brandl, T.; Mayor, M.; Berndt, R.; Gruber, M. Fragmentation and Distortion of Terpyridine-Based Spin-Crossover Complexes on Au(111). *J. Phys. Chem. C* **2019**, 123 (7), 4178–4185. <https://doi.org/10.1021/acs.jpcc.8b11242>.

(4) Pan, X.; Lawson, B.; Rustad, A. M.; Kamenetska, M. PH-Activated Single Molecule Conductance and Binding Mechanism of Imidazole on Gold. *Nano Lett.* **2020**, 20 (6), 4687–4692. <https://doi.org/10.1021/acs.nanolett.0c01710>.

### SESSION F.NM05.06: Semiconductors for Quantum

On Demand Abstracts Available for Viewing Starting Saturday Morning, November 21, 2020  
F-NM05

### 5:00 AM \*F.NM05.06.01

**Quantum Computing with Semiconductors—Spins Inside** Lieven Vandersypen; TU Delft, Netherlands

Quantum computation has captivated the minds of many for almost two decades. For much of that time, it was seen mostly as an extremely interesting scientific problem. In the last few years, we have entered a new phase as the belief has grown that a large-scale quantum computer can actually be built. Quantum bits encoded in the spin state of individual electrons in silicon quantum dot arrays, have emerged as a highly promising direction [1]. In this talk, I will present our vision of a large-scale spin-based quantum processor, and ongoing work to realize this vision.

First, we created local registers of spin qubits with sufficient control that we can program arbitrary sequences of operations. We show the creation of each of the Bell states with fidelities of 85-90% and the implementation of the four instances of the Deutsch-Jozsa and the Grover algorithms on two qubits [2].

Second, we have explored coherent coupling of spin qubits at a distance via two routes. In the first approach, the electron spins remain in place and are coupled via an intermediary degree of freedom. After showing this principle with an ancillary quantum dot as a coupler [3], we recently observed strong coupling of a single spin to a single microwave photon in a superconducting resonator [4]. In the second approach, spins are shuttled along a quantum dot array, preserving both the spin projection [5] and spin phase [6].

Third, in close collaboration with Intel, we have fabricated and measured quantum dots using all-optical lithography on 300 mm wafer, using industry-standard processing [7]. Qubit measurements are now underway. We expect that this industrial approach to nanofabrication will be critical for achieving the extremely high yield necessary for devices containing hundreds or thousands of qubits. Furthermore, we anticipate that the device stability and charge noise levels will eventually outperform those of devices made in university-style cleanrooms.

When combined, the progress along these various fronts can lead the way to scalable networks of high-fidelity spin qubit registers for computation and simulation.

- [1] L.M.K. Vandersypen, H. Bluhm, J.S. Clarke, A.S. Dzurak, R. Ishihara, A. Morello, D.J. Reilly, L.R. Schreiber, M. Veldhorst, Interfacing spin qubits in quantum dots and donors – hot, dense and coherent, *npj Quantum Information* 3, 34 (2017).
- [2] T. F. Watson, S. G. J. Philips, E. Kawakami, D. R. Ward, P. Scarlino, M. Veldhorst, D. E. Savage, M. G. Lagally, Mark Friesen, S. N. Coppersmith, M. A. Eriksson, L. M. K. Vandersypen, A programmable two-qubit quantum processor in silicon, *Nature* 555, 633-637 (2018)
- [3] T.A. Baart, T. Fujita, C. Reichl, W. Wegscheider, L.M.K. Vandersypen, Coherent spin-exchange via a quantum mediator, *Nature Nanotechnology*, 12, 26 (2017)
- [4] N. Samkharadze, G. Zheng, N. Kalhor, D. Brousse, A. Sammak, U. C. Mendes, A. Blais, G. Scappucci, L. M. K. Vandersypen, Strong spin-photon coupling in silicon, *Science* 359, 1123-1127 (2018)
- [5] T. A. Baart, M. Shafiei, T. Fujita, C. Reichl, W. Wegscheider, L. M. K. Vandersypen, Single-Spin CCD, *Nature Nanotechnology* 11, 330 (2016)
- [6] T. Fujita, T. A. Baart, C. Reichl, W. Wegscheider, L. M. K. Vandersypen, Coherent shuttle of electron-spin states, *npj Quantum Information* 3, 22 (2017)
- [7] R. Pillarisetty, H.C. George, T.F. Watson, L. Lampert, N. Thomas, S. Bojarski, P. Amin, R. Caudillo, E. Henry, N. Kashani, P. Keys, R. Kotlyar, F. Luthi, D. Michalak, K. Millard, J. Roberts, J. Torres, O. Zietz, T. Krähenmann, A.-M. Zwerver, M. Veldhorst, G. Scappucci, L.M.K. Vandersypen, and J.S. Clarke, 2019 IEEE IEDM San Francisco, pp. 31.5.1-31.5.4.

#### **5:15 AM \*F.NM05.06.02**

**Si/SiGe Heterostructures for Quantum Information Science** Clayton A. Jackson; HRL Laboratories, United States

Quantum information and computing are at the forefront of computer science, but their implementation relies on the identification and development of a suitable materials system. One such candidate is Si/SiGe. Much progress has been made in Si/SiGe heterostructures grown on metamorphic SiGe substrates as hosts to lithographically defined quantum dots. In this presentation we focus on the general structure and requirements of SiGe quantum dot heterostructures, the demands imposed by necessary dot performance, and advances in characterization methods for these materials.

#### **5:30 AM \*F.NM05.06.03**

**Effects of Coulomb Interactions in Silicon Quantum Dots** Susan Coppersmith<sup>1,2</sup>; <sup>1</sup>University of New South Wales, Australia; <sup>2</sup>University of Wisconsin–Madison, United States

Silicon is an attractive materials platform for developing large-scale quantum computers because of its compatibility with classical silicon electronics and its potential for scalability. Recent progress towards quantum computing in silicon has been impressive, but better understanding of the materials will enable improved controllability and predictability of qubit devices.

This talk will discuss some of the fundamental physics and materials science challenges that arise, focussing on the nontrivial interplay between Coulomb interactions and the valley degree of freedom in silicon quantum dots containing more than one electron. Prospects for further development will also be discussed.

#### **5:45 AM \*F.NM05.06.04**

**Exchange Control of Three Spins in Si Triple Quantum Dots** Seigo Tarucha; RIKEN, Japan

High-fidelity quantum operations of single and two spins as well as readout and initialization have recently been demonstrated for Si quantum dots. Among them exchange control between spins is an ingredient of quantum entanglement for implementing quantum algorithms, but the demonstration of entanglement has been limited to two-qubit entanglement mainly due to difficulties in controlling exchange couplings in a multi-qubit array. We use a triple quantum dot equipped

with a micro-magnet to control exchange couplings in two or three spin systems. We first measure the single qubit fidelity for three spins in the (1,1,1) charge state and obtain the values of 99.4 to 99.9 % for three spins. Then we use two spins to study exchange control of two qubits or singlet-triplet qubit drive. We use a resonant drive technique of the exchange interaction at the qubit frequency and obtained the fidelity of 99.6% thanks to the symmetric operation and a large micro-magnet Zeeman field gradient. Finally we use three spins to implement three-qubit entanglement. We precisely control exchange couplings between three spins and generate GHZ state. The GHZ state generation protocol will be useful to encode and decode a logical state for the bit-flip quantum error correction code.

#### **6:00 AM F.NM05.06.05**

**Theory of Single-Electron Transistors with Multiple Quantum Dots** Maicol A. Ochoa<sup>1,2</sup>, Keyi Liu<sup>1,2</sup>, Emily Townsend<sup>1,2</sup>, Michal Gawelczyk<sup>3</sup>, Michal Zielinski<sup>3</sup> and Garnett Bryant<sup>1,2</sup>; <sup>1</sup>National Institute of Standards and Technology, United States; <sup>2</sup>University of Maryland, United States; <sup>3</sup>Nicolaus Copernicus University, Poland

Donor-based quantum devices in silicon, manufactured with atomic precision, are a feasible alternative for the realization of universal quantum computing and analog quantum simulation. Protocols for operation, readout, and active control of these devices require a complete understanding of the quantum confinement effects, many-body interactions, transport characteristics, and response of the system to external fields. We report theoretical calculations on Si:P nanoscale transistors consisting of a single and multiple quantum dots, based on solutions of the Schrödinger-Poisson equations. In particular, we investigate the role of dopant location, dopant-dopant distance, and array orientation in the shape of the potential in different dopant arrays including  $2 \times n$  and  $n \times n$  arrays. We adopt a combined tight-binding description of the electronic properties of the Si:P substrate, and exact diagonalization techniques for electrons in the dopant array. The effect of external gates and source/drain potentials is accounted for by solving the Poisson equation with the finite element method under appropriate boundary conditions. Most importantly, we develop a way to describe transport through multi-electron, multidot quantum devices. Our simulations allow us to rationalize recent experimental measurements in these devices in terms of their stability diagrams, thus demonstrating that our approach provides an accurate description of single-electron transistors with multiple quantum dots.

#### **6:10 AM F.NM05.06.06**

**Alternative Gate Materials for Silicon Quantum Devices—Defects and Strain** Ryan Stein<sup>1</sup> and M. D. Stewart, Jr.<sup>2</sup>; <sup>1</sup>University of Maryland, United States; <sup>2</sup>National Institute of Standards and Technology, United States

Quantum dots (QD) in the silicon MOS system benefit from the use of palladium or platinum for gate materials because the small grain size of these metals compared to aluminum aids in shrinking the gate and dot dimensions. However, it is not clear what differences arise with respect to process-induced defect density and inhomogeneous strain. Here, we present measurements of oxide defect densities (fixed charge and interface trap density) as a function of forming gas anneal temperature for three different gate metals: Al, Ti/Pd, and Ti/Pt. We also investigate the concomitant effect of these anneals on the mechanical properties of the gate material, such as the intrinsic film stress ( $\sigma_0$ ) and coefficient of thermal expansion ( $\alpha$ ). Our results show that Ti/Pd and Ti/Pt result in much higher fixed charge density and higher, though comparable, interface trap densities when compared to Al with all three metals showing a minimum in interface trap density for a 30 minute anneal at 350C. Moreover, we find that  $\alpha$  is larger than the bulk value and that both  $\alpha$  and  $\sigma_0$  increase with temperature with  $\sigma_0 \approx 1$  GPa at 350 C for Pd. These results demonstrate that the forming gas anneal which minimizes electrical defects (inhomogeneous strain) strongly increases the effects of inhomogeneous strain (electrical defects).

#### **6:20 AM F.NM05.06.07**

**Tracking Interfacial Disorder in SiGe Qubit Material** Luis F. Pena, Justin C. Koepke and Ezra Bussman; Sandia National Laboratories, United States

Nano-scale quantum dot (QD) qubits in SiGe are exhibiting competitive quantum characteristics, e.g. long coherence times, required of future materials platforms for quantum information technologies. Qubits are intimately nested at semiconductor interfaces between Si and SiGe in layered heterostructures. A major challenge in developing the SiGe platform lies in understanding relationships between interface structure and quantum electronic properties. Specifically, atomic steps at Si/SiGe interfaces is theoretically predicted to strongly modulate a critical quantum property, the conduction band valley spitting. This atomic-scale interface structure-to-electronic-function relationship may be a determining factor in manufacturability of SiGe qubits. However, it is difficult to examine the relationship since it's exceedingly challenging to probe atomic structure at buried interfaces.

We characterize atomic-scale structural disorder at Si/SiGe qubit interfaces by using scanning tunneling microscopy in parallel with molecular beam epitaxial growth. We report a counterintuitive evolution of roughness and step spatial correlations during growth. We find interfaces are completely uncorrelated with Si sample miscut and take-on unique distributions at each interface, stemming from growth kinetics and strain effects. In addition, at the Si qubit interface, there are widely-ranging atomic step arrangements, at all length scales relevant for QDs reported in literature. This indicates that one should expect widely varying valley splittings and suppressed values measured in both QDs, and mesoscale electronic transport devices. Further, our measurements make it clear that sparse transmission electron and atomic force microscopy (AFM) measurements (the standard approach) will not suffice to evaluate these interfaces. For example, the Si qubit interface and other nearby interfaces have completely different structure and can't serve as proxies for one another to allow top-surface AFM to estimate the buried qubit interface structure. These results are meaningful toward elucidating structure-function relationships in SiGe QDs and a pathway to understanding the complex engineering required to leap beyond current device performance.

This work was performed, in part, at the Center for Integrated Nanotechnologies, an Office of Science User Facility operated for the U.S. Department of Energy (DOE) Office of Science. Sandia National Laboratories is a multimission laboratory managed and operated by National Technology & Engineering Solutions of Sandia, LLC, a wholly owned subsidiary of Honeywell International, Inc., for the United States DOE's National Nuclear Security Administration under contract DE-NA-0003525. The views expressed in the article do not necessarily represent the views of the U.S. Department of Energy or the United States Government.

**6:30 AM F.NM05.06.08**

**Growth of Nearly Atomically-Flat SiGe Layers on Thick SiGe Relaxed Buffers by UHV-CVD for Valley Splitting Enhancement** Weiguang Huo and James C. Sturm; Princeton University, United States

## Motivation

Spin qubits of electrons in Si are a leading route to implement quantum computing, due to silicon's weak spin-orbit coupling and the existence of stable zero nuclear spin isotopes. However, a fundamental challenge is the degeneracy of the conduction band minima, which is a decoherence source.

For electron qubits, a thin Si layer is typically grown on a  $\text{Si}_{0.7}\text{Ge}_{0.3}$  relaxed buffer for a tensile strain of 1.2%, which will break the cubic symmetry of Si and split its 6-fold degenerate valleys into four in-plane  $\Delta_4$  high-energy valleys and two out-of-plane  $\Delta_2$  low-energy valleys. This strain-induced valley splitting is a very large  $\sim 200$  meV. The two degenerate  $\text{Si}_{0.7}\text{Ge}_{0.3}$   $\Delta_2$  valleys are further split by the quantum well confinement potential, estimated to be 1 meV [1], sufficient for QC. However, experimental measurements are 10 times lower than this expectation [2], which seriously hinders the further development of Si-based QC. It is believed that a roughness as small as one atomic step at the SiGe/Si interface could cause this reduction in valley splitting, so that an atomically flat interface is required [1]. The typical roughnesses of relaxed SiGe layers in the literature are in the nm range or more, at least 10X too high. In this paper, we demonstrate the growth of an atomically flat relaxed  $\text{Si}_{0.7}\text{Ge}_{0.3}$  buffer layer, which could be the key to enhance the splitting of the two  $\Delta_2$  valleys in a thin Si layer grown on top of the SiGe. We also outline the fundamental mechanisms leading to SiGe roughness that must be suppressed.

## Methods

Conventional thick (3-micron) graded relaxed  $\text{Si}_{0.7}\text{Ge}_{0.3}$  relaxed buffers are first grown by CVD on Si (100) substrates. They are rough, so they are then chemically and mechanically polished to a surface roughness less than 0.2 nm. After wet acid cleaning, SiGe and Si layers are grown in a custom-built UHV-CVD system using silane and germane sources. The typical growth rates for Si and SiGe at 600°C are  $\sim 1$ -2 nm/min respectively. Oxygen and carbon contamination in Si and SiGe layers are all below  $5 \times 10^{17}$  cm<sup>-3</sup>, indicating clean layers. The roughness is characterized by a Bruker Dimension ICON3 Atomic Force Microscope (AFM) in tapping mode with a  $5 \mu\text{m} \times 5 \mu\text{m}$  scan size. The noise error is  $\sim 0.10$  nm RMS.

## Results

Important parameters affecting the growth of the SiGe layer are pre-growth "baking" of the polished relaxed SiGe in the UHV CVD chamber before growth and the growth temperature of the SiGe. Unlike the growth of Si on Si in UHV-CVD, we find that for growth on SiGe, baking is necessary to remove surface contamination, and thus layers grown after baking are

initially rough. The surface roughness is smoother as the regrowth interface contamination is reduced, from 3.4 nm RMS for 750°C baking to 0.46 nm RMS for 800°C baking, indicating that the cleanliness of the regrowth interface is important for layer roughness. The smoothest SiGe surface morphology occurs when the growth temperature is around 650°C, and the morphology gets rougher if the growth temperature is either lower or higher than 650°C. Growing SiGe at lower temperatures, adatoms from the gas source may not find minimum energy locations for step flow growth, possibly due to low adatom surface mobility, leading to roughness. At higher temperatures, multiple mechanisms may contribute to roughness, such as the re-evaporation process and the role of entropy. Silicon layers are consistently smoother than SiGe layers, and a nearly atomically flat relaxed SiGe (roughness = 0.17 nm RMS) is achieved by inserting a thin Si layer into the relaxed SiGe layer.

[1] Friesen, Mark, et al. Physical Review B 75.11 (2007): 115318.

[2] Borselli, Matthew G., et al. Applied Physics Letters 98.12 (2011): 123118.

#### 6:40 AM F.NM05.06.09

**Can AlO<sub>x</sub> SETs be Integrated with MOS Quantum Devices?** Yanxue Hong<sup>1,2</sup>, Ryan Stein<sup>1,2</sup>, N. M. Zimmerman<sup>2</sup>, M. D. Stewart, Jr.<sup>2</sup> and J.M. Pomeroy<sup>2</sup>; <sup>1</sup>University of Maryland, United States; <sup>2</sup>National Institute of Standards and Technology, United States

Plasma oxidation and ultra-high vacuum handling enable the formation of ultra-stable aluminum oxides (AlO<sub>x</sub>), demonstrated here using single-electron transistor (SET) measurements and improving prospects for broader implementation in quantum information applications. These devices exhibit remarkably mitigated charge offset drift (best  $\Delta Q_0 = 0.13 e \pm 0.01 e$  over  $\approx 7.6$  days) in our Al/AlO<sub>x</sub>/Al SETs, compared to previous SET results [1-4] with conventional, thermally oxidized tunnel barriers (best  $\Delta Q_0 = 0.43 e \pm 0.007 e$  over  $\approx 9$  days and most  $\Delta Q_0 \geq 1 e$  within one day). Slow, linear drift ( $< 0.025 e/day$ ) accounts for most of the charge offset drift in our devices and  $\Delta Q_0^{corr} = 0.07 e \pm 0.01 e$  over  $\approx 7.6$  days when the linear background is subtracted. Slow drift, combined with a control voltage feedback loop, allows good charge sensing as long as the control voltage activity does not obscure “real” charge transition events. The charge stability demonstrated here enables these Al/AlO<sub>x</sub>/Al SETs to be integrated as persistent charge sensors for projective spin-to-charge readout in qubit devices. For example, a signal-to-noise  $> 2$  can be achieved when the coupling capacitance is  $> 3.5$  aF between an AlO<sub>x</sub> SET and a Si MOS quantum dot with a self-capacitance  $\approx 50$  aF.

#### References

1. Zimmerman, N.M., et al., *Why the long-term charge offset drift in Si single-electron tunneling transistors is much smaller (better) than in metal-based ones: Two-level fluctuator stability*. Journal of Applied Physics, 2008. **104**(3): p. 033710.
2. Zimmerman, N.M. and W.H. Huber, *Microscope of glassy relaxation in femtogram samples: Charge offset drift in the single electron transistor*. Physical Review B, 2009. **80**(19): p. 195304.
3. Stewart, M.D. and N.M. Zimmerman, *Stability of Single Electron Devices: Charge Offset Drift*. Applied Sciences, 2016. **6**(7): p. 187.
4. Huber, W.H., S.B. Martin, and N.M. Zimmerman, *Long-term charge offset noise in Coulomb-Blockade devices*. Experimental Implementation of Quantum Computation; Clark, R., Ed.; Rinton Press, INC: Princeton, NJ, USA, 2001: p. 176-182.

SESSION F.NM05.07: Poster Session: Emerging Materials for Quantum Information Technologies  
On Demand Abstracts Available for Viewing Starting Saturday Morning, November 21, 2020  
5:00 AM - 8:00 AM  
F-NM05

#### F.NM05.07.01

**Observation of Strong Electron-Phonon and Electron-Photon Interactions in Topological Weyl Semimetals** Kunyan Zhang<sup>1</sup>, Tong Wang<sup>2</sup>, Xiaoqi Pang<sup>2</sup>, Fei Han<sup>3</sup>, Nguyen Tuan Hung<sup>2</sup>, Ahmad R. Nugraha<sup>2,4</sup>, Mingda Li<sup>3</sup>, Riichiro Saito<sup>2</sup> and Shengxi Huang<sup>1</sup>; <sup>1</sup>The Pennsylvania State University, United States; <sup>2</sup>Tohoku University, Japan; <sup>3</sup>Massachusetts Institute of Technology, United States; <sup>4</sup>Indonesian Institute of Sciences, Indonesia

Electron-phonon interaction plays an important role in the electronic properties of topological materials by affecting the dispersion and lifetime of phonon and electronic states. For example, Kohn anomaly describes the phonon softening

phenomenon when the dielectric screening from conducting electrons in a metal is disrupted. Another evidence of strong electron-phonon interaction is Fano resonance, the interference between discrete and continuous states, featured by an asymmetric Breit-Wigner-Fano lineshape. In this work, we present the anisotropic Kohn anomaly and Fano resonance in a type-II Weyl semimetal candidate LaAlSi by polarized Raman spectroscopy. The  $B_1$  phonon mode in our Raman spectra shows excitation-wavelength-dependent phonon-softening and lineshape asymmetry. In type-I Weyl semimetal TaP, abnormal symmetry breaking of another  $B_1$  mode in polarized Raman spectroscopy has been observed, attributed to the quantum interference of degenerate carrier pockets with different symmetries. The experimental observations combined with density-functional theory (DFT) calculations provide valuable insights into microscopy scattering pathways and transport properties of the type-II Weyl semimetal candidate LaAlSi and type-I Weyl semimetal TaP.

#### **F.NM05.07.02**

**1.5  $\mu\text{m}$  Telecom-Wavelength Single Photon Source of InAs/InP Quantum Dot via Strain-Controlled Growth** Youngho Ko<sup>1</sup>, Mireu Lee<sup>1,2</sup>, Hosung Kim<sup>1</sup>, Won Seok Han<sup>1</sup>, Je-Hyung Kim<sup>2</sup> and Jung Jin Ju<sup>1</sup>; <sup>1</sup>Electronics and Telecommunications Research Institute, Korea (the Republic of); <sup>2</sup>Ulsan National Institute of Science and Technology, Korea (the Republic of)

Owing to the rapid development of quantum information technology including quantum communication, quantum sensor, and quantum computer, realization of quantum light source, an essential element for the photonic quantum information applications, have been required. There have been numerous efforts to obtain single photon sources as a quantum light source by using various solid-state material platforms including semiconductor quantum dots (QDs), defect-based color centers in diamond and SiC, QDs in two-dimensional material of  $\text{WS}_2$  and  $\text{WSe}_2$ , and etc. III-V semiconductor QDs have been widely considered as a promising platform for the single photon source due to their various advantages of high generation efficiency of single photon, wavelength tunability, and favourable integration with various semiconductor-based photonic circuits. Single photon emission in 1.5  $\mu\text{m}$  telecom-wavelength range was quite important because of compatible with quantum communication and photonic integrated circuits of silicon photonics. However, single photon emission in telecom-wavelength range was still challenge. InAs QDs are normally grown by Stranski–Krastanov growth mode with molecular-beam epitaxy or metal organic chemical vapor deposition (MOCVD). Because the diameter and height of the self-assemble InAs QDs are determined by strain originated from lattice mismatch with host materials, it was difficult to obtain telecom-wavelength single photon emission from InAs/GaAs or InAs/InP QDs. In this study, we obtained 1.5  $\mu\text{m}$  telecom-wavelength single photon emission from InP-based InAs QDs by using strain-controlled layer of InAlGaAs. The single photon source was fabricated with circular bragg grating structure to obtain high collection efficiency of single photon emission. Moreover, we proposed integrated single photon devices to realize integrated quantum light source with photonic integrated circuits. For the strain control during the growth of InAs QDs, tensile-strained InAlGaAs layers as a host material were grown on the InP substrate. The InAs QDs were grown by Stranski–Krastanov growth mode in MOCVD. lattice-mismatched InAlGaAs on InP showed 0.74 % tensile strain with InP, which was characterized by x-ray diffraction measurement. We monitored the structural properties of InAs QDs by atomic force microscopy and transmission electron microscopy with changing the strain-controlled layers of InAlGaAs, InGaAs, and InP and with changing the thickness of strain-controlled layers. To optimize the size and density of the QD, InAs samples were grown with various growth condition including the temperature, growth rate, and the III/V ratio. We found that the size of InAs QDs were strongly dependent on the density and As flow was critical for emission efficiency of QD and wetting layer. Through systematic study, we could obtain low enough density of InAs QD from  $10^7/\text{cm}^2$  to  $10^9/\text{cm}^2$  for fabrication of single photon emitter. We carried out the micro-photoluminescence measurement at 3.4 K for optical analysis of QDs. The single QD emission peak was exhibited from 1.5 to 1.6  $\mu\text{m}$  wavelength. The second-order correlation function was measured for single photon analysis through Hanbury-Brown Twiss experiment. We designed circular bragg grating structures with InAs/InAlGaAs QD for collection efficiency and Purcell enhancement of cavity. Optical simulation of the QD in cavity was performed by finite-difference time domain simulation. The collection efficiency of the circular bragg grating structure was more than 80 % to objective lens of NA 0.7. We also designed the integrated single photon source with Si photonic circuit. InAlGaAs waveguide was designed as the nano tapered waveguide and  $\text{SiO}_2$  interlayer was adopted to efficiently couple the single photon emission with Si waveguide. The QD-based telecom-wavelength single photon source of high collection efficiency and integrated single photon source could provide a solution for on-chip quantum photonic devices.

#### **SYMPOSIUM F.NM06**



Spin Dynamics in Materials for Quantum Sensing, Optoelectronics and Spintronics  
November 21 - December 3, 2020

Symposium Organizers

Shunsuki Fukami, Tohoku University  
Ezekiel Johnston-Halperin, The Ohio State University  
Xiaoqin Li, The University of Texas at Austin  
Bernhard Urbaszek, Institut National des Sciences Appliquées de Toulouse

---

\* Invited Paper

SESSION Tutorial F.NM06: Spin Dynamics in Materials for Quantum Technologies—Experiment and Theory  
Session Chairs: Anais Dreau, Michael Flatte, Mikhail Glazov and Bernhard Urbaszek  
Sunday Afternoon, November 29, 2020  
F.NM06

**2:45 PM \***

**Quantum Technologies with Single Spin Defects in Semiconductors** Anais Dreau; CNRS - L2C, France

Optically-active spin defects in semiconductors are solid-state artificial atoms that can maintain their quantum properties over very long times, and sometimes up to room-temperature. A review of their appealing properties for quantum applications, such as ultra-sensitive nanoscale quantum sensors and quantum communication networks, will be presented. Current challenges towards large-scale implementation of quantum technologies and the exploration of novel platforms to isolate individual spin defects will be addressed.

**3:45 PM BREAK**

**4:00 PM \***

**Electron and Nuclear Spin Dynamics in Semiconductor Nano-Structures** Mikhail Glazov; Ioffe Institute, Russian Federation

Main spin relaxation mechanisms explained; interpreting spin dynamic in materials from optical spectroscopy and conclusions for material design

**5:00 PM BREAK**

**5:15 PM \***

**Exciton and Spin-Valley Dynamics in Atomically Thin Semiconductors** Bernhard Urbaszek; Institut National des Sciences Appliquées de Toulouse, France

Experimental techniques for accessing polarization dynamics in atomic monolayers; challenges in device designs for stable spin memory, access and read-out

**6:15 PM BREAK**

**6:30 PM \***

**New Materials and Devices for Quantum Coherent Technologies** Michael E. Flatte; University of Iowa, United States

How to meld the favorable properties of multiple materials or structures into hybrid coherent quantum systems that will outperform each of the constituents - achievements in material research so far and future challenges and prospects.

SESSION F.NM06.12: Live Keynote I: Spin Dynamics in Materials for Quantum Sensing, Optoelectronics and Spintronics  
Session Chairs: Ezekiel Johnston-Halperin and Bernhard Urbaszek  
Wednesday Afternoon, December 2, 2020  
F.NM06

**5:15 PM \*F.NM06.01.01**

**Chemistry for the Second Quantum Revolution** Daniel Laorenza<sup>1</sup>, Michael Wojnar<sup>1</sup>, Joseph Zadrozny<sup>2</sup> and Danna E. Freedman<sup>1</sup>; <sup>1</sup>Northwestern University, United States; <sup>2</sup>Colorado State University, United States

Chemical synthesis creates materials that are atomically precise, customizable, and reproducible. By bringing this toolkit to bear on the challenge of creating materials for quantum information science, we can design custom materials, each molecule geared towards a specific purpose. With these "designer qubits" it may be possible to imbue a qubit with water solubility for biological quantum sensing, create quantum memories with the careful placement of nuclear spins, or tune the emission frequency for quantum communication. Results will be presented on creating and understanding molecular qubits, with an emphasis on strategies to create qubits that can be integrated with established read-out approaches.

**5:30 PM \*F.NM06.01.03**

**Molecular Spin Qudits for Quantum Algorithms** Mario Ruben; Karlsruhe Institute of Technology, Germany

Metal complexes will be proposed to acting as active quantum units for Quantum Computing (QC). We report on the implementation of metal complexes into nanometre-sized (single-)molecular spintronic devices by a combination of bottom-up self-assembly and top-down lithography techniques. The controlled generation of magnetic molecular nanostructures on conducting surfaces/electrodes will be shown and persistence of their magnetic properties under confinement in Supramolecular Quantum Devices (SMQD) will be proven. The quantum properties (e.g.. superposition entanglement) of the metal complexes will be addressed at the single molecule level<sup>1-9</sup> to finally implement a quantum algorithm on a TbPc<sub>2</sub> Qudit performing quantum computing operations.<sup>10</sup>

References:

- [1] S. Kyatskaya et. al. *J. Am. Chem. Soc.* **2009**, *131*, 15143-15151.
- [2] M. Urdampilleta et al. *Nature Mater.* **2011**, *10*, 502-506.
- [3] J. Schwöbel et. al. *Nature Comms.* **2012**, *3*, 953-956.
- [4] R. Vincent et al. *Nature* **2012**, *488*, 357-360.
- [5] M. Ganzhorn et al. *Nature Nano.* **2013**, *8*, 165-169.
- [6] M. Ruben et. al. *Nature Nano.* **2013**, *8*, 377-389.
- [7] S. Wagner et. al. *Nature Nano.* **2013**, *8*, 575-579.
- [8] S. Thiele, et al. *Science* **2014**, *344*, 1135-1138.
- [9] M. Ganzhorn, et. al. *Nature Comms* **2016**, 11443.
- [10] C. Godfrin et al. *PRL* **2017**, *119*, 187702 (perspective article by A. Morello *Nature Nano* **2018**, *13*, 9-10).

**Recent Reviews:**

*Molecular spin qudits for quantum algorithms.*

E. Moreno-Pineda, C. Godfrin, F. Balestro, W. Wernsdorfer, M. Ruben. *Chem. Soc. Rev.* **2018**, *47*, 501.

*Synthetic Engineering of the Hilbert Space of Molecular Qudits: Isotopologue Chemistry*

W. Wernsdorfer, M. Ruben. *Adv. Mat.* **2019**, doi.org/10.1002/adma.201806687.

**5:45 PM \*F.NM06.02.01**

**Sensing and Controlling the Spin Sublattices of an Insulating Antiferromagnet by Electrical Means** Anand Bhattacharya; Argonne National Laboratory, United States

A central goal of antiferromagnetic spintronics is the ability to sense and control the magnetic state of an antiferromagnet. While the magnetic state of a metallic antiferromagnet (AF) may be inferred using magnetoresistance measurements, this is not an option for insulating AF materials. The spin Seebeck effect (SSE), where thermal gradients are used to drive magnon spin currents, has proven to be an effective probe [i] of AF order. Substantial spin currents have been measured using the

SSE in AF insulators Cr<sub>2</sub>O<sub>3</sub> [ii] and MnF<sub>2</sub> [iii], and even in geometrically frustrated antiferromagnets [iv]. In this talk, I will briefly review the antiferromagnetic spin Seebeck effect and present our latest results on epitaxial Pt/Cr<sub>2</sub>O<sub>3</sub> (0001)/Pt heterostructures. In our devices, the spin currents generated by thermal gradients are detected using the inverse spin Hall effect (ISHE) in thin films of Pt, grown both as an epitaxial underlayer beneath and as an overlayer on top of the Cr<sub>2</sub>O<sub>3</sub> film. Cr<sub>2</sub>O<sub>3</sub> is unique in that the spins on the top and bottom surfaces of the (0001) oriented film are uncompensated, and belong to separate magnetic sublattices, even in the presence of surface roughness. Using the ISHE in both top and bottom Pt layers [v], we find that the SSE is strongly sensitive to the respective sublattice magnetization. As a result, we are able to track the exact orientation of both sublattices upon application of a magnetic field, including during spin-flop processes. Furthermore, Cr<sub>2</sub>O<sub>3</sub> is a classic linear magnetoelectric, where an electric field applied in the [0001] direction can be used to tune the net magnetization [vii]. In this context, I will discuss how the application of electric fields in Pt/Cr<sub>2</sub>O<sub>3</sub>/Pt heterostructures can be used to tune magnon spin currents, generated using thermal gradients [viii].

[i] S. M. Rezende et al., *Phys. Rev. B* **93**, 014425 (2016).

[ii] S. Seki et al., *Phys. Rev. Lett.* **115**, 266601 (2015)

[iii] S. M. Wu et al., *Phys. Rev. Lett.* **116**, 097204 (2016)

[iv] S. M. Wu et al., *Phys. Rev. Lett.* **116**, 097204 (2015); C. Liu et al...

[v] Y. Luo et al., *arXiv*:1910.10340

[vii] D. N. Astrov, *Sov. Phys. JETP* **11**, 780 (1960).

[viii] C. Liu et al., in preparation (2020).

#### 6:00 PM \*F.NM06.03.02

**Driven Spin Systems with Protected Coherence in Commercially Available Silicon Carbide** Kevin Miao, Alexandre Bourassa, Christopher Anderson and [David Awschalom](#); University of Chicago, United States

Silicon carbide (SiC) is a host to a variety of robust, optically active quantum systems. Recent studies have shown that basally oriented *kh* divacancy defects in SiC possess a robust optical interface as well as exceptional spin coherence properties even in commercially available, naturally abundant SiC. We show that these excellent intrinsic properties can be further augmented and tuned by applying a periodic drive, giving rise to emergent phenomena unique to non-equilibrium quantum systems.

First, we demonstrate electrically driven coherent quantum interference in the optical transition of single *kh* divacancies [1]. By applying microwave frequency electric fields, we coherently drive the divacancy's excited-state orbitals and induce Landau-Zener-Stückelberg interference fringes in the resonant optical absorption spectrum. This result shows that the optical absorption spectrum of these divacancy defects can be rapidly reconfigured using localized electric field control, and reveals a highly responsive mechanism to potentially coherently interact with other electrically active quantum systems.

We then construct a robust qubit embedded in a decoherence-protected subspace, obtained by hybridizing an applied microwave drive with the ground-state electron spin of the *kh* divacancy [2]. This qubit is protected from magnetic, electric, and temperature fluctuations, which account for nearly all relevant decoherence channels in the solid state. This culminates in an increase of the qubit's inhomogeneous dephasing time by over four orders of magnitude (to >22 milliseconds), while its Hahn-echo coherence time approaches 64 milliseconds. Such an extension of inhomogeneous dephasing time opens up pathways to a vast array of hybrid quantum system applications. Furthermore, since this protocol requires few key platform-independent components, this result suggests that substantial coherence improvements can be achieved in a wide selection of quantum architectures.

This work was done in collaboration with Alexander L. Crook, Gary Wolfowicz, Joseph P. Blanton, Samuel J. Whiteley, Sam L. Bayliss, Hiroshi Abe, Takeshi Ohshima, Gergo Thiering, Péter Udvarhelyi, Viktor Ivády, and Adam Gali.

[1] K. C. Miao, A. Bourassa, C. P. Anderson, S. J. Whiteley, A. L. Crook, S. L. Bayliss, G. Wolfowicz, G. Thiering, P. Udvarhelyi, V. Ivády, H. Abe, T. Ohshima, Á. Gali, D. D. Awschalom, "Electrically driven optical interferometry with spins in silicon carbide," *Sci. Adv.* **5** (11), eaay0527 (2019)

[2] K. C. Miao, J. P. Blanton, C. P. Anderson, A. Bourassa, A. L. Crook, G. Wolfowicz, H. Abe, T. Ohshima, D. D. Awschalom, "Universal coherence protection in a solid-state spin qubit," *arXiv* 2005.06082 (2020)

#### 6:15 PM \*F.NM06.03.04

**Molecular States in the Silicon Vacuum—Deterministic Clusters of Donors and Acceptors in Silicon** Jianhua Zhu<sup>1</sup>, Wei Wu<sup>1</sup>, Nguyen Le<sup>2</sup>, Eran Ginossar<sup>2</sup> and Andrew Fisher<sup>1</sup>; <sup>1</sup>UCL (University College London), United Kingdom; <sup>2</sup>University of Surrey, United Kingdom

Advances in localised tip-induced lithography mean that the process of doping a semiconductor need no longer be random: instead, dopant atoms can be located in well-defined positions relative to one another. This has already been demonstrated for donors in silicon [1,2] and may in future be possible for other types of dopant. This opens the possibility of controlling the interactions between the dopants to form new deterministic devices, which in turn elevates the spin degree of freedom from a spectator into an important variable. As well as the established potential for spin-based quantum gates [3] a number of other applications can now be foreseen.

We have computed the excitation spectra of donor pairs and larger clusters [4] in silicon, using a combination of ab initio band-structure simulations and quantum chemistry techniques. The results show strong and characteristic changes in the character of the dominant excitation as a function of separation and spin state, raising the possibility optical detection and initialisation of the multi-donor spin state. We have also studied the application of controlled donor arrays as quantum simulators that can be probed by their transport properties [5]; in particular we have identified topological edge states and shown how their properties vary across the metal-insulator transition [6].

Finally, for acceptor clusters we have studied the consequences of the richer spin-orbit coupling present in the silicon valence band [7]. We find a complex interplay between the relative strengths of hopping and Coulomb interactions, the arrangement of the bond lengths, and the spin-orbit coupling. This can result in the emergence of novel kinds of topological state.

[1] Schofield, S. R., et al (2003). **Atomically precise placement of single dopants in Si.** *PHYSICAL REVIEW LETTERS*, 91 (13), ARTN 136104. doi:10.1103/PhysRevLett.91.136104

[2] Stock, T. J. Z., et al. (2020). **Atomic-Scale Patterning of Arsenic in Silicon by Scanning Tunneling Microscopy.** *ACS Nano*, acsnano.9b08943. doi:10.1021/acsnano.9b08943

[3] He, Y et al. (2019). **A two-qubit gate between phosphorus donor electrons in silicon.** *Nature* 571 p 371  
doi:10.1038/s41586-019-1381-2

[4] Wu, W., et al. (2018). **Excited states of defect linear arrays in silicon: A first-principles study based on hydrogen cluster analogs.** *Physical Review B*, 97 (3), ARTN 035205. doi:10.1103/PhysRevB.97.035205

[5] Le, N. H., et al. (2017). **Extended Hubbard model for mesoscopic transport in donor arrays in silicon.** *Physical Review B*, 96 (24), ARTN 245406. doi:10.1103/PhysRevB.96.245406

[6] Le, N. H., et al. (2020). **Topological phases of a dimerized Fermi–Hubbard model for semiconductor nano-lattices.** *npj Quantum Information*, 6 (1), 24. doi:10.1038/s41534-020-0253-9

[7] Zhu, J., et al. (2020). **Linear combination of atomic orbitals model for deterministically placed acceptor arrays in silicon.** *Physical Review B*, 101 (8), ARTN 085303. doi:10.1103/PhysRevB.101.085303

**6:30 PM \*F.NM06.04.01**

**Magnetoelectric Effects in Spin Crossovers and Metal-Organic Frameworks** Vivien Zapf; Los Alamos National Laboratory, United States

Magnetoelectric coupling is the coupling between magnetic order and the electric polarization in an insulator. To date it has been largely studied in inorganic oxides that show various types of ferromagnetic or antiferromagnetic order. Metal-organic frameworks and molecular compounds are a new and fertile direction to search for new magnetoelectric coupling mechanisms. I will talk about several recent results in which we couple spin crossovers to structure and electric polarization. I will also highlight multiferroic behavior in metal-organic frameworks. The experimental part of the work takes advantage of pulsed magnetic fields to perform high-sensitivity measurements and reach extended regions of the magnetic field-temperature phase diagram.

**6:45 PM \*F.NM06.10.01**

**Ultrastrong Magnonic Coupling in Canted Antiferromagnets** Takuma Makihara, Nicolas Marquez Peraca and Junichiro Kono; Rice University, United States

Light-matter coupling in the so-called ultrastrong coupling (USC) regime [1] has become an important general subject of modern science and technology. Many next-generation quantum technologies that exploit the extremely efficient light-matter interactions in the USC regime have been proposed. Further, a wealth of exotic phenomena has been predicted in the USC regime, such as quantum vacuum radiation or nonclassical ground states known as two-mode squeezed vacuums. The source

of these phenomena is the so-called counter-rotating terms in the Hamiltonian, which are typically negligible compared to the so-called co-rotating terms for weaker coupling strengths. USC has now been achieved in diverse platforms, but the exotic nature of the ground state due to the counter-rotating terms has not been explored. We have recently observed unusual matter-matter USC phenomena in rare-earth orthoferrites. First, we observed cooperative, Dicke-type coupling between a paramagnetic  $\text{Er}^{3+}$  spin ensemble and a single mode of terahertz magnons of ordered  $\text{Fe}^{3+}$  spins in  $\text{ErFeO}_3$  [2]. The data exhibited vacuum Rabi splitting values in the USC regime, indicating that rare-earth orthoferrites provide a rich playground in which to explore USC phenomena without light. Furthermore, we observed that magnons in  $\text{YFeO}_3$  display USC with a dominant role played by the counter-rotating terms. Our system is described by an unusual Hamiltonian, where: (i) the coupling strengths are tunable, (ii) the counter-rotating interactions dominate the co-rotating interactions, and (iii) the ground state is a magnonic two-mode squeezed vacuum with quantum fluctuation suppression up to 5.9 dB. These observations demonstrate that  $\text{YFeO}_3$  provides an extraordinary platform for both applied and fundamental studies of USC beyond the reaches of photonic platforms.

1. P. Forn-Diaz, L. Lamata, E. Rico, J. Kono, and E. Solano, "Ultrastrong Coupling Regimes of Light-Matter Interaction," *Rev. Mod. Phys.* **91**, 025005 (2019).

2. X. Li *et al.*, "Observation of Dicke Cooperativity in Magnetic Interactions," *Science* **361**, 794 (2018).

SESSION F.NM06.13: Live Keynote II: Spin Dynamics in Materials for Quantum Sensing, Optoelectronics and Spintronics

Session Chairs: Xiaoqin Li and Bernhard Urbaszek

Thursday Morning, December 3, 2020

F.NM06

### 11:30 AM \*F.NM06.05.01

**Electron and Nuclear Spin Dynamics in Semiconductor Nanosystems** Mikhail Glazov; Ioffe Institute, Russian Federation

Recently, the physicists and material scientists have experienced a new wave of interest in spin effects in solid-state systems. On the one hand, semiconductors and semiconductor nanosystems, allow one to perform benchtop studies of quantum and relativistic phenomena. On the other hand, the interest is supported by the prospects of realizing spin-based electronics where the electron or nuclear spins can play the role of quantum or classical information carriers. In my tutorial lecture, I will present the key aspects of multifaceted physics of interacting electron and nuclear spins in semiconductor-based low-dimensional structures. The hyperfine interaction of the charge carrier and nuclear spins increases in nanosystems compared with bulk materials. The enhanced coupling results in the efficient spin exchange between these two systems. It gives rise to beautiful and complex physics occurring in the ensemble of electrons and nuclei in semiconductors.

I will address the hyperfine interaction, nuclear magnetic resonance, dynamical nuclear polarization, spin-Faraday and -Kerr effects, processes of electron spin decoherence and relaxation, effects of electron spin precession mode-locking and frequency focusing, as well as fluctuations of electron and nuclear spins.

### 11:45 AM \*F.NM06.05.03

**Suppression of Nuclear Spin Fluctuations in (In,Ga)As/GaAs Quantum Dots Under Pulsed Excitation with GHz Frequency** E. Evers<sup>1</sup>, N.E. Kopteva<sup>1,2</sup>, Dmitri R. Yakovlev<sup>1,3</sup>, A. Greilich<sup>1</sup> and Manfred Bayer<sup>1,3</sup>; <sup>1</sup>Technische Universität Dortmund, Germany; <sup>2</sup>St. Petersburg State University, Russian Federation; <sup>3</sup>Russian Academy of Sciences, Russian Federation

One of the possible hybrid realizations of a qubit is the spin of an electron confined in a semiconductor quantum dot (QD), which is interacting with the surrounding nuclear spins. The prominent advantage of QDs is their strong optical dipole moment, which allows efficient coupling of photons to the confined electron spins according to the optical selection rules. The electron, on the other hand, is coupled to the nuclei of the QD crystal matrix by the hyperfine interaction. These couplings allow one to design schemes where the angular momentum of the photon is transferred to the nuclear spins using the electron as an auxiliary spin state. This may have significant advantages, as the electron spin coherence is limited to several microseconds at low temperatures, while the nuclear spin coherence can reach milliseconds.

To test the degree of control between the electron and the nuclear spin system, we present a model system of an ensemble of singly charged QDs. The use of an ensemble is justified in our case by the spectroscopic signal strength, which allows us to observe an averaged and integral response of many electron spins at the same time. It is also of interest for quantum memory applications. On the other hand, such an ensemble is usually strongly inhomogeneous, which leads to a strong variation of the

intrinsic parameters, like optical dipole moments, electron g-factor values, and strength of electron-nuclear spin interactions. This inhomogeneity can, however, be overcome in designed experiments, enabling effects such as spin mode-locking and nuclear-induced frequency focusing.

In previous studies on nuclei-induced frequency focusing in singly charged (In,Ga)As/GaAs QDs multiple precession modes were covered by the ensemble, as the nuclear fluctuations were of the same order as the mode separation in low external fields. Here we explore the degree of possible control of the nuclear surrounding using an inhomogeneous QD ensemble excited with a high repetition laser operated at 1 GHz. The GHz laser repetition frequency allows us to investigate the interaction of nuclear spin polarization and nuclear spin fluctuations with the electrons as the mode separation is an order of magnitude larger than the fluctuating nuclear field. It further allows us to use the effects of the strong electron-nuclear feedback and drive the inhomogeneous ensemble of electron spins to a single frequency precession. Additionally, we demonstrate the discretization of the total magnetic fields seen by the electron ensemble and show the effect of the reduction of the nuclear field fluctuations. While for fields lower than 0.6 T nuclear spin fluctuations inhibit the formation of a significant nuclear polarization, above the nuclear spin relaxation time becomes elongated such that the electron spins precess on the closest preferred frequency over a range of 128 mT. This leads to the observation of plateaus in the precession frequency as a function of the external magnetic field. The nuclear spin bath is constantly tuned, such that the phase synchronization condition is fulfilled while nuclear fluctuations are suppressed.

### 12:00 PM \*F.NM06.06.01

**The Physical Origins of Extreme Cross-Polarization Extinction in Confocal Resonant Spectroscopy** Khaled Karrai<sup>1</sup>, Meryem Benelajla<sup>1,2</sup>, Elena Kammann<sup>1</sup> and Bernhard Urbaszek<sup>2,1</sup>; <sup>1</sup>Attocube Systems AG, Germany; <sup>2</sup>Université de Toulouse, INSA-CNRS-UPS, LPCNO, France

In optical spectroscopy experiments, it is crucial to excite an emitter with a laser very close to its transition energy. Experiments under resonant excitation are essential for accessing the intrinsic optical and spin-polarization properties of large class of emitters<sup>1-6</sup>. Using linear cross-polarization in a confocal setup has been successfully employed as a dark-field method to carry out resonant fluorescence experiments to suppress scattered laser light, with the added benefit of high spatial resolution. Resonant fluorescence experiments allow crucial insights into light-matter coupling, such as the interaction of a single photon emitter with its environment, with optical cavities and also studying single defects in atomically thin materials such as WSe<sub>2</sub>. Dark-field confocal techniques allow developing single photon sources with high degrees of photon indistinguishability and longer coherence. In practice dark-field laser suppression is not just a spectroscopy tool, it is also a key part of more matured quantum technology systems. Despite many advances based on experiments in confocal microscopes with cross-polarization laser rejection, the physical mechanisms that make these experiments possible are not understood, hampering further progress in this field. The key figure of merit is the suppression of the excitation laser background by at least six orders of magnitude. Indeed a suppression by a factor of 10<sup>8</sup> up to 10<sup>11</sup> (this work) have been measured. But this is very surprising as mirrors and beam-splitter in such a system reduce the theoretical extinction limit to the 10<sup>3</sup> to 10<sup>4</sup> range. In this work we explain the physics behind the giant enhancement of the extinction ratio by up to eight orders of magnitude that make microscopy based on dark-field laser suppression possible. The measurements of resonant fluorescence are typically performed in an epifluorescence geometry, for which laser excitation and fluorescence collection are obtained through the same focusing lens. This involves necessarily the use of a beam-splitter orienting the back-reflected light containing the fluorescence towards a detection channel. In our work we identify two key ingredients that explain the giant amplification of the cross-polarization extinction ratio : (i) a reflecting surface (i.e. the beam-splitter) placed between a polarizer and analyzer, and (ii) a confocal arrangement. We demonstrate giant extinction ratios in our experiments for different mirrors (silver, gold, dielectric, beam-splitter cubes) and polarizers (Glan-Taylor, nanoparticle thin films). We demonstrate that behind this general observation lies the intriguing physics of the Imbert-Fedorov effect, which deviates a reflected light beam depending on its polarization helicity. We discover that a confocal arrangement not only amplifies the visibility of the Imbert-Fedorov effect dramatically, taking it from the nanometer to the micrometer scale, but also exploits conveniently the symmetry of the newly observed Imbert-Fedorov modes to insure that the cross-polarized laser beam is not coupled, explaining the near complete suppression of the laser background signal. In other words, we cannot treat the spatial (i.e. modal) and polarization properties of light separately in our dark-field confocal microscope analysis. In addition to new developments in dark-field microscopy our experiments provide powerful tools to understand spin-orbit coupling of light, in the broader context of topological photonics. Funding: European Union's Horizon 2020 research and innovation program, Marie Skłodowska-Curie grant agreement No 721394 ITN 4PHOTON.

<sup>1</sup> Aharonovich, I., *et al.* M. Nat. Phot. 10, 631 (2016)

<sup>2</sup> Högele, A. *et al.* Phys. Rev. Lett. 108, 197403 (2012)

<sup>3</sup> Paillard, M. *et al.* Phys. Rev. Lett. 86, 1634 (2001)

<sup>4</sup> Högele, A. *et al.* Phys. Rev. Lett. 93, 217401 (2004)

<sup>5</sup> Vamivakas, *et al.* Nat. Phys. 5, 198 (2009)

<sup>6</sup> Kaldewey, T. *et al.* Nat. Phot. 12, 68 (2018)

### 12:15 PM \*F.NM06.07.01

**Single Artificial Atoms in Silicon Emitting at Telecom Wavelengths** Anais Dreau; Laboratoire Charles Coulomb, CNRS & University of Montpellier, France

Given its unrivaled potential of integration and scalability, silicon is likely to become a key platform for large-scale quantum technologies. Individual electron-encoded artificial atoms either formed by impurities [1] or quantum dots [2, 3] have emerged as a promising solution for silicon-based integrated quantum circuits. However, single qubits featuring an optical interface needed for large-distance exchange of information [4] have not yet been isolated in such a prevailing semiconductor.

We show the first isolation of single optically-active point defects in a commercial silicon-on-insulator wafer implanted with carbon atoms [5]. These artificial atoms exhibit a bright, linearly polarized single-photon emission at telecom wavelengths suitable for long-distance propagation in optical fibers. Our results demonstrate that despite its small bandgap (~1.1 eV) a priori unfavorable towards such observation [6], silicon can accommodate point defects optically isolable at single scale, like in wide-bandgap semiconductors [7]. This work opens numerous perspectives for silicon-based quantum technologies, from integrated quantum photonics to quantum communications [8] and metrology.

[1] He, Y. *et al.*, Nature 571, 371 (2019).

[2] Watson, T. F. *et al.*, Nature 555, 633–637 (2018).

[3] Maurand, R. *et al.*, Nature Comm. 7, 13575 (2016).

[4] Hensen, B. *et al.*, Nature 526, 682–686 (2015).

[5] Redjem\*, W., Durand\*, A. *et al.*, arXiv : 2001.02136 (2020).

[6] Weber, J. R. *et al.*, PNAS 107, 8513–8518 (2010).

[7] Aharonovich, I., Englund, D. & Toth, M., Nature Photonics 10, 631–641 (2016).

[8] Wehner, S., Elkouss, D. & Hanson, R., Science 362, eaam9288 (2018).

### 12:30 PM \*F.NM06.08.01

**Ultrafast Excitation of Coherent Spin Waves in 2D Antiferromagnets** Xiao-Xiao Zhang; University of Florida, United States

The recently discovered atomically-thin magnetic crystals provide a unique playground to develop new approaches to manipulate magnetism. Rapid progresses have been made that demonstrate the potentials of utilizing 2D magnets to construct novel spintronics devices. However, their spin dynamics, which are crucial for microscopic understanding and determine the fundamental limit of spin manipulation, still remain elusive due to the difficulty of characterizing these micron-sized samples with conventional microwave techniques. In this talk, we will show how we can access and probe the collective spin-wave excitations in an antiferromagnetic bilayer CrI<sub>3</sub>, which allows us to extract magnetic anisotropy and exchange energy. In particular, we will demonstrate the gate tunability of magnon frequencies, which is unique for the 2D magnet system.

### 12:45 PM \*F.NM06.08.03

**Van der Waals Epitaxy of Transition Metal Dichalcogenides by MBE Application to the Study of the Valley Nernst Effect in WSe<sub>2</sub>** Minh-Tuan Dau<sup>1</sup>, Celine Vergnaud<sup>1</sup>, Alain Marty<sup>1</sup>, Frederic Bonell<sup>2</sup>, Cyrille Beigne<sup>1</sup>, Serge Gambarelli<sup>1</sup>, Vincent Maurel<sup>1</sup>, Thomas Guillet<sup>1</sup>, Timotee Journot<sup>3</sup>, Berangere Hyot<sup>3</sup>, Benjamin Grevin<sup>2</sup>, Hanako Okuno<sup>1</sup> and Matthieu Jamet<sup>1</sup>; <sup>1</sup>CEA Grenoble, France; <sup>2</sup>CNRS, France; <sup>3</sup>CEA-LETI, France

Semiconducting transition metal dichalcogenides (TMDCs) have gained a great attention because of their fascinating electronic and optical properties when downing the thickness to one monolayer. In the monolayer form, due to the breaking of inversion symmetry and strong spin-orbit coupling, the carriers in TMDCs carry a valley index noted K<sup>+</sup> or K<sup>-</sup>. This valley degree of freedom refers to local extrema in the band structure of TMDC monolayers at the K points of the two-dimensional Brillouin zone and it can be exploited to develop novel valleytronic devices. In MX<sub>2</sub> (M = Mo, W and X = S, Se) monolayers, the broken inversion symmetry and strong spin-orbit coupling originating from the d-orbitals of the transition metal atom align the electron spins near opposite valleys K<sup>+</sup> and K<sup>-</sup> to opposite out-of-plane directions thus preserving time reversal symmetry. The broken spatial inversion symmetry also generates large Berry curvatures near the K valleys, the Berry curvatures being opposite at opposite valleys. This effect gives rise to unconventional electronic properties such as the valley

Hall effect. An interesting growing field of investigation consists in coupling the valley physics with thermoelectrics. Several spin/valley-dependent thermoelectric effects have already been predicted theoretically in monolayer TMDCs such as the spin Nernst effect (thermoelectric counterpart of the spin Hall effect) and the valley Nernst effect (VNE). Hence, the experimental demonstration of those effects could give rise to a new field called valley caloritronics (by analogy with spin caloritronics) with the advantage that the coupled valley-spin degree of freedom is more robust than the spin with respect to external magnetic fields due to the large intrinsic spin-orbit coupling.

In this presentation, I will first review our recent results on the MBE growth of transition metal dichalcogenides on various substrates over large areas and explain the mechanisms underlying the van der Waals epitaxy regime [1]. Using this growth technique, we could study the interplay between thermoelectricity and the valley degree of freedom in monolayers of WSe<sub>2</sub>. For this purpose, high quality WSe<sub>2</sub> mono and multilayers were grown on epitaxial graphene on SiC. Using millimeter-sized samples, we were able to apply well-defined temperature gradients and demonstrate the very strong Seebeck response of this material. In a second step, we used the ferromagnetic resonance-spin pumping technique (FMR-SP) to (i) apply the temperature gradient by off centering the sample in the radio frequency (RF) cavity and (ii) address a single valley and break time reversal symmetry using the spin pumping through spin-valley coupling. For FMR-SP, we deposited in-situ the Al/Ni<sub>81</sub>Fe<sub>19</sub>/Al magnetic stack on top of the WSe<sub>2</sub> layer. The combination of a temperature gradient and the valley polarization lead to the valley Nernst effect in WSe<sub>2</sub> that we could detect electrically in the RF cavity. The Nernst coefficient we measured is in very good quantitative agreement with the predicted value [2]. This effect could be exploited to generate large transverse valley currents for valleytronics applications.

#### References

- [1] M.-T. Dau et al., ACS Nano 12, 2319 (2018).
- [2] M.-T. Dau et al., Nat. Commun. 10, 5796 (2019).

#### 1:00 PM \*F.NM06.09.02

##### **Optical and Microwave Spin Control of Donors in ZnO** Kai-Mei Fu; University of Washington, United States

Electrons bound to donors in silicon are electrically-controlled qubits with exceptional spin coherence properties. Here we seek to find analogous donor systems in direct band gap semiconductors which will enable an efficient optical interface to the donor electron spin qubit. We show that ZnO donors, optically coupled to donor-bound excitons, are particularly promising candidates [1]. Due to low spin-orbit coupling, we find donors exhibit longitudinal spin relaxation times up to 0.5 s at 1.5 K with relaxation fundamentally-limited by phonon interactions. Both lambda and near-cycling optical transitions exist which are suitable for optical spin initialization and readout. Spin-echo coherence times, which we determine via both optical and microwave control, are in the tens of microseconds and likely limited by nuclear spins in natural isotopic ZnO. These characteristics are all extracted from measurements on an ensemble of Ga donors in a commercial substrate. We will present ongoing efforts and challenges toward single donor isolation in nanowires, dual optical-microwave control of donors and two-laser coherent spin-spectroscopy in this emerging qubit platform.

- [1] X. Linpeng, M.L.K Viitaniemi, A. Vishnuradhan, Y. Kozuka, C.Johnson, M. Kawasaki, K.-M.C. Fu, Phys. Rev. Applied 10, 064061 (2018)

#### SESSION F.NM06.01: Quantum Magnets

On Demand Abstracts Available for Viewing Starting Saturday Morning, November 21, 2020  
F-NM06

#### 5:00 AM \*F.NM06.01.01

##### **Chemistry for the Second Quantum Revolution** Daniel Laurenza<sup>1</sup>, Michael Wojnar<sup>1</sup>, Joseph Zadrozny<sup>2</sup> and Danna E. Freedman<sup>1</sup>; <sup>1</sup>Northwestern University, United States; <sup>2</sup>Colorado State University, United States

Chemical synthesis creates materials that are atomically precise, customizable, and reproducible. By bringing this toolkit to bear on the challenge of creating materials for quantum information science, we can design custom materials, each molecule geared towards a specific purpose. With these "designer qubits" it may be possible to imbue a qubit with water solubility for biological quantum sensing, create quantum memories with the careful placement of nuclear spins, or tune the emission frequency for quantum communication. Results will be presented on creating and understanding molecular qubits, with an emphasis on strategies to create qubits that can be integrated with established read-out approaches.



### 5:15 AM \*F.NM06.01.03

**Molecular Spin Qudits for Quantum Algorithms** Mario Ruben; Karlsruhe Institute of Technology, Germany

Metal complexes will be proposed to act as active quantum units for Quantum Computing (QC). We report on the implementation of metal complexes into nanometre-sized (single-)molecular spintronic devices by a combination of bottom-up self-assembly and top-down lithography techniques. The controlled generation of magnetic molecular nanostructures on conducting surfaces/electrodes will be shown and persistence of their magnetic properties under confinement in Supramolecular Quantum Devices (SMQD) will be proven. The quantum properties (e.g., superposition entanglement) of the metal complexes will be addressed at the single molecule level<sup>1-9</sup> to finally implement a quantum algorithm on a TbPc<sub>2</sub> Qudit performing quantum computing operations.<sup>10</sup>

#### References:

- [1] S. Kyatskaya et al. *J. Am. Chem. Soc.* **2009**, *131*, 15143-15151.
- [2] M. Urdampilleta et al. *Nature Mater.* **2011**, *10*, 502-506.
- [3] J. Schwöbel et al. *Nature Comms.* **2012**, *3*, 953-956.
- [4] R. Vincent et al. *Nature* **2012**, *488*, 357-360.
- [5] M. Ganzhorn et al. *Nature Nano.* **2013**, *8*, 165-169.
- [6] M. Ruben et al. *Nature Nano.* **2013**, *8*, 377-389.
- [7] S. Wagner et al. *Nature Nano.* **2013**, *8*, 575-579.
- [8] S. Thiele, et al. *Science* **2014**, *344*, 1135-1138.
- [9] M. Ganzhorn, et al. *Nature Comms* **2016**, 11443.
- [10] C. Godfrin et al. *PRL* **2017**, *119*, 187702 (perspective article by A. Morello *Nature Nano* **2018**, *13*, 9-10).

#### Recent Reviews:

*Molecular spin qudits for quantum algorithms.*

E. Moreno-Pineda, C. Godfrin, F. Balestro, W. Wernsdorfer, M. Ruben. *Chem. Soc. Rev.* **2018**, *47*, 501.

*Synthetic Engineering of the Hilbert Space of Molecular Qudits: Isotopologue Chemistry*

W. Wernsdorfer, M. Ruben. *Adv. Mat.* **2019**, doi.org/10.1002/adma.201806687.

### 5:30 AM F.NM06.01.04

**Giant Phonon-Induced Effective Magnetic Fields in 4f Paramagnets** Dominik M. Juraschek and Prineha Narang; Harvard University, United States

A common approach to spin-based technologies is to manipulate the magnetic order of materials using ultrashort laser pulses, promising operation speeds that are orders of magnitude faster than in conventional spin-based devices. The electromagnetic field components of the radiation change electronic correlations and induce motions of the atoms that produce effective magnetic fields, which couple to the orbital and spin angular momentum of the electrons. A central challenge is to induce large fields that are able to quantitatively change the magnetic order, and usually they range on the order of a milli to a few tesla [1,2].

Here, we show that the extraordinarily strong spin-phonon coupling in the rare-earth trihalides allows the generation of effective magnetic fields of more than 100 tesla by driving circular lattice vibrations (phonons) in the material [3]. At these fields, the paramagnetic spins polarize, nearly reaching saturation, and the magnetization can be reversed by changing the handedness of circular excitation. Specifically, we use a combination of phenomenological modeling and first-principles calculations to predict the effective magnetic fields generated by the excitation of phonons and the subsequently induced magnetization for experimentally accessible pulse energies and temperatures. The phonon-induced magnetizations potentially enable entirely novel ways of ferroelectric or ferromagnetic switching.

- [1] Nova et al., *Nat. Phys.* *13*, 132 (2017)
- [2] Juraschek, Narang, and Spaldin, arXiv:1912.00129 (2019)
- [3] Juraschek and Narang, Under Review (2020)

5:00 AM \*F.NM06.02.01

**Sensing and Controlling the Spin Sublattices of an Insulating Antiferromagnet by Electrical Means** Anand Bhattacharya; Argonne National Laboratory, United States

A central goal of antiferromagnetic spintronics is the ability to sense and control the magnetic state of an antiferromagnet. While the magnetic state of a metallic antiferromagnet (AF) may be inferred using magnetoresistance measurements, this is not an option for insulating AF materials. The spin Seebeck effect (SSE), where thermal gradients are used to drive magnon spin currents, has proven to be an effective probe [i] of AF order. Substantial spin currents have been measured using the SSE in AF insulators  $\text{Cr}_2\text{O}_3$  [ii] and  $\text{MnF}_2$  [iii], and even in geometrically frustrated antiferromagnets [iv]. In this talk, I will briefly review the antiferromagnetic spin Seebeck effect and present our latest results on epitaxial Pt/ $\text{Cr}_2\text{O}_3$  (0001)/Pt heterostructures. In our devices, the spin currents generated by thermal gradients are detected using the inverse spin Hall effect (ISHE) in thin films of Pt, grown both as an epitaxial underlayer beneath and as an overlayer on top of the  $\text{Cr}_2\text{O}_3$  film.  $\text{Cr}_2\text{O}_3$  is unique in that the spins on the top and bottom surfaces of the (0001) oriented film are uncompensated, and belong to separate magnetic sublattices, even in the presence of surface roughness. Using the ISHE in both top and bottom Pt layers [v], we find that the SSE is strongly sensitive to the respective sublattice magnetization. As a result, we are able to track the exact orientation of both sublattices upon application of a magnetic field, including during spin-flop processes. Furthermore,  $\text{Cr}_2\text{O}_3$  is a classic linear magnetoelectric, where an electric field applied in the [0001] direction can be used to tune the net magnetization [vii]. In this context, I will discuss how the application of electric fields in Pt/ $\text{Cr}_2\text{O}_3$ /Pt heterostructures can be used to tune magnon spin currents, generated using thermal gradients [viii].

[i] S. M. Rezende et al., *Phys. Rev. B* **93**, 014425 (2016).

[ii] S. Seki et al., *Phys. Rev. Lett.* **115**, 266601 (2015)

[iii] S. M. Wu et al., *Phys. Rev. Lett.* **116**, 097204 (2016)

[iv] S. M. Wu et al., *Phys. Rev. Lett.* **116**, 097204 (2015); C. Liu et al...

[v] Y. Luo et al., *arXiv*:1910.10340

[vii] D. N. Astrov, *Sov. Phys. JETP* **11**, 780 (1960).

[viii] C. Liu et al., in preparation (2020).

5:15 AM F.NM06.02.02

**Transient Field- and Current-Induced Magneto-Transport in Epitaxial  $\alpha$ - $\text{Fe}_2\text{O}_3$ /Pt Heterostructures** Alexandra Churikova<sup>1</sup>, Angela Wittmann<sup>1</sup>, Norman Birge<sup>1,2</sup>, Larry Scipioni<sup>3</sup>, Adam Shepard<sup>3</sup>, Ty Newhouse-Illige<sup>3</sup>, James Greer<sup>3</sup> and Geoffrey Beach<sup>1</sup>; <sup>1</sup>Massachusetts Institute of Technology, United States; <sup>2</sup>Michigan State University, United States; <sup>3</sup>PVD Products, United States

Antiferromagnetic (AF) materials are candidates for next generation spintronic devices due to terahertz AF spin dynamics, high packing densities, and insensitivity to external magnetic fields. In AF insulators (AFIs), long spin diffusion lengths and predicted superfluid transport of spin currents are attractive for low-power device operation. The electrical control of AF domains has been attempted in AFIs with an adjacent heavy metal (HM) as a source of spin-orbit torque (SOT). Electrical detection of AF order via spin Hall magnetoresistance (SMR) has been developed, but due to heating artifacts in the HM, electrical detection methods must be supplemented by direct probing techniques. Hematite ( $\alpha$ - $\text{Fe}_2\text{O}_3$ ), an easy-plane AFI with triaxial anisotropy, is at the forefront of this effort, spurring discoveries of magnon-mediated long-distance spin transport, understanding of anisotropy-driven AF phase transitions, and an unambiguous control of the AF order by electrical current. Contrary to ferromagnets, where domain structure is governed by long-range demagnetizing fields, the domain structure in AFMs is controlled by “destressing fields” of magnetoelastic origin. **Here, we demonstrate that the destressing energy, rather than the anisotropy energy, governs the final state of the AF order in a low anisotropy AFI after the application of an external stimulus (applied current or magnetic field). We report the purely transient effect of electrical current and magnetic field application to the rotation of the AF vector in epitaxial  $\alpha$ - $\text{Fe}_2\text{O}_3$ /Pt bilayers. Implementing a combination of angle-dependent SMR and current pulsing methods, we probe, respectively, the full and partial re-orientation of AF domains. The current-induced rotation of the AF order within the  $\alpha$ - $\text{Fe}_2\text{O}_3$  domains is confirmed with full rotation to a monodomain state via external magnetic field (due to the low spin-flop transition). We find that approximately 20% of the maximal SMR signal is retained after the external magnetic field has been**

turned off and follows the angular symmetry of the saturated SMR (rather than the triaxial anisotropy). Meanwhile, a remanent SMR switching signal (~5% of the expected maximal SMR signal) remains after current pulsing along two of the three easy axes to rotate the AF order along each one. Therefore, a small fraction of the re-oriented domains retains their AF order even after the magnetic field (or, analogously, a current pulse) is turned off and the rest of the domains relax toward an equilibrium state. This finding is crucial to developing and engineering AFIs properties which would prevent such a relaxation following external stimulus—a key limitation to the stability of switched states in spintronic devices.

5:25 AM F.NM06.02.03

**Prominent Verwey Transition in Three-Dimensional Fe<sub>3</sub>O<sub>4</sub> Nanowire at 10 nm Length Scale** Azusa Hattori<sup>1</sup>, Rupali Rakshit<sup>2</sup>, Yasuhisa Naitoh<sup>3</sup>, Hisashi Shima<sup>3</sup>, Hiroyuki Akinaga<sup>3</sup> and Hidekazu Tanaka<sup>1</sup>; <sup>1</sup>Osaka Univ, Japan; <sup>2</sup>DST Inspire Faculty, India; <sup>3</sup>National Institute of Advanced Industrial Science and Technology, Japan

Nanostructured material is important because of low dimension fundamental physics and device application. The oldest magnetic material, magnetite (Fe<sub>3</sub>O<sub>4</sub>) undergoes a sharp Verwey transition with an abrupt change in its structure and electrical conductivity at about 120 K. To date, a variety of fabrication technique to realize high-quality nanostructures. However, the thin film and nanostructured configuration of Fe<sub>3</sub>O<sub>4</sub> are unable to show bulk-like Verwey transition due to a large number of unavoidable defects in them [1]. Three-dimensional (3D) Fe<sub>3</sub>O<sub>4</sub> epitaxial nanowires of 10 nm length scale have been constructed on a 3D-MgO nanotemplate using an original nanofabrication technique [2]. In spite of the high density of inevitable nanoscale defects, the ultrasmall Fe<sub>3</sub>O<sub>4</sub> nanowires exhibit a prominent Verwey transition at about 112 K with a maximum relative change in resistance of 9.5, which is six times larger than that of the thin-film configuration. Numerous measurements on a large number of Fe<sub>3</sub>O<sub>4</sub> nanowires grown concurrently on the same 3D-MgO nanotemplate reveal a dramatic difference in their electrical transport property with the presence/absence of the Verwey transition. A comparative study of Fe<sub>3</sub>O<sub>4</sub> wires of increasing volume and a thin film reveals that a profound change in the Verwey transition is observed only for wires with a volume of 10 nm<sup>3</sup> order. Moreover, a significant decrease in the sharpness of the resistance jump and the transition temperature (T<sub>MI</sub>) of the Verwey response is noticed with increasing volume of Fe<sub>3</sub>O<sub>4</sub>. This indicates the potency of the 3D nanofabrication technique in controlling nanoscale defects which is further reconfirmed through magnetoresistance (MR) measurement. A feature of the MR curve identifies the antiphase boundaries as a major source of defects. The occurrence of the smallest MR in the ultrasmall nanowire with the highest T<sub>MI</sub> and resistance change ratio proves that 3D isotropic spatial confinement into a length scale comparable to the average spacing between two antiphase boundaries enables the favourable control over nanoscale defects. Comparison of the Verwey transition properties of Fe<sub>3</sub>O<sub>4</sub> wires with increasing volume and thin film revealed that the efficient isolation of defects is only possible through isotropic 3D nanoconfinement at a length scale comparable to the average distance between two defects and also indicates the dependence of the Verwey response on the defect concentration. A simple statistical model satisfactorily illustrates the dependence of electrical transport properties on the volume of Fe<sub>3</sub>O<sub>4</sub> from the macroscale down to the nanoscale. Finally, an ultrasmall nanowire with a low defect concentration allows the estimation of the true coherent length of the fundamental quasiparticle, the trimeron, responsible for the Verwey transition.

[1] M. S. Senn et al., Nat. Lett., 481, 173 (2012), [2] R. Rakshit et al., Nano Lett., 19, 5003 (2019)

5:35 AM F.NM06.02.04

**A Novel Cubic-Fe/Pd Alloy Film Based Lithographically Patterned Hydrogen Gas Sensor with Enhanced FMR Signal Strength and Faster Response Time** Shahbaz Khan, Martin Saunders, Mariusz Martyniuk and Mikhail Kostylev; The University of Western Australia, Australia

The concept of Ferromagnetic resonance (FMR) based hydrogen gas sensing is a potential candidate for future hydrogen gas sensing technology. However, improvements of the FMR signal strength, response time, and stability of the employed sensing medium are required to make this novel concept competitive with established sensing platforms. Here, we proposed a novel cubic phased-Fe/Pd alloy film based hydrogen gas sensor (HGS), fabricated in a microwave waveguide like geometry. The fabricated devices show a superior FMR signal strength and a faster response time in ambient and H<sub>2</sub> environments in comparison with previous HGS based on continuous magnetic films. Moreover, upon annealing, the as sputtered Fe/Pd patterned devices undergo a structural phase transition from a tetragonal to a cubic phase. The transition is confirmed by careful analysis and interpretation of collected XRD and TEM data. Our findings suggest that the cubic phase of the Fe/Pd alloy film is thermally stable and offers high response times when compared to the tetragonal Fe/Pd film-based devices. This progress in the understanding of the fundamental principles behind the sensing process and the achieved enhancement in device performance represents a step forward towards the practical implementation of the FMR based sensing concept.

5:45 AM F.NM06.02.05

**Reversible Hydrogen-Ion Control of Room Temperature Antiferromagnetic State in  $\alpha$ -Fe<sub>2</sub>O<sub>3</sub>** [Hariom Jani](#) and T. Venky Venkatesan; National University of Singapore, Singapore

Antiferromagnetic insulators are a ubiquitous class of magnetic materials, holding the promise of low-dissipation spin-based computing devices that can display ultra-fast switching and are robust against stray fields. However, their imperviousness to magnetic fields also makes them difficult to control in a reversible and scalable manner. Here we demonstrate a novel ionic pathway to drive a 90° spin-reorientation reversibly in the most common antiferromagnetic insulator  $\alpha$ -Fe<sub>2</sub>O<sub>3</sub> (hematite) – now an emerging spintronic material that has recently been shown to host topological AFM textures (eg: half-skyrmions and bimerons) and long magnon-diffusion lengths. Our low-temperature catalytic-spillover process involves the incorporation (or removal) of hydrogen from  $\alpha$ -Fe<sub>2</sub>O<sub>3</sub>, post-growth, driving pronounced changes in its magnetic anisotropy, Néel-vector orientation and canted magnetism via electron injection and localized strains. We explain these effects with a detailed magnetic anisotropy model and first-principles calculations. Tailoring our work for future applications, we demonstrate control of the spin-state at room-temperature by reversibly doping hydrogen in Rh-substituted  $\alpha$ -Fe<sub>2</sub>O<sub>3</sub> and suggest pathways to build electric-field-controlled antiferromagnetic devices by deploying ionotronics.

**5:55 AM F.NM06.02.06**

**Thickness-Dependent Magnetic and Structural Properties of Epitaxial Fe Films** [Sangjae Lee](#)<sup>1</sup>, Valentina Bisogni<sup>2</sup>, Jonathan Pellicciari<sup>2</sup>, Frederick Walker<sup>1</sup> and Charles H. Ahn<sup>1</sup>; <sup>1</sup>Yale University, United States; <sup>2</sup>Brookhaven National Laboratory, United States

Manipulating spins in a ferromagnet spin channel using electrical current or voltage has received substantial attention in pursuit of more compact and energy-efficient memory and spintronic devices. As the technology focuses on nanoscale device applications, understanding the relationship between the dimensionality of the magnetic channel and magnetic and structural properties is crucial. We characterize the magnetic and structural properties of ferromagnetic thin films of  $\alpha$ -Fe (body-centered cubic, *bcc*) as a function of thickness, which are grown epitaxially on MgO substrates using molecular beam epitaxy (MBE). The out-of-plane dimensions of the Fe layers, measured with x-ray reflectivity, range from sub-nanometer to ~30nm. The MgO capping layer prevents the Fe layer from oxidation, as measured using x-ray absorption spectroscopy, and all films show saturation magnetization of ~2.1 $\mu_B$ /Fe at 100K, consistent with unoxidized bulk Fe. The lattice constant mismatch between the  $\alpha$ -Fe and the bulk MgO imposes a 3.7% tensile strain on Fe, resulting in a tetragonal distortion of the films for all thicknesses. Measurements of crystal truncation rods (CTRs) show strain relaxation of thicker Fe thin films while 3 unit cell thick Fe is coherently strained to the substrate. The synchrotron CTR measurements also show an unexpected expansion of the unit cell for ultra-thin Fe films, which does not strongly affect the magnetic properties. This work lays the groundwork for understanding how to control the spin excitations in ferromagnetic systems.

Work at Yale is supported by a grant from the Department of Energy, Basic Energy Sciences under grant number DE-SC0019211. This research used beamline 2-ID of the National Synchrotron Light Source II, a U.S. Department of Energy (DOE) Office of Science User Facility operated for the DOE Office of Science by Brookhaven National Laboratory under Contract No. DE-SC0012704.

SESSION F.NM06.03: Silicon Based Quantum Measurements  
On Demand Abstracts Available for Viewing Starting Saturday Morning, November 21, 2020  
F-NM06

**5:00 AM F.NM06.03.01**

**Transport Spin-Polarization of Pt/Magnetic Insulator Bilayers—Evidence for the Magnetic Proximity Effect** [Michael S. Osofsky](#)<sup>1</sup>, Joseph Prestigiacomo<sup>1</sup>, C S. Hellberg<sup>1</sup>, Peng Li<sup>2</sup>, Lauren Riddiford<sup>3</sup> and Yuri Suzuki<sup>3</sup>; <sup>1</sup>U.S. Naval Research Laboratory, United States; <sup>2</sup>Auburn University, United States; <sup>3</sup>Stanford University, United States

The anomalous Hall effect has been observed in non-magnetic metallic films with strong spin-orbit scattering that are in intimate contact with a magnetic insulator [1]. Two mechanisms have been proposed to explain this observation: the magnetic proximity effect (MPE) and a combination of the spin Hall effect and inverse spin Hall effect. Direct measurements of the local magnetization of the non-magnetic metal using spectroscopic techniques that are sensitive to local magnetic moments have been inconclusive. To definitively determine whether there is an MPE, point contact Andreev reflection (PCAR) measurements [2] were used to detect an induced transport spin polarization in Pt films deposited on yttrium iron

garnet and manganese aluminum ferrite films. The results will be compared to density functional theory calculations and can be used in the interpretation of measurements of spin currents.

The authors acknowledge the support of the Basic Research Office of the Assistant Secretary of Defense for Research and Engineering under the Vannevar Bush Faculty Fellowship (funded by the Office of Naval Research through grant N00014-15-1-0045).

## References

Z. Wang, C. Tang, R. Sachs, Y. Barlas, and J. Shi, Phys. Rev. Lett. **114**, 016603 (2015).  
R. J. Soulen, Jr., J. M. Byers, M. S. Osofsky, B. Nadgorny, T. Ambrose, S. F. Cheng, P. R. Broussard, C. T. Tanaka, J. Nowak, J. S. Moodera, A. Barry, and J. M. D. Coey, Science **282**, 85 (1998).

## 5:10 AM \*F.NM06.03.02

**Driven Spin Systems with Protected Coherence in Commercially Available Silicon Carbide** Kevin Miao, Alexandre Bourassa, Christopher Anderson and [David Awschalom](#); University of Chicago, United States

Silicon carbide (SiC) is a host to a variety of robust, optically active quantum systems. Recent studies have shown that basally oriented  $kh$  divacancy defects in SiC possess a robust optical interface as well as exceptional spin coherence properties even in commercially available, naturally abundant SiC. We show that these excellent intrinsic properties can be further augmented and tuned by applying a periodic drive, giving rise to emergent phenomena unique to non-equilibrium quantum systems.

First, we demonstrate electrically driven coherent quantum interference in the optical transition of single  $kh$  divacancies [1]. By applying microwave frequency electric fields, we coherently drive the divacancy's excited-state orbitals and induce Landau-Zener-Stückelberg interference fringes in the resonant optical absorption spectrum. This result shows that the optical absorption spectrum of these divacancy defects can be rapidly reconfigured using localized electric field control, and reveals a highly responsive mechanism to potentially coherently interact with other electrically active quantum systems.

We then construct a robust qubit embedded in a decoherence-protected subspace, obtained by hybridizing an applied microwave drive with the ground-state electron spin of the  $kh$  divacancy [2]. This qubit is protected from magnetic, electric, and temperature fluctuations, which account for nearly all relevant decoherence channels in the solid state. This culminates in an increase of the qubit's inhomogeneous dephasing time by over four orders of magnitude (to >22 milliseconds), while its Hahn-echo coherence time approaches 64 milliseconds. Such an extension of inhomogeneous dephasing time opens up pathways to a vast array of hybrid quantum system applications. Furthermore, since this protocol requires few key platform-independent components, this result suggests that substantial coherence improvements can be achieved in a wide selection of quantum architectures.

This work was done in collaboration with Alexander L. Crook, Gary Wolfowicz, Joseph P. Blanton, Samuel J. Whiteley, Sam L. Bayliss, Hiroshi Abe, Takeshi Ohshima, Gergo Thiering, Péter Udvarhelyi, Viktor Ivády, and Adam Gali.

[1] K. C. Miao, A. Bourassa, C. P. Anderson, S. J. Whiteley, A. L. Crook, S. L. Bayliss, G. Wolfowicz, G. Thiering, P. Udvarhelyi, V. Ivády, H. Abe, T. Ohshima, Á. Gali, D. D. Awschalom, "Electrically driven optical interferometry with spins in silicon carbide," *Sci. Adv.* **5** (11), eaay0527 (2019)

[2] K. C. Miao, J. P. Blanton, C. P. Anderson, A. Bourassa, A. L. Crook, G. Wolfowicz, H. Abe, T. Ohshima, D. D. Awschalom, "Universal coherence protection in a solid-state spin qubit," *arXiv* 2005.06082 (2020)

## 5:25 AM F.NM06.03.03

**Sensing Sub-Thermal Energies Through Low-Field DC Magnetoresistance of Neutral Divacancies in Silicon Carbide** [Stephen R. McMillan](#)<sup>1</sup> and Michael E. Flatté<sup>1,2</sup>; <sup>1</sup>University of Iowa, United States; <sup>2</sup>Technische Universiteit Eindhoven, Netherlands

The neutral divacancy in 4H-SiC has a spin-1 ground state that is highly sensitive to electrical and mechanical perturbations [1]. The long room temperature coherence times of these deep centers suggest that they are robust candidates for nanoscale quantum sensing [2]. Within the past five years optical readout of single divacancies in SiC has been demonstrated [3]. Electrical readout of single spins typically relies on Boltzmann distributed spin polarizations which necessitate operation at low temperatures and/or high magnetic fields to improve the quality of the single-shot protocol [4]. Recently ambient

electrical readout has been demonstrated on SiC defects using photocurrent detected magnetic resonance [5], relying on optical excitation to generate current. In contrast, we propose a time-averaged projective measurement technique that derives from local influences on the ground state coherent dynamics of the neutral divacancy. This provides resolution of processes corresponding to energy scales far below the thermal noise floor of the system without the need for optical hardware, AC fields, or large DC fields. We calculate the defect mediated current through a spin-polarized contact under a small ( $\sim$ mT) external magnetic field similar to previous calculations done on a spin-1/2 ground state [6]. We predict that measurement of the spin relaxation time is possible from analysis of the zero-field current and that spin-decoherence is discernible from the zero-field width. Magnetoresistive signatures also provide information on local electric and strain fields suggesting a path toward scalable, all-electric, room temperature quantum technology based on SiC. We acknowledge support for this work from DOE BES through grant number DE-SC0016379.

- [1] A. L. Falk, et al., *Phys. Rev. Lett.* 112, 187601 (2014)
- [2] A. L. Falk, et al., *Nat. Commun.* 4, 1819 (2013)
- [3] D. J. Christle, et al., *Nat. Mater.* 14, 160 (2015)
- [4] A. Morello, et al. *Nature* 467, 687(2010)
- [5] M. Niethammer, et al. *Nat. Commun.* 10, 5569 (2019)
- [6] S. R. McMillan, et al., arXiv:1907.05509 [cond-mat.mes-hall]

### 5:35 AM \*F.NM06.03.04

**Molecular States in the Silicon Vacuum—Deterministic Clusters of Donors and Acceptors in Silicon** Jianhua Zhu<sup>1</sup>, Wei Wu<sup>1</sup>, Nguyen Le<sup>2</sup>, Eran Ginossar<sup>2</sup> and Andrew Fisher<sup>1</sup>; <sup>1</sup>UCL (University College London), United Kingdom; <sup>2</sup>University of Surrey, United Kingdom

Advances in localised tip-induced lithography mean that the process of doping a semiconductor need no longer be random: instead, dopant atoms can be located in well-defined positions relative to one another. This has already been demonstrated for donors in silicon [1,2] and may in future be possible for other types of dopant. This opens the possibility of controlling the interactions between the dopants to form new deterministic devices, which in turn elevates the spin degree of freedom from a spectator into an important variable. As well as the established potential for spin-based quantum gates [3] a number of other applications can now be foreseen.

We have computed the excitation spectra of donor pairs and larger clusters [4] in silicon, using a combination of ab initio band-structure simulations and quantum chemistry techniques. The results show strong and characteristic changes in the character of the dominant excitation as a function of separation and spin state, raising the possibility optical detection and initialisation of the multi-donor spin state. We have also studied the application of controlled donor arrays as quantum simulators that can be probed by their transport properties [5]; in particular we have identified topological edge states and shown how their properties vary across the metal-insulator transition [6].

Finally, for acceptor clusters we have studied the consequences of the richer spin-orbit coupling present in the silicon valence band [7]. We find a complex interplay between the relative strengths of hopping and Coulomb interactions, the arrangement of the bond lengths, and the spin-orbit coupling. This can result in the emergence of novel kinds of topological state.

- [1] Schofield, S. R., et al (2003). **Atomically precise placement of single dopants in Si.** *PHYSICAL REVIEW LETTERS*, 91 (13), ARTN 136104. doi:10.1103/PhysRevLett.91.136104
- [2] Stock, T. J. Z., et al. (2020). **Atomic-Scale Patterning of Arsenic in Silicon by Scanning Tunneling Microscopy.** *ACS Nano*, acsnano.9b08943. doi:10.1021/acsnano.9b08943
- [3] He, Y et al. (2019). **A two-qubit gate between phosphorus donor electrons in silicon.** *Nature* 571 p 371 doi:10.1038/s41586-019-1381-2
- [4] Wu, W., et al. (2018). **Excited states of defect linear arrays in silicon: A first-principles study based on hydrogen cluster analogs.** *Physical Review B*, 97 (3), ARTN 035205. doi:10.1103/PhysRevB.97.035205
- [5] Le, N. H., et al. (2017). **Extended Hubbard model for mesoscopic transport in donor arrays in silicon.** *Physical Review B*, 96 (24), ARTN 245406. doi:10.1103/PhysRevB.96.245406
- [6] Le, N. H., et al. (2020). **Topological phases of a dimerized Fermi–Hubbard model for semiconductor nano-lattices.** *npj Quantum Information*, 6 (1), 24. doi:10.1038/s41534-020-0253-9
- [7] Zhu, J., et al. (2020). **Linear combination of atomic orbitals model for deterministically placed acceptor arrays in silicon.** *Physical Review B*, 101 (8), ARTN 085303. doi:10.1103/PhysRevB.101.085303

**5:00 AM \*F.NM06.04.01**

**Magnetoelectric Effects in Spin Crossovers and Metal-Organic Frameworks** Vivien Zapf; Los Alamos National Laboratory, United States

Magnetoelectric coupling is the coupling between magnetic order and the electric polarization in an insulator. To date it has been largely studied in inorganic oxides that show various types of ferromagnetic or antiferromagnetic order. Metal-organic frameworks and molecular compounds are a new and fertile direction to search for new magnetoelectric coupling mechanisms. I will talk about several recent results in which we couple spin crossovers to structure and electric polarization. I will also highlight multiferroic behavior in metal-organic frameworks. The experimental part of the work takes advantage of pulsed magnetic fields to perform high-sensitivity measurements and reach extended regions of the magnetic field-temperature phase diagram.

**5:15 AM F.NM06.04.02**

**Narrow-Gap Semiconductor Spintronics—Electron G-Tensor Engineering with Multilayer Structures** Antonio Ferreira da Silva<sup>1,2</sup>, Jhon E. Leon Padilla<sup>1</sup>, Marcelo A. Toloza Sandoval<sup>1</sup> and Jose Fernando D. Chubaci<sup>2</sup>; <sup>1</sup>Federal University of Bahia, Brazil; <sup>2</sup>São Paulo University, Brazil

Among the main trends for spintronic applications, narrow gap semiconductors provide a fertile ground to engineering the electron effective  $g$  factor, because of its strong dependency on the energy gap of the bulk material. Furthermore, it is well-known that in semiconductor heterostructures, the mesoscopic confinement also renormalizes the effective  $g$  factor by introducing extra anisotropies, transforming scalar  $g$  factors into tensors. In particular, for narrow-gap semiconductor layered structures, the electronic  $g$ -tensor is expressed as a diagonal matrix, where the diagonal elements correspond to configurations of magnetic-field longitudinal and transversal to the growth direction. Considering bound electrons in both, InAs- and InSb-based multilayer structures, we use an analytical and transparent envelope-function solution based on the Kane model for the bulk, to investigate the effective  $g$  tensor and the corresponding anisotropy, i.e., the difference between the longitudinal and transversal components. Following the prescription abovementioned, we 1) study the dependency between the obtained results and the bulk-band parameters, 2) study the fine-tuning of the effective  $g$ -factors (longitudinal and transversal) with the structural parameters, i.e., the thicknesses of the active layer and the tunneling barrier, in particular, we 3) explore the strongly interacting regime for thin active layers, for which the structure inversion asymmetry plays a fundamental role by inverting the signal of the  $g$ -factor anisotropy. Such results provide a clear understanding of the mechanisms of the  $g$ -factor renormalization in semiconductor nanostructures and can be useful in electron  $g$ -factor engineering.

This work was partially supported by the Office of Naval Research (Global office in South America, NICOP) Grant No.N62909-18-1-2121, FAPESP Grant No. 2014/03085-0, CAPES (No. PNPd 88882.306206/2018-01), CNPq Grant No.306145/2018-9, FAPESB Grants No. PNX 0007/2011 and INT 0003/2015.

**5:25 AM F.NM06.04.03**

**Spin Texture and Berry Curvature of Holes Confined in SiGe Quantum Well System** Tatsuki Tojo and Kyozauro Takeda; Waseda University, Japan

The spin-orbit interaction (SOI) is the relativistic correction, caused by the coupling between a spin  $\sigma$  and an effective magnetic field (EMF) of a charged carrier. Despite the necessity of understanding the characteristics in the SOI phenomena for holes as well as for electrons, the complexity of the valence band structure prevents us from our deep understanding of the SOI for holes. The SOIs are generally caused by symmetry breakings, such as the bulk-inversion-asymmetry (BIA) and the structure-inversion-asymmetry (SIA). Dresselhaus has studied intensively the BIA (Dresselhaus) SOI and revealed the characteristics for holes. Rashba has theoretically proposed that an electric field externally applied to quantum systems has potential to cause the SIA (Rashba) SOI.

In this presentation, we apply the Rashba external field to the two-dimensional (2D) SiGe mixed alloy quantum well (QW) system, and then study how the coexistence of the BIA and SIA SOIs influences the spin textures of holes. We particularly focus on the spin texture and Berry curvature of the heavy-mass holes (HHs), because it is our one more purpose how the inter-subband interaction influences them via the strongly anisotropic and non-parabolic eigenstates. Taking into account the in-planar crystal momentum as well as the particle one, we extend the  $k\mathbf{p}$  approach including the 2<sup>nd</sup>-order terms crossing

with those SIA and BIA SOIs and solve the  $kp$  perturbation equation under the virtual crystal approximation. By employing the solved Bloch periodic parts, we calculate the  $k$ -distribution of the in-plane spin of HHs. The SIA-BIA coexistence system changes the symmetry of the present SiGe 2D QW system characteristically. The electric-field application perpendicular to the 2D (001) plane causes the SIA whereas the alternating arrangement of Si and Ge heteroatoms causes the BIA. Eventually, the SIA and BIA SOIs strengthen the axial vectors cooperatively in the first and third quadrants of the Brillouin zone (BZ) whereas they compete and suppress themselves in the second and fourth quadrants. The present SIA and BIA SOIs resolve the spin degeneracy of HHs into the stabilized (HH<sup>+</sup>) and destabilized (HH<sup>-</sup>) one. Each spin texture exhibits the inequivalence between the [110] and [-110] directions, and both planes of (110) and (-110) are the mirror plane for an axial-vector spin. For the <110> direction, the HH spin orients to the tangent line of the equi-energy surface. However, except for this direction, the spin does not orient toward the tangential line. HHs basically orient their spins parallel to their own EMF. However, the EMF has a remarkable term to cause the directional discrepancy from the tangential line. In addition to this EMF characteristics, the EMF and spin correlate via the  $Is$  coupling. Consequently, the spin texture shows the characteristic  $k$ -distribution, significantly different from that found in 2D electron gas (2DEG). We further study the Berry curvature  $B^+$  for HH<sup>+</sup> and  $B^-$  for HH<sup>-</sup> influenced by the coexistence of SIA and BIA SOIs. HHs are energetically separated from other holes and the pair relation of  $B^+ = -B^-$  results. The coexistence of SIA and BIA SOIs multiply changes the sign of the Berry curvatures. Furthermore, the strong anisotropy and significant non-parabolicity of HHs distribute the Berry curvatures complicatedly. Nevertheless, the pair relation  $B^+ = -B^-$  is valid. We carry out the integration of the Berry curvature surrounded by the equi-energy contour  $E$ , and estimate the Berry phase  $\gamma(E)$  at an energy  $E$ . The resulting  $\gamma^+(E)$  causes a plateau of a half-integer  $1/2$  until  $E \sim 16\text{meV}$ ;  $\gamma^-(E)$  does that of  $-1/2$ . However, it suddenly changes the sign and an opposite plateau of  $-1/2$  ( $+1/2$ ) results in the higher energy region. This characteristic feature is peculiar to HHs not found in the 2DEG because the sign and  $k$ -distribution of the Berry curvature in the integral area are crucial for determining  $\gamma(E)$ . This feature influences the Chern number and Hall conductivity.

#### 5:35 AM F.NM06.04.04

**Late News: Zero-Bias Giant Rashba Spin-Orbit Coupling at Complex Oxide Interfaces** [Ganesh Ji Omar](#) and Ariando Ariando; National University of Singapore, Singapore

Following the second law of thermodynamics, the Landauer's principle dictates a fundamental physical limitation for the switching energy of complementary metal-oxide-semiconductor (CMOS). A primary solution in breaking this limitation is to utilize the spin-orbit coupling (SOC) effect, as it allows easy manipulation of spin currents. However, this SOC effect is often quite weak, especially in the absence of external voltage biases. We report a four-fold SOC enhancement at zero bias voltage and pronounced SOC evolution in correlated LaAlO<sub>3</sub>-SrTiO<sub>3</sub> heterostructures buffered by a carrier modulating LaFeO<sub>3</sub> layer. We use an entirely new approach to provide evidence of generating Rashba SOC. Correlating the magnetotransport data with first-principles calculations and high-resolution electron microscopy, we reveal that its origin lies in the asymmetric hybridization of the interfacial wavefunctions. Our results open hitherto unexplored avenues of generating and controlling Rashba coupling to design next-generation two-dimensional electron system based spin-orbitronic devices.

#### SESSION F.NM06.05: Electron and Nuclear Spintronics

On Demand Abstracts Available for Viewing Starting Saturday Morning, November 21, 2020

F-NM06

#### 5:00 AM \*F.NM06.05.01

**Electron and Nuclear Spin Dynamics in Semiconductor Nanosystems** [Mikhail Glazov](#); Ioffe Institute, Russian Federation

Recently, the physicists and material scientists have experienced a new wave of interest in spin effects in solid-state systems. On the one hand, semiconductors and semiconductor nanosystems, allow one to perform benchtop studies of quantum and relativistic phenomena. On the other hand, the interest is supported by the prospects of realizing spin-based electronics where the electron or nuclear spins can play the role of quantum or classical information carriers. In my tutorial lecture, I will present the key aspects of multifaceted physics of interacting electron and nuclear spins in semiconductor-based low-dimensional structures. The hyperfine interaction of the charge carrier and nuclear spins increases in nanosystems compared with bulk materials. The enhanced coupling results in the efficient spin exchange between these two systems. It gives rise to beautiful and complex physics occurring in the ensemble of electrons and nuclei in semiconductors.

I will address the hyperfine interaction, nuclear magnetic resonance, dynamical nuclear polarization, spin-Faraday and -Kerr



effects, processes of electron spin decoherence and relaxation, effects of electron spin precession mode-locking and frequency focusing, as well as fluctuations of electron and nuclear spins.

**5:15 AM \*F.NM06.05.03**

**Suppression of Nuclear Spin Fluctuations in (In,Ga)As/GaAs Quantum Dots Under Pulsed Excitation with GHz Frequency** E. Evers<sup>1</sup>, N.E. Kopteva<sup>1,2</sup>, Dmitri R. Yakovlev<sup>1,3</sup>, [A. Greulich](#)<sup>1</sup> and Manfred Bayer<sup>1,3</sup>; <sup>1</sup>Technische Universität Dortmund, Germany; <sup>2</sup>St. Petersburg State University, Russian Federation; <sup>3</sup>Russian Academy of Sciences, Russian Federation

One of the possible hybrid realizations of a qubit is the spin of an electron confined in a semiconductor quantum dot (QD), which is interacting with the surrounding nuclear spins. The prominent advantage of QDs is their strong optical dipole moment, which allows efficient coupling of photons to the confined electron spins according to the optical selection rules. The electron, on the other hand, is coupled to the nuclei of the QD crystal matrix by the hyperfine interaction. These couplings allow one to design schemes where the angular momentum of the photon is transferred to the nuclear spins using the electron as an auxiliary spin state. This may have significant advantages, as the electron spin coherence is limited to several microseconds at low temperatures, while the nuclear spin coherence can reach milliseconds.

To test the degree of control between the electron and the nuclear spin system, we present a model system of an ensemble of singly charged QDs. The use of an ensemble is justified in our case by the spectroscopic signal strength, which allows us to observe an averaged and integral response of many electron spins at the same time. It is also of interest for quantum memory applications. On the other hand, such an ensemble is usually strongly inhomogeneous, which leads to a strong variation of the intrinsic parameters, like optical dipole moments, electron g-factor values, and strength of electron-nuclear spin interactions. This inhomogeneity can, however, be overcome in designed experiments, enabling effects such as spin mode-locking and nuclear-induced frequency focusing.

In previous studies on nuclei-induced frequency focusing in singly charged (In,Ga)As/GaAs QDs multiple precession modes were covered by the ensemble, as the nuclear fluctuations were of the same order as the mode separation in low external fields. Here we explore the degree of possible control of the nuclear surrounding using an inhomogeneous QD ensemble excited with a high repetition laser operated at 1 GHz. The GHz laser repetition frequency allows us to investigate the interaction of nuclear spin polarization and nuclear spin fluctuations with the electrons as the mode separation is an order of magnitude larger than the fluctuating nuclear field. It further allows us to use the effects of the strong electron-nuclear feedback and drive the inhomogeneous ensemble of electron spins to a single frequency precession. Additionally, we demonstrate the discretization of the total magnetic fields seen by the electron ensemble and show the effect of the reduction of the nuclear field fluctuations. While for fields lower than 0.6 T nuclear spin fluctuations inhibit the formation of a significant nuclear polarization, above the nuclear spin relaxation time becomes elongated such that the electron spins precess on the closest preferred frequency over a range of 128 mT. This leads to the observation of plateaus in the precession frequency as a function of the external magnetic field. The nuclear spin bath is constantly tuned, such that the phase synchronization condition is fulfilled while nuclear fluctuations are suppressed.

**5:30 AM F.NM06.05.04**

**Spin-Phonon Relaxation from a Universal *Ab Initio* Density-Matrix Approach** [Yuan Ping](#); University of California Santa Cruz, United States

Designing new quantum materials with long-lived electron spin states urgently requires a general theoretical formalism and computational technique to reliably predict intrinsic spin relaxation times. We present a new, accurate and universal first-principles methodology based on Lindbladian dynamics of density matrices to calculate spin-phonon relaxation time of solids with arbitrary spin mixing and crystal symmetry<sup>1</sup>. This method describes contributions of Elliott-Yafet and D'yakonov-Perel' mechanisms to spin relaxation for systems with and without inversion symmetry on an equal footing. We show that intrinsic spin and momentum relaxation times both decrease with increasing temperature; however, for the D'yakonov-Perel' mechanism, spin relaxation time varies inversely with extrinsic scattering time. We predict large anisotropy of spin lifetime in transition metal dichalcogenides. The excellent agreement with experiments for a broad range of materials underscores the predictive capability of our method for properties critical to quantum information science. [1] J. Xu et al, *Nature Communications* **11**, 2780 (2020)

**5:40 AM F.NM06.05.05**

**Magnetocrystalline Anisotropy in Antiferromagnetic Fe<sub>2</sub>As—A First-Principles Study** [Kisung Kang](#), Kexin Yang, David Cahill and Andre Schleife; University of Illinois at Urbana-Champaign, United States

Antiferromagnetic tetragonal Fe<sub>2</sub>As attracts attention due to its easy-plane magnetism which might enable future usage in magnetic memory devices. Moreover, the possibility for electrical switching of the Néel vector is expected because of its metallicity. To understand the mechanism of switching for easy-plane magnetism, it is essential to know the magnetocrystalline anisotropy energy of antiferromagnetic Fe<sub>2</sub>As, which acts as an energy barrier. Using first-principles density functional theory, we study the contributions of spin-orbit interaction (SOI) and magnetic dipole-dipole interaction (MDD) to magnetocrystalline anisotropy. The tetragonal structure exhibits out-of-plane and in-plane anisotropy energy terms. The out-of-plane anisotropy, computed as a |K<sub>1</sub>| coefficient of 830 kJ/m<sup>3</sup>, originates from both SOI and MDD. The contribution of SOI is two times larger than that of MDD, and both show the same two-fold symmetry. Conversely, the in-plane MDD contribution is almost negligible and most of the anisotropy energy comes from SOI, which shows four-fold symmetry and a |K<sub>22</sub>| coefficient of 280 J/m<sup>3</sup>. This closely corresponds to the value of 150 J/m<sup>3</sup>, measured using torque magnetometry. Based on the calculated anisotropy energy, antiferromagnetic Fe<sub>2</sub>As shows potential for the switching process to occur, however, the results also indicate low thermal stability of the magnetic structure.

\*\* The Illinois Materials Research Science and Engineering Center is supported by the National Science Foundation MRSEC program under NSF Award Number DMR-1720633.

### 5:50 AM F.NM06.05.06

**Late News: Controlling Magnetic Order by Driving Phonons with Light** Ankit S. Disa<sup>1</sup>, Michael Fechner<sup>1</sup>, Michael Först<sup>1</sup>, Paolo G Radaelli<sup>2</sup> and Andrea Cavalleri<sup>1,2</sup>; <sup>1</sup>Max Planck Institute for the Structure and Dynamics of Matter, Germany; <sup>2</sup>University of Oxford, United Kingdom

The ability to strongly and deterministically manipulate magnetic order is crucial for applications ranging from spintronics to information storage. For example, strain engineering enables tuning of magnetic phases in a variety of complex systems. Combining this tunability with optical methods would enable novel optomagnetic technologies operating on ultrafast time scales. In this work, we demonstrate a route to dynamically mimic strain and create non-equilibrium magnetic properties by engineering the crystal structure with light. [1]. In particular, in the antiferromagnet CoF<sub>2</sub>, we induce a ferrimagnetic phase transition through selective THz excitation of optical phonons. The effect takes advantage of the coupling of the local magnetic moment to the crystal field environment, which statically leads to a net magnetization under uniaxial strain (piezomagnetism). Rather than strain, we exploit nonlinear, three-phonon coupling to drive the desired crystal field distortions [2]. Optical measurements reveal that, as a result, a bi-directional ferrimagnetic moment is generated on a time scale of few to hundreds of picoseconds. The generated moment is nearly three orders of magnitude larger than previously achieved by strain, demonstrating phonon-driven control of magnetic order beyond the elastic limit.

### References

- [1] A.S. Disa, M. Fechner, T. Nova, B. Liu, M. Först, D. Prabhakaran, P. Radaelli, A. Cavalleri, *Science* **394**, 1075 (2019).  
[2] P. Radaelli, *Physical Review B* **97**, 085145 (2018).

### SESSION F.NM06.06: Sensing Spin Qubits

On Demand Abstracts Available for Viewing Starting Saturday Morning, November 21, 2020

F-NM06

### 5:00 AM \*F.NM06.06.01

**The Physical Origins of Extreme Cross-Polarization Extinction in Confocal Resonant Spectroscopy** Khaled Karrai<sup>1</sup>, Meryem Benelajla<sup>1,2</sup>, Elena Kammann<sup>1</sup> and Bernhard Urbaszek<sup>2,1</sup>; <sup>1</sup>Attocube Systems AG, Germany; <sup>2</sup>Université de Toulouse, INSA-CNRS-UPS, LPCNO, France

In optical spectroscopy experiments, it is crucial to excite an emitter with a laser very close to its transition energy. Experiments under resonant excitation are essential for accessing the intrinsic optical and spin-polarization properties of large class of emitters<sup>1-6</sup>. Using linear cross-polarization in a confocal setup has been successfully employed as a dark-field method to carry out resonant fluorescence experiments to suppress scattered laser light, with the added benefit of high spatial resolution. Resonant fluorescence experiments allow crucial insights into light-matter coupling, such as the interaction of a single photon emitter with its environment, with optical cavities and also studying single defects in atomically thin materials such as WSe<sub>2</sub>. Dark-field confocal techniques allow developing single photon sources with high degrees of photon indistinguishability and longer coherence. In practice dark-field laser suppression is not just a spectroscopy tool, it is also a

key part of more matured quantum technology systems. Despite many advances based on experiments in confocal microscopes with cross-polarization laser rejection, the physical mechanisms that make these experiments possible are not understood, hampering further progress in this field. The key figure of merit is the suppression of the excitation laser background by at least six orders of magnitude. Indeed a suppression by a factor of  $10^8$  up to  $10^{11}$  (this work) have been measured. But this is very surprising as mirrors and beam-splitter in such a system reduce the theoretical extinction limit to the  $10^3$  to  $10^4$  range. In this work we explain the physics behind the giant enhancement of the extinction ratio by up to eight orders of magnitude that make microscopy based on dark-field laser suppression possible. The measurements of resonant fluorescence are typically performed in an epifluorescence geometry, for which laser excitation and fluorescence collection are obtained through the same focusing lens. This involves necessarily the use of a beam-splitter orienting the back-reflected light containing the fluorescence towards a detection channel. In our work we identify two key ingredients that explain the giant amplification of the cross-polarization extinction ratio : (i) a reflecting surface (i.e. the beam-splitter) placed between a polarizer and analyzer, and (ii) a confocal arrangement. We demonstrate giant extinction ratios in our experiments for different mirrors (silver, gold, dielectric, beam-splitter cubes) and polarizers (Glan-Taylor, nanoparticle thin films). We demonstrate that behind this general observation lies the intriguing physics of the Imbert-Fedorov effect, which deviates a reflected light beam depending on its polarization helicity. We discover that a confocal arrangement not only amplifies the visibility of the Imbert-Fedorov effect dramatically, taking it from the nanometer to the micrometer scale, but also exploits conveniently the symmetry of the newly observed Imbert-Fedorov modes to insure that the cross-polarized laser beam is not coupled, explaining the near complete suppression of the laser background signal. In other words, we cannot treat the spatial (i.e. modal) and polarization properties of light separately in our dark-field confocal microscope analysis. In addition to new developments in dark-field microscopy our experiments provide powerful tools to understand spin-orbit coupling of light, in the broader context of topological photonics. Funding: European Union's Horizon 2020 research and innovation program, Marie Skłodowska-Curie grant agreement No 721394 ITN 4PHOTON.

<sup>1</sup> Aharonovich, I., *et.al.* M. Nat. Phot. 10, 631 (2016)

<sup>2</sup> Högele, A. *et. al.* Phys. Rev. Lett. 108, 197403 (2012)

<sup>3</sup> Paillard, M. *et. al.* Phys. Rev. Lett. 86, 1634 (2001)

<sup>4</sup> Högele, A. *et. al.* Phys. Rev. Lett. 93, 217401 (2004)

<sup>5</sup> Vamivakas, *et.al.* Nat. Phys. 5, 198 (2009)

<sup>6</sup> Kaldewey, T. *et al.* Nat. Phot. 12, 68 (2018)

#### 5:15 AM F.NM06.06.02

**Photon Statistics as an Analytical Tool for Characterizing Solid-State Defects** Rebecca Fishman, Raj N. Patel, David Hopper, Tzu-Yung Huang and Lee Bassett; University of Pennsylvania, United States

Photon correlation spectroscopy is a powerful technique for measurement and analysis of optical dynamics. Historically, analysis of photon detection times enabled early studies of fundamental quantum mechanical phenomena in trapped atoms and ions and was used to probe dynamics in single-molecule spectroscopy. More recently, it has been applied to solid-state emitters to enable their characterization for quantum technological applications. The predominant use of photon statistics in solid-state systems is as an indicator of single-photon emission, a desirable property for applications such as quantum key distribution and quantum repeaters. However, a more comprehensive analysis of photon statistics can reveal even more characteristics of a system such as the electronic structure, multi-level optical dynamics, and responses to external fields. We discuss photon correlation spectroscopy as a measurement tool for solid-state emitters and outline important methods and considerations for proper acquisition and analysis of photon statistics. In particular, we explore the differences between the two most common measurement techniques, start-stop histogram and time-tagged-time-resolved mode, and we highlight the technical considerations in accounting for background fluorescence and detector jitter for robust characterization of single-photon emission. We also discuss how both an emitter's internal dynamics and experimental nonidealities must be taken into account in order to guarantee reliable measurements. Finally, we illustrate how the photon statistics framework can be used to characterize quantum emitters by applying it to known emitters like the diamond nitrogen-vacancy center and unknown emitters in hexagonal boron nitride. Through comparison of the measurements to optical-dynamics simulations, we posit an optical level diagram for the unknown emitters, advancing understanding of their electronic structure and optical dynamics.

#### 5:25 AM F.NM06.06.03

**Exploiting Spin Interaction within Magnetic Nanoparticles Toward Remote Spatially Resolved Temperature Sensing** Adam Biacchi, Thinh Q. Bui, Brianna B. dos Santos Correa, Cindi L. Dennis, Solomon I. Woods and Angela Hight Walker; National Institute of Standards and Technology, United States

Magnetic nanoparticles (MNPs) are an important class of low-dimensional materials displaying size-dependent magnetic

behavior. The controllable tunability of magnetic anisotropy introduced at nanoscale size regimes allows for nanoparticles of ferro/ferrimagnetic materials to be dispersed in a medium, with the addition of colloidal stabilizers, and still produce a significant collective response to a dynamic applied magnetic field. This strong response to external applied fields, while still maintaining colloidal dispersity, is the basis for employing these magnetic materials in biomedical applications such as imaging, sensing, drug delivery, and hyperthermia.

Magnetic nanothermometry is an emerging application of MNPs. While conventional remote thermometry can measure the temperature of a microscale spot only on an object's surface or in a small local region of an optically transparent material, magnetic nanothermometry is being developed to accurately measure temperature throughout a three-dimensional volume. This metrology is based on the temperature-dependent nature of the spin interaction within each particle, and the ability of applied AC magnetic fields to penetrate through many materials to probe the magnetization therein as a function of position. However, commercially available MNPs display only modest magnetic thermosensitivity, especially near room temperature; this response must be strengthened as a prerequisite to practical remote volumetric nanothermometry. Carefully designed doped or multi-domain nanoparticles, with a strong AC magnetic response and selective control of thermosensitive temperature ranges arising from magnetic exchange interactions, represent a potential route to overcome these limitations.

Here, we engineer MNPs specifically for room-temperature thermometry applications. Their synthesis relies on reproducible, easily scalable, solution chemistry routes and is tunable to afford colloidal particles of controlled size, structure, and composition. We exploit compositional doping and exchange coupling between core-shell magnetic heterostructures as means of controlling their temperature-dependent spin interaction. We find that these structurally complex MNPs based on ferrites show improved temperature-dependent change in their magnetization. Analysis conducted using X-ray scattering and diffraction, Raman spectroscopy, and high-resolution electron microscopies provide correlations between the nanoscale structure of these particles with their magnetic thermosensitivity. Finally, we use an AC magnetic particle spectrometer to measure the magnetization-dependence of these nanothermometers as a function of temperature in their local environment. Our results demonstrate that complex ferrite MNPs are a promising material platform for remote thermometric sensing based on temperature-dependent spin ordering under an applied magnetic field.

#### 5:35 AM F.NM06.06.04

**Nanoscale Structure of the Orbital Magnetic Moment of a Single Dopant Spin in a Semiconductor** Adonai R. Cruz<sup>1</sup> and Michael E. Flatté<sup>2,1</sup>; <sup>1</sup>Eindhoven University of Technology, Netherlands; <sup>2</sup>The University of Iowa, United States

The localized electron spin of a single impurity in a semiconductor is a promising system to realize quantum information schemes [1]. Coherent control of this spin depends on understanding the structure of the magnetic moment that couples the system with external fields. In this work we investigate the orbital contribution to the magnetic moment originated from the spin-orbit induced circulating current associated with the ground state of a single magnetic impurity in zincblende III-V semiconductor. This circulating current is dissipationless and represents an electron moving in a closed trajectory [2]. The orbital moment associated with the circulating current could be directly measured by the dc-magnetic field it produces through nanoscale magnetometry techniques provided by NV-centers in diamond [3].

In this project we developed a formalism employing Green's functions obtained by the Koster-Slater technique [4] with a  $sp^3d^5s^*$  empirical tight-binding Hamiltonian [5,6] to describe the host material. We calculated the circulating current and orbital moments of a single Mn dopant in GaAs. The spin-correlated orbital moments originates from the hybridization between the Mn( $d^5$ ) spin-polarized electrons and the As dangling bonds leading to  $t_2$ -symmetric triplet acceptor states in the band-gap above the valence band edge.

[1] Koenraad, P.M. and Flatté, M.E., Nature Materials 10, 1038 (2011).

[2] van Bree, J. and Silov, A.Yu and Koenraad, P.M. and Flatté, M. E., Phys. Rev. Lett. 112, 187201 (2014).

[3] Casola, F. and van der Sar, T. and Yacoby, A. Nature Reviews Materials, 3(1), 17088 (2018).

[4] Tang, J.M. and Flatté, M.E., Phys. Rev. Lett. 92, 047201 (2004).

[5] Jancu, J.M. and Scholz, R. and Beltram, F. and Bassani, F., Phys. Rev. B 57, 6493 (1998).

[6] Kortan, V.R. and Sahin, C. and Flatté, M.E., PRB 93, 220402(R) (2016).

\* This project has received funding from the European Union's Horizon 2020 research and innovation programme under the Marie Skłodowska-Curie grant agreement No 721394

**5:00 AM \*F.NM06.07.01**

**Single Artificial Atoms in Silicon Emitting at Telecom Wavelengths** Anais Dreau; Laboratoire Charles Coulomb, CNRS & University of Montpellier, France

Given its unrivaled potential of integration and scalability, silicon is likely to become a key platform for large-scale quantum technologies. Individual electron-encoded artificial atoms either formed by impurities [1] or quantum dots [2, 3] have emerged as a promising solution for silicon-based integrated quantum circuits. However, single qubits featuring an optical interface needed for large-distance exchange of information [4] have not yet been isolated in such a prevailing semiconductor.

We show the first isolation of single optically-active point defects in a commercial silicon-on-insulator wafer implanted with carbon atoms [5]. These artificial atoms exhibit a bright, linearly polarized single-photon emission at telecom wavelengths suitable for long-distance propagation in optical fibers. Our results demonstrate that despite its small bandgap (~1.1 eV) a priori unfavorable towards such observation [6], silicon can accommodate point defects optically isolable at single scale, like in wide-bandgap semiconductors [7]. This work opens numerous perspectives for silicon-based quantum technologies, from integrated quantum photonics to quantum communications [8] and metrology.

[1] He, Y. et al., Nature 571, 371 (2019).

[2] Watson, T. F. et al., Nature 555, 633–637 (2018).

[3] Maurand, R. et al., Nature Comm. 7, 13575 (2016).

[4] Hensen, B. et al., Nature 526, 682–686 (2015).

[5] Redjem\*, W., Durand\*, A. et al., arXiv : 2001.02136 (2020).

[6] Weber, J. R. et al., PNAS 107, 8513–8518 (2010).

[7] Aharonovich, I., Englund, D. & Toth, M., Nature Photonics 10, 631–641 (2016).

[8] Wehner, S., Elkouss, D. & Hanson, R., Science 362, eaam9288 (2018).

**5:15 AM F.NM06.07.02**

**Hybrid System of Giant Magnetostrictive Material and Diamond NV Color Centers for Mass Imaging** Ryota Kitagawa<sup>1</sup>, Soki Urashita<sup>1</sup>, Keigo Arai<sup>1</sup>, Kosuke Mizuno<sup>1</sup>, Hitoshi Ishiwata<sup>1,2</sup>, Yota Takamura<sup>1</sup>, Takayuki Iwasaki<sup>1</sup>, Shigeki Nakagawa<sup>1</sup> and Mutsuko Hatano<sup>1</sup>; <sup>1</sup>Tokyo Institute of Technology, Japan; <sup>2</sup>Japan Science and Technology Agency, Japan

Mass imaging technique for multiple length-scales from single cells to tissues is necessary for a wide range of applications such as the development of anti-cancer agents with fewer side effects[1,2]. Theoretical calculation demonstrated a hybrid sensor using nitrogen-vacancy (NV) centers combined with giant magnetostrictive(GMS) material as a promising platform for such application [3,4]. For the realization of the hybrid sensor, deposition of GMS material and vector imaging of GMS material with NV center is necessary. In this study, we performed imaging of stray magnetic field vectors produced by deposited GMS material using NV centers. Perpendicular magnetic anisotropy (PMA) in SmFe<sub>2</sub> was confirmed from both vibrating sample magnetometer (VSM) and vector imaging using NV center. SmFe<sub>2</sub> also could make sensitivity higher than GMS material with in-plane magnetic anisotropy due to its smaller anisotropic magnetic field.

SmFe<sub>2</sub> thin film with a thickness of 100 nm was deposited on a quartz substrate and Si/SiO<sub>2</sub> substrate with the facing target sputtering. M-H hysteresis curve was measured on SmFe<sub>2</sub> thin film using a VSM for testing PMA. Magnetostriction constant  $\lambda$ , directly related to the sensitivity of the hybrid sensor, was calculated from the change of the magnetic anisotropic energy density with bending stress of  $\pm 10$  MPa. Ensemble NV centers were fabricated on a IIa(100) diamond substrate by nitrogen ion implantation with implantation energy of 6 keV and  $2 \times 10^{13}$  cm<sup>-2</sup> concentration. SmFe<sub>2</sub> thin film was placed on top of the ensemble NV center for vector magnetic field measurement. The stray magnetic field was imaged by pulsed-optically detected magnetic resonance (ODMR) with a uniform bias magnetic field of approximately 5 mT solving degeneracy of NV energies.

M-H hysteresis measurements using VSM indicated the PMA of the deposited SmFe<sub>2</sub> thin-film and large magnetostriction constant of  $\lambda = -920$  ppm which is the same order as general GMS materials. ODMR measurements using NV centers revealed a magnetic field vector profile produced by the SmFe<sub>2</sub> thin-film with a spatial resolution of ~500 nm, a measurement field-of-view of 64  $\mu$ m x 64  $\mu$ m, and a magnetic field sensitivity of 50  $\mu$ T/Hz<sup>1/2</sup>. The stray field measured by NV centers was perpendicular to the surface, indicating that the SmFe<sub>2</sub> layer had PMA consistent with the VSM result. We

established essential techniques for constructing the hybrid system through deposition of  $\text{SmFe}_2$  and magnetic field vector imaging using NV centers. We aim a mass sensitivity of  $\sim 1 \text{ ng/Hz}^{1/2}$  (1% change in cell mass ( $\sim 1 \text{ ng}$ ) can be detected every 60 minutes) by optimizing the GMS thin film and the magnetic field sensitivity of NV center.

#### Acknowledgements

This study was supported in part by MEXT Q-LEAP JPMXS0118067395.

[1] G. Popescu et al., Lab Chip 14, 646 (2014).

[2] D. Martín et al., Nature 550, 500 (2017).

[3] Y. Takamura et al., Solid. State. Electron. 128, 194 (2017).

[4] J. Cai et al., Nat. Commun. 5, 1 (2014).

#### 5:25 AM F.NM06.07.03

**Predicted Strong Coupling of Solid-State Spins via a Single Magnon Mode** Denis R. Candido<sup>1,2,3</sup>, Gregory Fuchs<sup>3</sup>, Ezekiel Johnston-Halperin<sup>4</sup> and Michael E. Flatté<sup>1,2,5</sup>; <sup>1</sup>University of Iowa, United States; <sup>2</sup>The University of Chicago, United States; <sup>3</sup>Cornell University, United States; <sup>4</sup>The Ohio State University, United States; <sup>5</sup>Eindhoven University of Technology,, Netherlands

We propose [1] an approach to realize a hybrid quantum system composed of a diamond nitrogen-vacancy (NV) center spin coupled to a magnon mode of the low-damping, low-moment organic ferrimagnet vanadium tetracyanoethylene [2,3]. We derive an analytical expression for the spin-magnon cooperativity as a function of NV position under a micron-scale perpendicularly magnetized disk, and show that, surprisingly, the cooperativity will be higher using this magnetic material than in more conventional materials with larger magnetic moments, due to in part to the reduced demagnetization field. For reasonable experimental parameters, we predict that the spin-magnon-mode coupling strength is  $g \sim 10 \text{ kHz}$ . For isotopically pure  $^{12}\text{C}$  diamond we predict strong coupling of an NV spin to the unoccupied magnon mode, with cooperativity  $C \sim 6$  for a wide range of NV spin locations within the diamond, well within the spatial precision of NV center implantation. Thus our proposal describes a practical pathway for single-spin-state-to-single-magnon-occupancy transduction and for entangling NV centers over micron length scales.

The material is based on work supported by the U.S. Department of Energy, Office of Basic Energy Sciences, under Award Number DE-SC0019250.

[1] Denis R. Candido, Gregory D. Fuchs, Ezekiel Johnston-Halperin, Michael E. Flatté, arXiv:2003.04341 (Material for Quantum Technology -- <https://iopscience.iop.org/article/10.1088/2633-4356/ab9a55>)

[2] Na Zhu, Xufeng Zhang, I. H. Frøning, Michael E. Flatté and Hong X. Tang., Applied Physics Letters 109, 082402 (2016)

[3] A. Franson, et. al., APL Materials 7, 121113 (2019)

#### 5:35 AM F.NM06.07.04

**Optically Detected Magnetic Resonance Study of Spin Properties in the Pristine and Mn-Doped CdSe/CdS Seeded Nanorods** Joanna Dehnel, Yahel Barak, Itay Meir and Efrat Lifshitz; Technion Israel Institute of Technology, Israel

<div style="direction: ltr;">The discussed work deals with a control and characterization of spin degrees of freedom of photo-generated carriers in colloidal seeded nanorods (sNRs) - via magnetic doping. The material under consideration is CdSe/CdS:Mn sNRs, including diluted concentration of  $\text{Mn}^{2+}$  ions at the rod region. Magnetic doping was implemented extensively in colloidal quantum dots, but with a limited way in anisotropic structures, wherein the latter possess other significant properties (e.g., anisotropy and reduced Auger rates).

Our work reports a thorough investigation of spin degrees of freedom in the mentioned materials, monitored by an optically detected magnetic resonance (ODMR) spectroscopy tool, which provides a significant information on exact location of host carriers and dopants, as well as examine interactions between them.

More specifically, the comparison between the pristine structures (CdSe/CdS) and the magnetically doped derivative, CdSe/CdS:Mn, indicated that both include trapping of the photo-generated carriers at the interface between the seed and the rod. The trapped carriers are already unpaired spins that endow selective magneto-optical properties with extended radiative and spin-relaxation times. The dominant interaction with the magnetic dopant takes place along the seed/rod interface, leading to further enhancement of spin helicity and the radiative lifetime. Most importantly, the carrier-dopant interaction bestows an order of magnitude extension of spin-lattice relaxation time in doped sNRs with respect to that of the pristine material, with an extreme importance for practical applications. The extracted physical parameters from the ODMR experiments included: g-factors and their anisotropy, spin exchange interactions, angular momentum, carrier-dopant coupling constants, radiative and spin-lattice relaxation times.

The spin-properties in confined systems as mentioned here, undoubtedly can play an important role in the development of new spin-based technologies.

</div>

SESSION F.NM06.08: Spin Control in New 2D Materials  
On Demand Abstracts Available for Viewing Starting Saturday Morning, November 21, 2020  
F-NM06

**5:00 AM \*F.NM06.08.01**

**Ultrafast Excitation of Coherent Spin Waves in 2D Antiferromagnets** Xiao-Xiao Zhang; University of Florida, United States

The recently discovered atomically-thin magnetic crystals provide a unique playground to develop new approaches to manipulate magnetism. Rapid progresses have been made that demonstrate the potentials of utilizing 2D magnets to construct novel spintronics devices. However, their spin dynamics, which are crucial for microscopic understanding and determine the fundamental limit of spin manipulation, still remain elusive due to the difficulty of characterizing these micron-sized samples with conventional microwave techniques. In this talk, we will show how we can access and probe the collective spin-wave excitations in an antiferromagnetic bilayer CrI<sub>3</sub>, which allows us to extract magnetic anisotropy and exchange energy. In particular, we will demonstrate the gate tunability of magnon frequencies, which is unique for the 2D magnet system.

**5:15 AM F.NM06.08.02**

**Design of Giant Spin Hall Effect in Transition Metal Oxides** Priyamvada Jadaun, Leonard Register and Sanjay Banerjee; UT Austin, United States

Spin Hall effect (SHE), a mechanism by which materials convert a charge current into a spin current, has attracted significant attention owing to its novel physics and potential applications to spintronics, magnetic memory and spin logic devices. However, there have remained fundamental gaps in our understanding of the essential factors that control SHE in materials. Here we answer this important question, presenting a comprehensive theory of five rational design principles for achieving giant intrinsic SHE in transition metal oxides. Stemming from the inherently geometric nature of SHE, two of these design principles are weak crystal fields and the presence of structural distortions. Additionally, we discover that novel materials such as anti-perovskites are a highly promising class of materials for achieving giant SHE, with predicted SHE values reaching an order of magnitude larger than that reported for any oxide. We further examine the SHE values found in a variety of anti-perovskite oxides. Moreover, we derive three other design principles for enhancing SHE. Our findings shed light on the physics driving SHE, uncover technologically important SHE materials, and could help enhance and externally control SHE values.

**5:25 AM \*F.NM06.08.03**

**Van der Waals Epitaxy of Transition Metal Dichalcogenides by MBE Application to the Study of the Valley Nernst Effect in WSe<sub>2</sub>** Minh-Tuan Dau<sup>1</sup>, Celine Vergnaud<sup>1</sup>, Alain Marty<sup>1</sup>, Frederic Bonell<sup>2</sup>, Cyrille Beigne<sup>1</sup>, Serge Gambarelli<sup>1</sup>, Vincent Maurel<sup>1</sup>, Thomas Guillet<sup>1</sup>, Timotee Journot<sup>3</sup>, Berangere Hyot<sup>3</sup>, Benjamin Grevin<sup>2</sup>, Hanako Okuno<sup>1</sup> and Matthieu Jamet<sup>1</sup>; <sup>1</sup>CEA Grenoble, France; <sup>2</sup>CNRS, France; <sup>3</sup>CEA-LETI, France

Semiconducting transition metal dichalcogenides (TMDCs) have gained a great attention because of their fascinating electronic and optical properties when downing the thickness to one monolayer. In the monolayer form, due to the breaking of inversion symmetry and strong spin-orbit coupling, the carriers in TMDCs carry a valley index noted K<sup>+</sup> or K<sup>-</sup>. This valley degree of freedom refers to local extrema in the band structure of TMDC monolayers at the K points of the two-dimensional Brillouin zone and it can be exploited to develop novel valleytronic devices. In MX<sub>2</sub> (M = Mo, W and X = S, Se) monolayers, the broken inversion symmetry and strong spin-orbit coupling originating from the d-orbitals of the transition metal atom align the electron spins near opposite valleys K<sup>+</sup> and K<sup>-</sup> to opposite out-of-plane directions thus preserving time reversal symmetry. The broken spatial inversion symmetry also generates large Berry curvatures near the K valleys, the Berry curvatures being opposite at opposite valleys. This effect gives rise to unconventional electronic properties such as the valley Hall effect. An interesting growing field of investigation consists in coupling the valley physics with thermoelectrics. Several spin/valley-dependent thermoelectric effects have already been predicted theoretically in monolayer TMDCs such as the spin Nernst effect (thermoelectric counterpart of the spin Hall effect) and the valley Nernst effect (VNE). Hence, the experimental

demonstration of those effects could give rise to a new field called valley caloritronics (by analogy with spin caloritronics) with the advantage that the coupled valley-spin degree of freedom is more robust than the spin with respect to external magnetic fields due to the large intrinsic spin-orbit coupling.

In this presentation, I will first review our recent results on the MBE growth of transition metal dichalcogenides on various substrates over large areas and explain the mechanisms underlying the van der Waals epitaxy regime [1]. Using this growth technique, we could study the interplay between thermoelectricity and the valley degree of freedom in monolayers of WSe<sub>2</sub>. For this purpose, high quality WSe<sub>2</sub> mono and multilayers were grown on epitaxial graphene on SiC. Using millimeter-sized samples, we were able to apply well-defined temperature gradients and demonstrate the very strong Seebeck response of this material. In a second step, we used the ferromagnetic resonance-spin pumping technique (FMR-SP) to (i) apply the temperature gradient by off centering the sample in the radio frequency (RF) cavity and (ii) address a single valley and break time reversal symmetry using the spin pumping through spin-valley coupling. For FMR-SP, we deposited in-situ the Al/Ni<sub>81</sub>Fe<sub>19</sub>/Al magnetic stack on top of the WSe<sub>2</sub> layer. The combination of a temperature gradient and the valley polarization lead to the valley Nernst effect in WSe<sub>2</sub> that we could detect electrically in the RF cavity. The Nernst coefficient we measured is in very good quantitative agreement with the predicted value [2]. This effect could be exploited to generate large transverse valley currents for valleytronics applications.

#### References

- [1] M.-T. Dau et al., ACS Nano 12, 2319 (2018).  
[2] M.-T. Dau et al., Nat. Commun. 10, 5796 (2019).

#### 5:40 AM F.NM06.08.04

**Late News: Unusual Spin Physics and Charge Carrier Dynamics in Luminescent Dilute Organic Semiconductor for Spintronics Applications** Tejasvini Sharma, Naveen K. Tailor and Soumitra Satapathi; Indian Institute of Technology Roorkee, India

The pyrene derivatives have been widely investigated in the field of organic electronics and spintronics. However, the fundamental understanding of their excited state dynamics and spin physics remains elusive. Here, we present the temperature-dependent photoluminescence (PL) and electron spin resonance (ESR) study of a model fluorescent organic dilute semiconductor where organic fluorophore pyrene is incorporated in the insulating Poly-methyl methacrylate (PMMA) polymeric backbone as pendant unit (py-PMMA). We observe that lowering the temperature from 300K to 140K, the monomer fluorescence emission from py-PMMA gets blue-shifted, and their intensity enhances, which is attributed to less charge carrier scattering by lattice sites at low temperature. Interestingly, we observe additional higher energy peaks at 368 nm (~3.36 eV) below 70K in fluorescence emission, which is explained by the self-confined exciton-phonon coupling. The strong spin-orbit coupling was observed in our system by temperature-dependent electron spin resonance (TDESRS) spectroscopy, and spin relaxation time was calculated in order of picoseconds. The temperature-dependent intensity and bizarre linewidth behavior of the ESR signal are attributed to the phonon bottleneck effect. Our study provides the direction to examine and understand the electron-phonon interaction and spin-orbit coupling at low temperatures in organic polymers, which helps to design new organic devices in the field of spintronics.

SESSION F.NM06.09: Spin Control in II-VI and Related Materials  
On Demand Abstracts Available for Viewing Starting Saturday Morning, November 21, 2020  
F-NM06

#### 5:00 AM F.NM06.09.01

**Strain-Tunable Orbital Physics of Sr<sub>2</sub>CrReO<sub>6</sub> Epitaxial Films** Guillaume Marcaud<sup>1</sup>, Alex Taekyung Lee<sup>1</sup>, Sangjae Lee<sup>1</sup>, Adam Hauser<sup>2</sup>, Fengyuan Yang<sup>3</sup>, Diego Casa<sup>4</sup>, Mary Upton<sup>4</sup>, Thomas Gog<sup>4</sup>, Yilin Wang<sup>5</sup>, Mark P. Dean<sup>5</sup>, Frederick Walker<sup>1</sup>, Sohrab Ismail-Beigi<sup>1</sup>, Charles H. Ahn<sup>1</sup> and Ignace Jarrige<sup>5</sup>; <sup>1</sup>Yale University, United States; <sup>2</sup>The University of Alabama, United States; <sup>3</sup>The Ohio State University, United States; <sup>4</sup>Argonne National Laboratory, United States; <sup>5</sup>Brookhaven National Laboratory, United States

Rhenium-based double perovskites possess a rich array of properties including magnetic ordering at room temperature and an intricate interplay between structure, orbital ordering, and metal-insulator transitions (MIT). In particular, Sr<sub>2</sub>CrReO<sub>6</sub> (SCRO) possesses a high Curie temperature of T<sub>c</sub>=620K, a large strain-tunable magnetocrystalline anisotropy, and an insulating ground state with a bandgap of 0.21 eV. To determine the energy scale for the electronic interactions, we used resonant



inelastic X-ray scattering (RIXS) at the Re  $L_3$  edge for two strain states of SCRO thin films, compressive -1% on a  $(\text{LaAlO}_3)_{0.3}(\text{Sr}_2\text{AlTaO}_6)_{0.7}$  (LSAT) substrate and tensile +1% on a relaxed  $\text{SrCr}_{0.5}\text{Nb}_{0.5}\text{O}_3$  buffer layer on LSAT. We observe three Raman-like excitations around 150, 600 and 1000 meV on both samples and a broad fluorescence above 8 eV. All the Raman-like peaks show a strong dependence on strain, and only the lowest energy peak shows a temperature dependence. Using the exact diagonalization RIXS toolkit (EDRIXS) [2], we are able to assign the Raman-like features to Re  $d$  orbitals excitations. Implications of the observed experimental strain and temperature dependences on the physics of SCRO are discussed. .

[1] Hauser, A. J. et al. Fully ordered  $\text{Sr}_2\text{CrReO}_6$  epitaxial films: A high-temperature ferrimagnetic semiconductor. *Phys. Rev. B* **85**, 161201 (2012).

[2] Wang, Y. et al. EDRIXS : An open source toolkit for simulating spectra of resonant inelastic X-ray scattering. *Comp. Phys. Comm.* **243**, 151 (2019).

Work at Yale is supported by a grant from the Department of Energy, Basic Energy Sciences under grant number DE-SC0019211. Work was done at the Advanced Photon Source, a U.S. Department of Energy (DOE) Office of Science User Facility operated for the DOE Office of Science by Argonne National Laboratory under Contract No. DE-AC02-06CH11357.

### 5:10 AM \*F.NM06.09.02

**Optical and Microwave Spin Control of Donors in ZnO** Kai-Mei Fu; University of Washington, United States

Electrons bound to donors in silicon are electrically-controlled qubits with exceptional spin coherence properties. Here we seek to find analogous donor systems in direct band gap semiconductors which will enable an efficient optical interface to the donor electron spin qubit. We show that ZnO donors, optically coupled to donor-bound excitons, are particularly promising candidates [1]. Due to low spin-orbit coupling, we find donors exhibit longitudinal spin relaxation times up to 0.5 s at 1.5 K with relaxation fundamentally-limited by phonon interactions. Both  $\lambda$  and near-cycling optical transitions exist which are suitable for optical spin initialization and readout. Spin-echo coherence times, which we determine via both optical and microwave control, are in the tens of microseconds and likely limited by nuclear spins in natural isotopic ZnO. These characteristics are all extracted from measurements on an ensemble of Ga donors in a commercial substrate. We will present ongoing efforts and challenges toward single donor isolation in nanowires, dual optical-microwave control of donors and two-laser coherent spin-spectroscopy in this emerging qubit platform.

[1] X. Linpeng, M.L.K Viitaniemi, A. Vishnuradhan, Y. Kozuka, C.Johnson, M. Kawasaki, K.-M.C. Fu, *Phys. Rev. Applied* **10**, 064061 (2018)

### 5:25 AM F.NM06.09.03

**Direct Imaging of the AC Component of the Pumped Spin Polarization with Element Specificity** Santa Pile<sup>1</sup>, Martin Buchner<sup>1</sup>, Verena Ney<sup>1</sup>, Taddäus Schaffers<sup>1</sup>, Kilian Lenz<sup>2</sup>, Ryzard Narkowicz<sup>2</sup>, Jürgen Lindner<sup>2</sup>, Hendrik Ohldag<sup>3,4</sup> and Andreas Ney<sup>1</sup>; <sup>1</sup>Johannes Kepler Universität Linz, Austria; <sup>2</sup>Helmholtz-Zentrum Dresden-Rossendorf, Germany; <sup>3</sup>Stanford Linear Accelerator Center, United States; <sup>4</sup>Univ of California Santa Cruz, United States

In spintronics the generation and manipulation of pure spin currents is in the focus of research activities. Amongst the utilized fundamental effects is spin pumping where a precessing magnetization of a ferromagnet being at ferromagnetic resonance (FMR) transfers angular momentum to an adjacent nonferromagnetic layer [1]. The transfer of angular momentum into the nonferromagnetic layer can be described as a spin-current. The pumped spin current has a dc and an ac component corresponding to the reduction of the projection of the magnetization at FMR as well as the dynamic high-frequency magnetization, respectively. Spin pumping in a ferromagnet/nonferromagnet heterostructure is directly imaged with spatial resolution as well as element selectivity. The time-resolved detection in scanning transmission x-ray microscopy [2] allows to directly probe the spatial extent of the ac spin polarization in Co-doped ZnO which is generated by spin pumping from an adjacent permalloy microstrip complementing earlier results in Py/Co:ZnO heterostructures [3]. Comparing the relative phases of the dynamic magnetization component of the two constituents is possible and found to be antiphase. The correlation between the distribution of the magnetic excitation in the permalloy and the Co-doped ZnO reveals that laterally there is no one-to-one correlation. The observed distribution is rather complex, but integrating over larger areas clearly demonstrates that the spin polarization in the nonferromagnet extends laterally beyond the region of the ferromagnetic microstrip. Therefore the observations are better explained by a local spin pumping efficiency and a lateral propagation of the ac spin polarization in the nonferromagnet over the range of a few micrometers [4].

[1] Y. Tserkovnyak, A. Brataas, and G. E. W. Bauer, *Phys. Rev. Lett.* **88** (2002) 117601

[2] S. Bonetti et al., *Rev. Sci. Instrum.* **86** (2015) 093703; T. Schaffers et al. *Rev. Sci. Instrum.* **88** (2017) 093703

[3] M. Buchner et al. *J. Appl. Phys.* **127** (2020) 043901 (2020)

[4] S. Pile et al. arXiv 2005.08728

### 5:35 AM F.NM06.09.04

**Transition Metal-Vacancy Centers in Zinc Sulfide** Cuneyt Sahin and Michael E. Flatté; University of Iowa, United States

Wide bandgap semiconductors are essential to numerous commercial devices and have been extensively investigated due to their high optical transparency, controllable transport properties, carrier concentrations, and mobilities. Transition metal impurities and impurity-vacancy complexes in wide-gap semiconductors have also attracted both theoretical and experimental interest due to possible applications in single-photon emission with minimal decoherence [1], the possibility of robust exchange interactions of spin centers [2], and inducing also enhancing of the ferromagnetic order by doping [3]. Among various wide-gap semiconductors, zinc sulfide (ZnS) has been a platform for numerous applications such as display technologies, luminescent devices, nonlinear optical devices, solar cells, and other optoelectronic applications [4,5,6]. Furthermore, certain defects and defect-vacancy centers may provide a coherent, room-temperature interface between spins and photons in this host material.

Here we carry out the calculation of the electronic and structural properties of transition metal - vacancy complexes in ZnS within the density functional theory framework as implemented in the Vienna *ab initio* simulation package and projector-augmented wave approach. We simulate the host material ZnS as a 64 atom supercell and use a 2x2x2 Monkhorst-Pack k-point mesh for the sampling of the Brillouin zone. Perdew–Burke–Ernzerhof class of generalized gradient approximation is used for the treatment of the exchange-correlation potential. Both lattice constants and atomic positions are optimized with a convergence criterion of 1 meV. To fix the well-known band-gap problem of the density functional theory method, we use hybrid functionals resulting in a 3.65 eV gap, which agrees excellently with the experimental value.

Transition metal dopants are substitutionally replaced with a zinc atom, and the vacancy is formed at the neighboring sulfur atom. We then perform the ionic relaxations with a fixed lattice constant using the conjugate gradient algorithm. The defect formation energies are calculated following the formula of Ref. [7]. We have also calculated different charged states of the impurities in Zn-rich and S-rich conditions to establish the possibility of forming these impurities as a function of the Fermi level in the bandgap region. The charge transition levels are also computed from the relaxed final energies for different charged states. We have also included the charge corrections due to finite-size effects originating from the Coulomb interaction between impurities in the neighboring supercells using the Freysoldt-Neugebauer-Van de Walle scheme. [8]. Finally, we calculate the density of states, orbital projected densities, and electronic band structures of the system to identify states located in the bandgap and determine the characteristics of the impurities, such as deep vs. shallow. We conclude that ZnS is a strong candidate for a system in which impurity spin-light interfaces can be realized similarly to the nitrogen-vacancy color centers in diamond and divacancies in silicon carbide.

We acknowledge support from NSF DMREF Award No. DMR-1921877.

[1] M. Koperski, K. Nogajewski, A. Arora, V. Cherkez, P. Mallet, J.-Y. Veuillen, J. Marcus, P. Kossacki, and M. Potemski, *Nature Nanotechnology*, 10, 503-506 (2015)

[2] V. R. Kortan, C. Sahin, and M. E. Flatté, *Phys. Rev. B* 93, 220402(R) (2016)

[3] K. Sato and H. Katayama-Yoshida, *Jpn. J. Appl. Phys.*, 39, L555 (2000)

[4] X. Ma, J. Song, and Z. Yu, *Thin Solid Films*, 519(15),5043-5045 (2011)

[5] Y. Lun, Y. Lin, Y. Meng, and , and Y. Wang, *Ceramics International*, 40(6):8157–8163 (2014)

[6] X. Xu, S. Li, J. Chen, S. Cai, Z. Long, and X. Fang, *Adv. Funct. Mater.* 28 (36) 1802029 (2018)

[7] C. G. Van de Walle and J. Neugebauer, *J. Appl. Phys.* 95, 3851 (2004)

[8] C. Freysoldt, J. Neugebauer, and C. G. Van de Walle, *Phys. Rev. Lett.* 102, 016402 (2009)

### SESSION F.NM06.10: Quantum Magnonics

On Demand Abstracts Available for Viewing Starting Saturday Morning, November 21, 2020

F-NM06

### 5:00 AM \*F.NM06.10.01

**Ultrastrong Magnonic Coupling in Canted Antiferromagnets** Takuma Makihara, Nicolas Marquez Peraca and Junichiro Kono; Rice University, United States

Light-matter coupling in the so-called ultrastrong coupling (USC) regime [1] has become an important general subject of modern science and technology. Many next-generation quantum technologies that exploit the extremely efficient light-matter interactions in the USC regime have been proposed. Further, a wealth of exotic phenomena has been predicted in the USC regime, such as quantum vacuum radiation or nonclassical ground states known as two-mode squeezed vacuums. The source of these phenomena is the so-called counter-rotating terms in the Hamiltonian, which are typically negligible compared to the so-called co-rotating terms for weaker coupling strengths. USC has now been achieved in diverse platforms, but the exotic nature of the ground state due to the counter-rotating terms has not been explored. We have recently observed unusual matter-matter USC phenomena in rare-earth orthoferrites. First, we observed cooperative, Dicke-type coupling between a paramagnetic  $\text{Er}^{3+}$  spin ensemble and a single mode of terahertz magnons of ordered  $\text{Fe}^{3+}$  spins in  $\text{ErFeO}_3$  [2]. The data exhibited vacuum Rabi splitting values in the USC regime, indicating that rare-earth orthoferrites provide a rich playground in which to explore USC phenomena without light. Furthermore, we observed that magnons in  $\text{YFeO}_3$  display USC with a dominant role played by the counter-rotating terms. Our system is described by an unusual Hamiltonian, where: (i) the coupling strengths are tunable, (ii) the counter-rotating interactions dominate the co-rotating interactions, and (iii) the ground state is a magnonic two-mode squeezed vacuum with quantum fluctuation suppression up to 5.9 dB. These observations demonstrate that  $\text{YFeO}_3$  provides an extraordinary platform for both applied and fundamental studies of USC beyond the reaches of photonic platforms.

1. P. Forn-Diaz, L. Lamata, E. Rico, J. Kono, and E. Solano, "Ultrastrong Coupling Regimes of Light-Matter Interaction," *Rev. Mod. Phys.* **91**, 025005 (2019).

2. X. Li *et al.*, "Observation of Dicke Cooperativity in Magnetic Interactions," *Science* **361**, 794 (2018).

### 5:15 AM F.NM06.10.02

**First Principles Calculation of the Electronic Structure of  $\text{V}(\text{TCNE})_2$**  Yueguang Shi and Michael E. Flatté; The University of Iowa, United States

Over the past two decades there has been growing interest in organic magnetic materials, due to their potential applications in the field of magnonics and spintronics.[1,2,3,4] Vanadium tetracyanoethylene,  $\text{V}(\text{TCNE})_{x \approx 2}$ , is a room temperature ferrimagnetic semiconductor with a  $T_c \sim 600$  K [5] which has very low loss ferromagnetic resonance and spin-wave propagation[1, 2]. Previous first principles calculations of the electronic structure have indicated a substantially larger band gap (0.8 eV) than experimentally inferred (0.5 eV) [6,7], and that the band gap itself is an indirect gap with the valence maximum located at the (0,0,0.5) point and the conduction minimum at the (0,0.5,0) point. Our crystal axes are defined so that an equatorial TCNE ligand lies in the plane (0 0 1) and an apical ligand lies in (1 1 0) in a unit cell. The study of Ref. 6 used a local-orbital calculation with B3LYP hybrid functional. Here we explore the electronic structure using a plane-wave code VASP[8,9,10]. We have tried the following functionals: Perdew-Burke-Ernzerhof (PBE), PBE0, Becke, 3-parameter, Lee-Yang-Parr (B3LYP), Heyd-Scuseria-Ernzerhof (HSE06). The ferrimagnetic structure is studied using both collinear magnetic structure calculations and non-collinear calculations. We confirm that the structure of  $\text{VTCNE}$  has a triclinic unit cell with each V atom surrounded by 6 organic ligands, as found in Ref. 6. However, in contrast to the previous study we find a direct band gap of 0.4 eV located at the (0,0.5,0.5) point. This band gap better agrees with the experimental inference from the conductivity activation energy [7]. Further studies will explore the optical properties of this material and its magnetic dynamics, including anisotropy and magnetoelastic properties.

We acknowledge funding from NSF Grant No. DMR-1808742.

[1] H. Yu, M. Harberts, R. Adur, Y. Lu, P. C. Hammel, E. Johnston-Halperin, and A. J. Epstein, *Appl. Phys. Lett.* **105**, 012407 (2014).

[2] N. Zhu, X. Zhang, I. H. Froning, M. E. Flatté, E. Johnston-Halperin, and H. X. Tang, *Appl. Phys. Lett.* **109**, 082402 (2016).

[3] H. Liu, C. Zhang, H. Malissa, M. Groesbeck, M. Kavand, R. McLaughlin, S. Jamali, J. Hao, D. Sun, R. A. Davidson, L. Wojcik, J. S. Miller, C. Boehme, and X. V. Vardeny, *Nat. Mater.* **17**, 308–312 (2018).

[4] A. Franson, N. Zhu, S. Kurfman, M. Chilcote, D. R. Candido, K. S. Buchanan, M. E. Flatté, H. X. Tang, and E. Johnston-Halperin, *APL Materials* **7**, 121113 (2019).

[5] J. M. Manriquez, G. T. Yee, R. S. McLean, A. J. Epstein, and J. S. Miller, *Science* **252**, 1415 (1991).

[6] G. C. De Fusco, L. Pisani, B. Montanari, and N. M. Harrison, *Phys. Rev. B* **79**, 085201 (2009).

[7] V. N. Prigodin, P. R. Nandyala, K. I. Pokhodnya, J. S. Miller, and A. J. Epstein, *Adv. Mater.* **14**, 1230 (2002).

[8] G. Kresse and J. Hafner, *Phys. Rev. B* **47**, 558 (1993); *ibid.* **49**, 14 251 (1994).

[9] G. Kresse and J. Furthmüller, *Comput. Mat. Sci.* **6**, 15 (1996).

[10] G. Kresse and J. Furthmüller, *Phys. Rev. B* **54**, 11 169 (1996).

### 5:25 AM F.NM06.10.03

**High-Quality Magnetic Resonance in Cryogenic  $\text{V}[\text{TCNE}]_x$  Thin Films** Ezekiel Johnston-Halperin, Huma Yusuf,

Michael Chilcote, Seth Kurfman, Andrew Franson and Donley Cormode; The Ohio State University, United States

The ability to move beyond the study of isolated qubits to explore hybrid systems, i.e. where two or more component qubits coherently couple to yield new functionality, and to transduce and transmit quantum information is a key challenge for the emerging field of quantum information science and technology (QIST). Magnons (or spin-waves) provide an appealing avenue toward realizing this functionality as they can couple to a wide variety of spin-qubits using either exchange or dipole coupling, have coherence lengths from microns to millimeters, and can coherently transduce between spins, microwave photons, and phonons.

However, in order to fulfill this potential, materials with high quality-factor (high- $Q$ ), or low-loss, magnons are required. For almost half a century, we have been limited to yttrium iron garnet (YIG) despite substantial efforts to identify alternative materials. The molecule-based ferrimagnet vanadium tetracyanoethylene (V[TCNE] $_x$ ;  $x \sim 2$ ) has recently emerged as a compelling alternative to YIG. In contrast to other molecule-based materials, V[TCNE] $_x$  has a single-peaked, narrow magnetic resonance feature (less than 1 G at 10 GHz) and has a Curie temperature of over 600 K with sharp hysteresis switching to full saturation at room temperature. In addition to being magnetically robust, V[TCNE] $_x$  is a promising material for integration into solid-state quantum information systems due to its low damping ( $\alpha = (3.98 \pm 0.22) \times 10^{-5}$ ), high quality factor ( $Q$  up to 8,000) microwave resonance, ease of patterning, and compatibility with a wide variety of substrates.

Here we will discuss how V[TCNE] $_x$  can be exploited for applications in quantum information science. We report anomalous temperature dependent anisotropy in V[TCNE] $_x$  thin films, where we observe switching of magnetic easy-axis from in-plane at 300 K to out of plane at 25 K with a clear absence of anisotropy at 100 K. Further, we observe a reversion to room temperature anisotropy and linewidth values at a temperature of 5 K, validating V[TCNE] $_x$  for low temperature quantum applications. We will discuss applications of patterned V[TCNE] $_x$  magnon-resonators in a hybrid quantum device.

#### 5:35 AM F.NM06.10.04

**Spin Wave Dynamics in 1D Patterend Magnonic Crystals of V[TCNE] $_{x-2}$**  Kwangyul Hu<sup>1</sup> and Michael E. Flatté<sup>1,2</sup>; <sup>1</sup>University of Iowa, United States; <sup>2</sup>Eindhoven University of Technology, Netherlands

An organic semiconducting ferrimagnet, vanadium tetracyanoethylene (V[TCNE] $_{x-2}$ ) has a low magnetic damping and narrow ferromagnetic resonance linewidth[1-3], similar to a more commonly explored magnonic material, yttrium iron garnet (YIG)[4,5]. However, YIG requires high-temperature growth on a specific substrate, gadolinium gallium garnet, for high performance[6]. On the other hand, V[TCNE] $_{x-2}$  can be deposited on various rigid substrates at low temperature[1] without a substantial increase of damping. This allows integration of V[TCNE] $_{x-2}$  with other interesting materials.

Here we describe the spin wave dynamics in quasi one-dimensional patterned magnonic crystals of V[TCNE] $_{x-2}$  that can be formed by deposition of a uniform thickness film on a patterned substrate with ridges. The dispersion relations, linewidths and magnetization profiles are calculated by using the Landau-Lifshitz-Gilbert formalism[7,8]. For the structure, we considered alternatively aligned gratings on top and bottom of a thin film. Furthermore, we studied the symmetry of the magnon modes of this magnonic crystals under the influence of an arbitrarily oriented external magnetic field.

We acknowledge support from NSF EFRI NewLAW under Award No. EFMA-1741666.

[1] H. Yu, M. Harberts, R. Adur, Y. Lu, P. C. Hammel, E. Johnston-Halperin and A. J. Epstein, *Appl. Phys. Lett.* **105**, 012407 (2014).

[2] N. Zhu, X. Zhang, I. H. Froning, M. E. Flatté, E. Johnston-Halperin and H. X. Tang, *Appl. Phys. Lett.* **109**, 082402 (2016).

[3] H. Liu et al. *Nat. Mater.* **17**, 308-311 (2018).

[4] E. G. Spencer, R. C. LeCraw, and R. C. Linares, Jr, *Phys Rev.* **123**, 1937 (1961).

[5] C. Hauser et al. *Sci. Rep.* **6**, 20827 (2016).

[6] Y. Y. Sun, Y. Y. Song and M. Z. Wu, *Appl. Phys. Lett.* **101** 082405 (2012).

[7] G. Sietsema, T. Liu, M. E. Flatté, *SPIN*, **7** 1740012 (2017).

[8] R. A. Gallardo et al. *Phys. Rev. B*, **97**, 144405 (2018).

SESSION F.NM06.11: Poster Session: Spin Dynamics in Materials for Quantum Sensing, Optoelectronics and Spintronics  
On Demand Abstracts Available for Viewing Starting Saturday Morning, November 21, 2020

5:00 AM - 8:00 AM  
F-NM06

**F.NM06.11.02**

**Optical Control of Spin Transfer in Hybrid Perovskites-TMDC Heterostructures** [Anna Stadlbauer](#)<sup>1</sup>, Lissa Eyre<sup>1</sup>, Jonathan Zerhoch<sup>1</sup>, Sean A. Bourelle<sup>2</sup> and Felix Deschler<sup>1</sup>; <sup>1</sup>Walter Schottky Institute - Technical University of Munich, Germany; <sup>2</sup>University of Cambridge, United Kingdom

It is a fundamental question how material properties of heterostructures can control spin transfer. This work investigates how spin can be transferred in a heterosystem of a hybrid metal-halide perovskite and a 2D material, with focus on transition metal dichalcogenide (TMDC) layers. Metal halide perovskites and TMDC have already been combined in type II heterostructure devices such as photodetectors [1,2]. However, spin transfer has not yet been reported to the best of our knowledge, which would open up opportunities for optical control in spintronics applications.

Following our study of spin-exciton interactions and spin depolarization times in hybrid perovskites, we aim to investigate how the properties of the heterostructures control spin transfer. The most suitable 2D materials for this approach are semiconducting TMDCs due to their reported controllable valley degree of freedom [3,4]. To benefit from the coupling between spins and valleys in TMD layers, the components in the investigated heterosystem require not only a suitable combination of bandgaps and appropriate band alignment but also positions in k-space that fulfill the optical selection rules [3].

We analyze the obtained heterostructures with ultrafast time resolved photoluminescence spectroscopy, circularly polarized transient absorption spectroscopy and Faraday rotation to resolve the excitation and spin dynamics.

From our fundamental insights into the spin transfer in TMDC-perovskite-heterosystems, we anticipate to discover avenues and design guidelines for application of our for emerging spintronic technologies.

- [1] Ma, C. et al., *Adv. Mater.* **2016**, 28, 3683–3689
- [2] Shi et al., *Chem. Soc. Rev.*, **2018**, 47, 6046
- [3] Mak, K. et al. *Nature Photonics*, **2018**, 12, 451-460
- [4] Ciccarino, C., et al. *Nano Lett.*, **2018**, 18, 57809-5715

**SYMPOSIUM F.NM07**

---

Progress in Neuromorphic Computing Materials, Devices and Systems  
November 21 - November 21, 2020

Symposium Organizers

Simon Brown, University of Canterbury  
Ru Huang, Peking University  
Seyoung Kim, Pohang University of Science and Technology  
Hermann Kohlstedt, Christian-Albrechts-Universität zu Kiel  
Yun Seog Lee, Seoul National University  
Paolo Milani, INFN Sezione di Milano  
Ilia Valov, Research Center Juelich  
J. Joshua Yang, University of Southern California

---

\* Invited Paper

SESSION F.NM07.01: Neuromorphic Device and Application  
On Demand Abstracts Available for Viewing Starting Saturday Morning, November 21, 2020  
F-NM07

**5:00 AM \*F.NM07.01.01**

**Device Challenges for Neuromorphic Computing with Metal-Oxide Memristors** Dmitri Strukov; University of California, Santa Barbara, United States

There have been many demonstrations of nonvolatile memory devices, whose memory states can be continuously tuned, and early experimental results of utilizing such functionality in analog and mixed-signal computing, most notably in neuromorphic circuits. In my talk, I will discuss the major challenges in the quest of building practically useful mixed-signal neuromorphic circuits based on analog-grade memory devices, focusing on the simplest, in terms of device requirements, yet most common neuromorphic inference operation. I will conclude my talk by reviewing experimental results for neuromorphic circuits based on intergrated metal-oxide memristors, one of the most promising types of devices for this applicaiton, in the context of these challenges.

**5:15 AM \*F.NM07.01.02**

**Resistance Switching Memories as Artificial Synapses for Spiking Neural Networks** Sabina Spiga; CNR-IMM, Italy

Memristive devices have been receiving an increasing interest for a wide range of applications, such as storage class memory, in-memory computing and neuromorphic computing towards artificial intelligence at the edge. Indeed, neuro-inspired computing supported by memristive devices can pave the way to a revolution for an energy-efficient and area-efficient information processing that transcends von Neumann's computing. This goal can be achieved by developing computational substrates and engines able to mimicking the adaptation, interconnectivity, noise tolerance and energy efficiency of the human brain. Among the proposed memristive technologies, oxide-based resistance switching memory devices (RRAM) are based on redox reactions and electrochemical phenomena in oxides and are very promising because of low power consumption, fast switching times, scalability down to nm scale and CMOS compatibility. Therefore, they can be used as new hardware building blocks emulating electronic synapses in spiking neural networks (SNN) for real time and low power computation systems. In our work, we focus on the switching dynamics of HfO<sub>2</sub>-based RRAMs and on their implementation as electronic synapses in spiking neural networks (SNN). The conductance of the RRAM devices can be tuned either in a digital or in an analog fashion by using proper programming algorithms and by engineering the material stack. The device dynamics is used to emulate the biological potentiation (conductance increase) and depression (conductance decrease) processes, over several cycles. Moreover, the conductance value update can be achieved by a spike timing and rate dependent plasticity mechanism, which is demonstrated at hardware level, and that is exploited as learning rule in a SNN. System level simulation of SNN are implemented by using experimental RRAM characteristics for the synaptic nodes and neural equations derived from hardware CMOS implementation. The effect of device switching dynamics (linear and non-linear) and synaptic resolution on the SNN performances is discussed.

SESSION F.NM07.02: Novel Algorithm and Device for Neuromorphic Computing  
On Demand Abstracts Available for Viewing Starting Saturday Morning, November 21, 2020  
F-NM07

**5:00 AM F.NM07.02.02**

**A Statistical Analysis of Cu/SiO<sub>2</sub>/W Devices** Florian Maudet<sup>1</sup>, Veeresh Deshpande<sup>1</sup> and Catherine Dubourdieu<sup>1,2</sup>; <sup>1</sup>Helmholtz-Zentrum Berlin für Materialien und Energie, Germany; <sup>2</sup>Freie Universität Berlin, Germany

Resistance switching memories are promising candidates for low power consumption non-volatile memory applications owing to their dimensional scalability and fast switching speed. Furthermore, the possibility to obtain multiple stable states in such systems is of importance for applications in neuromorphic computing. Among the proposed systems, Cu/SiO<sub>2</sub> based memory devices have demonstrated very promising performances, including quantized conductance with a switching voltage as low as 250 mV and allow easy integration with CMOS technology [1]–[5]. It is known that in such systems the different states originate from the formation of a Cu filament in the SiO<sub>2</sub> solid electrolyte [4]. This offers opportunity to use the different quantum states that occur during the filament growth as different memory states. However, because of its

filamentary nature, the devices are very sensitive to local inhomogeneities like defects in the SiO<sub>2</sub> dielectric or interface roughness. As a result, the set/reset voltage can have significant device-to-device variations and the poor repeatability of the different states limits the advantage of such devices for potential applications. Additionally, the retention and endurance of these memories are also a limiting factor and needs to be improved. In order to quantify and understand the origin of the distribution of these characteristics, we present a broad statistical analysis of the current-voltage behavior of Cu/SiO<sub>2</sub>/W devices, as such data are missing in the literature. Several batches of samples were prepared, with several dies on each samples and tens of devices on each die. The influence of different voltage sweep rates on the set and reset voltages is investigated. Furthermore, the distribution of the quantum states occurring at different current is also studied by means of voltage-current measurements. We evidence half- and quarter G<sub>0</sub> conductance states. We will discuss the identification of key parameters that can be optimized to reduce device-to-device and sample-to-sample variability.

- [1] M. Wang *et al.*, “A novel CuSiO resistive memory in logic technology with excellent data retention and resistance distribution for embedded applications,” *Dig. Tech. Pap. - Symp. VLSI Technol.*, pp. 89–90, 2010.
- [2] S. P. Thermadam, S. K. Bhagat, T. L. Alford, Y. Sakaguchi, M. N. Kozicki, and M. Mitkova, “Influence of Cu diffusion conditions on the switching of Cu-SiO<sub>2</sub>-based resistive memory devices,” *Thin Solid Films*, vol. 518, no. 12, pp. 3293–3298, 2010.
- [3] S. Tappertzhofen, S. Menzel, I. Valov, and R. Waser, “Redox processes in silicon dioxide thin films using copper microelectrodes,” *Appl. Phys. Lett.*, vol. 99, no. 20, pp. 1–4, 2011.
- [4] S. R. Nandakumar, M. Minvielle, S. Nagar, C. Dubourdieu, and B. Rajendran, “A 250 mV Cu/SiO<sub>2</sub>/W Memristor with Half-Integer Quantum Conductance States,” *Nano Lett.*, vol. 16, no. 3, pp. 1602–1608, Mar. 2016.
- [5] A. Mehonic *et al.*, “Silicon Oxide (SiO<sub>x</sub>): A Promising Material for Resistance Switching?,” *Adv. Mater.*, vol. 30, no. 43, p. 1801187, Oct. 2018.

#### 5:10 AM F.NM07.02.04

**Resistive Switching in V3O5—A Promising Candidate for Neuromorphic Computing** Coline Adda, Min-Han Lee, Pavel Salev, Yoav Kalchheim and Ivan Schuller; University of California, San Diego, United States

Many neural networks are either implemented at the software level or in hardware using CMOS technology. While these have been shown to have unique functionalities, they are not easily scalable to large systems due to energetic considerations. Therefore, it is desirable to develop more energy-efficient solutions by implementing them directly in the hardware using the unique properties of quantum materials. In this fashion, neuronal and synaptic properties maybe implemented to emulate the behavior of biological systems. Recently, it has been shown that the volatile resistive switching in Mott Insulators could be used to implement Leaky, Integrate and Fire (LIF) neuron (“neuristor”) models although scaling of these systems maybe an issue. Very recent studies have shown that combining two physical phenomena may provide the basis for a scalable LIF neuristor. These were based on VO<sub>2</sub> and V<sub>2</sub>O<sub>3</sub>. In this work, we have synthesized and characterized another vanadium oxide, V<sub>3</sub>O<sub>5</sub>, which provides a higher transition temperature alternative. Its electrical properties were studied as a function of temperature, between 300 K and 450 K, across the metal-insulator transition. We show that V<sub>3</sub>O<sub>5</sub> presents the required characteristics as a potential hardware based thermal neuron, and therefore is a promising candidate for neuromorphic computing. Acknowledgements: This work was supported as part of the Quantum Materials for Energy Efficient Neuromorphic Computing (Q-MEEN-C) Energy Frontier Research Center (EFRC), funded by the U.S. Department of Energy, Office of Science, Basic Energy Sciences under Award # DE-SC0019273.

#### 5:20 AM F.NM07.02.05

**Scaled VO<sub>2</sub> Oscillators for Neural Network Applications** Elisabetta Corti<sup>1</sup>, Abhishek Khanna<sup>1,2</sup>, Fabian Konemman<sup>1</sup>, Kham Niang<sup>3</sup>, John Robertson<sup>3</sup>, Bernd Gotsmann<sup>1</sup> and Siegfried Karg<sup>1</sup>; <sup>1</sup>IBM Research, Switzerland; <sup>2</sup>University of Notre Dame, United States; <sup>3</sup>University of Cambridge, United Kingdom

Oscillatory Neural Networks are a novel, promising concept as hardware accelerator for neuromorphic computing. Systems of coupled oscillators present associative memory capabilities that can be used to implement tasks such as image recognition [1]. We fabricated compact electronic relaxation oscillators using the phase change properties of VO<sub>2</sub>, which undergoes a temperature driven metal-to-insulator Mott transition. We studied and developed fabrication techniques for the VO<sub>2</sub> coupled oscillators on a Si platform, to retain compatibility with CMOS process. VO<sub>2</sub> films were deposited with Atomic Layer Deposition on a SiO<sub>2</sub>/Si substrate. The as-deposited amorphous VO<sub>2</sub> films crystallize during a post-annealing treatment under oxygen flow at a temperature of 450° for 20 minutes. Typically, polycrystalline films with an average grain size between 80 and 50 nm [2] form on the SiO<sub>2</sub> surface. The annealed films show a phase transition at 340 K with a resistivity change of 2 to 3 orders of magnitude and a hysteresis width of about 10 K. The polycrystalline film was patterned with E-beam lithography and ICP etching to define scaled VO<sub>2</sub> oscillator structures, with dimensions between 200 and 500 nm. The oscillators are tested in their switching characteristics, and the variability impact on their coupling dynamics is addressed. In

particular, we investigated the phase transition of the polycrystalline devices using electrical characterization and Scanning Thermal Probe Microscopy (SThM) [3] on a single grain level. The temperature maps obtained with the SThM provide nanometer resolution and allow to observe the thermal signature of single grain switching in the scaled oscillator devices. Hence, the current path can be visualized in the insulating and metallic phases of the VO<sub>2</sub> device. The microscopic phase-change properties could be correlated with the characteristic waveforms of the oscillating pattern in a coupled oscillator system. In addition, a milli-second flash-anneal technique was tested and optimized to control the crystallization process. The average grain size could be reduced from 55 nm to 20 nm, resulting in more uniform electrical device characteristics and allowing further scaling of the VO<sub>2</sub> oscillators. The devices were tested in vacuum and coupled through external electrical components. A network of coupled oscillators locks in frequency and establishes programmable phase relations depending on the strength of the coupling [4,5]. We demonstrate the capability of the oscillator network coupled with an array of tunable resistors to perform image recognition. Experimental results of a three-coupled oscillator system and simulations on larger networks are shown illustrating the associative memory capabilities of the oscillating neural network. This work is supported by the HORIZON2020 PHASE-CHANGE SWITCH Project (Grant No. 737109). [1] F. Hoppensteadt and E. Izhikevich, *Phys. Rev. Lett.*, vol. 82, 2983-2986, 1999. [2] A. P. Peter et al, *Adv. Funct. Mater.*, 25: 679-686, 2015 [3] F. Menges et al., *Rev. Sci. Instr.*, vol.87, no. 7, pp. 074902, 2016 [4] N. Shukla et al., *J. Appl. Phys.*, vol. 117, no. 5, 2015. [5] E. Corti et al. 2018 IEEE International Conference on Rebooting Computing (ICRC), 2018, pp. 1-7. doi: 10.1109/ICRC.2018.8638626

### 5:30 AM F.NM07.02.06

#### **Tuning Mixed Small Polaron-Ionic Conductors for Multiple Resistance State Neuromorphic Device**

**Implementation** Dmitri Kalaev, Alon Vardi and Harry Tuller; Massachusetts Institute of Technology, United States

Natural Intelligence (NI) and Artificial Intelligence (AI) differ in their corresponding analog and digital implementations. One of the consequences of that distinction is the ability of NI to perform logic and memory operations at the local level, without spatially and functionally separating NI computing resources. This functional plasticity of basic units of NI, e.g. nerve cells, is attributed to explain NI's superior energy and time efficacy in task solving, in particular image and speech recognition/interpretation. Previous attempts to mimic NI analog functionality in digital hardware fall short in terms of dimensional scaling and power requirements. The proposed solution is to develop basic computational units that are better suited for NI tasks, e.g. analog. The main requirements for such devices are scalability down to a few nanometers and their ability to process and store data using minimal power consumption. One of the leading candidates for the realization of these goals is the 'memristive device'. In these two-terminal devices, the resistivity is a temporal function of an applied electrical field. Due to their inherent plasticity and scalability, memristive devices are envisioned to provide long-term solutions for hardware implementation of neuromorphic algorithms and energy efficient Deep Neural Networks (DNNs). We present simulation and experimental results for a possible implementation of devices with memristive characteristics. The device functionality is based on a non-stoichiometric oxide thin film, distinctively characterized by coupled ionic and electronic conductivity i.e. a mixed-ionic-electronic-conductor (MIEC). The modeling of the memristive device, in crossbar configuration, is based on the previous theoretical and experimental research on the thermodynamics and transport of oxygen vacancies in nonstoichiometric oxides<sup>1-3</sup> in conjunction with well-developed models of voltage pulse induced self-heating, similar to that used in phase change memories. The praseodymium doped cerium dioxide, Pr<sub>x</sub>Ce<sub>1-x</sub>O<sub>2-δ</sub>, was chosen as a test memristive material that is electronically conductive via small polarons and ionically conductive via oxygen vacancies with thermal activation energies of 0.4 eV and 0.8 eV, respectively.<sup>4</sup> The conductivities, in the latter, can be tuned by changing the praseodymium doping, *x*, and the oxygen deficiency, *δ*, levels. The device modelling shows that in order to achieve nano-second 'write' times and sufficient non-volatility of the 'read' resistance states, both electronic conduction by small polarons and high thermal activation energy of ionic transport, are essential. Finally, a new method for characterization of the ionic transport in MIECs over wide temperature limits, relevant to the memristive device operation temperature (from room temperature up to several hundred centigrade) and structure (crossbar device), will be presented.<sup>4</sup>

[1] S. R. Bishop, T. S. Stefanik, H. L. Tuller, *Phys. Chem. Chem. Phys.*, **2011**, 13, 10165.

[2] D. Kalaev, A. Rothschild, and I. Riess, *RSC Adv.*, **2017**, 7, 38059.

[3] D. Kalaev, H. L. Tuller, and I. Riess, *Solid State Ionics*, **2018**, 319, 291.

[4] D. Kalaev, T. Defferriere, C. Nicollet, T. Kadosh and H. L. Tuller, *Adv. Funct. Mater.*, **2019** (accepted).

### 5:40 AM F.NM07.02.07

#### **Kinetics of Electric Field-Driven Proton Diffusion and Corresponding Metal-Insulator Phase Transition on**

**NdNiO<sub>3</sub> Thin Film** Umar Sidik, Azusa Hattori and Hidekazu Tanaka; Institute of Scientific and Industrial Research, Osaka University, Japan

Resistive state change exploiting abrupt Mott phase transition in strongly correlated RNiO<sub>3</sub> (*R* = rare earth elements) has the



potential to enable high speed and densely scaled non-volatile memories for emerging neuromorphic computing applications [1]. While the metal-insulator phase transition can be triggered by electrostatic or thermal excitation, ion doping via chemical reactions as an emerging field can completely reconstruct the electronic band structures by introducing extremely high carrier density resulting in giant resistivity modulation. In recent years, the vast resistivity modulation in the  $RNiO_3$  family has been successfully demonstrated through this chemical route. For example, proton-doped  $SmNiO_3$  (SNO) thin film, where protons are dissociated from hydrogen molecules by utilizing Pt catalytic effect and then doped into the thin film, can lead to an  $\sim 10^8$  of colossal and reversible resistivity modulation at 300 K [2]. The colossal resistivity modulation is considered to be governed by proton motion in SNO, such as diffusion in the thin film. At the same time, the kinetics of such external control of proton diffusion, namely electric field, has not been clearly revealed. A comprehension of this matter is of relevance to the use of proton-doped correlated  $RNiO_3$  materials in emerging memory and neuromorphic computing pulls.

In this work, we prepared  $NdNiO_3$  (NNO) thin film resistor with different electrode materials (Pt and Au/Ti) and observed the effect of electric field-assisted hydrogenation. Because the hydrogen dissociates on the Pt but not on the Au/Ti electrode, by using this two-terminal resistor configuration, we were able to reveal that the resistivity modulation in NNO film during hydrogenation is associated with the proton diffusion controlled by the temperature ( $T$ ) and polarity-dependent electric field ( $V = \pm V$ ). To quantitatively investigate the correlation among them, simulations based on diffusion in semi-infinite solid were carried out for fitting of time-dependent diffusion coefficient ( $D_i$ ). The estimated  $D_i$  were plotted against  $T^{-1}$  and are in satisfactory agreement with the Arrhenius function of temperature. From this plot, we acquired the activation energy of proton diffusion under positive bias  $+V$  ( $E_{a(+)} = 0.55$  eV) and under negative bias  $-V$  ( $E_{a(-)} = 0.83$  eV) application. Then, a kinetic model based on the estimated  $E_{a(+)}$  and  $E_{a(-)}$  was proposed to describe the correlation between resistivity modulation and proton-lateral diffusion along the NNO channel region. Our kinetic model suggests that the polarities of electric field can ease or blockade the proton-lateral diffusion by decreasing or increasing the diffusion energy activation, respectively. From this relation, we extracted the unadulterated activation energy of proton diffusion ( $E_{a(0)}$ ) – which was about 0.69 eV and is slightly larger than that reported of 0.27-0.65 eV for SNO using a first-principles study [3]. The slight margin of that to our result is considered due to the discrepancy between the actual NNO film and the ideal SNO crystal structure. Generally, the value of  $E_{a(0)}$  is important to understand and estimate the significance of external and dynamic control effect, such as electric field in the solid-state proton-gated transistor. In this regard, we finally estimated the efficiency of electric field ( $\eta_{(E)}$ ) as a means to externally and dynamically control the proton-lateral diffusion in  $a$ -axis of NNO film following the established model. The estimated  $\eta_{(E)}$  was 20.38%, which means that despite the generally accepted thermal hopping and concentration gradient effect, electric field can simultaneously be a driving force to diffuse the positively charged proton in NNO film - with a contribution rate of about  $\sim 20\%$ . Our detail results and analysis will be discussed in the presentation.

[1] D. Ielmini *et al.*, John Wiley & Sons (2015).

[2] J. Shi *et al.*, Nat. Commun. **5.1** (2014) 1-9.

[3] C, Lan *et al.*, J. Comput. Electron. (2020).

SESSION F.NM07.03: Redox Devices for Neuromorphic Computing  
On Demand Abstracts Available for Viewing Starting Saturday Morning, November 21, 2020  
F-NM07

#### 5:00 AM \*F.NM07.03.01

#### **Resistive Switching Based on Small Cations and Oxygen Vacancies for Neuromorphic Computing, Consistent Switching and Proton Synapse** Bilge Yildiz; Massachusetts Institute of Technology, United States

Physical neural networks based on analog resistive switching processor arrays are promising for in-memory computing hardware which can implement machine learning algorithms at higher operating speed and lower energy cost. State-of-the-art analog resistive switches rely on the mechanism of either forming conductive filaments or inducing phase change. These processes suffer from poor repeatability or high energy consumption, respectively. The first part of this talk focuses on reducing the variability of the set/reset voltages using model systems of  $HfO_2$  grown on Nb:SrTiO<sub>3</sub> and Si/TiN substrates. We control the oxide microstructure via growth parameters and thermal treatment, to compare amorphous  $HfO_2$  films with nanocrystalline columnar-grained films with both single (-111) texture and multiple orientations. This work advances our understanding of the mechanisms behind device variability and achieving devices that meet the strict requirements of neuromorphic computing. The second part of the talk focuses on a deterministic charge controlled switching mechanism, that is small cation intercalation into active switching materials. Herein we demonstrate a three-terminal resistive switching device that consists of a channel of active material probed by two terminals (source and drain), a proton reservoir layer as gate terminal, and a proton conducting solid electrolyte separating the two. The device is made of entirely inorganic and CMOS

compatible materials. The electrical conductivity of the active material can be modulated by the precise control of proton intercalation, providing a highly reproducible resistive switching behavior. More than 100 states with an on/off ratio exceeding 200 have been demonstrated by a 5 ms wide gate current pulse train of  $\pm 1$  A. As the smallest cation, the shuffling of protons between the reservoir and the active material requires minimal energy. The energy consumption is only 3.5 fJ/m<sup>2</sup> per state, comparable with state-of-the-art demonstrations. The switching mechanism is probed by a combination of synchrotron X-ray spectroscopy methods. The advantages of this switching mechanism, namely, low energy dissipation and multi-state capability, are demonstrated.

#### 5:15 AM \*F.NM07.03.02

**Redox Transistors for Neuromorphic Computing** Elliot J. Fuller<sup>1</sup>, Scott Keene<sup>2</sup>, Armanas Melianas<sup>2</sup>, Sapan Agarwal<sup>1</sup>, Yiyang Li<sup>1</sup>, Yaakov Tuchman<sup>2</sup>, Christofer Bennet<sup>1</sup>, Matthew Marinella<sup>1</sup>, Alberto Salleo<sup>2</sup> and A. Talin<sup>1</sup>; <sup>1</sup>Sandia National Laboratories, United States; <sup>2</sup>Stanford University, United States

Efficiency bottlenecks inherent to conventional computing in executing neural algorithms have spurred the development of novel devices capable of “in-memory” computing. Commonly known as “memristors”, a variety of device concepts including conducting bridge, vacancy filament, phase change and other types have been proposed as promising elements in artificial neural networks for executing inference and learning algorithms. I will review the recent advances in memristor technology for neuromorphic computing and discuss strategies for addressing the most significant performance challenges, including ‘write’ asymmetry, high read/write currents, and endurance. As an alternative to two-terminal memristors, I will introduce the three-terminal electrochemical memory based on the redox transistor (RT) which uses a gate to tune the redox state of the channel. Charge-compensated redox reactions in the bulk of the transistor enable high-density synaptic weight storage. Decoupling the ‘read’ and ‘write’ operations with a third terminal enable low-energy operation without compromising analog performance. I will discuss the RT operating mechanisms using organic and inorganic materials, approaches for array integration, and prospects for achieving the device density and switching speeds necessary to make electrochemical memory competitive with established digital technology.

#### 5:30 AM \*F.NM07.03.03

**The Voltage-Triggered Transition in Mott Insulators—Mechanisms, Dynamics and Applications** Ivan Schuller; University of California, San Diego, United States

Volatile resistive switching, as observed in Mott materials, is a promising phenomenon which may allow for the implementation of artificial spiking neurons. Despite the technological potential and intense research efforts, many fundamental questions about the nature of this transition remain unsolved. The mechanism driving the insulator-metal (IMT) transition, the nature of the percolation process and the time dynamics still need to be addressed. In this talk, new insights about the resistive switching process in Mott insulators [1,2] will be shown:

**Underlying mechanism.** Two mechanisms may trigger the IMT: Joule heating and E-field destabilization of the Mott insulator. Which of these mechanisms is dominant depends on the material and defect concentration.

**Filamentary percolation.** Direct nanoscale imaging of the domain distribution during resistive switching, reveals the inhomogeneous nature of the percolation process.

**Dynamics.** We observe, for the first time, the switching process with temporal and spatial resolution. The presence of strain leads to slow dynamics both during filament formation and relaxation, with important consequences for the dynamic properties of Mott-based devices.

**Mimicking neuron functionalities.** We demonstrate that both charge build-up and heat transfer can be used to implement basic biological neuronal functions.

These results provide a deeper understanding of the voltage triggered IMT and the technical challenges to solve in order to implement it in a neuromorphic computing scheme.

This work was supported as part of the Quantum Materials for Energy Efficient Neuromorphic Computing (Q-MEEN-C) Energy Frontier Research Center (EFRC), funded by the U.S. Department of Energy, Office of Science, Basic Energy Sciences under Award # DE-SC0019273.

#### References:

Javier del Valle, Pavel Salev, Federico Tesler, Nicolas Vargas, Yoav Kalcheim, Paul Wang, Minhan Lee, Juan Trastoy, George Kassabian, Juan Gabriel Ramirez, Marcelo J. Rozenberg and Ivan K. Schuller, “*Subthreshold firing in Mott nanodevices*”, *Nature* **569**, 388 (2019)

Javier del Valle, Pavel Salev, Yoav Kalcheim and Ivan K. Schuller. “A caloritronics-based Mott neuristor”, *Scientific Reports-Nature* **10**, 4292 (2020)

5:45 AM F.NM07.03.04

**The Microstructure Observation of Brownmillerite Thin Film as the Memristive Device with *In Situ* TEM**

**Research** Hyounghyun Kim<sup>1</sup>, Ventaka R. Nallagatla<sup>2</sup>, Chang Uk Jung<sup>2</sup> and Miyoung Kim<sup>1</sup>; <sup>1</sup>Seoul National University, Korea (the Republic of); <sup>2</sup>Hankuk University of Foreign Studies, Korea (the Republic of)

Redox-based memristive devices are one of the most attractive candidates for future non-volatile memory applications and neuromorphic circuits. Many recent studies reported that resistive switching phenomena in transition metal oxides (TMO) by an external bias are associated with the migration of oxygen ions. Here, we study Sr<sub>2</sub>Fe<sub>2</sub>O<sub>5</sub> brownmillerite structure on the SrRuO<sub>3</sub>/SrTiO<sub>3</sub> substrate and Nb: SrTiO<sub>3</sub> substrate as a bottom electrode in order to understand the role of oxygen migration in resistive switching. Topotactic phase changes between the brownmillerite structure and perovskite structure appear by the oxygen ion migration. Using the fast ion path on the brownmillerite structure, it is possible to impede the random movements of oxygen vacancies. In-situ electric biasing holder was used to investigate the changes in atomic configurations as well as electronic structure caused by the transition of the oxygen vacancies. Electric biases were applied to the TEM samples directly in real time which makes it possible to compare the structure changes in the same TMO regions through SET and RESET cycles. To understand the mechanism of whether the oxygen ions are coming from the top or the bottom electrode in the topotactic phase change, the experiment was carried out with different kinds of bottom electrode. This provides a deeper understanding to control the oxygen ions of the redox-based memristive devices to improve and optimize performances.

5:55 AM F.NM07.03.06

***In Situ* Soft and Hard X-Ray Photoelectron Spectroscopy of Analogue Resistive Switching in HfO<sub>x</sub>-Based Memristive**

**Devices** Finn Zahari<sup>1</sup>, Matthias Kalläne<sup>1,1</sup>, Gitanjali Kolhatkar<sup>1</sup>, Christoph Schlueter<sup>2</sup>, Yury Matveyev<sup>2</sup>, Florian Diekmann<sup>1,1</sup>, Kai Rosnagel<sup>1,2</sup> and Hermann Kohlstedt<sup>1</sup>; <sup>1</sup>Christian-Albrechts-Universität zu Kiel, Germany; <sup>2</sup>Deutsches Elektronen-Synchrotron DESY, Germany

Analogue neuromorphic systems are attracting considerable attention for their potential in novel bio-inspired computing architectures. For this purpose, circuits presenting advantageous features such as low power dissipation and cognitive capabilities need to be developed. Double-barrier memristive devices (DBMDs) with the layer sequence Nb/AlO<sub>y</sub>/HfO<sub>x</sub>/Au are promising candidates for such applications. These devices can, e.g., be exploited to emulate the plastic behaviour of biological synapses in analogue electronic circuits. Their resistance can be varied by applying suitable voltage bias to the device electrodes, an effect known as resistive switching. While kinetic Monte Carlo simulations indicate that the drift of charged defects leads to a modulation of the Schottky barrier height and, hence, to resistive switching, experimental verification has been missing so far. Clearly, a deeper understanding of the resistive switching mechanism could pave the way towards tailoring of application specific devices. Here, we show that resistive switching in DBMDs is due to changes in the chemical composition of the HfO<sub>x</sub> layer. This is demonstrated using soft and hard x-ray photoelectron spectroscopy at photon energies of 1550 eV and 7000 eV, respectively. Corresponding experiments were performed at beamlines P04 and P22 of PETRA III (DESY, Hamburg, Germany). Using soft x-rays, Hf 4f core-level emissions from the buried HfO<sub>x</sub> layer were measured *in situ* for two different resistance states. Hard x-rays, on the other hand, were used to probe resistance state-dependent changes in the emissions from the buried metal oxides (Hf 3d<sub>5/2</sub>, Al 1s) under varying emission angle (15°, 41.4°, and 60°). Spectral shifts between bulk emissions and emissions from Au/HfO<sub>x</sub> and HfO<sub>x</sub>/AlO<sub>y</sub> interfaces were observed for the different resistance states and were analysed in terms of varying chemical composition and defect concentration in the device. The results suggest that the applied electric field induces oxygen vacancy motion in the HfO<sub>x</sub> layer, resulting in local oxygen concentration changes and a modification of the Schottky barrier height at the Au/HfO<sub>x</sub> interface. In addition, the AlO<sub>y</sub> composition is revealed to vary in the bulk, whereas the AlO<sub>y</sub> composition at the HfO<sub>x</sub>/AlO<sub>y</sub> interface appears not to be affected by the resistive switching. The experimental results therefore provide evidence that oxygen vacancy motion within the HfO<sub>x</sub> layer is directly related to the resistive switching in DBMDs. Engineering of the oxygen content in the HfO<sub>x</sub> layer is foreseen to enable a tailored device response.

6:05 AM F.NM07.03.07

**Electrochemical Redox Transistors as Analogue Memory in the Electronic and Optical Domains** Yiyang Li<sup>1</sup>, Jorik Van

de Groep<sup>2</sup>, Elliot J. Fuller<sup>1</sup>, Shiva Asapu<sup>3</sup>, Tomochika Kurita<sup>1</sup>, Sapan Agarwal<sup>1</sup>, J. Joshua Yang<sup>4</sup>, Mark L. Brongersma<sup>2</sup> and A. Talin<sup>1</sup>; <sup>1</sup>Sandia National Laboratories, United States; <sup>2</sup>Stanford University, United States; <sup>3</sup>University of Massachusetts Amherst, United States; <sup>4</sup>University of Southern California, United States

Neuromorphic in-memory computing can significantly decrease the energy consumption of important algorithms such as inference and backpropagation by eliminating the need to shuttle information from memory to processor. The key challenge is finding materials and devices that not only contain a large number of analogue non-volatile states but also have the ability to reliably switch between these states. We show how redox transistors, operating on the basis of electrochemical ion

insertion, can be used to dynamically tune the concentration of dopants in transition metal oxides. Such dynamic dopants are able to tune the electronic and optical properties of materials in a linear and analogue fashion and can be used to emulate synaptic weights in neural networks. We study the effect of lithium insertion into TiO<sub>2</sub> and WO<sub>3</sub>. In both cases, lithium acts as an n-type donor that adds an electron which localizes on the transition metal. This extra dopant changes the electronic and optical properties of the transition metal host. In the case of TiO<sub>2</sub>, we harness changes in electronic properties to create a low-voltage synaptic transistor based on electrochemical redox. This synaptic transistor has over 200 distinguishable analogue non-volatile states based on the lithium concentration; these were used to emulate the synaptic weights in a neural network. More importantly, it is possible to switch between neighboring states in a linear and symmetric fashion with low current and voltages. When implemented into a crossbar, simulations show that this allows for high training and classification accuracy, and significantly lower energy consumption than a digital processor. We also explore the case of lithium insertion into WO<sub>3</sub>. Here, we utilize changes in the optical refractive index that arise during lithium insertion, which alters the bandgap of WO<sub>3</sub>. These changes in bandgap combined with a resonant plasmonic structure enable a device with tunable, analogue optical response. Such system can be utilized for computing in the optical or the hybrid electronic-optical domains. References: Y. Li et al. "Dynamic tuning of gap plasmon resonances using a solid-state electrochromic device." *Nano Lett.* DOI: 10.1021/acs.nanolett.9b03143 Y. Li et al. "Low-voltage, CMOS free synaptic memory based on LiXTiO<sub>2</sub> redox transistors" *ACS Appl. Mater. Interfaces*, DOI: 10.1021/acsami.9b14338

#### 6:15 AM F.NM07.03.09

**Impedance Spectroscopy on Hafnium Oxide Based Memristive Devices** Richard Marquardt<sup>1</sup>, Jürgen Carstensen<sup>1</sup>, George Popkurov<sup>2,1</sup>, Finn Zahari<sup>1</sup>, Hermann Kohlstedt<sup>1</sup> and Martin Ziegler<sup>3</sup>; <sup>1</sup>Kiel University, Germany; <sup>2</sup>Bulgarian Academy of Science, Bulgaria; <sup>3</sup>Ilmenau University of Technology, Germany

Memristive devices for neuromorphic computing schemes for non-volatile memories are getting a rapidly increased amount of attention in the last couple of years. However, the requirements for the devices are sometimes very different for the different fields of applications. In neuromorphic electronics, memristive devices characterized by gradual resistance switch or multi-level resistance states are required, where bi-layer oxide systems have emerged as promising candidates for that field. An example for such a device structure is the double barrier Nb/Al/Al<sub>2</sub>O<sub>3</sub>/HfO<sub>x</sub>/Au memristive device, which possess a filamentary-free, homogenous interfacial resistive switching mechanism. The double layer device has a Al<sub>2</sub>O<sub>3</sub> tunnel barrier of 1.2 nm and an ultra-thin active HfO<sub>x</sub> layer of 3.5 nm. The key mechanism is due to mobile oxygen ions confined within the 3.5 nm thin HfO<sub>x</sub> layer which alter the Schottky barrier of the top HfO<sub>x</sub>/Au interface. To gain a deeper insight into the switching mechanism, impedance spectroscopy was applied to correlate the inner electronic and ionic processes with the observed *I-V* characteristics. In detail, potentiodynamic impedance spectroscopy (PDIS) and time resolved impedance spectroscopy (TRIS) were used in the course of this investigation. Evidence of ion motions at 1.8 V directly related to changes in Schottky barrier resistance has been found as the active mechanism. The results of the impedance analysis were translated into a more general model for memristive devices based on homogeneous ionic motion to map the physical processes during the switching of the memristive device.

SESSION F.NM07.04: Neuromorphic Device—Ferroelectric  
On Demand Abstracts Available for Viewing Starting Saturday Morning, November 21, 2020  
F-NM07

#### 5:00 AM \*F.NM07.04.01

**Ferroelectric Materials for Neuromorphic Device Applications** Jang-Sik Lee; Pohang University of Science and Technology, Korea (the Republic of)

Ferroelectric materials have spontaneous polarization states that can be maintained even without an external electric field. Delicate control of polarization is possible because domains in ferroelectric materials can be controlled by an applied electric field. Each polarization state of the ferroelectric layer can be confirmed by changes in channel conductance; to exploit this characteristic, ferroelectric materials have been evaluated as the dielectric layer in transistors. The conductance of channel material in ferroelectric transistor can be gradually controlled by the polarization of ferroelectric materials. These characteristics can be the solution to solve some problems in current synapse devices, such as a small on/off ratio, non-linear weight updates, and variations in electrical properties. Neuromorphic computing has attracted much attention due to its power-efficient data processing. To realize efficient neuromorphic hardware systems, the development of reliable and robust synaptic devices is essential. However, the limited performance of the synaptic devices remains as a challenge for realization

of neuromorphic hardware systems. Analog memory characteristics has been demonstrated in the ferroelectric thin-film transistor (FeTFT) based on oxide semiconductor and ferroelectric hafnium oxide layer. The conductance of the oxide semiconductor channel is modulated by controlling the polarization of the ferroelectric hafnium oxide layer. Conductance modulation characteristics of FeTFT were used to demonstrate potentiation and depression characteristics. The desired synaptic device characteristics, such as high linear weight update, small variation, and multiple states were achieved in FeTFTs. In addition, the possibility of FeTFT as a synaptic device in neural network was evaluated by artificial neural network simulation. This work can offer a possibility for FeTFT as a synaptic device to be used in neuromorphic hardware systems.

**5:15 AM \*F.NM07.04.02**

**Emerging Low-Dimensional Materials for Mid-Infrared Sensing and Detection** Han Wang; University of Southern California, United States

Emerging low dimensional materials, including both two-dimensional and quasi-one-dimensional materials, provide new optical and electronic properties attractive for developing novel detection and sensing functionalities in the mid-infrared wavelength, including dynamic bandgap tuning covering a broad spectral range in mid-IR, light polarization sensitivity and the ease for electronics integration. Many of these new features are available in the existing mid-IR devices based on traditional semiconductor materials. In this talk, the recent progress in our study of low-dimensional material based mid-IR detector and sensors will be discussed, focusing on layered materials black phosphorus, tellurene and quasi-one-dimensional material BaTiS<sub>3</sub>. The common and distinct characteristics of these emerging materials will be examined relating to their crystal structures, optical properties, and the device functionalities. Key performance metrics including the gain and detectivity will be benchmarked, and the new detection features including the polarization sensitivity are studied. I will also provide perspectives about how these new materials may change the future mid-infrared photonics technology.

**5:30 AM \*F.NM07.04.03**

**Memristors and Neuristors in Epitaxy Land—A Deeper Look in the Materials Properties** Beatriz Noheda<sup>1</sup>, Mart Salverda<sup>1</sup>, Yingfen Wei<sup>1</sup>, Pavan Nukala<sup>1</sup> and Sylvia Matzen<sup>2</sup>; <sup>1</sup>University of Groningen, Netherlands; <sup>2</sup>Université Paris-Saclay, France

The search for devices that can emulate the behavior of neurons and synapses, to be used in brain-inspired, in-memory or on-edge computing, is extending among different research fields with an increasing number of materials scientists involved in the quest. However, the number of materials that have been considered as the key elements in devices that are able to produce action potentials and provide tunable conductivity and/or resistive memory, is so far still restricted to the few materials that are compatible with CMOS integration. However, the need to limit the processing to low temperatures, often produces polycrystalline or amorphous materials that diminishes the control of the material's properties, reduce the device endurance and device-to-device reproducibility and obscure the understanding of the physical mechanisms at play. Thus, in order to acquire a better control of the final device, we propose that a detour into the world of epitaxial, single-crystalline materials should not be seen as a waste of resources but rather as a way to find a direct access to the key materials issues and their solution. In addition, the emergent efforts towards epitaxial growth of complex oxides by ALD[1] allows us to dream of a future of epitaxial oxide microelectronics for which we want to be prepared. In this talk, we will show two examples of epitaxial materials that show interesting neuromorphic features that, to our knowledge, have not been reported in other materials: the particular self-oscillating behavior of epitaxial TbMnO<sub>3</sub> [2] as a compact neuristor [3] and the synaptic plasticity of ferroelectric memristors and ferroelectric field-effect transistors (FeFETs) fabricated with epitaxial, rhombohedral, Hf<sub>0.5</sub>Zr<sub>0.5</sub>O<sub>2</sub>[4], a phase that is different from the ferroelectric phase of hafnia originally discovered[5], whose outstanding properties have put these materials in the spotlight.

H. H. Sonsteby et al. *Nature. Comm.* 11, 2872 (2020)

M. Salverda & B. Noheda, <https://arxiv.org/abs/2004.09903> <https://arxiv.org/abs/2004.09903>(under review in *Nat. Comm.*)

M. D. Pickett et al. *Nature Mat.* 12, 114 (2013); J. del Valle, *Scient. Rep.* 10, 4292 (2020)

Y. Wei et al, *Nature Mat.* 17, 1095 (2018); *Phys. Rev. Appl.* 12, 031001(2019); *npj Quan. Mat.* 4, 62 (2019); P. Nukala et al. *ACS Appl. Elect. Mat.* 1, 2585 (2019); [arxiv.org/abs/2005.01809](https://arxiv.org/abs/2005.01809) (to appear in the 50th Golden Anniversary Volume of *Ferroelectrics*, 2020)

T. S. Boescke et al. *Appl. Phys. Lett.* 99, 102903 (2011); S. Mueller, *et al. Adv. Funct. Mater.* 22, 2412 (2012)]

**5:45 AM F.NM07.04.05**

**From Synaptic to Neuronal Functionality Using Ferroelectric Tunnel Junctions** Sayani Majumdar<sup>1,2</sup>; <sup>1</sup>Aalto University, Finland; <sup>2</sup>VTT Technical Research Centre of Finland, Finland

Parallel information processing, energy efficiency and unsupervised learning make the human brain a model computing system for unstructured data handling. Oxide memristors, from filamentary to metal-insulator transition devices have been shown to emulate synaptic and neuronal functionalities in artificial neuromorphic circuits. However, challenges like non-linear conductance update, cycle-to-cycle and device-to-device variability and leakage current related issues in a dense crossbar structure are still not resolved. For neurons, often a circuit with multiple active or passive components are required which can complicate circuit designs in a large-scale neural network. In our earlier work, we reported solution-processable ferroelectric tunnel junctions (FTJs) with P(VDF-TrFE) copolymer barriers on semiconducting bottom electrode can show analog memristive behavior with a broad range of accessible conductance states and low energy dissipation of 100 fJ for the onset of depression and 1 pJ for the onset of potentiation by resetting small tunneling currents on nanosecond timescales. Key synaptic functions like programmable synaptic weight, long and short-term potentiation and depression, paired-pulse facilitation and depression, and Hebbian and anti-Hebbian learning through spike shape and timing-dependent plasticity are demonstrated. 1 In the current work, we demonstrate that by manipulating the carrier concentration of the semiconducting bottom electrode in FTJs, it is possible to control the dynamics of ferroelectric domain rotations in a way so that from synaptic devices they can act similar to neuronal devices. 2 These results offer a promising outlook for the FTJ memristors on semiconducting bottom electrodes as both synapse and neuron devices in artificial neural networks by controlling carrier doping concentrations only. References [1] S. Majumdar, H. Tan, Q. Qin and S. van Dijken. Adv. Electron. Mater. 5, 1800795 (2019). [2] S. Majumdar, H. Tan, I. Pande and S. van Dijken. APL Mater. 7, 091114 (2019).

**5:55 AM F.NM07.04.06**

**The Microstructure Observation of Brownmillerite Thin Film as the Memristive Device with *In Situ* TEM**

**Research** Hyoung Gyun Kim<sup>1</sup>, Ventaka R. Nallagatla<sup>2</sup>, Chang Uk Jung<sup>2</sup> and Miyoung Kim<sup>1</sup>; <sup>1</sup>Seoul National University, Korea (the Republic of); <sup>2</sup>Hankuk University of Foreign Studies, Korea (the Republic of)

Redox-based memristive devices are one of the most attractive candidates for future non-volatile memory applications and neuromorphic circuits. Many recent studies reported that resistive switching phenomena in transition metal oxides (TMO) by an external bias are associated with the migration of oxygen ions. Here, we study Sr<sub>2</sub>Fe<sub>2</sub>O<sub>5</sub> brownmillerite structure on the SrRuO<sub>3</sub>/SrTiO<sub>3</sub> substrate and Nb: SrTiO<sub>3</sub> substrate as a bottom electrode in order to understand the role of oxygen migration in resistive switching. Topotactic phase changes between the brownmillerite structure and perovskite structure appear by the oxygen ion migration. Using the fast ion path on the brownmillerite structure, it is possible to impede the random movements of oxygen vacancies. In-situ electric biasing holder was used to investigate the changes in atomic configurations as well as electronic structure caused by the transition of the oxygen vacancies. Electric biases were applied to the TEM samples directly in real time which makes it possible to compare the structure changes in the same TMO regions through SET and RESET cycles. To understand the mechanism of whether the oxygen ions are coming from the top or the bottom electrode in the topotactic phase change, the experiment was carried out with different kinds of bottom electrode. This provides a deeper understanding to control the oxygen ions of the redox-based memristive devices to improve and optimize performances.

SESSION F.NM07.05/F.SM05.02: Joint Session: Novel Materials for Neuromorphic Devices  
On Demand Abstracts Available for Viewing Starting Saturday Morning, November 21, 2020  
F-NM07

**5:00 AM \*F.NM07.05/F.SM05.02**

**One-Shot Regression and Classification with Crosspoint Memory Arrays** Daniele Ielmini<sup>1</sup>, Giacomo Pedretti<sup>1</sup>, Piergiulio Mannocci<sup>1</sup> and Zhong Sun<sup>2</sup>; <sup>1</sup>Politecnico di Milano, Italy; <sup>2</sup>Peking University, China

As artificial intelligence (AI) becomes a popular feature in industry, social networks, smart homes and transportation, there is an increasing need for AI accelerators in edge computing, to solve for excessive traffic to the cloud and ensure privacy and security of the processed data. In this frame, in-memory computing (IMC) has risen as low-power processing approach for data intensive problems. Matrix-vector multiplication (MVM) can be accelerated in crosspoint arrays by leveraging the Kirchhoff's law for current summation and the Ohm's law for voltage-conductance multiplication, as well as taking advantage of the parallelism in the memory array. Connecting the crosspoint array in a feedback loop also allows to accelerate inverse operations, i.e., one-step solutions of linear systems such as  $Ax = b$  where the  $N \times N$  matrix  $A$  is stored as conductance values in the array, vector  $b$  represents applied currents and solution vector  $x$  is the output voltage.  $O(1)$  complexity of eigenvector extraction and  $O(N)$  complexity of matrix inversion have been demonstrated, which outperforms

classical digital computing and even quantum computing.

In this work, we show that the same circuit concept can serve to accelerate regression and classification problems, which are two key problems of AI. Linear regression is solved within two coupled crosspoint arrays by computing the pseudo-inverse matrix in one step. M-dimensional linear regression allows to make predictions based on an existing data set or temporal sequence, thus enabling fast, energy efficient machine learning on the edge. The same circuit enables logistic regression, hence one-step classification within the crosspoint array, which allows for one-shot training of multiple layer perceptrons (MLP). The implications of these novel concepts for AI acceleration and the best technological implementation for data-intensive computing will be discussed.

#### **5:15 AM \*F.NM07.05/F.SM05.03**

**Progress in Analog DNN Hardware Accelerators Using Phase Change Materials** [Charles Mackin](#), Hsinyu Tsai, Prithish Narayanan, Stefano Ambrogio, Katie Spoon, Andrea Fasoli, Alexander Friz, An Chen and Geoffrey W. Burr; IBM, United States

Neuromorphic computing with analog memory can accelerate deep neural networks (DNNs) by enabling multiply-accumulate (MAC) operations to occur within memory. Analog memory, however, presents a number of device-level challenges having macro-implications on the achievable accuracy and reliability of these artificial neural networks. This talk focuses on the adverse effects of conductance drift in phase-change memory (PCM) on network reliability. It is shown that conductance drift can be effectively compensated in a variety of networks by applying a 'slope correction' technique to the squashing functions to maintain accuracy/reliability for a period of ~1 year. In addition to conductance drift, PCM poses considerable variability challenges, which impact the accuracy of the initial weights. This talk summarizes recent advances in optimizing initial weight programming, and provides evidence suggesting that the combination of 'slope correction' and programming optimization techniques may allow DNN acceleration using analog memory while maintaining software-equivalent accuracy with reasonable reliability.

#### **5:30 AM \*F.NM07.05/F.SM05.04**

**Atomic Memory and Computing Applications** [Deji Akinwande](#)<sup>1</sup> and Mario Lanza<sup>2</sup>; <sup>1</sup>The University of Texas at Austin, United States; <sup>2</sup>Soochow University, China

This talk will present our latest research adventures on 2D atomic nanomaterials towards greater scientific understanding and computing applications. In particular, the talk will highlight our work on non-volatile memory (atomristors) that can be employed in various applications including information storage, brain-inspired computing, and zero-power RF switches. Non-volatile memory device based on atomically-thin materials is an application of defects, and is a rapidly advancing field with rich physics that can be attributed to metal ion binding to native defects. The promising 2D materials for neuromorphic computing include MoS<sub>2</sub> and hBN. In particular, hBN memory devices feature very low switching energy, a relatively wide range of stable programmable resistance states, and good endurance and retention. Recent progress has also demonstrated wafer-scale integration of 2D memory devices with a prospect to leverage silicon electronics for fully integrated systems.

#### **5:45 AM F.NM07.05/F.SM05.05**

**High-Throughput Computational Screening to Identify Novel Proton Conducting Electrolytes for All-Solid-State Neuromorphic Devices** [Konstantin Klyukin](#), Pjotr Zguns, Ju Li and Bilge Yildiz; Massachusetts Institute of Technology, United States

Artificial electrochemical synapses based on the charge-driven proton intercalation demonstrate much promise toward brain-inspired neural computing [1]. Proton transport plays a critical role in these devices determining switching speed and reliability. Despite great attention and intensive experimental investigations, even the cutting-edge proton conductors still suffer from sluggish ion transport kinetics at low temperatures or are not compatible with current CMOS fabrication processes. Therefore, there is an urgent need for fast solid-state proton conductors operating below 100 °C, much required for rapidly growing proton-based neuromorphic computing applications.

In this work, we consider a large class of solid-state materials having hydrogen as a part of their nominal structure such as solid acids and inorganic hydrates. By considering different combinations of common acids and metal ions, it is possible to synthesize thousands of materials with widely varying structures and physicochemical properties, and yet many of them remain relatively unexplored for the ability to conduct protons. We performed a high-throughput computational screening of the available materials datasets to identify chemical compositions and structure types that are likely to have high proton mobility. To estimate proton conductivity, we used ab initio molecular dynamics simulations. We further correlated this data with simple structural features and built a classification model to preselect a small set of materials for more detailed

investigations. Based on our simulations, we identified promising materials and suggested effective strategies for improving proton conductivity.

## References

[1] Xiahui Yao, Konstantin Klyukin, Wenjie Lu, Murat Onen, Seungchan Ryu, Dongha Kim, Nicolas Emond, Iradwikanari Waluyo, Adrain Hunt, Jesus A. del Alamo, Ju Li, Bilge Yildiz, “Protonic Solid-State Electrochemical Synapse for Physical Neural Networks”, Nature Communications, in press, 2020.

### 5:55 AM F.NM07.05/F.SM05.06

#### **Metal-Insulator Transition Property for the Nano-Confined Electric Domain in the Strongly Correlated**

**NdNiO<sub>3</sub>** Azusa Hattori, Takashi Yamanaka, Akira Nanba and Hidekazu Tanaka; Osaka University, Japan

Strongly correlated metal oxide (SCMO), such as manganite, nickelate, and so on show first-order metal-insulator phase transition (MIT) with a change in conductivity by several orders magnitude. Since a discovery of the phase separation during MIT process, many researchers have been trying to capture a nanoscale electric domain and investigate its exotic properties. Typical SCMO material, rare earth Ni oxides (ReNiO<sub>3</sub>, Re = Nd, Sm, and Eu) having a perovskite structure, show giant resistance change due to MIT at a wide temperature range of 150 K to 500 K. In this family, bulk neodymium nickelate: NdNiO<sub>3</sub> (NNO) shows 1-2 orders resistance change through MIT at around 200 K [1]. Very recently, the coexistence of insulator and metal domains with a few hundred nm size was observed during the MIT process for NNO system [2]. This phase-separated phenomenon is also observed in typical SCMOs, such as VO<sub>2</sub> and manganite. The overall observed MIT property, i.e., the resistance change for a sample, is considered to be dominated by competing nanoscale electronic phases. A step resistance change due to the electronic phase confinement effect: increase in resistance change rate has been reported in nanoscale samples comparable to domain size [3]. Therefore, it is expected that the nanoscale NNO sample shows a step resistance change due to MIT property of single nanoscale electronic phases. In this study, we fabricated NNO nanowire structures with 50-200 nm widths and measured their transport properties.

The NNO thin films were fabricated on NdGaO<sub>3</sub>(110)( $a_{pc} = 0.3858$  nm), LSAT(100)( $a = 0.3868$  nm), and SrTiO<sub>3</sub>(100)( $a = 0.3858$  nm) substrates by pulsed laser deposition method. NNO nanowires with different wire widths from 50 nm to 500 nm were fabricated by electron beam (EB) lithography and Ar ion milling process. All films and nanowire samples showed the resistance changes corresponding to MIT, but the RT curves shape were quite different. While the thin film sample showed gradual resistance change, the nanowire sample showed some step resistance changes both in cooling and heating processes. This step changes indicate that the nano electronic phases are confined in the NNO nanowire and a single electric domain shows first-order MIT with a single-step change in electrical transport property. For example, we found that the 50 nm width nanowire on SrTiO<sub>3</sub> substrate showed the intermittent step-resistance change, implying the further confine electronic phases to a nanometer space. Interestingly, the nanowires on NdGaO<sub>3</sub>(110) and LSAT(100) substrates showed more prominent step resistance changes than that on SrTiO<sub>3</sub>(100) substrate, which imply the nano-confinement condition were affected by the strain. The  $dR/dT$  vs.  $T$  plot showed that the transition temperature distribution of each electronic phase in the nanowires were different. This is probably because the strains depending on the three different substrate effect where on the Ni-O-Ni angular distribution, which affected the MIT properties of NdNiO<sub>3</sub> nano-electronic phase. In the presentation, we will present the quantitative correlation between nano-spatial size and nano-confinement MIT properties. We will also discuss the revealed the MIT property for a single domain in a NNO nanowire and the strain effect for the nano-confined domains behaviors.

[1] G. Catalan *et al.*, Phys. Rev. B, 62, 7892 (2000), [2] G. Mattoni *et al.*, Nat. Commun., 7, 13141 (2016), [3] A. N. Hattori *et al.*, Nano Lett., 15, 4322 (2015).

### 6:05 AM F.NM07.05/F.SM05.07

#### **Ionic Liquid Regulated Silver Filament Formation in a Solid Polymer Electrolyte for Neuromorphic Applications** Zhongmou Chao, Ke Xu and Susan Fullerton; University of Pittsburgh, United States

Much progress has been made over the past decade using conductive bridge random access memory (CBRAM) to emulate both artificial synapses and artificial neurons for neuromorphic applications. However, the intrinsically stochastic switching process of metal filament formation and dissolution results in unreliable analog synaptic weight updating, while the non-volatile characteristic of CBRAM prevents the leaky integrate-and-fire function—a hallmark characteristic of an artificial neuron. We have previously reported that silver nanofilament growth dynamics in a polymer electrolyte can be regulated by the addition of ionic liquid (IL) by: (1) reducing stochasticity of the filament switching (shifting its formation time distribution from power-law to Gaussian) and (2) creating a competition between the formation of IL electrical double layers (EDL) and silver electrodeposition. The competition enables the tuning of filament growth dynamics from abrupt to gradual, with gradual growth introducing multiple well-defined resistance states—a feature necessary for emulating the



communications between neurons in an artificial neural network. We also observed a linear correspondence ( $R^2 = 0.95$ ) between nanofilament resistance states and program pulses, which is essential to improve learning accuracy in Deep Neural Networks (DNNs). Here, we report on silver filament formation and dissolution in response to presynaptic programming biases and focus on benchmarking the performance against the requirements for artificial synapses. The temporal stability of “abrupt growth” silver filaments is also studied. Lastly, we demonstrate a system integrating both gradual and abrupt silver filaments to implement some key artificial neuron functionalities.

**6:15 AM \*F.NM07.05/F.SM05.08**

**Computing with Memristive and Memcapacitive Devices** J. Joshua Yang; University of Southern California, United States

Memristive devices have become a promising candidate for unconventional computing(1) due to their attractive properties(2, 3). Computing can be implemented on a Resistive Neural Network (ResNN) with memristor synapses and neurons or a Capacitive Neural Network (CapNN) with memcapacitor synapses and neurons. For ResNNs as computing accelerators, we have built a dot-product engine based on a 128 x 64 1T1R crossbar array using traditional non-volatile memristors with 64 stable analog resistance levels(4). Accurate image compression and filtering have been demonstrated with such analog computing accelerator(4). In addition, we have demonstrated efficient and self-adaptive in-situ learning in a two-layer neural networks using such memristive arrays(5), which is expected to significantly improve the speed and energy efficiency of machine learning. A variety of neural networks based on such accelerators have been demonstrated, including reinforcement learning(6), LSTM(7), recurrent CNN(8) memristive networks. For ResNNs beyond accelerator applications, we developed diffusive memristors(9) with diffusion dynamics that is critical for neuromorphic functions. Based on the diffusive memristors, we have further developed artificial synapses(10) and neurons(11) to more faithfully emulate their bio-counterparts. We then integrated these artificial synapses and neurons into a small neural network, with which pattern classification and unsupervised learning have been demonstrated(11). For CapNNs, we have developed pseudo-memcapacitive devices based on the diffusive memristors. Capacitive synapses and neurons enabled by these memcapacitive devices have been developed and used to form a fully integrated CapNN(12), which has shown spiking signal classification and Hebbian-like learning functions. Moreover, the diffusive memristors can be used for cybersecurity(13, 14) and robotics applications(15). The requirements on device properties, and thus the corresponding challenges and solutions, are different for ResNNs and CapNNs, which will be discussed in detail in this talk. J. J. Yang, D. B. Strukov, D. R. Stewart, Memristive devices for computing. *Nature Nanotechnology* 8, 13-24 (2013). S. Pi et al., Memristor crossbar arrays with 6-nm half-pitch and 2-nm critical dimension. *Nature nanotechnology* 14, 35 (2019). Q. Xia, J. J. Yang, Memristive crossbar arrays for brain-inspired computing. *Nature materials* 18, 309 (2019). C. Li et al., Analogue signal and image processing with large memristor crossbars. *Nature Electronics* 1, 52 (2017). C. Li et al., Efficient and self-adaptive in-situ learning in multilayer memristive neural networks. *Nature communications* 9, 2385 (2018). Z. Wang et al., Reinforcement learning with analogue memristor arrays. *Nature Electronics* 2, 115 (2019). C. Li et al., Long short-term memory networks in memristor crossbar arrays. *Nature Machine Intelligence* 1, 49 (2019). Z. Wang et al., In situ training of feed-forward and recurrent convolutional memristor networks. *Nature Machine Intelligence* 1, 434-442 (2019). E. J. Fuller et al., Parallel programming of an ionic floating-gate memory array for scalable neuromorphic computing. *Science* 364, 570-574 (2019). Z. Wang et al., Memristors with diffusive dynamics as synaptic emulators for neuromorphic computing. *Nature Materials* 16, 101-108 (2017). Z. Wang et al., Fully memristive neural networks for pattern classification with unsupervised learning. *Nature Electronics* 1, 137-145 (2018). Z. Wang et al., Capacitive neural network with neuro-transistors. *Nature Communications* 9, 3208 (2018). H. Jiang et al., A Novel True Random Number Generator Based on a Stochastic Diffusive Memristor. *Nature communications* 8, 882 (2017). H. Jiang et al., Provable Key Destruction with Large Memristor Crossbars. *Nature Electronics* 1, 548 (2018). J. H. Yoon et al., An artificial nociceptor based on a diffusive memristor. *Nature Communications* 9, 417 (2018).

SESSION F.NM07.06: Neuromorphic Device—RRAM

On Demand Abstracts Available for Viewing Starting Saturday Morning, November 21, 2020

F-NM07

**5:00 AM \*F.NM07.06.02**

**Digital Memcomputing—From Logic to Dynamics to Topology** Massimiliano Di Ventra; University of California, San Diego, United States

Memcomputing [1, 2] is a novel physics-based approach to computation that employs memory to both process and store information on the same physical location. Its digital version [3, 4] is designed to solve combinatorial optimization problems.

A practical realization of digital memcomputing machines (DMMs) can be accomplished via circuits of non-linear, point-dissipative dynamical systems engineered so that periodic orbits and chaos can be avoided. A given logic problem is first mapped into this type of dynamical system whose point attractors represent the solutions of the original problem. A DMM then finds the solution via a succession of elementary instantons whose role is to eliminate solitonic configurations of logical inconsistency (“logical defects”) from the circuit [5, 6]. I will discuss the Physics behind memcomputing and show many examples of its applicability to various combinatorial optimization problems demonstrating its advantages over traditional approaches [7, 8]. Work supported in part by DARPA, DOE, MemComputing, Inc. (<http://memcpu.com/>), and CMRR.

- [1] M. Di Ventra and Y.V. Pershin, Computing: the Parallel Approach, *Nature Physics* 9, 200 (2013).
- [2] F. L. Traversa and M. Di Ventra, Universal Memcomputing Machines, *IEEE Transactions on Neural Networks and Learning Systems* 26, 2702 (2015).
- [3] M. Di Ventra and F.L. Traversa, Memcomputing: leveraging memory and physics to compute efficiently, *J. Appl. Phys.* 123, 180901 (2018).
- [4] F. L. Traversa and M. Di Ventra, Polynomial-time solution of prime factorization and NP-complete problems with digital memcomputing machines, *Chaos: An Interdisciplinary Journal of Nonlinear Science* 27, 023107 (2017).
- [5] M. Di Ventra, F. L. Traversa and I.V. Ovchinnikov, Topological field theory and computing with instantons, *Annalen der Physik* 529,1700123 (2017).
- [6] M. Di Ventra and I.V. Ovchinnikov, Digital memcomputing: from logic to dynamics to topology, *Annals of Physics* 409, 167935 (2019).
- [7] F. L. Traversa, P. Cicotti, F. Sheldon, and M. Di Ventra, Evidence of an exponential speed-up in the solution of hard optimization problems, *Complexity* 2018, 7982851 (2018).
- [8] F. Sheldon, F.L. Traversa, and M. Di Ventra, Taming a non-convex landscape with dynamical long-range order: memcomputing the Ising spin-glass, *Phys. Rev. E* 100, 053311 (2019).

#### **5:15 AM F.NM07.06.03**

**MoS<sub>2</sub>-Based LIF Neurons for Spiking Neural Networks** Durjoy Dev, Adithi Pandrahally Krishnaprasad Sharada, Mashiyat Sumaiya Shawkat, Yeonwoong Jung and Tania Roy; University of Central Florida, United States

Compared to all other neural networks, Spiking Neural Networks (SNN) mimic the brain most faithfully. Memristors are considered as promising candidates for realizing these SNNs because of their reduced complexity and nanoscale foot-print when compared to conventional complementary metal oxide semiconductor (CMOS) technology [1]. Volatile switching in memristors is used to emulate neurons in SNNs. In this work, we present neurons realized by memristors using chemical vapor deposited (CVD) MoS<sub>2</sub>. The neurons realized by volatile MoS<sub>2</sub> threshold switching memristors (TSM), facilitated by using Ag electrodes, exhibit the characteristics of a leaky integrate and fire (LIF) neuron. The LIF neurons exhibit temporal response modulated by circuit elements and input voltage pulses. The volatile switching is obtained due to the diffusion of Ag<sup>+</sup> ions into Au/MoS<sub>2</sub>/Ag stack. The device shows exceptional characteristics like high ON/OFF ratio of 106, low threshold voltage (~0.2 V), high compliance current (100  $\mu$ A), and a pulsed endurance of 107 switching cycles making it an exceptional candidate for artificial neuron application. The volatile switching characteristics are utilized to implement a LIF neuron. The TSM is integrated with a series resistor and parallel capacitor. The device shows continuous spiking when subjected to input pulses of amplitude of 0.5 V and duration of 5  $\mu$ s. The output spiking frequency of the neuron increases with increasing amplitude and pulse width. The variation in the spiking frequency follows the sigmoid activation function of ANN. The spiking frequency increases with an increase in the input pulse width. The spiking frequency decreases with increasing pulse interval. References: [1] P. Morella et al., *IEEE Custom Integrated Circuits Conference*, 2011.

#### **5:25 AM F.NM07.06.04**

**MoS<sub>2</sub>-Based Electronic Synapses for Unsupervised Learning** Adithi Pandrahally Krishnaprasad Sharada, Durjoy Dev, Mashiyat Sumaiya Shawkat, Yeonwoong Jung and Tania Roy; University of Central Florida, United States

Memristors are considered as promising candidates for realizing synapses for neuromorphic computing because of their reduced complexity and nanoscale foot-print when compared to conventional complementary metal oxide semiconductor (CMOS) technology. Non-volatile switching with multiple conductance states in memristors is employed to emulate synapses. In this work, we present synapses realized by memristors using chemical vapor deposited (CVD) MoS<sub>2</sub>. Graphene is used as electrode for this device. These synapses exhibit linear and symmetric weight update with identical pulses, considered to be the “holy grail” for unsupervised learning. The graphene/MoS<sub>2</sub> (G/M) synaptic device exhibits 4 distinct states in both DC potentiation and depression regimes. Additionally, it exhibits data retention for >10<sup>4</sup> s. For efficient unsupervised learning, the synapses should exhibit linear and symmetric weight update with identical input pulses and a high maximum/minimum conductance ratio (G<sub>max</sub>/G<sub>min</sub>). Resistive random-access memory (RRAM), phase change memory

(PCM) and ferroelectric field effect transistors (FeFET) have been used to emulate a synapse. But these devices exhibit non-linear weight update with identical pulses paired with reduced  $G_{max}/G_{min}$  ratio. Identical input voltage pulses with  $t_{ON}=500\ \mu s$  and amplitude of 6 V (-4 V) are applied to observe potentiation (depression) in the G/M synapse. With 25 input pulses applied for each regime, we obtain linear and symmetric weight update with an ideal symmetry of 0. The non-linearity factor (NLF) is 0 for both potentiation and depression regimes, and  $G_{max}/G_{min}$  is 16.5. These device characteristics are then incorporated in a pseudo-crossbar array of a 2-layer multi perceptron network with the help of the circuit macro model Neurosim1 to obtain online learning accuracy of 84.33 %. We benchmark our G/M synapse with other emerging synapse devices with respect to NLF, asymmetry,  $G_{max}/G_{min}$  and learning accuracy with Neurosim and show that our device is superior to all other emerging synaptic devices in all these categories. 1 P.-Y. Chen, X. Peng, and S. Yu, IEEE Transactions on Computer-Aided Design of Integrated Circuits and Systems 37 (12), 3067 (2018).

### 5:35 AM F.NM07.06.05

**A Stochastic Tantalum Disulfide Charge-Density-Wave Neuronal Oscillator** [Hefei Liu](#)<sup>1</sup>, Tong Wu<sup>2</sup>, Xiaodong Yan<sup>1</sup>, Jiangbin Wu<sup>1</sup>, Jing Guo<sup>2</sup> and Han Wang<sup>1,1</sup>; <sup>1</sup>University of Southern California, United States; <sup>2</sup>University of Florida, United States

Due to the unique physical properties, charge-density-wave (CDW) materials have been vastly investigated in the past half century, including the direct observation of atomic structure, phase transition, transport mechanism, and applications ranging from superconductor to electronic oscillator. As a layered CDW material, the CDW phase transition of 1T-TaS<sub>2</sub> can be incurred by external electric field at room temperature, accompanied by the significant decrease of resistance. The electric-field-driven phase transition makes a room temperature oscillator possible. Furthermore, the quench-and-melt dynamics leads to the random reconfiguration of CDW domains during phase transition, which implies the intrinsic stochasticity of the oscillator. Therefore, here we report a CDW stochastic neuronal oscillator based on 1T-TaS<sub>2</sub> thin film. Two working regimes, the regular and stochastic regimes, were found in this device. In stochastic regime, the CDW neuronal oscillator can generate spike trains with random interspike intervals following exponential, Gaussian and Gamma distribution with tunable parameters, closely matching the spike trains of biological neurons. Owing to the stochasticity, many key features of the Hodgkin-Huxley description of neurons can be realized in this compact two-terminal neuronal oscillator. Statistical analysis was conducted on the spike train generated by the CDW neuronal oscillator. By establishing a generalized linear model to describe the statistical distribution of interspike intervals and to quantify the correlation, we demonstrated that the artificial neuron resembles the neurons in the superior olivary complex of mammalian nervous system, in terms of its interspike interval distribution, the time-correlation of spiking behavior and its response to acoustic stimuli. The CDW oscillator can hence provide a new pathway, utilizing statistical features and pattern change in the interspike interval to transmit information, to the design of neuronal component for more sophisticated spiking neural networks and brain emulation.

### 5:45 AM F.NM07.06.06

**Improvement of Analog Resistive Switching Characteristics in TaOx-Based Synaptic Devices Through Complementary Resistive Switching** [Toshiki Miyatani](#), Yusuke Nishi and Tsunenobu Kimoto; Kyoto University, Japan

Neuromorphic chips which mimic the human brain working with extremely low power consumption of 20 W are intensively studied, because current artificial intelligence systems require enormous power consumption. Resistive switching (RS) cells as synaptic devices play an important role in neuromorphic chips by controlling the cell resistance continuously. However, conventional transition metal oxide-based RS cells often show an abrupt decrease in the cell resistance (set process) [1], which inhibits the continuous control of the cell resistance. In this paper, we report improvement of RS continuity in Ta<sub>2</sub>O<sub>5</sub>-based RS cells by suppressing the abrupt set process. We fabricated Pt/TaOx/Ta<sub>2</sub>O<sub>5</sub>/Pt stack cells on SiO<sub>2</sub>/Si substrates. A Pt layer was deposited by DC sputtering as a bottom electrode (BE). A Ta<sub>2</sub>O<sub>5</sub> layer and an O-deficient TaOx layer were deposited by reactive radio frequency sputtering. Pt top electrodes (TEs) with a diameter of 100  $\mu m$  were subsequently formed. The introduction of the TaOx layer caused diffusion of oxygen vacancies (VOs) from the TaOx layer to the Ta<sub>2</sub>O<sub>5</sub> layer. Consequently, the Ta<sub>2</sub>O<sub>5</sub> layer can be considered to consist of a VO-rich layer and a VO-poor layer for simplicity [2]. We measured electrical characteristics of the cells at room temperature with the TE grounded. We reported that two modes of bipolar RS (BRS), which show hysteresis curves of current-voltage (I-V) characteristics in opposite directions each other, were selectively obtained in a single Pt/TaOx/Ta<sub>2</sub>O<sub>5</sub>/Pt cell by appropriately adjusting a range of the applied voltage after a unique forming process [3]. One mode of BRS exhibits set and reset processes at positive and negative voltage, respectively, that is, RS characteristics in the direction of drawing the figure-eight. The other mode of BRS conversely presents RS characteristics in the counter direction. In this study, the maximum applied voltage after the forming was adjusted between the voltage of 1.0 V for the figure-eight BRS and that of 2.5 V for the counter figure-eight BRS. As a result, we demonstrated complementary RS (CRS) from  $\sim 1.5\ V$  to 1.5 V, in which a set process and a subsequent reset process occur symmetrically in both bias directions as the magnitude of the applied voltage increases. The CRS characteristics have been expected as one of

the ways to solve a sneak path problem. The typical CRS cell consist of anti-serially connected two BRS cells, and its characteristics can be generally interpreted by superposition of the two modes of BRS. However, we found that the stack structure of the VO-rich and VO-poor layers could exhibit stable CRS characteristics. This suggests that each of the two modes of BRS is dominated by RS phenomena which occur in the VO-rich and VO-poor layers. Moreover, we could separate two types of BRS operations with different polar for set and reset processes each other by changing the range of the applied voltage from 0.5 V to 1.0 V or from 1.0 V to 0.5 V after several CRS operations. Note that these RS characteristics were sufficiently gradual. Therefore, the cell resistance could be continuously controlled approximately between 0.2 k $\Omega$  and 1 k $\Omega$  by applying the appropriate voltage, indicating that analog RS characteristics were improved through CRS operations. The improvement of analog RS characteristics can be understood by the competition of a set process in the VO-rich layer and a reset process in the VO-poor layer, or vice versa, through the CRS operations. In other words, the CRS operations can be useful to not only suppress sneak pass current but to improve the continuity of RS. [1] D. Ielmini, *Microelectronic Engineering*, 190, 44 (2018). [2] T. Miyatani et al., *Jpn. J. Appl. Phys.*, 58, 090914 (2019). [3] T. Miyatani et al., *Mater. Res. Soc. Spring Meeting*, EP09.07.02 (2019).

#### 5:55 AM F.NM07.06.07

**Metal Oxide Based Three-Terminal Electrochemical Memory Devices Towards Energy Efficient Neuromorphic Computing Device** Dagil Ryu, Yangho Jeong, Hyunjoon Lee, Young Ho Chu and Yun Seog Lee; Seoul National University, Korea (the Republic of)

Deep neural network (DNN) based on the backpropagation (BP) has demonstrated outstanding performance in speech recognition, image detection, and natural language processing. Despite the great success, training of large DNNs is computationally intensive task that requires high energy consumption. To achieve massively parallel and energy-efficient DNN algorithms, in-memory computing with resistive memory devices such as RRAM, PCM, CBRAM, FRAM, etc., have been widely studied. These analog synaptic devices, however, have non-ideal characteristics including nonlinearity of conductance response, asymmetry, and variation originated from their operating mechanism or material properties, resulting in time consuming feedback programming scheme. In this contribution, we propose metal oxide based three-terminal electrochemical memory devices as artificial synapses for neuromorphic computing. Various metal oxides are employed as resistive channel material and a solid electrolyte deposited on the channel decouples the update and read operations. By injecting proton or oxygen ions into the channel, the conductance states of the channel can be tuned precisely. We investigate device structure designs and operation conditions for symmetrical programming with a wide range of states and long term stability through the reversible electrochemical intercalation or redox reaction with a charge control through the gate. More importantly, we discuss issues of the metal oxide based three-terminal electrochemical memory devices for CMOS process-compatibility and a large scale array fabrication.

SESSION F.NM07.07: Neuromorphic Device—New Concept and Novel Materials  
On Demand Abstracts Available for Viewing Starting Saturday Morning, November 21, 2020  
F-NM07

#### 5:00 AM F.NM07.07.01

**MoS<sub>2</sub>-Based Electronic Synapses for Unsupervised Learning** Adithi Pandrahally Krishnaprasad Sharada, Durjoy Dev, Mashiyat Sumaiya Shawkat, Yeonwoong Jung and Tania Roy; University of Central Florida, United States

Memristors are considered as promising candidates for realizing synapses for neuromorphic computing because of their reduced complexity and nanoscale foot-print when compared to conventional complementary metal oxide semiconductor (CMOS) technology. Non-volatile switching with multiple conductance states in memristors is employed to emulate synapses. In this work, we present synapses realized by memristors using chemical vapor deposited (CVD) MoS<sub>2</sub>. Graphene is used as electrode for this device. These synapses exhibit linear and symmetric weight update with identical pulses, considered to be the “holy grail” for unsupervised learning. The graphene/MoS<sub>2</sub> (G/M) synaptic device exhibits 4 distinct states in both DC potentiation and depression regimes. Additionally, it exhibits data retention for >10<sup>4</sup> s. For efficient unsupervised learning, the synapses should exhibit linear and symmetric weight update with identical input pulses and a high maximum/minimum conductance ratio (G<sub>max</sub>/G<sub>min</sub>). Resistive random-access memory (RRAM), phase change memory (PCM) and ferroelectric field effect transistors (FeFET) have been used to emulate a synapse. But these devices exhibit non-linear weight update with identical pulses paired with reduced G<sub>max</sub>/G<sub>min</sub> ratio. Identical input voltage pulses with t<sub>ON</sub>= 500  $\mu$ s and amplitude of 6 V (-4 V) are applied to observe potentiation (depression) in the G/M synapse. With 25 input pulses

applied for each regime, we obtain linear and symmetric weight update with an ideal symmetry of 0. The non-linearity factor (NLF) is 0 for both potentiation and depression regimes, and  $G_{max}/G_{min}$  is 16.5. These device characteristics are then incorporated in a pseudo-crossbar array of a 2-layer multi perceptron network with the help of the circuit macro model Neurosim1 to obtain online learning accuracy of 84.33 %. We benchmark our G/M synapse with other emerging synapse devices with respect to NLF, asymmetry,  $G_{max}/G_{min}$  and learning accuracy with Neurosim and show that our device is superior to all other emerging synaptic devices in all these categories. I P.-Y. Chen, X. Peng, and S. Yu, IEEE Transactions on Computer-Aided Design of Integrated Circuits and Systems 37 (12), 3067 (2018).

#### 5:10 AM F.NM07.07.02

**Tunable Volatile and Non-Volatile Resistive Switching of Non-Stoichiometric CuOx Nanowire for Selector and Memory Application** Chi-Hsin Huang<sup>1</sup>, Kosuke Matsuzaki<sup>2</sup> and Kenji Nomura<sup>1</sup>; <sup>1</sup>University of California, San Diego, United States; <sup>2</sup>Tokyo Institute of Technology, Japan

Resistive random-access memory (ReRAM)/memristive devices based on electrical resistance switching are highly expected to overcome persistent technological limitations in current memory technology and to develop next-generation nonvolatile memory because of its superior characteristics. These characteristics include high speed, high scalability, low power consumption, fast fabrication process, multistate storage, and compatibility with complementary metal-oxide semiconductor (CMOS). Particularly, nanowire-based resistive switching devices offer an ideal platform for a deeper understanding of resistive switching properties due to the confined nanostructure and the opportunity to develop nanoscale-memristive device for next-generation memory and neuromorphic computing. In addition, copper oxide is one of the attractive candidates for ReRAM/memristor due to the existing multiple oxidation states from “+2” to metal state (CuO, Cu<sub>4</sub>O<sub>3</sub>, Cu<sub>2</sub>O, Cu) for inducing resistive switching, which is believed to involve the phase transition with multiple oxidation state induced by redox reaction. In this work, we report the volatile and non-volatile resistive switching effect in p-type non-stoichiometric CuOx nanowires, which are fabricated using insulator CuO nanowires via a thermal-annealing technique with hydrogen atmosphere. These resistive switching modes were effectively controlled by the stability of conductive filament via the compliance current in the SET process. The non-volatile resistive switching exhibited low electric-field-induced switching, high ON/OFF ratio of 107, and long retention time of 104 seconds for ReRAM application. On the other hand, the volatile threshold switching was operated with low compliance current for selector application, and the device showed bidirectional operation, selectivity (104), low OFF-current (<100 pA), and stable reliability with endurance over 105 cycles under pulse operation. The presented work will discuss a nanoscale resistive switching mechanism based on hole-based conducting filament formation originated from the local redox reaction.

#### 5:20 AM F.NM07.07.03

**Photo Induced Synaptic Behaviors Emulated in Monolayer MoS2 Devices for Realizing Artificial Cogni-Retina** Molla Manjurul Islam, Sonali Das, Durjoy Dev, Adithi Pandrahally Krishnaprasad Sharada, Madison Manley and Tania Roy; University of Central Florida, United States

Neuromorphic computing, inspired by the human brain, provides efficient energy utilization, massive parallelism, flexible adaptive capability, and information processing and transmission. It has the potential to realize computational techniques requiring recognition, learning and decision making; fundamentally overcoming the bottleneck in von Neumann architectures.[1] Artificial synapses form the backbone of neuromorphic computing; emulating controlled functions related to learning and memory. Furthermore, to functionalize devices beyond their synaptic functions, it is essential to merge them with biometric sensing elements such as vision, auditory, touch and olfactory sensors. Optical stimuli in a synaptic device renders ultrafast computational speed due to high bandwidth, low crosstalk, and ultralow power consumption.[2] A photonic synaptic transistor based on 2D materials provides ultra-low power consumption along with flexibility and thickness scalability. Graphene, the first 2D material leads to a short photocarrier lifetime and high dark current due to its zero bandgap and is therefore unfavorable for use as an efficient synapse material. Unlike graphene, monolayer MoS<sub>2</sub> having a direct bandgap would allow a high absorption coefficient and efficient electron-hole pair generation under photoexcitation, becomes suitable in various neuromorphic applications. We demonstrate the concept of artificial cogni-retina; an optic-neural synaptic device that features synaptic and optical-sensing functions. It has the potential to replace bulky systems comprising of video camera and processing units. A MoS<sub>2</sub> based photonic synaptic transistor for emulating the superior and complex features of artificial cogni-retina is reported. The device finds application in prosthetic human eyes and robotic eyes in artificial intelligence based platforms of autonomous vehicles. The device shows synaptic behavior with high conductance ratio of 103 facilitated by gate tunability and a long-term memory of 104 s with an extremely low energy consumption (15 pJ/event). High quality large area (2cm×2cm) monolayer MoS<sub>2</sub> (grain size of 50 ?m) is grown on SiO<sub>2</sub>/Si substrate via CVD technique by maintaining the precursor at 950°C. As grown MoS<sub>2</sub> coated with PMMA is immersed in BOE to release the MoS<sub>2</sub> film by removing the underlying SiO<sub>2</sub>. The PMMA supported MoS<sub>2</sub> film is transferred to DI water bath and finally to

SiO<sub>2</sub>/p<sup>+</sup> silicon substrate with nickel source/drain contacts. The final sample is heated for increasing the adhesion of the transferred film, and the PMMA layer is etched by acetone followed by a forming gas annealing. MoS<sub>2</sub> is patterned to form the channels of the transistor by reactive ion etching in CF<sub>4</sub>. We explore the spectral response of our device, expressed through its photoresponsivity, over a wavelength of 400-700 nm for varying intensity. The negligible photoresponsivity obtained for wavelengths above 680 nm clearly depicts the bandgap of monolayer MoS<sub>2</sub> corresponding to 1.8 eV. The synaptic transistor exhibits excellent responsivity of 2×10<sup>3</sup> AW<sup>-1</sup> (EQE of 6×10<sup>5</sup> %) under illumination (450 nm, 10 ?W/cm<sup>2</sup>) for V<sub>G</sub> = 0 V and V<sub>D</sub> = 5 V. Both the responsivity and EQE of the device increase with gate voltage due to lowering of the barriers at the contacts. The device shows n-type behavior (ON/OFF current ratio of 10<sup>5</sup>) and under illumination, an enhancement in current is observed for both ON (V<sub>G</sub>>V<sub>TH</sub>) and OFF (V<sub>G</sub>>V<sub>GTH</sub>) states for all gate voltages. This indicates that the photocurrent dominates over thermionic and tunneling currents. Gate dependent potentiation and data retention of the device is observed by varying the gate bias. The device also demonstrates other essential synaptic behaviors, such as short-term potentiation (paired-pulse facilitation of 150%), spike-frequency dependent plasticity, spike-duration dependent plasticity. References [1] Q. Xia et al., Nature materials 2019, 18. [2] Z. Cheng et al., Science advances 2017, 3.

SESSION F.NM07.08: Neuromorphic Device—Neuron and Synapse  
On Demand Abstracts Available for Viewing Starting Saturday Morning, November 21, 2020  
F-NM07

#### 5:00 AM \*F.NM07.08.01

**Memristive Devices—From Atomistic Simulations to Circuit Modeling** Thomas Mussenbrock; Brandenburg University of Technology, Germany

Almost 40 years after Chua introduced his theory of memristive devices (nowadays aka resistive switching devices), they have been identified as promising candidates for non-volatile memory applications due to their distinct key features which are i) low power consumption, ii) passivity, and iii) scalability into the nanometer scale. Beyond these applications as non-volatile memories, memristive devices have turned out to be applicable as artificial synapses in neuromorphic circuits. Many of the available metal-oxide resistive switching devices rely on the stochastic phenomenon of creation and rupture of conductive metal filaments within a solid state electrolyte matrix. Inherent are initial electroforming procedures and distinct “on” and “off” states. The latter are in fact beneficial for memory applications. However, in the context of neuromorphic applications a more “analog” behavior is needed, rather than a purely “digital” behavior. To overcome these limitations, various kinds of interface-based resistive switching devices have been developed, tested, and applied. Although these devices are quite simple with respect to their structural compositions, the analog switching behavior itself - as a result of multiscale multiphysical phenomena - is in fact rather complex and not fully understood yet. This contribution is intended to provide an overview over our modeling and simulation approach in order to describe memristive devices on the human timescale, yet allowing for physical phenomena on the atomistic scale.

#### 5:15 AM \*F.NM07.08.02

**DNN Training Algorithm for Nonsymmetric Devices** Tayfun Gokmen; IBM T. J. Watson Research Center, United States

Resistive cross-point devices arrays that can simultaneously store and process data locally and all in parallel, are promising candidates for intensive deep neural network (DNN) training workloads. However, when the training is performed using the conventional state of the art learning algorithm, stochasticity gradient descent (SGD) using backpropagation (BP) algorithm, these array architectures must meet a set of stringent device requirements for the cross-point element. A key requirement is that the resistive devices must change conductance in a symmetrical fashion when subjected to positive and negative pulse stimuli. Here, we present an alternative training algorithm, so-called the Tiki-Taka algorithm, so that this stringent symmetry requirement of the cross-point element can be relaxed to a very large extend. We tested the validity of the Tiki-Taka algorithm on a range of network architectures such as fully connected, convolutional and LSTM networks. For all these networks, the Tiki-Taka algorithm with nonsymmetric devices characteristics results in training accuracies that are in par with the ones achieved with the conventional SGD algorithm with symmetric devices. Thanks to the relaxed device specification, this algorithmic improvement would enable earlier adaptation of crossbar-based hardware accelerators for DNN training workloads.

#### 5:25 AM F.NM07.08.03

**Towards Multilevel Phase Change Memory (PCM) Based on Engineered Multilayer Group III-Sb Alloys** Rubab Ume,

Haibo Gong, Vadim Tokranov, Michael Yakimov, Sandra Schujman, Devendra K. Sadana and Serge Oktyabrsky; SUNY Polytechnic Institute, United States

Phase change memory is currently considered as one of the promising candidates for the next-generation non-volatile memory devices and Resistive Processing Units for neuromorphic computing. Multilevel functionality of the PCM is a crucial next step in enhancing the bit density per unit cell. We investigated the potential of Tellurium-free group III-Sb alloys, specifically Al-Sb and Ga-Sb thin multilayer films deposited under UHV conditions by molecular beam epitaxy for obtaining multiple resistance states. Bulk films of group III-Sb binary alloys of different compositions showed intermediate resistance plateaus upon heating which is a promising first step to achieve multilevel functionality in PCMs. The resistance versus temperature curves of the multilayer films exhibited up to four distinct intermediate states that have the capability of stabilizing multiple PCM resistance levels and potentially reduce drift in PCM arrays. The calculated activation energy for crystallization ranged from 2.5-5.3 eV. Naturally transitions with the highest activation energies show projected data retention as high as 10 years at 160°C. Transmission Electron Microscopy (TEM) analysis of the samples revealed crystalline grain size of 30-100 nm upon annealing. TEM and X-Ray Diffraction (XRD) analysis of Ga-Sb samples annealed at different temperatures showed growth of crystallites mostly in A7 Antimony phase with further tendency to phase separation of Sb and GaSb phases. Initial pulse measurements were done on binary alloy mushroom PCM cells with TiN heater size of down to 100 nm. Test cells demonstrated reversible switching with a set/reset resistance ratio of ~100 for set voltage <1.5 V and pulse widths down to 200 ns. The multilayer film has the potential to be used similarly to the binary cell showing reversible switching. We believe the results obtained in this study demonstrate a path to enable multiple logic states in PCM materials.

#### 5:35 AM F.NM07.08.04

**Ionic Analog Synapses for Deep Learning Accelerators** Kevin Limanta, Ahmad Zubair and Tomas Palacios; Massachusetts Institute of Technology, United States

The need to reduce the power consumption of machine learning applications while improving performance has driven the development of specialized hardware accelerators. While digital CMOS-based accelerators have sped-up training and inference in neural networks, they have several limitations. Most notably, a spatially-separated memory and computation, volatile memory, and the lack of connectivity between nodes, all hinder the realization of ubiquitous, low-power deep learning accelerators. Alternatively, crossbar arrays of non-volatile memory (NVM) devices able to perform arithmetic (e.g. bit multiplication), are projected to be six orders of magnitude more energy-efficient than current state-of-the-art GPU accelerators. Borrowing bio-related terminology, these analog “synapses” perform in-memory computation, reducing the distance data travels and overall energy consumption. Unfortunately, current state-of-the-art analog “synaptic” devices based on resistive memories suffer from stochastic, asymmetric, and non-linear weight updates, detrimental to training accuracy. Meanwhile, electrochemical ion-based synaptic devices have been shown to be fast, energy-efficient, and exhibit symmetric, linear weight updates. However, the electrolytes for the electrochemical reaction are often CMOS incompatible and suffers from scalability.

Scalable, CMOS-compatible devices are needed for future large-scale production. In this project, we develop a MOS field-effect transistor(FET)-based analog synapse. Doping the SiO<sub>2</sub> gate oxide with protons by exposing the oxide to hydrogen plasma, allows non-volatile electrostatic control of the semiconductor channel conductance. Applying a short voltage pulse on the gate shifts the distribution of the protons, tuning the artificial neural network node weights. Ion trapping in the oxide maintains non-volatility. Electrostatics of a uniform sheet of ions predicts a linear relationship between the number of voltage pulses and the threshold voltage shift. Linear weight updates are expected, necessary for efficient training with crossbar array accelerators. Initially, we study the electrostatics and proton diffusion via Silvaco Atlas. Simulations predict a threshold voltage shift due to the presence of ions at different locations in the gate oxide. We then fabricate n-Si/ALD SiO<sub>2</sub>/Al MOS capacitors with proton doping, and characterized their ionic transport. We observe that the MOS gate stack exhibits hysteretic behavior below 2V, indicating non-volatility and low-voltage operation. C-V measurements estimate the ionic concentration to be 10<sup>12</sup>cm<sup>-2</sup>. To demonstrate switching characteristics, we fabricate and measure proton-doped GaN FETs as a quick testbed due to its simple fabrication and high carrier concentration. GaN has been intensively investigated as a BEOL material for future 3D integrated Si CMOS systems. Our results indicate that it could also be used for MOSFET synapses with proton-doped gate-oxides. These results are generalizable beyond GaN and they shed light on the feasibility of scalable, CMOS-compatible ionic devices for the next generation of neural network hardware accelerators.

#### 5:45 AM F.NM07.08.06

**2D Memtransistors and Gaussian Heterojunction Transistors as Artificial Synapses and Spiking Neurons** Vinod K.

Sangwan, Hong-Sub Lee, Megan Beck and Mark Hersam; Northwestern University, United States

Hardware implementation for neuromorphic computing aims to overcome the von Neumann bottleneck by co-locating memory and logic. In this context, resistive switches, phase-change devices, electrochemical systems, and complementary metal-oxide semiconductor (CMOS) transistors have been explored extensively for artificial synapses and spiking neurons in artificial neural networks. While each of these strategies has its attributes, none of them has clearly emerged as a universal approach for neuromorphic hardware, which suggests that alternatives should continue to be evaluated. For example, neuromorphic devices based on nanomaterials such as quantum dots, nanotubes, and two-dimensional (2D) monolayers have begun to show promise due to their controlled chemical composition, unique architectures, and compatibility with ultimate scaling and speed limits [1]. Furthermore, low-dimensional materials possess low dielectric screening that provides enhanced electrostatic control, thus allowing functions that better mimic a biological neuron [2]. In this presentation, recent advances in the development of artificial synapses and neurons based on 2D semiconductors and mixed-dimensional van der Waals heterojunctions will be discussed [3]. In particular, dual-gated memtransistors based on polycrystalline MoS<sub>2</sub> show novel synaptic responses in crossbar arrays [4]. The non-volatile memory states of these devices are tuned by both biasing history and the field-effect from the two gate terminals [5]. In this manner, the dual gates allow independent addressing of nodes in the crossbar by minimizing sneak currents in addition to facilitating tunability of synaptic weight update rules that resulted in a 94% recognition rate of hand-written digits using a multi-level perceptron model [4]. Since neuromorphic architectures require both artificial synapses and neurons, this talk will also introduce a Gaussian heterojunction transistor design that realizes the functionality of an integrate-and-fire neuron [6]. Specifically, dual-gated, self-aligned, mixed-dimensional *p-n* heterojunctions based on carbon nanotubes and MoS<sub>2</sub> operate as anti-ambipolar transistors where all parameters of the Gaussian transfer curves can be controlled by the applied gate potentials. These Gaussian heterojunction transistors enable a wide range of spiking behavior including constant spiking, latency, and bursting [6]. Since atomically thin dual-gated memtransistors and Gaussian heterojunction transistors are prepared using standard materials processing and fabrication schemes, they are well-poised to be integrated together and/or with traditional electronic devices for next-generation neuromorphic computing architectures.

## References

- [1] V. K. Sangwan and M. C. Hersam, *Nature Nanotechnology*, DOI: 10.1038/s41565-020-0647-z (2020).
- [2] M. E. Beck and M. C. Hersam, *ACS Nano*, **14**, 6498-6518 (2020).
- [3] D. Jariwala, T. J. Marks, and M. C. Hersam, *Nature Materials*, **16**, 170-181 (2017).
- [4] H.-S. Lee, V. K. Sangwan, H. Bergeron, H. Y. Jeong, K. Su, and M. C. Hersam, submitted, 2020.
- [5] V. K. Sangwan, H.-S. Lee, H. Bergeron, I. Balla, M. E. Beck, K.-S. Chen, and M. C. Hersam, *Nature*, **554**, 500-504 (2018).
- [6] M. E. Beck, A. Shylendra, V. K. Sangwan, S. Guo, W. A. Gaviria Rojas, H. Yoo, H. Bergeron, K. Su, A. R. Trivedi, and M. C. Hersam, *Nature Communications*, **11**, 1565 (2020).

## 5:55 AM F.NM07.08.07

**Scalable Method to Find the Shortest Path in a Graph with Circuits of Memristors** Alice Mizrahi<sup>1,2</sup>, Thomas Marsh<sup>1</sup>, Brian Hoskins<sup>1</sup> and Mark Stiles<sup>1</sup>; <sup>1</sup>National Institute of Standards and Technology, United States; <sup>2</sup>University of Maryland, United States

Biological systems have evolved to perform computing tasks while consuming little energy. Taking inspiration from the methods used by biological systems is therefore a promising path for building low energy computers, as demonstrated by the large body of work on neuromorphic computing. Here we propose to take inspiration from ant colonies, and in particular the way they are able to solve the shortest path in a graph problem without supervision, in a massively parallel way. Algorithms inspired from ant colonies have been proven useful for tackling the wide range of optimization problems that map to finding the shortest path between two given nodes in a graph. However, on conventional computers, they are mostly sequential and therefore the time and energy required to find the path scales with the size of the graph. Here propose a different approach: to implement this bio-inspired system directly in hardware, using circuits of memristors. The graph to study is constructed by interconnecting memristors so that the length of each edge of the graph is embodied by its number of memristors. When a voltage is applied across two nodes, the least resistive branch – i.e. the shortest path – between them receives more current than the other branches. This causes the memristors on the shortest path to turn on, attracting even more current. Our method leverages this reinforcement mechanisms intrinsic to memristors physics, in order to obtain a steady state where the memristors on the shortest path have a much higher conductance than the memristors on the rest of the graph. In consequence, the user can find the shortest path by a simple conductance measurement. Using numerical simulations, we



show that using a voltage ramp makes this method reliable. We validate it on graphs of different sizes and topologies. It is both valid for an experimentally derived memristor model and robust to device variability. We found that, contrary to conventional methods, the time and energy of the computation scale with the length of the shortest path rather than with the size of the graph. In consequence, this method is particularly attractive for solving large graphs with small path lengths (such as neural networks, social networks and power grids). Applying our method to these graphs opens the door to fast and low energy analysis of complex networks with wide ranges of applications.

#### 6:05 AM F.NM07.08.08

**A Bio-Inspired Perceptual Decision-Making Circuit Based on the Hassenstein-Reichardt Direction Detector** Tom Birkoben<sup>1</sup>, Mirko Hansen<sup>1</sup>, Marina Ignatov<sup>1</sup>, Martin Ziegler<sup>2</sup> and Hermann Kohlstedt<sup>1</sup>; <sup>1</sup>Faculty of Engineering, Kiel University, Germany; <sup>2</sup>Technische Universität Ilmenau, Germany

Decision-making belongs to one of the most prominent principles in the nerve system of living species. The crucial trade-off between time to decide (speed) and accuracy is essential for a creature to react to environmental stimuli and most importantly, relevant for survival. In-depth studies of coherent motion tasks in primates, based on two-choice decision experiments, led to a profound understanding of neuronal information processing and even bridged the gap to behavioural psychology. Three fundamental processing stages are needed to successfully perform a two-choice decision experiment based on a saccadic eye movement task: the neuronal representation of the sensory signal, the integration of the incoming stimuli and the comparison of the accumulated information to a threshold for a final decision. In accordance to the results of decision-making experiments with primates, an analogue electronic decision-making circuit was developed. Our concept study includes a LED-matrix showing moving light dots (i.e. the tasks screen in primate experiments), an array of photo diodes (i.e. retina of the primate, sensory evidence), a Hassenstein-Reichardt Detector (HRD) based motion detection (i.e. a correlation-type motion detector with a high biological relevance, based on an inhibitory circuit and delay lines) and finally a signal integration circuit. The latter stage represents the decision-making unit and is realised through an inhibitory mutual coupling of the accumulated signals. The entirely analogue circuit is based on integrate and fire relaxation oscillators to mimic firing neurons. We would like to emphasise that the presented real time decision-making system is closely related to biological information pathways in nerve systems. Neither a digital computer nor programming is necessary for decision-making, which might be an interesting approach for real time data processing in autonomous robots.

#### 6:15 AM F.NM07.08.09

**A-TiO<sub>2</sub> Nanoparticle Suspension Ink for Fully-Printed Electronic Synapses** Varvara Salonikidou<sup>1</sup>, Yasunori Takeda<sup>2</sup>, Jonathan England<sup>1</sup>, Shizuo Tokito<sup>2</sup> and Radu A. Sporea<sup>1</sup>; <sup>1</sup>University of Surrey, United Kingdom; <sup>2</sup>Yamagata University, Japan

Biomimetic electronic devices such as electronic synapses that emulate both short-term and long-term plasticity constitute an auspicious building block for neuromorphic computing systems and bioinspired electronic applications. The electronic synapse constitutes an energy efficient and versatile solution for new computing paradigms, however, to date such devices with well-controlled plasticity and synaptic behaviour are scarce. Most of the current fabrication processes are limited to conventional techniques, which are typically time-consuming and use ecologically harmful chemicals with considerable material waste. The present work aims on fully inkjet-printed MAM (metal-active-metal) electronic synapses. The fabrication technique introduces an alternative time- and cost-efficient method of low environmental impact. All of the layers are deposited in an additive manner without any material subtraction or chemical treatment. Active inks consisting of TiO<sub>2</sub> nanoparticle suspension developed in-house are presented and characterised in this work. The ink synthesis is based on low temperature and low complexity process that includes a mixture of solvents and acids. The active inks are analysed in terms of nanoparticle and morphological characteristics. Additionally, the resulted Z number  $[(\text{inertial force} \times \text{surface tension})^{1/2} / \text{viscous force}]$ , which defines the jettability of an ink, are defined experimentally. The formulations used seem to strongly affect the dispersity and sedimentation along with the nanoparticle size of the solution-ink, indicating a route to optimization for improved jettability, shelf life and in general ink robustness. The developed nanolayers of the fully-printed devices are in the range of 100-200 nm thickness, uniform and crack-free. Electrical characterisation of initial devices indicates low power ( $\mu\text{m}$  to 1 mA window of output current) and biomimetic properties of synaptic plasticity when trigger voltage pulses of 1 V are applied. The tuning of the active ink's rheological characteristics along with the investigation of the electrical framework under which the electronic devices respond synaptically present a favourable approach to alternative fabrication methods for versatile and flexible electronics.

**5:00 AM F.NM07.09.02**

**Analog Ionic Switches Based on LiCoO<sub>2</sub>/SiO<sub>2</sub>/TiO<sub>2</sub> Two-Terminal Devices for the Realization of Bio-Inspired Neural Functionalities Driven by the Reversible Li-Ion Migration** Panagiotis S. Ioannou<sup>1</sup>, Evripides Kyriakides<sup>1</sup>, Ioannis Giapintzakis<sup>1</sup> and Olivier Shcneegans<sup>2</sup>; <sup>1</sup>University of Cyprus, Cyprus; <sup>2</sup>CNRS, Centrale Supélec, France

Although in its embryonic state, bio-inspired computing has never been closer to its realization, due to the recent advances in neuromorphic hardware implementation with non-volatile, binary and analog, devices based on established and novel switching oxides. While binary or multibit information storing as synaptic weights, through the stimulated resistance modulation of such devices, enables in-memory computing and non-Von Neumann architectures, synaptic plasticity will enable direct emulation of biological neural activity. Bio-realistic synaptic plasticity can be facilitated through the pulse stimulation of devices with transient switching behaviour, with an internal timing mechanism through their inherent diffusive dynamics. Consequently temporal association of stimulating pulses, governs the triggered response of such devices, in a manner reminiscent of biological neural behaviour. Searching beyond filamentary resistive switching devices, diffusion based ionic switches, both in three-terminal and two-terminal configurations, receive noticeable attention. Robustness of non-filamentary switching mechanisms, along with unique switching characteristics and plasticity attributes, can expedite the integration of these devices in functional neural networks with bio-inspired capabilities. Cation-based ionic switches, and specifically Li ion diffusion driven switching oxides, attract reasonable attention in the neuromorphic community. Electrochemical relevancy of Li cation with cations such as Na, K and Ca, involved in the polarization/depolarization of neuron cells, apart from being philosophically sensational, disclose great potential for the realization of artificial neurons with synaptic plasticity. This work investigates the memristive/synaptic behaviour and underlying mechanism of two terminal, thin film battery-like, ionic switches based on LiCoO<sub>2</sub>-cathode, SiO<sub>2</sub> electrolyte and TiO<sub>2</sub> anode on a Si substrate. Acting as a self-doped p-type semiconductor, highly stoichiometric LiCoO<sub>2</sub> presents a reversible insulator to metal transition (IMT) upon electrochemical lithium removal. Each Li ion vacancy induces the oxidation of Co<sup>3+</sup> to Co<sup>4+</sup>, injecting an electron hole and consequently increasing the conductivity of Li-deficient LiCoO<sub>2</sub>. Controlling the Li concentration in the switching oxide, via voltage stimulated electrochemical migration of Li cations, through a solid electrolyte SiO<sub>2</sub> layer and storing them in a TiO<sub>2</sub> anode layer, the conductance of the battery-like stack can be tuned. The devices have been characterized by means of dc-cycling and non-abrupt, analog, switching with I-V hysteresis was recorded. Furthermore, non-symmetric, diode-like, characteristics with high rectification effect in reverse bias was evident, along with the rise and decay of an electromotive force after each potentiation. Pulse characterization of the devices lead to the observation of gradual conductance enhancement through a paired pulse facilitation mechanism. Diffusive dynamics of this system, were observed in the form of a decaying excitatory post synaptic current. Regardless, non-volatile multistate conductance enhancement was also monitored. Spike timing dependent plasticity functions were generated, through non-overlapping postsynaptic and presynaptic pulse-pair stimulation. Analog switching observed by these devices, in combination with the diffusive dynamics and the paired pulse facilitation mechanism, effectively facilitate the direct emulation of bio-inspired synaptic functionalities like STDP. Spontaneous state decay, in the form of an excitatory post synaptic current can be advantageous for the emulation of habituation processes observed in biological neurons. Finally non-filamentary switching with rectification characteristics can be beneficial upon device integration in dense cross-bar arrays, effectively enhancing durability and suppressing leakage currents respectively.

**5:10 AM F.NM07.09.04**

**Proton Intercalation in Solid-State Electrochemical Synapse for Energy-Efficient Neuromorphic Computing** Nicolas Emond, Xiahui Yao, Murat Onen, Seungchan Ryu, Jesus A. del Alamo, Ju Li and Bilge Yildiz; Massachusetts Institute of Technology, United States

Deep learning based on neural networks is a promising approach to accelerate machine learning applications. However, state-of-the-art processing units, based on Complementary Metal–Oxide–Semiconductor (CMOS) circuits, and computer systems based on von Neumann architecture, requires large memory space and high power consumption when simulating neural networks. Improvements in computing performance therefore requires designing novel scalable, fast and energy-efficient hardware structures with both processing and storage capabilities.

It has been demonstrated that crossbar-type arrays containing two-terminal resistive switches, whose electrical conductivity is electrically modulated, enable energy-efficient and fast-processing physical neural networks. Two main types of mechanisms

have been demonstrated in artificial intelligence applications to change the conductance of the switches, conductive-filament and phase-change mechanisms. A more recent concept, electrochemical cation intercalation-based resistive switches with three-terminal structures have the potential to circumvent issues faced by other mechanisms. Indeed, multistate capability and low energy consumption was recently demonstrated for inorganic Li-based<sup>1</sup> and organic proton-based<sup>2</sup> electrochemical devices. However, these devices also suffer from a scaling challenge as they are not compatible with current CMOS processes due to presence of Li and organic switching materials, respectively.

Our group is therefore working on the development of an all solid-state inorganic proton (H<sup>+</sup>) electrochemical intercalation resistive switch, which relies on a deterministic charge-controlled mechanism. Our initial design consists of a channel of active material, whose electronic conductivity is modulated through protonation/deprotonation, enabling for a continuum of resistance states<sup>3</sup>. A solid proton reservoir layer serves as the gate terminal while a proton conducting solid electrolyte separates the channel and the reservoir. Employing protons, the smallest cation, as the doping ion presents several advantages including high operation speed, good compatibility with Si technology and long lifetime.

Herein, I will first present our demonstration of this concept<sup>3</sup> for a device that includes tungsten trioxide (WO<sub>3</sub>) as an inorganic active channel material, and Pd-hydride as a solid hydrogen reservoir that is also used for gating the device. Hydrated Nafion is used as the polymer-based proton conducting electrolyte. The device has a very low energy consumption, nearly symmetrical protonation/deprotonation behavior and long cycling lifetime. While the channel and gate materials are CMOS-compatible, a challenge is to come up with CMOS-compatible inorganic proton conducting solid electrolytes. Another challenge is to find more insulating channel materials that can switch faster. I will therefore also present our work on the improvement of the device properties and integrability by exploring alternative materials for the active channel and the proton electrolyte. Vanadium pentoxide (V<sub>2</sub>O<sub>5</sub>), which is reported to efficiently intercalate small cations in its crystal structure along the (001) orientation (channel-like structure), and tantalum (Ta<sub>2</sub>O<sub>5</sub>) pentoxide, a potential two-phase system that could allow to fix the device open-circuit potential, are the two active materials studied within this context. On the other hand, nanocrystalline yttrium-doped barium zirconate (BZY), a state-of-the-art solid-state proton conducting ceramic, is considered as a possible alternative to replace Nafion polymer.

Fuller, E. J. *et al.* Li-Ion Synaptic Transistor for Low Power Analog Computing. *Adv. Mater.* **29**, 1604310 (2017).

van de Burgt, Y. *et al.* A Non-Volatile Organic Electrochemical Device as a Low-Voltage Artificial Synapse for Neuromorphic Computing. *Nat. Mater.* **16**, 414 (2017).

Yao, X. *et al.* Protonic Solid-State Electrochemical Synapse for Physical Neural Networks. Accepted in *Nat. Commun.* (2020).

#### 5:20 AM F.NM07.09.05

**Proton-Controlled Bimodal Operation of Tyrosine-Rich Peptide Memristor** Min-Kyu Song<sup>1</sup>, Seok Daniel Namgung<sup>2</sup>, Daehwan Choi<sup>1</sup>, Hyeohn Kim<sup>2</sup>, Hongmin Seo<sup>2</sup>, Misong Ju<sup>2</sup>, Yoon Ho Lee<sup>2</sup>, Taehoon Sung<sup>1</sup>, Yoon-Sik Lee<sup>2</sup>, Ki Tae Nam<sup>2</sup> and Jang-Yeon Kwon<sup>1</sup>; <sup>1</sup>Yonsei University, Korea (the Republic of); <sup>2</sup>Seoul National University, Korea (the Republic of)

With the advent of artificial intelligence(AI), neuromorphic computing inspired by efficient data processing in human brain has widely attracted immense research interest in various fields. Recent development of AI processor optimized for parallel computing including GPU, FPGA and ASIC has advanced AI-based industries including big data, autonomous vehicles, and internet of things. Nevertheless, CMOS based AI processor has theoretical limits of data bandwidth and energy efficient due to data shuttling between memory and computing units in terms of von Neumann bottleneck. Therefore, new concepts of electronic device have been proposed to mimic biological synapse responsible for both information storage and processing in human brain, termed in-memory computing. Memristors, a portmanteau of memory and resistor, is considered as one of the promising candidates for in-memory computing device because of its desirable properties as tunable resistance, non-volatility, low energy consumption, and fast operation. However, the key difference in working mechanism of biological synapses from artificial electron-based synthetic devices is the cooperative and multimodal activation process which includes the transfer of ions or molecules. In this study, we demonstrate bi-modal operation of peptide memristors, which is analogous to synaptic operation, by electronic and environmental inputs. Based on our understanding on coupling of electron and proton conduction, we designed sequence of amino acids in peptide to obtain controllability on resistive switching characteristics through proton injection by humidity control. As a result, the memristor based on Tyr-Tyr-Ala-Cys-Ala-Tyr-Tyr(Y7C) peptide operates not only by applying voltage inputs but also by applying humidity sweep without voltage sweep corresponding to signaling process by extracellular proton concentration in synapse.

Similar to previous reported electrochemical metallization memory, our peptide-based memory showed resistive switching characteristics owing to redox reactions of metal. However, we examined involvement of phenolic hydroxyl group of

tyrosine in resistive switching by introducing dehydroxylated tyrosine, phenylalanine, instead of tyrosine, resulting in 6-fold increment of set voltage. We assumed that electron transfer from tyrosine to Ag metal and vice versa through deprotonation and protonation promotes formation of Ag conductive filament. Thus, increasing relative humidity(RH) would promote resistive switching due to increased proton conduction in Y7C peptide. As a result, set voltage of peptide memristor showed linear dependency on RH values and, further, only humidity injection without voltage sweep induced reversible and non-volatile resistive switching, namely humidity mode of memristor was realized. Once transition from high resistive state to low resistive state is occurred by a forward RH sweep, the device maintained its state in wide range of RH condition for over  $10^4$  s, meaning data storage. To erase the data, a reverse RH sweep was applied and transition back to high resistive state was occurred in extremely low RH condition. On off resistance ratio reached up to  $10^4$ . Complementary bimodal operation of the peptide memristor was successfully carried out by writing data using humidity input and erasing data using voltage input in one device. Peptide film was characterized using circular dichroism(CD) analysis, nuclear magnetic resonance(NMR) spectroscopy and transmission electron microscopy(TEM). Proton conductivity of the peptide film was calculated by electrochemical impedance analysis(EIS). Proton involvement in the device was studied by kinetic isotope effect(KIE) of deuterium oxide vapor. This result suggests that proton can act as another control knob for neuromorphic computing devices and multimodal and biomimetic memory operation can be facilitated by material design, especially in tyrosine-rich peptide.

### 5:30 AM F.NM07.09.06

**Photo Induced Synaptic Behaviors Emulated in Monolayer MoS<sub>2</sub> Devices for Realizing Artificial Cogni-Retina** Molla Manjurul Islam, Sonali Das, Durjoy Dev, Adithi Pandrahally Krishnaprasad Sharada, Madison Manley and Tania Roy; University of Central Florida, United States

Neuromorphic computing, inspired by the human brain, provides efficient energy utilization, massive parallelism, flexible adaptive capability, and information processing and transmission. It has the potential to realize computational techniques requiring recognition, learning and decision making; fundamentally overcoming the bottleneck in von Neumann architectures.[1] Artificial synapses form the backbone of neuromorphic computing; emulating controlled functions related to learning and memory. Furthermore, to functionalize devices beyond their synaptic functions, it is essential to merge them with biometric sensing elements such as vision, auditory, touch and olfactory sensors. Optical stimuli in a synaptic device renders ultrafast computational speed due to high bandwidth, low crosstalk, and ultralow power consumption.[2] A photonic synaptic transistor based on 2D materials provides ultra-low power consumption along with flexibility and thickness scalability. Graphene, the first 2D material leads to a short photocarrier lifetime and high dark current due to its zero bandgap and is therefore unfavorable for use as an efficient synapse material. Unlike graphene, monolayer MoS<sub>2</sub> having a direct bandgap would allow a high absorption coefficient and efficient electron-hole pair generation under photoexcitation, becomes suitable in various neuromorphic applications. We demonstrate the concept of artificial cogni-retina; an optic-neural synaptic device that features synaptic and optical-sensing functions. It has the potential to replace bulky systems comprising of video camera and processing units. A MoS<sub>2</sub> based photonic synaptic transistor for emulating the superior and complex features of artificial cogni-retina is reported. The device finds application in prosthetic human eyes and robotic eyes in artificial intelligence based platforms of autonomous vehicles. The device shows synaptic behavior with high conductance ratio of 103 facilitated by gate tunability and a long-term memory of 104 s with an extremely low energy consumption (15 pJ/event). High quality large area (2cm×2cm) monolayer MoS<sub>2</sub> (grain size of 50 ?m) is grown on SiO<sub>2</sub>/Si substrate via CVD technique by maintaining the precursor at 950°C. As grown MoS<sub>2</sub> coated with PMMA is immersed in BOE to release the MoS<sub>2</sub> film by removing the underlying SiO<sub>2</sub>. The PMMA supported MoS<sub>2</sub> film is transferred to DI water bath and finally to SiO<sub>2</sub>/ p<sup>+</sup> silicon substrate with nickel source/drain contacts. The final sample is heated for increasing the adhesion of the transferred film, and the PMMA layer is etched by acetone followed by a forming gas annealing. MoS<sub>2</sub> is patterned to form the channels of the transistor by reactive ion etching in CF<sub>4</sub>. We explore the spectral response of our device, expressed through its photoresponsivity, over a wavelength of 400-700 nm for varying intensity. The negligible photoresponsivity obtained for wavelengths above 680 nm clearly depicts the bandgap of monolayer MoS<sub>2</sub> corresponding to 1.8 eV. The synaptic transistor exhibits excellent responsivity of  $2 \times 10^3$  AW<sup>-1</sup> (EQE of  $6 \times 10^5$  %) under illumination (450 nm,  $10$  ?W/cm<sup>2</sup>) for  $V_G = 0$  V and  $V_D = 5$  V. Both the responsivity and EQE of the device increase with gate voltage due to lowering of the barriers at the contacts. The device shows n-type behavior (ON/OFF current ratio of 105) and under illumination, an enhancement in current is observed for both ON ( $V_G > V_{TH}$ ) and OFF ( $V_G < V_{TH}$ ) states for all gate voltages. This indicates that the photocurrent dominates over thermionic and tunneling currents. Gate dependent potentiation and data retention of the device is observed by varying the gate bias. The device also demonstrates other essential synaptic behaviors, such as short-term potentiation (paired-pulse facilitation of 150%), spike-frequency dependent plasticity, spike-duration dependent plasticity. References [1] Q. Xia et al., Nature materials 2019, 18. [2] Z. Cheng et al., Science advances 2017, 3.

**5:00 AM \*F.NM07.10.01**

**Ionic Nanoarchitectonics for Creating Artificial Intelligence Devices** Kazuya Terabe, Takashi Tsuchiya and Tohru Tsuruoka; NIMS, Japan

At present days, an enormous number of semiconductor devices are used in information communications equipment. The memory and computational functions resulting from integration of semiconductor devices have progressed as a result of the development of ultrafine processing technologies, but it is said that this progress will slow down in the near future. Therefore, continued improvement of information communication equipment performance requires not only the further development of semiconductor devices, but also the creation of innovative devices that operate on new principles. Furthermore, development of Artificial Intelligence (AI) hardware such as a brain-type computer that operates with low power consumption and small size is expected in recent years. In order to realize such AI hardware, it will be necessary to create devices that achieve various unique functions such as brain ones. These devices will no longer be based on conventional semiconductors, which exhibit characteristics suitable for digital arithmetic processing. They will be based on new operating principles. One group such promising novel devices is the nanoionic device's group, these nanoionic devices operate by controlling local ion migration and electrochemical reactions instead of by electron and hole migration. The control of local ion migration allows for any reconstruction of internal and surface nanostructures of device materials, as well as heterointerface one. Namely, it is a nanoarchitecture of materials achieved by the control of ion migration (referred to as ionic nanoarchitectonics). The unique physical and chemical phenomena and functions are caused by the ionic nanoarchitectonics, and we can create interesting nanoionic devices with a variety of novel functions. So far, we have already made some nanoionic devices with diverse functions by using the ionic nanoarchitectonics. These devices include an atomic switch, decision-making devices, artificial synapse device, solid-state electric-double-layer transistor, multi-functional on-demand-type device, magnetization and magnetoresistance tuning device, and so on [1,2]. We believe that the ionic nanoarchitectonics is promising as a new method for creating AI devices.

[1] K. Terabe et al. *Nanoscale*, **8**, 13873, 2016

[2] T. Tsuchiya et al. *Science Adv.* **4**, eaau2057, 2018

**5:15 AM \*F.NM07.10.02**

**Memristive Stochastic Learning for Neuromorphic Computing** Martin Ziegler; TU Ilmenau, Germany

Memristive devices because of their non-volatile memory behavior and their relatively simple structure as an electronic counterpart to synapses for hardware-based artificial neural networks (neuromorphic circuits). An important behavior of devices is their inherent stochastic nature, which applies especially to devices. Here, the change in resistance is due to the formation and dissolution of electrically conductive paths in a solid state electrolyte, which result in changes in the resistance switching process and nondeterministic device behavior.

In this talk, a learning scheme is presented that uses the randomness of the switching process for neuronal-inspired computing. It is shown that the switching probability of ReRAM cells follows a Poisson distribution at a certain voltage and pulse width, the switching probability being controllable by the number, amplitude and width of the programming pulses. To demonstrate the power of stochastic learning for neuromorphic systems, a neural circuit for pattern recognition is presented, and one that mimics perceptual behavior.

**5:30 AM F.NM07.10.03**

**Resistive Switching Dynamics in Core-Shell Nanowire Networks for Neuromorphic Hardware Applications** Shangradhanva Eswara Vasisth and Juan Claudio Nino; University of Florida, United States

There is a recognized need to develop analog neuromorphic hardware to tackle the ever-increasing digital computation time and resources demanded by current artificial neural networks (ANNs). Here, we demonstrate novel neuromorphic architectures based on Ti/HfO<sub>2</sub>/Pt and Pt/HfO<sub>2</sub>/Pt memristive systems and discuss their electrical performance and their potential applications as ANNs. Current state-of-the-art systems are built on a crossbar array of memristors for neuromorphic computing. With a limit on the number of neurons and regular connectivity, the networks lack sparsity and randomness which results in high wiring cost and poor functional connectivity. To address these limitations, we have fabricated a random array of core-shell memristive wires to form the connectivity matrix for neuromorphic hardware. In the systems listed above,

the conductive core (Ti or Pt) serves as a conductive path or intermediate electrode with a memristive shell (HfO<sub>2</sub>) that can be electroformed with a set of top electrodes (Pt) deposited on the surface. These random nanowire networks are fabricated via electron-beam lithography on a 200 nm × 200 nm write field. Network quantifying simulations revealed a small-world coefficient of 2.89, the shortest path length of 3.61 and a clustering coefficient of 0.057. Remarkably, depending on the forming process, the individual core-shell wires can exhibit eight-wise (8W), counter eight-wise (C8W) bipolar resistive switching (BRS), and complementary resistive switching (CRS). At a low potential ranges ( $\pm 1.5$  V), the wires switch in a bipolar fashion between LRS ( $\sim 11.2$  k $\Omega$ ) and HRS ( $\sim 0.3$  M $\Omega$ ). Symmetric arrangement of layers in the wires along with 8W and C8W switching implies two memristors connected anti-serially. This configuration results in the wires exhibit CRS at higher potentials ( $\pm 2$  V). This ability to switch the devices via BRS or CRS enables us to dynamically control the read-write process. Moreover, due to the transient ON in CRS mode, both the currents and power consumption during the operation of the devices is comparatively lower. Given the low switching voltages, low processing temperatures and materials utilized, these neuromorphic devices can be considered CMOS compatible. In this presentation, the fabrication process, the memristive characteristics (endurance, resistance retention, pulse measurements, etc.), switching mechanism and synaptic characteristics (LTP, STP, and LTD) of the above-listed systems will be discussed in detail.

#### 5:40 AM F.NM07.10.04

##### **Polymer Linked Gold Nanoparticle Networks for Information Storage and Processing—A Molecular Dynamics Study** Xingfei Wei and Rigoberto Hernandez; Johns Hopkins University, United States

At the era of information technology, the growth of data is quickly moving beyond the processing capability of traditional silicon devices. New paradigms for data storage and processing are therefore needed. The answer may be hidden within the structure of your brain. We aim to construct nanoparticle networks inspired by the architecture of actual neural networks to perform brain-like computing. In this work, we show that polymer linked gold nanoparticle (AuNP) networks can function like neuronal networks in information storage and processing. Molecular dynamics (MD) simulations are used to realize their performance. A simple coarse-grained model (AuNP-PAH) is built, which contains one polyallylamine (PAH) chain of 200 repeating units wrapping on a 4 nm diameter citrate capped AuNP. A 2D network model with 100 AuNPs (10\*10\*1) and a 3D network model with 125 AuNPs (5\*5\*5) are constructed by replicating the simple AuNP-PAH structure. The network connection is formed by thermally heating and is also manipulated by an external electric field. The effect of the AuNP volume fraction on network formation will also be reported. We find that these AuNP-PAH networks can process through information differently from existing computing architectures.

#### 5:50 AM F.NM07.10.05

##### **Non-Ohmic Behavior and Resistive Switching of Au Cluster-Assembled Films Beyond the Percolation**

**Threshold** Paolo Milani<sup>1</sup>, Matteo Mirigliano<sup>1</sup>, Francesca Borghi<sup>1</sup>, Alessandro Podestà<sup>1</sup>, Aleandro Antidormi<sup>2</sup> and Luciano Colombo<sup>2</sup>; <sup>1</sup>Università degli Studi di Milano, Italy; <sup>2</sup>Università degli Studi di Cagliari, Italy

Networks based on nanoscale resistive switching junctions are considered promising for the fabrication of neuromorphic computing architectures [1]. To date random networks of nanowires, nanoparticles, and metal clusters embedded in a polymeric matrix or passivated by shell of ligands or oxide layers have been used to produce resistive switching systems. The strategies applied to tailor resistive switching behavior are currently based on the careful control of the volume fraction of the nanoscale conducting phase that must be fixed close to the electrical percolation threshold.

Here, by blending laboratory and computer experiments, we demonstrate that metallic nanostructured Au films fabricated by bare gold nanoparticles produced in the gas phase and with thickness well beyond the electrical percolation threshold, show a non-ohmic electrical behavior and complex and reproducible resistive switching. We observe that the nanogranular structure of the Au films does not evolve with thickness: this introduces a huge number of defects and junctions affecting the electrical transport and causing a dynamic evolution of the nanoscale electrical contacts under the current flow. To uncover the origin of the resistive switching behavior in Au cluster-assembled films, we developed a simple computational model for determining the evolution of a model granular film under bias conditions. The model exploits the information provided by experimental investigation about the nanoscale granular morphology of real films.

Our results show that metallic nanogranular materials have functional properties radically different from their bulk counterparts, in particular nanostructured Au films can be fabricated by assembling bare gold clusters which retain their individuality to produce an all-metal resistive switching system [2].

1 C. Minnai, A. Bellacicca, S. A. Brown, P. Milani, Sci. Rep. 7, 7955 (2017)

2 M. Mirigliano, et al., Nanotechnology 31, 234001 (2020)

#### 6:00 AM F.NM07.10.06

**Tunable Volatile and Non-Volatile Resistive Switching of Non-Stoichiometric CuOx Nanowire for Selector and Memory Application** Chi-Hsin Huang<sup>1</sup>, Kosuke Matsuzaki<sup>2</sup> and Kenji Nomura<sup>1</sup>; <sup>1</sup>University of California, San Diego, United States; <sup>2</sup>Tokyo Institute of Technology, Japan

Resistive random-access memory (ReRAM)/memristive devices based on electrical resistance switching are highly expected to overcome persistent technological limitations in current memory technology and to develop next-generation nonvolatile memory because of its superior characteristics. These characteristics include high speed, high scalability, low power consumption, fast fabrication process, multistate storage, and compatibility with complementary metal-oxide semiconductor (CMOS). Particularly, nanowire-based resistive switching devices offer an ideal platform for a deeper understanding of resistive switching properties due to the confined nanostructure and the opportunity to develop nanoscale-memristive device for next-generation memory and neuromorphic computing. In addition, copper oxide is one of the attractive candidates for ReRAM/memristor due to the existing multiple oxidation states from “+2” to metal state (CuO, Cu<sub>4</sub>O<sub>3</sub>, Cu<sub>2</sub>O, Cu) for inducing resistive switching, which is believed to involve the phase transition with multiple oxidation state induced by redox reaction. In this work, we report the volatile and non-volatile resistive switching effect in p-type non-stoichiometric CuOx nanowires, which are fabricated using insulator CuO nanowires via a thermal-annealing technique with hydrogen atmosphere. These resistive switching modes were effectively controlled by the stability of conductive filament via the compliance current in the SET process. The non-volatile resistive switching exhibited low electric-field-induced switching, high ON/OFF ratio of 107, and long retention time of 104 seconds for ReRAM application. On the other hand, the volatile threshold switching was operated with low compliance current for selector application, and the device showed bidirectional operation, selectivity (104), low OFF-current (<100 pA), and stable reliability with endurance over 105 cycles under pulse operation. The presented work will discuss a nanoscale resistive switching mechanism based on hole-based conducting filament formation originated from the local redox reaction.

**6:10 AM F.NM07.10.07**

**Dissolution of Conductive Filaments by Heat in NiO-Based Resistive Switching Cells** Yusuke Nishi and Tsunenobu Kimoto; Kyoto University, Japan

Resistive switching (RS) operations offer various useful applications for nonvolatile memories and neuromorphic computing. However, driving forces of the RS operations have remained unclear and controversial yet. We reported that conductance quantization in nickel-oxide (NiO)-based RS cells was observed upon a voltage sweep [1,2]. Moreover, not only conductance quantization but conductance fluctuations appeared in the cells by controlling amount of oxygen vacancies in NiO thin films [3]. In this study, disappearance conditions of conductance filaments are investigated through experiments and simulations.

A platinum (Pt) bottom electrode was deposited by sputtering on a silicon-dioxide/p-silicon substrate inserted by a titanium adhesion layer. An 80-nm-thick NiO layer as a resistance change material was subsequently deposited by radio-frequency reactive sputtering. The substrate temperature during sputtering was kept at 350°C. Pt top electrodes with a diameter of 100 μm were deposited on the NiO layer. As a result, a host of Pt/NiO/Pt RS cells were fabricated on the substrate. The first abrupt current jump by an initial voltage sweep to the cell made the cell conductance equivalent to the quantized conductance (2e<sup>2</sup>/h), indicating the formation of a conductive filament with a quantum point contact (QPC). Moreover, conductance fluctuations before and after the abrupt current jump were observed in several cells.

We investigated temperature dependences of cell conductance upon heating the sample. While the conductance in several cells did not change between before and after heating to 400 K, the conductance in other cells decreased by the quantized conductance at 370 K, which means that the conductive filament with a QPC is possibly ruptured by heat at a temperature of merely 370 K [1]. In the same manner, we found that the conductance fluctuations, which originate from the modification of oxygen-vacancy densities at grain boundaries in the NiO layer, possibly disappeared upon heating to, at least, 470 K [3]. In contrast, a fat filament with higher conductance than the quantized conductance created by the conventional forming remained unchanged upon heating to 600 K during a few days. These results indicate a relatively small heat is sufficient for the disappearance of the conductance quantization and fluctuations.

We estimated the temperature rise owing to Joule heat to destroy the conventional fat filament by rough simulation using solvers of heat transfer, electric current, and (particle) diffusion in commercial software COMSOL Multiphysics. The diameter of a cylindrical conductive filament and the diffusion coefficient of oxygen vacancies are assumed to be 10 nm and 10<sup>10</sup> m<sup>2</sup>/s, respectively. The simulation revealed that an applied voltage required for reaching the maximum temperature of 600 K in the filament was 0.34 V, independent of the voltage sweep rate in the range from 0.01 to 1000 V/s. The estimated voltages for reset increased from 0.68 to 1.16 V as the sweep rate increased, which agrees with our experiments to reset upon voltage sweeps. Moreover, the estimated temperature at reset was turned out to be over 680 K. These results indicate that the

temperature required for the diffusion of oxygen vacancies is higher than 600 K. Comparing the simulation to the above heat experiments, temperature required for dissolution of the conductive filament with a QPC is estimated to be lower than 600 K, irrespective of external heat or Joule heat.

The conductance quantization seemed to be a special form of the conductance fluctuations. Although the fluctuations may have poor thermostability at the present, the fluctuations imply the existence of multilevel resistances, which offers the possibility of multiple discrete weighting of synaptic devices.

[1] H. Sasakura et al., Appl. Phys. Lett. **107**, 233510 (2015).

[2] Y. Nishi et al., J. Mater. Res. **32**, 2631 (2017).

[3] Y. Nishi et al., J. Appl. Phys. **124**, 152134 (2018).

SESSION F.NM07.11: Poster Session: Neuromorphic Materials and Devices for Bioinspired Computing and Artificial Intelligence

On Demand Abstracts Available for Viewing Starting Saturday Morning, November 21, 2020

5:00 AM - 8:00 AM

F-NM07

**F.NM07.11.04**

**Energy-Effective Image Restoration Algorithms for Bioimages Enabled by Neuromorphic Computing at**

**Edge** Charlotte Reed<sup>1</sup>, Chanyeol Choi<sup>2</sup> and Jeehwan Kim<sup>2</sup>; <sup>1</sup>Independent Scholar, United States; <sup>2</sup>Massachusetts Institute of Technology, United States

The deep learning in medical image processing had a significant impact on computer-aided diagnosis for the last decade. Although the advanced medical image processing on deep learning allows improvements in image detection, recognition, segmentation, and registration, some of these applications still suffer from the low quality of input images directly from analogue sensors like photodetectors. Here we suggest that an energy-efficient neuromorphic computing platform where low-quality bioimages can be directly processed at edge without energy-hungry image signal processor (ISP). Even with a small convolutional kernel operation for image processing, a peak signal to noise ratio (PSNR) of images from GaAs detectors has been subsequently improved from 16.25 to 19.26 in ten random bio cell images with > 30 % energy savings compared to silicon-based ISP technology. In a segmentation task after image processing, a cell detection accuracy increases from 75 % to 95 % and an detection error rate decreases from 10 % to 2 %. We believe that our edge neuromorphic computing solution can offer fast image processing time and low energy consumption, and thus provide quick and reliable data while maintaining intuitive and safe image reading.

**F.NM07.11.06**

**Modelling Electronic-Thermal-Driven Electrical Conduction in Analog-Based Memristor for Neuromorphic Computing Applications**

Qishen Wang<sup>1</sup>, Karthekeyan Periasamy<sup>1</sup>, Yi Fu<sup>2</sup>, Ya-Ting Chan<sup>2</sup>, Cher-Ming Tan<sup>2</sup>, Natasa Bajalovic<sup>1</sup>, Jer-Chyi Wang<sup>2</sup> and Desmond Loke<sup>1</sup>; <sup>1</sup>Singapore University of Technology and Design, Singapore; <sup>2</sup>Chang Gung University, Taiwan

Device transport processes in the switching of analog-based memristors rely on device conduction mechanism, whose complexity still cannot be captured by traditional modelling approaches. Here we apply the concept of the unique combination of electronic and thermal considerations to modelling device conduction in such systems. The approach can fully account for the rich conduction behavior, as well as analog-type resistive switching, and is therefore, ideal for device films, composites and other geometries. Modelling of the analog-based memristor agrees well with experimental data and reveals conduction behavior not yet captured by conventional models. Fitting of device measurements even allows conduction properties to be extracted, which are subsequently harnessed to guide the prediction of analog-based memristors with improved device performance. Our hybrid approach, together with a simple calculation tool, now allows researchers with limited computation experience to perform realistic simulations.

**F.NM07.11.07**

**Dielectric Breakdown by Electric-Field Induced Phase Separation** Dimitrios Fraggedakis and Martin Bazant; Massachusetts Institute of Technology, United States



The control of the dielectric and conductive properties of device-level systems is important for increasing the efficiency of energy- and information-related technologies. In some cases, such as neuromorphic computing, it is desirable to increase the conductivity of an initially insulating medium by several orders of magnitude, resulting in effective dielectric breakdown. Here, we show that by tuning the value of the applied electric field in systems with variable electric permittivity and conductivity, e.g. ion intercalation materials, we can vary the device-level electrical conductivity by orders of magnitude. We attribute this behavior to the formation of filament-like conductive domains that percolate throughout the system.

#### F.NM07.11.08

##### **Correlation Between Depth Distribution of Chemical Compositions and Resistive Switching Characteristics in Metal/Ta<sub>2</sub>O<sub>5</sub>/Pt Cells** Toshiki Miyatani, Yusuke Nishi and Tsunenobu Kimoto; Kyoto University, Japan

Resistive switching cells are one of the strong candidates for synaptic devices thanks to analog controllability of the cell resistance. Many previous studies have reported continuous increase in the cell resistance when a voltage is applied to the cell, so-called gradual reset [1]. Nevertheless, the origin of the gradual reset is not clear because it is extremely difficult to determine an ultrafine region where resistive switching occurs. In this study, we investigated depth distribution of chemical compositions in the entire fabricated sample by high-resolution Rutherford backscattering spectrometry (HRRBS) without sample sputtering. Moreover, we discuss correlation between the depth distribution and electrical characteristics in TaO<sub>x</sub>-based resistive switching cells.

We fabricated two types of Metal/tantalum-oxide (Ta<sub>2</sub>O<sub>5</sub>)/platinum (Pt) stack structures on SiO<sub>2</sub>/Si substrates. As common fabrication processes, a Pt bottom electrode was deposited by DC sputtering. Then, a Ta<sub>2</sub>O<sub>5</sub> film was deposited by radio-frequency (RF) reactive sputtering. Finally, a metal layer was deposited by RF sputtering. We used nickel (Ni), titanium (Ti), and Ta as materials of the metal layer. As for one type of the Metal/Ta<sub>2</sub>O<sub>5</sub>/Pt structure, the metal layer covered a 5-nm-thick Ta<sub>2</sub>O<sub>5</sub> film. The thickness of the metal layer was 10 nm. For these samples, we investigated depth distribution of chemical compositions by the HRRBS. The depth distribution can be obtained without sample destruction, which means intrinsic data are not hidden by a knock-on effect. Moreover, the HRRBS has a higher depth resolution on the order of nanometers than the normal RBS. Then, the actual depth distributions were obtained by fitting energy spectra simulated from assumed depth distributions to experimental energy spectra. Note that RBS measurements at two scattering angles of 77 and 122 degrees improved accuracy in the depth distributions by a comparison of the obtained data each other in the same sample. As for the other type of the Metal/Ta<sub>2</sub>O<sub>5</sub>/Pt structure, the metal layer was deposited with a thickness of 20 nm and a diameter of 150 μm by using a mask as a top electrode on a 10-nm-thick Ta<sub>2</sub>O<sub>5</sub> film. We examined resistive switching characteristics for these Metal/Ta<sub>2</sub>O<sub>5</sub>/Pt cells at room temperature with the Pt bottom electrode grounded.

Comparing the depth distributions of the as-deposited Metal/Ta<sub>2</sub>O<sub>5</sub>/Pt samples, thickness of the oxygen diffusion area in the Metal/Ta<sub>2</sub>O<sub>5</sub> interface, which is less than 10 nm, increased in the order of Ni/Ta<sub>2</sub>O<sub>5</sub>/Pt, Ta/Ta<sub>2</sub>O<sub>5</sub>/Pt, and Ti/Ta<sub>2</sub>O<sub>5</sub>/Pt samples. The diffusion of oxygen from the Ta<sub>2</sub>O<sub>5</sub> film to the metal layer corresponds to supply of oxygen vacancies from the metal layer to the Ta<sub>2</sub>O<sub>5</sub> film. Here, the standard Gibbs energy of oxide formation of the metal layer is -4.39 eV (Ni), -7.92 eV (Ta), and -9.21 eV (Ti) [3], indicating that more oxygen vacancies tend to be supplied to the Ta<sub>2</sub>O<sub>5</sub> film as the magnitude of the standard Gibbs energy is higher.

The Ni/Ta<sub>2</sub>O<sub>5</sub>/Pt cells show relatively high initial resistance at 0.1 V of roughly 10<sup>12</sup> Ω before a forming process. On the other hand, the Ti/Ta<sub>2</sub>O<sub>5</sub>/Pt cells show lower initial resistance of about 10<sup>6</sup>-10<sup>9</sup> Ω because more oxygen vacancies are supplied to the Ta<sub>2</sub>O<sub>5</sub> film. Furthermore, when a negative voltage is applied to the Ni/Ta<sub>2</sub>O<sub>5</sub>/Pt cells, the cell resistance abruptly increases, approximately at -1 V from 100 Ω to 10 MΩ. In contrast, in the case of the Ti/Ta<sub>2</sub>O<sub>5</sub>/Pt cells, the cell resistance gradually increases from 1 kΩ to 100 kΩ when a voltage is applied from -1 V to -3 V.

These results suggest that the analog controllability of the cell resistance in the reset processes can be improved by supplying a larger number of oxygen vacancies to the Ta<sub>2</sub>O<sub>5</sub> film.

[1] D. Ielmini, *Microelectronic Engineering*, **190**, 44 (2018).

[2] T. Miyatani *et al.*, *MRS Advances*, **4**, 2601 (2019).

[3] C. Chen *et al.*, *J. Appl. Phys.*, **114**, 014502 (2013).

#### F.NM07.11.09

##### **Post Metallization Annealing Effect Utilizing Pt Gate Electrode for MFSFET with Ferroelectric Nondoped HfO<sub>2</sub> Formed by Ar/O<sub>2</sub>-Plasma Sputtering** Shun-ichiro Ohmi, Masakazu Kataoka and Masaki Hayashi; Tokyo Inst of

## Introduction

Ferroelectric nondoped HfO<sub>2</sub> has advantages compared to the doped HfO<sub>2</sub> in the reduction of crystallization temperature and threshold voltage ( $V_{TH}$ ) control to realize the Metal-Ferroelectrics-Si FET (MFSFET) [1,2]. We have reported that the ferroelectric nondoped HfO<sub>2</sub> formation on the Si(100) substrates by controlling the Ar/O<sub>2</sub> flow ratio during the reactive sputtering [3-5]. In this paper, we have investigated the effect of post metallization annealing (PMA) utilizing Pt gate electrode for the MFSFET with ferroelectric nondoped HfO<sub>2</sub> gate insulator.

## Experimental Procedure

After the active region patterning, n<sup>+</sup> source/drain (S/D) ion implantation was carried out followed by the activation annealing at 900°C/20 min in N<sub>2</sub> ambient. Then, the 1 nm thick Hf interlayer was deposited to improve the film quality followed by the 20 nm thick HfO<sub>2</sub> in-situ deposition at room temperature (RT) by the RF magnetron sputtering with the Ar/O<sub>2</sub>-plasma utilizing Hf target. The flow rate of Ar for Hf interlayer and Ar/O<sub>2</sub> for HfO<sub>2</sub> was 3.6 and 2.3/0.5 sccm, respectively, with the sputtering power of 60 W. Then, the 20 nm thick Pt gate electrode (G) was in-situ deposited at RT with the Ar flow rate of 4.4 sccm and the sputtering power of 80 W. Next, the S/D contact region was patterned followed by the Pt layer deposition for S/D. Then, PMA was carried out at 600°C/30 s in N<sub>2</sub> ambient followed by the G and S/D patterning. The gate length (L) and width (W) was 10/90 μm. The MFS diodes were fabricated in a same process, and the post deposition annealing (PDA) was also examined utilizing evaporated Al gate electrode for the comparison.

## Results and Discussion

The remnant polarization ( $2P_r$ ) of 2.5 μC/cm<sup>2</sup> was obtained from the P-V characteristics for the MFS diodes formed by the PMA process under the ±8 V sweep which is larger than the  $2P_r$  of 2.3 μC/cm<sup>2</sup> for the MFS diodes formed by the PDA process. From the C-V characteristics, the memory window (MW) was markedly increased from 0.22 V for the MFS diodes formed by the PDA process to 0.44 V for the MFS diodes formed by the PMA process. This is due to the enhancement of the orthorhombic phase HfO<sub>2</sub> formation by the PMA process which was confirmed by the grazing incident x-ray diffraction (GI-XRD) observation. The physical thicknesses were confirmed as 3.6 nm for SiO<sub>2</sub> interfacial layer (IL) and 20.8 nm for HfO<sub>2</sub> from the cross-sectional transmission electron microscopy (TEM) image. By considering the coercive voltage ( $V_c$ ) of 1.08 V extracted from the P-V characteristics, the coercive field ( $E_c$ ) was estimated as 0.52 MV/cm. The ferroelectric HfO<sub>2</sub> formation without doping realized the lower  $E_c$  compared to the reported data for the doped HfO<sub>2</sub>. Next, the MFSFET fabricated utilizing PMA process was evaluated. From the  $I_D$ - $V_G$  characteristic, MW of 0.41 V was obtained under the  $V_G$  sweep from -1 V to 3 V. The program and erase (P/E) characteristics were also examined. The MW obtained from the threshold voltage ( $V_{TH}$ ) difference of 0.41 V were also confirmed utilizing the P/E pulses of -5.5 V/100 ms and 6.5 V/100 ms, respectively. The MW of 0.15 V was obtained even at the P/E pulse width of 100 ns.

## Conclusions

In this paper, we investigated the effect of PMA for the device characteristics of MFSFET with ferroelectric nondoped HfO<sub>2</sub> formed by the Ar/O<sub>2</sub>-plasma sputtering. It was found that the small  $E_c$  was obtained for the 20 nm thick ferroelectric nondoped HfO<sub>2</sub>. Furthermore, the MW of 0.15 V was realized under the P/E pulse width of 100 ns with P/E voltages of -5.5 V and 6.5 V, respectively.

## Acknowledgements

This work was partially supported by JSPS KAKENHI Grant Number 19H00758, NEDO, JST, and CASIO Foundation.

## References

[1] T.S. Boscke *et al.*, *IEDM Tech. Dig.*, p. 547 (2011)., [2] F. Winkler *et al.*, *DRC Conf. Dig.*, p. 49, (2019)., [3] M.G. Kim, S. Ohmi *et al.*, *Jpn. J. Appl. Phys.*, **57**, 111UF09 (2018)., [4] S. Ohmi *et al.*, *Jpn. J. Appl. Phys.*, **58**, SIIB16 (2019)., [5] S. Ohmi *et al.*, *DRC Conf. Dig.* (2020). [to be presented]

## F.NM07.11.10

**“Metal-Organic Frameworks × Ionic Liquids” as an Electrolyte for Conductive Bridge Random Access Memory** Sang-Gyu Koh and Kentaro Kinoshita; Tokyo University of Science, Japan

Conductive bridge random access memory (CBRAM) is one of the most promising nanodevices for future information technology with applications not only for memory, but also for logic and neuromorphic computing because of its low power consumption and response times in the nanosecond range, as well as scalability down to the atomic level [1]. Recently, we

have reported that several drastic improvements for controllability of memory performance can be achieved by using ionic liquids (ILs) as a tunable solvent supplied into the grain boundaries of metal oxide film [2, 3]. We focused, as a next step, on the electrolyte engineering, in which the electrolyte should not be regarded as a diffusive medium for the migration of metal ions as ever but should be regarded as a porous body retaining ILs which mediates the ion migration in it. Metal-organic frameworks (MOFs), which is three-dimensional nanoporous materials composed of metal ions and organic ligands coordinated together, are the best candidate for the porous body retaining ILs without compromising their features owing to structural and functional flexibility in the design for uniformly sized nanopores, as well as relatively high thermal stability [4]. Although there are some reports so far that investigate the electrical characteristics of MOFs, most of their experiments has been done using pellet or polycrystalline film samples from which it is difficult to extract intrinsic bulk properties due to a lot of grain boundaries [5]. Moreover, ILs-loaded MOFs for the application of CBRAM has not yet been discussed so far. In this work, basic investigations in terms of electrical properties for HKUST-1 ( $\text{Cu}_3(1,3,5\text{-benzenetricarboxylic acid})_2$ ), which is to be easily synthesized and stable in air, were carried out using single crystalline sample. We clarified the dominant conduction mechanism of the HKUST-1 single crystals which include much less grain boundaries, by measuring the electrical conductivity as functions of a bias voltage, temperature and humidity. Ion conductivities of the IL ([*emin*][TFSI] (1-ethyl-3-methylimidazolium bis(trifluoromethylsulfonyl)-imide)) loaded into the nanopores of HKUST-1 single crystal were compared with that of bulk IL as a function of temperature using electrochemical impedance spectroscopy. The both activation energies extracted from the temperature dependence of ion conductivities were comparable, suggesting that the HKUST-1 enables to retain the IL without compromising its original property. We, furthermore, demonstrated by means of electromotive force measurement that the ionization of the electrochemically active electrode in a Ag/HKUST-1/Au structure under bias voltage, which is the first important step in CBRAM operation, was drastically promoted by loading the IL into the nanopores of HKUST-1. The ILs-loaded MOFs system provides a novel electrolyte which endow CBRAM with further improved memory performance.

[1] R. Waser *et al.*, *Adv. Mater.* 21, 2632 (2009).

[2] A. Harada *et al.*, *J. Mater. Chem. C* 4, 7215 (2016).

[3] K. Kinoshita *et al.*, *Jpn. J. Appl. Phys.* 56, 04CE13 (2017).

[4] I. Stassen *et al.*, *Chem. Soc. Rev.* 46, 3185 (2017).

[5] A. A. Talin *et al.*, *Science* 343, 66 (2014).

#### F.NM07.11.11

**Complex Electrical Spiking Activity in Resistive Switching Nanostructured Au Two-Terminal Devices** Paolo Milani<sup>1</sup>, Matteo Mirigliano<sup>1</sup>, Davide Decastri<sup>1</sup>, Alberto Pullia<sup>1</sup>, Alberto Casu<sup>2</sup> and Andrea Falqui<sup>2</sup>; <sup>1</sup>Università degli Studi di Milano, Italy; <sup>2</sup>King Abdullah University of Science and Technology, Saudi Arabia

Networks of nanoscale objects are subject of increasing interest as resistive switching systems for the fabrication of neuromorphic computing architectures. Nanostructured films of bare gold clusters produced in gas phase with thickness well beyond the electrical percolation threshold, show a non-ohmic electrical behavior and resistive switching resulting in groups of current spikes with irregular temporal organization [1]. Here we report the systematic characterization of the temporal correlations between single spikes and spiking rate power spectrum of nanostructured Au two-terminal devices consisting of a cluster-assembled film deposited between two planar electrodes. By varying the nanostructured film thickness we fabricated two different classes of devices with high and low initial resistance respectively. We show that the switching dynamics can be described by a power law distribution in low resistance devices whereas a bi-exponential behavior is observed in the high resistance ones [2]. The measured resistance of cluster-assembled films shows a  $1/f^\alpha$  scaling behavior in the range of analyzed frequencies. Our results suggest the possibility of using cluster-assembled Au films as components for neuromorphic systems where a certain degree of stochasticity is required.

1 M. Mirigliano, *et al.*, *Nanoscale Adv.* 1, 3119 (2019)

2 M. Mirigliano, *et al.*, *Nanotechnology* 31, 234001 (2020)

#### F.NM07.11.15

**Investigation and Characterization of the Annealing Effects on the Ferroelectric Behavior of BaTiO<sub>3</sub> Deposited by Pulsed Laser Deposition** Joshua Mayersky<sup>1</sup>, Albert Hilton<sup>2</sup>, Shanee Pacley<sup>3</sup>, Rashmi Jha<sup>1</sup> and Amber N. Reed<sup>3</sup>; <sup>1</sup>University of Cincinnati, United States; <sup>2</sup>KBR, United States; <sup>3</sup>Air Force Research Laboratory, United States

In pursuit of the goal of mimicking how the human brain learns and functions, emulation of synaptic plasticity, i.e. the ability of synapses to strengthen or weaken over time, is a critical requirement for the implementation of learning in neuromorphic systems. Finding the proper materials to synthesize nanoscale synapses and neurons that are reliable, durable, replicable and scalable remains a challenge. Recent developments on ferroelectric field effect transistor based non-volatile memory are

encouraging in this respect; in particular, their multiple threshold voltage states based on the polarization state of a ferroelectric oxide may offer a suitable structure for synaptic applications. This work investigates the ferroelectric behavior of BaTiO<sub>3</sub> (BTO) with and without annealing of the deposited film. 100 nm of BTO was deposited via Pulsed Laser Deposition (PLD) on a Niobium doped Strontium Titanate (Nb:STO) substrate. The process parameters included a temperature of 750 °C, an operating pressure of 10 mTorr under 35 sccm of O<sub>2</sub>, and a laser energy of 300 mJ. After deposition, the film was characterized via a coupled 2-theta-omega X-Ray Diffraction (XRD) scan; looking for the peak associated with the tetragonal phase of BTO. This was followed by characterizing the poling/switching characteristics using Piezoresponse Force Microscopy (PFM). Following these initial characterizations, the film was subjected to a 30 minute anneal at 850 °C in 100 Torr of O<sub>2</sub>. After this annealing step, the film was once again re-characterized using XRD and PFM. The BTO 2-Theta peak shifted from the annealed vs. non-annealed sample, to around 44.2 °, closer to the expected value for the tetragonal phase. A small region was then poled at +5 V, and the phase of the film monitored for the next 24 minutes. The poling did not result in any damage nor oxidation to the surface, which differed from the non-annealed BTO film. No degradation in the poled region was visible for the duration of measuring, whereas for the non-annealed film, the poled region started relaxing after 8 minutes. Finally, 100 nm of W was sputtered and patterned into 100 μm by 100 μm contact pads, and the film was subjected to electrical testing. This consisted of a forming sweep (PUND – Positive, Up, Negative, Down) of varying pulse lengths and amplitudes, followed by a hysteresis sweep of varying pulse lengths and amplitudes. For each test, an average was taken from 3 different devices. For a given forming sweep amplitude, pulse length, and a hysteresis sweep amplitude, an increasing pulse length of the hysteresis sweep resulted in an increase in the measured remnant polarization from 1.3 μC/cm<sup>2</sup> to 6 μC/cm<sup>2</sup>. Similarly, for all other variables constant, an increase in the pulse length of the forming sweep resulted in an increase in the remnant polarization from 3.53 μC/cm<sup>2</sup> to 5.73 μC/cm<sup>2</sup>. And again, all other variables constant, an increase in the forming amplitude resulted in an increased remnant polarization from 2.9E-3 μC/cm<sup>2</sup> to 5.9 μC/cm<sup>2</sup>. Here we demonstrate multiple, distinct polarization states of BTO as a function of the forming and hysteresis sweep pulse lengths and amplitudes.

#### F.NM07.11.16

**Late News: Modeling Resistive Switching in Nanogranular Metal Films** [Walter Tarantino](#) and Luciano Colombo; Università degli Studi di Cagliari, Italy

Nanogranular golden films present an interesting resistive switching behavior that can be exploited in the designing of components for neuromorphic computing. Its investigation has started only recently [Mirigliano *et al.* 2019, Mirigliano *et al.* 2020] and the underlying microscopical physical mechanisms are far from being clear. We address the challenge of its theoretical characterization from the limited information on the microscopic structure of the films with the tools of Effective Mean Theory, and present a model for thermally regulated local structural rearrangements that may explain the observed data.

### SYMPOSIUM F.SM01

---

Lessons from Nature—From Biology to Bioinspired Materials  
November 21 - December 4, 2020

#### Symposium Organizers

Sung Kang, Johns Hopkins University  
Boaz Pokroy, Technion-Israel Institute of Technology  
Nicolas Vogel, University Erlangen-Nürnberg  
Lauren Zarzar, The Pennsylvania State University

---

\* Invited Paper

SESSION F.SM01.10: Live Keynote I: Lessons from Nature—From Biology to Bioinspired Materials  
Session Chairs: Boaz Pokroy and Nicolas Vogel

Tuesday Morning, December 1, 2020  
F.SM01

**8:00 AM \*F.SM01.04.01**

**Skeletons with Eyes** Joanna Aizenberg; Harvard University, United States

The most finely tuned, rapidly responsive, and precisely directed optical systems currently known can be found on the surfaces of living organisms. Studies of brittlestars' tunable microlenses, sea sponges' optical fibers, butterflies' and beetles' intense colors, and squids' nearly perfect camouflage have revealed 3D architectures so intricately patterned down to the nanoscale that the topography itself controls the wavelengths and direction of reflected light. We are developing bioinspired, bottom-up self-assembly techniques that allow us to create comparably elaborate yet tunable hierarchical photonic structures, and integrate these into the design of a new class of dynamic, responsive optical materials.

**8:30 AM \*F.SM01.05.01**

**Organisms Manipulate Light with Nano-Scale Crystal Mirrors** Benjamin A. Palmer, Gan Zhang, Ofir Friedman, Anna Hirsch, Venkata J. Yallapragada, Dan Oron, Leor Kronik, Leslie Leiserowitz, Steve Weiner and Lia Addadi; Weizmann Institute of Science, Israel

Organisms construct 'devices' based on assemblies of organic nano-crystals with optical functions. The structure, polymorph, size, morphology and superstructural arrangement of the crystals determine the optical properties of the 'device'. All the crystals have unusually high refractive indexes in the directions along which the light penetrates the crystal. The controlled assembly of nano-crystals forms multilayer reflectors that create structural colors, or mirrors and light scattering layers that function to increase vision sensitivity in the eyes of the organisms. Scallops have tens of eyes, each containing a concave multi-layered mirror perfectly tiled with a mosaic of square guanine crystals, made up of composite twins, reflecting light to form images onto the overlying retinas [1]. Crustacean decapods such as shrimps, crayfish and lobsters possess compound eyes that contain two sets of mirrors, composed of isoxanthopterin crystals. The two mirrors have very different ultrastructures and functions that we can rationalize in terms of the optical performance of the eye [2,3]. The unusual zander fish eyes contain two layers of organic crystals: thin guanine crystals, form a reflective layer in the back of the eye, whereas block-shaped crystals of 7, 8-dihydroxanthopterin in the inner tapetum layer back-scatter light onto the retina, increasing the light sensitivity of the eye [4]. Finally, insects commonly known as jumping bristletails, form large amounts of xanthine crystals in their median and lateral ocelli [5]. The structure-function relations in this last example are still under investigation. In all these examples, the constituent molecules are mostly purines and pteridines, which raises the question of what molecular and structural characteristics of these crystals, favor their use for optical functions in organisms. Furthermore, the organization of the crystalline functional components is controlled from the crystal structure at the nanoscale to the complex 3D structure at the millimeter level, extending the interest in the relation between structure and optical properties to higher hierarchical levels.

[1] B.A. Palmer, G.J. Taylor, V. Brumfeld, D. Gur, M. Shemesh, N. Elad, A. Osherov, D. Oron, S. Weiner, L. Addadi: The Image Forming Mirror in the Eye of the Scallop. *Science* 358, 1172–1175 (2017).

[2] B.A. Palmer, A. Hirsch, V. Brumfeld, E.D. Aflalo, I. Pinkas, A. Sagi, S. Rozenne, D. Oron, L. Leiserowitz, L. Kronik, S. Weiner and L. Addadi: Isoxanthopterin: An Optically Functional Biogenic Crystal in the Eyes of Decapod Crustaceans. *PNAS*, 115, 10, 2299–2304 (2018).

[3] B.A. Palmer, V. J. Yallapragada, N. Schiffmann, E. Merary Wormser, N. Elad, E.D. Aflalo, A. Sagi, S. Weiner, L. Addadi, D. Oron: Highly Reflective Biogenic Materials from Core-Shell, Birefringent Nanospheres. *Nature Nanotechnology* 15, 138–144 (2020).

[4] G. Zhang, A. Hirsch, G. Shmul, L. Avram, N. Elad, V. Brumfeld, I. Pinkas, I. Feldman, R. Ben Asher, B. A. Palmer, L. Kronik, L. Leiserowitz, S. Weiner and L. Addadi: Guanine and 7, 8-dihydroxanthopterin reflecting crystals in the zander fish eye: crystal locations, compositions and structures, *J Am Chem Soc* 141, 19736–19745 (2019).

[5] A. Böhm and G. Pass: The ocelli of Archaeognatha (Hexapoda): functional morphology, pigment migration and chemical nature of the reflective tapetum, *The Journal of Experimental Biology* 19, 3039-3048 (2016).

### 9:00 AM \*F.SM01.01.01

**Bone—Deciphering the Tissue Organization and Materials Properties in 3D Using FIB SEM** Steve Weiner<sup>1</sup>, Emeline Raguin<sup>1</sup>, Neta Varsano<sup>1</sup>, Heden Haimov<sup>1</sup>, Lia Addadi<sup>1</sup> and Ron Shahar<sup>2</sup>; <sup>1</sup>Weizmann Institute of Science, Israel; <sup>2</sup>Hebrew University, Israel

Bone is both a tissue, comprising cells, vasculature and extracellular matrix, and a material comprising mainly mineral, collagen and water. It is thus a challenge to characterize bone's 3D structural organization in order to gain insights into how bone forms and functions. Focused ion beam-scanning electron microscopy (FIB SEM) can provide information at nanometer resolution to enable, for instance the identification of the collagen D-banding. At this resolution the spatial arrangement of fibrils can be assessed in volumes of thousands of microns cubed which can include tissue components. For example, examination of mineralized osteonal pig bone shows unidirectional collagen arrays oriented alternatively in different directions or changing direction progressively. These unidirectional arrays are separated by layers of collagen organized in a bidirectional patchwork motif. Earlier studies of demineralized lamellar bone showed that the layers with the patchwork motif stain heavily with osmium and Alcian Blue and have a disordered appearance.

Another example is the cryo- FIB SEM examination after cryo-fixation and under cryo-conditions, of the mineralized murine growth plate. It reveals the presence of a complex zone that includes blood vessels with mineral containing vesicles, blood vessel extremities surrounded by bone mineralizing matrix, and cartilage hypertrophic cells surrounded by ordered and disordered cartilage mineralizing matrix.

By exploiting the options for examining mineralized bone, demineralized bone matrix and the soft tissue components as well as the bone, FIB SEM can provide invaluable insights into bone organization. By combining FIB SEM in a correlative manner with 3D confocal light microscopy and microCT, it will be possible to address many fundamental questions in bone biology and mechanics.

Reznikov, N., Shahar, R. and Weiner, S. 2014. Bone hierarchical structure in three dimensions. *Acta Biomaterialia* 10, 3815-3826.

Haimov, H., Shimoni, E., Brumfeld, V., Shemesh, M., Varsano, N., Addadi, L. and Weiner, S. 2020. Mineralization pathways in the active murine epiphyseal growth plate. *Bone* 130, <https://doi.org/10.1016/j.bone.2019.115086>.

Raguin, E., Rechav, K., Brumfeld, V., Shahar, R. and Weiner, S. 2020. Unique three-dimensional structure of a fish mandible bone subjected to unusually high mechanical loads. *J. Structural Biol.* (in press).

### 9:30 AM \*F.SM01.01.03

**Osmotic Force Generation in Biological Materials** Peter Fratzl; Max Planck Institute of Colloids and Interfaces, Germany

Biological extracellular tissues are based on proteins, polysaccharides and, in certain cases, minerals. Their complex multiscale structure confers them a wide range of properties in accordance with the tissues' functions. While active functionality are usually attributed to cells, there are also examples of materials synthesized by living organisms, such as plant seeds, which fulfil an active function without living cells and work as mechanosensors and actuators. Water is an important component of all such extracellular tissues. While it is well known that the level of hydration determines the mechanical properties of many biological materials, it is less appreciated that water also plays an active role in generating forces within the materials. In particular water absorption and desorption provides actuation in a variety of plant seeds, including wild wheat, stone plant and banksia seed capsules. The shape change upon water uptake that provides the actuation is controlled by specific cellulose fibre architectures. In this way, well-controlled movements, such as bending, twisting or curling are programmed in these materials by structure of the underlying cellulose microarchitecture. The required deformation energy is provided by the absorption of water from the environment. Finally, the absorption of water to specific molecules and the resulting osmotic pressure is also providing internal stresses which control, for example, the mechanical behaviour of collagen in tendon, bone and dentin. The lecture will review general concepts for the roles of water in biological materials, both in the context of biology and of bioinspired engineering.

SESSION F.SM01.11: Live Keynote II: Lessons from Nature—From Biology to Bioinspired Materials  
Session Chairs: Sung Kang and Lauren Zarzar  
Wednesday Afternoon, December 2, 2020  
F.SM01

### 5:15 PM \*F.SM01.07.01

**3D Materials Systems as Bioelectronic Neural Interfaces and Bioinspired Passive Microfliers** John A. Rogers;

Northwestern University, United States

3D mesostructures represent essential, ubiquitous design features in biology, from the spherical constructs of living organoids to the aerodynamic shapes of swirling maple seeds. This talk presents our work in two corresponding areas of 3D materials engineering. The first focuses on mechanically compliant, 3D multifunctional neural interfaces to cortical spheroids and assembloids. Detailed studies of the spreading of coordinated bursting events and the cascades associated neuroregeneration represent two of the many opportunities in neuroscience research uniquely enabled by these platforms. The second area is in exploratory 3D materials architectures that mimic the aerodynamic features of gliding, spinning and twirling seeds that facilitate their dispersal. The talk will emphasize both basic and applied aspects of these two distinct classes of materials systems.

**5:39 PM \*F.SM01.07.04**

**Bio-Inspired Photosynthetic, Robotic and Bioactive Materials** [Samuel I. Stupp](#); Northwestern University, United States

The soft and hard materials that make up biological systems are a great source of inspiration in materials science for design of functional systems, particularly those that are critical in supporting the most intelligent processes in the plantae and animalia kingdoms. Great ideas from these systems include, the notion of self-assembly and reversible formation of structures, creating adaptive behaviors for specific environments, materials with capacity for self-repair, the engineering of autonomous motion, and the integration of multiple functions in a single structure, among many others. In this lecture bio-inspired synthetic systems are described based on supramolecular polymers as well as “hybrid bonding polymers (HBPs), which we define as materials that rationally integrate covalent and supramolecular polymers. HBPs are biomimetic structures critical in systems such as biological membranes, muscles, tendons, and the cytoskeleton. One of the systems to be described is based on supramolecular polymers that are highly dynamic and therefore strongly effective at signaling cells for regeneration. The lecture will also describe photosynthetic materials, inspired by leaves, in which HBPs are used to couple light harvesting assemblies and catalysts to make fuels. Finally robotic materials that emulate living creatures will be discussed in which HBPs or organic-metal hybrid hydrogels are configured to respond to light and magnetic fields in order to generate locomotion of macroscopic objects on surfaces.

**6:03 PM \*F.SM01.07.02**

**A Portable, Biologically-Inspired Platform for Color and Pattern Sensing and Display** [Leila Deravi](#); Northeastern University, United States

A small number of animals have the ability to actively change their visual appearance to perform important biological tasks. Cephalopods rank high on this list due to their ability to rapidly change color and texture - in some cases - for defense and signaling and have been a source of inspiration for the design of next generation adaptive systems. Recently, the electrochemical properties of the primary pigment found in cephalopod skin, xanthommatin, have been harnessed and applied in color-switching electrochromic displays with low power requirements. We describe the translation of this technology into a compact form factor that can sense and measure color from the environment then activate spatially patterned coloration with rapid (ca. seconds) response times. Our device uses reflectance-based sensors to measure color then triggers the formation of hue matched patterns by arrayed display components that can match and/or “hide” on surfaces of varying geometry, color, and luminous intensity. In future iterations of our approach, these principles may be applied to expand the palette of measured and displayed colors or to construct soft, deformable systems that can alter their optical signatures in response to environmental cues.

**6:27 PM \*F.SM01.02.01**

**Bio-Enabled Nanocomposites with Unique Physical Properties** [Vladimir Tsukruk](#); Georgia Institute of Technology, United States

Bio-enabled nanocomposites represent a novel class of functional bioderived materials, which uses principles of bioinspiration and biomimetic to design hierarchically organized hybrid materials with co-assembled biological and synthetic components to bring best of synthetic and biological worlds: versatile functions with responses to mechanical, optical, chemical, and light stimuli and mechanical strength, flexibility, biocompatibility, and environmental robustness [1, 2]. In first set of examples, we discuss uniformly aligned chiral bio-photonic films from a liquid crystal phase formed by a cellulose nanocrystal solution placed in a thin capillary [3]. This spatial and fluidic flow confinement facilitates homogeneous growth of chiral pseudo-layers parallel to the interface in contrast to the highly heterogeneous assembly of random tactoids. The resulting iridescence films show a narrower optical reflectance band and uniform birefringence over larger macroscopic regions than heterogeneous conventional drop-cast films. In another example, enhanced chiral properties of organized helical

patterned films with high asymmetry of circular polarization have been template-assembled via preferential orientation of high-aspect cellulose nanocrystals onto optical microgrids [4]. Bright chiral emission has been co-assembled in organized biopolymer photonic films from core-shell nanorods of cellulose nanocrystals and co-assembled carbon quantum dots mediated by polymer linkers [5]. Finally, co-assembly of cellulose nanocrystals with amorphous polysaccharides resulted in the formation of robust and flexible films with the preservation of the original structural photonic and fine control of the pitch length due to intimate intercalation of macromolecular backbones into the interstitial nanoscale pores of neighboring nematic monolayers [6].

- [1] R. Xiong, J. Luan, S. Kang, S. Singamaneni, V. V. Tsukruk, Natural Biopolymers for Organized Photonic Structures, *Chem. Soc. Review*, 2020, 49, 983.
- [2] R. Xiong, A. M. Grant, R. Ma, S. Zhang, V. V. Tsukruk, Naturally-derived biopolymer nanocomposite: interfacial design, properties and emerging applications, *Mat. Sci. & Eng. Reports*, 2018, 125, 1.
- [3] V. Cherpak, V.F. Korolovych, T. Turiv, D. Nepal, J. Kelly, T.J. Bunning, O.D. Lavrentovich, V.V. Tsukruk, Robust Chiral Organization of Cellulose Nanocrystals in Capillary Confinement, *Nano Lett.*, 2018, 118, 6770.
- [4] R. Xiong, S. Yu, S. Kang, K. M. Adstedt, D. Nepal, T. J. Bunning, V. V. Tsukruk, Integration of Optical Surface Structures with Chiral Nanocelluloses for Enhanced Chiroptical Properties, *Adv. Mater.*, 2019, 1905600.
- [5] R. Xiong, S. Yu, M. J. Smith, J. Zhou, M. Kreckler, L. Zhang, D. Nepal, T. J. Bunning, V. V. Tsukruk, Assembling Carbon Quantum Dots on Cellulose Nanocrystals for Chiral Luminescent Biophotonic Materials, *ACS Nano*, 2019, 13, 9074.
- [6] K. Adstedt, E. A. Popenov, K. J. Pierce, R. Xiong, R. Geryak, V. Cherpak, D. Nepal, T. J. Bunning, V. V. Tsukruk, Broad iridescence of natural polymer nanocomposites: chiral nanocrystals intercalated with amorphous polysaccharides, 2020, in press.

#### 6:51 PM \*F.SM01.02.03

**Exploiting Supramolecular Associations in Interpenetrating Networks and Elastomers** [LaShanda Korley](#) and Chase Thompson; University of Delaware, United States

Supramolecular interactions may hold the key to the development of network systems with tunable mechanics and modulated architecture, such as observed in the muscle protein titin. It is the dynamic nature of these physical associations that we have exploited in the design of tough supramolecular materials that super-impose covalent and non-covalent interactions to tailor tensile response. We have developed supramolecular elastomers and interpenetrating network (IPN) systems that probe the interplay of non-covalent and covalent interactions in structural organization and mechanical response. By tailoring physical associations via control of self-assembly and composition, we have demonstrated enhanced supramolecular dynamics driven by architecture and toughness enhancements due to phase behavior. Recently, non-covalent interaction strength, network regularity, and chemoresponsiveness have been utilized as handles to derive gradient materials and to induce actuation behavior. New insights into supramolecular nanocomposites are also highlighted.

SESSION F.SM01.12: Live Keynote III: Lessons from Nature—From Biology to Bioinspired Materials

Session Chairs: Sung Kang and Lauren Zarzar

Thursday Afternoon, December 3, 2020

F.SM01

#### 6:30 PM \*F.SM01.06.02

**Chemically Controlled Shape-Morphing of Elastic Sheets** [Anna C. Balazs](#)<sup>1</sup>, Raj K. Manna<sup>1</sup>, Oleg E. Shklyaev<sup>1</sup> and Howard A. Stone<sup>2</sup>; <sup>1</sup>University of Pittsburgh, United States; <sup>2</sup>Princeton University, United States

The shape-morphing of two-dimensional elastic materials into three-dimensional structures is a vital and ubiquitous transformation in biological systems, as evidenced, for example, by the morphogenesis in cells and tissues, the formation of well-defined curvatures in growing flowers and leaves, and reconfiguration of seedpods in the release of seeds. The functionality of such biological reconfigurations has inspired the development of synthetic shape-changing materials that are useful for soft robotics and soft actuators. Here, we use theory and simulation to devise a distinctive approach for driving shape changes of 2D elastic sheets in fluid-filled microchambers. The sheets are coated with catalyst to generate controllable fluid flows, which transform the sheets into complex 3D shapes. A given shape can be achieved by patterning the arrangement of the catalytic domains on the sheet and introducing the appropriate reactant to initiate a specific catalytic reaction. Moreover, a single sheet that encompasses multiple catalytic domains can be transformed into a variety of 3D



shapes through the addition of one or more reactants. Materials systems that morph on-demand into a variety of distinct structures can simplify manufacturing processes and broaden the utility of soft materials.

**7:00 PM \*F.SM01.06.01**

**Diffusiophoresis—From Physicochemical Effects to Biofilm Mitigation** Howard A. Stone; Princeton Univ, United States

Diffusiophoresis refers to the motion of colloid materials in concentration gradients. I describe some of our studies of these problems, using experiments and mathematical modeling, such as the influence of ion valence and the effect of multiple electrolytes. Also, we demonstrate that these effect can influence of the movement of bacteria. For example, I summarize our observations of the migration of wild-type *V. cholerae* and a mutant lacking flagella ( $\Delta$ flaA), as well as *S. aureus* and *P. aeruginosa*, near a dissolving CO<sub>2</sub> source, which shows that diffusiophoresis of bacteria is independent of shape and Gram stain. With long-time experiments, we show that CO<sub>2</sub>-driven diffusiophoresis can reduce surface contamination, which suggests that the mechanism can be applied to cleaning systems and anti-biofouling surfaces. This work involves contributions from Suin Shim, who investigated the diffusiophoretic response of bacteria, as well as Ankur Gupta, Jessica Wilson and others in my research group.

**7:30 PM \*F.SM01.05.02**

**Bioinspired Assembly and Collective Motion of Nanocomposite Hydrogel Sheets at Air/Water Interfaces** Ryan C. Hayward; University of Colorado Boulder, United States

We describe a platform of temperature-responsive hydrogel nanocomposites adsorbed at air/water interfaces that exhibit a variety of bioinspired non-equilibrium behaviors due to temperature gradients generated by illumination with visible light. In one example, we exploit spatial variations in thermally-induced deswelling of the gel particles to drive buckling of thin sheets into 3D shapes with non-zero Gaussian curvature. Similar to the mechanism exploited by numerous insects to climb menisci or drive clustering, pinning of the three-phase contact line at the sheet edges gives rise to capillary ‘multipole’ interactions between different objects, leading to assembly, repulsion, and even sustained rotational motion, depending on the geometry. In a second example, we exploit Marangoni forces resulting from temperature gradients to drive motion and interaction of planar particles, once again inspired by well-known strategies employed by aquatic insects. A simple method for Marangoni optical trapping is realized by shining appropriate patterns of light on the interface, enabling the definition of easily customized geometries in which to study coupled motion of multiple oscillators and spinners.

**8:00 PM \*F.SM01.01.04**

**Mapping the Phase Space of Protein Encapsulation via Complex Coacervation** Whitney C. Blocher McTigue, Xianci Zeng and Sarah L. Perry; University of Massachusetts Amherst, United States

The encapsulation of biomacromolecules is an important area of research, particularly in the context of medicine where increasing numbers of therapeutics are protein based. One particular encapsulation strategy takes advantage of the associative liquid-liquid phase separation phenomena known as complex coacervation. The self-assembly of complex coacervates is spontaneous, driven by electrostatic attractions and the entropic gains associated with the release of small ions upon complexation. Furthermore, coacervation enables the sequestration of therapeutic proteins and other cargo at high concentrations, and without the need for organic solvents.

A number of recent studies have highlighted strong parallels between the dense, polymer-rich droplets resulting from coacervation and membraneless organelles that have been observed in cells. Of particular interest is the ability of these liquid-liquid phase separated granules to recruit specific proteins, RNAs, and other biomolecules, either for storage in times of stress, or as a hub of catalytic activity. Inspired by these biological structures, we look to understand the design rules whereby complex coacervation can be used to encapsulate and potentially stabilize cargo proteins. Our work focuses on complex coacervation involving two oppositely-charged polypeptides and a cargo protein. The use of two-polymer coacervates allows for the encapsulation of even weakly charged proteins at a variety of different conditions, even near their isoelectric point. We look to map out range of conditions where both phase separation is observed, and the degree to which proteins are incorporated into the coacervate phase as a function of the composition of the two polymers and the encapsulated protein. Preliminary results suggest the potential for using the protein itself as a majority component of the coacervate to achieve incorporation at levels that could be used for therapeutic injection. We intend to use proof-of-concept studies with model proteins as a foundation upon which further research into therapeutic proteins can be built.

**8:00 AM \*F.SM01.01.02**

**A Study on the Mechanical Properties of a Natural and Chemically Functionalized Chitin Structure** Devis Montroni, Simona Fermani and Giuseppe Falini; Alma Mater Studiorum, University of Bologna, Italy

In this presentation two case of studies involving the use of the protein wrapped  $\beta$ -chitin matrix from the squid pen *Loligo vulgaris* are presented.

In the first one we addressed how the mechanical properties of the squid pen are related to intra- and inter- interactions among chitin and proteins. Chemical treatments were applied to modify the interactions involving proteins, through unfolding and/or degradation processes. The data analysis showed that chemical treatments did not modify the multi-scale hierarchical structure of the  $\beta$ -chitin matrix. This allowed to derive from the mechanical test analysis the following conclusions: (i) the maximum stress ( $\sigma_{\max}$ ) relies on the presence of the disulfide bonds; (ii) the Young's modulus (E) relies on the overall correct folding of the proteins; (iii) the whole removal of proteins induces a decrease of E ( $> 90\%$ ) and  $\sigma_{\max}$  ( $> 80\%$ ), and an increase in the maximum elongation. These observations indicate that in the chitin matrix the proteins act as a strengthener, which efficacy is controlled by the presence of disulfide bridges. This reinforcement links the chitin fibrils avoiding them to slide one on the other and maximizing their resistance and stiffness.<sup>1</sup>

In the second case of study the multi-scale hierarchical structure of the  $\beta$ -chitin matrix used as substrate to prepare new materials bio-inspired. Finding inspiration from the byssus, and with the aim to mimic its peculiar mechanical properties, we chemically functionalize the chitin matrix with catechols, the main functional group of the byssus. The obtained functionalized matrix preserves its multi-scale structural organization and is able to chelate reversibly Fe(III). Thus, it behaves as the byssus, acting as a metal cross-linkable matrix that upon metalation increases the Young's modulus, E ( $> 10$  times). This new material can be further cross-linked by oxidation of the catechols. This process generates an increase of the E ( $> 10$  times) and first failure stress ( $> 5$  times). The combination of oxidation and metalation of the functionalized matrix only slightly increases the mechanical properties. The produced stimulus responsive materials show that levels of complexity can be added to a multi-scale organized natural hierarchical matrix providing new properties.<sup>2</sup>

In conclusion we showed that the mechanical properties of the squid pen are controlled by the di-sulfide bonds and that its multi-scale organized  $\beta$ -chitin matrix can be chemically functionalized providing additional properties.

1. D. Montroni, F. Sparla, S. Fermani, G. Falini. (2020) *Acta Biomaterialia*, <https://doi.org/10.1016/j.actbio.2020.04.039>
2. D. Montroni, M. Palanca, K. Morellato, S. Fermani, L. Cristofolini, G. Falini. (2020) *Carbohydrate Polymers*, submitted

**8:30 AM \*F.SM01.07.03**

**Colour Engineering—Form Nature to Applications** Silvia Vignolini; University of Cambridge, United Kingdom

The most brilliant colours in nature are obtained by structuring transparent materials on the scale of the wavelength of visible light. By controlling/designing the dimensions of such nanostructures, it is possible to achieve extremely intense colourations over the entire visible spectrum without using pigments or colourants. Colour obtained through a structure, namely structural colour, is widespread in the animal and plant kingdom [1]. Such natural photonic nanostructures are generally synthesised in ambient conditions using a limited range of biopolymers.

In this seminar, I will review our recent advances to fabricate bio-mimetic photonic structures with cellulose and chitin and I will give examples of how to fabricate novel photonic materials based on chiral nematic architectures using low-cost polymers in ambient conditions [2-7].

[1] Kinoshita, S. et al. (2008). Physics of structural colours. Rep. Prog. Phys. 71(7), 076401.

[2] Narkevicius A, et al. (2019). Controlling the Self-Assembly Behavior of Aqueous Chitin Nanocrystal Suspensions, Biomacromolecules 20, 2830

[3] Chan C. L. et. al. (2019) Visual Appearance of Chiral Nematic Cellulose-Based Photonic Films: Angular and Polarization Independent Color Response with a Twist, Adv Mater 31, 1905151

[4] Frka-Petesic et al. (2019) Angular optical response of cellulose nanocrystal films explained by the distortion of the arrested suspension upon drying. Physical Review Materials 3, 045601

[5] Parker R. et al. (2018) The Self-Assembly of Cellulose Nanocrystals: Hierarchical Design of Visual Appearance. Adv Mat 30, 1704477

[6] Parker R. et al. (2016). Hierarchical Self-Assembly of Cellulose Nanocrystals in a Confined Geometry. ACS Nano, 10

(9), 8443–8449

[7] Liang H-L. et al. (2018). Roll-to-roll fabrication of touch-responsive cellulose photonic laminates, *Nat Com* 9, 4632

#### 9:00 AM \*F.SM01.02.02

**Bio-Inspired Hierarchical Porous Materials Made by 3D Printing** André R. Studart; ETH Zurich, Switzerland

Hierarchical porous materials are attractive structures for a variety of applications due to their enhanced mechanical efficiency and their high surface area with minimum permeability loss. Nature showcases remarkable examples of hierarchical porous materials that benefit from such unusual set of properties, including bamboo, bone, marine sponges and wood. However, synthetic porous materials have yet to reach the elaborate architectural design found in their biological counterparts. To fill this gap, processing routes that enable deliberate control over the material's porous structure at multiple length scales are highly demanded. In this talk, I will show how 3D printing technologies can be exploited to fabricate hierarchical porous materials with unprecedented mechanical efficiency and architectural control. The key feature of our approach is to design inks with an internal structure that serves as a template for the formation of tailored pores within the printed object. Using oil droplets, air bubbles or phase-separating mixtures as templating structures, this methodology enables independent tuning of porosity and pore sizes at multiple length scales. To demonstrate the potential of the process, we 3D printed complex-shaped parts with bioinspired multiscale porosity and enhanced mechanical efficiency that cannot be achieved through conventional fabrication technologies.

SESSION F.SM01.01: Multiscale Characterization of Biological Materials

On Demand Abstracts Available for Viewing Starting Saturday Morning, November 21, 2020

F-SM01

#### 5:00 AM \*F.SM01.01.01

**Bone—Deciphering the Tissue Organization and Materials Properties in 3D Using FIB SEM** Steve Weiner<sup>1</sup>, Emeline Raguin<sup>1</sup>, Neta Varsano<sup>1</sup>, Heden Haimov<sup>1</sup>, Lia Addadi<sup>1</sup> and Ron Shahar<sup>2</sup>; <sup>1</sup>Weizmann Institute of Science, Israel; <sup>2</sup>Hebrew University, Israel

Bone is both a tissue, comprising cells, vasculature and extracellular matrix, and a material comprising mainly mineral, collagen and water. It is thus a challenge to characterize bone's 3D structural organization in order to gain insights into how bone forms and functions. Focused ion beam-scanning electron microscopy (FIB SEM) can provide information at nanometer resolution to enable, for instance the identification of the collagen D-banding. At this resolution the spatial arrangement of fibrils can be assessed in volumes of thousands of microns cubed which can include tissue components. For example, examination of mineralized osteonal pig bone shows unidirectional collagen arrays oriented alternatively in different directions or changing direction progressively. These unidirectional arrays are separated by layers of collagen organized in a bidirectional patchwork motif. Earlier studies of demineralized lamellar bone showed that the layers with the patchwork motif stain heavily with osmium and Alcian Blue and have a disordered appearance.

Another example is the cryo- FIB SEM examination after cryo-fixation and under cryo-conditions, of the mineralized murine growth plate. It reveals the presence of a complex zone that includes blood vessels with mineral containing vesicles, blood vessel extremities surrounded by bone mineralizing matrix, and cartilage hypertrophic cells surrounded by ordered and disordered cartilage mineralizing matrix.

By exploiting the options for examining mineralized bone, demineralized bone matrix and the soft tissue components as well as the bone, FIB SEM can provide invaluable insights into bone organization. By combining FIB SEM in a correlative manner with 3D confocal light microscopy and microCT, it will be possible to address many fundamental questions in bone biology and mechanics.

Reznikov, N., Shahar, R. and Weiner, S. 2014. Bone hierarchical structure in three dimensions. *Acta Biomaterialia* 10, 3815-3826.

Haimov, H., Shimoni, E., Brumfeld, V., Shemesh, M., Varsano, N., Addadi, L. and Weiner, S. 2020. Mineralization pathways in the active murine epiphyseal growth plate. *Bone* 130, <https://doi.org/10.1016/j.bone.2019.115086>.

Raguin, E., Rechav, K., Brumfeld, V., Shahar, R. and Weiner, S. 2020. Unique three-dimensional structure of a fish mandible bone subjected to unusually high mechanical loads. *J. Structural Biol.* (in press).

#### 5:15 AM \*F.SM01.01.02

**A Study on the Mechanical Properties of a Natural and Chemically Functionalized Chitin Structure** Devis Montroni, Simona Fermani and Giuseppe Falini; Alma Mater Studiorum, University of Bologna, Italy

In this presentation two case of studies involving the use of the protein wrapped  $\beta$ -chitin matrix from the squid pen *Loligo vulgaris* are presented.

In the first one we addressed how the mechanical properties of the squid pen are related to intra- and inter- interactions among chitin and proteins. Chemical treatments were applied to modify the interactions involving proteins, through unfolding and/or degradation processes. The data analysis showed that chemical treatments did not modify the multi-scale hierarchical structure of the  $\beta$ -chitin matrix. This allowed to derive from the mechanical test analysis the following conclusions: (i) the maximum stress ( $\sigma_{\max}$ ) relies on the presence of the disulfide bonds; (ii) the Young's modulus ( $E$ ) relies on the overall correct folding of the proteins; (iii) the whole removal of proteins induces a decrease of  $E$  ( $> 90\%$ ) and  $\sigma_{\max}$  ( $> 80\%$ ), and an increase in the maximum elongation. These observations indicate that in the chitin matrix the proteins act as a strengthener, which efficacy is controlled by the presence of disulfide bridges. This reinforcement links the chitin fibrils avoiding them to slide one on the other and maximizing their resistance and stiffness.<sup>1</sup>

In the second case of study the multi-scale hierarchical structure of the  $\beta$ -chitin matrix used as substrate to prepare new materials bio-inspired. Finding inspiration from the byssus, and with the aim to mimic its peculiar mechanical properties, we chemically functionalize the chitin matrix with catechols, the main functional group of the byssus. The obtained functionalized matrix preserves its multi-scale structural organization and is able to chelate reversibly Fe(III). Thus, it behaves as the byssus, acting as a metal cross-linkable matrix that upon metalation increases the Young's modulus,  $E$  ( $> 10$  times). This new material can be further cross-linked by oxidation of the catechols. This process generates an increase of the  $E$  ( $> 10$  times) and first failure stress ( $> 5$  times). The combination of oxidation and metalation of the functionalized matrix only slightly increases the mechanical properties. The produced stimulus responsive materials show that levels of complexity can be added to a multi-scale organized natural hierarchical matrix providing new properties.<sup>2</sup>

In conclusion we showed that the mechanical properties of the squid pen are controlled by the di-sulfide bonds and that its multi-scale organized  $\beta$ -chitin matrix can be chemically functionalized providing additional properties.

1. D. Montroni, F. Sparla, S. Fermani, G. Falini. (2020) *Acta Biomaterialia*, <https://doi.org/10.1016/j.actbio.2020.04.039>

2. D. Montroni, M. Palanca, K. Morellato, S. Fermani, L. Cristofolini, G. Falini. (2020) *Carbohydrate Polymers*, submitted

### 5:30 AM \*F.SM01.01.03

**Osmotic Force Generation in Biological Materials** Peter Fratzl; Max Planck Institute of Colloids and Interfaces, Germany

Biological extracellular tissues are based on proteins, polysaccharides and, in certain cases, minerals. Their complex multiscale structure confers them a wide range of properties in accordance with the tissues' functions. While active functionality are usually attributed to cells, there are also examples of materials synthesized by living organisms, such as plant seeds, which fulfil an active function without living cells and work as mechanosensors and actuators. Water is an important component of all such extracellular tissues. While it is well known that the level of hydration determines the mechanical properties of many biological materials, it is less appreciated that water also plays an active role in generating forces within the materials. In particular water absorption and desorption provides actuation in a variety of plant seeds, including wild wheat, stone plant and banksia seed capsules. The shape change upon water uptake that provides the actuation is controlled by specific cellulose fibre architectures. In this way, well-controlled movements, such as bending, twisting or curling are programmed in these materials by structure of the underlying cellulose microarchitecture. The required deformation energy is provided by the absorption of water from the environment. Finally, the absorption of water to specific molecules and the resulting osmotic pressure is also providing internal stresses which control, for example, the mechanical behaviour of collagen in tendon, bone and dentin. The lecture will review general concepts for the roles of water in biological materials, both in the context of biology and of bioinspired engineering.

### 5:45 AM \*F.SM01.01.04

**Mapping the Phase Space of Protein Encapsulation via Complex Coacervation** Whitney C. Blocher McTigue, Xianci Zeng and Sarah L. Perry; University of Massachusetts Amherst, United States

The encapsulation of biomacromolecules is an important area of research, particularly in the context of medicine where increasing numbers of therapeutics are protein based. One particular encapsulation strategy takes advantage of the associative liquid-liquid phase separation phenomena known as complex coacervation. The self-assembly of complex coacervates is spontaneous, driven by electrostatic attractions and the entropic gains associated with the release of small ions upon complexation. Furthermore, coacervation enables the sequestration of therapeutic proteins and other cargo at high concentrations, and without the need for organic solvents.

A number of recent studies have highlighted strong parallels between the dense, polymer-rich droplets resulting from coacervation and membraneless organelles that have been observed in cells. Of particular interest is the ability of these liquid-liquid phase separated granules to recruit specific proteins, RNAs, and other biomolecules, either for storage in times of stress, or as a hub of catalytic activity. Inspired by these biological structures, we look to understand the design rules whereby complex coacervation can be used to encapsulate and potentially stabilize cargo proteins. Our work focuses on complex coacervation involving two oppositely-charged polypeptides and a cargo protein. The use of two-polymer coacervates allows for the encapsulation of even weakly charged proteins at a variety of different conditions, even near their isoelectric point. We look to map out range of conditions where both phase separation is observed, and the degree to which proteins are incorporated into the coacervate phase as a function of the composition of the two polymers and the encapsulated protein. Preliminary results suggest the potential for using the protein itself as a majority component of the coacervate to achieve incorporation at levels that could be used for therapeutic injection. We intend to use proof-of-concept studies with model proteins as a foundation upon which further research into therapeutic proteins can be built.

#### 6:00 AM F.SM01.01.05

**Analytical and Spectroscopic Studies of Ancient Silicified Plants—What Can We Learn?** Victor V. Volkov, Graham J. Hickman, Anna Sola Rabada and Carole C. Perry; Nottingham Trent University, United Kingdom

Inspiration from ancient plant species that abound wherever the ground is disrupted and can grow through concrete and bitumen. What can we learn in terms of mineral usage and reproduction?

Equisetum species are primitive vascular plants that benefit from the biogenesis of silica bio-organic inclusions in their tissues and participate in the annual biosilica turnover in local eco-systems. As means of Equisetum reproduction and propagation, spores are expected to reflect the evolutionary adaptation of the plants to the climatic conditions at different times of the year. Combining methods of Raman and scanning electron microscopy and assisted with density functional theory, we conducted material spatial-spectral correlations to characterize the distribution of biopolymers and silica based structural elements that contribute to the bio-mineral content of the elater. We propose the expansion of elater tips upon germination and the form of silica including encapsulated biopolymers are designed for ready dispersion, release of the polysaccharide-arginine rich content and to facilitate silica uptake to the developing plant. This behavior would help to condition local soil chemistry to facilitate competitive rooting potential and stem propagation. Further, X-ray and analytical electron microscopy studies of plant materials show an amazing array of minerals that can be isolated for use in applications as diverse as sensing, optics and catalysis.

#### 6:10 AM F.SM01.01.06

**Black Drum Fish's Teeth—Stiff and Wear-Resistant for Crushing Mollusk Shells** Zhifei Deng<sup>1</sup>, Hyunhae C. Loh<sup>2</sup>, Zian Jia<sup>1</sup>, Admir Masic<sup>2</sup>, Ron Shahar<sup>3</sup> and Ling Li<sup>1</sup>; <sup>1</sup>Virginia Polytechnic Institute and State University, United States; <sup>2</sup>Massachusetts Institute of Technology, United States; <sup>3</sup>The Hebrew University of Jerusalem, Israel

The black drum fish (*Pogonias Cromis*), being the largest durophagous sciaenid, has stiff, hard, and wear-resistant teeth on the powerful pharyngeal jaws to adapt to its almost exclusive diet on hard-shelled mollusks. With estimated biting force reaching 11,000 N at the largest body size (60 kg), the black drum fish's teeth have one of the highest bite force quotient (BFQ) among all living species. In this work, we aim to uncover the structural origins of such remarkable performance of these teeth via systematic structural, chemical and mechanical analysis across multiple length scales. The black drum fish's teeth consist of a stiff enameloid layer (90-110 GPa in reduced modulus  $E_r$ , and 3~7 GPa in hardness  $H$ ) and a softer inner dentin layer (20-50 GPa in  $E_r$ , and ~1 GPa in  $H$ ) separated by the dentin-enameloid-junction (DEJ). The gradient in microstructures from the enameloid (rods with increasing diameters and gradually twisted orientations) to the DEJ then to the dentin (parallel tubules with increasing curvy oscillation towards the interior), and the compositional gradient, *i.e.*, doping of Zn and F in the hydroxyapatite (HA) crystals in the enameloid layer *vs.* the Mg substitution in HA crystals in the dentin, contribute to the intricate gradient design of the teeth. The outer enameloid resists strong loadings; the DEJ deflects cracks to avoid catastrophic failure; and the inner dentin provides enhanced toughness. At the macroscale, the 90°-locking between the inner dentin and the bony plates provides additional bonding between the individual tooth and the pharyngeal jaw. Beyond critical loading, the tooth units first detach from the bony plates, which facilitates the erupting process of the new teeth from underneath.

#### 6:20 AM F.SM01.01.07

**From Nano to Macro—Artificial Muscles for Real-World Applications** Seyed M. Mirvakili and Robert Langer; Massachusetts Institute of Technology, United States

Actuators, also known as artificial muscles, are an integral part of daily life. From transportation means to biomedical devices, they all utilize actuators for one or more vital tasks. Cycle life, cost, output force, strain, energy density, power density, and efficiency are the key performance metrics that are used to evaluate the suitability of actuators for a specific application. The emerging field of soft actuators has been introducing new classes of stimuli-responsive materials that can mimic muscle's properties (*i.e.*, generating strain, changing stiffness). While these materials outperform the performance of the human muscle in one or more of the mentioned attributes, there is still no stimuli-responsive material that can beat the human muscle in all of them. In this talk, an overview of the field will be given and the current challenges and possible directions will be discussed.

#### 6:30 AM F.SM01.01.08

**Hierarchically Organized Liquid Crystal Structure of Ultra-Rigid Polymers Made with Coiled Coil Peptide Bundles** Kyunghee Kim<sup>1</sup>, Christopher Kloxin<sup>1</sup>, Jeffery G. Saven<sup>2</sup> and Darrin Pochan<sup>1</sup>; <sup>1</sup>University of Delaware, United States; <sup>2</sup>University of Pennsylvania, United States

Biomimetic assemblies using synthetic peptides facilitate a fabrication of nanoscale materials with desired structures, exhibiting several attractive features for biotechnological applications due to an ability to mimic structures and properties of nature. Sequence specificity in peptide building blocks allows designed nanostructures to have almost atomistic precision as in biological systems. Furthermore, higher-ordered materials with well-defined structures can be also produced through several processing methods such as sequential, hierarchical assembly or fiber spinning. The ability to precisely design and control the structure at the molecular level is crucial to construct new materials with well-designed structures at multiple length scales. This ability allows one to target desired properties such as the mechanical properties of the materials. Herein, peptide building blocks are employed to construct a hierarchically organized fiber material at macroscopic scale. The basic peptide building blocks are computationally designed to assemble into a cylindrical shape comprised of homotetrameric coiled coil bundles with an anti-parallel arrangement giving rise to a pair of reactive sites at each end of the bundles for further chemical reactivity. The bundles with complementary chemical functionality serve as supermonomer units and are directly connected to each other, resulting in hybrid physical/chemical peptide-based polymers. The polymeric chains exhibit highly rigid rod structure owing to a rigidity of constituent bundles and direct linkages between them through covalent interactions. Moreover, due to the unique physical characteristics, the rod chains in concentration solution exhibit liquid crystalline behavior. The resultant rigid rod-like polymers can further be assembled into a hierarchical organization on macroscopic scales via electrospinning processing, while preserving their unique rod-like structural characteristics. The organization of rods in concentrated liquid crystal solutions was characterized via polarized optical microscopy, x-ray and neutron scattering, and rheology in order to understand the control of liquid crystal behavior for the processing of concentrated solutions into fiber materials.

#### 6:40 AM F.SM01.01.09

**Nano-Mechanics Reveal Resilience in Nacre of Mollusk Shells and Pearls** Jiseok Gim<sup>1</sup>, Noah Schnitzer<sup>1</sup>, Laura Otter<sup>2</sup>, Yuchi Cui<sup>1</sup>, Alden Koch<sup>3</sup>, Sébastien Motreuil<sup>4</sup>, Frédéric Marin<sup>4</sup>, Stephan Wolf<sup>5</sup>, Dorrit Jacob<sup>2</sup>, Amit Misra<sup>1</sup> and Robert Hovden<sup>1,1</sup>; <sup>1</sup>University of Michigan, United States; <sup>2</sup>Macquarie University, Australia; <sup>3</sup>University of Michigan, United States; <sup>4</sup>Université de Bourgogne Franche-Comté (UBFC), France; <sup>5</sup>Friedrich-Alexander-University Erlangen-Nürnberg (FAU), Germany

The inherent tradeoff between strength and toughness inspires new design approaches to structural materials with high damage tolerance. Optimizing mechanical properties for predictable and non-catastrophic failure motivates novel design of modern high-performance structural materials. Among the diverse set of structural biominerals that straddle the gap between strength and toughness, nacre is the prototypical supermaterial. Nacre forms in many mollusk shells and is the primary structure of lustrous pearls. In nacre of both pearls and shells, we show a nanostructure that optimizes structural resilience. The biomineralization precisely controls secretion of organic and inorganic ingredients and hierarchically designs the combination of soft nanoscale organic components with inorganic nanograins that govern the formation of pearls and shells. After crack initiation, bulk nacre shows a 40-fold higher fracture toughness than the monolithic/single crystal calcium carbonate from which it is constructed. Thus, a central focus has been placed on understanding the principle mechanisms of nacre's excellent mechanical properties to inspire new designs of next-generation high-performance structural materials. However, nacre's ability to undergo limited deformation and dissipate critical stresses before fracture has not yet been quantified nor correlated with nanomechanical processes. Understanding nanomechanical responses across the 3D hierarchical architectures is critical to understanding how the individual nacre components work together to create properties greater than the sum of their parts (*i.e.* far exceeding the rule of mixtures). Our investigation of toughening strategies in nacre reveals nanomechanical deformation of organic interfaces, nanocrystallites, and organic inclusions as key to the increased damage-tolerance of nacre. High-resolution scanning /

transmission electron microscopy (S/TEM) combined with in-situ nano-indentation has been adapted to biomineral systems to allow sub-nanometer resolution imaging of the nanomechanical deformation processes and provide precise assessment of when and where fracture occurs. We show that during compressive indentation nacre undergoes non-destructive locking where inorganic tablets come into contact across organic interfaces. Remarkably, the completely locked interface recovers its original morphology without any deformation after releasing compression and retains its full mechanical strength. During compression, the aragonite grains and organic inclusions reversibly rotate and deform indicating nanoscale resilience of the nacre tablets. Prior to tablet locking, strain attenuates up to 80% between the decoupled tablets. However, by 3% engineering strain of the first tablet, the tablets have locked to redistribute stress continuously across the organic interface and the strain attenuation decreases. When fracture occurs, we show the organic components restrict crack propagation both within and between tablets, sustaining the overall macroscale architecture through multiple fractures to allow further structural loading. This allows nacre to absorb significantly greater mechanical energy than monolithic aragonite. This extends the damage tolerance of the superstructure beyond a single fracture. The present in situ S/TEM nanoindentation study illuminates nacre's distinct non-linear elastic deformation processes that provide high resilience.

#### 6:50 AM F.SM01.01.10

**The Benefits of Disorder in Biological Cellular Materials** Derek Aranguren van Egmond<sup>1,2</sup>, Glenn Hibbard<sup>1</sup> and Benjamin Hatton<sup>1</sup>; <sup>1</sup>University of Toronto, Canada; <sup>2</sup>National Research Council, Canada

Biological cellular materials, such as trabecular bone, sponge, and wood, typically exhibit disordered arrangements of pores that are neither fully random, nor perfectly ordered (hexagonal honeycomb). In fact, this degree of order/disorder has not been systematically quantified before. We have used equivalent Voronoi patterning to quantify the disorder (variation in cell size) for a wide range of biological and engineered cellular materials, through thresholds in cell nuclei spacing. We have identified a common range of disorder (pseudo-hexagonal in 2D) for biological materials ( $\delta$  of 0.5 to 0.8). Using 3D printed honeycomb models with systematically increasing disorder, we demonstrate that this range of 'pseudo-order' in 2D stochastic cellular solids exhibits a >30% increase in fracture toughness and equivalent strength compared to ordered (hexagonal) solids of the same density. This work demonstrates that there are significant improvements in defect tolerance for architected cellular solids having a certain degree of disorder. Highly ordered (hexagonal) arrays result in straight, catastrophic crack propagation, while too much disorder has highly branched cracks, but low strength. FEA models confirm a delocalization of damage during fracture. We suggest that the disorder in these biological materials may be optimal for the 'survivability' of fracture. We hypothesize that the delocalization of damage (cracks) limits their absolute size to that which is repairable through primary repair mechanisms, and provides an advantage for natural selection. We suggest that 'tailored disorder' in cellular solids represents a new design principle for the digital design of architected materials in general, to improve damage tolerance.

#### 7:00 AM F.SM01.01.11

**Transparent Nacre-Like Composites Toughened Through Mineral Bridges** Tommaso Magrini<sup>1</sup>, Simon Moser<sup>1</sup>, Madeleine Fellner<sup>2</sup>, Alessandro Lauria<sup>2</sup>, Florian Bouville<sup>3</sup> and André R. Studart<sup>1</sup>; <sup>1</sup>Complex Materials, Department of Materials, ETH Zürich, Switzerland; <sup>2</sup>ETH Zürich, Switzerland; <sup>3</sup>Imperial College London, United Kingdom

Bulk materials with remarkable mechanical properties have been developed by incorporating design principles of biological nacre into synthetic composites. However, this potential has not yet been fully leveraged for the fabrication of tough and strong materials that are also optically transparent.<sup>[1]</sup> In this work, a manufacturing route that enables the formation of nacre-like mineral bridges in a bioinspired composite consisting of glass platelets infiltrated with an index-matching polymer matrix is developed. By varying the pressure applied during compaction of the glass platelets, composites with tunable levels of mineral bridges and platelet interconnectivity can be easily fabricated.<sup>[2]</sup> The effect of platelet interconnectivity on the mechanical strength and fracture behavior of the bioinspired composites is investigated by performing state-of-the-art fracture experiments combined with in situ electron microscopy. The results show that the formation of interconnections between platelets leads to bulk transparent materials with an unprecedented combination of strength and fracture toughness. This unusual set of properties can potentially fulfil currently unmet demands in electronic displays and related technologies.

<sup>[1]</sup> T. Magrini et al., *Nature Communications* **2019**, 10, 2794

<sup>[2]</sup> T. Magrini et al., *Advanced Functional Materials* **2020**, 2002149

#### 7:10 AM F.SM01.01.12

**Understanding Synergy in the Nonlinear Mechanics of Composite (Bio)polymer Networks** Justin Tauber<sup>1</sup>, Simone Dussi<sup>1</sup>, Federica Burla<sup>2</sup>, Gijsje Koenderink<sup>3</sup> and Jasper van der Gucht<sup>1</sup>; <sup>1</sup>Wageningen University & Research, Netherlands; <sup>2</sup>AMOLF, Netherlands; <sup>3</sup>Delft University of Technology, Netherlands

Composite materials offer a unique opportunity to achieve novel (improved) material properties without the need for the development of new components. Sometimes, synergistic mechanics can be achieved, i.e. the mechanical properties of the composite are even better than the sum of the individual components. This synergy has been demonstrated within many material classes and on many length scales, from reinforced concrete to molecular polymeric composites [1,2,3] to the extracellular matrix supporting our tissues [4]. Here I will present our effort to rationalize the synergy observed in the non-linear mechanics of biopolymer composites [4] and in the fracture behaviour of generic elastic double networks [1], both containing a stiff polymer network embedded in a soft polymer matrix. We will show that the entanglement of these networks at the microscopic level is the key to the synergistic mechanics.

We look for mechanical synergy in composite biopolymer networks, inspired by the tuneable nonlinear mechanics of the extracellular matrix (ECM). In the ECM collagen is the main-component responsible for the nonlinear strain-stiffening response [5,6]. However, we show that hyaluronic acid (HA), the second most abundant biopolymer in the extracellular matrix, can significantly delay the strain-stiffening if the stiff collagen network is embedded in a much softer HA matrix [4]. Similarly, we show that the HA network enhances the linear elastic response of the collagen-HA composite. In both regimes the synergistic response is governed by mechanisms occurring at the microscopic level, but have a drastic effect on the macroscopic stress-strain response.

Experiments on synthetic double networks [2,3] show that a soft elastic matrix can not only have a significant effect on the elastic response of a stiff network, but also on the failure behaviour, shifting the failure response from brittle to ductile. By implementing bond breaking in a coarse-grained network simulation [1] we can demonstrate that the brittle-to-ductile transition can be captured by a simple force-balance between the two networks. Furthermore, our model predicts four mechanical regimes that are also observed in experiment. In particular, the simulations reveal that the four regimes are associated to differences in the microscopic failure response as well. Understanding these phenomena allows a better control over the synergistic failure response of double network materials.

Our findings not only elucidate how biology combines polymers with complementary properties to finely-tune the mechanics of living tissues, but also provide a new avenue for the design of synthetic elastic materials tuning their stress-strain response from the linear-regime until global failure.

## References

- [1] J. Tauber, S. Dussi, J. van der Gucht, Microscopic insights into the failure of elastic double networks, *Phys. Rev. Materials*, 4, 063603 (2020).
- [2] P. Millereau *et al.*, Mechanics of elastomeric molecular composites, *PNAS*, 115, 9110-9115 (2018).
- [3] S. Ahmed *et al.*, Brittle-ductile transition of double network hydrogels: Mechanical balance of two networks as the key factor, *Polymer*, 55, 914-923 (2014).
- [4] F. Burla/J. Tauber, S. Dussi, J. van der Gucht, G. H. Koenderink, Stress management in composite biopolymer networks, *Nat. Phys.*, 15, 549-553 (2019).
- [5] A. J. Licup *et al.*, Stress controls the mechanics of collagen networks, *PNAS*, 112, 9573-9578 (2015).
- [6] A. Sharma *et al.*, Strain-controlled criticality governs the nonlinear mechanics of fibre networks., *Nat. Phys.*, 12, 584-587 (2016).

## 7:20 AM F.SM01.01.13

**Dissipative Structures in Polysaccharide Solution by Water Evaporation** Kosuke Okeyoshi, Kulisara Budpud, Gargi Joshi and Tatsuo Kaneko; Japan Advanced Institute of Science and Technology, Japan

The air-water interface is expected to play an important role in establishing a universal model of dissipative structures in nature. Viscous fingering, as an example of fluidic flow, is an unstable situation that is widely known as *tears of wine*. This has been explained through the Marangoni effect, coffee ring effect, Saffman-Taylor instability, etc. However, due to the transitional nature of these phenomena, there are few strategies for immobilizing such fluidically regulated interfaces. Recently, such phenomena have been applied successfully to an immobilized structure by controlling the evaporation of a mixture of polymer and water.<sup>1</sup>

In this study, we present a brief discussion of “meniscus splitting phenomenon”. More precisely, an air-liquid interface is divided into multiple interfaces to partition a space. In particular, by using a mixture of polysaccharides and water, a macroscopic pattern following a specific rule could be confirmed. When the mixture is dried from a top open cell, the polymer forms deposits at specific positions to split the meniscus by bridging a millimeter-scale gap. Because water irreversibly evaporates from the liquid phase to the air phase through a gap, the air-liquid interface is in a nonequilibrium



state between polymer deposition and water evaporation. The interfacial instability is comparable to the mechanical instability of gels at the phase transition or to the skin layer of gel surfaces during shrinking. Furthermore, the deposited polymer film acts as vapor-sensitive materials. Here, the phenomenon and the material's behavior would be discussed from physicochemical viewpoints: polymer science, interface science, and colloidal science.

1. *Sci. Rep.* **2017**, *7*, 5615; *J. Colloid Interface Sci.* **2019**, *546*, 184; *Small*, in press; *Polymer J*, in press.

### 7:30 AM F.SM01.01.14

**Exploring the Growth and Form of Strontium Sulfate Biominerals Using X-Ray Nanotomography** Dawn Raja Somu<sup>1</sup>, Timothy Cracchiolo<sup>1</sup>, Imke Greving<sup>2</sup> and Vivian Merk<sup>1</sup>; <sup>1</sup>Florida Atlantic University, United States; <sup>2</sup>Helmholtz-Zentrum Geesthacht, Germany

Acantharia (*Acantharea*) are wide-spread marine protozoa, presenting one of the rare examples of strontium sulfate (SrSO<sub>4</sub>, celestite) mineralization in the biosphere. The unicellular organisms produce complex star-shaped skeletons with 20 spicules that radiate from the center according to a unique geometric pattern. Specifically, two quartets of polar spicules alternate with two quartets of tropical spicules and one quartet of equatorial spicules. It has been speculated that the crystallographic arrangement of the spicules stems from an interplay between crystallochemical and biological control, reconciling an optimum use of space at the spicular joint with the crystallographic requirements of an orthorhombic crystal lattice. The Acantharia class encompasses approximately 150 species with highly diverse, taxon-specific skeletal morphology, suggesting exquisite genetic regulation of the mineral deposition. Their sizes range from roughly 50 μm to 1 mm, depending on their developmental stage and origin. Exploring the three-dimensional skeletal architecture of the Acantharia is essential for understanding the underlying principles of biomineralization.

Synchrotron-based X-ray micro-computed tomography is a powerful method for visualizing nano-scale features without major sample preparation artefacts. Here, we used synchrotron-based nanotomography at the P05 imaging beamline (PETRA III, DESY, Hamburg, Germany) to resolve the complex internal morphology of Acantharian endoskeletons. Our analysis revealed pronounced morphological differences between taxa, suggesting species-specific crystal growth mechanisms. The study focused on how the spicules emanate from the central junction, as it might be the key to understanding inorganic morphogenesis. We used a correlative imaging approach, combining nanotomography with electron-optical investigations and Atomic Force Microscopy. Based on the experimental results, we hope to gain a deeper understanding of the skeletal development from rod-shaped, diametral crystals in juvenile Acantharia to well-developed skeletons in the adult organism. Interesting parallels might be drawn to smoothly curved, fenestrated spicules in subtropical sea urchins and marine sponges, whose skeletons are based on far more common biomineral systems. We will further discuss how bio-inspired model systems mimic the SrSO<sub>4</sub> crystallization in uncultured protists.

### 7:40 AM F.SM01.01.15

**Late News: The Different Destinies of DOPA—Spatiotemporal Regulation of Catechol Crosslinking During Mussel Byssus Formation** Tobias Priemel<sup>1</sup>, Ranveer Palia<sup>1</sup>, Margaryta Babych<sup>2</sup>, Christopher Thibodeaux<sup>1</sup>, Steve Bourgault<sup>2</sup> and Matthew J. Harrington<sup>1</sup>; <sup>1</sup>McGill University, Canada; <sup>2</sup>UQAM, Canada

Natural materials such as mussel byssal threads serve as inspiration for the design of new sustainable polymers. Byssal threads consist of proteins forming a complex hierarchical structure closely linked to the impressive mechanical properties including underwater adhesion, high toughness and self-healing. Each fiber forms within 5 min as a secretion of several proteins which self-assemble and crosslink into a rigid, yet extensible fiber. Interestingly, all proteins contain between 1 and 30 mol% of the post-translationally modified amino acid 3,4-dihydroxyphenylalanine (DOPA). The complex chemistry of DOPA enables a range of different interactions including metal coordination, oxidative crosslinking and hydrogen bonding. Evidence indicates that DOPA plays a key role in the post-secretion curing of the fibers though the details are still unclear. Here, we investigated the spatiotemporal regulation of DOPA cross-linking during thread assembly, using histological staining in combination with confocal Raman microspectroscopy. These methods were combined with induced thread formation to follow cross-linking at different stages of the formation process and in different parts of the thread. Results show that different parts of the thread utilize different DOPA interactions for crosslinking. Furthermore, these DOPA interactions are likely regulated by controlling their redox environment facilitating covalent crosslinking over DOPA-metal coordination or vice versa. These insights provide relevant physicochemical pathways for the design of mussel-inspired catechol-based polymers and could lead to the development of new sustainable materials with industrial and biomedical applications.

**5:00 AM \*F.SM01.02.01**

**Bio-Enabled Nanocomposites with Unique Physical Properties** Vladimir Tsukruk; Georgia Institute of Technology, United States

Bio-enabled nanocomposites represent a novel class of functional bioderived materials, which uses principles of bioinspiration and biomimetic to design hierarchically organized hybrid materials with co-assembled biological and synthetic components to bring best of synthetic and biological worlds: versatile functions with responses to mechanical, optical, chemical, and light stimuli and mechanical strength, flexibility, biocompatibility, and environmental robustness [1, 2]. In first set of examples, we discuss uniformly aligned chiral bio-photonic films from a liquid crystal phase formed by a cellulose nanocrystal solution placed in a thin capillary [3]. This spatial and fluidic flow confinement facilitates homogeneous growth of chiral pseudo-layers parallel to the interface in contrast to the highly heterogeneous assembly of random tactoids. The resulting iridescence films show a narrower optical reflectance band and uniform birefringence over larger macroscopic regions than heterogeneous conventional drop-cast films. In another example, enhanced chiral properties of organized helical patterned films with high asymmetry of circular polarization have been template-assembled via preferential orientation of high-aspect cellulose nanocrystals onto optical microgrids [4]. Bright chiral emission has been co-assembled in organized biopolymer photonic films from core-shell nanorods of cellulose nanocrystals and co-assembled carbon quantum dots mediated by polymer linkers [5]. Finally, co-assembly of cellulose nanocrystals with amorphous polysaccharides resulted in the formation of robust and flexible films with the preservation of the original structural photonic and fine control of the pitch length due to intimate intercalation of macromolecular backbones into the interstitial nanoscale pores of neighboring nematic monolayers [6].

- [1] R. Xiong, J. Luan, S. Kang, S. Singamaneni, V. V. Tsukruk, Natural Biopolymers for Organized Photonic Structures, *Chem. Soc. Review*, 2020, 49, 983.
- [2] R. Xiong, A. M. Grant, R. Ma, S. Zhang, V. V. Tsukruk, Naturally-derived biopolymer nanocomposite: interfacial design, properties and emerging applications, *Mat. Sci. & Eng. Reports*, 2018, 125, 1.
- [3] V. Cherpak, V.F. Korolovych, T. Turiv, D. Nepal, J. Kelly, T.J. Bunning, O.D. Lavrentovich, V.V. Tsukruk, Robust Chiral Organization of Cellulose Nanocrystals in Capillary Confinement, *Nano Lett.*, 2018, 118, 6770.
- [4] R. Xiong, S. Yu, S. Kang, K. M. Adstedt, D. Nepal, T. J. Bunning, V. V. Tsukruk, Integration of Optical Surface Structures with Chiral Nanocelluloses for Enhanced Chiroptical Properties, *Adv. Mater.*, 2019, 1905600.
- [5] R. Xiong, S. Yu, M. J. Smith, J. Zhou, M. Krecker, L. Zhang, D. Nepal, T. J. Bunning, V. V. Tsukruk, Assembling Carbon Quantum Dots on Cellulose Nanocrystals for Chiral Luminescent Biophotonic Materials, *ACS Nano*, 2019,13, 9074.
- [6] K. Adstedt, E. A. Popenov, K. J. Pierce, R. Xiong, R. Geryak, V. Cherpak, D. Nepal, T. J. Bunning, V. V. Tsukruk, Broad iridescence of natural polymer nanocomposites: chiral nanocrystals intercalated with amorphous polysaccharides, 2020, in press.

**5:15 AM \*F.SM01.02.02**

**Bio-Inspired Hierarchical Porous Materials Made by 3D Printing** André R. Studart; ETH Zurich, Switzerland

Hierarchical porous materials are attractive structures for a variety of applications due to their enhanced mechanical efficiency and their high surface area with minimum permeability loss. Nature showcases remarkable examples of hierarchical porous materials that benefit from such unusual set of properties, including bamboo, bone, marine sponges and wood. However, synthetic porous materials have yet to reach the elaborate architectural design found in their biological counterparts. To fill this gap, processing routes that enable deliberate control over the material's porous structure at multiple length scales are highly demanded. In this talk, I will show how 3D printing technologies can be exploited to fabricate hierarchical porous materials with unprecedented mechanical efficiency and architectural control. The key feature of our approach is to design inks with an internal structure that serves as a template for the formation of tailored pores within the printed object. Using oil droplets, air bubbles or phase-separating mixtures as templating structures, this methodology enables independent tuning of porosity and pore sizes at multiple length scales. To demonstrate the potential of the process, we 3D printed complex-shaped parts with bioinspired multiscale porosity and enhanced mechanical efficiency that cannot be achieved through conventional fabrication technologies.

### 5:30 AM \*F.SM01.02.03

**Exploiting Supramolecular Associations in Interpenetrating Networks and Elastomers** [LaShanda Korley](#) and Chase Thompson; University of Delaware, United States

Supramolecular interactions may hold the key to the development of network systems with tunable mechanics and modulated architecture, such as observed in the muscle protein titin. It is the dynamic nature of these physical associations that we have exploited in the design of tough supramolecular materials that super-impose covalent and non-covalent interactions to tailor tensile response. We have developed supramolecular elastomers and interpenetrating network (IPN) systems that probe the interplay of non-covalent and covalent interactions in structural organization and mechanical response. By tailoring physical associations via control of self-assembly and composition, we have demonstrated enhanced supramolecular dynamics driven by architecture and toughness enhancements due to phase behavior. Recently, non-covalent interaction strength, network regularity, and chemoresponsiveness have been utilized as handles to derive gradient materials and to induce actuation behavior. New insights into supramolecular nanocomposites are also highlighted.

### 5:45 AM F.SM01.02.04

**Direct Observation of Water Droplet by Scanning Electron Microscope** [Noriyuki Inoue](#)<sup>1</sup>, Shunsuke Asahina<sup>2</sup> and Natasha Erdman<sup>1</sup>; <sup>1</sup>JEOL USA, Inc., United States; <sup>2</sup>JEOL Ltd., Japan

A variety of materials developed in recent years have featured artificial water repellent surface structure inspired from organisms. However, an optical microscope cannot observe interfacial structural relationship with water droplet accurately due to problems of resolution and depth of focus. Therefore, we have applied the Scanning Electron Microscope (SEM) that can be used to observe the surface of specimen accurately. Traditionally, water droplets cannot be observed by SEM due to strict vacuum requirements for electron beam based imaging. Therefore, we have been developed a unique method called Aqua Cover method that allows observation of water directly in SEM [1].

SEM has a Low Vacuum (LV) mode that can facilitate imaging of water containing specimen. The chamber pressure of LV mode is able to reach several hundred Pa, but this pressure is insufficient to keep liquid water. There is also a method called Environmental SEM (ESEM). This method can maintain water droplets on a specimen by dew condensation. This is achieved by introducing the water vapor into the specimen chamber and cooling a specimen stage in LV mode. Although this method can make many tiny water droplets on the specimen surface, it cannot drop a water droplet directly at a specific site on the specimen surface. Unfortunately, tiny water droplets are also formed in crevices of uneven structures, so the Wenzel state is created even under the conditions that should be Cassie-Baxter state [2, 3]. From this reason, it is difficult to observe a behavior of sub mm to mm order water droplet, like a raindrop, on the specimen surface accurately, but it is important for development of fine structures and quality control in artificial water repellent materials.

As a method to solve this problem, Aqua Cover method that can keep the size of a water droplet from atmospheric pressure to pressure of LV mode and be observed by SEM is developed. Using this method, the interface relationship between water droplet dropped at atmospheric pressure and the specimen surface is observed by SEM and determined whether the water repellent state was Cassie-Baxter or Wenzel.

The experimental method is as follows: approximately 10 mm x 10 mm of lotus leaf was fixed on a 45 ° tilt specimen stub and installed on a cooling stage set at 0°C. 1 mL water droplet was then dropped onto the specimen surface. The Aqua Cover method was used for SEM observation at a specimen chamber pressure of 650 Pa and an accelerating voltage of 25 kV.

As a result of SEM Aqua Cover observation, air pockets were observed at the interface between surface unevenness structure and water droplet, so the state of this condition was determined to be Cassie-Baxter.

#### References

1. Inoue N, Takashima Y, Suga M, Suzuki T, Nemoto Y, and Takai O (2018). Observation of wet specimens sensitive to evaporation using scanning electron microscopy. *Microscopy*. **67**: 356-366.
2. Jung Y C, and Bhushan B (2008). Wetting behaviour during evaporation and condensation of water microdroplets on superhydrophobic patterned surfaces. *J. Microsc.* **229**: 127-140.
3. Darmanin T, and Guittars F (2015). Superhydrophobic and superoleophobic properties in nature. *Mater. Today* **18**: 273-285.

### 5:55 AM F.SM01.02.05

**Engineering the Seed Microenvironment** Benedetto Marelli, Hui Sun and [Augustine Zvinavashe](#); Massachusetts Institute of Technology, United States

Bioinspired by the tardigrade and bombyx mori we engineer the seed microenvironment to encapsulate, preserve and deliver *Rhizobium tropici*. Scientific discoveries in agriculture and sustainability are at the crossroads of material science,

biochemistry, agriculture and biology. They underpin the innovative technological solutions that will impact water, energy and food security (WEFS). These new technologies can then be implemented to address major societal problems that are linked to climate change, soil degradation and soil salinization. In particular, our objective is to augment agricultural outputs (*i.e.* crop yield and production) while decreasing inputs (*e.g.* water, energy, fertilizers, land, pesticides) by deploying plant-growth-promoting-bacteria (PGPBs) in the soil to alleviate plant stressors to be specific soil salinity. Using PGPBs as a substitute to synthetic fertilizer our design approach engineers the seed microenvironment by coating the seeds with PGPB laden biopolymers. PGPBs are well known to enhance crop production and protect plants from biotic and abiotic stresses, while decreasing the need for water and fertilizers. However, the bacteria's delicate nature has hindered their use in current agricultural practices. We use a silk and trehalose mixture that is able to encapsulate, protect, preserve and deliver *Rhizobium tropici* to *Phaseolus Vulgaris*. The coated *Phaseolus Vulgaris* seed are shown to be able to significantly alleviate soil salinity stress in Moroccan soil when compared with uncoated (control) *Phaseolus Vulgaris* seeds.

#### 6:05 AM F.SM01.02.06

**Enzymes—Efficient Biological Catalysts and Useful Tool for the Sustainable Degradation of Plastics?** Eva Krakor, Isabel Gessner and Sanjay Mathur; University of Cologne, Germany

Worldwide 350 to 400 million metric tons of synthetic polymers are produced every year and it is estimated that 5 to 13 million metric tons of plastic will enter the ocean every year. This leads to negative consequences for various ecosystems and the human and animal health. For the removal of plastic, enzymes have come into focus of recent research due to their high selectivity and catalytic efficiency under mild conditions and their sustainable alternative to toxic catalysts. Esterases and hydrolases such as lipase and cutinase, respectively, catalyze the hydrolysis of lipids and cutin, a complex hydrophobic polyester the main component of the plant cuticle.

Nevertheless, enzymes constitute an expensive catalyst making a reusable system where the enzymes are attached on the surface of magnetic particles a cost-efficient platform. Therefore, magnetic ellipsoidal-shaped  $\text{SiO}_2@\text{Fe}_3\text{O}_4$  particles were synthesized by coating ellipsoidal shaped  $\alpha\text{-Fe}_2\text{O}_3$  particles in a two-step sol-gel process with  $\text{SiO}_2$ . Afterwards the  $\alpha\text{-Fe}_2\text{O}_3$  core is reduced to magnetic  $\text{Fe}_3\text{O}_4$  in a  $\text{H}_2$ /argon atmosphere. Covalent immobilization of the enzyme was achieved by first modifying the particles with 3-(aminopropyl)triethoxysilane to obtain terminal amino groups which upon addition of glutaraldehyde formed a stable bond to the enzyme. The successful attachment of the enzyme was proven via Zeta potential, IR and CHNS measurements. Moreover, the activity of the enzyme was demonstrated using the optical conversion of 4-nitrophenyl acetate to 4-nitrophenol. This approach was extended to polymeric materials using polycaprolactone fiber mats which were analyzed regarding morphology changes upon enzymatic degradation.

#### 6:15 AM F.SM01.02.07

**Natural Layered Structures in Biogenic Magnesium Calcite Single Crystals** Alex Katsman and Boaz Pokroy; Technion - Israel Institute of Technology, Israel

Some calcitic biominerals have been shown to be formed through the crystallization of a Mg-rich amorphous calcium carbonate (Mg-ACC) precursor. Formation mechanisms of multiscale biogenic single crystal structures at ambient temperatures, in conditions of limited solid phase diffusion, remain largely incomprehensible. Based on experimental results, we develop a model describing the formation of the brittle star Mg-calcite nanostructure from an amorphous Mg-ACC precursor to a Mg-calcite nanostructure containing periodic layers with varying concentrations of coherent Mg-rich nano-inclusions. The formation route is rationalized in a two-step model: the first step involves spinodal decomposition of a liquid or gel-like Mg-ACC precursor into Mg-rich nanoparticles and a Mg-depleted amorphous matrix. The second step is the crystallization of the decomposed Mg-ACC precursor. The crystallization of Mg-depleted ACC matrix is accompanied by the exclusion of Mg ions into a diffusion zone adjacent to the crystallization front; after crystallization of a certain layer, the Mg concentration ahead of the layer exceeds the critical value above which the Mg-ACC matrix becomes unstable against spinodal decomposition. A secondary spinodal decomposition will then start and result in the formation of additional Mg-rich nano-domains. As a result, the density of Mg-rich nano-domains changes periodically and forms periodic layered structure inside magnesium calcite single crystals. The model was supported by our experimental results in synthetic Mg-calcite, which suggest a spinodal decomposition in the amorphous precursor. These new insights have significant implications for fundamental understanding of the biogenic layered structures formation.

#### 6:25 AM F.SM01.02.09

**Templated Crystallization of Structural Biopolymers for Tailored Hierarchical Materials** Hui Sun and Benedetto Marelli; Massachusetts Institute of Technology, United States

Living systems regulate the disorder to order transition of biomacromolecules to achieve complex materials with a variety of functionality and structural hierarchy, which has long been an inspiration for similar endeavors in synthetic materials. In particular, materials generation in nature often involves the use of templates to direct the assembly pathway and subsequent hierarchical organization of nanoscale building blocks, with the most prominent example being biomineralization that is ubiquitous in the natural world. The same principle underpins amyloid fibrils formation through pathogen (such as prions and misfolded A $\beta$  oligomers) templating, which follows a nucleation-elongation model. In this presentation, we introduce templated crystallization of structural biopolymers as a process to nanofabricate hierarchically structured materials up to centimeter scale, using silk fibroin as an example. The process involves the use of ordered peptide supramolecular assemblies as templates to drive a phase transformation of silk fibroin from unordered to ordered conformations, thereby enabling further assembly of the silk fibroin chains into nanostructured materials (i.e.  $\beta$ -sheeted nanofibrils). Multiple parameters including the relative concentration between silk fibroin and peptide seeds, silk fibroin molecular weight, pH and peptide conformation are investigated to fine tune the assembly kinetics and silk polymorphs. Combining the templated crystallization with various top-down fabrication such as soft lithography and printing enables (i) formation of different silk polymorphs at selected areas, generating free-standing patterned silk films, where the different molecular structures can be used to store or encrypt information; (ii) surface functionalization with topographical control over silk nanofibrils growth on pre-deposited peptide seeds; and (iii) three-dimensional manipulation of silk nanofibrils into macroscopic structures with customized shapes and controlled anisotropy. Together, these results pave the way for nanofabrication of a new generation of smart and adaptive materials built from the bottom up.

#### 6:35 AM F.SM01.02.11

**Late News: Accelerated Solar-Thermal Energy Harvesting Within Phase Change Materials Through Learning from Nature** Peng Tao, Chao Chang, Qinxian Ye, Xiaoxiang Li and Tao Deng; Shanghai Jiao Tong University, China

Converting abundant sunlight as storable heat within phase change materials (PCMs) is an attractive way to harness solar energy for a broad range of heating-related applications. Current PCMs, however, generally suffer from a low thermal conductivity, which seriously limits the solar-thermal energy harvesting (STEH) process. In nature, STEH is also vital for normal functioning of biological species, but they have developed different strategies. For example, butterflies rely on spreading their wings towards sunlight to absorb solar photons to quickly warm the body and dynamically folding their wings to mediate the body temperature. Inspired by such unique mechanism, we demonstrate dynamic movement of the solar-thermal converters along the melting solid/liquid interface as an effective strategy to accelerate transportation of solar photons within PCMs thereby achieving fast STEH. By magnetically tuning the distribution of Fe<sub>3</sub>O<sub>4</sub>@graphene nanoparticles within the paraffin composite the STEH rate was increased by  $\sim 3$  times. The low loading concentration requirement also enables the composites to fully retain and even slightly increase the fusion enthalpy of the PCMs. We further demonstrate rapid roll-to-roll STEH through illuminating the thin flexible form-stable composite PCM sheets while being continuously rolled. Due to shortened heat-diffusion distance and rollability of the composites, it achieves fast and uniform STEH within the bulk PCMs. The flexibility of charged composites also enables broad tuning of the discharging behavior, and provides the possibility to explore wearable thermotherapy and other flexible solar-thermal applications.

#### 6:45 AM F.SM01.02.12

**Late News: Hydroxycitrate-Controlled Brushite Crystallization in Aqueous Solution** Ma. Charlene C. Tapia<sup>1</sup>, Naoyuki Miyashita<sup>2,2</sup>, Wei Weilin<sup>2</sup>, Kazuki Miyata<sup>2,2</sup>, Takeshi Fukuma<sup>2,2</sup>, Jem Valerie Perez<sup>1</sup> and Bryan G. Alamani<sup>1</sup>; <sup>1</sup>University of the Philippines, Philippines; <sup>2</sup>Kanazawa University, Japan

Brushite is one of the most important polymorphs of calcium phosphate in the context of bio-inspired mineralization. It has been used as reconstruction materials, dental cements and in formulation chemistry. It is also a precursor of hydroxyapatite which is a common component of bones and teeth. Due to its wide application as a functional material and a precursor of other bioceramics, the control of its crystal morphology is important. The performance of a functional material significantly depends on its shape and surface properties. Fundamentally, carboxylates are known modifiers of crystal growth. One example is hydroxycitrate (HCA) which have effectively curbed and controlled calcium oxalate mineralization. Here we reported the effect of HCA in the crystal shape, aspect ratio and number density. The bulk crystallization was coupled with interfacial studies using atomic force microscopy to further evaluate its impact on the surface of brushite. Analysis shows a 50% reduction in the number of crystals formed and a change in brushite's morphology event at a very small inhibitor concentration (Ca/inhibitor=25000). Amplitude and Frequency Modulated AFM studies show that surface roughness increased through time in the presence of the HCA. Changes in the periodic features at near atomic resolution was also observed in the presence of HCA implying possible modifier-hydration layer interactions. Results obtained in this study may serve as a step in understanding the HCA's effect on brushite and in designing bio-inspired calcium phosphate materials and

precursors.

#### 6:55 AM F.SM01.02.13

**Late News: Emergent Behavior of Bioinspired Multicompartment Capsules Triggered by Temperature or Oxidants** Sai Nikhil Subraveti, Kerry DeMella and Srinivasa Raghavan; University of Maryland, United States

Life is an “emergent” property – i.e., one exhibited by living systems as a whole, but not by any of their individual parts. In a single eukaryotic cell, there exist internal compartments called organelles, such as the nucleus and mitochondria. While the organelles each have distinct functions, it is the overall cell that has the property of life – i.e., the whole is greater than the sum of the parts. Here, we describe our attempts to create millimeter-scale polymer capsules that exhibit emergent properties. In particular, we have created multicompartment capsules (MCCs) that have many internal compartments, each with distinct contents. We have also found ways to perfectly encapsulate (hermetically seal) aqueous solutes in a capsule core until an external stimulus is applied. The key to this property is to utilize hydrophobic shells that are impermeable to aqueous solutes. However, the shells can be degraded or made permeable by external triggers – either by heat or by oxidants that generate reactive oxygen species (ROS).

Using these concepts, we have activated multi-step or cascade reactions within MCCs. In one example, we use the MCC as a factory to synthesize fluorescent gold nanoclusters (AuNCs). Individual non-fluorescent reagents are encapsulated in internal compartments. When a stimulus is applied, the reagents leave the compartments and come into contact with each other, thus producing AuNCs. The overall MCC thereby displays an emergent property (fluorescence) that is not exhibited by any of its individual components. In a second example, we encapsulate a chemical fuel and catalytic particles in separate compartments. When the compartments are triggered to open up, the catalyst comes into contact with the fuel, which results in the production of oxygen gas. The gas causes the entire MCC to inflate, and this inflation is again a property that emerges from the interactions between the components of the MCC.

#### 7:05 AM F.SM01.02.14

**Late News: Dynamic Color-Change in Multi-Responsive Photonic Microspheres Formed by Hierarchical Assembly of Colloidal Nanogels** Golnaz Isapour; Massachusetts Institute of Technology, United States

Soft photonic materials formed from colloidal crystals are highly-desirable platforms for sensing and signaling in biomedical, chemical, and mechanical application scenarios<sup>1-3</sup>. A particularly accessible attribute of such materials is structural coloration; by using stimuli-responsive and reconfigurable colloidal crystals, dynamic coloration can be achieved, akin to the inspiring ability of chameleons to change their color appearance<sup>4</sup>. To date many concepts for the lab-scale creation of such photonic materials are known<sup>5</sup>, however a lack of efficient and scalable production methods with sufficient control of properties persists. In addition, in hybrid materials with multiple stimuli-responsive components, interactions among components tend to be overlooked. Here, we propose a simple and scalable method to prepare stimuli-responsive photonic hydrogel balls of several tens of microns in diameter, in which pH- responsive colloidal nanogels are embedded in a scaffolding hydrogel. We show a dynamic color-change spanning the entire visible spectral range through a variation of pH or temperature, which triggers the nanogels or the scaffolding hydrogel, respectively. We discuss the mutual swelling interactions between the colloidal nanogels and the scaffolding hydrogel. The response characteristics, such as timescale and spectral range of the photonic balls can be tuned by altering the composition, and responsive properties of the colloidal nanogel and the scaffolding hydrogel. These photonic hydrogel balls could be applied as optically interrogated sentinels in label-free multiplexed chemical, thermal, and mechanical sensing scenarios with sub-mm resolution. In addition, by employing modular assembly strategies, they can be used to form dynamic color-changing materials at scale.

(1) Zhao, Y.; Shang, L.; Cheng, Y.; Gu, Z. Spherical Colloidal Photonic Crystals. *Acc. Chem. Res.* **2014**, *47* (12), 3632–3642. <https://doi.org/10.1021/ar500317s>.

(2) Burgess, I. B.; Lončar, M.; Aizenberg, J. Structural Colour in Colourimetric Sensors and Indicators. *J. Mater. Chem. C* **2013**, *1* (38), 6075–6086. <https://doi.org/10.1039/C3TC30919C>.

(3) Chan, E. P.; Walish, J. J.; Urbas, A. M.; Thomas, E. L. Mechanochromic Photonic Gels. *Advanced Materials* **2013**, *25* (29), 3934–3947. <https://doi.org/10.1002/adma.201300692>.

(4) Teyssier, J.; Saenko, S. V.; van der Marel, D.; Milinkovitch, M. C. Photonic Crystals Cause Active Colour Change in Chameleons. *Nature Communications* **2015**, *6* (1), 6368. <https://doi.org/10.1038/ncomms7368>.

(5) Vogel, N.; Retsch, M.; Fustin, C.-A.; del Campo, A.; Jonas, U. Advances in Colloidal Assembly: The Design of Structure and Hierarchy in Two and Three Dimensions. *Chem. Rev.* **2015**, *115* (13), 6265–6311. <https://doi.org/10.1021/cr400081d>.

#### 7:15 AM F.SM01.02.15

**Late News: Structure, Assembly and Material Properties of Model Cephalopod Proteins** Preeta Pratakshya, Atrouli

Chatterjee, Rylan J. Kautz and Alon Gorodetsky; University of California, Irvine, United States

Cephalopods are known for their remarkable ability to camouflage by rapidly changing the color and reflectance of their skin, a property that is enabled by the presence of subcellular structures composed of unique structural proteins called reflectins. Given the critical role played by reflectins in regulating the optical behavior of these organisms, and their technological potential for the development of biophotonic and bioelectronic devices, these proteins have recently emerged as a desirable target for the design of novel functional biomaterials. However, the development of such materials has been impeded by a lack of complete understanding of the structure and assembly of this class of proteins. Here we will highlight the proteins' multi-faceted material properties within the context of bioelectronic and biophotonic platforms. Specifically, we will discuss how the structure and stimuli-responsive assembly of these proteins enables their electrical and optical functionality. Our findings not only underscore the potential of reflectins as functional materials but also hold relevance for the development of cephalopod-inspired bioelectronic technologies.

**7:25 AM F.SM01.02.16**

**Late News: 3D Nanostructure of Collagen Smectic Liquid Crystal Phase Used to Form Mussel Byssus**

**Threads** [Franziska Jehle](#)<sup>1,2</sup>, Tobias Priemel<sup>1</sup>, Peter Fratzl<sup>2</sup>, Luca Bertinetti<sup>2,3</sup> and Matthew J. Harrington<sup>1,2</sup>; <sup>1</sup>McGill University, Canada; <sup>2</sup>Max Planck Institute of Colloids and Interfaces, Germany; <sup>3</sup>B CUBE Center for Molecular Bioengineering TU Dresden, Germany

Marine mussels (*Mytilus* spp.) fabricate tough and self-healing collagenous biofibers known as byssal threads via self-assembly. The hierarchical organization of the protein building blocks comprising the fibers was previously demonstrated to be crucial for their outstanding mechanical properties. Evidence suggests that self-assembly of this hierarchical structure is aided by the storage of the collagenous precursor proteins as a colloidal liquid crystal (LC) phase within micron-scale secretory vesicles. Currently, however, very little is understood about the molecular level forces controlling LC phase formation. Here, we harnessed advanced electron microscopy methods to reconstruct the 3-dimensional LC nanostructure of the collagen precursors within the secretory vesicles with unprecedented detail, including visualization of specific LC defects. Specifically, we identified the presence of a lyotropic smectic LC phase that we posit arises from the block co-polymer-like primary structure of the specialized byssus collagen precursor, consisting of clear demarcations in hydrophathy and charge distribution. We further propose that terminal pH-responsive protein domains enriched in histidine provide the impetus for the fluid to fiber transition during thread formation. These findings may inspire new strategies for fabricating nanostructured soft materials with complex material properties through supramolecular self-assembly, which is relevant to ongoing efforts in sustainable polymers and tissue engineering.

SESSION F.SM01.03: Bio-Inspired Surfaces and Coatings

On Demand Abstracts Available for Viewing Starting Saturday Morning, November 21, 2020

F-SM01

**5:00 AM F.SM01.03.01**

**Frost-Free Surface Design Inspired by Macrot textured Leaves** Christian Machado and [K\\_yoo-Chul \(Ken\) Park](#); Northwestern University, United States

Numerous studies have focused on a low surface energy coating and a micro/nanoscale surface texture to design functional surfaces that delay frost formation and reduce ice adhesion. However, the scientific challenges for long-term icephobic surfaces have not been fully addressed because of degradation such as mechanical wearing. Inspired by the suppressed frost formation on concave regions of natural leaves, here we report findings on the frosting process on surfaces with various serrated structures. Dropwise condensation, the first stage of frosting, is enhanced on the peaks and suppressed in the valleys when the wavy surface is exposed to humid air, causing frosting to initiate from the peak. The condensed droplets in the valley are then evaporated, resulting in a non-frost band. The effects of surface topography on the frost pattern are systematically studied by varying the serrated geometry defined as the vertex angle, and numerically modeling the spatial distribution of diffusion flux of water vapor on the wavy surface. Under different ambient humidity levels, the magnitudes of diffusion flux at the non-frost boundaries of the surfaces are nearly identical, implying that the critical value of diffusion flux is the key to understanding the non-frost pattern.

**5:10 AM F.SM01.03.02**

**‘Antifouling’ Porous Lignocellulosic Biomass with Internal Microchannels as Solar Absorbers and Water Pumpers for Thermal Desalination** Chao Liu, Qiang Li, Pengcheng Luan and Hongli Zhu; Northeastern University, United States

Water pollution and freshwater shortages present two of most emerging societal challenging issues. Although many advances have been explored in obtaining clean water, such as reverse osmosis technologies, membrane treatments, ion exchange, and some multi-effect distillation systems, these technologies are still costly. Water desalination and purification from seawater and wastewater have been developed for addressing the globally growing need of clean water, among which solar-driven evaporation has drawn tremendous attention because it uses abundant solar energy and has a small environmental footprint. Conventional sunlight absorbers include carbon-based materials with strong light absorption abilities, heat localizing plasmonic nanoparticles, and hydrophilic sponges with carbonized surfaces. However, their relatively low energy conversion efficiencies, high cost, limited capacity for continuous steam generation, and salt accumulation induced efficiency decay have hindered the development. As a new solar technology, interface steam generation has great prospects for the application of desalination and fractionation. In this work, we report a sustainable, efficient and accessible solar evaporator with bilayer structure from lignocellulosic biomass. Loofah is a pervasive vegetable in our daily life. The mature loofah is comprised of natural fibers with high hydrophilicity, hierarchical macropores, and microchannels, which are essential features and structures for steam generators. We prepared a bilayer loofah-derived solar evaporator, which had a top carbonized layer that functioned as efficient solar absorbers with broad light absorption and high light trapping and a bottom loofah fiber layer for sufficient water pumping to the localized heating surface from different directions. During desalination, the salt concentration gradient of the macropores and microchannels allowed for efficient salt drainage in loofah and prevented the accumulation of salt on the surface of the evaporator, thus enabling the antifouling properties that provided the loofah solar evaporator a long-term stability. This economical light absorber and water-pumping natural fibers exhibited a steam generation rate of 1.42 kg m<sup>-2</sup> h<sup>-1</sup> and an efficiency of 89.9% under 1 Sun. This low-cost, abundant, and stable material from lignocellulose biomass thus have great potential for future large-scale solar steam applications.

**5:20 AM F.SM01.03.03**

**Antiviral and Antimicrobial Biomaterials Inspired by Mussel Adhesive Chemistry** Bruce Lee; Michigan Technological Univ, United States

Marine mussels secrete adhesive proteins that enable these organism to anchor themselves to various substrate (i.e., ship hull, rock) in a rough, intertidal zone. These mussel foot proteins contain a unique amino acid, L-3, 4 dihydroxyphenylalanine (DOPA), that is responsible for strong interfacial binding. Specifically, the catechol side chain of DOPA is capable of participating in reversible interactions and covalent crosslinking. Many investigators utilize the catechol adhesive moiety in designing biomimetic adhesives and coatings. In contrast to these applications, our lab has been developing antiviral and antimicrobial biomaterials utilizing the redox chemistry of catechol. Catechol generates reactive oxygen species (ROS), such as superoxide and hydrogen peroxide, when it becomes oxidized. The generated ROS was antimicrobial against both gram-negative (*Escherichia coli*) and gram-positive (*Staphylococcus epidermidis*) bacteria and reduced the infectivity of a non-enveloped porcine parvovirus and an enveloped bovine viral diarrhea virus. Most importantly, the generation of ROS can be easily activated by simple hydration of catechol-containing microgel or coating. Most recently, we chemically modified catechol with various halogens. These halogenated catechol demonstrated broad spectrum antimicrobial property against multiple strains of multidrug resistance bacteria. The combination of moisture-resistant adhesive property and inherent antimicrobial property greatly enhanced the potential for using catechol for designing multifunctional bioadhesives, wound dressings and coatings with antipathogenic properties.

**5:30 AM F.SM01.03.04**

**Bio-Inspired Active Skins for Surface Texture Morphing** Yujin Park and Kenneth J. Loh; University of California San Diego, United States

There has been tremendous interest in optimizing artificial surfaces that can continuously morph their surface texture for various purposes, such as camouflage, signaling, and hunting. In recent years, smart materials like stimuli-responsive polymers and hydrogels were leveraged to achieve surface texture morphing. However, their real-world applications are limited given their slow actuation and weak mechanical properties. Thus, the aim of this research is to broaden the current knowledge of surface texture morphing by designing instability-induced morphable structures using patterned, auxetic geometries. Our previous study introduced 3D-printed and thin-film-like Active Skins based on a star-reentrant geometry, and it was shown that unique patterns of out-of-plane deformations could be induced when uniaxial strains were applied. Moreover, geometrical imperfections or notches were introduced to program the surface morphing behavior of Active Skin in a desired manner. In this study, the geometrical dependence of surface morphing response (i.e., the nonlinear response of 3D-printed Active Skins) was characterized using both experiments and finite element model (FEM) simulations. First,



experimentally calibrated FEM simulations were employed to design the width and angles of the rib of unit cell geometries. Second, the locations of geometrical imperfections were selected by identifying regions where stress concentrations were greatest in the unit cell. Last, unit cells with these designed imperfections were replicated by 3D-printing. Both the experimental and FEM results confirmed that the Active Skins could deploy pre-programmed 3D features on-demand, reversibly, and effectively through a controlled buckling-induced deformation mechanism.

#### 5:40 AM F.SM01.03.06

**Bio-Inspired Vascularized Polymers Control Bacteria at Interfaces** Kayla Marquis, Benjamin Chasse and [Caitlin Howell](#); University of Maine, United States

Nearly all methods of introducing bioactive compounds to the surface of a substrate rely on application from above or fail over time due to depletion. In this work, we use a bio-inspired approach to deliver target molecules to an interface from below, making use of both theoretical modeling and experimental validation to rationally design customizable patterns and gradients. Mimicking the vascular systems of living organisms, networks of empty 3D-printed channels are filled with liquid containing the compound of interest, which flows through the vascular network and diffuses through the polymer, eventually reaching the substrate surface. In proof-of-principle experiments using *Escherichia coli* and *Bacillus subtilis* as model organisms, we demonstrate both theoretically and experimentally that the concentration of antibiotic and duration over which it is delivered to the surface can be controlled by varying the location of the vascular channels and concentration of the antibiotic solution inside. The result is a well-defined and predictable patterned response from the bacteria growing on the surface, a first step toward developing new types of adaptive antifouling surfaces and cell culture tools.

#### 5:50 AM F.SM01.03.07

**Compact Bio-Inspired Nanoscale Textures Reduce Contact Time of Bouncing Droplets** [Lin Wang](#), Ruoxi Wang, Jing Wang and Tak-Sing Wong; The Pennsylvania State University, University Park, United States

Many natural surfaces are capable of shedding water droplets rapidly, which has been attributed to the presence of low solid fraction ( $\Phi_s \sim 0.01$ ) (1) according to the classical wetting theories (2-4). However, recent high-resolution microscopic observations revealed the presence of unusual high solid fraction nanoscale textures on water-repellent insect surfaces. For example, superhydrophobic mosquito eyes, springtails, and cicada wings possess solid fractions ( $\Phi_s$ ) as high as 0.25 – 0.64 (5-7). In addition, the texture size on these insect surfaces is typically on the order of 100 – 300 nm. To understand why both high solid fraction and nanoscale textures are important for these superhydrophobic insect surfaces, we systematically designed and fabricated a series of textured surfaces with texture size varying from 100 nm to 30  $\mu\text{m}$  at solid fractions of 0.25 and 0.44, and investigated their static and dynamic wetting behaviors. Here we show that the contact time of bouncing droplets on high solid fraction surfaces can be reduced by reducing the texture size to nanometer scale. Specifically, we discovered that high solid fraction surfaces ( $\Phi_s \sim 0.44$ ) with texture size  $\sim 100$  nm could reduce the contact time by  $\sim 2.6$  ms compared to that with texture size  $> 300$  nm. This texture-size dependent contact time reduction on solid surfaces has not been observed previously, and cannot be explained by existing surface wetting theories. We showed theoretically that the reduction in droplet contact time can be attributed to the dominance of three-phase contact line tension (8) on compact nanoscale textures. Through pressure stability analysis and experiments, we have further shown that high solid fraction ( $\Phi_s > 0.25$ ) is an important requirement for insects to withstand high-speed impacting raindrops. Our results suggest that the compact and nanoscale textures on water repellent insect surfaces may work synergistically to repel and shed impacting raindrops rapidly, which could be an important survival strategy for flying insects. Technologically, the ability of compact nanoscale textured materials to repel high-speed impact of liquid droplets with reduced contact time may find use in a range of applications including fouling-resistant personal protective equipment (PPE), insect-sized flying robots, and miniaturized drones (9).

**Keywords:** contact time | drop impact | insects | nanoscale textures | pressure stability | superhydrophobic surfaces

#### References:

1. W. Barthlott, C. Neinhuis, Purity of the sacred lotus, or escape from contamination in biological surfaces. *Planta* **202**, 1-8 (1997).
2. A. B. D. Cassie, S. Baxter, Large contact angles of plant and animal surfaces. *Nature* **155**, 21-22 (1945).
3. A. B. D. Cassie, S. Baxter, Wettability of porous surfaces. *Trans. Faraday Soc.* **40**, 0546-0550 (1944).
4. R. N. Wenzel, Resistance of solid surfaces to wetting by water. *Ind. Eng. Chem.* **28**, 988-994 (1936).
5. X. Gao, X. Yan, X. Yao, L. Xu, K. Zhang, J. Zhang, B. Yang, L. Jiang, The dry-style antifogging properties of mosquito compound eyes and artificial analogues prepared by soft lithography. *Adv. Mater.* **19**, 2213-2217 (2007).
6. H. Gundersen, H. P. Leinaas, C. Thaulow, Surface structure and wetting characteristics of collembola cuticles. *PLoS ONE* **9**, e86783 (2014).

7. J. Oh, C. E. Dana, S. Hong, J. K. Román, K. D. Jo, J. W. Hong, J. Nguyen, D. M. Cropek, M. Alleyne, N. Miljkovic, Exploring the role of habitat on the wettability of cicada wings. *ACS Appl. Mater. Interfaces* **9**, 27173-27184 (2017).
8. J. W. Gibbs, *The scientific papers of J. Willard Gibbs*. (Dover Publications, New York, 1961).
9. L. Wang, R. Wang, J. Wang, T.-S. Wong, Compact nanoscale textures reduce contact time of bouncing droplets. *Sci. Adv.*, (2020), to appear.

#### 6:00 AM F.SM01.03.08

**Fabrication of Durable and Transparent Superhydrophobic Coatings Based on Novel Architecture Obtained by Pickering Emulsion Templating** Karthik Ananth Mani and Guy Mechrez; Agricultural Research Organization, Volcani Center, Israel

Despite the enormous research activity in the field of Pickering emulsions and the study of diverse emulsion systems such as O/W<sup>1</sup>, O/O<sup>2</sup>, W/O<sup>3</sup>, O/W/O, W/O/W<sup>4</sup>. There are only very few studies which presents the implementation of Pickering emulsions toward the development of superhydrophobic coatings and surfaces<sup>5-9</sup>. It is possible to obtain a hierarchical porous structure by application of Pickering emulsions on a given surface and evaporation of the solvents, this procedure is termed *emulsion templating*. Although that enormous amount of studies have previously reported the successful development of superhydrophobic coatings and surfaces, only very few of them exhibit significant durability and transparency that would be suitable for real life applications. The current study presents the development of highly durable and transparent superhydrophobic coating based on oil-in-oil (O/O) Pickering emulsions. The combination of superhydrophobicity with significant abrasion resistance and transparency is obtained due to the formation of unique structures of shranked colloidosomes on the surface of the coating. The coating is formed by emulsion templating of the O/O Pickering emulsion. The studied Pickering emulsions were applied on different types of polymeric substrates such as polypropylene and polycarbonate by using standard coating application methods including spin coating and roll coating.

#### References

- B. P. Binks, S. O. Lumsdon, *Phys. Chem. Chem. Phys.* 1999, 1, 3007.
- B. P. Binks, A. T. Tyowua, *Soft Matter* 2016, 12, 876.
- B. P. Binks, S. O. Lumsdon, *Langmuir* 2000, 16, 2539.
- Q. Gao, C. Wang, H. Liu, Y. Chen, Z. Tong, *Polym Chem* 2010, 1, 75.
- I. S. Bayer, A. Steele, P. J. Martorana, E. Loth, L. Miller, *Appl. Phys. Lett.* 2009, 94, 163902.
- I. S. Bayer, A. Steele, P. J. Martorana, E. Loth, *Appl. Surf. Sci.* 2010, 257, 823.
- A. Davis, S. Surdo, G. Caputo, I. S. Bayer, A. Athanassiou, *ACS Appl. Mater. Interfaces* 2018, 10, 2907.
- S. Naderizadeh, J. A. Heredia-Guerrero, G. Caputo, S. Grasselli, A. Malchiodi, A. Athanassiou, I. S. Bayer, *Adv. Mater. Interfaces* 2019, 6, 1801782.
- F. Li, Z. Wang, Y. Pan, X. Zhao, *Polymers* 2017, 9, 563.

#### 6:10 AM F.SM01.03.11

**Rational Design of Bio-Inspired Nanowire Architectures for Preventing Marine Biofouling** Jing Wang, Sudarat Lee, Ashley R. Bielinski, Kevin A. Meyer, Abhishek Dhyani, Alondra M. Ortiz-Ortiz, Anish Tuteja and Neil P. Dasgupta; University of Michigan, United States

Biofouling has a negative impact on human health and economic development. In particular, biofilms in the marine environment grow easily, adhere strongly on most surfaces, and continuously generate adhesive proteins from the living organisms in the film. They cause increased fuel penalty, attenuation of sensor signals, and more [1]. To overcome these challenges, several natural surfaces, including shark skin [2], crab eyes [3], and dragonfly wings [4], have shown reduced biofilm settlement, nucleation, and adhesion because of their micro- and nano- surface textures.

Inspired by natural surfaces, herein, we present the rational design and fabrication of ZnO/Al<sub>2</sub>O<sub>3</sub> core-shell nanowire (NW) architectures to significantly reduce marine biofouling (algae: cyanobacteria and diatoms) and further suppress the biofilm formation by tuning the NW geometry (length, spacing, branching) and surface chemistry [5]. Specifically, for hydrophilic NWs, we demonstrated algal fouling on NWs was only 40% of the fouling coverage on planar control surfaces when they were fully covered. These NWs outperform the surfaces with micrometer length-scale textures in marine fouling reduction under a multi-species fouling environment. Two mechanisms of the fouling reduction were summarized with geometric and mechanical effect of the NWs: (1) reduced effective settlement area, and (2) mechanical cell penetration. For superhydrophobic NWs, we demonstrated anti-biofouling performance for up to 22 days, which is one order of magnitude longer duration than what have been reported in the literature [6] under biofouling environment. A mass diffusion and thermodynamic model was developed to explain and predict the anti-fouling duration on NWs in the Cassie state. Furthermore, the nanowire surfaces are transparent across the visible spectrum, making them applicable to windows and oceanographic sensors. Through the rational control of surface nano-architectures, the coupled relationships between

wettability, transparency, and anti-biofouling performance are identified. We envision that the insights gained from the work can be used to systematically design surfaces that reduce marine biofouling in various industrial settings.

#### REFERENCES

- [1] J. A. Callow and M. E. Callow, "Trends in the development of environmentally friendly fouling-resistant marine coatings," *Nature Communications*, vol. 2, p. 244, 2011.
- [2] J. F. Schumacher, C. J. Long, M. E. Callow, J. A. Finlay, J. A. Callow, and A. B. Brennan, "Engineered nanoforce gradients for inhibition of settlement (attachment) of swimming algal spores," *Langmuir*, vol. 24, pp. 4931-4937, 2008.
- [3] G. Greco, T. S. Lanero, S. Torrassa, R. Young, M. Vassalli, A. Cavaliere, *et al.*, "Microtopography of the eye surface of the crab *Carcinus maenas*: an atomic force microscope study suggesting a possible antifouling potential," *Journal of the Royal Society Interface*, vol. 10, p. 20130122, 2013.
- [4] E. P. Ivanova, J. Hasan, H. K. Webb, G. Gervinskis, S. Juodkazis, V. K. Truong, *et al.*, "Bactericidal activity of black silicon," *Nature Communications*, vol. 4, p. 2838, 2013.
- [5] A. R. Bielinski, M. Boban, Y. He, E. Kazyak, D. H. Lee, C. Wang, *et al.*, "Rational design of hyperbranched nanowire systems for tunable superomniphobic surfaces enabled by atomic layer deposition," *ACS Nano*, vol. 11, pp. 478-489, 2017.
- [6] G. B. Hwang, K. Page, A. Patir, S. P. Nair, E. Allan, and I. P. Parkin, "The anti-biofouling properties of superhydrophobic surfaces are short-lived," *ACS Nano*, vol. 12, pp. 6050-6058, 2018.

#### 6:20 AM F.SM01.03.12

**Late News: Substrate-Mediated Colloidal Assembly for Templating Tunable Structural Color** Bianca C. Datta, Sunanda Sharma, Christine Ortiz and Neri Oxman; Massachusetts Institute of Technology, United States

To harness the spectacular functionality found in nature, scientists and engineers have developed a multitude of biomimetic and bio-inspired techniques, each with its own strengths and constraints. One classic example is structural color exhibited by organisms such as birds, insects, and cephalopods that produce compelling and vibrant visual displays, which provides a fascinating case study for exploring the role of material design on macroscale properties. Recent research has identified self-assembly of colloidal structures as a cheap, simple way to mimic aspects of this coloration, often using materials like polystyrene or silica as scattering elements.

Self-assembly of spherical and non-spherical particles is an appealing approach as it can be scalable, low cost, conducted under ambient and aqueous conditions, and versatile. There are many factors involved in the drying behavior of colloids which relate to self assembly and color visibility. Structure formation can be tuned by modulating particle composition, surface functionality, particle size and concentration, coating, solvent, substrate wettability and roughness, drying and deposition conditions, particle shape, and the temperature, humidity, and pH of the environment. By manipulating these conditions, the final colloidal assembly structure can be indirectly controlled, yielding a host of fascinating visual effects relevant to bio-inspired design. In this work, we examine the role of melanin for light absorption and polystyrene for light scattering in order to mimic the combination of pigment and structure found in nature, and ultimately demonstrate means to control patterns.

Here we explore the role of the substrate on evaporative dynamics and the interplay between pigment and structure in pattern formation. We influence the rate of the kinetics by tuning surface properties such as hydrophilicity, thereby controlling the color vibrancy. We observe the droplet behavior on different printed surfaces through optical microscopy and macroscopic imaging and demonstrate a visible difference in resulting patterns based on substrate wettability. We record the drying process to observe differences in the dynamics and relate kinetic processes to these final structures.

We utilize polystyrene microparticles with diameters from 173 – 500nm (Sigma Aldrich and Ted Pella), and eumelanin from cuttlefish ink (Sigma Aldrich and MP Biomedicals). By mixing polystyrene and melanin, we generate disordered structures in contrast to ordered structures formed by polystyrene alone, but take advantage of the absorptive properties of melanin to yield more saturated colors than typical amorphous colloidal systems. Polystyrene particle suspensions are mixed with melanin solutions at various ratios and evaporatively assembled on a variety of substrates with the ultimate goal of connecting initial droplet shape, contact angle and speed of evaporation, indirectly tuned using the substrate, to the resulting structure.

We thus present a comparison of drying behavior across several different surfaces, macro-patterning between pigment-based and structural responses to demonstrate color patterns, spectroscopic characterization of the performance of these assemblies on different surfaces, and novel insights about the dynamics of the drying process and the placement of absorbing melanin and scattering polystyrene on the dried surfaces. Properties such as reflectance, absorption, packing and organization, and global architectures are studied using a variety of methods, including timelapse imaging, scanning and transmission electron

microscopy, light microscopy, and angular spectroscopy. This work provides a path towards expanding the palette of achievable colors and patterns through bio-inspired design techniques. Such colloidal assemblies are of interest for optical devices, cosmetics, displays and inks, functional coatings, biocompatible products, sensors, and art elements.

#### 6:30 AM F.SM01.03.13

**Late News: Optical Manufacture and Application of Large-Area, Mechano-Responsive Photonic Sheets** Benjamin Miller, Helen Liu and Mathias Kolle; Massachusetts Institute of Technology, United States

Dynamic optical appearance plays a critical role for many animals that rely on adaptive camouflage or bright and varying color displays for their survival. The photonic materials used by these organisms are not just of interest to biologists, but have also captured the imagination of physicists, chemists, materials scientists, and engineers, who are trying to emulate their dynamic optical behavior in synthetic bio-inspired material systems. Mechanically-responsive soft photonic materials, for instance, represent a versatile material platform for colorimetric force sensing in a variety of different research and technology fields, including healthcare, robotics, and human-computer interaction. Existing fabrication approaches are varied, including self-assembly of colloids or liquid crystals, magnetically induced self-assembly, block copolymer self-assembly, sequential spin coating, and laser writing and interference lithography. However, the application of these materials has been limited by drawbacks relating to their optical quality, mechanical properties, limited scalability, or cost and complexity of manufacture. We have recently developed a new optical fabrication approach that is capable of tackling these challenges, harnessing the century-old technique of Lippmann photography combined with recent advances in holographic recording materials. This process can be performed using just a desktop projector, aluminum foil, and many off-the-shelf holographic recording materials, at low cost and over large areas. Our manufacturing approach also permits spatially patterning different photonic structures and mechanical properties, with micron-scale resolution. In principle, this technique can be extended to realize an almost unlimited range of pattern morphologies that we know from biological photonic materials. We anticipate that our mechano-responsive photonic sheets will facilitate a range of new applications, and we will demonstrate initial prototypes in the fields of human-computer interaction and robotics.

#### 6:40 AM F.SM01.03.14

**Late News: Mussels Fabricate Hard and Flexible Composite Coatings from Immiscible Multiprotein Coacervates** Franziska Jehle<sup>1,2</sup>, Elena Macias-Sanchez<sup>1</sup>, Sanja Sviben<sup>1</sup>, Peter Fratzl<sup>1</sup>, Luca Bertinetti<sup>1</sup> and Matthew J. Harrington<sup>1,2</sup>; <sup>1</sup>Max Planck Institute of Colloids and Interfaces, Germany; <sup>2</sup>McGill University, Canada

Mussel byssal threads are proteinaceous biofibers self-assembled by mussels in order to attach to surfaces at the rocky seashore. Byssal threads are protected by a thin cuticle that combines high hardness and extensibility, making it a useful role model for advanced flexible coatings. Cuticle mechanics have been shown to arise from DOPA-metal coordination cross-links, as well as from its composite micro- and nanostructure, which consists of biphasic granules within an amorphous matrix phase. Although the byssus cuticle has become an important source of bio-inspiration for producing tough, self-healing metallopolymers, the biochemical nature of the different cuticle structures and the assembly process by which the cuticle is formed are far from clear.

Here, we performed a compositional and ultrastructural investigation of the protein secretory vesicles used to fabricate cuticle and followed their self-assembly during cuticle formation utilizing advanced electron microscopy methods including FIB-SEM and STEM-EDX<sup>1</sup>. Findings suggest that the different proteins destined to form granules vs. matrix are pre-organized in a co-existing condensed fluid phase within secretory vesicles via phase separation of immiscible DOPA- and cysteine-rich precursors. During thread formation, the condensed fluid protein phases from multiple vesicles coalesce and solidify during secretion with the immiscible phases forming the matrix and granules, respectively. FIB-SEM 3D reconstruction of granule ultrastructure revealed a bicontinuous internal structure resembling a phase-separated block-copolymer, while elemental analysis with STEM-EDX exhibited an unusual partitioning of vanadium and iron between the DOPA-rich granules and cysteine-rich matrix, respectively, which may play a role in determining cuticle mechanics. These findings have direct relevance for production of nanostructured soft materials with complex and dynamic material properties.

1) Jehle, F., Macias-Sanchez, E., Sviben, S., Fratzl, P., Bertinetti, L. and Harrington, M. J. (2020) Biofabrication of functional meso-structured metallo-protein composites using co-existing condensed liquid phases. *Nature Communications*. 11, 862.

#### 6:50 AM F.SM01.03.15

**Bio-Inspired Swellable Hydrogel-Forming Double-Layered Adhesive Microneedle Protein Patch for Regenerative Internal/External Surgical Closure** Eun Young Jeon<sup>1,2</sup>, JungHo Lee<sup>1</sup>, Guenbae Lim<sup>1</sup>, Justin J. Chung<sup>2</sup> and Hyung Joon

Cha<sup>1</sup>; <sup>1</sup>Pohang University of Science and Technology, Korea (the Republic of); <sup>2</sup>Korea Institute of Science and Technology (KIST), Korea (the Republic of)

Significant tissue damage, scarring, and an intense inflammatory response remain the greatest concerns for conventional wound closure options, including sutures and staples. In particular, wound closure in internal organs poses major clinical challenges due to air/fluid leakage, local ischemia, and subsequent impairment of healing. Herein, to overcome these limitations, inspired by endoparasites that swell their proboscis to anchor to host's intestines, we developed a hydrogel-forming double-layered adhesive microneedle (MN) patch consisting of a swellable mussel adhesive protein (MAP)-based shell and a non-swellable silk fibroin (SF)-based core. By possessing tissue insertion capability (7-times greater than the force for porcine skin penetration), MAP-derived surface adhesion, and selective swelling-mediated physical entanglement, our hydrogel-forming adhesive MN patch achieved ex vivo superior wound sealing capacity against luminal leaks ( $139.7 \pm 14.1$  mmHg), which was comparable to suture ( $151.0 \pm 23.3$  mmHg), as well as in vivo excellent performance for wet and/or dynamic external and internal tissues. Collectively, our bioinspired adhesive MN patch can be successfully used in diverse practical applications ranging from vascular and gastrointestinal wound healing to transdermal delivery for proregenerative or anti-inflammatory agents to target tissues.

#### Acknowledgements

Financial support was provided by National Research Foundation of Korea (NRF) grant (NRF-2020R1C1C1012881) funded by the Ministry of Science and ICT (MSIT).

SESSION F.SM01.04: Multifunctional Materials and Structures  
On Demand Abstracts Available for Viewing Starting Saturday Morning, November 21, 2020  
F-SM01

#### **5:00 AM \*F.SM01.04.01**

**Skeletons with Eyes** Joanna Aizenberg; Harvard University, United States

The most finely tuned, rapidly responsive, and precisely directed optical systems currently known can be found on the surfaces of living organisms. Studies of brittlestars' tunable microlenses, sea sponges' optical fibers, butterflies' and beetles' intense colors, and squids' nearly perfect camouflage have revealed 3D architectures so intricately patterned down to the nanoscale that the topography itself controls the wavelengths and direction of reflected light. We are developing bioinspired, bottom-up self-assembly techniques that allow us to create comparably elaborate yet tunable hierarchical photonic structures, and integrate these into the design of a new class of dynamic, responsive optical materials.

#### **5:15 AM F.SM01.04.02**

**Chitin Nanocrystals Confined to a Polymer Microgel** Sujin Rebecca Lee, Elsa Reichmanis, Jung O Park and Mohan Srinivasarao; Georgia Institute of Technology, United States

Chitin is the second most abundant polysaccharide after cellulose, which can be extracted from exoskeletons of crustaceans and also from cell walls of fungi and insects. Similar to cellulose nanocrystals, chitin nanocrystals can be isolated through acid hydrolysis and form cholesteric phase. We investigate chitin nanocrystals confined to pnipam microgels using microfluidics device. The twisted structure of chitin nanocrystals are preserved within the polymer spheres, as characterized by optical microscopy. The droplet radius, R of the microgels can be adjusted by changing the volumetric flow rate of oil phase in a microfluidics device. Interestingly, the fabricated microgels shows bipolar structure with the shape of prolate spheroids. They exhibit swelling-deswelling behavior upon temperature change along the axis of helix.

#### **5:25 AM F.SM01.04.03**

**A Soft Lithography Method to Generate Arrays of Microstructures on Hydrogel Surfaces** Yolanda Vasquez<sup>1</sup>, Hasani G. Jayasinghe<sup>1</sup>, Mughees Khan<sup>2</sup> and Sundar V. Madihally<sup>1</sup>; <sup>1</sup>Oklahoma State University, United States; <sup>2</sup>Harvard University, United States

Research on synthetic mimics of microstructures found on natural organisms, such as the structured skin of the shark or the surface of the lotus leaf, have resulted in surfaces that dynamically change rigidity, adhesion, or wettability. Structured surfaces also have potential biomedical applications in tissue engineering and as drug delivery systems, sensors, and actuators. For the aforementioned biological applications, hydrogels are the materials of choice due to their biocompatibility,

biodegradability, and tunable mechanical properties. Generating patterns of intricate microstructures onto the hydrogel surfaces, however, is challenging because of the low mechanical strength, adhesion, or chemical incompatibility of hydrogels with various molds. Here, we report the use of a soft lithography technique to successfully pattern arrays of micropillars onto a poly(2-hydroxyethyl methacrylate) based hydrogel. The swelling of the hydrogel in solvents such as phosphate buffered saline, deionized water, 60% ethanol, and absolute ethanol, facilitates the reproducible replication of the pattern. Furthermore, the micropillar pattern promotes the attachment of HeLa cells onto this hydrogel which is not inherently adhesive when unpatterned.

#### 5:35 AM F.SM01.04.04

**Bioinspired Multiscale Pores and Channels** Xu Hou; Xiamen University, China

Nature provides a huge range of biological materials with various smart functions over millions of years of evolution and serves as a big source of bioinspiration for biomimetic materials that can bring impetus to the development of multifunctional materials and structures. From small biological ion channels to large oil pipelines, the structures with "Pore" and "Channel" are everywhere. Ion channels existing in living organisms play a significant role in maintaining balanced physiological conditions and serve as "smart" gates to ensure selective ionic transport. Pipelines, which are commonly used in chemical industry, food industry, agriculture, and energy-petroleum transportation, can be treated as macroscale channels. Multiscale pore and channel systems have been intensively explored and contributed to new developments in materials science, membrane science and technology, or micro/nanotechnology for analytical, biomedical, and energy applications. Stimulated by the achievements and the even larger potential of multiscale pore and channel systems, increasing research activities are devoted to important aspects such as energy saving, anti-fouling, anti-corrosion, and anti-blocking functionalities, switch ability and controllability integration of various functionalities, and good stability in such confined space. The most recent examples of mechanisms and strategies the learning from Nature are described, including bioinspired and smart multiscale pore/channel systems, especially building bioinspired liquid-based gating systems for bringing a new generation of design ideas of membrane separation technology; and bioinspired stimuli responsive micro/nanochannel systems for biomedical applications.

[1] Hou, X.\*, Natl. Sci. Rev. 2020, 7: 9.

[2] Hou, X.\*, et al., Angew. Chem. Int. Ed. 2019, 58: 3967.

[3] Hou, X.\*, et al., Adv. Mater. 2019, 31: 1805130.

[4] Hou, X.\*, et al., Sci. Adv. 2018, 4: eaao6724.

[5] Hou, X.\*, Adv. Mater. 2016, 28: 7049.

#### 5:45 AM F.SM01.04.05

**Bioinspired Cross-Linking of Preceramic Polymers via Metal Ion Coordination Bonding** Kara L. Martin<sup>1,2</sup>, Maria Parvulescu<sup>1,2</sup>, Pavel Mogilevsky<sup>1,2</sup> and Matthew Dickerson<sup>2</sup>; <sup>1</sup>UES, Inc., United States; <sup>2</sup>Air Force Research Laboratory, United States

The polychaete worms of the Nereididae family are distinguished by lightweight, conical teeth that exhibit a hardness level analogous to human dentin. While comparable in material properties to the mineral comprising dentin, the polychaete worm's teeth are proteinaceous material built from histidine rich proteins cross-linked with Zn<sup>+2</sup> ions through coordination chemistry. The exemplified material properties achieved through coordination cross-linking of such biomaterials has inspired us to extend this method of cross-linking to preceramic polymers. Preceramic polymers require rigorous cross-linking as a means to reduce volume shrinkage and mass loss during pyrolysis, and often require extensive thermal curing steps to prepare a green body viable for ceramitization. Coordination cross-linking offers a faster, dynamic platform to preparing preceramic green bodies. Herein, we report the functionalization of commercially available polysiloxane and polycarbosilane backbones with pyridyl-moieties and the subsequent coordination cross-linking of these polymers with Zn<sup>+2</sup> and Ti<sup>+4</sup> ions. The rapidly cross-linked materials were characterized with ATR-FTIR, oscillatory rheology, and thermal gravimetric analysis. The cross-linked green bodies were then pyrolyzed at 1400°C to ceramic materials, and characterized with XPS, XRD, and TEM. Ceramics generated from coordination cross-linked preceramic polymers represent the metal ion cross-linker, with Ti<sup>+4</sup> cross-linked polymers generating TiC/SiC, and Zn<sup>+2</sup> cross-linked materials generating SiC, as Zn<sup>+2</sup> evaporates between 1000–1200°C. Coordination cross-linking is a single dial that can adjust material characteristics before and after pyrolysis. Particularly, the viscoelastic properties, thermal stability, and ceramic yields at 800°C can be systematically changed with the loading equivalents of metal cross-linker and the ceramic composition can be changed by metal ion choice. To the best of our knowledge, this is the first example of silicon-based preceramic polymers cross-linked through pyridine-based metal ion coordination.

#### 5:55 AM F.SM01.04.06

**Design of Bio-Inspired Functional Nanomaterials and Their Applications** Nurxat Nuraje<sup>1,2</sup>; <sup>1</sup>Nazarbayev University, Kazakhstan; <sup>2</sup>Texas Tech University, United States

With learning and getting inspiration from Nature, many trivial scientific questions and industrial problems can be resolved via proper designing the materials and creating unique structures, which lead to emerging materials in the field of renewable energy, sensors, and nanomedicine. Mimicking nanotechnology existed in Nature, we are able to create unique assembled structures to improve certain properties of materials and device, and design tool box to generate functional emerging nanomaterials. The main goals of this research are to synthesize novel bio-inspired and biomimetic functional nanomaterials, characterize and investigate their properties, and apply them to understand fundamental science via creating their hierarchical nanostructured materials. Basic understanding from those above investigations are then applied to address problems in solar energy conversion, and coatings. This research will focus on the following topics: (a) synthesis of bio-inspired functional nanomaterials; (b) fabrication of unique nanoarchitectures to better understand fundamental science; and (c) Applying these unique nanomaterials and nanostructures to resolve the scientific and technical problems in energy harvesting and conversion, and functional coatings.

#### 6:05 AM F.SM01.04.08

**Late News: PEDOT:PSS Based Bilayer Actuators for Soft Robotics** Najathulla Bhagavathi Chalil, Mudrika Khandelwal and Atul S. Deshpande; Indian Institute of Technology Hyderabad, India

Poly(3,4-ethylenedioxythiophene) polystyrene sulfonate (PEDOT:PSS) is a well known conducting polymer preferred owing to high conductivity and processability. PEDOT:PSS on application of a potential bias attracts oppositely charged ions causing volume expansion. This reversible expansion is exploited to prepare bilayer actuator with bacterial cellulose as the substrate. A stable fish tail like deflection of over 5 mm was observed at 1 V. Effect of amount and properties of PEDOT:PSS on deflection is studied along with energy conversion efficiency. This electro-chemical actuator can have potential applications in biomimetic soft robotics.

SESSION F.SM01.05: Adaptive and Dynamic Materials and Structures  
On Demand Abstracts Available for Viewing Starting Saturday Morning, November 21, 2020  
F-SM01

#### 5:00 AM \*F.SM01.05.01

**Organisms Manipulate Light with Nano-Scale Crystal Mirrors** Benjamin A. Palmer, Gan Zhang, Ofir Friedman, Anna Hirsch, Venkata J. Yallapragada, Dan Oron, Leor Kronik, Leslie Leiserowitz, Steve Weiner and Lia Addadi; Weizmann Institute of Science, Israel

Organisms construct 'devices' based on assemblies of organic nano-crystals with optical functions. The structure, polymorph, size, morphology and superstructural arrangement of the crystals determine the optical properties of the 'device'. All the crystals have unusually high refractive indexes in the directions along which the light penetrates the crystal. The controlled assembly of nano-crystals forms multilayer reflectors that create structural colors, or mirrors and light scattering layers that function to increase vision sensitivity in the eyes of the organisms. Scallops have tens of eyes, each containing a concave multi-layered mirror perfectly tiled with a mosaic of square guanine crystals, made up of composite twins, reflecting light to form images onto the overlying retinas [1]. Crustacean decapods such as shrimps, crayfish and lobsters possess compound eyes that contain two sets of mirrors, composed of isoxanthopterin crystals. The two mirrors have very different ultrastructures and functions that we can rationalize in terms of the optical performance of the eye [2,3]. The unusual zander fish eyes contain two layers of organic crystals: thin guanine crystals, form a reflective layer in the back of the eye, whereas block-shaped crystals of 7, 8-dihydroxanthopterin in the inner tapetum layer back-scatter light onto the retina, increasing the light sensitivity of the eye [4]. Finally, insects commonly known as jumping bristletails, form large amounts of xanthine crystals in their median and lateral ocelli [5]. The structure-function relations in this last example are still under investigation. In all these examples, the constituent molecules are mostly purines and pteridines, which raises the question of what molecular and structural characteristics of these crystals, favor their use for optical functions in organisms. Furthermore, the organization of the crystalline functional components is controlled from the crystal structure at the nanoscale to the complex 3D structure at the millimeter level, extending the interest in the relation between structure and optical properties to higher

hierarchical levels.

[1] B.A. Palmer, G.J. Taylor, V. Brumfeld, D. Gur, M. Shemesh, N. Elad, A. Osherov, D. Oron, S. Weiner, L. Addadi: The Image Forming Mirror in the Eye of the Scallop. *Science* 358, 1172–1175 (2017).

[2] B.A. Palmer, A. Hirsch, V. Brumfeld, E.D. Aflalo, I. Pinkas, A. Sagi, S. Rozenne, D. Oron, L. Leiserowitz, L. Kronik, S. Weiner and L. Addadi: Isoxanthopterin: An Optically Functional Biogenic Crystal in the Eyes of Decapod Crustaceans. *PNAS*, 115, 10, 2299–2304 (2018).

[3] B.A. Palmer, V. J. Yallapragada, N. Schiffmann, E. Merary Wormser, N. Elad, E.D. Aflalo, A. Sagi, S. Weiner, L. Addadi, D. Oron: Highly Reflective Biogenic Materials from Core-Shell, Birefringent Nanospheres. *Nature Nanotechnology* 15, 138–144 (2020).

[4] G. Zhang, A. Hirsch, G. Shmul, L. Avram, N. Elad, V. Brumfeld, I. Pinkas, I. Feldman, R. Ben Asher, B. A. Palmer, L. Kronik, L. Leiserowitz, S. Weiner and L. Addadi: Guanine and 7, 8-dihydroxanthopterin reflecting crystals in the zander fish eye: crystal locations, compositions and structures, *J Am Chem Soc* 141, 19736–19745 (2019).

[5] A. Böhm and G. Pass: The ocelli of Archaeognatha (Hexapoda): functional morphology, pigment migration and chemical nature of the reflective tapetum, *The Journal of Experimental Biology* 19, 3039-3048 (2016).

#### 5:15 AM \*F.SM01.05.02

**Bioinspired Assembly and Collective Motion of Nanocomposite Hydrogel Sheets at Air/Water Interfaces** [Ryan C. Hayward](#); University of Colorado Boulder, United States

We describe a platform of temperature-responsive hydrogel nanocomposites adsorbed at air/water interfaces that exhibit a variety of bioinspired non-equilibrium behaviors due to temperature gradients generated by illumination with visible light. In one example, we exploit spatial variations in thermally-induced deswelling of the gel particles to drive buckling of thin sheets into 3D shapes with non-zero Gaussian curvature. Similar to the mechanism exploited by numerous insects to climb menisci or drive clustering, pinning of the three-phase contact line at the sheet edges gives rise to capillary ‘multipole’ interactions between different objects, leading to assembly, repulsion, and even sustained rotational motion, depending on the geometry. In a second example, we exploit Marangoni forces resulting from temperature gradients to drive motion and interaction of planar particles, once again inspired by well-known strategies employed by aquatic insects. A simple method for Marangoni optical trapping is realized by shining appropriate patterns of light on the interface, enabling the definition of easily customized geometries in which to study coupled motion of multiple oscillators and spinners.

#### 5:30 AM F.SM01.05.03

**Bioinspired Smart Materials—Sensing, Solar Harvesting and Soft Robotics** [Ximin He](#); University of California, Los Angeles, United States

From the cellular level up to the body system level, living organisms are able to sense and adapt to local environment for various functions, from detecting and transporting molecules in the complex bio-fluids to harvesting energy from the environment and generate motions to keep alive. These graceful capabilities arise from the coordination of the chemo-mechanical actions, such as the molecular configuration changes and micro/macroscopic mechanical motions. Stimuli-responsive hydrogels are a class of synthetic materials that can change their volume and physical properties in response to environmental cues including temperature, light, and specific molecules. Inspired by these unique abilities, we have developed a series of dynamic material systems based on hydrogels. This presentation will introduce several novel functionalities that this broad-based platform has demonstrated, ranging from beetle-inspired ultrafast colorimetric sensing of chemical and biological species (*Adv. Mater.* 2018; *Adv. Opt. Mater.* 2019), autonomous sorting of target molecules in complex biofluids or wastewater (*Nat. Chem.* 2015), and plant-mimetic adaptive light tracking and harvesting (*Nat. Nanotech.* 2019), as well as self-sensing actuators for soft robotics (*Sci. Robotics* 2019). Overall, the environment-adaptive, dynamic material systems would have broad impacts in areas ranging from wearable sensors to smart devices that regulate energy usage and fully autonomous soft robots.

#### 5:40 AM F.SM01.05.04

**Biorobotic Hybrid Heart—A Biomimetic Approach to Recreating the Heart’s Pumping Motion** [Clara Park](#) and Ellen Roche; Massachusetts Institute of Technology, United States



The heart is a uniquely challenging organ to recreate due to its dynamic three-dimensional (3D) motion and its detailed internal structures. Motivated by the lack of a synthetic or biological method to recapitulate both the complex motion and anatomical features of the heart, we recently developed a biorobotic hybrid heart that combines passive organic structures (intracardiac tissue) whose motion is driven by an active synthetic cardiac muscle. In this talk, we will describe a biomimetic design approach to programming the active synthetic cardiac muscles by replicating the intricate arrangements of cardiac fibers, which synchronously contract along to achieve efficient pumping motion of the heart. Instead of replicating the complex fiber structures directly in 3D, we took inspiration from the helical ventricular myocardial band theory – which proposes that the ventricle of the heart can be unraveled into a singular muscular band that is spirally arranged in the 3D space – to simplify the design and fabrication process of the synthetic cardiac muscles. We constructed a two-dimensional (2D) biomimetic matrix that has multiple linearly contracting pneumatic artificial muscles, which were oriented to match that of the muscle fibers in the unraveled heart tissue, in a soft elastomeric sheet. Then, the soft robotic matrix was rewrapped in a 3D helical fashion to recreate the hierarchical, functional architecture, and the global 3D motion of the ventricular cardiac muscle. Once assembled with the organic component, the biorobotic hybrid heart replicated the volumetric displacement of the heart at a physiological level upon cyclic actuation.

#### **5:50 AM F.SM01.05.06**

**Dynamic and Programmable Self-Assembly of Micro-Rafts at the Air-Water Interface** Wendong Wang, Gaurav Gardi, Vimal Kishore and Metin Sitti; Max-Planck-Institute, Germany

From the thermodynamic point of view, most materials are either in their equilibrium states, such as inorganic and organic crystals, or in kinetically trapped non-equilibrium states, such as porous materials. Life, on the other hand, is in dissipative non-equilibrium (or dynamic) state, with hierarchically ordered complex structures and highly coordinated functions. Developing dynamic materials systems where structural orders are sustained by continuous energy input and dissipation will not only introduce a new paradigm in materials science but also impact robotics. In the context of robotics, a micro-robot collective is a dynamic and programmable materials system, where fundamental physical and chemical principles guide the designs of local interactions and global behaviors. Here we show the collective patterns and behaviors of up to 250 micro-rafts spinning at the air-water interface and demonstrate the link between order and information in the collective motion. These micro-rafts display a rich variety of collective behaviors that resemble thermodynamic equilibrium phases such as gases, hexatics, and crystals. Moreover, they show emergent properties and functions when coupled with reconfigurable magnetic potentials. We devise information theoretical measures to quantify the information content of the spatiotemporal patterns and demonstrate their close relations with the order. Our findings are relevant for analyzing collective systems in nature and for designing collective robotic systems.

#### **6:00 AM F.SM01.05.07**

**In Pursuit of a Deeper Understanding of the Effects of Surface Flexibility on Ion Mobility** Veselina Marinova, Colin Freeman and John Harding; The University of Sheffield, United Kingdom

Crystallisation is an important process in a wide selection of problems – from the manufacture of pharmaceutical ingredients and inorganic materials to the prevention of scale formation and the production of minerals in living organisms. An understanding of the mechanisms which promote crystallisation can allow control over the formation of specific polymorphs, preventing the formation of crystals where it is undesirable, and tailoring crystalline materials for applications. In an uncontrolled environment, crystallisation typically occurs on foreign surfaces. Understanding the surface characteristics which promote and direct nucleation is key to the design and control of surface-aided crystallisation.

Compelling examples from literature show that flexible surfaces can strongly affect crystallisation rates. Self-assembled monolayers (SAMs) of alkenethiols, supported on gold or silver, can promote the nucleation of  $\text{CaCO}_3$  with a high degree of orientational specificity<sup>1,2,3</sup>. We use molecular dynamics simulations to understand the mechanisms through which defect-induced disorder in the flexible SAM of 16-mercaptohexadecanoic acid (16-MHDA) on an Au (111) surface can affect the ability of  $\text{Ca}^{2+}$  and  $\text{CO}_3^{2-}$  to form clusters.

To achieve this, we use molecular simulations to study possible defects in the monolayers through the removal of one or several surface atoms from the underlying Au (111) surface. This procedure forms step edges and vacancy islands which promote interactions between head groups of neighbouring chains through the offset created. As a reference case, we use an ordered SAM with a characteristic spacing of 0.498 nm between chains and a 30° angle of the carbon backbone with the underlying gold surface<sup>4</sup>. An all-atom AMBER<sup>5</sup> forcefield is used to reproduce the interactions between the alkenethiol chains, while a forcefield developed by Raiteri et al.<sup>6</sup> was used for an accurate representation of  $\text{CaCO}_3$  and its interactions

with water. The Schröder method was used to obtain the interactions between the SAM and the  $\text{Ca}^{2+}$  and  $\text{CO}_3^{2-}$  ions.

Our findings suggest that the presence of defects not only disrupts the local structure of the solvent, but in some cases can induce longer-ranged disorder effects, reducing the longevity of the solvent adsorbed state. The introduction of ions into the system reveals how the disrupted surface layer of the solvent affects ion mobility on and near the surfaces, shedding light on the role of defects in flexible surfaces on the formation of crystalline clusters. This is an important step towards the defining and understanding of effective nucleating agents.

## References

<sup>1</sup> Nielsen et al. *Farraday Discussion*, 2012, 159, 105-121

<sup>2</sup> Aisenberg et al. *Journal of the Chemical Society, Dalton Transactions*, 2000, 21, 3963-3968

<sup>3</sup> Tremel et al. *Handbook of Biomineralisation Chapter 12*, 2007, Wiley, 209-232

<sup>4</sup> Ulman et al. *Chem. Rev.* 1996, 96, 1533-1554

<sup>5</sup> Wang et al. *Journal of Computational Chemistry*, 2004, 25, 1157-1174

<sup>6</sup> Raiteri et al. *J. Am. Chem. Soc.*, 2010, 132, 17623-17634

## 6:10 AM F.SM01.05.08

**Learning from Viruses—Efficient Cellular Translocation and Accumulation of Nanoparticle-Based Carriers Using an Optimized Class of Cell-Penetrating Peptides** Isabel Gessner, Annika Klimpel, Eva Krakor, Merlin Klußmann, Ines Neundorf and Sanjay Mathur; University of Cologne, Germany

The discovery that viruses such as the Human Immunodeficiency Virus (HIV) contain proteins that allow the virus to overcome cellular barriers and achieve efficient cell penetration without need for a receptor represents a milestone in medicinal research. Since then, the Trans-Activator of Transcription (Tat) protein has been identified as first cell-penetrating peptide (CPP) and was linked to various cargos including large multimeric protein complexes to allow for their transport across cell membranes. The high translocation efficiency is thereby highly dependent on the sequence, secondary structure, and charge of the protein.

Given the increasing demand for intracellular delivery of nanoparticle-based therapeutics, we studied how the cell uptake of silica nanoparticles can be modulated after decoration with differently active CPPs. Employed CPPs were derived from antimicrobial peptide CAP18 and were systematically modified regarding the position of specific amino acids in their sequence. Interestingly, we found out that significant differences in uptake efficiency and intracellular accumulation of nanoparticle-CPP conjugates were observed depending on amphipathicity, alpha-helical structure formation and charge of the peptide, as well as the carrier size. These results demonstrate how we can learn from viruses to overcome current medicinal challenges, revealing the huge potential of sequential fine-tuning of CPPs and providing insights into their interaction with inorganic nanocarrier surfaces.

## 6:20 AM F.SM01.05.09

**Mechanistic Understanding of Metal-Coordination Bond Dissociation in Biological and Synthetic Materials for Tunable Mechanical Properties** Eesha Khare, Niels Holten-Andersen and Markus Buehler; Massachusetts Institute of Technology, United States

Metal-coordination complexes are emerging as a broad class of supramolecular crosslinks for use in advanced structural materials with tunable mechanical properties. Unlike conventional covalent bonds, these bonds have the capacity to reform after rupture, thereby enabling dynamic, tunable, and reversible (self-healing) mechanical properties. An increasing number of biological organisms, such as marine mussels (*Mytilus*) and marine worm jaws (*Nereis virens*), have been found to take advantage of these unique properties of metal-coordinate complexes in the secretion of loadbearing materials for complex extraorganismal functions. Inspired by the role of these bonds in biological materials, several studies have incorporated metal-coordination bonds as crosslinks in model hydrogel systems to tune dynamic mechanical properties over a broad spectrum of timescales. However, a deeper understanding of how microscopic behavior of metal-coordination bonds affect bulk mechanical properties is still missing, rendering predictive implementation in designing mechanical properties of materials a continued challenge.

This study presents a multiscale computational model of various metal-coordination complexes to elucidate how these complexes affect bulk mechanical properties of protein and synthetic metal-coordinated materials. First, we study how coordinating ligands specific to biological and synthetic contexts affect mechanical properties of the bulk material. Comparisons are drawn between imidazole, naturally found in marine mussels and worm jaws, and histidine, used in synthetic hydrogel studies, to demonstrate clear differences between biological and synthetic materials. Density functional

theory (DFT) and steered molecular dynamics (SMD) studies on individual coordination complexes reveal how the dissociation path of histidine-Ni<sup>2+</sup> or imidazole-Ni<sup>2+</sup> underpin bond lifetime and bulk material relaxation time. Second, we study how clusters of metal-coordination complexes affect bulk mechanical properties. To understand this effect, model systems with various coordination complexes are designed and tested. MD studies reveal that these different model systems significantly affect bulk relaxation time and strength. Results from studies on these model systems are qualitatively compared to metal-coordinate crosslinks in the *Nereis virens* marine worm jaw protein structure. This comparison may lend insight into how the structure of *Nereis* worm jaw optimizes the positioning of metal-coordination interactions for precise mechanical control. Altogether, this work proposes key design criteria for how metal-coordination chemistry can be advanced for biological applications with dynamic mechanical materials properties.

#### 6:30 AM F.SM01.05.10

**Mechanical Modulation of Lipid Membranes by Phospholipid Peroxidation** [Changjin Huang](#)<sup>1</sup>, Choon-Peng Chng<sup>1</sup>, Yoel Sadovsky<sup>2</sup> and K. Jimmy Hsia<sup>1</sup>; <sup>1</sup>Nanyang Technological University, Singapore; <sup>2</sup>Magee-Womens Research Institute, United States

The imbalance between the production of reactive oxygen species (ROS) by various mechanisms, including both internal metabolic processes and external environmental stimuli, and the endogenous antioxidant defences in mammalian cells often leads to oxidative stress and contributes to various pathological conditions, such as aging, neurodegenerations in Parkinson and Alzheimer diseases, and cancer. Under oxidative stress, the ROS initiates a series of oxidation reactions of cell membranes through the formation of hydroperoxides at the sites involving double-bonded carbon atoms along unsaturated fatty acid chains of phospholipids. Being hydrophilic in nature, the hydroperoxide group tends to migrate towards the water-membrane interface and changes to the internal structure of the lipid membrane. Despite the improved knowledge in the biological and chemical events during lipid peroxidation, how lipid peroxidation modulate the mechanics of lipid membranes remains largely elusive. In this study, we have investigated the peroxidation of polyunsaturated (more than one double-bond per fatty acid chain) phospholipids, a process involved in a recently identified form of programmed cell death, namely ferroptosis. By performing systematic coarse-grained molecular dynamics simulations, we have identified that lipid peroxidation affects the physical and mechanical properties of lipid membranes in an oxidation site-dependent manner. Our results show that the lipid peroxidation softens the membrane when the oxidation site is deep inside the hydrophobic core, while it tends to strengthen the membrane when the location of the oxidation is close to the water-membrane interface. Our study provides an insightful understanding on the modulation of membrane mechanics by lipid peroxidation.

#### 6:40 AM F.SM01.05.11

**Muscle-Inspired Highly Elastic Liquid Crystal Elastomer-Carbon Nanotube Composite Filaments as Programmed Actuators** Jiaqi Liu, [Yuchong Gao](#), Haihuan Wang, Ryan Poling-Skutvik, Chinedum Osuji and Shu Yang; University of Pennsylvania, United States

Many animals in nature possess musculoskeletal systems with astonishing actuation speed, strength, and adaptivity. To mimic their agile and forceful locomotion, liquid crystal elastomers (LCEs) are a promising candidate among all synthetic actuator materials, as they exhibit reversible and anisotropic deformation by multiple external stimuli. So far, most studies on LCEs have focused on accomplishing complex deformation in 2D thin films over centimeter scale areas with relatively small specific energy densities, which is different from the 1D fiber-based contraction mechanism of muscles. Herein, using an extrusion process, meter-long LCE composite filaments that are responsive to both infrared light and electrical fields are fabricated. In the composite filaments, a small quantity of cellulose nanocrystals (CNCs) is incorporated to facilitate the alignment of liquid crystal molecules along the long axis of the filament. Up to 2wt% carbon nanotubes (CNTs) is introduced into the LCE matrix without aggregation, which in turn greatly improves the mechanical property of filaments and their actuation speed, where the Young's modulus along the long axis reaches 40MPa, the electrothermal response time is within 10s. The maximum work capacity is 38J/kg with 2wt% CNT loading. Finally, shape transformation and locomotion in several soft robotics systems achieved by the dual responsive LCE/CNT composite filament actuators are demonstrated.

#### 6:50 AM F.SM01.05.12

**Peptidoglycan Isolated from *Bacillus subtilis* Spores Shows Extreme Stimuli-Responsive Actuation** [Zhi-Lun Liu](#)<sup>1,2</sup>, Haozhen Wang<sup>2,2</sup> and Xi Chen<sup>1,2</sup>; <sup>1</sup>The City College of New York, United States; <sup>2</sup>The City University of New York, United States

Actuators and artificial muscles require high-efficiency stimuli-responsive materials that transduce an energy form, such as electric voltage, thermal gradient, pneumatic pressure, or chemical potential, to their structural deformations. However, energy conversion efficiency of most man-made stimuli-responsive materials fail to compete with natural muscles, such as

human and insect muscles whose efficiencies reach 40 and 16%, respectively. Here, we report that peptidoglycan (PG) isolated from *Bacillus (B.) subtilis* spores exhibits powerfully humidity-responsiveness, and it efficiently transduces water's chemical potential energy into mechanical motions with an energy conversion efficiency of ~35%. We isolated PG from other protein-based components in spores by using several denaturing agents, and subsequently identified its structure by using a SEM and a liquid chromatography-electrospray ionization-mass spectrometry (LC-ESI-MS). Due to the lack of database of *B. subtilis* spore PG's chemical structure, we developed our own algorithm to deconvolute the LC-ESI-MS detected mass to charge ratio ( $m/z$ ) and identified 6 hydrolysates with an error less than 4 ppm. Our results suggest that our isolated PG are composed of long glycan chains that are loosely cross-linked by short peptide stems, forming a 3-dimensional amphiphilic hierarchical structure. When isolated PG is exposed to humidity changes or water gradients, we found that PG can forcefully swell and shrink. For example, when local relative humidity is increased from 5% to 90%, PG expands up to 50.1% of its original height with a swelling pressure of 302.17 MPa. Using a thermodynamic cycle, we characterized PG's energy density and power density which reach  $59.9 \text{ MJ m}^{-3}$  and  $5.9 \text{ MW m}^{-3}$ , respectively, exceeding that of all natural muscles. By using PG, we also created a large-scale bilayer structure that reversibly bends in response to RH changes, demonstrating the possibility of using PG to develop high-efficiency actuators.

#### 7:00 AM F.SM01.05.13

**Physical Implementation of Ant Colony Intelligence in Colloidal Particle System** Bokusui Nakayama and Toshiharu Saiki; Keio University, Japan

In the conventional computing paradigm based on the von Neumann architecture, a tremendous amount of data is transferred between memory and processor and the program operates on the data in a step-by-step fashion, which imposes a bottleneck in the speed and scalability of the architecture. A new paradigm beyond the von Neumann architecture is needed to address the problem fundamentally. The most promising approaches include implementation of swarm intelligence algorithm, like ant colony, to solve optimization problems. In order to implement natural computing algorithm into some physical systems, phase change materials (PCMs) are advantageous as a key platform due to its plasticity and threshold behavior (nonlinearity), which provide memory and processing functionalities, respectively. Based on the idea, we proposed an idea to implement an algorithm for Ising spin glass problem to the system of coupled plasmon particles interacting with PCM.

In this study, we attempt to implement ant pheromone algorithm. Ant colony optimization is a problem to find the shortest path between their nest and food using pheromone trails. Ants emit pheromone on the ground which works as a signal to attract other ants. If an ant follows the pheromone trail, it itself also emits more pheromone, thus emphasizing the trail. The more ants follow the trail, the pheromone deposition also increases (positive spiral). Pheromone strength decays over time due to the evaporation resulting in much less pheromone on less popular paths (negative spiral). These positive and negative spirals enable ants to find the shortest path autonomously.

In the experimental setup, polystyrene beads (PBs) with a diameter of 500 nm suspended in water were used to mimic the behavior of agent ants. The suspension was confined in a two-dimensional slit formed with two glass plates. A GeSbTe film, as a PCM, was deposited on the bottom glass plate. The PBs move around in Brownian motion on the GeSbTe film, which was initially in the amorphous phase. Under uniform light irradiation (sub-nanosecond-pulsed laser) over a wide area, the GeSbTe just beneath the PBs is crystallized due to the near-field lens effect of PB. The crystalline trail, which is expected to work as the pheromone trail, absorbs more light and becomes more heated than the amorphous background and thus a convection flow is formed such as to attract other PBs towards the crystalline trail. In addition to the convection flow, the electrostatic interaction between the PB and GeSbTe in the crystalline phase, the PBs trace the crystalline trail. By providing larger fluence pulses, the crystalline trail is amorphized, which is equivalent to the evaporation of pheromone. On this experimental platform, we demonstrated mimicking smart behavior of ants, which includes formation of trail by following a PB ahead and finding shortcut path through thermal communication of PBs.

#### 7:10 AM F.SM01.05.14

**Reconfigurable Microbots Folded from Simple Colloidal Chains** Tao Yang<sup>1</sup>, Brennan Sprinkle<sup>2</sup>, Yang Guo<sup>1</sup>, Jun Qian<sup>3</sup>, Daoben Hua<sup>3</sup>, Aleksandar Donev<sup>2</sup>, David Marr<sup>1</sup> and Ning Wu<sup>1</sup>; <sup>1</sup>Colorado School of Mines, United States; <sup>2</sup>New York University, United States; <sup>3</sup>Soochow University, China

Overcoming the reversible nature of low-Reynolds number flow, a variety of biomimetic micro-robotic propulsion schemes and devices capable of rapid transport have been developed. However, these approaches have been typically optimized for a specific function or environment and do not have the flexibility that many real organisms exhibit to thrive in complex microenvironments. Here, inspired by adaptable microbes and using a combination of experiment and simulation, we demonstrate that one-dimensional colloidal chains can fold into geometrically complex morphologies including helices, plectonemes, lassos, and coils and translate via multiple mechanisms that can be varied with applied magnetic field. With chains of multi-block asymmetry, the propulsion mode can be switched from surface-enabled to bulk, mimicking the motion

of organisms such as flagella-rotating bacteria, tail-whipping sperm, arching and stretching inchworms, and sidewinding snakes. We also demonstrate that reconfigurability enables navigation through three dimensional and narrow channels mimicking capillary blood vessels. Our results show that flexible microdevices based on simple chains can transform both shape and motility under varying magnetic fields, a capability we expect will be particularly beneficial in complex *in vivo* microenvironments.

#### 7:20 AM F.SM01.05.16

**Soft Robotic Rapid Actuation Using Vibrating Mesh Atomization** Han-Joo Lee and Kenneth J. Loh; University of California San Diego, United States

Conventional soft robotic structures are actuated by inflating the elastomer with a pneumatic pump. However, this method involves heavy, bulky pumps that should be tethered to the system with multiple tubes. More recently, soft actuation by liquid vaporization is receiving much attention, since it only requires a small heater and liquid embedded in the elastomer. The volume of the liquid expands during vaporization, which inflates and deforms the structure. Despite their benefits, they still face several limitations that have prevented their practical use. For instance, vaporization requires heating the embedded fluid in the structure to its boiling point, while actuation ceases when the system is tilted, and the heater is no longer in contact with the liquid. In addition, cooling the system to return the structure to its original shape takes a long time, thus limiting actuation frequency. In this study, these limitations were addressed by designing a soft robotic structure that actuates based on the principles of atomization and vaporization. First, a soaked wick was embedded in the soft elastomer structure in lieu of directly encasing liquid in cavities. A miniature piezoelectric ring transducer with a metal mesh in its center was positioned on the surface of the wick, thus making contact with the embedded fluid at all times and even when the system is tilted. Second, the piezoelectric ring was excited using a high-frequency electrical signal to vibrate the metal mesh while dispersing the embedded liquid into small droplets. These droplets were ejected into a small, embedded heater to enable rapid evaporation of the ejected droplets, which required significantly less temperature, power, and time than directly boiling the embedded fluid. A uniaxial motion bellows structure was fabricated with the soaked wick, piezoelectric ring with a metal mesh, and miniature heater. Their force and displacement performance were tested, characterized, and compared with conventional liquid vaporization. Overall, the developed method was shown to be faster, consumed less power, and enabled rapid cyclic motions as compared to actuation by boiling. The results also showed promising performance attributes comparable to pneumatic pumps but with the added benefits of being easier to miniaturize for portable or untethered soft robotic systems.

#### 7:30 AM F.SM01.05.17

**Regenerated *Bombyx Mori* Silk that Mimics Spider Silk's Superior Water Responsive Actuation** Yaewon Park<sup>1</sup>, Yeojin Jung<sup>1,2</sup> and Xi Chen<sup>1,2</sup>; <sup>1</sup>The City University of New York, United States; <sup>2</sup>The City College of New York, United States

Water-responsive (WR) materials that swell and shrink in response to changes in relative humidity or water gradient provide new engineering opportunities for adaptive structures, soft robotics, and sustainable energy. Spider dragline silk is a WR material that have demonstrated a significant actuation energy density of  $0.5 \text{ MJ m}^{-3}$ , which is higher than most stimuli-responsive materials used for actuators and artificial muscles. However, spider silk's low availability and the poor understanding of its structure-WR property relationship impede practical applications or *de novo* design of its mimetic structures. Here, using *Bombyx (B.) mori* silk that shares a similar supramolecular structure to that of spider silk proteins, we demonstrate tunable water-responsiveness of *B. mori* silk and found that a higher  $\beta$ -sheet crystallinity strongly correlates to a higher WR energy density. To mimic spider dragline silk's secondary structures and investigate its structure-WR relationship, we used a series of solvent treatments that allow us to control the crystallinity of regenerated *B. mori* silk. Surprisingly, when *B. mori* silk is processed to have a similar  $\beta$ -sheet content (48.6 %) as that of spider dragline silk, the *B. mori* silk possess a similar WR energy density ( $0.48 \text{ MJ m}^{-3}$ ) to spider silk. When *B. mori* silk's crystallinity was further increased to 57.6 %, its WR energy density reaches  $1.6 \text{ MJ m}^{-3}$ , surpassing that of all known natural muscles. Response time of WR *B. mori* silk could be reduced by rendering surface hydrophilicity and pore structures. As a proof-of-concept, we have demonstrated a regenerated *B. mori* silk muscle that can reversibly lift a load about 1200 times heavier than the silk's own weight.

#### 7:40 AM F.SM01.05.18

**Mimicking Nacre Through Magnetically Driven Self-Assembly of Colloids** Joelle Medinger and Marco Lattuada; University of Fribourg, Switzerland

Nature's intelligent design of composite materials leads to enhanced mechanical properties compared to the individual constituents, which can for example lead to a combination of high stiffness and toughness [1]. Nature design principles have

inspired scientists to fabricate reinforced synthetic materials by mimicking the architecture of biological systems. Nacre is one of the most studied systems [1-3]. It is a composite material formed of alternating layers of inorganic aragonite platelets intercalated by a biopolymer [4]. Nacre displays remarkably high mechanical properties going far beyond the rule of mixture of its constituents.

We tried to mimic this layered composite structure using silica as inorganic material. In order to obtain a layered porous and anisotropic silica network, we modified the conventional sol-gel process, which leads to porous silica monoliths, by adding superparamagnetic iron oxide nanoparticles (SPIONS) and applying an external rotating magnetic field during the sol-gel transition [5-6]. The magnetic nanoparticles will self-assemble into layered structures in the presence of a high frequency rotating field, aligned in the plane of rotation of the field. Silica having an affinity for the iron oxide nanoparticles will nucleate on them adopting the same structure as the SPIONS, which act as smart templates to dictate the final structure of the monolith, which is permanently fixed after gelation. The final inorganic-organic nacre inspired composite is created by filling the porous structure with a polymer. Compressions tests of the platelet-structured composite show the desired increase of the mechanical properties of the silica monolith.

[1] M. Meyers, P.Y. Chen, A. Lin, Y. Seki, *Progress in Materials Science*, 2008, **53**, 1.

[2] F. Barthelat, CM. Li, C. Comi and H.D. Espinosa, *Journal of Materials Research*, 2006, **21**, 1977.

[3] H. Zhao and L. Guo, *Advanced Materials*, 2017, **29**, 1702903.

[4] T. Niebel, F. Bouville, D. Kokkinis and A.R. Studart, *Journal of the Mechanics and Physics of Solids*, 2016, **96**, 133.

[5] M. Furlan and M. Lattuada, *Langmuir: the ACS journal of surfaces and colloids*, 2012, **28**, 12655.

[6] M. Furlan, B. Brand and M. Lattuada, *Soft Matter*, 2010, **6**, 5636.

#### 7:50 AM F.SM01.05.19

**Self-Regeneratable Living Material Produced from Microbial Cells** Avinash Manjula Basavanna<sup>1,2</sup>, Anna Duraj-Thatte<sup>1,2</sup> and Neel Joshi<sup>1,2</sup>; <sup>1</sup>Harvard University, United States; <sup>2</sup>Northeastern University, United States

Human-made materials are generally considered to be the resultant of heat-beat-treat strategies due to their energy-intensive, high temperature/pressure and harsh chemical treatments, whereas the biomaterials made by living cells are fabricated at ambient conditions from abundantly available benign components. Thus, drawing inspirations from nature and harnessing the unparalleled manufacturing capabilities restored in living cells could lead to the development of an ultimate materials technology. Just like a seed that can grow into a living wood, we envision that living cells can be engineered to fabricate living materials that have life-like properties. In this regard, we present a simple and versatile strategy to fabricate living materials from engineered microbial cells at ambient conditions. Remarkably, our living materials comprises of living cells and a fraction of the material can self-regenerate itself. This work opens up unprecedented avenues to integrate synthetic biology, materials engineering, microbiology, nanotechnology and biomimicry - to develop futuristic materials and systems for a sustainable world by employing microbial factories.

#### 8:00 AM F.SM01.05.20

**Bioinspired Materials with Self-Adaptable Mechanical Behaviors** Santiago Orrego<sup>1,2</sup>, Zhezhi Chen<sup>2</sup>, Urszula Krekora<sup>2</sup>, Decheng Hou<sup>2</sup>, Seung-Yeol Jeon<sup>2</sup>, Matthew Pittman<sup>2</sup>, Carolina Montoya<sup>1</sup>, Yun Chen<sup>2</sup> and Sung H. Kang<sup>2</sup>; <sup>1</sup>Temple University, United States; <sup>2</sup>Johns Hopkins University, United States

Nature produces outstanding materials for structural applications such as bones and woods that can adapt to their surrounding environment. For instance, bone regulates mineral quantity proportional to the amount of stress. It becomes stronger in locations subjected to higher mechanical loads. This leads to the formation of mechanically efficient structures for optimal biomechanical and energy-efficient performance. However, it has been a challenge for synthetic materials to change and adapt their structures and properties to address the changes in loading conditions. To address the challenge, we are inspired by the findings that bones are formed by the mineralization of ions from blood onto scaffolds. We report a material system that triggers mineral deposition from ionic solutions on organic scaffolds upon mechanical loadings so that it can self-adapt to mechanical loadings. For example, the mineralization rate within the material system could be modulated by controlling the loading condition, and a 30-180% increase in the modulus of the material was observed upon cyclic loadings whose range and rate of the property change could be modulated by varying the loading condition. We envision that our findings can open new strategies for making synthetic materials with self-adaptable mechanical properties.

Reference: S. Orrego, Z. Chen, U. Krekora, D. Hou, S.-Y. Jeon, M. Pittman, C. Montoya, Y. Chen, S. H. Kang, "Bioinspired materials with self-adaptable mechanical properties," **Advanced Materials**, 1906970 (2020).

**5:00 AM \*F.SM01.06.01**

**Diffusiophoresis—From Physicochemical Effects to Biofilm Mitigation** Howard A. Stone; Princeton Univ, United States

Diffusiophoresis refers to the motion of colloid materials in concentration gradients. I describe some of our studies of these problems, using experiments and mathematical modeling, such as the influence of ion valence and the effect of multiple electrolytes. Also, we demonstrate that these effect can influence of the movement of bacteria. For example, I summarize our observations of the migration of wild-type *V. cholerae* and a mutant lacking flagella ( $\Delta$ flaA), as well as *S. aureus* and *P. aeruginosa*, near a dissolving CO<sub>2</sub> source, which shows that diffusiophoresis of bacteria is independent of shape and Gram stain. With long-time experiments, we show that CO<sub>2</sub>-driven diffusiophoresis can reduce surface contamination, which suggests that the mechanism can be applied to cleaning systems and anti-biofouling surfaces. This work involves contributions from Suin Shim, who investigated the diffusiophoretic response of bacteria, as well as Ankur Gupta, Jessica Wilson and others in my research group.

**5:15 AM \*F.SM01.06.02**

**Chemically Controlled Shape-Morphing of Elastic Sheets** Anna C. Balazs<sup>1</sup>, Raj K. Manna<sup>1</sup>, Oleg E. Shklyaev<sup>1</sup> and Howard A. Stone<sup>2</sup>; <sup>1</sup>University of Pittsburgh, United States; <sup>2</sup>Princeton University, United States

The shape-morphing of two-dimensional elastic materials into three-dimensional structures is a vital and ubiquitous transformation in biological systems, as evidenced, for example, by the morphogenesis in cells and tissues, the formation of well-defined curvatures in growing flowers and leaves, and reconfiguration of seedpods in the release of seeds. The functionality of such biological reconfigurations has inspired the development of synthetic shape-changing materials that are useful for soft robotics and soft actuators. Here, we use theory and simulation to devise a distinctive approach for driving shape changes of 2D elastic sheets in fluid-filled microchambers. The sheets are coated with catalyst to generate controllable fluid flows, which transform the sheets into complex 3D shapes. A given shape can be achieved by patterning the arrangement of the catalytic domains on the sheet and introducing the appropriate reactant to initiate a specific catalytic reaction. Moreover, a single sheet that encompasses multiple catalytic domains can be transformed into a variety of 3D shapes through the addition of one or more reactants. Materials systems that morph on-demand into a variety of distinct structures can simplify manufacturing processes and broaden the utility of soft materials.

**5:30 AM F.SM01.06.03**

**Differential Growth and Shape Formation in Plant Organs** Changjin Huang<sup>1</sup>, Zilu Wang<sup>2</sup>, David Quinn<sup>2</sup>, Subra Suresh<sup>1</sup> and K. Jimmy Hsia<sup>1</sup>; <sup>1</sup>Nanyang Technological University, Singapore; <sup>2</sup>Carnegie Mellon University, United States

Morphogenesis is a phenomenon by which a wide variety of functional organs are formed in biological systems. In plants, morphogenesis is primarily driven by differential growth of tissues. Much effort has been devoted to identifying the role of genetic and biomolecular pathways in regulating cell division and cell expansion and in influencing shape formation in plant organs. However, general principles dictating how differential growth controls the formation of complex 3D shapes in plant leaves and flower petals remain largely unknown. Through quantitative measurements on live plant organs and detailed finite-element simulations, we show how the morphology of a growing leaf is determined by both the maximum value and the spatial distribution of growth strain. With this understanding, we develop a broad scientific framework for a morphological phase diagram that is capable of rationalizing four configurations commonly found in plant organs: twisting, helical twisting, saddle bending, and edge waving. We demonstrate the robustness of these findings and analyses by recourse to synthetic reproduction of all four configurations using controlled polymerization of a hydrogel. Our study points to potential approaches to innovative geometrical design and actuation in such applications as building architecture, soft robotics and flexible electronics.

**5:40 AM F.SM01.06.05**

**Effect of Ultraviolet Radiation on the Broadband Optical Properties of Synthetic Melanin Coatings** Anvay Patil<sup>1</sup>, Weiyao Li<sup>1</sup>, Xuhao Zhou<sup>2</sup>, Zhao Wang<sup>2</sup>, Ming Xiao<sup>1</sup>, Matthew Shawkey<sup>3</sup>, Nathan Gianneschi<sup>2,2</sup> and Ali Dhinojwala<sup>1</sup>; <sup>1</sup>The University of Akron, United States; <sup>2</sup>Northwestern University, United States; <sup>3</sup>Ghent University, Belgium

Melanin, a ubiquitous material present in all forms of the living kingdom, and its synthetic mimics have been extensively

studied owing to its intriguing properties like broadband absorption, ultraviolet (UV)-protection, and other multi-functional properties. In the recent decade, synthetic melanin (especially polydopamine) has been extensively employed to study structural color, optical filters and other optical applications. However, there is a lack of understanding on how the optical properties of these materials would be affected after intensive exposure to UV radiation (320-450 nm). In this work, we characterize the complex refractive index of synthetic melanin thin films using spectroscopic ellipsometer through the UV-NIR range, before- and after-UV treatment. Atomic force microscopy (AFM) is used as an independent technique, recording thickness changes to improve the fitting process of the ellipsometric parameters ( $\Delta$  and  $\Psi$ ) for derivation of the complex refractive index. This information has a crucial meaning in elucidating the optical properties of melanin and provides new prospective to melanin's UV protection behavior.

#### 5:50 AM F.SM01.06.06

**Enhancing the Toughness and Structural Safety of Eggshells—Effects of Defects and Soft Membrane** Zian Jia<sup>1</sup>, Zhifei Deng<sup>1</sup>, Leigh Kadlec<sup>1</sup>, Mary C. Stoddard<sup>2</sup> and Ling Li<sup>1</sup>; <sup>1</sup>Virginia Tech, United States; <sup>2</sup>Princeton University, United States

The eggs of birds and many reptiles are protected by hard eggshells composed mainly of calcium carbonate (~94 wt%). While the evolutionary success of birds and reptiles clearly suggests an effective biological design of eggshell, how eggshells achieve structural safety and robustness from such a thin shell with weak constituents is not fully understood. Even more puzzling is the observation that the inner side of eggshells is abundant with crack-like defects resulted from mammillary cones, which appear to weaken the eggshells. In this study, we developed a micromechanics model that takes microstructural defects, post-fracture deformation, and the underlying soft membrane of eggshell into account. With this model, we discover that membrane and crack-like defects play a critical role in amplifying the energy absorption and structural safety of eggshells. Impressively, the membrane can remain intact at displacements an order of magnitude greater than instances in which fracture is initiated in the hard shell. This improves the energy absorption by over 200%. On the other hand, the crack-like defects between mammillary cones accommodate the membrane deformation over a large area, enhancing the integrity of the membrane during post-fracture deformation. These findings are verified by three-point bending tests on both emu and hen eggshells, suggesting a general design strategy for eggshells. Such smart engineering of defects and a soft membrane in eggshell may further be adapted to the design of pressurized vessels and space capsules, where hard outer shells and structural safety are required simultaneously.

#### 6:00 AM F.SM01.06.07

**Investigating the Viscoelastic Behavior of Collagen Fibrils *via* Atomics Scale Modeling** Mario Milazzo<sup>1,2</sup>, Alessio David<sup>3</sup>, GangSeob Jung<sup>1</sup>, Serena Danti<sup>4,1,2</sup> and Markus Buehler<sup>1</sup>; <sup>1</sup>Massachusetts Institute of Technology, United States; <sup>2</sup>Scuola Superiore Sant'Anna, Italy; <sup>3</sup>Politecnico di Milano, Italy; <sup>4</sup>University of Pisa, Italy

Bone is mineralized tissue that constitutes the frame of the musculoskeletal system to support and protect body structures. In addition to other functions, bone plays a remarkable role in sound conduction. From a mechanic standpoint, bone is an anisotropic viscoelastic material, capable of transmitting and dissipating energy, preventing structural failures and their propagation.

We propose a computational study that aims at fully exploring the viscoelasticity of collagenous fibrils with different mineralization contents. We investigate the mechanical response of the tissue upon cyclic and impulsive loads to observe the viscoelastic phenomena from either shear or extensional strains *via* atomics scale modeling. We perform a sensitivity analysis that takes into account a number of benchmarks: intrafibrillar mineralization percentage, hydration state, and amplitude of the external load.

We prepare the building block of collagen (COL) fibrils, the so-called *D*-period of about 67 nm, composed of the overlap and gap region. The gap volume is the part where hydroxyapatite (HA), the mineral component of bone, is mostly accumulated. Based on the amount of HA, we define three structures for our study: COL/HA 100/0 (w/w%), for resembling pure collagenous tissues; COL/HA 80/20 and 60/40, to describe mineralized tissues.

We pre-process our structures based on the boundary conditions: full periodicity is used for the cyclic-loading study (CLS) while, concerning the investigation with impulsive loads (ILS), we apply the periodicity only to the axes that are transversal to the wave direction. We apply to the CLS a sinusoidal shear strain ( $\gamma$ ) with two amplitudes (*viz.*, 0.017 rad and 0.17 rad) ranging in 1-10 GHz frequency. As for the ILS, we cut the bonds along the loading axis in order to apply the impulsive load at one edge (*viz.*, a uniform displacement delivered in 2 ps with input velocities ranging between 100 m/s and 1000 m/s) and a fixed constraint to the opposite one. All the topologies are equilibrated *via* LAMMPS aiming at relaxing the structures and reaching the convergence of the potential energy and RMSD (Root-mean-square deviation).

Our results from the CLS show a growth of the elastic modulus ( $G'$ ) with the increase of the mineral percentage, which is more pronounced at low angular strains (up to 3000 MPa). The viscous part ( $G''$ ) increases with %HA at high values of  $\gamma$  (up to 40 MPa) while it is almost constant at low  $\gamma$ s, below 10 MPa. When considering the intrafibrillar water, the material



softens the elastic component with a wet/dry ratio that is almost 0.5, but increase considerably its viscosity, especially at high frequencies ( $G''$  up to 600 MPa). This behavior is also confirmed by the response of the material in ILS, in which water drastically reduces the relaxation times by one order of magnitude with respect to the dehydrated topologies, independently of the input velocity.

Our results may be used to improve the knowledge of the physiology of pure collagenous tissues or intrafibrillar mineralized tissues upon different conditions (e.g., traumas, diseases like osteoporosis or *osteogenesis imperfecta*). Moreover, although the main focus of this study is about the effect of the mineralization and hydration on the mechanical behavior of bone, our results are not limited to tissue engineering applications. From a materials science standpoint, our research may represent a contribution to the development of a larger class of bioinspired/biomimetic bone-like materials for impact loading, fatigue, prosthetics, and acoustic applications.

This work has received funding from the European Union's Horizon 2020 research and innovation program under the Marie Skłodowska-Curie grant agreement COLLHEAR No 794614.

#### 6:10 AM F.SM01.06.08

**Modeling Shape-Programmable and Reconfigurable Dielectric Elastomer Actuator Sheets** Bekir Aksoy and Herbert R. Shea; Ecole Polytechnique Federale Lausanne, Switzerland

Nature abounds with examples of living beings that can change their morphologies in complex ways to rapidly adapt to changing environmental conditions. Soft actuators able to generate programmable and reconfigurable shapes will enable the development of dynamic and adaptive systems. Simultaneously having both reconfigurability and high holding forces is a central challenge.

We report here a model and its experimental validation for a programmable soft material sheet that allows both dynamic control of shape and zero-power shape locking. The multimorph soft actuator combines the deformation mechanism of dielectric elastomers actuators (DEAs) with the multistability of heat-activated shape memory polymers (SMPs). Stretchable heaters are integrated to spatially tune the stiffness of SMP fibers. Spatial and temporal stiffness modulation allows us to actively define temporary soft axes. By controlling the location and the orientation of these axes, we use a single DEA covering the entire sheet to reach many distinct deformations. The shape can be fixed by cooling down the heated fibers when the target deformation is reached. This approach has potential to bridge the gap between soft and conventional robotics by offering both soft actuation state and load-bearing latched state.

The actuator sheets have an active area of 28 mm x 28 mm with a total thickness of less than 750  $\mu\text{m}$ . Two SMP layers in a grid pattern are bonded to the stack of the DEA and the heaters. Two sets of three heater arrays are aligned in different directions, allowing spatially varying temperature distribution. The six heaters reduce the Young's modulus of SMP segments by 250 times. By dynamically addressing a combination or a time sequence of these heaters, complex and different shape deformations are achieved upon DEA actuation. We previously demonstrated that this technique can be implemented in DEA grippers to augment their grasping ability to pick and place objects with different shapes that are not possible with a single shape transformation.[1]

The actuator sheets consist of several layers (up to 11 layers include including one or two DEA layers, SMP grids, heaters, and electrical and thermal insulator layers). This requires a carefully optimization of the design parameters to reach both large actuation deformation and high load-bearing capacity: thick SMP layers enable high blocking forces thanks to high stiffness in the glassy state, however they limit the deformation due to the non-zero stiffness in the rubbery state. We report here an analytical model that provides insights into the role of SMP thickness and as well as other design parameters on the device performance, e.g. the location of the DEA and the order of passive layers. The model couples the Maxwell pressure from a dielectric elastomer, beam deflection, and thermo-mechanical modeling of different materials. It accurately predicts the quasi-static behavior of the devices at different states of the actuator and the predictions agree well with the experimental results. The actuator sheet designed based on the model output can achieve a bending deflection of over  $300^\circ$  and can hold a force greater than 25 mN. It can be easily adapted to different scenarios where specific displacement and blocking force are needed.

This approach to shape-programmable sheets does not require joints or additional latching mechanisms, it can be easily integrated into a range of biomimetic soft robotics or wearable robotic applications.

[1] B. Aksoy and H. Shea, *Advanced Functional Materials*, 2020.

#### 6:20 AM F.SM01.06.09

**Modeling Zinc Ion Coordination in Structural Proteins, Including the *Nereis virens* Jaw Protein (Nvjp-1) and Amyloid- $\beta$  Peptides** Alby J. Joseph, Eesha Khare, Niels Holten-Andersen and Markus Buehler; Massachusetts Institute of Technology, United States

Nature has engineered biological materials with remarkable mechanical properties, including stiffness, toughness, and self-

healing properties. Transition metal coordination chemistry is an important component of proteinaceous materials that can impart such properties. Unlike conventional covalent bonds, metal coordination bonds are kinetically labile and tunable, enabling access to a wide range of dynamic mechanical properties. As such, coordination complexes have generated interest as a biomimetic strategy for engineering the mechanics of bioinspired artificial materials. For instance, Zn(II) metal-coordinated cross-linking is responsible for the high stiffness of the *Nereis* marine worm jaw (10-20 GPa), which is comparable to that of biomineralized materials. Interestingly, Zn(II) metal ion coordination can also play a structural and mechanical role in the assembly and aggregation of amyloid proteins. Natural amyloid peptides have the intrinsic capacity to self-assemble and form extraordinary fibrillar nanostructures rich in  $\beta$ -sheets with elastic moduli as high as 10-30 GPa. This aggregation has received much attention due to its pathological role in neurodegenerative disease, such as Alzheimer's Disease (AD). Given the remarkably high concentrations of Zn(II) (up to millimolar range) in the plaques of AD brains, experimental studies have sought to understand the effect of Zn(II) on amyloid- $\beta$  peptide aggregation; however, this still remains poorly understood.

This study aims to contribute to a mechanistic, molecular-level understanding of the role Zn(II) plays in the mechanics and assembly of structural proteins, such as *Nereis virens* jaw protein (Nvjp-1) and amyloid- $\beta$  (A $\beta$ ). Computational tools present a useful strategy to achieve this molecular-level understanding. Molecular dynamics simulation techniques, including replica exchange molecular dynamics (REMD) and steered molecular dynamics (SMD), are employed to study the concentration-dependent effect of Zn(II) metal ion coordination on the conformational free energy landscape and mechanical stability of these structural proteins. Through the comparison of structure-property relationships in Nvjp-1 and A $\beta$ , this work has the potential to inform the design and engineering of transition metal coordination complexes in bioinspired nanomaterials.

#### 6:30 AM F.SM01.06.10

**Late News: Coarse Grained Atomistic Simulations of Mechanical Behavior in Nacre-Inspired Composites** Raghavan Ranganathan and Param Punj Singh; Indian Institute of Technology Gandhinagar, India

The quest for improving mechanical properties of synthetic materials has been, unexpectedly, bolstered by the structure and organization of natural materials such as animal shells, bone, silk, etc. Among this class of biomaterials, the mollusk shell, also called as nacre has proved to be a fascinating material with superior toughness. Though the bulk (95%) of nacre is made up of the hard but brittle crystalline aragonite phase, the hierarchical "brick-and-mortar" nature of the microstructure of nacre held together by organic fillers is thought to be responsible for these superior properties.

Atomistic simulations on nacre-inspired materials have predominantly focused on expressing the inorganic and organic components via high-fidelity force fields that are computationally expensive and have limited scope for detailed structure-property elucidation. Here, we employ large-scale atomistic *coarse-grained* simulations of nacre-inspired microstructures, made up of crystalline grains that are held together by polymer chains. We show that coarse graining allows us to study the effect of several properties such as microstructure (grain morphology and size), polymer-crystal interactions and the effect of grafting. We explore tensile, compressive and viscoelastic behavior of these composites along with elucidation of nanoscale mechanisms. While being able to capture mechanisms for mechanical behavior reported in the literature qualitatively (such as the saw-tooth behavior in stress-strain curve under tensile loading), we show that our coarse grained models offer a promising alternative for efficient structure-property studies for design of novel biomimetic architectures.

SESSION F.SM01.07: Application and Design of Bio-Inspired Materials (e.g. Optics, Sensing, Actuation, Medicine)  
On Demand Abstracts Available for Viewing Starting Saturday Morning, November 21, 2020  
F-SM01

#### 5:00 AM \*F.SM01.07.01

**3D Materials Systems as Bioelectronic Neural Interfaces and Bioinspired Passive Microfliers** John A. Rogers; Northwestern University, United States

3D mesostructures represent essential, ubiquitous design features in biology, from the spherical constructs of living organoids to the aerodynamic shapes of swirling maple seeds. This talk presents our work in two corresponding areas of 3D materials engineering. The first focuses on mechanically compliant, 3D multifunctional neural interfaces to cortical spheroids and assembloids. Detailed studies of the spreading of coordinated bursting events and the cascades associated neuroregeneration represent two of the many opportunities in neuroscience research uniquely enabled by these platforms. The second area is in

exploratory 3D materials architectures that mimic the aerodynamic features of gliding, spinning and twirling seeds that facilitate their dispersal. The talk will emphasize both basic and applied aspects of these two distinct classes of materials systems.

**5:15 AM \*F.SM01.07.02**

**A Portable, Biologically-Inspired Platform for Color and Pattern Sensing and Display** Leila Deravi; Northeastern University, United States

A small number of animals have the ability to actively change their visual appearance to perform important biological tasks. Cephalopods rank high on this list due to their ability to rapidly change color and texture - in some cases - for defense and signaling and have been a source of inspiration for the design of next generation adaptive systems. Recently, the electrochemical properties of the primary pigment found in cephalopod skin, xanthommatin, have been harnessed and applied in color-switching electrochromic displays with low power requirements. We describe the translation of this technology into a compact form factor that can sense and measure color from the environment then activate spatially patterned coloration with rapid (ca. seconds) response times. Our device uses reflectance-based sensors to measure color then triggers the formation of hue matched patterns by arrayed display components that can match and/or “hide” on surfaces of varying geometry, color, and luminous intensity. In future iterations of our approach, these principles may be applied to expand the palette of measured and displayed colors or to construct soft, deformable systems that can alter their optical signatures in response to environmental cues.

**5:30 AM \*F.SM01.07.03**

**Colour Engineering—Form Nature to Applications** Silvia Vignolini; University of Cambridge, United Kingdom

The most brilliant colours in nature are obtained by structuring transparent materials on the scale of the wavelength of visible light. By controlling/designing the dimensions of such nanostructures, it is possible to achieve extremely intense colourations over the entire visible spectrum without using pigments or colourants. Colour obtained through a structure, namely structural colour, is widespread in the animal and plant kingdom [1]. Such natural photonic nanostructures are generally synthesised in ambient conditions using a limited range of biopolymers.

In this seminar, I will review our recent advances to fabricate bio-mimetic photonic structures with cellulose and chitin and I will give examples of how to fabricate novel photonic materials based on chiral nematic architectures using low-cost polymers in ambient conditions [2-7].

[1] Kinoshita, S. et al. (2008). Physics of structural colours. Rep. Prog. Phys. 71(7), 076401.

[2] Narkevicius A, et al. (2019). Controlling the Self-Assembly Behavior of Aqueous Chitin Nanocrystal Suspensions, Biomacromolecules 20, 2830

[3] Chan C. L. et al. (2019) Visual Appearance of Chiral Nematic Cellulose-Based Photonic Films: Angular and Polarization Independent Color Response with a Twist, Adv Mater 31, 1905151

[4] Frka-Petesic et al. (2019) Angular optical response of cellulose nanocrystal films explained by the distortion of the arrested suspension upon drying. Physical Review Materials 3, 045601

[5] Parker R. et al. (2018) The Self-Assembly of Cellulose Nanocrystals: Hierarchical Design of Visual Appearance. Adv Mat 30, 1704477

[6] Parker R. et al. (2016). Hierarchical Self-Assembly of Cellulose Nanocrystals in a Confined Geometry. ACS Nano, 10 (9), 8443–8449

[7] Liang H-L. et al. (2018). Roll-to-roll fabrication of touch-responsive cellulose photonic laminates, Nat Com 9, 4632

**5:45 AM \*F.SM01.07.04**

**Bio-Inspired Photosynthetic, Robotic and Bioactive Materials** Samuel I. Stupp; Northwestern University, United States

The soft and hard materials that make up biological systems are a great source of inspiration in materials science for design of functional systems, particularly those that are critical in supporting the most intelligent processes in the plantae and animalia kingdoms. Great ideas from these systems include, the notion of self-assembly and reversible formation of structures, creating adaptive behaviors for specific environments, materials with capacity for self-repair, the engineering of autonomous motion, and the integration of multiple functions in a single structure, among many others. In this lecture bio-inspired synthetic systems are described based on supramolecular polymers as well as “hybrid bonding polymers (HBPs), which we define as materials that rationally integrate covalent and supramolecular polymers. HBPs are biomimetic structures critical in systems such as biological membranes, muscles, tendons, and the cytoskeleton. One of the systems to be described is based on supramolecular polymers that are highly dynamic and therefore strongly effective at signaling cells for regeneration. The lecture will also describe photosynthetic materials, inspired by leaves, in which HBPs are used to couple light harvesting

assemblies and catalysts to make fuels. Finally robotic materials that emulate living creatures will be discussed in which HBPs or organic-metal hybrid hydrogels are configured to respond to light and magnetic fields in order to generate locomotion of macroscopic objects on surfaces.

#### 6:00 AM F.SM01.07.06

**Antibacterial Activity of Melanin Biopolymers Isolated from Horsehair Fibers** Tahmineh Rahmani Eliato, Joshua Smith, Young J. Kim and Cheryl Andam; University of New Hampshire, United States

Recent advances of biomaterials research have shown that biopolymers can be served as versatile materials in a variety of applications including structural, and electronics. Melanins are the broad class of biopolymers that can be found from many types of living organisms, including bacteria, fungi, plants, and animals. When melanin is extracted from different natural sources, or even synthesized *in vitro*, variability in the resulting macromolecular structures leads to different properties. There have been many studies that focus on the melanin isolated from the cuttlefish *Sepia officinalis* ink (*SepiaMel*) or synthetic melanin (*SynMel*). However, the properties of melanins sourced from dark-color fibers of mammalian fur are less studied, comparatively. Herein, we isolate melanins from dark-color horse fibers (*EquusMel*) using the acid hydrolysis method to investigate its structural and functional properties. Electron microscopy and X-ray scattering studies showed that *EquusMel* has a homogeneous elliptical shape in a sub-micron scale while *SepiaMel* exhibits a spherical nanostructure. *EquusMel* consists of chemical functionalities of pendant catechols and secondary amines that are similar to *SepiaMel* and *SynMel*. We hypothesized that well-ordered microstructure with chemical functionality of *EquusMel* can facilitate the generation of reactive oxygen species (ROS) within the hydrated condition. The antibacterial activity of melanins was tested against *Escherichia coli*. Our results reveal that *EquusMel* has considerable antibacterial activity due to its generation of ROS. After a four-hour incubation with *E. coli*, the bactericidal activity rate of *EquusMel* was 6.87%, 69.06%, 98.12%, and 100% at melanin concentrations of 2.5 mg/ml, 5 mg/ml, 20 mg/ml, and 150 mg/ml, respectively. Measurable levels of H<sub>2</sub>O<sub>2</sub> were detected in all samples, indicating the potential of *EquusMel* to generate ROS, which can damage bacterial cells. Facile extraction of melanins and their unique antibacterial property would make this biomaterial an ideal candidate for use as an antibacterial agent to mitigate bacteria colonization and biofilm formation. Potential applications in food packaging, filtration membranes, and medical device surfaces should be further explored.

#### 6:10 AM F.SM01.07.07

**Aqueous Synthesis of Bio-Templated Halide Perovskite Nanostructures with Complex Morphologies** Masoud Aminzare, Sara Mahshid and Noemie-Manuelle Dorval Courchesne; McGill University, Canada

Halide perovskites (HPs) have recently experienced unprecedented development as outstanding materials for optoelectronic applications. Because HPs are water soluble, they have been synthesized using organic solvents and ligands (mainly toxic solvents and materials), and thus, the aqueous synthesis routes and biological applications have been hardly considered. Nonetheless, preliminary studies demonstrate stabilization of HP nanocrystals in aqueous buffers by balancing solubility equilibrium. Here, we report the implementation of a sustainable and environmentally friendly aqueous synthesis, using biomaterials (proteins, natural biomolecules, etc.) as nucleation templates to produce novel HPs morphologies. Via this biomineralization approach, electrostatic forces together with hydrogen bindings contribute to interactions between inorganic crystals and bio-templates over multiple length scales, and the bio-templates act as biological scaffolds to assemble hierarchical structures. In this strategy, first, we form metal carbonates (MCO<sub>3</sub>, M = Ca, Ba) using different bio-templates with desirable nano- and microstructures. Second, we apply ion exchange reactions to introduce appropriate cations and halide groups to form the HPs while the original morphology is preserved. Consequently, we can engineer the structure of the HPs at the nano- and microscale to acquire a variety of complex structures that would be hardly attainable via other methods. In addition, working in aqueous media has the potential to improve the biocompatibility of HPs synthesis process, paving the way towards greener synthesis approach.

#### 6:20 AM F.SM01.07.09

**Bio-Inspired Luminescent Surfaces with Tailored Angular Emission for Compact Dark-Field Imaging Devices** Cecile Chazot<sup>1</sup>, Sara Nagelberg<sup>1</sup>, Christopher Rowlands<sup>2</sup>, Maik Scherer<sup>3</sup>, Igor Coropceanu<sup>1</sup>, Kurt Broderick<sup>1</sup>, Yunjo Kim<sup>1</sup>, Mounji Bawendi<sup>1</sup>, Peter So<sup>1</sup> and Mathias Kolle<sup>1</sup>; <sup>1</sup>Massachusetts Institute of Technology, United States; <sup>2</sup>Imperial College London, United Kingdom; <sup>3</sup>Papierfabrik Louisenthal, Germany

A comprehensive understanding of nature's strategies to manipulate light spectrally and spatially, gained through the ongoing efforts in the field of biological optics and photonics has repeatedly provided opportunities for the design of bio-inspired dynamic optical materials with utility in specific applications. Here, we demonstrate how insights into the optical mechanisms and structural designs underlying the wing coloration of the *Papilio blumei* butterfly have informed the

conception of a novel light management strategy that enables dark field imaging of low-contrast biological specimen. We simplify and downsize dark-field microscopy equipment by generating the high-angle illumination cone required for dark-field microscopy directly with a luminescent photonic substrate that relies on a structural design informed by the photonic structures found on *P. blumei*'s wing scales. The surfaces' light-emitting micro- and nanoscale components provide a controlled angular emission profile. We demonstrate the ability of these hierarchically structured luminescent surfaces to generate high-contrast dark-field images of micrometer-sized living organisms using standard optical microscopy equipment. This new type of substrate forms the basis for miniaturized lab-on-chip dark-field imaging devices that are compatible with simple and compact light microscopes.

#### 6:30 AM F.SM01.07.10

**Bio-Inspired Molecular Bridging in a Hybrid Perovskite Leads to Enhanced Stability and Tunable Properties** Arad Lang<sup>1,1</sup>, Iryna Polishchuk<sup>1,1</sup>, Eva Seknazi<sup>1,1</sup>, Jochen Feldmann<sup>2</sup>, Alexander Katsman<sup>1,1</sup> and Boaz Pokroy<sup>1,2</sup>; <sup>1</sup>Technion-Israel Institute of Technology, Israel; <sup>2</sup>Ludwig-Maximilians-Universität München, Israel

Biomaterials possess superior mechanical properties relatively to their synthetic counterparts. This, among else, is due to internal stresses induced by incorporation of organic molecules. Similarly, inorganic hosts, such as CaCO<sub>3</sub>, ZnO and Cu<sub>2</sub>O can synthetically incorporate single amino acids. This incorporation induces lattice strains and morphology changes, along with changes in the mechanical and optical properties of the host.

In this work, we wanted to expand our knowledge regarding this phenomenon to a more complicated non-oxide system: the hybrid organic-inorganic perovskite methylammonium lead bromide (MAPbBr<sub>3</sub>). Hybrid lead halide perovskites have demonstrated exceptionally high performance as the active materials in opto-electronic applications (*i.e.* photovoltaics, photodetectors and light emitting diodes). Their major set-back is their poor stability under ambient conditions, especially due to decomposition under humidity, which hinders their commercialization.

We grew MAPbBr<sub>3</sub> in the presence of all 20 common amino acids, in two growth routes: fast growth (low temperature), and slow growth (high temperature). We noticed that Lysine (Lys), possessing two NH<sub>3</sub><sup>+</sup> groups (similar to the MA<sup>+</sup> cations), is incorporated in a significant higher extent than all the other amino acids. We used high-resolution powder X-ray diffraction, together with *in-situ* cooling, to measure the lattice parameter of MAPbBr<sub>3</sub> grown with different amounts of Lys. Both lattice parameter and thermal expansion coefficient demonstrated a significant decrease with the increase of the amount of incorporated Lys. This decrease, along with the observed changes in the cubic-to-tetragonal phase transition temperature of the perovskite, suggest that Lys acts as a "molecular bridge", holding the crystal together. While all the Lys-containing samples showed an increase in the optical band gap, a drastic difference between slow and fast grown samples was observed. This difference can be attributed to the difference in incorporation mechanisms between the two growth routes. Moreover, electrochemical measurements of the perovskite dissolution kinetics revealed noticeable changes in the dissolution rate constants of MAPbBr<sub>3</sub> with and without incorporated Lys molecules. Specifically, when grown in high temperature (*i.e.* slow growth), MAPbBr<sub>3</sub> dissolution rate decreased in ~40% due to Lys incorporation.

#### 6:40 AM F.SM01.07.11

**Developing Extraordinary Mechanical Properties Through Machine Learning Enhanced Design of Bio-Inspired Composites** Ashish Ghimire<sup>1</sup>, Yu-Chuan Hsu<sup>2</sup>, Ya-Yun Tsai<sup>2</sup>, Chuin-Shan Chen<sup>2</sup>, Shu-Wei Chang<sup>2</sup> and Po-Yu Chen<sup>1</sup>; <sup>1</sup>National Tsing Hua University, Taiwan; <sup>2</sup>National Taiwan University, Taiwan

Natural organisms hold mastery over designing intricate structures in various length scales that exhibits remarkable mechanical properties, one such ingenious biomineral structure is nacre's brick and mortar like structure. In light of the demand for mechanically robust synthetic material, researchers have amply studied nacre. Here, we present an extensive exploit on nacre's structural features employing a machine learning model to predict composite design with high strength and toughness often mutually exclusive in artificial materials, over a large design space of  $3.6 \times 10^{10}$  including 320 topologies. The predicted models show multi-stage graceful failure with two major peaks in the tensile stress-strain curve, which are distinct from conventional brittle, ductile, or tough type deformation curves. The design guideline extracted from the predicted models is adapted to fabricate nacre inspired composites using a multi-material 3D printer. In addition to the composite with a rectangular tablet, an interlocking tablet design inspired by geometrically interlocking suture of the diatom is also synthesized. We report previously unseen and tunable work hardening phenomena and subsequent failure mechanisms in nacre inspired composites leading to the magnification of mechanical properties. Toughening mechanisms like crack reorientation during multi-stages failure under normal and shear stress, plastic deformation of soft phase, sliding and the interlocking of tablets and elastic deformation of the hard phase are elucidated by comparing experimental and simulation results. Interlocked tablet composites outperform the rectangular tablet composite in all regards, simulation results reveal that the geometry of interlocked tablets promotes higher normal stress concentrations on the tablets before the stress flow to the

soft interfaces leading to higher load-bearing capacity, delay of crack initiation, and gracious propagation which amplifies the overall mechanical properties reasonably. These novel observations provide significant new insights into developing synthetic composites with superior mechanical properties.

#### 6:50 AM F.SM01.07.12

**Fish Gill-Inspired Electrochemical Reactors for High Efficiency Redox Flow Systems** Andrew A. Wong<sup>1</sup>, Michael Aziz<sup>2</sup> and Eric B. Duoss<sup>1</sup>; <sup>1</sup>Lawrence Livermore National Laboratory, United States; <sup>2</sup>Harvard University, United States

Despite the wide variety of aquatic species on our planet, the microscopic architecture of gills in fish remains largely self-consistent, suggesting an evolutionary optimization [1]. These organs, used predominantly as gas exchange interfaces against an external, parallel-flowing aqueous solution, are used as inspiration for the design of a hierarchical electrochemical reactor. Leveraging insights from a new method for comparing porous electrodes used in redox flow batteries [2], this work explores the physical and electrochemical properties pertinent to enhancing the performance of these bio-inspired structures. Inspired by the high fidelity of the single-pass oxygen uptake inherent to ram ventilation in continuously moving fish, we explore the opportunities and limitations for high, single-pass electrochemical conversion. A computational model will be presented, applying these design principles to a liquid-fed CO<sub>2</sub> utilization system. The ohmic, kinetic, viscous, and mass transport loss limitations across a range of gill-like architectures and operating conditions will be discussed. This work provides a framework for applying bioinspired gas-exchange architectures to enhance the performance of electrochemical systems including flow batteries and CO<sub>2</sub> reactors for efficient energy conversion.

[1] Park, Keunhwan; Kim, Wonjung; Kim, Ho-Young. "Optimal lamellar arrangement in fish gills." *PNAS* 111 (22) 8067-8070 (2017).

[2] Wong, Andrew A.; Aziz, Michael J. "Method for Comparing Porous Carbon Electrode Performance in Redox Flow Batteries." (under review).

This work was performed under the auspices of the U.S. Department of Energy by Lawrence Livermore National Laboratory under Contract DE-AC52-07NA27344.

#### 7:00 AM F.SM01.07.13

**Hybrid Materials for Optoelectronics from Diatoms Microalgae** Gianluca M. Farinola<sup>1</sup>, Stefania R. Cicco<sup>2</sup>, Roberta Ragni<sup>1</sup>, Danilo Vona<sup>1</sup>, Gabriella Leone<sup>1</sup> and Gabriella Buscemi<sup>1</sup>; <sup>1</sup>University degli Studi-Bari Aldo Moro, Italy; <sup>2</sup>CNR-ICCOM, Italy

Diatoms are a large class of single cell microalgae combining photosynthetic activity with production of mesoporous biomineralized silica shells, called frustules [1]. Frustules exhibit features such as high surface area, transparency, mechanical resistance and periodic porosity, that make them appealing biomaterials for applications in photonics, sensing, optoelectronics and biomedicine [2]. Furthermore, *in vivo* and *in vitro* protocols enable frustules silica modification with functional molecules or nanoparticles. We have recently demonstrated that *in vivo* incorporation of organic [3] and organometallic emitters, such as iridium complexes [4], into *Coscinodiscus spp.* frustules represents a promising biotechnological route to biohybrid luminescent silica-based materials, whose properties result from the combination of the frustule nanostructures with the photoluminescence of incorporated molecules. We have also recently demonstrated that *Phaeodactylum tricornutum* diatom cells self-populate and propagate on transparent conductive ITO electrodes, either in the presence or in the absence of biochemical activators of adhesion. Our results demonstrate the suitability of diatoms as self-adherent microalgae capable of photocurrent production under eco-friendly conditions, paving the way to the development of a new generation of living photosynthetic organisms-based devices for optoelectronic applications.

[1] R. Ragni, S. R. Cicco, D. Vona, G. M. Farinola, in *Green Materials for Electronics* (Eds: M. Irimia-Valdu, E.D. Glowacky, N.S. Sariciftei, S. Bauer), Wiley-VCH, Germany 2017, 287.

[2] R. Ragni, S. R. Cicco, D. Vona and G. M. Farinola, *Adv. Mater.*, **1704289**, 1-23 (2017).

[3] R. Ragni, F. Scotognella, D. Vona, L. Moretti, E. Altamura, G. Ceccone, D. Mehn, S.-R. Cicco, F. Palumbo, G. Lanzani and G. M. Farinola, *Adv. Funct. Mater.*, **28** (24), 1706214-1706223 (2018).

[4] G. Della Rosa, D. Vona, A. Aloisi, R. Ragni, R. Di Corato, M. Lo Presti, S. R. Cicco, E. Altamura, A. Taurino, M. Catalano, G.-M. Farinola and R. Rinaldi, *ACS Sust. Chem. & Eng.*, **7**(2), 2207-2215 (2018).

#### 7:10 AM F.SM01.07.14

**Influence of Structural Disorder on the Optical Properties of Natural Bragg Mirrors** Sébastien R. Mouchet<sup>1,2</sup> and Pete

Vukusic<sup>1</sup>; <sup>1</sup>University of Exeter, United Kingdom; <sup>2</sup>University of Namur, Belgium

In the fabrication processes of photonic crystals, structural disorder arises in the synthesised structures from the limitations in the resolution of the synthesis processes. Such undesired disorder affects the optical properties of the fabricated photonic crystals. It must often be taken into account. Elucidating the influence of structural disorder helps reducing its optical effects and allows using it in technological applications.

Photonic structures found in the integuments of insects are interesting examples to investigate since they are known to be very tolerant of and resilient to structural or material defects and imperfections. The benefit and cost of these defects have not been so far comprehensively assessed.

In this contribution, we investigated the extent of structural disorder in Bragg mirrors occurring on the wings of beetles [1]. Some beetles exhibit indeed shiny iridescent colours ranging from violet to red thanks to such photonic structures. Due to structural disorder, variations in the optical response can be observed by optical microscopy. Using electron micrographs, we analysed the disorder in these photonic structures. We related this disorder to the optical properties, thanks to microspectrophotometric measurements of reflected light. We performed optical simulations for typical Bragg mirrors occurring in beetle wings. It allowed to assess the optical benefit and cost of structural disorder. This analysis showed that the optical response of natural Bragg mirrors in beetle wings is very resilient to disorder.

[1] J. A. Noyes, P. Vukusic, I. R. Hooper, Experimental method for reliably establishing the refractive index of buprestid beetle exocuticle, *Optics Express* 15, 2007.

#### 7:20 AM F.SM01.07.15

**Interacting Macromolecules Create a Distinct Chemical Environment Favorable for Calcite Nucleation** Leilah Krounbi<sup>1</sup>, Konrad Hedderick<sup>2</sup>, Zohar Eyal<sup>1</sup>, Lara Estroff<sup>2</sup> and Assaf Gal<sup>1</sup>; <sup>1</sup>Plant and Environmental Sciences, Weizmann Institute of Science, Israel; <sup>2</sup>Cornell University, United States

Organic macromolecules are a key ingredient in the formation of biogenic crystals. One example of biominerals formed in the presence of organic macromolecules is calcite scales, or coccoliths, created intracellularly by marine microalgae. Organic components associated with coccoliths can be divided into two groups, soluble coccolith-associated acidic polysaccharides (CAPs), and an insoluble organic plate-like structure called a base plate. Previous in vitro work has shown that these components cooperate to bind and localize calcium ions as a dense phase around the base plate, where calcite eventually crystallizes. However, the function and composition of this dense interphase in calcite nucleation in coccoliths is unknown. To further our understanding of the role of this dense Ca-rich interphase in calcite nucleation, we sought out a synthetic compound able to mimic the function of the biogenic macromolecules in vitro. Using scanning electron microscopy and dynamic light scattering, we have identified a polymer, poly(acrylic co-maleic acid), able to reproduce the particulate morphology of the CAP-calcium precipitates on the base plate. We also discovered that the precipitation of calcium with this polymer on the base plate commences at concentrations below the saturation point of calcium and polymer in solution. Thus, the base plate functions as a nucleator, engendering a chemical environment distinct from the bulk solution. Current experiments focus on nucleating calcite within the dense polymer-calcium phase on the base plate. Preliminary observations show precipitation of elongated calcium carbonate crystals growing from the base plate rim. We aim to identify the mechanism by which the organic components determine how living cells control calcite crystallization.

#### 7:30 AM F.SM01.07.16

**Interplay Between Order and Disorder in the Optical Response of Crosslinked Hydroxypropyl Cellulose-Based Photonic Films** Chun Lam Clement Chan<sup>1</sup>, Mélanie M. Bay<sup>1</sup>, Gianni Iacucci<sup>1</sup>, Roberto Vadrucchi<sup>1</sup>, Cyan A. Williams<sup>1</sup>, Gea T. van de Kerkhof<sup>1</sup>, Richard M. Parker<sup>1</sup>, Kevin Vynck<sup>2</sup>, Bruno Frka-Petescic<sup>1</sup> and Silvia Vignolini<sup>1</sup>; <sup>1</sup>University of Cambridge, United Kingdom; <sup>2</sup>CNRS, Institut d'Optique Graduate School, University of Bordeaux, France

Hydroxypropyl cellulose (HPC) is a cellulose derivative that combines the biocompatibility and edibility of cellulose and the processability of a water-soluble polymer. Therefore, it has found large industrial applications from coatings in pharmaceutical products to binder or thickening agent in food applications. Recently, HPC has also become a very attractive material for photonic applications due to its capability of forming a lyotropic chiral nematic liquid crystal phase in aqueous solution, which is responsible for a metallic and iridescent colour response. As a direct result of the chiral nematic phase, HPC, in fact, is capable of reflecting right-handed circular polarized light with specific colours and such colouration is usually strongly dependent of the direction of observation.

Here, we present a crosslinking method which allows us to drastically alter the visual appearance and photonic properties of

HPC, in terms of both angular and polarisation response. Specifically, we demonstrate that it is possible to achieve an angular independent colour reflection as well as a strong reflection of light with both handedness.

Our method not only allows us to preserve the photonic response of HPC in the absence of solvent, but highlights an approach to, using the same system, completely redesign the visual appearance of the material from iridescent and metallic to matte. With such control of appearance, we therefore demonstrate the potential of HPC as a biocompatible, biosourced photonic material that can replace traditional pigment and dyes.

#### 7:40 AM F.SM01.07.17

**Macropores in Bird Eggshells Give Rise to Mie Backscattering in the Ultraviolet Range** Mathieu Ladouce<sup>1</sup>, Tarek Barakat<sup>1</sup>, Bao-Lian Su<sup>1,2,3</sup>, Olivier Deparis<sup>1</sup> and Sébastien R. Mouchet<sup>1,4</sup>; <sup>1</sup>University of Namur, Belgium; <sup>2</sup>Wuhan University of Technology, China; <sup>3</sup>University of Cambridge, United Kingdom; <sup>4</sup>University of Exeter, United Kingdom

Eggshell is crucial for the reproduction and development of birds. The optical properties of the shells have an impact on biological functions such as heat and UV protection, recognition by the parents and camouflage. Whereas ultraviolet reflection by bird eggshells has been superficially described in the scientific literature [1,2], the physical origin of this phenomenon has remained poorly understood so far. In this contribution, macropores have been morphologically characterised by electron microscopy and mercury intrusion porosimetry in the eggshells of several breeds of domestic hens (*Gallus gallus domesticus*), one breed of duck and one breed of quail. They are located in the so-called “calcified shell” part of the eggshells (namely, at depths ranging from ca. 20  $\mu\text{m}$  and ca. 240  $\mu\text{m}$  from the shell outer surface). Two reflectance peaks (ca. 20-50%) were observed in the near UV range by spectrophotometric measurements from these eggshells. Progressively thinning down the cuticle of eggshells with ethylenediaminetetraacetic acid (EDTA) solutions allowed us to show that the so-called calcified shell is an efficient UV scattering structure whereas the cuticle partly absorbs UV radiation. Thanks to modelling relying on Mie scattering theory and an effective approach accounting for multiple scattering, we found the observed macropores were most likely giving rise to these peaks through Mie backscattering [3]. This optical response was discussed in terms of the visual sensation of chickens and human beings. Eggs displaying an achromatic visual appearance for humans appear chromatic for chickens. Fluorescence emission from the eggshells was measured and attributed to molecules of biliverdin IX $\alpha$  and protoporphyrin IX embedded within the shell. This emission is rather low in terms of quantum efficiencies and probably does not play any role in the visual appearance of the eggshells. In addition, electron microscopy imaging revealed the presence of pores within the so-called “calcified shell” part (i.e., between ca. 20  $\mu\text{m}$  and ca. 240  $\mu\text{m}$  deep from the outer surface). The average radii of these pores range from 120 to 160 nm, depending on the egg varieties. Mercury intrusion porosimetry allowed to highlight a distribution of pore radii around 175 nm. Spectral measurements of excitation and emission by fluorescence revealed the presence of fluorophores embedded in the shells. In addition, numerical and analytical predictions using scattering theory indicate that these pores are responsible for the optical response observed in the UV range. Due to the similarities between the pore size distributions observed among the eggshells of the investigated poultry eggshells, we expect Mie backscattering to be at the origin of the UV response from the eggshells of many other bird species.

[1] D. C. Fecheyr-Lippens, B. Igc, L. D’Alba, D. Hanley, A. Verdes, M. Holford, G. I. N. Waterhouse, T. Grim, M. E. Hauber and M. D. Shawkey, The cuticle modulates ultraviolet reflectance of avian eggshells, *Biology Open*, 2015, 4, 753-759.

[2] B. Igc, D. Fecheyr-Lippens, M. Xiao, A. Chan, D. Hanley, P. R. L. Brennan, T. Grim, G. I. N. Waterhouse, M. E. Hauber and M. D. Shawkey, A nanostructural basis for gloss of avian eggshells, *J. R. Soc. Interface*, 2015, 12, 20141210

[3] M. Ladouce, T. Barakat, B.-L. Su, O. Deparis and S. R. Mouchet, Scattering of ultraviolet light by avian eggshells, *Faraday Discussions*, 2020, accepted.

#### 7:50 AM F.SM01.07.18

**Methods for Iterative Design and Fabrication of Bio-Inspired Structural Color** Bianca C. Datta and Christine Ortiz; Massachusetts Institute of Technology, United States

Biological structures perform a variety of complex functions with a limited material set. One particularly exciting area of bio-inspired research is structural color, though present synthetic analogs are still limited, either by fabrication challenges or an incomplete understanding of structure-property relationships. Structural color not only provides a fascinating case study for exploring the role of material design on macroscale properties, but can provide insights on animal evolution, photonic devices, human and animal communication, signalling, and art. While this is a lively and active area of research, we are still finding the balance between what is physically possible and easy to fabricate and understanding the full extent of the color gamut that we can access. As replicating natural structurally-colored designs can be challenging and costly, we instead



explore methods for generating structures inspired by nature to create desired effects, while proposing surface designs that are physically producible with rapid prototyping. Interaction of light with Morpho butterfly structures is used as a starting point to determine key parameters and these principles are applied towards our simulations and designs. Methodologies for combined design, simulation, and material fabrication to generate colors through new structural surfaces are implemented. A computational inverse design methodology has been developed for the formulation of nanostructures exhibiting structural coloration, and opportunities for scalability are identified. A simple model based on scalar diffraction theory is used for the relationship between structural elements and optical response, where altering the surface changes the visible functionality. Through the use of larger scale optimization based on tiled repeat units and motifs, large scale arrays, displays, sensors, and art can be achieved. Simulated surfaces are then fabricated using two-photon polymerization, and optically characterized. We compare our simulations to fabricated structures using optical microscopy, scanning electron microscopy, and angular spectrometry to quantify reflected color and angular response. Through these methods, we contribute to an understanding of a) the limitations of this approach, b) the extent of the parameter or design space, c) the feasibility of this inverse design approach, and c) the limitations imposed by fabrication restrictions. By exploring different levers for production of structural color, the boundaries of our ability to mimic and expand upon natural color production are illuminated. This work provides an additional perspective on bio-inspired materials design with applications ranging from light harvesting and steering, to chemical sensing, high performance displays, responsive products and architecture. The limitations and trade-offs of our approach as it relates to scale-up and industrial use are discussed.

#### **8:00 AM F.SM01.07.19**

**Natural and Bioinspired Electronic Conductors from Supramolecular Protein Assemblies** Allon Hochbaum; University of California Irvine, United States

Electronic material properties are conventionally considered the domain of man-made materials and devices, but electronically conductive materials are also synthesized by some organisms as part of their native metabolic pathways. These biological conductors lack many of the structural characteristics typical of inorganic and organic conductors or semiconductors, and therefore represent an exciting new opportunity to study electron transport at the nexus of physics, chemistry, and biology. Well-studied microbes in oxygen-free environments, such as aquatic sediment, respire anaerobically by accessing alternative extracellular oxidants. This class of microbes displays a variety of mechanisms to shuttle spent electrons from inside the cell to remote electron acceptors. Some anaerobic bacteria, such as *Geobacter sulfurreducens*, synthesize protein supramolecular assemblies that exhibit inherent electronic conductivity and are key to their respiratory metabolism. Based on fundamental differences between the protein building blocks of these assemblies and the canonical building blocks of inorganic and organic conductors and semiconductors, it is clear that Nature has developed unique design principles for long-range electronic conductivity in amino acid materials. The biomolecular identity and supramolecular order underpinning biological conductive materials are poorly understood, as are the mechanisms by which these structures support electron transport. This talk will cover our ongoing work in the characterization of structure-function relationships in conductive protein and peptide materials. These efforts establish distinctive biomolecular design principles for long-range electron transport in self-assembling *de novo* peptide nanofibers, engineered biological materials, and native bacterial appendages. Such materials serve as an experimental platform to understand long-range charge transport in biological materials in general, and as promising technological platforms for bioelectronic interfaces.

#### **8:10 AM F.SM01.07.21**

**Platelet Heterogeneity Leads to Emergent Collective Behavior Enhancing Blood Clot Contraction** Yueyi Sun<sup>1</sup>, David Myers<sup>1,2</sup>, Wilbur Lam<sup>1,2</sup> and Alexander Alexeev<sup>1</sup>; <sup>1</sup>Georgia Institute of Technology, United States; <sup>2</sup>Emory University, United States

Blood clots are an active biomaterial in which anucleate cells, called platelets, can extend micrometer-long filopodia to impose contractile forces on the fibrin scaffold that lead to drastic macroscopic changes in clot volume and elastic modulus. Blood clots are involved in physiologic and pathologic processes, such as wound healing, fibrosis, and musculoskeletal contractures. We use experiments and mesoscale modeling to examine the biophysics of clot contraction by directly linking the microscale platelet movements to macroscale biomaterial properties and behavior. We find that the clot contraction is optimized through the intrinsic heterogeneity of platelets. When platelets within the clot are exposed to thrombin, they do not contract simultaneously as one can be expected, but rather contract over time at a sequential manner. We show that this temporal heterogeneity of platelets leads to emergent behaviors that significantly enhance the biomaterial volumetric contraction. We rationalize this surprising effect by the ability of heterogeneous platelets interact with fibers that are initially located out of their influence range. We show that only by accounting for platelet the cellular heterogeneity we are able to replicate the experimentally measured clot forces. This points to the importance of examining biomaterials as a 4D (space + time) system in which natural cellular heterogeneity can be harnessed to enhance the mechanical efficiency. Furthermore, our

results suggest a new direction of developing synthetic and hybrid stimuli-responsive composites in which engineered heterogeneity can serve to enrich the mechanical responses and shape transformations.

#### 8:20 AM F.SM01.07.22

**Rayleigh Blue—Elaboration and History** Anne Pillonnet<sup>1</sup>, Anne Goyer<sup>1</sup>, Amina Bensalah-Ledoux<sup>1</sup>, Cécile Le Luyer<sup>1</sup>, Davy Carole<sup>1</sup> and Romain Thomas<sup>2</sup>; <sup>1</sup>Univ of Lyon1-CNRS, France; <sup>2</sup>Université Paris Nanterre, France

The blue coloration in nature is mainly of non-pigmentary origin [1] and is known as Rayleigh or Tundall blue. This non-pigmentary or structural blue coloration is, for example, the blue color of the sky and mountains in the distance, the blue color of human or animal eyes, the blue color of feathers of some birds like *cotinga maynana*, a turquoise bird of Peru and Ecuador, for instance. The origin of this non-iridescence blue color is attributed to the constructive interference of scattered light from quasi-amorphous structures of self-assembly of mono-dispersed particles, typically closely packed air cavities in b-keratin for eyes or plum. Reproducing the phenomenon in thin film materials requires nanoparticles randomly dispersed in a transparent layer deposited on a highly absorbent dark film. The refractive index between the particles and the matrix must be different, thus pores containing air or contrary particles of high refractive index could be used. In our research work, the original idea to produce this coloration has originated from an encounter with a contemporary artist who intuitively realized for the first time this blue color from crushed white chalk, colorless oil and viscous black mineral peas collected in a natural resurgence. The using tools are only brushes, a mortar and a marble table to manually grind the materials. A collaboration with our scientific research laboratories made it possible to identify the optical phenomenon involved and to find a robust protocol to create this blue color in a reproducible and intense way, keeping the materials and the artist's tools and by optimizing the gestures [2]. The intensity of the produced blue color highlights the potentialities of using this coloring with simple materials and technologies for ecological and environmentally friendly coloring applications. Beyond this important issue, the intensity of this blue color has led to a discussion among the history of art, and the possibility that the ancient masters used this non-pigmentary blue coloring in their famous paintings at a time when the blue color was a major economic issue, before the advent of chemistry and the discovery of synthetic pigments and coloring [2]. Some ancient manuscripts mention it but, on the works it is not yet proven, knowing that this blue color is very fragile as it is very much linked to the architecture of the material and therefore very sensitive to ageing.

1 Andrew R Parker, *Review, Phil.Trans. R. Soc.* (2009) 364, 1759-1782

2 A. Goyer & al, *Arts et Science Journal*, 2019, 19, 3

#### 8:30 AM F.SM01.07.23

**Reconstructing *Bombyx mori* Silk Fibroin into a 3D Porous Microneedle Array for Detection of Food Bacteria** Doyoon Kim, Yunteng Cao, Dhanushkodi Mariappan, Michael S. Bono, A. John Hart and Benedetto Marelli; Massachusetts Institute of Technology, United States

Natural structures made of silk fibroins, such as cocoons and spider webs, have inspired researchers to utilize their mechanical properties and biocompatibility for various engineering applications. Recently, silk fibroins extracted from *Bombyx mori* silkworm cocoons have emerged as promising technical materials for food contact applications due to their non-toxic and edible nature, in addition to their tunable mechanical and chemical properties. Here, by leveraging water-based processing of *Bombyx mori* silk fibroin, we build a porous silk microneedle platform for the detection of bacteria in food. The microneedles can transport internal food fluid by capillary action to a colorimetric sensor on the backside of the array. We demonstrate detection of food contamination within 16h after injection of *E. coli* in fish fillets, by color-change of a polydiacetylene-based sensor printed onto the backside of the microneedle array. This response by *E. coli* contamination can be distinct from common food spoilage measured via an increase in sample pH. We also show that the microneedle sensor can pierce commercial food packaging, indicating the feasibility of successful adaptation of the technology downstream in current food supply chains. The platform developed in this study can contribute to food quality monitoring, which is critical to global food safety and to minimizing food loss and waste.

#### 8:40 AM F.SM01.07.24

**Structural Color as a Tool to Monitor Colloidal Cluster Formation** Junwei Wang, Chrameh Fru Mbah, Praveen Bommineni, Silvan Englisch, Thomas Przybilla, Erdmann Spiecker, Michael Engel and Nicolas Vogel; Friedrich-Alexander University Erlangen-Nürnberg, Germany

It is well-acknowledged that nature uses ordered nanostructures to generate vivid iridescent color such as opals. To mimic such structures, colloidal particles are widely used, due to their uniform and tunable sizes, to form colloidal crystals of densest closed-packed structure in bulk. Recent discoveries in butterfly scales reveal the role of isolated finite-size crystallites

as building blocks for their hierarchical structure. In this contribution, we present discrete colloidal clusters fabricated from self-assembly of colloidal particles encapsulated in emulsion droplets. Unusual equilibrium crystal structures with icosahedral, decahedral or fcc symmetry arise from the spherical droplet confinement. Combining simulations and electron tomography, we show that these colloidal clusters are in energy minima when the number of particles satisfies certain rules, leading to a “magic number” effect previously known only at subatomic and atomic length scale. We analyse their unique structural color resulting from the complex cluster structures, which can be used to monitor cluster rotation and colloid crystallization in spherical confinement in real-time. At last, we give examples of hierarchical structural design using colloidal clusters.

#### 8:50 AM F.SM01.07.26

**Membrane-Based Ionotronics Inspired by Neurons** Thomas B. Schroeder<sup>1</sup>, Varinder S. Takhar<sup>2</sup> and Joanna Aizenberg<sup>1</sup>; <sup>1</sup>Harvard University, United States; <sup>2</sup>University of Waterloo, Canada

Neurons generate electrical signals in response to chemical stimuli by altering the selective permeability of their membranes in the presence of an electrolyte gradient. After some integration, these signals move quickly along the length of the neuron before triggering a downstream chemical signal. Nervous systems, which are complex assemblies of these chemo-electro-chemical signaling units, are capable of guiding the autonomous function of animals.

Inspired by the architecture and biophysics of neurons, we present a hydrogel/organogel/hydrogel trilayer scheme capable of generating electrical potentials from chemical and optical signals. Energy is stored in an electrolyte gradient between the two aqueous compartments. Triggering the selective permeabilization of the initially insulating organogel membrane using stimuli-responsive chemistry causes a change in the electrical potential between the two aqueous domains on the order of 100 mV. We compare the spatial decrement of the signal along these membranes to the passive spread of an electrical potential in neurons. We further describe an electrochemical end effector intended to produce a chemical response spatially decoupled from the initial permeabilizing signal. We aim to interface this scheme with electrical detectors or network them to enable computation, feedback loops, or autonomous behavior.

#### SESSION F.SM01.08: Biomineralization

On Demand Abstracts Available for Viewing Starting Saturday Morning, November 21, 2020  
F-SM01

#### 5:00 AM F.SM01.08.01

**Late News: Helical Microstructures of the Mineralized Coralline Red Algae Determine their Mechanical Properties** Nuphar Bianco-Stein<sup>1</sup>, Iryna Polishchuk<sup>1</sup>, Gabriel Seiden<sup>2</sup>, Julie Villanova<sup>3</sup>, Alexander Rack<sup>3</sup>, Paul Zaslansky<sup>4</sup> and Boaz Pokroy<sup>1</sup>; <sup>1</sup>Technion–Israel Institute of Technology, Israel; <sup>2</sup>Moriah Scientific Consulting, Israel; <sup>3</sup>The European Synchrotron, France; <sup>4</sup>Charité–Universitätsmedizin Berlin, Germany

Biominerals produced by living organisms have superior properties compared to their synthetic counterparts. Even though biominerals are formed at ambient conditions and from a limited variety of available building blocks, they possess remarkable structures and often combine desired qualities such as low weight and improved mechanical properties. The coralline red algae secrete high-Mg calcite as a part of their skeleton, with Mg levels exceeding the thermodynamically stable one. They are highly prevalent around the world's oceans and contribute to reef ecology. The structure of these algae has not been widely studied previously and information on their nanostructure is largely missing.

In our attempt to gain a better understanding of nature's extraordinary designs, we study an articulated coralline red alga that resides in the shallow waters of the Mediterranean Sea. Because of its erect structure growing upright, this alga has to endure the great stresses applied to it by the sea waves. We explored its structure from the nano to the macroscale utilizing various state-of-the-art techniques such as synchrotron radiation nanotomography and high-resolution aberration-corrected TEM. We discovered that its structure is highly porous, with porosity levels reaching as high as 64 vol%. We showed that its structure is intricate and is hierarchical with several orders from the nano to the macroscale, formed by plate-like crystals with nanometric diameters. Surprisingly, we revealed its macrostructure is helical rather than cylindrical and proved that this configuration confers the alga great compliance, allowing it to be ~20% more compliant under compressive stress, as compared to a cylindrical structure with the same porosity.

The result is a sophisticated lightweight and compliant structure allowing the alga to sustain external stresses from its natural environment. This study can lead toward a better understanding of the structure-function relation of biomineralized

structures, and the synthesis of lightweight structures with improved mechanical properties.

SESSION F.SM01.09: Poster Session: Lessons from Nature—From Biology to Bioinspired Materials  
On Demand Abstracts Available for Viewing Starting Saturday Morning, November 21, 2020  
5:00 AM - 8:00 AM  
F-SM01

#### **F.SM01.09.01**

**Removal of Rare Earth Metal Ions from Contaminated Water by Sustainable Carboxycellulose Nanofibers Derived from Agave Through Nitro Oxidation Process** [Isha Brahmhatt](#)<sup>1,2</sup>, Sunil Sharma<sup>1</sup>, Priyanka Sharma<sup>1</sup>, Marc Nolan<sup>1</sup> and Benjamin Hsiao<sup>1</sup>; <sup>1</sup>Stony Brook University, The State University of New York, United States; <sup>2</sup>Ardley High School, United States

There is a growing need for rare earth metal ions such as lanthanides for use in electronics, fuel cells, and various other applications. These precious ions are currently derived by mining, causing major pollution and contamination in nearby water sources. As cellulose is the most abundant organic material, we derived carboxycellulose nanofibers from raw agave biomass using the simple nitro oxidation process for the removal of lanthanide ions. The nitro oxidation method converts untreated biomass to carboxycellulose nanofibers in a one step process using nitric acid and sodium nitrite. Zeta potential indicates that the fibers are highly electronegative (zeta potential -117.3 mV), and the conductometric titration method reveals that the fibers have a high carboxylate content (0.75 mmol/g). SEM measurements show that the fibers contain clearly visible fibrous structures. The TEM measurements of the fibers record fiber lengths of 55-690 nm and average fiber widths of 5-6 nm, and AFM data displayed an average thickness of 1.6 nm. The oxidation of the agave nanofibers was confirmed with <sup>13</sup>C CPMAS NMR data. The lower crystallinity of the agave nitro oxidized carboxycellulose nanofibers compared to raw agave was determined by WAXD. The nitro oxidation approach also offers beneficial reductions in the consumption of water and electric energy as well as the need for multi-chemicals when compared with conventional multiple-step processes at bench scale (e.g. TEMPO oxidation). Remediation studies on lanthanide ions showed a floc formation between the ions and nanofibers. The Langmuir isotherm generated from ICP-MS studies indicated a 285.7 mg/g adsorption capacity and over a 90% adsorption efficiency for all lanthanide concentrations, which supersedes current water purification mechanisms such as iron oxide beads (123.6 mg/g adsorption capacity). These results suggest that the agave nitro oxidized carboxycellulose nanofibers are effective for the removal of lanthanide ions for drinking water purification and lanthanide ion industry.

#### **F.SM01.09.02**

**Tremendously Enhancing Photodegradation Efficiency by Biomorphic Porous Carbon** [Weizhao Huang](#) and Hui Mei; Northwestern Polytechnical University, China

Traditional lab-based synthesis of photocatalyst are ineligible for urgent demand of exceptional recyclability and stability in industrially large-scale application resulting from the inevitably undergo agglomeration of powder-form catalysts. Immobilizing catalyst is an appealing strategy to obtain enhanced performance for solid support provides chemical, thermal, and mechanical stabilization to the catalytic species besides facilitating catalyst recovery. Carbonaceous materials with unique microstructure obtained by pyrolyzing renewable and environment-friendly nature plants have promising applications in areas such as battery and catalyst support. However, unexpected cracks accompanied by low oxidation resistance retard further development. In this study, a thin SiC coating for strengthening purpose was in-situ deposited on biomorphic porous carbon materials fabricated by pyrolyzing wood while maintaining low density. Continuously ordered microchannel structures from carbonized nature wood with a diameter of ca. 20 μm was completely replicated after depositing SiC coating, resulting in the good anisotropy in mechanical and thermal properties. The thin SiC coating was found to greatly increase compressive strength from 26.4 to 47.4 MPa and thermal conductivity from 0.49 to 14.94 W/m K in the axial direction with improved oxidation resistance of weight loss from 78.5% to 1.51%. In the radial direction, however, the increase of the two properties was lower due to the longitudinal microchannel structure. Feasibility of the biomorphic carbon serving as catalyst support with highly developed continuous channels was evaluated by loading typical molybdenum disulfide (MoS<sub>2</sub>). Result shows a significant improvement in both adsorption and photodegradation efficiency against the pure MoS<sub>2</sub>, which is because of the enlarged specific surface area of the catalyst.

#### **F.SM01.09.05**

**Bioinspired Design of Polymers for Protein Binding and Aggregation Modification** Sarah E. Morgan<sup>1</sup>, Ashleigh N. Bristol<sup>1</sup>, Lisa K. Kemp<sup>1</sup>, Shahid Karim<sup>2</sup> and Vijay Rangachari<sup>2</sup>; <sup>1</sup>The University of Southern Mississippi, United States; <sup>2</sup>University of Southern Mississippi, United States

Abnormal protein behaviors, such as aggregation or mislabeling as antigens, are involved in a range of disorders including Alzheimer's, Parkinson's, and celiac disease. Water-soluble polymers with functional motifs mimicking those in naturally occurring polymers provide an avenue to interrogate binding and assembly processes and can be designed to modify protein behavior. RAFT polymerization was employed for the synthesis of two different families of polymers, designed for the study of two different protein systems, to produce polymers with desired structures, targeted molecular weight, and low dispersity. Aggregation processes were evaluated with dynamic light scattering, GPC-MALLS, and fluorescence assays. FTIR and NMR were employed to determine hydrogen bonding patterns of the systems. Gliadin, a component of gluten and a known epitope, is implicated in celiac disease (CeD) and results in an inflammatory response in CeD patients when consumed. Stimuli-responsive polyelectrolytes with varying charged groups were employed as models to determine the effect of molecular weight and pendent group on non-covalent interaction modes with gliadin in vitro. The polymers exhibited pH dependent binding and alteration of gliadin secondary structure, providing a platform for therapeutic design of specific structure/binding interactions with food proteins. Glycopolymers with stereospecific pendent groups designed to mimic saccharide clusters in the GM1 ganglioside were prepared to analyze interactions with the amyloid  $\beta$  peptide associated with Alzheimer's disease. The A $\beta$ 42 assembly process was directly impacted by the stereochemistry of the pendent saccharide. Glycopolymer-silicone hydrogels prepared with varying hydrophobic/hydrophilic content and copolymer composition showed structure dependence of diffusion, rheology, and nanomechanical properties. These findings demonstrate the potential for design of selective glycopolymers for targeted molecular interactions for biomedical and personal care applications.

#### **F.SM01.09.06**

**Living Sorbents for Arsenic-Contaminated Drinking Water Remediation** Yidan Bi and Vicki L. Colvin; Brown University, United States

Arsenic is a pervasive contaminant in drinking water, and it has ranked the first on the Substance Priority List of Agency for Toxic Substances and Disease Registry (ATSDR) for more than two decades. Exposure to low-level arsenic in early life impairs children's cognitive development and buries the risk of developing a variety of cancers in young adulthood. To prevent the severe health effect of arsenic ingestion, materials with high arsenic removal capacity and fast treatment speed have been investigated. While these strategies are efficient for As(V), they are rendered ineffective when encountering the less abundant yet more toxic As(III), especially in the presence of competing ions. Solutions such as pretreatment or extensive removal of competing ions along with arsenic dramatically increase the operation cost and unnecessarily eliminate other benign species from water. Thus, there is a need for developing materials that can precisely capture arsenic from drinking water or even more complex beverage matrices and reduce the arsenic level below the EPA regulation (10 ppb) without altering the water chemistry.

In this work, we looked beyond the conventional physicochemical water treatment strategies and acquired insights from natural arsenic detoxification processes. The toxicity of As(III) originates from its high affinity to the cysteine residues in proteins. Natural organisms resolve this issue by expressing cysteine-rich peptides or proteins that can sequester As(III) in the cells. Inspired by this mechanism, we engineered a benign strain of *E. coli* to overexpress fusion proteins containing the binding pockets of two arsenic-binding proteins, ArsR and AfArsR, for improved arsenic scavenging competency. We also applied molecular biology tools to enhance the arsenic sorption capacity and accelerate the removal speed. One gram of these living sorbents can stoichiometrically immobilize milligrams of arsenic within a few hours. The high affinity of the proteins toward the substrate overcomes the selectivity barrier of inorganic sorbents like Bayoxide. For example, the living sorbents can bioaccumulate low levels of arsenic against common interfering species like phosphate, silicate, and natural organic matters, and the trapped As(III) does not leak to the water under these complicated conditions. In addition to remediating intractable matrices such as NSF challenge water, we found these living sorbents are adaptive to beverages including juice and wine, which were reported that are contaminated with arsenic but are not tightly regulated. Moreover, unlike the cumbersome inorganic material transportation, we propose that these living sorbents can be regenerated on-site after shipping the "seed material". We explored freeze-drying the biosorbents for storage and demonstrated that the reconstituted sorbents maintained arsenic-binding ability. To prevent secondary contamination after remediation, we explored tagging the bacterial cells with magnetic nanoparticles and found that the bacteria can be removed with a handhold magnet within a few minutes. This work provides the potential of applying renewable living sorbents for selective drinking water contaminant removal, and it is beneficial for the rural households and small communities who do not have access to the expensive and energy-consuming arsenic treatment technologies.

#### F.SM01.09.07

### **Strategic Design of Advanced Bioinspired and Biomimetic Membranes Conjugated with Graphene Oxide for Selective Ion Rejection** Sanju Gupta<sup>1,2</sup>; <sup>1</sup>CCNY-CUNY, United States; <sup>2</sup>Western Kentucky University, United States

Recent advances in synthetic membranes allow their use in fields as diverse as food and agriculture, industrial water treatment, potable water production, and bio-separation. Among the newly developed technologies, nanofiltration for liquids and more particularly for desalination of seawater or saline aquifers is the most recent one. However, limitations of current polymeric membranes call for the development of novel formulations that offer both high permeability (water flux) and ion differentiation (selectivity) usually considered antagonist features. We report the fabrication of membranes prepared from track-etched polymeric membranes as supports in which biological ion channels such as Gramicidin A, alpha-hemolysin are confined and ion-selective binding peptide motifs conjugated with graphene oxide as nanoporous hybrids. These bioinspired and biomimetic membranes are attracting widespread attention offering advantages including mechanical robustness, controlled pore dimension, and shape, modifiable surfaces for the desired efficiency. The permeability and selective ion transport are evaluated by ion diffusion kinetics, UV-Visible absorption spectroscopy, and nanofiltration while gaining insights into the role of key parameters including track-etch pore size, surface chemistry, and ion binding through solid-state nanopores or nanochannels. The proposed activity positively impacts the environment by integrating eco-friendly materials design, development, and deployment.

#### F.SM01.09.09

### **Biomimetic Musculoskeletal Polymer Nanocomposites for Magnetic Collective Swimming** Sukyong Won, Hee Eun Lee, Young Shik Cho, Seung Jae Yang and Jeong Jae Wie; Inha University, Korea (the Republic of)

In human musculoskeletal system, skeletal muscles attached to spongy bones play an essential role in exerting quick and powerful movement. Herein, we present a musculoskeletal design capable of agile magnetomotility of ternary polymeric nanocomposites. Inspired by protein actin in skeletal muscle, iron particles are attached to surface of helical porous carbon nanotube yarn (CNTY) owing to polydimethylsiloxane (PDMS) elastomer providing a fascia-like connective function. Under rotating 2D quadruple electromagnetic field, soft robots achieved agile rectangular orbital magnetomotility reaching up to 162 body length per second. Upon varying the frequency of the rotating magnetic field, the individual rectangular orbit of multiple soft robots is reconfigured into magnetic-assembled circular orbits. We will discuss magnetic swimming of collectively assembled soft robots that can manipulate vortex chirality of sustaining fluid.

#### F.SM01.09.10

### **Construction of Hybrid Soft Nanomaterials Composed of Supramolecular Nanostructures of DNA and Peptide Derivatives** Sayuri Higashi<sup>1</sup>, Aya Shibata<sup>1</sup>, Yoshiaki Kitamura<sup>1</sup>, Koichiro M. Hirosawa<sup>1</sup>, Kenichi G. Suzuki<sup>1</sup>, Kazunori Matsuura<sup>2,2</sup> and Masato Ikeda<sup>1,1,1</sup>; <sup>1</sup>Gifu University, Japan; <sup>2</sup>Tottori University, Japan

Under multi-component molecular conditions such as inside of living cells, fibrous proteins including actin filaments and microtubules are constructed based on orthogonal (self-sorted) self-assembling. Self-sorting enables plural supramolecular nanostructures to retain each property and function as well as their structures even under complex conditions. In artificial systems, construction of complex and discrete soft nanomaterials has received increasing attention in recent years, and only several self-sorting pairs of synthetic self-assembling (small) molecules and peptides have been reported. Meanwhile, the high-fidelity recognition based on Watson-Crick base pairing and programmable sequences of DNAs allows a variety of DNA nanostructures with controlled sizes and shapes to be constructed, and hybrid nanomaterials composed of DNA nanostructures have been pursued for a wide range of applications (*e.g.*, nanopores, scaffolds for catalytic reaction and protein assembly). However, much of these hybrid nanomaterials have been constructed based on co-assembly, and the orthogonal coexistence of DNA nanostructures with supramolecular nanostructures obtained by self-sorting with synthetic molecules has yet to be explored in detail.

To develop the hybrid nanomaterials composed of DNA nanostructures based on self-sorting phenomenon, we focused on nucleic acids and peptide derivatives as the component molecular pair. We recently constructed hybrid soft nanomaterials composed of DNA microspheres<sup>1</sup>, which can be obtained from three short single-stranded DNAs, and three different supramolecular nanostructures of semi-artificial glycopeptides<sup>2</sup> (helical nanofibers, straight nanoribbons, and flowerlike microaggregates) in single medium by a simple thermal annealing process.<sup>3</sup> Interestingly, both of supramolecular nanostructures exist orthogonally with only marginal impact on their morphology in single medium as a supramolecular hydrogel state. Noteworthy, to observe such self-sorted supramolecular nanostructures by fluorescence imaging, additional fluorochrome-labeled probes are required to synthesize. However, in this research, we have achieved the selective visualization of each supramolecular nanostructure by means of rational staining method focused on each selective

molecular-recognition property of DNAs and glycopeptides (e.g., intercalating agent, lectins, and saccharide-binding DNA aptamer) without additional probe developments. Furthermore, we have demonstrated the sequence-controlled degradation of the individual supramolecular nanostructures in response to distinctive bio-stimuli (i.e., enzyme and ssDNA), rendering these soft nanomaterials active against such stimuli. In this presentation, I would like to discuss the detail of these newly developed hybrid soft nanomaterials and underlying mechanism to form such unique superstructures and functions.

1. K. Matsuura, T. Yamashita, Y. Igami and N. Kimizuka, *Chem. Commun.* **2003**, 376–377.
2. T. Tsuzuki, M. Kabumoto, H. Arakawa and M. Ikeda, *Org. Biomol. Chem.*, **2017**, 15, 4595–4600.
3. S. L. Higashi, A. Shibata, Y. Kitamura, K. G. N. Suzuki, K. Matsuura and M. Ikeda, *Chem. Eur. J.*, **2019**, 25, 11955–11962.

#### **F.SM01.09.11**

**Self-Assembly of Positively Charged Computationally Designed Coiled Coil Peptide 'Bundlemer' Chains with Thiol-Michael Click Chemistry** Yao Tang<sup>1</sup>, Nairiti Sinha<sup>1</sup>, Rui Guo<sup>2</sup>, Jeffery G. Saven<sup>2</sup>, Christopher Kloxin<sup>1</sup> and Darrin Pochan<sup>1</sup>; <sup>1</sup>University of Delaware, United States; <sup>2</sup>University of Pennsylvania, United States

With the help of computational design, a series of peptides with a length of 29 amino acids were designed to be self-assembled into stable, tetrahedral, anti-parallel coiled coil peptide bundles with net charges ranging from 0 to +32. In this research, +4 charged peptides (leading to +16 charged coiled coil bundles) are synthesized via solid phase peptide synthesis (SPPS) with the N-termini of single peptides modified with cysteine or a non-natural maleimide. These peptides are self-assembled into 4 x 2nm cylindrical peptide bundles by non-covalent interactions and subsequently conjugated via Thiol-Michael 'click' chemistry to form coiled coil peptide bundle chains with extreme rigidity. Transmission electron microscopy (TEM) and circular dichroism (CD) spectroscopy are applied to investigate the effect of temperature, pH and solvent composition on the structure of coiled coil bundle chains. Polarized optical microscopy (POM) is applied to study the liquid crystalline behavior of conjugated peptide bundle chains. Small-angle X-ray scattering (SAXS) and small-angle neutron scattering (SANS) are utilized to characterize the size and structure of formed coiled coil peptide bundle chains. The effect of salt and pH on the solution behavior of the positively charged coiled coil chains will be also discussed. The self-assembled peptide bundles can be further used as building blocks to construct new 1-D and 2-D nanomaterials.

#### **F.SM01.09.13**

**Dialdehyde Cellulose and Cationic Dialdehyde Cellulose from Bamboo for Dyes Adsorption and Separation** Xiangyu Huang, Hongbin Zhuo, Pejman Hadi and Benjamin S. Hsiao; Stony Brook University, United States

In this study, bamboo-achieved cellulose is functionalized and upcycled into efficient, low-cost and environmental-friendly bio-adsorbents for dye adsorption and separation. Dialdehyde cellulose (DAC) was prepared through the chemical oxidation on cellulose surface via sodium periodate oxidation. Then, cationic Girard's reagent T (GT) was covalently crosslinked onto the backbone of cellulose molecules via the Schiff's base reaction between the amino groups of GT and the aldehyde groups on the DAC to form the cationic aldehyde cellulose (cDAC). The chemical structure and morphology of two bio-adsorbents were characterized. The adsorption behaviors of the functionalized DAC and cDAC possessed different available active sites (including aldehyde groups and quaternary ammonium cations) towards various dyes in the aqueous solution were investigated systematically. The effects of dye concentration, contact time and pH environment in the adsorption of the anionic Congo red (CR) and cationic Bismarck brown Y (BBY) were studied. The results showed that DAC could adsorb BBY more effectively while cDAC has a much higher adsorption capacity towards CR, this is due to the adsorption was dominated by both the static electric force and the chemical reaction between dyes and adsorbents. The adsorption process was found to happen promptly (within the first 10 minutes) and follow the pseudo-second-order model. Both DAC and cDAC were proved to exhibit great adsorption behaviors under a wide pH range. Furthermore, the adsorption performance of six different dyes onto DAC and cDAC were studied, separately. Their adsorption capacities varied significantly on CR, BBY, Brilliant cresyl blue (BCB), Acid green 25 (AG25), Acid brown M (ABM) and Alizarin red S (ARS), indicating the DAC and cDAC could adsorb dyes from aqueous system selectively owing to the different reactivity between dyes and the adsorbents' active sites. Based on the selective adsorption behavior towards different dyes, DAC and cDAC were proved to possess strong abilities for separating dye mixtures, such as: BBY-ARS, AG25-CR and BCB-CR.

#### **F.SM01.09.14**

**A Composite Superhydrophobic Bio-Membrane from Hydrophilic Biomass for Desalination via Membrane Distillation** Ritika Joshi<sup>1</sup>, Jackie Zheng<sup>1</sup>, Tom Lindstrom<sup>1,2</sup> and Benjamin Hsiao<sup>1</sup>; <sup>1</sup>Stony Brook University, United States; <sup>2</sup>Royal Institute of Technology, Sweden

Over 2 billion people live in countries experiencing high water stress (UN, 2018) and water crisis has become one of the biggest challenges for the world. Current desalination techniques necessitate complex infrastructure and high operating pressures, making them impractical in poor and technologically underdeveloped regions. Membrane distillation (MD) is an emerging water purification technique capable of purifying highly saline or contaminated water, which can help to alleviate water stress especially for the off-grid community. It is a thermally driven separation process employing a porous hydrophobic membrane which allows the passage of vapor molecules only. Currently used polymeric membranes in water filtration techniques have a large carbon footprint which makes it imperative to find an environmental and sustainable solution without compromising performance. In this study, a composite porous nanostructured cellulose based membrane was fabricated using carboxymethylated fibers (obtained from wood and non-wood plants like jute). The top barrier layer in this composite membrane is hydrophobic (mimicking lotus leaf) which prevents liquid penetration followed by a hydrophilic layer. The carboxymethylated cellulose fibers were cross-linked with wet strength additives to improve wet-integrity and water retention properties. The hydrophobic layer was developed by introducing micro-scale roughness using minerals like precipitated calcium carbonate followed by sizing with dimer giving high contact angle exceeding  $140^\circ$  to prevent wetting of the membrane. The porosity of the entire membrane is in the range of 70-80%. Different characterization techniques like infra-red spectroscopy, solid state NMR, scanning electron microscopy, thermo-gravimetric analysis, and contact angle were used to study membrane properties. The performance of composite membrane was evaluated using a laboratory scale direct contact membrane distillation (DCMD) system. Water flux and salt rejection were tested under a set of feed water temperatures ranging between 40-60°C keeping the permeate water temperature same at 20°C. Moreover, the fabricated cellulosic membrane exhibited a comparable performance to that of commercial hydrophobic PTFE membranes.

#### **F.SM01.09.15**

**Effect of Net Charge on Solution Structures of Polymerized Peptide Coiled-Coil ‘Bundlemers’** Yi Shi<sup>1</sup>, Rui Guo<sup>2</sup>, Jacquelyn Blum<sup>2</sup>, Jeffery G. Saven<sup>2</sup>, Christopher Kloxin<sup>1</sup> and Darrin Pochan<sup>1</sup>; <sup>1</sup>University of Delaware, United States; <sup>2</sup>University of Pennsylvania, United States

De Novo design of peptides for assembly into targeted nanostructure is being explored extensively in the self-assembly community with the help of computational methods. Various peptide structures and solution assembly behaviors have been achieved by computational design of the peptide molecule sequences. Previous work of our collaborative group has demonstrated that computationally designed anti-parallel, homotetrameric coiled-coil, or ‘bundlemers’, with N-terminal modifications can form nanomaterials ranging from 2-D materials with desired inter-bundle symmetry to polymer chain rigid rods via thiol-Michael reaction. In the case of concentrated rod solutions, birefringence was observed in concentrated rigid rod solutions which proved the presence of liquid crystal phases. In this current work, further study into controlling solution behavior of peptide rods was conducted with newly designed peptide sequences. Solution structure of highly net-charged bundlemers (-16 through -24 at pH 7) and bundlemers with parallel packing of constituent peptides were verified experimentally. Preliminary studies on liquid crystal behavior of rigid rods was investigated with these highly charged sequences due to their exterior charge repulsion, which can be controlled by ionic strength of solution and pH. Furthermore, semiflexible chains formed by conjugating coiled-coil and tetra-functional organic linkers as characterized via transmission electron microscopy and cryo-TEM. The semiflexible chains are expected to provide opportunities to achieve structures that resembles biological molecules.

#### **F.SM01.09.16**

**Interfacial Assembly of Bundlemers** Matthew Langenstein<sup>1</sup>, Rajkumar Misra<sup>1</sup>, Rui Guo<sup>2</sup>, Jeffery G. Saven<sup>2</sup>, Christopher Kloxin<sup>1</sup> and Darrin Pochan<sup>1</sup>; <sup>1</sup>University of Delaware, United States; <sup>2</sup>University of Pennsylvania, United States

Bundlemers are a series of computationally designed peptides that form monodisperse cylindrical particles through aqueous self-assembly into antiparallel homotetrameric coiled coils. Due to their robust coiled-coil-forming motif these peptidic colloids have extremely tunable surface chemistry mostly independent from their structure. Using this tunability, we have previously developed bundlemers that form predesigned 2D lattices, nanocages, and nanofibers through tailoring their surface chemistry and solution assembly conditions. Recently, we have used bundlemers as macromonomers to create stiff and extremely high aspect ratio supramolecular polymers through covalent chemistry between the neighboring bundlemer ends. As the library of bundlemers continues to grow, it is important to develop applications and processing methods to grow useful, disparate nanostructures out of these versatile building blocks. Drawing inspiration from carbon nanotubes, bundlemer brush nanoforests present an interesting potential nanostructure for the tuning of surface properties and the interaction of designed interfaces. By first templating a surface through the directed self-assembly of bundlemers onto a flat planar substrate, it should be possible to grow thin films of highly aligned supramolecular bundlemers brushes with tunable surface chemistry and packing structure. Ongoing work on the formation of the template layer has shown a dependence between deposition kinetics and electrostatic interactions between bundlemers. This presentation will overview the



characterization of bundlemer monolayers on a flat planar gold substrate as well as the impact of pH, ionic strength, and bundlemer surface charge on deposition kinetics through the use of atomic force microscopy, infrared reflection adsorption spectroscopy (IRRAS) and quartz crystal microgravimetry with dissipation monitoring (QCM-D).

#### **F.SM01.09.17**

**PEEU Fiber Mesh Elasticity and Its Regulatory Effects on Human Endothelial Cells** Xianlei Sun, Wingtai Tung, Weiwei Wang, Yue Liu, Jie Zou, Karl Kratz, Nan Ma and Andreas Lendlein; Institute of Biomaterial Science and Berlin-Brandenburg Centre for Regenerative Therapies, Helmholtz-Zentrum Geesthacht, Germany

Electrospinning technique enables the transformation of polymers into functional fiber/mesh architectures, with the comparable length scales to the native extracellular matrix<sup>1</sup>. Given the significant variation in local elastic properties of micro/nano fibers caused by the highly intersected and suspended architecture<sup>2</sup>, here we elucidated the correlation of the local mechanical properties of a fiber meshwork to its microscale network architecture, and investigated the influence of fiber mesh elasticity on the behavior of human umbilical vein endothelial cells (HUVECs).

The multiblock copolymers polyesteretherurethane (PEEU), containing poly( $\epsilon$ -caprolactone) (PCL) and poly(*p*-dioxanone) (PPDO) segments with different ratios (40-70wt% PPDO) were used to prepare the fiber meshes via electrospinning technique. The fiber diameter was not remarkably influenced by the copolymer composition, with the diameter below 2  $\mu$ m in all groups. The E-modulus of the fiber mesh at a dry state increased with the increase of PPDO percentage, according to the tensile tests. The three-point bending tests using an atomic force microscope (AFM) revealed a correlation between the local stiffness of a specific point on a single fiber and its position. HUVECs cultured on stiffer fiber meshes presented elongated F-actin filaments and spindle morphology, in comparison with their softer counterparts. The fiber mesh elasticity did not affect the initial HUVEC attachment, and a faster cell proliferation rate of HUVEC was shown on stiffer fibers. HUVEC pre-cultured on stiffer fiber meshes presented a faster migration velocity and an increased tube formation capacity than those from softer fibers, indicating a higher angiogenesis potential.

In summary, the functionality of HUVEC can be strongly regulated by the elasticity of fiber meshes. Mechanical characterization of the fibers at different scales, e.g. AFM for microscale in combination with tensile test for macroscale, could deepen our understanding on the cellular mechanosensing process and enable more meaningful substrate design towards favorable cell function.

#### **Reference**

1. Theocharis, A. D.; Skandalis, S. S.; Gialeli, C.; Karamanos, N. K., Extracellular matrix structure. *Adv Drug Deliver Rev* **2016**, *97*, 4-27.
2. Cronin-Golomb, M.; Sahin, O., High-resolution nanomechanical analysis of suspended electrospun silk fibers with the torsional harmonic atomic force microscope. *Beilstein J Nanotech* **2013**, *4*, 243-248.

#### **F.SM01.09.18**

**Bioinspired Novel-Tip-Shaped Micropillar Arrays for Selective Liquid Sliding Surfaces** Seongmin Kang, Ji Seong Choi and Joon Hyung An; Chungnam National University, Korea (the Republic of)

Recently, superomniphobic (meaning highly water and oil-repellent) surfaces have been extensively studied both theoretically and experimentally in the materials community with several remarkable findings. Considering a notable process towards springtail-inspired omniphobic surfaces, however, a robust liquid repelling surface that is capable of inducing a selective liquid sliding property has been rarely reported, which would have many potential applications in microfluidics, mobile market, electronic devices and precision industry. Here, we present for the first time a selective liquid sliding surface using a springtail-inspired mushroom-like re-entrant structure with a novel geometry of concave tip. By implementing a simple yet sturdy silicon fabrication and lithography method, the fabricated micropillar arrays displayed high structural fidelity. We investigated a design rule for the cap of the proposed structures, which resulted in not only superomniphobicity but also a selective liquid sliding property with DI water and mineral oil. We believe that our study makes a significant contribution to the literature because it proposes a novel springtail-inspired mushroom-like re-entrant structure that can induce a selective liquid sliding property between water and oil, which has not been accomplished before.

#### **F.SM01.09.19**

**Improving Control of Inverse Opal Surface Chemistry and Interactions with Fluids** Natalie Nicolas; Harvard University, United States

Inverse opal photonic crystals are bioinspired structurally colored porous materials that have been utilized in many applications including sensing, catalysis, and microfluidics. By modifying the surface chemistry and geometry of inverse opal pores to improve control over surface-fluid interactions in these materials, we can achieve highly localized effects and

dynamically alter the wetting point of inverse opal films. Several strategies were used to fine-tune the behavior of the inverse opal. The pore size and pore neck angle, which determine the threshold contact angle for fluid infiltration, were adjusted by atomic layer deposition. This technique provides sub-nanometer control of the pore radius and can be used in conjunction with surface chemical modification to change the wetting point of an inverse opal film. The surface chemistry of the pore, which controls the contact angle that a fluid forms with the surface, was patterned with multiple silanes. By taking advantage of the inherent disorder in self-assembled monolayers at features with a small radius of curvature, such as pore necks, controlled local patterns in surface chemistry were produced. For dynamic modulation of the contact angle, photoswitchable spiropyran and azobenzene molecules were attached to the pore surface. These molecules reversibly altered the hydrophobicity of the surface when their conformation was changed by exposure to ultraviolet or visible light. By understanding how pore geometry and surface chemistry contribute to the static and dynamic behavior of inverse opals and their interactions with fluids, we can more effectively utilize these structured materials.

#### **F.SM01.09.24**

**Late News: Investigation on the Partitioned Multilayers of the Wing Scale of *Papilio maackii* for Nature-Inspired Structural Coloration** Seungmuk Ji<sup>1</sup>, Deok-Jin Jeon<sup>1</sup>, Jihun Kang<sup>1</sup>, Seunghwan Moon<sup>1</sup>, Eunok Lee<sup>2</sup>, Jinhee Kim<sup>2</sup> and Jong-Souk Yeo<sup>1</sup>; <sup>1</sup>Yonsei University, Korea (the Republic of); <sup>2</sup>National Institute of Ecology, Korea (the Republic of)

Butterflies present a variety of brilliant colors on their wings based on pointillism. Pointillism is well-known drawing technique, however, to express colors, butterflies use very unique and diverse nanostructures such as tree-like multilayered ridges, chitin-air multilayers, photonic crystals, etc. Through investigating these photonic structures, we are able to come up with effective engineering strategies to produce vivid, durable, and eco-friendly colors. *Papilio maackii*, the alpine black swallowtail, is a butterfly that uses air-chitin partitioned multilayers to exhibit a blueish-green like color on its wing. Since it has scales that show various colors between blue to green, it has the advantage of studying how to control structural colors using multilayered structures.

In this work, we investigate the structural coloration of the wing scale of *Papilio maackii* according to its nanoscale multilayered. The color of the wing scales changes from blue to green, depending on the thickness of the chitin and air layer. We demonstrate by using finite difference time domain (FDTD) simulations that the chitin partitions in air-chitin mixed layers regulate the effective refractive index to improve the color contrast with low background intensities. Cross-sectional TEM investigations show that the thickness of the air-chitin mixed layers varies gradually, and when this gradual change is reflected in the simulation, it shows a more similar reflectance spectrum with that of the experimentally measured. We identify the presence of melanin on the colored scales, which is a light-absorbing pigment, by measuring Raman spectroscopy. FDTD simulations show that melanin can contribute to the intensity of the reflectance spectrum in the region of long wavelength. In order to realize the structural colors based on the partitioned multilayers, we use a method to coat polymeric nanoparticles and sol-gel glass thin films repeatedly. By using this method, the effects of inhomogeneity and volume fraction of air voids in the multilayered structure are experimentally examined.

This research was supported by National Research Foundation (NRF) grant funded by the Ministry of Education, under “Basic Science Research Program” (NRF-2017R1D1A1B04033182) and also supported by Research Program through the National Institute of Ecology (NIE-Basic Research-2020-18).

#### **F.SM01.09.20**

**Magnetic Field Alignment of Chitin Nanocrystals Confined to a Polymer Microgel** Sujin Rebecca Lee, Elsa Reichmanis, Jung O Park and Mohan Srinivasarao; Georgia Institute of Technology, United States

It is well documented that twist axis of cellulosic fiber aligns parallel to applied magnetic field. In here, we showed change in orientation of bio-derived cholesteric phase confined to microgel using low magnetic fields (0.5 – 1.2 T). As equilibrated on commercial magnet, droplets of chitin nanocrystal and superparamagnetic nanoparticles mixture possessed homeotropic anchoring and light induced polymerization of the monomer in droplets captured the phase into microgels. The helix orientation directly affected the texture of microgels under polarized optical microscopy. The exhibited structures of microgel were nested cup configuration of lamellar planes or bipolar structure even in the high chirality regime. Moreover, the microgels are responsive to temperature, as we used N-isopropyl acrylamide as a monomer. With temperature change we could observe swelling and de-swelling of nested cup structure which allowed us to understand the structure with more information. These findings give fundamental understanding bio-derived cholesteric materials and their self-assembly under confinement. Methodology for embedding twisted structure in polymer with bottom-up fabrication will give guideline for designing and controlling multifunctional nature-inspired programmable devices or materials with sustainable use of our resources.

#### F.SM01.09.22

**Late News: Biomimetic Moth-Eye Nanostructure with Improved Optical Properties and Facilitated Application to Optical Devices** Jiseong Choi, Joon Hyung An, Hyunjung Kim and Seongmin Kang; Chungnam National University, Korea (the Republic of)

Moth-eye inspired structure (MIS) has been regarded as important technology to enhance efficiency of optical device in biomimetic field. Since the nanostructures of the moth-eye surface gradually changed the refractive index from the air to devices, the MIS improved the optical properties of transmittance and reflectance. Despite these developments, film-based structures were difficult to apply and surface coating might damage to the surface of optical device during additional processes. Therefore, we fabricated three different sizes of MIS, 300 nm, 500 nm and 1000 nm, followed by optimizing materials and nanostructure size supported through two theoretical phenomena which are diffraction grating equation and double-slit effect. Then, optical devices were packaged by attaching polymer-based MIS without any treating and processing. As a result, the freestanding MIS composed of PDMS were identified to enhanced optical properties with over 94% transmittance and below 3.5% reflectance, compared to the MIS composed of PUA with substrate of PET film. In addition, PDMS-MIS attached to cell phone and ITO glass, which was used as substrate of optical devices, was proved that optical devices facilitated packaging as well as enhanced optical properties.

#### F.SM01.09.25

**Late News: Silk-Like Structure of Freshwater Mussel Byssus Fabricated via Shear-Induced Alpha to Beta Transition of Intermediate Filament-Like Precursors** Miriam Simmons and Matthew J. Harrington; McGill University, Canada

Freshwater invasive mussel species *Dreissena polymorpha* (zebra mussels) adhere themselves in underwater environments with a collection of protein-based fibers known as a byssus. The byssus of the zebra mussel is stronger, stiffer and faster to recover after deformation than those of the well-characterized marine mussels, but very little is known of its structure or composition. Here, we used a combination of Raman, FTIR and wide angle x-ray diffraction to elucidate the secondary structure of fresh and induced byssal fibres. Our data indicates that the secreted fibers are comprised of a mixture of parallel  $\beta$ -crystallites, similar to spider silk. Furthermore, investigation of the byssus biofabrication process indicates that the precursor proteins are stored in an  $\alpha$ -helical structure and transition from an  $\alpha$ -helix to  $\beta$ -sheet secondary structure during the formation process, similar to other structural proteins like intermediate filaments and keratin. This stress-induced transformation in secondary structure is being attributed to a coiled-coil protein predicted in the mussel transcriptome, and current efforts are aimed at extracting this protein to further understand its shear-induced phase transformation.

SESSION F.LP04.04: Live Poster Session: Soft Materials and Biomaterials (F.SM01, F.SM02 and F.SM03)

Session Chairs: Shaoting Lin and Yanxian Zhang

Wednesday Afternoon, December 2, 2020

7:30 PM - 9:30 PM

F.SM01

#### F.SM01.09.01

**Removal of Rare Earth Metal Ions from Contaminated Water by Sustainable Carboxycellulose Nanofibers Derived from Agave Through Nitro Oxidation Process** Isha Brahmhatt<sup>1,2</sup>, Sunil Sharma<sup>1</sup>, Priyanka Sharma<sup>1</sup>, Marc Nolan<sup>1</sup> and Benjamin Hsiao<sup>1</sup>; <sup>1</sup>Stony Brook University, The State University of New York, United States; <sup>2</sup>Ardley High School, United States

There is a growing need for rare earth metal ions such as lanthanides for use in electronics, fuel cells, and various other applications. These precious ions are currently derived by mining, causing major pollution and contamination in nearby water sources. As cellulose is the most abundant organic material, we derived carboxycellulose nanofibers from raw agave biomass using the simple nitro oxidation process for the removal of lanthanide ions. The nitro oxidation method converts untreated biomass to carboxycellulose nanofibers in a one step process using nitric acid and sodium nitrite. Zeta potential indicates that the fibers are highly electronegative (zeta potential -117.3 mV), and the conductometric titration method reveals that the fibers have a high carboxylate content (0.75 mmol/g). SEM measurements show that the fibers contain clearly visible fibrous

structures. The TEM measurements of the fibers record fiber lengths of 55-690 nm and average fiber widths of 5-6 nm, and AFM data displayed an average thickness of 1.6 nm. The oxidation of the agave nanofibers was confirmed with  $^{13}\text{C}$  CPMAS NMR data. The lower crystallinity of the agave nitro oxidized carboxycellulose nanofibers compared to raw agave was determined by WAXD. The nitro oxidation approach also offers beneficial reductions in the consumption of water and electric energy as well as the need for multi-chemicals when compared with conventional multiple-step processes at bench scale (e.g. TEMPO oxidation). Remediation studies on lanthanide ions showed a floc formation between the ions and nanofibers. The Langmuir isotherm generated from ICP-MS studies indicated a 285.7 mg/g adsorption capacity and over a 90% adsorption efficiency for all lanthanide concentrations, which supersedes current water purification mechanisms such as iron oxide beads (123.6 mg/g adsorption capacity). These results suggest that the agave nitro oxidized carboxycellulose nanofibers are effective for the removal of lanthanide ions for drinking water purification and lanthanide ion industry.

#### **F.SM01.09.02**

**Tremendously Enhancing Photodegradation Efficiency by Biomorphic Porous Carbon** Weizhao Huang and Hui Mei; Northwestern Polytechnical University, China

Traditional lab-based synthesis of photocatalyst are ineligible for urgent demand of exceptional recyclability and stability in industrially large-scale application resulting from the inevitably undergo agglomeration of powder-form catalysts. Immobilizing catalyst is an appealing strategy to obtain enhanced performance for solid support provides chemical, thermal, and mechanical stabilization to the catalytic species besides facilitating catalyst recovery. Carbonaceous materials with unique microstructure obtained by pyrolyzing renewable and environment-friendly nature plants have promising applications in areas such as battery and catalyst support. However, unexpected cracks accompanied by low oxidation resistance retard further development. In this study, a thin SiC coating for strengthening purpose was in-situ deposited on biomorphic porous carbon materials fabricated by pyrolyzing wood while maintaining low density. Continuously ordered microchannel structures from carbonized nature wood with a diameter of ca. 20  $\mu\text{m}$  was completely replicated after depositing SiC coating, resulting in the good anisotropy in mechanical and thermal properties. The thin SiC coating was found to greatly increase compressive strength from 26.4 to 47.4 MPa and thermal conductivity from 0.49 to 14.94 W/m K in the axial direction with improved oxidation resistance of weight loss from 78.5% to 1.51%. In the radial direction, however, the increase of the two properties was lower due to the longitudinal microchannel structure. Feasibility of the biomorphic carbon serving as catalyst support with highly developed continuous channels was evaluated by loading typical molybdenum disulfide ( $\text{MoS}_2$ ). Result shows a significant improvement in both adsorption and photodegradation efficiency against the pure  $\text{MoS}_2$ , which is because of the enlarged specific surface area of the catalyst.

#### **F.SM01.09.05**

**Bioinspired Design of Polymers for Protein Binding and Aggregation Modification** Sarah E. Morgan<sup>1</sup>, Ashleigh N. Bristol<sup>1</sup>, Lisa K. Kemp<sup>1</sup>, Shahid Karim<sup>2</sup> and Vijay Rangachari<sup>2</sup>; <sup>1</sup>The University of Southern Mississippi, United States; <sup>2</sup>University of Southern Mississippi, United States

Abnormal protein behaviors, such as aggregation or mislabeling as antigens, are involved in a range of disorders including Alzheimer's, Parkinson's, and celiac disease. Water-soluble polymers with functional motifs mimicking those in naturally occurring polymers provide an avenue to interrogate binding and assembly processes and can be designed to modify protein behavior. RAFT polymerization was employed for the synthesis of two different families of polymers, designed for the study of two different protein systems, to produce polymers with desired structures, targeted molecular weight, and low dispersity. Aggregation processes were evaluated with dynamic light scattering, GPC-MALLS, and fluorescence assays. FTIR and NMR were employed to determine hydrogen bonding patterns of the systems. Gliadin, a component of gluten and a known epitope, is implicated in celiac disease (CeD) and results in an inflammatory response in CeD patients when consumed. Stimuli-responsive polyelectrolytes with varying charged groups were employed as models to determine the effect of molecular weight and pendent group on non-covalent interaction modes with gliadin in vitro. The polymers exhibited pH dependent binding and alteration of gliadin secondary structure, providing a platform for therapeutic design of specific structure/binding interactions with food proteins. Glycopolymers with stereospecific pendent groups designed to mimic saccharide clusters in the GM1 ganglioside were prepared to analyze interactions with the amyloid  $\beta$  peptide associated with Alzheimer's disease. The A $\beta$ 42 assembly process was directly impacted by the stereochemistry of the pendent saccharide. Glycopolymer-silicone hydrogels prepared with varying hydrophobic/hydrophilic content and copolymer composition showed structure dependence of diffusion, rheology, and nanomechanical properties. These findings demonstrate the potential for design of selective glycopolymers for targeted molecular interactions for biomedical and personal care applications.

#### **F.SM01.09.06**

**Living Sorbents for Arsenic-Contaminated Drinking Water Remediation** Yidan Bi and Vicki L. Colvin; Brown University, United States

Arsenic is a pervasive contaminant in drinking water, and it has ranked the first on the Substance Priority List of Agency for Toxic Substances and Disease Registry (ATSDR) for more than two decades. Exposure to low-level arsenic in early life impairs children's cognitive development and buries the risk of developing a variety of cancers in young adulthood. To prevent the severe health effect of arsenic ingestion, materials with high arsenic removal capacity and fast treatment speed have been investigated. While these strategies are efficient for As(V), they are rendered ineffective when encountering the less abundant yet more toxic As(III), especially in the presence of competing ions. Solutions such as pretreatment or extensive removal of competing ions along with arsenic dramatically increase the operation cost and unnecessarily eliminate other benign species from water. Thus, there is a need for developing materials that can precisely capture arsenic from drinking water or even more complex beverage matrices and reduce the arsenic level below the EPA regulation (10 ppb) without altering the water chemistry.

In this work, we looked beyond the conventional physicochemical water treatment strategies and acquired insights from natural arsenic detoxification processes. The toxicity of As(III) originates from its high affinity to the cysteine residues in proteins. Natural organisms resolve this issue by expressing cysteine-rich peptides or proteins that can sequester As(III) in the cells. Inspired by this mechanism, we engineered a benign strain of *E. coli* to overexpress fusion proteins containing the binding pockets of two arsenic-binding proteins, ArsR and AfArsR, for improved arsenic scavenging competency. We also applied molecular biology tools to enhance the arsenic sorption capacity and accelerate the removal speed. One gram of these living sorbents can stoichiometrically immobilize milligrams of arsenic within a few hours. The high affinity of the proteins toward the substrate overcomes the selectivity barrier of inorganic sorbents like Bayoxide. For example, the living sorbents can bioaccumulate low levels of arsenic against common interfering species like phosphate, silicate, and natural organic matters, and the trapped As(III) does not leak to the water under these complicated conditions. In addition to remediating intractable matrices such as NSF challenge water, we found these living sorbents are adaptive to beverages including juice and wine, which were reported that are contaminated with arsenic but are not tightly regulated. Moreover, unlike the cumbersome inorganic material transportation, we propose that these living sorbents can be regenerated on-site after shipping the "seed material". We explored freeze-drying the biosorbents for storage and demonstrated that the reconstituted sorbents maintained arsenic-binding ability. To prevent secondary contamination after remediation, we explored tagging the bacterial cells with magnetic nanoparticles and found that the bacteria can be removed with a handhold magnet within a few minutes. This work provides the potential of applying renewable living sorbents for selective drinking water contaminant removal, and it is beneficial for the rural households and small communities who do not have access to the expensive and energy-consuming arsenic treatment technologies.

#### **F.S7M01.09.0**

**Strategic Design of Advanced Bioinspired and Biomimetic Membranes Conjugated with Graphene Oxide for Selective Ion Rejection** Sanju Gupta<sup>1,2</sup>; <sup>1</sup>CCNY-CUNY, United States; <sup>2</sup>Western Kentucky University, United States

Recent advances in synthetic membranes allow their use in fields as diverse as food and agriculture, industrial water treatment, potable water production, and bio-separation. Among the newly developed technologies, nanofiltration for liquids and more particularly for desalination of seawater or saline aquifers is the most recent one. However, limitations of current polymeric membranes call for the development of novel formulations that offer both high permeability (water flux) and ion differentiation (selectivity) usually considered antagonist features. We report the fabrication of membranes prepared from track-etched polymeric membranes as supports in which biological ion channels such as Gramicidin A, alpha-hemolysin are confined and ion-selective binding peptide motifs conjugated with graphene oxide as nanoporous hybrids. These bioinspired and biomimetic membranes are attracting widespread attention offering advantages including mechanical robustness, controlled pore dimension, and shape, modifiable surfaces for the desired efficiency. The permeability and selective ion transport are evaluated by ion diffusion kinetics, UV-Visible absorption spectroscopy, and nanofiltration while gaining insights into the role of key parameters including track-etch pore size, surface chemistry, and ion binding through solid-state nanopores or nanochannels. The proposed activity positively impacts the environment by integrating eco-friendly materials design, development, and deployment.

#### **F.SM01.09.09**

**Biomimetic Musculoskeletal Polymer Nanocomposites for Magnetic Collective Swimming** Sukyoung Won, Hee Eun Lee, Young Shik Cho, Seung Jae Yang and Jeong Jae Wie; Inha University, Korea (the Republic of)

In human musculoskeletal system, skeletal muscles attached to spongy bones play an essential role in exerting quick and

powerful movement. Herein, we present a musculoskeletal design capable of agile magnetomotility of ternary polymeric nanocomposites. Inspired by protein actin in skeletal muscle, iron particles are attached to surface of helical porous carbon nanotube yarn (CNTY) owing to polydimethylsiloxane (PDMS) elastomer providing a fascia-like connective function. Under rotating 2D quadruple electromagnetic field, soft robots achieved agile rectangular orbital magnetomotility reaching up to 162 body length per second. Upon varying the frequency of the rotating magnetic field, the individual rectangular orbit of multiple soft robots is reconfigured into magnetic-assembled circular orbits. We will discuss magnetic swimming of collectively assembled soft robots that can manipulate vortex chirality of sustaining fluid.

#### F.SM01.09.10

**Construction of Hybrid Soft Nanomaterials Composed of Supramolecular Nanostructures of DNA and Peptide Derivatives** Sayuri Higashi<sup>1</sup>, Aya Shibata<sup>1</sup>, Yoshiaki Kitamura<sup>1</sup>, Koichiro M. Hirose<sup>1</sup>, Kenichi G. Suzuki<sup>1</sup>, Kazunori Matsuura<sup>2,2</sup> and Masato Ikeda<sup>1,1,1</sup>; <sup>1</sup>Gifu University, Japan; <sup>2</sup>Tottori University, Japan

Under multi-component molecular conditions such as inside of living cells, fibrous proteins including actin filaments and microtubules are constructed based on orthogonal (self-sorted) self-assembling. Self-sorting enables plural supramolecular nanostructures to retain each property and function as well as their structures even under complex conditions. In artificial systems, construction of complex and discrete soft nanomaterials has received increasing attention in recent years, and only several self-sorting pairs of synthetic self-assembling (small) molecules and peptides have been reported. Meanwhile, the high-fidelity recognition based on Watson-Crick base pairing and programmable sequences of DNAs allows a variety of DNA nanostructures with controlled sizes and shapes to be constructed, and hybrid nanomaterials composed of DNA nanostructures have been pursued for a wide range of applications (*e.g.*, nanopores, scaffolds for catalytic reaction and protein assembly). However, much of these hybrid nanomaterials have been constructed based on co-assembly, and the orthogonal coexistence of DNA nanostructures with supramolecular nanostructures obtained by self-sorting with synthetic molecules has yet to be explored in detail.

To develop the hybrid nanomaterials composed of DNA nanostructures based on self-sorting phenomenon, we focused on nucleic acids and peptide derivatives as the component molecular pair. We recently constructed hybrid soft nanomaterials composed of DNA microspheres<sup>1</sup>, which can be obtained from three short single-stranded DNAs, and three different supramolecular nanostructures of semi-artificial glycopeptides<sup>2</sup> (helical nanofibers, straight nanoribbons, and flowerlike microaggregates) in single medium by a simple thermal annealing process.<sup>3</sup> Interestingly, both of supramolecular nanostructures exist orthogonally with only marginal impact on their morphology in single medium as a supramolecular hydrogel state. Noteworthy, to observe such self-sorted supramolecular nanostructures by fluorescence imaging, additional fluorochrome-labeled probes are required to synthesize. However, in this research, we have achieved the selective visualization of each supramolecular nanostructure by means of rational staining method focused on each selective molecular-recognition property of DNAs and glycopeptides (*e.g.*, intercalating agent, lectins, and saccharide-binding DNA aptamer) without additional probe developments. Furthermore, we have demonstrated the sequence-controlled degradation of the individual supramolecular nanostructures in response to distinctive bio-stimuli (*i.e.*, enzyme and ssDNA), rendering these soft nanomaterials active against such stimuli. In this presentation, I would like to discuss the detail of these newly developed hybrid soft nanomaterials and underlying mechanism to form such unique superstructures and functions.

1. K. Matsuura, T. Yamashita, Y. Igami and N. Kimizuka, *Chem. Commun.* **2003**, 376–377.

2. T. Tsuzuki, M. Kabumoto, H. Arakawa and M. Ikeda, *Org. Biomol. Chem.*, **2017**, 15, 4595–4600.

3. S. L. Higashi, A. Shibata, Y. Kitamura, K. G. N. Suzuki, K. Matsuura and M. Ikeda, *Chem. Eur. J.*, **2019**, 25, 11955–11962.

#### F.SM01.09.11

**Self-Assembly of Positively Charged Computationally Designed Coiled Coil Peptide 'Bundlemer' Chains with Thiol-Michael Click Chemistry** Yao Tang<sup>1</sup>, Nairiti Sinha<sup>1</sup>, Rui Guo<sup>2</sup>, Jeffery G. Saven<sup>2</sup>, Christopher Kloxin<sup>1</sup> and Darrin Pochan<sup>1</sup>; <sup>1</sup>University of Delaware, United States; <sup>2</sup>University of Pennsylvania, United States

With the help of computational design, a series of peptides with a length of 29 amino acids were designed to be self-assembled into stable, tetrahelical, anti-parallel coiled coil peptide bundles with net charges ranging from 0 to +32. In this research, +4 charged peptides (leading to +16 charged coiled coil bundles) are synthesized via solid phase peptide synthesis (SPPS) with the N-termini of single peptides modified with cysteine or a non-natural maleimide. These peptides are self-assembled into 4 x 2nm cylindrical peptide bundles by non-covalent interactions and subsequently conjugated via Thiol-Michael 'click' chemistry to form coiled coil peptide bundle chains with extreme rigidity. Transmission electron microscopy (TEM) and circular dichroism (CD) spectroscopy are applied to investigate the effect of temperature, pH and solvent composition on the structure of coiled coil bundle chains. Polarized optical microscopy (POM) is applied to study the liquid

crystalline behavior of conjugated peptide bundle chains. Small-angle X-ray scattering (SAXS) and small-angle neutron scattering (SANS) are utilized to characterize the size and structure of formed coiled coil peptide bundle chains. The effect of salt and pH on the solution behavior of the positively charged coiled coil chains will be also discussed. The self-assembled peptide bundles can be further used as building blocks to construct new 1-D and 2-D nanomaterials.

#### **F.SM01.09.13**

**Dialdehyde Cellulose and Cationic Dialdehyde Cellulose from Bamboo for Dyes Adsorption and Separation** Xiangyu Huang, Hongbin Zhuo, Pejman Hadi and Benjamin S. Hsiao; Stony Brook University, United States

In this study, bamboo-achieved cellulose is functionalized and upcycled into efficient, low-cost and environmental-friendly bio-adsorbents for dye adsorption and separation. Dialdehyde cellulose (DAC) was prepared through the chemical oxidation on cellulose surface via sodium periodate oxidation. Then, cationic Girard's reagent T (GT) was covalently crosslinked onto the backbone of cellulose molecules via the Schiff's base reaction between the amino groups of GT and the aldehyde groups on the DAC to form the cationic aldehyde cellulose (cDAC). The chemical structure and morphology of two bio-adsorbents were characterized. The adsorption behaviors of the functionalized DAC and cDAC possessed different available active sites (including aldehyde groups and quaternary ammonium cations) towards various dyes in the aqueous solution were investigated systematically. The effects of dye concentration, contact time and pH environment in the adsorption of the anionic Congo red (CR) and cationic Bismarck brown Y (BBY) were studied. The results showed that DAC could adsorb BBY more effectively while cDAC has a much higher adsorption capacity towards CR, this is due to the adsorption was dominated by both the static electric force and the chemical reaction between dyes and adsorbents. The adsorption process was found to happen promptly (within the first 10 minutes) and follow the pseudo-second-order model. Both DAC and cDAC were proved to exhibit great adsorption behaviors under a wide pH range. Furthermore, the adsorption performance of six different dyes onto DAC and cDAC were studied, separately. Their adsorption capacities varied significantly on CR, BBY, Brilliant cresyl blue (BCB), Acid green 25 (AG25), Acid brown M (ABM) and Alizarin red S (ARS), indicating the DAC and cDAC could adsorb dyes from aqueous system selectively owing to the different reactivity between dyes and the adsorbents' active sites. Based on the selective adsorption behavior towards different dyes, DAC and cDAC were proved to possess strong abilities for separating dye mixtures, such as: BBY-ARS, AG25-CR and BCB-CR.

#### **F.SM01.09.14**

**A Composite Superhydrophobic Bio-Membrane from Hydrophilic Biomass for Desalination via Membrane Distillation** Ritika Joshi<sup>1</sup>, Jackie Zheng<sup>1</sup>, Tom Lindstrom<sup>1,2</sup> and Benjamin Hsiao<sup>1</sup>; <sup>1</sup>Stony Brook University, United States; <sup>2</sup>Royal Institute of Technology, Sweden

Over 2 billion people live in countries experiencing high water stress (UN, 2018) and water crisis has become one of the biggest challenges for the world. Current desalination techniques necessitate complex infrastructure and high operating pressures, making them impractical in poor and technologically underdeveloped regions. Membrane distillation (MD) is an emerging water purification technique capable of purifying highly saline or contaminated water, which can help to alleviate water stress especially for the off-grid community. It is a thermally driven separation process employing a porous hydrophobic membrane which allows the passage of vapor molecules only. Currently used polymeric membranes in water filtration techniques have a large carbon footprint which makes it imperative to find an environmental and sustainable solution without compromising performance. In this study, a composite porous nanostructured cellulose based membrane was fabricated using carboxymethylated fibers (obtained from wood and non-wood plants like jute). The top barrier layer in this composite membrane is hydrophobic (mimicking lotus leaf) which prevents liquid penetration followed by a hydrophilic layer. The carboxymethylated cellulose fibers were cross-linked with wet strength additives to improve wet-integrity and water retention properties. The hydrophobic layer was developed by introducing micro-scale roughness using minerals like precipitated calcium carbonate followed by sizing with dimer giving high contact angle exceeding 140° to prevent wetting of the membrane. The porosity of the entire membrane is in the range of 70-80%. Different characterization techniques like infra-red spectroscopy, solid state NMR, scanning electron microscopy, thermo-gravimetric analysis, and contact angle were used to study membrane properties. The performance of composite membrane was evaluated using a laboratory scale direct contact membrane distillation (DCMD) system. Water flux and salt rejection were tested under a set of feed water temperatures ranging between 40-60°C keeping the permeate water temperature same at 20°C. Moreover, the fabricated cellulosic membrane exhibited a comparable performance to that of commercial hydrophobic PTFE membranes.

#### **F.SM01.09.15**

**Effect of Net Charge on Solution Structures of Polymerized Peptide Coiled-Coil 'Bundlers'** Yi Shi<sup>1</sup>, Rui Guo<sup>2</sup>, Jacquelyn Blum<sup>2</sup>, Jeffery G. Saven<sup>2</sup>, Christopher Kloxin<sup>1</sup> and Darrin Pochan<sup>1</sup>; <sup>1</sup>University of Delaware, United States; <sup>2</sup>University of Pennsylvania, United States

De Novo design of peptides for assembly into targeted nanostructure is being explored extensively in the self-assembly community with the help of computational methods. Various peptide structures and solution assembly behaviors have been achieved by computational design of the peptide molecule sequences. Previous work of our collaborative group has demonstrated that computationally designed anti-parallel, homotetrameric coiled-coil, or 'bundlers', with N-terminal modifications can form nanomaterials ranging from 2-D materials with desired inter-bundle symmetry to polymer chain rigid rods via thiol-Michael reaction. In the case of concentrated rod solutions, birefringence was observed in concentrated rigid rod solutions which proved the presence of liquid crystal phases. In this current work, further study into controlling solution behavior of peptide rods was conducted with newly designed peptide sequences. Solution structure of highly net-charged bundlers (-16 through -24 at pH 7) and bundlers with parallel packing of constituent peptides were verified experimentally. Preliminary studies on liquid crystal behavior of rigid rods was investigated with these highly charged sequences due to their exterior charge repulsion, which can be controlled by ionic strength of solution and pH. Furthermore, semiflexible chains formed by conjugating coiled-coil and tetra-functional organic linkers as characterized via transmission electron microscopy and cryo-TEM. The semiflexible chains are expected to provide opportunities to achieve structures that resembles biological molecules.

#### **F.SM01.09.16**

**Interfacial Assembly of Bundlers** Matthew Langenstein<sup>1</sup>, Rajkumar Misra<sup>1</sup>, Rui Guo<sup>2</sup>, Jeffery G. Saven<sup>2</sup>, Christopher Kloxin<sup>1</sup> and Darrin Pochan<sup>1</sup>; <sup>1</sup>University of Delaware, United States; <sup>2</sup>University of Pennsylvania, United States

Bundlers are a series of computationally designed peptides that form monodisperse cylindrical particles through aqueous self-assembly into antiparallel homotetrameric coiled coils. Due to their robust coiled-coil-forming motif these peptidic colloids have extremely tunable surface chemistry mostly independent from their structure. Using this tunability, we have previously developed bundlers that form predesigned 2D lattices, nanocages, and nanofibers through tailoring their surface chemistry and solution assembly conditions. Recently, we have used bundlers as macromonomers to create stiff and extremely high aspect ratio supramolecular polymers through covalent chemistry between the neighboring bundler ends. As the library of bundlers continues to grow, it is important to develop applications and processing methods to grow useful, disparate nanostructures out of these versatile building blocks. Drawing inspiration from carbon nanotubes, bundler brush nanoforests present an interesting potential nanostructure for the tuning of surface properties and the interaction of designed interfaces. By first templating a surface through the directed self-assembly of bundlers onto a flat planar substrate, it should be possible to grow thin films of highly aligned supramolecular bundler brushes with tunable surface chemistry and packing structure. Ongoing work on the formation of the template layer has shown a dependence between deposition kinetics and electrostatic interactions between bundlers. This presentation will overview the characterization of bundler monolayers on a flat planar gold substrate as well as the impact of pH, ionic strength, and bundler surface charge on deposition kinetics through the use of atomic force microscopy, infrared reflection adsorption spectroscopy (IRRAS) and quartz crystal microgravimetry with dissipation monitoring (QCM-D).

#### **F.SM01.09.17**

**PEEU Fiber Mesh Elasticity and Its Regulatory Effects on Human Endothelial Cells** Xianlei Sun, Wingtai Tung, Weiwei Wang, Yue Liu, Jie Zou, Karl Kratz, Nan Ma and Andreas Lendlein; Institute of Biomaterial Science and Berlin-Brandenburg Centre for Regenerative Therapies, Helmholtz-Zentrum Geesthacht, Germany

Electrospinning technique enables the transformation of polymers into functional fiber/mesh architectures, with the comparable length scales to the native extracellular matrix<sup>1</sup>. Given the significant variation in local elastic properties of micro/nano fibers caused by the highly intersected and suspended architecture<sup>2</sup>, here we elucidated the correlation of the local mechanical properties of a fiber meshwork to its microscale network architecture, and investigated the influence of fiber mesh elasticity on the behavior of human umbilical vein endothelial cells (HUVECs).

The multiblock copolymers polyesteretherurethane (PEEU), containing poly( $\epsilon$ -caprolactone) (PCL) and poly(*p*-dioxanone) (PPDO) segments with different ratios (40-70wt% PPDO) were used to prepare the fiber meshes via electrospinning technique. The fiber diameter was not remarkably influenced by the copolymer composition, with the diameter below 2  $\mu$ m in all groups. The E-modulus of the fiber mesh at a dry state increased with the increase of PPDO percentage, according to the tensile tests. The three-point bending tests using an atomic force microscope (AFM) revealed a correlation between the local stiffness of a specific point on a single fiber and its position. HUVECs cultured on stiffer fiber meshes presented elongated F-actin filaments and spindle morphology, in comparison with their softer counterparts. The fiber mesh elasticity did not affect the initial HUVEC attachment, and a faster cell proliferation rate of HUVEC was shown on stiffer fibers. HUVEC pre-cultured on stiffer fiber meshes presented a faster migration velocity and an increased tube formation capacity than those from softer fibers, indicating a higher angiogenesis potential.



In summary, the functionality of HUVEC can be strongly regulated by the elasticity of fiber meshes. Mechanical characterization of the fibers at different scales, e.g. AFM for microscale in combination with tensile test for macroscale, could deepen our understanding on the cellular mechanosensing process and enable more meaningful substrate design towards favorable cell function.

#### Reference

1. Theocharis, A. D.; Skandalis, S. S.; Gialeli, C.; Karamanos, N. K., Extracellular matrix structure. *Adv Drug Deliver Rev* **2016**, *97*, 4-27.
2. Cronin-Golomb, M.; Sahin, O., High-resolution nanomechanical analysis of suspended electrospun silk fibers with the torsional harmonic atomic force microscope. *Beilstein J Nanotech* **2013**, *4*, 243-248.

#### F.SM01.09.18

**Bioinspired Novel-Tip-Shaped Micropillar Arrays for Selective Liquid Sliding Surfaces** [Seongmin Kang](#), Ji Seong Choi and Joon Hyung An; Chungnam National University, Korea (the Republic of)

Recently, superomniphobic (meaning highly water and oil-repellent) surfaces have been extensively studied both theoretically and experimentally in the materials community with several remarkable findings. Considering a notable process towards springtail-inspired omniphobic surfaces, however, a robust liquid repelling surface that is capable of inducing a selective liquid sliding property has been rarely reported, which would have many potential applications in microfluidics, mobile market, electronic devices and precision industry. Here, we present for the first time a selective liquid sliding surface using a springtail-inspired mushroom-like re-entrant structure with a novel geometry of concave tip. By implementing a simple yet sturdy silicon fabrication and lithography method, the fabricated micropillar arrays displayed high structural fidelity. We investigated a design rule for the cap of the proposed structures, which resulted in not only superomniphobicity but also a selective liquid sliding property with DI water and mineral oil. We believe that our study makes a significant contribution to the literature because it proposes a novel springtail-inspired mushroom-like re-entrant structure that can induce a selective liquid sliding property between water and oil, which has not been accomplished before.

#### F.SM01.09.19

**Improving Control of Inverse Opal Surface Chemistry and Interactions with Fluids** [Natalie Nicolas](#); Harvard University, United States

Inverse opal photonic crystals are bioinspired structurally colored porous materials that have been utilized in many applications including sensing, catalysis, and microfluidics. By modifying the surface chemistry and geometry of inverse opal pores to improve control over surface-fluid interactions in these materials, we can achieve highly localized effects and dynamically alter the wetting point of inverse opal films. Several strategies were used to fine-tune the behavior of the inverse opal. The pore size and pore neck angle, which determine the threshold contact angle for fluid infiltration, were adjusted by atomic layer deposition. This technique provides sub-nanometer control of the pore radius and can be used in conjunction with surface chemical modification to change the wetting point of an inverse opal film. The surface chemistry of the pore, which controls the contact angle that a fluid forms with the surface, was patterned with multiple silanes. By taking advantage of the inherent disorder in self-assembled monolayers at features with a small radius of curvature, such as pore necks, controlled local patterns in surface chemistry were produced. For dynamic modulation of the contact angle, photoswitchable spiropyran and azobenzene molecules were attached to the pore surface. These molecules reversibly altered the hydrophobicity of the surface when their conformation was changed by exposure to ultraviolet or visible light. By understanding how pore geometry and surface chemistry contribute to the static and dynamic behavior of inverse opals and their interactions with fluids, we can more effectively utilize these structured materials.

#### F.SM01.09.20

**Magnetic Field Alignment of Chitin Nanocrystals Confined to a Polymer Microgel** [Sujin Rebecca Lee](#), Elsa Reichmanis, Jung O Park and Mohan Srinivasarao; Georgia Institute of Technology, United States

It is well documented that twist axis of cellulosic fiber aligns parallel to applied magnetic field. In here, we showed change in orientation of bio-derived cholesteric phase confined to microgel using low magnetic fields (0.5 – 1.2 T). As equilibrated on commercial magnet, droplets of chitin nanocrystal and superparamagnetic nanoparticles mixture possessed homeotropic anchoring and light induced polymerization of the monomer in droplets captured the phase into microgels. The helix orientation directly affected the texture of microgels under polarized optical microscopy. The exhibited structures of microgel were nested cup configuration of lamellar planes or bipolar structure even in the high chirality regime. Moreover, the microgels are responsive to temperature, as we used N-isopropyl acrylamide as a monomer. With temperature change we

could observe swelling and de-swelling of nested cup structure which allowed us to understand the structure with more information. These findings give fundamental understanding bio-derived cholesteric materials and their self-assembly under confinement. Methodology for embedding twisted structure in polymer with bottom-up fabrication will give guideline for designing and controlling multifunctional nature-inspired programmable devices or materials with sustainable use of our resources.

#### **F.SM01.09.22**

**Late News: Biomimetic Moth-Eye Nanostructure with Improved Optical Properties and Facilitated Application to Optical Devices** Jiseong Choi, Joon Hyung An, Hyunjung Kim and Seongmin Kang; Chungnam National University, Korea (the Republic of)

Moth-eye inspired structure (MIS) has been regarded as important technology to enhance efficiency of optical device in biomimetic field. Since the nanostructures of the moth-eye surface gradually changed the refractive index from the air to devices, the MIS improved the optical properties of transmittance and reflectance. Despite these developments, film-based structures were difficult to apply and surface coating might damage to the surface of optical device during additional processes. Therefore, we fabricated three different sizes of MIS, 300 nm, 500 nm and 1000 nm, followed by optimizing materials and nanostructure size supported through two theoretical phenomena which are diffraction grating equation and double-slit effect. Then, optical devices were packaged by attaching polymer-based MIS without any treating and processing. As a result, the freestanding MIS composed of PDMS were identified to enhanced optical properties with over 94% transmittance and below 3.5% reflectance, compared to the MIS composed of PUA with substrate of PET film. In addition, PDMS-MIS attached to cell phone and ITO glass, which was used as substrate of optical devices, was proved that optical devices facilitated packaging as well as enhanced optical properties.

#### **F.SM01.09.24**

**Late News: Investigation on the Partitioned Multilayers of the Wing Scale of *Papilio maackii* for Nature-Inspired Structural Coloration** Seungmuk Ji<sup>1</sup>, Deok-Jin Jeon<sup>1</sup>, Jihun Kang<sup>1</sup>, Seunghwan Moon<sup>1</sup>, Eunok Lee<sup>2</sup>, Jinhee Kim<sup>2</sup> and Jong-Souk Yeo<sup>1</sup>; <sup>1</sup>Yonsei University, Korea (the Republic of); <sup>2</sup>National Institute of Ecology, Korea (the Republic of)

Butterflies present a variety of brilliant colors on their wings based on pointillism. Pointillism is well-known drawing technique, however, to express colors, butterflies use very unique and diverse nanostructures such as tree-like multilayered ridges, chitin-air multilayers, photonic crystals, etc. Through investigating these photonic structures, we are able to come up with effective engineering strategies to produce vivid, durable, and eco-friendly colors. *Papilio maackii*, the alpine black swallowtail, is a butterfly that uses air-chitin partitioned multilayers to exhibit a blueish-green like color on its wing. Since it has scales that show various colors between blue to green, it has the advantage of studying how to control structural colors using multilayered structures.

In this work, we investigate the structural coloration of the wing scale of *Papilio maackii* according to its nanoscale multilayered. The color of the wing scales changes from blue to green, depending on the thickness of the chitin and air layer. We demonstrate by using finite difference time domain (FDTD) simulations that the chitin partitions in air-chitin mixed layers regulate the effective refractive index to improve the color contrast with low background intensities. Cross-sectional TEM investigations show that the thickness of the air-chitin mixed layers varies gradually, and when this gradual change is reflected in the simulation, it shows a more similar reflectance spectrum with that of the experimentally measured. We identify the presence of melanin on the colored scales, which is a light-absorbing pigment, by measuring Raman spectroscopy. FDTD simulations show that melanin can contribute to the intensity of the reflectance spectrum in the region of long wavelength. In order to realize the structural colors based on the partitioned multilayers, we use a method to coat polymeric nanoparticles and sol-gel glass thin films repeatedly. By using this method, the effects of inhomogeneity and volume fraction of air voids in the multilayered structure are experimentally examined.

This research was supported by National Research Foundation (NRF) grant funded by the Ministry of Education, under "Basic Science Research Program" (NRF-2017R1D1A1B04033182) and also supported by Research Program through the National Institute of Ecology (NIE-Basic Research-2020-18).

#### **F.SM01.09.25**

**Late News: Silk-Like Structure of Freshwater Mussel Byssus Fabricated via Shear-Induced Alpha to Beta Transition of Intermediate Filament-Like Precursors** Miriam Simmons and Matthew J. Harrington; McGill University, Canada

Freshwater invasive mussel species *Dreissena polymorpha* (zebra mussels) adhere themselves in underwater environments with a collection of protein-based fibers known as a byssus. The byssus of the zebra mussel is stronger, stiffer and faster to recover after deformation than those of the well-characterized marine mussels, but very little is known of its structure or composition. Here, we used a combination of Raman, FTIR and wide angle x-ray diffraction to elucidate the secondary structure of fresh and induced byssal fibres. Our data indicates that the secreted fibers are comprised of a mixture of parallel  $\beta$ -crystallites, similar to spider silk. Furthermore, investigation of the byssus biofabrication process indicates that the precursor proteins are stored in an  $\alpha$ -helical structure and transition from an  $\alpha$ -helix to  $\beta$ -sheet secondary structure during the formation process, similar to other structural proteins like intermediate filaments and keratin. This stress-induced transformation in secondary structure is being attributed to a coiled-coil protein predicted in the mussel transcriptome, and current efforts are aimed at extracting this protein to further understand its shear-induced phase transformation.

#### F.SM02.05.01

**Hydrated Poly(ether urethane) Semi-Interpenetrating Network with High Lubricity and Mechanical Properties Under Physiologically Relevant Loading for Cartilage Replacement Applications** Shimon Unterman, Mushtaq Al Zuhairi and Iraklis C. Kourtis; Hyalex Orthopaedics, United States

Orthopaedic biomaterials for use as bearings against cartilage in diarthrodial joints face the dual challenges of being able to withstand high multiaxial loads while minimizing coefficient of friction and wear. High lubricity in aqueous conditions has been achieved with hydrogels such as poly(vinyl alcohol) (PVA), but mechanical properties of these hydrated polymeric networks have typically been inferior to native cartilage. Conversely, high mechanical properties can be achieved with other engineered materials but with increased cartilage wear. This study describes a novel biomimetic hydrated semi-interpenetrating network (IPN) based on poly(ether urethane) (PEU) that was previously implanted in a rabbit cartilage repair model<sup>1</sup>. The frictional and mechanical properties compare favorably with native cartilage.

A tunable semi-IPN of PEU and a cross-linked polyelectrolyte network was synthesized. Similar to proteoglycans in hyaline cartilage, the polyelectrolyte caused the semi-IPN to swell in water, imparting the high lubricity of a hydrophilic polymer network, while the PEU imparted high stiffness and strength, resembling the collagen type II of cartilage. Upon completion of synthesis, the semi-IPN was a translucent, highly hydrated, qualitatively slippery material. The semi-IPN passed standard ISO 10993 biocompatibility testing.

The semi-IPN was evaluated for coefficient of friction (COF) using a pin-on-disk friction tester with  $\sim 1$  MPa normal loading in aqueous conditions against a fused silica counterface, yielding a COF of  $< 0.05$ ; typical cartilage COFs have been reported as  $< 0.01$ - $0.04$ <sup>2</sup>. The mechanical properties were measured in tension, compression, tear, and shear in physiologically relevant conditions (simulated body fluid at 37° C) and compared to known properties of articular cartilage and PVA orthopaedic hydrogels. Compressive and tensile moduli at physiologic loads were  $> 40$  MPa, stiffer than PVA orthopaedic hydrogels<sup>4</sup> and considerably closer to the modulus of cartilage<sup>3</sup> than traditional joint replacement materials like ultra-high molecular weight polyethylene (UHMWPE) and cobalt chrome alloys (CoCr). Tensile strength was  $> 30$  MPa (cartilage: 3.75 MPa<sup>5</sup>), tear strength was  $> 40$  N/mm (cartilage: 1.21 N/mm<sup>6</sup>), shear strength was  $> 20$  MPa (cartilage: 7.25 MPa<sup>5</sup>), and the material did not fail in the measured compression range ( $> 180$  MPa; cartilage: 35.7 MPa<sup>7</sup>). By design the material strength exceeded that of native cartilage, in order to ensure long term performance without adversely impacting adjacent or opposing cartilage.

Hydrated semi-IPNs based on PEU and a polyelectrolyte network offer an attractive combination of mechanical strength, stiffness, and lubricity under physiologic loads. The semi-IPN properties, which closely mimic or exceed the high strength and low friction of native cartilage, provide a promising and novel platform for cartilage replacement applications.

1. Bichara DA; Unterman S; Schmidt MB. *Orthopedic Research Society* (2020 Annual Meeting).
2. Forster, H. & Fisher, J. *Proc. Inst. Mech. Eng. Part H J. Eng. Med.* **210**, 109–118 (1996).
3. Setton, L. A., Elliott, D. M. & Mow, V. C. *Osteoarthr. Cartil.* **7**, 2–14 (1999).
4. Stammen, J. A., Williams, S., Ku, D. N. & Gulberg, R. E. *Biomaterials* **22**, 799–806 (2001).
5. Kumar, P. et al. *Nihon Seikeigeka Gakkai Zasshi* **65**, 1070–7 (1991).
6. Chin-Purcell, M. V & Lewis, J. L. *J. Biomech. Eng.* **118**, 545–56 (1996).
7. Kerin, A. J., Wisnom, M. R. & Adams, M. A. *Proc. Inst. Mech. Eng. Part H J. Eng. Med.* **212**, 273–280 (1998).

#### F.SM02.05.04

**An Investigation of Timolol Introduction on Three Hydrogel-Based Drug Delivery Devices for Glaucoma Treatment** Nicole Mortensen and Jeffrey S. Bates; The University of Utah, United States

Contact lenses can be used as drug delivery systems because they are cross-linked, water-soluble, biocompatible hydrogels. Glaucoma is the second largest cause of blindness worldwide that increases the interocular pressure (IOP) of the eye. Topical eye drops of timolol is a common treatment that lowers IOP. The number of patients who become bilaterally blind every year is high due to the inefficiencies of eye drops and low patient adherence. In this study, three hydrogel-based contact lenses were analyzed on their uptake and release concentrations, reversibility, drug concentration profile over 12 hours, as well as their optical and mechanical properties. Synthesized molecular imprinted and soaked, non-imprinted, hydroxyethyl methacrylate (HEMA) based hydrogels resulted in having an uptake and release concentration dependent on the loading solution concentration it was left to soak in. Soaking Acuvue contact lenses resulted in having an uptake and release concentration independent of the timolol loading solution concentration. It released significantly higher concentrations than a daily dosage of timolol. All three hydrogel-based contact lenses successfully delivered timolol for 12 hours and could be reused up to six times. The synthesized HEMA hydrogels lacked in optical and mechanical properties that were to ensure comfort and prevent vision problems when used as a contact lens. As a result, further optimization is needed. Using contact lenses to deliver glaucoma medication has the potential to become a more efficient method of treatment that will increase patient adherence by eliminating barriers within glaucoma therapy created by eye drop medication.

#### **F.SM02.05.05**

**Versatile 3D Printing of Hydrogels by Pluronic** Kusuma Betha Cahaya Imani and Jinhwan Yoon; Pusan National University, Korea (the Republic of)

In recent years, there's an increase of study regarding 3D printing of soft materials, because of its importance for development of new technologies such as wearable electronic devices and artificial human organs, which require both non-rigid property and precise positioning. For 3D printing of soft materials study, it is required to choose a material which has enough viscosity but also can be easily extruded without clogging, and for that, pluronic is one of the most widely used materials. Pluronic is a thermo-responsive triblock copolymers consisting of poly(propylene oxide) (PPO) and poly(ethylene oxide) (PEO), as the hydrophobic center and hydrophilic side blocks respectively. This structure allows pluronic to form spherical micelles above its critical micelle temperature (CMT) within aqueous solution, which is suitable for 3D printing. Upon deposition on a substrate, by controlling the extruder and bath, pluronic can quickly change its phase, preventing the ink from flowing out of the intended position and retaining the desired 3D shape. In this study, pluronic F127 ((PEO)<sub>99</sub>-(PPO)<sub>65</sub>-(PEO)<sub>99</sub>) is synthesized into pluronic F-dimethacrylate (FDMA) to prepare hydrogels for extrusion-based 3D printing. This work can be further developed to have 3D printed hydrogels with conductive property or controllable elastic modulus. The synthesis of FDMA is simple and it has the prospect for applications in various fields.

#### **F.SM02.05.07**

**The Effect of Fibrin on the Osteogenic Differentiation of Human Dental Pulp Stem Cells** Kao Li<sup>1</sup>, Evan Cheng<sup>2</sup>, Tianjian Bai<sup>3</sup>, Jake D. Feldman<sup>4</sup>, Alyssa Kim<sup>5</sup> and Juyi Li<sup>1</sup>; <sup>1</sup>Stony Brook University, The State University of New York, United States; <sup>2</sup>Syosset High School, United States; <sup>3</sup>Huron High School, United States; <sup>4</sup>Plainview-Old Bethpage John F. Kennedy High School, United States; <sup>5</sup>New Hyde Park Memorial High School, United States

In addition to having non-toxic degradation products, being cytocompatible, and causing the formation of an extracellular matrix, fibrin, a major plasma protein, has been found to be highly suitable in supporting dental tissue formation and improving cell-dentin interactions[1]. This study sought to determine the effects of fibrin on the proliferation and differentiation of dental pulp stem cells, DPSCs, an investigation with potential applications in osteogenic regenerative therapy. Prior studies for in-vitro cultures of DPSCs directly on fibrin clots failed due to rapid fibrinolysis of the substrates prior to differentiation. Here we demonstrate the construction of a gelatin/fibrin scaffold, which is not enzymatically degraded at least during the 28 days required for DPSC differentiation. Furthermore, since gelatin is easily bioprinted it also offers an effective scaffold for fibrinogen, which is then rapidly cross-linked after extrusion, maintaining its shape. Gelatin-fibrinogen hydrogels were created using 9% w/v gelatin and 4 mg/mL bovine fibrinogen cross-linked by 2 different concentration of mTG (microbial transglutaminase) and 2units/ml thrombin, respectively. The gels were media exchanged and cells were cultured in osteogenic media, but without dexamethasone, the standard inducer of osteogenic differentiation. On Days 8 and 28, confocal microscopy indicated that strong tissue formation was occurring on both substrates. RT-PCR was performed at day 8 and 28 to measure the upregulation of genes associated with differentiation; ALP, COL1, and OCN. Even though this set of genes was upregulated on all samples, relative to cells plated on TCP controls, the levels for ALP and OCN for cells plated on the for gelatin-fibrinogen mixture were two and three times higher, respectively, than those for cells plated on pure gelatin confirming the regenerative potential of fibrin clots.

#### **F.SM02.05.08**

**Dual-Network Hydrogels Reinforced with Field-Responsive Hydroxyapatite Exhibiting High Strength and Stiffness**

**While Fully Hydrated** Morgan Pfaff and Jessica Faust; Northeastern University, United States

Modern medicine is seeking stronger composite materials for artificial bone graft applications that are both osteoconductive and exhibit high strength. Alginate-calcium phosphate (CaP) hydrogels have been studied as a potential material, but lack the strength required for artificial bone grafts. Here, we suggest using an alginate-gelatin dual-network embedded with magnetically-aligned CaP rods to significantly increase the overall strength of the material. CaP rods were prepared through hydrothermal precipitation and functionalized with iron oxide nanoparticles. These rods were incorporated into uncrosslinked dual-network solution and aligned under a magnetic field with constant heat and vibration. After alignment, the gelatin was thermally crosslinked at room temperature and the alginate ionically crosslinked in 10% calcium chloride solution. Tensile samples were analyzed using dynamic mechanical analysis. Preliminary results show superior mechanical strength in the dual network films compared to alginate- and gelatin-only hydrogels. The mechanical strength is further increased with higher concentrations of CaP rods. Alignment orientation also impacts hydrogel mechanics, with parallel alignment providing greatest strength and perpendicular alignment the greatest elasticity. The results of this study indicate that an osteoconductive alginate-gelatin hydrogel with high strength is possible with magnetically-aligned reinforcement and is a promising material for bone graft applications.

#### **F.SM02.05.09**

**Thermo-Responsive Artificial Perspiration Membrane** Jeong Hun Kim<sup>1</sup>, Junsoo Kim<sup>1</sup>, Solyee Im<sup>1</sup>, Sang Moon Kim<sup>2</sup>, Jong Pil Im<sup>1</sup>, Jiyong Woo<sup>1</sup> and Seung Eon Moon<sup>1</sup>; <sup>1</sup>Electronics and Telecommunications Research Institute, Korea (the Republic of); <sup>2</sup>Incheon National University, Korea (the Republic of)

Thermal management is essential for living organisms and electronic devices to survive and maintain their functions. However, it has been challenging to develop a flexible cooling devices for flexible electronics or biological systems because conventional coolers are bulky and require rigid batteries. In nature, however, the skin helps to maintain the body temperature constantly by dissipating the heat through the perspiration. Inspired by nature, we introduce an artificial perspiration membrane which automatically regulates evaporation rate at water-air interface depending on temperature. This membrane consists of a valve structure and a rigid frame; the valve is made of silicone-coated thermo-responsive hydrogels and the frame is made of plastics. Those two components are stably bonded by copolymerization. By designing the shape of the valve and the mechanical constraint, we were able to control the area where evaporation occurs depending on temperature. As a result, the valves in the membrane open in a hot environment, which facilitates the evaporation of water, and the valves close in a cool environment, which suppresses the evaporation of water, mimicking cooling function of perspiration in a flexible manner. Our work shows the potential value of a bio-inspired, membrane-type, and automatic cooling device that can solve heat problems in artificial skin devices.

The thermo-responsive hydrogel is patterned with pinwheel-like shape and supported by backbone through copolymerizing at the interface to control the evaporation area depending on the temperature. The stretchable rubber is selectively coated to prevent the unintended evaporation through the hydrogel while securing the water path for swelling. Consequently, the water surface at open state is about 6 times greater than that of close state with fast transition rate (~1 s). The evaporation rate is automatically controlled depending on the temperature with 30% of evaporation reduction at lower temperature. Our study on a smart membrane that can automatically regulate cooling power without external power source may solve thermal problems in wearable or artificial skin devices.

#### **F.SM02.05.11**

**Enhancing Osteogenic Differentiation of Mesenchymal Stem Cells Using Injectable Microporous Hydrogel** Seth Edwards and Kyung Jae Jeong; University of New Hampshire, United States

Mesenchymal stem cell (MSC) delivery and subsequent differentiation into bone forming cells has promising implications for the future of bone repair. Use of hydrogel as a delivery vehicle is advantageous in order to enhance cell retention, and provide a scaffold to facilitate new bone growth. Here we describe a microporous injectable hydrogel for encapsulation of MSCs with the intent to improve proliferation and subsequent osteogenic differentiation. Physically crosslinked microgels are formed by thermal crosslinking of gelatin in a water in oil emulsion. Bulk scaffold formation involves chemical crosslinking of gelatin by nontoxic enzymatic reaction. Enzymatic crosslinking of gelatin provides prolonged strengthening of the bulk gel, and provides a covalent mechanism for tissue adhesion. A hydrated suspension of microgels and cells can be injected for noninvasive cell delivery, and the scaffold can crosslink *in situ*, encapsulating delivered cells in the pore space. This hydrogel provides an advantageous environment for MSC growth and differentiation due to the large interstitial space between microgels, which improved cell spreading and proliferation when examined by confocal microscopy, and improved osteogenic differentiation when examined using alizarin red S stain and high resolution micro computed tomography.

### F.SM02.05.12

**A Smart LEA for Dynamic Adjustments to Brain Aneurysm Embolization and Healing\*** Juyi Li<sup>1</sup>, Robert Wong<sup>1</sup>, Aaron Slutsky<sup>2</sup>, Daniel Cohn<sup>2</sup>, Chandramouli Sadasivan<sup>1</sup>, Anya Chabria<sup>3</sup>, Jessica Guo<sup>4</sup>, Varun Nimmagadda<sup>5</sup>, Tyler Shern<sup>6</sup>, Stephanie Tarrab<sup>7</sup>, Jeffrey Zhang<sup>8</sup>, Emily Zhou<sup>9</sup>, Jeffrey Huang<sup>10</sup>, Ikshu Pandey<sup>11</sup> and Miriam H. Rafailovich<sup>1</sup>; <sup>1</sup>Stony Brook University, The State University of New York, United States; <sup>2</sup>The Hebrew University of Jerusalem, Israel; <sup>3</sup>The Wheatley School, United States; <sup>4</sup>Ward Melville High School, United States; <sup>5</sup>Novi High School, United States; <sup>6</sup>Mission San Jose High School, United States; <sup>7</sup>Yeshivah of Flatbush Joel Braverman High School, United States; <sup>8</sup>Centerville High School, United States; <sup>9</sup>The Harker School, United States; <sup>10</sup>University of Pennsylvania, United States; <sup>11</sup>Johns Hopkins University, United States

Brain aneurysms are focal, pathological dilations that mostly form at branch points of the cerebral vasculature. These weak-wall structures can rupture leading to hemorrhagic stroke with mortality and morbidity rates as high as 40% and 25%, respectively. More than 60% of aneurysms are currently treated with minimally invasive endovascular/interventional methods. Most of these methods involve the permanent implantation of metallic devices such as intrasaccular coils and meshes or endovascular flow diversion. These implants reduce blood flow velocity within the aneurysm and thus promote clot formation within the aneurysmal sac, which is converted to fibrous tissue over a period of several months. However, current devices show unfavorable primary outcomes in 20% to 30% of cases on average and success rates are substantially lower depending on aneurysm type and location. In this project, we discuss the development of an injectable, multi-functional, reverse thermo-responsive, *in situ* cross-linkable, shape-conforming, intrasaccular porous scaffold. This scaffold changes dynamically to enhance the associated wound healing process which follows obduration. The scaffold is engineered to work with the natural blood flow and promotes vascular remodeling and endothelialization followed by personalized biodegradation, at the end of the process, leaving no residue behind. This research program harnesses the unique behavior of a family of reverse thermo-responsive (RTR) polymers to generate a novel Biodegradable Intrasaccular Polymeric Device, displaying enhanced clinical performance. The aqueous solutions of these polymers display low viscosity at in-physiological temperatures and are gels at 37 degrees. The device is an easily syringable, low viscosity multi-component aqueous solution comprising: [a] a cross-linkable RTR component that forms a robust and homogeneously porous scaffold for controlled intrasaccular thrombosis, [b] a leachable RTR-displaying component acting as the porogen, [c] an iodine-rich radiopaque agent, [d] a polymerizable (RGD)-containing oligopeptide that will *in situ* co-polymerize with the other components, aimed at accelerating the generation of an endothelial cell layer at the aneurysm neck, [e] inclusion of basic Fibroblast Growth Factor (bFGF) in the cross-linked component to promote thrombus organization and intrasaccular fibrosis/remodeling, and [f] a cross-linkable oligopeptide containing the matrix metalloprotease (MMP)-degradable leucine-glycine motif that will be *in situ* co-crosslinked with the RTR components, to impart to the polymer device to degrade in a personalized, patient-specific manner, as a function of the healing process. This process represents a major step in treatment of aneurysms, which shortens optimize brain aneurysm treatment with short procedure times, require no chronic anti-platelet medications, promote endothelialization of the parent-vessel interface, enhance aneurysm 'sac' fibrosis, and degrade in a patient-specific manner to leave no trace of the pathology or the treatment, with lower costs.

\*Authors 3-10 contributed equally to this work.

We gratefully acknowledge support from the Louis Morin Charitable Trust

[1]Taschner CA, Chapot R, Costalat V, Machi P, Courtheoux P, Barreau X, et al. Second-Generation Hydrogel Coils for the Endovascular Treatment of Intracranial Aneurysms: A Randomized Controlled Trial. **Stroke**. 2018;49(3):667-74.

[2]Sosnik A, Cohn D. Reverse thermo-responsive poly (ethylene oxide) and poly (propylene oxide) multiblock copolymers. **Biomaterials**. 2005;26(4):349-57.

### F.SM02.05.13

**Late News: Using Coarse-Grained Molecular Dynamics to Model Hydrogel Viscosity** Kyle R. Shi<sup>1</sup>, Hannah Even<sup>2</sup>, Shoumik Saha<sup>3</sup> and Dilip Gersappe<sup>3</sup>; <sup>1</sup>Dublin High School, United States; <sup>2</sup>Staples High School, United States; <sup>3</sup>Stony Brook University, The State University of New York, United States

**Hydrogels are systems of hydrophilic polymers that swell when placed in a solvent to form a gel-like structure. When nanocomposites are added to hydrogels, they can enhance their properties by crosslinking the polymers. Hydrogels have shown promise as an environmentally friendly substitute to cement as soil stabilizers, mechanically improving the strength of the soil. While past studies have found a positive relationship between clay nanocomposite concentration and hydrogel viscosity with a qualitative stress-autocorrelation function, specific mechanical properties and structure formation of these hydrogels remain unknown. Our research aims to learn more about the properties of hydrogels with rigid rod-shaped clay nanocomposites and explore the possibility of determining more quantitative**

trends on viscosity by simulating shear stress on the hydrogel system, imitating realistic soil movement on the hydrogels. We performed Molecular Dynamics simulations in order to understand the rheological properties of hydrogels. The concentration of the nanocomposite and the shear rate were varied and different polymer-nanocomposite interaction energies were used in order to determine the effects of these factors on the viscosity of hydrogels. The results show a clear shear thinning behavior in these systems and reflect similar trends to previous studies. Our results can be used to predict an optimum hydrogel composition in different conditions for soil stability.

We gratefully acknowledge support from the Louis Morin Charitable Trust.

#### F.SM02.05.14

**Late News: Optically Active Nanoengineered Fibrous Scaffolds for Cardiac Cell Monitoring** Stijn Jooken<sup>1</sup>, Olivier Deschaume<sup>1</sup>, Olga Krylychkina<sup>2</sup>, Yovan de Coene<sup>1</sup>, Thierry Verbiest<sup>1</sup>, Koen Clays<sup>1</sup>, Geert Callewaert<sup>3</sup> and Carmen Bartic<sup>1</sup>; <sup>1</sup>KU Leuven, Belgium; <sup>2</sup>imec, Belgium; <sup>3</sup>KU Leuven KULAK, Belgium

In cardiac tissue engineering the incorporation of nanoparticles (NPs) such as plasmonic NPs, carbon nanotubes or magnetic particles was shown to improve the function of in vitro cardiac patches in terms of cell viability, electrical signal coupling, beat synchronicity, etc. [1,2]. Moreover, it has also allowed to locally deliver stimuli to cells and guide cell behavior, for instance, by heating of plasmonic NPs[3].

In this work, we created a smart scaffold capable of optically reporting cardiomyocyte activity *in situ* (electrical and contractile) by incorporating voltage-sensitive semiconductor quantum dots (QDs) in 2D scaffolds and 3D hydrogels.

We have characterized the fluorescence voltage sensitivity of Type I CdSe/ZnS QDs and pseudo-Type II CdSe/CdS rods, investigated in a controlled environment, under single and two photon optical excitation. Then, QDs were incorporated in 2D scaffolds of collagen nanofibers and used two-photon fluorescence microscopy to readout of the activity of cultured primary cardiomyocytes [4]. The method was validated in a pharmacological assay where the drugs epinephrine and blebbistatin were used for their combined chronotropic and inotropic effects. Finally, the concept is extended to 3D by incorporating QD-labeled collagen fibers in 3D hydrogel constructs.

[1] Baei, P. *et al.* Electrically Conductive Gold Nanoparticle-Chitosan Thermosensitive Hydrogels for Cardiac Tissue Engineering. *Mater. Sci. Eng. C* **2016**, *63*, 131–141.

[2] Yu, H. *et al.* Mechanically and Electrically Enhanced CNT-Collagen Hydrogels As Potential Scaffolds for Engineered Cardiac Constructs. *ACS Biomater. Sci. Eng.* **2017**.

[3] Baffou, G. *et al.* Photoinduced Heating of Nanoparticle Arrays. *ACS Nano* **2013**, *7* (8), 6478–6488.

[4] Jooken, S. *et al.* Quantum Dot-Functionalized Extracellular Matrices for in Situ Monitoring of Cardiomyocyte Activity. *ACS Appl. Nano Mater.* **2020**.

#### F.SM02.05.15

**Late News: Gelation-Based Naked-Eye Detection of Glucose via Dual-Enzyme Cascade Reaction** Jisoo Lee and Seonki Hong; DGIST, Korea (the Republic of)

Many efforts have been conducted to develop bioassays in point-of-care settings for rapid and convenient biomarker detection. Among them, the colorimetric-based system has been emerging due to the advantages in simple read-out through the naked-eye without requiring any expensive devices. However, it has still been challenging to simplify the labor-intensive multiple steps required to improve the limit of detection and remove the background color which may interfere with the detection signal.

Herein, we report a gelation-based bioassay mediated by a cascade reaction of two enzymes. We reasoned that biomarker-specific gelation can provide a detectable signal through the naked-eye even in the presence of the background color biospecimens such as blood and urine. Gelation is triggered by the quinone tanning reaction of catechol-conjugated polyethylene glycols via horseradish peroxidase (HRP) in the presence of hydrogen peroxide (H<sub>2</sub>O<sub>2</sub>). Therefore, we coupled another enzyme, glucose oxidase (GOx), that produces the H<sub>2</sub>O<sub>2</sub> depending on the concentration of glucose to initiate the HRP-mediated gelation.

In our system, parameters adjusting the gelation time include the concentration of enzymes (HRP and GOx), catechol content conjugated to the polymeric precursor, the concentration of polymeric precursor, and the pH. In the experiment using H<sub>2</sub>O<sub>2</sub> as a positive control to glucose/GOx system, the gelation time dramatically decreased down to 1 minute as the HRP concentration increased up to 1 U/mL. In the HRP/GOx dual-enzyme system, 0.25 U/mL of HRP was sufficient to achieve successful gelation within 80 minutes with 10-100 U/mL of GOx in the presence of 10 mM glucose. The best conditions of

other parameters for the fastest gelation were observed at 83% of catechol content, 5wt% of the precursor, and pH 7. Finally, as low as 16 mM of glucose was detectable through the naked-eye within 20 minutes of gelation time.

With the advantage of the cascade reaction of two enzymes, we expect improvement in the detection sensitivity. In addition, single-step glucose detection is allowed without requiring washing steps due to the enzymes' intrinsic specificity.

#### **F.SM02.05.16**

**Late News: A Clock-Like Hydrogel That Visually Indicates Time** So Hyun Ahn, Srinivasa Raghavan and William E. Bentley; University of Maryland, United States

Microcapsules can be used to monitor the local micro-environment *in vivo*, e.g., within the gastro-intestinal (GI) tract. For example, when molecular signals are released into the GI, the payload within the microcapsules could undergo a color change in response to the signal. While the nature of the signal is often the key piece of information in such experiments, the *time* at which the signal is released could be another vital aspect. To obtain information regarding time, there is the need for a gel-like material that could function like a 'clock' – i.e., exhibit systematic changes at regular time intervals.

Here, we report a simple 'clock' construct based on self-destructing structures embedded in an agarose gel. For this, we fabricate capsules of alginate crosslinked by  $\text{Ca}^{2+}$  and containing the enzyme alginate lyase. This enzyme severs alginate chains, thereby causing the capsule to degrade over a period of time. The higher the enzyme concentration, the lower the degradation time. Capsules with different concentrations of enzyme are embedded in an agarose gel to create our 'clock'. Capsule degradation proceeds in a sequential manner, and visual inspection of the gel (i.e., the capsules that remain intact) reveals the time elapsed from the start of the experiment. To facilitate visual clarity, we embed colored or fluorescent nanoparticles in each of the capsules. Moreover, the degradation rate can be varied using pH, temperature, and other variables that affect the enzymatic activity. Variations of the above simple clock include: (a) one that is activated by an external trigger; and (b) one that locks-in the elapsed time at a particular juncture.

#### **F.SM03.05.01**

**Beyond Elastic Limit of Piezoelectric Ceramic with 3D Hollow ZnO Nanostructures** Hoon Kim, Seokjung Yun, Kisun Kim, Wonsik Kim, Jeongjae Ryu, Hyeon Gyun Nam, Seung Min J. Han, Seokwoo Jeon and Seungbum Hong; Korea Advanced Institute of Science and Technology, Korea (the Republic of)

Piezoelectric materials are suitable for haptic technology as they can convert mechanical stimuli into electrical signals and vice-versa. However, owing to their disadvantageous mechanical properties such as brittleness (in ceramics) and a low piezoelectric coefficient (in polymers), it is still a challenge to use them in haptic technology. Here, we present a truss-like 3D hollow zinc oxide (ZnO) nanostructure that shows a drastically improved elastic strain limit while maintaining a piezoelectric coefficient similar to that of single-crystal ZnO. The ZnO hollow nanostructures were fabricated by proximity field nanopatterning (PnP) and atomic layered deposition (ALD) at four different process temperatures from 90 to 300°C. The piezoelectric properties were visualized and analyzed through dual AC resonance tracking piezoresponse force microscopy (PFM). The piezoelectric coefficient was approximately 9.2 pm/V. Furthermore, we measured the measured elastic strain limit of approximately 10% using the nanopillar compression test, which was at least 3 times greater than the prior report. The extended elastic limit of the 3D hollow structure was further supported by finite element simulations. We envision that our ZnO hollow nanostructure can be used in enhanced haptic devices, which mimic the human sense of touch.

#### **F.SM03.05.02**

**Highly Crystalline PCL Ultrathin Films as Thermally Switchable Biomaterial Coatings** Shivam Saretia<sup>1,2</sup>, Rainhard Machatschek<sup>1,2</sup> and Andreas Lendlein<sup>1,2</sup>; <sup>1</sup>Helmholtz-Zentrum Geesthacht, Germany; <sup>2</sup>University of Potsdam, Germany

Degradable semi-crystalline polymers are a class of materials that modern regenerative medicine heavily relies on. While their formulation into nanostructured devices can be advantageous to tailor functional properties such as cellular uptake kinetics and degradation behaviour, it is difficult to assess and control the morphology, crystallinity and organization of nanostructured polymer materials by common preparation methods.

The Langmuir technique overcomes most of the drawbacks concerning preparation and investigation of nanostructured polymer materials. Here, ultrathin films at the air-liquid interface serve as model systems for polymer devices and interfaces, which can be manipulated and observed in a straightforward way. In particular, the semi-crystalline morphology, including crystal size, number density, thickness, and melting temperature can be precisely adjusted. By transferring the layers to solid substrates, functional biomaterial interfaces with unique properties can be created. For example, via enzymatic degradation of



the amorphous chains, a semi-crystalline Langmuir film can be converted into an almost entirely crystalline film with a thickness of a few nanometers. The preparation and analysis of these highly functional, entirely crystalline thin films based on oligo( $\epsilon$ -caprolactone)s (OCL) with different end-groups is of particular interest. Poly( $\epsilon$ -caprolactone) (PCL) is established in clinical applications with a relatively low melting point and well documented enzymatic degradability<sup>1</sup>. The melting temperature of PCL or OCL crystals can be adjusted via the crystallization temperature to be very close to physiological conditions, producing a polymer coating that changes a broad variety of its functional properties upon application of a small thermal stimulus.

For example, highly crystalline films of hydroxyl and methacrylate end capped linear OCL are prepared by degrading its amorphous phase by the enzyme *Pseudomonas cepacia* lipase (0.007 mg mL<sup>-1</sup>) at constant surface pressure of  $\sim 7$  mN m<sup>-1</sup> on air-water interface at room temperature. The thickness of the OCL crystals in the film can be adjusted in the range of  $\sim 6$  to 8 nm, resulting in a melting temperature between  $\sim 30$  to 40 °C at the air-water interface. Upon melting, the elastic moduli of the film are drastically altered. Further, functional end groups are expelled from the crystals and therefore accumulated at the crystalline surface. Upon melting, these end-groups are buried in the amorphous phase, resulting in a change of the chemical composition of the material surface. Moreover, the degradability of the thin film increases significantly upon melting, meaning that the lifetime of the material can be adjusted via its thermal history. In addition, the barrier properties of the thin film depend on its crystallinity, with polymer crystals being considered impenetrable for small molecules.

Here, we demonstrate the fabrication and behaviour of these thermally switchable OCL crystals coatings, which are of interest for applications such as barrier layers, substrates modulating stem cell adhesion, or coatings with on-demand acceleration of degradability. Another possible application are friction reducing coatings, for example on sutures. Here, the temperature at the suture-tissue interface does not increase as long as the heat generated by frictional forces is absorbed by the melting enthalpy of the crystals.

### F.SM03.05.03

**Late News: Functionalised Capacitive Microfluidic Force Sensors for Orthopaedic Surgery** [Liam Ives](#)<sup>1</sup>, Qingshen Jing<sup>1</sup>, Alizée Pace<sup>1</sup>, Anke Husmann<sup>1</sup>, Vikas Khanduja<sup>1</sup>, Jehangir Cama<sup>2</sup> and Sohini Kar-Narayan<sup>1</sup>; <sup>1</sup>University of Cambridge, United Kingdom; <sup>2</sup>University of Exeter, United Kingdom

The correct balance of forces on the hip joint during total hip arthroplasty (THA) is essential for implant longevity and to prevent the need for revision surgery. This has become increasingly important since the average age of a THA patient is decreasing, hence these implants must survive greater activity levels and correspondingly higher stresses than those typically found in older, less active patients. Currently, the lifetime of an implant positioned purely by a surgeon's judgement is approximately 15 years. Quantitative force feedback during surgery could provide more accurate implant positioning, increasing the average lifetime. However, there are currently no force sensors capable of providing this information within the small and complex geometry of the hip joint.

Here, we solve this unmet clinical need by presenting a thin, conformable and flexible microfluidic capacitive force sensor, which can be incorporated into the surgical process without significant modification to existing implants. The sensor consists of a deformable microfluidic chip bonded to a flexible substrate, on which interdigitated electrodes are incorporated, and that can operate in confined spaces to give accurate force readings from joints. The sensor operates by monitoring the change in capacitance of the electrodes as the fluid in the microfluidic channel is displaced in response to an applied force. Multiple sensors were incorporated into a model hip implant geometry, and a bespoke mechanical testing rig was built to simulate loading of the acetabular cup from the femoral head at different angles. The experimental results were validated using finite element modelling. This was used to optimise the sensor geometry for the production of sensitive devices that can withstand the high forces required for surgery. Our novel microfluidic-based force sensing technology can potentially be adapted for application in joints either for sensor-assisted orthopaedic surgery, or for gathering telemetric data from joints before, during and/or after surgery. Such biocompatible and implantable force sensors will contribute significantly to several clinical drivers, through providing quantitative feedback to the attending clinician, and could also serve to underpin robot-assisted orthopaedic surgery in the future.

## SYMPOSIUM F.SM02

---

Hydrogel Technology for Humans and Machines  
November 21 - December 2, 2020

Symposium Organizers

Costantino Creton, ESPCI Paris  
Yuhang Hu, Georgia Institute of Technology  
Xuanhe Zhao, Massachusetts Institute of Technology  
Jie Zheng, University of Akron

Symposium Support

**Silver**  
Science Robotics | AAAS

---

\* Invited Paper

SESSION F.SM02.06: Live Keynote and Oral I: Hydrogel Technology for Humans and Machines  
Session Chairs: Costantino Creton and Yuhang Hu  
Tuesday Afternoon, December 1, 2020  
F.SM02

**1:45 PM \*F.SM02.01.01**

**Formulating Bioinks and Bioink Processing Methods for Tissue Bioprinting** Yu Shrike Zhang; Harvard Medical School, United States

Over the last decade, three-dimensional bioprinting has offered great versatility to fabricate biomimetic volumetric tissues that are both structurally and functionally relevant to their native counterparts. The technology enables precise control over the composition, spatial distribution, and architecture of the bioprinted constructs, facilitating recapitulation of the delicate shapes and structures of targeted organs and tissues. This talk will discuss our recent efforts on developing various cytocompatible and cell-instructive bioink formulations, as well as their processing methods, for the fabrication of engineered tissues towards regenerative medicine and tissue model engineering applications, using a series of established or customized bioprinting strategies.

**2:00 PM \*F.SM02.02.01**

**Chemical and Topological Design of Mussel-Inspired Polymers—A Single-Molecule Adhesion Perspective** Yiran Li<sup>1</sup>, Peyman Delparastan<sup>2</sup>, Jing Cheng<sup>2</sup>, Haoqi Wang<sup>1</sup>, Kelsey DeFrates<sup>2</sup>, Yi Cao<sup>1</sup> and Phillip B. Messersmith<sup>2,3</sup>; <sup>1</sup>Nanjing University, China; <sup>2</sup>University of California, Berkeley, United States; <sup>3</sup>Lawrence Berkeley National Laboratory, United States

In mussels, the adhesive proteins that are instrumental for attachment to wet surfaces are known to contain high levels of 3,4-dihydroxy-L-alanine (DOPA), often located adjacent to amino residues such as lysine (Lys). The special synergistic relationship between catechols and amines is a subject of high interest, not only for understanding native proteins but also for informing the design of bioinspired polymer systems. Other research groups have shown that catechol and amine functional groups act synergistically to enhance adhesion at wet surfaces, however reports of catechol-amine interfacial phenomena on a single molecule level have been limited. In this talk we will describe single molecule force spectroscopy (SMFS) measurements that are providing new insights into interactions between Lys-DOPA peptides and various surfaces. Of particular interest is the impact of chemical composition (DOPA and Lys), peptide length and topology (i.e. distribution of adhesive elements along a polymer) on interfacial adhesion to a wet substrate. The results may inform the future design of novel polymer adhesives, including adhesive hydrogels, pressure sensitive adhesives and high-strength thermoset adhesives.

**2:15 PM \*F.SM02.02.02**

**Smart Material and Adhesive Utilizing Mussel Adhesive Chemistry** Bruce Lee; Michigan Technological Univ, United States

Marine mussels secrete adhesive proteins that enable these organism to anchor themselves to various substrate (i.e., ship hull,

rock) in a rough, intertidal zone. These mussel foot proteins contain a unique amino acid, L-3, 4 dihydroxyphenylalanine (DOPA), that is responsible for strong interfacial binding and curing of the proteins. The catechol side chain of DOPA is capable of participating in various stimuli responsive, reversible interactions, dictated by its oxidation state. In this presentation, I will describe our efforts in utilizing these interactions in designing various types of smart biomaterial. We have incorporated catechol-metal ion coordination bond to design hydrogel actuators that can fold into various 3-dimensional shapes. We have also utilized catechol-boronic acid complexation chemistry to design moisture-resistant smart adhesive with tunable adhesive properties. Most recently, we demonstrated the feasibility of using applied electricity to directly deactivate catechol-based adhesive that is bonded to a surface.

### **2:30 PM \*F.SM02.04.01**

**Evolution of Self-Oscillating Polymer Gels as Life-Like Softmachines** Ryo Yoshida; The University of Tokyo, Japan

In living systems, there are many autonomous and oscillatory phenomena to sustain life such as heart beating. We developed “self-oscillating” polymer gels that undergo spontaneous cyclic swelling–deswelling changes without any on–off switching of external stimuli, as with heart muscle. The self-oscillating gels were designed by utilizing the Belousov-Zhabotinsky (BZ) reaction, an oscillating reaction, as a chemical model of the TCA cycle. We have systematically studied these self-oscillating polymer gels since they were first reported in 1996. Potential applications of the self-oscillating polymers and gels include several kinds of functional material systems such as biomimetic actuators, mass transport systems and functional fluids. For example, it was demonstrated that an object was autonomously transported in the tubular self-oscillating gel by the peristaltic pumping motion similar to an intestine. Further, self-oscillating polymer brush surface like cilia, vesicles or colloidosomes undergoing cell-like autonomous shape oscillations with buckling, was prepared. Besides, autonomous sol-gel oscillation and amoeba-like motion was realized utilizing well-designed block copolymer solution. In this presentation, our recent progress on the self-oscillating polymer gels is summarized.

### **2:45 PM \*F.SM02.04.02**

**HASEL Artificial Muscles—Versatile High-Performance Actuators for Bioinspired Robotics** Christoph Keplinger; University of Colorado-Boulder, United States

Robots today rely on rigid components and electric motors based on metal and magnets, making them heavy, unsafe near humans, expensive and ill-suited for unpredictable environments. Nature, in contrast, makes extensive use of soft materials and has produced organisms that drastically outperform robots in terms of agility, dexterity, and adaptability. To create a new generation of soft, life-like robots that reproduce the vast capabilities of biological systems, we need to develop actuators that replicate the astonishing all-around actuation performance of biological muscle. Hydraulically Amplified Self-healing ELectrostatic (HASEL) transducers are a new class of self-sensing, high-performance muscle-mimetic actuators, which are electrically driven and harness a mechanism that couples electrostatic and hydraulic forces to achieve a wide variety of actuation modes. Current designs of HASEL artificial muscles exceed actuation stress of 0.3 MPa, linear strain of 100%, specific power of 600W/kg, efficiency of 30% and bandwidth of 100Hz; all these metrics match or exceed the capabilities of biological muscle. This talk gives an overview over the latest developments, including materials systems, modeling, new designs of actuators, fabrication techniques, and creation of untethered soft robotic devices.

### **3:00 PM \*F.SM02.04.03**

**Non-Equilibrium Signal Integration in Hydrogels** Peter Korevaar, Nadir Kaplan and Joanna Aizenberg; Harvard University, United States

Materials that perform complex chemical signal processing are ubiquitous in living systems. Their synthetic analogs would transform developments in biomedicine, catalysis, and many other areas. By drawing inspiration from biological signaling dynamics, we show how simple hydrogels have a previously untapped capacity for non-equilibrium chemical signal processing and integration. Using a common polyacrylic acid hydrogel, with divalent cations and acid as representative stimuli, we demonstrate the emergence of non-monotonic osmosis-driven spikes and waves of expansion/contraction, as well as traveling color waves. These distinct responses emerge from different combinations of rates and sequences of arriving stimuli. A non-equilibrium continuum theory we developed quantitatively captures the nonmonotonic osmosis-driven deformation waves and determines the onset of their emergence in terms of the input parameters. These results suggest that simple hydrogels, already built into numerous systems, have a much larger sensing space than currently employed.

### **3:15 PM F.SM02.01.02**

**3D Printing of Jammed Double Network Granular Hydrogels with Superior Mechanical Properties** Matteo Hirsch,

Alvaro Charlet and Esther Amstad; EPFL, Switzerland

Hydrogels are among the first biomaterials expressly designed for their use in biomedicine. However, state-of-the-art applications of hydrogels are severely limited because of their mechanical properties. Most hydrogels are either too soft or too brittle to be used for load-bearing applications. To overcome this shortcoming, double network (DN) hydrogels composed of two interpenetrating polymeric networks have been introduced. These DN hydrogels are composed of a highly crosslinked network, the filler, responsible for the stiffness of the hydrogel and a second loosely crosslinked one, the matrix, that regulates the toughness of the material. Despite this great improvement in mechanics, composition and structural complexity found in soft natural tissues remain yet to be matched. Indeed, soft natural materials possess locally varying compositions and structures that are well-defined over many length scales. By contrast, synthetic hydrogels typically have an ill-defined microstructure and their composition is most often homogeneous. To obtain a better structural control, we introduce a novel 3D printing approach to fabricate strong and tough soft materials, namely double network granular hydrogels (DNGHs). This is achieved with an ink composed of microgels that are swollen in a monomer-containing solution. Upon printing and post-curing, the monomers are converted into a percolating network, yielding a solid DNGH. These DNGHs possess mechanical properties that are superior to reported additive manufactured hydrogels. In this work, we demonstrate that this technique enables printing macroscopic strong and tough objects with a high shape fidelity. Because this new technology employs a microgel-based ink, it significantly extends the choice of materials that can be additive manufactured. Moreover, the modularity of the jamming approach allows for the combination of different ink in the same printing process, resulting in mechanically robust stimuli responsive structures.

### 3:25 PM F.SM02.01.03

**Programmable Living Hydrogels for Gut Therapeutics and 3D Printing** [Anna Duraj-Thatte](#)<sup>1,2</sup>, Avinash Manjula Basavanna<sup>1,2</sup> and Neel Joshi<sup>1,2</sup>; <sup>1</sup>Harvard University, United States; <sup>2</sup>Northeastern University, United States

Over the last few decades, living cells have been employed as factories to make organic molecules, polymers, drugs, and fuels. Lately, living cells are being engineered to make materials and/or to modulate its properties, giving rise to an exciting field of Living Materials. Earlier work has shown that engineered living materials (ELMs) can bind to nanoparticles, catalyze reactions, and modulate conductivity amongst others.

Herein, we present a versatile strategy for the fabrication of living hydrogels directly from the bacterial culture by a simple filtration protocol. This hydrogel comprises of *E. coli* embedded in an extracellular matrix of engineered protein fibers. Genetic programming enables the hydrogels to be customized to interact and adhere to different tissues of the gastrointestinal tract. The designed mucoadhesive and anti-inflammatory hydrogels can be sprayed directly in the gut serving as an innovative wound healing strategy for the gut lumen.

By genetic engineering, we have also developed a functional microbial ink for 3D printing of living materials. This microbial ink is produced from engineered bacteria and can also be embedded with desired microbes to enable the printing of complex 3D architectures having various functions like sensing and sequestration.

Thus, we demonstrate the very first examples of microbial ink for 3D printing and the biomedical application of living materials. This unique platform of genetically programmable living hydrogels provides unprecedented opportunities to harvest the characteristics of living systems and thereby enables advanced applications of living materials.

### 3:35 PM F.SM02.02.03

**Electrically Conductive Bioadhesive Interface for Bioelectronics** [Jue Deng](#)<sup>1,2</sup>, Hyunwoo Yuk<sup>1</sup>, Claudia Varela<sup>1</sup>, Jingjing Wu<sup>1,2</sup>, Xiaoyu Chen<sup>1</sup>, Ellen Roche<sup>1</sup>, Chuanfei Guo<sup>2</sup> and Xuanhe Zhao<sup>1</sup>; <sup>1</sup>Massachusetts Institute of Technology, United States; <sup>2</sup>Southern University of Science and Technology, China

Reliable functions of bioelectronic devices require conformal, stable, and conductive interfaces with biological tissues. Integrating bioelectronic devices with native tissues usually relies on physical attachment or surgical suturing. Whilst these conventional methods face challenges such as non-conformal contact, unstable fixation, tissue damage and/or scar formation. Here we present a new class of bioadhesive electronic devices capable of compatibly and robustly integrating with various wet dynamic tissues, offering a promising solution beyond suturing and physical attachment to address the aforementioned challenges. The bioadhesive electronics are enabled by a new nanocomposite interface that can provide rapid (adhesion formation within five seconds), robust (interfacial toughness over 400 J m<sup>-2</sup>), and on-demand detachable adhesion of bioelectronic devices on diverse wet tissues. The nanocomposite interface is electrically conductive (conductivity over 2.6 S

m<sup>-1</sup>) to allow bi-directional bioelectronic communications. We demonstrate applicability, mechanical and electrical stability, biocompatibility, and bioelectronic recording and stimulation functionalities of the bioadhesive electronics based on ex vivo porcine and in vivo rat models. This study provides a new powerful platform for diverse bioelectronics to address the long-standing challenges in human-machine interface.

SESSION F.SM02.07: Live Keynote and Oral II: Hydrogel Technology for Humans and Machines

Session Chairs: Xinyue Liu and Jie Zheng

Wednesday Morning, December 2, 2020

F.SM02

**8:00 AM \*F.SM02.03.02**

**Linking Molecular Behavior to Macroscopic Properties in Ideal Dynamic Covalent Hydrogels** Mark W. Tibbitt; ETH Zürich, Switzerland

Dynamic covalent chemistry has emerged as an elegant molecular design strategy to engineer functional polymer networks that combine advantageous properties of both chemically and physically cross-linked materials. Dynamic covalent networks (DCvNs) are increasingly used in advanced materials design with applications ranging from recyclable thermosets to self-healing hydrogels. However, the relationship between the underlying chemistry at the junctions of DCvNs and their macroscopic properties is still not fully understood. In this presentation, we will outline a robust framework to predict how complex network behavior in DCvNs emerges from the chemical landscape of the dynamic chemistry at the junction. We use ideal dynamic covalent boronic ester-based hydrogels as model DCvNs. We will describe physical models that explain how viscoelastic properties, as measured by shear rheometry, are linked to the molecular behavior of the dynamic junction, quantified via fluorescence and NMR spectroscopy and DFT calculations. Additionally, shear rheometry is combined with Eyring Transition State Theory to quantify the kinetics and thermodynamics of network rearrangements, enabling a mechanistic understanding including preferred reaction pathways for dynamic covalent chemistries. We apply this approach to corroborate the ‘loose-bolt’ postulate for the reaction mechanism in Wulff-type boronic acids. These findings, grounded in molecular principles, advance our understanding and rational design of dynamic polymer networks, improving our ability to predict, design, and leverage their unique properties for future applications. We will also discuss applications of these materials for the thermal stabilization of biologics and as tunable viscoelastic materials.

**8:15 AM \*F.SM02.03.03**

**Non-Linear Mechanics and Failure of Composite Fibre Gels** Jasper van der Gucht; Wageningen University & Research, Netherlands

Living tissues show an extraordinary adaptiveness to strain, which is crucial for their proper biological functioning. The physical origin of this mechanical behaviour has been widely investigated using reconstituted networks of collagen fibres, the principal load-bearing component of tissues. However, collagen fibres in tissues are embedded in a soft hydrated polysaccharide matrix which generates substantial internal stresses whose effect on tissue mechanics is unknown. Here, by combining mechanical measurements and computer simulations, we show that networks composed of collagen fibres and a hyaluronan matrix exhibit synergistic mechanics characterized by an enhanced stiffness and delayed strain-stiffening. We demonstrate that the polysaccharide matrix has a dual effect on the composite response involving both internal stress and elastic reinforcement. Moreover, the matrix has a pronounced effect on fracture of the networks, leading to enhanced toughness and a transition from brittle to ductile behaviour. Our findings elucidate how tissues can tune their strain-sensitivity over a wide range and provide a novel design principle for synthetic materials with programmable mechanical properties.

[1] F. Burla, J. Tauber, S. Dussi, J. van der Gucht, G.H. Koenderink, *Nature Physics*, 15, 549 (2019)

[2] S. Dussi, J. Tauber, J. van der Gucht, *Physical Review Letters* 124 (2020), 018002

[3] F. Burla, S. Dussi, C. Martinez-Torres, J. Tauber, J. van der Gucht\*, G.H. Koenderink, *PNAS* 117 (2020), 8326

**8:30 AM \*F.SM02.03.04**

**Self-Assembly to Build Hydrogels and Insights into Their Morphology** Cécile A. Dreiss; King's College London, United Kingdom

Interest in hydrogels over the past couple of decades has exploded for a wide range of biomedical applications, including drug delivery, and tissue engineering.<sup>1</sup> There is a huge interest in building these supramolecular structures from non-covalent interactions, e.g. hydrogen bonds, host-guest interactions, which provide an easy tailoring of dynamic properties, impart shear-thinning and thus injectability and self-healing, making them more amenable to biomedical applications. Our group focuses on harnessing and understanding simple gelation processes in materials that come from renewable sources or are easily accessible. We exploit hybrid gelation processes to the cross-linking process,<sup>2</sup> spontaneous self-assembly in mixtures of modified polymers and surfactants,<sup>3</sup> formation of pseudopolyrotaxanes with cyclodextrins,<sup>4</sup> and thermally-triggered gelation.<sup>5</sup> In this talk I will present some of our recent work on self-assembled gels and in particular how we use small-angle neutron scattering to elucidate the spatial organisation of the networks that sustain the rheological properties, and ultimately build towards a rationale for hydrogel formulations.

- [1] C. A. Dreiss (2020) *Curr. Opin Colloid Interface Sci.* 48, 1; C. Salzechner et al. (2020) *Adv. Healthcare Mat.* 9, 4, 1901134; da Silva & Dreiss (2016) *Polym. Int.* 65, 268  
[2] M.A. da Silva et al. (2017) *J. Pol. Sci. B.* 55, 1850; M. A. da Silva (2015) *Biomacromolecules* 16, 1401; M. A. da Silva et al. (2015) *Biomacromolecules* 16, 1401.  
[3] N. Zoratto et al. (2019) *J. Colloid Interface Sci.*, 556, 301  
[4] M. Serres-Gómez et al. (2018) *Langmuir*, 34, 10591  
[5] J. Puig-Rigall et al. (2017) *J. Colloid Int. Sci.* 524, 42

#### 8:45 AM \*F.SM02.03.05

##### **Viscoelastic Properties of Supramolecular Gels and Mixtures Based on Hydrogen Bonding** Dimitri Vlassopoulos<sup>1,2</sup>; <sup>1</sup>FORTH, Greece; <sup>2</sup>University of Crete, Greece

Understanding and tailoring the self-assembly of supramolecular moieties is a challenging subject with potential implications in materials engineering and biological function. Here we discuss two problems associated with the viscoelastic properties of (i) hydrogel mixtures due to competitive interactions and (ii) organogels due to the presence of traces of humidity.

Concerning the former, we investigated a class of binary hydrogels made by mixing fibrillar supramolecular polymers that are formed from two compounds: 1,3,5-benzene-tricarboxamide decorated with aliphatic chains terminated by tetra(ethylene glycol) (BTA) and a 20 kg/mol telechelic poly(ethylene glycol) decorated with the same hydrogen bonding BTA motif on both ends (BTA-PEG-BTA). We found that the respective single-compound-based supramolecular systems form very different networks which exhibit drastically different rheology. More strikingly, mixing the compounds results in a non-monotonic dependence of modulus and viscosity on composition, suggesting a competition between interactions of the two compounds, which can then be used to fine-tune the mechanical properties.

The latter problem concerns the self-assembly of supramolecular moieties in organic solvents which is affected by the presence of trace amounts of water in the monomeric state that induce competitive association and change the helicity of the assembled structure. We investigated an organogel in dodecane (biphenyl tricarboxamide, BPTA) and found that water affects the self-assembled structure by changing the persistence length and contour length of the fiber. The content of water in the fiber changed with temperature, bequeathing the linear and nonlinear viscoelastic properties with unusual temperature responsiveness. For instance, as the temperature increased from 15 to 35°C, the relaxation time of the system varied non-monotonically with temperature. This stems from the fact that the system loses its reversible and dynamic character for temperatures above 35°C where water does not mediate the association of BPTA units.

These findings are discussed in the context of existing theories of living polymers and of the perspective of designing gels with desired and tunable properties.

Work in collaboration with E. Vereroudakis (Crete), N.J. Van Zee (ESPCI, Paris), E. Del Gado (Georgetown) and E.W. Meijer (T. U. Eindhoven).

#### 9:00 AM \*F.SM02.04.04

##### **Polymer Gels for Autonomous Motion and Mesoscale Assembly** Alfred J. Crosby; University of Massachusetts Amherst, United States

Nature is masterful at using limited components and basic driving forces to achieve complex tasks, such as high power movement and multi-structure assembly, across a broad range of size scales. The materials that enable these achievements often rely upon the integration of phases that allow for internal transport, elastic energy storage, system protecting dissipation, and tunable sensitivity to interfacial interactions. Accordingly, polymer gels, which combine liquid phases with shear-sustaining macromolecular network structures, offer a robust materials platform for transferring lessons from nature into synthetic engineered devices. Here, we describe two examples from our research group of how to take advantage of

mesoscale structural asymmetry, mechanics, liquid transport, and interfacial interactions to achieve new engineered capabilities. The first example takes inspiration from multiple examples in nature, including mantis shrimp and trap-jaw ants, that use Latch-Mediated Spring Actuation (LaMSA) to achieve high power, impulsive movements. We demonstrate how transient metastable deformations associated with swelling and deswelling of a polymer gel can be exploited to generate mechanical bi-stability, giving rise to multiple, self-repeating, snap-through movements. We introduce models to quantitatively describe these mechanisms and harness them to develop autonomous jumping devices. In a related manner, the second example describes the use of structural asymmetry to mediate swelling/deswelling processes and elastic restoring forces to control the motion and assembly of mesoscale polymer gel ribbons. Collectively, both examples provide new insight into how polymer gel properties, related to elasticity, diffusion, and interfacial forces, can combine with purposeful structural design to yield complex tasks, which can be used in the development of microscale robots and new adaptable composite materials.

#### 9:15 AM F.SM02.03.09

**Intrinsic Fracture Energy of Soft Mechanical Metamaterials** [Dongchang Zheng](#)<sup>1,2</sup>, Shaoting Lin<sup>1</sup>, Liu Wang<sup>1</sup> and Xuanhe Zhao<sup>1,1</sup>; <sup>1</sup>Massachusetts Institute of Technology, United States; <sup>2</sup>University of Science and Technology of China, China

Diverse soft metamaterials have been developed for energy-absorbing, tunable thermal expansion, soft actuator, etc. Although various functional properties of soft metamaterials have been investigated, their fatigue properties have not been studied yet, which hinders the translation of soft metamaterials into real applications. With 3D printing techniques, we control the geometrical parameters of soft metamaterials. Fracture tests and simulations are conducted to measure the S-N curve of a single printing filament and fatigue threshold of 3D printed soft metamaterials. We show that the fatigue threshold of soft metamaterials is linearly proportional to the fiber's diameter and strain energy density limit, but independent of its length. Constitutive relation of the materials and geometrical shapes determine the prefactor of such proportion relations. The results are intrinsically different from the classical Lake-Thomas theory for polymer networks, leading to a generalized theory for predicting soft metamaterials' fatigue threshold. The capability of the theory correlating the fatigue property of a single filament and entire topological networks is critical for the design of durable soft metamaterials. This theory inspires us to manufacture sinusoidal structure metamaterials, whose fatigue threshold increase dramatically.

#### 9:25 AM F.SM02.04.15

**Surface Engineering of Hydrogels for Solar Water Purification** [Youhong Guo](#) and Guihua Yu; The University of Texas at Austin, United States

Water scarcity has been an increasingly severe threat to our society. Solar vapor generation provides a sustainable means for desalination and water purification technologies. With highly tunable structures, unique polymer-water interactions, and ease of integration with functional materials, hydrogels show great potential for efficient solar water purification. The rational design and engineering of hydrogel surfaces have a substantial impact on the interfacial solar water vaporization process. Here, we will discuss effective ways to tailor the surface topography and wetting states of hydrogel solar evaporators to accelerate the solar vapor generation rate. Specifically, the nanotextured topography of the surface can be fabricated by a liquid-liquid interface-guided gelation process, resulting in an increased heat flux at the sharply dimpled hydrogel-air interface. In addition, hydrogel evaporators with inhomogeneous surface wettability demonstrate an ultrahigh evaporation rate with synergistic contributions from both wetting regions. Molecular dynamics simulation reveals the surface-modulated escaping behavior of water molecules. By applying hydrophilic polymers as building blocks, the hydrogel evaporators have been endowed with multifunctionalities, such as antifouling and complex contaminants removal, to improve both quantity and quality of collected water. Together with an easy-to-employ and portable purification prototype, hydrogels are an emerging materials platform for high-performance yet cost-effective water purification applications.

#### 9:35 AM F.SM02.03.11

**Late News: Mesoscale Modeling of Controlled Degradation in Hydrogels** [Vaibhav A. Palkar](#), Chandan K. Choudhury and Olga Kuksenok; Clemson University, United States

Hydrogel based soft materials with chemical functionalities that allow controlled degradation of the polymer are utilized as active stimuli responsive platforms for numerous applications. As one example, a hydrogel with multiple degradable functional groups that degrade in response to different wavelengths of light enables sequential release of drugs from the network. Herein, we present Dissipative Particle Dynamics (DPD) based simulations of degradation in tetra-arm polyethylene glycol (tetra-PEG [1]) hydrogels. Controlled degradation can be introduced in these gels via several chemical pathways [2,3].

In our DPD model we use the modified segmental repulsive potential (mSRP [4]) to avoid unphysical polymer chain crossing and we first establish model parameters that mimic the hydrophilicity of PEG. Further, we use our recently developed framework [5] to introduce controlled degradation in these gels and measure the fraction of degradable bonds intact during degradation. Our method allows modeling of first order degradation kinetics in these gels. We track the evolution of mass loss from bulk degrading gels and note the occurrence of a slow mass loss regime due to erosion followed by a fast regime due to reverse gelation of the polymer network. We quantify the reverse gel point of these gels by tracking the size of the second largest cluster during degradation. We focus on the effect of finite size on mass loss and reverse gel point calculations and compare these effects with previously developed scaling [6]. The reverse gel point for tetra-PEG hydrogels measured from our simulations corresponds well with the value obtained from percolation theory on a diamond lattice.

#### References:

1. Sakai, T., Matsunaga, T., Yamamoto, Y., Ito, C., Yoshida, R., Suzuki, S., Sasaki, N., Shibayama, M., & Chung, U. I. (2008). Design and fabrication of a high-strength hydrogel with ideally homogeneous network structure from tetrahedron-like macromonomers. *Macromolecules*, 41(14), 5379-5384.
2. Li, X., Tsutsui, Y., Matsunaga, T., Shibayama, M., Chung, U. I., & Sakai, T. (2011). Precise control and prediction of hydrogel degradation behavior. *Macromolecules*, 44(9), 3567-3571.
3. Azagarsamy, M. A., McKinnon, D. D., Alge, D. L., & Anseth, K. S. (2014). Coumarin-based photodegradable hydrogel: Design, synthesis, gelation, and degradation kinetics. *ACS Macro Letters*, 3(6), 515-519.
4. Sirk, T. W., Slizoberg, Y. R., Brennan, J. K., Lisal, M., & Andzelm, J. W. (2012). An enhanced entangled polymer model for dissipative particle dynamics. *The Journal of chemical physics*, 136(13), 134903.
5. Palkar, V., Choudhury, C. K., & Kuksenok, O. (2020). Development of Dissipative Particle Dynamics framework for modeling hydrogels with degradable bonds. *MRS Advances*, 5(17), 927-934.
6. Lin, T. S., Wang, R., Johnson, J. A., & Olsen, B. D. (2018). Topological structure of networks formed from symmetric four-arm precursors. *Macromolecules*, 51(3), 1224-1231.

#### SESSION F.SM02.01: 3D/4D Printing of Hydrogels

On Demand Abstracts Available for Viewing Starting Saturday Morning, November 21, 2020  
F-SM02

##### 5:00 AM \*F.SM02.01.01

**Formulating Bioinks and Bioink Processing Methods for Tissue Bioprinting** Yu Shrike Zhang; Harvard Medical School, United States

Over the last decade, three-dimensional bioprinting has offered great versatility to fabricate biomimetic volumetric tissues that are both structurally and functionally relevant to their native counterparts. The technology enables precise control over the composition, spatial distribution, and architecture of the bioprinted constructs, facilitating recapitulation of the delicate shapes and structures of targeted organs and tissues. This talk will discuss our recent efforts on developing various cytocompatible and cell-instructive bioink formulations, as well as their processing methods, for the fabrication of engineered tissues towards regenerative medicine and tissue model engineering applications, using a series of established or customized bioprinting strategies.

##### 5:15 AM F.SM02.01.02

**3D Printing of Jammed Double Network Granular Hydrogels with Superior Mechanical Properties** Matteo Hirsch, Alvaro Charlet and Esther Amstad; EPFL, Switzerland

Hydrogels are among the first biomaterials expressly designed for their use in biomedicine. However, state-of-the-art applications of hydrogels are severely limited because of their mechanical properties. Most hydrogels are either too soft or too brittle to be used for load-bearing applications. To overcome this shortcoming, double network (DN) hydrogels composed of two interpenetrating polymeric networks have been introduced. These DN hydrogels are composed of a highly crosslinked network, the filler, responsible for the stiffness of the hydrogel and a second loosely crosslinked one, the matrix, that regulates the toughness of the material. Despite this great improvement in mechanics, composition and structural complexity found in soft natural tissues remain yet to be matched. Indeed, soft natural materials possess locally varying compositions and structures that are well-defined over many length scales. By contrast, synthetic hydrogels typically have an ill-defined microstructure and their composition is most often homogeneous. To obtain a better structural control, we introduce a novel



3D printing approach to fabricate strong and tough soft materials, namely double network granular hydrogels (DNGHs). This is achieved with an ink composed of microgels that are swollen in a monomer-containing solution. Upon printing and post-curing, the monomers are converted into a percolating network, yielding a solid DNGH. These DNGHs possess mechanical properties that are superior to reported additive manufactured hydrogels. In this work, we demonstrate that this technique enables printing macroscopic strong and tough objects with a high shape fidelity. Because this new technology employs a microgel-based ink, it significantly extends the choice of materials that can be additive manufactured. Moreover, the modularity of the jamming approach allows for the combination of different ink in the same printing process, resulting in mechanically robust stimuli responsive structures.

#### 5:25 AM F.SM02.01.03

**Programmable Living Hydrogels for Gut Therapeutics and 3D Printing** [Anna Duraj-Thatte](#)<sup>1,2</sup>, Avinash Manjula Basavanna<sup>1,2</sup> and Neel Joshi<sup>1,2</sup>; <sup>1</sup>Harvard University, United States; <sup>2</sup>Northeastern University, United States

Over the last few decades, living cells have been employed as factories to make organic molecules, polymers, drugs, and fuels. Lately, living cells are being engineered to make materials and/or to modulate its properties, giving rise to an exciting field of Living Materials. Earlier work has shown that engineered living materials (ELMs) can bind to nanoparticles, catalyze reactions, and modulate conductivity amongst others.

Herein, we present a versatile strategy for the fabrication of living hydrogels directly from the bacterial culture by a simple filtration protocol. This hydrogel comprises of *E. coli* embedded in an extracellular matrix of engineered protein fibers. Genetic programming enables the hydrogels to be customized to interact and adhere to different tissues of the gastrointestinal tract. The designed mucoadhesive and anti-inflammatory hydrogels can be sprayed directly in the gut serving as an innovative wound healing strategy for the gut lumen.

By genetic engineering, we have also developed a functional microbial ink for 3D printing of living materials. This microbial ink is produced from engineered bacteria and can also be embedded with desired microbes to enable the printing of complex 3D architectures having various functions like sensing and sequestration.

Thus, we demonstrate the very first examples of microbial ink for 3D printing and the biomedical application of living materials. This unique platform of genetically programmable living hydrogels provides unprecedented opportunities to harvest the characteristics of living systems and thereby enables advanced applications of living materials.

#### 5:35 AM F.SM02.01.05

**Late News: Development of the Thermomechanical Properties of the Gelatin/Siloxane Hybrid Material as Bioink** [Bryan Valenzuela](#); Universidad Autónoma de Ciudad Juárez, Mexico

Bioinks are hydrogels that have the ability to encapsulate cells and promote their proliferation, there are compound and hybrid bioinks of the following natural materials, synthetic polymers, bioceramics, metallic nanoparticles. Composite bioinks are materials where their chemical structure and properties are combined in homogeneous way, otherwise, the hybrid bioinks have a chemical structure and properties combined in heterogeneous way, even in some hybrids bioinks, it is possible to observe different phases of this components.

At use gelatin/siloxane hybrid material in a room temperature, is possible to observe the organic (gelatin) and inorganic (siloxane) phase which is a tremendous advantage. It is important to remark the presence of these phase offers thermomechanical properties that facilitate its funcionalization as bioink.

Siloxane is a direct derivate of silicon dioxide gel that is biocompatible and non - cytotoxic, properties that allows cell culture deposition and encapsulation, gelatin is a material derived from collagen which consist of a biopolymer of three aminoacids (arginine, glycine and lysine).

The funcionalization of siloxane and gelatin by means of magnetic stirring allows the interaction of the amine groups (NH<sup>+</sup>) of gelatin and the hydroxyl groups (OH<sup>-</sup>) of the siloxane.

The lost of water through the oxidation of the siloxane allows the modulation of thermomechanical properties of the gelatin/siloxane hybrid material, through physical treatments such as UV radiation and heat treatments in the range of fifty degrees centigrade (50C) to seventy degrees centigrade (70C), forming the siloxane bonds that improve the termomechanical properties of the material such viscosity and mechanical compression.

The gelatin/siloxane hybrid material possesses a viscosity that can be modulated by heat treatments in the range of thirty-two degrees centigrade (32C) to forty-two degrees centigrade (42C).

*The viscosity of the gelatin/siloxane hybrid material is related to the concentration of dispersed siloxane particles.*

This relationship permit that at temperature in the range of four degrees centigrade (4C) to fifteen degrees centigrade (15C), the material reticulates by forming fibers that help maintain the fidelity and mechanical properties necessary to use the gelatin/siloxane hybrid material as bioink.

The aforementioned thermomechanical properties of the gelatin/siloxane hybrid material provide the support of being used as bioink. The gelatin/siloxane hybrid material let the cultivation of various cell lines such as: (carotid artery cells, liver, myocytes, cardiomyocytes among others).

In function on its thermomechanical properties. The degradation of siloxane inhibits certain enzymes in bacterial metabolism that generate antibacterial properties.

3D bioprinting is a technique for biofabrication of three - dimensional structures that, through layered printing technology, allows manufacture constructs for the deposit or seeding of cell cultures. The BIO X bioprinter (Cellink®) is a bioprinter with a resolution in the range of 10 to 100 µm depending on the bioink used and the printing syringe nozzle. Is one of the most user - friendly bioprinters on the market, in addition to allow the use of composite and hybrid bioinks depending on the printing parameters (nozzle size, applied pressure, printing speed, head and print bed temperature), however, bioprinters are highly sophisticated and precise equipment, therefore, to determine the printing parameters of a bioink it is imperative to perform mathematical analysis.

In conclusion, this work deals with the development of a bioprinting process specifically of the gelatin/siloxane hybrid material that, thanks to the mathematical model used, generates a better mechanical performance of the printed constructs with the assistance of the BIO X bioprinter (Cellink®) and provides a look to the futures with the first tests of a bioprinter that combines extrusion and injection technology.

#### SESSION F.SM02.02: Gel Adhesion

On Demand Abstracts Available for Viewing Starting Saturday Morning, November 21, 2020

F-SM02

##### 5:00 AM \*F.SM02.02.01

**Chemical and Topological Design of Mussel-Inspired Polymers—A Single-Molecule Adhesion Perspective** Yiran Li<sup>1</sup>, Peyman Delparastan<sup>2</sup>, Jing Cheng<sup>2</sup>, Haoqi Wang<sup>1</sup>, Kelsey DeFrates<sup>2</sup>, Yi Cao<sup>1</sup> and Phillip B. Messersmith<sup>2,3</sup>; <sup>1</sup>Nanjing University, China; <sup>2</sup>University of California, Berkeley, United States; <sup>3</sup>Lawrence Berkeley National Laboratory, United States

In mussels, the adhesive proteins that are instrumental for attachment to wet surfaces are known to contain high levels of 3,4-dihydroxy-L-alanine (DOPA), often located adjacent to amino residues such as lysine (Lys). The special synergistic relationship between catechols and amines is a subject of high interest, not only for understanding native proteins but also for informing the design of bioinspired polymer systems. Other research groups have shown that catechol and amine functional groups act synergistically to enhance adhesion at wet surfaces, however reports of catechol-amine interfacial phenomena on a single molecule level have been limited. In this talk we will describe single molecule force spectroscopy (SMFS) measurements that are providing new insights into interactions between Lys-DOPA peptides and various surfaces. Of particular interest is the impact of chemical composition (DOPA and Lys), peptide length and topology (i.e. distribution of adhesive elements along a polymer) on interfacial adhesion to a wet substrate. The results may inform the future design of novel polymer adhesives, including adhesive hydrogels, pressure sensitive adhesives and high-strength thermoset adhesives.

##### 5:15 AM \*F.SM02.02.02

**Smart Material and Adhesive Utilizing Mussel Adhesive Chemistry** Bruce Lee; Michigan Technological Univ, United States

Marine mussels secrete adhesive proteins that enable these organism to anchor themselves to various substrate (i.e., ship hull, rock) in a rough, intertidal zone. These mussel foot proteins contain a unique amino acid, L-3, 4 dihydroxyphenylalanine (DOPA), that is responsible for strong interfacial binding and curing of the proteins. The catechol side chain of DOPA is capable of participating in various stimuli responsive, reversible interactions, dictated by its oxidation state. In this presentation, I will describe our efforts in utilizing these interactions in designing various types of smart biomaterial. We have incorporated catechol-metal ion coordination bond to design hydrogel actuators that can fold into various 3-dimensional shapes. We have also utilized catechol-boronic acid complexation chemistry to design moisture-resistant smart adhesive with tunable adhesive properties. Most recently, we demonstrated the feasibility of using applied electricity to directly deactivate catechol-based adhesive that is bonded to a surface.

### 5:30 AM F.SM02.02.03

**Electrically Conductive Bioadhesive Interface for Bioelectronics** Jue Deng<sup>1,2</sup>, Hyunwoo Yuk<sup>1</sup>, Claudia Varela<sup>1</sup>, Jingjing Wu<sup>1,2</sup>, Xiaoyu Chen<sup>1</sup>, Ellen Roche<sup>1</sup>, Chuanfei Guo<sup>2</sup> and Xuanhe Zhao<sup>1</sup>; <sup>1</sup>Massachusetts Institute of Technology, United States; <sup>2</sup>Southern University of Science and Technology, China

Reliable functions of bioelectronic devices require conformal, stable, and conductive interfaces with biological tissues. Integrating bioelectronic devices with native tissues usually relies on physical attachment or surgical suturing. Whilst these conventional methods face challenges such as non-conformal contact, unstable fixation, tissue damage and/or scar formation. Here we present a new class of bioadhesive electronic devices capable of compatibly and robustly integrating with various wet dynamic tissues, offering a promising solution beyond suturing and physical attachment to address the aforementioned challenges. The bioadhesive electronics are enabled by a new nanocomposite interface that can provide rapid (adhesion formation within five seconds), robust (interfacial toughness over 400 J m<sup>-2</sup>), and on-demand detachable adhesion of bioelectronic devices on diverse wet tissues. The nanocomposite interface is electrically conductive (conductivity over 2.6 S m<sup>-1</sup>) to allow bi-directional bioelectronic communications. We demonstrate applicability, mechanical and electrical stability, biocompatibility, and bioelectronic recording and stimulation functionalities of the bioadhesive electronics based on ex vivo porcine and in vivo rat models. This study provides a new powerful platform for diverse bioelectronics to address the long-standing challenges in human-machine interface.

### 5:40 AM F.SM02.02.04

**Multi-Functional Bioadhesive Platforms for Translational Tissue Adhesive Technologies** Hyunwoo Yuk and Xuanhe Zhao; Massachusetts Institute of Technology, United States

Tools to close and repair wounds in our body are the first set of medical devices in human history. Despite the long history even started from the pre-historic use sutures, the standard care to close wounds still mostly rely on the traditional methods such as sutures and surgical staplers. These old standard cares have faced numerous lingering challenges including slow or complex procedure, leakage, and tissue damage with a huge cost to our society: each year, over millions of people suffer and perish due to the leakages of sealed incisions of organs, failures of prompt hemostasis, and chronic open wounds. Considering the fact that how the entire world has been suffered from the less than 1M death toll by the COVID-19, the degree of the clinical and societal burden from the limitations of current tissue closure and repair technologies is startlingly grave.

Tissue adhesives including tissue sealants and hemostatic agents have been the most recent technologies to address these challenges. However, translational benefits of the tissue adhesives in clinical applications have still been in the nascent state due to the long list of limitations of existing tissue adhesive technologies including 1) slow adhesion formation, 2) weak bonding, 3) low biocompatibility, 4) poor mechanical match with tissues, 5) incompatibility to body fluids like blood, 6) lack of triggerable on-demand detachment, 7) lack of programmable modulation of wounded tissues, and/or 8) poor compatibility to emerging surgical techniques such as minimally invasive surgeries (MIS). In this talk, we will introduce our set of recent advances to translational tissue adhesive technologies based on various yet highly synergistic multi-functional bioadhesive platforms to address all of the abovementioned limitations. We will first briefly summarize the unmet clinical demands in existing tissue adhesives with associated scientific backgrounds for the mechanistic source of the challenges. Then, we will introduce our multi-functional bioadhesive platforms to satisfy the unmet clinical demands with corresponding clinical applications that we are exploring with collaboration with leading clinical experts.

### 5:50 AM F.SM02.02.05

**Multifunctional Tissue Sealant for Minimally Invasive Surgery** Sarah Wu<sup>1</sup>, Hyunwoo Yuk<sup>1</sup>, Jingjing Wu<sup>1</sup>, Christoph Nabzdyk<sup>2</sup> and Xuanhe Zhao<sup>1</sup>; <sup>1</sup>Massachusetts Institute of Technology, United States; <sup>2</sup>Mayo Clinic, United States

Methods for tissue sealing and repair in minimally invasive surgery (MIS) represent a significant challenge in the shift toward less invasive procedures. Traditional surgical sutures and stapling devices are often difficult to maneuver precisely in MIS, and these pointwise modalities of sealing can cause tissue damage and lead to anastomotic leakage. While tissue adhesives offer the potential to overcome these limitations, existing adhesives have significant drawbacks; for example, they can be easily washed out in dynamic physiological environments, are prone to fouling in the presence of blood and body fluids, exhibit slow and/or weak adhesion to wet tissue, and may induce unfavorable inflammatory responses. Here, we propose a novel multifunctional bioadhesive designed to achieve controllable tissue adhesion in diverse physiological environments. The bioadhesive takes the form of a conformable patch and is realized by a synergistic combination of three

functional layers: 1) a hydrophobic liquid overlayer for protection against blood and body fluids, 2) a micro-textured bioadhesive layer for rapid and robust pressure-triggered adhesion, and 3) a zwitterionic anti-fouling layer for mitigation of foreign-body response and postoperative adhesion formation. The patch can be adapted to integrate with existing MIS tools, giving it the potential to advance a wide range of surgical procedures.

#### 6:00 AM F.SM02.02.06

**Strain Programmable Bioadhesive Patch for Accelerated Diabetic Wound Closure and Healing** Heejung Roh<sup>1</sup>, Hyunwoo Yuk<sup>1</sup>, Georgios Theocharidis<sup>2</sup>, Aristidis Veves<sup>2</sup> and Xuanhe Zhao<sup>1</sup>; <sup>1</sup>Massachusetts Institute of Technology, United States; <sup>2</sup>Harvard, United States

Impaired wound healing capability and consequent chronic wounds such as diabetic foot ulcers (DFU) are devastating complications in diabetic patients with rapidly growing clinical and economic burdens in aging societies, recording over 750,000 new DFU each year. Furthermore, significant clinical outcomes including lower extremity amputations are readily induced, resulting in the total annual cost of treatment of DFU and amputations at over 11 billion dollars. Given the rapidly growing patients across the world and the deleterious economic costs including a critical reduction in quality of lives, the treatment of diabetic wounds is one of the major current and future clinical challenges in need of effective solutions.

Despite various therapeutic strategies including several skin scaffolds and growth factor-based treatments that have been introduced and clinically tested for treatment of DFU in the last few decades, their benefits are rather limited as more than 50% of treated DFU patients fail to respond. This lack of effective treatment along with the gravity of the problem highlights the critical importance of developing new therapeutic solutions for diabetic wound healing.

Mechanical modulation of wounded or scarred skin has been a promising strategy to repair and remodel healthy skin in both animal models and human clinical trials. Given the previous animal studies indicating the reduced degree of contractibility of the wound as one of the sources of impaired wound healing in diabetes patients, such mechanical modulation is an attractive treatment route for diabetic wounds. However, the potential therapeutic benefits of the mechanical modulation approach have not been well investigated for chronic wounds such as DFU due to several technical limitations. Existing wound dressings and bandages for mechanical reinforcement or stimuli lack capabilities to 1) form rapid and robust adhesion on wet wounded skin and 2) precisely program mechanical contraction, limiting their use only for passive mechanical coverage, uncontrolled contraction, and/or fully closed wounds. These limitations have prevented the use of a mechanical modulation approach for chronic wounds such as DFU, leaving this potential therapeutic strategy untapped.

In this work, we report a strain programmable bioadhesive patch capable of rapid and fully programmable contraction and stress remodeling of wet wounded skins as a promising therapeutic platform for chronic diabetic wounds. The strain programmable bioadhesive patch synergistically combines a novel hydration-based shape-memory mechanism and the dry-crosslinking mechanism to simultaneously achieve rapid, robust, and on-demand detachable adhesion as well as predictable mechanical modulation when on wet wounded skin tissues. The strain programmable bioadhesive patch takes the form of a thin flexible film consisting of non-adhesive elastomer backing in the rubbery state (Young's modulus ~ 1 MPa) and a dry bioadhesive in the glassy state (Young's modulus ~ 5 GPa) with the programmed strain. Once hydrated by the native physiological fluids or moisture from the wounded tissue, the patch rapidly and robustly adheres to the underlying tissue by the bioadhesive while releasing its programmed strain to provide mechanical contraction to the wound.

To validate the proposed strain programmable bioadhesive patch and its efficacy on diabetic wound contraction and healing, we have performed systematic mechanical analysis (mechanical properties, adhesion performance, theoretical and FEM-based framework for predictable strain programming and mechanical modulation of a wound), in vitro and in vivo biocompatibility, and in vivo diabetic wound healing based on ex vivo porcine and in vivo diabetic mice models. The current study not only provides a promising solution for the treatment of chronic wounds but also offers insights into the development of technologies for programmable mechanical modulation of biological tissues.

#### 6:10 AM F.SM02.02.07

**Late News: Biocompatible Hydrogel Ostomy Adhesive** William Pan<sup>1</sup>, Beverly Matsuda<sup>1</sup> and Hyunwoo Yuk<sup>2</sup>; <sup>1</sup>Northwood High School, United States; <sup>2</sup>Massachusetts Institute of Technology, United States

Ostomies are digestive and excretory surgeries where waste is redirected to the outside of the abdomen, requiring a bag to catch excretion. Current methods use adhesives to create adhesion for 24-hour usage of the ostomy bag. However, current adhesives are weak and unstable, and often lead to leakages of ostomy effluents resulting various clinical complications including irritant dermatitis and infection. Despite these challenges, no commercially-available product can provide strong

enough adhesion nor mechanical softness to prevent skin damage from ostomy leaks. In this work, we introduce a hydrogel ostomy adhesive (HOA) made from a tough double-network hydrogel based on polyacrylamide and sodium alginate that can be strongly adhered onto the skin for over 24 hours and prevent leaks by maintaining fluid-tight sealing against regular bodily movements. The adhesion of HOA to abdominal skin is achieved by the topological adhesion formed by a biopolymer chitosan solution. The HOA's capability to form robust adhesion of ostomy bag is demonstrated based on *ex vivo* porcine skin and *in vivo* human skin in comparison with existing commercially-available ostomy bag adhesives.

#### 6:20 AM F.SM02.02.08

**Late News: Electrically Induced Adhesion of Polyelectrolyte Hydrogels to Animal and Plant Tissues** [Leah K. Borden](#), Uma J. Kokilepersaud and Srinivasa Raghavan; University of Maryland, United States

This talk will present studies from our lab on the electrically induced adhesion of hydrogels to various soft matter. The basic phenomenon involves crosslinked acrylate hydrogels made with either anionic or cationic co-monomers. When a rectangular strip of a cationic gel (connected to an anode) is contacted for just a few seconds with a strip of anionic gel (connected to a cathode) within an electric field of  $\sim 2\text{-}4$  V/mm, the two gel strips form a strong adhesive bond. When the polarity of the electrodes is reversed, the phenomenon is reversed, i.e., the gels can be easily detached.

While the above phenomenon of 'electro-adhesion' has been reported before for hydrogels, we show that it is much more general and widespread. Specifically, we can substitute either of the above gel strips with gels of various geometrical structures made using charged biopolymers such as chitosan or alginate. The same electro-adhesion works in resealing punctures in gel tubes thereby preventing gas and liquids from leaking out of these punctured structures. As an extreme case, two severed pieces of a tube can be stuck back together using a gel strip that spans both cut segments. In turn, electro-adhesion can also be applied for the pick-up and drop-off of soft cargo, and for the sorting of small cargo. Most interestingly, the same phenomenon also works with certain animal and plant tissues – that is, we show that cationic gels can be electro-adhered to these tissues. We thereby demonstrate that cuts or tears in tissues can be electro-sealed using gel strips.

#### SESSION F.SM02.03: Mechanics and Physics of Gels

On Demand Abstracts Available for Viewing Starting Saturday Morning, November 21, 2020  
F-SM02

#### 5:00 AM \*F.SM02.03.02

**Linking Molecular Behavior to Macroscopic Properties in Ideal Dynamic Covalent Hydrogels** [Mark W. Tibbitt](#); ETH Zürich, Switzerland

Dynamic covalent chemistry has emerged as an elegant molecular design strategy to engineer functional polymer networks that combine advantageous properties of both chemically and physically cross-linked materials. Dynamic covalent networks (DCvNs) are increasingly used in advanced materials design with applications ranging from recyclable thermosets to self-healing hydrogels. However, the relationship between the underlying chemistry at the junctions of DCvNs and their macroscopic properties is still not fully understood. In this presentation, we will outline a robust framework to predict how complex network behavior in DCvNs emerges from the chemical landscape of the dynamic chemistry at the junction. We use ideal dynamic covalent boronic ester-based hydrogels as model DCvNs. We will describe physical models that explain how viscoelastic properties, as measured by shear rheometry, are linked to the molecular behavior of the dynamic junction, quantified via fluorescence and NMR spectroscopy and DFT calculations. Additionally, shear rheometry is combined with Eyring Transition State Theory to quantify the kinetics and thermodynamics of network rearrangements, enabling a mechanistic understanding including preferred reaction pathways for dynamic covalent chemistries. We apply this approach to corroborate the 'loose-bolt' postulate for the reaction mechanism in Wulff-type boronic acids. These findings, grounded in molecular principles, advance our understanding and rational design of dynamic polymer networks, improving our ability to predict, design, and leverage their unique properties for future applications. We will also discuss applications of these materials for the thermal stabilization of biologics and as tunable viscoelastic materials.

#### 5:15 AM \*F.SM02.03.03

**Non-Linear Mechanics and Failure of Composite Fibre Gels** [Jasper van der Gucht](#); Wageningen University & Research,

Netherlands

Living tissues show an extraordinary adaptiveness to strain, which is crucial for their proper biological functioning. The physical origin of this mechanical behaviour has been widely investigated using reconstituted networks of collagen fibres, the principal load-bearing component of tissues. However, collagen fibres in tissues are embedded in a soft hydrated polysaccharide matrix which generates substantial internal stresses whose effect on tissue mechanics is unknown. Here, by combining mechanical measurements and computer simulations, we show that networks composed of collagen fibres and a hyaluronan matrix exhibit synergistic mechanics characterized by an enhanced stiffness and delayed strain-stiffening. We demonstrate that the polysaccharide matrix has a dual effect on the composite response involving both internal stress and elastic reinforcement. Moreover, the matrix has a pronounced effect on fracture of the networks, leading to enhanced toughness and a transition from brittle to ductile behaviour. Our findings elucidate how tissues can tune their strain-sensitivity over a wide range and provide a novel design principle for synthetic materials with programmable mechanical properties.

[1] F. Burla, J. Tauber, S. Dussi, J. van der Gucht, G.H. Koenderink, *Nature Physics*, 15, 549 (2019)

[2] S. Dussi, J. Tauber, J. van der Gucht, *Physical Review Letters* 124 (2020), 018002

[3] F. Burla, S. Dussi, C. Martinez-Torres, J. Tauber, J. van der Gucht\*, G.H. Koenderink, *PNAS* 117 (2020), 8326

#### 5:30 AM \*F.SM02.03.04

**Self-Assembly to Build Hydrogels and Insights into Their Morphology** Cécile A. Dreiss; King's College London, United Kingdom

Interest in hydrogels over the past couple of decades has exploded for a wide range of biomedical applications, including drug delivery, and tissue engineering.<sup>1</sup> There is a huge interest in building these supramolecular structures from non-covalent interactions, e.g. hydrogen bonds, host-guest interactions, which provide an easy tailoring of dynamic properties, impart shear-thinning and thus injectability and self-healing, making them more amenable to biomedical applications.

Our group focuses on harnessing and understanding simple gelation processes in materials that come from renewable sources or are easily accessible. We exploit hybrid gelation processes to the cross-linking process,<sup>2</sup> spontaneous self-assembly in mixtures of modified polymers and surfactants,<sup>3</sup> formation of pseudopolyrotaxanes with cyclodextrins,<sup>4</sup> and thermally-triggered gelation.<sup>5</sup> In this talk I will present some of our recent work on self-assembled gels and in particular how we use small-angle neutron scattering to elucidate the spatial organisation of the networks that sustain the rheological properties, and ultimately build towards a rationale for hydrogel formulations.

[1] C. A. Dreiss (2020) *Curr. Opinion Colloid Interface Sci.* 48, 1; C. Salzlechner et al. (2020) *Adv. Healthcare Mat.* 9, 4, 1901134; da Silva & Dreiss (2016) *Polym. Int.* 65, 268

[2] M.A. da Silva et al. (2017) *J. Pol. Sci. B.* 55, 1850; M. A. da Silva (2015) *Biomacromolecules* 16, 1401; M. A. da Silva et al. (2015) *Biomacromolecules* 16, 1401.

[3] N. Zoratto et al. (2019) *J. Colloid Interface Sci.*, 556, 301

[4] M. Serres-Gómez et al. (2018) *Langmuir*, 34, 10591

[5] J. Puig-Rigall et al. (2017) *J. Colloid Int. Sci.* 524, 42

#### 5:45 AM \*F.SM02.03.05

**Viscoelastic Properties of Supramolecular Gels and Mixtures Based on Hydrogen Bonding** Dimitri Vlassopoulos<sup>1,2</sup>; <sup>1</sup>FORTH, Greece; <sup>2</sup>University of Crete, Greece

Understanding and tailoring the self-assembly of supramolecular moieties is a challenging subject with potential implications in materials engineering and biological function. Here we discuss two problems associated with the viscoelastic properties of (i) hydrogel mixtures due to competitive interactions and (ii) organogels due to the presence of traces of humidity.

Concerning the former, we investigated a class of binary hydrogels made by mixing fibrillar supramolecular polymers that are formed from two compounds: 1,3,5-benzene-tricarboxamide decorated with aliphatic chains terminated by tetra(ethylene glycol) (BTA) and a 20 kg/mol telechelic poly(ethylene glycol) decorated with the same hydrogen bonding BTA motif on both ends (BTA-PEG-BTA). We found that the respective single-compound-based supramolecular systems form very different networks which exhibit drastically different rheology. More strikingly, mixing the compounds results in a non-monotonic dependence of modulus and viscosity on composition, suggesting a competition between interactions of the two compounds, which can then be used to fine-tune the mechanical properties.

The latter problem concerns the self-assembly of supramolecular moieties in organic solvents which is affected by the presence of trace amounts of water in the monomeric state that induce competitive association and change the helicity of the

assembled structure. We investigated an organogel in dodecane (biphenyl tricarboxamide, BPTA) and found that water affects the self-assembled structure by changing the persistence length and contour length of the fiber. The content of water in the fiber changed with temperature, bequeathing the linear and nonlinear viscoelastic properties with unusual temperature responsiveness. For instance, as the temperature increased from 15 to 35°C, the relaxation time of the system varied non-monotonically with temperature. This stems from the fact that the system loses its reversible and dynamic character for temperatures above 35°C where water does not mediate the association of BPTA units.

These findings are discussed in the context of existing theories of living polymers and of the perspective of designing gels with desired and tunable properties.

Work in collaboration with E. Vereroudakis (Crete), N.J. Van Zee (ESPCI, Paris), E. Del Gado (Georgetown) and E.W. Meijer (T. U. Eindhoven).

#### 6:00 AM F.SM02.03.06

**Amphiphilic Interfacial Hydrogel Films for Biocompatible Emulsion Stabilization** Joerg G. Werner<sup>1,2</sup>, Brendan Deveney<sup>2</sup>, John Heyman<sup>2</sup>, Julie Bouchon<sup>2</sup> and David Weitz<sup>2</sup>; <sup>1</sup>Boston University, United States; <sup>2</sup>Harvard University, United States

Aqueous droplets dispersed in fluorinated oils have found a wide variety of applications as biomimetic compartments for the isolation and analysis of cells and biomolecules. Advances in microfluidic manipulation of emulsion drops has enabled biological assays and diagnostics on the single cell and single molecule level at high throughput. Despite the significant advancements in the field of droplet microfluidics, some challenges remain. The stability of especially large drops over 50 microns in diameter is a key issue for applications involving long incubation periods necessary for cell proliferation or organoid growth, as well as thermal stresses experienced in thermocycling for polymerase chain reaction (PCR). Here we report our recently developed approach for stabilizing water-in-fluorocarbon emulsion drops with biocompatible interfacial films that contain a water-facing hydrogel and an oil-facing fluoropolymer that are cross-linked with dynamic covalent bonds. We combine fluorocarbon-soluble random copolymers that contain boronic acid moieties with biocompatible and hydrophilic polymers dispersed in microfluidics-derived water-in-fluorocarbon emulsion droplets. The dynamic covalent chemistry of boronic acids enables the formation of an amphiphilic interfacial thin film around the drop without the use of charged species that often inhibit or interfere with biologic functionalities such as enzyme activity. The amphiphilic interfacial film contains an inert polyol hydrogel facing the water drop and a highly fluorinated outer layer, providing armor to coalescence even in surfactant-free environments. We demonstrate the successful application of our armored droplets for in-drop (RT)-PCR with repeated thermocycling to 96 °C without drop coalescence or inter-drop diffusion even for drops as large as 200 microns, as well as the expansion of cells in 375 micron-sized drops incubated for 96 hours. The strength of the interfacial film is tunable by the choice of complexing polymer and copolymer composition. Our strategy of oil-soluble, boronic acid-containing copolymers for interfacial film formation and droplet stabilization is transferrable to water-hydrocarbon emulsions. Furthermore, tunable adhesive strength between the armored drops enables additive drop assemblies, producing filaments of aqueous microdroplets that are of interest to the hierarchically shape-guided growth of organoids and other cell colonies.

#### 6:10 AM F.SM02.03.07

**Anisotropic Double Network Hydrogels Based on Semi-Rigid Polyelectrolyte Physical Networks** Daniel R. King, Riku Takahashi, Takuma Ikai, Kazuki Fukao, Takayuki Kurokawa and Jian Ping Gong; Hokkaido University, Japan

Many biomaterials possess unique structures that result in anisotropic mechanical properties, along with high strength, toughness, and water content. Applying the double network principle to develop tough hydrogels that possess these features with different polymer chemistries is important for the potential application of hydrogel materials. Synthesis of the two interpenetrating networks with contrasting structure and physical properties required for double networks usually involves a two-step polymerization process. First, the sacrificial network is fabricated, followed by the stretchable, weak network. In this work, we present a new method to synthesize tough double network hydrogels by post-physical crosslinking of linear, semi-rigid polyelectrolytes entrapped in a chemically crosslinked neutral network. This has been achieved through a one-pot polymerization method. Owing to their semi-rigid structure, poly(2,2'-disulfonyl-4,4'-benzidine terephthalamide) (PBDT) can form a brittle physical network above their overlap concentration in multi-valent  $ZrCl_2O$  ion solutions without macroscopic phase separation, within the flexible neutral network. The double network hydrogels thus prepared exhibit high modulus (~1.7 MPa), strength (~1.3 MPa), fracture strain (~7.3), and strain energy density (~5.9 MJ/m<sup>3</sup>), while containing over 80% water. These materials also exhibit modest self-healing ability (~51% after 30 minutes), demonstrating an additional benefit of a physical sacrificial network. Furthermore, applying pre-stretch prior to physical crosslinking allows for the fabrication of an oriented sacrificial network. The anisotropic hydrogels demonstrate a Young's modulus anisotropy ratio

of close to 3. The method presented here is simpler than the conventional two-step polymerization of traditional double network hydrogels and could be applied to develop tough hydrogels from rigid polyelectrolytes, including biopolymers such as DNA, HA, and chondroitin sulfate.

#### 6:20 AM F.SM02.03.08

##### **Coformulation with Water to Improve the Properties of Gelatin-Supported Deep Eutectic Solvent Gel Electrolytes** Rachel E. Owyung, Sameer Sonkusale and Matthew Panzer; Tufts University, United States

Ionic skin devices aim to mimic their biological counterparts for wearable devices and soft robotic applications by sensing touch due to a capacitive change upon deformation. Commonly, salts are added to hydrogels to create ionic conductors that are supported by mechanically compliant polymer networks for these devices. However, hydrogel systems are often unstable with respect to liquid evaporation and can require additional chemical crosslinks to improve gel mechanical stiffness and toughness.

Our group recently demonstrated gelatin-supported deep eutectic solvent (DES) gels using a 1:2 molar ratio of choline chloride (ChCl) and ethylene glycol (EG) as nonvolatile gel electrolyte alternatives. Compared to a hydrogel with the same gelatin content (22 wt.%), the DES gel demonstrated remarkably improved stretchability (fracture strain improved from 40% to 320%) and toughness (improved from 2.1 to 133 kJ/m<sup>3</sup>). As these gels were supported only by noncovalent cross-links formed via gelatin self-assembly (*e.g.* triple helices), there was a clear synergistic effect of both ChCl and EG on the gelatin scaffold to improve DES gel mechanical properties relevant to ionic skin applications. However, there is still a need to better understand how the solvent dictates *in situ* gelation.

In this work, we probe the inherent interactions between the solid and liquid components within these gels by exploring the effects of the organic hydrogen bond donor (HBD) of the DES as well as coformulation with 25 mol% water on the resulting gelatin self-assembly. These gel electrolytes were characterized to determine their tensile properties, ionic conductivities, and thermal transitions in order to probe interactions between ChCl, HBD, and water and the gelatin scaffold.

We have observed that varying the HBD identity within DES/water mixture gels enables tuning of the Young's modulus by up to a six-fold increase: from 7 kPa (1,2-propanediol) to 42 kPa (glycerol) for a fixed gelatin content (20 wt.%).

Additionally, DES/water mixture gels exhibit notable improvements in toughness and ionic conductivity versus their "dry" DES gel counterparts. Toughness was increased from 23 to 68 kJ/m<sup>3</sup> for ethylene glycol-based gels and ionic conductivity increased from 3.3 to 5.2 mS/cm. Similar improvements to toughness and conductivity were found for glycerol-based DES gels, with water addition increasing gel toughness from 46 to 198 kJ/m<sup>3</sup> and ionic conductivity from 0.9 to 1.2 mS/cm.

The results of this work demonstrate that water-in-DES mixtures can synergistically improve ion transport and mechanical properties within DES/water mixture gel electrolytes, and that proper materials selection of the liquid electrolyte and polymer scaffold system can lead to greater tunability of gel properties relevant to ionic skin device applications.

#### 6:30 AM F.SM02.03.09

##### **Intrinsic Fracture Energy of Soft Mechanical Metamaterials** Dongchang Zheng<sup>1,2</sup>, Shaoting Lin<sup>1</sup>, Liu Wang<sup>1</sup> and Xuanhe Zhao<sup>1,1</sup>; <sup>1</sup>Massachusetts Institute of Technology, United States; <sup>2</sup>University of Science and Technology of China, China

Diverse soft metamaterials have been developed for energy-absorbing, tunable thermal expansion, soft actuator, etc.

Although various functional properties of soft metamaterials have been investigated, their fatigue properties have not been studied yet, which hinders the translation of soft metamaterials into real applications. With 3D printing techniques, we control the geometrical parameters of soft metamaterials. Fracture tests and simulations are conducted to measure the S-N curve of a single printing filament and fatigue threshold of 3D printed soft metamaterials. We show that the fatigue threshold of soft metamaterials is linearly proportional to the fiber's diameter and strain energy density limit, but independent of its length. Constitutive relation of the materials and geometrical shapes determine the prefactor of such proportion relations. The results are intrinsically different from the classical Lake-Thomas theory for polymer networks, leading to a generalized theory for predicting soft metamaterials' fatigue threshold. The capability of the theory correlating the fatigue property of a single filament and entire topological networks is critical for the design of durable soft metamaterials. This theory inspires us to manufacture sinusoidal structure metamaterials, whose fatigue threshold increase dramatically.

#### 6:40 AM F.SM02.03.10

##### **Noninvasive Study of Hydrogel Re-Swelling Inside Soft Tissues** Michael Shur, Kangling Wu, Outman Akouissi and Stephanie P. Lacour; Ecole Polytechnique Federale de Lausanne, Switzerland

Neural tissues are extremely soft with kPa-range modulus. Hydrogels offer a unique opportunity to design neural interfaces



with biomimetic mechanical properties. Some designs which utilize hydrogels either as coating or bulk material, such as penetrating intracortical probes, require de-hydration of the hydrogel before the time of implantation to prevent any buckling during insertion and to minimize the hydrogel delamination due to shear forces. Once inserted into the brain the hydrogel absorbs moisture from the tissue, swells and provides a tissue-like interface.

We report on the re-swelling process and assess the mechanical properties of the hydrogel in as-prepared and post re-swelling conditions, comparing thermal and freeze drying as de-hydration methods. We studied polyacrylamide (PAAm) hydrogel with increasing monomer concentrations (3 to 6% AAm), which correspond to shear storage moduli ( $G'$ ) in the 120 to 750 Pa range. We found that the recovery of  $G'$  and of the swelling capacity depends on the initial composition of the hydrogel. Following either thermal or freeze-drying process, the softest hydrogel (3% AAm) displays only 40% swelling capacity recovery and a 3.5 times increase in storage modulus, compared to its initial properties. Stiffer hydrogels were found to be less sensitive to the de-hydration process with a 2 to 2.8  $G'$  increase factor.

Next we studied the re-swelling kinetics and normal forces associated to the process, both in free and constrained swelling scenario (mimicking the implant-tissue interface). Finite element simulation extended the analysis to help quantify the mechanical stresses that are being exerted on the neural tissue during the re-swelling stage. Preliminary results indicate that these stresses may reach up to several tens of kPa for a 100 $\mu$ m thick hydrogel coating, being applied on the surrounding during a constrained re-swelling process of a 300 Pa hydrogel.

These preliminary results indicate hydrogel dynamics should be taken into account when designing in vivo probes and suggest that the soft material in vivo may display stiffer properties than those in vitro. We believe this work provides important insights on hydrogel-tissue interface and inherent limitations associated with the use of ultra-soft hydrogels for implantable neural interfaces.

#### 6:50 AM F.SM02.03.11

**Late News: Mesoscale Modeling of Controlled Degradation in Hydrogels** Vaibhav A. Palkar, Chandan K. Choudhury and Olga Kuksenok; Clemson University, United States

Hydrogel based soft materials with chemical functionalities that allow controlled degradation of the polymer are utilized as active stimuli responsive platforms for numerous applications. As one example, a hydrogel with multiple degradable functional groups that degrade in response to different wavelengths of light enables sequential release of drugs from the network. Herein, we present Dissipative Particle Dynamics (DPD) based simulations of degradation in tetra-arm polyethylene glycol (tetra-PEG [1]) hydrogels. Controlled degradation can be introduced in these gels via several chemical pathways [2,3]. In our DPD model we use the modified segmental repulsive potential (mSRP [4]) to avoid unphysical polymer chain crossing and we first establish model parameters that mimic the hydrophilicity of PEG. Further, we use our recently developed framework [5] to introduce controlled degradation in these gels and measure the fraction of degradable bonds intact during degradation. Our method allows modeling of first order degradation kinetics in these gels. We track the evolution of mass loss from bulk degrading gels and note the occurrence of a slow mass loss regime due to erosion followed by a fast regime due to reverse gelation of the polymer network. We quantify the reverse gel point of these gels by tracking the size of the second largest cluster during degradation. We focus on the effect of finite size on mass loss and reverse gel point calculations and compare these effects with previously developed scaling [6]. The reverse gel point for tetra-PEG hydrogels measured from our simulations corresponds well with the value obtained from percolation theory on a diamond lattice.

#### References:

1. Sakai, T., Matsunaga, T., Yamamoto, Y., Ito, C., Yoshida, R., Suzuki, S., Sasaki, N., Shibayama, M., & Chung, U. I. (2008). Design and fabrication of a high-strength hydrogel with ideally homogeneous network structure from tetrahedron-like macromonomers. *Macromolecules*, 41(14), 5379-5384.
2. Li, X., Tsutsui, Y., Matsunaga, T., Shibayama, M., Chung, U. I., & Sakai, T. (2011). Precise control and prediction of hydrogel degradation behavior. *Macromolecules*, 44(9), 3567-3571.
3. Azagarsamy, M. A., McKinnon, D. D., Alge, D. L., & Anseth, K. S. (2014). Coumarin-based photodegradable hydrogel: Design, synthesis, gelation, and degradation kinetics. *ACS Macro Letters*, 3(6), 515-519.
4. Sirk, T. W., Slizoberg, Y. R., Brennan, J. K., Lisal, M., & Andzelm, J. W. (2012). An enhanced entangled polymer model for dissipative particle dynamics. *The Journal of chemical physics*, 136(13), 134903.
5. Palkar, V., Choudhury, C. K., & Kuksenok, O. (2020). Development of Dissipative Particle Dynamics framework for modeling hydrogels with degradable bonds. *MRS Advances*, 5(17), 927-934.
6. Lin, T. S., Wang, R., Johnson, J. A., & Olsen, B. D. (2018). Topological structure of networks formed from symmetric four-arm precursors. *Macromolecules*, 51(3), 1224-1231.

SESSION F.SM02.04: Soft Machines and Devices  
On Demand Abstracts Available for Viewing Starting Saturday Morning, November 21, 2020  
F-SM02

**5:00 AM \*F.SM02.04.01**

**Evolution of Self-Oscillating Polymer Gels as Life-Like Softmachines** Ryo Yoshida; The University of Tokyo, Japan

In living systems, there are many autonomous and oscillatory phenomena to sustain life such as heart beating. We developed “self-oscillating” polymer gels that undergo spontaneous cyclic swelling–deswelling changes without any on–off switching of external stimuli, as with heart muscle. The self-oscillating gels were designed by utilizing the Belousov-Zhabotinsky (BZ) reaction, an oscillating reaction, as a chemical model of the TCA cycle. We have systematically studied these self-oscillating polymer gels since they were first reported in 1996. Potential applications of the self-oscillating polymers and gels include several kinds of functional material systems such as biomimetic actuators, mass transport systems and functional fluids. For example, it was demonstrated that an object was autonomously transported in the tubular self-oscillating gel by the peristaltic pumping motion similar to an intestine. Further, self-oscillating polymer brush surface like cilia, vesicles or colloidosomes undergoing cell-like autonomous shape oscillations with buckling, was prepared. Besides, autonomous sol-gel oscillation and amoeba-like motion was realized utilizing well-designed block copolymer solution. In this presentation, our recent progress on the self-oscillating polymer gels is summarized.

**5:15 AM \*F.SM02.04.02**

**HASEL Artificial Muscles—Versatile High-Performance Actuators for Bioinspired Robotics** Christoph Keplinger; University of Colorado-Boulder, United States

Robots today rely on rigid components and electric motors based on metal and magnets, making them heavy, unsafe near humans, expensive and ill-suited for unpredictable environments. Nature, in contrast, makes extensive use of soft materials and has produced organisms that drastically outperform robots in terms of agility, dexterity, and adaptability. To create a new generation of soft, life-like robots that reproduce the vast capabilities of biological systems, we need to develop actuators that replicate the astonishing all-around actuation performance of biological muscle. Hydraulically Amplified Self-healing ELectrostatic (HASEL) transducers are a new class of self-sensing, high-performance muscle-mimetic actuators, which are electrically driven and harness a mechanism that couples electrostatic and hydraulic forces to achieve a wide variety of actuation modes. Current designs of HASEL artificial muscles exceed actuation stress of 0.3 MPa, linear strain of 100%, specific power of 600W/kg, efficiency of 30% and bandwidth of 100Hz; all these metrics match or exceed the capabilities of biological muscle. This talk gives an overview over the latest developments, including materials systems, modeling, new designs of actuators, fabrication techniques, and creation of untethered soft robotic devices.

**5:30 AM \*F.SM02.04.03**

**Non-Equilibrium Signal Integration in Hydrogels** Peter Korevaar, Nadir Kaplan and Joanna Aizenberg; Harvard University, United States

Materials that perform complex chemical signal processing are ubiquitous in living systems. Their synthetic analogs would transform developments in biomedicine, catalysis, and many other areas. By drawing inspiration from biological signaling dynamics, we show how simple hydrogels have a previously untapped capacity for non-equilibrium chemical signal processing and integration. Using a common polyacrylic acid hydrogel, with divalent cations and acid as representative stimuli, we demonstrate the emergence of non-monotonic osmosis-driven spikes and waves of expansion/contraction, as well as traveling color waves. These distinct responses emerge from different combinations of rates and sequences of arriving stimuli. A non-equilibrium continuum theory we developed quantitatively captures the nonmonotonic osmosis-driven deformation waves and determines the onset of their emergence in terms of the input parameters. These results suggest that simple hydrogels, already built into numerous systems, have a much larger sensing space than currently employed.

**5:45 AM \*F.SM02.04.04**

**Polymer Gels for Autonomous Motion and Mesoscale Assembly** Alfred J. Crosby; University of Massachusetts Amherst, United States

Nature is masterful at using limited components and basic driving forces to achieve complex tasks, such as high power movement and multi-structure assembly, across a broad range of size scales. The materials that enable these achievements often rely upon the integration of phases that allow for internal transport, elastic energy storage, system protecting dissipation, and tunable sensitivity to interfacial interactions. Accordingly, polymer gels, which combine liquid phases with shear-sustaining macromolecular network structures, offer a robust materials platform for transferring lessons from nature into synthetic engineered devices. Here, we describe two examples from our research group of how to take advantage of mesoscale structural asymmetry, mechanics, liquid transport, and interfacial interactions to achieve new engineered capabilities. The first example takes inspiration from multiple examples in nature, including mantis shrimp and trap-jaw ants, that use Latch-Mediated Spring Actuation (LaMSA) to achieve high power, impulsive movements. We demonstrate how transient metastable deformations associated with swelling and deswelling of a polymer gel can be exploited to generate mechanical bi-stability, giving rise to multiple, self-repeating, snap-through movements. We introduce models to quantitatively describe these mechanisms and harness them to develop autonomous jumping devices. In a related manner, the second example describes the use of structural asymmetry to mediate swelling/deswelling processes and elastic restoring forces to control the motion and assembly of mesoscale polymer gel ribbons. Collectively, both examples provide new insight into how polymer gel properties, related to elasticity, diffusion, and interfacial forces, can combine with purposeful structural design to yield complex tasks, which can be used in the development of microscale robots and new adaptable composite materials.

#### **6:00 AM F.SM02.04.05**

**Bioinspired Self-Healing Protein Hydrogels for Soft Machines** Abdon Pena-Francesch<sup>1,2</sup>, Melik C. Demirel<sup>3</sup> and Metin Sitti<sup>1</sup>; <sup>1</sup>Max Planck Institute for Intelligent Systems, Germany; <sup>2</sup>University of Michigan, United States; <sup>3</sup>The Pennsylvania State University, United States

Recent research efforts have focused on developing soft, flexible, compliant materials for robotics, biointerfacing, and biosensing applications. Because of their intrinsic softness, these materials are susceptible to cut, puncture, scratch, and/or tear damage that compromise their physical integrity, and therefore self-healing properties are indispensable for soft machines and devices operating in dynamic environments. However, current self-healing materials have shortcomings that limit their practical application, such as low healing strength (below MPa) and long healing times (hours). Here, we introduce high-strength bioinspired synthetic proteins that self-heal micro- and macro-scale mechanical damage within a second by local heating. These protein hydrogels are systematically optimized to improve their hydrogen-bonded nanostructure and network morphology, with programmable healing properties (23 MPa strength after 1 second of healing) surpassing those found in other natural and synthetic soft materials by several orders of magnitude. Such healing performance opens new opportunities for bioinspired materials design, and addresses current limitations in self-healing materials for soft robotics and wearable technology.

#### **6:10 AM F.SM02.04.06**

**Coiled pH-Responsive and Athermal Polymer Artificial Muscles** Sevketcan Sarikaya<sup>1</sup>, Frank Gardea<sup>2</sup> and Mohammad Naraghi<sup>1</sup>; <sup>1</sup>Texas A&M University, United States; <sup>2</sup>U.S. Army Combat Capabilities Development Command Army Research Laboratory South, United States

The interest in artificial muscles has been expanding due to the shortcomings of traditional motors and actuators, such as piezoelectric actuators and shape memory alloys. Stiffness incompatibility with human bodies and IR-detectable actuation mechanisms are among the limitations of the traditional actuators. Soft matter and polymers, including hydrogels, as artificial muscles offer great potential to enhance robotic applications where lightweight and flexible structures are desired. Upon application of an external stimulus, polymer artificial muscles can expand or contract, similar to a mammalian muscle, replicating comparable stroke and stiffness, which enables safe interactions with humans. pH is one of the stimuli which provides a silent and athermal motion to artificial muscles. pH-driven polymer gels can lead to significant swelling and deswelling behaviors when exposed to acid and basic environments and provide muscle-like actuation when in a fiber form. In this work, we investigated the actuation behaviors of polyacrylonitrile (PAN) gel fibers by exploiting structural adjustments in which a simple but efficient method, twisting and coiling approach was applied. In this manner, the material response –dimensional change with change in pH- was enhanced with the peculiar structural design of a coil, leading to drastically augmented strokes. Here, we first characterized electrospun PAN nanofibers and commercially available PAN microfibrils in terms of fabrication conditions. In this step, the variables of thermal stabilization and hydrolysis, resulting in a PAN pH-responsive gel, were tested in order to obtain optimum actuation conditions. Aligned micro and electrospun nanofibers prepared with different fabrication conditions were actuated at various levels of mechanical loading. A maximum of ~54% actuation was achieved under no stress and it was found that higher thermal stabilization results in lower actuation. Radius and overall volume change of pH-responsive single PAN microfiber were measured. Next, as-received PAN

microfibers were highly twisted and coiled to produce volume-change induced actuation. Coiled PAN fibers yielded a promising actuation performance compared to their linear and aligned counterparts. Analytical models relating material response to structural responses were studied. This work shows that pH-responsive PAN gel fibers can be further enhanced in terms of actuation performance through structural design.

#### 6:20 AM F.SM02.04.07

**Development of a Bilayered Hydrogel with Cartilage-Mimicking Mechanical and Lubrication Properties** Lorenzo Vannozzi<sup>1,2</sup>, Diego Trucco<sup>1,2,3</sup>, Eti Teblum<sup>4</sup>, Madina Telkhozhayeva<sup>4</sup>, Saverio Affatato<sup>3</sup>, Gina Lisignoli<sup>3</sup>, Gilbert D. Nessim<sup>4</sup> and Leonardo Ricotti<sup>1,2</sup>; <sup>1</sup>Scuola Superiore Sant'Anna, Italy; <sup>2</sup>Scuola Superiore Sant'Anna, Italy; <sup>3</sup>IRCCS Istituto Ortopedico Rizzoli, Italy; <sup>4</sup>Bar Ilan Institute for Nanotechnology and Advanced Materials, Israel

Recently, new tissue engineering approaches are being developed as an alternative to traditional treatments for articular cartilage (AC) repair. Being an avascular tissue, AC has a limited ability to heal from defects caused by traumas and/or degenerative diseases. Materials in the form of hydrogels are particularly attractive as owing to their biocompatibility, degradability, and ability to homogeneously mix with cells and smart nanomaterials. Hydrogels can be injectable, thus to easily fill defects with different shapes, thus repairing the articular cartilage in a minimally invasive way. Several tissue engineering approaches have been proposed to restore the AC native properties [1]. This specialized tissue provides a low-friction surface for articulation, guaranteeing shock-absorption and wear-resistance [2]. Despite the noticeable efforts spent in the recent years, there is still a high difficulty to reproduce *in vitro* the mechanical and lubrication properties of AC.

We developed a bilayered hydrogel made of blends of Gellan Gum (GG) and Polyethylene glycol diacrylate (PEGDA), able to mimic the mechanical and lubrication features of AC. Graphene Oxide (GO) was used as an effective lubricant agent [3]. GG (1.5 % wt. in deionized water) was mixed with PEGDA (Mn: 575) at different concentration (10 and 15 % wt. for top and bottom layer, respectively). The photocrosslinking was enabled by the addition of Irgacure 2959 (0.1 % wt.) and different UV light exposure time (5 and 10 min) have been tested. Then, samples were immersed in magnesium chloride (MgCl<sub>2</sub>, 1 % wt. in deionized water) for 10 min and/or culture medium (DMEM) for 24 h to enable the ionic crosslinking. Mechanical compression tests allowed to determine the optimal crosslinking parameters. We found two combination of crosslinking able to match the compression Young's modulus of the human AC, which ranges from  $0.28 \pm 0.16$  MPa to  $0.73 \pm 0.26$  MPa, respectively for its superficial and deep layer [4]. We achieved the targeted range of Young's modulus values for the top ( $0.18 \pm 0.06$  MPa) and bottom ( $0.80 \pm 0.15$  MPa) layers of AC by combining photo (5 min) and ionic crosslinking with MgCl<sub>2</sub>. The contribution of ionic crosslinking with MgCl<sub>2</sub> was also more effective than the UV exposure time for the improvement of the toughness and fracture stress/strain of the hydrogels, important features of AC. GO nanosheets were synthesized as described in [5] and added to the top layer solution (0.01 % wt.). The hydrogels with and without GO were analyzed with a custom setup (flat-on-flat geometry) made of using a MCR 102 rheometer equipped with the Tribocell T-PTD200 and a Peltier temperature control. Tribological analyses demonstrated that the non-doped formulation possessed a smaller friction factor (~0.03) in the static regime than the doped formulation (~0.04), while the presence of GO led the friction factor to smaller values in the kinetic regime, as opposed to the bare hydrogel in which that value progressively increased.

In summary, we demonstrated the achievement of the target compressive Young's modulus of AC layers and the improved lubricant behavior provided by the presence of GO in the kinetic regime of compression, which is important for guaranteeing low friction in the articulation during daily life activities. These results are extremely promising in view of the fabrication of a multi-layered synthetic implant for restoring AC defects.

#### ACKNOWLEDGMENTS

This work received funding from the European Union's Horizon 2020 research and innovation program, grant agreement No 814413, project ADMAIORA.

#### REFERENCES

- [1] J. W. Reboledo et al. *Adv. Healthc. Mater.*, 5, 2191, 2016.
- [2] A. J. Sophia Fox et al. *Sports Health*, 1: 461, 2009.
- [3] Y. Meng et al. *J. Phys. Chem. A*, 122: 3157, 2018.
- [4] R. Krishnan et al. *J. Biomech. Eng.*, 125: 569, 2003.
- [5] O. Marciano et al. *Langmuir*, 32: 11672, 2016.

#### 6:30 AM F.SM02.04.08

**Fabrication of Hydrogel Objects and Devices in Liquids with Focused Electron Beams** Andrei A. Kolmakov; National Institute of Standards and Technology, United States

Electron/X-ray focused beams fabrication of hydrogels with submicron resolution and rate inside liquid precursor solutions

would be highly demanded development which, however, is hard to realize due to the vacuum incompatibility of liquid samples. In this contribution, we resolve this impediment and demonstrate a technique for in-liquid focused beam induced crosslinking of hydrogels using fluidic enclosures equipped with electron/x-ray transparent windows. Being inspired by continuous liquid interface production 3D printing technology (CLIP)[1], we developed an alternative method of controllable delamination of the e-beam printed layer from the supporting membrane. Our approach is based on electrochemical quenching of the crosslinking process at the electrified membrane-solution interface. The potential of this technique for sensorics, bioelectronics, interfacing, and drug delivery is demonstrated via in situ addressable immobilization of live-cell, synthesis of nanocomposite hydrogels, and microfabrication of photonic sensors[2].

[1] J. R. Tumbleston *et al.*, "Continuous liquid interface production of 3D objects," *Science*, vol. 347, no. 6228, pp. 1349-1352, 2015.

[2] T. Gupta *et al.*, "Focused Electron and X-ray Beam Crosslinking in Liquids for Nanoscale Hydrogels 3D Printing and Encapsulation," *arXiv preprint arXiv:1904.01652*, 2019.

#### 6:40 AM F.SM02.04.09

**Fatigue Resistant Hydrogel Fiber for Light Delivery** Xinyue Liu, Siyuan Rao and Xuanhe Zhao; Massachusetts Institute of Technology, United States

Light technologies have enabled numerous biomedical devices to assess health and treat disease, among which optical fibers permit light transmission between the external world and human nervous system. The peripheral nervous system flexes with the human body during movement, while silica-based optical fibers with limited deformability constrain the natural movement of the nerves, impeding light delivery in freely moving animals. On the other side, the high compliance, high water content, and biocompatibility make hydrogels an ideal material candidate for optic devices, especially for those in close contact with biological organisms. However, existing hydrogel optical fibers suffer from low mechanical stability, poor coupling with external optics, and severe light leakage. Here, we present a fatigue-resistant hydrogel-based optically stimulating technology (FAR-HOST) that utilizes nanocrystalline hydrogels as optical fibers for optogenetic control in the peripheral nervous system. The hydrogel optical fibers are soft and stretchable to conform to the flexible substrates, and meanwhile the formation of polymeric nanocrystals in hydrogels confers fatigue-resistance to these hydrogel materials against repeated movements. In addition, hydrogels with polymeric nanocrystals exhibit a relatively high refractive index that minimizes interfacial light leakage, and high transparency that reduces light absorption or scattering, synergistically contributing to efficient light transmission. In vitro and in vivo results demonstrate that using FAR-HOST to exert optogenetic control over the sciatic nerve, revealing its potentials diagnostic imaging, health monitoring, and neuromodulation.

#### 6:50 AM F.SM02.04.10

**Hydrogel Embedded Quantum Dot-Transcription Factor Sensor for Quantitative Progesterone Detection** Mingfu Chen<sup>1</sup>, Chloe Gazon<sup>1</sup>, Prerana Sensharma<sup>1</sup>, Thuy Nguyen<sup>1</sup>, Yunpeng Feng<sup>1</sup>, Margaret Chern<sup>1</sup>, R Baer<sup>1</sup>, Nitinun Varongchayakul<sup>1</sup>, Katherine Cook<sup>1</sup>, Sébastien Lecommandoux<sup>2</sup>, Catherine Klapperich<sup>1</sup>, James Galagan<sup>1</sup>, Allison M. Dennis<sup>1</sup> and Mark Grinstaff<sup>1</sup>; <sup>1</sup>Boston University, United States; <sup>2</sup>Univ. Bordeaux, France

Immobilization of biosensors in or on a functional material is critical for subsequent device development and translation to wearable technology. Here we present the development and assessment of an immobilized quantum dot - transcription factor - nucleic acid complex for progesterone detection as a first step toward such device integration. The sensor is composed of a polyhistidine-tagged transcription factor linked to a quantum dot and a fluorophore-modified cognate DNA, and embedded within a hydrogel as an immobilization matrix. The hydrogel is optically transparent, soft, and flexible as well as traps the quantum dot - transcription factor DNA assembly but allows free passage of the analyte, progesterone. Upon progesterone exposure, DNA dissociates from the quantum dot - transcription factor DNA assembly resulting in an attenuated ratiometric fluorescent output via Förster resonance energy transfer. The sensor performs in a dose-dependent manner with a limit of detection of 55 nM. Repeat analyte measurements are also similarly successful. Our approach combines a systematically characterized hydrogel as an immobilization matrix and a transcription factor - DNA binding as a recognition/ transduction element, offering a promising framework for future biosensor devices based upon allosteric transcription factor.

#### 7:00 AM F.SM02.04.11

**Interference-Assisted Wide-Range Plasmonic Coloration of Single Gold Nanoparticles and Its Dynamic Control** Bokusui Nakayama, Keiko Esashika, Yuki Hiruta and Toshiharu Saiki; Keio University, Japan

The main challenges in conventional color printing involve protecting ink from fading and enabling it to be rewritable. As for color displays, a liquid crystal display, for example, suffers from high power consumption and small viewing angle.

Alternatively, as seen in stained glass and peacock feathers, some of the historical artifacts and natural livings exhibit rich colors, whose principle include localized surface plasmon resonance (LSPR) and/or interference effects. Recently novel color printing and displays based on these effects have been widely demonstrated.

Towards plasmonic color display at video frame rate, dynamic modulation of plasmonic coloration by using volume phase transition of responsive polymer gels has been proposed [1,2]. In these studies, a hydrogel with drastic volume responsibility to an external field was employed for fine tuning of gap distance of neighboring metal nanostructures to control of LSPR.

The color modulation range, however, is still unsatisfied and far behind from practical use.

In this study, we propose a new method to widen the wavelength range of plasmonic coloration by exploiting interference between illuminating white light and LSPR scattering light. The sample consists of gold nanoparticles (AuNP;  $\Phi = 80$  nm) dispersed in Poly(N-isopropylacrylamide) (PNIPAM) hydrogel, which was sandwiched between two coverslips (Fig. 1 inset). Under bright-field microscope observation, back-scattered light from AuNP interferes with white light reflected back from the bottom coverslip. Depending on the distance between AuNP and the bottom coverslip, the relative phase of interfering lights differs for individual AuNPs and they appear in different colors in a wide-range (Fig. 1). In addition, we can control the AuNP-coverslip distance via volume phase transition of PNIPAM induced by temperature control (Fig. 2 inset). Figure 2 demonstrates continuous color tuning of a single AuNP, broadly covering the chromatic diagram, upon heating and cooling of PNIPAM.

#### 7:10 AM F.SM02.04.12

##### **Novel Integration of Fabric-Based Hydrogel Electrodes and Pressure Sensors in Smart Eyewear** S. Zohreh

Homayounfar, Soha Rostaminia, Ali Kiaghadi, Deepak Ganesan and Trisha Andrew; University of Massachusetts, Amherst, United States

There is a significant interest in measuring biopotential signals (such as ECG and EOG) unobtrusively via novel textile-based electronics. Herein, electrodes are the interface who receives the charges in the ionic form from the body and injects them as electrons through wires. A fundamental challenge to be addressed to reliably measure biopotential parameters with fabric-based electrodes is whether we can design an electrode that has the signal quality of traditional wet electrodes and the comfort of dry electrodes. The crucial role of a hydrogel in an electrode, specifically in reducing the motion artifact, is undeniable. However, fabricating a hydrogel which can be stably grafted to the underneath plate and, more importantly, can be fully recovered after being dried out is still a great challenge among scientists. In this study, we developed a mechanically stable hydrogel as the electrolyte on our bioelectrode by taking advantage of initiated Chemical Vapor Deposition (iCVD). Our first-of-its-kind hydrogel electrodes successfully address all known drawbacks of conventional “wet” electrodes, in addition to affording high signal to noise ratio during long-term data acquisition, displaying wash-stability, breathability, no skin irritation, and being capable of further miniaturization for embedding into any wearable platforms. The functionality of these electrodes has been successfully approved by being incorporated into an eye-mask to detect eye movement (EOG). To capture additional physiological measures that are complementary to eye movement information captured by the electrodes, we embedded a fabric-based pressure sensor for pulse detection along the strap of the eyewear which let the wearer’s pulse to be imperceptibly measured, simultaneously with any eye movement. We anticipate that the ability to track pulse along with eye movement in a single device will enable a host of cutting-edge biomedical, psychological and psycho-social studies, in addition to improving the accuracy and usability of gaming and virtual reality headsets.

#### 7:20 AM F.SM02.04.13

##### **PEDOT:PSS/pNIPAAm Hydrogel-Based Electrodes for the Monitoring of the Capture and Release of Label-Free**

**Biomarkers** Janire Saez<sup>1</sup>, Maite Garcia-Hernandez<sup>2</sup>, Achilleas Savva<sup>1</sup>, Lourdes Basabe-Desmots<sup>2,3</sup>, Fernando Benito-Lopez<sup>2</sup> and Roisin Owens<sup>1</sup>; <sup>1</sup>University of Cambridge, United Kingdom; <sup>2</sup>University of the Basque Country, Spain; <sup>3</sup>IKERBASQUE, Spain

Circulating Tumor Cells (CTCs) are responsible for inducing metastasis when they exit from a primary tumor, they travel through blood and invade another healthy tissue. They are considered as crucial biomarkers of the prognosis of cancer patients, but they are normally found in low concentrations in the first stages of the disease and their detection and is still a challenge. Therefore, the development of biosensors capable of not only detecting, but also collecting pure CTCs is of great interest for the scientific community and society in general. Stimuli responsive materials are gaining interest for cell capture and release, specifically, poly(N-isopropylacrylamide) (pNIPAAm), which changes its configuration in response to variations in temperature above and below 32 °C in a range able to preserve cell viability. In parallel, the extensive use of conducting polymers (CPs) in the bioengineering field is enabling important advances in cell applications. This is thanks to their properties such as optical transparency, amenability to surface functionalization, high biocompatibility and chemical stability,

high conductivity/weight ratio, high porosity and very good electrical and physical properties. The additional ability of CPs to be turned into mechanically soft hydrogels opened exciting new possibilities to integrate electrically conducting materials within thermoresponsive polymers and create biosensors. Here, we report a hybrid functional, conductive and thermoresponsive copolymer, based on poly(3,4-ethylenedioxythiophene) / poly(styrene sulfonate) (PEDOT:PSS) blended with pNIPAAm. The material is capable of performing label free, non-invasive cell capture, release, and simultaneous electrical monitoring of the process of cell capture and release. This technology opens a new possibility for detecting and collecting CTC biomarkers in early stage cancers for further analysis to improve patient prognosis.

#### 7:30 AM F.SM02.04.14

**Rewiring Bacterial Electron Transfer for Computational Living Materials** [Austin J. Graham](#), Christopher M. Dundas, Gina Partipilo, Thomas FitzSimons, Adrienne M. Rosales and Benjamin K. Keitz; The University of Texas at Austin, United States

#### **Rewiring Bacterial Electron Transfer for Computational Living Materials**

Austin J. Graham<sup>1,2</sup>, Christopher M. Dundas<sup>1</sup>, Gina Partipilo<sup>1</sup>, Thomas M. FitzSimons<sup>1,2</sup>, Adrienne M. Rosales<sup>1,2</sup>, Benjamin K. Keitz<sup>1,2</sup>

<sup>1</sup>McKetta Department of Chemical Engineering, University of Texas at Austin, Austin, TX

<sup>2</sup>Center for the Dynamics and Control of Materials, University of Texas at Austin, Austin, TX

Keywords: living materials, synthetic biology, genetic logic

Qualities exhibited by living systems, including self-regulation, self-healing, morphology control, and environmental responsiveness, are highly attractive from a material design perspective. Collectively, these capabilities all arise from the ability of living systems to perform computation. However, traditional biological materials, such as biofilms and tissues, are generally less robust and more difficult to engineer than synthetic materials. Next-generation materials must bridge the computational abilities of natural systems with the precision of synthetic systems. These designs will require programming of genetic and transcriptional responses whose outputs can control non-biological material properties. Towards these goals, living materials are a class of materials defined by their incorporation of autonomous cells that use biological functions to control material properties. Our group recently demonstrated that leveraging extracellular electron transfer (EET) from the organism *Shewanella oneidensis* enables control over the redox equilibrium of metal catalysts to polymerize and cross-link synthetic materials via atom-transfer radical polymerization<sup>1,2</sup>. Using this method, we report the production of hydrogel living materials in which *S. oneidensis* controls the cross-linking of methacrylated hyaluronic acid<sup>3</sup>. Cross-linking by genetic knockouts demonstrated that hydrogel formation was closely coupled to the expression of specific EET proteins, as gelation kinetics and stiffness correlated to the number of removed EET genes. Furthermore, strains complemented with an inducible EET gene showed inducer-dependent cross-linking activity and hydrogel mechanics, including both gel microstructure and bulk properties. Modeling gene expression using an activating Hill Function yielded quantitative prediction of hydrogel storage modulus, demonstrating control over material properties using design principles from synthetic biology. Genetic circuits controlling different EET genes also yielded networks with tunable properties depending on the choice of gene, demonstrating traditional buffer gate logic. By coupling EET activity to cross-link density, we have engineered a platform that utilizes autonomous bacterial metabolism to design computational materials that cross-link in response to environmental cues using genetic logic. Next, we will further demonstrate the general applicability of EET-controlled catalysis for computational material synthesis, cross-linking fully synthetic polymer networks using thiol-ene and CuAAC click chemistries. Genetic control over these chemistries will significantly expand the synthetic capability of microorganisms. Finally, more sophisticated Boolean logic, such as NOT, AND, and OR gates will enable more advanced living material computation for applications in biosensing, tissue engineering, and additive manufacturing.

1. G. Fan\*, C.M. Dundas, **A.J. Graham**, N.A. Lynd, B.K. Keitz. “*Shewanella oneidensis* as a living electrode for controlled radical polymerization.” *Proc. Natl. Acad. Sci. U.S.A.* **115**(18): 4559–4564 (2018).

2. G. Fan, **A.J. Graham**, J. Kolli, N.A. Lynd, B.K. Keitz. “Aerobic Radical Polymerization Mediated by Microbial Metabolism.” *Nat. Chem.* (in press, 2020). DOI: 10.1038/s41557-020-0460-1.

3. **A.J. Graham**, C.M. Dundas, A. Hillsley, D.K. Kasprak, A.M. Rosales, B.K. Keitz. “Genetic Control of Radical Cross-linking in a Semisynthetic Hydrogel.” *ACS Biomater. Sci. Eng.* **6**(3): 1375–1386 (2020).

#### 7:40 AM F.SM02.04.15

**Surface Engineering of Hydrogels for Solar Water Purification** [Youhong Guo](#) and Guihua Yu; The University of Texas at Austin, United States

Water scarcity has been an increasingly severe threat to our society. Solar vapor generation provides a sustainable means for desalination and water purification technologies. With highly tunable structures, unique polymer-water interactions, and ease of integration with functional materials, hydrogels show great potential for efficient solar water purification. The rational design and engineering of hydrogel surfaces have a substantial impact on the interfacial solar water vaporization process. Here, we will discuss effective ways to tailor the surface topography and wetting states of hydrogel solar evaporators to accelerate the solar vapor generation rate. Specifically, the nanotextured topography of the surface can be fabricated by a liquid-liquid interface-guided gelation process, resulting in an increased heat flux at the sharply dimpled hydrogel-air interface. In addition, hydrogel evaporators with inhomogeneous surface wettability demonstrate an ultrahigh evaporation rate with synergistic contributions from both wetting regions. Molecular dynamics simulation reveals the surface-modulated escaping behavior of water molecules. By applying hydrophilic polymers as building blocks, the hydrogel evaporators have been endowed with multifunctionalities, such as antifouling and complex contaminants removal, to improve both quantity and quality of collected water. Together with an easy-to-employ and portable purification prototype, hydrogels are an emerging materials platform for high-performance yet cost-effective water purification applications.

**7:50 AM F.SM02.04.16**

**Tough Hydrogel-Based Biocontainment of Engineered Organisms for Continuous, Self-Powered Sensing and Computation** Tzu-Chieh Tang<sup>1</sup>, Eleonore Tham<sup>1</sup>, Xinyue Liu<sup>1</sup>, Kevin Yehl<sup>1</sup>, Alexis Rovner<sup>2</sup>, Hyunwoo Yuk<sup>1</sup>, Farren Isaacs<sup>3</sup>, Xuanhe Zhao<sup>1</sup> and Timothy Lu<sup>1</sup>; <sup>1</sup>Massachusetts Institute of Technology, United States; <sup>2</sup>Harvard University, United States; <sup>3</sup>Yale University, United States

Genetically modified microorganisms (GMMs) can enable a wide range of important applications, including environmental sensing, precision therapeutics, and responsive materials. However, the containment of GMMs to prevent environmental escape and satisfy regulatory requirements is a bottleneck for real-world use. While biochemical strategies have been developed to restrict unwanted growth and replication of GMMs in the environment, there is a need for deployable physical containment technologies to achieve redundant, multi-layered, and robust containment. In addition, form factors that enable easy retrieval would be useful for environmental sensing. To address this challenge, we developed a hydrogel-based encapsulation system for GMMs that incorporates a biocompatible multilayer tough shell and an alginate-based core. This DEployable Physical COntainment Strategy (DEPCOS) allows no detectable GMM escape, bacteria to be protected against environmental insults including antibiotics and low pH, controllable lifespan, and easy retrieval of genetically recoded bacteria. To highlight the versatility of a DEPCOS, we demonstrate that robustly encapsulated cells can execute useful functions, including performing cell-cell communication with other encapsulated bacteria and sensing heavy metals in water samples from the Charles River. We envision that our multilayered physical and chemical containment strategy will facilitate the realization of a wide range of real-world applications for 'living' biosensors.

**8:00 AM F.SM02.04.18**

**Late News: Robust and Flexible Gel-Sheet That Can Rapidly Absorb Water and Blood** Hema Choudhary, Srinivasa Raghavan and Matthew Dowling; University of Maryland, College Park, United States

Superabsorbent polymer gels that can absorb a significant amount of water are widely used in materials such as diapers and for keeping soil moist. These gels are typically in the form of microscale beads. The same gels can also be made as macroscopic solids (e.g., a sheet or cube), but these solids take a long time (~ 24 h) to swell in water. For a large, solid gel to swell rapidly, it is necessary to make it porous, but porous gels tend to be fragile.

Here, we present a simple and low-cost approach to create solid gels that are both porous and highly robust. Our approach involves the polymerization of a foamed monomer solution, with the bubbles of the foam being stabilized by novel polymers. The final dried material is typically in the form of a sheet (thickness ~ 1 mm, length and width from 1 to 100 cm). The sheet is flexible and robust; it can be rolled up like a paper towel and cut into patches of desired size. When added to water, the gel-sheet absorbs 150 times its weight in water within 30 s, and the swollen sheet can be lifted up by hand.

We expect this type of superabsorbent material to have many applications, one of which is in stopping bleeding from severe wounds. In that regard, our gel-sheet is able to rapidly absorb whole blood – up to 60 times its weight within a minute. Moreover, due to the presence of the polymer stabilizers, the blood tends to remain immobilized in the swollen gel. Data from experiments with bleeding models in animals will be presented.

**8:10 AM F.SM02.04.19**

**Late News: 2D Material-Integrated Hydrogels as Multifunctional Protective Skins for Soft Robots** Lin Jing and Po-Yen



Chen; National University of Singapore, Singapore

The deployment of soft robotic technologies for rescue and navigation missions are expected to provide safe object-machine interactions and substantially reduce the risks associated with operation staff. Yet, most of the reported soft robots were made of soft matter with insufficient material stability to support normal robotic operations in extreme environments. Installation of conventional protective modules/exoskeletons onto soft robots inevitably compromises their compliant/complex actuations and increases their energy consumption rates. Herein, we developed a set of soft robotic skins composed of two-dimensional materials (2DM) and gelatin hydrogels, featuring with skin-like multifunctionality (including stretchability, thermoregulation, threat protection, strain sensation). The 2DM-integrated hydrogel skins (2DM/H) enabled the protected soft robots to execute designated missions upon exposure to various environmental threats. All 2DM/H robotic skins demonstrated autonomic perspiration behaviors and maintained mild machine temperatures under high heat. By adopting different 2DM units (including graphene oxide (GO), montmorillonite (MMT), titanium carbide (MXene)), the 2DM/H-protected grippers performed soft grasping missions in organic liquids (GO/H), open fire (MMT/H), electromagnetic radiation and biocontamination (MXene/H). Furthermore, through blending MXene into the hydrogel layer, the MXene-blended hydrogel skin (M-H) was strain sensitive and capable of providing piezoresistive signals in real-time. We next applied conformal GO/M-H skin onto a soft gripper, which demonstrated the ultimate integration of skin-mimicking capabilities to handle irregular objects in hot organic liquids. Two demonstrations were finally presented: a dual-bellows walker robot with MMT/H skin performed a vision-guided search mission in an open fire, and a GO/H-protected batoid robot conducted autonomous underwater locomotion/navigation upon serious DCM spills.

#### **8:20 AM F.SM02.04.20**

**Late News: A Smart Skin for Hydrogels That Regulates the Entry and Exit of Solutes** Sai Nikhil Subraveti and Srinivasa Raghavan; University of Maryland, United States

Many applications of hydrogels rely on their ability to deliver encapsulated solutes such as drugs or dyes to an external medium. However, a problem in many such applications is that, the moment the gel is placed in contact with water, the solutes rapidly leak out by diffusion. Ideally, there should be a way to regulate the release of solutes – i.e., to ensure zero release until a desired time, and thereafter, for the release to be ‘switched on’. Moreover, it would be even better if this was a repeatable switch, i.e., if the gel could be cycled many times between the on and off states. Such a perfect, cyclical on-off release of contents from hydrogels has never been achieved to our knowledge.

We address this challenge by taking inspiration from structures found in nature such as fruits and vegetables, which have a hydrophobic skin that envelops and protects their water-rich core. We have found a way to synthesize a soft hydrophobic skin around any gel. The initial skin completely prevents hydrophilic solutes from leaking out of the gel into the external solution. The skin is also equipped with redox-responsive properties. That is, in the presence of oxidants, the skin becomes hydrophilic, thereby ‘turning on’ the release of solutes out of the gel. Conversely, solute release can be ‘turned off’ at any time by adding a reducing agent that reverts the skin to its hydrophobic state. Thus, our smart skin enables regulated (on-off) release of solutes out of a gel, and this concept is likely to be useful in many applications.

SESSION F.SM02.05: Poster Session: Hydrogel Technology for Humans and Machines  
On Demand Abstracts Available for Viewing Starting Saturday Morning, November 21, 2020  
5:00 AM - 8:00 AM  
F-SM02

#### **F.SM02.05.01**

**Hydrated Poly(ether urethane) Semi-Interpenetrating Network with High Lubricity and Mechanical Properties Under Physiologically Relevant Loading for Cartilage Replacement Applications** Shimon Unterman, Mushtaq Al Zuhairi and Iraklis C. Kourtis; Hyalex Orthopaedics, United States

Orthopaedic biomaterials for use as bearings against cartilage in diarthrodial joints face the dual challenges of being able to withstand high multiaxial loads while minimizing coefficient of friction and wear. High lubricity in aqueous conditions has been achieved with hydrogels such as poly(vinyl alcohol) (PVA), but mechanical properties of these hydrated polymeric networks have typically been inferior to native cartilage. Conversely, high mechanical properties can be achieved with other engineered materials but with increased cartilage wear. This study describes a novel biomimetic hydrated semi-

interpenetrating network (IPN) based on poly(ether urethane) (PEU) that was previously implanted in a rabbit cartilage repair model<sup>1</sup>. The frictional and mechanical properties compare favorably with native cartilage.

A tunable semi-IPN of PEU and a cross-linked polyelectrolyte network was synthesized. Similar to proteoglycans in hyaline cartilage, the polyelectrolyte caused the semi-IPN to swell in water, imparting the high lubricity of a hydrophilic polymer network, while the PEU imparted high stiffness and strength, resembling the collagen type II of cartilage. Upon completion of synthesis, the semi-IPN was a translucent, highly hydrated, qualitatively slippery material. The semi-IPN passed standard ISO 10993 biocompatibility testing.

The semi-IPN was evaluated for coefficient of friction (COF) using a pin-on-disk friction tester with ~1 MPa normal loading in aqueous conditions against a fused silica counterface, yielding a COF of < 0.05; typical cartilage COFs have been reported as <0.01-0.04<sup>2</sup>. The mechanical properties were measured in tension, compression, tear, and shear in physiologically relevant conditions (simulated body fluid at 37° C) and compared to known properties of articular cartilage and PVA orthopaedic hydrogels. Compressive and tensile moduli at physiologic loads were > 40 MPa, stiffer than PVA orthopaedic hydrogels<sup>4</sup> and considerably closer to the modulus of cartilage<sup>3</sup> than traditional joint replacement materials like ultra-high molecular weight polyethylene (UHMWPE) and cobalt chrome alloys (CoCr). Tensile strength was > 30 MPa (cartilage: 3.75 MPa<sup>5</sup>), tear strength was > 40 N/mm (cartilage: 1.21 N/mm<sup>6</sup>), shear strength was > 20 MPa (cartilage: 7.25 MPa<sup>5</sup>), and the material did not fail in the measured compression range (>180 MPa; cartilage: 35.7 MPa<sup>7</sup>). By design the material strength exceeded that of native cartilage, in order to ensure long term performance without adversely impacting adjacent or opposing cartilage.

Hydrated semi-IPNs based on PEU and a polyelectrolyte network offer an attractive combination of mechanical strength, stiffness, and lubricity under physiologic loads. The semi-IPN properties, which closely mimic or exceed the high strength and low friction of native cartilage, provide a promising and novel platform for cartilage replacement applications.

1. Bichara DA; Unterman S; Schmidt MB. *Orthopedic Research Society* (2020 Annual Meeting).
2. Forster, H. & Fisher, J. *Proc. Inst. Mech. Eng. Part H J. Eng. Med.* **210**, 109–118 (1996).
3. Setton, L. A., Elliott, D. M. & Mow, V. C. *Osteoarthr. Cartil.* **7**, 2–14 (1999).
4. Stammen, J. A., Williams, S., Ku, D. N. & Guldborg, R. E. *Biomaterials* **22**, 799–806 (2001).
5. Kumar, P. et al. *Nihon Seikeigeka Gakkai Zasshi* **65**, 1070–7 (1991).
6. Chin-Purcell, M. V & Lewis, J. L. *J. Biomech. Eng.* **118**, 545–56 (1996).
7. Kerin, A. J., Wisnom, M. R. & Adams, M. A. *Proc. Inst. Mech. Eng. Part H J. Eng. Med.* **212**, 273–280 (1998).

#### **F.SM02.05.04**

**An Investigation of Timolol Introduction on Three Hydrogel-Based Drug Delivery Devices for Glaucoma Treatment** Nicole Mortensen and Jeffrey S. Bates; The University of Utah, United States

Contact lenses can be used as drug delivery systems because they are cross-linked, water-soluble, biocompatible hydrogels. Glaucoma is the second largest cause of blindness worldwide that increases the interocular pressure (IOP) of the eye. Topical eye drops of timolol is a common treatment that lowers IOP. The number of patients who become bilaterally blind every year is high due to the inefficiencies of eye drops and low patient adherence. In this study, three hydrogel-based contact lenses were analyzed on their uptake and release concentrations, reversibility, drug concentration profile over 12 hours, as well as their optical and mechanical properties. Synthesized molecular imprinted and soaked, non-imprinted, hydroxyethyl methacrylate (HEMA) based hydrogels resulted in having an uptake and release concentration dependent on the loading solution concentration it was left to soak in. Soaking Acuvue contact lenses resulted in having an uptake and release concentration independent of the timolol loading solution concentration. It released significantly higher concentrations than a daily dosage of timolol. All three hydrogel-based contact lenses successfully delivered timolol for 12 hours and could be reused up to six times. The synthesized HEMA hydrogels lacked in optical and mechanical properties that were to ensure comfort and prevent vision problems when used as a contact lens. As a result, further optimization is needed. Using contact lenses to deliver glaucoma medication has the potential to become a more efficient method of treatment that will increase patient adherence by eliminating barriers within glaucoma therapy created by eye drop medication.

#### **F.SM02.05.05**

**Versatile 3D Printing of Hydrogels by Pluronic** Kusuma Betha Cahaya Imani and Jinhwan Yoon; Pusan National University, Korea (the Republic of)

In recent years, there's an increase of study regarding 3D printing of soft materials, because of its importance for development of new technologies such as wearable electronic devices and artificial human organs, which require both non-

rigid property and precise positioning. For 3D printing of soft materials study, it is required to choose a material which has enough viscosity but also can be easily extruded without clogging, and for that, pluronic is one of the most widely used materials. Pluronic is a thermo-responsive triblock copolymers consisting of poly(propylene oxide) (PPO) and poly(ethylene oxide) (PEO), as the hydrophobic center and hydrophilic side blocks respectively. This structure allows pluronic to form spherical micelles above its critical micelle temperature (CMT) within aqueous solution, which is suitable for 3D printing. Upon deposition on a substrate, by controlling the extruder and bath, pluronic can quickly change its phase, preventing the ink from flowing out of the intended position and retaining the desired 3D shape. In this study, pluronic F127 ((PEO)<sub>99</sub>-(PPO)<sub>65</sub>-(PEO)<sub>99</sub>) is synthesized into pluronic F-dimethacrylate (FDMA) to prepare hydrogels for extrusion-based 3D printing. This work can be further developed to have 3D printed hydrogels with conductive property or controllable elastic modulus. The synthesis of FDMA is simple and it has the prospect for applications in various fields.

#### **F.SM02.05.07**

**The Effect of Fibrin on the Osteogenic Differentiation of Human Dental Pulp Stem Cells** Kao Li<sup>1</sup>, Evan Cheng<sup>2</sup>, Tianjian Bai<sup>3</sup>, Jake D. Feldman<sup>4</sup>, Alyssa Kim<sup>5</sup> and Juyi Li<sup>1</sup>; <sup>1</sup>Stony Brook University, The State University of New York, United States; <sup>2</sup>Syosset High School, United States; <sup>3</sup>Huron High School, United States; <sup>4</sup>Plainview-Old Bethpage John F. Kennedy High School, United States; <sup>5</sup>New Hyde Park Memorial High School, United States

In addition to having non-toxic degradation products, being cytocompatible, and causing the formation of an extracellular matrix, fibrin, a major plasma protein, has been found to be highly suitable in supporting dental tissue formation and improving cell-dentin interactions[1]. This study sought to determine the effects of fibrin on the proliferation and differentiation of dental pulp stem cells, DPSCs, an investigation with potential applications in osteogenic regenerative therapy. Prior studies for in-vitro cultures of DPSCs directly on fibrin clots failed due to rapid fibrinolysis of the substrates prior to differentiation. Here we demonstrate the construction of a gelatin/fibrin scaffold, which is not enzymatically degraded at least during the 28 days required for DPSC differentiation. Furthermore, since gelatin is easily bioprinted it also offers an effective scaffold for fibrinogen, which is then rapidly cross-linked after extrusion, maintaining its shape. Gelatin-fibrinogen hydrogels were created using 9% w/v gelatin and 4 mg/mL bovine fibrinogen cross-linked by 2 different concentration of mTG (microbial transglutaminase) and 2units/ml thrombin, respectively. The gels were media exchanged and cells were cultured in osteogenic media, but without dexamethasone, the standard inducer of osteogenic differentiation. On Days 8 and 28, confocal microscopy indicated that strong tissue formation was occurring on both substrates. RT-PCR was performed at day 8 and 28 to measure the upregulation of genes associated with differentiation; ALP, COL1, and OCN. Even though this set of genes was upregulated on all samples, relative to cells plated on TCP controls, the levels for ALP and OCN for cells plated on the for gelatin-fibrinogen mixture were two and three times higher, respectively, than those for cells plated on pure gelatin confirming the regenerative potential of fibrin clots.

#### **F.SM02.05.08**

**Dual-Network Hydrogels Reinforced with Field-Responsive Hydroxyapatite Exhibiting High Strength and Stiffness While Fully Hydrated** Morgan Pfaff and Jessica Faust; Northeastern University, United States

Modern medicine is seeking stronger composite materials for artificial bone graft applications that are both osteoconductive and exhibit high strength. Alginate-calcium phosphate (CaP) hydrogels have been studied as a potential material, but lack the strength required for artificial bone grafts. Here, we suggest using an alginate-gelatin dual-network embedded with magnetically-aligned CaP rods to significantly increase the overall strength of the material. CaP rods were prepared through hydrothermal precipitation and functionalized with iron oxide nanoparticles. These rods were incorporated into uncrosslinked dual-network solution and aligned under a magnetic field with constant heat and vibration. After alignment, the gelatin was thermally crosslinked at room temperature and the alginate ionically crosslinked in 10% calcium chloride solution. Tensile samples were analyzed using dynamic mechanical analysis. Preliminary results show superior mechanical strength in the dual network films compared to alginate- and gelatin-only hydrogels. The mechanical strength is further increased with higher concentrations of CaP rods. Alignment orientation also impacts hydrogel mechanics, with parallel alignment providing greatest strength and perpendicular alignment the greatest elasticity. The results of this study indicate that an osteoconductive alginate-gelatin hydrogel with high strength is possible with magnetically-aligned reinforcement and is a promising material for bone graft applications.

#### **F.SM02.05.09**

**Thermo-Responsive Artificial Perspiration Membrane** Jeong Hun Kim<sup>1</sup>, Junsoo Kim<sup>1</sup>, Solyee Im<sup>1</sup>, Sang Moon Kim<sup>2</sup>, Jong Pil Im<sup>1</sup>, Jiyong Woo<sup>1</sup> and Seung Eon Moon<sup>1</sup>; <sup>1</sup>Electronics and Telecommunications Research Institute, Korea (the Republic of); <sup>2</sup>Incheon National University, Korea (the Republic of)

Thermal management is essential for living organisms and electronic devices to survive and maintain their functions. However, it has been challenging to develop a flexible cooling devices for flexible electronics or biological systems because conventional coolers are bulky and require rigid batteries. In nature, however, the skin helps to maintain the body temperature constantly by dissipating the heat through the perspiration. Inspired by nature, we introduce an artificial perspiration membrane which automatically regulates evaporation rate at water-air interface depending on temperature. This membrane consists of a valve structure and a rigid frame; the valve is made of silicone-coated thermo-responsive hydrogels and the frame is made of plastics. Those two components are stably bonded by copolymerization. By designing the shape of the valve and the mechanical constraint, we were able to control the area where evaporation occurs depending on temperature. As a result, the valves in the membrane open in a hot environment, which facilitates the evaporation of water, and the valves close in a cool environment, which suppresses the evaporation of water, mimicking cooling function of perspiration in a flexible manner. Our work shows the potential value of a bio-inspired, membrane-type, and automatic cooling device that can solve heat problems in artificial skin devices.

The thermo-responsive hydrogel is patterned with pinwheel-like shape and supported by backbone through copolymerizing at the interface to control the evaporation area depending on the temperature. The stretchable rubber is selectively coated to prevent the unintended evaporation through the hydrogel while securing the water path for swelling. Consequently, the water surface at open state is about 6 times greater than that of close state with fast transition rate (~1 s). The evaporation rate is automatically controlled depending on the temperature with 30% of evaporation reduction at lower temperature. Our study on a smart membrane that can automatically regulate cooling power without external power source may solve thermal problems in wearable or artificial skin devices.

#### **F.SM02.05.11**

**Enhancing Osteogenic Differentiation of Mesenchymal Stem Cells Using Injectable Microporous Hydrogel** Seth Edwards and Kyung Jae Jeong; University of New Hampshire, United States

Mesenchymal stem cell (MSC) delivery and subsequent differentiation into bone forming cells has promising implications for the future of bone repair. Use of hydrogel as a delivery vehicle is advantageous in order to enhance cell retention, and provide a scaffold to facilitate new bone growth. Here we describe a microporous injectable hydrogel for encapsulation of MSCs with the intent to improve proliferation and subsequent osteogenic differentiation. Physically crosslinked microgels are formed by thermal crosslinking of gelatin in a water in oil emulsion. Bulk scaffold formation involves chemical crosslinking of gelatin by nontoxic enzymatic reaction. Enzymatic crosslinking of gelatin provides prolonged strengthening of the bulk gel, and provides a covalent mechanism for tissue adhesion. A hydrated suspension of microgels and cells can be injected for noninvasive cell delivery, and the scaffold can crosslink *in situ*, encapsulating delivered cells in the pore space. This hydrogel provides an advantageous environment for MSC growth and differentiation due to the large interstitial space between microgels, which improved cell spreading and proliferation when examined by confocal microscopy, and improved osteogenic differentiation when examined using alizarin red S stain and high resolution micro computed tomography.

#### **F.SM02.05.12**

**A Smart LEA for Dynamic Adjustments to Brain Aneurysm Embolization and Healing\*** Juyi Li<sup>1</sup>, Robert Wong<sup>1</sup>, Aaron Slutsky<sup>2</sup>, Daniel Cohn<sup>2</sup>, Chandramouli Sadasivan<sup>1</sup>, Anya Chabria<sup>3</sup>, Jessica Guo<sup>4</sup>, Varun Nimmagadda<sup>5</sup>, Tyler Shern<sup>6</sup>, Stephanie Tarrab<sup>7</sup>, Jeffrey Zhang<sup>8</sup>, Emily Zhou<sup>9</sup>, Jeffrey Huang<sup>10</sup>, Ikshu Pandey<sup>11</sup> and Miriam H. Rafailovich<sup>1</sup>; <sup>1</sup>Stony Brook University, The State University of New York, United States; <sup>2</sup>The Hebrew University of Jerusalem, Israel; <sup>3</sup>The Wheatley School, United States; <sup>4</sup>Ward Melville High School, United States; <sup>5</sup>Novi High School, United States; <sup>6</sup>Mission San Jose High School, United States; <sup>7</sup>Yeshivah of Flatbush Joel Braverman High School, United States; <sup>8</sup>Centerville High School, United States; <sup>9</sup>The Harker School, United States; <sup>10</sup>University of Pennsylvania, United States; <sup>11</sup>Johns Hopkins University, United States

Brain aneurysms are focal, pathological dilations that mostly form at branch points of the cerebral vasculature. These weak-wall structures can rupture leading to hemorrhagic stroke with mortality and morbidity rates as high as 40% and 25%, respectively. More than 60% of aneurysms are currently treated with minimally invasive endovascular/interventional methods. Most of these methods involve the permanent implantation of metallic devices such as intrasaccular coils and meshes or endovascular flow diversion. These implants reduce blood flow velocity within the aneurysm and thus promote clot formation within the aneurysmal sac, which is converted to fibrous tissue over a period of several months. However, current devices show unfavorable primary outcomes in 20% to 30% of cases on average and success rates are substantially lower depending on aneurysm type and location. In this project, we discuss the development of an injectable, multi-functional, reverse thermo-responsive, *in situ* cross-linkable, shape-conforming, intrasaccular porous scaffold. This scaffold changes dynamically to enhance the associated wound healing process which follows obduration. The scaffold is engineered to work with the natural blood flow and promotes vascular remodeling and endothelialization followed by personalized

biodegradation, at the end of the process, leaving no residue behind. This research program harnesses the unique behavior of a family of reverse thermo-responsive (RTR) polymers to generate a novel Biodegradable Intracascular Polymeric Device, displaying enhanced clinical performance. The aqueous solutions of these polymers display low viscosity at in-physiological temperatures and are gels at 37 degrees. The device is an easily syringable, low viscosity multi-component aqueous solution comprising: [a] a cross-linkable RTR component that forms a robust and homogeneously porous scaffold for controlled intracascular thrombosis, [b] a leachable RTR-displaying component acting as the porogen, [c] an iodine-rich radiopaque agent, [d] a polymerizable (RGD)-containing oligopeptide that will *in situ* co-polymerize with the other components, aimed at accelerating the generation of an endothelial cell layer at the aneurysm neck, [e] inclusion of basic Fibroblast Growth Factor (bFGF) in the cross-linked component to promote thrombus organization and intracascular fibrosis/remodeling, and [f] a cross-linkable oligopeptide containing the matrix metalloprotease (MMP)-degradable leucine-glycine motif that will be *in situ* co-crosslinked with the RTR components, to impart to the polymer device to degrade in a personalized, patient-specific manner, as a function of the healing process. This process represents a major step in treatment of aneurysms, which shortens optimize brain aneurysm treatment with short procedure times, require no chronic anti-platelet medications, promote endothelialization of the parent-vessel interface, enhance aneurysm 'sac' fibrosis, and degrade in a patient-specific manner to leave no trace of the pathology or the treatment, with lower costs.

\*Authors 3-10 contributed equally to this work.

We gratefully acknowledge support from the Louis Morin Charitable Trust

[1]Taschner CA, Chapot R, Costalat V, Machi P, Courtheoux P, Barreau X, et al. Second-Generation Hydrogel Coils for the Endovascular Treatment of Intracranial Aneurysms: A Randomized Controlled Trial. **Stroke**. 2018;49(3):667-74.

[2]Sosnik A, Cohn D. Reverse thermo-responsive poly (ethylene oxide) and poly (propylene oxide) multiblock copolymers. **Biomaterials**. 2005;26(4):349-57.

#### F.SM02.05.13

**Late News: Using Coarse-Grained Molecular Dynamics to Model Hydrogel Viscosity** Kyle R. Shi<sup>1</sup>, Hannah Even<sup>2</sup>, Shoumik Saha<sup>3</sup> and Dilip Gersappe<sup>3</sup>; <sup>1</sup>Dublin High School, United States; <sup>2</sup>Staples High School, United States; <sup>3</sup>Stony Brook University, The State University of New York, United States

**Hydrogels are systems of hydrophilic polymers that swell when placed in a solvent to form a gel-like structure. When nanocomposites are added to hydrogels, they can enhance their properties by crosslinking the polymers. Hydrogels have shown promise as an environmentally friendly substitute to cement as soil stabilizers, mechanically improving the strength of the soil. While past studies have found a positive relationship between clay nanocomposite concentration and hydrogel viscosity with a qualitative stress-autocorrelation function, specific mechanical properties and structure formation of these hydrogels remain unknown. Our research aims to learn more about the properties of hydrogels with rigid rod-shaped clay nanocomposites and explore the possibility of determining more quantitative trends on viscosity by simulating shear stress on the hydrogel system, imitating realistic soil movement on the hydrogels. We performed Molecular Dynamics simulations in order to understand the rheological properties of hydrogels. The concentration of the nanocomposite and the shear rate were varied and different polymer-nanocomposite interaction energies were used in order to determine the effects of these factors on the viscosity of hydrogels. The results show a clear shear thinning behavior in these systems and reflect similar trends to previous studies. Our results can be used to predict an optimum hydrogel composition in different conditions for soil stability.**

**We gratefully acknowledge support from the Louis Morin Charitable Trust.**

#### F.SM02.05.14

**Late News: Optically Active Nanoengineered Fibrous Scaffolds for Cardiac Cell Monitoring** Stijn Jooke<sup>1</sup>, Olivier Deschaume<sup>1</sup>, Olga Krylychkina<sup>2</sup>, Yovan de Coene<sup>1</sup>, Thierry Verbiest<sup>1</sup>, Koen Clays<sup>1</sup>, Geert Callewaert<sup>3</sup> and Carmen Bartic<sup>1</sup>; <sup>1</sup>KU Leuven, Belgium; <sup>2</sup>imec, Belgium; <sup>3</sup>KU Leuven KULAK, Belgium

In cardiac tissue engineering the incorporation of nanoparticles (NPs) such as plasmonic NPs, carbon nanotubes or magnetic particles was shown to improve the function of *in vitro* cardiac patches in terms of cell viability, electrical signal coupling, beat synchronicity, etc. [1,2]. Moreover, it has also allowed to locally deliver stimuli to cells and guide cell behavior, for instance, by heating of plasmonic NPs[3].

In this work, we created a smart scaffold capable of optically reporting cardiomyocyte activity *in situ* (electrical and contractile) by incorporating voltage-sensitive semiconductor quantum dots (QDs) in 2D scaffolds and 3D hydrogels.

We have characterized the fluorescence voltage sensitivity of Type I CdSe/ZnS QDs and pseudo-Type II CdSe/CdS rods, investigated in a controlled environment, under single and two photon optical excitation. Then, QDs were incorporated in 2D scaffolds of collagen nanofibers and used two-photon fluorescence microscopy to readout of the activity of cultured primary cardiomyocytes [4]. The method was validated in a pharmacological assay where the drugs epinephrine and blebbistatin were used for their combined chronotropic and inotropic effects. Finally, the concept is extended to 3D by incorporating QD-labeled collagen fibers in 3D hydrogel constructs.

[1] Baei, P. *et al.* Electrically Conductive Gold Nanoparticle-Chitosan Thermosensitive Hydrogels for Cardiac Tissue Engineering. *Mater. Sci. Eng. C* **2016**, *63*, 131–141.

[2] Yu, H. *et al.* Mechanically and Electrically Enhanced CNT-Collagen Hydrogels As Potential Scaffolds for Engineered Cardiac Constructs. *ACS Biomater. Sci. Eng.* **2017**.

[3] Baffou, G. *et al.* Photoinduced Heating of Nanoparticle Arrays. *ACS Nano* **2013**, *7* (8), 6478–6488.

[4] Jookan, S. *et al.* Quantum Dot-Functionalized Extracellular Matrices for in Situ Monitoring of Cardiomyocyte Activity. *ACS Appl. Nano Mater.* **2020**.

#### F.SM02.05.15

**Late News: Gelation-Based Naked-Eye Detection of Glucose via Dual-Enzyme Cascade Reaction** Jisoo Lee and Seonki Hong; DGIST, Korea (the Republic of)

Many efforts have been conducted to develop bioassays in point-of-care settings for rapid and convenient biomarker detection. Among them, the colorimetric-based system has been emerging due to the advantages in simple read-out through the naked-eye without requiring any expensive devices. However, it has still been challenging to simplify the labor-intensive multiple steps required to improve the limit of detection and remove the background color which may interfere with the detection signal.

Herein, we report a gelation-based bioassay mediated by a cascade reaction of two enzymes. We reasoned that biomarker-specific gelation can provide a detectable signal through the naked-eye even in the presence of the background color biospecimens such as blood and urine. Gelation is triggered by the quinone tanning reaction of catechol-conjugated polyethylene glycols via horseradish peroxidase (HRP) in the presence of hydrogen peroxide (H<sub>2</sub>O<sub>2</sub>). Therefore, we coupled another enzyme, glucose oxidase (GOx), that produces the H<sub>2</sub>O<sub>2</sub> depending on the concentration of glucose to initiate the HRP-mediated gelation.

In our system, parameters adjusting the gelation time include the concentration of enzymes (HRP and GOx), catechol content conjugated to the polymeric precursor, the concentration of polymeric precursor, and the pH. In the experiment using H<sub>2</sub>O<sub>2</sub> as a positive control to glucose/GOx system, the gelation time dramatically decreased down to 1 minute as the HRP concentration increased up to 1 U/mL. In the HRP/GOx dual-enzyme system, 0.25 U/mL of HRP was sufficient to achieve successful gelation within 80 minutes with 10–100 U/mL of GOx in the presence of 10 mM glucose. The best conditions of other parameters for the fastest gelation were observed at 83% of catechol content, 5wt% of the precursor, and pH 7. Finally, as low as 16 mM of glucose was detectable through the naked-eye within 20 minutes of gelation time.

With the advantage of the cascade reaction of two enzymes, we expect improvement in the detection sensitivity. In addition, single-step glucose detection is allowed without requiring washing steps due to the enzymes' intrinsic specificity.

#### F.SM02.05.16

**Late News: A Clock-Like Hydrogel That Visually Indicates Time** So Hyun Ahn, Srinivasa Raghavan and William E. Bentley; University of Maryland, United States

Microcapsules can be used to monitor the local micro-environment *in vivo*, e.g., within the gastro-intestinal (GI) tract. For example, when molecular signals are released into the GI, the payload within the microcapsules could undergo a color change in response to the signal. While the nature of the signal is often the key piece of information in such experiments, the *time* at which the signal is released could be another vital aspect. To obtain information regarding time, there is the need for a gel-like material that could function like a 'clock' – i.e., exhibit systematic changes at regular time intervals.

Here, we report a simple 'clock' construct based on self-destructing structures embedded in an agarose gel. For this, we fabricate capsules of alginate crosslinked by Ca<sup>2+</sup> and containing the enzyme alginate lyase. This enzyme severs alginate chains, thereby causing the capsule to degrade over a period of time. The higher the enzyme concentration, the lower the degradation time. Capsules with different concentrations of enzyme are embedded in an agarose gel to create our 'clock'. Capsule degradation proceeds in a sequential manner, and visual inspection of the gel (i.e., the capsules that remain intact) reveals the time elapsed from the start of the experiment. To facilitate visual clarity, we embed colored or fluorescent

nanoparticles in each of the capsules. Moreover, the degradation rate can be varied using pH, temperature, and other variables that affect the enzymatic activity. Variations of the above simple clock include: (a) one that is activated by an external trigger; and (b) one that locks-in the elapsed time at a particular juncture.

### **SYMPOSIUM F.SM03**

---

Materials and Mechanics Challenges in Haptics for Human–Machine Interfaces  
November 21 - December 2, 2020

#### Symposium Organizers

Rebecca Kramer-Bottiglio, Yale University  
Darren Lipomi, University of California, San Diego  
Yigit Menguc, Facebook  
Benjamin Tee, National University of Singapore

---

\* Invited Paper

SESSION F.SM03.06: Live Panel Discussion I: Haptic Actuators  
Session Chairs: Yigit Menguc and Benjamin Tee  
Tuesday Afternoon, December 1, 2020  
F.SM03

**7:30 PM PANEL DISCUSSION**

**8:30 PM CHARLES DHONG, PANELIST**

**8:30 PM MICHAEL TOLLEY, PANELIST**

**8:30 PM FABRIZIO SERGI, PANELIST**

SESSION F.SM03.07: Live Panel Discussion II: Haptics in VR and AR  
Session Chairs: Yigit Menguc and Benjamin Tee  
Tuesday Afternoon, December 1, 2020  
F.SM03

**8:30 PM PANEL DISCUSSION**

**9:30 PM JAMES COLGATE, PANELIST**

**9:30 PM TANIA MORIMOTO, PANELIST**

**9:30 PM LAURE KAYSER, PANELIST**

SESSION F.SM03.08: Live Panel Discussion III: Haptic Materials  
Session Chairs: Rebecca Kramer-Bottiglio and Darren Lipomi  
Wednesday Morning, December 2, 2020  
F.SM03

**11:30 AM PANEL DISCUSSION**

**12:30 PM CARMEL MAJIDI, PANELIST**

**12:30 PM MARTIN KALTENBRUNNER, PANELIST**

**12:30 PM HERBERT SHEA, PANELIST**

SESSION F.SM03.09: Live Panel Discussion IV: Wearable Haptic Devices  
Session Chairs: Rebecca Kramer-Bottiglio and Darren Lipomi  
Wednesday Afternoon, December 2, 2020  
F.SM03

**12:30 PM PANEL DISCUSSION**

**1:30 PM NANSHU LU, PANELIST**

**1:30 PM MARCIA O'MALLEY, PANELIST**

**1:30 PM HEATHER CULBERTSON, PANELIST**

SESSION F.SM03.01: Haptic Actuators  
On Demand Abstracts Available for Viewing Starting Saturday Morning, November 21, 2020  
F-SM03

**5:00 AM \*F.SM03.01.01**

**Soft Electrically-Driven Actuators for Wearable Haptics** Herbert R. Shea; Ecole Polytechnique Federale de Lausanne, Switzerland, Switzerland

For virtual reality (VR) to be truly immersive, the sense of touch must be stimulated: a tennis ball should feel light and rubbery, a wall must be impenetrable, a lightswitch must click when pressed. Why don't we have haptic suits with thousands of individual actuators (taxels) when every smartphone display has millions of individually addressed pixels? Generating localized forces on the human body in a comfortable and safe way is a major challenge for soft actuation: both fast motion and high forces are needed, yet the device must conform to the human body, and consume low power.

I will present some approaches developed in my lab for flexible actuators combining high strain and high force, operating at high speed, and that do not rely on external compressed air or vacuum supplies. Due to its high energy density, we have focused on electrostatic actuation, using high electric fields to deform elastomers or textile structures.

For kinesthetic feedback, which can be described as controlling the motion of joint, we have focused on textile-based brakes, only 1 mm thick, that can block the motion of two sliding strips in a few milliseconds[1]. By coating conductive textile strips with high permittivity dielectrics, we developed a clutch that blocks up to 20 N pulling force per square centimeter of active region, for a power consumption of under 2 mW. We integrated these clutches into thin gloves. Users wearing them are much more accurate when manipulating virtual objects and feel deeper immersion. We will report a new fabrication method allowing for even higher forces for use in full-body kinesthetic haptics, blocking shoulder and elbow motion to allow feeling virtual objects as being heavy, and virtual tables as blocking hand motion.

Cutaneous feedback requires dense arrays of actuators to locally stimulate to skin to provide the illusion of touching an



object. We use our fingers to identify objects by sliding our fingertips over them, and we know if a glass is about to slip out of our hand by sensing shear forces. Simulate this in VR requires being able to generate normal and shear forces with high spatial resolution. We have developed arrays of sub-mm thick flexible actuators that generate over 60% strain and operate at over 300 Hz. A 6 mm diameter actuator generates 300 mN normal force and 500  $\mu\text{m}$  displacement. This is achieved using fluidically coupled electrostatic zipping and a combination of flexible polymers with high breakdown field and silicone elastomers that allow for high displacement[2]. We have made 5x5 arrays, mounted them directly on the arm and on consumer products, and report on user feedback for notification, control and navigation.

By use of thin dielectrics, high permittivity films, and low stiffness electrodes, we have reduced the drive voltage of Dielectric Elastomer Actuators (DEAs) to 400 V, a level at which we can use SMD components for compact control electronics[3]. We report “feel-through” untethered cutaneous haptics, with DEA actuators only 18  $\mu\text{m}$  thick, so thin the user does not feel them mounted on his or her fingertip when they are off. However, when the 3 mm diameter devices are turned on, the user feels localized pulsation that allows receiving rich haptic information.

I will close by going over the challenge of integrating these technologies in a glove or suit, and the promise of this field.

[1] R. Hinchet and H. Shea, “High Force Density Textile Electrostatic Clutch,” *Advanced Materials Technologies*, vol. 5, p. 1900895, 2019, doi: 10.1002/admt.201900895.

[2] E. Leroy, R. Hinchet, and H. Shea, “Multimode Hydraulically Amplified Electrostatic Actuators for Wearable Haptics,” *Advanced Materials*, 2020. in press.

[3] X. Ji *et al.*, “An autonomous untethered fast soft robotic insect driven by low-voltage dielectric elastomer actuators,” *Science Robotics*, vol. 4, no. 37, 2019, doi: 10.1126/scirobotics.aaz6451.

### 5:30 AM F.SM03.01.02

**Scaling of Hydraulically Amplified Electrostatic Zipping Actuators (HAXELs)** Edouard Leroy and Herbert R. Shea; École Polytechnique Fédérale de Lausanne, Switzerland

Haptic interfaces for virtual reality (VR) or augmented reality (AR) require dense arrays of actuators to provide realistic feedback to the user. These actuators must be fast (<20 ms), generate large static forces (>100 mN) and displacements (>300  $\mu\text{m}$ ) while being easy to integrate in lightweight, comfortable interfaces. The actuator mechanical compliance should be close to that of skin. Conventional actuation technologies such as electromagnetic, piezoelectric or pneumatic either provide only vibratory feedback or are difficult to integrate in low-profile interfaces. Flexible electrostatic actuators such as our HAXEL devices offer effective solutions to these challenges.

HAXELs are hydraulically amplified zipping electrostatic actuators, less than one millimeter in thickness, designed for integration into textile-based haptic interfaces for VR or AR scenarios. In previous work [1], we reported 6 mm x 6 mm HAXEL actuators that can produce up to 300 mN force and 500  $\mu\text{m}$  displacement (i.e. 60% strain). We report here the modeling and experimental results on scaling HAXELs down to 3 mm and up to 50 mm diameter, for applications in wearable haptics and in soft robotics.

Each HAXEL consists of a fluid-filled cavity whose shell is made of a non-stretchable polymer in the outer regions and of a stretchable elastomer for the central region. Electrodes are patterned in both top and bottom polymer shells. When a voltage is applied to the annular electrodes, they are pulled together by Maxwell pressure, starting to zip at the outer regions where the electric field is highest. As the top and bottom polymer regions are pulled together, the fluid is rapidly forced into the stretchable region, forming a raised bump. To obtain high power density (>100 W/kg), we use high permittivity layers based on PVDF terpolymers.

These actuators can easily be felt by users and provide both normal force and shear force by using segmented electrodes to drive the fluid in-plane. Using a flexible 5x5 matrix of HAXELs, users can obtain information about the location and texture of a virtual object. HAXELs could lead to lightweight and comfortable gloves, sleeves or full-body suits delivering realistic haptic feedback.

Different locations on our bodies have different sensitivity thresholds for feeling force and displacement, and different pitch discrimination. On fingertips we can feel pins 0.8 mm apart, while on our back the distance is roughly 5 mm. It is necessary to adapt the size of the taxels to body location and to the targeted VR application.

The force and displacement characteristics of HAXELs from 3 mm x 3 mm up to 50 mm x 50 mm are discussed and compared to a finite element model that accounts for coupled electrostatics and mechanics using nonlinear material models. Both static and dynamic characteristics are studied as they are equally important for haptic feedback. The measured static displacements range from 100  $\mu\text{m}$  to several mm while the forces range from tens of mN to over 1 N. Good agreement between the model and the experiment is shown, validating the finite element model as a tool for future designs. Optimized electrode shape, cavity shape and effect of materials choice on actuation voltage and generated force, displacement and device dynamics are presented.

Although HAXEL actuators were initially designed for haptics, they can find applications in other areas such as microfluidics

as dense arrays of valves or to rapidly reconfigure channels, and for soft robotic as matrices of high force actuators for locomotion or grasping.

[1] E. Leroy, R. Hinchet, H. Shea, "Multimode Hydraulically Amplified Electrostatic Actuators for Wearable Haptics", *Advanced Materials*, 2020, in press.

#### 5:45 AM F.SM03.01.04

**A Dynamic Electrically-Driven Soft Valve for the Control of Mesoscale Fluidic Flows** [Siyi Xu](#)<sup>1</sup>, Yufeng Chen<sup>2</sup>, Nak-Seung Patrick Hyun<sup>1</sup> and Robert Wood<sup>1</sup>; <sup>1</sup>Harvard University, United States; <sup>2</sup>Massachusetts Institute of Technology, United States

Soft valves for hydraulic actuators that based on meso-scale channels have been designed in various forms, primarily fluid-driven or electrically-driven, with promise for the control of soft robots. Fluid-driven valves are often tethered to external pressure sources that limit, for example, robot locomotion. Electrically-driven valves based on electrostatic forces exhibit a large hysteresis and slow response times. In our work, we present a dynamic electrically-driven soft valve made of ultra high power density dielectric elastomer actuators (DEAs). These dynamic DEAs are actuated at 200Hz or above, with low damping ( $\tan(\delta) < 0.34$  at 100Hz) and a short response time (in less than 10 milliseconds). Dynamic actuation produces 300% greater blocked force compared to quasi-static operation with the same DEAs due to higher driving voltages and greater than five times increase in free displacement at the actuator resonance. The channel, on the contrary, is cast with a dissipative material. The viscoelasticity difference between the actuator and the channel materials makes it possible to achieve both pressure and flow control with the dynamic DEAs. The valve performance can be tuned by the input voltage, the driving frequency, and the active area of the DEAs. This dynamic electrically-driven soft valve, as a component of a soft fluidic robot, enables effective control of 1.5psi flow pressure in soft channels. The novel dynamic design represents a substantial performance improvement over existing quasi-steady DEA valves, and will enable effective control of future meso-scale hydraulic robots.

#### 6:00 AM \*F.SM03.01.05

**fMRI-Compatible Force Controlled Robots and Their Application in Motor Neuroscience** [Fabrizio Sergi](#); University of Delaware, United States

Can we use robots to help humans learn a new motor skill, or to improve performance of a motor task? If so, what are the neural substrates that enable humans to improve motor skill learning or execution when they interact physically with external agents? These are fundamental motor neuroscience questions, which have or will have special relevance in multiple domains, such as human augmentation, surgical training, athletics, and neurorehabilitation. In this talk, I will present the development of methods that can help address these questions, which combine MRI-compatible robotics with functional neuroimaging and advanced biosignal processing, and will present two applications of these methods in fundamental motor neuroscience research.

Over the past years, my lab has developed a new class of MRI-compatible robots that can be used in conjunction with functional Magnetic Resonance Imaging to study the neural substrates involved in the neural control of movements during physical interaction with external agents. Specifically, I will present two systems, the MR-SoftWrist, a 2 DOF wrist exoskeleton capable of force feedback designed to study neural substrates involved in the control of wrist movements during externally imposed forces, and the MR-StretchWrist, a 1DOF wrist robot designed to apply velocity-controlled perturbations to the wrist to condition stretch reflexes and study their neural correlates using fMRI.

The development of these robots is complicated by the magnetic fields of MRI, which pose challenges from the standpoint of materials selection for robot components, electrodes for measuring biosignals associated with motor tasks, as well as biosignal processing. To achieve MRI-compatibility, our current solution is to include piezoelectric ultrasonic motors for actuators, shielding and filtering of sensor signals, and use non-magnetic metal for all robot parts. However, because piezoelectric motors are intrinsically high-impedance actuators, we have developed custom solutions based on series elastic actuation and nonlinear passivity-based force control for reducing actuator impedance. Moreover, we have recently developed a novel method for measuring artifact-free electromyographic signals during MRI which enables for the first time collection of biosignals during arm movements under fMRI using a novel set of electrodes and nonlinear interference estimation algorithms. Validation experiments demonstrate that the biosignals measured during MRI are not significantly different than those measured in normal lab conditions.

In this talk, I will also present the application of MRI-compatible robots to establish the neural correlates involved in the neural control of movements. In one experiment, we exposed 30 healthy individuals to lateral force perturbations during

point-to-point wrist movements to elicit adaptation to this condition. By analyzing resting state fMRI data measured before and after motor execution and before and after adaptation, we were able to identify areas involved in creating and processing the memory related to movement execution under force perturbations. In a second experiment, we used the MR-StretchWrist to apply perturbations to the wrist along the flexion/extension axes and condition long-latency responses. Long-latency responses are interesting components of motor control because they gracefully blend fast reaction times of spinal reflexes with sophisticated modulation capabilities of voluntary control. In our first experiment with the MR-StretchWrist, we were able to determine the somatotopic organization of long-latency responses of flexor and extensor muscles in the brainstem for the first time in-vivo in humans. The observed organization is partially consistent with animal models, with activity primarily in the ipsilateral medulla for flexors and in the contralateral pons for extensors, but also include other areas, such as the midbrain and bilateral pontomedullary contributions.

#### **6:30 AM F.SM03.01.06**

**Electroactive Artificial Muscles Actuators for Human-Machine Interaction and Soft Robotics** Maduran Palaniswamy, Shardul Panwar, Ty Ebling, Max Herzog, Erin Rutledge and Michael P. Rowe; Toyota Research Institute of North America, United States

Electroactive artificial muscles have been a scientific novelty soft actuator for many years, but of little practical use because they lack substantial force output or large-enough displacement. Significant advancements in constituent materials, actuator design and assembly of component artificial muscles for devices have now allowed the transition of this interesting technology into actual consideration for real-world applications in haptics, human-machine interactions and soft robotics. The electroactive artificial muscles discussed here are, fundamentally, flexible capacitors that give a mechanical response when an electrical potential is applied to them. As with any capacitor, greater force is expressed with an inverse squared relationship to the thickness of the electrical insulation used to space the positive and negative electrodes. As insulation thickness is reduced, output force from the artificial muscle is increased. We have determined that particular acrylic polymer blends exhibit an impressively high resistance to electrical breakdown per-micron-thickness of material in these systems, when compared to other polymers including: polypropylenes, polyesters, polyimides and silicone polymers. Electrical insulation polymer optimization was found to be able to reduce electrode spacing by x4, which can manifest in up to a x16 increase in force. It was found that this increased force is lost if the artificial muscle stiffness is not tuned correctly. Too much stiffness immobilizes the muscle whereas a lower value would result in the muscle not able to transfer the elevated force being generated. This optimization was accomplished through specific layering of biaxially oriented polypropylene (BOPP). With these marked material improvements, forces of nearly 7N were generated for 0.5mm of displacement from an artificial muscle that is only ~350 microns thick in a resting state are achieved. A single stack of artificial muscles is rarely capable of generating the necessary force for real-world applications. The exceptional artificial muscles discussed here are uniquely capable of functioning by arranging the individual artificial muscles are arranged in an overlapping closest-packed tessellated pattern. This original system-level optimization still further improves artificial muscle force output by an additional x4; setting these original ensembles of artificial muscles apart from related technology in the field of soft robotics research. These flexible actuators hold the promise to proliferate the automotive industry and beyond for haptics in general because they are light weight, quiet, compliant, thin, simple to implement and new.

#### SESSION F.SM03.02: Haptic Materials

On Demand Abstracts Available for Viewing Starting Saturday Morning, November 21, 2020

F-SM03

#### **5:00 AM \*F.SM03.02.01**

**Liquid Metal Architectures for Wearable Energy Harvesting and Storage** Carmel Majidi; Carnegie Mellon University, United States

Wearable technologies for human-machine interaction (HMI) require on-board sources of energy to power sensors for tactile or physiological monitoring, actuators for haptic feedback, and electronics for signal processing and communication. For many emerging haptic/HMI applications, miniature battery technologies (e.g. coin cells, LiPo) are inadequate – operation over sustained durations instead depends on larger batteries or methods of harvesting energy from the body or environment. However, in order to be compatible with the human body, such energy storage and harvesting systems should be soft and stretchable so that they can deform with the surrounding tissue and not impair natural motion.

In this talk, I will highlight progress in creating soft, highly stretchable batteries and energy harvesting devices using liquid metal (LM) alloys. Eutectic gallium indium (EGaIn) is selected as the LM alloy due to its enabling combination of high electrical conductivity and fluidic deformability. In particular, I will focus on the following LM architectures: (i) soft-matter batteries composed of EGaIn and ionic gel that can be stretched to >300% strain; (ii) LM-polymer composites for thermoelectric and triboelectric energy harvesting; and (iii) dielectric elastomer generators composed of an LM-polymer dielectric and thin-film EGaIn coating. To demonstrate their potential role in future haptics/HMI, I will present examples of how these LM-based technologies are used for powering wearable sensors and electronics.

#### 5:30 AM F.SM03.02.02

**Liquid Metal-Based Strain-Insensitive Conductors for Stretchable Electronic Circuits** [Shanliangzi Liu](#)<sup>1,2</sup>, Dylan Shah<sup>2</sup> and Rebecca Kramer-Bottiglio<sup>2</sup>; <sup>1</sup>Purdue University, United States; <sup>2</sup>Yale University, United States

Gallium-based liquid metals have shown great potential in applications such as soft and stretchable electronics due to their high conductivity and intrinsic softness. However, liquid metal-based bulk conductors are typically sensitive to strain and therefore not be suitable for stretchable interconnects. Additionally, reliably interfacing liquid metal with conventional, rigid electronics often requires cumbersome fabrication processes. In this work, we present a liquid metal-based biphasic conductor with high conductivity, extreme stretchability (>1000%), negligible resistance change when strained, cyclic stability, and a reliable interface with rigid electronics. The biphasic material is a mixture of liquid metal and crystalline solids, which are produced by thermally processing liquid metal particles. We use a scalable transfer-printing process to create various multilayer circuit board assemblies that maintain their performance when stretched. This technique enables facile and direct conversion of existing PCB designs into soft and stretchable forms for applications in soft robotics and wearable devices.

#### 5:45 AM \*F.SM03.02.03

**Conductive Polymers as Electro-Active Materials for Haptics** [Laure V. Kayser](#); University of Delaware, United States

Conductive polymers have been extensively used as flexible and transparent alternatives to inorganic conductors in transistors, light-emitting diodes, and solar cells. These “classic” applications, however, do not take advantage of some of the unique features of conductive polymers such as their ionic conductivity and our ability to tune their physical and mechanical properties via chemical modification. These features really shine in the developing area of bioelectronics: the interface between electronic materials and devices, and biological systems. In particular, I will highlight in this talk our efforts in using conductive polymers for haptics, to study or stimulate the human sense of touch.

The most widely-used conductive polymer is doped poly(3,4-ethylenedioxythiophene) (PEDOT), commercially available in water as a polyelectrolyte complex with poly(styrene sulfonate) (PSS). PEDOT:PSS, however, often requires the use of additives to modify its electronic and mechanical properties leading to potentially unstable and unsafe materials. Instead, we are using PSS copolymers to modify the intrinsic properties of PEDOT:PSS without additives. In particular, we have synthesized stretchable conductive polymers which served as electro-tactile materials to simulate rough and smooth surfaces in virtual reality. I will also share our preliminary research in the development of PEDOT:PSS conductive copolymers that can dynamically change their mechanical properties under applied voltages: electro-active actuators.

#### 6:15 AM F.SM03.02.04

**Designing Magnetorheological Fluids with 2D Materials for Soft Robotics** [Abigail L. Rendos](#)<sup>1</sup>, Kevin McDonald<sup>1</sup>, Ran Li<sup>1</sup>, Stephanie Woodman<sup>1,2</sup>, Xi Ling<sup>1</sup>, Tommaso Ranzani<sup>1</sup> and Keith A. Brown<sup>1</sup>; <sup>1</sup>Boston University, United States; <sup>2</sup>Yale, United States

Smart fluids are suspensions of functional particles in which an applied field drastically changes the fluid's properties. For example, magnetic microparticles in solution can form magnetorheological fluids (MRFs) that solidify upon the application of a magnetic field because of the formation of rigid particle chains. By virtue of being a fluid, these materials could provide an empowering path to realizing tunable actuators in soft robotic systems for human interactions. To test this idea, we successfully use an MRF as the active fluid in a soft actuator and gripper. Despite this success, the efficacy of MRF is inversely proportional to its density, which is commonly high on account of containing a high volume fraction of iron. As a path to realizing more efficient MRFs, we hypothesized that the inclusion of ultra-high aspect ratio 2D materials could provide the needed increase in yield stress without requiring a high volume fraction of dense iron particles. Thus, we explored 2D material sheets as additives in an MRF and tested its response to magnetic fields in shear mode, where the fluid is sheared between two plates, and in valve mode, where a pressure gradient pushes the fluid through a tube. While the addition of the 2D material did not affect performance in shear mode, its presence increased the pressure difference seen in

valve mode at low flow rates. To explain these seemingly contradictory results, we propose a model based on the 2D material improving the yield stress by averaging out the shear stress over length scales commensurate with the particle size. This discovery can be used to rationally design MRFs for valve mode operation, which is important to their successful incorporation into soft robotics. These advances motivate further exploration of MRFs in soft robotics and reveal the influence of highly anisotropic additives on MRF performance.

### 6:30 AM \*F.SM03.02.05

**Sustainable, Bioderived and Degradable Soft Materials for Human Machine Interfaces** Martin Kaltenbrunner; Johannes Kepler University, Austria

Nature inspires a wide range of bio-mimetic systems ranging from soft robotic actuators to perceptive electronic skins that enhance and support our life. The growing demand on assistive, medical and bioelectronic technologies however raises concerns on the ecological footprint of this emerging platforms, as they are often designed for a defined, limited operational lifetime. Introducing a key feature essential to nature - biodegradability - will enable soft electronic and robotic devices that reduce (electronic) waste and are paramount for a sustainable future.

We here introduce materials and methods such as tough yet biodegradable biogels for soft systems that facilitate a broad range of applications, from transient wearable electronics to metabolizable soft robots. These embodiments are highly stretchable, are able to heal and are resistant to dehydration with unchanged mechanical properties for more than one year on the shelf. Our forms of soft electronics and robots are built from resilient gelatin-based gels with tunable, extreme mechanical properties that uniquely combine performance and durability with degradability. They are engineered for long-term operation in ambient conditions without fatigue, sustaining more than 350 000 actuation cycles and even operate under water for extended periods of time, but fully degrade after use through biological triggers. Electronic skins that measure pressure, strain, temperature and humidity serve as human-friendly on-skin interfaces or equip robotic systems with sensory feedback. Such advances in the synthesis of biodegradable, mechanically tough and stable gels that do not compromise in performance when compared to their non-degradable counterparts may bring bionic soft systems a step closer to nature and enable human-friendly technologies with reduced ecological footprint.

M. Baumgartner, F. Hartmann, M. Drack, D. Preninger, D. Wirthl, R. Gerstmayr, L. Lehner, G. Mao, R. Pruckner, S. Demchyshyn, L. Reiter, M. Strobel, T. Stockinger, D. Schiller, S. Kimeswenger, F. Greibich, G. Buchberger, E. Bradt, S. Hild, S. Bauer, M. Kaltenbrunner, "Resilient yet entirely degradable gelatin-based biogels for soft robots and electronics", *Nature Materials* (2020)

### 7:00 AM \*F.SM03.02.06

**Materials Control of Tactile Sensations** Charles Dhong; University of Delaware, United States

For the sense of sight, we can purchase high definition screens to recreate nearly any image. There is no equivalent technology for the sense of touch. However, the accurate and rich recreation of tactile sensations could have broad implications in human machine interfaces, virtual reality, and health.

Touch is a complex event. As a finger and object make contact, a rich variety of mechanical vibrations are produced, which contributes to the subtlety and object identification behind every day tactile experiences. In this talk, we will discuss how we can use materials control at interfaces to create new tactile sensations by controlling friction and adhesion. We will share our work on screening and characterizing tactile materials, demonstrating that tactile perception cannot be predicted from material properties alone. We also share our complementary work on building a fundamental basis for tactile perception, enabled by materials control over tactile stimuli. Establishing a fundamental basis for touch could help unify our understanding of touch and help recreate arbitrary tactile sensations through a combination of more basic units.

### 7:15 AM F.SM03.02.07

**Development of Soft Robotic Morphing Nanocomposite PVDF/SWCNT and PVDF/BNNT** Ji Eun Lee<sup>1</sup>, Ryan Nam<sup>1</sup>, Michael Jakubinek<sup>2</sup>, Behnam Ashrafi<sup>2</sup> and H.E. Naguib<sup>1</sup>; <sup>1</sup>University of Toronto, Canada; <sup>2</sup>National Research Council, Canada

Stimuli responsive polymers and composites have garnered attention in the development of novel actuators due to their ability to respond to various stimuli such as light, heat, electric field, magnetic field, and more. Compared to traditional electric motors, these actuators offer advantages such as conformability, better biomimicking ability, lower cost, and higher power-to-weight ratio. These advantages also are ideal for the field of soft robotics, creating flexible morphing structures that

is able to move with more degrees of freedom than conventional stiff robotics. Piezoelectric materials, with external stimuli of electric field, the morphing device in use can respond with great speed and accuracy.

The current study investigates the development of a nanocomposite with 1D nanofillers single-walled carbon nanotubes (SWCNT) and boron nitride nanotubes (BNNT) in a piezoelectric polymer Polyvinylidene Fluoride (PVDF) matrix. The addition of nanotubes will: (i) increase piezoelectric property for enhanced actuation with its alignment, (ii) lower applied power due to conductive nanofiller percolation, and (iii) enhance mechanical property to withstand the environmental conditions of various actuation applications. Due to its high aspect ratio and conductivity, PVDF/SWCNT samples after stretching had high polar  $\beta$  crystal content of 80% and high conductivity ( $>10$ -6 S/cm). This resulted in high deflection magnitude at low applied electric field. At 0.5 wt.% PVDF/SWCNT stretched resulted in a maximum deflection of 570 $\mu$ m at 5.88 V/mm. With PVDF/BNNT, the samples after electric poling whilst lower in  $\beta$  crystal content, had higher deflection magnitude due to the higher overall dipole moment. PVDF/BNNT stretched and poled had  $\beta$  crystal content 12% lower than that of only stretched but 520% increase in deflection magnitude (from 50 $\mu$ m to 260 $\mu$ m) With an increase in conductivity and piezoelectric property, the material's actuation can be performed with greater displacement and lower power. With the addition of nanotube which provided constraints for alignment, percolation, and enhancement of mechanical properties, flexible morphing devices were developed. The choice of nanotube is important to optimize specific properties (i.e., electrical) but both nanofillers exhibited great morphing magnitude to various electric fields applied. This study provides insight to future research utilizing piezoelectric materials for actuation application in soft robotics.

#### 7:25 AM F.SM03.02.08

**Hard-Magnetic Elastica** Liu Wang, Yoonho Kim and Xuanhe Zhao; Massachusetts Institute of Technology, United States

Recently, *ferromagnetic soft continuum robots* – a type of slender, thread-like robots that can be steered magnetically – have demonstrated the capability to navigate through the brain's narrow and winding vasculature, offering a range of captivating applications such as robotic endovascular neurosurgery. Composed of soft polymers with embedded hard-magnetic particles as distributed actuation sources, ferromagnetic soft continuum robots produce large-scale elastic deflections through magnetic torques and/or forces generated from the intrinsic magnetic dipoles under the influence of external magnetic fields. This unique actuation mechanism based on distributed intrinsic dipoles yields better steering and navigational capabilities at much smaller scales, which differentiate them from previously developed continuum robots. To account for the presence of intrinsic magnetic polarities, this emerging class of magnetic continuum robots provides a new type of active structure – *hard-magnetic elastica* – which means a thin, elastic strip or rod with hard-magnetic properties. In this work, we present a nonlinear theory for hard-magnetic elastica, which allows accurate prediction of large deflections induced by the magnetic body torque and force in the presence of an external magnetic field. From our model, explicit analytical solutions can be readily obtained when the applied magnetic field is spatially uniform. Our model is validated by comparing the obtained solutions with both experimental results and finite element simulations. The validated model is then used to calculate required magnetic fields for the robot's end tip to reach a target point in space, which essentially is an inverse problem challenging to solve with a linear theory or finite-element simulation. Providing facile routes to analyze nonlinear behavior of hard-magnetic elastica, the presented theory can be used to guide the design and control of the emerging class of magnetically steerable soft continuum robots.

#### 7:35 AM F.SM03.02.09

**Mixed-Conducting Particulate Composites for High Resolution Human-Machine Interfaces** Patricia Jastrzebska-Perfect<sup>1,2</sup>, Han Yu<sup>1</sup>, Jennifer Gelinis<sup>1</sup> and Dion Khodagholy<sup>1</sup>; <sup>1</sup>Columbia University, United States; <sup>2</sup>Massachusetts Institute of Technology, United States

Human-machine interfaces require soft, biocompatible materials that can provide high spatiotemporal resolution-coupling with bioelectronic devices. Here, we introduce an organic mixed-conducting particulate composite material (MCP) that enables highly-resolvable coupling by varying particle size and density. MCP-based high performance anisotropic films are pattern-free, scalable, and biocompatible. MCP enabled facile and effective electronic bonding between soft and rigid electronics, permitting recording of neurophysiological data at the resolution of individual neurons from freely moving rodents and from the surface of the human brain through a small opening in the skull. We also acquired high spatiotemporal resolution electrophysiological signals non-invasively by directly interfacing MCP with human skin. MCP provides a single material solution to facilitate development of bioelectronic devices that can safely acquire, transmit, and process complex biological signals.

#### 7:45 AM \*F.SM03.02.10

**High-Sensitivity and Wide-Range Capacitive Pressure Sensors Enabled by the Hybrid Response of Conductive Foams** Kyoung-Ho Ha<sup>1</sup>, Weiyi Zhang<sup>2</sup>, Seungmin Kang<sup>1</sup> and Nanshu Lu<sup>1</sup>; <sup>1</sup>The University of Texas at Austin, United

States; <sup>2</sup>Tianjin University, China

Soft pressure sensors with high sensitivity over a wide pressure range are required for various applications such as electronic skins for human-mimetic robotics and electronic tattoos for digitizing human body. In the last decade, most research aiming at increasing the sensitivity of capacitive pressure sensors focused on developing dielectric materials with added air gaps and/or higher dielectric constants. After extensive research, sensitivity has been significantly improved at low pressure range, e.g. 1 kPa, but drops drastically as the pressure increases. To overcome this challenge, we present a novel soft capacitive pressure sensor employing an electrically conductive foam capable of both piezoresistive and piezocapacitive responses. The foam is made out of functionalized carbon nanotubes and Ecoflex and can be inexpensively fabricated without MEMS technology. The foam is 600- $\mu\text{m}$  thick, 85% porous, and open cell with tubular ligaments. An ultrathin dielectric layer was added between the conductive foam and the electrode to ensure the whole device is still capacitive. The sensor has a modulus of 2 kPa and an initial impedance of 47 M $\Omega$  with a phase angle of  $-86^\circ$ . This capacitive sensor exhibits a sensitivity of 1.95 kPa<sup>-1</sup> within 0-1 kPa, 1.06 kPa<sup>-1</sup> within 1-5 kPa, 0.88 kPa<sup>-1</sup> within 5-10 kPa, 0.52 kPa<sup>-1</sup> within 10-30 kPa, and 0.35 kPa<sup>-1</sup> within 30-50 kPa of pressure ranges. The hybrid response is fully understood through a simplified circuit model, which has been validated by the experimental measurements. We have successfully applied this sensor to measure subtle mechanophysiology on human body, including the pulse waves on the neck and the seismocardiogram on the chest.

#### 8:00 AM F.SM03.02.11

**Mechanics Guided Designs of Stretchable Nanowire Conductors** Shuang Wu, Yuxuan Liu, Shanshan Yao and Yong Zhu; North Carolina State University, United States

There are two main strategies to develop stretchable conductors based on the materials used – nanocomposites with synthesized nanomaterials dispersed into a polymer matrix and deposited thin films exploiting mechanics guided structural design. Both strategies have seen remarkable progresses in developing highly conductive and stretchable conductors. However, so far the mechanical design strategy has been mainly applied to the deposited thin films. It would be interesting to exploit this strategy for the nanocomposites. Here we present two mechanical designs – delaminated buckle and horseshoe – for developing highly conductive and stretchable silver nanowire conductors. In the first design, a polymer composite film (with a thin layer of silver nanowires encased) was bonded to a pre-stretched elastomer substrate. Upon releasing the prestrain, a partially delaminated wavy geometry of the composite film is created. During the evolution of the buckle delamination, the blisters pop up randomly but self-adjust into a uniform distribution, which effectively reduces the local strain in the silver nanowires. The resistance change of the conductor is less than 3% with the applied strain up to 100%. In the second design, the polymer film was patterned into a horseshoe shape and bonded to an elastomer substrate. We found that the substrate thickness and bonding strength can dictate the deformation modes of the polymer film. For thin substrate and weak bonding, the resistance change of the conductor is less than 1% with the applied strain up to 100%.

SESSION F.SM03.03: Haptics in Virtual and Augmented Reality  
On Demand Abstracts Available for Viewing Starting Saturday Morning, November 21, 2020  
F-SM03

#### 5:00 AM \*F.SM03.03.01

**Toward the Haptic Display of Texture** James E. Colgate; Northwestern University, United States

An important problem in the field of haptics is the recording and playback (or similarly, composition and display) of *texture*. This problem is by no means unique to haptics: texture is a vital component of computer-generated graphics and it has been studied in the auditory domain as well (think of crickets chirping or wind blowing through leaves). Haptics, however, presents unique challenges.

Consider the problem of recording: what signals should be measured? While an argument can be made for measuring material and geometric properties of the textured surface, very little progress has been made toward realistic playback on the basis of such information. One reason is that the perception of texture requires contact and, typically, relative movement. This interaction causes the skin to deform whereupon various specialized mechanoreceptors capture aspects of that deformation including localized strain, skin stretch, and vibration. Arguably, the right signals to record are the same ones that the mechanoreceptors respond to. Indeed, measurements of normal and lateral force, movement speed, and skin vibration, have generally proved more useful than measurements of surface properties when it comes to playback. Playback, however,

is limited in two additional respects: one, the ability of the haptic display to physically create spatiotemporal patterns of skin deformation similar to those caused by real world interaction; two, the ability of the display to control those patterns as a function of state variables such as finger pressure and speed.

In this talk, I'll discuss the issues of recording and playback in the context of electroadhesive variable friction haptic displays. The talk will necessarily begin with a discussion of fingertip mechanics, including the roles of moisture and stratum corneum plasticization, in regulating friction; and then go on to a discussion of electroadhesion in which the material properties of both the skin and the countersurface are highly significant.

Electroadhesion is a technology that provides very good temporal control (bandwidth from DC up to several tens of kHz ... well beyond the tactile range), but limited spatial resolution (the touch surface remains flat at all times and actuation is typically synchronous across the full fingerpad). This puts rather stringent limitations on playback, the perceptual consequences of which are sometimes surprising. I'll review a number of studies we have performed to explore and expand the gamut of variable friction textures.

Ultimately, the gamut of an electroadhesive display, especially one built on a rigid surface, is limited. Properties such as hardness/softness, warmth/coolness, as well as coarseness (i.e., 2.5D shape), are unlikely to be realized without advances in the underlying display technology. While it is certainly possible that electroadhesion could be combined with other existing actuation methods (e.g., vibrotactile, pin arrays, thermoelectric, etc.) to expand the range of stimuli, the pathway toward an elegant, robust, and cost-effective solution is not evident. Instead, a pathway rooted in the development of novel "haptic materials" is more appealing. I will close this talk by discussing some of the characteristics such materials should possess.

#### **5:30 AM \*F.SM03.03.02**

**Wireless Sensing for Medical Continuum Robots** Tania Morimoto; University of California, San Diego, United States

Continuum robots are promising for medical interventions due to their ability to traverse around obstacles in confined spaces and conform to highly curved paths. In addition, their inherent structural compliance offers improved safety and adaptability, which is critical for interactions with sensitive structures inside the body. Real-time information about robot shape and applied forces is important for enabling more advanced control methods, ensuring safety, and creating new human-machine interfaces with haptic feedback. Yet the small size, and in particular, the highly limited space for routing wires through these robots, introduces a number of challenges for sensing and makes the integration of standard sensors difficult, especially if measurements along the entire robot length are required. To begin addressing these challenges, we are developing both wireless localization and force sensing methods compatible with continuum robots. This talk will first focus on a permanent-magnet based method for the localization of the tip of a growing robot (also known as a vine robot). The approach combines analytical and machine learning techniques to localize the robot tip in 5 degrees of freedom without requiring any significant modifications of the robot. The second part of the talk will focus on a new wireless force sensor based on backscatter tags. When a force is applied, the sensor deforms, creating contact between two conductive traces, which results in the reflection of electromagnetic waves on the edges of this contact area. The reflected waves will have a phase change that is dependent on the amount of contact between the traces, and can be used to determine the magnitude and location of the applied force. The development of these sensors is important to enable user interfaces with improved control and haptic feedback.

#### **6:00 AM F.SM03.03.03**

**Visualizing Strain of the Body Movement with Highly Responsible Hierarchical Thermochromism** Byeonghak Park and Tae-il Kim; Sungkyunkwan University, Korea (the Republic of)

As eidetic signal recognition has become important, displaying mechanical signals visually has imposed huge demands for simple readability and without complex signal processing. Such visualization of mechanical signals has been used in delicate urgent medical or safety-related industries. Accordingly, chromic materials have been considered to facilitate the visualization with multiple colors and simple process, yet the response and recovery time is very long, so that rapid regular signals are unable to be detected, i.e., physiological signals, such as respiration. Here, we suggest the simple visualization of low strain ~2 %, with ultrasensitive crack-based strain sensors with a hierarchical thermochromic layer. The sensor shows a gradient color change from red to white color in each strain, which is attributed to the hierarchical property, and the thermal response (recovery) time is dramatically minimized within < 0.3 s, as the hierarchical membrane was inspired by termite mounds for efficient thermal management. The fast recovery property can be taken advantage of in medical fields, such as monitoring regular respiration, and the color changes can be delicately monitored with high accuracy by software on a mobile phone.



**5:00 AM F.SM03.04.01**

**Soft Magnetic Actuators for Wearable Tactile Feedback** [Alex J. Mazursky](#) and Pedro Lopes; University of Chicago, United States

Recent developments in wearable devices brought technology much closer to the user's skin in the form of interactive fabrics, electronic skins, interactive tattoos, and more. However, these devices are typically only used for user input and do not provide haptic feedback in response to interactions. In fact, while we have seen many advances in the materials that make up wearable devices, the haptic feedback included in most wearables is, typically, based on off-the-shelf actuators such as linear resonant actuators that, due to their rigidity, cannot conform to the soft, flexible, and dynamic human body. To tackle this, we created a haptic device based on stretchable magnets. Our haptic device has two components: (1) a silicone skin doped with permanent magnetic micro powder (NdFeB) allowing it to display tunable magnetic polarity, and (2) a fingernail-worn device that includes an electromagnetic coil, 9-DOF IMU, and microcontroller. Users interact with our wearable haptic device by touching or dragging their finger over the magnetic silicone skin. Our device senses the proximity to the magnetic layer (via its IMU) and actuates the coil, causing the magnetic skin to oscillate—creating haptic vibrations on the user's skin. Using this mechanism, we can render a wide range of haptic sensations such as detents, button presses, or textures. We believe our device is especially suited for on-body gestures, such as thumb-to-index pinching (popularized by Google's Soli or Microsoft's HoloLens, to cite a few) or to expand haptic output to different areas of the body where rigid devices are uncomfortable. Lastly, we studied our device's dynamic performance via modal analysis and users' perception of tactile feedback by means of psychophysical studies.

**5:15 AM \*F.SM03.04.02**

**Wireless Multimodal E-Tattoos Capable of Long-Term Operation** [Nanshu Lu](#); The University of Texas at Austin, United States

Merging human body with electronics and machines can enable internet of health (IoH), human-machine interface (HMI), as well as augmented human capabilities. However, bio-tissues are soft, curvilinear and dynamic whereas wafer-based electronics are hard, planar, and rigid. Over the past decade, stretchable electronics have emerged as a result of new materials development, structural design and manufacturing processes. In particular, epidermal electronics, a.k.a. electronic tattoos (e-tattoos), represent a class of stretchable circuits, sensors, and stimulators that are ultrathin, ultrasoft and skin-conformable. This talk will introduce a dry and freeform (subtractive) “cut-solder-paste” process for the rapid prototyping of modular and reconfigurable e-tattoos. This method is applicable for thin film metals, polymers, ceramics, as well as 2D materials and can easily incorporate integrated circuits to the stretchable e-tattoos. Electrically conductive open cell foams with hybrid piezoresistive and piezocapacitive responses has been applied as high-sensitivity mechanical transducer. The e-tattoos can laminate at different locations of the human skin for the synchronous and continuous tracking of electrophysiology (ECG, EEG, EMG, EOG), mechanophysiology (respiration, seismocardiogram, blood pressure, etc.), as well as thermophysiology etc.. In addition to sensing, the e-tattoos can also be used as personalized treatment and therapeutic devices. For wireless operation, we leverage near field communication (NFC) for wireless and Bluetooth low energy (BLE) for wireless data transfer. A wireless charging-on-the-go strategy enables the long-term (e.g., 3 days) operation of the e-tattoo.

**5:45 AM \*F.SM03.04.04**

**Wearable Haptics—Device Design Opportunities and Challenges** [Marcia K. O'Malley](#); William Marsh Rice University, United States

Wearable haptics refers to systems worn on the body or integrated into clothing that can provide haptic feedback to the wearer in a wide range of forms, such as vibrotactile, cutaneous, skin stretch, pressure, and kinesthetic feedback. The potential for wearable haptics is supported by technological advancements in sensing and actuation that allow for the design and deployment of flexible materials, fabrics, and small-footprint actuators that can augment and enhance human performance. While rigid and grounded haptic feedback devices have been explored as a means to train new motor skills, rehabilitate movement coordination after neurological injury, and even augment human force output capabilities in tasks such

as lifting or running, the application space is limited due to the weight and scale of such devices. Wearable haptic devices seek to overcome the limitations of rigid and grounded haptic devices.

Vibrotactile haptic feedback is ubiquitous for notifications and alerts in portable devices such as phones, smart watches, and fitness trackers, but the set of possible notifications is limited by the nature of the eccentric motors so often used to deliver such cues. In recent years, my group has been shifting to wearable haptic systems that provide multiple haptic modalities of feedback to the user, including vibration, skin stretch, pressure, and kinesthetic feedback, all packaged in bands that can be worn on the arm, or in hybrid rigid-soft exosuits that can apply forces directly to the limbs. We are particularly interested in applications where the provision of such feedback has a measurable impact on human performance.

In this talk, I will present some of our wearable haptic systems, describe our target applications, and highlight the distinguishing features our hardware while identifying opportunities for improvement. Two systems that I will discuss leverage multi-sensory haptic cues that are displayed directly on the user's arm. Tasbi is a wearable haptic device that provides squeeze and vibration feedback for haptically enhanced augmented and virtual reality interactions. MISSIVE incorporates skin stretch, squeeze and vibration cues presented simultaneously to the user in distinct patterns. The use of multisensory cues allows us to design large discrete cue sets while maintaining a small and wearable form factor. With MISSIVE, we demonstrated language transmission via haptic phonemes, or units of sound encoded as haptic cues consisting of vibration, radial squeeze, and lateral skin stretch components. I will also present two wearable exosuit systems for upper limb movement assistance and rehabilitation, a glove, and an upper limb garment. Using cable-based actuation systems that enable remote placement of actuators, rigid spines precisely located for load transfer and cable management, and soft goods for compliant human-machine interfacing, these devices offer the potential for improved wearability compared to their rigid robotic counterparts, and feasible integration into the performance of everyday functional tasks.

#### **6:15 AM \*F.SM03.04.05**

**Minimizing Haptic Hardware in Wearable Devices** Heather Culbertson; University of Southern California, United States

Wearable haptic devices present many challenges in actuator selection and design. In addition to providing a sufficiently strong signal to be easily felt by the user, the actuators must also not encumber the user's motion. Ideally the actuators should be small, thin, lightweight, flexible, low power, and provide multiple degrees of actuation. An actuator with all these properties is not currently available commercially, forcing haptic designers to make decisions regarding trade-offs between magnitude, resolution, degrees of freedom, and workspace among many others. These limitations motivate our research towards providing complex haptic signals using minimal hardware. We approach this problem from two directions by using haptic illusions and by creating novel actuators that can provide multiple haptic sensations simultaneously.

Haptic illusions seek to fool our sense of touch into thinking we are feeling something different than what is being displayed by taking advantage of the inexactness of our perception. In our research, we employ haptic illusions to allow small, lightweight actuators to create sensations that would normally require actuators that are impractical for a wearable device. I will discuss two haptic illusions and their uses: asymmetric vibrations for generating ungrounded forces and sequential indentation for creating lateral motions.

I will also present our work in creating multi-modal hardware, which allows for complex haptic sensations using minimal actuator size and weight. Our PATCH (Pump-Actuated Thermal Compression Haptic) device presents simultaneous thermal and pressure cues. The PATCH system is actuated by using pumps to fill fabric actuators with water of varying temperature. The actuators are lightweight, flexible, and provide a wide range of haptic cues.

#### **6:45 AM F.SM03.04.06**

**High-Resolution Liquid Metal Patterning for Stretchable and Ultra-Transparent Electronic Interfaces** Haotian Chen, Laurent Dejace and Stephanie P. Lacour; École Polytechnique Fédérale de Lausanne, Switzerland

Integrated wearable electronics capable of providing biophysical information on complex and dynamic systems have attracted interests in diverse fields such as healthcare and robotics. Gallium and gallium-based liquid metals stand out for their excellent combination of electrical conductivity and mechanical deformability. However, liquid metals feature complex physical and chemical properties that pose challenges to the fabrication of miniaturized soft and stretchable circuits. Herein, we present a manufacturing approach to form ultrathin (1.5  $\mu\text{m}$ ) and high-resolution (2.2  $\mu\text{m}$ ) liquid metal features with high surface density over large surface areas (wafer scale). Based on a combination of soft lithography, selective wetting, Ion Beam Etching and thermal evaporation of gallium, the process enables a range of channel designs and geometries with unprecedented aspect ratios ( $> 10'000$ ) that can be used to form liquid metal based stretchable electronic conductors with

unrivaled transparency.

We demonstrate conducting grids of  $w = 2.2 \mu\text{m}$  width and variable pitch ( $p = 100.2, 50.2, 29.2, 15.2 \mu\text{m}$ ) that can reversibly stretch to 100 %. Adjusting the density of the narrow lines across the PDMS substrate offer tunability in the patterned metallic grid. In the relaxed state, the liquid metal grids display optical transmittances at 550 nm wavelength of 69.3 %, 80.2 %, 86.9 %, and 89.6 % for  $p = 15.2 \mu\text{m}, 29.2 \mu\text{m}, 50.2 \mu\text{m}, 100.2 \mu\text{m}$  with sheet resistance of 4.8 Ohm/sq., 6.4 Ohm/sq., 8.8 Ohm/sq., 12.5 Ohm/sq. respectively. The accuracy and the robustness of the patterning technique are demonstrated by stretching the most transparent structure ( $p = 100.2 \mu\text{m}$ ) to 100 % deformation. The combination of high electrical conductivity (12.5 Ohm/sq.), optical transparency (89.6 %) and mechanical deformability (100 %) ranks these soft and stretchable liquid metal grids amongst the best performing transparent conductors reported to date.

SESSION F.SM03.05: Poster Session: Materials for Haptics  
On Demand Abstracts Available for Viewing Starting Saturday Morning, November 21, 2020  
5:00 AM - 8:00 AM  
F-SM03

#### F.SM03.05.01

**Beyond Elastic Limit of Piezoelectric Ceramic with 3D Hollow ZnO Nanostructures** Hoon Kim, Seokjung Yun, Kisun Kim, Wonsik Kim, Jeongjae Ryu, Hyeon Gyun Nam, Seung Min J. Han, Seokwoo Jeon and Seungbum Hong; Korea Advanced Institute of Science and Technology, Korea (the Republic of)

Piezoelectric materials are suitable for haptic technology as they can convert mechanical stimuli into electrical signals and vice-versa. However, owing to their disadvantageous mechanical properties such as brittleness (in ceramics) and a low piezoelectric coefficient (in polymers), it is still a challenge to use them in haptic technology. Here, we present a truss-like 3D hollow zinc oxide (ZnO) nanostructure that shows a drastically improved elastic strain limit while maintaining a piezoelectric coefficient similar to that of single-crystal ZnO. The ZnO hollow nanostructures were fabricated by proximity field nanopatterning (PnP) and atomic layered deposition (ALD) at four different process temperatures from 90 to 300°C. The piezoelectric properties were visualized and analyzed through dual AC resonance tracking piezoresponse force microscopy (PFM). The piezoelectric coefficient was approximately 9.2 pm/V. Furthermore, we measured the measured elastic strain limit of approximately 10% using the nanopillar compression test, which was at least 3 times greater than the prior report. The extended elastic limit of the 3D hollow structure was further supported by finite element simulations. We envision that our ZnO hollow nanostructure can be used in enhanced haptic devices, which mimic the human sense of touch.

#### F.SM03.05.02

**Highly Crystalline PCL Ultrathin Films as Thermally Switchable Biomaterial Coatings** Shivam Saretia<sup>1,2</sup>, Rainhard Machatschek<sup>1,2</sup> and Andreas Lendlein<sup>1,2</sup>; <sup>1</sup>Helmholtz-Zentrum Geesthacht, Germany; <sup>2</sup>University of Potsdam, Germany

Degradable semi-crystalline polymers are a class of materials that modern regenerative medicine heavily relies on. While their formulation into nanostructured devices can be advantageous to tailor functional properties such as cellular uptake kinetics and degradation behaviour, it is difficult to assess and control the morphology, crystallinity and organization of nanostructured polymer materials by common preparation methods.

The Langmuir technique overcomes most of the drawbacks concerning preparation and investigation of nanostructured polymer materials. Here, ultrathin films at the air-liquid interface serve as model systems for polymer devices and interfaces, which can be manipulated and observed in a straightforward way. In particular, the semi-crystalline morphology, including crystal size, number density, thickness, and melting temperature can be precisely adjusted. By transferring the layers to solid substrates, functional biomaterial interfaces with unique properties can be created. For example, via enzymatic degradation of the amorphous chains, a semi-crystalline Langmuir film can be converted into an almost entirely crystalline film with a thickness of a few nanometers. The preparation and analysis of these highly functional, entirely crystalline thin films based on oligo( $\epsilon$ -caprolactone)s (OCL) with different end-groups is of particular interest. Poly( $\epsilon$ -caprolactone) (PCL) is established in clinical applications with a relatively low melting point and well documented enzymatic degradability<sup>1</sup>. The melting temperature of PCL or OCL crystals can be adjusted via the crystallization temperature to be very close to physiological conditions, producing a polymer coating that changes a broad variety of its functional properties upon application of a small thermal stimulus.

For example, highly crystalline films of hydroxyl and methacrylate end capped linear OCL are prepared by degrading its amorphous phase by the enzyme *Pseudomonas cepacia* lipase ( $0.007 \text{ mg mL}^{-1}$ ) at constant surface pressure of  $\sim 7 \text{ mN m}^{-1}$  on air-water interface at room temperature. The thickness of the OCL crystals in the film can be adjusted in the range of  $\sim 6$  to  $8 \text{ nm}$ , resulting in a melting temperature between  $\sim 30$  to  $40 \text{ }^\circ\text{C}$  at the air-water interface. Upon melting, the elastic moduli of the film are drastically altered. Further, functional end groups are expelled from the crystals and therefore accumulated at the crystalline surface. Upon melting, these end-groups are buried in the amorphous phase, resulting in a change of the chemical composition of the material surface. Moreover, the degradability of the thin film increases significantly upon melting, meaning that the lifetime of the material can be adjusted via its thermal history. In addition, the barrier properties of the thin film depend on its crystallinity, with polymer crystals being considered impenetrable for small molecules.

Here, we demonstrate the fabrication and behaviour of these thermally switchable OCL crystals coatings, which are of interest for applications such as barrier layers, substrates modulating stem cell adhesion, or coatings with on-demand acceleration of degradability. Another possible application are friction reducing coatings, for example on sutures. Here, the temperature at the suture-tissue interface does not increase as long as the heat generated by frictional forces is absorbed by the melting enthalpy of the crystals.

### F.SM03.05.03

**Late News: Functionalised Capacitive Microfluidic Force Sensors for Orthopaedic Surgery** [Liam Ives](#)<sup>1</sup>, [Qingshen Jing](#)<sup>1</sup>, [Alizée Pace](#)<sup>1</sup>, [Anke Husmann](#)<sup>1</sup>, [Vikas Khanduja](#)<sup>1</sup>, [Jehangir Cama](#)<sup>2</sup> and [Sohini Kar-Narayan](#)<sup>1</sup>; <sup>1</sup>University of Cambridge, United Kingdom; <sup>2</sup>University of Exeter, United Kingdom

The correct balance of forces on the hip joint during total hip arthroplasty (THA) is essential for implant longevity and to prevent the need for revision surgery. This has become increasingly important since the average age of a THA patient is decreasing, hence these implants must survive greater activity levels and correspondingly higher stresses than those typically found in older, less active patients. Currently, the lifetime of an implant positioned purely by a surgeon's judgement is approximately 15 years. Quantitative force feedback during surgery could provide more accurate implant positioning, increasing the average lifetime. However, there are currently no force sensors capable of providing this information within the small and complex geometry of the hip joint.

Here, we solve this unmet clinical need by presenting a thin, conformable and flexible microfluidic capacitive force sensor, which can be incorporated into the surgical process without significant modification to existing implants. The sensor consists of a deformable microfluidic chip bonded to a flexible substrate, on which interdigitated electrodes are incorporated, and that can operate in confined spaces to give accurate force readings from joints. The sensor operates by monitoring the change in capacitance of the electrodes as the fluid in the microfluidic channel is displaced in response to an applied force. Multiple sensors were incorporated into a model hip implant geometry, and a bespoke mechanical testing rig was built to simulate loading of the acetabular cup from the femoral head at different angles. The experimental results were validated using finite element modelling. This was used to optimise the sensor geometry for the production of sensitive devices that can withstand the high forces required for surgery. Our novel microfluidic-based force sensing technology can potentially be adapted for application in joints either for sensor-assisted orthopaedic surgery, or for gathering telemetric data from joints before, during and/or after surgery. Such biocompatible and implantable force sensors will contribute significantly to several clinical drivers, through providing quantitative feedback to the attending clinician, and could also serve to underpin robot-assisted orthopaedic surgery in the future.

## SYMPOSIUM F.SM04

---

Degradable and Self-Healing Electronic Materials for Biological Interfaces  
November 21 - December 3, 2020

### Symposium Organizers

Po-Yen Chen, National University of Singapore  
Fabio Cicoira, Ecole Polytechnique de Montreal

Noemie-Manuelle Dorval Courchesne, McGill University  
Jadranka Travas-Sejdic, Univ of Auckland

Symposium Support

**Bronze**

Polytechnique Montreal Chemical Engineering Department  
University of Auckland

---

\* Invited Paper

SESSION F.SM04.07: Live Keynote I: Degradable and Self-Healing Electronic Materials for Biological Interfaces  
Session Chairs: Fabio Cicoira and Jadranka Travas-Sejdic  
Tuesday Afternoon, December 1, 2020  
F.SM04

**12:00 PM \*F.SM04.01.01**

**How Can We Approach *In Vivo* Bioelectronics Challenges with Stretchable Electronics?** János Vörös; ETH Zurich, Switzerland

A new class of electronic devices based on stretchable materials can interact with the soft human body in an unprecedented manner. They are highly suitable for epidermal electronics because they can be designed to conform closely to and with the irregular shape of the skin, providing an improved functional interface even during motion, while being imperceptible to the user.<sup>1,2</sup>

But does the stretchability also provide benefits for *in vivo* applications? This lecture will systematically discuss the challenges and possibilities for *in vivo* bioelectronics<sup>3</sup>:

The first part will discuss our progress on using metal nanowires embedded in PDMS that can be processed using regular photolithography or filtration to realize stretchable conductive leads down to 10 micrometer resolution. Stretchable and biocompatible transparent microelectrode arrays can thus be realized that enable stimulation and recording of brain activity directly from the cortex both electronically and optically.<sup>4,5</sup>

The technology also allows for creating strain sensors with up to 500% stretchability and Gauge factors of over 100 that can be used as smart and passive RFID tags to measure the filling level of the bladder in handicapped users, or to record the volume of the heart during operation.<sup>6,7</sup> Here, advanced imaging with coherent X-rays in combination with machine learning based data evaluation helped to provide a full theoretical understanding of the strain-response and to build a model with predictive value.<sup>8</sup>

The biggest challenge of *in vivo* bioelectronics remains the lack of understanding of the brain. Stretchable electronics can be used to create well-defined, *in vitro* neuron networks of human iPSC-derived neurons that can be stimulated and recorded in a closed-loop fashion enabling a new approach, i.e. bottom-up neuroscience.<sup>9</sup>

Trends in epidermal stretchable electronics for noninvasive long-term healthcare applications, H. Han, et al., Automation and Smart Technology, 2017.

Skin Conformal Polymer Electrodes for Clinical ECG and EEG Recordings; F. Stauffer, et al. Adv. H. Mat. 2018

A guide towards long-term functional electrodes interfacing neuronal tissue, A.F. Renz et al, J. Neur. Eng. 2018.

High-Density Stretchable Electrode Grids for Chronic Neural Recording; K. Tybrandt et al., Adv. Materials, 2018.

Opto-e-dura: a soft, stretchable ECoG array for multimodal, multi-scale neuroscience; A.F. Renz et al., Adv. H. Mat. 2020, submitted.

Soft Electronic Strain Sensor with Chipless Wireless Readout: Toward Real-Time Monitoring of Bladder Volume; F. Stauffer, et al.; Advanced Materials Technologies, 2018.

Continuous heart volume monitoring by fully implantable soft strain sensor; B.L. Zambrano et al., Adv. H. Mat. 2020, submitted.

Visualizing and Analyzing 3D Metal Nanowire Networks for Stretchable Electronics; C. Forró, et al., Adv. Theory and Simulations, 2020, in press.

Modular microstructure design to build neural structures with defined functional connectivity; C. Forró, et al.; Biosensors and Bioelectronics, 2018

### 12:30 PM \*F.SM04.04.01

**Large-Area Printable and Flexible Electronic Biosensors for Label-Free Single-Molecule Detection** Luisa Torsi<sup>1,2</sup>; <sup>1</sup>University of Bari A. Moro, Italy; <sup>2</sup>Åbo Akademi University, Finland

Detecting a marker or a pathogen at the physical limit is the new frontier in medical analysis as it endows the clinicians with the attacker's advantage over life-threatening diseases such as tumours and pandemics. It is also received that label-free and electronic transductions can be conveniently fast and wieldy. Within this field different transducing approaches are pursued. They involve a transducing interface functionalized with biological recognition elements, such as antibodies or DNA probes, that endow the device with recognition properties by selectively capturing the analyte e.g. an antigen or a genomic marker, respectively. One recently proposed approach involves a large interface hosting trillions of highly-packed bio-recognition elements. The challenge is indeed that of measuring one single molecule in a large volume such as for instance 100 ml. This means being able to deploy a technology that can detect  $10 - 20 \cdot 10^{-21}$  mole  $l^{-1}$  (zeptomolar).

Mimicking cell's behaviour, ecently proposed approach involves a large interface hosting trillions of highly-packed bio-recognition elements. This is called, the "**Single Molecule with a large Transistor (SiMoT)**" technology that was proposed to sense a solution with markers present at extremely low concentrations. It is based on an Electrolyte Gated Organic filed-effect transistor operated in deionized water, with a gate that has an area of ca.  $0.5 \text{ cm}^2$ , hosting  $10^{12}$  antibodies or genomic probes. The SiMoT platform has been proven to perform label-free and selective detection at the physical limit in real biofluids of protein biomarkers such as: human Immunoglobulin G, Immunoglobulin M, C-reactive protein, MUC1 and HIV1 p24 antigen as well as genomic markers such as miR-182-5p and KRAS. Indeed, the widely applicable method used to conjugate the recognition elements to the gate electrode, makes the SiMoT platform suitable for the detection of different classes of markers and pathogens reaching world record detections limits for label-free protein detection.

### 1:00 PM \*F.SM04.03.02

**Self-Assembled Bioinspired Nanostructures for Green Electronics** Nurit Ashkenasy; Ben Gurion University of the Negev, Israel

Self-assembling peptides that are inherently biodegradable and biocompatible are extremely suitable for use in devices that adhere on, or even implanted into, the human body in order to monitor and regulate biological functions. The challenge for incorporating these materials in bioelectronic devices is the optimization of their electronic properties for the desired application. In this talk I will present peptide design rules that can be used to prepare electron and/ or proton conducting peptide based materials. Specifically, I will discuss the influence of aromatic side chains (both natural and non-natural) on electron conductivity.<sup>1,2</sup> I will further present enhancement of proton conduction in these films by the incorporation of protonating side chains, which can lead to extremely high proton conductivity values in these materials.<sup>3,4</sup> I will finally discuss the control of conductivity, thermal stability and biodegradability of self-assembling peptide nanostructures by peptide backbone motifs. These studies demonstrate the great potential of using peptide building blocks for the fabrication of green electronic materials.

### References

1. Ashkenasy, N.; Horne, W. S.; Ghadiri, M. R., Design of Self-Assembling Peptide Nanotubes with Delocalized Electronic States. *Small* **2006**, *2*, 99-102.
2. Ivnitski, D.; Amit, M.; Silberbush, O.; Atsmon-Raz, *et al.*, The Strong Influence of Structure Polymorphism on the Conductivity of Peptide Fibrils. *Angewandte Chemie-Int. Ed.* **2016**, *55*, 9988-9992.
3. Amit, M.; Appel, S.; Cohen, R.; Cheng, G.; *et al.*, Hybrid Proton and Electron Transport in Peptide Fibrils. *Adv. Funct. Mater.* **2014**, *24*, 5873-5880.
4. Silberbush, O.; Amit, M.; Roy, S.; Ashkenasy, N., Significant Enhancement of Proton Transport in Bioinspired Peptide Fibrils by Single Acidic or Basic Amino Acid Mutation. *Adv. Funct. Mater.* **2017**, *27*, 1604624.

SESSION F.SM04.08: Live Keynote II: Degradable and Self-Healing Electronic Materials for Biological Interfaces

Session Chairs: Po-Yen Chen and Noemie-Manuelle Dorval Courchesne

Wednesday Afternoon, December 2, 2020

F.SM04

### 7:30 PM \*F.SM04.02.01

**Multifunctional Fibers as Bioelectronic Interfaces** Polina Anikeeva; Massachusetts Institute of Technology, United States

The ability to seamlessly integrate a diversity of electronic and optical materials within the flexible thermally-drawn fibers has recently enabled their applications as biocompatible and multifunctional tools for neural recording, modulation, and tissue repair. In this talk, I will highlight the advances in multimaterial fiber-based interfaces with neural tissue and illustrate how integration of active electronics and elastomers may allow for expanding the application domain of these devices toward probing physiology of other electroactive organs deep within the body. Furthermore, this talk will discuss the materials innovation to permit combinatorial thermal drawing and lithographic patterning within fibers that will further expand the geometries of fiber-based bioelectronic interfaces.

**8:00 PM \*F.SM04.03.01**

**Optimizing Synergy Between Materials and Cell Microenvironments Using Functional Polyesters** Milica Radisic; University of Toronto, Canada

Material based technologies play an integral role in many medical treatment strategies, including joint replacements, vascular stents, drug delivery methods, contact lenses and medical sutures. The application of successful technologies continues to grow, with an estimated market size of \$130 billion USD by 2020. Although successes are notable, a number of biomaterial-based devices are limited in application by non-specific material properties to tissue type and undesired inflammation at the device interface. In application, polyester materials have traditionally been an effective polymer strategy, with successes in tissue engineering scaffolds and a variety of biomedical devices. Leveraging advantageous polyester degradability and well understood chemical synthesis, these materials serve as a strong functional platform to further optimize material-cell microenvironments. In this talk, I will describe the development of polyesters that (a) exhibit controllable mechanical properties to mimic the elastic properties of cardiac tissue extracellular matrix (ECM) and (b) incorporate a biomimetic moiety of mammalian immunity to recapitulate mechanistic inflammation regulation at the material surface.

Development of engineered cardiac tissue requires material scaffolds that match the elastic behavior of cardiac ECM. Using polycondensation techniques to incorporate unsaturated carbonyl groups into elastic polyester material gels, we generated materials that can be molded into intricate designs with secondary crosslinking to generate constructs with highly tunable elasticity. By adapting material synthesis conditions (i.e. monomer ratios, reaction time), elastic mechanical behavior was highly tunable across a range of soft biomaterial applications. Material applicability was highlighted in a number of micro-designed elastomeric scaffold supports for engineered tissue, both for *in vitro* organ-on-a-chip and *in vivo* cardiac patch technologies, wherein the two-step synthesis process allowed for micro molding into intricate shapes prior to gelation. With biomaterial application *in vivo*, inflammation at the biomaterial surface limits device application. To tackle this, we looked to itaconate, a powerful small molecule metabolite of innate immunity that has recently emerged as a regulator of innate immune inflammation. This molecule has been previously limited therapeutically by short circulation times. To circumvent this, itaconate was incorporated directly into material backbones to impart biomimetic small molecule modulation, with quantified hydrolytic degradation release from polyester chains. Harnessing hydrolytic degradation release from polyester backbones, itaconate polymers resulted in the mechanism specific immunoregulatory properties on macrophage polarization *in vitro*. In a functional assay, the polymer-released itaconate inhibited bacterial growth on acetate. Translation to an *in vivo* model of biomaterial associated inflammation, intraperitoneal injection of ITA polymers demonstrated a rapid resolution of inflammation in comparison to a control polymer silicone, demonstrating the value of sustained biomimetic presentation of itaconate. Using scalable polyester synthesis techniques, we have demonstrated the power of instructive biomaterial technologies as functional modulators of the cell microenvironment.

**8:30 PM \*F.SM04.07.04**

**Pushing the Limits of Elasticity in Soft-Matter Electronics** Carmel Majidi; Carnegie Mellon University, United States

In order for machines and electronics to interface with biological tissue, they should be soft and elastic – i.e. remain functional when stretched and then return to their natural length when unloaded. In recent years, there has been tremendous progress in creating conductive elastomers and gels that are capable of extreme stretchability and which have been successfully utilized as bioelectronic interfaces. These include material architectures that are self-healing and can restore electrical and/or mechanical functionality when torn or punctured.

In this talk, I will review recent efforts to create mechanically robust, stretchable electronics using a variety of soft material architectures. In particular, I will focus on the following approaches: (i) silver-hydrogel composites that exhibit an unprecedented combination of mechanical compliance and electrical conductivity; (ii) biphasic compositions of silver nanoparticles and eutectic gallium-indium (EGaIn) liquid metal alloy for ultrathin “epidermal” electronics; and (iii) EGaIn-polymer composites capable of high electrical conductivity, extreme stretchability, negligible electromechanical coupling, and a variety of self-healing properties. To demonstrate their potential role in future bioelectronic applications, I will present

examples of how these soft material architectures are used as electrodes for physiological monitoring (e.g. EMG, ECG) and as electrical interconnects for highly stretchable digital circuits.

#### 9:00 PM \*F.SM04.05.01

**Fabrication of 3D Monolithic Architecture Electrodes Based on Conducting Polymer Microstructures** Youngseok Kim and Myung-Han Yoon; Gwangju Institute of Science and Technology, Korea (the Republic of)

The conventional bioelectronic interfaces have been based on either 2-D thin films or 1-D fibers/wires which limit 3-D scalability as well as volume-/mass-dependent performance. Moreover, biological tissues and organs typically exhibit 3D arbitrary curvatures with wet surface, which impeded the close physical contact between the target tissue/organ and bioelectronic interfaces, leading to the low efficiency in bioelectric signal recording and/or stimulation. In this research, we report on 3D monolithic architectures with arbitrary shapes by employing conducting polymer microstructures as building blocks. Such arbitrary 3D structures were constructed by performing the seamless fusion of separate conducting polymer microstructures without using binder or adhesive. The resultant 3D structures exhibited decent mechanical robustness, high water stability, and outstanding biocompatibility, while the sheet resistance was reduced below 1 Ohm/square and the gravimetric capacitance was increased up to 79 F/g by taking advantage of cumulative mass loading and structural fusion. Finally, we demonstrated that 3D conductive mesh electrodes could be attached to the wet surface of biological organs/tissues such as heart and sciatic nerves without glue or clamp and efficiently record/stimulate bioelectrical signals *in vivo*.

SESSION F.SM04.01: Biodegradable and Biointegrated Electronics  
On Demand Abstracts Available for Viewing Starting Saturday Morning, November 21, 2020  
F-SM04

#### 5:00 AM \*F.SM04.01.01

**How Can We Approach *In Vivo* Bioelectronics Challenges with Stretchable Electronics?** János Vörös; ETH Zurich, Switzerland

A new class of electronic devices based on stretchable materials can interact with the soft human body in an unprecedented manner. They are highly suitable for epidermal electronics because they can be designed to conform closely to and with the irregular shape of the skin, providing an improved functional interface even during motion, while being imperceptible to the user.<sup>1,2</sup>

But does the stretchability also provide benefits for *in vivo* applications? This lecture will systematically discuss the challenges and possibilities for *in vivo* bioelectronics<sup>3</sup>:

The first part will discuss our progress on using metal nanowires embedded in PDMS that can be processed using regular photolithography or filtration to realize stretchable conductive leads down to 10 micrometer resolution. Stretchable and biocompatible transparent microelectrode arrays can thus be realized that enable stimulation and recording of brain activity directly from the cortex both electronically and optically.<sup>4,5</sup>

The technology also allows for creating strain sensors with up to 500% stretchability and Gauge factors of over 100 that can be used as smart and passive RFID tags to measure the filling level of the bladder in handicapped users, or to record the volume of the heart during operation.<sup>6,7</sup> Here, advanced imaging with coherent X-rays in combination with machine learning based data evaluation helped to provide a full theoretical understanding of the strain-response and to build a model with predictive value.<sup>8</sup>

The biggest challenge of *in vivo* bioelectronics remains the lack of understanding of the brain. Stretchable electronics can be used to create well-defined, *in vitro* neuron networks of human iPSC-derived neurons that can be stimulated and recorded in a closed-loop fashion enabling a new approach, i.e. bottom-up neuroscience.<sup>9</sup>

Trends in epidermal stretchable electronics for noninvasive long-term healthcare applications, H. Han, et al., Automation and Smart Technology, 2017.

Skin Conformal Polymer Electrodes for Clinical ECG and EEG Recordings; F. Stauffer, et al. Adv. H. Mat. 2018

A guide towards long-term functional electrodes interfacing neuronal tissue, A.F. Renz et al, J. Neur. Eng. 2018.

High-Density Stretchable Electrode Grids for Chronic Neural Recording; K. Tybrandt et al., Adv. Materials, 2018.



Opto-e-dura: a soft, stretchable ECoG array for multimodal, multi-scale neuroscience; A.F. Renz et al., Adv. H. Mat. 2020, submitted.

Soft Electronic Strain Sensor with Chipless Wireless Readout: Toward Real-Time Monitoring of Bladder Volume; F. Stauffer, et al.; Advanced Materials Technologies, 2018.

Continuous heart volume monitoring by fully implantable soft strain sensor; B.L. Zambrano et al., Adv. H. Mat. 2020, submitted.

Visualizing and Analyzing 3D Metal Nanowire Networks for Stretchable Electronics; C. Forró, et al., Adv. Theory and Simulations, 2020, in press.

Modular microstructure design to build neural structures with defined functional connectivity; C. Forró, et al.; Biosensors and Bioelectronics, 2018

#### **5:30 AM F.SM04.01.04**

##### **Biocompatible and Biodegradable Solid-State Electrolyte Based Organic Transistors and Their Integrated Circuits** Young Jin Jo and Tae-il Kim; Sungkyunkwan University, Korea (the Republic of)

Organic Electronics are essential components of bio-integrated electronics for wearable electronics, electronic skins and soft robotics. However, there are a variety of obstacles like mechanical properties similar to biological surface (skin, tissues and organs), reliability of electrical characteristics under deformations, biocompatibility, biodegradability and low-voltage operation of electronics to apply organic electronics to biomedical devices. One of the candidates to reduce the operating voltage is using electrolyte as dielectrics in organic transistors as known as electrolyte-gated transistors (EGTs). Electrolytes can dramatically reduce operating voltage of organic electronics due to high capacitance from the electrical double layers, but liquid electrolyte requires harsh passivation layer to prevent it from escaping from the devices in the biological environment. Also, ion gel based on synthetic organic compound and polymers has not been proved as being biocompatible and biodegradable. Here, we suggest solid-state electrolytes based on natural compound such as gelatin, levan polysaccharide for organic electronics. Gelatin is a semi-solid electrolyte and a sort of natural, protein-based hydrogel with great biocompatibility and biodegradability. Moreover, thermo-responsive behavior of gelatin hydrogels can realize fabrication of organic electronics with printing method by solution process. We fabricated organic electrochemical transistors (OECT) and simple logic circuits by all printing-process with gelatin hydrogels. We also utilized choline as the biocompatible and biodegradable ionic compound to cast solid electrolyte by coupling with levan polysaccharide (Levan-based Solid-state Electrolyte, LSE). This electrolyte is flexible and highly transparent, also can be served as substrate for organic electronics. Therefore, we fabricated organic transistor on free-standing LSE films directly and we also utilized LSE based organic transistors for biomedical device due to their flexibility, biocompatibility and biodegradability, especially recording electrocardiogram by attaching on biological surface.

#### **5:40 AM F.SM04.01.05**

##### **Biodegradable Device with Energy Harvesting Operation** Abdulilah M. Mayet; King Khalid University, Saudi Arabia

Low power consumption devices and hygienic material are the heist concern in biomedical devices. Our innovative material amorphous tungsten nitride (WN<sub>x</sub>) is one of the optimal solutions for both demand characteristics. Fabricating amorphous WN<sub>x</sub> based nanoelectromechanical (NEM) switches that can be used to obtain power by reusing the stored potential energy in a bent NEM switch to power the next logic operation could solve the power consumption issue. we exhibit the power dissipated in silicon CMOS adiabatic circuit and compare it with the power dissipated in an energy reversible adiabatic NEM switch fabricated with amorphous metal. Besides, amorphous WN<sub>x</sub> can provide an effective solution to nano-scaled devices and systems, as the absence of significantly larger grains and associated boundaries during subtractive etching provides more uniform architecture. Therefore, we are reporting dissolution characteristics and biocompatibility of an amorphous WN<sub>x</sub> – which has a grain-less molecular structure. Tungsten nitride's structure contributes to corrosion resistance, high endurance, smooth surface, low contact wear, and exacerbation resistance. Here, we report its dissolution characteristics and mechanism in groundwater (GW), deionized (DI) water, and saline. Complete dissolution times were analyzed for different size features, between the nanoscale and macroscale. As an example, we have fabricated an amorphous WN<sub>x</sub> based nanoelectromechanical (NEMS) switch to demonstrate nanoscale structures. We also fabricated an accelerometer to show a microscale device and a temperature sensor to display a large surface area macroscopic dimensions. The dissolution rate for all devices is approximately 20-60 nm/hour, at room temperature, in groundwater. The successful and complete dissolution of WN<sub>x</sub> based devices highlights the versatile nature and simple chemistry of amorphous WN<sub>x</sub> film and its utility in transient electronic applications. Besides, we reported the material amorphous WN<sub>x</sub> based devices could be used in sub-dermal implants for biodegradable function. We aim to insulate transdermal wires connected to an externally mounted miniaturized wireless potentiostat for data transmission. This biodegradable function will prevent bacteria from forming biofilms along transdermal

wires, or seeding haematogenously, with the potential to migrate within the body and to provoke immune-mediated pathological tissue reactions. Another application is to use the amorphous WN<sub>x</sub> as a stent or tubular support placed temporarily inside a blood vessel, canal, or duct to aid healing or relieve an obstruction which degrades gradually by the time with no need for extraction surgery.

#### 5:50 AM F.SM04.01.06

**Protein-Based Multifunctional Bio-Nanocomposite—A Conformal Coating for Perishable Fruits** Yufei Cui, Seohui Jung, Pulickel Ajayan and Muhammad Rahman; Rice University, United States

Hunger and chronic undernourishment impact over 800 million people, which equals 10.7% of the world population. While countries are increasingly making efforts to reduce poverty and hunger by pursuing sustainable energy and agricultural practices, a third of the food produced around the globe still never consumed and thus wasted. Reducing food shortages is vital in this effort and is often addressed by the development of genetically modified produce or chemical additives and inedible coatings to extend freshness, which creates additional health and environmental concerns. Hence, a novel material needed to be developed that is both protective of fresh produce, biocompatible, and biodegradable while at the same time brings economical and environmental sustainability. Herein, a multifunctional bio-nanocomposite comprised largely of egg-derived polymers and cellulose nanomaterials as a conformal coating onto fresh produce that slows down food decay by retarding ripening, dehydration, and microbial invasion is reported. Chemical composition and morphology of the composite were characterized by Infrared Spectra, TEM, and AFM. Affinity to multiple fruit surfaces and hydrophilicity of the coating was measured by the sessile droplet test. The composite forms a uniform coating of approximately 18 μm thick on fruits, as measured through confocal microscopy. The coating's effectiveness against fruit ripening was tested on representative climacteric and non-climacteric fruits: strawberries, bananas, avocados, and papayas. Through time-elapse photos, fruit stiffness measurement, and weight loss measurement of bare and coated fruits over time, the coating showed an extension of fruit freshness by more than a week. The dried coating film showed comparably low water vapor transmission rate and oxygen permeability rate among common packaging materials, and thus these distinct barrier properties likely contributed to the retarding of fruit ripening. Moreover, the coating film eliminated the bacteria on top within 24 hrs, displaying excellent antimicrobial property and thus prevent the microbial attack on fruit surfaces. Additionally, the coating is edible, washable, and made from readily available inexpensive or waste materials, making it a promising economic alternative to commercially available fruit coatings. This green coating composite also provides a potential solution to combat food wastage that is rampant in the world.

SESSION F.SM04.02: Bioelectronic Interfaces with Living Systems

On Demand Abstracts Available for Viewing Starting Saturday Morning, November 21, 2020  
F-SM04

#### 5:00 AM \*F.SM04.02.01

**Multifunctional Fibers as Bioelectronic Interfaces** Polina Anikeeva; Massachusetts Institute of Technology, United States

The ability to seamlessly integrate a diversity of electronic and optical materials within the flexible thermally-drawn fibers has recently enabled their applications as biocompatible and multifunctional tools for neural recording, modulation, and tissue repair. In this talk, I will highlight the advances in multimaterial fiber-based interfaces with neural tissue and illustrate how integration of active electronics and elastomers may allow for expanding the application domain of these devices toward probing physiology of other electroactive organs deep within the body. Furthermore, this talk will discuss the materials innovation to permit combinatorial thermal drawing and lithographic patterning within fibers that will further expand the geometries of fiber-based bioelectronic interfaces.

#### 5:15 AM F.SM04.02.02

**Polydopamine Interfaces for Integration of Photosynthetic Enzymes on Electrodes** Gianluca M. Farinola<sup>1</sup>, Gabriella Buscemi<sup>1</sup>, Roberta Ragni<sup>1</sup>, Francesco Milano<sup>2</sup>, Danilo Vona<sup>1</sup> and Massimo Trotta<sup>3</sup>; <sup>1</sup>University degli Studi-Bari Aldo Moro, Italy; <sup>2</sup>CNR-ISPA, Italy; <sup>3</sup>CNR-IPCF, Italy

The reaction center (RC) photoenzyme from *Rhodospirillum rubrum* photosynthetic bacterium is a membranespanning protein capable to convert solar energy into charge separated states with efficiency close to 100%. The photogenerated electron-hole pairs can be exploited to produce photocurrents and the suitability of RC for photoconversion in electronic and

electrochemical devices is well established [1,2].

However, the electronic interface of RC with electrodes and the photoenzyme stability after integration in devices still require optimization to improve the efficiency of the photocurrent production [3]. Enzyme stability can be improved by encapsulation in soft structures, such as vesicles [4] and polymersomes [5]. Electron transfer between RC and electrode surface can occur either directly or through electrochemical mediators. In the first case a suitable immobilization strategy is required [6]. Although in the second case the RC can be dispersed in solution, higher photocurrents are produced if it is immobilized onto the electrode. To this aim, various protocols are reported in literature, and we have recently demonstrated that modification under mild temperature and pH conditions of RC with biomimetic and adhesive polymers, such as polydopamine, is a very promising method to improve the electrode/protein interface without altering the enzyme photoactivity [7].

[1] F. Milano, A. Punzi, R. Ragni, M. Trotta, G. M. Farinola, *Adv. Funct. Mater.*, **29**, 1805521, (2019).

[2] A.J. McCormick, P. Bombelli, R. W. Bradley, R. Thorne, T. Wenzel, C. J. Howe *Energy Environ. Sci.*, **8**, 1092-1109, (2015).

[3] H. Yuk, B. Lu, X. Zhao, *Chem. Soc. Rev.*, **48**, 1642-1667 (2019)

[4] E. Altamura, F. Milano, M. Trotta, P. Stano, F. Mavelli, *Advances in Bionanomaterials*, Lecture Notes in Bioengineering, Springer, 97-109 (2018).

[5] R. R. Tangorra, A. Operamolla, F. Milano, O. Hassan Omar, J. Henrard, R. Comparelli, F. Italiano, A. Agostiano, V. De Leo, R. Marotta, A. Falqui, G.M. Farinola, Trotta M., *Photochem Photobiol Sci.*, **14**(10), 1844-52 (2015).

[6] M. Chatzipetrou, F. Milano, L. Giotta, D. Chirizzi, M. Trotta, M. Massauti, M.R. Guascito, I. Zergioti, *Electrochemistry Communications*, **64**, 46-50 (2016)

[7] M. Lo Presti, M.M. Giangregorio, R. Ragni, L. Giotta, M. R. Guascito, R. Comparelli, E. Fanizza, R. R. Tangorra, A. Agostiano, M. Losurdo, G. M. Farinola, F. Milano, M. Trotta *Adv. Electron. Mater.* 2000140, (2020)

#### 5:25 AM F.SM04.02.03

**Cephalopod-Inspired Optical Engineering of Human Cells** Alon Gorodetsky, Atrouli Chatterjee, [Aleeza Farrukh](#) and Georgii Bogdanov; University of California, Irvine, United States

Although many animals have evolved intrinsic transparency for the purpose of concealment, the development of dynamic, that is, controllable and reversible, transparency for living human cells and tissues has remained elusive to date. By drawing inspiration from the structures and functionalities of adaptive cephalopod skin cells, we have designed and engineer human cells that contain reconfigurable protein-based photonic architectures and, as a result, possess tunable transparency-changing and light-scattering capabilities. Our findings may lead to the development of unique biophotonic and bioelectronic tools for applications in materials science and bioengineering, as well as ultimately facilitate an improved understanding of various biological systems.

#### 5:35 AM F.SM04.02.04

**Protein-Based Conductive Biopolymers** [Nadav Amdursky](#); Technion-Israel Institute of Technology, Israel

Biological charge transfer processes are based on the controlled transport of charges (electrons, protons, ions) across specific pathways within proteins from the nm-scale up to the  $\mu\text{m}$  scale. With this biological inspiration, we report here on a new family of conductive and free-standing biological materials. We are using different types of proteins as building blocks to form various types of materials, which were later functionalized in a bioinspired fashion to exhibit efficient electron transport on the centimeter length scales. With this in mind, we focus only on proteins that can be produced in bulk quantities and in low cost from raw materials, in which most of our work to date has been focused on the bovine serum albumin protein. Following the formation of the biopolymer, we show that it can be functionalized in different ways for the formation of efficient ionomers with measured ionic conduction of  $>10$  mS/cm at room temperature or for the formation of light responsive materials. Due to the protein-based nature of our materials, it enables us to explore the governing factors and mechanisms of long-range biological charge transport. Nonetheless, our new protein-based biopolymers have several attractive properties for their possible integration in various applications. Our materials are environmentally friendly, they possess inherent biodegradability and their formation obeys to most principals of green chemistry. In terms of their mechanical properties, they have high elastic modulus of  $\sim 160$  MPa, but at the same time, they are highly stretchable, capable of stretching more than 4 times their length. They have high resistance to harsh organic solvents and acids, they are very easy to form, and have a very low price tag with materials cost of around  $\$1/\text{cm}^2$ . Currently, our main targeted application for our new family of materials is for biological interfaces, while other lines of applications include the use of our biopolymers for biomedical application (tissue engineering) and for energy applications such as membranes for fuel cells.

5:45 AM \*F.SM04.02.05

**Programming *E. coli* for Production of Protein Nanowires for Sustainable Electronics** [Derek Lovley](#); University of Massachusetts, United States

Microbially produced electrically conductive protein nanowires (e-PNs) are a revolutionary ‘green’ electronic material with substantial sustainability and functional advantages over traditional materials such as silicon nanowires and carbon nanotubes. e-PNs are produced from renewable feedstocks, with 100-fold less energy demand than that required for producing silicon nanowires or carbon nanotubes. No toxic chemicals are required for e-PN fabrication and the final product is biocompatible, environmentally benign, and recyclable. Yet, e-PNs are remarkably robust, maintaining function even under harsh CMOS-compatible fabrication conditions. e-PNs can be processed into thin-film electronics, nanocables, and flexible conductive composites. However, development of applications has been slowed by the fact that bacteria and archaea known to naturally produce e-PNs are slow-growing anaerobes that are difficult to mass culture. We resolved this bottleneck by designing a nonpathogenic strain of *E. coli* (strain GPN) that expresses abundant e-PNs from synthetic variants of the e-PN monomer gene from *Geobacter* species (ACS Synthetic Biology 9:647-654 (2020)). Advantages of strain GPN for e-PN fabrication include: 1) rapid, and scalable mass-culture under aerobic conditions; 2) ‘plug and play’ simplicity for the design and expression of e-PNs with novel functionalities; and 3) a versatile *E. coli* genetic toolbox for the introduction of genetic circuits that control the expression of multiple monomer genes introduced into the same strain to fabricate e-PNs with advanced sensing and electronic features. When coupled with a newly developed, simplified filtration method for harvesting e-PNs, *E. coli* strain GPN ensures a ready supply of e-PNs for diverse electronics applications. Examples of recently developed novel applications for e-PNs include devices that generate electricity from the ambient humidity in air (Nature 578:550-554 (2020)); neuromorphic memory devices that operate at biological voltages (Nature Communications 11:1861 (2020)); and electronic sensors with high selectivity and sensitivity (Nano Research 13:1479-1484 (2020)). These and other applications are being further optimized by tailoring e-PN properties to specific applications. For example, e-PN conductivity has been tuned over a million-fold by designing genes for synthetic e-PNs with modified amino acid composition. Peptides can be displayed on the outer surface of e-PNs by expressing novel monomer genes designed to add the desired peptide to the carboxyl end of the e-PN monomer (ACS Synthetic Biology 8:1809-1817 (2019)). These peptide decorations can function as ligands to specifically bind analytes of interest for sensor applications or to enhance interactions of e-PNs with other materials. More than one ligand can be added to the same wire and the stoichiometry of the ligands on the wires can be controlled with genetic circuits. Newly designed e-PNs fabricated with *E. coli* strain GPN and their potential applications will be discussed.

6:00 AM F.SM04.02.07

**Smart Nanostructured Multifunctional Biomaterials as Next Generation Cochlear Implant** [Serena Danti](#)<sup>1,2</sup>, Mario Milazzo<sup>1</sup>, Bahareh Azimi<sup>2</sup>, Andrea Lazzeri<sup>2</sup>, Markus Buehler<sup>1</sup> and Stefano Berrettini<sup>2</sup>; <sup>1</sup>Massachusetts Institute of Technology, United States; <sup>2</sup>University of Pisa, Italy

About 466 million people are estimated to suffer from disabling hearing loss. When the transduction mechanism (i.e., sensory cells and/or neurons) is damaged, sensorineural hearing loss (SNHL) occurs. Up to now, severe SNHL is only possible using complex electronic implants, i.e., cochlear implants (CIs). Conventional CIs suffer from some important disadvantages impacting the quality of life and hearing after implantation and for such reasons a new class of CIs is desirable. The ear sensory cells, hair cells, act as biological transducers in the organ of Corti, where they convert the mechanical vibration of the basilar membrane into stimulation of the underlying spiral ganglion neurons. By exploiting the mechanical tonotopy still present in deaf cochleae, piezoelectric materials in contact with the basilar membrane could potentially enable a fine-tuning process of the sound vibrations, thus providing a better quality of hearing versus discretized electrodes in electronic CIs. Piezoelectric CIs would thus represent an innovative and smart solution: they work in a biomimetic fashion, are self-powered and fully implantable, less expensive (material-based) than bionic CIs and a-magnetic (i.e., MRI-compatible). In our hypothesis, a tissue engineering-aided nanostructured piezoelectric device and its proper surgical implantation can promote direct contact with spiral ganglion neurons, thus reducing the necessary electric output for neural stimulation and finally achieving sufficient sensitivity. Specifically, we move forward the primitive concept of bulk-structured piezoelectric CIs by designing a new device based on ultrafine fibers produced via electrospinning to be precisely delivered and provided with a nano/microscale resolution to be intimately and efficiently integrated with the cochlear microenvironment. Ceramic materials with a perovskite-like structure, possess higher piezoelectric properties than those of piezopolymers (e.g., polyvinylidene fluoride, PVDF), but are very rigid and difficult to process. To gain the multifunctionality of the nanofibrous device, we study the immunomodulatory and antibacterial properties of nanoceramics to be incorporated inside piezoelectric

polymeric fibers. In fact, reducing the fibrotic tissue formation would allow the best electric delivery by the piezoelectric materials.

We investigate lithium niobate as a potential candidate material for next-generation CIs. Lithium niobate nanoparticles resulted otocompatible *in vitro* with OC-k3 cells, enhanced human beta-defensin (HBD-2) in HaCaT epithelial cells, and also showed direct antibacterial activity against *P. aeruginosa*. The LiNbO<sub>3</sub> ability of modulating the expression of IL-6 and IL-8 could play a beneficial role *in vivo*, by reducing the extent or duration of a post-implant inflammatory response. These nanoparticles were efficiently incorporated into PVDF-trifluoroethylene P(VDF-TrFE) fibers via electrospinning. Aligned composite fibers at 20% (w/w%) of lithium niobate showed an enhanced piezoelectric response, namely  $90 \pm 2$  mV, with respect to their random counterparts, namely  $40 \pm 4$  mV, under an applied load of 2.12 N. These composite fibrous structures supported SHSY-5Y neural-like cell growth *in vitro*.

Electroactive materials combining nanotechnology and tissue engineering show promise for cochlear stimulation and otoprotection.

This study was supported by MISTI funds 2016 (MIT-UNIPi project NANOSPARKS).

SESSION F.SM04.03: Bio-inspired and Bio-derived Electronics  
On Demand Abstracts Available for Viewing Starting Saturday Morning, November 21, 2020  
F-SM04

#### 5:00 AM \*F.SM04.03.01

**Optimizing Synergy Between Materials and Cell Microenvironments Using Functional Polyesters** Milica Radisic;  
University of Toronto, Canada

Material based technologies play an integral role in many medical treatment strategies, including joint replacements, vascular stents, drug delivery methods, contact lenses and medical sutures. The application of successful technologies continues to grow, with an estimated market size of \$130 billion USD by 2020. Although successes are notable, a number of biomaterial-based devices are limited in application by non-specific material properties to tissue type and undesired inflammation at the device interface. In application, polyester materials have traditionally been an effective polymer strategy, with successes in tissue engineering scaffolds and a variety of biomedical devices. Leveraging advantageous polyester degradability and well understood chemical synthesis, these materials serve as a strong functional platform to further optimize material-cell microenvironments. In this talk, I will describe the development of polyesters that (a) exhibit controllable mechanical properties to mimic the elastic properties of cardiac tissue extracellular matrix (ECM) and (b) incorporate a biomimetic moiety of mammalian immunity to recapitulate mechanistic inflammation regulation at the material surface.

Development of engineered cardiac tissue requires material scaffolds that match the elastic behavior of cardiac ECM. Using polycondensation techniques to incorporate unsaturated carbonyl groups into elastic polyester material gels, we generated materials that can be molded into intricate designs with secondary crosslinking to generate constructs with highly tunable elasticity. By adapting material synthesis conditions (i.e. monomer ratios, reaction time), elastic mechanical behavior was highly tunable across a range of soft biomaterial applications. Material applicability was highlighted in a number of micro-designed elastomeric scaffold supports for engineered tissue, both for *in vitro* organ-on-a-chip and *in vivo* cardiac patch technologies, wherein the two-step synthesis process allowed for micro molding into intricate shapes prior to gelation.

With biomaterial application *in vivo*, inflammation at the biomaterial surface limits device application. To tackle this, we looked to itaconate, a powerful small molecule metabolite of innate immunity that has recently emerged as a regulator of innate immune inflammation. This molecule has been previously limited therapeutically by short circulation times. To circumvent this, itaconate was incorporated directly into material backbones to impart biomimetic small molecule modulation, with quantified hydrolytic degradation release from polyester chains. Harnessing hydrolytic degradation release from polyester backbones, itaconate polymers resulted in the mechanism specific immunoregulatory properties on macrophage polarization *in vitro*. In a functional assay, the polymer-released itaconate inhibited bacterial growth on acetate. Translation to an *in vivo* model of biomaterial associated inflammation, intraperitoneal injection of ITA polymers demonstrated a rapid resolution of inflammation in comparison to a control polymer silicone, demonstrating the value of sustained biomimetic presentation of itaconate. Using scalable polyester synthesis techniques, we have demonstrated the power of instructive biomaterial technologies as functional modulators of the cell microenvironment.

#### 5:15 AM \*F.SM04.03.02

**Self-Assembled Bioinspired Nanostructures for Green Electronics** Nurit Ashkenasy; Ben Gurion University of the

Negev, Israel

Self-assembling peptides that are inherently biodegradable and biocompatible are extremely suitable for use in devices that adhere on, or even implanted into, the human body in order to monitor and regulate biological functions. The challenge for incorporating these materials in bioelectronic devices is the optimization of their electronic properties for the desired application. In this talk I will present peptide design rules that can be used to prepare electron and/ or proton conducting peptide based materials. Specifically, I will discuss the influence of aromatic side chains (both natural and non-natural) on electron conductivity.<sup>1,2</sup> I will further present enhancement of proton conduction in these films by the incorporation of protonating side chains, which can lead to extremely high proton conductivity values in these materials.<sup>3,4</sup> I will finally discuss the control of conductivity, thermal stability and biodegradability of self-assembling peptide nanostructures by peptide backbone motifs. These studies demonstrate the great potential of using peptide building blocks for the fabrication of green electronic materials.

#### References

1. Ashkenasy, N.; Horne, W. S.; Ghadiri, M. R., Design of Self-Assembling Peptide Nanotubes with Delocalized Electronic States. *Small* **2006**, *2*, 99-102.
2. Ivnitski, D.; Amit, M.; Silberbush, O.; Atsmon-Raz, *et al.*, The Strong Influence of Structure Polymorphism on the Conductivity of Peptide Fibrils. *Angewandte Chemie-Int. Ed.* **2016**, *55*, 9988-9992.
3. Amit, M.; Appel, S.; Cohen, R.; Cheng, G.; *et al.*, Hybrid Proton and Electron Transport in Peptide Fibrils. *Adv. Funct. Mater.* **2014**, *24*, 5873-5880.
4. Silberbush, O.; Amit, M.; Roy, S.; Ashkenasy, N., Significant Enhancement of Proton Transport in Bioinspired Peptide Fibrils by Single Acidic or Basic Amino Acid Mutation. *Adv. Funct. Mater.* **2017**, *27*, 1604624.

#### 5:30 AM F.SM04.03.03

**Electrical and Mechanical Self-Healing of Genetically Engineered Conductive Curli Fiber Films** Daniel Modafferi, Catrina Huyer, Juliana Ferraro, Sophia Roy and Noemie-Manuelle Dorval Courchesne; McGill University, Canada

The expanding use of electronics in all aspects of society broadens their use towards novel medical applications but also raises new environmental and health concerns. Medical electronic devices need to be able to store, harvest and transfer electric charges, while benefitting from physical properties harmonious with their biological interface, such as flexibility, stretchability and self-healing. One strategy to obtain both electrical and biocompatible properties is to use biological materials, which have the added benefit of being biodegradable, while having a much lower carbon footprint than other electronic materials like metals and organic polymers. Evolution has already generated biological materials, proteins, able to transfer electronic charges over long distances. Drawing inspiration from theoretical understanding of how electrons can be transferred in some native protein fibers through aromatic amino acids, fibrous proteins have been genetically engineered to exhibit conductivity. Curli fibers, which are grown naturally in the ubiquitous and very scalable *Escherichia coli*, are formed by the self-assembly of beta-helical CsgA monomers. Mutating a row of amino acids along the helix to aromatic residues confers conductivity to the dry amyloid film.

These proteins' ability to self-assemble through non-covalent bonds and their dispersibility in water are good indicators for self-healing properties. Here, we tested the conductive and mechanical properties of genetically engineered conductive curli fiber films. Specifically, we evaluated whether they can regenerate from different tears and scratches, simply by rehydrating the film in water. We drop-cast conductive curli fibers between electrodes to form films of various thicknesses and cut at different sizes. We used SEM imaging to observe the mechanical healing of the drop-cast film. We further performed cycles of cuts and healing to observe longer-term reusability of the material. Next, to reveal the flexibility of a free-standing film, we performed tensile tests. We were able to reattach two pieces of film back together to determine the material's resistance to breaks, and to quantify the regeneration of the electrical properties in doing so. We found that the material can recover almost entirely with micron-scale cut sizes, even for protein films as thin as 2  $\mu\text{m}$ . These self-healing properties we defined show potential for use of conductive curli fibers as composites, or even pure materials, in wearable medical devices.

#### 5:40 AM F.SM04.03.04

**Photovoltage Generation in Organic-Biological Hybrid Architectures** Massimo Trotta<sup>1</sup>, Michele Di Lauro<sup>2</sup>, Gioacchino Calandra Sebastianella<sup>3</sup>, Anna De Salvo<sup>2</sup>, Gabriella Buscemi<sup>4</sup>, Danilo Vona<sup>4</sup>, Fabio Biscarini<sup>2</sup> and Gianluca M. Farinola<sup>4</sup>; <sup>1</sup>Consiglio Nazionale delle Ricerche, Italy; <sup>2</sup>Istituto Italiano di Tecnologia, Italy; <sup>3</sup>Universita di Modena e Reggio Emilia, Italy; <sup>4</sup>Università degli Studi di Bari Aldo Moro, Italy

Solar energy transduction performed by photosynthetic organisms is the paramount process that ensures power to all metabolic activities on planet Earth[1]. Exploiting the highly efficient capability of the photosynthetic organisms to convert

visible and near infrared radiations into energy forms viable to human beings is a dream that accompanies man-kind since the visionary and wishful speech by Giacomo Ciamician at the beginning of XX century[2].

In the last two decades, vast literature tackles the use of photosynthesis in energy conversion using several approaches ranging from the use of the isolated enzymatic machinery responsible of light photoconversion [3] to complex systems that exploit photosynthetic microorganisms[4].

The most recent advances regarding photovoltage generation and the subsequent current amplification in Light-modulated Electrolyte-gated organic transistors[5,6] will be presented. These hybrid systems, based on the unique coupling of photosynthetic materials or organisms with the peculiarities offered by the platform of organic electronics will be presented. The potential of these architectures will be discussed in view of the interaction of the photosynthetic apparatus employed in the voltage generation with the organic electronic device of choice.

[1] Nicola Armaroli, Vincenzo Balzani, Nick Serpone. *Powering Planet Earth: Energy Solutions for the Future* (2013) Wiley-VCH

[2] Giacomo Ciamician. *The Photochemistry of the Future* (1912) **Science** **36**(926) 385-94

[3] Ravi, SK, Rawding, P, Elshahawy, AM, Huang, K, Sun, W, Zhao, F, Wang, J, Jones, MR & Tan, SC, *Photosynthetic apparatus of Rhodospirillum rubrum exhibits prolonged charge storage*. (2019) **Nature Comm.** **10**(902).

[4] F. Milano, A. Punzi, R. Ragni, M. Trotta, G.M. Farinola, *Photonics and Optoelectronics with Bacteria: Making Materials from Photosynthetic Microorganisms* (2018) **Adv. Funct. Mat.** **29**(21) 1805521.

[5] M. Di Lauro, S. la Gatta, C.A. Bortolotti, V. Beni, V. Parkula, S. Drakopoulou, M. Giordani, M. Berto, F. Milano, T. Cramer, M. Murgia, A. Agostiano, G.M. Farinola, M. Trotta, F. Biscarini *A Bacterial Photosynthetic Enzymatic Unit Modulating Organic Transistors with Light*. **Adv. Electr. Mat.** **6**(1) 1900888

[6] M. Di Lauro, G. Buscemi, M. Bianchi, A. De Salvo, M. Berto, S. Carli, G.M. Farinola, Luciano Fadiga, F. Biscarini, and M. Trotta. *Photovoltage generation in enzymatic bio-hybrid architectures*. (2020) **MRS Advances** **5**(18-19), 985-990.

SESSION F.SM04.04: Flexible, Soft and Self-Healing Electronics

On Demand Abstracts Available for Viewing Starting Saturday Morning, November 21, 2020

F-SM04

#### 5:00 AM \*F.SM04.04.01

**Large-Area Printable and Flexible Electronic Biosensors for Label-Free Single-Molecule Detection** Luisa Torsi<sup>1,2</sup>; <sup>1</sup>University of Bari A. Moro, Italy; <sup>2</sup>Åbo Akademi University, Finland

Detecting a marker or a pathogen at the physical limit is the new frontier in medical analysis as it endows the clinicians with the attacker's advantage over life-threatening diseases such as tumours and pandemics. It is also received that label-free and electronic transductions can be conveniently fast and wieldy. Within this field different transducing approaches are pursued. They involve a transducing interface functionalized with biological recognition elements, such as antibodies or DNA probes, that endow the device with recognition properties by selectively capturing the analyte e.g. an antigen or a genomic marker, respectively. One recently proposed approach involves a large interface hosting trillions of highly-packed bio-recognition elements. The challenge is indeed that of measuring one single molecule in a large volume such as for instance 100 ml. This means being able to deploy a technology that can detect  $10^{-20}$  mole l<sup>-1</sup> (zeptomolar).

Mimicking cell's behaviour, recently proposed approach involves a large interface hosting trillions of highly-packed bio-recognition elements. This is called, the "**S**ingle **M**olecule with a large **T**ransistor (SiMoT)" technology that was proposed to sense a solution with markers present at extremely low concentrations. It is based on an Electrolyte Gated Organic field-effect transistor operated in deionized water, with a gate that has an area of ca. 0.5 cm<sup>2</sup>, hosting 10<sup>12</sup> antibodies or genomic probes. The SiMoT platform has been proven to perform label-free and selective detection at the physical limit in real biofluids of protein biomarkers such as: human Immunoglobulin G, Immunoglobulin M, C-reactive protein, MUC1 and HIV1 p24 antigen as well as genomic markers such as miR-182-5p and KRAS. Indeed, the widely applicable method used to conjugate the recognition elements to the gate electrode, makes the SiMoT platform suitable for the detection of different classes of markers and pathogens reaching world record detections limits for label-free protein detection.

#### 5:15 AM \*F.SM04.04.02

**Pushing the Limits of Elasticity in Soft-Matter Electronics** Carmel Majidi; Carnegie Mellon University, United States

In order for machines and electronics to interface with biological tissue, they should be soft and elastic – i.e. remain functional when stretched and then return to their natural length when unloaded. In recent years, there has been tremendous progress in creating conductive elastomers and gels that are capable of extreme stretchability and which have been successfully utilized as bioelectronic interfaces. These include material architectures that are self-healing and can restore electrical and/or mechanical functionality when torn or punctured.

In this talk, I will review recent efforts to create mechanically robust, stretchable electronics using a variety of soft material architectures. In particular, I will focus on the following approaches: (i) silver-hydrogel composites that exhibit an unprecedented combination of mechanical compliance and electrical conductivity; (ii) biphasic compositions of silver nanoparticles and eutectic gallium-indium (EGaIn) liquid metal alloy for ultrathin “epidermal” electronics; and (iii) EGaIn-polymer composites capable of high electrical conductivity, extreme stretchability, negligible electromechanical coupling, and a variety of self-healing properties. To demonstrate their potential role in future bioelectronic applications, I will present examples of how these soft material architectures are used as electrodes for physiological monitoring (e.g. EMG, ECG) and as electrical interconnects for highly stretchable digital circuits.

### 5:30 AM F.SM04.04.03

**Organic Electrochemical Sensing Transistors Fabricated on Soft Bioresorbable Substrates** Nicolas Fumeaux, Silvia Demuru and Danick Briand; EPFL, Switzerland

Transient electronics have gained attention in the recent years, showing great promise to reduce electronic waste, enabling devices that can disintegrate for data security purposes or novel biomedical implants which eliminate the need for re-operation. In this work, we focus on the latter, also called “bioresorbable electronics”, devices that will naturally dissolve or be degraded into benign byproducts in the body. Materials such as dissolvable metals, degradable semi-conductors, polymers and dielectrics have been proposed. However, due to their properties, these materials are often not compatible with processes that involve high temperature or harsh chemicals, making them challenging to pattern. Printing techniques show great promise to address this challenge and could pave the road to personalized implants based on digital additive manufacturing, but require joint optimization of the ink formulation, the printing conditions and the post-treatment. In this work, we leverage the potential of these techniques to deposit functional materials on bioresorbable elastomeric substrates, poly(glycerol sebacate) (PGS) and poly(octamethylene maleate (anhydride) citrate) (POMaC) as well as on a biopolymer derived from silkworms, silk fibroin. Bioresorbable elastomers are of particular interest, as they enable the development of low-profile transient bioelectronics, in that they can conform to the shape and curves of internal organs and minimize immune response. We focus on the manufacturing of poly(3,4-ethylenedioxythiophene) polystyrene sulfonate (PEDOT:PSS)-based organic electrochemical transistors (OECTs). OECTs, generally based on a conducting polymeric channel gated through an aqueous electrolyte, have generated a lot of attention recently for the detection of multiple biomolecules and ions and high signal-to-noise ratio electrophysiological recordings.

PGS and POMaC were synthesized as described in previous publications, spin-coated on silicon wafers onto sacrificial layers and formed into free-standing films after thermal curing. Silk fibroin was purified as described previously, blade-cast and treated with water vapor for 24h. The suitability of the transient polymers as substrates for printed electronics was assessed and compared with a conventional substrate, polyimide. Degradable inks based on respectively zinc and carbon pastes were developed and evaluated for the creation of contacts and interconnects and silk fibroin inks were formulated to be used as a dielectric layer. Various manufacturing methods such as screen printing and direct ink writing were investigated for the patterning of these inks, as well as post-treatments that are compatible with the relatively low thermal resistance of the bioresorbable substrates. The degradation behavior of the printed patterns was assessed in phosphate buffered saline (PBS). Inks based on aqueous dispersions of PEDOT:PSS were patterned using inkjet printing and the conductivity of the polymer was compared on the degradable substrates and polyimide. The behavior of the resulting OECTs on transient substrates was characterized in PBS and found to be in line with the state of the art considering channel dimensions. A preliminary test to demonstrate the ion sensing capabilities of the organic transistors was conducted with different concentrations of potassium chloride (KCl). The work presented here represents a step forward in the facile manufacturing of bioresorbable implantable sensors. The fabrication scheme used in this work leverages different methods of material deposition, and, while combining fabrication approaches may be advantageous in some cases, we aim to develop fully printed devices. This could allow to create personalizable implants made of bioresorbable materials, for example for regeneration or diagnosis applications, in a scalable and customized manner.



#### 5:40 AM F.SM04.04.04

**Tracking Anticancer Drug Activity at Attomolar Concentrations in Cellular Lysates with Bioinspired Electrochemical Devices** Jason D. Slinker<sup>1</sup>, Ashan Wettasinghe<sup>1</sup>, Naveen Singh<sup>2</sup>, David Boothman<sup>2</sup> and Edward Motea<sup>2</sup>; <sup>1</sup>The University of Texas at Dallas, United States; <sup>2</sup>Indiana University School of Medicine, United States

The immunotherapy market surpassed 75 billion USD in 2019, and many emerging drugs also leverage the body's immune system. Among these immunotherapies, many current and future cancer treatments utilize DNA damage. To follow these DNA damaging immunotherapies, we have applied bioinspired electrochemical devices for real-time measurements of DNA damaging drugs in cellular lysates. We have shown these devices to quantify concentration-dependent drug activity, identify therapeutic concentration windows of cancer-selective activity, and mechanistically correlate damage activity with cancer cell death. Recently, we have shown these devices to detect an onset of activity of a deoxyniboquinone derivative at 100 attomolar levels in approximately 100 microliters of cellular media. This device is ready to be implemented as a standard tool for analyzing the drug activity of cancer-selective treatments in the lab, enabling quantitative identification of effective drugs for patients while minimizing side effects.

SESSION F.SM04.05: Synthesis of Bio-active and Bio-derived Nanocomposites  
On Demand Abstracts Available for Viewing Starting Saturday Morning, November 21, 2020  
F-SM04

#### 5:00 AM \*F.SM04.05.01

**Fabrication of 3D Monolithic Architecture Electrodes Based on Conducting Polymer Microstructures** Youngseok Kim and Myung-Han Yoon; Gwangju Institute of Science and Technology, Korea (the Republic of)

The conventional bioelectronic interfaces have been based on either 2-D thin films or 1-D fibers/wires which limit 3-D scalability as well as volume-/mass-dependent performance. Moreover, biological tissues and organs typically exhibit 3D arbitrary curvatures with wet surface, which impeded the close physical contact between the target tissue/organ and bioelectronic interfaces, leading to the low efficiency in bioelectric signal recording and/or stimulation. In this research, we report on 3D monolithic architectures with arbitrary shapes by employing conducting polymer microstructures as building blocks. Such arbitrary 3D structures were constructed by performing the seamless fusion of separate conducting polymer microstructures without using binder or adhesive. The resultant 3D structures exhibited decent mechanical robustness, high water stability, and outstanding biocompatibility, while the sheet resistance was reduced below 1 Ohm/square and the gravimetric capacitance was increased up to 79 F/g by taking advantage of cumulative mass loading and structural fusion. Finally, we demonstrated that 3D conductive mesh electrodes could be attached to the wet surface of biological organs/tissues such as heart and sciatic nerves without glue or clamp and efficiently record/stimulate bioelectrical signals *in vivo*.

#### 5:15 AM F.SM04.05.02

**Multifunctional Biodegradable Films with Engineered Properties—A Kirigami-Inspired Approach** Sayantan Pradhan and Vamsi Yadavalli; Virginia Commonwealth University, United States

Multifunctional surfaces that can conformally adhere to complex interfaces, degrade at a controllable rate and invoke minimal reaction within the body can be used for soft and implantable electronics, wound healing, tissue engineering, neural interfacing and *in vivo* disease diagnostics. Designing interfaces for applications at dynamic, non-planar biological environments is a problem of great interest. Recently, “kirigami”- the Japanese art of paper cutting has been proposed as a unique strategy to engineer flexibility and stretchability by introducing patterned defects or cuts. We discuss how the concepts of kirigami can be applied to form photolithographically patterned cuts in flexible, mechanically robust silk proteins for the fabrication of biofunctional films.[1] These macroscale films are optically transparent and possess tuneable degradation and engineered flexibility with precisely defined microscale cuts. The kirigami cutting is formed using the technique of “protein photolithography” using silk fibroin as a route to multiscale fabrication.[2,3] Tensile tests performed on these films show a remarkable improvement in mechanical properties in comparison to pristine films. Using numerical modelling, the mechanical behavior of the silk kirigami films can be predicted as a function of different cut geometry. We show that these films can be used as multilayer, biodegradable cell culture substrates as a result of the biocompatibility of the substrate biomaterial. Finally, by incorporating the conducting polymer polyaniline (PANI) in the silk composite, we are able to make multifunctional conducting silk kirigami films. The films demonstrate excellent linear

conductive behavior ( $\mu\text{S}$  range) over a voltage range of  $-0.5$  to  $+0.5$  V. The films are able to maintain their conductivity under severe mechanical flexure and deformations. These results indicate that silk kirigami can provide exceptional bioinspired and biodegradable structures towards flexible and stretchable biodevices.

#### References:

- [1] S Pradhan, L Ventura, F Agostinacchio, M Xu, E Barbieri, A Motta, NM Pugno, VK Yadavalli. ACS Appl. Mater. Interfaces. 12(11),12436-44, 2020.
- [2] NE Kurland, T Dey, C Wang, SC Kundu, VK Yadavalli, Adv. Mater. 26, 4431-4437, 2014.
- [3] M Xu, S Pradhan, F. Agostinacchio, RK Pal, G Greco, B Mazzolai, NM Pugno, A Motta, VK Yadavalli, Adv. Mater. Interfaces, 6, 1801822, 2019

#### 5:25 AM F.SM04.05.04

##### **Hierarchically Structured Silver Nanosattellite Particles for Highly Conductive Healable Putty-Like**

**Nanocomposites** Faseela Kizhakke Palakkamkuzhiyil, Daewoo Suh, Wonjoon Kim, Chanyong Park, Jang Gyun Lim, Sungwon Seo, Moon Ki Kim, Hyungpil Moon and Seunghyun Baik; Sungkyunkwan University, Korea (the Republic of)

Healable and deformable conductive materials have received considerable attention for future electronics such as artificial human skin, internet of things, and bioelectronics. However, their practical applications are impeded by low electrical conductivity and irreversible conductivity degradation after breaking/healing cycles. Here we report a highly conductive completely reversible electron tunneling-assisted percolation network of silver nanosattellite particles for putty-like moldable and healable nanocomposites [1]. The hierarchically structured silver nanosattellite particles with a bimodal size (medium: 164 nm, small: 3.7 nm) distribution are generated by the radical and reactive oxygen species-mediated vigorous etching and reduction reaction of silver flakes using tetrahydrofuran peroxide in a healable silicone rubber matrix. The silver nanosattellite network dramatically increases electrical conductivity by  $\sim 5$  orders of magnitude, achieving an unusually high conductivity (1020 S/cm) in putty-like nanocomposites with excellent moldability [1]. The silver nanosattellite particles are uniformly and densely distributed with an interparticle distance of 3.1 nm, and the close work function match between silver and silicone enables electron tunneling. This leads to a completely reversible reconstruction of the percolation network, achieving  $\sim 100\%$  electrical healing efficiency after 1000 breaking/healing cycles [1]. Moreover, the conductivity is stable even after 1000 water immersion cycles and 6-month exposure to ambient air. An emergency electronics repair demonstration is also performed by a robot using the nanocomposites [1]. A recent progress in our laboratory will also be introduced. Reference: [1] Suh et al., Nature Communications 11, 2252 (2020). <https://doi.org/10.1038/s41467-020-15709-8>

#### 5:35 AM \*F.SM04.05.05

**Self-Healing Tandem Repeat Proteins Inspired by Squid Ring Teeth** Melik C. Demirel, Oguzhan Colak and Abdon Penafrancesch; The Pennsylvania State University, United States

Production of repetitive polypeptides that comprise one or more tandem copies of a single unit with distinct amorphous and ordered regions have been an interest for the last couple of decades. The self-healing performance of tandem repeat polypeptides creates new opportunities for the design of bioinspired and biosynthetic materials that were not possible previously, and addresses current limitations in self-healing soft materials. In this talk, we review programmable design, structure, and properties of functional materials and composites from squid-inspired tandem repeat proteins, with applications in bioelectronics. Protein based self-healing materials provides a rich architecture that can micro-phase-separate to form periodic nanostructures with enhanced physicochemical properties via directed or natural evolution that often exceed those of conventional synthetic polymers. These materials show hydrogen-bonded nanostructure and network morphology, with programmable healing properties (2–23 MPa strength after 1 s of healing) that surpass by several orders of magnitude those of other natural and synthetic soft materials.

SESSION F.SM04.06: Poster Session: Degradable and Self-Healing Electronic Materials for Biological Interfaces  
On Demand Abstracts Available for Viewing Starting Saturday Morning, November 21, 2020  
5:00 AM - 8:00 AM  
F-SM04

#### F.SM04.06.01

**Programmable Photomechanical Jumping of Polymer Monoliths** Jisoo Jeon<sup>1</sup>, Jun-Chan Choi<sup>2</sup>, Hyeok Lee<sup>3</sup>, Woongbi Cho<sup>1</sup>, Jae Gwang Kim<sup>1</sup>, Jae-Won Lee<sup>2</sup>, Kyung-Il Joo<sup>2,4</sup>, M. Cho<sup>3</sup>, Hak-Rin Kim<sup>2</sup> and Jeong Jae Wie<sup>1</sup>; <sup>1</sup>Inha University, Korea (the Republic of); <sup>2</sup>Kyungpook National University, Korea (the Republic of); <sup>3</sup>Seoul National University, Korea (the Republic of); <sup>4</sup>Electronics and Telecommunications Research Institute, Korea (the Republic of)

Controlled jumping is a unique motion in nature and robotics to achieve rapid mobility and to avoid obstacles as well as rough terrains. One key challenge is the introduction of a remote powering system for untethered miniaturized robots as they have to work to overcome their own body mass without an internal power system. Toward light-fueled jumping, we synthesize photo-responsive polymer monoliths where spring-like molecular geometry is implemented via self-assembly of liquid crystalline polymer networks (LCNs). Upon light irradiation, the spring-like self-assembled photo-responsive molecules induce non-isometric structures providing unprecedented photomechanical jumping by an instantaneous energy release. The experimental jumping behavior is supported by a finite element method (FEM) simulation for quantitative analysis. The jumping capability of the soft robotic LCN reaches 15.5 body length (BL) height, and 880 BL/s take-off velocity. In addition, we demonstrate rotational axis- and angle-controlled jumping by programming the molecular alignment and macroscopic design. Finally, the controlled light irradiation provides continuous and directional jumping of soft robotic LCNs.

#### **F.SM04.06.02**

**A Protein Based Polymer Film for Bio-Electronic Interfacing** Ramesh Nandi, Yuval Agam and Nadav Amdursky; Technion-Israel Institute of Technology, Israel

Human machine interfacing is a long challenge for researchers, in last few decades we have witnessed emerging of different materials and electrodes for the purpose. Successful interfacing of human body with machine involves coupling of ionic and electronic signal at the interface. In addition to the successful interfacing of the ionic and electronic signals, any conductive material for biological interfacing should be stretchable, flexible, stable in aqueous or humid environment, bio-compatible and bio-degradable. Developing a single material having all these properties is a challenge by itself. However, conductive polymers are one of the promising materials for this purpose due to their organic carbon-based nature. Over the years, many different types of conducting organic polymers have been emerged using different synthetic organic analogues, however, the development of a synthetic polymer that fits all the above-mentioned criteria is still consider a challenge for researchers. Inspired by natural electron and ion transfer processes mediated mainly by proteins, here we present a novel conductive polymer made out of 100% natural Bovine Serum Albumin (BSA) protein, which is a side product of bovine industry, cheap and available in large scale. The polymer film is free-standing, transparent, stretchable, and highly stable in aqueous environment. Moreover, it is bio-compatible and biodegradable due to its biological nature, the synthesis method is within one pot and energy-efficient process and there is no need for any post-synthetic purification. This polymer film can efficiently record brain (electroencephalogram) and heart signal (electroencephalogram) from the human body in a non-invasive way with several other potential applications. While considering its novelty, our polymer can be considered a new class of materials in the field of bioelectronics.

**Keywords:** Biological Interfacing, Conductive Polymers, Polymer Film, electroencephalogram, electroencephalogram.

#### **F.SM04.06.03**

**Diffusivity Modulation of Planer Lipid Bilayer Mediated by Self-Assembled Peptides** Yoshiki Nakamura, Hironaga Noguchi, Mirano Tsukiiwa and Yuhei Hayamizu; Tokyo Institute of Technology, Japan

Two-dimensional (2D) materials represented by graphene have been studied for biosensor applications owing to their excellent electronic properties and high specific surface areas. Lipid bilayer biosensors based on the 2D materials as supporting substrates have gained wide interest as a platform for highly-sensitive biosensing with inserted membrane proteins. For stable formation of a lipid film on the surface of 2D materials, it is essential to control the hydrophobicity of the surface which is correlated to the affinity of the surface with the lipid film. Moreover, it is important to control the lateral diffusivity of the lipid membrane for understanding interaction dynamics of biomolecules embedded into the membrane. In this study, to address this, we utilized self-assembled peptides as an adhesive layer for immobilization of planar lipid bilayer on h-BN, an insulative 2D material which is transparent in visible region. In our recent research, we developed a series of peptides which have an ability to form uniform monomolecular thick peptide thin film in a self-assembly manner [1]. More recently, peptides with a repeated amino acid sequence of glycine (G) and alanine (A) inspired by silk proteins have been demonstrated to form stable  $\beta$ -sheet structures on the surface of two-dimensional materials [2]. In this study, we utilized three types of peptides containing additional hydrophilic amino acids with the GA repeat sequence. These peptides formed self-assembled structures on h-BN surface and act as an adhesive layer to form a planar lipid bilayer. Self-assembled peptides

were prepared by dropping an aqueous peptide solution onto the surface of transferred h-BN on a substrate of Si/SiO<sub>2</sub> or cover glass, and it was incubated at room temperature for 1 hour. Then, planar lipid membranes were prepared by the rupture method, where DOPC vesicle suspension in 10 mM PB was placed on the sample with the self-assembled peptides, and it was incubated at room temperature for 1 hour or more. The morphology of lipid membranes on the surface was observed by atomic force microscopy (AFM). Furthermore, to investigate the fluidity of lipid molecules in the membrane, DOPC was mixed with 1% 14:0 NBD PE (lipid molecule tagged with a fluorophore). The lateral diffusion constant of the lipid membrane was measured by the photobleaching after fluorescence recovery (FRAP) method. AFM observations showed that lipid bilayer can be formed on a h-BN surface with high coverage, indicating that self-assembled peptides support the lipid bilayer as a molecular scaffold with a controlled hydrophilicity. The FRAP results showed that the diffusion constants of lipid bilayers depend on peptide sequences. These results revealed the importance of the peptide design to control the physical properties of the planar lipid bilayer on 2D material, which could be essential to develop lipid-based biosensors with 2D materials.

#### Reference

- [1] Y. Hayamizu, et al., Scientific rep 2016, 6:33778  
[2] P. Li, et al., ACS Appl. Mater. Interfaces 2019, 11, 20670–20677

#### F.SM04.06.04

**The Porphyrin Ring Rather Than the Metal Ion Dictates Long-Range Electron Transport Across Proteins Suggesting Coherence-Assisted Mechanism** Yuval Agam and Nadav Amdursky; Technion–Israel Institute of Technology, Israel

The fundamental biological process of electron transport (ET) takes place across proteins with common ET pathways of several nanometers. Recent discoveries from the bacterial world push this limit and show long-range extracellular ET over several micrometers. Here, we aim in deciphering how protein-bound intramolecular cofactors can facilitate such long-range ET. In contrast to natural systems, our protein-based platform enables us to modulate important factors associated with ET in a facile manner, such as the type of the cofactor and its quantity within the protein. We chose here the biologically-relevant porphyrin molecule as the electron mediator. We use electrochemical impedance measurements (EIS) as well as three-terminal field effect transistor (FET) measurements to explore the role of the porphyrin variant in mediating ET. Using different porphyrins with different metal centers, or lacking a metal center, we show that the metal redox center has no role in ET, and that ET is mediated solely by the conjugated backbone of the molecule. We further support these results with advanced density functional theory (DFT) calculations of the variants. We discuss several mechanisms accounting to possible contribution of coherent processes during the ET. Our results suggest that our high measured ET efficiency is probably due to coherence-assisted ET mechanism. Our work can help understand the participation of heme molecules in common long-range biological ET and introduce the possibility of using the protein-based platform as a tool for the investigation of different systems.

#### F.SM04.06.06

**Improvement of Adhesion and Osseointegration of Nanocomposite Biomembranes for Medical Implants** Soyeon Kim, youngjoon Han, Chungik Oh, Hojoon Lee and Seungbum Hong; Korea Advanced Institute of Science and Technology, Korea (the Republic of)

Medical societies dedicated to treating musculoskeletal diseases are facing challenges due to an unprecedented increase in the aging population around the globe. As such, it is getting more important to develop novel class of materials that could assist the self-healing process of rigid body tissues. Hydroxyapatite (HAp, Ca<sub>10</sub>(PO<sub>4</sub>)<sub>6</sub>(OH)<sub>2</sub>), one of the most common form of naturally-occurring calcium orthophosphates, is actively investigated as a viable candidate as it integrates easily with the surrounding tissue, induced by its similarity with the main components and structure of human bones and teeth. To this end, it is most desirable that we fabricate HAp-based ceramic-polymer medical nanocomposites that significantly improves the unique mechanical and electrical properties of the host filler particles. However, the interface between the ceramic filler and the polymer matrix is very unstable due to the large discrepancy in their dielectric and bonding characteristics, which leads to the agglomeration of the ceramic particles inside the mixture. In order to resolve this issue, we sought to modify the HAp surface using mussel-inspired adhesive protein layer known as polydopamine (PDA) to reduce the interfacial energy between the two materials. Based on the result of our surface modification, we incorporated the PDA-coated HAp particles into a ferroelectric polymer membrane known as poly(vinylidene fluoride-co-trifluoroethylene) a.k.a. P(VDF-TrFE) to form a biocompatible nanocomposite that promotes electrochemical stimulus without any external bias. Our measurements suggests that the P(VDF-TrFE)/HAp nanocomposite has a high potential as a coating agent for a wide range of medical implants

#### F.SM04.06.07

**Transparent and Conductive F-Doped SnO<sub>2</sub> Nanostructured Thin Films by Sequential Nebulizer Spray Pyrolysis** T. M. W. J. Bandara<sup>1</sup>, A. A. A. P. Aththanayake<sup>1</sup>, G. R. A. Kumara<sup>2</sup>, P. Samarasekara<sup>1</sup>, Ajith DeSilva<sup>3</sup> and K. Tennakone<sup>2,4</sup>; <sup>1</sup>University of Peradeniya, Sri Lanka; <sup>2</sup>National Institute of Fundamental Studies, Sri Lanka; <sup>3</sup>University of West Georgia, United States; <sup>4</sup>Georgia State University, United States

Transparent conductive oxides (TCO) are a key component in many optoelectronic applications such as solar cells, flat panel displays, sensors, touch screens, light-emitting diodes, frost-resistant surfaces, and smart windows. The high electronic conductivity and high optical transmission are essential properties of TCOs for these applications. Owing to chemical inertness and high-temperature tolerance of F-doped tin oxide (FTO) films, they also have much demand in a variety of electrochemical devices. In this work, transparent and electrically conductive FTO thin films are prepared on soda-lime glass substrates. The films are fabricated by sequential nebulized spray pyrolysis with the help of a homemade low-cost spray gun. The surface morphology of the films is analyzed using scanning electron microscopy (SEM). It is found that surface is homogeneous and FTO crystallite sizes are in the order of ~10 nm. XRD pattern of the FTO films exhibits  $2\theta$  peaks for corresponding SnO<sub>2</sub> crystal planes at 26.64° (110), 33.90° (101), 37.95° (200), 51.87° (211), 56.17° (200), 60.05° (310), 61.89° (301). The crystallite sizes calculated from XRD data are in agreement with that of SEM. Optical transparency and bandgap energies are evaluated by UV visible spectroscopy. The FTO films with 15  $\Omega$  cm<sup>-2</sup> sheet resistance are used to prepare quasi-solid-state dye-sensitized solar cells with a TiO<sub>2</sub> photoelectrode. The solar cell showed a ~ 5% energy conversion efficiency with high short-term stability.

#### **F.SM04.06.08**

**Autonomic Self-Healing of PEDOT:PSS Achieved via Polyethylene Glycol Addition** Yang Li<sup>1</sup>, Xinda Li<sup>1</sup>, Shiming Zhang<sup>2</sup> and Fabio Cicoira<sup>1</sup>; <sup>1</sup>Polytechnique Montreal, Canada; <sup>2</sup>University of California, Los Angeles, United States

Self-healing electronic materials are of primary interest for bioelectronics and sustainable electronics. In this work we report autonomic self-healing of films obtained from mixtures of the conducting polymer poly(3,4-ethylenedioxythiophene) doped with polystyrene sulfonate (PEDOT:PSS) and polyethylene glycol (PEG). The presence of PEG in PEDOT:PSS films decreases the elastic modulus and increases the elongation at break, thus leading to a softer material with enhanced self-healing characteristics. In situ imaging of the cutting/healing process shows that the healing mechanism is likely due to flowing back of the material to the damaged area right after the cutting.

#### **F.SM04.06.10**

**Comparative Analysis of Neurogenic Differentiation *In Vitro* from Human Dental Pulp Stem Cells Using PLA and P4VP** Haijiao Liu, Kuan-Che Feng, Ya-Chen Chuang, Juyi Li, Marcia Simon and Miriam H. Rafailovich; Stony Brook University, The State University of New York, United States

Millions of people acquire spinal cord or traumatic brain injuries and over 5000 related deaths each year. There is currently no effective way to treat nervous system injuries. Besides, nerve cells do not regenerate in the body. Human dental pulp stem cells (hDPSCs) are important oral mesenchymal stem cells with strong proliferation and multidirectional differentiation functions. Due to their capability to differentiate into neurons, hDPSCs play an important role in dentin repair and regeneration, which provides a new approach for regeneration treatment of traumatic brain injuries in clinical applications. However, the specific mechanisms involved in the neurogenic differentiation process of hDPSCs are still unclear and require further research. To address the issue, hDPSCs were differentiated into neurons using two different polymers, PLA and P4VP. Using these two polymers, we cultured hDPSCs on substrates under eight different conditions, PLA, P4VP, flat film, fiber, with Graphene and without Graphene. hDPSCs were cultured by neurobasal A media, consisting of 100 U/ml penicillin, 1 x B27 supplement, 100  $\mu$ g/mL streptomycin, 20 ng/mL epidermal growth factor, and 40 ng/mL basic fibroblast growth factor (FGF) was used. After 7,14,21,28 days, we observed nerve cells numbers and differentiation by SEM and optical microscopy. For 28 days nerve cells, we used PCR technology to detect NES, TUBB3 and NEFM primer. Confocal Microscopy showed multiple layers on most substrates; more elongated cells directly on the substrate surface. SEM showed uniform fibers with no deformities, even with graphene. The results also show that greater elongation of DPSCs on PLA fibers, upregulation of neurogenic markers was slightly higher on flat surfaces than fibrous surfaces. Graphene was shown to be insignificant in neurogenic differentiation. Therefore, the substrates coated with PLA fibers with Graphene may help millions of people restore nerve cells injure cases annually.

#### **F.SM04.06.11**

**Synthesis and Characterization of Cellulose Nanofiber Reinforced Aromatic Polyamide Membranes** Rodolfo Cruz-Silva<sup>1,1</sup>, Kazuo Izu<sup>1</sup>, Jun Maeda<sup>1</sup>, Shigeru Saito<sup>1</sup>, Aaron Morelos-Gomez<sup>1,1</sup>, Celia Aguilar<sup>1,2</sup>, Yoshihiro Takizawa<sup>1</sup>, Yamanaka

Ayaka<sup>3</sup>, Syogo Tejima<sup>3</sup>, Kazunori Fujisawa<sup>1,1</sup>, Kenji Takeuchi<sup>1,1</sup>, Takuya Hayashi<sup>1,1</sup>, Toru Noguchi<sup>1,1</sup>, Akira Isogai<sup>4</sup> and Morinobu Endo<sup>1,1</sup>; <sup>1</sup>Shinshu University, Japan; <sup>2</sup>Universidad Autonoma de Nuevo Leon, Mexico; <sup>3</sup>Research Organization for Information Science and Technology, Japan; <sup>4</sup>The University of Tokyo, Japan

Cellulose nanofibers have attracted great attention in recent years. Cellulose is an abundant biopolymer that combines not only structural functions with excellent mechanical properties and is also closely related to water transport functions in plants. Here, we show that aromatic polyamide reinforced with TEMPO-oxidized crystalline cellulose nanofibers shows better chlorine resistance, permeation, and antifouling as compared to plain polyamide membranes. Synthesis was carried out by interfacial polymerization over a supported polysulfone membrane. Membranes were conditioned and tested for desalination against 3.5% sodium chloride salt solution. Fouling tests were carried out using bovine serum albumin as foulant model. Molecular dynamics studies show that cellulose nanofibers reduce the matrix mobility and improve the hydrophilicity without affecting the chemical composition of the surface layer of the membrane. Infrared and X-ray photoelectron spectroscopy results show a strong interaction between the carboxylic groups of the CNF surface and the m-phenyldiamine monomer. Membrane morphology was studied by several microscopic techniques, such as SEM, TEM, AFM and laser confocal scanning microscopy. Molecular dynamics simulations show that m-phenyldiamine/cellulose nanofiber provides the matrix with higher water affinity improving the membrane permeation without affecting the salt rejection. CNF shows great potential as a novel nanoreinforcing material for the preparation of nanocomposite aromatic polyamide membranes with improved properties.

SESSION F.LP05.02: Live Poster Session: Soft Materials and Biomaterials (F.SM04, F.SM05, F.SM06, F.SM07 and F.SM08)

Session Chairs: Po-Yen Chen, Fabio Cicoira, Derfogail Delcassian, Kaitlyn Sadtler and Mark Tibbitt  
Thursday Morning, December 3, 2020  
8:00 AM - 10:00 AM  
F.SM04

#### **F.SM04.06.01**

**Programmable Photomechanical Jumping of Polymer Monoliths** Jisoo Jeon<sup>1</sup>, Jun-Chan Choi<sup>2</sup>, Hyeok Lee<sup>3</sup>, Woongbi Cho<sup>1</sup>, Jae Gwang Kim<sup>1</sup>, Jae-Won Lee<sup>2</sup>, Kyung-Il Joo<sup>2,4</sup>, M. Cho<sup>3</sup>, Hak-Rin Kim<sup>2</sup> and Jeong Jae Wie<sup>1</sup>; <sup>1</sup>Inha University, Korea (the Republic of); <sup>2</sup>Kyungpook National University, Korea (the Republic of); <sup>3</sup>Seoul National University, Korea (the Republic of); <sup>4</sup>Electronics and Telecommunications Research Institute, Korea (the Republic of)

Controlled jumping is a unique motion in nature and robotics to achieve rapid mobility and to avoid obstacles as well as rough terrains. One key challenge is the introduction of a remote powering system for untethered miniaturized robots as they have to work to overcome their own body mass without an internal power system. Toward light-fueled jumping, we synthesize photo-responsive polymer monoliths where spring-like molecular geometry is implemented via self-assembly of liquid crystalline polymer networks (LCNs). Upon light irradiation, the spring-like self-assembled photo-responsive molecules induce non-isometric structures providing unprecedented photomechanical jumping by an instantaneous energy release. The experimental jumping behavior is supported by a finite element method (FEM) simulation for quantitative analysis. The jumping capability of the soft robotic LCN reaches 15.5 body length (BL) height, and 880 BL/s take-off velocity. In addition, we demonstrate rotational axis- and angle-controlled jumping by programming the molecular alignment and macroscopic design. Finally, the controlled light irradiation provides continuous and directional jumping of soft robotic LCNs.

#### **F.SM04.06.02**

**A Protein Based Polymer Film for Bio-Electronic Interfacing** Ramesh Nandi, Yuval Agam and Nadav Amdursky; Technion-Israel Institute of Technology, Israel

Human machine interfacing is a long challenge for researchers, in last few decades we have witnessed emerging of different materials and electrodes for the purpose. Successful interfacing of human body with machine involves coupling of ionic and electronic signal at the interface. In addition to the successful interfacing of the ionic and electronic signals, any conductive material for biological interfacing should be stretchable, flexible, stable in aqueous or humid environment, bio-compatible and bio-degradable. Developing a single material having all these properties is a challenge by itself. However, conductive

polymers are one of the promising materials for this purpose due to their organic carbon-based nature. Over the years, many different types of conducting organic polymers have been emerged using different synthetic organic analogues, however, the development of a synthetic polymer that fits all the above-mentioned criteria is still consider a challenge for researchers. Inspired by natural electron and ion transfer processes mediated mainly by proteins, here we present a novel conductive polymer made out of 100% natural Bovine Serum Albumin (BSA) protein, which is a side product of bovine industry, cheap and available in large scale. The polymer film is free-standing, transparent, stretchable, and highly stable in aqueous environment. Moreover, it is bio-compatible and biodegradable due to its biological nature, the synthesis method is within one pot and energy-efficient process and there is no need for any post-synthetic purification. This polymer film can efficiently record brain (electroencephalogram) and heart signal (electroencephalogram) from the human body in a non-invasive way with several other potential applications. While considering its novelty, our polymer can be considered a new class of materials in the field of bioelectronics.

**Keywords:** Biological Interfacing, Conductive Polymers, Polymer Film, electroencephalogram, electroencephalogram.

#### **F.SM04.06.03**

**Diffusivity Modulation of Planer Lipid Bilayer Mediated by Self-Assembled Peptides** Yoshiki Nakamura, Hironaga Noguchi, Mirano Tsukiiwa and Yuhei Hayamizu; Tokyo Institute of Technology, Japan

Two-dimensional (2D) materials represented by graphene have been studied for biosensor applications owing to their excellent electronic properties and high specific surface areas. Lipid bilayer biosensors based on the 2D materials as supporting substrates have gained wide interest as a platform for highly-sensitive biosensing with inserted membrane proteins. For stable formation of a lipid film on the surface of 2D materials, it is essential to control the hydrophobicity of the surface which is correlated to the affinity of the surface with the lipid film. Moreover, it is important to control the lateral diffusivity of the lipid membrane for understanding interaction dynamics of biomolecules embedded into the membrane. In this study, to address this, we utilized self-assembled peptides as an adhesive layer for immobilization of planar lipid bilayer on h-BN, an insulative 2D material which is transparent in visible region. In our recent research, we developed a series of peptides which have an ability to form uniform monomolecular thick peptide thin film in a self-assembly manner [1]. More recently, peptides with a repeated amino acid sequence of glycine (G) and alanine (A) inspired by silk proteins have been demonstrated to form stable  $\beta$ -sheet structures on the surface of two-dimensional materials [2]. In this study, we utilized three types of peptides containing additional hydrophilic amino acids with the GA repeat sequence. These peptides formed self-assembled structures on h-BN surface and act as an adhesive layer to form a planar lipid bilayer. Self-assembled peptides were prepared by dropping an aqueous peptide solution onto the surface of transferred h-BN on a substrate of Si/SiO<sub>2</sub> or cover glass, and it was incubated at room temperature for 1 hour. Then, planar lipid membranes were prepared by the rupture method, where DOPC vesicle suspension in 10 mM PB was placed on the sample with the self-assembled peptides,, and it was incubated at room temperature for 1 hour or more. The morphology of lipid membranes on the surface was observed by atomic force microscopy (AFM). Furthermore, to investigate the fluidity of lipid molecules in the membrane, DOPC was mixed with 1% 14:0 NBD PE (lipid molecule tagged with a fluorophore). The lateral diffusion constant of the lipid membrane was measured by the photobleaching after fluorescence recovery (FRAP) method. AFM observations showed that lipid bilayer can be formed on a h-BN surface with high coverage, indicating that self-assembled peptides support the lipid bilayer as a molecular scaffold with a controlled hydrophilicity. The FRAP results showed that the diffusion constants of lipid bilayers depend on peptide sequences. These results revealed the importance of the peptide design to control the physical properties of the planar lipid bilayer on 2D material, which could be essential to develop lipid-based biosensors with 2D materials.

#### Reference

- [1] Y. Hayamizu, et al., Scientific rep 2016, 6:33778
- [2] P. Li, et al., ACS Appl. Mater. Interfaces 2019, 11, 20670–20677

#### **F.SM04.06.04**

**The Porphyrin Ring Rather Than the Metal Ion Dictates Long-Range Electron Transport Across Proteins Suggesting Coherence-Assisted Mechanism** Yuval Agam and Nadav Amdursky; Technion–Israel Institute of Technology, Israel

The fundamental biological process of electron transport (ET) takes place across proteins with common ET pathways of several nanometers. Recent discoveries from the bacterial world push this limit and show long-range extracellular ET over several micrometers. Here, we aim in deciphering how protein-bound intramolecular cofactors can facilitate such long-range ET. In contrast to natural systems, our protein-based platform enables us to modulate important factors associated with ET in a facile manner, such as the type of the cofactor and its quantity within the protein. We chose here the biologically-relevant porphyrin molecule as the electron mediator. We use electrochemical impedance measurements (EIS) as well as three-

terminal field effect transistor (FET) measurements to explore the role of the porphyrin variant in mediating ET. Using different porphyrins with different metal centers, or lacking a metal center, we show that the metal redox center has no role in ET, and that ET is mediated solely by the conjugated backbone of the molecule. We further support these results with advanced density functional theory (DFT) calculations of the variants. We discuss several mechanisms accounting to possible contribution of coherent processes during the ET. Our results suggest that our high measured ET efficiency is probably due to coherence-assisted ET mechanism. Our work can help understand the participation of heme molecules in common long-range biological ET and introduce the possibility of using the protein-based platform as a tool for the investigation of different systems.

#### **F.SM04.06.06**

**Improvement of Adhesion and Osseointegration of Nanocomposite Biomembranes for Medical Implants** Soyeon Kim, youngjoon Han, Chungik Oh, Hojoon Lee and Seungbum Hong; Korea Advanced Institute of Science and Technology, Korea (the Republic of)

Medical societies dedicated to treating musculoskeletal diseases are facing challenges due to an unprecedented increase in the aging population around the globe. As such, it is getting more important to develop novel class of materials that could assist the self-healing process of rigid body tissues. Hydroxyapatite (HAp,  $\text{Ca}_{10}(\text{PO}_4)_6(\text{OH})_2$ ), one of the most common form of naturally-occurring calcium orthophosphates, is actively investigated as a viable candidate as it integrates easily with the surrounding tissue, induced by its similarity with the main components and structure of human bones and teeth. To this end, it is most desirable that we fabricate HAp-based ceramic-polymer medical nanocomposites that significantly improves the unique mechanical and electrical properties of the host filler particles. However, the interface between the ceramic filler and the polymer matrix is very unstable due to the large discrepancy in their dielectric and bonding characteristics, which leads to the agglomeration of the ceramic particles inside the mixture. In order to resolve this issue, we sought to modify the HAp surface using mussel-inspired adhesive protein layer known as polydopamine (PDA) to reduce the interfacial energy between the two materials. Based on the result of our surface modification, we incorporated the PDA-coated HAp particles into a ferroelectric polymer membrane known as poly(vinylidene fluoride-co-trifluoroethylene) a.k.a. P(VDF-TrFE) to form a biocompatible nanocomposite that promotes electrochemical stimulus without any external bias. Our measurements suggests that the P(VDF-TrFE)/HAp nanocomposite has a high potential as a coating agent for a wide range of medical implants

#### **F.SM04.06.07**

**Transparent and Conductive F-Doped  $\text{SnO}_2$  Nanostructured Thin Films by Sequential Nebulizer Spray Pyrolysis** T. M. W. J. Bandara<sup>1</sup>, A. A. A. P. Aththanayake<sup>1</sup>, G. R. A. Kumara<sup>2</sup>, P. Samarasekara<sup>1</sup>, Ajith DeSilva<sup>3</sup> and K. Tennakone<sup>2,4</sup>; <sup>1</sup>University of Peradeniya, Sri Lanka; <sup>2</sup>National Institute of Fundamental Studies, Sri Lanka; <sup>3</sup>University of West Georgia, United States; <sup>4</sup>Georgia State University, United States

Transparent conductive oxides (TCO) are a key component in many optoelectronic applications such as solar cells, flat panel displays, sensors, touch screens, light-emitting diodes, frost-resistant surfaces, and smart windows. The high electronic conductivity and high optical transmission are essential properties of TCOs for these applications. Owing to chemical inertness and high-temperature tolerance of F-doped tin oxide (FTO) films, they also have much demand in a variety of electrochemical devices. In this work, transparent and electrically conductive FTO thin films are prepared on soda-lime glass substrates. The films are fabricated by sequential nebulized spray pyrolysis with the help of a homemade low-cost spray gun. The surface morphology of the films is analyzed using scanning electron microscopy (SEM). It is found that surface is homogeneous and FTO crystallite sizes are in the order of  $\sim 10$  nm. XRD pattern of the FTO films exhibits  $2\theta$  peaks for corresponding  $\text{SnO}_2$  crystal planes at  $26.64^\circ$  (110),  $33.90^\circ$  (101),  $37.95^\circ$  (200),  $51.87^\circ$  (211),  $56.17^\circ$  (200),  $60.05^\circ$  (310),  $61.89^\circ$  (301). The crystallite sizes calculated from XRD data are in agreement with that of SEM. Optical transparency and bandgap energies are evaluated by UV visible spectroscopy. The FTO films with  $15 \Omega \text{ cm}^{-2}$  sheet resistance are used to prepare quasi-solid-state dye-sensitized solar cells with a  $\text{TiO}_2$  photoelectrode. The solar cell showed a  $\sim 5\%$  energy conversion efficiency with high short-term stability.

#### **F.SM04.06.08**

**Autonomic Self-Healing of PEDOT:PSS Achieved via Polyethylene Glycol Addition** Yang Li<sup>1</sup>, Xinda Li<sup>1</sup>, Shiming Zhang<sup>2</sup> and Fabio Cicoira<sup>1</sup>; <sup>1</sup>Polytechnique Montreal, Canada; <sup>2</sup>University of California, Los Angeles, United States

Self-healing electronic materials are of primary interest for bioelectronics and sustainable electronics. In this work we report autonomic self-healing of films obtained from mixtures of the conducting polymer poly(3,4-ethylenedioxythiophene) doped with polystyrene sulfonate (PEDOT:PSS) and polyethylene glycol (PEG). The presence of PEG in PEDOT:PSS films decreases the elastic modulus and increases the elongation at break, thus leading to a softer material with enhanced self-



healing characteristics. In situ imaging of the cutting/healing process shows that the healing mechanism is likely due to flowing back of the material to the damaged area right after the cutting.

#### **F.SM04.06.10**

**Comparative Analysis of Neurogenic Differentiation *In Vitro* from Human Dental Pulp Stem Cells Using PLA and P4VP** Haijiao Liu, Kuan-Che Feng, Ya-Chen Chuang, Juyi Li, Marcia Simon and Miriam H. Rafailovich; Stony Brook University, The State University of New York, United States

Millions of people acquire spinal cord or traumatic brain injuries and over 5000 related deaths each year. There is currently no effective way to treat nervous system injuries. Besides, nerve cells do not regenerate in the body. Human dental pulp stem cells (hDPSCs) are important oral mesenchymal stem cells with strong proliferation and multidirectional differentiation functions. Due to their capability to differentiate into neurons, hDPSCs play an important role in dentin repair and regeneration, which provides a new approach for regeneration treatment of traumatic brain injuries in clinical applications. However, the specific mechanisms involved in the neurogenic differentiation process of hDPSCs are still unclear and require further research. To address the issue, hDPSCs were differentiated into neurons using two different polymers, PLA and P4VP. Using these two polymers, we cultured hDPSCs on substrates under eight different conditions, PLA, P4VP, flat film, fiber, with Graphene and without Graphene. hDPSCs were cultured by neurobasal A media, consisting of 100 U/ml penicillin, 1 x B27 supplement, 100 µg/mL streptomycin, 20 ng/mL epidermal growth factor, and 40 ng/mL basic fibroblast growth factor (FGF) was used. After 7,14,21,28 days, we observed nerve cells numbers and differentiation by SEM and optical microscopy. For 28 days nerve cells, we used PCR technology to detect NES, TUBB3 and NEFM primer. Confocal Microscopy showed multiple layers on most substrates; more elongated cells directly on the substrate surface. SEM showed uniform fibers with no deformities, even with graphene. The results also show that greater elongation of DPSCs on PLA fibers, upregulation of neurogenic markers was slightly higher on flat surfaces than fibrous surfaces. Graphene was shown to be insignificant in neurogenic differentiation. Therefore, the substrates coated with PLA fibers with Graphene may help millions of people restore nerve cells injure cases annually.

#### **F.SM04.06.11**

**Synthesis and Characterization of Cellulose Nanofiber Reinforced Aromatic Polyamide Membranes** Rodolfo Cruz-Silva<sup>1,1</sup>, Kazuo Izu<sup>1</sup>, Jun Maeda<sup>1</sup>, Shigeru Saito<sup>1</sup>, Aaron Morelos-Gomez<sup>1,1</sup>, Celia Aguilar<sup>1,2</sup>, Yoshihiro Takizawa<sup>1</sup>, Yamanaka Ayaka<sup>3</sup>, Syogo Tejima<sup>3</sup>, Kazunori Fujisawa<sup>1,1</sup>, Kenji Takeuchi<sup>1,1</sup>, Takuya Hayashi<sup>1,1</sup>, Toru Noguchi<sup>1,1</sup>, Akira Isogai<sup>4</sup> and Morinobu Endo<sup>1,1</sup>; <sup>1</sup>Shinshu University, Japan; <sup>2</sup>Universidad Autonoma de Nuevo Leon, Mexico; <sup>3</sup>Research Organization for Information Science and Technology, Japan; <sup>4</sup>The University of Tokyo, Japan

Cellulose nanofibers have attracted great attention in recent years. Cellulose is an abundant biopolymer that combines not only structural functions with excellent mechanical properties and is also closely related to water transport functions in plants. Here, we show that aromatic polyamide reinforced with TEMPO-oxidized crystalline cellulose nanofibers shows better chlorine resistance, permeation, and antifouling as compared to plain polyamide membranes. Synthesis was carried out by interfacial polymerization over a supported polysulfone membrane. Membranes were conditioned and tested for desalination against 3.5% sodium chloride salt solution. Fouling tests were carried out using bovine serum albumin as foulant model. Molecular dynamics studies show that cellulose nanofibers reduce the matrix mobility and improve the hydrophilicity without affecting the chemical composition of the surface layer of the membrane. Infrared and X-ray photoelectron spectroscopy results show a strong interaction between the carboxylic groups of the CNF surface and the m-phenylenediamine monomer. Membrane morphology was studied by several microscopic techniques, such as SEM, TEM, AFM and laser confocal scanning microscopy. Molecular dynamics simulations show that m-phenylenediamine/cellulose nanofiber provides the matrix with higher water affinity improving the membrane permeation without affecting the salt rejection. CNF shows great potential as a novel nanoreinforcing material for the preparation of nanocomposite aromatic polyamide membranes with improved properties.

#### **F.SM05.06.03**

**Mood Identification by Facial Subtle Movement Analysis** Fan Yang<sup>1</sup>, Jordan Saadon<sup>1</sup>, Ryan Burgert<sup>1</sup>, Selma Mohammad<sup>1</sup>, Miriam H. Rafailovich<sup>1</sup>, Charles Mikell<sup>1</sup>, Sima Mofakham<sup>1</sup>, Wade Boohar<sup>2</sup>, Sophia Cai<sup>3</sup> and Amisha Agrawal<sup>4</sup>; <sup>1</sup>Stony Brook University, United States; <sup>2</sup>Olathe North High School, United States; <sup>3</sup>Barrington High School, United States; <sup>4</sup>University High School, United States

Research into mood and emotion has often been dependent on self-report, highlighting the need for a more objective measure of mood state. However, until recently, it has been nearly impossible for machines to match the speed and accuracy of the

average person in interpreting faces. In this study, we used digital image speckle correlation (DISC), a technique which was originally used to study the mechanical properties of materials by tracking their deformations, to assess an individual's mood state based on the analysis of facial microexpressions. Ten healthy volunteers were shown a set of ten happy and ten sad images while being videotaped. Upon measuring facial movements in response to happy and sad images, we conducted detailed Shannon entropy and Principal Component Analysis (PCA) to identify facial maps for different mood states. Within and across subjects, happy and sad images elicited spatially distinct changes in facial expression. PCA and entropy calculations on facial movement reliably distinguished the subject's underlying mood. Furthermore, we characterized key changes in facial expression which reliably signal changes in mood state across all individuals. DISC-based analysis of the face was capable of determining an individual's mood with high specificity across multiple test subjects, suggesting that automated camera-based methods may be both robust and economical in clinical monitoring settings. It also showed promising potentials in brain study together with electroencephalogram as subtle facial movements were also found in epilepsy and comatose patients using DISC.

#### **F.SM06.05.02**

**The Effects of Bioprinting on the Structure, Function and Survival of Organotypic Skin** Kimberly Lu, Olias Christie, Michael Cottone, Philip Cottone, Michael Gozelski, Juyi Li, Robert Wong and Miriam H. Rafailovich; Stony Brook University, United States

With the advancement of 3D printing in the 21st century, prospective treatments for regenerative medicine, cosmetology, and material science are actively being explored<sup>1,2</sup>. This research aims to investigate the feasibility of 3D bioprinting technology in producing viable skin tissue. In order to achieve this, a novel procedure for the construction of dermal and epidermal organotypics was developed. This evaluation was performed by comparing organotypic skin samples consisting of non-printed epidermal and dermal layers (NN), non-printed epidermal and printed dermal layers (NP), printed epidermal and non-printed dermal layers (PN), and printed epidermal and dermal layers (PP). The assessment of claudin and filaggrin immunohistochemical staining of the samples suggest a revision to the methodology in which printing the epidermal layer at a lower pressure while printing the dermal layer at a relatively higher pressure may lead to improved cellular function and overall integrity of the organotypic skin-equivalent. These results demonstrate the potential of bioprinting as a novel technique for producing a skin equivalent product, which may serve as an alternative to conventional tissue engineering methods.

1. Chang R, Nam J, Sun W: Effects of dispensing pressure and nozzle diameter on cell survival from solid freeform fabrication-based direct cell writing. *Tissue Eng Part A* 2008, 14(1):41-48.
2. Chien S: Effects of disturbed flow on endothelial cells. *Ann Biomed Eng* 2008, 36(4):554-562.

#### **F.SM06.05.04**

**Late News: Synthesis of Alginate Microgels with a Polymer Shell—A Simple Way to Protect Encapsulated Cells** So Hyun Ahn, Srinivasa Raghavan and William E. Bentley; University of Maryland, United States

Microgels of biopolymers such as alginate are widely used to encapsulate cells and other biological payloads. Alginate is an attractive material for cell encapsulation because spherical gels are easily created by contacting aqueous droplets of sodium alginate with divalent cations such as  $\text{Ca}^{2+}$ . Alginate chains in the gel become crosslinked by  $\text{Ca}^{2+}$  cations into a 3-D network. When alginate gels are placed in a buffer, however, the  $\text{Ca}^{2+}$  crosslinks are eliminated by exchange with  $\text{Na}^+$ , thereby weakening and degrading the gels. With time, encapsulated cells are released into the external solution.

Here, we describe a simple solution to the above problem, which involves forming alginate gels enveloped by a thin shell of a covalently crosslinked gel. The shell is formed via free-radical polymerization using conventional monomers such as acrylamide (AAm) or acrylate derivatives, including polyethylene glycol-diacrylate (PEGDA). The entire process is performed in a single step at room temperature (or  $37^\circ\text{C}$ ) under mild, aqueous conditions. It involves combining the alginate solution with a radical initiator, which is then introduced as droplets into a reservoir containing  $\text{Ca}^{2+}$  and monomers. Within minutes, the droplets are converted into alginate-polymer microcapsules with a core of alginate and a shell of the polymer (AAm or PEGDA). The stability of these microcapsules under physiological conditions is compared with that of conventional alginate/ $\text{Ca}^{2+}$  microgels. The latter swell and degrade when placed in buffer or in chelators like sodium citrate, whereas the former remain stable under all conditions.

We also show that a various types of cells can be safely encapsulated in these hybrid beads. We encapsulate both mammalian cell and different strains of genetically engineered bacteria in these microcapsules and find that the cells remain viable and

functional over time. In particular, engineered 'reporter' bacterial cells respond to different molecular signals from the external solution such as IPTG, AI-1 and hydrogen peroxide. The cells are retained in the hydrogel capsules throughout the study which is a crucial aspect for studying cell's response to molecular cues in a robust manner. Moreover, multiple sets of capsules each containing different strains can be synthesized and co-cultured to study cell-cell communication, providing an ideal platform for studying *in vitro* signaling events. Lastly, a variation of the synthesis technique is performed to generate multilayered microcapsules with a liquid core surrounded by concentric layers of alginate and AAm gels.

#### **F.SM06.05.05**

**Late News: Analysis and Mechanical Compression Model of a Three-Component Scaffold Composed of Polycaprolactone-Hydroxyapatite-Graphene Oxide for Tissue Engineering** Javier Ortiz Ortiz, Georgina Carbajal de la Torre, Marco Antonio Espinosa Medina, Nancy Nelly Zurita Méndez and Lourdes Ballesteros-Almanza; Universidad Michoacana de San Nicolas de Hidalgo, Mexico

The use of multiple materials has helped in the development of tissue engineering. The use of polymeric matrices and biomaterials added to particular materials offers specific solutions both due to the interaction of the biomaterials and the mechanical properties of the generated biomaterial. In this work, the mechanical properties of compression of a three-component scaffolds for tissue engineering composed of polycaprolactone (PCL), hydroxyapatite (HA), and graphene oxide (GO) are shown. Scaffolds were subjected to compression on the Cell Scale™ brand Univert™ testing machine. Once the experimental data had been obtained, the stress-strain curve was obtained, also the compression mechanical behavior model was performed using the Levenberg-Marquardt least-squares algorithm in the Comsol Multiphysics™ software. To explain the compression phenomenon, scanning electron microscopy analyzes are performed where scaffolds are observed before being compressed and also after compression.

#### **F.SM06.05.07**

**Late News: Determination of the Physical and Mechanical Properties of the Nopal Fiber (Opuntia ficus-indica) and Availability as a Biopolymer** Isai Pérez Servín, Rosa E. Pérez Sánchez, Georgina Carbajal de la Torre, Ruy Ortíz Rodríguez, Héctor E. Martínez Flores and Javier Ortiz Ortiz; Universidad Michoacana de San Nicolás de Hidalgo, Mexico

Nopal is a cactus that is distributed in different agroclimatic zones in a wild and cultivated way, due to its high forage potential, it has been destined to be used in the food, agricultural and pharmaceutical industry, however, when the cladode nopal reaches certain maturity, its use in the previously mentioned scopes is no longer viable, due to its high availability of fiber and lignin; this content of fiber in nopal could be implemented in the cosmetic and medical scopes as a biopolymer. The present study shows the physical and mechanical properties of nopal fiber components, and its thermographic analysis as an approach to determine its suitability and availability to fulfill the function of a biopolymer. An acid/alkaline extraction with potassium hydroxide (KOH; 1%) at 50° C was performed on the nopal sample previously dried. After the extraction, the sample was dried in a vacuum oven and its size was reduced by grinding. Mechanical tests were performed on nopal fibers in the Cell Scale Univert testing machine to obtain stress-strain curves. From the thermographic analysis, the kinetic drying model describing the process necessary for finite element modeling was proposed. The evaluation of the physical and mechanical characteristics allows us to determine the use and viability of nopal fiber as a biomaterial.

#### **F.SM07.05.04**

**Human Primary Macrophages Upregulate M1 Phenotype Markers in Response to Chemically Modified Alginates** Erin O'Brien<sup>1</sup>, Stephen T. Nestor<sup>2</sup>, Arturo Vegas<sup>2</sup> and Kara Spiller<sup>1</sup>; <sup>1</sup>Drexel University, United States; <sup>2</sup>Boston University, United States

**Introduction:** Angiogenesis is largely directed by macrophages, immune cells that can change their phenotype in response to external stimuli. Macrophages precisely control the timing and dosage of angiogenic growth factors, and also direct the innate immune response to biomaterials. Therefore, biomaterial-mediated macrophage modulation is an attractive strategy to recover dysfunctional angiogenesis. Macrophage phenotypes encompass a wide spectrum, but *in vitro* are commonly categorized as M0 before activation, then M1 or M2 post-activation, with several identified subtypes under the M2 umbrella. Although each phenotype's exact role in angiogenesis is not well understood, there is a growing body of evidence suggesting that early M1 macrophages initiate blood vessel sprouting, and subsequent M2 activity stabilizes these structures. Recent studies also indicate that M1 macrophages that switch to an M2 phenotype may have enhanced angiogenic properties. Furthermore, in pathologies where angiogenesis is inhibited, such as chronic wounds, M1 macrophages are insufficiently activated and fail to switch to an M2 phenotype. Thus, biomaterial strategies that seek to recover dysfunctional angiogenesis should aim to initially promote a robust M1 macrophage phenotype.

Previous work from Vegas et al. established a library of alginate hydrogels modified with chemical functionalities, then

ranked it by inflammatory activity, as measured by levels of cathepsin activity in vivo. This study was conducted to test the capabilities of the inflammatory alginate hydrogels to promote an M1 phenotype in primary human macrophages in vitro. Here we seeded M0 macrophages onto alginate hydrogels, then used Nanostring, a high-throughput gene expression assay, to measure expression of M1 markers, M2 markers, and genes associated with angiogenesis or fibrosis.

**Methods:** 5 types of alginate hydrogels were fabricated by the Vegas lab at Boston University: 3 inflammatory, 1 anti-inflammatory, and 1 non-modified. Primary monocytes were purchased from the Human Immunology Core at the University of Pennsylvania and cultured with 20 ng/mL of macrophage colony stimulating factor (MCSF) to induce differentiation into macrophages. On day 5, 200,000 macrophages were seeded onto each 5 mm section of hydrogel in a 24-well plate. Samples were incubated for 1 hour at 37°C to allow cell attachment. 800 µL of complete media with MCSF was added to each scaffold-containing well. M0 and M1 control samples were refreshed with complete media with MCSF. 100 ng/mL of human recombinant IFN $\gamma$  and LPS were added to the M1 control samples to induce M1 activation. On day 7, media was removed and scaffolds were mechanically degraded and lysed. RNA was extracted and quantified. For samples with at least 20 ng/µL of RNA, 100 ng were hybridized with a 72-gene custom Nanostring Codeset targeting M1, M2, angiogenic, and fibrotic genes. Nanostring sample preparation and reading was conducted according to Nanostring's standard protocol.

**Results:** Nanostring gene counts were normalized to the Nanostring in-house controls and fold changes over the M0 controls were calculated. Of the M1 markers measured, two (CD80 and CCL2) were upregulated in macrophages seeded on the inflammatory alginate hydrogels. Interestingly, these genes were also highly upregulated in macrophages seeded on non-modified alginate, and were even upregulated in macrophages seeded on anti-inflammatory alginate, though to a lesser extent.

**Conclusion:** These findings show that alginate hydrogels may be able to induce an M1-like phenotype in macrophages, via upregulation of CD80 and CCL2. However, proinflammatory modification of these hydrogels did not seem to enhance this upregulation. Instead, the results of this study suggest that alginate may be a naturally inflammatory material. Further investigation of the inflammatory properties of alginate are necessary to explore its potential as an M1 phenotype-promoting biomaterial.

#### **F.SM07.05.05**

**New Class of Biodegradable Drug Delivery Vehicles** [Eva Krakor](#), Isabel Gessner, Veronika W. Wulff, Astrid Schauss, Uwe Ruschewitz and Sanjay Mathur; University of Cologne, Germany

The field of nanoparticles for biomedical applications has become one of the most promising and most studied topics in the last years because it offers potential enhancement in pharmaceuticals, medical imaging and diagnosis, cancer treatment, implantable materials and tissue regeneration. In terms of therapeutic applications, especially drug delivery vehicles have been intensively studied. In this case, hollow particles have aroused tremendous interest due to their unique properties such as large surface areas, low densities and high loading capacities due to a protected hollow core. The transport of therapeutic, which can be either, encapsulated, covalently attached or adsorbed onto hollow particles, has been shown to be highly beneficial for multiple reasons compared to simple drug administration e.g., the cargo is protected against enzymatic degradation and the total drug administration can be reduced, which minimizes the risk of side effects.

HMSC were synthesized through a hard template-based method. First, ellipsoidal hematite particles were synthesized in a solvothermal process and coated with silica in a sol gel process afterwards. The iron oxide core was removed by etching resulting in HMSC. The porosity of as-prepared particles was analyzed using nitrogen adsorption-desorption method revealing a pore size of circa 4 nm and a high surface area of 308.8 m<sup>2</sup>/g. Cytotoxicity was determined using cell viability test (MTT) towards human kidney cells (HEK293) which clearly demonstrates that no reduction of cell viability was observed even at high concentrations of 100 µg/ml. Uptake studies using confocal microscopy were carried out using human cervical cancer cells (HeLa) which could show the successful internalization over a period of 24 hours. For testing their capability as drug delivery vehicle, a hydrophilic antibiotic (ciprofloxacin) and a hydrophobic anticancer (curcumin) compound were loaded and a pH dependent release under physiological conditions at 37°C was monitored via UV-Vis spectroscopy. After the drug release a reduction in shell thickness of HMSC was confirmed via SEM and TEM images. This study demonstrates the suitability of as-prepared hollow silica capsules as drug delivery vehicles for a broad range of drugs, hydrophobic as well as hydrophilic. Furthermore, it would be possible to modify the surface of drug loaded HMSC with proteins, e.g. antibodies as they are often used in immunotherapeutic regimens.

#### **F.SM07.05.06**

**Nanoparticle Synthesis by Engineered *E. coli* Cells Transformed with a Phytochelatin Synthase Gene** [Haley Hill](#), Manjula Bomma, Zhigang Xiao and Qunying Yuan; Alabama A&M University, United States

In this study, the phytochelatin synthase gene of *Rhizobium tropici* was assembled by PCR, inserted into pUC19 vector, and further transformed into *E. coli* DH5 $\alpha$  cells. Our preliminary data showed that these engineered *E. coli* DH5 $\alpha$  cells synthesized

more selenium nanoparticles than DH5 $\alpha$  cells transformed with pUC19 vector. The scanning electron microscope (SEM) examination of the nanoparticles revealed that the nanoparticles produced by both groups of cells had a size of 100-200nm with a spherical conformation, compositional analysis using Energy-dispersive X-ray spectroscopy identified that the nanoparticles only contain selenium. The capacity of phytochelatin synthase gene transformed bacteria to produce other metallic nanoparticles, including silver and gold will be tested and the physical properties of the nanoparticles will be further analyzed using the transmission electron microscope (TEM) analysis. The research results will be reported in the MRS meeting.

#### **F.SM07.05.08**

**Late News: Vitamin Lipid Nanoparticles Enable Adoptive Macrophage Transfer for the Treatment of Multidrug-Resistant Bacterial Sepsis** Xucheng Hou and Xinfu Zhang; OSU college of pharmacy, United States

Sepsis, a condition caused by severe infections, affects more than 30 million people worldwide every year and remains the leading cause of death in hospitals. Moreover, antimicrobial resistance has become an additional challenge in the treatment of sepsis, and thus, alternative therapeutic approaches are urgently needed. Macrophages are one of the most efficient pathogen scavengers. Indeed, in septic patients, impaired macrophages seem to be primarily responsible for insufficient antimicrobial defense. Nevertheless, immunostimulatory agents for reversing deactivated macrophages did not significantly improve the patient survival in clinical trials. This may be attributed to that immunostimulatory agents are not able to completely restore the function of impaired macrophages. Moreover, many bacteria, such as *Staphylococcus aureus* and *Escherichia coli*, have evolved immune escape mechanisms for thwarting phagolysosomal killing, resulting in intracellular survival. In addition, the prevalence of antibiotic resistance contributes to recurrent infections. Based on these research findings, we hypothesized that adoptive transfer of macrophages containing antimicrobial peptides linked to cathepsin B in the lysosomes (MACs) may enable the immunocompromised sepsis host to boost innate immunity, prevent bacterial immune evasion, and eliminate multi-drug resistant (MDR) bacteria.

To test our hypothesis, we first designed the AMP-CatB mRNA encoding an antimicrobial peptide IB367 (AMP-IB367), a cathepsin B (CatB), and a CatB-sensitive linker. AMP-IB367 is a broad-spectrum AMP with rapid bactericidal activity. CatB, an endogenous lysosomal protein, is first translated as an inactive precursor in the cytoplasm. After translocation into the lysosome, the precursor is processed into mature CatB. Here, the CatB is incorporated to transport the AMP-IB367 into lysosomes, where the linker is cleaved by CatB and thus the APM-IB367 is released. When phagosomes encapsulating bacteria fuse with lysosomes, the ingested bacteria are exposed to both pre-stored AMP-IB367 and lysosomal antimicrobial components. Although immune evasion strategies may protect MDR bacteria from phagolysosomal killing mechanisms, the AMP-IB367 is able to kill these bacteria. In order to equip macrophages with the AMP-CatB mRNA, we synthesized a series of vitamin-derived lipid nanomaterials. We found that the mRNA delivery efficiency of V<sub>C</sub>LNPs was 10-fold better than Lipofectamine 3000 and 50-fold better than electroporation in RAW264.7 macrophages. After optimizing the molar ratio of V<sub>C</sub>-Lipid:DOPE:Cholesterol and the mass ratio of V<sub>C</sub>-Lipid:mRNA, we identified the optimal V<sub>C</sub>LNPs formulation with improved mRNA delivery efficiency over 7-fold than its initial formulation. Because V<sub>C</sub>LNPs were also effective to deliver mRNA in bone-marrow-derived macrophages (BMDMs), we chose BMDMs for further antibacterial studies because of the clinical translatability. In vitro bactericidal results showed that MACs eliminated over 80% multi-drug resistant *Staphylococcus aureus* (MDRSA) or multi-drug resistant *Escherichia coli* (MDR E.coli) at 12 h. Next, we tested the therapeutic effects of MACs in MDRSA- and MDR E.coli-induced sepsis mice with immunosuppression. Analysis of blood at 24 h showed that MACs were more effective in cleaning bacteria than PBS-BMDMs. Furthermore, survival rate of MACs (83%) was significantly higher than that of PBS-BMDM group (40%).

In summary, we have developed macrophages containing antimicrobial peptides linked to cathepsin B in the lysosomes (MACs) via V<sub>C</sub>LNPs-mediated delivery of mRNA. Our results prove the concept that adoptive transfer of MACs beneficially reduce bacterial burden and improve survival in MDR bacteria-induced sepsis mice with immunosuppression by restoring innate immune defense, preventing bacterial immune evasion, and eradicating infections.

#### **F.SM07.05.09**

**Late News: TiO<sub>2</sub> Increases Bacterial Infection by Altering the Distribution of Cholesterol on Cell Membrane** Fan Yang<sup>1</sup>, Yan Xu<sup>1</sup>, Stephen Walker<sup>1</sup>, Wonhwa Cho<sup>2</sup>, Tatsiana Mironava<sup>1</sup> and Miriam H. Rafailovich<sup>1</sup>; <sup>1</sup>Stony Brook University, United States; <sup>2</sup>University of Illinois at Chicago, United States

According to the National Nanotechnology Initiative of America, titanium dioxide (TiO<sub>2</sub>) is one of the most commonly manufactured nanoparticles. These nanoparticles are widely used in food, pharmaceutical, cosmetic and chemical industries

as pigments, catalysts, and photovoltaic sources. The latter property is also exploited in water purification where UV-irradiated TiO<sub>2</sub> is a common anti-bacterial agent. However, there is no consensus on the toxicological profile of TiO<sub>2</sub> nanoparticles (NPs), and multiple concerns have surfaced on the potential harmful effects on human health<sup>1</sup>. Experiments conducted on HeLa cells indicated that cells cultured with 0.1 mg/ml rutile and anatase TiO<sub>2</sub> NPs for 24 hrs prior to exposure to *Staphylococcus aureus* (*S. aureus*) had 350 and 250% respectively more bacteria per cell, while macrophages exposed to TiO<sub>2</sub> NPs ingested 40% fewer *S. aureus*, further increasing the risk of infection when present in vivo<sup>2</sup>. The particles were observed to sequester within the cytoplasm of phagocytes simply occupying space which would normally be used for ingesting bacteria. Ingestion of TiO<sub>2</sub> NPs in HeLa cells resulted in an increase in membrane rigidity and extracellular LDH which was attributed to the increase in bacteria<sup>2</sup>.

Another possible explanation may be in the concentration distribution of membrane cholesterol. Specifically, we demonstrate an increase in cholesterol concentration of the outer plasma membrane leaflet accompanied by the decrease in cholesterol inner leaflet concentration. Alteration of the inner/outer leaflet cholesterol ratio may also explain the increase in bacterial infectivity NPs since *S. aureus* requires cholesterol for proper membrane attachment and virulence. This effect was absent in ABCA1 knockout HeLa cells suggesting an interaction between TiO<sub>2</sub> and the ABCA, a known cholesterol membrane efflux regulatory protein that facilitates cholesterol transport across the cellular membrane. The hypothesis has also been confirmed by the RT-PCR data detecting the RNA expressions of ABCA1 and ABCG1. We found that compared to the control group, cells exposed to TiO<sub>2</sub> for 24 hrs had higher RNA expression levels to 240% and 170% for ABCA1 and ABCG1, respectively. These data indicate that cells exposed to TiO<sub>2</sub> NPs have altered cholesterol distribution within their membranes, which results in increased rigidity and enhanced bacterial infection. Further work is in progress to evaluate this effect in cells obtained from healthy human tissue.

<sup>1</sup>Pan, Zhi, et al. "Adverse effects of titanium dioxide nanoparticles on human dermal fibroblasts and how to protect cells." *Small* 5.4 (2009): 511-520.

<sup>2</sup>Xu, Yan, et al. "Exposure to TiO<sub>2</sub> nanoparticles increases Staphylococcus aureus infection of HeLa cells." *Journal of nanobiotechnology* 14.1 (2016): 34.

#### F.SM07.05.10

##### **Late News: Influence of Surface Topography and Modulus on Fibrinogen Adsorption and Subsequent Cell Response** [Jie Li](#) and Kyla Sask; McMaster University, Canada

**Introduction:** Protein adsorption to a material is a complex process which causes thrombus formation, infection, and inflammation and can lead to failure of devices<sup>1</sup>. Surface properties such as chemistry, topography, and mechanics influence protein adsorption and structural changes. Fibrinogen plays a dominant role in mediating platelet and leukocyte interactions with surfaces and its degree of unfolding can impact the extent of cell activation<sup>2</sup>. Macrophages are essential in the immune response to biomaterials and the effect of protein conformational changes on their activation is not fully understood. This work aims to characterize protein adsorption and conformational changes on planar and patterned polydimethylsiloxane (PDMS) with varying elastic moduli and determine the relationship to macrophage response.

**Methods:** Microscale patterns were designed with three sizes of the following height : groove width : ridge width ratio: (1) 20:20:10  $\mu\text{m}$ ; (2) 20:20:20  $\mu\text{m}$  and; (3) 10:10:10  $\mu\text{m}$ . Photolithography and soft lithography are used with PDMS substrates of varying mixing ratios of Sylgard 184 and 527 to investigate the combined effect of surface topography and elastic modulus on fibrinogen adsorption and degree of unfolding. A micro-BCA assay was used to determine the amounts of fibrinogen adsorption (2.0 mg/mL in PBS) on PDMS with the range of stiffnesses. An antibody binding assay using a primary antibody to the fibrinogen gamma chain was developed to quantify the amount of fibrinogen adsorbed with exposure of the gamma chain. This assay will be extended to determine RGD density and further conformational changes of protein on PDMS. We are in the process of further interrogating the role of protein conformation on immune cell interactions using the RAW 264.7 macrophage cell line.

**Results:** Micropattern designs of three dimensions were prepared for photolithography and soft lithography. Contact angle measurements of PDMS substrates with varying stiffnesses indicated that ratios had relatively similar surface wettabilities with the 1:5 ratio slightly more and the 1:1 ratio slightly less hydrophobic. According to the BCA assay results, the 1:1 ratio of Syl 184 & 527 PDMS polymers adsorbed the most fibrinogen with an average of  $10.50 \pm 0.26 \mu\text{g}/\text{cm}^2$ , while the 1:5 ratio of Syl 184 & 527 adsorbed the least with an average of  $8.88 \pm 0.48 \mu\text{g}/\text{cm}^2$ . The antibody binding assay was completed and is being optimized to compare absorbance values based on the amount of fibrinogen determined from the BCA assay. This will provide an indication of changes in orientation and conformation as a result of varying surface topography and modulus.

**Discussion and Conclusions:** This work focuses on understanding the mechanisms underlying protein adsorption and subsequent cellular regulation abilities of microstructures and elastic modulus. The designed micropatterns provide a way to investigate the combined effect of topography and stiffness on protein adsorption and macrophage adhesion. The BCA assay indicates that varying the surface modulus has an influence on fibrinogen adsorption. The antibody binding assay will

investigate whether protein conformational changes play a role in this varied amount. Future work is being completed to determine the establishment of macrophage focal adhesions and cytokine secretion profiles in response to micropatterned topography and elastic modulus. Controlling these surface properties provides a method to monitor macrophage activation and regulation of immune cell response.

#### References:

1. I Firkowska Boden., et al. *Advanced healthcare materials*, 7 (1), p.1700995, 2018.
2. P Koeqler., et al. *Advanced drug delivery reviews* 64 (15) pp.1820-1839, 2012.

#### F.SM07.05.11

**Robust Immune Suppressing Nanoparticles to Overcome Multidrug Resistance in Breast Cancer** Haneen Omar and Abdulaziz Almalik; King Abdulaziz City for Science and Technology, Saudi Arabia

Multidrug resistance (MDR), accounting for therapeutic failure, remains a major challenge to manage cancer effectively. Currently, there are only a few strategies that are executed to conquer MDR by restoring chemosensitivity. In this respect, we report an immune suppressing nanoparticle decorated with alpha-1 acid glycoprotein (AGP), an anti-inflammatory protein, to serve as an effective chemoresistant reversal agent to modulate MDR and resensitize aggressive breast tumour cells. Hyaluronic acid-chitosan nanoparticles decorated with AGP (AGP-HA NPs) were synthesized by a sequential ionic gelation method consisting of spray drying and AGP-surface adsorption. The morphology, size, surface charge density, and composition of the synthesized NPs were characterized by utilizing SEM, DLS, Zeta potential, and FTIR, respectively. We have investigated the potential efficacy of AGP-HA NPs in reversing the MDR phenotype of MDA-MB-231 in response to anti-cancer drug doxorubicin (DOX). Our findings showed synergistic antitumor effects between HA and AGP protein as evident from the significantly enhanced efficacy of DOX post switching drug resistance phenotype of the cells to chemosensitive phenotype. Overall, our results suggest that AGP-HA NPs represent a viable and effective treatment option to strengthen the anticancer effects of chemotherapeutic agents and potentially contribute to improving the survival rate of patients with metastatic breast cancer.

#### F.SM07.05.13

**pH-sensitive Nanoparticles Based Oral Drug Delivery for the Treatment of Inflammatory Bowel Disease** Eden M. Jacob and Sakthi Kumar; Toyo University, Japan

The role of nanomedicine as an enhanced pharmaceutical strategy to deliver drugs has been studied for quite a few decades. The emergence of pH-sensitive nanoscale particles is beneficial due to its ability to release its cargo only at a high pH environment of the colon, which helps for direct targeting of the inflamed tissues in inflammatory bowel disease (IBD). Hence, we have designed the formulation of biodegradable polymer poly (lactic-co-glycolic acid) nanoparticles coated with Eudragit® S100 (EPNPs) for the delivery of novel polyphenolic compounds to reduce the inflammation caused by proinflammatory cytokines. The EPNPs were prepared by a single emulsion solvent evaporation technique and were characterized for shape and surface morphology using a scanning electron microscope (SEM) and transmission electron microscopy (TEM). The *in vitro* drug release was investigated using phosphate buffer saline (PBS) simulating different gut pH. The *in vitro* cytotoxicity of the EPNPs also evaluated and found to be highly biocompatible in nature. The inhibition of proinflammatory cytokines production also conducted using lactate dehydrogenase (LDH) assay. The characterization of EPNPs using SEM and TEM revealed spherical shape and smooth surface of the nanoparticles and was found to be 200-300nm in size. The EPNPs showed substantial improvement in the release of the drug, specifically at colonic pH. Results suggested that pH-sensitive EPNP nanoparticles as a promising candidate in the oral delivery to the colonic inflamed tissues.

#### F.SM07.05.14

**Two is Better Than One—A Comprehensive Study on the Synergistic Effects of Co-Delivery of Paclitaxel and Parthenolide in Discoidal Bicelle, *In Vitro* and *In Vivo*** Armin Rad, Mu-Ping Nieh and Xiuling Lu; University of Connecticut, United States

Combinatory modulation of the physical and biochemical characteristics of nanocarrier delivery systems is an emergent topic in the field of nanomedicine. Here, using the combined effects of incorporation of active targeting moieties, nanoscale morphology and shape, and physical properties for anti-cancer drugs function. We investigated a novel complex made of lipid bicelles nanocarrier for the efficient delivery of a combination of Paclitaxel (PTX). In addition, we hypothesized that Parthenolide (PTL) can be used as a chemosensitizers to restore the proper apoptotic signaling and to overcome chemotherapy resistance in human lung and breast cancer cells. We synthesized and characterized self-assembled bicelles

(nanodiscs) and nanovesicles which were made up of short- (DHPC) and long-chain (DPPC) lipids encapsulating PTL and PTX molecules. By using simultaneous self-assembly encapsulation, we have encapsulated Parthenolide and Paclitaxel as two cancer drugs. Dynamic light scattering, small angle X-ray scattering (SAXS), Fluorescence-activated cell sorting (FACS), and fluorescence confocal optical microscopy (FCOM) were used to quantify and visualize the cellular uptake of folate-conjugated NPs, respectively and *in vivo* subcutaneous rat studies were performed to investigate the samples. Self-assembled lipid discoidal and vesicular nanoparticles with low-polydispersity ~30 nm size range and identical chemical compositions were synthesized, characterized, and correlated with *in vitro* cancer cellular internalization, *in vivo* tumor accumulation and cancer treatments. Folate targeted nanodiscs not only have shown a higher tumor uptake and therapeutic efficiency, but also exhibited well-defined size, robust formation, and high-efficiency encapsulation of hydrophobic molecules, which enable the scalable manufacturing of a generalized *in vivo* multimodal delivery platform. A comprehensive evaluation of different effective factors, such as loading rate, surface chemistry, nanocarriers shapes, and drug combination ratios were evaluated and a comprehensive regiment for an effective treatment is introduced. The negatively charged bicelles with a PTL:PTX:Lipid molar ratio of 2.5:1:500 yielded a discoidal shape with a uniform diameter of 30 nm and a bilayer thickness of 5 nm, indicated the best anti-cancer function against both regular and drug resistive lung and breast cancer cells. SAXS analysis was also performed to provide insight into how the hydrophobic PTL and PTX molecules interact within the bicelles. Further, flow cytometry followed by confocal microscopy analyses substantiates the superior transfection efficiency of bicelles. We further analyzed how the co-encapsulation and molar ratios of drug and nanocarrier may affect the anti-cancer efficiency *in vivo* and *in vitro*. Several important discoveries in this report are summarized below. Detailed structural analysis and loading capacity of bicelles with two hydrophobic drug molecules, PTX and PTL, are performed. The structural variation of discs strongly depends on the molecular size and shape of the payload. Generally speaking, bicelle shows great potential as a nanocarrier for hydrophobic drug molecules. Both *in vitro* and *in vivo* studies on A549 cell line using drug-loaded bicelles indicate high efficacy (high cellular uptake, low IC<sub>50</sub> and MIC<sub>90</sub>) for cancer treatment. Moreover, we demonstrate strong synergy with PTX and PTL with IC<sub>50</sub> and MIC<sub>90</sub> are magnitudes lower than those of the free drugs in DMSO or Cremophor EL. The significant synergetic effect is observed in the MDR A549 cell line as well. The research outcome aims to provide an efficacious nanocarrier platform, which can potentially be generalized for transporting therapeutics and diagnostics to other types of cancers or diseased cells.

<!--[endif]----><!--[endif]---->

#### **F.SM08.09.01**

**Microfabricated Porous PTFE Membrane for Separation in Biomedical Uses** Masashi Maruyama, Mitsuya Yamamoto and Hirotaka Sakuma; Hitachi Ltd, Japan

Porous membranes with well-defined pore structures find plenty of uses in research and industrial areas. Well-defined pore structures afford sharp selectivity in filtration and thus applications in biomedical uses are also expected such as cell/spheroid separation and immunoprotection. Track-etching is a well-known technology to fabricate porous membranes with relatively defined pores, but undesired overlapped spots result in loss of selectivity. Against the background, we developed a novel microfabrication methodology to prepare porous membrane with strictly defined pores. We successfully developed porous PTFE membrane with 5-10 um thickness with tunable pore sizes. We will discuss the potential applications of microfabricated PTFE membranes in biomedical uses.

#### **F.SM08.09.03**

**Designed Organization of Proteins in Multidimensional Arrays with Preserved Biological Functionality** Shih-Ting Wang<sup>1</sup>, Brian Minevich<sup>2</sup>, Jianfang Liu<sup>3</sup>, Honghu Zhang<sup>1</sup>, Dmytro Nykypanchuk<sup>1</sup>, James Byrnes<sup>1</sup>, Wu Liu<sup>1</sup>, Lev Bershadsky<sup>1</sup>, Qun Liu<sup>1</sup>, Tong Wang<sup>4</sup>, Gang Ren<sup>3</sup> and Oleg Gang<sup>1,2</sup>; <sup>1</sup>Brookhaven National Laboratory, United States; <sup>2</sup>Columbia University, United States; <sup>3</sup>Lawrence Berkeley National Laboratory, United States; <sup>4</sup>The City College of New York, United States

An ability to control the assembly of functional proteins with designable organizations and an unpresented density in multidimensional space, provides routes to the next-generation nano-systems, biomaterials and complex biomolecular scaffolds. To achieve this, DNA nanotechnology offers exciting opportunities to modulate assembly processes with nano-scale resolution and spatial addressability. In this work, we developed a protein encapsulation strategy combined with the DNA programmable assembly for a bottom-up fabrication of biologically functional protein arrays with 2D and 3D prescribed organizations. We showed that ferritin, an iron storage protein, was integrated with DNA frames, of which each vertex and their internal space were encoded with addressable strands to program the protein position and vertex-to-vertex interconnection. Such designed arrays allow to maintain a biological activity of ferritin in the nanoscale lattices at relevant environments, and meanwhile, small molecules can access the iron core of ferritin within the 3D array and convert it into a core-less form, apoferritin. Our study, through the use of *in situ* small angle X-ray scattering, electron microscopy and



tomographic modelling, revealed the complex arrangement of designed protein arrays and their ability to perform functions within 3D arrays, thus confirming a new strategy for creating bio-active protein-containing materials.

#### **F.SM08.09.04**

**Late News: Polymer-Ceramic Scaffold for Bone Tissue Applications** Katia Mendoza-Calderón<sup>1</sup>, Nancy Nelly Zurita Méndez<sup>2</sup>, Javier Ortiz Ortiz<sup>2</sup>, Marco Antonio Espinosa Medina<sup>2</sup> and Georgina Carbajal de la Torre<sup>2</sup>; <sup>1</sup>Tecnológico Nacional de México., Mexico; <sup>2</sup>Universidad Michoacana de San Nicolás de Hidalgo, Mexico

Defects in bone tissue have been more common in recent years, based on this a section has been dedicated in the area of biomaterials for research. Currently, knowledge about new biomaterials has led to the discovery of sets of precursors that work effectively in the recovery of damaged tissue, which must meet certain requirements to be recognized as biomaterials, that is, they must be biocompatible, biodegradable, non-toxic, have mechanical resistance, as well as the appropriate density, weight, shape and size. Once these characteristics are known, it has been decided to experiment with three basic precursors in bone regeneration. The work that was carried out aims to manufacture three-dimensional matrices using precursors such as hydroxyapatite, polylactic acid and polycaprolactone. The characterizations were carried out to verify the purity of such biomaterials. Differential Scanning Calorimetry for both tests in a nitrogen/air atmosphere (80/20) at a temperature range of 100 °C to 1000 °C with a heating of 10 °C/min; on the other hand, for polylactic acid an analysis was carried out using Fourier Transform Infrared Spectrometry. Once the results were obtained, the scaffolding was manufactured using leaching and solvent casting techniques. With this, two groups of samples were developed with concentrations of 30% HAp -10% PLA -60% PCL and 10% HAp - 10% PLA - 80% PCL, they were mixed with an organic solvent and sodium chloride. The resulting scaffolds were subjected to mechanical compression and tension tests. Obtaining promising results for application in bone tissue.

#### **F.SM08.09.05**

**A Study of Silver Nanoparticles Control with Three Biocompatible Reducing Substances** Qixing Liu<sup>1</sup>, Arthur McClelland<sup>2</sup> and Tingying (Helen) Zeng<sup>3,4</sup>; <sup>1</sup>Zhejiang University, China; <sup>2</sup>Harvard University, United States; <sup>3</sup>Academy for Advanced Research and Development, United States; <sup>4</sup>Massachusetts Institute of Technology, United States

Silver nanoparticles play a significant role in public health. They have been proven to be effective substrates for high-intensity surface-enhanced Raman spectroscopy (SERS) in biomedical applications. The nanoparticles are able to detect organic molecules at nanomolar concentration and has the potential for early disease detection or virus killing. Since SERS technology has gained traction in public health uses recently, the synthesis of AgNPs which is considered as the essential and fundamental key of applications, has attracted numerous researchers. In this study, we propose a green, wet-chemical way to control the synthesis of AgNPs and explore three different reducing agents under similar conditions. Sodium citrate, L-cysteine, and oxalic acid, all used as reducing agents, are respectively added into the AgNO<sub>3</sub> aqueous solution where the Ag<sup>+</sup> concentration is 2.5mmol/L in room temperature. L-cysteine, a specially selected amino acid, exists in every group acting as the capping agent to restrict the aggregation and control the size of nanoparticles. According to the surface-enhanced Raman spectrum and SEM images, sodium citrate demonstrates the best reducing ability under the same concentration of the carboxy group and can be used for a quick synthesis. On the other hand, the particle size of oxalic acid carpets is more controlled regardless of concentration. It is suitable for precise synthesis associated with the time when the surface-enhanced Raman spectrum indicates the size growth of silver nanoparticles as time increases. Some mechanisms during the process are revealed as well. After analyzing the spectrum, we deem that Ag<sup>+</sup> ion combines with carboxy groups more easily than sulfur in this system. Consequently, these three reducing agents exhibit their unique advantages which provide us with various selections for the synthesis of silver nanoparticles under different requirements for different applications in public health.

#### **Acknowledgment**

The first author is grateful to the Academy for Advanced Research and Development (AARD, website: [www.ardacademy.org](http://www.ardacademy.org); contact email: [admissions@ardacademy.org](mailto:admissions@ardacademy.org)) for the Intern Research Sponsorship through the collaboration with the Center for Nanoscale Systems at Harvard University.

## SYMPOSIUM F.SM05

---

Brain-Inspired Information Processing—From Novel Material Concepts for Neuromorphic Computing to Sensing, Manipulation and Local Processing of Biological Signals  
November 21 - December 2, 2020

### Symposium Organizers

Paschalis Gkoupidenis, Max Planck Institute for Polymer Research  
Dion Khodagholy, Columbia University  
Duygu Kuzum, University of California, San Diego  
Yoeri van de Burgt, Eindhoven University of Technology

---

\* Invited Paper

SESSION F.SM05.07: Live Keynote I: Organic Neuromorphic Materials and Devices  
Session Chairs: Paschalis Gkoupidenis and Yoeri van de Burgt  
Tuesday Afternoon, December 1, 2020  
F.SM05

### **5:15 PM \*F.SM05.07.01**

**Polymer-Based Artificial Synapses—Using Protons and Electrons to Impart Plasticity to Semiconductors** Alberto Salleo; Stanford University, United States

The brain can perform massively parallel information processing while consuming only ~1- 100 fJ per synaptic event. I will describe a novel electrochemical neuromorphic device (ENODE) that switches at record-low energy (<0.1 fJ projected, <10 pJ measured) as well as voltage (< 1mV, measured), and displays a large number of distinct, non-volatile conductance states within a ~1 V operating range. The tunable resistance behaves very linearly, allowing blind updates in a neural network when operated with the proper access device. ENODEs also display outstanding endurance achieving over  $10^9$  switching events with very little degradation. I will describe our recent efforts at scaling and materials selection, allowing us to reach 20 ns write pulses and operation at high temperature (up to 120°C). These properties are very promising in terms of the ability to integrate with Si electronics to demonstrate online learning and inference. ENODEs are electrochemical devices where gated proton drift induces changes in the electronic states of a semiconductor channel. The peculiarities of the physics of these devices will be discussed along with their consequences on device design and performance.

### **5:45 PM \*F.SM05.07.02**

**Electron Transport and Complex Dynamics in 2D Nanoparticle-Molecule Networks—A Platform for Reservoir Computing** Dominique Vuillaume; IEMN-CNRS, France

2D networks of interconnected nano-objets (nanowires, nanoparticles, molecules) are experimentally and theoretically explored to implement unconventional computing machines, and especially reservoir computing [1-9]. 2D networks of molecularly functionalized nanoparticles (NPs) (hereafter called NMN : nanoparticle molecule network) have emerged as an interesting approach in molecular electronics to understand fundamental electron transport mechanisms [10].

I will describe the study of NMN approaches using functional molecules self-assembled in high density 2D networks with topological structures that are intrinsically similar to the structure of a "reservoir computing". NMNs equipped with molecules which can change their electronic properties upon a given excitation (optical, chemical, ionic) are interesting to study multifunctional systems at the nanoscale (<100 nm).

I will discuss several key features of the electronic properties of these 2D networks of molecularly functionalized nanoparticles to assess their possible use for reservoir computing: highly non-linear electron transport, variability, complex/rich dynamics (harmonic, interharmonic, intermodulation distortions), co-tunneling, noise and plasmonic response [9-12]. I will also discuss the electron transport properties of some molecules of interest for the chemical and biochemical sensing with these NMNs reservoir computing approaches, combining sensing and computing in a single nanoscale device. These approaches, without direct analogs in semiconductor nanoelectronics, would open new perspectives to molecular electronics in unconventional computing.

1. Tour, J. M.; van Zandt, W. L.; Husband, C. P.; Husband, S. M.; Wilson, L. S.; Franzon, P. D.; Nackashi, D. P. *IEEE Trans. Nanotechnol.* 2002, 1, (2), 100-109.
2. Sköldbberg, J.; Wendin, G. *Nanotechnology* 2007, 18, (48), 485201.
3. Bose, S. K.; Lawrence, C. P.; Liu, Z.; Makarenko, K. S.; van Damme, R. M. J.; Broersma, H. J.; van der Wiel, W. G. *Nature Nanotech* 2015, 10, 1048-1053.
4. Roychowdhury, V. P.; Janes, D. B.; Bandyopadhyay, S.; Wang, X. *IEEE Transactions on Electron Devices* 1996, 43, 1688-1699.
5. Sillin, H. O.; Aguilera, R.; Shieh, H.-H.; Avizienis, A. V.; Aono, M.; Stieg, A. Z.; Gimzewski, J. K. *Nanotechnology* 2013, 24, (38), 384004.
6. Maass, W.; Natschläger, T.; Markram, H. *Neural Computation* 2002, 14, 2531-2560.
7. Jeager, H.; Haas, H. *Science (New York, NY)* 2004, 304, (5667), 78-80.
8. Tanaka, H.; Akai-Kasaya, M.; TermehYousefi, A.; Hong, L.; Fu, L.; Tamukoh, H.; Tanaka, D.; Asai, T.; Ogawa, T. *Nature Communications* 2018, 9, (1), 2693.
9. Viero, Y.; Guerin, D.; Alibart, F.; Lenfant, S.; Vuillaume, D. *Adv. Func. Mater.* 2018, 28, 1801506.
10. Liao, J.; Blok, S.; van der Molen, S. J.; Diefenbach, S.; Holleitner, A. W.; Schönenberger, C.; Vladyka, A.; Calame, M. *Chem. Soc. Rev.* 2015, 44, 999-1014.
11. Viero, Y.; Copie, G.; Guerin, D.; Krzeminski, C.; Vuillaume, D.; Lenfant, S.; Cleri, F. *J. Phys. Chem. C* 2015, 119, 21173-21183.
12. Stievenard, D.; Guerin, D.; Lenfant, S.; Leveque, G.; Nijhuis, C. A.; Vuillaume, D. *Nanoscale* 2018, 10, 23122-23130.

#### 6:15 PM \*F.SM05.07.03

**Physically Flexible and Biological Compatible Demonstration of an Organic Electronics Axon-Hillock Neural Circuit** Mohammad Javad Mirshojaeian Hosseini<sup>1</sup>, Elisa Donati<sup>2</sup>, Tomoyuki Yokota<sup>3</sup>, Sunghoon Lee<sup>3</sup>, Giacomo Indiveri<sup>2</sup>, Takao Someya<sup>3</sup> and Robert A. Nawrocki<sup>1</sup>; <sup>1</sup>Purdue University, United States; <sup>2</sup>Institute of Neuroinformatics, Switzerland; <sup>3</sup>The University of Tokyo, Japan

Spiking Neural Networks (SNN) provide distributed computational capability and emulate the brain processing principles based on spike frequency and pulse width [1]. Because of being intrinsically compatible with brain signaling, one of the target applications of SNN hardware implementation, known as neuromorphic systems [2], are Brain-Computer Interfaces (BCI) [3]. With a handful of exceptions [4], such implementations have typically been implemented using silicon technology, which is physically hard and rigid, and non-biocompatible, resulting in a permanent damage to the brain's soft tissue. Organic electronics offer physical softness and flexibility, biocompatibility, and low-cost, large-area fabrication, to directly interface with biological tissues [5].

We report on the fabrication of a physically flexible, organic electronics, spiking integrate-and-fire Axon-Hillock (AH) neural circuit. Organic Field-Effect Transistors (OFETs) are fabricated on top of a flexible, 50  $\mu\text{m}$  Polyimide substrate. OFETs' architecture is bottom-gate top-contact, and fabricated through thermal deposition of Ti (3 nm)/Au (50 nm) as the gate electrode, 60 nm of Parylene as the dielectric, 30 nm of dinaphtho[2,3b:2',3'-f]thieno[3,2-b]thiophene (DNNT) as the p-type and N,N'-bis(n-octyl)-x:y,dicyanoperylene<sub>3,4:9,10</sub>-bis(dicarboximide) (PDI8-CN2) as the n-type semiconductor. A 50 nm layer of Au serves as the source and the drain electrodes. A layer of Parylene encapsulates the structure. Non-circuit-integrated commercial resistors and capacitors are used to accelerate the characterization and the fabrication process. All integrated all-organic circuit is beyond the scope of this work and would increase the complexity of the process.

The results show that the AH circuit with 500 nA input current can produce spikes with a range of frequencies. Given the membrane capacitance ( $C_{mem}$ ) of 15 nF and feedback capacitance ( $C_{feedback}$ ) of 47 nF, the spiking frequency reaches 670 mHz. The frequency can be lowered by increasing capacitance values to  $C_{mem} = 33$  nF and  $C_{feedback} = 100$  nF, respectively, to 370 mHz. Decreasing capacitance to  $C_{mem} = 2.2$  nF and  $C_{feedback} = 6.8$  nF, will result in a higher spiking rate (5 Hz), but will also increase the influence of power line noise and parasitic capacitance. The frequency-current ( $F-I$ ) transfer function shows the dynamics of the neuron. By increasing the input current, the  $F-I$  curve will saturate indicating an upper bound of frequency spikes. The computational ability of the neuron is also demonstrated with a basic summation of two unitary excitatory synaptic events. The static and dynamic power dissipation is recorded and is limited to 0.4  $\mu\text{W}$  and 40  $\mu\text{W}$ , respectively.

We believe that this work is the first demonstration of a functioning organic electronics integrate-and-fire spiking neuron, paving the way for future implantable BMIs. Beyond neuroscientific applications, this technology can also be used in slow processes, such as temperature measurement, which are intrinsically difficult for ultra-fast silicon devices to achieve, as well as physically flexible large-area applications.

- [1] F. Rieke and D. Warland, "Spikes: Exploring the Neural Code," *MIT Press*, 1999.
- [2] R. Nawrocki, et al., "A mini review of neuromorphic architectures and implementations," *IEEE Transactions on Electron Devices*, vol. 63 (10), 2016.
- [3] F. Boi, et al., "A Bidirectional Brain-Machine Interface Featuring a Neuromorphic Hardware Decoder," *Frontiers in Neuroscience*, vol. 10 (563), 2016.
- [4] R. Nawrocki, et al., "Neurons in polymer: Hardware neural units based on polymer memristive devices and polymer transistors," *IEEE Transactions on Electron Devices*, vol. 61 (10), 2014.
- [5] G. Schwartz, et al., "Flexible polymer transistors with high-pressure sensitivity for application in electronic skin and health monitoring," *Nature Communications*, vol. 4 (1), 2013.

#### 6:45 PM \*F.SM05.07.04

**Memory and Learning in Biomolecular Soft Materials** [Charles P. Collier](#)<sup>1</sup>, Joseph S. Najem<sup>2</sup>, Richard S. Williams<sup>3</sup>, Graham Taylor<sup>4</sup>, Md S. Hasan<sup>5</sup>, Ryan Weiss<sup>6</sup>, Stephen A. Sarles<sup>6</sup>, Garrett Rose<sup>6</sup>, Alex Belianinov<sup>1</sup> and Catherine Schuman<sup>1</sup>; <sup>1</sup>Oak Ridge National Laboratory, United States; <sup>2</sup>The Pennsylvania State University, United States; <sup>3</sup>Texas A&M University, United States; <sup>4</sup>T&T Scientific, United States; <sup>5</sup>The University of Mississippi, United States; <sup>6</sup>The University of Tennessee, Knoxville, United States

Neuromorphic elements have been predominantly solid-state devices which simulate the resistive and capacitive behaviors needed for neural networks and brain-inspired computing, but in non-brain-like ways. This talk will describe ways we are integrating lipid and polymer bilayer membranes with micro- and nanofabrication to develop fundamentally new types of neuromorphic elements that have the composition (biomolecules), structure (biomembranes), and switching mechanism (voltage-sensitive ion channels) of real biological synapses, and operate at lower power than the current state-of-the-art. Our devices consist of insulating, nm-thick lipid or polymer-based bilayer membranes that assemble at the interfaces of two or more aqueous droplets in oil, and that have demonstrated both memristive and memcapacitive behaviors, including memory resistance and capacitance, synaptic functions such as paired-pulse facilitation and depression, spike rate dependent plasticity, voltage-dependent inactivation and recovery, and charging hysteresis. These behaviors are linked to electrostriction, an electromechanical phenomenon that encompasses both electrowetting and electrocompression in the membrane, which are changes in membrane area and thickness due to charging in the presence of electric fields. Electrostriction results in a voltage-dependent capacitive susceptibility that replaces the more familiar concept of static capacitance, which, up to now, has dominated electrophysiological descriptions and characterizations of biomembranes. In this picture, biomembranes are not just equivalent RC circuits dependent only on ionic currents controlled by the conductance (resistance) of ion channels. Large capacitive currents from small voltage inputs can be generated as well for the development of neuromorphic computing elements exhibiting both short-term and long-term synaptic plasticity.

SESSION F.SM05.08: Live Keynote II: Bioelectronics and Smart Adaptive Biointerfaces

Session Chairs: Paschalis Gkoupidenis and Yoeri van de Burgt

Wednesday Morning, December 2, 2020

F.SM05

#### 11:30 AM \*F.SM05.08.01

**Merging Bio-Sensing and Neuromorphic Computing with Organic Electro Chemical Transistors** [Fabien Alibert](#)<sup>1,2</sup>, Mahdi Ghazal<sup>1</sup>, Kamila Janzakova<sup>1</sup>, Ankush Kumar<sup>1</sup>, Anna Susloparova<sup>1</sup>, Sophie Halliez<sup>3</sup>, Morvane Colin<sup>3</sup>, Luc Buée<sup>3</sup>, David Guérin<sup>1</sup>, Thomas Dargent<sup>1</sup>, Yannick Coffinier<sup>1</sup> and Sébastien Pecqueur<sup>1</sup>; <sup>1</sup>IEMN-CNRS, France; <sup>2</sup>LN2-3IT, Canada; <sup>3</sup>Jean Pierre Aubert Research Center, France

Most of today's strategies to interface biology with electronic hardware are based on layered architectures where the front-end of sensing is optimized separately from the back-end for processing/computing signals. Alternatively, biological systems are capitalizing on distributed architecture where both sensing and computing are mix together and co-optimized. In this talk, we will present our strategy to implement bio-sensing of electroactive cells in a neuromorphic perspective. We will present how organic electrochemical transistors can be used to record electrical signals from neural cells. We will show various strategies capitalizing on the versatility of organic materials synthesis and organic device fabrication to tune and adapt the functionalities of such bio-sensors. We will then present how these strategies can be efficiently used to realize computing functions directly at the interface with biology. Notably, we will illustrate how a network of ionic sensors can implement the

reservoir computing concept, a powerful neuromorphic computing approach of particular interest for dynamical signal processing.

**12:00 PM \*F.SM05.08.02**

**Scalable, Soft and Stretchable Optoelectronics and Neuromorphic Sensing Architectures in Human-Machine Interfaces** Benjamin C. Tee; National University of Singapore, Singapore

Human-machine interfaces will continue to be critical to advance applications in healthcare, robotics and consumer electronics. Having a cross-disciplinary approach to materials innovation, especially with regards to soft materials<sup>1</sup> will effectively address the mechanical constraints when interfacing with humans. In this talk, I will discuss some of the new material platforms we are developing for more robust human-machine interactions, such as self-healing stretchable optoelectronics devices<sup>2</sup>. Such optoelectronic devices might be employed in optogenetic neural interfaces. At the same time, I will also present our efforts in brain inspired scalable neuromorphic architectures for electronic skins<sup>3</sup>. Such system architectures can be broadly applied in various applications with high impact potential for wearables, brain-machine interfaces, prosthetics and robotics.

1. **Soft Electronically Functional Polymeric Composite Materials for a Flexible and Stretchable Digital Future**, B. C. K. Tee\*, J. Ouyang, *Advanced Materials*, 1802560, 2018.
2. **A transparent, self-healing and high-k dielectric for low-field-emission stretchable optoelectronics**, Y. J. Tan, H. Godaba, G. Chen, S. T. M. Tan, G. Wan, G. Li, P. M. Lee, Y. Cai, S. Li, R. F. Shepherd, J. S. Ho & B. C. K. Tee\*, *Nature Materials*, 2019.
3. **A neuro-inspired artificial peripheral nervous system for scalable electronic skins**, WW Lee, Y. J. Tan, H. Yao, S. Li, H. H. See, M. Hon, K. A. Ng, B. Xiong, J. S. Ho and B. C. K. Tee\*, *Science Robotics*, 2019.

**12:30 PM \*F.SM05.08.03**

**Designing Biomimetic Electronic Interfaces** Francesca Santoro; Istituto Italiano di Tecnologia, Italy

The interface between biological cells and non-biological materials has profound influences on cellular activities, chronic tissue responses, and ultimately the success of medical implants and bioelectronic devices. The optimal coupling between cells, i.e. neurons, and materials is mainly based on surface interaction, electrical communication and sensing.

In the last years, many efforts have been devoted to the engineering of materials to recapitulate both the environment (i.e. dimensionality, curvature, dynamicity) and the functionalities (i.e. long and short term plasticity) of the neuronal tissue to ensure a better integration of the bioelectronic platform and cells.

On the one hand, here we explore how the transition from planar to pseudo-3D nanopatterned inorganic and organic materials have introduced a new strategy of integrating bioelectronic platforms with biological cells under static and dynamic conditions. Although a spontaneous penetration does not occur, adhesion processes are such that a very intimate contact can be achieved. On the other hand, we investigate how organic semiconductors can be exploited for recapitulating electrical neuronal functions such as long term and short term potentiation. In this way, both the topology and the material functionalities can be exploited for achieving in vitro biohybrid platforms for neuronal network interfacing.

**1:00 PM \*F.SM05.08.04**

**New Materials and Device Concepts for Organic Electrochemical Transistors** Jonathan Rivnay; Northwestern University, United States

Organic electrochemical transistors (OECTs) have gained considerable interest for applications in bioelectronics, power electronics, circuits and neuromorphic computing. Their defining characteristic is the bulk-modulation of channel conductance owing to the facile penetration of ions into the (semi)conducting polymeric channel. For this reason, their device scaling relies on film thickness, enabling finer size scale devices, and unique form factors. Despite recent progress and a rapidly expanding library of new materials, the understanding of stability and transport/coupling of ionic and electronic carriers remain largely unexplored. We highlight recent synthetic and processing approaches used to tailor device properties and stability, as well as new opportunities enabled by such advances. We demonstrate how the reliance on bulk transport allows for relaxed fabrication demands and production of simple multi-device circuit concepts for analog signal processing. Finally, by studying the role of additives on charging, trapping, and structural re-arrangement, we can gain insight into the next generation of non-volatile organic mixed conductors for neuromorphic hardware. The implementation of OECT-based sensing and circuits holds particular promise in brain-inspired bioelectronics – the role of materials design and development is critical for their success.

**5:00 AM \*F.SM05.01.01**

**Polymer-Based Artificial Synapses—Using Protons and Electrons to Impart Plasticity to Semiconductors** Alberto Salleo; Stanford University, United States

The brain can perform massively parallel information processing while consuming only ~1- 100 fJ per synaptic event. I will describe a novel electrochemical neuromorphic device (ENODE) that switches at record-low energy (<0.1 fJ projected, <10 pJ measured) as well as voltage (< 1mV, measured), and displays a large number of distinct, non-volatile conductance states within a ~1 V operating range. The tunable resistance behaves very linearly, allowing blind updates in a neural network when operated with the proper access device. ENODEs also display outstanding endurance achieving over  $10^9$  switching events with very little degradation. I will describe our recent efforts at scaling and materials selection, allowing us to reach 20 ns write pulses and operation at high temperature (up to 120°C). These properties are very promising in terms of the ability to integrate with Si electronics to demonstrate online learning and inference. ENODEs are electrochemical devices where gated proton drift induces changes in the electronic states of a semiconductor channel. The peculiarities of the physics of these devices will be discussed along with their consequences on device design and performance.

**5:30 AM \*F.SM05.01.02**

**Electron Transport and Complex Dynamics in 2D Nanoparticle-Molecule Networks—A Platform for Reservoir Computing** Dominique Vuillaume; IEMN-CNRS, France

2D networks of interconnected nano-objects (nanowires, nanoparticles, molecules) are experimentally and theoretically explored to implement unconventional computing machines, and especially reservoir computing [1-9]. 2D networks of molecularly functionalized nanoparticles (NPs) (hereafter called NMN : nanoparticle molecule network) have emerged as an interesting approach in molecular electronics to understand fundamental electron transport mechanisms [10].

I will describe the study of NMN approaches using functional molecules self-assembled in high density 2D networks with topological structures that are intrinsically similar to the structure of a "reservoir computing". NMNs equipped with molecules which can change their electronic properties upon a given excitation (optical, chemical, ionic) are interesting to study multifunctional systems at the nanoscale (<100 nm).

I will discuss several key features of the electronic properties of these 2D networks of molecularly functionalized nanoparticles to assess their possible use for reservoir computing: highly non-linear electron transport, variability, complex/rich dynamics (harmonic, interharmonic, intermodulation distortions), co-tunneling, noise and plasmonic response [9-12]. I will also discuss the electron transport properties of some molecules of interest for the chemical and biochemical sensing with these NMNs reservoir computing approaches, combining sensing and computing in a single nanoscale device. These approaches, without direct analogs in semiconductor nanoelectronics, would open new perspectives to molecular electronics in unconventional computing.

1. Tour, J. M.; van Zandt, W. L.; Husband, C. P.; Husband, S. M.; Wilson, L. S.; Franzon, P. D.; Nackashi, D. P. *IEEE Trans. Nanotechnol.* 2002, 1, (2), 100-109.
2. Sköldbberg, J.; Wendin, G. *Nanotechnology* 2007, 18, (48), 485201.
3. Bose, S. K.; Lawrence, C. P.; Liu, Z.; Makarenko, K. S.; van Damme, R. M. J.; Broersma, H. J.; van der Wiel, W. G. *Nature Nanotech* 2015, 10, 1048-1053.
4. Roychowdhury, V. P.; Janes, D. B.; Bandyopadhyay, S.; Wang, X. *IEEE Transactions on Electron Devices* 1996, 43, 1688-1699.
5. Sillin, H. O.; Aguilera, R.; Shieh, H.-H.; Avizienis, A. V.; Aono, M.; Stieg, A. Z.; Gimzewski, J. K. *Nanotechnology* 2013, 24, (38), 384004.
6. Maass, W.; Natschläger, T.; Markram, H. *Neural Computation* 2002, 14, 2531-2560.
7. Jeager, H.; Haas, H. *Science (New York, NY)* 2004, 304, (5667), 78-80.
8. Tanaka, H.; Akai-Kasaya, M.; TermehYousefi, A.; Hong, L.; Fu, L.; Tamukoh, H.; Tanaka, D.; Asai, T.; Ogawa, T. *Nature Communications* 2018, 9, (1), 2693.
9. Viero, Y.; Guerin, D.; Alibart, F.; Lenfant, S.; Vuillaume, D. *Adv. Func. Mater.* 2018, 28, 1801506.

10. Liao, J.; Blok, S.; van der Molen, S. J.; Diefenbach, S.; Holleitner, A. W.; Schöenberger, C.; Vladyka, A.; Calame, M. *Chem. Soc. Rev.* 2015, 44, 999-1014.
11. Viero, Y.; Copie, G.; Guerin, D.; Krzeminski, C.; Vuillaume, D.; Lenfant, S.; Cleri, F. *J. Phys. Chem. C* 2015, 119, 21173-21183.
12. Stievenard, D.; Guerin, D.; Lenfant, S.; Leveque, G.; Nijhuis, C. A.; Vuillaume, D. *Nanoscale* 2018, 10, 23122-23130.

#### 6:00 AM \*F.SM05.01.03

**Evolvable Organic Electrochemical Transistors for Neuromorphic Applications** Simone Fabiano; Linköping University, Sweden

Organic electrochemical transistors (OECTs) are in a stage of rapid development as novel applications that make use of these versatile devices continue to emerge. OECTs are characterized by the coupling of both ionic and electronic inputs to modulate transistor channel conductance. This attribute renders OECTs ideal for interfacing electronics with biological systems, which make use of ionic and biochemical currents and gradients for signaling. Here we will present a new concept of OECT that evolves with use. The transistor channel can be formed, modulated, and obliterated under operation. The strength of the transistor response to a given stimulus can be modulated within a range that spans several orders of magnitude, introducing behaviors analogous to neuroplasticity into electronic systems. This evolvable transistor can be incorporated into a simple circuit that mimics classical conditioning. Also, we will present several biomimetic logic circuits that link sensory inputs to the growth of the transistor channel, thus to achieve higher order processes like self-regulation and coincidence detection. OECTs that physically and electronically evolve under operation will bring about a new paradigm of machine learning based on evolvable organic electronics.

#### 6:30 AM F.SM05.01.05

**Governing Conducting-Polymer Micro-Objects' Fractality for Unconventional Computing** Ankush Kumar<sup>1</sup>, Kamila Janzakova<sup>1</sup>, Yannick Coffinier<sup>1</sup>, David Guérin<sup>1</sup>, Fabien Alibert<sup>1,2</sup> and Sébastien Pecqueur<sup>1</sup>; <sup>1</sup>Institut d'Électronique, Microélectronique et Nanotechnologie (IEMN), CNRS, UMR 8520, F-59652, France; <sup>2</sup>Laboratoire Nanotechnologies & Nanosystèmes (LN2), CNRS, Université de Sherbrooke, Canada

Electropolymerization is an interesting bottom-up strategy to structure conducting materials at the micro/nano-scale in liquid phase that offers a wide morphological versatility. Since the geometry of these structures governs their electrochemical properties, it is fundamental to decipher the mechanisms that rule the polymer assembling upon the electrically-programmed growth to use this phenomenon as a neuro-inspired building block for unconventional information processing. Herein, we investigate various electrical parameters of electropolymerization affecting the conducting polymer network geometry. We find that various structures such as dendrites, trees, fractals as well as low-fractality cables can be obtained between the two-wire electrodes, based on applied voltage amplitude, biasing symmetry, bias frequency, the concentration of monomers and electrode configurations. We qualitatively and quantitatively study the relationship between the electrical parameters affecting geometrical parameters of the conducting polymer network as well as electropolymerization dynamics through video and image processing. The systematic analysis shows that an increase in applied voltage leads to higher growth rate, more branches, and lower surface to bulk ratio. At the other hand, an increase in bias frequency leads to higher growth rate, smaller number of branches, and higher surface to volume ratio. In order to model the experimental phenomena, we simulate a simplified version of the problem with two bipolar metal electrodes and an electrolyte filled with dilute moving particles at random positions, reflecting the monomers in the liquid phase. The wire electrodes are biased with AC frequency and the spacio-temporal potential map is evaluated by solving the Laplace equation. The motion of the monomer particles is controlled by the electric field and by random Brownian motion. The particles that happen to touch the electrodes are stuck to the electrodes, with a certain probability of sticking. The stuck particles are incorporated into the electrode, and the potential is recalculated for the motion of the particles. The simulations are tested for different AC applied voltages, frequency, duty cycles, and voltage offsets. The increase in applied voltage leads to higher sticking probability; resulting in a higher growth rate, multiple branches, and higher density, which goes well with the experiments. Further, the effect of frequency, which is not so intuitive, shows that higher AC frequency, favors linear cable like growth, while lower frequency leads to more isotropic growth, while voltage offset and non-equal duty cycle lead to asymmetrical growth, in accordance with experiments. In addition, the effect of electrode spacing, different electrode designs, electrical pulse shapes and the concentration of particles, are also studied. The study helps in visualizing the motion of particles in different electrical conditions, which is not possible to probe experimentally. Some subtle experimental features, such as the effect of preferential growth on the tips, and broadening of the electrode before touching, are observed in the modeling studies. Thus, we find that the different network architectures are associated with different Laplace end diffusion fields governing the monomers motion and in turn electropolymerized network geometry. Such unconventional engineering route could have a variety of applications from neuromorphic engineering to bottom-up computing strategies.

#### 6:45 AM \*F.SM05.01.06

##### **Physically Flexible and Biological Compatible Demonstration of an Organic Electronics Axon-Hillock Neural Circuit**

Mohammad Javad Mirshojaeian Hosseini<sup>1</sup>, Elisa Donati<sup>2</sup>, Tomoyuki Yokota<sup>3</sup>, Sunghoon Lee<sup>3</sup>, Giacomo Indiveri<sup>2</sup>, Takao Someya<sup>3</sup> and Robert A. Nawrocki<sup>1</sup>; <sup>1</sup>Purdue University, United States; <sup>2</sup>Institute of Neuroinformatics, Switzerland; <sup>3</sup>The University of Tokyo, Japan

Spiking Neural Networks (SNN) provide distributed computational capability and emulate the brain processing principles based on spike frequency and pulse width [1]. Because of being intrinsically compatible with brain signaling, one of the target applications of SNN hardware implementation, known as neuromorphic systems [2], are Brain-Computer Interfaces (BCI) [3]. With a handful of exceptions [4], such implementations have typically been implemented using silicon technology, which is physically hard and rigid, and non-biocompatible, resulting in a permanent damage to the brain's soft tissue. Organic electronics offer physical softness and flexibility, biocompatibility, and low-cost, large-area fabrication, to directly interface with biological tissues [5].

We report on the fabrication of a physically flexible, organic electronics, spiking integrate-and-fire Axon-Hillock (AH) neural circuit. Organic Field-Effect Transistors (OFETs) are fabricated on top of a flexible, 50  $\mu\text{m}$  Polyimide substrate. OFETs' architecture is bottom-gate top-contact, and fabricated through thermal deposition of Ti (3 nm)/Au (50 nm) as the gate electrode, 60 nm of Parylene as the dielectric, 30 nm of dinaphtho[2,3b:2',3'-f]thieno[3,2-b]thiophene (DNFTT) as the p-type and N,N'-bis(n-octyl)-x:y,dicyanoperylene3,4:9,10-bis(dicarboximide) (PDI8-CN2) as the n-type semiconductor. A 50 nm layer of Au serves as the source and the drain electrodes. A layer of Parylene encapsulates the structure. Non-circuit-integrated commercial resistors and capacitors are used to accelerate the characterization and the fabrication process. All integrated all-organic circuit is beyond the scope of this work and would increase the complexity of the process.

The results show that the AH circuit with 500 nA input current can produce spikes with a range of frequencies. Given the membrane capacitance ( $C_{mem}$ ) of 15 nF and feedback capacitance ( $C_{feedback}$ ) of 47 nF, the spiking frequency reaches 670 mHz. The frequency can be lowered by increasing capacitance values to  $C_{mem} = 33$  nF and  $C_{feedback} = 100$  nF, respectively, to 370 mHz. Decreasing capacitance to  $C_{mem} = 2.2$  nF and  $C_{feedback} = 6.8$  nF, will result in a higher spiking rate (5 Hz), but will also increase the influence of power line noise and parasitic capacitance. The frequency-current ( $F-I$ ) transfer function shows the dynamics of the neuron. By increasing the input current, the  $F-I$  curve will saturate indicating an upper bound of frequency spikes. The computational ability of the neuron is also demonstrated with a basic summation of two unitary excitatory synaptic events. The static and dynamic power dissipation is recorded and is limited to 0.4  $\mu\text{W}$  and 40  $\mu\text{W}$ , respectively.

We believe that this work is the first demonstration of a functioning organic electronics integrate-and-fire spiking neuron, paving the way for future implantable BMIs. Beyond neuroscientific applications, this technology can also be used in slow processes, such as temperature measurement, which are intrinsically difficult for ultra-fast silicon devices to achieve, as well as physically flexible large-area applications.

[1] F. Rieke and D. Warland, "Spikes: Exploring the Neural Code," *MIT Press*, 1999.

[2] R. Nawrocki, et al., "A mini review of neuromorphic architectures and implementations," *IEEE Transactions on Electron Devices*, vol. 63 (10), 2016.

[3] F. Boi, et al., "A Bidirectional Brain-Machine Interface Featuring a Neuromorphic Hardware Decoder," *Frontiers in Neuroscience*, vol. 10 (563), 2016.

[4] R. Nawrocki, et al., "Neurons in polymer: Hardware neural units based on polymer memristive devices and polymer transistors," *IEEE Transactions on Electron Devices*, vol. 61 (10), 2014.

[5] G. Schwartz, et al., "Flexible polymer transistors with high-pressure sensitivity for application in electronic skin and health monitoring," *Nature Communications*, vol. 4 (1), 2013.

#### 7:15 AM \*F.SM05.01.07

**Bio-Inspired Neuromorphic Electronics for Artificial Nervous Systems** Tae-Woo Lee; Seoul National University, Korea (the Republic of)

Neuromorphic electronics have handled complex real-world problems such as visual information, speech recognition, and body motion control with compressibility, fault tolerance, and high energy efficiency. These neuromorphic electronics have been investigated to develop artificial nervous system systems that mimic biological nervous systems. Mimicking the learning and memory functions of the human brain has been a major focus so far in neurological electronics. Further, the functional integration of artificial synapses with sensing/motor elements would be a core technology for applications of



human-like robotics and neuroprosthetics, enabling the emulation of sensing and responding behaviors in biological systems. In biology, sensations such as vision, hearing, touch, taste, and smell and responding with muscles are related with peripheral nerves.

Herein, bio-inspired neuromorphic electronics for artificial nervous systems were covered. Artificial synapse-based sensory and motor electronic nerves are developed by integrating with sensory and motor organs. Firstly, pressure sensors (artificial mechanoreceptors), organic ring oscillators (artificial nerve fibers), and synaptic transistors were integrated to emulate the functions and operating principles of biological counterparts. By connecting this artificial pressure-sensory nerve to biological motor nerves in a detached cockroach leg, a hybrid reflex arc system was realized. In addition, a stretchable photo-sensitive sensorimotor nervous system composed of a photo-sensitive detector (an artificial photoreceptor) and a stretchable artificial synapse with a polymer actuator (an artificial muscle). In addition, a retina-inspired photo-sensitive synaptic transistor was developed by using ultraviolet-responsive 2-dimensional carbon nitride nanodot layers as a floating gate to selectively detect and process ultraviolet light exposure information. Lastly, for an artificial auditory system, organic artificial synapse was connected to a triboelectric sensor. Our bio-inspired neuromorphic systems can be used for neuromorphic computing, humanoid soft robots, and neural prostheses.

### 7:30 AM \*F.SM05.01.09

**Memory and Learning in Biomolecular Soft Materials** Charles P. Collier<sup>1</sup>, Joseph S. Najem<sup>2</sup>, Richard S. Williams<sup>3</sup>, Graham Taylor<sup>4</sup>, Md S. Hasan<sup>5</sup>, Ryan Weiss<sup>6</sup>, Stephen A. Sarles<sup>6</sup>, Garrett Rose<sup>6</sup>, Alex Belianinov<sup>1</sup> and Catherine Schuman<sup>1</sup>; <sup>1</sup>Oak Ridge National Laboratory, United States; <sup>2</sup>The Pennsylvania State University, United States; <sup>3</sup>Texas A&M University, United States; <sup>4</sup>T&T Scientific, United States; <sup>5</sup>The University of Mississippi, United States; <sup>6</sup>The University of Tennessee, Knoxville, United States

Neuromorphic elements have been predominantly solid-state devices which simulate the resistive and capacitive behaviors needed for neural networks and brain-inspired computing, but in non-brain-like ways. This talk will describe ways we are integrating lipid and polymer bilayer membranes with micro- and nanofabrication to develop fundamentally new types of neuromorphic elements that have the composition (biomolecules), structure (biomembranes), and switching mechanism (voltage-sensitive ion channels) of real biological synapses, and operate at lower power than the current state-of-the-art. Our devices consist of insulating, nm-thick lipid or polymer-based bilayer membranes that assemble at the interfaces of two or more aqueous droplets in oil, and that have demonstrated both memristive and memcapacitive behaviors, including memory resistance and capacitance, synaptic functions such as paired-pulse facilitation and depression, spike rate dependent plasticity, voltage-dependent inactivation and recovery, and charging hysteresis. These behaviors are linked to electrostriction, an electromechanical phenomenon that encompasses both electrowetting and electrocompression in the membrane, which are changes in membrane area and thickness due to charging in the presence of electric fields. Electrostriction results in a voltage-dependent capacitive susceptibility that replaces the more familiar concept of static capacitance, which, up to now, has dominated electrophysiological descriptions and characterizations of biomembranes. In this picture, biomembranes are not just equivalent RC circuits dependent only on ionic currents controlled by the conductance (resistance) of ion channels. Large capacitive currents from small voltage inputs can be generated as well for the development of neuromorphic computing elements exhibiting both short-term and long-term synaptic plasticity.

### 7:45 AM F.SM05.01.01

**Late News: Self-Assembled Oligoethylene Glycols for Air-Stable Molecular Electronics and In Operando Modulation** Xinkai Qiu and Ryan C. Chiechi; University of Groningen, Netherlands

Self-assembled monolayers (SAMs) are widely used to engineer the surface properties of metals. The relatively simple and versatile chemistry of metal-thiolate bonds makes thiolate SAMs the preferred option in a range of applications, yet fragility and a tendency to oxidize in air limit their long-term use. In our recently published paper in Nature Materials, we report the formation of thiol-free self-assembled mono- and bilayers of glycol ethers, which bind to the surface of coinage metals through the spontaneous chemisorption of glycol ether-functionalized fullerenes. As-prepared assemblies are bilayers presenting fullerene cages at both the substrate and ambient interface. Subsequent exposure to functionalized glycol ethers displaces the topmost layer of glycol ether-functionalized fullerenes, and the resulting assemblies expose functional groups to the ambient interface. These layers exhibit the key properties of thiolate SAMs, yet they are stable to ambient conditions for several weeks, as shown by the performance of tunneling junctions formed from SAMs of alkyl-functionalized glycol ethers. Glycol ether-functionalized spiropyrans incorporated into mixed monolayers lead to reversible, light-driven conductance switching. Self-assemblies of glycol ethers are drop-in replacements for thiolate SAMs that retain all of their useful properties while avoiding the drawbacks of metal-thiolate bonds.<sup>[1]</sup>

In a follow-up work, we demonstrate the reconfiguration of molecular tunneling junctions while in operation via the self-assembly of bilayers of glycol ethers. We use well-established functional groups to modulate the magnitude and direction of

rectification in assembled tunneling junctions by exposing them to solutions containing different glycol ethers. Variable temperature measurements reveal that rectification occurs by a bias-dependent tunneling-hopping mechanism and that glycol ethers, besides being unusually efficient tunneling medium, behave identically to alkanes. We fabricated memory bits from crossbar junctions prepared by injecting eutectic Ga-In in microfluidic channels. Two 8-bit registers were able to perform logical AND operations on bit strings encoded into chemical packets as microfluidic droplets that alter the composition of the crossbar junctions through self-assembly to effect memristor-like properties. This proof-of-concept work demonstrates the potential for fieldable molecular-electronic devices based on tunneling junctions of self-assembled monolayers and bilayers.<sup>[2]</sup>

[1] Qiu, X., Ivasyshyn, V., Qiu, L., Enache, M., Dong, J., Rousseva, S., Portale, G., Stöhr, M., Hummelen, J.C. and Chiechi, R.C. "Thiol-free self-assembled oligoethylene glycols enable robust air-stable molecular electronics." *Nat. Mater.* **19**, 330-337 (2020).

[2] Qiu, X., Rousseva, S., Ye, G., Hummelen, J.C. and Chiechi, R.C. "Stochastic computing via in operando modulation of rectification in molecular tunneling junctions." ChemRxiv, 2020.

SESSION F.SM05.02/F.NM07.05: Joint Session: Novel Materials for Neuromorphic Devices  
On Demand Abstracts Available for Viewing Starting Saturday Morning, November 21, 2020  
F-SM05

#### 5:00 AM \*F.SM05.02/F.NM07.05.02

**One-Shot Regression and Classification with Crosspoint Memory Arrays** Daniele Ielmini<sup>1</sup>, Giacomo Pedretti<sup>1</sup>, Piergiulio Mannocci<sup>1</sup> and Zhong Sun<sup>2</sup>; <sup>1</sup>Politecnico di Milano, Italy; <sup>2</sup>Peking University, China

As artificial intelligence (AI) becomes a popular feature in industry, social networks, smart homes and transportation, there is an increasing need for AI accelerators in edge computing, to solve for excessive traffic to the cloud and ensure privacy and security of the processed data. In this frame, in-memory computing (IMC) has risen as low-power processing approach for data intensive problems. Matrix-vector multiplication (MVM) can be accelerated in crosspoint arrays by leveraging the Kirchhoff's law for current summation and the Ohm's law for voltage-conductance multiplication, as well as taking advantage of the parallelism in the memory array. Connecting the crosspoint array in a feedback loop also allows to accelerate inverse operations, i.e., one-step solutions of linear systems such as  $Ax = b$  where the  $N \times N$  matrix  $A$  is stored as conductance values in the array, vector  $b$  represents applied currents and solution vector  $x$  is the output voltage.  $O(1)$  complexity of eigenvector extraction and  $O(N)$  complexity of matrix inversion have been demonstrated, which outperforms classical digital computing and even quantum computing.

In this work, we show that the same circuit concept can serve to accelerate regression and classification problems, which are two key problems of AI. Linear regression is solved within two coupled crosspoint arrays by computing the pseudo-inverse matrix in one step.  $M$ -dimensional linear regression allows to make predictions based on an existing data set or temporal sequence, thus enabling fast, energy efficient machine learning on the edge. The same circuit enables logistic regression, hence one-step classification within the crosspoint array, which allows for one-shot training of multiple layer perceptrons (MLP). The implications of these novel concepts for AI acceleration and the best technological implementation for data-intensive computing will be discussed.

#### 5:30 AM \*F.SM05.02/F.NM07.05.03

**Atomic Memory and Computing Applications** Deji Akinwande<sup>1</sup> and Mario Lanza<sup>2</sup>; <sup>1</sup>The University of Texas at Austin, United States; <sup>2</sup>Soochow University, China

This talk will present our latest research adventures on 2D atomic nanomaterials towards greater scientific understanding and computing applications. In particular, the talk will highlight our work on non-volatile memory (atomristors) that can be employed in various applications including information storage, brain-inspired computing, and zero-power RF switches. Non-volatile memory device based on atomically-thin materials is an application of defects, and is a rapidly advancing field with rich physics that can be attributed to metal ion binding to native defects. The promising 2D materials for neuromorphic computing include MoS<sub>2</sub> and hBN. In particular, hBN memory devices feature very low switching energy, a relatively wide range of stable programmable resistance states, and good endurance and retention. Recent progress has also demonstrated wafer-scale integration of 2D memory devices with a prospect to leverage silicon electronics for fully integrated systems.

6:00 AM F.SM05.02/F.NM07.05.04

**High-Throughput Computational Screening to Identify Novel Proton Conducting Electrolytes for All-Solid-State Neuromorphic Devices** Konstantin Klyukin, Pjotr Zguns, Ju Li and Bilge Yildiz; Massachusetts Institute of Technology, United States

Artificial electrochemical synapses based on the charge-driven proton intercalation demonstrate much promise toward brain-inspired neural computing [1]. Proton transport plays a critical role in these devices determining switching speed and reliability. Despite great attention and intensive experimental investigations, even the cutting-edge proton conductors still suffer from sluggish ion transport kinetics at low temperatures or are not compatible with current CMOS fabrication processes. Therefore, there is an urgent need for fast solid-state proton conductors operating below 100 °C, much required for rapidly growing proton-based neuromorphic computing applications.

In this work, we consider a large class of solid-state materials having hydrogen as a part of their nominal structure such as solid acids and inorganic hydrates. By considering different combinations of common acids and metal ions, it is possible to synthesize thousands of materials with widely varying structures and physicochemical properties, and yet many of them remain relatively unexplored for the ability to conduct protons. We performed a high-throughput computational screening of the available materials datasets to identify chemical compositions and structure types that are likely to have high proton mobility. To estimate proton conductivity, we used ab initio molecular dynamics simulations. We further correlated this data with simple structural features and built a classification model to preselect a small set of materials for more detailed investigations. Based on our simulations, we identified promising materials and suggested effective strategies for improving proton conductivity.

#### References

[1] Xiahui Yao, Konstantin Klyukin, Wenjie Lu, Murat Onen, Seungchan Ryu, Dongha Kim, Nicolas Emond, Iradwikanari Waluyo, Adrain Hunt, Jesus A. del Alamo, Ju Li, Bilge Yildiz, "Protonic Solid-State Electrochemical Synapse for Physical Neural Networks", Nature Communications, in press, 2020.

6:15 AM F.SM05.02/F.NM07.05.05

**Metal-Insulator Transition Property for the Nano-Confined Electric Domain in the Strongly Correlated NdNiO<sub>3</sub>** Azusa Hattori, Takashi Yamanaka, Akira Nanba and Hidekazu Tanaka; Osaka University, Japan

Strongly correlated metal oxide (SCMO), such as manganite, nickelate, and so on show first-order metal-insulator phase transition (MIT) with a change in conductivity by several orders magnitude. Since a discovery of the phase separation during MIT process, many researchers have been trying to capture a nanoscale electric domain and investigate its exotic properties. Typical SCMO material, rare earth Ni oxides (ReNiO<sub>3</sub>, Re = Nd, Sm, and Eu) having a perovskite structure, show giant resistance change due to MIT at a wide temperature range of 150 K to 500 K. In this family, bulk neodymium nickelate: NdNiO<sub>3</sub> (NNO) shows 1-2 orders resistance change through MIT at around 200 K [1]. Very recently, the coexistence of insulator and metal domains with a few hundred nm size was observed during the MIT process for NNO system [2]. This phase-separated phenomenon is also observed in typical SCMOs, such as VO<sub>2</sub> and manganite. The overall observed MIT property, i.e., the resistance change for a sample, is considered to be dominated by competing nanoscale electronic phases. A step resistance change due to the electronic phase confinement effect: increase in resistance change rate has been reported in nanoscale samples comparable to domain size [3]. Therefore, it is expected that the nanoscale NNO sample shows a step resistance change due to MIT property of single nanoscale electronic phases. In this study, we fabricated NNO nanowire structures with 50-200 nm widths and measured their transport properties.

The NNO thin films were fabricated on NdGaO<sub>3</sub>(110)( $a_{pc} = 0.3858$  nm), LSAT(100)( $a = 0.3868$  nm), and SrTiO<sub>3</sub>(100)( $a = 0.3858$  nm) substrates by pulsed laser deposition method. NNO nanowires with different wire widths from 50 nm to 500 nm were fabricated by electron beam (EB) lithography and Ar ion milling process. All films and nanowire samples showed the resistance changes corresponding to MIT, but the RT curves shape were quite different. While the thin film sample showed gradual resistance change, the nanowire sample showed some step resistance changes both in cooling and heating processes. This step changes indicate that the nano electronic phases are confined in the NNO nanowire and a single electric domain shows first-order MIT with a single-step change in electrical transport property. For example, we found that the 50 nm width nanowire on SrTiO<sub>3</sub> substrate showed the intermittent step-resistance change, implying the further confine electronic phases to a nanometer space. Interestingly, the nanowires on NdGaO<sub>3</sub>(110) and LSAT(100) substrates showed more prominent step resistance changes than that on SrTiO<sub>3</sub>(100) substrate, which imply the nano-confinement condition were affected by the strain. The  $dR/dT$  vs.  $T$  plot showed that the transition temperature distribution of each electronic phase in the nanowires were different. This is probably because the strains depending on the three different substrate effect where on the Ni-O-Ni angular distribution, which affected the MIT properties of NdNiO<sub>3</sub> nano-electronic phase. In the presentation, we will present

the quantitative correlation between nano-spatial size and nano-confinement MIT properties. We will also discuss the revealed the MIT property for a single domain in a NNO nanowire and the strain effect for the nano-confined domains behaviors.

[1] G. Catalan *et al.*, Phys. Rev. B, 62, 7892 (2000), [2] G. Mattoni *et al.*, Nat. Commun., 7, 13141 (2016), [3] A. N. Hattori *et al.*, Nano Lett., 15, 4322 (2015).

#### 6:30 AM F.SM05.02/F.NM07.05.06

##### **Ionic Liquid Regulated Silver Filament Formation in a Solid Polymer Electrolyte for Neuromorphic Applications** Zhongmou Chao, Ke Xu and Susan Fullerton; University of Pittsburgh, United States

Much progress has been made over the past decade using conductive bridge random access memory (CBRAM) to emulate both artificial synapses and artificial neurons for neuromorphic applications. However, the intrinsically stochastic switching process of metal filament formation and dissolution results in unreliable analog synaptic weight updating, while the non-volatile characteristic of CBRAM prevents the leaky integrate-and-fire function—a hallmark characteristic of an artificial neuron. We have previously reported that silver nanofilament growth dynamics in a polymer electrolyte can be regulated by the addition of ionic liquid (IL) by: (1) reducing stochasticity of the filament switching (shifting its formation time distribution from power-law to Gaussian) and (2) creating a competition between the formation of IL electrical double layers (EDL) and silver electrodeposition. The competition enables the tuning of filament growth dynamics from abrupt to gradual, with gradual growth introducing multiple well-defined resistance states—a feature necessary for emulating the communications between neurons in an artificial neural network. We also observed a linear correspondence ( $R^2 = 0.95$ ) between nanofilament resistance states and program pulses, which is essential to improve learning accuracy in Deep Neural Networks (DNNs). Here, we report on silver filament formation and dissolution in response to presynaptic programming biases and focus on benchmarking the performance against the requirements for artificial synapses. The temporal stability of “abrupt growth” silver filaments is also studied. Lastly, we demonstrate a system integrating both gradual and abrupt silver filaments to implement some key artificial neuron functionalities.

#### 6:45 AM \*F.SM05.02/F.NM07.05.07

##### **Progress in Analog DNN Hardware Accelerators Using Phase Change Materials** Charles Mackin, Hsinyu Tsai, Prithvi Narayanan, Stefano Ambrogio, Katie Spoon, Andrea Fasoli, Alexander Friz, An Chen and Geoffrey W. Burr; IBM, United States

Neuromorphic computing with analog memory can accelerate deep neural networks (DNNs) by enabling multiply-accumulate (MAC) operations to occur within memory. Analog memory, however, presents a number of device-level challenges having macro-implications on the achievable accuracy and reliability of these artificial neural networks. This talk focuses on the adverse effects of conductance drift in phase-change memory (PCM) on network reliability. It is shown that conductance drift can be effectively compensated in a variety of networks by applying a ‘slope correction’ technique to the squashing functions to maintain accuracy/reliability for a period of  $\sim 1$  year. In addition to conductance drift, PCM poses considerable variability challenges, which impact the accuracy of the initial weights. This talk summarizes recent advances in optimizing initial weight programming, and provides evidence suggesting that the combination of ‘slope correction’ and programming optimization techniques may allow DNN acceleration using analog memory while maintaining software-equivalent accuracy with reasonable reliability.

#### 7:15 AM \*F.SM05.02/F.NM07.05.08

##### **Computing with Memristive and Memcapacitive Devices** J. Joshua Yang; University of Southern California, United States

Memristive devices have become a promising candidate for unconventional computing(1) due to their attractive properties(2, 3). Computing can be implemented on a Resistive Neural Network (ResNN) with memristor synapses and neurons or a Capacitive Neural Network (CapNN) with memcapacitor synapses and neurons. For ResNNs as computing accelerators, we have built a dot-product engine based on a 128 x 64 1T1R crossbar array using traditional non-volatile memristors with 64 stable analog resistance levels(4). Accurate image compression and filtering have been demonstrated with such analog computing accelerator(4). In addition, we have demonstrated efficient and self-adaptive in-situ learning in a two-layer neural networks using such memristive arrays(5), which is expected to significantly improve the speed and energy efficiency of machine learning. A variety of neural networks based on such accelerators have been demonstrated, including reinforcement learning(6), LSTM(7), recurrent CNN(8) memristive networks. For ResNNs beyond accelerator applications, we developed diffusive memristors(9) with diffusion dynamics that is critical for neuromorphic functions. Based on the diffusive memristors, we have further developed artificial synapses(10) and neurons(11) to more faithfully emulate their bio-counterparts. We then integrated these artificial synapses and neurons into a small neural network, with which pattern

classification and unsupervised learning have been demonstrated(11). For CapNNs, we have developed pseudo-memcapacitive devices based on the diffusive memristors. Capacitive synapses and neurons enabled by these memcapacitive devices have been developed and used to form a fully integrated CapNN(12), which has shown spiking signal classification and Hebbian-like learning functions. Moreover, the diffusive memristors can be used for cybersecurity(13, 14) and robotics applications(15). The requirements on device properties, and thus the corresponding challenges and solutions, are different for ResNNs and CapNNs, which will be discussed in detail in this talk. J. J. Yang, D. B. Strukov, D. R. Stewart, Memristive devices for computing. *Nature Nanotechnology* 8, 13-24 (2013). S. Pi et al., Memristor crossbar arrays with 6-nm half-pitch and 2-nm critical dimension. *Nature nanotechnology* 14, 35 (2019). Q. Xia, J. J. Yang, Memristive crossbar arrays for brain-inspired computing. *Nature materials* 18, 309 (2019). C. Li et al., Analogue signal and image processing with large memristor crossbars. *Nature Electronics* 1, 52 (2017). C. Li et al., Efficient and self-adaptive in-situ learning in multilayer memristive neural networks. *Nature communications* 9, 2385 (2018). Z. Wang et al., Reinforcement learning with analogue memristor arrays. *Nature Electronics* 2, 115 (2019). C. Li et al., Long short-term memory networks in memristor crossbar arrays. *Nature Machine Intelligence* 1, 49 (2019). Z. Wang et al., In situ training of feed-forward and recurrent convolutional memristor networks. *Nature Machine Intelligence* 1, 434-442 (2019). E. J. Fuller et al., Parallel programming of an ionic floating-gate memory array for scalable neuromorphic computing. *Science* 364, 570-574 (2019). Z. Wang et al., Memristors with diffusive dynamics as synaptic emulators for neuromorphic computing. *Nature Materials* 16, 101-108 (2017). Z. Wang et al., Fully memristive neural networks for pattern classification with unsupervised learning. *Nature Electronics* 1, 137-145 (2018). Z. Wang et al., Capacitive neural network with neuro-transistors. *Nature Communications* 9, 3208 (2018). H. Jiang et al., A Novel True Random Number Generator Based on a Stochastic Diffusive Memristor. *Nature communications* 8, 882 (2017). H. Jiang et al., Provable Key Destruction with Large Memristor Crossbars. *Nature Electronics* 1, 548 (2018). J. H. Yoon et al., An artificial nociceptor based on a diffusive memristor. *Nature Communications* 9, 417 (2018).

SESSION F.SM05.03: Novel Materials for Neuromorphic Devices  
 On Demand Abstracts Available for Viewing Starting Saturday Morning, November 21, 2020  
 F-SM05

#### 5:00 AM \*F.SM05.03.01

**Memristive Materials and Devices for Unconventional Computing** J. Joshua Yang; University of Southern California, United States

Memristive devices<sup>1</sup> have become a promising candidate for energy-efficient and high-throughput unconventional computing<sup>2</sup>, which is a key enabler for artificial intelligent systems in the big data and IoT era<sup>3</sup>. The computing can be implemented on a Resistive Neural Network<sup>4</sup> with memristive synapses<sup>5</sup> and neurons<sup>6</sup> or a Capacitive Neural Network<sup>7,8</sup> with memcapacitive synapses and neurons. In this talk, I will first briefly introduce the promises and challenges of memristive materials and devices for such applications. I will then discuss a few examples selected from our recent experimental demonstrations of unconventional computing using memristive networks with different levels of bio-inspiration: first, deep learning accelerators<sup>9</sup> with supervised online learning<sup>10</sup>; second, neuromorphic computing for pattern classification with unsupervised learning<sup>6</sup>; last, other computing applications, such as reinforcement learning<sup>11</sup> for decision making, artificial nociceptors for robotics<sup>12</sup>, provable key destruction<sup>13</sup> and true random number generators<sup>14</sup> for cybersecurity.

1. Yang, J. J., Strukov, D. B. & Stewart, D. R. Memristive devices for computing. *Nature Nanotechnology* 8, 13-24 (2013).
2. Xia, Q. & Yang, J. J. Memristive crossbar arrays for brain-inspired computing. *Nature materials* 18, 309-323 (2019).
3. Wang, Z. *et al.* Resistive switching materials for information processing. *Nature Reviews Materials*, 1-23 (2020).
4. Wang, Z. *et al.* In situ training of feed-forward and recurrent convolutional memristor networks. *Nature Machine Intelligence* 1, 434-442 (2019).
5. Wang, Z. *et al.* Memristors with diffusive dynamics as synaptic emulators for neuromorphic computing. *Nature Materials* 16, 101-108 (2017).
6. Wang, Z. *et al.* Fully memristive neural networks for pattern classification with unsupervised learning. *Nature Electronics* 1, 137-145 (2018).
7. Wang, Z. *et al.* Capacitive neural network with neuro-transistors. *Nature Communications* 9, 3208 (2018).
8. Li, C. *et al.* Long short-term memory networks in memristor crossbar arrays. *Nature Machine Intelligence* 1, 49-57 (2019).
9. Li, C. *et al.* Analogue signal and image processing with large memristor crossbars. *Nature Electronics* 1, 52 (2018).
10. Li, C. *et al.* Efficient and self-adaptive in-situ learning in multilayer memristive neural networks. *Nature communications* 9, 2385 (2018).
11. Wang, Z. *et al.* Reinforcement learning with analogue memristor arrays. *Nature Electronics* 2, 115 (2019).

12. Yoon, J. H. *et al.* An artificial nociceptor based on a diffusive memristor. *Nature communications* **9**, 417 (2018).
13. Jiang, H. *et al.* A provable key destruction scheme based on memristive crossbar arrays. *Nature Electronics* **1**, 548-554 (2018).
14. Jiang, H. *et al.* A Novel True Random Number Generator Based on a Stochastic Diffusive Memristor. *Nature communications* **8**, 882 (2017).

### 5:30 AM \*F.SM05.03.02

#### **Development of Neuristors and Synaptors Using Quantum Materials for Energy Efficient Neuromorphic Computing** Ivan Schuller; University of California, San Diego, United States

The Quantum Materials for Energy Efficient Neuromorphic Computing (QMEENC) Energy Frontiers Research Center (EFRC) is a highly collaborative effort dedicated to the development of quantum materials based implementation of energy efficient devices that will form the basis for neuromorphic computing. This project is currently two parallel approaches based on charge, using highly correlated oxides, and spin, using spin torque oscillators. We are also developing hybrid concepts, which take advantage of the functional properties of both approaches.

In addition to the general description of the QMEENC approach, I will describe the first implementation of energy efficient neuristors (that emulates neuronal functionalities) and a synaptors (that emulates synaptic functionalities), based on heterostructures, which incorporate strongly correlated oxides.

This work was supported as part of the Quantum Materials for Energy Efficient Neuromorphic Computing an Energy Frontiers Research Center funded by the U.S. Department of Energy, Office of Science, Basic Energy Sciences under Award # DE-SC0019273.

### 6:00 AM \*F.SM05.03.03

#### **Robust Resistive and Mem-Devices Using Organometallic Molecules- Ideal Candidates for Neuromorphic Devices** Thirumalai Venkatesan<sup>1,2</sup>, Sreetosh Goswami<sup>3</sup> and Sreebrata Goswami<sup>3</sup>; <sup>1</sup>Azometrix, United States; <sup>2</sup>National University of Singapore, Singapore; <sup>3</sup>NUS, Singapore

Artificial intelligence (AI) has been heralded as the flagbearer of the fourth industrial revolution. But it comes with a cost and that is computing power. It is projected that by 2040, we will need more computing energy than the total energy we can produce now. So, we need devices that can offer higher computing/ storage density with low energy consumption like neuronal computation. We are addressing these challenges using a molecular-electronic route. Historically, organic electronic devices have stimulated scientific excitement in OLEDs but are yet to make any other significant technological impact. The reasons behind their limited success are their poor robustness, stability, endurance and most importantly, the lack of mechanistic understanding that restricts the emergence of approaches to solve these problems. We have overcome each of these difficulties in our memristors based on transition metal complexes of azo-aromatic ligands that exhibit high reproducibility (~350 devices), fast switching ( $\leq 30$  ns), excellent endurance ( $\sim 10^{12}$  cycles), stability ( $> 10^6$  s) and scalability (down to  $\sim 60\text{nm}^2$ )<sup>1-5</sup>. Using *in-situ* Raman spectroscopy we are able to track the electronic changes in molecules *in-operando* at every point of our voltage sweep providing a clear picture of our molecular mechanism that enables us to do different molecular and device engineering to achieve targeted functionalities. Using devices of this genre we are addressing the existing computing challenges *via* three routes,

**By designing devices with ultra-low power:** We can design memristors with switching voltage as low as 70mV, with energy  $\sim 36\text{aJ}/60\text{nm}^2$ . The current and voltage levels of these devices meet the requirements specified in ITRS road map.

**By designing memristors and memcapacitors with multiple discrete plateaus<sup>3</sup>:** We have developed memristors with 3- 4 distinct conducting plateaus which also shows mem-capacitance. Their concomitant occurrence is enabled by symmetry breaking of our film-molecules driven by voltage, a new paradigm in condensed matter physics.

**Brain inspired computing:** Using devices that exhibit concomitant memristive and memcapacitive functions we can simulate biological actions such as neuronal action potential and even cardiac myocyte pulsing.

#### **References**

1. Goswami S, Matula AJ, Rath SP, Hedström S, Saha S, Annamalai M, et al. Robust resistive memory devices using solution-processable metal-coordinated azo aromatics, *Nature materials* 2017, 16(12): 1216.
2. Valov I, Kozicki M. Non-volatile memories: Organic memristors come of age, *Nature materials* 2017, 16(12): 1170.
3. Sreetosh Goswami, Santi P. Rath, Damien Thompson, Svante Hedström, Meenakshi Annamalai, Rajib Pramanick, B. Robert Ilic, Soumya Sarkar, Christian A. Nijhuis, Jens Martin, Sreebrata Goswami, and T. Venkatesan, A Ternary Resistive Memory Device Based on Charge Disproportionate Molecular Redox, *Nature Nanotechnology*, (2020)
4. Sreetosh Goswami, Sreebrata Goswami and T. Venkatesan, An Organic approach to low energy memory and Brain

Inspired Electronics, 7(2), 021303 **Applied Physics Reviews- Invited (2020)**

5. Sreetosh Goswami, R. Stanley Williams, Damien Thompson, Sreebrata Goswami and T. Venkatesan, Colossal current and voltage tunability in an organic memristors via electrode engineering, **Applied Materials Today (2020)**

**6:30 AM F.SM05.03.04**

**Acting Like a Synapse—A Biohybrid Neuromorphic Platform Combining Electronical and Optical Readouts** Giovanni Maria Matrone<sup>1</sup>, Claudia Lubrano<sup>1</sup>, Valeria Criscuolo<sup>1</sup>, Csaba Forro<sup>2</sup>, Yoeri van de Burgt<sup>3</sup> and Francesca Santoro<sup>1</sup>; <sup>1</sup>Istituto Italiano di Tecnologia, Italy; <sup>2</sup>Stanford University, United States; <sup>3</sup>Technische Universiteit Eindhoven, Netherlands

In biological neural networks communication relies on electric signals in the form of action potentials (APs) that trigger the release of neurotransmitters at the synapses, thus influencing the mechanisms of synaptic plasticity that regulates over time the transmission efficiency across the synaptic cleft. Indeed, progress over the last few years designing artificial neuromorphic systems (ANS)<sup>1</sup> has paved the way to a rapid improvement of the current machine learning (ML) processes but, focusing mainly on replicating electrical signal transmission, has limited a direct communication with biological systems<sup>2</sup>. Electrical to chemical signal transduction is essential to fully replicate brain functions and establish in future an active interaction with biological tissues<sup>3</sup>. Biohybrid interfaces are emerging since they promise to couple the activity of biological neural cells with neuromorphic artificial devices, enabling sensing and stimulation through two ways communication.

In this context, the conductive polymer mixture PEDOT: PSS can be exploited for the electrochemical detection of electroactive neurotransmitters<sup>4</sup> (i.e. dopamine, norepinephrine, ascorbic acid) through redox reactions while providing a suitable biocompatible interface with cells and neurons<sup>5</sup>. Here, we present the design of a novel electrochemical neuromorphic organic device (ENODE) capable of identifying multiple neurotransmitters simultaneously present. Additionally, through modular microfluidic channels, different flow regimes are regulated in order to replicate the condition of exocytosis displayed by a real synapse. Hence, the platform allows to transduce the neurotransmitters-mediated chemical signal, eliciting an output that is stored and read as a change in the polymer's conductance, a neuromorphic phenomenon that replicates neuronal's short-term and long-term plasticity<sup>6</sup>. Moreover, by exploiting PEDOT:PSS electrochromism, the system's readout is alternatively monitored as a variation of the polymer's transmittance and since this is intimately related to its conductance modulation, a novel dual output system to refine feedback regulation in closed-loop operations is presented. Hence, this platform allows to fully recapitulate synaptic plasticity and being conceivable as a bio-hybrid interface through direct coupling with neural tissues, it promises to move from a mere recording of biological functions to a dynamic interactive control.<sup>7</sup>

1. Furber, S. Large-scale neuromorphic computing systems. *J. Neural Eng.* **13**, 051001 (2016).
2. van Doremaele, E. R. W., Gkoupidenis, P. & van de Burgt, Y. Towards organic neuromorphic devices for adaptive sensing and novel computing paradigms in bioelectronics. *J. Mater. Chem. C* **7**, 12754–12760 (2019).
3. Markram, H. A history of spike-timing-dependent plasticity. *Front. Synaptic Neurosci.* **3**, (2011).
4. Gualandi, I. *et al.* Textile Organic Electrochemical Transistors as a Platform for Wearable Biosensors. *Sci. Rep.* **6**, 33637 (2016).
5. Asplund, M. *et al.* Toxicity evaluation of PEDOT/biomolecular composites intended for neural communication electrodes. *Biomed. Mater.* **4**, 045009 (2009).
6. Abbott, L. F. & Regehr, W. G. Synaptic computation. *Nature* **431**, 796–803 (2004).
7. Keene, S. T., Lubrano, C., Kazemzadeh, S., Melianas, A., Tuchman, Y., Polino, G., Scognamiglio, P., Cinà, L., Salleo, A., van de Burgt, Y., Santoro, F. A biohybrid synapse with neurotransmitter-mediated plasticity. *Nat. Mater.* (2020).

**6:45 AM F.SM05.03.05**

**Elucidating Microstructure-Dependent Synaptic Plasticity of Ion-Gel Gated Semi-Crystalline Polymer Synaptic Transistors** Gyeong-Tak Go<sup>1</sup>, Yeongjun Lee<sup>1</sup>, Dae-Gyo Seo<sup>1</sup>, Mingyuan Pei<sup>2</sup>, Wanhee Lee<sup>1</sup>, Hoichang Yang<sup>2</sup> and Tae-Woo Lee<sup>1</sup>; <sup>1</sup>Seoul National University, Korea (the Republic of); <sup>2</sup>Inha University, Korea (the Republic of)

Organic synaptic transistors using intrinsic organic semiconductors have emerged to overcome the limitation of conventional electronics by demonstrating various synaptic functions. Although organic synaptic transistors have succeeded in mimic biological synapses, especially short-term plasticity, devices emulated only limited long-term plasticity with short retention behaviors. The long-term retention behavior is essential for non-volatile and long-term memory characteristic in neuromorphic computing. Correlating the synaptic responses with the microstructures of polymer semiconductor is a crucial step to achieve long-term retention. The fundamental study on synaptic responses related to microstructures of organic materials has not been discovered yet. Here, we show that the long-term retention in ion-gel gated organic synaptic transistors (IGOSTs) can be achieved by controlling the microstructure of organic semiconductors. We controlled the crystallinity of

poly(3-hexylthiophene-2,5-diyl) (P3HT) in films spun-cast on bare and self-assembled monolayer, before and after thermal treatments. The long-term retention has been significantly prolonged in the IGOSTs, which tends to be elongated as the crystallinity of the semiconductor increased. The microstructure and crystallinity are determined by grazing-incidence X-ray diffraction, optical analyses, and atomic force microscopy. We also evaluate the synaptic current decay behaviors according to a de-doping mechanism of the polymer semiconductor over time. We simulated the recognition of handwritten digits of IGOSTs based on highly-crystalline P3HT, thus achieved higher classification accuracy (>92%) compared with IGOSTs based on low-crystalline P3HT. Our study provides fundamental information about the effects of microstructure on the synaptic responses and strategy to design the IGOSTs for neuromorphic electronics.

SESSION F.SM05.04: Biointerfaces and Neuromorphic Sensing  
On Demand Abstracts Available for Viewing Starting Saturday Morning, November 21, 2020  
F-SM05

**5:00 AM \*F.SM05.04.01**

**Designing Biomimetic Electronic Interfaces** [Francesca Santoro](#); Istituto Italiano di Tecnologia, Italy

The interface between biological cells and non-biological materials has profound influences on cellular activities, chronic tissue responses, and ultimately the success of medical implants and bioelectronic devices. The optimal coupling between cells, i.e. neurons, and materials is mainly based on surface interaction, electrical communication and sensing.

In the last years, many efforts have been devoted to the engineering of materials to recapitulate both the environment (i.e. dimensionality, curvature, dynamicity) and the functionalities (i.e. long and short term plasticity) of the neuronal tissue to ensure a better integration of the bioelectronic platform and cells.

On the one hand, here we explore how the transition from planar to pseudo-3D nanopatterned inorganic and organic materials have introduced a new strategy of integrating bioelectronic platforms with biological cells under static and dynamic conditions. Although a spontaneous penetration does not occur, adhesion processes are such that a very intimate contact can be achieved. On the other hand, we investigate how organic semiconductors can be exploited for recapitulating electrical neuronal functions such as long term and short term potentiation. In this way, both the topology and the material functionalities can be exploited for achieving in vitro biohybrid platforms for neuronal network interfacing.

**5:30 AM \*F.SM05.04.02**

**Merging Bio-Sensing and Neuromorphic Computing with Organic Electro Chemical Transistors** [Fabien Alibert](#)<sup>1,2</sup>, [Mahdi Ghazal](#)<sup>1</sup>, [Kamila Janzaková](#)<sup>1</sup>, [Ankush Kumar](#)<sup>1</sup>, [Anna Susloparova](#)<sup>1</sup>, [Sophie Halliez](#)<sup>3</sup>, [Morvane Colin](#)<sup>3</sup>, [Luc Buée](#)<sup>3</sup>, [David Guérin](#)<sup>1</sup>, [Thomas Dargent](#)<sup>1</sup>, [Yannick Coffinier](#)<sup>1</sup> and [Sébastien Pecqueur](#)<sup>1</sup>; <sup>1</sup>IEMN-CNRS, France; <sup>2</sup>LN2-3IT, Canada; <sup>3</sup>Jean Pierre Aubert Research Center, France

Most of today's strategies to interface biology with electronic hardware are based on layered architectures where the front-end of sensing is optimized separately from the back-end for processing/computing signals. Alternatively, biological systems are capitalizing on distributed architecture where both sensing and computing are mix together and co-optimized. In this talk, we will present our strategy to implement bio-sensing of electroactive cells in a neuromorphic perspective. We will present how organic electrochemical transistors can be used to record electrical signals from neural cells. We will show various strategies capitalizing on the versatility of organic materials synthesis and organic device fabrication to tune and adapt the functionalities of such bio-sensors. We will then present how these strategies can be efficiently used to realize computing functions directly at the interface with biology. Notably, we will illustrate how a network of ionic sensors can implement the reservoir computing concept, a powerful neuromorphic computing approach of particular interest for dynamical signal processing.

**6:00 AM \*F.SM05.04.03**

**Organic Memristive Devices for Learning Mimicking and Interfacing with Nervous Cells** [Victor Erokhin](#); IMEM-CNR, Italy

Organic memristive devices contain a heterojunction of conducting polymer and solid electrolyte. Similarly to nervous systems, these elements combine memory and processing functions. Their working principle is based on the significant difference of the polyaniline resistance in reduced and oxidized states [1, 2]. These devices have been successfully applied for the construction of artificial neuron networks at the hardware level [3,4]. The device can be realized on flexible supports



and its properties are similar to synapse behavior, what has allowed realization of electrical circuits, mimicking learning of simple animals (pond snail) [5] and classical conditioning (Pavlov dog learning) according to STDP-like algorithm [6,7]. Its biocompatibility was demonstrated by the realization of hybrid systems, where slim mould *Physarum polycephalum* was interfaced with organic memristive devices [8].

Long- and short-term potentiation and depression of these devices depends not only on the number of passed pulses, but also on the frequency of their application [9].

Finally, we will consider a first step towards the realization of synapse prosthesis, describing experiments on the coupling of two live nervous cells from the rat cortex via organic memristive device [10]. Nervous cells were contacted by patch clamp electrodes, allowing to avoid artifacts. It has been demonstrated that the plasticity of the device electrical properties is similar to that of chemical synapses in living beings.

1. V. Erokhin, T. Berzina, and M.P. Fontana. Hybrid electronic device based on polyaniline-polyethylenoxide junction. *J. Appl. Phys.*, **97**, 064501 (2005).
2. V. Erokhin and M.P. Fontana. Thin film electrochemical memristive systems for bio-inspired computation. *J. Computational Theor. Nanosci.*, **8**, 313-330 (2011).
3. V.A. Demin, A.V. Emelyanov, S. Battistoni, G. Baldi, S. Iannotta, P.K. Kashkarov, and M.V. Kovalchuk. Hardware elementary perceptron based on polyaniline memristive devices. *Org. Electronics*, **25**, 16-20 (2015).
4. A.V. Emelyanov, D.A. Lapkin, V.A. Demin, S. Battistoni, G. Baldi, A. Dimonte, A.N. Korovin, S. Iannotta, P.K. Kashkarov, and M.V. Kovalchuk. First step towards the realization of a double layer perceptron based on organic memristive devices. *AIP Adv.*, **6**, 111301 (2016).
5. V. Erokhin, T. Berzina, P. Camorani, A. Smerieri, D. Vavoulis, J. Feng, and M.P. Fontana. Material memristive device circuits with synaptic plasticity: Learning and memory. *BioNanoScience*, **1**, 24-30 (2011).
6. A.A. Minnekhanov, A.V. Emelyanov, D.A. Lapkin, K.E. Nikiryu, B.S. Shvetsov, A.A. Nesmelov, V.V. Rylkov, V.A. Demin, and V.V. Erokhin. Parylene based memristive devices with multilevel resistive switching for neuromorphic applications. *Sci. Rep.*, **9**, 10800 (2019).
7. N.V. Prudnikov, D.A. Lapkin, A.V. Emelyanov, A.A. Minnekhanov, Y.N. Malakhova, S.N. Chvalun, V.A. Demin, and V.V. Erokhin. Associative STDP-like learning of neuromorphic circuits based on polyaniline memristive microdevices. *J. Phys. D: Appl. Phys.* in press <https://doi.org/10.1088/1361-6463/ab9262> (2020).
8. A. Cifarelli, T. Berzina, and V. Erokhin. Bio-organic memristive device: Polyaniline – *Physarum polycephalum* interface. *Physica Status Solidi C*, **12**, 218-221 (2015).
9. S. Battistoni, V. Erokhin, and S. Iannotta. Frequency driven organic memristive devices for neuromorphic short and long term plasticity. *Org. Electronics*, **65**, 434-438 (2019).
10. E. Juzekaeva, A. Nasretidinov, S. Battistoni, T. Berzina, S. Iannotta, R. Khazipov, V. Erokhin, and M. Mukhtarov. Coupling cortical neurons through electronic memristive synapse. *Adv. Mater. Technol.*, **4**, 1800350 (2019).

#### 6:30 AM F.SM05.04.04

**Engineering of Synaptic Plasticity of Ion-Gel Gated Synaptic Transistors for Neuromorphic Computing and Artificial Sensory Nerves** Dae-Gyo Seo<sup>1</sup>, Yeongjun Lee<sup>1,2</sup>, Hoichang Yang<sup>3</sup>, Changduk Yang<sup>4</sup>, Sang-Woo Kim<sup>5</sup> and Tae-Woo Lee<sup>1</sup>; <sup>1</sup>Seoul National University, Korea (the Republic of); <sup>2</sup>Samsung Advanced Institute of Technology, Korea (the Republic of); <sup>3</sup>Inha University, Korea (the Republic of); <sup>4</sup>Ulsan National Institute of Science and Technology, Korea (the Republic of); <sup>5</sup>Sungkyunkwan University, Korea (the Republic of)

Unlike the inorganic neuromorphic electronics which can only implement the long-term plasticity, the organic neuromorphic electronics have paid attention due to promising applications from next-generation computing to neuroprosthetics by implementing not only the long-term potentiation (LTP) but also the short-term potentiation (STP). Recently, conjugated polymers such as poly(3-hexylthiophene-2,5-diyl) (P3HT) with electrolyte dielectrics have been studied to implement high-density computing and memory systems using less energy. Parallely, diketopyrrolopyrroles (DPPs) based artificial synaptic devices have shown promising applications from neuroprosthetics to soft robotics. However, recently studied organic-based artificial synapses only focused on emulating the single function of the biological counterparts; either memory or signal transitions.

In this study, we introduce the engineering of synaptic properties by modulating morphological characteristics of organics semiconductors (OSCs) with fixed presynaptic spike forms in artificial synaptic devices without changing the OSCs. By achieving this, the relation between the morphology of the film and the synaptic property has been revealed. Changing the morphological property of the OSCs, resulted in the clear transition from STP dominant synaptic property to LTP dominant synaptic properties. Furthermore, artificial neural networks (ANNs) simulation and artificial auditory sensory nervous system were successfully demonstrated. This achievement is an imperative step toward the development of versatile neuromorphic electronics and promising for various neuromorphic electronics applications from neuromorphic computing to neural

prosthetics, bio-interface devices, and soft robotics which can immensely expand the field of neuromorphic electronics by providing an understanding of the mechanisms of synaptic properties.

[1] D.-G. Seo, et al., *Nano Energy* **2019**, *65*, 104035 [2] Y. Kim, et al., *Science*. **2018**, *360*, 998 [3] Y. Lee, et al., *Sci. Adv.* **2018**, *4*, eaat7387 [4] W. Xu, et al., *Sci. Adv.* **2016**, *2*, e1501326

#### 6:45 AM \*F.SM05.04.05

##### **Scalable, Soft and Stretchable Optoelectronics and Neuromorphic Sensing Architectures in Human-Machine Interfaces** Benjamin C. Tee; National University of Singapore, Singapore

Human-machine interfaces will continue to be critical to advance applications in healthcare, robotics and consumer electronics. Having a cross-disciplinary approach to materials innovation, especially with regards to soft materials<sup>1</sup> will effectively address the mechanical constraints when interfacing with humans. In this talk, I will discuss some of the new material platforms we are developing for more robust human-machine interactions, such as self-healing stretchable optoelectronics devices<sup>2</sup>. Such optoelectronic devices might be employed in optogenetic neural interfaces. At the same time, I will also present our efforts in brain inspired scalable neuromorphic architectures for electronic skins<sup>3</sup>. Such system architectures can be broadly applied in various applications with high impact potential for wearables, brain-machine interfaces, prosthetics and robotics.

1. **Soft Electronically Functional Polymeric Composite Materials for a Flexible and Stretchable Digital Future**, B. C. K. Tee\*, J. Ouyang, *Advanced Materials*, 1802560, 2018.

2. **A transparent, self-healing and high-k dielectric for low-field-emission stretchable optoelectronics**, Y. J. Tan, H. Godaba, G. Chen, S. T. M. Tan, G. Wan, G. Li, P. M. Lee, Y. Cai, S. Li, R. F. Shepherd, J. S. Ho & B. C. K. Tee\*, *Nature Materials*, 2019.

3. **A neuro-inspired artificial peripheral nervous system for scalable electronic skins**, WW Lee, Y. J. Tan, H. Yao, S. Li, H. H. See, M. Hon, K. A. Ng, B. Xiong, J. S. Ho and B. C. K. Tee\*, *Science Robotics*, 2019.

#### 7:15 AM \*F.SM05.04.06

##### **New Materials and Device Concepts for Organic Electrochemical Transistors** Jonathan Rivnay; Northwestern University, United States

Organic electrochemical transistors (OECTs) have gained considerable interest for applications in bioelectronics, power electronics, circuits and neuromorphic computing. Their defining characteristic is the bulk-modulation of channel conductance owing to the facile penetration of ions into the (semi)conducting polymeric channel. For this reason, their device scaling relies on film thickness, enabling finer size scale devices, and unique form factors. Despite recent progress and a rapidly expanding library of new materials, the understanding of stability and transport/coupling of ionic and electronic carriers remain largely unexplored. We highlight recent synthetic and processing approaches used to tailor device properties and stability, as well as new opportunities enabled by such advances. We demonstrate how the reliance on bulk transport allows for relaxed fabrication demands and production of simple multi-device circuit concepts for analog signal processing. Finally, by studying the role of additives on charging, trapping, and structural re-arrangement, we can gain insight into the next generation of non-volatile organic mixed conductors for neuromorphic hardware. The implementation of OECT-based sensing and circuits holds particular promise in brain-inspired bioelectronics – the role of materials design and development is critical for their success.

#### 7:45 AM F.SM05.04.07

##### **Cellular Lensing and Near Infrared Fluorescent Nanosensor Arrays for Real-Time Chemical Efflux Cytometry** Sooyeon Cho, Xun Gong, Volodymyr Koman and Michael Strano; Massachusetts Institute of Technology, United States

Nanosensor arrays have proven to be powerful tools to measure single biological cells and organisms, achieving spatial and temporal precision even at the single molecule level. However, there has not been a way of extending this approach to statically relevant numbers of living cells and organisms. Herein, we design and fabricate a high throughput nanosensor array in a microfluidic channel that addresses this limitation, creating a Nanosensor Chemical Cytometry (NCC) for the first time. We show that one can utilize the cell itself as a lens and optical element to extract much more information from the nanosensor array on a per cell basis at high throughput. An array of nIR fluorescent single walled carbon nanotube (SWNT) sensors is deposited along a microfluidic channel through which a population of flowing cells is guided. As an example, the array can detect, in real time, the H<sub>2</sub>O<sub>2</sub> efflux of monocytes at attomole sensitivity at a rate of 10 cells/min. We show that the cells themselves can function as Gaussian lenses, projecting informative excitation profiles onto the nanosensor array. This

allows for cross-correlation of the cellular diameter, effective refractive index, and eccentricity with chemical efflux and creates a chemical cytometer for the measurement of cellular heterogeneity with unprecedented precision. For example, we study distinct H<sub>2</sub>O<sub>2</sub> efflux rates between 330 and 624 atmole/cell per min in cell size ranges of 271 and 263 μm<sup>2</sup>, eccentricity values between 0.405 and 0.363 and RI values between 1.383 and 1.377 for pristine and activated monocytes, respectively. Hence, we show that this new nanotechnology based tool has significant potential to answer important questions in cellular immunology, cell manufacturing and biopharmaceutical research.

#### 8:00 AM F.SM05.04.08

**3D Nanoarchitecture Materials for Synergistic Electrical/Optical Multimodal Sensing Capability** Hyeuk Jin Han<sup>1,2</sup>, Seunghee H. Cho<sup>2</sup>, Sangjun Han<sup>2</sup>, Ji-Soo Jang<sup>2</sup>, Gyu Rac Lee<sup>2</sup>, Eugene Cho<sup>2</sup>, Il Doo Kim<sup>2</sup>, Min Seok Jang<sup>2</sup>, Harry Tuller<sup>3</sup>, Judy Cha<sup>1</sup> and Yeon Sik Jung<sup>2</sup>; <sup>1</sup>Yale University, United States; <sup>2</sup>Korea Advanced Institute of Science and Technology, Korea (the Republic of); <sup>3</sup>Massachusetts Institute of Technology, United States

To detect chemical or biological molecules, it is crucial that sensor devices can differentiate various target molecules. However, in general, each sensing methods are geared towards one aspect for sensing while sacrificing others due to their particular limitations. For example, gas sensors based on metal oxide have high sensitivity while having low identification ability. On the other hand, surface-enhanced Raman spectroscopy is a representative label-free and selective detection method that can identify target molecules but often lack quantitative sensing capability, especially for gaseous targets. Herein, we introduce a label-free electrical/optical multimodal sensor based on systematically assembled 3D nanoarchitecture with multifunctional materials for optimizing the structure effect. It combines several sensing modalities and sensing elements via the integration of semiconducting nanowire frameworks and dual-functioning metallic nanoparticles. Our multimodal sensor can successfully estimate the mixed gas compositions selectively and quantitatively in the sub-100 ppm level, even in a mixture of gaseous aromatic compounds with similar molecular structures by providing complementary information. Our approach not only provides the sensitivity but also has the ability to differentiate the target molecules. Potentially, a multimodal sensor could be an application to early diagnosis of many diseases and the rapid detection of toxic chemicals and explosives

SESSION F.SM05.05/F.FL01.06: Joint Session: Bioelectronics and Sensing  
On Demand Abstracts Available for Viewing Starting Saturday Morning, November 21, 2020  
F-SM05

#### 5:00 AM \*F.SM05.05/F.FL01.06.01

**Electron Transporting Polymers for Biological Interfacing** Sahika Inal; King Abdullah University of Science and Technology (KAUST), Saudi Arabia

Fluidity, mobility, and resistivity are key characteristics of native membranes in our cells where cation channels regulate numerous molecular mechanisms (e.g., the excitation of neurons). Interfacing with biomimetic membranes via electronic devices promises to expand our understanding of the function of these membranes in disease states. The challenge is to form supported lipid bilayer (SLBs) on (semi)conducting films while sustaining high sensitivity and operational stability. In this talk, I will show the traits of n-type organic semiconductors for such biological interfaces. I will show the very first ion channel sensor based on an n-type, accumulation mode, microscale organic electrochemical transistor (OECT), which interfaces an SLB embedded with a pore-forming protein. The polymer is particularly sensitive to divalent cations, endowing the system with biomimetic properties. The side-chain engineering of semiconducting polymers prompts the development of next-generation bioelectronic hybrids where electron-transporting polymers establish bilateral electronic communication with living systems.

#### 5:30 AM \*F.SM05.05/F.FL01.06.02

**Thin-Film Organic Electrochemical Devices for Applied Neural Control—Capacitive and Faradaic Effects** Eric Glowacki; Linköping University, Sweden

A great demand exists for minimally-invasive neuromodulation technologies to enable next-generation bioelectronic medicine. We report on our developments of ultrathin organic (opto)electronic devices for neurostimulation. All of these

devices rely on far red/near infrared irradiation in the tissue transparency window to actuate nanoscale organic semiconductor components. Our flagship technology is the organic electrolytic photocapacitor (OEPC) – a device that mimics biphasic current-pulse neurostimulation and thus transduces an optical signal into directly-evoked action potentials in neurons. These devices are not only wireless, but also 100-1000 times thinner than most existing technologies. We will discuss chronic implants capable of stimulating peripheral nerves (sciatic and vagus) when actuated from outside of the body using diode lasers. We have observed stable operation in rodent models for at least 100 days. As a different approach, we will report on favorable harnessing of DC electrochemistry effects, normally considered spurious and undesired. Specifically, we show how electrochemical generation of low doses of hydrogen peroxide can be used to reversibly stimulate M-type potassium channels, providing a novel method of controlling neural excitability.

#### **6:00 AM F.SM05.05/F.FL01.06.03**

**Enhancement-Mode Ion-Based Transistors for *In Vivo* Electrophysiology and Real-Time Data Processing** Claudia Cea, Georgios Spyropoulos, Jennifer Gelinis and Dion Khodagholy; Columbia University, United States

Bioelectronic devices must have high speed and high performance to interact with the often rapid, low amplitude signals generated by neural tissue. They should also be capable of forming complementary logic and analog circuits to allow acquisition, processing and manipulation of a biological environment. However, the lack of readily available p-type polymers for use in enhancement mode transistors and their complicated synthesis significantly limits the investigation and application of such devices in bioelectronics. Here, we develop an enhancement mode ion-gated transistor (e-IGT) that functions based on a reversible redox reaction and hydrated ion reservoirs within the conducting polymer channel to enable long-term stable operation and shortened ion transit time. We combined a highly conductive poly(3, 4-ethylenedioxythiophene) doped with polystyrene sulfonate (PEDOT:PSS) and a reducing agent polyethylenimine (PEI) to enable doping of the polymer in an aqueous environment. The transistor operates as following: (1) the protonated PEI bonds with the PSS- and de-dopes the PEDOT:PSS chain resulting in an initial off-state of the transistor, (2) a subsequent application of negative gate voltage dopes the PEDOT:PSS switching the channel on. To determine an optimal transistor configuration and material composition, we microfabricated transistor arrays of varying geometrical parameters. The high-transconductance and high-speed of the e-IGTs resulted in a gain bandwidth product that is several orders of magnitude above other ion-based transistors. We used these transistors to acquire a wide range of electrophysiological signals, including in vivo recording of neural action potentials. Furthermore, we combined E-IGTs with d-IGTs to create a real-time non-linear rectifier to accurately detect epileptic discharges in vivo. In conclusion, E-IGTs offer a safe, reliable, and high performance building block for chronically implanted bioelectronics, with spatiotemporal resolution to the scale of individual neurons.

#### **6:15 AM F.SM05.05/F.FL01.06.04**

**Organic Electrochemical Transistors Based on Electropolymerized Dendritic Structures** Kamila Janzakova<sup>1</sup>, Mahdi Ghazal<sup>1</sup>, Ankush Kumar<sup>1</sup>, Yannick Coffinier<sup>1</sup>, David Guérin<sup>1</sup>, Sébastien Pecqueur<sup>1</sup> and Fabien Alibert<sup>1,2</sup>; <sup>1</sup>University of Lille, France; <sup>2</sup>Laboratoire Nanotechnologies & Nanosystèmes (LN2), Canada

One of the neuromorphic engineering aims is using nanoelectronics' materials and devices to reproduce key features that are used by the brain for computing. Currently, neuromorphic engineering has explored standard silicon-based technologies (i.e. such as complementary metal-oxide-semiconductor) or more emerging material and devices (iono-electronic materials and resistive memory devices, for example). Most of these technologies are still bounded to a top down approach. However, brain computing largely rely on bottom-up processes. For instance, interconnectivity between cells and formation of communication pathway in neural networks result principally from bottom-up organization. Here, we show how dendritic growth of organic conductive polymers (PEDOT) can be used to mimic structural branching observed in neural network. Conducting-polymer based dendritic structures with different morphology are synthesized in a two-electrode setup by pulsed voltage-driven electropolymerization derived from state-of-the-art bipolar AC-electrochemical synthetic methods. We show how various AC signals can lead to a large variety of dendritic structures and PEDOT morphologies. In a second part, such dendritic structures are used to implement functional OECTs. More importantly, we focus on the transconductance and memory effects that can be obtained in such dendritic OECTs such as short term plasticity. We report on the relationship between dendrites morphologies and STP time constant. This work paves the way to new approaches for neuromorphic engineering, such as structural plasticity and neural network topology exploration.

#### **6:30 AM \*F.SM05.05/F.FL01.06.05**

**Forming Input/Output (i/o) Interfaces with Excitable Cells And Tissue Using Nanocarbons** Tzahi Cohen-Karni; Carnegie Mellon University, United States

We focus on developing a new class of nanoscale materials and novel strategies for the investigation of biological entities at multiple length scales, from the molecular level to complex cellular networks. Our highly flexible bottom-up nanomaterials synthesis capabilities allow us to form unique hybrid-nanomaterials that can be used in various input/output bioelectrical interfaces. For example, we have developed several bioelectrical platforms based on graphene, a two-dimensional (2D) atomically thin carbon allotrope. We have demonstrated recording of the electrical activity of excitable cells with graphene-based ultra-microelectrodes as small as the size of an axon ca. 2 μm in size. Using graphene-based hybrid-nanomaterials, we have formed remote, non-genetic bioelectrical interfaces with excitable cells and modulated cellular and network activity with high precision and low needed power. We have also developed a breakthrough bioelectrical interface, a 3D self-rolled biosensor arrays (3D-SR-BAs) of either active field effect transistors or passive microelectrodes to measure both cardiac and neural spheroids electrophysiology in 3D. Our approach enables electrophysiological investigation and monitoring of the complex signal transduction in 3D cellular assemblies toward an organ-on-an-electronic-chip (organ-on-e-chip) platform for tissue maturation investigations and development of drugs for disease treatment. In summary, the exceptional synthetic control and flexible assembly of nanomaterials provide powerful tools for fundamental studies and applications in life science and open up the potential to seamlessly merge either nanomaterials-based platforms or unique nanosensor geometries and topologies with cells, fusing nonliving and living systems together.

**7:00 AM \*F.SM05.05/F.FL01.06.06**

**High-Resolution Bioelectronic Interfaces Enabled by Nanoscale Soft Conductors** Flavia Vitale; University of Pennsylvania, United States

The rapid rise of bioelectronics has enabled a number of innovative approaches to treat neurological disorders, restore and repair lost functions, and modulate neural circuitry to control mood and behavior. The vast majority of bioelectronic interfaces, however, still rely on traditional noble metal and silicon materials, which are expensive to source and process and are intrinsically inadequate to address the mechanical, chemical, and electrical properties of excitable circuits in the body. To establish bioelectronic technologies as the clinical standard, significant innovations in materials and fabrication strategies are still required to achieve safety, softness, biocompatibility, and long-term stability. Nanostructured materials are uniquely positioned to address these challenges because they combine high electrical conductivity with intrinsically high mass-specific surface area and mechanical flexibility. Furthermore, they can interact with biological systems on a molecular scale and can be easily integrated within scalable solution-based processing, thus allowing easy modulation of their electronic and optical properties.

In this talk I will present the ongoing work in my lab to leverage the unique properties of nanostructured materials and engineer novel bioelectronic interfaces for sensing and stimulating neural and neuromuscular circuits. Specifically, I will describe the fundamental electronic, electrochemical, and mechanical properties of 2D transition metal carbides nanomaterials (a.k.a. MXenes) and how these translate into significant impedance and noise reduction when MXenes are integrated bioelectronic interfaces. Then, I will present *ad hoc*, scalable, rapid manufacturing processes developed in my lab to translate the exceptional material properties at the molecular scale into high-resolution, low impedance bioelectronic interfaces that are also compatible with clinical neuroimaging modalities, such as magnetic resonance imaging (MRI) and computerized tomography (CT). Finally, to illustrate the potential of MXene-based bioelectronics, I will present different examples of applications in both implantable and wearable interfaces.

**7:30 AM F.SM05.05/F.FL01.06.07**

**Late News: Spatiotemporal Response of Organic Electrochemical Transistors** Dimitrios Koutsouras<sup>1</sup>, Morteza Hassanpour Amiri<sup>1</sup>, Katharina Lieberth<sup>1</sup>, Kamal Asadi<sup>1</sup>, Fabrizio Torricelli<sup>2</sup>, Paul W. Blom<sup>1</sup> and Paschal Gkoupidenis<sup>1</sup>; <sup>1</sup>Max Planck Institute for Polymer Research, Germany; <sup>2</sup>University of Brescia, Italy

Organic electrochemical transistors (OECTs) have recently attracted tremendous attention in the scientific community due to their unique set of features. Especially, the lack of an insulating layer that separates gate from channel, like in conventional field effect transistors, and their feature to support electrolyte gating open new pathways in the field of bioelectronics. In particular, they render the device ideal for measurements in the aqueous environments that dominate the biological world. Additionally, they provide extra possibilities in terms of the device architecture as the gating electrode can be patterned on the same plane as the conducting channel. In a set up like that, what is of extreme interest is the effect of the gate position with respect to the channel. In this work, the spatiotemporal response of a poly(3,4 ethylenedioxythiophene) polystyrene sulfonate (PEDOT:PSS) OECT is examined and its device physics is studied. This work opens new routes for exploiting the physics of multi terminal OECT devices in bioelectronics, sensing and neuromorphic electronics.

SESSION F.SM05.06: Poster Session: Organic Neuromorphic Materials and Devices  
On Demand Abstracts Available for Viewing Starting Saturday Morning, November 21, 2020  
5:00 AM - 8:00 AM  
F-SM05

### F.SM05.06.03

**Mood Identification by Facial Subtle Movement Analysis** Fan Yang<sup>1</sup>, Jordan Saadon<sup>1</sup>, Ryan Burgert<sup>1</sup>, Selma Mohammad<sup>1</sup>, Miriam H. Rafailovich<sup>1</sup>, Charles Mikell<sup>1</sup>, Sima Mofakham<sup>1</sup>, Wade Boohar<sup>2</sup>, Sophia Cai<sup>3</sup> and Amisha Agrawal<sup>4</sup>; <sup>1</sup>Stony Brook University, United States; <sup>2</sup>Olathe North High School, United States; <sup>3</sup>Barrington High School, United States; <sup>4</sup>University High School, United States

Research into mood and emotion has often been dependent on self-report, highlighting the need for a more objective measure of mood state. However, until recently, it has been nearly impossible for machines to match the speed and accuracy of the average person in interpreting faces. In this study, we used digital image speckle correlation (DISC), a technique which was originally used to study the mechanical properties of materials by tracking their deformations, to assess an individual's mood state based on the analysis of facial microexpressions. Ten healthy volunteers were shown a set of ten happy and ten sad images while being videotaped. Upon measuring facial movements in response to happy and sad images, we conducted detailed Shannon entropy and Principal Component Analysis (PCA) to identify facial maps for different mood states. Within and across subjects, happy and sad images elicited spatially distinct changes in facial expression. PCA and entropy calculations on facial movement reliably distinguished the subject's underlying mood. Furthermore, we characterized key changes in facial expression which reliably signal changes in mood state across all individuals. DISC-based analysis of the face was capable of determining an individual's mood with high specificity across multiple test subjects, suggesting that automated camera-based methods may be both robust and economical in clinical monitoring settings. It also showed promising potentials in brain study together with electroencephalogram as subtle facial movements were also found in epilepsy and comatose patients using DISC.

## SYMPOSIUM F.SM06

---

Biofabrication for Emulating Biological Tissues  
November 21 - December 2, 2020

### Symposium Organizers

Mario Alvarez, Tecnologico de Monterrey  
Tim Woodfield, University of Otago  
Yu Shrike Zhang, Harvard Medical School  
Weijia Zhang, Fudan University

### Symposium Support

#### **Gold**

National Science Foundation

#### **Bronze**

Allevi, Inc.

---

\* Invited Paper

SESSION F.SM06.06: Live Keynote I: Biofabrication for Emulating Biological Tissues  
Session Chairs: Grissel Trujillo de Santiago, Tim Woodfield and Yu Shrike Zhang

Tuesday Afternoon, December 1, 2020  
F.SM06

**1:45 PM \*F.SM06.02.01**

**Converged Biofabrication Technologies for the Generation of Osteochondral Implants with Long-Term Functionality** Jos Malda<sup>1,2</sup>; <sup>1</sup>UMC Utrecht, Netherlands; <sup>2</sup>Utrecht University, Netherlands

A major challenge in the application of regenerative medicine strategies is the replication of the complexity and functionality of living tissues. Biofabrication techniques, such as inkjet, extrusion, or light-assisted printing, can result in living structures that further replicate the 3D architecture and organization of native tissue. Recent developments have resulted in the availability of a plethora of bioinks, new printing approaches, and the technological advancement of established techniques. However, it remains largely unknown which materials and technical parameters are essential for the fabrication of intrinsically hierarchical cell-material constructs that truly mimic biological function of tissues. Moreover, it is unlikely that any of these technologies used individually would be able to replicate this complexity and functionality. Hence, we previously urged the field to shift its focus from materials and technologies toward the biological development of the resulting constructs.

This is illustrated by an example from the field of orthopaedics, in particular the treatment of osteochondral defects in a large (equine) animal model. Driven by the observations that the collagen structure provides articular cartilage with its extraordinary mechanical properties and that this structure does not recover once damaged, we evaluated the performance of a biofabricated composite osteochondral implant designed to provide long-term mechanical resistance, comparing implants cell-seeded with cell-free implants. The implants were composed of a gelatin methacryloyl cartilage phase, reinforced with precisely patterned melt electro-written polycaprolactone micrometer-scale fibers and displaying a zonal, cartilage-mimetic architecture. This structure was firmly integrated with a room temperature-setting calcium phosphate cement-based bone anchor via a converged melt electrowriting-extrusion-based printing approach. Cell-containing implants were pre-cultured in vitro and samples were then implanted orthotopically in ponies for 6 months. The reinforcement of the cartilage phase enhanced both the compressive and shear properties of the implants considerably, closer to native values than achieved before.

Abundant deposition of glycosaminoglycan- and type II collagen-rich tissue was observed in vitro, which was maintained during the 6-month in vivo implantation period, showing that the composite architecture, comprising multi-scale printing of hydrogel, microfibers and ceramic materials had provided the required mechanical stability and integration of the implant within the subchondral bone to allow survival of the implant in the mechanically challenging environment of the equine knee joint over an extensive period of time while retaining its mechanical characteristics. Our findings underscore the hypothesis that the mechanical stability is more determining for the success of the implant than the presence of cells. This observation is of great translational importance and highlights the aptness of advanced (bio)fabrication and 3D printing technologies for functional tissue restoration in the harsh articular environment.

**2:15 PM \*F.SM06.03.01**

**Strategies to Engineer a Functional Kidney Proximal Tubule** Rosalinde Mascreeuw; University of Utrecht, Netherlands

In patients with severe kidney disease, renal clearance is compromised resulting in the accumulation of a plethora of endogenous waste molecules that cannot be removed by current dialysis techniques, the most often applied treatment. These uremic retention solutes, also named uremic toxins, are a heterogeneous group of organic compounds of which many are too large to be filtered and/or are protein-bound. Their renal excretion depends largely on renal tubular secretion by which the binding is shifted towards the free fraction that can be eliminated. To facilitate this process, kidney proximal tubule cells are equipped with a range of transport proteins that cooperate in cellular uptake and urinary excretion. In recent years, we and others have invested in the development of bioengineered kidney tubules that could potentially restore this essential function. For this, well characterized human kidney proximal tubule cells were combined with functionalized, living membranes. This presentation addresses these developments in the context of functional kidney tubule engineering. Furthermore, hurdles to take before a safe implementation of bioengineered kidneys in clinics becomes a realistic option will be discussed.

**2:45 PM \*F.SM06.01.01**

**Biomaterials for the Early Detection and Treatment of Disease** Joyce Y. Wong; Boston University, United States

To engineer and build tissues, one requires an understanding of key relationships between cell behavior and the underlying substrate. In native tissues, extracellular matrix proteins are in the form of fibrous networks, sheets, and fibers. Our laboratory has been developing methods to form extracellular matrix fiber alloys and cell sheets. Over the past few years, we

have been investigating the role of composition and processing conditions of various extracellular matrix fibers and alloy fibers on mechanical properties and biological properties. These fibers are also critical components of tissues such as blood vessels. We have also determined the role of mechanical strain on binding of different antibodies and peptide-functionalized contrast agents to these fibers. Importantly, we discovered that composition can be tuned to stabilize extracellular matrix proteins in fiber forms, which is especially useful with compositions where it is difficult to process the proteins into fibers. Through an integrated computational and experimental approach, we have discovered relationships between hydrophobicity and protein fiber forming capability and stability. Moreover, we have verified that the protein alloy fibers support cell adhesion and allow one to tune the mechanical properties of the fiber. This is of significance as the mechanical properties of the substrate play an important role in modulating cell behavior, e.g. cell migration and proliferation. We have also developed several methods to generate a layered tissue patch that mimics the cellular organization of native vessels and a bioMEMS device that can be used to assess physiological function of these tissue-engineered constructs with patient data input.

### **3:15 PM \*F.SM06.03.03**

**Engineering the Microenvironment That will Enable a Long-Term Bioprosthetic Ovary Transplant** Monica M. Laronda<sup>1,2</sup>; <sup>1</sup>Ann and Robert H. Lurie Children's Hospital of Chicago, United States; <sup>2</sup>Northwestern University, United States

The ovaries contain a finite resource of potential eggs and sex hormone-producing cells, and therefore, life-saving cancer treatments that irradiate or chemically induce cell death within the ovaries will likely result in premature ovarian insufficiency (POI) with reduced ovarian hormones and infertility. The option to have biological children, is a key quality of life measure for cancer survivors. Women with POI will experience co-morbidities associated with loss of ovarian hormones and a shorter life expectancy. The only method for fertility preservation for pediatric patients, who do not yet make eggs, is ovarian tissue cryopreservation (OTC). This tissue can then be transplanted back to restore fertility and hormone function. However, only 20 – 30% of transplants result in livebirth and it produces an average of 2 – 5 years of hormone restoration, leaving many without biological children and decades of post-cancer survival without essential hormone production. One major contributor to the shortened function of transplanted ovarian tissue is the significant spike in activation of the ovarian reserve (primordial follicles, containing the oocytes and hormone-producing cells) and subsequent depletion, at least in part, due to the disruption in the microenvironment. Additionally, some patients have metastatic disease within the ovary and therefore cannot use that tissue in its current form. Therefore, a safe, long-term solution for fertility and hormone restoration would involve isolating the ovarian cells that are essential for function from potential cancer cells and housing them in a microenvironment that maintains the bank of potential eggs and prolongs hormone production. We have defined the architectures of a 3D printed scaffold that support the necessary cell-cell contacts between the oocyte and the surrounding hormone producing support cells. This bioprosthetic ovary of the 3D printed gelatin scaffold with isolated ovarian follicles restored fertility and hormone function and supported livebirths and rearing of offspring in mice. To advance this research through the next steps toward translation to the clinic, we must define the follicular microenvironment that will enable a regulated recruitment of eggs from the ovarian reserve and support a safe, effective and long-term transplant. We have mapped the matrix composition across the ovarian compartments and the stiffness of tissue components in ovaries of large mammals. Our novel proteomics screen and analysis has enabled us to identify new matrix proteins within the ovary and pinpoint proteins of interest that may control primordial follicle activation or quiescence. We have additionally defined the physical properties of the ovarian compartments, where the cortical (outer) region is denser and stiffer than the medullary (inner) region. We have developed decellularized ovary extracellular matrix inks and are investigating the roles of specific biochemical and physical cues on primordial follicle quiescence and activation. A bioprosthetic ovary, defined by these microenvironment properties, would improve current options for fertility and hormone restoration for women.

### **3:30 PM \*F.SM06.02.03**

**Using Chaotic Advection for Facile High-Throughput Fabrication of Ordered Multilayer Micro- and Nanostructures—Continuous Chaotic Printing** Grissel Trujillo de Santiago, Edna Johana Bolívar-Monsalve, Carlos Ceballos-González, Carolina Chávez-Madero, Mohamadmahdi Samandari, Diego Armando Sandoval Salaiza, Yu Shrike Zhang and Mario M. Alvarez; Tecnológico de Monterrey, Mexico

Today, tissue engineering evolves exponentially and provides real solutions to create biological models and solve clinical problems. However, we still face challenges that hinder its full potential to generate complex and large-size tissues and organs. Here we present advances in chaotic bioprinting, an additive manufacturing technique that enables the creation of complex biological structures at an unprecedented level of resolution and throughput.

Continuous chaotic printing uses chaotic advection for deterministic and continuous extrusion of fibers with internal multilayered structures. Two free-flowing materials are coextruded through a printhead containing a miniaturized Kenics static mixer (KSM) composed of multiple helicoidal elements. This produces a fiber with a well-defined internal multilayer



microarchitecture at high-throughput ( $>1.0 \text{ m min}^{-1}$ ). The number of mixing elements and the printhead diameter determine the number and thickness of the internal lamellae, which are generated according to successive bifurcations that yield a vast amount of inter-material surface area ( $\sim 10^2 \text{ cm}^2 \text{ cm}^{-3}$ ) at high resolution ( $\sim 10 \text{ }\mu\text{m}$ ). This creates a new opportunity to produce structures with extremely high surface area to volume (SAV). Comparison of experimental and computational results demonstrates that continuous chaotic 3D printing is a robust process with predictable output. The simplicity and high resolution of continuous chaotic printing strongly supports its potential use in novel applications.

Here, we illustrate the application of continuous chaotic bioprinting into the fabrication of complex multi-layered bacterial microcosmoi. We demonstrate that the degree of resolution achieved within these constructs can be finely controlled up to the range of a few microns of separation between layers and that the degree of interface between bacterial layers greatly matters for competition.

We also demonstrate the application of tissue-like structures in which living layers of muscle cells evolve into a coherent segment of muscle. Lumina can be easily built into these constructs by using a combination of sacrificial and permanent inks and a multi-port modification to the chaotic printhead.

We are currently exploring more applications of chaotic printing into tissue engineering such as the fabrication of vascularized cancer models, and multi-cell type tissue-like architectures where distinctive mammalian cell layers share a high amount of common interface.

Different fields, outside biosciences and technologies, are also in pursuit of simple and robust ways to create multilayered and multi-material structures to attain functionalities that monolithic materials do not exhibit. We envision that chaotic printing may be applied to technological scenarios such as the fabrication of batteries, superconductors, super catalytic surfaces, and 3D microfluidic reactors.

SESSION F.SM06.07: Live Keynote II: Biofabrication for Emulating Biological Tissues

Session Chairs: Tim Woodfield and Yu Shrike Zhang

Wednesday Afternoon, December 2, 2020

F.SM06

#### 5:15 PM \*F.SM06.04.01

**Growth, Characterization and Application of Self-Organized Microvascular Networks for Models of Disease** Roger Kamm; Massachusetts Institute of Technology, United States

Methods now exist to create single- or multi-organ engineered living systems that can be used to model a variety of disease processes. Aside from providing new insights into disease mechanisms, these systems can also be used to screen new drugs to treat the disease, or even to identify different therapeutic strategies for sub-populations possessing different genetic profiles. Here we present several models that require a microvascular network, modeling different stages of metastatic cancer. In one set of studies, circulating tumor cells are introduced via side channels into the microvascular bed, where they arrest, become activated and undergo transendothelial migration. Model systems include the brain, muscle, placenta and bone marrow, each showing distinctive characteristics. These or others can be used to model drug delivery to a developing tumor, either primary or metastatic.

Microfluidic devices used in these studies are, for the most part, simple, single layer systems that can be cast in a single piece of PDMS, forming channels and gel compartments by bonding to a coverslip. Alternatively, systems can be injection molded in tissue culture plastics. Microphysiological systems (MPS) can be either 'engineered' or self-organize using the same capabilities of developing organisms. Our approach is to rely, as much as possible, on the innate capabilities of the cells to interact to form the structures of a particular organ. Cells or cell assemblies/organoids are mixed in hydrogel solution and injected into one or more adjacent compartments allowing for direct signaling or physical contact between the multiple different cell types. Many of these systems contain microvascular networks that can be perfused via side channels, with pumping by simple low-pressure diaphragm pumps, directly connected to the MPS to minimize media volumes. The role of circulating immune cells can also be studied, as these, too, arrest in the vascular beds and extravasate into the surrounding gel matrix.

Results will be shown first demonstrating the form and function of the microvascular beds. Then several examples will be taken from the systems mentioned above to illustrate different applications, and to demonstrate the flexibility of the underlying platform. Future directions will be discussed including the challenges ahead in generating perfusable organoids.

#### 5:45 PM \*F.SM06.03.02

**Stem Cell-Derived Models to Study Human Neural System Development** Jianping Fu; University of Michigan-Ann Arbor, United States

Neurulation is a key developmental process that gives rise to the neural tube (NT), the precursor structure of the central nervous system (CNS). Neurulation is initiated after the gastrulation by a neural induction process, during which the dorsal ectoderm is specified into a patterned tissue containing the neural plate (NP) and the non-neural ectoderm (NNE) separated by the neural plate border (NPB). After neural induction, the NP folds and fuses to form the tubular NT. The development of the NT continues with differentiation of distinct classes of neuronal progenitor cells located at defined positions within the NT along both the anterior-posterior (AP) and dorsal-ventral (DV) axes. In this talk, I will discuss the recent research activities in my group to leverage the developmental potential and self-organization property of human pluripotent stem cells (hPSCs) in conjunction with 2D and 3D bioengineering tools to achieve the development of spatially patterned multicellular tissues that mimic certain aspects of early human neurulation process, including neural induction, AP and DV patterning of the NT. These stem cell-derived models offer promising trackable systems to study neural development and disease.

**6:15 PM \*F.SM06.01.02**

**Bioelectronic Devices and Materials for Engineered, 3D Hybrid Tissues** Brian Timko; Tufts University, United States

Hybrid bioelectronic systems offer unique advantages to achieve two-way electronic communication with living cells and tissues. Bioelectronic devices are readily multiplexed and form seamless, stable interfaces with surrounding cells and tissues, representing a distinct advantage over conventional systems such as patch clamp and optical dyes. First, we will present an overview of our recent heart-on-a-chip platform which integrated both extra- and intracellular devices for monitoring cardiac electrophysiology during episodes of acute hypoxia. This system allowed us to monitor not only cell-cell communication (e.g., wavefront propagation) but also action potentials at several spatially-distinct regions simultaneously. Next, we will discuss prospects for flexible bioelectronic scaffolds for achieving hybrid, 3D cardiac or brain systems. We developed a Photo-crosslinkable Silk Fibroin (PSF) derivative which was compatible with conventional photolithography processes and enabled flexible scaffolds with well-defined geometries and cm-scale uniformity. Our freestanding PSF-based scaffolds supported bioelectronic devices, provided excellent electrical passivation, and adhered both cardiac and neuron model cells. Finally, we will discuss recent work to develop stimulation elements for spatially-selective neural activation. Taken together, these research directions open new avenues for engineered, bioelectronics-innervated cardiac and brain systems. We will discuss prospects for merging our bioelectronic devices with state-of-the-art tissue engineering techniques.

**6:30 PM \*F.SM06.02.02**

**Extracellular Matrix-Derived Printable Biomaterials for Engineering Human Tissues** Jinah Jang; Pohang University of Science and Technology, Korea (the Republic of)

The recent development of bioengineering enables to create human tissues by integrating various native microenvironments, including tissue-specific cells, biochemical and biophysical cues. A significant transition of 3D bioprinting technology into the biomedical field helps to improve the function of engineered tissues by recapitulating physiologically relevant geometry, complexity, and vascular network. Bioinks, used as printable biomaterials, facilitate dispensing of cells through a dispenser as well as support their viability and function by providing engineered extracellular matrix. The successful construction of functional human tissues requires accurate environments that are able to mimic the biochemical and biophysical properties of the target tissue. This talk will cover my research interests in building 3D human tissues and organs to understand, diagnose, and treat various intractable diseases, particularly for cardiovascular diseases and diabetes. A development of tissue-derived decellularized extracellular matrix bioink will be mainly discussed as a straightforward strategy to provide biological and biophysical phenomena into engineered tissues. I will also discuss the development of a 3D vascularized stem cell patch that is generated by integrating the concept of tissue engineering and the developed platform technologies. Combined with recent advances in human pluripotent stem cell technologies, printed human tissues could serve as an enabling platform for studying complex physiology in tissue and organ contexts of individuals.

**7:00 PM \*F.SM06.04.02**

**Microfluidic Organs-on-Chips** Yuanjin Zhao; Southeast University, China

In biological research, the interaction of biomolecules, cells and materials is an eternal topic. Many technologies have been employed to construct three-dimensional micro- and nano- hierarchical structure of materials. However, it is still a challenge to combine the artificially controllable biomaterials and the complicated biomolecular interaction/cell living unit, and thus to realize the regulation and control of the cell culture by using these materials. Moreover, it is necessary to develop a biotechnology for cell research to real-time and accurately monitor the interaction of the biomolecules/cells and the

biomaterials, which could effectively reveal the biological mechanism of the cell behavior. In this point, we proposed to generate the desired functional materials by using microfluidic methods. Based on this technology, we have created a series of novel biomaterials, which showed demonstrated values in cells culture and organs-on-chips construction.

SESSION F.SM06.01: Bioanalysis of Engineered Tissues and Tissue Models  
On Demand Abstracts Available for Viewing Starting Saturday Morning, November 21, 2020  
F-SM06

**5:00 AM \*F.SM06.01.01**

**Biomaterials for the Early Detection and Treatment of Disease** Joyce Y. Wong; Boston University, United States

To engineer and build tissues, one requires an understanding of key relationships between cell behavior and the underlying substrate. In native tissues, extracellular matrix proteins are in the form of fibrous networks, sheets, and fibers. Our laboratory has been developing methods to form extracellular matrix fiber alloys and cell sheets. Over the past few years, we have been investigating the role of composition and processing conditions of various extracellular matrix fibers and alloy fibers on mechanical properties and biological properties. These fibers are also critical components of tissues such as blood vessels. We have also determined the role of mechanical strain on binding of different antibodies and peptide-functionalized contrast agents to these fibers. Importantly, we discovered that composition can be tuned to stabilize extracellular matrix proteins in fiber forms, which is especially useful with compositions where it is difficult to process the proteins into fibers. Through an integrated computational and experimental approach, we have discovered relationships between hydrophobicity and protein fiber forming capability and stability. Moreover, we have verified that the protein alloy fibers support cell adhesion and allow one to tune the mechanical properties of the fiber. This is of significance as the mechanical properties of the substrate play an important role in modulating cell behavior, e.g. cell migration and proliferation. We have also developed several methods to generate a layered tissue patch that mimics the cellular organization of native vessels and a bioMEMS device that can be used to assess physiological function of these tissue-engineered constructs with patient data input.

**5:15 AM \*F.SM06.01.02**

**Bioelectronic Devices and Materials for Engineered, 3D Hybrid Tissues** Brian Timko; Tufts University, United States

Hybrid bioelectronic systems offer unique advantages to achieve two-way electronic communication with living cells and tissues. Bioelectronic devices are readily multiplexed and form seamless, stable interfaces with surrounding cells and tissues, representing a distinct advantage over conventional systems such as patch clamp and optical dyes. First, we will present an overview of our recent heart-on-a-chip platform which integrated both extra- and intracellular devices for monitoring cardiac electrophysiology during episodes of acute hypoxia. This system allowed us to monitor not only cell-cell communication (e.g., wavefront propagation) but also action potentials at several spatially-distinct regions simultaneously. Next, we will discuss prospects for flexible bioelectronic scaffolds for achieving hybrid, 3D cardiac or brain systems. We developed a Photo-crosslinkable Silk Fibroin (PSF) derivative which was compatible with conventional photolithography processes and enabled flexible scaffolds with well-defined geometries and cm-scale uniformity. Our freestanding PSF-based scaffolds supported bioelectronic devices, provided excellent electrical passivation, and adhered both cardiac and neuron model cells. Finally, we will discuss recent work to develop stimulation elements for spatially-selective neural activation. Taken together, these research directions open new avenues for engineered, bioelectronics-innervated cardiac and brain systems. We will discuss prospects for merging our bioelectronic devices with state-of-the-art tissue engineering techniques.

**5:30 AM F.SM06.01.03**

**“All Electric” Ion Pumps as Artificial Cell Membranes** Gideon Segev<sup>1</sup>, Rylan J. Kautz<sup>2</sup>, Shane Ardo<sup>2,2,2</sup>, David Larson<sup>3,3</sup>, Joel W. Ager<sup>3,3,4</sup> and Francesca Maria Toma<sup>3,3</sup>; <sup>1</sup>Tel Aviv University, Israel; <sup>2</sup>University of California, Irvine, United States; <sup>3</sup>Lawrence Berkeley National Laboratory, United States; <sup>4</sup>University of California, Berkeley, United States

Ion pumps are devices that use external power to introduce a net ionic flux. For example, in the photosynthetic process, light is used to pump protons up a concentration gradient which will be used in sequential steps to generate fuels. Although every cell membrane is essentially an ion pump, an artificial ion pump that can operate in steady state with no associated redox reactions is yet to be demonstrated. In this contribution we report a first of its kind “all electric”, ion pump based on a ratcheting mechanism.

Electronic ratchets are devices that utilize modulation in a spatially varying electric field to drive steady state current. Similar to peristaltic pumps, where the pump mechanism is not in direct contact with the pumped fluid, electronic ratchets induce net ionic current with no direct charge transport between the power source and the pumped charge carriers. Thus, electronic ratchets can be used to pump ions in steady state with no electrochemical reactions between the power source and the pumped ions resulting in an “all electric” ion pump.

Porous capacitor based ion pumps were fabricated by coating the two surfaces of nano-porous alumina wafers with gold. The electric field within the nano-pores is modulated by oscillating the capacitors voltage. Thus, when immersed in solution, ions within the pores experience a modulating electric field resulting in ratchet based ion pumping. The device pumping performance was studied both theoretically and experimentally for various input signals, geometries and solutions. It is shown that different ions can be pumped selectively by tuning the input signal frequency.

#### 5:40 AM F.SM06.01.05

**Label-Free Monitoring and Manipulation of Microfluidic Water-in-Oil Droplets** Christoph Frey<sup>1,2</sup>, Jonas Pfeil<sup>3</sup>, Tobias Neckernuss<sup>3</sup>, Daniel Geiger<sup>3</sup>, Klaus Weishaupt<sup>1,2</sup>, Ilia Platzman<sup>1,2</sup>, Othmar Marti<sup>3</sup> and Joachim Spatz<sup>1,2,4</sup>; <sup>1</sup>Max Planck Institute for Medical Research, Germany; <sup>2</sup>University of Heidelberg, Germany; <sup>3</sup>University of Ulm, Germany; <sup>4</sup>Max Planck School Matter to Life, Germany

The advantages of droplet-based microfluidics are evident: multiple lab functions can be integrated on a single chip, sample consumption is minimal and objects like cells can be studied in an isolated environment, thus offering high precision at high throughput. A key point for end-user applications is the availability of powerful but easy-to-implement methods for real-time analysis and automatized manipulation of the droplets. We developed an optical device, consisting of a fast camera with an integrated data processing unit that uses smart algorithms for label-free real-time monitoring and active manipulation of passing droplets. The device continuously analyzes up to 10000 frames per second in real-time. In bright-field images parameters like size, brightness, granularity, circumference and speed of the droplets and their content are analyzed and can be used to manipulate the passing droplets based on their properties. We demonstrate the capabilities of our device by measuring different droplet production parameters and the label-free detection of cells encapsulated in droplets. Furthermore, we performed field-mediated, label-free sorting of cell containing droplets from empty droplets. Therefore, peripheral electronics consisting of a function generator and high-voltage amplifier that are connected to a sorting electrode are controlled by our device. Decision making is based on predefined parameter ranges that are compared to the measurement results of the droplets right before the sorting gate. Similarly, in another experiment we demonstrate efficient separation of droplets of different size. We envision that our novel device will be a useful tool for the online monitoring of passing droplets, enhancing the possibilities and dissemination of label-free methods for screening and manipulation in lab-on-a-chip systems.

#### 5:50 AM F.SM06.01.06

**PEDOT:Hyaluronic Acid and Collagen-Based Scaffolds for Electroactive Monitoring of Cellular Processes** Janire Saez<sup>1</sup>, Antonio Dominguez-Alfaro<sup>2,3</sup>, David Mecerreyes<sup>3,4</sup> and Roisin Owens<sup>1</sup>; <sup>1</sup>University of Cambridge, United Kingdom; <sup>2</sup>CIC biomaGUNE, Spain; <sup>3</sup>POLYMAT Research Centre, Spain; <sup>4</sup>IKERBASQUE, Spain

3D cell cultures to create biomimetic environments are finding numerous applications in drug discovery, regenerative medicine, and cancer research, among many other fields. 3D cultures often rely on scaffolds, typically made of polymeric and biopolymeric materials, which support cell attachment and favour tissue development. These scaffolds possess certain structural and mechanical properties, such as porosity and stiffness, that mimic the extracellular matrix providing a similar microenvironment to that found in vivo. However, these scaffolds are typically passive, merely providing a templated support. We have been focusing on electroactive scaffolds capable of electrically monitoring cellular processes (eg. cell growth, migration) by following a synthetic biology approach. Porous conducting polymer scaffolds made of PEDOT (poly(3,4-ethylenedioxythiophene): HA (Hyaluronic acid) and/or collagen dispersions were obtained by the freeze-drying method, fine-tuning the chemophysical and mechanical properties of the scaffold to render the system suitable for a variety of biological applications. We demonstrate that these scaffolds, apart from being a cell growth support, are capable of electrically monitoring cell growth. Current work is focusing on understanding the role of cancer cell migration through the scaffolds, in addition to the typical mechanical and biochemical cues present in 3D scaffolds.

SESSION F.SM06.02: Bioprinting in Tissue Model Fabrication  
On Demand Abstracts Available for Viewing Starting Saturday Morning, November 21, 2020  
F-SM06

**5:00 AM \*F.SM06.02.01**

**Converged Biofabrication Technologies for the Generation of Osteochondral Implants with Long-Term Functionality** Jos Malda<sup>1,2</sup>; <sup>1</sup>UMC Utrecht, Netherlands; <sup>2</sup>Utrecht University, Netherlands

A major challenge in the application of regenerative medicine strategies is the replication of the complexity and functionality of living tissues. Biofabrication techniques, such as inkjet, extrusion, or light-assisted printing, can result in living structures that further replicate the 3D architecture and organization of native tissue. Recent developments have resulted in the availability of a plethora of bioinks, new printing approaches, and the technological advancement of established techniques. However, it remains largely unknown which materials and technical parameters are essential for the fabrication of intrinsically hierarchical cell-material constructs that truly mimic biological function of tissues. Moreover, it is unlikely that any of these technologies used individually would be able to replicate this complexity and functionality. Hence, we previously urged the field to shift its focus from materials and technologies toward the biological development of the resulting constructs.

This is illustrated by an example from the field of orthopaedics, in particular the treatment of osteochondral defects in a large (equine) animal model. Driven by the observations that the collagen structure provides articular cartilage with its extraordinary mechanical properties and that this structure does not recover once damaged, we evaluated the performance of a biofabricated composite osteochondral implant designed to provide long-term mechanical resistance, comparing implants cell-seeded with cell-free implants. The implants were composed of a gelatin methacryloyl cartilage phase, reinforced with precisely patterned melt electro-written polycaprolactone micrometer-scale fibers and displaying a zonal, cartilage-mimetic architecture. This structure was firmly integrated with a room temperature-setting calcium phosphate cement-based bone anchor via a converged melt electrowriting-extrusion-based printing approach. Cell-containing implants were pre-cultured in vitro and samples were then implanted orthotopically in ponies for 6 months. The reinforcement of the cartilage phase enhanced both the compressive and shear properties of the implants considerably, closer to native values than achieved before.

Abundant deposition of glycosaminoglycan- and type II collagen-rich tissue was observed in vitro, which was maintained during the 6-month in vivo implantation period, showing that the composite architecture, comprising multi-scale printing of hydrogel, microfibers and ceramic materials had provided the required mechanical stability and integration of the implant within the subchondral bone to allow survival of the implant in the mechanically challenging environment of the equine knee joint over an extensive period of time while retaining its mechanical characteristics. Our findings underscore the hypothesis that the mechanical stability is more determining for the success of the implant than the presence of cells. This observation is of great translational importance and highlights the aptness of advanced (bio)fabrication and 3D printing technologies for functional tissue restoration in the harsh articular environment.

**5:15 AM \*F.SM06.02.02**

**Extracellular Matrix-Derived Printable Biomaterials for Engineering Human Tissues** Jinah Jang; Pohang University of Science and Technology, Korea (the Republic of)

The recent development of bioengineering enables to create human tissues by integrating various native microenvironments, including tissue-specific cells, biochemical and biophysical cues. A significant transition of 3D bioprinting technology into the biomedical field helps to improve the function of engineered tissues by recapitulating physiologically relevant geometry, complexity, and vascular network. Bioinks, used as printable biomaterials, facilitate dispensing of cells through a dispenser as well as support their viability and function by providing engineered extracellular matrix. The successful construction of functional human tissues requires accurate environments that are able to mimic the biochemical and biophysical properties of the target tissue. This talk will cover my research interests in building 3D human tissues and organs to understand, diagnose, and treat various intractable diseases, particularly for cardiovascular diseases and diabetes. A development of tissue-derived decellularized extracellular matrix bioink will be mainly discussed as a straightforward strategy to provide biological and biophysical phenomena into engineered tissues. I will also discuss the development of a 3D vascularized stem cell patch that is generated by integrating the concept of tissue engineering and the developed platform technologies. Combined with recent advances in human pluripotent stem cell technologies, printed human tissues could serve as an enabling platform for studying complex physiology in tissue and organ contexts of individuals.

**5:30 AM \*F.SM06.02.03**

**Using Chaotic Advection for Facile High-Throughput Fabrication of Ordered Multilayer Micro- and Nanostructures—Continuous Chaotic Printing** Grissel Trujillo de Santiago, Edna Johana Bolívar-Monsalve, Carlos Ceballos-González, Carolina Chávez-Madero, Mohamadmahdi Samandari, Diego Armando Sandoval Salaiza, Yu Shrike

Zhang and Mario M. Alvarez; Tecnológico de Monterrey, Mexico

Today, tissue engineering evolves exponentially and provides real solutions to create biological models and solve clinical problems. However, we still face challenges that hinder its full potential to generate complex and large-size tissues and organs. Here we present advances in chaotic bioprinting, an additive manufacturing technique that enables the creation of complex biological structures at an unprecedented level of resolution and throughput.

Continuous chaotic printing uses chaotic advection for deterministic and continuous extrusion of fibers with internal multilayered structures. Two free-flowing materials are coextruded through a printhead containing a miniaturized Kenics static mixer (KSM) composed of multiple helicoidal elements. This produces a fiber with a well-defined internal multilayer microarchitecture at high-throughput ( $>1.0 \text{ m min}^{-1}$ ). The number of mixing elements and the printhead diameter determine the number and thickness of the internal lamellae, which are generated according to successive bifurcations that yield a vast amount of inter-material surface area ( $\sim 10^2 \text{ cm}^2 \text{ cm}^{-3}$ ) at high resolution ( $\sim 10 \text{ }\mu\text{m}$ ). This creates a new opportunity to produce structures with extremely high surface area to volume (SAV). Comparison of experimental and computational results demonstrates that continuous chaotic 3D printing is a robust process with predictable output. The simplicity and high resolution of continuous chaotic printing strongly supports its potential use in novel applications.

Here, we illustrate the application of continuous chaotic bioprinting into the fabrication of complex multi-layered bacterial microcosmoi. We demonstrate that the degree of resolution achieved within these constructs can be finely controlled up to the range of a few microns of separation between layers and that the degree of interface between bacterial layers greatly matters for competition.

We also demonstrate the application of tissue-like structures in which living layers of muscle cells evolve into a coherent segment of muscle. Lumina can be easily built into these constructs by using a combination of sacrificial and permanent inks and a multi-port modification to the chaotic printhead.

We are currently exploring more applications of chaotic printing into tissue engineering such as the fabrication of vascularized cancer models, and multi-cell type tissue-like architectures where distinctive mammalian cell layers share a high amount of common interface.

Different fields, outside biosciences and technologies, are also in pursuit of simple and robust ways to create multilayered and multi-material structures to attain functionalities that monolithic materials do not exhibit. We envision that chaotic printing may be applied to technological scenarios such as the fabrication of batteries, superconductors, super catalytic surfaces, and 3D microfluidic reactors.

#### 5:45 AM F.SM06.02.04

***In Situ* Printing of Nanoengineered Osteogenic Hybrid Materials for the Treatment of Bone Defects** Adnan Memic<sup>1</sup>, Azadeh Mostafavi<sup>2</sup>, Tuerdimaimaiti Abudula<sup>1</sup>, Carina Russell<sup>2</sup>, Ebrahim Mostafavi<sup>3</sup>, Tyrell Williams<sup>2</sup>, Numan Salah<sup>1</sup>, Ahmed Alshahrie<sup>1</sup>, Seth Harris<sup>2</sup>, Seyed Masoud M. Basri<sup>4</sup>, Yogendra Mishra<sup>5</sup>, Thomas J. Webster<sup>3</sup> and Ali Tamayol<sup>6</sup>; <sup>1</sup>King Abdulaziz University, Saudi Arabia; <sup>2</sup>University of Nebraska–Lincoln, United States; <sup>3</sup>Northeastern University, United States; <sup>4</sup>American University of Sharjah, United Arab Emirates; <sup>5</sup>University of Southern Denmark, Denmark; <sup>6</sup>University of Connecticut, United States

Bone defects are commonly caused by traumatic injuries and tumor removal and critically sized defects overwhelm the regenerative capacity of the native tissue. Reparative strategies such as auto, xeno, and allografts have proven to be insufficient to cure these defects. For the first time, we introduce the use of handheld melt spun three dimensional printers that can deposit scaffolding materials directly within the defect site to properly fill the cavity. Engineered composite filaments were generated from poly(caprolactone) doped with zinc oxide nanoparticles and hydroxyapatite microparticles. The use of PCL-based materials allowed low-temperature printing to avoid overheating of the surrounding tissues. The *in situ* printed scaffolds showed moderate adhesion to the bone tissue, which can prevent scaffold dislocation. The printed scaffolds showed to be osteoconductive and supported the osteodifferentiation of mesenchymal stem cells. Biocompatibility of the scaffolds upon *in situ* printing subcutaneously in mice showed promising results.

SESSION F.SM06.03: Biofabrication for Tissue Emulation

On Demand Abstracts Available for Viewing Starting Saturday Morning, November 21, 2020

F-SM06

#### 5:00 AM \*F.SM06.03.01

**Strategies to Engineer a Functional Kidney Proximal Tubule** Rosalinde Masereeuw; University of Utrecht, Netherlands

In patients with severe kidney disease, renal clearance is compromised resulting in the accumulation of a plethora of endogenous waste molecules that cannot be removed by current dialysis techniques, the most often applied treatment. These uremic retention solutes, also named uremic toxins, are a heterogeneous group of organic compounds of which many are too large to be filtered and/or are protein-bound. Their renal excretion depends largely on renal tubular secretion by which the binding is shifted towards the free fraction that can be eliminated. To facilitate this process, kidney proximal tubule cells are equipped with a range of transport proteins that cooperate in cellular uptake and urinary excretion. In recent years, we and others have invested in the development of bioengineered kidney tubules that could potentially restore this essential function. For this, well characterized human kidney proximal tubule cells were combined with functionalized, living membranes. This presentation addresses these developments in the context of functional kidney tubule engineering. Furthermore, hurdles to take before a safe implementation of bioengineered kidneys in clinics becomes a realistic option will be discussed.

**5:15 AM \*F.SM06.03.02**

**Stem Cell-Derived Models to Study Human Neural System Development** Jianping Fu; University of Michigan-Ann Arbor, United States

Neurulation is a key developmental process that gives rise to the neural tube (NT), the precursor structure of the central nervous system (CNS). Neurulation is initiated after the gastrulation by a neural induction process, during which the dorsal ectoderm is specified into a patterned tissue containing the neural plate (NP) and the non-neural ectoderm (NNE) separated by the neural plate border (NPB). After neural induction, the NP folds and fuses to form the tubular NT. The development of the NT continues with differentiation of distinct classes of neuronal progenitor cells located at defined positions within the NT along both the anterior-posterior (AP) and dorsal-ventral (DV) axes. In this talk, I will discuss the recent research activities in my group to leverage the developmental potential and self-organization property of human pluripotent stem cells (hPSCs) in conjunction with 2D and 3D bioengineering tools to achieve the development of spatially patterned multicellular tissues that mimic certain aspects of early human neurulation process, including neural induction, AP and DV patterning of the NT. These stem cell-derived models offer promising trackable systems to study neural development and disease.

**5:30 AM \*F.SM06.03.03**

**Engineering the Microenvironment That will Enable a Long-Term Bioprosthetic Ovary Transplant** Monica M. Laronda<sup>1,2</sup>; <sup>1</sup>Ann and Robert H. Lurie Children's Hospital of Chicago, United States; <sup>2</sup>Northwestern University, United States

The ovaries contain a finite resource of potential eggs and sex hormone-producing cells, and therefore, life-saving cancer treatments that irradiate or chemically induce cell death within the ovaries will likely result in premature ovarian insufficiency (POI) with reduced ovarian hormones and infertility. The option to have biological children, is a key quality of life measure for cancer survivors. Women with POI will experience co-morbidities associated with loss of ovarian hormones and a shorter life expectancy. The only method for fertility preservation for pediatric patients, who do not yet make eggs, is ovarian tissue cryopreservation (OTC). This tissue can then be transplanted back to restore fertility and hormone function. However, only 20 – 30% of transplants result in livebirth and it produces an average of 2 – 5 years of hormone restoration, leaving many without biological children and decades of post-cancer survival without essential hormone production. One major contributor to the shortened function of transplanted ovarian tissue is the significant spike in activation of the ovarian reserve (primordial follicles, containing the oocytes and hormone-producing cells) and subsequent depletion, at least in part, due to the disruption in the microenvironment. Additionally, some patients have metastatic disease within the ovary and therefore cannot use that tissue in its current form. Therefore, a safe, long-term solution for fertility and hormone restoration would involve isolating the ovarian cells that are essential for function from potential cancer cells and housing them in a microenvironment that maintains the bank of potential eggs and prolongs hormone production. We have defined the architectures of a 3D printed scaffold that support the necessary cell-cell contacts between the oocyte and the surrounding hormone producing support cells. This bioprosthetic ovary of the 3D printed gelatin scaffold with isolated ovarian follicles restored fertility and hormone function and supported livebirths and rearing of offspring in mice. To advance this research through the next steps toward translation to the clinic, we must define the follicular microenvironment that will enable a regulated recruitment of eggs from the ovarian reserve and support a safe, effective and long-term transplant. We have mapped the matrisome composition across the ovarian compartments and the stiffness of tissue components in ovaries of large mammals. Our novel proteomics screen and analysis has enabled us to identify new matrisome proteins within the ovary and pinpoint proteins of interest that may control primordial follicle activation or quiescence. We have additionally defined the physical properties of the ovarian compartments, where the cortical (outer) region is denser and stiffer than the medullary (inner) region. We have developed decellularized ovary extracellular matrix inks and are investigating the roles of specific biochemical and physical cues on primordial follicle quiescence and activation. A bioprosthetic ovary, defined by these microenvironment properties, would improve current options for fertility and hormone restoration for women.

#### 5:45 AM F.SM06.03.04

**Impact of Drying Time and Temperature on Lyophilized Silk Fibroin Scaffold Structural Properties** Alycia Abbott,  
Mattea E. Gravina and Jeannine M. Coburn; Worcester Polytechnic Institute, United States

Lyophilized silk fibroin (silk) scaffolds have been used to develop 3D models for multiple disease states.<sup>1</sup> Silk is a natural, biocompatible, FDA approved biomaterial that allows a high degree of control over physical properties.<sup>2</sup> Lyophilization of different silk solutions produces porous scaffolds with varying pore sizes and Young's moduli.<sup>3</sup> However, the effect of varying the drying time and temperature during lyophilization on pore size, pore shape, and bulk modulus is not well described. Understanding the impact of drying time and temperature conditioning on silk scaffold structural properties will allow better definition of lyophilization protocols and tailoring of silk scaffolds to specific disease states.

Silk fibroin was extracted from *B. Mori* silkworm cocoons as previously described.<sup>1</sup> Solutions of 3, 6, 9, and 12% silk (w/v) were created by concentrating silk solution or diluting with water. Rate-controlled lyophilization cycles were used to create porous scaffolds (15.6 mm diameter). Primary drying times (18 h – 1 week) and drying temperatures (-45°C to -15°C) were explored to determine the impact on pore size, pore shape, and Young's modulus. Shelf and sample temperatures were recorded during lyophilization. Pores were evaluated through fluorescent and scanning electron microscopy of scaffolds cut into 200 µm thick sections. An ImageJ protocol was developed to evaluate pore size and shape. Scaffolds were hydrated (impact on secondary structures was examined through FTIR), biopsied (6 mm) and compressed between two parallel plates. The Young's modulus of the scaffolds was determined through uniaxial compression testing on an Instron (2mm/min to 50% strain). Young's modulus was calculated from the stress-strain curve.

Not all lyophilization runs produced viable scaffolds from all silk concentrations. Higher silk percentages (9 and 12%) were shown to require longer drying times than lower silk percentages (3 and 6%). A gradient of pore sizes was seen throughout scaffolds with smaller pores being present in the outermost regions. Pore size was non-normally distributed when imaged at low magnifications (4x) but was normally distributed at high magnifications (500x) suggesting multiple scales may be important for pore evaluation. Due to low average circularity values, Feret diameter, area, and perimeter were used to compare scaffolds instead of treating pores as spheres. Preliminary data suggests silk concentration had a greater impact on pore size and shape than drying time and temperature. Young's moduli values increased as silk concentration increased in agreement with previous literature.<sup>3</sup> Young's moduli values for each silk concentration were significantly different from each other silk concentration ( $p < 0.01$ ). Scaffolds fabricated from the same silk concentration but with stepwise temperature drying had significantly lower Young's moduli (6%,  $p < 0.001$ ; 12%,  $p < 0.0001$ ) than scaffolds dried at a constant temperature.

The impact of lyophilization parameters on Young's modulus, and pore size and shape for four different silk formulations were evaluated. The Young's moduli of scaffolds increased as silk concentration increased. Drying temperature significantly affected the Young's moduli of scaffolds with the same silk concentration. Changes in silk concentration had a larger impact on pore size and shape than lyophilization parameters, although analysis is still ongoing. These results begin to demonstrate the impact of drying time and temperature on silk scaffold properties. This knowledge can be used to tailor lyophilization protocols to produce silk scaffolds with specific properties, such as a soft matrix with a desired pore range for tissue engineering applications.

1.D.N. Rockwood, Nat Protoc.6,1612-31 (2011). 2. J.E. Brown, Adv Healthc Mater.6, 1600762(2017) 3. M. Amirikia, Biologicals.57,1-8(2019)

#### SESSION F.SM06.04: On-Chip Tissue Recapitulation

On Demand Abstracts Available for Viewing Starting Saturday Morning, November 21, 2020

F-SM06

#### 5:00 AM \*F.SM06.04.01

**Growth, Characterization and Application of Self-Organized Microvascular Networks for Models of Disease** Roger Kamm; Massachusetts Institute of Technology, United States

Methods now exist to create single- or multi-organ engineered living systems that can be used to model a variety of disease processes. Aside from providing new insights into disease mechanisms, these systems can also be used to screen new drugs to treat the disease, or even to identify different therapeutic strategies for sub-populations possessing different genetic profiles. Here we present several models that require a microvascular network, modeling different stages of metastatic cancer. In one set of studies, circulating tumor cells are introduced via side channels into the microvascular bed, where they arrest,



become activated and undergo transendothelial migration. Model systems include the brain, muscle, placenta and bone marrow, each showing distinctive characteristics. These or others can be used to model drug delivery to a developing tumor, either primary or metastatic.

Microfluidic devices used in these studies are, for the most part, simple, single layer systems that can be cast in a single piece of PDMS, forming channels and gel compartments by bonding to a coverslip. Alternatively, systems can be injection molded in tissue culture plastics. Microphysiological systems (MPS) can be either 'engineered' or self-organize using the same capabilities of developing organisms. Our approach is to rely, as much as possible, on the innate capabilities of the cells to interact to form the structures of a particular organ. Cells or cell assemblies/organoids are mixed in hydrogel solution and injected into one or more adjacent compartments allowing for direct signaling or physical contact between the multiple different cell types. Many of these systems contain microvascular networks that can be perfused via side channels, with pumping by simple low-pressure diaphragm pumps, directly connected to the MPS to minimize media volumes. The role of circulating immune cells can also be studied, as these, too, arrest in the vascular beds and extravasate into the surrounding gel matrix.

Results will be shown first demonstrating the form and function of the microvascular beds. Then several examples will be taken from the systems mentioned above to illustrate different applications, and to demonstrate the flexibility of the underlying platform. Future directions will be discussed including the challenges ahead in generating perfusable organoids.

#### **5:15 AM \*F.SM06.04.02**

**Microfluidic Organs-on-Chips** Yuanjin Zhao; Southeast University, China

In biological research, the interaction of biomolecules, cells and materials is an eternal topic. Many technologies have been employed to construct three-dimensional micro- and nano- hierarchical structure of materials. However, it is still a challenge to combine the artificially controllable biomaterials and the complicated biomolecular interaction/cell living unit, and thus to realize the regulation and control of the cell culture by using these materials. Moreover, it is necessary to develop a biotechnology for cell research to real-time and accurately monitor the interaction of the biomolecules/cells and the biomaterials, which could effectively reveal the biological mechanism of the cell behavior. In this point, we proposed to generate the desired functional materials by using microfluidic methods. Based on this technology, we have created a series of novel biomaterials, which showed demonstrated values in cells culture and organs-on-chips construction.

#### **5:30 AM F.SM06.04.03**

**Heart-on-a-Chip Model with Integrated Extra- and Intracellular Bioelectronics for Monitoring Cardiac Electrophysiology Under Acute Hypoxia** Olurotimi A. Bolonduro and Brian Timko; Tufts University, United States

Cardiovascular disease is the leading cause of death in the US, with many cases attributed to cardiac ischemia. Cardiac ischemia occurs when an artery supplying blood to the heart is partially or fully blocked. This results in reduced blood flow to downstream tissue, gradually transforming normoxic blood (21% O<sub>2</sub>) into hypoxic blood (<5% O<sub>2</sub>). If hypoxic conditions are present for an extended period of time, a myocardial infarction (MI) may occur, leading to abnormal cardiac electrophysiology, loss of function, and tissue death. Despite the effects of ischemic stresses on cardiac electrophysiology, there are few tools that enable multiplexed, real-time studies of cardiac function under ischemia-like conditions.

Herein, we present a heart-on-a-chip model with integrated bioelectronics for studying the effects of acute hypoxia on cardiac function. This model consisted of a PDMS microfluidic channel, cell culture area, and extra- and intracellular recording elements that provided complementary electrophysiological readouts from cardiac model cells. The microfluidic channel enabled rapid modulation of medium oxygenation within the reservoir, which mimicked oxygenation regimes induced by an onset or removal of a coronary occlusion. Basic functionality of the microfluidic channel was confirmed with immunohistochemistry; reversibly-activated hypoxia-related transduction pathways were activated and visualized within the cardiomyocytes.

Our platform provided multiplexed bioelectronic readouts from up to 16 spatially-distinct locations. Extracellular recording elements consisted of 30-micron Au pads and provided stable, continuous readouts of wavefront propagation. Intracellular recording elements penetrated the cytosol following highly-localized electroporation, providing readouts that followed the action potential. A hypoxic regime applied over a 6-hour window caused an initial period of tachycardia followed by a reduction in beat rate and eventually arrhythmia; disruption of wavefronts and continuous reduction in propagation speed from  $19 \pm 5$  mm/s to  $< 13 \pm 8$  mm/s; and narrowing of the AP. Moreover, multiplexed recordings of APs allowed us to observe heterogeneities between cells under both normoxic and hypoxic conditions, highlighting a clear advantage of our platform over traditional techniques such as patch clamp.

The noninvasive nature of our platform enables a wide range of studies relevant to MI and could also be extended to incorporate other elements of ischemia including acidosis, hyperkalemia, nutrient deprivation, and waste accumulation. Moreover, our multiplexing capabilities could be expanded to larger and denser arrays for more complex biological systems including hypoxic gradients. Ultimately, our platform could yield fundamental insights into cardiac signaling pathways and/or provide a high-throughput platform for assessing therapeutics.

#### 5:40 AM F.SM06.04.04

**Perfusion Bioreactor Enabled Bone Metastasis Prostate Cancer Testbed** [Haneesh Jasuja](#), Kalpana Katti and Dinesh Katti; North Dakota State University, United States

The International Agency for Research on Cancer (IARC) of the World Health Organization reports 1,276,106 incidences and 358,989 fatalities resulting from prostate cancer world wide in 2018. Prostate cancer is the second leading cause of cancer death among men in the United States. Prostate cancer has the propensity to migrate to or metastasize to bone. Although curative treatments are available for primary prostate cancer tumors, advanced-stage prostate cancer that has metastasized to bone often results in a poor prognosis. The primary cause of morbidity due to prostate cancer is the metastasis to bone. The effects of various biochemical factors in the bone microenvironment have been demonstrated in the disease progression to metastasis; however, the role of physical factors such as mechanical cues induced by the interstitial fluid flow around the bone is poorly explored. It has been established that interstitial flow has a pro-migratory and biomechanical stimulatory effect on cancer cell invasion. To address this issue, we designed a 3D *in-vitro* model to evaluate the progression of prostate cancer cells at metastasis condition, colonizing the bone site under dynamic conditions. In this study, we developed a 3D dynamic *in-vitro* model employing nanoclay-polycaprolactone-hydroxyapatite scaffolds and a specially designed perfusion bioreactor. Initially, we differentiated human mesenchymal stem cells (hMSCs) on scaffolds under dynamic culturing conditions to duplicate an accurate bone-like microenvironment. Next, we utilized these bone mimetic scaffolds to grow prostate cancer cells under identical dynamic conditions to recapitulate prostate cancer metastasis to bone. Finally, we performed various cellular assays and immunocytochemistry studies to establish the feasibility of dynamic culture. We observed a significant increase in bone growth under dynamic culture conditions evaluated by bone-related biomarkers (ALP, RUNX2, and OCN) compared to static culture. We also noticed upregulation in E-cadherin and downregulation of vimentin levels under dynamic conditions that confirms the occurrence of mesenchymal to epithelial (MET) transition of prostate cancer cells at the metastatic bone site. We further examined the influence of fluid-induced mechanical cues on cells by monitoring alteration in orientation and morphology of hMSCs and prostate cancer cells. Overall, we observed significant differences in cellular morphology and gene expressions of bone cells and prostate tumors grown under flow conditions. The established perfusion bioreactor based 3D dynamic *in-vitro* model can be further utilized to elucidate the mechanisms of prostate cancer metastasis and screen novel drug therapies geared towards bone metastasis prostate cancer.

#### 5:50 AM F.SM06.04.05

**Spatially Controlled Stem Cell Differentiation via Morphogen Gradients—A Comparison of Static and Dynamic Microfluidic Platforms** [Kiara W. Cui](#), Leeya Engel, Carolyn Dundes, Tina Nguyen, Kyle Loh and Alexander Dunn; Stanford University, United States

The ability to harness the processes by which complex tissues arise during embryonic development would improve our ability to engineer complex tissue-like constructs *in vitro*—a long-standing goal of tissue engineering and regenerative medicine. In embryos, uniform populations of stem cells are exposed to spatial gradients of diffusible extracellular signaling proteins, known as morphogens. Varying levels of these signaling proteins induce stem cells to differentiate into distinct cell types at different positions along the gradient, thus creating spatially patterned tissues.

Here, we describe two straightforward and easy-to-adopt microfluidic strategies to expose human pluripotent stem cells (hPSCs) *in vitro* to spatial gradients of desired differentiation-inducing extracellular signals. Both approaches afford a high degree of control over the distribution of extracellular signals while preserving the viability of the cultured stem cells. The first microfluidic platform is commercially available and entails static culture, whereas the second microfluidic platform requires fabrication and dynamic fluid exchange. In each platform, we first computationally modeled the spatial distribution of differentiation-inducing extracellular signals. Then, we used each platform to expose hPSCs to a gradient of these signals (in this case, inducing a cell type known as the primitive streak), resulting in a regionalized culture with differentiated primitive streak (PS) cells predominately localized on one side and undifferentiated stem cells at the other side of the device. By combining this approach with a fluorescent reporter for differentiated cells and live-cell fluorescence imaging, we characterized the spatial and temporal dynamics of primitive streak differentiation within the induced signaling gradients. We

envision that microfluidic approaches to create precisely controlled morphogen gradients will add to the stem cell and developmental biology toolkit, and may eventually pave the way to create increasingly spatially patterned tissue-like constructs *in vitro*.

SESSION F.SM06.05: Poster Session: Biofabrication for Emulating Biological Tissues  
On Demand Abstracts Available for Viewing Starting Saturday Morning, November 21, 2020  
5:00 AM - 8:00 AM  
F-SM06

#### **F.SM06.05.02**

**The Effects of Bioprinting on the Structure, Function and Survival of Organotypic Skin** Kimberly Lu, Olias Christie, Michael Cottone, Philip Cottone, Michael Gozelski, Juyi Li, Robert Wong and Miriam H. Rafailovich; Stony Brook University, United States

With the advancement of 3D printing in the 21st century, prospective treatments for regenerative medicine, cosmetology, and material science are actively being explored<sup>1,2</sup>. This research aims to investigate the feasibility of 3D bioprinting technology in producing viable skin tissue. In order to achieve this, a novel procedure for the construction of dermal and epidermal organotypics was developed. This evaluation was performed by comparing organotypic skin samples consisting of non-printed epidermal and dermal layers (NN), non-printed epidermal and printed dermal layers (NP), printed epidermal and non-printed dermal layers (PN), and printed epidermal and dermal layers (PP). The assessment of claudin and filaggrin immunohistochemical staining of the samples suggest a revision to the methodology in which printing the epidermal layer at a lower pressure while printing the dermal layer at a relatively higher pressure may lead to improved cellular function and overall integrity of the organotypic skin-equivalent. These results demonstrate the potential of bioprinting as a novel technique for producing a skin equivalent product, which may serve as an alternative to conventional tissue engineering methods.

1. Chang R, Nam J, Sun W: Effects of dispensing pressure and nozzle diameter on cell survival from solid freeform fabrication-based direct cell writing. *Tissue Eng Part A* 2008, 14(1):41-48.
2. Chien S: Effects of disturbed flow on endothelial cells. *Ann Biomed Eng* 2008, 36(4):554-562.

#### **F.SM06.05.04**

**Late News: Synthesis of Alginate Microgels with a Polymer Shell—A Simple Way to Protect Encapsulated Cells** So Hyun Ahn, Srinivasa Raghavan and William E. Bentley; University of Maryland, United States

Microgels of biopolymers such as alginate are widely used to encapsulate cells and other biological payloads. Alginate is an attractive material for cell encapsulation because spherical gels are easily created by contacting aqueous droplets of sodium alginate with divalent cations such as  $\text{Ca}^{2+}$ . Alginate chains in the gel become crosslinked by  $\text{Ca}^{2+}$  cations into a 3-D network. When alginate gels are placed in a buffer, however, the  $\text{Ca}^{2+}$  crosslinks are eliminated by exchange with  $\text{Na}^+$ , thereby weakening and degrading the gels. With time, encapsulated cells are released into the external solution.

Here, we describe a simple solution to the above problem, which involves forming alginate gels enveloped by a thin shell of a covalently crosslinked gel. The shell is formed via free-radical polymerization using conventional monomers such as acrylamide (AAm) or acrylate derivatives, including polyethylene glycol-diacrylate (PEGDA). The entire process is performed in a single step at room temperature (or 37°C) under mild, aqueous conditions. It involves combining the alginate solution with a radical initiator, which is then introduced as droplets into a reservoir containing  $\text{Ca}^{2+}$  and monomers. Within minutes, the droplets are converted into alginate-polymer microcapsules with a core of alginate and a shell of the polymer (AAm or PEGDA). The stability of these microcapsules under physiological conditions is compared with that of conventional alginate/ $\text{Ca}^{2+}$  microgels. The latter swell and degrade when placed in buffer or in chelators like sodium citrate, whereas the former remain stable under all conditions.

We also show that a various types of cells can be safely encapsulated in these hybrid beads. We encapsulate both mammalian cell and different strains of genetically engineered bacteria in these microcapsules and find that the cells remain viable and functional over time. In particular, engineered 'reporter' bacterial cells respond to different molecular signals from the external solution such as IPTG, AI-1 and hydrogen peroxide. The cells are retained in the hydrogel capsules throughout the

study which is a crucial aspect for studying cell's response to molecular cues in a robust manner. Moreover, multiple sets of capsules each containing different strains can be synthesized and co-cultured to study cell-cell communication, providing an ideal platform for studying *in vitro* signaling events. Lastly, a variation of the synthesis technique is performed to generate multilayered microcapsules with a liquid core surrounded by concentric layers of alginate and AAm gels.

#### F.SM06.05.05

**Late News: Analysis and Mechanical Compression Model of a Three-Component Scaffold Composed of Polycaprolactone-Hydroxyapatite-Graphene Oxide for Tissue Engineering** Javier Ortiz Ortiz, Georgina Carbajal de la Torre, Marco Antonio Espinosa Medina, Nancy Nelly Zurita Méndez and Lourdes Ballesteros-Almanza; Universidad Michoacana de San Nicolas de Hidalgo, Mexico

The use of multiple materials has helped in the development of tissue engineering. The use of polymeric matrices and biomaterials added to particular materials offers specific solutions both due to the interaction of the biomaterials and the mechanical properties of the generated biomaterial. In this work, the mechanical properties of compression of a three-component scaffolds for tissue engineering composed of polycaprolactone (PCL), hydroxyapatite (HA), and graphene oxide (GO) are shown. Scaffolds were subjected to compression on the Cell Scale™ brand Univert™ testing machine. Once the experimental data had been obtained, the stress-strain curve was obtained, also the compression mechanical behavior model was performed using the Levenberg-Marquardt least-squares algorithm in the Comsol Multiphysics™ software. To explain the compression phenomenon, scanning electron microscopy analyzes are performed where scaffolds are observed before being compressed and also after compression.

#### F.SM06.05.07

**Late News: Determination of the Physical and Mechanical Properties of the Nopal Fiber (*Opuntia ficus-indica*) and Availability as a Biopolymer** Isaí Pérez Servín, Rosa E. Pérez Sánchez, Georgina Carbajal de la Torre, Ruy Ortíz Rodríguez, Héctor E. Martínez Flores and Javier Ortiz Ortiz; Universidad Michoacana de San Nicolás de Hidalgo, Mexico

Nopal is a cactus that is distributed in different agroclimatic zones in a wild and cultivated way, due to its high forage potential, it has been destined to be used in the food, agricultural and pharmaceutical industry, however, when the cladode nopal reaches certain maturity, its use in the previously mentioned scopes is no longer viable, due to its high availability of fiber and lignin; this content of fiber in nopal could be implemented in the cosmetic and medical scopes as a biopolymer. The present study shows the physical and mechanical properties of nopal fiber components, and its thermographic analysis as an approach to determine its suitability and availability to fulfill the function of a biopolymer. An acid/alkaline extraction with potassium hydroxide (KOH; 1%) at 50° C was performed on the nopal sample previously dried. After the extraction, the sample was dried in a vacuum oven and its size was reduced by grinding. Mechanical tests were performed on nopal fibers in the Cell Scale Univert testing machine to obtain stress-strain curves. From the thermographic analysis, the kinetic drying model describing the process necessary for finite element modeling was proposed. The evaluation of the physical and mechanical characteristics allows us to determine the use and viability of nopal fiber as a biomaterial.

### SYMPOSIUM F.SM07

---

Biomaterials for Studying and Controlling the Immune System  
November 21 - December 2, 2020

#### Symposium Organizers

Eric Appel, Stanford University  
Derfogail Delcassian, Nottingham University  
Evan Scott, Northwestern University  
Kara Spiller, Drexel University

---

\* Invited Paper

SESSION F.SM07.06: Live Keynote I: Immunoengineering for Improving Vaccines and Cancer Immunotherapies  
Session Chairs: Eric Appel and Derfogail Delcassian  
Tuesday Morning, December 1, 2020  
F.SM07

**8:00 AM \*F.SM07.03.02**

**Enhancing Vaccine Immunity via a Nanoparticle Adjuvant That Alters Lymph Flow and Lymph Node Permeability** Darrell Irvine; Massachusetts Institute of Technology, United States

Adjuvants play critical roles in shaping the immune response to vaccines. Here we describe a novel nanoparticle adjuvant, saponin-MPLA nanoparticles (SMNP), formed by the immunostimulatory compound saponin, the Toll like receptor (TLR)-4 agonist monophosphoryl lipid A (MPLA), cholesterol, and phospholipids. These components self-assemble into striking ~40 nm diam. cage-like structures reminiscent of ISCOMs (Immunostimulatory complexes) previously reported for saponin/phospholipid complexes, but have synergistic immunostimulatory properties from the combined action of saponins and MPLA. SMNP exhibited striking potency in both mouse and non-human primate (NHP) preclinical animal models of vaccination with a variety of subunit vaccines. Protein vaccines adjuvanted with SMNP elicited robust germinal center B cell and Tfh responses, leading to strong serum IgG responses and (in NHPs) HIV tier 2 neutralizing antibody responses. Strikingly, SMNP exhibited distinctive mechanisms of action, altering lymph flow and promoting antigen entry into draining lymph nodes, in a manner dependent on co-assembly of MPLA and saponin together in the same nanoparticle. Altogether, these findings suggest SMNP may be a promising novel adjuvant for subunit vaccines in settings of HIV, COVID-19, and other infectious diseases.

**8:30 AM Q&A**

**8:45 AM BREAK**

SESSION F.SM07.07: Live Panel Discussion I: Immunoengineering for Improving Vaccines and Cancer Immunotherapies  
Session Chairs: Eric Appel and Derfogail Delcassian  
Tuesday Morning, December 1, 2020  
F.SM07

**9:00 AM SUSAN THOMAS, PANELIST**

**9:00 AM DARRELL IRVINE, PANELIST**

**9:00 AM LI TANG, PANELIST**

**9:00 AM JOEL COLLIER, PANELIST**

**9:00 AM PAULA HAMMOND, PANELIST**

**9:00 AM PANEL DISCUSSION**

SESSION F.SM07.08: Live Keynote II: Biomaterials for Studying and Controlling the Immune System  
Session Chairs: Evan Scott and Kara Spiller  
Wednesday Afternoon, December 2, 2020  
F.SM07

**7:30 PM \*F.SM07.02.02**

**Microenvironmental Control of Bioengineered Immune Tissues with Microfluidics** Rebecca R. Pompano; University of

Virginia, United States

A critical element of the immune system is tissue-level spatial organization. Cells and extracellular matrix elements are all highly organized in the lymph node, spleen, and thymus, as well as in the peripheral organs where immune cells infiltrate. Furthermore, secreted molecules are arranged in local patterns that depend on diffusion and interstitial flow. To begin to probe the functional outcomes of this intricate organizational structure, our laboratory has focused on combining live tissues and engineered biomaterials with microfluidic and micropatterning for fluidic and spatial control. We have developed microsystems to deliver drugs locally to specific regions of spatially structured tissues, to co-culture multiple structured organs under recirculating flow, and to begin to build a micropatterned lymph node. Here we will discuss our recent progress towards modeling complex immune function outside the body, to gain insight into the spatiotemporal dynamics of inflammation and immunity.

**8:00 PM Q&A**

**8:15 PM BREAK**

SESSION F.SM07.09: Live Panel Discussion II: Biomaterials for Studying and Controlling the Immune System  
Wednesday Afternoon, December 2, 2020  
F.SM07

**8:30 PM PANEL DISCUSSION**

**9:30 PM LONNIE SHEA, PANELIST**

**9:30 PM BENJAMIN KESELOWSKY, PANELIST**

**9:30 PM ANKUR SINGH, PANELIST**

**9:30 PM REBECCA POMPANO, PANELIST**

**9:30 PM CHRISTOPHER JEWELL, PANELIST**

SESSION F.SM07.01: Directing and Understanding Immune Tolerance and Responses to Implants  
On Demand Abstracts Available for Viewing Starting Saturday Morning, November 21, 2020  
F-SM07

**5:00 AM \*F.SM07.01.01**

**Biomaterials as Tools to Study and Manipulate Immune Signaling** Christopher M. Jewell; University of Maryland, United States

Our research combines immunology and biomaterials to understand the interactions between synthetic materials and immune tissues, and to design more selective therapeutic vaccines for cancer and autoimmunity. This presentation will highlight our recent efforts toward these goals combining materials science and bioengineering tools, cell culture, animal models, and samples from human patients. In one example I will discuss new degradable polymer depots that could improve the selectivity of therapies for autoimmune diseases such as multiple sclerosis and diabetes by locally reprogramming the function of lymph nodes – tissues that coordinate immune function. A second area will present the lab's efforts to self-assemble immune signals into modular nanostructures. This rational design approach allows activation of programmable combinations and levels of immune pathways triggered. Modular control over these aspects of immune signaling could help improve the efficacy of vaccines for cancer and infectious disease, and enhance the efficiency of vaccine translation.

### 5:15 AM \*F.SM07.01.02

**Intravenous Nanoparticle Delivery for Reprogramming Immune Cells and Modulating Inflammatory Disease** Lonnie Shea<sup>1,1</sup>, Eiji Saito<sup>1</sup>, Yining Zhang<sup>1</sup> and Jonghyuck Park<sup>2</sup>; <sup>1</sup>University of Michigan–Ann Arbor, United States; <sup>2</sup>University of Kentucky, United States

**Introduction:** Inflammatory monocytes and neutrophils contribute to deleterious inflammatory disease and tissue damage in a number of pathological conditions, such as trauma, viral infection, autoimmune disease, sepsis, and cancer. Tissue destruction results from the influx of these inflammatory monocytes and neutrophils, which secrete pro-inflammatory cytokines, reactive oxygen species (ROS). Critically, a number of agents such as steroids or cytokine-depleting antibodies are associated with unfavorable side effects, such as sepsis, gastrointestinal bleeding, and thromboembolism, indicating that improved methods are needed. Systemic depletion of neutrophils or monocytes has either not altered or has had a small effect on outcomes. Because monocytes and neutrophils are necessary for wound healing and tissue regeneration after injury, reprogramming the immune response could be a more effective strategy to minimize loss of function and enable repair.

**Results:** Herein, we describe our efforts at employing NPs to reprogram inflammatory cells intravascularly, which can alter their trafficking and polarization. NPs (500 nm diameter, zeta potential < -30 mV) and intercept the immune cells prior to their extravasation and redirect some to the spleen, with a fraction trafficking to the site of trauma or disease. Importantly, the NPs are attenuating the innate response yet do not alter the adaptive immune response and also support enhanced regeneration and functional recovery at sites of trauma or disease. These particles have been applied to models of viral infection and spinal cord injury to limit injury and tissue degeneration, and in models of metastatic cancer to alter metastasis.

**Conclusions:** NP infusion can reduce inflammation resulting in increasing tissue regeneration and normal tissue function. NPs-mediated rapid reprogramming of innate immune cells has a sustained impact on microenvironment modulation, which initiates a cascade of events, including induction of gene expression profiles associated with regeneration. Collectively, this strategy of targeting the innate immune cells in the vasculature prior to their extravasation to a injury or disease site may have broad applications to attenuating inflammation-mediated tissue damage.

**Acknowledgements:** This study was supported by the National Institutes of Health (NIH) R01 EB013198 and R01 AI148076.

**Conflicts:** LDS serves as a consultant and has a financial interest in Cour Pharmaceutical.

### 5:30 AM \*F.SM07.01.03

**Tissue-Anchored Enzyme for Immuno-Metabolic Suppression** Benjamin Keselowsky; University of Florida, United States

This presentation highlights results from our molecular based approaches to direct the immune system toward tolerance and suppression. We have developed tissue-anchored enzymes – chimeric enzyme-carbohydrate binding fusion proteins in order to direct localized immunometabolism toward suppression. Specifically, indoleamine 2,3 dioxygenase, which depletes tryptophan through the kynurenine pathway, is fused to galectin 3, which binds extracellular glycans and affords prolonged tissue retention. This approach has provided potent, confined metabolic programming promoting tissue homeostasis in multiple inflammation models including osteoarthritis and periodontal disease.

### 5:45 AM F.SM07.01.05

**The Plasticity of Primary Human Macrophages When Interacting with Tissue-Engineered Blood Vessels** Beatriz Hernaez Estrada<sup>1,2</sup>, Edorta Santos Vizcaino<sup>2,3</sup>, Rosa M. Hernandez<sup>2,3</sup> and Kara Spiller<sup>1</sup>; <sup>1</sup>Drexel University, United States; <sup>2</sup>University of the Basque Country, Spain; <sup>3</sup>Biomedical Research Networking, Spain

**Introduction:** Deficient vascularization of engineered tissues is one of the major causes of inadequate tissue integration and function *in vivo*. A potential solution to this problem is the implantation of pre-vascularized biomaterials, such as those prepared from human adipose microvascular endothelial cells (HAMECS) and adipose-derived mesenchymal stromal cells (MSC) [1-2]. However, these pre-vascularized constructs will encounter an inflammatory environment upon implantation, and it is not known how this will affect the engineered blood vessels. Macrophages, the primary cells of the inflammatory response, are key regulators of tissue vascularization and integration of implanted biomaterials. Even though macrophages can exist as different phenotypes, each with distinct effects on blood vessels, they are also very plastic cells that are able to switch phenotypes depending on microenvironmental stimuli [3]. In the first phase of wound healing, macrophages are primarily pro-inflammatory (M1), whereas the second stage is characterized by a pro-wound resolution phenotype (M2). M2 macrophages can be derived from non-activated (M0) macrophages or they may switch from M1 (resulting in M1-M2). The diversity of these populations and their crosstalk with blood vessels are not known. Therefore, the purpose of this study was to assess the phenotypic subsets of primary human macrophages polarized to pro-inflammatory (M1) and pro-wound

resolution (M2 and M1-M2) phenotypes, and how they change when cultured with 3D tissue-engineered human blood vessels *in vitro*.

**Methods:** Tissue-engineered blood vessels were formed by co-culturing HAMECs and MSCs within porous gelatin scaffolds (Surgifoam®). M0, M1, M2 and M1-M2 primary macrophages were seeded alone on the scaffolds or in co-culture with the engineered blood vessels as previously described [3]. Then, the scaffolds were digested to generate a single cell suspension and stained with a 10-marker flow cytometry panel: macrophage general marker (CD45), M1 macrophage markers (CCR7, HLA-DR, CD83, CD38 and PD-L1), and M2 macrophage markers (CD206, CD209, CD163 and CXCR4). Data were acquired on BD Fortessa™ flow cytometer. Live, single and CD45 positive cells from all the different conditions were down sampled and merged into a single expression matrix prior to dimensionality reduction analysis in FlowJo®. Cluster analysis was done using manual gating or different plugins such as FlowSom.

**Results:** Using this approach, we were able to differentiate the effect of the biomaterial itself from the effects of interactions with blood vessels on macrophage phenotype. While macrophages polarized to the different phenotypes were relatively homogenous in 2D culture, after 24 hours in 3D culture, even without tissue-engineered blood vessels, they became a heterogeneous population comprising 3-4 main clusters, each comprising cells that expressed varying levels of each marker. Following crosstalk with tissue-engineered blood vessels, the prior polarization states of the macrophages affected their response. In particular, M1 and M1-M2 macrophages became enriched in clusters characterized by high levels of M1 markers (such as CD38, CD80 and CD38), while M2 and M0 macrophages became enriched in clusters that were predominant in M2 markers (such as CD206, CD163 and CXCR4).

**Conclusions:** These findings suggest that macrophage phenotype is strongly affected by co-culture with tissue-engineered blood vessels in a way that depends on the prior polarization state of the macrophages.

**Acknowledgements:** This project was supported by NHLBI HL130037 to KLS. The NanoBioCel group acknowledges SAF2017-82292-R (MINECO/AEI/FEDER, UE). B.Hernaez thanks the Basque Government for the PhD grant. Flow cytometry was conducted in Sidney Kimmel Cancer Center Flow Cytometry Facility (Philadelphia)

**References:** [1]Freiman et al. Stem Cell Research & Therapy (2016) [2]Ben-Shaul et al. PNAS (2019) [3]Graney, P.L. et al. Science Advances (2020)

#### 5:55 AM F.SM07.01.06

**De novo Design of Functional Zwitterionic Biomimetic Material for Immunomodulation** Bowen Li<sup>1</sup> and Shaoyi Jiang<sup>2</sup>; <sup>1</sup>Massachusetts Institute of Technology, United States; <sup>2</sup>Cornell University, United States

Super-hydrophilic zwitterionic polymers are a class of non-fouling materials capable of effectively resisting any nonspecific interactions with biological systems. Beyond conventional zwitterionic polymers that are biologically inert, we have designed a functional zwitterionic polymer by achieving a tradeoff between the non-specific interaction for non-fouling property and the specific interaction for bioactive functionality. Built from phosphoserine, an immune-signaling molecule in nature, this zwitterionic polymer exhibits both non-fouling and immunomodulatory properties. Conjugation of this zwitterionic polymer to uricase, a highly immunogenic enzyme, shows to proactively eradicate all the unwanted immune response, outperforming the inert zwitterionic polymers. On the other hand, this polymer could significantly prolong the half-life of uricase *in vivo*, overcoming the innate drawback of phosphoserine in inducing accelerated clearance. As the first demonstration of a non-fouling zwitterionic material with build-in immunomodulatory functionality, this work not only provides new insights into the fundamental design of biomaterials, but also contains far-reaching implications for broad biomedical applications including drug delivery, implants and cell therapy.

SESSION F.SM07.02: Directing and Understanding the Immune System  
On Demand Abstracts Available for Viewing Starting Saturday Morning, November 21, 2020  
F-SM07

#### 5:00 AM \*F.SM07.02.01

**Materials-Based Organoids to Model Immunity in Aged and Young Individuals Against Antibiotic-Resistant Bacteria** Ankur Singh; Georgia Institute of Technology, United States

Antibiotic-resistant bacteria are a major and rising global health threat. Although this threat affects all ages, pediatric patients, and aged individuals are at increased risk of antibiotic-resistant bacterial infections. Of concern are *Klebsiella*



*pneumoniae* (*K. pneumoniae*) that fail to induce in vivo germinal center B cell responses, which facilitate antibody production to fight infection. Immunotherapies using antibodies targeting antibiotic-resistant bacteria are emerging as promising alternatives, however, they cannot be efficiently derived ex vivo, necessitating the need for immune technologies to develop therapeutics. In this talk, I will discuss how organoid polymer functionality and mode of *Klebsiella pneumoniae* membrane antigen presentation regulates ex vivo germinal center epigenetics in young and aged B cells. In this work, polyethylene glycol (PEG)-based immune organoids are developed to elucidate the effects of polymer endpoint chemistry, integrin ligands, and mode of *K. pneumoniae* antigen presentation on germinal center B cell phenotype and epigenetics, to better define the lymph node microenvironment factors regulating ex vivo germinal center dynamics. Notably, both PEG vinyl sulfone or acrylate fail to sustain primary immune cells, but functionalization with maleimide (PEG-4MAL) leads to B cell expansion and germinal center-like induction. Single cell RNA sequencing analysis of lymph node stromal and bulk sequencing of germinal center B cells show niche associated heterogeneity of integrin-related genes. Incorporation of niche-mimicking peptides reveals that collagen-1 promotes germinal center-like dynamics and epigenetics. PEG-4MAL organoids elucidate the impact of *K. pneumoniae* outer membrane-embedded protein antigen versus soluble antigen presentation on germinal centers and preserve the response across young and aged mice. Finally, I will discuss ongoing efforts to engineer immune organoids from primary B cells from non-human primates and humans.

#### 5:15 AM \*F.SM07.02.02

**Microenvironmental Control of Bioengineered Immune Tissues with Microfluidics** Rebecca R. Pompano; University of Virginia, United States

A critical element of the immune system is tissue-level spatial organization. Cells and extracellular matrix elements are all highly organized in the lymph node, spleen, and thymus, as well as in the peripheral organs where immune cells infiltrate. Furthermore, secreted molecules are arranged in local patterns that depend on diffusion and interstitial flow. To begin to probe the functional outcomes of this intricate organizational structure, our laboratory has focused on combining live tissues and engineered biomaterials with microfluidic and micropatterning for fluidic and spatial control. We have developed microsystems to deliver drugs locally to specific regions of spatially structured tissues, to co-culture multiple structured organs under recirculating flow, and to begin to build a micropatterned lymph node. Here we will discuss our recent progress towards modeling complex immune function outside the body, to gain insight into the spatiotemporal dynamics of inflammation and immunity.

#### 5:30 AM F.SM07.02.03

**Cell- and Fluid-Sampling Microneedle Arrays for Minimally Invasive Monitoring of Tissue-Resident Immunity** Sasan Jalili-Firoozinezhad<sup>1</sup>, Coralie M. Backlund<sup>1</sup>, Daniel Garafola<sup>1,1,1</sup>, Mariane Melo<sup>2</sup>, Paula T. Hammond<sup>1,1,3</sup> and Darrell Irvine<sup>1,4,3</sup>; <sup>1</sup>Massachusetts Institute of Technology, United States; <sup>2</sup>Massachusetts Institute of Technology and Harvard University, United States; <sup>3</sup>Institute for Soldier Nanotechnologies, MIT, United States; <sup>4</sup>Department of Biological Engineering, MIT, United States

Immune monitoring approaches in human patients and animal models primarily rely on peripheral blood analysis, as the standard method for immunophenotyping. Although this strategy mirrors important information of the immune responses of the host, blood draws fail to track major immune cell populations preferentially residing in peripheral tissues, including barrier tissues such as the skin. Moreover, invasive approaches for sampling and analyzing immune cell populations from lymph nodes or skin are apparatus intensive and require special training for use. On the other hand, minimally invasive methods for quantitative monitoring of the immune status of the skin or other barrier tissues could provide valuable information in the context of patients with genetic and acquired immunodeficiency disorders, organ transplants, and vaccination, but such approaches are currently lacking. To overcome these challenges, we developed microneedle (MN) skin patches, coated with an ionically-crosslinked biocompatible polymer, which swells upon skin insertion, absorbing interstitial fluid (ISF) and enabling migration of cells into the patch in a minimally invasive, cost-effective manner. These MN arrays were used to monitor antigen-specific tissue-resident lymphocytes in the OVA-vaccinated and LPS-infected C57Bl/6 mice skin. We demonstrated that by applying the patches to skin for 12 hours, several thousand live cells are recovered without immunizing or altering pre-existing T cell or B cell responses against target antigens. In response to local intradermal LPS injection, without prior vaccination, MN arrays were able to sample more abundant lymphocytes and inflammatory cytokines compared to naïve, untreated mice. Our data strongly suggest that the sampling MN skin patches could be harnessed as a powerful tool to quantitatively elucidate immune signatures of infectious or autoimmune diseases in the future.

#### 5:40 AM F.SM07.02.04

**Detecting Cancer Biomarkers Using Single-Molecule Techniques for Future Liquid Biopsy Applications** Keshani G.

Pattiya Arachchillage, Subrata Chandra and Juan M. Artes Vivancos; University of Massachusetts, Lowell, United States

Cancer is one of the most frequent causes of death globally, and cancer biomarkers are promising for detecting cancers early.<sup>1</sup> This disease kills more than 8 million people per year, and most probably, we may need to expect this number to increase by more than 50% in the coming decades.<sup>1</sup> Early diagnosed cancers are relatively easier to treat and cure. There are various techniques to screen cancers as early as possible. Liquid biopsy is a promising approach since it is used to diagnose tumor-specific biomarkers non-invasively.<sup>2</sup> Moreover, it can detect genetic material (circulating tumor nucleic acids, ctNA), which is important in various applications, including cancer screening.<sup>3,2</sup> Detecting ctNA in the blood is challenging, because of the low ctNA concentration and the low frequency of mutations compared to wild-type sequences.<sup>2</sup> Nanotechnology methods can help to address this challenge. In particular, the Scanning Tunneling Microscopic (STM)-assisted break junctions method (STM-BJ)<sup>4</sup> has recently allowed the first demonstration of detection and identification of RNA via single-molecule conductance.<sup>3</sup> This is an ideal method for liquid biopsy since it is non-invasive and could be helpful to detect cancers without the use of surgery.<sup>2</sup> Early detection of the genetic material in cancer biomarkers, such as ctDNA and ctRNA<sup>2</sup>, through liquid biopsy using nanotechnology may help save many lives from cancer patients.

In this work, we focus on characterizing ctNAs and investigate an effective method for their ultra-sensitive detection in complex samples. The main hypothesis of the study is that the sequences of ctNAs can be used to detect cancers as the literature supports.<sup>5</sup> The selected biomarkers are KRAS, BRAF, and Nras, in agreement with data from the Pan-Cancer Analysis of Whole Genomes (PCAWG) Consortium of the International Cancer Genome Consortium (ICGC) and The Cancer Genome Atlas (TCGA).<sup>5,6</sup> We use STMBJ to measure and compare the conductivity of these ctNAs, comparing the conductivity of wild type and mutated biomarker sequences of different lengths. Detecting electrical fingerprints from biomarkers will greatly impact the early detection of cancers, allowing beginning treatments early, potentially saving many lives.

#### References

1. Campbell PJ, Getz G, Korbel JO, et al. Pan-cancer analysis of whole genomes. *Nature*. 2020;578(7793):82-93. doi:10.1038/s41586-020-1969-6
2. Das J, Kelley SO. High-Performance Nucleic Acid Sensors for Liquid Biopsy Applications. *Angew Chemie - Int Ed*. 2019. doi:10.1002/anie.201905005
3. Li Y, Artés JM, Demir B, et al. Detection and identification of genetic material via single-molecule conductance. *Nat Nanotechnol*. 2018;13(12):1167-1173. doi:10.1038/s41565-018-0285-x
4. Xu B, Tao NJ. Measurement of single-molecule resistance by repeated formation of molecular junctions. *Science (80- )*. 2003;301(5637):1221-1223. doi:10.1126/science.1087481
5. Rheinbay E, Nielsen MM, Abascal F, et al. Analyses of non-coding somatic drivers in 2,658 cancer whole genomes. *Nature*. 2020;578(7793):102-111. doi:10.1038/s41586-020-1965-x
6. Detection of BRAF mutation in thyroid papillary carcinomas by mutant allele-specific PCR amplification (MASA) in: *European Journal of Endocrinology* Volume 154 Issue 2 (2006). <https://ej.ebioscientifica.com/view/journals/eje/154/2/1540341.xml>. Accessed June 8, 2020.

#### **5:50 AM F.SM07.02.05**

**Late News: Engineering a Dynamic Host-Guest Substrate for Cytotoxic T Cell Activation** Rui Li<sup>1</sup>, Yingrui Deng<sup>2</sup>, Boguang Yang<sup>2</sup>, Cai Liang<sup>2</sup>, Oi Lan Kathy Lui<sup>2</sup> and Liming Bian<sup>2</sup>; <sup>1</sup>New York University, United States; <sup>2</sup>The Chinese University of Hong Kong, Hong Kong

In immunotherapy, cytotoxic T cells orchestrate an organized macromolecular assembly of T cell receptors (TCRs) in the immunological synapse (IS) to successfully commit antigen recognition and effector functions. Shortly after the contact of T cells with the APCs or cancer cells, the complex of the ligated TCR and costimulatory molecules will dynamically cluster in the IS. Initially, the TCR-CD3-pMHC complexation would generate biochemical and mechano-cues, augmented by the CD28 co-stimulation through the PI3K signaling pathway. Then the ligated TCRs transfer to the central SMAC to trigger the downstream tyrosine kinase cascades. Eventually, the dynamic interactions between the TCR clusters and the actomyosin cytoskeleton lead to the maturation of the IS and the full activation of T cells. Recent researches have shown that the enhanced flexibility of the immunoreceptors would improve the T cell activation and proliferation through an enhanced mechanosensing of the TCR. Lambert et al. showed that the CD4+/CD8+ T cell populations showed an elevated proliferation and robust cytokine production with a decrease in the rigidity of PDMS stimulating microsphere. Moreover, an artificial T cell-stimulating matrix with two stimulating signals and low mechanical stiffness was reported to better promote the CD3 clustering, T cell proliferation, and cytotoxic functionality of the CD8+ T cells. Though not yet fully proven, the high flexibility and mobility of the stimulating ligands should contribute to the augmented outcomes of the activated T cell. Inspired by this idea, we emulated the dynamic process of TCR ligation and clustering by utilizing the supramolecular host-

guest interactions to conjugate the activating ligands onto an APC-mimetic substrate, where the cyclodextrin-modified ligands are likely to be relocated under the retrograde actin flow-mediated force during the TCR clustering. First, we synthesized the adamantane-modified methacrylated hyaluronic acid (MeHA-ADA) macromers and separately conjugated the anti-CD3 $\epsilon$  (stimulation signal 1) and anti-CD28 (co-stimulation signal 2) antibodies to the  $\beta$ -cyclodextrins. Then both signal molecules attach to the backbones of MeHA-ADA through the non-covalent reversible interactions between the  $\beta$ -cyclodextrins and adamantanes. Control substrates were fabricated by chemically crosslinking the antibodies onto the macromer through thiol-ene reactions. The dynamic host-guest T cell activating substrate was characterized to have similar mechanical stiffness and to bear the non-significantly different amounts of antibodies and RGD peptides compared with those of the control substrates. Then the freshly isolated murine naïve CD8<sup>+</sup> T cells were cultured on all substrates for 7 days before the verification of their effects on T cell activation and proliferation. The RT-qPCR results showed that the expression levels of IFN $\gamma$ , IL-2, TNF $\alpha$ , and NFATc1 were significantly promoted in the CD8<sup>+</sup> T cells cultured on the dynamic host-guest substrate compared to those of the control substrates and free-adding antibodies. Besides, the flow cytometry results showed that the surface markers of activated T cells, CD44 and CD69, were significantly elevated on the T cells cultured on dynamic host-guest substrates. Furthermore, over 68% of the naïve T cells cultured on the dynamic host-guest substrates differentiate into the CD45R<sup>+</sup> effector T cells and CD45R<sup>+</sup>/CD62L<sup>+</sup> effector memory T cells, accompanied by robust proliferation and cytokine secretion. These results indicate that the reversible nature of supramolecular interactions offers great prospects for the design of T cell-activating platforms, combining the soft mechanical properties of the lymphoid tissues and complex ligand presentation of the APC membrane to promote the activation of cytotoxic T cells for the future clinical use. Our work provides valuable insights for the biomimetic design of platforms with wide therapeutic applications in immunotherapy.

#### 6:00 AM F.SM07.02.06

**Late News: Spatial Organization of CpG-Nanoconstructs Influences Targeting of Toll-Like Receptors** [Kwahun Lee](#) and Teri W. Odom; Northwestern University, United States

Nanoparticle-based constructs have shown enhanced performance when delivering immunostimulatory molecules in cancer immunotherapy – an emerging approach to treat cancer. Their endosomal organization, however, has received little attention for targeting intracellular receptors. This talk will describe how the spatial organization of endosome-targeted constructs can influence their ability to induce downstream cell signaling. As a model system, Toll-like receptor 9 activation of macrophage induced by CpG-constructs will be examined. First, we will discuss how endosomal organizations of these constructs can be controlled by the surface curvature. Second, the spatial organizations will be correlated with immunostimulatory activity of the constructs. Finally, we will describe the implications and promises of these results for different targeted-delivery systems.

#### 6:10 AM F.SM07.02.07

**Late News: Antigen Functionalized Nanomaterials for the Study and Regulation of the Mechanical Activity of NK Cells and T Cells** [Mark Schwartzman](#); Ben-Gurion University of the Negev, Israel

The immune activity of cytotoxic lymphocytes cells is regulated by many chemical and physical cues, whose integration mechanism is still obscure. As other lymphocytes, Cytotoxic lymphocytes act in a highly heterogeneous and diverse environment, with rapidly and abruptly changing physical properties and chemical compositions. Here, we engineered a new nanoscale platform which allows to control and integrate chemical, mechanical, and spatial stimuli for Natural Killer (NK) cells, and screen the individual and cumulative effect of these stimuli on NK cell morphology and cytotoxic activity. This platform is based on nanowires produced from the bottom-up, which are confined within micron-scale stimulating domains. These domains mimic to a certain extent professional antigen-presenting cells, such as dendritic cells. The nanowires within the domains provide the mechanical stimulation of NK cells, as we recently reported [1]. Whether the enhanced activation is due to the high compliance of the ultra-flexible nanowires to the mechanical forces, or to the nanoscale topography that the nanowires impose on the cell membrane, is still unclear.

To address this question here, we compared NK cells stimulated on domains of nanowires with different diameters. These nanowires comply differently to the mechanical forces applied by NK cells while producing similar topographical environments. In our platform, we also mimicked the spatial discontinuity of antigens into nanosized clusters, by selective immobilization onto the nanowire tips. We seeded primary NK cells on these heterogeneous surfaces and found two distinct subpopulations split by physical location: either on the top of the nanowire islands or between the islands. The two subpopulations vastly differed in morphological features of the cells, including circularity, length, spreading, and orientation. Furthermore, the cells in the two subpopulations were different in their activation levels, which we quantified *via* expression of lysosomal Lysosomal-associated membrane protein 1 (LAMP-1): only cells belonging to the subpopulation sitting on atop the nanowire islands showed enhanced activation. Finally, we showed that by independently varying nanowire flexibility *via* their diameter, as well as the presence of stimulating antigens, the degree of activation of NK cells could be

fine-tuned.

To further explore the effect of the nanowire flexibility on the activation of cytotoxic lymphocytes, we synthesized nanowires with systematically varied length – from 2 microns to 20 microns, chemically coated them with antigens, and used them as a stimulation platform for primary NK cells and T cells. In both cases, we found that the activation of these cells assessed via the expression of LAMP-1 and the release of interferon-gamma increased with the increase in the nanowire length. These results confirm that the nanoscale mechanical compliance of the interface between NK cells and T cells plays a critical role in their immune stimulation.

Our novel platform demonstrates an unprecedented level of simultaneous control over chemical and physical stimuli, with an unparalleled spatial resolution at the nanometric scale. The observed immune response of NK cells to the fine variations in both physical and chemical stimuli provides an important insight into the mechanism of their cytotoxic activity. Besides, the demonstrated microenvironment for NK cell stimulation, which is engineered with features that independently tune chemical and physical stimuli, paves the way to future technologies for the *ex vivo* expansion and activation of cytotoxic lymphocytes in immunotherapy.

[1] Le Saux et al, G. Le Saux, N. Bar Hanin\*, A. Edri, U. Hadad, A. Porgador, and M. Schwartzman *Adv. Mater.* 31,1805954 (2019)

SESSION F.SM07.03: Materials Approaches to Modulating Vaccine Responses  
On Demand Abstracts Available for Viewing Starting Saturday Morning, November 21, 2020  
F-SM07

**5:00 AM \*F.SM07.03.01**

**Delivering Molecular Self-Assemblies for Immunotherapies—Tabletization and Mucosal Delivery** Sean H. Kelly, Emmanuel Opolot, Yaoying Wu, Ajay K. Varadhan and Joel Collier; Duke University, United States

The control or eradication of numerous infectious diseases relies on widespread vaccination, which in turn currently depends on cold chain continuity and the availability of trained medical personnel across the globe. Supramolecular vaccines based on short peptides have been previously found to be highly thermally stable, potentially reducing requirements for a continuous cold chain. Here we describe recent efforts to render peptide self-assemblies immunogenic when delivered via mucosal routes, along with additional strategies for designing easily administered and stable tabletized forms that are immunogenic sublingually (under the tongue). Combinations of self-assembly, modification with the mucus-inert polymers polyethylene glycol (PEG) or proline-alanine-serine peptides (PAS), mucosal adjuvants, and sublingual delivery enabled systemic immune responses against short peptide epitopes, which otherwise are poorly immunogenic sublingually. Stabilized self-assemblies were formulated into highly porous, thermally stable, and easily administered tablets which rapidly dissolved under the tongue to deliver peptide self-assemblies and elicit systemic immune responses. In mice, sublingual immunizations with tabletized self-assembling peptides elicited antibody responses against both model epitopes and an epitope from *M. tuberculosis*. Further, the tablets' immunogenicity was not diminished after being heated for 1 week at 45 degrees C, in contrast to traditional carrier-based vaccines that were thermally sensitive. Together these strategies are aimed at reducing barriers for global vaccine distribution and administration by reducing dependence on continuous cold chains and highly trained medical personnel.

**5:15 AM \*F.SM07.03.02**

**Enhancing Vaccine Immunity via a Nanoparticle Adjuvant That Alters Lymph Flow and Lymph Node Permeability** Darrell Irvine; Massachusetts Institute of Technology, United States

Adjuvants play critical roles in shaping the immune response to vaccines. Here we describe a novel nanoparticle adjuvant, saponin-MPLA nanoparticles (SMNP), formed by the immunostimulatory compound saponin, the Toll like receptor (TLR)-4 agonist monophosphoryl lipid A (MPLA), cholesterol, and phospholipids. These components self-assemble into striking ~40 nm diam. cage-like structures reminiscent of ISCOMs (Immunostimulatory complexes) previously reported for saponin/phospholipid complexes, but have synergistic immunostimulatory properties from the combined action of saponins and MPLA. SMNP exhibited striking potency in both mouse and non-human primate (NHP) preclinical animal models of vaccination with a variety of subunit vaccines. Protein vaccines adjuvanted with SMNP elicited robust germinal center B cell and Tfh responses, leading to strong serum IgG responses and (in NHPs) HIV tier 2 neutralizing antibody responses. Strikingly, SMNP exhibited distinctive mechanisms of action, altering lymph flow and promoting antigen entry into draining lymph nodes, in a manner dependent on co-assembly of MPLA and saponin together in the same nanoparticle. Altogether,

these findings suggest SMNP may be a promising novel adjuvant for subunit vaccines in settings of HIV, COVID-19, and other infectious diseases.

#### 5:30 AM F.SM07.03.03

**Enhancing the Stability and Potency of Innate Activators Through Polymeric Nanoparticle Delivery** Emily Gale, Gillie Roth, Anton Smith and Eric A. Appel; Stanford University, United States

Immunomodulatory therapies such as cancer immunotherapies and prophylactic vaccines often depend on adjuvants to drive potent and directed immune responses. Innate immune receptor agonists have become a popular category of adjuvants due to their specificity and robust effects. A subset of these agonists (e.g. CpG ODN, poly(I:C), and cyclic dinucleotides) are nucleic acid derivatives that activate cytosolic or endosomal receptors in immune cells, including several classes of dendritic cells (DCs). Stimulated DCs can then present antigen and stimulate naïve T cells for generation of the appropriate adaptive immune response. Unfortunately, these agonists are susceptible to degradation by nucleases *in vivo*, and thus enhanced stabilization and targeting should prolong their function and enhance their effect. We hypothesized that encapsulation of these negatively charged agonists in cationic polymeric nanoparticles would provide an increased agonist half-life and promote targeting to intracellular compartments of immune cells. Here, I discuss the development of methods to encapsulate nucleic acid agonists in biodegradable cationic poly(beta amino-ester) (PBAEs) nanoparticles as well as the specific particle properties (*i.e.*, size, surface charge, polymer chemistry) that lead to a 13-fold increase in innate immune cell activation as measured by type I interferon production. By controlling stability, targeting, and release profiles of this promising class of nucleic acid agonists, we were able to direct the downstream adaptive immune response to a subunit vaccine, significantly enhancing both antibody concentration (1.5-fold) and affinity (14-fold). This nanoparticle platform can be used for the delivery of a range of therapeutic and stimulatory nucleic acids for improved cancer immunotherapies and infectious disease vaccines.

Cancer immunotherapy can also be augmented with innate immune cell-targeting adjuvants to elicit potent immune activation and a strong anti-cancer response. Despite their potential in both vaccines and as part of cancer immunotherapies, many small molecule toll-like receptor (TLR) agonists have been limited clinically due to their extreme potency and lack of pharmacokinetic control, causing systemic toxicity from unregulated systemic cytokine release. In this work, we overcome these shortcomings by generating PEG-PLA nanoparticles presenting potent TLR7/8a moieties on their surface. The NP platform allows precise control of TLR7/8a valency and resulting surface presentation through self-assembly using nanoprecipitation. We hypothesized that the pharmacokinetic profile of the nanoparticles would minimize systemic toxicity, localizing TLR7/8a presentation to the tumor bed and tumor draining lymph nodes. In conjunction with anti-programmed death-ligand 1 (anti-PD-L1) checkpoint blockade, peritumoral injection of TLR7/8a nanoparticles slowed tumor growth, extended survival, and decreased systemic toxicity in comparison to the free TLR7/8a in a murine colon adenocarcinoma model. These nanoparticles constitute a modular platform for controlling pharmacokinetics of small molecule immunostimulatory molecules, resulting in increased potency and decreased toxicity. Together both of these studies demonstrate the value of polymer nanoparticle delivery systems for targeted delivery of different adjuvants (many of which have not made it to the clinic due to toxicity or poor stability) to enhance safety and efficacy for use in either prophylactic vaccines or as part of cancer immunotherapies.

#### 5:40 AM \*F.SM07.03.04

**Spatial Control Over Innate Immune Activation by Imidazoquinoline TLR7/8 Agonists Through Lipid Polymer Amphiphile Conjugation** Bruno G. De Geest; Ghent University, Belgium

Uncontrolled systemic inflammatory immune triggering has hampered the clinical translation of several classes of small-molecule immunomodulators, such as imidazoquinoline TLR7/8 agonists for vaccine design and cancer immunotherapy. By taking advantage of the inherent serum-protein-binding property of lipid motifs and their tendency to accumulate in lymphoid tissue, we designed amphiphilic lipid-polymer conjugates that suppress systemic inflammation but provoke potent lymph-node immune activation. This work provides a rational basis for the design of lipid-polymer amphiphiles for optimized lymphoid targeting.

#### 5:55 AM F.SM07.03.05

**Microneedle Based Vaccines for Viral Infections** Divakara SSM Uppu<sup>1</sup>, Michelle Turvey<sup>1</sup>, Abdul RM Sharif<sup>1</sup>, Katell Bidet<sup>1</sup>, Yanpu He<sup>2</sup>, Jianzhu Chen<sup>1,2,2</sup> and Paula T. Hammond<sup>1,2,2</sup>; <sup>1</sup>Singapore-MIT Alliance for Research and Technology (SMART), Singapore; <sup>2</sup>Massachusetts Institute of Technology, United States

In the current era of the COVID-19 pandemic, there is no greater need than vaccines. Dengue, a mosquito-borne viral disease,

is a neglected disease in the tropical world, where an estimated 2.5 billion people live at risk of infection each year<sup>1</sup>. To date, no safe and effective vaccine exists for Dengue. Most virus vaccines are live-attenuated vaccines (LAVs) containing a weakened virus that produce an effective immune response. However, LAVs typically suffer from safety limitations and, more importantly, require cold chain storage<sup>2</sup>. In contrast to LAVs, protein-based subunit vaccines are considered safer. However, subunit proteins as vaccine antigens are typically poorly immunogenic and require adjuvants that require both co-delivery and controlled release for maximum efficacy<sup>3</sup>. In this talk, I will describe our efforts to achieve cold chain independence and vaccine delivery using biomaterials.

Here, we design and formulate microneedle-based intradermal vaccines based on the live virus as well as subunit proteins for protection against the Dengue virus. Microneedles are miniaturized needles (100  $\mu\text{m}$  to 1mm) typically assembled as an array and applied onto the skin. Specifically, I will talk about the design and development of (i) LAV<sup>2</sup> and (ii) protein subunit<sup>3</sup> microneedle-based vaccines using the Dengue virus as a model system. In the first part of my talk, I will discuss the development of polymeric matrix to formulate the LAV vaccine on microneedles for improving the viability at room temperature for up to 4 weeks without loss of efficacy. During the second part, I will talk about developing polymeric multilayer thin films on microneedles encapsulating a subunit vaccine (protein antigen and two adjuvants) for achieving controlled release from days to weeks.

#### References

1. Bhatt S *et al.* *Nature*, **2013**, 496, 504-507.
2. Turvey ME *et al.*, *Bioeng. Transl. Med.*, **2019**, 4, e10127.
3. DSSM Uppu *et al.*, *J. Control. Release.*, **2020**, 317, 130.

#### 6:05 AM \*F.SM07.03.06

##### **Mimicry of Glycoprotein-Independent HIV Targeting of Myeloid Cells with Lipid-Wrapped Polymer**

**Nanoparticles** Behnaz Eshaghi<sup>1</sup>, Suryaram Gummuluru<sup>2</sup> and Bjoern Reinhard<sup>1</sup>; <sup>1</sup>Boston University, United States; <sup>2</sup>Boston University Medical School, United States

Human Immunodeficiency Virus (HIV) transfers from special, non-endolysosomal compartments in myeloid dendritic cells and macrophages to T cells in a process called trans-infection. It has been demonstrated that lipid-wrapped gold nanoparticles that contain the ganglioside, GM3, can recapitulate viral segregation in non-endolysosomal compartments in CD169-expressing dendritic cells and macrophages, and some findings suggest that GM3-presenting nanoparticles can even reconstitute a virological synapse after addition of T cells. However, for a number of reasons, including low payload and their non-degradable nature, gold nanoparticles are not ideal for exploiting the GM3-CD169 mediated accumulation of nanoparticles at the contact between antigen presenting cells and T cells for important applications. In this presentation, we will provide an overview of our recent progress in utilizing lipid-wrapped polymer nanoparticles as HIV-mimicking nanoparticles. We have assembled GM3-presenting, lipid-wrapped polymer nanoparticles with different polymer cores. Due to differences in the core composition, the NP had different glass transition temperatures that resulted in different stiffnesses at physiological temperatures. We mapped the intracellular distribution of the nanoparticles in CD169-expressing macrophages through confocal microscopy. Our findings suggest that in addition to the presentation of the ganglioside GM3 in the membrane around the nanoparticle core, the stiffness of the core plays an important role for successfully mimicking viral behavior. We found that while soft nanoparticles (Young's modulus of < 100 MPa) exclusively enter an endolysosomal pathway, for nanoparticles with a stiff core (Young's modulus  $\approx$ 1.4 GPA) a significant fraction of cells shows a different trafficking pattern that results in a segregation in non-endolysosomal compartments. The staining patterns of these compartments resemble those of virus containing compartments (VCCs) known to be reservoir sites for HIV.

SESSION F.SM07.04: Materials Approaches for Improving Cancer Immunotherapies  
On Demand Abstracts Available for Viewing Starting Saturday Morning, November 21, 2020  
F-SM07

#### 5:00 AM \*F.SM07.04.01

**Engineering Smart Technologies for Next-Generation Vaccines and Immunotherapies** John T. Wilson; Vanderbilt University, United States

Interventions that engage the power and specificity of the immune system have enormous potential to improve human health, yet the efficacy, safety, and utility of many promising immunomodulatory agents is limited by critical drug delivery barriers. This talk will describe current research in my laboratory focused on engineering nanostructured polymeric materials for intracellular delivery of immunomodulatory proteins, nucleic acids, and small molecules. Specifically, I will discuss our recent efforts in developing environmentally-responsive “smart” materials that open access cytosolic immunoregulatory machinery and how these materials can be leveraged to improve responses to cancer immunotherapy and infectious disease vaccines.

**5:15 AM \*F.SM07.04.02**

**Polymeric, Microparticle-Loaded Hydrogels Serve as Depots for Lactate and Mimic the 'Cold' Tumor Microenvironment** Jamal Lewis; University of California, Davis, United States

Immunotherapeutic approaches are effective by either harnessing the ability of the host immune system to recognize and eliminate cells that display tumor antigens, providing external stimuli to ramp up the destruction of tumor cells in an antigen-specific manner, or by negating the ability of the tumor cells to inhibit host immune cell activation. The latter option is particularly attractive as it avoids constitutive activation of immune cells, which can result in collateral damage to healthy tissues. This can be accomplished by exploiting molecular signals within the tumor microenvironment (TME), so that the tumor shifts from being “immunologically cold” and immune-evasive to “immunologically hot” and susceptible to immune elimination (e.g. checkpoint inhibitor - Keytruda®; anti-PD-1). Although these new immunotherapeutic approaches are a significant improvement on more conventional therapies, they still fail to rid the patient of tumor burden in most cases. As such, active research is underway to uncover other molecules that engender the ‘cold’ climate of the TME. One molecule that is ubiquitous in the TME and now emerging as a major source of immune suppression is lactate. Lactic acid is an intermediate in glucose metabolism and at physiological pHs is found as the conjugate base, lactate. Lactate is surprisingly both a byproduct and energy source for cancer cells, depending on the availability of oxygen. Within the TME, lactate drives the differentiation of immunosuppressive cell subsets, such as myeloid derived suppressor cells, which have the ability to prevent the maturation of dendritic cells (DCs), thereby halting subsequent anti-tumor adaptive immune responses. Lactate also impairs the differentiation of monocytes into macrophages (MΦ) and DCs and the LPS maturation of MΦs and DCs in the TME. Evidently, lactate immunometabolism is critical to the host’s immune response to cancer. However, we lack a defined model to replicate lactate conditions seen in the TME. *In vitro* models of solid tumors vary in complexity and range from tumor-derived cell lines to 3D models of the tumor microenvironment. More often than not, these models fail to recapitulate the complex milieu of immune factors and immune cells that are present in the *in vivo* setting and crucial to evaluating the efficacy of immunotherapies. Moreover, current cancer models fail to isolate the effects of lactate alone, which can conflate interpretation of results and leaves the efficacy of therapeutic strategies targeting lactate unanswered. Moreover, a combinatorial model, where lactate can be incorporated in combination with other molecules/ conditions of interest (e.g. hypoxia) is highly desired. Biomaterials offer a potential strategy to recapitulate the biochemistry of the TME, including lactate bioavailability. Here, we engineered a TME-mimicking system that is able to replicate one critical component of the TME, endogenous lactate levels, to understand the direct effect of localized lactate concentrations on immune cells. This system utilizes peptide hydrogels loaded with GM-CSF and degradable lactate-based polymeric microparticles. The hydrogel environment encapsulates the microparticles in a hydrated peptide mesh which allows for its hydrolysis into monomeric lactate and the subsequent accumulation of lactate in the hydrogel. Additionally, GM-CSF, a suppressive secretory chemokine produced by many tumors, serves to recruit innate immune cells to the hydrogel. Such a platform is expandable, where lactate and other immunogenic moieties can be investigated together. Moreover, the isolated effects of lactate on immune cells *in vivo* can provide evidence for targeting this molecule in immunotherapies.

**5:30 AM \*F.SM07.04.03**

**Engineered Biomaterials for Overcoming Transport Barriers in the Tumor Immune Microenvironment to Enhance Cancer Immunotherapy** Susan N. Thomas; Georgia Institute of Technology, United States

The transport of fluids, biomolecules and cells from the tumor microenvironment to draining lymph nodes and into the circulation is facilitated by the concerted influence of the blood and lymphatic vascular systems. Our efforts to characterize the impact of these transport processes on disease progression, in particular by regulating both metastasis and adaptive immunity, as well as to develop therapeutic approaches for tumor therapy that mitigate these effects by leveraging engineered biomaterials, will be described.

**5:45 AM F.SM07.04.04**

**Injectable Hydrogel Reservoirs Alter CD40 Agonist Antibody Pharmacokinetics to Improve Safety and Efficacy** Santiago Correa, Emily Gale, Aaron T. Mayer, Zunyu Xiao, Joseph L. Mann and Eric A. Appel; Stanford, United States

States

Immunotherapy can be made safer and more effective by using materials approaches to control the spatial and temporal exposure to immuno-stimulants. We previously described a polymer-nanoparticle (PNP) based hydrogel that is biocompatible, long lasting, and injectable<sup>1,2</sup>, traits that we hypothesized would improve controlled local delivery of immunotherapy. Here, we report that PNP hydrogels prolong the local exposure to CD40 agonist antibody (CD40 mAb), improving tolerability and therapeutic efficacy in the B16 model of melanoma.

We used positron emission tomography (PET) imaging to confirm hydrogel delivery altered CD40 mAb pharmacokinetics over the course of 12 days. Compared to dose-matched local bolus injections, hydrogels redistributed antibody exposure to the injection site and the tumor draining lymph node, increasing CD40 mAb AUC by 96% and 35%, respectively. As anticipated, hydrogel delivery reduced CD40 mAb loss to off-target antigen sinks such as the liver and the spleen, where CD40 mAb AUC decreased by 15% and 23%, respectively.

Consistent with these findings, we observed reduced toxicity in mice treated with hydrogels. In particular, mice treated with CD40 hydrogels had attenuated weight loss and recovered their weight more quickly than bolus controls. Serum cytokine analyses confirmed that hydrogels mitigated cytokine storm compared to dose-matched local bolus controls. Toxic side effects were further diminished by reducing the dose of CD40 mAb in the hydrogels, but reduced dose did not impair antitumor efficacy. Overall, these results indicate that delivery via PNP gel improves safety and maintains efficacy of CD4 mAb at low doses.

This approach did not require modifying cargo in any way, thus we anticipate hydrogel delivery will also improve the safety of other potent biologics, including cytokines and bispecific antibodies. Overall, PNP hydrogels may provide a highly translatable solution to the problem of immune-related adverse effects.

## References

1. Appel, E.A. et al. Self-assembled hydrogels utilizing polymer-nanoparticle interactions. *Nat Commun* **6**, 6295 (2015).
2. Stapleton, L.M. et al. Use of a supramolecular polymeric hydrogel as an effective post-operative pericardial adhesion barrier. *Nat Biomed Eng* **3**, 611-620 (2019).

## 5:55 AM F.SM07.04.05

**Noninvasive Imaging of Tumor-Infiltrating Immune Cells Using Rare-Earth Nanoparticles to Monitor Response to Cancer Immunotherapy** Swati Kataria<sup>1,2</sup> and Angela Belcher<sup>1,2</sup>; <sup>1</sup>Massachusetts Institute of Technology, United States; <sup>2</sup>Koch Institute for Integrative Cancer Research at MIT, United States

Cancer immunotherapy is fast emerging as the most promising treatment approach for a number of cancers, fueled by the breakthrough success of immune checkpoint inhibitors which promote immune-mediated clearance of tumors. However, the response rates to checkpoint inhibitors remain limited to 10-40% of patients, and it is a significant clinical challenge to identify candidates for treatment to minimize immunotherapy-related adverse events. Studies have shown that the presence of tumor-infiltrating lymphocytes (such as CD8+ T-cells, which drive tumor-cell killing) is one of the strongest prognostic factors predicting overall survival across a large number of cancers. Tumor biopsies have shown that during immunotherapy, responders exhibit an influx of activated CD8+ T-cells to the tumor site, while non-responding tumors continue to exclude them. Thus, the ability to visualize the distribution of tumor-infiltrating lymphocytes before and during treatment will allow us to observe and monitor the response status to therapy. However, it is a significant challenge to image and track immune cells in-vivo because they are relatively sparse and highly mobile. There is a need to develop new tools that can non-invasively assess the evolving immune composition of the tumor microenvironment, allowing evaluation of therapy-induced responses in real time.

Imaging in the near-infrared window (NIR-II 1000nm-1700nm) has generated growing excitement in recent years for deep-tissue optical imaging approaches. Biological tissue in this spectral range exhibits reduced scattering of photons and autofluorescence, enabling for high resolution imaging of deep tissue structures. Rare-earth nanoparticles (RENPs) have emerged as superior imaging agents due to their emission bands in regions of near-zero tissue autofluorescence (1300-1700nm), high photostability, and low intrinsic toxicity in a variety of animal models. We leverage advances in near-infrared imaging technologies using rare-earth nanoparticles to target and image immune cells in tumors as markers for therapeutic response. To achieve this, we synthesized small but ultra-bright rare-earth nanoparticles (sodium ytterbium fluoride doped



with erbium, cerium and zinc), and tailored the size and brightness during synthesis to enable observation of microscale features in-vivo. We then used a custom PEG-rich lipid formulation to make the nanoparticles serum-stable, and conjugated targeting antibodies on the surface to target immune cells of interest. We then performed both ex-vivo and in-situ labeling of immune cells in a murine melanoma tumor model, known for its poor response to immunotherapy. We demonstrate the ability of these nanoparticles to non-invasively image trafficking of labeled immune cells to the tumor in subsets of mice undergoing checkpoint inhibitor therapy (anti-PD1), indicating immune-mediated anti-tumor activity. Our work focuses on one key immune-cell sub-type (CD8+ T-cells), but the modularity of rare-earth nanoparticles makes them ideal tools for multiplexing, allowing future studies that simultaneously image multiple cell types in tumors for a more complex understanding of tumor-immune dynamics.

#### **6:05 AM \*F.SM07.04.06**

**Making Cold Tumors Hot—Nano-Layered Particles for Systemic Cytokine Delivery** Antonio Barberio, Sean Smith, Darrell Irvine and Paula T. Hammond; Massachusetts Institute of Technology, United States

Although immunotherapies have been highly effective for some forms of cancer, it has generally worked best in tumors in which there are significant numbers of leukocytes present that enable immune activation. Unfortunately, there are numerous aggressive cancer types which do not present with significant immune cell infiltration. These tumors tend to show little or no response to check point inhibitors or other therapies that block the regulatory response of the immune system; furthermore, such tumors are often also poor responders to Car-T and other more established immuno-therapeutic approaches. Cytokines can be potent immune stimulators that upregulate the innate immune response within a tumor microenvironment, causing a cascade of inflammatory signaling that can lead to activation of antigen presenting cells, and ultimately, the infiltration of tumor-specific CD8+ T cells and NK cells to the tumor site. This effect of creating a localized cytokine storm within the tumor can lead to a much more effective immune response against tumor cells; however delivery of cytokines, particularly highly potent and effective ones such as IL-12 can be difficult due to patient safety concerns. Release of cytokine to the blood stream can lead to harmful off-target effects, and these kinds of effects have made these proteins difficult to introduce as promising immunotherapies for patients. We have developed a modular nanoparticle approach using liposomal core particles and layering them with an electrostatic layer-by-layer (LBL) process in a simple and elegant method of constructing highly tailored ultrathin polymer coatings. The resulting LbL nanoparticles (NPs) have negatively charged outer layers that present polyelectrolytes such as dextran sulfate or hyaluronic acid in a hydrated brush arrangement that enables hydration, steric repulsion, colloidal and serum stability, and specific or non-specific targeting. We have determined a subset of polyanion outer layers that have high affinity and selectivity for ovarian cancer cells and, based on the polyanion composition, will cause trafficking either to the outer surface or to intracellular compartments in ovarian cancer cells. We have used this unique ability to control trafficking to create LbL NPs that can deliver IL-12 from the outer surfaces of ovarian cancer cells, thus generating highly localized depots that efficiently release cytokine and upregulate the immune response in high grade serous ovarian cancer, a cancer which has not previously benefitted from immunotherapeutic approaches. In vitro and in vivo results will be discussed, as well as release mechanisms, toxicity studies and clinical outlook for these targeted systems.

#### **6:20 AM \*F.SM07.04.07**

**Metabolic and Chemical Immunoengineering Enhances Anti-Tumor Immunity** Li Tang; École polytechnique fédérale de Lausanne (EPFL), Switzerland

Cancer immunotherapy represented by immune checkpoint blockades has achieved remarkable clinical success. However, an outstanding challenge is that a great majority of patients fail to respond to this therapy. This is in part due to the fact that tumor infiltrating lymphocytes (TILs) become exhausted and eventually incapable to control tumor progression. Among exhausted CD8+ TILs, a subpopulation, termed terminally exhausted CD8+ T-cells, have superior cytotoxicity but largely reduced proliferation capacity, and are known to be the direct contributors to the anti-tumor cytotoxicity. However, this subpopulation does not respond to immune checkpoint blockades or most current immunotherapies and are difficult to expand and maintain with their cytotoxicity. In the first part of the talk, I will discuss a new metabolic immunoengineering approach that expands the terminally exhausted CD8+ TILs and sustains their cytotoxic functions leading to eradication of established solid tumors and durable cures in a majority of treated mice when combined with adoptive T-cell transfer immunotherapies. Next, I will discuss a new cancer vaccine platform we developed recently for personalized neoantigen vaccine delivery, termed polycondensate neoepitope (PNE). PNE is a redox-responsive vaccine made through a reversible polycondensation reaction of peptide neoantigens and adjuvants together with a tracelessly responsive linker-monomer. Peptide-based neoantigens with diverse sequences and structures could be co-polymerized with molecular adjuvants to form PNEs of high loading capacity for vaccine delivery without adding any carriers. The redox-responsive PNEs with controlled molecular weights and sizes efficiently targeted and accumulated in draining lymph nodes, and greatly promoted the antigen capture and cross-presentation by professional antigen presenting cells. Mice immunized with PNEs showed markedly

enhanced antigen-specific T cell response and the protective immunity against the tumor cell challenge.

#### 6:35 AM F.SM07.04.08

**Engineering Biomaterials to Overcome Hypoxia-Driven Immunosuppression and Boost Cytotoxic T Cells** Thibault Colombani<sup>1</sup>, Loek Eggermont<sup>1</sup>, Stephen Hatfield<sup>1</sup>, Mahboobeh Rezaeeyazdi<sup>1</sup>, Adnan Memic<sup>1,2</sup>, Michail Stikovskiy<sup>1</sup> and Sidi A. Bencherif<sup>1,3</sup>; <sup>1</sup>Northeastern University, United States; <sup>2</sup>King Abdulaziz University, Saudi Arabia; <sup>3</sup>Harvard University, United States

Hypoxia, a state of low oxygen tension, is one of the major obstacles in the treatment of solid tumors due to its inhibitory potential on cytotoxic immune cells. Targeting hypoxia-driven immunosuppression is a promising approach to prevent tumor escape from immunosurveillance. Biomaterials with a capacity to produce oxygen and be delivered near a tumor bed represent a viable strategy for reversing local hypoxia. This approach could boost effector functions of antitumor T cells, and potentially reinforce current cancer immunotherapies. Recently, we engineered injectable oxygen-generating biomaterials, known as cryogels. Oxygen-generating cryogels (O<sub>2</sub>-cryogels), with their unique physical features, including mechanical robustness and syringe injectability, were designed to release oxygen in a controlled and sustained fashion. We found that local oxygenation from O<sub>2</sub>-cryogels downregulated hypoxia-inducible gene expression in hypoxic murine melanoma and reduced the accumulation of immunosuppressive metabolites such as extracellular adenosine. Strikingly, O<sub>2</sub>-cryogels released the break on the tumoricidal function of hypoxic T cells against melanoma in a very short time (< 4h). Mechanistically, O<sub>2</sub>-cryogels *i*) enhanced T cell–tumor cell interactions; *ii*) increased T cell-mediated production of cytotoxic proteins (perforin and granzyme B) fatal to tumor cells; and, as a result, *iii*) restored the killing ability of antigen-specific T cells. Collectively, O<sub>2</sub>-cryogels provide a unique platform to expand our understanding on how hypoxia affects immune cells and may leverage emergent cancer immunotherapies to circumvent hypoxia-driven immunosuppressive mechanisms and achieve more predictable and favorable outcomes.

Acknowledgement: This work was supported by Northeastern University Seed Grant/Proof of Concept Tier 1 Research Grant and NSF CAREER award (DMR 1847843).

#### 6:45 AM F.SM07.04.09

**Establishing the Role of Matrix Viscoelasticity on Cancer-Macrophage Migration and Phenotype** Kolade Adebawale and Ovijit Chaudhuri; Stanford University, United States

Increased tumor stiffness and alterations in viscoelasticity has been implicated in cancer progression. Viscoelastic materials exhibit stress relaxation, which results in resistance to a deformation relaxing over time. Emerging evidence indicates that macrophage immune cells play a key role in regulating cancer progression and can constitute up to 50% of the tumor mass. Macrophages migrate into the tumor microenvironment where they can polarize to a cancer supporting (anti-inflammatory) or cancer inhibiting (pro-inflammatory) phenotype. Current work has demonstrated the impact of 2D elastic substrates on macrophage phenotype. However, the impact of viscoelasticity on macrophage polarization and migration in 3D is unknown. Here, we develop an alginate-collagen based matrix that has tunable viscoelastic properties to examine how matrix viscoelasticity impacts macrophage migration and phenotype. The choice of collagen as the biochemical ligand is to mimic the stromal matrix where immune cells are typically found. Importantly, the viscoelastic properties are tuned independent of polymer concentration and Young's modulus by varying the molecular weight and crosslinking of the gels, allowing for the impact of matrix viscoelasticity to be specifically demonstrated. Specifically, we can tune the characteristic stress relaxation times from ~100 to 5,000 seconds while keeping the initial Young's modulus of all the materials at ~2kPa. U937 pro-monocytic cells lines were encapsulated in the 3D alginate-collagen matrix and cell migration was assessed using confocal time-lapse microscopy. The results demonstrate enhanced cell migration with faster matrix stress relaxation. Ongoing studies are examining the impact of matrix viscoelasticity on U937 polarization as well as elucidate the biophysical mechanisms of U937 immune cell migration.

#### 6:55 AM F.SM07.04.11

**Engineering Innate Immune Mediated Cancer Cell Killing by Antibody Recruiting Macromolecules** Bruno G. De Geest and Annemiek Uvyen; Ghent University, Belgium

Binding of monoclonal antibodies (mAbs) onto a cell surface triggers antibody-mediated effector killing by innate immune cells through complement activation (CDC), antibody-dependent cellular cytotoxicity (ADCC) and antibody-dependent phagocytosis (ADCP). As an alternative to mAbs, synthetic systems that can recruit endogenous antibodies from the blood stream to a cancer cell surface could be of great relevance. Herein, we explore antibody-recruiting polymers (ARmacro) as a

novel class of immunotherapy. ARmacro consist of a cell-binding motif linked to a polymer that contains multiple small molecule antibody-binding motifs such as dinitrophenol and rhamnose along its backbone or at dangling chain ends. As a proof of concept, we employ a lipid anchor that inserts into the phospholipid cell membrane or a cteloocyte that covalently conjugates to the glycocalyx of metabolically azide-labeled cells. We demonstrate that macro allow for high avidity antibody binding and drive antibody recruitment to treated cells for several days. Furthermore, we show that macro-treated cancer cells are prone to antibody-mediated killing through phagocytosis by macrophages.

7:05 AM F.SM07.04.12

**Development of Platelet-Based Drug Delivery System** Brian Schnoor and Anne-Laure Papa; George Washington University, United States

**Introduction:** The interactions between platelets and circulating tumor cells (CTCs) facilitate the survival and dissemination of these cells during the metastatic cascade by cushioning the CTCs and thus protecting them from both shear stress and the immune response [1-3]. We recently demonstrated that drug free-platelet decoys display an anti-metastatic effect on disseminating cancer cells *in vivo* by providing an anti-platelet effect [4]. The goal of this current study is to design a platelet-based drug delivery system capable of targeting CTC clusters, which are multicellular assemblies of CTCs and platelets, consolidated by fibrin. Developing novel therapeutic strategies to abate the enhanced metastatic potential of these clusters (as opposed to single CTCs) is essential to limit metastatic dissemination and increase CTC vulnerability in the circulation. A system leveraging the effect of decoy platelets while incorporating a drug delivery component could effectively target and dissociate CTC clusters.

**Materials and Methods:** For the development of this cellular engineering system, the FDA-approved therapeutic agent Tissue Plasminogen Activator (TPA) was immobilized on the surface of a Lyophilized Platelet (LP) carrier. The LP carrier was chosen because it preserves platelet surface structures while inhibiting platelet function. This system was characterized by flow cytometry and a fluorescence assay to determine the carrier decoration level and drug loading. The loading method was optimized for incubation time and component concentration. Flow cytometry was used to determine the availability of GP IIb/IIIa receptors, integral to the system's interaction with CTCs. Finally, fibrinolytic and clot lysis activity of the system was measured using a fluorescent assay and an absorbance assay, respectively.

**Results and Discussion:** The results demonstrated that TPA was successfully loaded onto the LP carrier with a high level of decoration (97.8% decorated LP) and loading efficiency (38.5%). Flow cytometry confirmed that the GP IIb/IIIa receptors needed for the system to interact with cancer cells were available for CTC binding. The fibrinolytic assessment demonstrated that TPA retained its effectiveness when loaded onto the system. The fluorescent assay indicated that the rate of fibrinolysis was maintained for loaded TPA and the clot lysis assay showed almost identical curves for absorbance. These results demonstrate that the loading was successful, and the system components retained their functionality.

**Conclusions:** Through an optimized loading procedure, a platelet-based delivery system for TPA targeting CTC clusters was created. This is an important step in developing a method to delay metastasis by targeting CTC clusters. Moreover, this system can be adapted toward other conditions requiring a fibrinolytic response. With minor alterations, this system could treat strokes by targeting and lysing dangerous clots. To create a viable system, the effectiveness of the system will need to be assessed *in vitro* and *in vivo*, however, these results demonstrate the viability of this approach for multiple medical applications.

**Acknowledgments:** This work has been supported by the George Washington University startup funds and the Department of Defense Breast Cancer Research Program Expansion Award (W81XWH-19-1-0667).

#### References:

- [1] L. Erpenbeck and M. P. Schön, "Deadly allies: the fatal interplay between platelets and metastasizing cancer cells," *Blood*, vol. 115, no. 17, pp. 3427–3436, Apr. 2010.
- [2] N. M. Bambace and C. E. Holmes, "The platelet contribution to cancer progression," *J. Thromb. Haemost.*, vol. 9, no. 2, pp. 237–249, Feb. 2011.
- [3] L. J. Gay and B. Felding-Habermann, "Contribution of platelets to tumour metastasis," *Nat. Rev. Cancer*, vol. 11, no. 2, pp. 123–134, Feb. 2011.
- [4] A.-L. Papa *et al.*, "Platelet decoys inhibit thrombosis and prevent metastatic tumor formation in preclinical models," *Sci Transl Med*, vol. 11, no. 479, 13 2019.

SESSION F.SM07.05: Poster Session: Biomaterials for Studying and Controlling the Immune System  
On Demand Abstracts Available for Viewing Starting Saturday Morning, November 21, 2020  
5:00 AM - 8:00 AM  
F-SM07

#### F.SM07.05.04

##### **Human Primary Macrophages Upregulate M1 Phenotype Markers in Response to Chemically Modified**

**Alginates** Erin O'Brien<sup>1</sup>, Stephen T. Nestor<sup>2</sup>, Arturo Vegas<sup>2</sup> and Kara Spiller<sup>1</sup>; <sup>1</sup>Drexel University, United States; <sup>2</sup>Boston University, United States

**Introduction:** Angiogenesis is largely directed by macrophages, immune cells that can change their phenotype in response to external stimuli. Macrophages precisely control the timing and dosage of angiogenic growth factors, and also direct the innate immune response to biomaterials. Therefore, biomaterial-mediated macrophage modulation is an attractive strategy to recover dysfunctional angiogenesis. Macrophage phenotypes encompass a wide spectrum, but in vitro are commonly categorized as M0 before activation, then M1 or M2 post-activation, with several identified subtypes under the M2 umbrella. Although each phenotype's exact role in angiogenesis is not well understood, there is a growing body of evidence suggesting that early M1 macrophages initiate blood vessel sprouting, and subsequent M2 activity stabilizes these structures. Recent studies also indicate that M1 macrophages that switch to an M2 phenotype may have enhanced angiogenic properties. Furthermore, in pathologies where angiogenesis is inhibited, such as chronic wounds, M1 macrophages are insufficiently activated and fail to switch to an M2 phenotype. Thus, biomaterial strategies that seek to recover dysfunctional angiogenesis should aim to initially promote a robust M1 macrophage phenotype.

Previous work from Vegas et al. established a library of alginate hydrogels modified with chemical functionalities, then ranked it by inflammatory activity, as measured by levels of cathepsin activity in vivo. This study was conducted to test the capabilities of the inflammatory alginate hydrogels to promote an M1 phenotype in primary human macrophages in vitro. Here we seeded M0 macrophages onto alginate hydrogels, then used Nanostring, a high-throughput gene expression assay, to measure expression of M1 markers, M2 markers, and genes associated with angiogenesis or fibrosis.

**Methods:** 5 types of alginate hydrogels were fabricated by the Vegas lab at Boston University: 3 inflammatory, 1 anti-inflammatory, and 1 non-modified. Primary monocytes were purchased from the Human Immunology Core at the University of Pennsylvania and cultured with 20 ng/mL of macrophage colony stimulating factor (MCSF) to induce differentiation into macrophages. On day 5, 200,000 macrophages were seeded onto each 5 mm section of hydrogel in a 24-well plate. Samples were incubated for 1 hour at 37°C to allow cell attachment. 800 µL of complete media with MCSF was added to each scaffold-containing well. M0 and M1 control samples were refreshed with complete media with MCSF. 100 ng/mL of human recombinant IFN $\gamma$  and LPS were added to the M1 control samples to induce M1 activation. On day 7, media was removed and scaffolds were mechanically degraded and lysed. RNA was extracted and quantified. For samples with at least 20 ng/µL of RNA, 100 ng were hybridized with a 72-gene custom Nanostring Codeset targeting M1, M2, angiogenic, and fibrotic genes. Nanostring sample preparation and reading was conducted according to Nanostring's standard protocol.

**Results:** Nanostring gene counts were normalized to the Nanostring in-house controls and fold changes over the M0 controls were calculated. Of the M1 markers measured, two (CD80 and CCL2) were upregulated in macrophages seeded on the inflammatory alginate hydrogels. Interestingly, these genes were also highly upregulated in macrophages seeded on non-modified alginate, and were even upregulated in macrophages seeded on anti-inflammatory alginate, though to a lesser extent.

**Conclusion:** These findings show that alginate hydrogels may be able to induce an M1-like phenotype in macrophages, via upregulation of CD80 and CCL2. However, proinflammatory modification of these hydrogels did not seem to enhance this upregulation. Instead, the results of this study suggest that alginate may be a naturally inflammatory material. Further investigation of the inflammatory properties of alginate are necessary to explore its potential as an M1 phenotype-promoting biomaterial.

#### F.SM07.05.05

**New Class of Biodegradable Drug Delivery Vehicles** Eva Krakor, Isabel Gessner, Veronika W. Wulff, Astrid Schauss, Uwe Ruschewitz and Sanjay Mathur; University of Cologne, Germany

The field of nanoparticles for biomedical applications has become one of the most promising and most studied topics in the last years because it offers potential enhancement in pharmaceuticals, medical imaging and diagnosis, cancer treatment, implantable materials and tissue regeneration. In terms of therapeutic applications, especially drug delivery vehicles have been intensively studied. In this case, hollow particles have aroused tremendous interest due to their unique properties such as large surface areas, low densities and high loading capacities due to a protected hollow core. The transport of therapeutic, which can be either, encapsulated, covalently attached or adsorbed onto hollow particles, has been shown to be highly beneficial for multiple reasons compared to simple drug administration e.g., the cargo is protected against enzymatic degradation and the total drug administration can be reduced, which minimizes the risk of side effects.

HMSC were synthesized through a hard template-based method. First, ellipsoidal hematite particles were synthesized in a

solvothermal process and coated with silica in a sol gel process afterwards. The iron oxide core was removed by etching resulting in HMSC. The porosity of as-prepared particles was analyzed using nitrogen adsorption-desorption method revealing a pore size of circa 4 nm and a high surface area of 308.8 m<sup>2</sup>/g. Cytotoxicity was determined using cell viability test (MTT) towards human kidney cells (HEK293) which clearly demonstrates that no reduction of cell viability was observed even at high concentrations of 100 µg/ml. Uptake studies using confocal microscopy were carried out using human cervical cancer cells (HeLa) which could show the successful internalization over a period of 24 hours. For testing their capability as drug delivery vehicle, a hydrophilic antibiotic (ciprofloxacin) and a hydrophobic anticancer (curcumin) compound were loaded and a pH dependent release under physiological conditions at 37°C was monitored via UV-Vis spectroscopy. After the drug release a reduction in shell thickness of HMSC was confirmed via SEM and TEM images. This study demonstrates the suitability of as-prepared hollow silica capsules as drug delivery vehicles for a broad range of drugs, hydrophobic as well as hydrophilic. Furthermore, it would be possible to modify the surface of drug loaded HMSC with proteins, e.g. antibodies as they are often used in immunotherapeutic regimens.

#### **F.SM07.05.06**

**Nanoparticle Synthesis by Engineered *E. coli* Cells Transformed with a Phytochelatin Synthase Gene** Haley Hill, Manjula Bomma, Zhigang Xiao and Qunying Yuan; Alabama A&M University, United States

In this study, the phytochelatin synthase gene of *Rhizobium tropici* was assembled by PCR, inserted into pUC19 vector, and further transformed into *E coli* DH5 $\alpha$  cells. Our preliminary data showed that these engineered *E coli* DH5 $\alpha$  cells synthesized more selenium nanoparticles than DH5 $\alpha$  cells transformed with pUC19 vector. The scanning electron microscope (SEM) examination of the nanoparticles revealed that the nanoparticles produced by both groups of cells had a size of 100-200nm with a spherical conformation, compositional analysis using Energy-dispersive X-ray spectroscopy identified that the nanoparticles only contain selenium. The capacity of phytochelatin synthase gene transformed bacteria to produce other metallic nanoparticles, including silver and gold will be tested and the physical properties of the nanoparticles will be further analyzed using the transmission electron microscope (TEM) analysis. The research results will be reported in the MRS meeting.

#### **F.SM07.05.08**

**Late News: Vitamin Lipid Nanoparticles Enable Adoptive Macrophage Transfer for the Treatment of Multidrug-Resistant Bacterial Sepsis** Xucheng Hou and Xinfu Zhang; OSU college of pharmacy, United States

Sepsis, a condition caused by severe infections, affects more than 30 million people worldwide every year and remains the leading cause of death in hospitals. Moreover, antimicrobial resistance has become an additional challenge in the treatment of sepsis, and thus, alternative therapeutic approaches are urgently needed. Macrophages are one of the most efficient pathogen scavengers. Indeed, in septic patients, impaired macrophages seem to be primarily responsible for insufficient antimicrobial defense. Nevertheless, immunostimulatory agents for reversing deactivated macrophages did not significantly improve the patient survival in clinical trials. This may be attributed to that immunostimulatory agents are not able to completely restore the function of impaired macrophages. Moreover, many bacteria, such as *Staphylococcus aureus* and *Escherichia coli*, have evolved immune escape mechanisms for thwarting phagolysosomal killing, resulting in intracellular survival. In addition, the prevalence of antibiotic resistance contributes to recurrent infections. Based on these research findings, we hypothesized that adoptive transfer of macrophages containing antimicrobial peptides linked to cathepsin B in the lysosomes (MACs) may enable the immunocompromised sepsis host to boost innate immunity, prevent bacterial immune evasion, and eliminate multi-drug resistant (MDR) bacteria.

To test our hypothesis, we first designed the AMP-CatB mRNA encoding an antimicrobial peptide IB367 (AMP-IB367), a cathepsin B (CatB), and a CatB-sensitive linker. AMP-IB367 is a broad-spectrum AMP with rapid bactericidal activity. CatB, an endogenous lysosomal protein, is first translated as an inactive precursor in the cytoplasm. After translocation into the lysosome, the precursor is processed into mature CatB. Here, the CatB is incorporated to transport the AMP-IB367 into lysosomes, where the linker is cleaved by CatB and thus the AMP-IB367 is released. When phagosomes encapsulating bacteria fuse with lysosomes, the ingested bacteria are exposed to both pre-stored AMP-IB367 and lysosomal antimicrobial components. Although immune evasion strategies may protect MDR bacteria from phagolysosomal killing mechanisms, the AMP-IB367 is able to kill these bacteria. In order to equip macrophages with the AMP-CatB mRNA, we synthesized a series of vitamin-derived lipid nanomaterials. We found that the mRNA delivery efficiency of V<sub>C</sub>LNPs was 10-fold better than Lipofectamine 3000 and 50-fold better than electroporation in RAW264.7 macrophages. After optimizing the molar ratio of V<sub>C</sub>-Lipid:DOPE:Cholesterol and the mass ratio of V<sub>C</sub>-Lipid:mRNA, we identified the optimal V<sub>C</sub>LNPs formulation with improved mRNA delivery efficiency over 7-fold than its initial formulation. Because V<sub>C</sub>LNPs were also effective to deliver mRNA in bone-marrow-derived macrophages (BMDMs), we chose BMDMs for further antibacterial studies because of the

clinical translatability. In vitro bactericidal results showed that MACs eliminated over 80% multi-drug resistant *Staphylococcus aureus* (MDRSA) or multi-drug resistant *Escherichia coli* (MDR E.coli) at 12 h. Next, we tested the therapeutic effects of MACs in MDRSA- and MDR E.coli-induced sepsis mice with immunosuppression. Analysis of blood at 24 h showed that MACs were more effective in cleaning bacteria than PBS-BMDMs. Furthermore, survival rate of MACs (83%) was significantly higher than that of PBS-BMDM group (40%).

In summary, we have developed macrophages containing antimicrobial peptides linked to cathepsin B in the lysosomes (MACs) via V<sub>C</sub>LNPs-mediated delivery of mRNA. Our results prove the concept that adoptive transfer of MACs beneficially reduce bacterial burden and improve survival in MDR bacteria-induced sepsis mice with immunosuppression by restoring innate immune defense, preventing bacterial immune evasion, and eradicating infections.

#### F.SM07.05.09

**Late News: TiO<sub>2</sub> Increases Bacterial Infection by Altering the Distribution of Cholesterol on Cell Membrane** [Fan Yang](#)<sup>1</sup>, Yan Xu<sup>1</sup>, Stephen Walker<sup>1</sup>, Wonhwa Cho<sup>2</sup>, Tatsiana Mironava<sup>1</sup> and Miriam H. Rafailovich<sup>1</sup>; <sup>1</sup>Stony Brook University, United States; <sup>2</sup>University of Illinois at Chicago, United States

According to the National Nanotechnology Initiative of America, titanium dioxide (TiO<sub>2</sub>) is one of the most commonly manufactured nanoparticles. These nanoparticles are widely used in food, pharmaceutical, cosmetic and chemical industries as pigments, catalysts, and photovoltaic sources. The latter property is also exploited in water purification where UV-irradiated TiO<sub>2</sub> is a common anti-bacterial agent. However, there is no consensus on the toxicological profile of TiO<sub>2</sub> nanoparticles (NPs), and multiple concerns have surfaced on the potential harmful effects on human health<sup>1</sup>. Experiments conducted on HeLa cells indicated that cells cultured with 0.1 mg/ml rutile and anatase TiO<sub>2</sub> NPs for 24 hrs prior to exposure to *Staphylococcus aureus* (*S. aureus*) had 350 and 250% respectively more bacteria per cell, while macrophages exposed to TiO<sub>2</sub> NPs ingested 40% fewer *S. aureus*, further increasing the risk of infection when present in vivo<sup>2</sup>. The particles were observed to sequester within the cytoplasm of phagocytes simply occupying space which would normally be used for ingesting bacteria. Ingestion of TiO<sub>2</sub> NPs in HeLa cells resulted in an increase in membrane rigidity and extracellular LDH which was attributed to the increase in bacteria<sup>2</sup>.

Another possible explanation may be in the concentration distribution of membrane cholesterol. Specifically, we demonstrate an increase in cholesterol concentration of the outer plasma membrane leaflet accompanied by the decrease in cholesterol inner leaflet concentration. Alteration of the inner/outer leaflet cholesterol ratio may also explain the increase in bacterial infectivity NPs since *S. aureus* requires cholesterol for proper membrane attachment and virulence. This effect was absent in ABCA1 knockout HeLa cells suggesting an interaction between TiO<sub>2</sub> and the ABCA, a known cholesterol membrane efflux regulatory protein that facilitates cholesterol transport across the cellular membrane. The hypothesis has also been confirmed by the RT-PCR data detecting the RNA expressions of ABCA1 and ABCG1. We found that compared to the control group, cells exposed to TiO<sub>2</sub> for 24 hrs had higher RNA expression levels to 240% and 170% for ABCA1 and ABCG1, respectively. These data indicate that cells exposed to TiO<sub>2</sub> NPs have altered cholesterol distribution within their membranes, which results in increased rigidity and enhanced bacterial infection. Further work is in progress to evaluate this effect in cells obtained from healthy human tissue.

<sup>1</sup>Pan, Zhi, et al. "Adverse effects of titanium dioxide nanoparticles on human dermal fibroblasts and how to protect cells." *Small* 5.4 (2009): 511-520.

<sup>2</sup>Xu, Yan, et al. "Exposure to TiO<sub>2</sub> nanoparticles increases *Staphylococcus aureus* infection of HeLa cells." *Journal of nanobiotechnology* 14.1 (2016): 34.

#### F.SM07.05.10

**Late News: Influence of Surface Topography and Modulus on Fibrinogen Adsorption and Subsequent Cell Response** [Jie Li](#) and Kyla Sask; McMaster University, Canada

**Introduction:** Protein adsorption to a material is a complex process which causes thrombus formation, infection, and inflammation and can lead to failure of devices<sup>1</sup>. Surface properties such as chemistry, topography, and mechanics influence protein adsorption and structural changes. Fibrinogen plays a dominant role in mediating platelet and leukocyte interactions with surfaces and its degree of unfolding can impact the extent of cell activation<sup>2</sup>. Macrophages are essential in the immune response to biomaterials and the effect of protein conformational changes on their activation is not fully understood. This work aims to characterize protein adsorption and conformational changes on planar and patterned polydimethylsiloxane (PDMS) with varying elastic moduli and determine the relationship to macrophage response.

**Methods:** Microscale patterns were designed with three sizes of the following height : groove width : ridge width ratio: (1)

20:20:10  $\mu\text{m}$ ; (2) 20:20:20  $\mu\text{m}$  and; (3) 10:10:10  $\mu\text{m}$ . Photolithography and soft lithography are used with PDMS substrates of varying mixing ratios of Sylgard 184 and 527 to investigate the combined effect of surface topography and elastic modulus on fibrinogen adsorption and degree of unfolding. A micro-BCA assay was used to determine the amounts of fibrinogen adsorption (2.0 mg/mL in PBS) on PDMS with the range of stiffnesses. An antibody binding assay using a primary antibody to the fibrinogen gamma chain was developed to quantify the amount of fibrinogen adsorbed with exposure of the gamma chain. This assay will be extended to determine RGD density and further conformational changes of protein on PDMS. We are in the process of further interrogating the role of protein conformation on immune cell interactions using the RAW 264.7 macrophage cell line.

**Results:** Micropattern designs of three dimensions were prepared for photolithography and soft lithography. Contact angle measurements of PDMS substrates with varying stiffnesses indicated that ratios had relatively similar surface wettabilities with the 1:5 ratio slightly more and the 1:1 ratio slightly less hydrophobic. According to the BCA assay results, the 1:1 ratio of Syl 184 & 527 PDMS polymers adsorbed the most fibrinogen with an average of  $10.50 \pm 0.26 \mu\text{g}/\text{cm}^2$ , while the 1:5 ratio of Syl 184 & 527 adsorbed the least with an average of  $8.88 \pm 0.48 \mu\text{g}/\text{cm}^2$ . The antibody binding assay was completed and is being optimized to compare absorbance values based on the amount of fibrinogen determined from the BCA assay. This will provide an indication of changes in orientation and conformation as a result of varying surface topography and modulus.

**Discussion and Conclusions:** This work focuses on understanding the mechanisms underlying protein adsorption and subsequent cellular regulation abilities of microstructures and elastic modulus. The designed micropatterns provide a way to investigate the combined effect of topography and stiffness on protein adsorption and macrophage adhesion. The BCA assay indicates that varying the surface modulus has an influence on fibrinogen adsorption. The antibody binding assay will investigate whether protein conformational changes play a role in this varied amount. Future work is being completed to determine the establishment of macrophage focal adhesions and cytokine secretion profiles in response to micropatterned topography and elastic modulus. Controlling these surface properties provides a method to monitor macrophage activation and regulation of immune cell response.

#### References:

1. I Firkowska Boden., et al. *Advanced healthcare materials*, 7 (1), p.1700995, 2018.
2. P Koegler., et al. *Advanced drug delivery reviews* 64 (15) pp.1820-1839, 2012.

#### F.SM07.05.11

**Robust Immune Suppressing Nanoparticles to Overcome Multidrug Resistance in Breast Cancer** Haneen Omar and Abdulaziz Almalik; King Abdulaziz City for Science and Technology, Saudi Arabia

Multidrug resistance (MDR), accounting for therapeutic failure, remains a major challenge to manage cancer effectively. Currently, there are only a few strategies that are executed to conquer MDR by restoring chemosensitivity. In this respect, we report an immune suppressing nanoparticle decorated with alpha-1 acid glycoprotein (AGP), an anti-inflammatory protein, to serve as an effective chemoresistant reversal agent to modulate MDR and resensitize aggressive breast tumour cells. Hyaluronic acid-chitosan nanoparticles decorated with AGP (AGP-HA NPs) were synthesized by a sequential ionic gelation method consisting of spray drying and AGP-surface adsorption. The morphology, size, surface charge density, and composition of the synthesized NPs were characterized by utilizing SEM, DLS, Zeta potential, and FTIR, respectively. We have investigated the potential efficacy of AGP-HA NPs in reversing the MDR phenotype of MDA-MB-231 in response to anti-cancer drug doxorubicin (DOX). Our findings showed synergistic antitumor effects between HA and AGP protein as evident from the significantly enhanced efficacy of DOX post switching drug resistance phenotype of the cells to chemosensitive phenotype. Overall, our results suggest that AGP-HA NPs represent a viable and effective treatment option to strengthen the anticancer effects of chemotherapeutic agents and potentially contribute to improving the survival rate of patients with metastatic breast cancer.

#### F.SM07.05.13

**pH-sensitive Nanoparticles Based Oral Drug Delivery for the Treatment of Inflammatory Bowel Disease** Eden M. Jacob and Sakthi Kumar; Toyo University, Japan

The role of nanomedicine as an enhanced pharmaceutical strategy to deliver drugs has been studied for quite a few decades. The emergence of pH-sensitive nanoscale particles is beneficial due to its ability to release its cargo only at a high pH environment of the colon, which helps for direct targeting of the inflamed tissues in inflammatory bowel disease (IBD). Hence, we have designed the formulation of biodegradable polymer poly (lactic-co-glycolic acid) nanoparticles coated with Eudragit® S100 (EPNPS) for the delivery of novel polyphenolic compounds to reduce the inflammation caused by proinflammatory cytokines. The EPNPs were prepared by a single emulsion solvent evaporation technique and were characterized for shape and surface morphology using a scanning electron microscope (SEM) and transmission electron

microscopy (TEM). The *in vitro* drug release was investigated using phosphate buffer saline (PBS) simulating different gut pH. The *in vitro* cytotoxicity of the EPNPs also evaluated and found to be highly biocompatible in nature. The inhibition of proinflammatory cytokines production also conducted using lactate dehydrogenase (LDH) assay. The characterization of EPNPs using SEM and TEM revealed spherical shape and smooth surface of the nanoparticles and was found to be 200-300nm in size. The EPNPs showed substantial improvement in the release of the drug, specifically at colonic pH. Results suggested that pH-sensitive EPNP nanoparticles as a promising candidate in the oral delivery to the colonic inflamed tissues.

#### F.SM07.05.14

**Two is Better Than One—A Comprehensive Study on the Synergistic Effects of Co-Delivery of Paclitaxel and Parthenolide in Discoidal Bicelle, *In Vitro* and *In Vivo*** Armin Rad, Mu-Ping Nieh and Xiuling Lu; University of Connecticut, United States

Combinatory modulation of the physical and biochemical characteristics of nanocarrier delivery systems is an emergent topic in the field of nanomedicine. Here, using the combined effects of incorporation of active targeting moieties, nanoscale morphology and shape, and physical properties for anti-cancer drugs function. We investigated a novel complex made of lipid bicelles nanocarrier for the efficient delivery of a combination of Paclitaxel (PTX). In addition, we hypothesized that Parthenolide (PTL) can be used as a chemosensitizers to restore the proper apoptotic signaling and to overcome chemotherapy resistance in human lung and breast cancer cells. We synthesized and characterized self-assembled bicelles (nanodiscs) and nanovesicles which were made up of short- (DHPC) and long-chain (DPPC) lipids encapsulating PTL and PTX molecules. By using simultaneous self-assembly encapsulation, we have encapsulated Parthenolide and Paclitaxel as two cancer drugs. Dynamic light scattering, small angle X-ray scattering (SAXS), Fluorescence-activated cell sorting (FACS), and fluorescence confocal optical microscopy (FCOM) were used to quantify and visualize the cellular uptake of folate-conjugated NPs, respectively and *in vivo* subcutaneous rat studies were performed to investigate the samples. Self-assembled lipid discoidal and vesicular nanoparticles with low-polydispersity ~30 nm size range and identical chemical compositions were synthesized, characterized, and correlated with *in vitro* cancer cellular internalization, *in vivo* tumor accumulation and cancer treatments. Folate targeted nanodiscs not only have shown a higher tumor uptake and therapeutic efficiency, but also exhibited well-defined size, robust formation, and high-efficiency encapsulation of hydrophobic molecules, which enable the scalable manufacturing of a generalized *in vivo* multimodal delivery platform. A comprehensive evaluation of different effective factors, such as loading rate, surface chemistry, nanocarriers shapes, and drug combination ratios were evaluated and a comprehensive regiment for an effective treatment is introduced. The negatively charged bicelles with a PTL:PTX:Lipid molar ratio of 2.5:1:500 yielded a discoidal shape with a uniform diameter of 30 nm and a bilayer thickness of 5 nm, indicated the best anti-cancer function against both regular and drug resistive lung and breast cancer cells. SAXS analysis was also performed to provide insight into how the hydrophobic PTL and PTX molecules interact within the bicelles. Further, flow cytometry followed by confocal microscopy analyses substantiates the superior transfection efficiency of bicelles. We further analyzed how the co-encapsulation and molar ratios of drug and nanocarrier may affect the anti-cancer efficiency *in vivo* and *in vitro*. Several important discoveries in this report are summarized below. Detailed structural analysis and loading capacity of bicelles with two hydrophobic drug molecules, PTX and PTL, are performed. The structural variation of discs strongly depends on the molecular size and shape of the payload. Generally speaking, bicelle shows great potential as a nanocarrier for hydrophobic drug molecules. Both *in vitro* and *in vivo* studies on A549 cell line using drug-loaded bicelles indicate high efficacy (high cellular uptake, low IC<sub>50</sub> and MIC<sub>90</sub>) for cancer treatment. Moreover, we demonstrate strong synergy with PTX and PTL with IC<sub>50</sub> and MIC<sub>90</sub> are magnitudes lower than those of the free drugs in DMSO or Cremophor El. The significant synergetic effect is observed in the MDR A549 cell line as well. The research outcome aims to provide an efficacious nanocarrier platform, which can potentially be generalized for transporting therapeutics and diagnostics to other types of cancers or diseased cells.

<!--![endif]----><!--![endif]---->

#### SYMPOSIUM F.SM08

---

Regenerative Engineering and Synthetic Biology  
November 21 - December 3, 2020



Symposium Organizers

Akhilesh Gaharwar, Texas A&M University  
Kaitlyn Sadtler, National Institute of Health  
Mark Tibbitt, ETH Zürich  
Dimitrios Zeugolis, National University of Ireland, Galway

---

\* Invited Paper

SESSION F.SM08.10: Live Panel Discussion I: Engineering Tools for Regenerative Engineering  
Tuesday Morning, December 1, 2020  
F.SM08

**11:30 AM PANEL DISCUSSION: ENGINEERING TOOLS FOR REGENERATIVE ENGINEERING**

**12:30 PM COLE DEFOREST, PANELIST**

**12:30 PM PAULA HAMMOND, PANELIST**

**12:30 PM APRIL KLOXIN, PANELIST**

**12:30 PM DAVE MOONEY, PANELIST**

SESSION F.SM08.11: Live Lightning/Flash Talks: Regenerative Engineering and Synthetic Biology  
Tuesday Afternoon, December 1, 2020  
F.SM08

**12:30 PM INTRODUCTION**

**12:35 PM F.SM08.01.03**

**Harnessing the Secreted Extracellular Matrix to Direct Cell Responses for Percutaneous Devices** Nicholas G. Fischer, David De Jong and Conrado Aparicio; University of Minnesota, United States

Native extracellular matrixes (ECM) acts as signaling repositories to regulate cell behavior and function. Installation of implantable medical devices disrupts these matrices and destroys spatiotemporal presentation and interaction of cells with microenvironmental cues. Regeneration of tissue niches is critical for long-term stability and integration of medical devices in patients. Here, we present a new, broadly-applicable physicochemical strategy for percutaneous devices to leverage secreted, nascent ECM for instructing epithelial cell behavior. We synthesized a set of photopolymerizable polymers with catechol and structurally-similar moieties, easily applied to percutaneous device surfaces like catheters, dental restorative materials, or orthopaedic implants, with systematically varied physicochemical properties but similar bulk mechanical properties. Tuning surface physicochemical properties, specifically charge and polarity, enabled us to tune keratinocyte hemidesmosome formation, adhesive structures that anchor cells to ECM, formation and downstream signaling. A series of inhibitor and knock-down experiments demonstrated the bioinstructive effect of our materials on elaborated ECM, laminin332 in particular, in an integrin-dependent manner. We propose our biostructure polymers direct cell responses via modulation of laminin332's structure in the pericellular ECM. Finally, we challenged our engineered materials in a course of experiments, including *ex vivo*, meant to reflect the harsh environment experienced during clinical therapeutic use and showed our materials retain their mechanical and bioinstructive properties. Taken together, we present a strategy to leverage the secreted matrix, via surface physicochemical properties, for control of ECM-mediated signals toward enhancing biological responses critical for long-term stability and integration of percutaneous medical devices.

**12:46 PM F.SM08.04.02**

**Shifting Macrophage Phenotype to Encourage Angiogenesis in Murine Hindlimb Ischemia Model** Greg Risser<sup>1</sup>, Dong

Li<sup>2</sup>, Samuel Sung<sup>1</sup> and Kara Spiller<sup>1</sup>; <sup>1</sup>Drexel University, United States; <sup>2</sup>Shanghai Jiao Tong University, China

**Introduction:** Therapeutic angiogenesis is a promising treatment for ischemic tissue disorders and for vascularizing biomaterials in regenerative medicine. Macrophages are important regulators of angiogenesis, playing distinct roles in different stages of angiogenesis due to their diverse phenotypes. Interleukin 4 (IL-4)-stimulated macrophages (M2) play a role in the later stage of angiogenesis, likely by stabilizing and supporting new blood vessels, although their precise functions are not known. Biomaterials that control macrophages may be advantageous compared to strategies targeting other cell types because macrophages regulate many different cell types involved in angiogenesis and tissue repair. However, macrophages are highly plastic cells that can easily change their phenotype upon encountering different stimuli at a wound site. Consequently, a localized drug delivery system is necessary to release polarizing signals to macrophages in a sustained manner to maintain and promote phenotype. As a potent stimulator of the pro-angiogenic M2 phenotype, IL-4 was encapsulated in poly(lactic-co-glycolic acid) (PLGA) microparticles for sustained release. To test their effects on macrophage phenotype and angiogenesis, the microparticles were co-delivered with fluorescent macrophages into a murine model of hindlimb ischemia three days post-surgery.

**Materials and Methods:** Using double emulsion, IL-4 was encapsulated into PLGA microparticles (30-40  $\mu$ m). Green fluorescent protein-labeled (GFP+) murine bone marrow derived macrophages were gathered and cultured to an M2 phenotype via stimulation with IL-4. These macrophages and microparticles were injected intramuscularly into the calf of a hindlimb ischemia murine model 3 days post injury. Mice were sacrificed two days later, and their calves harvested for flow cytometry analysis and immunohistochemistry (IHC). Using collagenase to digest the muscle, a single cell solution of the calf was stained with multiple macrophage phenotype markers (F4/80, CD206, ARG1, CD38, CD86) and Live/ Dead (L/D) markers. Separately, the solution was also stained with F4/80 and endothelial cell marker CD31. Flow data were analyzed using tSNE dimensionality reduction and Phenograph and FlowSOM clustering algorithms. Calf muscle sections were stained with DAPI and CD31, and images were analyzed with CellProfiler for CD31+ structures. All animal studies were approved by the Drexel Institutional Animal Use and Care Committee.

**Results and Discussion:** The number of GFP- macrophages was very high while the number of recovered GFP+ macrophages was exceedingly low, indicating that any effects of microparticles on angiogenesis and macrophage phenotype was caused by host macrophages. IL-4 releasing microparticles caused macrophages to take on a complex phenotypic profile. IL-4 affected macrophages were highest in clusters expressing both M1 and M2 markers. Additionally, treatment with IL-4 releasing microparticles increased the amount of endothelial cells (F4/80-CD31+), suggesting angiogenesis. Analysis of CD31+ structures showed that IL-4-releasing microparticles increased the density of vessels of 5-18  $\mu$ m in diameter, while small capillaries (2-5  $\mu$ m diameter) were unaffected. IL-4 release from the microparticles may have cause the M2 macrophages to help support recently created blood vessels, thereby increasing the number of larger structures.

**Conclusions:** This study shows that IL-4 releasing microparticles can control macrophage phenotype to support the development of blood vessels *in vivo*.

12:57 PM F.SM08.06.02

**Naturally-Derived, Powder-Based Lung Tissue Sealant for Pleural Defects Utilizing a Murine Model** Patrick N. Charron, Spencer Fenn, Minara Aliyeva, Nirav Daphtary and Rachael Oldinski; University of Vermont, United States

**Introduction:** Damage to the pleural tissue lining the lungs can occur in a multitude of ways, resulting in fluid leak into the pleural cavity, which, left untreated, can result in mortality. Historically such cases were treated via pleurodesis. Recent developments of lung tissue sealants serve as alternatives, but few options are available. While popular sealant tests can deliver qualitative pass/fail data, there is lack of quantitative *in vivo* methods to characterize sealing capabilities of these materials, particularly for pleural applications. In addition, commercial products have failed due to poor design and administration. Herein, we describe our development of a powder sealant capable of adhering to tissue and crosslinking to form an elastic hydrogel, circumventing limitations of current tissue sealants.

**Experimental methods:** Methacrylated alginate (AMA) was synthesized and characterized via <sup>1</sup>H-NMR spectroscopy. To enable gelation, visible green light crosslinkers were incorporated into the polymer solution. A sodium ion exchange was performed, the solution was lyophilized, and the product was processed into a powder. To investigate physical material properties, gelation kinetics and the viscosities of reconstituted solutions were collected at 37C, via an oscillatory time sweep at 10% radial strain and 1 Hz during exposure to green light. Quantitative *in vitro* experiments: dynamic burst pressure experiments were conducted using a custom-built burst pressure testing device, using a modified ASTM F2392 standard. Quantitative *in vivo* experiments: a murine model was developed in which we controlled respiratory dynamics to

test sealant mechanics. Mice were anesthetized with pentobarbital sodium, tracheostomized, and paralyzed using pancuronium. Body temperature was maintained by keeping the animal under a lamp. Mice were connected to a computer-controlled small animal mechanical ventilator (flexiVent, Scireq) and ventilated. A series of deep inflation maneuvers (Total Lung Capacity and Trapezoidal deep inflation waveform) and a composite signal comprising of mutually prime frequencies ranging from 0-20 Hz were performed to establish baseline for the animal prior to injury. The thoracic cavity of the animal was opened and lungs were punctured, followed by another series of baseline measurements to calibrate testing mechanics and verify injury. The injury was treated by the application of the AMA powder and tests were repeated to compare lung mechanics pre-injury and post-repair, allowing for real-time pressure data collection of lung mechanics during sealant testing. After testing, animals underwent euthanasia.

**Results:** After acute traumatic injury using a murine model, there was a loss in pressure, confirming the injury model. Successful post-repair (i.e., application of the AMA powder, hydration and crosslinking) tests indicated that the sealant maintained physiologically-relevant lung pressure and returned lung capacity to pre-injury values, and that the sealant did not fail. A failure in the patch would result in a failure to hold pressure. Initial results show physiologically relevant burst pressure values (i.e. 30 cmH<sub>2</sub>O) for the powder sealant collected during *in vitro* testing.

**Conclusions:** The data indicates efficacy of a novel powder-based elastic sealant for recapitulating lung mechanics post injury. During an *in vitro* burst pressure experiment, the powder formed a crosslinked sealant capable of maintaining physiological pressure before failure. The powder-based sealant has the advantages of adhering to tissue upon application *in situ* and subsequent hydration, remaining in place while crosslinking via light exposure took place. Future work will explore long term *in vivo* studies to investigate lung tissue healing after repair with the novel powder sealant material.

**Acknowledgements:** This work was funded in part by NIH R01EB020964 (Oldinski) and the University of Vermont.

**Disclosure of Interest:** None Declared.

#### 1:08 PM F.SM08.07.03

**Late News: Microbial Biofactories—Production of Nanomaterials with Biomedical Applications** Catherine P. O'Connell, David Medina and Thomas J. Webster; Northeastern University, United States

Antimicrobial resistance to antibiotics (AMR) and drug-resistant cancer are two of the main concerns that the healthcare system is facing nowadays [1,2]. Current chemotherapy treatments and antibiotic-based therapies are becoming ineffective or have plenty of drawbacks that are increasing the prevalence of resistance in both hospital and community settings. Therefore, new alternatives are needed, and nanotechnology might offer a suitable answer.

Although different nanomaterials are being used as a method to fight pathogens and cancer, traditionally synthesized nanoparticles present drawbacks, such as the production of toxic by-products, increased cytotoxicity in the cell and lack of selectivity. Consequently, green nanotechnology appears as an alternative approach, which employs living organisms and biomolecules as raw materials in a cost-effective and environmentally-friendly approach [3]. Among all these methods, microbially-produced nanomaterials have presented a significant potential, rendering nanomaterials with a powerful antimicrobial activity that can be tailored to the infection.

With the objective to demonstrate the antimicrobial and biocompatibility efficacy of bacterial-produced nanoparticles in skin bacterial infections, top pathogenic strains found in cutaneous wounds were employed for the synthesis of metalloid selenium nanoparticles (SeNPs), including Methicillin-resistant *Staphylococcus aureus* or *Pseudomonas aeruginosa*. Once generated, the SeNPs were analyzed in terms of their physicochemical features and the composition was extensively studied. After purification, the SeNPs were used as antimicrobial and anticancer agents through colony counting unit and MTS assays, respectively, as well as characterized for the mechanisms of death associated to their activities. At the same time, low cytotoxicity was demonstrated over the same range of antimicrobial efficiency.

Consequently, microbiological agents were successfully used as a biofactories for the generation of SeNPs of different compositions with biomedical properties. Therefore, bacteria were presented as a suitable approach for the synthesis of nanomaterials in a green fashion, overcoming the limitations of traditional nanotechnology.

#### References

- [1] Ventola, C. Lee. *Pharmacy and Therapeutics* 40.4 (2015): 277–283.
- [2] Katz, Steven J. *Journal of Oncology Practice* 9.3 (2013): 114–115.
- [3] De la Guardia, Miguel. *BioImpacts: BI* 4.1 (2014): 1–2.

**1:19 PM F.SM08.08.02**

**Biomaterial-Guided Recruitment of Endothelial Progenitor Cells for Vascular Regeneration** Mohamed A. Elkhodiry<sup>1</sup>, Omar Bashth<sup>1</sup>, Gaetan Laroche<sup>2,3</sup>, Jean-François Tanguay<sup>4,5</sup> and Corinne A. Hoesli<sup>1</sup>; <sup>1</sup>McGill University, Canada; <sup>2</sup>Université Laval, Canada; <sup>3</sup>Centre de Recherche du CHU de Québec, Canada; <sup>4</sup>Montreal Heart Institute, Canada; <sup>5</sup>Université de Montréal, Canada

Endogenous endothelial progenitor cell (EPC) recruitment to sites of vascular injury is a multi-step process mediated by selectins, chemokines, and extracellular matrix (ECM) proteins. New vascular implants with surface-immobilized capture antibodies targeting circulating EPCs have shown clinical promise in accelerating the formation of neo-endothelium to cover the implant. The absence of subsequent adhesion-based signaling needed for EPC proliferation and differentiation could explain the lack of long-term improvement in vascular re-stenosis and overall vascular recovery. Antibodies can mimic the cell tethering effect of selectins but lack necessary EPC signaling effects introduced by cytokines and ECM proteins. We have previously shown that ECM-derived peptides, such as RGD, can promote the adhesion and enhance the clonal expansion of EPC-derived endothelial colony forming cells (ECFCs) via integrin based signaling. In this study, we developed a novel bifunctional surface modification strategy to produce surfaces that combine immobilized capture-antibodies and surface grafted ECM-derived peptides with controlled surface concentrations and ligand orientation. We hypothesize that this bifunctional strategy would further accelerate the re-endothelialization process while maximizing downstream endothelial function and vascular recovery via an integrin-dependent process.

Peripheral blood from 22 adult human donors was used to obtain donor-specific ECFCs. Aminated culture surfaces were modified by either the covalent conjugation of a customized RGD peptide, immobilization of vascular endothelial growth factor receptor-2 (VEGFR-2) antibody, or combining both biomolecules at different ratios using an optimized process. Unmodified surfaces were used as a negative control. Surface concentration of the peptide and antibody were analyzed using fluorescence microscopy and an enzyme-linked immunosorbent assay. First, the expanded ECFCs were seeded under static conditions and cell adhesion was studied using immunocytochemistry. ECFC interactions with the bifunctional surfaces were then interrogated under more physiologically relevant dynamic flow conditions in a microchannel perfusion loop at 1 dyn/cm<sup>2</sup> wall shear stress and analyzed through live cell imaging followed by immunocytochemistry.

Surfaces with immobilized anti-VEGFR-2 antibodies displayed significantly enhanced ECFC capture potential compared to RGD and unmodified controls as quantified by the number of adhered cells under both static and dynamic conditions. Average ECFC spreading and focal adhesion formation were significantly increased on RGD surfaces compared to the anti-VEGFR-2 and unmodified controls under both static and dynamic conditions. Total endothelial coverage and the total number of focal adhesions were maximized on the bifunctional surfaces combining the anti-VEGFR-2 and RGD due to a combined increase in both cell number and cell spreading. By increasing the peptide concentration on the bifunctional surfaces, ECFC spreading was increased without significantly affecting the number of adhered cells. These results suggest an additive (i.e. independent) effect of capture antibodies on ECFC tethering vs. RGD peptides on subsequent ECFC spreading and integrin-dependent cell signaling.

To our knowledge, this is the first study showcasing the ability of a bifunctional antibody/peptide surface modification strategy in promoting ECFC capture and adhesion. Our results also display a clear distinction between the mechanisms by which human-derived ECFCs react to immobilized capture antibodies and conjugated ECM-peptides. This strategy creates sequential steps of EPC trafficking to mimic endogenous processes of vascular healing which can potentially create an effective regenerative capacity for vascular implants.

SESSION F.SM08.12: Live Panel Discussion II: Immunoengineering: Opportunities and Challenges  
Session Chairs: Kaitlyn Sadtler and Mark Tibbitt  
Thursday Afternoon, December 3, 2020  
F.SM08

**3:00 PM PANEL DISCUSSION: IMMUNOENGINEERING: OPPORTUNITIES AND CHALLENGES**

**3:40 PM JENNIFER ELISSEEFF, PANELIST**

**3:40 PM JAMAL LEWIS, PANELIST**

**3:40 PM KARA SPILLER, PANELIST**

SESSION F.SM08.13: Live Panel Discussion III: Tissue Regeneration: Where Do We Stand, Where Are We Going  
Session Chairs: Kaitlyn Sadtler and Mark Tibbitt  
Thursday Afternoon, December 3, 2020  
F.SM08

**3:40 PM PANEL DISCUSSION: TISSUE REGENERATION: WHERE DO WE STAND, WHERE ARE WE GOING**

**4:20 PM JASON BURDICK, PANELIST**

**4:20 PM CHRIS CHEN, PANELIST**

**4:20 PM IVAN MARTIN, PANELIST**

**4:20 PM TATIANA SEGURA, PANELIST**

SESSION F.SM08.14: Live Panel Discussion IV: Synthetic Biology and Engineering Development  
Session Chairs: Kaitlyn Sadtler and Mark Tibbitt  
Thursday Afternoon, December 3, 2020  
F.SM08

**4:20 PM PANEL DISCUSSION: SYNTHETIC BIOLOGY AND ENGINEERING DEVELOPMENT**

**5:00 PM ELENA MARTINEZ, PANELIST**

**5:00 PM ED BOYDEN, PANELIST**

**5:00 PM CELESTE NELSON, PANELIST**

SESSION F.SM08.01: Biomaterials as Instructive Environments  
On Demand Abstracts Available for Viewing Starting Saturday Morning, November 21, 2020  
F-SM08

**5:00 AM \*F.SM08.01.01**

**Designing Soft Biomaterials with Multiscale Properties as Instructive Synthetic Extracellular Matrices** [April M. Kloxin](#); University of Delaware, United States

The biophysical and biochemical properties of the extracellular matrix (ECM) (e.g., mechanics, multiscale structure, receptor-binding sites) are essential for the function and regeneration of connective tissues throughout the body, from the collagen-rich loose irregular connective tissue of the lung to the dense regular connective tissue of tendon and ligament. To study the complex process of connective tissue healing outside of the body toward ultimately directing it in vivo, we have designed soft biomaterials, engineered synthetic hydrogels, that mimic key aspects of the collagen-rich ECM found in the early stages of tissue healing. These materials are constructed by bottom-up assembly of multifunctional collagen mimetic peptides (mfCMPs) designed with hydrogen bonding blocks and sticky ends for the formation of nano- and micro-fibrils and decorated with reactive handles for covalent crosslinking and labeling to control mechanical properties and bioactivity. We have established robust, scalable workflows for synthesis of these materials to facilitate their use in translational applications. Wound healing human mesenchymal stem cells (hMSCs) encapsulated within these materials exhibit good viability (over 85%) and significant elongation during 3D culture, with deposition of cell-secreted collagen I. Further, in response to a

chemokine gradient, hMSCs exhibit directional invasion and increased motility within these materials relative to hydrogels without mfCMPs. Our on-going investigations demonstrate the relevance of these collagen mimetic materials for fundamental studies to examine cell responses in fibrous wound-healing microenvironments and for translational studies to implement these materials as scaffolds for enhanced tissue regeneration.

#### 5:15 AM F.SM08.01.02

**Investigation of How Cell-Cell Communication in Regulating Dental Pulp Stem Cells Proliferation and Differentiation** Ya-Chen Chuang<sup>1</sup>, Haijiao Liu<sup>1</sup>, Marcia Simon<sup>1</sup>, Chang-Yong Nam<sup>2</sup> and Miriam H. Rafailovich<sup>1</sup>; <sup>1</sup>Stony Brook University, The State University of New York, United States; <sup>2</sup>Brookhaven National Laboratory, United States

Stem cells isolated from the dental pulp (dental pulp stem cells (DPSCs)) were shown the pluripotent differentiation properties, where the differentiation lineage can be regulated by both soluble and non-soluble factors. In our previous studies, we have shown that substrate modulus can trigger DPSCs to biomineralize when the modulus is higher than a critical value. However, the incomplete differentiation and amorphous particle-like mineral deposits were observed on flat hard substrates. Surface coating with TiO<sub>2</sub>, on the other hand, was found to be able to induce osteogenic differentiation and hard tissue formation, regardless of substrate moduli. Instead of directly inducing the differentiation by substrate properties, lateral signals, cell-cell communication was also found to be important to regulate cell functions. Therefore, half-coating the polybutadiene (PB) substrates with TiO<sub>2</sub> by atomic layer deposition (ALD) were used to study DPSCs communication between cultures on TiO<sub>2</sub> coating and non-coating region of the substrate. The results showed that the cell proliferation was improved and biomineralization was induced from the cultures on the non-coating region, indicating the ability of lateral signal transduction in DPSCs. However, amorphous particle-like mineral deposits were present on the non-coating region while collagen fibers templated minerals were observed on the TiO<sub>2</sub> coating region. Hence, even though proliferation and biomineralization could be induced without directly contact with TiO<sub>2</sub>-coated surface, while the ability to form fibers templated minerals, the structure required for bone or dentin tissue formation, is a function of surface properties, particularly the role of TiO<sub>2</sub> to nucleate banded collagen fibers in enabling hard tissue formation.

This study address the importance of both integrin signals from substrate properties and transmembrane signals from cell-cell contact are important to investigate due to the dynamic *in vivo* environment, and was found to be able to regulate DPSCs proliferation and differentiation.

#### 5:25 AM F.SM08.01.03

**Harnessing the Secreted Extracellular Matrix to Direct Cell Responses for Percutaneous Devices** Nicholas G. Fischer, David De Jong and Conrado Aparicio; University of Minnesota, United States

Native extracellular matrixes (ECM) acts as signaling repositories to regulate cell behavior and function. Installation of implantable medical devices disrupts these matrices and destroys spatiotemporal presentation and interaction of cells with microenvironmental cues. Regeneration of tissue niches is critical for long-term stability and integration of medical devices in patients. Here, we present a new, broadly-applicable physicochemical strategy for percutaneous devices to leverage secreted, nascent ECM for instructing epithelial cell behavior. We synthesized a set of photopolymerizable polymers with catechol and structurally-similar moieties, easily applied to percutaneous device surfaces like catheters, dental restorative materials, or orthopaedic implants, with systematically varied physicochemical properties but similar bulk mechanical properties. Tuning surface physicochemical properties, specifically charge and polarity, enabled us to tune keratinocyte hemidesmosome formation, adhesive structures that anchor cells to ECM, formation and downstream signaling. A series of inhibitor and knock-down experiments demonstrated the bioinstructive effect of our materials on elaborated ECM, laminin332 in particular, in an integrin-dependent manner. We propose our biostructure polymers direct cell responses via modulation of laminin332's structure in the pericellular ECM. Finally, we challenged our engineered materials in a course of experiments, including *ex vivo*, meant to reflect the harsh environment experienced during clinical therapeutic use and showed our materials retain their mechanical and bioinstructive properties. Taken together, we present a strategy to leverage the secreted matrix, via surface physicochemical properties, for control of ECM-mediated signals toward enhancing biological responses critical for long-term stability and integration of percutaneous medical devices.

#### 5:35 AM \*F.SM08.01.04

**Functional Biomaterials from Functionalized Proteins—User-Programmable Hydrogels to Probe and Direct 4D Stem Cell Fate** Cole DeForest; University of Washington, United States

The extracellular matrix directs stem cell function through a complex choreography of biomacromolecular interactions in a tissue-dependent manner. Far from static, this hierarchical milieu of biochemical and biophysical cues presented within the native cellular niche is both spatially complex and ever changing. As these pericellular reconfigurations are vital for tissue

morphogenesis, disease regulation, and healing, *in vitro* culture platforms that recapitulate such dynamic environmental phenomena would be invaluable for fundamental studies in stem cell biology, as well as in the eventual engineering of functional human tissue. In this talk, I will discuss some of our group's recent success in reversibly modifying both the chemical and physical aspects of synthetic cell culture platforms with user-defined spatiotemporal control, emphasizing new material strategies that are genetically encoded. Results will highlight our ability to modulate intricate cellular behavior including stem cell differentiation, protein secretion, and cell-cell interactions in 4D.

#### 5:50 AM F.SM08.01.05

**Vibrational Spectroscopy of the Electropolymerization of Poly(3,4-ethylenedioxythiophene) Copolymers** Shrirang S. Chhatre, David Bruce Chase and David C. Martin; University of Delaware, United States

Various functionalized polythiophenes, particularly poly(3,4-ethylenedioxythiophene) (PEDOT), have been investigated as tissue interfacing materials in medical devices and implants. Polythiophenes have the ability to communicate both electronically and ionically; thus, allowing it to communicate both with implanted electronic devices and electrolytically-active organs. They possess mechanical properties intermediate to hard inorganic electronics and soft wet tissue. Additionally, they are mechanically and chemically stable. These features make PEDOTs prime candidates for neural regeneration applications. However, despite the continued interest in PEDOT, there are still many unanswered questions. A major challenge is the relative insolubility of PEDOTs in most major solvents which prevents an accurate analysis of the degree of polymerization.

PEDOT and its copolymers, including the polymer formed from the carboxyl-substituted monomer P(EDOT-acid), have received specific attention because of their chemical stability and excellent charge transport properties. We have been investigating the use of vibrational spectroscopic techniques along with Gaussian molecular simulations to obtain a better understanding of the polymerization process. This complements ongoing research in our laboratory using in-situ Transmission Electron Microscopy (TEM) and hot stage optical microscopy (OM).

We were able to collect a Gel Permeation Chromatogram of P(EDOT-acid) thus allowing us for the first time to associate the vibrational spectra of a polymer with its molecular weight. Complimenting this with Density Functional Theory calculations and experimental vibrational spectroscopy (Raman and FTIR) data for various oligomers we are able to develop a deeper understanding about the chemistry and the material properties of these materials. We are examining the influence of chain length and conformation on the experimental and simulated vibrational spectra of PEDOT and P(EDOT-acid) oligomers. We have identified characteristic peaks associated with the reactive hydrogens on the thiophene ring that allow us to monitor the process of polymerization. We have specifically studied the vibrational modes associated with the reactive protons and conjugation of the thiophene network. The  $3110\text{ cm}^{-1}$  thiophene C-H stretch peak is of particular interest, since it decreases with intensity as the monomers react. In addition, we have monitored the peak at  $1422\text{ cm}^{-1}$  associated with the C=C stretch and the peaks at  $835\text{-}1184\text{ cm}^{-1}$  associated with backbone conjugation. The peaks at  $1540\text{ cm}^{-1}$  and  $1570\text{ cm}^{-1}$  are associated with the quinoidal structure of the PEDOT. These clues provide insight into the changes occurring during the polymerization reaction. By correlating these spectroscopic results with data using microscopy, we are developing a deeper understanding of the thiophene electropolymerization reaction.

#### SESSION F.SM08.02: Biomaterials for Regeneration

On Demand Abstracts Available for Viewing Starting Saturday Morning, November 21, 2020  
F-SM08

#### 5:00 AM \*F.SM08.02.01

**Biomaterial Approaches to Endogenous Tissue Repair in the Heart** Jason Burdick; University of Pennsylvania, United States

Heart disease is the leading cause of mortality across the world and myocardial infarctions (MIs) are individually linked to at least 50% of deaths. During MI, blood supply to cardiac tissue is compromised, initiating a tissue remodeling response, which includes the loss of contractile cardiomyocytes and the replacement of healthy tissue with non-contractile fibrotic tissue. One goal in the treatment of MI is the replacement of these lost cardiomyocytes to improve cardiac function; however, cell-based therapies have not been successful to do this. An alternative to cell delivery is to promote endogenous cardiomyocyte proliferation using growth factors, small molecules, and gene transfer. Specifically, microRNA-based therapies that target cardiomyocyte proliferation have great potential for the treatment of MI, including the miR-302/367 cluster.

We developed an injectable hyaluronic acid (HA) hydrogel for the local and sustained delivery of miR-302 mimics to the heart. The hydrogel is based on the assembly of HA through modification with host-guest chemical groups, namely cyclodextrin (host) and adamantane (guest). These modifications permit the fabrication of shear-thinning and self-healing hydrogels that can be injected into cardiac tissue. The miR-302 mimics released from hydrogels *in vitro* over a week and promoted cardiomyocyte proliferation and a single injection of the hydrogel in the mouse heart led to local and sustained cardiomyocyte proliferation for two weeks. After MI, miR-302 hydrogel delivery caused local clonal proliferation and increased cardiomyocyte numbers in the border zone of Confetti mice. Further, the hydrogel delivered miR-302 decreased cardiac end-diastolic (39%) and end-systolic (50%) volumes and improved ejection fraction (32%) and fractional shortening (64%) four weeks after MI and injection, compared to controls. This is quite promising towards the development of new therapies in cardiac regeneration and we are currently investigating other delivered therapeutics, such as extracellular vesicles.

To better understand the action of molecules on tissues, *in vitro* models are needed. However, current models are limited in the engineering of functional tissue models with requisite cell densities and heterogeneity to appropriately model cell and tissue behaviors, such as cardiac tissue after MI. To address this, we developed a new bioprinting approach to transfer cellular spheroids into self-healing support hydrogels at high resolution, enabling their patterning and fusion into high-cell density microtissues of prescribed spatial organization. We bioprinted induced pluripotent stem cell-derived cardiac microtissue models with spatially controlled cardiomyocyte and fibroblast cell ratios to replicate the structural and functional features of scarred cardiac tissue that arise following MI, including reduced contractility and irregular electrical activity. The bioprinted *in vitro* model was then combined with functional readouts to probe how various pro-regenerative microRNA treatment regimes influenced tissue regeneration and recovery of function as a result of cardiomyocyte proliferation. This method is useful for a range of biomedical applications, including the development of precision models to mimic diseases and for the screening of drugs, particularly where high cell densities and heterogeneity are important.

#### 5:15 AM F.SM08.02.03

**Late News: Influence of Composition of  $\beta$ -TCP and Borate Bioglass Scaffolds on Cell Proliferation of Adipose Tissue-Derived Mesenchymal Stem Cells—Osteogenic Differentiation** Carlos Paucar, Natalia Jaramillo, Ana I. Moreno, Valentina Ospina and Claudia Garcia; National University of Colombia, Colombia

Cell proliferation and osteogenic differentiation of mesenchymal stem cells were evaluated in contact with biodegradable and bioactive ceramic scaffolds. These structures were generated by 3D printing with Schwarz D geometry based on periodic minimum surfaces (TPMS). For its printing, composition by weight of the ceramic paste was used was 66.5% calcium phosphate  $\beta$ -TCP or 66.5% calcium phosphate with Magnesium  $\beta$ -TCP / Mg, 28.5% Bioglass Borate (BGBS), 3% Atapulgit and 2% of water. The osteogenic differentiation of mesenchymal stem cells (hMSC) from human adipose tissue (ADSCs) was performed. The scaffolds were characterized by X-ray diffraction (XRD) and infrared spectroscopy (FTIR), morphology, porosity and interconnectivity of the pores by scanning electron microscopy (SEM), degradability was tested by ISO 10993-14 standard, *in vitro* bioactivity by means of immersion tests in SBF by Kokubo test in different time intervals, cell proliferation and osteogenic differentiation by means of alkaline phosphatase activity.

The structural results showed calcium phosphate associated with its respective crystalline phases ( $\beta$ -TCP) and ( $\beta$ -TCP)/Mg, in addition to the amorphous character of Bioglass Borate (BGBS). Calcium phosphate scaffold with Magnesium ( $\beta$ -TCP)/Mg showed better degradability and bioactivity compared to the ( $\beta$ -TCP) scaffold. Both scaffolds showed porosity and interconnectivity of pores. As for the mesenchymal stem cells from adipose tissue, they showed good adhesion and cell proliferation in contact with the scaffolds, being the scaffolds doped with Mg a better promoter of cell proliferation, in addition to this; they do not generate any cytotoxic effect in the cells, and finally the differentiation to an osteogenic environment was verified by means of alkaline phosphatase activity. As a result of this study, the 3D printed scaffolds showed good performance on cells proliferation of adipose tissue derived mesenchymal stem cells and the influence of magnesium is crucial for the development of osteogenic differentiation

#### 5:25 AM \*F.SM08.02.04

**Annealed Hydrogel Microparticle (MAP) Scaffolds, Immune Response, and Regenerative Wound Healing** Tatiana Segura; Duke University, United States

Injectable materials that can conform to the shape of a desired space are used in a variety of fields including medicine. The ability to fill a tissue defect with an injectable material can be used for example to deliver drugs, augment tissue volume, or



promote repair of an injury. This talk will explore the development of injectable materials that are based on assembled particle building blocks, for tissue repair. We find that using microparticle building blocks to build the scaffold generates a porous network by the space left behind between adjacent building blocks. Due to the injectability of this microporous material we have explored its wide applicability to tissue repair applications ranging from skin to brain wounds. In this talk, I will describe how MAP scaffolds can modulate the wound healing immune response and lead to regenerative wound healing.

SESSION F.SM08.03: Bottom-Up Biology and Multicellular Assembly  
On Demand Abstracts Available for Viewing Starting Saturday Morning, November 21, 2020  
F-SM08

**5:00 AM \*F.SM08.03.01**

**Development of Biomimetic Models of Intestinal Tissue—Guiding Cellular Self-Organization Through Biofabrication Techniques** Elena Martinez; University of Barcelona, Barcelona, Spain

Epithelial tissues contain three-dimensional (3D) microstructures that guide cell self-organization at the tissue level. In the small intestine, crypts and finger-like villi microstructures improve its absorbance function, provide specific microenvironments and compartmentalize cell types [1–3]. Despite its physiological relevance, tissue architecture and multicellular population are neglected in the standard in vitro models, thus compromising their predictive capabilities [4]. Our efforts in addressing these shortcomings by including key elements to mimic the native tissue in vitro will be discussed in this talk. First, this will include strategies to promote cell's self-organization capabilities giving rise to crypt-villus domains on 2D monolayers [5], and strategies to engineer cell spatial positioning through micropatterning. Then, our approach to include the 3D architecture of the tissue will be addressed. In here, light-based biofabrication techniques to produce 3D villus-like structures [6,7] will be discussed. Finally, I will introduce our biofabrication proposal to produce tissue engineered models that include the epithelial and the stromal compartments [8]. Improving the prediction capabilities of cell-based assays is a growing strategy to lead to more efficient drug development processes. As 2D-based systems are showing their limits, new 3D strategies are gaining acceptance among the scientific community [9]. Our approaches aim to further accelerate this trend by providing feasible strategies to routinely incorporate 3D multicellular structures at the tissue level in cell culture systems.

- [1] G.J. Tortora, B.H. Derrickson, Principles of Anatomy and Physiology, 14th Ed., Wiley Global Education (2014).
- [2] M.N. Marsh, J.A. Swift, Gut, 10 940–949 (1969).
- [3] P. Kelly, I. Menzies, R. Crane, I. Zulu, C. Nickols, R. Feakins, J. Mwansa, V. Mudenda, M. Katubulushi, S. Greenwald, M. Farthing, Am. J. Trop. Med. Hyg. 70, 412–419 (2004)
- [4] Torras, N., García-Díaz, M., Fernández-Majada, V., Martínez, E. Front. Bioeng. Biotech. 6, 197 (2018)
- [5] Altay, G.; Larrañaga, E.; Tosi, S.; Barriga, F.M.; Batlle, E.; Fernandez-Majada, V.; Martinez, E., Scientific Reports 9(1), 10140 (2019).
- [6] Castaño, AG; Garcia-Diaz, M; Torras, N; Altay, G; Comelles, J; Martinez, E. Biofabrication 11(2) 025007 (2019).
- [7] Altay, G.; Tosi, S.; García-Díaz, M.; Martínez, E. Front. Bioeng. and Biotech. 8, 294 (2020).
- [8] Vila, A., Torras, N., Castaño, A.G., García-Díaz, M., Comelles, J., Pérez-Berezo, T., Corregidor, C., Castaño, Ó., Engel, E., Fernández-Majada, V., Martínez, E. Biofabrication 12 (2), 025008, (2020).
- [9] Martínez, E.; St-Pierre JF.; Variola, F. Advances in Physics:X, 4:1, 1622451 (2019).

**5:15 AM \*F.SM08.03.02**

**Engineering Epithelial Development** Celeste Nelson; Princeton Univ, United States

The morphogenetic patterning that generates three-dimensional (3D) tissues requires dynamic concerted rearrangements of individual cells with respect to each other. We have developed microfluidic approaches to investigate the mechanical forces and downstream signaling responsible for generating the airways of the lung. I will discuss how we combine these experimental techniques with computational models to uncover the physical forces that drive development of complex epithelial geometries. I will also describe efforts to uncover and actuate the different physical mechanisms used to build the airways in lungs from birds, mammals, and reptiles.

**5:30 AM F.SM08.03.03**

**Late News: Au Patterned Arrays and Spatially Controlled Bacterial Cell Organization Reveal Filamentous Cell**

**Interconnections in Multicellular Assemblies of *Xylella fastidiosa*** [Silambarasan Anbumani](#)<sup>1</sup>, Richard Jannisen<sup>2</sup>, Aldeliane M. da Silva<sup>1</sup>, Mariana de Souza e. Silva<sup>3</sup>, A. A. von Zuben<sup>1</sup>, Hernandes F. Carvalho<sup>1</sup>, Alessandra Alves de Souza<sup>3</sup> and Monica A. Cotta<sup>1</sup>; <sup>1</sup>University of Campinas, Brazil; <sup>2</sup>Delft University of Technology, Netherlands; <sup>3</sup>Agronomic Institute of Campinas, Brazil

Spatially controlled arrangement of bacterial adhesion and microcolonies (clusters of cells) has the great potential to unveil the dynamics of multicellular systems and especially complex biological phenomena such as cell-cell communication<sup>1</sup>. We present here a simple Au/SiO<sub>2</sub> device to spatially control bacterial cluster formation so that the basic biofilm framework can be studied in detail. Gold (Au) surfaces are biocompatible, chemically inert, and commonly used in diverse biomedical applications. On the other hand, thiol groups, which strongly interact with Au, are key functional molecules involved in adhesion mechanisms of several bacteria<sup>2</sup>, including a plant pathogen *Xylella fastidiosa*.

In this work, Au patterned SiO<sub>2</sub> substrates have been prepared with direct laser writing lithography for selective bacterial adhesion of *X. fastidiosa*. The bacterial adhesion and aggregation were specifically tuned with well-defined geometry of Au array and different disk spacings. Ordered nucleated clusters on the Au patterned samples allowed us an extensive analysis for cell length populations with different growth time that represent unambiguous length distribution of typical cells (~3-4 μm) and filamentous cells (>9 μm) of *X. fastidiosa*<sup>3</sup>. Two filamentous cell populations are observed which relate well to the geometric distances between first and second neighbors in the disk array. Further, Au arrays with smaller spacings and closely organized clusters present larger fractions of filamented cells, when compared to Au arrays with larger spacings. We readily observed adjacent bacterial clusters interconnected by filamentous cells which predominantly depend on cluster sizes and disk distances. Upon continued growth, the clusters were interconnected by multiple filamentous cells that facilitate the macro-scale biofilm architecture of *X. fastidiosa*<sup>3</sup>. The results indirectly confirm quorum sensing based chemical signaling involved in the formation of filamentous cells associated with bacterial clusters of *X. fastidiosa*. The present approach based on Au patterned arrays is not only promising to understand various complex phenomenon of multicellular assembly but also offers new directions to engineering biological system.

#### References:

1. Chen, F, *et al.* Bacterial photolithography: patterning Escherichia coli biofilms with high spatial control using photocleavable adhesion molecules. *Adv. Biosyst.* **3**, 1800269 (2019).
2. Newton, G. L. *et al.* Distribution of thiols in microorganisms: mycothiol is a major thiol in most actinomycetes. *J. Bacteriol.* **178**, 1990–1995 (1996).
3. Janissen, R. *et al.* Spatiotemporal distribution of different extracellular polymeric substances and filamentation mediate *Xylella fastidiosa* adhesion and biofilm formation. *Sci. Rep.* **5**, 9856 (2015).

#### SESSION F.SM08.04: Immune-Engineering

On Demand Abstracts Available for Viewing Starting Saturday Morning, November 21, 2020  
F-SM08

#### 5:00 AM \*F.SM08.04.01

**Advances in Engineering Particles for Immunotherapy of Autoimmune Disease** [Jamal Lewis](#); University of California, Davis, United States

Current paradigms for the treatment of autoimmune diseases (e.g. rheumatoid arthritis [RA]) are woefully inadequate, often missing the mark on desired physiological responses and not targeting the root cause of the disease. Predictably, novel approaches to re-establish immune homeostasis in patients afflicted by autoimmune conditions are now under intense investigation. Notably, we are developing an array of multifunctional, biomaterial-based ‘anti-vaccines’ that can be easily administered to remediate some of the prevalent autoimmune diseases. In this talk, I will focus on two particulate systems currently under development in my lab, which attempt to control critical cellular and humoral mediators that engender conditions such as RA and autoimmune autism. Previously, our group demonstrated that subcutaneous injection of a dual-sized, biodegradable PLGA MP regulatory vaccine (REGvac), comprising two ~1 μm phagocytosable MPs (Vit D3 and collagen-II (coll-II)-loaded MPs) and two ~30 μm non-phagocytosable MPs (TGF-β1-loaded MPs and GM-CSF-loaded MPs), resulted in remission of the characteristic symptoms of RA. In this iteration, we used a singly encapsulated formulation of the REGvac, meaning each microparticle had one agent. To increase the translatability of this system we re-engineered this REGvac and applied it to a more rigorous model of RA, the collagen-induced arthritis/citrullinated fibrinogen induced

arthritis model (CIA/FIA). Further, we co-encapsulated each factor previously described in the REGvac into one small microparticle containing coll-II, citrullinated fibrinogen (cit fib) and Vit D3, and one large particle containing TGF- $\beta$ 1 and GM-CSF (*Duo* REGvac). Additionally, we tuned the release of each of the factors, fabricating the small MP from an increased molecular weight PLGA polymer and the large MP from a lower molecular weight PLGA polymer. This co-encapsulated formulation allows for the spatiotemporal control over delivery of each factor. The quick release of GM-CSF and TGF- $\beta$ 1 allows for rapid infiltration and recruitment of DCs to the injection site hours after the injection. The slower release of encapsulated factors from the small MP allows for a higher therapeutic payload to be delivered inside the cell. Moreover, Vit D3 co-encapsulation with antigen allows for tolerogenic cues to be delivered directly with antigen in a spatiotemporal context. We describe our efforts to improve the REGvac system and assess its ability to intervene in late stage RA in the CIA/FIA model. We are also heavily invested in developing a nanoparticle-based prophylactic for Maternal Autoantibody-related (MAR) autism. We previously demonstrated that LDH B peptide-functionalized citrate-coated dextran iron oxide nanoparticles (DIONPs) [Systems for Nanoparticle-based Autoantibody Reception and Entrapment (SNARE)] are capable of capturing LDH B autoantibodies from mothers of children with MAR autism *in vitro*. Further, we found that SNAREs intravenously injected in C57BL/6j pregnant dams demonstrated slow clearance from the blood (24 hours) and deposited in the liver and the lungs confirmed via histology and magnetic resonance imaging (MRI) analyses. Here, we investigated the ability of SNAREs to capture MAR autoantibodies in immunized pregnant dams. Remarkably, a single injection of 100 mg/kg SNAREs led to a 62% reduction of LDH B autoantibody maternal blood titer within 4 hours and 54% within 24 hours of injection with dampened titer levels for 5 days thereafter. The ability of SNAREs to capture MAR LDH B autoantibodies *in vivo* sets the basis for investigating its efficacy to prevent disease in a MAR autism mouse model.

#### 5:15 AM F.SM08.04.02

**Shifting Macrophage Phenotype to Encourage Angiogenesis in Murine Hindlimb Ischemia Model** Greg Risser<sup>1</sup>, Dong Li<sup>2</sup>, Samuel Sung<sup>1</sup> and Kara Spiller<sup>1</sup>; <sup>1</sup>Drexel University, United States; <sup>2</sup>Shanghai Jiao Tong University, China

**Introduction:** Therapeutic angiogenesis is a promising treatment for ischemic tissue disorders and for vascularizing biomaterials in regenerative medicine. Macrophages are important regulators of angiogenesis, playing distinct roles in different stages of angiogenesis due to their diverse phenotypes. Interleukin 4 (IL-4)-stimulated macrophages (M2) play a role in the later stage of angiogenesis, likely by stabilizing and supporting new blood vessels, although their precise functions are not known. Biomaterials that control macrophages may be advantageous compared to strategies targeting other cell types because macrophages regulate many different cell types involved in angiogenesis and tissue repair. However, macrophages are highly plastic cells that can easily change their phenotype upon encountering different stimuli at a wound site. Consequently, a localized drug delivery system is necessary to release polarizing signals to macrophages in a sustained manner to maintain and promote phenotype. As a potent stimulator of the pro-angiogenic M2 phenotype, IL-4 was encapsulated in poly(lactic-co-glycolic acid) (PLGA) microparticles for sustained release. To test their effects on macrophage phenotype and angiogenesis, the microparticles were co-delivered with fluorescent macrophages into a murine model of hindlimb ischemia three days post-surgery.

**Materials and Methods:** Using double emulsion, IL-4 was encapsulated into PLGA microparticles (30-40  $\mu$ m). Green fluorescent protein-labeled (GFP+) murine bone marrow derived macrophages were gathered and cultured to an M2 phenotype via stimulation with IL-4. These macrophages and microparticles were injected intramuscularly into the calf of a hindlimb ischemia murine model 3 days post injury. Mice were sacrificed two days later, and their calves harvested for flow cytometry analysis and immunohistochemistry (IHC). Using collagenase to digest the muscle, a single cell solution of the calf was stained with multiple macrophage phenotype markers (F4/80, CD206, ARG1, CD38, CD86) and Live/ Dead (L/D) markers. Separately, the solution was also stained with F4/80 and endothelial cell marker CD31. Flow data were analyzed using tSNE dimensionality reduction and Phenograph and FlowSOM clustering algorithms. Calf muscle sections were stained with DAPI and CD31, and images were analyzed with CellProfiler for CD31+ structures. All animal studies were approved by the Drexel Institutional Animal Use and Care Committee.

**Results and Discussion:** The number of GFP- macrophages was very high while the number of recovered GFP+ macrophages was exceedingly low, indicating that any effects of microparticles on angiogenesis and macrophage phenotype was caused by host macrophages. IL-4 releasing microparticles caused macrophages to take on a complex phenotypic profile. IL-4 affected macrophages were highest in clusters expressing both M1 and M2 markers. Additionally, treatment with IL-4 releasing microparticles increased the amount of endothelial cells (F4/80-CD31+), suggesting angiogenesis. Analysis of CD31+ structures showed that IL-4-releasing microparticles increased the density of vessels of 5-18  $\mu$ m in diameter, while small capillaries (2-5  $\mu$ m diameter) were unaffected. IL-4 release from the microparticles may have cause the M2 macrophages to help support recently created blood vessels, thereby increasing the number of larger structures.

**Conclusions:** This study shows that IL-4 releasing microparticles can control macrophage phenotype to support the development of blood vessels *in vivo*.

**5:25 AM \*F.SM08.04.03**

**Immunomodulatory Biomaterials for Limb Salvage** Kara Spiller; Drexel University, United States

Lower limb amputations are a major source of morbidity and mortality throughout the world. They principally result from a trifecta of atherosclerosis, limb ischemia, and the formation of non-healing chronic wounds. At the core of these afflictions is dysregulated behavior of macrophages, which are critical regulators of homeostatic tissue turnover and the healing of injured tissues. Therefore, biomaterials that can correct dysfunctional macrophage behavior hold promise for promoting wound healing in patients at risk for amputation.

In successful wound healing, macrophages transition from a population that is largely pro-inflammatory (M1) to a heterogeneous population of macrophages associated with the resolution of inflammation and wound healing (M2), although the extent of the diversity of this M2 population is not known. Because M1 macrophages normally switch to M2, and because chronic wounds are characterized by deficiencies in M1 as well as M2 activation, we investigated the consequences of prior M1 polarization on subsequent M2 polarization. M2 macrophages that were derived from M1 macrophages exhibited a distinct gene, protein, and functional signature compared to M2 macrophages derived directly from unactivated macrophages, suggesting that M1 polarization is an important regulator of M2 activation. These findings, in combination with our previous work describing important roles for M1 macrophages in initiating angiogenesis, indicate that immunomodulatory biomaterials should allow for a robust M1 phase prior to mediating a transition to M2. To investigate this concept, we developed PLGA microparticles that released IL4, a main cytokine responsible for promoting a key M2 subtype. When administered locally to the site of injury at 3 days following injury in a murine hindlimb ischemia model, these microparticles increased the number of larger blood vessels without affecting the number of small blood vessels. These findings support a potential role for M2 macrophages in the maturation stage of angiogenesis. Then, because patients at risk for amputation may suffer from impaired immune cell trafficking, we designed a biomaterial-mediated macrophage cell therapy strategy to control the phenotype of macrophages following their administration, a long-standing problem in macrophage cell therapy due to the inherent plasticity of these cells. In a proof-of-concept study, the anti-inflammatory drug dexamethasone was incorporated into PLGA microparticles and loaded into human peripheral blood-derived monocytes via phagocytosis. The microparticles were retained intracellularly for several weeks *in vitro* and they did not interfere with monocyte-to-macrophage differentiation nor subsequent phagocytosis of tissue debris or bacteria. After 7 days in pro-inflammatory media, macrophages containing dexamethasone-loaded microparticles decreased expression of pro-inflammatory genes, increased expression of M2 genes associated with dexamethasone treatment, and decreased secretion of the potent pro-inflammatory cytokine tumor necrosis factor-alpha (TNF $\alpha$ ), even in the presence of pro-inflammatory stimuli.

Collectively, these studies highlight the importance of temporal control over macrophage phenotype, and suggest that immunomodulatory biomaterials that target macrophages may be effective in treatments designed to rescue angiogenesis and wound repair.

**5:40 AM INVITED PRESENTATION BY JENNIFER ELISSEEFF**

**5:40 AM INVITED PRESENTATION BY DAVID MOONEY**

**5:40 AM F.SM08.04.05**

**C-MEMS Based Label-Free Electrochemical Aptasensors for Turn-on and Turn-off Detections of Cancer Biomarkers** Shahrzad Forouzanfar, Fahmida Alam, Nezh Pala and Chunlei Wang; Florida International University, United States

Cancer is referred to as a group of diseases in which abnormal growth of cells interferes with the function of vital organs and finally stops the body from functioning. Cancer patients have higher chances of survival if their cancer diseases are diagnosed in the early stage of development. Detection of cancer via cancer biomarkers is one of the well-established ways for early diagnosis of cancer diseases. Cancer biomarker is referred to as any substance that can indicate the presence of cancer in a body. Thus far, many cancer biomarkers have been discovered, which can be collected from tissue, blood, and urine. Among the cancer biomarkers detectable from blood, platelet-derived growth factor-BB (PDGF-BB) has been associated with development and metastasis of various malignant tumors in vital organs including breast, brain, ovarian, pancreas, and liver. A feasible means for early detection of cancers is developing point-of-care biosensors based on DNA aptamers, which are referred to as aptasensors. Various advanced technologies have been investigated for developing cancer biomarker aptasensors, including optical, piezoelectric, and electrochemical based techniques. Among the developed technologies,

label-free electrochemical aptasensors are highly compelling since they can reduce the cost and complications of sample preparation, and the electrochemical cells can be efficiently miniaturized and integrated with available lab-on-chips and MEMS technologies. Nevertheless, the sensing performance of the label-free electrochemical cancer aptasensors, including selectivity, limit of detection, and dynamic range requires further enhancements to be at similar levels to clinical testing. In the light of the importance of PDGF-BB detection and demanded enhancements for label-free electrochemical aptasensors, we have developed label-free electrochemical aptasensors based on photoresist derived carbon microelectrodes. The active electrode of this aptasensor was synthesized via well-established C-MEMS (carbon microelectromechanical systems) fabrication technology. C-MEMS platforms have unique features such as high resolution, low background capacitance, high stability when they exposed to different physical/chemical treatments, biocompatibility, and good electrical conductivity. The applied C-MEMS fabrication in this study includes photopatterning of SU-8 25 negative photoresist-based microelectrodes and carbonization of the developed microelectrodes at high temperatures and oxygen-free tube furnaces. The carbonized microelectrodes were functionalized utilizing oxygen plasma oxidation pretreatment to introduce carboxyl groups to the surfaces of the carbon microelectrodes. The PDGF-BB affinity aptamers were covalently immobilized via amid binding of amino-tag terminated aptamers and carboxyl groups covered carbon surfaces. The Fourier-transform infrared spectroscopy (FTIR) confirmed the successful carboxyl group functionalization of the C-MEMS microelectrodes and covalent immobilization of affinity aptamers via amide binding. Cyclic voltammetry (CV) and electrochemical impedance spectroscopy (EIS) were used for characterizing the C-MEMS based aptasensors in different stages of development and sensing performances. The turn-on sensing strategy was implemented via measuring the charge transfer resistance ( $R_{CT}$ ) from EIS Nyquist plots, which yielded to wide sensing linear range of 0.005 – 50 nM with a high sensitivity of  $14.82 \times 10^3 \Omega \cdot (\text{Log}(M))^{-1}$  and low limit of detection of 1.9 pM (S/N=3). The turn-off sensing strategy was applied via measuring capacitance from CV curves, which conceded to a wide linear response range of 0.01 – 50 nM with a high sensitivity of  $29.97 \text{ mF} \cdot \text{cm}^{-2} \cdot (\text{Log}(M))^{-1}$  and low limit of detection of 7 pM (S/N=3) toward the PDGF-BB. The developed label-free electrochemical aptasensor exhibited good selectivity, stability, and repeatability, which is highly promising for point-of-care cancer diagnosis technologies.

SESSION F.SM08.05: Nanotechnology for Regeneration  
On Demand Abstracts Available for Viewing Starting Saturday Morning, November 21, 2020  
F-SM08

#### 5:00 AM INVITED PRESENTATION BY PAULA HAMMOND

##### 5:00 AM F.SM08.05.02

**Light-Driven *In Situ* Gelation of Self-Assembled Hydrogels for Drug Delivery** Hung Pang Lee and Akhilesh K. Gaharwar; Texas A&M University, United States

In situ gelation of hydrogels via near-infrared (NIR) light can implant drug reservoirs at deep tumor tissues with minimal invasion. Ultraviolet or visible light is often used for photocrosslinking but has limited application for deep tissue therapy due to the shallow penetration depths. NIR is of particular interest because of the therapeutic window where light has its maximum depth of penetration in tissue. However, NIR-triggered formation of hydrogels is rarely reported due to limited tools of NIR photochemistry. In this study, we demonstrate in situ gelation by combining with a NIR-responsive photothermal agent, molybdenum disulfide ( $\text{MoS}_2$ ), with a temperature-responsive phase transition polymer, poly(*N*-isopropyl acrylamide) (PNIPAm). Molybdenum is thiophilic, and sulfur has a strong affinity toward forming disulfide bonds, together they offer facile binding centers for thiolated molecules. Therefore, thiolated-PNIPAm is synthesized to form crosslinks with defect-rich  $\text{MoS}_2$  nanosheets. Moreover, dynamic polymer-nanoparticle interactions can be leveraged to control the formation of hydrogels spatiotemporally. With the increase in temperature by the photothermal effect of  $\text{MoS}_2$ , the hydrophobic interactions of  $\text{MoS}_2$  nanosheets and PNIPAm chains are strengthened, and thus facilitate the gelation. Further, the combinatorial chemo-photothermal therapy of the  $\text{MoS}_2$  hydrogels showed significant inhibition of cancer cells, indicating its effective role in chemotherapy. Overall, the hazardous-free gelling behavior of the  $\text{MoS}_2$  hydrogels has strong potential for a range of biomedical applications, including phototherapy, 3D printing, and therapeutic delivery.

##### 5:10 AM F.SM08.05.04

**Maximizing Magnetic Heating of Iron Oxide Nanoparticle for Wireless Neuromodulation** Gloria Lesly J. Miranda, Rohini Trevi G., Jason Giuliani and Gabriela Romero Uribe; University of Texas at San Antonio, United States

Neurological disorders such as Epilepsy and Parkinson's (PD) are associated with the alteration of neural signals. Current techniques to modulate neural activity such as implantable microelectronic devices, pharmacological agents or optical stimulation, are nonspecific to cell-type and damaging to biological tissues<sup>1-3</sup>. Recently, magnetic hyperthermia has been proposed in neuromodulation as a wireless technology that could reach deep into brain due to the weak magnetic properties and low electrical conductivity of brain tissues<sup>4</sup>. This technology is highly dependent of the hysteresis power loss of magnetic nanoparticles (MNPs) under an applied alternating magnetic field (AMF). Thus, maximizing magnetic heating of MNPs will allow a more efficient energy conversion with lower cytotoxic effects.

Here, we investigate the magnetic heating properties of core and core-shell cubic MNPs for neuromodulation applications. Core MNPs are composed of Fe and Zn ( $\text{Fe}_2\text{O}_4\text{Zn}$ ) at different molar compositions were synthesized to obtain nanoparticles (NPs) with different sizes (28 to 89 nm). It was observed that  $\text{Fe}_2\text{O}_4\text{Zn}$  NPs coercivity ( $H_c$ ) increases with NPs size up to a saturation point due to a change in the multi-magnetic domains. On the other hand, it was found that the hybridization of  $\text{Fe}_2\text{O}_4\text{Zn}$  NPs with a Fe-Co shell ( $\text{CoFe}_2\text{O}_4$ ) allowed us to control their  $H_c$ . Hybridization with Fe-Co shell can enhance  $\text{Fe}_2\text{O}_4\text{Zn}$  NPs  $H_c$  from 13 to 170 times depending on the shell molar composition. After optimization,  $\text{Fe}_2\text{O}_4\text{Zn}$  NPs (28, 35 and 55 nm) and  $\text{Fe}_2\text{O}_4\text{Zn-CoFe}_2\text{O}_4$  NPs (with different Co concentration) were functionalized with polyacrylic acid (PAA) to stabilize them in biological fluids. Calorimetry studies were done to evaluate the specific power loss (SLP) of these MNPs when exposed to an AMF. SLP measurements were consistent with  $H_c$  values (dependent on size and Co concentration). Electrokinetic potential and polydispersity of MNPs in different biological fluids was assed using dynamic light scattering, and revealing high colloidal stability in phosphate buffer and media with high concentration of proteins. The cytotoxicity of these MNPs with and without AMFs was evaluated with a MTT Assay, where it was observed that MNPs functionalized with PAA (MNPs/PAA) with or without AMF cause no cytotoxic effects.

Finally, we tested our MNPs/PAA with the highest SLP and  $H_c$  to evoke neural activity in neurons expressing the heat-sensitive ion channel TRPV1. We isolated primary hippocampal neurons from new-born rats. After 1 week of culturing, we label the neurons with the Calcium indicator Fluo-4 in order to monitor neural activity through Calcium influx. Hippocampal neurons were exposed to cubic MNPs (with and without shell) and AMFs. Neural activity was recorded in real time using a calcium fluorescence imaging. We were able to evoke neural activity with all the MNPs tested. The heat dissipated by our MNPs was enough to trigger the response of the heat-sensitive transmembrane ion channels expressed on hippocampal neurons. The most remarkable achievement from this preliminary stimulation results was our ability to excite neural activity using 50X and 100X less the amount of MNPs in comparison with previously reported work<sup>4</sup>. This finding corroborates our hypothesis for maximizing hysteretic losses by magnetic anisotropy. Moreover, the optimized MNPs phase transfer procedure allowed us to reduce the possibility of agglomeration and bulk heating.

## References

1. Polikov, V. S., *et al.*, *J. Neurosci. Methods* **148**, 1–18 (2005).
2. Strazielle, N, *et al.*, *Mol. Pharm.* **10**, 1473–1491 (2013).
3. Roet, M. *et al.*, *Prog. Neurobiol.* **177**, 1–14 (2019).
4. Chen, R., *et al.*, *Science* **347**, 1477–1480 (2015).

SESSION F.SM08.06: Regenerative Medicine

On Demand Abstracts Available for Viewing Starting Saturday Morning, November 21, 2020

F-SM08

### 5:00 AM \*F.SM08.06.01

**Engineered Tissues—Replacement Parts or Germs of Regeneration?** Ivan Martin; University Hospital Basel, Switzerland

Cellular grafts for the regeneration of cartilage and bone have been engineered using a variety of cell sources, scaffolds and manufacturing systems. Clinical implementation of some of these approaches by the own group has led to promising outcome results (Fulco+, *Lancet* 2014; Mumme+, *Lancet* 2016; Saxer+, *Stem Cells* 2016), but is still associated with manufacturing and robustness challenges. Alternative strategies have been conceived to gain repeatability of processes, by delivering signals capable to recapitulate developmental events, with proofs of principle in the context of bone and cartilage regeneration (Scotti+, *PNAS* 2013; Occhetta+, *PNAS* 2018). Along this line, it was identified that regeneration-inductive signals may not require living cells to be efficiently delivered, but could be encoded in cell-laid and subsequently devitalized extracellular matrices (Bourgine+, *PNAS* 2014; Bourguin+, *Adv Funct Mater* 2017). The combination of multiple cytokines and morphogens, physiologically presented by a set of extracellular matrix molecules, would synergistically potentiate their effects. This new class of off-the-shelf biomaterials, which would function by offering the primordial template for the

development of the target tissue, may offer an alternative strategy to synthetic matrices. These cell-free extracellular matrices, as germs for de novo tissue development, could be generated based on highly standardized processes, thanks to the use of cell lines and bioreactor-based systems, and at the same time customized to address specific disease stages and patient profiles, in a perspective of personalized medicine (Haumer+, Adv Drug Del Rev 2017).

#### 5:15 AM F.SM08.06.02

**Naturally-Derived, Powder-Based Lung Tissue Sealant for Pleural Defects Utilizing a Murine Model** Patrick N. Charron, Spencer Fenn, Minara Aliyeva, Nirav Daphtary and Rachael Oldinski; University of Vermont, United States

**Introduction:** Damage to the pleural tissue lining the lungs can occur in a multitude of ways, resulting in fluid leak into the pleural cavity, which, left untreated, can result in mortality. Historically such cases were treated via pleurodesis. Recent developments of lung tissue sealants serve as alternatives, but few options are available. While popular sealant tests can deliver qualitative pass/fail data, there is lack of quantitative *in vivo* methods to characterize sealing capabilities of these materials, particularly for pleural applications. In addition, commercial products have failed due to poor design and administration. Herein, we describe our development of a powder sealant capable of adhering to tissue and crosslinking to form an elastic hydrogel, circumventing limitations of current tissue sealants.

**Experimental methods:** Methacrylated alginate (AMA) was synthesized and characterized via <sup>1</sup>H-NMR spectroscopy. To enable gelation, visible green light crosslinkers were incorporated into the polymer solution. A sodium ion exchange was performed, the solution was lyophilized, and the product was processed into a powder. To investigate physical material properties, gelation kinetics and the viscosities of reconstituted solutions were collected at 37C, via an oscillatory time sweep at 10% radial strain and 1 Hz during exposure to green light. **Quantitative *in vitro* experiments:** dynamic burst pressure experiments were conducted using a custom-built burst pressure testing device, using a modified ASTM F2392 standard. **Quantitative *in vivo* experiments:** a murine model was developed in which we controlled respiratory dynamics to test sealant mechanics. Mice were anesthetized with pentobarbital sodium, tracheostomized, and paralyzed using pancuronium. Body temperature was maintained by keeping the animal under a lamp. Mice were connected to a computer-controlled small animal mechanical ventilator (flexiVent, Scireq) and ventilated. A series of deep inflation maneuvers (Total Lung Capacity and Trapezoidal deep inflation waveform) and a composite signal comprising of mutually prime frequencies ranging from 0-20 Hz were performed to establish baseline for the animal prior to injury. The thoracic cavity of the animal was opened and lungs were punctured, followed by another series of baseline measurements to calibrate testing mechanics and verify injury. The injury was treated by the application of the AMA powder and tests were repeated to compare lung mechanics pre-injury and post-repair, allowing for real-time pressure data collection of lung mechanics during sealant testing. After testing, animals underwent euthanasia.

**Results:** After acute traumatic injury using a murine model, there was a loss in pressure, confirming the injury model. Successful post-repair (i.e., application of the AMA powder, hydration and crosslinking) tests indicated that the sealant maintained physiologically-relevant lung pressure and returned lung capacity to pre-injury values, and that the sealant did not fail. A failure in the patch would result in a failure to hold pressure. Initial results show physiologically relevant burst pressure values (i.e. 30 cmH<sub>2</sub>O) for the powder sealant collected during *in vitro* testing.

**Conclusions:** The data indicates efficacy of a novel powder-based elastic sealant for recapitulating lung mechanics post injury. During an *in vitro* burst pressure experiment, the powder formed a crosslinked sealant capable of maintaining physiological pressure before failure. The powder-based sealant has the advantages of adhering to tissue upon application *in situ* and subsequent hydration, remaining in place while crosslinking via light exposure took place. Future work will explore long term *in vivo* studies to investigate lung tissue healing after repair with the novel powder sealant material.

**Acknowledgements:** This work was funded in part by NIH R01EB020964 (Oldinski) and the University of Vermont.

**Disclosure of Interest:** None Declared.

#### 5:25 AM F.SM08.06.04

**Late News: The Influence of Conductivity and Mechanical Properties on the Neurogenic Differentiation of Dental Pulp Stem Cells** Samuel Liu<sup>1</sup>, Shivek Narang<sup>2</sup>, Kuan-Che Feng<sup>3</sup>, Haijiao Liu<sup>3</sup>, Marcia Simon<sup>4</sup> and Miriam H. Rafailovich<sup>3</sup>; <sup>1</sup>Olathe North High School, United States; <sup>2</sup>Stanford Online High School, United States; <sup>3</sup>Stony Brook University, United States; <sup>4</sup>Stony Brook University, The State University of New York, United States

**Currently, the central nervous system is unable to effectively repair itself or regenerate neurons when affected by damage. Dental pulp stem cells (DPSCs) are pluripotent stem cells which are promising candidates in**

neuroregenerative medicine due to their ability to differentiate into functional neurons and accessibility via human third molars. Polybutadiene (PB) is a biocompatible polymer, whose modulus can be regulated by changing film thickness or adding inorganic particles. We have shown that when DPSCs are cultured in biomineralizing media containing beta glycerol phosphate and plated on PB they can adjust their modulus to follow that of the underlying substrate such that when the modulus exceeded a critical value, upregulation of the mineralizing gene, OCN, and hydroxyapatite deposition was observed. Further differentiation along a biomineralizing lineage was observed with the addition of titania nanoparticles [1]. Here we wish to explore whether these factors are also important in determining differentiation when the DPSCs are cultured in neurogenic media with and without graphene (G) and graphene oxide (GO) platelets. PB films, 250 nm (thin) and 2500 nm (thick) films with and without G were spun cast out of toluene onto silicon wafers. GO was floated onto the spun cast films from the air/water interface. The samples were annealed at 180C in ultra-high vacuum. Atomic Force Microscopy (AFM) analysis indicated that the G platelets were encapsulated and well distributed within the thick PB films. Aggregation of the graphene platelets, protruding from the film surfaces, were observed in the thin films. The GO films uniformly coated the thin and thick PB substrates. The relative modulus of the cells and substrates were also measured using scanning modulated force microscopy (SMFM). The results indicated that as previously observed, the thin films were 4.7 times harder than the thick films, and the addition of graphene increased their moduli approx. 6 fold, while maintaining the ratio. The modulus of the cells was also measured after 3 days in culture. Surprisingly the cells plated on the soft PB substrates, with and without graphene, were 1.5 times as hard as those plated on the harder thin PB and PB+G substrates, in contrast to previous results on DPSCs in osteogenic media. After 21 days, Real-Time Polymerase Chain Reaction (RT-PCR) was used to identify mRNA levels of neuronal markers which were compared to those measured for the culture after one day in culture. The results indicated no significant differences between hard and soft PB overlaid with GO, despite the significant differences in substrate and cell modulus, indicating that mechanical differences of either the substrate or the cells were not a factor in inducing differentiation. A significant result was observed only on the thick PB plus graphene substrate where the cells showed downregulation of early and intermediate neuronal markers NES and TUBB3, and upregulation of mature neuronal marker NEFM, suggesting that the presence of graphene enhanced neurogenic differentiation. Since graphene is highly conductive, while graphene oxide is not, these results indicate that the enhanced conductivity of the substrate due to the encapsulated particles may be the determining factor in enabling differentiation which is consistent with previous observations that graphene enhanced neuronal communication.

[1] Chuang, Ya-Chen, et al. "TiO<sub>2</sub> Nanoparticles Synergize with Substrate Mechanics to Improve Dental Pulp Stem Cells Proliferation and Differentiation." *Materials Science and Engineering: C*, vol. 118, 2021, p. 111366., doi:10.1016/j.msec.2020.111366.

We gratefully acknowledge support from the Louis Morin Charitable Trust.

SESSION F.SM08.07: Synthetic Biology

On Demand Abstracts Available for Viewing Starting Saturday Morning, November 21, 2020

F-SM08

5:00 AM \*F.SM08.07.01

**Tools for Controlling and Observing Complex Biological Systems** Ed Boyden; Massachusetts Institute of Technology, United States

To enable the understanding and repair of complex biological systems such as the brain, we are creating novel optical tools that enable molecular-resolution maps of large scale systems, as well as technologies for observing and controlling high-speed physiological dynamics in such systems. First, we have developed a method for imaging large 3-D specimens with nanoscale precision, by embedding them in a swellable polymer, homogenizing their mechanical properties, and exposing them to water – which causes them to expand isotropically manyfold. This method, which we call expansion microscopy (ExM), enables scalable, inexpensive diffraction-limited microscopes to do large-volume nanoscopy, in a multiplexed fashion – important, for example, for brain mapping. Second, we have developed a set of genetically-encoded reagents, known as optogenetic tools, that when expressed in specific neurons, enable their electrical activities to be precisely driven or silenced in response to millisecond timescale pulses of light. Finally, we are developing novel reagents, such as fluorescent voltage indicators, and systems, such as novel microscope architectures, to enable the imaging of fast physiological processes in 3-D with millisecond precision. In this way we aim to enable the systematic mapping, control, and dynamical observation of complex biological systems like the brain.



## 5:15 AM INVITED PRESENTATION BY CHRISTOPHER VOIGT

### 5:30 AM F.SM08.07.03

**Late News: Microbial Biofactories—Production of Nanomaterials with Biomedical Applications** Catherine P. O'Connell, David Medina and Thomas J. Webster; Northeastern University, United States

Antimicrobial resistance to antibiotics (AMR) and drug-resistant cancer are two of the main concerns that the healthcare system is facing nowadays [1,2]. Current chemotherapy treatments and antibiotic-based therapies are becoming ineffective or have plenty of drawbacks that are increasing the prevalence of resistance in both hospital and community settings. Therefore, new alternatives are needed, and nanotechnology might offer a suitable answer.

Although different nanomaterials are being used as a method to fight pathogens and cancer, traditionally synthesized nanoparticles present drawbacks, such as the production of toxic by-products, increased cytotoxicity in the cell and lack of selectivity. Consequently, green nanotechnology appears as an alternative approach, which employs living organisms and biomolecules as raw materials in a cost-effective and environmentally-friendly approach [3]. Among all these methods, microbially-produced nanomaterials have presented a significant potential, rendering nanomaterials with a powerful antimicrobial activity that can be tailored to the infection.

With the objective to demonstrate the antimicrobial and biocompatibility efficacy of bacterial-produced nanoparticles in skin bacterial infections, top pathogenic strains found in cutaneous wounds were employed for the synthesis of metalloid selenium nanoparticles (SeNPs), including Methicillin-resistant *Staphylococcus aureus* or *Pseudomonas aeruginosa*. Once generated, the SeNPs were analyzed in terms of their physicochemical features and the composition was extensively studied. After purification, the SeNPs were used as antimicrobial and anticancer agents through colony counting unit and MTS assays, respectively, as well as characterized for the mechanisms of death associated to their activities. At the same time, low cytotoxicity was demonstrated over the same range of antimicrobial efficiency.

Consequently, microbiological agents were successfully used as a biofactories for the generation of SeNPs of different compositions with biomedical properties. Therefore, bacteria were presented as a suitable approach for the synthesis of nanomaterials in a green fashion, overcoming the limitations of traditional nanotechnology.

#### References

- [1] Ventola, C. Lee. *Pharmacy and Therapeutics* 40.4 (2015): 277–283.
- [2] Katz, Steven J. *Journal of Oncology Practice* 9.3 (2013): 114–115.
- [3] De la Guardia, Miguel. *BioImpacts: BI* 4.1 (2014): 1–2.

## SESSION F.SM08.08: Vascular Engineering

On Demand Abstracts Available for Viewing Starting Saturday Morning, November 21, 2020  
F-SM08

### 5:00 AM \*F.SM08.08.01

**Engineering Vasculature Using Physical and Structural Cues** Christopher Chen; Boston University, United States

A major barrier in tissue engineering is a lack of understanding of how to integrate vascular networks into 3D tissue constructs. Without perfusable vascular networks, large constructs containing living cells develop necrotic cores due to nutrient, oxygen, and waste diffusion limitations. To address this challenge, we have developed approaches to generate perfusable vascular networks that support 3D culture of assembled constructs, provide a means to study how to regulate vascular remodeling and angiogenesis, and improve the integration of such vasculature to host circulation in implanted constructs. We demonstrate a critical role for material properties such as stiffness or degradability, and also an important role for the organization of materials and cells to provide functional perfusable vasculature. Ultimately, these approaches will inform how we establish solutions to generate functional vascular beds for engineered tissues both in vitro and in vivo.

### 5:15 AM F.SM08.08.02

**Biomaterial-Guided Recruitment of Endothelial Progenitor Cells for Vascular Regeneration** Mohamed A. Elkhodiry<sup>1</sup>,

Omar Bashth<sup>1</sup>, Gaetan Laroche<sup>2,3</sup>, Jean-François Tanguay<sup>4,5</sup> and Corinne A. Hoesli<sup>1</sup>; <sup>1</sup>McGill University, Canada; <sup>2</sup>Université Laval, Canada; <sup>3</sup>Centre de Recherche du CHU de Québec, Canada; <sup>4</sup>Montreal Heart Institute, Canada; <sup>5</sup>Université de Montréal, Canada

Endogenous endothelial progenitor cell (EPC) recruitment to sites of vascular injury is a multi-step process mediated by selectins, chemokines, and extracellular matrix (ECM) proteins. New vascular implants with surface-immobilized capture antibodies targeting circulating EPCs have shown clinical promise in accelerating the formation of neo-endothelium to cover the implant. The absence of subsequent adhesion-based signaling needed for EPC proliferation and differentiation could explain the lack of long-term improvement in vascular re-stenosis and overall vascular recovery. Antibodies can mimic the cell tethering effect of selectins but lack necessary EPC signaling effects introduced by cytokines and ECM proteins. We have previously shown that ECM-derived peptides, such as RGD, can promote the adhesion and enhance the clonal expansion of EPC-derived endothelial colony forming cells (ECFCs) via integrin based signaling. In this study, we developed a novel bifunctional surface modification strategy to produce surfaces that combine immobilized capture-antibodies and surface grafted ECM-derived peptides with controlled surface concentrations and ligand orientation. We hypothesize that this bifunctional strategy would further accelerate the re-endothelialization process while maximizing downstream endothelial function and vascular recovery via an integrin-dependent process.

Peripheral blood from 22 adult human donors was used to obtain donor-specific ECFCs. Aminated culture surfaces were modified by either the covalent conjugation of a customized RGD peptide, immobilization of vascular endothelial growth factor receptor-2 (VEGFR-2) antibody, or combining both biomolecules at different ratios using an optimized process. Unmodified surfaces were used as a negative control. Surface concentration of the peptide and antibody were analyzed using fluorescence microscopy and an enzyme-linked immunosorbent assay. First, the expanded ECFCs were seeded under static conditions and cell adhesion was studied using immunocytochemistry. ECFC interactions with the bifunctional surfaces were then interrogated under more physiologically relevant dynamic flow conditions in a microchannel perfusion loop at 1 dyn/cm<sup>2</sup> wall shear stress and analyzed through live cell imaging followed by immunocytochemistry.

Surfaces with immobilized anti-VEGFR-2 antibodies displayed significantly enhanced ECFC capture potential compared to RGD and unmodified controls as quantified by the number of adhered cells under both static and dynamic conditions. Average ECFC spreading and focal adhesion formation were significantly increased on RGD surfaces compared to the anti-VEGFR-2 and unmodified controls under both static and dynamic conditions. Total endothelial coverage and the total number of focal adhesions were maximized on the bifunctional surfaces combining the anti-VEGFR-2 and RGD due to a combined increase in both cell number and cell spreading. By increasing the peptide concentration on the bifunctional surfaces, ECFC spreading was increased without significantly affecting the number of adhered cells. These results suggest an additive (i.e. independent) effect of capture antibodies on ECFC tethering vs. RGD peptides on subsequent ECFC spreading and integrin-dependent cell signaling.

To our knowledge, this is the first study showcasing the ability of a bifunctional antibody/peptide surface modification strategy in promoting ECFC capture and adhesion. Our results also display a clear distinction between the mechanisms by which human-derived ECFCs react to immobilized capture antibodies and conjugated ECM-peptides. This strategy creates sequential steps of EPC trafficking to mimic endogenous processes of vascular healing which can potentially create an effective regenerative capacity for vascular implants.

### 5:25 AM F.SM08.08.03

**Bioelectronic Tissue Engineered Vasculature for Monitoring Cell Behavior** Alexander J. Boys, Charalampos Pitsalidis and Roisin Owens; University of Cambridge, United Kingdom

Monitoring vascular permeability represents a significant challenge in materials science. The study of vascular permeabilization is of great interest to the scientific community in its relevance to extravasation during tumor growth, transport across the blood-brain barrier, etc. However, studying vascular permeability *in vitro* requires development of materials systems that not only support cell growth but also produce real-time data on cell behavior. Native vasculature consists of a tube with an interior lining of barrier-forming cells called endothelial cells. These cells selectively allow transport of different factors, of which small molecules and ions primarily pass through intercellular junctions. In this study, we developed a bioelectronic platform for vascular tissue engineering to actively monitor the integrity of the vascular membrane during culture.

Previously, we developed bioelectronic monitoring systems for gauging various cellular phenomena. These systems have frequently used conductive polymers, such as poly(ethylene dioxythiophene):poly(styrene sulfonate) (PEDOT:PSS), which are biocompatible and ion-sensitive. These polymers can be designed for use as electrodes or transistors to monitor local ion flux. As cells deposit extracellular matrix (ECM) and form intercellular junctions, these structures inhibit ion flow, which can be sensed using conductive polymeric devices. These polymers can also be fabricated as porous scaffolds through ice templating to support cell growth.

To produce this vascular monitoring system, we constructed a bioelectronic device, which can simultaneously promote and monitor the development of a vascular membrane. This device was constructed using a porous, electroactive PEDOT:PSS scaffold to support cell culture with surrounding electrical architecture to monitor ion flux into the scaffolds. We produced tissue engineered vasculature by seeding fibroblasts onto the top of the scaffold. These cells were allowed to proliferate, producing a bed of ECM on top of and within the pores of the scaffold. Subsequently, vascular endothelial cells were deposited on top of this culture and allowed to proliferate. After a period of static culture, the devices were placed on an orbital shaker to mimic blood flow. During the following culture period, the devices were monitored using impedance spectroscopy to gauge the formation of a vascular membrane.

Over the course of the culture period, we observed a continuous increase in impedance, indicative of the deposition of ECM and the formation of vascular junctions. At the termination of culture, we found the scaffolds showed complete coverage and junctional formation across the entirety of the 6 mm scaffolds. We will now seek to apply biological factors that affect vascular permeability, such as TNF- $\alpha$ , to promote extravasation in the tissue engineered cultures allowing for determination of the efficacy of using this system to monitor vascular permeabilization. This system provides a platform for studying various physiological phenomena associated with transport through the vascular wall and highlights the capabilities of *in vitro* bioelectronic tissue engineering.

#### 5:35 AM F.SM08.08.04

**Superparamagnetic Iron Oxide Nanoparticles Modulate Platelet Functions** Regina K. Kottana<sup>1</sup>, Lionel Maurizi<sup>2</sup>, Brian Schnoor<sup>1</sup>, Kenise Morris<sup>1</sup>, Nadine Millot<sup>2</sup> and Anne-Laure Papa<sup>1</sup>; <sup>1</sup>The George Washington University, United States; <sup>2</sup>University of Bourgogne Franche-Comté, France

**Introduction:** Platelets play a role in hemostasis and are the first responders to arrest bleeding during an injury [1]. Therefore, any aberration in their function can cause bleeding or thrombus formation. Nanoparticles (NPs) when present in the bloodstream interact with the different components of blood and have been shown to modulate platelet functions [2,3]. However, these interactions are not well understood. In this study, we are using six formulations of PVA (polyvinyl alcohol) coated-SPIONs based on differences in molecular weight (M.W.) and charge of the polymer coating to study the effect caused by their presence on platelet function of activation and aggregation, and additionally, we have explored possible mechanisms to explain the observed effect.

**Materials and Methods:** Human platelet-rich plasma was obtained from healthy donor blood. Platelet activation and aggregation were assessed in the presence of PVA-SPIONs with 12 kDa and 31 kDa PVA, as well as positive, neutral, or negative surface charges, by using flow cytometry and light transmission aggregometry. The agonist adenosine diphosphate was used to induce platelet activation and aggregation. Platelets were incubated with up to 500  $\mu$ g/mL PVA-SPIONs. ELISAs were used to quantify the presence of plasma proteins fibrinogen and von-Willebrand factor (vWF) in platelet-poor plasma incubated with SPIONs. Fibrinogen and vWF binding to platelet GPIIb-IIIa was also studied using flow cytometry, while their structural integrity with SPION incubation was assessed by UV-vis.

**Results and Discussion:** Platelets were activated in the presence of positively charged SPIONs at 500  $\mu$ g/mL, irrespective of M.W. of PVA. A dose-dependent inhibitory effect was also observed on platelet aggregation when platelets were incubated with SPIONs. This antiplatelet effect was independent of the M.W. and surface charge of the PVA-SPIONs. Therefore, we tested three hypotheses to explain this antiplatelet effect. Based on the important role of plasma proteins fibrinogen and vWF in platelet aggregation and the formation of protein corona due to the adsorption of proteins on the surface of NPs [4], we tested if the proteins were significantly adsorbed on the surface of the NP, thus depleting them from the plasma for potential platelet aggregation. Although adsorption of proteins was observed, there was no significant decrease in the concentration of available proteins for platelet aggregation. Next, we tested if the NPs interfere with the normal process of fibrinogen and/or vWF binding to platelet GPIIb-IIIa. In agreement with our platelet activation study, there was an increase in binding of fibrinogen to the receptor GPIIb-IIIa when the PRP was incubated with positively charged SPIONs. In addition, there was no change in the binding efficiency for both fibrinogen and vWF with other SPION formulations. Lastly, we investigated whether the PVA-SPIONs would interfere with the protein structure, and thus with their role in platelet aggregation.

**Conclusions:** PVA-SPIONs induced an inhibitory effect on platelet aggregation regardless of their size and charge. Our results suggest that the inhibitory effect could be ascribed to a change in fibrinogen conformation, induced by the presence of these nanoparticles, thus impairing the platelet-platelet bridging ability of the protein.

**Acknowledgments:** This work has been supported by the George Washington University startup funds.

#### References:

- [1] M. A. Packham, "Role of platelets in thrombosis and hemostasis," *Can. J. Physiol. Pharmacol.*, 72, 3, 278–284, 1994.
- [2] S. Shrivastava, T. Bera, S. K. Singh, G. Singh, P. Ramachandrarao, D. Dash, "Characterization of antiplatelet properties of silver nanoparticles," *ACS Nano*, 3, 6, 1357–1364, 2009.
- [3] U. Sakulkhu, M. Mahmoudi, L. Maurizi, J. Salaklang, H. Hofmann, "Protein corona composition of superparamagnetic iron oxide nanoparticles with various physico-chemical properties and coatings," *Sci. Rep.*, 4, 5020, 2014.

SESSION F.SM08.09: Poster Session: Regenerative Engineering and Synthetic Biology  
On Demand Abstracts Available for Viewing Starting Saturday Morning, November 21, 2020  
5:00 AM - 8:00 AM  
F-SM08

**F.SM08.09.01**

**Microfabricated Porous PTFE Membrane for Separation in Biomedical Uses** Masashi Maruyama, Mitsuya Yamamoto and Hirotaka Sakuma; Hitachi Ltd, Japan

Porous membranes with well-defined pore structures find plenty of uses in research and industrial areas. Well-defined pore structures afford sharp selectivity in filtration and thus applications in biomedical uses are also expected such as cell/spheroid separation and immunoprotection. Track-etching is a well-known technology to fabricate porous membranes with relatively defined pores, but undesired overlapped spots result in loss of selectivity. Against the background, we developed a novel microfabrication methodology to prepare porous membrane with strictly defined pores. We successfully developed porous PTFE membrane with 5-10  $\mu\text{m}$  thickness with tunable pore sizes. We will discuss the potential applications of microfabricated PTFE membranes in biomedical uses.

**F.SM08.09.03**

**Designed Organization of Proteins in Multidimensional Arrays with Preserved Biological Functionality** Shih-Ting Wang<sup>1</sup>, Brian Minevich<sup>2</sup>, Jianfang Liu<sup>3</sup>, Honghu Zhang<sup>1</sup>, Dmytro Nykypanchuk<sup>1</sup>, James Byrnes<sup>1</sup>, Wu Liu<sup>1</sup>, Lev Bershadsky<sup>1</sup>, Qun Liu<sup>1</sup>, Tong Wang<sup>4</sup>, Gang Ren<sup>3</sup> and Oleg Gang<sup>1,2</sup>; <sup>1</sup>Brookhaven National Laboratory, United States; <sup>2</sup>Columbia University, United States; <sup>3</sup>Lawrence Berkeley National Laboratory, United States; <sup>4</sup>The City College of New York, United States

An ability to control the assembly of functional proteins with designable organizations and an unpresented density in multidimensional space, provides routes to the next-generation nano-systems, biomaterials and complex biomolecular scaffolds. To achieve this, DNA nanotechnology offers exciting opportunities to modulate assembly processes with nano-scale resolution and spatial addressability. In this work, we developed a protein encapsulation strategy combined with the DNA programmable assembly for a bottom-up fabrication of biologically functional protein arrays with 2D and 3D prescribed organizations. We showed that ferritin, an iron storage protein, was integrated with DNA frames, of which each vertex and their internal space were encoded with addressable strands to program the protein position and vertex-to-vertex interconnection. Such designed arrays allow to maintain a biological activity of ferritin in the nanoscale lattices at relevant environments, and meanwhile, small molecules can access the iron core of ferritin within the 3D array and convert it into a core-less form, apoferritin. Our study, through the use of *in situ* small angle X-ray scattering, electron microscopy and tomographic modelling, revealed the complex arrangement of designed protein arrays and their ability to perform functions within 3D arrays, thus confirming a new strategy for creating bio-active protein-containing materials.

**F.SM08.09.04**

**Late News: Polymer-Ceramic Scaffold for Bone Tissue Applications** Katia Mendoza-Calderón<sup>1</sup>, Nancy Nelly Zurita Méndez<sup>2</sup>, Javier Ortiz Ortiz<sup>2</sup>, Marco Antonio Espinosa Medina<sup>2</sup> and Georgina Carbajal de la Torre<sup>2</sup>; <sup>1</sup>Tecnológico Nacional de México., Mexico; <sup>2</sup>Universidad Michoacana de San Nicolás de Hidalgo, Mexico

Defects in bone tissue have been more common in recent years, based on this a section has been dedicated in the area of biomaterials for research. Currently, knowledge about new biomaterials has led to the discovery of sets of precursors that work effectively in the recovery of damaged tissue, which must meet certain requirements to be recognized as biomaterials, that is, they must be biocompatible, biodegradable, non-toxic, have mechanical resistance, as well as the appropriate density, weight, shape and size. Once these characteristics are known, it has been decided to experiment with three basic precursors in bone regeneration. The work that was carried out aims to manufacture three-dimensional matrices using precursors such as hydroxyapatite, polylactic acid and polycaprolactone. The characterizations were carried out to verify the purity of such biomaterials. Differential Scanning Calorimetry for both tests in a nitrogen/air atmosphere (80/20) at a temperature range of 100 °C to 1000 °C with a heating of 10 °C/min; on the other hand, for polylactic acid an analysis was carried out using

Fourier Transform Infrared Spectrometry. Once the results were obtained, the scaffolding was manufactured using leaching and solvent casting techniques. With this, two groups of samples were developed with concentrations of 30% HAp -10% PLA -60% PCL and 10% HAp - 10% PLA - 80% PCL, they were mixed with an organic solvent and sodium chloride. The resulting scaffolds were subjected to mechanical compression and tension tests. Obtaining promising results for application in bone tissue.

#### **F.SM08.09.05**

**A Study of Silver Nanoparticles Control with Three Biocompatible Reducing Substances Qixing Liu<sup>1</sup>, Arthur McClelland<sup>2</sup> and Tingying (Helen) Zeng<sup>3,4</sup>; <sup>1</sup>Zhejiang University, China; <sup>2</sup>Harvard University, United States; <sup>3</sup>Academy for Advanced Research and Development, United States; <sup>4</sup>Massachusetts Institute of Technology, United States**

Silver nanoparticles play a significant role in public health. They have been proven to be effective substrates for high-intensity surface-enhanced Raman spectroscopy (SERS) in biomedical applications. The nanoparticles are able to detect organic molecules at nanomolar concentration and has the potential for early disease detection or virus killing. Since SERS technology has gained traction in public health uses recently, the synthesis of AgNPs which is considered as the essential and fundamental key of applications, has attracted numerous researchers. In this study, we propose a green, wet-chemical way to control the synthesis of AgNPs and explore three different reducing agents under similar conditions. Sodium citrate, L-cysteine, and oxalic acid, all used as reducing agents, are respectively added into the AgNO<sub>3</sub> aqueous solution where the Ag<sup>+</sup> concentration is 2.5mmol/L in room temperature. L-cysteine, a specially selected amino acid, exists in every group acting as the capping agent to restrict the aggregation and control the size of nanoparticles. According to the surface-enhanced Raman spectrum and SEM images, sodium citrate demonstrates the best reducing ability under the same concentration of the carboxy group and can be used for a quick synthesis. On the other hand, the particle size of oxalic acid carpets is more controlled regardless of concentration. It is suitable for precise synthesis associated with the time when the surface-enhanced Raman spectrum indicates the size growth of silver nanoparticles as time increases. Some mechanisms during the process are revealed as well. After analyzing the spectrum, we deem that Ag<sup>+</sup> ion combines with carboxy groups more easily than sulfur in this system. Consequently, these three reducing agents exhibit their unique advantages which provide us with various selections for the synthesis of silver nanoparticles under different requirements for different applications in public health.

#### **Acknowledgment**

The first author is grateful to the Academy for Advanced Research and Development (AARD, website: [www.ardacademy.org](http://www.ardacademy.org); contact email: [admissions@ardacademy.org](mailto:admissions@ardacademy.org)) for the Intern Research Sponsorship through the collaboration with the Center for Nanoscale Systems at Harvard University.

### **SYMPOSIUM F.SF01**

---

Materials for Extreme Conditions (MEC)  
November 21 - December 4, 2020

#### Symposium Organizers

Alexander Goncharov, Carnegie Inst of Washington

Ke Han, Florida State Univ

Florence Lecouturier, CNRS-LNCMI

Wenge Yang, Center for High Pressure Science & Technology Advanced Research

---

\* Invited Paper

SESSION F.SF01.10: Live Keynote I: Materials for Extreme Conditions (MEC)  
Session Chairs: Alexander Goncharov, Muhammad Musaddique Ali Rafique and Yang Ren  
Wednesday Afternoon, December 2, 2020  
F.SF01

**5:15 PM \*F.SF01.01.01**

**Stress Induced Mesoscale Assembly of Nanoparticles for Active Nanostructures** Hongyou Fan; Sandia National Laboratories, United States

Due to the size- and shape-dependent properties, nanoparticles have been successfully used as functional building blocks to fabricate 1-3D ordered assemblies for the development of artificial metamaterials. At ambient pressure, entropy driven self-assembly of monosized or binary nanoparticles generally results in polycrystalline 2- or 3D close-packed arrangements, and extensive efforts have been made to develop structural perfection of nanoparticle arrays or 'single crystal-like' domain structures with precise long range order for their definite advantages for electron transport. To date, fabrications of ordered nanoparticle assemblies have been relied on specific interparticle chemical or physical interactions such as van der Waals interactions, dipole-dipole interaction, chemical reactions, etc. Recently we have discovered a pressure-induced assembly method to engineer nanoparticle assembly at mesoscale and to fabricate new nanoparticle architectures without relying on specific nanoparticle interactions. We show that under a hydrostatic pressure field, the unit cell dimension of a 3D ordered nanoparticle arrays can be manipulated to reversibly shrink, allowing fine-tuning of interparticle separation distance. Under uniaxial pressure field, nanoparticles are forced to contact and coalesce, forming hierarchical nanostructures. Depending on the orientation of the initial nanoparticle arrays, 1-3D ordered nanostructures including nanorod, nanowire, and nanoporous network can be fabricated through the pressure-induced self-assembly method. Guided by computational simulations, we were able to rationalize the pressure-induced self-assembly of nanoparticle arrays for predictable nanostructures. Moreover, we discovered for the first time a transition from an ordered polycrystalline nanoparticle mesophase to quasi-single crystalline nanoparticle lattices induced by PDA process. Exerting pressure-dependent control over the structure of nanoparticle arrays provides a unique and robust system to understand collective chemical and physical characteristics and to develop novel electronic and photonic behavior for energy transduction related applications.

Sandia National Laboratories is a multimission laboratory managed and operated by National Technology and Engineering Solutions of Sandia, LLC., a wholly owned subsidiary of Honeywell International, Inc., for the U.S. Department of Energy's National Nuclear Security Administration under contract DE-NA0003525.

**5:27 PM \*F.SF01.01.02**

**Supercritical Elasticity and Its Potential Applications in Extreme Conditions** Haiyang Chen<sup>1</sup>, Yan-Dong Wang<sup>1</sup> and Yang Ren<sup>2</sup>; <sup>1</sup>University of Science and Technology Beijing, China; <sup>2</sup>Argonne National Laboratory, United States

Developing elastic materials for technological applications in extreme conditions has been a challenging task. Normal metals have an elastic strain limit rarely exceeding 1%. A large pseudo-elastic strain up to 10% can be achieved in the so-called shape-memory alloys (SMAs). However, the intrinsic hysteresis and temperature sensitivity of the first-order phase transformation significantly hinder their usage in many critical areas. We recently discovered a new type elasticity: supercritical elasticity (SCE), in NiCoFeGa single crystals, which exhibit a large elasticity up to 15.2% strain, with non-hysteretic mechanical responses, a small temperature dependence and high-energy-storage capability and cyclic stability over a wide temperature and composition range [Chen et al., Nature Materials, (2020). <https://doi.org/10.1038/s41563-020-0645-4>]. Such a giant SCE is conceived to work even down to absolute zero Kelvin. In situ synchrotron X-ray diffraction measurements show that the SCE is correlated with a stress-induced continuous variation of lattice parameter accompanied by structural fluctuation. Neutron diffraction and electron microscopy observations reveal an unprecedented microstructure consisting of atomic-level entanglement of ordered and disordered crystal structures, which can be manipulated to tune the SCE. The discovery of the giant SCE and associated the entangled structure paves the way for exploiting elastic strain engineering and development of related functional materials for a wide variety of high-performance engineering applications, ranging from deep-space and deep-sea exploration to intelligent robotics.

**5:39 PM \*F.SF01.01.05**

**Pressure-Induced Dramatic Changes in Electronically Low-Dimensional Metal Halides** Xujie Lu, Songhao Guo, Hui Luo, Yongsheng Zhao and Wenge Yang; Center for High Pressure Science & Technology Advanced Research, China

Metal halide perovskites are promising for advanced photovoltaic and optoelectronic applications. Solar cells and light-emitting diodes based on metal halides have achieved an impressive power conversion efficiency of 25.2% and a high external quantum efficiency of over 20%, respectively. Importantly, exceptional structural tunability enables enhanced and/or emergent properties. By using appropriate organic and inorganic components, many perovskite variants with 2D, 1D, and 0D structures on the molecular level have been obtained. These electronically low-dimensional metal halides have exhibited rich emergent properties and significantly expanded the scope of halide perovskites, while critical challenges remain. Future design of high-performance metal halides calls for a deeper understanding of the structure-property relationships. In this talk, we will present our recent efforts in using external pressure to tune the structures and physical properties of low-dimensional metal halides. Using state-of-the-art high-pressure techniques coupled with *in situ* synchrotron-based and in-laboratory property measurements, we characterized the changes in their structural, electronic, and optical properties. Pressure-enhanced properties such as higher photoluminescence quantum yields, as well as pressure-induced novel phenomena including emergent photocurrent, were observed. Our findings demonstrate that high pressure is able to realize enhanced and/or emergent properties of various metal halides, and further our understanding of the underlying mechanisms.

**5:51 PM \*F.SF01.01.13**

**Heterostructured Materials—Strain Gradient Near Interface and Its Dislocation Mechanisms** Yuntian T. Zhu<sup>1,2</sup>; <sup>1</sup>Southeast University, China; <sup>2</sup>City University of Hong Kong, China

Recently, heterostructures are found to produce unprecedented combination of strength and ductility that is considered impossible from our textbook knowledge and materials history. Heterostructured (HS) materials consist of domains with dramatic strength differences. The superior mechanical properties have been attributed to back-stress strengthening and back-stress work hardening, which are related to strain gradient near the heterogeneous domain interfaces. Here I'll discuss *in-situ* observations of strain gradient evolution near the domain interface and the dislocation mechanisms for the formation of strain gradient. It is found that contrary to our conventional understanding, negative strain gradient was developed near the interface. It is also observed under in-situ TEM that the Frank-Read dislocation sources are dynamically created and destroyed although postmortem examinations do not observe many Frank Read sources. These observations provide a new piece of scientific foundation for heterostructured materials, which is becoming a hot research field.

**6:15 PM BREAK**

SESSION F.SF01.11: Live Lightning/Flash Talks I: Materials for Extreme Conditions (MEC)  
Session Chairs: Alexander Goncharov, Muhammad Musaddique Ali Rafique and Yang Ren  
Wednesday Afternoon, December 2, 2020  
F.SF01

**6:30 PM F.SF01.01.03**

**Initiation of the CuO/Al Thermite Reaction Through High-Velocity Microparticle Impact Testing** Carlos Parra<sup>1,2</sup>, Yuchen Sun<sup>3,3</sup>, David A. Veysset<sup>3</sup>, Digvijay R. Yadav<sup>4</sup>, Kelvin Xie<sup>4</sup> and Zachary Cordero<sup>3</sup>; <sup>1</sup>Rice University, United States; <sup>2</sup>Escuela Superior Politecnica del Litoral, ESPOL, Ecuador; <sup>3</sup>Massachusetts Institute of Technology, United States; <sup>4</sup>Texas A&M University, United States

Thermite reactions between a metallic fuel and a solid oxide can be thermally or mechanically activated. The ignition temperature in a thermally activated thermite reaction generally increases with heating rate but is ultimately limited by the onset of melting of the lower melting point constituent. In mechanically activated thermite reactions, there is often a structure-sensitive threshold pressure required to drive the reaction. Historically, thermally activated thermite reactions have been explained using diffusion-based reaction mechanisms while mechanically activated thermite reactions have been described using deformation-based mechanical mixing models. Here we probe mechanically activated thermite reactions at a single well-defined heterophase interface using a combination of hydrocode simulations and laser-induced particle impact testing, where a CuO powder particle strikes an aluminum target at supersonic velocities. No reactions are observed through *in situ* imaging; however, post-mortem characterization of embedded CuO particles reveals a thin nanocrystalline Al<sub>2</sub>O<sub>3</sub> reaction layer, with a thickness roughly equal to that of a molten lubricating layer predicted to form during penetration. These results suggest that local melting at hot spots drives the ultrafast reactions observed in mechanically activated thermite

reactions and that thermally and mechanically activated thermite reactions may in fact result from the same underlying mechanisms.

#### 6:32 PM F.SF01.01.04

**Silica-Titania Nanocomposite Based Fiber Optic Sensor for Aromatic Hydrocarbons Detection** Shumaila Islam and Adil Alshoabi; King Faisal University, Saudi Arabia

Surface stability of deposited sensing material is becoming a crucial issue in the field of opto-chemical sensor technology due to cracks/stresses. Porous silica-titania (ST) nanocomposite coating material is synthesized and doped with CdTe as transducers for sensing cyclic compounds. Ultra-thin coatings are obtained, ~11 nm for ST nanocomposite, and 5 nm for encapsulated and heat-treated samples. BET analysis shows large surface area  $\sim 441 \text{ m}^2/\text{g} \pm 3 \text{ m}^2/\text{g}$  and pore diameter 58 Å of ST nanocomposite. It decreases down to  $\sim 410 \text{ m}^2/\text{g} \pm 2 \text{ m}^2/\text{g}$ , and pore diameter to 24 Å, after encapsulation. However, after heat treatment, it again increases up to  $419 \text{ m}^2/\text{g} \pm 2 \text{ m}^2/\text{g}$  and pore diameter to 38 Å. The sensitivity of 71.37 counts per unit change in the carbon chain with correlation determination coefficient  $R^2 \sim 0.89$  at 468 nm is observed. The prepared sensor device shows excellent stability, signal-to-noise ratio, and good reversibility towards different hydrocarbons and non-hydrocarbons (inorganic materials).

#### 6:34 PM F.SF01.01.08

**Modeling and Experimental Studies of Neat and Metal-Doped Stishovite, Coesite and Quartz Under High Pressure** Iskander G. Batyrev, Michael C. Golt and Rosario C. Sausa; CCDC Army Research Laboratory, United States

The results of a comparative study of neat and doped silicon dioxide polymorphs (Fe, Ni or Cu) obtained by density functional theory (DFT) at 0 K and at ambient pressure, 10 GPa, and 20 GPa are presented. The metal atoms are introduced at substitutional and octahedral interstitial sites of the crystal, and the relaxed structures are analyzed and ranked according to the enthalpy. Changes in the enthalpy of the neat and doped crystals are estimated at selected temperatures using quantum mechanics molecular dynamics (DFT-MD). We report the modeled enthalpy of the neat and doped crystals, as well as the dependency of the unit-cell parameters, band gaps, and Raman-active modes on pressure, and compare some of these results to those obtained experimentally using a diamond anvil cell. In addition, we present our search results of the high-pressure phases of silicon dioxide using DFT - based evolutionary simulations and report on the stability of the silica phases, as evaluated by convex-hull construction.

Funding Acknowledgement: This work was supported in part by a grant of computer time from the DOD High-Performance Computing Modernization Program at the ARL, Navy, AFRL, and ERDC DoD Supercomputing Resource Centers.

#### 6:36 PM F.SF01.01.07

**Shear Localization in Molecular Crystal Cyclotetramethylene-Tetranitramine ( $\beta$ -HMX)** Mohammad Jane Alam Khan and Catalin Picu; Rensselaer Polytechnic Institute, United States

Cyclotetramethylene-Tetranitramine ( $\beta$ -HMX) is an energetic molecular crystal widely used as a constituent for plastic bonded explosives (PBXs). At high pressures encountered under shock conditions, dislocation motion is inhibited and plastic deformation takes place primarily by shear localization. Atomistic simulations of shear localization are performed in  $\beta$ -HMX under isothermal-isobaric conditions. The post localization flow stress for different pressures (0 to 15 GPa) and strain rates ( $10^7$  to  $10^{10} \text{ s}^{-1}$ ) and at different temperatures of the shear band is investigated. The flow stress decreases linearly with temperature and increases quadratically with the pressure and exponentially with the strain rates. Shear thinning is observed, i.e. the viscosity decreases with increasing the strain rate. It is concluded that the flow stress increases exponentially with the density of the amorphous shear band and hence it can be described as a function of this single variable. The pressure, temperature and strain rates control the flow stress through the density.

The critical stress for shear localization (CSSL) was investigated for different strain rates at different pressures. The critical stress depends significantly on pressure and weakly on strain rates.

#### 6:38 PM F.SF01.01.16

**Friction and Dislocation Motion Using Objective Molecular Dynamics** Gunjan Pahlani<sup>1</sup>, Ananya Renuka Balakrishna<sup>2,1</sup> and Richard D. James<sup>1</sup>; <sup>1</sup>University of Minnesota, United States; <sup>2</sup>University of Southern California, United States

Atomic features, such as surface roughness and dislocations, affect the mechanical strength and plastic deformation of materials under high shear rates. The precise role of how these atomic features influence the wear and tear of materials under nonequilibrium settings is not well understood. We use Objective Molecular Dynamics (OMD) to investigate the links



between atomic features and high shear rates. This method has two advantages over traditional MD simulations: First, it simplifies solutions by exploiting the group invariance of the equations of molecular dynamics. For example, in OMD only a modest number of atoms are simulated (typically, 50-1000) and the motions of the other, typically infinite, set of atoms (the non-simulated atoms) are given by the group action on the simulated atoms. Second, it provides a framework for modeling continuum loads at an atomic scale. For example, a Lagrangian velocity gradient tensor is introduced to describe affine motion of simulated atoms. In today's talk, we demonstrate these advantages of OMD through two examples: 1) frictional behavior of sliding surfaces, and 2) dislocation movement under shear stress. Both of these computations were done under high shear rates, and demonstrate how atomic features, such as rough surfaces, edge dislocations, and vacancies, affect mechanical deformation. Broadly, we present a theoretical framework to explore the interplay between extreme mechanical loads at the continuum scale and mechanical deformation at the atomic scale.

**6:40 PM F.SF01.01.18**

**Superhard Conductive Rhenium Nitride Thin Films via Magnetic Field-Assisted CVD from Volatile Rhenium**

**Precursors** Michael Frank, Lasse Jurgensen, David Graf, Daniel Stadler, Isabel Gessner and Sanjay Mathur; University of Cologne, Germany

Rhenium nitride is a promising candidate as superhard conductor. Different rhenium-to-nitrogen ratios and several phases result in challenging synthetic strategies for phase pure rhenium nitride. Novel heteroleptic rhenium(I) compounds, [*fac*-Re(I)(CO)<sub>3</sub>(L)] (e.g., L= *tfb*-*dmpda*, (*N,N*-(4,4,4-trifluorobut-1-en-3-on)-dimethyl propylene diamine)), containing preformed Re–N bonds act as efficient precursors for selective growth of polycrystalline rhenium nitride (ReN) films by vapor phase deposition. This is the first known access to synthesize phase pure rhenium nitride by single source precursor approach without the need of additional gases. Interdependence of materials strength and thin film orientation is strongly influenced by external magnetic fields. Deposition of ReN films in presence of an external magnetic field showed an orientation effect with preferred growth of crystallites along  $\langle 100 \rangle$  direction.

**6:42 PM F.SF01.01.19**

**Synthesis of Molecular Metallic Barium Superhydride—Pseudocubic BaH<sub>12</sub>** Dmitrii Semenov<sup>1</sup>, Wuhao Chen<sup>2</sup>,

Alexander Kvashnin<sup>1</sup>, Xiaoli Huang<sup>2</sup>, Alexander F. Goncharov<sup>3</sup>, Artem Oganov<sup>1,4</sup> and Tian Cui<sup>2,5</sup>; <sup>1</sup>Skolkovo Institute of Science and Technology, Russian Federation; <sup>2</sup>Jilin University, China; <sup>3</sup>Carnegie Institution of Washington, United States; <sup>4</sup>Northwestern Polytechnical University, China; <sup>5</sup>Ningbo Institute of Materials Technology and Engineering, Chinese Academy of Sciences, China

Inspired by recent progress in chemistry of compressed polyhydrides [1-2] and the discovery of high-temperature superconductivity above 250 K in the La–H system [3-4], we experimentally studied the high-pressure chemistry of Ba hydrides in four independent DACs. We successfully synthesized novel barium superhydride BaH<sub>12</sub> with a pseudocubic crystal structure, stabilized in the pressure range of 75–173 GPa. The compound was obtained by laser-heating of metallic barium with an excess of ammonia borane compressed to 173, 160, 146, and 90 GPa. The Ba sublattice structure of BaH<sub>12</sub> was resolved using the X-ray synchrotron diffraction, evolutionary structure prediction, and several postprocessing Python scripts, including an XRD matching algorithm. The *ab initio* calculations confirm a small distortion of the ideal *fcc*-barium sublattice to space group *Cmc*2<sub>1</sub> (or even *P*2<sub>1</sub>), determined by the presence of additional weak reflections in the diffraction patterns. Discovered BaH<sub>12</sub> has unique combination of molecular H<sub>2</sub> and H<sub>3</sub> fragments formed due to Peierls-type distortion of one-dimensional H-chains, metallic conductivity, and even superconductivity with  $T_C = 20$  K at 140 GPa, and one of the highest hydrogen content (>92 mol %) among all metal hydrides synthesized so far. Discovered barium dodecahydride is also the first known example of molecular metal amid polyhydrides with one-dimensional conductivity and superconductivity, realized in the H sublattice without its atomization. The results of these experiments confirm that the comparative stability of superhydrides increases with the growth of the period number of a hydride-forming element in the periodic table. [5]

References:

- [1] D. Semenov et al. *Mat. Today* 2020, **33**, 36.
- [2] D. Zhou et al. *J. Am. Chem. Soc.* 2020, **142**, 6, 2803–2811.
- [3] M. Somayazulu et al. *Phys. Rev. Lett.* 2019, **122**, 027001.
- [4] A. Drozdov et al. *Nature* 2019, **569**, 528.
- [5] D. Semenov et al. *Cur. Op. in Sol. State and Mat. Sci.* 2020, **24**, 2, 100808.

**6:46 PM F.SF01.01.11**

**Thermal Stability of XeF<sub>2</sub> at High Pressures** Elena Bykova<sup>1</sup>, Maxim Bykov<sup>2</sup>, S. Chariton<sup>3</sup>, V. Prakapenka<sup>3</sup> and Alexander

F. Goncharov<sup>1</sup>; <sup>1</sup>Earth and Planets Laboratory, United States; <sup>2</sup>Howard University, United States; <sup>3</sup>Argonne National Laboratory, United States

Xenon is quite a reactive noble gas, and xenon difluoride (XeF<sub>2</sub>) being stable at ambient conditions is used in organic synthesis as fluorinating agent. Formation of XeF<sub>2</sub> is possible because xenon is bonded to highly electronegative fluorine atoms that take electrons from xenon filled outermost electron shell, forming cation Xe<sup>2+</sup>.

High-pressure behavior of XeF<sub>2</sub> (sp. gr. *I4/mmm*) is still under debate. Early powder X-ray diffraction and Raman experiments propose that XeF<sub>2</sub> should transform from a molecular compound to extended graphite-like layer structure at 50 GPa, and then above 70 GPa to a metallic fluorite structure. Contrary, the later experimental studies suggest just slight decrease in XeF<sub>2</sub> lattice symmetry, first to *Immm* and then to *Pnma* structure at 28 GPa and 59 GPa, respectively. Theoretical calculations predict that XeF<sub>2</sub> becomes unstable above 81 GPa, while high pressures should stabilize other xenon–fluorine compounds, such as XeF<sub>4</sub>, XeF<sub>6</sub> and Xe<sub>2</sub>F.

In order to resolve this issues, we investigated thermal stability of XeF<sub>2</sub> at pressures up to 54 GPa by means of single crystal X-ray diffraction in laser-heated diamond anvil cells. Single-crystal XRD opens the way to determine not only crystal structure of the material at truly extreme conditions, but also allows to refine its chemical composition. We report here the crystal structures of novel fluorides xenon, synthesized at high-pressure and high temperature conditions. In particular, the crystal structures of XeF<sub>4</sub> and Xe<sub>3</sub>F<sub>2</sub>, that both formed under heating-induced disproportionation of XeF<sub>2</sub> at 54 GPa. Similarly to ambient pressure structure, XeF<sub>4</sub> is a molecular compound composed of XeF<sub>4</sub> units with square planar geometry. Xe<sub>3</sub>F<sub>2</sub> is not known at ambient conditions, and its structure is formed by isolated Xe atoms and linear XeF<sub>2</sub> molecules.

#### 6:48 PM F.SF01.01.14

##### **Effects of Ultrahigh Strain and Strain Rates on the Heterogeneous Microstructural Evolution of Cold-Sprayed Coatings** Yu Zou; University of Toronto, Canada

Cold spray, initially a coating technique, is being touted as a ‘near-net shape’ manufacturing technology that minimizes material waste by virtue of the high rate of deposition. During the cold spray process, metallic bulk components can be produced by spraying metal powders at high velocity, generating bonding through severe plastic deformation at temperatures well below the melting point of the powders. To fully understand the cold spray processing of metal powders, we systematically compare and study the microstructure evolution in Cu, Ni, Al, Ti, Ti-6Al-4V samples prepared by cold spray using electron backscatter diffraction (EBSD), transmission electron microscopy (TEM) and nanoindentation. We show complex microstructure in these powder particles after cold spraying: nanocrystalline, nanotwins, annealing twins, gradient grains, deformation bands, dynamic/static recovery and recrystallization. The effects of gas temperature and powder velocity on the microstructure and mechanical properties in the cold sprayed samples are also discussed. Of particular interest are grain refinement, recrystallization and particle/particle bonding mechanisms of the cold sprayed powders.

#### 6:50 PM F.SF01.01.20

##### **Late News: Atomic-Scale Insight into Melting of BCC Tungsten Under Shear Stresses by Extended Finnis-Sinclair Potential—Molecular Dynamics Simulation** Dulat Akzhigitov, Tamerlan Srymbetov, Boris Golman, Christos Spitas and Zhandos Utegulov; Nazarbayev University, Kazakhstan

Understanding melting processes in refractory materials under external stresses is important and can be of particular interest in harsh environment applications ranging from aerospace to nuclear and fusion energy where these materials have to simultaneously withstand the effect of high temperatures and complex stress states in such ways, that a melting process might be initiated in extreme conditions. However, most if not all of the prior research was focused on melting phenomena in the presence of hydrostatic compression.

In our work, we investigate the melting phenomenon in BCC tungsten under different shear stress types. We explore these relationships numerically by molecular dynamics simulations employing extended Finnis-Sinclair potential [1-2] and solid-liquid coexistence method and validate our results with theoretical and experimental findings previously reported in the literature for a hydrostatic compression case.

Regarding other stress states, no similar results have been reported yet for bcc tungsten. The melting behaviour was investigated for all studied stress states and compared both quantitatively and qualitatively on the basis of equivalent strain, least-square atomic-scale strain invariants, maximum shear stress, radial distribution function (RDF), thermal expansion and Lindemann melting criterion. For the majority of shear stress states, an abrupt decline of stress-induced melting point values was detected after certain critical stress values, which was explored with regard to the change of an RDF’s amplitude of the first peak. New high-temperature thermo-mechanical results are correlated with intricate structural changes taking place on the atomic scale during metal-melt phase transition.

## Acknowledgements

The authors acknowledge the funding support of FDCR Grant No. 110119FD4501 by Nazarbayev University, Grant No. AP05130446 and State-Targeted Program No. BR05236454 by Kazakhstan Ministry of Education and Science.

## References

- [1] Akzhigitov D, Srymbetov T, Golman B, Spitas C and Utegulov Z N 2020 Melting of tungsten under uniaxial and shear stresses: molecular dynamics simulation *Modelling Simul. Mater. Sci. Eng.* [in press] <https://doi.org/10.1088/1361-651X/abaf39>
- [2] Dai X D, Kong Y, Li J H and Liu B X 2006 Extended Finnis–Sinclair potential for bcc and fcc metals and alloys *Journal of Physics: Condensed Matter* <https://doi.org/10.1088/0953-8984/18/19/008>

## 6:52 PM F.SF01.01.21

### Late News: *In Situ* Characterization of Dynamic Deformation of AZ31B Magnesium Alloys at High Strain Rate Impact Using 3D-Digital Image Correlation Technique Francis Tetteh; York University, Canada

The deployment of Magnesium (Mg) alloys have increased significantly in the automotive, aerospace, and defense industries due to their lightweight structural integrity. In structural applications, these materials components are exposed to a wide range of strain rates such as explosive forming, high-speed impact, and shock loadings. These alloy components are placed in extreme loading environments where high strain rates are commonly achieved. Therefore, the evolution of failure mechanisms from strain localization and formation of adiabatic Shear Bands (ASBs) and the mechanical behavior at high strain rates is of desirable interest by the aerospace and automotive industries. The deformation behavior of Mg has extensively been studied under low strain rate loadings. However, the high strain rate deformation still requires further investigation. Deformation and damage accumulation in Mg alloys at high strain rate loading conditions such as impact is not fully understood. Thus, the correlation between the accuracy of the reported mechanical data and microstructural features that leads to the credence of failure mechanisms within Mg is not well understood. It is therefore critical to extending the understanding of the mechanism of failure of Mg at high strain rates of loadings by exploiting other techniques. In this work, the dynamic mechanical impact response and ASBs nucleation of heat-treated AZ31B Mg alloys at different strain rates and impact momentums are characterized in-situ during impact at room temperature using the Direct Impact Hopkinson Pressure Bar (DIHPB) coupled with an in-situ 3D Digital Image Correlation (DIC) and high speed and high-resolution thermal imaging techniques. DIC provides an independent measurement of surface strains directly on test specimens during deformation to monitor stain evolution and strain localization. It is found that the flow stress increased gradually to (~50 %) with increasing strain rates and impact momentums and the AZ31B Mg exhibits strain rate sensitivity at dynamic loadings. This is due to an increasingly selective grain refinement under dynamic compression. Evaluation of DIC results indicated that strain occurrence is linear at the onset of deformation but becomes heterogeneous at the later stage of deformation with multiple nucleation sites of strain localization leading to ASB at ~80% of the specimen length after ~340 us of deformation. The region of peak non-linearity of maximum strain concentration leads to ASB formation with characteristic fine grains, voids, and crack initiation. At most, ~22 °C temperature rise is observed. The temperature rise is, however, lower with respect to the homologous temperature of Mg, and a hence higher degree of strain hardening behavior is induced after deformation. These results suggest that ASB forms in AZ31B Mg alloy despite its brittle nature that leads to crack initiation and ultimate failure under high strain rates and large strains of deformation and can be used to extend the understanding of the mechanism of failure in Mg alloys.

## 6:54 PM OPEN DISCUSSION

SESSION F.SF01.12: Live Keynote II: Materials for Extreme Conditions (MEC)

Session Chairs: G. Grissonnanche, Florence Lecouturier and Sergei Zherlitsyn

Thursday Morning, December 3, 2020

F.SF01

## 8:00 AM \*F.SF01.02.04

**High Strength—High Conductivity Materials for High Field Magnets** Francois Debray, Olivier Jay and Florence Lecouturier; UGA-INSA-UPS-CNRS, France

Magnetic field is a powerful tool to study new materials and new processes. The highest magnetic field generated with superconducting magnets made of NbTi and Nb<sub>3</sub>Sn windings is 23.5 T. During the last years, technological breakthroughs have confirmed the feasibility of superconducting magnets generating more than 30 T thanks to the integration of high temperature superconductors. Still, higher magnetic fields are only available through copper-based magnets. Steady high magnetic field can be generated during several hours and implies a large electrical power (typically 30 MW for 40 T) whereas pulsed magnetic field can reach 100 T for some milliseconds with negligible power consumption. The French High Magnetic Field Facility (LNCMI) is developing both technologies, on its pulsed field site in Toulouse and its steady field site in Grenoble. Optimizing the high field magnets requires to search for the best material and associated shaping process for the realization of these highly constrained machines. The main high field magnet constraints are the mechanical constraints due to Lorentz forces and the thermal constraints coming from Joule losses.

For steady field magnets, copper alloys with high strength and high electrical conductivity are required for an operating temperature that can reach 150°C. To keep the windings of the magnet at a temperature acceptable for a given alloy a high velocity water flow is injected in it to manage heat fluxes as high as 10 MW.m<sup>-2</sup>. Steady high field resistive magnets used two technologies: the Bitter and the polyhelix one. Bitter magnets are made of thin plates (from 0.2 to 1 mm) up to 1000 mm in diameter. In this shape Copper alloys with a high content of Silver (18 wt.%, yield strength up to 1000 MPa and electrical conductivity at room temperature of 50 MS.m<sup>-1</sup>) have been industrialized by one company worldwide up to 250 mm in diameter. For larger diameters, copper plates with a possible addition of a low content of Silver are proposed by different companies with yield strength ranging from 400 to 450 MPa and a conductivity around 58 MS.m<sup>-1</sup>. For the polyhelix technology, the LNCMI has set a R&D program to replace forged tubes (CuCrZr) with limited mechanical properties. Copper alloy tubes prepared by the Cold Spray technology are now in operation on the high field facility in Grenoble.

For pulsed field magnets, the highest priority is set on the mechanical properties of conductors at cryogenic temperature which have to cope with the increasingly severe mechanical constraints at fields beyond 60 T. To avoid excessive heating, the duration of the current that passes through a magnet is reduced to the order of 10-100 milliseconds. The LNCMI Toulouse disposes of several capacitor banks with a total energy of 22 MJ able to produce non-destructive fields over 60 T in 28 mm and close to 100 T in 8 mm bore. Beyond 100 T, it also features a Megagauss installation that makes use of dynamic effects in exploding copper single-turn coils to produce 200 T on a microsecond time scale. "In-house" copper/stainless steel macrocomposite conductors for wire wound pulsed field magnets generating magnetic fields up to 80 T are developed. High strength multiscale Cu/Nb nanocomposite wires produced by severe plastic deformation by ADB (Accumulative Drawing and Bundling) process are dedicated to the production of magnetic field over 90 T. New innovative composite copper based conductors, processed by powder metallurgy, reinforced with carbon nanotube or silver nanowires- are under development to reach non-destructive pulsed fields over 100 T.

#### **8:12 AM \*F.SF01.02.02**

**Materials Requirements for Ultra-High-Field Magnets at the National High Magnetic Field Laboratory Mark D. Bird; Florida State University, United States**

Ultra-High-Field (UHF) electromagnets require high current densities in high magnetic field with resulting intense Lorentz forces. A central part of developing higher field magnets is managing the Lorentz forces to keep stress and strain within the materials' allowables.

The simplest UHF magnets are dc resistive ones. DC operations UHF results in maximum performance being presently attained by high-strength copper and its alloys. Fatigue performance has started to emerge as a challenge in CuAg nano-composites. Pulsed resistive magnets are able to mix high-strength conductors and reinforcing materials with both high strength and high stiffness by appropriately adjusting the pulse length. High strength copper and a number of its alloys are productively employed, as are metallic and polymer/epoxy composite reinforcements. The highest field superconducting magnets employ the high-temperature superconducting (HTS) materials along with high strength reinforcement.

The present state of the art of material requirements for UHF magnets is briefly presented along with challenges for next-generation systems.

#### **8:24 AM \*F.SF01.02.03**

**Understanding Requirements of Advanced Magnet Materials to go Beyond 100 Tesla Doan Nguyen and Do T. Vo; Los Alamos National Laboratory, United States**

High magnetic fields have a long history of uncovering fundamentally important information about materials. They take their place among e.g. X-ray and neutron techniques, as a critically important tool of condensed matter physicists. The National High Magnetic Field Laboratory's Pulsed Field Facility at Los Alamos National Laboratory is one of few research centers in

the world that can create and use ultra-high pulsed magnetic field for scientific research. The facility houses several types of non-destructive pulsed magnets which can provide the peak fields ranging from 60 tesla to 100 tesla for users. However, present frontiers in quantum matter, including topological matter and superconductivity, require magnetic fields beyond 100 tesla and several high field facilities around the world are currently working toward that ambitious goal. The power and stored energy required to generate a magnetic field increase exponentially with the field amplitude. Therefore the better conductors with higher mechanical strength and electrical conductivity are required to nondestructively generate magnetic fields above 100 tesla with acceptable risk and cost. Finite Element Modeling (FEM) simulations and our in-house mid-plane pulsed magnet design codes were employed to understand the requirements of advanced magnet materials to practically achieve magnetic fields beyond 100 tesla.

#### **8:36 AM \*F.SF01.02.01**

**Material Requirements for Pulsed Magnets at the HLD** Sergei Zherlitsyn, Thomas Herrmannsdoerfer and Joachim Wosnitza; Helmholtz-Zentrum Dresden-Rossendorf (HZDR), Germany

The Dresden High Magnetic Field Laboratory (HLD) is a pulsed-field user facility, which provides external and in-house researchers with the possibility to perform a broad range of experiments in pulsed magnetic fields [1]. The HLD develops, manufactures, and operates the non-destructive pulsed magnets for the field range up to 90 T and beyond. A design of the magnets requires high-strength, high-conductivity wires with selected cross-sections and high-strength reinforcement materials. Currently some test coils are fabricated at the HLD for a prototype triple-coil magnet for magnetic fields of about 100 T. We will discuss the choice of materials for this pulsed magnet, material-based limitations, long standing experience with available materials, and material challenges for generating even higher magnetic fields by the non-destructive pulsed magnets.

[1] <http://www.hzdr.de/hld>

#### **8:48 AM BREAK**

#### **8:52 AM \*F.SF01.02.06**

**Ultra-High Local Plasticity Induced by Room-Temperature Restoration in High-Strength Nanocomposite** Rongmei Niu and Ke Han; Florida State Univ, United States

We subject an aged Cu-24 wt%Ag ingot to heavily cold drawing to develop a nanocomposite. The as-drawn wire is composed of Cu-rich proeutectic components and Ag-rich eutectic components. A fine lamellar structure are developed in the proeutectic component embedded a high density of Ag fibers. The average lamellar spacing is  $20\pm 6$  nm. Ag fiber width is below 5nm. The eutectic component has a relative coarse structure with Ag grain size around 100 nm. This bimodal size distributed Ag fibers yield ultra-high bending plasticity—up to 59% bending strain at the outermost edge-- 15 times the tensile elongation of the wire (3.6%). During our bending tests, dynamic recovery and partial recrystallization occur primarily in the eutectic component, and are more frequently at the inner edge than the outer edge. The high bending strain causes some of the thick Ag fibers to become discontinuous and lose their original alignment. This structural evolution increases local plasticity, resulting in unexpectedly high achievable bending strain. This is unusual in nano-sized, Ag-fiber-reinforced high-strength composite.

#### **9:04 AM \*F.SF01.02.05**

**Properties of Copper-Silver Alloys Obtained by the Cold Spray Process** Christophe Verdy<sup>1</sup>, Olivier Jay<sup>2</sup> and Francois Debray<sup>2</sup>; <sup>1</sup>LERMPS, ICB, UMR 6303, CNRS, Univ. Bourgogne Franche-Comté, UTBM, France; <sup>2</sup>Univ. Grenoble Alpes, INSA Toulouse, Univ. Toulouse Paul Sabatier, EMFL, CNRS, LNCMI, France

The cold spray process was developed at the end of the 20th century and his principle is mainly based on the kinetic energy transmitted to micron size particles to allow their deposition. The particles remain solid and the deposits are generated by the particles impacting the substrate at high velocity. Working at low temperature, below the melting point of the deposited material, appears particularly interesting for deposition of oxygen sensitive materials like copper alloys. In comparison with conventional thermal spray processes, cold spray can retain the original properties of powder feedstock (grain size, nanostructured particles), prevent the adverse influence on the underlying substrate materials, and can produce very thick coatings due to compressive stresses.

To spray oxygen sensitive material like copper alloys, it is preferable to select an inert gas as propellant gas for cold spray deposition. Nitrogen is mainly used but, as the gas velocity is strongly linked to the gas mass, gases with low atomic weight like hydrogen or helium are particularly interesting to reach high velocities. Among those gases, helium is much better from

the human safety point of view but its price is very high due to limited amounts on earth. A closed loop avoiding costly helium losses was implemented. Thus, deposition efficiency of cold spray copper alloys higher than 96 %, porosity below 0.1 % and oxygen content below 150 ppm were obtained. High deposition rates up to 7 kg/h were also reached.

Copper silver alloys present attractive mechanical properties combined with high thermal conductivity suitable for many applications like high field magnets. In the present work, CrCrZr and CuAg with various Ag percentage deposits were manufactured by cold spray using helium as propellant gas. The work hardening mechanisms are involved by comparison with classically forged materials. A large tailoring of the material's properties can be obtained through specific heat treating. Residual stresses are very low after heat treating and allow machining helices without deformation. This process now allows to produce tubes for polyhelix magnets at LNCMI with a major performance gain.

**9:16 AM \*F.SF01.02.07**

**A Powder Metallurgy Route Involving Spark Plasma Sintering Towards High-Strength Wires for DC or Pulsed Resistive Magnets** Christophe Laurent<sup>1</sup>, Simon Tardieu<sup>1,2</sup>, David Mesguich<sup>1</sup>, Antoine Lonjon<sup>1</sup>, Nelson Ferreira<sup>2</sup>, Geoffroy Chevallier<sup>2</sup>, Arnaud Proietti<sup>1</sup>, Claude Estournes<sup>2</sup> and Florence Lecouturier<sup>2</sup>; <sup>1</sup>Université Toulouse 3 Paul Sabatier, France; <sup>2</sup>CNRS, France

There is a demand for stronger yet lighter conducting copper wires in high-technology domains of global interest where weight is at a premium, such as power and aerospace engineering as well as in niche applications, such as materials for high-field magnets.

Many proposed solutions involve the preparation of copper-matrix composite wires or copper-rich alloyed wires with ultrafine but complex microstructures. Wires are prepared by wire-drawing billets (cylinders). This is a severe plastic deformation method and may be followed by appropriate thermal treatments. There are many variants but the importance of the characteristics of the cylinder is not to be neglected. The usual routes for cylinder preparation involve melting-solidification at some point, and therefore a relatively high temperature, either for alloying or for the preparation of the pure copper sample to be used in a composite.

We have proposed an alternative method based on powder metallurgy routes, involving the consolidation of a suitable powder into a cylinder by sintering at a relatively low temperature. This is done by spark plasma sintering (SPS), which has several advantages over pressureless sintering and hot-pressing, including rapid heating and cooling rates. Therefore, lower sintering temperatures and shorter holding times make it possible to avoid grain growth and prepare copper cylinders with micrometer-sized grains, typically ten times lower than conventional copper cylinders.

SPS typically differs from hot-pressing by the application of a dc pulsed current to the pressing die and powder compact, while a uniaxial pressure is simultaneously applied. Interestingly, cylinders with only about 90% of their full density were found suitable for the rest of the study, because a too high density hampers the deformability of the cylinder during wire-drawing, resulting in sample breaking.

The basics of SPS will be presented and we will show several examples of the preparation of wires of pure copper, carbon nanotube - copper composites and silver nanowire - copper composites. The microstructure of the powders, cylinders (typically 8 mm in diameter and 33 mm long) and wires will be presented as well as the mechanical properties and electrical resistivity of the wires measured at 293 K and 77 K.

**9:28 AM \*F.SF01.02.09**

**Application of the Nanostructured Cu-Nb *In Situ* Microcomposites as Strengthening Elements in High Strength Cu-Matrix Composites** V. Pantsyrny<sup>1,2</sup>; <sup>1</sup>Nanoelectro LLC, Russian Federation; <sup>2</sup>Bochvar Institute of Inorganic Materials, Russian Federation

Advanced electrical and electronic devices sometimes require that conductor's material properties should be counteracting, e.g. high electrical conductivity and high mechanical strength. Traditional high strength Cu-matrix composites consists of Cu-based matrix, which contains a uniformly distributed nanoscaled particles of intermetallic compounds or oxides. The required microstructure is usually formed by the doping of the initial Cu matrix alloy by the combination of elements which would form the intermetallic compounds during the aging heat treatment at specific temperature range of 300-500 ° C (Cu-Zr-Nb; Cu-Ni-Si; Cu-Cr-Zr alloys) or to form fine oxides through the process of internal oxidation (Cu-Al alloys). These submicron particles of oxides and intermetallic compounds altogether with increase of ultimate strength lead to substantial decrease of fatigue properties. The paper describes the alternative approach to development of the advanced high strength Cu-matrix composites with the application of the plastic nanostructured Cu-Nb *in situ* microcomposites as a strengthening element. As an example the principally new design of composite Contact Wire for high speed railways has been proposed to attain at least 20% better combination of ultimate tensile strength (610-660 MPa) and high conductivity (more than 80% IACS). Composite conductor contains the bundles of nanostructured anomalously high strength Cu-Nb filamentary cores and outer layer made of low doped high conductivity Cu-Zr-Nb alloy with improved tribological properties. The microcomposite

Contact Wire has very high fatigue properties due to filamentary architecture of microstructure of Cu-Nb strengthening component. This Contact wire was designed for the use in the scope of Overhead Contact Line CS-400 for railways with the speeds of 400 km per hour. The results of laboratory complex tests of contact wire are presented.

SESSION F.SF01.13: Live Lightning/Flash Talks II: Materials for Extreme Conditions (MEC)  
Thursday Morning, December 3, 2020  
F.SF01

#### 9:40 AM F.SF01.02.11

**New High Strength Silver Nanowire-Copper Composite Conductors by Spark Plasma Sintering and Wire-Drawing for High Field Magnets** Simon Tardieu<sup>1,2</sup>, David Mesguich<sup>2</sup>, Antoine Lonjon<sup>2</sup>, Florence Lecouturier<sup>1</sup>, Nelson Ferreira<sup>1</sup>, Geoffroy Chevallier<sup>2,3</sup>, Arnaud Proietti<sup>4</sup>, Claude Estournès<sup>2,3</sup> and Christophe Laurent<sup>2</sup>; <sup>1</sup>LNCMI, France; <sup>2</sup>CIRIMAT, France; <sup>3</sup>Plateforme Nationale CNRS de Frittage Flash, France; <sup>4</sup>Centre de Microcaractérisation Raimond Castaing, France

LNCMI-Toulouse produces some of the most intense non-destructive pulsed magnetic fields in the world with a European record of 98.8 Tesla and aims at reaching more than 100 Tesla. The generation of pulsed magnetic fields higher than 60 T requires the use of coils wound of wires with exceptional properties. The wires need a high conductivity to limit the heating and they must have a high strength to be able to resist the Lorentz forces. The Lorentz forces are tangential to the coil and proportional to the square of the magnetic field. The resulting von Mises stress is 1 GPa at 60 T and higher than 2.2 GPa at 100 T.

Classical methods for strengthening copper wires involve the preparation of composite wires, such as copper-stainless steel (Cu-SS) and copper-niobium (Cu-Nb) or alloyed wires such as copper/silver (Cu/Ag). Cu-Nb and Cu/Ag wires present a nanostructured microstructure with fine and elongated grains. Cu-Nb microstructure is made up of pure Cu and pure Nb grains, while the Cu/Ag microstructure presents Cu-rich and Ag-rich solid solution. These wires exhibit a UTS value higher than 1 GPa but they are distinguished by their high resistivity. The aim of this work is the preparation of composite wires based on pure Cu and pure Ag.

LNCMI and CIRIMAT explore the design and preparation of novel Cu-based nanocomposite wires with the use of powder metallurgy, spark plasma sintering (SPS) and wire-drawing at room temperature. This preparation method is adapted to the preparation of Ag-Cu composite wires. Ag nanowires (200 nm in diameter and 30  $\mu\text{m}$  in length) were synthesized and mixed with a commercial micrometric (about 1  $\mu\text{m}$ ) Cu powder. Samples containing 1, 5 and 10 vol. % Ag were prepared. Cu and Ag-Cu cylinders (diameter 8 mm, length 33 mm) are prepared by SPS. Cylinders are sintered at 400, 500 or 600 °C. The so-obtained cylinders serve as precursors to wire-drawing. Their diameter is reduced by wire-drawing at room temperature, in several passes, thus producing progressively finer wires (diameter in the range 1 - 0.2 mm).

The wires show a lamellar microstructure with ultrafine Cu grains (200 - 700 nm for a 0.5 mm diameter wire) elongated over several micrometers. The Ag nanowires are dispersed along the grain boundaries of Cu. Cu and Ag grains exhibit major  $\langle 111 \rangle$  and minor  $\langle 100 \rangle$  orientations like most of wire-drawn face centered cubic metals.

The electrical resistivity and tensile strength were measured at 293 K and 77 K. The tensile strength for the composite wires is more than twice the value measured for the corresponding pure Cu wires. Interestingly, the wires containing only 1 vol.% Ag offer the best combination of high strength (1100 MPa at 77 K) and low electrical resistivity (0.50  $\mu\Omega\cdot\text{cm}$  at 77 K).

We have obtained wires with excellent mechanical properties while greatly reducing the electrical resistivity compared to Cu/Ag alloy. The present 1 vol. % Ag-Cu composite wires compare favorably with Cu/Ag alloy wires containing about 20 times more Ag.

#### 9:42 AM F.SF01.02.12

**Enhanced Properties of High-Strength Reinforcement Materials for High-Field Magnets** Ke Han, Rongmei Niu, Jun Lu and Vince Toplosky; Florida State University, United States

Nanostructured reinforcement materials, which have been successfully used in high field magnets and at cryogenic

temperatures, reach their most desirable strength level when their scale of microstructure is below 100 nanometers. This refined microstructure can be achieved by plastic deformation and heat treatment, which create obstacles, such as dislocations and precipitates, for dislocation motions. Both deformation and heat treatment also introduce microstructure and property anisotropy. Investigating both anisotropy and microstructure changes helps us to understand the plasticity of these materials, particularly at cryogenic temperatures. The goal of our research is to relate microstructural scale and anisotropy to the mechanical and physical properties of these materials. This presentation describes microstructure in different orientations, with emphasis on the impact of high anisotropy and fine microstructure on properties. This work was performed at the National High Magnetic Field Laboratory, which is supported by the National Science Foundation Cooperative Agreement No. DMR-1644779 and the State of Florida.

## 9:44 AM OPEN DISCUSSION

SESSION F.SF01.14: Live Keynote III: Materials for Extreme Conditions (MEC)  
Friday Afternoon, December 4, 2020  
F.SF01

### 4:00 PM \*F.SF01.03.02

#### **Giant Thermal Hall Conductivity from Phonons in the Pseudogap Phase of Cuprate Superconductors G.**

Grissonnanche<sup>1</sup>, A. Legros<sup>1,2</sup>, S. Thériault<sup>1</sup>, S. Badoux<sup>1</sup>, E. Lefrançois<sup>1</sup>, M.-E. Boulanger<sup>1</sup>, V. Zlatko<sup>1</sup>, M. Lizaire<sup>1</sup>, F. Laliberté<sup>1</sup>, A. Gourgout<sup>1</sup>, J.-S. Zhou<sup>3</sup>, S. Pyon<sup>4</sup>, T. Takayama<sup>4</sup>, H. Takagi<sup>4</sup>, S. Ono<sup>5</sup>, N. Doiron-Leyraud<sup>1</sup> and L. Taillefer<sup>1,6</sup>; <sup>1</sup>Université de Sherbrooke, Canada; <sup>2</sup>CEA Saclay, France; <sup>3</sup>The University of Texas at Austin, United States; <sup>4</sup>The University of Tokyo, Japan; <sup>5</sup>Central Research Institute of Electric Power Industry, Japan; <sup>6</sup>Canadian Institute for Advanced Research, Canada

The nature of the pseudogap phase of cuprates remains a major puzzle. Although there are indications that this phase breaks various symmetries, there is no consensus on its fundamental nature [1].

Fermi-surface, transport and thermodynamic signatures of the pseudogap phase are reminiscent of a transition into a phase with antiferromagnetic order, but evidence for an associated long-range magnetic order is still lacking. Here we report measurements of the thermal Hall conductivity  $\kappa_{xy}$  in the normal state of four different cuprates and show that a large negative  $\kappa_{xy}$  signal is a property of the pseudogap phase, appearing with the onset of that phase at the critical doping  $p^*$  [2]. It is also a property of the Mott insulator at  $p \approx 0$ , where  $\kappa_{xy}$  has the largest reported magnitude of any insulator. Since this negative  $\kappa_{xy}$  signal grows as the system becomes increasingly insulating electrically, it cannot be attributed to conventional mobile charge carriers. Nor is it due to magnons, since it exists in the absence of magnetic order.

In order to identify the heat carriers responsible for this negative  $\kappa_{xy}$ , we turn to transverse heat transport along the c-axis:  $\kappa_{zy}$ . Here we show that the thermal Hall conductivity at  $p = 0$  is roughly isotropic, being nearly the same for heat transport parallel and normal to the  $\text{CuO}_2$  planes, *i.e.*  $\kappa_{zy}(T) \approx \kappa_{xy}(T)$ . This shows that the negative thermal Hall response must come from phonons, these being the only heat carriers able to move as easily normal and parallel to the planes. At  $p > p^*$ , we observe no c-axis Hall signal, *i.e.*  $\kappa_{zy}(T) = 0$ , showing that phonons have zero Hall response outside the pseudogap phase. The microscopic mechanism by which phonons become chiral in cuprates remains to be identified. This intrinsic phonon Hall effect provides a new window on quantum materials and it may explain the thermal Hall signal observed in other topologically nontrivial insulators [4].

[1] Proust & Taillefer, *Annu. Rev. Condens. Matter Phys.* **10**, 409 (2019).

[2] Grissonnanche *et al.*, *Nature* **571**, 376 (2019).

[3] Grissonnanche *et al.*, *Nature Physics (to appear)*; arXiv:2003.00111 (2020).

[4] Kasahara *et al.*, *Nature* **559**, 227 (2018).

### 4:12 PM \*F.SF01.03.01

**Superconducting Superhydrides—Novel Materials and Possible Applications** Maddury S. Somayazulu; Argonne National Laboratory, United States

Since the prediction of metallization and superconductivity of hydrogen and hydrogen-rich materials at high pressures [1,2], there has been a sustained effort to make advances in high pressure sciences (theory, experiments and techniques) to realize this dream. In comparison to the much larger research landscape spawned by the discovery of high  $T_c$  cuprate



superconductors, the high pressure (and high temperature) superconductivity field has been slow to encapsulate the attention of many. Partly, this has to do with the paucity of experimental probes that can be broguth to bear and to a major extent, it is the question of transitioning discovery to application. Nevertheless, the discovery of superconductivity in H<sub>3</sub>S, YH<sub>6</sub> and LaH<sub>10</sub> /3,4,5/ and the phenomenal rise in transition temperatures has begged the question of revisiting these two questions. These discoveries have been aided by theoretical predictions and those can be used to make technological feasibility a likelihood /6-9/. However, there are experimental limitations that need to be surmounted to understand the physics and chemistry of these materials that constitute and important feedback to these simulations /10,11/. This talk will aim at connecting these dots and discus the rapidly evolving picture we have of these fascinating materials.

#### References:

1. Ashcroft, N. W., Metallic hydrogen: A high-temperature superconductor? Phys. Rev. Lett. (1968) **21**, 1748.
2. Ashcroft, N. W., Hydrogen Dominant Metallic Alloys: High Temperature Superconductors? Phys. Rev. Lett. (2004) **92**, 187002.
3. Drozdov, A. P., et. al, Conventional Superconductivity at 203 Kelvin at High Pressures in the Sulfur Hydride System. Nature, (2015) **525**, 7567
4. Kong, P., et. al, Superconductivity up to 243 K in yttrium hydrides under high pressure. (2019) arXiv:1909.10482
5. Somayazulu. M. S., et. al, Evidence for Superconductivity above 260 K in Lanthanum Superhydride at Megabar Pressures. Phys. Rev. Lett, (2019) **122**, 027001.
6. Y. Li, et. al, The Metallization and Superconductivity of Dense Hydrogen Sulfide, J. Chem. Phys. (2014) **140**, 174712.
7. Hanyu Liu et. al, Potential high-*T<sub>c</sub>* superconducting lanthanum and yttrium hydrides at high pressure, PNAS (2017), **114**, 6990.
8. Ying Sun et. al, Route to a Superconducting Phase above Room Temperature in Electron-Doped Hydride Compounds under High Pressure, Phys. Rev. Lett., (2019) **123**, 097001.
9. Jose A Flores-Livas et. al, A Perspective on Conventional High-Temperature Superconductors at High Pressure: Methods and Materials, (2019) arXiv:1905.06693
10. Shirin Mozaffari et. al, Superconducting phase diagram of H3S under high magnetic fields, Nat. Comm. (2019), 10. 2522. 10.1038/s41467-019-10552-y.
11. A. D. Grokowiak et. al, Hot Hydride Superconductivity above 550 K, (2020) arXiv:2006.03004

#### 4:24 PM \*F.SF01.04.01

**Plasma Facing Materials by Self Interstitial Solid Solution Strengthening** Muhammad Musaddique Ali Rafique; Eastern Engineering Solutions LLC, United States

Bubble – a precursor of undersense nanostructure or fuzz formation is crystal lattice defect and is approached by Frenkel pair formation mechanism. One needs to have crystal lattice that inhibits Frenkel Pair generation by ejection of W self-interstitial atom by He cluster and its bonding with vacancy. However, this mechanism is very commonly observed in nuclear materials. It is applicable in conventional nuclear materials where  $\alpha$  and  $\beta$  particles,  $\gamma$  rays and neutron flux strike the material. Plasma does not constitute of aforementioned and thus it is not very applicable mechanism. In the present study, author addresses this problem of development of plasma facing materials by primitive method of self-interstitial solid solution strengthening. Actual mechanism of bubble formation in studied and a suitable lattice is selected and proposed which inhibits possible Frenkel pair generation thus inherently promotes formation of plasma facing material.

#### 4:36 PM \*F.SF01.08.01

**Helium Compounds and Their Dynamical Properties Under Extreme Conditions** Jian Sun; Nanjing University, China

Helium is the most inert element in the periodic table and generally considered to be unreactive under ambient conditions. On the other hand, helium is one of the main components of giant icy planets' atmosphere. It is unclear whether the helium can diffuse into the depths and react with the mantle materials (water, ammonia and methane). In this talk, I will introduce some of our recent theoretical predictions on helium compounds, including helium-water, helium-ammonia, helium-methane and helium-alkali metal oxides/sulfides, etc [1-4], using our own machine learning accelerated crystal structure search method [5]. In addition, we also found that some of these compounds exhibit exotic dynamical properties at high pressure and high temperature, including the superionic, plastic states and their co-existence.

#### REFERENCE

Hao Gao, Cong Liu, Andreas Hermann, Richard J. Needs, Chris J. Pickard, Hui-Tian Wang, Dingyu Xing, and Jian Sun\*, "Coexistence of plastic and partially diffusive phases in a helium-methane compound", **Natl. Sci. Rev.** (2020). DOI: 10.1093/nsr/nwaa064

Cong Liu, Hao Gao, Andreas Hermann, Yong Wang, Maosheng Miao, Chris J. Pickard, Richard J. Needs, Hui-Tian Wang, Dingyu Xing, and **Jian Sun\***, “Plastic and Superionic Helium Ammonia Compounds under High Pressure and High Temperature”, **Phys. Rev. X** 10, 021007 (2020).

Cong Liu, Hao Gao, Yong Wang, Richard J. Needs, Chris J. Pickard, **Jian Sun\***, Hui-Tian Wang\*, Dingyu Xing, “Multiple superionic states in helium-water compounds”, **Nature Physics** 15, 1065 (2019).

Hao. Gao, **Jian Sun\***, Chris. J. Pickard, Richard. J. Needs, “Prediction of pressure-induced stabilization of noble-gas-atom compounds with alkali oxides and alkali sulfides”, **Phys. Rev. Mater.** 3, 015002 (2019).

Kang Xia, Hao Gao, Cong Liu, Jianan Yuan, **Jian Sun\***, Hui-Tian Wang\*, Dingyu Xing, “A novel superhard tungsten nitride predicted by machine-learning accelerated crystal structure search”, **Sci. Bull.** 63, 817 (2018).

#### 4:48 PM \*F.SF01.02.10

**Thermomechanical Stability of Metallic Interfaces Containing 3D Character** **Nathan Mara**<sup>1</sup>, Justin Y. Cheng<sup>1</sup>, Shuozhi Xu<sup>2</sup>, Youxing Chen<sup>3</sup>, Jonathan Poplawsky<sup>4</sup>, Nan Li<sup>5</sup>, Kevin Baldwin<sup>5</sup> and Irene Beyerlein<sup>2</sup>; <sup>1</sup>University of Minnesota, United States; <sup>2</sup>University of California, Santa Barbara, United States; <sup>3</sup>University of North Carolina at Charlotte, United States; <sup>4</sup>Oak Ridge National Laboratory, United States; <sup>5</sup>Los Alamos National Laboratory, United States

2-dimensional (2-D) sharp interfaces with distinct boundaries demarcating an abrupt discontinuity in material properties in nanolayered composites have been studied for almost twenty years and are responsible for enhanced behaviors such as strength, radiation damage tolerance, and deformability. However, 2-D interfaces have their limitations with respect to deformability and toughness. 3-D interfaces are defined as heterophase interfaces that extend out of plane into the two crystals on either side and are chemically, crystallographically, and/or topologically divergent, in three dimensions, from both crystals they join. Here, we focus on the thermal stability and mechanical behavior of nanolayered Cu/Nb containing interfaces with 3-D character. By co-sputtering the bimaterial interfaces between the constituent pure phases, the resulting compositional gradient gives rise to new interphase boundary structures, which have been analyzed and quantified via S/TEM and Atom Probe Tomography. Micropillar compression results show that the strength of Cu/Nb nanocomposites containing 3-D interfaces is significantly greater than those containing 2-D interfaces. Mechanical anisotropy, as well as shear banding is observed during pillar compression with retention of continuous layers across the shear band. We will present our recent results on deformation of such 3-D interfaces and structures, and describe their structural evolution mechanistically through the use of atomistic simulations.

#### 5:00 PM BREAK

SESSION F.SF01.15: Live Lightning/Flash Talks III: Materials for Extreme Conditions (MEC)  
Friday Afternoon, December 4, 2020  
F.SF01

#### 5:05 PM F.SF01.03.03

**Self-Regulation of Current Sharing in High-Temperature Superconducting Cables by Temperature-Dependent Resistivity Switching in Vanadium Oxide Coatings** **Sachin V. Muley**<sup>1,2</sup>, Aurora Cecilia Araujo Martinez<sup>1,3</sup>, Zhenuai Yang<sup>1,4</sup>, Xiaorong Wang<sup>1</sup>, Qing Ji<sup>1</sup> and Andre Anders<sup>1,5,6</sup>; <sup>1</sup>Lawrence Berkeley National Laboratory, United States; <sup>2</sup>University of Wisconsin–Madison, United States; <sup>3</sup>University of Guanajuato, Mexico; <sup>4</sup>Harbin Institute of Technology, China; <sup>5</sup>Leibniz Institute of Surface Engineering, Germany; <sup>6</sup>Universität Leipzig, Germany

The high-temperature superconductors (HTS), e.g., RE-Ba<sub>2</sub>Cu<sub>3</sub>O<sub>x</sub> (RE = rare earth) can sustain significant transport current at high background magnetic field and elevated temperatures, enabling various applications including fusion energy generation, next generation high-energy physics particle accelerators, and medical accelerators for carbon therapy. However, reliable protection against catastrophic superconducting-to-normal transitions (quenches) remains to be addressed for successful applications of HTS magnet technology. To address this issue, we investigated the potential of vanadium oxide (VO<sub>x</sub>) coatings as a temperature-dependent switching medium to self-regulate current sharing. VO<sub>x</sub> coatings (1.70 ≤ x ≤ 2.07) were deposited by reactive cathodic arc deposition on insulating glass and commercial REBCO tapes to study their electrical properties. The process gas was monitored *in situ* by a residual gas analyzer. Effects of varying process parameters such as argon-to-oxygen ratio and substrate manipulator speed on coating properties were studied. The coatings were X-ray amorphous but Raman spectrometry showed short-range crystalline ordering. Hall effect measurements found a decrease in resistivity of VO<sub>x</sub> by at least three orders of magnitude when the temperature increased from 80 to 300 K. The coating

process did not damage the REBCO tapes as evidenced by a negligible change in critical current after versus before coating. The results from current-sharing experiments and circuit analysis suggest that the VO<sub>x</sub> coating can effectively self-regulate current sharing in REBCO magnets and enable self-protection during quenches. This work was supported by the Office of Science, Office of Fusion Energy Sciences, U.S. Department of Energy under Contract No. DE-AC02-05CH11231 and the Laboratory Directed Research and Development (LDRD) funding from the Lawrence Berkeley National Laboratory provided by the Director. Work at the Molecular Foundry was supported by the Office of Science, Office of Basic Energy Sciences, of the U.S. Department of Energy under Contract No. DE-AC02-05CH11231.

#### 5:07 PM F.SF01.04.03

**Swift Heavy Ion Irradiation Effects in Pre-Damaged Gallium Nitride** Kristina Tomić Luketić<sup>1</sup>, René Heller<sup>2</sup>, Shavkat Akhmadaliev<sup>2</sup>, Henning Lebius<sup>3</sup>, Abdenacer Benyagoub<sup>3</sup>, Isabelle Monnet<sup>3</sup>, Corneliu Ghica<sup>4</sup>, Ferdinand Scholz<sup>5</sup>, Oliver Rettig<sup>5</sup>, Branko Šantić<sup>1</sup>, Stjepko Fazinić<sup>1</sup> and Marko Karlušić<sup>1</sup>; <sup>1</sup>Ruder Boskovic Institute, Croatia; <sup>2</sup>Helmholtz-Zentrum Dresden-Rossendorf, Germany; <sup>3</sup>Normandie Univ, ENSICAEN, UNICAEN, CEA, CNRS, CIMAP, France; <sup>4</sup>National Institute of Materials Physics, Romania; <sup>5</sup>Institute of Functional Nanosystems, Germany

\*Corresponding author: marko.karlusic@irb.hr

When a beam of swift heavy ions (SHI) impinges onto a material, the formation of defects called ion tracks is possible as a result, either in the bulk or on the surface of the material. As a consequence, effects produced by means of SHI irradiation that lead to structural changes of the material can be used to modify the properties of the material via defects engineering. SHI damage introduction to materials can result in complex behavior, especially in radiation harsh environments. To assess the final damage of the material, the effect of the energy deposition from the ions to the atoms within the material must be taken under consideration. Deposition of energy occurs through two main channels: either to the electronic subsystem of the material (electronic stopping power) or to the nuclei (nuclear stopping power). Here we investigate the influence of ion beams with different stopping powers, used in a sequence, on defects formation. It is known that sequential irradiation of ion beams can lead to the SHIBIEC effect (Swift Heavy Ion Beam Induced Epitaxial Crystallization) i.e. the annealing of defects that occurs during the second irradiation step. Alternatively, the anti-SHIBIEC effect is also possible, i.e. the enhanced defect formation during the second step of irradiation.

Sequential ion irradiation of GaN has not been investigated so far. This material is an important semiconductor for high-power electronics. The results presented here are of importance for basic research in this field as well. In our previous work [1], we found no evidence of ion track formation in the bulk after SHI irradiation using 23 MeV I and 90 MeV Xe beams. However, recently we were able to introduce additional disorder into moderately damaged GaN crystals using the same 23 MeV I and 90 MeV Xe beams, in cases where GaN samples have been pre-irradiated with 2 MeV Au or with 900 MeV Xe ion beams. Two different ion beams are expected to introduce damage into GaN either by nuclear or electronic stopping, respectively [2,3]. We observe the difference in total damage in the material depending on the fluence of the beams applied. In this contribution, we report new results of sequential ion irradiation of GaN based on RBS/c (Rutherford Backscattering Spectroscopy in Channeling) and TEM (Transmission Electron Microscopy) measurements.

[1] M. Karlušić et al., Response of GaN to energetic ion irradiation - conditions for ion track formation, J. Phys. D: Appl. Phys. 48 (2015) 325304

[2] S.O. Kucheyev et al., Ion implantation into GaN, Mat. Sci. Eng. 33 (2001) 51

[3] M. Sall et al., Track formation in III-N semiconductors irradiated by swift heavy ions and fullerene and re-evaluation of the inelastic thermal spike model, J. Mater. Sci. (2015) 50:5214–5227

#### 5:09 PM F.SF01.04.06

**Plasma-Assisted Atomic Layer Annealing as a Low-Temperature Technique Enabling Crystalline Growth of  $\beta$ -Ga<sub>2</sub>O<sub>3</sub> Films for Wearable/Flexible Electronics** Saidjafarzoda Ilhom<sup>1</sup>, Adnan Mohammad<sup>1</sup>, Deepa R. Shukla<sup>1</sup>, John Grasso<sup>1</sup>, Brian Willis<sup>1</sup>, Ali Okyay<sup>2</sup> and Necmi Biyikli<sup>1</sup>; <sup>1</sup>The University of Connecticut, United States; <sup>2</sup>Stanford University, United States

The rapid evolution in technology and its integration with humans requires the development of novel processes that enable the incorporation of the crucial electronic materials, such as the wide bandgap semiconductors (Ga<sub>2</sub>O<sub>3</sub> and GaN) into the wearable electronic systems. Wide bandgap semiconductors form the building blocks of the current high-power high-frequency electronics and the upcoming mmWave fifth-generation (5G) device technologies. To make such technologies integrable with wearable/flexible systems, it is critical that high quality and in particular as-grown crystalline thin films of these materials can be produced on highly temperature-sensitive substrates at very low temperatures.

In this work, we report on the low-temperature, as-grown crystalline Ga<sub>2</sub>O<sub>3</sub> films on various substrates (Si, sapphire, glass,

and Kapton) via a hollow-cathode plasma-ALD system. Triethylgallium (TEG) and Ar/O<sub>2</sub> plasma were employed as metal precursor and oxygen co-reactant, respectively. Growth experiments have been performed at 160 – 240 °C substrate temperature and 30 – 200 W rf-power range. Additionally, each unit AB-type ALD-cycle was followed by an in situ Ar-plasma annealing treatment, which consisted of Ar-plasma exposure for 20 seconds scanned over 50 – 300 W rf-power. Both in situ and ex situ ellipsometry were employed to measure the thickness and optical properties of the films. The thickness of the films without Ar-annealing stage, ranged between 20.74 – 39.30 nm and as-grown refractive indices were between 1.75 – 1.67 within the scanned plasma power range. X-ray diffraction (XRD) showed that Ga<sub>2</sub>O<sub>3</sub> films grown without in situ plasma annealing exhibited amorphous structure irrespective of both substrate temperature and rf-power. However, with the in situ Ar-annealing phase incorporated, the thickness of the films ranged between 22.9 – 31.4 nm with refractive indices of 1.75 – 1.79. The increased refractive index (1.79) and reduced thickness gain (31.4 nm) at 250 W Ar-annealing power indicates possible densification and crystallization of the films. Indeed, XRD and XRR confirmed that in situ Ar-plasma treated films grow in a monoclinic β-Ga<sub>2</sub>O<sub>3</sub> crystal phase with further improving crystallinity and film density (from 5.07 to 5.80 g/cm<sup>3</sup>) with increasing Ar-annealing plasma power. Additionally, we will discuss the impact of varying in situ Ar-annealing plasma chemistries (Ar-only, O<sub>2</sub>-only, and Ar/O<sub>2</sub>) coupled with x-ray photoelectron spectroscopy (XPS) measurements, which will provide additional insight into the elemental composition of the films that might help to understand the changes in the structural, optical, and electrical properties. A future outlook will be provided to overcome the challenges to achieve device quality layers on temperature-sensitive flexible substrates.

#### 5:11 PM F.SF01.04.05

**Late News: Novel Defect-Fluorite Pyrochlore Sodium Niobate Nanoparticles—Solution-Phase Synthesis and Analysis of Neutron Tolerance** Rana Faryad Ali and Byron Gates; Simon Fraser University, Canada

Materials possessing a defect-fluorite pyrochlore structure can have a range of useful properties that are sought after, which include radiation tolerance, nuclear waste immobilization, and phase stability at elevated temperatures. In this study, we demonstrate for the first time the synthesis and a detailed analysis of defect-fluorite pyrochlore sodium niobate (NaNbO<sub>3</sub>) nanoparticles. This analysis included an investigation into the stability of these nanoparticles at elevated temperatures, as well as to neutron irradiation. A surfactant-assisted solvothermal method was used to prepare nanoparticles of NaNbO<sub>3</sub>. This solution-phase approach results in the formation of crystalline nanoparticles of a defect-fluorite pyrochlore NaNbO<sub>3</sub> at relatively low temperatures. The products had an average diameter of ~74 ± 11 nm. The nanoparticles adopted a defect-fluorite pyrochlore phase and matched the cubic space group. This pyrochlore form of NaNbO<sub>3</sub> was stable up to at least 500 °C. The nanoparticles transformed into the cubic and rhombohedral perovskite phases of NaNbO<sub>3</sub>, along with the introduction of a pseudo-hexagonal Nb<sub>2</sub>O<sub>5</sub> at higher temperatures. These defect-fluorite pyrochlore nanoparticles of NaNbO<sub>3</sub> also exhibited a resistance to radiation induced amorphization. The dimensions, phase, and crystallinity of the defect-fluorite pyrochlore nanoparticles after exposure to a flux of neutrons were comparable to the as-synthesized product. The thermal stability and radiation tolerance of these pyrochlore nanoparticles could be useful in the design of thermally resilient materials, high temperature catalysts, and durable materials for the handling and storage of radioactive waste.

#### 5:13 PM F.SF01.05.03

**Molecular Layer Deposition Approach for Synthesis of SiAlCO Polymer Derived Ceramic (PDC) Thin Films** Kristina Ashurbekova<sup>1</sup>, Karina Ashurbekova<sup>2</sup>, Iva Saric<sup>3</sup>, Evgenii Modin<sup>2</sup>, Mladen Petradić<sup>3</sup>, Aziz Abdulgatov<sup>1</sup>, Mato Knez<sup>2,4</sup> and Ilmutdin Abdulgatov<sup>1</sup>; <sup>1</sup>Dagestan State University, Russian Federation; <sup>2</sup>CIC nanoGUNE, Spain; <sup>3</sup>University of Rijeka, Croatia; <sup>4</sup>IKERBASQUE, Basque Foundation for Science, Spain

Organosilicon polymer derived ceramic (PDC) materials and its derivatives have gained interest as an emerging class of materials capable of providing mechanical stability and heat dissipation upon operation in extreme environments. PDC's found various applications such as electrode material for Li-ion batteries, ultra-high temperature composites and others [1]. Being X-ray amorphous, PDC's consist of nanodomains of different structures and compositions, demonstrating nanoscale heterogeneity that influence their unique mechanical, chemical and functional properties. Conventionally, PDC coatings are prepared by wet-chemical dipping, spinning thermal-spraying or by plasma-assisted chemical vapor deposition (CVD), followed by high temperature pyrolysis [2].

In this work, molecular layer deposited (MLD) hybrid organic-inorganic films serve as precursors for the synthesis of SiAlCO PDC composite coatings. Alumina-polysiloxane films were grown using sequential surface reactions between 1,3,5,7-tetravinyl-1,3,5,7-tetramethylcyclotetrasiloxane (V<sub>4</sub>D<sub>4</sub>) and trimethylaluminum (TMA). The deposition was conducted at temperatures between 120 and 220 °C. *In-situ* quartz crystal microbalance (QCM) monitoring showed linear mass increase with the number of MLD cycles with the highest mass gain rate of 24 ng/cm<sup>2</sup>/cycle at 180 °C. The QCM study revealed a self-limiting surface chemistry. An infrared analysis (FTIR) of the deposited films showed vibrational features characteristic of organosilicon polymers: Si-CH<sub>3</sub>, Si-O-Si, Si-CH=CH<sub>2</sub> and Si-O-Al peaks. High-resolution transmission

electron microscopy (HRTEM) imaging confirmed the conformal nature of the deposited MLD film.

In order to increase mass yield during the polymer-to-ceramic transformation, cross-linking of the growing polymer chains is needed. Cross-linking was achieved at 200°C by introducing a third precursor, di-tert-butyl peroxide (TBPO), into the MLD cycle, following a  $V_4D_4$ /TBP/TMA sequence. A positive mass gain after TBPO dosing, observed by QCM, indicates the formation of radicals and cross-linking. The cross-linking occurs through the activation of the vinyl groups. Characteristic signals, related to the generated polyethylene chains, were identified by ATR-FTIR and XPS. The formed Si-C-C-Si units are expected to improve the mechanical and thermal properties of the cross-linked SiAlCO PDCs, since the Si-C and C-C bonds are not affected by thermal depolymerization reactions.

X-ray and optical characterization techniques were employed to analyze the structural changes and composition of the films after pyrolysis. After pyrolysis at 900°C in an Ar atmosphere, the composite thin film remained amorphous. The resulting film contained uniformly distributed Si, Al, O, and C. Raman spectroscopy showed presence of graphitic carbon within the film. This MLD-derived SiAlCO thin film is expected to have exceptional uniformity, high temperature stability, creep, and corrosion resistance.

[1] P. Colombo, et al., *J. Am. Ceram. Soc.*, 93 (7), 1805–1837 (2010)

[2] G. Borroso, et al, *J. Mater. Chem. A.*, 7 (5), 1936–1963 (2019)

#### 5:15 PM F.SF01.05.04

**Late News: Size-Controlled Formation and Functionalization of Superparamagnetic Magnetite Nanoparticles with Enhanced Colloidal Stability at Extreme High Salinity Condition** Wei Wang, Hooisweng Ow, Sehoon Chang and Bora Yoon; Aramco Services Company: Aramco Research Center-Boston, United States

Magnetic nanoparticles (MNPs) have attracted significant attention in the oil industry in the past decade due to their potential applications including reservoir sensing and mapping, enhanced oil recovery, drilling and completion improvement, oil-water separation in produced water, oil spill clean-up, and directional transport and local heating. For these specific applications, the dispersity and stability of the MNPs in suspension are of great importance. Surface coating and specific functionalization of the MNPs are typically used to improve their stability and to reduce aggregation for the successful use of the nanoparticles. However, many of the well-established methods and procedures of surface coating chemistry for lab applications are not suitable for harsh environmental conditions such as at extreme high salinity for industrial oil applications. In this research, we synthesized magnetite MNPs with tuned particle sizes to optimize their superparamagnetic properties, and developed a new procedure for surface functionalization to enhance their colloidal stability at high salinity. The functionalized magnetite MNPs have been characterized by XRD, HR-TEM, cryo-TEM, dynamic light scattering and zeta potentials. Colloidal stabilities have been studied in a wide pH range and salinity with 5000-230000 ppm of TDS (Total Dissolved Solids). The results have demonstrated that the covalently bonded zwitterionic functional groups and cross-linked saccharide highly enhance the colloidal stability in high salinity brines.

#### 5:17 PM F.SF01.06.01

**Strain-Coupled Electronic Polarization in Semiconducting Oxides Under Extreme Electric Field** Yen-Ting Chi<sup>1</sup>, Mostafa Youssef<sup>2,1</sup>, Bilge Yildiz<sup>1</sup> and Krystyn Van Vliet<sup>1</sup>; <sup>1</sup>Massachusetts Institute of Technology, United States; <sup>2</sup>The American University in Cairo, Egypt

The polarization response of ionic and electronic defects in complex oxides under high electric field is critical for applications such as memristors and ferroelectrics, but historically challenging to model or measure. Here we developed a localized Hubbard U approach that resolves the dilemma of maintaining in-gap localized defect states for an oxygen vacancy while simultaneously retaining non-linear dielectric behavior of perovskite oxides. With this approach, we obtained accurate dielectric constant and electronic configuration for SrTiO<sub>3</sub> under electric field, using density functional theory and Berry phase calculations. We identified a direct relationship between oxygen vacancy polarizability and lattice strain, which can be generalized to other materials with similar crystal structure. For example, a neutral oxygen vacancy in BaTiO<sub>3</sub> and in SrTiO<sub>3</sub> strained to exhibit the same lattice constants showed identical polarization behavior under the same electric field. To trace the site polarizability difference between defected crystals and their defect-free counterparts, we utilized maximally localized Wannier functions to obtain the site-decomposed polarization. These simulations illustrated that not only the vacant site, but also the neighboring ions around the vacancy have significant influence on the system polarization with field applied either parallel or perpendicular to the Ti – V<sub>O</sub><sup>x</sup> – Ti chain. Together, this model and identification of driving factors in defect displacement under electric field contribute generalizable approaches to study and optimize materials in memristors, ferroelectrics, electrocaloric refrigeration and flash sintering.

#### 5:19 PM F.SF01.07.01

**High-Temperature and Abrasion Resistant Selective Solar Absorber** Yanpei Tian, Xiaojie Liu and Yi Zheng; Northeastern University, United States

Selective solar absorbers with high performance are the key to concentrated solar power systems. Optical metamaterials are emerging as a promising strategy to enhance selective photon absorption, however, the high-temperature resistance (500 C) remains as one of the main challenges for practical applications. Here, a multilayered metamaterial system ( $\text{Al}_2\text{O}_3/\text{W}/\text{SiO}_2/\text{W}$ ) based on metal-insulator-metal resonance effect has been demonstrated with high solar absorptance over 92%, low thermal emittance loss below 6%, and significant high-temperature resistance: it has been proved that the optical performance remains 94% after 1-hour thermal annealing under ambient environment up to 500 C, and 94% after 96-hour thermal cycle test at 400 C. Outdoor tests demonstrate that a peak temperature rise (193.5 C) can be achieved with unconcentrated solar irradiance and surface abrasion resistance test yields that SSAs have a robust resistance to abrasion attack for engineering applications.

**5:21 PM F.SF01.07.02**

**Deformation Mechanisms of Alumina-Forming Austenitic Stainless Steels for High Temperature Applications** Andrew Peterson; Dartmouth College, United States

Alumina-forming austenitic stainless steels (AFAs) are a class of alloys that are showing promise for use in high temperature applications, particularly for use in power generation. AFAs have been shown to demonstrate good high temperature strength, great oxidation resistance due to a protective alumina scale, and are cheaper than nickel-base alloys. While showing great promise, these alloys need to continue to be studied and improved to be practical for use. In particular, the deformation behavior of these alloys is not well understood. The austenitic matrix can contain various precipitates, including:  $\text{L}_{12}$  structured precipitates, B2 precipitates, Laves precipitates, carbides, and others. The grain boundary (GB) also can become covered by Laves and/or B2 precipitates. In a complex alloy with different types and sizes of precipitates, it can be difficult to determine what effect each of these precipitates are having on the high temperature strength.

In this work, we studied the deformation mechanisms in the model AFA alloy Fe-20Cr-30Ni-2Nb-5Al (at%). This alloy displays many characteristics of AFA alloys, and thus is a good alloy for scientific studies. This alloy contains  $\text{L}_{12}$ , Laves, and B2 precipitates in the matrix as well as Laves and B2 precipitates on the GBs. Creep tests, high temperature tensile tests, and high temperature strain-rate jump tests were performed on this alloy after various heat treatments to determine the deformation mechanisms – including strain-rate jump tests with and without  $\text{L}_{12}$  precipitates (but otherwise similar microstructures) to determine the effect of these precipitates on the high temperature strength. In addition, tests were performed on alloys with different grain size, but otherwise similar microstructure, to determine the effect of GB precipitation. Analysis of the stress – strain rate relationships was used to predict deformation mechanisms and to fit the experimental data to models. In addition, transmission electron microscopy (TEM) and scanning electron microscopy (SEM) were performed on samples after mechanical testing to determine deformation behavior. In-situ straining experiments in the TEM and SEM were also performed. This study found that nano-sized  $\text{L}_{12}$  precipitates provided the majority of the strengthening in this alloy. At low stresses dislocations by-passed these particles by climb, and at high stresses dislocations started to form Orowan loops around the particles. While dislocations piled up at larger Laves and B2 precipitates, these precipitates were not as effective at strengthening the alloy. In addition, work was performed to determine if there was a GB strengthening effect due to coverage of the GB by precipitates.

#### **Acknowledgements**

This research was supported by National Science Foundation (NSF) Grant DMR 1708091.

**5:23 PM F.SF01.07.03**

**$\text{Zn}_x\text{Fe}_{3-x}\text{O}_4$  Nanoparticles—Structural and Magnetic Behaviour Evolution After Thermal Treatment up to 1400 °C** Angelika Kmita<sup>1</sup>, Jan Zukrowski<sup>1</sup>, Juliusz Kuciakowski<sup>1,2</sup>, Marianna Marciszko-Wiackowska<sup>1</sup>, Antoni Zywczyk<sup>1</sup>, Dorota Lachowicz<sup>1</sup>, Marta Gajewska<sup>1</sup> and Marcin Sikora<sup>1</sup>; <sup>1</sup>AGH University of Science and Technology, Academic Centre for Materials and Nanotechnology, Poland; <sup>2</sup>AGH University of Science and Technology, Faculty of Physics and Applied Computer Science, Poland

Zinc ferrite nanoparticles are currently of much interest for their potential applications in extreme conditions like high temperature: e.g. in metal casting, in water splitting reaction for  $\text{H}_2$  production (solar fuels) or as high - temperature desulfurizing sorbents [1-3]. Bulk  $\text{ZnFe}_2\text{O}_4$  (ZF) should have paramagnetic nature around room temperature, when it is the normal spinel with  $\text{Zn}^{2+}$  incorporated mostly in the tetrahedral lattice sites. In the case of nanoparticles, the situation is more complex due to high probability of inversion in the cation distribution between octahedral and tetrahedral sites, which may lead to ferrimagnetism or superparamagnetism [4-6]. It was suggested that during heating  $\text{Zn}^{2+}$  ions can move from

tetrahedral site to octahedral site whereas  $\text{Fe}^{3+}$  ions redistribute within the octahedral and tetrahedral sites in order to reduce the strain [7]. It was also speculated the possibility of reduction of  $\text{Fe}^{3+}$  to  $\text{Fe}^{2+}$  during high temperature treatment. In order to verify these hypotheses we have performed a comprehensive study of structural and magnetic properties of stoichiometric and non-stoichiometric zinc ferrite  $\text{Zn}_x\text{Fe}_{3-x}\text{O}_4$  (NZF) nanoparticles synthesized using co-precipitation and thermal decomposition method [2, 8] as well as their evolution after thermal treatment. Nanoparticles with different zinc to iron ratio were obtained and systematically probed with volume (XRD, VSM, TG/DSC), microscopic (TEM) and element sensitive probes (ICP-OES, Mossbauer spectroscopy, XPS, XAFS). Magnetic studies proved paramagnetic response of stoichiometric ZF nanoparticles, while a superparamagnetic behaviour is observed in strongly non-stoichiometric (as synthesized) nanoparticles. After thermal treatment at 1400 °C in inert atmosphere, significant changes in the saturation magnetization were observed in the case of NZF. This is related with an increase of the amount of formally  $\text{Fe}^{2+}$  ions. The estimated saturation magnetization of as synthesized NZF nanoparticles, of approx. 50 emu/g, is increased upon thermal treatment (at 1400 °C in inert atmosphere) up to approx. 130 emu/g. As such we have confirmed that zinc concentration and method of synthesis plays important role in magnetic properties of non-stoichiometric zinc ferrite nanoparticles. Moreover, the reduction of  $\text{Fe}^{3+}$  to  $\text{Fe}^{2+}$  during high temperature treatment has been observed in NZF nanoparticles annealed in inert atmosphere.

**Acknowledgements:** This work was supported by the National Science Centre, Poland, Grant No: 2016/23/D/ST8/00013.

#### References

1. H. Kaneko, T. Kodama, N. Gokon, et al., *Solar Energy.*, Vol. 76, p.317 (2004)
2. A. Kmita, D. Lachowicz, J. Zukrowski, et al., *Materials.*, Vol. 12, p.1048 (2019)
3. A. Kmita, A. Pribulova, M. Holtzer et al. *Archives of Metallurgy and Materials.*, Vol. 61, p.2141 (2016)
4. W. Szczerba, J. Zukrowski, M. Przybylski, et al., *Physical Chemistry Chemical Physics.*, Vol. 18, p.25221 (2018)
5. S. J. Stewart, I.A. Al-Omari, F.R. Sives, et al. *Journal of Alloys and Compounds.*, Vol. 495, p.506 (2010)
6. G. Muscas, N. Yaacoub, G. Concas, et al., *Nanoscale.*, Vol.7, 13576-13585 (2015)
7. J. Philip, G. Gnanaprakash, G. Panneerselvam, et al., *Journal of Applied Physics.*, Vol. 102, 054305 (2007)
8. D. Lachowicz, R. Wirecka, W. Gorka-Kumik, et al., *Physical Chemistry Chemical Physics.*, Vol. 21, 23473 (2019)

#### 5:25 PM F.SF01.07.04

**The Influence of Lattice Defects and Recombination on Thermal Transport in Single Crystal Actinide Oxides** Cody A. Dennett and David H. Hurley; Idaho National Laboratory, United States

Actinide and lanthanide fluorite oxides,  $\text{UO}_2$ ,  $\text{CeO}_2$ ,  $\text{ThO}_2$ , form an important class of ceramic energy materials with applications ranging from nuclear fuels to solid oxide fuel cells. Of these systems,  $\text{ThO}_2$  (thoria), has been the least explored and offers unique features including an extremely high melting temperature and a fixed tetravalent oxidation state. Many potential application environments for thoria include high radiation fields or temperatures which either promote or directly generate lattice defects. Such defects drastically influence thermal transport, a controlling safety and performance property in many applications. To date, little experimentally-validated understanding has been generated on the role of defect formation and clustering on thermal transport in thoria due to the lack of high-quality starting material in which these effects may be explored. In this work, high-quality oriented single crystals of thoria are grown using hydrothermal synthesis and then exposed to proton irradiation at both room temperature and 600C. The thermal conductivity of the defected surface layer in these crystals is measured using an all-optical spatial domain thermoreflectance (SDTR) technique and sub-electron-microscopy-resolution defects are characterized using Raman spectroscopy. Together, these methods provide important initial insight into the types of defects formed under ionizing radiation, defect clustering, and how these defects impact thermal transport in high-quality thoria.

#### 5:27 PM F.SF01.08.07

**Tailoring Nanopomposites with Enhanced Failure Tolerance by Interface Engineering** Daniel Kiener<sup>1</sup>, Michael Wurmshuber<sup>1</sup>, Inas Issa<sup>1</sup>, Michael Burtscher<sup>1</sup>, Mingyue Zhao<sup>1</sup> and Christoph Gammer<sup>2</sup>; <sup>1</sup>Montanuniversität Leoben, Austria; <sup>2</sup>Erich Schmid Institute of Materials Science, Austrian Academy of Sciences, Austria

Designing ever stronger nanostructured materials that can even withstand harsh environments has become a major goal in the last decades. However, the increase in strength commonly comes hand in hand with a severe reduction in ductility, which at the same time also limits the toughness of these materials. Due to the high fraction of interfaces in such nanostructured materials, it is safe to assume that the processes limiting ductility and toughness as well as their response to harsh environments are controlled by the respective interface structures. However, a detailed understanding is at this point still lacking.

Bulk nanostructured materials were synthesized by severe plastic deformation and subject to tailored interface modifications. To investigate the structural properties of these nanomaterials at high stress and strain, we utilize quantitative miniaturized

deformation and fracture experiments performed in situ in scanning or transmission electron microscopes. These highly resolved techniques not only allow to measure material performance, but also to directly identify the underlying deformation and failure mechanisms at the same time.

Using this experimental approach, we will first address the nanoscale processes taking place during deformation and fracture of bcc nanocrystalline metals with modified interfaces. Building on this, the discussion will be extended to the behavior of nanocomposite structures and the influence of an irradiative environment.

#### 5:29 PM F.SF01.08.02

**Crystal Chemical Design of Novel High Energy Density Polynitrides** Maxim Bykov<sup>1,2</sup>, Elena Bykova<sup>2</sup>, Mohammad Mahmood<sup>1</sup>, Leonid Dubrovinsky<sup>3</sup> and Alexander F. Goncharov<sup>2</sup>; <sup>1</sup>Howard University, United States; <sup>2</sup>Carnegie Institution for Science, United States; <sup>3</sup>University of Bayreuth, Germany

The high-pressure chemistry of nitrogen and nitrogen-rich compounds have been in a focus of many studies in the recent years due to both fundamental and practical interest and due to the improvement of high-pressure synthetic and characterization techniques. Poly-nitrogen compounds are usually considered as potential high energy density materials (HEDM) due to the remarkable difference in the average bond energy between the single N–N bond, the double N=N bond, and the triple N≡N bond. Numerous polynitrogen compounds with various nitrogen polymeric networks were theoretically predicted, but there are only a very few experimental attempts to obtain such compounds.

In the present work we have systematically studied reactions between transition metals and nitrogen at pressures up to 130 GPa in laser-heated diamond anvil cells. Despite very high synthesis pressure Hf, W, Re and Os react with nitrogen forming porous metal-inorganic frameworks Hf<sub>4</sub>N<sub>22</sub>, WN<sub>10</sub>, ReN<sub>10</sub> and Os<sub>5</sub>N<sub>34</sub> of various topologies. The frameworks are built of metals interconnected via polymeric nitrogen linkers, while the pores are filled with dinitrogen molecules N<sub>2</sub>. Lighter transition metals (Fe) form non-porous polynitrides featuring polymeric nitrogen chains, while alkali metals react with nitrogen at extreme conditions with the formation of pentazolate salts. In this contribution we will discuss novel synthetic routes to energetic polynitrogen compounds and crystal-chemical rules governing their formation.

#### 5:31 PM F.SF01.08.08

**Late News: Multi-Scale Structural Response of Pyrochlore Oxides to Far-from-Equilibrium Processing** Eric O'Quinn<sup>1</sup>, Devon L. Drey<sup>1</sup>, Antonio Fuentes<sup>2</sup> and Maik Lang<sup>1</sup>; <sup>1</sup>University of Tennessee, United States; <sup>2</sup>Cinvestav-Unidad Saltillo, Mexico

Swift heavy ion irradiation and high-energy ball milling are far-from-equilibrium processing techniques which provide access to a unique phase space not achievable by means of traditional synthesis approaches. High-resolution neutron total scattering experiments were utilized to gain fundamental insight into the multi-scale structural details of A<sub>2</sub>B<sub>2</sub>O<sub>7</sub> pyrochlore oxides prepared by these extreme conditions and their subsequent evolution under high-temperature treatment. Pair distribution function analysis revealed unconventional atomic arrangements characterized by an unexpectedly high degree of local order. For instance, the atomic arrangement of ball-milled titanate pyrochlore oxides is nearly identical to the same pyrochlore composition synthesized by solid-state reaction and subsequently amorphized by intense ion irradiation (1). Interestingly, the same atomic arrangement is found in pyrochlore oxides that exhibit distinct long-range radiation responses (order-disorder *versus* crystalline-amorphous) (2). These phenomena are proposed to be the result of fundamental chemical rules which stringently dictate the atomic configuration in disordered materials (3, 4). This description provides insight into far-from-equilibrium processing of oxides and helps to better elucidate the structural properties and heterogeneity of disordered complex oxides from the local atomic arrangement to the macroscale.

1. E. C. O'Quinn *et al.*, Advanced characterization technique for mechanochemically synthesized materials: neutron total scattering analysis. *J. Mater. Sci.* **53**, 13400–13410 (2018).
2. J. Shamblin *et al.*, Similar local order in disordered fluorite and aperiodic pyrochlore structures. *Acta Mater.* **144**, 60–67 (2018).
3. D. Drey, Disorder in Ho<sub>2</sub>Ti<sub>2-x</sub>Zr<sub>x</sub>O<sub>7</sub>: Pyrochlore to Defect Fluorite Solid Solution Series. *RSC Adv.* **In Press** (2020).
4. E. C. O'Quinn *et al.*, Predicting short-range order and correlated phenomena in disordered crystalline materials. *Sci. Adv.* **6**, 1–8 (2020).

#### 5:33 PM F.SF01.08.03

**Improved Dielectric Properties of Na<sub>1/2</sub>Y<sub>1/2</sub>Cu<sub>3</sub>Ti<sub>4</sub>O<sub>12</sub> Ceramics Synthesized by Ball-Milling and Reactive Sintering** Hicham Kotb and Adil Alshoaibi; King Faisal University, Saudi Arabia



Na<sub>1/2</sub>Y<sub>1/2</sub>Cu<sub>3</sub>Ti<sub>4</sub>O<sub>12</sub> (NYCTO) ceramics with giant dielectric constant ( $\epsilon'$ ) were synthesized by simple reactive sintering. NYCTO nanopowder was first synthesized using high energy ball-mill. Then the pelletized powder was sintered in air at temperatures in the range 975 °C to 1050 °C for 10–20 h. The obtained ceramics showed pure CaCu<sub>3</sub>Ti<sub>4</sub>O<sub>12</sub> (CCTO)-like cubic phase as revealed by x-ray diffraction measurements. Field effect-SEM observations showed that the grain size increases from 2  $\mu$ m to 5  $\mu$ m with increasing sintering temperature. NYCTO samples sintered at temperatures higher than 975 °C showed giant dielectric constant (10<sup>3</sup>–10<sup>4</sup>) over most of the frequency range. The minimum dielectric loss ( $\tan\delta$ ) of ~0.055 at 300 K has been approved for the ceramic sample sintered at 1050 °C. Impedance and modulus spectra of the current samples showed two relaxations related to semiconductor (grain) and high resistance (grain-boundaries) elements. The activation energy for conduction located in the range 0.1–0.5 eV highlighted the role of single ionized oxygen vacancies in the dielectric properties of the investigated NYCTO ceramics.

#### 5:35 PM F.SF01.08.04

**Simulations of Hydrogen Retention in Polycrystalline Tungsten** [Brandon Laufer](#) and Karl D. Hammond; University of Missouri, United States

Tungsten will be the plasma-facing material in the ITER divertor. Hydrogen blistering has been observed in plasma-facing materials, but to date, all electronic structure and molecular mechanics simulations have indicated that hydrogen atoms repel one another in perfect crystals. The influence of grain boundaries on hydrogen retention is also not well-understood. We conducted simulations intended to elucidate the mechanisms of blister formation. These studies were accelerated using direct implantation, as we have used in the past for helium, so that computational time ordinarily required to simulate hydrogen atoms that reflect is instead used to simulate diffusion. Consistent with prior observations, we observe that hydrogen is generally repelled by other hydrogen atoms in single-crystal tungsten and we observe neither self-clustering nor cluster growth of any kind. Near grain boundaries, however, the excess volume present allows hydrogen to cluster. Eventually, sufficient hydrogen concentration can build up and weaken the grain boundary, possibly resulting in delamination of the grains and forming a blister.

#### 5:37 PM F.SF01.08.05

**Electric Current and Field Effects on the Microstructural Development of Al Doped ZnO** [Claudia Gorynski](#) and Markus Winterer; University Duisburg-Essen, Germany

The present work focuses on understanding the microstructural development during sintering of nanopowders under pressure and electric fields/currents. For this purpose, a method has been developed which combines flash sintering (FS) and spark plasma sintering (SPS) [1]. This FS-SPS combination enables us to combine the advantages of both techniques: to force the electric current through the sample (FS) and to sinter pellet-shaped samples under mechanical loads (SPS). We explored the novel device on the model material Al doped ZnO and discovered a different microstructure, compared to conventional SPS. Grain growth and second phase formation were emphasized by FS-SPS. It remains controversial if the observed microstructure is a result of an intrinsic electric current/field effect or of a temperature-distribution. However, this method helps to understand mechanisms involved in electric current or field assisted sintering techniques and possibly produces new microstructures and, hence, materials.

#### Acknowledgement:

We acknowledge the support from the German Research Foundation (DFG, Deutsche Forschungsgemeinschaft)—Priority Programme (SPP, Schwerpunktprojekt) 1959/1 “Manipulation of matter controlled by electric and magnetic fields: Toward novel synthesis and processing routes of inorganic materials” with Project Nos. WI 981/16-1 and WO 577/13-1.

#### References:

[1] C. Gorynski, U. Anselmi-Tamburini and M. Winterer, Rev. Sci. Instrum. **91**, 015112 (2020); doi: 10.1063/1.5119059

SESSION F.SF01.01: High Pressure/Stress/Strain

On Demand Abstracts Available for Viewing Starting Saturday Morning, November 21, 2020

F-SF01

#### 5:00 AM \*F.SF01.01.01

**Stress Induced Mesoscale Assembly of Nanoparticles for Active Nanostructures** [Hongyou Fan](#); Sandia National

Laboratories, United States

Due to the size- and shape-dependent properties, nanoparticles have been successfully used as functional building blocks to fabricate 1-3D ordered assemblies for the development of artificial metamaterials. At ambient pressure, entropy driven self-assembly of monosized or binary nanoparticles generally results in polycrystalline 2- or 3D close-packed arrangements, and extensive efforts have been made to develop structural perfection of nanoparticle arrays or 'single crystal-like' domain structures with precise long range order for their definite advantages for electron transport. To date, fabrications of ordered nanoparticle assemblies have been relied on specific interparticle chemical or physical interactions such as van der Waals interactions, dipole-dipole interaction, chemical reactions, etc. Recently we have discovered a pressure-induced assembly method to engineer nanoparticle assembly at mesoscale and to fabricate new nanoparticle architectures without relying on specific nanoparticle interactions. We show that under a hydrostatic pressure field, the unit cell dimension of a 3D ordered nanoparticle arrays can be manipulated to reversibly shrink, allowing fine-tuning of interparticle separation distance. Under a uniaxial pressure field, nanoparticles are forced to contact and coalesce, forming hierarchical nanostructures. Depending on the orientation of the initial nanoparticle arrays, 1-3D ordered nanostructures including nanorod, nanowire, and nanoporous network can be fabricated through the pressure-induced self-assembly method. Guided by computational simulations, we were able to rationalize the pressure-induced self-assembly of nanoparticle arrays for predictable nanostructures. Moreover, we discovered for the first time a transition from an ordered polycrystalline nanoparticle mesophase to quasi-single crystalline nanoparticle lattices induced by PDA process. Exerting pressure-dependent control over the structure of nanoparticle arrays provides a unique and robust system to understand collective chemical and physical characteristics and to develop novel electronic and photonic behavior for energy transduction related applications.

Sandia National Laboratories is a multimission laboratory managed and operated by National Technology and Engineering Solutions of Sandia, LLC., a wholly owned subsidiary of Honeywell International, Inc., for the U.S. Department of Energy's National Nuclear Security Administration under contract DE-NA0003525.

#### 5:15 AM \*F.SF01.01.02

**Supercritical Elasticity and Its Potential Applications in Extreme Conditions** Haiyang Chen<sup>1</sup>, Yan-Dong Wang<sup>1</sup> and Yang Ren<sup>2</sup>; <sup>1</sup>University of Science and Technology Beijing, China; <sup>2</sup>Argonne National Laboratory, United States

Developing elastic materials for technological applications in extreme conditions has been a challenging task. Normal metals have an elastic strain limit rarely exceeding 1%. A large pseudo-elastic strain up to 10% can be achieved in the so-called shape-memory alloys (SMAs). However, the intrinsic hysteresis and temperature sensitivity of the first-order phase transformation significantly hinder their usage in many critical areas. We recently discovered a new type elasticity: supercritical elasticity (SCE), in NiCoFeGa single crystals, which exhibit a large elasticity up to 15.2% strain, with non-hysteretic mechanical responses, a small temperature dependence and high-energy-storage capability and cyclic stability over a wide temperature and composition range [Chen et al., Nature Materials, (2020). <https://doi.org/10.1038/s41563-020-0645-4>]. Such a giant SCE is conceived to work even down to absolute zero Kelvin. In situ synchrotron X-ray diffraction measurements show that the SCE is correlated with a stress-induced continuous variation of lattice parameter accompanied by structural fluctuation. Neutron diffraction and electron microscopy observations reveal an unprecedented microstructure consisting of atomic-level entanglement of ordered and disordered crystal structures, which can be manipulated to tune the SCE. The discovery of the giant SCE and associated the entangled structure paves the way for exploiting elastic strain engineering and development of related functional materials for a wide variety of high-performance engineering applications, ranging from deep-space and deep-sea exploration to intelligent robotics.

#### 5:30 AM F.SF01.01.03

**Initiation of the CuO/Al Thermite Reaction Through High-Velocity Microparticle Impact Testing** Carlos Parra<sup>1,2</sup>, Yuchen Sun<sup>3,3</sup>, David A. Veysset<sup>3</sup>, Digvijay R. Yadav<sup>4</sup>, Kelvin Xie<sup>4</sup> and Zachary Cordero<sup>3</sup>; <sup>1</sup>Rice University, United States; <sup>2</sup>Escuela Superior Politecnica del Litoral, ESPOL, Ecuador; <sup>3</sup>Massachusetts Institute of Technology, United States; <sup>4</sup>Texas A&M University, United States

Thermite reactions between a metallic fuel and a solid oxide can be thermally or mechanically activated. The ignition temperature in a thermally activated thermite reaction generally increases with heating rate but is ultimately limited by the onset of melting of the lower melting point constituent. In mechanically activated thermite reactions, there is often a structure-sensitive threshold pressure required to drive the reaction. Historically, thermally activated thermite reactions have been explained using diffusion-based reaction mechanisms while mechanically activated thermite reactions have been

described using deformation-based mechanical mixing models. Here we probe mechanically activated thermite reactions at a single well-defined heterophase interface using a combination of hydrocode simulations and laser-induced particle impact testing, where a CuO powder particle strikes an aluminum target at supersonic velocities. No reactions are observed through *in situ* imaging; however, post-mortem characterization of embedded CuO particles reveals a thin nanocrystalline Al<sub>2</sub>O<sub>3</sub> reaction layer, with a thickness roughly equal to that of a molten lubricating layer predicted to form during penetration. These results suggest that local melting at hot spots drives the ultrafast reactions observed in mechanically activated thermite reactions and that thermally and mechanically activated thermite reactions may in fact result from the same underlying mechanisms.

#### 5:40 AM F.SF01.01.04

**Silica-Titania Nanocomposite Based Fiber Optic Sensor for Aromatic Hydrocarbons Detection** Shumaila Islam and Adil Alshoaibi; King Faisal University, Saudi Arabia

Surface stability of deposited sensing material is becoming a crucial issue in the field of opto-chemical sensor technology due to cracks/stresses. Porous silica-titania (ST) nanocomposite coating material is synthesized and doped with CdTe as transducers for sensing cyclic compounds. Ultra-thin coatings are obtained, ~11 nm for ST nanocomposite, and 5 nm for encapsulated and heat-treated samples. BET analysis shows large surface area ~441 m<sup>2</sup>/g ± 3 m<sup>2</sup>/g and pore diameter 58 Å of ST nanocomposite. It decreases down to ~410 m<sup>2</sup>/g ± 2 m<sup>2</sup>/g, and pore diameter to 24 Å, after encapsulation. However, after heat treatment, it again increases up to 419 m<sup>2</sup>/g ± 2 m<sup>2</sup>/g and pore diameter to 38 Å. The sensitivity of 71.37 counts per unit change in the carbon chain with correlation determination coefficient R<sup>2</sup> ~0.89 at 468 nm is observed. The prepared sensor device shows excellent stability, signal-to-noise ratio, and good reversibility towards different hydrocarbons and non-hydrocarbons (inorganic materials).

#### 5:50 AM \*F.SF01.01.05

**Pressure-Induced Dramatic Changes in Electronically Low-Dimensional Metal Halides** Xujie Lu, Songhao Guo, Hui Luo, Yongsheng Zhao and Wenge Yang; Center for High Pressure Science & Technology Advanced Research, China

Metal halide perovskites are promising for advanced photovoltaic and optoelectronic applications. Solar cells and light-emitting diodes based on metal halides have achieved an impressive power conversion efficiency of 25.2% and a high external quantum efficiency of over 20%, respectively. Importantly, exceptional structural tunability enables enhanced and/or emergent properties. By using appropriate organic and inorganic components, many perovskite variants with 2D, 1D, and 0D structures on the molecular level have been obtained. These electronically low-dimensional metal halides have exhibited rich emergent properties and significantly expanded the scope of halide perovskites, while critical challenges remain. Future design of high-performance metal halides calls for a deeper understanding of the structure-property relationships. In this talk, we will present our recent efforts in using external pressure to tune the structures and physical properties of low-dimensional metal halides. Using state-of-the-art high-pressure techniques coupled with *in situ* synchrotron-based and in-laboratory property measurements, we characterized the changes in their structural, electronic, and optical properties. Pressure-enhanced properties such as higher photoluminescence quantum yields, as well as pressure-induced novel phenomena including emergent photocurrent, were observed. Our findings demonstrate that high pressure is able to realize enhanced and/or emergent properties of various metal halides, and further our understanding of the underlying mechanisms.

#### 6:05 AM F.SF01.01.07

**Shear Localization in Molecular Crystal Cyclotetramethylene-Tetranitramine ( $\beta$ -HMX)** Mohammad Jane Alam Khan and Catalin Picu; Rensselaer Polytechnic Institute, United States

Cyclotetramethylene-Tetranitramine ( $\beta$ -HMX) is an energetic molecular crystal widely used as a constituent for plastic bonded explosives (PBXs). At high pressures encountered under shock conditions, dislocation motion is inhibited and plastic deformation takes place primarily by shear localization. Atomistic simulations of shear localization are performed in  $\beta$ -HMX under isothermal-isobaric conditions. The post localization flow stress for different pressures (0 to 15 GPa) and strain rates (10<sup>7</sup> to 10<sup>10</sup> s<sup>-1</sup>) and at different temperatures of the shear band is investigated. The flow stress decreases linearly with temperature and increases quadratically with the pressure and exponentially with the strain rates. Shear thinning is observed, i.e. the viscosity decreases with increasing the strain rate. It is concluded that the flow stress increases exponentially with the density of the amorphous shear band and hence it can be described as a function of this single variable. The pressure, temperature and strain rates control the flow stress through the density. The critical stress for shear localization (CSSL) was investigated for different strain rates at different pressures. The critical stress depends significantly on pressure and weakly on strain rates.

6:15 AM F.SF01.01.08

**Modeling and Experimental Studies of Neat and Metal-Doped Stishovite, Coesite and Quartz Under High**

**Pressure** Iskander G. Batyrev, Michael C. Golt and Rosario C. Sausa; CCDC Army Research Laboratory, United States

The results of a comparative study of neat and doped silicon dioxide polymorphs (Fe, Ni or Cu) obtained by density functional theory (DFT) at 0 K and at ambient pressure, 10 GPa, and 20 GPa are presented. The metal atoms are introduced at substitutional and octahedral interstitial sites of the crystal, and the relaxed structures are analyzed and ranked according to the enthalpy. Changes in the enthalpy of the neat and doped crystals are estimated at selected temperatures using quantum mechanics molecular dynamics (DFT-MD). We report the modeled enthalpy of the neat and doped crystals, as well as the dependency of the unit-cell parameters, band gaps, and Raman-active modes on pressure, and compare some of these results to those obtained experimentally using a diamond anvil cell. In addition, we present our search results of the high-pressure phases of silicon dioxide using DFT - based evolutionary simulations and report on the stability of the silica phases, as evaluated by convex-hull construction.

Funding Acknowledgement: This work was supported in part by a grant of computer time from the DOD High-Performance Computing Modernization Program at the ARL, Navy, AFRL, and ERDC DoD Supercomputing Resource Centers.

6:25 AM F.SF01.01.11

**Thermal Stability of XeF<sub>2</sub> at High Pressures** Elena Bykova<sup>1</sup>, Maxim Bykov<sup>2</sup>, S. Chariton<sup>3</sup>, V. Prakapenka<sup>3</sup> and Alexander F. Goncharov<sup>1</sup>; <sup>1</sup>Earth and Planets Laboratory, United States; <sup>2</sup>Howard University, United States; <sup>3</sup>Argonne National Laboratory, United States

Xenon is quite a reactive noble gas, and xenon difluoride (XeF<sub>2</sub>) being stable at ambient conditions is used in organic synthesis as fluorinating agent. Formation of XeF<sub>2</sub> is possible because xenon is bonded to highly electronegative fluorine atoms that take electrons from xenon filled outermost electron shell, forming cation Xe<sup>2+</sup>.

High-pressure behavior of XeF<sub>2</sub> (sp. gr. *I4/mmm*) is still under debate. Early powder X-ray diffraction and Raman experiments propose that XeF<sub>2</sub> should transform from a molecular compound to extended graphite-like layer structure at 50 GPa, and then above 70 GPa to a metallic fluorite structure. Contrary, the later experimental studies suggest just slight decrease in XeF<sub>2</sub> lattice symmetry, first to *Immm* and then to *Pnma* structure at 28 GPa and 59 GPa, respectively. Theoretical calculations predict that XeF<sub>2</sub> becomes unstable above 81 GPa, while high pressures should stabilize other xenon-fluorine compounds, such as XeF<sub>4</sub>, XeF<sub>6</sub> and Xe<sub>2</sub>F.

In order to resolve this issues, we investigated thermal stability of XeF<sub>2</sub> at pressures up to 54 GPa by means of single crystal X-ray diffraction in laser-heated diamond anvil cells. Single-crystal XRD opens the way to determine not only crystal structure of the material at truly extreme conditions, but also allows to refine its chemical composition. We report here the crystal structures of novel fluorides xenon, synthesized at high-pressure and high temperature conditions. In particular, the crystal structures of XeF<sub>4</sub> and Xe<sub>3</sub>F<sub>2</sub>, that both formed under heating-induced disproportionation of XeF<sub>2</sub> at 54 GPa. Similarly to ambient pressure structure, XeF<sub>4</sub> is a molecular compound composed of XeF<sub>4</sub> units with square planar geometry. Xe<sub>3</sub>F<sub>2</sub> is not known at ambient conditions, and its structure is formed by isolated Xe atoms and linear XeF<sub>2</sub> molecules.

6:45 AM \*F.SF01.01.13

**Heterostructured Materials—Strain Gradient Near Interface and Its Dislocation Mechanisms** Yuntian T.

Zhu<sup>1,2</sup>; <sup>1</sup>Southeast University, China; <sup>2</sup>City University of Hong Kong, China

Recently, heterostructures are found to produce unprecedented combination of strength and ductility that is considered impossible from our textbook knowledge and materials history. Heterostructured (HS) materials consist of domains with dramatic strength differences. The superior mechanical properties have been attributed to back-stress strengthening and back-stress work hardening, which are related to strain gradient near the heterogeneous domain interfaces. Here I'll discuss *in-situ* observations of strain gradient evolution near the domain interface and the dislocation mechanisms for the formation of strain gradient. It is found that contrary to our conventional understanding, negative strain gradient was developed near the interface. It is also observed under *in-situ* TEM that the Frank-Read dislocation sources are dynamically created and destroyed although postmortem examinations do not observe many Frank Read sources. These observations provide a new piece of scientific foundation for heterostructured materials, which is becoming a hot research field.

7:00 AM F.SF01.01.14

**Effects of Ultrahigh Strain and Strain Rates on the Heterogeneous Microstructural Evolution of Cold-Sprayed Coatings** Yu Zou; University of Toronto, Canada

Cold spray, initially a coating technique, is being touted as a 'near-net shape' manufacturing technology that minimizes material waste by virtue of the high rate of deposition. During the cold spray process, metallic bulk components can be produced by spraying metal powders at high velocity, generating bonding through severe plastic deformation at temperatures well below the melting point of the powders. To fully understand the cold spray processing of metal powders, we systematically compare and study the microstructure evolution in Cu, Ni, Al, Ti, Ti-6Al-4V samples prepared by cold spray using electron backscatter diffraction (EBSD), transmission electron microscopy (TEM) and nanoindentation. We show complex microstructure in these powder particles after cold spraying: nanocrystalline, nanotwins, annealing twins, gradient grains, deformation bands, dynamic/static recovery and recrystallization. The effects of gas temperature and powder velocity on the microstructure and mechanical properties in the cold sprayed samples are also discussed. Of particular interest are grain refinement, recrystallization and particle/particle bonding mechanisms of the cold sprayed powders.

#### 7:10 AM F.SF01.01.16

**Friction and Dislocation Motion Using Objective Molecular Dynamics** [Gunjan Pahlani](#)<sup>1</sup>, Ananya Renuka Balakrishna<sup>2,1</sup> and Richard D. James<sup>1</sup>; <sup>1</sup>University of Minnesota, United States; <sup>2</sup>University of Southern California, United States

Atomic features, such as surface roughness and dislocations, affect the mechanical strength and plastic deformation of materials under high shear rates. The precise role of how these atomic features influence the wear and tear of materials under nonequilibrium settings is not well understood. We use Objective Molecular Dynamics (OMD) to investigate the links between atomic features and high shear rates. This method has two advantages over traditional MD simulations: First, it simplifies solutions by exploiting the group invariance of the equations of molecular dynamics. For example, in OMD only a modest number of atoms are simulated (typically, 50-1000) and the motions of the other, typically infinite, set of atoms (the non-simulated atoms) are given by the group action on the simulated atoms. Second, it provides a framework for modeling continuum loads at an atomic scale. For example, a Lagrangian velocity gradient tensor is introduced to describe affine motion of simulated atoms. In today's talk, we demonstrate these advantages of OMD through two examples: 1) frictional behavior of sliding surfaces, and 2) dislocation movement under shear stress. Both of these computations were done under high shear rates, and demonstrate how atomic features, such as rough surfaces, edge dislocations, and vacancies, affect mechanical deformation. Broadly, we present a theoretical framework to explore the interplay between extreme mechanical loads at the continuum scale and mechanical deformation at the atomic scale.

#### 7:20 AM F.SF01.01.18

**Superhard Conductive Rhenium Nitride Thin Films via Magnetic Field-Assisted CVD from Volatile Rhenium Precursors** [Michael Frank](#), Lasse Jurgensen, David Graf, Daniel Stadler, Isabel Gessner and Sanjay Mathur; University of Cologne, Germany

Rhenium nitride is a promising candidate as superhard conductor. Different rhenium-to-nitrogen ratios and several phases result in challenging synthetic strategies for phase pure rhenium nitride. Novel heteroleptic rhenium(I) compounds, [*fac*-Re(I)(CO)<sub>3</sub>(L)] (e.g., L= tfb-dmpda, (*N,N*-(4,4,4-trifluorobut-1-en-3-on)-dimethyl propylene diamine)), containing preformed Re-N bonds act as efficient precursors for selective growth of polycrystalline rhenium nitride (ReN) films by vapor phase deposition. This is the first known access to synthesize phase pure rhenium nitride by single source precursor approach without the need of additional gases. Interdependence of materials strength and thin film orientation is strongly influenced by external magnetic fields. Deposition of ReN films in presence of an external magnetic field showed an orientation effect with preferred growth of crystallites along  $\langle 100 \rangle$  direction.

#### 7:30 AM F.SF01.01.19

**Synthesis of Molecular Metallic Barium Superhydride—Pseudocubic BaH<sub>12</sub>** [Dmitrii Semenov](#)<sup>1</sup>, Wuhao Chen<sup>2</sup>, Alexander Kvashnin<sup>1</sup>, Xiaoli Huang<sup>2</sup>, Alexander F. Goncharov<sup>3</sup>, Artem Oganov<sup>1,4</sup> and Tian Cui<sup>2,5</sup>; <sup>1</sup>Skolkovo Institute of Science and Technology, Russian Federation; <sup>2</sup>Jilin University, China; <sup>3</sup>Carnegie Institution of Washington, United States; <sup>4</sup>Northwestern Polytechnical University, China; <sup>5</sup>Ningbo Institute of Materials Technology and Engineering, Chinese Academy of Sciences, China

Inspired by recent progress in chemistry of compressed polyhydrides [1-2] and the discovery of high-temperature superconductivity above 250 K in the La-H system [3-4], we experimentally studied the high-pressure chemistry of Ba hydrides in four independent DACs. We successfully synthesized novel barium superhydride BaH<sub>12</sub> with a pseudocubic crystal structure, stabilized in the pressure range of 75–173 GPa. The compound was obtained by laser-heating of metallic barium with an excess of ammonia borane compressed to 173, 160, 146, and 90 GPa. The Ba sublattice structure of

BaH<sub>12</sub> was resolved using the X-ray synchrotron diffraction, evolutionary structure prediction, and several postprocessing Python scripts, including an XRD matching algorithm. The ab initio calculations confirm a small distortion of the ideal fcc-barium sublattice to space group *Cmc*2<sub>1</sub> (or even *P*2<sub>1</sub>), determined by the presence of additional weak reflections in the diffraction patterns. Discovered BaH<sub>12</sub> has unique combination of molecular H<sub>2</sub> and H<sub>3</sub> fragments formed due to Peierls-type distortion of one-dimensional H-chains, metallic conductivity, and even superconductivity with  $T_C = 20$  K at 140 GPa, and one of the highest hydrogen content (>92 mol %) among all metal hydrides synthesized so far. Discovered barium dodecahydride is also the first known example of molecular metal amid polyhydrides with one-dimensional conductivity and superconductivity, realized in the H sublattice without its atomization. The results of these experiments confirm that the comparative stability of superhydrides increases with the growth of the period number of a hydride-forming element in the periodic table. [5]

#### References:

- [1] D. Semenov et al. *Mat. Today* 2020, **33**, 36.
- [2] D. Zhou et al. *J. Am. Chem. Soc.* 2020, **142**, 6, 2803–2811.
- [3] M. Somayazulu et al. *Phys. Rev. Lett.* 2019, **122**, 027001.
- [4] A. Drozdov et al. *Nature* 2019, **569**, 528.
- [5] D. Semenov et al. *Cur. Op. in Sol. State and Mat. Sci.* 2020, **24**, 2, 100808.

#### 7:40 AM F.SF01.01.20

**Late News: Atomic-Scale Insight into Melting of BCC Tungsten Under Shear Stresses by Extended Finnis-Sinclair Potential—Molecular Dynamics Simulation** Dulat Akzhigitov, Tamerlan Srymbetov, Boris Golman, Christos Spitas and Zhandos Utegulov; Nazarbayev University, Kazakhstan

Understanding melting processes in refractory materials under external stresses is important and can be of particular interest in harsh environment applications ranging from aerospace to nuclear and fusion energy where these materials have to simultaneously withstand the effect of high temperatures and complex stress states in such ways, that a melting process might be initiated in extreme conditions. However, most if not all of the prior research was focused on melting phenomena in the presence of hydrostatic compression.

In our work, we investigate the melting phenomenon in BCC tungsten under different shear stress types. We explore these relationships numerically by molecular dynamics simulations employing extended Finnis-Sinclair potential [1-2] and solid-liquid coexistence method and validate our results with theoretical and experimental findings previously reported in the literature for a hydrostatic compression case.

Regarding other stress states, no similar results have been reported yet for bcc tungsten. The melting behaviour was investigated for all studied stress states and compared both quantitatively and qualitatively on the basis of equivalent strain, least-square atomic-scale strain invariants, maximum shear stress, radial distribution function (RDF), thermal expansion and Lindemann melting criterion. For the majority of shear stress states, an abrupt decline of stress-induced melting point values was detected after certain critical stress values, which was explored with regard to the change of an RDF's amplitude of the first peak. New high-temperature thermo-mechanical results are correlated with intricate structural changes taking place on the atomic scale during metal-melt phase transition.

#### Acknowledgements

The authors acknowledge the funding support of FDCR Grant No. 110119FD4501 by Nazarbayev University, Grant No. AP05130446 and State-Targeted Program No. BR05236454 by Kazakhstan Ministry of Education and Science.

#### References

- [1] Akzhigitov D, Srymbetov T, Golman B, Spitas C and Utegulov Z N 2020 Melting of tungsten under uniaxial and shear stresses: molecular dynamics simulation *Modelling Simul. Mater. Sci. Eng.* [in press] <https://doi.org/10.1088/1361-651X/abaf39>
- [2] Dai X D, Kong Y, Li J H and Liu B X 2006 Extended Finnis–Sinclair potential for bcc and fcc metals and alloys *Journal of Physics: Condensed Matter* <https://doi.org/10.1088/0953-8984/18/19/008>

#### 7:50 AM F.SF01.01.21

**Late News: In Situ Characterization of Dynamic Deformation of AZ31B Magnesium Alloys at High Strain Rate Impact Using 3D-Digital Image Correlation Technique** Francis Tetteh; York University, Canada

The deployment of Magnesium (Mg) alloys have increased significantly in the automotive, aerospace, and defense industries due to their lightweight structural integrity. In structural applications, these materials components are exposed to a wide

range of strain rates such as explosive forming, high-speed impact, and shock loadings. These alloy components are placed in extreme loading environments where high strain rates are commonly achieved. Therefore, the evolution of failure mechanisms from strain localization and formation of adiabatic Shear Bands (ASBs) and the mechanical behavior at high strain rates is of desirable interest by the aerospace and automotive industries. The deformation behavior of Mg has extensively been studied under low strain rate loadings. However, the high strain rate deformation still requires further investigation. Deformation and damage accumulation in Mg alloys at high strain rate loading conditions such as impact is not fully understood. Thus, the correlation between the accuracy of the reported mechanical data and microstructural features that leads to the credence of failure mechanisms within Mg is not well understood. It is therefore critical to extending the understanding of the mechanism of failure of Mg at high strain rates of loadings by exploiting other techniques. In this work, the dynamic mechanical impact response and ASBs nucleation of heat-treated AZ31B Mg alloys at different strain rates and impact momentums are characterized in-situ during impact at room temperature using the Direct Impact Hopkinson Pressure Bar (DIHPB) coupled with an in-situ 3D Digital Image Correlation (DIC) and high speed and high-resolution thermal imaging techniques. DIC provides an independent measurement of surface strains directly on test specimens during deformation to monitor stain evolution and strain localization. It is found that the flow stress increased gradually to (~50 %) with increasing strain rates and impact momentums and the AZ31B Mg exhibits strain rate sensitivity at dynamic loadings. This is due to an increasingly selective grain refinement under dynamic compression. Evaluation of DIC results indicated that strain occurrence is linear at the onset of deformation but becomes heterogeneous at the later stage of deformation with multiple nucleation sites of strain localization leading to ASB at ~80% of the specimen length after ~340 us of deformation. The region of peak non-linearity of maximum strain concentration leads to ASB formation with characteristic fine grains, voids, and crack initiation. At most, ~22 °C temperature rise is observed. The temperature rise is, however, lower with respect to the homologous temperature of Mg, and a hence higher degree of strain hardening behavior is induced after deformation. These results suggest that ASB forms in AZ31B Mg alloy despite its brittle nature that leads to crack initiation and ultimate failure under high strain rates and large strains of deformation and can be used to extend the understanding of the mechanism of failure in Mg alloys.

#### SESSION F.SF01.02: High Magnetic Field

On Demand Abstracts Available for Viewing Starting Saturday Morning, November 21, 2020  
F-SF01

##### 5:00 AM \*F.SF01.02.01

**Material Requirements for Pulsed Magnets at the HLD** Sergei Zherlitsyn, Thomas Herrmannsdoerfer and Joachim Wosnitza; Helmholtz-Zentrum Dresden-Rossendorf (HZDR), Germany

The Dresden High Magnetic Field Laboratory (HLD) is a pulsed-field user facility, which provides external and in-house researchers with the possibility to perform a broad range of experiments in pulsed magnetic fields [1]. The HLD develops, manufactures, and operates the non-destructive pulsed magnets for the field range up to 90 T and beyond. A design of the magnets requires high-strength, high-conductivity wires with selected cross-sections and high-strength reinforcement materials. Currently some test coils are fabricated at the HLD for a prototype triple-coil magnet for magnetic fields of about 100 T. We will discuss the choice of materials for this pulsed magnet, material-based limitations, long standing experience with available materials, and material challenges for generating even higher magnetic fields by the non-destructive pulsed magnets.

[1] <http://www.hzdr.de/hld>

##### 5:15 AM \*F.SF01.02.02

**Materials Requirements for Ultra-High-Field Magnets at the National High Magnetic Field Laboratory** Mark D. Bird; Florida State University, United States

Ultra-High-Field (UHF) electromagnets require high current densities in high magnetic field with resulting intense Lorentz forces. A central part of developing higher field magnets is managing the Lorentz forces to keep stress and strain within the materials' allowables.

The simplest UHF magnets are dc resistive ones. DC operations results in maximum performance being presently attained by high-strength copper and its alloys. Fatigue performance has started to emerge as a challenge in CuAg nano-composites.

Pulsed resistive magnets are able to mix high-strength conductors and reinforcing materials with both high strength and high stiffness by appropriately adjusting the pulse length. High strength copper and a number of its alloys are productively employed, as are metallic and polymer/epoxy composite reinforcements. The highest field superconducting magnets employ the high-temperature superconducting (HTS) materials along with high strength reinforcement. The present state of the art of material requirements for UHF magnets is briefly presented along with challenges for next-generation systems.

#### 5:30 AM \*F.SF01.02.03

**Understanding Requirements of Advanced Magnet Materials to go Beyond 100 Tesla** Doan Nguyen and Do T. Vo; Los Alamos National Laboratory, United States

High magnetic fields have a long history of uncovering fundamentally important information about materials. They take their place among e.g. X-ray and neutron techniques, as a critically important tool of condensed matter physicists. The National High Magnetic Field Laboratory's Pulsed Field Facility at Los Alamos National Laboratory is one of few research centers in the world that can create and use ultra-high pulsed magnetic field for scientific research. The facility houses several types of non-destructive pulsed magnets which can provide the peak fields ranging from 60 tesla to 100 tesla for users. However, present frontiers in quantum matter, including topological matter and superconductivity, require magnetic fields beyond 100 tesla and several high field facilities around the world are currently working toward that ambitious goal. The power and stored energy required to generate a magnetic field increase exponentially with the field amplitude. Therefore the better conductors with higher mechanical strength and electrical conductivity are required to nondestructively generate magnetic fields above 100 tesla with acceptable risk and cost. Finite Element Modeling (FEM) simulations and our in-house mid-plane pulsed magnet design codes were employed to understand the requirements of advanced magnet materials to practically achieve magnetic fields beyond 100 tesla.

#### 5:45 AM \*F.SF01.02.04

**High Strength—High Conductivity Materials for High Field Magnets** Francois Debray, Olivier Jay and Florence Lecouturier; UGA-INSA-UPS-CNRS, France

Magnetic field is a powerful tool to study new materials and new processes. The highest magnetic field generated with superconducting magnets made of NbTi and Nb<sub>3</sub>Sn windings is 23.5 T. During the last years, technological breakthroughs have confirmed the feasibility of superconducting magnets generating more than 30 T thanks to the integration of high temperature superconductors. Still, higher magnetic fields are only available through copper-based magnets. Steady high magnetic field can be generated during several hours and implies a large electrical power (typically 30 MW for 40 T) whereas pulsed magnetic field can reach 100 T for some milliseconds with negligible power consumption. The French High Magnetic Field Facility (LNCMI) is developing both technologies, on its pulsed field site in Toulouse and its steady field site in Grenoble. Optimizing the high field magnets requires to search for the best material and associated shaping process for the realization of these highly constrained machines. The main high field magnet constraints are the mechanical constraints due to Lorentz forces and the thermal constraints coming from Joule losses.

For steady field magnets, copper alloys with high strength and high electrical conductivity are required for an operating temperature that can reach 150°C. To keep the windings of the magnet at a temperature acceptable for a given alloy a high velocity water flow is injected in it to manage heat fluxes as high as 10 MW.m<sup>2</sup>. Steady high field resistive magnets used two technologies: the Bitter and the polyhelix one. Bitter magnets are made of thin plates (from 0.2 to 1 mm) up to 1000 mm in diameter. In this shape Copper alloys with a high content of Silver (18 wt.%, yield strength up to 1000 MPa and electrical conductivity at room temperature of 50 MS.m<sup>-1</sup>) have been industrialized by one company worldwide up to 250 mm in diameter. For larger diameters, copper plates with a possible addition of a low content of Silver are proposed by different companies with yield strength ranging from 400 to 450 MPa and a conductivity around 58 MS.m<sup>-1</sup>. For the polyhelix technology, the LNCMI has set a R&D program to replace forged tubes (CuCrZr) with limited mechanical properties. Copper alloy tubes prepared by the Cold Spray technology are now in operation on the high field facility in Grenoble.

For pulsed field magnets, the highest priority is set on the mechanical properties of conductors at cryogenic temperature which have to cope with the increasingly severe mechanical constraints at fields beyond 60 T. To avoid excessive heating, the duration of the current that passes through a magnet is reduced to the order of 10-100 milliseconds. The LNCMI Toulouse disposes of several capacitor banks with a total energy of 22 MJ able to produce non-destructive fields over 60 T in 28 mm and close to 100 T in 8 mm bore. Beyond 100 T, it also features a Megagauss installation that makes use of dynamic effects in exploding copper single-turn coils to produce 200 T on a microsecond time scale. "In-house" copper/stainless steel macrocomposite conductors for wire wound pulsed field magnets generating magnetic fields up to 80 T are developed. High strength multiscale Cu/Nb nanocomposite wires produced by severe plastic deformation by ADB (Accumulative Drawing



and Bundling) process are dedicated to the production of magnetic field over 90 T. New innovative composite copper based conductors, processed by powder metallurgy, reinforced with carbon nanotube or silver nanowires- are under development to reach non-destructive pulsed fields over 100 T.

#### 6:00 AM \*F.SF01.02.05

**Properties of Copper-Silver Alloys Obtained by the Cold Spray Process** Christophe Verdy<sup>1</sup>, Olivier Jay<sup>2</sup> and Francois Debray<sup>2</sup>; <sup>1</sup>LERMPS, ICB, UMR 6303, CNRS, Univ. Bourgogne Franche-Comté, UTBM, France; <sup>2</sup>Univ. Grenoble Alpes, INSA Toulouse, Univ. Toulouse Paul Sabatier, EMFL, CNRS, LNCMI, France

The cold spray process was developed at the end of the 20th century and his principle is mainly based on the kinetic energy transmitted to micron size particles to allow their deposition. The particles remain solid and the deposits are generated by the particles impacting the substrate at high velocity. Working at low temperature, below the melting point of the deposited material, appears particularly interesting for deposition of oxygen sensitive materials like copper alloys. In comparison with conventional thermal spray processes, cold spray can retain the original properties of powder feedstock (grain size, nanostructured particles), prevent the adverse influence on the underlying substrate materials, and can produce very thick coatings due to compressive stresses.

To spray oxygen sensitive material like copper alloys, it is preferable to select an inert gas as propellant gas for cold spray deposition. Nitrogen is mainly used but, as the gas velocity is strongly linked to the gas mass, gases with low atomic weight like hydrogen or helium are particularly interesting to reach high velocities. Among those gases, helium is much better from the human safety point of view but its price is very high due to limited amounts on earth. A closed loop avoiding costly helium losses was implemented. Thus, deposition efficiency of cold spray copper alloys higher than 96 %, porosity below 0.1 % and oxygen content below 150 ppm were obtained. High deposition rates up to 7 kg/h were also reached.

Copper silver alloys present attractive mechanical properties combined with high thermal conductivity suitable for many applications like high field magnets. In the present work, CrCrZr and CuAg with various Ag percentage deposits were manufactured by cold spray using helium as propellant gas. The work hardening mechanisms are involved by comparison with classically forged materials. A large tailoring of the material's properties can be obtained through specific heat treating. Residual stresses are very low after heat treating and allow machining helices without deformation. This process now allows to produce tubes for polyhelix magnets at LNCMI with a major performance gain.

#### 6:15 AM \*F.SF01.02.06

**Ultra-High Local Plasticity Induced by Room-Temperature Restoration in High-Strength Nanocomposite** Rongmei Niu and Ke Han; Florida State Univ, United States

We subject an aged Cu-24 wt%Ag ingot to heavily cold drawing to develop a nanocomposite. The as-drawn wire is composed of Cu-rich proeutectic components and Ag-rich eutectic components. A fine lamellar structure are developed in the proeutectic component embedded a high density of Ag fibers. The average lamellar spacing is 20±6 nm. Ag fiber width is below 5nm. The eutectic component has a relative coarse structure with Ag grain size around 100 nm. This bimodal size distributed Ag fibers yield ultra-high bending plasticity—up to 59% bending strain at the outermost edge-- 15 times the tensile elongation of the wire (3.6%). During our bending tests, dynamic recovery and partial recrystallization occur primarily in the eutectic component, and are more frequently at the inner edge than the outer edge. The high bending strain causes some of the thick Ag fibers to become discontinuous and lose their original alignment. This structural evolution increases local plasticity, resulting in unexpectedly high achievable bending strain. This is unusual in nano-sized, Ag-fiber-reinforced high-strength composite.

#### 6:30 AM \*F.SF01.02.07

**A Powder Metallurgy Route Involving Spark Plasma Sintering Towards High-Strength Wires for DC or Pulsed Resistive Magnets** Christophe Laurent<sup>1</sup>, Simon Tardieu<sup>1,2</sup>, David Mesguich<sup>1</sup>, Antoine Lonjon<sup>1</sup>, Nelson Ferreira<sup>2</sup>, Geoffroy Chevallier<sup>2</sup>, Arnaud Proietti<sup>1</sup>, Claude Estournes<sup>2</sup> and Florence Lecouturier<sup>2</sup>; <sup>1</sup>Université Toulouse 3 Paul Sabatier, France; <sup>2</sup>CNRS, France

There is a demand for stronger yet lighter conducting copper wires in high-technology domains of global interest where weight is at a premium, such as power and aerospace engineering as well as in niche applications, such as materials for high-field magnets.

Many proposed solutions involve the preparation of copper-matrix composite wires or copper-rich alloyed wires with ultrafine but complex microstructures. Wires are prepared by wire-drawing billets (cylinders). This is a severe plastic deformation method and may be followed by appropriate thermal treatments. There are many variants but the importance of the characteristics of the cylinder is not to be neglected. The usual routes for cylinder preparation involve melting-

solidification at some point, and therefore a relatively high temperature, either for alloying or for the preparation of the pure copper sample to be used in a composite.

We have proposed an alternative method based on powder metallurgy routes, involving the consolidation of a suitable powder into a cylinder by sintering at a relatively low temperature. This is done by spark plasma sintering (SPS), which has several advantages over pressureless sintering and hot-pressing, including rapid heating and cooling rates. Therefore, lower sintering temperatures and shorter holding times make it possible to avoid grain growth and prepare copper cylinders with micrometer-sized grains, typically ten times lower than conventional copper cylinders.

SPS typically differs from hot-pressing by the application of a dc pulsed current to the pressing die and powder compact, while a uniaxial pressure is simultaneously applied. Interestingly, cylinders with only about 90% of their full density were found suitable for the rest of the study, because a too high density hampers the deformability of the cylinder during wire-drawing, resulting in sample breaking.

The basics of SPS will be presented and we will show several examples of the preparation of wires of pure copper, carbon nanotube - copper composites and silver nanowire - copper composites. The microstructure of the powders, cylinders (typically 8 mm in diameter and 33 mm long) and wires will be presented as well as the mechanical properties and electrical resistivity of the wires measured at 293 K and 77 K.

#### 7:00 AM \*F.SF01.02.09

**Application of the Nanostructured Cu-Nb *In Situ* Microcomposites as Strengthening Elements in High Strength Cu-Matrix Composites** V. Pantsyrny<sup>1,2</sup>; <sup>1</sup>Nanoelectro LLC, Russian Federation; <sup>2</sup>Bochvar Institute of Inorganic Materials, Russian Federation

Advanced electrical and electronic devices sometimes require that conductor's material properties should be counteracting, e.g. high electrical conductivity and high mechanical strength. Traditional high strength Cu-matrix composites consists of Cu-based matrix, which contains a uniformly distributed nanoscaled particles of intermetallic compounds or oxides. The required microstructure is usually formed by the doping of the initial Cu matrix alloy by the combination of elements which would form the intermetallic compounds during the aging heat treatment at specific temperature range of 300-500 °C (Cu-Zr-Nb; Cu-Ni-Si; Cu-Cr-Zr alloys) or to form fine oxides through the process of internal oxidation (Cu-Al alloys). These submicron particles of oxides and intermetallic compounds altogether with increase of ultimate strength lead to substantial decrease of fatigue properties. The paper describes the alternative approach to development of the advanced high strength Cu-matrix composites with the application of the plastic nanostructured Cu-Nb *in situ* microcomposites as a strengthening element. As an example the principally new design of composite Contact Wire for high speed railways has been proposed to attain at least 20% better combination of ultimate tensile strength (610-660 MPa) and high conductivity (more than 80% IACS). Composite conductor contains the bundles of nanostructured anomalously high strength Cu-Nb filamentary cores and outer layer made of low doped high conductivity Cu-Zr-Nb alloy with improved tribological properties. The microcomposite Contact Wire has very high fatigue properties due to filamentary architecture of microstructure of Cu-Nb strengthening component. This Contact wire was designed for the use in the scope of Overhead Contact Line CS-400 for railways with the speeds of 400 km per hour. The results of laboratory complex tests of contact wire are presented.

#### 7:15 AM \*F.SF01.02.10

**Thermomechanical Stability of Metallic Interfaces Containing 3D Character** Nathan Mara<sup>1</sup>, Justin Y. Cheng<sup>1</sup>, Shuozhi Xu<sup>2</sup>, Youxing Chen<sup>3</sup>, Jonathan Poplawsky<sup>4</sup>, Nan Li<sup>5</sup>, Kevin Baldwin<sup>5</sup> and Irene Beyerlein<sup>2</sup>; <sup>1</sup>University of Minnesota, United States; <sup>2</sup>University of California, Santa Barbara, United States; <sup>3</sup>University of North Carolina at Charlotte, United States; <sup>4</sup>Oak Ridge National Laboratory, United States; <sup>5</sup>Los Alamos National Laboratory, United States

2-dimensional (2-D) sharp interfaces with distinct boundaries demarcating an abrupt discontinuity in material properties in nanolayered composites have been studied for almost twenty years and are responsible for enhanced behaviors such as strength, radiation damage tolerance, and deformability. However, 2-D interfaces have their limitations with respect to deformability and toughness. 3-D interfaces are defined as heterophase interfaces that extend out of plane into the two crystals on either side and are chemically, crystallographically, and/or topologically divergent, in three dimensions, from both crystals they join. Here, we focus on the thermal stability and mechanical behavior of nanolayered Cu/Nb containing interfaces with 3-D character. By co-sputtering the bimaterial interfaces between the constituent pure phases, the resulting compositional gradient gives rise to new interphase boundary structures, which have been analyzed and quantified via S/TEM and Atom Probe Tomography. Micropillar compression results show that the strength of Cu/Nb nanocomposites containing 3-D interfaces is significantly greater than those containing 2-D interfaces. Mechanical anisotropy, as well as shear banding is observed during pillar compression with retention of continuous layers across the shear band. We will

present our recent results on deformation of such 3-D interfaces and structures, and describe their structural evolution mechanistically through the use of atomistic simulations.

#### 7:30 AM F.SF01.02.11

**New High Strength Silver Nanowire-Copper Composite Conductors by Spark Plasma Sintering and Wire-Drawing for High Field Magnets** Simon Tardieu<sup>1,2</sup>, David Mesguich<sup>2</sup>, Antoine Lonjon<sup>2</sup>, Florence Lecouturier<sup>1</sup>, Nelson Ferreira<sup>1</sup>, Geoffroy Chevallier<sup>2,3</sup>, Arnaud Proietti<sup>4</sup>, Claude Estournès<sup>2,3</sup> and Christophe Laurent<sup>2</sup>; <sup>1</sup>LNCMI, France; <sup>2</sup>CIRIMAT, France; <sup>3</sup>Plateforme Nationale CNRS de Frittage Flash, France; <sup>4</sup>Centre de Microcaractérisation Raimond Castaing, France

LNCMI-Toulouse produces some of the most intense non-destructive pulsed magnetic fields in the world with a European record of 98.8 Tesla and aims at reaching more than 100 Tesla. The generation of pulsed magnetic fields higher than 60 T requires the use of coils wound of wires with exceptional properties. The wires need a high conductivity to limit the heating and they must have a high strength to be able to resist the Lorentz forces. The Lorentz forces are tangential to the coil and proportional to the square of the magnetic field. The resulting von Mises stress is 1 GPa at 60 T and higher than 2.2 GPa at 100 T.

Classical methods for strengthening copper wires involve the preparation of composite wires, such as copper-stainless steel (Cu-SS) and copper-niobium (Cu-Nb) or alloyed wires such as copper/silver (Cu/Ag). Cu-Nb and Cu/Ag wires present a nanostructured microstructure with fine and elongated grains. Cu-Nb microstructure is made up of pure Cu and pure Nb grains, while the Cu/Ag microstructure presents Cu-rich and Ag-rich solid solution. These wires exhibit a UTS value higher than 1 GPa but they are distinguished by their high resistivity. The aim of this work is the preparation of composite wires based on pure Cu and pure Ag.

LNCMI and CIRIMAT explore the design and preparation of novel Cu-based nanocomposite wires with the use of powder metallurgy, spark plasma sintering (SPS) and wire-drawing at room temperature. This preparation method is adapted to the preparation of Ag-Cu composite wires. Ag nanowires (200 nm in diameter and 30  $\mu\text{m}$  in length) were synthesized and mixed with a commercial micrometric (about 1  $\mu\text{m}$ ) Cu powder. Samples containing 1, 5 and 10 vol. % Ag were prepared. Cu and Ag-Cu cylinders (diameter 8 mm, length 33 mm) are prepared by SPS. Cylinders are sintered at 400, 500 or 600  $^{\circ}\text{C}$ . The so-obtained cylinders serve as precursors to wire-drawing. Their diameter is reduced by wire-drawing at room temperature, in several passes, thus producing progressively finer wires (diameter in the range 1 - 0.2 mm).

The wires show a lamellar microstructure with ultrafine Cu grains (200 - 700 nm for a 0.5 mm diameter wire) elongated over several micrometers. The Ag nanowires are dispersed along the grain boundaries of Cu. Cu and Ag grains exhibit major  $\langle 111 \rangle$  and minor  $\langle 100 \rangle$  orientations like most of wire-drawn face centered cubic metals.

The electrical resistivity and tensile strength were measured at 293 K and 77 K. The tensile strength for the composite wires is more than twice the value measured for the corresponding pure Cu wires. Interestingly, the wires containing only 1 vol.% Ag offer the best combination of high strength (1100 MPa at 77 K) and low electrical resistivity (0.50  $\mu\Omega\cdot\text{cm}$  at 77 K).

We have obtained wires with excellent mechanical properties while greatly reducing the electrical resistivity compared to Cu/Ag alloy. The present 1 vol. % Ag-Cu composite wires compare favorably with Cu/Ag alloy wires containing about 20 times more Ag.

#### 7:40 AM F.SF01.02.12

**Enhanced Properties of High-Strength Reinforcement Materials for High-Field Magnets** Ke Han, Rongmei Niu, Jun Lu and Vince Toplosky; Florida State University, United States

Nanostructured reinforcement materials, which have been successfully used in high field magnets and at cryogenic temperatures, reach their most desirable strength level when their scale of microstructure is below 100 nanometers. This refined microstructure can be achieved by plastic deformation and heat treatment, which create obstacles, such as dislocations and precipitates, for dislocation motions. Both deformation and heat treatment also introduce microstructure and property anisotropy. Investigating both anisotropy and microstructure changes helps us to understand the plasticity of these materials, particularly at cryogenic temperatures. The goal of our research is to relate microstructural scale and anisotropy to the mechanical and physical properties of these materials. This presentation describes microstructure in different orientations, with emphasis on the impact of high anisotropy and fine microstructure on properties.

This work was performed at the National High Magnetic Field Laboratory, which is supported by the National Science Foundation Cooperative Agreement No. DMR-1644779 and the State of Florida.

**5:00 AM \*F.SF01.03.01**

**Superconducting Superhydrides—Novel Materials and Possible Applications** Maddury S. Somayazulu; Argonne National Laboratory, United States

Since the prediction of metallization and superconductivity of hydrogen and hydrogen-rich materials at high pressures /1,2/, there has been a sustained effort to make advances in high pressure sciences (theory, experiments and techniques) to realize this dream. In comparison to the much larger research landscape spawned by the discovery of high  $T_c$  cuprate superconductors, the high pressure (and high temperature) superconductivity field has been slow to encapsulate the attention of many. Partly, this has to do with the paucity of experimental probes that can be broguth to bear and to a major extent, it is the question of transitioning discovery to application. Nevertheless, the discovery of superconductivity in  $H_3S$ ,  $YH_6$  and  $LaH_{10}$  /3,4,5/ and the phenomenal rise in transition temperatures has begged the question of revisiting these two questions. These discoveries have been aided by theoretical predictions and those can be used to make technological feasibility a likelihood /6-9/. However, there are experimental limitations that need to be surmounted to understand the physics and chemistry of these materials that constitute and important feedback to these simulations /10,11/. This talk will aim at connecting these dots and discus the rapidly evolving picture we have of these fascinating materials.

References:

1. Ashcroft, N. W., Metallic hydrogen: A high-temperature superconductor? Phys. Rev. Lett. (1968) **21**, 1748.
2. Ashcroft, N. W., Hydrogen Dominant Metallic Alloys: High Temperature Superconductors? Phys. Rev. Lett. (2004) **92**, 187002.
3. Drozdov, A. P., et. al, Conventional Superconductivity at 203 Kelvin at High Pressures in the Sulfur Hydride System. Nature, (2015) **525**, 7567
4. Kong, P., et. al, Superconductivity up to 243 K in yttrium hydrides under high pressure. (2019) arXiv:1909.10482
5. Somayazulu. M. S., et. al, Evidence for Superconductivity above 260 K in Lanthanum Superhydride at Megabar Pressures. Phys. Rev. Lett, (2019) **122**, 027001.
6. Y. Li, et. al, The Metallization and Superconductivity of Dense Hydrogen Sulfide, J. Chem. Phys. (2014) **140**, 174712.
7. Hanyu Liu et. al, Potential high- $T_c$  superconducting lanthanum and yttrium hydrides at high pressure, PNAS (2017), **114**, 6990.
8. Ying Sun et. al, Route to a Superconducting Phase above Room Temperature in Electron-Doped Hydride Compounds under High Pressure, Phys. Rev. Lett., (2019) **123**, 097001.
9. Jose A Flores-Livas et. al, A Perspective on Conventional High-Temperature Superconductors at High Pressure: Methods and Materials, (2019) arXiv:1905.06693
10. Shirin Mozaffari et. al, Superconducting phase diagram of  $H_3S$  under high magnetic fields, Nat. Comm. (2019), 10. 2522. 10.1038/s41467-019-10552-y.
11. A. D. Grokowiak et. al, Hot Hydride Superconductivity above 550 K, (2020) arXiv:2006.03004

**5:15 AM \*F.SF01.03.02**

**Giant Thermal Hall Conductivity from Phonons in the Pseudogap Phase of Cuprate Superconductors** G. Grissonnanche<sup>1</sup>, A. Legros<sup>1,2</sup>, S. Thériault<sup>1</sup>, S. Badoux<sup>1</sup>, E. Lefrancois<sup>1</sup>, M.-E. Boulanger<sup>1</sup>, V. Zatkan<sup>1</sup>, M. Lizaire<sup>1</sup>, F. Laliberté<sup>1</sup>, A. Gourgout<sup>1</sup>, J.-S. Zhou<sup>3</sup>, S. Pyon<sup>4</sup>, T. Takayama<sup>4</sup>, H. Takagi<sup>4</sup>, S. Ono<sup>5</sup>, N. Doiron-Leyraud<sup>1</sup> and L. Taillefer<sup>1,6</sup>; <sup>1</sup>Université de Sherbrooke, Canada; <sup>2</sup>CEA Saclay, France; <sup>3</sup>The University of Texas at Austin, United States; <sup>4</sup>The University of Tokyo, Japan; <sup>5</sup>Central Research Institute of Electric Power Industry, Japan; <sup>6</sup>Canadian Institute for Advanced Research, Canada

The nature of the pseudogap phase of cuprates remains a major puzzle. Although there are indications that this phase breaks various symmetries, there is no consensus on its fundamental nature [1].

Fermi-surface, transport and thermodynamic signatures of the pseudogap phase are reminiscent of a transition into a phase with antiferromagnetic order, but evidence for an associated long-range magnetic order is still lacking. Here we report measurements of the thermal Hall conductivity  $\kappa_{xy}$  in the normal state of four different cuprates and show that a large

negative  $\kappa_{xy}$  signal is a property of the pseudogap phase, appearing with the onset of that phase at the critical doping  $p^*$ [2]. It is also a property of the Mott insulator at  $p \approx 0$ , where  $\kappa_{xy}$  has the largest reported magnitude of any insulator. Since this negative  $\kappa_{xy}$  signal grows as the system becomes increasingly insulating electrically, it cannot be attributed to conventional mobile charge carriers. Nor is it due to magnons, since it exists in the absence of magnetic order. In order to identify the heat carriers responsible for this negative  $\kappa_{xy}$ , we turn to transverse heat transport along the c-axis:  $\kappa_{zy}$ . Here we show that the thermal Hall conductivity at  $p = 0$  is roughly isotropic, being nearly the same for heat transport parallel and normal to the  $\text{CuO}_2$  planes, *i.e.*  $\kappa_{zy}(T) \approx \kappa_{xy}(T)$ . This shows that the negative thermal Hall response must come from phonons, these being the only heat carriers able to move as easily normal and parallel to the planes. At  $p > p^*$ , we observe no c-axis Hall signal, *i.e.*  $\kappa_{zy}(T) = 0$ , showing that phonons have zero Hall response outside the pseudogap phase. The microscopic mechanism by which phonons become chiral in cuprates remains to be identified. This intrinsic phonon Hall effect provides a new window on quantum materials and it may explain the thermal Hall signal observed in other topologically nontrivial insulators [4].

[1] Proust & Taillefer, *Annu. Rev. Condens. Matter Phys.* **10**, 409 (2019).

[2] Grissonnanche *et al.*, *Nature* **571**, 376 (2019).

[3] Grissonnanche *et al.*, *Nature Physics (to appear)*; arXiv:2003.00111 (2020).

[4] Kasahara *et al.*, *Nature* **559**, 227 (2018).

### 5:30 AM F.SF01.03.03

**Self-Regulation of Current Sharing in High-Temperature Superconducting Cables by Temperature-Dependent Resistivity Switching in Vanadium Oxide Coatings** Sachin V. Muley<sup>1,2</sup>, Aurora Cecilia Araujo Martinez<sup>1,3</sup>, Zhenuai Yang<sup>1,4</sup>, Xiaorong Wang<sup>1</sup>, Qing Ji<sup>1</sup> and Andre Anders<sup>1,5,6</sup>; <sup>1</sup>Lawrence Berkeley National Laboratory, United States; <sup>2</sup>University of Wisconsin–Madison, United States; <sup>3</sup>University of Guanajuato, Mexico; <sup>4</sup>Harbin Institute of Technology, China; <sup>5</sup>Leibniz Institute of Surface Engineering, Germany; <sup>6</sup>Universität Leipzig, Germany

The high-temperature superconductors (HTS), e.g., RE-Ba<sub>2</sub>Cu<sub>3</sub>O<sub>x</sub> (RE = rare earth) can sustain significant transport current at high background magnetic field and elevated temperatures, enabling various applications including fusion energy generation, next generation high-energy physics particle accelerators, and medical accelerators for carbon therapy. However, reliable protection against catastrophic superconducting-to-normal transitions (quenches) remains to be addressed for successful applications of HTS magnet technology. To address this issue, we investigated the potential of vanadium oxide (VO<sub>x</sub>) coatings as a temperature-dependent switching medium to self-regulate current sharing. VO<sub>x</sub> coatings ( $1.70 \leq x \leq 2.07$ ) were deposited by reactive cathodic arc deposition on insulating glass and commercial REBCO tapes to study their electrical properties. The process gas was monitored *in situ* by a residual gas analyzer. Effects of varying process parameters such as argon-to-oxygen ratio and substrate manipulator speed on coating properties were studied. The coatings were X-ray amorphous but Raman spectrometry showed short-range crystalline ordering. Hall effect measurements found a decrease in resistivity of VO<sub>x</sub> by at least three orders of magnitude when the temperature increased from 80 to 300 K. The coating process did not damage the REBCO tapes as evidenced by a negligible change in critical current after versus before coating. The results from current-sharing experiments and circuit analysis suggest that the VO<sub>x</sub> coating can effectively self-regulate current sharing in REBCO magnets and enable self-protection during quenches. This work was supported by the Office of Science, Office of Fusion Energy Sciences, U.S. Department of Energy under Contract No. DE-AC02-05CH11231 and the Laboratory Directed Research and Development (LDRD) funding from the Lawrence Berkeley National Laboratory provided by the Director. Work at the Molecular Foundry was supported by the Office of Science, Office of Basic Energy Sciences, of the U.S. Department of Energy under Contract No. DE-AC02-05CH11231.

SESSION F.SF01.04: Materials Under Plasma/Radiation/Laser

On Demand Abstracts Available for Viewing Starting Saturday Morning, November 21, 2020

F-SF01

### 5:00 AM \*F.SF01.04.01

**Plasma Facing Materials by Self Interstitial Solid Solution Strengthening** Muhammad Musaddique Ali Rafique; Eastern Engineering Solutions LLC, United States

Bubble – a precursor of undersense nanostructure or fuzz formation is crystal lattice defect and is approached by Frenkel pair formation mechanism. One needs to have crystal lattice that inhibits Frenkel Pair generation by ejection of W self-interstitial

atom by He cluster and its bonding with vacancy. However, this mechanism is very commonly observed in nuclear materials. It is applicable in conventional nuclear materials where  $\alpha$  and  $\beta$  particles,  $\gamma$  rays and neutron flux strike the material. Plasma does not constitute of aforementioned and thus it is not very applicable mechanism. In the present study, author addresses this problem of development of plasma facing materials by primitive method of self-interstitial solid solution strengthening. Actual mechanism of bubble formation is studied and a suitable lattice is selected and proposed which inhibits possible Frenkel pair generation thus inherently promotes formation of plasma facing material.

#### 5:15 AM F.SF01.04.03

**Swift Heavy Ion Irradiation Effects in Pre-Damaged Gallium Nitride** Kristina Tomić Luketić<sup>1</sup>, René Heller<sup>2</sup>, Shavkat Akhmadaliev<sup>2</sup>, Henning Lebius<sup>3</sup>, Abdenacer Benyagoub<sup>3</sup>, Isabelle Monnet<sup>3</sup>, Corneliu Ghica<sup>4</sup>, Ferdinand Scholz<sup>5</sup>, Oliver Rettig<sup>5</sup>, Branko Šantić<sup>1</sup>, Stjepko Fazinić<sup>1</sup> and Marko Karlušić<sup>1</sup>; <sup>1</sup>Ruder Boskovic Institute, Croatia; <sup>2</sup>Helmholtz-Zentrum Dresden-Rossendorf, Germany; <sup>3</sup>Normandie Univ, ENSICAEN, UNICAEN, CEA, CNRS, CIMAP, France; <sup>4</sup>National Institute of Materials Physics, Romania; <sup>5</sup>Institute of Functional Nanosystems, Germany

\*Corresponding author: marko.karlusic@irb.hr

When a beam of swift heavy ions (SHI) impinges onto a material, the formation of defects called ion tracks is possible as a result, either in the bulk or on the surface of the material. As a consequence, effects produced by means of SHI irradiation that lead to structural changes of the material can be used to modify the properties of the material via defects engineering. SHI damage introduction to materials can result in complex behavior, especially in radiation harsh environments. To assess the final damage of the material, the effect of the energy deposition from the ions to the atoms within the material must be taken under consideration. Deposition of energy occurs through two main channels: either to the electronic subsystem of the material (electronic stopping power) or to the nuclei (nuclear stopping power). Here we investigate the influence of ion beams with different stopping powers, used in a sequence, on defects formation. It is known that sequential irradiation of ion beams can lead to the SHIBIEC effect (Swift Heavy Ion Beam Induced Epitaxial Crystallization) i.e. the annealing of defects that occurs during the second irradiation step. Alternatively, the anti-SHIBIEC effect is also possible, i.e. the enhanced defect formation during the second step of irradiation.

Sequential ion irradiation of GaN has not been investigated so far. This material is an important semiconductor for high-power electronics. The results presented here are of importance for basic research in this field as well. In our previous work [1], we found no evidence of ion track formation in the bulk after SHI irradiation using 23 MeV I and 90 MeV Xe beams. However, recently we were able to introduce additional disorder into moderately damaged GaN crystals using the same 23 MeV I and 90 MeV Xe beams, in cases where GaN samples have been pre-irradiated with 2 MeV Au or with 900 MeV Xe ion beams. Two different ion beams are expected to introduce damage into GaN either by nuclear or electronic stopping, respectively [2,3]. We observe the difference in total damage in the material depending on the fluence of the beams applied. In this contribution, we report new results of sequential ion irradiation of GaN based on RBS/c (Rutherford Backscattering Spectroscopy in Channeling) and TEM (Transmission Electron Microscopy) measurements.

[1] M. Karlušić et al., Response of GaN to energetic ion irradiation - conditions for ion track formation, J. Phys. D: Appl. Phys. 48 (2015) 325304

[2] S.O. Kucheyev et al., Ion implantation into GaN, Mat. Sci. Eng. 33 (2001) 51

[3] M. Sall et al., Track formation in III-N semiconductors irradiated by swift heavy ions and fullerene and re-evaluation of the inelastic thermal spike model, J. Mater. Sci. (2015) 50:5214–5227

#### 5:25 AM F.SF01.04.05

**Late News: Novel Defect-Fluorite Pyrochlore Sodium Niobate Nanoparticles—Solution-Phase Synthesis and Analysis of Neutron Tolerance** Rana Faryad Ali and Byron Gates; Simon Fraser University, Canada

Materials possessing a defect-fluorite pyrochlore structure can have a range of useful properties that are sought after, which include radiation tolerance, nuclear waste immobilization, and phase stability at elevated temperatures. In this study, we demonstrate for the first time the synthesis and a detailed analysis of defect-fluorite pyrochlore sodium niobate (NaNbO<sub>3</sub>) nanoparticles. This analysis included an investigation into the stability of these nanoparticles at elevated temperatures, as well as to neutron irradiation. A surfactant-assisted solvothermal method was used to prepare nanoparticles of NaNbO<sub>3</sub>. This solution-phase approach results in the formation of crystalline nanoparticles of a defect-fluorite pyrochlore NaNbO<sub>3</sub> at relatively low temperatures. The products had an average diameter of  $\sim 74 \pm 11$  nm. The nanoparticles adopted a defect-fluorite pyrochlore phase and matched the cubic space group. This pyrochlore form of NaNbO<sub>3</sub> was stable up to at least 500 °C. The nanoparticles transformed into the cubic and rhombohedral perovskite phases of NaNbO<sub>3</sub>, along with the introduction of a pseudo-hexagonal Nb<sub>2</sub>O<sub>5</sub> at higher temperatures. These defect-fluorite pyrochlore nanoparticles of

NaNbO<sub>3</sub> also exhibited a resistance to radiation induced amorphization. The dimensions, phase, and crystallinity of the defect-fluorite pyrochlore nanoparticles after exposure to a flux of neutrons were comparable to the as-synthesized product. The thermal stability and radiation tolerance of these pyrochlore nanoparticles could be useful in the design of thermally resilient materials, high temperature catalysts, and durable materials for the handling and storage of radioactive waste.

#### 5:35 AM F.SF01.04.06

**Plasma-Assisted Atomic Layer Annealing as a Low-Temperature Technique Enabling Crystalline Growth of  $\beta$ -Ga<sub>2</sub>O<sub>3</sub> Films for Wearable/Flexible Electronics** Saidjafarzoda Ilhom<sup>1</sup>, Adnan Mohammad<sup>1</sup>, Deepa R. Shukla<sup>1</sup>, John Grasso<sup>1</sup>, Brian Willis<sup>1</sup>, Ali Okyay<sup>2</sup> and Necmi Biyikli<sup>1</sup>; <sup>1</sup>The University of Connecticut, United States; <sup>2</sup>Stanford University, United States

The rapid evolution in technology and its integration with humans requires the development of novel processes that enable the incorporation of the crucial electronic materials, such as the wide bandgap semiconductors (Ga<sub>2</sub>O<sub>3</sub> and GaN) into the wearable electronic systems. Wide bandgap semiconductors form the building blocks of the current high-power high-frequency electronics and the upcoming mmWave fifth-generation (5G) device technologies. To make such technologies integrable with wearable/flexible systems, it is critical that high quality and in particular as-grown crystalline thin films of these materials can be produced on highly temperature-sensitive substrates at very low temperatures.

In this work, we report on the low-temperature, as-grown crystalline Ga<sub>2</sub>O<sub>3</sub> films on various substrates (Si, sapphire, glass, and Kapton) via a hollow-cathode plasma-ALD system. Triethylgallium (TEG) and Ar/O<sub>2</sub> plasma were employed as metal precursor and oxygen co-reactant, respectively. Growth experiments have been performed at 160 – 240 °C substrate temperature and 30 – 200 W rf-power range. Additionally, each unit AB-type ALD-cycle was followed by an in situ Ar-plasma annealing treatment, which consisted of Ar-plasma exposure for 20 seconds scanned over 50 – 300 W rf-power. Both in situ and ex situ ellipsometry were employed to measure the thickness and optical properties of the films. The thickness of the films without Ar-annealing stage, ranged between 20.74 – 39.30 nm and as-grown refractive indices were between 1.75 – 1.67 within the scanned plasma power range. X-ray diffraction (XRD) showed that Ga<sub>2</sub>O<sub>3</sub> films grown without in situ plasma annealing exhibited amorphous structure irrespective of both substrate temperature and rf-power. However, with the in situ Ar-annealing phase incorporated, the thickness of the films ranged between 22.9 – 31.4 nm with refractive indices of 1.75 – 1.79. The increased refractive index (1.79) and reduced thickness gain (31.4 nm) at 250 W Ar-annealing power indicates possible densification and crystallization of the films. Indeed, XRD and XRR confirmed that in situ Ar-plasma treated films grow in a monoclinic  $\beta$ -Ga<sub>2</sub>O<sub>3</sub> crystal phase with further improving crystallinity and film density (from 5.07 to 5.80 g/cm<sup>3</sup>) with increasing Ar-annealing plasma power. Additionally, we will discuss the impact of varying in situ Ar-annealing plasma chemistries (Ar-only, O<sub>2</sub>-only, and Ar/O<sub>2</sub>) coupled with x-ray photoelectron spectroscopy (XPS) measurements, which will provide additional insight into the elemental composition of the films that might help to understand the changes in the structural, optical, and electrical properties. A future outlook will be provided to overcome the challenges to achieve device quality layers on temperature-sensitive flexible substrates.

#### SESSION F.SF01.05: Corrosion

On Demand Abstracts Available for Viewing Starting Saturday Morning, November 21, 2020  
F-SF01

#### 5:00 AM F.SF01.05.03

**Molecular Layer Deposition Approach for Synthesis of SiAlCO Polymer Derived Ceramic (PDC) Thin Films** Kristina Ashurbekova<sup>1</sup>, Karina Ashurbekova<sup>2</sup>, Iva Saric<sup>3</sup>, Evgenii Modin<sup>2</sup>, Mladen Petravić<sup>3</sup>, Aziz Abdulagatov<sup>1</sup>, Mato Knez<sup>2,4</sup> and Ilmutdin Abdulagatov<sup>1</sup>; <sup>1</sup>Dagestan State University, Russian Federation; <sup>2</sup>CIC nanoGUNE, Spain; <sup>3</sup>University of Rijeka, Croatia; <sup>4</sup>IKERBASQUE, Basque Foundation for Science, Spain

Organosilicon polymer derived ceramic (PDC) materials and its derivatives have gained interest as an emerging class of materials capable of providing mechanical stability and heat dissipation upon operation in extreme environments. PDC's found various applications such as electrode material for Li-ion batteries, ultra-high temperature composites and others [1]. Being X-ray amorphous, PDC's consist of nanodomains of different structures and compositions, demonstrating nanoscale heterogeneity that influence their unique mechanical, chemical and functional properties. Conventionally, PDC coatings are prepared by wet-chemical dipping, spinning thermal-spraying or by plasma-assisted chemical vapor deposition (CVD), followed by high temperature pyrolysis [2].

In this work, molecular layer deposited (MLD) hybrid organic-inorganic films serve as precursors for the synthesis of

SiAlCO PDC composite coatings. Alumina-polysiloxane films were grown using sequential surface reactions between 1,3,5,7-tetravinyl-1,3,5,7-tetramethylcyclotetrasiloxane ( $V_4D_4$ ) and trimethylaluminum (TMA). The deposition was conducted at temperatures between 120 and 220 °C. *In-situ* quartz crystal microbalance (QCM) monitoring showed linear mass increase with the number of MLD cycles with the highest mass gain rate of 24 ng/cm<sup>2</sup>/cycle at 180 °C. The QCM study revealed a self-limiting surface chemistry. An infrared analysis (FTIR) of the deposited films showed vibrational features characteristic of organosilicon polymers: Si-CH<sub>3</sub>, Si-O-Si, Si-CH=CH<sub>2</sub> and Si-O-Al peaks. High-resolution transmission electron microscopy (HRTEM) imaging confirmed the conformal nature of the deposited MLD film.

In order to increase mass yield during the polymer-to-ceramic transformation, cross-linking of the growing polymer chains is needed. Cross-linking was achieved at 200°C by introducing a third precursor, di-tert-butyl peroxide (TBPO), into the MLD cycle, following a  $V_4D_4$ /TBP/TMA sequence. A positive mass gain after TBPO dosing, observed by QCM, indicates the formation of radicals and cross-linking. The cross-linking occurs through the activation of the vinyl groups. Characteristic signals, related to the generated polyethylene chains, were identified by ATR-FTIR and XPS. The formed Si-C-C-Si units are expected to improve the mechanical and thermal properties of the cross-linked SiAlCO PDCs, since the Si-C and C-C bonds are not affected by thermal depolymerization reactions.

X-ray and optical characterization techniques were employed to analyze the structural changes and composition of the films after pyrolysis. After pyrolysis at 900°C in an Ar atmosphere, the composite thin film remained amorphous. The resulting film contained uniformly distributed Si, Al, O, and C. Raman spectroscopy showed presence of graphitic carbon within the film. This MLD-derived SiAlCO thin film is expected to have exceptional uniformity, high temperature stability, creep, and corrosion resistance.

[1] P. Colombo, et al., *J. Am. Ceram. Soc.*, 93 (7), 1805–1837 (2010)

[2] G. Borroso, et al, *J. Mater. Chem. A.*, 7 (5), 1936–1963 (2019)

#### 5:10 AM F.SF01.05.04

**Late News: Size-Controlled Formation and Functionalization of Superparamagnetic Magnetite Nanoparticles with Enhanced Colloidal Stability at Extreme High Salinity Condition** Wej Wang, Hooisweng Ow, Sehoon Chang and Bora Yoon; Aramco Services Company; Aramco Research Center-Boston, United States

Magnetic nanoparticles (MNPs) have attracted significant attention in the oil industry in the past decade due to their potential applications including reservoir sensing and mapping, enhanced oil recovery, drilling and completion improvement, oil-water separation in produced water, oil spill clean-up, and directional transport and local heating. For these specific applications, the dispersity and stability of the MNPs in suspension are of great importance. Surface coating and specific functionalization of the MNPs are typically used to improve their stability and to reduce aggregation for the successful use of the nanoparticles. However, many of the well-established methods and procedures of surface coating chemistry for lab applications are not suitable for harsh environmental conditions such as at extreme high salinity for industrial oil applications. In this research, we synthesized magnetite MNPs with tuned particle sizes to optimize their superparamagnetic properties, and developed a new procedure for surface functionalization to enhance their colloidal stability at high salinity. The functionalized magnetite MNPs have been characterized by XRD, HR-TEM, cryo-TEM, dynamic light scattering and zeta potentials. Colloidal stabilities have been studied in a wide pH range and salinity with 5000-230000 ppm of TDS (Total Dissolved Solids). The results have demonstrated that the covalently bonded zwitterionic functional groups and cross-linked saccharide highly enhance the colloidal stability in high salinity brines.

SESSION F.SF01.06: Electrical Field

On Demand Abstracts Available for Viewing Starting Saturday Morning, November 21, 2020

F-SF01

#### 5:00 AM F.SF01.06.01

**Strain-Coupled Electronic Polarization in Semiconducting Oxides Under Extreme Electric Field** Yen-Ting Chi<sup>1</sup>, Mostafa Youssef<sup>2,1</sup>, Bilge Yildiz<sup>1</sup> and Krystyn Van Vliet<sup>1</sup>; <sup>1</sup>Massachusetts Institute of Technology, United States; <sup>2</sup>The American University in Cairo, Egypt

The polarization response of ionic and electronic defects in complex oxides under high electric field is critical for applications such as memristors and ferroelectrics, but historically challenging to model or measure. Here we developed a localized Hubbard U approach that resolves the dilemma of maintaining in-gap localized defect states for an oxygen vacancy



while simultaneously retaining non-linear dielectric behavior of perovskite oxides. With this approach, we obtained accurate dielectric constant and electronic configuration for SrTiO<sub>3</sub> under electric field, using density functional theory and Berry phase calculations. We identified a direct relationship between oxygen vacancy polarizability and lattice strain, which can be generalized to other materials with similar crystal structure. For example, a neutral oxygen vacancy in BaTiO<sub>3</sub> and in SrTiO<sub>3</sub> strained to exhibit the same lattice constants showed identical polarization behavior under the same electric field. To trace the site polarizability difference between defected crystals and their defect-free counterparts, we utilized maximally localized Wannier functions to obtain the site-decomposed polarization. These simulations illustrated that not only the vacant site, but also the neighboring ions around the vacancy have significant influence on the system polarization with field applied either parallel or perpendicular to the Ti – V<sub>O</sub><sup>x</sup> – Ti chain. Together, this model and identification of driving factors in defect displacement under electric field contribute generalizable approaches to study and optimize materials in memristors, ferroelectrics, electrocaloric refrigeration and flash sintering.

SESSION F.SF01.07: High Temperatures  
On Demand Abstracts Available for Viewing Starting Saturday Morning, November 21, 2020  
F-SF01

**5:00 AM F.SF01.07.01**

**High-Temperature and Abrasion Resistant Selective Solar Absorber** Yanpei Tian, Xiaojie Liu and Yi Zheng;  
Northeastern University, United States

Selective solar absorbers with high performance are the key to concentrated solar power systems. Optical metamaterials are emerging as a promising strategy to enhance selective photon absorption, however, the high-temperature resistance (500 C) remains as one of the main challenges for practical applications. Here, a multilayered metamaterial system (Al<sub>2</sub>O<sub>3</sub>/W/SiO<sub>2</sub>/W) based on metal-insulator-metal resonance effect has been demonstrated with high solar absorptance over 92%, low thermal emittance loss below 6%, and significant high-temperature resistance: it has been proved that the optical performance remains 94% after 1-hour thermal annealing under ambient environment up to 500 C, and 94% after 96-hour thermal cycle test at 400 C. Outdoor tests demonstrate that a peak temperature rise (193.5 C) can be achieved with unconcentrated solar irradiance and surface abrasion resistance test yields that SSAs have a robust resistance to abrasion attack for engineering applications.

**5:10 AM F.SF01.07.02**

**Deformation Mechanisms of Alumina-Forming Austenitic Stainless Steels for High Temperature Applications** Andrew Peterson; Dartmouth College, United States

Alumina-forming austenitic stainless steels (AFAs) are a class of alloys that are showing promise for use in high temperature applications, particularly for use in power generation. AFAs have been shown to demonstrate good high temperature strength, great oxidation resistance due to a protective alumina scale, and are cheaper than nickel-base alloys. While showing great promise, these alloys need to continue to be studied and improved to be practical for use. In particular, the deformation behavior of these alloys is not well understood. The austenitic matrix can contain various precipitates, including: L<sub>12</sub> structured precipitates, B<sub>2</sub> precipitates, Laves precipitates, carbides, and others. The grain boundary (GB) also can become covered by Laves and/or B<sub>2</sub> precipitates. In a complex alloy with different types and sizes of precipitates, it can be difficult to determine what effect each of these precipitates are having on the high temperature strength. In this work, we studied the deformation mechanisms in the model AFA alloy Fe-20Cr-30Ni-2Nb-5Al (at%). This alloy displays many characteristics of AFA alloys, and thus is a good alloy for scientific studies. This alloy contains L<sub>12</sub>, Laves, and B<sub>2</sub> precipitates in the matrix as well as Laves and B<sub>2</sub> precipitates on the GBs. Creep tests, high temperature tensile tests, and high temperature strain-rate jump tests were performed on this alloy after various heat treatments to determine the deformation mechanisms – including strain-rate jump tests with and without L<sub>12</sub> precipitates (but otherwise similar microstructures) to determine the effect of these precipitates on the high temperature strength. In addition, tests were performed on alloys with different grain size, but otherwise similar microstructure, to determine the effect of GB precipitation. Analysis of the stress – strain rate relationships was used to predict deformation mechanisms and to fit the experimental data to models. In addition, transmission electron microscopy (TEM) and scanning electron microscopy (SEM) were performed on samples after mechanical testing to determine deformation behavior. In-situ straining experiments in the TEM and SEM were also performed. This study found that nano-sized L<sub>12</sub> precipitates provided the majority of the strengthening in this alloy. At low stresses dislocations by-passed these particles by climb, and at high stresses dislocations

started to form Orowan loops around the particles. While dislocations piled up at larger Laves and B2 precipitates, these precipitates were not as effective at strengthening the alloy. In addition, work was performed to determine if there was a GB strengthening effect due to coverage of the GB by precipitates.

#### Acknowledgements

This research was supported by National Science Foundation (NSF) Grant DMR 1708091.

#### 5:20 AM F.SF01.07.03

**Zn<sub>x</sub>Fe<sub>3-x</sub>O<sub>4</sub> Nanoparticles—Structural and Magnetic Behaviour Evolution After Thermal Treatment up to 1400 °C** Angelika Kmita<sup>1</sup>, Jan Zukrowski<sup>1</sup>, Juliusz Kuciakowski<sup>1,2</sup>, Marianna Marciszko-Wiackowska<sup>1</sup>, Antoni Zywczyk<sup>1</sup>, Dorota Lachowicz<sup>1</sup>, Marta Gajewska<sup>1</sup> and Marcin Sikora<sup>1</sup>; <sup>1</sup>AGH University of Science and Technology, Academic Centre for Materials and Nanotechnology, Poland; <sup>2</sup>AGH University of Science and Technology, Faculty of Physics and Applied Computer Science, Poland

Zinc ferrite nanoparticles are currently of much interest for their potential applications in extreme conditions like high temperature: e.g. in metal casting, in water splitting reaction for H<sub>2</sub> production (solar fuels) or as high - temperature desulfurizing sorbents [1-3]. Bulk ZnFe<sub>2</sub>O<sub>4</sub> (ZF) should have paramagnetic nature around room temperature, when it is the normal spinel with Zn<sup>2+</sup> incorporated mostly in the tetrahedral lattice sites. In the case of nanoparticles, the situation is more complex due to high probability of inversion in the cation distribution between octahedral and tetrahedral sites, which may lead to ferrimagnetism or superparamagnetism [4-6]. It was suggested that during heating Zn<sup>2+</sup> ions can move from tetrahedral site to octahedral site whereas Fe<sup>3+</sup> ions redistribute within the octahedral and tetrahedral sites in order to reduce the strain [7]. It was also speculated the possibility of reduction of Fe<sup>3+</sup> to Fe<sup>2+</sup> during high temperature treatment. In order to verify these hypotheses we have performed a comprehensive study of structural and magnetic properties of stoichiometric and non-stoichiometric zinc ferrite Zn<sub>x</sub>Fe<sub>3-x</sub>O<sub>4</sub> (NZF) nanoparticles synthesized using co-precipitation and thermal decomposition method [2, 8] as well as their evolution after thermal treatment. Nanoparticles with different zinc to iron ratio were obtained and systematically probed with volume (XRD, VSM, TG/DSC), microscopic (TEM) and element sensitive probes (ICP-OES, Mossbauer spectroscopy, XPS, XAFS). Magnetic studies proved paramagnetic response of stoichiometric ZF nanoparticles, while a superparamagnetic behaviour is observed in strongly non-stoichiometric (as synthesized) nanoparticles. After thermal treatment at 1400 °C in inert atmosphere, significant changes in the saturation magnetization were observed in the case of NZF. This is related with an increase of the amount of formally Fe<sup>2+</sup> ions. The estimated saturation magnetization of as synthesized NZF nanoparticles, of approx. 50 emu/g, is increased upon thermal treatment (at 1400 °C in inert atmosphere) up to approx. 130 emu/g. As such we have confirmed that zinc concentration and method of synthesis plays important role in magnetic properties of non-stoichiometric zinc ferrite nanoparticles. Moreover, the reduction of Fe<sup>3+</sup> to Fe<sup>2+</sup> during high temperature treatment has been observed in NZF nanoparticles annealed in inert atmosphere.

**Acknowledgements:** This work was supported by the National Science Centre, Poland, Grant No: 2016/23/D/ST8/00013.

#### References

1. H. Kaneko, T. Kodama, N. Gokon, et al., *Solar Energy.*, Vol. 76, p.317 (2004)
2. A. Kmita, D. Lachowicz, J. Zukrowski, et al., *Materials.*, Vol. 12, p.1048 (2019)
3. A. Kmita, A. Pribulova, M. Holtzer et al. *Archives of Metallurgy and Materials.*, Vol. 61, p.2141 (2016)
4. W. Szczerba, J. Zukrowski, M. Przybylski, et al., *Physical Chemistry Chemical Physics.*, Vol. 18, p.25221 (2018)
5. S. J. Stewart, I.A. Al-Omari, F.R. Sives, et al. *Journal of Alloys and Compounds.*, Vol. 495, p.506 (2010)
6. G. Muscas, N. Yaacoub, G. Concas, et al., *Nanoscale.*, Vol.7, 13576-13585 (2015)
7. J. Philip, G. Gnanaprakash, G. Panneerselvam, et al., *Journal of Applied Physics.*, Vol. 102, 054305 (2007)
8. D. Lachowicz, R. Wirecka, W. Gorka-Kumik, et al., *Physical Chemistry Chemical Physics.*, Vol. 21, 23473 (2019)

#### 5:30 AM F.SF01.07.04

**The Influence of Lattice Defects and Recombination on Thermal Transport in Single Crystal Actinide Oxides** Cody A. Dennett and David H. Hurley; Idaho National Laboratory, United States

Actinide and lanthanide fluorite oxides, UO<sub>2</sub>, CeO<sub>2</sub>, ThO<sub>2</sub>, form an important class of ceramic energy materials with applications ranging from nuclear fuels to solid oxide fuel cells. Of these systems, ThO<sub>2</sub> (thoria), has been the least explored and offers unique features including an extremely high melting temperature and a fixed tetravalent oxidation state. Many potential application environments for thoria include high radiation fields or temperatures which either promote or directly generate lattice defects. Such defects drastically influence thermal transport, a controlling safety and performance property in many applications. To date, little experimentally-validated understanding has been generated on the role of defect formation and clustering on thermal transport in thoria due to the lack of high-quality starting material in which these effects may be

explored. In this work, high-quality oriented single crystals of thoria are grown using hydrothermal synthesis and then exposed to proton irradiation at both room temperature and 600C. The thermal conductivity of the defected surface layer in these crystals is measured using an all-optical spatial domain thermorefectance (SDTR) technique and sub-electron-microscopy-resolution defects are characterized using Raman spectroscopy. Together, these methods provide important initial insight into the types of defects formed under ionizing radiation, defect clustering, and how these defects impact thermal transport in high-quality thoria.

SESSION F.SF01.08: Other Extreme Environment  
On Demand Abstracts Available for Viewing Starting Saturday Morning, November 21, 2020  
F-SF01

#### 5:00 AM \*F.SF01.08.01

**Helium Compounds and Their Dynamical Properties Under Extreme Conditions** Jian Sun; Nanjing University, China

Helium is the most inert element in the periodic table and generally considered to be unreactive under ambient conditions. On the other hand, helium is one of the main components of giant icy planets' atmosphere. It is unclear whether the helium can diffuse into the depths and react with the mantle materials (water, ammonia and methane). In this talk, I will introduce some of our recent theoretical predictions on helium compounds, including helium-water, helium-ammonia, helium-methane and helium-alkali metal oxides/sulfides, etc [1-4], using our own machine learning accelerated crystal structure search method [5]. In addition, we also found that some of these compounds exhibit exotic dynamical properties at high pressure and high temperature, including the superionic, plastic states and their co-existence.

#### REFERENCE

Hao Gao, Cong Liu, Andreas Hermann, Richard J. Needs, Chris J. Pickard, Hui-Tian Wang, Dingyu Xing, and Jian Sun\*, "Coexistence of plastic and partially diffusive phases in a helium-methane compound", **Natl. Sci. Rev.** (2020). DOI: 10.1093/nsr/nwaa064

Cong Liu, Hao Gao, Andreas Hermann, Yong Wang, Maosheng Miao, Chris J. Pickard, Richard J. Needs, Hui-Tian Wang, Dingyu Xing, and Jian Sun\*, "Plastic and Superionic Helium Ammonia Compounds under High Pressure and High Temperature", **Phys. Rev. X** 10, 021007 (2020).

Cong Liu, Hao Gao, Yong Wang, Richard J. Needs, Chris J. Pickard, Jian Sun\*, Hui-Tian Wang\*, Dingyu Xing, "Multiple superionic states in helium-water compounds", **Nature Physics** 15, 1065 (2019).

Hao. Gao, Jian Sun\*, Chris. J. Pickard, Richard. J. Needs, "Prediction of pressure-induced stabilization of noble-gas-atom compounds with alkali oxides and alkali sulfides", **Phys. Rev. Mater.** 3, 015002 (2019).

Kang Xia, Hao Gao, Cong Liu, Jianan Yuan, Jian Sun\*, Hui-Tian Wang\*, Dingyu Xing, "A novel superhard tungsten nitride predicted by machine-learning accelerated crystal structure search", **Sci. Bull.** 63, 817 (2018).

#### 5:15 AM F.SF01.08.02

**Crystal Chemical Design of Novel High Energy Density Polynitrides** Maxim Bykov<sup>1,2</sup>, Elena Bykova<sup>2</sup>, Mohammad Mahmood<sup>1</sup>, Leonid Dubrovinsky<sup>3</sup> and Alexander F. Goncharov<sup>2</sup>; <sup>1</sup>Howard University, United States; <sup>2</sup>Carnegie Institution for Science, United States; <sup>3</sup>University of Bayreuth, Germany

The high-pressure chemistry of nitrogen and nitrogen-rich compounds have been in a focus of many studies in the recent years due to both fundamental and practical interest and due to the improvement of high-pressure synthetic and characterization techniques. Poly-nitrogen compounds are usually considered as potential high energy density materials (HEDM) due to the remarkable difference in the average bond energy between the single N–N bond, the double N=N bond, and the triple N≡N bond. Numerous polynitrogen compounds with various nitrogen polymeric networks were theoretically predicted, but there are only a very few experimental attempts to obtain such compounds.

In the present work we have systematically studied reactions between transition metals and nitrogen at pressures up to 130 GPa in laser-heated diamond anvil cells. Despite very high synthesis pressure Hf, W, Re and Os react with nitrogen forming porous metal-inorganic frameworks Hf<sub>4</sub>N<sub>22</sub>, WN<sub>10</sub>, ReN<sub>10</sub> and Os<sub>5</sub>N<sub>34</sub> of various topologies. The frameworks are built of metals interconnected via polymeric nitrogen linkers, while the pores are filled with dinitrogen molecules N<sub>2</sub>. Lighter transition metals (Fe) form non-porous polynitrides featuring polymeric nitrogen chains, while alkali metals react with nitrogen at extreme conditions with the formation of pentazolite salts. In this contribution we will discuss novel synthetic

routes to energetic polynitrogen compounds and crystal-chemical rules governing their formation.

#### 5:25 AM F.SF01.08.03

##### **Improved Dielectric Properties of $\text{Na}_{1/2}\text{Y}_{1/2}\text{Cu}_3\text{Ti}_4\text{O}_{12}$ Ceramics Synthesized by Ball-Milling and Reactive Sintering** Hicham Kotb and Adil Alshoaibi; King Faisal University, Saudi Arabia

$\text{Na}_{1/2}\text{Y}_{1/2}\text{Cu}_3\text{Ti}_4\text{O}_{12}$  (NYCTO) ceramics with giant dielectric constant ( $\epsilon'$ ) were synthesized by simple reactive sintering. NYCTO nanopowder was first synthesized using high energy ball-mill. Then the pelletized powder was sintered in air at temperatures in the range 975 °C to 1050 °C for 10–20 h. The obtained ceramics showed pure  $\text{CaCu}_3\text{Ti}_4\text{O}_{12}$  (CCTO)-like cubic phase as revealed by x-ray diffraction measurements. Field effect-SEM observations showed that the grain size increases from 2  $\mu\text{m}$  to 5  $\mu\text{m}$  with increasing sintering temperature. NYCTO samples sintered at temperatures higher than 975 °C showed giant dielectric constant (103–104) over most of the frequency range. The minimum dielectric loss ( $\tan\delta$ ) of ~0.055 at 300 K has been approved for the ceramic sample sintered at 1050 °C. Impedance and modulus spectra of the current samples showed two relaxations related to semiconductor (grain) and high resistance (grain-boundaries) elements. The activation energy for conduction located in the range 0.1–0.5 eV highlighted the role of single ionized oxygen vacancies in the dielectric properties of the investigated NYCTO ceramics.

#### 5:35 AM F.SF01.08.04

##### **Simulations of Hydrogen Retention in Polycrystalline Tungsten** Brandon Laufer and Karl D. Hammond; University of Missouri, United States

Tungsten will be the plasma-facing material in the ITER divertor. Hydrogen blistering has been observed in plasma-facing materials, but to date, all electronic structure and molecular mechanics simulations have indicated that hydrogen atoms repel one another in perfect crystals. The influence of grain boundaries on hydrogen retention is also not well-understood. We conducted simulations intended to elucidate the mechanisms of blister formation. These studies were accelerated using direct implantation, as we have used in the past for helium, so that computational time ordinarily required to simulate hydrogen atoms that reflect is instead used to simulate diffusion. Consistent with prior observations, we observe that hydrogen is generally repelled by other hydrogen atoms in single-crystal tungsten and we observe neither self-clustering nor cluster growth of any kind. Near grain boundaries, however, the excess volume present allows hydrogen to cluster. Eventually, sufficient hydrogen concentration can build up and weaken the grain boundary, possibly resulting in delamination of the grains and forming a blister.

#### 5:45 AM F.SF01.08.05

##### **Electric Current and Field Effects on the Microstructural Development of Al Doped ZnO** Claudia Gorynski and Markus Winterer; University Duisburg-Essen, Germany

The present work focuses on understanding the microstructural development during sintering of nanopowders under pressure and electric fields/currents. For this purpose, a method has been developed which combines flash sintering (FS) and spark plasma sintering (SPS) [1]. This FS-SPS combination enables us to combine the advantages of both techniques: to force the electric current through the sample (FS) and to sinter pellet-shaped samples under mechanical loads (SPS). We explored the novel device on the model material Al doped ZnO and discovered a different microstructure, compared to conventional SPS. Grain growth and second phase formation were emphasized by FS-SPS. It remains controversial if the observed microstructure is a result of an intrinsic electric current/field effect or of a temperature-distribution. However, this method helps to understand mechanisms involved in electric current or field assisted sintering techniques and possibly produces new microstructures and, hence, materials.

#### Acknowledgement:

We acknowledge the support from the German Research Foundation (DFG, Deutsche Forschungsgemeinschaft)—Priority Programme (SPP, Schwerpunktprojekt) 1959/1 “Manipulation of matter controlled by electric and magnetic fields: Toward novel synthesis and processing routes of inorganic materials” with Project Nos. WI 981/16-1 and WO 577/13-1.

#### References:

[1] C. Gorynski, U. Anselmi-Tamburini and M. Winterer, Rev. Sci. Instrum. **91**, 015112 (2020); doi: 10.1063/1.5119059

#### 5:55 AM F.SF01.08.07

##### **Tailoring Nanocomposites with Enhanced Failure Tolerance by Interface Engineering** Daniel Kiener<sup>1</sup>, Michael Wurmshuber<sup>1</sup>, Inas Issa<sup>1</sup>, Michael Burtscher<sup>1</sup>, Mingyue Zhao<sup>1</sup> and Christoph Gammer<sup>2</sup>; <sup>1</sup>Montanuniversity Leoben,

Austria; <sup>2</sup>Erich Schmid Institute of Materials Science, Austrian Academy of Sciences, Austria

Designing ever stronger nanostructured materials that can even withstand harsh environments has become a major goal in the last decades. However, the increase in strength commonly comes hand in hand with a severe reduction in ductility, which at the same time also limits the toughness of these materials. Due to the high fraction of interfaces in such nanostructured materials, it is safe to assume that the processes limiting ductility and toughness as well as their response to harsh environments are controlled by the respective interface structures. However, a detailed understanding is at this point still lacking.

Bulk nanostructured materials were synthesized by severe plastic deformation and subject to tailored interface modifications. To investigate the structural properties of these nanomaterials at high stress and strain, we utilize quantitative miniaturized deformation and fracture experiments performed in situ in scanning or transmission electron microscopes. These highly resolved techniques not only allow to measure material performance, but also to directly identify the underlying deformation and failure mechanisms at the same time.

Using this experimental approach, we will first address the nanoscale processes taking place during deformation and fracture of bcc nanocrystalline metals with modified interfaces. Building on this, the discussion will be extended to the behavior of nanocomposite structures and the influence of an irradiative environment.

#### 6:05 AM F.SF01.08.08

**Late News: Multi-Scale Structural Response of Pyrochlore Oxides to Far-from-Equilibrium Processing** Eric O'Quinn<sup>1</sup>, Devon L. Drey<sup>1</sup>, Antonio Fuentes<sup>2</sup> and Maik Lang<sup>1</sup>; <sup>1</sup>University of Tennessee, United States; <sup>2</sup>Cinvestav-Unidad Saltillo, Mexico

Swift heavy ion irradiation and high-energy ball milling are far-from-equilibrium processing techniques which provide access to a unique phase space not achievable by means of traditional synthesis approaches. High-resolution neutron total scattering experiments were utilized to gain fundamental insight into the multi-scale structural details of  $A_2B_2O_7$  pyrochlore oxides prepared by these extreme conditions and their subsequent evolution under high-temperature treatment. Pair distribution function analysis revealed unconventional atomic arrangements characterized by an unexpectedly high degree of local order. For instance, the atomic arrangement of ball-milled titanate pyrochlore oxides is nearly identical to the same pyrochlore composition synthesized by solid-state reaction and subsequently amorphized by intense ion irradiation (1). Interestingly, the same atomic arrangement is found in pyrochlore oxides that exhibit distinct long-range radiation responses (order-disorder *versus* crystalline-amorphous) (2). These phenomena are proposed to be the result of fundamental chemical rules which stringently dictate the atomic configuration in disordered materials (3, 4). This description provides insight into far-from-equilibrium processing of oxides and helps to better elucidate the structural properties and heterogeneity of disordered complex oxides from the local atomic arrangement to the macroscale.

1. E. C. O'Quinn *et al.*, Advanced characterization technique for mechanochemically synthesized materials: neutron total scattering analysis. *J. Mater. Sci.* **53**, 13400–13410 (2018).
2. J. Shamblin *et al.*, Similar local order in disordered fluorite and aperiodic pyrochlore structures. *Acta Mater.* **144**, 60–67 (2018).
3. D. Drey, Disorder in  $Ho_2Ti_{2-x}Zr_xO_7$ : Pyrochlore to Defect Fluorite Solid Solution Series. *RSC Adv.* **In Press** (2020).
4. E. C. O'Quinn *et al.*, Predicting short-range order and correlated phenomena in disordered crystalline materials. *Sci. Adv.* **6**, 1–8 (2020).

SESSION F.SF01.09: Poster Session: Materials for Extreme Conditions (MEC)  
On Demand Abstracts Available for Viewing Starting Saturday Morning, November 21, 2020  
5:00 AM - 8:00 AM  
F-SF01

#### F.SF01.09.04

**Gallium Nitride Nanowire Field Effect Transistor for High Temperature Applications** Kasif Teker and Mustafa A. Yildirim; Istanbul Sehir University, Turkey

Wide bandgap (WBG) semiconductor-based electronics are becoming the center of interest due to their ability to operate at high temperatures and high voltages. Gallium Nitride (GaN), as one of the WBG semiconductors, is a strong candidate that

can meet expectations in high-temperature electronic applications such as military systems, automotive and aerospace control units, gas and oil exploration drilling systems. The superior physical properties of GaN nanowires such as high direct bandgap, high breakdown voltage, and high thermal conductivity, as well as high surface area to volume ratio, make it even more significant material for harsh environments. In this work, we investigate the electrical transport properties of a back-gated single GaN nanowire field-effect transistor (GaNNW-FET) at elevated temperatures.

In order to analyze transport properties ( $I_{DS}$ - $V_{DS}$  and  $I_{DS}$ - $V_{GS}$ ), electrical measurements were performed at temperatures ranging from room temperature to as high as 350°C. The device performs very well until 250°C, whereas it shows some reduction in current values beyond 300°C. In fact, the drain current increases by 2.1, 13.6 and 19.7 times at the temperatures of 100°C and 200°C, 250°C, respectively, with respect to room temperature current at the same bias voltage of 1 V. The enhancement of current is likely due to the reduction of contact resistance between the nanowire and electrodes as well as an increase in thermally excited carrier concentration. On the other hand, degradation of current is likely due to the increase in lattice scattering, lowering the carrier mobility, of the GaN nanowire. Moreover, the influence of high temperature on important transport properties such as transconductance, carrier concentration and carrier mobility will be presented in details. The device offers the following unique advantages: (i) stable operation at high temperatures (at 350°C), (ii) exhibiting an on/off current ratio of  $5.5 \times 10^2$  and a high transconductance value of 3.09  $\mu\text{S}$  at 350°C indicating a good gating effect even at high temperatures, and (iii) offering solutions not only for high-power but also for low-power circuit and photonic applications at high temperature ambients ( $> 300^\circ\text{C}$ ). In summary, GaNNW-FET proves to be an excellent device capable of operating at high temperatures enabling the development of high-performance nanoelectronic/photonic devices especially for harsh conditions.

#### **F.SF01.09.06**

**Mechanical Response of Engineered Segmented Copolymer Coatings to the Growing Tin Whiskers Under Harsh Environments** Preeth Sivakumar<sup>1</sup>, Surbhi Du<sup>2</sup>, John Daye<sup>2</sup>, Matt Selter<sup>2</sup> and Junghyun Cho<sup>1,1</sup>; <sup>1</sup>Binghamton University, The State University of New York, United States; <sup>2</sup>Honeywell Federal Manufacturing & Technologies, National Security Campus, United States

Electrical short circuits caused by the growing tin whiskers can be mitigated by applying a polymeric conformal coating over the whisker-prone tin (Sn) surface which is now common in Pb-free electronics. These conformal coatings should be mechanically adaptable to resist the metallic whisker nucleation and growth while providing enough toughness to avoid cracking ahead of the growing tin whiskers. Importantly, the delamination of conformal coating would provide a space for tin whisker activities that will ultimately result in the vertical growth of tin whisker and its penetration through the coating; hence, the adhesion strength of the conformal coating to tin surface plays an important role. The selection of a conformal coating should consider all these mechanical characteristics because these coatings will be exposed to extreme environmental conditions over a long period. In this study, silicone rubbers were added to the polyurethane-based conformal coatings to form phase-separated nanosized domains for enhanced toughness, which were tested under high temperature and high humidity (HTHH) exposure (85°C/85% relative humidity). Furthermore, in an effort to increase the adhesion of these coatings to the tin surface, silane coupling agents were also applied to the tin surface. The effect of long-term exposure with temperature and moisture (up to 5000 hours) on the chemical degradation of the polymeric coating and its adhesion to the tin surface was examined using Fourier transform infrared spectroscopy (FTIR), Raman spectroscopy, and thermogravimetric analysis (TGA). Mechanical degradation of the nanocomposite coatings under HTHH conditions was evaluated at various length scales by universal testing machine and indentation techniques. In particular, interplays between the degradation of aged conformal coating and the growing tin whiskers under highly compressive stress in the tin layer are highlighted to understand the effectiveness of the conformal coating for tin whisker mitigation. For this, cross-sectional SEM images were obtained from the microtome-sliced coated tin coupons to monitor the growth of tin whiskers under various time stages under HTHH. This study, therefore, provides a potential source of developing an effective polymer coating strategy under harsh environments with optimal mechanical and adhesion properties that can well prevent or entrap the growth of tin whiskers and nodules beneath its coating.

(Honeywell Federal Manufacturing & Technologies, LLC operates the Kansas City National Security Campus for the United States Department of Energy / National Nuclear Security Administration under Contract Number DE-NA0002839)

#### **F.SF01.09.07**

**Seebeck Coefficient of Boride at Ultra-High Temperatures Over 2000 Celsius** Yucheng Lan, Kit Sze, Mikel Tucker and Saroj Pramanik; Morgan State University, United States

Thermoelectric materials have been widely employed to convert heat into electricity and thermocouples. The state-of-art

materials are usually working below 1000 Celsius. Here, a boride with a thermally stable structure up to 3000°C is synthesized. The Seebeck coefficient (thermopower) of the boride is characterized over 2000 Celsius. The phonon/electron transports are investigated under extreme conditions. The investigation would explore applications of thermoelectric materials at ultra-high temperatures.

#### F.SF01.09.08

**Late News: Precipitates Distribution on Susceptibility to Shear Band Formation of Heat Treated 7050 Aluminium Alloy** Francis Tetteh and Solomon Boakye-Yiadom; York University, Canada

The goal of this work was to investigate the influence of grain boundary (GB) precipitates on the susceptibility of 7050 Aluminium alloy to Adiabatic shear band (ASB) during high strain rates using a Direct Impact Hopkinson Pressure Bar (DIHPB). It is demonstrated continuous distributed GB precipitates increase the propensity of ASB formation whereas discontinuously distributed GB precipitates coupled with large precipitation free zones decreases susceptibility to ASB formation of 7050 Aluminium. It is apparent that precipitates within the initial microstructure of 7050 Aluminium before deformation undergo fragmentation and/or dissolution during the occurrence of ASBs at high strain rate deformation.

#### F.SF01.09.09

**Late News: DFT Study of "Unlayered-Graphene Solid" Formation in Liquid Carbon Droplets at Low Pressures** Chathuri Silva<sup>1</sup>, Philip Chrostoski<sup>1</sup> and P. Fraundorf<sup>1,2</sup>; <sup>1</sup>University of Missouri St. Louis, United States; <sup>2</sup>Washington University in St. Louis, United States

At ambient and lower pressures elemental carbon sublimates to vapor near 4000K, even though quenched carbon droplets have been reported in laboratory laser ablation studies [1,2]. However, a subset of meteoritic carbon particles from red giant atmospheres show an “unlayered-graphene solid” core/graphite-rim structure [3,4], likely following condensation of super-cooled carbon droplets from the vapor phase, which nucleated ~40-Å graphene sheets (about 10<sup>19</sup>/cc) on randomly-oriented 5-member rings before solidification and subsequent coating with a graphite rim. Similar core-rim particles (with ~15-Å sheets) can be formed by slow cooling of carbon vapor in the lab [5,6].

The difficulty of experimentation under extreme conditions in a lab remains as a challenge to study the properties of liquid carbon. Therefore, we investigated nucleation and growth of carbon rings and graphene sheets using density functional theory (DFT). Our computations target growth of carbon rings & graphene sheets at the experimental 1.8g/cc density estimate, by relaxing randomized positions of liquid-like 13/20/30/40/60/100-carbon atom clusters in a cubic supercell. Inter-atom distances characteristic of covalent vs. metallic interactions (with a gap in 1.7Å -2.0Å range) allow us to identify covalent “bonds” with small separation. Local energy minima at T = 0K show a mix of sp<sup>2</sup> and sp coordination numbers, plus few sp<sup>3</sup> as in the literature which reports that liquid carbon favors sp coordination at lower densities, sp<sup>3</sup> coordination at higher densities, and a mix of sp and sp<sup>2</sup> coordination at intermediate densities [7-11].

The formation of rings continues to be the same trend in all different sizes of atom clusters, where the ring sizes vary from triangle to heptagon but pentagons are more abundant than hexagons as possible nucleation seeds, also consistent with previous reports [10,11]. The properties of unlayered graphene sheets in a frozen liquid matrix, e.g. as a diffusion barrier, should be interesting to explore further both experimentally and computationally. Further work remains to see if such ab initio studies can confirm that abundant pentagonal rings at this density, during slow cooling of the liquid, can nucleate the growth of faceted pentacones as suggested by electron phase-contrast imaging of the presolar cores [12].

#### References

- [1] D. Kasuya et al., (2002) *J. Phys. Chem B* **106**, 4947.
- [2] W.A. De Heer et al., (2005) *Science* **307**:5711, pp. 907–910.
- [3] P. Fraundorf and M. Wackenhut (2002) *Ap. J. Lett.* **578**(2): L153-156
- [4] T. Kevin Croat et al., (2014) *Elements* **10**, 441-446.
- [5] P. Fraundorf et al., (2019) HAL-02238804.
- [6] P. Fraundorf et al., (2020). *Microscopy and Microanalysis*, 1-4. doi:10.1017/S1431927620022953
- [7] Christopher B. Cannella and Nir Goldman (2015), *J.Phys.Chem* **119**, 29-31.
- [8] J. R. Morris et al., (1995) *Phys. Rev. B* **52**.
- [9] Christine J. Wu et al., (2002), *Phys.Rev.Lett* **89**,135701
- [10] N. A. Marks et al., (2002) *Phys. Rev. B* **65**, 075411.
- [11] Volker L. Deringer and Gábor Csányi (2017) *Phys. Rev. B* **95**, 094203.
- [12] Eric Mandell, "Electron Beam Characterization of Carbon Nanostructures" (2007) Ph.D. Dissertation at UM-St Louis/Rolla.

#### F.SF01.09.10

**Late News: Pressure-Induced Phase Transformations in Iron Carbon Under Hydrostatic Compression** Hoang Thien Luu and Nina Gunkelmann; Clausthal University of Applied Technology, Germany

Pressure-induced phase transformations from body-centered cubic to hexagonal close-packed iron occur at pressures above 13 GPa. The contribution of alloying elements may change the transition pressure. Several studies have documented the role of different alloying elements on diffusionless phase transitions. However, iron-carbon under high pressure conditions has not been analyzed in detail, although carbon forms the basis of modern steels. This study aims to determine the influence of interstitial carbon on the transformation mechanism. We performed molecular dynamics simulations using the Embedded Atom Method (EAM) to explore the potential relationship between carbon and the phase transition in iron. Our results show that octahedral sites are energetically favorable for interstitial carbon atoms. We find that carbon atoms tend to be trapped in tetrahedral sites during the transformation, which results in an increasing threshold pressure.

#### F.SF01.09.11

**Late News: Molecular Dynamics Study of Shock Waves in Iron—On the Role of Plasticity** Hoang Thien Luu<sup>1</sup>, Ramon J. Ravelo<sup>2</sup>, Martin Rudolph<sup>3</sup>, Eduardo M. Bringa<sup>4</sup>, Timothy C. Germann<sup>5</sup>, David Rafaja<sup>3</sup> and Nina Gunkelmann<sup>1</sup>; <sup>1</sup>Clausthal University of Applied Technology, Germany; <sup>2</sup>The University of Texas at El Paso, United States; <sup>3</sup>TU Bergakademie Freiberg, Germany; <sup>4</sup>University of Mendoza, Argentina; <sup>5</sup>Los Alamos National Laboratory, United States

Shock compression is widely used to investigate the mechanical responses of iron under dynamic loading. With shock waves, it is possible to investigate new, previously undiscovered regimes of material dynamics for the discovery of materials inaccessible at ambient conditions. It has been long known that  $\alpha$ -iron transforms to  $\epsilon$ -iron under high pressure. Recently, molecular dynamics simulations have shown that plasticity occurs just before the parent phase transforms into  $\epsilon$ -iron. To provide insights into the interplay of elastic and plastic activities during shocks in iron, we performed atomistic simulations of shock compression of nanocrystalline iron with a mean grain size of 20 nm comprising a total number of 267.5 million atoms. We observed elastic and plastic deformations before the phase transformation takes place. The plastic state is metastable and highly depends on the deformation rate. After a relaxation process of a few picoseconds, the structure transforms into a quasi-3D compressed state in which the new phase is stable. We found that with increasing ramp time of the piston, plastic relaxation is stronger.

Analysis of the X-ray diffraction patterns calculated from the atomistic structure using the Debye equation revealed pronounced anisotropy of the line broadening in hcp Fe that is due to stacking faults and dislocations.

SESSION F.LP06.02: Live Poster Session: Structural and Functional Materials (F.SF01, F.SF02, F.SF03 and F.SF04)

Session Chairs: Ke Han, Chuan Liu and Yongmin Liu

Friday Morning, December 4, 2020

8:00 AM - 10:00 AM

F.SF01

#### F.SF01.09.04

**Gallium Nitride Nanowire Field Effect Transistor for High Temperature Applications** Kasif Teker and Mustafa A. Yildirim; Istanbul Sehir University, Turkey

Wide bandgap (WBG) semiconductor-based electronics are becoming the center of interest due to their ability to operate at high temperatures and high voltages. Gallium Nitride (GaN), as one of the WBG semiconductors, is a strong candidate that can meet expectations in high-temperature electronic applications such as military systems, automotive and aerospace control units, gas and oil exploration drilling systems. The superior physical properties of GaN nanowires such as high direct bandgap, high breakdown voltage, and high thermal conductivity, as well as high surface area to volume ratio, make it even more significant material for harsh environments. In this work, we investigate the electrical transport properties of a back-gated single GaN nanowire field-effect transistor (GaN<sub>NW</sub>-FET) at elevated temperatures.

In order to analyze transport properties ( $I_{DS}$ - $V_{DS}$  and  $I_{DS}$ - $V_{GS}$ ), electrical measurements were performed at temperatures ranging from room temperature to as high as 350°C. The device performs very well until 250°C, whereas it shows some reduction in current values beyond 300°C. In fact, the drain current increases by 2.1, 13.6 and 19.7 times at the temperatures of 100°C and 200°C, 250°C, respectively, with respect to room temperature current at the same bias voltage of 1 V. The



enhancement of current is likely due to the reduction of contact resistance between the nanowire and electrodes as well as an increase in thermally excited carrier concentration. On the other hand, degradation of current is likely due to the increase in lattice scattering, lowering the carrier mobility, of the GaN nanowire. Moreover, the influence of high temperature on important transport properties such as transconductance, carrier concentration and carrier mobility will be presented in details. The device offers the following unique advantages: (i) stable operation at high temperatures (at 350°C), (ii) exhibiting an on/off current ratio of  $5.5 \times 10^2$  and a high transconductance value of 3.09  $\mu\text{S}$  at 350°C indicating a good gating effect even at high temperatures, and (iii) offering solutions not only for high-power but also for low-power circuit and photonic applications at high temperature ambients ( $> 300^\circ\text{C}$ ). In summary, GaNNW-FET proves to be an excellent device capable of operating at high temperatures enabling the development of high-performance nanoelectronic/photonic devices especially for harsh conditions.

#### **F.SF01.09.06**

**Mechanical Response of Engineered Segmented Copolymer Coatings to the Growing Tin Whiskers Under Harsh Environments** Preeth Sivakumar<sup>1</sup>, Surbhi Du<sup>2</sup>, John Daye<sup>2</sup>, Matt Selter<sup>2</sup> and Junghyun Cho<sup>1,1</sup>; <sup>1</sup>Binghamton University, The State University of New York, United States; <sup>2</sup>Honeywell Federal Manufacturing & Technologies, National Security Campus, United States

Electrical short circuits caused by the growing tin whiskers can be mitigated by applying a polymeric conformal coating over the whisker-prone tin (Sn) surface which is now common in Pb-free electronics. These conformal coatings should be mechanically adaptable to resist the metallic whisker nucleation and growth while providing enough toughness to avoid cracking ahead of the growing tin whiskers. Importantly, the delamination of conformal coating would provide a space for tin whisker activities that will ultimately result in the vertical growth of tin whisker and its penetration through the coating; hence, the adhesion strength of the conformal coating to tin surface plays an important role. The selection of a conformal coating should consider all these mechanical characteristics because these coatings will be exposed to extreme environmental conditions over a long period. In this study, silicone rubbers were added to the polyurethane-based conformal coatings to form phase-separated nanosized domains for enhanced toughness, which were tested under high temperature and high humidity (HTHH) exposure (85°C/85% relative humidity). Furthermore, in an effort to increase the adhesion of these coatings to the tin surface, silane coupling agents were also applied to the tin surface. The effect of long-term exposure with temperature and moisture (up to 5000 hours) on the chemical degradation of the polymeric coating and its adhesion to the tin surface was examined using Fourier transform infrared spectroscopy (FTIR), Raman spectroscopy, and thermogravimetric analysis (TGA). Mechanical degradation of the nanocomposite coatings under HTHH conditions was evaluated at various length scales by universal testing machine and indentation techniques. In particular, interplays between the degradation of aged conformal coating and the growing tin whiskers under highly compressive stress in the tin layer are highlighted to understand the effectiveness of the conformal coating for tin whisker mitigation. For this, cross-sectional SEM images were obtained from the microtome-sliced coated tin coupons to monitor the growth of tin whiskers under various time stages under HTHH. This study, therefore, provides a potential source of developing an effective polymer coating strategy under harsh environments with optimal mechanical and adhesion properties that can well prevent or entrap the growth of tin whiskers and nodules beneath its coating.

(Honeywell Federal Manufacturing & Technologies, LLC operates the Kansas City National Security Campus for the United States Department of Energy / National Nuclear Security Administration under Contract Number DE-NA0002839)

#### **F.SF01.09.07**

**Seebeck Coefficient of Boride at Ultra-High Temperatures Over 2000 Celsius** Yucheng Lan, Kit Sze, Mikel Tucker and Saroj Pramanik; Morgan State University, United States

Thermoelectric materials have been widely employed to convert heat into electricity and thermocouples. The state-of-art materials are usually working below 1000 celsius. Here, a boride with a thermally stable structure up to 3000°C is synthesized. The Seebeck coefficient (thermopower) of the boride is characterized over 2000 Celsius. The phonon/electron transports are investigated under extreme conditions. The investigation would explore applications of thermoelectric materials at ultra-high temperatures.

#### **F.SF01.09.08**

**Late News: Precipitates Distribution on Susceptibility to Shear Band Formation of Heat Treated 7050 Aluminium Alloy** Francis Tetteh and Solomon Boakye-Yiadom; York University, Canada

The goal of this work was to investigate the influence of grain boundary (GB) precipitates on the susceptibility of 7050 Aluminium alloy to Adiabatic shear band (ASB) during high strain rates using a Direct Impact Hopkinson Pressure Bar (DIHPB). It is demonstrated continuous distributed GB precipitates increase the propensity of ASB formation whereas discontinuously distributed GB precipitates coupled with large precipitation free zones decreases susceptibility to ASB formation of 7050 Aluminium. It is apparent that precipitates within the initial microstructure of 7050 Aluminium before deformation undergo fragmentation and/or dissolution during the occurrence of ASBs at high strain rate deformation.

#### F.SF01.09.09

**Late News: DFT Study of "Unlayered-Graphene Solid" Formation in Liquid Carbon Droplets at Low Pressures** Chathuri Silva<sup>1</sup>, Philip Chrostoski<sup>1</sup> and P. Fraundorf<sup>1,2</sup>; <sup>1</sup>University of Missouri St. Louis, United States; <sup>2</sup>Washington University in St. Louis, United States

At ambient and lower pressures elemental carbon sublimates to vapor near 4000K, even though quenched carbon droplets have been reported in laboratory laser ablation studies [1,2]. However, a subset of meteoritic carbon particles from red giant atmospheres show an "unlayered-graphene solid" core/graphite-rim structure [3,4], likely following condensation of super-cooled carbon droplets from the vapor phase, which nucleated ~40-Å graphene sheets (about 10<sup>19</sup>/cc) on randomly-oriented 5-member rings before solidification and subsequent coating with a graphite rim. Similar core-rim particles (with ~15-Å sheets) can be formed by slow cooling of carbon vapor in the lab [5,6].

The difficulty of experimentation under extreme conditions in a lab remains as a challenge to study the properties of liquid carbon. Therefore, we investigated nucleation and growth of carbon rings and graphene sheets using density functional theory (DFT). Our computations target growth of carbon rings & graphene sheets at the experimental 1.8g/cc density estimate, by relaxing randomized positions of liquid-like 13/20/30/40/60/100-carbon atom clusters in a cubic supercell. Inter-atom distances characteristic of covalent vs. metallic interactions (with a gap in 1.7Å -2.0Å range) allow us to identify covalent "bonds" with small separation. Local energy minima at T = 0K show a mix of sp<sup>2</sup> and sp coordination numbers, plus few sp<sup>3</sup> as in the literature which reports that liquid carbon favors sp coordination at lower densities, sp<sup>3</sup> coordination at higher densities, and a mix of sp and sp<sup>2</sup> coordination at intermediate densities [7-11].

The formation of rings continues to be the same trend in all different sizes of atom clusters, where the ring sizes vary from triangle to heptagon but pentagons are more abundant than hexagons as possible nucleation seeds, also consistent with previous reports [10,11]. The properties of unlayered graphene sheets in a frozen liquid matrix, e.g. as a diffusion barrier, should be interesting to explore further both experimentally and computationally. Further work remains to see if such ab initio studies can confirm that abundant pentagonal rings at this density, during slow cooling of the liquid, can nucleate the growth of faceted pentacones as suggested by electron phase-contrast imaging of the presolar cores [12].

#### References

- [1] D. Kasuya et al., (2002) *J. Phys. Chem B* **106**, 4947.
- [2] W.A. De Heer et al., (2005) *Science* **307**:5711, pp. 907–910.
- [3] P. Fraundorf and M. Wackenhut (2002) *Ap. J. Lett.* **578**(2): L153-156
- [4] T. Kevin Croat et al., (2014) *Elements* **10**, 441-446.
- [5] P. Fraundorf et al., (2019) HAL-02238804.
- [6] P. Fraundorf et al., (2020). *Microscopy and Microanalysis*, 1-4. doi:10.1017/S1431927620022953
- [7] Christopher B. Cannella and Nir Goldman (2015), *J.Phys.Chem* **119**, 29-31.
- [8] J. R. Morris et al., (1995) *Phys. Rev. B* **52**.
- [9] Christine J. Wu et al., (2002), *Phys.Rev.Lett* **89**,135701
- [10] N. A. Marks et al., (2002) *Phys. Rev. B* **65**, 075411.
- [11] Volker L. Deringer and Gábor Csányi (2017) *Phys. Rev. B* **95**, 094203.
- [12] Eric Mandell, "Electron Beam Characterization of Carbon Nanostructures" (2007) Ph.D. Dissertation at UM-St Louis/Rolla.

#### F.SF01.09.10

**Late News: Pressure-Induced Phase Transformations in Iron Carbon Under Hydrostatic Compression** Hoang Thien Luu and Nina Gunkelmann; Clausthal University of Applied Technology, Germany

Pressure-induced phase transformations from body-centered cubic to hexagonal close-packed iron occur at pressures above 13 GPa. The contribution of alloying elements may change the transition pressure. Several studies have documented the role of different alloying elements on diffusionless phase transitions. However, iron-carbon under high pressure conditions has not been analyzed in detail, although carbon forms the basis of modern steels. This study aims to determine the influence of interstitial carbon on the transformation mechanism. We performed molecular dynamics simulations using the Embedded

Atom Method (EAM) to explore the potential relationship between carbon and the phase transition in iron. Our results show that octahedral sites are energetically favorable for interstitial carbon atoms. We find that carbon atoms tend to be trapped in tetrahedral sites during the transformation, which results in an increasing threshold pressure.

#### F.SF01.09.11

**Late News: Molecular Dynamics Study of Shock Waves in Iron—On the Role of Plasticity** Hoang Thien Luu<sup>1</sup>, Ramon J. Ravelo<sup>2</sup>, Martin Rudolph<sup>3</sup>, Eduardo M. Bringa<sup>4</sup>, Timothy C. Germann<sup>5</sup>, David Rafaja<sup>3</sup> and Nina Gunkelmann<sup>1</sup>; <sup>1</sup>Clausthal University of Applied Technology, Germany; <sup>2</sup>The University of Texas at El Paso, United States; <sup>3</sup>TU Bergakademie Freiberg, Germany; <sup>4</sup>University of Mendoza, Argentina; <sup>5</sup>Los Alamos National Laboratory, United States

Shock compression is widely used to investigate the mechanical responses of iron under dynamic loading. With shock waves, it is possible to investigate new, previously undiscovered regimes of material dynamics for the discovery of materials inaccessible at ambient conditions. It has been long known that  $\alpha$ -iron transforms to  $\epsilon$ -iron under high pressure. Recently, molecular dynamics simulations have shown that plasticity occurs just before the parent phase transforms into  $\epsilon$ -iron. To provide insights into the interplay of elastic and plastic activities during shocks in iron, we performed atomistic simulations of shock compression of nanocrystalline iron with a mean grain size of 20 nm comprising a total number of 267.5 million atoms. We observed elastic and plastic deformations before the phase transformation takes place. The plastic state is metastable and highly depends on the deformation rate. After a relaxation process of a few picoseconds, the structure transforms into a quasi-3D compressed state in which the new phase is stable. We found that with increasing ramp time of the piston, plastic relaxation is stronger.

Analysis of the X-ray diffraction patterns calculated from the atomistic structure using the Debye equation revealed pronounced anisotropy of the line broadening in hcp Fe that is due to stacking faults and dislocations.

#### F.SF02.09.01

**Molecular Dynamics Features for Predicting Metallic Glass Critical Casting Thickness** Lane E. Schultz, Benjamin T. Afflerbach, Izabela Szlufarska and Dane Morgan; University of Wisconsin-Madison, United States

Determining metal compositions that have good Glass Forming Ability (GFA), and in particular that yield bulk metallic glasses through cooling, has been an outstanding grand challenge in metallic glass research. Previous attempts to predict GFA for metals often include some functional form of  $T_g$ ,  $T_x$ , and  $T_i$ , known as the glass transition, the onset of crystallization, and the liquidus temperatures, respectively. For example, the reduced glass transition temperature,  $T_{rg}=T_g/T_i$ , is a well-known GFA indicator. Another well-known GFA indicator is the liquid fragility,  $m$ , which is measured by finding the slope of viscosity as a function of temperature near  $T_g$  for an alloy. Multiple researchers have shown that direct measures of GFA, in particular the critical cooling rate ( $R_c$ ) and critical casting diameter ( $d_{max}$ ), can be written as relatively simple functions of  $T_g$ ,  $T_x$ ,  $T_i$ , and  $m$  [1, 2]. However, these relationships have limited applicability for new materials discovery because a material must be synthesized and measured in order to obtain these features, and they cannot be readily predicted accurately from molecular simulations. However, there are other characteristic temperatures and kinetic properties that have similar physics to that represented in the above features and which are accessible to molecular simulations.

Our study explores to what extent characteristic temperatures of metallic alloys readily accessible to molecular dynamics (MD) can be correlated with  $d_{max}$ . We use MD to predict a set of characteristic temperatures  $\{T_i\}$  for 73 metal alloys and fit  $d_{max}$  as a function of  $\{T_i\}$  using experimental  $d_{max}$  values for 19 of the alloys. We find a 3-fold cross-validation root mean squared error (RMSE) score of 0.512 for the model, well below the standard deviation of 0.848 for the 19  $d_{max}$  values. The remaining 54 alloys are used as a test set and the  $d_{max}$  predictions are used to determine if the alloy should form a glass under melt spinning, and this categorization was then compared to experimental results. We find a maximum F1 score of 0.75 for the categorization model. These cross-validation and F1 scores suggest that the model has significant predictive ability, providing a potential pathway to predicting  $d_{max}$  directly from MD.

#### References

- [1] W. L. Johnson, J. H. Na and M. D. Demetriou, "Quantifying the origin of metallic glass formation," *Nature Communications*, vol. 7, no. 1, p. 10313, 20 12 2016.
- [2] Z. Long, H. Wei, Y. Ding, P. Zhang, G. Xie and A. Inoue, "A new criterion for predicting the glass-forming ability of bulk metallic glasses," *Journal of Alloys and Compounds*, vol. 475, no. 1-2, pp. 207-219, 2009.

#### F.SF02.09.02

**Direct Measurement of Critical Cooling Rates in Metallic Glass Forming Alloys Through a Combinatorial Strategy** Naijia Liu<sup>1</sup>, Tianxing Ma<sup>2</sup>, Chaoqun Liao<sup>3</sup>, Shaofan Zhao<sup>3</sup>, Jonathan P. Singer<sup>2</sup> and Jan Schroers<sup>1</sup>; <sup>1</sup>Yale University, United States; <sup>2</sup>Rutgers, The State University of New Jersey, United States; <sup>3</sup>Qian Xuesen Laboratory of Space Technology, China

Critical Cooling Rate ( $R_c$ ) is the lowest rate a liquid can be cooled to avoid crystallization and vitrify into a glass. While it is a key factor to quantify the glass forming ability (GFA), direct measurement of Critical Cooling Rate ( $R_c$ ) of metallic glass has been cumbersome and challenging and only determined for a few alloys.

The development of science and technologies raise demand for new materials including new Bulk Metallic Glasses. However, it has been estimated that only about 10% of the composition space of potential BMG formation has been considered thus far. To address the large potential compositional space more effectively, combinatorial approaches have been used for the fabrication of large number of alloys in thin film alloy libraries. But attempts to directly quantify critical cooling rates of alloys in such libraries have been limited to the as-sputtered state which forms under a cooling rate exceeding  $10^8$  K/s. Although scientifically important, this high cooling rate is not able to probe practical BMGs, of which the  $R_c$  is always below  $10^3$  K/s. Some progress was made recently by reheating the thin films and reducing the cooling rate to  $\sim 10^5$  K/s. However, this is with a still high cooling rate range.

We will report a fast screening method which is based on Single Pulse Laser Annealing to directly measure  $R_c$  in thin film alloy libraries. Cooling rates ranging from  $10^2$  to  $10^6$  K/s can be realized during solidification of the alloys. To demonstrate this method, we determined  $R_c$  for a large number of alloys in the Al-Ge-Ni system, and identified the best glass forming composition as  $Al_{51}Ge_{35}Ni_{14}$  with a critical cooling rate of  $10^4$  K/s.

#### F.SF02.09.03

**Accelerated Discovery and Mechanical Property Characterization of Bioresorbable Amorphous Alloys Using High-Throughput Methods** Amit Datye, Sebastian A. Kube, Jan Schroers and Udo Schwarz; Yale University, United States

Bioresorbable materials have been of increased interest in the last two decades due to their potentially transforming impact on human body implants. However, even with a large number of groups working on it, there is data available only for a very small number of alloy compositions (<20) in the ternary amorphous alloy systems of magnesium (Mg)–zinc (Zn)–calcium (Ca) and iron (Fe)–Mg–Zn. The optimal alloy compositions for biomedical applications should be chosen from a large variety of available alloys with best combination of mechanical properties (modulus, strength, hardness) and biological response (in-situ degradation rates, cell adhesion and proliferation). This research presents high-throughput screening of more than 150 different compositions each in two different bioresorbable alloy systems. We demonstrate that this new approach will allow future researchers to develop patient- and implant-specific bioresorbable alloys based on specific application requirements. As a first step towards establishing a database designed to enable such targeted material selection, amorphous alloy composition libraries were fabricated employing a combinatorial magnetron sputtering approach where Mg, Zn, and Ca/Fe are co-deposited from separate sources onto a silicon wafer substrate, followed by composition analysis using energy dispersive X-ray spectroscopy and X-ray diffraction measurements and mechanical properties characterization using nanoindentation.

[1] Amit Datye et al., Journal of Materials Chemistry B 7, 5392 (2019).

#### F.SF02.09.04

**Coupling Among Shear Band Initiation, Propagation and Sliding During Plastic Deformation of Metallic Glass Under Constrained Deformation** Zenon H. Melgarejo<sup>1</sup>, Joseph E. Jakes<sup>2</sup> and Donald S. Stone<sup>1</sup>; <sup>1</sup>University of Wisconsin-Madison, United States; <sup>2</sup>Forest Biopolymer Science and Engineering, USDA Forest Products Lab, United States

When, in the regime of inhomogeneous flow, a metallic glass is constrained during plastic deformation, all aspects of the kinetics of shear banding, including initiation, advance of the tip, and "shear," or displacement across its thickness, become coupled. An example is the indentation experiment, in which surrounding material, loaded elastically, constrains deformation within the plastic zone and leads to a self-similar, hemispherical pattern of shear bands falling along multiple orientations surrounding the indent. Likewise, in metallic glass composites the reinforcement phases introduce constraints because they disrupt shear band propagation and shear. In each case, the effect of the constraint is to introduce a back stress, which leads to an increase in deformation resistance similar to kinematic hardening in crystalline composites. From indentation experiments, we can measure the

strength of this coupling in terms of a "hardening modulus," the magnitude of which can be determined from the fluctuations in slope of the load-depth curve during serrated loading. It is expected that the hardening modulus will depend on both material properties and the geometry of the constraint.

Using nanoindentation experiments with a Berkovich indenter, we measure the hardening modulus in ZrCuAl metallic glass ribbons and ingots across 2 decades of strain rate during loading and 6 decades of strain rate during constant load creep. Hardening modulus is nearly independent of load despite a size effect in the serrations. Relaxing the glass near T influences the hardening modulus. The magnitude of the constraint is the same during constant load creep and during loading. Work arguments allow us to arrive at a model for coupled deformation, from which we estimate the magnitude of the constraint modulus in terms of the shear modulus of the glass, G. We compare this estimate with experimentally measured values.

#### **F.SF02.09.05**

**Bicontinuous Nanoporous Design Induced Homogenization of Strain Localization in Metallic Glasses** Chang Liu and Paulo Branicio; University of Southern California, United States

Bicontinuous nanoporous metallic glasses (MG) synergize the outstanding properties of MGs and open cell nanoporous materials. The low-density and high-specific-surface-area of bicontinuous nanoporous structures have the potential to enhance the applicability of MGs in catalysis, sensors, and lightweight structural designs. In this work we generated stochastic bicontinuous structure using an efficient direct method based on Cahn's idea and Fibonacci grids. We then perform molecular-dynamics simulations of tensile loading on a bicontinuous nanoporous  $\text{Cu}_{64}\text{Zr}_{36}$  and characterize the deformation mechanisms dictating its elastic and plastic response preceding failure. Results indicate an anomalous MG mechanical behavior featuring extensive plastic deformation preceding a typically ductile failure. Results show progressive necking of ligaments aligned with the loading direction and progressive alignment of randomly oriented ligaments during the loading. Failure occurs by fracture following successive necking and rupture of ligaments. This work indicates that a bicontinuous nanoporous design is able to effectively delocalize strain localization in a bulk MG by utilizing the size effect of MG nanopillars and nanowires that induces a brittle to ductile transition in their mechanical behavior as ligament sizes are reduced to less than 100 nm.

#### **F.SF02.09.06**

**Tuning the Mechanical Properties of Shape Memory Metallic Glass Composites with Brick and Mortar Designs** Suyue Yuan and Paulo Branicio; University of Southern California, United States

The intricate deformation and failure of a shape memory alloy-bulk metallic glass composites (BMGC) under tensile loading is investigated with large-scale molecular dynamics simulations. By carefully choosing the volume fraction and the arrangement of the crystalline phase the failure of the BMGC is shifted from the propagation of a critical shear band in the amorphous matrix to yield and failure of the crystalline second phase. Results show that a brick and mortar design with staggered crystalline bricks (stg-BMGC) is able to further synergize the mechanical properties of the amorphous and crystalline phases. By effectively distributing the local stress and preventing the generation of a critical shear band the stg-BMGC design displays enhanced ductility while preserving the strength of the metallic glass matrix.

#### **F.SF03.12.01**

**Thermal Behaviors of Hydrocarbon-Coated Aluminum Nanoparticles as Energetic Metamaterials in Combustion Applications—A ReaxFF Molecular Dynamics Study** Sungwook Hong, Roxanne Esparza and Ryan Parlier; California State University, Bakersfield, United States

Aluminum nanoparticles (ANPs) have been considered attractive additives for combustible applications because the ANPs possess a high energy density with an increased burning rate, owing to an increased surface area-to-volume ratio.<sup>1</sup> Unfortunately, use of the ANPs is limited by two factors: (1) ANPs can be readily sintered; and (2) ANPs can be easily oxidized, prior to the combustion process due to their high reactivity, degrading the combustion performance. To resolve this issue, synthesis of metamaterials, using ANPs and hydrocarbon has been suggested. For example, ANPs could be effectively coated by hydrocarbon precursors to improve its combustion performance.<sup>2,3</sup> The previous studies reported that the hydrocarbon-coated ANPs are less reactive at low temperatures and they became susceptible to the oxidation at higher temperatures, suggesting that the hydrocarbon coating is essential for the ANPs to be used as combustible materials.<sup>4,5</sup> However, a molecular-level understanding of thermal behaviors of the hydrocarbon-coated ANPs has yet to be achieved. Here we perform reactive molecular dynamics (RMD) simulations based on ReaxFF<sup>6</sup> to investigate effects of hydrocarbon coating on the combustion process of the ANPs including sintering and oxidation processes. Our RMD

simulations reveal molecular-level reaction steps for the combustion process of the bare/hydrocarbon coated ANPs. As such, our RMD simulations will help guide an experimental design of a novel energetic metamaterial using ANPs and hydrocarbon, providing a valuable input for the community of solid-fuel propellants.

S.H. and R.P. acknowledge a start-up funding from School of Natural Science, Mathematics and Engineering at California State University, Bakersfield (CSUB). A.M. acknowledges a funding support from Student Research Scholar (SRS) program at CSUB.

## References

- [1] Yetter, R. A.; Risha, G. A.; Son, S. F. Metal Particle Combustion and Nanotechnology. *Proc. Combust. Inst.* **2009**, 32, 1819–1838
- [2] Park, K.; Rai, A.; Zachariah, M. Characterizing the Coating and Size-Resolved Oxidative Stability of Carbon-Coated Aluminum Nanoparticles by Single-Particle Mass-Spectrometry. *J. Nanopart. Res.* **2006**, 8, 455–464.
- [3] Guo, L.; Song, W.; Hu, M.; Xie, C.; Chen, X. Preparation and Reactivity of Aluminum Nanopowders Coated by Hydroxyl-Terminated Polybutadiene (Htpb). *Appl. Surf. Sci.* **2008**, 254, 2413–2417.
- [4] Park, K.; Rai, A.; Zachariah, M. Characterizing the Coating and Size-Resolved Oxidative Stability of Carbon-Coated Aluminum Nanoparticles by Single-Particle Mass-Spectrometry. *J. Nanopart. Res.* **2006**, 8, 455–464.
- [5] Hong, S. and van Duin A. Atomistic-Scale Analysis of Carbon Coating and Its Effect on the Oxidation of Aluminum Nanoparticles by ReaxFF-Molecular Dynamics Simulations. *J. Phys. Chem. C* **2016**, 120, 9464–9474
- [6] Senftle, T. P.; Hong, S.; Islam, M. M.; Kylasa, S. B.; Zheng, Y.; Shin, Y. K.; Junkermeier, C.; Engel-Herbert, R.; Janik, M. J.; Aktulga, H. M. The ReaxFF Reactive Force-Field: Development, Applications and Future Directions. *npj Comput. Mater.* **2016**, 2, 15011.

## F.SF03.12.02

**Computational Design of Energetic Metamaterials Using Graphene-Supported Aluminum Nanoparticles—A ReaxFF Molecular Dynamics Study** [Ryan Parlier](#), Andrew Martinez and Sungwook Hong; California State University, Bakersfield, United States

Aluminum nanoparticles (ANPs) have attracted a great amount of interest owing to their high energy density, high reaction rate, earth abundance, and low toxicity.<sup>1</sup> ANPs have been considered effective energetic materials. Unfortunately, ANPs are easily oxidized at room temperature, leading to oxide layers on their surfaces. Those oxide layers work as a dead weight. Therefore, it is vitally important to design a novel metamaterial that improves the combustion performance of ANPs. Recent studies show that adding graphene oxide and graphene fluoride improves the combustion performance of ANPs.<sup>2,3</sup> This is mainly due to a synergistic effect between graphene sheets and ANPs. For example, oxygen molecules could be easily dissociated when they get closer to both graphene sheets and ANPs. As such, we hypothesize that graphene-supported ANPs, which could be considered novel energetic metamaterials, provide a remarkable combustion performance. Here we simulate the oxidation of graphene-supported ANPs using reactive molecular dynamics (RMD) simulations based on ReaxFF.<sup>4</sup> Our RMD simulations reveal atomic-level reaction mechanism for the improved oxidation process of graphene-supported ANPs. As such, the RMD results will help guide an experimental design of a novel energetic metamaterial using graphene sheets and ANPs, providing a valuable input for the community of energetic metamaterials.

S.H. and R.P. acknowledge a start-up funding from School of Natural Science, Mathematics and Engineering at California State University, Bakersfield (CSUB). A.M. acknowledges a funding support from Student Research Scholar (SRS) program at CSUB.

## References

- [1] Yetter, R. A.; Risha, G. A.; Son, S. F. Metal Particle Combustion and Nanotechnology. *Proc. Combust. Inst.* **2009**, 32, 1819–1838
- [2] Jiang, Y.; Deng, S.; Hong, S.; Zhao, J.; Huang, S.; Wu, C.-C.; Gottfried, J. L.; Nomura, K.-i.; Li, Y.; Tiwari, S.; Kalia, R. K.; Vashishta, P.; Nakano, A.; Zheng, X. Energetic Performance of Optically Activated Aluminum/Graphene Oxide Composites. *ACS Nano* **2018**, 12, 11366–11375.
- [3] Jiang, Y.; Deng, S.; Hong, S.; Tiwari, S.; Chen, H.; Nomura, K.; Kalia, R. K.; Nakano, A.; Vashishta, P.; Zachariah, M.; Zheng, X. Synergistically Chemical and Thermal Coupling between Graphene Oxide and Graphene Fluoride for Enhancing Aluminum Combustion. *ACS Appl. Mater. Interfaces* **2020**, 12, 7451–7458
- [4] Senftle, T. P.; Hong, S.; Islam, M. M.; Kylasa, S. B.; Zheng, Y.; Shin, Y. K.; Junkermeier, C.; Engel-Herbert, R.; Janik, M. J.; Aktulga, H. M. The ReaxFF Reactive Force-Field: Development, Applications and Future Directions. *npj Comput.*

Mater. 2016, 2, 15011.

### F.SF03.12.03

**Spin-Valley Locked Edge States in Staggered Chiral Photonic Crystal** Yeseul Kim, Minkyung Kim and Junsuk Rho; Pohang University of Science and Technology, Korea (the Republic of)

Topological phases of matters, firstly investigated in condensed matter physics, have been extended to other wave physics such as photonics. In this poster presentation, we present spin-valley locking of edge states in a chiral photonic crystal in the two-dimensional honeycomb lattice. Using a coupled dipole method, we demonstrate bulk band structure with a band gap, which is spanned by the spin-valley locked edge states. The staggered chirality breaks the inversion symmetry and the chirality provides the spin-valley locking characteristics.

### F.SF03.12.06

**Late News: Computational Synthesis of Novel Energetic Metamaterials Using Metal Nanoparticles and Hydrocarbon Precursors for Combustion Applications** Roxanne Esparza and Sungwook Hong; California State University, Bakersfield, United States

The use of aluminum nanoparticles (ANPs) in combustion applications has attracted a great amount of attention owing to their high energy density with an increased burning rate.<sup>1</sup> Unfortunately, due to the nature of ANPs' high reactivity, the ANPs are easily sintered, leading to an increase in their particle size, and thus lowering the combustion efficiency. In order to tackle this issue, recent efforts have been made to synthesize novel metamaterials, using ANPs and hydrocarbon precursors. For example, ANPs could be effectively coated by hydrocarbon precursors to lower their reactivity, thus preventing sintering effects of ANPs. However, an effect of precursor types of hydrocarbon on sintering behaviors of ANPs has yet to be understood at the atomic level. Here we perform reactive molecular dynamics (RMD) simulations based on ReaxFF<sup>2</sup> to investigate computational synthesis of energetic metamaterials using ANPs and carbon precursors. In particular, we employed different types of carbon precursors to evaluate the sintering behaviors of ANPs. Our RMD simulations suggest detailed reaction steps for the sintering process of the bare/hydrocarbon coated ANPs. As such, our RMD simulations will help provide a valuable input for experimental synthesis of a novel metamaterial using ANPs and hydrocarbon for combustion application.

S.H. and R.E. acknowledge a start-up funding from School of Natural Science, Mathematics and Engineering at California State University, Bakersfield (CSUB).

### References

[1] Yetter, R. A.; Risha, G. A.; Son, S. F. Metal Particle Combustion and Nanotechnology. Proc. Combust. Inst. 2009, 32, 1819–1838

[2] Senftle, T. P.; Hong, S.; Islam, M. M.; Kylasa, S. B.; Zheng, Y.; Shin, Y. K.; Junkermeier, C.; Engel-Herbert, R.; Janik, M. J.; Aktulga, H. M. The ReaxFF Reactive Force-Field: Development, Applications and Future Directions. npj Comput. Mater. 2016, 2, 15011.

### F.SF03.12.07

**Late News: Humidity-Dependent Flaw Sensitivity in the Crack Propagation Resistance of 3D-Printed Nano-Ceramics** Edoardo M. Rossi<sup>1</sup>, Jens Bauer<sup>2</sup> and Marco Sebastiani<sup>1</sup>; <sup>1</sup>Università degli Studi Roma Tre, Italy; <sup>2</sup>University of California, United States

Pyrolytic 3D-printed carbon nano-ceramics currently emerge as a class of lightweight materials with exceptional mechanical strength and stiffness, being characterized by feature-sizes well below the capabilities of the highest-resolution 3D additive manufacturing techniques alone. Despite the increasing applications, their use is hampered by the lack of knowledge on their mechanical reliability. Few studies have investigated their intrinsic mechanical properties: important characteristics, like hardness and fracture toughness, and their dependency on environmental conditions, which can be relevant for a thorough understanding of the complex mechanical behaviour of additively manufactured pyrolytic carbon structures, are unknown. In this work, we present nanoindentation splitting of TPP-DLW-derived pyrolytic carbon micro-pillar specimens, characterized by a diameter of 5.3  $\mu\text{m}$  and a height-to-diameter ratio of two, as a straight-forward method to measure the fracture toughness and nanoindentation continuous stiffness measurements for the assessment of the elastic modulus and hardness. Micro-pillars with and without SEM detectable surface flaws, absent of STEM-detectable internal defects, were

tested at two extremal intervals of the environmental relative humidity, humid air was used to adjust RH at values greater than 60% and dry nitrogen at room pressure ensured RH levels below 5%, to investigate the impact of pyrolysis-induced surface flaws and the interplayed effects with the testing environment on the mechanical reliability of the 3D printed nanoceramics. We show that TPP-derived pyrolytic carbon can achieve 500% increased fracture toughness over macroscopic forms of vitreous carbon, which typically lies in the range of 0.5-1.4 MPam<sup>0.5</sup>, with values up to 3.1 MPam<sup>0.5</sup>. However, experiments at RH > 60% revealed a detrimental effect of high relative humidity environments on the fracture toughness of the pyrolytic carbon nano-ceramic structures, causing embrittlement due to liquid diffusion ascribed to the presence of only a few, nanometer-sized, which probably promotes crack propagation under external loading due to chemically induced structural weakening of the glassy carbon structure. While comparable effects are less relevant in macro-size ceramics, this study demonstrates that reliability and durability of micro- and nano-architected ceramic metamaterials and devices require toughening design approaches which focus on size-dependent surface effects. The observed humidity effect can have a remarkable impact on the scale-up of such nano-architected metamaterial in a wide range of applications, especially biomedical and micro-fluidics fields.

#### **F.SF03.12.08**

**Late News: Infrared Reflecting/Transmitting Smart Glass For Energy Efficient Windows** Mark Altwerger, Yashashvini Andugula, Harry Efstathiadis and Iulian Gherasoiu; SUNY Polytechnic Institute CNSE, United States

Low-e glass panes are not well adapted for use in regions where the predominant heat that passes through windows has its origin indirect solar radiation. Almost 49% of solar energy is distributed in the spectrum from 0.7-2.5 $\mu$ m for which low-e glass-pane reflectivity is below 10%. This is the case with 14% of the contiguous U.S. according to NREL. The metamaterial that we propose is a robust, thin-film structure that has the ability to reflect near-infrared heat radiation (NIR) with  $\lambda$  0.7-10 $\mu$ m while transmitting more than 90% of the visible light intensity. The ability to reflect NIR and transmit selected wavelength range is obtained through the field-enhanced electron concentration of moderately doped metal oxide thin films. Approximately 48% of the total energy produced in the U.S. or 18.6 billion kWh is spent on heating and cooling. Therefore, the ability to retrofit this technology onto existing buildings is of considerable interest. Electrical and optical characterization demonstrate the synthesis of state-of-the-art materials with properties suitable for the fabrication of smart glass devices.

#### **F.SF04.07.01**

**Low-Voltage IGZO Thin-Film Transistors Using SAM Surface Modification on Ta<sub>2</sub>O<sub>5</sub> as the Gate Dielectric** Navid Mohammadian and Leszek A. Majewski; The University of Manchester, United Kingdom

Low-voltage, high-performance thin-film transistors (TFTs) have been getting tremendous attention over recent years due to the increasing demand for low-power, portable electronic devices and sensor arrays. However, reducing the power consumption of TFTs is an extremely challenging task [1]. High- $\kappa$  dielectric materials are thought to play an essential role in applications where a low-power device operation is needed.

In particular, tantalum pentoxide (Ta<sub>2</sub>O<sub>5</sub>) is a very promising candidate due to the high dielectric constant in the bulk ( $\kappa_{\text{bulk}} \sim 27$ ) and as a thin-film ( $\kappa_{\text{thin-film}} \sim 20$ ). These values are at least two times larger than that of Al<sub>2</sub>O<sub>3</sub> ( $\kappa_{\text{bulk}} \sim 9$ ) and five times larger than that of SiO<sub>2</sub> ( $\kappa_{\text{bulk}} \sim 3.9$ ) [2]. As a result, Ta<sub>2</sub>O<sub>5</sub> has been abundantly used in electrolytic capacitors, DRAM devices, and recently in solution-processed inorganic semiconductor thin-film transistors as a promising gate dielectric for low-power electronics [3].

whereas high-k insulators introduce undesirable effects at the semiconductor-insulator interface which generally leads to increased trapping which causes a rise of V<sub>TH</sub> and SS, as well as lowers the field-effect mobility of charge carriers in TFTs [4]. To overcome both issues in low voltage organic thin-film transistors (OTFTs) passivating of the high-k metal oxides surfaces with self-assembled monolayer (SAM) compounds is routinely used [5]. Although modification of ultra-thin ( $d \leq 20$  nm) metal oxide gate dielectrics with SAMs is currently a common process in organic TFTs [6], this approach has not yet been explored in metal oxide semiconductor transistors.

In this talk, low-voltage a-IGZO TFTs using solution-deposited, OTS-modified Ta<sub>2</sub>O<sub>5</sub> operating at 1 V are presented. The optimised devices display threshold voltages V<sub>TH</sub> around 0.4 V, subthreshold swings (SS) below 90 mV/dec, current on/off ratios larger than 10<sup>5</sup>, and field-effect mobility in excess of 2.3 cm<sup>2</sup>/Vs. The morphology and dielectric properties of both pristine and OTS-treated thin Ta<sub>2</sub>O<sub>5</sub> films have been studied. It is shown that the proposed approach has a high potential to enable the design of stable, low-voltage organic semiconductor circuitry in a highly reproducible manner.

#### References

[1] R. P. Ortiz, A. Facchetti, and T. J. Marks, "High-k organic, inorganic, and hybrid dielectrics for low-voltage organic



field-effect transistors,” *Chem. Rev.*, vol. 110, no. 1, pp. 205–239, 2010.

[2] S. Ezhilvalavan and T. Y. Tseng, “Preparation and properties of tantalum pentoxide (Ta<sub>2</sub>O<sub>5</sub>) thin films for ultra large scale integrated circuits (ULSIs) application -- A review,” *J. Mater. Sci. Mater. Electron.*, vol. 10, no. 1, pp. 9–31, Mar. 1999.

[3] N. Mohammadian, S. Faraji, S. Sagar, B. C. Das, M. L. Turner, and L. A. Majewski, “One-Volt, Solution-Processed Organic Transistors with Self-Assembled Monolayer-Ta<sub>2</sub>O<sub>5</sub> Gate Dielectrics,” *Materials (Basel)*, vol. 12, no. 16, p. 2563, 2019.

[4] Q. Wang, W. Wang, S. Jin, H. Zhu, and N. T. Zhang, “Quality-optimized joint source selection and power control for wireless multimedia D2D communication using stackelberg game,” *IEEE Trans. Veh. Technol.*, vol. 64, no. 8, pp. 3755–3769, 2015.

[5] P. Barquinha *et al.*, “Low-temperature sputtered mixtures of high- $\kappa$  and high bandgap dielectrics for GIZO TFTs,” *J. Soc. Inf. Disp.*, vol. 18, no. 10, pp. 762–772, 2010.

[6] P. Sista *et al.*, “Enhancement of OFET performance of semiconducting polymers containing benzodithiophene upon surface treatment with organic silanes,” *J. Polym. Sci. Part A Polym. Chem.*, vol. 49, no. 10, pp. 2292–2302, 2011.

#### F.SF04.07.02

##### **Direct Langmuir-Blodgett Deposition of Few-Layered 2H WSe<sub>2</sub> Flakes for Electrical Characterization** Madina

Telkhozhayeva<sup>1</sup>, Rajashree Konar<sup>1</sup>, Eti Teblum<sup>1</sup>, Hagit Aviv<sup>1</sup>, Maria Tkachev<sup>2</sup>, Olga Girshevitz<sup>2</sup>, Yaakov Tischler<sup>1</sup> and Gilbert D. Nessim<sup>1</sup>; <sup>1</sup>Bar-Ilan University, Israel; <sup>2</sup>Institute of Nanotechnology and Advanced Materials, Bar-Ilan University, Israel

Two-dimensional (2D) semiconductors have attracted extensive research interest due to their unique size, atomic thickness and band structure. In this respect, transition metal di-chalcogenides (TMDCs) are leading candidates because of strong in-plane chemical bonds and out-of-plane weak interactions. This allows them to be exfoliated into so-called 2D flakes, which can be micrometers wide but less than a nanometer thick. Among them, 2H-WSe<sub>2</sub> as a layered 2D material demonstrates remarkable properties such as low thermal conductivity, high carrier mobility, and direct band-gap, thus offering a suitable platform for next generation nanoscale devices [1-2].

Liquid-phase exfoliation (LPE) of bulk TMDCs can yield high-quality semiconducting flakes dispersed in commonly used solvents. Although a considerable number of research with LPE methods towards 2H-WSe<sub>2</sub> has been conducted, there are lack of reports on controlled organization of these exfoliated flakes on substrates. This step is crucial since produced 2H-WSe<sub>2</sub> flakes tend to restack into a bulk structure via van der Waals interactions, which significantly limit device applications. Langmuir-Blodgett (LB) assembly is an effective and easily integrated approach for arranging 2D flakes into highly ordered single-layer and multilayered films with controllable thickness, well-defined structure, and homogeneity.

Here, we present a cost-effective and facile technique for the controlled processing of 2D 2H-WSe<sub>2</sub> dispersions into uniform close-packed flakes via the LB method. Bulk 2H-WSe<sub>2</sub>, synthesized using an atmospheric-pressure chemical vapor deposition (AP-CVD) technique, was exfoliated into mono- to few-layered 2H-WSe<sub>2</sub> flakes using low-boiling solvent (ethanol) at high-frequency bath sonication system. The compression of the liquid-exfoliated WSe<sub>2</sub> flakes on the water sub-phase was used to form a continuous layer, which was subsequently transferred onto a pretreated substrate. UV-Vis, Raman, AFM, HRSEM and HRTEM prove that the as-deposited material is successfully exfoliated from bulk 2H-WSe<sub>2</sub> into mono- to few-layered flakes. Furthermore, we studied the electrical properties of the FIB-fabricated 2H-WSe<sub>2</sub> flake device using a two-probe current versus voltage (I-V) measurements. The proposed technique provides a simple path to assemble structures of solution-processed 2D semiconductors avoiding the challenges related to high cost and high temperature processing for further applications in electronics and optoelectronics.

#### References

[1] Sahin *et al.*, *Phys. Rev. B*, 2013, 87, 165409.

[2] Allain *et al.*, *ACS Nano*, 2014, 8, 7180-7185.

#### F.SF04.07.03

**Effect of DUV Curing on Low-Temperature Synthesis of IZO Semiconductor-Based TFTs** Alessio Mancinelli<sup>1</sup>, Sami Bolat<sup>2</sup>, Jaemin Kim<sup>1</sup>, Yaroslav E. Romanyuk<sup>2</sup> and Danick Briand<sup>1</sup>; <sup>1</sup>EPFL, Switzerland; <sup>2</sup>Empa–Swiss Federal Laboratories for Materials Science and Technology, Switzerland

Solution processing is an attractive alternative to standard vacuum fabrication techniques for the large-area manufacturing of metal-oxide (MO<sub>x</sub>) based electron devices. In this frame, thin-film transistors (TFTs), which serve as the essential electronics building blocks, have to be primarily addressed. Furthermore, when these TFTs are realized on flexible substrates, many

potential applications such as displays, chemical sensors, and conformable wearable devices, could be envisioned. However, the need for high-temperature sintering processes ( $T > 350\text{ }^{\circ}\text{C}$ ) has restrained thus far their commercial diffusion. The necessity for temperature-resistant polyimide as a substrate has restrained their field of application mainly to displays (e.g. indium gallium zinc oxide (IGZO) on polyimide). More economic and environmental-friendly substrates such as PET, cellulose, and biopolymers will become essential in future daily life applications requiring cheap and perhaps disposable devices. Among others, smart label sensors for temperature and chemical monitoring of food, realized directly in the packaging could be enabled. Accordingly, the development of a production process compatible with such thermosensitive substrates has to be addressed.

One of the key challenges for the full exploitation of these devices is the reduction of the thermal budget required for the  $\text{MO}_x$  synthesis. Our approach is based on the use of deep ultraviolet light (DUV) to promote the sol-gel synthesis reaction and therefore reduce the thermal budget of the process. The energetic photons generated by the DUV lamp are used to photo-activated the chemical reactions and initiating the M–O–M bond formation inside the deposited thin film. The quality of the  $\text{MO}_x$  layer is further enhanced by the heat treatment which eliminates the undesired reaction residuals and densifies the film. Similar photonic processes for solution-processed metal-oxide transistors have been mainly based on indium oxide ( $\text{InO}_x$ ) as semiconductor material. The more convenient chemistry of  $\text{InO}_x$  facilitates its solution processing at low-temperature. However, the films obtained from these compounds can suffer from unstable behaviour and operation at negative voltages. We report on TFTs based on a solution-processed indium zinc oxide (IZO) semiconductor utilizing a DUV enhanced curing, which enables a reduction of the processing temperature. A parametric analysis of the curing parameters has been carried out in to investigate the minimal conditions required to achieve performing devices. In this frame, we compared the efficiency of a post-annealing step in with in-situ combined DUV exposure and heating). Furthermore, the curing processes have been investigated using two different DUV light sources evaluating the different outcomes: a single-wavelength (172 nm) emitting excimer lamp and a broader emitting DUV lamp (184 nm/253 nm). The electrical characteristics of the TFT have been extracted and used to establish optimal curing conditions. Notably using DUV, short curing times as low as 10 minutes at  $200\text{ }^{\circ}\text{C}$  (e.g. 5 min DUV + 5 min post-annealing @  $200\text{ }^{\circ}\text{C}$ ) achieved mobility of  $3\text{ cm}^2/\text{Vs}$ . Higher mobility values ( $>15\text{ cm}^2/\text{Vs}$ ) have been achieved with prolonged processes ( $>80\text{ min}$ ). While a temperature reduction to  $180\text{ }^{\circ}\text{C}$  yielded  $\sim 1\text{ cm}^2/\text{Vs}$ . The effects of the different curing protocols on the chemical composition of the IZO films have been studied using Fourier-transform infrared spectroscopy and X-ray photoelectron spectroscopy. The IZO semiconductor has been eventually paired with a printed high-k  $\text{MO}_x$  dielectric film, cured using the same methodology, to realize fully solution-processed  $\text{MO}_x$  TFTs, with as ultimate goal producing full printed TFTs. The identification of the most effective tool, combined with a fine-tuning of the parameters, allows to the DUV enhanced curing to diminish the thermal budget required to process IZO TFTs, paving the way for its further implementation on temperature-sensitive substrates.

#### **F.SF04.07.04**

**Uniform and Stable Aerosol-Jet Printing of Carbon Nanotube Thin-Film Transistors** [Shiheng Lu](#), Joanne Zheng, Jorge Cardenas, Nicholas Williams, Yuh-Chen Lin and Aaron D. Franklin; Duke University, United States

Carbon nanotube thin-film transistors (CNT-TFTs) have attracted intensive attention due to their potential use in various applications, including display backplanes and sensing systems. Device uniformity, which is largely determined by the homogeneity and reproducibility of CNT thin films, is essential for large-scale manufacturing and practical applications. Here, we demonstrate an aerosol-jet printing approach to realizing CNT-TFTs with device characteristics that are among the most uniform of CNT-based transistors to date. The key enabling factors include proper ink formulation, polymer surfactant removal via rapid thermal anneal (RTA), and careful ink temperature control. Terpineol was added as a secondary solvent, and both optical and atomic force microscopy (AFM) reveal that the addition of this nonvolatile and viscous component efficiently suppresses the unwanted coffee-ring effect. The effectiveness of RTA-based polymer removal was supported by AFM results. It was discovered that a lower CNT ink temperature during printing offers higher ink output, increased CNT density, larger field-effect mobility, as well as enhanced device uniformity. This ink temperature-device uniformity relationship was further examined by fabricating batches of CNT-TFTs at a range of different ink temperatures, which revealed that low ink temperature (e.g.,  $8\text{ }^{\circ}\text{C}$ ) not only benefits uniformity of devices printed within a short period of time ( $\sim 70\text{ s}$ ), but also improves long-term ( $\sim 1\text{ h}$ ) printing stability. A set of several dozen CNT-TFTs printed from a CNT ink at  $8\text{ }^{\circ}\text{C}$  exhibited a mobility of  $12.5 \pm 0.5\text{ cm}^2\text{ V}^{-1}\text{ s}^{-1}$ , with a relative standard deviation  $\sigma(\mu_h) / \mu_h$  as small as 4%. These results unveil the role that ink temperature and other critical processing factors play in aerosol jet printed films and have the potential to address device uniformity issues that have previously plagued the utility of printed CNT thin films.

#### **F.SF04.07.05**

**Fine-Tuning of Molecular Conformations for High-Speed Organic Photodetectors with Enhanced Charge Transport** [Jisoo Shin](#), Sungyoung Yun, Hye Sung Choi, Taejin Choi, Younhee Lim, Seon-Jeong Lim, Kyung-Bae Park and

Sunghan Kim; Samsung Advanced Institute of Technology, Korea (the Republic of)

Organic semiconductors have the advantages of high absorption coefficients and wavelength selectivity compared with those of inorganic materials. As such, organic photodetectors (OPDs) are emerging as the next candidates for commercialized organic electronic devices, organic CMOS image sensors (OCISs). Wavelength-selective OPDs are applicable to the three-dimensional (3D) stacked structure that can replace the existing CMOS image sensors for the expansion of the light-input surface area by maximizing the photons absorbed effectively by each pixel, leading to high sensitivity and resolution since they can absorb selective wavelength from incident light without color filters.

To realize these advantages, systematic approach for molecular design of OPDs and optimized device architecture has been reported by our group recently. Noteworthy, through recent years of research on OPDs, the improvement of charge transport properties is also indispensable for commercialization of high-speed image sensors. Compared to silicon CMOS image sensors, some charges are slowly transported and remain in organic layer, then slow decays of photocurrent induced image lags closely related to remaining charges (RCs) in OCISs.

Here, combined with simulation and experiment, we designed and synthesized novel push-pull type molecules with different moieties by tuning the molecular conformations, which showed improved optical properties as well as charge carrier mobility. According to the improved device performance, we experimentally find out that charge transport properties including RCs are closely related to molecular structure with introduction of carbon-bridge and various types of side group. The effect of molecular conformations on the optoelectronic properties of high-speed OPDs will be discussed in detail.

#### **F.SF04.07.06**

##### **Unsubstituted and Fluorinated CoPc Nanowires, Ultrathin Films and Composites for Room Temperature ppb**

**Environmental Gas Monitoring in Highly Humid Terrains** Soraya Flores<sup>1</sup>, Jean Gonzalez<sup>1</sup>, Juan Cintron<sup>1</sup>, Dalice M. Piñero Cruz<sup>1</sup>, Jose Hernandez<sup>1</sup>, Nerida deJesus<sup>2</sup>, Ruben E. Diaz-Rivera<sup>2</sup> and Luis F. Fonseca<sup>1</sup>; <sup>1</sup>University of Puerto Rico at Río Piedras, United States; <sup>2</sup>University of Puerto Rico at Mayagüez, United States

Metallo Phthalocyanines (MPc) have been widely studied as promising material to develop sensitive gas sensor devices. In particular, its electrical response when exposed to gas analytes encourages its use in chemiresistors. This is so because they show some characteristics that can be exploited for the development of very sensitive gas sensors. When compared with other semiconductors, such as metal oxides, their baseline resistivity is relatively high and can change orders of magnitude when exposed to the sensing gas, which can be easily tuned through the incorporation of substituents in the periphery of the Pc platform. Moreover, there is little difference between their room temperature and higher temperature response. Recent publications report reproducible single digit parts-per-million sensitivities at room temperature, usually when preparing the material at the nanoscale.

This work summarizes advances in the synthesis, solution preparation, and gas sensing applications of CoPc and fluorinated CoPc nanowires and films with thicknesses below 20nm. In this case, room temperature parts-per-billion response is reported. Novel sensors prototypes based on F<sub>16</sub>CoPc composites activated with Pt nanoclusters show significant reduction in their sensor response time. The report includes a systematic comparison with unsubstituted CoPc, and the response to different reducing and oxidizing gases. These new prototypes will be optimized for the detection of environmental contaminants in areas with high atmospheric relative humidity.

#### **F.SF04.07.07**

##### **Metal Oxide Nanostructure Patterns via Modified Immersion Transfer Printing for Internal Light Extraction of**

**Quantum Dot Light-Emitting Diodes** Moohyun Kim, Eugene Cho, Jeong Min Shin, Min Seok Jang and Yeon Sik Jung; Korea Advanced Institute of Science and Technology, Korea (the Republic of)

Quantum dot light-emitting diodes (QLEDs) are considered as next-generation displays due to the outstanding advantages of quantum dots (QDs) such as large color gamut by narrow emission, high brightness, solution-processability and potential long term stability. The performance of QLED is characterized by external quantum efficiency (EQE), which is the multiplication of internal quantum efficiency (IQE) and light out-coupling efficiency ( $EQE = IQE \times \text{light out-coupling efficiency}$ ). Recent progress has improved EQE of QLEDs for red, green and blue color to about 20%, which is on the level of commercial phosphorescent organic light-emitting diodes (OLEDs). Considering that the light out-coupling efficiency of a typical multilayer structure device is 20%, it can be seen that the IQE of QLEDs reached 100%. Therefore, research on light out-coupling efficiency or light extraction of QLEDs has been gaining attention to further improve the EQE.

In OLEDs, light is commonly extracted through corrugated structure or photonic crystal like internal light extraction nanostructure. Generally, these nanostructures are located between the multilayer structure and transparent electrode to interact with the target wavelength. However, applying this strategy for enhancement of QLEDs has difficulty even though the structural similarity of the multilayer structure. This is because multilayer structure of QLEDs is fabricated based on

solution process while OLEDs are fabricated through vacuum deposition. Therefore, in QLED, the light extraction nanostructure strongly affects the morphology of the multilayer device causing degradation of the operation characteristic. Furthermore, very narrow QDs emission with 30nm of full-width at half maximum (FWHM) suggests the need for more advanced technique with finer and more precise nanostructures.

In this study, we demonstrate a metal oxide ( $\text{MoO}_3$ ) nanostructure fabricated by modifying immersion transfer printing (iTP) method for internal light extraction of QLEDs.  $\text{MoO}_3$  was applied as the internal light extraction material on the basis of high refractive index value ( $n$ ) of 2.1 at 520 nm and semiconducting properties as a hole transport layer in optoelectronic devices. iTP is introduced as the fabrication method for its compatibility with the solution processed QLEDs and capability for forming high resolution  $\text{MoO}_3$  nanostructure. Previously reported iTP, which uses hydrophobic particles, was modified to compensate for the incompatibility between hydrophilic  $\text{MoO}_3$  particles and PDMS brushed substrates. PDMS-PS co-brush system was applied to control the surface affinity as a way to achieve  $\text{MoO}_3$  incorporation onto the Si template. In addition, PDMS/PS bilayer was used as the picking carrier polymer to increase the transfer yield of the  $\text{MoO}_3$  nanostructure. As a result, nanoscale line patterns with widths of 1000, 350, and 50 nm in large areas are well demonstrated. Finite-difference time-domain (FDTD) simulations are conducted to help design the precise size and shape of the pattern for light extraction to optimize the QLED internal light extraction. QLED was fabricated based on this design and showed improvement in the performance of the QLED device.

#### F.SF04.07.10

##### **Examining the Impact of Air Exposure and Temperature Variation on N- and P-Type Polymer Charge Transport for Transistor and Photovoltaic Applications** Samantha Brixi and Benoit Lessard; University of Ottawa, Canada

Enhancing device stability is essential to the widespread commercial adoption of organic electronic devices. Interactions of organic semiconductors with their environment often lead to degradation of device performance; therefore, it is important to understand how such devices as organic thin-film transistors and organic photovoltaics are affected by these interactions. This allows scientists and engineers to both choose appropriate applications for these materials and guide the development of new materials with enhanced stability. Polymers are of particular interest due to their capacity to be processed in solution for a new generation highly scalable and inexpensive electronic devices from sensors to solar cells. We have studied the stability of p- and n-type materials of interest for transistor and photovoltaic applications in environments relevant to commercial applications of these materials, including exposure to air, vacuum, and varied temperatures. In all cases, significant degradation could be observed. After 18 days of air exposure for p-type materials P3HT and PBDB-T, a 95% loss in hole mobility ( $\mu_h$ ) was observed for P3HT, while PBDB-T only experienced a  $\mu_h$  loss of 42%.<sup>1</sup> For n-type polymers studied, a loss in electron mobility ( $\mu_e$ ) of 99% was observed for N2200 exposed to air for two weeks, while an 84%  $\mu_e$  loss was observed for PIBDFBT-37.<sup>2</sup> Preliminary studies on polymers in organic photovoltaics indicate similar trends, but the degradation of charge transport properties does not give the full picture. We plan to further explore the impact of polymer degradation and charge transport on the stability of organic photovoltaics and transistors.

1. Brixi, *et al.*, 2018, J. Mater. Chem. C, 6, 11972-11979

2. Brixi, *et al.*, 2020, Sci. Rep., 10, 4014

#### F.SF04.07.11

##### **Dielectrophoretic Assembly of Single Nanowires for Advanced Characterisation Nanoscale Standards** Maxim Shkunov<sup>1</sup>, Sebastian Wood<sup>2</sup>, Ruth Rawcliffe<sup>1</sup>, Filipe Richeimer<sup>2</sup>, Tomas Peach<sup>1</sup> and Fernando Castro<sup>2</sup>; <sup>1</sup>University of Surrey, United Kingdom; <sup>2</sup>National Physical Laboratory, United Kingdom

Nano-characterisation techniques, including confocal microscopy, atomic force microscopy (AFM) and tip enhanced Raman scattering (TERS), rely on the ability of each instrument to resolve nano-scale features without distortions and artefacts, however, reference samples allowing to perform fully quantitative characterisation of their responses are not available. Calibration of lateral and depth resolution of advanced scanning-probe microscopy methods is currently very challenging and calls for the development of nanoscale standards with features in 10-200 nm range with various morphological and optoelectronic characteristics.

We demonstrate the development of solution-based, single-nanowire-based reference samples, where easily identifiable device positions each contain a semiconducting nanowire with a particular set of properties. Key parameters that are considered include: diameter and length, Raman response, photoluminescence and conductivity. The devices are self-assembled from a wide range of solution-processed semiconducting nanowires, including Si, Ge, InAs, InP, GaN, Ge/Si. Individual nanowires are positioned in pre-defined locations using electric-field assisted process, dielectrophoresis (DEP), by applying controllable DEP signal voltage and frequency. Nanowires are characterised, and various response metrics are analysed using conducting-AFM, confocal Raman, TERS and other techniques to establish which nanowire materials provide

highly distinguishable responses, necessary for reference standards. Challenges in identifying most suitable nanowire materials, including their spectroscopic characteristics (e.g. Raman) and morphological features (e.g. diameters) are discussed and several reference samples for the characterisation of lateral and vertical resolution of nanoscale scanning probe techniques are suggested.

#### **F.SF04.07.13**

##### **Effect of Oxygen Pressure on Optical and Electrical Properties of Single-Crystalline Cu<sub>2</sub>O Fabricated by Pulsed Laser Deposition** Jan Lancok, [Lenka Volfova](#), Premysl Fitl and Michal Novotny; Czech Academy of Sciences, Czechia

Copper oxide Cu<sub>2</sub>O is an important and well known p-type transition metal oxide semiconductor material, which has already been employed in the fabrication of electronic devices. For example Cu<sub>2</sub>O has been used in thin photovoltaic devices, resistive switching, transistors, gas sensors or catalysts. The films were fabricated by Pulsed Laser Deposition from CuO ceramic target by means of Nd:YAG laser operated at 266 nm wavelength. MgO(100) substrates were mounted on substrate holder 5 cm away from the target and maintained at temperature in the range 500-700 °C. Our attention was mainly focused on the influence of the oxygen pressure, which was varied between 10<sup>-5</sup> Pa and 1 Pa, on the structural and following on optical and electrical properties. The investigation of the plasma was carried out by Optical emission spectroscopy. The surface morphology and composition were characterised by AFM and XPS, respectively. The crystalline quality of the films were characterised by means of XRD and following by TEM and HRTEM, which confirmed the epitaxial growth of the films in low oxygen pressure up to 0.1 Pa. When the oxygen pressure exceeded 0.1 Pa the growing films started to be polycrystalline and the CuO phase also appeared. Because we focused on utilization of the Cu<sub>2</sub>O films as gas sensors, the near ambient pressure photoelectron spectroscopy was carried out to investigation of surfaces composition in the presence of gasses and vapours such as ethanol, hydrogen and NO<sub>2</sub>.

#### **F.SF04.07.14**

##### **Thermal Dedoping of Doped Poly (3-hexylthiophene) for Multimodal Temperature Sensing** [Hemanth Maddali](#)<sup>1</sup> and Deirdre O'Carroll<sup>1,2</sup>; <sup>1</sup>Rutgers, The State University of New Jersey, United States; <sup>2</sup>Rutgers University, United States

Conjugated polymers have a wide range of applications in optoelectronic devices and in numerous sensing technologies. Conjugated polymers that have thermally activated optical or electrical responses have garnished interest due to their potential as thermal sensors. These thermochromic properties are often introduced via doping. In this study, we investigate the use of electrochemically doped poly(3-hexylthiophene) (P3HT) thin films as multimodal temperature sensors. P3HT thin films spin coated on indium-tin oxide coated glass substrates are electrochemically doped using tetrabutylammonium perchlorate (TBAP) dissolved in acetonitrile. The pristine P3HT thin films, which are purple in color, exhibit a color change to blue, upon doping. The doped P3HT thin films are then heated under vacuum at 140<sup>0</sup> C and the color of the thin films reverts from blue to purple indicating thermally activated dedoping. UV-visible absorbance spectra of pristine, doped and dedoped P3HT thin films show that the change in optical absorption properties upon doping is reversed due to thermally activated dedoping. Energy dispersive X-ray spectroscopy (EDS) reveal the presence of dopant molecules (TBAP) distributed throughout the doped P3HT film. Upon dedoping, the EDS maps show almost negligible levels of the dopant molecules. This further proves that heating of doped P3HT thin films triggers dedoping and causes the distinctive thermochromic response, i.e., a color change from blue to purple. The electrical properties of doped and dedoped films are also expected to result in a significantly different current upon application of voltage. This warrants fabrication of a current-based temperature sensor that would perform colorimetrically and electrically.

#### **F.SF04.07.15**

##### **A 13.56 MHz Rectifier Based on Fully Inkjet Printed Organic Diodes** [Fabrizio A. Viola](#) and Mario Caironi; Istituto Italiano di Tecnologia - IIT, Italy

The increasing diffusion of portable and wearable technologies results in a growing interest in electronic devices having features such as flexibility, lightness-in-weight, transparency and wireless operation. Organic electronics was proposed as a potential candidate to fulfill such needs, in particular targeting pervasive Radio-Frequency (RF) applications. Still, limitations in terms of device performances at RF, particularly severe when large-area and scalable fabrication techniques are employed, have largely precluded the achievement of such an appealing scenario. In this work, we demonstrate a high-frequency rectifier based on fully inkjet printed organic Schottky diodes fabricated through scalable large-area methods on plastic. The inkjet printing of the organic semiconductor, the core of the diode structure, has been carefully optimized in order to obtain a low series resistance, which is mandatory to improve the diode cut off frequency. Moreover, the employed materials in the presented device have been chosen to finely tune the barriers formed at metal-semiconductor interface, in order to increase the rectification ratio of the diode: the obtained value is higher than 10<sup>6</sup> which is, to the best of our knowledge, the highest

value ever reported with a fully printed structure. Furthermore, we show, as a proof-of-concept, how a rectifier circuit integrating the fully printed diode, can successfully supply power to a polymer micro-electronic circuit printed on a plastic foil with a similar process. In particular, by rectifying a 13.56 MHz AC voltage the rectifier enables the correct operation of a D-Flip Flop, which is a fundamental logic building block for serialization elements. The possibility of harvesting electrical power from RF waves and delivering it to a cheap flexible substrate through a simple printed circuitry paves the way to a plethora of appealing distributed electronic applications.

#### **F.SF04.07.16**

**Thermally Stable Au Decorated Silica-Titania Mesoporous Nanocomposite for pH Sensing Evaluation** Shumaila Islam and Adil Alshoaibi; King Faisal University, Pakistan

Herein, doping/decoration of gold nanoparticles (AuNPs) within mesoporous silica-titania nanocomposite is achieved via a facile and co-assembly sol-gel method. Polyethylene glycol is used as a co-structure-directing agent. For sensing analysis, a mixture of organic dyes i.e., bromophenol blue, phenol red, and cresol red is encapsulated in the AuST nanocomposite matrix. FESEM/EDX analysis shows a crack-free surface, porous network and uniform distribution of Au, Ti, Si, along with dye species. FTIR and XRD suggested the heterogeneous chemical bonding and crystallite size 24 nm after encapsulation. AuST nanocomposite shows thermally stable behavior after 450 °C even after co-dyes encapsulation. High surface area  $322 \pm 2.5$  m<sup>2</sup>/g, pore diameter 30.2 Å, and pore volume 0.24 cm<sup>3</sup>/g, average surface roughness 10 nm, and refractive index 1.29 is advantageous for good sensing response at pH 1–12. The sensitivity is measured as 10 counts/pH at 441 nm. Moreover, good reversible response, fast response time 2.1 sec in acidic media, and 0.9 sec in basic media is observed.

#### **F.SF04.07.17**

**Late News: Hybrid Surface Treatment of Elastomer Substrates for Robust and Reliable Integration of Rigid Components with Inkjet-Printed Stretchable Circuits** Hyungsoo Yoon, Byeongmoon Lee, Sujin Jeong and Yongtaek Hong; Seoul National University, Korea (the Republic of)

Stretchable electronics has emerged as a next-generation technology that goes beyond rigid and flexible electronics to enable novel form-free devices and provide advanced user-experiences. Integration of rigid integrated circuit (IC) chips and inkjet-printed circuits on pre-strained elastomers has been regarded as one of the most powerful methods for fabricating stretchable multifunctional systems due to their unique advantages such as a facile and low-cost process, and a high degree of customizability. However, direct inkjet-printing on elastomers is challenging due to their low surface energy that causes dewetting. Furthermore, the super-hydrophobic surface shows poor adhesion with inkjet-printed metal films as well as conductive adhesives for chip bonding, significantly limiting system stability under deformation. Therefore, appropriate surface modification is indispensable for the robust implementation of inkjet-printing-based stretchable hybrid electronic system. Surface modification of elastomers has been realized by oxygen-plasma or ultraviolet/ozone (UVO) treatments. Both methods render the surface of the elastomers wettable by creating a large number of hydrophilic groups on it, where well-defined patterns can be formed by inkjet-printing. However, the methods have several limitations when applied to inkjet-printing on pre-strained elastomers. Plasma-treated elastomers undergo fast hydrophobic recovery due to the molar migration from the bulk to the surface, resulting in unstable wettability, uneven patterns, and poor adhesion. Alternatively, the UVO treatment provides improved stability and uniformity. However, a thick layer of the elastomer from the surface is stiffened by UV energy, which causes a large strain mismatch between the thick stiff surface and soft bulk. Consequently, the pre-stretched elastomer cannot completely return to its original dimension, restricting the maximum stretchability of the system far behind compared to the applied pre-strain. Therefore, a new surface modification strategy that simultaneously offers stable wetting and a high level of adhesion without compromising their stretchability is highly required.

In this work, we demonstrate robust stretchable hybrid electronic system based-on inkjet-printing and hybrid surface modification of polydimethylsiloxane (PDMS). The surface treatment offers stable wettability and great adhesion and preserves the substrate stretchability. Specifically, the pre-strained PDMS (mixed at 10:1) is exposed with oxygen-plasma to form hydroxyl groups and poly-L-lysine (PLL) solution (aqueous solution, 0.1% (w/v) in H<sub>2</sub>O) is sequentially drop-casted on the plasma-treated PDMS. After that, the PDMS is rinsed with deionized (DI) water. Abundant amine groups functionalized on the surface of the PDMS enable stable wetting and good adhesion for inkjet-printing process. Furthermore, the modified surface shows remarkable adhesion with conductive epoxy, allowing robust IC chip bonding on the printed stretchable circuits. To investigate the effect of the hybrid surface treatment, we compare three biaxially pre-stretched PDMS substrates that undergo UVO, oxygen-plasma, and oxygen-plasma with PLL treatments, respectively. The plasma-treated PDMS results in uneven patterns and poor adhesion due to its instability and fast hydrophobic recovery. While the UVO-treated PDMS only shows stretchability of 19% when it is pre-stretched ~70%, the PDMS with hybrid surface treatment restores its original dimension, i.e., it shows the same stretchability as the pre-strain value. Finally, a series of stretchable hybrid electronic

systems are demonstrated with their mechanical robustness, including stretchable LED displays, which proves the superiority of our hybrid surface treatment. The detailed methods and results will be discussed at the conference.

This research was supported by Samsung Research Funding & Incubation Center of Samsung Electronics under Project Number SRFC-IT1801-07.

#### F.SF04.07.18

**Late News: Implementing ITO-Free Transparent Conductive Electrodes in Flexible Organic and Hybrid Light-Emitting Diodes** Felix Hermerschmidt<sup>1</sup>, Lukas Kinner<sup>1,2</sup>, Theodoros Dimopoulos<sup>2</sup> and Emil List-Kratochvil<sup>1,3</sup>; <sup>1</sup>Humboldt-Universität zu Berlin, Germany; <sup>2</sup>Austrian Institute of Technology, Austria; <sup>3</sup>Helmholtz-Zentrum Berlin, Germany

We utilize 25% of our total electricity consumption for lighting and display applications. To address this consumption, several efficient lighting technologies have been targeted. Inorganic solid-state lighting together with organic light-emitting diodes (OLEDs) are the candidates spearheading the lighting revolution of the 21st century. However, while OLEDs have shown commercial success in rigid display applications, a number of challenges remain to be overcome in order to fulfil their full potential.

Among these are the continued quest for stable emitter materials and to improve strategies for the outcoupling of light from the device. Additionally, energy, temperature and cost efficient processing methods need to be targeted in order to fabricate the transparent conductive electrodes (TCEs) needed for device operation.

Today, transparent conductive oxides, and in particular indium tin oxide (ITO), represent the dominant class of TCEs. ITO combines high transparency (>85% in the visible wavelength range) with low sheet resistance (ca.  $10 \Omega \text{ sq}^{-1}$ ) when deposited on glass. As a result, most optoelectronic devices utilize ITO as the transparent electrode. However, ITO has some inherent limits in its range of applications. It is mechanically unstable upon bending, while its scarcity translates to a volatile and high price. It is therefore desirable to replace ITO with other transparent conductive electrodes [1].

Of particular interest are low temperature processes (<130 °C), since these are compatible with the use of temperature-sensitive and low cost flexible substrates, such as polyethylene terephthalate (PET). In this contribution we highlight our recent work on the design, fabrication and characterization of a number of different low temperature processes using, among others, inkjet printing and spray coating to produce TCEs [2,3]. These approaches are based on Ag and Cu nanoparticle, particle-free and nanowire inks. We will show that the developed ITO-free electrodes on PET show superior optical, electrical and mechanical performance compared to PET/ITO reference samples.

[1] Hermerschmidt et al., Adv. Mater. Technol. 4 (2019) 1800474.

[2] Hermerschmidt et al., Adv. Mater. Technol. 3 (2018) 1800146.

[3] Kinner et al., Phys. Status Solidi RRL (2020) 2000305.

#### F.SF04.07.20

**Late News: Organic Radiation Dosimeter for X-Ray, Gamma and Neutron Detection** Zachary Lamport<sup>1</sup>, Marco R. Cavallari<sup>2</sup>, Michael Bardash<sup>3</sup> and Ioannis Kymissis<sup>1</sup>; <sup>1</sup>Columbia University, United States; <sup>2</sup>Federal University for Latin American Integration, Brazil; <sup>3</sup>QEL System Services, Inc., United States

In many professions, ionizing radiation is either a by-product of some process or is itself utilized, posing a significant hazard to those in the surrounding area. Workers will usually be required to wear a personal radiation dosimeter which measures and integrates the cumulative radiation dose experienced such that either prolonged or flash exposures are recorded and analyzed for the safety of the wearer. For personal dosimeter badges, the sensing element is usually made of relatively high-Z elements which absorb radiation differently than the lighter elements found in the human body.<sup>1,2</sup> An all-organic radiation dosimeter could more closely approximate the effect of radiation on biological tissues. Another added benefit of such organic-based devices is that they can be made quite cheaply and on a lightweight, flexible substrate. These factors together with the burgeoning IoT systems could allow for a more robust detector network in areas relevant to homeland security. Here, we report on an all-organic radiation dosimeter using the conducting polymer poly(3,4-ethylenedioxythiophene)-poly(styrenesulfonate) (PEDOT:PSS)<sup>3</sup> as both the detector region and conductive traces patterned on a polyethylene naphthalate (PEN) substrate. Ionizing radiation incident on a central PEDOT:PSS pad induces a static charge in the air, the PEDOT:PSS itself, and the underlying PEN substrate that is measured as a voltage by the connected op-amp voltage follower.<sup>4-6</sup> Two organic field-effect transistors (OFETs) with the PEDOT:PSS source and drain, respectively, connected to the central PEDOT:PSS region allow for an initial biasing of the central pad, as the semiconductor 6,13-bis(triisopropylsilyl)ethynyl) pentacene (TIPS-pentacene) functions as two very large resistors. The OFETs allow for a very small amount of current to flow through the ungated semiconductor in order to place the central pad at a desired voltage, from which any deviations are measured. To clear the charge from the central pad, one or both of the OFETs can be turned on through the respective PEDOT:PSS gate electrode underneath a parylene dielectric. We show reproducible and reliable

measurements of the radiation dosimeters subjected to a wide range of exposure energies of both X-ray and gamma rays using wide and focused beams resulting in an approximate detection limit of 5 mRad/hour. In addition, there is very strong evidence that the PEDOT:PSS-based devices can detect neutrons from a shielded and unshielded beryllium-encased plutonium source at a dose of 620 mRad/hour. This represents a significant step forward in the production of cheap, reusable radiation dosimeters made with materials of similar radiation cross-section to the human body.

1. Beckerle, P. & Ströbele, H. Charged particle detection in organic semiconductors. *Nucl. Instruments Methods Phys. Res. Sect. A* **449**, 302–310 (2000).
2. Fraboni, B. *et al.* Organic Semiconducting Single Crystals as Next Generation of Low-Cost, Room-Temperature Electrical X-ray Detectors. *Adv. Mater.* **24**, 2289–2293 (2012).
3. Schrote, K. & Frey, M. W. Effect of irradiation on poly(3,4-ethylenedioxythiophene):poly(styrenesulfonate) nanofiber conductivity. *Polymer*. **54**, 737–742 (2013).
4. Bardash, M. An organic semiconductor device for detecting ionizing radiation on a cellular level. *Organic Semiconductors in Sensors and Bioelectronics III* (Vol. 7779, p. 77790F). International Society for Optics and Photonics. 77790F (2010). doi:10.1117/12.861999.
5. Bardash, M. Solid state tissue equivalent detector, main component for a light-weight tissue equivalent microdosimeter. U.S. Patent 8,350,225 (2013).
6. Cavallari, M. R., Bardash, M. & Kymissis, I. Fully organic solid state tissue equivalent radiation dose (SSTED) detector (Conference Presentation). in *Organic and Hybrid Sensors and Bioelectronics XII* (eds. Shinar, R., Kymissis, I. & List-Kratochvil, E. J.) 4 (SPIE, 2019). doi:10.1117/12.2530701.

#### F.SF04.07.21

**Late News: Highly Conformable Pressure-Sensitive Thin-Film Transistors Using Capacitance Modulation via Nanostructured Surface Morphology of AgNWs** Hayun Kim, Byeongmoon Lee, Hyunuk Oh, Hyunjun Yoo and Yongtaek Hong; Seoul National University, Korea (the Republic of)

Electronic skin that can map pressure distribution on arbitrary surfaces has gained tremendous significance for its wide range of use in various fields such as skin prosthesis, artificial nerve systems for soft robotics, and advanced human-machine interfaces. To keep pace with these trends, many studies have focused on reporting high-performance pressure sensors and their passive-matrix array using novel materials and structures. Among various types of pressure sensors, capacitive pressure sensors with engineered microstructures offer significant potential owing to their high sensitivity, fast response time, and great mechanical flexibility. However, previous works on capacitive pressure sensors mainly focused on the performance of a single sensor, and their application to a high-resolution array was challenging because of their complex structure and fabrication process. Therefore, reported sensor arrays using capacitive pressure sensors generally showed low spatial fidelity due to the crosstalk among pixels and low pixel density. Furthermore, to exploit the capacitance change in practical applications, the circuit requires a capacitance-to-current converter that can limit the design freedom and make the system unstable on complex 3-dimensional surfaces. Therefore, device-scale integration between capacitive pressure sensors and thin-film transistors (TFTs) is highly desirable for capacitance-to-current conversion and further active-matrix applications. Although a few studies have reported pressure-sensitive thin-film transistors, they usually suffer from complex fabrication processes and limited flexibility due to their sophisticated structures such as sidewall spacers to make air gaps in dielectric layers.

In this work, we propose a facile and large-area compatible method for pressure-sensitive TFTs (PSTFTs) and their application to flexible sensor arrays. Our PSTFT is based on all-inkjet-printed single-wall carbon nanotube (SWCNT) TFTs, where a silver nanowire (AgNW) gate electrode with nanostructured surface morphology softly touch the top surface of the dielectric layer. The fabrication process of the PSTFT is fairly simple, highly customizable, and cost-effective. The SWCNT active channel, silver (Ag) source and drain electrodes, and poly(4-vinylphenol) (PVP) dielectric layer were sequentially inkjet-printed on a surface-engineered polyethylene naphthalate (PEN) substrate. The AgNW gate electrode was then formed on another flexible substrate by spray-coating. The 3D nanostructures in the AgNW random network form nano-scale air gaps between the gate electrode and dielectric. These nanoscale air gaps are key to the capacitance modulation in the PSTFTs. When the vertical pressure is applied to the top gate electrode, as the air gaps disappear and the contact area between the gate electrode and dielectric increased, the capacitance between the gate electrode and active layer drastically increases without any supporting spacer. Our PSTFT showed well-split transfer curves with on-off ratios of from 1 to  $1.3 \times 10^4$  according to the applied pressure. When the pressure reached 700 kPa, the TFT showed  $1.3 \times 10^4$  on/off ratio. We further demonstrate the feasibility of our approach by mounting the highly conformable sensor array on human skin to read out the change of the pressure such as finger touch and joint flexure. This study provides a new pathway to map pressure distribution using capacitive pressure sensors without any crosstalk among adjacent pixels, which can be further applied to any type of deformable substrates with potential applications such as skin-mounted device, deforming soft robotics, and



display. The detailed methods and results will be discussed later.

This work was supported by the Technology Innovation Program (No.20008801, Development of muscular function management solution based on electronic skin with EMG IMU and Strain sensor) funded By the Ministry of Trade, Industry & Energy(MOTIE, Korea).

## SYMPOSIUM F.SF02

---

Bulk Metallic Glasses  
November 21 - December 4, 2020

### Symposium Organizers

Katharine Flores, Washington University in St. Louis  
Alan Lindsay Greer, University of Cambridge  
Yanhui Liu, Yale University  
Jan Schroers, Yale University

---

\* Invited Paper

SESSION F.SF02.10: Live Keynote I: Bulk Metallic Glasses  
Session Chairs: Alan Lindsay Greer and Jan Schroers  
Thursday Morning, December 3, 2020  
F.SF02

### 11:30 AM WELCOME

#### 11:35 AM \*F.SF02.08.01

**Vitrification Kinetics versus Alpha-Process in Metallic Glass-Formers** Isabella Gallino<sup>1</sup>, Daniele Cangialosi<sup>2,3</sup>, Beatrice Ruta<sup>4</sup>, Xavier Monnier<sup>2</sup> and Ralf Busch<sup>1</sup>; <sup>1</sup>Saarland University, Germany; <sup>2</sup>Donostia International Physics Center, Spain; <sup>3</sup>Centro de Fisica de Materiales (CSIC-UPV/EHU), Spain; <sup>4</sup>Universite Claude Bernard Lyon 1, France

Understanding how glasses form remains a challenge in material science. Vitrification is the thermal transition from a supercooled liquid in metastable equilibrium into a non-equilibrium glass. One of the major questions is whether vitrification in viscous liquids is related to sluggish atomic mobility exclusively *via* the primary structural  $\alpha$ -relaxation process or rather other atomic motions play a role. Here, we present experimental evidences that multicomponent bulk metallic glasses can display heterogeneity of vitrification kinetics and that the cooling rate dependency of the vitrification kinetics is decoupled from the temperature dependence of the  $\alpha$ -relaxation [1-3]. The evidences are based on exhaustive studies of the atomic mobility of an Au-based metallic glass former by dynamic mechanical analysis (DMA), x-ray photon correlation spectroscopy (XPCS), and fast scanning calorimetry (FSC); the latest by means of a step response analysis *via* the temperature and frequency dependence of the complex specific heat. The vitrification kinetics is characterized in FSC in terms of the limiting fictive temperature, i.e., the temperature at which a glass formed after cooling at a given rate would be at equilibrium. The separation of these two aspects of the glassy dynamics (vitrification kinetics and  $\alpha$ -process) becomes more pronounced at larger undercooling, suggesting a larger contribution of additional dynamical processes to the vitrification process, which are not connected to the  $\alpha$ -process. The observed heterogeneity of vitrification kinetics hints toward the existence of multiple relaxation mechanisms, which are observed during aging experiments [3].

[1] X. Monnier, D. Cangialosi, B. Ruta, R. Busch, I. Gallino, *Sci. Adv.* 6 (2020) eaay1454

[2] S. Hechler, B. Ruta, ... R. Busch and I. Gallino, *Phys. Rev. Mat.*, 2 (2018) 085603

[3] I. Gallino, D. Cangialosi, et al., *Acta Mater.*, 144 (2019) 400

#### 11:55 AM \*F.SF02.08.02

**Tracing Structural Dynamics in Metallic Glasses During Cryogenic Cycling** Robert Maass<sup>1,2</sup>; <sup>1</sup>University of Illinois at Urbana-Champaign, United States; <sup>2</sup>Federal Institute for Materials Research and Testing (BAM), Germany

Highly unrelaxed structural states of metallic glasses have often advantageous mechanical properties. Since metallic glasses continuously relax with time (age) or inherently are well relaxed after processing, methods to uniformly rejuvenate the material are needed. One approach that has received attention is the so-called cryogenic-cycling method, during which a metallic glass is repeatedly immersed into liquid nitrogen. In some cases, cryogenic cycling is truly efficient in increasing the stored excess enthalpy of metallic glasses, but it does not seem to be universally applicable to all alloys and structural states. The origins for these differences remain unclear due to our limited understanding of the underlying structural evolution. In order to shed more light onto the fundamental structural processes of cryogenic cycling, we pursue in-situ x-ray photon correlation spectroscopy (XPCS) to trace the atomic-scale structural dynamics of a Zr-based metallic glass in two different structural states (ribbon and bulk metallic glass). This method allows calculating the relaxation times as a function of time throughout the thermal cycling. It is found that the investigated glasses exhibit heterogeneous structural dynamics at 300 K, which changes to monotonic aging at 78 K. Cryogenic cycling homogenizes the relaxation time distribution for both structural states. This effect is much more pronounced in the ribbon, which is the only structural state that rejuvenates upon cycling. We furthermore reveal how fast atomic-scale dynamics is correlated with long-time average structural relaxation times irrespective of the state, and that the ribbon exhibits unexpected additional fast atomic-scale relaxation in comparison to the plate material. Overall, a picture emerges that points towards heterogeneities in fictive temperature as a requirement for cryogenic energy storage.

#### 12:15 PM BREAK

#### 12:30 PM \*F.SF02.01.05

**The Non-Equilibrium Origin of a Brittle-to-Ductile Transition in Metallic Glasses** Eran Bouchbinder<sup>1</sup>, Manish Vasoya<sup>2,1</sup>, Christopher Rycroft<sup>3</sup>, Jittisa Ketkaew<sup>4</sup> and Jan Schroers<sup>4</sup>; <sup>1</sup>Weizmann Institute of Science, Israel; <sup>2</sup>Texas A&M University, United States; <sup>3</sup>Harvard University, United States; <sup>4</sup>Yale University, United States

Understanding the fracture toughness of glasses is a fundamental problem of prime theoretical and practical importance. We develop a theory of the notch fracture toughness of glasses using a non-equilibrium thermodynamic approach to the elastoplastic deformation of glassy materials. We show that the notch fracture toughness results from a competition between the initial plastic relaxation timescale, which depends on initial non-equilibrium structural state of the glass (e.g. its age and its preparation protocol), and an effective loading timescale, which depends on the notch radius, the system's geometry and the external loading rate. The initial glass structure, which controls the initial plastic relaxation timescale, is characterized by a non-equilibrium (effective/fictive) temperature. The theory predicts a rather abrupt increase in the toughness – a brittle-to-ductile transition – as a function of the ratio between these two timescales. Novel experiments on various Bulk Metallic Glasses (BMGs), which allow to carefully controlling the initial structural state of the glass and accurately measure the toughness, verify the theoretical predictions. In particular, they show that BMGs can be significantly toughened by carefully controlling their initial non-equilibrium state. These results highlight the importance of timescales competition and far from steady-state plastic deformation dynamics for understanding the toughness of glasses, and open up the way for a broader usage of BMGs as tough, highly-reproducible structural materials.

#### 12:50 PM \*F.SF02.03.07

**Effects of Testing Temperature and Sample-Size on Tensile Deformation of Metallic Glass** Golden Kumar and Chandra Sekhar Meduri; University of Texas at Dallas, United States

Deformation of nanoscale metallic glasses has attracted increasing attention but remains controversial due to difficulty in fabrication and testing of small samples. Here, we report the effects of systematic variation in sample-size and testing temperature. Pt-based metallic glass samples with varying diameters (100 nm -500 nm) were prepared by thermoplastic drawing. Multiple samples were deformed at different temperatures and the fracture morphologies were characterized using SEM. The results show that the fraction of vein-like morphology decreases with decreasing sample size and mirror-like fracture surface was observed in samples smaller than about 2 nm in diameter. With further decreasing diameter, transition from shear-localized to necking was observed and the extent of neck increased with decreasing sample diameter. The lowering in temperature had similar effect as decrease in sample diameter. This temperature-size equivalence is discussed in terms of temperature rise and formation of liquid-like layer in shear bands.

#### 1:10 PM \*F.SF02.01.02

**Concept of Defects in Glasses and Liquids** Takeshi Egami<sup>1,2</sup>; <sup>1</sup>University of Tennessee, United States; <sup>2</sup>Oak Ridge National

Laboratory, United States

In crystals atomic mobility in transport and deformation is governed by structural defects, such as vacancies and dislocations. This was carried over to the study of glasses and liquids, and various defect-like concepts have been proposed, including free-volume, cooperatively rearranging region and shear-transformation-zone (STZ). However, whereas in crystals defects are topologically protected by the lattice and preserve their identity after motion, the same does not apply for liquid and glass. For this reason, today these defects in glass are considered to be transient; they do not pre-exist and disappear after the action. In this talk this view is advanced even further to suggest that the dynamics in liquid and glass is governed not by defects but by the structural medium-range order (MRO) of the bulk. The MRO is defined by the coherence length which characterizes the decay of the oscillation in the pair-distribution function (PDF) beyond the first peak. Because the higher-order peaks of the PDF are broad,  $\sim 1 \text{ \AA}$  in width, the MRO does not describe the order at the atomic level. It represents the strength of the coarse-grained density wave, represented by the first peak in the structure function,  $S(Q)$ . We show that the coherence volume is proportional to the fragility coefficient,  $m$ , at the glass transition temperature,  $T_g$ , and also to the activation energy of viscosity above  $T_g$ . In crystal atoms are mobile only at defects of which density is low. But in liquid all atoms are mobile and participate in transport. Whereas the defect-like sites have a higher propensity to start deformation or atomic transport, as soon as deformation starts extensive atomic rearrangement ensues, and the structure of the final state is very different from the initial one. Furthermore, at the saddle point of transition the effective temperature becomes so high that the system locally melts for a short time, and the system locally loses its thermal history. Therefore, the mobility is not determined by the initial structure but by the resistance to local collective motion which is determined by the MRO. For this reason, the structural coherence, which is a bulk property in equilibrium, controls the dynamics in liquid and glass. Defects are relevant only as outliers in the equilibrium statistical distribution where action could start.

SESSION F.SF02.11: Live Keynote II: Bulk Metallic Glasses  
Session Chairs: Katharine Flores and Jan Schroers  
Friday Afternoon, December 4, 2020  
F.SF02

### 6:30 PM WELCOME

#### 6:35 PM \*F.SF02.01.01

#### **Multiscale Modeling of Plastic Flow and Failure in Amorphous Solids—The Role of Effective (Fictive) Temperature as a Measure of Disorder** Michael L. Falk; Johns Hopkins University, United States

We have undertaken to develop multiscale models of plastic flow and failure processes in amorphous solids, materials that exhibit a complete lack of crystalline order. In this we have taken metallic glass as an exemplar material and applied molecular dynamics simulation to examine the physics at the atomic scale. This has allowed us to uncover the statistics of the shear transformation zone (STZ) defects that control plastic deformation. We have then sought to relate this defect structure to statistical mechanics models of “effective temperature” that characterize the degree of glass disorder in an effort to build a constitutive model of plastic deformation. The constitutive model has been incorporated into a high-fidelity viscoplastic finite differencing scheme that adapts techniques originally developed for solving the Navier-Stokes equation. A novel machine learning algorithm then utilizes the atomistic data to guide the parameterization of the constitutive model so as to inform the continuum method. In doing so we have begun to ask some fundamental questions about the concept of “effective temperature.”

The concept of fictive-temperature has long been utilized to characterize the processing dependence of glass structure, and has recently been shown to be predictive of metallic glass ductility. Some theories have hypothesized that it is actually a real temperature related to the configurational degrees of freedom of the glass, i.e. an “effective-temperature,” notably the shear-transformation-zone (STZ) and soft-glassy-rheology (SGR) theories. We derive a thermodynamic integration scheme for calculating effective-temperature based on a 2-temperature hypothesis. To test this scheme we simulate a binary Cu-Zr metallic glass modeled with an EAM potential. Measures of the energy fluctuations associated with both the fast and slow degrees of freedom are measured during the glass quench. The resulting effective-temperature is consistent with estimates of fictive-temperature obtained from simulation in more heuristic ways. The results indicate that effective-temperature can be understood as a purely structural quantity. The method provides a means to measure the effective-temperature in the absence of fluctuations induced by shear and without resorting computationally expensive and impractical methods for explicitly measuring the configurational entropy.

#### 6:55 PM \*F.SF02.02.04

**Metallic Glass Stability and Surface Dynamics** Sachin V. Muley<sup>1</sup>, Debaditya Chatterjee<sup>1</sup>, Carter Francis<sup>1</sup>, Ajay Annamareddy<sup>1</sup>, Chengrong Cao<sup>1</sup>, Jittisa Ketkaew<sup>2</sup>, Jan Schroers<sup>2</sup>, John Perepezko<sup>1</sup>, Dane Morgan<sup>1</sup> and Paul M. Voyles<sup>1</sup>; <sup>1</sup>University of Wisconsin, United States; <sup>2</sup>Yale University, United States

Metallic glasses can have widely varying thermodynamic and kinetic stability at constant composition depending on their processing history. For bulk glasses, fast quenching or post-synthesis deformation result in a high free energy, less stable states and slow quenching or post-synthesis sub- $T_g$  annealing result in low free energy, more stable states.

For thin films and nanostructures, surfaces play a larger role. We have used electron correlation microscopy experiments and molecular dynamics simulations to show that metallic glass surfaces have approximately ten times faster dynamics than the bulk at the same temperature for temperatures near  $T_g$ . The fast surface layer has a glass transition temperature that is suppressed with respect to the bulk by  $\sim 20$  K. We have extended the understanding of diffusion in supercooled liquids based on caging and hopping of atoms to surfaces to explain this behavior.

Enhanced surface dynamics enable deposition of highly stable thin films, since every atom at some point has been a surface atom and the surface layer maintains sufficient mobility for the atoms to find low-energy configurations even at temperatures well below the bulk  $T_g$ . We have deposited  $Zr_{65}Cu_{27.5}Al_{7.5}$  metallic glass thin films with varying stability by varying the deposition rate at a substrate temperature of  $0.7T_g$ . The stability of the films is demonstrated by calorimetry and creates changes in films' modulus and hardness. We show using electron nanodiffraction that more stable films have greater nanometer-scale structural order, demonstrated by an increase in Friedel speckle pairs associated with Bragg diffraction from ordered structures. Analysis of rotational symmetries in nanodiffraction patterns show that the order is dominated by icosahedra, but that crystal-like rotational symmetries are also present. The ability to create glasses with widely varying stability at constant composition enables disentangling the influence of atomic rearrangements created by processing and changes in chemistry.

#### 7:15 PM \*F.SF02.07.01

**Additive Manufacturing and Deposition of Bulk Glass Forming Alloys and Composites—Progress and Outlook** Douglas C. Hofmann<sup>1</sup>, Punnathat Bordeenithikasem<sup>1</sup>, Samad Firdosy<sup>1</sup>, Andre Pate<sup>1</sup> and Daniel East<sup>2</sup>; <sup>1</sup>NASA JPL/Caltech, United States; <sup>2</sup>Commonwealth Scientific and Industrial Research Organisation, Australia

Additive manufacturing (AM) has emerged as a unique method for producing highly specialized metal alloys and composites. The high cooling rates and customizable cooling rates afforded by AM are particularly useful in the creation of bulk metallic glasses (BMGs) and BMG metal matrix composites. While AM allows for net-shaped fabrication of even the weakest glass-forming alloys, macroscale parts still suffer from embrittlement due to annealing, porosity, partial crystallization and oxygen. In contrast, thin coatings and overlays made from BMGs and BMG composites may be ideal for some wear-resistant applications. This talk will provide an overview of how BMG printing and deposition technologies might be matured and infused into applications. It will cover Fe-based, Zr-based, Cu-based, and Ti-based BMG alloys.

#### 7:35 PM BREAK

#### 7:50 PM \*F.SF02.05.01

**Syntheses and Features of Pseudo-High Entropy Bulk Metallic Glasses** Akihisa Inoue<sup>1,2,3</sup>, Fanli Kong<sup>2</sup>, Baolong Shen<sup>1</sup>, Shengli Zhu<sup>3</sup> and Alan Lindsay Greer<sup>4</sup>; <sup>1</sup>China University of Mining and Technology, China; <sup>2</sup>Josai International University, Japan; <sup>3</sup>Tianjin University, China; <sup>4</sup>University of Cambridge, United Kingdom

Since the first synthesis of a bulk metallic glass (BMG) by copper mold casting in 1989, a large number of BMGs with centimeter-size diameter were synthesized in a variety of multicomponent alloy systems such as La, Mg, Zr, Ti, Hf, Fe, Co, Ni, Cu, Pd, Pt and Au metal bases. These BMGs are composed of multicomponent with negative and nearly zero heats of mixing and significant atomic size mismatches, while there has been little information on the influence of additional metallic elements with positive heat of mixing on the formation, thermal stability, crystallization behavior and fundamental properties for BMGs. Very recently, the pseudo-high entropy (PHE) BMGs containing solute atomic pairs with positive heats of mixing, which are different from the component rule for ordinary BMGs, have attracted an increasing interest because of their unique properties<sup>1</sup>. In particular, the PHE BMGs exhibit two exothermic peaks on the continuously heating DSC curve

and the temperature interval between the two peaks is as large as 200-400 K. Besides, no crystalline phase is observed even after annealing for 1-5 h at the temperatures well above the first exothermic peak. The unusual high stability to the progress in crystallization has been reported for various PHE BMGs such as Zr-Al-(Ni,Cu)-Nb, Zr-Al-(Ni,Cu)-Ag, Zr-Al-(Co,Cu)-Ag, Zr-(Fe,Co,Ni,Cu), Ti-Zr-(Cu,Pd)-Nb and Fe-Cr-Mo-C-B-Y systems. These results indicate the possibility of developing a heat resistant BMG by utilizing this novel phenomenon. Here we present the formation, thermal stability, crystallization behavior and mechanical properties of PHE BMGs and to investigate the criterion for the synthesis of BMGs with ultrahigh thermal stability.

1) A. Inoue, F.L. Kong, S.L. Zhu, A.L. Greer, Multicomponent bulk metallic glasses with elevated-temperature resistance, MRS Bull. 44 (2019) 867-872.

**8:10 PM \*F.SF02.04.01**

**The Controlled Large-Area Synthesis of Freestanding Two-Dimensional Metallic-Glass Nanosheets/Nanostructures** Yong Yang; City University of Hong Kong, China

The rise of nanotechnology has been propelled by low dimensional metals. Albeit the long-perceived importance, synthesis of freestanding metallic nanomembranes (or the so-called 2D metals), however, has been mainly restricted to elemental metals with a very limited in-plane size ( $< 10 \mu\text{m}$ ). In this talk, I would like to talk about the development of a low-cost method to synthesize 2D metals through polymer surface buckling enabled exfoliation (PSBEE). The 2D metals so obtained could be as chemically complex as conventional metallic glasses while possessing in-plane dimensions at the scale of bulk metals ( $> 1 \text{cm}$ ). With our approach, we successfully synthesized a variety of 2D metallic glasses with controllable geometries and morphologies. Interestingly, our results clearly show that, as the thickness of the 2D metallic glasses reduces to a few nanometers, its modulus is significantly reduced to only a fraction of the modulus of their bulk counterparts. Aside from rather low elastic modulus, these 2D metallic glasses also exhibit unusual properties, such as good stretchability and tunable optical properties. Finally, we demonstrate that 2D ceramic glasses and 2D metallic composites can be also fabricated through PSBEE aside from 2D metallic glasses.

SESSION F.SF02.01: Modeling Structure and Properties

On Demand Abstracts Available for Viewing Starting Saturday Morning, November 21, 2020

F-SF02

**5:00 AM \*F.SF02.01.01**

**Multiscale Modeling of Plastic Flow and Failure in Amorphous Solids—The Role of Effective (Fictive) Temperature as a Measure of Disorder** Michael L. Falk; Johns Hopkins University, United States

We have undertaken to develop multiscale models of plastic flow and failure processes in amorphous solids, materials that exhibit a complete lack of crystalline order. In this we have taken metallic glass as an exemplar material and applied molecular dynamics simulation to examine the physics at the atomic scale. This has allowed us to uncover the statistics of the shear transformation zone (STZ) defects that control plastic deformation. We have then sought to relate this defect structure to statistical mechanics models of “effective temperature” that characterize the degree of glass disorder in an effort to build a constitutive model of plastic deformation. The constitutive model has been incorporated into a high-fidelity viscoplastic finite differencing scheme that adapts techniques originally developed for solving the Navier-Stokes equation. A novel machine learning algorithm then utilizes the atomistic data to guide the parameterization of the constitutive model so as to inform the continuum method. In doing so we have begun to ask some fundamental questions about the concept of “effective temperature.”

The concept of fictive-temperature has long been utilized to characterize the processing dependence of glass structure, and has recently been shown to be predictive of metallic glass ductility. Some theories have hypothesized that it is actually a real temperature related to the configurational degrees of freedom of the glass, i.e. an “effective-temperature,” notably the shear-transformation-zone (STZ) and soft-glassy-rheology (SGR) theories. We derive a thermodynamic integration scheme for calculating effective-temperature based on a 2-temperature hypothesis. To test this scheme we simulate a binary Cu-Zr metallic glass modeled with an EAM potential. Measures of the energy fluctuations associated with both the fast and slow degrees of freedom are measured during the glass quench. The resulting effective-temperature is consistent with estimates of fictive-temperature obtained from simulation in more heuristic ways. The results indicate that effective-temperature can be understood as a purely structural quantity. The method provides a means to measure the effective-temperature in the absence

of fluctuations induced by shear and without resorting computationally expensive and impractical methods for explicitly measuring the configurational entropy.

### 5:30 AM \*F.SF02.01.02

**Concept of Defects in Glasses and Liquids** Takeshi Egami<sup>1,2</sup>; <sup>1</sup>University of Tennessee, United States; <sup>2</sup>Oak Ridge National Laboratory, United States

In crystals atomic mobility in transport and deformation is governed by structural defects, such as vacancies and dislocations. This was carried over to the study of glasses and liquids, and various defect-like concepts have been proposed, including free-volume, cooperatively rearranging region and shear-transformation-zone (STZ). However, whereas in crystals defects are topologically protected by the lattice and preserve their identity after motion, the same does not apply for liquid and glass. For this reason, today these defects in glass are considered to be transient; they do not pre-exist and disappear after the action. In this talk this view is advanced even further to suggest that the dynamics in liquid and glass is governed not by defects but by the structural medium-range order (MRO) of the bulk. The MRO is defined by the coherence length which characterizes the decay of the oscillation in the pair-distribution function (PDF) beyond the first peak. Because the higher-order peaks of the PDF are broad,  $\sim 1 \text{ \AA}$  in width, the MRO does not describe the order at the atomic level. It represents the strength of the coarse-grained density wave, represented by the first peak in the structure function,  $S(Q)$ . We show that the coherence volume is proportional to the fragility coefficient,  $m$ , at the glass transition temperature,  $T_g$ , and also to the activation energy of viscosity above  $T_g$ . In crystal atoms are mobile only at defects of which density is low. But in liquid all atoms are mobile and participate in transport. Whereas the defect-like sites have a higher propensity to start deformation or atomic transport, as soon as deformation starts extensive atomic rearrangement ensues, and the structure of the final state is very different from the initial one. Furthermore, at the saddle point of transition the effective temperature becomes so high that the system locally melts for a short time, and the system locally loses its thermal history. Therefore, the mobility is not determined by the initial structure but by the resistance to local collective motion which is determined by the MRO. For this reason, the structural coherence, which is a bulk property in equilibrium, controls the dynamics in liquid and glass. Defects are relevant only as outliers in the equilibrium statistical distribution where action could start.

### 6:00 AM F.SF02.01.03

**The Energy Landscape Governs Ductility in Bulk Metallic Glasses** Longwen Tang and Mathieu Bauchy; University of California, Los Angeles, United States

Depending on their thermal history, bulk metallic glasses can fail in a brittle or ductile fashion. However, the nature of the link between structure and propensity for ductility has remained elusive. Here, based on molecular dynamics simulations, we investigate how the degree of structural disorder affects the fracture of bulk metallic glasses. As expected, we observe that structural disorder results in an increase in ductility. By applying the activation-relaxation technique (an open-ended saddle point search algorithm), we demonstrate that the propensity for ductility is controlled by the topography of the energy landscape. Interestingly, we observe a power-law relationship between the particle non-affine displacement upon fracture and the average local energy barrier. This reveals that the dynamics of the atoms upon fracture is encoded in the static energy landscape, i.e., before any load is applied. Besides bulk metallic glasses, this relationship is shown to apply to several classes of non-crystalline materials (oxide glasses, amorphous solids, and colloidal gels), which suggests that it may be a generic feature of disordered materials.

### 6:15 AM F.SF02.01.04

**Structural Relaxation and Mechanical Properties of Model Glass Systems at the Micro-Second Timescale** Peter M. Derlet<sup>1</sup> and Robert Maass<sup>2</sup>; <sup>1</sup>Paul Scherrer Institute, Switzerland; <sup>2</sup>University of Illinois at Urbana-Champaign, United States

It is now possible to routinely perform atomistic simulations at the microsecond timescale. In the present work, we exploit this for a model binary Lennard-Jones glass to study structural relaxation at a timescale spanning several tens of microseconds, and the collective plastic shear activity under simple shear spanning six orders of magnitude strain rate. It is found that at these longer time-scales, significant mobility and relaxation occurs. Under load, such structural activity during collective and system-spanning plasticity plays an important role, producing a rich spectrum of atomic-scale activity in terms of spatial and temporal correlation, both in the elastic and plastic regimes of deformation.

### 6:30 AM \*F.SF02.01.05

**The Non-Equilibrium Origin of a Brittle-to-Ductile Transition in Metallic Glasses** Eran Bouchbinder<sup>1</sup>, Manish Vasoya<sup>2,1</sup>, Christopher Rycroft<sup>3</sup>, Jittisa Ketkaew<sup>4</sup> and Jan Schroers<sup>4</sup>; <sup>1</sup>Weizmann Institute of Science, Israel; <sup>2</sup>Texas A&M University, United States; <sup>3</sup>Harvard University, United States; <sup>4</sup>Yale University, United States

Understanding the fracture toughness of glasses is a fundamental problem of prime theoretical and practical importance. We develop a theory of the notch fracture toughness of glasses using a non-equilibrium thermodynamic approach to the elastoplastic deformation of glassy materials. We show that the notch fracture toughness results from a competition between the initial plastic relaxation timescale, which depends on initial non-equilibrium structural state of the glass (e.g. its age and its preparation protocol), and an effective loading timescale, which depends on the notch radius, the system's geometry and the external loading rate. The initial glass structure, which controls the initial plastic relaxation timescale, is characterized by a non-equilibrium (effective/fictive) temperature. The theory predicts a rather abrupt increase in the toughness – a brittle-to-ductile transition – as a function of the ratio between these two timescales. Novel experiments on various Bulk Metallic Glasses (BMGs), which allow to carefully controlling the initial structural state of the glass and accurately measure the toughness, verify the theoretical predictions. In particular, they show that BMGs can be significantly toughened by carefully controlling their initial non-equilibrium state. These results highlight the importance of timescales competition and far from steady-state plastic deformation dynamics for understanding the toughness of glasses, and open up the way for a broader usage of BMGs as tough, highly-reproducible structural materials.

#### 7:00 AM F.SF02.01.06

**Towards a Better Atomistic Understanding of Deformation and Relaxation Mechanisms in Metallic Glasses** Daniel Sopp<sup>1,2</sup> and Jurgen H. Eckert<sup>1,3</sup>; <sup>1</sup>Erich Schmid Institute, Austria; <sup>2</sup>Technical University of Darmstadt, Germany; <sup>3</sup>Montanuniversität Leoben, Austria

Over time, a variety of environmental descriptors have been proposed to identify and characterize the atomic scale heterogeneities and to guide us towards an inherent structure-property relationship for metallic glasses. By using the STZ-vortex coupling the atomic-level mechanisms underlying elastic and plastic deformation in metallic glasses are disclosed. Removing the thermal noise by simulating athermal quasistatic shearing processes even small elastic/structural fluctuations can be identified and analysed. Given to complex morphology and a long range signature of STZs the activation of low number of events could strongly perturb the initial configuration and explain the observed weak correlations between structure and dynamics. The rotation field calculation reveals that elastic and plastic STZs have similar signature but different dynamics. Additionally, the observed deformation mechanisms have significant implications for understanding relaxation phenomena in amorphous metals and allow distinguishing between the different relaxation mechanisms. These results highlight that the classical definition of STZ should be reconsidered and a full understanding of this elementary event must be assured as they play a decisive role in controlling plasticity in metallic glasses

#### 7:15 AM F.SF02.01.07

**Machine Learning for the Analysis of Deformation Experiments on Colloidal Glasses** Agnese Curatolo<sup>1</sup>, Seong Ho Pahng<sup>1</sup>, Katharine E. Jensen<sup>2</sup>, Michael P. Brenner<sup>1</sup>, David Weitz<sup>1</sup> and Frans Spaepen<sup>1</sup>; <sup>1</sup>Harvard University, United States; <sup>2</sup>Williams College, United States

Plastic deformation of glasses is governed by local shear transformation zones (STZs). We need to know their concentration, their size, their transformation rate, how they nucleate, whether they are reversible or not, and if there are correlations between them. STZs can be studied by deforming colloidal glasses and tracking the particles in space and time. As modeling systems, colloidal glasses have the advantage of being dynamic, three-dimensional and large (>50,000 particles). The data in this study were obtained during cyclic deformation in pure shear up to  $10^{-5} \text{ s}^{-1}$  between 0 and 10%. To study how the dynamics and properties of the STZs are related to the evolution of the glassy structure, we have employed three machine learning techniques: Support Vector Machines (SVM), Convolutional Neural Networks (CNN) and Graph Neural Networks (GNN). We will discuss how these methods can be applied to experimental data with physical boundary conditions. We use them to predict the evolution of local strain, which particles are most likely to move, and which particles undergo irreversible rearrangements. The results of the three methods for each of these tasks will be compared.

#### 7:30 AM F.SF02.01.09

**Effective Quantification of Liquid Structure in Metallic Alloys and Its Relation to Glass-Forming Ability** Porter Weeks and Katharine Flores; Washington University in St. Louis, United States

Recent research<sup>1-3</sup> has proposed that structural order present in the liquid is related to glass-forming ability in metallic alloys suggesting that high order in the metallic liquid makes crystallization easier due to the lack of atomic motion needed for this process to occur in comparison to a liquid with little order in the liquid. However, the effective quantification of this liquid structure is extremely challenging due to the inherent long-range disorder present. While Voronoi tessellation is a common method for describing the short-range order of disordered systems, there are many drawbacks to this technique. Namely,

Voronoi indices describe the topology of the polyhedral volume associated with a particular atom, but provide little insight into the relative similarity of the various polyhedra that make up the material. That is, a minor distortion in atomic positions may result in vastly different Voronoi indices without dramatically impacting the local environment of an atom or the overall degree of ordering in the system. A more rigorous approach would ask if local environments are *similar enough* to be considered the same. Here, we show that a density-based machine learning approach (HDBSCAN) provides such characterization of structure in the liquid. Out of this method emerge groups of atoms with similar atomic arrangements. The relative degree of order is described by the variance in the group sizes; a low variance indicates that most atoms belong to a small number of groups, implying a high degree of order. To demonstrate the effectiveness of this approach, we analyze the structures of simulated Cu-Zr and Al-Sm alloys to show that this variance is inversely correlated to experimentally observed glass-forming ability. This work has the potential to fundamentally change our understanding of glass formation. While the historical approach to glass formation is to consider the competition between the thermodynamic driver and the kinetic mobility of atoms within the super-cooled liquid, this data suggests that the ease of glass formation in a given material is predetermined in the liquid state, before ever reaching the melting point or the glass transition temperature.

<sup>1</sup>N. A. Mauro, M. Blodgett, M. L. Johnson, A. J. Vogt, and K. F. Kelton, “A structural signature of liquid fragility,” *Nat. Commun.*, vol. 5, Aug. 2014.

<sup>2</sup>X. J. Liu *et al.*, “Static atomic-scale structural heterogeneity and its effects on glass formation and dynamics of metallic glasses,” *Intermetallics*, vol. 101, pp. 133–143, Oct. 2018.

<sup>3</sup>J. Wang, A. Agrawal, and K. Flores, “Are hints about glass forming ability hidden in the liquid structure?,” *Acta Mater.*, vol. 171, pp. 163–169, Jun. 2019.

#### 7:45 AM F.SF02.01.10

**Late News: Predicting Plastic Events via the Local Yield Stress Method in 3D Model Glasses** [Dihui Ruan](#)<sup>1</sup>, Sylvain Patinet<sup>2</sup> and Michael L. Falk<sup>1</sup>; <sup>1</sup>Johns Hopkins University, United States; <sup>2</sup>ESPCI, France

**Within the context of the ‘shear transformation zone’ model, the local yield stress (LYS) method provides a straightforward assessment of the local elastoplastic response for the sake of identifying shear transformation zone defects in amorphous materials. Here, for the first time in 3D, we study as-quenched binary Lennard-Jones glasses using the LYS method. We first systematically vary the size of the LYS probing region. At an optimal LYS probing region size ~5 atomic diameters in radius, high correlations are confirmed between the incremental stress required to trigger the local plasticity (i.e., the local yield stress) and the locations of the plastic events. When local probing is limited to align with the loading applied at the boundary, the averaged correlations remain positive until 1/3 of the yielding strain (200 plastic events). At the location of the first plastic event, the anisotropy of the local yield surface is systematically investigated by varying a unit strain tensor which determines the orientation and triaxiality of the local probing. The results indicate that the lowest local yield stress is not necessary to align with the loading on the boundary, but can be inferred by projecting the stress applied on the boundary onto the local yield surface. Thus, the predictivity of the local yield stress method for locating the plastic events may be enhanced by more completely sampling the local yield surface at each local probing region.**

SESSION F.SF02.02: Structural Characterization

On Demand Abstracts Available for Viewing Starting Saturday Morning, November 21, 2020  
F-SF02

#### 5:00 AM F.SF02.02.02

**Atomic-Resolution Observation of Crystal Growth in Metallic Glass Nanorods** [Yujun Xie](#)<sup>1,2,3</sup>, Sungwoo Sohn<sup>1</sup>, Jan Schroers<sup>1</sup> and Judy Cha<sup>1</sup>; <sup>1</sup>Yale University, United States; <sup>2</sup>Lawrence Berkeley National Laboratory, United States; <sup>3</sup>University of California, Berkeley, United States

Crystallization induced microstructure plays a central role in tailoring materials properties, yet our understanding of its formation process is limited due to its complexity. Classical crystallization theories assume that nucleation and growth are separate processes in which thermodynamically unstable clusters fluctuate in the nucleation stage, but do not participate in the later growth. Here, we apply in situ aberration-corrected transmission electron microscopy (TEM) technique to directly observe the crystal growth of metallic glass nanorods at the atomic resolution and test the classical theories. Surprisingly, we



show that, at the atomic scale, the isothermal growth rate for a single crystalline phase is asymmetric upon thermal history. This observation is in direct contrast to what would be expected based on classical theories. We further observe that the asymmetric growth rate depends on the diameter of the nanorod. Thus, our *in situ* TEM observations mark departure from classical theories in metallic glass system<sup>1,2,3</sup>.

1. Sohn, S., Jung, Y., Xie, Y., Osuji, C., Schroers, J. and Cha, J.J., 2015. Nanoscale size effects in crystallization of metallic glass nanorods. *Nature communications*, 6, p.8157.
2. Sohn, S.\*, Xie, Y\*, Jung, Y., Schroers, J. and Cha, J.J., 2017. Tailoring crystallization phases in metallic glass nanorods via nucleus starvation. *Nature communications*, 8(1), pp.1-8. (co-first author)
3. Xie, Y., Sohn, S., Wang, M., Xin, H., Jung, Y., Shattuck, M.D., O'Hern, C.S., Schroers, J. and Cha, J.J., 2019. Supercluster-coupled crystal growth in metallic glass forming liquids. *Nature communications*, 10(1), pp.1-9.

### 5:10 AM F.SF02.02.03

***In Situ* Heating TEM Study on Structural Evolution of Metallic Glasses** Yuan Tian and Mingwei Chen; Johns Hopkins University, United States

Metastable metallic glasses experience significant structural evolution and phase transition in supercooled liquid regions at high temperatures. In this research, we employed a MEMS based ultra-stable heating stage to *in situ* investigate the coalescence and crystallization of metallic glasses in a Cs-corrected high-resolution transmission electron microscope. The atomic-scale *in situ* observations reveal the significant kinetic difference between crystals and glasses in particle coalescence, demonstrating that the fast surface dynamics of metallic glasses is associated with the isotropic atomic structure and supercooling state. On the other hand, the kinetics-controlled crystallization process at temperatures close to  $T_g$  is found to be manipulated by both liquid diffusivity and chemical defects at liquid/crystal interfaces. These results provide new insights into the relation between structural stability and surface/interface dynamics of metallic glasses.

### 5:20 AM \*F.SF02.02.04

**Metallic Glass Stability and Surface Dynamics** Sachin V. Muley<sup>1</sup>, Debadya Chatterjee<sup>1</sup>, Carter Francis<sup>1</sup>, Ajay Annamareddy<sup>1</sup>, Chengrong Cao<sup>1</sup>, Jittisa Ketkaew<sup>2</sup>, Jan Schroers<sup>2</sup>, John Perepezko<sup>1</sup>, Dane Morgan<sup>1</sup> and Paul M. Voyles<sup>1</sup>; <sup>1</sup>University of Wisconsin, United States; <sup>2</sup>Yale University, United States

Metallic glasses can have widely varying thermodynamic and kinetic stability at constant composition depending on their processing history. For bulk glasses, fast quenching or post-synthesis deformation result in a high free energy, less stable states and slow quenching or post-synthesis sub- $T_g$  annealing result in low free energy, more stable states.

For thin films and nanostructures, surfaces play a larger role. We have used electron correlation microscopy experiments and molecular dynamics simulations to show that metallic glass surfaces have approximately ten times faster dynamics than the bulk at the same temperature for temperatures near  $T_g$ . The fast surface layer has a glass transition temperature that is suppressed with respect to the bulk by  $\sim 20$  K. We have extended the understanding of diffusion in supercooled liquids based on caging and hopping of atoms to surfaces to explain this behavior.

Enhanced surface dynamics enable deposition of highly stable thin films, since every atom at some point has been a surface atom and the surface layer maintains sufficient mobility for the atoms to find low-energy configurations even at temperatures well below the bulk  $T_g$ . We have deposited  $Zr_{65}Cu_{27.5}Al_{7.5}$  metallic glass thin films with varying stability by varying the deposition rate at a substrate temperature of  $0.7T_g$ . The stability of the films is demonstrated by calorimetry and creates changes in films' modulus and hardness. We show using electron nanodiffraction that more stable films have greater nanometer-scale structural order, demonstrated by an increase in Friedel speckle pairs associated with Bragg diffraction from ordered structures. Analysis of rotational symmetries in nanodiffraction patterns show that the order is dominated by icosahedra, but that crystal-like rotational symmetries are also present. The ability to create glasses with widely varying stability at constant composition enables disentangling the influence of atomic rearrangements created by processing and changes in chemistry.

### 5:35 AM F.SF02.02.05

**Electron Correlation Microscopy Measurements of Metallic Glass Surface Dynamics** Debaditya Chatterjee<sup>1</sup>, Ajay Annamareddy<sup>1</sup>, Jittisa Ketkaew<sup>2,3</sup>, Jan Schroers<sup>3</sup>, Dane Morgan<sup>1</sup> and Paul M. Voyles<sup>1</sup>; <sup>1</sup>University of Wisconsin–Madison, United States; <sup>2</sup>Supercool Metals, United States; <sup>3</sup>Yale University, United States

We have applied electron correlation microscopy (ECM) to study near-surface layer dynamics in metallic glass forming liquids as a function of temperature using *in situ* heating. Previous ECM studies showed that the near-surface layer relaxation dynamics in Pt<sub>57.5</sub>Cu<sub>14.7</sub>Ni<sub>5.3</sub>P<sub>22.5</sub> metallic glass nanowires are an order of magnitude faster than bulk dynamics at the same temperature [1]. We have performed ECM experiments with higher spatial resolution and at temperatures lower than the bulk glass transition temperature, where the surface layer dynamics are still active but the bulk is vitrified. Our investigations reveal a ~1 nm layer with faster dynamics near the surface of the nanowire, which has a glass transition temperature 20 K lower than the bulk. Coating the nanowire with a thin layer of amorphous carbon suppresses the fast near-surface layer, which indicates that access to free volume available at the surface is responsible for the enhanced mobility.

Parallel investigations were performed via molecular dynamics simulations on a Ni<sub>80</sub>P<sub>20</sub> system. Simulated Ni<sub>80</sub>P<sub>20</sub> has a ~1 nm thick surface layer with faster dynamics and a glass transition temperature suppressed by 40 K compared to the bulk. With the surface layer held immobile in the simulation, the near-surface layer dynamics become slower than the bulk, but speed up with distance away from the surface, converging to the bulk dynamics. Based on these observations, we will briefly present a mechanism of diffusion in supercooled liquids based on caging and hopping of atoms, and how caging barriers control atomic diffusion and relaxation phenomena even in the near-surface region.

[1] Zhang, P., Maldonis, J.J., Liu, Z. et al. Spatially heterogeneous dynamics in a metallic glass forming liquid imaged by electron correlation microscopy. Nat Commun 9, 1129 (2018). <https://doi.org/10.1038/s41467-018-03604-2>

#### SESSION F.SF02.03: Mechanical Properties

On Demand Abstracts Available for Viewing Starting Saturday Morning, November 21, 2020

F-SF02

##### 5:00 AM \*F.SF02.03.01

**Effects of Minor Alloying on Stability and Mechanical Properties of Al-Based Metallic Glasses** Izabela Szlufarska, Vrishank Jambur, Jianqi Xi, Chaiyapat Tangpatjaroen, George Bokas, Dane Morgan and John Perepezko; University of Wisconsin, United States

While minor alloying is used extensively to manipulate stability and mechanical properties of metallic glasses (MGs), a mechanistic understanding of these effects is still lacking, limiting rational design of new MGs. In crystalline metals, alloying elements can, for instance, pin dislocations and thereby have a large effect on the overall mechanical response, but MGs do not have a long-range order and they do not exhibit dislocation plasticity. It is therefore puzzling how a small amount of impurities can lead to significant changes in mechanical properties of an amorphous material. To understand the role of minor alloying on stability and mechanical properties of MGs, we have investigated Al-Sm glasses microalloyed with transition metal (TM) elements. Al-based glasses were chosen because of the many excellent properties of these materials, such as light weight, high specific strength, good corrosion resistance, and thermoplastic forming ability.

We have found experimentally that TMs increase both the glass forming ability (GFA) and the strength of Al-Sm-TM glasses, and we have used atomistic simulations to discover the underlying mechanisms for these effects. First, we have found that in the binary Al-Sm glasses, the experimentally determined GFA (quantified based on the critical cooling rate) is correlated with a local topology determined from classical molecular dynamics (MD) simulations. Specifically, the GFA was found to be higher for glasses that have a higher fraction of icosahedral clusters. We have then used this topological descriptor combined with *ab initio* MD simulations to predict ternary Al-Sm-TM glasses with high GFA. The predictions were then verified experimentally. This result shows that, similarly to what has been reported in commonly studied Cu-Zr MGs, the topology plays a dominant role in determining stability of Al-Sm MGs. The results also demonstrate that *ab initio* simulations can be used directly to design new glass compositions with high GFA.

Interestingly, we have found the topology to be correlated with mechanical strength of binary Al-Sm glasses, but not with the strength of Al-Sm-TM glasses. A commonly accepted explanation for the strengthening of MGs with minor alloying is based on the impurity-induced increase in the topological order and a more efficient packing of atoms. It has been confirmed to be

the case for instance in Cu-Zr glasses and by us in Al-Sm binary glasses. However, in the case of Al-Sm-TM, we discovered that a small amount of impurities can increase the strength of MGs by changing the chemical bond strength alone. In fact, we find that the favorable changes in the chemical bond strength overcome the effect of impurity-induced unfavorable changes in the topological order.

Our results are important for design of new MGs, as they demonstrate that the effect of bond chemistry and the effect of topology should be separated from each other and they could potentially compete with each other in controlling mechanical response of MGs. These results also highlight the importance of investigating structure-property relations in a number of different MGs, beyond the Cu-Zr model system, in order to extract generally applicable trends.

**5:15 AM \*F.SF02.03.02**

**Coupling Between MRO Structure and Local Plasticity of Metallic Glasses** Gerhard H. Wilde; University of Muenster, Germany

Plastic deformation of metallic glasses is usually carried by local plastic instabilities, eventually leading to shear banding that is coupled to work softening. As a result, metallic glasses often show macroscopically brittle behaviour, thus limiting practical applications. This short description already signifies that plastic deformation of metallic glasses inherently involves vastly different length scales from the scale of locally ordered regions (so-called medium range order, MRO) to the macroscopic and system-spanning dimensions of shear bands. In this contribution, emphasis is laid on the local MRO structure of metallic glasses and specifically its modifications upon applying an external shear stress.

For this reason, the MRO structure of both as-cast and deformed states of different metallic glasses were analysed using variable resolution fluctuation electron microscopy. After deformation, significant changes of the MRO structure were observed inside the shear bands and also inside the adjacent matrix; the MRO structure was altered in terms of types, sizes and volume fractions. The changes in the matrix upon deformation confirm the existence of a shear affected zone around shear bands.

To understand the coupling between medium range order structure and local deformation behaviour further, sputtered nanolaminates of a binary metallic glass,  $\text{Cu}_{40}\text{Zr}_{60}$ , and nanocrystalline Cu were synthesized and subsequently co-deformed. The nanolaminates deform in shear zones, including nanocrystalline Cu layers, amorphous layers and the surrounding matrix. Due to the confinement of the glass, large plastic strains can be realized without premature macroscopic failure, allowing to assess deformation states in one sample that have carried between several ten percent and up to several hundred percent of strain. Analyses of nanobeam-diffraction patterns reveal an extraordinary modification of the MRO structure of amorphous  $\text{Cu}_{40}\text{Zr}_{60}$  after deformation. This transformation shows similarities to a reverse martensitic transformation in the corresponding crystal from the B19 to the B2 structure, as shown by fluctuation electron microscopy and a symmetry analysis of nanobeam-diffraction patterns. Since the local ordered domain size surprisingly stays similar, this phenomenon is attributed to transformation-induced plasticity of the local units in the glass that carry the shear.

The current work illustrates the significance of the MRO structure for the deformation of metallic glasses and further suggests that the plasticity of monolithic BMGs might be improved by tailoring the topological order based on MRO types, sizes and volume fractions.

**5:30 AM F.SF02.03.03**

**Structure of Shear Bands in a Zr-Based Bulk Metallic Glass** Chaoyang Liu<sup>1</sup> and Robert Maass<sup>1,2</sup>; <sup>1</sup>University of Illinois at Urbana-Champaign, United States; <sup>2</sup>Federal Institute for Materials Research and Testing (BAM), Germany

Damage accumulation as a function of plastic strain is well understood in crystalline metals but not in metallic glasses, where strain localizes into nano-scale shear bands. Here we aim at revealing how the nanoscale and mesoscopic signature of strain localization evolves during deformation. Using high-energy x-ray tomography, we first address how the gradual emergence of shear-band cavities leads to a large reduction in the load bearing area as a function of strain (Scripta Materialia 170 (2019) 29). Determining the true flow stress on the basis of the tomography data indicates significantly larger stresses than the yield stress of the material. This apparent strain hardening can be rationalized by taking into account the shear-plane roughness and its contribution to the friction condition between the two shearing sample parts. As a second step, we pay attention to the shear band itself with the interest in tracing any structural or chemical changes as a function of shear strain. To this end, we use a combination of high-angle annular dark-field scanning transmission electron microscopy (HAADF-STEM), synchrotron-based nano-beam x-ray fluorescence, atom probe tomography (APT), scanning electron nano-beam diffraction (SEND) and energy-dispersive x-ray spectroscopy (EDS). Apparent chemical changes in the shear band are found that can be shown to be due to the density change of the shear band relative to the matrix (Scripta Materialia 169 (2019) 23). We further discuss if the shear-band width and density change are related and how they depend on position (Acta Materialia 140 (2017) 206). Finally, we provide first evidence for that the locally admitted shear strain determines the locally determined density

change of the shear-band material. This body of work highlights the locally varying complexity of shear-band structure in bulk metallic glasses.

#### 5:40 AM F.SF02.03.04

**Revealing the Role of Cluster Connectivity in Plastic Deformation of Pd-Si Metallic Glasses** Sinan Liu<sup>1</sup>, Jiacheng Ge<sup>1</sup>, Xun-Li Wang<sup>2</sup>, Yang Ren<sup>3</sup> and Si Lan<sup>1</sup>; <sup>1</sup>Nanjing University of Science and Technology, China; <sup>2</sup>City University of Hong Kong, China; <sup>3</sup>Argonne National Laboratory, United States

It would be interesting to study the atomic-scale structure response to deformation for better understanding the structure-property relationship for metallic glasses. The atomic-scale structure evolution during plastic deformation of Pd<sub>82</sub>Si<sub>18</sub> metallic glasses was studied using the high-energy X-ray pair-distribution function. Our experimental results revealed that the change of the cluster connectivity on the medium-range length scale plays an essential role during plastic deformation. It was found that the transformation between 2-atom and 3-atom connection modes would be responsible for the densification process during tension. Our findings would be helpful in deepening the understanding of the plastic deformation mechanism of metallic glasses.

#### 5:50 AM \*F.SF02.03.05

**Atomic-Scale Details of Structural Relaxation, Rejuvenation and Plasticity of Metallic Glasses from Anelastic Deformation** Michael Atzmon<sup>1</sup>, Tianjiao Lei<sup>1</sup>, Luis Rangel DaCosta<sup>1</sup>, Jie Shen<sup>2</sup>, Ming Liu<sup>2</sup>, Alan Lindsay Greer<sup>3</sup>, Yonghao Sun<sup>2</sup> and Wei Hua Wang<sup>2</sup>; <sup>1</sup>University of Michigan, United States; <sup>2</sup>Institute of Physics, Chinese Academy of Sciences, China; <sup>3</sup>University of Cambridge, United Kingdom

Current understanding of plastic deformation of crystalline solids has benefitted greatly from electron-microscopic imaging of lattice defects. In the absence of periodicity, atomic-scale imaging of glasses is far more limited. However, similar to crystalline materials, physical analogs have provided important initial insights. Bubble-raft experiments by Argon et al. indicated that time-dependent deformation of a glass, permanent or reversible, is accommodated by localized rearrangements, termed shear transformations. Using Eshelby's theory of deformation of inclusions embedded in an elastic medium, Argon developed a theory of thermally activated, stress-biased, shear transformation kinetics. It is based on a single size of a shear transformation zone (STZ). Since the activation free energy for a shear transformation is proportional to the STZ volume, the spread in time constants associated with different STZ sizes can be significant. Dynamic-mechanical analysis results have, indeed, demonstrated a range of time constants. However, with the loss modulus peak associated with a single time constant being a Cauchy function, details cannot be readily resolved.

We have used quasi-static anelastic relaxation measurements spanning more than ten orders of magnitude of time,  $10^{-3}$  –  $6 \times 10^7$  s. Non-instrumented curvature measurements at stable room temperature, with automated curvature determination from images, provide relaxation curves with small error bars. The inverse problem of obtaining relaxation-time spectra from the seemingly featureless experimental curves was solved computationally. The spectra exhibited distinct peaks, which we showed to correspond to an atomically-quantized hierarchy of STZs. The resolution level achieved is assisted by the relatively low temperature of the experiment. Using Argon's theory, the spectra yield the volume of each STZ type as well as the volume fraction occupied by the corresponding potential STZs.

We have used the methodology detailed above to obtain the following results:

- 1) At small radii of curvature, for which the strain is large and the anelastic strain rate is not linear in the stress, we obtained the transformation shear strain and volume of the largest STZs independently. The value of the former is 0.18, in agreement with physical analogs. This result indicates that reports of STZ volume values of hundreds of atoms are unrealistically high, as they were based on a transformation strain value equal to the much-smaller macroscopic yield strain.
- 2) Structural relaxation increases each of the time constants and reduces the volume fraction occupied by the largest active potential STZs. The former effect is a result of an increase in shear modulus. Rejuvenation by cryogenic cycling reverses the increase in time constants, suggesting a reversal of densification. However, the volume fraction occupied by the largest active potential STZs is not restored.
- 3) Some metallic glasses exhibit a distinct high-frequency  $\beta$  relaxation. While it has been suggested to correspond to a mechanism distinct from that of the  $\alpha$  relaxation, we find that both  $\alpha$  and  $\beta$  are consistent with the STZ model. However, they exhibit different properties – either the STZ volume increment in the hierarchy or the corresponding shear modulus is different for the two mechanical relaxation modes. Both possibilities are consistent with composition fluctuations.
- 4) While it has been suggested that an intense  $\beta$  relaxation correlates with alloy plasticity, a comparison between La<sub>70</sub>Cu<sub>15</sub>Al<sub>15</sub> and La<sub>70</sub>Ni<sub>15</sub>Al<sub>15</sub> shows the opposite – the former exhibits far greater plasticity and its  $\beta$  relaxation intensity is smaller. We find that the overall anelastic response, which is equal to the integrated area of the relaxation-time spectrum, can be used as a predictor of plasticity.

This work was funded by the U.S. National Science Foundation, Grant DMR-1708043

**6:05 AM \*F.SF02.03.06**

**Tailoring Shear Banding in Bulk Metallic Glasses and Composites** [Jurgen H. Eckert](#)<sup>1,2</sup>; <sup>1</sup>Erich Schmid Institute of Materials Science, Austrian Academy of Sciences, Austria; <sup>2</sup>Montanuniversitaet Leoben, Austria

Shear banding is the main mechanism dominating plastic deformation of bulk metallic glasses (BMGs). Under constrained loading conditions, such as bending or compression, BMGs generally deform through serrated flow at room temperature. A serration event is accomplished by fast nucleation and propagation, together with the arrest of a shear band. A shear band forms by cooperative shear of nanometer-size shear transformation zones (STZ), developing into a highly localized deformation band with a thickness of ~10 nm. The dynamics of serrated flow in BMGs have been intensively studied, and the cumulative distribution of shear-avalanche sizes follows a universal power-law relation multiplied by an exponentially decaying scaling function as depicted by the mean-field theory. In contrast, under uniaxial tension, BMGs exhibit almost zero plasticity due to the fast runaway of a detrimental shear band.

In order to improve the tensile plasticity of BMGs, bulk metallic glass composites (BMGCs) containing *in-situ* formed crystals during solidification have been developed. Zr/Ti-based BMGCs containing beta-Zr/Ti phases and CuZr-based BMGCs containing B2 CuZr phases are the two most intensively investigated kinds of BMGCs. Generally, macroscopic serrated flow of BMGCs under tension disappears, because the shear bands are well restricted in the inter-crystalline glassy regions. BMGCs often exhibit strain-softening, because hardening caused by dislocation entanglement in the crystals cannot sufficiently compensate shear-softening in the glassy matrix. Recent research has shown that this drawback can be overcome and strain-hardening can be obtained *via* incorporating deformation-induced phase transformations or twinning of metastable crystals.

This talk explores the possibilities for tuning shear band initiation and propagation in metallic glasses and composites considering structural heterogeneity, phase transformation and size effects for glasses and composites with different composition and inherent stability. The findings will be discussed with respect to short- and medium-range order modulation, local stress and strain states, and their impact on shear band nucleation, bifurcation, blunting and modulation of cooperative shear events in the presence of crystals or triggered by the precipitation of secondary phases. The structure changes will be correlated with plastic deformability and strain-hardening capacity, and the effectiveness of composition tuning and structure modulation for ductility improvement will be discussed to derive guidelines for property optimization.

**6:20 AM \*F.SF02.03.07**

**Effects of Testing Temperature and Sample-Size on Tensile Deformation of Metallic Glass** [Golden Kumar](#) and Chandra Sekhar Meduri; University of Texas at Dallas, United States

Deformation of nanoscale metallic glasses has attracted increasing attention but remains controversial due to difficulty in fabrication and testing of small samples. Here, we report the effects of systematic variation in sample-size and testing temperature. Pt-based metallic glass samples with varying diameters (100 nm -500 nm) were prepared by thermoplastic drawing. Multiple samples were deformed at different temperatures and the fracture morphologies were characterized using SEM. The results show that the fraction of vein-like morphology decreases with decreasing sample size and mirror-like fracture surface was observed in samples smaller than about 2 nm in diameter. With further decreasing diameter, transition from shear-localized to necking was observed and the extent of neck increased with decreasing sample diameter. The lowering in temperature had similar effect as decrease in sample diameter. This temperature-size equivalence is discussed in terms of temperature rise and formation of liquid-like layer in shear bands.

**6:35 AM \*F.SF02.03.08**

**Plastic Deformation of Metallic Glasses Under Triaxial Stress State at Room Temperature** [Yi Li](#)<sup>1</sup> and Alan Lindsay Greer<sup>2</sup>; <sup>1</sup>Institute of Metal Research, China; <sup>2</sup>University of Cambridge, United Kingdom

Usually, plastic deformation of large-sized metallic glasses (MGs) is highly localized into shear bands under uniaxial stress state. Because of this, the plastic deformation is heterogeneous and strain softening would occur. Over the past few years, we have studied the plastic behaviour of metallic glasses under triaxial stress state. Under this condition, shear banding is suppressed, and metallic glasses are capable homogeneous plastic flow at room temperature under either tension or compression. Our talk will present a summary on the mechanical behaviour of BMGs in a deep notched cylindrical bar. We will show that the plasticity and strength of Zr-based BMG can be significantly enhanced by suppressing shear banding under tension condition due to strain hardening and densification (e.g. free volume annihilation) due to mechanical relaxation. Meanwhile, the samples also exhibit different fracture behaviour with new fracture features. Under the compression

condition, however, metallic glasses can be rejuvenated and extreme softening is seen in the sample. Such softened glass enables subsequent strain hardening. The mechanism for these observations will be discussed in terms of annihilation and generation of free volume under triaxial stress state.

#### 6:50 AM F.SF02.03.09

**Strain-Hardening in Metallic Glasses** [Alan Lindsay Greer](#)<sup>1</sup> and Yi Li<sup>2</sup>; <sup>1</sup>University of Cambridge, United Kingdom; <sup>2</sup>Chinese Academy of Sciences, China

Conventional polycrystalline alloys show strain-hardening. This is a key factor underpinning their usefulness in structural applications, delocalizing plastic deformation, enabling ductility, and preventing catastrophic failure. In contrast, metallic glasses (MGs) generally show strain-softening, leading to extreme localization of plastic flow in thin (10–20 nm) shear bands. This shear banding leads to early catastrophic failure in tension, and to unsightly surface steps when significant plastic strains can be achieved in other deformation modes, notably bending.

There have been many attempts at ‘shear-band engineering’, mainly to stimulate as many shear bands as possible to promote more uniform plastic flow, and by such means uniquely high damage tolerance has been achieved [1]. Nevertheless, shear-banding is the key obstacle to the wider use of MGs in mechanical applications [2]. Elimination of shear bands would be highly desirable. Yet there is the concern that shear-banding might be inevitable, given that the yield stress of MGs is a high fraction of the theoretical strength, so that any capacity for hardening must be limited.

In recent years, there has been a focus on the range of MG states that can be obtained at a given composition. As annealing and relaxation often lead to embrittlement, there is particular interest in the reverse process (‘rejuvenation’), by which the MG is taken to higher-energy, less dense states. It is speculated that a sufficiently rejuvenated MG could show strain-hardening [3], but it has been unclear whether the required rejuvenation could be achieved without destabilizing the MG against, for example, crystallization.

Thermomechanical processing, particularly in compression, can induce extreme rejuvenation in significant (mm-scale) volumes of MG [4]. When these rejuvenated volumes are subjected to uniaxial stress, in tension or compression, they do show strain-hardening, and correspondingly shear-banding is suppressed [5]. With this finding, it is possible that the aim of MG research should shift from shear-band engineering to the elimination of shear bands.

The first well accepted explanation of strain-hardening in polycrystalline metals was that proposed by G.I. Taylor in 1934 [6]: plastic strain involves the generation of dislocations, and as the imposed macroscopic strain increases, internal local strain gradients increasingly impede the motion of those dislocations. In general terms, this has remained the only explanation for strain-hardening until that now offered for MGs. In Taylor’s model, it is intrinsic that strain-hardening involves increased defect density and a higher energy for the system. In contrast, the strain-hardening of MGs involves a lower energy and, effectively a decreased density of defects. We survey the strain-hardening rate of metallic materials, and find that this is particularly high for MGs.

[1] M.D. Demetriou, M.E. Launey, G. Garrett, J.P. Schramm, D.C. Hofmann, W.L. Johnson, R.O. Ritchie, *Nature Mater.* 10 (2011) 123–128.

[2] A.L. Greer, Y. Q. Cheng and E. Ma, *Mater. Sci. Eng. R* 74 (2013) 71–132.

[3] Y.H. Sun, A. Concustell, A.L. Greer, *Nature Rev. Mater.* 1 (2016) 16039.

[4] J. Pan, Y.X. Wang, Q. Guo, D. Zhang, A.L. Greer, Y. Li, *Nature Comm.* 9 (2018) 560.

[5] J. Pan, Yu.P. Ivanov, W.H. Zhou, Y. Li, A.L. Greer, *Nature* 578 (2020) 559–562.

[6] G.I. Taylor, *Proc. R. Soc. Lond. A* 145 (1934) 362–387.

#### 7:00 AM F.SF02.03.10

**Engineering Structure Defects for Controlled Mechanical Behaviors in 3D-Printed Bulk Metallic Glasses** [Shuai Wei](#); Aarhus University, Denmark

In the last decades, researchers have been developing amorphous metals with bulk size, so-called bulk metallic glasses (BMGs) through carefully designing the alloy compositions and the quenching processes. Although the critical cooling rates required to bypass crystallization have been much reduced, BMGs still suffer from the constraints in dimensions and geometries when they are produced by casting. Here, we use the selective laser melting (SLM) technique to 3D-print the near-net-shape bulk metallic glasses. Their microstructures and mechanical properties are characterized. The defects such as porosity, pore size and morphology are analyzed in the relation with their tensile fracture behaviors of large-scale fully

amorphous 3D-printed BMGs. The results show that the characteristics of porosity in 3D-printed BMGs play a crucial role in the ultimate tensile strength (UTS). The UTS decreases drastically from  $\sim 1.5$  GPa for pore-free samples to  $\sim 1.25$  GPa for samples with a porosity of 0.26%. Yet, the Young's modulus is found to be insensitive in the low-porosity regime. Finite element simulations show different deformation behaviors of pore-free and pore-containing models, where the former fractures with multi shear bands initiated at the material weak point, while the latter experiences plastic deformation around pores with the shear transformation zone (STZs) perpendicular to the normal stress. The understanding of microstructure defects enables us to engineer the defects for controlled tensile fracture behaviors in 3D-printed BMGs.

#### 7:10 AM F.SF02.03.11

**Micro- and Macroplasticity Mechanisms in Polymer-Supported Thin-Film Metallic Glasses** Oleksandr Glushko<sup>1</sup>, Christoph Gammer<sup>2</sup>, Christian Mitterer<sup>1</sup> and Jurgen H. Eckert<sup>1</sup>; <sup>1</sup>Montanuniversität Leoben, Austria; <sup>2</sup>Erich Schmid Institute of Materials Science, Austrian Academy of Sciences, Austria

The in-depth understanding of the mechanisms of plastic deformation in metallic glasses is still missing despite years of dedicated experimental and theoretical effort. Here we demonstrate how polymer-supported films can be utilized to capture different stages of shear band formation and propagation opening new perspectives to uncover plasticity mechanisms in metallic glasses.

By means of in-situ resistance measurements, in-situ optical microscopy as well as quasi-in-situ SEM and FIB characterization, different stages of evolution of shear bands and cracks with increasing strain are detected and described. Two distinct types of shear bands appear in polymer-supported sputter deposited Pd<sub>80</sub>Si<sub>20</sub> and Au<sub>60</sub>Ag<sub>20</sub>Si<sub>20</sub> metallic glasses with increasing strain: (i) the "out-of-plane" shear bands (the direction of shear is not in the film plane) which are formed at about 2% strain and develop quickly into through-thickness cracks and (ii) in-plane shear bands (the direction of shear is within the film plane) which appear after crack density saturation (at about 10% strain) and do not lead to crack formation. If the film thickness is above 500-700 nm the propagation of single out-of-plane shear bands which do not develop into cracks is observed. If the film thickness is reduced below 15 nm, the formation of shear bands is generally suppressed and the film can deform up to strains of about 6% elasto-plastically (i.e. without cracking) showing formation of homogeneously distributed short nanocracks at higher strains. It is demonstrated, that with increasing applied strain, new in-plane shear bands can easily intersect the existing ones, whereupon the intersected shear bands become inactive and cannot carry further plastic deformation. This mechanism can lead to effective strain hardening of metallic glasses. Furthermore, the existence of droplet-like extrusion directly on top of the traces of in-plane shear bands provides a direct evidence of specific material state characterized by high free volume and low viscosity during the shear banding event.

Reported results demonstrate that polymer-supported films offer an alternative way to investigate plasticity of metallic glasses through higher control over generation, propagation and topology of shear bands. It is believed that new insights into such controversial topics as the propagation mode, propagation speed as well as temperature of operating shear bands can be gained.

#### 7:20 AM F.SF02.03.12

**Traction Rheoscopy of Colloidal Glass** J. Z. Terdik, David Weitz and Frans Spaepen; Harvard University, United States

Micron sized colloidal particles, which interact with nearly hard-sphere potentials, can be used to form dense amorphous packings using a variety of well established techniques. Due to the large size and slow dynamics of colloidal particles, confocal microscopy can be used to measure the 3D structure and dynamics of these densely packed colloidal glasses. For example, previous work has directly visualized, as a function of applied strain, both the inhomogeneous particle level rearrangements that occur within a colloidal glass, and the emergence of continuum elastic strain fields that surround these rearrangements. While microscopic visualization of colloidal glasses provides real-space information not readily obtainable in atomic systems, measuring the stress response of colloidal glasses, in addition to visualization, is a significant challenge. The large, micron-size of the colloidal particles and their thermal interactions produce solids with exceptionally small elastic moduli on the order to 10-100 mPa. We introduce a new technique, traction rheoscopy, to directly measure the mechanical response of these highly compliant colloidal glasses under simple shear strain while simultaneously visualizing their microstructure. The method consists of placing a bilayer of colloidal glass atop a well calibrated soft polymer gel of similar shear modulus. The composite bilayer undergoes strain-controlled shear; shear stresses are inferred from the displacement of embedded tracer particles in the calibrated polymer gel. Using these stress measurements, we show that under applied shear the colloidal glass goes through as sequence of reversible and irreversible microscopic rearrangements as the stress develops correlated spatial heterogeneities. The stress measurements with simultaneous real space visualization of the particle dynamics corroborate previously reported microscopic flow mechanisms and present new insight into the shear response of the colloidal glass.

### 7:30 AM F.SF02.03.13

**Microstructural Dependence of Shear Localization in Metallic Glass Composites** Jonathan M. Gentile<sup>1</sup>, Douglas Stauffer<sup>2</sup>, Douglas C. Hofmann<sup>3</sup> and Jason R. Trelewicz<sup>1,1</sup>; <sup>1</sup>Stony Brook University, The State University of New York, United States; <sup>2</sup>Hysitron Products, United States; <sup>3</sup>California Institute of Technology, United States

Metallic glass composites employ extrinsic approaches to improving the ductility and toughness of classically brittle amorphous alloys through the introduction of a distributed crystalline phase upon solidification. The crystalline heterogeneities have been shown to distribute the process of shear localization in the amorphous matrix while simultaneously promoting dislocation plasticity, manifesting as a more homogeneous plastic response. Although studies have demonstrated such mechanisms, there exists a disparity in the effective mechanical length scales of delocalization as well as a lack of a definitive approach for quantifying the crossover from incipient to homogeneous flow as a function of the underlying composite microstructural length scales. Here, we use nanoindentation combined with a bonded interface indentation technique to quantify individual shear banding events and map the role of composite microstructure on the shift in the governing yield criterion. Our results reveal a reduction in the stress required to nucleate a shear band when mechanical length scales were coincident with the composite microstructural length scales, i.e., the nucleating shear band interacts with the amorphous-crystalline interfaces. At larger indentation depths producing a fully developed plastic zone, a reduction in the propensity for shear localization was observed and attributed to strain accommodation by the crystalline dendrites suppressing shear band propagation. A crossover from the shear plane to maximum shear stress yield criterion is uncovered at a crystalline fraction of approximately 60%, thus signaling an effective transition from incipient to homogeneous flow as the dominant deformation mode of the composite.

SESSION F.SF02.04: Nanostructures and Nanoforming  
On Demand Abstracts Available for Viewing Starting Saturday Morning, November 21, 2020  
F-SF02

### 5:00 AM \*F.SF02.04.01

**The Controlled Large-Area Synthesis of Freestanding Two-Dimensional Metallic-Glass Nanosheets/Nanostructures** Yong Yang; City University of Hong Kong, China

The rise of nanotechnology has been propelled by low dimensional metals. Albeit the long-perceived importance, synthesis of freestanding metallic nanomembranes (or the so-called 2D metals), however, has been mainly restricted to elemental metals with a very limited in-plane size ( $< 10 \mu\text{m}$ ). In this talk, I would like to talk about the development of a low-cost method to synthesize 2D metals through polymer surface buckling enabled exfoliation (PSBEE). The 2D metals so obtained could be as chemically complex as conventional metallic glasses while possessing in-plane dimensions at the scale of bulk metals ( $> 1 \text{ cm}$ ). With our approach, we successfully synthesized a variety of 2D metallic glasses with controllable geometries and morphologies. Interestingly, our results clearly show that, as the thickness of the 2D metallic glasses reduces to a few nanometers, its modulus is significantly reduced to only a fraction of the modulus of their bulk counterparts. Aside from rather low elastic modulus, these 2D metallic glasses also exhibit unusual properties, such as good stretchability and tunable optical properties. Finally, we demonstrate that 2D ceramic glasses and 2D metallic composites can be also fabricated through PSBEE aside from 2D metallic glasses.

### 5:15 AM F.SF02.04.02

**Thermal Drawing of Structured Nanoscale Metallic Glass Fibers** Inès Richard<sup>1</sup>, Wei Yan<sup>2,1</sup>, Güven Kurtuldu<sup>3</sup>, Nicholas D. James<sup>1</sup>, Giuseppe Schiavone<sup>1</sup>, Stephanie P. Lacour<sup>1</sup>, Vasiliki Tileli<sup>1</sup>, Grégoire Courtine<sup>1</sup>, Jörg F. Löffler<sup>3</sup> and Fabien Sorin<sup>1</sup>; <sup>1</sup>Ecole Polytechnique Federale de Lausanne, Switzerland; <sup>2</sup>Massachusetts Institute of Technology, United States; <sup>3</sup>ETH Zürich, Switzerland

Micro- and nanoscale metallic glass systems offer exciting opportunities for both fundamental research and applications in healthcare, micro-engineering, optics and electronics. In addition to their functional attributes, exceptional mechanical properties and corrosion resistance, a singular feature of bulk metallic glasses (BMGs) is their ability to be processed in the supercooled liquid state thanks to their sluggish crystallization kinetics and relatively low viscosity. However, thus far the scientific challenges and technological opportunities associated with exploiting viscous deformation to realize advanced micro- and nanoscale MG architectures remain to a large extent unexplored. Moreover, integrating nano-scale MG structures



into well-functioning devices still poses great challenges.

Here, we present a scalable method to produce fibers containing continuous and well-ordered micro- and nanoscale Pt-based MG conductors via their thermal co-drawing in the supercooled liquid state within a polymer matrix [1]. Designing the parts in a macroscopic scaled-up preform enables the fabrication of structured MGs with arbitrary transverse geometries and controllable feature size down to a few tens of nanometers, previously unachievable. This approach allows us to deepen our fundamental understanding of deformation and size effects on crystallization kinetics, and engineer innovative MG-based devices within advanced fibers and smart textiles.

First, we discuss how we selected the right combination of MG and polymer for a successful co-drawing. *In situ* heating transmission electron microscopy (TEM) on drawn MG ribbons is then presented to reveal the influence of the thermal drawing process on the crystallization kinetics, which ultimately determines the achievable feature size. After establishing this fundamental understanding, we show a variety of complex MG nanostructures in flexible polymer matrices. Finally, we demonstrate the potential of BMGs in comparison to more traditional drawable materials by presenting applications in optoelectronic and neuroscience. We show that the MG ribbons can serve as electrodes to enhance the performance of optoelectronics fibers and fabrics. We then present two implantable MG-based fiber probes integrating multiple MG conductors, and in one case a microfluidic channel for local chemical delivery. Chronic experiments in rats show the ability to elicit robust behavioral responses when delivering electrical neurostimulation in deep structures, to record neuronal activity during unconstrained locomotion, and to deliver pharmacological agents to manipulate local circuits.

#### Reference

[1] W. Yan, I. Richard et al., Structured nanoscale metallic glass fibres with extreme aspect ratios, *Nature Nanotech.*, 2020 (Accepted, in Press)

#### 5:25 AM F.SF02.04.03

**Nanomolding Far and Close to Equilibrium and Its Mechanism** [Naijia Liu](#), Guannan Liu, Arindam Raj, Sungwoo Sohn and Jan Schroers; Yale Univeristy, United States

Tremendous effort has been taken during the last two decades in the development of nano fabrication techniques for materials exhibiting desirable functional properties. However, both bottom-up and top-down fabrication approaches are limited in some critical aspects such as material choice, geometry, and scalability.

A highly versatile and widely used fabrication method is molding, which is generally associated with a soft state of a material. Nanomolding has been realized, based on creep flow, for polymers, gels, and some glasses that soften at elevated temperatures, but not for crystalline materials that remain hard in their crystalline state.

Recently, we discovered that nanomolding is possible with crystalline materials. Processing usually around  $\sim 0.5 T_m$ , such thermomechanical nanomolding (TMNM) results in very high aspect ratio up to 1000 and nanowires as small as 5 nm in diameter. It offers itself as a versatile nanomolding technique for metals, alloys and even ordered phases.

By tracking the atomic moving in TMNM with multilayer samples and analyzing scaling experiments, we studied the underlying mechanism to be based on interface atomic diffusion and dislocation. They dominate TMNM in different temperature ranges as an interface diffusion mechanism works most effectively with a temperature above  $\sim 0.4 T_m$  and a dislocation mechanism works at lower temperature. A diffusion dominated mechanism is also found effective to form nanowires through amorphous phases (BMGs), with a processing temperature below  $T_g$ .

We will discuss the underlying mechanisms in TMNM, and their effect on structure and composition of formed nanowires in solid solutions, ordered phases and amorphous phases (BMGs).

#### SESSION F.SF02.05: Glass Formation

On Demand Abstracts Available for Viewing Starting Saturday Morning, November 21, 2020

F-SF02

#### 5:00 AM \*F.SF02.05.01

**Syntheses and Features of Pseudo-High Entropy Bulk Metallic Glasses** [Akihisa Inoue](#)<sup>1,2,3</sup>, Fanli Kong<sup>2</sup>, Baolong Shen<sup>1</sup>, Shengli Zhu<sup>3</sup> and Alan Lindsay Greer<sup>4</sup>; <sup>1</sup>China University of Mining and Technology, China; <sup>2</sup>Josai International University, Japan; <sup>3</sup>Tianjin University, China; <sup>4</sup>University of Cambridge, United Kingdom

Since the first synthesis of a bulk metallic glass (BMG) by copper mold casting in 1989, a large number of BMGs with centimeter-size diameter were synthesized in a variety of multicomponent alloy systems such as La, Mg, Zr, Ti, Hf, Fe, Co,

Ni, Cu, Pd, Pt and Au metal bases. These BMGs are composed of multicomponent with negative and nearly zero heats of mixing and significant atomic size mismatches, while there has been little information on the influence of additional metallic elements with positive heat of mixing on the formation, thermal stability, crystallization behavior and fundamental properties for BMGs. Very recently, the pseudo-high entropy (PHE) BMGs containing solute atomic pairs with positive heats of mixing, which are different from the component rule for ordinary BMGs, have attracted an increasing interest because of their unique properties<sup>1</sup>). In particular, the PHE BMGs exhibit two exothermic peaks on the continuously heating DSC curve and the temperature interval between the two peaks is as large as 200-400 K. Besides, no crystalline phase is observed even after annealing for 1-5 h at the temperatures well above the first exothermic peak. The unusual high stability to the progress in crystallization has been reported for various PHE BMGs such as Zr-Al-(Ni,Cu)-Nb, Zr-Al-(Ni,Cu)-Ag, Zr-Al-(Co,Cu)-Ag, Zr-(Fe,Co,Ni,Cu), Ti-Zr-(Cu,Pd)-Nb and Fe-Cr-Mo-C-B-Y systems. These results indicate the possibility of developing a heat resistant BMG by utilizing this novel phenomenon. Here we present the formation, thermal stability, crystallization behavior and mechanical properties of PHE BMGs and to investigate the criterion for the synthesis of BMGs with ultrahigh thermal stability.

1) A. Inoue, F.L. Kong, S.L. Zhu, A.L. Greer, Multicomponent bulk metallic glasses with elevated-temperature resistance, MRS Bull. 44 (2019) 867-872.

#### 5:15 AM \*F.SF02.05.02

**Core-Shell Energy State of Icosahedral Clusters Inside Undercooled Metallic Liquids and Its Relationship with Glass-Forming Ability** Donghua Xu; Oregon State University, United States

This presentation will start by introducing the new Cu-based bulk metallic glasses (CBMGs) in the Cu-Zr-Hf-Al system that my group has developed recently. These new CBMGs are free of rare earths, precious metals or toxic elements, and yet possess the highest glass-forming ability known to any copper-based alloys. The presentation will then shift to focus on a computation study of the energy state of icosahedral clusters inside undercooled metallic liquids in some simpler metallic systems, in order to gain fundamental insights into glass formation and glass-forming ability.

Icosahedral clusters have been experimentally confirmed to exist in undercooled metallic liquids. Their existence is generally understood using the argument about an isolated icosahedron Frank made almost 70 years ago. This argument establishes an icosahedron as the most energy-efficient packing for an isolated 13-atom cluster, but fails to consider the effects of surrounding atoms in a liquid and temperature on the energy state of the cluster. The argument suggests core stabilization as the main mechanism for the origin of icosahedral clusters - since the core of an isolated cluster has lower potential energy than the shell.

Using large scale atomistic simulations and statistical analysis of several BCC (body-centered-cubic) and FCC (face-centered-cubic) metals, we have found that the shells of icosahedrons spontaneously formed inside deeply undercooled metallic liquids or glasses in fact have lower (averaged) potential energy than the cores. The shell potential energy deficiency occurs only to the icosahedral clusters but not to the equilibrium-crystal clusters, and, for icosahedral clusters, this deficiency grows with decreasing temperature. Compared with FCC metals, BCC metals exhibit greater potential energy deficiency on the icosahedral shells and produce significantly more icosahedral clusters upon liquid quenching, which explains the higher tendency of BCC metals to be vitrified observed in ultrafast cooling experiments. Inspecting the potential energy deficiency on the icosahedral shells through computation could provide a new avenue to the search for amorphous metals (i.e. metallic glasses) with high glass forming ability and processability.

#### 5:30 AM \*F.SF02.05.03

**Glass Formation in Binary Alloys with Different Atomic Symmetries** Corey O'Hern; Yale University, United States

Prediction of the glass forming ability (GFA) of alloys remains a major challenge. We are not able to predict the composition dependence of the GFA of even binary alloys. To investigate the effect of each element's propensity to form particular crystal structures on glass formation, we focus on binary alloys composed of elements with the same size, but different atomic symmetries using the patchy-particle model. For mixtures with atomic symmetries that promote different crystal structures, the minimum critical cooling rate  $R_c$  is only a factor of 5 lower than that for the pure substances. For mixtures with different atomic symmetries that promote local crystalline and icosahedral order, the minimum  $R_c$  is more than 3 orders of magnitude lower than that for pure substances. Results for  $R_c$  for the patchy-particle model are in agreement with those from embedded atom method simulations and sputtering experiments of NiCu, TiAl, and high entropy alloys.

#### 5:45 AM F.SF02.05.04

**Machine Learning Predictions of Glass Forming Ability from Compositional Information** Benjamin T. Afflerbach, Lane E. Schultz, Carter Francis, Paul M. Voyles, Izabela Szlufarska and Dane Morgan; University of Wisconsin–Madison, United States

Bulk metallic glasses (BMGs) are generally defined as a subset of metallic glasses which can be synthesized with dimensions exceeding 1 mm while maintaining their amorphous structure. Metallic glasses possess a wide range of mechanical, magnetic, and chemical properties making them exciting for many commercial applications, particularly if they can be made in larger sizes as is possible for BMGs. Unfortunately, today there is no robust method for determining which new alloy compositions will yield BMGs without synthesizing and cooling the alloy, greatly inhibiting materials design in this area. Perhaps the most direct measure of glass forming ability (GFA) is critical cooling rate ( $R_c$ ), which is the slowest rate at which a glass can be cooled and stay fully amorphous. In this work we focus on predicting  $R_c$  from easily obtained compositional information using machine learning. There are on the order of 100 measured values of  $R_c$  in the literature, which is too little data to machine learn  $R_c$  as a function of composition. In this work we dramatically extend this database by using other sources of approximate  $R_c$  values derived from robust correlations, including correlation of  $R_c$  with (i) characteristics temperatures (about 480 new values), (ii) critical casting diameters (about 550 new values), and (iii) results of melt spinning experiments (about 2000 new values). We obtain a database of 2884 approximate  $R_c$  values which we used to build a Random Forest model for  $R_c$  as a function of elemental properties, which in turn can be derived from composition. This model is validated and then used to predict GFA on several new glassy alloys. 5-fold cross validation performance of the model gives RMSE errors of around 0.66 log(K/s) in  $R_c$  (30% of the  $R_c$  database standard deviation of 2.4 log units). This value is low enough to design BMGs if it can be maintained across new systems, but we will also show that the model has significant challenges in treating new compositions.

**5:55 AM F.SF02.05.05**

**Metastability in Multicomponent Alloys—Solid Solution and Glass Formation** Sebastian A. Kube and Jan Schroers; Yale University, United States

While metastability is undoubtedly a key-characteristic of metallic glasses, its role is often underappreciated for multicomponent alloys in general, and High Entropy Alloys (HEAs) in particular. The HEA field has long focused on equilibrium conditions, aiming to stabilize single-phase solid solutions (SPSS). However, the high entropy effect is often insufficient to fully stabilize SPSS, yielding only few, mostly metastable SPSS. While the prospective space of favorable SPSS formation is smaller than commonly assumed, only larger degrees of metastability can open up the vast High Entropy Alloy space. We argue that HEAs form metastable SPSS through polymorphic solidification upon rapid cooling. To quantify a HEA's metastability, we propose the critical cooling rate of SPSS formation  $R_c^{SPSS}$ , which is analogous to the critical cooling rate of glass formation  $R_c^{Glass}$ . On this unified basis, we can compare multicomponent alloys by their metastability and tendency to form SPSS or glasses, which is determined by their underlying atomic dispersity.

**6:05 AM \*F.SF02.05.06**

**Sulfur Bearing Bulk Metallic Glass** Ralf Busch, Alexander Kuball, Oliver Gross and Benedikt Bochtler; Univ of Saarland, Germany

Metallic glasses constitute a class of engineering materials having an enormous potential for many fields of application due to their superior properties. Here, we report on a new family of sulfur-bearing bulk metallic glasses. So far, sulfur was not considered as alloying element for the synthesis of bulk metallic glasses. We observe bulk glass formation in a variety of sulfur-containing systems, including titanium-based bulk glass-forming systems with an extremely high titanium content of 70 at.%. These findings allow the development of a whole new class of amorphous metals, having good processability and consisting of alloying elements suitable for industrial applications.

SESSION F.SF02.06: BMGs for the Energy Transition  
On Demand Abstracts Available for Viewing Starting Saturday Morning, November 21, 2020  
F-SF02

**5:00 AM \*F.SF02.06.02**

**Electrochemical Hydrogen Storage and Evolution in Metallic Glasses** Baran Sarac<sup>1</sup>, Yurii P. Ivanov<sup>2</sup>, Tolga Karazehir<sup>3</sup>, A. Sezai Sarac<sup>4</sup>, Alan Lindsay Greer<sup>2</sup> and Jurgen H. Eckert<sup>5</sup>; <sup>1</sup>Erich Schmid Institute of Materials Science (ÖAW),

Austria; <sup>2</sup>Cambridge University, United Kingdom; <sup>3</sup>Adana Alparslan Turkes Science and Technology University, Turkey; <sup>4</sup>Istanbul Technical University, Turkey; <sup>5</sup>Montanuniversität Leoben, Austria

Among the novel advanced metallic alloy systems, metallic glass (MG) is a potential candidate for long-term use hydrogen interactions owing to its loosely packed structure promoting the number of interaction sites. The hydrogen storage and electrocatalytic activity of Pd-Si-based MG nanofilms and Si/SiO<sub>2</sub> hybrid structures were evaluated by combining electrochemical (chronoamperometry, cyclic voltammetry, electrochemical impedance spectroscopy), structural (aberration-corrected high-resolution transmission electron microscopy, X-ray diffraction), composition (X-ray photoelectron spectroscopy, energy dispersive X-ray) and morphologic (scanning electron microscopy, atomic force microscopy) techniques. Recently we have shown that maximum total hydrogen charge stored in Pd-Si-Au MG nanofilm is equal to that in polycrystalline Pd films with 1 μm thickness [1]. Hydrogen to Palladium ratio of Pd-Si-Cu MG was found to be 1.56 (c.f. 0.61 in polycrystalline Pd + Si/SiO<sub>2</sub> of the same film thickness) [2, 3]. The volume expansion of a palladium hydride unit cell obtained from HRTEM images due to hydrogenation of the Pd-MG nanofilms is around 6 times larger than that of the Pd-polycrystalline counterpart hydrogenated under the same conditions. The same Pd-Cu-Si MG based hybrid structure has a Tafel slope of 109 mV/dec, which is less than the half of the crystalline PdNF electrode of the same thickness. Besides, it shows the highest overpotential at 10 mA/cm<sup>2</sup>, indicating a better electrocatalytic activity [4]. We have also established a general evaluation criterion with practicality in assessment and high accuracy for electrocatalytic reactions applicable to different metallic alloy systems.

[1] Sarac, et al., Chem. Eur. J., DOI: 10.1002/chem.202001596

[2] Sarac, et al., ACS Appl. Energy Mater., 1 (2018) 2630-2646.

[3] Sarac, et al., Mater. Horiz., 6 (2019) 1481-1487.

[4] Sarac, et al., Electrocatalysis, 11 (2020) 94-109.

#### SESSION F.SF02.07: Additive Manufacturing

On Demand Abstracts Available for Viewing Starting Saturday Morning, November 21, 2020  
F-SF02

##### 5:00 AM \*F.SF02.07.01

**Additive Manufacturing and Deposition of Bulk Glass Forming Alloys and Composites—Progress and Outlook** Douglas C. Hofmann<sup>1</sup>, Punnathat Bordeenithikasem<sup>1</sup>, Samad Firdosy<sup>1</sup>, Andre Pate<sup>1</sup> and Daniel East<sup>2</sup>; <sup>1</sup>NASA JPL/Caltech, United States; <sup>2</sup>Commonwealth Scientific and Industrial Research Organisation, Australia

Additive manufacturing (AM) has emerged as a unique method for producing highly specialized metal alloys and composites. The high cooling rates and customizable cooling rates afforded by AM are particularly useful in the creation of bulk metallic glasses (BMGs) and BMG metal matrix composites. While AM allows for net-shaped fabrication of even the weakest glass-forming alloys, macroscale parts still suffer from embrittlement due to annealing, porosity, partial crystallization and oxygen. In contrast, thin coatings and overlays made from BMGs and BMG composites may be ideal for some wear-resistant applications. This talk will provide an overview of how BMG printing and deposition technologies might be matured and infused into applications. It will cover Fe-based, Zr-based, Cu-based, and Ti-based BMG alloys.

#### SESSION F.SF02.08: Dynamics and Transitions

On Demand Abstracts Available for Viewing Starting Saturday Morning, November 21, 2020  
F-SF02

##### 5:00 AM \*F.SF02.08.01

**Vitrification Kinetics versus Alpha-Process in Metallic Glass-Formers** Isabella Gallino<sup>1</sup>, Daniele Cangialosi<sup>2,3</sup>, Beatrice Ruta<sup>4</sup>, Xavier Monnier<sup>2</sup> and Ralf Busch<sup>1</sup>; <sup>1</sup>Saarland University, Germany; <sup>2</sup>Donostia International Physics Center, Spain; <sup>3</sup>Centro de Fisica de Materiales (CSIC-UPV/EHU), Spain; <sup>4</sup>Universite Claude Bernard Lyon 1, France

Understanding how glasses form remains a challenge in material science. Vitrification is the thermal transition from a supercooled liquid in metastable equilibrium into a non-equilibrium glass. One of the major questions is whether vitrification in viscous liquids is related to sluggish atomic mobility exclusively *via* the primary structural  $\alpha$ -relaxation process or rather other atomic motions play a role. Here, we present experimental evidences that multicomponent bulk metallic glasses can display heterogeneity of vitrification kinetics and that the cooling rate dependency of the vitrification kinetics is decoupled from the temperature dependence of the  $\alpha$ -relaxation [1-3]. The evidences are based on exhaustive studies of the atomic mobility of an Au-based metallic glass former by dynamic mechanical analysis (DMA), x-ray photon correlation spectroscopy (XPCS), and fast scanning calorimetry (FSC); the latest by means of a step response analysis *via* the temperature and frequency dependence of the complex specific heat. The vitrification kinetics is characterized in FSC in terms of the limiting fictive temperature, i.e., the temperature at which a glass formed after cooling at a given rate would be at equilibrium. The separation of these two aspects of the glassy dynamics (vitrification kinetics and  $\alpha$ -process) becomes more pronounced at larger undercooling, suggesting a larger contribution of additional dynamical processes to the vitrification process, which are not connected to the  $\alpha$ -process. The observed heterogeneity of vitrification kinetics hints toward the existence of multiple relaxation mechanisms, which are observed during aging experiments [3].

[1] X. Monnier, D. Cangialosi, B. Ruta, R. Busch, I. Gallino, *Sci. Adv.* 6 (2020) eaay1454

[2] S. Hechler, B. Ruta, ...R. Busch and I. Gallino, *Phys. Rev. Mat.*, 2 (2018) 085603

[3] I. Gallino, D. Cangialosi, et al., *Acta Mater.*, 144 (2019) 400

#### 5:15 AM \*F.SF02.08.02

**Tracing Structural Dynamics in Metallic Glasses During Cryogenic Cycling** Robert Maass<sup>1,2</sup>; <sup>1</sup>University of Illinois at Urbana-Champaign, United States; <sup>2</sup>Federal Institute for Materials Research and Testing (BAM), Germany

Highly unrelaxed structural states of metallic glasses have often advantageous mechanical properties. Since metallic glasses continuously relax with time (age) or inherently are well relaxed after processing, methods to uniformly rejuvenate the material are needed. One approach that has received attention is the so-called cryogenic-cycling method, during which a metallic glass is repeatedly immersed into liquid nitrogen. In some cases, cryogenic cycling is truly efficient in increasing the stored excess enthalpy of metallic glasses, but it does not seem to be universally applicable to all alloys and structural states. The origins for these differences remain unclear due to our limited understanding of the underlying structural evolution. In order to shed more light onto the fundamental structural processes of cryogenic cycling, we pursue in-situ x-ray photon correlation spectroscopy (XPCS) to trace the atomic-scale structural dynamics of a Zr-based metallic glass in two different structural states (ribbon and bulk metallic glass). This method allows calculating the relaxation times as a function of time throughout the thermal cycling. It is found that the investigated glasses exhibit heterogeneous structural dynamics at 300 K, which changes to monotonic aging at 78 K. Cryogenic cycling homogenizes the relaxation time distribution for both structural states. This effect is much more pronounced in the ribbon, which is the only structural state that rejuvenates upon cycling. We furthermore reveal how fast atomic-scale dynamics is correlated with long-time average structural relaxation times irrespective of the state, and that the ribbon exhibits unexpected additional fast atomic-scale relaxation in comparison to the plate material. Overall, a picture emerges that points towards heterogeneities in fictive temperature as a requirement for cryogenic energy storage.

#### 5:30 AM F.SF02.08.03

**Surface Dynamics Measurement on a Gold Based Metallic Glass** Chengrong Cao, Lian Yu and John Perepezko; University of Wisconsin-Madison, United States

The surface diffusion kinetics has been measured on an Au<sub>60</sub>Cu<sub>15.5</sub>Ag<sub>7.5</sub>Si<sub>17</sub> metallic glass using the method of surface grating decay from room temperature up to 20 K below the glass transition temperature ( $T_g$ ). In the early stage of gratings decay the surface diffusion coefficients were evaluated as varying in the range from  $10^{-20}$  to  $10^{-18}$  m<sup>2</sup>/s over the temperature range of measurement and the corresponding average activation energy is about 0.67 eV. During longer time annealing the surface gratings decay rate slowed down significantly. The slowing of the initial decay was a result of the surface dynamics and influenced by the surface segregation of silicon at long time which induced a surface crystallization of a silicon-rich phase.

#### 5:40 AM \*F.SF02.08.04

**Ultrafast Calorimetry Experiments on Bulk Metallic Glasses—Studying Phase Transitions in Slow Motion** Jörg F. Löffler; ETH Zurich, Switzerland

Metallic materials generally show rapid nucleation and growth kinetics, which makes studies of their phase transitions and metastable phase formation generally more difficult. Bulk metallic glasses (BMGs), on the other hand, reveal very sluggish crystallization kinetics. By applying ultrafast differential scanning calorimetry to slowly transforming BMG-forming systems

at heating and cooling rates of several 10,000 K/s, we are able to determine phase transitions of metallic systems more or less in slow motion. In this way we find that many metallic systems reveal solid-to-solid phase transitions that proceed via melting of a metastable phase [1]. Ultrafast calorimetry also allows us to interrupt rapid cooling after (metastable) phase formation and then to "up-quench" the frozen structure via rapid heating. Via surpassing the metastable-to-stable solid phase transition, the formed metastable phase can then be fully melted and its thermophysical properties, such as temperature and enthalpy of melting, be investigated in detail [2]. In this way, we are able to discover hidden transient phases, determine the stochastics of nucleation [3], and study multistep crystallization and melting pathways in metals. In fact, we show that even simple binary alloys can reveal multiple melting points [4]. Applying ultrafast calorimetry, we are thus able to construct energy-temperature diagrams including metastable phases, with the final aim of generating complete metastable phase diagrams.

[1] S. Pogatscher, D. Leutenegger, J. E. K. Schawe, P. J. Uggowitzer, J. F. Löffler, 'Solid-solid phase transitions via melting in metals', *Nature Comm.* **7** (2016) 11113.

[2] G. Kurtuldu, K. F. Shamlaye, J. F. Löffler, 'Metastable quasicrystal-induced nucleation in a bulk glass-forming liquid', *PNAS* **115** (2018) 6123 – 6128.

[3] J. E. K. Schawe, J. F. Löffler, 'Existence of multiple critical cooling rates which generate different types of monolithic metallic glass', *Nature Comm.* **10** (2019) 1337.

[4] G. Kurtuldu, J. F. Löffler, 'Multistep crystallization and melting pathways in the free-energy landscape of a Au-Si eutectic alloy', *Adv. Science* (2020), doi:10.1002/advs.201903544.

### 5:55 AM F.SF02.08.06

#### **Sputtering of Zr-Based Metallic Glasses to Vary Kinetic Stability, Icosahedral Ordering and Mechanical**

**Properties** Sachin V. Muley<sup>1</sup>, Chengrong Cao<sup>1</sup>, Debaditya Chatterjee<sup>1</sup>, Carter Francis<sup>1</sup>, Felix P. Lu<sup>2</sup>, Mark Ediger<sup>3</sup>, John Perepezko<sup>1</sup> and Paul M. Voyles<sup>1</sup>; <sup>1</sup>University of Wisconsin-Madison, United States; <sup>2</sup>The University of Chicago, United States; <sup>3</sup>University of Wisconsin-Madison, United States

Thermodynamic and kinetic stabilities in glasses can be varied by physical vapor deposition. We investigated the structure and properties in Zr-Cu-Ni-Al and Zr-Cu-Al thin films sputtered from single alloy targets as a function of substrate temperature and deposition rate. For both compositions, we discovered a pseudo-phase boundary between amorphous and crystalline films as a function of rate and temperature. A semi-quantitative model based on surface-diffusion limited crystallization predicts the amorphous / crystalline growth boundary. Kinetic stability in  $Zr_{65}Cu_{27.5}Al_{7.5}$  metallic glass thin films, as indicated by their glass transition onset temperature, was significantly increased by lowering deposition rate at constant temperature. The most kinetically stable film's reduced modulus was 20% higher than a glass of the same composition quenched from the liquid by melt spinning, consistent with increased density and improved thermodynamic stability. Fluctuation electron microscopy and angular correlations in coherent electron nanodiffraction reveal that the more stable glasses show enhanced icosahedral medium range structural order. Our results suggest that enhanced nanoscale icosahedral order contributes to resistance of glass to both glass transition and mechanical deformation.

SESSION F.SF02.09 Poster Session: Bulk Metallic Glasses

On Demand Abstracts Available for Viewing Starting Saturday Morning, November 21, 2020

5:00 AM - 8:00 AM

F-SF02

### F.SF02.09.01

**Molecular Dynamics Features for Predicting Metallic Glass Critical Casting Thickness** Lane E. Schultz, Benjamin T. Afflerbach, Izabela Szlufarska and Dane Morgan; University of Wisconsin-Madison, United States

Determining metal compositions that have good Glass Forming Ability (GFA), and in particular that yield bulk metallic glasses through cooling, has been an outstanding grand challenge in metallic glass research. Previous attempts to predict GFA for metals often include some functional form of  $T_g$ ,  $T_x$ , and  $T_l$ , known as the glass transition, the onset of crystallization, and the liquidus temperatures, respectively. For example, the reduced glass transition temperature,  $T_{rg}=T_g/T_l$ , is a well-known GFA indicator. Another well-known GFA indicator is the liquid fragility,  $m$ , which is measured by finding the slope of viscosity as a function of temperature near  $T_g$  for an alloy. Multiple researchers have shown that direct measures of GFA, in particular the critical cooling rate ( $R_c$ ) and critical casting diameter ( $d_{max}$ ), can be written as relatively simple functions of  $T_g$ ,  $T_x$ ,  $T_l$ , and  $m$  [1, 2]. However, these relationships have limited applicability for new materials discovery

because a material must be synthesized and measured in order to obtain these features, and they cannot be readily predicted accurately from molecular simulations. However, there are other characteristic temperatures and kinetic properties that have similar physics to that represented in the above features and which are accessible to molecular simulations.

Our study explores to what extent characteristic temperatures of metallic alloys readily accessible to molecular dynamics (MD) can be correlated with  $d_{max}$ . We use MD to predict a set of characteristic temperatures  $\{T_i\}$  for 73 metal alloys and fit  $d_{max}$  as a function of  $\{T_i\}$  using experimental  $d_{max}$  values for 19 of the alloys. We find a 3-fold cross-validation root mean squared error (RMSE) score of 0.512 for the model, well below the standard deviation of 0.848 for the 19  $d_{max}$  values. The remaining 54 alloys are used as a test set and the  $d_{max}$  predictions are used to determine if the alloy should form a glass under melt spinning, and this categorization was then compared to experimental results. We find a maximum F1 score of 0.75 for the categorization model. These cross-validation and F1 scores suggest that the model has significant predictive ability, providing a potential pathway to predicting  $d_{max}$  directly from MD.

#### References

- [1] W. L. Johnson, J. H. Na and M. D. Demetriou, "Quantifying the origin of metallic glass formation," *Nature Communications*, vol. 7, no. 1, p. 10313, 20 12 2016.
- [2] Z. Long, H. Wei, Y. Ding, P. Zhang, G. Xie and A. Inoue, "A new criterion for predicting the glass-forming ability of bulk metallic glasses," *Journal of Alloys and Compounds*, vol. 475, no. 1-2, pp. 207-219, 2009.

#### F.SF02.09.02

**Direct Measurement of Critical Cooling Rates in Metallic Glass Forming Alloys Through a Combinatorial Strategy** Naijia Liu<sup>1</sup>, Tianxing Ma<sup>2</sup>, Chaoqun Liao<sup>3</sup>, Shaofan Zhao<sup>3</sup>, Jonathan P. Singer<sup>2</sup> and Jan Schroers<sup>1</sup>; <sup>1</sup>Yale University, United States; <sup>2</sup>Rutgers, The State University of New Jersey, United States; <sup>3</sup>Qian Xuesen Laboratory of Space Technology, China

Critical Cooling Rate ( $R_c$ ) is the lowest rate a liquid can be cooled to avoid crystallization and vitrify into a glass. While it is a key factor to quantify the glass forming ability (GFA), direct measurement of Critical Cooling Rate ( $R_c$ ) of metallic glass has been cumbersome and challenging and only determined for a few alloys.

The development of science and technologies raise demand for new materials including new Bulk Metallic Glasses. However, it has been estimated that only about 10% of the composition space of potential BMG formation has been considered thus far. To address the large potential compositional space more effectively, combinatorial approaches have been used for the fabrication of large number of alloys in thin film alloy libraries. But attempts to directly quantify critical cooling rates of alloys in such libraries have been limited to the as-sputtered state which forms under a cooling rate exceeding  $10^8$  K/s. Although scientifically important, this high cooling rate is not able to probe practical BMGs, of which the  $R_c$  is always below  $10^3$  K/s. Some progress was made recently by reheating the thin films and reducing the cooling rate to  $\sim 10^5$  K/s. However, this is with a still high cooling rate rage.

We will report a fast screening method which is based on Single Pulse Laser Annealing to directly measure  $R_c$  in thin film alloy libraries. Cooling rates ranging from  $10^2$  to  $10^6$  K/s can be realized during solidification of the alloys. To demonstrate this method, we determined  $R_c$  for a large number of alloys in the Al-Ge-Ni system, and identified the best glass forming composition as  $Al_{51}Ge_{35}Ni_{14}$  with a critical cooling rate of  $10^4$  K/s.

#### F.SF02.09.03

**Accelerated Discovery and Mechanical Property Characterization of Bioresorbable Amorphous Alloys Using High-Throughput Methods** Amit Datye, Sebastian A. Kube, Jan Schroers and Udo Schwarz; Yale University, United States

Bioresorbable materials have been of increased interest in the last two decades due to their potentially transforming impact on human body implants. However, even with a large number of groups working on it, there is data available only for a very small number of alloy compositions (<20) in the ternary amorphous alloy systems of magnesium (Mg)–zinc (Zn)–calcium (Ca) and iron (Fe)–Mg–Zn. The optimal alloy compositions for biomedical applications should be chosen from a large variety of available alloys with best combination of mechanical properties (modulus, strength, hardness) and biological response (in-situ degradation rates, cell adhesion and proliferation). This research presents high-throughput screening of more than 150 different compositions each in two different bioresorbable alloy systems. We demonstrate that this new approach

will allow future researchers to develop patient- and implant-specific bioresorbable alloys based on specific application requirements. As a first step towards establishing a database designed to enable such targeted material selection, amorphous alloy composition libraries were fabricated employing a combinatorial magnetron sputtering approach where Mg, Zn, and Ca/Fe are co-deposited from separate sources onto a silicon wafer substrate, followed by composition analysis using energy dispersive X-ray spectroscopy and X-ray diffraction measurements and mechanical properties characterization using nanoindentation.

[1] Amit Datye et al., Journal of Materials Chemistry B 7, 5392 (2019).

#### **F.SF02.09.04**

**Coupling Among Shear Band Initiation, Propagation and Sliding During Plastic Deformation of Metallic Glass Under Constrained Deformation** Zenon H. Melgarejo<sup>1</sup>, Joseph E. Jakes<sup>2</sup> and Donald S. Stone<sup>1</sup>; <sup>1</sup>University of Wisconsin-Madison, United States; <sup>2</sup>Forest Biopolymer Science and Engineering, USDA Forest Products Lab, United States

When, in the regime of inhomogeneous flow, a metallic glass is constrained during plastic deformation, all aspects of the kinetics of shear banding, including initiation, advance of the tip, and "shear," or displacement across its thickness, become coupled. An example is the indentation experiment, in which surrounding material, loaded elastically, constrains deformation within the plastic zone and leads to a self-similar, hemispherical pattern of shear bands falling along multiple orientations surrounding the indent. Likewise, in metallic glass composites the reinforcement phases introduce constraints because they disrupt shear band propagation and shear. In each case, the effect of the constraint is to introduce a back stress, which leads to an increase in deformation resistance similar to kinematic hardening in crystalline composites. From indentation experiments, we can measure the strength of this coupling in terms of a "hardening modulus," the magnitude of which can be determined from the fluctuations in slope of the load-depth curve during serrated loading. It is expected that the hardening modulus will depend on both material properties and the geometry of the constraint.

Using nanoindentation experiments with a Berkovich indenter, we measure the hardening modulus in ZrCuAl metallic glass ribbons and ingots across 2 decades of strain rate during loading and 6 decades of strain rate during constant load creep. Hardening modulus is nearly independent of load despite a size effect in the serrations. Relaxing the glass near T influences the hardening modulus. The magnitude of the constraint is the same during constant load creep and during loading. Work arguments allow us to arrive at a model for coupled deformation, from which we estimate the magnitude of the constraint modulus in terms of the shear modulus of the glass, G. We compare this estimate with experimentally measured values.

#### **F.SF02.09.05**

**Bicontinuous Nanoporous Design Induced Homogenization of Strain Localization in Metallic Glasses** Chang Liu and Paulo Brancio; University of Southern California, United States

Bicontinuous nanoporous metallic glasses (MG) synergize the outstanding properties of MGs and open cell nanoporous materials. The low-density and high-specific-surface-area of bicontinuous nanoporous structures have the potential to enhance the applicability of MGs in catalysis, sensors, and lightweight structural designs. In this work we generated stochastic bicontinuous structure using an efficient direct method based on Cahn's idea and Fibonacci grids. We then perform molecular-dynamics simulations of tensile loading on a bicontinuous nanoporous  $\text{Cu}_{64}\text{Zr}_{36}$  and characterize the deformation mechanisms dictating its elastic and plastic response preceding failure. Results indicate an anomalous MG mechanical behavior featuring extensive plastic deformation preceding a typically ductile failure. Results show progressive necking of ligaments aligned with the loading direction and progressive alignment of randomly oriented ligaments during the loading. Failure occurs by fracture following successive necking and rupture of ligaments. This work indicates that a bicontinuous nanoporous design is able to effectively delocalize strain localization in a bulk MG by utilizing the size effect of MG nanopillars and nanowires that induces a brittle to ductile transition in their mechanical behavior as ligament sizes are reduced to less than 100 nm.

#### **F.SF02.09.06**

**Tuning the Mechanical Properties of Shape Memory Metallic Glass Composites with Brick and Mortar Designs** Suyue Yuan and Paulo Brancio; University of Southern California, United States

The intricate deformation and failure of a shape memory alloy-bulk metallic glass composites (BMGC) under tensile loading is investigated with large-scale molecular dynamics simulations. By carefully choosing the volume fraction and the arrangement of the crystalline phase the failure of the BMGC is shifted from the propagation of a critical shear band in the amorphous matrix to yield and failure of the crystalline second phase. Results show that a brick and mortar design with



staggered crystalline bricks (stg-BMGC) is able to further synergize the mechanical properties of the amorphous and crystalline phases. By effectively distributing the local stress and preventing the generation of a critical shear band the stg-BMGC design displays enhanced ductility while preserving the strength of the metallic glass matrix.

## SYMPOSIUM F.SF03

---

New Frontiers in the Design, Fabrication and Application of Metamaterials  
November 21 - December 4, 2020

### Symposium Organizers

Jennifer Dionne, Stanford University  
Yongmin Liu, Northeastern University  
Justus Ndukaife, Vanderbilt University  
Shuang Zhang, Univ of Birmingham

### Symposium Support

**Gold**  
Science | AAAS

---

\* Invited Paper

SESSION F.SF03.13: Live Keynote I: New Frontiers in the Design, Fabrication and Application of Metamaterials  
Session Chairs: Jennifer Dionne, Yongmin Liu and Justus Ndukaife  
Thursday Afternoon, December 3, 2020  
F.SF03

### 3:00 PM OPENING REMARKS

#### 3:02 PM \*F.SF03.04.01

**Multifunctional Structured Light with Flat Optics** Federico Capasso and [Ahmed Dorrah](#); Harvard University, United States

Flat optics based on metasurfaces holds promise for the design of a new class of diffractive optical component that circumvents the limits of refractive as well as Fresnel optics, in terms of control of aberrations, compactness and multifunctionality. Here we highlight the enhanced functions enabled by metasurface flat optics in structuring light. Optical elements coupling the spin and orbital angular momentum (SAM/OAM) of light have found a range of applications in classical and quantum optics. Q-plate type devices based on dielectric metasurfaces have shown superior performance in terms of singularity definition and ability to generate fractional and high OAM beams. A far more general spin to orbital angular momentum scheme has been recently demonstrated based on novel metasurface optical elements (J-plates) not limited to conjugate converted states, which are used to generate new complex structured light. The J-plate, with J referring to the photon's total angular momentum (TAM), is a metasurface device that imparts two arbitrary OAM states on an arbitrary orthogonal basis of spin states. When these J-plates are cascaded in series, they can generate several single quantum number beams and versatile superpositions thereof. Moreover, in contrast to previous spin-orbit-converters, the output polarization states of cascaded J-plates are not constrained to be the conjugate of the input states. Cascaded J-plates are also demonstrated to produce vector vortex beams and complex structured light, providing new ways to control TAM states of light

Metasurfaces hold major potential for multi-functionality, which may play a pivotal role in the next-generation compact nanodevices. OAM from lasers holds the promise for compact, at-the-source solutions to fuel applications from imaging to communications. However, conjugate symmetry between circular spin and opposite helicity OAM states from conventional

spin-orbit (SO) approaches, as well as low purity modes, has meant that complete control of light's angular momentum from lasers has remained elusive. Recent work on metasurface-enhanced lasers that overcomes this limitation will be discussed, including the demonstration of new high-purity OAM states with quantum numbers reaching  $l = 100$ , and non-symmetric vector vortex beams that lase simultaneously on independent OAM states as much as  $\Delta l = 90$  apart. This laser conveniently emits in the visible, producing new OAM states of light as well as all previously reported OAM modes from lasers, offering a compact and power-scalable source that harnesses intra-cavity structured metasurfaces for the creation of arbitrary chiral states of structured light.

Finally, recent work on beams with light structured along the propagation direction will be presented, where the polarization or the OAM of the beam changes along the propagation direction.

### 3:18 PM \*F.SF03.04.02

**Multifunctional Nonlocal Metasurfaces** [Nanfang Yu](#), Stephanie Malek and Adam C. Overig; Columbia University, United States

Diffractive photonic devices manipulate light via local and nonlocal optical modes. Local devices, such as metasurfaces, can shape a wavefront at multiple selected wavelengths, but inevitably modify light across the spectrum; nonlocal devices, such as grating filters, offer great frequency selectivity but limited spatial control. In this talk, I will introduce a rational design paradigm using quasi-bound states in the continuum to realize multifunctional nonlocal devices: metasurfaces that produce narrowband spatially tailored wavefronts at multiple selected wavelengths and yet are otherwise transparent.

I will show an experimental demonstration of dielectric metalenses that focus light only for narrowband resonances and leave the rest of the spectrum unaffected. Our resonant metasurfaces can be cascaded to achieve multifunctional behavior with each metasurface independently shaping the wavefront for a distinct resonance resonant wavelength.

These devices may expand the capabilities of multifunctional meta-optics to include active or nonlinear wavefront shaping. Scaled to visible wavelengths, our resonant metalenses may prove useful for augmented reality applications as compact and highly transparent multi-color see-through lenses.

### 3:34 PM \*F.SF03.01/F.SF05.01.01

**Aqueous Synthesis of 3D Nano-architected Ceramics and Metals—Nano-Architected TiO<sub>2</sub> PhCs** [Julia R. Greer](#); California Institute of Technology, United States

Additive manufacturing (AM), or 3D printing, represents a set of processes that enable layer-by-layer fabrication of complex structures using a wide range of materials that include ceramics, polymers, and metals. AM has allowed exploiting novel material properties, especially those that arise at the nano-scale, that do not occur in conventional materials, revolutionizing the production of complex parts for aerospace, military, automotive, optical, and medical applications. Facilitating these technologies requires a fabrication process to create a variety of functional materials in 3D, however the material choice for AM at the nano- and micro-scale is limited. A conspicuous example is a lack of AM processes for high refractive index ( $n$ ), low absorption materials with nano-sized dimensions, which are typically required for microoptics and device applications. To harness the beneficial properties of 3D nano-architected meta-materials, it is critical to assess their properties at each relevant scale while capturing overall structural complexity. We present the fabrication and synthesis of nano- and micro-architected materials using 3D (two-photon and interference) lithography, as well as characterization of their properties as a function of architecture, constituent materials, and microstructural detail. We focus on additive manufacturing of complex, multi-component and multi-material architectures comprised of metal oxides, metals, and hydrogels that are derived from (metal) salt-based, aqueous photoresin synthesis. The discussion will focus on each representative materials system (metals, oxides, and hydrogels), with a detailed overview of titanium dioxide, with critical feature dimensions between 150 and 600 nm and  $<1\%$  porosity. Using the described methodology, we created 3D dielectric photonic crystals (PhCs) out of rutile TiO<sub>2</sub> patterned into woodpile face-centered tetragonal (FCT) architectures with beam dimensions of 300-600nm and lateral periods of 0.8-1.5  $\mu\text{m}$ . We use Plane Wave Expansion (PWE) simulations and Fourier Transform Infrared Spectroscopy (FTIR) to demonstrate the full photonic bandgaps centered at 1.8-2.9  $\mu\text{m}$ . This fundamental research provides insights into the range of possible, often *transient* attainable chemical compositions, microstructures and architectures of chemically-derived, 3D-architected ceramics and metals, enabling advances in multiple technologies, i.e. 3D MEMS, micro-optics, and prototyping of 3D PhCs.

### 3:50 PM \*F.SF03.05.01

**Design and Additive Manufacturing of Intelligent Metamaterials** [Xiaoyu Zheng](#); University of California, Los Angeles, United States

Metamaterials represent the concept of utilizing artificial material building blocks to create desirable properties derived from three-dimensional layout and compositions. While novel topologies can now be realized via additive manufacturing, the lack of processable materials, multi-material gradients, speed and scalabilities have stymied its further adoption. In this talk, I will outline a suite of new material design and manufacturing routes, enabled by additive manufacturing of topologies, multi-scale features and multi-material cues. Attention is focused on how additive manufacturing techniques will enable processing the unprocessable, from structural composites to functional and stimuli-responsive multi-materials. This unleashes new design freedoms for rapid material property discovery and product realizations; where electrical, thermo, mechanical behaviors and their couplings can be inversely designed and tailored by an end-user at will. I will present a few examples, where structural, electronic and energy transduction materials are 3D architected into a compact form factor, without requiring multiple processing stages such as printing, embedding or wiring. Next, we will present their new applications, such as ultralight and strong materials, self-sensing materials, microsystems for robotics, air and maritime sensing, transducers, wave guiding and telecommunications.

#### 4:06 PM BREAK

#### 4:10 PM \*F.SF03.10.01

##### **Engineering Light-Matter Interactions in Semiconductor Nanowire Photodetectors and in Optical Nanotweezers** Kenneth Crozier; The University of Melbourne, Australia

We present recent studies in which engineering the interaction between light and nanoscale materials has been pursued for applications in photodetectors and in optical tweezers.

We review our recent work that demonstrates that the absorption spectrum of a photodetector can be controlled via waveguide resonances in semiconductor nanowires [1-6]. We discuss the physical interpretation for this phenomenon [1]. We review work in which p-i-n photodiodes were incorporated into vertically oriented silicon nanowires, and then used for colour imaging [2-5]. We also review recent work on extending this concept to the short-wave infrared via Ge nanowires [6]. We describe recent work in which we demonstrated chip-scale microspectrometers based on arrays of nanowire photodetector pixels [7] and an interleaved design with a “fishnet” pattern [8].

We also describe our work on optical trapping with plasmonic nanoapertures [9] and with all-dielectric (silicon) nanoantennas [10,11]. Fluorescence microscopy is used to track the position of, and emission from, individual trapped nanoparticles. The nanoparticles consist of fluorescent polystyrene nanospheres with diameters of 20 nm and 100 nm and streptavidin-coated CdSe/ZnS quantum dots. We observe the Brownian motion of the trapped nanoparticles using fluorescence imaging. Other experiments reported include the two-photon excitation of fluorescence from trapped nanoparticles, and the trapping of multiple nanoparticles simultaneously. We also discuss our recent work on an algorithmic approach to the design of plasmonic nanoapertures for optical tweezers [12].

#### References

1. K. Seo, M. Wober, P. Steinvurzel, E. Schonbrun, Y. Dan, T. Ellenbogen, K.B. Crozier, *Nano Letters* **11**, 1851 (2011)
2. H. Park, Y. Dan, K. Seo, Y.J. Yu, P.K. Duane, M. Wober, K.B. Crozier, *Nano Letters* **14**, 1804 (2014)
3. H. Park, K. Seo, K.B. Crozier, *Applied Physics Letters* **101**, 193107 (2012)
4. H. Park and K.B. Crozier, *Sci. Rep.* **3**, 2460 (2013)
5. H. Park and K. B. Crozier, *ACS Photonics* **2**, 544 (2015)
6. A. Solanki, S. Li, H. Park, and K.B. Crozier, *ACS Photonics* **5**, 520 (2018)
7. J. Meng, J.J. Cadusch, and K.B. Crozier, *Nano Letters* **20**, 320 (2020)
8. J.J. Cadusch, J. Meng, B. Craig, and K.B. Crozier, *Optica* **6**, 1171 (2019)
9. Z. Xu, W. Song, K. B. Crozier, *ACS Photonics* **5**, 2850 (2018)
10. Z. Xu, W. Song, K. B. Crozier, *ACS Photonics* **5**, 4993 (2018)
11. Z. Xu, K. B. Crozier, *Opt. Express* **27**, 4034 (2019)
12. N. Li, J. Cadusch, and K. Crozier, *Optics Letters* **44**, 5250-5253 (2019)

#### 4:26 PM \*F.SF03.06.01

**Parametric Oscillation of Electromagnetic Waves in Momentum Band Gaps of a Spatiotemporal Crystal** Seojoo Lee<sup>1</sup>, Jagang Park<sup>1</sup>, Hyukjoon Cho<sup>1</sup>, Yifan Wang<sup>2</sup>, Brian Kim<sup>2</sup>, Chiara Daraio<sup>2</sup> and Bumki Min<sup>1</sup>; <sup>1</sup>Korea Advanced Institute of Science and Technology, Korea (the Republic of); <sup>2</sup>California Institute of Technology, United States

Photonic crystals have revolutionized the field of photonics with their unique capabilities of dispersion and energy band gap

engineering, such as the demonstration of extreme group and phase velocities, topologically-protected photonic edge states, and the control of spontaneous emission of photons. On the other hand, time-variant media have shown their distinct functionalities including nonreciprocal propagation, frequency conversion, and amplification of light. However, these phenomena in time-variant media have mostly been investigated for the cases where spatiotemporal modulation is in the form of a simple harmonic wave. Here, we extend the type of spatiotemporal modulation so that time-variant and spatially-discrete photonic crystal structures, or spatiotemporal crystals, can be analyzed. The design of spatiotemporal crystals allows the engineering of momentum band gap, within which the parametric amplification occurs. As a potential platform for the construction of a parametric oscillator, a finite-sized spatiotemporal crystal is proposed and analyzed. The parametric oscillation is initiated by the energy and momentum conversion of an incident wave and the subsequent amplification by parametric gain within the momentum band gap. The oscillation process dominates over frequency mixing interactions above a transition threshold determined by the balance between gain and loss. Furthermore, the asymmetric formation of momentum band gaps can be realized by spatial phase control of temporal modulation, which leads to the directional radiation of oscillations at distinct frequencies. The proposed structure would enable simultaneous engineering of energy and momentum band gaps and provide a guideline to the implementation of advanced dispersion-engineered parametric oscillators.

**4:42 PM \*F.SF03.11.01**

**Metadevices Based on Integration of Microsystems and Metamaterials** Xin Zhang; Boston University, United States

Metamaterials, a major type of artificially engineered materials, exhibits unprecedented and controllable effective properties, including electric permittivity and magnetic permeability, and have boosted the development of optical and photonic devices. Metamaterials are composed of arrays of subwavelength unit cells. The effective properties of metamaterials are mainly determined by the structural design of the constituting subwavelength unit cells rather than their chemical composition. The design-driven properties enable versatile designs of their electromagnetic properties. Recent research has shifted to construct reconfigurable, tunable, and nonlinear metamaterials towards the development of metamaterial devices via integrating actuation mechanisms and quantum materials with meta-atoms. Microelectromechanical systems (MEMS) provide a powerful platform for manipulating the effective properties of metamaterials and the integration of multiple functions with metamaterials. In this talk, I will introduce the fundamentals of metamaterials, approaches to integrate MEMS with metamaterials, functional metamaterial devices from the synergy, and outlooks for metamaterial-enabled devices. Specifically, I will talk about terahertz devices based on the tunable metamaterials for dynamic control of the magnitude, phase, wave front, and polarization by MEMS-driven metamaterial unit cells. Terahertz detectors based on nonlinear terahertz metamaterials will be introduced. In addition, I will discuss the recent advances in the metamaterials for magnetic resonance imaging (MRI) based on the controllable nonlinearity in metamaterials. The implementation of intelligent metamaterials to boost the signal to noise ratio of clinical MRI, which will be translated to improvement in image quality and efficiency. The implementation of nonreciprocal devices based on nonlinearity will also be presented. Besides electromagnetic metamaterials, I will also present the construction of acoustic metamaterials for sound wave manipulation. The acoustic lens to focus sound waves based on the horn-like space coiling structures will be discussed. The ultra-open metamaterial for noise mitigation will also be presented. The future of metamaterials will be outlooked. Based on the MEMS and advanced manufacture technology, multifunctional metamaterial in electromagnetic and acoustic domains will be developed to yield functional devices to achieve functions that are not achievable by nature materials.

**4:58 PM CLOSING REMARKS**

SESSION F.SF03.14: Live Keynote II: New Frontiers in the Design, Fabrication and Application of Metamaterials  
Session Chairs: Jennifer Dionne, Yongmin Liu, Justus Ndukaife and Shuang Zhang  
Friday Morning, December 4, 2020  
F.SF03

**11:30 AM OPENING REMARKS**

**11:32 AM \*F.SF03.07.02**

**Non-Hermitian Symmetry and Topology in Photonics** Liang Feng; University of Pennsylvania, United States

Symmetry and topology are fundamental notions existing in all kinds of natural systems, from spiral galaxies and hurricanes to amino acids in molecules and non-trivial topologically protected electronic states in condensed matter. A stream of linearly polarized photons is typically topologically trivial, nevertheless, its full-vector nature intrinsically endows light with full capability of creating and carrying unique symmetry and topology. Most notably, the intrinsic capability of photonics of superposing non-Hermitian eigenstates through optical gain and loss provides a powerful toolbox for exploring the symmetry paradigms that were deemed challenging in condensed matter systems. Such investigations of symmetry and topology in photonics are revolutionizing the design principles in optical sciences. We have discovered new synthetic photonic materials, geometries, and field profiles that systematically enable the exploration of symmetry and topology in photonics. As such, the elusive symmetries can simplify the design of photonic meta-atoms and unit cells to reshape the density of states of photons in a topological and ultraflexible manner, which leads to on-demand meta-control of light emission, transmission, scattering and detection [1], thereby sustaining the ever-expanding information explosion for information processing, communication and computing.

For example, we have demonstrated one of the most striking benefits: the creation of eigenstate degeneracies such as exceptional points intrinsically associated with non-Hermitian Hamiltonians. This breaks the natural symmetry between reciprocal counterpropagating resonant modes in a micro-cavity to conduct unidirectional light-matter interaction carrying the large orbital angular momentum for structured light emission. Such a symmetry-driven approach allowed us to create the first microlaser source carrying the desired spin and orbital chirality as unique information carriers [2-4], giving rise to a new dimension of storing and processing information in photon's chiral degree of freedom. In addition to expanding the information dimensions to address the upcoming information explosion, flexible reconfiguration of topological pathways can offer a completely new paradigm for high-density photonics routing. However, the desired topological robustness unfortunately diminishes the hope of topological tunability. To overcome this fundamental limitation, we perform non-Hermitian symmetry to enable a new kind of topological states into the bulk of the topological insulator with a uniform topology, for the first time [5]. Without "battling" against topological protection, the new non-Hermitian topological states facilitate robust transmission links in the entire footprint to route optical signal to any desired output port. The ports-to-footprint ratio is at least 2 orders of magnitude higher than the state-of-the-art. Hence, our research addresses grand challenges in fundamental quantum physics and also enables entirely new optical sciences and photonic technologies, which advances and benefits both fields simultaneously.

L. Feng, R. El-Ganainy, L. Ge, Non-Hermitian photonics based on parity-time symmetry. *Nat. Photon.* **11**, 752-762 (2017).

P. Miao *et al.* Orbital angular momentum microlaser. *Science* **353**, 464-467 (2016).

Z. Zhang *et al.* Tunable topological charge vortex microlaser. *Science* **368**, 760-763 (2020).

Z. Ji *et al.* Photocurrent detection of the orbital angular momentum of light. *Science* **368**, 763-767 (2020).

H. Zhao *et al.* Non-Hermitian topological light steering. *Science* **365**, 1163-1166 (2019).

#### 11:48 AM \*F.SF03.09.01

**Twisted Polaritonics** [Andrea Alù](#); City University of New York, United States

In this talk, we discuss our recent progress in the area of twistrionics with light based on twisted metasurfaces or twisted van-der-Waals bilayers, which support topological transitions at photonic magic angles. The unusual interplay between coupled hyperbolic polaritons and the rotation angle between them enables unusual transitions from hyperbolic to elliptical propagation, which can be predicted by counting the number of intersections between the polariton bands of the two individual surfaces when isolated. During the talk, we discuss the unusual phenomena supported by these structures, and their opportunities for nano-imaging and information transport.

#### 12:04 PM \*F.SF03.08.02

**Topological Anomalies Made Visible** [Henning Schomerus](#); Lancaster University, United Kingdom

Topological photonics and mechanics aim to replicate fermionic symmetries as feats of precision engineering. Here I show how to enhance these systems via effects such as gain, loss and nonlinearities that do not have a direct electronic counterpart. This leads to a topological mechanism of mode selection [1,2,3], formation of compactons in flat band condensates [4] and sonic metamaterials [5], topological response of lasers [6] and robotic metamaterials [7], and practical applications such as for receiver protectors [8]. Common to them all are structured intensity distributions of the topological modes which are associated with topological anomalies and supersymmetry [9,10,11], normally abstract concepts that become directly visible in experiments.

[1] Topologically protected midgap states in complex photonic lattices, H. Schomerus, *Opt. Lett.* **38**, 1912 (2013).

[2] Selective enhancement of topologically induced interface states in a dielectric resonator chain, C. Poli, M. Bellec, U.

- Kuhl, F. Mortessagne, H. Schomerus, Nat. Commun. 6, 6710 (2015).
- [3] Topological Hybrid Silicon Microlasers, H. Zhao et al., Nat. Commun. 9, 981 (2018).
- [4] Exciton-polaritons in a two-dimensional Lieb lattice with spin-orbit coupling, C. E. Whittaker et al., Phys. Rev. Lett. 120, 097401 (2018).
- [5] Sonic Landau Levels and Synthetic Gauge Fields in Mechanical Metamaterials, H. Abbaszadeh, A. Souslov, J. Paulose, H. Schomerus, and V. Vitelli, Phys. Rev. Lett. **119**, 195502 (2017).
- [6] Topological dynamics and excitations in lasers and condensates with saturable gain or loss, S. Malzard, E. Cancellieri, and H. Schomerus, Opt. Express 26, 22506-22518 (2018).
- [7] Nonreciprocal response theory of non-Hermitian mechanical metamaterials: Response phase transition from the skin effect of zero modes, H. Schomerus, Phys. Rev. Research **2**, 013058 (2020)
- [8] Self-Shielded Topological Receiver Protectors, M. Reisner et al., Phys. Rev. Applied **13**, 034067 (2020).
- [9] Topological tight-binding models from nontrivial square roots, J. Arkininstall, M. H. Teimourpour, L. Feng, R. El-Ganainy, and H. Schomerus, Phys. Rev. B **95**, 165109 (2017).
- [10] Supersymmetric Polarization Anomaly in Photonic Discrete-Time Quantum Walks, S. Barkhofen, L. Lorz, T. Nitsche, C. Silberhorn, and H. Schomerus, Phys. Rev. Lett. **121**, 260501 (2018).
- [11] Observation of supersymmetric pseudo-Landau levels in strained microwave graphene, M. Bellec, C. Poli, U. Kuhl, F. Mortessagne, and H. Schomerus, Light: Science and Applications (in press); arXiv:2001.10287.

#### 12:20 PM \*F.SF03.07.04

**Active Topological Photonics on the Nanoscale** Gennady Shvets, Minwoo Jung and Ran Gladstein Gladstone; Cornell University, United States

Topological photonics enables unusual and robust properties of electromagnetic waves, including reflections-free photon propagation along strongly curved interfaces and localization at the corners and other discontinuities of photonic structures. One of the key remaining challenges include bringing topological photonics to the nanoscale and making it active/reconfigurable. In this talk, I will describe our group's progress on using two-dimensional materials such as electrostatically-gated graphene to accomplish these goals. The concept of a metagate – a structured metallic gate used to imprint topologically-complex chemical potential landscape onto graphene – will be introduced. Examples of lower- and higher-order topological structures that, respectively, confine graphene surface plasmon polaritons to edges and corners, will be presented, and the prospects for their experimental realization will be discussed. A novel regime of quantum landscaping, where periodic patterns of chemical potential simultaneously modify electronic and photonic propagation bands, will be introduced and exemplified using meta-gated graphene.

#### 12:36 PM BREAK

#### 12:40 PM \*F.SF03.09.02

**Photonics Inverse Design** Jelena Vuckovic; Stanford University, United States

Combining state of the art optimization and machine learning techniques with high speed electromagnetic solvers offers a new approach to "inverse" design and implement classical and quantum photonic circuits with superior properties, including robustness to errors in fabrication and environment, compact footprints, novel functionalities, and high efficiencies. We illustrate this with a number of demonstrated devices in silicon, diamond, and silicon carbide, including wavelength and polarization splitters and converters, power splitters, couplers, nonreciprocal switches and routers, on chip laser driven particle accelerators, and efficient quantum emitter-photon interfaces.

#### 12:56 PM \*F.SF03.08.01

**Revealing the Energy Spectrum of Plasmonic Hot-Carriers via Single Molecule Transport Measurements** Vladimir Shalaev<sup>1</sup>, Harsha Reddy<sup>1</sup>, Kun Wang<sup>2</sup>, Zhaxylyk Kudyshev<sup>1</sup>, Linxiao Zhu<sup>2</sup>, Shen Yan<sup>2</sup>, Andrea Vezzoli<sup>3</sup>, Simon Higgins<sup>3</sup>, Vikram Gavini<sup>2</sup>, Alexandra Boltasseva<sup>1</sup>, Pramod Reddy<sup>2</sup> and Edgar Meyhofer<sup>2</sup>; <sup>1</sup>Purdue University, United States; <sup>2</sup>University of Michigan–Ann Arbor, United States; <sup>3</sup>University of Liverpool, United Kingdom

The generation of hot-carriers in plasmonic nanostructures, via plasmon decay, is of great current interest as hot-carriers play key roles in applications like photocatalysis, energy harvesting and in novel photodetection schemes that circumvent band-gap limitations. However, experimental quantification of steady-state energy distributions of hot-carriers in plasmonic nanostructures, which is critical for systematic progress, has not been possible. In this talk, we will describe our recent experimental advances that have enabled the direct measurement of hot-carrier energy distributions under steady-state conditions [1]. Specifically, we will explain how a scanning probe-based technique that records charge transport through

single molecular junctions, when combined with nanoplasmonic experimental methods, can be leveraged to directly quantify hot-carrier energy distributions in a key model system—a thin gold film that supports propagating surface plasmon polaritons. Furthermore, key physical insights from our measurements on the role of Landau damping in producing hot-carriers and the contributions of different plasmonic modes towards hot-carrier generation will be discussed. Finally, we will outline how these experimental advances could potentially be leveraged to quantify hot-carrier distributions in plasmonic nanoparticles and other nanophotonic devices.

## References:

[1] H. Reddy, K. Wang, Z. Kudyshev, L. Zhu, S. Yan, A. Vezzoli, S. J. Higgins, V. Gavini, A. Boltasseva, P. Reddy, V. M. Shalaev, and E. Meyhofer, “Determining plasmonic hot-carrier energy distributions via single molecule transport measurements,” *Science*, 10.1126/science.abb3457, 2020.

### 1:12 PM \*F.SF03.11.02

**Tunable Chiral Optical Properties in Semiconductor Nanocrystals and Metamaterials** Vivian Ferry; University of Minnesota Twin Cities, United States

Optical nanomaterials offer the ability to bend, twist, guide, and confine light in nanoscale dimensions. Among these materials, chiral nanostructures particularly show promise for applications ranging from polarization manipulation to 3D displays, sensing, and spin-selective transport. Compared to their molecular counterparts, chiral nanomaterials exhibit orders of magnitude stronger dissymmetry factors, but have only been realized in a limited set of materials systems. We have recently demonstrated different strategies to tune and manipulate the polarization response of chiral metamaterials that combine metallic nanostructures, dielectric materials, and semiconductor nanocrystals. By controlling the refractive index of the dielectric components in different architectures, we show that the sign of the circular dichroism can be reversed, and the polarization and directionality of the outcoupled luminescence from nearby nanocrystals can be controlled. To create light-emitting metamaterials, it is additionally useful to create nanostructured elements comprised entirely of photoluminescent materials. We have recently developed patterning methods to transform semiconductor nanocrystals into patterned nanocrystal solids, realizing lateral feature sizes as small as 30 nm and heights in excess of 100 nm without degradation of the photoluminescence. We show that by designing the shape of the nanocrystal solid at this length scale and controlling connectivity between the nanocrystals, the refractive index and nanostructure absorptivity can be tailored. This work points to new strategies to design dynamically tunable metamaterials and control nanoscale light-matter interactions.

### 1:28 PM CLOSING REMARKS

SESSION F.SF03.01/F.SF05.01: Keynote Session

On Demand Abstracts Available for Viewing Starting Saturday Morning, November 21, 2020  
F-SF03

### 5:00 AM \*F.SF03.01/F.SF05.01.01

**Aqueous Synthesis of 3D Nano-architected Ceramics and Metals—Nano-Architected TiO<sub>2</sub> PhCs** Julia R. Greer; California Institute of Technology, United States

Additive manufacturing (AM), or 3D printing, represents a set of processes that enable layer-by-layer fabrication of complex structures using a wide range of materials that include ceramics, polymers, and metals. AM has allowed exploiting novel material properties, especially those that arise at the nano-scale, that do not occur in conventional materials, revolutionizing the production of complex parts for aerospace, military, automotive, optical, and medical applications. Facilitating these technologies requires a fabrication process to create a variety of functional materials in 3D, however the material choice for AM at the nano- and micro-scale is limited. A conspicuous example is a lack of AM processes for high refractive index (n), low absorption materials with nano-sized dimensions, which are typically required for microoptics and device applications. To harness the beneficial properties of 3D nano-architected meta-materials, it is critical to assess their properties at each relevant scale while capturing overall structural complexity. We present the fabrication and synthesis of nano- and micro-architected materials using 3D (two-photon and interference) lithography, as well as characterization of their properties as a function of architecture, constituent materials, and microstructural detail. We focus on additive manufacturing of complex, multi-component and multi-material architectures comprised of metal oxides, metals, and hydrogels that are derived from

(metal) salt-based, aqueous photoresin synthesis. The discussion will focus on each representative materials system (metals, oxides, and hydrogels), with a detailed overview of titanium dioxide, with critical feature dimensions between 150 and 600 nm and <1% porosity. Using the described methodology, we created 3D dielectric photonic crystals (PhCs) out of rutile TiO<sub>2</sub> patterned into woodpile face-centered tetragonal (FCT) architectures with beam dimensions of 300-600nm and lateral periods of 0.8-1.5  $\mu\text{m}$ . We use Plane Wave Expansion (PWE) simulations and Fourier Transform Infrared Spectroscopy (FTIR) to demonstrate the full photonic bandgaps centered at 1.8-2.9  $\mu\text{m}$ . This fundamental research provides insights into the range of possible, often *transient* attainable chemical compositions, microstructures and architectures of chemically-derived, 3D-architected ceramics and metals, enabling advances in multiple technologies, i.e. 3D MEMS, micro-optics, and prototyping of 3D PhCs.

#### SESSION F.SF03.02: New Photonic Structures

On Demand Abstracts Available for Viewing Starting Saturday Morning, November 21, 2020  
F-SF03

##### 5:00 AM \*F.SF03.02.01

**Some New Physics We Can Learn from Quasi-1D Structures** C.T. Chan; The Hong Kong University of Science and Technology, Hong Kong

We will use some examples to illustrate that quasi-1D systems which have very simple structures can give rise to interesting phenomena that are similar to those observed in topological materials.

A unique and very useful property of topological materials is the existence of topological edge modes which are guaranteed to exist by the topological invariants of the bulk through a bulk-edge correspondence. These topological edge modes or surface states support one-way transport that cannot be interrupted by disorder, and such robustness is probably the most sought after property of topological materials. The topological materials usually require a careful design and many have complex structures. Here, we give one example in which many topological properties of one-way edge modes can be realized in very simple quasi-1D photonic waveguides subjected to simple boundary conditions. These properties include the robustness of transport against imperfections and the ability to go around sharp corners. It appears that under some specific conditions, a certain boundary condition can emulate the existence of a material which carries a gap with some specific non-trivial topological characteristics. The same principle work for acoustic waves. The design principle also allows us to realize waveguides which have desirable characteristics such as being single-mode and have linear dispersion, in addition to being robust against disorder.

In the quest for topological materials, momentum space nodal points such as Weyl and Dirac points have attracted much attention. Realizing such nodal points require 3D/2D structures. However, some interesting nodal points can also be obtained using simple quasi-1D systems. For example, we will see that nexus points of nodal lines can be realized in 1D stacks of ordinary dielectric material layers with misaligned optical axes. Hidden symmetries give rise to interesting band crossings and new type of multifold nodal points. We will see that a fractional periodicity of different components of the permittivity tensor can manifest hidden symmetries of the Maxwell's equations. The hidden symmetries cannot be described using the standard space group theory. Such systems carry a new kind of protected band crossings (Kramers-like nodal lines) which are topological features unique to photonic systems. Such systems carry triply degenerate nodal points as the nexuses of several nodal lines enforced by the hidden symmetry, which can be viewed as a new kind of magnetic monopoles terminating Berry flux strings in the momentum space. In the vicinity of the triple nexus points, the iso-frequency surfaces has spin-1 Dirac-like conical dispersion. This implies that the nexus point can serve as a new platform for probing spin-1 physics. Breaking the hidden symmetry give rise to Type-II and Type-III nodal rings in photonic systems.

##### 5:15 AM \*F.SF03.02.02

**B<sub>1</sub><sup>+</sup> Homogenization in 7T Brain MRI with Inversely-Designed Metasurfaces** Namkyoo Park and Hansol Noh; Seoul National University, Korea (the Republic of)

##### Abstract

Offering enhanced SNR, contrast, and spatial resolution, ultra-high field (UHF,  $B_0 \geq 7\text{T}$ ) MRI has shown its potential for clinical diagnostics, such as evaluation of strokes, Alzheimer's, and Parkinson's disease [1-4]. However, at the Larmor frequency corresponding to  $B_0$  above 7 Tesla, the effective wavelength of the  $B_1^+$  field becomes smaller than the dimension of the head, leading to the spatial phase variation and inhomogeneity of  $B_1^+$  fields inside. For the mitigation of this



detrimental  $B_1^+$  inhomogeneity creating uneven contrast and the variation of SNR in the UHF MRI image, various approaches have been investigated, such as parallel transmission techniques (PTx), high permittivity material (HPM) structures, and metasurfaces. While PTx improves  $B_1^+$  homogeneity in the whole brain, hardware complexity, and the need for real-time SAR assessment prevents its clinical 7T practice [5,6]. Structures with metallic inclusions, such as metasurfaces and hybridized meta-atoms (HMAs) have also been reported to manipulate field profiles at subwavelength scales [7,8], but often resulted in deterioration of the global  $B_1^+$  homogeneity over the ROI.

In this talk, we propose and present an inverse-design of metasurfaces addressing the *global*  $B_1^+$  homogeneity over the region of interest (ROI) in the whole axial planes. Approximating MRI environments as a 2D system governed by the Helmholtz equation, we inversely obtain permittivity distributions of cylindrical metasurfaces enclosing the head at proximity. With the metasurface constructed of cylindrical HPMs of different permittivity, stacked along the superior direction, it is numerically confirmed that the proposed metasurface excite the target fields near the surfaces and ROI in both approximated and real MRI environments. When tested with an actual anatomical head model (MIDA), it is found that the CV (coefficient of variation) and Max-to-min ratios of  $B_1^+$  in the ROI are reduced on average by 40% and 33% respectively, along with SAR reduction in the head by 34% (average) and 44% (peak). Since the  $B_1^+$  distribution itself is globally homogenized, the proposed structure is expected to be most useful in spin-echo based imaging in UHF MRI, such as T2-weighted imaging and diffusion-weighted imaging in the whole brain.

## References

- [1] G. Barisano, et al., The British Journal of Radiology, vol. 92, no. 1094, p. 20180492, 2019.
- [2] P. Balchandani, et al., American Journal of Neuroradiology, vol. 36, no. 7, pp. 1204–1215, 2014.
- [3] M. Inglese, et al., Expert Review of Neurotherapeutics, vol. 18, no. 3, pp. 221–230, 2018.
- [4] B. R. Knowles, et al., Clinical and Translational Radiation Oncology, vol. 18, pp. 87–97, 2019.
- [5] C. M. Deniz, et al., Topics in Magnetic Resonance Imaging, vol. 28, no. 3, pp. 159–171, 2019.
- [6] O. Kraff, et al., Journal of Magnetic Resonance Imaging, vol. 46, no. 6, pp. 1573–1589, 2017.
- [7] R. Schmidt, et al., Scientific Reports, Vol. 7, no. 1, 1678, 2017.
- [8] M. Dubois, et al., Physical Review X, vol. 8, no. 3, 031083, 2018.

## 5:30 AM F.SF03.02.03

### Nanoparticle Supercrystals Formed by Covalent Bonding Interaction in Conjunction with Slow Solvent

**Evaporation** [Jiwhan Kim](#)<sup>1</sup>, Jahar Dey<sup>1</sup>, Aminah Umar<sup>1,2</sup>, Sang-Jo Lee<sup>1</sup>, Jae-Min Ha<sup>1</sup> and Sung-Min Choi<sup>1</sup>; <sup>1</sup>Korea Advanced Institute of Science and Technology, Korea (the Republic of); <sup>2</sup>University of Indonesia, Indonesia

Nanoparticle supercrystals (NPSCs) are of great interest as materials with new emergent properties. The emergent properties of NPSCs through collective interaction between nanoparticles provide new opportunities for a wide range of applications such as plasmonics, photonics, electronics, magnetics, and catalysis. Different types of intermolecular interactions such as hydrogen bonding, van der Waal's interaction, and electrostatic interaction have been used for fabricating NPSCs of various crystal symmetries and lattice parameters. However, the limited structural stability of NPSCs fabricated by the intermolecular forces still remains a major hurdle for realizing their potential applications.

The covalent bonding, which shares electrons to form stable organic molecules of various structures, is the most representative intramolecular force much stronger than the intermolecular forces such as van der Waals and hydrogen bonding interactions. Recently, the precision and versatility of covalent chemistry has been successfully established through covalent bonding of various large crystal structures such as metal-organic frameworks and covalent organic frameworks. Considering all these successes, covalent bonding interaction can be an excellent choice for fabricating more stable NPSCs. However, the covalent bonding interaction has not been successfully explored as a main driving force for the formation of highly ordered NPSCs yet.

Here, we report a new method to fabricate highly stable and highly ordered three-dimensional NPSCs by using covalent bonding interaction in conjunction with the slow solvent evaporation process, and demonstrated using isotropic and anisotropic building blocks. In this method, the NPSCs stabilized by covalent bonding are highly stable in solvents of different polarity ranging from water to toluene as well as dried states and at temperature up to 160 °C. Considering the diverse combined choices of covalent bonding reactions, ligand molecules with different chain lengths and physicochemical properties, and nanoparticles may allow the designed synthesis of NPSCs for potential applications. In addition to high strength and the large library of covalent chemistry, the low cost of organic ligands molecules used in this method makes the NPSCs induced by covalent bonding interaction highly versatile and economic, providing new opportunities for the fabrication and applications of NPSCs.

## 5:40 AM F.SF03.02.04

### Atomic Network Adjustment in Amorphous Silicon for Optimizing Metasurface in the Visible Spectrum [Younghwan](#)

Yang, Gwanho Yoon and Junsuk Rho; Pohang University of Science and Technology, Korea (the Republic of)

This work suggests an adjustable index of hydrogenated-amorphous silicon for obtaining high-efficiency metasurface in the visible by modulating chemical equilibrium of deposition. Hydrogenated-amorphous silicon has been widely used for metasurface since it has cost-effective, CMOS-compatible fabrication methods. Also, hydrogenated-amorphous silicon exhibit a high index  $\sim 3.0$  at the visible frequency, which induces optical property modulation with geometrical structures on thin film. Based on these advantages, many practical metasurface have been reported such as metalenses, meta-hologram, and structural color filters. However, hydrogenated-amorphous silicon suffers from low-efficiency in high-frequency range because it has a bandgap tail in the visible. The bandgap tail is known to be the main obstacle to be transparent materials, so high-efficient metasurface is limited by inherent material properties of silicons. Here, this work explores atomic structure networks of hydrogenated amorphous silicon to modulate complex refractive index, which enables high-efficiency metasurface in the visible spectrum. The adjustability of the refractive index achieved with varying deposition conditions of plasma-enhanced chemical vapor deposition, which affect bonding states and their hydrogenation. It is revealed that substrate temperature and atmospheric pressure are the main factor to change bonding states and hydrogenation. By changing the deposition conditions, atomic structures were verified, and it is confirmed by X-ray diffraction and transmission electron microscopy. Substrate temperature and atmospheric pressure are the main factor to change bonding states and hydrogenation. Optimized pressure creates micro/nano crystallinity in hydrogenated silicon, which reduces the extinction coefficient. Another parameter affects hydrogen contents, which reduce dangling bonds of silicon. These phenomena change the bandgap tail of silicon, it induce high refractive index coverage when chemical equilibrium is manipulated. As a result, the refractive index can modify between 2.6 and 4.2; the extinction coefficient can be lower than 0.1 at the wavelength of 450 nm. Also, the adjusted hydrogenated-amorphous silicon has near-zero absorption at the wavelength of 532 nm and 635 nm, which is comparable to normal transparent materials (TiO<sub>2</sub>, GaN, etc). Furthermore, conversion efficiency for visible range metasurface was calculated with an optimized complex refractive index, resulting in 96.6%, 90.9%, and 64.7% at the wavelength of 635 nm, 532 nm, and 450 nm, respectively. Those results can alter materials of metasurface from conventional, transparent dielectrics (TiO<sub>2</sub>, GaN, etc) to hydrogenated amorphous silicon. Also, the high adjustability of the complex refractive index of silicon with simple steps can be useful for low-cost fabricatable, versatile metasurfaces. At last, the experimental demonstration was also conducted to verify high-efficiency metasurface composed of optimized materials. Optimized refractive index with suitable geometrical parameters achieves 64% at the wavelength of 635 nm, 65% at the one of 532 nm, and 42% at one of 450 nm, which have been not reported yet. Considering the simple fabrication steps with adjustability compared to other dielectrics, hydrogenated amorphous silicon will be a promising material for the practical application of metasurfaces.

SESSION F.SF03.03: Structural Color and Optical Display Using Metasurfaces  
On Demand Abstracts Available for Viewing Starting Saturday Morning, November 21, 2020  
F-SF03

**5:00 AM \*F.SF03.03.01**

**Electrically-Controlled Digital Metasurface Device for Light Projection Displays** Na Liu<sup>1,2</sup>; <sup>1</sup>University of Stuttgart, Germany; <sup>2</sup>Max Planck Institute for Solid State Research, Germany

The fast development of nanophotonics urges breakthrough concepts and design principles to create functional devices for diverse optical applications. In particular, the advent of metasurfaces has revolutionized nanophotonics, enabling a variety of opportunities. Metasurfaces, which comprise subwavelength optical antennas in ultrathin layers, identify a class of flat optical devices with exceptional control over the propagation of light.[1] Despite the exciting progress, a specific research focus - dynamic optical metasurfaces,[2] which probably also provide the most important link to the real-world optical applications, still awaits endeavors. They allow for active manipulation of light beams and enable fascinating optical functions, including dynamic beam steering, focusing and shaping, as well as optical vortex generations, imaging, and sensing. However, the reported schemes have been mostly limited to simultaneous tuning of the resonance frequencies or amplitudes of all the metasurface antennas.[3, 4] They also suffer from poor device control with low intensity modulation and narrow operating band. Thus, there is still plenty of room to advance this research focus, especially at visible frequencies.

We demonstrate a strategy to realize dynamic optical metasurfaces by tailoring their spatial frequencies via modulation of both the geometric and propagation phases at visible frequencies. In particular, we showcase electrically-controlled digital metasurface devices (DMSDs) for light projection displays. The DMSD consists of metasurface pixels in an  $M \times N$  array. Each metasurface pixel contains gold nanorods arranged in a rectangular lattice. In some preselected (odd or even) columns,

the nanorods are covered with a dielectric material. The sample is subsequently encapsulated in a thin liquid crystal (LC) cell. The dynamic function of the metasurface pixels is enabled by electrically controlling the relative phase between the neighboring odd and even columns via LCs on the millisecond time scale. In principle, each metasurface pixel can be designed to generate a specific dynamic holographic pattern in the far field. Particularly for light projection display applications, each metasurface pixel that can be electrically switched between '1' and '0' states is individually addressed by an electrode, forming an anomalous reflection spot that can be turned on and off with high contrast in the projection screen. As a result, programmable images are dynamically generated and displayed. [5]

#### References

- Yu, N. *et al.* Light Propagation with phase discontinuities: generalized laws of reflection and refraction. *Science* **334**, 333–337 (2011).
- Shaltout, A. M., Shalaev, V. M. & Brongersma, M. L. Spatiotemporal light control with active metasurfaces. *Science* **364**, eaat3100 (2019).
- Li, S.-Q. *et al.* Phase-only transmissive spatial light modulator based on tunable dielectric metasurface. *Science* **364**, 1087–1090 (2019).
- Zubritskaya, I., Maccaferri, N., Inchausti Ezeiza, X., Vavassori, P. & Dmitriev, A. Magnetic Control of the Chiroptical Plasmonic Surfaces. *Nano Lett.* **18**, 302–307 (2018).
- J. X. Li, P. Yu, S. Zhang, and N. Liu, *Electrically-controlled digital metasurface device for light projection displays*. *Nature Communications* **11**, 3574 (2020).

#### 5:15 AM F.SF03.03.02

**Highly Reflective Subtractive Colors Based on Silver Nanodisk Metasurfaces** Jolie Blake<sup>1</sup>, Stefano Rossi<sup>2</sup>, Oliver Olsson<sup>1</sup>, Marika Gugole<sup>1</sup>, Kunli Xiong<sup>1</sup>, Magnus Jonsson<sup>2</sup> and Andreas Dahlin<sup>1</sup>; <sup>1</sup>Chalmers University of Technology, Sweden; <sup>2</sup>Linköping University, Sweden

Plasmonic structural colors generated by metasurfaces have emerged as feasible alternatives to traditional pigment-based printing. Despite extensive studies, producing structural colors from nanostructured metasurfaces in metal-insulator-metal (MIM) configuration still presents some challenges. One major hurdle is pixel fabrication that does not rely on expensive lithographic methods but can still controllably produce saturated and bright colors. We report highly reflective cyan, magenta and yellow (CMY) color pixels based on silver metasurfaces, using a wide-area fabrication technique suitable for upscaling. Through numerical simulations we demonstrate that the colors achieved are as a result of resonances more characteristic of Fabry-Pérot than gap- surface plasmon modes due to the thick spacer layer.

#### SESSION F.SF03.04: Multifunctional Metasurfaces

On Demand Abstracts Available for Viewing Starting Saturday Morning, November 21, 2020  
F-SF03

#### 5:00 AM \*F.SF03.04.01

**Multifunctional Structured Light with Flat Optics** Federico Capasso and [Ahmed Dorrah](#); Harvard University, United States

Flat optics based on metasurfaces holds promise for the design of a new class of diffractive optical component that circumvents the limits of refractive as well as Fresnel optics, in terms of control of aberrations, compactness and multifunctionality. Here we highlight the enhanced functions enabled by metasurface flat optics in structuring light. Optical elements coupling the spin and orbital angular momentum (SAM/OAM) of light have found a range of applications in classical and quantum optics. Q-plate type devices based on dielectric metasurfaces have shown superior performance in terms of singularity definition and ability to generate fractional and high OAM beams. A far more general spin to orbital angular momentum scheme has been recently demonstrated based on novel metasurface optical elements (J-plates) not limited to conjugate converted states, which are used to generate new complex structured light. The J-plate, with J referring to the photon's total angular momentum (TAM), is a metasurface device that imparts two arbitrary OAM states on an arbitrary orthogonal basis of spin states. When these J-plates are cascaded in series, they can generate several single quantum number beams and versatile superpositions thereof. Moreover, in contrast to previous spin-orbit-converters, the output polarization states of cascaded J-plates are not constrained to be the conjugate of the input states. Cascaded J-plates are also demonstrated to produce vector vortex beams and complex structured light, providing new ways to control TAM states of light

Metasurfaces hold major potential for multi-functionality, which may play a pivotal role in the next-generation compact nanodevices. OAM from lasers holds the promise for compact, at-the-source solutions to fuel applications from imaging to communications. However, conjugate symmetry between circular spin and opposite helicity OAM states from conventional spin-orbit (SO) approaches, as well as low purity modes, has meant that complete control of light's angular momentum from lasers has remained elusive. Recent work on metasurface-enhanced lasers that overcomes this limitation will be discussed, including the demonstration of new high-purity OAM states with quantum numbers reaching  $l = 100$ , and non-symmetric vector vortex beams that lase simultaneously on independent OAM states as much as  $\Delta l = 90$  apart. This laser conveniently emits in the visible, producing new OAM states of light as well as all previously reported OAM modes from lasers, offering a compact and power-scalable source that harnesses intra-cavity structured metasurfaces for the creation of arbitrary chiral states of structured light.

Finally, recent work on beams with light structured along the propagation direction will be presented, where the polarization or the OAM of the beam changes along the propagation direction.

#### 5:15 AM \*F.SF03.04.02

**Multifunctional Nonlocal Metasurfaces** Nanfang Yu, Stephanie Malek and Adam C. Overig; Columbia University, United States

Diffractive photonic devices manipulate light via local and nonlocal optical modes. Local devices, such as metasurfaces, can shape a wavefront at multiple selected wavelengths, but inevitably modify light across the spectrum; nonlocal devices, such as grating filters, offer great frequency selectivity but limited spatial control. In this talk, I will introduce a rational design paradigm using quasi-bound states in the continuum to realize multifunctional nonlocal devices: metasurfaces that produce narrowband spatially tailored wavefronts at multiple selected wavelengths and yet are otherwise transparent.

I will show an experimental demonstration of dielectric metalenses that focus light only for narrowband resonances and leave the rest of the spectrum unaffected. Our resonant metasurfaces can be cascaded to achieve multifunctional behavior with each metasurface independently shaping the wavefront for a distinct resonance resonant wavelength.

These devices may expand the capabilities of multifunctional meta-optics to include active or nonlinear wavefront shaping. Scaled to visible wavelengths, our resonant metalenses may prove useful for augmented reality applications as compact and highly transparent multi-color see-through lenses.

#### 5:30 AM F.SF03.04.03

**Sensitivity of Plate-Lattice Metamaterials to Geometric Imperfections** Fani Derveni<sup>1</sup>, Andrew Gross<sup>2</sup>, Kara Peterman<sup>1</sup> and Simos Gerasimidis<sup>1</sup>; <sup>1</sup>University of Massachusetts Amherst, United States; <sup>2</sup>University of South Carolina, United States

Structural requirements have pushed lightweight materials with advantageous material properties to the forefront of engineering practice. As a result, it has become necessary to enhance the breadth of design options with a new generation of lightweight materials offering high strength, high stiffness, and high energy absorption capacity. The accelerated progress of additive manufacturing has enabled the fabrication of intricate architectures which are used today to design new materials. These materials, also called architected materials, exhibit mechanical properties which are dictated primarily by their pattern rather than their composition and therefore the design of their architectures has received great attention. The fabrication capabilities gained from additive manufacturing has opened up a new space for design exploration based on these architectural forms. Until today, there have been numerous architected lattice materials with extraordinary properties such as negative Poisson's ratio, negative stiffness, multi-stability, negative thermal expansion and others. Very recently, a new generation of architected materials has emerged in the form of plate-lattice materials in which plates are patterned in different configurations to create a cellular geometry. Recent findings have shown that plate-lattice materials are not only significantly stiffer and stronger than truss-lattices, but also able to attain the theoretical Hashin Shtrikman and Suquet bounds for isotropic materials. The objective of this work is to explore the imperfection sensitivity of a variety of isotropic and anisotropic plate-lattice architectures of cubic symmetry, such as Simple Cubic (SC), Body-Centered Cubic (BCC), Face-Centered Cubic (FCC) and their isotropic combinations (SC-BCC and SC-FCC). Three-dimensional shell computational models with periodic boundary conditions are used to study the buckling behavior. Short and long wavelength buckling modes are observed by increasing the tessellation size of plate-lattices under axial compression for a range of relative densities between 0.05% (ultra-thin) and 25%. Geometric imperfections are incorporated in the model by varying imperfections of modal shapes. The main goal of this work is to provide accurate knockdown factors for plate-lattice materials with geometric imperfections and to characterize fundamental behavior of these plate-lattice metamaterials with a potential use in new generation structural applications.

**5:40 AM F.SF03.04.04**

**Multidimensional and Multifunctional Metalenses Based on Photonic Spin Hall Effect** Renchao Jin<sup>1,2</sup>, Zheng-Gao Dong<sup>2</sup> and Yongmin Liu<sup>1,1</sup>; <sup>1</sup>Northeastern University, United States; <sup>2</sup>Southeast University, China

Metasurfaces are composed of arrays of subwavelength meta-atoms, which have demonstrated many exciting opportunities to control the amplitude, phase and polarization of incident light. Metasurfaces with circularly polarized sensitivity has attracted wide attention, because of the manifestation of the photonic spin Hall effect (PSHE)[1]. Pancharatnam-Berry (PB) phase is the frequently used method to control the phase of circularly polarized light. However, most metasurfaces based on the PB phase only work for circularly polarized light with one specific spin, hindering the simultaneous and independent control of left-handed circularly polarized (LCP) light and right-handed circularly polarized (RCP) light [2].

In this talk, we demonstrate that utilizing both the PB phase and the propagation phase, we can rationally control the phase for each spin state of light [3]. The PB phase provides opposite phase modulation for LCP and RCP light, and it is determined by the in-plane rotation angle of meta-atoms [4,5]. In contrast, the propagation phase provides the same phase modulation regardless of the polarization of incident light and rotation angle of meta-atoms. Therefore, combing the PB phase and propagation creates a flexible way to realize simultaneous phase control of LCP and RCP light. As proof-of-concept demonstrations, here we numerically and experimentally realize the independent focusing and manipulation of both spins of light by V-antenna metasurfaces. Our multidimensional metalens is able to focus light of different spins at designated positions along both transverse and longitudinal directions. It can be used as a polarization analyzer to distinguish the polarization state of incident light. In addition, our multifunctional metalens can act either as a convex lens or an axicon, depending on the spin of light. The demonstrated multidimensional and multifunctional metalens has versatile potentials in spin-dependent nanophotonics, ranging from optical imaging and micro/nano-object manipulation to optical sensing.

## SESSION F.SF03.05: Mechanical Metamaterials

On Demand Abstracts Available for Viewing Starting Saturday Morning, November 21, 2020  
F-SF03

**5:00 AM \*F.SF03.05.01**

**Design and Additive Manufacturing of Intelligent Metamaterials** Xiaoyu Zheng; University of California, Los Angeles, United States

Metamaterials represent the concept of utilizing artificial material building blocks to create desirable properties derived from three-dimensional layout and compositions. While novel topologies can now be realized via additive manufacturing, the lack of processable materials, multi-material gradients, speed and scalabilities have stymied its further adoption. In this talk, I will outline a suite of new material design and manufacturing routes, enabled by additive manufacturing of topologies, multi-scale features and multi-material cues. Attention is focused on how additive manufacturing techniques will enable processing the unprocessable, from structural composites to functional and stimuli-responsive multi-materials. This unleashes new design freedoms for rapid material property discovery and product realizations; where electrical, thermo, mechanical behaviors and their couplings can be inversely designed and tailored by an end-user at will. I will present a few examples, where structural, electronic and energy transduction materials are 3D architected into a compact form factor, without requiring multiple processing stages such as printing, embedding or wiring. Next, we will present their new applications, such as ultralight and strong materials, self-sensing materials, microsystems for robotics, air and maritime sensing, transducers, wave guiding and telecommunications.

**5:15 AM F.SF03.05.02**

**Extreme Mechanical Resilience in Nanolabyrinthine Self-Assembled Metamaterials** Carlos Portela<sup>1,2</sup>, A Vidyasagar<sup>2</sup>, Sebastian Krödel<sup>3</sup>, Tamara Weissenbach<sup>3</sup>, Daryl Yee<sup>2</sup>, Julia R. Greer<sup>2</sup> and Dennis Kochmann<sup>3</sup>; <sup>1</sup>Massachusetts Institute of Technology, United States; <sup>2</sup>California Institute of Technology, United States; <sup>3</sup>ETH Zürich, Switzerland

Lightweight materials with tailorable properties have attracted attention for decades, yet stiff materials that can resiliently tolerate extreme forces and deformation, while being manufactured at large scales, have remained a rare find. Bio-inspired designs such as hierarchical foams and atomic-lattice-mimicking trusses have achieved optimal combinations of mechanical parameters but suffer from limited mechanical tunability, limited long-term stability, and low throughput volumes. Most mechanical metamaterials have relied on symmetry, periodicity, and lack of defects to achieve the desired mechanical response, resulting in sub-optimal mechanical response under the presence of inevitable defects. Shell-type designs, which

can mitigate stress concentrations and flaws, have come with high densities and limited recoverability.

We exploit non-periodic ceramic shell architectures of ultralow density (reaching 4 mg/cm<sup>3</sup>) whose engineered curvature distribution achieves close-to-optimal stiffness scaling and, moreover, whose careful combination of topology, geometry and base material results in mechanical resilience superior to previous mechanical metamaterials. We present a method for scalable fabrication of these materials, guided by natural spinodal decomposition, which results in shell-based ceramic architectures with thicknesses down to ~10 nm and overall sample volumes of up to a few cubic centimeters. We show the capability of these architectures to maintain more than 50% of their original stiffness and strength after ten cycles of compression up to 30% while exhibiting no visible permanent deformation. Guided by simulations, we show how controlling the material morphology leads to the (an)isotropic material response whose directional stiffness distribution, impressively, remains constant over a wide range of shell thicknesses, as demonstrated experimentally. Our approach highlights pathways to harness self-assembly methods in the design and scalable fabrication of novel metamaterials with both tunable high stiffness and unsurpassed recoverability, simultaneously unachievable by previously reported mechanical metamaterials.

SESSION F.SF03.06: New Concepts of Metamaterials  
On Demand Abstracts Available for Viewing Starting Saturday Morning, November 21, 2020  
F-SF03

**5:00 AM \*F.SF03.06.01**

**Parametric Oscillation of Electromagnetic Waves in Momentum Band Gaps of a Spatiotemporal Crystal** Seojoo Lee<sup>1</sup>, Jagang Park<sup>1</sup>, Hyukjoon Cho<sup>1</sup>, Yifan Wang<sup>2</sup>, Brian Kim<sup>2</sup>, Chiara Daraio<sup>2</sup> and Bumki Min<sup>1</sup>; <sup>1</sup>Korea Advanced Institute of Science and Technology, Korea (the Republic of); <sup>2</sup>California Institute of Technology, United States

Photonic crystals have revolutionized the field of photonics with their unique capabilities of dispersion and energy band gap engineering, such as the demonstration of extreme group and phase velocities, topologically-protected photonic edge states, and the control of spontaneous emission of photons. On the other hand, time-variant media have shown their distinct functionalities including nonreciprocal propagation, frequency conversion, and amplification of light. However, these phenomena in time-variant media have mostly been investigated for the cases where spatiotemporal modulation is in the form of a simple harmonic wave. Here, we extend the type of spatiotemporal modulation so that time-variant and spatially-discrete photonic crystal structures, or spatiotemporal crystals, can be analyzed. The design of spatiotemporal crystals allows the engineering of momentum band gap, within which the parametric amplification occurs. As a potential platform for the construction of a parametric oscillator, a finite-sized spatiotemporal crystal is proposed and analyzed. The parametric oscillation is initiated by the energy and momentum conversion of an incident wave and the subsequent amplification by parametric gain within the momentum band gap. The oscillation process dominates over frequency mixing interactions above a transition threshold determined by the balance between gain and loss. Furthermore, the asymmetric formation of momentum band gaps can be realized by spatial phase control of temporal modulation, which leads to the directional radiation of oscillations at distinct frequencies. The proposed structure would enable simultaneous engineering of energy and momentum band gaps and provide a guideline to the implementation of advanced dispersion-engineered parametric oscillators.

**5:15 AM F.SF03.06.02**

**3D Chiral Self-Assembly of Spheres and Tetrahedra** Daniel B. Straus and Robert J. Cava; Princeton University, United States

The design of new chiral materials usually requires stereoselective organic synthesis to create molecules with chiral centers. Less commonly, achiral molecules can self-assemble into chiral materials, despite the absence of intrinsic molecular chirality. Here, we demonstrate the assembly of high-symmetry molecules into a chiral van der Waals structure by synthesizing crystals of C<sub>60</sub>(SnI<sub>4</sub>)<sub>2</sub> from icosahedral buckminsterfullerene (C<sub>60</sub>) and tetrahedral SnI<sub>4</sub> molecules through spontaneous self-assembly. The SnI<sub>4</sub> tetrahedra template the Sn atoms into a chiral cubic three-connected net of the SrSi<sub>2</sub> type that is held together by van der Waals forces. Our results represent the remarkable emergence of a self-assembled chiral material from two of the most highly symmetric molecules, demonstrating that almost any molecular, nanocrystalline, or engineered precursor can be considered when designing chiral assemblies.

### 5:25 AM F.SF03.06.03

**Synthesis and Characterization of Nanoscale 3-Dimensional Metamaterials** Grace Pakeltis<sup>1</sup>, C. Praise Anyanwu<sup>2</sup>, Juan C. Idrobo<sup>3</sup>, David Masiello<sup>2</sup>, Jason Fowlkes<sup>1,3</sup> and Philip D. Rack<sup>1,3</sup>; <sup>1</sup>The University of Tennessee, Knoxville, United States; <sup>2</sup>University of Washington, United States; <sup>3</sup>Oak Ridge National Laboratory, United States

Metamaterials have been of great interest in the field of photonics due to their ability to realize intriguing new properties unachievable in natural materials. Advances in metamaterial design and characterization have led to advancing from the microwave region to terahertz and optical frequency to realize artificial magnetism, negative refractive index, and superlenses. One of the most common elements in metamaterial design is the split ring resonator. While much work has been devoted to optically modeling and characterizing planar plasmonic SRR arrays, there has yet to be a robust strategy for synthesizing 3 dimensional SRR structures. Enhanced functionality should be possible by extending into the third dimension. In this study, we illustrate a nanoscale synthesis process which utilizes a hybrid of direct-write 3D nanoprinting and thin film deposition to fabricate free-standing split ring resonators for the investigation of 3D metamaterials. Focused electron beam induced deposition is used to deposit non-plasmonic 3D scaffolds, which are subsequently isolated with a conformal SiO<sub>2</sub> layer and coated with a plasmonic materials, specifically Au, to create functional 3D metamaterials. A variety of single coupled SRR structures were fabricated and low-loss electron energy loss spectroscopy was utilized to characterize their full plasmonic spectra with nanoscale resolution. Complementary electron discrete dipole approximation simulations were performed to elucidate the resultant consequent electric and magnetic field distributions. This work demonstrates the flexibility FEBID scaffolds offer for the advancement of new 3D devices for applications and fundamental studies of metamaterials.

### SESSION F.SF03.07: Topological Photonics

On Demand Abstracts Available for Viewing Starting Saturday Morning, November 21, 2020  
F-SF03

### 5:00 AM \*F.SF03.07.01

**Novel Valley Manipulation in Photonic Crystals** Baile Zhang; Nanyang Technological University, Singapore

The valley degree of freedom (DOF) has recently been introduced into photonic crystals as a new way to manipulate electromagnetic waves, similar to how electrons are manipulated in valleytronic materials. Compared to the photonic pseudospin that requires complex construction such as ring resonators and bianisotropic metamaterials, the valley DOF originates from the underlying lattice symmetry, which does not rely on strong spin-orbit coupling and thus can be easily integrated in a photonic crystal setup. In this talk, I will introduce some of our recent works on valley manipulation.

First of all, the topological valley edge states have been realized in many photonic crystals. We firstly implemented a valley photonic crystal at microwave frequencies based on a four band model, and demonstrated the spin-valley locking feature. A very interesting phenomenon is the perfect out-coupling of valley edge states because of the valley conservation at the zigzag interface.

Secondly, we constructed an unpaired Dirac point at a single valley. It is well known that a photonic graphene exhibits two Dirac cones at two valleys. Therefore, in order to probe features of 2D Dirac particles, special precautions must be taken to ensure that only one valley is excited. Depending on the system geometry, this is not always possible, because defects and interfaces can give rise to strong intervalley scattering. Here we will discuss the construction of an unpaired Dirac point at only one valley. Some unique photonic phenomena such as the nonreciprocal reflection and angular selectivity are discussed. This unpaired single Dirac cone is inspired by the famous Haldane model, where the inversion symmetry breaking and time reversal symmetry breaking compete to open a topological bandgap.

Thirdly, we found that another mechanism that can be utilized to manipulate valley is via loss and gain, or non-Hermiticity. By modifying the Haldane model, it can be seen that the loss/gain can participate in the completion between inversion symmetry breaking and time reversal symmetry breaking, and drive the Haldane-type topological transition. In particular, the loss/gain can displace the Dirac points in momentum space. So the modulation of loss/gain can induce a uniform effective magnetic field and thus Landau levels, similar to the effect of strain engineering, but without lattice deformation.

Finally, these valley photonic crystals have found device applications such as the on-chip communication and electrically

pumped lasers.

**5:15 AM \*F.SF03.07.02**

**Non-Hermitian Symmetry and Topology in Photonics** Liang Feng; University of Pennsylvania, United States

Symmetry and topology are fundamental notions existing in all kinds of natural systems, from spiral galaxies and hurricanes to amino acids in molecules and non-trivial topologically protected electronic states in condensed matter. A stream of linearly polarized photons is typically topologically trivial, nevertheless, its full-vector nature intrinsically endows light with full capability of creating and carrying unique symmetry and topology. Most notably, the intrinsic capability of photonics of superposing non-Hermitian eigenstates through optical gain and loss provides a powerful toolbox for exploring the symmetry paradigms that were deemed challenging in condensed matter systems. Such investigations of symmetry and topology in photonics are revolutionizing the design principles in optical sciences. We have discovered new synthetic photonic materials, geometries, and field profiles that systematically enable the exploration of symmetry and topology in photonics. As such, the elusive symmetries can simplify the design of photonic meta-atoms and unit cells to reshape the density of states of photons in a topological and ultraflexible manner, which leads to on-demand meta-control of light emission, transmission, scattering and detection [1], thereby sustaining the ever-expanding information explosion for information processing, communication and computing.

For example, we have demonstrated one of the most striking benefits: the creation of eigenstate degeneracies such as exceptional points intrinsically associated with non-Hermitian Hamiltonians. This breaks the natural symmetry between reciprocal counterpropagating resonant modes in a micro-cavity to conduct unidirectional light-matter interaction carrying the large orbital angular momentum for structured light emission. Such a symmetry-driven approach allowed us to create the first microlaser source carrying the desired spin and orbital chirality as unique information carriers [2-4], giving rise to a new dimension of storing and processing information in photon's chiral degree of freedom. In addition to expanding the information dimensions to address the upcoming information explosion, flexible reconfiguration of topological pathways can offer a completely new paradigm for high-density photonics routing. However, the desired topological robustness unfortunately diminishes the hope of topological tunability. To overcome this fundamental limitation, we perform non-Hermitian symmetry to enable a new kind of topological states into the bulk of the topological insulator with a uniform topology, for the first time [5]. Without "battling" against topological protection, the new non-Hermitian topological states facilitate robust transmission links in the entire footprint to route optical signal to any desired output port. The ports-to-footprint ratio is at least 2 orders of magnitude higher than the state-of-the-art.

Hence, our research addresses grand challenges in fundamental quantum physics and also enables entirely new optical sciences and photonic technologies, which advances and benefits both fields simultaneously.

L. Feng, R. El-Ganainy, L. Ge, Non-Hermitian photonics based on parity-time symmetry. *Nat. Photon.* **11**, 752-762 (2017).

P. Miao *et al.* Orbital angular momentum microlaser. *Science* **353**, 464-467 (2016).

Z. Zhang *et al.* Tunable topological charge vortex microlaser. *Science* **368**, 760-763 (2020).

Z. Ji *et al.* Photocurrent detection of the orbital angular momentum of light. *Science* **368**, 763-767 (2020).

H. Zhao *et al.* Non-Hermitian topological light steering. *Science* **365**, 1163-1166 (2019).

**5:30 AM \*F.SF03.07.04**

**Active Topological Photonics on the Nanoscale** Gennady Shvets, Minwoo Jung and Ran Gladstein Gladstone; Cornell University, United States

Topological photonics enables unusual and robust properties of electromagnetic waves, including reflections-free photon propagation along strongly curved interfaces and localization at the corners and other discontinuities of photonic structures. One of the key remaining challenges include bringing topological photonics to the nanoscale and making it active/reconfigurable. In this talk, I will describe our group's progress on using two-dimensional materials such as electrostatically-gated graphene to accomplish these goals. The concept of a metagate – a structured metallic gate used to imprint topologically-complex chemical potential landscape onto graphene – will be introduced. Examples of lower- and higher-order topological structures that, respectively, confine graphene surface plasmon polaritons to edges and corners, will be presented, and the prospects for their experimental realization will be discussed. A novel regime of quantum landscaping, where periodic patterns of chemical potential simultaneously modify electronic and photonic propagation bands, will be introduced and exemplified using meta-gated graphene.



**5:00 AM \*F.SF03.08.01**

**Revealing the Energy Spectrum of Plasmonic Hot-Carriers via Single Molecule Transport Measurements** Vladimir Shalaev<sup>1</sup>, Harsha Reddy<sup>1</sup>, Kun Wang<sup>2</sup>, Zhaxylyk Kudyshev<sup>1</sup>, Linxiao Zhu<sup>2</sup>, Shen Yan<sup>2</sup>, Andrea Vezzoli<sup>3</sup>, Simon Higgins<sup>3</sup>, Vikram Gavini<sup>2</sup>, Alexandra Boltasseva<sup>1</sup>, Pramod Reddy<sup>2</sup> and Edgar Meyhofer<sup>2</sup>; <sup>1</sup>Purdue University, United States; <sup>2</sup>University of Michigan–Ann Arbor, United States; <sup>3</sup>University of Liverpool, United Kingdom

The generation of hot-carriers in plasmonic nanostructures, via plasmon decay, is of great current interest as hot-carriers play key roles in applications like photocatalysis, energy harvesting and in novel photodetection schemes that circumvent band-gap limitations. However, experimental quantification of steady-state energy distributions of hot-carriers in plasmonic nanostructures, which is critical for systematic progress, has not been possible. In this talk, we will describe our recent experimental advances that have enabled the direct measurement of hot-carrier energy distributions under steady-state conditions [1]. Specifically, we will explain how a scanning probe-based technique that records charge transport through single molecular junctions, when combined with nanoplasmonic experimental methods, can be leveraged to directly quantify hot-carrier energy distributions in a key model system—a thin gold film that supports propagating surface plasmon polaritons. Furthermore, key physical insights from our measurements on the role of Landau damping in producing hot-carriers and the contributions of different plasmonic modes towards hot-carrier generation will be discussed. Finally, we will outline how these experimental advances could potentially be leveraged to quantify hot-carrier distributions in plasmonic nanoparticles and other nanophotonic devices.

**References:**

[1] H. Reddy, K. Wang, Z. Kudyshev, L. Zhu, S. Yan, A. Vezzoli, S. J. Higgins, V. Gavini, A. Boltasseva, P. Reddy, V. M. Shalaev, and E. Meyhofer, “Determining plasmonic hot-carrier energy distributions via single molecule transport measurements,” *Science*, 10.1126/science.abb3457, 2020.

**5:15 AM \*F.SF03.08.02**

**Topological Anomalies Made Visible** Henning Schomerus; Lancaster University, United Kingdom

Topological photonics and mechanics aim to replicate fermionic symmetries as feats of precision engineering. Here I show how to enhance these systems via effects such as gain, loss and nonlinearities that do not have a direct electronic counterpart. This leads to a topological mechanism of mode selection [1,2,3], formation of compactons in flat band condensates [4] and sonic metamaterials [5], topological response of lasers [6] and robotic metamaterials [7], and practical applications such as for receiver protectors [8]. Common to them all are structured intensity distributions of the topological modes which are associated with topological anomalies and supersymmetry [9,10,11], normally abstract concepts that become directly visible in experiments.

- [1] Topologically protected midgap states in complex photonic lattices, H. Schomerus, *Opt. Lett.* 38, 1912 (2013).  
[2] Selective enhancement of topologically induced interface states in a dielectric resonator chain, C. Poli, M. Bellec, U. Kuhl, F. Mortessagne, H. Schomerus, *Nat. Commun.* 6, 6710 (2015).  
[3] Topological Hybrid Silicon Microlasers, H. Zhao et al., *Nat. Commun.* 9, 981 (2018).  
[4] Exciton-polaritons in a two-dimensional Lieb lattice with spin-orbit coupling, C. E. Whittaker et al., *Phys. Rev. Lett.* 120, 097401 (2018).  
[5] Sonic Landau Levels and Synthetic Gauge Fields in Mechanical Metamaterials, H. Abbaszadeh, A. Souslov, J. Paulose, H. Schomerus, and V. Vitelli, *Phys. Rev. Lett.* 119, 195502 (2017).  
[6] Topological dynamics and excitations in lasers and condensates with saturable gain or loss, S. Malzard, E. Cancellieri, and H. Schomerus, *Opt. Express* 26, 22506-22518 (2018).  
[7] Nonreciprocal response theory of non-Hermitian mechanical metamaterials: Response phase transition from the skin effect of zero modes, H. Schomerus, *Phys. Rev. Research* 2, 013058 (2020)  
[8] Self-Shielded Topological Receiver Protectors, M. Reisner et al., *Phys. Rev. Applied* 13, 034067 (2020).  
[9] Topological tight-binding models from nontrivial square roots, J. Arkininstall, M. H. Teimourpour, L. Feng, R. El-Ganainy, and H. Schomerus, *Phys. Rev. B* 95, 165109 (2017).  
[10] Supersymmetric Polarization Anomaly in Photonic Discrete-Time Quantum Walks, S. Barkhofen, L. Lorz, T. Nitsche,

C. Silberhorn, and H. Schomerus, Phys. Rev. Lett. **121**, 260501 (2018).

[11] Observation of supersymmetric pseudo-Landau levels in strained microwave graphene, M. Bellec, C. Poli, U. Kuhl, F. Mortessagne, and H. Schomerus, Light: Science and Applications (in press); arXiv:2001.10287.

### 5:30 AM F.SF03.08.03

**A Trajectory Model of Quantum Mechanical Tunneling for Comparisons to Electromagnetic Wave Propagation Through a Barrier** Kevin L. Jensen<sup>1</sup>, Nina Riga<sup>2</sup>, Donald Shiffler<sup>2</sup>, Rebecca Seviour<sup>3</sup> and Joel L. Lebowitz<sup>4</sup>; <sup>1</sup>Naval Research Laboratory, United States; <sup>2</sup>Air Force Research Laboratory, United States; <sup>3</sup>University of Huddersfield, United Kingdom; <sup>4</sup>Rutgers, The State University of New Jersey, United States

Quantum mechanical (QM) tunneling and transit time effects are increasingly important to attosecond and nanoscale physics for which quasi-classical trajectory interpretations are useful [1] to characterize electron emission. Modeling electron transport with particle-based methods may possibly benefit from using a Wigner distribution function (WDF), which is a quantum distribution with a trajectory interpretation that has analogs to a classical distribution of particles. The WDF is therefore potentially useful to describing tunneling and other purely quantum mechanical behaviors like resonant transmission [2, 3]. An exploration of the trajectory interpretation, however, is made difficult because there are few analytically solvable cases on which to test the methods, investigate the trajectory behavior, and relate to dielectric structure experiments examining the relationship between QM tunneling and electromagnetic wave propagation through a barrier that are progressing in tandem and described by N. M. Riga, et al. (this conference).

In this work, the WDF for an exactly solvable system for closed boundary conditions [4] gives both analytic trajectories and time-dependent behavior, and is described. Changes in the eigenstates associated with a step-potential lead to trajectories whose tunneling behavior is examined. Open boundary conditions are required to consider current flow and are required for the emission models, but require numerical approaches to the time evolution behavior for even simple barriers (in contrast to exact solutions to Schrodinger's Eq. [5]). Our methods and findings are presented and compared to alternate methods for thin barriers using analytic models [6].

1. M.F. Ciappina, J.A. Perez-Hernandez, A.S. Landsman, W.A. Okell, et al., Attosecond physics at the nanoscale, Rep. Prog. Phys. 80, 054401 (2017).

2. F. A. Buot, K.L. Jensen, Lattice Weyl-wigner Formulation of Exact Many-body Quantum-transport Theory and Applications to Novel Solid-state Quantum-based Devices, Phys. Rev. B 42, 9429 (1990).

3. S. Dries, B. Fons, M. Wim, Classical trajectories: A powerful tool for solving tunneling problems, Physica A: Statistical Mechanics and its Applications 391, 78 -81 (2012).

4. K.L. Jensen, D.A. Shiffler, N.M. Riga, et al., Analytic Wigner distribution function for a split potential well, J. Appl. Phys. 126, 144301 (2019); K.L. Jensen, D.A. Shiffler, J.L. Lebowitz, et al., Analytic Wigner distribution function for tunneling and trajectory models, J. Appl. Phys. 125, 114303 (2019).

5. O. Costin, R. Costin, I. Jauslin, J.L. Lebowitz, Solution of the time dependent Schrodinger equation leading to Fowler-Nordheim field emission, J. Appl. Phys. 124, (2018).

6. K. L. Jensen, A. Shabaev, S. G. Lambrakos, et al., Analytic Model of Electron Transport Through and Over Non-Linear Barriers, (accepted for publication, J. Appl. Phys, 2020).

### 5:40 AM F.SF03.08.04

**Local Valley-Hall Effect for Photons** Dia'aaldin Bisharat and Dan Sevenpiper; University of California, San Diego, United States

In recent years, there has been extensive research on photonic topological insulators (PTIs), motivated by the prospect of backscattering-immune wave propagation. One way to realize PTIs is by altering the crystalline symmetry of the lattice to emulate the quantum valley-Hall effect. This relies on the valley degree of freedom (DOF) that is readily available in photonic crystals (PhCs) with C<sub>6v</sub> symmetry. Typically, however, the lattice is reduced to C<sub>3v</sub> symmetry, causing a transition of the system to the valley topological phase (characterized by half-integer Chern numbers of opposite signs associated with the positive and negative halves of the Brillouin zone, respectively). This enables the occurrence of valley-polarized modes exhibiting backscattering-immune wave propagation in the absence of inter-valley scattering disorder. Here, we propose a local-valley approach that maintains C<sub>6v</sub> symmetry yet supports robust valley-polarized modes.

To differentiate our approach from the typical valley-based approach, consider the example of a hexagonal lattice of dielectric rods. In the typical approach, the rods are usually deformed into triangular shape and the edge modes are observed at the interface between two PhCs, where the triangles in one PhC are facing the opposite way with respect to those in the other PhC. In comparison, in the proposed approach, the rods have cylindrical shape and the edge modes are observed along one row of rods that are misaligned with respect to the original lattice like in common line defect waveguides. Note that the preserved rotational symmetry of the unit cell means that the edge states in the later approach must reside in an intrinsic

bandgap of the PhC that is different than that associated with  $C_{3v}$  symmetry. In both approaches, the edge modes are the results of linking opposite orbital angular momentum vortices across the waveguide region. In addition, the proposed edge modes exhibit the expected unidirectional wave excitation and robust wave transmission through sharp zigzag-shaped bends. Moreover, we show that our proof-of-concept platform is in fact an analogue of bilayer graphene system with AB/BA stacking regions. Hence, we reveal that the sole criterion for supporting valley-polarized states is breaking the mirror inversion symmetry locally, i.e. only near the waveguide region. Attractively, the proposed approach leads to simple implementation, benefiting practical applications and easier fabrication at optical frequencies compared to existing valley-type PTIs.

SESSION F.SF03.09: Novel Approaches for Photonic Design  
On Demand Abstracts Available for Viewing Starting Saturday Morning, November 21, 2020  
F-SF03

**5:00 AM \*F.SF03.09.01**

**Twisted Polaritonics** [Andrea Alù](#); City University of New York, United States

In this talk, we discuss our recent progress in the area of twistronics with light based on twisted metasurfaces or twisted van-der-Waals bilayers, which support topological transitions at photonic magic angles. The unusual interplay between coupled hyperbolic polaritons and the rotation angle between them enables unusual transitions from hyperbolic to elliptical propagation, which can be predicted by counting the number of intersections between the polariton bands of the two individual surfaces when isolated. During the talk, we discuss the unusual phenomena supported by these structures, and their opportunities for nano-imaging and information transport.

**5:15 AM \*F.SF03.09.02**

**Photonics Inverse Design** [Jelena Vuckovic](#); Stanford University, United States

Combining state of the art optimization and machine learning techniques with high speed electromagnetic solvers offers a new approach to "inverse" design and implement classical and quantum photonic circuits with superior properties, including robustness to errors in fabrication and environment, compact footprints, novel functionalities, and high efficiencies. We illustrate this with a number of demonstrated devices in silicon, diamond, and silicon carbide, including wavelength and polarization splitters and converters, power splitters, couplers, nonreciprocal switches and routers, on chip laser driven particle accelerators, and efficient quantum emitter-photon interfaces.

**5:30 AM F.SF03.09.03**

**Probabilistic Representation and Inverse Design of Metasurfaces Based on a Deep Generative Model** [Yihao Xu](#), Wei Ma and Yongmin Liu; Northeastern University, United States

Over the past decades, the study of metamaterials and metasurfaces has brought enormous success in modern photonics. With rationally designed sub-wavelength units, known as meta-atoms, one can manipulate light in a desired and prescribed manner. Although modern numerical methods can accurately simulate the optical responses of complex structures, the full-wave simulation methods such as FEM and FDTD still require a lot of time and computational resources, especially when parameter sweeping in a huge design space is required to inversely retrieve the optimal structure according to certain optical responses. In the traditional research approach, researchers need to adjust the geometric/material parameters through experience repeatedly until the simulated optical responses meet the requirements to the maximum. This process still takes enormous time even for experienced researchers when the design problem is challenging.

Very recently, data-driven approaches, such as deep learning, have been applied to design various photonic structures, including metamaterials, metasurfaces, photonic crystals and plasmonic nanostructures<sup>1-4</sup>. To better reveal the implicit structure-property relationship and thus facilitate metasurface designs, we proposed to represent metasurfaces and model the inverse design problem in a probabilistically generative manner with the help of variational autoencoders (VAE), which not only enable to efficiently and elegantly investigate the complex structure-optical response relationship in an interpretable way, but solve the one-to-many mapping issue that is tough in a deterministic model<sup>2</sup>. Moreover, to avoid vast full-wave simulation when collecting data, a semi-supervised learning strategy is developed that allows the model to utilize unlabeled

data in addition to labeled data in an end-to-end training network<sup>5</sup>. We demonstrate that the self-supervised deep learning model can effectively utilize randomly generated unlabeled data during training, with the total test loss and prediction accuracy improved by about 15% compared with the fully supervised counterpart. On a data-driven basis, the proposed deep generative model can serve as a comprehensive and efficient tool that prompts the design, characterization, and even novel discovery in the research domain of metasurface, and photonics in general.

#### References

- 1 Ma, W., Cheng, F. & Liu, Y. Deep-Learning-Enabled On-Demand Design of Chiral Metamaterials. *ACS Nano* **12**, 6326-6334, doi:10.1021/acsnano.8b03569 (2018).
- 2 Ma, W., Cheng, F., Xu, Y., Wen, Q. & Liu, Y. Probabilistic Representation and Inverse Design of Metamaterials Based on a Deep Generative Model with Semi-Supervised Learning Strategy. *Adv. Mater.* **31**, e1901111, doi:10.1002/adma.201901111 (2019).
- 3 Liu, Z., Zhu, D., Rodrigues, S. P., Lee, K. T. & Cai, W. Generative Model for the Inverse Design of Metasurfaces. *Nano Lett.* **18**, 6570-6576, doi:10.1021/acs.nanolett.8b03171 (2018).
- 4 Asano, T. & Noda, S. Optimization of photonic crystal nanocavities based on deep learning. *Opt. Express* **26**, 32704-32717, doi:10.1364/OE.26.032704 (2018).
- 5 Wei, M. & Yongmin, L. A data-efficient self-supervised deep learning model for design and characterization of nanophotonic structures. *SCIENCE CHINA Physics, Mechanics & Astronomy*.

#### 5:40 AM F.SF03.09.04

**Active Learning with Multi-Objective Optimization for 3D-Printed Acoustic Metamaterials Combining Simulations and Experiments** [Karsten Bruening](#)<sup>1</sup>, Wan Shou<sup>2</sup>, Mina Konaković Luković<sup>2</sup>, Beichen Li<sup>2</sup>, Kui Wu<sup>2</sup>, Xianchen Xu<sup>3</sup>, Jun Amano<sup>1</sup> and Wojciech Matusik<sup>2,2</sup>; <sup>1</sup>Konica Minolta Laboratory USA, United States; <sup>2</sup>Massachusetts Institute of Technology, United States; <sup>3</sup>University of Missouri–Kansas City, United States

3D-printing and additive manufacturing enable much larger design spaces than conventional manufacturing methods (e.g. subtractive manufacturing, injection molding). This applies to the geometry as well as to the materials, with some 3D-printers offering multi-material printing with continuous variation in composition. Without the bounds from “design for manufacturing”, more complex designs become possible and are not penalized by manufacturability. In fact, complex designs are often favored over geometrically simple designs (e.g. structured infill vs. solid infill). This freedom of design leads to a vast design space which can be hard to navigate. Even simple objects with 5 to 10 design parameters, resulting in a design space of an equally large number of dimensions, require sophisticated methods to fully take advantage of the design freedom and find the design with optimum performance. Typically, the optimal design is found by searching the design space using simulation and the optimal simulated outcome is manufactured.

In this work, we add an additional layer of optimization. We use simulation to narrow down the design candidates to a set which is Pareto-optimal. Then, we take these designs as seeds for experimental optimization. The simulation as well as the experimental optimization use active learning based on multi-objective Gaussian processes Bayesian optimization. For the experimental optimization, we perform active learning in batches, filling the print volume with a set of Pareto-optimal candidate designs, which maximize the acquisition function, enabling efficient experimental iteration over candidate designs. This approach of combining simulation and experiments is particularly useful because often simulations do not accurately represent the real-life object performance, e.g. due to simplifying assumptions, difficult to characterize material parameters etc.

In this paper, we use the outlined approach to optimize the sound transmission loss (STL) spectrum of an acoustic metamaterial. The objectives are to maximize STL at certain frequencies, while keeping the material thickness in the deep subwavelength regime (e.g. 20 mm thickness, vs. 343 mm wavelength for  $f = 1000$  Hz). We achieve the optimal design by starting with a conceptual idea, e.g. a combination of membranes with Helmholtz resonators, or using an array of multi-membrane cells producing phase shifts that lead to a desirable interference in the outgoing wave field. This conceptual idea has 5 to 10 design variables (e.g. membrane size, resonator size). These design variables are then optimized using active learning with multi-objective Gaussian processes Bayesian optimization. Our framework incorporates NSGA-II (Non-dominated Sorting Genetic Algorithm II) optimization implemented in Matlab and Python. The workflow seamlessly integrates with COMSOL simulation and creates STL files for printing. Experimental measurements are performed on an impedance tube, which is a fairly quick and simple measurement (~ 3 min per sample), such that a large number of samples can be measured.

Ultimately, we optimized acoustic metamaterials for various applications. We obtained and experimentally validated superior properties compared to state-of-the-art acoustic insulators. This optimization framework combining simulations and experiments can be adapted to various design problems in materials science.

**5:00 AM \*F.SF03.10.01**

**Engineering Light-Matter Interactions in Semiconductor Nanowire Photodetectors and in Optical Nanotweezers** Kenneth Crozier; The University of Melbourne, Australia

We present recent studies in which engineering the interaction between light and nanoscale materials has been pursued for applications in photodetectors and in optical tweezers.

We review our recent work that demonstrates that the absorption spectrum of a photodetector can be controlled via waveguide resonances in semiconductor nanowires [1-6]. We discuss the physical interpretation for this phenomenon [1]. We review work in which p-i-n photodiodes were incorporated into vertically oriented silicon nanowires, and then used for colour imaging [2-5]. We also review recent work on extending this concept to the short-wave infrared via Ge nanowires [6]. We describe recent work in which we demonstrated chip-scale microspectrometers based on arrays of nanowire photodetector pixels [7] and an interleaved design with a "fishnet" pattern [8].

We also describe our work on optical trapping with plasmonic nanoapertures [9] and with all-dielectric (silicon) nanoantennas [10,11]. Fluorescence microscopy is used to track the position of, and emission from, individual trapped nanoparticles. The nanoparticles consist of fluorescent polystyrene nanospheres with diameters of 20 nm and 100 nm and streptavidin-coated CdSe/ZnS quantum dots. We observe the Brownian motion of the trapped nanoparticles using fluorescence imaging. Other experiments reported include the two-photon excitation of fluorescence from trapped nanoparticles, and the trapping of multiple nanoparticles simultaneously. We also discuss our recent work on an algorithmic approach to the design of plasmonic nanoapertures for optical tweezers [12].

References

1. K. Seo, M. Wober, P. Steinvurzel, E. Schonbrun, Y. Dan, T. Ellenbogen, K.B. Crozier, *Nano Letters* **11**, 1851 (2011)
2. H. Park, Y. Dan, K. Seo, Y.J. Yu, P.K. Duane, M. Wober, K.B. Crozier, *Nano Letters* **14**, 1804 (2014)
3. H. Park, K. Seo, K.B. Crozier, *Applied Physics Letters* **101**, 193107 (2012)
4. H. Park and K.B. Crozier, *Sci. Rep.* **3**, 2460 (2013)
5. H. Park and K. B. Crozier, *ACS Photonics* **2**, 544 (2015)
6. A. Solanki, S. Li, H. Park, and K.B. Crozier, *ACS Photonics* **5**, 520 (2018)
7. J. Meng, J.J. Cadusch, and K.B. Crozier, *Nano Letters* **20**, 320 (2020)
8. J.J. Cadusch, J. Meng, B. Craig, and K.B. Crozier, *Optica* **6**, 1171 (2019)
9. Z. Xu, W. Song, K. B. Crozier, *ACS Photonics* **5**, 2850 (2018)
10. Z. Xu, W. Song, K. B. Crozier, *ACS Photonics* **5**, 4993 (2018)
11. Z. Xu, K. B. Crozier, *Opt. Express* **27**, 4034 (2019)
12. N. Li, J. Cadusch, and K. Crozier, *Optics Letters* **44**, 5250-5253 (2019)

**5:15 AM F.SF03.10.03**

**Experimental Investigation on an Interfacial Structure for Solar-Driven Water Desalination** Xiaojie Liu, Yanpei Tian, Fangqi Chen and Yi Zheng; Northeastern University, United States

Solar-driven interfacial steam generation for desalination has attracted broad attention. However, a significant challenge still exists for achieving a fast evaporation rate and high quality of water together with the low-cost and simple-to-manufacture device to provide a feasible solar-driven steam generation system. In this study, a novel "blackest" paint Black 3.0 serving as a perfect solar absorber is introduced into the hot-pressed melamine foam networks, constructing the blackest (99% absorptance in the solar region) and self-floating evaporation device. The features of effective solar absorptance and salt-rejection capability contribute to a high evaporation rate at  $2.48 \text{ kg m}^{-2} \text{ h}^{-1}$  under one sun ( $1 \text{ kW m}^{-2}$ ). This feature shines remarkable lights on a facilely fabricated, robust, high-efficient, and cost-effective solar steam generation system.

**5:25 AM F.SF03.10.04**

**Assembling and Orienting Gold Nano-Triangles and Nano-Octahedra at the Vapor/Aqueous Interface and in the Bulk Solution** Hyeong Jin Kim<sup>1</sup>, Md Mir Hossen<sup>1</sup>, Andrew C. Hillier<sup>1</sup>, David Vaknin<sup>1</sup>, Wenjie Wang<sup>2</sup> and Surya K. Mallapragada<sup>1</sup>; <sup>1</sup>Iowa State University, United States; <sup>2</sup>Ames Laboratory, United States

Here, we report on anisotropic nanostructure assemblies at the vapor/aqueous interface and in the bulk solution. Gold nano-triangles and octahedra were synthesized and functionalized with poly(ethylene) glycol (both polymer-grafted nanostructures are referred to as PEG-AuNSts). Synchrotron-based grazing incidence small angle X-ray scattering and liquid surface X-ray reflectivity showed that PEG-AuNSts were populated at the vapor/aqueous interface with preferred orientation at the surface by introducing salts or polyelectrolytes which can induce interpolymer complexation between grafted-polymer and polyelectrolytes at low pH level. The resulting assemblies of PEG-AuNSts were further investigated by regulating the concentration of electrolytes and solution pH. Similar strategies were also used to create the three-dimensional assemblies of PEG-AuNSts in the bulk solution. Solution small angle X-ray scattering revealed that controlled assemblies could be achieved by the interplay of temperature, salt concentration, and interpolymer complexation.

SESSION F.SF03.11: Applications of Metamaterials  
On Demand Abstracts Available for Viewing Starting Saturday Morning, November 21, 2020  
F-SF03

**5:00 AM \*F.SF03.11.01**

**Metadevices Based on Integration of Microsystems and Metamaterials** Xin Zhang; Boston University, United States

Metamaterials, a major type of artificially engineered materials, exhibits unprecedented and controllable effective properties, including electric permittivity and magnetic permeability, and have boosted the development of optical and photonic devices. Metamaterials are composed of arrays of subwavelength unit cells. The effective properties of metamaterials are mainly determined by the structural design of the constituting subwavelength unit cells rather than their chemical composition. The design-driven properties enable versatile designs of their electromagnetic properties. Recent research has shifted to construct reconfigurable, tunable, and nonlinear metamaterials towards the development of metamaterial devices via integrating actuation mechanisms and quantum materials with meta-atoms. Microelectromechanical systems (MEMS) provide a powerful platform for manipulating the effective properties of metamaterials and the integration of multiple functions with metamaterials. In this talk, I will introduce the fundamentals of metamaterials, approaches to integrate MEMS with metamaterials, functional metamaterial devices from the synergy, and outlooks for metamaterial-enabled devices. Specifically, I will talk about terahertz devices based on the tunable metamaterials for dynamic control of the magnitude, phase, wave front, and polarization by MEMS-driven metamaterial unit cells. Terahertz detectors based on nonlinear terahertz metamaterials will be introduced. In addition, I will discuss the recent advances in the metamaterials for magnetic resonance imaging (MRI) based on the controllable nonlinearity in metamaterials. The implementation of intelligent metamaterials to boost the signal to noise ratio of clinical MRI, which will be translated to improvement in image quality and efficiency. The implementation of nonreciprocal devices based on nonlinearity will also be presented. Besides electromagnetic metamaterials, I will also present the construction of acoustic metamaterials for sound wave manipulation. The acoustic lens to focus sound waves based on the horn-like space coiling structures will be discussed. The ultra-open metamaterial for noise mitigation will also be presented. The future of metamaterials will be outlooked. Based on the MEMS and advanced manufacture technology, multifunctional metamaterial in electromagnetic and acoustic domains will be developed to yield functional devices to achieve functions that are not achievable by nature materials.

**5:15 AM \*F.SF03.11.02**

**Tunable Chiral Optical Properties in Semiconductor Nanocrystals and Metamaterials** Vivian Ferry; University of Minnesota Twin Cities, United States

Optical nanomaterials offer the ability to bend, twist, guide, and confine light in nanoscale dimensions. Among these materials, chiral nanostructures particularly show promise for applications ranging from polarization manipulation to 3D displays, sensing, and spin-selective transport. Compared to their molecular counterparts, chiral nanomaterials exhibit orders of magnitude stronger dissymmetry factors, but have only been realized in a limited set of materials systems. We have recently demonstrated different strategies to tune and manipulate the polarization response of chiral metamaterials that combine metallic nanostructures, dielectric materials, and semiconductor nanocrystals. By controlling the refractive index of

the dielectric components in different architectures, we show that the sign of the circular dichroism can be reversed, and the polarization and directionality of the outcoupled luminescence from nearby nanocrystals can be controlled. To create light-emitting metamaterials, it is additionally useful to create nanostructured elements comprised entirely of photoluminescent materials. We have recently developed patterning methods to transform semiconductor nanocrystals into patterned nanocrystal solids, realizing lateral feature sizes as small as 30 nm and heights in excess of 100 nm without degradation of the photoluminescence. We show that by designing the shape of the nanocrystal solid at this length scale and controlling connectivity between the nanocrystals, the refractive index and nanostructure absorptivity can be tailored. This work points to new strategies to design dynamically tunable metamaterials and control nanoscale light-matter interactions.

#### 5:30 AM F.SF03.11.03

**Aluminized Polymethylpentene Thin Film for High-Effective Radiative Cooling** Yanpei Tian, Xiaojie Liu and Yi Zheng; Northeastern University, United States

The radiative cooling phenomenon relies on the atmospheric transparency window to dissipate heat from the earth into outer space, which is an energy-saving cooling technique. This work demonstrates a highly effective aluminized Polymethylpentene (PMP) thin-film thermal structure. The emissivity of aluminized PMP thin films matches perfectly to the atmospheric transparency window so as to minimize parasitic heat losses. This photon-to-cooling structure yields a highest-to-date temperature drop of 8.5 K in comparison to the ambient temperature and a corresponding radiative cooling power of 193 W/m<sup>2</sup> during a one-day cycle. The easy-to-manufacture feature of an aluminized PMP thin film makes it a practically scalable radiative cooling method.

#### 5:40 AM F.SF03.11.04

**Radiative Cooling in the Earth's Glow Using Commonplace Materials** Jyotirmoy Mandal<sup>1</sup>, Sagar Mandal<sup>2</sup>, John Brewer<sup>1</sup>, Arvind Ramachandran<sup>3</sup> and Aaswath P. Raman<sup>1</sup>; <sup>1</sup>University of California, Los Angeles, United States; <sup>2</sup>Independent Researcher, United States; <sup>3</sup>Arizona State University, United States

Passive daytime radiative cooling involves solar reflection and thermal emission into the cold outer space through the atmospheric transmission windows. Due to its passive nature and net cooling effect, it is a promising alternative or complement to electrical cooling.<sup>1-2</sup> For efficient radiative cooling of objects, an unimpeded view of the sky is ideal. However, the view of the sky is often limited - for instance, the walls of buildings have > 50% of their field of view subtended by the earth. Moreover, objects on earth become sources of heat under sunlight. Therefore, vertical building facades with hot terrestrial objects in view experience reduced cooling or heating, even with materials optimized for heat loss into the sky.<sup>2-3</sup>

We show that by using materials with selective long-wavelength infrared (LWIR) emittances, walls and roofs can radiatively cool to considerably lower temperatures than achievable by using broadband thermal emitters like paints and recent designs.<sup>2</sup> Promisingly, selective LWIR emitters can be scalably manufactured from common polymers, ceramics and composites, with some being sufficiently ubiquitous to be sourced from waste. The materials are suitable for use on both opaque and transparent building envelopes, making them applicable on both walls and windows. Cooling enhancements (theoretical and demonstrated) achieved by such commonplace materials offer a remarkable opportunity for untapped energy savings in buildings.

[1] A. Raman et. al., Nature 515, 541 (2014)

[2] J. Mandal et. al., Science 362, 315 (2018)

[3] Y. Zhai et. al. Science 355, 1062–1066 (2017)

*Acknowledgments: Jyotirmoy Mandal was supported by Schmidt Science Fellows, in partnership with the Rhodes Trust.*

SESSION F.SF03.12: Poster Session: New Frontiers in the Design, Fabrication and Application of Metamaterials  
On Demand Abstracts Available for Viewing Starting Saturday Morning, November 21, 2020

5:00 AM - 8:00 AM

F-SF03

#### F.SF03.12.01

**Thermal Behaviors of Hydrocarbon-Coated Aluminum Nanoparticles as Energetic Metamaterials in Combustion Applications—A ReaxFF Molecular Dynamics Study** Sungwook Hong, Roxanne Esparza and Ryan Parlier; California State University, Bakersfield, United States

Aluminum nanoparticles (ANPs) have been considered attractive additives for combustible applications because the ANPs possess a high energy density with an increased burning rate, owing to an increased surface area-to-volume ratio.<sup>1</sup> Unfortunately, use of the ANPs is limited by two factors: (1) ANPs can be readily sintered; and (2) ANPs can be easily oxidized, prior to the combustion process due to their high reactivity, degrading the combustion performance. To resolve this issue, synthesis of metamaterials, using ANPs and hydrocarbon has been suggested. For example, ANPs could be effectively coated by hydrocarbon precursors to improve its combustion performance.<sup>2,3</sup> The previous studies reported that the hydrocarbon-coated ANPs are less reactive at low temperatures and they became susceptible to the oxidation at higher temperatures, suggesting that the hydrocarbon coating is essential for the ANPs to be used as combustible materials.<sup>4,5</sup> However, a molecular-level understanding of thermal behaviors of the hydrocarbon-coated ANPs has yet to be achieved. Here we perform reactive molecular dynamics (RMD) simulations based on ReaxFF<sup>6</sup> to investigate effects of hydrocarbon coating on the combustion process of the ANPs including sintering and oxidation processes. Our RMD simulations reveal molecular-level reaction steps for the combustion process of the bare/hydrocarbon coated ANPs. As such, our RMD simulations will help guide an experimental design of a novel energetic metamaterial using ANPs and hydrocarbon, providing a valuable input for the community of solid-fuel propellants.

S.H. and R.P. acknowledge a start-up funding from School of Natural Science, Mathematics and Engineering at California State University, Bakersfield (CSUB). A.M. acknowledges a funding support from Student Research Scholar (SRS) program at CSUB.

## References

- [1] Yetter, R. A.; Risha, G. A.; Son, S. F. Metal Particle Combustion and Nanotechnology. *Proc. Combust. Inst.* **2009**, 32, 1819–1838
- [2] Park, K.; Rai, A.; Zachariah, M. Characterizing the Coating and Size-Resolved Oxidative Stability of Carbon-Coated Aluminum Nanoparticles by Single-Particle Mass-Spectrometry. *J. Nanopart. Res.* **2006**, 8, 455–464.
- [3] Guo, L.; Song, W.; Hu, M.; Xie, C.; Chen, X. Preparation and Reactivity of Aluminum Nanopowders Coated by Hydroxyl-Terminated Polybutadiene (Htpb). *Appl. Surf. Sci.* **2008**, 254, 2413–2417.
- [4] Park, K.; Rai, A.; Zachariah, M. Characterizing the Coating and Size-Resolved Oxidative Stability of Carbon-Coated Aluminum Nanoparticles by Single-Particle Mass-Spectrometry. *J. Nanopart. Res.* **2006**, 8, 455–464.
- [5] Hong, S. and van Duin A. Atomistic-Scale Analysis of Carbon Coating and Its Effect on the Oxidation of Aluminum Nanoparticles by ReaxFF-Molecular Dynamics Simulations. *J. Phys. Chem. C.* **2016**, 120, 9464–9474
- [6] Senftle, T. P.; Hong, S.; Islam, M. M.; Kylasa, S. B.; Zheng, Y.; Shin, Y. K.; Junkermeier, C.; Engel-Herbert, R.; Janik, M. J.; Aktulga, H. M. The ReaxFF Reactive Force-Field: Development, Applications and Future Directions. *npj Comput. Mater.* **2016**, 2, 15011.

## F.SF03.12.02

**Computational Design of Energetic Metamaterials Using Graphene-Supported Aluminum Nanoparticles—A ReaxFF Molecular Dynamics Study** Ryan Parlier, Andrew Martinez and Sungwook Hong; California State University, Bakersfield, United States

Aluminum nanoparticles (ANPs) have attracted a great amount of interest owing to their high energy density, high reaction rate, earth abundance, and low toxicity.<sup>1</sup> ANPs have been considered effective energetic materials. Unfortunately, ANPs are easily oxidized at room temperature, leading to oxide layers on their surfaces. Those oxide layers work as a dead weight. Therefore, it is vitally important to design a novel metamaterial that improves the combustion performance of ANPs. Recent studies show that adding graphene oxide and graphene fluoride improves the combustion performance of ANPs.<sup>2,3</sup> This is mainly due to a synergistic effect between graphene sheets and ANPs. For example, oxygen molecules could be easily dissociated when they get closer to both graphene sheets and ANPs. As such, we hypothesize that graphene-supported ANPs, which could be considered novel energetic metamaterials, provide a remarkable combustion performance. Here we simulate the oxidation of graphene-supported ANPs using reactive molecular dynamics (RMD) simulations based on ReaxFF.<sup>4</sup> Our RMD simulations reveal atomic-level reaction mechanism for the improved oxidation process of graphene-supported ANPs. As such, the RMD results will help guide an experimental design of a novel energetic metamaterial using graphene sheets and ANPs, providing a valuable input for the community of energetic metamaterials.



S.H. and R.P. acknowledge a start-up funding from School of Natural Science, Mathematics and Engineering at California State University, Bakersfield (CSUB). A.M. acknowledges a funding support from Student Research Scholar (SRS) program at CSUB.

### References

- [1] Yetter, R. A.; Risha, G. A.; Son, S. F. Metal Particle Combustion and Nanotechnology. *Proc. Combust. Inst.* **2009**, 32, 1819–1838
- [2] Jiang, Y.; Deng, S.; Hong, S.; Zhao, J.; Huang, S.; Wu, C.-C.; Gottfried, J. L.; Nomura, K.-i.; Li, Y.; Tiwari, S.; Kalia, R. K.; Vashishta, P.; Nakano, A.; Zheng, X. Energetic Performance of Optically Activated Aluminum/Graphene Oxide Composites. *ACS Nano* **2018**, 12, 11366–11375.
- [3] Jiang Y.; Deng, S.; Hong, S.; Tiwari, S.; Chen, H.; Nomura, K.; Kalia, R. K.; Nakano, A.; Vashishta, P.; Zachariah, M.; Zheng, X. Synergistically Chemical and Thermal Coupling between Graphene Oxide and Graphene Fluoride for Enhancing Aluminum Combustion. *ACS Appl. Mater. Interfaces* **2020**, 12, 7451–7458
- [4] Senftle, T. P.; Hong, S.; Islam, M. M.; Kylasa, S. B.; Zheng, Y.; Shin, Y. K.; Junkermeier, C.; Engel-Herbert, R.; Janik, M. J.; Aktulga, H. M. The ReaxFF Reactive Force-Field: Development, Applications and Future Directions. *npj Comput. Mater.* 2016, 2, 15011.

### F.SF03.12.03

**Spin-Valley Locked Edge States in Staggered Chiral Photonic Crystal** Yeseul Kim, Minkyung Kim and Junsuk Rho; Pohang University of Science and Technology, Korea (the Republic of)

Topological phases of matters, firstly investigated in condensed matter physics, have been extended to other wave physics such as photonics. In this poster presentation, we present spin-valley locking of edge states in a chiral photonic crystal in the two-dimensional honeycomb lattice. Using a coupled dipole method, we demonstrate bulk band structure with a band gap, which is spanned by the spin-valley locked edge states. The staggered chirality breaks the inversion symmetry and the chirality provides the spin-valley locking characteristics.

### F.SF03.12.06

**Late News: Computational Synthesis of Novel Energetic Metamaterials Using Metal Nanoparticles and Hydrocarbon Precursors for Combustion Applications** Roxanne Esparza and Sungwook Hong; California State University, Bakersfield, United States

The use of aluminum nanoparticles (ANPs) in combustion applications has attracted a great amount of attention owing to their high energy density with an increased burning rate.<sup>1</sup> Unfortunately, due to the nature of ANPs' high reactivity, the ANPs are easily sintered, leading to an increase in their particle size, and thus lowering the combustion efficiency. In order to tackle this issue, recent efforts have been made to synthesize novel metamaterials, using ANPs and hydrocarbon precursors. For example, ANPs could be effectively coated by hydrocarbon precursors to lower their reactivity, thus preventing sintering effects of ANPs. However, an effect of precursor types of hydrocarbon on sintering behaviors of ANPs has yet to be understood at the atomic level. Here we perform reactive molecular dynamics (RMD) simulations based on ReaxFF<sup>2</sup> to investigate computational synthesis of energetic metamaterials using ANPs and carbon precursors. In particular, we employed different types of carbon precursors to evaluate the sintering behaviors of ANPs. Our RMD simulations suggest detailed reaction steps for the sintering process of the bare/hydrocarbon coated ANPs. As such, our RMD simulations will help provide a valuable input for experimental synthesis of a novel metamaterial using ANPs and hydrocarbon for combustion application.

S.H. and R.E. acknowledge a start-up funding from School of Natural Science, Mathematics and Engineering at California State University, Bakersfield (CSUB).

### References

- [1] Yetter, R. A.; Risha, G. A.; Son, S. F. Metal Particle Combustion and Nanotechnology. *Proc. Combust. Inst.* 2009, 32, 1819–1838
- [2] Senftle, T. P.; Hong, S.; Islam, M. M.; Kylasa, S. B.; Zheng, Y.; Shin, Y. K.; Junkermeier, C.; Engel-Herbert, R.; Janik, M. J.; Aktulga, H. M. The ReaxFF Reactive Force-Field: Development, Applications and Future Directions. *npj Comput. Mater.* 2016, 2, 15011.

### F.SF03.12.07

**Late News: Humidity-Dependent Flaw Sensitivity in the Crack Propagation Resistance of 3D-Printed Nano-Ceramics** Edoardo M. Rossi<sup>1</sup>, Jens Bauer<sup>2</sup> and Marco Sebastiani<sup>1</sup>; <sup>1</sup>Università degli Studi Roma Tre, Italy; <sup>2</sup>University of California, United States

Pyrolytic 3D-printed carbon nano-ceramics currently emerge as a class of lightweight materials with exceptional mechanical strength and stiffness, being characterized by feature-sizes well below the capabilities of the highest-resolution 3D additive manufacturing techniques alone. Despite the increasing applications, their use is hampered by the lack of knowledge on their mechanical reliability. Few studies have investigated their intrinsic mechanical properties: important characteristics, like hardness and fracture toughness, and their dependency on environmental conditions, which can be relevant for a thorough understanding of the complex mechanical behaviour of additively manufactured pyrolytic carbon structures, are unknown. In this work, we present nanoindentation splitting of TPP-DLW-derived pyrolytic carbon micro-pillar specimens, characterized by a diameter of 5.3  $\mu\text{m}$  and a height-to-diameter ratio of two, as a straight-forward method to measure the fracture toughness and nanoindentation continuous stiffness measurements for the assessment of the elastic modulus and hardness. Micro-pillars with and without SEM detectable surface flaws, absent of STEM-detectable internal defects, were tested at two extremal intervals of the environmental relative humidity, humid air was used to adjust RH at values greater than 60% and dry nitrogen at room pressure ensured RH levels below 5%, to investigate the impact of pyrolysis-induced surface flaws and the interplayed effects with the testing environment on the mechanical reliability of the 3D printed nanoceramics. We show that TPP-derived pyrolytic carbon can achieve 500% increased fracture toughness over macroscopic forms of vitreous carbon, which typically lies in the range of 0.5-1.4 MPam<sup>0.5</sup>, with values up to 3.1 MPam<sup>0.5</sup>. However, experiments at RH > 60% revealed a detrimental effect of high relative humidity environments on the fracture toughness of the pyrolytic carbon nano-ceramic structures, causing embrittlement due to liquid diffusion ascribed to the presence of only a few, nanometer-sized, which probably promotes crack propagation under external loading due to chemically induced structural weakening of the glassy carbon structure. While comparable effects are less relevant in macro-size ceramics, this study demonstrates that reliability and durability of micro- and nano-architected ceramic metamaterials and devices require toughening design approaches which focus on size-dependent surface effects. The observed humidity effect can have a remarkable impact on the scale-up of such nano-architected metamaterial in a wide range of applications, especially biomedical and micro-fluidics fields.

### F.SF03.12.08

**Late News: Infrared Reflecting/Transmitting Smart Glass For Energy Efficient Windows** Mark Altwerger, Yashashvini Andugula, Harry Efstathiadis and Iulian Gherasoiu; SUNY Polytechnic Institute CNSE, United States

Low-e glass panes are not well adapted for use in regions where the predominant heat that passes through windows has its origin indirect solar radiation. Almost 49% of solar energy is distributed in the spectrum from 0.7-2.5 $\mu\text{m}$  for which low-e glass-pane reflectivity is below 10%. This is the case with 14% of the contiguous U.S. according to NREL. The metamaterial that we propose is a robust, thin-film structure that has the ability to reflect near-infrared heat radiation (NIR) with  $\lambda$  0.7-10 $\mu\text{m}$  while transmitting more than 90% of the visible light intensity. The ability to reflect NIR and transmit selected wavelength range is obtained through the field-enhanced electron concentration of moderately doped metal oxide thin films. Approximately 48% of the total energy produced in the U.S. or 18.6 billion kWh is spent on heating and cooling. Therefore, the ability to retrofit this technology onto existing buildings is of considerable interest. Electrical and optical characterization demonstrate the synthesis of state-of-the-art materials with properties suitable for the fabrication of smart glass devices.

## SYMPOSIUM F.SF04

---

Solution-Processed Semiconductors and Devices for Form-free Displays, Logic and Sensors  
November 21 - December 4, 2020

### Symposium Organizers

Thomas Anthopoulos, King Abdullah University of Science and Technology  
Chuan Liu, Sun Yat-sen University

\* Invited Paper

SESSION F.SF04.08: Live Keynote I: Solution-Processed Semiconductors and Devices for Form-free Displays, Logic and Sensors

Session Chairs: Chuan Liu and Yong-Young Noh  
Thursday Afternoon, December 3, 2020  
F.SF04

**6:30 PM \*F.SF04.01.17**

**Hybrid Fabrication Techniques for Bioelectronics** George G. Malliaras; University of Cambridge, United Kingdom

While lithography provides unparalleled control over dimensions, additive manufacturing techniques enable unique design flexibility. Here we consider the merits of hybrid fabrication involving the combined use of lithography and various additive manufacturing techniques in bioelectronics. We examine examples ranging from implantable sensors to neuromorphic transistors and discuss various fabrication strategies, showing the hybrid approaches offer several advantages.

**6:50 PM \*F.SF04.01.04**

**Graphene-Templated Growth of Organic Semiconductors for Organic Electronics** Kilwon Cho; Pohang University of Science and Technology, Korea (the Republic of)

High-performance organic electronic devices require organic semiconductor (OSC) thin films to possess desired microstructures. An effective approach is use of graphene as a template for controlling growth behavior of OSC crystals. Unlike on ordinary substrates, the growth modes of OSCs on graphene are not only determined by the graphitic surface structure but also electronic characteristics of graphene. In this talk, I will discuss how OSC molecules assemble on graphene surface under the influence of graphene's doping effect. Also I will discuss a result that the OSC films grown on a graphene template under an optimized condition provide favorable vertical and lateral transport pathways for charge carriers and excitons in organic transistor and photovoltaic devices

**7:10 PM \*F.SF04.01.08**

**Linking Microstructure to Transport at Several Lengthscales in Conjugated Polymers** Alberto Salleo; Stanford University, United States

Carrier mobility in conjugated polymers continues to increase with recent reports of field-effect mobilities exceeding 10 cm<sup>2</sup>/V.s. Charge transport is intrinsically dependent on processes occurring across multiple lengthscales. In order to access order parameters at the molecular scale we use charge modulation spectroscopy combined with theory. This technique allows us to further differentiate field-induced and doping-induced charges and study how their delocalization depends on local structure and disorder. Furthermore, we study the mesoscale organization of polymers using new techniques in the transmission electron microscope. By combining 4D STEM and HRTEM we are able to study the microstructure across a range of length-scales in real space and reciprocal space. These techniques are used on homopolymers and donor-acceptor copolymers and allow to extract information about the microstructure that is typically not visible by inspection. Such multiscale studies of microstructure are instrumental in guiding our understanding of charge transport in conjugated polymers.

**7:30 PM \*F.SF04.04.02**

**Amplified Spontaneous Emission and Lasing in Quasi-2D Perovskites** Franky So and Kenan Gundogdu; North Carolina State University, United States

Recently, metal-halide perovskite materials are considered as a promising candidate for lasing applications. Compared to 3D and other low-dimensional perovskites, quasi-2D perovskites are a better gain media due to its unique properties such as large binding energy and self-assembled quantum wells. Specifically, efficient energy funneling from low-dimensional domains to high-dimensional domains will not only enhance the radiative recombination but also facilitate population

inversion.

In this presentation, we will discuss the fundamental requirements for population inversion in perovskites in the context of material dimensionality and morphology. We will also present our recent work on laser cavity design and processing for optimum laser performance.

**7:50 PM \*F.SF04.06.01**

**Various Solution Processing Methods for Boosting Electrical Performance of Metal-Oxide-Based Thin-Film**

**Transistors and Phototransistors** I Sak Lee, Dong Hyun Choi, Dongwoo Kim and Hyun Jae Kim; Yonsei Univ, Korea (the Republic of)

Oxide thin-film transistors (TFTs) have attracted much attention for next-generation electronics because of their superior performance compared with conventional a-Si TFTs such as high mobility and optical transmittance in the visible light. Particularly, solution process is a promising technique for the oxide TFT fabrication method for being a low-cost method with high composition controllability, high throughput, and various application. In this study, we propose various researches to improve the electrical and optical performances in oxide TFTs. Furthermore, we suggest a solution-processed oxide absorption layer (SAL) to enable detection of visible light for oxide phototransistors.

**Voltage-Based Ambi-Ionic Migration (VAM) for Modulating Active Layer**

The voltage-based ambi-ionic modulation (VAM) technique allows specific ions to migrate into the active layer by applying bias, easily modulating the active layer. Also, the potassium superoxide ( $\text{KO}_2$ ) solution is employed in oxide thin-film transistors (TFTs) as a source of potassium ( $\text{K}^+$ ) ions and highly reactive superoxide radical ( $\text{O}_2^{\cdot-}$ ) ions. By applying external bias, the  $\text{K}^+$  and  $\text{O}_2^{\cdot-}$  ions rapidly migrate into the active layer, directly changing its electrical properties and chemical composition. Through the VAM technique, various metal-oxide-based devices such as oxide TFTs can perform better.

**Multifunctional Heterogeneous Organic (MHO) Passivation Layer for Oxide TFT**

We propose a highly flexible and reliable multifunctional heterogeneous organic (MHO) passivation layer composed of stacked diketopyrrolopyrrole (DPP)-polymer and parylene-C films for improving the stability of oxide TFTs under various ambient environments and mechanical stress. The presented MHO passivation layer leads to high-performance oxide TFTs by: (1) protecting them from external reactive molecules, (2) blocking light to the oxide layer, and (3) improving their electrical characteristics. As a result, oxide TFTs with MHO passivation layer exhibit higher stability in ambient environment and under light. Moreover, since the MHO passivation layer can be deposited at room temperature and exhibits high mechanical stability, it could be practical in the fabrication of flexible/wearable devices.

**Selective modulation of electrical characteristics by electro-hydro-dynamic printing**

A simple fabrication method for homojunction-structured Al-doped indium–tin oxide (ITO) thin-film transistors (TFTs) using an electro-hydro-dynamic (EHD) jet-printed  $\text{Al}_2\text{O}_3$  passivation layer with a specific line ( $W_{\text{Al}_2\text{O}_3}$ ) is proposed. After EHD jet-printing, the specific region of ITO where  $\text{Al}_2\text{O}_3$  is printed changes from a conducting film to a semiconducting film while  $\text{Al}_2\text{O}_3$  acts as passivation layer. The channel length of the fabricated TFTs is defined by  $W_{\text{Al}_2\text{O}_3}$  which is easily changed with varying EHD jet printing conditions, replacing masks with varying patterns. Consequently, the proposed approach is promising as a low-cost and flexible manufacturing system for multi-item small-lot-sized production of Internet of Things devices.

**Solution-Processed Oxide Absorption Layer (SAL) for Visible-Light Detecting Phototransistor**

We propose a solution-processed oxide absorption layer (SAL) for visible-light (532 and 635 nm) detection for indium–gallium–zinc oxide (IGZO) phototransistors. The SAL was deposited onto the sputtered IGZO using precursor solutions composed of the same atomic configuration of sputtered IGZO, resulting in superior interface characteristics. We artificially generated sub-gap states in the SAL using a low temperature (200°C) annealing, minimizing the degradation of the electrical characteristics of TFT. These sub-gap states in SALs improved the photoelectron generation under long-wavelength visible-light despite the wide bandgap of IGZO (over 3.0 eV). As a result, the IGZO phototransistors with SALs have both superior optoelectronic characteristics and high optical transparency.

**8:10 PM \*F.SF04.05.03**

**Design Requirements for Flexible TFT-Based Logic Applications** Kris Myny<sup>1,2</sup>; <sup>1</sup>imec, Belgium; <sup>2</sup>KU Leuven, Belgium

In last decades, the research on flexible logic circuits based on thin-film transistors (TFTs) have been increasingly growing as technologies tend to stabilize enabling application-oriented research. Although backplane applications such as active matrix displays and 2-D imager arrays are the main driver for technology developments, logic applications also benefit from

increased performance. In this invited presentation, I will elaborate on several design requirements for TFT-based logic circuits and link them to technology and material requirements.

The focus of this work will be in the direction of flexible IoT applications, ranging from radio-frequency communication chips to sensor readout circuitry to monitor vital parameters. All demonstrated flexible integrated circuits have been realized in a dual-gate self-aligned a-IGZO TFT technology. The main advantage of a self-aligned transistor is the strongly reduced parasitic overlap capacitance between gate and source-drain contacts, enabling faster circuit blocks consuming less power. Consequently, we have demonstrated a flexible IGZO-based NFC communication tag connecting to an NFC-enabled smartphone [1]. In recent work, we have been updating our design libraries with substantially lower power consumption and realized a capacitive tag that communicates directly with the touchscreen of a smartphone as an enabler for the Internet-of-Everything [2]. This tag has been made self-powered by integrating a flexible Perovskite photovoltaic cell that captures the energy from the smartphone screen which powers the chip.

The dual-gate self-aligned transistor provides a designer with an additional benefit, namely the presence of an extra gate. The backgate can be employed for several different purposes: to increase the transconductance, to improve the output resistance or to control the threshold voltage. Most of these design considerations are mainly interesting for analogue circuits, for example to improve the gain of an operational amplifier. As a third case in this presentation, I will discuss our recent achievements on a flexible ECG patch with NFC compatibility for healthcare monitoring patches [3]. Finally, as the newest technology developments move in the direction of increased charge carrier mobilities, matching p-types and low-temperature polysilicon and oxides (LTPO), I will elaborate on the future enabling opportunities for TFT-based logic circuits and applications.

#### References

- [1] K. Myny, “The development of flexible integrated circuits based on thin-film transistors”, *Nature Electronics* 1, pp. 30-39 (2018)
- [2] N. Papadopoulos, et al.; “Touchscreen tags based on thin-film electronics for the Internet of Everything”, *Nature Electronics* 2, pp. 606-611 (2019)
- [3] M. Zulqarnain, et al.; “A flexible ECG patch with NFC compatible RF communication”, accepted to *Flexible Electronics* (npg)

*Acknowledgement* – I would like to thank my coworkers at imec and TNO/Holst centre; M. Zulqarnain and E. Cantatore from TUE for their valuable contributions to this work. Part of this work has received funding from the European Research Council (ERC) under the European Union's Horizon 2020 research and innovation program under grant agreement No 716426 (FLICs project).

SESSION F.SF04.09: Live Keynote II: Solution-Processed Semiconductors and Devices for Form-free Displays, Logic and Sensors

Session Chairs: Thomas Anthopoulos and Jana Zaumseil  
Friday Afternoon, December 4, 2020  
F.SF04

#### 1:45 PM \*F.SF04.01.01

**Flexible Semiconductors Films by Molecular Design, Nanostructure Synthesis and Porous Morphologies** Antonio Facchetti<sup>1,2</sup>; <sup>1</sup>Northwestern University, United States; <sup>2</sup>Flexterra Corp, United States

In this presentation we report the development of novel semiconductors, as well as thin-film engineering, for flexible and stretchable organic and inorganic (electrochemical) transistors and sensors. In particular we show that “ultra-soft” polymers comprising naphthalenediimide units co-polymerized with “rigid” and “flexible” organic units can change how charge transport is affected by mechanical stress, demonstrating that polymer backbone composition is more important than film degree of texturing. Furthermore, molecular design of polymers enables plasticization of a small molecule semiconductor film used in thin-film transistors. In addition, we report new “soft” transistor architectures using porosity as key element enhancing mechanical flexibility and tuned charge transport. Finally, metaloxide semiconductor nanostructures are fabricated in a very simple way and enable TFT and several types of sensors which can be monolithically integrated. These devices can better sense analytes, intercalate ions, and be chemically doped.

### 2:05 PM \*F.SF04.02.01

**Water-Based and Defect-Free 2D-Inks for Printed Electronics** [Cinzia Casiraghi](#); University of Manchester, United Kingdom

2-Dimensional materials (2DMs) are very attractive building blocks for the next generation electronics, which require low cost and flexible devices that can be easily integrated onto substrates such as paper and plastic. The atomically thin nature of 2DMs enables mechanical flexibility, high sensitivity, easy functionalization, and allows one to stack together different 2DMs to fabricate multifunctional heterostructure-based devices.

In this talk I will show a general formulation approach to make water-based, defect-free and biocompatible 2DM-based inks suitable for fabrication of a wide range of fully printed devices, such as photodetectors, capacitors and transistors, on paper and plastic [1-3].

Furthermore, printed 2DM-based devices can be easily coupled with printed RFID tags made of graphene, enabling the development of a wireless and battery-free multisensing platform on paper [4-6]. Finally, the inks can be easily combined with polycrystalline 2DMs produced by chemical vapour deposition, allowing quick fabrication of complex circuits on paper, such as high-gain inverters, logic gates and current mirrors [7].

If time allows, I will also introduce a new C-based, highly resilient and flexible substrate for printed electronics, specifically designed for applications that involve repeated strain, where paper cannot be used because the increasing fatigue in the cellulose substrate leads to failure of the device. We will show that this highly resilient substrate can sustain over 50k bending cycles without failure, in contrast to paper, which starts failing already after 5k cycles [5].

[1] McManus et al, Nature Nano, 12, 343 (2017)

[2] Worsley et al, ACS Nano, 2018, DOI: 10.1021/acsnano.8b06464

[3] Lu et al, ACS nano 13 (10), 11263 (2019)

[4] Leng et al, 2D Materials 7 (2), 024004 (2020)

[5] Worsley et al, submitted

[6] Casiraghi et al, Carbon 129, 462 (2018)

[7] Conti et al, arXiv preprint arXiv:1911.06233

### 2:25 PM \*F.SF04.02.02

**Progress Towards Reproducible, Robust, and Recyclable Printed Electronics** [Aaron D. Franklin](#); Duke University, United States

The promises of a printed electronics revolution continue to be hindered by challenges in the performance, reproducibility, and broad utility of printed devices. Inks from nanoscale materials have received increasing attention for their potential to overcome some of these hurdles, particularly in yielding direct-printed thin films meeting target electrical performance, air stability, and process compatibility. While many commercial options now exist for conducting inks, accessibility of versatile and robust semiconducting and insulating inks remains a challenge. In this talk, the recent progress on, and benefits of, semiconducting carbon nanotube (CNT) inks will be reviewed, particularly in the context of direct-write, aerosol jet-printed electronic devices. Proper control of ink properties and printing process, including factors such as ink temperature and printing time, can yield semiconducting CNT thin films with relatively high mobility, uniformity, and reproducibility. In addition, two attractive options for direct-write printed insulating inks will be discussed: hexagonal boron nitride (hBN) and crystalline nanocellulose (CNC). It will be shown how the appropriate design of these nanomaterial-based inks can enable the printing of fully recyclable electronics, where the constituent nanomaterials can be reclaimed and reused after initial printing and use in electronic devices.

### 2:45 PM \*F.SF04.03.01

**Laser Printing of Functional Materials** [Oana D. Jurchescu](#); Wake Forest University, United States

The past decades have witnessed a commendable progress in the development of materials for low-cost flexible electronics. New products that are beyond reach with current technologies can soon become a mainstay in our lives if these materials reach the necessary standards for performance and stability. The development of processing techniques that can address the manufacturability – scalability – sustainability – performance balance represents the next key step in the integration of these materials into next-generation electronic devices. In this presentation, I will introduce the use of laser printing, a rapid, scalable, environmentally friendly and low-cost manufacturing technique for deposition and patterning of various functional materials on flexible substrates. The first example focuses on organic semiconductors, and I will discuss the fabrication and characterization of organic thin-film transistors placed on plastic and paper. Aerosol spray laser lithography was used to

define the electrodes, in conjunction with different metal inks: the pattern was created using a regular toner, which was subsequently selectively removed. We created a grid of transistor devices with variable channel lengths and widths and obtained good charge carrier mobilities and an excellent tolerance to bending. Next, I will describe the use of laser printing for the fabrication of metal halide perovskite films. The electrical properties of the laser printed films were comparable with those of the spin-coated layers, despite the fact that the microstructure consists of randomly oriented crystallites. The current-voltage characteristics exhibit negligible hysteresis and the electrical properties of the films are very stable under ambient conditions due to the fact that a vertical separation of the toner components results in an encapsulating the perovskite layer by the other toner components. Our work introduces an exciting new avenue for the fabrication of stable perovskite devices that is scalable and devoid of hazardous solvents.

### **3:05 PM \*F.SF04.03.02**

**Processing Fundamentals for Self-Aligned Flexible Printed Electronics** Krystopher Jochem, Motao Cao, Panayiotis Kollipoulos, Xiaochen Ma, Satish Kumar, Daniel Frisbie and Lorraine F. Francis; University of Minnesota Twin Cities, United States

Continuous, roll-to-roll (R2R) printing processes are attractive for manufacturing of flexible electronics. Two common challenges with R2R are reaching small feature sizes and achieving precise registration of multiple functional layers in devices such as transistors. This presentation will cover our efforts to overcome these issues using Self-Aligned Capillarity-Assisted Lithography for Electronics (or SCALE). SCALE has two steps. In the first step, R2R imprinting is used to create a multilevel open network of reservoirs, capillaries and device structures into a UV-curable coating deposited on a flexible substrate. In the second step, electronically functional inks are then delivered sequentially into the reservoirs on this imprinted substrate by inkjet printing, and capillarity pulls inks into capillaries and device structures. Since the imprint stamps are fabricated from high-resolution, Si master patterns created by photolithography, the features created in the imprint resin are also high-resolution, at the micron scale. The single imprinting step also simultaneously creates all the structural features needed to control the flow and deposition of multiple inks, resulting in self-alignment of multiple materials in complex multilayer devices.

To-date we have developed SCALE methods to create conductive networks, resistors, capacitors, diodes and transistors. For example, to manufacture high aspect ratio (thickness/width) SCALE conductive networks, we used a combination of inkjet delivery of a silver particle-free ink into reservoirs of the imprinted substrate, followed by capillary flow and thermal annealing to convert the ink to a silver seed layer and lastly electroless copper plating to build conductor thickness in capillary channels. By optimizing processing conditions and understanding the fundamentals of capillary flow, narrow (e.g., 10  $\mu\text{m}$ ), high aspect ratio ( $>1$ ), low resistance ( $\sim 1$  ohm per cm of conductor length) embedded conductive traces were created. This presentation will show advances in device architecture and performance, and explore the key processing steps. Special attention will be given to continuous roll-to-roll processes.

### **3:25 PM \*F.SF04.04.01**

**Organic Infrared Sensors and Energy Storage Capacitors Based on Narrow Bandgap Polymers** Tse Nga Ng<sup>1</sup>, Ning Li<sup>1</sup>, Lulu Yao<sup>1</sup>, Kaiping Wang<sup>1</sup> and Jason D. Azoulay<sup>2</sup>; <sup>1</sup>University of California San Diego, United States; <sup>2</sup>University of Southern Mississippi, United States

Narrow bandgap polymers are used to realize infrared photodetectors that is relevant to a variety of applications including environmental monitoring and medical diagnosis. To achieve high detectivity in detectors, it is critical to reduce the device noise. This talk presents experimental and modeling studies on the noise current in exemplar organic bulk heterojunction photodiodes, with 10 donor-acceptor combinations spanning wavelength between 800 and 1600 nm. A significant reduction of the noise and higher detectivity were found in devices using non-fullerene acceptors (NFAs) in comparison to those using fullerene derivatives. The low noise in NFA blends was attributed to a sharp drop off in the distribution of bandtail states, as revealed by variable-temperature density-of-states measurements. Taking disorder into account, we developed a general physical model to explain the dependence of thermal noise on the effective bandgap and bandtail spread.

The narrow bandgap polymers are also Faradaic materials for energy storage and present opportunities to create energy dense supercapacitors. The vast majority of conducting polymers are p-type, and here we present promising n-type polymers that are stable when operating within a large potential window (3V), with a best-in-class energy densities (30.4 Wh/kg at a 1 A/g discharge rate), and a long cycle life (90% capacitance retention after 5000 cycles) critical to energy storage and management. This work demonstrates the application of a new class of stable and tunable redoxactive material to realize high-endurance energy storage devices for flexible printed systems.

**5:00 AM \*F.SF04.01.01**

**Flexible Semiconductors Films by Molecular Design, Nanostructure Synthesis and Porous Morphologies** Antonio Facchetti<sup>1,2</sup>; <sup>1</sup>Northwestern University, United States; <sup>2</sup>Flexterra Corp, United States

In this presentation we report the development of novel semiconductors, as well as thin-film engineering, for flexible and stretchable organic and inorganic (electrochemical) transistors and sensors. In particular we show that “ultra-soft” polymers comprising naphthalenediimide units co-polymerized with “rigid” and “flexible” organic units can change how charge transport is affected by mechanical stress, demonstrating that polymer backbone composition is more important than film degree of texturing. Furthermore, molecular design of polymers enables plasticization of a small molecule semiconductor film used in thin-film transistors. In addition, we report new “soft” transistor architectures using porosity as key element enhancing mechanical flexibility and tuned charge transport. Finally, metaloxide semiconductor nanostructures are fabricated in a very simple way and enable TFT and several types of sensors which can be monolithically integrated. These devices can better sense analytes, intercalate ions, and be chemically doped.

**5:15 AM \*F.SF04.01.02**

**Material, Process and Device Issues in Solution Processed Semiconductor Products** Yue Kuo; Texas A&M Univ, United States

The general trend in semiconductor fabrications is the low thermal budget because of limitations on the minimum device dimension or the substrate material. For example, in IC fabrication, the process temperature can change the dopant redistribution, which directly affects the junction and interface properties. In large area flat panel displays, the glass substrate can only tolerate a low temperature, i.e., below the softening temperature. Since the solution process method can deposit thin films at a low temperature, it is compatible with various rigid or flexible substrates. Currently, there are many efforts in applying the solution process method to fabricate semiconductor products.

Among many types of low temperature prepared devices, thin film transistors (TFTs) are probably most popular because they have been critical components in the flat panel displays for 3 decades [1]. TFTs can also be used in a broad range of non-display products, such as chemical, gaseous, solution, bio, magnetic, and optical sensors as well as imagers, memories, and circuit drivers [2,3]. In TFTs, the semiconductor layers can be made of small or large organic molecules or inorganic silicon, metal oxide, or compound materials. The dielectric layer can also be made of organic or inorganic materials. However, in spite of many reports on solution process fabricated TFTs, no commercial products are available on the market. In this paper, a detailed analysis of some critical issues in this kind of device will be presented. For the device performance part, the bulk and interface defects, which may be of chemical or physical nature, are key factors to be improved. For the reliability part, the long-term stability, such as shifts of characteristics under the operation condition, will be addressed. Many disadvantageous material properties in the low temperature solution processed thin films and stacked structures can be improved with a low thermal budget pulsed rapid thermal annealing process [4,5]. A discussion on this method will be included in this presentation, too.

[1] Y. Kuo, ECS Interface, 22(1), 55-60 (2013).

[2] Y. Kuo, Amorphous Silicon Thin Film Transistors, Kluwer Academic Publishers, Norwell, MA, 2004.

[3] Y. Kuo, Polycrystalline Silicon Thin Film Transistors, Kluwer Academic Publishers, Norwell, MA, 2004.

[4] Y. Kuo and C. H. Lin, ECS 237th Meeting, Abstract # 130648, May 10-15, 2020.

[5] Y. Kuo, and C.-C. Lin, MRS Proc. Symp., 1426, 269-274 (2012).

**5:30 AM F.SF04.01.03**

**Narrowband-Absorption-Type Organic Photodetectors Based on Solution-Processed Fullerene-Free Bulk Heterojunctions** Vincenzo Pecunia, Kai Xia and Yang Cao; Soochow University, China

Organic semiconductors have attracted considerable interest for spectrally-selective light sensing (i.e., narrowband



photodetection), which is relevant to manifold applications—e.g., colorimetry, healthcare monitoring, biology, chemical fingerprinting.<sup>1</sup> The attractiveness of organic semiconductors for narrowband photodetection is especially due to the capability of many such compounds to absorb light precisely over the spectral range of interest, thereby enabling filterless narrowband-absorption-type organic photodetectors (OPDs). However, it has been generally challenging to date to realize such OPDs while achieving good spectral selectivity. This has been primarily due to the widespread use of fullerenes as electron acceptors, which bring along a detrimental shallow absorption tail through the visible range.<sup>2</sup> Additionally, while solution-based methods have been recognized as key to developing low-cost and/or free-form photodetectors and imagers, narrowband-absorption-type OPDs comprising solution-based active layers have thus far struggled to deliver high photoconversion efficiency.<sup>3</sup>

In this study we show that non-fullerene acceptors (NFAs) provide an attractive route to high-performance solution-processed OPDs with narrowband-absorption-type capability. We discuss the viability and general applicability of this approach by presenting the NFA-based solutions we have developed for narrowband-absorption-type OPDs selectively responding in the green range and the far-red range. In particular, we have studied two solution-processible NFAs: a benzodithiophene-based compound with narrowband absorption in the far-red range (solid-state spectral absorbance width of 132 nm) and a subphthalocyanine-based compound with narrowband absorption in the green range (solid-state spectral absorbance width of 80 nm). In both cases, we have explored solution-deposited photoactive layers consisting of bulk-heterojunctions in which the NFAs are combined with donors that are either transparent or that also selectively absorb in the target spectral range.

By tailoring our solution-processed NFA-based photoactive layers, we have achieved narrowband-absorption-type photodetection with cutting-edge performance. In self-powered operation, our NFA-based OPDs for the far-red range deliver the highest specific detectivity to date ( $1.4 \times 10^{13}$  Jones) of all narrowband-absorption-type far-red-selective OPDs, and concurrently achieve the narrowest spectral width (141 nm) of all solution-processed implementations.<sup>4</sup> Moreover, our green-selective NFA-based OPDs deliver a spectral width of 130 nm with an external quantum efficiency up to 40%, which is the highest to date for green-selective solution-processed narrowband-absorption-type OPDs. Our OPDs additionally show a linear response over an optical power range greater than four orders of magnitude, and exhibit a fast response compatible with a wealth of relevant applications. The versatility of our NFA-based narrowband-absorption-type approach marks an important step in the realization of solution-processible OPDs towards high-performance and low-cost colour sensors and imagers, and additionally motivate dedicated synthetic efforts in NFA research targeting narrowband OPD applications.

1 V. Pecunia, *Organic Narrowband Photodetectors: Materials, devices and applications*, Institute of Physics Publishing, Bristol, UK, 2019.

2 R. D. Jansen-van Vuuren, A. Armin, A. K. Pandey, P. L. Burn and P. Meredith, *Adv. Mater.*, 2016, 4766–4802.

3 V. Pecunia, *J. Phys. Mater.*, 2019, 2, 042001.

4 K. Xia, Y. Li, Y. Wang, L. Portilla and V. Pecunia, *Adv. Opt. Mater.*, 2020, 1902056.

#### 5:40 AM \*F.SF04.01.04

**Graphene-Templated Growth of Organic Semiconductors for Organic Electronics** Kilwon Cho; Pohang University of Science and Technology, Korea (the Republic of)

High-performance organic electronic devices require organic semiconductor (OSC) thin films to possess desired microstructures. An effective approach is use of graphene as a template for controlling growth behavior of OSC crystals. Unlike on ordinary substrates, the growth modes of OSCs on graphene are not only determined by the graphitic surface structure but also electronic characteristics of graphene. In this talk, I will discuss how OSC molecules assemble on graphene surface under the influence of graphene's doping effect. Also I will discuss a result that the OSC films grown on a graphene template under an optimized condition provide favorable vertical and lateral transport pathways for charge carriers and excitons in organic transistor and photovoltaic devices

#### 5:55 AM \*F.SF04.01.05

**Understanding Printing Physics for Controlled Conformation, Aggregation and Alignment of Conjugated Polymers** Ying Diao; University of Illinois at Urbana-Champaign, United States

Controlled morphology evolution via directed assembly has played a central role in the development of modern electronic, optical and clean energy materials. In comparison to conventional 'hard' materials, organic electronics can be easily processed into diverse form factors by low-cost, high-throughput methods such as roll-to-roll printing and 3D printing. The printing conditions intimately couple with the assembly process and sensitively modulate the solid-state properties in the

fabricated devices. A major challenge in this field lies in controlling the nucleation, growth, aggregation and alignment of conjugated polymers during solution printing and coating, which critically impact the printed device performance by orders of magnitude. The rapid printing process creates a complex environment with coupled physics that drive the polymer assembly far from equilibrium. Yet little is known of the non-equilibrium molecular assembly pathways and the printing physics so essential to tuning molecular conformation and multiscale morphology and the resulting intrachain and interchain charge transport properties of printed organic semiconductors.

In our work, we elucidate fundamental printing physics through finite element simulations and free energy modeling. By doing so, we are able to decipher non-equilibrium assembly pathways and control multi-scale assembly of semiconducting polymers. We further establish processing-structure-property relationship by performing printing experiments, morphology and device characterizations. We observe unexpected flow-induced morphology and electronic transition that accompanies change in printing regimes. We elucidate that printing flow in a moving, drying meniscus can drastically alter the polymer assembly pathways by flow-induced conformation change. We further design bioinspired assembly processes learning from biosystems, allowing molecules to put themselves together cooperatively into highly ordered structures otherwise not possible. High degree of morphology control from molecular to device scale further enables new insights into charge transport properties of semiconducting polymers and realizes advanced electronic devices such as printed 2D monolayer devices and ultrasensitive chemical sensors.

#### 6:10 AM F.SF04.01.06

##### **Monolithic Integration of Organic Light-Emitting Transistors and Organic Photodiodes for a New Class of**

**Optoplasmonic Devices in Biosensing** Mario Prosa<sup>1</sup>, Emilia Benvenuti<sup>1</sup>, Michael Toerker<sup>2</sup>, David Kallweit<sup>3</sup>, Paola Pellacani<sup>4</sup>, Laura Lopez-Sanchez<sup>4</sup>, Margherita Bolognesi<sup>1</sup>, Lucia Fornasari<sup>4</sup>, Franco Marabelli<sup>5</sup> and Stefano Toffanin<sup>1</sup>; <sup>1</sup>Consiglio Nazionale delle Ricerche (CNR), Italy; <sup>2</sup>Fraunhofer FEP, Germany; <sup>3</sup>CSEM, Switzerland; <sup>4</sup>Plasmore Srl, Italy; <sup>5</sup>University of Pavia, Italy

The implementation of different organic optoelectronic devices in a single architecture may represent a winning approach for the development of compact, highly-sensitive and -selective sensors.

Here, the monolithic integration of organic photodiodes (OPDs) onto organic light-emitting transistors (OLETs) is demonstrated, discussed and validated as a new platform for biosensing. While OLETs combine electrical switching characteristics with light generation capability, the deposition of OPDs directly onto the source electrodes of the OLETs provides the light-sensing ability to the whole multifunctional system, as a result of the spectral compatibility between OLETs and OPDs.

The potential of the platform is demonstrated in a real sensing application by depositing a nanoplasmonic grating on the top side of the encapsulating glass of the OLET+OPD chip. The nanoplasmonic thin film, which has been suitably designed and developed, has the ability to change the spectral reflectivity if a variation of the refractive index occurs on the top surface. The effectiveness of the new detection scheme is validated by proving that the OPD photocurrent, generated as a consequence of the light emitted by the OLET and then reflected by the nanoplasmonic grating, changes by a factor  $10^{-9}$  A when exposing the sensing surface from water to alcoholic solutions at different concentrations.

#### 6:20 AM F.SF04.01.07

**A sub 150-nm, Ultrathin, Ultraflexible, Fully Solution Processed Organic Field Effect Transistor** Fabrizio A. Viola and Mario Caironi; Istituto Italiano di Tecnologia - IIT, Italy

In recent decades, a rising interest in flexible electronic devices has led to an increasing request for novel fabrication technologies for a large set of possible applications such as prosthetics, human-robot interaction, and rehabilitation. In this field, one of the major goals is the fabrication of flexible electronic devices by means of unconventional and highly compliant materials. In particular, organic materials have attracted significant interest in the scientific and industrial community due to their intrinsic mechanical characteristics and to the possibility to process them at very low temperatures at low costs, enabling new potential applications not achievable with inorganic counterparts.

In this work, we demonstrate that is possible to fabricate an all solution processed organic field effect transistor with a total thickness lower than 150 nm, which is the thinnest organic transistor ever fabricated, by adopting an approach based on solution-assisted delamination of freestanding ultra-thin layers of a well-known polymer insulator, namely poly(vinyl formal) (PVF). Thanks to the peculiar characteristics of the employed materials, the device shows an excellent transparency, together with an extremely high level of conformability. In fact, the proposed device is able to sustain bending to extremely small curvature radii and to conform on complex 3D surfaces, such as human skin, which makes it non-invasive and completely imperceptible, opening to a multitude of possible applications of our approach in several fields, from wearable electronics to implantable-electronics. The device fabrication relies entirely on solutions process techniques (such as spin-coating and ink-

jet printing) and can be potentially up-scaled to an industrial size. Moreover, the devices show very reliable electrical performances, with mobility up to 0.18 cm<sup>2</sup>/Vs, and a very good reproducibility, which are requirements particularly challenging when large-area fabrication techniques and solution processed materials are employed.

### 6:30 AM \*F.SF04.01.08

**Linking Microstructure to Transport at Several Lengthscales in Conjugated Polymers** Alberto Salleo; Stanford University, United States

Carrier mobility in conjugated polymers continues to increase with recent reports of field-effect mobilities exceeding 10 cm<sup>2</sup>/V.s. Charge transport is intrinsically dependent on processes occurring across multiple lengthscales. In order to access order parameters at the molecular scale we use charge modulation spectroscopy combined with theory. This technique allows us to further differentiate field-induced and doping-induced charges and study how their delocalization depends on local structure and disorder. Furthermore, we study the mesoscale organization of polymers using new techniques in the transmission electron microscope. By combining 4D STEM and HRTEM we are able to study the microstructure across a range of length-scales in real space and reciprocal space. These techniques are used on homopolymers and donor-acceptor copolymers and allow to extract information about the microstructure that is typically not visible by inspection. Such multiscale studies of microstructure are instrumental in guiding our understanding of charge transport in conjugated polymers.

### 6:45 AM \*F.SF04.01.09

**Thermoelectric Energy Conversion Devices of Electrochemically Doped Polymer Films** Taishi Takenobu; Nagoya University, Japan

Thermoelectric energy conversion is one of the key technologies for energy harvesting devices to convert waste heat into electric power, and vice versa. Particularly, for IoT (Internet of Things) society based on wearable electronics, flexible large-scale thermoelectric conversion devices are highly required. Therefore, as the active semiconductors of these devices, organic conducting polymers are strong candidates due to their low-temperature solution processability, compatibility with large-area deposition techniques, and intrinsic robust mechanical properties. However, the thermoelectric transport mechanism of these materials is still unclear due to their unique disordered nature, in particular the poor interconnectivity between crystalline domains. Here, we investigated their thermoelectric and carrier transport properties using the electrochemical doping technique and successfully maximized their performances [1].

In thermoelectric energy conversion devices, the Seebeck coefficient (= thermopower,  $S$ ), which is the proportional constant to the voltage generation against an induced temperature gradient, is a significant factor in designing thermoelectric devices. Importantly, according to the Mott equation,  $S$  is proportional to the energy derivative of the electronic density of states at around Fermi energy; therefore, it is critically important to control the energy band filling. Conventionally, the band filling is tuned by chemical doping and, in most materials, it is very difficult to establish precisely controllable doping methods. Another important factor for thermoelectric energy conversion devices is the thermoelectric power factor  $S^2\sigma$  ( $\sigma$  is conductivity). It should be strongly emphasized that the power factor has to be optimized to maximize the electric power output of thermoelectric devices. Consequently, this is a key parameter for applications. However, it is widely known that there is a trade-off between  $S$  and  $\sigma$  in terms of carrier density,  $n$ . Although  $\sigma$  is almost linearly proportional to  $n$ ,  $S$  decreases with increasing  $n$ . Therefore, again, it is necessary to maximize  $S^2\sigma$  by tuning  $n$ .

To overcome this limit, we developed electrochemical doping technique [2-6] and combined this technique with thermoelectric measurements [1, 7-12]. In particular, we applied this method into semicrystalline PBTTT and donor-acceptor copolymers [1]. As the results, we successfully maximized their power factor and clarified the behind physics.

- [1] H. Tanaka, T. Takenobu, *et al.*, *Sci. Adv.*, 6, eaay8065 (2020)
- [2] K. Matsuki, J. Pu, and T. Takenobu, *Adv. Funct. Mater.*, 1908641 (2020)
- [3] Q. Liu, T. Takenobu, *et al.*, *Adv. Electron. Mater.*, 6, 1901414 (2020)
- [4] Y. Kawasugi, T. Takenobu, *et al.*, *Sci. Adv.*, 5, eaav7282 (2019)
- [5] M.-H. Chiu, T. Takenobu, *et al.*, *Adv. Matter.*, 31, 1900861 (2019)
- [6] J. Pu, T. Takenobu, *et al.*, *ACS Nano*, 13, 9218 (2019)
- [7] K. Kanahashi, J. Pu, and T. Takenobu, *Adv. Energy Mater.*, 1902842 (2019)
- [8] K. Kanahashi, T. Takenobu, *et al.*, *npj 2D Mater. Appl.* 3, 44 (2019)
- [9] J. Pu, T. Takenobu, *et al.*, *Phys. Rev. B* 94, 014312 (2016)
- [10] Shimizu, T. Takenobu, *et al.*, *SMALL* 12, 3388 (2016)

[11] Y. Kawasugi, T. Takenobu, *et al.*, Appl. Phys. Lett. 109, 233301 (2016).

[12] K. Yanagi, T. Takenobu, *et al.*, Nano Lett. 14, 6437-6442 (2014)

#### 7:00 AM F.SF04.01.10

**Physical Image of Organic Vertical Transistors with Conductive-Network Electrodes** Chuan Liu, Zihao Chen, Kairong Huang, Sujuan Hu and Xiaoci Liang; Sun Yat-sen University, China

Organic vertical transistors with conductive-network electrodes composed of carbon- or metal-based nanowires or meshes have been gaining increasing attention in recent years and several comprehensive reviews have been published [1, 2]. Differing from planar field-effect transistors (FETs) or thin-film transistors (TFTs), the conduction of the carriers in such devices occurs through vertical channels that are controlled by the gate field from the gaps between the nanowires or from the holes within the metal films [3]. Because of their submicron channel length, vertical transistors based on organic semiconductors (e.g., polymers or small molecules) with carbon-nanotube electrodes or metal meshes exhibit a large current density that can be used to drive light-emitting diodes [4]. The device structure also show great potential on flexibility, high degree of intergration. In addition, the layer-by-layer structure can be deposited by state-of-the-art printing technologies in industrial printing lines established for organic light-emitting diodes. However, the devices lack concise physical images to understand the operations and explicit design rules to achieve the necessary performance, such as sharp subthreshold swing, a large on: off ratio and and saturation in the high drain voltage ( $V_D$ ).

Here, we develop a device theory with concise physical images, which are generally applicable for devices with organic or inorganic semiconductors. The simplified solution of Poisson's equation reveals that the electrostatic potential at the semiconductor-dielectric interface is controlled by both the gate and drain field, behaving like a plucked string. The spacing between electrodes and the capacitance ratio between dielectrics and semiconductors are critical for achieving strong gate tunability of the interfacial potential, which can be maximized to achieve a sharp turn-on property toward the Boltzmann limit in the subthreshold regime. Above the threshold, the conduction channels in devices with Schottky contacts can change from the "L type" to "I type", or vice versa, during scanning and the current-voltage relations can be well described by modifying classical transistor equations. The derived theories and equations agree well with the numerically simulated devices and reported experiments, revealing the physical images and providing explicit rules for designing, fabricating, and characterizing such transistors.

[1] J. Liu, Z. Qin, H. Gao, H. Dong, J. Zhu, and W. Hu, Vertical organic field-effect transistors, Adv. Mater. 29, 1808453 (2019).

[2] H. Kleemann, K. Krechan, A. Fischer, and K. Leo, A review of vertical organic transistors, Adv. Funct. Mater. 1907113 (2020).

[3] X. Fang, C.-H. Lin, Y.-T. Sun, H.-T. Chin, H.-W. Zan, H.-F. Meng, S.-F. Horng, and L. A. Wang, A solvent-free lift-off method for realizing vertical organic transistors with low leakage current and high ON/OFF ratio, Org. Electron. 31, 227 (2016).

[4] F. M. Sawatzki, D. H. Doan, H. Kleemann, M. Liero, A. Glitzky, T. Koprucki, and K. Leo, Balance of Horizontal and Vertical Charge Transport in Organic Field-Effect Transistors, Phys. Rev. Appl. 10, 034069 (2018).

[5] C. Liu, Z. Chen, K. Huang, S. Hu, X. Liang, and J. Chen, Vertical Transistors with Conductive-Network Electrodes: A Physical Image and What It Tells. Phys. Rev. Appl. 13, 054066. (2020)

#### 7:10 AM F.SF04.01.11

**Soft Electronics and Materials for Ear to Brain Engineering** Georgios Spyropoulos; Ghent University, Belgium

Responsive modulation of neural networks is increasingly being used to treat patients with auditory-neurological disorders and neuropsychiatric diseases. Yet, current technology burdens neurostimulation tools with bulky, non-biocompatible electrical components that require rigid encapsulation for long-term implantation in body. Recently, we created a novel transistor architecture (internal ion-gated organic electrochemical transistors; IGT) that can be an efficient building block for integrated bioelectronics. These transistors include all the key features required for safe, efficient, and prolonged use of transistors in biological environments: i) they are made out of biocompatible and stable materials; ii) they are soft and conformable; iii) they show high speed and amplification to detect potentially low-amplitude ionic signals of the body; iv) they can perform certain computations.

Here, I am presenting the vision of our newly founded lab towards designing, based on that emerging technology, and developing novel fully implantable, contained and responsive neural interface devices that will allow long-term acquisition and closed-loop manipulation of neural circuits with high spatiotemporal resolution over extended period of time to reveal neural dynamics in the auditory-neurological pathway.

#### 7:20 AM \*F.SF04.01.12

**Monolayer Organic Field-Effect Transistors with Extremely High Current Density** Paddy K. L. Chan; University of Hong Kong, Hong Kong

In this talk, I will focus on the high performance monolayer organic crystal and utilize it to develop an OFET with record high current density. The semiconductor is based on the solution processable DNNT derivatives and the deposition method is solution shearing. Among the four derivatives, the best performance for the contact resistance is 25 ohm-cm at  $V_{DS} = -1$  V, under a gate bias of -85V. The monolayer crystal could conduct unprecedentedly high density of current up to 19  $\mu\text{A}/\mu\text{m}$  per channel width which is corresponding to 1.2 MA/cm<sup>2</sup> normalized by channel cross-section area. This current density is significantly higher than the reported values of other OFETs and also comparable with the inorganic transistors. Operating the OFETs with a high current density, however, would induce significant heating effect and a temperature rise of 110 K is obtained in the channel area. This inevitable wasted heat in the high power operation would lead to the thermal damage in the OFETs especially at the metal/organic contact interface. To suppress the thermal damage, a reduced voltage pulse width down to 10  $\mu\text{s}$  and duty cycle down to 1% would still operate the device properly. Our work suggests that (i) monolayer crystal is a favored configuration in lowering the contact resistance; (ii) molecularly thin semiconductor could still conduct enormous amount of current; and (iii) thermal management is critical for future studies on OFETs, especially those with outstanding performance. Lastly, I will demonstrate how can use this high current density OFETs to drive different electronic devices such as LEDs and buzzers.

**7:35 AM \*F.SF04.01.13**

**Printing Blends of Small Molecule Semiconductors with Insulating Polymers to Fabricate High Performing and Stable OFETs for Sensing Applications** A. Tamayo<sup>1</sup>, Tommaso Salzillo<sup>1</sup>, Antonio Campos<sup>1</sup>, Inés Temiño<sup>1</sup>, Sergi Riera-Galindo<sup>1</sup>, Simona Ricci<sup>1</sup>, Adara Babuji<sup>1</sup>, Raul Santiago<sup>2</sup>, Stefan T. Bromley<sup>2</sup>, Carmen Ocal<sup>1</sup>, Esther Barrena<sup>1</sup>, Remy Jouclas<sup>3</sup>, Christian Ruzie<sup>3</sup>, Guillaume Schweicher<sup>3</sup> and Marta Mas-Torrent<sup>1</sup>; <sup>1</sup>Institut de Ciència de Materials de Barcelona (ICMAB-CSIC), Spain; <sup>2</sup>Universitat de Barcelona, Spain; <sup>3</sup>Université Libre de Bruxelles (ULB), Belgium

Printing organic small molecule semiconductors by solution shearing for the fabrication of highly performing organic field-effect transistors (OFETs) is currently of major technological interest. However, two challenging issues remain unsolved in order to implement these devices in real applications: reproducibility and long-term stability. The blending of the organic semiconducting molecules (OSC) with insulating binding polymers has proved to be an efficient route to ensure the formation of homogenous films over large areas with high device-to-device reproducibility. However, since molecules are bound together through weak van der Waals interactions, they are prone to polymorphism. Slight differences between polymorphs can lead to dramatic changes in their mobilities. Further, some technologically desirable polymorphs are metastable but can degrade with time to the most thermodynamically stable form, thus impacting device performance. Recently, we have shown that the use of blends of OSCs with polymers by Bar-Assisted Meniscus Shearing (BAMS) gives rise to highly crystalline films.[1] In addition, the control of the deposition parameters (coating speed and temperature) as well as the modification of the ink formulation can be used as tools to tune the thin films morphology and the formation of thermodynamic and Kinetic polymorphs.[2] In a recent publication, we have also demonstrated that the blending approach can also be exploited to trap metastable polymorphs, which can lead to devices with both improved performance and long-term stability.[3]

The devices fabricated with this methodology have been applied for the development of X-ray detectors [4], biosensors[5] and for recording the activity of cells[6].

[1] I. Temiño, F.G.Del Pozo, A.Murugan, S. Galindo, J. Puigdollers, M. Mas-Torrent, Adv. Mater. Technol. 2016, 1,1600090.

[2] S. Galindo, A. Tamayo, F. Leonardi, M. Mas-Torrent, Adv. Funct. Mater., 2017, 27,1700526.

[3] T. Salzillo, A. Campos, A. Babuji, R. Santiago, S. T. Bromley, C. Ocal, E. Barrena, R. Jouclas, C. Ruzie, G. Schweicher, Y. H. Geerts, M. Mas-Torrent, Adv. Funct. Mater., 2020, 2007115.

[4] I. Temiño, L. Basiricò, I. Fratelli, A. Tamayo, A. Ciavatti, M. Mas-Torrent, B. Fraboni, Nature Communications 2020, 11:2136.

[5] S. Ricci, S. Casalini, V. Parkula, M. Selvaraj, D. Deniz, P. Greco, F. Biscarini, M. Mas-Torrent, Biosensors and Bioelectronics 2020, 167, 112433.

[6] A. Kyndiah, F. Leonardi, C. Tarantino, T. Cramer, R. Millan-Solsona, E. Garreta, N. Montserrat, M. Mas-Torrent, G. Gomila, Biosensors and Bioelectronics 2020, 150, 111844.

**7:50 AM F.SF04.01.14**

**Late News: Hydroresistive Flexible Organic Molecular Metal** Raphael Pfattner<sup>1,2</sup>, Victor Lebedev<sup>1</sup>, Elena Laukhina<sup>2</sup>, Marta Mas-Torrent<sup>1,2</sup>, Vladimir Laukhin<sup>1,3</sup>, Concepcio Rovira<sup>1,2</sup> and Jaume Veciana<sup>1,2</sup>; <sup>1</sup>Materials Science Institute of

Barcelona (ICMAB-CSIC), Spain; <sup>2</sup>Networking Research Center on Bioengineering, Biomaterials and Nanomedicine (CIBER-BBN), Spain; <sup>3</sup>Institucio Catalana de Recerca i Estudis Avancats (ICREA), Spain

The first [BEDT-TTF = bis(ethylenedithio)-tetrathiafulvalene based quasi-two-dimensional organic superconductor  $\beta$ -(BEDT-TTF) $_2$ I $_3$ ] was first reported back in 1984.<sup>[1]</sup> Soon it became clear that ion radical salts (IRSs) derived from BEDT-TTF exhibit tuneable electronic band structures; therefore, such molecules are excellent building blocks for engineering a rich and diverse family of organic crystalline metals and semiconductors. Electronic band structures of BEDT-TTF-based molecular conductors originate from ordered arrangements, such as stacks and layers, leading to metallic charge-transfer salts with partially filled bands.<sup>[2]</sup>

One interesting characteristic of BEDT-TTF-based crystalline conductors is the very deformable molecular and crystal structure with strong electron–electron and electron–phonon couplings. Thanks to this, their anisotropic electronic structures exhibit many fascinating electronic and structural phase transitions caused by lattice deformations, which can be controlled by external stimuli such as light, temperature, strain, pressure, and humidity, among others. Nevertheless, it is necessary to engineer these crystals into a proper material for sensing applications. This was done by forming polycrystalline layers of IRSs, derived from BEDT-TTF-based conductors, in nanocomposite bilayer (BL) films a strategy that allows combining electrical properties of IRSs with classical properties of insulating polymers, like flexibility, transparency, and solution processability.

Developing smart materials that can respond to an external stimulus is of major interest in artificial sensing devices able to read information about the physical, chemical and/or biological changes produced in our environment. Additionally, if these materials can be deposited or integrated on flexible, transparent substrates, their appeal is greatly increased. Such properties can be further tuned by choosing the nature of the IRSs enabling high sensitivity towards strain, pressure, temperature or even contactless radiation sensing i.e. bolometers.<sup>[3,4]</sup> In a very recent example, bilayer films, composed of conducting polycrystalline layers of two dimensional BEDT-TTF-IRSs, hydroresistive sub-micron sized crystals on top of a polymeric host matrix permit to electrically monitor relative humidity in a stable and fully reversible fashion.<sup>[5]</sup> This sensor platform enables the combination of high electrical performance of single crystals with processing properties of polymers towards a simple, low-cost and highly sensitive platform for applications in robotics, biomedicine and human health care.

[1] E. B. Yagubskii, I. F. Shchegolev, V. N. Laukhin, P. A. Kononovich, M. V. Kartsovnik, A. V. Zvarykina, L. I. Buravov, JETP Lett. 1984, 39, 12.

[2] J. M. Williams, J. R. Ferraro, R. J. Thorn, K. D. Carlson, U. Geiser, H. H. Wang, A. M. Kini, M.-H. Whangbo, Organic Superconductors

(Including Fullerenes): Synthesis, Structure, Properties and Theory; Prentice Hall: Englewood Cliffs, NJ, 1992.

[3] E. Laukhina, R. Pfattner, L. R. Ferreras, S. Galli, M. Mas-Torrent, N. Masciocchi, V. Laukhin, C. Rovira, J. Veciana. Advanced Materials, 2009, 21, 1-5.

[4] R. Pfattner, V. Lebedev, E. Laukhina, S. Chaitanya Kumar, A. Esteban-Martin, V. Ramaiah-Badarla, M. Ebrahim-Zadeh, F. Pelayo García

de Arquer, G. Konstantatos, V. Laukhin, C. Rovira, J. Veciana. Advanced Electronic Materials, 2015, 1, 1500090.

[5] R. Pfattner, E. Laukhina, L. Ferlauto, F. Liscio, S. Milita, A. Crespi, V. Lebedev, M. Mas-Torrent, V. Laukhin, C. Rovira, J. Veciana, ACS

Applied Electronic Materials 2019, 1, 1781.

#### **8:00 AM \*F.SF04.01.17**

**Hybrid Fabrication Techniques for Bioelectronics** George G. Malliaras; University of Cambridge, United Kingdom

While lithography provides unparalleled control over dimensions, additive manufacturing techniques enable unique design flexibility. Here we consider the merits of hybrid fabrication involving the combined use of lithography and various additive manufacturing techniques in bioelectronics. We examine examples ranging from implantable sensors to neuromorphic transistors and discuss various fabrication strategies, showing the hybrid approaches offer several advantages.

#### **8:15 AM \*F.SF04.01.18**

**Printed Polymer Field-Effect Transistors and Rectifiers Operating at Radio-Frequencies** Mario Caironi; Istituto Italiano di Tecnologia, Italy

Organic electronics has been developed for many novel applications towards large area and flexible electronics, but it has been traditionally considered only for low frequency applications. However roadmaps towards GHz operation have been

recently proposed, exploiting improved electronic properties and optimized electronic device architectures. Such frequency range would be appealing for example to enable local area networks interconnecting large-area distributed and wearable sensors. Towards such applications, manufacturing processes comprising high-throughput printing techniques would be very appealing, although limitations in spatial resolution and in the control of electronic properties add a further obstacle to an already very challenging roadmap. In this contribution I will report on our progress in developing printed electronic devices capable of operating at radio-frequencies, targeting the High-Frequency range. In particular, I will show direct-written polymer field-effect transistors (FETs) operating above 20 MHz at low-voltage on plastic substrates, and fully inkjet printed diodes enabling rectifiers on plastic at 13.56 MHz. Finally, I will show recent results on FETs targeting the Ultra-High Frequency range, where local communication would be feasible.

SESSION F.SF04.02: Nano

On Demand Abstracts Available for Viewing Starting Saturday Morning, November 21, 2020  
F-SF04

**5:00 AM \*F.SF04.02.01**

**Water-Based and Defect-Free 2D-Inks for Printed Electronics** [Cinzia Casiraghi](#); University of Manchester, United Kingdom

2-Dimensional materials (2DMs) are very attractive building blocks for the next generation electronics, which require low cost and flexible devices that can be easily integrated onto substrates such as paper and plastic. The atomically thin nature of 2DMs enables mechanical flexibility, high sensitivity, easy functionalization, and allows one to stack together different 2DMs to fabricate multifunctional heterostructure-based devices.

In this talk I will show a general formulation approach to make water-based, defect-free and biocompatible 2DM-based inks suitable for fabrication of a wide range of fully printed devices, such as photodetectors, capacitors and transistors, on paper and plastic [1-3].

Furthermore, printed 2DM-based devices can be easily coupled with printed RFID tags made of graphene, enabling the development of a wireless and battery-free multisensing platform on paper [4-6]. Finally, the inks can be easily combined with polycrystalline 2DMs produced by chemical vapour deposition, allowing quick fabrication of complex circuits on paper, such as high-gain inverters, logic gates and current mirrors [7].

If time allows, I will also introduce a new C-based, highly resilient and flexible substrate for printed electronics, specifically designed for applications that involve repeated strain, where paper cannot be used because the increasing fatigue in the cellulose substrate leads to failure of the device. We will show that this highly resilient substrate can sustain over 50k bending cycles without failure, in contrast to paper, which starts failing already after 5k cycles [5].

[1] McManus et al, Nature Nano, 12, 343 (2017)

[2] Worsley et al, ACS Nano, 2018, DOI: 10.1021/acsnano.8b06464

[3] Lu et al, ACS nano 13 (10), 11263 (2019)

[4] Leng et al, 2D Materials 7 (2), 024004 (2020)

[5] Worsley et al, submitted

[6] Casiraghi et al, Carbon 129, 462 (2018)

[7] Conti et al, arXiv preprint arXiv:1911.06233

**5:15 AM \*F.SF04.02.02**

**Progress Towards Reproducible, Robust, and Recyclable Printed Electronics** [Aaron D. Franklin](#); Duke University, United States

The promises of a printed electronics revolution continue to be hindered by challenges in the performance, reproducibility, and broad utility of printed devices. Inks from nanoscale materials have received increasing attention for their potential to overcome some of these hurdles, particularly in yielding direct-printed thin films meeting target electrical performance, air stability, and process compatibility. While many commercial options now exist for conducting inks, accessibility of versatile and robust semiconducting and insulating inks remains a challenge. In this talk, the recent progress on, and benefits of, semiconducting carbon nanotube (CNT) inks will be reviewed, particularly in the context of direct-write, aerosol jet-printed electronic devices. Proper control of ink properties and printing process, including factors such as ink temperature and printing time, can yield semiconducting CNT thin films with relatively high mobility, uniformity, and reproducibility. In

addition, two attractive options for direct-write printed insulating inks will be discussed: hexagonal boron nitride (hBN) and crystalline nanocellulose (CNC). It will be shown how the appropriate design of these nanomaterial-based inks can enable the printing of fully recyclable electronics, where the constituent nanomaterials can be reclaimed and reused after initial printing and use in electronic devices.

### 5:30 AM F.SF04.02.03

**Ambipolar Printed-Carbon-Nanotube Transistors with Self-Assembled-Monolayer Nanodielectrics for Low-Power and Low-Voltage Electronics** Luis Portilla<sup>1,2</sup>, Jianwen Zhao<sup>2</sup> and Vincenzo Pecunia<sup>1</sup>; <sup>1</sup>Soochow University, China; <sup>2</sup>Suzhou Institute of Nanotech and Nano-bionics, China

Easy-to-fabricate, low-power and low-voltage thin-film-transistors (TFTs) that allow robust (complementary/complementary-like) circuit integration are highly sought-after for the development of off-the-grid smart sensors for the Internet of Things (IoT) ecosystem (1). Semiconducting single walled carbon nanotubes (sc-SWCNT) are a promising semiconductor material for TFTs with high field-effect mobilities and capable of low-voltage operation (2). However, fabricating sc-SWCNT TFT electronics with complementary (CMOS) characteristics typically requires complex fabrication processes, due to the several materials solutions (e.g. selective doping, different contact metals, multiple capping layers) required to this end, which also result in extra process steps (3). In this talk, we present our findings on the capability of ambipolar semiconducting single-walled carbon nanotube network (sc-SWCNTN) TFTs to deliver electronics that is easy-to-fabricate, low-power, (ultra-)low-voltage, and complementary-like. Our ambipolar TFTs comprise a sc-SWCNTN active layer deposited and patterned via aerosol-jet printing—with a maximum processing temperature of 120 °C—atop self-assembled monolayer (SAM)/AlO<sub>x</sub> hybrid nanodielectrics. These TFTs exhibit symmetric ambipolar characteristics with balanced electrons and hole mobilities in the neighborhood of 10 cm<sup>2</sup> V<sup>-1</sup> s<sup>-1</sup>, along with an onset voltage near 0 V and threshold voltages of < 1 V, all which enables these devices to operate within a voltage range of ~ 1 V.

The significance of our ambipolar sc-SWCNTN devices for low-voltage TFT electronics is assessed both experimentally and theoretically. We firstly discuss the impact of two key TFT parameters—subthreshold slope and flatband voltage—on the voltage and power requirements of circuits based on our ambipolar sc-SWCNTN TFTs. Moreover, by connecting our sc-SWCNTN TFTs in CMOS fashion, we demonstrate experimentally that the resultant inverters and NAND gates deliver CMOS-like performance with positive noise margins at supply voltages (V<sub>DD</sub>) as low as 0.5 V and up to 2 V. On the high end of this V<sub>DD</sub> range, inverter gates achieve gains > 80 V/V and bandwidths exceeding 100 kHz. Additionally, on the low end of this V<sub>DD</sub> range, inverters are able to operate with subnanowatt static power dissipation, which is well aligned with the power requirements of off-the-grid applications. Importantly, in addition to its cutting-edge capabilities, our CMOS-like integration comes with the inherent advantage of using one single semiconductor for both *n*-channel and *p*-channel conduction, which allows a streamlined fabrication process compared to alternative approaches reported in the literature (e.g., involving dopants, different capping layers, different source and drain contact materials). In summary, we demonstrate that the combination of printed sc-SWCNTs and hybrid SAM nanodielectrics provides an attractive route to the realization of ambipolar sc-SWCNT TFT CMOS-like circuits for low-voltage/(ultra-)low power electronics.

#### References

1. J. A. Cardenas, J. B. Andrews, S. G. Noyce, A. D. Franklin, Carbon nanotube electronics for IoT sensors. *Nano Futur.* **4**, 012001 (2020).
2. P. Prakash, K. Mohana Sundaram, M. Anto Bennet, A review on carbon nanotube field effect transistors (CNTFETs) for ultra-low power applications. *Renew. Sustain. Energy Rev.* **89**, 194–203 (2018).
3. Y. Yang, L. Ding, J. Han, Z. Zhang, L.-M. Peng, High-Performance Complementary Transistors and Medium-Scale Integrated Circuits Based on Carbon Nanotube Thin Films. *ACS Nano.* **11**, 4124–4132 (2017).

#### SESSION F.SF04.03: Printing Process

On Demand Abstracts Available for Viewing Starting Saturday Morning, November 21, 2020

F-SF04

### 5:00 AM \*F.SF04.03.01

**Laser Printing of Functional Materials** Oana D. Jurchescu; Wake Forest University, United States

The past decades have witnessed a commendable progress in the development of materials for low-cost flexible electronics.



New products that are beyond reach with current technologies can soon become a mainstay in our lives if these materials reach the necessary standards for performance and stability. The development of processing techniques that can address the manufacturability – scalability – sustainability – performance balance represents the next key step in the integration of these materials into next-generation electronic devices. In this presentation, I will introduce the use of laser printing, a rapid, scalable, environmentally friendly and low-cost manufacturing technique for deposition and patterning of various functional materials on flexible substrates. The first example focuses on organic semiconductors, and I will discuss the fabrication and characterization of organic thin-film transistors placed on plastic and paper. Aerosol spray laser lithography was used to define the electrodes, in conjunction with different metal inks: the pattern was created using a regular toner, which was subsequently selectively removed. We created a grid of transistor devices with variable channel lengths and widths and obtained good charge carrier mobilities and an excellent tolerance to bending. Next, I will describe the use of laser printing for the fabrication of metal halide perovskite films. The electrical properties of the laser printed films were comparable with those of the spin-coated layers, despite the fact that the microstructure consists of randomly oriented crystallites. The current-voltage characteristics exhibit negligible hysteresis and the electrical properties of the films are very stable under ambient conditions due to the fact that a vertical separation of the toner components results in an encapsulating the perovskite layer by the other toner components. Our work introduces an exciting new avenue for the fabrication of stable perovskite devices that is scalable and devoid of hazardous solvents.

#### 5:15 AM \*F.SF04.03.02

**Processing Fundamentals for Self-Aligned Flexible Printed Electronics** Krystopher Jochem, Motao Cao, Panayiotis Kolliopoulos, Xiaochen Ma, Satish Kumar, Daniel Frisbie and Lorraine F. Francis; University of Minnesota Twin Cities, United States

Continuous, roll-to-roll (R2R) printing processes are attractive for manufacturing of flexible electronics. Two common challenges with R2R are reaching small feature sizes and achieving precise registration of multiple functional layers in devices such as transistors. This presentation will cover our efforts to overcome these issues using Self-Aligned Capillarity-Assisted Lithography for Electronics (or SCALE). SCALE has two steps. In the first step, R2R imprinting is used to create a multilevel open network of reservoirs, capillaries and device structures into a UV-curable coating deposited on a flexible substrate. In the second step, electronically functional inks are then delivered sequentially into the reservoirs on this imprinted substrate by inkjet printing, and capillarity pulls inks into capillaries and device structures. Since the imprint stamps are fabricated from high-resolution, Si master patterns created by photolithography, the features created in the imprint resin are also high-resolution, at the micron scale. The single imprinting step also simultaneously creates all the structural features needed to control the flow and deposition of multiple inks, resulting in self-alignment of multiple materials in complex multilayer devices.

To-date we have developed SCALE methods to create conductive networks, resistors, capacitors, diodes and transistors. For example, to manufacture high aspect ratio (thickness/width) SCALE conductive networks, we used a combination of inkjet delivery of a silver particle-free ink into reservoirs of the imprinted substrate, followed by capillary flow and thermal annealing to convert the ink to a silver seed layer and lastly electroless copper plating to build conductor thickness in capillary channels. By optimizing processing conditions and understanding the fundamentals of capillary flow, narrow (e.g., 10  $\mu\text{m}$ ), high aspect ratio ( $>1$ ), low resistance ( $\sim 1$  ohm per cm of conductor length) embedded conductive traces were created. This presentation will show advances in device architecture and performance, and explore the key processing steps. Special attention will be given to continuous roll-to-roll processes.

#### 5:30 AM F.SF04.03.04

**Ink Engineering for Color-Selective Printed Organic Photodiodes and Filterless Multichannel Visible Light Communication** Noah Strobel<sup>1,2</sup>, Nikolaos Droseros<sup>3</sup>, Wolfgang Köntges<sup>4</sup>, Mervin Seiberlich<sup>1,2</sup>, Manuel Pietsch<sup>1,2</sup>, Stefan Schliske<sup>1,2</sup>, Rasmus Schroeder<sup>4</sup>, Ulrich Lemmer<sup>1,2</sup>, Martin Pfannmöller<sup>4</sup>, Natalie Banerji<sup>3</sup> and Gerardo Hernandez-Sosa<sup>1,2</sup>; <sup>1</sup>Karlsruhe Institute of Technology, Germany; <sup>2</sup>InnovationLab, Germany; <sup>3</sup>University of Bern, Switzerland; <sup>4</sup>Universität Heidelberg, Germany

Organic photodiodes (OPDs) are particularly well suited for future optical sensing technologies in the fields of mobile, wearable and skin-like electronics as they enable chemically tunable optoelectronic performance and fabrication by digital printing techniques on mechanically compliant substrates.<sup>(1)</sup> However, OPDs have typically utilized active layers developed for photovoltaic applications exhibiting broad absorption range and lacking the spectral selectivity necessary in fields like imaging or communication which require optical detectors that can distinguish between different wavelengths. To solve this, common approaches have relied on device engineering methods which result in devices with increased fabrication complexity.

This work introduces a general solution for inkjet-printing wavelength-selective bulk-heterojunction (BHJ) photodetectors through engineering of the ink formulation and demonstrate its potential for Visible Light Communication (VLC).<sup>(2)</sup> Non-fullerene acceptors (NFAs) are incorporated in a transparent semiconductor polymer donor matrix to narrow and tune the response in the visible range without optical filters or light-management techniques. In this approach, the device spectral response solely depends on the choice of the NFA while the polymer donor dictates the rheological properties of the ink. Thus, this approach effectively decouples the optical response from the viscoelastic ink properties, simplifying process development. A thorough morphological and spectroscopic investigation of the novel BHJ systems finds excellent charge-carrier dynamics enabling responsivities up to  $230 \text{ mA W}^{-1}$ . This state-of-the-art response combined with high bandwidths  $>1.5 \text{ MHz}$ , allows effective application in a VLC system. In this system, the complementary color-selectivity of the devices enables successful demultiplexing of simultaneously transmitted optical signals without the need of any additional optical filters or light-management techniques.

(1) N. Strobel, M. Seiberlich, R. Eckstein, U. Lemmer, G. Hernandez-Sosa, Organic photodiodes: printing, coating, benchmarks, and applications. *Flex. Print. Electron.* **4**, 043001 (2019).

(2) N. Strobel, N. Droseros, W. Köntges, M. Seiberlich, M. Pietsch, S. Schliske, F. Lindheimer, R. R. Schröder, U. Lemmer, M. Pfannmöller, N. Banerji, G. Hernandez-Sosa, Color-Selective Printed Organic Photodiodes for Filterless Multichannel Visible Light Communication. *Adv. Mater.* **32**, 1908258 (2020).

#### 5:40 AM F.SF04.03.05

**Late News: High Yield Manufacturing of Fully Screen Printed Organic Electrochemical Transistors** Marzieh Zabihipour<sup>1</sup>, Roman Lassnig<sup>2</sup>, Jan Strandberg<sup>2</sup>, Magnus Berggren<sup>1</sup>, Simone Fabiano<sup>1</sup>, Isak Engquist<sup>1</sup> and Peter Andersson Ersman<sup>2</sup>; <sup>1</sup>Linköping University, Sweden; <sup>2</sup>RISE Research Institutes of Sweden, Sweden

The potential of the screen printing method for large-scale production of organic electrochemical transistors (OECTs), combining high production yield with low cost, is here demonstrated. Fully screen printed OECTs of  $1 \text{ mm}^2$  area, based on poly(3,4-ethylenedioxythiophene) doped with poly(styrenesulfonate) (PEDOT:PSS), have been manufactured on flexible PET substrates. The goal of this project effort has been to explore and develop the printing processing to enable high yield and stable transistor parameters, targeting miniaturized digital OECT circuits for large scale integration (LSI). Of the 760 OECTs manufactured in one batch on a PET sheet, only 2 devices were found malfunctioning, thus achieving an overall manufacturing yield of 99.7 %. A drain current ON/OFF ratio at least equal to 400 was applied as the strict exclusion principle for the yield, motivated by proper operation in LSI circuits. This consistent performance of low-footprint OECTs allows for the integration of PEDOT:PSS-based OECTs into complex logic circuits operating at high stability and accuracy.

#### SESSION F.SF04.04: Optoelectrics

On Demand Abstracts Available for Viewing Starting Saturday Morning, November 21, 2020

F-SF04

#### 5:00 AM \*F.SF04.04.01

**Organic Infrared Sensors and Energy Storage Capacitors Based on Narrow Bandgap Polymers** Tse Nga Ng<sup>1</sup>, Ning Li<sup>1</sup>, Lulu Yao<sup>1</sup>, Kaiping Wang<sup>1</sup> and Jason D. Azoulay<sup>2</sup>; <sup>1</sup>University of California San Diego, United States; <sup>2</sup>University of Southern Mississippi, United States

Narrow bandgap polymers are used to realize infrared photodetectors that is relevant to a variety of applications including environmental monitoring and medical diagnosis. To achieve high detectivity in detectors, it is critical to reduce the device noise. This talk presents experimental and modeling studies on the noise current in exemplar organic bulk heterojunction photodiodes, with 10 donor-acceptor combinations spanning wavelength between 800 and 1600 nm. A significant reduction of the noise and higher detectivity were found in devices using non-fullerene acceptors (NFAs) in comparison to those using fullerene derivatives. The low noise in NFA blends was attributed to a sharp drop off in the distribution of bandtail states, as revealed by variable-temperature density-of-states measurements. Taking disorder into account, we developed a general physical model to explain the dependence of thermal noise on the effective bandgap and bandtail spread.

The narrow bandgap polymers are also Faradaic materials for energy storage and present opportunities to create energy dense

supercapacitors. The vast majority of conducting polymers are p-type, and here we present promising n-type polymers that are stable when operating within a large potential window (3V), with a best-in-class energy densities (30.4 Wh/kg at a 1 A/g discharge rate), and a long cycle life (90% capacitance retention after 5000 cycles) critical to energy storage and management. This work demonstrates the application of a new class of stable and tunable redoxactive material to realize high-endurance energy storage devices for flexible printed systems.

#### 5:15 AM \*F.SF04.04.02

**Amplified Spontaneous Emission and Lasing in Quasi-2D Perovskites** Franky So and Kenan Gundogdu; North Carolina State University, United States

Recently, metal-halide perovskite materials are considered as a promising candidate for lasing applications. Compared to 3D and other low-dimensional perovskites, quasi-2D perovskites are a better gain media due to its unique properties such as large binding energy and self-assembled quantum wells. Specifically, efficient energy funneling from low-dimensional domains to high-dimensional domains will not only enhance the radiative recombination but also facilitate population inversion.

In this presentation, we will discuss the fundamental requirements for population inversion in perovskites in the context of material dimensionality and morphology. We will also present our recent work on laser cavity design and processing for optimum laser performance.

#### 5:30 AM F.SF04.04.03

**Solution-Processed Photoelectrochemical (PEC)-Type Photodetectors Based on Layered Metal Monochalcogenides (GaS, GaSe, GeSe)** Gabriele Bianca<sup>1,2</sup>, Marilena I. Zappia<sup>3,4</sup>, Sebastiano Bellani<sup>1,3</sup>, Michele Serri<sup>1</sup>, Leyla Najafi<sup>1,3</sup>, Nicola Curreli<sup>1</sup>, Beatriz Martin-Garcia<sup>1</sup>, Reinier Oropesa-Nunez<sup>3</sup>, David Sedmidubsky<sup>5</sup>, Vittorio Pellegrini<sup>1,3</sup>, Zdenek Sofer<sup>5</sup>, Anna Cupolillo<sup>4</sup> and Francesco Bonaccorso<sup>1,3</sup>; <sup>1</sup>Istituto Italiano di Tecnologia, Italy; <sup>2</sup>Università degli Studi di Genova, Italy; <sup>3</sup>Bedimensional Spa, Italy; <sup>4</sup>Università della Calabria, Italy; <sup>5</sup>University of Chemistry and Technology Prague, Czechia

The conversion of light energy into electricity and chemical fuels through photoelectrochemical (PEC) cells represents a powerful strategy for sustainable fuel and chemical generation, environmental remediation (*i.e.*, pollutant degradation), advanced analytical systems (*i.e.*, chemical sensors) for environmental and biological monitoring, as well as innovative self-powered photodetectors. In particular, aqueous PEC cells, including water splitting ones, are emerging for the development of cheap, easily fabricated, environmentally friendly self-powered photodetectors with high spectral responsivity. In this context, two-dimensional (2D) materials, including either single- and few-layer flake forms, are continually attracting utmost interest as potential advanced photo(electro)catalysts. Recently, group-III and group-IV transition metal monochalcogenides, which can be exfoliated in 2D form due to their low cleavage energy (typically  $< 0.5 \text{ J m}^{-2}$ ), have been theoretically predicted to be water splitting photocatalysts. In fact, their 2D nature intrinsically guarantees that the charge carriers are directly photogenerated at the interface with the electrolyte, where redox reactions take place before they recombine. Moreover, their electronic structure can be tuned by controlling the number of the layers to fulfil the fundamental requirements for water splitting photocatalysts, *i.e.*: 1) conduction band minimum (CBM) energy ( $E_{\text{CBM}}$ )  $>$  reduction potential of  $\text{H}^+/\text{H}_2$  ( $E(\text{H}^+/\text{H}_2)$ ); 2) valence band maximum (VBM) energy ( $E_{\text{VBM}}$ )  $<$  reduction potential of  $\text{O}_2/\text{H}_2\text{O}$  ( $E(\text{O}_2/\text{H}_2\text{O})$ ). Among them, low-cost and environmentally friendly layered gallium sulfide (GaS), gallium selenide (GaSe) and germanium selenide (GeSe) are promising materials candidate for optoelectronic devices due to their properties: tunable electronic structure, strong visible-light absorbance, significant photoresponse due to direct-bandgap transitions, photoferroelectricity and environmental stability. Here, we report the first experimental characterization of the PEC water splitting activity of single-/few-layer flakes of GaS, GaSe and GeSe produced in form inks by scalable liquid-phase exfoliation (LPE) approach in non-toxic solvents. The as-produced dispersions were deposited by spray-coating technique to conceive solution-processed self-powered PEC-type photodetectors. The PEC behaviour of MCs-based photoelectrodes was evaluated in different aqueous media, ranging from acidic to alkaline solutions: 0.5 M  $\text{H}_2\text{SO}_4$  (pH 0.3), 1 M  $\text{Na}_2\text{SO}_4$  (pH 6), 1 M KCl (pH 6.5), 1 M KOH (pH 14) under different illumination wavelengths in the visible spectral range, namely 455, 505 and 625 nm. Moreover, due to its large band gap, GaS was also tested under UV radiation (275 nm) obtaining an UV photodetector without using any visible light filter. Instead, GaSe and GeSe photoelectrodes show a responsivity up to  $\sim 0.16 \text{ A W}^{-1}$  and  $\sim 0.32 \text{ A W}^{-1}$ , respectively, upon 455 nm illumination at light intensity up to  $63.5 \mu\text{W cm}^{-2}$ . The obtained performances are superior to those of several self-powered and low-voltage solution-processed photodetectors, approaching the ones of self-powered commercial UV-Vis photodetectors. Our results can open the way towards the use of 2D metal monochalcogenides in innovative PEC systems, (bio)sensors and other innovative optoelectronics devices.

#### 5:40 AM F.SF04.04.04

**Mantis-Shrimp Inspired Multispectral and Polarimetric Imaging Achieved Using Highly Polarized Organic**

**Photodetectors** [Harry Schrickx](#)<sup>1</sup>, Ali Altaqui<sup>1</sup>, Pratik Sen<sup>1</sup>, Jeromy Rech<sup>2</sup>, Jin-Woo Lee<sup>3</sup>, Michael Escuti<sup>1</sup>, Wei You<sup>2</sup>, Bumjoon J. Kim<sup>3</sup>, Robert Kolbas<sup>1</sup>, Michael Kudenov<sup>1</sup> and Brendan T. O'Connor<sup>1</sup>; <sup>1</sup>North Carolina State University, United States; <sup>2</sup>University of North Carolina at Chapel Hill, United States; <sup>3</sup>Korea Advanced Institute of Science and Technology, Korea (the Republic of)

Multispectral and polarimetric imaging provides invaluable information undetectable by the human eye, leading to significant advancements in fields that include biomedical imaging, astronomy, and agriculture. Current methods for snapshot multispectral and polarization imaging require an array of adjacent pixels to create a super-pixel, where each pixel serves to measure a subset of the optical information. However, this super-pixel suffers from significant spatial and sampling error. To overcome these limitations, we introduce a new detector strategy inspired by stomatopods, or mantis shrimp. Mantis shrimp display one of the most intricate vision systems in nature, featuring 16 types of photoreceptor cells capable of perceiving light ranging from UV to far-red, as well as polarized light. We refer to our sensor as a Stomatopod-Inspired Multispectral and POLarization (SIMPOL) sensor. The SIMPOL sensor leverages two key technologies: (1) polarization sensitive semitransparent organic photovoltaics (P-OPVs), and (2) folded retarder (FR) films. The FRs enable finely tuned polarization rotation for different wavelengths of light. The P-OPVs then preferentially sense light polarized with a specific orientation. By pairing the P-OPVs and FRs, we create a versatile sensing platform for narrow optical bandwidth detection and polarization sensing. The SIMPOL detector design consists of a cascading series of P-OPVs and FRs and share many features of the mantis shrimp eye, enabling the realization of multispectral and polarization sensing in a single pixel for the first time.

The function of the SIMPOL sensor is critically dependent on the performance of the P-OPVs, which are required to be highly polarized, and highly transparent along the non-absorbing electric field orientation. The polarization sensitivity of these devices is achieved by orienting the polymer semiconductors in the plane of the film. Here, we introduce a strategy of high temperature rubbing on a low molecular weight all-polymer bulk heterojunction film to achieve a high degree of in-plane alignment. We demonstrate a blend of PBnDT-FTAZ and P(NDI2OD-T2) subjected to the high temperature rubbing results in dichroic ratios of over 18 and photocurrent ratios of over 7 when under orthogonally polarized illumination. This represents the most polarization sensitive OPVs demonstrated to date. The SIMPOL sensor consists of six stacked P-OPVs enabling the detection of four spectral channels with a spectral resolution of up to 16.9 nm, while simultaneously measuring the linear polarization state of the light. We demonstrate the potential of the SIMPOL detector by imaging a scene that includes broad spectral and polarization features, representing a significant advancement in spectral and polarization imaging.

#### SESSION F.SF04.05: Industry and Circuits

On Demand Abstracts Available for Viewing Starting Saturday Morning, November 21, 2020

F-SF04

#### 5:00 AM \*F.SF04.05.01

**Renect Progress in the Design of Shape Free Displays** [Jongho Hong](#), Jae Min Shin, Sang-Woo Kim, Jangyeol Yoon, Sung-Chan Jo, Changhee Lee and Jinoh Kwag; Samsung Display, Korea (the Republic of)

Recently, the development of the existing flat panel display technology has reached an extreme level, interest in the new display form factor has been increased more than ever. Since those researches began, foldable display, which has been successful in establishing itself in the mobile display market since 2019. In addition to the design aspect, it succeeded in receiving the customer's choice in terms of functionality, such as the expansion of the screen, and is expected to continue to develop in the future. Rollable display technology is also expected to be applied to various products in near future beyond the research level.

In the last decade, stretchable display technologies have attracted much attention as a next step after foldable and rollable displays. A stretchable display capable of realizing a free-form that is impossible with existing display technology is expected to be applied as a field of new products. Free-form display, as a high potential and challenging research field, have brought interest to the issue of how to make stretchable behavior that offer both durable and reliable characteristics with conventional and/or newly developed electronic materials. Although there were several efforts to make intrinsic stretchable display based on soft materials with stretchable electronics, the resolution of pixel images and long-life stability should be improved.

We report on the latest advances in stretchable display based on OLED technology and discuss the recent progress in the design of stretchable display by comparing the key design consideration in terms of substrate, materials, and geometries. We will also introduce the freeform stretchable display based on low temperature poly-silicon (LTPS) active-matrix OLED

(AMOLED) technology. This research has introduced a stretchable display that operates normally without degradation of image quality even after convex or concave static formed shaping using a low-temperature vacuum thermoforming process. In addition, repetitive deformation was applied in a vertical direction to stretch the center of the display panel while the panel was in operation. After applying tensile elongation up to 50,000 cycles using a repetitive stretching machine, no significant difference was observed in the color coordinate measurement depending on the deformation.

#### 5:15 AM \*F.SF04.05.02

**Conformable Imager for Biometric Data Measurement** Tomoyuki Yokota and Takao Someya; The University of Tokyo, Japan

With the rapid aging of Japanese society, how to increase quality of life (QoL) while controlling rising medical expenses has become an urgent issue. To solve this difficult issue, the acquisition and utilization of biological information using new technologies such as wearable devices is more expected. In particular, self-care and home medical care, in which patients and their families are responsible for their own health, are considered as one of the way to solving the issues of a super-aging society. Indeed, wearable sensors that can constantly monitor health conditions and home-use blood pressure monitors with communication functions are being introduced to the market one after another to prepare for the advent of a self-care era. On the other hand, when designing a new insurance system or incentive system using biometric information from wearable sensors, it is important issue how to confirm whether data measured at home is the patient's own. Furthermore, the risk of patient mix-ups must be reduced as more wearable devices come to be used in hospitals and welfare facilities in the future. Therefore, measuring vital signs simultaneously with biometric authentication of the user is an urgent issue.

We have developed a sheet-type image sensor that enables high-resolution and high-speed reading. This sheet-type image sensor can take the high-resolution image of fingerprints and veins used for biometric authentication. In addition, the same sheet-type imager can measure the pulse wave which is one of the vital signs, and its distribution.

Although there are many reports of sheet-type image sensors, it has not been achieved both high-resolution imaging and high-speed readout, and static biometric data and dynamic vital signs cannot be measured by one sheet-type image sensor. This is because high-sensitivity photodetectors and high-speed switching elements could not be integrated on a polymer substrate without damaging of the switching elements.

The developed sheet-type image sensor is fabricated by densely integrating a high-efficiency readout circuit using an active matrix of a low-temperature polysilicon thin film transistor and a photodetector that uses a highly efficient organic semiconductor as a photosensitive layer. The resolution of the image sensor achieves 508 dots per inch (dpi) required for fingerprint authentication, and the organic photodetector consists of bulk hetero structure organic layer which has high photosensitivity to near infrared light with a wavelength of 850 nanometers (external quantum efficiency of 50% or more). It is easy to integrate the sheet-type image sensor into equipment and attach it to curved surfaces due to the thickness of the polymer base material is 10 micrometers, and the total thickness of the sheet-type image sensor is 15 micrometers (Figure 1). By developing a process technology that integrates photodetectors and thin-film transistors without damage to each other, it has become possible to realize a sheet-type image sensor that achieves both high-resolution imaging and high-speed reading. Evaluation of vein and fingerprint images taken by this sheet-type image sensor showed that the contrast difference of the veins was less than 5% compared to images using a general CMOS imager. We confirmed that the conformable imager has high image quality equivalent to that of conventional CMOS imagers.

Since the sheet-type image sensor is thin and bendable, it can be easily integrated into wearable devices, and it is possible to measure health condition and perform biometric authentication at the same time. As a result, it is expected that prevention of "spoofing" and patient from being mixed up.

#### 5:30 AM \*F.SF04.05.03

**Design Requirements for Flexible TFT-Based Logic Applications** Kris Myny<sup>1,2</sup>; <sup>1</sup>imec, Belgium; <sup>2</sup>KU Leuven, Belgium

In last decades, the research on flexible logic circuits based on thin-film transistors (TFTs) have been increasingly growing as technologies tend to stabilize enabling application-oriented research. Although backplane applications such as active matrix displays and 2-D imager arrays are the main driver for technology developments, logic applications also benefit from increased performance. In this invited presentation, I will elaborate on several design requirements for TFT-based logic circuits and link them to technology and material requirements.

The focus of this work will be in the direction of flexible IoT applications, ranging from radio-frequency communication chips to sensor readout circuitry to monitor vital parameters. All demonstrated flexible integrated circuits have been realized in a dual-gate self-aligned a-IGZO TFT technology. The main advantage of a self-aligned transistor is the strongly reduced parasitic overlap capacitance between gate and source-drain contacts, enabling faster circuit blocks consuming less power.

Consequently, we have demonstrated a flexible IGZO-based NFC communication tag connecting to an NFC-enabled smartphone [1]. In recent work, we have been updating our design libraries with substantially lower power consumption and realized a capacitive tag that communicates directly with the touchscreen of a smartphone as an enabler for the Internet-of-Everything [2]. This tag has been made self-powered by integrating a flexible Perovskite photovoltaic cell that captures the energy from the smartphone screen which powers the chip.

The dual-gate self-aligned transistor provides a designer with an additional benefit, namely the presence of an extra gate. The backgate can be employed for several different purposes: to increase the transconductance, to improve the output resistance or to control the threshold voltage. Most of these design considerations are mainly interesting for analogue circuits, for example to improve the gain of an operational amplifier. As a third case in this presentation, I will discuss our recent achievements on a flexible ECG patch with NFC compatibility for healthcare monitoring patches [3]. Finally, as the newest technology developments move in the direction of increased charge carrier mobilities, matching p-types and low-temperature polysilicon and oxides (LTPO), I will elaborate on the future enabling opportunities for TFT-based logic circuits and applications.

### References

- [1] K. Myny, “The development of flexible integrated circuits based on thin-film transistors”, Nature Electronics 1, pp. 30-39 (2018)
- [2] N. Papadopoulos, et al.; “Touchscreen tags based on thin-film electronics for the Internet of Everything”, Nature Electronics 2, pp. 606-611 (2019)
- [3] M. Zulqarnain, et al.; “A flexible ECG patch with NFC compatible RF communication”, accepted to Flexible Electronics (npg)

*Acknowledgement* – I would like to thank my coworkers at imec and TNO/Holst centre; M. Zulqarnain and E. Cantatore from TUE for their valuable contributions to this work. Part of this work has received funding from the European Research Council (ERC) under the European Union's Horizon 2020 research and innovation program under grant agreement No 716426 (FLICs project).

### 5:45 AM F.SF04.05.04

**Patchable 3D Motion Tracking Magneto-Interactive Electroluminescence Display** Seung Won Lee, Chanho Park, Hyeokjung Lee, Kyuho Lee and Cheolmin Park; Yonsei University, Korea (the Republic of)

Development of a human-interactive display that enables the simultaneous sensing, visualisation, and memorisation of a magnetic field has attracted significant attention because it offers control and easy access to information that is rarely available. This study demonstrates a magneto-interactive electroluminescent display patchable on skin, which is capable of sensing, visualising, and storing magnetic field information, thereby enabling 3D motion tracking. For this purpose, a magnetic field-dependent conductive gate is employed in an alternating current electroluminescent (EL) display, which is used to produce non-volatile and rewritable magnetic field-dependent EL display. By constructing mechanically flexible arrays of non-volatile magneto-interactive EL displays, a skin-patchable and pixelated platform is realised. The unique feature of magnetic field varying along the z-axis enables the 3D motion tracking (monitoring and memorisation) on 2D pixelated display. This 3D motion tracking display is successfully used as a non-destructive surgery-path guiding display, wherein a pathway for a surgical robotic arm with a magnetic probe is visualised and recorded on a display patched on the abdominal skin of a rat, thereby helping the robotic arm to find an optimal pathway without damage incurred on the path to the surgery spot.

SESSION F.SF04.06: Oxide and Inorganics

On Demand Abstracts Available for Viewing Starting Saturday Morning, November 21, 2020  
F-SF04

### 5:00 AM \*F.SF04.06.01

**Various Solution Processing Methods for Boosting Electrical Performance of Metal-Oxide-Based Thin-Film Transistors and Phototransistors** I Sak Lee, Dong Hyun Choi, Dongwoo Kim and Hyun Jae Kim; Yonsei Univ, Korea (the Republic of)

Oxide thin-film transistors (TFTs) have attracted much attention for next-generation electronics because of their superior performance compared with conventional a-Si TFTs such as high mobility and optical transmittance in the visible light. Particularly, solution process is a promising technique for the oxide TFT fabrication method for being a low-cost method with high composition controllability, high throughput, and various application. In this study, we propose various researches to improve the electrical and optical performances in oxide TFTs. Furthermore, we suggest a solution-processed oxide absorption layer (SAL) to enable detection of visible light for oxide phototransistors.

#### Voltage-Based Ambi-Ionic Migration (VAM) for Modulating Active Layer

The voltage-based ambi-ionic modulation (VAM) technique allows specific ions to migrate into the active layer by applying bias, easily modulating the active layer. Also, the potassium superoxide ( $\text{KO}_2$ ) solution is employed in oxide thin-film transistors (TFTs) as a source of potassium ( $\text{K}^+$ ) ions and highly reactive superoxide radical ( $\text{O}_2^{\bullet-}$ ) ions. By applying external bias, the  $\text{K}^+$  and  $\text{O}_2^{\bullet-}$  ions rapidly migrate into the active layer, directly changing its electrical properties and chemical composition. Through the VAM technique, various metal-oxide-based devices such as oxide TFTs can perform better.

#### Multifunctional Heterogeneous Organic (MHO) Passivation Layer for Oxide TFT

We propose a highly flexible and reliable multifunctional heterogeneous organic (MHO) passivation layer composed of stacked diketopyrrolopyrrole (DPP)-polymer and parylene-C films for improving the stability of oxide TFTs under various ambient environments and mechanical stress. The presented MHO passivation layer leads to high-performance oxide TFTs by: (1) protecting them from external reactive molecules, (2) blocking light to the oxide layer, and (3) improving their electrical characteristics. As a result, oxide TFTs with MHO passivation layer exhibit higher stability in ambient environment and under light. Moreover, since the MHO passivation layer can be deposited at room temperature and exhibits high mechanical stability, it could be practical in the fabrication of flexible/wearable devices.

#### Selective modulation of electrical characteristics by electro-hydro-dynamic printing

A simple fabrication method for homojunction-structured Al-doped indium–tin oxide (ITO) thin-film transistors (TFTs) using an electro-hydro-dynamic (EHD) jet-printed  $\text{Al}_2\text{O}_3$  passivation layer with a specific line ( $W_{\text{Al}_2\text{O}_3}$ ) is proposed. After EHD jet-printing, the specific region of ITO where  $\text{Al}_2\text{O}_3$  is printed changes from a conducting film to a semiconducting film while  $\text{Al}_2\text{O}_3$  acts as passivation layer. The channel length of the fabricated TFTs is defined by  $W_{\text{Al}_2\text{O}_3}$  which is easily changed with varying EHD jet printing conditions, replacing masks with varying patterns. Consequently, the proposed approach is promising as a low-cost and flexible manufacturing system for multi-item small-lot-sized production of Internet of Things devices.

#### Solution-Processed Oxide Absorption Layer (SAL) for Visible-Light Detecting Phototransistor

We propose a solution-processed oxide absorption layer (SAL) for visible-light (532 and 635 nm) detection for indium–gallium–zinc oxide (IGZO) phototransistors. The SAL was deposited onto the sputtered IGZO using precursor solutions composed of the same atomic configuration of sputtered IGZO, resulting in superior interface characteristics. We artificially generated sub-gap states in the SAL using a low temperature (200°C) annealing, minimizing the degradation of the electrical characteristics of TFT. These sub-gap states in SALs improved the photoelectron generation under long-wavelength visible-light despite the wide bandgap of IGZO (over 3.0 eV). As a result, the IGZO phototransistors with SALs have both superior optoelectronic characteristics and high optical transparency.

#### 5:15 AM \*F.SF04.06.02

**Electron and Hole Transport in Methyl Ammonium Lead Iodide** Mohammad Sajedi Alvar, Gert-Jan Wetzelaer and Paul W. Blom; Max Planck Institute for Polymer Research, Germany

Hybrid organic-inorganic perovskites are promising materials for the application in solar cells and light-emitting diodes. However, the basic current-voltage behavior for electrons and holes is still poorly understood in these semiconductors due to their mixed electronic-ionic character. To develop an experimentally-validated numerical device model, it is therefore necessary to isolate individual physical phenomena. We investigate the dynamics of ion motion in methyl ammonium lead iodide ( $\text{MAPbI}_3$ ) by impedance spectroscopy and electric displacement as a function of frequency. The displacement response is fully reproduced by a numerical device model that enables us to determine the frequency-dependent dielectric constant, the ion concentration and the ion diffusion coefficient. These validated ion dynamics are applied to analyze space-charge-limited electron and hole currents in  $\text{MAPbI}_3$ . We demonstrate that the frequency dependence of the permittivity plays a crucial role in the analysis of space-charge-limited currents and their dependence on voltage scan rate. Our mixed electronic-ionic device model accurately reproduces the current-voltage characteristics of single-carrier devices, showing that in  $\text{MAPbI}_3$  transport of electrons dominates over holes.

### 5:30 AM F.SF04.06.03

**High-Performance Carbon-Free Solution-Processed Oxide TFTs Fabricated by Direct Patterning** Masashi Miyakawa, Mitsuru Nakata, Hiroshi Tsuji and Yoshiki Nakajima; NHK Science & Technology Research Laboratories, Japan

Facile solution-processing of metal oxide thin-film transistors (TFTs) is a promising alternative to conventional vacuum-processing and offers various advantages, such as low cost, large-area fabrication capability, and process simplicity.<sup>1</sup> The patterning of such films is necessary for device integration; however, most solution-processing is still conducted using traditional photolithographic patterning processes. A simple and reliable direct patterning method is a key technological requirement to maximize the advantages of solution-processing.<sup>2</sup> We have previously reported a direct patterning method for an aqueous In-Ga-Zn oxide (IGZO) precursor.<sup>3</sup>

A direct patterning method to obtain high-performance carbon-free oxide TFTs using In-Zn oxide (IZO) and In-oxide (InO) will be presented. Direct patterning is achieved by selective photoreaction of water molecules as a precursor solvent and nitrate ligands under ultraviolet irradiation without organic photosensitive additives. This environmentally-friendly chemical etching process uses a non-toxic organic acid (citric acid), followed by annealing at 350 °C, to obtain carbon-free oxide films of IZO and InO. TFTs with these oxide films on SiO<sub>2</sub> dielectrics that were fabricated by the direct patterning method and with sputtered Mo electrodes exhibited high mobilities of 11.5±1.6 cm<sup>2</sup>/Vs for IZO and 39.0±1.9 cm<sup>2</sup>/Vs for InO. The InO TFTs with solution-processed dielectrics using siloxane materials also exhibited good switching characteristics and a mobility of more than 30 cm<sup>2</sup>/Vs. X-ray reflectivity and X-ray diffraction analysis of the InO film density and crystallinity indicated denser and larger crystallinity in the photo-patterned oxide films. Efficient photooxidation by optimization of the deposition conditions and precursor concentrations during UV exposure resulted in higher quality solution-processed oxide films.

1. E. Fortunato, P. Barquinha and R. Martins, *Adv Mater* **24** (22), 2945-2986 (2012).
2. H. S. Lim, Y. S. Rim and H. J. Kim, *Sci Rep* **4**, 4544 (2014).
3. M. Miyakawa, M. Nakata, H. Tsuji and Y. Fujisaki, *Sci Rep* **8** (1) (2018).

SESSION F.SF04.07: Poster Session: Solution-Processed Semiconductors and Devices for Form-free Displays, Logic and Sensors

On Demand Abstracts Available for Viewing Starting Saturday Morning, November 21, 2020

5:00 AM - 8:00 AM

F-SF04

### F.SF04.07.01

**Low-Voltage IGZO Thin-Film Transistors Using SAM Surface Modification on Ta<sub>2</sub>O<sub>5</sub> as the Gate Dielectric** Navid Mohammadian and Leszek A. Majewski; The University of Manchester, United Kingdom

Low-voltage, high-performance thin-film transistors (TFTs) have been getting tremendous attention over recent years due to the increasing demand for low-power, portable electronic devices and sensor arrays. However, reducing the power consumption of TFTs is an extremely challenging task [1]. High- $\kappa$  dielectric materials are thought to play an essential role in applications where a low-power device operation is needed.

In particular, tantalum pentoxide (Ta<sub>2</sub>O<sub>5</sub>) is a very promising candidate due to the high dielectric constant in the bulk ( $\kappa_{\text{bulk}} \sim 27$ ) and as a thin-film ( $\kappa_{\text{thin-film}} \sim 20$ ). These values are at least two times larger than that of Al<sub>2</sub>O<sub>3</sub> ( $\kappa_{\text{bulk}} \sim 9$ ) and five times larger than that of SiO<sub>2</sub> ( $\kappa_{\text{bulk}} \sim 3.9$ ) [2]. As a result, Ta<sub>2</sub>O<sub>5</sub> has been abundantly used in electrolytic capacitors, DRAM devices, and recently in solution-processed inorganic semiconductor thin-film transistors as a promising gate dielectric for low-power electronics [3].

whereas high- $\kappa$  insulators introduce undesirable effects at the semiconductor-insulator interface which generally leads to increased trapping which causes a rise of V<sub>TH</sub> and SS, as well as lowers the field-effect mobility of charge carriers in TFTs [4]. To overcome both issues in low voltage organic thin-film transistors (OTFTs) passivating of the high- $\kappa$  metal oxides surfaces with self-assembled monolayer (SAM) compounds is routinely used [5]. Although modification of ultra-thin ( $d \leq 20$  nm) metal oxide gate dielectrics with SAMs is currently a common process in organic TFTs [6], this approach has not yet been explored in metal oxide semiconductor transistors.

In this talk, low-voltage a-IGZO TFTs using solution-deposited, OTS-modified Ta<sub>2</sub>O<sub>5</sub> operating at 1 V are presented. The optimised devices display threshold voltages V<sub>TH</sub> around 0.4 V, subthreshold swings (SS) below 90 mV/dec, current on/off ratios larger than 10<sup>5</sup>, and field-effect mobility in excess of 2.3 cm<sup>2</sup>/Vs. The morphology and dielectric properties of both



pristine and OTS-treated thin Ta<sub>2</sub>O<sub>5</sub> films have been studied. It is shown that the proposed approach has a high potential to enable the design of stable, low-voltage organic semiconductor circuitry in a highly reproducible manner.

#### References

- [1] R. P. Ortiz, A. Facchetti, and T. J. Marks, "High-k organic, inorganic, and hybrid dielectrics for low-voltage organic field-effect transistors," *Chem. Rev.*, vol. 110, no. 1, pp. 205–239, 2010.
- [2] S. Ezhilvalavan and T. Y. Tseng, "Preparation and properties of tantalum pentoxide (Ta<sub>2</sub>O<sub>5</sub>) thin films for ultra large scale integrated circuits (ULSIs) application -- A review," *J. Mater. Sci. Mater. Electron.*, vol. 10, no. 1, pp. 9–31, Mar. 1999.
- [3] N. Mohammadian, S. Faraji, S. Sagar, B. C. Das, M. L. Turner, and L. A. Majewski, "One-Volt, Solution-Processed Organic Transistors with Self-Assembled Monolayer-Ta<sub>2</sub>O<sub>5</sub> Gate Dielectrics," *Materials (Basel)*, vol. 12, no. 16, p. 2563, 2019.
- [4] Q. Wang, W. Wang, S. Jin, H. Zhu, and N. T. Zhang, "Quality-optimized joint source selection and power control for wireless multimedia D2D communication using stackelberg game," *IEEE Trans. Veh. Technol.*, vol. 64, no. 8, pp. 3755–3769, 2015.
- [5] P. Barquinha *et al.*, "Low-temperature sputtered mixtures of high- $\kappa$  and high bandgap dielectrics for GIZO TFTs," *J. Soc. Inf. Disp.*, vol. 18, no. 10, pp. 762–772, 2010.
- [6] P. Sista *et al.*, "Enhancement of OFET performance of semiconducting polymers containing benzodithiophene upon surface treatment with organic silanes," *J. Polym. Sci. Part A Polym. Chem.*, vol. 49, no. 10, pp. 2292–2302, 2011.

#### F.SF04.07.02

**Direct Langmuir-Blodgett Deposition of Few-Layered 2H WSe<sub>2</sub> Flakes for Electrical Characterization** Madina Telkhozhayeva<sup>1</sup>, Rajashree Konar<sup>1</sup>, Eti Teblum<sup>1</sup>, Hagit Aviv<sup>1</sup>, Maria Tkachev<sup>2</sup>, Olga Girshevit<sup>2</sup>, Yaakov Tischler<sup>1</sup> and Gilbert D. Nessim<sup>1</sup>; <sup>1</sup>Bar-Ilan University, Israel; <sup>2</sup>Institute of Nanotechnology and Advanced Materials, Bar-Ilan University, Israel

Two-dimensional (2D) semiconductors have attracted extensive research interest due to their unique size, atomic thickness and band structure. In this respect, transition metal di-chalcogenides (TMDCs) are leading candidates because of strong in-plane chemical bonds and out-of-plane weak interactions. This allows them to be exfoliated into so-called 2D flakes, which can be micrometers wide but less than a nanometer thick. Among them, 2H-WSe<sub>2</sub> as a layered 2D material demonstrates remarkable properties such as low thermal conductivity, high carrier mobility, and direct band-gap, thus offering a suitable platform for next generation nanoscale devices [1-2].

Liquid-phase exfoliation (LPE) of bulk TMDCs can yield high-quality semiconducting flakes dispersed in commonly used solvents. Although a considerable number of research with LPE methods towards 2H-WSe<sub>2</sub> has been conducted, there are lack of reports on controlled organization of these exfoliated flakes on substrates. This step is crucial since produced 2H-WSe<sub>2</sub> flakes tend to restack into a bulk structure via van der Waals interactions, which significantly limit device applications. Langmuir-Blodgett (LB) assembly is an effective and easily integrated approach for arranging 2D flakes into highly ordered single-layer and multilayered films with controllable thickness, well-defined structure, and homogeneity.

Here, we present a cost-effective and facile technique for the controlled processing of 2D 2H-WSe<sub>2</sub> dispersions into uniform close-packed flakes via the LB method. Bulk 2H-WSe<sub>2</sub>, synthesized using an atmospheric-pressure chemical vapor deposition (AP-CVD) technique, was exfoliated into mono- to few-layered 2H-WSe<sub>2</sub> flakes using low-boiling solvent (ethanol) at high-frequency bath sonication system. The compression of the liquid-exfoliated WSe<sub>2</sub> flakes on the water sub-phase was used to form a continuous layer, which was subsequently transferred onto a pretreated substrate. UV-Vis, Raman, AFM, HRSEM and HRTEM prove that the as-deposited material is successfully exfoliated from bulk 2H-WSe<sub>2</sub> into mono- to few-layered flakes. Furthermore, we studied the electrical properties of the FIB-fabricated 2H-WSe<sub>2</sub> flake device using a two-probe current versus voltage (I-V) measurements. The proposed technique provides a simple path to assemble structures of solution-processed 2D semiconductors avoiding the challenges related to high cost and high temperature processing for further applications in electronics and optoelectronics.

#### References

- [1] Sahin *et al.*, *Phys. Rev. B*, 2013, 87, 165409.
- [2] Allain *et al.*, *ACS Nano*, 2014, 8, 7180-7185.

#### F.SF04.07.03

**Effect of DUV Curing on Low-Temperature Synthesis of IZO Semiconductor-Based TFTs** Alessio Mancinelli<sup>1</sup>, Sami

Bolat<sup>2</sup>, Jaemin Kim<sup>1</sup>, Yaroslav E. Romanyuk<sup>2</sup> and Danick Briand<sup>1</sup>; <sup>1</sup>EPFL, Switzerland; <sup>2</sup>Empa–Swiss Federal Laboratories for Materials Science and Technology, Switzerland

Solution processing is an attractive alternative to standard vacuum fabrication techniques for the large-area manufacturing of metal-oxide (MO<sub>x</sub>) based electron devices. In this frame, thin-film transistors (TFTs), which serve as the essential electronics building blocks, have to be primarily addressed. Furthermore, when these TFTs are realized on flexible substrates, many potential applications such as displays, chemical sensors, and conformable wearable devices, could be envisioned. However, the need for high-temperature sintering processes ( $T > 350\text{ }^{\circ}\text{C}$ ) has restrained thus far their commercial diffusion. The necessity for temperature-resistant polyimide as a substrate has restrained their field of application mainly to displays (e.g. indium gallium zinc oxide (IGZO) on polyimide). More economic and environmental-friendly substrates such as PET, cellulose, and biopolymers will become essential in future daily life applications requiring cheap and perhaps disposable devices. Among others, smart label sensors for temperature and chemical monitoring of food, realized directly in the packaging could be enabled. Accordingly, the development of a production process compatible with such thermosensitive substrates has to be addressed.

One of the key challenges for the full exploitation of these devices is the reduction of the thermal budget required for the MO<sub>x</sub> synthesis. Our approach is based on the use of deep ultraviolet light (DUV) to promote the sol-gel synthesis reaction and therefore reduce the thermal budget of the process. The energetic photons generated by the DUV lamp are used to photo-activated the chemical reactions and initiating the M–O–M bond formation inside the deposited thin film. The quality of the MO<sub>x</sub> layer is further enhanced by the heat treatment which eliminates the undesired reaction residuals and densifies the film. Similar photonic processes for solution-processed metal-oxide transistors have been mainly based on indium oxide (InO<sub>x</sub>) as semiconductor material. The more convenient chemistry of InO<sub>x</sub> facilitates its solution processing at low-temperature. However, the films obtained from these compounds can suffer from unstable behaviour and operation at negative voltages. We report on TFTs based on a solution-processed indium zinc oxide (IZO) semiconductor utilizing a DUV enhanced curing, which enables a reduction of the processing temperature. A parametric analysis of the curing parameters has been carried out in to investigate the minimal conditions required to achieve performing devices. In this frame, we compared the efficiency of a post-annealing step in with in-situ combined DUV exposure and heating). Furthermore, the curing processes have been investigated using two different DUV light sources evaluating the different outcomes: a single-wavelength (172 nm) emitting excimer lamp and a broader emitting DUV lamp (184 nm/253 nm). The electrical characteristics of the TFT have been extracted and used to establish optimal curing conditions. Notably using DUV, short curing times as low as 10 minutes at 200 °C (e.g. 5 min DUV + 5 min post-annealing @ 200 °C) achieved mobility of 3 cm<sup>2</sup>/Vs. Higher mobility values (>15 cm<sup>2</sup>/Vs) have been achieved with prolonged processes (>80 min). While a temperature reduction to 180 °C yielded ~1 cm<sup>2</sup>/Vs. The effects of the different curing protocols on the chemical composition of the IZO films have been studied using Fourier-transform infrared spectroscopy and X-ray photoelectron spectroscopy. The IZO semiconductor has been eventually paired with a printed high-k MO<sub>x</sub> dielectric film, cured using the same methodology, to realize fully solution-processed MO<sub>x</sub> TFTs, with as ultimate goal producing full printed TFTs. The identification of the most effective tool, combined with a fine-tuning of the parameters, allows to the DUV enhanced curing to diminish the thermal budget required to process IZO TFTs, paving the way for its further implementation on temperature-sensitive substrates.

#### F.SF04.07.04

**Uniform and Stable Aerosol-Jet Printing of Carbon Nanotube Thin-Film Transistors** Shiheng Lu, Joanne Zheng, Jorge Cardenas, Nicholas Williams, Yuh-Chen Lin and Aaron D. Franklin; Duke University, United States

Carbon nanotube thin-film transistors (CNT-TFTs) have attracted intensive attention due to their potential use in various applications, including display backplanes and sensing systems. Device uniformity, which is largely determined by the homogeneity and reproducibility of CNT thin films, is essential for large-scale manufacturing and practical applications. Here, we demonstrate an aerosol-jet printing approach to realizing CNT-TFTs with device characteristics that are among the most uniform of CNT-based transistors to date. The key enabling factors include proper ink formulation, polymer surfactant removal via rapid thermal anneal (RTA), and careful ink temperature control. Terpineol was added as a secondary solvent, and both optical and atomic force microscopy (AFM) reveal that the addition of this nonvolatile and viscous component efficiently suppresses the unwanted coffee-ring effect. The effectiveness of RTA-based polymer removal was supported by AFM results. It was discovered that a lower CNT ink temperature during printing offers higher ink output, increased CNT density, larger field-effect mobility, as well as enhanced device uniformity. This ink temperature-device uniformity relationship was further examined by fabricating batches of CNT-TFTs at a range of different ink temperatures, which revealed that low ink temperature (e.g., 8 °C) not only benefits uniformity of devices printed within a short period of time (~70 s), but also improves long-term (~1 h) printing stability. A set of several dozen CNT-TFTs printed from a CNT ink at 8 °C exhibited a mobility of  $12.5 \pm 0.5\text{ cm}^2\text{ V}^{-1}\text{ s}^{-1}$ , with a relative standard deviation  $\sigma(\mu_h) / \mu_h$  as small as 4%. These results unveil

the role that ink temperature and other critical processing factors play in aerosol jet printed films and have the potential to address device uniformity issues that have previously plagued the utility of printed CNT thin films.

#### **F.SF04.07.05**

**Fine-Tuning of Molecular Conformations for High-Speed Organic Photodetectors with Enhanced Charge Transport** Jisoo Shin, Sungyoung Yun, Hye Sung Choi, Taejin Choi, Younhee Lim, Seon-Jeong Lim, Kyung-Bae Park and Sunghan Kim; Samsung Advanced Institute of Technology, Korea (the Republic of)

Organic semiconductors have the advantages of high absorption coefficients and wavelength selectivity compared with those of inorganic materials. As such, organic photodetectors (OPDs) are emerging as the next candidates for commercialized organic electronic devices, organic CMOS image sensors (OCISs). Wavelength-selective OPDs are applicable to the three-dimensional (3D) stacked structure that can replace the existing CMOS image sensors for the expansion of the light-input surface area by maximizing the photons absorbed effectively by each pixel, leading to high sensitivity and resolution since they can absorb selective wavelength from incident light without color filters.

To realize these advantages, systematic approach for molecular design of OPDs and optimized device architecture has been reported by our group recently. Noteworthy, through recent years of research on OPDs, the improvement of charge transport properties is also indispensable for commercialization of high-speed image sensors. Compared to silicon CMOS image sensors, some charges are slowly transported and remain in organic layer, then slow decays of photocurrent induced image lags closely related to remaining charges (RCs) in OCISs.

Here, combined with simulation and experiment, we designed and synthesized novel push-pull type molecules with different moieties by tuning the molecular conformations, which showed improved optical properties as well as charge carrier mobility. According to the improved device performance, we experimentally find out that charge transport properties including RCs are closely related to molecular structure with introduction of carbon-bridge and various types of side group. The effect of molecular conformations on the optoelectronic properties of high-speed OPDs will be discussed in detail.

#### **F.SF04.07.06**

**Unsubstituted and Fluorinated CoPc Nanowires, Ultrathin Films and Composites for Room Temperature ppb Environmental Gas Monitoring in Highly Humid Terrains** Soraya Flores<sup>1</sup>, Jean Gonzalez<sup>1</sup>, Juan Cintron<sup>1</sup>, Dalice M. Piñero Cruz<sup>1</sup>, Jose Hernandez<sup>1</sup>, Nerida deJesus<sup>2</sup>, Ruben E. Diaz-Rivera<sup>2</sup> and Luis F. Fonseca<sup>1</sup>; <sup>1</sup>University of Puerto Rico at Río Piedras, United States; <sup>2</sup>University of Puerto Rico at Mayagüez, United States

Metallo Phthalocyanines (MPc) have been widely studied as promising material to develop sensitive gas sensor devices. In particular, its electrical response when exposed to gas analytes encourages its use in chemiresistors. This is so because they show some characteristics that can be exploited for the development of very sensitive gas sensors. When compared with other semiconductors, such as metal oxides, their baseline resistivity is relatively high and can change orders of magnitude when exposed to the sensing gas, which can be easily tuned through the incorporation of substituents in the periphery of the Pc platform. Moreover, there is little difference between their room temperature and higher temperature response. Recent publications report reproducible single digit parts-per-million sensitivities at room temperature, usually when preparing the material at the nanoscale.

This work summarizes advances in the synthesis, solution preparation, and gas sensing applications of CoPc and fluorinated CoPc nanowires and films with thicknesses below 20nm. In this case, room temperature parts-per-billion response is reported. Novel sensors prototypes based on F<sub>16</sub>CoPc composites activated with Pt nanoclusters show significant reduction in their sensor response time. The report includes a systematic comparison with unsubstituted CoPc, and the response to different reducing and oxidizing gases. These new prototypes will be optimized for the detection of environmental contaminants in areas with high atmospheric relative humidity.

#### **F.SF04.07.07**

**Metal Oxide Nanostructure Patterns via Modified Immersion Transfer Printing for Internal Light Extraction of Quantum Dot Light-Emitting Diodes** Moohyun Kim, Eugene Cho, Jeong Min Shin, Min Seok Jang and Yeon Sik Jung; Korea Advanced Institute of Science and Technology, Korea (the Republic of)

Quantum dot light-emitting diodes (QLEDs) are considered as next-generation displays due to the outstanding advantages of quantum dots (QDs) such as large color gamut by narrow emission, high brightness, solution-processability and potential long term stability. The performance of QLED is characterized by external quantum efficiency (EQE), which is the multiplication of internal quantum efficiency (IQE) and light out-coupling efficiency (EQE = IQE × light out-coupling efficiency). Recent progress has improved EQE of QLEDs for red, green and blue color to about 20%, which is on the level of commercial phosphorescent organic light-emitting diodes (OLEDs). Considering that the light out-coupling efficiency of a

typical multilayer structure device is 20%, it can be seen that the IQE of QLEDs reached 100%. Therefore, research on light out-coupling efficiency or light extraction of QLEDs has been gaining attention to further improve the EQE.

In OLEDs, light is commonly extracted through corrugated structure or photonic crystal like internal light extraction nanostructure. Generally, these nanostructures are located between the multilayer structure and transparent electrode to interact with the target wavelength. However, applying this strategy for enhancement of QLEDs has difficulty even though the structural similarity of the multilayer structure. This is because multilayer structure of QLEDs is fabricated based on solution process while OLEDs are fabricated through vacuum deposition. Therefore, in QLED, the light extraction nanostructure strongly effects the morphology of the multilayer device causing degradation of the operation characteristic. Furthermore, very narrow QDs emission with 30nm of full-width at half maximum (FWHM) suggests the need for more advanced technique with finer and more precise nanostructures.

In this study, we demonstrate a metal oxide ( $\text{MoO}_3$ ) nanostructure fabricated by modifying immersion transfer printing (iTP) method for internal light extraction of QLEDs.  $\text{MoO}_3$  was applied as the internal light extraction material on the basis of high refractive index value ( $n$ ) of 2.1 at 520 nm and semiconducting properties as a hole transport layer in optoelectronic devices. iTP is introduced as the fabrication method for its compatibility with the solution processed QLEDs and capability for forming high resolution  $\text{MoO}_3$  nanostructure. Previous reported iTP, which uses hydrophobic particles, was modified to compensate for the incompatibility between hydrophilic  $\text{MoO}_3$  particles and PDMS brushed substrates. PDMS-PS co-brush system was applied to control the surface affinity as a way to achieve  $\text{MoO}_3$  incorporation onto the Si template. In addition, PDMS/PS bilayer was used as the picking carrier polymer to increase the transfer yield of the  $\text{MoO}_3$  nanostructure. As a result, nanoscale line patterns with widths of 1000, 350, and 50 nm in large areas are well demonstrated. Finite-difference time-domain (FDTD) simulations are conducted to help design the precise size and shape of the pattern for light extraction to optimize the QLED internal light extraction. QLED was fabricated based on this design and showed improvement in the performance of the QLED device.

#### F.SF04.07.10

##### **Examining the Impact of Air Exposure and Temperature Variation on N- and P-Type Polymer Charge Transport for Transistor and Photovoltaic Applications** Samantha Brix and Benoit Lessard; University of Ottawa, Canada

Enhancing device stability is essential to the widespread commercial adoption of organic electronic devices. Interactions of organic semiconductors with their environment often lead to degradation of device performance; therefore, it is important to understand how such devices as organic thin-film transistors and organic photovoltaics are affected by these interactions. This allows scientists and engineers to both choose appropriate applications for these materials and guide the development of new materials with enhanced stability. Polymers are of particular interest due to their capacity to be processed in solution for a new generation highly scalable and inexpensive electronic devices from sensors to solar cells. We have studied the stability of p- and n-type materials of interest for transistor and photovoltaic applications in environments relevant to commercial applications of these materials, including exposure to air, vacuum, and varied temperatures. In all cases, significant degradation could be observed. After 18 days of air exposure for p-type materials P3HT and PBDB-T, a 95% loss in hole mobility ( $\mu_h$ ) was observed for P3HT, while PBDB-T only experienced a  $\mu_h$  loss of 42%.<sup>1</sup> For n-type polymers studied, a loss in electron mobility ( $\mu_e$ ) of 99% was observed for N2200 exposed to air for two weeks, while an 84%  $\mu_e$  loss was observed for PIBDFBT-37.<sup>2</sup> Preliminary studies on polymers in organic photovoltaics indicate similar trends, but the degradation of charge transport properties does not give the full picture. We plan to further explore the impact of polymer degradation and charge transport on the stability of organic photovoltaics and transistors.

1. Brix, *et al.*, 2018, J. Mater. Chem. C, 6, 11972-11979

2. Brix, *et al.*, 2020, Sci. Rep., 10, 4014

#### F.SF04.07.11

##### **Dielectrophoretic Assembly of Single Nanowires for Advanced Characterisation Nanoscale Standards** Maxim Shkunov<sup>1</sup>, Sebastian Wood<sup>2</sup>, Ruth Rawcliffe<sup>1</sup>, Filipe Richheimer<sup>2</sup>, Tomas Peach<sup>1</sup> and Fernando Castro<sup>2</sup>; <sup>1</sup>University of Surrey, United Kingdom; <sup>2</sup>National Physical Laboratory, United Kingdom

Nano-characterisation techniques, including confocal microscopy, atomic force microscopy (AFM) and tip enhanced Raman scattering (TERS), rely on the ability of each instrument to resolve nano-scale features without distortions and artefacts, however, reference samples allowing to perform fully quantitative characterisation of their responses are not available. Calibration of lateral and depth resolution of advanced scanning-probe microscopy methods is currently very challenging and calls for the development of nanoscale standards with features in 10-200 nm range with various morphological and optoelectronic characteristics.

We demonstrate the development of solution-based, single-nanowire-based reference samples, where easily identifiable

device positions each contain a semiconducting nanowire with a particular set of properties. Key parameters that are considered include: diameter and length, Raman response, photoluminescence and conductivity. The devices are self-assembled from a wide range of solution-processed semiconducting nanowires, including Si, Ge, InAs, InP, GaN, Ge/Si. Individual nanowires are positioned in pre-defined locations using electric-field assisted process, dielectrophoresis (DEP), by applying controllable DEP signal voltage and frequency. Nanowires are characterised, and various response metrics are analysed using conducting-AFM, confocal Raman, TERS and other techniques to establish which nanowire materials provide highly distinguishable responses, necessary for reference standards. Challenges in identifying most suitable nanowire materials, including their spectroscopic characteristics (e.g. Raman) and morphological features (e.g. diameters) are discussed and several reference samples for the characterisation of lateral and vertical resolution of nanoscale scanning probe techniques are suggested.

#### **F.SF04.07.13**

##### **Effect of Oxygen Pressure on Optical and Electrical Properties of Single-Crystalline Cu<sub>2</sub>O Fabricated by Pulsed Laser Deposition** Jan Lancok, Lenka Volfova, Premysl Fitl and Michal Novotny; Czech Academy of Sciences, Czechia

Copper oxide Cu<sub>2</sub>O is an important and well known p-type transition metal oxide semiconductor material, which has already been employed in the fabrication of electronic devices. For example Cu<sub>2</sub>O has been used in thin photovoltaic devices, resistive switching, transistors, gas sensors or catalysts. The films were fabricated by Pulsed Laser Deposition from CuO ceramic target by means of Nd:YAG laser operated at 266 nm wavelength. MgO(100) substrates were mounted on substrate holder 5 cm away from the target and maintained at temperature in the range 500-700 °C. Our attention was mainly focused on the influence of the oxygen pressure, which was varied between 10<sup>-5</sup> Pa and 1 Pa, on the structural and following on optical and electrical properties. The investigation of the plasma was carried out by Optical emission spectroscopy. The surface morphology and composition were characterised by AFM and XPS, respectively. The crystalline quality of the films were characterised by means of XRD and following by TEM and HRTEM, which confirmed the epitaxial grown of the films in low oxygen pressure up to 0.1 Pa. When the oxygen pressure exceeded 0.1 Pa the growing films started to be polycrystalline and the CuO phase also appeared. Because we focused on utilization of the Cu<sub>2</sub>O films as gas sensors, the near ambient pressure photoelectron spectroscopy was carried out to investigation of surfaces composition in the presence of gasses and vapours such as ethanol, hydrogen and NO<sub>2</sub>.

#### **F.SF04.07.14**

##### **Thermal Dedoping of Doped Poly (3-hexylthiophene) for Multimodal Temperature Sensing** Hemanth Maddali<sup>1</sup> and Deirdre O'Carroll<sup>1,2</sup>; <sup>1</sup>Rutgers, The State University of New Jersey, United States; <sup>2</sup>Rutgers University, United States

Conjugated polymers have a wide range of applications in optoelectronic devices and in numerous sensing technologies. Conjugated polymers that have thermally activated optical or electrical responses have garnished interest due to their potential as thermal sensors. These thermochromic properties are often introduced via doping. In this study, we investigate the use of electrochemically doped poly(3-hexylthiophene) (P3HT) thin films as multimodal temperature sensors. P3HT thin films spin coated on indium-tin oxide coated glass substrates are electrochemically doped using tetrabutylammonium perchlorate (TBAP) dissolved in acetonitrile. The pristine P3HT thin films, which are purple in color, exhibit a color change to blue, upon doping. The doped P3HT thin films are then heated under vacuum at 140<sup>o</sup> C and the color of the thin films reverts from blue to purple indicating thermally activated dedoping. UV-visible absorbance spectra of pristine, doped and dedoped P3HT thin films show that the change in optical absorption properties upon doping is reversed due to thermally activated dedoping. Energy dispersive X-ray spectroscopy (EDS) reveal the presence of dopant molecules (TBAP) distributed throughout the doped P3HT film. Upon dedoping, the EDS maps show almost negligible levels of the dopant molecules. This further proves that heating of doped P3HT thin films triggers dedoping and causes the distinctive thermochromic response, i.e., a color change from blue to purple. The electrical properties of doped and dedoped films are also expected to result in a significantly different current upon application of voltage. This warrants fabrication of a current-based temperature sensor that would perform colorimetrically and electrically.

#### **F.SF04.07.15**

##### **A 13.56 MHz Rectifier Based on Fully Inkjet Printed Organic Diodes** Fabrizio A. Viola and Mario Caironi; Istituto Italiano di Tecnologia - IIT, Italy

The increasing diffusion of portable and wearable technologies results in a growing interest in electronic devices having features such as flexibility, lightness-in-weight, transparency and wireless operation. Organic electronics was proposed as a potential candidate to fulfill such needs, in particular targeting pervasive Radio-Frequency (RF) applications. Still, limitations in terms of device performances at RF, particularly severe when large-area and scalable fabrication techniques are employed,

have largely precluded the achievement of such an appealing scenario. In this work, we demonstrate a high-frequency rectifier based on fully inkjet printed organic Schottky diodes fabricated through scalable large-area methods on plastic. The inkjet printing of the organic semiconductor, the core of the diode structure, has been carefully optimized in order to obtain a low series resistance, which is mandatory to improve the diode cut off frequency. Moreover, the employed materials in the presented device have been chosen to finely tune the barriers formed at metal-semiconductor interface, in order to increase the rectification ratio of the diode: the obtained value is higher than  $10^6$  which is, to the best of our knowledge, the highest value ever reported with a fully printed structure. Furthermore, we show, as a proof-of-concept, how a rectifier circuit integrating the fully printed diode, can successfully supply power to a polymer micro-electronic circuit printed on a plastic foil with a similar process. In particular, by rectifying a 13.56 MHz AC voltage the rectifier enables the correct operation of a D-Flip Flop, which is a fundamental logic building block for serialization elements. The possibility of harvesting electrical power from RF waves and delivering it to a cheap flexible substrate through a simple printed circuitry paves the way to a plethora of appealing distributed electronic applications.

#### **F.SF04.07.16**

**Thermally Stable Au Decorated Silica-Titania Mesoporous Nanocomposite for pH Sensing Evaluation** Shumaila Islam and Adil Alshoaibi; King Faisal University, Pakistan

Herein, doping/decoration of gold nanoparticles (AuNPs) within mesoporous silica-titania nanocomposite is achieved via a facile and co-assembly sol-gel method. Polyethylene glycol is used as a co-structure-directing agent. For sensing analysis, a mixture of organic dyes i.e., bromophenol blue, phenol red, and cresol red is encapsulated in the AuST nanocomposite matrix. FESEM/EDX analysis shows a crack-free surface, porous network and uniform distribution of Au, Ti, Si, along with dye species. FTIR and XRD suggested the heterogeneous chemical bonding and crystallite size 24 nm after encapsulation. AuST nanocomposite shows thermally stable behavior after 450 °C even after co-dyes encapsulation. High surface area  $322 \pm 2.5$  m<sup>2</sup>/g, pore diameter 30.2 Å, and pore volume 0.24 cm<sup>3</sup>/g, average surface roughness 10 nm, and refractive index 1.29 is advantageous for good sensing response at pH 1–12. The sensitivity is measured as 10 counts/pH at 441 nm. Moreover, good reversible response, fast response time 2.1 sec in acidic media, and 0.9 sec in basic media is observed.

#### **F.SF04.07.17**

**Late News: Hybrid Surface Treatment of Elastomer Substrates for Robust and Reliable Integration of Rigid Components with Inkjet-Printed Stretchable Circuits** Hyungsoo Yoon, Byeongmoon Lee, Sujin Jeong and Yongtaek Hong; Seoul National University, Korea (the Republic of)

Stretchable electronics has emerged as a next-generation technology that goes beyond rigid and flexible electronics to enable novel form-free devices and provide advanced user-experiences. Integration of rigid integrated circuit (IC) chips and inkjet-printed circuits on pre-strained elastomers has been regarded as one of the most powerful methods for fabricating stretchable multifunctional systems due to their unique advantages such as a facile and low-cost process, and a high degree of customizability. However, direct inkjet-printing on elastomers is challenging due to their low surface energy that causes dewetting. Furthermore, the super-hydrophobic surface shows poor adhesion with inkjet-printed metal films as well as conductive adhesives for chip bonding, significantly limiting system stability under deformation. Therefore, appropriate surface modification is indispensable for the robust implementation of inkjet-printing-based stretchable hybrid electronic system. Surface modification of elastomers has been realized by oxygen-plasma or ultraviolet/ozone (UVO) treatments. Both methods render the surface of the elastomers wettable by creating a large number of hydrophilic groups on it, where well-defined patterns can be formed by inkjet-printing. However, the methods have several limitations when applied to inkjet-printing on pre-strained elastomers. Plasma-treated elastomers undergo fast hydrophobic recovery due to the molar migration from the bulk to the surface, resulting in unstable wettability, uneven patterns, and poor adhesion. Alternatively, the UVO treatment provides improved stability and uniformity. However, a thick layer of the elastomer from the surface is stiffened by UV energy, which causes a large strain mismatch between the thick stiff surface and soft bulk. Consequently, the pre-stretched elastomer cannot completely return to its original dimension, restricting the maximum stretchability of the system far behind compared to the applied pre-strain. Therefore, a new surface modification strategy that simultaneously offers stable wetting and a high level of adhesion without compromising their stretchability is highly required.

In this work, we demonstrate robust stretchable hybrid electronic system based-on inkjet-printing and hybrid surface modification of polydimethylsiloxane (PDMS). The surface treatment offers stable wettability and great adhesion and preserves the substrate stretchability. Specifically, the pre-strained PDMS (mixed at 10:1) is exposed with oxygen-plasma to form hydroxyl groups and poly-L-lysine (PLL) solution (aqueous solution, 0.1% (w/v) in H<sub>2</sub>O) is sequentially drop-casted on the plasma-treated PDMS. After that, the PDMS is rinsed with deionized (DI) water. Abundant amine groups functionalized on the surface of the PDMS enable stable wetting and good adhesion for inkjet-printing process. Furthermore, the modified

surface shows remarkable adhesion with conductive epoxy, allowing robust IC chip bonding on the printed stretchable circuits. To investigate the effect of the hybrid surface treatment, we compare three biaxially pre-stretched PDMS substrates that undergo UVO, oxygen-plasma, and oxygen-plasma with PLL treatments, respectively. The plasma-treated PDMS results in uneven patterns and poor adhesion due to its instability and fast hydrophobic recovery. While the UVO-treated PDMS only shows stretchability of 19% when it is pre-stretched ~70%, the PDMS with hybrid surface treatment restores its original dimension, *i.e.*, it shows the same stretchability as the pre-strain value. Finally, a series of stretchable hybrid electronic systems are demonstrated with their mechanical robustness, including stretchable LED displays, which proves the superiority of our hybrid surface treatment. The detailed methods and results will be discussed at the conference.

This research was supported by Samsung Research Funding & Incubation Center of Samsung Electronics under Project Number SRFC-IT1801-07.

#### F.SF04.07.18

**Late News: Implementing ITO-Free Transparent Conductive Electrodes in Flexible Organic and Hybrid Light-Emitting Diodes** Felix Hermerschmidt<sup>1</sup>, Lukas Kinner<sup>1,2</sup>, Theodoros Dimopoulos<sup>2</sup> and Emil List-Kratochvil<sup>1,3</sup>; <sup>1</sup>Humboldt-Universität zu Berlin, Germany; <sup>2</sup>Austrian Institute of Technology, Austria; <sup>3</sup>Helmholtz-Zentrum Berlin, Germany

We utilize 25% of our total electricity consumption for lighting and display applications. To address this consumption, several efficient lighting technologies have been targeted. Inorganic solid-state lighting together with organic light-emitting diodes (OLEDs) are the candidates spearheading the lighting revolution of the 21st century. However, while OLEDs have shown commercial success in rigid display applications, a number of challenges remain to be overcome in order to fulfil their full potential.

Among these are the continued quest for stable emitter materials and to improve strategies for the outcoupling of light from the device. Additionally, energy, temperature and cost efficient processing methods need to be targeted in order to fabricate the transparent conductive electrodes (TCEs) needed for device operation.

Today, transparent conductive oxides, and in particular indium tin oxide (ITO), represent the dominant class of TCEs. ITO combines high transparency (>85% in the visible wavelength range) with low sheet resistance (ca. 10  $\Omega$  sq<sup>-1</sup>) when deposited on glass. As a result, most optoelectronic devices utilize ITO as the transparent electrode. However, ITO has some inherent limits in its range of applications. It is mechanically unstable upon bending, while its scarcity translates to a volatile and high price. It is therefore desirable to replace ITO with other transparent conductive electrodes [1].

Of particular interest are low temperature processes (<130 °C), since these are compatible with the use of temperature-sensitive and low cost flexible substrates, such as polyethylene terephthalate (PET). In this contribution we highlight our recent work on the design, fabrication and characterization of a number of different low temperature processes using, among others, inkjet printing and spray coating to produce TCEs [2,3]. These approaches are based on Ag and Cu nanoparticle, particle-free and nanowire inks. We will show that the developed ITO-free electrodes on PET show superior optical, electrical and mechanical performance compared to PET/ITO reference samples.

[1] Hermerschmidt et al., Adv. Mater. Technol. 4 (2019) 1800474.

[2] Hermerschmidt et al., Adv. Mater. Technol. 3 (2018) 1800146.

[3] Kinner et al., Phys. Status Solidi RRL (2020) 2000305.

#### F.SF04.07.20

**Late News: Organic Radiation Dosimeter for X-Ray, Gamma and Neutron Detection** Zachary Lamport<sup>1</sup>, Marco R. Cavallari<sup>2</sup>, Michael Bardash<sup>3</sup> and Ioannis Kymissis<sup>1</sup>; <sup>1</sup>Columbia University, United States; <sup>2</sup>Federal University for Latin American Integration, Brazil; <sup>3</sup>QEL System Services, Inc., United States

In many professions, ionizing radiation is either a by-product of some process or is itself utilized, posing a significant hazard to those in the surrounding area. Workers will usually be required to wear a personal radiation dosimeter which measures and integrates the cumulative radiation dose experienced such that either prolonged or flash exposures are recorded and analyzed for the safety of the wearer. For personal dosimeter badges, the sensing element is usually made of relatively high-Z elements which absorb radiation differently than the lighter elements found in the human body.<sup>1,2</sup> An all-organic radiation dosimeter could more closely approximate the effect of radiation on biological tissues. Another added benefit of such organic-based devices is that they can be made quite cheaply and on a lightweight, flexible substrate. These factors together with the burgeoning IoT systems could allow for a more robust detector network in areas relevant to homeland security. Here, we report on an all-organic radiation dosimeter using the conducting polymer poly(3,4-ethylenedioxythiophene)-poly(styrenesulfonate) (PEDOT:PSS)<sup>3</sup> as both the detector region and conductive traces patterned on a polyethylene naphthalate (PEN) substrate. Ionizing radiation incident on a central PEDOT:PSS pad induces a static charge in the air, the PEDOT:PSS itself, and the underlying PEN substrate that is measured as a voltage by the connected op-amp voltage

follower.<sup>4-6</sup> Two organic field-effect transistors (OFETs) with the PEDOT:PSS source and drain, respectively, connected to the central PEDOT:PSS region allow for an initial biasing of the central pad, as the semiconductor 6,13-bis(triisopropylsilylethynyl) pentacene (TIPS-pentacene) functions as two very large resistors. The OFETs allow for a very small amount of current to flow through the ungated semiconductor in order to place the central pad at a desired voltage, from which any deviations are measured. To clear the charge from the central pad, one or both of the OFETs can be turned on through the respective PEDOT:PSS gate electrode underneath a parylene dielectric. We show reproducible and reliable measurements of the radiation dosimeters subjected to a wide range of exposure energies of both X-ray and gamma rays using wide and focused beams resulting in an approximate detection limit of 5 mRad/hour. In addition, there is very strong evidence that the PEDOT:PSS-based devices can detect neutrons from a shielded and unshielded beryllium-encased plutonium source at a dose of 620 mRad/hour. This represents a significant step forward in the production of cheap, reusable radiation dosimeters made with materials of similar radiation cross-section to the human body.

1. Beckerle, P. & Ströbele, H. Charged particle detection in organic semiconductors. *Nucl. Instruments Methods Phys. Res. Sect. A* **449**, 302–310 (2000).
2. Fraboni, B. *et al.* Organic Semiconducting Single Crystals as Next Generation of Low-Cost, Room-Temperature Electrical X-ray Detectors. *Adv. Mater.* **24**, 2289–2293 (2012).
3. Schrote, K. & Frey, M. W. Effect of irradiation on poly(3,4-ethylenedioxythiophene):poly(styrenesulfonate) nanofiber conductivity. *Polymer.* **54**, 737–742 (2013).
4. Bardash, M. An organic semiconductor device for detecting ionizing radiation on a cellular level. *Organic Semiconductors in Sensors and Bioelectronics III* (Vol. 7779, p. 77790F). International Society for Optics and Photonics. 77790F (2010). doi:10.1117/12.861999.
5. Bardash, M. Solid state tissue equivalent detector, main component for a light-weight tissue equivalent microdosimeter. U.S. Patent 8,350,225 (2013).
6. Cavallari, M. R., Bardash, M. & Kymissis, I. Fully organic solid state tissue equivalent radiation dose (SSTED) detector (Conference Presentation). in *Organic and Hybrid Sensors and Bioelectronics XII* (eds. Shinar, R., Kymissis, I. & List-Kratochvil, E. J.) 4 (SPIE, 2019). doi:10.1117/12.2530701.

#### F.SF04.07.21

**Late News: Highly Conformable Pressure-Sensitive Thin-Film Transistors Using Capacitance Modulation via Nanostructured Surface Morphology of AgNWs** Hayun Kim, Byeongmoon Lee, Hyunuk Oh, Hyunjun Yoo and Yongtaek Hong; Seoul National University, Korea (the Republic of)

Electronic skin that can map pressure distribution on arbitrary surfaces has gained tremendous significance for its wide range of use in various fields such as skin prosthesis, artificial nerve systems for soft robotics, and advanced human-machine interfaces. To keep pace with these trends, many studies have focused on reporting high-performance pressure sensors and their passive-matrix array using novel materials and structures. Among various types of pressure sensors, capacitive pressure sensors with engineered microstructures offer significant potential owing to their high sensitivity, fast response time, and great mechanical flexibility. However, previous works on capacitive pressure sensors mainly focused on the performance of a single sensor, and their application to a high-resolution array was challenging because of their complex structure and fabrication process. Therefore, reported sensor arrays using capacitive pressure sensors generally showed low spatial fidelity due to the crosstalk among pixels and low pixel density. Furthermore, to exploit the capacitance change in practical applications, the circuit requires a capacitance-to-current converter that can limit the design freedom and make the system unstable on complex 3-dimensional surfaces. Therefore, device-scale integration between capacitive pressure sensors and thin-film transistors (TFTs) is highly desirable for capacitance-to-current conversion and further active-matrix applications. Although a few studies have reported pressure-sensitive thin-film transistors, they usually suffer from complex fabrication processes and limited flexibility due to their sophisticated structures such as sidewall spacers to make air gaps in dielectric layers.

In this work, we propose a facile and large-area compatible method for pressure-sensitive TFTs (PSTFTs) and their application to flexible sensor arrays. Our PSTFT is based on all-inkjet-printed single-wall carbon nanotube (SWCNT) TFTs, where a silver nanowire (AgNW) gate electrode with nanostructured surface morphology softly touch the top surface of the dielectric layer. The fabrication process of the PSTFT is fairly simple, highly customizable, and cost-effective. The SWCNT active channel, silver (Ag) source and drain electrodes, and poly(4-vinylphenol) (PVP) dielectric layer were sequentially inkjet-printed on a surface-engineered polyethylene naphthalate (PEN) substrate. The AgNW gate electrode was then formed on another flexible substrate by spray-coating. The 3D nanostructures in the AgNW random network form nano-scale air gaps between the gate electrode and dielectric. These nanoscale air gaps are key to the capacitance modulation in the PSTFTs. When the vertical pressure is applied to the top gate electrode, as the air gaps disappear and the contact area between the gate electrode and dielectric increased, the capacitance between the gate electrode and active layer drastically



increases without any supporting spacer. Our PSTFT showed well-split transfer curves with on-off ratios of from 1 to  $1.3 \times 10^4$  according to the applied pressure. When the pressure reached 700 kPa, the TFT showed  $1.3 \times 10^4$  on/off ratio. We further demonstrate the feasibility of our approach by mounting the highly conformable sensor array on human skin to read out the change of the pressure such as finger touch and joint flexure. This study provides a new pathway to map pressure distribution using capacitive pressure sensors without any crosstalk among adjacent pixels, which can be further applied to any type of deformable substrates with potential applications such as skin-mounted device, deforming soft robotics, and display. The detailed methods and results will be discussed later.

This work was supported by the Technology Innovation Program (No.20008801, Development of muscular function management solution based on electronic skin with EMG IMU and Strain sensor) funded By the Ministry of Trade, Industry & Energy(MOTIE, Korea).

## SYMPOSIUM F.SF05

---

Advanced Materials for Additive Manufacturing  
November 21 - December 4, 2020

### Symposium Organizers

Yat Li, University of California, Santa Cruz  
Juana Mendenhall, Morehouse College  
Artur Moreira Pinto, Universidade do Porto  
Marcus Worsley, Lawrence Livermore National Laboratory

### Symposium Support

**Platinum**  
National Science Foundation - Award #2028092

---

\* Invited Paper

SESSION F.SF05.08: Live Panel Discussion I: New Technologies Enabled by Additive Manufacturing  
Session Chairs: Yat Li and Marcus Worsley  
Wednesday Afternoon, December 2, 2020  
F.SF05

**7:30 PM PANEL DISCUSSION**

**9:30 PM ERIC DUOSS, PANELIST**

**9:30 PM XIAOYU ZHENG, PANELIST**

**9:30 PM MICHAEL MCALPINE, PANELIST**

**9:30 PM JULIA GREER, PANELIST**

SESSION F.SF05.09: Live Panel Discussion II: Opportunities and Challenges in Architected Materials  
Session Chairs: Yat Li and Marcus Worsley  
Thursday Morning, December 3, 2020  
F.SF05

**8:00 AM PANEL DISCUSSION**

**10:00 AM DONG LIN, PANELIST**

**10:00 AM ANDRE STUDART, PANELIST**

**10:00 AM BRIAN DERBY, PANELIST**

**10:00 AM SUBRAMANIAN RAMAKRISHNAN, PANELIST**

SESSION F.SF05.10: Live Panel Discussion III: Future of Bioprinting  
Session Chairs: Juana Mendenhall and Artur Moreira Pinto  
Friday Afternoon, December 4, 2020  
F.SF05

**6:30 PM PANEL DISCUSSION**

**8:30 PM MIGUEL CASTILHO, PANELIST**

**8:30 PM SARAH HEILSHORN, PANELIST**

**8:30 PM ANNE MEYER, PANELIST**

**8:30 PM MONICA MOYA, PANELIST**

SESSION F.SF05.01/F.SF03.01: Keynote Session  
On Demand Abstracts Available for Viewing Starting Saturday Morning, November 21, 2020  
F-SF01

**5:00 AM \*F.SF05.01/F.SF03.01.01.01**

**Aqueous Synthesis of 3D Nano-architected Ceramics and Metals—Nano-Architected TiO<sub>2</sub> PhCs** Julia R. Greer;  
California Institute of Technology, United States

Additive manufacturing (AM), or 3D printing, represents a set of processes that enable layer-by-layer fabrication of complex structures using a wide range of materials that include ceramics, polymers, and metals. AM has allowed exploiting novel material properties, especially those that arise at the nano-scale, that do not occur in conventional materials, revolutionizing the production of complex parts for aerospace, military, automotive, optical, and medical applications. Facilitating these technologies requires a fabrication process to create a variety of functional materials in 3D, however the material choice for AM at the nano- and micro-scale is limited. A conspicuous example is a lack of AM processes for high refractive index (n), low absorption materials with nano-sized dimensions, which are typically required for microoptics and device applications. To harness the beneficial properties of 3D nano-architected meta-materials, it is critical to assess their properties at each relevant scale while capturing overall structural complexity. We present the fabrication and synthesis of nano- and micro-architected materials using 3D (two-photon and interference) lithography, as well as characterization of their properties as a function of architecture, constituent materials, and microstructural detail. We focus on additive manufacturing of complex, multi-component and multi-material architectures comprised of metal oxides, metals, and hydrogels that are derived from (metal) salt-based, aqueous photorefin synthesis. The discussion will focus on each representative materials system (metals, oxides, and hydrogels), with a detailed overview of titanium dioxide, with critical feature dimensions between 150 and 600 nm and <1% porosity. Using the described methodology, we created 3D dielectric photonic crystals (PhCs) out of rutile TiO<sub>2</sub> patterned into woodpile face-centered tetragonal (FCT) architectures with beam dimensions of 300-600nm and lateral periods

of 0.8-1.5  $\mu\text{m}$ . We use Plane Wave Expansion (PWE) simulations and Fourier Transform Infrared Spectroscopy (FTIR) to demonstrate the full photonic bandgaps centered at 1.8-2.9  $\mu\text{m}$ . This fundamental research provides insights into the range of possible, often *transient* attainable chemical compositions, microstructures and architectures of chemically-derived, 3D-architected ceramics and metals, enabling advances in multiple technologies, i.e. 3D MEMS, micro-optics, and prototyping of 3D PhCs.

SESSION F.SF05.02: 3D Printed Materials for Applications  
On Demand Abstracts Available for Viewing Starting Saturday Morning, November 21, 2020  
F-SF05

**5:00 AM \*F.SF05.02.01**

**3D Printing Functional Materials and Devices** Michael C. McAlpine; University of Minnesota Twin Cities, United States

The ability to three-dimensionally interweave biological and functional materials could enable the creation of devices possessing personalized geometries and functionalities. Indeed, interfacing active devices with biology in 3D could impact a variety of fields, including biomedical devices, regenerative biomedicines, bioelectronics, smart prosthetics, and human-machine interfaces. Biology, from the molecular scale of DNA and proteins, to the macroscopic scale of tissues and organs, is three-dimensional, often soft and stretchable, and temperature sensitive. This renders most biological platforms incompatible with the fabrication and material processing methods that have been developed and optimized for functional electronics, which are typically planar, rigid and brittle. A number of strategies have been developed to overcome these dichotomies. Our approach is to utilize extrusion-based multi-material 3D printing, which is an additive manufacturing technology that offers freeform, autonomous fabrication. This approach addresses the challenges presented above by (1) using 3D printing and imaging for personalized device architectures; (2) employing ‘nano-inks’ as an enabling route for introducing a diverse palette of functionalities; and (3) combining 3D printing of biological and functional inks on a common platform to enable the interweaving of these two worlds, from biological to electronic. 3D printing is a multiscale platform, allowing for the incorporation of functional nanoscale inks, the printing of microscale features, and ultimately the creation of macroscale devices. This blending of 3D printing, functional materials, and ‘living’ inks may enable next-generation 3D printed devices.

**5:15 AM \*F.SF05.02.03**

**Manufacturing Molecules for the New Carbon Economy** Eric B. Duoss; Lawrence Livermore National Laboratory, United States

Material properties are governed by the chemical composition and spatial arrangement of constituent elements at multiple length scales. This fundamentally limits material properties with respect to each other creating trade-offs when selecting materials for a specific application. For example, strength and density are inherently linked so that, in general, the denser the material, the stronger it is in bulk form. We are combining advanced micro-architected design with additive manufacturing techniques to create material systems and devices with previously unachievable property combinations. We have demonstrated designer properties resulting from architected materials in polymers, metals, ceramics, and combinations thereof for unprecedented control of structural, mechanical, thermal, chemical, and functional properties. Our manufacturing techniques can generate designed structures which are highly three-dimensional and composed of micro- and nano-scale features with multiple constituent materials in the same structure. In this talk, I will discuss our advanced modeling, materials, and manufacturing methods with focus on applying these approaches to cellular fluidics—a novel 3D fluidic control and delivery platform—and printed electrochemical reactors for CO<sub>2</sub> reduction reactions. This work was performed under the auspices of the U.S. Department of Energy by Lawrence Livermore National Laboratory under Contract DE-AC52-07NA27344.

**5:30 AM F.SF05.02.04**

**3D Printed Electrodes with Periodic Pores for Fast Bubble Transport During High-Rate Alkaline Water Electrolysis** Tianyi Kou; University of California, Santa Cruz, United States

Water electrolysis has been gaining century-long attention as a hydrogen production technique due to its simplicity and effectiveness. Coupling with renewable energy, water electrolysis paves the way for clean and sustainable hydrogen generation without worsening the depletion of fossil fuels and degradation of ecosystems. Particularly, alkaline water

electrolysis (AWE) is one mature industrial strategy, and megawatt-level stacks have been well established in the market recently owing to many of the following advantages. The less corrosive nature of alkaline electrolyte compared to acid media allows for the use of non-platinum catalysts which significantly lowers the cost of AWE. In addition, the low vapor pressure of alkaline media is helpful in realizing high-purity hydrogen gas production. AWE generally exhibits a decent energy efficiency of about 80-85% at mid-high current densities of 100-200 mA/cm<sup>2</sup>, but the efficiency drops significantly when increasing the current to 400 mA/cm<sup>2</sup> or higher. The considerable energy efficiency loss is related with the both limited intrinsic and extrinsic activity of electrodes. In spite of recent efforts in developing intrinsically active electrodes for AWS with facile proton-coupled electron transfer (PCET) and fast reaction kinetics, it is equally urgent to promote the extrinsic activity of electrodes at high current densities. Three-dimensional (3D) porous electrodes, such as commercial Ni foam, have been routinely used for as AWS electrode substrate because of their high surface area and ability in enhancing the mass diffusion of electrolyte. Nonetheless, the large amount of gas bubbles generated at high current densities are unfavorable to be released out of the 3D Ni foam due to the disordered pore arrangement. The sluggish bubble transport and release behavior of gas bubbles in 3D Ni foam block the efficient reactant diffusion and cause high ohmic loss, leading to substantial high overpotentials and low energy efficiency. Through an additive manufacturing strategy, we prepared a 3D printed Ni electrode with periodical pore structures as the substrate of AWS electrodes. The pore channels aligning with the buoyancy direction is believed to facilitate the upward movement of gas bubbles, and therefore enhance their diffusion and release out of the 3D electrodes. By growing intrinsically active AWS catalyst of carbon doped NiO on the 3D printed Ni, the electrodes exhibit much higher extrinsic activity than the counterparts supported on Ni foam. A high current density of 1000 mA/cm<sup>2</sup> can be obtained in 1.0 M KOH at low overpotentials of 245 and 425 mV for HER and OER, respectively. The work provides a new strategy of enhancing extrinsic activity of AWS electrodes at practically high current densities through pore structure engineering.

#### 5:40 AM F.SF05.02.06

**3D Printed Self-Supporting Elastomeric Structures for Multifunctional Microfluidics** [Ruitao Su](#)<sup>1</sup>, Jiaxuan Wen<sup>1</sup>, Qun Su<sup>1</sup>, Michael S. Wiederoder<sup>2</sup>, Joshua R. Uzarski<sup>2</sup>, Steven Koester<sup>1</sup> and Michael C. McAlpine<sup>1</sup>; <sup>1</sup>University of Minnesota Twin Cities, United States; <sup>2</sup>U.S. Army Combat Capabilities Development Command Soldier Center, United States

Due to the advantages of small sample volumes and well-controlled microenvironments, microfluidic devices have enabled exciting applications such as lab-on-a-chip diagnostics, point-of-care systems, organ-on-a-chip, nanomaterial synthesis, and bioassays. Soft lithography is a widely employed device fabrication method that can achieve sub-micron resolution using the elastomer polydimethylsiloxane (PDMS). Yet, the requirement of microfabrication facilities, stamp distortions, as well as time-consuming manual steps such as PDMS molding, layer alignment and bonding imposes constraints on the use of soft lithography to produce ubiquitous and widely deployable microfluidic devices. Additive manufacturing, or 3D printing, techniques have recently emerged as promising complements or alternatives to augment the manufacturability of microfluidic devices. 3D printing methods such as stereolithography (SL) and multi-jet modeling (MJM) utilize photo-curable polymers to create well-defined micro channels with feature sizes below 100  $\mu\text{m}$  and a range of components for fluid manipulation. However, due to the potential for contamination from either the residual precursor resins or sacrificial supporting materials, directly printing microfluidic structures onto substrates that contain pre-deposited 3D structures or electronic sensing elements is challenging for SL and MJM. The degree of automation of SL and MJM is also compromised due to necessary post-processing steps to remove residual precursor and supporting materials from the channels. In addition, microfluidic devices printed by SL and MJM with photo-curable polymers have low elasticity and cannot be aligned to existing structures. Microfluidic device fabrication methods can be further enhanced by directly integrating microfluidic structures with electronic sensors and curvilinear surfaces as well as improving automation.

Here, we introduce an automatable extrusion-based printing methodology that can directly align and print elastomeric microfluidic structures onto planar and curvilinear substrates with minimal post-processing. By selecting a silicone-based ink of proper viscosity and controlling the profiles of printed overhung structures, self-supporting walls were realized and further enclosed to form hollow structures such as channels and chambers. Since the microfluidic spanning distance is in the sub-millimeter regime, a sufficiently small bending moment results that the as-printed walls can withstand, rendering this method highly suitable for printing microfluidic structures. Printing toolpaths can then be specifically designed to create leakage-free transitions between channels and chambers, T-shaped intersections and overlapping channels. The mechanical equilibrium states of the 3D printed silicone structures eliminate the need for supporting materials and rigid exterior covers that are conventionally required to build hollow structures with viscoelastic materials. Multi-material mixers were fabricated by integrating printed herringbone ridges to achieve high mixing efficiency in an enclosed microfluidic channel. Further, seamless integration of microfluidics and sensing microelectrodes was realized via synchronous alignment and printing onto the micro-chip. High-throughput and real-time impedance measurements of NaCl solutions were demonstrated with the 3D printed salinity sensor array. Most compellingly, we conformably printed 3D microfluidic networks that were integrated with valves on a spherical surface, demonstrating a novel device form-factor that can be potentially extended to freeform surfaces

such as the human body as microfluidics-based wearable health sensors. The devices demonstrated in this work serve as a proof of concept for the automatable capabilities of extrusion-based 3D printing to fabricate self-supporting and aligned multifunctional microfluidic structures.

[This document has been authorized for unlimited public release. PAO number U20-2128.]

#### 5:50 AM F.SF05.02.07

**3D Printed Soft Robots with Self-Healing, Reconfigurable and Conducting Capabilities** Eliot Gomez<sup>1</sup>, Shiwanka Wanasinghe<sup>2</sup>, Obed Dodo<sup>2</sup>, Michael F. Durstock<sup>3</sup>, Dominik Konkolewicz<sup>2</sup> and Carl Thrasher<sup>3</sup>; <sup>1</sup>UES, Inc., United States; <sup>2</sup>Miami University, United States; <sup>3</sup>Wright-Patterson Air Force Base, United States

3D printing with light-based vat photopolymerization (VP-3DP) can make challenging geometries (e.g. overhangs, cavities, channels) with soft elastic materials, resulting in great strides in soft robotics. As printing speeds and resolution improve, soft robotics still face challenges to produce large-scale features via VP-3DP due to a limited build area and the need for structural supports for complex features. In an effort to bridge this gap, we have developed tunable photopolymerizable resin systems amenable to VP-3DP to produce self-healing elastomers. Materials consist of dynamically exchangeable moieties that can be printed with wide-ranging moduli (e.g. elastic to rigid). Printed parts have high elongations (up to 2,000% strain); the capacity to self-heal to elastic or rigid parts; and reset permanent shape via bond exchange with applied heat. By printing these materials into small modular structures and utilizing their capacity for dynamic bond exchange, we demonstrate the facile construction of highly complex, reconfigurable, and macro-sized soft robotic actuators. We then combine these soft robotic actuators with self-healing conductors in the form of bulk liquid metal or Polymerized Liquid Metal Networks for embedded strain sensing, joule heating, and power delivery in a self-healable soft robot.

#### 6:00 AM F.SF05.02.08

**3D Printing of 0D/1D/2D Materials into Complex Architectures** Kun Fu; University of Delaware, United States

Carbon nanomaterials, including 0D carbon nanopowders, 1D carbon nanotubes, and 2D graphene, exhibit scaling effect and exceptional properties with great interest in structural and functional applications. The integration of carbon nanomaterials and architectural features at multiple length scales into structural mechanics and functional materials has significantly shifted the paradigm of materials engineering toward materials by design with structural and functional capabilities. Three-dimensional carbon multiscale architectures featuring the characteristics of both the constituent CNT material, which brings the effects of its feature nanoscale resolution and properties, as well as the structures across multiscale lengths offer breakthrough advances in many applications including ultra-light structural materials, energy storage, and biomedical devices. However, there is no effect approach to assemble those carbon nanomaterials into macro-scale structures with desired architecture while ensuring scaling properties. Therefore, it is highly anticipated to develop new manufacturing technology to handle nanomaterials and assemble them into large-scale structure with complex architectural features in a fast and efficient way.

In my talk, I will introduce our recent work on additive manufacturing of three-dimensional carbon-based multiscale architectures, and demonstrate its applications in electrochemical energy storage. Our method will retain the properties of carbon nanomaterials and there no additional binder or polymer in the final 3D components. We have demonstrated that carbon nanomaterials, including 0D carbon nanopowders, 1D carbon nanotubes, and 2D graphene, could be all processed into complex three-dimensional multiscale carbon architectures.

#### 6:10 AM F.SF05.02.09

**3D-Printed Pseudocapacitive Electrodes Enable Efficient Electron and Ion Transport at High Mass Loadings** Bin Yao<sup>1</sup>, Marcus A. Worsley<sup>2</sup> and Yat Li<sup>1</sup>; <sup>1</sup>University of California, Santa Cruz, United States; <sup>2</sup>Lawrence Livermore National Laboratory, United States

High mass loading and efficient charge transport are two crucial but often mutually exclusive characteristics of supercapacitors. 3D printing has emerged as a new tool to fabricate high-performance electrodes for energy storage devices. The interconnected conductive pathways in the printed 3D structures allow efficient electron transport. The periodic large pores in the 3D printed structures provide a short cut for electrolyte ions to the electrode surface. This efficient electron transport and ion diffusion in 3D printed electrodes enables fast charging and discharging even for thick electrodes at high mass loadings without sacrificing their gravimetric and volumetric capacitive performance, which successfully addresses the long-term challenge in this area. In this talk, I will present a millimeter-thick 3D-printed graphene aerogel electrode that could support pseudocapacitive manganese oxide (MnO<sub>2</sub>) up to 180 mg cm<sup>-2</sup>. The ultrahigh mass loading and efficient kinetic process enable them a record-high areal capacitance of 44.13 F cm<sup>-2</sup> for supercapacitors. More importantly, the 3D-printed graphene/MnO<sub>2</sub> electrode can simultaneously achieve excellent capacitance normalized to area, gravimetry, and volume,

which is the trade-off for most electrodes. Furthermore, by pairing the 3D-printed graphene aerogel/MnO<sub>2</sub> as a cathode and surface-functionalized graphene aerogel as an anode, the assembled asymmetric supercapacitor (ASC) could further be extended to 2V. This high mass loading-ASC could achieve a remarkable energy density of 0.65 mWh cm<sup>-2</sup> at an ultrahigh power density of 164.5 mW cm<sup>-2</sup>, outperforming all the previously reported supercapacitor devices operated at the same power density. These works have successfully proved the feasibility of fabricating pseudocapacitive electrodes *via* a 3D printing method, which might revolutionize the conventional fabrication process of commercial supercapacitors.

#### 6:20 AM F.SF05.02.10

**A Low-Maintenance Soil Moisture Sensor Fabricated with Ecofriendly and Biodegradable Materials** Yongkun Sui<sup>1</sup>, Madhur Atreya<sup>1</sup>, Subash Dahal<sup>2</sup>, Rajiv Khosla<sup>2</sup> and Gregory L. Whiting<sup>1</sup>; <sup>1</sup>University of Colorado Boulder, United States; <sup>2</sup>Colorado State University, United States

Every year in the United States, hundreds of billions dollars are spent on farm production. The two largest farming costs are related to crop input and labor. The cost on labor can be reduced by mechanization. However, because of the heterogeneity of farmlands, farmers face a challenge of reduced resource efficiency after switching to large-scale farming. To further reduce the cost by improving the resource efficiency, precision agriculture (PA) technologies has been widely adopted since the early 1990s. PA technologies use various sensors to measure temporal and site-specific environment, soil, and crop data. The currently available commercial sensors fabricated using conventional components are cost-prohibitive, therefore the deployment density and data resolution are limited.

Recently, additive manufacturing (AM), owing to its reduced material wastage, fast prototyping, and lower equipment cost features, has been used to fabricate sensors for PA applications. Various AM techniques such as inkjet-printing, screen-printing, stencil-printing, and extrusion-printing have been used to fabricate soil and environment sensors. Of the two, soil sensors probably benefit the most from low fabrication costs because accommodating the spatial and temporal heterogeneity of soil requires a high sensor density. For instance, soil moisture level could be different between two sampling spots at 2.5 m apart. Deploying sensors at this high density is obviously infeasible. In reality, only 1 sensor is deployed per hectare which is insufficient for high-resolution PA applications.

Researches have tried several printing approaches to reduce the fabrication cost of soil moisture sensors in order to improve the measuring resolution. Most printed soil moisture sensors use interdigitated electrodes to measure the dielectric constant of soil at different moisture levels. The electrodes are typically printed using silver or copper inks on polymer substrates. These printed sensors have demonstrated reliable performances in laboratory environments; however, still pose two challenges: (1) the sensors are made of non-degradable materials therefore require labor-intensive retrievals to avoid accumulation in the field, (2) the conductive components (i.e. silver or copper) are toxic to soil microbes and crops.

In this work, we report on a printed soil moisture sensor made of biodegradable and ecofriendly materials. The sensor is comprised of a slowly degradable hydrophobic encapsulant and rapidly degradable functional components (i.e. the electrodes and substrates). This combination of materials allows the sensor to function in soil for an extended period then rapidly fail after the encapsulant is decomposed by soil microbes. The rapid breakdown facilitates easy assessment of each sensor's service life so that the maintenance effort can be reduced. The sensor will eventually decompose completely hence eliminates the needs of labor-intensive retrievals. Ecotoxicity tests show that the sensor materials do not hinder the crop growth. Sensors with encapsulants of different thickness were fabricated and their sensitivities as a function of volumetric water content (VWC) were measured. The long-term stability of the sensor was assessed by accelerating the degradation under controlled temperature. Finally, the breakdown of the sensor was characterized with an extended accelerated test.

#### 6:30 AM F.SF05.02.11

**Developing Ceramic AM to Unlock Enhanced Thermal Storage by Swirling Two-Phase Flow in a Package Integrated Cyclone COoler (PICCO)—A Case Study** Cathleen A. Hoel<sup>1</sup>, Rinaldo Miorini<sup>1</sup>, Hendrik De Bock<sup>1</sup> and Darin Sharar<sup>2</sup>; <sup>1</sup>GE Research, United States; <sup>2</sup>U.S. Army Research Laboratory, United States

Power electronic devices have a driving demand to both decrease in size and weight while increasing in performance, which requires next generation thermal management methods. GE Research and the US Army Research Lab have teamed up to explore the concept of utilizing a 3D printed ceramic cooling channel with an internal swirler to enable efficient use of two-phase flow in a Package Integrated Cyclone COoler (PICCO). This work will describe the challenges and learnings associated with 3D printing the ceramic swirler in alumina by stereolithography. Processing effects were evaluated including printing orientation, substrate effects, and slurry grade. Design effects were evaluated including support structures, addition of fillets and geometric non-uniformities.

Research was sponsored by the U.S. Army Research Laboratory's Sensors and Electron Devices Directorate (SEDD) and was accomplished under Cooperative Agreement Number W911NF1920276. The views and conclusions contained in this document are those of the authors and should not be interpreted as representing the official policies, either expressed or

implied, of the U.S. Army Research Laboratory's Sensors and Electron Devices Directorate (SEDD) or the U.S. Government. The U.S. Government is authorized to reproduce and distribute reprints for Government purposes notwithstanding any copyright notation herein.

#### **6:40 AM F.SF05.02.12**

**Metallic 3D Printing—Implications to Customized Prosthetic Implants** Sze Yi Mak<sup>1</sup> and Ching Hang Bob Yung<sup>2</sup>; <sup>1</sup>The University of Hong Kong, Hong Kong; <sup>2</sup>Koln 3D Technology (Medical) Limited, Hong Kong

Medical devices such as artificial implants and prostheses are commonly made of metallic materials, for instance, Cobalt-Chromium alloy, Titanium alloy and stainless steel, for they demonstrate satisfactory biomechanical properties and biocompatibility. The introduction of additive manufacturing has brought the design and fabrication of medical device into a new era, customizing not only shape but also porosity, internal design and surface finishing. Here we present the use of novel Integrated Machining Direct Metal Laser Sintering (IM-DMLS) 3D printing technology to enable hybrid fabrication of prosthetic implant customizing to specific bone anatomy to a dimensional accuracy of  $\pm 0(10)$  microns. Subsequent fine polishing results in a surface roughness (Ra) in micron to submicron range. Tailoring the internal structure of prosthetic implant reduces the weight of implant while preserving good biomechanical properties. Furthermore, we demonstrate the feasibility to form Cobalt-Chromium alloy scaffolds with tunable lattice size and porosity in the biological-relevant range which allows osseointegration. Our work has prominent potential in medical applications of customized medical devices that benefits patients in terms of better bone-implant integration in long term and improved patient experience of size fitting and weight reduction.

SESSION F.SF05.03: Additive Manufacturing of Functional Materials  
On Demand Abstracts Available for Viewing Starting Saturday Morning, November 21, 2020  
F-SF05

#### **5:00 AM \*F.SF05.03.01**

**3D Printing of Aerogels** Dong Lin, Halil Tetik and Nasrullah Shah; Kansas State University, United States

Aerogels are highly porous structures produced by replacing the liquid solvent of a gel by air without causing a collapse in the solid network. Unlike conventional fabrication methods, additive manufacturing has been proposed to fabricate aerogels having complex geometries with designed pore morphologies, which can be advantageous for various applications. However, the fabrication of Aerogels with tailored macrostructures by scalable and controllable methods remains a big challenge. The vision of tailoring the architecture of aerogels for broad applications, including separation, all-solid-state batteries, micro pressure sensors, electrodes, and electrochemical catalyst templates, has stimulated the research on 3D printing of aerogels. Herein, we propose a printing methodology that combines multi-nozzle drop-on-demand inkjet printing of nanomaterials suspension with freeze casting for rapid printing of 3D aerogels architectures to achieve several key qualities, namely, pure, continuous, boundary-free, controlled microstructure, and truly 3D architectures (e.g., 3D truss with overhang structures). To date, we have successfully printed world's lightest material via 3D printing through the proposed technique.

#### **5:15 AM \*F.SF05.03.02**

**Electrochemically Active Architected Materials by Additive Manufacturing** Xiaoxing Xia<sup>1</sup>, Julia R. Greer<sup>2</sup>, Claudio V. Di Leo<sup>3</sup>, Carlos M. Portela<sup>2</sup>, Dennis Kochmann<sup>4</sup>, Eric B. Duoss<sup>1</sup> and Sarah E. Baker<sup>1</sup>; <sup>1</sup>Lawrence Livermore National Laboratory, United States; <sup>2</sup>California Institute of Technology, United States; <sup>3</sup>Georgia Institute of Technology, United States; <sup>4</sup>ETH Zürich, Switzerland

Architected materials are a new class of engineered materials with carefully controlled internal structures that give rise to properties that differ from or surpass those of their constituent materials. Additive manufacturing provides an extraordinary opportunity to rationally design the structure and the chemical composition of architected materials across multiple length scales to optimize properties and functionalities for a variety of applications. These functional architected materials are capable of decoupling critical trade-offs to reach new regions of the material property space and enabling exotic properties that rarely exist in classical materials. Electrochemistry describes the mutual interaction between electricity and chemical reactions, which enables electrically controlled and oftentimes reversible release/storage of energy through electrochemical reactions in, for example, batteries, fuel cells and electrodeposition processes. Designing an electrochemical system is a multi-faceted engineering challenge with trade-offs and constraints such as ion transport through electrolyte, electron

transport inside both electrodes, active electrode surface area, chemical reversibility, and mechanical/chemical stability of electrodes and products during reaction. Recent development in high resolution additive manufacturing has enabled an unprecedented degree of structural control at length scales relevant to electrochemical transport kinetics and thus open up possibilities to rationally design material architectures that improve the performance of these electrochemical systems.

Recently, we created additively manufactured architected materials that can respond to and facilitate electrochemical reactions in the local environment. We developed novel fabrication methods based on a suite of 3D printing methods such as two-photon lithography and stereolithography and various physical and chemical post-processing techniques to create architected materials with multi-level design freedom including feature sizes, structural geometries, and material compositions, which resonates with the entangled challenges in electrochemical systems. We demonstrated that additive manufacturing provides a new platform to design 3D-architected electrodes for batteries and electrochemical reactors for CO<sub>2</sub> reduction with enhanced transport kinetics and mechanical stability. Furthermore, we presented a new class of electrochemically reconfigurable architected materials that could transform their structures in a programmable, reversible and non-volatile fashion, which provide new vistas for designing mechanical metamaterials with tunable phononic bandgaps and deployable micro-devices for biomedical applications. The multi-scale and multi-physics nature of these electrochemically active architected materials prompted us to develop a toolset of in situ microscopy techniques and various simulation frameworks to capture and analyze their dynamic behaviors undergoing electrochemical reactions in order to provide an in-depth understanding of the underlying mechanisms as well as design principles generalizable for other functional architected material systems.

**5:30 AM \*F.SF05.03.03**

**Multi-Functional Materials for Additive Manufacturing—Electromechanical Materials for Self-Sensing and Actuation** Xiaoyu Zheng; University of California Los Angeles, United States

While considerable progress has made in additive manufacturing of structural materials, including polymer, metal and ceramics, adding multi-functionality into the material pallet is compelling. However, such efforts has been challenged by the trade-off between active properties and manufacturability. In this talk, I will present the additive manufacturing of a suite of electro-mechanical coupling materials (e.g. piezoelectric materials and electronic integration) for energy transduction, where electrical and mechanical behaviors and their couplings can be inversely designed and tailored by an end-user at will. This unleashes new design freedoms for rapid material property discovery and functional product realizations. I will discuss a suite of all-in-one transducers and their new applications, including self-sensing autonomous materials, microsystems for robotics, as well as air and maritime self-sensing system.

**5:45 AM F.SF05.03.06**

**3D Printing of Hydroxypropyl Cellulose Liquid Crystal—Towards Tunable and Sustainable Photonic Structures** Chun Lam Clement Chan, Iek Man Lei, Yan Yan Shery Huang and Silvia Vignolini; University of Cambridge, United Kingdom

As we move towards more sustainable manufacturing systems, cellulosic materials are extremely promising due to their biocompatible and sustainable characteristics. Hydroxypropyl cellulose (HPC) is a biocompatible cellulose derivative capable of self-assembling into a lyotropic chiral nematic phase in aqueous solution, which can then reflect vibrant colourations.

We report here a functionalised photocrosslinkable HPC ink compatible with 3D printing. We demonstrate that we can 3D print solid materials with a large variety of shapes, and that the HPC retains its liquid crystalline state and therefore, its colouration after the printing. The final colour of the material can be tuned on-line during printing either by changing the amount of water in the ink formulation or by altering the temperature at which the ink is photo-crosslinked. Our developed system, therefore, allows us to extend beyond the limits of traditional multi-color printing systems based on dyes, as it allows to create materials with colours across the visible range using a single feedstock.

**5:55 AM F.SF05.03.08**

**Additive Manufacturing of Functional Materials via Photopolymer Complex Synthesis** Daryl Yee and Julia R. Greer; California Institute of Technology, United States

Over the past decade, additive manufacturing has emerged as one of the most powerful manufacturing tools available today. Vat photopolymerization techniques, in particular, are especially promising as they are capable of achieving high resolutions



and throughputs. However, the fabrication of non-polymeric materials with this technique still remains a challenge in the field — ceramics can be fabricated using vat photopolymerization but are often either based on photosensitive slurries that can be challenging to use and have poor resolutions or on inorganic-organic photoresins that are limited in composition achievable and require some complex synthesis. Metals, in general, have not been explored with vat photopolymerization techniques.

To address these, we introduce the concept of architected “chemical reactors” and demonstrate how we can use this general idea to adapt the field of materials chemistry to additive manufacturing. We present a novel technique called photopolymer complex synthesis that combines solution combustion synthesis with vat photopolymerization to address the issues mentioned above and enable the additive manufacturing of both complex metal oxides and metals. In brief, aqueous metal-ion containing homogenous photoresins are prepared and used with photolithography, in conjunction with post-processing techniques to fabricate architected metal oxide or metal structures. As examples of this technique, we fabricated and characterized zinc oxide (ZnO) and lithium cobalt oxide (LCO) architected structures with sub-micron and sub-millimetre features respectively. Compression of the ZnO structures resulted in an electromechanical response, and electrochemical cycling of the LCO structures showed efficient performance as a lithium ion battery cathode. We also demonstrate the fabrication and characterization of metal structures made from copper and cupronickel alloys. Characterization of these structures using X-ray diffraction, energy-dispersive spectroscopy and transmission electron microscopy indicate that the structures are indeed comprised of the appropriate material, highlighting the utility of photopolymer complex synthesis as a facile and accessible method for the fabrication of these metal oxide and metal materials.

#### **6:05 AM F.SF05.03.10**

**Aerosol Jet Printing of Battery Separator Membranes** Andrew L. Fassler<sup>1,2</sup>, Ryan R. Kohlmeyer<sup>1,2,3</sup>, Gregory Horrocks<sup>1</sup> and Michael F. Durstock<sup>1</sup>; <sup>1</sup>Air Force Research Laboratory, United States; <sup>2</sup>UES, Inc, United States; <sup>3</sup>Xerion Advanced Battery Corp, United States

Additive manufacturing of batteries offers great potential for the future of power integration into electronics and devices, such as in thin film and flexible devices where battery packaging physically prevents intimate incorporation. Additionally, printing technologies open up new design spaces for batteries such as in distributed power supplies and utilization of unused negative space around other features within a device. To achieve this, additive manufacturing approaches must be developed that permit the deposition of battery component materials with fine feature sizes and with control over complex 3D topologies and thin film morphologies.

We demonstrate the use of aerosol jet printing approaches for the deposition and control of 3D printed battery component materials. The printed ink is atomized into micro-droplets and entrained into a flowing carrier gas. This flow is then focused at the printing nozzle where it exits in a high speed collimated stream. This process couples high resolution feature sizes (10-100  $\mu\text{m}$ ) with a large working distance, making it ideal for incorporating batteries into minute spaces and on non-planar structures. However, the complexity of the aerosol jet process puts specific constraints on the inks in order to maintain proper atomization.

Here we focus on controlling the separator/electrolyte membrane morphology, which is known to be one of the most critical challenges in 3D printed battery systems. A relatively high level of separator porosity is required to maintain a high ionic conductivity, however these features must be small enough in size to prevent dendritic growth and shorting. We achieve this porosity control through a drying induced phase separation process. A mixed solvent system with carefully controlled relative evaporation rates is used together with a variety of polymer/nanoparticle host materials. This leads to instability in the ink upon drying thereby causing phase separation into polymer poor and polymer rich phases, creating porosity upon solidification. This approach enables the deposition of extremely uniform separator films with fine porosity control. In this study, we examine printing the separator material both on flat substrates and directly onto rough graphite anodes as a means of printing Li-ion batteries. We explore how the printing processes directly impacts battery performance and demonstrate how intimate contact between the electrode and separator at this interface can impact dendrite growth, a key safety concern in Li-ion batteries.

#### **6:15 AM F.SF05.03.12**

**Bamboo Fibre-Reinforced Mycelium Composites for Sustainable Structures** Hortense Le Ferrand<sup>1</sup>, Nazanin Saeidi<sup>2,3</sup>, Eugene Soh<sup>1</sup> and Zhi Yong Chew<sup>1</sup>; <sup>1</sup>Nanyang Technological University, Singapore; <sup>2</sup>ETH Zürich, Singapore; <sup>3</sup>KIT, Germany

Mycelium-bound composites are promising materials for sustainable packaging, insulation, fashion, architecture. They consist in exploiting a living organism, a fungus, to develop its intricate mycelium network to form a composite material. To date, moulding is the main fabrication process explored for mycelium-bound composites that strongly limits the ability to

design complex shapes that could widen the range of applications. As an alternative, extrusion printing is a facile and low energy-cost process that has not been explored yet but that could offer with design freedom and structural properties. In this study, we combine bamboo microfibrils, chitosan, and mycelium from *Ganoderma Lucidum* to establish a composite mixture that is workable, extrudable and buildable. All those components are issued from agricultural waste, which is key in obtaining interesting composites that are also sustainable. We studied the impact of bamboo fibre size, chitosan concentration, pH and ratio to determine the optimum growth condition for the mycelium as well as highest mechanical stiffness and building capability. The resulting materials that we fabricated have thus low energy costs, are sustainable, and present mechanical properties that makes the process promising for structural applications. The printing method now allows the investigation of complex structures for more optimal mycelium growth thanks to the design of 3D porous structures allowing spreading of the loads and high surface contact with oxygen.

#### SESSION F.SF05.04: Bioprinting

On Demand Abstracts Available for Viewing Starting Saturday Morning, November 21, 2020  
F-SF05

##### 5:00 AM \*F.SF05.04.01

**3D Bioprinting Using UNiversal Orthogonal Network (UNION) Bioinks** [Sarah C. Heilshorn](#); Stanford University, United States

Three-dimensional (3D) bioprinting is a promising technology to produce living, tissue-like structures, but a current lack of diversity in bioink materials is a major limitation. A cell's phenotype is directly influenced by its surrounding microenvironment; thus, ideally each cell type would be printed in its own customizable bioink. To fulfill this need for a universally applicable bioink strategy, we developed a versatile, bioorthogonal crosslinking mechanism that is completely cell compatible and works with any type of biopolymer. We term this family of materials UNiversal, Orthogonal Network (UNION) bioinks. To prepare these materials, the biopolymer backbone is modified with either an azide or a bicyclononyne (BCN) group. The functionalized polymer is mixed with cells to create a bioink, and then extruded into a support bath containing soluble, multifunctional crosslinkers modified with the partner bioorthogonal reactive group. As demonstration of UNION bioink versatility, gelatin, hyaluronic acid (HA), recombinant elastin-like protein (ELP), and polyethylene glycol (PEG) were each used as backbone polymers to create inks with storage moduli spanning 200 to 10,000 Pa. Because UNION bioinks are crosslinked by a common chemistry, multiple materials can be printed together to form a unified, cohesive structure. This approach is compatible with any support bath that enables diffusion of the UNION crosslinker. Both matrix-adherent human corneal mesenchymal stromal cells and non-matrix-adherent human induced pluripotent stem cell-derived neural progenitor spheroids were printed with UNION bioinks. The cells retained high viability and expressed characteristic phenotypic markers after printing. Thus, UNION bioinks are a versatile strategy to expand the toolkit of customizable materials available for 3D bioprinting.

##### 5:15 AM \*F.SF05.04.02

**3D Printing of Engineered Bacteria for the Production of Biofilms-on-a-Chip** [Anne S. Meyer](#); University of Rochester, United States

In order to create crisp, defined patterns of biologically-created materials, new technologies need to be developed and implemented. The Meyer lab is developing first-of-their-kind DIY bacterial 3D printers that can deposit engineered bacteria in specific three-dimensional patterns using simple devices and chemistries. Our affordable, easy-to-build bacterial 3D printers have fully automated, coordinated control of the pumps and printhead, allowing for high spatial resolution (<mm-scale) printing of bacteria onto wet or dry surfaces. Our printers mix an alginate-containing bacterial culture with a calcium chloride solution upon printing, triggering cross-linking of the alginate molecules to form a stable, biocompatible scaffold to support the bacteria. After printing, the bacteria survive for several weeks and can be induced to produce a variety of biomaterials. We are applying our printer to the fabrication of engineered biofilms, groups of bacteria that live within a spatially structured polymer matrix. We use our 3D printer to deposit engineered *E. coli* that are able to produce CsgA fibrils, or curli fibrils, the major protein component of biofilm polymer matrices. These engineered bacteria can stick to the printing surface even upon attempting to dissolve the printing scaffold, creating free-standing, stably patterned biofilms. Our patterned biofilms develop emergent properties analogous to those seen in natural biofilms, including resistance to anti-bacterial treatment and oxygen depletion within the biofilm interior. These model biofilms will be crucial for future development of anti-biofilm strategies, for which no reproducible model biofilm test system is currently available, as well as

for the reliable production of beneficial living materials, which could be applied for water and soil purification or mineral extraction.

**5:30 AM \*F.SF05.04.03**

**Additively Manufactured Architected Synthetic Biofilms** William Hynes, Karen Dubbin, Javier Alvarado and Monica Moya; Lawrence Livermore National Laboratory, United States

Bio-active materials integrated with living cells are capable of sensing and responding to a wide range of environmental stimuli and show great promise in biological and chemical sensing applications. The field of bioprinting has typically been geared towards mimicking biology for the purpose of creating human ex-vivo tissues and little work aimed at engineering materials to perform a synthetic function. In this work we engineer hybrid materials composed of living and non-living materials to structure and support the viability and function of living microbes through the fabrication of artificial biofilms

We have previously demonstrated the ability to additively manufacture three-dimensional living tissues using optimized scaffolding materials that sustain the long-term viability of living cells and are amenable to creating diverse living constructs with high degrees of cellular organization. Using the 3D structuring capabilities of LLNL's BioPuSL system (a custom-built biological projection micro-stereolithography), we demonstrate the viable patterning and subsequent growth of *E. coli* bacteria within 3D bioprinted, bacterial-laden engineered biofilms. We show how altering biofilm 3D architecture influences the mass-transport to govern the target application of metal ion absorption. This approach of incorporating sensing cells within novel substrates and architecture designs can enable the development of a new generation of biological generated functional materials with many applications from biosensors to the production of biofuels and bioproducts.

This work was performed under the auspices of the U.S. Department of Energy by Lawrence Livermore National Laboratory under Contract DE-AC52-07NA27344. LLNLCONF-760584.

**5:45 AM \*F.SF05.04.04**

**Electrohydrodynamic Printing to Achieve the Next Generation of Functional Biomaterials** Miguel Castilho<sup>1,2</sup>; <sup>1</sup>UMC Utrecht, Netherlands; <sup>2</sup>Eindhoven University of Technology, Netherlands

AM technology is a rapidly growing biomaterial processing technique that has an enormous potential for (bio)medical applications such as tissue engineering and regenerative medicine, however greater resolution is required for the next generation of biomedical materials. Melt electro (spinning) writing (MEW) is one such unique AM process that has gained the spotlight in regenerative medicine due to its potential to engineer highly-ordered fibrous scaffolds, capable of replicating extracellular microenvironment functions. Highly resolved porous constructs fabricated in this manner have great utility for both *in vitro* and *in vivo* applications and represents the cutting-edge of 3D printing in biomedical applications. This talk will highlight some of latest developments in such high-resolution 3D MEW processing. This includes developments in processing parameters, functional designs, modelling biomechanics of MEW fibre constructs, and bioactive and hydrogel-based materials for MEW. A particular focus will be placed on the application of MEW constructs for cartilage and cardiac muscle regeneration. The second part of the presentation discusses an even more enticing feature in advancing MEW technology: the convergency of MEW with other 3D printing technologies, e.g. extrusion-based printing, in a single printing platform. The simultaneous use of MEW with other complementary 3D printing processes allows the strategic arrangement of multiple material compositions and operation at different length scales, from sub-micron to centimetre scale, not possible with any single component deposition method. Applications of this novel multitechnology fabrication in soft tissue engineering will be discussed.

**6:00 AM F.SF05.04.05**

**3D Printing of Living Microbial Fuel Cell Anode** Megan Freyman, Tianyi Kou, Shanwen Wang and Yat Li; University of California, Santa Cruz, United States

3D printing helps to provide further control on electrode design. By using 3D printing to tune the geometry, porosity and dimensions of the structure, mass transport to functional microbes or sites in the structure can be improved. By embedding living microbes directly into the ink we can create 3D printed structures to help harness the activity of microbes and use them in functional devices. Here we demonstrate the incorporation of the living bacteria *Shewanella Oneidensis* MR-1 (*S. Oneidensis* MR-1) directly into an ink used for creating 3D printed structures. By incorporating *S. Oneidensis* MR-1 into a sodium alginate-cellulose ink we showed that *S. Oneidensis* MR-1 survives the 3D printing process through the prominent degradation of methyl orange azo dye from the surrounding solution in the presence of the living 3D printed structure. The viability was further confirmed using confocal microscopy. By incorporating carbon black into this ink we further

demonstrate the direct printing of a living microbial fuel cell (MFC) anode. Electrochemical measurements showed there was good charge transfer between the *S. Oneidensis* MR-1 and the electrode surface. To our knowledge, this is the first report on implementing 3D printed bacteria structure as a living electrode for an MFC system. The capability of printing living and functional 3D bacterial structure could open up new possibilities in design and fabrication of microbial devices as well as fundamental research on the interaction between different bacterial strains, electrode materials, and surrounding environments.

#### 6:10 AM F.SF05.04.06

**High Fidelity 3D Printable Materials with Spatio-Temporally Tunable Degradation for Tissue Engineering** Archish Muralidharan, Robert McLeod and Stephanie Bryant; University of Colorado Boulder, United States

In order to advance the state-of-the-art of tissue engineering, there is a need for degradable materials with adequate mechanical properties, tunable degradation, and the ability to form biologically relevant complex geometries. The overarching goal of this work is to 3D print personalized stiff structural scaffold which can be infilled with a soft cellular niche hydrogel, satisfying the conflicting design requirement of both a soft matrix to promote neo-tissue growth and a stiff scaffold to withstand physiological loads. To achieve this goal, mechanical integration of these two materials is needed to enable transfer of biomechanical cues and prevent delamination at the interface and engineer the scaffold to degrade at pre-engineered rates.

In our previous study, a relationship between the exposure conditions during 3D printing and the local mesh size of the network formed was established (*Muralidharan et. al. Adv. Mater Technol. 2019*). Control over mesh size of the 3D printed polymer network ranging from 1.3nm to 11.5nm was achieved. Mesh size ultimately controls the transport of second material (soft hydrogel) into the printed network, and integration distances ranging from 10s of microns to millimeters in 3D printed parts were demonstrated.

This study aimed to develop 3D printable degradable materials with high fidelity and predictable properties through two specific objectives: **1) Design and develop 3D printable materials with controlled degradation.** The synthesis of traditional multifunctional macromers that form degradable networks commonly involves multiple functionalization and purification steps, which makes the development of large numbers of polymers with diverse properties difficult. Poly ( $\beta$ -amino esters) (PBAEs) are an attractive biomaterial for degradable materials that has one-step synthesis with no further purification steps and tunable degradation. Linear macromers based on diacrylate-terminated PBAEs were synthesized by reacting 1° amines (RNH<sub>2</sub>) with diacrylates. 3D printable poly ( $\beta$ -amino ester) based acrylate terminated macromers were subsequently photopolymerized and characterized for degradation. Through rational selection of acrylates and amines used to synthesize the PBAEs, the hydrophobicity of the network can be controlled. This directly influences the degradation mechanism (i.e. bulk vs surface degradation). We demonstrate degradation profiles with an exponential decay in mechanical properties over time, evident of bulk erosion, to networks with minimal change in mechanical properties, evident of surface erosion. Mass loss was measured over time in an accelerated degradation solution of 1M NaOH. The degradation profiles ranged from linear mass loss to systems where mass loss is slow at early times and accelerates as the network degrades. The polymers with similar modulus of 8-10MPa, exhibited a wide range of degradation rate from 100% mass loss within 90 min to 100% mass loss in 10 days to minimal mass loss over 45 days. These variations, achieved through simple chemical modifications, illustrate the versatility of these PBAE based polymers. **2) High resolution 3D printing using PBAE macromers.** Through high resolution projection microstereolithography based 3D printing, customized medical image derived geometries with precisely prescribed microarchitectures can be produced. The high molecular weight macromers limit the diffusion of propagating radical into dark during 3D printing, thus allowing high fidelity features as low as 20 $\mu$ m. Moreover, the spatio-temporal degradation control was demonstrated with three orders of magnitude variation in degradation rates. In summary, with an advanced toolbox of synthetic and manufacturing methodologies in hand, we can rationally design and manufacture polymer materials with specific properties.

#### 6:20 AM F.SF05.04.07

**High-Throughput Methods for Materials Creation, Selection and Identification Leading to the Production of Personalised Cell Instructive Biomedical Devices via Ink Jet Based 3D Printing** Ricky Wildman, Yinfeng He, Morgan Alexander, Derek Irvine, Paul Williams, Zuoxin Zhou, Richard Hague, Christopher Tuck, Jeni Lockett, Jean Dubern and Andrew Hook; University of Nottingham, United Kingdom

3D printing has been widely investigated for biomedical applications and attracted considerable attention as a cost-effective manufacturing technique to produce bespoke devices for patients. However, it is still facing many challenges for realizing this target due to a lack of suitable materials. At the University of Nottingham, we have developed a methodology that allows

us to rapidly identify printable formulations for use with inkjet 3D printing, selected from libraries of materials with cell instructive behaviour. We show how we can exploit this high throughput approach to quickly identify useful, printable materials with potential for scale up and for the production of multimaterial, multifunctional devices. We will show how we used this method to produce devices composed of formulations that can inhibit biofilm formation (*Pseudomonas Aeruginosa* and *Staphylococcus aureus*) by more than 90% in comparison with commonly used devices made from silicone rubber. We go on to show how the design and manufacture of these multimaterial devices can be coupled to design optimisation approaches that generate compositional maps of materials that tell us where to put which materials in order to get a precise mechanical response. As a result, we are able to show that we can select for material, shape and the distribution of material composition to create bespoke implants or other devices that offer significantly reduced infection mortality rate during application, as well as offering all the personalisation benefits that come with 3D printing. We have carried out a range of characterizations that show our devices are capable of safe use and retain their efficacious properties both *in vitro* and *in vivo*.

#### 6:30 AM F.SF05.04.08

**Microstructural Control of Polymers Achieved Using Controlled Phase Separation During 3D Printing with Oligomer Libraries—Dictating Drug Release for Personalized Subdermal Implants** Laura A. Ruiz Cantu, Gustavo F. Trindade, Zuoxin Zhou, Vincenzo Taresco, Laurence Burroughs, Elizabeth Clark, Felicity Rose, Morgan Alexander, Christopher Tuck, Richard Hague, Clive J Roberts, Derek Irvine and Ricky Wildman; The University of Nottingham, United Kingdom

In developing 3D printed implants, we face considerable challenges in defining which materials to utilize and what combinations to adopt to personalize their performance. A pertinent example is the long-term subdermal contraceptive implant. This is usually cylindrical with a size (maximum diameter 2 mm, length range 1 to 4 cm) defined by a combination of implantation method and anatomical positioning. Currently, such devices are manufactured by a process which heats a blend of polymer and active pharmaceutical ingredient (API) to around 100°C. However, current systems are not personalizable, nor is it possible to combine multiple drugs into a single treatment. One route to achieving personalization is through 3D printing. Ink jet based 3D printing, offers multiple benefits including its scalability, high resolution and importantly, drop by drop deposition that can provide both control over material properties at the microscale as well as the ability to co-deposit multiple materials (drugs).

In this study, we show that ink jet 3D printing of polymer blends gives rise to controllable phase separation that can be used to tailor the release of drugs. We predicted phase separation using high throughput screening combined with a model based on the Flory-Huggins interaction parameter, and were able to show that drug release from 3D printed structures can be predicted from observations based on single drops of mixtures.

Here, we report the creation of a library of multicomponent biodegradable inks, whose diversity of physicochemical properties allows for the range of phase separation behaviour required for tailoring drug release. We show that, by understanding the mechanisms that drive formation of this microstructure, we can predict microstructure that arises out of the ink jet printing process and reliably design and manufacture implants for tailored release. The screen considers the behavior of formulations designed for the release of drugs from 3D printed constructs and uses single drops screening (SDS) to characterize behavior in large, printed constructs.

We observed microstructure in larger-scale printed material that is similar to the drops but not evident in cast materials. We show that, by understanding both this microstructuring and the material composition characteristics, we can design and manufacture implants exhibiting tailored release that does not require varying the implant geometry. This is an important advance for implants that need to be delivered by cannula, where the shape is highly constrained and thus the usual geometrical freedoms associated with 3D printing cannot be exploited, bringing a hitherto unseen level of understanding to emergent material properties of 3D printing.

#### 6:40 AM F.SF05.04.09

**Multifunctional Artificial Artery from Direct 3D Printing with Built-In Ferroelectricity and Tissue-Matching Modulus for Real-Time Sensing and Occlusion Monitoring** Jun Li, Yin Long, Fan Yang and Xudong Wang; University of Wisconsin–Madison, United States

Treating vascular grafts failure often requires complex surgery procedures and associates with a high mortality rate. Real-time monitoring vascular system could enable quick and reliable identification of complications and initiate safer treatments in the early stage. In this work, electric field-assisted 3D printing technology was developed to fabricate *in situ*-poled ferroelectric artificial arteries that offered battery-free real-time blood pressure sensing and occlusion monitoring capability.

The complex functional artery architecture was made possible by the development of a printable ferroelectric bio-composite which could be quickly polarized during printing and reshaped into devised objects. Synergistic effect from the ferroelectric potassium sodium niobate (KNN) particles and the ferroelectric polyvinylidene fluoride (PVDF) polymer matrix yielded a superb piezoelectric performance (bulk-scale  $d_{33} > 12 \text{ pC N}^{-1}$ , confirmed by piezometer) on a par with that of commercial ferroelectric polymers. The sinusoidal architecture brought the mechanical modulus down to the same level of human blood vessels. The desired piezoelectric and mechanical properties of the 3D-printed artificial artery provided an excellent sensitivity to pressure change ( $0.306 \text{ mV/mmHg}$ ,  $R^2 > 0.99$ ) within the range of human blood pressure (11.25 to 225.00 mmHg). The high pressure sensitivity and the ability to detect subtle vessel motion pattern change enabled early detection of partial occlusion (e.g., thrombosis), allowing for preventing grafts failure. This work demonstrated a promising strategy of incorporating multi-functionality to artificial biological systems for smart healthcare systems.

#### **6:50 AM F.SF05.04.10**

**Support-Enabled Three-Dimensional Printing of Bacteria** Marco Riccardo Binelli, Patrick A. Rühls, Giovanni Pisaturo and André R. Studart; ETH Zürich, Switzerland

The three-dimensional localization of bacterial cultures provides a valuable tool for studying the behavior of microbes and for generating engineered living materials, but remains a challenging feat to achieve. Recent efforts have been made to confine bacteria into printable hydrogel matrices, mainly focusing on sustaining the growth of microbes while ensuring adequate material properties for 3D printing. At times, though, the rheological features required for conventional direct ink writing do not match the needs of the bacterial strain of choice and hinder the growth of the microorganisms. To circumvent this obstacle, we developed a 3D printing approach that allows us to directly deposit bacteria suspensions into a matrix that both supports free-form printing and allows oxygen diffusion. In our approach, we choose bacteria that have a potential for functional applications or for the synthesis of materials. Amongst these, bacteria capable of synthesizing bacterial cellulose such as *G. xylinus* are of particular interest as they are able to produce personalized biomaterials with outstanding properties such as biocompatibility, tensile strength, and high chemical purity. The rheological behavior of the matrix selected to host such bacteria must prevent the shape-distorting effects of surface tension and gravity. Moreover, when a needle ploughs through the support matrix, it is necessary to ensure a rapid closure of the groove behind the tip to maintain the resolution of the print. Using this approach, we are able to print freeform bacteria suspensions and, when using *G. xylinus*, directly form complex 3D cellulose structures. The use of bacteria to directly grow functional materials in accurate 3D shapes opens the way to a new generation of tailorable living materials, which do not only perform the designed function but also retain the ability to regenerate and respond to environmental stimuli. We envision this new paradigm to be of interest for a wide variety of applications as, for instance, wound dressing and drug delivery.

SESSION F.SF05.05: Developments in AM Materials, Techniques and Processes  
On Demand Abstracts Available for Viewing Starting Saturday Morning, November 21, 2020  
F-SF05

#### **5:00 AM \*F.SF05.05.01**

**Additive Manufacturing of Hierarchical Materials Using Self-Assembly Inks** André R. Studart; ETH Zurich, Switzerland

Additive manufacturing (AM) offers new opportunities to shape functional materials into complex three-dimensional geometries that are not accessible via conventional fabrication technologies. The layer-by-layer approach used in AM processes also allows us to build artificial structures in a similar way to the methods used by living organisms to grow complex hierarchical materials with unusual sets of properties. Living organisms strongly rely on self-assembly processes to create such functional hierarchical structures. In this talk, I will show how additive manufacturing can be combined with self-assembly processes to fabricate macroscopic functional objects with structural features spanning over multiple length scales. The underlying concept is to exploit the shaping capabilities of AM to define the structure of the object at the macroscale ( $> 1 \text{ mm}$ ), while implementing self-assembly strategies within the feedstock ink to achieve structural control at the sub-millimeter scale. Alike biological materials, the 3D objects manufactured through this approach exhibit properties that emerge primarily from the hierarchical structure rather than the specific chemistry of its constituents. This provides an attractive route towards the design and fabrication of functional materials with enhanced performance using more sustainable chemical resources.

#### **5:15 AM \*F.SF05.05.02**

**Complex Materials Design for Multidimensional Additive Processing** Subramanian Ramakrishnan and Tarik Dickens; Florida Agricultural and Mechanical University, United States

The ability to pattern multiple materials, on micrometer length scales, in three dimensions is critical for several technological applications including composites, microfluidics, photonics, and tissue engineering. The aim of the recently established NSF CREST Center at Florida A&M University is to promote additive manufacturing of novel device structures with an effort towards ab-initio fundamental understanding of material-property relationships that govern the working forces behind high-rate processing applications, and thus low-cost energy products. It is our goal to develop a materials-to-manufacturing framework for research in 3D printing of structures and devices for a wide variety of applications. We aim to (1) gain a fundamental understanding of the materials assembly and additive processing through a combination of experiments and theory; (2) develop and use novel processing/characterization tools for the proposed materials/devices; and (3) use AM to layer-by-layer process these structures/devices. The three main subprojects in the center include - (1) Nanostructured lightweight magnetic materials for shielding/sensing applications. (2) Nanostructured materials for energy applications and (3) Nanostructured Materials for Biological Applications. In this talk, I will detail recent developments in the CREST on these particular sub projects – flow and field assisted processing of multifunctional nanocomposites – where we use combined flow and magnetic fields to orient nickel nanorods, direct printability and performance of 3D conductive graphite structures – where we use extrusion printing to fabricate graphitic structures with enhanced electrical and thermal conductivities, microscopic origin of elasticity and yielding in colloidal gels – where we use a combination of rheology and x-ray scattering to get a microscopic view of macroscopic properties and characterization and printability of Sodium alginate-Gelatin hydrogel for bioprinting non small cell lung cancer cells (NSCLC) co-culture. Research is tightly integrated with education of minority students at FAMU which is the only HBCU to offer a PhD in chemical and industrial engineering.

**5:30 AM \*F.SF05.05.03**

**Novel Inks Based on Capillary Suspensions for Additive Manufacturing with 2D Materials** Brian Derby; University of Manchester, United Kingdom

Current state-of-the-art graphene inks for extrusion based additive manufacturing (AM) typically contain large quantities of polymers and other additives that require removal through post processing heat treatment to allow access to many functionalities of the 2D materials. Alternative routes, e.g. freeze casting, require complex multiple steps under thermal control to allow printability. Here, an alternative route to additive manufacturing with 2D materials is proposed, based on the concept of the capillary suspension. Capillary suspensions can form when a solid phase is suspended in a mixture of two immiscible solvents, one of which (the minor phase of the mixture) strongly wets the particles in suspension. The microstructure of a capillary suspension leads to a Bingham behavior, with low resistance to flow above a critical stress when the capillary bridges within the suspension are ruptured and is thus ideally suited to extrusion based AM. A capillary suspension containing 20 wt.% graphene in aqueous suspension, with carboxymethyl cellulose as dispersant, is transformed to a capillary suspension through the addition of 5% octanol. The resulting ink has fluid properties compatible with 3D printing and simple lattice structures are produced with strength sufficient strength for handling after air drying. Similar inks and demonstrator structures with 2D BN in suspension have also been produced. The graphene structures have open porosity of 69%, a compression strength of 1.3 MPa and electrical conductivity of  $250 \text{ Sm}^{-1}$ . The stability of the ink is shown to be controlled by the relative wetting angle with the two fluids and particle size and aspect ratio.

**5:45 AM F.SF05.05.04**

**3D Printable Sustainable Biocomposites from Corn Starch and Husks** Yijie Jiang and Md. Nurul Islam; University of North Texas, United States

There are increasing research interests in natural materials and composites for sustainable additive manufacturing. Natural materials, such as cellulose fibers, have been used as reinforcement fillers in petroleum-based matrix polymers. However, the hydrophilic cellulose fibers are incompatible with many synthetic hydrophobic polymers, leading to weak interfacial bonding and poor mechanical properties. More importantly, the majority of these composites remains not recyclable or degradable. Manufacturing pure natural materials into mechanically-robust engineering materials can benefit in both environmental and economic perspectives associated with the replacement of petroleum-based materials. The natural resources are renewable, biodegradable, and inexpensive. For example, corn is the largest agricultural product in the US with an annual output over 300 million tons. Processing this large amount of corn results in more than 200 million tons of waste, such as husks and cobs. Although there are emerging researches using natural materials, such as rice and protein, to develop 3D printable materials, limitations on printable materials and their mechanical properties exist. Here, we develop 3D printable biocomposites entirely from corn products and waste, namely starch and cellulose fibers from husks. We extract cellulose microfibrils from corn

husks via an alkalization process to achieve controlled dimension and structures. The cellulose fibers are distributed into compatible matrices derived from corn starch, to formulate 3D printable biocomposites using an extrusion-based direct ink writing (DIW) method. We perform a systematic design of experiments to investigate the ink formula, processing steps, and resulted mechanical properties to establish process-structure-property relationships and obtain the optimal mechanical properties. The results indicate comparable stiffness and strength compared with other 3D printed thermoplastics. Since our biocomposites consist of purely natural components, they have potential applications in medical and food area.

#### 5:55 AM F.SF05.05.05

##### **4D Printing of High-Performance Shape-Memory Isotropic Thermoset via Fused Deposition Modelling—Print the Unprintable** Qiyi Chen and Rigoberto Advincula; Oak Ridge National Laboratory, United States

Fused deposition modeling (FDM), as one of the most dominant 3D printing techniques, has been increasingly applied in various fields, yet it suffers from the anisotropic performance in the printed materials and the difficulty to print thermoset polymer. Here, we present an unprecedented 4D printing process that achieves, for the first time, FDM printability of highly isotropic thermoset polymer with excellent shape memory behavior and superb thermo-mechanical performance. A specially modified Epoxy-benzoxazine/carbon nanotube hybrid resin was formulated that behaves as a low-temperature thermoplastic allowing FDM printing, and a high-temperature thermoset achieving covalently crosslinked structure. The cross-layer reaction fuses individual layers into an integrity, thus eliminating layer delamination induced by FDM to offer isotropic mechanical properties regardless of the printing orientations. The highly crosslinked epoxy-benzoxazine network offers excellent shape memory behavior with fast recovery rate (full recovery in 80 s) and large recovery degree (98%), as well as outstanding mechanical strength and thermal stability that are superior over most FDM printed polymer.

#### 6:05 AM F.SF05.05.06

##### **A Time-Saving and Cost-Effective Method to Process New Alloys by Laser Powder Bed Fusion** Paolo Fino, Alberta Aversa, Alessandra Martucci, Fabrizio Marinucci, Federico Bosio, Federica Bondioli, Diego Manfredi and Mariangela Lombardi; Politecnico di Torino, Italy

Nowadays, there are only a limited number of commercial alloy systems for Laser Powder Bed Fusion (LPBF), i.e. pure titanium and Ti6Al4V alloys, stainless steels, nickel-based superalloys, Al-Si alloys, cobalt chromium and recently high-entropy alloys. At the same time, developing new alloy compositions is now becoming a key challenge to address in the additive manufacturing field. However, the development of new alloys for LPBF generally requires high economical investments. In fact, the starting powders have a high cost because of they must present high sphericity and specific particle size distribution to guarantee good flowability and to prevent the formation of porosities in the final parts. In addition, finding the right window for the main process parameters is a core procedure for adopting novel alloy compositions for LPBF. There are many process parameters that can affect the final density of the parts:

considering a fixed value for the layer thickness, selected on the basis of the powder mean size and distribution, part quality depends from laser power, scan speed, hatching distance and scanning strategy. The traditional Design Of Experiment (DOE) approaches for defining the operating process windows are time consuming and expensive requiring the manufacturing of several matrices of massive samples.

Recently in literature it has been demonstrated that the proper P and v values for can be determined via the Single Scan Tracks (SSTs) approach, which requires small quantity of powders with respect to the manufacturing of massive samples. In fact, SSTs are useful for the evaluation of the melting and consolidation behaviour of the material by changing laser power and scan speed, but without considering the effect of the hatching distance. For this reason, according to the traditional approaches SST analyses must be followed by matrices of massive samples with different hatching distances with a consequent increase of the employed powders.

In this work, a novel method to define LPBF process parameter of new alloys through SSTs is proposed. At first, a power - speed operating window is easily defined. Then, the proper hatching distance is designed considering to have an optimum overlap among adjacent scan tracks. In this way, massive samples can be directly produced by using the best P-v combinations, avoiding many experiments. In particular, in the first jobs a range of P-v values for which stable and regular SSTs are identified. For the SST characterization an automated and fast method is set up by developing a code for analysing SST images, also avoiding the subjectivity of each researcher in measuring SST features. After that, the measurement of SST width allows to directly select the hatching distance to ensure a good overlapping. In this way the manufacturing of dense samples can be easily carried out by employing a small quantity of powder and time.

#### 6:15 AM F.SF05.05.07

##### **Additive Manufacturing of Conductive Polymer Using Stereolithography—Effects of Multi-Walled Carbon Nanotubes Reinforcement on Electrical Properties and Dimensional Accuracy** Daniel D. Lim<sup>1,2</sup>, Jaemin Lee<sup>1</sup> and



Wonjoon Choi<sup>1</sup>; <sup>1</sup>Korea University, Korea (the Republic of); <sup>2</sup>University of California, Berkeley, United States

Stereolithography (SLA) 3D printing is often used to fabricate complex 3D structures requiring precise and clean surface finish due to its geometrical accuracy compared to other additive manufacturing methods. However, photopolymer resin used in the SLA has limited mechanical, electrical, and thermal properties. Nanofibers or nanoparticles were used as fillers to improve these properties, and studies showed that adding Carbon Nanotubes (CNT) as reinforcement enhanced the electrical conductivity of the resin, but these lacked in the analysis of the geometrical accuracy performance.

In this study, we evaluated the effect of CNT concentration on electrical conductivity, curing conditions, and dimensional accuracy. Polyurethane acrylate resin was mixed with varying MWCNT concentration from 0 weight percentage (wt%) to 0.8 wt%, and structures were printed using a desktop masked SLA 3D printer. Electrical conductivity was measured using a four-point probe method and dimensional accuracy was evaluated with the geometrical benchmark model.

From the measured data, 0.6 wt% was the maximum concentration of MWCNT that performed a high precision level of SLA method, which also showed 0.033 S/m of electrical conductivity. We applied these findings to fabricate complex multi-material 3D circuit and capacitive sensor.

#### 6:25 AM F.SF05.05.08

**Electrohydrodynamic Redox 3D Printing—Broadening the Materials Range for Multi-Material Additive Manufacturing at the Submicron Scale** Alain Reiser, Lukas Koch, Maxence Menétrey, Mirco Nydegger and Ralph Spolenak; ETH Zurich, Switzerland

Many emerging applications in microscale engineering require the fabrication of three-dimensional architectures in inorganic materials. Small-scale additive manufacturing (AM) aspires to provide access to these geometries with feature sizes in the micro- and submicrometer range. Yet, the synthesis of device-grade inorganic materials is still a challenge for AM [1] – a major handicap for its incorporation in advanced micro- and nanofabrication processes.

Here, we present our latest advances in electrohydrodynamic redox printing (EHD-RP), focusing on the broadening of the materials range and the optimization of the deposited microstructure. EHD-RP has previously been shown to enable the direct, ink-free fabrication of polycrystalline multi-metal 3D structures with a resolution of 250 nm and a feature size of  $\approx 100$  nm [2]. The electrochemical concept can result in excellent as-printed materials quality printed at speeds that outperform alternative electrochemical techniques by one order of magnitude. Additionally, as a most unique feature, EHD-RP has demonstrated nanoscale multi-metal printing with unprecedented detail. Yet, until now, the materials available to EHD-RP have been limited to copper, silver, and gold.

In this talk, we will discuss our latest findings on microstructure optimization in copper. Further, we will present our efforts to expand the printable materials palette to different metals, including alloys and magnetic metals, as well as semiconductors and insulators. We will show that the method is compatible with different sources of ions (sacrificial anodes and salt solutions) and will discuss the role of the solvent. The results present a further step towards the additive deposition of inorganic materials of high quality by microscale AM.

[1] Reiser, A., Koch, L., Dunn, K. A., Matsuura, T., Iwata, F., Fogel, O., Kotler, Z., Zhou, N., Charipar, K., Piqué, A., Rohner, P., Poulidakos, D., Lee, S., Seol, S. K., Utke, I., Nisselroy, C., Zambelli, T., Wheeler, J. M., Spolenak, R., Metals by Micro-Scale Additive Manufacturing: Comparison of Microstructure and Mechanical Properties. *Adv. Funct. Mater.* **1910491**, 1910491 (2020).

[2] Reiser, A., Lindén, M., Rohner, P., Marchand, A., Galinski, H., Sologubenko, A. S., Wheeler, J. M., Zenobi, R., Poulidakos, D., Spolenak, R., Multi-metal electrohydrodynamic redox 3D printing at the submicron scale. *Nat. Commun.* **10**, 1853 (2019).

[3] Reiser, A., Hirt, L., Spolenak, R. & Zambelli, T. Additive Manufacturing of Metal Structures at the Micrometer Scale. *Adv. Mater.* **29**, 1604211 (2017).

#### 6:35 AM F.SF05.05.09

**Engineering a Biodegradable, Electrically Conductive Polymer Nanocomposite via 3D Printing** Yiwei Fang, Xianghao Zuo, Yuan Xue, Yichen Guo and Miriam H. Rafailovich; Stony Brook University, United States

The consistent growth of electronic devices is one poses one of the most serious ecological challenges of the decade. The rapid pace of innovation correlates with rapid obsolescence of existing devices. Disposal of these devices often poses problems since the electronic circuitry is often printed using toxic heavy metals and other hazardous chemicals which are harmful to both global environment and human health. To address these issues we have engineered a new degradable,

environmentally sustainable, and electronically and thermally conductive nanocomposite, which could be extruded into filaments and used for 3-D printing of circuits and antennas. We blended poly (butylene adipate-co-butylene terephthalate) (PBAT) with a semi-crystalline harder polymer, poly (lactic acid) (PLA), and added graphene nano-platelets (GNPs) as filler. PLA and PBAT are incompatible and phase segregate, but the interfacial tension between GNPs and PLA is even higher than that of the two polymers, and hence the GNPs are sequestered only within the PBAT phase, and do not segregate at the polymer interfaces. The blend is also ductile and easily extruded into filaments for 3-D printing. TEM imaging of the filaments showed that the additional confinement during extrusion further aligned the GNPs allowing them to form percolated rope-like structures within the matrix. Electrical and thermal conductivity measurements indicated that samples formed via 3D printing had better thermal and electrical properties than those formed via molding, without sacrificing the mechanical performance. Compared with molded PBAT/PLA/GNPs at 20% graphene loading, printed electrical conductivity significantly increased from 2.49S/m to 597 S/m, thermal conductivity increased from 0.664W/mK to 1.794W/mK, while the Young's Modulus increased from 867MPa to 1258Mpa.

#### **6:45 AM F.SF05.05.11**

**Ink Design Strategies for the Direct Ink Writing of Energy Devices** Stefano Tagliaferri, Apostolos Panagiotopoulos, Heather Au, Pierpaolo Modugno, Magdalena Titirici and Cecilia Mattevi; Imperial College London, United Kingdom

3D printing is gaining importance for the fabrication of energy devices with superior performance, controllable dimension and customized shape. The complex architectures enabled by printing processes are able to enhance electron and mass transport and provide high surface area, which constitute fundamental features for energy systems. Among extrusion-based techniques, Direct Ink Writing offers the possibility to print a wide range of different materials, and it is suitable for the multi-material deposition of full energy devices, such as supercapacitors and rechargeable batteries.

Despite the great potential held by 3D printing processes, the fabrication of full devices via Direct Ink Writing is bound to the formulation of printable inks from energy materials. Inks must meet specific rheological requirements to be printable, which include high shear-thinning behaviour during flow, solid-like response at rest and fast recovery of the elastic properties after extrusion. The ink design strategy must be carefully optimized to simultaneously obtain high printability and achieve favourable electrochemical properties.

Here the most common ink formulation strategies for energy devices are discussed, highlighting the role played by the different ink components to achieve high printability and their impact on the electrochemical performance of the final device. Viable ink formulations for the fabrication of sodium-ion batteries are presented, giving insight into the connection between rheological behaviour and printability.

#### **6:55 AM F.SF05.05.12**

**PDMS-Rich Domain on the Electrical Properties of 3D-Printed CNT/PDMS Foam Nanocomposites** Chao Liu and Junjun Ding; Alfred University, United States

The carbon nanotube (CNT)/polydimethylsiloxane (PDMS) composite has been studied and fabricated as soft electronics, such as strain sensors, supercapacitors, and electrodes, due to its excellent flexibility and electrical conductivity. An engineered foam structure provides the capability of large-scale deformation as stretchable devices and also affects the percolation threshold of CNT concentration in the CNT/PDMS foam composites. It has been investigated that PDMS-rich domains form at the surface of the composites, where limited reinforcements distribute in this region. However, little research has been focused on the influence of this domain on the electrical conductivity of composites. In this work, we present the effect of the PDMS-rich domain on the CNT/PDMS foam nanocomposites. The material extrusion 3D printing method is used to fabricate the composites due to its advantage of free design to form the scaffold model. The foam structure is built by introducing a foaming agent into CNT/PDMS composite ink as feedstock for material extrusion 3D printing. Electrical pathways formed by interconnected CNTs increase due to PDMS-rich regions at the surface of micropores in the foam structure. Therefore, we hypothesize that the percolation threshold of CNT concentration in the foam composites decreases compared to that in the solid composites. The percolation threshold is inversely proportional to the density of micropores in the foam structure. It is also noted that the electrical conductivity of CNT/PDMS foam composites is higher than the solid composites at identical CNT concentrations. We will compare this hypothesis to our achieved foam structure fabricated using a sacrificial material (sodium chloride). This study provides a broader insight into the mechanism of electrical conductivity in polymer-based foam nanocomposites.

#### **7:05 AM F.SF05.05.13**

**Process Development of WC-Ni Cemented Carbide Composites via Laser Powder Bed Fusion** B. Reeja Jayan, Jack Beuth and Edgar Mendoza Jimenez; Carnegie Mellon University, United States

In this work, laser powder bed fusion (LPBF) is used for the additive manufacturing of composite samples consisting of tungsten carbide particles with a nickel binder. Such process can become a viable low-energy alternative to the conventional production of ceramic-metal composites for applications including tooling, electronics, and wear components. Single track experiments are used to evaluate the melting behavior of the composite material. Samples are then printed with of process parameters that adequately melted the material. The density, microstructure, and functional properties of these samples are measured. Highly dense (>98%) samples are successfully manufactured and analyzed as a function of LPBF parameters. Macro- and microdefects resulting from the laser processing are also discussed. A methodical approach to evaluate an acceptable processing region is presented and used to investigate the feasibility of additively manufacturing tungsten carbide-nickel composites via LPBF.

**7:15 AM F.SF05.05.14**

**Selective Laser Melting of Metal Matrix Composites** [Ethan Parsons](#); MIT Lincoln Laboratory, United States

Aluminum metal matrix composites (MMCs) are highly desirable materials for precision aerospace applications, where stiffness and low mass are critical, but they are rarely used because of their cost and machining difficulty. In these applications, components typically have complex geometries and are produced in small numbers. Therefore, processing metal matrix composites additively would be the ideal solution, but MMCs with high ceramic content are not commercially available for AM. Here, using purely mechanical methods and readily available constituent powders, we fabricate composite feedstock powders optimized for laser powder bed fusion in a cost-effective, scalable manner. We demonstrate that these powders can be laser consolidated to nearly 100% relative density, providing a potential pathway for the broader adoption of these high-performance yet underused materials.

**7:25 AM F.SF05.05.15**

**Structure and Tensile Behavior of Nanocrystalline Laminar Composites Fabricated by Ultrasonic Additive Manufacturing** [Austin A. Ward](#)<sup>1</sup> and Zachary Cordero<sup>2,1</sup>; <sup>1</sup>Rice University, United States; <sup>2</sup>Massachusetts Institute of Technology, United States

Ultrasonic additive manufacturing combines layer-by-layer ultrasonic welding of foils with CNC machining to produce net-shape components without melting the feedstock. The solid-phase nature of ultrasonic additive manufacturing makes it attractive for building bulk nanocrystalline metals; however, the high hardness of nanostructured materials makes it difficult to achieve the plastic flow necessary for welding without excessive frictional heating, which could compromise their grain structure. Here, we circumvent this processing challenge by creating laminar composites comprising nanocrystalline NiCo feedstock alternated with soft Al interlayers which accommodate the deformation required for bonding. During the layer deposition process, the NiCo grain structure was preserved and the Al asperities completely conformed to the NiCo surface. TEM chemical analysis of the NiCo/Al interfaces combined with thermodynamic calculations reveals a 100 nm interdiffusion zone containing several intermetallic phases. Tensile testing of the composites and the monolithic NiCo shows that an improved energy absorption in the laminates is realized in part through delocalized damage mechanisms. Ultimately, we couple this experimental work with process models that quantitatively illustrate the tradeoff between frictional heating induced- grain growth and interfacial plastic flow, theoretically validating the addition of softer interlayers as a processing strategy for nanostructure preservation.

**7:35 AM F.SF05.05.16**

**Voxel-Scale Conversion Mapping Informs Intrinsic Resolution in Stereolithographic Additive Manufacturing** [Tobin Brown](#), Callie Higgins and Jason Killgore; National Institute of Standards and Technology, United States

In stereolithography (SLA), diffusion of reactive species between light and dark regions of the printing plane limits the achievable resolution. Partially crosslinked macromolecules diffuse away from initiating regions, leading to overpolymerization in dark zones and loss of print fidelity. Additionally, gradients within polymerized regions cause mechanical heterogeneity in the final part. These processes occur on the individual voxel scale and below, so bulk measurement techniques such as photorheology and infrared spectroscopy are unable to adequately measure them, and new measurement techniques are needed. As resolution requirements for new applications push the limits of scalable single-photon processes, the ability to meet this demand hinges on an increased understanding of the fundamental photopolymerization processes involved.

In this talk, I will describe an atomic force microscopy (AFM) technique to directly map the generation and diffusion of

polymeric species during stereolithography. We use an AFM cantilever with a nanocylinder extending from the tip, and when the cylindrical probe is inserted into a resin, the drag on the cylinder can be used to measure the local viscosity of the liquid, and in turn, the local extent of reaction. Vibrating the cantilever at one of its resonance frequencies ( $10^4$  Hz -  $10^7$  Hz) affords high temporal resolution. Computational fluid dynamics modeling indicates that the fluid motion induced by the oscillating cantilever is localized within 1  $\mu\text{m}$  of the probe. Employing a custom-built instrument, we can direct arbitrary light patterns from a spatial light modulator to the imaging plane of the AFM to achieve photopolymerization. By translating the tip and light pattern relative to one another, the full spatial evolution of the reaction profile can be measured.

We employed this technique to measure the reaction dynamics during SLA photopolymerization of a thiol-ene resin. The thiol-ene click reaction has some advantages over the photopolymerization of acrylate resins, including reduced shrinkage stress and insensitivity to oxygen inhibition. We find a non-reciprocal dependence of the reaction on light intensity; increasing the light intensity decreases the efficiency of the reaction, likely by increasing the bi-radical termination rate. Thus, at constant light dose, lower light intensities lead to increased conversion in the reaction volume, even accounting for increased time for diffusion. This disproves a common assumption in stereolithography, namely that gelation depends solely on the light dose, often referred to as the “critical dose.”

Mapping the spatial evolution of the polymer conversion profile also allows us to easily identify the diffusion length scales during the reaction, and we measure polymer accumulation 20  $\mu\text{m}$  away from the illuminated region within one second of light exposure, identifying the relevant length scale of our process. We then created an open ring test structure (inner diameter = 15  $\mu\text{m}$ , outer diameter = 45  $\mu\text{m}$ ) based on this finding to determine the effect that diffusion plays on the resolution of a printed part. Consistent with our measurements of the reaction profile, we observe significant overpolymerization in the ring center, leading to gelation and loss of fidelity to the projected mask. This new technique provides adequate spatial (1  $\mu\text{m}$ ) and temporal (<1 ms) resolution for modern stereolithography applications, and it can be used to predict the ultimate printing resolution and rapidly determine the optimal exposure conditions for a given resin.

**7:45 AM F.SF05.05.17**

**Late News: Additive Manufacturing of Reversible Covalent Polymer Networks for Self-Healing Soft Robotic Applications** [Joost Brancart](#), Ellen Roels, Seppe Terryn, Bram Vanderborght and Guy Van Assche; Vrije Universiteit Brussel, Belgium

Dynamic covalent chemistries have attracted much attention to create reversibly crosslinked covalent polymer networks that show improved processability compared to irreversibly crosslinked networks. Two types of dynamic covalent mechanisms exist: (i) dissociative reversible reactions where the covalent bonds dissociate upon application of the corresponding stimulus, such as heat or light and (ii) associative exchange reactions where a certain functional group can exchange bonds with existing covalent bonds. These dynamic covalent chemistries have also become very popular to create self-healing materials that are able to reform broken bonds to recover the functional properties of materials and hence increase the service lifetime of structures and systems by recovering their functional performance.

The thermally reversible Diels-Alder cycloaddition reaction between furan and maleimide functional groups is a widely studied reversible covalent chemistry for creating thermally reversible covalent polymer networks. While scientific articles reporting synthesis of new reversible polymer networks are numerous, accurate knowledge of the reaction kinetics and thermodynamics of the dynamically reversible equilibrium reaction and the structure and property development of derived stimuli-responsive materials are much less widespread. Such knowledge allows to design and optimize the functional properties of the materials in view of intended applications and to tailor the processability of the reversible polymer networks. Heating the thermally reversible polymer networks based on the Diels-Alder reaction shifts the reaction equilibrium towards the gradual breaking of the cycloadduct crosslinks in the network. At a certain point so many bonds are broken that the material undergoes a solid-liquid transition, referred to as degelation, as the network structure is broken down. This reversible gel transition was employed to create filaments for the 3D printing of 3D structures for flexible, compliant components for a self-healing soft robotic gripper.

The dynamically reversible chemistry, choice of monomers and resulting polymer network architecture determine the (thermo)mechanical properties, thermoresponsive behaviour and healing capabilities of the created reversible covalent polymer networks. Optima need to be sought between (i) reasonably fast reaction kinetics for fast and efficient damage healing at moderate temperatures, (ii) reasonable processing and manufacturing conditions and (iii) adequate mechanical properties and structural stability required for the intended application. Stress relaxation is desirable property to make materials tougher, relieving stress before microscopic defects can grow into macroscopic cracks and ultimately lead to failure, while creep behaviour during application can't be allowed. Recycling and reprocessing of materials are desirable from an ecological viewpoint, while the materials should also be able to withstand static and dynamic loading in a considerable range of environmental conditions.

7:55 AM F.SF05.05.19

**Late News: Direct-Write 3D Printing from Solution for Tunable Structural Color of Bottlebrush Block Copolymers** [Bijal Patel](#) and Ying Diao; University of Illinois at Urbana-Champaign, United States

Additive manufacturing of functional polymers remains limited by the challenge of precisely controlling multiscale hierarchical assembly during processing. In this work, we address this challenge by integrating nonequilibrium self-assembly of densely grafted bottle brush block copolymers with a highly versatile direct-write 3D printing approach. We demonstrate that programmatic variation of printing conditions enables control of peak reflected wavelength for bottlebrush photonic crystals across a range of 403 to 626 nm (blue to red) with a single ink material. We further demonstrate spatial and functional patterning of photonic crystals to achieve colorful prints of chameleon patterns through on-the-fly tuning of assembly kinetics during printing. Via scanning electron microscopy and synchrotron small-angle X-ray scattering analysis of printed films, we then clarify the microstructural underpinning of this phenomena as tuning of lamellar domain d-spacing (total thickness of A+B block) over a range of greater than 30 nm, which we attribute to modulation of polymer conformation during printing. Finally, we establish the role of kinetic trapping of metastable microstructures as the mechanism for domain size control based on *in situ* optical microscopy and solvent-vapor annealing experiments. Thus, we demonstrate a new method for tunable block copolymer photonics without synthetic variation. Furthermore, we present a hardware and software integrated 3D printing scheme that can serve as a test bed for functional property modulation for a variety of functional polymeric and material systems.

SESSION F.SF05.06: Mechanical Behaviour of 3D Printed Materials  
On Demand Abstracts Available for Viewing Starting Saturday Morning, November 21, 2020  
F-SF05

5:00 AM \*F.SF05.06.01

**Aqueous Synthesis of 3D Nano-architected Ceramics and Metals—Nano-Architected TiO<sub>2</sub> PhCs** [Julia R. Greer](#); California Institute of Technology, United States

Additive manufacturing (AM), or 3D printing, represents a set of processes that enable layer-by-layer fabrication of complex structures using a wide range of materials that include ceramics, polymers, and metals. AM has allowed exploiting novel material properties, especially those that arise at the nano-scale, that do not occur in conventional materials, revolutionizing the production of complex parts for aerospace, military, automotive, optical, and medical applications. Facilitating these technologies requires a fabrication process to create a variety of functional materials in 3D, however the material choice for AM at the nano- and micro-scale is limited. A conspicuous example is a lack of AM processes for high refractive index (n), low absorption materials with nano-sized dimensions, which are typically required for microoptics and device applications. To harness the beneficial properties of 3D nano-architected meta-materials, it is critical to assess their properties at each relevant scale while capturing overall structural complexity. We present the fabrication and synthesis of nano- and micro-architected materials using 3D (two-photon and interference) lithography, as well as characterization of their properties as a function of architecture, constituent materials, and microstructural detail. We focus on additive manufacturing of complex, multi-component and multi-material architectures comprised of metal oxides, metals, and hydrogels that are derived from (metal) salt-based, aqueous photorefin synthesis. The discussion will focus on each representative materials system (metals, oxides, and hydrogels), with a detailed overview of titanium dioxide, with critical feature dimensions between 150 and 600 nm and <1% porosity. Using the described methodology, we created 3D dielectric photonic crystals (PhCs) out of rutile TiO<sub>2</sub> patterned into woodpile face-centered tetragonal (FCT) architectures with beam dimensions of 300–600nm and lateral periods of 0.8–1.5 μm. We use Plane Wave Expansion (PWE) simulations and Fourier Transform Infrared Spectroscopy (FTIR) to demonstrate the full photonic bandgaps centered at 1.8–2.9 μm. This fundamental research provides insights into the range of possible, often *transient* attainable chemical compositions, microstructures and architectures of chemically-derived, 3D-architected ceramics and metals, enabling advances in multiple technologies, i.e. 3D MEMS, micro-optics, and prototyping of 3D PhCs.

5:15 AM F.SF05.06.02

**Bridging Micro-Mechanical and Macromechanical Properties of Titanium Alloys Made by Additive**

**Manufacturing** Yu Zou; University of Toronto, Canada

Dual-phase titanium alloys, incorporating  $\alpha$  and  $\beta$  phases with contrasting mechanical properties, exhibit balanced and comprehensive mechanical performance, which is suitable for many structural applications, especially in aerospace and biomedical sectors. Laser melting deposition (LMD, one of the primary additive manufacturing methods) provides an ideal method to efficiently fabricate metallic components with complex geometries, as well as controlling microstructure. The complex phases, microstructure, and related phase/grain boundaries significantly influence the deformation and fracture behavior of AM-produced titanium parts. So far, the correlation between the microscale mechanics of individual phases/grains and global mechanics of AM-produced parts has been poorly understood. This thesis will focus on analyzing the micromechanical properties of  $\alpha+\beta$  titanium alloys, including hardness/modulus in different phases, micro-compression/tension/bending tests, towards a better understanding the role of micromechanical properties of each phase and interfaces on plastic deformation and damage behavior of bulk materials. Thus, the goal of this work is to bridge the microscale and macroscale mechanical properties in additive manufactured titanium alloys.

**5:25 AM F.SF05.06.04**

**Electromechanical Behavior of Additively Manufactured Polycrystalline Zinc Oxide** Rebecca Gallivan<sup>1</sup>, Daryl Yee<sup>1</sup>, Julia R. Greer<sup>1</sup>, Zachary Aitken<sup>2</sup>, Antoine Chamoun-Farah<sup>3</sup> and Yong-Wei Zhang<sup>2</sup>; <sup>1</sup>California Institute of Technology, United States; <sup>2</sup>Institute of High Performance Computing, A\*STAR, Singapore; <sup>3</sup>Washington University, United States

Sub-micron resolution oxide materials have immense potential in the fabrication of various nanotechnologies. Zinc oxide (ZnO) is of particular interest due to its piezoelectric properties and its application as sensors in microelectromechanical systems (MEMS). We have recently developed a technique called Photopolymer Complex Synthesis that enables the creation of nano-architected polycrystalline ZnO with feature sizes of 250nm. We achieve this by first patterning zinc ion-containing aqueous photoresins using two-photon lithography and subsequently calcining them at a variety of temperatures to give ZnO. *In-situ* microcompression experiments with concurrent electrical measurements on these architected ZnO structures demonstrate an electromechanical response, i.e. a voltage drop is observed during compression of the structure. Since ZnO exhibits an intrinsic piezoelectricity effect primarily along the c-axis of the crystal, some net crystallographic alignment is necessary for any piezoelectric effect to be observed in polycrystalline ZnO. However, TEM analysis of these polycrystalline ZnO architectures show that they have a homogeneous random crystal orientation. Thus, a more in-depth study of this material and its microstructure-property relationship is necessary to understand the emergence of the observed electromechanical properties.

By adopting a statistical approach that accounts for the random nature of this microstructure, we show through analytical models and experimental results the role of relative length scales, i.e. the microstructure grain size compared to the architecture feature size, in this observed phenomenon. Our findings also demonstrate that microstructure can be used to tune the piezoelectric response of these structures and highlights the possibility of exploiting localized strain in complex architectures. Investigation of this unique processing of ZnO demonstrates not only the specific properties of this architected material, but highlights the importance of microstructural investigation in novel micro-scale 3D printing materials. Additionally, this fundamental exploration provides an insight into the underlying mechanisms of electromechanical behavior in intrinsic polycrystalline piezoelectrics and lays the foundation for future design and engineering of these materials at the nanoscale.

**5:35 AM F.SF05.06.05**

**Limits of Mechanical Stability in Nanoscale Direct Laser Writing** Elaheh Sedghamiz, Modan Liu and Wolfgang Wenzel; Karlsruhe Institute of Technology, Germany

Three-dimensional direct laser writing (3D-DLW) is an indispensable tool to high accuracy structuring and fabricating of 3D micro- and nano-objects via polymerization processes induced by direct laser writing. Over the past decade, this technology has become a well-established lithography tool for fabricating 3D geometries directly on functional substrates. This capability provided the possibility for a wide range of applications in photonics, microfluidics, mechanical microstructures, and cell scaffolds.

As the dimensions of the printed structures shrink it remains a challenge to control the stiffness of the fabricated structure by changing the many conditions influencing direct laser writing condition. We therefore developed a nanoscale simulation approach as an alternative to physical experiments to optimize the 3D writing process and reduce the number of experiments. This approach enables a systematic studies of how various writing parameters affect the structure and stiffness of the fabricated polymer network. We employ a coarse grained molecular dynamics (MD) method to simulate direct laser writing

of 3D polymer networks from a monomer pool, where monomers react irreversibly according to reaction rate constants, which results in 3D objects being printed voxel by voxel.

Simulations show that the degree of monomer conversion increases with higher laser power or, correspondingly, higher exposure times and saturates towards high writing powers/ high exposure times. Nonetheless, the laser power has a more pronounced effect on the degree of monomer conversion and mechanical properties than exposure time. We investigate the physical parameters and mechanical stability of the resulting structures and find optimize the parameters to write 3D polymer networks with high mechanical stability. This approach allows us to tune the mechanical properties of the 3D printed objects exploiting the fine interplay between laser power, exposure time and also aspect ratio of the printed objects to meet the requirements for different applications.

#### 5:45 AM F.SF05.06.06

**Mechanical Properties of 3D-Printed Elastomeric Foams** [Ali Alperen Bakir](#)<sup>1</sup> and Sezer Ozerinc<sup>2</sup>; <sup>1</sup>The University of Nottingham, United Kingdom; <sup>2</sup>Middle East Technical University, Turkey

Fused deposition modeling (FDM) is one of the most widely used additive manufacturing techniques for the production of plastic parts. Until recently, prototyping activities had been the main application of FDM, where mechanical properties of printed structures are of minor importance. However, with the decreasing costs of FDM-based manufacturing, and improvements in filament technologies, the manufacturing of functional load-bearing components has become feasible for many applications. This new application route requires a better understanding of the process-mechanical property relationships in FDM-produced parts. Parameters such as nozzle temperature, raster orientation, print orientation, and infill ratio directly affect the strength and ductility of FDM parts. There have been many studies on this topic in the last decade, mostly focusing on the widely used filament materials such as ABS and PLA. In the meantime, new advances in filament technology have made elastomers available for FDM. Low stiffness and extreme elongation capabilities of elastomers provide new 3D printing opportunities for a wide range of structural applications. Further advancement in the field has recently enabled the printing of elastomeric foams by using the readily available FDM printers. Mechanical properties conventional elastomeric foams are well-characterized in the literature; however, there is no study in the literature about the mechanical behavior of 3D-printed elastomeric foams to our knowledge.

In this work, we investigate the process-property relationships of an elastomeric filament designed to foam during extrusion, providing a low-density and porous structure. We focused on the effect of infill ratio, layer thickness, feed rate, and nozzle temperature on the mechanical properties. An Ultimaker 2+ FDM printer produced tensile dogbone specimens by using Varioshore TPU natural filament manufactured by Colorfabb (Netherlands). Scanning electron microscopy characterized the microstructure of the specimens, and conventional tensile mechanical testing quantified the mechanical properties. Increasing nozzle temperature, increasing layer thickness, and decreasing feed rate promote foaming and provides a lower density structure. As the extent of foaming increases, the elastic modulus, strength, and elongation at failure decrease. After the characterization step, we combined the excellent capability of FDM in producing custom cellular structures with the intrinsically low stiffness of the elastomeric foam and demonstrated the fabrication of extremely compliant cellular structures. Compression testing results of these model structures demonstrate the enormous potential of the foaming filament technology for the generation of novel compliant structures.

#### 5:55 AM F.SF05.06.07

**Microstructure Modeling of Uniform Droplet Sprayed Deposits for Mg Alloy-Based Additive Manufacturing** Nikolaos Kostoglou<sup>1</sup>, Hiroki Fukuda<sup>2</sup>, Emre I. Gunduz<sup>3</sup>, Claus Rebholz<sup>4</sup>, Teiichi Ando<sup>5</sup> and [Charalabos C. Doumanidis](#)<sup>6</sup>; <sup>1</sup>Montanuniversitat Leoben, Austria; <sup>2</sup>Fukuda Metal Foil & Powder Co Ltd, Japan; <sup>3</sup>Naval Postgraduate School, United States; <sup>4</sup>University of Cyprus, Cyprus; <sup>5</sup>Northeastern University, United States; <sup>6</sup>Vin University, Viet Nam

This article addresses modeling of the solidifying material structure during 3D welding/printing of fully dense Mg alloy products by fused deposition of molten droplets from a uniform droplet spray source on a motorized X-Y table substrate. The resulting crystallite size distribution is simulated by a solidification model consisting of nucleation/fragmentation and constrained growth description, calibrated via structural data from a single droplet splat. This is enabled by a semi-analytical thermal modeling framework, based on superposition of moving Green's and Rosenthal functions for the temperature field from a Gaussian source distribution, in which the deposit solid geometry and heat transfer boundary conditions are accounted for by mirror source images of modulated efficiency. The simulation model is implemented for layered ellipsoidal deposit sections on planar substrates by multi-pass spraying, and its predictions are validated against measured crystal size by image analysis of experimental micrographs of a Mg<sub>97</sub>ZnY<sub>2</sub> alloy, to an error margin of  $\pm 15\%$ . The computationally efficient simulation provides insight to the deposit microstructure, and is intended as a process observer in a closed-loop, adaptive control scheme based on infrared temperature measurements.

**6:05 AM F.SF05.06.08**

**Multi-Modal Synchrotron Analysis for the Design of Corrosion Resistant Additively Manufactured Stainless Steels** David J. Sprouster, Gary P. Halada and Jason R. Trelewicz; Stony Brook University, United States

Additive manufacturing processes produce materials with hierarchical microstructures containing fusion boundaries at the macroscale, irregular grains and grain boundaries at the microscale, and subgrain dislocation structures at the nanoscale. In 316L stainless steels, corrosion performance has been discussed in the context of chemical heterogeneities formed in the presence of these hierarchical microstructures. However, the large variability in reported measurements underscores the need for statistically significant microstructural data, which is often difficult to access via electron microscopy alone. In this presentation, we explore multi-modal synchrotron x-ray techniques for quantifying hierarchical microstructures and their connection to the underlying chemical distribution in 316L stainless steel. Our results show that the dislocation density depends on the printing conditions and ultimately influences chemical distribution at the nanoscale with implications for the formation of deleterious second phases from a corrosion perspective. On this basis, corrosion rates and pit densities are discussed to build a connection between printing conditions and corrosion performance vis-à-vis microstructural and chemical information from correlative electron microscopy and synchrotron characterization experiments. A decreased pitting potential and loss of passive behavior accompanied by elongated regions of pitting attack were attributed to Cr depletion degrading passive film formation with Mn carbides serving as initiation sites for localized attack.

**6:15 AM F.SF05.06.11**

**The Effect of Part Printing Angle Normal to the Print Bed for Fused Filament Fabrication of 17-4 PH Stainless-Steel Metal Additive Manufacturing** Tawaddod Alkindi, Mozah Alyammahi and Rahmat Agung Susantyoko; DEWA R&D Center, Dubai Electricity and Water Authority, United Arab Emirates

Additive Manufacturing (AM) has been developed expeditiously in the past years, and the application domain and material range are broadening steadily. The 3D printing era has started in 1987 when the first commercial 3D printer was released utilizing stereolithography technique. Ever since, new AM processes are introduced and implemented to face current challenges and accommodate the new requirements in the manufacturing field along the way of 3D printing development. In opposition to subtractive manufacturing techniques that include material removal to obtain the desired shape, additive manufacturing (AM) is a process where joining of materials takes a place to create three-dimensional (3D) objects from 3D model data. The printed designs are made by adding subsequent layers generated from computer-aided design. The ultimate advantage of AM is that it gives the user the ability to create bespoke designs of both different geometric and different materials. However, AM is a very diversified term that comprises different methods such as direct metal laser sintering, fused filament fabrication (FFF), stereolithography, powder bed fusion, selective laser melting (SLM), and binder jetting. The 3D printing of metallic materials is based on the layered consolidation of feedstock materials in the form of: i) powder, ii) wire, or iii) sheet while using various energy sources to form complex structures and designs. Metal printing methods are categorized as electron- beam-based, arc-based, laser-based, welding-based, and ultrasonic. However, the most common energy sources for metal 3D printing are electron beams and lasers. Laser-based metal 3D printing processes are classified into laser sintering (LS), laser melting (LM), and laser metal deposition (LMD). LS is a powder bed fusion technique where a scanning laser is used to consolidate the layers of metal powder sequentially. The LM is another powder bed fusion technique involving the consolidation of metal powders using high-intensity lasers. All equipment setup, configuration, and processing methodology are similar in LS and LM, but in LM, the powder is almost or completely melted to produce a dense structure. LM enables the production of metal parts with a considerably high level of microstructural homogeneity when compared with LS. In LMD, the feedstock material is either a wire or powder. In powder-based LMD, a pressurized gas transfers the powder through a nozzle into a melt pool created by a laser beam on a substrate. The laser and powder integrated system deposits the material while following a specified path. In wire-based LMD, a wire is continuously fed into the path of the laser, while the tip of the wire is continuously melted to make deposits on a substrate. The FFF technique for printing metallic parts is a particular interest in the investigation of this work due to acceptable printing resolution and relatively low-cost process compared to LS, LM, and LMD costs. To our knowledge, no one has reported the effect of printing angles to the tensile property for metal FFF process. We will use the Markforged Metal X 3D printer using 17-PH stainless steel material in this work. The 3D printing consists of 3 steps: FFF 3D printing of metal-binder filament, washing to remove the binder, and sintering to achieve metal mechanical property. We will use Eiger software to import and slice the STL file of the sample design. We will use standard tensile test sample ASTM D638 V. This work will investigate the effect of 3D printing angles on the mechanical properties of the printed samples. The default orientation in the printer is zero for X, Y, and Z, which corresponds to sample X0Y0Z0. We will do experiments of five different print angles of 0, 30, 45, 60, and 90 degrees normal to the surface. Finally, we will measure and discuss the tensile properties (stress, strain, Young's modulus and yield) of the 17-4 PH stainless steel using Instron 3367 apparatus.



#### 6:25 AM F.SF05.06.13

**Late News: Mechanical Testing of Stereolithographically Fabricated Polymer-Graphene Composites** Kalaimani Markandan and Changquan Lai; Nanyang Technological University, Singapore

The emergence of 3D printing has allowed for the rapid prototyping of complex geometries that were previously inaccessible using traditional manufacturing techniques. Amongst these additive manufacturing techniques, stereolithography stands out in terms of the surface smoothness, isotropy in properties and fabrication speed it can provide. The materials that can be 3D printed with stereolithography, however, are limited and fairly weak in mechanical properties. Here, we aim to improve the mechanical performance of stereolithographically printed polymers through the addition of graphene fillers. The effects of filler concentration, post-fabrication baking and loading direction on the quasistatic and dynamic mechanical properties of the composite were investigated. It was found that the graphene platelets were selectively aligned along the print axis, the graphene platelets were well-dispersed up to a concentration of ~ 0.05 wt% and post-print bake has the effect of increasing the degree of cure in the PMMA polymer resin up to 120°C, beyond which it would begin to degrade. As a result of such optimization, polymers reinforced with as little as 0.02 wt. % graphene were found to increase their stiffness by 88.3 % and strength by 115.2 %. Split-Hopkinson pressure bar tests also showed that these composites had higher specific strengths and specific energy absorption compared to other lightweight materials such as syntactic ceramic foams and Al alloys (in both bulk and foam form factors).

SESSION F.SF05.07: Poster Session: Advanced Materials for Additive Manufacturing  
On Demand Abstracts Available for Viewing Starting Saturday Morning, November 21, 2020  
5:00 AM - 8:00 AM  
F-SF05

#### F.SF05.07.04

**Tunable Elongation-at-Break of Tensile Mechanical Properties of Stereolithography Additive Manufacturing Through Control of Printing Orientations** Mozah Alyammahi, Rahmat Agung Susantyoko and Tawaddod Alkindi; DEWA R&D Center, Dubai Electricity and Water Authority, United Arab Emirates

Additive manufacturing (AM) spread widely not only for prototyping but also for the production of end-use products. Quality control is a vital importance in the production of parts. One of the challenges of quality control in AM technology - such as fused deposition modeling (FDM) - is that the mechanical strength of the 3d-printed part could be anisotropic (not uniform). The part's printing orientation could affect the mechanical strength of 3d-printed parts. Among the AM technology spectrum, the stereolithography (SLA) process is known to be able to produce parts with relatively uniform mechanical strength (isotropic).

Many studies were done using FFF 3D printing method. However, to our knowledge, only very few studies had done to investigate the effect of printing orientation on the elongation-at-break of 3d-printed parts using SLA technology. Moreover, previous studies only experimented with a limited amount of samples and orientations. Therefore, strength and elongation-at-break need to be examined in detail and with more variations of print orientation. For this purpose, this study investigated the influence of part's printing orientation to the tensile mechanical properties (tensile-stress-at-max-load, tensile-strength-at-break, tensile-stress-at-yield, young-modulus, elongation-at-break) of SLA technology. This work covered a large number of orientations (27 printing orientations) testing five different mechanical properties.

We used Form 2 3D printer to 3D print with White photopolymer resin of FLGPWH04 material. We used Preform 3.03.1 software to set the sample positions. The samples were oriented with respect to x, y, and z axes according to the software axes. Permutation-with-repetition of 3 different angles (0°, 45°, and 90°) with respect to 3 different axes resulted in 27 part's printing orientations. Furthermore, we printed 3 samples for each orientation with for a total of 81 samples for all orientations. The printed samples were washed in isopropyl alcohol (IPA) for 20 minutes. Afterward, we carefully removed the support structures from the samples using a tweezer; followed by drying and curing process at 60 °C for a total of 20 minutes (samples were flipped every 10 minutes).

We followed the ASTM D638 V standard tensile test design. Each printed sample was kept at the same time (13 days) before the tensile testing to avoid time impact on the properties. Then we performed the tensile testing using Instron 3367. In Bluehill LE 3.77 software, the sizes were entered for each sample. It took the measurements while the test was running and calculated the strain, stress, modulus, and yield. The raw data from the samples compiled in Microsoft Excel.

The results showed relatively uniform isotropy of the tensile-stress-at-max-load and it has 3.8% relative standard deviation.

In addition, tensile-strength-at-break, tensile-stress-at-yield, and young-modulus has 4.15%, 5.67% and 7.94% relative standard deviation, respectively. In contrast, a relatively large anisotropy of elongation-at-break has been observed with 21% relative standard deviation. The sample printed vertically (90 degrees normal to the bed) elongated to an average of 10% whereas the sample printed horizontally (0 degrees normal to the bed) elongated to an average of 15%. One hypothesis that explains this behavior is that printing vertically created many layers comparing to printing horizontally. Thus, the high number of interfaces layers make the part elongate less. The results show that the elongation-at-break could vary and could be tuned in SLA technology; a new finding in this research field.

We recommend that the designer of SLA parts to consider the part's printing orientation depending on the possible application (whether the application requires large elongation-at-break or short elongation-at-break). By knowing the effect of printing orientation, high-quality parts could be produced consistently according to the application's requirement.

#### **F.SF05.07.05**

**Enhanced Toughness in Ceramic-Reinforced Polymer Composites with Herringbone Architectures** Robert Zando, Ataollah Mesgarnejad, Chunzhou Pan, Sandra Shefelbine, Alain Karma and Randall M. Erb; Northeastern University, United States

A common design rule in synthetic particle-filled composites is to align all reinforcing particles parallel with the primary stress and thereby perpendicular to a likely fracture. Doing so can often result in crack deflection, which is commonly touted as evidence that a material has enhanced fracture toughness. In reality, as soon as the crack deflection occurs, the material is fracturing along an "easy axis". Much better is for the crack not to deflect and be forced to propagate forward along a "hard axis" spending much more energy to grow. Geometric conditions alone can create T-stress that confine the crack to propagate straight along a hard-direction. However, real-world applications of filled composites often dictate geometric design and put toughness at risk. Instead, designed texturing of reinforcing particles has the potential to steer cracks along a "hard axis" without reliance on geometric loading conditions. Recent advances in the field of composite manufacturing techniques, make such architectures possible, allowing the creation of microstructures which can locally tune the fracture toughness anisotropy. In the studies presented, we explore a unique variant of this principle through the creation of an alignment architecture reminiscent of the spine of a herringbone fish, designed to trap a fracture along the boundary between two regions of distinct particle alignment. This robs the fracture of a preferred direction of initial fracture deflection, delaying the initiation of fracture formation, and forces it along a "hard" direction of fracture initiation, effectively raising both its initial and overall fracture resistance significantly beyond monolithically aligned composite polymer systems. However, while this custom microstructure proved successful in demonstrating this method of boosting mechanical performance over traditional monolithic systems in principle, it remains limited in application by the necessity of a fracture initiating at or near the boundary between two alignment regions. Without filling this pre-condition, the fracture would initiate in a manner similar to a monolithic alignment system.

To overcome this limitation, we applied these principles to generate a new class of beautiful herringbone mosaics that provide isotropic toughness in 2D. This structure was composed of a series of hexagonal unit cells, further divided into a series of triangular sub-cells, each with herringbone patterns. Mechanical testing of these samples determined that this structure not only demonstrated superior initial fracture toughness to monolithic samples, but that this effect was approximately isotropic, showing superior mechanical performance over the highest performing monolithic samples regardless of the direction of the tensile force relative to the microstructure placement. In applications in which the geometric design of a particle-filled composite is constrained, texturing materials with herringbone mosaics provide a meaningful route toward boosting isotropic toughness through microstructural design alone.

#### **F.SF05.07.06**

**Lightweight Cellular Metal Composites with Zero and Tunable Thermal Expansion Enabled by Ultrasonic Additive Manufacturing** Ethan Parsons; MIT Lincoln Laboratory, United States

In aerospace applications, variations of temperature caused by changing environmental conditions or generation of heat is a common problem. The resulting thermal strains cause separation and alignment errors in optical systems, and stresses due to mismatches of thermal expansion at material interfaces cause failure of components and structures. Because minimizing weight, cost, and lead time are also critical requirements, lightweight, easily machined metals are attractive for aerospace applications, but these materials all have substantial coefficients of thermal expansion. Previous work has shown that the superposition of two metals with dissimilar coefficients of thermal expansion in periodic cellular configurations can result in a composite material with zero effective thermal expansion. However, fabrication of these material architectures typically is either impossible or requires manual assembly. Here, we propose methods to design and fabricate cellular metal composites with tunable thermal expansion and optimized specific stiffness that can be manufactured at useful scales entirely with automated methods. Samples were manufactured with ultrasonic additive manufacturing and computer-controlled machining,

and thermal expansion was measured optically. The results demonstrate the practical fabrication of cellular metal composites with zero or negative thermal expansion in one direction, tunable thermal expansion in a second direction, and structural performance indices competitive with the indices of conventional aerospace alloys.

#### **F.SF05.07.08**

##### **The Effects of Solidification Rates on Grain Refinement Capacity of TiC in Directionally Solidified Ti6Al4V**

**Alloy Naoki Date**<sup>1</sup>, Shunya Yamamoto<sup>1</sup>, Yoshimi Watanabe<sup>2</sup>, Shizuka Nakano<sup>3,4</sup>, Naoko Sato<sup>3</sup> and Shinsuke Suzuki<sup>1,1</sup>; <sup>1</sup>Waseda University, Japan; <sup>2</sup>Nagoya Institute of Technology, Japan; <sup>3</sup>National Institute of Advanced Industrial Science and Technology, Japan; <sup>4</sup>Henry Monitor Inc., Japan

In additive manufacturing, a titanium alloy Ti6Al4V is the most widely used and was reported to form columnar grains during process. However, columnar grains are generally regarded to be unfavorable since their presence can impart solidification defects and mechanical property anisotropy. Therefore, fine equiaxed microstructures are desired. Recently more or less 0.3vol% addition of TiC particles resulted in grain refinement of Ti6Al4V during Laser-based powder bed fusion of metals[1]. Furthermore it was clarified that TiC particles partially melted in molten Ti6Al4V and the residual TiC particles generated fine and equiaxed grains from the heterogeneous nuclei during directional solidification of Ti6Al4V[2]. Although equiaxed grains can be obtained at high solidification rates in general, the effect has not been clear in an alloy with TiC. In this study, as a fundamental research for additive manufacturing, we aimed to reveal the effects of solidification rate, which varies the amount of melted TiC and the degree of constitutional undercooling.

Ti6Al4V powder (with 2.0vol% TiC and without TiC) in a Ti6Al4V sheath was melted and directionally solidified with a floating zone melting method at various solidification rates  $V(=1,3,5,10,15\text{mm/min})$ . During the process, the temperature around the melt pool was measured using a two-color pyrometer. Microscopic images on the cross section through the center of directionally solidified samples were obtained to evaluate the numbers and equivalent diameter of the prior  $\beta$  grains. The area fractions of the precipitate and matrix were analyzed by an image processing software, and the carbon contents in them were analyzed by Electron Probe Micro Analyzer(EPMA) to estimate the amount of the melted TiC. Also using phase field method, microstructure evolution of Ti6Al4V during solidification was simulated and constitutional undercooling around solidification front was estimated.

From microstructural observations, the number of fine equiaxed prior  $\beta$  grains increased by TiC addition except at 1mm/min and the total number of grains increased as solidification rate increased. Also with TiC added microstructure, precipitation appeared in the prior  $\beta$  grains regardless of solidification rates. EPMA analysis results showed that the precipitation was  $\text{Ti}_2\text{C}$  and the area percentage of  $\text{Ti}_2\text{C}$  decreased with increasing solidification rate. Estimating carbon amount from  $\text{Ti}_2\text{C}$  fraction, carbon amount derived from melted TiC is 0.262 mass% at 1mm/min and 0.178 mass% at 15mm/min. Considering total carbon amount 0.270 mass% from 2.0vol% added TiC, carbon amount derived from melted TiC is smaller when solidification rate is higher. From phase field simulation, constitutional undercooling around solidification front was larger as solidification rates increased. From above, it is considered that at a higher solidification rate, the amount of melted TiC particles is smaller, and the amount of residual potent heterogeneous nucleus TiC particles is larger at a large constitutional undercooling .

#### References

- [1] Y.Watanabe *et al.*, *Metall. Mater. Trans. A*, 51(2020)1345.
- [2] S.Yamamoto *et al.*, *Metall. Mater. Trans. A*, 50(2019)3174.

#### **F.SF05.07.09**

##### **4D Printing with Elastic Hinge Using Shape Memory Polymer and Elastomer via Fused Deposition Modeling 3D Printer Shunsuke Yamamura and Eiji Iwase; Waseda University, Japan**

Recently, many researchers have studied 4D printing by fused deposition modeling (FDM)-3D printer using thermoplastic material including shape memory polymer (SMP) [1]. 4D printing is 3D printing with shape-shifting-function triggered by material shrinkage and/or expansion. A conventional 4D-printed device by FDM-3D printer is, however, difficult to deform after shape-shifting, because thermoplastic material is rigid below the glass transition temperature. Therefore, a conventional 4D-printed device is not possible to use as an origami stretchable device which is deformed by origami-deformation of elastic hinges [2].

In this study, we proposed a 4D printing device with a hybrid hinge. The hybrid hinge has a structure in which a self-folding hinge made of SMP and soft hinges made of elastomer are arranged in series. By applying heat to the 3D printed device with

a hybrid hinge, the self-folding hinge works to form a folded structure. The elastic deformation after self-folded can be realized not by a self-folded hinge but by soft hinges made of an elastomer with wide elastic range. In order to confirm the elasticity of hybrid hinge, we evaluated a change of folding angle when the devices were repeatedly bent. As a comparison to our proposed device with a hybrid hinge, we prepared a device without a hybrid hinge, i.e. without soft hinges. In the device without a hybrid hinge, we confirmed that the folding angle changed at one cycle bending due to plastic deformation of SMP. On the contrary, the bending angle of the device with a hybrid hinge did not change by a repetition of bending deformation. Finally, we demonstrated an origami stretchable device with multiple hybrid hinges. We fabricated miura-ori as origami stretchable device. Unlike a previous demonstration of miura-ori using 4D printing via FDM-3D printer, our fabricated device can be deformed from folded shape to deployed shape by external force even under room temperature at 25°C.

In conclusions, our proposed hybrid hinge was confirmed as an effective way to realize the 4D printing with elastic hinge. We believe that our proposed way will accelerate the development of stretchable origami device.

[1] Teunis van Manen *et al.*, *Materials Horizons*, vol. 4, pp. 1064-1069, 2017.

[2] Shuguang Li *et al.*, *Proceedings of the National Academy of Sciences*, vol. 114, pp. 13132-13137, 2017.

#### **F.SF05.07.10**

**3D Printing of Poly-Ether-Ether-Ketone (PEEK) and Reinforced Peek Materials and Its Mechanical Properties with Post Heat Treatments** Kyung-hyun Kim, Hyeon-Sik Ahn, Dong-Hwan Kim, Ae-Sun Oh and Hyun-Cheol Bae; Electronics and Telecommunications Research Institute, Korea (the Republic of)

3D printing or additive manufacturing has great attention in recent years as it allows the manufacturing of complex shapes and various geometries. Specially, these techniques have various application fields, which are making prototypes for electronics, aerospace, automotive, and so on. For 3D printing technology to be applied to electric vehicles, it needs to be light, high strength and high thermal stability. Many researchers are working on high-temperature, high-strength materials such as PEEK and composites to increase strength.

Therefore, we have designed a hybrid organic-inorganic composite material, which are glass fiber, carbon fiber, and modified PEEK, for high-temperature, high-strength materials stability. We successfully made organic-inorganic 3D printing filaments using a mini-extruder machine for fused deposition modelling (FDM) printer. Also, we studied thermal and mechanical properties of 3D printed samples with or without post heat treatment at 250°C for 1 hr. These printed samples were measured by thermal mechanical analyzer (TMA), bending strength and tensile strength with micro-universal testing machine. Surface morphology and the crystallinity of PEEK of those are measured by scanning electron microscope (SEM) and the Differential Scanning Calorimetry (DSC) method.

We will present the detailed experiment results and other analysis results for improved 3D printed samples.

This work was partly supported by the National Research Council of Science & Technology (NST) grant by the Korea government (MSIP) (No. CRC-19-02-ETRI) and the Technology Innovation Program (No. 20005139) funded by the Ministry of Trade, Industry & Energy (MOTIE, Korea)

#### **F.SF05.07.11**

**Synthesis of Polyetherimide(PEI)-Based Photocurable Resin for Biocompatible DLP Stereolithography 3D Printing Process** Jae hwan Chung, Hee Jeong Park, Hyejin Kim and Dong hyun Lee; Dankook University, Korea (the Republic of)

3D printing, commonly known as additive manufacturing, is a manufacturing process of producing three dimensional objects having complex features through layer by layer printing. The 3D printing technique has been developed rapidly and applied to various industrial fields since it was proposed in 1980s. Even though there are many 3D printing techniques introduced so far, the photocuring 3D printing which is based on photopolymerization of photo-sensitive materials is becoming more important due to its high printing speed, high precision and smooth surface of products. However, the materials which are mainly utilized in the photocuring 3D printing often encounter limited mechanical properties which are originated from their own nature. Thus, it is necessary to design photo-sensitive materials satisfying the requirements. Recently, poly(ethylene glycol) diacrylate(PEGMA) which is commonly a highly biocompatible photocurable material is widely used in the photocuring 3D printing for biomaterials, dental materials, biomimetics, and tissue engineering and so on despite its poor mechanical and thermal properties. Thus, there are many demand to overcome the disadvantages of PEGDA and to find suitable materials for the fields. Here, we report the polyetherimide-based photocurable resin for biocompatible 3D printing. Polyetherimide(PEI) is one of engineering plastics, which has superior mechanical strength, long-term thermal stability, excellent chemical resistance and good biocompatibility. By integrating those properties of polyetherimide to advanced biocompatible 3D printing, we synthesized a polyetherimide-based photocurable resin for DLP stereolithography 3D printing. To synthesize the polyetherimide-based resin condensation reaction between dianhydrides of BPADA and diamines

of 3,5-diaminobenzoic acid under the nitrogen flow are conducted to produce amic acid groups in chain backbones and chain ends. As thermal imidization of the reactants is then proceeded in sequential 3 steps of 60°C for 2 hours, 110°C for 2 hours and 205°C for 4 hours, the amic acid groups are successfully converted to imide linkages. It is noted that the carboxylic acid of diamono acid are still remained after the imidization. After cooling down to the 30°C, glycidil methacrylate (GMA) is additionally grafted to the PEI molecules by the reaction with the carboxylic acids in presence of tetraethylammonium bromide (TEAB), triethylamine and hydroquinone under the nitrogen flow of 100°C. The GMA groups impart the photochemical reactivity to in the PEI molecules. After the precipitation in distilled water and filtration, PEI-g-GMA powder is obtained and dried in vacuum oven at 40°C for 24 hours. To prepare the photocurable resin for 3D printing, the synthesized PEI-g-GMA is mixed with crosslinkers(PEGDA), reactive diluents(1-vinyl-2-pyrrolidinone(NVP) and photo initiators(Igarure819<sup>®</sup>). To test the biocompatible property of our resins, three dimensional specimens are printed with the photocurable resins prepared here, by precisely adjusting light dosage and compositions of the mixtures. It is found that the specimens are printed in 0.4 seconds of exposure time and 30 μm of layer thickness. The printed specimens are rinsed with isopropanol and post-cured in a UV light chamber. The photocurable resin and the printed specimens are characterized by using universal test machine(UTM), differential scanning calorimeter(DSC), thermal gravimetric analysis(TGA), FT-IR and H<sup>1</sup>-NMR spectroscopy. In addition, the molecular weight of PEI-g-GMA is estimated by end group analysis based on H<sup>1</sup>-NMR data.

#### F.SF05.07.13

***In Situ* Microbeam X-Ray Scattering and Infra-Red Imaging of Polypropylene/Graphene Nanoplatelet Nanocomposites During Additive Manufacturing** Yu-Chung Lin<sup>1</sup>, Aniket M. Raut<sup>1</sup>, Yuval Shmueli<sup>1</sup>, Steve N. Nitodas<sup>1</sup>, Guillaume Freychet<sup>2</sup>, Mikhail Zhernenkov<sup>2</sup> and Miriam H. Rafailovich<sup>1</sup>; <sup>1</sup>SUNY Stony Brook University, United States; <sup>2</sup>Brookhaven National Laboratory, United States

The fused deposition modeling (FDM) is an advanced 3D printing technique in which the thermoplastic polymer is melted and extruded by the shear force coming from the nozzle to create layer by layer structure according to the user input file. Compared to the conventional molding, a major challenge of the FDM process is the highly nonequilibrium thermal gradients that impact the filament fusion and the thermo-mechanical and electrical integrity of the materials produced. Furthermore, since these gradients are poorly understood, structure/property models predicting the outcome of printing have been difficult to establish. In order to visualize the gradients, while probing the internal structure of the printed samples, we designed an apparatus which can simultaneously profile both macrostructure and microstructure during printing, as a function of time, using synchrotron X-ray scattering, and together with infrared thermal imaging. This information is then combined with Raman spectroscopy, rheology, and DMA studies, in order to understand the evolution of the internal structure and its corresponding influence on the properties of the materials. We had previously applied these techniques to crystalline polymers, PLA and iPP [1]. Here, we extend these measurements to the study of the internal structure of FDM printed Polypropylene (PP)/Graphene Nanoplatelet (GNPs) nanocomposites. Micro-beam wide-angle scattering analysis showed that the GNPs cluster towards the center of the filament during extrusion from the nozzle when the GNP concentration is higher than 10%. Previous studies had demonstrated that iPP interacts strongly with graphene [2], and hence the segregation of the GNP away from the interface facilitates chain diffusion across the interfaces, consistent with the high impact toughness observed. Thermal imaging confirms the non-uniform distribution, with the highest conductivity, 267% increase, occurring along the center of the fibers. Hence incorporation of GNP and the subsequent alignment enables the printing of oriented thermal or conductors. In operando time-dependent small angle scattering analysis of the filament during extrusion shows the interesting correlated motion of the GNPs, which stops abruptly once the temperature is below the melting point. This confirms the gel-like state which occurs with the GNP in the iPP melt state and drives the particles along the velocity gradient in the moving nanocomposite stream.

1. Shmueli, Y., et al., *Compos. Sci. Technol*, 2020. 196, 108227

2. Kai, Y., et al., *Nanocomposites*, 2015. 1(3) p. 126-137.

#### F.SF05.07.15

**Optimizing the Mechanical Properties of 3D Printed Binary Mixtures of PLA and Polyolefins** Yu-Chung Lin<sup>1</sup>, Larry J. Huang<sup>2</sup>, Richard Li<sup>3</sup>, Addison Liu<sup>4</sup>, Nikita Salunke<sup>5</sup>, Zimei Du<sup>1</sup>, Amhed Shata<sup>1</sup>, Henry Takizawa<sup>1</sup>, Mustafa Zaidi<sup>1</sup>, Daniel Luo<sup>6</sup>, Yuval Shmueli<sup>1</sup>, Miriam H. Rafailovich<sup>1</sup> and Steve N. Nitodas<sup>1</sup>; <sup>1</sup>SUNY Stony Brook University, United States; <sup>2</sup>Wilton High Svhol, United States; <sup>3</sup>Conestoga High School, United States; <sup>4</sup>Unionville High School, United States; <sup>5</sup>Evergreen Valley High School, United States; <sup>6</sup>Monroe-Woodbury High School, United States

Poly(lactic acid) (PLA) is commonly used for 3D-printing, nevertheless it is characterized by poor self-adhesion. The quick cooling rate of PLA does not allow enough time for the fibers in the filament to properly penetrate across an interface and form strong polymer chains. As a result, adhesion is inhibited and the overall strength of prints is reduced, making 3D-printed

PLA a nonviable material for load bearing applications. This work aims at tackling this problem with a binary polymer blend of PLA combined with a polyolefin, more specifically high-density polyethylene (HDPE) or isotactic polypropylene (iPP). HDPE has superior self-adhesive properties to PLA and a lower surface energy than PLA. This coupled with its low glass transition temperature causes the HDPE to segregate towards the surface of the filament, forming an outer shell during extrusion. We hypothesized that a shell thickness of three radii of gyration will provide a polymer chain long enough to enhance the interpenetration of fibers between layers while keeping phase separation to a minimum. Three radii of gyration are theoretically found at a mass composition of 0.36 wt% HDPE/99.64 wt% PLA. The binary composite showing the highest improvement in mechanical properties, as compared to neat PLA, was 0.25 wt% HDPE/99.75 wt% PLA. This supports the hypothesis that the addition of a small loading of HDPE can improve the mechanical properties of a 3D-print by manipulating the polymer structure via migration of HDPE to the surface of PLA, as also verified by water contact angle measurements and secondary-ion mass spectrometry. Improved interlayer diffusion was also observed when adding low concentrations of iPP to PLA. The inherent immiscibility of PLA and iPP, as a result of the lower surface energy of the latter, allows for an enhanced filament structure: when present at low concentrations, iPP migrates to the surface of the extruded PLA matrix as well, creating a filament characterized by a PLA core and an iPP shell, as confirmed by water contact angle goniometry. Mechanical testing showed that in comparison to the pure PLA control, an optimized filament of 99 wt.% PLA/1 wt.% iPP displayed a 66% increase in toughness. Optical microscopy validated this data, revealing indistinguishable filament-to-filament interfaces in the optimized composite as opposed to pure PLA

#### **F.SF05.07.18**

**Late News: Rheological Study of 3D Printable Thermoelectric Inorganic Materials** Hyejin Ju, Jung-Eun Lee and Han Gi Chae; Ulsan National Institute of Science and Technology, Korea (the Republic of)

The thermoelectric(TE) generator is a solid-state device that directly converts the flow rate (temperature difference) into electrical energy. This TE energy transformation offers a unique solution for producing electricity from waste heat. For enhancing the efficiency of the TE generator, 3d printing method to produce TE materials are needed with geometries suitable for heat sources. Herein, in order to attain high-quality 3D printing of TE inorganic materials, a comprehensive evaluation of appropriate rheological properties and methodologies for formulating inorganic inks is required. For 3D printing, the most important feature is the thixotropy that implies time-dependent shear thinning property.

In this study, we analyzed the rheological behavior of the  $\text{Bi}_2\text{Te}_3$ -based and  $\text{Cu}_2\text{Se}$ -based TE inorganic inks to assess printability and 3D structural retention concerning the content of ion binder which has a strong electrostatic interaction among their particles. Moreover, for evaluating the thixotropy, 3D printing was imitated using a rheometer by three-interval thixotropy test (3ITT) under the nonlinear viscoelastic region.

In static state, the inks showed Bingham plot and it becomes solid like property with increasing ion binder content. Especially, the 3ITT indicated that in  $\text{Bi}_2\text{Te}_3$  based ink without ion binder, storage modulus( $G'$ ) increased dramatically when subjected to stress over the 10 Pa. It implied that the particles are aggregated and turned into unstable states. Using quantitative functions such as degree of structural deformation(De), Degree of structural recovery(Rec), we numerically examined the degree of ink recovery after high shear stress. Both inks have generally shown similar rheological characteristics. Phase stability is improved when binder content increases, but above a certain binder concentration the particle aggregation occurs, and recovery rate and printability are reduced. Thus, it is essential to find the optimum ion binder concentration of inorganic ink suitable for 3D printing. These results were able to demonstrate that ion binder of 25wt% in  $\text{Bi}_2\text{Te}_3$ -based ink and 50wt% in  $\text{Cu}_2\text{Se}$ -based ink were the optimized ion binder conditions for high-quality 3d printing TE materials.

#### **F.SF05.07.19**

**Late News: Direct Ink Writing of Dehydrofluorinated Poly(vinylidene difluoride) to Fabricate Porous Films** Beenish Imtiaz, Nick A. Shepelin, Sandra Kentish and Amanda V. Ellis; The University of Melbourne, Australia

Poly(vinylidene fluoride) (PVDF) has been used extensively as a membrane material for water treatment. It can be easily processed into porous films with high mechanical strength directly from the solution. However, the chemical instability of PVDF remains an issue, particularly in the caustic environments found during the membrane cleaning process, which consequently decreases the lifetime of PVDF membranes. Despite possessing high mechanical strength, PVDF membranes exhibit decreased applicability for low-fouling piezoelectric separation applications, owing to a low electroactive phase following deposition. For the use as piezoelectric membranes, it is important to maximize the electroactive phase, in order to produce vibrations through the application of AC voltage. Moreover, the techniques currently used to enhance the electroactive phase in PVDF, such as poling, mechanical stretching, and quenching, result in the instability and hinder high-temperature separation applications in piezoelectric PVDF membranes.

To overcome these issues, PVDF can be chemically modified to make dehydrofluorinated PVDF (dPVDF). This

modification has multiple benefits. The primary advantage of this modified material is the presence of pendant alkene moieties, which can be used for further post modification strategies to fabricate smart and reactive membranes that respond to external stimuli, such as pH, temperature or electric potential, in order to mitigate fouling. An additional advantage of this material is an increased electroactive phase relative to PVDF, which makes it a promising candidate for low-fouling piezoelectric membrane applications.

Here, for the first time, we present the fabrication of porous dPVDF films by direct ink writing (DIW) and subsequent phase inversion. The dPVDF solutions in *N,N*-dimethylacetamide (DMAc) exhibited Bingham behavior at polymer concentrations between 7 wt% and 15 wt%, and thus could be DIW to produce continuous films. The dPVDF inks (dPVDF (15 wt% in DMAc), and 5, 15, 30 wt% PVP), were subsequently DIW into continuous films, and phase inverted in deionized water (non-solvent) to produce porous films. The porosity of the dPVDF films was confirmed using helium beam ion microscopy. The presence of alkene moieties in the dPVDF and dPVDF porous films was confirmed through attenuated total reflection – Fourier transform infrared (ATR-FTIR) spectroscopy and Raman spectroscopy. An increase in electroactive phase fraction was observed in the DIW films, confirming the enhancement in piezoelectric characteristics. The DIW porous dPVDF membranes presented herein show exceptional promise for the production of piezoelectric membranes and the subsequent utilization as separation membranes in harsh environments.

#### F.SF05.07.20

**Late News: Investigating and Comparing the Resistance to Tensile Testing of Molded and 3D Printed PLA/PP Polymer Blends** Daniel Luo<sup>1,2</sup>, Yu-Chung Lin<sup>2</sup> and Miriam H. Rafailovich<sup>2</sup>; <sup>1</sup>Monroe Woodbury High School, United States; <sup>2</sup>Stony Brook University, The State University of New York, United States

When 3D printing, the quick cooling rate of PLA does not allow enough time for the filament to properly diffuse across an interface<sup>1</sup>, which inhibits adhesion and reduces the overall strength of prints. We aimed to tackle this problem by adding low concentrations of polypropylene (PP) to PLA to create a 3D-printing filament with improved interlayer diffusion.<sup>2</sup> Our hypothesis is when a PLA/PP blend is formed through 3D printing, PP migrates to the surface of the filaments due to its lower surface energy and lower glass transition temperature, forming a core-shell structure that produces pseudo-"self-healing"<sup>2</sup> by fusing fibers. Due to PP's lower surface tension compared to PLA (30.7 mN/m vs 44 mN/m)<sup>5</sup>, PP will travel to the surface of the fibers when extruded, displacing air pockets formed when the fibers crack.<sup>3,4</sup> Previous testing shows that 1% PP blends are the most resistant to tensile testing, and this study seeks to determine if the PP/PLA blend produced by molding or 3D printing is more effective, and which concentration of PP is most resistant to tensile testing.

To find how the core-shell structure impacted the physical properties of the blends, the ratio of the Volume of the Shell vs. Volume of the Fiber and Shell thickness were both plotted against the Volume fraction of PP. Radius of gyration ( $R_g$ ) of PLA and PP were also calculated. By using the thickness of the shell and the diameter of the fiber, the number of  $R_g$ s of PLA and PP in each core-shell sample was found.

5 groups differing in PP % by weight were used to compare which concentration of PP in a PLA/PP blend best resisted tensile testing: 0%, 0.5%, 1%, 2.5%, and 5%. After preparation, the Young's Modulus, UTS (Ultimate Tensile Strength), and Elongation at Break were analyzed. The Young's Modulus of the molded samples showed that the Pure PLA had the highest Young's Modulus, meaning that the molded samples did not exhibit "self-healing". The results for the 0.5% PP, 1% PP, 2.5% PP, 5% PP, and Pure PLA 3D printed samples indicate that 0.5% PP has a higher Young's Modulus compared to 1% and Pure PLA, making it more reliable for 3D printing. The contact angle measurements indicate that even a small % of PP in a blend produces a contact angle similar to pure PP, meaning that adding PP lowers the surface tension of the blend, therefore in the 3D printed blends PP travels to the fibers' surface and produces "self-healing".

In conclusion, this study shows that the optimal concentrations for making a PLA/PP blend for 3D printing is 99.5% PLA/0.5% PP. It also shows that compared to the 3D printed blends, the molded blends do not strengthen the blends to the same extent during tensile testing.

<sup>1</sup> Liu, Zengguang, et al. "A Critical Review of Fused Deposition Modeling 3D Printing Technology in Manufacturing Poly(lactic Acid) Parts." *International Journal of Advanced Manufacturing Technology*, vol. 102, no. 9-12, Springer Science and Business Media LLC, 2019, pp. 2877–89, doi:10.1007/s00170-019-03332-x.

<sup>2</sup> Peng, Fang, et al. "3D Printing with Core-Shell Filaments Containing High or Low Density Polyethylene Shells." *ACS Applied Polymer Materials*, vol. 1, no. 2, American Chemical Society, Feb. 2019, pp. 275–85, doi:10.1021/acsapm.8b00186.

<sup>3</sup> Mehrabi Mazidi, Majid, et al. "Highly-Toughened Poly(lactide)- (PLA) Based Ternary Blends with Significantly Enhanced Glass Transition and Melt Strength: Tailoring the Interfacial Interactions, Phase Morphology, and Performance." *Macromolecules*, vol. 51, no. 11, American Chemical Society, June 2018, pp. 4298–314, doi:10.1021/acs.macromol.8b00557.

<sup>4</sup> "Polymer Properties Database." *Surface Tension*, polymerdatabase.com/polymer%20physics/sigma.html.

<sup>5</sup> Guo, Yichen, et al. "Enhancing Impact Resistance of Polymer Blends via Self-Assembled Nanoscale Interfacial Structures." *Macromolecules*, vol. 51, no. 11, American Chemical Society, June 2018, pp. 3897–910, doi:10.1021/acs.macromol.8b00297.

We gratefully acknowledge support from the Louis Morin Charitable Trust.

#### F.SF05.07.21

**Late News: A Design of 3D-Printable, Biodegradable, Flame Resistant Polymer/Clay Nanocomposite** Yiwei Fang<sup>1</sup>, Christian Apostol<sup>2</sup>, Jiale Lu<sup>3</sup>, Lawrence Zhao<sup>4</sup>, Yuan Xue<sup>1</sup>, Yichen Guo<sup>1</sup> and Miriam H. Rafailovich<sup>1</sup>; <sup>1</sup>Stony Brook University, United States; <sup>2</sup>Ward Melville High School, United States; <sup>3</sup>Princeton International School of Mathematics and Science, United States; <sup>4</sup>University Laboratory High School, United States

Here we designed a non-toxic and environmental sustainable polymer nanocomposite PLA/PBAT/APP/RDP-Clay which achieved good flame resistance and balanced mechanical properties with the addition of 3wt% ammonium phosphate (APP) and 2wt% resorcinol diphenyl phosphate (RDP)-coated montmorillonite clays (C-Na<sup>+</sup>). Polylactic acid (PLA) received attention due to its biodegradability and mechanical properties. However, its poor impact strength and flammability largely limits its application in wide range of areas. In our previous study<sup>1</sup>, APP was found to be rigid and made the impact strength of PLA even worse. We were able to increase the ductility without affecting flammability of the PLA/APP composite by decreasing the APP concentration to only 2 wt% with the addition of only 0.12wt%RDP. Hence, poly(butylene adipate-co-butylene terephthalate)(PBAT), a ductile and biodegradable polymer, is introduced to balanced impact strength. But PBAT was found to be a poor efficient carbon source in APP intumescent system. For PLA/PBAT(75/25) over 10wt% APP/RDP is required to make PLA/PBAT(75/25) resisted to combustion, while pure PLA only need 2wt%APP/RDP. The huge increase for the use of APP not only increase the cost but also sacrificing the desired impact strength. According to Contact Angle Measurement and work of adhesion ( $W_a$ ) between related materials, APP is more affinity to PBAT than PLA which possibly draw part of APP into PBAT phase and decrease the overall flame retardancy. In order to minimize this effect, 2wt%RDP coated sodium clay(C-Na<sup>+</sup>) is added to reduce the interfacial energy between PLA and PBAT which decrease PBAT domain size. Compatibilization was further confirmed by observation of a 32% decrease (from 2.53 $\mu$ m to 1.73 $\mu$ m) in PBAT domain size via Scanning Electron Microscopy. With 2wt%RDP-clay into the composites, we achieved a V-0 designation with a low loading of APP(3wt%). This was attributed to the decreased PBAT domain size, increasing the efficiency of APP to decrease the heat release in the combustion at a reduced overall concentration. From Thermogravimetric Analysis (TGA) result, the reaction mechanism was confirmed by the presence of intumescent char. Which is a byproduct of the reaction in the solid state. The increased ductility below T<sub>g</sub> and viscosity in the melt enables fiber drawing and comparison of the combustibility upon FDM printing, which will be discussed.

We gratefully acknowledge support from the Louis Morin Charitable Trust.

1. Y. Xue, X. Zuo, L. Wang, Y. Zhou, Y. Pan, J. Li, Y. Yin, D. Li, R. Yang, M.H. Rafailovich and Y. Guo: Enhanced flame retardancy of poly(lactic acid) with ultra-low loading of ammonium polyphosphate. *Composites Part B: Engineering* **196**, 108124 (2020).

SESSION F.LP06.04: Live Poster Session: Structural and Functional Materials (F.SF05, F.SF07 and F.SF08)  
Session Chairs: Yat Li and Juana Mendenhall  
Friday Afternoon, December 4, 2020  
1:45 PM - 3:45 PM  
F.SF05

#### F.SF05.07.04

**Tunable Elongation-at-Break of Tensile Mechanical Properties of Stereolithography Additive Manufacturing Through Control of Printing Orientations** Mozah Alyammahi, Rahmat Agung Susantyoko and Tawaddod Alkindi; DEWA R&D Center, Dubai Electricity and Water Authority, United Arab Emirates

Additive manufacturing (AM) spread widely not only for prototyping but also for the production of end-use products. Quality control is a vital importance in the production of parts. One of the challenges of quality control in AM technology - such as fused deposition modeling (FDM) - is that the mechanical strength of the 3d-printed part could be anisotropic (not uniform).



The part's printing orientation could affect the mechanical strength of 3d-printed parts. Among the AM technology spectrum, the stereolithography (SLA) process is known to be able to produce parts with relatively uniform mechanical strength (isotropic).

Many studies were done using FFF 3D printing method. However, to our knowledge, only very few studies had done to investigate the effect of printing orientation on the elongation-at-break of 3d-printed parts using SLA technology. Moreover, previous studies only experimented with a limited amount of samples and orientations. Therefore, strength and elongation-at-break need to be examined in detail and with more variations of print orientation. For this purpose, this study investigated the influence of part's printing orientation to the tensile mechanical properties (tensile-stress-at-max-load, tensile-strength-at-break, tensile-stress-at-yield, young-modulus, elongation-at-break) of SLA technology. This work covered a large number of orientations (27 printing orientations) testing five different mechanical properties.

We used Form 2 3D printer to 3D print with White photopolymer resin of FLGPWH04 material. We used Preform 3.03.1 software to set the sample positions. The samples were oriented with respect to x, y, and z axes according to the software axes. Permutation-with-repetition of 3 different angles (0°, 45°, and 90°) with respect to 3 different axes resulted in 27 part's printing orientations. Furthermore, we printed 3 samples for each orientation with for a total of 81 samples for all orientations. The printed samples were washed in isopropyl alcohol (IPA) for 20 minutes. Afterward, we carefully removed the support structures from the samples using a tweezer; followed by drying and curing process at 60 °C for a total of 20 minutes (samples were flipped every 10 minutes).

We followed the ASTM D638 V standard tensile test design. Each printed sample was kept at the same time (13 days) before the tensile testing to avoid time impact on the properties. Then we performed the tensile testing using Instron 3367. In Bluehill LE 3.77 software, the sizes were entered for each sample. It took the measurements while the test was running and calculated the strain, stress, modulus, and yield. The raw data from the samples compiled in Microsoft Excel.

The results showed relatively uniform isotropy of the tensile-stress-at-max-load and it has 3.8% relative standard deviation. In addition, tensile-strength-at-break, tensile-stress-at-yield, and young-modulus has 4.15%, 5.67% and 7.94% relative standard deviation, respectively. In contrast, a relatively large anisotropy of elongation-at-break has been observed with 21% relative standard deviation. The sample printed vertically (90 degrees normal to the bed) elongated to an average of 10% whereas the sample printed horizontally (0 degrees normal to the bed) elongated to an average of 15%. One hypothesis that explains this behavior is that printing vertically created many layers comparing to printing horizontally. Thus, the high number of interfaces layers make the part elongate less. The results show that the elongation-at-break could vary and could be tuned in SLA technology; a new finding in this research field.

We recommend that the designer of SLA parts to consider the part's printing orientation depending on the possible application (whether the application requires large elongation-at-break or short elongation-at-break). By knowing the effect of printing orientation, high-quality parts could be produced consistently according to the application's requirement.

#### **F.SF05.07.05**

**Enhanced Toughness in Ceramic-Reinforced Polymer Composites with Herringbone Architectures** Robert Zando, Ataollah Mesgarnejad, Chunzhou Pan, Sandra Shefelbine, Alain Karma and Randall M. Erb; Northeastern University, United States

A common design rule in synthetic particle-filled composites is to align all reinforcing particles parallel with the primary stress and thereby perpendicular to a likely fracture. Doing so can often result in crack deflection, which is commonly touted as evidence that a material has enhanced fracture toughness. In reality, as soon as the crack deflection occurs, the material is fracturing along an "easy axis". Much better is for the crack not to deflect and be forced to propagate forward along a "hard axis" spending much more energy to grow. Geometric conditions alone can create T-stress that confine the crack to propagate straight along a hard-direction. However, real-world applications of filled composites often dictate geometric design and put toughness at risk. Instead, designed texturing of reinforcing particles has the potential to steer cracks along a "hard axis" without reliance on geometric loading conditions. Recent advances in the field of composite manufacturing techniques, make such architectures possible, allowing the creation of microstructures which can locally tune the fracture toughness anisotropy. In the studies presented, we explore a unique variant of this principle through the creation of an alignment architecture reminiscent of the spine of a herringbone fish, designed to trap a fracture along the boundary between two regions of distinct particle alignment. This robs the fracture of a preferred direction of initial fracture deflection, delaying the initiation of fracture formation, and forces it along a "hard" direction of fracture initiation, effectively raising both its initial and overall fracture resistance significantly beyond monolithically aligned composite polymer systems. However, while this custom microstructure proved successful in demonstrating this method of boosting mechanical performance over traditional monolithic systems in principle, it remains limited in application by the necessity of a fracture initiating at or near the boundary between two alignment regions. Without filling this pre-condition, the fracture would initiate in a manner similar to a monolithic alignment system.

To overcome this limitation, we applied these principles to generate a new class of beautiful herringbone mosaics that

provide isotropic toughness in 2D. This structure was composed of a series of hexagonal unit cells, further divided into a series of triangular sub-cells, each with herringbone patterns. Mechanical testing of these samples determined that this structure not only demonstrated superior initial fracture toughness to monolithic samples, but that this effect was approximately isotropic, showing superior mechanical performance over the highest performing monolithic samples regardless of the direction of the tensile force relative to the microstructure placement. In applications in which the geometric design of a particle-filled composite is constrained, texturing materials with herringbone mosaics provide a meaningful route toward boosting isotropic toughness through microstructural design alone.

#### **F.SF05.07.06**

##### **Lightweight Cellular Metal Composites with Zero and Tunable Thermal Expansion Enabled by Ultrasonic Additive Manufacturing** Ethan Parsons; MIT Lincoln Laboratory, United States

In aerospace applications, variations of temperature caused by changing environmental conditions or generation of heat is a common problem. The resulting thermal strains cause separation and alignment errors in optical systems, and stresses due to mismatches of thermal expansion at material interfaces cause failure of components and structures. Because minimizing weight, cost, and lead time are also critical requirements, lightweight, easily machined metals are attractive for aerospace applications, but these materials all have substantial coefficients of thermal expansion. Previous work has shown that the superposition of two metals with dissimilar coefficients of thermal expansion in periodic cellular configurations can result in a composite material with zero effective thermal expansion. However, fabrication of these material architectures typically is either impossible or requires manual assembly. Here, we propose methods to design and fabricate cellular metal composites with tunable thermal expansion and optimized specific stiffness that can be manufactured at useful scales entirely with automated methods. Samples were manufactured with ultrasonic additive manufacturing and computer-controlled machining, and thermal expansion was measured optically. The results demonstrate the practical fabrication of cellular metal composites with zero or negative thermal expansion in one direction, tunable thermal expansion in a second direction, and structural performance indices competitive with the indices of conventional aerospace alloys.

#### **F.SF05.07.08**

##### **The Effects of Solidification Rates on Grain Refinement Capacity of TiC in Directionally Solidified Ti6Al4V Alloy** Naoki Date<sup>1</sup>, Shunya Yamamoto<sup>1</sup>, Yoshimi Watanabe<sup>2</sup>, Shizuka Nakano<sup>3,4</sup>, Naoko Sato<sup>3</sup> and Shinsuke Suzuki<sup>1,1</sup>; <sup>1</sup>Waseda University, Japan; <sup>2</sup>Nagoya Institute of Technology, Japan; <sup>3</sup>National Institute of Advanced Industrial Science and Technology, Japan; <sup>4</sup>Henry Monitor Inc., Japan

In additive manufacturing, a titanium alloy Ti6Al4V is the most widely used and was reported to form columnar grains during process. However, columnar grains are generally regarded to be unfavorable since their presence can impart solidification defects and mechanical property anisotropy. Therefore, fine equiaxed microstructures are desired. Recently more or less 0.3vol% addition of TiC particles resulted in grain refinement of Ti6Al4V during Laser-based powder bed fusion of metals[1]. Furthermore it was clarified that TiC particles partially melted in molten Ti6Al4V and the residual TiC particles generated fine and equiaxed grains from the heterogeneous nuclei during directional solidification of Ti6Al4V[2]. Although equiaxed grains can be obtained at high solidification rates in general, the effect has not been clear in an alloy with TiC. In this study, as a fundamental research for additive manufacturing, we aimed to reveal the effects of solidification rate, which varies the amount of melted TiC and the degree of constitutional undercooling.

Ti6Al4V powder (with 2.0vol% TiC and without TiC) in a Ti6Al4V sheath was melted and directionally solidified with a floating zone melting method at various solidification rates  $V(=1,3,5,10,15\text{mm/min})$ . During the process, the temperature around the melt pool was measured using a two-color pyrometer. Microscopic images on the cross section through the center of directionally solidified samples were obtained to evaluate the numbers and equivalent diameter of the prior  $\beta$  grains. The area fractions of the precipitate and matrix were analyzed by an image processing software, and the carbon contents in them were analyzed by Electron Probe Micro Analyzer(EPMA) to estimate the amount of the melted TiC. Also using phase field method, microstructure evolution of Ti6Al4V during solidification was simulated and constitutional undercooling around solidification front was estimated.

From microstructural observations, the number of fine equiaxed prior  $\beta$  grains increased by TiC addition except at 1mm/min and the total number of grains increased as solidification rate increased. Also with TiC added microstructure, precipitation appeared in the prior  $\beta$  grains regardless of solidification rates. EPMA analysis results showed that the precipitation was  $\text{Ti}_2\text{C}$  and the area percentage of  $\text{Ti}_2\text{C}$  decreased with increasing solidification rate. Estimating carbon amount from  $\text{Ti}_2\text{C}$  fraction, carbon amount derived from melted TiC is 0.262 mass% at 1mm/min and 0.178 mass% at 15mm/min. Considering total carbon amount 0.270 mass% from 2.0vol% added TiC, carbon amount derived from melted TiC is smaller when

solidification rate is higher. From phase field simulation, constitutional undercooling around solidification front was larger as solidification rates increased. From above, it is considered that at a higher solidification rate, the amount of melted TiC particles is smaller, and the amount of residual potent heterogeneous nucleus TiC particles is larger at a large constitutional undercooling.

#### References

- [1] Y.Watanabe *et al.*, *Metall. Mater. Trans. A*, 51(2020)1345.
- [2] S.Yamamoto *et al.*, *Metall. Mater. Trans. A*, 50(2019)3174.

#### F.SF05.07.09

##### **4D Printing with Elastic Hinge Using Shape Memory Polymer and Elastomer via Fused Deposition Modeling 3D Printer** Shunsuke Yamamura and Eiji Iwase; Waseda University, Japan

Recently, many researchers have studied 4D printing by fused deposition modeling (FDM)-3D printer using thermoplastic material including shape memory polymer (SMP) [1]. 4D printing is 3D printing with shape-shifting-function triggered by material shrinkage and/or expansion. A conventional 4D-printed device by FDM-3D printer is, however, difficult to deform after shape-shifting, because thermoplastic material is rigid below the glass transition temperature. Therefore, a conventional 4D-printed device is not possible to use as an origami stretchable device which is deformed by origami-deformation of elastic hinges [2].

In this study, we proposed a 4D printing device with a hybrid hinge. The hybrid hinge has a structure in which a self-folding hinge made of SMP and soft hinges made of elastomer are arranged in series. By applying heat to the 3D printed device with a hybrid hinge, the self-folding hinge works to form a folded structure. The elastic deformation after self-folded can be realized not by a self-folded hinge but by soft hinges made of an elastomer with wide elastic range. In order to confirm the elasticity of hybrid hinge, we evaluated a change of folding angle when the devices were repeatedly bent. As a comparison to our proposed device with a hybrid hinge, we prepared a device without a hybrid hinge, i.e. without soft hinges. In the device without a hybrid hinge, we confirmed that the folding angle changed at one cycle bending due to plastic deformation of SMP. On the contrary, the bending angle of the device with a hybrid hinge did not change by a repetition of bending deformation. Finally, we demonstrated an origami stretchable device with multiple hybrid hinges. We fabricated miura-ori as origami stretchable device. Unlike a previous demonstration of miura-ori using 4D printing via FDM-3D printer, our fabricated device can be deformed from folded shape to deployed shape by external force even under room temperature at 25°C.

In conclusions, our proposed hybrid hinge was confirmed as an effective way to realize the 4D printing with elastic hinge. We believe that our proposed way will accelerate the development of stretchable origami device.

- [1] Teunis van Manen *et al.*, *Materials Horizons*, vol. 4, pp. 1064-1069, 2017.
- [2] Shuguang Li *et al.*, *Proceedings of the National Academy of Sciences*, vol. 114, pp. 13132-13137, 2017.

#### F.SF05.07.10

##### **3D Printing of Poly-Ether-Ether-Ketone (PEEK) and Reinforced Peek Materials and Its Mechanical Properties with Post Heat Treatments** Kyung-hyun Kim, Hyeon-Sik Ahn, Dong-Hwan Kim, Ae-Sun Oh and Hyun-Cheol Bae; Electronics and Telecommunications Research Institute, Korea (the Republic of)

3D printing or additive manufacturing has great attention in recent years as it allows the manufacturing of complex shapes and various geometries. Specially, these techniques have various application fields, which are making prototypes for electronics, aerospace, automotive, and so on. For 3D printing technology to be applied to electric vehicles, it needs to be light, high strength and high thermal stability. Many researchers are working on high-temperature, high-strength materials such as PEEK and composites to increase strength.

Therefore, we have designed a hybrid organic-inorganic composite material, which are glass fiber, carbon fiber, and modified PEEK, for high-temperature, high-strength materials stability. We successfully made organic-inorganic 3D printing filaments using a mini-extruder machine for fused deposition modelling (FDM) printer. Also, we studied thermal and mechanical properties of 3D printed samples with or without post heat treatment at 250°C for 1 hr. These printed samples were measured by thermal mechanical analyzer (TMA), bending strength and tensile strength with micro-universal testing machine. Surface morphology and the crystallinity of PEEK of those are measured by scanning electron microscope (SEM) and the Differential Scanning Calorimetry (DSC) method.

We will present the detailed experiment results and other analysis results for improved 3D printed samples.

This work was partly supported by the National Research Council of Science & Technology (NST) grant by the Korea

government (MSIP) (No. CRC-19-02-ETRI) and the Technology Innovation Program (No. 20005139) funded by the Ministry of Trade, Industry & Energy (MOTIE, Korea)

#### F.SF05.07.11

##### **Synthesis of Polyetherimide(PEI)-Based Photocurable Resin for Biocompatible DLP Stereolithography 3D Printing Process** Jae hwan Chung, Hee Jeong Park, Hyejin Kim and Dong hyun Lee; Dankook University, Korea (the Republic of)

3D printing, commonly known as additive manufacturing, is a manufacturing process of producing three dimensional objects having complex features through layer by layer printing. The 3D printing technique has been developed rapidly and applied to various industrial fields since it was proposed in 1980s. Even though there are many 3D printing techniques introduced so far, the photocuring 3D printing which is based on photopolymerization of photo-sensitive materials is becoming more important due to its high printing speed, high precision and smooth surface of products. However, the materials which are mainly utilized in the photocuring 3D printing often encounter limited mechanical properties which are originated from their own nature. Thus, it is necessary to design photo-sensitive materials satisfying the requirements. Recently, poly(ethylene glycol) diacrylate(PEGMA) which is commonly a highly biocompatible photocurable material is widely used in the photocuring 3D printing for biomaterials, dental materials, biomimetics, and tissue engineering and so on despite its poor mechanical and thermal properties. Thus, there are many demand to overcome the disadvantages of PEGMA and to find suitable materials for the fields. Here, we report the polyetherimide-based photocurable resin for biocompatible 3D printing. Polyetherimide(PEI) is one of engineering plastics, which has superior mechanical strength, long-term thermal stability, excellent chemical resistance and good biocompatibility. By integrating those properties of polyetherimide to advanced biocompatible 3D printing, we synthesized a polyetherimide-based photocurable resin for DLP stereolithography 3D printing. To synthesize the polyetherimide-based resin condensation reaction between dianhydrides of BPADA and diamines of 3,5-diaminobenzoic acid under the nitrogen flow are conducted to produce amic acid groups in chain backbones and chain ends. As thermal imidization of the reactants is then proceeded in sequential 3 steps of 60°C for 2 hours, 110°C for 2 hours and 205°C for 4 hours, the amic acid groups are successfully converted to imide linkages. It is noted that the carboxylic acid of diamino acid are still remained after the imidization. After cooling down to the 30°C, glycidyl methacrylate (GMA) is additionally grafted to the PEI molecules by the reaction with the carboxylic acids in presence of tetraethylammonium bromide (TEAB), triethylamine and hydroquinone under the nitrogen flow of 100°C. The GMA groups impart the photochemical reactivity to in the PEI molecules. After the precipitation in distilled water and filtration, PEI-g-GMA powder is obtained and dried in vacuum oven at 40°C for 24 hours. To prepare the photocurable resin for 3D printing, the synthesized PEI-g-GMA is mixed with crosslinkers(PEGDA), reactive diluents(1-vinyl-2-pyrrolidinone(NVP) and photo initiators(Igarure819®). To test the biocompatible property of our resins, three dimensional specimens are printed with the photocurable resins prepared here, by precisely adjusting light dosage and compositions of the mixtures. It is found that the specimens are printed in 0.4 seconds of exposure time and 30 µm of layer thickness. The printed specimens are rinsed with isopropanol and post-cured in a UV light chamber. The photocurable resin and the printed specimens are characterized by using universal test machine(UTM), differential scanning calorimeter(DSC), thermal gravimetric analysis(TGA), FT-IR and H<sup>1</sup>-NMR spectroscopy. In addition, the molecular weight of PEI-g-GMA is estimated by end group analysis based on H<sup>1</sup>-NMR data.

#### F.SF05.07.13

##### ***In Situ* Microbeam X-Ray Scattering and Infra-Red Imaging of Polypropylene/Graphene Nanoplatelet Nanocomposites During Additive Manufacturing** Yu-Chung Lin<sup>1</sup>, Aniket M. Raut<sup>1</sup>, Yuval Shmueli<sup>1</sup>, Steve N. Nitodas<sup>1</sup>, Guillaume Freychet<sup>2</sup>, Mikhail Zhernenkov<sup>2</sup> and Miriam H. Rafailovich<sup>1</sup>; <sup>1</sup>SUNY Stony Brook University, United States; <sup>2</sup>Brookhaven National Laboratory, United States

The fused deposition modeling (FDM) is an advanced 3D printing technique in which the thermoplastic polymer is melted and extruded by the shear force coming from the nozzle to create layer by layer structure according to the user input file. Compared to the conventional molding, a major challenge of the FDM process is the highly nonequilibrium thermal gradients that impact the filament fusion and the thermo-mechanical and electrical integrity of the materials produced. Furthermore, since these gradients are poorly understood, structure/property models predicting the outcome of printing have been difficult to establish. In order to visualize the gradients, while probing the internal structure of the printed samples, we designed an apparatus which can simultaneously profile both macrostructure and microstructure during printing, as a function of time, using synchrotron X-ray scattering, and together with infrared thermal imaging. This information is then combined with Raman spectroscopy, rheology, and DMA studies, in order to understand the evolution of the internal structure and its corresponding influence on the properties of the materials. We had previously applied these techniques to crystalline polymers, PLA and iPP [1]. Here, we extend these measurements to the study of the internal structure of FDM printed Polypropylene (PP)/Graphene Nanoplatelet (GNPs) nanocomposites. Micro-beam wide-angle scattering analysis showed that

the GNPs cluster towards the center of the filament during extrusion from the nozzle when the GNP concentration is higher than 10%. Previous studies had demonstrated that iPP interacts strongly with graphene [2], and hence the segregation of the GNP away from the interface facilitates chain diffusion across the interfaces, consistent with the high impact toughness observed. Thermal imaging confirms the non-uniform distribution, with the highest conductivity, 267% increase, occurring along the center of the fibers. Hence incorporation of GNP and the subsequent alignment enables the printing of oriented thermal or conductors. In operando time-dependent small angle scattering analysis of the filament during extrusion shows the interesting correlated motion of the GNPs, which stops abruptly once the temperature is below the melting point. This confirms the gel-like state which occurs with the GNP in the iPP melt state and drives the particles along the velocity gradient in the moving nanocomposite stream.

1. Shmueli, Y., et al., *Compos. Sci. Technol*, 2020. 196, 108227

2. Kai, Y., et al., *Nanocomposites*, 2015. 1(3) p. 126-137.

#### **F.SF05.07.15**

**Optimizing the Mechanical Properties of 3D Printed Binary Mixtures of PLA and Polyolefins** Yu-Chung Lin<sup>1</sup>, Larry J. Huang<sup>2</sup>, Richard Li<sup>3</sup>, Addison Liu<sup>4</sup>, Nikita Salunke<sup>5</sup>, Zimei Du<sup>1</sup>, Amhed Shata<sup>1</sup>, Henry Takizawa<sup>1</sup>, Mustafa Zaidi<sup>1</sup>, Daniel Luo<sup>6</sup>, Yuval Shmueli<sup>1</sup>, Miriam H. Rafailovich<sup>1</sup> and Steve N. Nitodas<sup>1</sup>; <sup>1</sup>SUNY Stony Brook University, United States; <sup>2</sup>Wilton High Svhol, United States; <sup>3</sup>Conestoga High School, United States; <sup>4</sup>Unionville High School, United States; <sup>5</sup>Evergreen Valley High School, United States; <sup>6</sup>Monroe-Woodbury High School, United States

Poly(lactic acid) (PLA) is commonly used for 3D-printing, nevertheless it is characterized by poor self-adhesion. The quick cooling rate of PLA does not allow enough time for the fibers in the filament to properly penetrate across an interface and form strong polymer chains. As a result, adhesion is inhibited and the overall strength of prints is reduced, making 3D-printed PLA a nonviable material for load bearing applications. This work aims at tackling this problem with a binary polymer blend of PLA combined with a polyolefin, more specifically high-density polyethylene (HDPE) or isotactic polypropylene (iPP). HDPE has superior self-adhesive properties to PLA and a lower surface energy than PLA. This coupled with its low glass transition temperature causes the HDPE to segregate towards the surface of the filament, forming an outer shell during extrusion. We hypothesized that a shell thickness of three radii of gyration will provide a polymer chain long enough to enhance the interpenetration of fibers between layers while keeping phase separation to a minimum. Three radii of gyration are theoretically found at a mass composition of 0.36 wt% HDPE/99.64 wt% PLA. The binary composite showing the highest improvement in mechanical properties, as compared to neat PLA, was 0.25 wt% HDPE/99.75 wt% PLA. This supports the hypothesis that the addition of a small loading of HDPE can improve the mechanical properties of a 3D-print by manipulating the polymer structure via migration of HDPE to the surface of PLA, as also verified by water contact angle measurements and secondary-ion mass spectrometry. Improved interlayer diffusion was also observed when adding low concentrations of iPP to PLA. The inherent immiscibility of PLA and iPP, as a result of the lower surface energy of the latter, allows for an enhanced filament structure: when present at low concentrations, iPP migrates to the surface of the extruded PLA matrix as well, creating a filament characterized by a PLA core and an iPP shell, as confirmed by water contact angle goniometry. Mechanical testing showed that in comparison to the pure PLA control, an optimized filament of 99 wt.% PLA/1 wt.% iPP displayed a 66% increase in toughness. Optical microscopy validated this data, revealing indistinguishable filament-to-filament interfaces in the optimized composite as opposed to pure PLA

#### **F.SF05.07.18**

**Late News: Rheological Study of 3D Printable Thermoelectric Inorganic Materials** Hyejin Ju, Jung-Eun Lee and Han Gi Chae; Ulsan National Institute of Science and Technology, Korea (the Republic of)

The thermoelectric (TE) generator is a solid-state device that directly converts the flow rate (temperature difference) into electrical energy. This TE energy transformation offers a unique solution for producing electricity from waste heat. For enhancing the efficiency of the TE generator, 3d printing method to produce TE materials are needed with geometries suitable for heat sources. Herein, in order to attain high-quality 3D printing of TE inorganic materials, a comprehensive evaluation of appropriate rheological properties and methodologies for formulating inorganic inks is required. For 3D printing, the most important feature is the thixotropy that implies time-dependent shear thinning property.

In this study, we analyzed the rheological behavior of the Bi<sub>2</sub>Te<sub>3</sub>-based and Cu<sub>2</sub>Se-based TE inorganic inks to assess printability and 3D structural retention concerning the content of ion binder which has a strong electrostatic interaction among their particles. Moreover, for evaluating the thixotropy, 3D printing was imitated using a rheometer by three-interval thixotropy test (3ITT) under the nonlinear viscoelastic region.

In static state, the inks showed Bingham plot and it becomes solid like property with increasing ion binder content. Especially, the 3ITT indicated that in Bi<sub>2</sub>Te<sub>3</sub> based ink without ion binder, storage modulus(G') increased dramatically when subjected to stress over the 10 Pa. It implied that the particles are aggregated and turned into unstable states. Using

quantitative functions such as degree of structural deformation(De), Degree of structural recovery(Rec), we numerically examined the degree of ink recovery after high shear stress. Both inks have generally shown similar rheological characteristics. Phase stability is improved when binder content increases, but above a certain binder concentration the particle aggregation occurs, and recovery rate and printability are reduced. Thus, it is essential to find the optimum ion binder concentration of inorganic ink suitable for 3D printing. These results were able to demonstrate that ion binder of 25wt% in Bi<sub>2</sub>Te<sub>3</sub>-based ink and 50wt% in Cu<sub>2</sub>Se-based ink were the optimized ion binder conditions for high-quality 3d printing TE materials.

#### F.SF05.07.19

**Late News: Direct Ink Writing of Dehydrofluorinated Poly(vinylidene difluoride) to Fabricate Porous Films** [Beenish Imtiaz](#), Nick A. Shepelin, Sandra Kentish and Amanda V. Ellis; The University of Melbourne, Australia

Poly(vinylidene fluoride) (PVDF) has been used extensively as a membrane material for water treatment. It can be easily processed into porous films with high mechanical strength directly from the solution. However, the chemical instability of PVDF remains an issue, particularly in the caustic environments found during the membrane cleaning process, which consequently decreases the lifetime of PVDF membranes. Despite possessing high mechanical strength, PVDF membranes exhibit decreased applicability for low-fouling piezoelectric separation applications, owing to a low electroactive phase following deposition. For the use as piezoelectric membranes, it is important to maximize the electroactive phase, in order to produce vibrations through the application of AC voltage. Moreover, the techniques currently used to enhance the electroactive phase in PVDF, such as poling, mechanical stretching, and quenching, result in the instability and hinder high-temperature separation applications in piezoelectric PVDF membranes.

To overcome these issues, PVDF can be chemically modified to make dehydrofluorinated PVDF (dPVDF). This modification has multiple benefits. The primary advantage of this modified material is the presence of pendant alkene moieties, which can be used for further post modification strategies to fabricate smart and reactive membranes that respond to external stimuli, such as pH, temperature or electric potential, in order to mitigate fouling. An additional advantage of this material is an increased electroactive phase relative to PVDF, which makes it a promising candidate for low-fouling piezoelectric membrane applications.

Here, for the first time, we present the fabrication of porous dPVDF films by direct ink writing (DIW) and subsequent phase inversion. The dPVDF solutions in *N,N*-dimethylacetamide (DMAc) exhibited Bingham behavior at polymer concentrations between 7 wt% and 15 wt%, and thus could be DIW to produce continuous films. The dPVDF inks (dPVDF (15 wt% in DMAc), and 5, 15, 30 wt% PVP), were subsequently DIW into continuous films, and phase inverted in deionized water (non-solvent) to produce porous films. The porosity of the dPVDF films was confirmed using helium beam ion microscopy. The presence of alkene moieties in the dPVDF and dPVDF porous films was confirmed through attenuated total reflection – Fourier transform infrared (ATR-FTIR) spectroscopy and Raman spectroscopy. An increase in electroactive phase fraction was observed in the DIW films, confirming the enhancement in piezoelectric characteristics. The DIW porous dPVDF membranes presented herein show exceptional promise for the production of piezoelectric membranes and the subsequent utilization as separation membranes in harsh environments.

#### F.SF05.07.20

**Late News: Investigating and Comparing the Resistance to Tensile Testing of Molded and 3D Printed PLA/PP Polymer Blends** [Daniel Luo](#)<sup>1,2</sup>, Yu-Chung Lin<sup>2</sup> and Miriam H. Rafailovich<sup>2</sup>; <sup>1</sup>Monroe Woodbury High School, United States; <sup>2</sup>Stony Brook University, The State University of New York, United States

When 3D printing, the quick cooling rate of PLA does not allow enough time for the filament to properly diffuse across an interface<sup>1</sup>, which inhibits adhesion and reduces the overall strength of prints. We aimed to tackle this problem by adding low concentrations of polypropylene (PP) to PLA to create a 3D-printing filament with improved interlayer diffusion.<sup>2</sup> Our hypothesis is when a PLA/PP blend is formed through 3D printing, PP migrates to the surface of the filaments due to its lower surface energy and lower glass transition temperature, forming a core-shell structure that produces pseudo-"self-healing"<sup>2</sup> by fusing fibers. Due to PP's lower surface tension compared to PLA (30.7 mN/m vs 44 mN/m)<sup>5</sup>, PP will travel to the surface of the fibers when extruded, displacing air pockets formed when the fibers crack.<sup>3,4</sup> Previous testing shows that 1% PP blends are the most resistant to tensile testing, and this study seeks to determine if the PP/PLA blend produced by molding or 3D printing is more effective, and which concentration of PP is most resistant to tensile testing.

To find how the core-shell structure impacted the physical properties of the blends, the ratio of the Volume of the Shell vs. Volume of the Fiber and Shell thickness were both plotted against the Volume fraction of PP. Radius of gyration ( $R_g$ ) of PLA and PP were also calculated. By using the thickness of the shell and the diameter of the fiber, the number of  $R_g$ s of PLA and PP in each core-shell sample was found.

5 groups differing in PP % by weight were used to compare which concentration of PP in a PLA/PP blend best resisted tensile testing: 0%, 0.5%, 1%, 2.5%, and 5%. After preparation, the Young's Modulus, UTS (Ultimate Tensile Strength), and Elongation at Break were analyzed. The Young's Modulus of the molded samples showed that the Pure PLA had the highest Young's Modulus, meaning that the molded samples did not exhibit "self-healing". The results for the 0.5% PP, 1% PP, 2.5 % PP, 5% PP, and Pure PLA 3D printed samples indicate that 0.5% PP has a higher Young's Modulus compared to 1% and Pure PLA, making it more reliable for 3D printing. The contact angle measurements indicate that even a small % of PP in a blend produces a contact angle similar to pure PP, meaning that adding PP lowers the surface tension of the blend, therefore in the 3D printed blends PP travels to the fibers' surface and produces "self-healing".

In conclusion, this study shows that the optimal concentrations for making a PLA/PP blend for 3D printing is 99.5% PLA/0.5% PP. It also shows that compared to the 3D printed blends, the molded blends do not strengthen the blends to the same extent during tensile testing.

<sup>1</sup> Liu, Zengguang, et al. "A Critical Review of Fused Deposition Modeling 3D Printing Technology in Manufacturing Polymeric Parts." *International Journal of Advanced Manufacturing Technology*, vol. 102, no. 9-12, Springer Science and Business Media LLC, 2019, pp. 2877–89, doi:10.1007/s00170-019-03332-x.

<sup>2</sup> Peng, Fang, et al. "3D Printing with Core-Shell Filaments Containing High or Low Density Polyethylene Shells." *ACS Applied Polymer Materials*, vol. 1, no. 2, American Chemical Society, Feb. 2019, pp. 275–85, doi:10.1021/acsapm.8b00186.

<sup>3</sup> Mehrabi Mazidi, Majid, et al. "Highly-Toughened Polylactide- (PLA) Based Ternary Blends with Significantly Enhanced Glass Transition and Melt Strength: Tailoring the Interfacial Interactions, Phase Morphology, and Performance." *Macromolecules*, vol. 51, no. 11, American Chemical Society, June 2018, pp. 4298–314, doi:10.1021/acs.macromol.8b00557.

<sup>4</sup> "Polymer Properties Database." *Surface Tension*, polymerdatabase.com/polymer%20physics/sigma.html.

<sup>5</sup> Guo, Yichen, et al. "Enhancing Impact Resistance of Polymer Blends via Self-Assembled Nanoscale Interfacial Structures." *Macromolecules*, vol. 51, no. 11, American Chemical Society, June 2018, pp. 3897–910, doi:10.1021/acs.macromol.8b00297.

We gratefully acknowledge support from the Louis Morin Charitable Trust.

#### F.SF05.07.21

**Late News: A Design of 3D-Printable, Biodegradable, Flame Resistant Polymer/Clay Nanocomposite** Yiwei Fang<sup>1</sup>, Christian Apostol<sup>2</sup>, Jiale Lu<sup>3</sup>, Lawrence Zhao<sup>4</sup>, Yuan Xue<sup>1</sup>, Yichen Guo<sup>1</sup> and Miriam H. Rafailovich<sup>1</sup>; <sup>1</sup>Stony Brook University, United States; <sup>2</sup>Ward Melville High School, United States; <sup>3</sup>Princeton International School of Mathematics and Science, United States; <sup>4</sup>University Laboratory High School, United States

Here we designed a non-toxic and environmental sustainable polymer nanocomposite PLA/PBAT/APP/RDP-Clay which achieved good flame resistance and balanced mechanical properties with the addition of 3wt% ammonium phosphate (APP) and 2wt% resorcinol diphenyl phosphate (RDP)-coated montmorillonite clays (C-Na<sup>+</sup>). Polylactic acid (PLA) received attention due to its biodegradability and mechanical properties. However, its poor impact strength and flammability largely limits its application in wide range of areas. In our previous study<sup>1</sup>, APP was found to be rigid and made the impact strength of PLA even worse. We were able to increase the ductility without affecting flammability of the PLA/APP composite by decreasing the APP concentration to only 2 wt% with the addition of only 0.12wt%RDP. Hence, poly(butylene adipate-co-butylene terephthalate)(PBAT), a ductile and biodegradable polymer, is introduced to balanced impact strength. But PBAT was found to be a poor efficient carbon source in APP intumescent system. For PLA/PBAT(75/25) over 10wt% APP/RDP is required to make PLA/PBAT(75/25) resisted to combustion, while pure PLA only need 2wt%APP/RDP. The huge increase for the use of APP not only increase the cost but also sacrificing the desired impact strength. According to Contact Angle Measurement and work of adhesion ( $W_a$ ) between related materials, APP is more affinity to PBAT than PLA which possibly draw part of APP into PBAT phase and decrease the overall flame retardancy. In order to minimize this effect, 2wt%RDP coated sodium clay(C-Na<sup>+</sup>) is added to reduce the interfacial energy between PLA and PBAT which decrease PBAT domain size. Compatibilization was further confirmed by observation of a 32% decrease (from 2.53 $\mu$ m to 1.73 $\mu$ m) in PBAT domain size via Scanning Electron Microscopy. With 2wt%RDP-clay into the composites, we achieved a V-0 designation with a low loading of APP(3wt%). This was attributed to the decreased PBAT domain size, increasing the efficiency of APP to decrease the heat release in the combustion at a reduced overall concentration. From Thermogravimetric Analysis (TGA) result, the reaction mechanism was confirmed by the presence of intumescent char. Which is a byproduct of the reaction in the solid state. The increased ductility below  $T_g$  and viscosity in the melt enables fiber drawing and comparison of the combustibility upon FDM printing, which will be discussed.

We gratefully acknowledge support from the Louis Morin Charitable Trust.

1. Y. Xue, X. Zuo, L. Wang, Y. Zhou, Y. Pan, J. Li, Y. Yin, D. Li, R. Yang, M.H. Rafailovich and Y. Guo: Enhanced flame retardancy of poly(lactic acid) with ultra-low loading of ammonium polyphosphate. *Composites Part B: Engineering* **196**, 108124 (2020).

#### F.SF07.06.01

**Construction of an EAM Type Inter-Atomic Potential Model for Describing Metallic Polytype Structures** Shinya Ogane<sup>1</sup>, Taku Miyakawa<sup>2,1</sup> and Koji Moriguchi<sup>1,2</sup>; <sup>1</sup>Graduate School of Environmental Studies, Tohoku University, Japan; <sup>2</sup>R&D Laboratories, Nippon Steel Corporation, Japan

Polytypism is a special case of polymorphism when the two polymorphs differ only in the stacking of identical two-dimensional sheets or layers. The polytypes are characterized by a stacking sequence with a given repeating unit along a directional axis (c-axis) and are theoretically possible to have endless permutations of the sequences. Among these polytypes, the crystalline systems composed of close-packed (CP) layers have especially attracted attention on their fundamental and technological properties for many years. While these polytypes are often experimentally observed in wide-bandgap semiconductors, SiC systems are particularly known to show several hundred polytypes [1]. Since some SiC polytypes located around the ground state are energetically degenerated with about  $\Delta T = 2\text{K}$  [1], it is difficult to control the phase stability during the growth of single crystals with the desired stacking polymorphism. For this reason, a variety of physical perspectives are being investigated in order to establish better single crystal growing techniques [2, 3]. In addition, the long period stacking ordered (LPSO) Mg alloys with light weight, high specific strength, and high heat resistance are also recently drawing attention as a metallic system with similar polytypism to that in SiC [4, 5].

We have proposed a computational method coupled with three theoretical tools (PGA: polytype generation algorithm; FPC-DFT: first-principles calculations based on the density functional theory; and ANNNI: axial next-nearest-neighbor Ising model), which can make us possible to efficiently investigate the structural energetics for diverse nonequivalent polytypes [1]. In our recent study [5], we have systematically evaluated the static energetics of metallic polytypes for a wide variety of elements based on the same computational method proposed by the authors [1]. For all these elemental systems, the atomistic geometry, energetics, and electronic structure for all polytypes with up to the periodic stacking length of  $L=13$  (165 kinds of polytypes in total) have been carefully calculated based on the DFT within the GGA [5]. Using the ANNNI model extracted from the GGA calculations, we have shown from the perspective of static structural energetics that the interlayer interaction among CP layers is one of the important factors for the polytype formation [5].

Not only the static energetics but also the dynamical aspect generally affects the polytype selection during the crystal growth processes [2, 3]. It is, therefore, important to elucidate the polytype formation mechanism from the viewpoint of dynamics associated. Since the molecular dynamics (MD) simulations have become a powerful computational tool to understand and predict the structural, thermodynamic and dynamic properties of materials, the direct MD observation of dynamical aspects for the polytype growth is expected to greatly advance our understanding on the polytype selection. While the state-of-the-art potentials are often fitted to many databases including a large set of atomic configurations calculated by FPC-DFT [6], we have found that the potential models proposed so far cannot describe the accurate polytypes energetics. In the present study, we are, therefore, developing an Embedded Atom Method (EAM) type potential [6] which can be used for the dynamical simulations of metallic polytype structures focusing on the lanthanum (La) system. The basic properties and transferability of the EAM type potential model constructed in the present work will be discussed.

[1] K. Moriguchi, et al., *J. Mater. Res.* **28**, 7 (2013).

[2] K. Kusunoki, Doctoral thesis: Nagoya University, 10725 (2014).

[3] K. Moriguchi et al., NIPPON STEEL & SUMITOMO METAL TECHNICAL REPORT 117, 56 (2017).

[4] E. Abe et al., *Phil. Mag. Lett.* **91**, 690 (2011).

[5] T. Miyakawa and K. Moriguchi, 236th ECS Meeting Abstracts, Vol. MA2019-02, 2417 (2019).

[6] K. Moriguchi and M. Igarashi, *Phys Rev B* **74**, 024111 (2006) and references therein.

#### F.SF07.06.02

**Phase Equilibria and Crystal Structures of Highly Ordered Intermetallic Compounds of  $\text{Fe}_2\text{Al}_5$  Phases with the Framework Structure of  $\eta$ - $\text{Fe}_2\text{Al}_5$  Phase** Tetsuya Hamada, Ryutaro Sakai, Kodai Niitsu and Haruyuki Inui; Kyoto University, Japan

Hot dipped Zn-Al alloy coated steel is widely used in the field of automobile. It is well known that the coated layer is mainly composed of the  $\text{Fe}_2\text{Al}_5$  intermetallic compound. This compound has been considered to be the orthorhombic  $\eta$  phase (space



group  $Cmcm$ ). On the other hand, our group has recently found that the layer phase often crystallizes into highly ordered atomic arrangement most likely termed as the  $\eta'''$  phase even during short-term dipping. Besides, recent researches address there exists several ordered phases similar to the  $\eta'''$  phase with the framework structure of  $\eta$  phase<sup>[1]</sup>. According to Burkhardt's study<sup>[2]</sup>, the  $\eta$  phase is composed of a full occupied framework structure (4 Fe and 8 Al atoms) and partially occupied chains along the  $c$ -axis (6 Al sites). The  $c$ -axis chain is considered to allow chemical tenability and various kinds of atomic orderings; the formation of various kinds of ordered phases is considered to be responsible for how Fe and Al atoms order in the  $c$ -axis chain sites. However, the crystal structures of some of these ordered phases are still controversial and phase equilibrium among them are not consolidated.

In this study, we have examined the phase equilibrium among these phases and refined their crystal structures. Experiments are carried out with scanning electron microscope, energy dispersive spectroscopy, X-ray diffraction, transmission electron microscope, scanning transmission electron microscope and synchrotron X-ray diffraction. There are some invariant reactions: the  $\eta$  phase is found to dissolve into the  $\eta'''$  and  $\eta^m$  phases at around 350 °C while the  $\eta$  phase has been thought to be stable at low temperature. Some of the other phases are found to have highly ordered long-period structures with periodic antiphase boundaries.

Reference: [1] H. Becker et al., *Intermetallics*, **93**, (2018) 251-262.

[2] U. Burkhardt et al., *Acta Cryst*, **B50**, (1994) 313-316.

### F.SF07.06.03

**ANNNI Model Descriptions on Structural Energetics for a Wide Variety of Metallic Polytypes Composed of Close-Packed Layers** Koji Moriguchi<sup>1,2</sup>, Taku Miyakawa<sup>2,1</sup>, Shinya Ogane<sup>1</sup>, Kazumasa Tsutsui<sup>2</sup> and Yuta Tanaka<sup>2</sup>; <sup>1</sup>Tohoku University, Japan; <sup>2</sup>Nippon Steel Corporation, Japan

The local inhomogeneity such as defect, surface, interface, and nanostructure often assumes an important role for developing sophisticated materials since the functionalities of materials usually originate from the spatial inhomogeneity in the associated systems. In this work, among the many phenomena related to inhomogeneity in materials, we will report our computational research on the phenomenon called "Polytypism". Polytypism is a special case of polymorphism where two polymorphs differ only in the stacking sequences of the same two-dimensional sheets or layers.

Many crystalline compounds can be considered to be composed of one or more structural units. When these units can be stacked in different ways to form stable or metastable phases, the resulting phases are known as polytypes. Among the polytypes for these compounds, the silicon carbide (SiC) systems have been the most attractive and motivated tremendous amounts of theoretical and experimental investigations on their fundamental and technological properties for many years. Many SiC polytypes located around the ground state have been found to be energetically degenerated with energy of about  $\Delta T = 2K$  [1]. It is, therefore, very difficult to control the phase stability during the growth of a single crystal in order to obtain the desired stacking polytype in SiC systems. For this reason, a variety of physical perspectives are being investigated in order to establish better single crystal growing techniques [2]. In addition, the long period stacking ordered (LPSO) Mg alloys with light weight, high specific strength, and high heat resistance are also recently drawing attention as a metallic system with similar polytypism to that in SiC [3]. For both systems, the physical mechanism behind polytype selection is not yet fully understood and remains challenging issues to be solved.

In this situation, we have proposed a computational method coupled with three theoretical tools (PGA: polytype generation algorithm; FPC-DFT: first-principles calculations based on the density functional theory; and ANNNI: axial next-nearest-neighbor Ising model), which can make us possible to efficiently investigate the structural energetics for diverse nonequivalent close-packed (CP) polytypes [1, 4]. In the present work, the static energetics of a wide variety polytypes for 17 kinds of metallic elements (M=Be, Mg, Sc, Y, Co, Zn, Cu, Ag, Au, Ni, Pd, Pt, Al, Ca, Sr, Ba, and La) is systematically evaluated based on the same computational method proposed by the authors [1, 4]. For all these elemental systems, the atomistic geometry, energetics, and electronic structure for all polytypes with up to the periodic stacking length of  $L=13$  (165 kinds of polytypes in total) have been carefully calculated based on the DFT within the GGA. The equilibrium theories based on the ANNNI model that is well known in the field of statistical mechanics have played an efficient role in the study of the origins of polytypism [5, 6]. In this work, the ANNNI model including interactions up to the third-nearest neighbor layer with the four-spin term [6] is adopted for the systems considered. Using the ANNNI model extracted from the GGA calculations, we will describe the inter-layer interactions, the phase diagrams of ANNNI model with interactions up to third-nearest neighbor, and the stability of stacking faults for each element. The relation to polytypism in the metallic systems considered will be also discussed.

[1] K. Moriguchi, et al., *J. Mater. Res.* **28**, 7 (2013).

- [2] K. Moriguchi et al., NIPPON STEEL & SUMITOMO METAL TECHNICAL REPORT 117, 56 (2017).  
 [3] E. Abe et al., Phil. Mag. Lett, 91, 690 (2011).  
 [4] T. Miyakawa and K. Moriguchi, 236th ECS Meeting Abstracts, Vol. MA2019-02, 2417 (2019).  
 [5] E. Rodriguez-Horta, E. Estevez-Rams, R. Lora-Serrano and R. Neder, Acta Cryst. A73, 377 (2017) and references therein.  
 [6] J. J. A. Shaw and V. Heine, J. Phys.: Condens. Matter 2, 4351 (1990).

#### F.SF07.06.04

**Microstructure Characterization of As-Cast and Directionally Solidified Near-Eutectic Mo–Si–B Alloys** LinYE Zhu<sup>1</sup>, Shuntaro Ida<sup>1</sup>, Georg Hasemann<sup>2</sup>, Manja Krueger<sup>2</sup> and Kyosuke Yoshimi<sup>1</sup>; <sup>1</sup>Tohoku University, Japan; <sup>2</sup>Otto-von-Guericke University Magdeburg, Germany

Mo–Si–B-based alloys have been developed as ultrahigh temperature material candidates for high-pressure turbine blades. Recently, Hasemann et al. reported that a Mo–Si–B alloy with Mo<sub>ss</sub> + T<sub>2</sub> + Mo<sub>3</sub>Si eutectic prepared by directional solidification (DS) has substantially improved creep resistance compared with a powder metallurgy (PM) processed alloy. It was found that a homogenous microstructure with preferentially orientated grains through DS can ameliorate mechanical performance, however, the effect of DS on the microstructure evolution of Mo–Si–B alloy is still not clear. In this study, phase constitution and microstructure of as-cast and directionally solidified near-eutectic Mo–Si–B alloys are investigated to clarify the microstructure evolution caused by DS.

Alloys with the nominal composition of Mo–17Si–7B (at.%) corresponding to the Mo<sub>ss</sub> + T<sub>2</sub> + Mo<sub>3</sub>Si eutectic point were prepared by arc-melting (as-cast alloy) and crucible-free zone melting (directionally solidified alloy) in an Ar atmosphere. The microstructure of the as-cast alloy consisted of primary Mo<sub>ss</sub> dendrites and two eutectics of Mo<sub>3</sub>Si + T<sub>2</sub> and Mo<sub>ss</sub> + Mo<sub>3</sub>Si + T<sub>2</sub> in cellular or dendritic growth, while the directionally solidified alloy was almost composed of a uniform and well-aligned Mo<sub>ss</sub> + Mo<sub>3</sub>Si + T<sub>2</sub> eutectic phase in cellular growth. The electron backscatter diffraction (EBSD) results showed that in the as-cast alloy only <100> orientation of the T<sub>2</sub> phase preferentially grew along the solidification direction while the other Mo<sub>ss</sub> and Mo<sub>3</sub>Si phases had no apparent orientation. However, the <001> growth direction of Mo<sub>3</sub>Si phase parallel to the solidification direction became much stronger by the directional solidification. The coupled growth of <001>Mo<sub>ss</sub>//<100>T<sub>2</sub>//<001>Mo<sub>3</sub>Si in the directionally solidified alloy presumably had an effect on the mechanical properties because of the texture. No habit relationship between the phases was found in both alloys possibly because the lattice parameters of constituent phases are greatly different and the system cannot minimize interfacial energy by atomic arrangement.

#### F.SF07.06.05

**Energy Barrier of the Initial Stage Microstructure Formation in Martensitic Transformation of TiNi Shape Memory Alloy** Kazuya Nagahira, Takeshi Teramoto and Katsushi Tanaka; Kobe University, Japan

The self-accommodation microstructure, which is the martensitic microstructure of the shape memory alloy, is constructed by a plate-like martensite variant. Recently, formation process of the self-accommodation microstructure during the martensitic transformation have been reported in the several shape memory alloy systems. In TiNi shape memory alloy, specific variant pairs including {11-1} type-I twinning interface are frequently observed in the initial stage of martensitic transformation. In this study, we refer the variant pair that formed in the initial stage of martensitic transformation as initial stage microstructure (ISM). This result suggests that there is a selection rule for the self-accommodation microstructure in the initial stage of martensitic transformation. The selection rule of ISM is important for understanding self-accommodation microstructure because it represents a mechanism of variant selection in the absence of the influence of other variants. In the present study, we have performed evaluations of energy barrier of the formation of ISM in order to elucidate the factors that determine the selection rule of ISM in TiNi shape memory alloy.

The energy barrier of the formation of ISM is the sum of the interfacial energy of the twin interface included in ISM and the elastic strain energy for the ISM formation. In the TiNi shape memory alloy, 8 types of twin orientation relations and corresponding variant pairs exist. It is considered that the variant pair with the smallest energy barrier is selectively formed as ISM. The interfacial energy of twin interface was evaluated by the first-principles calculation using VASP (Vienna Ab initio Simulation Package) code. The elastic interaction energy to form a variant pair was evaluated by a micro-mechanics proposed by Eshelby.

Since interfacial energy of {11-1} type-I twin and elastic interaction energy of the variant pair including {11-1} type-I twin are relatively small among the twin interfaces considered, it is supposed that the energy barrier of the variant pair including {11-1} type-I twin is smaller than others. These results indicate suggests that the variant pair with a small energy barrier is selectively formed as the initial stage of martensitic transformation.

#### F.SF07.06.06

**Transient Liquid Phase Bonding of Bi-Ni Intermetallics for High-Temperature Electronics** Hamid Fallahdoost and Junghyun Cho; State University of New York at Binghamton, United States

Transient liquid phase bonding (TLPB) has been used as a bonding process that joins dissimilar materials by employing an interlayer that provides a lower melting process. It shows the potential to be used in high temperature electronics (operated or exposed over 200°C), where there are no clear lead (Pb)-free solder options available. During the reflow process for electronics components, the interlayer melts and the constituents of the interlayer and its joining materials diffuse each other, subsequently making a homogenous intermetallic bond via isothermal solidification. Once formed, it results in a higher melting point than the bonding temperature. This research investigates such a TLPB system made of a nickel (Ni) bonding surface and a bismuth (Bi) interlayer, which can serve as a Pb-free solder alternative for high-temperature electronics. Upon melting of Bi on Ni, intermetallic phases ( $\text{Bi}_3\text{Ni}$ ,  $\text{BiNi}$ ) nucleate and grow by consuming a Ni layer on the substrate or the die side. Intermetallic reactions and microstructure developments were studied under various reflow conditions including temperature and time on three sets of the sandwiched assemblies: 1) Si die Sputtered Ni (1  $\mu\text{m}$ -thick)/Bi/Si die; 2) Si die/Bi/Ni foil (0.5 mm-thick); 3) Ni foil/Bi/Ni foil. As such bonds constitute the structural joints in electronic packaging, mechanical properties of the intermetallic bonds and their long-term microstructural developments under high temperature aging and thermal cycling (-55°C to 200°C) were investigated by shear testing and cross-sectional microstructure analyses of the sandwiched samples. It was shown that temporal evolution of two intermetallic phases composed of faster  $\text{Bi}_3\text{Ni}$  and slower  $\text{BiNi}$ , along with the remaining Bi, are responsible for mechanical performances of TLPB. This presentation will also discuss about optimal microstructure development for the TLPB, which is critical to offset the defects and brittleness of the intermetallic phases.

#### F.SF07.06.07

**Microstructure and Crystallographic Orientation Relationships in Directionally Solidified  $\text{NbSi}_2/\text{Nb}_5\text{Si}_3$  Eutectic Composites with Mo Addition** Haruka Uemura, Kosei Takeda, Kyosuke Kishida and Haruyuki Inui; Kyoto University, Japan

Eutectic composites composed of intermetallics and/or ceramics with very high eutectic temperatures have been considered as attractive materials for ultra-high temperature structural applications because of their high melting temperature, high structural stability and good mechanical properties. Recently, we have systematically investigated microstructure-property relationship of  $\text{MoSi}_2/\text{Mo}_5\text{Si}_3$  eutectic composites with very high eutectic temperature of 1900 °C and have revealed that their high-temperature strength and room-temperature fracture toughness can be improved simultaneously by optimization of microstructure and interface properties through controlling growth condition and ternary/quaternary alloying. These previous results open a new possibility to develop novel structural materials endowed with excellent high-temperature strength and good room-temperature fracture toughness by utilizing interphase boundaries. In the present study, we focused on  $\text{NbSi}_2/\text{Nb}_5\text{Si}_3$  eutectic composites (eutectic temperature  $\sim 1900$  °C for binary) as a new target system and investigated microstructure variation of directionally solidified (DS) ingots of the eutectic composites as a function of ternary Mo addition. When Mo is alloyed more than 2 at. %, DS ingots are conformed to composed of  $\text{C40-(Nb,Mo)Si}_2$  and  $\text{D8}_m\text{-(Nb,Mo)}_5\text{Si}_3$ , which indicates that the  $\text{D8}_m$  (high temperature) to  $\text{D8}_l$  (low temperature) phase transformation that occurs in binary  $\text{Nb}_5\text{Si}_3$ , is suppressed by the Mo addition. A fine eutectic microstructure of the so-called script-lamellar type, which is similar to those observed in  $\text{MoSi}_2/\text{Mo}_5\text{Si}_3$  DS eutectic composites, is confirmed to develop for the Mo-alloyed  $\text{NbSi}_2/\text{Nb}_5\text{Si}_3$  DS eutectic composites. Crystallographic orientation relationships between C40 and  $\text{D8}_m$  phases as well as their preferential growth directions are identified by electron backscattered diffraction (EBSD) in scanning electron microscopy and transmission electron microscopy (TEM).

#### F.SF07.06.08

**Evaluation of Mechanical Properties for Constituent Phases by Nano-indentation Method in  $\gamma$ -TiAl Alloys** Sota Taniguchi, Yotaro Okada, Ryosuke Yamagata, Hirotoyo Nakashima and Masao Takeyama; Tokyo Institute of Technology, Japan

Nano-indentation method is a powerful tool to evaluate the mechanical properties of each phase in materials consisting of multi-phase microstructures. If the mechanical properties of each phase can be evaluated correctly, then we can predict the mechanical properties of bulk materials having different amounts of the phases, which would allow us to construct the design principle for materials integration (MI) to solve inverse problems. However, there are a number of factors affecting the properties by this method, since the machine is so sensitive to the specimen itself such as surface conditions, as well as the machine itself such as specimen set-ups and tip of the indenters. In this study, titanium aluminide alloys were selected to evaluate the mechanical properties of the constituent phases since the alloys consist of three phases of b-Ti (bcc),  $\alpha_2\text{-Ti}_3\text{Al}$

(D0<sub>19</sub> with hcp based) and g-TiAl (L1<sub>0</sub> with fcc based). In addition, we recently revealed that the introduction of an appropriate amount of the b phase is effective in improving the fracture toughness as well as tensile properties. Thus, it is very important to build up the mechanical property database for each phase in equilibrium each other in order to construct the construction of MI platform for inverse problems. The alloy studies are Ti-Al-Cr ternary alloys. These alloys were homogenized first in the b single phase region, and then heat treated in the three-phase region at 1173 K to reach the equilibrium state, based on our phase diagram study. The specimens were mechanically polished, followed by electro-polishing. Before and after the indentation test, the microstructure and orientation analysis of each phase were performed by FE-SEM and EBSD. Nano-indentation tests were performed to evaluate the Young's modulus and hardness using a continuous stiffness measurement (CSM) method with a frequency of 110 Hz using a Berkovich type indenter made of diamond. The advantage of the CSM method allows us to evaluate the properties continuously as a function of indentation depth. The results were compared with those obtained from the Oliver-Pharr method. Both properties are found to be sensitive to the indentation depth and sampling distance, depending on the phases as well as orientation. The details of the appropriate conditions will be discussed, in conjunction with the O-P method. This work was supported by Council for Science, Technology and Innovation (CSTI), Cross-ministerial Strategic Innovation Promotion Program (SIP), "Material Integration" for revolutionary design system of structural materials.

#### **F.SF07.06.09**

**Effect of Si in Solution on the Crystal Structure of  $\sigma$  Phase ( $tP30$ ) in Fe-Cr Binary Alloys** Eitaro Maeda and Masao Takeyama; Tokyo Institute of Technology, Japan

FeCr- $\sigma$  with a crystal structure of  $tP30$  (ordered tetragonal phase) is one of the TCP phases and often observed in heat resistant materials. This phase is considered as a harmful phase to deteriorate mechanical properties of the materials. However this phase could be a strengthening phase, just like Laves phase, if the phase stability can be increased by alloying. In the previous study, we have found that the lattice parameters of both  $a$  and  $c$  become either larger or smaller by the addition of M in solution, depending on the size of atomic radius of M relative to those of Fe ( $r_{Fe}=1.274 \text{ \AA}$ ) and Cr ( $r_{Cr}=1.282 \text{ \AA}$ ) as usual, except Fe addition. In case of the excess addition of Fe in solution, the  $a$  axis becomes smaller whereas the  $c$  axis becomes larger. We attributed the unusual anisotropic lattice parameter change to the site occupancy change in five sub-lattice sites (M1, M2, M3, M4, M5) of the  $\sigma$  phase, based on the Rietveld analysis; the occupancy of Cr atom in M5 sub-lattice site increase with increasing excess Fe atoms. In this study, we picked up non-transition element Si as the third element since it has larger atomic radius ( $r_{Si}=1.322 \text{ \AA}$ ) and is known as strong  $\sigma$  stabilizer, and investigated the lattice parameter change with Si in solution.

The alloys studies are Fe-(50-x/2)Cr-xSi (at. %) where x=5, 10. They were prepared by arc melting to 30g button ingot, and homogenized in the  $\sigma$  single-phase region. Phase identification was conducted by powder XRD techniques and the lattice parameters were calculated from obtained XRD profiles. The obtained XRD profiles were further analyzed by means of Rietveld method to determine the structural change of  $\sigma$  phase as well as site occupation of the elements. Microstructures were examined by SEM and hardness was measured by micro Vickers hardness machine. We confirmed that both alloys with 5 and 10 at.% Si exhibit  $\sigma$  single phase with almost the same hardness of 12 GPa. It is interesting to note that, just like Fe addition, the anisotropic behavior of the lattice parameters was obtained; the  $a$  axis decreases whereas the  $c$  axis increases with increasing in Si content. However, Rietveld analysis suggested that this anisotropic behavior is different from that in Fe case related to the site occupancy change of M5 sub-lattice site. The detailed mechanism of this anisotropic behavior and the crystal structure change will be discussed in conjunction with the  $c/a$  ratio and unit cell volume of the  $\sigma$  phase.

#### **F.SF07.06.10**

**Towards High-Throughput First-Principles High-Temperature Thermodynamic Modeling** Siya Zhu and Axel van de Walle; Brown University, United States

We demonstrate how widely used high-throughput first-principles calculation frameworks for novel phase discovery can be augmented to enable phase stability predictions above absolute zero and yield informative phase diagrams at a fraction of the computational cost of traditional methods. The approach is based on a combination of (i) the special quasirandom structures formalism, extended to account for possible short-range order, (ii) carefully selected lattice dynamics calculations (iii) efficient molecular dynamics modeling of liquid phases that leverage high-quality experimental thermodynamic for elemental liquids and (iv) the CALPHAD approach for free energy modeling. As an example, we investigate the Ni-Re system, where earlier calculations predicted the presence of novel D0<sub>19</sub> and D1<sub>a</sub> phases. We find that, in spite of their stability at 0K, these intermetallic compounds become unstable at high temperature. These findings also prove helpful in guiding the search for alloys that provide cost effective substitutes for rhenium as a structural material.

#### **F.SF07.06.11**

**Development of a Thermodynamic Database for CALPHAD Simulations of CoNiCrAlY Metallic Coatings** Marlena Ostrowska<sup>1</sup>, Yao Wang<sup>1,2</sup> and Gabriele Cacciamani<sup>1</sup>; <sup>1</sup>University of Genoa, Italy; <sup>2</sup>Centre of Excellence for Advanced Materials, China

High temperature materials, such as superalloys, are often covered with metallic coatings in order to protect the substrate from oxidation and to extend its working life. The phases present in the coatings, partly determined by the alloy composition, play an important role in the material properties. Among them, several are beneficial for the properties while some phases are detrimental during service. Co and Ni are the major elements in the metallic coatings. The appropriate amounts of Al, Cr and Y are added to improve their overall performance and to meet the demanding industrial requirements. In general Al-Co-Cr-Ni alloys are adopted as the main coatings for superalloys and small amounts of Y are added to improve oxide scale adherence. However, it is very difficult to predict how phase stabilities are affected by the addition of each element in multi-component alloys, without performing computational simulations.

A reliable thermodynamic database containing Al, Co, Cr, Ni and Y has been developed to support the design of CoNiCrAlY coatings, following the CALPHAD approach. All binary and ternary subsystems are included in the database. Most of the ternary subsystems, due to the lack of consistent thermodynamic description in the literature, were assessed by our group, namely Al-Co-Ni [1], Al-Cr-Ni [2], Co-Cr-Ni [3] and several ternary systems containing yttrium, such as Al-Co-Y, Al-Cr-Y, Al-Ni-Y and Co-Ni-Y (paper in preparation).

The new database was used to simulate a few commercial alloys used as metallic coatings protecting gas turbine blades. The calculated phase compositions were then confronted with the available experimental data from the literature for the following coatings: PWA270 (Ni-21%Co-18%Cr-12.7%Al-0.17%Y), PWA286 (Ni-21.1%Co-17.1%Cr-12.7%Al-0.61%Y) at 1000°C [4] and the Co-based coating Co-28.6Ni-21.2Cr-15.6Al-0.4Y at 1150°C [5] (in at%). The good agreement between calculated and experimental data was evident, therefore, the present database can be reliably used to predict phase equilibria in alloy coatings already in use or to support the design of new alloys with improved performance. In particular, to find the temperature range in which undesired phases (e.g.  $\sigma$ ) are stable and investigate the influence of each element on the phase stability.

- [1] Y. Wang, G. Cacciamani, Experimental investigation and thermodynamic assessment of the Al-Co-Ni system, *Calphad Comput. Coupling Phase Diagrams Thermochem.* 61 (2018) 198–210. doi:10.1016/j.calphad.2018.03.008.
- [2] Y. Wang, G. Cacciamani, Thermodynamic modeling of the Al-Cr-Ni system over the entire composition and temperature range, *J. Alloys Compd.* 688 (2016) 422–435. doi:10.1016/j.jallcom.2016.07.130.
- [3] G. Cacciamani, G. Roncallo, Y. Wang, E. Vacchieri, A. Costa, Thermodynamic modelling of a six component (C-Co-Cr-Ni-Ta-W) system for the simulation of Cobalt based alloys, *J. Alloys Compd.* 730 (2018) 291–310. doi:10.1016/j.jallcom.2017.09.327.
- [4] M. Hasegawa, M. Iwashita, Y. Kubota, P. Dymáček, F. Dobeš, Microstructure evolution under high temperature deformation of CoNiCrAlY bond coat alloy, *Mater. Sci. Eng. A.* 756 (2019) 237–247. doi:10.1016/j.msea.2019.04.030.
- [5] O. Zubacheva, Plasma-Sprayed and Physically Vapor Deposited Thermal Barrier Coatings: Comparative Analysis of Thermoelastic Behavior Based on Curvature Studies, RWTH Aachen University, 2004. <http://sylvester.bth.rwth-aachen.de/dissertationen/2004/203/>.

**F.SF07.06.12**

**Influences of Loading Axis Orientation and Specimen Shape on Kink-Band Formation in Single Crystals of Mg-Zn-Y LPSO Phase Investigated by Micropillar Compression Tests** Kohei Okage, Kyosuke Kishida and Haruyuki Inui; Kyoto University, Japan

Mg-TM(transition metal)-RE(rare earth) ternary alloys containing a precipitation phase with a long-period stacking-ordered (LPSO) structure have received considerable attentions as a new light-weight structural material endowed with high strength and good ductility simultaneously. Such attractive mechanical properties are believed to be caused by heavily kinked structure of platelet precipitates of Mg-LPSO phase developed during hot extrusion process. Formation of the kinked structure in HCP metals with a relatively high  $c/a$  ratio has been interpreted generally with the dislocation-based kink band formation mechanisms such as the Hess and Barrett model, Frank-Stroh model, and Gilman model, which considered different trigger mechanisms for the activation of basal slip when the loading axis is (nearly) parallel to the basal planes, i.e., elastic buckling, stress concentration caused by pre-existing or pre-introduced defects, and a slight tilt of basal plane, respectively. However, the actual controlling factors for the kink-band formation in Mg-LPSO phases have not been fully clarified yet. In the present study, we investigated compression deformation behavior of Mg-LPSO single crystals as a function of loading axis orientation, specimen shape and stacking sequence of the LPSO structure (18R and 14H-type) by utilizing micropillar compression methodology in order to clarify the dominant controlling factors for the kink-band formation in Mg-LPSO phases.

### F.SF07.06.13

**The Effect of Forming Internal Electric Field in Seebeck Effect** Momoka Sakamoto<sup>1</sup>, Rikuto Sasaoka<sup>2</sup>, Chiho Inoue<sup>2</sup> and Shinji Munetoh<sup>2</sup>; <sup>1</sup>Chikushigaoka High School, Japan; <sup>2</sup>Kyushu University, Japan

In the Seebeck effect in p-type semiconductor, the voltage can be generated by the diffusion of excited carrier in high temperature side to low temperature side in impurity level. However, carriers in a valence band rediffuse to high temperature side because of electric potential difference, and the value of voltage drop at equilibrium. On the other hand, the block of rediffusing carrier can generate larger the value of voltage. In this study, we combined two different fermi level of p-type semiconductors, the light boron doped silicon and the heavy boron doped silicon, in order to form internal electric field in the interface with Spark Plasma Sintering. This process has formed the barrier of energy for prevention of carrier rediffusion. We found that the synthesized sample's voltage increased in comparison with the light boron doped silicon and the heavy boron doped silicon. It is indicated that voltage can increase by forming internal electric field, with the sample combined different fermi level p-type semiconductors.

### F.SF07.06.14

**Late News: The Influence of the Powder Metallurgy Precursor on the Microstructure and Mechanical Properties of a Porous Cu-Al-Ni Alloy** Maria T. Malachevsky<sup>1,2</sup>, Alberto Baruj<sup>1,2</sup>, Graciela Bertolino<sup>1,2</sup> and Ignacio Papuccio<sup>3</sup>; <sup>1</sup>Centro Atomico Bariloche - CNEA, Argentina; <sup>2</sup>CONICET, Argentina; <sup>3</sup>Facultad de Ciencias Exactas -UNCPBA, Argentina

Shape memory alloys are able to stand large deformations and to recover their shape afterwards. Depending on the temperature, the shape recovery could take place after heating or by the so-called pseudoelastic behavior. These particular properties make these smart materials good candidates for applications such as damping or actuation. Cu-based shape memory alloys are commercially attractive due to their relatively low cost compared to Ni-Ti alloys. Multiple research efforts have focused on expanding their potential applications by adding features that can improve the material. Porous shape memory alloys were developed in an effort to combine the shape recovery and energy dissipation properties with reduced density and weight. However, most polycrystalline Cu-based shape memory alloys are prone to intergranular fracture both in compact and porous samples. Reducing the material grain size could decrease the stress concentration at grain boundaries and help to avoid fracture. This can be achieved by alloying with other elements or by selecting an appropriate manufacturing method. As a possible fabrication route, we used powder metallurgy starting from a small particle size.

Among Cu-based shape memory alloys, Cu-Al-Ni alloys are an alternative with good properties and low cost. In this work, we explored the fabrication of porous Cu-14Al-3Ni by conventional powder metallurgy, starting from mechanically pre-alloyed powder and a mixture of the elemental metal powders. For preparing the pre-alloyed powder, we employed a high-energy Frisch Pulverisette 7 planetary mill, processing under Argon at 700 rpm for 3 hours. The resulting powder was analyzed by means of X-Ray Diffraction (XRD). The XRD pattern showed no presence of Al or Ni while the Cu peaks were shifted to lower angles indicating the solid solution of both Al and Ni in the structure. The Cu peaks were also significantly widened due to the strain resulting from the high-energy milling. Some peaks of  $\gamma$ -Cu<sub>9</sub>Al<sub>4</sub> were detected, as well as small CW peaks resulting from the milling media contamination. The other precursor was prepared by hand mixing the elementary powders in an agate mortar. Both precursors were mixed with 1 wt.% mixture of PVA and PVB as a binder and, after drying, 30 vol.% ammonium bicarbonate was added as space holder. Cylindrical samples were prepared by uniaxial cold pressing at 700 MPa. After sintering at 1000 °C, the samples were solution-treated for 24 h at 900 °C under Ar. After the treatment, they were water-quenched to obtain the martensitic phase.

The samples prepared with the milled powder were investigated by XRD. After sintering, the phases detected were  $\alpha$ ,  $\gamma$ -Cu<sub>9</sub>Al<sub>4</sub> and AlNi. The heat treated samples consisted of the shape memory phase 18R accompanied by  $\alpha$  and AlNi. The presence of AlNi in the sintered sample suggests that the alloy resulted short of both elements and consequently the solution treatment was performed in the  $\alpha$ - $\beta$  two-phase field. After quenching,  $\alpha$  remained as a secondary phase. Meanwhile, the samples prepared with the hand mixed precursor consisted of the 18R and 2H shape memory phases.

X-ray microtomography images of the porous samples were acquired with an Xradia Micro XCT-200 microscope. The samples prepared with the pre-alloyed precursor presented internal cracks indicating that the presence of the brittle  $\gamma$ -Cu<sub>9</sub>Al<sub>4</sub> phase reduced the powder compressibility. The lower density prevented their mechanical characterization. On the other hand, samples prepared with the hand mixed precursor were well sintered allowing their complete characterization. Compression uniaxial tests were performed and the shape memory behavior was corroborated. Samples recovered 100% from a 7% strain and 98.56% from 11.5% strain when heated to 140 °C. The obtained grain size is about 30  $\mu$ m.

### F.SF07.06.16

**Computational Study of Radiation Damage in Bilayer Nanostructures** Cameron Hopper<sup>1</sup>, Raghuram Santhanpuram<sup>1</sup>, Elton Chen<sup>2</sup>, Remi Dingreville<sup>2</sup> and Arun K. Nair<sup>1</sup>; <sup>1</sup>University of Arkansas–Fayetteville, United States; <sup>2</sup>Sandia National

Laboratories, United States

Neutron and ion radiation damage materials used in radioactive environments, such as nuclear reactors. This type of radiation can cause atoms to be moved around in the atomic structure or removed entirely, causing defects and damage to accumulate in the material, which leads to lower mechanical strength. Since these defects are on the atomic level, it can be hard to detect. We propose examining two different types of interfaces: bilayer interfaces, specifically Silicon-Aluminum and Silicon-Gold, as well as crystalline-amorphous interfaces to investigate whether these types of interfaces can help develop radiation-resistant materials. Using molecular dynamics, we will model these bilayer and amorphous structures as well introduce radiation in the form of Frenkel pairs to our system. To analyze the mechanical strength at different levels of radiation damage, yield surface calculations will be performed by subjecting the samples to biaxial and uniaxial tension and compression tests to determine the yield points. Different defect absorption mechanisms at the interface will also be discussed.

#### **F.SF07.06.17**

**Late News: Understanding the Interaction Between Grain Boundary Precipitation and Creep Cavitation of Type 316H Stainless Steel During In-Service Aging** Siqi He<sup>1</sup>, Hao Shang<sup>1</sup>, Antonio Fernandez-Caballero<sup>2</sup>, Alexander Warren<sup>1</sup>, David Knowles<sup>1</sup>, Peter Flewitt<sup>1</sup> and Tomas Martin<sup>1</sup>; <sup>1</sup>University of Bristol, United Kingdom; <sup>2</sup>University of Oxford, United Kingdom

Creep cavitation is an important degradation mechanism for metallic components used at an elevated temperature. Stress, temperature and microstructure all play a role in the initiation of creep cavities, and the formation mechanism of cavities can depend heavily on local phase and chemistry. In this work, the relationship between microstructural evolution due to long term thermal ageing and creep cavitation is explored in an ex-service AISI type 316H stainless steel sample from an advanced gas-cooled nuclear reactor boiler header after 65,000 hours at 490 to 530°C. The microstructure of the ex-service specimen has been investigated by secondary electron microscopy, focused-ion beam cross sectioning, electron backscatter diffraction and transmission electron microscopy.  $M_{23}C_6$  precipitates,  $\alpha$ -ferrite precipitates and creep cavities are observed at grain boundaries, with increased precipitation and cavitation at random grain boundaries, and an absence of creep cavities at coincidence site lattice (CSL) 3 boundaries. The  $\alpha$ -ferrite precipitates grow during in-service exposure at grain boundaries with a Kurdjumov-Sachs orientation relationship to at least one neighbouring austenite matrix grain. The creep cavities were observed to initiate at the intergranular  $M_{23}C_6$  and  $\alpha$  ferrite precipitates. Based on the orientation relationship of the ferrite precipitates with the austenite matrix, some creep cavities are initiated after the ferrite precipitates have formed. The influence of microstructure changes on creep cavitation of materials during in-service aging and the implications for more reliable predictions of lifetime for components operating at high temperature are discussed.

### **SYMPOSIUM F.SF06**

---

High-Entropy and Compositionally Complex Alloys  
November 21 - November 21, 2020

#### Symposium Organizers

Easo George, Oak Ridge National Laboratory  
Uwe Glatzel, Universität Bayreuth  
Haruyuki Inui, Kyoto University  
Celine Varvenne, CINaM CNRS Aix-Marseille University

---

\* Invited Paper

SESSION F.SF06.01: Functional and Other Properties  
On Demand Abstracts Available for Viewing Starting Saturday Morning, November 21, 2020  
F-SF06

### 5:00 AM \*F.SF06.01.01

**From High Entropy Alloys to Complex Concentrated Alloys—How to Tune Multiple Properties** Mathilde Laurent-Brocq<sup>1</sup>, D. Mereib<sup>1</sup>, T. Rieger<sup>1</sup>, Loic Perriere<sup>1</sup>, J. Monnier<sup>1</sup>, Y. Danard<sup>1</sup>, C. Vary<sup>1</sup>, H. Ben Kahla<sup>1</sup>, B. Villeroy<sup>1</sup>, Jean-Marc Joubert<sup>1</sup>, I. Guillot<sup>1</sup>, D. Mercier<sup>2</sup>, X.A. Wang<sup>2</sup>, P. Marcus<sup>2</sup>, M. Roussel<sup>3</sup> and A. Facco<sup>3</sup>; <sup>1</sup>Université Paris Est Créteil, CNRS, ICMPE, UMR 7182, France; <sup>2</sup>Chimie ParisTech, PSL University, CNRS, Institut de Recherche de Chimie Paris, Physical Chemistry of Surfaces Group, France; <sup>3</sup>Manoir Industries, France

Since the discovery of the face-centered-cubic (fcc) single-phased CoCrFeMnNi and the proposal of the concept of high entropy alloys (HEA) in 2004, the understanding of the thermodynamic and mechanical behavior of those alloys has greatly increased. Indeed, it is now possible to reliably map the stable phases in the Co-Cr-Fe-Mn-Ni system using the CALPHAD method [1] and to calculate the solid-solution strengthening [2]. So today, modelling tools are available to “investigate the unexplored central region of multi-component space” [3]. It is time to go pass single-phase materials and/or equimolar quinary compositions and look for complex concentrated alloys. To do so, two different approaches will be presented. First, the objective is to identify compositions of solid-solution to resist to severe environment (like high temperature and corrosive environment). The strategy consists in: (i) identifying criteria which are relevant for the targeted properties (like the yield strength, the Cr content or the cost) ; (ii) mapping those criteria for the entire composition space ; (iii) selecting compositions ; (iv) performing an experimental validation by processing, microstructural characterization and properties measurements. This will be presented for the Co-Cr-Fe-Mn-Ni and Co-Cr-Fe-Mo-Ni systems.

Second, the objective is to create a chemical architecturation within the CoCrFeMnNi alloy in order to strengthen it while preserving its ductility. More specifically, a mixture of pure Ni and CoCrFeMnNi powders is sintered in order to create chemical gradients at the interfaces of both phases [4]. The microstructure of these innovative chemically architected alloys will be characterized in detail. Then it will be shown how the width of the gradient can be controlled by varying the processing parameters and how it influences the mechanical properties. Finally, the different strengthening contributions will be sorted out and analyzed.

[1] Bracq, G., Laurent-Brocq, M., Perrière, L., Pirès, R., Joubert, J.-M., and Guillot, I., *Acta Materialia*, **2017**. 128: p. 327-336.

[2] Bracq, G., Laurent-Brocq, M., Varvenne, C., Perrière, L., Curtin, W.A., Joubert, J.M., and Guillot, I., *Acta Materialia*, **2019**. 177: p. 266-279.

[3] Cantor, B., Chang, I.T.H., Knight, P., and Vincent, A.J.B., *Materials Science and Engineering: A*, **2004**. 375–377: p. 213-218.

[4] Laurent-Brocq, M., Mereib, D., Garcin, G., Monnier, J., Perrière, L., and Villeroy, B., *Journal of Alloys and Compounds*, **2020**. 835: p. 155279.

### 5:15 AM \*F.SF06.01.02

**Corrosion of Single Phase Compositionally Complex NiFeCrMnCo Alloys** Gerald S. Frankel<sup>1</sup>, Tianshu Li<sup>1</sup>, Sarita Sahu<sup>1</sup>, John Scully<sup>2</sup> and Angela Gerard<sup>2</sup>; <sup>1</sup>The Ohio State University, United States; <sup>2</sup>University of Virginia, United States

The corrosion resistance of several single phase, non-equiatomic, NiFeCrMnCo compositionally complex alloys (CCAs) containing a range of Cr content from 6-22% was investigated in chloride solutions. Comparison was made to NiCr and FeCr binary alloys with similar Cr contents as the CCAs. The oxide film character and the localized corrosion performance, including susceptibility to crevice and pitting corrosion, were studied utilizing in-situ electrochemical and ex-situ surface-sensitive techniques. An NiFeCrMnCo CCA with only 6% Cr was found to exhibit passivity and breakdown by pitting corrosion. Crystallographic pit morphology was observed in most of these CCAs, suggesting a difficulty in precipitation of a salt film, which would result in polished pit surfaces. The crystallographic pit morphology indicates that the pit growth was under charge-transfer/ohmic control. The passive film composition, thickness, and elemental valence states, and fate of each element were studied for the CCA with 22% Cr by in-situ atomic emission spectro-electrochemistry, ex-situ X-ray photoelectron spectroscopy, and atom probe tomography. It demonstrated slightly better corrosion resistance than the binary Ni-24Cr alloy. Passive films on the HEA contained primarily Cr, and small amounts of Ni, Fe and Mn, while dissolution of Ni, Fe, Co was observed. Metallic Ni was enriched at the passive film-metal interface. Enrichment of Cr in the passive film occurred to a greater extent in the HEA than for the Ni-Cr binary alloy. Enrichment factors were determined and the origins of enrichment were assessed.



### 5:30 AM F.SF06.01.03

**Hydrogen Storage by Ti-V-Cr Based Multi Component Alloys** Etsuo Akiba, Rika Hayashi and Shota Itano; Kyushu University, Japan

Ti-V-Cr based hydrogen absorbing alloys these have BCC structure absorb hydrogen up to 3 wt% that is the highest among materials working under ambient conditions [1]. However, they have a potential to store hydrogen around 4 wt% because more than 1wt% of hydrogen in the hydrogenated alloys cannot be released at room temperature. To improve hydrogen capacity, the number of constituent elements is increased to make multi component alloys. Equimolar multi component alloys are called as high entropy alloys or multi principal element alloys. It has been reported a five-element equimolar high entropy alloy TiZrNbHfTa absorbed hydrogen at 300°C [2]. We tried to prepare four or five element Ti-V-Cr based alloys with equimolar or near-equimolar compositions because they are lighter than the reported high entropy alloys consisted of heavy elements and expected to absorb hydrogen under ambient conditions. Hydrogen absorbing performance was measured at room temperature. Some of four and five element alloys with BCC structure prepared in this study reversibly absorb and desorb hydrogen at room temperature.

[1] E. Akiba, H. Iba, *Intermetallics*, 6, 461-470 (1996).

[2] C. Zlotea, M.A. Sow, G. Ek, J. -P. Couzinié, L. Perrière, I. Guillot, J. Bourgon, K. T. Møller, T. R. Jensen, E. Akiba, M. Sahlberg, *J. Alloys Comp.*, 775, 667-674 (2019).

### 5:40 AM F.SF06.01.04

**Synthesis, Mechanical Properties, and High Temperature Stability of the Spinel High Entropy Oxide**

**(Mg<sub>0.2</sub>Ni<sub>0.2</sub>Co<sub>0.2</sub>Cu<sub>0.2</sub>Zn<sub>0.2</sub>)Al<sub>2</sub>O<sub>4</sub>** Brianna Musico<sup>1</sup>, Joshua Smith<sup>1</sup>, Quinton Wright<sup>1</sup>, Claudia Rawn<sup>1</sup>, Kurt E. Sickafus<sup>1</sup>, David Mandrus<sup>1,2</sup> and Veerle Keppens<sup>1</sup>; <sup>1</sup>The University of Tennessee, Knoxville, United States; <sup>2</sup>Oak Ridge National Laboratory, United States

Reports on the unique properties achieved with HEAs, including improved mechanical properties, has motivated the application of the multi-component approach to oxide materials, expanding the available compositional space and providing greater flexibility to meet the demands of today's advanced materials. We have applied this methodology to an alumina based spinel oxide, resulting in the synthesis of polycrystalline (Mg<sub>0.2</sub>Ni<sub>0.2</sub>Co<sub>0.2</sub>Cu<sub>0.2</sub>Zn<sub>0.2</sub>)Al<sub>2</sub>O<sub>4</sub>. Samples were made by either the solid state reaction method or the polymeric steric entrapment (PSE) technique, and in-situ High Temperature X-Ray Diffraction (HTXRD) was used to compare the phase transformation behavior and investigate the high temperature phase stability. Resonant Ultrasound Spectroscopy (RUS) has been used to evaluate the elastic behavior of a dense polycrystalline pellet sample, allowing for a comparison of the mechanical properties of the multicomponent (Mg<sub>0.2</sub>Ni<sub>0.2</sub>Co<sub>0.2</sub>Cu<sub>0.2</sub>Zn<sub>0.2</sub>)Al<sub>2</sub>O<sub>4</sub> to those of the traditional MgAl<sub>2</sub>O<sub>4</sub> spinel.

### 5:50 AM F.SF06.01.05

**Electrical Resistivity Change of CrMnFeCoNi High-Entropy Alloy by Electropulsing and Annealing** Hisanori Tanimoto, Ryo Hozumi and Mari Kawamura; University of Tsukuba, Japan

High-entropy alloys (HEAs) are a new class of metallic materials because of their unique properties; high strength and ductility at low temperatures, texture stability due to sluggish diffusion of atoms at elevated temperatures, and so on. HEAs are solid solution and the constitute atoms form a lattice but the chemical atomic arrangement is totally disordered. It is pointed out that, however, some local inhomogeneity or structure are existed in HEAs to accommodate the large local strains and hence assist the stability of HEAs [1]. Amorphous alloys are another type of random system where the atom positions are chemically and topologically disordered. Existence of local structures in amorphous alloys and the characteristic dynamic response were suggested by several studies. We found that the resistivity of amorphous (a-) ZrCu alloys was decreased to less than 60% of the initial value after passing an electric pulse (electropulsing). In the experiment, the current exponentially decayed with the time constant of ~3 ms from the initial current density of ~0.6 GA/m<sup>2</sup> [2]. Further, nanocrystallites of ZrCu, the high-temperature intermetallic compound phase, were revealed from the X-ray diffraction measurement and transmission electron microscopy. These observations suggested that that crystalline-like local structures in a-ZrCu are embedded in the amorphous alloys and transformed to nanocrystallites through collective motions of the local structures excited by electropulsing. The information on the local structure and its dynamical behavior can be surveyed from the electropulsing experiment.

In the present study, the electropulsing experiments were performed for CrMnFeCoNi HEA in the as-prepared state and annealed state. The phase separation of CrMnFeCoNi HEA was reported after annealing below 1073 K [3]. It is expected that the local structure is developed by annealing below 1073 K and the texture change or phase separation are accelerated by electropulsing. For CrMnFeCoNi HEA in the as-prepared state, no decrease in the resistivity and no secondary phase formation were observed after electropulsing up to 1.4 GA/m<sup>2</sup>. By annealing at 1023 K for 1 hour, the resistivity of

CrMnFeCoNi HEA showed an increase by 10 % from that in the as-prepared state. The resistivity increased by annealing showed a slight recovery by electropulsing up to 1.2 GA/m<sup>2</sup>; the resistivity became 8% larger than that in the as-prepared state. It is noted that no texture change and no new phase formation were detected by the XRD measurements after the present annealing and subsequent electropulsing. The increase in the resistivity by annealing indicates some local structure formation toward the phase separation, whereas the slight recovery of the increased resistivity by electropulsing disappearance of the local structure induced by annealing. These results suggest that in CrMnFeCoNi HEA, local structures which are dynamically unstable and easily transform to other states are not exited or considerably stable if existed.

#### Reference

- J. Dinga et. al., PNAS 115, (2018), 8919–8924.  
H. Tanimoto et. al., Mater. Trans. 61 (2020) 878-883.  
B. Schuh et. al., Acta Mater, 96 (2015) 258.

#### 6:00 AM F.SF06.01.09

**Designing High Entropy Oxides as Effective Catalysts for Pollution Abatement** Christopher Riley<sup>1</sup>, James Park<sup>1</sup>, Stephen Percival<sup>1</sup>, Andrew De La Riva<sup>2</sup>, Abhaya Datye<sup>2</sup> and Stan Chou<sup>1</sup>; <sup>1</sup>Sandia National Laboratories, United States; <sup>2</sup>The University of New Mexico, United States

High entropy oxides (HEOs) offer great potential to innovate fields involving applied materials. However, the development of HEOs for use as heterogeneous catalysts is still lacking, due in part to current HEO production methods. Common synthetic techniques involve physically mixing individual metal oxides and heating the mixture to high temperatures (>1000 °C), which allows for interdiffusion and achievement of phase pure structures. However, high temperature synthetic routes sinter HEOs into low surface area materials, rendering them inactive in catalyzed gas-phase reactions. Here, we explore a sol-gel synthesis of HEOs conducted at much lower temperatures (500 °C). The resulting HEOs contain primarily rare earth elements and are made with uniform structure, high surface area, and high catalytic activity for CO oxidation. Incorporation of multiple dopant elements into the fluorite phase HEOs facilitates the transfer of reactive lattice oxygen to CO reactant via a Mars van Krevelen mechanism. Further, the high surface area of these materials leads to a high number of active sites for CO oxidation. The sol-gel synthesis presented herein is broadly applicable and enables the design of HEOs as effective catalysts.

Sandia National Laboratories is a multimission laboratory managed and operated by National Technology & Engineering Solutions of Sandia, LLC, a wholly owned subsidiary of Honeywell International Inc., for the U.S. Department of Energy's National Nuclear Security Administration under contract DE-NA0003525.

#### 6:10 AM F.SF06.01.10

**A Novel B2-Ordered Fe<sub>30</sub>Co<sub>40</sub>Mn<sub>15</sub>Al<sub>15</sub> Medium-Entropy Alloy with Outstanding Soft Magnetic Properties and High Thermal Stability** Youxiong Ye, Scott D. Lish, Markus W. Wittmann and Ian Baker; Dartmouth College, United States

Thus far, soft magnetic behavior in high-entropy alloys has only been observed in disordered single-phase microstructures (e.g., FCC or BCC) or a mixture of disordered and ordered structures (e.g., FCC/BCC + B2/L2<sub>1</sub>/L1<sub>2</sub>). Here, we have reported, for the first time, a novel single-phase B2-ordered Fe<sub>30</sub>Co<sub>40</sub>Mn<sub>15</sub>Al<sub>15</sub> medium-entropy alloy with potential use as a soft magnet. The microstructure and deformation mechanisms were examined using transmission electron microscopy. The effects of annealing at 600, 800 and 1000 °C on phase stability, mechanical behavior and magnetic behavior were studied. Outstanding soft magnetic properties were obtained for the as-cast alloy, i.e., a high saturation magnetization of ~156 emu/g, a high Curie temperature of ~810 °C, and a very low coercivity of ~2.6 Oe, which are superior to values previously reported for medium- and high-entropy alloys. The alloy exhibited excellent microstructural, mechanical, and magnetic stability upon long time (> 3 days) annealing at up to 600 °C. Furthermore, high temperature magnetic measurements revealed a gentle decrease in the saturation magnetization and almost unchanged coercivity at temperatures up to 700 °C, suggesting its potential for high-temperature applications as a soft magnet. The work was supported by NIST grant 60NANB2D0120.

#### 6:20 AM F.SF06.01.11

**Multicomponent Pyrochlore Solid Solutions with Uranium Incorporation—New Perspective of Materials Design for Nuclear Applications** Kun Yang and Jie Lian; Rensselaer Polytechnic Institute, United States

Compositionally complex pyrochlore oxide solid solutions with and without uranium incorporation were fabricated by solid state reaction and consolidated by sparking plasma sintering. The as-sintered compositionally complex pyrochlore oxide with distinct mixing entropy varies from medium to high were considered and their thermal and mechanical properties were

compared to baseline single component rare-earth titanate pyrochlore ( $A_2Ti_2O_7$ ). The medium entropy pyrochlore oxides have lower thermal conductivity than its high entropy counterpart. The measured thermal conductivity increases by increasing the A-site mixing entropy and decreasing a modified size disorder parameter, and thus the size disorder and mixing entropy could be good indicators for predicting thermal conductivity of multicomponent pyrochlore solid solutions. Uranium incorporation in general reduces hardness and fracture toughness as compared with single component compositions due to the significant low hardness and fracture toughness for  $UO_2$ . High entropy pyrochlore with uranium displays the highest thermal conductivity among all of the multicomponent pyrochlore solid solutions with significantly better mechanical properties than  $UO_2$ . This work opens up the possibility of designing multicomponent oxide solid solutions by controlling their chemical disorder/mixing entropy to achieve acceptable thermal-mechanical properties and desired radiation and corrosion performance for potential nuclear waste form and inert matrix fuel applications.

SESSION F.SF06.02: Local Structural Order and Disorder  
On Demand Abstracts Available for Viewing Starting Saturday Morning, November 21, 2020  
F-SF06

**5:00 AM F.SF06.02.01**

**Effect of Short Range Order on Physical Properties for Cr-Co-Ni Medium Entropy Alloy** Katsushi Tanaka, Takeshi Teramoto, Yusuke Ito and Kentaro Kitasumi; Kobe University, Japan

Short range ordering (SRO) in Cr-Co-Ni medium entropy alloy is considered as an important phenomenon for understanding its physical properties. Recent works indicate that slowly cooled alloy from 1273 K exhibits relatively higher yield stresses and higher stacking fault energies. The knowledges of the thermodynamic condition and kinetics of the formation of SRO are required to understand the physical and mechanical properties of the alloy, but are still open question. In the present study, we have successfully confirmed that an atomic scale rearrangement occurs by annealings at the temperatures below 873 K, which may be attributed as the formation of SRO. The SRO disappears when the specimen is annealed at the temperatures of 973 K or higher. We will show experimental results indicating the development of SRO in Cr-Co-Ni medium entropy alloy and variations of other physical properties such as lattice constant, elastic properties and yield stress.

**5:10 AM F.SF06.02.02**

**Local Structural Disorder Revealed by EXAFS Measurements in Medium-Entropy Alloy CrCoNi** Noriaki Hanasaki<sup>1</sup>, Masaharu Oda<sup>1</sup>, Kodai Niitsu<sup>2</sup>, Kazuki Ehara<sup>2</sup>, Hiroaki Nitani<sup>3</sup>, Hitoshi Abe<sup>3</sup> and Haruyuki Inui<sup>2</sup>; <sup>1</sup>Dept. of Physics, Osaka University, Japan; <sup>2</sup>Kyoto University, Japan; <sup>3</sup>KEK, Japan

High-entropy alloys are promising materials for the high strength and ductility. As the origin of these important properties, the lattice distortion, sluggish diffusion, and cocktail effect have been discussed. The previous studies suggested that the yield strength is proportional to the atomic displacement theoretically. Thus, it is essential to clarify the local structure in this class of alloys experimentally. We investigated the local structure in the medium-entropy alloy CrCoNi by the measurements of the EXAFS (extended x-ray absorption fine structure) for the Cr, Co, Ni-K edges, whose spectra were obtained accurately by recording the transmitted x-ray beam. We found that the Debye-Waller factor in the Cr atom is larger than those in the Co and Ni atoms, suggesting that the Cr atom has a guest-like character inducing the local structural disorder in CrCoNi. Our result is consistent with the previous studies suggesting that the atomic displacement tends to be larger in the atom having the lower atomic number. We will discuss the local structure and the annealing effect on the basis of the EXAFS results.

**5:20 AM F.SF06.02.04**

**Local Structure and Carbon Vacancies in High Entropy Carbides** Abinash Kumar<sup>1</sup>, Mohammad Delower Hossain<sup>2</sup>, Jon-Paul Maria<sup>2</sup> and James M. LeBeau<sup>1</sup>; <sup>1</sup>Massachusetts Institute of Technology, United States; <sup>2</sup>The Pennsylvania State University, United States

High entropy ceramics- a chemically disorder crystal with four or more metals randomly distributed in the cation sublattice and either carbon, oxygen or boron populates the anion sublattice. These new materials displayed remarkable properties such as high hardness, low thermal conductivity and reversible electrochemical energy storage behavior [1-3]. The local structure in the chemically disorder crystal affects the properties which demands a nanoscale probe to establish the structure property relationship. Scanning transmission electron microscopy (STEM) provides the opportunity to map the local structure in high entropy materials with variation in local chemistry or in presence of point, line and planar defects in the crystal.

High entropy carbide thin films were synthesized by using reactive radio frequency (RF) magnetron sputtering and carbon content in the samples were regulated by flowing 99.99% methane gas during deposition. Two thin films having a 10% C vacancy and a stoichiometric high entropy carbide were characterized by a combination of STEM imaging and spectroscopy techniques. The low magnification TEM and STEM images reveals formation of stacking faults in the carbon deficient sample. The clustering of carbon vacancies instigated the stacking faults in the materials which is substantiated by EELS mapping in STEM mode. Segregation of carbon vacancies are preferred due to the reduced energy penalty by the formation of stacking faults compared to the random distribution as explored by first principle calculation in binary transition metal carbides [4]. In comparison, the stoichiometric high entropy samples are free from any kind of point or line defects. We observed a broad distribution of the cation-cation bond distances in both samples which are corroborated by the pair distribution generated from density function theory calculation of the chemically disorder crystal. The atomic size mismatch among the constituents of the high entropy carbide cations contributed to the wider distribution. High-angle annular dark field (HAADF) STEM imaging of stoichiometric sample show variation in the intensity of the metal atomic columns with alternate plane of higher and lower intensity. Such variation can be associated with the presence of nanoscale cation ordering in the sample. We will further discuss using statistical tools how such variation in elemental distribution lead to change in local strain which may have profound effect on strengthening of the materials.

References:

- [1] P. Sarker et al., Nature Communications 9 (2018)
- [2] X. Yan et al., Journal of the American Ceramic Society 101 (2018)
- [3] A. Sarkar et al., Nature Communications 9 (2018)
- [4] H. Ding et al., Journal of the European Ceramic Society 34 (2014)

#### 5:30 AM F.SF06.02.05

**Characterizing the Extent of Short-Range Order in a Lightweight FeMnAlC Steel Alloy Using STEM** Michael Xu, Hyun Seok Oh, Cem Tasan and James M. LeBeau; Massachusetts Institute of Technology, United States

Compared with many other steel alloys, highly alloyed FeMnAlC lightweight steels have been shown to have a unique combination of strength and ductility, which has gained interest for automotive applications [1-3]. One of the potential reasons for these enhanced properties has been attributed to the growth of ordered  $\kappa$ -carbides in the austenitic matrix upon aging [3-5]. A particularly important deformation mechanism for high strain-hardening rate alloys is short-range order (SRO)-linked planar glide [6]. Thus, in order to understand the role that local atomic structure may ultimately have on material properties, it becomes crucial to characterize and correlate short-range ordering with deformation mechanisms.

In this presentation, we will show the direct imaging of atomically ordered clusters within the austenite matrix with scanning transmission electron microscopy (STEM). Using Revolving STEM (RevSTEM) imaging, atom column indexing, intensity correlation, and analysis [7,8], we first show direct evidence for nanosized ordered clusters in FeMnAlC, suggesting  $L1_2$ -type ordering of the substitutional atoms in agreement with  $\kappa$ -carbide. We then map the extent of ordering with respect to the introduced plastic strain, and the evolution of crystallographic defects such as dislocations and twin boundaries, to provide insights on the behavior of defects in relation to short-range ordering. Finally, we will examine the effect of aging treatments on these phenomena [9].

References:

- [1] H. Kim et al., Sci. Technol. Adv. Mater. 14 (2013), 014205.
- [2] J.D. Yoo et al., Mater. Sci. Eng. A 508 (2009), p. 234-240.
- [3] H. Kim et al., Sci. Technol. Adv. Mater., vol. 14, no. 1 (2013).
- [4] W. K. Choo et al., Acta Mater., vol. 45, no. 12 (1997), p. 4877-4885.
- [5] S.-D. Kim et al., Sci. Rep. 9 (2019), 15171.
- [6] V. Gerold and H.P. Karnthaler, Acta Metall. 37 (1989), p. 2177-83.
- [7] C. Niu et al., Appl. Phys. Lett. 106 (2015), 161906.
- [8] X. Sang and J. M. LeBeau, Ultramicroscopy 138 (2014), p. 28.
- [9] We acknowledge support for this work from the National Science Foundation (CMMI-1922206).

#### 5:40 AM F.SF06.02.06

**Experimental Determination of the Effective Atomic Radius of the Constituent Elements in Cr-Mn-Fe-Co-Ni High Entropy Alloy** Takeshi Teramoto, Momoko Narasaki and Katsushi Tanaka; Kobe University, Japan

Solid solution strengthening is the major strengthening mechanism for its yield stress in high entropy alloys (HEA). In order

to understand the solid solution strengthening mechanism, lattice distortions caused by the difference in effective atomic radii of the constituent elements have recently been discussed theoretically such as first-principles calculations and Goldschmidt radius. However, no experimental study has been reported to determine the effective atomic radii of the constituent elements in HEA. In this study, the effective atomic radii of the constituent elements in the Cr-Mn-Fe-Co-Ni alloys have been experimentally determined. The effective atomic radii are estimated by applying a rigid sphere model to the effective atomic volumes of the constituent elements determined by an X-ray diffraction. As a result of comparing the derived effective atomic radii with the previously reported theoretical ones, the experimentally determined effective atomic radii show different trends in terms of the absolute values and the order. It has been reported that there is a correlation between the yield stress and the mean square atomic displacement (MSAD) parameter caused by the difference in the atomic radii. However the present study shows there is no correlation between the yield stress and the lattice strains estimated from the experimentally determined atomic radii. These results suggest that the difference in atomic radii is not directly related to the solution strengthening mechanism of HEAs.

#### 5:50 AM F.SF06.02.07

**Combinatorial Exploration of High Entropy Alloys** Sebastian A. Kube<sup>1</sup>, Pamela Banner<sup>1</sup>, Sungwoo Sohn<sup>1</sup>, David Uhl<sup>2</sup>, Amit Datye<sup>1</sup>, Suchismita Sarker<sup>3</sup>, Apurva Mehta<sup>3</sup> and Jan Schroers<sup>1</sup>; <sup>1</sup>Yale University, United States; <sup>2</sup>Southern Connecticut State University, United States; <sup>3</sup>SLAC National Accelerator Laboratory, United States

High Entropy Alloys (HEAs) are inherently complex and span a vast composition space, across which single-phase solid solutions (SPSS) potentially form. Using combinatorial co-sputtering and high-throughput EDX and synchrotron XRD, we consistently fabricate and characterize large numbers of distinct quinary HEAs. By mining a first data set comprising ~2,500 quinary HEAs based on the elements Al, Cr, Mn, Fe, Co, Ni, and Cu, we show that resulting crystal structures are determined by the combination of the BCC/FCC element content and the atomic size difference. We further reveal a BCC preference effect: The BCC structure becomes increasingly favorable with increasing atomic size difference, because of its ability to accommodate atoms of various sizes more efficiently than FCC. Finally, we present our new expanded data set comprising 10,000 ternary and quinary compositions based on 20 different elements. We place special emphasis on the metastable character of these alloys: Given the high cooling rates involved (~10<sup>10</sup> K/s), SPSS and glasses are obtained through polymorphic solidification and can be studied across exceptionally wide composition ranges.

#### 6:00 AM F.SF06.02.08

**Magnetically Driven Short-Range Order in the CrCoNi System** Flynn Walsh<sup>1,2</sup>, Robert Ritchie<sup>1,2</sup> and Mark Asta<sup>1,2</sup>; <sup>1</sup>Lawrence Berkeley National Laboratory, United States; <sup>2</sup>University of California, Berkeley, United States

The presence, nature, and impact of chemical short-range order in the CrCoNi multi-principal element alloy are all topics of current interest and debate, especially in the context of the system's role as a model for related high-entropy alloys. While the ordering of this material has been previously analyzed in terms of purely chemical relationships, first-principles calculations reveal that its origins are fundamentally magnetic. Specifically, the dominant interaction is found to be repulsion among like-spin Cr nearest neighbors, which is complemented by a preference to form a second-nearest neighbor sublattice of Cr with moments opposing those of ferromagnetic Co. Magnetically aligned pairs of Co and Cr atoms are additionally calculated to be unfavorable, emphasizing the need to analyze the ordering of this material in spin-polarized terms. Models of order following these principles are used to explain anomalous experimental measurements concerning both net magnetization and atomic volumes across a range of compositions, demonstrating the effects of both short-range order and magnetic interactions with implications for a broader class of high-entropy alloys containing multiple principal 3d elements.

#### 6:10 AM F.SF06.02.09

**Order-Disorder Transition Behaviors in Lightweight High-Entropy Alloys** Rui Feng<sup>1,2</sup>, Chuan Zhang<sup>3</sup>, Michael Gao<sup>4,5</sup>, Zongrui Pei<sup>4,6</sup>, Fan Zhang<sup>3</sup>, Yan Chen<sup>2</sup>, Dong Ma<sup>2</sup>, Ke An<sup>2</sup>, Jonathan Poplawsky<sup>2</sup>, Yang Ren<sup>7</sup>, Michael Widom<sup>8</sup>, Jeffery Hawk<sup>4</sup> and Peter Liaw<sup>1</sup>; <sup>1</sup>The University of Tennessee, Knoxville, United States; <sup>2</sup>Oak Ridge National Laboratory, United States; <sup>3</sup>Computherm, LLC, United States; <sup>4</sup>National Energy Technology Laboratory, United States; <sup>5</sup>Leidos Research Support Team, United States; <sup>6</sup>ORISE, United States; <sup>7</sup>Argonne National Laboratory, United States; <sup>8</sup>Carnegie Mellon University, United States

The much larger compositional space afforded by high-entropy alloys (HEAs) compared to traditional alloys, opens new opportunities to develop high-performance materials. Here the CALculation of PHase Diagrams (CALPHAD)-based high-throughput computational method (HTCM) is used to screen lightweight HEAs in the Al-Cr-Fe-Mn-Ti system that contain nanoscale L<sub>21</sub> precipitates within the body-centered-cubic (BCC) matrix for cost-effective high-temperature applications. The order-disorder transition behaviors and their effects on the microstructures and mechanical properties of these newly-

designed lightweight high-entropy alloys (LWHEAs) are understood by *in-situ* neutron scattering and advanced microcopies, *ab-initio* molecular dynamics (AIMD), and Monte-Carlo (MC) simulations. The fundamental understanding of the order-disorder transition behaviors of these LWHEAs explains the different microstructural and mechanical responses among them, which provides in-depth insights into the discovery of advanced precipitation-strengthened structural materials by the HEA concept.

#### **Acknowledgment**

P.K.L. very much appreciates the support of the U.S. Army Research Office project numbers of W911NF-13-1-0438 and W911NF-19-2-0049 and the support from the National Science Foundation under grant DMR-1611180 and 1809640. M.C.G. acknowledges the support of the US Department of Energy's Fossil Energy Cross-Cutting Technologies Program at the National Energy Technology Laboratory (NETL) under the RSS contract, 89243318CFE000003. M.W. was supported through DOE grant SC-0014506 for the development of simulation methods. Atom probe tomography (APT) was conducted at Oak Ridge National Laboratory (ORNL)'s Center for Nanophase Materials Sciences (CNMS), which is a U.S. Department of Energy (DOE) Office of Science User Facility. The Neutron-scattering work was carried out at the Spallation Neutron Source (SNS), which is the U.S. DOE user facility at ORNL, sponsored by the Scientific User Facilities Division, Office of Basic Energy Sciences.

#### **6:20 AM F.SF06.02.11**

**Asymmetry of Element-Specific Lattice Distortion in 3D Transition Metal Based Complex Concentrated Alloys** Hyun Seok Oh<sup>1</sup>, Khorgolkhuu Odbadrakh<sup>2</sup>, Yuji Ikeda<sup>3,4</sup>, Sai Mu<sup>5</sup>, Fritz Koermann<sup>3,6</sup>, Chengjun Sun<sup>7</sup>, Hye Sang Ahn<sup>8</sup>, Kook Noh Yoon<sup>8</sup>, Duancheng Ma<sup>9</sup>, Cem Tasan<sup>1</sup>, Takeshi Egami<sup>10</sup> and Eun Soo Park<sup>8</sup>; <sup>1</sup>Massachusetts Institute of Technology, United States; <sup>2</sup>University of Tennessee and Oak Ridge National Laboratory, United States; <sup>3</sup>Max-Planck-Institut für Eisenforschung, Germany; <sup>4</sup>University of Stuttgart, Germany; <sup>5</sup>Oak Ridge National Laboratory, United States; <sup>6</sup>Delft University of Technology, Netherlands; <sup>7</sup>Argonne National Laboratory, United States; <sup>8</sup>Seoul National University, Korea (the Republic of); <sup>9</sup>Friedrich-Alexander-Universität, Germany; <sup>10</sup>The University of Tennessee, Knoxville, United States

Lattice distortion has been regarded as one of the four core effects of complex concentrated and high entropy alloys. Recently, it was shown that atomic-level pressure (or the misfit volume) in 3d transition metal element (V, Cr, Mn, Fe, Co, Ni)-based complex concentrated alloys (3d CCAs) with face-centered cubic structure originates from charge transfer between neighboring atoms, which suggests the electronic origin of lattice distortion, rather than a classical mechanical view mainly based on atomic size arguments. Here we show that the magnitude of the local lattice distortion of a specific element is strongly affected by its electronegativity. The trend is only little affected in the presence of short-range order. This study provides an important link between atomistic properties (electronegativity) and physical properties in 3d CCA, and rationalizes the proposed relation between lattice distortion and complexity-induced properties in 3d CCAs.

#### **6:30 AM F.SF06.02.13**

**Role of Local Chemical Order in Orientation Relationship Determination in an Al<sub>0.3</sub>CoCrFeNi High Entropy Alloy** Elaf A. Anber<sup>1</sup>, Daniel Foley<sup>1</sup>, Diana Farkas<sup>2</sup>, Peter Liaw<sup>3</sup> and Mitra L. Taheri<sup>1</sup>; <sup>1</sup>Johns Hopkins University, United States; <sup>2</sup>Virginia Tech, United States; <sup>3</sup>The University of Tennessee, United States

High entropy alloys (HEAs) have attracted the major interest due to their novel mechanical and structural properties. Local chemical ordering (LCO) plays an important role in determining thermal and electrical conductivity of solid solutions, diffusion, and passivity of alloys containing elements that are electrochemically active. Here, we describe that the change in LCO may promote formation of a distinct-uncommon crystal orientation relationship (OR) with the matrix. In this study, we examined the role of LCO on the OR of BCC precipitates in annealed Al<sub>0.3</sub>CoCrFeNi via using in-situ and ex-situ TEM heating techniques, where we report a new BCC-ORs due to local chemical fluctuations. These studies were coupled with Extended Electron Energy Loss Fine Structure (EXELFS) and Energy-dispersive X-ray spectroscopy (EDS). Overall, the LCO associated with ORs offers new opportunities to tune properties, enabling a more predictive view of phase transformation in this class of alloys.

SESSION F.SF06.03: Mechanical Behavior

On Demand Abstracts Available for Viewing Starting Saturday Morning, November 21, 2020  
F-SF06

#### 5:00 AM \*F.SF06.03.02

**Strength and Toughness in TRIP, TWIP and Dual-Phase CrMnFeCoNi High-Entropy Alloys** Bernd Gludovatz<sup>1</sup>, Hyun Seok Oh<sup>2</sup>, Eun Soo Park<sup>2</sup> and Robert Ritchie<sup>3,4</sup>; <sup>1</sup>UNSW Sydney, Australia; <sup>2</sup>Seoul National University, Korea (the Republic of); <sup>3</sup>Lawrence Berkeley National Laboratory, United States; <sup>4</sup>University of California, Berkeley, United States

Compositionally complex alloys, often termed high-entropy alloys (HEAs), are alloy systems with at least five principal elements in (near-)equiatomic ratios that are promising candidates for the development of materials with enhanced damage tolerance, i.e., that is a good combination of strength and toughness, which is key for the increasing complexity of energy-efficient and safety-critical applications. Despite containing elements with different crystal structures, the most studied HEA to date, the Cantor alloy CrMnFeCoNi, is a single-phase face-centered cubic (FCC) material that has been shown to exhibit strength levels above 1 GPa and fracture toughness values well above 200 MPa.m<sup>1/2</sup> at room temperature. Interestingly, the alloy's strength, ductility and fracture toughness improve simultaneously with decreasing temperatures, a trend that is the opposite for most other materials. This is achieved through a combination of sequentially triggered deformation mechanisms including planar dislocation slip, rapid motion of partial dislocations, near-tip crack bridging and deformation-induced nano-twinning. Based on our work on this alloy we will examine compositionally modified variations of this material that were designed with the aim to gradually lower stacking-fault energy. We will show how their failure resistance develops in the same temperature range when compositionally triggered deformation mechanisms such as transformation induced plasticity (TRIP) or twinning induced plasticity (TWIP) are enabled and additionally compare their behavior to a similar alloy that contains a second phase. Using a combination of advanced electron microscopy imaging techniques, we will show how deformation modes such as planar dislocation slip, deformation-induced nano-twinning, and transformation-induced plasticity control mechanical properties and highlight the importance of controlled triggering of each individual mechanism.

#### 5:15 AM F.SF06.03.03

**Dynamic Amorphization, Inverse Hall Petch Behavior and the Tribological Properties of High Entropy Alloys** Morgan R. Jones, Brendan Nation, Ping Lu, Andrew Kustas, Michael Chandross and Nicolas Argibay; Sandia National Laboratories, United States

We report on tribological investigations with an additively manufactured (AM) equiatomic CoCrFeMnNi high entropy alloy. As this work highlights, AM HEAs are a promising combination of advanced and processing techniques for next-generation structural and multi-functional devices, including applications where high-consequence and low volume drive design and qualification. The tribological, mechanical, and microstructural properties for this HEA in a range of environments are studied, including ultra-high vacuum (UHV), to highlight environment-dependent frictional and wear properties. We showed that low friction ( $\mu < 0.4$ ) and high wear resistance ( $K \sim 10^{-6} \text{ mm}^3/\text{Nm}$ ) are achievable with unlubricated high entropy alloys in inert environments and establish evidence of inverse Hall-Petch behavior by a recently proposed process of dynamic amorphization. We also discuss the origin of impressive wear resistance, linked to extreme grain refinement, that was achievable even in inert environments.

Sandia National Laboratories is a multimission laboratory managed and operated by National Technology & Engineering Solutions of Sandia, LLC, a wholly owned subsidiary of Honeywell International Inc., for the U.S. Department of Energy's National Nuclear Security Administration under contract DE-NA0003525. -or- if you have a character limit, you may use: SNL is managed and operated by NTESS under DOE NNSA contract DE-NA0003525.

#### 5:25 AM F.SF06.03.04

**High Entropy Alloy Displays Unique Strengthening and Deformation Pathways** Simon Tsianikas<sup>1</sup>, Yujie Chen<sup>1</sup>, Zonghan Xie<sup>1</sup>, Jiwon Jeong<sup>2</sup> and Siyuan Zhang<sup>2</sup>; <sup>1</sup>The University of Adelaide, Australia; <sup>2</sup>Max Planck Institute for Eisenforschung, Germany

Most of high entropy alloys (HEAs) with body centered cubic (BCC) structure suffer from limited plasticity at room temperature, which hinders their practical applications. To tackle this challenge, a Fe<sub>49.5</sub>Mn<sub>30</sub>Co<sub>10</sub>Cr<sub>10</sub>B<sub>0.5</sub> high entropy alloy with body centered cubic (BCC) structure was prepared by closed field unbalanced magnetron sputtering. The coating exhibits an excellent combination of strength and ductility (~ 2.8 GPa yield strength and ~ 40% compressive strain), which can be attributed to the synergy of multiple strengthening mechanisms, including transformation induced plasticity (TRIP) and twinning induced plasticity (TWIP) effect, compositional fluctuations, grain boundary engineering, grain refinement, and nanolaminate strain partitioning. A two-step phase transformation; namely, BCC to hexagonal closed packed (HCP) and then to face centered cubic (FCC) structure, was identified under applied load. On one hand, the phase transformation from BCC

to HCP and then to FCC structure, along with the formation of heterogeneous, bi-modal microstructure, works to absorb the strain and mitigate the stress concentration in the alloy. On the other hand, the increased phase boundaries generated by phase transformation pose as additional barriers to dislocation movements, providing extra strain hardening. The results of this work demonstrates that the two-step phase transformation is an effective mechanism that imparts the new HEA with appreciable damage tolerance while maintaining high strength.

#### 5:35 AM F.SF06.03.08

**Influence of Creep Tests Temperature on Sluggish Diffusion of the Single Crystalline High and Medium Entropy Alloys CrMnFeCoNi and CrCoNi** Christian Gadelmeier, Sebastian Haas and Uwe Glatzel; University of Bayreuth, Germany

The equiatomic, face centered cubic (fcc), single phase high and medium entropy alloys CrMnFeCoNi and CrCoNi are perfect candidates for the study of solid solution hardening in a statistically distributed crystal lattice. Both alloys show extraordinary properties compared to conventional alloys like nickel-based superalloys or steels, which is not expected for single face fcc materials. Previous investigations on CrMnFeCoNi and CrCoNi alloys have concentrated almost exclusively on polycrystalline structures.

This work focuses on the determination of the entropy effects of mechanical deformation on single crystalline (SX) single phase fcc alloys with 5, 3 and 1 component. Any influences such as grain size, grain boundary sliding and diffusion or effects due to precipitation can be isolated. Targeted creep tests under vacuum made it possible to eliminate the influence of oxidation at higher temperatures. These ideal conditions allow a direct comparison to study the solid solution strengthening effect towards to a higher configurational entropy depending on the temperature. Therefore, the alloys with different configurational entropy CrMnFeCoNi (Sconf = 1.61 J/(mol\*K), CrCoNi (Sconf = 1.10 J/(mol\*K), and pure nickel (Sconf = 0 J/(mol\*K), were chosen.

All alloys were cast in single crystalline state by using induction casting under argon atmosphere for further characterization. For the mechanical testing the miniature specimens are manufactured by electrical discharge machining (EDM) and tested in a radiation-heated vacuum creep device with a maximum temperature tolerance less than  $\pm 1$  °C. A main part of this work concentrated on the investigation of the dislocations in the alloys. This was realized over a wider temperature range from 700 °C to 1200 °C. Using stress levels of 2 MPa, the results of the creep tests provide quite different behavior of sluggish diffusion in the three tested alloys. The reason for this discrepancy was examined in more detail by electron channelling contrast imaging (ECCI) and transmission electron microscopy (TEM). Especially for this purpose some creep tests were interrupted and cooled down to room temperature under load, to examine the dislocation structure in the samples.

#### 5:45 AM F.SF06.03.09

**Discovery and Design of Fatigue-Resistant High-Entropy Alloys** Weidong Li, Peter Liaw and Shuying Chen; The University of Tennessee, Knoxville, United States

Fatigue resistance is a crucial requirement to the novel high-entropy alloys when they come to engineering applications, as many metal structures used in practice are failed by cyclic loading. Here, a thorough analysis of the information on the low-cycle fatigue, high-cycle fatigue, crack-growth rates, and fatigue mechanisms in the high-entropy alloy literature unveils a guideline through which the discovery and design of fatigue-resistant high-entropy alloys can be facilitated. Overall, multi-phase alloys, particularly the metastable ones, are favorable to fatigue resistance over single-phase alloys. Suggestions are proposed in the end to accelerate the discovery and design of candidates for fatigue-resistant applications.

#### 5:55 AM F.SF06.03.10

**Microstructure Evolution and Mechanical Properties at Intermediate to Elevated Temperatures of Refractory Mo-V-Nb-W-Ti High-Entropy Alloys** Maximilian Regenberg, Georg Hasemann, Markus Wilke, Thorsten Halle and Manja Krueger; Institute for Materials and Joining Technology, Germany

High-entropy alloys (HEAs) can either be defined as solid solution alloys containing at least 5 elements in equiatomic or near-equiatomic composition, or as alloys with high configurational entropies (larger than 1.5R), regardless of the number of elements involved [1]. In the present study we report on an alloy design route for refractory high-entropy alloys (RHEAs) based on equimolar Mo-V-Nb alloys with additions of W and Ti. In general, our work was motivated by Senkov et al. [2, 3] who investigated refractory HEAs based on Mo-Nb-W-Ta and Mo-V-Nb-W-Ta. Also to be noted is the US Patent published by Bei [4] in which a multi-component solid solution alloy with high entropy of mixing, namely Mo-V-Nb-W-Ti, has been mentioned. Senkov et al. investigated their alloys experimentally and showed that they have a single-phase body-centered



cubic (bcc) structure. It is assumed that the patented alloy Mo-V-Nb-W-Ti also consists of a single-phase bcc structure. The aim of our present experimental work was to produce and analyze a refractory high-entropy alloy of aforesaid composition with a single-phase structure and a reduced density, compared to Senkov's alloys, by replacing one and/or both of the heavy elements W and Ta with Ti. For this purpose, a systematic alloy design involving four- and five-element compositions was used. SEM (scanning electron microscopy) analysis have shown that Mo-V-Nb-xW-yTi ( $x=0, 20$ ;  $y=5, 10, 15, 20, 25$ ) is in fact a RHEA with a bcc dendritic structure. Furthermore, the Ti-concentration of the experimental alloys was varied within the composition interval between 5 at.% and 35 at.% as it is defined by Yeh [5], for each principle elements in HEAs, to obtain the influence of Titanium on the microstructure evolution. Additionally, compressive tests at elevated temperatures (in a range of 400-1100 °C) will be carried out to evaluate the influence of the different alloying elements and the Ti-fraction, on the mechanical properties. The observations of the present work are then compared to the published results on similar alloys from the group of K. F. Yao et al. and critically discussed [6, 7].

- [1] M. C. Gao, P. K. Liaw, J. W. Yeh, and Y. Zhang, *High-entropy alloys: Fundamentals and applications*, book, 2016.
- [2] O. N. Senkov, G. B. Wilks, D. B. Miracle, C. P. Chuang, and P. K. Liaw, "Refractory high-entropy alloys," *Intermetallics*, vol. 18, no. 9, pp. 1758–1765, 2010, doi: 10.1016/j.intermet.2010.05.014.
- [3] O. N. Senkov, G. B. Wilks, J. M. Scott, and D. B. Miracle, "Mechanical properties of Nb<sub>25</sub>Mo<sub>25</sub>Ta<sub>25</sub>W<sub>25</sub> and V<sub>20</sub>Nb<sub>20</sub>Mo<sub>20</sub>Ta<sub>20</sub>W<sub>20</sub> refractory high entropy alloys," *Intermetallics*, vol. 19, no. 5, pp. 698–706, 2011, doi: 10.1016/j.intermet.2011.01.004.
- [4] H. Bei, "Multi-component solid solution alloys having high mixing entropy," USA Patent No US 2013/0108502 A1. 2013.
- [5] J. W. Yeh, "Alloy design strategies and future trends in high-entropy alloys," *Jom*, vol. 65, no. 12, pp. 1759–1771, 2013, doi: 10.1007/s11837-013-0761-6.
- [6] Z. D. Han *et al.*, "Effect of Ti additions on mechanical properties of NbMoTaW and VNbMoTaW refractory high entropy alloys," *Intermetallics*, vol. 84, pp. 153–157, 2017, doi: 10.1016/j.intermet.2017.01.007.
- [7] Z. D. Han *et al.*, "Microstructures and mechanical properties of TixNbMoTaW refractory high-entropy alloys," *Mater. Sci. Eng. A*, vol. 712, no. December 2017, pp. 380–385, 2018, doi: 10.1016/j.msea.2017.12.004.

#### 6:05 AM F.SF06.03.12

**Dynamic Behavior of CrMnFeCoNi High-Entropy Alloy** Zezhou Li<sup>1,2</sup>, Shiteng Zhao<sup>3</sup>, Carlos J. Ruestes<sup>4</sup>, Wen Yang<sup>1</sup>, Bingfeng Wang<sup>5</sup>, Yong Liu<sup>5</sup>, Nathan Mara<sup>2</sup>, Robert Ritchie<sup>3</sup> and Marc A. Meyers<sup>1</sup>; <sup>1</sup>University of California, San Diego, United States; <sup>2</sup>University of Minnesota, Twin Cities, United States; <sup>3</sup>Lawrence Berkeley National Laboratory, United States; <sup>4</sup>Universidad Nacional de Cuyo, Argentina; <sup>5</sup>Central South University, China

High impact resistance of the annealed and pre-deformed equiatomic CrMnFeCoNi high-entropy alloys (HEAs) is expected from their excellent high-strain-rate plasticity. Its underlying deformation mechanisms under dynamic loading have been identified by both experiments and simulation. The microstructures of alloys after dynamic loading have been revealed by (high-resolution) transmission electron microscopy. The high strain-hardening ability of the CrMnFeCoNi HEA (enabled by solid-solution hardening, forest dislocation hardening, twinning hardening, and phase transformation), a marked strain-rate sensitivity and modest thermal softening, result in an excellent resistance to shear localization. For the annealed CrMnFeCoNi alloy, a shear strain of  $\sim 7$  has been discovered as required for the shear-band propagation (using a hat-shaped specimen that enables one single shear band to initiate and grow). Additionally, the pre-deformed CrMnFeCoNi alloy obtains an even higher absorbed impact strain energy (under similar loading conditions). The remarkable high-strain-rate plasticity is significant for its structural applications.

#### 6:15 AM F.SF06.03.13

**Deformation by "Faulting" in Complex Concentrated Alloys?** Shaolou Wei and Cem Tasan; Massachusetts Institute of Technology, United States

Crystalline defects are of fundamental importance in understanding and thereby tailoring the macroscopic mechanical responses of complex concentrated alloys (CCAs). Particularly in the context of microstructural metastability engineering, appreciable interest has aggregated in transformation-induced plasticity or twinning effect. However, the inherent operative unit for the foregoing deformation mechanism, stacking faults, has not yet drawn abundant attention. By investigating a CoCrNiW CCA, we will reveal in this presentation a lesser-explored deformation "faulting" response. Through coupled in-situ synchrotron and electron channeling contrast imaging (ECCI) experiments, we will show that it is the nucleation of extensive stacking faults that is acting as the major plasticity carrier within this CCA, providing macroscopic strain hardenability, and thereby suppressing the formation of the blocky HCP-martensite. We will demonstrate through

computational thermodynamic approach that this sort of faulting mechanism is largely ascribed to a negative intrinsic stacking fault energy, for which our in-situ ECCI deformation experiment will reveal a direct validation. Broader insights into the role of multi-layer generalized stacking fault energy landscape will also be discussed in a sense to complement the current thermodynamic-guided design strategy of metastable CCAs or high-entropy alloys.

#### 6:25 AM F.SF06.03.16

**Late News: High-Temperature Tensile Creep Properties and Microstructure of a CrMnFeCoNi High Entropy Alloy** Mingwei Zhang<sup>1</sup>, Easo P. George<sup>2,3</sup> and Jeffrey C. Gibeling<sup>1</sup>; <sup>1</sup>University of California, Davis, United States; <sup>2</sup>Oak Ridge National Laboratory, United States; <sup>3</sup>The University of Tennessee, Knoxville, United States

High entropy alloys (HEAs) can exhibit good combinations of mechanical properties, thermal stability, and corrosion resistance that are critical for high-temperature applications. However, their suitability for service at elevated temperatures under creep conditions has not been explored in detail. In addition to understanding how the special attributes of the concentrated solid solution matrix influence creep, knowledge of the creep properties and deformation mechanisms of the HEA is a prerequisite for further consideration of engineering the material for creep resistance through precipitation or dispersion strengthening. In the present study, constant stress creep tests on an FCC single-phase CrMnFeCoNi were conducted under vacuum between 1023 K and 1173 K. The stress exponent was found to be  $3.7 \pm 0.1$  over all temperatures and stresses. The apparent activation energy of creep was determined to be lower than that for lattice self-diffusion. No significant change in grain size and texture was observed during creep deformation. The steady-state creep microstructure is characterized by highly entangled dislocations networks without subgrain boundary formation. This structure resembles that of low and room temperature deformation at high plastic strain for CrMnFeCoNi and is unlike the creep microstructure of conventional alloys. This observation suggests that the dislocations in CrMnFeCoNi feature more rapid multiplication than in Class A alloys and more sluggish recovery than in Class M alloys.

#### 6:35 AM F.SF06.03.17

**Late News: A High Entropy Alloy for High Temperature Applications** Kevin Garber and Bhaskar S. Majumdar; New Mexico Tech, United States

We report our investigation of high entropy alloys (HEA) for use in the range 600 – 900C, for turbine engine applications. The goal was to evaluate whether the high configurational entropy of HEAs would permit high temperature strengths that were competitive with superalloys while offering a lower density. CALPHAD based alloy design relied on forming a high volume fraction of L1<sub>2</sub> precipitates in an fcc matrix for high temperature strength and creep resistance, while minimizing brittle phases and reducing density. Samples of screened alloys were prepared by arc melting and suction cast into 3 mm diameter rods. Compression tests of the final alloy ( $\Delta S_{\text{config}}=1.62$ ) up to 871 C revealed that it had a 0.2% offset yield strength of 950 MPa at 750 C, which is not only competitive with most superalloys ( $\Delta S_{\text{config}} \leq 1.3$ ) but bettered the best high temperature HEA to date. The density was approximately 7.9 gm/cc, giving the alloy specific strength advantage over existing superalloys. TEM revealed important composition trends in the precipitate phase, and possibly a result of high alloy content influencing atomic partitioning. The microstructure and mechanical properties will be discussed.

SESSION F.SF06.04: Microstructure Evolution and Properties  
On Demand Abstracts Available for Viewing Starting Saturday Morning, November 21, 2020  
F-SF06

#### 5:00 AM \*F.SF06.04.01

**Effect of Phase Stability on Nanograin Formation and in Fcc High-Entropy Alloys** Koichi Tsuchiya<sup>1,2</sup> and Jein Lee<sup>3</sup>; <sup>1</sup>National Institute for Materials Science, Japan; <sup>2</sup>University of Tsukuba, Japan; <sup>3</sup>Pusan National University, Korea (the Republic of)

FCrMnFeCoNi high-entropy alloy, known as Cantor alloy, exhibits enhanced ductility and high fracture toughness at cryogenic temperatures. This anomalous damage tolerance was attributed to the formation of nanotwins at lower temperatures. Such study motivated the extensive investigations on fcc high/medium entropy alloys, but major effort has been on the search for new compositions and mechanical properties, while the effect of phase transformation on mechanical properties or microstructure formation is not well-understood.

In the present study, a series of high-entropy alloys with different fcc/hcp phase stability was designed and the deformation behavior and microstructures were investigated. They were also subjected to severe plastic deformation (SPD) by high-pressure torsion (HPT). The process of grain refinement was compared for different alloys.

Ingots of Cr<sub>20</sub>Mn<sub>20</sub>Fe<sub>20</sub>Co<sub>40-x</sub>Ni<sub>x</sub> (x=0~20) was prepared by high-frequency melting. They were then hot forged and rolled into bars. They are heat treated at 1473 K for 48 hrs followed by water quench. In as-quenched condition, the samples with 0~10mol%Ni were composed of hcp phase and fcc phase, while others are in a fcc single phase state.

Room temperature tensile tests revealed that yield stress does not depend on Ni content while tensile strength and total elongation depends strongly on Ni content. The best strength-elongation balance was obtained in the 10Ni and 15Ni samples. X-ray diffraction and EBSD revealed deformation induced fcc-hcp transformation (5Ni) and pronounced twinning (10Ni), both of them led to pronounced work hardening. Sample with hcp phase exhibited higher strength but lower ductility than those of fcc single phase samples.

The 10 mmΦ disks of 0~20Ni alloys were deformed by HPT under an applied compressive stress of 5 GPa up to 10 rotations of the anvils. For the samples with 15~20Ni, HPT led to a drastic increase in the value of micro Vickers hardness (Hv). Hv was about 125 in an as-quenched sample; it increased to about 320Hv in the center of the disk and to about 420Hv at peripheral positions even after 0.25 rotation. This can be attributed to rapid progress of grain refinement. BSD-SEM observations revealed that pronounced formation of lamellar structures with about 100 nm width separated by nanotwins. The formation of lamellar limits the mean-free path of dislocations and accelerate dislocation density increase which leads to formation of equiaxed nanograins (~50 nm) by continuous dynamic recrystallization. The observed behavior was similar to low stacking fault materials such as SUS316 or Cu-Al alloys. It was found the with decreasing Ni content and volume fraction of fcc phase resulted in less pronounced hardening and grain refinement by HPT deformation, which may be due to limited number of slip systems in hcp. <gdiv></gdiv>

5:15 AM \*F.SF06.04.03

**Microstructural Formation and Thermal Stability in Refractory Metal High Entropy Superalloy Systems** Nicholas Jones; University of Cambridge, United Kingdom

In just ten years, research that evolved from equiatomic combinations of refractory metal elements has led to the discovery of a new class of materials that has great potential for high temperature service. The so called refractory metal high entropy superalloys (RMHES) exhibit fine-scale two-phase microstructures comprising small coherent cuboidal precipitates of one phase within a matrix of the other. Visually, these microstructures are similar to those of Ni-based superalloys, and the similarities continue in that both phases have cubic structures with similar lattice parameters and one phase is a superlattice structure of the other. However, there are two key differences between RMHES and conventional superalloys. First, RMHES are based on a body centred unit cell and not the face centred form, which may have implications for a range of material properties. Second, in current RMHES, the matrix phase has the ordered CsCl (B2) structure whilst the precipitates are a disordered *bcc* solid solution phase, the inverse configuration to that found in Ni-based systems. The presence of an ordered matrix leads to concerns with respect to ductility and toughness, both of which are key parameters for many industrial applications. Despite this, initial mechanical property data from these alloys is extremely promising with the state-of-the-art material, AlMo<sub>0.5</sub>NbTa<sub>0.5</sub>TiZr, exhibiting a 0.2% proof stress of 2 GPa at room temperature and ~1.6 GPa at 800°C. In addition, the incorporation of a significant quantity of Al, Ti and Zr means that the density of this alloy is 7.4 g.cm<sup>-3</sup>, well below that of Ni-base superalloys. As such, RMHES show great potential as an alternative or complementary option to conventional Ni-base superalloys for elevated temperature service.

However, there is still a huge amount to learn about these new materials and several aspects of their metallurgy require further investigation. In particular, work is required to understand the microstructural formation pathway, to elucidate the mechanism by which the two phases form and evaluate whether their configuration can be inverted. Similarly, it is critical to assess the stability of the fine-scale two-phase microstructure during prolonged exposure to likely service temperatures, particularly given the detrimental effect that topologically close packed phases are known to have on the properties of other high temperature alloys.

One of the challenges in studying the microstructural formation and stability of these materials is their inherent compositional complexity, which makes it difficult to identify the effects of individual alloying elements. As such, our approach has been to elucidate the critical mechanisms through the characterisation of key compositionally simpler constituent systems.

Consequently, this talk will present data from a number of systematically varying alloy series, that build in complexity from ternary to senary systems. The results of these studies will be used to discuss how the fine-scale microstructure observed in these alloys arises, identify the role of specific key elements and determine the phase equilibria, and hence stability, of the microstructure following long duration thermal exposures. Such information will be critical in the continued development of RMHES and the determination of a commercially viable high temperature alloy.

**5:30 AM F.SF06.04.06**

**Visualizing Phase Stability in High Entropy Alloys** Daniel Evans, Jiadong Chen and Wenhao Sun; University of Michigan–Ann Arbor, United States

The identification of promising solid-solution regions in High Entropy Alloy composition space is hindered by the lack of suitable tools to visualize stability relationships in high-component systems. Traditional phase diagrams use barycentric coordinates to represent composition axes, requiring  $D = (N - 1)$  spatial dimensions to visualize an  $N$  component system. This means that systems with  $\geq 4$  components cannot be visualized on traditional phase diagram axes. We propose forgoing barycentric composition axes in favor of two energy axes: a formation-energy axis and a ‘reaction energy’ axis. These two dimensional visualizations are successful in capturing complex stability relationships in  $N \geq 5$  component systems. By constructing temperature-dependent phase stability graphs, we show that these visual tools can both rationalize high-level qualitative statements regarding the quench-ability of metastable HEA solid-solutions as well as illuminate details about compositional phase-separation.

**5:40 AM F.SF06.04.07**

**Is My Alloy Single Phase? A Simulated X-Ray Diffraction Study of the Detection Limit of Secondary Phases in High-Entropy Alloys** Howie Joress, Brian L. DeCost and Jason R. Hattrick-Simpers; National Institute of Standards and Technology, United States

In the high-entropy alloy (HEA) community, it is often a goal to find compositions that are stable as single phases. This single-phase label is often applied based on interpretation of powder x-ray diffraction (XRD), specifically the lack of a detectable peak not indexable to the HEA phase. While scientifically important in general, accuracy of these labels is particularly crucial for accurate machine learning based models in these systems. Depending on many factors, including background levels, signal-to-noise ratio (SNR), grain size and other peak broadening effects, and peak overlap, detection of these secondary phase peaks can be quite difficult. For instance, we show that in a compositionally varying NbTiTa film, the portion of the film in which we can identify the presence of a secondary phase varies considerably based on XRD collection time (and thereby SNR). To quantify this effect in a broad way, we simulated XRD patterns from a common HEA phase with a distinct secondary phase, varying sample and measurement factors including SNR, phase fraction, peak spacing, peak widths, and background level. Each pattern is fit with two models, an HEA specific model and a two phase model having at least one extra peak compared to the HEA model. We then use a Bayesian information criterion based on these fits to apply a single-phase and dual-phase label to the simulated data, so that we can clarify the role of each nuisance factor on the detection limit for secondary phases. We demonstrate that under realistic sample and diffraction conditions, even with idealized simulated data, a secondary phase can remain obscured even at the several percent phase fraction level. We hope this data set can act as a guide for understanding a reasonable lower limit for phase detection and will facilitate a conversation leading to improved standards for data quality when applying phase labels in the HEA space and beyond.

**5:50 AM F.SF06.04.09**

**A High-Throughput Investigation of the Compositional Effects on Phase Stability and Mechanical Properties in Nb-Ti-V-Zr** Mu Li, Zhaohan Zhang, Arashdeep S. Thind, Guodong Ren, Rohan Mishra and Katharine Flores; Washington University in St. Louis, United States

Refractory complex concentrated alloys (RCCAs) open new opportunities for high-temperature structural applications that require a combination of high strength, high melting point, good ductility, low density etc. Despite the vast compositional space due to the presence of multiple principal elements, current design of RCCAs is mostly focused on equiatomic compositions to increase stability of single solid solution BCC phase, and to avoid formation of brittle intermetallic phases. Nevertheless, the knowledge of what competing phases are and their stability dependence on each element is yet to be broadened to optimize the development of RCCAs. In this work, we start with an equiatomic NbVZr alloy, which is one of the two multi-phase-forming ternary compositions in the Nb-Ti-V-Zr system. Besides a BCC majority phase, we identified two Laves phases, cubic C15 and hexagonal C14 phases, of which C14 was previously reported to be unstable. With first principles calculations, we determine the stable composition for each phase, and a good consistency is found with the experimental results. The Laves phases are more compliant than BCC, but they strengthen the material, as measured by nanoindentation. Ongoing work expands the scope to non-equiatomic compositions to better understand elemental effects on the alloy’s phase selection and properties. We apply combinatorial methods to synthesize Nb-Ti-V-Zr compositional libraries via direct laser deposition, which facilitates the high-throughput identification of different phases, microstructures and mechanical properties as a function of composition. This work also provides guidelines for exploration of compositional effects in all RCCA systems; a complete knowledge of the role each element plays will significantly expedite the design of

RCCA candidates for high-temperature applications.

#### 6:00 AM F.SF06.04.10

##### **Late News: High Temperature Crystal Structure and Microstructure Evolution in High-Entropy Alloys CoCrFeNiX (X = Al, Ti, Cu, Mn) Produced by Mechanical Alloying** Alexander S. Rogachev<sup>1,2</sup>, Dmitrii Y. Kovalev<sup>1</sup>, Sergei G.

Vadchenko<sup>1</sup>, Nikolai A. Kochetov<sup>1</sup>, Natalia Shkodich<sup>1</sup>, Alexander S. Shchukin<sup>1</sup>, Kirill V. Kuskov<sup>2</sup>, Anna V. Panteleeva<sup>2</sup> and Alex Mukasyan<sup>3</sup>; <sup>1</sup>Russian Academy of Sciences, Russian Federation; <sup>2</sup>National University of Science and Technology “MISIS”, Russian Federation; <sup>3</sup>University of Notre Dame, United States

High-entropy alloys (HEA) were initially regarded as stable single-phase disordered solid solutions with fcc or bcc structures stabilized by increased configurational entropy [1,2]. Later, a question about possible metastability of these phases arose [3], and currently the most of the known HEAs recognized as metastable materials [4]. Decomposition of the metastable HEA phases results in (i) precipitation of new phases (intermetallic,  $\sigma$ -,  $\eta$ -, etc.) and (ii) crystal structure changes in the initial major multicomponent phase. Both these effects are equally important for understanding stability and metastability of HEAs. However, most of the known up-to-now works derive metastability of HEAs from the experimentally observed precipitation of secondary phases after annealing, and less attention was paid to evolution of the matrix phase, which commonly remains multicomponent. Thus, a question arises concerning “final destination” of major fcc and bcc high-entropy phases after long-term annealing: will they finally transform into stable HEA or decay down to simple ordered phases, such as intermetallic and binary (ternary) solid solutions?

A task of this work is to reveal *in situ* fine crystal structure transformations in the major fcc and bcc phases of the 3d-transition metals high-entropy alloys CoCrFeNiX, where X = Al, Ti, Cu, or Mn.

A uniform high entropy alloys were produced in a powdered form by fast (90-120 min) mechanical alloying in the planetary mill. The powders were annealed at different temperatures, up to 1473 K in vacuum, with simultaneous X-ray diffraction analysis. Compacted bulk samples were obtained using Spark Plasma Sintering (SPS) method. Structure and properties of the powders and bulk samples were studied with XRD, SEM, EDS, TEM and other methods.

Several specific transformations of crystal structure and microstructure were detected for different studied HEAs. They involve shrinking and expansion of crystal lattice, co-existence of two FCC phases, transformations of BCC into FCC phase, and, possibly, martensitic-like transformation of cubic into tetragonal phase. Shrinking of the atomic structures were detected for all phases after annealing in the temperature range 873 – 1273 K for 5 – 6 h. A drift of the (111) peak regarding to (200) peak of the fcc phase CoCrFeNiAl at 1273 K allow assumption of weak martensitic transformations: high-temperature cubic phase turns into slightly tetragonal ( $c/a = 1.00123$ ) phase at room temperature. Despite of the structural transformations, the alloys remains multi-principal elemental (high-entropy) after annealing.

This research was done at the expense of grant from Russian Science Foundation (Project No. 20-13-00277). Use of the Spark Plasma Sintering set-up was possible due to support from the Ministry of Education and Science of the Russian Federation under the Competitiveness Enhancement Program of NUST MISiS (Grant no. K2-2020-015).

References.

- [1] J.-W. Yeh, S.-K. Chen, S.J. Lin, J.-Y. Gan, T.-S. Chin, T.-T. Shun, C.-H. Tsau, S.-Y. Chang, *Adv. Eng. Mater.* 6(5) (2004) 299-303.
- [2] B. Cantor, I.T.H. Chang, P. Knight, A.J.B. Vincent, *Mater. Sci. Eng. A* 375-377 (2004) 213-218.
- [3] B. Cantor, *Ann. Chim. Sci. Mat.* 32(3) (2007) 245-256.
- [4] S.A. Kube, J. Schroers, *Scripta Mater.* 186 (2020) 392-400.

SESSION F.SF06.05: Theory, Simulation and Modeling

On Demand Abstracts Available for Viewing Starting Saturday Morning, November 21, 2020

F-SF06

#### 5:00 AM \*F.SF06.05.01

##### **Machine Learning-Assisted *Ab Initio* Exploration of High-Entropy Alloys** Alexander Shapeev; Skoltech, Russian Federation

High-entropy alloys possess unique properties such as long decomposition time of their metastable random solution phase. Being favorable from the point of view of applications, this property also manifests a challenge to their experimental study: it requires long annealing times to observe alloy decomposition. This opens avenues for application of *ab initio* methods which, in their turn, encounter the problem of large supercells and long simulation times which are beyond the capabilities of

modern supercomputers. Machine learning hence comes to the stage as a tool to accelerate ab initio calculations through learning from a limited number or relatively small-scale calculations and using the efficient machine-learned model in full-scale simulations.

Application of machine learning, in its turn, faces difficulties originating from the vast configurational space of high-entropy alloys. Indeed, there are about 300 different nearest-neighbor atomic environments in an fcc-based binary alloy (after applying symmetries), while this number for a five-component alloy is about 25 million. Such a large configurational space is harder to cover in interatomic interaction models, which typically manifests in degradation of their accuracy. For instance, when using cluster expansion - a data-driven model used to model configurational lattice entropy - it gets harder to maintain the meV accuracy of the model with adding more and more elements into the model. Also, the accuracy of interatomic potentials that are used to model alloys at vibrational time scales, degrade with increasing chemical complexity.

In my talk I will present some of the latest developments in machine learning-assisted ab initio modeling of entropic effects in high-entropy alloys. Namely, I will show how one can use machine-learning interatomic potentials to accurately study elastic properties, thermal expansion, short-range order, and stability of phases of prototypical medium-entropy and high-entropy alloys.

**5:15 AM \*F.SF06.05.02**

**Estimation of Material Parameters in High-Entropy Alloy by Adjoint Method Derived from Phase-Field**

**Method** Toshiyuki Koyama; Nagoya University, Japan

Recently, high-entropy alloys (HEAs) have attracted attention as a new category of advanced metal materials, and large amount of effort are concentrated to explore the solid solution single phase of HEAs because of their excellent mechanical properties. Latest development of HEAs extends not only to structural materials but also high-performance functional materials. Although attention is often paid on the single phase HEAs, the most important contribution of HEAs to physical metallurgy and alloy engineering must be its application to the matrix phase of multi-phase microstructures, i.e. the HEAs are utilized as a matrix phase of structural materials with multi-phase microstructures. High strength and good ductility of HEAs provide ideal properties as a matrix phase of microstructure, and there is a great choice because of a large variety of HEAs, the element combination in HEAs with considering the composition variation is almost infinite. Up until now, alloy systems have been categorized into Fe-based alloys, Ni-based alloys and so on, focusing on the principle element in the matrix phase. Therefore, so to speak, "HEA-based alloys" must be the ultimate alloy system in the history of metallurgy.

In order to carry forward the development of "HEA-based alloys", it is convenient that we are able to utilize the conventional approaches for alloy design based on phase diagrams and phase transformations. However, we always encounter the difficulty because the phase diagram of multi-component alloy systems, in particular high composition region in the phase diagram, is unknown in many cases, and the most of phase transformations observed in multi-component alloy systems is quite complicated. Therefore, the fundamental issues to boost up materials design in the field of HEAs are (1) the effective and accurate assessment of phase diagrams and Gibbs energies in the wide composition range of multi-component alloy systems, and (2) the rapid optimization of materials properties and microstructures within the diverse space of materials parameters and process conditions. In order to overcome these issues, we focused on the following three targets in this study: (i) First-principles calculation on the phase diagram of HEAs and re-assessment of the Gibbs energy database with Calphad approach, (ii) Comprehensive evaluation of materials parameters in Gibbs energy functions and diffusion mobility functions based on the phase-field method with data assimilation techniques by using the kinetic data of microstructures, and (iii) Effective optimization of materials properties and microstructures accelerated by several machine learning techniques. The objective of this study is to provide the efficient strategy in materials science and engineering to handle HEAs on a daily basis.

In particular, as the phase-field method coupled with data science technique is an interesting topic in this approach, the recent results obtained from this study are demonstrated in the presentation. We applied one of the data assimilation techniques "Adjoint method" to the phase-field theory, which derives the adjoint equations in conjunction with phase-field method, and the thermodynamic parameters in Gibbs energy function and the atom diffusivities in HEAs are estimated from the experimental data of composition profiles of HEAs, which is obtained by the conventional diffusion couple investigation on HEAs. As a result, materials parameters are reasonably and efficiently determined in this methodology. It should be emphasized that the inverse problem implemented with phase-field method is quite useful because there are a lot of materials parameters and process conditions utilized in phase-field simulations, and the large amount of experimental microstructure data required for data assimilation process is now available due to the recent development of material characterization devices and techniques.

**5:30 AM \*F.SF06.05.03**

**Atomic Scale Computational Investigations of Dislocations in bcc High Entropy Alloys** Sheng Yin<sup>1,2</sup>, Yunxing Zuo<sup>3</sup>, Jun Ding<sup>4</sup>, Robert Ritchie<sup>1,2</sup>, Shyue Ping Ong<sup>3</sup> and Mark Asta<sup>1,2</sup>; <sup>1</sup>University of California, Berkeley, United States; <sup>2</sup>Lawrence Berkeley National Laboratory, United States; <sup>3</sup>University of California, San Diego, United States; <sup>4</sup>Xi'an Jiaotong University, China

In traditional body-centered cubic (bcc) metals, the core properties of screw dislocations play a critical role in plastic deformation at low temperatures. Recently, much attention has been focused on refractory high-entropy alloys (RHEAs), which also possess bcc crystal structures. In this presentation we present results on dislocation core structures and their mobilities in bcc HEAs, including effects of chemical short-range order (SRO) in these multiple principal element alloys. Specifically, using density functional theory (DFT), we investigate the distribution of dislocation core structures and energies in MoNbTaW RHEAs alloys, and how they are influenced by SRO. The average values of the core energies in the RHEA are found to be larger than those in the corresponding pure constituent bcc metals, and are relatively insensitive to the degree of SRO. However, the presence of SRO is shown to have an effect on narrowing the distribution of dislocation core energies and decreasing the spatial heterogeneity of these energies in the RHEA. It is argued that the consequences for the mechanical behavior of HEAs is a change in the energy landscape of the dislocations which would likely heterogeneously inhibit their motion. We also present results of molecular dynamics simulations using a machine-learning potential for MoNbTaW RHEAs, that is shown to reproduce well the DFT results for distribution of core energies. The simulations investigate dislocation motion for both screw and edge dislocations, and are analyzed in terms of the nature of the mechanisms of motion and pinning induced by spatial heterogeneities in the RHEA. This research was supported by the US Department of Energy, Office of Science, Office of Basic Energy Sciences, Materials Sciences and Engineering Division, under contract no. DE-AC02-05-CH11231 within the Damage-Tolerance in Structural Materials (KC 13) program.

**5:45 AM F.SF06.05.07**

**Continuous Modeling of Dislocations in Random fcc Alloys** Ali Rida<sup>1</sup>, David Rodney<sup>2</sup>, Enrique Martinez<sup>3</sup> and Pierre-Antoine Geslin<sup>1</sup>; <sup>1</sup>INSA LYON, France; <sup>2</sup>Université Claude Bernard Lyon 1, France; <sup>3</sup>Los Alamos National Laboratory, United States

The motion of dislocations and their interactions with obstacles control the mechanical behavior of metals and alloys. In disordered random alloys such as binary solid solutions or high entropy alloys, the random distribution of atoms generates internal stresses that impede the motion of dislocations, leading to improved mechanical properties. Understanding the interactions between dislocations and this structural environment is crucial to better predict the mechanical properties of the alloys.

In this context, we investigated the behavior of a dislocation evolving in a random solid solution by means of a continuous elastic model based on previous work [1]. In a first step, using micro-elasticity theory, we derived general expressions for the spatial correlations of the stress and displacement fields emerging from elastic interactions of different atoms in random alloys. This approach is based on the definition of eigenstrains associated with each atomic lattice site in a linear elastic medium. In particular, we show that in the case of isotropic elasticity the spatial correlations of the displacement and stress fields follow  $1/d$  and  $1/d^3$  behaviors respectively.

In a second step, the influence of the random solid solution is assessed by relaxing a dislocation line in a noisy stress environment. The nature of the noise (amplitude and spatial correlations) is carefully implemented using the developed analytic expressions to mimic the stress environment of atomistic random solid solutions. This approach allows us to characterize the shape of the dislocation represented as a power spectrum, as well as model quantitatively the dislocation behavior in a random structural environment without integrating the dynamics of individual atoms. Finally, the results obtained from the continuous model are compared with atomistic simulations performed in Al<sub>50</sub>-Mg<sub>50</sub> random alloys, and the assumptions used in previous models in the literature [2] are discussed in light of the present findings.

#### REFERENCES

- [1] P.A. Geslin, D. Rodney. "Thermal fluctuations of dislocations reveal the interplay between their core energy and long-range elasticity." *Physical Review B* 98 (2018), 174115.
- [2] C. Varvenne, A. Luque, W.A. Curtin. "Theory of strengthening in fcc high entropy alloys." *Acta Materialia* 118 (2016),164-176.

**5:55 AM F.SF06.05.08**

**Machine Learning Formation Enthalpy of Compositionally Complex Intermetallics** Zhaohan Zhang, Mu Li, Katharine Flores and Rohan Mishra; Washington University in St. Louis, United States

Strengthening high entropy alloys (HEAs) via secondary intermetallic phases has been proven to be an effective approach experimentally. However, the design of intermetallic phases in HEAs for property enhancement is challenging due to the limited understanding of intermetallics in compositionally complex space. While density-functional-theory (DFT)-based methods have promoted design of binary and ternary intermetallics, they are not amenable for rapidly screening the vast combinatorial space of HEAs. In this work, we have developed a machine learning model to accelerate the discovery of intermetallics by predicting their formation enthalpy given only the composition. The model uses easily accessible elemental properties as descriptors and has a mean absolute error (MAE) of  $\sim 0.044$  eV/atom for a testing set of binary alloys. We use the ML model to successfully identify new binary intermetallics that are subsequently confirmed using DFT. The model trained with binary intermetallics can predict ternary intermetallics with a MAE of  $\sim 0.057$  eV/atom without further training. We further extend this model to multi-element systems and guide the prediction of compositionally complex intermetallics that may form in HEAs.

Acknowledgements: This work was supported by the National Science Foundation through grant number DMR-1809571.

#### 6:05 AM F.SF06.05.12

**Late News: Theory and Simulation of Interdiffusion in Multicomponent Systems—A Challenge** Andrei V. Nazarov<sup>1,2</sup>; <sup>1</sup>National Research Nuclear University MEPhI, Russian Federation; <sup>2</sup>Institute for Theoretical and Experimental Physics named by A.I. Alikhanov of National Research Center "Kurchatov Institute", Russian Federation

Multi-principal-element alloys (high-entropy alloys) have attracted worldwide attention because they open up a vast compositional space in which different kinds of materials may be discovered [1] and the understanding of the diffusion kinetics in HEAs is of fundamental significance [2]. We examine the interdiffusion in multicomponent systems using the approach analogically to one developed earlier for description of interdiffusion in binary alloys [3-5]. In opposite to traditional theory this approach takes into consideration an active role of vacancies, equilibrium distribution of which is not supposed, therefore there are contributions in equations for component fluxes, conditioned by vacancy concentration gradient. We have developed the system of diffusion equations for components and vacancies after substituting the expressions for fluxes in the equations of a continuity. Solutions of the equations show that the vacancy concentration's deviation from the equilibrium one equalize the fluxes of components [3] and component profiles are determined by interdiffusion coefficient. This coefficient [3-5] differs from traditional one (Darken's approach).

A direct generalization of the theory to the case of multicomponent systems meets with serious mathematical complexities. Therefore, we developed a new version of the equations linearization of the original system. The system of linearized equations is solved and we have found a relation between the interdiffusion coefficients and the corresponding tracer diffusion coefficients. Interdiffusion coefficient equations significantly differ from traditional one (Darken's approach). Then we numerically simulate interdiffusion in some alloys and analyze interdiffusion in high-entropy alloys, a possibility of sluggish diffusion in these alloys and the reasons of this effect. Using results the applicability of the quasi-binary approximation is analyzed in calculating the diffusion coefficients in multicomponent alloys.

[1] B. Cantor, I.T.H. Chang, P. Knight, A.J.B. Vincent, *Mater. Sci. Eng. A* **375-377**, 213 (2004).

[2] D. Gaertner, K. Abrahams, J. Kottke, V.A.Esin, I. Steinbach, G.Wilde, S.V. Divinski, *Acta Mater.* **166**, 357 (2019).

[3] A.V. Nazarov, K.P. Gurov, *Phys. Metals and Metallography* **37**, 41 (1974).

[4] A.V. Nazarov, K.P. Gurov, *Phys. Metals and Metallography* **38**, 30 (1974).

[5] A.V. Nazarov, K.P. Gurov, *Phys. Metals and Metallography* **45**, 185 (1979).

SESSION F.SF06.06: Poster Session: High-Entropy and Compositionally Complex Alloys  
On Demand Abstracts Available for Viewing Starting Saturday Morning, November 21, 2020

5:00 AM - 8:00 AM

F-SF06

#### F.SF06.06.01

**The Effects of Ti and Si on Mechanical Properties of CoCrFeMnNi-Based Face-Centered Cubic Single-Phase Alloy** Syuki Yamanaka, Ken-ichi Ikeda and Seiji Miura; Hokkaido University, Japan

Cantor alloy, which is a face-centered cubic (fcc) high entropy alloy composed of the equiatomic ratio of Co, Cr, Fe, Mn, and Ni, has been attracting attentions as structural materials because of its good strength–ductility balance. By introducing a



secondary strengthening phase to the Cantor-based fcc matrix, the development of materials with an excellent balance of strength and ductility is expected. We selected Ti and Si as additive elements. We investigated the phase equilibrium of Ti or Si added Cantor alloy and found that these elements introduce some secondary phases such as Laves phase,  $\alpha$ Mn structure phase, and  $\beta$ Mn structure phase. However, as the basis of alloy designing with these phases as precipitates, it is quite important to reveal the effect of additive elements on the mechanical properties of the matrix phase. In the present study, the effect of Ti or Si addition on mechanical properties of Cantor-based fcc single-phase alloys were investigated. Several (Co, Cr, Fe, Mn, Ni) -Si and (Co, Cr, Fe, Mn, Ni) -Ti alloys were prepared by arc melting or induction melting. The ratio of Co, Cr, Fe, Mn, and Ni was selected and kept to be equiatomic. Each alloy sealed in evacuated silica tubes was annealed at 1000 °C for 168 hours. After homogenization, all the alloys were identified as fcc single-phase alloys by using XRD and FE-EPMA. The Vickers hardness was investigated with a load of 4.9 N. After machining from the cold-rolled sheets, the dog-bone-shaped specimens for tensile tests were annealed at 1000 °C for 15 minutes, and fully recrystallized fcc single-phase specimens with a grain size of  $\sim 40 \mu\text{m}$  were obtained, regardless of the composition. The tensile test was performed with an engineering strain rate of  $1.0 \times 10^{-3} \text{ s}^{-1}$  at room temperature. It was found that the Vickers hardness increased with either element addition. The increase in hardness of the Ti-added alloy was greater than that of the Si-added alloy. Furthermore, the ductility was improved by Si addition, while Ti addition does not show significant improvement. It was suggested that Ti is an alloying element that improves strength, while Si improves both strength and elongation of the matrix phase.

### F.SF06.06.03

**Plastic Deformation of Single Crystals of a Cr-Fe-Co-Ni Equiatomic Medium Entropy Alloy** Ashif Equbal and Kazuki Ehara; Kyoto University, Japan

Medium/high entropy alloys are a class of complex compositional solid solution alloys with equiatomic or nearly equiatomic compositions, which prefers to form single-phase solid solution. Some of these alloys exhibit exceptional mechanical properties. For example, their strength, ductility and fracture toughness increase with decreasing temperature. Cr-Fe-Co-Ni equiatomic solid solution alloy is one such alloy with face-centered cubic (FCC) structure, which has been reported to exhibit exceptional strength in polycrystalline materials. However, the detailed mechanisms behind the exceptional mechanical properties of Cr-Fe-Co-Ni equiatomic alloy remain unclear in many aspects, primarily because of the lack of fundamental studies using single crystals. In this study, we prepared single crystals of the Cr-Fe-Co-Ni equiatomic solid solution alloy by directional solidification in an optical floating zone furnace, and investigated the deformation behavior of the [-123]-oriented single crystals under uniaxial tensile and compressive loading over a wide temperature range (13K to 1073K). Temperature dependence of the activation volume were investigated by strain rate change compression tests ( $1 \times 10^{-5}$  to  $5 \times 10^{-3} \text{ s}^{-1}$ ). Stress-strain curves obtained from tensile tests at low temperatures indicate the presence of twinning deformation, also found in Cr-Mn-Fe-Co-Ni and Cr-Co-Ni equiatomic solid solution alloys. This is considered to reflect a relatively low stacking fault energy for the Cr-Fe-Co-Ni equiatomic alloy. We also compared the critical resolved shear stress (CRSS) of the Cr-Fe-Co-Ni equiatomic alloy with Cr-Mn-Fe-Co-Ni and Cr-Co-Ni equiatomic alloys. The CRSS value increases significantly with decreasing temperature down to 0 K, and with increasing temperature above 873 K. Activation volume of the Fe-Cr-Co-Ni equiatomic alloy is found to be much lower than those of binary FCC solid solution alloys, which is consistent with quinary HEA and ternary MEA.

### F.SF06.06.04

**Solute Concentration Effect on Stacking Fault Energy in CoFeCrNi<sub>x</sub>Mn<sub>y</sub> HEAs** Eryo Wada<sup>1</sup>, Tatsuya Fukushi<sup>1</sup> and Naoyuki Hashimoto<sup>2</sup>; <sup>1</sup>Graduate School of Engineering, Hokkaido University, Japan; <sup>2</sup>Faculty of Engineering, Hokkaido University, Japan

The high entropy alloys (HEAs) have unique properties such as a high radiation resistance and corrosion resistance at elevated temperatures compared with conventional nuclear component materials. This attractive property could make HEAs candidates for high temperature nuclear reactor components. However, the studies on their microstructural evolution and mechanical property change under irradiation, especially at elevated temperatures, is very limited. FCC-type nuclear fission and/or fusion materials have lower stacking fault energies (SFE), and these materials would form stacking fault-type defects, such as stacking fault tetrahedron (SFT) especially in Cu alloy and Ni base alloys and Frank loops in matrix, when irradiated in a wide temperature range. Those stacking fault-type defects, especially Frank loops, would increase the yield strength and decrease the elongation of materials. Therefore, the control of SFE would be a key of less degradation of FCC-type materials under irradiation. In this study, we investigated the effect of Mn and Ni concentration on the stacking fault energy (SFE) in CoFeCrNi<sub>x</sub>Mn<sub>y</sub> high entropy alloys. The TEM observation of the deformed alloys indicated that the SFE of CoFeCrNi<sub>x</sub>Mn<sub>y</sub> seemed to be increased with increasing Mn and Ni concentration. Furthermore, the tensile properties of the alloys appeared to have a relationship with SFE, especially in the yield strength and total elongation. From these results, it is

suggested that  $\text{CoFeCrNi}_x\text{Mn}_y$  could be well-designed by controlling the stacking fault energy with optimized Mn and Ni concentration.

#### **F.SF06.06.06**

**Plastic Deformation Behavior of a Ti-Zr-Nb-Hf-Ta Equiatomic Solid Solution Alloy** Shutaro Matsuura, Kyosuke Kishida, Kodai Niitsu and Haruyuki Inui; Kyoto University, Japan

Recently, high-entropy alloys (HEAs) with the body-centered cubic (BCC) structure have received considerable attentions as new structural materials because of their attractive mechanical properties, such as superior strength retention at elevated temperatures of V-Nb-Mo-Ta-W equiatomic alloy and its derivatives and good low-temperature ductility observed for Ti-Zr-Nb-Hf-Ta equiatomic alloy. However, the underlying mechanisms endowing these BCC-HEAs with attractive mechanical properties are largely unknown mostly because of the lack of experimental results for these BCC-HEAs. It is thus quite important to investigate fundamental deformation behavior of these BCC-HEAs. In the present study, we have prepared polycrystalline ingots of the Ti-Zr-Nb-Hf-Ta equiatomic alloy by arc-melting, cold-rolling and subsequent heat-treatment. Compression tests of polycrystalline specimens were carried out at room temperature and 77 K and orientation dependence of slip plane was investigated through trace analysis of apparent slip planes appeared on the surfaces of compressed polycrystalline specimens. In addition, micropillar compression tests of single crystals fabricated from the polycrystalline ingots were carried out as a function of specimen size and loading axis orientations in order to clarify the size and orientation dependence of critical resolved shear stress.

#### **F.SF06.06.07**

**Research and Development of FeCrNiMn-Based HEAs for Nuclear Reactor** Tatsuya Fukushi<sup>1</sup>, Eryo Wada<sup>1</sup> and Naoyuki Hashimoto<sup>2</sup>; <sup>1</sup>Graduate school of Engineering, Hokkaido University, Japan; <sup>2</sup>Faculty of Engineering, Hokkaido University, Japan

In order to operate advanced nuclear power reactors safely and efficiently, it is essential to develop new structural materials with high irradiation resistance, especially at higher temperatures. The development of structural materials for nuclear reactors has been mainly focused on highly reliable steel materials such as austenitic stainless steels and low alloy steels. While, in recent years, high entropy alloys (HEAs) have attracted attention as a high radiation resistance material at high temperatures. In this study, we investigated the effects of Mn and Ni composition on the change of mechanical property and microstructure development in FeCrNiMn-based alloys under irradiation.

The results of the present study indicate that the stacking fault energy of FeCrNiMn-based alloys seemed to be increased with increasing Mn and Ni concentration. Furthermore, the ion-irradiation to the alloys resulted in the formation of plane defects such as stacking fault tetrahedra and frank loops. The number density and the average size of these defects appeared to have a strong relationship with stacking fault energy of each alloy. From these results, it is suggested that FeCrNiMn-based alloys could be improved to a higher irradiation resistant alloys with an appropriate stacking fault energy by controlling Mn and Ni concentration.

#### **F.SF06.06.08**

**Understanding and Tuning Lattice Distortion in an Entropy Stabilized Oxide, (MgCoNiCuZn)O<sub>5</sub>** Jonathan Kaufman and Keivan Esfarjani; University of Virginia, United States

Lattice distortion in high entropy alloys is postulated to have major effects on these alloys and their properties. There are limited studies that look at the effect of lattice distortion on entropy stabilized oxides. In this study, the entropy stabilized oxide,  $\text{MgCoNiCuZnO}_5$  is explored to understand the lattice distortion in this system. This work uses molecular dynamics to identify the explicit distances that each atom and atom type distorts from its parent rocksalt crystal structure. Through manipulation of the Buckingham interatomic potentials used to define the structure, effectively changing the alloy composition, changes in the lattice distortion are understood. This entropy stabilized oxide can be optimized to either increase or decrease the total lattice distortion in the system by changing the atomic composition or by replacing certain elements with alternative elements. The effective bond length between metal and oxygen as opposed to bond strength, charge, or mass, is the main factor that causes the distortion of this system.

#### **F.SF06.06.14**

**Late News: New High-Entropy Alloys: Preliminary Study of Their Properties for a Possible Use as Material for Medical Instruments** Pedro Pablo Socorro Perdomo<sup>1</sup>, Ionelia Voiculescu<sup>2</sup>, Viviana Lucero Baldevenites<sup>1</sup>, Nestor Florido Suarez<sup>1</sup> and Julia C. Mirza Rosca<sup>1</sup>; <sup>1</sup>Universidad de Las Palmas de Gran Canaria, Spain; <sup>2</sup>University Politehnica of Bucharest, Romania

The alloys have been traditionally held using a base metal and others in lesser proportion in order to improve the properties of the former. However, at the end of the 20th century a new concept of alloys emerged totally revolutionary based on the mixing of multiple components in fractions identical or similar molars and it was not until 1996 when the concepts of "high-entropy alloys" (HEAs) and "multi-principal-element alloys" (MPEAs), which were perfected and extended in 2004 in publications by Jien-Wei Yeh (Taiwan) and Brian Cantor (UK) (Yeh *et al.*, 2004)(Zhang, 2019)

The behavior of two new high entropy alloys named BioHEA 1 (FeMoTaTiZr) and BioHEA 2 (NbMoTaTiZr) containing chemical elements that exhibit relatively low bio-toxicity for the human body has been obtained and characterized in order to use them for medical instruments, such as surgical blades, saws or cutters.

Vacuum arc remelting (VAR) process was used for the manufacture of the high-entropy alloys by using the MRF ABJ 900 VAR at ERAMET Laboratory (Romania). Highly pure powders of Mo, Ta, Ti, Zr, Nb and Fe (99.9%) were used and classified according to ASTM B214-16. Eventual losses of material by vaporization are to be heeded, so as the theoretical chemical elements assimilations degree into the melt. Both conditions are taken into account for the charge. The alloys obtained were melted in VAR unit up to seven times making use of Argon as inert atmosphere, so that an adequate homogeneity could be achieved.

The experimental alloys were microstructurally characterized to highlight the phase's types and the distribution of chemical elements in the dendritic formations.

The corrosion properties of the HEAs were evaluated using a potentiodynamic polarization method, open circuit potential, pitting potential and repassivation potential. Also the electrochemical impedance spectroscopy (EIS) technique was used. The alloys were immersed in SBS (Simulated Body Fluid) during one week and the corrosion parameters were registered. Analysis of the impedance spectra was carried out by fitting different equivalent circuits to the experimental data. Two equivalent circuits, with one time constant and two time constants respectively, can be satisfactory used for fitting the spectra: one time constant represents the characteristics of the passive film and the second one is for the charge transfer reactions.

We concluded that the low corrosion rates, low corrosion currents and high polarization resistance attest the good stability of these high entropy alloys in simulated biological environment.

#### References:

- Yeh, J. W. *et al.* (2004) "Nanostructured high-entropy alloys with multiple principal elements: Novel alloy design concepts and outcomes," *Advanced Engineering Materials*, 6(5), pp. 299-303+274. doi: 10.1002/adem.200300567.
- Zhang, Y. (2019) *High-Entropy Materials A Brief Introduction*. doi: 10.1007/978-981-13-8526-1.
- ASTM B214-16, Standard Test Method for Sieve Analysis of Metal Powders, ASTM International, West Conshohocken, PA, 2016. (2016) doi:10.1520/B0214-16.

### SYMPOSIUM F.SF07

---

Processing Structure-Property Relationship of Advanced Intermetallic-Based Alloys for Structural and Functional Applications

November 21 - December 4, 2020

#### Symposium Organizers

Manja Krueger, Forschungszentrum Jülich GmbH and RWTH Aachen University

Soumya Nag, GE Global Research

Matthew Willard, Case Western Reserve University

Hiroyuki Yasuda, Osaka University

#### Symposium Support

**Bronze**

General Electric Research

---

\* Invited Paper

SESSION F.SF07.07: Live Keynote I: Processing Structure-Property Relationship of Advanced Intermetallic-Based Alloys for Structural and Functional Applications

Session Chairs: Manja Krueger, Soumya Nag, Matthew Willard and Hiroyuki Yasuda

Wednesday Morning, December 2, 2020

F.SF07

### 11:30 AM OPENING REMARKS

#### 11:35 AM \*F.SF07.01.01

**Microstructural Heterogeneity and Post Processing Effects on Mechanical Properties of Ti-48Al-2Cr-2Nb Additively Manufactured by Electron Beam Melting (EBM)** [John Lewandowski](#)<sup>1</sup>, Ayman Salem<sup>2</sup>, Dan Satko<sup>2</sup>, Mohsen Seifi<sup>1,3</sup> and S.L. Semiatin<sup>3</sup>; <sup>1</sup>Case Western Reserve University, United States; <sup>2</sup>Materials Resources LLC, United States; <sup>3</sup>Air Force Research Laboratory, United States

Both cast and wrought titanium aluminide alloys have been studied for more than two decades because of attractive properties that include low density, high specific strength, high specific stiffness and oxidation resistance up to about 700°C. Electron beam melting provides another processing approach to produce net shape components, although little work has been conducted to examine processing-microstructure-property relationships. This work examines as-deposited  $\gamma$ -TiAl (Ti-48Al-2Cr-2Nb) specimens made by Arcam AB and post-processed materials. Mechanical behavior studies on as-deposited, HIPed, and HIPed + Vacuum heat treated conditions included Vickers micro-hardness, compression, fracture toughness and fatigue crack growth testing. In addition, microstructural details were investigated over a range of scales using various microscopy tools. The presentation will summarize this evolving work on the characterization of AM  $\gamma$  TiAl and provide some comparison to other conventional (e.g. as-cast, wrought)  $\gamma$ -TiAl alloys.

#### 12:00 PM \*F.SF07.01.02

**TiAl Blades Produced by EBM—Industrialization Challenges** Michele Coppola, Gianfranco Vallillo, Veronica Malerba and [Silvia Sabbadini](#); GE AVIO, Italy

Electron Beam Melting has proven to be a technology capable of producing high quality Titanium Aluminide blades and is currently being applied to additively manufacture Low Pressure Turbine airfoils for the GE9x: the largest, most powerful and fuel-efficient commercial aircraft engine in its class, which incorporates GE's most advanced technologies developed over the last decade.

While providing several benefits such as being capable to process a highly reactive alloy such as TiAl, producing sound parts and reducing development time, this additive manufacturing technology has also posed many challenges related to its industrialization and scale-up.

This article is aimed at giving an overview of the main technical areas that had to be addressed to advance EBM from a lab scale to a mass production environment and to guarantee material and process control when it comes to part certification. One of the main areas of attention was to identify Key Process Variables, determine the associate tolerance band and their impact on desired characteristics of finished parts, such as mechanical (e.g., static strength, fatigue, fracture), metallurgical, physical, or chemical properties.

A significant part of this effort was focused on gaining a good understanding of the defects that can be generated by the additive process and that are different from traditional manufacturing routes such as casting and forging. Additionally, the impact of such defects on material properties, their detectability and acceptance limits are key items to be considered.

Process quality control is another crucial focus area, including part-to-part, build-to-build, machine-to-machine variations, machine qualification, powder handling and correlation between batch coupons and parts. Destructive and non-destructive tests and statistical process control are also part of this effort.

As of now more than 10000 blades have been produced and most certification engine tests have been completed, which makes a great contribution to pushing further the additive technology development and usage.

### 12:25 PM BREAK

#### 12:40 PM \*F.SF07.02.02

**Insights into TiAl Processing by *In Situ* Characterisation** [Florian Pyczak](#)<sup>1,2</sup>, Katja Hauschildt<sup>1</sup>, Marcus W. Rackel<sup>1</sup> and

Andreas Stark<sup>1</sup>; <sup>1</sup>Helmholtz-Zentrum Geesthacht, Germany; <sup>2</sup>Brandenburg University of Technology Cottbus-Senftenberg, Germany

TiAl-alloys are a typical example that advanced modern lightweight materials have an increasingly complex chemical composition and phase constitution. Accordingly, a sophisticated and complete characterisation of the material is necessary to fully comprehend their behaviour and properties for knowledge-based alloy and process development. Unfortunately, many processing methods for TiAl as well as their operation itself take place at high temperature making their direct monitoring and characterisation difficult. In addition, it is also of interest to investigate the material behaviour if other external loads as for example an applied stress are present in parallel.

In the contribution examples for the direct monitoring and characterisation of the processing of TiAl alloys using *in situ* specimen environments and high energy X-ray diffraction at synchrotron sources are shown. The processes can be rather simple as for example a heat treatment at a certain annealing temperature where the phase composition and its development are monitored (e.g. [1]). But, also complex processing scenarios like hot forming [1,2] or a transient liquid phase bonding process [3] can be directly investigated by those methods. In the former case the texture development during the hot forming is observed while in the latter case the solidification of the joining zone and the subsequent phase transformations are investigated to understand the microstructure formation.

Simple heat treatment, hot forming, transient liquid phase bonding and many other processes for TiAl alloys have in common that phase constitution, texture or microstructure react very sensitively to changes of applied temperature and/or stress. They normally change significantly when the stress is removed or the specimen is cooled down at the end of the processing step. Due to these reasons it is not possible to unambiguously reconstruct the situation at processing temperature and/or under stress based on subsequent material characterisation at room temperature or in absence of the mechanical load. In situ characterisation as presented here is the only means to acquire the full picture and get insight into crucial process details under processing conditions.

#### References:

- [1] Pyczak, F., Rackel, M., Gabrisch, H., Halici, D., Lorenz, U., Schreyer, A., Stark, A., In-situ monitoring of thermal treatments and hot deformation of a g-TiAl alloy by high energy X-ray diffraction, 123HIMAT-2015 Proceedings (2015) 323-326.
- [2] Stark, A., Rackel, M., Tchouaha Tankoua, A., Oehring, M., Schell, N., Lottermoser, L., Schreyer, A., Pyczak, F., In situ High-Energy X-Ray Diffraction during Hot-Forming of a Multiphase TiAl Alloy, Metals 5 (2015) 2252-2265.
- [3] Hauschildt, K., Stark, A., Burmester, H., Tietze, U., Schell, N., Müller, M., Pyczak, F., Phase Transformations in the Brazing Joint during Transient Liquid Phase Bonding of a g-TiAl Alloy Studied with In Situ High-Energy X-Ray Diffraction, Materials Science Forum 941 (2018) 943-948.

#### 1:05 PM \*F.SF07.01.06

**Intermetallic Titanium Aluminides** Helmut Clemens and Svea Mayer; Montanuniversitaet Leoben, Austria

Intermetallic TiAl alloys based on the  $\gamma$ -TiAl phase are already used as engineering lightweight high-temperature materials in aircraft and automotive engines. Thereby, they partly substitute the twice as heavy Ni-base superalloys. Present applications are, for example, blades in the low-pressure turbine of advanced aero-engines, turbine wheels for turbocharger systems of car diesel engines and engine parts used in racing sport applications. All the applications mentioned above require balanced mechanical properties, i.e. certain ductility at room temperature as well as defined creep strength at elevated temperatures. In the framework of this presentation the alloy design strategies, which have been applied for the development of so-called process adapted TiAl alloys will be explained. Besides the considerations which have led to the selected alloying elements, the heat treatments conducted subsequent to conventional hot-forging and additive manufacturing are discussed. In this context it will be shown that a combination of computer-aided alloy design and novel characterization techniques, e.g. in-situ high-energy X-ray and neutron diffraction, has accelerated both alloy and process development as well as the understanding of this class of alloys sustainably.

SESSION F.SF07.08: Live Keynote II: Processing Structure-Property Relationship of Advanced Intermetallic-Based Alloys for Structural and Functional Applications

Session Chairs: Manja Krueger, Soumya Nag, Matthew Willard and Hiroyuki Yasuda

Thursday Afternoon, December 3, 2020

F.SF07

### 3:00 PM \*F.SF07.04.01

**A Hexagonal Close Packed Multi-Principal-Element Alloy Identified Computationally** Mark Asta<sup>1,2</sup>, Daryl Chrzan<sup>1</sup>, Qijun Hong<sup>3</sup>, Lu Jiang<sup>1</sup>, Andrew Minor<sup>1,2</sup>, Velimir Radmilovic<sup>4</sup>, Julian E. Sabisch<sup>5</sup>, Ruoshi Sun<sup>3</sup> and Axel van de Walle<sup>3</sup>; <sup>1</sup>University of California, Berkeley, United States; <sup>2</sup>Lawrence Berkeley National Laboratory, United States; <sup>3</sup>Brown University, United States; <sup>4</sup>University of Belgrade, Serbia; <sup>5</sup>Sandia National Laboratories, United States

In this work we consider the design of alloys that can mimic the excellent combination of room temperature and high-temperature mechanical properties displayed by the refractory elemental metal rhenium, but with reduced cost. Experimental investigations of the deformation mechanisms and microstructures in this material highlight the important role of {11-21} deformation twinning, and high-resolution electron microscopy combined with first-principles calculations offer insights into the origin of the dominance of this twin system. These considerations lead to a design principle that trades off average valence electron count and cost considerations, identifying a promising pool of candidate substitute alloys in the Mo-Ru-Ta-W quaternary system. We demonstrate how this design principles is combined with a computational thermodynamics model of phase stability, based on high-throughput ab initio calculations, to further narrow down the search and lead to the identification of alloys that maintain rhenium's desirable hcp crystal structure. The predictions of this modeling are validated through comparisons to known binary phase diagram sections and corroborated by experimental synthesis and structural characterization demonstrating multi-principle-element hcp solid-solution samples selected from a promising composition range. Additional theoretical calculations and initial mechanical properties measurements will be presented to assess the potential performance of these alloys for high temperature applications.

### 3:25 PM \*F.SF07.05.01

**Exploding, Weeping and Reversible Phase Transformations on the Way to a Shape Memory Ceramic** Hanlin Gu<sup>1</sup>, Justin Jetter<sup>2</sup>, Jascha Rohmer<sup>2</sup>, Eckhard Quandt<sup>2</sup> and Richard D. James<sup>1</sup>; <sup>1</sup>University of Minnesota, United States; <sup>2</sup>University of Kiel, Germany

The systematic tuning of the lattice parameters to achieve improved kinematic compatibility between phases is an effective strategy for improving the reversibility, and lowering the hysteresis, of solid-solid phase transformations. We present an apparently paradoxical example in which tuning to near perfect compatibility leads to a high degree of irreversibility in oxides of ZrHfYNb, as manifested by violently explosive behavior. Tuning lattice parameters slightly away from near perfect compatibility gives an intermediate “weeping” behavior, in which the polycrystal slowly and steadily falls apart at the grain boundaries. Finally, tuning to satisfy a condition we term the equidistance condition results in reversible behavior with the lowest hysteresis in this system. We give evidence that these observations are explained by a more careful analysis of compatibility of the polycrystal. These results show an extreme diversity of behavior, from reversible to explosive, is possible in a chemically homogeneous system by manipulating conditions of compatibility.

### 3:50 PM \*F.SF07.05.06

**Intermetallic Compounds—A Versatile Class of Materials Meets Interesting Catalytic Challenges** Marc Armbrüster; Chemnitz University of Technology, Germany

Heterogeneous catalysis is dominated by two material properties, i.e. the electronic structure (ligand effect) and the arrangement of the atoms (geometric effect). A priori, any material offering altered electronic or structural properties is of interest for heterogeneous catalysis. While intermetallic compounds fulfil these criteria, they offer three advantages compared to substitutional alloys: i) stability, caused by the chemical bonding, which can prevent segregation or decomposition in reactive atmosphere, ii) a wide range of chemical potential of the involved (transition)metals and iii) peculiar combinations of electronic and crystal structure. Since intermetallic compounds are thermodynamically stable and available in a wide range of materials, covering nanoparticles, polycrystalline materials as well as large single crystals, they can serve as platform materials to address catalytic challenges.

The stability allows studying their intrinsic properties in many environments, while the different available chemical potentials can be used to adjust the redox properties to the needs of the reaction in question. Systematic study of the geometric effects in reactions is possible by exploiting the large variety of available crystal structures. The use of isostructural substitutional series or compounds with different valence electron concentration allows addressing the electronic effect (ligand effect) on a reaction. Since only the filling degree of the electronic structure is changes, while the crystal structure and thus the electronic scaffold is kept, the electronic effect can be studied with only minor influence of the geometric effect. Like the metallic elements and the substitutional alloys, intermetallic compounds possess electrical conductivity, allowing electrochemical

studies. The versatility of intermetallic compounds created a vivid and active community and in the contribution, several examples will be presented to elaborate the possibilities - and the requirements - for catalytic studies on this class of materials.

SESSION F.SF07.09: Live Keynote III: Processing Structure-Property Relationship of Advanced Intermetallic-Based Alloys for Structural and Functional Applications  
Session Chairs: Manja Krueger, Soumya Nag, Matthew Willard and Hiroyuki Yasuda  
Friday Morning, December 4, 2020  
F.SF07

**8:00 AM \*SF07.01.05|**

**Current Activities on Powder Processed TiAl Alloys for Jet Engine Applications in Japan** Masao Takeyama; Tokyo Institute of Technology, Japan

A five-year National project of “*Structural Materials for Innovation (SM<sup>4</sup>I)*” in *Cross-ministerial Strategic Innovation Promotion Program (SIP)* starting from 2014 in Japan ended in 2018, and the following another 5-year project of “*Materials Integration for Revolutionary Design System of Structural Materials*” in the SIP II Program has started in 2018. For both programs I have been committed to as the technical leader and take responsibility for the alloy design and development of TiAl alloys, in collaboration with universities and industries. In the first program, the focus was placed on the design/process principles of innovative wrought and cast TiAl alloys to be used for LPT blades, based on the thermodynamics and kinetics of multi-components titanium aluminide systems, and we have successfully proposed and developed new alloys. In the second program, however, we have focused on construction of inverse design principle for innovative TiAl alloys with required properties available for both MIM (metal injection molding) and AM (additive manufacturing) processes, in collaboration with Kobe Steel, Ltd., Osaka Yakin Kogyo Co., Ltd, Mitsubishi Heavy Industries Aero Engine and Osaka University. The degree of freedom of the microstructure design in MIM and AM processes is much wider than that in wrought and cast processes, but attention has to be paid to impurity levels of oxygen and carbon picked up by processing routes of powdering, injection molding and sintering in case of MIM. In this talk, we first show you how oxygen affects the phase equilibria among  $\beta$ -Ti,  $\alpha$ -Ti ( $\alpha_2$ -Ti<sub>3</sub>Al) and  $\gamma$ -TiAl phases, and eventually affects the microstructures created through the phase transformations, based on our phase diagram studies. You have to be careful for alloy development under powder processes if you use currently existing thermodynamic databases. None of them works. The microstructure can significantly be changed from the fully  $\alpha_2/\gamma$  lamellae to the  $\beta/\gamma$  grained, depending on oxygen level, even the major alloy elements as well as the heat treatment routes are the same. Current progress on this project, especially how important the  $\beta$  phase plays in role in improving mechanical properties for both MIM and AM, based on our novel customized powders, will be presented. A part of this study has been carried under the research of SIP II in JST (Japan Science and Technology Agency).

**8:50 AM BREAK**

**9:05 AM \*F.SF07.03.01**

**High Temperature Creep Behavior of MoSiBTiC Alloy** Kyosuke Yoshimi, Ryuta Yanagiya, Shiho Kamata, Shuntaro Ida and Nobuaki Sekido; Tohoku University, Japan

High temperature creep behavior of TiC-added Mo-Si-B alloy was studied in the temperature range of 1400 - 1600°C and the stress range of 75 – 300 MPa. Creep strain under constant applied stress control was measured by directly reading the change in specimen gage length using CMOS image sensors. 4 stages were observed on the creep curves. That is, I. instantaneous strain, II. primary creep, III. secondary creep with the minimum creep rate and IV. tertiary creep with acceleration. The minimum creep rates showed a good linear relationship with applied stress in the Norton plot, and the obtained stress exponent,  $n$ , was about 3.5, indicating power-law creep. The minimum creep rates also showed a good linear relationship with inverse temperature in the Arrhenius plot, and the obtained apparent creep activation energy,  $Q_c$ , was about 497 kJ/mol. The value is in good agreement with the activation energy of Mo self-diffusion (488 kJ/mol), strongly suggesting that Mo self-diffusion is the rate-controlling process of creep deformation of the MoSiBTiC alloy under the conditions. Instantaneous strain varied from  $10^{-4}$  to  $10^{-2}$  depending on stress and temperature. To reach a  $10^{-2}$  instantaneous strain, some mechanisms in addition to an elastic strain should be considered to operate. Careful SEM observations indicated that micro-cracking in

coarse  $T_2$  phase and interfacial separation appeared to occur during the increase in instantaneous strain. Those weakening mechanisms would cause the large instantaneous strain. From the perspective of high temperature applications, the time for creep strain to reach 1% is one of the guidelines for development. Therefore, suppressing the occurrence of those weakening mechanisms through microstructure control as well as the increase in strain-hardening coefficient of Mo solid solution is important for improving the high temperature creep strength of the MoSiBTiC alloy especially in a small creep strain.

9:30 AM \*F.SF07.05.09

**Relationship Between Thermoelectric Properties and Phase Interfaces Formed on a Multiscale by Phase Separation in the Same Ordered Structure Phases** Yoshisato Kimura<sup>1</sup>, Yaw Wang Chai<sup>1</sup> and Yonghoon Lee<sup>2</sup>; <sup>1</sup>Tokyo Institute of Technology, Japan; <sup>2</sup>KELK Ltd., Japan

Thermoelectric power generation is an appealing approach for conserving energy and preserving the global environment. Thermoelectric properties are sensitively affected by microstructure of materials which changes during high temperature fabrication processing and practical long term operations. Improvement of thermoelectric performance can be achieved by microstructure control. We focus on the formation of interfaces on a multi-scale according to the phase separation between the same ordered structure phases in two alloy systems. One is phase separation between half-Heusler structure TiNiSn–(Zr,Hf)NiSn according to the miscibility gap, and the other is that between anti-fluorite structure  $Mg_2Si$ – $Mg_2Sn$  during coring microstructure formation. Objective of the present work is to understand the formation mechanism of interfaces by the phase separation, and evaluate the effects of interfaces on thermoelectric properties focusing on the electrical and thermal conduction.

Half-Heusler MNiSn (M = Hf, Zr, Ti) are excellent n-type thermoelectric materials. The present author's group reported the phase separation between TiNiSn and ZrNiSn, and TiNiSn and HfNiSn from a random solid solution MNiSn phase. The existence of a miscibility gap was suggested at temperatures higher than 1273 K. The relaxed lattice misfit, evaluated using XRD measurement, is about 3.2% between TiNiSn and ZrNiSn, and 2.5% between TiNiSn and HfNiSn, respectively. These values are quite large compared with 0.6% between ZrNiSn and HfNiSn. Considering the elastically constrained phase interface, a quite large elastic energy can be the driving force of the phase separation. Sharp grain boundaries between Ti-rich and Zr-rich half-Heusler phases can be observed in solidified microstructure of (Ti,Zr)NiSn alloys using SEM. On the other hand, it is very hard to observe a constrained interface. Diffuse interface can be barely observed using TEM in a (Ti,Zr)NiSn alloy after the heat treatment, annealed in the two-phase field for phase separation. Excellent electrical power factor exceeding  $5 \text{ mWm}^{-1}\text{K}^{-2}$  can be achieved while the lattice thermal conductivity is effectively reduced around  $3 \text{ Wm}^{-1}\text{K}^{-1}$  in Ti-rich (Ti,Zr)NiSn alloy according to the effect of solid solution together with the effect of interfaces introduced by phase separation.

Microstructure development in the  $Mg_2Si$ – $Mg_2Sn$  pseudo-binary system is characterized by the peritectic reaction. The Mg–Si–Sn ternary phase diagram was evaluated experimentally focusing on the reaction scheme and solidification sequence. It has been found that the gradient composition layered structure is formed in  $Mg_2(Si_x,Sn_{1-x})$  alloys on a micro-scale during the solidification process. Dominant mechanism is the phase separation of  $Mg_2(Si,Sn)$  solid solution phase into Si-rich  $Mg_2Si(Si,Sn)$  and Sn-rich  $Mg_2(Sn,Si)$  phases during the coring structure development. Phase separation is occurred leaving phase interfaces to release the large elastic energy stored due to quite large lattice misfit. The constrained lattice misfit between Si-rich  $Mg_2Si(Si,Sn)$  and Sn-rich  $Mg_2(Sn,Si)$  phases has been evaluated about 5% based on the powder XRD measurements, and the semi-coherent interfaces with interfacial dislocation networks can be observed using TEM. Each layer of the gradient composition layered microstructure is consisting of nano- to micro-scale poly-crystal grains having a compositional gradient of Si/Sn composition ratio. The lattice thermal conductivity can effectively be reduced lower than  $2 \text{ Wm}^{-1}\text{K}^{-1}$  in a  $Mg_2(Si_{0.75},Sn_{0.25})$  alloy which contains high density of phase interfaces of gradient composition layered microstructure. Note that the dominant mechanism for the reduction of thermal conductivity is attributed to the phono scattering based on the solid solution effect in  $Mg_2(Si_x,Sn_{1-x})$  phase grains and layers.

SESSION F.SF07.01: Titanium Aluminides, Novel Processing  
On Demand Abstracts Available for Viewing Starting Saturday Morning, November 21, 2020  
F-SF07

5:00 AM \*F.SF07.01.01

**Microstructural Heterogeneity and Post Processing Effects on Mechanical Properties of Ti-48Al-2Cr-2Nb Additively Manufactured by Electron Beam Melting (EBM)** John Lewandowski<sup>1</sup>, Ayman Salem<sup>2</sup>, Dan Satko<sup>2</sup>, Mohsen Seifi<sup>1,3</sup> and S.L. Semiatin<sup>3</sup>; <sup>1</sup>Case Western Reserve University, United States; <sup>2</sup>Materials Resources LLC, United States; <sup>3</sup>Air Force



Research Laboratory, United States

Both cast and wrought titanium aluminide alloys have been studied for more than two decades because of attractive properties that include low density, high specific strength, high specific stiffness and oxidation resistance up to about 700°C. Electron beam melting provides another processing approach to produce net shape components, although little work has been conducted to examine processing-microstructure-property relationships. This work examines as-deposited  $\gamma$ -TiAl (Ti-48Al-2Cr-2Nb) specimens made by Arcam AB and post-processed materials. Mechanical behavior studies on as-deposited, HIPed, and HIPed + Vacuum heat treated conditions included Vickers micro-hardness, compression, fracture toughness and fatigue crack growth testing. In addition, microstructural details were investigated over a range of scales using various microscopy tools. The presentation will summarize this evolving work on the characterization of AM  $\gamma$  TiAl and provide some comparison to other conventional (e.g. as-cast, wrought)  $\gamma$ -TiAl alloys.

#### 5:15 AM \*F.SF07.01.02

**TiAl Blades Produced by EBM—Industrialization Challenges** Michele Coppola, Gianfranco Vallillo, Veronica Malerba and Silvia Sabbadini; GE AVIO, Italy

Electron Beam Melting has proven to be a technology capable of producing high quality Titanium Aluminide blades and is currently being applied to additively manufacture Low Pressure Turbine airfoils for the GE9x: the largest, most powerful and fuel-efficient commercial aircraft engine in its class, which incorporates GE's most advanced technologies developed over the last decade.

While providing several benefits such as being capable to process a highly reactive alloy such as TiAl, producing sound parts and reducing development time, this additive manufacturing technology has also posed many challenges related to its industrialization and scale-up.

This article is aimed at giving an overview of the main technical areas that had to be addressed to advance EBM from a lab scale to a mass production environment and to guarantee material and process control when it comes to part certification. One of the main areas of attention was to identify Key Process Variables, determine the associate tolerance band and their impact on desired characteristics of finished parts, such as mechanical (e.g., static strength, fatigue, fracture), metallurgical, physical, or chemical properties.

A significant part of this effort was focused on gaining a good understanding of the defects that can be generated by the additive process and that are different from traditional manufacturing routes such as casting and forging. Additionally, the impact of such defects on material properties, their detectability and acceptance limits are key items to be considered. Process quality control is another crucial focus area, including part-to-part, build-to-build, machine-to-machine variations, machine qualification, powder handling and correlation between batch coupons and parts. Destructive and non-destructive tests and statistical process control are also part of this effort.

As of now more than 10000 blades have been produced and most certification engine tests have been completed, which makes a great contribution to pushing further the additive technology development and usage.

#### 5:30 AM F.SF07.01.03

**Microstructure and Tensile Properties of  $\beta$ -Containing TiAl Alloy Additively Manufactured by Electron Beam Melting** Ken Cho<sup>1</sup>, Hajime Kawabata<sup>1</sup>, Hirotaka Odo<sup>1</sup>, Tatsuhiro Hayashi<sup>1</sup>, Hiroyuki Y. Yasuda<sup>1</sup>, Masao Takeyama<sup>2</sup> and Takayoshi Nakano<sup>1</sup>; <sup>1</sup>Osaka University, Japan; <sup>2</sup>Tokyo Institute of Technology, Japan

Intermetallic TiAl alloys that exhibit low density, high strength at high temperatures and excellent oxidation resistance are used for low pressure turbine (LPT) blades of an aero engine. In recent years, the alloys containing the  $\beta$  phase have attracted much attention due to their good mechanical properties at operation temperature of LPT blades. In this study, rectangular rods of  $\beta$ -containing Ti-Al-Cr alloy were fabricated by electron beam melting (EBM) which is one of the suitable manufacturing processes for the TiAl alloys. Surface morphology, internal defect, microstructure and mechanical properties of these rods were investigated focusing on input energy density of the EBM process. We found that the microstructure of the samples is strongly influenced by the input energy density. The rods fabricated at low energy densities contain fine  $\alpha_2/\gamma$  lamellar structure with the  $\beta/\gamma$  cells discontinuously precipitated at the lamellar colony boundary. On the other hand, the  $\alpha_2/\beta/\gamma$  mixed structure composed of the  $\alpha_2/\gamma$  lamellar and ( $\beta+\gamma$ ) structures can be obtained at high energy densities. The variation in microstructure is caused by the difference in solidification process and temperature distribution in the vicinity of the melt pool during the EBM process. We also found that the tensile properties of the alloys depend strongly on the volume fraction of the  $\alpha_2/\gamma$  lamellar structure, the  $\beta/\gamma$  cells and the  $\beta$  phase. The strength of the alloys prepared under the optimum condition demonstrate at room temperature and 1023 K is higher than that of Ti-48Al-2Cr-2Nb alloy and comparable to that of Ti-Al-Nb-Mo-B (TNM) alloy.

This work was supported by Council for Science, Technology and Innovation(CSTI), Cross-ministerial Strategic Innovation Promotion Program (SIP), “Materials integration” for revolutionary design system of structural materials” (Funding agency: JST).

#### 5:40 AM F.SF07.01.04

##### **Microstructure Evolution and Mechanical Properties of TiAl/TiAlNb Gradient Alloys Produced by Laser Direct Metal Deposition** Yu Zou; University of Toronto, Canada

TiAl/Ti<sub>2</sub>AlNb dual alloys exhibit potential applications on aircraft engines, but manufacturing of such alloys needs to achieve an appropriate gradient transition between these two alloys. Here, we deposited -TiAl alloy on a AlNb substrate using the direct metal deposition (DMD) technique and analyzed their graded zone near the interface. Our results show that the transition zone mainly consists of three characteristic layers: the first layer possesses a small amount of and phases disspreading in the matrix. In the the second layer, directional dendrites ( phases as dendrite core and phases as dendrite arms) are developed in matrix. The third layer exhibits equiaxial (+) colony with fully lamellar microstructure, which is similar to the microstructure of the -TiAl alloy. We also preformed nanoindentation tests on different phases and layers to revel their mechanical properties. The relationship between nanoindentation results and characteristic microstructure has been identified.

Key words: intermetallics; direct metal deposition; microstructure; nanoindentation; mechanical properties.

#### 5:50 AM \*F.SF07.01.05

##### **Current Activities on Powder Processed TiAl Alloys for Jet Engine Applications in Japan** Masao Takeyama; Tokyo Institute of Technology, Japan

A five-year National project of “*Structural Materials for Innovation (SM<sup>4</sup>I)*” in *Cross-ministerial Strategic Innovation Promotion Program (SIP)* starting from 2014 in Japan ended in 2018, and the following another 5-year project of “Materials Integration for Revolutionary Design System of Structural Materials” in the SIP II Program has started in 2018. For both programs I have been committed to as the technical leader and take responsibility for the alloy design and development of TiAl alloys, in collaboration with universities and industries. In the first program, the focus was placed on the design/process principles of innovative wrought and cast TiAl alloys to be used for LPT blades, based on the thermodynamics and kinetics of multi-components titanium aluminide systems, and we have successfully proposed and developed new alloys. In the second program, however, we have focused on construction of inverse design principle for innovative TiAl alloys with required properties available for both MIM (metal injection molding) and AM (additive manufacturing) processes, in collaboration with Kobe Steel, Ltd., Osaka Yakin Kogyo Co., Ltd, Mitsubishi Heavy Industries Aero Engine and Osaka University. The degree of freedom of the microstructure design in MIM and AM processes is much wider than that in wrought and cast processes, but attention has to be paid to impurity levels of oxygen and carbon picked up by processing routes of powdering, injection molding and sintering in case of MIM. In this talk, we first show you how oxygen affects the phase equilibria among  $\beta$ -Ti,  $\alpha$ -Ti ( $\alpha_2$ -Ti<sub>3</sub>Al) and  $\gamma$ -TiAl phases, and eventually affects the microstructures created through the phase transformations, based on our phase diagram studies. You have to be careful for alloy development under powder processes if you use currently existing thermodynamic databases. None of them works. The microstructure can significantly be changed from the fully  $\alpha_2/\gamma$  lamellae to the  $\beta/\gamma$  grained, depending on oxygen level, even the major alloy elements as well as the heat treatment routes are the same. Current progress on this project, especially how important the  $\beta$  phase plays in role in improving mechanical properties for both MIM and AM, based on our novel customized powders, will be presented. A part of this study has been carried under the research of SIP II in JST (Japan Science and Technology Agency).

#### 6:05 AM \*F.SF07.01.06

##### **Intermetallic Titanium Aluminides** Helmut Clemens and Svea Mayer; Montanuniversitaet Leoben, Austria

Intermetallic TiAl alloys based on the  $\gamma$ -TiAl phase are already used as engineering lightweight high-temperature materials in aircraft and automotive engines. Thereby, they partly substitute the twice as heavy Ni-base superalloys. Present applications are, for example, blades in the low-pressure turbine of advanced aero-engines, turbine wheels for turbocharger systems of car diesel engines and engine parts used in racing sport applications. All the applications mentioned above require balanced mechanical properties, i.e. certain ductility at room temperature as well as defined creep strength at elevated temperatures. In the framework of this presentation the alloy design strategies, which have been applied for the development of so-called process adapted TiAl alloys will be explained. Besides the considerations which have led to the selected alloying elements, the heat treatments conducted subsequent to conventional hot-forging and additive manufacturing are discussed. In this context it will be shown that a combination of computer-aided alloy design and novel characterization techniques, e.g. in-situ

high-energy X-ray and neutron diffraction, has accelerated both alloy and process development as well as the understanding of this class of alloys sustainably.

#### **6:20 AM F.SF07.01.08**

**Applying a Softening Adapted Acceleration to the Hot Deformation of TNM-B1** Mark Eisentraut, Johan A. Stendal, Sebastian Bolz, Marcus Bambach and Sabine Weiß; Brandenburg University of Technology Cottbus-Senftenberg, Germany

Hot isostatically forged TiAl turbine blades made of TNM-B1 are commercially used in aircraft engines, as they offer significantly lower weight than the traditional nickel-based blades while exhibiting similar strength. Like other TiAl alloys, TNM-B1 displays high peak stress followed by a strong softening behavior (i.e. stress reduction) during hot deformation. This softening can be used to accelerate the deformation process by reducing the processing time and in turn the costs for TNM-B1 parts. In order to avoid increased damage during the accelerated process, a pre-heat treatment (HT) for the hot isostatically pressed material (HIP) is required. To simulate the accelerated forming process, hot compression tests were performed with a DIL805A/D/T dilatometer from TA Instruments (New Castle, Delaware, USA) with different strain rates (0.0013, 0.005, 0.01 and 0.05) and temperatures ( $T=1150, 1175$  and  $1200^{\circ}\text{C}$ ). Deformation of the heat-treated state revealed lower flow stress (in both, peak stresses and steady state stresses) and fewer voids compared to the HIP state. The compression test data were used to develop material and temperature specific strain rate profiles based on a material model presented in [Stendal, J.A et al., Applying machine learning to the phenomenological flow stress modeling of TNM-B1. *Metals* 9 (2019) 220]. Subsequently, hot compression tests were performed with different strain rate profiles (starting strain rates 0.0013 and 0.0052) for the HIP and the HT state. The results were evaluated with regard to their microstructure, deformation, and damage behavior. A reduction of the processing time for all tested strain rate profiles by factors 2-3 could be achieved compared to constant strain rates. Furthermore, the results indicated that the deformation with strain rate profiles (compared to constant strain rates) did not significantly change the resulting microstructure or damage tolerance of the HT state.

Maybe also HEXRD results of the strain rate profiles can be presented to show in detail that the accelerated forming process can lead to the same results as the constant forming process.

#### **6:30 AM F.SF07.01.09**

**Diffusion Bonding of  $\gamma$ -TiAl Parts** Marcus W. Rackel, Dirk Matthiessen, Jonathan D. Paul, Andreas Stark and Florian Pyczak; Helmholtz-Zentrum Geesthacht, Germany

In modern aero engines,  $\gamma$ -TiAl alloys can be used as a replacement for Ni-base super alloys for certain components such as low-pressure turbine blades, due to  $\gamma$ -TiAl alloys having about half the density of superalloys. Nevertheless, due to the relative novelty of  $\gamma$ -TiAl, not the whole variety of processes available for established materials has been fully investigated. One possibility for a joining or repair process is diffusion bonding. Diffusion bonding can be used to repair components by replacing damaged or worn sections without significantly modifying the microstructure. For Ni-base super alloys, diffusion bonding and brazing are well-established repair processes that are used to extend the life cycle of turbine blades. For  $\gamma$ -TiAl alloys, such repair processes are not commercially available.

In the current work diffusion bonding of two commercially used  $\gamma$ -TiAl alloys, Ti-48Al-2Nb-2Cr (4822) alloy and Ti-43.5Al-4Nb-1Mo-0.2B (TNM) alloy, (all compositions in at.%), was as a possible repair technique. The microstructure developed during diffusion bonding and the corresponding mechanical properties after bonding have been determined at room and elevated temperatures. Furthermore, the use of different surface treatments before bonding, such as wire cutting, grinding, drilling and turning as well as various geometric arrangements were examined.

For successful diffusion bonding temperatures above  $1000^{\circ}\text{C}$  had to be applied to produce sound joints in both alloys. The TNM alloy showed changes in the substrate microstructure (e.g. lamellar coarsening) after bonding at high temperatures close to the  $\gamma$ -solvus temperature. In contrast, there seemed to be no significant microstructural changes in the substrate of the cast 4822 alloy, except for some grain growth at and across the bonded joint.

By optimising the diffusion bonding parameters, it was possible to reach tensile strengths and ductilities in diffusion bonded samples that were comparable to those of the base material. Through optimisation of the surface treatment, it was also possible to produce solid joints for various geometric arrangements and improve the overall quality of the joint.

SESSION F.SF07.02: Titanium Aluminides, Microstructure and Mechanical Properties  
On Demand Abstracts Available for Viewing Starting Saturday Morning, November 21, 2020  
F-SF07

## 5:00 AM \*F.SF07.02.02

**Insights into TiAl Processing by *In Situ* Characterisation** Florian Pyczak<sup>1,2</sup>, Katja Hauschildt<sup>1</sup>, Marcus W. Rackel<sup>1</sup> and Andreas Stark<sup>1</sup>; <sup>1</sup>Helmholtz-Zentrum Geesthacht, Germany; <sup>2</sup>Brandenburg University of Technology Cottbus-Senftenberg, Germany

TiAl-alloys are a typical example that advanced modern lightweight materials have an increasingly complex chemical composition and phase constitution. Accordingly, a sophisticated and complete characterisation of the material is necessary to fully comprehend their behaviour and properties for knowledge-based alloy and process development. Unfortunately, many processing methods for TiAl as well as their operation itself take place at high temperature making their direct monitoring and characterisation difficult. In addition, it is also of interest to investigate the material behaviour if other external loads as for example an applied stress are present in parallel.

In the contribution examples for the direct monitoring and characterisation of the processing of TiAl alloys using *in situ* specimen environments and high energy X-ray diffraction at synchrotron sources are shown. The processes can be rather simple as for example a heat treatment at a certain annealing temperature where the phase composition and its development are monitored (e.g. [1]). But, also complex processing scenarios like hot forming [1,2] or a transient liquid phase bonding process [3] can be directly investigated by those methods. In the former case the texture development during the hot forming is observed while in the latter case the solidification of the joining zone and the subsequent phase transformations are investigated to understand the microstructure formation.

Simple heat treatment, hot forming, transient liquid phase bonding and many other processes for TiAl alloys have in common that phase constitution, texture or microstructure react very sensitively to changes of applied temperature and/or stress. They normally change significantly when the stress is removed or the specimen is cooled down at the end of the processing step. Due to these reasons it is not possible to unambiguously reconstruct the situation at processing temperature and/or under stress based on subsequent material characterisation at room temperature or in absence of the mechanical load. *In situ* characterisation as presented here is the only means to acquire the full picture and get insight into crucial process details under processing conditions.

### References:

- [1] Pyczak, F., Rackel, M., Gabrisch, H., Halici, D., Lorenz, U., Schreyer, A., Stark, A., In-situ monitoring of thermal treatments and hot deformation of a g-TiAl alloy by high energy X-ray diffraction, 123HIMAT-2015 Proceedings (2015) 323-326.
- [2] Stark, A., Rackel, M., Tchouaha Tankoua, A., Oehring, M., Schell, N., Lottermoser, L., Schreyer, A., Pyczak, F., In situ High-Energy X-Ray Diffraction during Hot-Forming of a Multiphase TiAl Alloy, Metals 5 (2015) 2252-2265.
- [3] Hauschildt, K., Stark, A., Burmester, H., Tietze, U., Schell, N., Müller, M., Pyczak, F., Phase Transformations in the Brazing Joint during Transient Liquid Phase Bonding of a g-TiAl Alloy Studied with In Situ High-Energy X-Ray Diffraction, Materials Science Forum 941 (2018) 943-948.

## 5:15 AM F.SF07.02.03

**Effect of Microstructure Factor on Room-Temperature Fracture Toughness of  $\beta$ -Ti Phase Containing  $\gamma$ -TiAl Based Alloys** Ryosuke Yamagata, Hirotoyo Nakashima and Masao Takeyama; Tokyo Institute of Technology, Japan

In order to clarify the effect of microstructure factor on the fracture toughness in  $\beta$  phase containing  $\gamma$ -TiAl based alloys, the room-temperature fracture toughness of these alloys have been investigated, because the room-temperature fracture toughness is a quite important material property for jet engine application materials. In addition, it is essentially important to understand the relationship between microstructure factor and alloy properties for not only predicting alloy properties from microstructure feature but also solving the inverse problem which means to propose the optimal microstructure feature from the required properties.

The microstructure of alloys studied were intentionally controlled from the nearly  $\alpha_2$ -Ti<sub>3</sub>Al/ $\gamma$  lamellae to  $\beta$ -Ti/ $\gamma$  grained, through the  $\beta/\gamma$  lamellae using the cellular reaction of  $\alpha_2 + \gamma \rightarrow \beta + \gamma$  in Ti-Al-Cr ternary system alloys. The fracture toughness was evaluated by an instrumented three-point bend test using a chevron-notched square-bar specimen with 30 mm in a span length under the cross-head speed of 0.05 mm/min. The  $K_{IC}$  was calculated using a maximum force in the load-displacement curve on the bend tests and the shape factor of chevron-notched specimen. Some of the specimens were also tested under the higher test speed. The results were compared with the  $\Delta K_{th}$  and Paris slope those obtained by compact tension (CT) test. We found that the existence of the  $\beta$ -Ti phase is effective in increasing the fracture toughness. Based on these results, methodology to predict the fracture toughness is discussed.

This work was supported by Council for Science, Technology and Innovation (CSTI), Cross-ministerial Strategic Innovation

Promotion Program (SIP), “Material Integration” for revolutionary design system of structural materials.

#### 5:25 AM F.SF07.02.04

**A New Method for Determining the Brittle-Ductile Transition Temperature of a TiAl Intermetallic** Sarper Nizamoglu, Karl-Heinz Lang and Martin Heilmaier; Karlsruhe Institute of Technology–Institute for Applied Materials, Germany

Intermetallic materials typically change their deformation behavior from brittle to ductile at a certain temperature called the brittle-ductile transition temperature (BDTT). This specific temperature can be determined by tensile or bending test results conducted at different temperature steps. In order to find the effect of strain rate on the BDTT, these experiments should be repeated at different strain rates. In order to reduce the amount of specimens for finding the BDTT a new methodology is studied. Experiments with particular loading strategies were performed on a fully lamellar Ti-48Al-2Nb-0.7Cr-0.3Si alloy in order to find the BDTT by using a single specimen. For this methodology cyclic loading is applied isothermally under strain control. The same loading block is then repeated on the specimen at different temperatures. The change in plastic strain with increasing temperature is then used for determining the BDTT of the specimen. In the next step a study is conducted to find the effect of strain rate on the BDTT also by using a single specimen. The same methodology as for finding the BDTT is used, but the cyclic loading was applied at different strain rates in a temperature step. Additional dwell times at constant total strains were introduced to identify the BDTT at very low plastic strain rates. The BDTT's of the TiAl alloy at different strain rates determined by this new methodology are compared in an Arrhenius plot from which the activation energy for brittle-ductile transition can be found.

#### 5:35 AM F.SF07.02.05

**Nano-Indentation Modulus and Hardness of  $\beta$ -Ti/ $\alpha_2$ -Ti<sub>3</sub>Al/ $\gamma$ -TiAl in Ti-Al-Cr System** Yotaro Okada, Sota Taniguchi, Ryosuke Yamagata, Hirotoyo Nakashima and Masao Takeyama; Tokyo Institute of Technology, Japan

Microstructures of  $\beta$ -solidifying TiAl alloys typically consists of  $\beta$ -Ti,  $\alpha_2$ -Ti<sub>3</sub>Al, and  $\gamma$ -TiAl three phases. We have revealed that fatigue crack growth resistance and ductility could improve by introduction of  $\beta$  phase. However, in order to evaluate and estimate the properties of a bulk material more quantitatively, it is essential to measure the properties of each phase. Nano-indentation method is appropriate to evaluate properties of individual phase in multi-phase material. In this study, Young's modulus and hardness of  $\beta$ ,  $\alpha_2$ , and  $\gamma$  phases have been investigated using nano-indentation in Ti-Al-Cr system. The alloys were heat-treated based on our phase diagram study. Young's modulus and hardness were measured by nano-indentation tests with continuous stiffness measurement mode. Crystallographic orientation analysis was performed before measurements with electron backscatter diffraction technique in order to identify the effect of orientation on the properties. In Ti-44Al-4Cr (at.%) equilibrated at 1373 K, the Young's modulus and hardness of all phases vary depending on the crystallographic orientation. In  $\beta$  and  $\gamma$  phases with (001) orientation, the Young's modulus is 136 and 146 GPa respectively, and the hardness is 7.0 and 3.0 GPa at room temperature. The hardness of  $\beta$  phase is more than twice as much as that of  $\gamma$  phase.  $\beta$  phase is harder than  $\gamma$  phase even at 1073 K although  $\beta$  phase is often considered to be soft at high temperature. This work was supported by Council for Science, Technology and Innovation (CSTI), Cross-ministerial Strategic Innovation Promotion Program (SIP), “Material Integration” for revolutionary design system of structural materials.

#### 5:45 AM F.SF07.02.06

**Effect of Interstitial Carbon and Oxygen in Solution on the Phase Equilibria Among  $\beta/\alpha/\alpha_2/\gamma$  Phases in TiAl Alloys** Hirotoyo Nakashima and Masao Takeyama; Tokyo Institute of Technology, Japan

Phase equilibria among  $\beta$ -Ti,  $\alpha$ -Ti,  $\alpha_2$ -Ti<sub>3</sub>Al and  $\gamma$ -TiAl phases has been examined experimentally in order to reveal the effect of interstitial carbon and oxygen in Ti-Al binary and Ti-Al-M (M:  $\beta$  stabilizing elements) ternary systems. Alloys with carbon/oxygen content from 0.13 (base) to 1.5 at. % were prepared by vacuum arc melting into button ingots. Those ingots were homogenized at the  $\beta$  or  $\alpha$  single-phase region, and then equilibrated at temperature range from 1573 K to 1073 K for up to 2 months. Chemical compositions of the metal elements in the phases present in equilibrated samples were analyzed by conventional wavelength dispersive spectroscopy (WDS). Carbon and oxygen contents in phases were analyzed by Soft X-ray Emission Spectroscopy (SXES).

In Ti-Al binary system, both carbon and oxygen partition into the  $\alpha$  (or  $\alpha_2$ ) against  $\gamma$  phase, and the  $\alpha+\gamma$  two-phase region expands toward both lower and higher Al content side. Oxygen content in  $\gamma$  phase in equilibrium with  $\alpha$  is clearly smaller than that of carbon, and thus the partition coefficient of oxygen between  $\alpha/\gamma$  is almost twice higher. In Ti-Al-M ternary systems, interstitial elements also partition into the  $\alpha$  (or  $\alpha_2$ ) against  $\gamma$  and  $\beta$  phases. By adding interstitials into the ternary alloys, the  $\beta+\alpha+\gamma$  three-phase coexisting region shift towards the higher M content side. At the same time, the terminal composition of the  $\beta$  phase increases with increasing interstitial content in the alloy, especially in case of oxygen. Detailed difference between the effect of carbon and oxygen will be discussed.

This work was supported by Council for Science, Technology and Innovation (CSTI), Cross-ministerial Strategic Innovation Promotion Program (SIP), "Material Integration" for revolutionary design system of structural materials.

#### 5:55 AM F.SF07.02.07

**Phase Equilibria in Ternary Ti–Al–Nb Alloys** Benedikt Distl, Martin Palm and Frank Stein; Max-Planck-Institute für Eisenforschung GmbH, Germany

Development of next-generation TiAl-based alloys for high-temperature, high-strength applications such as turbine blades relies on computational methods like CALPHAD modelling for alloy and microstructure design. To achieve the goal of further increased service temperatures, an exact knowledge of phase equilibria and microstructures is essential and plays an important role in determining the high-temperature mechanical properties of respective alloys. Therefore, a dataset of reliable experimental results is needed to improve the accuracy of the modelling. The Ti–Al–Nb system is the essential system for alloys such as TNM, TNB or 4822 which are currently used for low pressure turbine blades. However, there are only few results in the literature about the Ti–Al–Nb system regarding phase equilibria below 1000°C, and there is a variety of different and contradicting experimental results for temperatures of 1000°C and above. Based on these data, reliable predictions from CALPHAD modelling is difficult. For further development of TiAl-based alloys the existing CALPHAD database should therefore be improved. Another factor complicating the matter is the not fully understood formation of ternary O- ( $Ti_2NbAl$ ) and  $\omega$ - phase ( $Ti_4NbAl_3$ ) from ( $\beta Ti$ ) and  $\alpha_2$  ( $Ti_3Al$ ), respectively, which depend on a variety of factors. Since these phases are important for the mechanical properties of these alloys, research presented here aims to clarify the uncertainties in phase equilibria in Ti-Al-Nb alloys. The research is carried out within the scope of the EU-funded project ADVANCE which is part of the Clean Sky 2 research initiative. The aim of the project is to improve an existing database for TiAl-based alloys for speeding up the development of next-generation alloys based on titanium aluminides. The project is carried out in collaboration with Helmholtz-Zentrum-Geesthacht (Germany), Montanuniversität Leoben (Austria), and Thermo-Calc Software (Sweden).

#### 6:05 AM F.SF07.02.08

**The Effect of Zr Addition on High Temperature Phase Transformation and Microstructure of TiAl Alloys** Fabian Kathöfer and Florian Pyczak; Helmholtz-Zentrum Geesthacht, Germany

Titanium aluminide alloys (TiAl) are widely recognized for their potential as aero engine components due to their combination of similar service temperature and lower density than conventional metallic systems as for example Ni-base superalloys. However, an improved understanding of the microstructure formation and phase transformation during the production of TiAl parts is necessary to adapt the process parameters for hot forming. Fortunately, an appropriate tuning of the alloy composition can provide good deformation capabilities. For instance, the addition of Zirconium (Zr), a  $\beta$ -stabilizing element, lowers the phase transformation temperatures of the 'softer' disordered  $\alpha$  and  $\beta$  phases and has other additional beneficial effects e.g. solution strengthening of TiAl alloys. In order to determine appropriate TiAl-Zr compositions thermodynamic calculations were performed using Thermo-Calc Software ('TCTH v1' database). Based on these, samples with selected compositions were produced by arc melting and afterwards heat treated for chemical homogenization. The thermodynamic behavior during heating was investigated by differential scanning calorimetry (DSC) using a NETZSCH DSC 404 F3 Pegasus. Additionally, high-energy synchrotron X-Ray diffraction (HEXRD) was performed in-situ to observe the phase changes during heating. Both measurement methods reveal that thermodynamic calculations based on currently available databases for TiAl-Zr alloys can only show tendencies how phase transitions change with increasing or decreasing Zr content, but do not allow accurate predictions of transition temperatures.

#### 6:15 AM F.SF07.02.09

**Influence of Oxidation Protective Coatings on the Fatigue Behaviour of Ti-48Al-2Cr-2Nb** Christoph Breuner<sup>1</sup>, Stefan Guth<sup>1</sup>, Karl-Heinz Lang<sup>1</sup>, Peter-Philipp Bauer<sup>2</sup> and Martin Heilmaier<sup>1</sup>; <sup>1</sup>Karlsruhe Institute of Technology, Germany; <sup>2</sup>German Aerospace Center, Germany

Due to their good oxidation resistance and excellent specific mechanical properties at elevated temperatures, intermetallic Titanium Aluminides are candidate materials to replace Ni-base alloys in high temperature turbine applications. One promising example of Titanium Aluminides is Ti-48Al-2Cr-2Nb (at-%) which is already used for low-pressure turbine blades. Although its duplex microstructure is stable up to a temperature of 850 °C, the alloy is limited to temperatures below 700 °C since oxidation rates increase dramatically at higher temperatures. One possibility to reduce oxidation and increase the operation temperature are oxidation protective coatings. However, these coatings are typically very brittle and therefore unfavourable for fatigue loading. In this study, the influence of oxide layers and oxidation protective coatings on the fatigue lifetime of Ti-48Al-2Cr-2Nb at 750 °C are investigated. Stress-controlled fatigue tests were conducted on coated and

uncoated samples that were pre-oxidised for 300 h at 850 °C as well as on untreated samples. The results indicate that for low stress amplitudes the lifetimes for coated, uncoated pre-oxidised and untreated samples are comparable. Above a certain stress amplitude the S-N-curves for coated and uncoated-pre-oxidised samples are much flatter than for untreated material. I. e. lifetimes of coated and uncoated pre-oxidised materials decrease much more with increasing stress amplitude than lifetimes of untreated samples. The behaviour is discussed based on cyclic deformation analysis and damage observations and explanations are proposed.

SESSION F.SF07.03: Ultra-High Temperature Alloys  
On Demand Abstracts Available for Viewing Starting Saturday Morning, November 21, 2020  
F-SF07

#### 5:00 AM \*F.SF07.03.01

**High Temperature Creep Behavior of MoSiBTiC Alloy** Kyosuke Yoshimi, Ryuta Yanagiya, Shiho Kamata, Shuntaro Ida and Nobuaki Sekido; Tohoku University, Japan

High temperature creep behavior of TiC-added Mo-Si-B alloy was studied in the temperature range of 1400 - 1600°C and the stress range of 75 – 300 MPa. Creep strain under constant applied stress control was measured by directly reading the change in specimen gage length using CMOS image sensors. 4 stages were observed on the creep curves. That is, I. instantaneous strain, II. primary creep, III. secondary creep with the minimum creep rate and IV. tertiary creep with acceleration. The minimum creep rates showed a good linear relationship with applied stress in the Norton plot, and the obtained stress exponent,  $n$ , was about 3.5, indicating power-law creep. The minimum creep rates also showed a good linear relationship with inverse temperature in the Arrhenius plot, and the obtained apparent creep activation energy,  $Q_c$ , was about 497 kJ/mol. The value is in good agreement with the activation energy of Mo self-diffusion (488 kJ/mol), strongly suggesting that Mo self-diffusion is the rate-controlling process of creep deformation of the MoSiBTiC alloy under the conditions. Instantaneous strain varied from  $10^{-4}$  to  $10^{-2}$  depending on stress and temperature. To reach a  $10^{-2}$  instantaneous strain, some mechanisms in addition to an elastic strain should be considered to operate. Careful SEM observations indicated that micro-cracking in coarse  $T_2$  phase and interfacial separation appeared to occur during the increase in instantaneous strain. Those weakening mechanisms would cause the large instantaneous strain. From the perspective of high temperature applications, the time for creep strain to reach 1% is one of the guidelines for development. Therefore, suppressing the occurrence of those weakening mechanisms through microstructure control as well as the increase in strain-hardening coefficient of Mo solid solution is important for improving the high temperature creep strength of the MoSiBTiC alloy especially in a small creep strain.

#### 5:15 AM F.SF07.03.02

**Creep Performance of Pesting-Resistant Mo-Si-Ti Alloys** Alexander Kauffmann, Martin Heilmaier and Susanne Obert; Karlsruhe Institute of Technology–Institute for Applied Materials, Germany

High-temperature structural materials require not only high solidus temperatures and acceptable densities, but especially good creep and oxidation resistance. The improvement in efficiency of high-temperature applications requires the development of alternates to Ni-based superalloys with operating temperatures higher than 1100 °C and densities lower than 8.5 g/cm<sup>3</sup>. Ti macro-alloyed Mo-Si-based alloys have shown great potential due to their high solidus temperatures in the range of 1800 °C and considerably reduced densities down to 6 to 7 g/cm<sup>3</sup>, while possessing a competitive creep resistance compared to state-of-the-art single crystalline Ni-based superalloys [1]. However, the oxidation behaviour is typically characterised by catastrophic mass loss at temperatures below 1000 °C caused by volatilisation of MoO<sub>3</sub>, known as ‘*peisting*’ [1]. In order to achieve peisting-stability in Mo-Si-Ti alloys, a threshold of Ti content of 43 at% needs to be exceeded [2]. The attained fine-scaled microstructures are either fully eutectic (alloy Mo-20Si-52.8Ti (at%) comprising Mo solid solution Mo<sub>SS</sub> and (Ti,Mo)<sub>5</sub>Si<sub>3</sub> [1]) or eutectic-eutectoid (alloy Mo-21Si-43.4Ti, comprising Mo<sub>SS</sub>, (Ti,Mo)<sub>5</sub>Si<sub>3</sub> and (Mo,Ti)<sub>5</sub>Si<sub>3</sub> [2]) and possess a solidus temperature-dependent creep resistance. Thus, the creep behaviour is determined by the Ti to Mo ratio, while the Ti content is pre-defined in order to ensure peisting-stability. With the aim of improving the creep resistance of those alloys, several alloy design approaches are pursued: (i) adjustment of the Mo content accordingly to the required Ti threshold, (ii) variation of the microstructural length scale including artificially coarsened microstructures and (iii) potential strengthening phases like Mo<sub>SS</sub> and (Mo,Ti)<sub>5</sub>Si<sub>3</sub>. It is found that both targets, peisting-stability and creep resistance are met by an intermediate alloy Mo-21.6Si-44.2Ti comprising a eutectic-eutectoid matrix with a small volume fraction of primary solidified (Mo,Ti)<sub>5</sub>Si<sub>3</sub> (< 5 vol%). Moreover, the alloy Mo-26Si-40Ti with almost 30 vol% primary solidified (Mo,Ti)<sub>5</sub>Si<sub>3</sub> was created, which reveals a further improved creep resistance at 1200 °C and still provides peisting-stability.

[1] D. Schliephake, A. Kauffmann, X. Cong, C. Gombola, M. A. Azim, B. Gorr, H.-J. Christ, M. Heilmaier, *Intermetallics*. 2019, 104, 133-142.

[2] S. Obert, A. Kauffmann, M. Heilmaier, *Acta Materialia*. 2020, 184, 132-142.

#### 5:25 AM F.SF07.03.03

**Oxidation Resistance of Additively Manufactured Mo-Si-B Alloys** [Julia Becker](#)<sup>1</sup>, Janett Schmelzer<sup>1</sup>, Manja Krueger<sup>1</sup>, Georg Hasemann<sup>1</sup>, David Fichtner<sup>2</sup>, Christoph Heinze<sup>2</sup> and Sven Schmigalla<sup>3</sup>; <sup>1</sup>Otto von Guericke University, Germany; <sup>2</sup>Siemens AG, Germany; <sup>3</sup>Institute für Korrosions- und Schadensanalyse, Germany

Mo-Si-B alloys are high-performance materials that exhibit excellent mechanical properties at ultra-high temperatures (> 1200°C), thus enabling their use in demanding load scenarios. Especially ternary Mo-Si-B alloys, which consist of a Mo solid solution matrix with intermetallic phases (Mo<sub>3</sub>Si and Mo<sub>5</sub>SiB<sub>2</sub>), offer the potential to replace the currently used nickel base superalloys, whose operating temperature is limited to a maximum of 1150°C.

However, the production of such Mo-Si-B alloys is difficult due to the very high melting temperatures of over 2000 °C and the complex solidification behavior. A possible way of production is a multi-stage powder metallurgical process. The development of a single-stage process for the production of Mo-Si-B alloys represents a new challenge.

Additive manufacturing processes such as the powder bed-based Laser Powder Bed Fusion (L-PBF) and the powder nozzle-based Directed Energy Deposition (DED) offer unique new possibilities for near-net-shape production with targeted adjustment of fine-grained microstructures or chemically graded materials.

Initial findings show that it is possible to produce near-eutectic Mo-Si-B alloys using the L-PBF process. These alloys show excellent creep properties and reduced brittle-ductile transition temperatures compared to other Mo-Si-B alloys with a silicide matrix.

Besides the mechanical properties at elevated temperatures, oxidation resistance is another decisive factor for the use of Mo-Si-B alloys. Current work is being carried out to investigate the behavior under cyclic oxidation conditions. The mass loss curves of the additively manufactured Mo-Si-B alloys show that, compared to nickel-based alloys, comparatively high mass losses occur, which can be explained by the microstructures formed by additive processing. However, the AM alloys show an improved oxidation resistance compared with powder metallurgically produced Mo-Si-B alloys having a solid solution matrix.

#### 5:35 AM F.SF07.03.04

**Off-Stoichiometric Effect on Elastic and Plastic Properties of TiC Phase in Mo-Ti-C Ternary System** [Shuntaro Ida](#), Nobuaki Sekido and Kyosuke Yoshimi; Tohoku University, Japan

TiC is a promising carbide for ultrahigh temperature applications not only as a dispersion-strengthening phase but also as structural components. One of the biggest problems with this phase is its poor fracture toughness at room temperature. Interestingly, TiC phase has a wide compositional range away from stoichiometry like intermetallics, which can influence its elastic and plastic properties. Therefore, it is important to understand changes in the elastic and plastic properties of TiC phase in relation to off-stoichiometry and structural point defects. In this work, the effects of off-stoichiometry and Mo substitution on the elastic and plastic properties of TiC phase at room temperature were investigated for Mo-Ti-C ternary alloys in the Mo/TiC two-phase region. Multiple alloys on the same tie lines at 2073 K were made based on the Mo-Ti-C ternary phase diagram. The elastic moduli of the TiC phases with different terminal compositions in the two-phase region were estimated from the elastic moduli of the alloys obtained experimentally based on the rule of mixture by the Voigt model. The Young's modulus and shear modulus of the TiC phase increase with Mo substitution, but decrease from off-stoichiometry toward the metal-rich side. The change in the elastic moduli of the TiC phase is more effective by the off-stoichiometry than by the Mo substitution. The increase in Young's modulus and the decrease in shear modulus may improve fracture toughness since the increase in yield stress and the improvement of plastic deformability increase the energy absorbed during crack propagation. The TiC phase in the Ti-C binary system, which has the lowest shear modulus and Young's modulus, exhibits better toughness at room temperature than other TiC phases. The decrease in shear modulus appears to be a more important factor in improving the toughness of the TiC phase at room temperature.

#### 5:45 AM F.SF07.03.05

**Additive Manufacturing of a Near-Eutectic V-9Si-5B Alloy for High-Temperature Application** [Janett Schmelzer](#)<sup>1</sup>, Silja-Katharina Rittinghaus<sup>2</sup> and Manja Krueger<sup>1</sup>; <sup>1</sup>Otto-von-Guericke-University Magdeburg, Germany; <sup>2</sup>Fraunhofer - Institute for Laser Technology, Germany

There nearly is no other industry placing such high demands on materials as aircraft construction. Due to the mature design of the aircraft engines, further competition will take place with innovative materials and manufacturing processes. In the



vicinity of the combustor, where engine parts are burdened with temperatures higher than 500 °C, Ni-based superalloys have been state-of-the-art for many years. However, Ni-based superalloys come along with a high density (~ 8.5 g/cm<sup>3</sup>). Weight reduction is an important issue to achieve the target of increased thermodynamic efficiency including less fuel consumption and a reduced amount of exhaust emissions. To this end, research activities focus on new light-weight materials with good high-temperature properties to increase the thrust-to-weight ratio in aircraft engines by replacing Ni-based superalloys. Vanadium points out as an interesting candidate, since it offers the lowest density ( $\rho = 6.11 \text{ g/cm}^3$ ) in comparison to other high-melting metals. Moreover, alloyed with Si and B a multi-phase microstructure, consisting of a vanadium solid solution ( $V_{ss}$ ) phase next to the intermetallic phases  $V_3Si$  and  $V_5SiB_2$  [1,2] forms, which offers a low ductile-brittle-transition as well as enhanced high-temperature strength and creep resistance next to an improved oxidation resistance [1]. However, conventional ingot metallurgical processing of V–Si–B material and subsequent machining is energy- and time-consuming due to the different behavior of the ductile solid solution phase and the brittle silicides. This work presents the first study on the feasibility of printing pre-alloyed near-eutectic V-9Si-5B powder material via directed energy deposition (DED) as a method for additive manufacturing. Tailored V-9Si-5B powder material was produced by means of a gas atomization process. A novel setup for the DED experiments was developed and an overview of the production parameters for manufacturing of crack-free specimens is given. The microstructural evolution of the three-phase V-9Si-5B alloy is described by means of SEM, EBSD and STEM analyses during the entire process chain, i.e. the gas atomization of the powder material, the consolidation via DED and the heat treatment of the compacts. First mechanical tests demonstrate the high hardness and the competitive creep resistance of the AM V-9Si-5B material in comparison to other three-phase V-based alloys.

[1] M. Krüger, *Scripta Mater.* **2019**, 121, 75–78.

[2] G. Hasemann, M. Krüger, M. Palm, F. Stein, *Mater Sci Forum.* **2018**, 941, 827-832.

#### 5:55 AM F.SF07.03.06

**Properties of Laser-Based Additively Manufactured Mo-Si-B Alloys** Manja Krueger; Otto von Guericke University, Germany

Additive manufacturing (AM) of Mo-Si-B alloys is very challenging due to their high melting temperatures above 2000 °C and their possible oxide formation reactions during processing. Additionally, multi-phase Mo-Si-B alloys are brittle up to ~ 950 °C, which is critical in terms of possible crack formation during fast cooling in AM processes.

In this presentation we will demonstrate that laser-based AM can be applied to produce dense Mo-Si-B bodies using tailored gas atomized powders. Therefore, the alloys Mo-9Si-8B, Mo-13.5Si-7.5B and Mo-16.5Si-7.5B were selected, which have different concentrations of silicide phases. We show how the modified processes Laser Powder Bed Fusion (LPBF) and Direct Energy Deposition (DED) lead to homogeneous and crack-free bulk materials with a low porosity of < 1%. The microstructure of these materials will be compared to microstructures derived from powder metallurgical (PM) processes and the properties of the AM and PM materials will be comparatively assessed. It will be demonstrated that the hardness, the brittle-ductile-transition-temperature (BDTT) and the creep response of AM Mo-Si-B materials are quite competitive with PM Mo-Si-B materials.

#### 6:05 AM F.SF07.03.07

**Micropillar Compression Deformation of Transition-Metal Disilicides with the C40 Structure** Kyosuke Kishida and Haruyuki Inui; Kyoto University, Japan

Transition-metal disilicides,  $TMSi_2$  (TM = Nb, Cr, Ta and V) with the hexagonal C40 structure have received considerable attention as base materials of a new-class of ultra-high temperature structural materials for more than three decades because of their high melting points, attractive mechanical properties at high temperatures and relatively low density. In these hexagonal C40 silicides, only basal slip has been confirmed to be operative at high temperatures above 400 °C in pristine single crystalline specimens. Among these four C40 silicides,  $CrSi_2$  exhibits quite peculiar slip behavior of synchroshear-type, while the other three silicides deforms with normal slip. Recently, we have investigated room-temperature plastic deformation behavior of various hard and brittle intermetallics, such as  $TM_5Si_3$  type silicides, laves phase, sigma phase, by micropillar compression methodology and have confirmed the dislocation activations in most of these hard and brittle intermetallics even at room temperature in the micropillar form. In the present study, room-temperature deformation behavior of single crystals of various transition-metal disilicides  $TMSi_2$  (TM = V, Cr, Nb and Ta) with the C40 structure was investigated by the micropillar compression method as a function of the loading axis orientation and specimen size in order to clarify the details of operative slip systems and to evaluate their CRSS values at room temperature. Dissociation schemes of the identified dislocations were investigated by transmission electron microscopy imaging of dislocation microstructures and atomic-resolution scanning transmission electron microscopy imaging of their core structure. Although plastic flow is

observed only at high temperatures for most  $\text{TMSi}_2$  in the bulk form, basal slip was confirmed to be operative at room temperature in the four C40-TMSi<sub>2</sub> in the micropillar form. The CRSS value for each slip system exhibits ‘smaller is stronger’ behavior following an inverse power-law relationship with the power-law exponents depending on slip systems and materials. Deformation mechanisms of these TMSi<sub>2</sub> at room temperature will be discussed based on the comparison with those previously obtained for bulk-sized single crystals at elevated temperatures.

#### 6:15 AM F.SF07.03.08

**V<sub>SS</sub>-V<sub>3</sub>B<sub>2</sub> Eutectic Alloys—Microstructure and Compression Properties** Christopher Müller, Georg Hasemann, Maximilian Regenberg and Manja Krueger; Otto-von-Guericke-University, Germany

Due to their low density in combination with a high melting point, vanadium-based alloys provide great potential as a new type of structural lightweight material for high temperature applications. Based on the promising V-Si-B system, the microstructural evolution and room temperature deformability in different binary eutectic V<sub>SS</sub> (V solid solution)-V<sub>3</sub>B<sub>2</sub> alloys were determined. In particular, it was investigated how the binary eutectic trough (V<sub>SS</sub>-V<sub>3</sub>B<sub>2</sub>) is affected by alloying with silicon and how the resulting phase fractions affect the compression properties at room temperature. These aspects were systematically investigated for the first time.

Different binary V-B and ternary V-Si-B alloys were produced by conventional arc-melting. Scanning Electron Microscopy (SEM) and X-ray Diffraction (XRD) methods were used to examine the as-cast microstructures as well as to identify phases and to determine phase fractions. Microhardness measurements and room temperature compression tests were carried out to determine the mechanical properties in dependence of the respective phase fractions.

The results were compared with the current literature in order to estimate the contributions of the various phases to the resulting compressive strengths and to re-evaluate the information available on solidification processes in the V-Si-B system. The results indicate that the V<sub>SS</sub> phase controls the plastic deformability in the V<sub>SS</sub>-V<sub>3</sub>B<sub>2</sub> eutectic microstructure whereas the intermetallic V<sub>3</sub>B<sub>2</sub> phase acts as second phase strengthener. With increasing silicon addition, the eutectic composition is shifted to lower boron concentrations. Compared to the calculated liquidus projection of the V-Si-B system, the present experimental results also suggest a much larger binary eutectic trough than recently reported in the literature.

#### 6:25 AM F.SF07.03.09

**Microstructure Evolution and Mechanical Properties of Eutectic V-Si-B Alloys** Georg Hasemann<sup>1</sup>, Christopher Müller<sup>1</sup>, Weiguang Yang<sup>2</sup>, Maximilian Regenberg<sup>1</sup> and Manja Krueger<sup>1</sup>; <sup>1</sup>Otto-von-Guericke University Magdeburg, Germany; <sup>2</sup>Forschungszentrum Jülich GmbH, Germany

The solidification behavior of arc-melted alloys in the V-rich portion of the ternary V-Si-B alloy system has been experimentally investigated. A detailed microstructure analysis of several as-cast alloys based on SEM observations, EDS/WDS and EBSD measurements was carried out. As a result, different solidification reactions in the V-rich V-Si-B system were identified. On the two binary boundary systems V-Si and V-B those reactions were attributed to primary V<sub>SS</sub>, V<sub>3</sub>Si, V<sub>5</sub>Si<sub>3</sub>, V<sub>3</sub>B<sub>2</sub> and VB. Furthermore, a primary solidification reaction within the ternary system was attributed to V<sub>5</sub>SiB<sub>2</sub>. As a result, the new data allows a reconstruction of the liquidus surface of the V-Si-B phase diagram. Furthermore, a V<sub>SS</sub>-V<sub>3</sub>Si-V<sub>5</sub>SiB<sub>2</sub> ternary eutectic reaction was identified and its composition was investigated experimentally. The V-based ternary eutectic is isomorph to the well-known Mo-Si-B system and the Mo<sub>SS</sub>-Mo<sub>3</sub>Si-Mo<sub>5</sub>SiB<sub>2</sub> ternary eutectic. However, the V-based ternary eutectic has a solid solution character since V<sub>SS</sub> forms the major phase as compared to the intermetallic character of the Mo-base eutectic with the Mo<sub>3</sub>Si phase as the major phase. This will have advantages considering low temperature deformability and fracture toughness.

By carrying out this work special attention had been paid to the eutectic reactions in the binary V-Si and V-B systems as well as in the ternary V-Si-B system. Thus, the binary eutectic compositions of V<sub>SS</sub>-V<sub>3</sub>Si and V<sub>SS</sub>-V<sub>3</sub>B<sub>2</sub> had been re-investigated carefully, since they represent important anchor points for the liquidus projection in the ternary system.

Besides the microstructure evolution, room temperature compression tests were carried out to get first insights in the alloys compressive yield stress and deformability. Silicon was found to act as a strong solid solution strengthener without embrittling the V<sub>SS</sub> phase, even at its maximum Si solubility of about 7 at.%.

#### 5:00 AM \*F.SF07.04.01

**A Hexagonal Close Packed Multi-Principal-Element Alloy Identified Computationally** Mark Asta<sup>1,2</sup>, Daryl Chrzan<sup>1</sup>, Qijun Hong<sup>3</sup>, Lu Jiang<sup>1</sup>, Andrew Minor<sup>1,2</sup>, Velimir Radmilovic<sup>4</sup>, Julian E. Sabisch<sup>5</sup>, Ruoshi Sun<sup>3</sup> and Axel van de Walle<sup>3</sup>; <sup>1</sup>University of California, Berkeley, United States; <sup>2</sup>Lawrence Berkeley National Laboratory, United States; <sup>3</sup>Brown University, United States; <sup>4</sup>University of Belgrade, Serbia; <sup>5</sup>Sandia National Laboratories, United States

In this work we consider the design of alloys that can mimic the excellent combination of room temperature and high-temperature mechanical properties displayed by the refractory elemental metal rhenium, but with reduced cost. Experimental investigations of the deformation mechanisms and microstructures in this material highlight the important role of {11-21} deformation twinning, and high-resolution electron microscopy combined with first-principles calculations offer insights into the origin of the dominance of this twin system. These considerations lead to a design principle that trades off average valence electron count and cost considerations, identifying a promising pool of candidate substitute alloys in the Mo-Ru-Ta-W quaternary system. We demonstrate how this design principles is combined with a computational thermodynamics model of phase stability, based on high-throughput ab initio calculations, to further narrow down the search and lead to the identification of alloys that maintain rhenium's desirable hcp crystal structure. The predictions of this modeling are validated through comparisons to known binary phase diagram sections and corroborated by experimental synthesis and structural characterization demonstrating multi-principle-element hcp solid-solution samples selected from a promising composition range. Additional theoretical calculations and initial mechanical properties measurements will be presented to assess the potential performance of these alloys for high temperature applications.

#### 5:15 AM F.SF07.04.02

**Deformation Microstructure of an L1<sub>2</sub> Intermetallic High Entropy Alloy** Rachel D. Osmundsen and Ian Baker; Thayer School of Engineering at Dartmouth College, United States

In the search for single-phase high entropy alloys (HEAs), intermetallic HEAs have been largely neglected. Intermetallic HEAs are often components of multi-phase HEAs that have good structural properties, so, it is critical to understand their deformation microstructures. This work shows that the HEA Al<sub>8.8</sub>Co<sub>18.1</sub>Cr<sub>21.7</sub>Fe<sub>20.2</sub>Ni<sub>31.1</sub>, which is the L1<sub>2</sub> phase of the AlCoCrFeNi<sub>2.1</sub> eutectic system, can be cast as a single ordered phase. The deformation microstructure was examined in the transmission electron microscope using weak-beam dark-field imaging on samples compressed to ~3% plastic strain. Deformation occurred on the {111}<110> slip system and stacking faults, dipole nets, and large macrokinks were observed. The stacking fault energy was estimated and dissociated dislocations identified through careful tilting experiments. Tensile tests were performed on the alloy in both the disordered and strongly ordered states. The difference in tensile properties between the two is thus due to features unique to the ordered state, such as antiphase boundary (APB) tubes. Additionally, magnetization curves were taken with a vibrating sample magnetometer to measure the change in magnetization with APB tube formation. The formation of APB tubes changes the local chemical environment, including where ferromagnetic elements sit in relation to one another. The formation of APB tubes in ordered Al<sub>8.8</sub>Co<sub>18.1</sub>Cr<sub>21.7</sub>Fe<sub>20.2</sub>Ni<sub>31.1</sub> is compared to other binary alloys, with a focus on Ni<sub>3</sub>Fe. This work was supported by the U.S. Department of Energy, Basic Energy Sciences, under award #DE-SC0018962.

#### 5:25 AM F.SF07.04.03

**Development of Fe–Al–Nb(–B) Alloys for High-Temperature Structural Applications** Angelika Gedsun and Martin Palm; Max-Planck-Institut für Eisenforschung GmbH, Germany

For high-temperature structural applications, e.g. compressor blades in steam turbines, novel sustainable and heat resistant materials are required. Fe–Al based alloys show significant longevity due to their outstanding corrosion and wear resistance additionally to their low density and good mechanical properties.

Fe–Al based alloys are becoming more interesting for industrial applications, not at least because they are an economically efficient alternative to replace Cr-steels and Ni-based superalloys in specific applications. Moreover, standard processing techniques can be applied for their large-scale production [1, 2].

Through recent developments, especially the creep resistance could be improved by different alloying concepts [2]. E.g., incoherent precipitates such as borides or Laves phase or coherent precipitates can significantly enhance the mechanical properties.

In Fe–Al–Ta the formation of the stable hexagonal C14 Laves phase is preceded by the formation of the coherent metastable L2<sub>1</sub> Heusler phase, which improves strength and creep resistance up to 750°C. Through thermomechanical processing, heat treatment or doping, microstructures with fine scaled and homogeneously distributed Laves phase precipitates inside the Fe–Al matrix and at grain boundaries were obtained [3].

For further optimization, Ta was replaced by Nb in the present research.

In the Fe–Al–Nb system, the controlled distribution of the stable Laves phase within the Fe–Al matrix and at grain boundaries could also be achieved when the formation of the incoherent Laves phase is preceded by the formation of the coherent metastable Heusler phase.

Further investigations focus on the morphology of Laves phase precipitates at grain boundaries and their coarsening.

[1] C. G. McKamey, Iron aluminides, Phys. Metall. Process. Internet. Compd. Springer (1996) 351-391

[2] M. Palm, F. Stein, and G. Dehm, Iron Aluminides, Annu. Rev. Mater. Res. 49 (2019) 297-326

[3] P. Prokopčáková, M. Švec, and M. Palm, Microstructural evolution and creep of Fe–Al–Ta alloys, Int. J. Mater. Res. 107 (2016) 396-405

#### 5:35 AM F.SF07.04.04

**Predict Homogeneous Crystal Nucleation Rate from Melts with a Steep Composition Gradient—A Computational Study of NiAl Intermetallic Formation** Peng Yi, Tim Weihs and Michael L. Falk; Johns Hopkins University, United States

Reactions at interfaces between different solid (crystalline or amorphous) materials are critical processing steps for a variety of applications including microelectronics, superconducting magnet wires, coatings on turbine blades, and reactive materials.[1] Due to the highly non-equilibrium nature of interfaces, phase formation at these interfaces is complicated and difficult to predict. It is well established experimentally that the first phase to form through an interfacial reaction need not be the most stable phase predicted by the phase diagram. As an example, DSC and TEM experiments in the Ni/Al multilayer system have suggested that the formation of intermetallic phases can be suppressed by a high heating rate, [2, 3] or by reducing the interspacing between the layers.[4, 5] Different heating rate or interspacing lead to different composition gradient across the interface, which strongly affects the thermodynamics and kinetics of the nucleation process.

We studied homogeneous nucleation of the non-stoichiometric NiAl-B2 intermetallic compound from deeply undercooled amorphous melts with an imposed composition gradient.[6] Data from MD simulations permits quantification of the nucleation rate of the intermetallic phase and indicates that nucleation proceeds in a polymorphous mode. The nucleation rate decreases with increasing gradient, and nucleation is completely suppressed above a critical gradient, as suggested by Desré and co-workers[7]. Based on an argument of crystal nucleus stability, a simple estimate provides good prediction of the critical gradient. A modified classical nucleation model parameterized with thermodynamic and kinetic quantities calculated independently predicts the nucleation rates and their variation with the imposed gradient, matching the MD results very well. This model can be used to compute the nucleation rates for different intermetallic compounds at an interface for the prediction of the phase formation sequence.

#### References:

1. Adams, D.P., *Reactive multilayers fabricated by vapor deposition: A critical review*. Thin Solid Films, 2015. **576**: p. 98-128.
2. Trenkle, J.C., et al., *Phase transformations during rapid heating of Al/Ni multilayer foils*. Applied physics letters, 2008. **93**(8): p. 081903.
3. Grapes, M.D., et al., *A detailed study of the Al3Ni formation reaction using nanocalorimetry*. Thermochemica Acta, 2017. **658**: p. 72-83.
4. Edelstein, A.S., et al., *Intermetallic phase formation during annealing of Al/Ni multilayers*. Journal of Applied Physics, 1994. **76**(12): p. 7850-7859.
5. Blobaum, K.J., et al., *Al/Ni formation reactions: characterization of the metastable Al9Ni2 phase and analysis of its formation*. Acta Materialia, 2003. **51**(13): p. 3871-3884.
6. Yi, et al., *Predict homogeneous crystal nucleation rate from melts with a steep composition gradient*, (to be submitted).
7. Desré, P.J. and A.R. Yavari, *Suppression of crystal nucleation in amorphous layers with sharp concentration gradients*. Physical Review Letters, 1990. **64**(13): p. 1533-1536.

#### 5:45 AM F.SF07.04.05

**Study of the Initial Stages of Precipitation of Alloy 718 During Conventional versus Direct Ageing** Vitor V. Rielli<sup>1</sup>, Felix Theska<sup>1</sup>, Flora Godor<sup>2</sup>, Aleksandar Stanojevic<sup>2</sup>, Bernd Oberwinkler<sup>2</sup> and Sophie Primig<sup>1</sup>; <sup>1</sup>UNSW Sydney,

Australia; <sup>2</sup>voestalpine BÖHLER Aerospace GmbH & Co KG, Austria

Recent global events have been negatively affecting the air transport market exposing the great need for operational excellence and efficiency due to optimal utilization of materials [1]. Better aircrafts with more efficient engines will push materials to the limit, and as a vital alloy for turbine discs, Alloy 718, a Ni-based superalloy, must have its properties improved in order to withstand higher temperatures and workloads. Direct ageing is a common processing route where solution annealing between forging and ageing is omitted, producing yield strength increases up to 10% in comparison to conventional ageing [2]. Several mechanisms are responsible for this behaviour, such as changes in  $\gamma$ -matrix grain size,  $\delta$  phase fraction, dislocation density, and mainly the configuration of  $\gamma'$  and  $\gamma''$  precipitates [3]. An investigation regarding the nucleation and growth of these precipitates during the early stages of precipitation during direct ageing was published recently [4] and it has found that the presence of dislocations enabled the formation of  $\gamma''$  precipitates during air cooling from forging and an accelerated growth during direct ageing. A comparison between the evolution of the nanoscale precipitates during direct ageing of materials water quenched after forging and conventionally aged materials is still lacking. In this study through the use of atom probe microscopy and TEM in-situ heating, a holistic analysis of the precipitation of  $\gamma'$  and  $\gamma''$  is given and the effects on the mechanical properties are investigated.

[1] M. Hader, <https://www.rolandberger.com/en/Point-of-View/COVID-19-How-we-will-need-to-rethink-the-aerospace-industry.html>. Accessed 10/06/2020

[2] C. Krueger, The Minerals, Metals and Materials Society, 1989

[3] F. Theska, A. Stanojevic, B. Oberwinkler, S.P. Ringer, S. Primig, Acta Mater. 156 (2018) 116–124.

[4] F. Theska, K. Nomoto, F. Godor, B. Oberwinkler, A. Stanojevic, S.P. Ringer, S. Primig, Acta Mater. 188 (2020) 492-503.

#### 5:55 AM F.SF07.04.06

##### **Experimental and Calculation Approach for Phase Equilibria Among $\gamma$ /TCP/GCP *oP6* Phases at Elevated Temperatures** Ryota Nagashima, Hirotoyo Nakashima and Masao Takeyama; Tokyo Institute of Technology, Japan

Strengthening of Ni-base superalloys are in principle designed using GCP (Geometrically Closed- packed) phase of  $\text{Ni}_3\text{Al}$ - $\gamma'$  ( $L_{12}$ ), however game-changing microstructural design principle without relying on  $\gamma'$  phase will be needed for further development of the alloys. We are currently constructing a novel microstructure design principle, using thermodynamically stable TCP (Topologically Close-packed phase) or  $\alpha$ -W for grain boundaries, together with GCP (Geometrically Close-packed phase) other than  $\gamma'$  phase for grain interiors, based on grain boundary precipitation strengthening mechanism. One of the promising systems is Ni-Cr-Mo ternary system, where TCP phases of NiMo,  $\mu$  and P together with GCP phases of  $\text{Ni}_3\text{Mo}$ ,  $\text{Ni}_4\text{Mo}$  and  $\text{Ni}_2\text{Cr}$  (*oP6*) exist. We have clarified that *oP6* phase becomes extremely stable by Mo in solution at over 1073 K which is stable at 873 K in Ni-Cr binary system. Thus, there exist three-phase regions of  $\gamma/\text{NiMo}/\text{oP6}$  and  $\gamma/\text{P}/\text{oP6}$ , unlike the phase diagram calculated based on commercially available thermodynamic databases. Moreover, *oP6* phase precipitates coherently with tweed-like morphology and possess an orientation relationship of  $\{110\}_{\gamma}/\{100\}_{\text{oP6}}$ ,  $\langle 001 \rangle_{\gamma}/\langle 010 \rangle_{\text{oP6}}$ , just like precipitation behavior of  $\gamma'$  particles in ordinary Ni-based superalloys. In contrast, the TCP phases preferentially precipitate at the grain boundaries. On the other hand, in Ni-Cr-W ternary system, g phase equilibrates with  $\alpha$ -W phase. By partially replaced Mo by W, there arises another possibility of  $\gamma/\alpha\text{-W}/\text{oP6}$  three-phase region. Since W is the same transition metals of VIb group with Cr and Mo, *oP6* phase stability is expected to increase by W. In order to evaluate the possibility for utilizing a novel microstructure design principle for Ni-based alloys having TCP phase at grain boundaries and GCP phase other than  $\gamma'$  phase within grain interiors, in this study phase equilibria among  $\gamma$ /TCP or  $\alpha$ -W/GCP *oP6* phases in Ni-Cr-M (M: Mo, W) ternary and Ni-Cr-Mo-W quaternary systems, have been experimentally examined at elevated temperatures. Since it is not easy to clarify the phase diagram based on only experimental, we assess the thermodynamic model for each phase and optimize the interaction parameters to calculate the phase diagram in good agreement with experimentally determined phase diagram. Novel microstructure design using TCP or  $\alpha$ -W and *oP6* phases has been suggested based on the phase equilibria.

#### 6:05 AM F.SF07.04.07

##### **The Effects of RE-RE Substitution on the Phase Stability of LPSO Phase in Mg Alloys** Seiji Miura<sup>1</sup>, Futoshi Miyakawa<sup>1</sup>, Ken-ichi Ikeda<sup>1</sup>, Satoshi Takizawa<sup>1</sup>, Toshiaki Horiuchi<sup>2</sup>, Satoshi Minamoto<sup>3</sup> and Takaomi Itoi<sup>4</sup>; <sup>1</sup>Hokkaido University, Japan; <sup>2</sup>Hokkaido University of Science, Japan; <sup>3</sup>National Institute for Materials Science, Japan; <sup>4</sup>Chiba University, Japan

An LPSO (long period stacking ordered) phase appearing in Mg alloys has been attracting attention as a strengthening phase. The phase is composed of transition elements (TM) such as Zn, Ni, Cu and Al, together with rare-earth elements (RE) such as Y, Dy and Gd. Many investigations have been dedicated to understand the stability of LPSO phases, however, still the reason of the formation type of Mg alloys with LPSO phases are not well understood. In a previous study, the effect of substitution of TM elements in a Mg-Al-Zn-Gd quaternary system from  $\text{Mg}_{85}\text{Al}_6\text{Gd}_9$  to  $\text{Mg}_{85}\text{Zn}_6\text{Gd}_9$  was investigated and found that

the formation type of Mg alloys changes from Type II -> Type I -> Type II <sup>(1)</sup>. For a further discussion, it is needed to investigate the substitution behavior of rare-earth elements. Especially there are several rare-earth elements which do not form LPSO phases. In the present study it is attempted to confirm the existence of stable phases around the LPSO to understand the substitution behavior of Mg-Zn-RE LPSO phase.

Quaternary alloys, the total weight of each sample is approximately 30 g, were prepared by melting Mg blocks (99.95 wt.% purity), Zn blocks (99.5 wt.% purity) and several RE metal blocks (99.9 wt.% purity) in a graphite crucible placed in a high-frequency furnace under argon atmosphere, and casting into a mild steel mold. All the alloys sealed in glass tubes under argon atmosphere were annealed for up to 1000 h at 673 K or 723 K and then quenched into water. Phases in the samples were identified by X-ray diffraction (XRD, PHILIPS, X'Pert-MPD), and by wavelength dispersive X-ray spectrometer (WDS) equipped with field emission electron probe microanalyzer (FE-EPMA, JEOL, JXA-8530F).

It was found that almost no Ce substitutes for Y in Mg-Zn-Y-Ce based LPSO, while almost no Y substitutes for Ce in the Mg<sub>12</sub>Ce phase. These phases co-exist in Mg<sub>85</sub>Zn<sub>6</sub>Y<sub>4.5</sub>Ce<sub>4.5</sub> alloy, suggesting that the stable Mg<sub>12</sub>Ce is one of the reasons why the limited amount of Ce can be solved into the LPSO phase.

#### Reference

(1) Formation of LPSO Phases in As-Cast Mg-Al-Zn-Gd Quaternary Alloys, K. Masaoka, T. Yamada, T. Horiuchi, T. Itoi and S. Miura, Japan Institute of Metals, VOL.83, (2019)257-263, Materials Transactions, VOL.61 (2020) 849-855.

#### Acknowledgments

A part of this work was supported by JSPS KAKENHI for Scientific Research on Innovative Areas "MFS Materials Science" (Grant Numbers JP18H05482). A part of this work was conducted at Hokkaido University, supported by "Nanotechnology Platform" Program of the Ministry of Education, Culture, Sports, Science and Technology (MEXT), Japan.

#### 6:15 AM F.SF07.04.11

**Tribomechanical Investigation of TiC-Reinforced Tribaloy T400 Suspension-Powder Plasma-Sprayed Composite Biocompatible Coating** Moumita Mistri<sup>1</sup>, Shrikant Joshi<sup>2</sup>, Kantesh Balani<sup>1</sup> and Kamal Kar<sup>1,1</sup>; <sup>1</sup>Indian Institute of Technology Kanpur, India; <sup>2</sup>University West, Sweden

Tribaloy T400 (CoCrMoSi) alloy is considered as a potential candidate in impeding the wear-assisted surface material loss from engineering modules operating at a temperature as high as 800 °C. In this report, a hybrid suspension-powder plasma spray technique has been employed to deposit TiC (d<sub>50</sub>= 2.2 μm)-reinforced T400 (average powder size = ~10-45 μm) composite coating for such application. A uniform and adherent T400-TiC coating of thickness ~100 μm revealed in microstructural analysis infers favorable higher densification (ImageJ Pro analysis) characteristic to suspension plasma spray. Dendritic Laves CoMoSi/Co<sub>3</sub>Mo<sub>2</sub>Si and hard intermetallic Co<sub>7</sub>Mo<sub>6</sub>/Co<sub>2</sub>Mo<sub>7</sub> phases of T400, along with the corresponding TiC phases, are confirmed in phase analysis. Synergistic reinforcement of TiC has further elicited an enhancement in elastic modulus (of ~184.5 GPa) by ~36%, and Vickers hardness (of ~11.5 GPa) by ~82% in comparison to that of T400 (~135.2 GPa, and ~6.3 GPa respectively); which unambiguously elucidates the consequent increase in plasticity index by ~26.7% and a drop in maximum displacement amplitude (h<sub>max</sub>) by ~19.8% in T400-TiC. A subsequent decreased fretting wear contact diameter, hence an improved damage tolerance, in T400-TiC compared to T400 alone is noted from a contact area-based wear model postulated herein. Further, with synergistic cell viability in L929 fibroblast, TiC reinforcement in T400 is ascertained to accommodate heavy-duty in-situ load-bearing application with substantially improved micro-hardness via retaining the smaller grain size, and a subsequent fretting wear augmentation through carbide phase strengthening.

SESSION F.SF07.05: Functional Intermetallics

On Demand Abstracts Available for Viewing Starting Saturday Morning, November 21, 2020

F-SF07

#### 5:00 AM \*F.SF07.05.01

**Exploding, Weeping and Reversible Phase Transformations on the Way to a Shape Memory Ceramic** Hanlin Gu<sup>1</sup>, Justin Jetter<sup>2</sup>, Jascha Rohmer<sup>2</sup>, Eckhard Quandt<sup>2</sup> and Richard D. James<sup>1</sup>; <sup>1</sup>University of Minnesota, United States; <sup>2</sup>University of Kiel, Germany

The systematic tuning of the lattice parameters to achieve improved kinematic compatibility between phases is an effective strategy for improving the reversibility, and lowering the hysteresis, of solid-solid phase transformations. We present an

apparently paradoxical example in which tuning to near perfect compatibility leads to a high degree of irreversibility in oxides of ZrHfYNb, as manifested by violently explosive behavior. Tuning lattice parameters slightly away from near perfect compatibility gives an intermediate “weeping” behavior, in which the polycrystal slowly and steadily falls apart at the grain boundaries. Finally, tuning to satisfy a condition we term the equidistance condition results in reversible behavior with the lowest hysteresis in this system. We give evidence that these observations are explained by a more careful analysis of compatibility of the polycrystal. These results show an extreme diversity of behavior, from reversible to explosive, is possible in a chemically homogeneous system by manipulating conditions of compatibility.

**5:15 AM F.SF07.05.02**

**Giant Compressive Superelastic Deformation of a [001]-Oriented SrNi<sub>2</sub>P<sub>2</sub> Micropillar via Double Lattice Collapse and Expansion** Shuyang Xiao; University of Connecticut, United States

Shape memory materials or superelastic crystalline solids have the capability to recover their original shape even after the large amount of deformation is applied. The shape recovery of these materials usually occurs through a reversible phase transformation between martensitic and austenitic phase, which is a shear process. However, their elastic performance is limited by the energetics and geometry of the phase transformation, limiting their application range. Therefore, it is desirable to seek out a new material that can overcome this limit through a completely different superelasticity mechanism. In this presentation, we report our first discovery of the giant superelasticity in a novel intermetallic compound SrNi<sub>2</sub>P<sub>2</sub> via the double lattice collapse and expansion, which correspond to making and breaking P-P bonds in two different co-existing crystal structures.

*In-situ* uni-axial compression on [001]-oriented SrNi<sub>2</sub>P<sub>2</sub> micropillars revealed superelasticity with a remarkably huge elastic limit over 17%, which is one of the highest elastic limits ever reported for crystalline solids, via sudden lattice collapse and expansion. This sudden structural collapse corresponds to the first order phase transition. The collapsed tetragonal phase transition, which results from making P-P bonds during the uni-axial compression, is the main mechanism of superelasticity and differs entirely from the shear process of martensitic-austenitic transition of conventional crystalline superelastic materials. Density Functional Theory (DFT) simulation, X-ray diffraction measurement, and High-Resolution Transmission Electron Microscopy analysis have confirmed that SrNi<sub>2</sub>P<sub>2</sub> consists of two different crystal structures. DFT calculations of uniaxial deformation of each crystal structure showed that these structures are collapsed at different stresses, leading to double lattice collapse and expansion, which are also shown as double-steps in both loading and unloading curves in stress-strain data. No fatigue damage was observed after 10,000 cycles of superelastic deformation because a simple making and breaking bond mechanism is not associated with any shear-based plastic deformation process such as dislocation plasticity or deformation twinning. Therefore, SrNi<sub>2</sub>P<sub>2</sub> is expected to be strongly fatigue-resistant. Up to our knowledge, this is the first report that shows the co-existence of two different superelastic ThCr<sub>2</sub>Si<sub>2</sub>-type structures in a single material and their unique double lattice collapse and expansion. By considering that ThCr<sub>2</sub>Si<sub>2</sub>-type structure is one of the most populous crystal structures (over 2500 compounds), therefore, our results are believed to make a significant impact in fundamental understanding of superelasticity of ThCr<sub>2</sub>Si<sub>2</sub>-structured intermetallic compounds.

**5:25 AM F.SF07.05.03**

**Heterogeneity of Multiscale Deformation in Notched Martensitic Shape Memory Alloys** Partha P. Paul<sup>1,2</sup>, Harshad Paranjape<sup>3</sup>, Darren Pagan<sup>4</sup>, Nobumichi Tamura<sup>5</sup> and L. Catherine Brinson<sup>6</sup>; <sup>1</sup>Stanford Synchrotron Radiation Lightsource, United States; <sup>2</sup>Northwestern University, United States; <sup>3</sup>Confluent Medical Technologies, United States; <sup>4</sup>Cornell University, United States; <sup>5</sup>Lawrence Berkeley National Laboratory, United States; <sup>6</sup>Duke University, United States

The low symmetry martensite phase in Nickel-Titanium (NiTi) shape memory alloy (SMA) has a hierarchical microstructure with micro-scale crystallites, which themselves consist of nano-laminates with an internal twin structure. The martensite phase deforms inelastically through reorientation of the twin structure. Furthermore, structural features in the specimens such as cracks or notches interact with the microstructure, influencing the deformation of martensite. We explore this complex interaction between structure and microstructure during tensile loading in martensitic NiTi specimens, with machined notches [1, 2].

In this work, using multi-scale experiments and macro-scale modeling, we demonstrate that the deformation of martensite in NiTi at the macro scale in a notched specimen is largely determined by the structural features, and the hierarchical nature of the microstructure plays a smaller role. Digital image correlation is used to obtain macro (specimen)-scale strain fields while macro-scale modeling is used to isolate the effect of notch geometry from the inherent microstructural anisotropy in the heterogeneous deformation field. At the micro-scale, in-situ, high-energy x-ray diffraction measurements at two spatial resolutions (3D x-ray diffraction microscopy and microdiffraction) indicate that the martensite microstructure continuously evolves during tensile loading and unloading. This spatial evolution of the martensitic microstructure is also spatially

heterogeneous, with respect to the notch. This observation is counter to the intuition of martensite twins reorienting to large domains of the most favored crystallographic variant at larger loads. Finally, the nano-laminate twin structure persists despite the large imposed deformation and the presence of stress concentrating features such as a notch, primarily due to the non-uniaxial stress field induced by the notch in its vicinity. Nanoscale characterization (using TEM) reveals nanocrystallization of martensite close to the notch on the fracture surface, and a persistence of twins away from the notch on the fracture surface.

These results can guide modeling of fracture-related deformation phenomena in NiTi martensite phase. This persistence of a nano-laminate structure rather than coarsening into large domains of individual variants indicates that the deformation field around cracks/notches in martensite may be modeled for fracture-related phenomena with adequate accuracy using coarse-grained models, without a compelling need for computationally expensive martensite single-variant-scale models.

#### References:

[1] P. Paul et. al, In-situ, microscale characterization of heterogeneous deformation around notch in martensitic Shape Memory Alloy, *Materials Science and Engineering: A*, 771, pp 138605 (2020).

[2] P. Paul et. al, Heterogeneity and Inelasticity of Deformation in a Notched Martensitic NiTi Shape Memory Alloy Specimen, *Acta Materialia* (2020).

#### 5:35 AM F.SF07.05.04

**Supercooled Austenite-Martensite Transformations in CuZr-Based Thin-Film Shape Memory Alloys** Yucong Miao and Joost Vlassak; Harvard University, United States

CuZr-based alloys are being investigated as potential shape memory alloys for use in high-temperature applications. Previous studies on bulk samples of these alloys have reported typical athermal martensitic transformations where the degree of transformation to martensite is independent of time, and is a function of temperature and strain only. Here we report that in sputter-deposited CuZr, CuZrNi and CuZrCo thin-film samples, the austenitic phase can be supercooled below the martensite finish temperature  $M_f$  and then transforms to martensite in an explosive process that converts the entire sample in microseconds. This explosive transformation behavior is characterized by the following observations: 1) The transformation takes place at a critical temperature below  $M_f$ , causing a sudden temperature spike. 2) The critical temperature has a narrow distribution and decreases slightly with cooling rate. 3) Whether the transformation occurs explosively depends on the temperature history of the sample above the austenite finish temperature  $A_f$ . If the sample is quenched immediately on heating above  $A_f$ , the martensite forms gradually on cooling below the martensite start temperature  $M_s$ ; if the sample is allowed to dwell above  $A_f$  for a few seconds, the martensite forms explosively. We suggest that austenite supercooling in thin-film samples is due to a lack of heterogeneous nucleation sites, while the gradual transformation is facilitated by the presence of defects. Transmission electron microscopy of CuZrCo samples suggests that the defects may be residual martensite above the austenite finish temperature. Kinetics measurements using nanocalorimetry reveals that the reverse transformation of this residual martensite can be described by an interface mobility model that takes into account the free energy difference between the two phases.

#### 5:45 AM \*F.SF07.05.06

**Intermetallic Compounds—A Versatile Class of Materials Meets Interesting Catalytic Challenges** Marc Armbrüster; Chemnitz University of Technology, Germany

Heterogeneous catalysis is dominated by two material properties, i.e. the electronic structure (ligand effect) and the arrangement of the atoms (geometric effect). A priori, any material offering altered electronic or structural properties is of interest for heterogeneous catalysis. While intermetallic compounds fulfil these criteria, they offer three advantages compared to substitutional alloys: i) stability, caused by the chemical bonding, which can prevent segregation or decomposition in reactive atmosphere, ii) a wide range of chemical potential of the involved (transition)metals and iii) peculiar combinations of electronic and crystal structure. Since intermetallic compounds are thermodynamically stable and available in a wide range of materials, covering nanoparticles, polycrystalline materials as well as large single crystals, they can serve as platform materials to address catalytic challenges.

The stability allows studying their intrinsic properties in many environments, while the different available chemical potentials can be used to adjust the redox properties to the needs of the reaction in question. Systematic study of the geometric effects in reactions is possible by exploiting the large variety of available crystal structures. The use of isostructural substitutional series or compounds with different valence electron concentration allows addressing the electronic effect (ligand effect) on a reaction. Since only the filling degree of the electronic structure is changes, while the crystal structure and thus the electronic scaffold is kept, the electronic effect can be studied with only minor influence of the geometric effect. Like the metallic elements and the substitutional alloys, intermetallic compounds possess electrical conductivity, allowing electrochemical



studies. The versatility of intermetallic compounds created a vivid and active community and in the contribution, several examples will be presented to elaborate the possibilities - and the requirements - for catalytic studies on this class of materials.

#### 6:00 AM F.SF07.05.07

**High Performance NiFe Permanent Magnets** Ian Baker<sup>1</sup>, Nour Hayek<sup>1</sup>, Ty P. Teodori<sup>1</sup>, Xiaobin Guo<sup>1</sup>, Rachel D. Osmundsen<sup>1</sup>, Cynthia Bundi<sup>1</sup>, Elisa Giraso<sup>1</sup>, Jonathan D. Bonilla Toledo<sup>1</sup>, Damien Fabrègue<sup>2</sup>, Patrice Chantrenne<sup>2</sup>, Si Chen<sup>3</sup>, Yang Ren<sup>3</sup>, Liang Wang<sup>4</sup>, Gheorghe Gurau<sup>5</sup>, Heung Nam Han<sup>6</sup>, Ju-Won Park<sup>6</sup>, Gerard Ludtka<sup>7</sup> and Bart Murphy<sup>7</sup>; <sup>1</sup>Dartmouth College, United States; <sup>2</sup>INSA Lyon, France; <sup>3</sup>Argonne National Laboratory, United States; <sup>4</sup>Beijing Institute of Technology, China; <sup>5</sup>Universitatea "Dunarea de Jos" Galati, Romania; <sup>6</sup>Seoul National University, Korea (the Republic of); <sup>7</sup>Oak Ridge National Laboratory, United States

Demand for high-performance permanent magnets for motors is increasing rapidly for applications such as wind turbine generators and motors in electric and hybrid cars. Sm-Co and Nd-Fe-B magnets are generally used for such challenging applications. While these rare earth (RE) magnets have the highest energy product  $(BH)_{max}$  of any material, they are not without problems such as corrosion and brittle fracture. Other important issues are that over 95% of REs are produced in China, and that there are no US-owned manufacturers of RE magnets. There has also been substantial price volatility with the RE elements. Finally, RE mining has been associated with severe environmental degradation. In this project we aimed to establish a low-cost method to produce bulk L1<sub>0</sub>-structured NiFe, which has magnetic properties comparable to the best RE magnets. Replacing the latter in electric motors in electric/hybrid cars and wind turbines will not only lead to large cost reductions, and hence greater adoption of these technologies with associated energy reductions, but the reduction in RE metal production will also lead to substantial environmental benefits and reduction in energy usage in their production. The key issue is that the transformation from the high temperature f.c.c. phase to the L1<sub>0</sub>-structured phase occurs at around 600 K and, thus, is exceedingly slow. We attempted several paths to produce the transformation to the equilibrium room-temperature L1<sub>0</sub>-structured, i.e. the incorporation of a large supersaturation of vacancies followed by annealing; cold rolling (including at 77 K) followed by conventional annealing, electro-pulse annealing or high magnetic field processing; and high pressure torsion processing followed by annealing. We also looked at carbon doping, which can lead to the formation of a martensitic phase upon quenching. It is quite difficult to determine if the L1<sub>0</sub> phase has formed since the superlattice reflections are weak and the lattice parameters of the L1<sub>0</sub> and f.c.c. phases are both 0.3585 nm. Thus, both synchrotron XRD and neutron diffraction were used to identify the phases, while EBSPs/orientation imaging in a SEM was used to determine the extent of recrystallization. The results of these different processing methods will be outlined. Funding at Dartmouth was provided by the Irving Institute for Energy and Society, the Women in Science Program, the First-Year Research in Engineering program, and the Presidential Scholars program.

#### 6:10 AM \*F.SF07.05.09

**Relationship Between Thermoelectric Properties and Phase Interfaces Formed on a Multiscale by Phase Separation in the Same Ordered Structure Phases** Yoshisato Kimura<sup>1</sup>, Yaw Wang Chai<sup>1</sup> and Yonghoon Lee<sup>2</sup>; <sup>1</sup>Tokyo Institute of Technology, Japan; <sup>2</sup>KELK Ltd., Japan

Thermoelectric power generation is an appealing approach for conserving energy and preserving the global environment. Thermoelectric properties are sensitively affected by microstructure of materials which changes during high temperature fabrication processing and practical long term operations. Improvement of thermoelectric performance can be achieved by microstructure control. We focus on the formation of interfaces on a multi-scale according to the phase separation between the same ordered structure phases in two alloy systems. One is phase separation between half-Heusler structure TiNiSn–(Zr,Hf)NiSn according to the miscibility gap, and the other is that between anti-fluorite structure Mg<sub>2</sub>Si–Mg<sub>2</sub>Sn during coring microstructure formation. Objective of the present work is to understand the formation mechanism of interfaces by the phase separation, and evaluate the effects of interfaces on thermoelectric properties focusing on the electrical and thermal conduction.

Half-Heusler MNiSn (M = Hf, Zr, Ti) are excellent n-type thermoelectric materials. The present author's group reported the phase separation between TiNiSn and ZrNiSn, and TiNiSn and HfNiSn from a random solid solution MNiSn phase. The existence of a miscibility gap was suggested at temperatures higher than 1273 K. The relaxed lattice misfit, evaluated using XRD measurement, is about 3.2% between TiNiSn and ZrNiSn, and 2.5% between TiNiSn and HfNiSn, respectively. These values are quite large compared with 0.6% between ZrNiSn and HfNiSn. Considering the elastically constrained phase interface, a quite large elastic energy can be the driving force of the phase separation. Sharp grain boundaries between Ti-rich and Zr-rich half-Heusler phases can be observed in solidified microstructure of (Ti,Zr)NiSn alloys using SEM. On the other hand, it is very hard to observe a constrained interface. Diffuse interface can be barely observed using TEM in a (Ti,Zr)NiSn

alloy after the heat treatment, annealed in the two-phase field for phase separation. Excellent electrical power factor exceeding  $5 \text{ mWm}^{-1}\text{K}^{-2}$  can be achieved while the lattice thermal conductivity is effectively reduced around  $3 \text{ Wm}^{-1}\text{K}^{-1}$  in Ti-rich (Ti,Zr)NiSn alloy according to the effect of solid solution together with the effect of interfaces introduced by phase separation.

Microstructure development in the  $\text{Mg}_2\text{Si-Mg}_2\text{Sn}$  pseudo-binary system is characterized by the peritectic reaction. The Mg-Si-Sn ternary phase diagram was evaluated experimentally focusing on the reaction scheme and solidification sequence. It has been found that the gradient composition layered structure is formed in  $\text{Mg}_2(\text{Si}_x, \text{Sn}_{1-x})$  alloys on a micro-scale during the solidification process. Dominant mechanism is the phase separation of  $\text{Mg}_2(\text{Si}, \text{Sn})$  solid solution phase into Si-rich  $\text{Mg}_2\text{Si}(\text{Si}, \text{Sn})$  and Sn-rich  $\text{Mg}_2(\text{Sn}, \text{Si})$  phases during the coring structure development. Phase separation is occurred leaving phase interfaces to release the large elastic energy stored due to quite large lattice misfit. The constrained lattice misfit between Si-rich  $\text{Mg}_2\text{Si}(\text{Si}, \text{Sn})$  and Sn-rich  $\text{Mg}_2(\text{Sn}, \text{Si})$  phases has been evaluated about 5% based on the powder XRD measurements, and the semi-coherent interfaces with interfacial dislocation networks can be observed using TEM. Each layer of the gradient composition layered microstructure is consisting of nano- to micro-scale poly-crystal grains having a compositional gradient of Si/Sn composition ratio. The lattice thermal conductivity can effectively be reduced lower than  $2 \text{ Wm}^{-1}\text{K}^{-1}$  in a  $\text{Mg}_2(\text{Si}_{0.75}, \text{Sn}_{0.25})$  alloy which contains high density of phase interfaces of gradient composition layered microstructure. Note that the dominant mechanism for the reduction of thermal conductivity is attributed to the phono scattering based on the solid solution effect in  $\text{Mg}_2(\text{Si}_x, \text{Sn}_{1-x})$  phase grains and layers.

#### 6:25 AM F.SF07.05.10

**Effect of Different Inclusion Species on the Thermoelectric Transport and Mechanical Properties of the Zintl Phase  $\text{Yb}_{14}\text{MnSb}_{11}$**  Giacomo Cerretti, Sabah Bux and Jean-Pierre Fleurial; NASA Jet Propulsion Laboratory, United States

Composite materials are conceptualized with the intent of obtaining a final material with improved characteristics. In thermoelectrics this has been achieved for organic-inorganic composites where conducting materials embedded in polymeric matrixes improved the thermoelectric properties. A completely different situation is the combination of two inorganic compounds. Although according to some studies a thermoelectric composite cannot have better properties than its constituents, a study from Bergman and Fel (1999) proved that the enhancement of the figure of merit of a composite material is possible under specific conditions. The purpose of this work is to show the effect of different kind of metal inclusions on the electronic and thermal property of  $\text{Yb}_{14}\text{MnSb}_{11}$ .  $\text{Yb}_{14}\text{MnSb}_{11}$ , with a zT of about 1.2 at 1200 K, is already the most performing p-type material for high temperature thermoelectric applications. Our intent is to further increase its thermoelectric performance by decoupling the electronic transport properties ( $\sigma$ , S). Transition metals are characterized by a metallic electrical conductivity, but some of them still show a relatively high Seebeck coefficient. Therefore, the selected metal inclusions are expected to provide a boost to the electrical conductivity, while affecting only marginally S. Another important aspect of compositing with metal inclusions is the improvement of mechanical properties and fracture toughness, a fundamental aspect in terms of device fabrication. To verify the validity of our assumptions, we synthesized samples with different inclusion density, always remaining largely below percolation limit. The samples have been chemically, electrically, thermally, and mechanically characterized and the obtained results will be shown and compared with the baseline of the Jet Propulsion Laboratory for the  $\text{Yb}_{14}\text{MnSb}_{11}$  ATEC (Advanced ThermoElectric Converter).

#### 6:35 AM F.SF07.05.11

**Synthesis of P-Type BaCuSi Clathrate for Thermoelectric Materials** Chiho Inoue, Shinji Munetoh, Masahide Yasuda, Yuichiro Magami and Zilong Zhang; The Kyushu University, Japan

BaCuSi clathrate samples for p-type thermoelectric materials were synthesized with various initial composition of Cu ratio. Cu ratio in the samples increased with initial composition Cu ratio. However, volume of BaCuSi clathrate phases in their samples decreased with the increase of initial composition of Cu ratio. Those phases cannot be detected their accurate electrical properties because of their small grain size. In this study, we synthesized the sample by using CZ method to obtain the larger phase. It was found that the Cu ratio in the CZ sample was smaller than the sample without CZ method. The CZ sample with a large grain size can be obtained with heavy Cu doping sample. The CZ sample successfully showed p-type properties.

#### 6:45 AM F.SF07.05.12

**Processing and Defects Responsible for Embrittlement in P-Type PbTe Thermoelectric Materials** James P. Male<sup>1</sup>, Riley Hanus<sup>2,1</sup>, Naomi Pieczulewski<sup>1</sup>, Raphael P. Hermann<sup>3</sup> and G. Snyder<sup>1</sup>; <sup>1</sup>Northwestern University, United States; <sup>2</sup>Georgia Institute of Technology, United States; <sup>3</sup>Oak Ridge National Laboratory, United States

Heavily-doped, p-type PbTe thermoelectric materials reach the heat-to-electricity conversion efficiency necessary for

improved space power generation or waste heat recovery. However, unexplained brittle behavior at high electronic doping levels occurs in p-type PbTe, but not in n-type PbTe. This distinctively asymmetric trend restricts the thermoelectric community's best-performing materials for practical use. Our mechanical and elastic property measurements on single crystal and polycrystalline PbTe contradict previously suggested explanations for embrittlement, such as bond stiffening from PbTe's  $\Sigma$  band. We also show certain dopants break the previously established mechanical trend. Strain measurements through neutron powder diffraction show that ball milling can double the amount of strain in undoped PbTe beyond unstrained samples. Introducing extrinsic p-type dopants increases the strain by another factor of two and better maintains strain at high temperatures. We propose that increased dislocation strain from typical processing methods is linked to embrittlement. Further, by analyzing extrinsic doping efficiency, we note a link between strain and both extrinsic dopant defects and intrinsic compensating defects. Introducing dislocation strain, as is often done to reduce thermal conductivity and increase thermoelectric efficiency, thus appears to also be detrimental for mechanical properties in p-type PbTe. This study seeks to explore the link between these properties and offers routes to tune them through phase boundary mapping, choice of dopant, and intrinsic defect engineering.

#### 6:55 AM F.SF07.05.13

##### **Modeling Atomic Displacement and Ionic Charges in Filled Skutterudite via Resonant X-Ray Dynamical**

**Diffraction** Rafaela F. Penacchio<sup>1</sup>, Maurício B. Estradiote<sup>1</sup>, Adriana Valerio<sup>1</sup>, Marli R. Cantarino<sup>1</sup>, Fernando A. Garcia<sup>1</sup>, Sergio L. Morelhao<sup>1</sup>, Stefan W. Kycia<sup>2</sup>, Guilherme A. Calligaris<sup>3</sup> and Claudio M. Remédios<sup>4</sup>; <sup>1</sup>University of Sao Paulo, Brazil; <sup>2</sup>University of Guelph, Canada; <sup>3</sup>Brazilian Synchrotron Light Laboratory, Brazil; <sup>4</sup>Universidade Federal do Pará, Brazil

Thermoelectric properties of the materials originate from thermal conduction by free charge carriers instead of by collective lattice vibrations (phonons). Understanding the scattering mechanism, or dissipation, of phonons allows the engineering of materials with higher coefficient of Seebeck [1], i.e. higher difference of electric potential created for a given thermal gradient. In skutterudite type of thermoelectric materials, dissipation of phonons are attributed to localized, low frequency and anharmonic vibrations of heavy ions of the lanthanide family introduced into the large voids of the crystalline structure. Since most of these materials can be synthesized in the form of high quality single crystals, we have the possibility of revisiting the phonon scattering mechanism through x-ray phase measurements via dynamic diffraction effects [2]. Structure factor phases are susceptible to the differences between the vibration amplitudes of the atoms (root mean square atomic displacements), or in other words, phase values are invariants with temperature only when all occupied sites of the unit cell have the same Debye-Waller factor.

Structure factor calculation in model structures revealed suitable Bragg reflections and x-ray energies to resolve the difference in atomic vibrations as a functions of temperature. It also revealed a giant resonant phase shift for the whole family of filled skutterudites RFe<sub>4</sub>P<sub>12</sub> (R=Ce, La, Nd, Pr, Sm). By exploiting this resonant phase shift with synchrotron x-rays at different temperatures in CeFe<sub>4</sub>P<sub>12</sub>, we were able to demonstrated that rattling of Ce alone inside the icosahedral cage is not enough to explain phonon scattering and that the whole cage of 12 P is taking part of scattering mechanism.

[1] G. J. Snyder, E. S. Toberer. Complex thermoelectric materials. Nat. Mater. 7, 105-114 (2008).

doi = 10.1038/nmat2090

[2] S. L. Morelhão, C. M. R. Remédios, G. A. Calligaris, G. Nisbet. X-ray dynamical diffraction in amino acid crystals: a step towards improving structural resolution of biological molecules via physical phase measurements. J. Appl. Cryst. 50, (2017). doi: 10.1107/S1600576717004757

SESSION F.SF07.06: Poster Session: Processing Structure-Property Relationship of Advanced Intermetallic-Based Alloys for Structural and Functional Applications

On Demand Abstracts Available for Viewing Starting Saturday Morning, November 21, 2020

5:00 AM - 8:00 AM

F-SF07

#### F.SF07.06.01

##### **Construction of an EAM Type Inter-Atomic Potential Model for Describing Metallic Polytype Structures Shinya**

Ogane<sup>1</sup>, Taku Miyakawa<sup>2,1</sup> and Koji Moriguchi<sup>1,2</sup>; <sup>1</sup>Graduate School of Environmental Studies, Tohoku University, Japan; <sup>2</sup>R&D Laboratories, Nippon Steel Corporation, Japan

Polytypism is a special case of polymorphism when the two polymorphs differ only in the stacking of identical two-dimensional sheets or layers. The polytypes are characterized by a stacking sequence with a given repeating unit along a directional axis (*c*-axis) and are theoretically possible to have endless permutations of the sequences. Among these polytypes, the crystalline systems composed of close-packed (CP) layers have especially attracted attention on their fundamental and technological properties for many years. While these polytypes are often experimentally observed in wide-bandgap semiconductors, SiC systems are particularly known to show several hundred polytypes [1]. Since some SiC polytypes located around the ground state are energetically degenerated with about  $\Delta T = 2\text{K}$  [1], it is difficult to control the phase stability during the growth of single crystals with the desired stacking polymorphism. For this reason, a variety of physical perspectives are being investigated in order to establish better single crystal growing techniques [2, 3]. In addition, the long period stacking ordered (LPSO) Mg alloys with light weight, high specific strength, and high heat resistance are also recently drawing attention as a metallic system with similar polytypism to that in SiC [4, 5].

We have proposed a computational method coupled with three theoretical tools (PGA: polytype generation algorithm; FPC-DFT: first-principles calculations based on the density functional theory; and ANNNI: axial next-nearest-neighbor Ising model), which can make us possible to efficiently investigate the structural energetics for diverse nonequivalent polytypes [1]. In our recent study [5], we have systematically evaluated the static energetics of metallic polytypes for a wide variety of elements based on the same computational method proposed by the authors [1]. For all these elemental systems, the atomistic geometry, energetics, and electronic structure for all polytypes with up to the periodic stacking length of  $L=13$  (165 kinds of polytypes in total) have been carefully calculated based on the DFT within the GGA [5]. Using the ANNNI model extracted from the GGA calculations, we have shown from the perspective of static structural energetics that the interlayer interaction among CP layers is one of the important factors for the polytype formation [5].

Not only the static energetics but also the dynamical aspect generally affects the polytype selection during the crystal growth processes [2, 3]. It is, therefore, important to elucidate the polytype formation mechanism from the viewpoint of dynamics associated. Since the molecular dynamics (MD) simulations have become a powerful computational tool to understand and predict the structural, thermodynamic and dynamic properties of materials, the direct MD observation of dynamical aspects for the polytype growth is expected to greatly advance our understanding on the polytype selection. While the state-of-the-art potentials are often fitted to many databases including a large set of atomic configurations calculated by FPC-DFT [6], we have found that the potential models proposed so far cannot describe the accurate polytypes energetics. In the present study, we are, therefore, developing an Embedded Atom Method (EAM) type potential [6] which can be used for the dynamical simulations of metallic polytype structures focusing on the lanthanum (La) system. The basic properties and transferability of the EAM type potential model constructed in the present work will be discussed.

[1] K. Moriguchi, et al., *J. Mater. Res.* 28, 7 (2013).

[2] K. Kusunoki, Doctoral thesis: Nagoya University, 10725 (2014).

[3] K. Moriguchi et al., NIPPON STEEL & SUMITOMO METAL TECHNICAL REPORT 117, 56 (2017).

[4] E. Abe et al., *Phil. Mag. Lett.*, 91, 690 (2011).

[5] T. Miyakawa and K. Moriguchi, 236th ECS Meeting Abstracts, Vol. MA2019-02, 2417 (2019).

[6] K. Moriguchi and M. Igarashi, *Phys Rev B* 74, 024111 (2006) and references therein.

#### F.SF07.06.02

**Phase Equilibria and Crystal Structures of Highly Ordered Intermetallic Compounds of  $\text{Fe}_2\text{Al}_5$  Phases with the Framework Structure of  $\eta$ - $\text{Fe}_2\text{Al}_5$  Phase** Tetsuya Hamada, Ryutaro Sakai, Kodai Niitsu and Haruyuki Inui; Kyoto University, Japan

Hot dipped Zn-Al alloy coated steel is widely used in the field of automobile. It is well known that the coated layer is mainly composed of the  $\text{Fe}_2\text{Al}_5$  intermetallic compound. This compound has been considered to be the orthorhombic  $\eta$  phase (space group *Cmcm*). On the other hand, our group has recently found that the layer phase often crystallizes into highly ordered atomic arrangement most likely termed as the  $\eta'''$  phase even during short-term dipping. Besides, recent researches address there exists several ordered phases similar to the  $\eta'''$  phase with the framework structure of  $\eta$  phase<sup>[1]</sup>. According to Burkhardt's study<sup>[2]</sup>, the  $\eta$  phase is composed of a full occupied framework structure (4 Fe and 8 Al atoms) and partially occupied chains along the *c*-axis (6 Al sites). The *c*-axis chain is considered to allow chemical tenability and various kinds of atomic orderings; the formation of various kinds of ordered phases is considered to be responsible for how Fe and Al atoms order in the *c*-axis chain sites. However, the crystal structures of some of these ordered phases are still controversial and phase equilibrium among them are not consolidated.

In this study, we have examined the phase equilibrium among these phases and refined their crystal structures. Experiments are carried out with scanning electron microscope, energy dispersive spectroscopy, X-ray diffraction, transmission electron

microscope, scanning transmission electron microscope and synchrotron X-ray diffraction. There are some invariant reactions : the  $\eta$  phase is found to dissolve into the  $\eta''$  and  $\eta^m$  phases at around 350 °C while the  $\eta$  phase has been thought to be stable at low temperature. Some of the other phases are found to have highly ordered long-period structures with periodic antiphase boundaries.

Reference: [1] H. Becker et al., *Intermetallics*, **93**, (2018) 251-262.

[2] U. Burkhardt et al., *Acta Cryst*, **B50**, (1994) 313-316.

#### F.SF07.06.03

**ANNNI Model Descriptions on Structural Energetics for a Wide Variety of Metallic Polytypes Composed of Close-Packed Layers** Koji Moriguchi<sup>1,2</sup>, Taku Miyakawa<sup>2,1</sup>, Shinya Ogane<sup>1</sup>, Kazumasa Tsutsui<sup>2</sup> and Yuta Tanaka<sup>2</sup>; <sup>1</sup>Tohoku University, Japan; <sup>2</sup>Nippon Steel Corporation, Japan

The local inhomogeneity such as defect, surface, interface, and nanostructure often assumes an important role for developing sophisticated materials since the functionalities of materials usually originate from the spatial inhomogeneity in the associated systems. In this work, among the many phenomena related to inhomogeneity in materials, we will report our computational research on the phenomenon called "Polytypism". Polytypism is a special case of polymorphism where two polymorphs differ only in the stacking sequences of the same two-dimensional sheets or layers.

Many crystalline compounds can be considered to be composed of one or more structural units. When these units can be stacked in different ways to form stable or metastable phases, the resulting phases are known as polytypes. Among the polytypes for these compounds, the silicon carbide (SiC) systems have been the most attractive and motivated tremendous amounts of theoretical and experimental investigations on their fundamental and technological properties for many years. Many SiC polytypes located around the ground state have been found to be energetically degenerated with energy of about  $\Delta T = 2K$  [1]. It is, therefore, very difficult to control the phase stability during the growth of a single crystal in order to obtain the desired stacking polytype in SiC systems. For this reason, a variety of physical perspectives are being investigated in order to establish better single crystal growing techniques [2]. In addition, the long period stacking ordered (LPSO) Mg alloys with light weight, high specific strength, and high heat resistance are also recently drawing attention as a metallic system with similar polytypism to that in SiC [3]. For both systems, the physical mechanism behind polytype selection is not yet fully understood and remains challenging issues to be solved.

In this situation, we have proposed a computational method coupled with three theoretical tools (PGA: polytype generation algorithm; FPC-DFT: first-principles calculations based on the density functional theory; and ANNNI: axial next-nearest-neighbor Ising model), which can make us possible to efficiently investigate the structural energetics for diverse nonequivalent close-packed(CP) polytypes [1, 4]. In the present work, the static energetics of a wide variety polytypes for 17 kinds of metallic elements (M=Be, Mg, Sc, Y, Co, Zn, Cu, Ag, Au, Ni, Pd, Pt, Al, Ca, Sr, Ba, and La) is systematically evaluated based on the same computational method proposed by the authors [1, 4]. For all these elemental systems, the atomistic geometry, energetics, and electronic structure for all polytypes with up to the periodic stacking length of  $L=13$  (165 kinds of polytypes in total) have been carefully calculated based on the DFT within the GGA. The equilibrium theories based on the ANNNI model that is well known in the field of statistical mechanics have played an efficient role in the study of the origins of polytypism [5, 6]. In this work, the ANNNI model including interactions up to the third-nearest neighbor layer with the four-spin term [6] is adopted for the systems considered. Using the ANNNI model extracted from the GGA calculations, we will describe the inter-layer interactions, the phase diagrams of ANNNI model with interactions up to third-nearest neighbor, and the stability of stacking faults for each element. The relation to polytypism in the metallic systems considered will be also discussed.

[1] K. Moriguchi, et al., *J. Mater. Res.* **28**, 7 (2013).

[2] K. Moriguchi et al., *NIPPON STEEL & SUMITOMO METAL TECHNICAL REPORT* **117**, 56 (2017).

[3] E. Abe et al., *Phil. Mag. Lett.*, **91**, 690 (2011).

[4] T. Miyakawa and K. Moriguchi, *236th ECS Meeting Abstracts*, Vol. MA2019-02, 2417 (2019).

[5] E. Rodriguez-Horta, E. Estevez-Rams, R. Lora-Serrano and R. Neder, *Acta Cryst.* **A73**, 377 (2017) and references therein.

[6] J. J. A. Shaw and V. Heine, *J. Phys.: Condens. Matter* **2**, 4351 (1990).

#### F.SF07.06.04

**Microstructure Characterization of As-Cast and Directionally Solidified Near-Eutectic Mo–Si–B Alloys** Linye Zhu<sup>1</sup>, Shuntaro Ida<sup>1</sup>, Georg Hasemann<sup>2</sup>, Manja Krueger<sup>2</sup> and Kyosuke Yoshimi<sup>1</sup>; <sup>1</sup>Tohoku University, Japan; <sup>2</sup>Otto-von-Guericke

University Magdeburg, Germany

Mo–Si–B-based alloys have been developed as ultrahigh temperature material candidates for high-pressure turbine blades. Recently, Hasemann et al. reported that a Mo–Si–B alloy with  $\text{Mo}_{\text{ss}} + \text{T}_2 + \text{Mo}_3\text{Si}$  eutectic prepared by directional solidification (DS) has substantially improved creep resistance compared with a powder metallurgy (PM) processed alloy. It was found that a homogenous microstructure with preferentially orientated grains through DS can ameliorate mechanical performance, however, the effect of DS on the microstructure evolution of Mo–Si–B alloy is still not clear. In this study, phase constitution and microstructure of as-cast and directionally solidified near-eutectic Mo–Si–B alloys are investigated to clarify the microstructure evolution caused by DS.

Alloys with the nominal composition of Mo–17Si–7B (at.%) corresponding to the  $\text{Mo}_{\text{ss}} + \text{T}_2 + \text{Mo}_3\text{Si}$  eutectic point were prepared by arc-melting (as-cast alloy) and crucible-free zone melting (directionally solidified alloy) in an Ar atmosphere. The microstructure of the as-cast alloy consisted of primary  $\text{Mo}_{\text{ss}}$  dendrites and two eutectics of  $\text{Mo}_3\text{Si} + \text{T}_2$  and  $\text{Mo}_{\text{ss}} + \text{Mo}_3\text{Si} + \text{T}_2$  in cellular or dendritic growth, while the directionally solidified alloy was almost composed of a uniform and well-aligned  $\text{Mo}_{\text{ss}} + \text{Mo}_3\text{Si} + \text{T}_2$  eutectic phase in cellular growth. The electron backscatter diffraction (EBSD) results showed that in the as-cast alloy only  $\langle 100 \rangle$  orientation of the  $\text{T}_2$  phase preferentially grew along the solidification direction while the other  $\text{Mo}_{\text{ss}}$  and  $\text{Mo}_3\text{Si}$  phases had no apparent orientation. However, the  $\langle 001 \rangle$  growth direction of  $\text{Mo}_3\text{Si}$  phase parallel to the solidification direction became much stronger by the directional solidification. The coupled growth of  $\langle 001 \rangle \text{Mo}_{\text{ss}} / \langle 100 \rangle \text{T}_2 / \langle 001 \rangle \text{Mo}_3\text{Si}$  in the directionally solidified alloy presumably had an effect on the mechanical properties because of the texture. No habit relationship between the phases was found in both alloys possibly because the lattice parameters of constituent phases are greatly different and the system cannot minimize interfacial energy by atomic arrangement.

#### F.SF07.06.05

**Energy Barrier of the Initial Stage Microstructure Formation in Martensitic Transformation of TiNi Shape Memory Alloy** Kazuya Nagahira, Takeshi Teramoto and Katsushi Tanaka; Kobe University, Japan

The self-accommodation microstructure, which is the martensitic microstructure of the shape memory alloy, is constructed by a plate-like martensite variant. Recently, formation process of the self-accommodation microstructure during the martensitic transformation have been reported in the several shape memory alloy systems. In TiNi shape memory alloy, specific variant pairs including  $\{11\bar{1}\}$  type-I twinning interface are frequently observed in the initial stage of martensitic transformation. In this study, we refer the variant pair that formed in the initial stage of martensitic transformation as initial stage microstructure (ISM). This result suggests that there is a selection rule for the self-accommodation microstructure in the initial stage of martensitic transformation. The selection rule of ISM is important for understanding self-accommodation microstructure because it represents a mechanism of variant selection in the absence of the influence of other variants. In the present study, we have performed evaluations of energy barrier of the formation of ISM in order to elucidate the factors that determine the selection rule of ISM in TiNi shape memory alloy.

The energy barrier of the formation of ISM is the sum of the interfacial energy of the twin interface included in ISM and the elastic strain energy for the ISM formation. In the TiNi shape memory alloy, 8 types of twin orientation relations and corresponding variant pairs exist. It is considered that the variant pair with the smallest energy barrier is selectively formed as ISM. The interfacial energy of twin interface was evaluated by the first-principles calculation using VASP (Vienna Ab initio Simulation Package) code. The elastic interaction energy to form a variant pair was evaluated by a micro-mechanics proposed by Eshelby.

Since interfacial energy of  $\{11\bar{1}\}$  type-I twin and elastic interaction energy of the variant pair including  $\{11\bar{1}\}$  type-I twin are relatively small among the twin interfaces considered, it is supposed that the energy barrier of the variant pair including  $\{11\bar{1}\}$  type-I twin is smaller than others. These results indicate suggests that the variant pair with a small energy barrier is selectively formed as the initial stage of martensitic transformation.

#### F.SF07.06.06

**Transient Liquid Phase Bonding of Bi-Ni Intermetallics for High-Temperature Electronics** Hamid Fallahdoost and Junghyun Cho; State University of New York at Binghamton, United States

Transient liquid phase bonding (TLPB) has been used as a bonding process that joins dissimilar materials by employing an interlayer that provides a lower melting process. It shows the potential to be used in high temperature electronics (operated or exposed over 200°C), where there are no clear lead (Pb)-free solder options available. During the reflow process for electronics components, the interlayer melts and the constituents of the interlayer and its joining materials diffuse each other, subsequently making a homogenous intermetallic bond via isothermal solidification. Once formed, it results in a higher melting point than the bonding temperature. This research investigates such a TLPB system made of a nickel (Ni) bonding

surface and a bismuth (Bi) interlayer, which can serve as a Pb-free solder alternative for high-temperature electronics. Upon melting of Bi on Ni, intermetallic phases ( $\text{Bi}_3\text{Ni}$ ,  $\text{BiNi}$ ) nucleate and grow by consuming a Ni layer on the substrate or the die side. Intermetallic reactions and microstructure developments were studied under various reflow conditions including temperature and time on three sets of the sandwiched assemblies: 1) Si die Sputtered Ni (1  $\mu\text{m}$ -thick)/Bi/Si die; 2) Si die/Bi/Ni foil (0.5 mm-thick); 3) Ni foil/Bi/Ni foil. As such bonds constitute the structural joints in electronic packaging, mechanical properties of the intermetallic bonds and their long-term microstructural developments under high temperature aging and thermal cycling (-55°C to 200°C) were investigated by shear testing and cross-sectional microstructure analyses of the sandwiched samples. It was shown that temporal evolution of two intermetallic phases composed of faster  $\text{Bi}_3\text{Ni}$  and slower  $\text{BiNi}$ , along with the remaining Bi, are responsible for mechanical performances of TLPB. This presentation will also discuss about optimal microstructure development for the TLPB, which is critical to offset the defects and brittleness of the intermetallic phases.

#### F.SF07.06.07

**Microstructure and Crystallographic Orientation Relationships in Directionally Solidified  $\text{NbSi}_2/\text{Nb}_5\text{Si}_3$  Eutectic Composites with Mo Addition** Haruka Uemura, Kosei Takeda, Kyosuke Kishida and Haruyuki Inui; Kyoto University, Japan

Eutectic composites composed of intermetallics and/or ceramics with very high eutectic temperatures have been considered as attractive materials for ultra-high temperature structural applications because of their high melting temperature, high structural stability and good mechanical properties. Recently, we have systematically investigated microstructure-property relationship of  $\text{MoSi}_2/\text{Mo}_5\text{Si}_3$  eutectic composites with very high eutectic temperature of 1900 °C and have revealed that their high-temperature strength and room-temperature fracture toughness can be improved simultaneously by optimization of microstructure and interface properties through controlling growth condition and ternary/quaternary alloying. These previous results open a new possibility to develop novel structural materials endowed with excellent high-temperature strength and good room-temperature fracture toughness by utilizing interphase boundaries. In the present study, we focused on  $\text{NbSi}_2/\text{Nb}_5\text{Si}_3$  eutectic composites (eutectic temperature ~1900 °C for binary) as a new target system and investigated microstructure variation of directionally solidified (DS) ingots of the eutectic composites as a function of ternary Mo addition. When Mo is alloyed more than 2 at. %, DS ingots are conformed to composed of  $\text{C40-(Nb,Mo)Si}_2$  and  $\text{D8}_m\text{-(Nb,Mo)}_5\text{Si}_3$ , which indicates that the  $\text{D8}_m$  (high temperature) to  $\text{D8}_l$  (low temperature) phase transformation that occurs in binary  $\text{Nb}_5\text{Si}_3$ , is suppressed by the Mo addition. A fine eutectic microstructure of the so-called script-lamellar type, which is similar to those observed in  $\text{MoSi}_2/\text{Mo}_5\text{Si}_3$  DS eutectic composites, is confirmed to develop for the Mo-alloyed  $\text{NbSi}_2/\text{Nb}_5\text{Si}_3$  DS eutectic composites. Crystallographic orientation relationships between C40 and  $\text{D8}_m$  phases as well as their preferential growth directions are identified by electron backscattered diffraction (EBSD) in scanning electron microscopy and transmission electron microscopy (TEM).

#### F.SF07.06.08

**Evaluation of Mechanical Properties for Constituent Phases by Nano-indentation Method in  $\gamma\text{-TiAl}$  Alloys** Sota Taniguchi, Yotaro Okada, Ryosuke Yamagata, Hirotoyo Nakashima and Masao Takeyama; Tokyo Institute of Technology, Japan

Nano-indentation method is a powerful tool to evaluate the mechanical properties of each phase in materials consisting of multi-phase microstructures. If the mechanical properties of each phase can be evaluated correctly, then we can predict the mechanical properties of bulk materials having different amounts of the phases, which would allow us to construct the design principle for materials integration (MI) to solve inverse problems. However, there are a number of factors affecting the properties by this method, since the machine is so sensitive to the specimen itself such as surface conditions, as well as the machine itself such as specimen set-ups and tip of the indenters. In this study, titanium aluminide alloys were selected to evaluate the mechanical properties of the constituent phases since the alloys consists of three phases of b-Ti (bcc),  $\text{a}_2\text{-Ti}_3\text{Al}$  ( $\text{D0}_{19}$  with hcp based) and g-TiAl ( $\text{L1}_0$  with fcc based). In addition, we recently revealed that the introduction of an appropriate amount of the b phase is effective in improving the fracture toughness as well as tensile properties. Thus, it is very important to build up the mechanical property database for each phase in equilibrium each other in order to construct the construction of MI platform for inverse problems. The alloy studies are Ti-Al-Cr ternary alloys. These alloys were homogenized first in the b single phase region, and then heat treated in the three-phase region at 1173 K to reach the equilibrium state, based on our phase diagram study. The specimens were mechanically polished, followed by electro-polishing. Before and after the indentation test, the microstructure and orientation analysis of each phase were performed by FE-SEM and EBSD. Nano-indentation tests were performed to evaluate the Young's modulus and hardness using a continuous stiffness measurement (CSM) method with a frequency of 110 Hz using a Berkovich type indenter made of diamond. The advantage of the CSM method allows us to evaluate the properties continuously as a function of indentation

depth. The results were compared with those obtained from the Oliver-Pharr method. Both properties are found to be sensitive to the indentation depth and sampling distance, depending on the phases as well as orientation. The details of the appropriate conditions will be discussed, in conjunction with the O-P method. This work was supported by Council for Science, Technology and Innovation (CSTI), Cross-ministerial Strategic Innovation Promotion Program (SIP), “Material Integration” for revolutionary design system of structural materials.

#### F.SF07.06.09

**Effect of Si in Solution on the Crystal Structure of  $\sigma$  Phase ( $tP30$ ) in Fe-Cr Binary Alloys** Eitaro Maeda and Masao Takeyama; Tokyo Institute of Technology, Japan

FeCr- $\sigma$  with a crystal structure of  $tP30$  (ordered tetragonal phase) is one of the TCP phases and often observed in heat resistant materials. This phase is considered as a harmful phase to deteriorate mechanical properties of the materials. However this phase could be a strengthening phase, just like Laves phase, if the phase stability can be increased by alloying. In the previous study, we have found that the lattice parameters of both  $a$  and  $c$  become either larger or smaller by the addition of M in solution, depending on the size of atomic radius of M relative to those of Fe ( $r_{Fe}=1.274 \text{ \AA}$ ) and Cr ( $r_{Cr}=1.282 \text{ \AA}$ ) as usual, except Fe addition. In case of the excess addition of Fe in solution, the  $a$  axis becomes smaller whereas the  $c$  axis becomes larger. We attributed the unusual anisotropic lattice parameter change to the site occupancy change in five sub-lattice sites (M1, M2, M3, M4, M5) of the  $\sigma$  phase, based on the Rietveld analysis; the occupancy of Cr atom in M5 sub-lattice site increase with increasing excess Fe atoms. In this study, we picked up non-transition element Si as the third element since it has larger atomic radius ( $r_{Si}=1.322 \text{ \AA}$ ) and is known as strong  $\sigma$  stabilizer, and investigated the lattice parameter change with Si in solution.

The alloys studies are Fe-(50-x/2)Cr-xSi (at. %) where x=5, 10. They were prepared by arc melting to 30g button ingot, and homogenized in the  $\sigma$  single-phase region. Phase identification was conducted by powder XRD techniques and the lattice parameters were calculated from obtained XRD profiles. The obtained XRD profiles were further analyzed by means of Rietveld method to determine the structural change of  $\sigma$  phase as well as site occupation of the elements. Microstructures were examined by SEM and hardness was measured by micro Vickers hardness machine. We confirmed that both alloys with 5 and 10 at.% Si exhibit  $\sigma$  single phase with almost the same hardness of 12 GPa. It is interesting to note that, just like Fe addition, the anisotropic behavior of the lattice parameters was obtained; the  $a$  axis decreases whereas the  $c$  axis increases with increasing in Si content. However, Rietveld analysis suggested that this anisotropic behavior is different from that in Fe case related to the site occupancy change of M5 sub-lattice site. The detailed mechanism of this anisotropic behavior and the crystal structure change will be discussed in conjunction with the  $c/a$  ratio and unit cell volume of the  $\sigma$  phase.

#### F.SF07.06.10

**Towards High-Throughput First-Principles High-Temperature Thermodynamic Modeling** Siya Zhu and Axel van de Walle; Brown University, United States

We demonstrate how widely used high-throughput first-principles calculation frameworks for novel phase discovery can be augmented to enable phase stability predictions above absolute zero and yield informative phase diagrams at a fraction of the computational cost of traditional methods. The approach is based on a combination of (i) the special quasirandom structures formalism, extended to account for possible short-range order, (ii) carefully selected lattice dynamics calculations (iii) efficient molecular dynamics modeling of liquid phases that leverage high-quality experimental thermodynamic for elemental liquids and (iv) the CALPHAD approach for free energy modeling. As an example, we investigate the Ni-Re system, where earlier calculations predicted the presence of novel  $D0_{19}$  and  $D1_9$  phases. We find that, in spite of their stability at 0K, these intermetallic compounds become unstable at high temperature. These findings also prove helpful in guiding the search for alloys that provide cost effective substitutes for rhenium as a structural material.

#### F.SF07.06.11

**Development of a Thermodynamic Database for CALPHAD Simulations of CoNiCrAlY Metallic Coatings** Marlena Ostrowska<sup>1</sup>, Yao Wang<sup>1,2</sup> and Gabriele Cacciamani<sup>1</sup>; <sup>1</sup>University of Genoa, Italy; <sup>2</sup>Centre of Excellence for Advanced Materials, China

High temperature materials, such as superalloys, are often covered with metallic coatings in order to protect the substrate from oxidation and to extend its working life. The phases present in the coatings, partly determined by the alloy composition, play an important role in the material properties. Among them, several are beneficial for the properties while some phases are detrimental during service. Co and Ni are the major elements in the metallic coatings. The appropriate amounts of Al, Cr and Y are added to improve their overall performance and to meet the demanding industrial requirements. In general Al-Co-Cr-Ni alloys are adopted as the main coatings for superalloys and small amounts of Y are added to improve oxide scale adherence.



However, it is very difficult to predict how phase stabilities are affected by the addition of each element in multi-component alloys, without performing computational simulations.

A reliable thermodynamic database containing Al, Co, Cr, Ni and Y has been developed to support the design of CoNiCrAlY coatings, following the CALPHAD approach. All binary and ternary subsystems are included in the database. Most of the ternary subsystems, due to the lack of consistent thermodynamic description in the literature, were assessed by our group, namely Al-Co-Ni [1], Al-Cr-Ni [2], Co-Cr-Ni [3] and several ternary systems containing yttrium, such as Al-Co-Y, Al-Cr-Y, Al-Ni-Y and Co-Ni-Y (paper in preparation).

The new database was used to simulate a few commercial alloys used as metallic coatings protecting gas turbine blades. The calculated phase compositions were then confronted with the available experimental data from the literature for the following coatings: PWA270 (Ni-21%Co-18%Cr-12.7%Al-0.17%Y), PWA286 (Ni-21.1%Co-17.1%Cr-12.7%Al-0.61%Y) at 1000°C [4] and the Co-based coating Co-28.6Ni-21.2Cr-15.6Al-0.4Y at 1150°C [5] (in at%). The good agreement between calculated and experimental data was evident, therefore, the present database can be reliably used to predict phase equilibria in alloy coatings already in use or to support the design of new alloys with improved performance. In particular, to find the temperature range in which undesired phases (e.g.  $\sigma$ ) are stable and investigate the influence of each element on the phase stability.

[1] Y. Wang, G. Cacciamani, Experimental investigation and thermodynamic assessment of the Al-Co-Ni system, *Calphad Comput. Coupling Phase Diagrams Thermochem.* 61 (2018) 198–210. doi:10.1016/j.calphad.2018.03.008.

[2] Y. Wang, G. Cacciamani, Thermodynamic modeling of the Al-Cr-Ni system over the entire composition and temperature range, *J. Alloys Compd.* 688 (2016) 422–435. doi:10.1016/j.jallcom.2016.07.130.

[3] G. Cacciamani, G. Roncallo, Y. Wang, E. Vacchieri, A. Costa, Thermodynamic modelling of a six component (C-Co-Cr-Ni-Ta-W) system for the simulation of Cobalt based alloys, *J. Alloys Compd.* 730 (2018) 291–310. doi:10.1016/j.jallcom.2017.09.327.

[4] M. Hasegawa, M. Iwashita, Y. Kubota, P. Dymáček, F. Dobeš, Microstructure evolution under high temperature deformation of CoNiCrAlY bond coat alloy, *Mater. Sci. Eng. A.* 756 (2019) 237–247. doi:10.1016/j.msea.2019.04.030.

[5] O. Zubacheva, Plasma-Sprayed and Physically Vapor Deposited Thermal Barrier Coatings: Comparative Analysis of Thermoelastic Behavior Based on Curvature Studies, RWTH Aachen University, 2004. <http://sylvester.bth.rwth-aachen.de/dissertationen/2004/203/>.

#### F.SF07.06.12

**Influences of Loading Axis Orientation and Specimen Shape on Kink-Band Formation in Single Crystals of Mg-Zn-Y LPSO Phase Investigated by Micropillar Compression Tests** Kohei Okage, Kyosuke Kishida and Haruyuki Inui; Kyoto University, Japan

Mg-TM(transition metal)-RE(rare earth) ternary alloys containing a precipitation phase with a long-period stacking-ordered (LPSO) structure have received considerable attentions as a new light-weight structural material endowed with high strength and good ductility simultaneously. Such attractive mechanical properties are believed to be caused by heavily kinked structure of platelet precipitates of Mg-LPSO phase developed during hot extrusion process. Formation of the kinked structure in HCP metals with a relatively high  $c/a$  ratio has been interpreted generally with the dislocation-based kink band formation mechanisms such as the Hess and Barrett model, Frank-Stroh model, and Gilman model, which considered different trigger mechanisms for the activation of basal slip when the loading axis is (nearly) parallel to the basal planes, i.e., elastic buckling, stress concentration caused by pre-existing or pre-introduced defects, and a slight tilt of basal plane, respectively. However, the actual controlling factors for the kink-band formation in Mg-LPSO phases have not been fully clarified yet. In the present study, we investigated compression deformation behavior of Mg-LPSO single crystals as a function of loading axis orientation, specimen shape and stacking sequence of the LPSO structure (18R and 14H-type) by utilizing micropillar compression methodology in order to clarify the dominant controlling factors for the kink-band formation in Mg-LPSO phases.

#### F.SF07.06.13

**The Effect of Forming Internal Electric Field in Seebeck Effect** Momoka Sakamoto<sup>1</sup>, Rikuto Sasaoka<sup>2</sup>, Chiho Inoue<sup>2</sup> and Shinji Munetoh<sup>2</sup>; <sup>1</sup>Chikushigaoka High School, Japan; <sup>2</sup>Kyushu University, Japan

In the Seebeck effect in p-type semiconductor, the voltage can be generated by the diffusion of excited carrier in high temperature side to low temperature side in impurity level. However, carriers in a valence band rediffuse to high temperature side because of electric potential difference, and the value of voltage drop at equilibrium. On the other hand, the block of rediffusing carrier can generate larger the value of voltage. In this study, we combined two different fermi level of p-type semiconductors, the light boron doped silicon and the heavy boron doped silicon, in order to form internal electric field in the

interface with Spark Plasma Sintering. This process has formed the barrier of energy for prevention of carrier rediffusion. We found that the synthesized sample's voltage increased in comparison with the light boron doped silicon and the heavy boron doped silicon. It is indicated that voltage can increase by forming internal electric field, with the sample combined different fermi level p-type semiconductors.

#### F.SF07.06.14

**Late News: The Influence of the Powder Metallurgy Precursor on the Microstructure and Mechanical Properties of a Porous Cu-Al-Ni Alloy** Maria T. Malachevsky<sup>1,2</sup>, Alberto Baruj<sup>1,2</sup>, Graciela Bertolino<sup>1,2</sup> and Ignacio Papuccio<sup>3</sup>; <sup>1</sup>Centro Atómico Bariloche - CNEA, Argentina; <sup>2</sup>CONICET, Argentina; <sup>3</sup>Facultad de Ciencias Exactas -UNCPBA, Argentina

Shape memory alloys are able to stand large deformations and to recover their shape afterwards. Depending on the temperature, the shape recovery could take place after heating or by the so-called pseudoelastic behavior. These particular properties make these smart materials good candidates for applications such as damping or actuation. Cu-based shape memory alloys are commercially attractive due to their relatively low cost compared to Ni-Ti alloys. Multiple research efforts have focused on expanding their potential applications by adding features that can improve the material. Porous shape memory alloys were developed in an effort to combine the shape recovery and energy dissipation properties with reduced density and weight. However, most polycrystalline Cu-based shape memory alloys are prone to intergranular fracture both in compact and porous samples. Reducing the material grain size could decrease the stress concentration at grain boundaries and help to avoid fracture. This can be achieved by alloying with other elements or by selecting an appropriate manufacturing method. As a possible fabrication route, we used powder metallurgy starting from a small particle size.

Among Cu-based shape memory alloys, Cu-Al-Ni alloys are an alternative with good properties and low cost. In this work, we explored the fabrication of porous Cu-14Al-3Ni by conventional powder metallurgy, starting from mechanically pre-alloyed powder and a mixture of the elemental metal powders. For preparing the pre-alloyed powder, we employed a high-energy Frisch Pulverisette 7 planetary mill, processing under Argon at 700 rpm for 3 hours. The resulting powder was analyzed by means of X-Ray Diffraction (XRD). The XRD pattern showed no presence of Al or Ni while the Cu peaks were shifted to lower angles indicating the solid solution of both Al and Ni in the structure. The Cu peaks were also significantly widened due to the strain resulting from the high-energy milling. Some peaks of  $\gamma$ -Cu<sub>9</sub>Al<sub>4</sub> were detected, as well as small CW peaks resulting from the milling media contamination. The other precursor was prepared by hand mixing the elementary powders in an agate mortar. Both precursors were mixed with 1 wt.% mixture of PVA and PVB as a binder and, after drying, 30 vol.% ammonium bicarbonate was added as space holder. Cylindrical samples were prepared by uniaxial cold pressing at 700 MPa. After sintering at 1000 °C, the samples were solution-treated for 24 h at 900 °C under Ar. After the treatment, they were water-quenched to obtain the martensitic phase.

The samples prepared with the milled powder were investigated by XRD. After sintering, the phases detected were  $\alpha$ ,  $\gamma$ -Cu<sub>9</sub>Al<sub>4</sub> and AlNi. The heat treated samples consisted of the shape memory phase 18R accompanied by  $\alpha$  and AlNi. The presence of AlNi in the sintered sample suggests that the alloy resulted short of both elements and consequently the solution treatment was performed in the  $\alpha$ - $\beta$  two-phase field. After quenching,  $\alpha$  remained as a secondary phase. Meanwhile, the samples prepared with the hand mixed precursor consisted of the 18R and 2H shape memory phases.

X-ray microtomography images of the porous samples were acquired with an Xradia Micro XCT-200 microscope. The samples prepared with the pre-alloyed precursor presented internal cracks indicating that the presence of the brittle  $\gamma$ -Cu<sub>9</sub>Al<sub>4</sub> phase reduced the powder compressibility. The lower density prevented their mechanical characterization. On the other hand, samples prepared with the hand mixed precursor were well sintered allowing their complete characterization. Compression uniaxial tests were performed and the shape memory behavior was corroborated. Samples recovered 100% from a 7% strain and 98.56% from 11.5% strain when heated to 140 °C. The obtained grain size is about 30  $\mu$ m.

### SYMPOSIUM F.SF08

---

Defect-Dominated Plasticity and Chemistry in Metals and Alloys  
November 21 - December 4, 2020

#### Symposium Organizers

Christian Brandl, The University of Melbourne  
Daniel Gianola, University of California, Santa Barbara

\* Invited Paper

SESSION F.SF08.12: Live Keynote: Defect-Dominated Plasticity and Chemistry in Metals and Alloys  
Session Chairs: Christian Brandl and Daniel Gianola  
Thursday Afternoon, December 3, 2020  
F.SF08

**6:30 PM \*F.SF08.10.01**

**Structural and Chemical Atomic Complexity of Lattice Defects—From Defect Phase Diagrams to Material Properties** [Sandra Korte-Kerzel](#)<sup>1</sup>, Tilmann Hickel<sup>2</sup>, Liam Huber<sup>2</sup>, Jorg Neugebauer<sup>2</sup>, Dierk R. Raabe<sup>2</sup>, Stefanie Sandlöbes<sup>1</sup> and Mira Todorova<sup>2</sup>; <sup>1</sup>RWTH Aachen University, Germany; <sup>2</sup>Max Planck Institut für Eisenforschung, Germany

The design of new metallic materials is essential in fulfilling the promise of emerging and improving key technologies from efficient energy conversion over lightweight transport to safe medical devices. Over the last decades, two approaches in materials physics have proven immensely successful in the design of new metallic materials: Firstly, thermodynamic descriptions of crystalline phases have enabled materials scientists and engineers to tailor and process alloys to obtain a desired internal structure at the microscale. Secondly, better understanding and manipulation of the crystal defects, which govern the material's strength, formability and corrosion resistance, has led to the development of new alloying and processing concepts that provide some of the most advanced high-performance alloys in operation today. However, to date, these two concepts remain essentially decoupled.

Our vision is to bridge the gap between these existing and powerful approaches by bringing them together in one new conceptual framework, which will consider defects and their thermodynamic stability in a holistic manner. Consequently, a new material design concept originating from the atomic scale will be accessible to materials physicists and engineers which jointly considers the local crystalline structure of defects (structural complexity), the atomic distribution of each element among the different types of phases and defects (chemical complexity) and the stability of defects under the given conditions, such as bulk composition, temperature and applied stress or electrode potential. We will show here, how these can be linked by defect phase diagrams, which will describe the transition between and the coexistence of defect phases. This structural and chemical complexity at the atomic scale naturally exists in all materials. On this basis, we believe that a new physical description of metallic materials will be possible and will provide a powerful toolbox for future design of engineering materials with tailored properties regarding concurrent mechanisms and properties, such as mechanical and corrosion performance of engineering materials.

**7:00 PM \*F.SF08.06.01**

**Grain Boundary Migration—Coupling Modes and Disconnections** [Nicolas Combe](#)<sup>1,2</sup>; <sup>1</sup>CEMES - UPR 8011, France; <sup>2</sup>University Toulouse III, France

In specific conditions, grain boundary (GB) migration occurs in poly-crystalline materials as an alternative vector of plasticity compared to the usual dislocation activity. The shear-coupled GB migration, the expected most efficient GB based mechanism, couples the GB motion to an applied shear stress. For a given GB, several migration mechanisms referred as coupling modes can occur.

Both experimental and theoretical studies have evidenced that the migration of the GB occurs through the nucleation and motion of disconnections [1-3]. Disconnections are GB defects that have both a step and a dislocation (Burgers Vector) character. They can homogeneously or heterogeneously nucleate [4-6].

We use atomistic simulations (especially the Nudge Elastic Band method) on symmetric tilt grain boundary in FCC materials to evidence these disconnections and to characterize both their structural and energetic properties. In this study, we focus on homogeneous disconnections nucleation. Investigating the <100> and <110> coupling modes, we evidence the disconnections characteristics dependence on the grain boundary disorientation. Besides, we evidence the operation of specific disconnections involving coupling modes different from the usually observed <100> and <110> coupling modes.

[1] A. Rajabzadeh et al., *Philosophical Magazine*, 93, 1299 (2013)

[2] A. Rajabzadeh et al., *Phys. Rev. Lett.*, 110, 265507 (2013)

[3] A. Rajabzadeh et al., *Acta Mat.*, 77, 223-235 (2014)

[4] N. Combe, et al., *Phys. Rev. B*, **93**, 024109 (2016)

[5] N. Combe, et al., *Phys. Rev. M*, **1**, 033605 (2017)

[6] N. Combe, et al. *Phys. Rev. M*, **3**, 060601 (2019)

### 7:30 PM \*F.SF08.10.03

**The Coupling of Plasticity and Mass Transfer in Al Alloys** Christopher Hutchinson; Monash University, Australia

High strength Al alloys exploit solid state precipitation to tailor their mechanical response. This precipitation requires two ingredients: a thermodynamic driving force and atomic mobility. For a given alloy chemistry, the heat treatment (precipitation) temperature is chosen as a compromise between having sufficient driving force for precipitation and sufficient atomic mobility so that the precipitation reaction occurs in a reasonable time and results in a ‘not too coarse’ precipitate distribution. It is this compromise that frames the competition between nucleation, growth and coarsening that constrains the possible precipitate distributions and hence mechanical responses.

This talk demonstrates a new approach that uses small amplitude cyclic plasticity at room temperature as a means of continually pumping vacancies into the system to achieve atomic mobility under conditions of high thermodynamic driving force. The approach is self-regulating (in both space and particle size) and results in extremely fine-scale inhomogeneous solid solutions. Such structures lead to combinations of strength and elongation that exceed those of conventionally precipitate strengthened alloys, without the presence of precipitate free zones.

Since the approach does not use thermal treatments, it somewhat decouples control of the thermodynamic driving force and atomic mobility. This provides a means to fully alter the competition between precipitate nucleation, growth and coarsening and new microstructures, with new combinations of properties are obtained. Examples of both monotonic and cyclic properties are demonstrated.

### 8:00 PM \*F.SF08.04.01

**Cryo Atom Probe—Measuring Hydrogen in Steels via Deuterium Charging** Julie Cairney, Yi-Sheng Chen and Ingrid McCarroll; University of Sydney, Australia

Hydrogen in steel is associated with a catastrophic failure mode, known as hydrogen embrittlement. This phenomenon is abrupt and is initiated at the atomic level. Although the exact mechanisms are still subject to debate [1], some mitigation strategies are available, including minimizing hydrogen ingress with surface coatings, or controlling hydrogen diffusion within via the introduction of microstructural ‘traps’, e.g. second phase precipitates such as niobium carbide [2]. It is believed that the incorporation of fine, distributed traps can reduce the mobility of detrimental hydrogen atoms and mitigate the macroscale embrittlement. However, as hydrogen is difficult to examine at fine scale, the experimental evidence is lacking for further optimization of the microstructural design.

Atom probe tomography is a powerful technique that can provide accurate 3D maps showing the position and identity of atoms. H is easily detected but, because it is so mobile, researchers are never sure whether it arises from the sample or the chamber itself. It has recently been demonstrated [3] that this issue can be tackled by charging samples with deuterium (D), the less common stable isotope of H, and cooling the specimen to cryogenic temperatures immediately after charging to slow diffusion. This approach allows the D to serve as a marker for H, so that the location of the H atoms can be determined unambiguously.

The University of Sydney has recently installed a suite of tools that allow the preparation and transfer of samples into and between instruments via ultra-high vacuum cryogenic transfer. These facilities include a purpose-built controlled-atmosphere glovebox (Microscopy Solutions), a Zeiss Auriga scanning electron microscope-focused ion beam (SEM-FIB) equipped with a custom-designed cryogenic stage (also Microscopy Solutions), and a CAMECA laser-assisted local electrode atom probe (LEAP) equipped with a Vacuum and Cryo Transfer Module (VCTM) on the load lock, all which are connected by a Ferrovac UHV suitcase. This new specimen treatment chamber allows specimens to be charged with D in a gaseous environment, at various temperatures, quenched to cryogenic conditions and then transferred to the atom probe for analysis. This talk will include an overview of this system as well as atom probe data from deuterated steel samples, including direct observation of deuterium at trapping sites, such as dislocations, grain boundaries and precipitates in martensitic steels [4].

### References:

[1] I.M. Robertson et al., *Metall Mater Trans A*, **46a**, 2323-2341 (2015).

[2] H. Bhadeshia, *ISIJ International*, **56**, 24-36 (2016).

[3] Y.S. Chen *et al.*, Science 355 (2017) 1196-1199.

[4] Y.S. Chen *et al.*, Science 367 (2020) 171-175.

SESSION F.SF08.13: Live Panel Discussion: Defect-Dominated Plasticity and Chemistry in Metals and Alloys

Session Chairs: Daniel Kiener and Stefanie Sandlöbes

Friday Morning, December 4, 2020

F.SF08

**11:30 AM \*F.SF08.10.02**

**Controlling the Structure of Interfaces and Dislocations to Directly Alter Mechanical Response** Timothy J. Rupert;

University of California, Irvine, United States

Both grain boundaries and dislocations have been recently shown to experience structural transitions between defect states known as complexions. In this talk, we discuss how one can manipulate the natural variations in stress, chemistry, and atomic structure near grain boundaries and dislocations to stabilize these defects and use them as tailorable features. We also demonstrate how different complexions can alter the mechanical properties of materials on the nanoscale. For grain boundary complexions, we focus on nanocrystalline metals, where such features have the largest effect due to the high grain boundary density. We isolate the materials and processing conditions which can cause the strength and ductility of these materials to be simultaneously augmented, as well as report on small-scale mechanical testing and atomistic modeling techniques to study grain boundary mechanics. For linear complexions, our work uncovers how nanoscale phases restricted to the region along a dislocation line direction can affect plasticity, encompassing both initial yield and subsequent flow. Alloy choice is shown to be very important, as various responses ranging from softening to strong hardening are predicted. As a whole, this work demonstrates that our field is on the precipice of a new age, where defects can be manipulated and designed rather than simply tolerated.

**11:55 AM PANEL DISCUSSION INTRODUCTION**

**12:00 PM JULIE CAIRNEY , PANELIST**

**12:05 PM TING ZHU, PANELIST**

**12:10 PM SANDRA KORTE-KERZEL, PANELIST**

**12:15 PM PANEL DISCUSSION**

SESSION F.SF08.01: Complex Defect Structures

On Demand Abstracts Available for Viewing Starting Saturday Morning, November 21, 2020

F-SF08

**5:00 AM \*F.SF08.01.01**

**2D and 3D EBSD Studies of Alpha Variant Selection During Electron Powder Bed Fusion of Ti-6Al-4V** Sophie Primig, Ryan W. Demott and Nima Haghdadi; UNSW Sydney, Australia

Ti-6Al-4V is one of the most commonly used alloys for additive manufacturing (AM) due to its applications as orthopaedic implants and aerospace components which can uniquely benefit from the advantages of AM. However, the inherent inhomogeneity and cyclic thermal loading in additive manufacturing processes significantly complicate the microstructural evolution of this alloy. The current understanding of the microstructural evolution in Ti-6Al-4V is based on traditional processing and cannot adequately predict its behaviour during AM.

Analysis of different interfaces (prior beta grain boundaries, alpha inter-variant boundaries) formed during AM of Ti-6Al-4V can clarify the competition between different modes of alpha variant selection in determining the final microstructure. Here,

traditional 2D characterization methods are often insufficient for uncovering complex, interconnected microstructural features that arise from solid-solid phase transformations during AM.

In this work, Ti-6Al-4V blocks were produced using different scanning strategies during electron beam powder bed fusion and characterized using 2D and 3D electron backscatter diffraction. This revealed that the microstructure is more complex, and that alpha laths are more interconnected than previously believed. For example, inter-variant boundary character distributions showed significant evidence of different variant selection mechanisms as a function of the position in the build and the scanning strategy. Some of these variant selection mechanisms are more desirable than others. Understanding the complexity of the microstructure in 3D provides new insights into the fundamental phenomena behind the microstructural evolution of titanium alloys in AM, and will help to give recommendations for optimising process design.

Acknowledgements: Funding by the AUSMURI program, Department of Industry, Innovation and Science, Australia is acknowledged. Samples were provided by Prof. Suresh Babu and Miss Sabina Kumar, The University of Tennessee, Knoxville.

#### **5:15 AM F.SF08.01.03**

**A Novel Technique to Synthesize Metallic Films with Controlled Heterogeneous Microstructures and Its Tensile Deformation Behavior** Rohit Berlia and Jagannathan Rajagopalan; Arizona State University, United States

Materials with heterogeneous microstructures have been shown to exhibit a superior combination of strength and toughness compared to homogeneous nanostructured or coarse-grained materials. However, only a limited progress has been made in producing heterogeneous microstructures with good repeatability and robust control of key microstructural parameters such as grain size dispersion, texture or spatial distribution of grains. In this work, we report a novel technique to synthesize metallic films with highly tailored heterogeneous microstructures using magnetron sputtering. The technique is capable of precisely controlling the volume fraction, in-plane texture, spatial arrangement, morphology and connectivity of two or more sets of grains. Using this technique, we synthesized bimodal films of pure metals like aluminum, copper, iron and nickel where the mean size of smaller grains is around 30-300 nm while the coarser grains have a mean size exceeding 5  $\mu\text{m}$ . The microstructure of these films was characterized by a combination of X-ray diffraction, electron backscattered diffraction and transmission electron microscopy to reveal the grain size dispersion, texture and orientation distribution. Mechanical characterization via uniaxial tensile loading-unloading was performed on bimodal Fe films with varying volume fraction and spatial arrangement of nanocrystalline and coarse grains using MEMS stages. Films with higher volume fraction of coarse grains showed enhanced strain hardening capability and a better combination of strength, ductility and toughness. This method enables the optimization of microstructural parameters (volume fraction of fine and coarse grains, texture, morphology, etc.), to obtain films with superior mechanical properties.

#### **5:25 AM F.SF08.01.04**

**Slip-Twin Transfer Across Phase Boundaries—An *In Situ* Investigation of a Ti-Al-V-Fe ( $\alpha+\beta$ ) Alloy** Shaolou Wei, Gaoming Zhu and Cem Tasan; Massachusetts Institute of Technology, United States

Microstructural plastic strain distribution evolution is highly heterogeneous even in single-phase alloys. One of the important factors that govern this heterogeneity is slip/twin transfer across grain/phase boundaries. In this regard, the fundamentals of transfer across grain boundaries have drawn significant attention in the literature, while the understanding of phase boundaries remains comparatively limited. ( $\alpha+\beta$ ) titanium alloys provide a profound platform to explore these phenomena, since: (i) both of the present phases can exhibit plastic deformation at similar microscopic strain levels; (ii) both slip and mechanically-induced twinning can be triggered to accommodate plastic strain. By integrating in-situ EBSD/SEM testing, crystallographic calculations, and microstructure-based strain mapping approach, we aim to address the following three propositions in this presentation: (1) could deformation transfer take place in the form between mechanical twinning in the  $\alpha$ -phase and dislocation glide in the  $\beta$ -phase? (2) What parameters would be rational indicators to quantify the propensity for the incipience of this event? (3) What micro-mechanical consequences are associated with the slip-twin transfer activity? Broader indications for mechanistically-guided microstructural design concept will also be discussed.

SESSION F.SF08.02: Dislocation

On Demand Abstracts Available for Viewing Starting Saturday Morning, November 21, 2020  
F-SF08

**5:00 AM \*F.SF08.02.01**

**Integrating Computational Modeling and *In Situ* Experiment to Decipher Microscopic Deformation Mechanisms** Ting Zhu; Georgia Institute of Technology, United States

With recent advances in computational modeling and in situ experimental technologies, there have been increased efforts to combine these approaches to understand microscopic deformation mechanisms in metals and alloys. In this talk, I will present our recent studies that integrate in situ electron microscopy and diffraction experiments with crystal plasticity and atomistic simulations for gaining a deep understanding of microscopic deformation processes. For example, we have combined in situ synchrotron X-ray diffraction experiments with crystal plasticity simulations to investigate the microscale residual stresses in additively manufactured stainless steel. We have also combined in situ transmission electron microscopy experiments and atomistic simulations to study the effects of atomic structures and elemental distributions on the exceptional mechanical properties of high-entropy alloys. In addition, we have used this strategy to reveal the grain boundary deformation atom by atom, step by step, thus uncovering the unexpected grain boundary sliding mechanisms in real time.

**5:15 AM F.SF08.02.02**

**Plastic Deformation of Cr Single Crystals in Triple-Q State Compressed at 77 K** Jakub Holzer<sup>1,2</sup>, Zdeněk Chlup<sup>1</sup>, Tomáš Kruml<sup>1</sup> and Roman Gröger<sup>1,2</sup>; <sup>1</sup>The Czech Academy of Sciences, Czechia; <sup>2</sup>Central European Institute of Technology, Czechia

A series of compression tests on chromium single crystals at 77 K was carried out in order to investigate the slip activity in the first 2-4% of plastic strain. Macroscopic samples of about 3×3×10 mm were polished mechanically and electrolytically and their orientations prior to and after deformation were determined by electron backscatter diffraction to assess the magnitudes and directions of crystal rotations. The crystals compressed in the direction close to [001] deformed primarily by slip on the most highly stressed (-101)[111] and (101)[-111] systems. Loading the crystals in the directions close to the [011]-[-111] edge of the stereographic triangle resulted in preferential twinning on {112}<111> systems. For loading in the center-triangle direction, the slip morphology was dominated by anomalous slip on the low-stressed (0-11) plane in contrast to the prediction of the Schmid law. Diffraction contrast imaging in TEM reveals the presence of [100] screw junctions between intersecting 1/2[111] and 1/2[-111] screw dislocations. Using molecular statics simulations, we show that this junction is not removed under the applied stress. Instead, the three dislocations move on the (0-11) plane, which results in the anomalous slip.

**5:25 AM F.SF08.02.03**

**Dislocation Interactions During Shear Deformation of a Colloidal Crystal** Seongsoo Kim, Ilya Svetlizky, David Weitz and Frans Spaepen; Harvard University, United States

Understanding dislocation interactions at different length scales, from atomistic to macroscopic, is important in the study of work hardening, fatigue and crack formation. Colloidal systems, in which particles can be tracked by confocal microscopy in 3D-space and time during deformation, provide the opportunity to study dislocations and their interactions over a wide size scale, from the particle to the sample level. The colloidal crystals in this work consist of micrometer-size hard spheres dispersed in a liquid, which have been sedimented onto a template to form a face-centered cubic single crystal. When the crystal is sheared, dislocations nucleate, glide, react and often form Lomer-Cottrell locks. We supplement these observations with measurements of the local stress and strain fields and identify the zipping-unzipping mechanism of the locks.

**5:35 AM F.SF08.02.04**

**Multi-Scale Visualization with Machine Learning of Dislocation Networks in Colloidal Single Crystals** Ilya Svetlizky, Seongsoo Kim, Seong Ho Pahng, Agnese Curatolo, Michael P. Brenner, David Weitz and Frans Spaepen; Harvard University, United States

Understanding the formation and evolution of dislocation networks and their effect on the mechanical properties of solids is challenging, as it spans a vast hierarchy of length and time scales. Hard-sphere colloidal suspensions provide a unique model system to address this difficulty: the micrometer size of the suspended particles both slows down their motion and allows them to be visualized by optical microscopy. At high density, these colloidal particles form face-centered cubic crystals with non-zero stiffness, which allows us to use them to study the principles of crystalline plasticity. Here we present simultaneous multi-scale visualization of dislocation networks. At the single particle level the structure of the dislocations and their interactions are visualized by laser confocal microscopy. To visualize the large-scale collective

dislocation dynamics we developed a laser diffraction imaging technique inspired by the classical TEM imaging methods in atomic systems. The flexibility in manipulating visible light, in contrast to electrons, allows us to image under multiple diffraction conditions almost instantaneously. We designed a deep convolutional neural network to address the inverse problem of inferring the structure of the dislocation network from the multiple complex diffraction images. We will show that the neural network reliably reconstructs the spatial positions of the dislocations and their Burgers vectors by testing the results with in-situ confocal microscopy data on a smaller portion of the sample. We demonstrate the success of our method by applying it to the network of misfit dislocations formed via during particle sedimentation on a strained substrate.

#### 5:45 AM F.SF08.02.05

***In Situ* Nanomechanics of Crystalline Metallic Nanowires** Guangming Cheng<sup>1</sup>, Sheng Yin<sup>2</sup>, Gunther Richter<sup>3</sup>, Huajian Gao<sup>4,2</sup> and Yong Zhu<sup>1</sup>; <sup>1</sup>North Carolina State University, United States; <sup>2</sup>Brown University, United States; <sup>3</sup>Max Planck Institute for Intelligent Systems, Germany; <sup>4</sup>Nanyang Technological University, Singapore

Metallic nanowires have been widely used in a variety of nanoengineering applications, including nanoelectromechanical systems, nanosensors, transparent electrodes, optoelectronics, and flexible and stretchable electronics. Mechanical behaviors of metallic NWs play a crucial role in reliability of the nanowire-based devices. Here I will present our recent work on in-situ nanomechanics of crystalline metallic nanowires inside transmission electron microscope (TEM) in three case studies. First, we report competition of deformation mechanisms (twinning and slip) in single-crystalline metallic nanowires. We found that the competition depends on the cross-sectional shape of the nanowire, which affects the change of surface energy associated with each deformation mechanism. Second, we found unexpectedly, through careful cross-sectional TEM study, that most of the synthesized single-crystalline nanowires include a central twin boundary along the entire length of the nanowire, so we call them bi-twinned nanowires. We also found two competing deformation mechanisms – localized dislocation slip and delocalized plasticity via an anomalous tensile detwinning mechanism – depending on the volume ratio between the two twin variants and the cross-sectional aspect ratio. The mechanism of the observed tensile detwinning was investigated. Finally, we found that the twin boundary can cause interesting recoverable plasticity and Bauschinger effect.

#### SESSION F.SF08.03: Dislocation and Alloying

On Demand Abstracts Available for Viewing Starting Saturday Morning, November 21, 2020

F-SF08

#### 5:00 AM F.SF08.03.02

**Effect of Stacking Fault Energy and Solute Atoms on Microstructural Evolutions of Cu, Ag and Cu-Al Alloys Processed by Equal Channel Angular Pressing** Mayu Asano, Motohiro Yuasa and Hiroyuki Miyamoto; Doshisha University, Japan

The stacking fault energy (SFE) changes with an addition of solute atoms for FCC metals. Tendency to form deformation twins and stacking faults increases with decreasing SFEs and affects the mechanical properties. In severe plastic deformation (SPD), alloying elements generally enhance grain refinement by inhibiting dynamic recovery and accumulating dislocations leading to smaller grain size than that in pure FCC metals. The role of alloying elements on grain refinement has two possibilities. The first is the formation of extended dislocations on decreasing SFE with the addition of solute atoms. The second is the segregation of solute atoms at dislocations and stacking faults. Both the two effects can suppress the dynamic recovery and retard the formation of grain boundaries until the significant dislocation densities is accumulated. Previous studies have focused only on the effect of SFEs on grain refinement and do not take the effect of segregation of solute atoms into consideration. In these cases, it is not obvious which one is the major effect. The purpose of this study is to investigate the relative importance of the effect of SFEs and solute atoms on microstructural evolutions for ultrafine grained (UFG) materials. Pure copper, pure silver, Cu-4.6at%Al and Cu-6.8at%Al were selected (SFEs are about 41, 22, 37 and 23 mJ/m<sup>2</sup>, respectively). UFG structures were formed by ECAP at the same homologous temperature so that the effect of temperature on thermal activation can be eliminated. Samples processed from one to eight passes through Route Bc at 5mm/min for pure metals and 1mm/min for alloys. Microstructural evolutions were observed by EBSD, TEM and XRD. The microstructural investigation is focused on variation of the subgrain or grain size, the distribution of grain boundary misorientations and the dislocation density. The results show that grain size significantly decreases at initial stage of pressing while it saturates at the final stage of pressing. The final grain size after eight passes for Cu, Ag, Cu-4.6at%Al and Cu-6.8at%Al were 325, 268, and 251 and 76 nm. It is found by comparing Ag and Cu-6.8at%Al, that grain size of the Cu-6.8at%Al was smaller than that of Ag despite the same SFE. It seems that the final grain size is determined by the ultimate cell size because cell boundaries lose



mobility once they transformed to sharper grain boundaries by dynamic recovery. It is assumed the solute effect is greater to inhibit the transformation of cell boundaries than the effect of stacking faults, which result in smaller effect of SFE than solute atoms on grain refinement.

#### **5:10 AM F.SF08.03.04**

**Connecting Short Range Order into Mechanical Response in High Entropy Alloys** Daniel Foley<sup>1</sup>, James Hart<sup>1</sup>, Elaf A. Anber<sup>1</sup>, Robert Ritchie<sup>2</sup>, Andrew Minor<sup>2</sup>, Mark Asta<sup>2</sup>, Flynn Walsh<sup>2</sup>, Douglas E. Spearot<sup>3</sup> and Mitra L. Taheri<sup>1</sup>; <sup>1</sup>Johns Hopkins University, United States; <sup>2</sup>UC Berkeley/Lawrence Berkeley National Laboratory, Berkeley, United States; <sup>3</sup>University of Florida, United States

This talk reviews recent work complex systems local structure evolution in high entropy alloys (HEAs). Despite their nominal chemical disorder, several studies have reported short range order (SRO) in HEAs – i.e. preferential bonding, local elemental enrichment and/or clustering – and such SRO may have broad implications for HEA performance. To tackle this problem, a suite of spatially resolved, electron imaging, diffraction, and spectroscopy techniques is leveraged to correlate local order with microstructural evolution and related dislocation phenomena. Microstructures of HEAs subjected to a variety of deformation regimes and quantified using diffraction-based techniques. In these samples, the extent to which SRO controls localized dislocation-based phenomena during microstructural evolution is discussed. The techniques presented allow for the direct observation of the interplay between chemistry and microstructure, and thus, provides us with key tuning knobs for future HEA development.

SESSION F.SF08.04: Dislocation and Impurity  
On Demand Abstracts Available for Viewing Starting Saturday Morning, November 21, 2020  
F-SF08

#### **5:00 AM \*F.SF08.04.01**

**Cryo Atom Probe—Measuring Hydrogen in Steels via Deuterium Charging** Julie Cairney, Yi-Sheng Chen and Ingrid McCarroll; University of Sydney, Australia

Hydrogen in steel is associated with a catastrophic failure mode, known as hydrogen embrittlement. This phenomenon is abrupt and is initiated at the atomic level. Although the exact mechanisms are still subject to debate [1], some mitigation strategies are available, including minimizing hydrogen ingress with surface coatings, or controlling hydrogen diffusion within via the introduction of microstructural ‘traps’, e.g. second phase precipitates such as niobium carbide [2]. It is believed that the incorporation of fine, distributed traps can reduce the mobility of detrimental hydrogen atoms and mitigate the macroscale embrittlement. However, as hydrogen is difficult to examine at fine scale, the experimental evidence is lacking for further optimization of the microstructural design.

Atom probe tomography is a powerful technique that can provide accurate 3D maps showing the position and identity of atoms. H is easily detected but, because it is so mobile, researchers are never sure whether it arises from the sample or the chamber itself. It has recently been demonstrated [3] that this issue can be tackled by charging samples with deuterium (D), the less common stable isotope of H, and cooling the specimen to cryogenic temperatures immediately after charging to slow diffusion. This approach allows the D to serve as a marker for H, so that the location of the H atoms can be determined unambiguously.

The University of Sydney has recently installed a suite of tools that allow the preparation and transfer of samples into and between instruments via ultra-high vacuum cryogenic transfer. These facilities include a purpose-built controlled-atmosphere glovebox (Microscopy Solutions), a Zeiss Auriga scanning electron microscope-focused ion beam (SEM-FIB) equipped with a custom-designed cryogenic stage (also Microscopy Solutions), and a CAMECA laser-assisted local electrode atom probe (LEAP) equipped with a Vacuum and Cryo Transfer Module (VCTM) on the load lock, all which are connected by a Ferrovac UHV suitcase. This new specimen treatment chamber allows specimens to be charged with D in a gaseous environment, at various temperatures, quenched to cryogenic conditions and then transferred to the atom probe for analysis. This talk will include an overview of this system as well as atom probe data from deuterated steel samples, including direct observation of deuterium at trapping sites, such as dislocations, grain boundaries and precipitates in martensitic steels [4].

#### **References:**

- [1] I.M. Robertson *et al.*, *Metall Mater Trans A*, **46a**, 2323-2341 (2015).  
[2] H. Bhadeshia, *ISIJ International*, **56**, 24-36 (2016).  
[3] Y.S. Chen *et al.*, *Science* 355 (2017) 1196-1199.  
[4] Y.S. Chen *et al.*, *Science* 367 (2020) 171-175.

#### 5:15 AM F.SF08.04.04

**Atomistic and Mesoscopic Modeling of Plasticity in Carbon Steels** Arnaud Allera<sup>1,2</sup>, Fabienne Ribeiro<sup>1</sup>, Michel Perez<sup>3</sup>, Jaime Marian<sup>4</sup> and David Rodney<sup>2</sup>; <sup>1</sup>Institut de Radioprotection et de Sûreté Nucléaire, France; <sup>2</sup>Univ Lyon, Université Claude Bernard Lyon 1, CNRS, France; <sup>3</sup>Univ Lyon, INSA-Lyon, France; <sup>4</sup>University of California, Los Angeles, United States

The vessel of pressurized water reactors operated in nuclear plants consists mainly of ferritic steels (Fe-C alloys). During operation, these components are subjected to extreme conditions (600 K, 155 bar, irradiation, ...) that affect their microstructural evolution and induce hardening and embrittlement, which can significantly impact the safety of the plant. In particular, the carbon atoms tend to diffuse and segregate over time, forming Cottrell atmospheres around dislocations and modifying their core structure [1].

The aim of this work is to establish a link between microstructural evolution and plastic properties. This requires to refine our understanding of the glide of screw dislocations in ferritic steels, in the presence of carbon solute atoms and at different scales. A number of state-of-the-art Fe-C interatomic potentials from the literature were tested on different alloy and dislocation properties, including carbon-carbon and carbon-dislocation binding energies, the screw dislocation core structure and Peierls potential. While none of the potentials fully agrees with *ab initio* reference data, we propose a combination of the two that perform best [2] [3].

This new potential is used in molecular dynamics (MD) simulations to study the glide of screw dislocations pinned by random solute atoms. It is evidenced that (1) short range interactions between solute and dislocation core atoms prevail compared to mid-range elastic interactions, (2) that the dislocation adopts a 3D structure due to its interaction with carbon atoms in different neighboring octahedral positions and (3) that the dislocation is very strongly pinned when the distance between carbon atoms decreases below a few tens of Burgers vectors. The simulated time scale is then extended to model static and dynamic strain ageing with a kinetic Monte Carlo approach parameterized on the DFT and EAM calculations. This work paves the way for the development of a general mobility law for dislocations in aged steels.

- [1] Ventelon L. *et al.* *Phys. Rev. B*. 91 (2015).  
[2] Veiga, R. G., Becquart, C. S., & Perez, M. *Comput. Materials Science*, 82 (2014).  
[3] Proville, L., Rodney, D., & Marinica, M. C. *Nature Materials*, 11 (2012).

#### SESSION F.SF08.05: Dislocation and Temperature

On Demand Abstracts Available for Viewing Starting Saturday Morning, November 21, 2020  
F-SF08

#### 5:00 AM F.SF08.05.01

**Thermomechanical Conversion in Metals—Constraints from a Two-Temperature Dislocation Plasticity Model** Charles Lieou<sup>1</sup> and Curt Bronkhorst<sup>2</sup>; <sup>1</sup>Los Alamos National Laboratory, United States; <sup>2</sup>University of Wisconsin–Madison, United States

Using two-temperature thermodynamics, we derive an important constraint on the Taylor-Quinney coefficient, which quantifies the fraction of plastic work that is converted into heat during plastic deformation. We show that the Taylor-Quinney coefficient is a function of a thermodynamically defined effective temperature that measures the configurational disorder in the material, and increases as deformation progresses. Finite-element analysis of a recent experiment on the AA6016-T4 aluminum alloy, using the thermodynamic dislocation theory (TDT) of Langer *et al.*, shows good agreement between theory and experiment for both stress-strain behavior and temporal evolution of the temperature.

#### 5:10 AM F.SF08.05.02

**TiAl Embrittlement at High Temperatures** Camille Thenot<sup>1</sup>, Jean-Philippe Monchoux<sup>1</sup>, Damien Connetable<sup>2</sup> and Pierre

Sallot<sup>3</sup>; <sup>1</sup>CEMES CNRS UPR 8011, France; <sup>2</sup>CIRIMAT CNRS UMR 5085, INP UPS, ENSIACET, France; <sup>3</sup>SAFRAN Tech, France

Titanium-Aluminum alloys (TiAl) are very interesting for applications in turbomachines because of their low density (3.8 - 4.2 g.cm<sup>-3</sup>) and of their high mechanical strength at high temperatures. However, when exposing TiAl alloys to high temperatures, a catastrophic loss of ductility is observed. Here, we study the role of oxygen in this phenomenon. For this purpose, we investigate the nature of the TiAl-oxygen solid solution (diluted O atoms, or forming clusters), we determine the oxygen diffusion mechanisms and study the interactions between the dislocations and the oxygen atoms. The nature of the solute solution and the diffusion mechanisms have been investigated theoretically using atomistic calculations (DFT), and the dislocation-oxygen interactions have been studied experimentally by characterizations at the microscopic scale (TEM). In the experimental part, tensile test on Ti<sub>48</sub>Al<sub>48</sub>W<sub>2</sub>B<sub>0.08</sub> alloys have been carried out on samples exposed in air at 800°C for 500h, to characterize the embrittlement phenomenon. It was shown that the embrittlement comes from oxygen penetration in a surface layer 10 μm to 100 μm thick. Then, to evaluate the influence of oxygen on the bulk mechanical properties, tensile tests on alloys with low and high oxygen concentrations have been performed. Results showed that the alloy with high bulk oxygen concentration has a lower ductility than the alloy with lower oxygen content, as classically observed in TiAl alloys. TEM observations showed the presence of pinning points on the dislocations, which may have an impact on the alloy ductility. Based on these results, our hypothesis is that TiAl embrittlement at high temperature occurs by a loss of ductility of the superficial diffusion layer.

In the numerical part, DFT simulations were used to study the interactions between clusters of one to 6 oxygen atoms with lattice defects such as vacancies and antisites at the atomic scale. We identified which type of complex defect (defect + oxygen cluster) would be the most probable and in which concentration, depending on the temperature. However, these clusters of 1 to 6 oxygen atoms are much smaller than the clusters pinning the dislocations, which should be composed of about 10<sup>9</sup> oxygen atoms, according to the first evaluations based on the TEM images. Nevertheless, both the two clusters may have an impact on the mechanical properties. The small clusters are likely to decrease the diffusivity of oxygen in TiAl by acting as traps, which would lead to decrease oxygen penetration, and thus to diminish embrittlement. On the contrary, the big clusters, which pin the dislocations, probably contribute to increase the strength and to lower the ductility in the surface layer, which increase embrittlement.

#### 5:20 AM F.SF08.05.03

**Dislocation Motion and Cross-Slip in f.c.c. Metals—Atomistic Simulations** Eyal Oren, Ohad Grinbaum, Eyal Yahel and Guy Makov; Ben-Gurion University of the Negev, Israel

Dynamic properties of dislocations are both of fundamental importance in understanding and modelling plasticity and mechanical deformation of solids and are required for constructing mesoscale dislocation dynamics simulations. However, these properties are not easily accessible by experimental means due to the short time-scales. Molecular dynamics provides a tool for studying the dynamics of dislocations at the short time and length scales, which are difficult to access by experimental means, but requires careful convergence for physical meaning. We have studied the dynamics of dislocation glide and of dislocation cross-slip in FCC crystals of Al, Cu, Ni and Ag to elucidate the effect of chemical species on the dislocation properties. Highly converged simulations were performed on long dislocations in large FCC crystal supercells with full periodic boundary conditions, incorporating a dislocation dipole with zero net Burgers vector. Kinematics were studied by accelerating dislocations at constant stress and temperature. The relation between stress and terminal velocity at cryogenic and room temperatures for both screw and edge dislocations was obtained. A transition from viscous behaviour to near sonic asymptotic behaviour was identified and the velocity dependence of the drag force was characterised. At higher stresses a shift into the transonic regime occurs and the mechanism and stability of this transition is examined. The thermally activated process of cross-slip was simulated multiple times creating statistical data from which the kinematics and kinetics were deduced and from which the activation parameters were calculated. The effects of stresses in the cross-slip and glide planes on the activation volumes were determined. Finally, the rate-controlling step of the cross-slip process was identified producing insight into the cross-slip mechanism.

[1] E. Oren, E. Yahel, G. Makov, Kinetics of dislocation cross-slip : A molecular dynamics study, *Comput. Mater. Sci.* 138 (2017) 246–254. doi:10.1016/j.commatsci.2017.06.039.

[2] E. Oren, E. Yahel, G. Makov, Dislocation kinematics : a molecular dynamics study in Cu, *Model. Simul. Mater. Sci. Eng.* 025002 (2017). doi:10.1088/1361-651X/aa52a7.

#### 5:30 AM F.SF08.05.04

**Plasticity in Small-Sized Crystals Through Diffusion-Mediated Surface Defects** Xiang Wang, Sixue Zheng and Scott X. Mao; University of Pittsburgh, United States

Due to the small scale and high surface-to-volume ratio of nanometer-sized metallic crystals, it is generally believed that surface surface-related deformation mechanisms govern the plasticity of nanocrystals at atomic scale. As the sample size of the nanocrystals goes further down to sub-ten nanometer, strong surface diffusion activities took place and mediated plastic deformation. However, thus far, much less is known about the yielding and plastic flow mechanisms at atomic scale in small-sized nanocrystals where surface atomic diffusion is activated. Here, by performing in-situ transmission electron microscope tensile tests of Ag NWs and Pt NWs, it was revealed that the yield strength-size relationship changed from “smaller is stronger” to “smaller is weaker” with decreasing the sample diameters of Ag NWs, while Pt NWs showed traditional “Hall-Petch” size-dependent behavior. This difference arose from surface atomic diffusion activities in Ag NWs, which may increase dislocation nucleation sites and the probability of surface defect interaction, thereby lowering critical surface dislocation nucleation stress. The coupled displacive-diffusive plasticity was quantitatively investigated by analyzing the lattice stress-applied strain evolution in nanowires at atomic scale. This work provides new insights into the atomic-scale mechanisms of diffusion-assisted dislocation nucleation and diffusion-mediated plastic deformation process with displacive plasticity in small-sized materials.

#### 5:40 AM F.SF08.05.05

**Probing the Small-Scale Plasticity of an Icosahedral Quasicrystal, i-Al-Pd-Mn, at Moderate Temperatures** Yu Zou; University of Toronto, Canada

Quasicrystalline materials possess a remarkable structure that does not exhibit crystallographically legitimate periodicity in certain crystallographic directions. Despite their special configuration and many related useful properties, the major drawback of these quasiperiodic structures is extreme brittleness of the materials at temperatures below about  $0.75 T/T_m$  ( $T_m$ -the melting point) which hugely handicaps their practical implementation in the moderate temperature region. Here, we study the mechanical behavior of a typical icosahedral quasicrystal (i-Al-Pd-Mn) using a micro-thermomechanical technique over the temperature range of 25-500 °C, which has never been explored before. A couple of interesting phenomena have been observed, including micro-pillar shrinkage, phase transformations, grain refinement, and thermally induced transition from brittle fracture to serrated and homogeneous plastic flows. Furthermore, we discuss the multiple underlying mechanisms on the deformation behavior of the quasicrystal in this temperature regime, including surface evaporation/diffusion, diffusion-enhanced plasticity, dislocation activities, and grain boundary rotation/sliding. Our study bridges the gap between room temperature and high temperature plasticity in quasicrystals and also demonstrates a new opportunity to study complex intermetallic phases in broad size and temperature regimes.

#### 5:50 AM F.SF08.05.06

**High-Temperature Bulk Dislocation Dynamics in Aluminum** Leora Dresselhaus-Marais<sup>1</sup>, Grethe Winther<sup>2</sup>, Marylesa Howard<sup>3</sup>, Arnulfo Gonzalez<sup>3</sup>, Sean R. Breckling<sup>3</sup>, Can Yildirim<sup>4</sup>, Philip Cook<sup>5</sup>, Mustafacan Kutsal<sup>2,6</sup>, Luis Zepeda-Ruiz<sup>1</sup>, Amit Samanta<sup>1</sup>, Carsten Detlefs<sup>6</sup>, Jon Eggert<sup>1</sup>, Hugh Simons<sup>2</sup> and Henning F. Poulsen<sup>2</sup>; <sup>1</sup>Lawrence Livermore National Laboratory, United States; <sup>2</sup>Technical University of Denmark, Denmark; <sup>3</sup>Nevada National Security Site, United States; <sup>4</sup>CEA Grenoble, France; <sup>5</sup>Universität für Bodenkultur Wien, Austria; <sup>6</sup>European Synchrotron Radiation Facility, France

Establishing the appropriate thermal pathways to tune a metal's microstructure and generate the appropriate continuum response requires a quantitative view of high-temperature annealing. The dislocation motion and interactions that are known to dictate microstructural changes in metals depend strongly on temperature, however, the necessary time-resolved measurements have been elusive, especially near the melt. We use time-resolved dark-field X-ray microscopy to directly image dislocation motion at temperatures spanning the final 7% to  $T_m$ . Our real-time movies resolve the creep-dominated dislocation motion and interactions deep beneath any surface in single-crystal, showing dynamics that has previously been limited to theory. Quantitative analysis of the temperature-dependent dislocation mobility in these findings present opportunities to test and refine dislocation models that have previously relied on indirect measurements and multi-scale models for validation.

This work was performed in part under the auspices of the U.S. Department of Energy by Lawrence Livermore National Laboratory under Contract DE-AC52-07NA27344.

**5:00 AM \*F.SF08.06.01**

**Grain Boundary Migration—Coupling Modes and Disconnections** Nicolas Combe<sup>1,2</sup>; <sup>1</sup>CEMES - UPR 8011, France; <sup>2</sup>University Toulouse III, France

In specific conditions, grain boundary (GB) migration occurs in poly-crystalline materials as an alternative vector of plasticity compared to the usual dislocation activity. The shear-coupled GB migration, the expected most efficient GB based mechanism, couples the GB motion to an applied shear stress. For a given GB, several migration mechanisms referred as coupling modes can occur.

Both experimental and theoretical studies have evidenced that the migration of the GB occurs through the nucleation and motion of disconnections [1-3]. Disconnections are GB defects that have both a step and a dislocation (Burgers Vector) character. They can homogeneously or heterogeneously nucleates [4-6].

We use atomistic simulations (especially the Nudge Elastic Band method) on symmetric tilt grain boundary in FCC materials to evidence these disconnections and to characterize both their structural and energetic properties. In this study, we focus on homogeneous disconnections nucleation. Investigating the  $\langle 100 \rangle$  and  $\langle 110 \rangle$  coupling modes, we evidence the disconnections characteristics dependence on the grain boundary disorientation. Besides, we evidence the operation of specific disconnections involving coupling modes different from the usually observed  $\langle 100 \rangle$  and  $\langle 110 \rangle$  coupling modes.

[1] A. Rajabzadeh et al., *Philosophical Magazine*, 93, 1299 (2013)

[2] A. Rajabzadeh et al., *Phys. Rev. Lett.*, 110, 265507 (2013)

[3] A. Rajabzadeh et al., *Acta Mat.*, 77, 223-235 (2014)

[4] N. Combe, et al., *Phys. Rev. B*, 93, 024109 (2016)

[5] N. Combe, et al., *Phys. Rev. M*, 1, 033605 (2017)

[6] N. Combe, et al. *Phys. Rev. M*, 3, 060601 (2019)

**5:15 AM F.SF08.06.03**

**Atomistic Insight into the Deformation Map of Grain Boundary** Qi Zhu and Jiangwei Wang; Zhejiang University, China

Grain boundary (GB) migration is a prevalent plastic deformation mode in nanocrystalline and polycrystalline materials, and a systematic insight of GB migration is vital to the development of novel materials through GB engineering. However, current understanding on the atomistic mechanism of GB-dominated plasticity remains largely elusive. Here, we combine state-of-the-art in situ TEM nanomechanical testing and atomistic simulations to investigate the atomistic dynamics of shear-induced GB migration in Au nanocrystals. Using the  $\langle 110 \rangle$  tilt GBs as examples, we demonstrate that the shear-induced GB migration is fundamentally accommodated by GB defects, including disconnections (high angle GB) and geometrically necessary dislocations (low angle GB). In the high angle range (as exemplified by the  $\Sigma 11(113)$  GB), we unambiguously reveal a disconnection-mediated GB migration mechanism under shear loading, where the nucleation, propagation and dynamic interactions of various disconnections dominate the GB migration. Moreover, the migrating  $\Sigma 11(113)$  GB can readily accommodate intragranular lattice defects (including dislocation and stacking fault), where the pre-existing disconnections interact with the residual disconnections generated on the GB. This disconnection-mediated dynamic is further proved to be universal among different high angle GB structures, where triple junctions can serve as effective nucleation and annihilation sites of disconnections. In contrast, low angle GBs with dislocation characters typically migrate via conservative gliding of intrinsic GB dislocations. The fully reversible motion of such coherent GBs can be achieved under shear loading cycles in Au nanocrystals, due to the suppression of heterogeneous surface nucleation of lattice defects and robust structural stability throughout GB motion. Inspired by these scientific insights, we propose a GB engineering protocol to realize controllable plastic reversibility in metallic nanocrystals. This reversible deformation via conservative GB migration is retained in a broad class of face-centered cubic metals with low stacking fault energies when tuning the GB misorientation, external geometry and loading conditions over a wide range. Above results enable us to establish a full deformation map of  $\langle 110 \rangle$  tilt GBs, providing novel insights into the GB-dominated plasticity in nanocrystalline materials. This talk is based on our recent works: In situ atomistic observation of disconnection-mediated grain boundary migration. *Nat. Commun.* **10**, 156 (2019); Metallic nanocrystals with low-angle grain boundary for controllable plastic reversibility. *Nat. Commun.* (2020, accepted); In situ atomistic observation of grain boundary migration subjected to defect interaction. (under review).

**5:25 AM F.SF08.06.04**

**A Comparative Study of Electromigration in Nanowires with Twin Boundaries** Mohammad Waliullah and Rodrigo Bernal; The University of Texas at Dallas, United States

Electromigration is a critical failure mode of metallic interconnects in the semiconductor industry, and in the emerging fields of flexible and wearable electronics. This failure can be attributed to the diffusion of metallic atoms due to momentum transfer of electrons flowing through the interconnect when a high current density is applied. The diffusion eventually leads to formation of voids and hence a time-dependent increase of electrical resistance of the interconnect. Since it is a diffusion process, the microstructure of the interconnect is one of the controlling factors of electromigration. Twin boundaries, in contrast to grain boundaries, can have the potential to reduce diffusion of atoms and consequentially improve electromigration performance both in electronic chips and in flexible electronics. Note that in nanostructured flexible electronics, it is common to have nanowires with twin boundaries, acting as interconnects. Unfortunately, very few studies have been conducted about the diffusion performance of these interconnects. No literature is available about the collective effect of twin boundaries throughout the interconnect. Moreover, some of the studies said that twinning slows down the diffusion and hence void growth [1], [2] and some said that twinning does not necessarily hinders void growth [3]. Given these conflicting reports, there is clearly a need for a systematic study of diffusion through twinned interconnects.

In this work, we investigated electromigration failure of penta-twinned silver nanowires, with diameters ranging from 50 nm to 80 nm to understand the diffusion process during electromigration of twinned interconnects. Samples were prepared by random deposition of nanowires on a substrate containing gold electrodes fabricated by photolithography. The nanowires were connected with the electrodes by e-beam lithography. The electrodes were then connected to a printed circuit board (PCB) through a wirebonding package. Under a fixed current density and temperature, the resistance was measured using 4-point measurement method so that it can be measured continuously without the influence of contact resistances. The currents were applied in an automated fashion to test a large number of nanowires. The failure criterion was set as 10% increase in resistance which is widely used in the electronics industry. Resistance vs. time plots were obtained in different temperatures, which were fitted to a mathematical model combining the theory of electromigration diffusion flux and the theory of void growth. The fit produces a diffusivity product, independent of temperature, for twin boundaries and the activation energy required for atomic fluxes through twin boundaries. These parameters enable a comparison between the diffusion through twinned interconnects and the published data for diffusion through other microstructures of interconnects currently used in the electronics industry. The results of this study should also allow reliability calculations to be made for novel electronic devices that utilize twinned metallic interconnects, such as wearable electronics that use nanowires as flexible conductors.

#### References

- [1] K. Chen, W. Wu, C. Liao, L. Chen and K. Tu, "Observation of atomic diffusion at twin-modified grain boundaries in copper," *Science*, vol. 321, no. 5892, pp. 1066-1069, 2008.
- [2] H. Chem, C. Huang, C. Wang, W. Wu, C. Liao, L. Chen and K. Tu, "Optimization of the nanotwin- induced zigzag surface of copper by electromigration," *Nanoscale*, vol. 8, no. 5, pp. 2584-2588, 2016.
- [3] Y. Oh, S. Kim, M. Kim, S. Lee and Y. Kim, "Preferred diffusion paths for copper electromigration by in situ transmission electron microscopy," *Ultramicroscopy*, vol. 181, no. Supplement C, pp. 160-164, 2017.

SESSION F.SF08.07: Grain Boundary and Alloying  
On Demand Abstracts Available for Viewing Starting Saturday Morning, November 21, 2020  
F-SF08

#### 5:00 AM F.SF08.07.02

**Grain Boundary Solute Segregation Beyond the Dilute Limit** Malik Wagih and Christopher Schuh; Massachusetts Institute of Technology, United States

Beyond the dilute limit, solute segregation to grain boundaries is known to be concentration dependent. The classic explanation for this effect comes from the Fowler-Guggenheim approach, which solely attributes this dependence to increasing solute-solute interactions at grain boundaries e.g. as solute concentration increases, a strong solute-solute repulsion at grain boundaries will reduce the segregation tendency of additional solute atoms. However, there is a second, less

understood, contribution to this concentration dependence: the gradual exhaustion of favorable segregation sites. Grain boundaries have a complex environment with a variety of site-types available for segregation, and a spectrum of solute binding “segregation” energies. Segregation will first occur at the most favorable sites, forcing the next round of solute atoms to compete for less favorable sites, which reduces their tendency to segregate. In this work, we outline a computational and analytical framework to delineate, for the first time, both contributions to the concentration dependence of solute segregation: 1) the spectrality of site energies in grain boundaries and 2) solute-solute interactions.

#### 5:10 AM F.SF08.07.03

##### **Exploring Grain Boundary Failure in Technically Pure and Micro-Doped Molybdenum via Bending Experiments S.**

**Jakob<sup>1</sup>, T. Weissenböck<sup>1</sup>, A. Hohenwarter<sup>1</sup>, A. Lorich<sup>2</sup>, W. Knabl<sup>2</sup>, R. Pippan<sup>3</sup>, Helmut Clemens<sup>1</sup> and V. Maier-Kiener<sup>1</sup>; <sup>1</sup>Montanuniversitaet Leoben, Austria; <sup>2</sup>Plansee SE, Austria; <sup>3</sup>Austrian Academy of Sciences, Austria**

Interfaces, such as grain boundaries, are crucial for the mechanical properties of metallic materials. Especially in refractory metals like tungsten and molybdenum, grain boundaries are often the weakest link regarding the materials' strength and ductility. These metals are inherently susceptible for intergranular failure and suffer from a limited deformation capability at low temperatures. An advanced approach for the improvement of the interfaces is segregation engineering, e.g. the addition of cohesion enhancing elements segregating to the grain boundaries.

In this work, three-point-bending tests are conducted on recrystallized commercially pure and microdoped molybdenum at temperatures between -40°C and room temperature. The early stages of intergranular crack formation are examined on the specimen surface which is under tension close to the final fracture plane. The occurring grain separations are investigated regarding their distinct features, for instance the crystallography of the adjacent grains or the frequency of open grain boundaries. Doping of molybdenum with elements such as carbon and/or boron is known to suppress intercrystalline failure. Therefore, the presented grain boundary characterization methods will be applied to extract mechanical changes caused by these segregations.

#### SESSION F.SF08.08: Grain Boundary and Dislocation

On Demand Abstracts Available for Viewing Starting Saturday Morning, November 21, 2020  
F-SF08

#### 5:00 AM \*F.SF08.08.01

**Simulations of Grain Boundary-Dislocation Interactions in FCC Nickel Eric R. Homer<sup>1</sup>, David Page<sup>1</sup>, Devin Adams<sup>1</sup>, Ricky Wyman<sup>1</sup>, David Fullwood<sup>1</sup> and Robert Wagoner<sup>2</sup>; <sup>1</sup>Brigham Young University, United States; <sup>2</sup>The Ohio State University, United States**

Grain boundary-dislocation interactions play a crucial role in the deformation behavior of polycrystalline materials. While it is well known that grain boundaries can respond in a variety of ways to imposed deformation, the criteria for each response is not well known. We present work focused on determining the criteria for nucleation of dislocations from a grain boundary as well as efforts to determine the criteria for transmission of dislocations through a grain boundary. The nucleation simulations of a single grain boundary find unique criteria for every slip system, which include non-Schmid effects. The transmission simulations sample a larger population of grain boundaries and find more variation in the observed geometric criteria and resolved shear stresses. We also detail current efforts to examine the evolving criteria as repeated dislocations impact a grain boundary.

#### 5:15 AM F.SF08.08.03

**Detwinning-Governed Size Effect in Zirconia Based Ceramics Haolu Zhang<sup>1</sup>, Justin Jetter<sup>2</sup>, Hanlin Gu<sup>3</sup>, Richard D. James<sup>3</sup>, Eckhard Quandt<sup>2</sup> and Julia R. Greer<sup>1</sup>; <sup>1</sup>California Institute of Technology, United States; <sup>2</sup>University of Kiel, Germany; <sup>3</sup>University of Minnesota, United States**

Unlike dislocation-driven size-effect in single-crystalline materials at the nanoscale, the effect of sample dimensions on the strength of twin-containing materials, especially that of ceramics, still lacks universal understanding. Previous work has demonstrated >5% plastic strain in Zirconia-based ceramics via twinning. Using diffraction methods and *in-situ* nanomechanical experiments, we uncover the microstructure-strength relationship in these twin-containing ionic crystals and reveal contributing factors to the competition between twinning and slip as the major plasticity carrier. The prominent twinning-governed size-dependence was compared to that reported for metals, where the uncanny similarities between these

drastically different material systems shed light on an universal scaling relationship that can be tied back to the well-known “smaller-is-stronger” slip-governed size-effect.

#### 5:25 AM F.SF08.08.04

**Defect-Induced Hall-Petch Softening in Nanocrystalline-Nanotwinned Metals** Frederic Sansoz<sup>1</sup>, Morris Wang<sup>2</sup>, Xing Ke<sup>1</sup>, Jianchao Ye<sup>2</sup>, Zhiliang Pan<sup>1,3</sup>, Jaime Marian<sup>4</sup> and Ryan Ott<sup>5</sup>; <sup>1</sup>University of Vermont, United States; <sup>2</sup>Lawrence Livermore National Laboratory, United States; <sup>3</sup>Guilin University of Electronic Technology, China; <sup>4</sup>University of California, Los Angeles, United States; <sup>5</sup>Ames Laboratory, United States

Strengthening of metals through nanoscale grain boundaries and coherent twin boundaries is manifested by a maximum strength—a phenomenon known as Hall-Petch breakdown. Different softening mechanisms are generally considered to occur for nanocrystalline and nanotwinned materials. Here, we synthesized nanotwinned Ag metals with hardness 3.05 GPa, i.e. 42% higher than the previous record, by segregating trace concentrations of Cu impurity (<1.0 wt.%) to grain boundaries and twin boundary defects. The grain diameter and twin spacings were 45 nm and 3.6 nm, respectively, which is well below the current limits for pure Ag, making it possible to explore plasticity mechanisms in nanostructures that approach those only studied by atomistic simulation. In this presentation, hybrid Monte-Carlo and Molecular-Dynamics simulations reveal three distinct strength regions as twin spacing decreases, delineated by positive Hall-Petch strengthening to grain-boundary-dictated (near-zero Hall-Petch slope) mechanisms, and to softening (negative Hall-Petch slope) induced by twin-boundary defects. Both our experiments and simulations find that an ideal maximum strength is reached for a range of twin spacings below 7 nm in pure and Cu-segregated nanotwinned Ag. We present a continuum theory predicting the softening behavior from kink motion in twin boundaries applicable to pure metals and segregated alloys containing nanoscale twins.

#### 5:35 AM F.SF08.08.05

**Mechanistic Competition Between Grain Boundary and Dislocation Plasticity in Grain Boundary Doped Aluminum Alloys** Wenbo Wang and Jason R. Trelewicz; Stony Brook University, United States

Grain boundary doping has been widely leveraged for the stabilization of nanocrystalline materials. Depending on the dopant species and concentrations, a range of mechanisms have been demonstrated for stabilizing the nanocrystalline grain structure that include thermodynamic contributions often driving alloy design criteria and kinetic pinning forces inhibiting grain boundary motion at elevated temperatures. The presence of deliberately designed solute heterogeneities has implications for the mechanical behavior with a number of studies reporting grain boundary segregated nanocrystalline alloys with significantly enhanced strength relative to their unalloyed counterparts. In this presentation, we use molecular dynamics simulations of nanocrystalline Al containing Mg doped grain boundaries to quantify the mechanisms responsible for this unexpected increase in strength in the context of fundamental changes in grain boundary properties upon alloying. We find that grain boundary microplasticity at low strains is suppressed by solute enrichment producing more stable interfacial configurations, which delays the onset of grain boundary-mediated dislocation slip and promotes an increase in strength. Following the yield point, the interaction of lattice dislocations with grain boundary solute atoms reduces the strain accommodated through dislocation plasticity, thus shifting plastic strain accommodation to the grain boundaries and augmenting flow behavior relative to pure nanocrystalline aluminum.

### SESSION F.SF08.09: Interfaces

On Demand Abstracts Available for Viewing Starting Saturday Morning, November 21, 2020  
F-SF08

#### 5:00 AM F.SF08.09.02

**Multiscale Characterization of Cu/Nb Nanocomposites with Novel 3D Interfaces** Ze Zhou Li<sup>1</sup>, Justin Y. Cheng<sup>1</sup>, Shuozhi Xu<sup>2</sup>, Jonathan Poplawsky<sup>3</sup>, Kevin Baldwin<sup>4</sup>, Irene Beyerlein<sup>2</sup> and Nathan Mara<sup>1</sup>; <sup>1</sup>University of Minnesota, Twin Cities, United States; <sup>2</sup>University of California, Santa Barbara, United States; <sup>3</sup>Oak Ridge National Laboratory, United States; <sup>4</sup>Los Alamos National Laboratory, United States

We present our latest results mainly focusing on elevated temperature microstructural stability of Cu/Nb nanocomposites containing 3-D interfaces. Cu/Nb nanocomposites with atomically sharp 2-D interfaces that exhibit outstanding thermomechanical stability have been examined intensively for over two decades. Their strength is enhanced by defect-interface interactions such that dislocations are blocked from traversing Cu/Nb sharp interfaces. We have investigated the



relationship between atomic structure, mechanical behavior, and thermal stability in Cu/Nb nanocomposites with novel 3-D interfaces. We have shown that the mechanical properties (such as the strength) of Cu/Nb nanocomposites can be further improved by the introduction of chemical, crystallographic, and/or topological variations in all 3 dimensions at heterophase interfaces. Structural characterization employed a combined atom probe tomography (APT) and transmission electron microscopy (TEM) approach. These techniques complement each other very well. While it is possible to observe chemical inhomogeneities in 3-D interfaces with APT, it does not render atomic-resolution information and is prone to magnification artifacts caused by differences in atomic vaporization rates in multi-component samples. However, high-resolution TEM provides atomic-scale information to probe the existence of amorphous regions, metastable alloys, or third-crystal phase precipitates in the 3D interfaces, and help to identify the relevant structure and possible deformation mechanisms. Additionally, we carried out thermal stability studies, incorporating static annealing and differential scanning calorimetry (DSC) scans. Annealed samples were investigated by TEM to uncover the structural evolution associated with thermally perturbed 3D interfaces, while enthalpy changes by DSC analysis were used to identify the onset of thermally-induced structural changes. These correlated studies determined the thermal stability of 3-D interfaces, and how post-deposition annealing can be used to manipulate 3-D interface morphology and possibly enable optimal mechanical performance.

#### SESSION F.SF08.10: Phase Transformation

On Demand Abstracts Available for Viewing Starting Saturday Morning, November 21, 2020  
F-SF08

##### 5:00 AM \*F.SF08.10.01

##### **Structural and Chemical Atomic Complexity of Lattice Defects—From Defect Phase Diagrams to Material**

**Properties** [Sandra Korte-Kerzel](#)<sup>1</sup>, Tilmann Hickel<sup>2</sup>, Liam Huber<sup>2</sup>, Jorg Neugebauer<sup>2</sup>, Dierk R. Raabe<sup>2</sup>, Stefanie Sandlöbes<sup>1</sup> and Mira Todorova<sup>2</sup>; <sup>1</sup>RWTH Aachen University, Germany; <sup>2</sup>Max Planck Institut für Eisenforschung, Germany

The design of new metallic materials is essential in fulfilling the promise of emerging and improving key technologies from efficient energy conversion over lightweight transport to safe medical devices. Over the last decades, two approaches in materials physics have proven immensely successful in the design of new metallic materials: Firstly, thermodynamic descriptions of crystalline phases have enabled materials scientists and engineers to tailor and process alloys to obtain a desired internal structure at the microscale. Secondly, better understanding and manipulation of the crystal defects, which govern the material's strength, formability and corrosion resistance, has led to the development of new alloying and processing concepts that provide some of the most advanced high-performance alloys in operation today. However, to date, these two concepts remain essentially decoupled.

Our vision is to bridge the gap between these existing and powerful approaches by bringing them together in one new conceptual framework, which will consider defects and their thermodynamic stability in a holistic manner. Consequently, a new material design concept originating from the atomic scale will be accessible to materials physicists and engineers which jointly considers the local crystalline structure of defects (structural complexity), the atomic distribution of each element among the different types of phases and defects (chemical complexity) and the stability of defects under the given conditions, such as bulk composition, temperature and applied stress or electrode potential. We will show here, how these can be linked by defect phase diagrams, which will describe the transition between and the coexistence of defect phases. This structural and chemical complexity at the atomic scale naturally exists in all materials. On this basis, we believe that a new physical description of metallic materials will be possible and will provide a powerful toolbox for future design of engineering materials with tailored properties regarding concurrent mechanisms and properties, such as mechanical and corrosion performance of engineering materials.

##### 5:15 AM \*F.SF08.10.02

**Controlling the Structure of Interfaces and Dislocations to Directly Alter Mechanical Response** [Timothy J. Rupert](#);  
University of California, Irvine, United States

Both grain boundaries and dislocations have been recently shown to experience structural transitions between defect states known as complexions. In this talk, we discuss how one can manipulate the natural variations in stress, chemistry, and atomic structure near grain boundaries and dislocations to stabilize these defects and use them as tailorable features. We also demonstrate how different complexions can alter the mechanical properties of materials on the nanoscale. For grain boundary complexions, we focus on nanocrystalline metals, where such features have the largest effect due to the high grain boundary density. We isolate the materials and processing conditions which can cause the strength and ductility of these materials to be

simultaneously augmented, as well as report on small-scale mechanical testing and atomistic modeling techniques to study grain boundary mechanics. For linear complexions, our work uncovers how nanoscale phases restricted to the region along a dislocation line direction can affect plasticity, encompassing both initial yield and subsequent flow. Alloy choice is shown to be very important, as various responses ranging from softening to strong hardening are predicted. As a whole, this work demonstrates that our field is on the precipice of a new age, where defects can be manipulated and designed rather than simply tolerated.

### 5:30 AM \*F.SF08.10.03

**The Coupling of Plasticity and Mass Transfer in Al Alloys** Christopher Hutchinson; Monash University, Australia

High strength Al alloys exploit solid state precipitation to tailor their mechanical response. This precipitation requires two ingredients: a thermodynamic driving force and atomic mobility. For a given alloy chemistry, the heat treatment (precipitation) temperature is chosen as a compromise between having sufficient driving force for precipitation and sufficient atomic mobility so that the precipitation reaction occurs in a reasonable time and results in a 'not too coarse' precipitate distribution. It is this compromise that frames the competition between nucleation, growth and coarsening that constrains the possible precipitate distributions and hence mechanical responses.

This talk demonstrates a new approach that uses small amplitude cyclic plasticity at room temperature as a means of continually pumping vacancies into the system to achieve atomic mobility under conditions of high thermodynamic driving force. The approach is self-regulating (in both space and particle size) and results in extremely fine-scale inhomogeneous solid solutions. Such structures lead to combinations of strength and elongation that exceed those of conventionally precipitate strengthened alloys, without the presence of precipitate free zones.

Since the approach does not use thermal treatments, it somewhat decouples control of the thermodynamic driving force and atomic mobility. This provides a means to fully alter the competition between precipitate nucleation, growth and coarsening and new microstructures, with new combinations of properties are obtained. Examples of both monotonic and cyclic properties are demonstrated.

### 5:45 AM F.SF08.10.04

**Coupling Plasticity and Precipitation in Magnesium Alloys Using Hot Compression** Suhas Eswarappa Prameela<sup>1</sup>, Joey Chen<sup>1</sup>, Yannick Hollenweiger<sup>2</sup>, Steven Lavenstein<sup>1</sup>, Burigede Liu<sup>3</sup>, Roshan Plamthottam<sup>1</sup>, Peng Yi<sup>1</sup>, Kaushik Bhattacharya<sup>3</sup>, Jaafar El-Awady<sup>1</sup>, Michael L. Falk<sup>1</sup>, Dennis Kochmann<sup>2</sup> and Tim Weihs<sup>1</sup>; <sup>1</sup>Johns Hopkins University, United States; <sup>2</sup>ETH Zürich, Switzerland; <sup>3</sup>California Institute of Technology, United States

Simple aging of Magnesium alloys often yields inadequate precipitation hardening response compared to Aluminum alloys. Deformation induced precipitation is one viable strategy to overcome this problem. Using defects, one can severely alter the nucleation and growth of desired second phases and thereby tune their number density, size, shape, orientation, and spatial distribution. Through simple compression experiments on rolled, large-grained Magnesium-Aluminum alloys, we show how solid-solid phase transformations are altered in grain interiors and along grain boundaries after only 10% plastic strain and at four, relatively low temperatures (25C, 100C, 150C, and 200C). With ex situ TEM, we detail the nanoscale Mg<sub>17</sub>Al<sub>12</sub> intermetallic precipitates that form with a fully solutionized Mg-9Al matrix after compression. With crystal plasticity simulations, we link the inhomogeneity of these nano precipitates to the heterogeneity of deformation gradients within the samples. Finally, we explore the underlying mechanisms behind this deformation induced precipitation.

### 5:55 AM F.SF08.10.05

**Precipitate Nucleation Facilitated by Defects During Deformation in Magnesium Alloys** Peng Yi and Michael L. Falk; Johns Hopkins University, United States

Magnesium has great potential as a lightweight material, and there are great interests in designing Mg alloys with enhanced mechanical properties. However, precipitate strengthening in the Mg alloys is much less effective as compared to Al alloys, due to the low number density of the precipitates in the Mg alloys and their highly anisotropic morphology. One promising method to overcome this limitation is dynamic processing, e.g. hot compression and ECAE, which could enhance nanoscale precipitation to achieve a higher precipitation strengthening effect.[1] This enhancement is achieved through precipitate nucleation facilitated by defects generated during deformation, including dislocations and vacancies.

We performed molecular dynamics (MD) simulations on nucleation of gamma-Mg<sub>17</sub>Al<sub>12</sub> precipitates in Mg-Al solid solution. The critical nucleus size, and the Gibbs free energy calculated for solids under non-hydrostatic stress field, were used to

estimate the interfacial free energy using the classical nucleation theory (CNT). Dislocations and vacancy clusters significantly reduce the critical nucleus sizes and the nucleation barriers of the precipitates, mainly by reducing the precipitate-matrix interfacial free energies. A macroscopic strain hardening model to predict the dislocations multiplication for precipitate nucleation enhancement compared favorably with ECAE experiments.[2] Vacancy diffusion and clustering were also simulated using a continuum model parameterized using MD and kinetic Monte Carlo simulations. The temporal and spatial distributions of vacancy clusters are also consistent with the non-uniformity of the precipitate particles observed in dynamic processing experiments.

#### References:

1. Ma, X.L., et al., *Dynamic precipitation and recrystallization in Mg-9wt.%Al during equal-channel angular extrusion: A comparative study to conventional aging*. Acta Materialia, 2019. **172**: p. 185-199.
2. Prameela, S.E., et al., *Deformation assisted nucleation of continuous nanoprecipitates in Mg-Al alloys*. Materialia, 2020. **9**: p. 100583.

SESSION F.SF08.11: Poster Session: Defect-Dominated Plasticity and Chemistry in Metals and Alloys  
On Demand Abstracts Available for Viewing Starting Saturday Morning, November 21, 2020  
5:00 AM - 8:00 AM  
F-SF08

#### F.SF08.11.03

**Computational Study of Radiation Damage in Bilayer Nanostructures** Cameron Hopper<sup>1</sup>, Raghuram Santhanapuram<sup>1</sup>, Elton Chen<sup>2</sup>, Remi Dingreville<sup>2</sup> and Arun K. Nair<sup>1</sup>; <sup>1</sup>University of Arkansas–Fayetteville, United States; <sup>2</sup>Sandia National Laboratories, United States

Neutron and ion radiation damage materials used in radioactive environments, such as nuclear reactors. This type of radiation can cause atoms to be moved around in the atomic structure or removed entirely, causing defects and damage to accumulate in the material, which leads to lower mechanical strength. Since these defects are on the atomic level, it can be hard to detect. We propose examining two different types of interfaces: bilayer interfaces, specifically Silicon-Aluminum and Silicon-Gold, as well as crystalline-amorphous interfaces to investigate whether these types of interfaces can help develop radiation-resistant materials. Using molecular dynamics, we will model these bilayer and amorphous structures as well introduce radiation in the form of Frenkel pairs to our system. To analyze the mechanical strength at different levels of radiation damage, yield surface calculations will be performed by subjecting the samples to biaxial and uniaxial tension and compression tests to determine the yield points. Different defect absorption mechanisms at the interface will also be discussed.

#### F.SF08.11.04

**Late News: Understanding the Interaction Between Grain Boundary Precipitation and Creep Cavitation of Type 316H Stainless Steel During In-Service Aging** Siji He<sup>1</sup>, Hao Shang<sup>1</sup>, Antonio Fernandez-Caballero<sup>2</sup>, Alexander Warren<sup>1</sup>, David Knowles<sup>1</sup>, Peter Flewitt<sup>1</sup> and Tomas Martin<sup>1</sup>; <sup>1</sup>University of Bristol, United Kingdom; <sup>2</sup>University of Oxford, United Kingdom

Creep cavitation is an important degradation mechanism for metallic components used at an elevated temperature. Stress, temperature and microstructure all play a role in the initiation of creep cavities, and the formation mechanism of cavities can depend heavily on local phase and chemistry. In this work, the relationship between microstructural evolution due to long term thermal ageing and creep cavitation is explored in an ex-service AISI type 316H stainless steel sample from an advanced gas-cooled nuclear reactor boiler header after 65,000 hours at 490 to 530°C. The microstructure of the ex-service specimen has been investigated by secondary electron microscopy, focused-ion beam cross sectioning, electron backscatter diffraction and transmission electron microscopy.  $M_{23}C_6$  precipitates,  $\alpha$ -ferrite precipitates and creep cavities are observed at grain boundaries, with increased precipitation and cavitation at random grain boundaries, and an absence of creep cavities at coincidence site lattice (CSL) 3 boundaries. The  $\alpha$ -ferrite precipitates grow during in-service exposure at grain boundaries with a Kurdjumov-Sachs orientation relationship to at least one neighbouring austenite matrix grain. The creep cavities were observed to initiate at the intergranular  $M_{23}C_6$  and  $\alpha$  ferrite precipitates. Based on the orientation relationship of the ferrite precipitates with the austenite matrix, some creep cavities are initiated after the ferrite precipitates have formed. The influence of microstructure changes on creep cavitation of materials during in-service aging and the implications for more

reliable predictions of lifetime for components operating at high temperature are discussed.

## SYMPOSIUM F.X

---

Frontiers of Materials Research  
November 30 - December 4, 2020

---

\* Invited Paper

SESSION F.X.01  
Monday Afternoon, November 30, 2020  
Symposium X

### 4:00 PM \*F.X.01.01

**Efficient Recycling and Regeneration of E-Mobility Components and Materials** [Anke Weidenkaff](#)<sup>1,2</sup>; <sup>1</sup>Fraunhofer Research Institution for Materials Recycling and Resource Strategies IWKS, Germany; <sup>2</sup>Technical University of Darmstadt, Germany

A sustainable future e-mobility requires an efficient circularity of the energy converters with a programmable long lifetime. Electrochemical energy conversion processes in batteries, fuel cells and electrolyzers require full reversibility of local effects, defect formations, phase segregations and redox reactions. Therefore, regenerative or self-repairing materials have to be developed to produce long-lasting devices.

The design of sustainable high performance materials is based on theoretical predictions, life cycle assessment and a profound knowledge on composition-structure-property relationships, defect chemistry, ion mobility assessment and the criticality analysis of applied elements to improve the cycle life of future batteries, fuel cells and electrolyzers.

#### Biography:

Since October 1, 2018, Prof. Dr. Anke Weidenkaff has been head of Fraunhofer IWKS in Hanau and Alzenau. In addition, Anke Weidenkaff is professor at the Technical University of Darmstadt. Her principal areas of research and expertise are materials science and resource strategies, including the development, synthesis and characterization of sustainable materials for energy conversion and storage. Her current work focuses on regenerative, self-healing materials and the development of next-generation process technologies for fast and efficiently closed material cycles. Anke Weidenkaff completed her PhD degree in Chemistry at ETH Zürich in 2000, received the Venia Legendi for Solid State Chemistry and Materials Science from the University of Augsburg in 2006 and became section head at Empa as well as associated professor at the University of Bern, Switzerland. She was chair holder for Materials Chemistry and director of the Institute for Materials Science at the University of Stuttgart from 2013-2018, was president of the European Thermoelectric Society (ETS), elected member of the E-MRS Executive Committee and chair of the E-MRS spring meeting 2019. In 2011, she was awarded with the Kavli Foundation Lectureship prize. She also served on expert panels of the German Science Foundation DFG and on expert panels of the European Research Council (ERC) and is member of the German Advisory Council on Global Change (WBGU). Until present, Anke Weidenkaff published some 250 SCI rated publications on materials research in energy conversion technologies.

SESSION F.X.02  
Wednesday Afternoon, December 2, 2020  
Symposium X

**2:45 PM DANIEL ANDERSON, MASSACHUSETTS INSTITUTE OF TECHNOLOGY**

SESSION F.X.03  
Thursday Afternoon, December 3, 2020  
Symposium X

**1:45 PM \*F.X.03.01**

**Intellectual Property Filing Strategy, Portfolio Management and Licensing of Material-Related Technologies** Frederick Mau; Toyota Motor North America, Inc., United States

A key understanding of intellectual property strategies is essential to build meaningful intellectual property portfolios for material-related technologies. Intellectual property portfolios typically consist of a combination of both patents and trade secret/know-how information. Unlike other technologies, patent filings for material-related technologies such as batteries, catalysts and functionalized materials require additional data, description and documentation to ensure broad protection of the underlying technology. While patent application filings for mechanical, electrical and software technologies do require a detailed description of the structure and operation of the technology to enable recreation by one of skill in the art, material-related technologies additionally require demonstration of a strong understanding of the underlying mechanism behind the invention coupled with strong support of laboratory data. Any shortcoming in this area will result in narrow protection covering only the specific aspects of the invention supported by the data provided. This presentation will focus on best practices to ensure proper intellectual property protection for material-related technologies. Additionally, we will discuss how to build intellectual property portfolios around fundamental technologies with an eye toward protection of commercial interests and licensing.

**Biography**

Mau has the position of Intellectual Property Counsel with Toyota Motor North America, Inc. His job responsibilities include all patent filing, prosecution and patent portfolio management (domestic & foreign) for all Advanced Research, Vehicle Engineering and Manufacturing business units within North America. Furthermore, Mau handles and/or advises on many other Intellectual property-related matters, which may include patent disputes, patent clearance studies, open source software, intellectual property matters relating to contracts, business establishment and support of IP lobbying efforts for Toyota Government Affairs. In addition to his role as Intellectual Property Counsel for TMNA, Mau also oversees the licensing activity for Toyota IP Solutions as Director of Patent Licensing.

SESSION F.X.04  
Friday Morning, December 4, 2020  
Symposium X

**10:15 AM \*F.X.04.01**

**Extreme Wave Interactions in Metamaterials with Broken Symmetries** Andrea Alù; The City University of New York, United States

In this talk, I discuss our recent discoveries in electromagnetics, nano-optics and acoustics showing how suitably tailored *meta-atoms* and their arrangements open exciting avenues to enable extreme phenomena and new technology based on light, radio-waves and sound. In particular, I discuss venues in which broken symmetries play a pivotal role in establishing emerging phenomena in metamaterials, from geometrical asymmetries and generalized forms of chirality, to time-reversal symmetry breaking and parity-time symmetry. Our work shows how symmetry concepts offer interesting tools to break Lorentz reciprocity and realize isolation without the need of magnetic bias, based on broken time-reversal symmetry induced by mechanical motion, spatio-temporal modulation and/or nonlinearities. Broken symmetries in space and space-time open

also the opportunity to induce topological order in metamaterials. The opportunities offered by hybrid metamaterials combining classical photonic material platforms with 2D and quantum materials characterized by exotic lattice symmetries will also be discussed. Finally, the role of parity-time symmetry and non-Hermitian physics in enabling broadband wave manipulations beyond the limits of passive systems will be outlined. In the talk, I will outline the impact of these concepts from basic science to practical technology, from classical waves to quantum phenomena.

Biography:

Andrea Alù is the founding director of the Photonics Initiative at the CUNY Advanced Science Research Center, Einstein Professor of Physics at the CUNY Graduate Center, and Professor of Electrical Engineering at The City College of New York. He is affiliated with the Wireless Networking and Communications Group and the Applied Research Laboratories, both based at the University of Texas at Austin, where he is a Senior Research Scientist and Adjunct Professor. His research interests span over a broad range of technical areas, including applied electromagnetics, nano-optics and nanophotonics, microwave, THz, infrared, optical and acoustic metamaterials and metasurfaces, plasmonics, nonlinearities and nonreciprocity, cloaking and scattering, acoustics, optical nanocircuits and nanoantennas. Since 2014, Dr. Alù has been also serving as Chief Technology Officer of Silicon Audio RF Circulator, a company that holds the exclusive license of a few inventions stemming from Alù's lab around magnetic-free technology for non-reciprocal devices.

## SYMPOSIUM F.IMRC

---

International Materials Research Congress (IMRC) Winners  
November 21 - November 21, 2020

---

\* Invited Paper

SESSION F.IMRC: Poster Session: International Materials Research Congress (IMRC) Winners  
On Demand Abstracts Available for Viewing Starting Saturday Morning, November 21, 2020  
5:00 AM - 7:00 AM  
On Demand

### F.IMRC.01

**High Open-Circuit Voltage ( $V_{OC}$ ) in Dye-Sensitized Solar Cells (DSSC) by the Incorporation of ZnO/Au Nanoflowers into  $TiO_2$  Photoanodes** Susana Borbón; Universidad Autónoma de Nuevo León, UANL, Mexico

Dye-sensitized solar cells (DSSCs) are a promising alternative to the currently commercialized photovoltaic devices; they are semi-transparent, can be assembled on flexible substrates and have a good performance even under diffuse light.

Furthermore, the fabrication process is simple, and the materials used are low-cost, making it a potentially economic technology. The most used semiconductor oxides in DSSCs are  $TiO_2$  and ZnO. Both have a wide band-gap, are non-toxic, abundant and can be synthesized in varied morphologies; however, ZnO has a higher electron mobility. Despite its superior properties, ZnO DSSC does not surpass the efficiency of those composed of  $TiO_2$ . Therefore, it is desirable to fuse the properties of both semiconductors to obtain superior devices.

In this work we report on the enhancement of the open-circuit voltage ( $V_{OC}$ ) of about 100 mV of a DSSC with an electrode composed of  $TiO_2$  and ZnO nanoflowers. The proportion of ZnO nanoflowers was varied from 5, 10 to 15%, being the rest  $TiO_2$ . Moreover, to increase the short-circuit current ( $J_{SC}$ ) we incorporated Au nanoparticles to the most efficient  $TiO_2/ZnO$  composition. The addition of the Au nanoparticles was achieved by decoration of the ZnO nanoflowers by a chemical reduction process in three different proportions. The ZnO/Au nanoflowers were characterized by field-emission scanning electron microscopy (FE-SEM), energy-dispersive spectroscopy (EDS) and inductively-coupled plasma optical emission spectroscopy (ICP-OES). The DSSCs were characterized by measuring the current-voltage (I-V) curves, electrochemical

impedance (EIS) and intensity modulated photovoltage and photocurrent spectroscopies (IMVS/IMPS). The results demonstrate that the coupling of TiO<sub>2</sub> and ZnO increases the recombination resistance ( $R_{CT}$ ) and the electron lifetime ( $t_{1/2}$ ) due to the improved charge carrier separation and electron-hole transfer, resulting in a larger  $V_{OC}$ . The incorporation of Au nanoparticles showed a beneficial effect on the  $J_{SC}$  due to its photocharging effect, especially for low Au loading. The most efficient DSSC consisted of a photoanode with 5% of ZnO nanoflowers decorated with 418 ppm of Au nanoparticles, and achieved an efficiency of 2.79% with a  $V_{OC}$  of 886 mV and a  $J_{SC}$  of 4.55 mAcm<sup>-2</sup>.

### F.IMRC.02

#### **Evolution of Phase Transition H<sub>2</sub>Ti<sub>3</sub>O<sub>7</sub>-Anatase and Its Effect on Physicochemical Adsorption and Photocatalytic Degradation** Facundo Ruiz and Ana Laura Ruiz Castillo; Universidad Autónoma de San Luis Potosí, UASLP, Mexico

Titanate nanotubes (NTs) were synthesized by the hydrothermal method and later calcined at temperatures between 100 – 500 °C. The calcined NTs were characterized and evaluated for the physicochemical adsorption of safranin dye and photocatalytic degradation of caffeine. The materials calcined at low temperatures possess a tubular structure and H<sub>2</sub>Ti<sub>3</sub>O<sub>7</sub> crystalline phase, which is transformed into anatase nanoparticles at 400°C. The NTs treated at 100 °C showed the highest adsorption capacity (94 %). Safranin is adsorbed through an ion-exchange mechanism, following a Langmuir isotherm model and a pseudo-second-order kinetic model. While NTs calcined at lower temperatures are better for adsorption, the photocatalytic degradation of caffeine increased in samples calcined at higher temperatures with a maximum removal of 72%. The photocatalytic behavior of the NT samples confirms that the crystalline anatase structure in conjunction with structural OH groups enhanced the photocatalytic activity. The addition of isopropanol as a scavenger demonstrated the important role of the •OH radicals in the photocatalytic process. NTs calcined at 300 °C were efficient for both adsorption and photocatalytic processes. Due to its efficiency, this sample was reused after dye adsorption for the photocatalytic degradation of caffeine under visible light due to its enhanced absorbance in the visible region. This research work demonstrates the potential of NTs for wastewater purification.

### F.IMRC.03

**Change in the Rectification Ratio in Metal- ZnO:Ti Thin Structures at Low Magnetic Field** Lucía Ivonne Juárez Amador<sup>1</sup>, Miguel Galván Arellano<sup>2</sup>, Karen Ailed Neri Espinoza<sup>3</sup>, José Alberto Andraca Adame<sup>4</sup>, Gabriel Romero Paredes<sup>2</sup> and Ramón Peña Sierra<sup>2</sup>; <sup>1</sup>Programa de Doctorado en Nanociencias y Nanotecnología Centro de Investigación y de Estudios Avanzados del IPN - CINVESTAV, Mexico; <sup>2</sup>CINVESTAV- IPN, Mexico; <sup>3</sup>Instituto Politécnico Nacional, IPN, Mexico; <sup>4</sup>Instituto Politécnico Nacional, UPIIH, Mexico

Magnetoresistance and rectification are two fundamental physical properties in magneto- electronics devices (MED) fabricated with diluted magnetic oxide semiconductors (DMOs). The MED have great potential in the new generation magneto- optical devices based on DMOs as ZnO or SnO<sub>2</sub>. This study was directed to analyse the magnetoresistance effects in metal- DMOs structures. The DMOs films are titanium (Ti) doped Zinc oxide (TZO) grown by Magnetron Sputtering technique. TZO thin films were obtained at room temperature using co- sputtering process for both Ni and ZnO targets was performed using two separate power sources. The DC power of the Ti target material was 5, 10, 15 and 25 W, respectively while the radio frequency (RF) power of the Zinc Oxide (ZnO) target material was set to 150 W. The structural characteristics of the films can be further controlled with additional annealing stages at 250 and, 350 °C in N<sub>2</sub> atmosphere by 30 min until the samples reach the usual electrical insulating character of separated ZnO films. The required annealing period to get insulating layers varies with the thickness of the Ti ion film and the film nanostructure. The ZnO:Ti ion films are formed by nanocrystallites of ~ 20 nm in size with (002) and (004) orientation and are stressed along the c- parameter according to X- ray diffraction measurements. The electrical resistivity of the films was varied from 7.69 to 392 Ω-cm, the electron concentration from 1020 to 1016 cm<sup>-3</sup>, for a range of carrier mobility from 1.57 to 14 cm<sup>2</sup>/V- s. The band gap energy of the films was of ~ 3.3 eV with transmittance of ~90% to ~95 % of in the visible region. The changes observed in the rectification ratio are attributed to the titanium doping by metal transition character. Change in the structure saturation current were also observed, this change can be explained by the dangling bonds at the metal- DMO interface. The I- V curves present the rectifying effect due to the intrinsic space- charge region in the junction Metal- TZO. For the zero- magnetic field I- V curve, the current is about 1.51 x 10<sup>-9</sup> A at 4.38 V. On the other hand, when H=0.55T, at the same voltage bias 4.38 V the current is shifted down- ward to 3.06 x 10<sup>-10</sup> A.